JOURNAL OF AGRICULTURAL AND FOOD CHEMISTRY

Article

pubs.acs.org/JAFC

Comparative Analysis of Phenolic Content and Profile, Antioxidant Capacity, and Anti-inflammatory Bioactivity in Wild Alaskan and Commercial *Vaccinium* Berries

Mary H. Grace,[†] Debora Esposito,[†] Kriya L. Dunlap,[§] and Mary Ann Lila*[,†]

[†]Plants for Human Health Institute, Food Bioprocessing and Nutrition Sciences Department, North Carolina State University, North Carolina Research Campus, 600 Laureate Way, Kannapolis, North Carolina 28081, United States

[§]Department of Chemistry and Biochemistry, University of Alaska—Fairbanks, 900 Yukon Drive, Fairbanks, Alaska 99775, United States

ABSTRACT: Wild Alaskan *Vaccinium* berries, *V. vitis-idaea* (lowbush cranberry) and *V. uliginosum* (bog blueberry), were investigated in parallel with their commercial berry counterparts, *V. macrocarpon* (cranberry) and *V. angustifolium* (lowbush blueberry). Lowbush cranberry accumulated about twice the total phenolics (624.4 mg/100 g FW) and proanthocyanidins (278.8 mg/100 g) content as commercial cranberries, but A-type proanthocyanidins were more prevalent in the latter. Bog blueberry anthocyanin and total phenolic contents of 220 and 504.5 mg/100 g, respectively, significantly exceeded those of the lowbush blueberry. Chlorogenic acid, however, was quite high in lowbush blueberry (83.1 mg/100 g), but undetected in bog blueberry, and the proanthocyanidins of lowbush blueberry had significantly higher levels of polymerization. Antioxidant capacity (DPPH, APTS, and FRAP) correlated with phenolic content for each berry. A polyphenol-rich fraction from lowbush cranberry exhibited dose-dependent inhibition of LPS-elicited induction of IL-1β in RAW 264.7 cells, indicative of strong anti-inflammatory activity. These results corroborate the historic use of wild Alaskan berries as medicinally important foods in Alaska Native communities.

KEYWORDS: *Vaccinium vitis-idaea, V. uliginosum, V. macrocarpon, V. angustifolium, phenolics, antioxidant, anti-inflammatory*

INTRODUCTION

Epidemiological studies have shown that increased consumption of fruits and vegetables correlates with improved cardiovascular health as well as reduced risk of cancer, stroke, degenerative diseases, loss of functionality associated with aging, and more.[1−3] Whereas fruits and vegetables are rich sources of vitamins and minerals, recent attention in biomedical research has focused heavily on phenolic components, flavonoids in particular, for their antioxidant, anti-inflammatory, and other health-relevant bioactivities.[4−6] Although not fully understood, these health-promoting effects have been mainly related to interactions between the phenolic compounds and several key enzymes, signaling cascades involving cytokines and regulatory transcription factors, and antioxidant systems.[7]

Many types of wild berries are indigenous to Alaska, and seasonal harvests are major community events, especially in rural Alaska Native villages. Wild Alaskan berries are delicious fresh, frozen, dried, or turned into any number of tasty creations: jams, muffins, fruit leathers, sauces, and agutuk (otherwise known as Alaskan/Eskimo ice cream, made from seal oil and berries).[8] People commonly harvest berries of the *Vaccinium* genus, blueberries, lowbush cranberries, and other wild berries, when the berries are ripe in July, August, and September and use them for both food and medicine. The summer season is short, and the day length of summer is dramatically longer than that found at lower latitudes, which can have a profound impact on the phytochemical composition and content of the fruits.[9]

The genus *Vaccinium* includes several popular commercial berry species, including lowbush, highbush, and rabbiteye blueberries, domesticated cranberries, and lingonberries. In general, *Vaccinium* berry fruits are widely renowned for their health benefits, reportedly due to their high concentrations of phenolic compounds and/or the presence of specific, particularly potent polyphenolic compounds that may interact (additively or synergistically) to ameliorate human health conditions.[10]

The influence of the growing environment on both phenolic concentrations and profiles has been previously described,[11,12] which could condition the health-relevant potency of berries from wild and cultivated regimes. However, the composition and merits of most wild *Vaccinium* selections have not been well documented. In this study, we comparatively examined two wild Alaskan berry species, lowbush cranberry (*Vaccinium vitis-idaea*, also known as lingonberry or cowberry in many other parts of the world) and bog blueberry (*Vaccinium uliginosum*, also known as alpine blueberry or bilberry), and their corresponding commercial counterparts, American cranberry (*Vaccinium macrocarpon*) and lowbush blueberry (*Vaccinium angustifolium*), because considerable baseline data have already been generated for the latter two commercially cultivated species. *V. vitis-idaea* and *V. uliginosum* are among the most significant wild berries in Nordic countries, Russia, and other circumpolar regions, and their phenolic profiles have been

Special Issue: 2013 Berry Health Benefits Symposium

Received: August 27, 2013
Revised: November 11, 2013
Accepted: November 12, 2013
Published: November 12, 2013

ACS Publications © 2013 American Chemical Society

investigated previously.[13,14] However, only scant analysis has been conducted to determine phytochemical profiles or anti-inflammatory bioactivity of these species in Alaska. Streamlined and sophisticated analytical protocols were applied to rigorously establish and cross-compare the phytochemical profiles and antioxidant capacities of these berries to provide information on their potential suitability for different applications. Also, the effect of berry extracts on the expression of four well-known genetic biomarkers of inflammation was investigated in vitro in a lipopolysaccharide-stimulated murine RAW 264.7 macrophage model.

MATERIALS AND METHODS

Reagents and Materials. Reference compounds procyanidin A2 (PAC-A2), procyanidin B2 (PAC-B2), catechin, and epicatechin were purchased from Chromadex (Irvine, CA, USA). 4-Dimethylamino-cinnamaldehyde (DMAC), Folin−Ciocalteu reagent, 2,2-diphenyl-1-picrylhydrazyl (DPPH), 6-hydroxy-2,5,7,8-tetramethylchroman-2-carboxylic acid (Trolox), 2,2′-azinobis(3-ethylbenzothiazoline-6-sulfonic acid) diammonium salt (ABTS), 2,2′-azobis(2-methylpropionamidine) dihydrochloride (AAPH), phosphate buffer, 2,4,6-tri(2-pyridyl)-*s*-triazine (TPTZ), iron(III) chloride hexahydrate, and fluorescein sodium salt (FL) were purchased from Sigma-Aldrich Inc. (St. Louis, MO, USA). All organic solvents were of HPLC grade and obtained from VWR International (Suwanee, GA, USA).

Berry Sources. Wild Alaskan lowbush cranberry (*V. vitis-idaea* L.) and bog blueberry (*V. uliginosum* L.) were handpicked when fully ripe from the vicinity of Fairbanks, AK, USA. Lowbush cranberry was collected at latitude 64.8 N, longitude 147.7 W, in September 2012. Bog blueberry was collected at latitude 65.5 N, longitude 145.4 W, in July 2012. A total of 3 kg of fruit was collected from each species in the growing region over a 1 week period. Berries were immediately stored at −80 °C before freeze-drying. Freeze-dried berries were ground before sampling and analysis. A composite sample of commercially grown lowbush blueberries (*V. angustifolium* Aiton) was obtained from the Wild Blueberry Association of North America (Old Town, ME, USA). The blueberries were a composite of fruits from all major growing sites in Canada (Prince Edward Island, New Brunswick, Nova Scotia, Quebec) and the United States (Maine). The composite was made in the fall 2012, frozen by Cherryfield Foods, Inc., at −15 °C (Cherryfield, ME, USA), and subsequently stored at −80 °C. American cranberries (*V. macrocarpon* Ait) were obtained from The Cranberry Network, LLC (Wisconsin Rapids, WI, USA) in fall 2012 and stored at −80 °C. Commercial berries (5 kg each) were freeze-dried and then ground prior to sampling and extraction. Dry matter (DM) percentage was calculated on the basis of the difference between berry fresh weight (FW) and the weight after freeze-drying (FD). All extractions were performed on the freeze-dried material, and results were calculated on a fresh weight basis by considering the water content in each berry.

Extraction and Polyphenol Enrichment. Freeze-dried ground berry fruits (2.5 g × 3 replicates) were blended (Waring, Inc., Torrington, CT, USA) with 30 mL of acidified 70% aqueous methanol (0.5% acetic acid) for 2 min. The mixture was centrifuged (Sorvall RC-6 plus, Asheville, NC, USA) for 20 min at 4000 rpm, and the supernatant was transferred to 100 mL volumetric flasks. The extraction of the pellet was repeated two more times and the combined extracts were brought to a final volume of 100 mL. Samples of crude extracts (CE) were filtered, using a 0.20 μm PTFE syringe filter (Fisher Scientific, Pittsburgh, PA, USA), before analysis using HPLC, LC-MS, and MS/MS, and antioxidant capacity bioassays. An aliquot of the crude extract (2 mL) was dried down completely before testing for anti-inflammatory activity, as described below. The crude extract (50 mL) was evaporated to about 2 mL before loading onto two SPE cartridges (Supelclean LC-18, 12 mL) preconditioned with methanol and then acidified water (0.01% HCl). Each cartridge was washed with 50 mL of acidified water before elution with 100% methanol until all color eluted off. The methanol extract was evaporated and freeze-dried to get the polyphenol-rich fraction (PRE), which was subjected to HPLC, LC-MS analyses, and anti-inflammatory bioassays.

Determination of Total Phenolics, Anthocyanins, and Proanthocyanidins. The CE from each berry was diluted to appropriate concentrations for analysis. Total phenolics (TP) were determined with Folin−Ciocalteu reagent according to the method of Singleton.[15] Concentrations were expressed as milligrams per liter gallic acid equivalents based on a created gallic acid standard curve. Total monomeric anthocyanin (ANC) content was measured by using the pH differential spectrophotometric method,[16] using a Shimadzu UV-2450 (Tokyo, Japan) spectrophotometer. ANC concentration was calculated as milligrams per liter cyanidin 3-*O*-glucoside equivalents. Total proanthocyanidins (PAC) concentration was determined colorimetrically using the DMAC method in a 96-well plate as previously described.[17] A series of dilutions of standard procyanidin A2 dimer were prepared in 80% ethanol ranging from 1 to 100 μg/mL. Blank, standard, and diluted samples were analyzed in triplicates. The plate reader protocol was set to read the absorbance (640 nm) of each well in the plate every minute for 30 min (SpectraMax M3, Sunnyvale, CA, USA). Concentration of PAC in the solution was expressed as milligrams per liter procyanidin A2 equivalent.

Reversed Phase HPLC and LC-ESI-MS Analysis. HPLC analyses for anthocyanins were conducted using an Agilent 1200 HPLC (Agilent Technologies, Santa Clara, CA, USA), according to our previously published protocol.[18] Quantification of anthocyanins was performed using the peak areas recorded at 520 nm to construct the calibration curve for cyanidin-3-*O*-glucoside.

HPLC for chlorogenic acid was performed using a Phenomenex Synergi 4 μm Hydro-RP 80A column (250 mm × 4.6 mm × 5 μm; Torrance, CA, USA). The mobile phase consisted of 2% acetic acid in distilled H_2O (solvent A) and 0.5% acetic acid in 50% acetonitrile in water (solvent B). The flow rate was set at 1 mL/min with a step gradient of 10, 15, 25, 55, 100, and 10% of solvent B at 0, 13, 20, 50, 54, and 60 min, respectively. Quantification was performed from the peak areas recorded at 280 nm to the calibration curve obtained with reference standard.

LC-MS analysis was performed using a Shimadzu LC-MS-IT-TOF instrument equipped with a Prominence HPLC system. The LC separation was performed using a Shim-pack XR-ODS column (50 mm × 3.0 mm × 2.2 μm) at 40 °C with a binary solvent system composed of 0.1% formic acid in water (A) and methanol (B). Compounds were eluted into the ion source at a flow rate of 0.35 mL/min with a step gradient of B of 5−8% (0−5 min), 8−14% (10 min), 14% (15 min), 20% (25 min), 25% (85 min), 5% (35 min), and 5% (40 min). Ionization was performed using an ESI source in the negative ion mode. Compounds were characterized and identified by their MS, MS/MS spectra, and LC retention times and by comparison with available reference samples and our previous analyses.[18,19]

Normal Phase HPLC−Fluorescence Analysis of Proanthocyanidins. HPLC analyses were conducted using an Agilent 1200 HPLC with fluorescence detector (FLD) and photodiode array detector (DAD). Proanthocyanidin separation was performed according to the method of Wallace and Giusti,[20] using a Develosil Diol column, 250 mm × 4.6 mm × 5 μm (Phenomenex). PAC were identified by comparison with available standards, our previous analyses,[18] reported literature,[20] and LC-ESI-MS. Quantification of proanthocyanidin was calculated using peak areas and a calibration curve for PAC-A2, and amounts were expressed as PAC-A2 equivalents.

Free Radical Scavenging (DPPH Assay). The radical scavenging activity was measured using the stable DPPH and Trolox as reference substances.[21] Samples were diluted 10 times with 80% methanol before mixing with the reagent. An aliquot (100 μL) of each sample was pipetted into 3.9 mL of DPPH solution (0.08 M in 95% ethanol) to initiate the reaction. After a reaction time of 3 h at ambient temperature, the reaction had reached completion. The decrease in absorbance of DPPH free radicals was read at 515 nm against ethanol as a blank using a Shimadzu UV-2450 spectrophotometer. Trolox (0, 100, 200, 300, 400, and 500 μM) was used as a standard antioxidant

Table 1. Polyphenol Content, Radical Scavenging Capacity (DPPH, ABTS), and Ferric Reducing Capacity (FRAP) of Wild Alaskan and Commercial *Vaccinium* Species[a]

berry fruit	dry matter (%)	ANC[b] (mg/100 g FW)	PAC[c] (mg/100 g FW)	ChA[d] (mg/100 g FW)	TP[e] (mg/100 g FW)	DPPH (μM TE/g FW)	ABTS (μM TE/g FW)	FRAP (μM $FeSO_4$/g FW)
cranberry (*V. macrocarpon*)	24.6 ± 0.5^A	76.6 ± 3.2^C	132.7 ± 5.7^B	12.2 ± 0.2^C	350.5 ± 16.1^C	37.8 ± 0.1^B	35.8 ± 2.5^C	57.9 ± 4.1^D
lowbush cranberry[f] (*V. vitis-idaea*)	21.3 ± 0.5^B	194.6 ± 6.4^B	278.8 ± 19.6^A	18.3 ± 0.9^B	624.4 ± 34.2^A	51.3 ± 2.2^A	69.3 ± 2.2^A	122.2 ± 4.6^A
lowbush blueberry (*V. angustifolium*)	16.0 ± 0.1^D	189.8 ± 8.0^B	71.2 ± 3.3^C	83.1 ± 1.0^A	371.3 ± 2.2^C	39.8 ± 1.2^B	40.1 ± 2.1^C	68.5 ± 4.3^C
bog blueberry[f] (*V. uliginosum*)	18.4 ± 0.3^C	220.0 ± 11.9^A	85.5 ± 5.9^C	ND[g]	504.5 ± 32.2^B	46.5 ± 4.5^A	51.4 ± 0.1^B	100.3 ± 2.1^B

[a]Means with different letters within the same column are significantly different at $p < 0.05$. [b]ANC, anthocyanins, quantified by pH differential assay as cyanidin-3-glucoside. [c]PAC, proanthocyanidins, quantified by DMAC assay as procyanidin A2. [d]ChA, chlorogenic acid, quantified by HPLC using reference standard. [e]TP, total phenolics, quantified by Folin−Ciocalteu assay as gallic acid equivalent. [f]Wild species collected from Alaska. [g] ND, not detected.

compound. Analysis was performed in triplicate for each sample and each concentration of standard. The antioxidant activity was reported in micromoles of Trolox equivalents per gram fresh weight (μmol TE/g FW).

Free Radical Scavenging (ABTS Assay). The ABTS assay was performed as described by Re[22] and is based on the reduction of $ABTS^{\bullet+}$ radicals by antioxidants in the berry extracts. ABTS radical cation ($ABTS^{\bullet+}$) was produced by reacting ABTS solution (7 mM) with 2.45 mM potassium persulfate (final concentration) and allowing the mixture to stand in the dark at room temperature for 12−16 h before use. For the assay, the $ABTS^{\bullet+}$ solution was diluted in deionized water or ethanol to an absorbance of 0.7 (±0.02) at 734 nm. After the addition of 100 μL of berry extract solutions to 3 mL of $ABTS^{\bullet+}$ solution, the absorbance reading was taken at 30 °C 10 min after initial mixing (A_E). All determinations were carried out in triplicate. The antioxidant activity was reported in micromoles of Trolox equivalents per gram fresh weight (μmol TE/g FW).

Ferric Reducing Antioxidant Power (FRAP) Assay. This method is based on the reduction, at low pH, of a colorless ferric complex (Fe^{3+}−tripyridyltriazine) to a blue-colored ferrous complex (Fe^{2+}−tripyridyltriazine) by the action of electron-donating antioxidants. The ferric reducing power of berry extracts was performed in a 96-well microplate using the FRAP assay[23] with minor modifications. The working FRAP reagent was prepared daily by mixing 10 volumes of 30 mM acetate buffer, pH 3.6, with 1 volume of 10 mM TPTZ in 40 mM hydrochloric acid and with 1 volume of 20 mM $FeCl_3$. A standard curve was prepared using various concentrations of $FeSO_4 \cdot 7H_2O$. All solutions were used on the day of preparation. FRAP solution (175 μL) freshly prepared and warmed at 37 °C was added to three replicates of each sample (25 μL), whereas the same volume of acetate buffer was added to the fourth one (blank). The reaction mixture was incubated for 30 min at 37 °C, and then the absorbance was measured at 593 nm. The absorbance of the blank was subtracted from the absorbance of the samples. In this assay, the reducing capacity of the extracts tested was calculated with reference to the reaction signal given by a Fe^{2+} solution. FRAP values were expressed as micromoles of Fe^{2+} per gram of fresh berry.

Macrophage Cell Culture. The mouse macrophage cell line RAW 264.7 (ATCC TIB-71, obtained from American Type Culture Collection, Livingstone, MT, USA) was maintained in Dulbecco's modified Eagle's medium (DMEM, Life Technologies, Grand Island, NY, USA), supplemented with 100 IU/mL penicillin/100 μg/mL streptomycin (Fisher) and 10% fetal bovine serum (Life Technologies) at a density not exceeding 5×10^5 cells/mL and maintained at 37 °C in a humidified incubator with 5% CO_2.

Anti-inflammatory in Vitro Assay. Cells were subcultured by TrypLE (Life Technologies) when dishes reached up to 90% confluence with a 1:5 ratio in fresh medium. Cells were seeded in 24-well plates (5×10^5 cells/well) 24 h prior to treatment. The cells were then treated in triplicates with berry extracts at predetermined doses for 1 h before elicitation with LPS at 1 μg/mL for an additional 4 h. For every experiment, one positive control (cells treated with dexamethasone (Dex) at 10 μM) and one negative control (cells treatment with vehicle) were included. Three replicates were made for both the treatments and the controls. At the end of the treatment period, cells were harvested in TRIzol reagent (Life Technologies) for subsequent cellular RNA extraction.

Cell Viability Assay and Dose Range Determination. RAW 264.7 cells were seeded in a 96-well plate for the viability assay. Cell viability was measured by the 3-(4,5-dimethylthiazol-2-yl)-2,5-diphenyltetrazolium bromide (MTT) assay[24] in triplicate and quantified spectrophotometrically at 550 nm using a SynergyH1 microplater reader (BioTek). The concentrations of test reagents that showed no changes in cell viability compared with that vehicle (ethanol) were selected for further studies.

Total RNA Extraction, Purification, and cDNA Synthesis. The total RNA was isolated from RAW macrophages using TRIzol reagent (Life Technologies) following the manufacturer's instructions. RNA was quantified spectrophotometrically using the SynergyH1/Take 3 (BioTek, Winooski, VT, USA). The cDNAs were synthesized using 2 μg of RNA for each sample using commercially available high-capacity cDNA Reverse Transcription kit (Life Technologies), following the manufacturer's protocol on an ABI GeneAMP 9700 (Life Technologies).

Quantitative PCR Analysis. The resulting cDNA was amplified by real-time quantitative PCR using SYBR green PCR Master Mix (Life Technologies). To avoid interference due to genomic DNA contamination, only intron-overlapping primers were selected using Primer Express version 2.0 software (Applied Biosystems, Foster City, CA, USA) as follows: β-actin, forward primer, 5′-AAC CGT GAA AAG ATG ACC CAG AT-3′, reverse primer, 5′-CAC AGC CTG GAT GGC TAC GT-3′; COX2, forward primer, 5′-TGG TGC CTG GTC TGA TGA TG-3′, reverse primer, 5′-GTG GTA ACC GCT CAG GTG TTG-3′; iNOS, forward primer, 5′-CCC TCC TGA TCT TGT GTT GGA-3′, reverse primer, 5′-TCA ACC CGA GCT CCT GGA A-3′; IL6, forward primer, 5′-TAG TCC TTC CTA CCC CAA TTT CC-3′, reverse primer, 5′-TTG GTC CTT AGC CAC TCC TTC-3′; and IL1β, forward primer, 5′-CAA CCA ACA AGT GAT ATT CTC CAT G-3′, reverse primer, 5′-GAT CCA CAC TCT CCA GCT GCA-3′. Quantitative PCR (qPCR) amplifications were performed on an ABI 7500 Fast real time PCR (Life Technologies) using 1 cycle at 50 °C for 2 min and 1 cycle of 95 °C for 10 min, followed by 40 cycles of 15 s at 95 °C and 1 min at 60 °C. The dissociation curve was completed with 1 cycle of 1 min at 95 °C, 30 s at 55 °C, and 30 s at 95 °C. mRNA expression was analyzed using the ΔΔCT method and normalized with respect to the expression of the β-actin housekeeping genes using 7500 Fast System SDS software v 1.3.0 (Life Technologies). A value of <1.0 indicates transcriptional down-regulation (inhibition of gene expression) compared with LPS, which shows maximum genetic induction (1.0). Therefore, lower values indicate greater anti-inflammatory activity. Values of >1.0 imply overexpression of the particular gene in excess of LPS stimulation. Amplification of specific transcripts was further confirmed by obtaining melting curve profiles. A 2-fold change in gene expression was

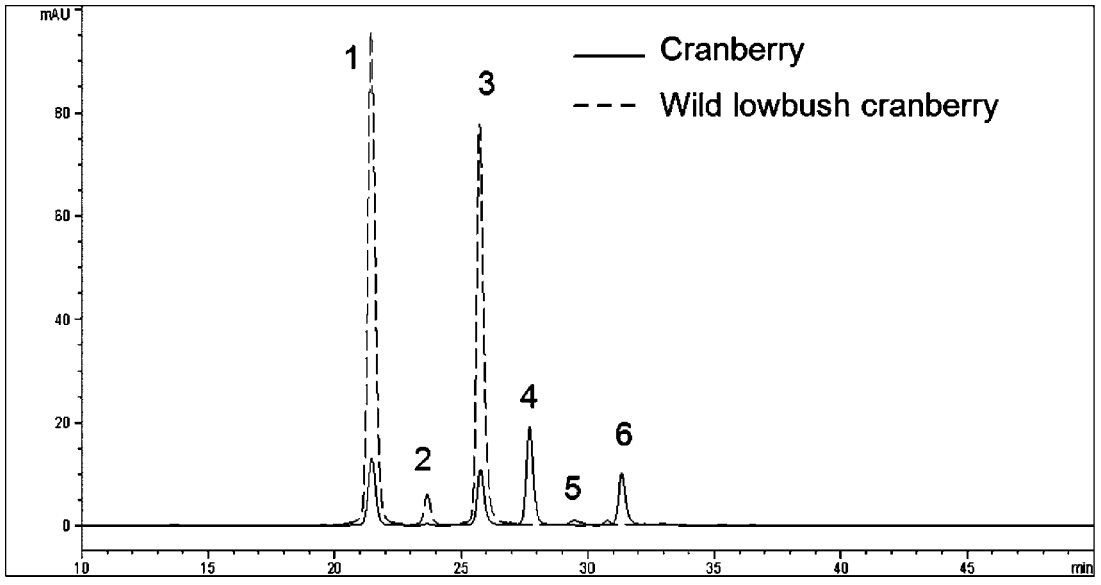

Figure 1. Reversed phase HPLC chromatograms for anthocyanins (A_{520}) in crude extracts of commercial cranberry (*V. macrocarpon*) and wild Alaskan lowbush cranberry (*V. vitis-idaea*).

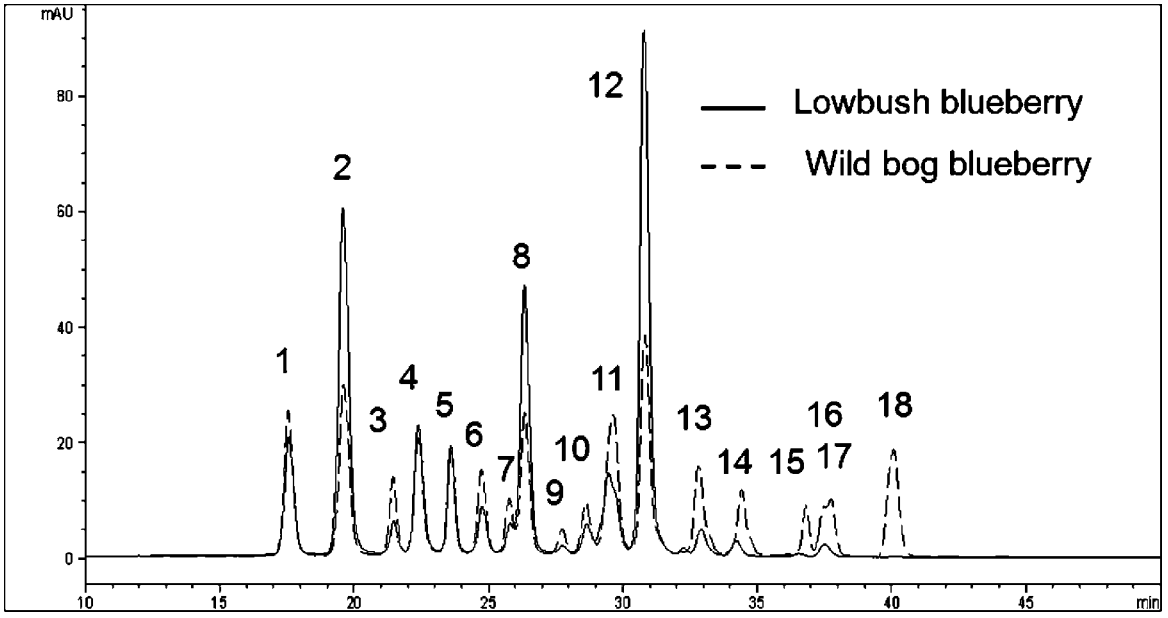

Figure 2. Reversed phase HPLC chromatograms for anthocyanins (A_{520}) in crude extracts of commercial lowbush blueberry (*V. angustifolium*) and wild Alaskan bog blueberry (*V. uliginosum*).

determined to be sufficient to eliminate background noise; therefore, 2-fold or higher values were used as a reliable estimation of relative expression ratio.[25]

Statistical Analysis. Statistical analyses were performed using Prism 4.0 (GraphPad Software, San Diego, CA, USA). Data were analyzed by one-way ANOVA with treatment as a factor. Post hoc analyses of differences between individual experimental groups were made using Dunnett's multiple-comparison tests.

RESULTS AND DISCUSSION

Total Monomeric Anthocyanins, Proanthocyanidins, Total Phenolics, and Chlorogenic Acid. Dry matter (DM) content of the berries used in this study ranged from 16% for commercial lowbush blueberry (*V. angustifolium*) to 24.6% for commercial American cranberry (*V. macrocarpon*). Wild Alaskan lowbush cranberry (*V. vitis-idaea*) and bog blueberry (*V. uliginosum*) contained 21.3 and 18.4% DM, respectively (Table 1).

Total anthocyanins (ANC) measured by pH differential assay indicated that the wild Alaskan lowbush cranberry contained levels of ANC (194.6 ± 6.4 mg/100 g FW) comparable to those of the commercial lowbush blueberry (189.8 ± 8.0 mg/100 g) but less than the wild Alaskan bog blueberry (220.0 ± 11.9 mg/100 g), whereas commercial cranberry contained significantly lower ANC concentration (76.6 ± 3.2 mg/100 g) (Table 1). ANC content of wild lowbush cranberry was >2.5-fold higher than that of commercial cranberry. In another study, *V. vitis-idaea* from Canada exhibited 1.4-fold greater ANC content than that of commercial cranberry, measured using the same assay.[26] Conversely, other researchers estimated that *V. vitis-idaea*

grown in Finland contained less ANC than European cranberry (257.0 and 299.3 mg/100 g, respectively, estimated by HPLC and based on dry weight).[27] In our comparison, bog blueberry from Alaska accumulated the highest ANC concentration, which is within the same range for this species grown in northern Europe (155−256 mg/100 g FW).[14,28]

Proanthocyanidins, measured spectrophotometrically by DMAC assay, exhibited highest levels in wild Alaskan lowbush cranberry (278.8 ± 19.6 mg/100 g FW), which was comparable to the PAC content of the same species in Finland (260 mg/100 g FW).[27] Commercial cranberry contained 132.7 ± 5.7 mg/100 g FW PAC, about half the PAC concentration of wild lowbush cranberry from Alaska. Wild Alaskan bog blueberry and commercial lowbush blueberry showed much lower levels of PAC (85.5 ± 5.9 and 71.2 ± 3.3 mg/100 g, respectively) with no significant difference at $P < 0.05$. Chlorogenic acid was highly accumulated in commercial lowbush blueberry (83.1 ± 1.0 mg/100g) but not detected in Alaskan bog blueberry. Wild Alaskan lowbush cranberry and commercial cranberry contained 18.3 ± 0.9 and 12.2 ± 0.2 mg/100 g chlorogenic acid, respectively. Total phenolics (TP) measured using Folin−Ciocalteu assay and expressed as gallic acid equivalents were much higher for Alaskan lowbush cranberry (624.4 ± 34.2 mg/100 g) than for the other three species and were comparable to same species grown in Canada.[26] Second to lowbush cranberry, the Alaskan bog blueberry exhibited TP of 504.5 ± 32.2 mg/100 g, whereas both the commercial berries, cranberry and lowbush blueberry, contained 350.5 ± 16.1 and 371.3 ± 2.2 mg/100 g, respectively, with no significant differences (Table 1).

Anthocyanin Profiles of Berries. The HPLC-DAD chromatograms of anthocyanins for all four berries are illustrated in Figures 1 and 2. Commercial cranberry is known to contain six anthocyanins, which are the galactosides, glucosides, and arabinosides of both cyanidin (peaks 1−3, 44%) and peonidin (peaks 4−6, 56%) (Table 2).[29] Wild Alaskan lowbush cranberry displayed only cyanidin glycosides as the dominant anthocyanin, with nondetectable levels of peonidins. This agrees with the results reported on the same species grown in Finland.[30] Environmental, geographical, or other factors in the northernmost latitudes of Finland were linked to higher relative content of cyanidin glycosides. Cyanidin glycosides were also present in slightly higher concentration in blueberries from the northern latitudes (Norway and Sweden), whereas delphinidin glycosides were better represented in the berries from southern latitudes (Italy, Poland, and Romania).[31] The HPLC chromatograms of Alaskan bog berry and commercial lowbush blueberry (Figure 2), and percentage of each anthocyanin (Table 2) indicated that the glucosides of delphinidin, petunidin, and malvidin (peaks 2, 8, and 12) were highly represented in wild bog blueberry (21.6, 14.8, and 29.2%, respectively) as compared to commercial lowbush blueberry (11.0, 4.3, and 13.1%, respectively). On the other hand, although lowbush blueberry contained a total of 17.4% acylated anthocyanins, none of these derivatives were detected in wild bog blueberry, which concurs with a previous report on *V. uliginosum* recently collected from different regions of Alaska.[9]

Proanthocyanin Profiles of Berries. Normal phase HPLC with fluorescence detection was able to separate proanthocyanin components in the berry extracts according to their degree of polymerization (Figures 3 and 4). Commercial cranberry had higher percentages of A-type dimers and trimers (23.2 and 12.1%, respectively) than B-type analogues (9.2 and 3.6%, respectively). Wild lowbush cranberry exhibited a higher percentage of B-type dimers (16.5%) and trimers (12.8%) than A-type analogues (7.8 and 2.6%, respectively). Comparison of wild bog blueberry to commercial lowbush blueberry revealed the former accumulated higher percentages of A-type dimers (13.7%) and trimers (11.7%) than the latter (2.0% and under the limit of detection, respectively). Among all of the berries, commercial lowbush blueberry contained the highest percentage of polymeric proanthocyanidins (25.1%) (Table 3).

Table 2. Anthocyanin Composition in Wild Alaskan and Commercial *Vaccinium* Species Measured Using RP-HPLC and UV Detection at 520 nm[a]

		% of total ANC	
peak (Figure 1)	anthocyanin	cranberry (*V. macrocarpon*)	lowbush cranberry[b] (*V. vitis-idaea*)
1	Cn-3-gal	23.4	54.5
2	Cn-3-glu	0.7	3.2
3	Cn-3-ara	20.0	42.2
4	Pn-3-gal	34.6	ND
5	Pn-3-glu	2.6	ND
6	Pn-3-ara	18.7	ND
		% of total ANC	
peak (Figure 2)	anthocyanin	lowbush blueberry (*V. angustifolium*)	bog blueberry[b] (*V. uliginosum*)
1	Dp-3-gal	8.8	6.4
2	Dp-3-glu	11.0	21.6
3	Cn-3-gal	3.8	1.4
4	Dp-3-ara	6.3	7.1
5	Cn-3-glu	4.8	4.7
6	Pt-3-gal	4.6	2.4
7	Cn-3-ara	2.6	1.3
8	Pt-3-glu	4.3	14.8
9	Pn-3-gal	5.7	0.5
10	Pt-3-ara	1.9	1.8
11	Mv-3-gal	8.0	7.2
12	Mv-3-glu	13.1	29.2
13	Mv-3-ara	7.9	1.7
14	Dp-3-(6″-acetoyl)-glu	4.2	ND
15	Cn-3-(6″-acetoyl)-glu	2.6	ND
16	Mv-3-(6″-acetoyl)-gal	1.8	ND
17	Pt-3-(6″-acetoyl)-glu	2.5	ND
18	Mv-3-(6″-acetoyl)-glu	6.3	ND

[a]Compounds were quantified on the basis of peak area measurements. Cn, cyanidin; Pn, peonidin; Dp, delphinidin; Pt, petunidin; Mv, malvidin; gal, galactoside; glu, glucoside; ara, arabinoside. [b]Wild species collected from Alaska.

Phenolic Profile of Berries by LC-ESI-TOF-MS^n. On the basis of extracted ion chromatogram (EIC), catechin predominated in wild lowbush cranberry, whereas epicatechin predominated in commercial cranberry and Alaskan bog blueberry. PAC-A2 was prominent in commercial cranberry (Tables 3 and 4). PAC-B1 was prominent in wild lowbush cranberry and commercial lowbush blueberry, whereas PAC-B2 was present in commercial cranberry, lowbush bluberries, and bog blueberries but weak in wild lowbush cranberry (Table 4). Procyanidin A-type trimers were highly detected in all berries except commercial lowbush blueberry, which showed very weak signal. Chlorogenic acid was very prominent in commercial lowbush blueberry compared to the three other berries.

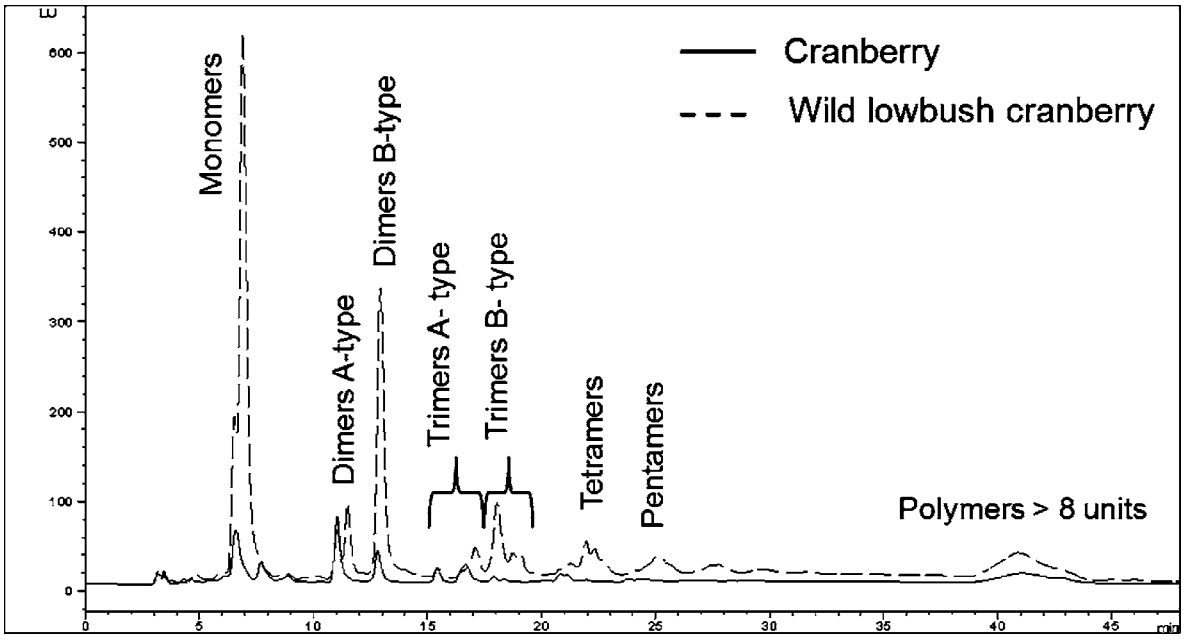

Figure 3. Normal phase HPLC-FLD chromatograms for proanthocyanidins (excitation, 230 nm; emission, 320 nm) in crude extracts of commercial cranberry (*V. macrocarpon*) and wild Alaskan lowbush cranberry (*V. vitis-idaea*).

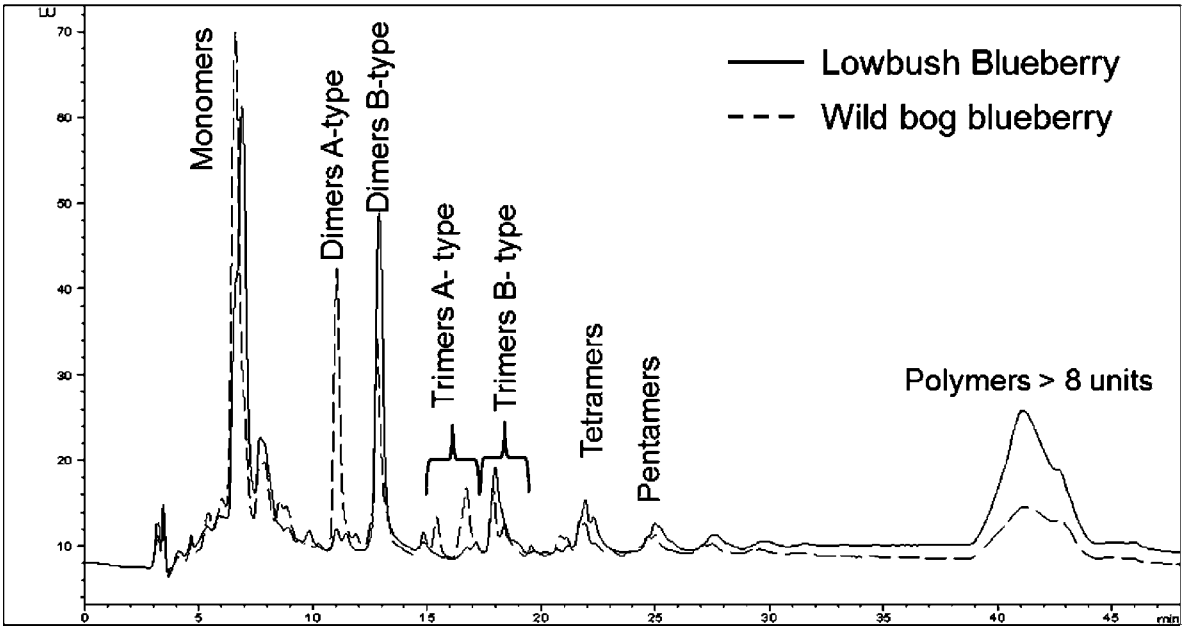

Figure 4. Normal phase HPLC-FLD chromatograms for proanthocyanidins (excitation, 230 nm; emission, 320 nm) in crude extracts of commercial lowbush blueberry (*V. angustifolium*) and wild Alaskan bog blueberry (*V. uliginosum*).

Commercial cranberry contained quercetin, myricetin, syringetin, and laricitrin glycosides, whereas wild lowbush cranberry was deficient in the last two flavonol glycosides. Commercial lowbush blueberry displayed quercetin, myricetin, and syringetin glycosides with no laricitrin, compared to wild bog blueberry, which contained the four flavonol glycosides. Additional results are shown in Table 4.

Antioxidant Capacity. The relative antioxidant capacity as measured by DPPH, ABTS, and FRAP assays mirrors the polyphenolic content of the investigated berries. Table 1 shows that wild lowbush cranberry had the highest radical scavenging activity in the three antioxidant capacity assays performed here (51.3 ± 2.2 and 69.3 ± 2.2 μM TE/g FW for DPPH and ABTS assays, respectively, and 122.2 ± 4.6 μM Fe^{+}/g for FRAP assay). DPPH, APTS, and FRAP assay results correlated well with the total phenolic content of the four investigated berries (R^2 = 0.98, 0.99, and 0.997, respectively). A previous study on the antioxidant capacity of Alaskan wild berries utilizing the H-ORAC$_{FL}$ assay indicated that lowbush cranberry collected from interior and south-central Alaska had about 2.5-fold the activity as wild bog blueberry from the same regions.[32]

A cleanup procedure was conducted on the crude extract, using a C18 RP-SPE cartridge (Supelco), to remove sugars, pectins, and lipophilic material and to concentrate polyphenolic compounds. Anthocyanins were more concentrated in the commercial lowbush blueberry polyphenol-rich (PPR) fraction

Table 3. Proanthocyanidin Composition in Wild Alaskan and Commercial *Vaccinium* Species Measured Using Normal Phase HPLC and Fluorescence Detection, Excitation and Emission at 230 and 320 nm, Respectively

	% of total proanthocyanidins			
proanthocyanidin	cranberry (*V. macrocarpon*)	lowbush cranberry[a] (*V. vitis-idaea*)	lowbush blueberry (*V. angustifolium*)	bog blueberry[a] (*V. uliginosum*)
monomers	21.8	32.4	32.4	28.6
dimers A-type	23.2	7.8	2.0	13.7
dimers B-type	9.2	16.5	18.4	13.4
trimers A-type	12.1	2.6	ND	11.7
trimers B-type	3.6	12.8	8.2	7.1
tetramers	6.9	7.1	7.2	5.9
pentamers−heptamers	4.6	10.8	6.8	3.4
polymers >8 units	18.8	9.8	25.1	15.2

[a]Wild species collected from Alaska.

Table 4. Proanthocyanidin Oligomers, Phenolic Acids, and Flavonoids in Wild Alaskan and Commercial *Vaccinium* Species Identified by LC-ESI-MS^n in Negative Ion Mode

compound	MS $[M-1]^-$ m/z	MS/MS m/z	UV λ (nm)	Rt (min)	cranberry	lowbush cranberry[a]	lowbush blueberry	bog blueberry[a]
catechin	289	245, 203	278	10.58	D^{weak}[b]	D	D	D^{weak}
epicatechin	289	245, 203	278	17.68	D	D^{weak}	D	D
procyanidin B1	577	407, 289	233, 278	9.50	D^{weak}	D	D	D^{weak}
procyanidin B2	577	407, 289	243, 278	13.60	D	D^{weak}	D	D
procyanidin A2	575	289	232, 278	23.00	D	D	D^{weak}	D
dimer A-type	575	289	233, 278	19.90	D^{weak}	D	D^{weak}	D^{weak}
trimer B-type	865	407	240, 277	multiple peaks	D	D	D	D
trimer A-type	863	575, 423	241, 241	multiple peaks	D	D	D^{weak}	D
chlorogenic acid	353		241, 325	12.84	D^{weak}	D^{weak}	D	ND[b]
feruloylquinic acid	267		322	23.26	ND	ND	D	ND
malonyl-caffeoylquinic acid	439	395. 411	281	17.47	D	ND	ND	ND
quercetin	301	229. 041	268, 355	25.36	D	D	D	D
quercetin-3-rut	609	463, 301	255, 355	25.30	D	D	D	D
quercetin-3-gal/glc	463	301. 03	254, 353	24.30	D	D	D	D
quercetin-3-arab	433	301	256, 356	24.45	D	D	D	D
quercetin-3-acetoyl-rha	489	447, 301	253, 353	25.34	ND	ND	D	ND
myricetin-3-gal/glu	479	316, 271	260, 359	20.30, 23.60	D	D	D	D
myricetin-3-ara	449	316	358	24.04	D	ND	ND	D
syringetin-3-O-glu	507	344, 301	252, 353	24.90	D	ND	D	D
syringetin-ara	477	344	245, 354	25.26	D	ND	D	D
laricitrin glu	493	331	260, 360	24.04	D	ND	ND	D
laricitrin ara	463	331	254, 353	24.27	D^{weak}	ND	ND	D

[a]Wild species collected from Alaska. [b]D, detected; ND, not detected.

Table 5. Polyphenol Content of Crude and Polyphenol-rich Fractions Used in the Anti-inflammatory Activity Assay[a]

	crude extract (mg/g)			polyphenol-rich fraction (mg/g)		
berry extract	ANC[b]	PAC[c]	TP[d]	ANC[b]	PAC[c]	TP[d]
cranberry (*V. macrocarpon*)	4.7^{C}	8.6^{B}	22.7^{C}	52.1^{C}	96.3^{BC}	905
lowbush cranberry[e] (*V. vitis-idaea*)	12.6^{B}	17.6^{A}	39.3^{A}	68.2^{C}	215.6^{A}	1030^{A}
lowbush blueberry (*V. angustifolium*)	14.6^{A}	5.5^{C}	28.5^{B}	193.1^{A}	103.3^{B}	883
bog blueberry[e] (*V. uliginosum*)	13.8^{AB}	5.5^{C}	32.7^{B}	156.9^{B}	69.3^{C}	723^{B}

[a]Means with different letters within the same column are significantly different at $p < 0.05$. [b]ANC, anthocyanins, quantified by pH differential assay as cyanidin-3-*O*-glucoside. [c]PAC, proanthocyanidins, quantified by DMAC assay as procyanidin A2. [d]TP, total phenolics, quantified by Folin−Ciocalteu assay as gallic acid equivalent; [e]Wild species collected from Alaska.

(193.1 mg/g), whereas PAC were highest in wild lowbush cranberry PPR fraction (215.6 mg/g). The PPR contained an average of 30-fold the concentrations of TP in the crude extracts (see Table 5 for concentrations of ANC, PAC, and TP in crude and PPR extracts). The PPR was tested alongside the dried crude extract for anti-inflammatory activity.

Anti-inflammatory Assay. Many studies have suggested that exposure of mammalian cells to the main component of the outer membrane of the Gram-negative bacteria, lipopolysaccharide (LPS), can lead to release of pro-inflammatory cytokines and in turn activate inflammatory cascades including cytokines, lipid mediators, and adhesion molecules such as interleukin-1β (IL-1β), cyclooxygenase-2 (COX-2), inducible

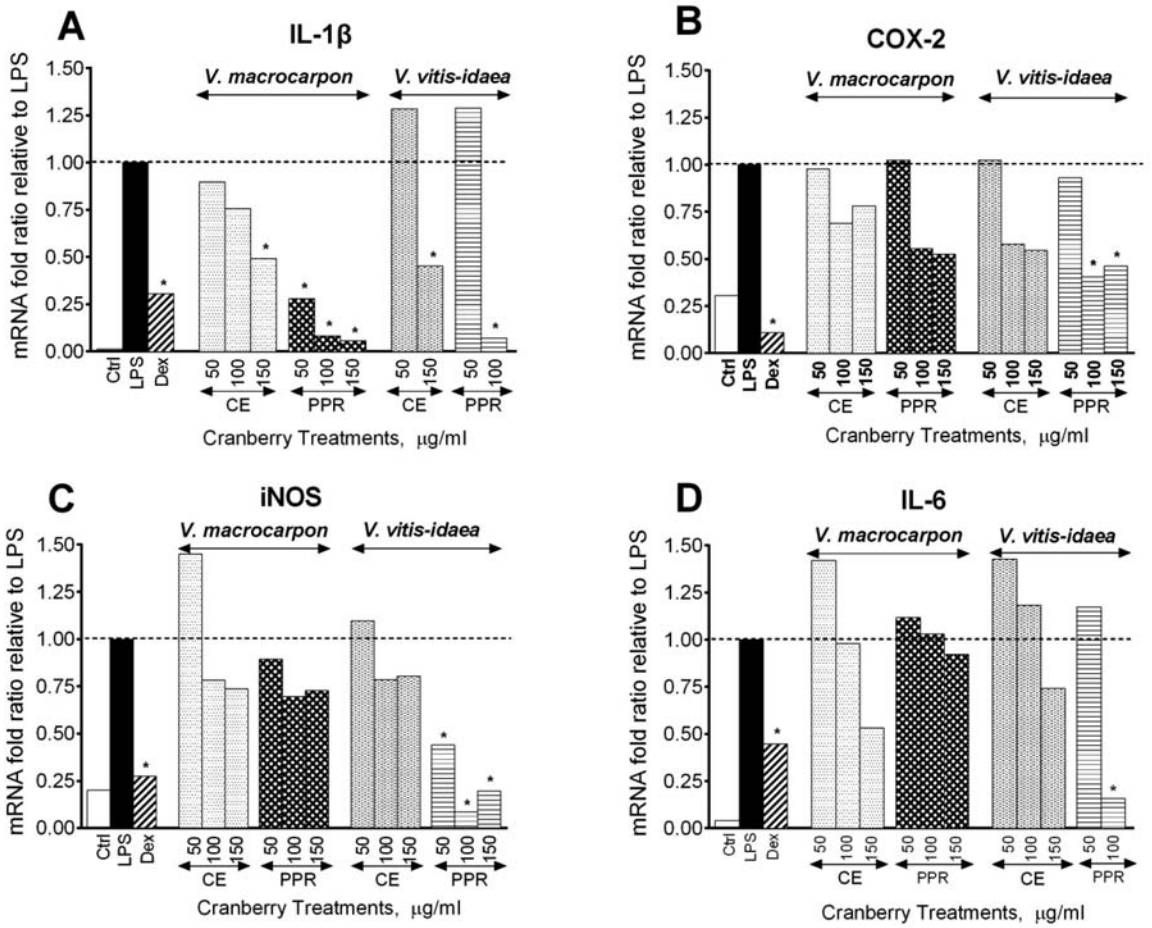

Figure 5. Anti-inflammatory bioactivity of wild Alaskan and commercial *Vaccinium* crude extracts (CE) and polyphenol-rich fractions (PPR); effects on the expression of the inflammatory biomarker genes in the LPS-stimulated RAW264.7 macrophages at 50, 100, and 150 μg/mL. Genes involved in the acute-phase response, inflammatory response, and humoral immune responses are represented: IL-1β assay (A), COX-2 assay (B), iNOS assay (C), and IL-6 assay (D). Changes in gene expression were measured by comparing mRNA quantity relative to LPS. A value of <1.0 indicates transcriptional down-regulation (inhibition of gene expression) compared with LPS, which shows maximum genetic induction (1.0). Therefore, lower values indicate greater anti-inflammatory activity. Ctrl, cells treatment with vehicle only; Dex, dexamethasone at 10 μM used as positive control.

nitric oxide synthase (iNOS), and interleukin-6 (IL-6). These four well-known genetic biomarkers involved in the acute-phase response, inflammatory response, and humoral immune responses were investigated in vitro in the LPS-stimulated murine RAW 264.7 macrophage model. The in vitro experiments were designed to quantify the relative amount of transcripts for target genes within the total RNA in individual cell batches undergoing dose-dependent treatments (50, 100, and 150 μg/mL) with four CE and four PPR fractions. For each assay, three control sets were monitored. The negative control (no LPS treatment) maintained a constant amount of transcripts for all constitutively expressed genes and served as a reference baseline; the induction control (treated with LPS) showed the maximum up-regulation of the marker genes; and the positive control (treated with LPS and Dex) served as a reference for the effectiveness of the assay.[31] Because noncytotoxic doses were predetermined by the MTT assay (data not shown), the observed changes in gene expression (genetic down-regulation) were not due to cell death.

On the basis of gene expression results, wild lowbush cranberry exhibited a potent anti-inflammatory activity in the macrophage cell culture based on a 2-fold or higher change in biomarker gene expression relative to the LPS-stimulated controls (Figures 5 and 6). In some instances, 10-fold reduction was observed in pro-inflammatory gene expression similar to or exceeding that of the positive control (Figures 5A and 6A). PPR fractions of cranberry and lowbush blueberry effectively inhibited LPS-elicited induction of pro-inflammatory inducible cytokine IL-1β and two enzyme coding genes cyclooxygenase-2 (Cox2) and nitric oxide synthase (Figure 5B,C).

Determination of pharmacologically relevant and attainable doses for polyphenol-rich cranberry extracts in vivo will be an important next step toward developing novel preventive or clinical applications based on cranberry supplementation. Cranberry polyphenols are a complex mixture composed of monomeric catechins, epicatechins, polymeric proanthocyanidins (with and without additional substitutions), and multiple anthocyanins (Tables 1 and 2). Whereas anthocyanins are known for their low bioavailability, monomeric proanthocyanidins from fruits have been known to reach systemic circulation at the level of 50−80 μg/mL of plasma,[33] which is comparable to the low and intermediate level doses used in this study. It is therefore likely that the in vitro anti-inflammatory effects of wild lowbush[33] cranberry will be observed in vivo in circulating macrophages and especially in resident intestinal macrophages that receive higher exposure to dietary poly-

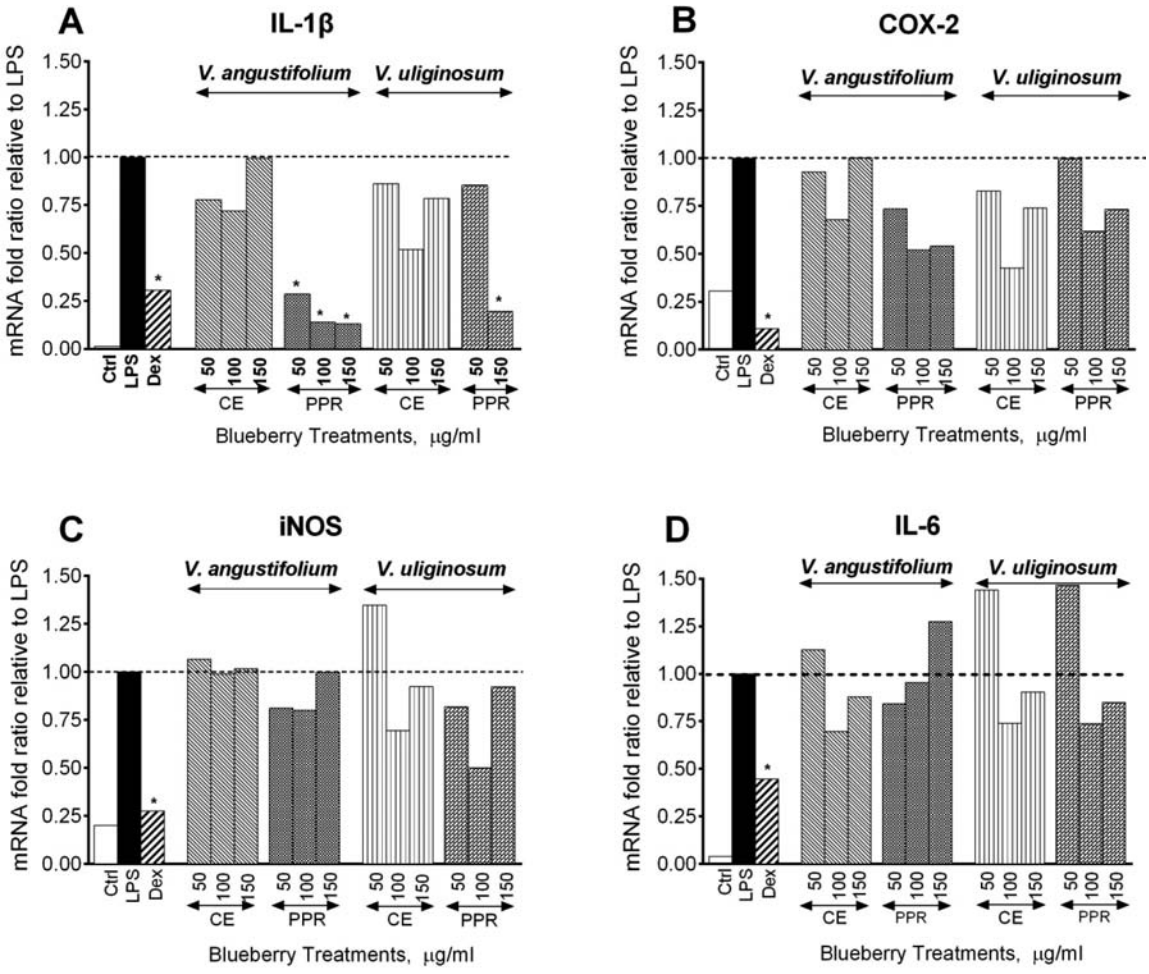

Figure 6. Anti-inflammatory bioactivity of wild Alaskan and commercial *Vaccinium* crude extracts (CE) and polyphenol-rich fractions (PPR); effects on the expression of the inflammatory biomarker genes in the LPS-stimulated RAW264.7 macrophages at 50, 100, and 150 μg/mL. Genes involved in the acute-phase response, inflammatory response, and humoral immune responses are represented: IL-1β assay (A), COX-2 assay (B), iNOS assay (C), and IL-6 assay (D). Changes in gene expression were measured by comparing mRNA quantity relative to LPS. A value of <1.0 indicates transcriptional down-regulation (inhibition of gene expression) compared with LPS, which shows maximum genetic induction (1.0). Ctrl, cells treatment with vehicle only; Dex, dexamethasone at 10 μM used as positive control.

phenols.[34] All PPR fractions were highly enriched with ANC, PAC, and TP, with the Alaskan lowbush cranberry showing the highest concentration of PAC (215.6 mg/g, Table 5). Lowbush blueberry PPR extract contained the highest ANC content among all berries and higher levels of PAC compared to bog blueberry. The anti-inflammatory capacity of the berries is likely to be conditioned by the combination of flavonoid phytochemicals contained in the extracts, as has been noted in previous research.[35]

In summary, wild Alaskan lowbush cranberry and commercial American cranberry are both rich in PAC, comprising about 45 and 38% of TP, respectively. The PAC content in wild lowbush cranberry was >2-fold higher than that in commercial cranberry. Compositional analyses indicated that commercial cranberry accumulates a richer concentration of procyanidin A-type dimers and trimers, whereas wild lowbush cranberry accumulates predominantly B-type dimers and trimers (>2 times that of A-type). Wild Alaskan lowbush cranberry is characterized by high levels of the flavan-ol catechin (32.4% of proanthocyanidin content) compared to commercial cranberry, in which epicatechins comprise most of the monomer content (21.8%). Cranberry A-type procyanidins are known to inhibit the attachment of uropathogenic *Escherichia coli* to uroepithelial and vaginal cells,[36] whereas wild lowbush cranberry has not been well evaluated for antiadhesion capacity. Alaskan bog blueberry demonstrated higher levels of all phenolic groups investigated and higher antioxidant capacity than commercial lowbush blueberry. Bog blueberry lacks acylated anthocyanins but contains higher levels of procyanidin A-type than lowbush blueberry. Investigations on acylated anthocyanins indicated that they may be less easily absorbed/less bioavailable than the nonacylated forms, a phenomenon which has been linked to their greater hydrophobicity.[37,38] Thus, compositional differences between berry sources may affect their biological activities. Alaskan wild berries are rich sources of antioxidants, based on their polyphenolic content and antioxidant capacity. Although wild berries in Alaska have limited accessibility, distribution, and availability and could not compete in commercial markets with cultivated berries, the enhanced accumulation of heath-beneficial wild berry constituents may represent a novel opportunity for development of Alaskan berries as a potential new niche market commodity, an American-grown specialty functional food to compete in the same market as several other exotic berry species currently in vogue.[39]

AUTHOR INFORMATION

Corresponding Author

*(M.A.L.) Phone: (704) 250-5407. Fax: (704) 250-5409. E-mail: maryann_lila@ncsu.edu.

Funding

This work is supported by the National Institute of General Medical Sciences of the National Institutes of Health under Award P20GM103395 at the University of Alaska—Fairbanks and UNC General Administration funding. The content is solely the responsibility of the authors and does not necessarily represent the official views of the National Institutes of Health.

Notes

The authors declare no competing financial interest.

REFERENCES

(1) Ames, B. N.; Shigenaga, M. K.; Hagen, T. M. Oxidants, antioxidants, and the degenerative diseases of aging. *Proc. Natl. Acad. Sci. U.S.A.* **1993**, *90*, 7915−7922.

(2) Dai, Q.; Borenstein, A. R.; Wu, Y.; Jackson, J. C.; Larson, E. B. Fruit and vegetable juices and Alzheimer's disease: the Kame Project. *Am. J. Med.* **2006**, *119*, 751−759.

(3) Joshipura, K. J.; Ascherio, A.; Manson, J. E.; Stampfer, M. J.; Rimm, E. B.; Speizer, F. E.; Hennekens, C. H.; Spiegelman, D.; Willett, W. C. Fruit and vegetable intake in relation to risk of ischemic stroke. *JAMA, J. Am. Med. Assoc.* **1999**, *282*, 1233−1239.

(4) He, X.; Liu, R. H. Cranberry phytochemicals: isolation, structure elucidation, and their antiproliferative and antioxidant activities. *J. Agric. Food Chem.* **2006**, *54*, 7069−7074.

(5) Cirico, T. L.; Omaye, S. Additive or synergetic effects of phenolic compounds on human low density lipoprotein oxidation. *Food Chem. Toxicol.* **2006**, *44*, 510−516.

(6) Duthie, G. G.; Gardner, P. T.; Kyle, J. A. Plant polyphenols: are they the new magic bullet? *Proc. Nutr. Soc.* **2003**, *62*, 599−603.

(7) Pan, M.; Lai, C.; Ho, C. Anti-inflammatory activity of natural dietary flavonoids. *Food Funct.* **2010**, *1*, 15−31.

(8) Stanek, S.; Butcher, B. Collecting and using Alaska's wild berries and other wild products. *Alaska Cooperative Extension Publication FNH-00120*, 1998.

(9) Kellogg, J.; Wang, J.; Flint, C.; Ribnicky, D.; Kuhn, P.; De Mejia, E. G.; Raskin, I.; Lila, M. A. Alaskan wild berry resources and human health under the cloud of climate change. *J. Agric. Food Chem.* **2010**, *58*, 3884−3900.

(10) Seeram, N.; Adams, L. S.; Hardy, M. L.; Heber, D. Total cranberry extract versus its phytochemical constituents: antiproliferative and synergistic effects against human tumor cell lines. *J. Agric. Food Chem.* **2004**, *52*, 2512−2517.

(11) Howard, L. R.; Clark, J. R.; Brownmiller, C. Antioxidant capacity and phenolic content in blueberries as affected by genotype and growing season. *J. Sci. Food Agric.* **2003**, *83*, 1238−1247.

(12) Lila, M. A. The nature-versus-nurture debate on bioactive phytochemicals: the genome versus terroir. *J. Agric. Food Chem.* **2006**, *86*, 2510−2515.

(13) Ek, S.; Kartimo, H.; Mattila, S.; Tolonen, A. Characterization of phenolic compounds from lingonberry (*Vaccinium vitis-idaea*). *J. Agric. Food Chem.* **2006**, *54*, 9834−9842.

(14) Lätti, A. K.; Jaakola, L.; Riihinen, K. R.; Kainulainen, P. S. Anthocyanin and flavonol variation in bog bilberries (*Vaccinium uliginosum* L.) in Finland. *J. Agric. Food Chem.* **2010**, *58*, 427−433.

(15) Singleton, V. L.; Orthofer, R.; Lamuela-Raventós, R. M. Analysis of total phenols and other oxidation substrates and antioxidants by means of Folin-Ciocalteu reagent. *Methods Enzymol.* **1999**, *299*, 152−178.

(16) Lee, J.; Durst, R. W.; Wrolstad, R. E. Determination of total monomeric anthocyanin pigment content of fruit juices, beverages, natural colorants, and wines by the pH differential method: collaborative study. *J. AOAC Int.* **2005**, *88*, 1269−1278.

(17) Prior, R. L.; Fan, E.; Ji, H.; Howell, A.; Nio, C.; Payne, M. J.; Reed, J. Multi-laboratory validation of a standard method for quantifying proanthocyanidins in cranberry powders. *J. Sci. Food Agric.* **2010**, *90*, 1473−1478.

(18) Grace, M. H.; Guzman, I.; Roopchand, D. E.; Moskal, K.; Cheng, D. M.; Pogrebnyak, N.; Raskin, I.; Howell, A.; Lila, M. A. Stable binding of alternative protein-enriched food matrices with concentrated cranberry bioflavonoids for functional food applications. *J. Agric. Food Chem.* **2013**, *61*, 6856−6864.

(19) Grace, M. H.; Ribnicky, D. M.; Kuhun, P.; Poulev, A.; Logendra, S.; Yousef, G. G.; Raskin, I.; Lila, M. A. Hypoglygemic activity of a novel anthocyanin-rich formulation from lowbush blueberry, *Vaccinium angustifolium* Aiton. *Phytomedicine* **2009**, *16*, 406−415.

(20) Wallace, T. C.; Giusti, M. M. Extraction and normal-phase HPLC-fluorescence-electrospray MS characterization and quantification of procyanidins in cranberry extracts. *J. Food Sci.* **2010**, *75*, C690−C696.

(21) Truong, V. D.; McFeeters, R. F.; Thompson, R. T.; Dean, L. L.; Shofran, B. Phenolic acid content and composition in leaves and roots of common commercial sweetpotato (*Ipomoea batatas* L.) cultivars in the United States. *J. Food Sci.* **2007**, *72*, C343−C349.

(22) Re, R.; Pellegrini, N.; Proteggente, A.; Pannala, A.; Yang, M.; Rice-Evans, C. Antioxidant activity applying an improved ABTS• radical cation decolorization assay. *Free Radical Biol. Med.* **1999**, *26*, 1231−1237.

(23) Szeto, Y. T.; Tomlinson, B.; Benzie, I. F. F. Total antioxidant and ascorbic acid content of fresh fruits and vegetables: implications for dietary planning and food preservation. *Br. J. Nutr.* **2002**, *87*, 55−59.

(24) Mosmann, T. Rapid colorimetric assay for cellular growth and survival: application to proliferation and cytotoxicity assays. *J. Immunol. Methods* **1983**, *65*, 55−63.

(25) Karlen, Y.; McNair, A.; Perseguers, S.; Mazza, C.; Mermod, N. Statistical significance of quantitative PCR. *BMC Bioinf.* **2007**, *8*, 131.

(26) Zheng, W.; Wang, S. Y. Oxygen radical absorbing capacity of phenolics in blueberries, cranberries, chokeberries, and lingonberries. *J. Agric. Food Chem.* **2003**, *51*, 502−509.

(27) Kylli, P.; Nohynek, L.; Puupponen-Pimiä, R.; Westerlund-Wikström, B.; Leppänen, T.; Welling, J.; Moilanen, E.; Heinonen, M. Lingonberry (*Vaccinium vitis-idaea*) and European cranberry (*Vaccinium microcarpon*) proanthocyanidins: isolation, identification, and bioactivities. *J. Agric. Food Chem.* **2011**, *59*, 3373−3384.

(28) Anderson, ØM. Anthocyanins in fruits of *Vaccinium uliginosum* L. (bog whortleberry). *J. Food Sci.* **1987**, *52*, 665−666.

(29) Grace, M. H.; Massey, A. R.; Mbeunkui, F.; Yousef, G. G.; Lila, M. A. Comparison of health-relevant flavonoids in commonly consumed cranberry products. *J. Food Sci.* **2012**, *77*, H176−H183.

(30) Määttä-Riihinen, K. R.; Kamal-Eldin, A.; Mattila, P. H.; González-Paramás, A. M.; Riitta, T. A. R. Distribution and contents of phenolic compounds in eighteen Scandinavian berry species. *J. Agric. Food Chem.* **2004**, *52*, 4477−4486.

(31) Martinelli, E. M.; Baj, A.; Bombardelli, E. Computer-aided evaluation of liquid-chromatographic profiles for anthocyanins in *Vaccinium myrtillus* fruits. *Anal. Chim. Acta* **1986**, *191*, 275−281.

(32) Leiner, R., H; Holloway, P. S.; Neal, D. B. Antioxidant capacity and quercetin levels in Alaska wild berries. *Int. J. Fruit Sci.* **2006**, *6*, 83−91.

(33) Agarwal, C.; Singh, R. P.; Agarwal, R. Grape seed extract induces apoptotic death of human prostate carcinoma DU145 cells via caspases activation accompanied by dissipation of mitochondrial membrane potential and cytochrome c release. *Carcinogenesis* **2002**, *23*, 1869−1876.

(34) Magrone, T.; Jirillo, E. The interplay between the gut immune system and microbiota in health and disease: nutraceutical intervention for restoring intestinal homeostasis. *Curr. Pharm. Des.* **2013**, *19*, 1329−1342.

(35) Cuevas-Rodriguez, E. O.; Dia, V. P.; Yousef, G. G.; Garcia-Saucedo, P. A.; Lopez-Medina, J.; Paredes-Lopez, O.; Gonzalez de Mejia, E.; Lila, M. A. Inhibition of pro-inflammatory responses and

antioxidant capacity of Mexican blackberry (*Rubus* spp.) extracts. *J. Agric. Food Chem.* **2010**, *58*, 9542−9548.
(36) Howell, A. B.; Reed, J. D.; Krueger, C. G.; Winterbottom, R.; Cunningham, D. G.; Leahy, M. A-type cranberry proanthocyanidins and uropathogenic bacterial anti-adhesion activity. *Phytochemistry* **2005**, *66*, 2281−2291.
(37) Charron, C. S.; Clevidence, B. A.; Britz, S. J.; Novotny, J. A. effect of dose size on bioavailability of acylated and nonacylated anthocyanins from red cabbage (*Brassica oleracea* L. var. capitata). *J. Agric. Food Chem.* **2007**, *55*, 5354−5362.
(38) Charron, C. S.; Kurilich, A. C.; Clevidence, B. A.; Simon, P. W.; Harrison, D. J.; Britz, S. J.; Baer, D. J.; Novotny, J. A. Bioavailability of anthocyanins from purple carrot juice: effects of acylation and plant matrix. *J. Agric. Food Chem.* **2009**, *57*, 1226−1230.
(39) Kellog, J.; Higgs, C.; Lila, M. A. Prospects for commercialization of an Alaskan native wild resource as a commodity crop. *J. Entrepreneurship* **2011**, *20*, 77−101.

JOURNAL OF AGRICULTURAL AND FOOD CHEMISTRY

Article

pubs.acs.org/JAFC

Changes in Chokeberry (*Aronia melanocarpa* L.) Polyphenols during Juice Processing and Storage

Kail Wilkes, Luke R. Howard,* Cindi Brownmiller, and Ronald L. Prior

Department of Food Science, University of Arkansas, 2650 North Young Avenue, Fayetteville, Arkansas 72704, United States

Supporting Information

ABSTRACT: Chokeberries are an excellent source of polyphenols, but their fate during juice processing and storage is unknown. The stability of anthocyanins, total proanthocyanidins, hydroxycinnamic acids, and flavonols at various stages of juice processing and over 6 months of storage at 25 °C was determined. Flavonols, total proanthocyanidins, and hydroxycinnamic acids were retained in the juice to a greater extent than anthocyanins, with losses mostly due to removal of seeds and skins following pressing. Anthocyanins were extensively degraded by thermal treatments during which time levels of protocatechuic acid and phloroglucinaldehyde increased, and additional losses occurred following pressing. Flavonols, total proanthocyanidins, and hydroxycinnamic acids were well retained in juices stored for 6 months at 25 °C, whereas anthocyanins declined linearly. Anthocyanin losses during storage were paralleled by increased polymeric color values, indicating that the small amounts of anthocyanins remaining were present in large part in polymeric forms.

KEYWORDS: *anthocyanins, chokeberries, flavonols, hydroxycinnamic acids, juice, processing, proanthocyanidins, storage*

INTRODUCTION

Chokeberries (*Aronia melanocarpa*) are gaining popularity as a result of their exceptional content of polyphenols. The berries are exceptionally rich in anthocyanins, which are responsible for the deep purple color. Chokeberry anthocyanins consist mainly of cyanidin glycosides (glucoside, xyloside, galactoside, and arabinoside), but the galactoside and arabinoside generally account for >75% of total anthocyanins.[1] Chokeberries are also rich in proanthocyanidins (PACs), which impart a very astringent taste. The proanthocyanidin profile of the berries is complex, ranging from monomers to decamers and to exceptionally high levels of polymers.[1] The berries also contain high levels of hydroxycinnamic acids (chlorogenic acid and neochlorogenic acid) and considerable levels of flavonols, mostly quercetin derivatives.[2−5] As a result of their exceptional polyphenol composition, chokeberries are thought to play an important role in protection against many chronic diseases. There is accumulating evidence that chokeberries or polyphenolic-rich extracts from chokeberries possess cardioprotective, hepatoprotective, antidiabetic, and anticarcinogenic effects.[6−10]

Due to their astringent taste, chokeberries are commonly processed and consumed in various shelf-stable forms including juices, nectars, wines, and liqueurs. Unfortunately, chokeberry processing has been shown to result in marked losses of anthocyanins.[11−13] Several studies have reported on the concentration of polyphenols in chokeberries, pomace, and juice, but results are expressed on a dry weight basis and do not provide any indications of actual concentrations in the three fractions as weights of the berries, juice, and pomace were not measured or taken into account.[3,13]

In addition to anthocyanin losses during juice processing, further extensive losses of anthocyanins during storage have been reported in other anthocyanin-rich berries.[14−16] Anthocyanin losses in these studies were paralleled by increased polymeric color values indicating anthocyanin−tannin polymers were formed during storage; these polymers are resistant to bleaching in the presence of potassium metabisulfite. Because chokeberries are particularly rich in polyphenols, we suspect that similar losses of anthocyanins and possibly other polyphenols occur during juice processing and storage. The objective of this study was to determine the fate of chokeberry anthocyanins, total PACs, hydroxycinnamic acids, and flavonols during various stages of juice processing and throughout 6 months of storage at ambient temperature.

MATERIALS AND METHODS

Frozen Berries. Frozen chokeberries (*A. melanocarpa* cv. Viking) were obtained from Mae's Health and Wellness (Omaha, NE, USA). The berries grown outside Davenport, NE, USA, were harvested at commercial ripeness and frozen within 4 hours after harvest. They were then transported overnight under refrigeration to the University of Arkansas, Food Science Department. Upon receipt, the berries were stored at −20 °C for <2 weeks prior to processing.

Chemicals and Reagents. A mixture of 3-*O*-*β*-glucoside standards of delphinidin, cyanidin, petunidin, peonidin, pelargonidin, and malvidin was obtained from Polyphenols Laboratories (Sandnes, Norway). HPLC grade methanol, acetone, formic acid, and acetic acid were obtained from Sigma-Aldrich (St. Louis, MO, USA). Chlorogenic acid, rutin, protocatechuic acid, phloroglucinaldehyde, (+)-catechin, 4-dimethylaminocinnamaldehyde, and quercetin were also obtained from Sigma-Aldrich.

Juice Processing. Chokeberries were processed into nonclarified juice as previously described.[14] The juice processing scheme with five sampling points indicated is shown in Figure 1. Frozen berries were

Special Issue: 2013 Berry Health Benefits Symposium

Received: September 24, 2013
Revised: November 22, 2013
Accepted: November 26, 2013
Published: November 26, 2013

ACS Publications © 2013 American Chemical Society

dx.doi.org/10.1021/jf404281n | J. Agric. Food Chem. 2014, 62, 4018−4025

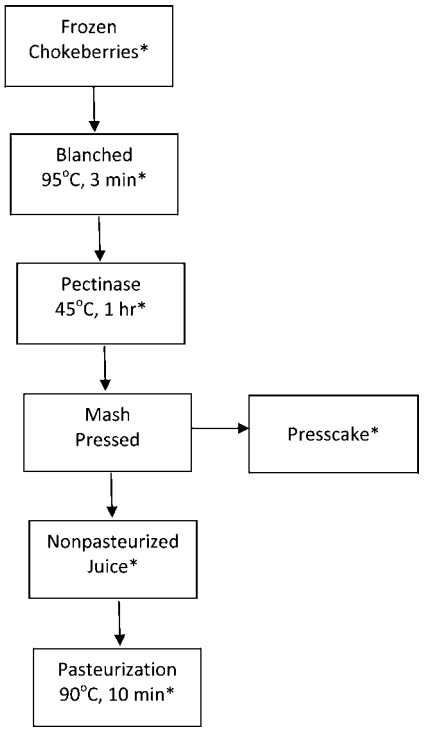

Figure 1. Flowchart of chokeberry juice processing with sampling points indicated by asterisks.

simultaneously heated and mixed with a Mixco Batch mixer (Avon, NY, USA) in a large steam kettle until the berry mash reached a temperature of 95 °C. After 3 min of incubation, the mash was allowed to cool to 40 °C prior to depectinization. Pectinex Smash XXL (Novozyme, Bagsvared, Denmark) was added at a concentration of 0.0827 mL/kg, and the mash was incubated for 1 h at 40 °C. Complete depectinization was verified by the negative alcohol precipitation test where no flocculation of pectin was observed following the addition of 2 volumes of 96% ethanol (v/v) to 1 volume of juice. The mash was then pressed in a 25 L Enrossi bladder press (Enoagricol Rossi, s.r.l., Calzolaro, Italy) operated at 20 psi to separate the juice from the presscake. The nonclarified juice was dispensed into 6 oz glass bottles and heated in a steam box (American Sterilizer Co., Erie, PA, USA) until the juice temperature monitored using a thermocouple reached 90 °C. The bottle caps were tightened, and the juices were allowed to cool overnight. Samples of each juice treatment were stored in the dark at 25 °C. Five samples were taken at each sampling point during the juicing process, and five bottles of juice were sampled after 1, 2, 3, 4, 5, and 6 months of storage at 25 °C.

Extraction of Polyphenols. For isolation of anthocyanins, hydroxycinnamic acids, and flavonols, five samples each of frozen and blanched berries, enzyme-treated mash, and presscake were homogenized with 20 mL of methanol/water/acetic acid (60:37:3, v/v/v) using a EuroTurrax T18 tissuemizer (Tekmar-Dohrman Corp., Mason, OH, USA) and then filtered through MiraCloth (Calbiochem, La Jolla, CA, USA). The residue was collected, the extraction repeated two more times, and the volume of the extracts adjusted to 100 mL with extraction solvent. The same protocol was used to isolate PACs except acetone/water/acetic acid (70:29.5:0.5, v/v/v) was used as extraction solvent. Juice samples were analyzed directly and required no extraction.

HPLC Analysis of Anthocyanins and Hydroxycinnamic Acids. Methanol/water/acetic acid extracts (8 mL) were dried using a SpeedVac concentrator (ThermoSavant, Holbrook, NY, USA) and resuspended in 1 mL of 3% formic acid in water. The reconstituted samples were passed through 0.45 μm PTFE syringe filters prior to HPLC analysis. Anthocyanin monoglycosides and hydroxycinnamic acids were separated by reverse phase HPLC on a Symmetry C_{18} column (Waters Corp., Milford, MA, USA) according to the method described by Cho et al.[17] Anthocyanins were monitored at 520 nm and hydroxycinnamic acids at 320 nm. Anthocyanin glycosides were quantified as cyanidin 3-glucoside equivalents and hydroxycinnamic acids as chlorogenic acid equivalents using external calibration curves of authentic standards. Protocatechuic acid and phloroglucinaldehyde were monitored at 280 nm and quantified using external calibration curves of authentic standards.

HPLC and HPLC-MS Analysis of Flavonols. Methanol/water/acetic acid extracts extracts (8 mL) were dried using a SpeedVac concentrator and resuspended in 1 mL of 50% methanol in water. The reconstituted samples were passed through 0.45 μm PTFE syringe filters prior to HPLC analysis. Individual flavonols were separated by reverse phase HPLC on an Aqua C_{18} column (Phenomenex, Torrance, CA, USA) according to the method described by Cho et al.[18] Flavonol peaks were monitored at 360 nm and quantified as rutin equivalents using external calibration curves of an authentic standard. Quercetin was quantified using an external calibration curve of an authentic standard. The identification of flavonols was performed by HPLC-MS using the HPLC conditions described above, except the HPLC system was interfaced to a Bruker Esquire LC-MS ion trap mass spectrometer (Billerica, MA, USA). Mass spectral analysis was conducted in negative ion electrospray mode using conditions previously described in Cho et al.[18]

Percent Polymeric Color Analysis. Percent polymeric color of methanol/water/acetic acid extracts from samples taken throughout juice processing and juices was determined using the spectrophotometric assay of Giusti and Wrolstad.[19] Absorbance values of two matching samples, one treated with water (control) and the other with potassium metabisulfite, were recorded at 420, 520, and 700 nm. Potassium metabisulfite was used to bleach the monomeric anthocyanins present in the juices, whereas polymeric anthocyanins resistant to bleaching remain colored. The ratio of the absorbance value of the potassium metabisulfite bleached sample to the control sample (nonbleached) × 100 reflects percent polymeric color.

Total Proanthocyanidin Analysis. Total PACs were measured by the 4-dimethylaminocinnamaldehyde (DMAC) assay of Prior et al.[20] The absorbance (640 nm) of samples in 96-well plates was measured every min for 30 min on a BioTek Synergy HT (Winooski, VT, USA) plate reader. Catechin was used as standard with results expressed as milligrams of catechin equivalents per 100 g berry fresh weight.

Calculations. To account for dilution and concentration effects, anthocyanin, flavonol, proanthocyanidin, hydroxycinnamic acid, and phenolic acid concentrations were converted to original berry weight to allow comparison of all samples on an equivalent basis. The following equation was used:

$$C_{berry} = C_{product} \times R$$

C_{berry} = concentration on original berry weight basis, R = mass of the product divided by mass of original berry, and $C_{product}$ = concentration in the product.

Statistical Analysis. The effects of processing and storage on anthocyanin, hydroxycinnamic acid, flavonol, total proanthocyanidin, and phenolic acid concentrations and percent polymeric color were determined by one-way analysis of variance (ANOVA) using JMP 8.0 (Cary, NC, USA). Differences between means (n = 5) were determined by Student's t test (α = 0.05).

RESULTS AND DISCUSSION

Polyphenol Composition of Chokeberries and Juice. Cyanidin 3-galactoside (cyd 3-gal), cyanidin 3-glucoside (cyd 3-glu), cyanidin 3-arabinoside (cyd 3-ara), and cyanidin 3-xyloside (cyd 3-xyl) were identified and quantified by HPLC (Supporting Information Figure S1), and the results are presented in Table 1. These anthocyanins were previously identified in chokeberry juice by HPLC-MS using identical HPLC conditions described above.[21] Cyd 3-gal and cyd 3-ara

Table 1. Concentrations of Anthocyanins, Hydroxycinnamic Acids, and Total Proanthocyanidins (PACs) and Percent Polymeric Color throughout Chokeberry Juice Processing[a]

processing step	anthocyanins (mg/100 g berry FW)					hydroxycinnamic acids (mg/100 g berry FW)			% polymeric color	total PACs (mg/100 g berry FW)
	cyanidin 3-galactoside	cyanidin 3-glucoside	cyanidin 3-arabinoside	cyanidin 3-xyloside	total	neochlorogenic acid	chlorogenic acid	total		
frozen	424.7 ± 9.6 a	19.8 a	154.7 a	20.1 ± 0.9 a	619.2 ± 16.5 a	46.2 ± 1.0 a	70.2 ± 1.9 b	116.4 ± 2.7 b	16.2 b	845.2 ± 25.6 b
blanched	205.5 ± 5.5 b (48%)	10.9 ± 0.3 b (55%)	57.5 ± 1.2 b (37%)	7.3 ± 0.2 b (36%)	281.2 ± 7.2 b (45%)	46.8 ± 1.1 a (101%)	80.2 ± 1.6 a (114%)	127.0 ± 2.6 a (109%)	7.4 e	868.6 ± 7.4 b (103%)
enzyme	190.7 ± 0.8 c (45%)	10.5 ± 0.1 b (53%)	54.2 ± 0.5 b (35%)	6.9 ± 0.0 b (35%)	262.4 ± 1.4 b (42%)	45.1 ± 0.2 a (98%)	77.2 ± 0.4 a (110%)	122.2 ± 0.5 a (105%)	10.1 de	940.7 ± 29.1 a (111%)
juice, NP[b]	77.1 ± 0.7 e (18%)	4.6 ± 0.0 d (23%)	20.4 ± 0.2 d (13%)	2.7 ± 0.0 c (13%)	104.8 ± 1.0 d (17%)	30.1 ± 0.0 b (65%)	47.7 ± 0.1 c (68%)	77.9 ± 0.2 c (67%)	13.4 bc	392.6 ± 8.6 e (62%)
presscake	99.8 ± 1.8 d (23%)	5.4 ± 0.1 c (27%)	29.3 ± 0.6 c (19%)	3.7 ± 0.1 c (18%)	138.3 ± 2.6 c (22%)	14.9 ± 0.1 d (32%)	28.8 ± 0.3 d (41%)	43.7 ± 0.3 d (38%)	12.2 cd	524.2 ± 13.4 c (46%)
juice, P[b]	32.4 ± 0.6 f (8%)	2.3 ± 0.0 e (12%)	6.3 ± 0.1 e (4%)	0.9 ± 0.0 d (4%)	42.0 ± 0.8 e (7%)	27.9 ± 0.7 c (61%)	45.9 ± 1.2 c (65%)	73.9 ± 1.9 c (63%)	29.4 a	464.8 ± 20.8 d (55%)

[a]Mean values ($n = 5$) within a column with different letters are significantly different ($p \leq 0.05$). Values in parentheses represent percent retention compared with frozen berries. [b]NP, nonpasteurized; P, pasteurized.

were the major anthocyanins in the chokeberry samples and juices, confirming previous results.[1−4] Two hydroxycinnamic acids, neochlorogenic acid (NCA) and chlorogenic acid (CA), were present in the berries and juices (Supporting Information Figure S2 and Table 1). The high concentrations of NCA and CA in chokeberry samples and juices confirm previous findings.[3,4] Eight flavonols were identified by HPLC and HPLC-MS (Supporting Information Figure S3) and included the following derivatives of quercetin: two dihexosides (m/z 625/301), vicianoside (arabinosyl-glucoside) (m/z 595/301), robinobioside (rhamnosyl-galactoside) (m/z 609/301), rutinoside (rhamnosyl-glucoside) (m/z 609/301), galactoside (m/z 463/301), glucoside (m/z 463/301), and aglycone (m/z 301). All of these compounds have previously been identified in chokeberries.[4,5] The quantities of individual flavonols in samples taken throughout juice processing are presented in Table 2. The relative abundance of quercetin derivatives in frozen berries was similar to findings of Mikulic-Petkovsek,[5] who reported that galactoside was the predominant quercetin derivative followed by glucoside, rutinoside, vicianoside, robinobioside, and dihexosides. The amount of total flavonols in frozen chokeberries in our study, 33.9 mg/100 g FW, falls within the range of values (26−71 mg/100 g FW) previously reported for fresh chokeberries.[4,5]

Processing Changes in Chokeberry Polyphenols and Percent Polymeric Color. *Anthocyanins.* Anthocyanins were readily degraded during the two thermal treatments, blanching and pasteurization, as well as physical removal of the presscake (Table 1). Cyd pentosides (ara and xyl) were more susceptible to degradation during blanching (63 and 64% losses, respectively) than cyd hexosides (gal and glu, 52 and 45% losses, respectively). A similar trend was observed in response to pasteurization with cyd 3-ara and cyd 3-xyl, each incurring 69% losses, whereas cyd 3-gal and cyd 3-glu showed 58 and 50% losses, respectively, compared with levels found in nonpasteurized juice. Our results are consistent with previous studies reporting anthocyanin hexosides to be more stable than pentosides.[12,21,22] Following pasteurization, the juices contained only 8, 12, 4, 4, and 7% of the levels of cyd 3-gal, cyd 3-glu, cyd 3-ara, cyd 3-xyl, and total anthocyanins found in frozen chokeberries. A major loss of anthocyanins also occurred during the pressing operation when presscake containing seeds and skins was removed from the mash. The presscake contained 52, 51, 54, and 54% of the levels of cyd 3-gal, cyd 3-glu, cyd 3ara, and cyd 3-xyl found in the enzyme-treated mash, respectively, with most of the balance transferred to the juice. These results indicate that chokeberry presscake is an excellent source of anthocyanins and may be useful as a substrate for recovering natural pigments. The anthocyanin losses observed in response to thermal treatments were much higher than those previously reported for blueberry,[14] blackberry,[15] and black raspberry[19] juices processed under similar conditions. The extensive anthocyanin losses observed in this study could be due to several factors. It is clear that thermal treatments had a detrimental effect on anthocyanins. We observed significant increases in two HPLC peaks following blanching that were identified as protocatechuic acid (PCA) and phloroglucinaldehyde (PGA) (Figure 2), and the concentrations of these two compounds increased upon thermal treatments (Figure 3). Levels of PCA and PGA increased by 343 and 400% after blanching, by 30 and 24% from blanched berries to enzyme treated mash, and by 29 and 7% from nonpasteurized to pasteurized juice. The formation of PCA and PGA in response

Table 2. Concentrations of Flavonols throughout Chokeberry Juice Processing[a]

	flavonols (mg/100 g berry FW)								
processing step	quercetin 3-dihexoside	quercetin 3-dihexoside	quercetin 3-vicianoside	quercetin 3-robinobioside	quercetin 3-rutinoside	quercetin 3-galactoside	quercetin 3-glucoside	quercetin	total
frozen	3.0 ± 0.2 b	1.4 ± 0.1 b	4.0 ± 0.2 b	3.5 ± 0.2 a	3.9 ± 0.1 b	10.6 ± 0.5 a	7.6 ± 0.3 a	0.74 ± 0.0 a	34.7 ± 1.4 a
blanched	3.6 ± 0.1 a (120%)	1.6 ± 0.0 a (114%)	4.5 ± 0.1 a (115%)	3.1 ± 0.1 b (89%)	4.1 ± 0.1 ab (105%)	10.2 ± 0.2 a (96%)	7.2 ± 0.1 a (95%)	0.66 ± 0.0 b (89%)	35.0 ± 0.6 a (101%)
enzyme	4.1 ± 0.2 a (137%)	1.7 ± 0.0 a (121%)	4.8 ± 0.0 a (123%)	3.3 ± 0.0 ab (94%)	4.3 ± 0.0 a (110%)	10.6 ± 0.1 a (100%)	7.5 ± 0.1 a (99%)	0.71 ± 0.0 a (96%)	36.9 ± 0.2 a (106%)
juice, NP[b]	2.2 ± 0.0 c (73%)	1.0 ± 0.0 c (71%)	3.1 ± 0.0 c (79%)	2.1 ± 0.0 c (60%)	2.8 ± 0.0 c (72%)	5.7 ± 0.0 b (54%)	4.2 ± 0.0 b (55%)	0.19 ± 0.0 d (26%)	21.3 ± 0.0 b (61%)
presscake	1.6 ± 0.0 d (53%)	0.7 ± 0.0 d (50%)	1.9 ± 0.0 e (49%)	1.4 ± 0.0 e (40%)	1.7 ± 0.0 e (44%)	5.2 ± 0.1 bc (49%)	3.6 ± 0.0 c (47%)	0.66 ± 0.0 b (89%)	16.7 ± 0.2 c (48%)
juice, P[b]	2.3 ± 0.3 c (77%)	0.9 ± 0.1 cd (64%)	2.6 ± 0.2 d (67%)	1.7 ± 0.2 d (49%)	2.3 ± 0.2 d (59%)	4.5 ± 0.4 c (42%)	3.5 ± 0.3 c (46%)	0.31 ± 0.0 c (42%)	18.2 ± 1.8 c (52%)

[a]Mean values (n = 5) within a column with different letters are significantly different ($p \leq 0.05$). Values in parentheses represent percent retention compared with frozen berries. [b]NP, nonpasteurized; P, pasteurized.

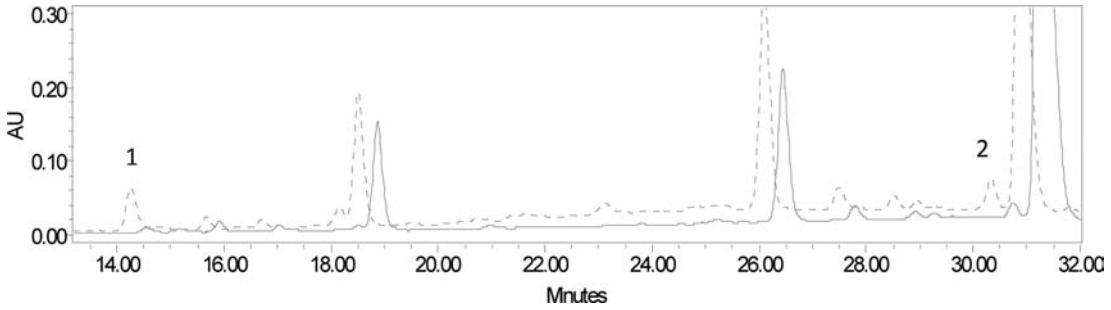

Figure 2. HPLC chromatogram (260 nm) of frozen (solid line) and blanched (dashed line) chokeberry extracts. Peaks: 1, protocatechuic acid; 2, phloroglucinaldehyde.

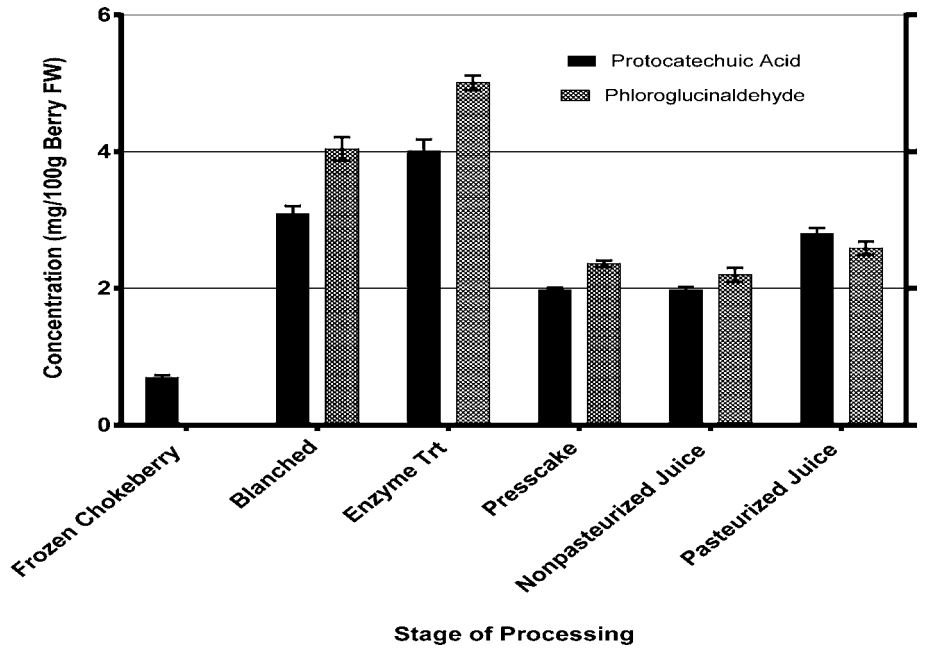

Figure 3. Concentrations of protocatechuic acid and phloroglucinaldehyde throughout chokeberry juice processing. Bars represent standard errors of the mean (n = 5). Bars with different letters are significantly different ($p \leq 0.05$).

to thermal treatments is consistent with the scheme of cyanidin 3-glycoside degradation proposed by Sadilova et al.[23] According to Sadilova et al.,[23] the first step of pH-dependent thermal degradation of cyanidin at pH 3.5, which is similar to the pH of chokeberries used in this study, involves opening of the pyrilium ring and chalcone glycoside formation. The next step involves deglycosylation to yield chalcone, which degrades quickly in the presence of heat to protocatechuic acid, 4-hydroxybenzoic acid, and phloroglucinaldehyde. We did not detect 4-hydroxybenzoic acid in our chromatograms, which is consistent with results reported for heated elderberry extracts that are also rich in cyd glycosides.[23] However, the increases in

dx.doi.org/10.1021/jf404281n | J. Agric. Food Chem. 2014, 62, 4018−4025

Table 3. Concentrations of Anthocyanins, Hydroxycinnamic Acids, and Total Proanthocyanidins (PACs) and Percent Polymeric Color throughout Chokeberry Juice Storage at 25 °C[a]

	anthocyanins (mg/100 g berry FW)					hydroxycinnamic acids (mg/100 g berry FW)				
storage time (months)	cyanidin 3-galactoside	cyanidin 3-glucoside	cyanidin 3-arabinoside	cyanidin 3-xyloside	total	neochlorogenic acid	chlorogenic acid	total	% polymeric color	total PACs (mg/100 g berry FW)
1	22.2 ± 0.8 a (69%)	1.6 ± 0.1 a (70%)	4.1 ± 0.21 a (65%)	0.58 ± 0.0 a (64%)	28.6 ± 1.1 a (68%)	27.5 ± 1.1 a (99%)	45.2 ± 1.7 a (98%)	72.7 ± 2.8 a (98%)	34.8 d	447.8 ± 8.7 ab (97%)
2	18.1 ± 0.3 b (56%)	1.3 ± 0.0 b (57%)	3.3 ± 0.1 b (52%)	0.51 ± 0.0 b (57%)	23.3 ± 0.4 b (55%)	27.9 ± 0.6 a (100%)	46.3 ± 1.2 a (101%)	74.3 ± 1.8 a (101%)	34.4 d	450.8 ± 10.1 a (96%)
3	15.1 ± 0.1 c (47%)	1.1 ± 0.0 c (48%)	2.7 ± 0.0 c (43%)	0.43 ± 0.0 c (48%)	19.3 ± 0.2 c (46%)	28.3 ± 0.2 a (101%)	47.0 ± 0.5 a (102%)	75.3 ± 0.7 a (102%)	37.5 c	425.7 ± 14.8 abc (92%)
4	10.0 ± 0.6 d (31%)	0.7 ± 0.0 d (30%)	1.8 ± 0.1 d (29%)	0.30 ± 0.0 d (33%)	12.8 ± 0.8 d (30%)	22.9 ± 1.2 b (82%)	37.7 ± 2.0 b (82%)	60.6 ± 3.2 b (82%)	40.4 b	413.2 ± 13.8 bc (89%)
5	5.5 ± 1.2 e (17%)	0.5 ± 0.1 e (22%)	1.0 ± 0.2 e (16%)	0.22 ± 0.0 e (24%)	7.3 ± 0.4 e (17%)	18.9 ± 2.6 c (68%)	31.2 ± 4.4 bc (68%)	50.1 ± 7.0 bc (68%)	39.9 b	409.9 ± 12.8 c (88%)
6	5.6 ± 0.3 e (17%)	0.4 ± 0.0 e (17%)	1.0 ± 0.0 e (16%)	0.21 ± 0.0 e (23%)	7.2 ± 1.5 e (17%)	18.4 ± 1.1 c (66%)	30.4 ± 1.8 c (66%)	48.9 ± 2.9c (66%)	44.5 a	406.0 ± 9.2 c (87%)

[a]Mean values (n = 5) within a column with different letters are significantly different ($p \leq 0.05$). Values in parentheses represent percent retention compared with pasteurized juice.

cyd degradation products PCA and PGA during processing accounted for only about 3% of the losses in total anthocyanins that occurred during processing. The presence of ascorbic acid and pro-oxidant metals in the chokeberries may have played a role in anthocyanin degradation.[24] Enzymes such as polyphenol oxidase and peroxidase are also reported to cause degradation of anthocyanins,[25−27] but the frozen chokeberries used in this study were immediately blanched to inactivate enzymes. The extensive loss of anthocyanins during blanching was most likely due to the long time it took the 23 kg batch of frozen chokeberries to heat to the blanching temperature of 95 °C and then cool to 40 °C. In an additional experiment involving a 5.4 kg batch of chokeberries, in which it took 12 min for the frozen berries to heat to 95 °C and 3 min to cool to 40 °C, we observed a 25% loss of anthocyanins. Because chokeberry anthocyanins appear to be very heat labile, use of a blanching treatment prior to depectinization may be counterproductive, especially if the berries contain low polyphenol oxidase activity.

Percent Polymeric Color. Percent polymeric color values decreased in response to blanching and enzyme treatments, which may indicate cleavage of some anthocyanin−tannin linkages (Table 1). The major change in polymeric color occurred when juice was pasteurized, from 13.4% in non-pasteurized juice to 29.4% in pasteurized juice. According to Kunsagi-Mate et al.[28] the formation of anthocyanin−tannin polymers is slow at room temperature due to the high activation energy of the reaction, but is accelerated at elevated temperatures. Hence, the increased polymeric color values observed following pasteurization may reflect higher levels of anthocyanin−tannin polymers, which may account for some of the losses of monomeric anthocyanins.

Hydroxycinnamic Acids. The level of NCA did not change in response to blanching, whereas the level of CA increased by 14%, indicating CA was not completely extracted from frozen berries (Table 1). Significant losses of HCAs occurred during the pressing operation. The presscake contained 33 and 37% of the levels of NCA and CA found in enzyme-treated mash, respectively, whereas the NP juice contained 67 and 62% of NCA and CA, respectively. Levels of NCA and CA were minimally affected by pasteurization with CA and total HCAs showing no losses and NCA showing a 7% loss compared with the value for NP juice. Following pasteurization, the juices contained 60, 65, and 63% of the levels of NCA, CA, and total HCAs found in frozen chokeberries, respectively.

Total Proanthocyanidins. The levels of total PACs were stable upon blanching, but increased by 11% following the enzyme treatment (Table 1). Disruption of cell wall polysaccharides presumably allowed for enhanced extraction of the PACs following enzyme treatment. The major loss of total PACs occurred during the pressing operation. The presscake contained 60% of the levels of total PACs found in enzyme-treated mash, whereas the NP juice contained 46%. Surprisingly, PACs increased 17% in response to pasteurization. This may be due to disruption of cell wall polysaccharide−proanthocyanidin complexes, which allowed more PACs to react with the DMAC reagent. It is also possible that pasteurization resulted in depolymerization of large molecular weight PACs to monomers, which are reported to react more readily with the DMAC reagent than polymers.[20]

Flavonols. Levels of quercetin dihexosides, vicianoside, robinobioside, and rutinoside showed modest increases (11−20%) in response to either blanching or enzyme treatment, compared with values for frozen berries, whereas levels of the

Table 4. Concentrations of Flavonols throughout Chokeberry Juice Storage at 25 °C[a]

	flavonols (mg/100 g berry FW)								
storage time (months)	quercetin 3-dihexoside	quercetin 3-dihexoside	quercetin 3-vicianoside	quercetin 3-robinobioside	quercetin 3-rutinoside	quercetin 3-galactoside	quercetin 3-glucoside	quercetin	total
1	2.3 ± 0.2 a (100%)	0.9 ± 0.0 a (100%)	2.9 ± 0.1 a (112%)	2.0 ± 0.1 a (118%)	2.7 ± 0.1 a (117%)	5.0 ± 0.2 a (111%)	3.9 ± 0.2 a (111%)	0.35 ± 0.0 b (113%)	19.7 ± 0.9 ab (108%)
2	2.4 ± 0.1 a (104%)	0.9 ± 0.0 a (100%)	3.1 ± 0.0 a (119%)	2.0 ± 0.0 a (118%)	2.8 ± 0.0 a (122%)	5.2 ± 0.0 a (116%)	4.0 ± 0.0 a (114%)	0.39 ± 0.0 ab (126%)	20.9 ± 0.2 a (115%)
3	2.3 ± 0.1 a (100%)	1.0 ± 0.0 a (111%)	3.2 ± 0.0 a (123%)	2.1 ± 0.0 a (124%)	2.9 ± 0.0 a (126%)	5.3 ± 0.0 a (118%)	4.1 ± 0.0 a (117%)	0.40 ± 0.0 a (129%)	21.3 ± 0.2 a (117%)
4	2.1 ± 0.1 a (91%)	1.0 ± 0.0 a (111%)	3.1 ± 0.0 a (119%)	2.1 ± 0.0 a (124%)	2.9 ± 0.0 a (126%)	5.2 ± 0.0 a (116%)	4.1 ± 0.0 a (117%)	0.40 ± 0.0 a (129%)	20.9 ± 0.1 a (115%)
5	1.6 ± 0.2 b (70%)	0.8 ± 0.1 b (89%)	2.5 ± 0.3 b (96%)	1.7 ± 0.2 b (100%)	2.4 ± 0.3 b (104%)	4.2 ± 0.5 b (93%)	3.3 ± 0.3 b (94%)	0.35 ± 0.0 b (113%)	16.7 ± 1.8 b (92%)
6	1.5 ± 0.2 b (65%)	0.8 ± 0.1 b (89%)	2.5 ± 0.3 b (96%)	1.6 ± 0.2 c (94%)	2.4 ± 0.3 b (104%)	4.1 ± 0.4 b (91%)	3.2 ± 0.3 b (91%)	0.35 ± 0.0 b (113%)	16.5 ± 1.8 b (91%)

[a]Mean values (n = 5) within a column with different letters are significantly different ($p \leq 0.05$). Values in parentheses represent percent retention compared with pasteurized juice.

two major quercetin conjugates, galactoside and glucoside, and total flavonols were stable (Table 2). Significant losses of flavonol glycosides occurred during the pressing operation, with 39−49% of the compounds being retained in the presscake, whereas 54−64% were expressed into the juice. The less polar quercetin hexosides (galactoside and glucoside) were retained to a greater extent in the presscake (48 and 49%) than the more polar quercetin diglycosides (39 and 41%). Additionally, the majority of the nonpolar quercetin aglycone was retained in the presscake, whereas only 27% was expressed into the juice. Pasteurization did not affect levels of the two quercetin hexosides, but other derivatives decreased by 16−21% in response to pasteurization. Although present at low level, the concentration of quercetin aglycone increased by 63% in response to pasteurization, indicating that some sugar conjugates were cleaved from the quercetin glycosides in response to thermal treatment. Overall, total flavonol levels decreased by 15% in response to pasteurization.

Storage Changes in Chokeberry Polyphenols and Percent Polymeric Color. *Anthocyanins.* Levels of cyd 3-gal, cyd 3-glu, cyd 3-ara, cyd 3-xyl, and total anthocyanins in juices declined in a linear fashion over 1−5 months of storage at 25 °C, but levels appeared to stabilize from 5 to 6 months (Table 3). After 6 months of storage, the juices lost 75, 75, 76, 64, and 75% of the levels of cyd 3-gal, cyd 3-glu, cyd 3-ara, cyd 3-xyl, and total anthocyanins, respectively, found in juices after 1 month of storage. These results are consistent with other studies reporting marked losses of anthocyanins during ambient-temperature storage of chokeberry juice,[21,29] nectars, and purees.[11] The type of sugar attached had little effect on anthocyanin stability during long-term storage, which contrasts with results observed in response to thermal treatments during processing, where hexosides showed greater retention than pentosides (Table 1). Consistent with our findings, Hellstrom et al.[29] reported no differences in stability of chokeberry anthocyanin glycosides stored at 4, 9, and 21 °C over 12 weeks of storage. The mechanisms responsible for anthocyanin degradation during storage have not been well elucidated, but may be associated with water nucleophilic attack at the 2-position of the anthocyanin nucleus, resulting in decolorization,[30] or the formation of anthocyanin−tannin polymers.[31] Levels of PCA and PGA were stable for up to 3 months of storage and then declined about 30% from 3 to 6 months of storage (data not shown), indicating that anthocyanins were not degraded into phenolic acids during ambient temperature storage.

Percent Polymeric Color. Percent polymeric color values of the juices increased (from 34.8 to 44.5%) from 1 to 6 months of storage, and these values were inversely correlated with anthocyanins (r = −0.81) (Table 3). These changes indicate that some losses of anthocyanins throughout storage may be due to the formation of anthocyanin−epicatechin polymers that are resistant to bleaching by potassium metabisulfite in the polymeric color assay. However, it is also possible that the anthocyanin−epicatechin polymers formed in the juices during processing were more resistant to degradation during storage. The anthocyanin−epicatechin polymers appeared to play an important role in color stability as the juices retained a dark purple color despite marked losses of monomeric anthocyanins.

Hydroxycinnamic Acids. In contrast to anthocyanins, levels of NCA, CA, and total HCAs were stable from 1 to 3 months of storage (Table 3), but levels declined by about 30% from 3 to 6 months of storage. Levels of chlorogenic acid in blueberry and chokeberry juices were also found to be relatively stable over long-term storage at ambient temperature.[29,32]

Total Proanthocyanidins. Levels of total PACs were stable (>90% retention) from 1 to 6 months of storage (Table 3). The stability of PACs over storage contrasts with the marked decline in anthocyanins and increase in percent polymeric color values observed from 1 to 6 months of storage. These results indicate that PACs did not react with anthocyanins to any great extent to form polymeric pigments throughout storage. This finding supports the hypothesis that polymeric pigments formed during processing are more resistant to degradation than monomeric anthocyanins and play an important role in color stability.

Flavonols. Quercetin glycosides and aglycone were stable from 1 to 4 months of storage at 25 °C, but levels decreased by 17−29% from 4 to 6 months (Table 4). Total flavonol levels decreased by 21% from 4 to 6 months of storage at 25 °C. Levels of quercetin followed the same trend as quercetin glycosides, indicating that losses of glycosides from 4 to 6 months of storage were not due to cleavage of sugar moieties. The losses of flavonols late during storage may be due to physical binding to insoluble solids, resulting in precipitation, or oxidation to quinones.

In summary, juice processing had a much greater effect on polyphenol losses in chokeberries than did storage of juices at 25 °C. Anthocyanins were more susceptible to losses during

processing than flavonols, total PACs, and hydroxycinnamic acids as a result of thermal degradation, evident by increased levels of protocatechuic acid and phloroglucinaldehyde, and polymerization, evident by increased polymeric color values. The juice pressing step resulted in losses of all polyphenols due to physical removal of skins, but anthocyanins and total PACs were retained in the presscake to a greater extent than hydroxycinnamic acids and flavonols. Flavonols, total PACs, and hydroxycinnamic acids were well retained over 6 months of storage at 25 °C compared with anthocyanins, which degraded in a linear manner up to 5 months. Losses of anthocyanins during storage were accompanied by increased polymeric color values, indicating that the small amounts of anthocyanins remaining after long-term storage were present largely in polymeric forms. The polymeric forms of anthocyanins appear to be more stable than monomeric anthocyanins and likely play an important role in color stability. Novel, cost-effective treatments are needed to stabilize anthocyanins during chokeberry juice processing and storage.

■ ASSOCIATED CONTENT

Ⓢ Supporting Information

HPLC chromatograms used to identify and quantify anthocyanins (Figure S1), hydroxycinnamic acids (Figure S2), and flavonols (Figure S3). This material is available free of charge via the Internet at http://pubs.acs.org.

■ AUTHOR INFORMATION

Corresponding Author

*(L.R.H.) Phone: (479) 575-2978. Fax: (479) 575-6936. E-mail: lukeh@uark.edu.

Notes

The authors declare no competing financial interest.

■ ACKNOWLEDGMENTS

We thank Mae's Health and Wellness for providing the frozen chokeberries used in this study.

■ REFERENCES

(1) Wu, X.; Gu, L.; Prior, R. L.; McKay, S. Characterization of anthocyanins and proanthocyanidins in some cultivars of *Ribes*, *Aronia*, and *Sambucus* and their antioxidant capacity. *J. Agric. Food Chem.* **2004**, *52*, 7846−7856.

(2) Bermúdez-Soto, M. J.; Tomás-Barberán, F. A. Evaluation of commercial red fruit juice concentrates as ingredients for antioxidant functional juices. *Eur. Food Res. Technol.* **2004**, *219*, 133−141.

(3) Oszmianski, J.; Wojdylo, A. Aronia melanocarpa phenolics and their antioxidant activities. *Eur. Food Res. Technol.* **2005**, *221*, 809−815.

(4) Slimestad, R.; Torskangerpoll, K.; Nateland, H. S.; Johannessen, T.; Giske, N. H. Flavonoids from black chokeberries, *Aronia melanocarpa*. *J. Food Compos. Anal.* **2005**, *18*, 61−68.

(5) Mikulic-Petkovsek, M.; Slatnar, A.; Stampar, F.; Veberic, R. HPLC-MS identification and quantification of flavonol glycosides in 28 wild and cultivated berry species. *Food Chem.* **2012**, *135*, 2138−2146.

(6) Zhao, C.; Giusti, M. M.; Malik, M.; Moyer, M. P.; Magnuson, B. A. Effects of commercial anthocyanin-rich extracts on colonic cancer and nontumorigenic colonic cell growth. *J. Agric. Food Chem.* **2004**, *52*, 6122−6128.

(7) Kulling, S. E.; Rawel, H. M. Chokeberry (*Aronia melanocarpa*) − a review on the characteristic components and potential health effects. *Planta Med.* **2008**, *74*, 1625.

(8) Broncel, M.; Kozirog, M.; Duchnowicz, P.; Koter-Michalak, M.; Sikora, J.; Chojnowska-Jezierska, J. *Aronia melanocarpa* extract reduces blood pressure, serum endothelium, lipid, and oxidative stress marker levels in patients with metabolic syndrome. *Med. Sci. Monit.* **2010**, *16*, CR28−CR34.

(9) Jurgoński, A.; Juśkiewicz, J.; Zduńczyk, Z. Ingestion of black chokeberry fruit extract leads to intestinal and systemic changes in a rat model of prediabetes and hyperlipidemia. *Plant Foods Hum. Nutr.* **2008**, *63*, 176−182.

(10) Denev, P.; Kratchanov, C.; Ciz, M.; Lojek, A.; Kratchanova, M. Bioavailability and antioxidant activity of black chokeberry (*Aronia melanocarpa*) polyphenols: *in vitro* and *in vivo* evidences and possible mechanisms of action: a review. *Comp. Rev. Food Sci. Saf.* **2012**, *11*, 471−489.

(11) Georgiev, D.; Ludneva, D. Possibilities for production of nectars and purees from fruits of black chokeberry (*Aronia melanocarpa*). *ISHS Acta Hortic.* **2009**, *825*, 595−598.

(12) Trošt, K.; Golic-Wondra, M.; Prošek, M.; Milivojevič, L. Anthocyanin degradation of blueberry-aronia nectar in glass compared with carton during storage. *J. Food Sci.* **2008**, *73*, S405−S411.

(13) Mayer-Miebach, E.; Adamiuk, M.; Behsnilian, D. Stability of chokeberry bioactive polyphenols during juice processing and stabilization of a polyphenol-rich material from the by-product. *Agriculture* **2012**, *2*, 244−258.

(14) Brownmiller, C.; Howard, L. R.; Prior, R. L. Processing and storage effects on monomeric anthocyanins, percent polymeric color, and antioxidant capacity of processed blueberry products. *J. Food Sci.* **2008**, *73*, H72−H79.

(15) Hager, T. J.; Howard, L. R.; Prior, R. L. Processing and storage effects on monomeric anthocyanins, percent polymeric color, and antioxidant capactiy of processed blackberry products. *J. Agric. Food Chem.* **2008**, *56*, 689−695.

(16) Hager, A.; Howard, L. R.; Prior, R. L.; Brownmiller, C. Procesing and storage effects on monomeric anthocyanins, percent polymer color, and antioxidant capacity of processed black raspberry products. *J. Food Sci.* **2008**, *73*, H134−H140.

(17) Cho, M. J.; Howard, L. R.; Prior, R. L.; Clark, J. R. Flavonoid glycosides and antioxidant capacity of various blackberry, blueberry, and red grape genotypes determined by high-performance liquid chromatography/mass spectrometry. *J. Sci. Food Agric.* **2004**, *84*, 1771−1782.

(18) Cho, M. J.; Howard, L. R.; Prior, R. L.; Clark, J. R. Flavonol glycosides and antioxidant capacity of various blackberry and blueberry genotypes determined by high-performance liquid chromatography/mass spectrometry. *J. Sci. Food Agric.* **2005**, *85*, 2149−2158.

(19) Giusti, M. M.; Wrolstad, R. E. Characterization and measurement of anthocyanins with UV-visible spectroscopy. In *Current Protocols in Food Analytical Chemistry*; Wrolstad, R. E., Ed.; Wiley: New York, NY, USA, 2001; pp F1.2.1−F1.2.13.

(20) Prior, R. L.; Fan, E.; Ji, H.; Howell, A.; Nio, C.; Payne, M. J.; Reed, J. D. Multi-laboratory validation of a standard method for quantifying procyanidins in cranberry powders. *J. Sci. Food Agric.* **2010**, *90*, 1473−1478.

(21) Howard, L. R.; Brownmiller, C. R.; Prior, R. L.; Mauromoustakos, A. Improved stability of chokeberry juice anthocyanins by β-cyclodextrin addition and refrigeration. *J. Agric. Food Chem.* **2013**, *61*, 693−699.

(22) Ichiyanagi, T.; Oikawa, K.; Tateyama, C.; Konishi, T. Acid mediated hydrolysis of blueberry anthocyanins. *Chem. Pharm. Bull.* **2001**, *49*, 114−123.

(23) Sadilova, E.; Carle, R.; Stintzing, F. C. Thermal degradation of anthocyanins and its impact on color and *in vitro* antioxidant capacity. *Mol. Nutr. Food Res.* **2007**, *51*, 1461−1471.

(24) Skrede, G.; Wrolstad, R. E. Chapter 3. Flavonoids from berries and grapes. In *Functional Foods: Biochemical and Processing Aspects*, 1st ed.; Shi, J., Mazza, G., Maguer, M., Eds.; CRC Press: Boca Raton, FL, USA, 2002; Vol. 2 pp 71−133.

(25) Kader, F.; Rovel, B.; Girardin, M.; Metche, M. Mechanism of browning in fresh highbush blueberry fruit (*Vaccinium corymbosum* L.). Partial purification and characterization of blueberry polyphenol oxidase. *J. Sci. Food Agric.* **1997**, *73*, 513−516.

(26) Kader, F.; Rovel, B.; Girardin, M.; Metche, M. Mechanism of browning in fresh highbush blueberry fruit (*Vaccinium corymbosum* L.). Role of blueberry polyphenol oxidase, chlorogenic acid and anthocyanins. *J. Sci. Food Agric.* **1997**, *74*, 31−34.
(27) Kader, F.; Irmouli, M.; Nicolas, J. P.; Metche, M. Involvement of blueberry peroxidase in the mechanisms of anthocyanin degradation in blueberry juice. *J. Food Sci.* **2002**, *67*, 910−915.
(28) Kunsági-Máté, S.; May, B.; Tschiersch, C.; Fetzer, D.; Horváth, I.; Kollár, L.; Nikfardjam, M. P. Transformation of stacked $\pi-\pi$-stabilized malvidin-3-*O*-glucoside — catechin complexes towards polymeric structures followed by anisotropy decay study. *Food Res. Int.* **2011**, *44*, 23−27.
(29) Hellstrom, J.; Mattila, P.; Karjalainen, R. Stability of anthocyanins in berry juices stored at different temperatures. *J. Food Compos. Anal.* **2013**, *31*, 12−19.
(30) Castaneda-Ovando, A.; Pacheco-Hernandez, M. L.; Paez-Hernandez, E.; Rodriguez, J.; Galan-Vidal, C. Chemical studies of anthocyanins: a review. *Food Chem.* **2009**, *113*, 859−871.
(31) Howard, L. R.; Prior, R. L.; Liyanage, R.; Lay, J. O. Processing and storage effect on berry polyphenols: challenges and implication for bioactive properties. *J. Agric. Food Chem.* **2012**, *60*, 6678−6693.
(32) Brownmiller, C.; Howard, L. R.; Prior, R. L. Processing and storage effects on blueberry (*Vaccinium corymbosum* L.) polyphenolics. *Acta Hortic.* **2009**, *841*, 347−354.

JOURNAL OF AGRICULTURAL AND FOOD CHEMISTRY

Review

pubs.acs.org/JAFC

Pro-oxidative and Antioxidative Controls and Signaling Modification of Polyphenolic Phytochemicals: Contribution to Health Promotion and Disease Prevention?

Kai On Chu,[†,‡] Sun-On Chan,[#] Chi Pui Pang,[†] and Chi Chiu Wang*[,‡]

[†]Department of Ophthalmology and Visual Sciences, The Chinese University of Hong Kong in Hong Kong Eye Hospital, Kowloon, Hong Kong

[‡]Department of Obstetrics and Gynaecology, The Chinese University of Hong Kong in Prince of Wales Hospital, Shatin, New Territories, Hong Kong

[#]School of Biomedical Sciences, The Chinese University of Hong Kong, Shatin, New Territories, Hong Kong

ABSTRACT: Polyphenolic phytochemicals (PPs) have been extensively studied as potential nutriceuticals for maintenance of health and treatment of cancer, inflammation, and neurodegeneration. However, the reported beneficial outcomes are inconsistent. The biological activities of PPs have been attributed to their pro-oxidative and antioxidative actions and effects on signaling mechanisms and epigenomic modifications. These diversified properties were described or postulated on the basis of a variety of experimental studies using cell culture and animal models, even though most have not been replicated and results are not validated. This review attempts to give an overview of biological properties of PPs, based on the coherent results from relevant studies, and evaluate critically the experimental conditions and possible artifacts. Complicated molecular mechanisms and multitargeting genomic interactions of PPs are discussed, with a view that reasonable mechanistic propositions are usually obtained from well-designed in vivo studies.

KEYWORDS: *phytochemical polyphenols, antioxidation, pro-oxidation, signaling, epigenetic*

INTRODUCTION

Polyphenolic phytochemicals (PPs) are bioactive secondary metabolites found in a variety of plants. These compounds have diversified chemical structures and properties and are formed by one or more six-carbon aromatic rings with at least two hydroxyl groups. According to the structure and position in the biosynthetic pathways,[1−3] they can be classified into three major classes: (1) hydroxycinnamic acids, (2) chalcone, and (3) flavonoids, which include flavonols, flavones, isoflavones, flavanones, procyanidins, and anthocyanins/cyanidin (Figure 1). Although hydroxycinnamic acid has only one hydroxyl group, it shares common functional properties with other polyphenols.

PPs are commonly found in different species of plants and are involved in many biological activities essential for survival. They contribute to the color in leaves, flowers, and fruits, attracting insects and facilitating reproduction and dissemination. They protect plants against pathogens, repel insect attacks, and minimize harmful effects of ultraviolet light. They act also as antioxidants to scavenge free radicals generated during photosynthesis.[4,5]

Most polyphenols are flavonoids. Their nuclear structures are composed of two aromatic rings, A and B, linked to an oxygenated heterocyclic ring C. They are further divided into subclasses according to the extent of hydrogenation and the position of the heterocyclic ring. Polyphenols are commonly found in fruits and vegetables. Various types of quercetin glucoside derivatives are commonly found in onion, broccoli, lemon, and grapefruit,[6−8] whereas rutin is rich in asparagus and buckwheat.[9,10] Isoflavones are found in soy milk, beans, and vegetable proteins;[6,11] anthocyanidins in red and bluish cherries;[6,12] proanthocyanidins in grape seed and red wine;[13,14] ellagic acid derivatives in grapes and strawberries;[15−17] catechins in green and black tea;[6,18] and kaempferol glycosides and derivatives in broccoli and radish[19,20] (Table 1). Other important polyphenol groups are phenylpropanoids (e.g., hydroxycinnamic acid), stilbenoids (e.g., resveratrol), and benzoic acids.

Structural Properties. The potent antioxidant property of polyphenols is mainly attributed to the chemical structures. Polyphenols contain an ortho-diol or trihydroxyl group in the B ring and a meta-5,7-dihydroxyl group in the A ring. The diol group forms a complex with metal ions, allowing the polyphenol to scavenge catalytic ions and prevent free radical generation.[21,22] The 2,3-double bond conjugates with keto groups in the C ring. Hydroxyl groups are present at the 3- and 5-positioned for efficient hydroxylation without steric hindrances.[23−25] The hydroxyl group maintains chemical stability by delocalizing electrons captured from free radicals and reacts with peroxyl radicals to form anthocyanin-like compounds,[26] seven-member B-ring anhydride dimers, and ring-fission compounds. In addition, some flavonoids are both lipophilic and hydrophilic, enabling them to dissolve at the interface between plasma membrane and aqueous layer.[25,27] Therefore, they can quench the propagation of free radicals formed during

Received: August 29, 2013
Revised: March 7, 2014
Accepted: April 19, 2014
Published: April 20, 2014

ACS Publications © 2014 American Chemical Society

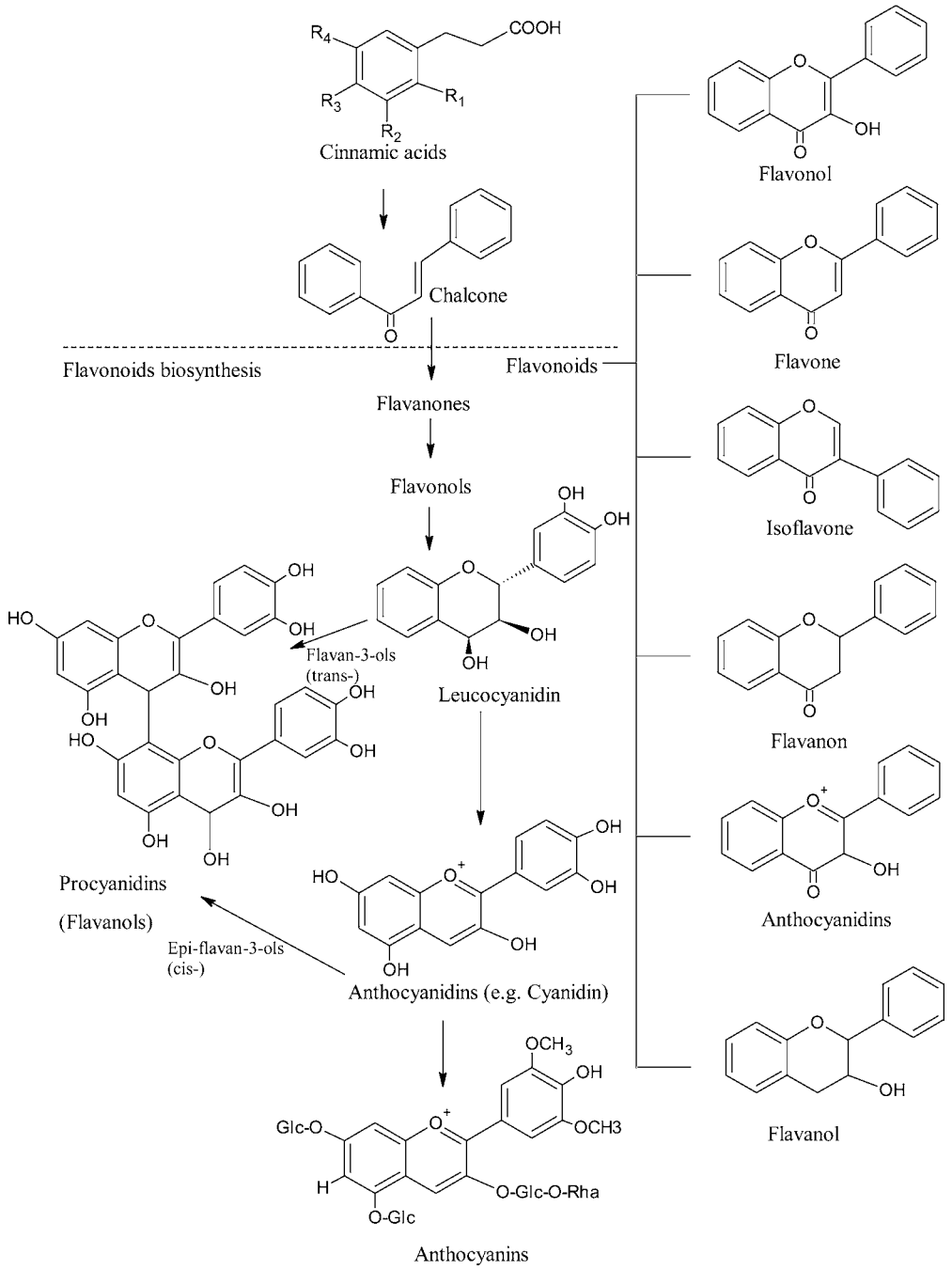

Figure 1. Basic structures of the skeletons of polyphenols.

Table 1. Phytochemicals and Their Natural Sources

phytochemicals	natural sources	refs
quercetin glucoside derivatives	onions, broccoli, lemon, and grapefruit	6−8
rutin	asparagus and buckwheat	9, 10
isoflavones	soy milk, beans, and vegetable proteins	6, 11
anthocyanidins	red and bluish cherries	6, 12
proanthocyanidins	grape seed and red wine	13, 14
ellagic acid derivatives	grapes and strawberries	15−17
catechins	green and black tea	6, 18
kaempferol glycosides and derivatives	broccoli and radish	19, 20

lipid peroxidation. They also regenerate oxidized α-tocopherol in the lipid membrane and oxidize ascorbic acid and glutathione in the aqueous layer.[28,29]

Different mathematical methods for structure−activity relationships have been used to predict the antioxidant and pro-oxidant properties of flavonoids. Antioxidative potency and inhibitory effect on matrix metalloproteinase (MMP) expression are related positively to the number of OH groups on the B ring (e.g., in myricetin, queretin, kaempferol, luteolin, apigenin, and chrysin), as determined by diphenyl-2-picrylhydrazine (DPPH) and xanthine/xanthine oxidase assays.[30,31] Fukumoto and colleagues[32] also used β-carotene bleaching and HPLC to study the antioxidative activity of polyphenolic compounds and found PPs with more hydroxyl groups and less

dx.doi.org/10.1021/jf500080z | J. Agric. Food Chem. 2014, 62, 4026−4038

glycosylation demonstrate higher antioxidative activities. Quantitative structure−activity relationship (QSAR) models are applied to correlate physical properties of polyphenols with pro-oxidant activity. The cytotoxicity is associated with single electron oxidation in polyphenols.[33,34] Hydrophobicity, in terms of partition coefficient (w/o), is also found correlated to apoptosis and cytotoxicity.[35,36] The three-dimensional (3D) topographic structure has been used to predict the effect of PPs on caspase-mediated apoptotic activity.[37] Comparative molecular field analysis (CoMFA) and comparative molecular similarity indices analysis (CoMSIA) have shown positive correlation of steric and hydrophobic fields of different phenols with caspase-mediated apoptosis. Substituents with larger hydrophobicity at position 2 and less hydrophobicity at position 4 favor the activity, whereas substituents with more electronegativity at position 4 and less electronegativity at position 3 also increase the activity. On the other hand, the position of hydroxyl groups, dipole moment magnitude, and the shape of molecules also correlate with the inhibition of lipid peroxidation and antioxidation observed in melatonin derivatives and flavonoids.[38,39] The 3D structure of flavonoid has also been related to the radical-scavenging activity.[40,41] The energy of the highest occupied molecular orbital and the energy of heat formation both contribute significantly to the radical-scavenging activity. These may explain why flavonoids with 3′,4′-dihydroxy groups at the B ring, a 3-OH group, or an increased number of −OH groups show higher radical-scavenging activity. The methyl or *o*-glucoside substituent does not affect the activity. In summary, the concentration, physicochemical property, and physical and topological structures are important factors influencing the antioxidant, pro-oxidant, and enzyme modulatory properties of polyphenols.

BENEFICIAL EFFECTS OF POLYPHENOLIC PHYTOCHEMICALS TO HUMAN HEALTH

Epidemiological Studies. Epidemiological studies, however, do not indicate conclusive results on beneficial effects of PP consumption on human health. There are difficulties in interpreting results of case-control studies, likely caused by differences in confounding factors, variations in quantifying dietary PP consumption, lack of objective biomarker measurements, differences in disease etiology, geographic location and population, and genetic polymorphism and heterogeneity.[42] Nevertheless, there are strong links between PP intake and reduced incidence of cardiovascular disease and cancer.[43] Also, over 200 case-control studies and cohort studies have shown associations between tea consumption and reduced risk for colon, lung, stomach, breast, prostate, ovarian, pancreatic, kidney, and bladder cancers.[42] However, the results reported in these studies are rather inconsistent.[44] More epidemiological studies and intervention trials are needed to confirm the direct beneficial effects of PPs.

Animal Studies. Well-designed intervention studies may provide a better understanding of beneficial effects of PPs.[45−47] For cancer prevention, most in vivo studies are carried out in animal disease models. In particular, many studies have shown that tea polyphenols are able to inhibit tumorigenesis during the initiation, promotion, and progression stage of cancers.[48] Cancer models of the alimentary canal have been investigated extensively with positive results.[44] The anti-carcinogenic effectiveness is possibly due to direct exposure of high concentration of PPs to the tissues along the alimentary tract. Tea polyphenols inhibit the spontaneous development of small intestinal tumors in a dose-dependent manner, which is associated with an increased E-cadherin signaling and reduced expression of nuclear β-catenin, MYC (transcription factor regulating gene), phospho-Akt (protein kinase B), phospho-ERK1 (extracellular-signal-regulated kinases 1), and phospho-ERK2.[49] Skin and lung cancers are also studied with favorable outcomes. In a mouse model of adenocarcinoma, a high dose of green tea extract (0.5% Polyphenon E) is given daily to mice for 52 weeks. This treatment has shown to inhibit cell proliferation, increase apoptosis, and decrease levels of phosphorylated transcription factors Jun, ERK1 and ERK2.[50] Co-treatment of tea polyphenols and lipid-lowering agent Atorvastatin can down-regulate the anti-apoptotic proteins, induce myeloid leukemia cell differentiation protein (MCl1) and B-cell lymphoma-extra-large protein (Bcl-XL), and so stimulate apoptosis in a synergistic inhibitory manner both in vivo and in vitro.[51]

Cell Culture Studies. Under certain circumstances, flavonoids are pro-oxidative, especially at high doses and in the presence of metal ions.[52,53] It has been reported that a lot of food contains polyphenols, especially flavonoids (quercetin, myricetin, kaepferol, and caffeic acid) that exert pro-oxidant effects.[54−57] Although the pro-oxidant property of polyphenols has been postulated to prevent colon cancers,[58,59] pro-oxidation can induce mitochondrial dysfunction, leading consequently to apoptosis of cancer cells and mobilization of endogenous catalytic copper, which induces oxidative damage of proteins, DNA, mitochondria, and lipids inside the cell.[60,61] Although these reactions occur mainly in in vitro condition, diseases that involve increased systemic ion overload, such as hemochromatosis,[107] may result in serious internal lesions if highly reducing polyphenols are administered to reduce the free ion loading.[62]

BIOLOGICAL PROPERTIES OF POLYPHENOLIC PHYTOCHEMICALS

Antioxidation. PPs can scavenge directly the reactive oxygen species (ROS) and chelate divalent metal ions to reduce the oxidative activity. PPs also exert indirect antioxidant effects through induction of endogenous protective antioxidative enzymes. This indirect activity acts primarily through activation of nuclear factor-erythroid-2-related factor 2 (Nrf2), which stimulates antioxidative enzymes such as glutathione peroxidase (GPx), glutathione *S*-transferase, catalase, NAD(P)H:quinone oxidoreductase-1 (NQO1), and/or phase II enzymes.[63] Notably, these indirect activities involve up-regulation of antioxidant enzymes or cytoprotective proteins[64] and provide more efficient antioxidant actions in vivo.[65,66] Although PPs are strong antioxidants in vitro, their direct free radical neutralization activity is reported in only a small number of in vivo studies, because of the limited bioavailability[67] and the presence of excessive oxidative stress.

Pro-oxidation. PPs can be oxidized to generate ROS in cell culture medium that results in cell death.[68] This pro-oxidant effect appears to be responsible for the induction of apoptosis in cancer cell studies. The pro-oxidant activity is most prominent under experimental conditions such as high pH and excessive availability of transition metal ions and oxygen molecules,[69] which cause chemical instability, depletion of cellular GSH, and mobilization of cellular copper ions.[65] The ROS generation may subsequently activate Nrf2 antioxidant-responsive element pathway to induce production of antioxidative and detoxifying enzymes.[70] Nuclear factor kappa-light-chain-enhancer of activated B cells (NF-κB) has

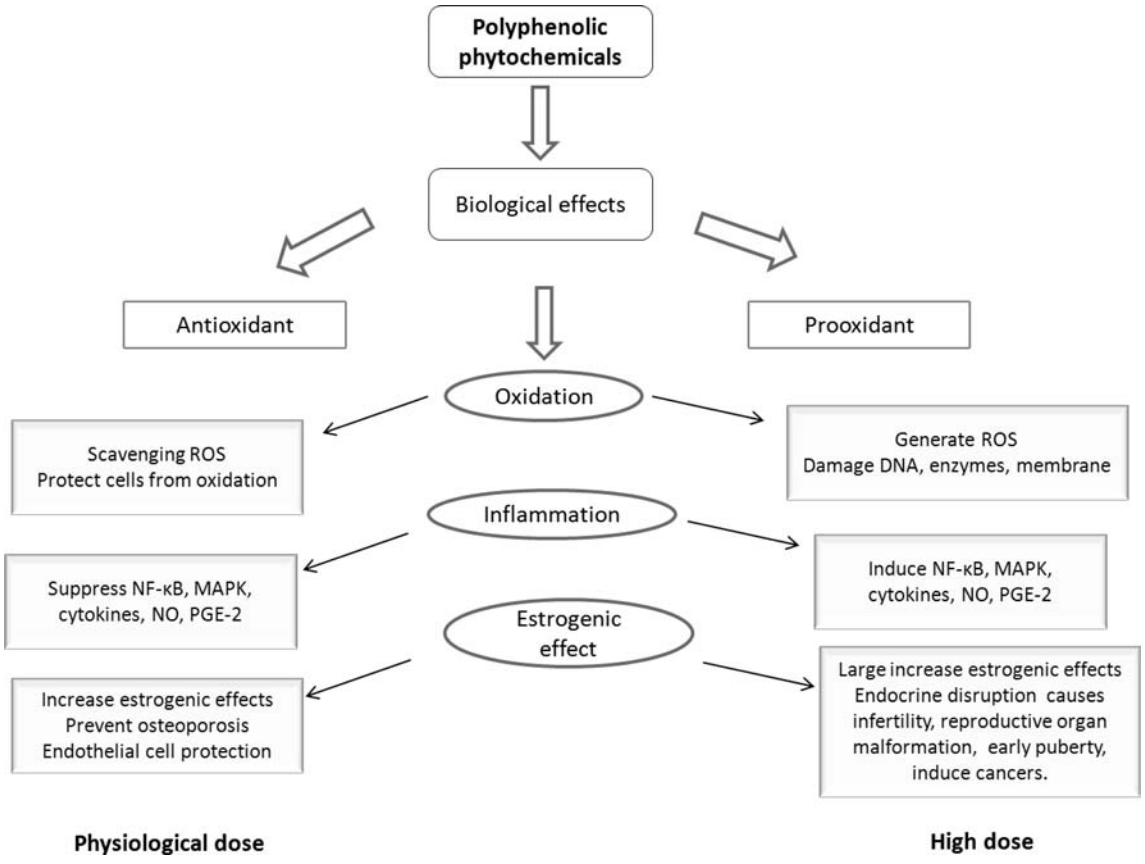

Figure 2. Schematic diagram shows PPs exhibit different biological effects under different dosages.

been described as a redox-regulated transcription factor because it is activated by oxidative stress and inhibited by various antioxidants. Interactions between these NRF2 and NF-κB occur likely because their upstream signaling molecules, such as mitogen-activated protein kinases (MAPK), phosphatidylinositide 3-kinases (PI3K), and protein kinase C (PKC), are closely regulated.[71]

Inflammation Inhibition. PPs may act as inflammation modulatory agents by down-regulating NF-κB and inducing inflammatory cytokine release through ROS generation.[72] Oxidized low-density lipoprotein (LDL) is a major constituent of atherogenic plaques on the vascular wall that induce macrophage foam cell formation and thrombotic activity.[73] PPs inhibit oxidation of LDL[74] and modulate the inflammatory process through inhibition of mitogen-activated protein (MAP) kinases, NF-κB, and tumor necrosis factor alpha (TNF-α) and induction of vascular cell adhesion molecules (VCAM) and c-Jun N-terminal kinase activity.[75]

Interaction with Signaling Molecules and Enzymes. EGCG has been studied extensively and shown to be an enzyme inhibitor in the phosphorylation of proteins and kinases such as JNK, JUN, MEK1, MEK2, ERK1, ERK2, and ETS domain-containing protein (ELK1). The inhibition is associated with activator protein 1 (AP1) transcriptional activity and cell transformation.[76,77] Cyclin-dependent kinase 2 (CDK2) and CDK4, which are associated with cell cycle at G0 and G1 phases, are inhibited by EGCG.[78] EGCG has also been reported to inhibit the chymotryptic activity of 20S proteasomes, leading to G0 and G1 cell cycle arrest and accumulation of p27 and NF-κB inhibitor (IκB).[79] EGCG also increases the expression of tissue inhibitor of metalloproteases 1 (TIMP1) and TIMP2[80] and activates dihydrofolate reductase, glucose-6-phosphate dehydrogenase, and glyceraldehyde-3-phosphate dehydrogenase.[63] Moreover, green tea extract, in which EGCG is the major polyphenol, also up-regulates γ-glutamyltransferase, glutamate cysteine ligase, hemoxygenase-1, and glutathione *S*-transferase P.[81,82] On the other hand, curcumin prevents hematogenous breast cancer metastases in immunodeficient mice through reduction of NF-κB activity and down-regulation of AP-1 to suppress MMPs expression.[83]

Many studies have demonstrated an inhibitory effect of EGCG on EGF receptor signaling pathways, which are frequently overexpressed in cancers and associated with poor prognosis.[84] Phosphorylation of hepatocyte growth factor receptor (HGFR) and AKT1, which are important in epithelial-mesenchymal transition in tumorigenesis and metastasis, has been shown to be completely blocked by EGCG.[85] EGCG also decreases the RNA and peptide level of vascular endothelial growth factor A (VEGFA), disrupts VEGFA-induced VEGFR2 dimerization, and suppresses the downstream PI3K activity.[86] In prostate cancer models, tea polyphenols suppress cell proliferation and increase apoptosis through inhibition of VEGF-A, MMPs, and insulin-like growth factor 1 (IGF1) signaling pathways.[87,88] Currently, more than 20 human trials with tea polyphenol preparations have been planned or conducted. However, only a few have been completed or have yielded clear and consistent conclusions.[89]

The eight hydroxyl groups of EGCG can serve as hydrogen bond donors. EGCG has been shown to bind to salivary proline-rich proteins, fibronectin, fibrinogen, histidine-rich glycoproteins, metastases associated 67 kDa laminin receptor, and the BH3 pocket of anti-apoptosis Bcl-2 proteins.[90] Using a

Sepharose 4B column, 2D electrophoresis, and MALDI-TOF mass spectroscopy, EGCG is reported to bind directly to vimentin, insulin-like growth factor 1 receptor (IGF1R), proto-oncogene tyrosine-protein kinase (FYN), glucose-regulated proteins (GRP78), and zeta-chain-associated protein kinase 70 (ZAP70), which are associated with cell cycle regulation, cell proliferation, and cell survival.[63] In addition, EGCG can physically bind to nucleic acids, suggesting that DNA and RNA are also targets of tea polyphenols.[91]

Epigenomic Modulation. PPs function as potent modulators for mammalian epigenetic regulation through DNA methylation, histone acetylation, and histone deacetylation.[92] EGCG inhibits both DNA methyltransferase (DNMT) and histone acetyltransferase (HAT), leading to DNA demethylation and histone H3 and H4 deacetylation in human telomerase-reverse transcriptase (hTERT) promoter, respectively. These events affect epigenomic regulation and chromatin restructuring that result in hTERT down-regulation and telomerase inhibition, leading ultimately to cell apoptosis.[93,94] Inhibition of DNMT also causes demethylation of hypermethylated promoters of tumor suppressor gene such as inhibitors of CDK4A (INK4A), retinoic acid receptor-β, the DNA repair genes MutL homologue 1 (MLH1), and methylguanine methyltransferase.[95] Such epigenetic inhibition of estrogen receptors is mainly due to hypomethylation of hTERT promotor, deacetylation of histone by DNMT, and HAT inhibition.[96] EGCG causes chromatin remodeling by histone acetylation and DNA methylation to reactivate ERα receptor of breast cancer cells; that is, antiestrogen treatment is possible.

EGCG can also suppress DNA methylation, DNMT, and histone deacetylase (HDAC) activity. It lowers DNMT expression and increases histone acetylation. These effects lead to suppression of cancer proliferation.[97−99] EGCG also modulates immunity, possibly through epigenetic regulation of T cells, to suppress autoimmune diseases.[100] Curcumin also produces necrosis and apoptosis of cancer cells through epigenetic regulation of HAT, HDAC, DNMT, and miRNA to modulate gene expression.[101−103] The epigenetic inhibition also targets the upstream phosphodiesterase, which hydrolyzes signaling molecules such as cAMP and cGMP, resulting in antiproliferation of melanoma cells.[104]

CONTROVERSY OF BIOLOGICAL EFFECTS OF POLYPHENOLS

Oxidative stress is the result of overproduction of oxygen-derived free radicals caused by ultraviolet light exposure, allergen, pollution, smoking, emotional stress, intensive exercise,[105,106] and excessive fat and carbohydrate consumption.[107−109] Even normal cellular metabolism can generate oxygen-derived reactive species that need antioxidants for neutralization.

Controversy on Antioxidation and Pro-oxidation Properties. PPs are known for their antioxidative effects, which are presumably beneficial to health. Many diseases are attributed to chronic exposure to oxygen-derived radical species, for example, cardiovascular diseases,[110] cancers,[111] and neurodegenerative disorders.[112] Antioxidant treatment, in particular PP, has been proposed to alleviate these diseases by free radical neutralization. These antioxidative properties have been demonstrated in many studies. For example, quercetin (a flavonoid) protects rat H41E cells against H_2O_2-induced cytotoxicity at low doses (10−25 μM).[113] γ-Resorcyclic acid and hydrobenzoic acid[114] remove excess ions at low pH by chelating ions and forming stable complexes. Green tea can inhibit lipoprotein oxidation induced by Cu^{2+} ion.[115] However, these antioxidative effects have been demonstrated only in cell culture experiments.[116]

Table 2. Key Publications of Biological Mechanisms of Polyphenols

mechanism	contents	refs
antioxidation	• reaction mechanisms of different polyphenols scavenging free radical and oxidized to different compounds	21, 26
	• indirect antioxidant increase anti-oxidative enzymatic and signaling activities	64
	• bioavailability of polyphenols	67
pro-oxidation	• polyphenols generate ROS present in culture medium	125, 126
	• pro-oxidation appears at high concentration PPs and ions	69, 70
	• pro-oxidative effect provokes enzymatic and signaling molecular activation	70, 71
inflammation	• pro-oxidative effect provokes enzymatic and signaling molecular activation	74
modulation signaling and enzymes	• PPs involve different signaling pathways and regulation enzymes	76, 79, 81, 82
epigenomic modulation	• pro-oxidative effect provokes enzymatic and signaling molecular activation	92, 94, 102

In contrast, many cell culture studies instead show polyphenols exhibit pro-oxidant properties, particularly when they are applied at high doses.[117,118] For example, quercetin at 50 μM promotes superoxide production in cell culture condition.[117] The survival rate, viability, thiol level, total antioxidative capacity, and antioxidative enzyme activities are all reduced under this high dose.[118] The cytotoxic effect is probably caused by DNA damage and apoptosis as a result of ROS production through autoxidation at high concentration.[119,120] However, the toxicity is not observed even at an oral dose as high as 2000 mg/kg in mice, probably because of low bioavailability and the high metabolic rate in the animals.[121]

Moreover, instead of chelating metal ions, a high level of strong antioxidant PPs (e.g., 50 μM−1 mM EGCG) can induce a pro-oxidative effect in the presence of metal ions.[119,122,123] EGCG induces DNA fragmentation in cells as a result of oxidative damage[119] by hydrogen or electron donation to catalytic metal ions, for example, Fe^{3+} and Cu^{2+}, that generates free radicals via the Fenton reaction.[107] In addition, PPs, including EGCG, can generate free radicals, superoxides, and hydrogen peroxide species in cell culture medium, for example, Dulbecco's modified Eagle medium (DMEM).[124−126] Oxidative stress may be arbitrarily induced in the surrounding medium instead of through the intracellular biological processes in some cell culture experiments.

Extrapolation of Results from Cell Culture Studies. Many beneficial effects of PPs and their association with antioxidant and pro-oxidant properties have been proposed on the basis of studies in cultured cell lines. It has been speculated from experimental conditions that cannot be recapitulated in in vivo conditions. For example, to demonstrate the pro-oxidative effect, high concentrations of PPs are added into the culture

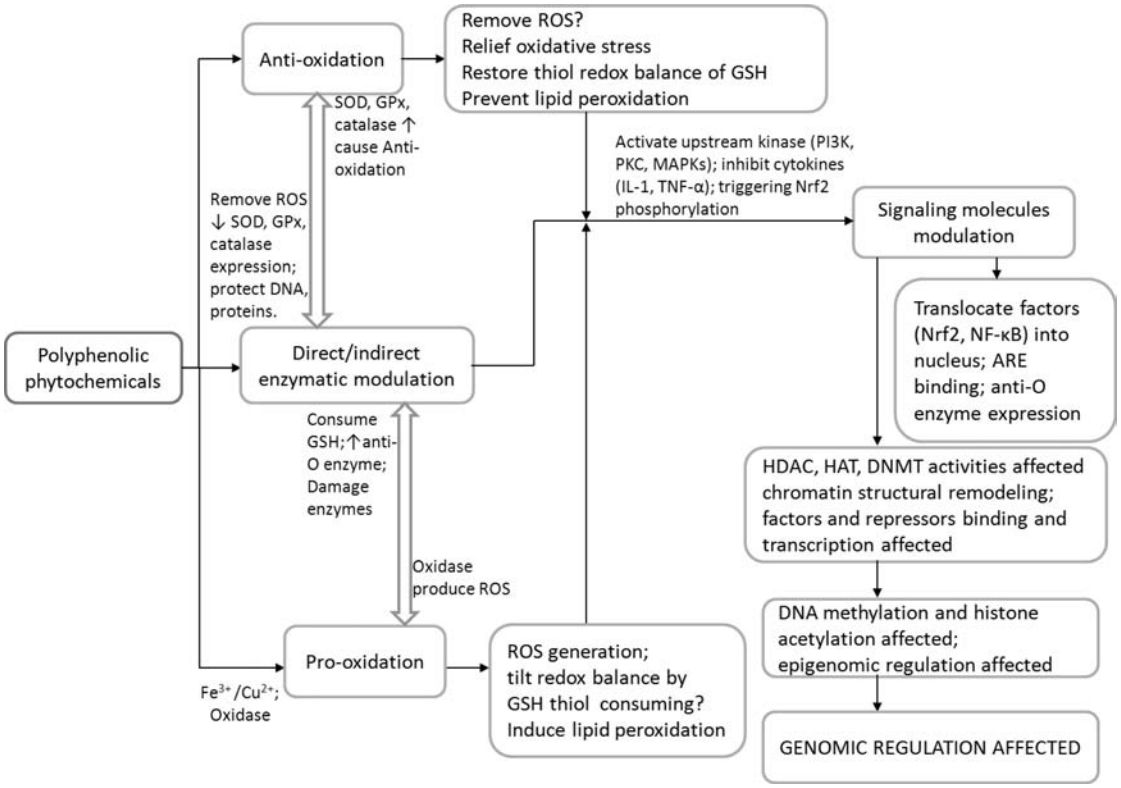

Figure 3. Schematic diagram shows the possible interactions between different mechanisms affecting the final genomic regulation. Polyphenolic phytochemicals can act as antioxidants or prooxidants under different conditions to tilt the redox status that affects signaling molecules response, modify the epigenetic regulation, and eventually affect genomic expression. On the other hand, they can directly bind to regulatory enzymes or indirectly influence their activities that induce the signaling cascades and eventually affect the genomic regulation.

medium.[127] An extraordinarily high concentration (250 μM) of flavonoid (quercetin and fisetin) has been used to show that flavonoid can induce DNA damage and apoptosis.[113] However, this high level of flavonoid cannot be reached in physiological conditions in vivo. Moreover, because most flavonoids are not completely water-soluble, to achieve such a high concentration the researchers have to dissolve the compounds in dimethyl sulfoxide (DMSO).[128] The solvent may enhance membrane permeability to increase the intracellular concentration of PPs. Practically, this method cannot be applied for human treatment. For the green tea extract, Polyphenon E, which has been used for clinical trial in humans suffering from colon cancer, the maximum dose, 1200 mg of EGCG, tested produces only a C_{max} of EGCG in plasma at about 7.3 μM for a transient period.[129] The bioavailability of PP is actually limited in in vivo condition. On the other hand, some researchers apply strong reducing antioxidants to high concentration of free ions, such as Fe^{3+} and Cu^{2+}, to investigate their pro-oxidative potential.[62,119] Again, this condition is not achievable under normal physiological conditions because almost all catalytic ions are bound onto proteins, cofactors, and enzymes. Only a low concentration of free ions (e.g., ~10^{-18} M intracellular Cu^{2+})[130] is available. Flavonoids at such low ion concentrations would act as chelators instead[131] (Figure 2).

Controversy in Reaction Kinetics and Pharmacokinetics of Polyphenols. The scavenging property of PPs has been questionable because the rate of free radical generation is very fast (rate constant ranged from 8.29×10^6 M^{-1} s^{-1} for phenol to 4.03×10^9 M^{-1} s^{-1} for catechol) when compared to scavenging rates of polyphenols (~4×10^3 M^{-1} s^{-1}).[132,133] Therefore, the free radicals are expected to have damaged surrounding molecules before they are captured by the polyphenol. In addition, from the pharmacokinetic point of view, it remains suspicious that whether the low in vivo concentration of PPs, for example, a plasma level of green tea (0.1−0.7 μmol/L for an intake of 90−150 mg catechins), cocoa (0.25−0.7 μmol/L for an intake of 70−165 mg cocoa procyanidins), or red wine (0.09 μmol/L flavonoids for an intake of 35 mg polyphenols),[134,135] is able to neutralize the surge in production of free radicals from the chain reaction. Furthermore, only a transient and modest increase in total antioxidant activity is reported in the plasma of humans[136] and rats,[137] even after administration of a substantial dose of green tea extract (GTE), probably caused by a limited bioavailability[138] and strong redox buffering in plasma.[139]

Controversy in Experimental Design. It is still unclear whether PPs have any direct antioxidant effects in vivo.[140] To confirm the antioxidative protection of EGCG, some studies precondition the retinal pigment epithelial cells with high concentrations of EGCG (~100 μM) before exposure to oxidative stress induced by H_2O_2 in the cell culture.[141] However, the results showed that the antioxidative enzyme and protein kinase levels (superoxide dismutase, catalase, and protein kinase C) are increased after addition of EGCG, indicating that EGCG, on the contrary, acts as a pro-oxidant during the preconditioning period, inducing expression of antioxidative enzymes to adapt and defend against later oxidative insult through receptor binding.[142,143] These pro-oxidative phenomena have been demonstrated in other studies, showing that endogenous antioxidative systems are induced in normal tissues to protect against later carcinogenic insults.[58] The preconditioning involves direct activation of NF-κB

without association with antioxidation. Furthermore, EGCG has been supplemented to a cancer cell culture to study its antioxidative effects. However, the anticancer effect is abolished after the addition of SOD and catalase, which is consistent with its pro-oxidative role.[144] These findings show that many in vitro experimental designs suffer from hypothesis-driven biases and may overlook some basic properties of experimental parameters.

Further investigations would be needed to confirm whether these effects can be extrapolated to in vivo situations or used for therapeutic application. The partial pressure of oxygen is much lower in the in vivo environment than in cell culture medium. The physiological composition of biological fluid is different from the medium. The bioavailability of polyphenols cannot be achieved to the same level as in the cell culture condition. The pH and redox buffering capacity is more effective in in vivo condition than in culture condition. Moreover, compartmental barriers appear in vivo. Digestion and metabolic transformations occur in vivo but not in vitro. In fact, our unpublished results showed that both antioxidative and pro-oxidative effects coexist in the rat eye after administration of green tea extract. The oxidative status depends on the type of tissues and the EGCG dosage. In short, the biological effects of PPs in vivo are the results of complex and interacting mechanisms, suggesting that animal models should be used to investigate the biological properties of PPs rather than using cell culture models.

Moreover, to understand the biological effects of a particular PP isolated from natural products in vivo, it is more appropriate to compare the effects of a genetically modified natural product without the PPs with the same natural product that contains a high concentration of those PPs. This type of experimental design includes the effect of matrix present in the natural products. With the recent advanced targeting genome editing technologies,[145] such as single guided RNA cleavage, these mutants are easily generated nowadays to facilitate in vivo analysis.

Biological Differences between Compounds Present in Natural Products and Purified Form. Epidemiological studies demonstrate that constant intake of polyphenols from a natural diet offers many health benefits.[146−149] These results imply that long-term administration of PPs at low dose from natural sources (e.g., 143 mg of flavonoids per 100 g of apple[150]) provides beneficial health effects. It is different from taking isolated polyphenols because no apparent health benefits or even harms are reported in long-term administration.[151,152] This discrepancy may be attributed to the presence of plant matrix and synergic effects of different PPs from natural products. It is supported by a study in the rat that the heart is protected from ischemia-reperfusion injury after taking mutated anthocyanin deficient maize added with concentrated anthocyanins compared to the pure mutant maize.[153] Although some animal models of diseases showed that purified polyphenols, such as quercetin, rutin, and EGCG, alleviate oxidative damages induced by ischemia-reperfusion and other interventions,[154,155] other studies reported carcinogenicity and toxicity in rodents on high-dose and long-term administration.[156,157] Therefore, the source, dosage, duration of administration, and animal model are important factors to determine whether the effects are beneficial or harmful.

Interactions with Signaling Molecules. Recently, the biological effects of polyphenols have been attributed to their interactions with signaling molecules. Examples include inhibition of phosphorylation of mitogen activated protein (MAP) kinase,[158] AP-1, and ELK-1/2 through direct competitive binding on the proline-rich site.[159] The importance of this interaction is further supported by congeners with similar chemical properties. EGCG and its related compound theaflavin-3,3′-digallate inhibit the MEK1 and Raf-1 pathways, respectively, suggesting that the effects are independent of redox status but with their specific structures. The interaction can involve direct binding or indirect signaling modulation.[84] Interestingly, the IC_{50} doses reported in these studies are about 0.1 μM, which is close to the physiological level of PPs.

Flavonoids have been shown to bind to many key binding sites including the ATPase binding site, which affects a number of signaling molecules such as calcium plasma membrane ATPase and protein kinases,[160] which are involved in the regulation of many cellular processes. This may explain why PPs affect a wide range of biological activities, which could be beneficial in one instance and harmful in others. For example, the estrogen-like activity of isoflavones through binding to β-estradiol receptors can relieve menopause symptoms but induce breast and prostate cancer.[161,162]

These biological activities likely involve multiple molecular mechanisms rather than single receptors or molecular targets. Apart from antioxidative and pro-oxidative mechanisms, PPs also inhibit inflammation, enzyme activities, and signal transduction pathways, resulting in the suppression of cell proliferation and enhancement of apoptosis, as well as inhibition of cell invasion, angiogenesis, and metastasis in cancer cells. PPs have been shown to bind directly to several receptors[163,164] and signaling molecules,[165] and also inhibit the functions of key receptors,[166] kinases,[167] proteinases, and other enzymes.[168,169] These results may explain why PPs have such a variety of biological effects[80,95,170−172] and account for the fact that addition of SOD or catalase in the cell culture experimental studies cannot abolish completely PPs' actions.[173] However, evidence of direct interactions with receptors and enzymes comes largely from cell culture studies that involve high concentrations of PPs (5−100 μM) and defined experimental conditions. These direct interactions may not reflect the actions in physiological condition as nonspecific binding may occur at high concentration, and the polyphenol per se may be modified in the culture environment. For example, EGCG is epimerized to GCG when SOD is added.[174] This epimerized product inhibits epidermal growth receptor (EGFR) phosphorylation that may complicate the outcome of the experiment.[175]

Epigenomic Modulation. In addition to enzymatic and signaling regulation, polyphenols also exert antioxidative action through genomic and epigenomic regulations. EGCG is involved in the epigenetic regulation of apoptosis in cancer cells, which involves upstream inhibition of HAT and DNMT epigenetic mechanisms[176] that eventually affect the gene expression of antioxidative enzymes. As PPs are known to act as effective antioxidants, they may regulate functions of cellular epigenome through their antioxidative effects on the redox status.[177] PPs also act as pro-oxidants in the presence of Fe^{3+} and oxygen or in concert with oxidases to induce oxidative stress, which in turn cause modulation of cellular epigenome through oxidant and thiol-redox signaling. PPs are also known to involve in biotransformation into metabolites catalyzed by the cellular phase I and phase II xenobiotic-metabolizing enzymes, which may regulate the cellular epigenome through signaling cascades.

Summary. The complex properties and possible actions of polyphenols are summarized in Table 2 and Figure 3. Again, most molecular and genomic studies are conducted in cell culture studies. Whether these mechanisms reflect the biological processes in animals remains to be determined in future experiments.

PROSPECTIVES

Although aglycones can be absorbed from the small intestine, most natural polyphenols are esterified with glycosides. They need to be hydrolyzed by intestinal enzymes or colonic microflora before absorption.[178] Flavonoids are conjugated by methylation, sulfation, and glucuronidation in the small intestine, liver, and colon.[179] The remaining flavonoids in the colon are metabolized extensively by microflora to form small phenolic derivatives such as protocatechuic acid.[180] The hydrolyzed aglycones and breakdown products are absorbed into the colon and excreted into the bile in enteroheptic circulation.[179] Therefore, the bioavailability of polyphenols is low, and the systemic concentration of biochemical metabolites is usually far higher than that of their parent compounds.

To investigate the candidates and mechanisms contributing to the actual therapeutic effect, animal models should be the main tool for investigations instead of cell culture models, in which many essential parameters contributing to biological mechanisms cannot be replicated. Because of extensive biotransformation, the metabolites should be investigated as well as their parent compounds to find the effective constituents and understand the actual structure−activity relationship occurring in vivo. With the advanced development of high-throughput and sensitive LC-MS, GC-MS, and bioinformatics, a metabolomic approach may help to identify potential PPs and their metabolites as candidate drugs for various pathological processes.[181] Some biomarkers and indices such as oxidative stress level,[182] nitrogen oxidase synthetase, and COX pathways[183] have been established and evaluated extensively in rodents. High-sensitivity proteomic techniques should be used to detect changes of these biomarkers in a single sample, which can more likely help hunt down true candidates that contribute proper target responses for in vivo protection.

Discovery of PPs with multitargeting properties brings forth treatments with more therapeutic potential than those using a one-target−one-drug approach.[184] These drugs regulate relevant pathways simultaneously to achieve desirable biological effects, which are more effective, and the dosage and side effects are minimal. Moreover, an in vivo high-throughput screening (HTS) approach may help to characterize pharmacokinetics properties of PPs.[185,186] This approach involves giving a mixture of compounds with different scaffold structures into an animal disease model. By means of computational deconvolution technique, the lead compound with major action can be identified.[187] With these innovative technologies, the lead PP candidates and their underlying mechanisms in therapeutic treatments can soon be unraveled.

AUTHOR INFORMATION

Corresponding Author

*(C.C.W.) Department of Obstetrics and Gynaecology, The Chinese University of Hong Kong, The Prince Wales Hospital, Shatin, N.T., Hong Kong. Phone: (852) 26323099. Fax: (852) 26360008. E-mail: ccwang@cuhk.edu.hk.

Notes

The authors declare no competing financial interest.

ABBREVIATIONS USED

AP1: activator protein 1
Bcl-XL: B-cell lymphoma-extra-large protein
CDK2: cyclin-dependent kinase 2
DNMT: deoxyribonucleic acid (DNA) methyltransferase
DPPH: diphenyl-2-picrylhydrazine
ERK1: extracellular-signal-regulated kinases 1
FYN: proto-oncogene tyrosine-protein kinase
GRP78: glucose-regulated proteins
HAT: histone acetyltransferase
HDAC: histone deacetylase
HGFR: hepatocyte growth factor receptor
hTERT: human telomerase-reverse transcriptase
IGF1: insulin-like growth factor 1
IGF1R: insulin-like growth factor 1 receptor
LDL: low-density lipoprotein
MAPK: mitogen-activated protein kinases
MCl1: myeloid leukemia cell differentiation protein
MMP: metalloproteinase
MYC: transcription factor regulating gene
NF-κB: nuclear factor kappa-light-chain-enhancer of activated B cells
Nrf2: nuclear factor-erythroid-2-related factor 2
Phospho-Akt: protein kinase B
PI3K: phosphatidylinositide 3-kinases
PKC: protein kinase C
PPs: polyphenolic phytochemicals
QSAR: quantitative structure−activity relationship
ROS: reactive oxygen species
TIMP1: inhibitor of metalloproteinases 1
TNF-α: tumor necrosis factor alpha
VCAM: vascular cell adhesion molecules
VEGF-A: vascular endothelial growth factor A
ZAP70: zeta-chain-associated protein kinase 70

REFERENCES

(1) Bravo, L. Polyphenols: chemistry, dietary sources, metabolism, and nutritional significance. *Nutr. Rev.* **1998**, *56*, 317−333.
(2) Lepiniec, L.; Debeaujon, I.; Routaboul, J. M.; Baudry, A.; Pourcel, L.; Nesi, N.; Caboche, M. Genetics and biochemistry of seed flavonoids. *Annu. Rev. Plant Biol.* **2006**, *57*, 405−430.
(3) Henry-Kirk, R. A.; McGhie, T. K.; Andre, C. M.; Hellens, R. P.; Allan, A. C. Transcriptional analysis of apple fruit proanthocyanidin biosynthesis. *J. Exp. Bot.* **2012**, *63*, 5437−5450.
(4) Gould, K. S.; Lister, C. Flavonoid functions in plants. In *Flavonoids, Chemistry, Biochemistry and Applications*; Andersen, O. M., Markham, K. R., Eds.; CRC Press: Boca Raton, FL, USA, 2006; pp 397−442.
(5) Ibanez, S.; Gallet, C.; Després, L. Plant insecticidal toxins in ecological networks. *Toxins (Basel)* **2012**, *4*, 228−243.
(6) Nichols, J. A.; Katiyar, S. K. Skin photoprotection by natural polyphenols: anti-inflammatory, antioxidant and DNA repair mechanisms. *Arch. Dermatol. Res.* **2010**, *302*, 71−83.
(7) Gattuso, G.; Barreca, D.; Gargiulli, C.; Leuzzi, U.; Caristi, C. Flavonoid composition of citrus juices. *Molecules* **2007**, *12*, 1641−1673.
(8) Vallejo, F.; Tomás-Barberán, F. A.; Ferreres, F. Characterisation of flavonols in broccoli (*Brassica oleracea* L. var. *italica*) by liquid chromatography-UV diode-array detection-electrospray ionisation mass spectrometry. *J. Chromatogr., A* **2004**, *1054*, 181−193.
(9) Danila, A. M.; Kotani, A.; Hakamata, H.; Kusu, F. Determination of rutin, catechin, epicatechin, and epicatechin gallate in buckwheat

Fagopyrum esculentum Moench by micro-high-performance liquid chromatography with electrochemical detection. *J. Agric. Food Chem.* **2007**, *55*, 1139−1143.
(10) Wang, M.; Tadmor, Y.; Wu, Q. L.; Chin, C. K.; Garrison, S. A.; Simon, J. E. Quantification of protodioscin and rutin in asparagus shoots by LC/MS and HPLC methods. *J. Agric. Food Chem.* **2003**, *51*, 6132−6136.
(11) Malenčić, D.; Cvejić, J.; Miladinović, J. Polyphenol content and antioxidant properties of colored soybean seeds from central Europe. *J. Med. Food.* **2012**, *15*, 89−95.
(12) Wu, X.; Gu, L.; Prior, R. L.; McKay, S. Characterization of anthocyanins and proanthocyanidins in some cultivars of *Ribes*, *Aronia*, and *Sambucus* and their antioxidant capacity. *J. Agric. Food Chem.* **2004**, *52*, 7846−7856.
(13) Monagas, M.; Gómez-Cordovés, C.; Bartolomé, B.; Laureano, O.; Ricardo da Silva, J. M. Monomeric, oligomeric, and polymeric flavan-3-ol composition of wines and grapes from *Vitis vinifera* L. cv. Graciano, Tempranillo, and Cabernet Sauvignon. *J. Agric. Food Chem.* **2003**, *51*, 6475−6481.
(14) Bak, M. J.; Jun, M.; Jeong, W. S. Procyanidins from wild grape (*Vitis amurensis*) seeds regulate ARE-mediated enzyme expression via Nrf2 coupled with p38 and PI3K/Akt pathway in HepG2 cells. *Int. J. Mol. Sci.* **2012**, *13*, 801−818.
(15) Lee, J. H.; Johnson, J. V.; Talcott, S. T. Identification of ellagic acid conjugates and other polyphenolics in muscadine grapes by HPLC-ESI-MS. *J. Agric. Food Chem.* **2005**, *53*, 6003−6010.
(16) Abe, L. T.; Lajolo, F. M.; Genovese, M. I. Potential dietary sources of ellagic acid and other antioxidants among fruits consumed in Brazil: jabuticaba (*Myrciaria jaboticaba* (Vell.) Berg). *J. Sci. Food Agric.* **2012**, *92*, 1679−1687.
(17) Pinto, M. D. S.; Lajolo, F. M.; Genovese, M. I. Bioactive compounds and quantification of total ellagic acid in strawberries (*Fragaria* × *ananassa* Duch.). *Food Chem.* **2008**, *107*, 1629−1635.
(18) Rahim, A. A.; Nofrizal, S.; Saad, B. Rapid tea catechins and caffeine determination by HPLC using microwave-assisted extraction and silica monolithic column. *Food Chem.* **2014**, *147*, 262−268.
(19) Somerset, S. M.; Johannot, L. Dietary flavonoid sources in Australian adults. *Nutr. Cancer* **2008**, *60*, 442−449.
(20) Lin, L. Z.; Sun, J.; Chen, P.; Harnly, J. UHPLC-PDA-ESI/HRMS/MS(n) analysis of anthocyanins, flavonol glycosides, and hydroxycinnamic acid derivatives in red mustard greens (*Brassica juncea* Coss variety). *J. Agric. Food Chem.* **2011**, *59* (22), 12059−12072.
(21) Valcic, S.; Burr, J. A.; Timmermann, B. N.; Liebler, D. C. Antioxidant chemistry of green tea catechins. New oxidation products of (−)-epigallocatechin gallate and (−)-epigallocatechin from their reactions with peroxyl radicals. *Chem. Res. Toxicol.* **2000**, *13*, 801−810.
(22) Aqil, F.; Gupta, A.; Munagala, R.; Jeyabalan, J.; Kausar, H.; Sharma, R. J.; Singh, I. P.; Gupta, R. C. Antioxidant and antiproliferative activities of anthocyanin/ellagitannin-enriched extracts from *Syzygium cumini* L. (Jamun, the Indian blackberry). *Nutr. Cancer* **2012**, *64*, 428−438.
(23) Moalin, M.; Strijdonck, G. P.; Beckers, M.; Hagemen, G.; Borm, P.; Bast, A.; Haenen, G. R. A planar conformation and the hydroxyl groups in the B and C rings play a pivotal role in the antioxidant capacity of quercetin and quercetin derivatives. *Molecules* **2011**, *16*, 9636−9650.
(24) Kumar, S.; Pandey, A. K. Chemistry and biological activities of flavonoids: an overview. *Sci. World J.* **2013**, DOI: 10.1155/2013/162750.
(25) Thavasi, V.; Leong, L. P.; Bettens, R. P. Investigation of the influence of hydroxy groups on the radical scavenging ability of polyphenols. *J. Phys. Chem. A* **2006**, *110*, 4918−4923.
(26) Tanaka, T.; Matsuo, Y.; Kouno, I. Chemistry of secondary polyphenols produced during processing of tea and selected foods. *Int. J. Mol. Sci.* **2010**, *11*, 14−40.
(27) Scheidt, H. A.; Pampel, A.; Nissler, L.; Gebhardt, R.; Huster, D. Investigation of the membrane localization and distribution of flavonoids by high-resolution magic angle spinning NMR spectroscopy. *Biochim. Biophys. Acta* **2004**, *1663*, 97−107.
(28) Rahman, K. Studies on free radicals, antioxidants, and co-factors. *Clin. Interv. Aging* **2007**, *2*, 219−236.
(29) Masella, R.; Di Benedetto, R.; Vari, R.; et al. Novel mechanisms of natural antioxidant compounds in biological systems: involvement of glutathione and glutathione-related enzymes. *J. Nutr. Biochem.* **2005**, *16*, 577−586.
(30) Sim, G. S.; Lee, B. C.; Cho, H. S.; Lee, J. W.; Kim, J. H.; Lee, D. H.; Kim, J. H.; Pyo, H. B.; Moon, D. C.; Oh, K. W.; Yun, Y. P.; Hong, J. T. Structure activity relationship of antioxidative property of flavonoids and inhibitory effect on matrix metalloproteinase activity in UVA-irradiated human dermal fibroblast. *Arch. Pharm. Res.* **2007**, *30*, 290−298.
(31) Yi, L.; Chen, C. Y.; Jin, X.; Zhang, T.; Zhou, Y.; Zhang, Q. Y.; Zhu, J. D.; Mi, M. T. Differential suppression of intracellular reactive oxygen species-mediated signaling pathway in vascular endothelial cells by several subclasses of flavonoids. *Biochimie* **2012**, *94*, 2035−2044.
(32) Fukumoto, L. R.; Mazza, G. Assessing antioxidant and prooxidant activities of phenolic compounds. *J. Agric. Food Chem.* **2000**, *48*, 3597−3604.
(33) Nemeikaite-Ceniene, A.; Imbrasaite, A.; Sergediene, E.; Cenas, N. Quantitative structure-activity relationships in prooxidant cytotoxicity of polyphenols: role of potential of phenoxyl radical/phenol redox couple. *Arch. Biochem. Biophys.* **2005**, *441*, 182−190.
(34) Grellier, P.; Nemeikaite-Ceniene, A.; Sarlauskas, J.; Cenas, N. Role of single-electron oxidation potential and lipophilicity in the antiplasmodial in vitro activity of polyphenols: comparison to mammalian cells. *Z. Naturforsch. C* **2008**, *63*, 445−450.
(35) Selassie, C. D.; Kapur, S.; Verma, R. P.; Rosario, M. Cellular apoptosis and cytotoxicity of phenolic compounds: a quantitative structure-activity relationship study. *J. Med. Chem.* **2005**, *48*, 7234−7242.
(36) Hakimuddin, F.; Paliyath, G.; Meckling, K. Selective cytotoxicity of a red grape wine flavonoid fraction against MCF-7 cells. *Breast Cancer Res. Treat.* **2004**, *85*, 65−79.
(37) Wang, Y.; Zhang, H.; Lin, Y.; Zhao, Q.; Liu, H.; Zhang, Z.; Xia, Q.; Zhu, B.; Lin, Z. 3D-QSAR studies on caspase-mediated apoptosis activity of phenolic analogues. *J. Mol. Model.* **2011**, *17*, 1−8.
(38) Rasulev, B. F.; Abdullaev, N. D.; Syrov, V. N.; Leszczynski, J. A quantitative structure-activity relationship (QSAR) study of the antioxidant activity of flavonoids. *QSAR Comb. Sci.* **2005**, *24*, 1056−1065.
(39) Durand, A. C.; Farce, A.; Carato, P.; Dilly, S.; Yous, S.; Berthelot, P.; Chavatte, P. Quantitative structure-activity relationships studies of antioxidant hexahydropyridoindoles and flavonoid derivatives. *J. Enzyme Inhib. Med. Chem.* **2007**, *22*, 556−562.
(40) Om, A.; Kim, J. H. A quantitative structure-activity relationship model for radical scavenging activity of flavonoids. *J. Med. Food* **2008**, *11*, 29−37.
(41) Yi, L.; Jin, X.; Chen, C. Y.; Fu, Y. J.; Zhang, T.; Chang, H.; Zhou, Y.; Zhu, J. D.; Zhang, Q. Y.; Mi, M. T. Chemical structures of 4-oxo-flavonoids in relation to inhibition of oxidized low-density lipoprotein (LDL)-induced vascular endothelial dysfunction. *Int. J. Mol. Sci.* **2011**, *12*, 5471−5489.
(42) Ju, J.; Lu, G.; Lambert, J. D.; Yang, C. S. Inhibition of carcinogenesis by tea constituents. *Semin. Cancer Biol.* **2007**, *17*, 395−402.
(43) Stevenson, D. E.; Hurst, R. D. Polyphenolic phytochemicals − just antioxidants or much more? *Cell. Mol. Life Sci.* **2007**, *64*, 2900−2916.
(44) Yang, C. S.; Ju, J.; Lu, G.; Xiao, H.; Hao, X.; Sang, S.; Lambert, J. D. Cancer prevention by tea and tea polyphenols. *Asia Pac. J. Clin. Nutr.* **2008**, *17* (Suppl. 1), 245−248.
(45) Khan, N.; Mukhtar, H. Tea polyphenols for health promotion. *Life Sci.* **2007**, *81*, 519−33.
(46) Chacko, S. M.; Thambi, P. T.; Kuttan, R.; Nishigaki, I. Beneficial effects of green tea: a literature review. *Chin. Med.* **2010**, *5*, 13.

(47) de Pascual-Teresa, S.; Moreno, D. A.; García-Viguera, C. Flavanols and anthocyanins in cardiovascular health: a review of current evidence. *Int. J. Mol. Sci.* **2010**, *11*, 1679−1703.
(48) Khan, N.; Adhami, V. M.; Mukhtar, H. Review: Green tea polyphenols in chemoprevention of prostate cancer: preclinical and clinical studies. *Nutr. Cancer* **2009**, *61*, 836−481.
(49) Ju, J.; Hong, J.; Zhou, J. N.; Pan, Z.; Bose, M.; Liao, J.; Yang, G. Y.; Liu, Y. Y.; Hou, Z.; Lin, Y.; Ma, J.; Shih, W. J.; Carothers, A. M.; Yang, C. S. Inhibition of intestinal tumorigenesis in Apcmin/+ mice by (−)-epigallocatechin-3-gallate, the major catechin in green tea. *Cancer Res.* **2005**, *65*, 10623−10631.
(50) Lu, G.; Liao, J.; Yang, G.; Reuhl, K. R.; Hao, X.; Yang, C. S. Inhibition of adenoma progression to adenocarcinoma in a 4-(methylnitrosamino)-1-(3-pyridyl)-1-butanone-induced lung tumorigenesis model in A/J mice by tea polyphenols and caffeine. *Cancer Res.* **2006**, *66*, 11494−11501.
(51) Lu, G.; Xiao, H.; You, H.; Lin, Y.; Jin, H.; Snagaski, B.; Yang, C. S. Synergistic inhibition of lung tumorigenesis by a combination of green tea polyphenols and atorvastatin. *Clin. Cancer Res.* **2008**, *14*, 4981−4988.
(52) Bouayed, J. Polyphenols: a potential new strategy for the prevention and treatment of anxiety and depression. *Curr. Nutr. Food Sci.* **2010**, *6*, 13−18.
(53) Raza, H.; John, A. Green tea polyphenol epigallocatechin-3-gallate differentially modulates oxidative stress in PC12 cell compartments. *Toxicol. Appl. Pharmacol.* **2005**, *207*, 212−220.
(54) Suh, K. S.; Chon, S.; Oh, S.; Kim, S. W.; Kim, J. W.; Kim, Y. S.; Woo, J. T. Prooxidative effects of green tea polyphenol (−)-epigallocatechin-3-gallate on the HIT-T15 pancreatic β cell line. *Cell Biol. Toxicol.* **2010**, *26*, 189−199.
(55) Maurya, D. K.; Devasagayam, T. P. Antioxidant and prooxidant nature of hydroxycinnamic acid derivatives ferulic and caffeic acids. *Food Chem. Toxicol.* **2010**, *48*, 3369−3373.
(56) Kristinová, V.; Mozuraityte, R.; Storrø, I.; Rustad, T. Antioxidant activity of phenolic acids in lipid oxidation catalyzed by different prooxidants. *J. Agric. Food Chem.* **2009**, *57*, 10377−10385.
(57) Simić, A.; Manojlović, A.; Šegan, D.; Todorović, M. Electrochemical behavior and antioxidant and prooxidant activity of natural phenolics. *Molecules* **2007**, *12*, 2327−2340.
(58) Lambert, J. D.; Elias, R. J. The antioxidant and pro-oxidant activities of green tea polyphenols: a role in cancer prevention. *Arch. Biochem. Biophys.* **2010**, *501*, 65−72.
(59) Yuan, J. H.; Li, Y. Q.; Yang, X. Y. Inhibition of epigallocatechin gallate on orthotopic colon cancer by upregulating the Nrf2-UGT1A signal pathway in nude mice. *Pharmacology* **2007**, *80*, 269−278.
(60) Galati, G.; O'Brien, P. J. Potential toxicity of flavonoids and other dietary phenolics: significance for their chemopreventive and anticancer properties. *Free Radical Biol. Med.* **2004**, *37*, 287−303.
(61) Azmi, A. S.; Bhat, S. H.; Hadi, S. M. Resveratrol-Cu(II) induced DNA breakage in human peripheral lymphocytes: implications for anticancer properties. *FEBS Lett.* **2005**, *579*, 3131−3135.
(62) Decker, E. A. Phenolics: prooxidants or antioxidants? *Nutr. Rev.* **1997**, *55*, 396−398.
(63) Wu, T. Y.; Khor, T. O.; Saw, C. L.; Loh, S. C.; Chen, A. I.; Lim, S. S.; Park, J. H.; Cai, L.; Kong, A. N. Anti-inflammatory/Anti-oxidative stress activities and differential regulation of Nrf2-mediated genes by non-polar fractions of tea *Chrysanthemum zawadskii* and licorice *Glycyrrhiza uralensis*. *AAPS J.* **2011**, *13*, 1−13.
(64) Vauzour, D. Dietary polyphenols as modulators of brain functions: biological actions and molecular mechanisms underpinning their beneficial effects. *Oxid. Med. Cell. Longev.* **2012**, DOI: 10.1155/2012/914273.
(65) Hu, M. L. Dietary polyphenols as antioxidants and anticancer agents: more questions than answers. *Chang Gung Med. J.* **2011**, *34*, 449−460.
(66) Celik, G.; Semiz, A.; Karakurt, S.; Arslan, S.; Adali, O.; Sen, A. A comparative study for the evaluation of two doses of ellagic acid on hepatic drug metabolizing and antioxidant enzymes in the rat. *Biomed. Res. Int.* **2013**, DOI: 10.1155/2013/358945.
(67) D'Archivio, M.; Filesi, C.; Varì, R.; Scazzocchio, B.; Masella, R. Bioavailability of the polyphenols: status and controversies. *Int. J. Mol. Sci.* **2010**, *1*, 1321−1342.
(68) Yang, G. Y.; Liao, J.; Kim, K.; Yurkow, E. J.; Yang, C. S. Inhibition of growth and induction of apoptosis in human cancer cell lines by tea polyphenols. *Carcinogenesis* **1998**, *19*, 611−616.
(69) Dai, J.; Mumper, R. J. Plant phenolics: extraction, analysis and their antioxidant and anticancer properties. *Molecules* **2010**, *15*, 7313−7352.
(70) Na, H. K.; Surh, Y. J. Modulation of Nrf2-mediated antioxidant and detoxifying enzyme induction by the green tea polyphenol EGCG. *Food Chem. Toxicol.* **2008**, *46*, 1271−1278.
(71) Zhu, W.; Oxford, G. S. Phosphoinositide-3-kinase and mitogen activated protein kinase signaling pathways mediate acute NGF sensitization of TRPV1. *Mol. Cell. Neurosci.* **2007**, *34*, 689−700.
(72) Huang, S. M.; Wu, C. H.; Yen, G. C. Effects of flavonoids on the expression of the pro-inflammatory response in human monocytes induced by ligation of the receptor for AGEs. *Mol. Nutr. Food Res.* **2006**, *50*, 129−139.
(73) Soulat, T.; Philippe, C.; Bal dit Sollier, C.; Brezillon, C.; Berge, N.; Teissedre, P. L.; Callebert, J.; Rabot, S.; Drouet, L. Wine constituents inhibit thrombosis but not atherogenesis in C57BL/6 apolipoprotein E-deficient mice. *Br. J. Nutr.* **2006**, *96*, 290−298.
(74) Wahyudi, S.; Sargowo, D. Green tea polyphenols inhibit oxidized LDL-induced NF-κB activation in human umbilical vein endothelial cells. *Acta Med. Indones.* **2007**, *39*, 66−70.
(75) Xiao, J.; Song, J.; Hodara, V.; Ford, A.; Wang, X. L.; Shi, Q.; Chen, L.; Vandeberg, J. L. Protective effects of resveratrol on TNF-α-induced endothelial cytotoxicity in baboon femoral arterial endothelial cells. *J. Diabetes Res.* **2013**, DOI: 10.1155/2013/185172.
(76) Dong, Z.; Ma, W.; Huang, C.; Yang, C. S. Inhibition of tumor promoter-induced activator protein 1 activation and cell transformation by tea polyphenols, (−)-epigallocatechin gallate, and theaflavins. *Cancer Res.* **1997**, *57*, 4414−4419.
(77) Bachmeier, B.; Nerlich, A. G.; Iancu, C. M.; Cilli, M.; Schleicher, E.; Vené, R.; Dell'Eva, R.; Jochum, M.; Albini, A.; Pfeffer, U. The chemopreventive polyphenol *Curcumin* prevents hematogenous breast cancer metastases in immunodeficient mice. *Cell Physiol. Biochem.* **2007**, *19*, 137−152.
(78) Gupta, S.; Hussain, T.; Mukhtar, H. Molecular pathway for (−)-epigallocatechin-3-gallate-induced cell cycle arrest and apoptosis of human prostate carcinoma cells. *Arch. Biochem. Biophys.* **2003**, *410*, 177−185.
(79) Nam, S.; Smith, D. M.; Dou, Q. P. Ester bond-containing tea polyphenols potently inhibit proteasome activity in vitro and in vivo. *J. Biol. Chem.* **2001**, *276*, 13322−13330.
(80) Zhen, M. C.; Huang, X. H.; Wang, Q.; Sun, K.; Liu, Y. J.; Li, W.; Zhang, L. J.; Cao, L. Q.; Chen, X. L. Green tea polyphenol epigallocatechin-3-gallate suppresses rat hepatic stellate cell invasion by inhibition of MMP-2 expression and its activation. *Acta Pharmacol. Sin.* **2006**, *27*, 1600−1607.
(81) Shen, G.; Xu, C.; Hu, R.; Jain, M. R.; Nair, S.; Lin, W.; Yang, C. S.; Chan, J. Y.; Kong, A. N. Comparison of (−)-epigallocatechin-3-gallate elicited liver and small intestine gene expression profiles between C57BL/6J mice and C57BL/6J/Nrf2 (−/−) mice. *Pharm. Res.* **2005**, *22*, 1805−1820.
(82) Chow, H. H.; Hakim, I. A.; Vining, D. R.; Crowell, J. A.; Tome, M. E.; Ranger-Moore, J.; Cordova, C. A.; Mikhael, D. M.; Briehl, M. M.; Alberts, D. S. Modulation of human glutathione s-transferases by polyphenon E intervention. *Cancer Epidemiol. Biomarkers Prev.* **2007**, *16*, 1662−1666.
(83) Bachmeier, B.; Nerlich, A. G.; Iancu, C. M.; Cilli, M.; Schleicher, E.; Vené, R.; Dell'Eva, R.; Jochum, M.; Albini, A.; Pfeffer, U. The chemopreventive polyphenol curcumin prevents hematogenous breast cancer metastases in immunodeficient mice. *Cell Physiol. Biochem.* **2007**, *19*, 137−152.
(84) Pan, M. H.; Lin, C. C.; Lin, J. K.; Chen, W. J. Tea polyphenol (−)-epigallocatechin 3-gallate suppresses heregulin-β1-induced fatty acid synthase expression in human breast cancer cells by inhibiting

phosphatidylinositol 3-kinase/Akt and mitogen-activated protein kinase cascade signaling. *J. Agric. Food Chem.* **2007**, *55*, 5030−5037.
(85) Bigelow, R. L.; Cardelli, J. A. The green tea catechins, (−)-epigallocatechin-3-gallate (EGCG) and (−)-epicatechin-3-gallate (ECG), inhibit HGF/Met signaling in immortalized and tumorigenic breast epithelial cells. *Oncogene* **2006**, *25*, 1922−1930.
(86) Rodriguez, S. K.; Guo, W.; Liu, L.; Band, M. A.; Paulson, E. K.; Meydani, M. Green tea catechin, epigallocatechin-3-gallate, inhibits vascular endothelial growth factor angiogenic signaling by disrupting the formation of a receptor complex. *Int. J. Cancer* **2006**, *118*, 1635−1644.
(87) Yang, C. S.; Wang, X.; Lu, G.; Picinich, S. C. Cancer prevention by tea: animal studies, molecular mechanisms and human relevance. *Nat. Rev. Cancer* **2009**, *9*, 429−439.
(88) Adhami, V. M.; Siddiqui, I. A.; Ahmad, N.; Gupta, S.; Mukhtar, H. Oral consumption of green tea polyphenols inhibits insulin-like growth factor-I-induced signaling in an autochthonous mouse model of prostate cancer. *Cancer Res.* **2004**, *64*, 8715−8722.
(89) http://www.cancer.gov/CLINICALTRIALS.
(90) Tachibana, H.; Koga, K.; Fujimura, Y.; Yamada, K. A receptor for green tea polyphenol EGCG. *Nat. Struct. Mol. Biol.* **2004**, *11*, 380−381.
(91) Kuzuhara, T.; Sei, Y.; Yamaguchi, K.; Suganuma, M.; Fujiki, H. DNA and RNA as new binding targets of green tea catechins. *J. Biol. Chem.* **2006**, *281*, 17446−17456.
(92) Malireddy, S.; Kotha, S. R.; Secor, J. D.; Gurney, T. O.; Abbott, J. L.; Maulik, G.; Maddipati, K. R.; Parinandi, N. L. Phytochemical antioxidants modulate mammalian cellular epigenome: implications in health and disease. *Antioxid. Redox Signal.* **2012**, *17*, 327−339.
(93) Berletch, J. B.; Liu, C.; Love, W. K.; Andrews, L. G.; Katiyar, S. K.; Tollefsbol, T. O. Epigenetic and genetic mechanisms contribute to telomerase inhibition by EGCG. *J. Cell Biochem.* **2008**, *103*, 509−519.
(94) Meeran, S. M.; Patel, S. N.; Chan, T. H.; Tollefsbol, T. O. A novel prodrug of epigallocatechin-3-gallate: differential epigenetic hTERT repression in human breast cancer cells. *Cancer Prev. Res. (Phila.)* **2011**, *4*, 1243−1254.
(95) Fang, M. Z.; Wang, Y.; Ai, N.; Hou, Z.; Sun, Y.; Lu, H.; Welsh, W.; Yang, C. S. Tea polyphenol (−)-epigallocatechin-3-gallate inhibits DNA methyltransferase and reactivates methylation-silenced genes in cancer cell lines. *Cancer Res.* **2003**, *63*, 7563−7570.
(96) Li, Y.; Yuan, Y. Y.; Meeran, S. M.; Tollefsbol, T. O. Synergistic epigenetic reactivation of estrogen receptor-α (ERα) by combined green tea polyphenol and histone deacetylase inhibitor in ERα-negative breast cancer cells. *Mol. Cancer* **2010**, *9*, 274.
(97) Mittal, A.; Piyathilake, C.; Hara, Y.; Katiyar, S. K. Exceptionally high protection of photocarcinogenesis by topical application of (−)-epigallocatechin-3-gallate in hydrophilic cream in SKH-1 hairless mouse model: relationship to inhibition of UVB-induced global DNA hypomethylation. *Neoplasia* **2003**, *5*, 555−565.
(98) Nandakumar, V.; Vaid, M.; Katiyar, S. K. (−)-Epigallocatechin-3-gallate reactivates silenced tumor suppressor genes, Cip1/p21 and p16INK4a, by reducing DNA methylation and increasing histones acetylation in human skin cancer cells. *Carcinogenesis* **2011**, *32*, 537−544.
(99) Nihal, M.; Roelke, C. T.; Wood, G. S. Anti-melanoma effects of vorinostat in combination with polyphenolic antioxidant (−)-epigallocatechin-3-gallate (EGCG). *Pharm. Res.* **2010**, *27*, 1103−1114.
(100) Wong, C. P.; Nguyen, L. P.; Noh, S. K.; Bray, T. M.; Bruno, R. S.; Ho, E. Induction of regulatory T cells by green tea polyphenol EGCG. *Immunol. Lett.* **2011**, *139*, 7−13.
(101) Huang, J.; Plass, C.; Gerhauser, C. Cancer chemoprevention by targeting the epigenome. *Curr. Drug Targets* **2011**, *12*, 1925−1956.
(102) Kang, J.; Chen, J.; Shi, Y.; Jia, J.; Zhang, Y. Curcumin-induced histone hypoacetylation: the role of reactive oxygen species. *Biochem. Pharmacol.* **2005**, *69*, 1205−1213.
(103) Reuter, S.; Gupta, S. C.; Park, B.; Goel, A.; Aggarwal, B. B. Epigenetic changes induced by curcumin and other natural compounds. *Genes Nutr.* **2011**, *6*, 93−108.
(104) Abusnina, A.; Keravis, T.; Yougbaré, I.; Bronner, C.; Lugnier, C. Anti-proliferative effect of curcumin on melanoma cells is mediated by PDE1A inhibition that regulates the epigenetic integrator UHRF1. *Mol. Nutr. Food Res.* **2011**, *55*, 1677−1689.
(105) Rosa, E. F.; Takahashi, S.; Aboulafia, J.; Nouailhetas, V. L.; Oliveira, M. G. Oxidative stress induced by intense and exhaustive exercise impairs murine cognitive function. *J. Neurophysiol.* **2007**, *98*, 1820−1826.
(106) Vollaard, N. B.; Shearman, J. P.; Cooper, C. E. Exercise-induced oxidative stress: myths, realities and physiological relevance. *Sports Med.* **2005**, *35*, 1045−1062.
(107) Valko, M.; Leibfritz, D.; Moncol, J.; Cronin, M. T.; Mazur, M.; Telser, J. Free radicals and antioxidants in normal physiological functions and human disease. *Int. J. Biochem. Cell Biol.* **2007**, *39*, 44−84.
(108) Bloomer, R. J.; Fisher-Wellman, K. H. Systemic oxidative stress is increased to a greater degree in young, obese women following consumption of a high fat meal. *Oxid. Med. Cell. Longev.* **2009**, *2*, 19−25.
(109) Souza, C. G.; Moreira, J. D.; Siqueira, I. R.; Pereira, A. G.; Rieger, D. K.; Souza, D. O.; Souza, T. M.; Portela, L. V.; Perry, M. L. Highly palatable diet consumption increases protein oxidation in rat frontal cortex and anxiety-like behavior. *Life Sci.* **2007**, *81*, 198−203.
(110) Elahi, M. M.; Kong, Y. X.; Matata, B. M. Oxidative stress as a mediator of cardiovascular disease. *Oxid. Med. Cell. Longev.* **2009**, *2*, 259−269.
(111) Lee, K. W.; Lee, H. J.; Lee, C. Y. Vitamins, phytochemicals, diets, and their implementation in cancer chemoprevention. *Crit. Rev. Food Sci. Nutr.* **2004**, *44*, 437−452.
(112) Halliwell, B. Oxidative stress and neurodegeneration: where are we now? *J. Neurochem.* **2006**, *97*, 1634−1658.
(113) Wätjen, W.; Michels, G.; Steffan, B.; Niering, P.; Chovolou, Y.; Kampkötter, A.; Tran-Thi, Q. H.; Proksch, P.; Kahl, R. Low concentrations of flavonoids are protective in rat H4IIE cells whereas high concentrations cause DNA damage and apoptosis. *J. Nutr.* **2005**, *135*, 525−531.
(114) Moran, J. F.; Klucas, R. V.; Grayer, R. J.; Abian, J.; Becana, M. Complexes of iron with phenolic compounds from soybean nodules and other legume tissues: prooxidant and antioxidant properties. *Free Radical Biol. Med.* **1997**, *22*, 861−870.
(115) Hodgson, J. M.; Puddey, I. B.; Croft, K. D.; Burke, V.; Mori, T. A.; Caccetta, R. A.; Beilin, L. J. Acute effects of ingestion of black and green tea on lipoprotein oxidation. *Am. J. Clin. Nutr.* **2000**, *71*, 1103−1107.
(116) Choi, J. S.; Choi, Y. J.; Shin, S. Y.; Li, J.; Kang, S. W.; Bae, J. Y.; Kim, D. S.; Ji, G. E.; Kang, J. S.; Kang, Y. H. Dietary flavonoids differentially reduce oxidized LDL-induced apoptosis in human endothelial cells: role of MAPK- and JAK/STAT-signaling. *J. Nutr.* **2008**, *138*, 983−990.
(117) De Marchi, U.; Biasutto, L.; Garbisa, S.; Toninello, A.; Zoratti, M. Quercetin can act either as an inhibitor or an inducer of the mitochondrial permeability transition pore: a demonstration of the ambivalent redox character of polyphenols. *Biochim. Biophys. Acta* **2009**, *1787*, 1425−1432.
(118) Robaszkiewicz, A.; Balcerczyk, A.; Bartosz, G. Antioxidative and prooxidative effects of quercetin on A549 cells. *Cell Biol. Int.* **2007**, *31*, 1245−1250.
(119) Rietjens, I. M.; Boersma, M. G.; van der Woude, H.; Jeurissen, S. M.; Schutte, M. E.; Alink, G. M. Flavonoids and alkenylbenzenes: mechanisms of mutagenic action and carcinogenic risk. *Mutat. Res.* **2005**, *574*, 124−138.
(120) Chang, Y. F.; Chi, C. W.; Wang, J. J. Reactive oxygen species production is involved in quercetin-induced apoptosis in human hepatoma cells. *Nutr. Cancer* **2006**, *55*, 201−209.
(121) Utesch, D.; Feige, K.; Dasenbrock, J.; Broschard, T. H.; Harwood, M.; Danielewska-Nikiel, B.; Lines, T. C. Evaluation of the potential in vivo genotoxicity of quercetin. *Mutat. Res.* **2008**, *654*, 38−44.

(122) Azam, S.; Hadi, N.; Khan, N. U.; Hadi, S. M. Prooxidant property of green tea polyphenols epicatechin and epigallocatechin-3-gallate: implications for anticancer properties. *Toxicol In Vitro* **2004**, *18*, 555−561.
(123) Yin, J. J.; Fu, P. P.; Lutterodt, H.; Zhou, Y. T.; Antholine, W. E.; Wamer, W. Dual role of selected antioxidants found in dietary supplements: crossover between anti- and pro-oxidant activities in the presence of copper. *J. Agric. Food Chem.* **2012**, *60*, 2554−2561.
(124) Hong, J.; Lu, H.; Meng, X.; Ryu, J. H.; Hara, Y.; Yang, C. S. Stability, cellular uptake, biotransformation, and efflux of tea polyphenol (−)-epigallocatechin-3-gallate in HT-29 human colon adenocarcinoma cells. *Cancer Res.* **2002**, *62*, 7241−7246.
(125) Nakagawa, H.; Hasumi, K.; Woo, J. T.; Nagai, K.; Wachi, M. Generation of hydrogen peroxide primarily contributes to the induction of Fe(II)-dependent apoptosis in Jurkat cells by (−)-epigallocatechin gallate. *Carcinogenesis* **2004**, *25*, 1567−1574.
(126) Babich, H.; Schuck, A. G.; Weisburg, J. H.; Zuckerbraun, H. L. Research strategies in the study of the pro-oxidant nature of polyphenol nutraceuticals. *J. Toxicol.* **2011**, DOI: 10.1155/2011/467305.
(127) Yin, S. T.; Tang, M. L.; Deng, H. M.; Xing, T. R.; Chen, J. T.; Wang, H. L.; Ruan, D. Y. Epigallocatechin-3-gallate induced primary cultures of rat hippocampal neurons death linked to calcium overload and oxidative stress. *Naunyn Schmiedebergs Arch. Pharmacol.* **2009**, *379*, 551−564.
(128) Du, G. J.; Zhang, Z.; Wen, X. D.; Yu, C.; Calway, T.; Yuan, C. S.; Wang, C. Z. Epigallocatechin gallate (EGCG) is the most effective cancer chemopreventive polyphenol in green tea. *Nutrients* **2012**, *4*, 1679−1691.
(129) Chow, H. H.; Hakim, I. A. Pharmacokinetic and chemoprevention studies on tea in humans. *Pharmacol. Res.* **2011**, *64*, 105−112.
(130) Rae, T. D.; Schmidt, P. J.; Pufahl, R. A.; Culotta, V. C.; O'Halloran, T. V. Undetectable intracellular free copper: the requirement of a copper chaperone for superoxide dismutase. *Science* **1999**, *284*, 805−808.
(131) Weinreb, O.; Amit, T.; Mandel, S.; Youdim, M. B. Neuroprotective molecular mechanisms of (−)-epigallocatechin-3-gallate: a reflective outcome of its antioxidant, iron chelating and neuritogenic properties. *Genes Nutr.* **2009**, *4*, 283−296.
(132) Ali, H. M.; Abo-Shady, A.; Eldeen, H. A. S.; Soror, H. A.; Shousha, W. G.; Abdel-Barry, O. A.; Saleh, A. M. Structural features, kinetics and SAR study of radical scavenging and antioxidant activities of phenolic and anilinic compounds. *Chem. Central J.* **2013**, *7*, 53.
(133) Priyadarsini, K. I.; Khopde, S. M.; Kumar, S. S.; Mohan, H. Free radical studies of ellagic acid, a natural phenolic antioxidant. *J. Agric. Food Chem.* **2002**, *50*, 2200−2206.
(134) Manach, C.; Scalbert, A.; Morand, C.; Rémésy, C.; Jiménez, L. Polyphenols: food sources and bioavailability. *Am. J. Clin. Nutr.* **2004**, *79*, 727−747.
(135) Iwasaki, M.; Inoue, M.; Sasazuki, S.; Miura, T.; Sawada, N.; Yamaji, T.; Shimazu, T.; Willett, W. C.; Tsugane, S. Plasma tea polyphenol levels and subsequent risk of breast cancer among Japanese women: a nested case-control study. *Breast Cancer Res. Treat.* **2010**, *124*, 827−834.
(136) Hakim, I. A.; Harris, R. B.; Chow, H. H.; Dean, M.; Brown, S.; Ali, I. U. Effect of a 4-month tea intervention on oxidative DNA damage among heavy smokers: role of glutathione S-transferase genotypes. *Cancer Epidemiol. Biomarkers Prev.* **2004**, *13*, 242−249.
(137) Chu, K. O.; Chan, K. P.; Wang, C. C.; Chu, C. Y.; Li, W. Y.; Choy, K. W.; Rogers, M. S.; Pang, C. P. Green tea catechins and their oxidative protection in the rat eye. *J. Agric. Food Chem.* **2010**, *58*, 1523−1534.
(138) Chung, F. L.; Schwartz, J.; Herzog, C. R.; Yang, Y. M. Tea and cancer prevention: studies in animals and humans. *J. Nutr.* **2003**, *133*, 3268S−3274S.
(139) Apak, R.; Güçlü, K.; Ozyürek, M.; Karademir, S. E.; Altun, M. Total antioxidant capacity assay of human serum using copper(II)-neocuproine as chromogenic oxidant: the CUPRAC method. *Free Radical Res.* **2005**, *39*, 949−961.
(140) Halliwell, B.; Rafter, J.; Jenner, A. Health promotion by flavonoids, tocopherols, tocotrienols, and other phenols: direct or indirect effects? Antioxidant or not? *Am. J. Clin. Nutr.* **2005**, *81*, 268S−276S.
(141) Ruginǎ, D.; Adela, P.; Momeu, C. Epigallocatechin gallate antioxidant effect in retinal pigment epithelial cells. *Bull. UASVM, Agric.* **2008**, *65*, 1843−5246.
(142) Gundimeda, U.; McNeill, T. H.; Elhiani, A. A.; Schiffman, J. E.; Hinton, D. R.; Gopalakrishna, R. Green tea polyphenols precondition against cell death induced by oxygen-glucose deprivation via stimulation of laminin receptor, generation of reactive oxygen species, and activation of protein kinase Cε. *J. Biol. Chem.* **2012**, *287*, 34694−34708.
(143) Akhlaghi, M.; Bandy, B. Dietary green tea extract increases phase 2 enzyme activities in protecting against myocardial ischemia-reperfusion. *Nutr. Res. (N. Y.)* **2010**, *30*, 32−39.
(144) Li, G. X.; Chen, Y. K.; Hou, Z.; Xiao, H.; Jin, H.; Lu, G.; Lee, M. J.; Liu, B.; Guan, F.; Yang, Z.; Yu, A.; Yang, C. S. Pro-oxidative activities and dose-response relationship of (−)-epigallocatechin-3-gallate in the inhibition of lung cancer cell growth: a comparative study in vivo and in vitro. *Carcinogenesis* **2010**, *31*, 902−910.
(145) Ran, F. A.; Hsu, P. D.; Lin, C. Y.; Gootenberg, J. S.; Konermann, S.; Trevino, A. E.; Scott, D. A.; Inoue, A.; Matoba, S.; Zhang, Y.; Zhang, F. Double nicking by RNA-guided CRISPR Cas9 for enhanced genome editing specificity. *Cell* **2013**, *154*, 1380−1389.
(146) Pandey, K. B.; Rizvi, S. I. Plant polyphenols as dietary antioxidants in human health and disease. *Oxid. Med. Cell. Longev.* **2009**, *2*, 270−278.
(147) Dauchet, L.; Amouyel, P.; Dallongeville, J. Fruit and vegetable consumption and risk of stroke: a meta-analysis of cohort studies. *Neurology* **2005**, *65*, 1193−1197.
(148) Knekt, P.; Jarvinen, R.; Reunanen, A.; Maatela, J. Flavonoid intake and coronary mortality in Finland: a cohort study. *BMJ* **1996**, *312*, 478−481.
(149) van Duijnhoven, F. J.; Bueno-De-Mesquita, H. B.; Ferrari, P.; et al. Fruit, vegetables, and colorectal cancer risk: the European Prospective Investigation into Cancer and Nutrition. *Am. J. Clin. Nutr.* **2009**, *89*, 1441−1452.
(150) Eberhardt, M. V.; Lee, C. Y.; Liu, R. H. Antioxidant activity of fresh apples. *Nature* **2000**, *405*, 903−904.
(151) Rice-Evans, C. Flavonoid antioxidants. *Curr. Med. Chem.* **2001**, *8*, 797−807.
(152) Liu, R. H. Health benefits of fruit and vegetables are from additive and synergistic combinations of phytochemicals. *Am. J. Clin. Nutr.* **2003**, *78*, 517S−520S.
(153) Toufektsian, M. C.; de Lorgeril, M.; Nagy, N.; Salen, P.; Donati, M. B.; Giordano, L.; Mock, H. P.; Peterek, S.; Matros, A.; Petroni, K.; Pilu, R.; Rotilio, D.; Tonelli, C.; de Leiris, J.; Boucher, F.; Martin, C. Chronic dietary intake of plant-derived anthocyanins protects the rat heart against ischemia-reperfusion injury. *J. Nutr.* **2008**, *138*, 747−752.
(154) Kebieche, M.; Lakroun, Z.; Lahouel, M.; Bouayed, J.; Meraihi, Z.; Soulimani, R. Evaluation of epirubicin-induced acute oxidative stress toxicity in rat liver cells and mitochondria, and the prevention of toxicity through quercetin administration. *Exp. Toxicol. Pathol.* **2009**, *61*, 161−167.
(155) Itagaki, S.; Oikawa, S.; Ogura, J.; Kobayashi, M.; Hirano1, T.; Iseki, K. Protective effects of quercetin-3-rhamnoglucoside (rutin) on ischemia-reperfusion injury in rat small intestine. *Food Chem.* **2010**, *118*, 426−429.
(156) Ito, N.; Fukushima, S.; Hagiwara, A.; Shibata, M.; Ogiso, T. Carcinogenicity of butylated hydroxyanisole in F344 rats. *J. Natl. Cancer Inst.* **1983**, *70*, 343−352.
(157) Branen, A. L. Toxicology and biochemistry of butylated hydroxyanisole and butylated hydroxytoluene. *J. Am. Oil Chem. Soc.* **1975**, *52*, 59−63.

(158) Sen, T.; Dutta, A.; Chatterjee, A. Epigallocatechin-3-gallate (EGCG) downregulates gelatinase-B (MMP-9) by involvement of FAK/ERK/NFκB and AP-1 in the human breast cancer cell line MDA-MB-231. *Anticancer Drugs* **2010**, *21*, 632−644.
(159) Yang, J.; Han, Y.; Sun, H.; Chen, C.; He, D.; Guo, J.; Yu, C.; Jiang, B.; Zhou, L.; Zeng, C. (−)-Epigallocatechin gallate suppresses proliferation of vascular smooth muscle cells induced by high glucose by inhibition of PKC and ERK1/2 signalings. *J. Agric. Food Chem.* **2011**, *59*, 11483−11490.
(160) Williams, R. J.; Spencer, J. P.; Rice-Evans, C. Flavonoids: antioxidants or signaling molecules? *Free Radical Biol. Med.* **2004**, *36*, 838−849.
(161) Ososki, A. L.; Kennelly, E. J. Phytoestrogens: a review of the present state of research. *Phytother. Res.* **2003**, *17*, 845−869.
(162) Mennen, L. I.; Walker, R.; Bennetau-Pelissero, C.; Scalbert, A. Risks and safety of polyphenol consumption. *Am. J. Clin. Nutr.* **2005**, *81*, 326S−329S.
(163) Fujimura, Y.; Sumida, M.; Sugihara, K.; Tsukamoto, S.; Yamada, K.; Tachibana, H. Green tea polyphenol (−)-EGCG sensing motif on the 67-kDa laminin receptor. *PLoS One* **2012**, DOI: 10.1371/journal.pone.0037942.
(164) Williamson, M. P.; McCormick, T. G.; Nance, C. L.; Shearer, W. T. (−)-Epigallocatechin gallate, the main polyphenol in green tea, binds to the T-cell receptor, CD4: potential for HIV-1 therapy. *J. Allergy Clin. Immunol.* **2006**, *118*, 1369−1374.
(165) Bharrhan, S.; Chopra, K.; Arora, S. K.; Toor, J. S.; Rishi, P. Down-regulation of NF-κB signalling by polyphenolic compounds prevents endotoxin-induced liver injury in a rat model. *Innate Immun.* **2012**, *18*, 70−79.
(166) Kwon, J. Y.; Seo, S. G.; Heo, Y. S.; Yue, S.; Cheng, J. X.; Lee, K. W.; Kim, K. H. Piceatannol, natural polyphenolic stilbene, inhibits adipogenesis via modulation of mitotic clonal expansion and insulin receptor-dependent insulin signaling in early phase of differentiation. *J. Biol. Chem.* **2012**, *287*, 11566−11578.
(167) Zang, M.; Xu, S.; Maitland-Toolan, K. A.; Zuccollo, A.; Hou, X.; Jiang, B.; Wierzbicki, M.; Verbeuren, T. J.; Cohen, R. A. Polyphenols stimulate AMP-activated protein kinase, lower lipids, and inhibit accelerated atherosclerosis in diabetic LDL receptor-deficient mice. *Diabetes* **2006**, *55*, 2180−2191.
(168) Armour, S. M.; Baur, J. A.; Hsieh, S. N.; Land-Bracha, A.; Thomas, S. M.; Sinclair, D. A. Inhibition of mammalian S6 kinase by resveratrol suppresses autophagy. *Aging (Albany, N. Y.).* **2009**, *1*, 515−528.
(169) Schloms, L.; Smith, C.; Storbeck, K. H.; Marnewick, J. L.; Swart, P.; Swart, A. C. Rooibos influences glucocorticoid levels and steroid ratios in vivo and in vitro: a natural approach in the management of stress and metabolic disorders? *Mol. Nutr. Food Res.* **2014**, *58*, 537−549.
(170) Boulay, A.; Masson, R.; Chenard, M. P.; El Fahime, M.; Cassard, L.; Bellocq, J. P.; Sautès-Fridman, C.; Basset, P.; Rio, M. C. High cancer cell death in syngeneic tumors developed in host mice deficient for the stromelysin-3 matrix metalloproteinase. *Cancer Res.* **2001**, *61*, 2189−2193.
(171) Liu, J. D.; Chen, S. H.; Lin, C. L.; Tsai, S. H.; Liang, Y. C. Inhibition of melanoma growth and metastasis by combination with (−)-epigallocatechin-3-gallate and dacarbazine in mice. *J. Cell Biochem.* **2001**, *83*, 631−642.
(172) Berger, S. J.; Gupta, S.; Belfi, C. A.; Gosky, D. M.; Mukhtar, H. Green tea constituent (−)-epigallocatechin-3-gallate inhibits topoisomerase I activity in human colon carcinoma cells. *Biochem. Biophys. Res. Commun.* **2001**, *288*, 101−105.
(173) Umeda, D.; Tachibana, H.; Yamada, K. Epigallocatechin-3-*O*-gallate disrupts stress fibers and the contractile ring by reducing myosin regulatory light chain phosphorylation mediated through the target molecule 67 kDa laminin receptor. *Biochem. Biophys. Res. Commun.* **2005**, *333*, 628−635.
(174) Sang, S.; Lee, M. J.; Hou, Z.; Ho, C. T.; Yang, C. S. Stability of tea polyphenol (−)-epigallocatechin-3-gallate and formation of dimers and epimers under common experimental conditions. *J. Agric. Food Chem.* **2005**, *53*, 9478−9484.
(175) Hou, Z.; Sang, S.; You, H.; Lee, M. J.; Hong, J.; Chin, K. V.; Yang, C. S. Mechanism of action of (−)-epigallocatechin-3-gallate: auto-oxidation-dependent inactivation of epidermal growth factor receptor and direct effects on growth inhibition in human esophageal cancer KYSE 150 cells. *Cancer Res.* **2005**, *65*, 8049−8056.
(176) Siow, R. C.; Mann, G. E. Dietary isoflavones and vascular protection: activation of cellular antioxidant defenses by SERMs or hormesis? *Mol. Aspects Med.* **2010**, *31*, 468−477.
(177) Hitchler, M. J.; Domann, F. E. Redox regulation of the epigenetic landscape in cancer: a role for metabolic reprogramming in remodeling the epigenome. *Free Radical Biol. Med.* **2012**, *53*, 2178−2187.
(178) Pandey, K. B.; Rizvi, S. I. Plant polyphenols as dietary antioxidants in human health and disease. *Oxid. Med. Cell. Longev.* **2009**, *2*, 270−278.
(179) Landete, J. M. Updated knowledge about polyphenols: functions, bioavailability, metabolism, and health. *Crit. Rev. Food Sci. Nutr.* **2012**, *52*, 936−948.
(180) Kay, C. D.; Kroon, P. A.; Cassidy, A. The bioactivity of dietary anthocyanins is likely to be mediated by their degradation products. *Mol. Nutr. Food Res.* **2009**, *53* (Suppl. 1), S92−S101.
(181) Gu, P.; Chen, H. Modern bioinformatics meets traditional Chinese medicine. *Brief Bioinform.* **2013**, DOI: 10.1093/bib/bbt063.
(182) Mellor, D. D.; Madden, L. A.; Smith, K. A.; Kilpatrick, E. S.; Atkin, S. L. High-polyphenol chocolate reduces endothelial dysfunction and oxidative stress during acute transient hyperglycaemia in type 2 diabetes: a pilot randomized controlled trial. *Diabetes Med.* **2013**, *30*, 478−483.
(183) Umesalma, S.; Sudhandiran, G. Differential inhibitory effects of the polyphenol ellagic acid on inflammatory mediators NF-κB, iNOS, COX-2, TNF-αa, and IL-6 in 1,2-dimethylhydrazine-induced rat colon carcinogenesis. *Basic Clin. Pharmacol. Toxicol.* **2010**, *107*, 650−655.
(184) Paolini, G. V.; Shapland, R. H.; van Hoorn, W. P.; Mason, J. S.; Hopkins, A. L. Global mapping of pharmacological space. *Nat. Biotechnol.* **2006**, *24*, 805−815.
(185) Armishaw, C. J.; Singh, N.; Medina-Franco, J. L.; Clark, R. J.; Scott, K. C.; Houghten, R. A.; Jensen, A. A. A synthetic combinatorial strategy for developing α-conotoxin analogs as potent α7 nicotinic acetylcholine receptor antagonists. *J. Biol. Chem.* **2010**, *285*, 1809−1821.
(186) Carroll, F. I.; Houghten, R. A. From rapid in vitro screening to rapid in vivo screening in the drug discovery process. *Neuropsychopharmacology* **2009**, *34*, 251−252.
(187) Medina-Franco, J. L.; Giulianotti, M. A.; Welmaker, G. S.; Houghten, R. A. Shifting from the single to the multitarget paradigm in drug discovery. *Drug Discov. Today* **2013**, *18*, 495−501.

JOURNAL OF AGRICULTURAL AND FOOD CHEMISTRY

Review

pubs.acs.org/JAFC

Interactive Association between Biopolymers and Biofunctions in Carinata Seeds as Energy Feedstock and Their Coproducts (Carinata Meal) from Biofuel and Bio-oil Processing before and after Biodegradation: Current Advanced Molecular Spectroscopic Investigations

Peiqiang Yu,*[,†,‡] Hangshu Xin,[‡] Yajing Ban,[‡] and Xuewei Zhang[†]

[†]Department of Animal Science, Tianjin Agricultural University, 22 Jinjin Road, Tianjin 300384, China

[‡]Department of Animal and Poultry Science, College of Agriculture and Bioresources, University of Saskatchewan, 51 Campus Drive, Saskatoon, Saskatchewan S7N 5A8, Canada

ABSTRACT: Recent advances in biofuel and bio-oil processing technology require huge supplies of energy feedstocks for processing. Very recently, new carinata seeds have been developed as energy feedstocks for biofuel and bio-oil production. The processing results in a large amount of coproducts, which are carinata meal. To date, there is no systematic study on interactive association between biopolymers and biofunctions in carinata seed as energy feedstocks for biofuel and bioethanol processing and their processing coproducts (carinata meal). Molecular spectroscopy with synchrotron and globar sources is a rapid and noninvasive analytical technique and is able to investigate molecular structure conformation in relation to biopolymer functions and bioavailability. However, to date, these techniques are seldom used in biofuel and bioethanol processing in other research laboratories. This paper aims to provide research progress and updates with molecular spectroscopy on the energy feedstock (carinata seed) and coproducts (carinata meal) from biofuel and bioethanol processing and show how to use these molecular techniques to study the interactive association between biopolymers and biofunctions in the energy feedstocks and their coproducts (carinata meal) from biofuel and bio-oil processing before and after biodegradation.

KEYWORDS: *carinata, molecular structure, biopolymer functions, nutrient profiles, molecular spectroscopy application, nutrient utilization, coproducts, biofuel/bio-oil processing*

INTRODUCTION

Carinata Seeds as Energy Feedstocks for Biofuel and Bio-oil Processing. With the development of environmentally friendly biofuel industry and bio-oil industry, vegetable oil is extracted from oilseed crops and widely utilized for biofuel and food oil production, because these oilseeds are renewable, nontoxic, nutritive sources and the biofuel made from them has lower emissions (e.g., particulates, carbon monoxide, hydrocarbons) than the normal fuel from petroleum.[1]

Brassica carinata (or Ethiopia mustard), which originates in Ethiopia, is an oilseed crop with development potential for the dry western Canadian prairie because of its good tolerance of heat and drought climate, high-salt[2] or clay soil, and its more productive character, compared with canola, which prefers to grow in a cooler environment with good moisture.[2−4] Recently, Ban and Yu[3] summarized growth conditions of carinata in comparison with canola.

Carinata seeds have a lower oil content (26−40%) compared with canola *Brassica napus*, and *Brassica carinata* has less oleic acid (28%) than *B. napus* (62%).[4−6] In addition, the linoleic and linolenic acid contents of carinata seeds are higher than those of *B. napus*.[4−7] With the development of the high oleic acid and low linolenic acid *B. carinata* germplasm,[8] the oil extracted from those seeds could be utilized for the food-grade oil industry.[3]

Similar to canola seeds, carinata seed and carinata meal still contain some antinutrients, which may inhibit the bioactivities of digestive enzymes and so decrease the digestibility and absorption of some important nutrients.[5,6,9] These antinutrients include erucic acids, glucosinolates, and condensed tannins. The structures of these antinutrients could be found on the Web[3] (http://en.wikipedia.org/wiki).

The oil extracted from canola seeds has <2% erucic acid (monounsaturated 22:1 omega-9 fatty acid with formula $CH_3(CH_2)_7CH{=}CH(CH_2)_{11}COOH$),[10] and for the whole canola seeds, the glucosinolates are around 16 μmol/g and the condensed tannins are 1.5−3.0 g/100 g.[9] A previous study showed that conventional carinata has a higher concentration of glucosinolates.[4] In our preliminary recent study,[5] we reported the antinutrient levels in carinata yellow and brown lines on the basis of a few samples.

Carinata Meal as Coproducts from Biofuel and Bio-oil Processing. With the rapid development of biofuel and bio-oil processing industries and the widely utilized oil seeds (e.g., carinata) in Canada, a large amount of coproducts, products after bio-oil extraction and biofuel processing, is generated. The carinata meal is regarded to be a good source of protein (48%) for animal feed, compared with canola meal (40%) in a

Received: January 2, 2014
Revised: March 30, 2014
Accepted: April 15, 2014
Published: April 28, 2014

 © 2014 American Chemical Society

preliminary study for CFIA.[11] However, the metabolizable protein contents of carinata are still in question in comparison with canola meal.

Many research projects have been done on the application of both canola seeds and canola meal in the ruminant feed industry[12−17] and the monogastric feed industry.[18,19] However, few papers from other research groups could be found in the literature on carinata seeds and their coproducts (carinata meal) for their physiochemical or nutrient structure profiles and biopolymer functions as well as structure associated with nutritive degradation and digestion, so the quality of the carinata seeds and carinata meal from biofuel and bio-oil production is still unknown.

Molecular Spectroscopic Studies on Carinata Seeds and Their Coproducts from Biofuel and Bio-oil Processing. The true nutritive values of feeds are associated with both chemical composition and internal molecular structure, because the nutrient bioavailability and fermentation features are influenced by internal structure.[20,21] However, the inherent structures of feed samples are usually destroyed during the conventional "wet chemical analysis" methods (e.g., AOAC[22,23]), and the wet chemical analysis fails to link chemical composition to inherent structure.[20,24]

In recent publications,[24−26] cutting edge Synchrotron radiation based Fourier Transform Infrared Microspectroscopy (SR-IMS) has been applied as a rapid and noninvasive advanced technique to reveal the structure of feedstuff on a molecular basis within intact tissue. With six components (electron gun, linear accelerator, booster ring, storage ring, beamlines, and experimental stations), the synchrotron could turn electrons into extreme bright light and then show inherent structure of biological tissues.[27] This synchrotron-based technique is capable of showing four kinds of tissue information (tissue structure, tissue chemistry, tissue environment, and tissue composition) within different layers at the same time.[25,27,28] Several studies have been done with the successful application of this synchrotron technique to reveal molecular structure and structure changes by different treatments of various feedstuff in our laboratories.[20,21,29,30] With the development and application of this technique, the relationship between molecular structure and biological functions could be explained from the revealed differences in spectra from SR-IMS according to the previous research.[31−33] However, to date, few studies have been found on molecular structure in relation to biofunctions and bioavailability of nutrients in carinata seeds and carinata meal except our preliminary study.

Aims of This Review. This paper aims to provide research progress and updates in molecular spectroscopy on the energy feedstock (carinata seed) and the coproducts (carinata meal) from biofuel and bioethanol processing and show how to use the molecular techniques to study the interactive association between biopolymers and biofunctions in carinata seeds and their coproducts (carinata meal) from biofuel and bio-oil processing before and after biodegradation using a system approach.

Our research program with several projects aims to (1) systematically study the structure, physicochemical, and nutrition features of the yellow and brown types of carinata seeds for biofuel and bio-oil production as well as the coproducts after the processing compared with canola seeds and canola meal in terms of (a) molecular structural spectral features by synchrotron SR-IMS and ATR-FT/IR techniques, (b) special chemical compounds and chemical profiles, (c) protein and carbohydrate fractions and their contributions to rumen bypassed protein and carbohydrate (d) energy values in beef and dairy production, (e) rumen degradation kinetics/rumen fermentation characteristics, and (f) intestinal availability of primary nutrients and true nutrient supply to dairy cattle; and (2) explore the relationship between new line structure and nutrient availability to assist further development of new lines of carinata seeds for the biofuel, bio-oil, and animal feed industries.[3]

CURRENT CARINATA BIOFUEL AND BIO-OIL PROCESSING AND THEIR COPRODUCT PRODUCTION

Biofuel Process and Coproduct Production. The biofuel process of carinata seed is similar to that of rapeseed. Reference 34 provides a schematic graph to clearly show detailed biofuel processing from rapeseeds.[34] As stated in GEA,[34] "Bio-fuel from rapeseed oil seed is one of the most promising biofuels. In contrast to bio-diesel, Bio-fuel from rapeseed oil is a chemically unmodified vegetable oil. Transesterification is not required and the basic molecular structure of the vegetable oil can be retained, to allow it to be used in the engines of trucks, airplanes or agricultural vehicles converted to use rapeseed oil",[34] so do carinata seeds.

Bio-oil Processing and Coproduct Production. The bio-oil process of carinata seed for human consumption is similar to that of rapeseed, too. Reference 35 also provides a very good schematic graph to show bio-oil processing from rapeseeds.[35] The detailed processing procedure has been reported in many papers with some modifications in the procedure. We do not repeat it here.

CURRENT BIOFUNCTION/NUTRITION STUDIES ON CARINATA AS ENERGY FEEDSTOCKS AND COPRODUCTS (CARINATA MEAL) FROM BIOFUEL AND BIO-OIL PROCESSING

Synchrotron-Based Molecular Spectroscopy for Molecular Structure Studies of Carinata Seed as Energy Feedstocks for Biofuel and Bio-oil Processing. Synchrotron radiation based infrared microspectroscopy (SR-IMS), as a rapid and noninvasive advanced technique, has several advantages and is capable of showing four kinds of tissue information: structure, chemistry, environment, and composition.[24,26,28] To date, no study has been found on molecular structure in relation to biofunctions and nutrient availability in carinata seeds and carinata meal in other laboratories. Currently we are trying to apply synchrotron-based technology (the SR-IMS technique) to compare newly developed yellow-type and brown-type carinata seeds.

Brief Procedure for Synchrotron Study. Carinata seeds are cut into thin cross sections and then transferred to spectral IR windows for the SR-IMS study. Then a microscope linked to a digital camera from the window in the synchrotron centers takes photomicrographs of the cross section of the sample tissues.[25,32] Our previous paper[25] provided a detailed description of the methodology and procedure. The synchrotron infrared spectra are obtained in the mid-IR region (ca. 4000−800 cm^{-1}) with an aperture setting of 10 × 10 μm and 128−256 co-added scans at a spectral resolution of 4 cm^{-1}.

Univariate Molecular Spectral Analysis. The parameters shown on the spectrum could be analyzed for the band intensities, integrated intensities, band frequencies, and band intensity ratios.[36] OMNIC software (Spectra Tech., Madison,

WI, USA) is used to analyze the spectral data. Several parameters of carbohydrate and protein functional groups are detected as the following: structural carbohydrate peak height and area (SCHO with theoretical baseline of ca. 1487−1190 cm^{-1}); cellulosic compound peak height and area (CELC with theoretical baseline of ca. 1306−1191 cm^{-1}); total carbohydrate peak height and area (CHO with theoretical baseline of ca. 1198−896 cm^{-1}); protein amide I and II height and area (theoretical baseline of ca. 1728−1478 cm^{-1}; peaks are amonbetween ca. 1728−1576 and 1576−1478 cm^{-1}); α-helix and β-sheet peak height and area (peaks within ca. 1662−1650 and ca. 1636−1620 cm^{-1}, theoretically). The detailed peak intensity height and area ratios would be calculated.

Multivariate Molecular Spectral Analysis. The multivariate data analysis creates spectral corrections and maps according to all of the spectral information. Statistica 8.0 software (StatSoft Inc., Tulsa, OK, USA) is used to analyze the differences of carbohydrate-related and protein-related molecular conformation between carinata seeds and canola seeds in our preliminary study. The multivariate analyses agglomerative hierarchical cluster analysis (AHCA) and principal component analyses (PCA).[37−39] In AHCA, distance matrix and then the two most similar IR spectra (minimal distance) within the distance matrix are calculated. Then new "hierarchical group" (or "cluster") is obtained by combining these spectra, and spectral distances between all remaining spectra and the new cluster are recalculated. The results of the spectral data set would be shown as dendrograms. In PCA, the original variables are transformed to the uncorrelated variables called "principal components" (PCs), of which the first few account for >95% of the variance, to reduce the amount of linear combinations (PCs) with the same information.[37−39]

Infrared Molecular Spectroscopy of ATR-FT/IR for Molecular Structure Studies on Biofuel and Bio-oil Coproducts (Carinata Meals). The carbohydrate, protein, and lipid molecular spectra of the carinata meal and canola meal can be studied by infrared molecular spectroscopy of ATR-FT/IR or DRIFT.[5,11,40−46] Brief procedure is as follows: Sample spectral data are collected using the FT/IR with ATR (JASCO Corp., Tokyo, Japan). All of the samples are ground through a 0.25 mm screen two times. Then the IR spectra are obtained under the mid-IR region (ca. 4000−800 cm^{-1}) with 64 or 128 co-added scans at a spectral resolution of 4 cm^{-1}. For univariate molecular spectral analysis, the parameters shown on the spectrum can be analyzed for the band intensities, integrated intensities, band frequencies, and band intensity ratios.[36] OMNIC 7.3 (Spectra Tech., Madison, WI, USA) is used to analyze the spectral data. Several parameters of carbohydrate and protein functional groups are detected as follows:[5,11,41−43] structural carbohydrate peak height and area (SCHO with theoretical baseline of ca. 1487−1190 cm^{-1}); cellulosic compound peak height and area (CELC with theoretical baseline of ca. 1306−1191 cm^{-1}); total carbohydrate peak height and area (CHO with theoretical baseline of ca. 1198−896 cm^{-1}); protein amide I and II height and area (theoretical baseline of ca. 1728−1478 cm^{-1}, peaks between ca. 1728−1576 and ca. 1576−1478 cm^{-1}); α-helix and β-sheet peak height and area (peaks within ca. 1662−1650 and ca. 1636−1620 cm^{-1}, theoretically). For multivariate molecular spectral analysis, the multivariate data analysis creates spectral corrections and maps according to all of the spectral information. Statistica 8.0 software (StatSoft Inc.) is used to analyze the differences of carbohydrate-related and protein-related molecular conformation using the multivariate analyses.[39] For the detailed application, please see the following sections.

Wet Chemical Profile Studies. To access the chemical profiles and nutrient value of energy feedstocks and coproducts, analysis of their constituent compositions is essential. The most common method of nutrient constituent evaluation is proximate analysis, which separates nutrients that are required by the animal. With the proximate analysis, water, crude protein, crude fat, fiber, nonfiber carbohydrate, minerals, etc., can be measured. In this way, the magnitude of differences in chemical profiles can be detected.[11] Brief analysis procedures are as follows: The samples are ground and screened to a final particle size of 1 or 0.5 mm for the following chemical analyses. All of the samples are analyzed in duplicate and repeated if the error exceeds 5%. Detailed compositions and methods were dry matter (DM, %, AOAC official method 930.15), ash (% DM, AOAC official method 942.05), EE (or crude fat, % DM, AOAC official method 954.02), and crude protein (% DM, AOAC official method 984.13) analyzed by the procedures of AOAC.[22,23] Different types of fiber and lignin [acid detergent fiber (ADF, % DM, % NDF), neutral detergent fiber (NDF, % DM), acid detergent lignin (ADL, % DM, % NDF)] are analyzed by the procedures in Van Soest et al.[47] Samples are incubated with bicarbonate−phosphate buffer and filtered through Whatman filter paper for analyzing total soluble crude protein (SCP, % CP, % DM). The nonprotein nitrogen (NPN, % SCP, % CP, % DM) content is obtained by precipitating true protein in the filtrate with trichloroacetic acid (TCA, 10%) and determined as the difference between total N and the N content of the residue after filtration. Acid detergent insoluble protein (ADICP, % CP, % DM) and neutral detergent insoluble protein (NDICP, % CP, % DM) are measured according to the procedures of Licitra et al.[48] Starch (% DM, % NFC, % CHO) is analyzed using the Megazyme Starch Assay Kit. The nonstructural carbohydrates (NSC) or nonfibrous carbohydrates (NFC) (% DM, % CHO), fatty acids (FA, % DM), and NDFn (N adjusted) are calculated according to the formula of NRC dairy.[49] NSC is measured by enzymatic methods (Smith, 1981). NFC = 100 − (% NDF + % CP + % fat + % ash); FA = EE − 1; NDFn = NDF − NDICP). The detailed chemical profiles of carinata seed and meals have been reported recently.[11,41]

Biodegradation and Bioavailability Prediction Using the Cornell Net Carbohydrate and Protein System (CNCPS) Based on Chemical Profiles in Energy Feedstocks and Coproducts. The CNCPS is a mathematical model developed on the basis of animals, feeds, management conditions, and different environmental conditions. The protein fractions are partitioned according to CNCPS 6.1.[50−52] The characterizations of the protein fraction can be divided as fraction PA (nonprotein N), fraction PB (true protein), and PC (unavailable protein). In fraction PB, there are fraction PB1 (rapidly degraded protein with degradation rate of 1.20−4.00/h), PB2 (intermediately degraded protein with degradation rate of 0.03−0.16/h), and PB3 (slowly degraded protein with degradation rate of 0.0006−0.0055/h) divided according to the differences on ruminal degradation rates. Fraction PB1 is degraded in the rumen, fraction PB2 is insoluble in buffer but soluble in neutral detergent, and fraction PB3 is soluble only in acid detergent. Fraction PB2 can be estimated with the differences between buffer-insoluble protein and fraction PB3. Fraction PC is considered to be undergradable protein (like ADICP) because it is highly resistant to microbes and

mammalian enzymes. The CHO fraction is partitioned based on CNCPS 6.1 into fraction CA1 (volatile fatty acids, VFA), fraction CA2 (lactic acid), fraction CA3 (other organic acids), fraction CA4 (sugars), fraction CB1 (starch), fraction CB2 (soluble fiber), fraction CB3 (available neutral detergent fiber, NDF), and fraction CC (unavailable NDF).

In the CNCPS 6.1 model, rumen degraded and bypassed protein as well as bypassed CHO will be estimated on the basis of the contribution from each fraction. The following parameters will be determined: RDPA, RDPB1, RDPB2, RDPB3, total RDP = RDPB1 + RDPB2 + RDPB3, where RDPA is ruminally degraded protien A fraction, RDPB1 is ruminally degraded PB1, RDPB2 (g/day) is ruminally degraded PB2, RDPB3 is ruminally degraded PB3, and total RDP is ruminally degraded peptides/protein REPB1, REPB2, REPB3, and REPC, where REPB1 is ruminally escaped protein B1, REPB2 is ruminally escaped protein B2, REPB3 is ruminally escaped protein B3, and REPC is ruminally escaped protein C. RDCA is ruminally degraded CA, RDCB1 is ruminally degraded CB1, and RDCB2 is ruminally degraded CB2. RECA is ruminally escaped carbohydrate A, RECB1 is ruminally escaped carbohydrate B1, RECB2 is ruminally escaped carbohydrate B2, and RECC is ruminally escaped carbohydrate C. The fraction studies in carinata seed and carinata meals by CNCPS system have been reported recently from our laboratories.[11,41]

Energy Evaluation. In the NRC-2001 model, energy requirements for maintenance and milk production are described on the premise of metabolic body size (NE_m), tissue (NE_g), and milk (NE_L) composition. The feed energy values are also expressed on the basis of feed NE_m, NE_g, and NE_L values. In feeds, the total digestible nutrient (TDN) and digestible energy (DE), metabolizable energy (ME), and net energy (NE) are used to estimate available energy according to the NRC dairy 2001. Gross energy is measured using a Parr adiabatic bomb calorimeter (model 1200, Parr Instrument Co., Moline, IL, USA). Using the NRC 2001 system, tdNDF, tdNFC, tdCP, tdFA (% DM), TDN_{1X}, ME_{3X}, NE_m, NE_g, and NE_{Lp} can be determined. Detailed energy studies in energy feedstock (carinata seeds) and coproducts (carinata meals) have been reported recently from our laboratories.[5,11,41−43]

In Situ Technique for Degradation Kinetic Study. In situ incubation is a widely used method of evaluating ruminant feed according to the rate and extent of degradation. This involves suspension of tested feed material in the rumen, allowing for contact between the tested feed and actual rumen environment.[53] The rate and extent of rumen degradation of particular test feed are evaluated by the analysis of in situ residue samples after incubation. This fractionates nutrients into three fractions depending on their rumen availability. These fractions are soluble, potentially degradable, and undegradable fractions, named A, B, and C or S, D, and U, respectively.[54,55]

Brief Procedure. The samples are ground through 3 mm screens or using a roller (coarsely ground); then ca. 7 g of DM is placed into each nylon bag with the pore size of approximately 40 μm and subsequently put into the rumen. The rumen incubation is performed according to the schedule of "gradual addition − all out" for 48, 24, 12, 8, 4, 2, and 0 h. After that, all of the bags should be pulled out and washed in cool water without detergent and then dried at 55 °C for 48 h (including the 0 h bags). Later, the dried samples will be pooled and stored at 4 °C.[54]

The rumen degradation parameters can be estimated according to the modified first-order kinetics model[56−58] and NRC model.[49] The soluble fraction (S), undegradable fraction (U), and potentially degradable fraction (D) and the degradation rate in % h^{-1} (K_d) and the lag time (T_0) can be calculated on the basis of the first-order kinetic models to fit the fermentation or disappearance curves (goodness of fit) using the nonlinear and logarithmic-linear mathematical models.[56,59,60]

Gamage[61] summarized the potential sources of variation associated with the in situ nylon bag technique as animal, bag, substrate, temporal, procedural aspects and mathematical component, bag pore size, sample to bag ratio, particle size, bag incubation sequence, relative location of nylon bags suspended in the rumen, feeding frequency, diet composition, type of animal used, washing after incubation, and selection of mathematical model. In our preliminary study, we reported detailed kinetics studies in carinata seed and meals and their rumen residues.[5,11,41−46]

Intestinal Digestion Estimation. Intestinal digestibility of rumen undegraded feed protein (% RUP) is estimated by a three-step in vitro procedure (using in situ 12 or 16 h rumen incubation residue).[62] A brief procedure is as follows: (1) If using 16 h rumen incubation, nylon bags need to be filled with feed samples and then incubated in the rumen for 16 h. (2) After 16 h of rumen incubation, the residue is weighed to contain about 15 mg of N and put into a 50 mL centrifugation tube. Then 10 mL of 0.1 N HCl solution containing 1 g/L of pepsin is added into the tube, and the weighed residue is incubated for 1 h at 38 °C. (3) After incubation, the pH is neutralized by adding 0.5 mL of 1 N NaOH and 13.5 mL of pancreatin solution (pH 7.8, 0.5 M KH_2PO_4 buffer containing 50 ppm of thymol and 3 g/L pancreatin). The tube is vortexed and incubated at 38 °C in a shaker water bath for 24 h. All of the samples should be vortexed every 8 h. (4) Then 3 mL of a 100% (w/v) trichloroacetic acid solution is added to the tube immediately to stop the enzymatic action precipitating undigested protein. The tube is vortexed and kept for 15 min. (5) The samples are centrifuged at 10000*g* for 15 min and analyzed for soluble N in the supernatant. Pepsin−pancreatin digestion of protein is calculated as trichloroacetic acid-soluble N divided by sample nitrogen content (bag residues).[62] This technique has been used to estimated intestinal digestion of protein in energy feedstock (carinata seed) and coproducts (carinata meals).[5,11,41−46]

Modeling Truly Absorbable Protein Supply to the Small Intestine. To model true protein digested and absorbed in the small intestine, three models are most widely used, TDN-based NRC-2001 model in North America and non-TDN-based model DVE/OEB model[57,58,63] and PDI system in Europe. These models have been developed on the basis of the many previously developed nutritional models and incorporate some new approaches.[54,64−66] There is an updated version of DVE/OEB protein evaluation system, which is DVE-2010. Based on truly absorbable protein supply or metabolizable protein value, the feed milk vaule (FMV) will be determined.[15,49] Detailed comparisons among the three models have been reported.[64,66−68]

In our recent study,[43] we used modeling approaches to determine metabolizable protein supply of carinata meal to dairy cattle in comparison with conventional canola meal and found that "the value of true protein digested in the intestine predicted by the DVE/OEB system was 153 g/kg DM in carinata meal, which was similar to that in canola meal. Carinata meal had a positive degraded protein balance (+248 g/kg DM)", which has been reported.[43]

CURRENT MOLECULAR STRUCTURE STUDIES ON CARINATA AS ENERGY FEEDSTOCKS AND THEIR COPRODUCTS FROM BIOFUEL AND BIO-OIL PROCESSING

Study Interactive Association between Biopolymers and Biofunctions in Carinata Meal -Coproducts from Biofuel and Bio-oil Processing before and after Rumen Biodegradation. *Application 1 of Molecular Spectroscopy To Study the Relationship between CHO Structure and CHO Availability in Carinata Meal (Coproducts).* Molecular analyses with FTIR technique with attenuated total reflectance (ATR) and chemometrics may enable detection of structural features on a molecular basis. In this study,[11] we used FTIR-ATR spectroscopy in our laboratory to "investigate spectral features of carbohydrate conformation in carinata meal and investigate differences in carbohydrate molecular functional group spectral intensities after in situ ruminal fermentation at 0, 12, 24, and 48 h compared to conventional canola meal as a reference". Our measured parameters included[11] SCHO (mainly associated with hemicellulosic and cellulosic compounds; region and baseline ca. 1483−1184 cm^{-1}), cellulosic compounds (CELC, region and baseline ca. 1304−1184 cm^{-1}), total carbohydrates (CHO, region and baseline ca. 1193−889 cm^{-1}) as well as the spectral ratios calculated on the basis of respective spectral intensity data of carbohydrates. In this study we also published a typical ATR-FTIR molecular spectrum of carinata meal in the mid-IR region ca. 4000−800 cm^{-1}; please check our previous paper for the spectral graph.[11] In this study, we reported that "the spectral profiles of carinata meal were different from that of canola meal in CHO 2nd peak area (center at ca. 1091 cm^{-1}, region: 1102−1083 cm^{-1}) and functional group peak intensity ratios such as SCHO 1st peak (ca. 1415 cm^{-1}) to 2nd peak (ca. 1374 cm^{-1}) height ratio, CHO 1st peak (ca. 1149 cm^{-1}) to 3rd peak (ca. 1032 cm^{-1}) height ratio, CELC to total CHO area ratio and STCHO to CELC area ratio. The results indicated that carinata meal may not in full accord with canola meal in carbohydrate utilization and availability in ruminants. Almost all the spectral parameters were decreased during 48 h ruminal degradation in both carinata meal and canola meal."[11]

Application 2 of Molecular Spectroscopy To Study the Relationship between Protein Structure and Protein Availability in Carinata Meal (Coproducts). To date, no study in other laboratories was found on nutritive values and molecular structural characteristics associated with protein biopolymers of carinata meal from biofuel and bio-oil processing.[41] In this project,[41] we investigated the possible relationship between protein intrinsic structural features and nutrient profiles of carinata meal in comparison with conventional canola meal. We found that "carinata meal had 20−31% greater IR absorbance in protein amide I height and area as well as α-helix and β-sheet heights than canola meal. But agglomerative hierarchical cluster analysis and principal component analysis indicated these two types of the meals could not be distinguished completely within protein spectrum region (ca. 1728−1478 cm^{-1})."[41] We also observed some close correlations between protein structural parameters and protein nutrient profiles and subfractions" as reported in our individual project publication.[41]

Application 3 of Molecular Spectroscopy To Study Rumen Residue of Canola Meal (Coproducts). No study was found on whether protein structure changes during rumen fermentation from other research teams. In these studies,[41,42] we characterized protein structure spectral changes in carinata meal during ruminal fermentation using the FTIR technique. We wanted to find out "1) whether protein amide profile and protein 2nd structure profile changed after ruminal fermentation at 0, 12, 24, and 48 h in carinata meal and canola meal; 2) whether there were some correlation between protein spectral parameters and chemical profile in in situ rumen residue samples".[41,42] In the publications, we reported that "Protein structure spectral features in both carinata meal and canola meal were altered as incubation time increased and linear and curvilinear relationships on amide II height and area, height and area ratio of amide I and II as well as height ratio of α-helix and β-sheet were observed within 48 h ruminal fermentation. The amide I height and area as well as α-helix height and β-sheet height were in the highest level of IR absorbance at 0 h and then gradually declined linearly by 30−38% after 48 h incubation. We found that not only quantities decreased but also inherent structure changed in protein chemical make-up during ruminal fermentation. Strong correlations were found between protein spectral parameters and some basic nutrients profile such as CP (positively) and NDF (negatively). And multivariate spectral analysis showed that rumen residues from carinata meal (were) not distinguished from those from canola meal, suggesting some relationship in structural make-up exhibited between them within protein region during 48 h rumen fermentation".[41,42]

Study Interactive Association between Biopolymers and Biofunctions in Carinata Seeds as Feedstock for Biofuel and Bio-oil Processing. *Application 4 of Molecular Spectroscopy To Study the Relationship between CHO Structure and CHO Availability in Energy Feedstock (Carinata Seeds).* In this study,[41] we investigated the correlations between carbohydrate structural features and nutritional profiles in yellow and brown types of carinata seeds, with comparison to common canola seed as a reference. The key findings in this study were reported as follows: "carinata lines showed significantly different IR intensities in structural carbohydrate (SCHO), cellulosic compounds (CELC) and total CHO profiles from Canola seeds. The changes of CELC and CHO peak intensities were highly related with some changes in CHO chemical profile, energy values and NDF degradation kinetics in carinata and canola seeds."[41]

Application 5 of Molecular Spectroscopy To Study the Relationship between Protein Structure and Protein Availability in Carinata Seeds (as Energy Feedstock). In this study,[44] we detected "the correlations between protein intrinsic structural features and most important nutritional profiles of DVE, OEB and FMV values in three lines of carinata in yellow and brown seed coats, with comparison to canola seed as a control reference".[44] We found "significant differences in protein amide II peak height, amide I peak area and β-sheet height among the different carinata lines. However, multivariate spectral analyses indicated a similarity in protein structural make-up in these four kinds of oilseed. Not very strong correlations showed in our study implied that the limited sample size and narrow range in biological and spectral variation might be (a) response (to) the weak relationships between chemical profile and mid-IR spectral data." Nutritive values of DVE, OEB, and FMV from carinata seed and canola seed and multivariates molecular spectral analysis among the carinata lines were graphically presented in this publication.[44]

Application 6 of Molecular Spectroscopy To Study the Lipid-Related Chemical Functional Spectral Profile in Carinata Seeds (as Energy Feedstock). To date, information

dx.doi.org/10.1021/jf405809m | J. Agric. Food Chem. 2014, 62, 4039−4047

is lacking on the lipid molecular structural characteristics in relation to contents of oil, fatty acids, and antinutritional compounds in *B. carinata*.[5] In this study,[5] we investigated (1) oil content and fatty acid profile; glucosinolate profile, total polyphenols, and condensed tannins; and lipid-related inherent molecular structures in terms of CH stretching bands, unsaturated lipid bands (ULB) and lipid ester C═O carbonyl (LECC) bands in seeds from yellow-seeded and brown-seeded carinata lines [for typical ATR-FTIR molecular spectrum of carinata seeds and canola seed as a reference control in the mid-IR region ca. 4000−800 cm^{-1}, please see our publication[5]]; and (2) the relationship between the molecular spectral data and the contents of oil, fatty acids, and antinutritional compounds in the oilseeds.[69−71]

In this study, we reported that "brown-seeded carinata had lower contents of oil, C17:0, C18:0, C20:1, C20:2n-6, C24:1n-9 and total saturated fatty acids, and higher contents of C22:0, C22:1n-9 and C24:0 than yellow-seeded carinata. However, the contents of glucosinolates, polyphenols and condensed tannins were not different between the yellow and brown seeds. There were marked differences between carinata and canola seeds in the contents of oil, fatty acids profile, glucosinolates profile and polyphenols. The yellow seeds had lower peak heights of asymmetric CH_2 and symmetric CH_2, however, no changes were found in other spectral parameters. The absorbed peak intensities of CH stretchings, ULB and LECC of both types of carinata seeds were markedly stronger than those of canola seeds. The multivariate, cluster and principal component analyses showed no significant differences in the lipids molecular structures between the yellow-seeded and brown-seed carinata seed; whereas, the molecular structures of canola seeds were fully distinguished from both types of carinata seeds in the regions of CH stretchings and ULB. The lipid-related spectral bands intensities were strongly correlated to oil content, fatty acids, glucosinolates and polyphenols. The regression equations gave relatively high predictive power for the estimation of oil (R^2 = 0.99); all measured fatty acids (R^2 > 0.80), except C14:0, C20:3n-3, C22:2n-9 and C22:2n-6; 3-butenyl, 2-OH-3-butenyl, 4-OH-3-CH_3-indolyl and total glucosinolates (R^2 > 0.686) and total polyphenols (R^2 = 0.935)."[5] (For a detailed typical ATR-FTIR lipid molecular spectrum of carinata seeds and canola seed, please check our publication.)[5]

Application 7 of Molecular Spectroscopy To Study Heat-Induced Molecular Structure Change in Lipid-Related Chemical Functional Spectral Profile in Carinata Seeds (as Energy Feedstock). In this study,[46] we explored the effect of different autoclave heating times (30, 60, and 90 min) on fatty acid supply and molecular stability in carinata seed. In this work,[42] heat-induced molecular structure changes in lipid-related chemical functional spectral profile in carinata seeds detected by FTIR-ATR were presented graphically.[42] We reported that "autoclaving treatments decreased total fatty acids content in a linear fashion in carinata seed as heating time increased; and reduced concentrations were observed in C18:3n3, C20:1, C22:1n9, monounsaturated fatty acids (MUFA), polyunsaturated fatty acids (PUFA), omega 3 (ω-3) and 9 (ω-9) fatty acids. Correspondingly, the heated seeds showed dramatic reductions in all the peak intensities within lipid-related spectral regions. Results from agglomerative hierarchical cluster analysis (AHCA) and principal component analysis (PCA) indicated that the raw oilseed had different structural make-up from the autoclaved seeds in both CH_3 and CH_2 asymmetric and symmetric stretching region (ca. 2999−2800 cm^{-1}) and lipid ester C═O carbonyl region (ca. 1787−1706 cm^{-1}). However, the oilseeds heated for 30, 60, and 90 min were not grouped into separate classes or ellipses in all the lipid-related regions, indicating that there still exhibited similarities in lipid biopolymer conformations among autoclaved carinata seeds. Moreover, strong relationships observed in our study implied that lipid-related spectral parameters might have a potential to predict some fatty acids content in oilseed samples like *B. carinata*. However, more data from (a) large sample size and diverse range would be necessary and helpful to draw up a final conclusion."

All of the above results are based on limited samples in our laboratory, an experiment with a large sample size with detailed and systematical studies is on the way to confirming our findings in our preliminary study and exploring new findings in our large-scale study. For example, carinata meals with a higher crude protein content but contained less metabolizable protein supply for dairy cattle and had lower feed milk values when compared with conventional canola meals. These results should be checked and confirmed again. The correlation between inherent structures and nutrient biofunctions and bioavailability are inconclusive and should be studied with a large range of sample sizes. To improve nutrient availability predictions in energy feedstock and coproducts, the new concept of digestion in various functional groups could be tested in the new studies. In summary, this paper reviewed (1) the carinata seeds as energy feedstocks, biofuel and bio-oil processing procedures, and their processing coproducts; (2) potential synchrotron-based, globar-based molecular sepctroscopy and conventional evaluation methods on energy feestock (new carinata seeds) and coproducts (carinata meal) from biofuel and bio-oil processing; and (3) interactive association between biopolymers and biofunctions in carinata seeds and carinata meal, coproducts from biofuel and bio-oil processing before and after rumen biodegradation, and how molecular structural changes affect nutrient bioavailability and biofunctions.

AUTHOR INFORMATION

Corresponding Author

*(P.Y.) Mail: Professor and Ministry of Agriculture Strategic Research Chair, College of Agriculture and Bioresources, University of Saskatchewan, 6D10 Agriculture Building, 51 Campus Drive, Saskatoon, SK, Canada S7N 5A8. Phone: (306) 966-4132. E-mail: peiqiang.yu@usask.ca.

Funding

We acknowledge financial support from the Saskatchewan Ministry of Agriculture Strategic Feed Research Chair (P.Y.) Program, the Natural Sciences and Engineering Research Council of Canada (NSERC, both CRD and ID grants), SaskCanola (Saskatchewan Canola Development Commission), the Saskatchewan-ADF fund, and the Federal and Provincial Growing Forward 2 Program as well as the Thousand-Talent-People Award Program in Tianjin.

Notes

The authors declare no competing financial interest.

ACKNOWLEDGMENTS

We thank Agrisoma, Dr. Kevin Falk (AAFC, Saskatoon), and Colleen Christensen (University of Saskatchewan) for providing study samples.

ABBREVIATIONS USED

amide I intensity under amide I band (ca. 1718−1579 cm^{-1}) in this study
amide II intensity under amide II band (ca.1579−1488 cm^{-1}) in this study
ADF acid detergent fiber
ADICP acid detergent insoluble crude protein
ADIN acid detergent insoluble nitrogen
ADL acid detergent lignin
AHCA agglomerative hierarchical cluster analysis
ATR-FT/IR attenuated total reflectance Fourier transform infrared spectroscopy
CA1 volatile fatty acids
CA2 lactic acid
CA3 other organic acids
CA4 sugars
CA rapidly degradable soluble sugar fraction (K_d = 200−350% per h) defined by CNCPS
CB1 intermediately degradable carbohydrate subfraction (K_d = 20−50% per h) defined by CNCPS
CB2 slowly degradable carbohydrate subfraction (K_d = 2−10% per h) defined by CNCPS
CC unfermentable carbohydrate subfraction defined by CNCPS
CELC cellulosic compounds
CHO total carbohydrate
CNCPS Cornell Net Carbohydrate and Protein System
CP crude protein
D potential degradable fraction in the in situ ruminal incubation
DE digestible energy
$DE_{1\times}$ digestible energy at maintenance
$DE_{3\times}$ (DE_p) digestible energy at three times maintenance (i.e., production level)
DM dry matter
DRIFT diffuse reflectance infrared Fourier transform spectroscopy
dRUP estimated intestinal digestibility of RUP
DVE truly absorbed protein in the small intestine defined by DVE/OEB system
EE ether extract
FA fatty acid
FMV feed milk vaule
FTIR Fourier transform infrared spectroscopy
H_1630 β-sheet peak height (ca. 1630 cm^{-1})
H_1655 α-helix peak height (ca. 1655 cm^{-1})
IDP estimated intestinal digestibility of RUP
IR infrared
K_d degradation rate
K_p passage rate
LECC lipid ester C═O carbonyl
ME metabolizable energy
$ME_{3\times}$ (ME_p) metabolizable energy at 3 times maintenance (i.e., production level)
MP metabolizable protein
MUFA monounsaturated fatty acids
NDF neutral detergent fiber
NDFn nitrogen-free neutral detergent fiber (NDFn = NDF − NDICP)
NDICP neutral detergent insoluble crude protein
NE_g net energy for growth
$NE_{L3\times}$ (NE_{Lp}) net energy for lactation at 3 times maintenance (i.e., production level)
NE_m net energy for maintenance in growing animals
NFC nonfiber carbohydrate
NPN nonprotein nitrogen
NSC nonstructural carbohydrate
OEB degraded protein balance
OM organic matter
PA nonprotein nitrogen defined by CNCPS (K_d is assumed to be infinity)
PB1 rapidly degradable protein subfraction defined by CNCPS (K_d = 120−400% per h)
PB2 intermediately degradable protein subfraction defined by CNCPS (K_d = 3−16% per h)
PB3 slowly degradable protein subfraction defined by CNCPS (K_d = 0.06−0.55% per h
PC undegradable protein subfraction defined by CNCPS
PCA principal component analysis
PUFA polyunsaturated fatty acids
RDCA ruminally degraded carbohydrate A
RDCB1 ruminally degraded carbohydrate B1
RDCB2 ruminally degraded carbohydrate B2
RDPA ruminally degraded protein A
RDPB1 ruminally degraded protein/peptide B1
RDPB2 ruminally degraded protein/peptide B2
RDPB3 ruminally degraded protein/peptide B3
RDP ruminally degraded peptides
RECA ruminally escaped carbohydrate A
RECB1 ruminally escaped carbohydrate B1
RECB2 ruminally escaped carbohydrate B2
RECC ruminally escaped carbohydrate CC
REPB1 ruminally escaped protein B1
REPB2 ruminally escaped protein B2
REPB3 ruminally escaped protein B3
S potential soluble fraction in the in situ ruminal incubation
SCHO structural carbohydrates
SCP soluble crude protein
SR-IMS synchrotron-based Fourier transform infrared microspectroscopy
T_0 lag time
TCA trichloroacetic acid
tdCP truly digestible crude protein
tdFA truly digestible fatty acid
TDN total digestible nutrients
$TDN_{1\times}$ total digestible nutrients at maintenance
$TDN_{3\times}$ total digestible nutrients at 3 times maintenance (i.e., production level)
tdNDF truly digestible neutral detergent fiber
tdNFC truly digestible nonfiber carbohydrate
U potential undegradable fraction in the in situ ruminal incubation
ULB unsaturated lipid bands

REFERENCES

(1) Bouaid, A.; Martinez, M.; Aracil, J. Production of biodiesel from bioethanol and *Brassica* carinata oil: oxidation stability study. *Bioresour. Technol.* **2009**, *100*, 2234−2239.
(2) Canam, T.; Li, X.; Holowachuk, J.; Yu, M.; Xia, J.; Mandal, R.; Krishnamurthy, R.; Bouatra, S.; Sinelnikov, I.; Yu, B.; Grenkow, L.; Wishart, D. S.; Steppuhn, H.; Falk, K. C.; Dumonceaux, T. J.; Gruber, M. Y. Differential metabolite profiles and salinity tolerance between two genetically related brown-seeded and yellow-seeded *Brassica carinata* lines. *Plant Sci.* **2013**, *198*, 17−26.
(3) Ban, Y.; Yu, P. *Structure, Physicochemical, Nutrition Characterization of Newly Developed Yellow- or Brown-Types of AAFC Carinata Lines/ Germplasms for Bio-Fuel/ Bio-Oil Production in Comparison with*

Canola Seeds and Meal. Thesis Research Proposal, University of Saskatchewan, Canada, 2013.
(4) Rakow, G.; Getinet, A. *Brassica carinata* an oilseed crop for Canada (abstract). International Symposium *Brassica*. *Acta Hortic.* **1998**, *495*, 419−426.
(5) Xin, H.; Yu, P. Detect changes in lipid-related structure of brown- and yellow-seeded *Brassica carinata* seed during rumen fermentation in relation to basic chemical profile using ATR-FT/IR molecular spectroscopy with chemometrics. *Spectrochim. Acta Part A: Mol. Biomol. Spectrosc.* **2013**.
(6) Xin, H.; Khan, N.; Falk, K. C.; Yu, P. Lipid molecular structural characteristics of *Brassica carinata* seeds: relationship with oil content, fatty acids profile and anti-nutritional compounds. *J. Agric. Food Chem.* **2013**.
(7) Getinet, A.; Rakow, G.; Raney, J. P.; Downey, R. K. Development of zero erucic acid Ethiopian mustard through an interspecific cross with zero erucic acid Oriental mustard. *Can. J. Plant Sci.* **1994**, *74*, 793−795.
(8) Velasco, L.; Nabloussi, A.; De Haro, A.; Fernández-Martínez, J. M. Development of high-oleic, low-linolenic acid Ethiopian-mustard (*Brassica carinata*) germplasm. *Theor. Appl. Genet.* **2003**, *107*, 823−830.
(9) Khattab, R.; Goldberg, E.; Lin, L.; Thiyam, U. Quantitative analysis and free-radical-scavenging activity of chlorophyll, phytic acid, and condensed tannins in canola. *Food Chem.* **2010**, *122*, 1266−1272.
(10) Raymer, P. L. Canola: an emerging oilseed crop. *Trends in New Crops and New Uses*; Janick, J., Whipkey, A., Eds.; ASHS Press: Alexandria, VA, USA, 2002.
(11) Xin, H.; Yu, P. Chemical profile, energy values, protein molecular structure characteristics of bio-fuel and bio-oil co-products (carinata meal) in comparison with canola meal. *J. Agric. Food Chem.* **2013**, *61*, 3926−3933.
(12) Chichlowski, M. W.; Schroeder, J. W.; Park, C. S.; Keller, W. L.; Schimek, D. E. Altering the fatty acids in milk fat by including canola seed in dairy cattle diets. *J. Dairy Sci.* **2005**, *88*, 3084−3094.
(13) Sánchez, J. M.; Claypool, D. W. Canola meal as a protein supplement in dairy rations. *J. Dairy Sci.* **1988**, *66*, 80−85.
(14) Chibisa, G. E.; Christensen, D. A.; Mutsvangwa, T. Effects of replacing canola meal as the major protein source with wheat dried distillers grains with solubles on ruminal function, microbial protein synthesis, omasal flow, and milk production in cows. *J. Dairy Sci.* **2012**, *95*, 824−841.
(15) Theodoridou, K.; Yu, P. Metabolic characteristics of the proteins in yellow-seeded and brown-seeded canola meal and presscake in dairy cattle: comparison of three systems (PDI, DVE, NRC) in nutrient supply and feed milk value (FMV). *J. Agric. Food Chem.* **2013**, *61*, 2820−2830.
(16) Theodoridou, K.; Yu, P. Application potential of ATR-FT/IR molecular spectroscopy in animal nutrition: reveal protein molecular structures of canola meal and presscake, as affected by heat processing methods, in relationship with their protein digestive behaviour and utilization for dairy cattle. *J. Agric. Food Chem.* **2013**, *61*, 5449−5458.
(17) Thedoridou, K.; Vail, S.; Yu, P. Explore protein molecular structure in endosperm tissues in newly developed black and yellow type canola seeds by using synchrotron-based Fourier transform infrared microspectroscopy. *Spectrochim. Acta Part A: Mol. Biomol. Spectrosc.* **2014**, *120*, 421−427.
(18) Castell, G.; Falk, L. Effects of dietary canola seed on pig performance and backfat composition. *Can. J. Anim. Sci.* **1980**, *60*, 795−797.
(19) Hilton, J. W.; Slinger, S. J. Digestibility and utilization of canola meal in practical-type diets for rainbow trout (*Salmo gairdneri*). *Can. J. Fish. Aquat. Sci.* **1986**, *43*, 1149−1155.
(20) Yu, P. Study of barley grain molecular structure for ruminants using DRIFT, FTIR-ATR and synchrotron radiation infrared micro-spectroscopy (SR-IMS): a review. *J. Phys.: Conf. Ser.* **2012**, *359*, 012008.
(21) Yu, P. Board Invited Review: Sensitivity and responses of functional groups to feed processing on a molecular basis. *J. Anim. Sci. Biotechnol.* **2012**, *3*, 40.
(22) AOAC. *Official Methods of Analysis of the Association of Official Analytical Chemists*, 15th ed.; AOAC: Arlington, VA, USA, 1990; Vol. II.
(23) AOAC. *Official Methods of Analysis of AOAC International*, 18th ed.; AOAC International: Gaithersburg, MD, USA, 2005.
(24) Yu, P. Application of advanced synchrotron radiation-based fourier transform infrared (SR-FTIR) microspectroscopy to animal nutrition and feed science: a novel approach. *Br. J. Nutr.* **2004**, *92*, 869−885.
(25) Yu, P.; McKinnon, J. J.; Christensen, C. R. Chemical imaging of microstructure of plant tissues within cellular dimension using synchrotron infrared microspectroscopy. *J. Agric. Food Chem.* **2003**, *51*, 6062−6067.
(26) Miller, L. M.; Dumans, P. Chemical imaging of biological tissue with synchrotron infrared light. *Biochim. Biophys. Acta* **2006**, *1758*, 846−857.
(27) Yu, P. Novel approach for protein research. In *Protein Research Progress*; Nova Science Publishers: Hauppauge, NY, USA, 2008; pp 207−231.
(28) Budevska, B. O. Applications of vibrational spectroscopy in life, pharmaceutical and natural sciences. In *Handbook of Vibrational Spectroscopy*; Wiley: New York, 2002; 5, pp 3720−3732.
(29) Zhang, X.; Yu, P. Using ATR-FT/IR molecular spectroscopy to detect effects of blend DDGS inclusion level on the molecular structure spectral and metabolic characteristics of the proteins in hulless barley. *Spectrochim. Acta Part A: Mol. Biomol. Spectrosc.* **2012**, *95*, 53−63.
(30) Yu, P. Effect of heat processing methods on spectral images of biological tissues (yellow canola seed protein) using advanced synchrotron-based infrared technique. *Biomed. Spectrosc. Imaging (Netherlands)* **2012**, *1* (2), 147−157.
(31) Doiron, K. J.; Yu, P.; Christensen, C. R.; Christensen, D. A.; McKinnon, J. J. Detecting molecular changes in Vimy flaxseed protein structure using synchrotron FTIRM and DFTIR spectroscopic techniques: structural and biochemical characterization. *Spectroscopy* **2009**, *23*, 307−322.
(32) Yu, P.; Christensen, C. R.; Christensen, D. A.; McKinnon, J. J. Ultrastructural-chemical makeup of yellow-seeded (*Brassica rapa*) and brown-seeded (*Brassica napus*) canola within cellular dimensions, explored with synchrotron reflection FTIR microspectroscopy. *Can. J. Plant Sci.* **2005**, *85*, 533−541.
(33) Yu, P.; Theodoridou, K.; Xin, H.; Huang, P. Y.; Lee, Y. C.; Wood, B. R. Synchrotron-based microspectroscopic study on the effects of heat treatments on cotyledon tissues in yellow-type canola (*Brassica*) seeds. *J. Agric. Food Chem.* **2013**, *61*, 7234−7241.
(34) GEA. Bio-fuel processing; http://www.westfalia-separator.com/applications/renewable-resources/fuel-from-rapeseed-oil.html (retrieved online Dec 27, 2013).
(35) GEA. Bio-oil processing; http://www.westfalia-separator.com/applications/renewable-resources/rapeseed-oil.html (retrieved online Dec 27, 2013).
(36) Yu, P. Synchrotron IR microspectroscopy for protein structure analysis: potential and questions. *Spectroscopy* **2006**, *20*, 229−251.
(37) Jolliffe, I. T. *Principal Component Analysis*; Springer-Verlag: New York, 1986; 487 pp.
(38) Jain, A. K.; Dubes, R. C. *Algorithms for Clustering Data*; Prentice-Hall: Upper Saddle River, NJ, USA, 1988; 320 pp.
(39) Yu, P. Applications of hierarchical cluster analysis (CLA) and principal component analysis (PCA) in feed structure and feed molecular chemistry research, using synchrotron-based fourier transform infrared (FTIR) microspectroscopy. *J. Agric. Food Chem.* **2005a**, *53*, 7115−7127.
(40) Chalmers, J. M.; Griffiths, P. R. *Handbook of Vibrational Spectroscopy*; Wiley: New York, 2002; Vol. 5.
(41) Xin, H.; Yu, P. Detect changes in protein structure of carinata meal during rumen fermentation in relation to basic chemical profiles

and comparison with canola meal using ATR-FT/IR molecular spectroscopy with chemometrics. *Spectrochim. Acta Part A: Mol. Biomol. Spectrosc.* **2013**, *112*, 318−325.
(42) Xin, H.; Yu, P. Using ATR-FT/IR to detect carbohydrate-related molecular structure features of carinata meal and their in situ residues of ruminal fermentation in comparison with canola meal. *Spectrochim. Acta Part A: Mol. Biomol. Spectrosc.* **2013**, *114*, 599−606.
(43) Xin, H.; Yu, P. Rumen degradation, intestinal and total digestion characteristics and metabolizable protein supply of carinata meal in comparison with canola meal to dairy cows. *Anim. Feed Sci. Technol.* **2013**, in review.
(44) Xin, H.; Falk, K. C.; Yu, P. Studies on *Brassica carinata* seed. 1. Protein molecular structure in relation to protein nutritive values and metabolic characteristics. *J. Agric. Food Chem.* **2013**, *61*, 10118−10126.
(45) Xin, H.; Falk, K. C.; Yu, P. Studies on *Brassica carinata* seed. 2. Carbohydrate molecular structure in relation to carbohydrate chemical profile, energy values and biodegradation characteristics. *J. Agric. Food Chem.* **2013**, *61*, 10127−10134.
(46) Xin, H.; Zhang, Y.; Yu, P. Implication of modified molecular structure of lipid through heat-related process to fatty acids supply in *Brassica carinata* seed. *J. Agric. Food Chem.* **2013**, in review.
(47) Van Soest, P. J.; Robertson, J. B.; Lewis, B. A. Methods for dietary fiber, neutral detergent fiber, and nonstarch polysaccharides in relation to animal nutrition. *J. Dairy Sci.* **1991**, *74*, 3583−3597.
(48) Licitra, G.; Hernandez, T. M.; Van Soest, P. J. Standardization of procedures for nitrogen fractionation of ruminant feeds. *Anim. Sci. Feed Technol.* **1996**, *57*, 347−358.
(49) NRC (National Research Council). *Nutrient Requirements of Dairy Cattle*; National Academy Press: Washington, DC, USA, 2001.
(50) Sniffen, C. J.; O'Connor, J. D.; Van Soest, P. J.; Fox, D. G.; Russell, J. B. A net carbohydrate and protein system for evaluating cattle diets: II. carbohydrate and protein availability. *J. Anim. Sci.* **1992**, *70*, 3562−3577.
(51) Lanzas, C.; Sniffen, C. J.; Seo, S.; Tedeschi, L. O.; Fox, D. G. A revised CNCPS feed carbohydrate fractionation scheme for formulating rations for ruminants. *Anim. Feed Sci. Technol.* **2007**, *136*, 167−190.
(52) Fox, D. G.; Tedeschi, L. O.; Tylutki, T. P.; Russell, J. B.; Van Amburgh, M. E.; Chase, L. E.; Pell, A. N.; Overton, T. R. The Cornell Net Carbohydrate and Protein System model for evaluating herd nutrition and nutrient excretion. *Anim. Feed Sci. Technol.* **2004**, *112*, 29−78.
(53) Nocek, J. E. *In situ* and other methods to estimate ruminal protein and energy digestibility: a review. *J. Dairy Sci.* **1988**, *71*, 2051−2069.
(54) Yu, P.; Goelema, J. O.; Tamminga, S. Using the DVE/OEB model to determine optimal conditions of pressure toasting on horse beans (*Vicia faba*) for the dairy feed industry. *Anim. Feed Sci. Technol.* **2000**, *86*, 165−176.
(55) Gamage, I. H.; Jonker, A.; Christensen, D. A.; Yu, P. Metabolic characteristic of proteins and biomolecular spectroscopic profiles in different batches of feedstock (wheat) and their co-products (wheat dried distillers grain with solubles) from the same bioethanol processing plant. *J. Dairy Sci.* **2012**, *95*, 6695−6715.
(56) Ørskov, E. R.; McDonald, I. The estimation of protein degradability in the rumen from incubation measurements weighted according to rate of passage. *J. Agric. Sci.* **1979**, *92*, 499−503.
(57) Tamminga, S.; Van Straalen, W. M.; Subnel, A. P. J.; Meijer, R. G. M.; Steg, A.; Wever, C. J. G.; Blok, M. C. The Dutch protein evaluation system: the DVE/OEB-system. *Livest. Prod. Sci.* **1994**, *40*, 139−155.
(58) Tamminga, S.; Brandsma, G. G.; Dijksta, J.; Duinkerken, G. V.; Vuuren A. M. V.; Blok, M. C. Protein evaluation for ruminants: the DVE/OEB 2007 system. CVB documentation report 53, CVB, Lelystad, 2007.
(59) Robinson, P. H.; Fadel, J. G.; Tamminga, S. Evaluation of mathematical models to describe neutral detergent residue in terms of its susceptibility to degradation in the rumen. *Anim. Feed Sci. Technol.* **1986**, *15*, 249−271.
(60) Dhanoa, M. S. On the analysis of dracon bag data for low degradability feeds (research note). *Grass Forage Sci.* **1988**, *43*, 441−444.
(61) Gamage, I. H. *Structural, Chemical and Nutrient Characterization of Original Feed Stock and Co-Products from a Newly Built Biofuel Plant In Saskatchewan*. Thesis, University of Saskatchewan, Canada, 2013.
(62) Calsamiglia, S.; Stern, M. D. A three-step in vitro procedure for estimating intestinal digestion of protein in ruminants. *J. Anim. Sci.* **1995**, *73*, 1459−1465.
(63) Van Duinkerken, G.; Blok, M. C.; Bannink, A.; Cone, J. W.; Dijkstra, J.; Van Vuuren, A. M.; Tamminga, S. Update of the Dutch protein evaluation system for ruminants: the DVE/OEB2010 system. *J. Agric. Sci.* **2011**, *149*, 351−367.
(64) Yu, P.; Christensen, D. A.; McKinnon, J. J. Comparison of the national research council-2001 model with the Dutch system (DVE/OEB) in the prediction of nutrient supply to dairy cows from forages. *J. Dairy Sci.* **2003**, *86*, 2178−2192.
(65) Yu, P.; Meier, J. A.; Christensen, D. A.; Rossnagel, B. G.; McKinnon, J. J. Using the NRC-2001 model and the DVE/OEB system to evaluate nutritive values of Harrington (malting-type) and Valier (feed-type) barley for ruminants. *Anim. Feed Sci. Technol.* **2003**, *107*, 45−60.
(66) Yu, P. Prediction of protein supply to ruminants from concentrates: comparison of the NRC-2001 model with the DVE/OEB system. *J. Sci. Food Agric.* **2005**, *85*, 527−538.
(67) Nuez-Ortín, W. G.; Yu, P. Modelling the metabolic characteristics of proteins in dairy cattle from co-products of bioethanol processing: comparison of the NRC 2001 model with the DVE/OEB system. *J. Sci. Food Agric.* **2010**, *91*, 405−411.
(68) Gamage, I. H.; Yu, P. Short communication: comparison of newly developed DVE/OEB_{2010} system and NRC_{2001} model in modeling metabolic characteristics of proteins. *J. Dairy Sci.* **2013**, *96*, 5908−5913.
(69) CLS Web, 2013; http://www.lightsource.ca/.
(70) Yu, P.; Block, H.; Niu, Z.; Doiron, K. Rapid characterization of molecular chemistry and nutrient make-up and microlocalization of internal seed tissue. *J. Synchrotron Radiat.* **2007**, *14*, 382−390.
(71) Tylutki, T. P.; Fox, D. G.; Durbal, V. M.; Tedeschi, L. O.; Russell, J. B.; Van Amburgh, M. E.; Overton, T. R.; Chase, L. E.; Pell, A. N. Cornell Net Carbohydrate and Protein System: a model for precision feeding of dairy cattle. *Anim. Feed Sci. Technol.* **2008**, *143*, 174−202.

JOURNAL OF AGRICULTURAL AND FOOD CHEMISTRY

Review

pubs.acs.org/JAFC

Diacetyl: Occurrence, Analysis, and Toxicity

Takayuki Shibamoto*

Department of Environmental Toxicology, University of California, Davis, California 95616, United States

ABSTRACT: Diacetyl possesses a butter-like flavor and has been widely used as a flavoring agent. It forms from sugars and lipids via various bacteria and heat treatment in various foods and beverages, such as milk. The toxicity of diacetyl, especially when inhaled, has recently attracted the attention not only of consumers but also of regulatory agencies. Even though accurate quantitative analysis of diacetyl is extremely important in evaluating its possible adverse effects, precise quantitative analysis of diacetyl in foods and beverages, as well as in ambient air, is considerably difficult because it is highly reactive and soluble in water. Among the many analytical methods developed for measuring diacetyl, preparation of 2,3-dimethylquinoxaline followed by gas chromatography has been most commonly used in the analysis of various foods, beverages, and air samples. This mini-review summarizes the formation mechanisms, analytical methods, occurrence, and toxicity of diacetyl.

KEYWORDS: *diacetyl, α-dicarbonyl compounds, inhalation toxicity, lipids, sugars*

INTRODUCTION

Diacetyl is a degradation product of various food components, including fatty acids/triglycerides, carbohydrates/sugars, and proteins/amino acids. Formation of diacetyl from sugar degradation had already been reported by the middle of the past century.[1] Around that time, diacetyl was found in lipid peroxidation products.[2,3] More recent research has shown that diacetyl forms by the action of lactic bacteria.[4] Diacetyl is also known to form as a natural product of the action of microorganisms during fermentation in some food products, such as yogurt[5] and fermented soybeans.[6] Consequently, diacetyl has been found in many foods and beverages, particularly in dairy products.

Diacetyl is listed in the FDA's GRAS (generally regarded as safe) list and has been used widely in the preparation of butter and related food products, at levels of 6−9 μg/g, because it possesses a unique, butter-like flavor with an odor threshold of 50 ppb.[7,8] On the other hand, NIOSH proposed limits on diacetyl exposure for factory workers, who might be exposed to vapor-phase diacetyl in related production factories.[9−11] Toxicities associated with diacetyl, such as interacting with other factors to cause lung damage[12] and playing a role in oxidative stress, have also been reported.[13] Determination of toxicity is the first avenue to establishing the safety level of chemicals. Establishing regulatory values of diacetyl, however, is rather difficult because sufficient information, such as actual levels in foods and beverages, vapor-phase levels, formation mechanisms, and toxicities, is required before the safety level can be set. This information is not yet completely known.

A number of reviews involved in specific issues of diacetyl, such as analytical and biochemical considerations,[14] foodborne microorganisms,[15] respiratory sensitizer,[16] and brewery fermentation,[17] have been published. However, virtually no reviews providing sufficient information on the occurrence, toxicity, and analytical method of diacetyl are available.

Analysis of diacetyl is not easy because it is highly reactive, volatile, and water-soluble. The mainstream practice in diacetyl analysis is therefore to prepare a stable compound, such as 2,3-dimethylquinoxaline, and then analyze it using gas chromatography.[18] Various less commonly used methods, such as colorimetric,[19] fluorometric,[20] GC-MS,[5] GC-ECD,[21] and HPLC-UVD analyses,[22,23] have also been reported. The recent development of LC-MS analysis may provide an ideal analytical method for diacetyl in the near future.

CHEMISTRY AND FORMATION MECHANISMS OF DIACETYL

Physical Nature. Diacetyl (CAS Registry No. 431-03-8) is a simple α-dicarbonyl compound with a molecular weight of 86.0892. Another common name for diacetyl is 2,3-butanedione. It is a yellow liquid at room temperature and soluble in most organic solvents and water. Its melting point is between −2 and −4 °C, and its boiling point is 88 °C.

Chemical Formation. Many carbonyl compounds, including diacetyl, are known to be formed from lipids upon oxidation. Figure 1 summarizes the generally recognized proposed formation pathways of carbonyl compounds from lipids, which were reported in the early 1980s.[24,25] It has also been known since the 1960s that sugars degrade into many low-molecular-weight carbonyl compounds including diacetyl.[1,26] Formation of diacetyl in milk by heat treatment had already been demonstrated in the late 1960s.[27] Figure 2 shows the proposed formation pathways of diacetyl from sucrose. In these pathways, the first step is tautomerization of a free sugar group, followed by cleavage at keto−enol bonding in acidic or alkaline solution.[28] A recent study reported that higher levels of diacetyl were formed from sugars in acidic or basic solutions than in neutral solutions.[29]

In addition to the formation pathways of α-dicarbonyl compounds shown in Figures 1 and 2, there is a pathway by which a lipid or sugar produces various low-molecular-weight radicals, such as $^{\bullet}CH_3$, $^{\bullet}C{=}O$, and $^{\bullet}C{=}O(CH_3)$, and these radicals subsequently combine to yield diacetyl. This pathway

Received: February 4, 2014
Revised: April 14, 2014
Accepted: April 16, 2014
Published: April 16, 2014

ACS Publications © 2014 American Chemical Society

dx.doi.org/10.1021/jf500615u | J. Agric. Food Chem. 2014, 62, 4048−4053

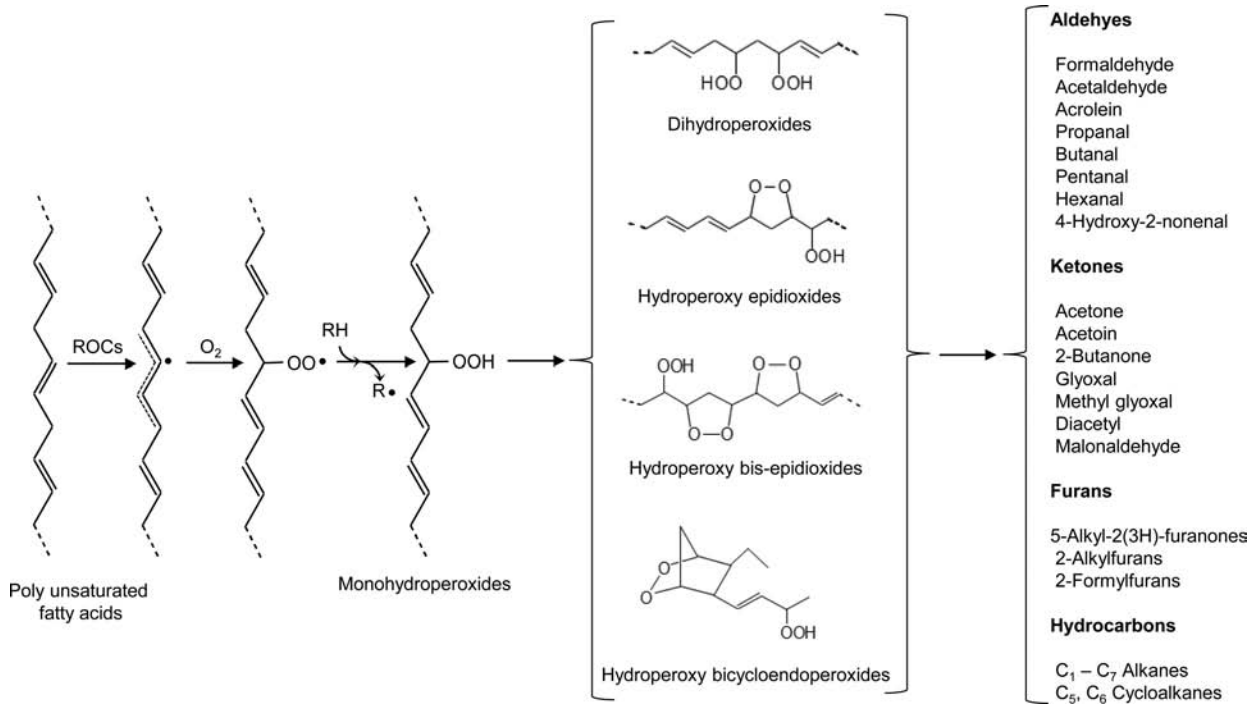

Figure 1. Generally recognized proposed formation pathways of carbonyl compounds from lipids.

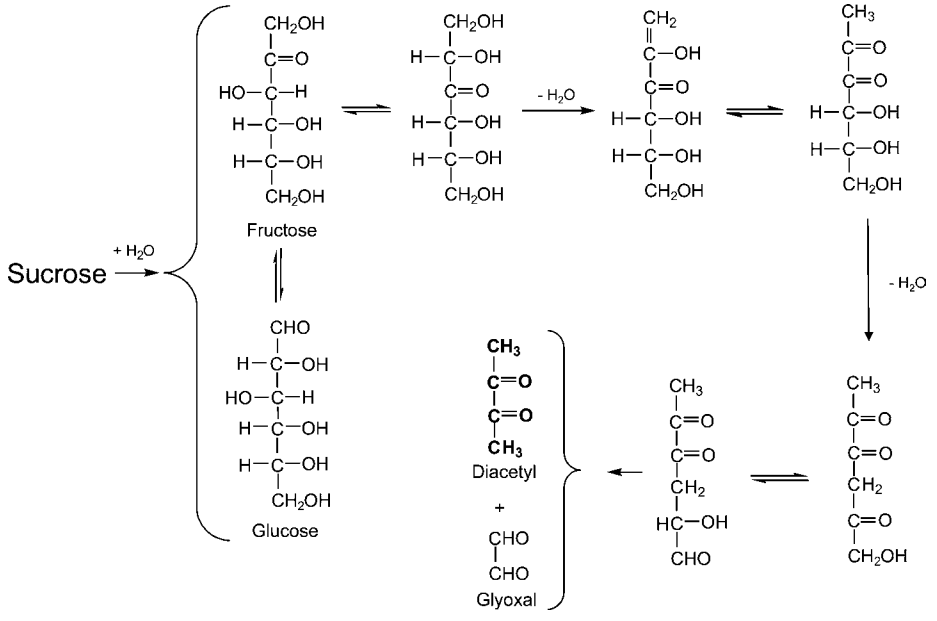

Figure 2. Proposed formation pathways of diacetyl from sucrose.

could be proposed when the reaction systems absorb high levels of energy from exposure to high temperatures, as in cooking or photoirradiation.[30] In fact, when cod liver oil was irradiated by UV, 27.23 nmol/mg glyoxal and 5.72 nmol/mg methylglyoxal were formed, suggesting that the radicals listed above combined to produce these diacetyl analogues.[31]

Maillard Reaction. The Maillard reaction is one of the most important reactions that form carbonyl compounds, including diacetyl, in foods. The Maillard reaction occurs between carbonyl compounds, such as sugars and lipids, and nitrogen-containing compounds, such as amino acids. It is generally recognized that nitrogen comes from an amino acid via Strecker degradation.[32] The sources of carbonyl compounds are sugars and lipids.[33] Formation of diacetyl from a Maillard model system consisting of L-rhamonse and ammonia was reported in the late 1970s.[34] Despite the fact that carbonyl compounds do not contain a nitrogen atom, amine compounds react with a sugar or a lipid to promote the formation of carbonyl compounds, including diacetyl,[35] suggesting that amine compounds act as catalysts for sugar or lipid degradation. Maltose, for example, degraded into diacetyl through an Amadori product intermediate when it was incubated with L-lysine.[36] In this study, diacetyl was recovered as a quinoxaline derivative ranging from 0.08 to 0.14 mmol/mol maltose.

Bacterial Formation. Formation of diacetyl by bacterial treatment may follow the pathway shown in Figures 1 and 2

dx.doi.org/10.1021/jf500615u | J. Agric. Food Chem. 2014, 62, 4048−4053

Table 1. Diacetyl Found in Various Foods and Beverages

sample	level (μg/g)	objective of analysis	analytical method	ref
heated milk	0.005−0.38	volatiles (19)[a]	GC-MS, direct	27
oxidized sardine oil	1.6−3.1	α-dicarbonyls	6-chloroquinoxaline/GC-ECD	42
fermented soybean	NR[b]	volatiles (45)	GC-MS, direct	6
brandy, vinegar, wine, butter	2.1−0.3	α-dicarbonyls	polarography	43
fermented soybean curds	0.02−0.12	volatiles (92)	GC-MS-FID direct	44
wine	0.5−10 mg/L	α-dicarbonyls	quinoxaline/HPLC-UV, GC-MS, GC-NPD	23
cheese	4.52	organic acids, diacetyl	HPLC-UV or RI	45
fresh milk	NR	volatiles (71)	GC-MS, GC-FID, direct	46
orange juice	<0.10	diacetyl	polarography	47
whiting, mackerel, cod	NR	volatiles (86)	SPME/GC-MS, direct	48
roasted coffee	2.72	α-dicarbonyls	HPLC-DAD, direct	49
sweet cream butter	0−0.078	volatiles (21)	GC-MS direct	50
goat's milk jack cheese	5.97−13.68	volatiles (26)	GC-headspace analyzer, direct	51
yogurt	200−3000	volatiles (49)	GC-FID direct	5
artichoke juice	0−179 mmol/L	diacetyl, acetoin	polarography	37
beer	0.034−0.110	diacetyl	6-nitroquinoxaline/HPLC-UV	52
selected dairy products	1.2−22000	volatiles (11)	GC-MS, direct	53

[a]Number of chemicals reported. [b]NR, not reported in the reference.

because the processes are mild compared with thermal degradation. There have been many reports on the formation of diacetyl by various bacteria.[37] Lactic bacteria were used to enhance butter flavor by inducing diacetyl.[38] *Lactobacillus casei* was also used to increase the capacity to synthesize diacetyl from lactose in whey permeate.[39] A low level of citrate contained in cheeses was proposed to produce diacetyl by *Streptococcus diacetylactis*.[40] One interesting study reported that diacetyl could be used as a microbial spoilage marker for meat products using PTR-MS.[41] The amount of diacetyl produced in Jerusalem artichoke juice by the action of 10 *Lactobacillus* strains ranged from 0 to 179 μmol/L.[37]

ANALYSIS OF DIACETYL IN FOODS AND BEVERAGES

Analytical Methods. Table 1 shows typical reports on diacetyl in foods and beverages along with the analytical methods used. In this table, unit amounts were harmonized to micrograms per gram because the units used in the original papers were varied (e.g., ppm, mg/kg, and μg/g). However, some units, such as milligrams per liter and millimoles per milliliter, which could not be changed to mcirograms per gram are shown as they were in the original papers.

The colorimetric method involves formation of color from diacetyl and a color reagent prepared with creatine and β-naphthol, after which its UV absorption at 525 nm is measured.[37] One study demonstrated that the detection and quantification limits of HPLC were 0.002 and 0.006 mg/L, respectively.[23]

There are two types of diacetyl analysis. In the first, diacetyl is included as one component of the volatile chemicals found in foods and beverages. The second analysis is specific to α-dicarbonyl compounds, including diacetyl. As mentioned above, due to its high reactivity and water solubility, it is difficult to conduct a quantitative analysis of diacetyl. The use of appropriate derivatives to perform quantitative determination of this type of chemical is a commonly recognized method of analysis. One of the most widely used derivatives for diacetyl is 2,3-dimethylquinoxaline, which is a product of diacetyl and 2,3-phenylenediamine.[18] Figure 3 shows the reaction between α-dicarbonyl compounds and 2,3-phenylenediamine to form a corresponding quinoxaline derivative. This reaction occurs readily under mild conditions in a slightly basic solution at room temperature.[31] Quinoxalines themselves were reported as flavor chemicals in heat-treated foods in the early 1970s.[54] Diacetyl has been quantified in various foods and beverages using this quinoxaline derivative. For example, 2.72 μg/g diacetyl was reported in roasted coffee using this derivative.[49]

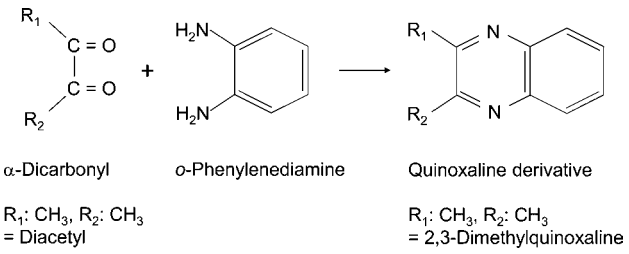

Figure 3. Reaction between α-dicarbonyl compounds and 2,3-phenylenediamine to form a corresponding quinoxaline derivative.

One study showed that 6-nitro-2,3-dimethylquinoxaline derived from diacetyl with 4-nitro-*o*-phenylenediamine yielded better separation in an HPLC column than 2,3-dimethylquinoxaline when diacetyl was analyzed in beer samples by HPLC-UVD.[52] In addition to the method reported in the above references, the OSHA has summarized the recommended sample preparation and analytical methods of diacetyl.[55,56]

Diacetyl Found in Foods. The presence of diacetyl in various fruits, such as apples[57] and pineapples,[58] has been known since the 1960s. When analyzed as one of the volatile components of food and beverage samples, diacetyl has been directly observed by gas chromatography and GC-MS without the use of derivatives. The quantity of diacetyl has therefore generally been reported as a GC peak area percentage rather than an absolute amount. When diacetyl is analyzed for assessment of flavor characteristics or toxicity evaluation, it is necessary to analyze the absolute amount present in samples. Quantitative analysis of trace levels of highly reactive and volatile chemicals such as diacetyl, however, is rather difficult.[18] There are many reports of the presence of diacetyl in foods and beverages, but only a few studies have reported the levels of diacetyl. The presence of diacetyl and 70 other volatile

dx.doi.org/10.1021/jf500615u | J. Agric. Food Chem. 2014, 62, 4048−4053

chemicals was reported in fresh milk, for example, but without quantitative analysis.[46] On the other hand, analysis of a volatile sample recovered from fermented soybean curds using a simultaneous steam distillation and extraction apparatus resulted in a quantitative measure of 0.001−0.17 μg/g diacetyl.[44] Diacetyl found in 12 brands of beer using a slightly modified quinoxaline derivative ranged from 0.034 to 0.11 μg/g.[52]

Diacetyl has been found to be one of the volatile chemicals that contributes the characteristic butter flavor to various foods and beverages. It was reported as one of the most intense volatile compounds, for example, in the aroma of pasteurized AA butter.[55] These reports indicate that diacetyl is also present in the headspace of food and beverage samples. Determination of diacetyl in the vapor phase has therefore become important in assessing the flavor quality of butter and related products as well as in evaluating its inhalation toxicity.

Among over 120 volatile compounds reported in yogurt, diacetyl was described as one of the major chemicals contributing to the characteristic yogurt flavor.[5] Starter distillates, which are used as ingredients in the formulation of various foods, such as cottage cheese, margarine, and sour cream, contained 1.2−22000 μg/g diacetyl in their headspace when analyzed using SPME and GC-MS.[53] Amounts (5−600 ppb) of diacetyl vaporized from beer at high temperature were monitored using an automatic flow system after diacetyl was derivatized into 2,3-dimethylquinoxaline.[59] Vapor-phase diacetyl in cigarette smoke analyzed using quinoxaline derivative resulted in measurements of 301−433 mg/cigarette in 14 brands of cigarette.[60] Recently, between 13.9 and 2835.7 ng/g of diacetyl were reported in the headspace of heated butter and cheese samples using a unique simultaneous purging and extraction apparatus.[29]

The headspace from spoiled fish samples was successively trapped using a SPME fiber made of carboxen/polydimethylsiloxane.[48] Analysis of the trapped sample by GC-MS resulted in the identification of 86 volatile compounds, including diacetyl. The absolute amounts of the volatiles, however, were not reported in this article due to the difficulty of performing quantitative analysis using SPME.[61] Later, diacetyl in the headspace of goat's milk jack cheese during the aging process was successfully determined using static headspace GC with an internal standard.[51]

TOXICITY OF DIACETYL

Diacetyl toxicity (mutagenicity) was first reported in 1979 as a positive finding in an Ames assay.[62] Later, mutagenicity of diacetyl was reported using a mammalian cell gene mutation assay in L5178Y mouse lymphoma cells.[63] Another early study demonstrated that various carbonyl compounds, including diacetyl, induced chromosome loss when they were combined with subacute concentrations of propionitrile.[64]

Since the recent publication of comprehensive studies of the respiratory toxicity of diacetyl using C57BBI/6 mice,[65] occupational health issues among workers in plants associated with diacetyl vapor, such as butter-flavoring production plants, have received much attention.[11] Diacetyl has been produced in large amounts (228,000 pounds in 2005) for use as a flavoring agent in food products. It has recently been linked to bronchiolitis obliterans occurring among factory workers.[10]

A recent review indicated that diacetyl is associated with chronic forms of diffuse parenchymal lung disease.[66] When human epithelial lung cells were exposed to diacetyl vapor, increases in some disease indicators, including inflammatory mediators, IL-6, and TNF-α, were observed.[67] Another recent study indicated that diacetyl aggregated amyloid-β, which is associated with Alzheimer's disease.[68] The same authors proposed, on the basis of the identification of a diacetyl/2-deoxyguanosine adduct, that diacetyl forms this adduct with the guanosine residue of DNA, which leads to cell death.[69]

Since the inhalation toxicity of diacetyl was first reported, many studies have focused on occupational lung disease among factory workers. A study using experimental mice demonstrated that diacetyl induced dose-dependent irritation in the respiratory tract and that sensory irritation in humans was estimated to occur at levels >20 μg/g.[70] After NIOSH investigated lung disease associated with the butter flavoring used in popcorn, the safety level of diacetyl in ambient air was targeted for restriction by some regulatory agencies. When the inhalation toxicity of a given chemical is assessed, it is extremely important to know the exact amount of that chemical inhaled by the target subjects, whether animal or human. A detailed discussion of diacetyl toxicities associated with occupational health, such as bronchiolitis obliterans,[71] is not within the scope of this mini-review.

CONCLUSIONS

Diacetyl is known as a flavor chemical possessing a butter-like flavor, and it is found in various foods and beverages. It has begun to receive attention as a possible cause of certain lung diseases in the past 5 years. The toxicity of α-dicarbonyl compounds glyoxal and methylglyoxal has been reported frequently, but reports on diacetyl toxicity were very infrequent until the 2000s. After NIOSH reported its inhalation toxicity, limits on diacetyl became a pressing need to protect factory workers. It is therefore important to know the formation mechanisms and occurrence of diacetyl to assess the safety of foods and beverages as well as indoor air containing diacetyl.

AUTHOR INFORMATION

Corresponding Author

*Phone: (530) 752-4523. Fax: (530) 752-3394. E-mail: tshibamoto@ucdavis.edu.

Notes

The authors declare no competing financial interest.

ABBREVIATIONS USED

CAS, Chemical Abstracts Service; DAD, diode array detector; FDA, U.S. Food and Drug Administration; FID, flame ionization detector; GC-EC, gas chromatograph−electron capture detector; GC-MS, gas chromatography−mass spectrometry; GC-NPD, gas chromatograph−nitrogen phosphorus detector; GRAS, generally regarded as safe; HPLC-UVD, high-performance liquid chromatograph−ultraviolet detector; IL, interleukin; LC-MS, liquid chromatography−mass spectrometry; NIOSH, National Institute of Occupational Safety and Health; OSHA, Occupational Safety and Health Administration; PTR-MS, proton-transfer-reaction mass spectrometry; SPME, solid phase microextraction; TNF-α, tumor necrosis factor alpha

REFERENCES

(1) Hodge, J. Origin of flavor in foods: nonenzymatic browning reactions. In *Chemistry and Physiology of Flavors*; Schultz, H. W., Day,

E. A., Libbey, L. M., Eds.; AVI Publishing: Westport, CT, USA, 1967; pp 465−491.
(2) Johnson, C. B.; Holman, R. T. Mass spectrometry of lipids. II. Monoglycerides, their diacetyl derivatives and their trimethylsilyl ethers. *Lipids* **1966**, *1*, 371−380.
(3) Pamplona, R. Advanced lipoxidation end-products. *Chem.−Biol. Interact.* **2011**, *192*, 14−20.
(4) Malherbe, S.; Menichelli, E.; du Toit, M.; Tredoux, A.; Muller, N.; Naes, T.; Nieuwoudt, H. The relationships between consumer liking, sensory and chemical attributes of *Vitis vinifera* L. cv. Pinotage wines elaborated with different *Oenococcus oeni* starter cultures. *J. Sci. Food Agric.* **2013**, *93*, 2829−2840.
(5) Cheng, H. Volatile flavor compounds in yogurt: a review. *Crit. Rev. Food Sci. Nutr.* **2010**, *50*, 938−950.
(6) Owens, J. D.; Allagheny, N.; Kipping, G.; Ames, J. M. Formation of volatile compounds during *Bacillus subtilis* fermentation of soya beans. *J. Sci. Food Agric.* **1997**, *74*, 132−140.
(7) Selfridge, T. B.; Amerine, M. A. Odor thresholds and interactions of ethyl acetate and diacetyl in an artificial wine medium. *Am. J. Enol. Vitic.* **1978**, *29*, 1−6.
(8) Arctander, S. *Perfume and Flavor Chemicals*; self-published: Montclair, CA, USA, 1969.
(9) White, K. L.; Hekkila, K.; Williams, R.; Levin, L.; Lockey, J. E.; Rice, C. Diacetyl exposures at four microwave popcorn plants. *J. Occup. Environ. Hyg.* **2010**, *7*, 185−193.
(10) Martyny, J. W.; Van Dyke, M. V.; Arbuckle, S.; Towle, M.; Rose, C. S. Diacetyl exposures in the flavor manufacturing industry. *J. Occup. Environ. Hyg.* **2008**, *5*, 679−688.
(11) Kanwal, R.; Kullman, G.; Fedan, K. B.; Kreiss, K. Occupational lung disease risk and exposure to butter-flavoring chemicals after implementation of controls to a microwave popcorn plant. *Public Health Rep.* **2011**, *126*, 480−494.
(12) Kovacic, P.; Cooksy, A. L. Electron transfer as potential cause of diacetyl toxicity in popcorn lung disease. *Rev. Environ. Contam. Toxicol.* **2010**, *204*, 133−1348.
(13) Kovacic, P.; Cooksy, A. L. Role of diacetyl metabolite in alcohol toxicity and addiction via electron transfer and oxidative stress. *Arch. Toxicol.* **2005**, *79*, 123−128.
(14) Wainwright, T. Diacetyl—a review: part I—analytical and biochemical considerations: part II—brewing experience. *J. Inst. Brew.* **1973**, *79*, 451−470.
(15) Jay, J. M. Effect of diacetyl on foodborne microorganisms. *J. Food Sci.* **1982**, *47*, 1829−1831.
(16) Dworak, J. J.; Roberts, D. W.; Calter, M. A.; Fields, C. A.; Borak, J. Is diacetyl a respiratory sensitizer? A reconsideration using QSAR, QMM, and competition experiments. *Chem. Res. Toxicol.* **2013**, *26*, 631−633.
(17) Krogerus, K.; Gibson, B. R. 125th anniversary review: diacetyl and its control during brewery fermentation. *J. Inst. Brew.* **2013**, *119*, 86−97.
(18) Shibamoto, T. Analytical methods for trace levels of reactive carbonyl compounds formed in lipid peroxidation systems. *J. Pharm. Biomed. Anal.* **2006**, *41*, 12−25.
(19) Guymon, J. F.; Crowell, E. A. The formation of acetoin and diacetyl during fermentation and the leaves found in wines. *Am. J. Enol. Vitic.* **1965**, *16*, 85−91.
(20) Voulgaropoulos, A.; Soilis, T.; Andricopoulos, N. Fluorimetric determination of diacetyl in wines after condensation with 3,4-diaminoanisole. *Am. J. Enol. Vitic.* **1991**, *42*, 73−75.
(21) Martineau, B.; Acree, T. E.; Henick-Kling, T. Effect of wine type on the detection threshold for diacetyl. *Food Res. Int.* **1995**, *28*, 139−143.
(22) Kavadze, A. V.; Rodopulo, A. K.; Egorov, I. A. α-Diketones and α-hydroxyketones in wines. *Appl. Biochem. Microbiol.* **1977**, *13*, 150−154.
(23) de Revel, G.; Pripis-Nicolau, L.; Barbe, J.-C.; Bertrand, A. The detection of α-dicarbonyl compounds in wine by formation of quinoxaline derivatives. *J. Sci. Food Agric.* **2000**, *80*, 102−108.
(24) Frankel, E. N. Lipid oxidation. *Prog. Lipid Res.* **1980**, *19*, 1−22.
(25) Frankel, E. N. Volatile lipid oxidation products. *Prog. Lipid Res.* **1982**, *22*, 1−13.
(26) Gobert, J.; Glomb, M. A. Degradation of glucose: Reinvestigation of reactive α-dicarbonyl compounds. *J. Agric. Food Chem.* **2009**, *57*, 8591−8597.
(27) Scanlan, R. A.; Lindsay, R. C.; Libbey, L. M.; Day, E. A. Heat-induced volatile compounds in milk. *J. Dairy Sci.* **1968**, *51*, 1001−1007.
(28) West, E. S.; Todd, W. R.; Mason, H. S.; van Bruggen, J. T. Carbohydrates, or the saccharides. In *Textbook of Biochemistry*, IV ed.; Macmillan: London, UK, 1966; pp 173−260.
(29) Jiang, Y.; Hengel, M.; Pan, C.; Seiber, J. N.; Shibamoto, T. Determination of toxic α-dicarbonyl compounds, glyoxal, methylglyoxal, and diacetyl released to the headspace of lipid commodities upon heat treatment. *J. Agric. Food Chem.* **2013**, *61*, 1067−1071.
(30) Yasuhara, A.; Tanaka, Y.; Hengel, M.; Shibamoto, T. Gas chromatographic investigation of acrylamide formation in browning model systems. *J. Agric. Food Chem.* **2003**, *51*, 3999−4003.
(31) Niyati-Shirkhodaee, F.; Shibamoto, T. Gas chromatographic analysis of glyoxal and methylglyoxal formed from lipids and related compounds upon ultraviolet irradiation. *J. Agric. Food Chem.* **1993**, *41*, 227−230.
(32) Strecker, A. Notiz über eine Eigenthumliche Oxydation durch Alloxan. *Ann. Chem.* **1862**, *123*, 363−365.
(33) Whitfield, F. B. Volatiles from interactions of Maillard reactions and lipids. *Crit. Rev. Food Sci. Nutr.* **1992**, *31*, 1−58.
(34) Shibamoto, T.; Bernhard, R. A. Formation of heterocyclic compounds from the reaction of L-rhamnose with ammonia. *J. Agric. Food Chem.* **1978**, *26*, 183−187.
(35) Yaylayan, V. A.; Keyhani, A. Origin of 2,3-pentanedione and 2,3-butanedione in D-glucose/L-ananine Maillard model systems. *J. Agric. Food Chem.* **1999**, *47*, 3280−3284.
(36) Smuda, M.; Glomb, M. A. Novel insights into the Maillard catalyzed degradation of maltose. *J. Agric. Food Chem.* **2011**, *59*, 13254−13264.
(37) Zalán, Z.; Hudácek, J.; Tóh-Markus, M.; Husová, E.; Solichová, K.; Hegyi, F.; Plocková, M.; Chumchalová, J.; Halász, A. Sensorically and antimicrobially active metabolite production of *Lactobacillus* strands on Jerusalem artichoke juice. *J. Sci. Food Agric.* **2011**, *91*, 672−679.
(38) Escamilla-Hurtado, M. L.; Tomasini-Campocosio, A.; Valdes-Martinez, S.; Soriano-Santos, J. Diacetyl formation by lactic bacteria. *Rev. Latinoam. Microbiol.* **1996**, *38*, 129−137.
(39) Nadal, I.; Rico, J.; Perez-Martinez, G.; Yebra, M.; Monedero, V. Diacetyl and acetoin production from whey permeate using engineered *Lactobacillus casei*. *J. Ind. Microbiol. Biotechnol.* **2009**, *36*, 1233−1237.
(40) Fox, P. F.; Lucey, J. A.; Cogan, T. M. Glycolysis and related reactions during cheese manufacture and ripening. *Crit. Rev. Food Sci. Nutr.* **1990**, *29*, 237−253.
(41) Holm, E. S.; Adamsen, A. P.; Feilberg, A.; Schafer, A.; Lokke, M. M.; Petersen, M. A. Quality changes during storage of cooked and sliced meat products measured with PTR-MS and HS-GC-MS. *Meat Sci.* **2013**, *95*, 302−310.
(42) Hirayama, T.; Yamada, N.; Nohara, M.; Fukui, S. The existence of the 1,2-dicarbonyl compounds glyoxal, methylglyoxal and diacetyl in autoxidized edible oils. *J. Sci. Food Agric.* **1984**, *35*, 1357−1362.
(43) Rodrigues, J. A.; Barros, A. A.; Rodrigues, P. G. Differential pulse polarographic determination of α-dicarbonyl compounds in foodstuffs after derivatization with *o*-phenylenediamine. *J. Agric. Food Chem.* **1999**, *47*, 3219−3222.
(44) Chung, H. Y. Volatile flavor components in red fermented soybean (*Glycine max*) curds. *J. Agric. Food Chem.* **2000**, *48*, 1803−1809.
(45) Zeppa, G.; Conterno, L.; Gerbi, V. Determination of organic acids, sugars, diacetyl, and acetoin in cheese by high-performance liquid chromatography. *J. Agric. Food Chem.* **2001**, *49*, 2722−2726.

(46) Bendall, J. G. Aroma compounds of fresh milk from New Zealand cows fed different diets. *J. Agric. Food Chem.* **2001**, *49*, 4825−4832.
(47) Esteve, M. J.; Frigola, A.; Rodrigo, M. C.; Rodrigo, M. Use of polarography as a quality control method for determining diacetyl in citrus and vegetable juice, yoghurt and butter. *Food Addit. Contam.* **2002**, *19*, 519−523.
(48) Duflos, G.; Marcel-Coin, V.; Cornu, M.; Antinelli, J.-F. Determination of volatile compounds to characterize fish spoilage using headspace/mass spectrometry and solid-phase microextraction/gas chromatography/mass spectrometry. *J. Sci. Food Agric.* **2006**, *86*, 600−611.
(49) Daglia, M.; Patetti, A.; Aceti, C.; Sordelli, B.; Spini, V.; Gazzani, G. Isolation and determination of α-dicarbonyl compounds by RP-HPLC-DAD in green and roasted coffee. *J. Agric. Food Chem.* **2007**, *55*, 8877−8882.
(50) Lozano, P. R.; Miracle, E. R.; Krause, A. J. Effect of cold storage and packaging material on the major aroma components of sweet cream butter. *J. Agric. Food Chem.* **2007**, *55*, 7840−7846.
(51) Attaie, R. Quantification of volatile compounds in goat milk Jack cheese using static headspace gas chromatography. *J. Dairy Sci.* **2008**, *92*, 2435−2443.
(52) Li, P.; Zhu, Y.; He, S.; Fan, J.; Hu, Q.; Cao, Y. Development and validation of high-performance liquid chromatography method for the determination of diacetyl in beer using 4-nitro-*o*-phenylenediamine as the derivatization reagent. *J. Agric. Food Chem.* **2012**, *60*, 3013−3019.
(53) Rincon-Delgadillo, M. I.; Lopez-Hernandez, A.; Wijayam, I.; Rankin, S. A. Diacetyl levels and volatile profiles of commercial starter distillates and selected dairy foods. *J. Dairy Sci.* **2012**, *95*, 1128−1139.
(54) Mussinan, C.; Wilson, R. A.; Katz, I. Isolation and identification of pyrazines present in pressure-cooked beef. *J. Agric. Food Chem.* **1973**, *21*, 871−872.
(55) Simmons, M.; Hendricks, W. Sampling and analytical methods: acetoin/diacetyl, PV1013. https://www.osha.gov/dts/sltc/methods/validated/1013/1013.html (accessed Dec 4, 2013).
(56) Shah, Y. C. Sampling and analytical methods: diacetyl, PV2118. https://www.osha.gov/dts/sltc/methods/partial/t-pv2118/t-pv2118.html (accessed Dec 4, 2013).
(57) Drawer, F.; Heimann, W.; Emberger, R.; Tressl, R. Uber die Biolgenese von Aromastoffen bei Pflanzen und Fruchten-III. *Phytochemistry* **1968**, *7*, 881−883.
(58) Connell, D. W. Volatile flavouring constituents of the pineapple. I. Some esters alcohols, and carbonyl compounds. *Aust. J. Chem.* **1964**, *17*, 130−140.
(59) Rodrigues, P. G.; Rodrigues, J. A.; Barros, A. A.; Lapa, R. A.; Lima, J. L.; Machado Cruz, J. M.; Ferreira, A. A. Automatic flow system with voltammetric detection for diacetyl monitoring during brewing process. *J. Agric. Food Chem.* **2002**, *50*, 3647−3653.
(60) Fujioka, K.; Shibamoto, T. Determination of toxic carbonyl compounds in cigarette smoke. *Environ. Toxicol.* **2006**, *21*, 47−54.
(61) Fujioka, K.; Shibamoto, T. Improved malonaldehyde assay using headspace solid-phase microextraction and its application to the measurement of the antioxidant activity of phytochemicals. *J. Agric. Food Chem.* **2005**, *53*, 4708−4713.
(62) Bjeldanes, L. F.; Chew, H. Mutagenicity of 1,2-dicarbonyl compounds: maltol, kojic acid, diacetyl and related substances. *Mutat. Res.* **1979**, *67*, 367−371.
(63) Whittaker, P.; Clarke, J. J.; San, R. H.; Begley, T. H.; Dunkel, V. C. Evaluation of the butter flavoring chemical diacetyl and a fluorochemical paper additive for mutagenicity and toxicity using the mammalian cell gene mutation assay in L5178Y mouse lymphoma cells. *Food Chem. Toxicol.* **2008**, *46*, 2928−2933.
(64) Zimmermann, F. K.; Mohr, A. Formaldehyde, glyoxal, urethane, methyl carbamate, 2,3-butanedione, 2,3-hexanedione, ethyl acrylate, dibromoacetonitrile and 2-hydroxypropionitrile induce chromosome loss in *Saccharomyces cerevisiae*. *Mutat. Res.* **1992**, *270*, 151−166.
(65) Morgan, D. L.; Flake, G. P.; Kirby, P. J.; Palmer, S. M. Respiratory toxicity of diacetyl in C57BL/6 mice. *Toxicol. Sci.* **2008**, *103*, 169−180.
(66) Sauler, M.; Gulati, M. Newly recognized occupational and environmental causes of chronic terminal airways and parenchymal lung disease. *Clin. Chest Med.* **2012**, *33*, 667−680.
(67) Anderson, S. E.; Jackson, L. G.; Franko, J.; Wells, J. R. Evaluation of dicarbonyls generated in a simulated indoor air environment using an in vitro exposure system. *Toxicol. Sci.* **2010**, *115*, 453−461.
(68) More, S. S.; Vartak, A. P.; Vince, R. The butter flavorant, diacetyl, exacerbates β-amyloid cytotoxicity. *Chem. Res. Toxicol.* **2012**, *25*, 2083−2091.
(69) More, S. S.; Raza, A.; Vince, R. The butter flavorant, diacetyl, forms a covalent adduct with 2-deoxyguanosine, uncoils DNA, and leads to cell death. *J. Agric. Food Chem.* **2012**, *60*, 3311−3317.
(70) Larsen, S. T.; Alarie, Y.; Hammer, M.; Nielsen, G. D. Acute airway effects of diacetyl in mice. *Inhal. Toxicol.* **2009**, *21*, 1123−1128.
(71) Potera, C. Still searching for better butter flavoring. *Environ. Health Perspect.* **2012**, *120*, A457.

JOURNAL OF AGRICULTURAL AND FOOD CHEMISTRY

Article

pubs.acs.org/JAFC

Interaction of Moderate UV-B Exposure and Temperature on the Formation of Structurally Different Flavonol Glycosides and Hydroxycinnamic Acid Derivatives in Kale (*Brassica oleracea* var. *sabellica*)

Susanne Neugart,*[,†] Michaela Fiol,[‡] Monika Schreiner,[†] Sascha Rohn,[§] Rita Zrenner,[†] Lothar W. Kroh,[‡] and Angelika Krumbein[†]

[†]Leibniz-Institute of Vegetable and Ornamental Crops Grossbeeren/Erfurt e.V., Theodor-Echtermeyer-Weg 1, 14979 Grossbeeren, Germany

[‡]Institut of Food Technology and Food Chemistry, Technische Universität Berlin, Gustav-Meyer-Allee 25, 13355 Berlin, Germany

[§]Hamburg School of Food Science, Institute of Food Chemistry, Universität Hamburg, Grindelallee 117, 20146 Hamburg, Germany

ABSTRACT: Kale has a high number of structurally different flavonol glycosides and hydroxycinnamic acid derivatives. In this study we investigated the interaction of moderate UV-B radiation and temperature on these compounds. Kale plants were grown at daily mean temperatures of 5 or 15 °C and were exposed to five subsequent daily doses (each 0.25 kJ m^{-2} d^{-1}) of moderate UV-B radiation at 1 d intervals. Of 20 phenolic compounds, 11 were influenced by an interaction of UV-B radiation and temperature, e.g., monoacylated quercetin glycosides. Concomitantly, enhanced mRNA expression of *flavonol 3′- hydroxylase* showed an interaction of UV-B and temperature, highest at 0.75 kJ m^{-2} and 15 °C. Kaempferol glycosides responded diversely and dependent on, e.g., the hydroxycinnamic acid residue. Compounds containing a catechol structure seem to be favored in the response to UV-B. Taken together, subsequent exposure to moderate UV-B radiation is a successful tool for enhancing the flavonoid profile of plants, and temperature should be considered.

KEYWORDS: *Brassica oleracea, UV-B, flavonoids, flavonol glycosides, hydroxycinnamic acids, flavonol 3′-hydroxylase*

INTRODUCTION

Ultraviolet-B (UV-B) radiation (280−315 nm) is a naturally occurring part of solar radiation. However, with depletion of the stratospheric ozone layer, enhanced levels of UV-B radiation are now reaching the earth's surface.[1] In response to these higher levels of UV-B radiation, plants induce the biosynthesis of phenolic compounds, such as flavonoids and hydroxycinnamic acids,[2] which act as shielding components and antioxidants in the defense against reactive oxygen species (ROS).[3,4] Phenolic compounds containing a catechol structure have also been reported to exhibit an especially high antioxidant activity.[5]

Kale (*Brassica oleracea* var. *sabellica*) has a large number of naturally occurring flavonol glycosides and hydroxycinnamic acid derivatives[6−10] and is cultivated mainly in Central and Northern Europe as well as in North America. As a leafy vegetable that has a large exposed surface area, it is an ideal model crop to study the effect of radiation on the biosynthesis of its phenolic compounds.[9] In kale, a total of 71 flavonol glycosides have been tentatively identified by HPLC-DAD−MS^n, including 27 non-acylated, 30 monoacylated, and 14 diacylated glycosides based on the flavonol aglycons quercetin, kaempferol, and isorhamnetin, respectively (Figure 1a).[9] Seven of these 71 compounds have been further identified with NMR in a previous study.[10] A general structure of a complex diacylated flavonol tetraglycoside is shown in Figure 2. The main flavonol glycosides in kale are non-acylated and monoacylated quercetin and kaempferol glycosides; the majority of other flavonol glycosides are acylated with hydroxycinnamic acids (Figure 1b).[9] Acylation of flavonol glycosides leads to a shift of the light-absorbing π-electron system band II in the flavonol structure to lower wavelengths.[11] For instance, in kale, acylated flavonol glycosides have absorption maxima between 328 and 340 nm,[9] which make this vegetable an interesting plant for investigating the influence of UV-B radiation on phenolic compounds. The main

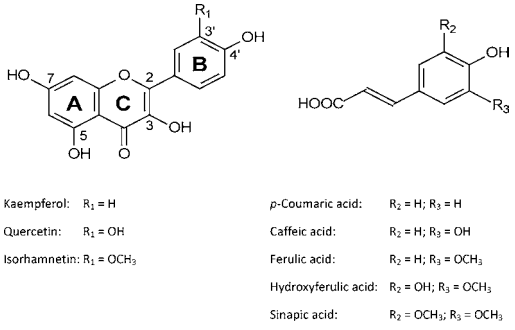

Figure 1. Structure of flavonol aglycons (a, left) and hydroxycinnamic acids (b, right) present in flavonol glycosides and hydroxycinnamic acid derivatives of kale.

Received: August 29, 2013
Revised: March 20, 2014
Accepted: March 22, 2014
Published: March 22, 2014

ACS Publications © 2014 American Chemical Society

dx.doi.org/10.1021/jf4054066 | *J. Agric. Food Chem.* 2014, 62, 4054−4062

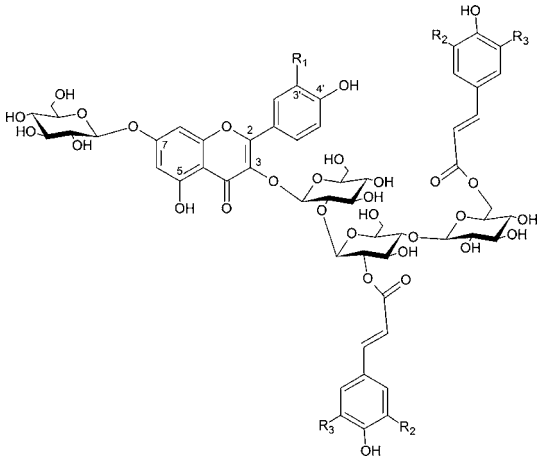

Figure 2. Kaempferol-3-*O*-disinapoyl-triglucoside-7-*O*-glucoside (R1 = H; R2 = MeOH; R3 = MeOH) in kale was identified by mass spectrometry (MS)[9] and nuclear magnetic resonance (NMR) spectroscopy.[10]

hydroxycinnamic acid derivatives in kale, namely, caffeoylquinic acid (chlorogenic acid), disinapoyl-gentiobiose, and sinapoyl-feruloyl-gentiobiose, provide antioxidant properties and have been further identified with NMR in a previous study.[5,10] The absorption maxima of hydroxycinnamic acids range from 318 to 328 nm, thereby suggesting that in kale plants they take an active response when exposed to UV-B radiation.

UV-B radiation is able to modify the flavonoid profile of different plant species. In the majority of studies ambient subsequent doses of UV-B radiation led to an enhanced quercetin to kaempferol ratio in comparison to UV-B exclusion for days up to weeks[12−14] and a study with high doses of additional UV-B radiation[15] in annual vegetables and ornamentals. Mainly quercetin glycosides can be enhanced by UV-B radiation in *Arabidopsis* (*Arabidopsis thaliana*).[16,17] However, only a small number of studies have assessed the effects of moderate UV-B exposure during cultivation,[18] and most of these applied additional UV-B for one week or more. Moderate UV-B radiation is defined as being less than 5 kJ m^{-2} d^{-1}.[19] In a recent study on kale examining the changes in flavonol glycoside profile to single doses of moderate UV-B radiation (less than 1 kJ m^{-2} d^{-1} UV-B_{BE} (biologically effective UV-B radation)), the quercetin and kaempferol glycosides as well as the hydroxycinnamic acid derivatives responded dose- and structure-dependently.[20] However, there is still a lack of knowledge on the interaction of UV-B radiation with other ecophysiological parameters such as temperature. Even though several investigations showed an effect of UV-B in combination with temperature on the flavonoid glycosides in pak choi (*Brassica campestris* L. ssp. *chinensis* var. *communis*)[21] and in willow (*Salix myrsinifolia*).[22] In contrast, an increase in caffeoylquinic acid in willow and arnica (*Arnica montana*) was reported only upon a temperature decrease independent of the UV-B dose applied.[22,23] Finally, although low temperature[24] and high UV-B levels[25] have been reported to modify the gene expression coding for key enzymes of flavonol biosynthesis, such as flavanone 3β-hydroxylase, flavonol synthase, and flavonol 3′-hydroxylase, a study examining the effects of interaction of UV-B radiation and temperature has not yet been performed.

The aims of this study were (I) to investigate whether, in contrast to a single dose of moderate UV-B, subsequent levels of targeted moderate UV-B radiation during cultivation of kale can enhance levels of flavonol glycosides and hydroxycinnamic acid derivatives, (II) to determine the effect of the flavonol glycoside structure in response to subsequent doses of moderate UV-B radiation, (III) for the first time to assess whether there are any interactive effects due to UV-B radiation and temperature on the biosynthesis of flavonol glycosides and hydroxycinnamic acid derivatives to find growing conditions that reveal a high concentration of health-promoting phenolics, and (IV) to perform corresponding gene expression studies to ascertain which key genes, namely, flavanone 3β-hydroxylase, flavonol synthase, and flavonol 3′-hydroxylase, involved in flavonol biosynthesis are up- or downregulated by moderate UV-B radiation treatment.

MATERIAL AND METHODS

Reagents and Standard Solutions. Methanol and the standards quercetin-3-*O*-glucoside, kaempferol-3-*O*-glucoside, and caffeoylquinic acid were purchased from Roth (Karlsruhe, Germany), acetic acid was purchased from Merck (Darmstadt, Germany), and acetonitrile was purchased from J. T. Baker (Griesheim, Germany). All reagents were of HPLC-grade quality.

Plant Material and Experimental Design. Kale (*B. oleracea* var. *sabellica*) plants of the cv. Winterbor (by Bruno Nebelung, Norken, Germany) were sown on Jan 3, 2010 (experiment I) and on Jan 10, 2010 (experiment II). All plants were grown up to the four- to five-leaf stage under greenhouse conditions (20 °C and ambient light). In the greenhouse, two experiments were conducted with equal UV-B radiation conditions at different daily mean temperatures (5 ± 1 °C (experiment I) and 15 ± 1 °C (experiment II)). For both experiments, the plants were cultivated in potting soil (Einheitserde type 1, Fitz Kausek GmbH & Co. KG, Mittenwalde, Germany) and set in a randomized block design spaced 0.02 m × 0.02 m away from each other. Water supply was given as needed by the plants, and fertilization was given as nutrient solution (pH 6.4, 41 mg L^{-1} P, 43 mg L^{-1} Mg, 154 mg L^{-1} NO_3, 205 mg L^{-1} Ca, 230 mg L^{-1} K, 280 mg L^{-1} SO_4, 0.82 mg L^{-1} Zn). The plants were exposed to one to five subsequent consecutive daily doses of 0.5 kJ m^{-2} d^{-1} UV-B radiation for 1 h with acclimatization intervals of 23 h. UV-B radiation was supplied by five UV-B fluorescent light sources (TL 40W 12 RS, Philips, Hamburg, Germany), and the distance of the UV-B lamps from the plants was 60 cm. UV-B radiation was determined using a UV-B sensor (type DK-UVB 1.3-051, deka Sensor + Technologie, Teltow, Germany) with a spectral range of 265−315 nm. Compared to that of Sangtarash et al.,[19] the UV-B dose administered is moderate, and the total dose given within 5 d was 2.5 kJ m^{-2} UV-B. The corresponding biologically effective UV-B radiation treatment level of 0.25 kJ m^{-2} d^{-1} UV-B_{BE} (total dose 1.25 kJ m^{-2} UV-B_{BE}) was calculated with the generalized plant weighting function according to Caldwell.[26] Environmental conditions were 5 °C and 93 μmol m^{-2} s^{-1} photosynthetic photon flux density (PPFD) for experiment I and 15 °C and 272 μmol m^{-2} s^{-1} PPFD for experiment II. Both experiments were carried out in the greenhouse in February 2010 at Grossbeeren, Germany (52.37° N, 13.33° E) under partly overcast skies. Three plants per replication and three biological replications per treatment were harvested from the block of plants every day after an acclimatization period of 24 h following the UV-B treatment.

Sample Preparation. For each replication, the leaves (excluding the middle rib) taken from three four- to five-leaf stage plants were frozen in liquid nitrogen, stored until lyophilization at −40 °C, lyophilized, and then ground to a powder. The samples were stored in darkness at room temperature until they were required for analysis. To analyze flavonol glycosides and hydroxycinnamic acid derivatives, the samples were extracted as described[20] with the following modifications. In analytical duplicates, 20 mg of freeze-dried and ground powder was extracted with 600 μL of 60% aqueous methanol for 1 h with high agitation at room temperature. Samples were centrifuged at 19000*g* for 10 min, and the supernatants were collected in a new tube.

dx.doi.org/10.1021/jf4054066 | J. Agric. Food Chem. 2014, 62, 4054−4062

Table 1. Influence of Ultraviolet-B (UV-B, kJ m^{-2} $UV\text{-}B_{BE}$) and Temperature (T, °C) on Quercetin Glycosides (mg g^{-1} of dry matter) in Juvenile Kale Plants[a]

			non-acylated triglucoside		monoacylated triglucoside		monoacylated tri- and tetraglucoside		diacylated tetraglucoside	
			Q-3-*O*-soph-7-*O*-D-glc[b]		Q-3-*O*-fer-soph-7-*O*-D-glc[b]	Q-3-*O*-hfer-soph-7-*O*-D-glc[b]			Q-3-*O*-Disin-triglc-7-*O*-D-glc[b]	
UV-B			***		***	***	***		*	
T			ns		***	***	***		ns	
UV-B × T			ns		*	***	*		ns	
	main effect									
UV-B	0.25		0.04 ± 0.021	a	0.17 ± 0.051	0.32 ± 0.139	0.36 ± 0.089		0.09 ± 0.012	a
	0.5		0.07 ± 0.027	ab	0.15 ± 0.036	0.27 ± 0.095	0.36 ± 0.067		0.13 ± 0.034	ab
	0.75		0.13 ± 0.029	bc	0.26 ± 0.080	0.27 ± 0.079	0.57 ± 0.150		0.14 ± 0.030	b
	1.0		0.14 ± 0.080	c	0.33 ± 0.177	0.33 ± 0.043	0.70 ± 0.367		0.10 ± 0.013	ab
	1.25		0.12 ± 0.048	bc	0.47 ± 0.233	0.40 ± 0.082	0.99 ± 0.440		0.10 ± 0.024	ab
T	5		0.09 ± 0.032	a	0.21 ± 0.093	0.28 ± 0.117	0.46 ± 0.158		0.11 ± 0.019	
	15		0.11 ± 0.074	a	0.34 ± 0.210	0.35 ± 0.062	0.73 ± 0.434		0.11 ± 0.034	
T	UV-B									
5		0.25	0.06 ± 0.002		0.21 ± 0.051	ab	0.19 ± 0.042	ab	0.43 ± 0.036	ab	0.09 ± 0.017	
		0.5	0.07 ± 0.022		0.14 ± 0.039	a	0.18 ± 0.017	a	0.31 ± 0.044	a	0.10 ± 0.010	
		0.75	0.12 ± 0.041		0.19 ± 0.006	ab	0.22 ± 0.077	abc	0.45 ± 0.063	ab	0.12 ± 0.031	
		1.0	0.09 ± 0.028		0.20 ± 0.059	ab	0.34 ± 0.034	bcd	0.43 ± 0.102	ab	0.10 ± 0.011	
		1.25	0.10 ± 0.032		0.32 ± 0.162	abc	0.45 ± 0.098	d	0.70 ± 0.188	ab	0.11 ± 0.001	
15		0.25	0.03 ± 0.009		0.14 ± 0.019	a	0.44 ± 0.034	d	0.28 ± 0.040	a	0.10 ± 0.006	
		0.5	0.07 ± 0.054		0.17 ± 0.033	a	0.35 ± 0.041	bcd	0.40 ± 0.050	a	0.15 ± 0.032	
		0.75	0.14 ± 0.012		0.33 ± 0.045	abc	0.31 ± 0.065	abcd	0.69 ± 0.096	ab	0.15 ± 0.027	
		1.0	0.19 ± 0.084		0.47 ± 0.132	bc	0.31 ± 0.056	abcd	0.98 ± 0.316	bc	0.11 ± 0.017	
		1.25	0.13 ± 0.064		0.61 ± 0.218	c	0.35 ± 0.009	cd	1.28 ± 0.442	c	0.09 ± 0.032	

[a]The concentration of the quercetin glycosides was quantitated as quercetin-3-*O*-glucoside equivalents. Values with the same letters are not significantly different (Tukey's HSD test ($n = 3$) is calculated at $p \leq 0.05$) for each quercetin glycoside. Key: *, significant at $p \leq 0.05$; **, significant at $p \leq 0.01$; ***, significant at $p \leq 0.005$; ns, not significant. Abbreviations: Q, quercetin; soph, sophorose; glc, glucose; diglc, diglucoside; triglc, triglucoside; fer, feruloyl; hfer, hydroxyferuloyl; sin, sinapoyl; disin, disinapoyl. [b]The compound was tentatively identified by HPLC-DAD−MS^n as shown by Schmidt et al.[9] [c]The compound was identified with NMR as shown by Fiol et al.[10]

The extraction procedure was repeated with 400 and 200 μL for 20 and 10 min, respectively. The supernatants were added together and were evaporated to dryness while being rotated. The residue was dissolved in 200 μL of distilled water. The extract was then filtered through Corning Costar Spin-X plastic centrifuge tube filters with a cellulose acetate mambrane (Sigma-Aldrich Chemical Co., St. Louis, MO) for HPLC analysis.

HPLC-DAD−ESI-MS^n. The HPLC-DAD−ESI-MS^n method for the tentative identification[9] and quantitation[20] of the flavonol glycosides and hydroxycinnamic acid derivatives in kale was done with an HPLC series 1100 by Agilent (Waldbronn, Germany) consisting of a degaser, binary pump, autosampler, column oven, and photodiode array detector. An ion trap (Agilent series 1100 MSD) with an ESI ion source in negative ionization mode was used as the mass spectrometer. The parameters for HPLC-DAD−ESI-MS^n have been previously described.[20] Mass fragments for the identification of the compounds have been previously given.[9] The main flavonol glycosides (10 compounds) and structurally related minor flavonol glycosides (7 compounds) and hydroxycinnamic acid derivatives (3 compounds) were selected for the investigation (Tables 1−5). The standards quercetin-3-*O*-glucoside (for quercetin glycosides), kaempferol-3-*O*-glucoside (for kaempferol glycosides), and caffeoylquinic acid (for hydroxycinnamic acid derivatives) were used to obtain an external calibration curve ranging from 0.1 to 10 mg 100 mL^{-1} for a semiquantitative approach. The variation coefficient for the reproducibility of the major flavonoid glycosides was 0.7−3.3% for the extraction and 0.5−3.4% for the HPLC analysis. The variation coefficient for the reproducibility of the hydroxycinnamic acid derivatives was 1.5−1.9% for the extraction and 1.0−1.7% for the HPLC analysis.

Gene Expression Analysis by Semiquantitative Real-Time PCR. The RNA extraction was carried out as previously described by Neugart et al.[27] Quantitative two-step RT-PCR was performed using a SYBRR Green 1 protocol in 96-well reaction plates on an Applied Biosystems 7500 real-time PCR system according to Neugart et al.[27] Data were exported to LinReg software[28] to determine the PCR amplification efficiency for each primer pair. Relative transcript levels were normalized on the basis of expression of an invariant control orthologous to At3g18780 (ACT2) AF044573 using the equation $2 - \Delta CT$.[29] Quantitative PCR was performed on three biological replicates measured in analytical duplicates for each gene, and nontemplate controls were included.

Statistical Analysis. All data were statistically analyzed by a two-factorial ANOVA. Fisher's F test was performed to assess the main effect of the factors UV-B radiation and temperature and their interactions followed by a comparison of the factor levels using Tukey's HSD test. For nonsignificant interactions, the means of the levels of the main factors were separated, while for significant interactions, all combinations of the factor levels were compared. Residuals were tested for Gaussian distribution using the Kolmogorov−Smirnov test. All tests were conducted at a significance level of 5%. Calculations were performed using Statistica for Windows (version 9.0, Statsoft Inc., Tulsa, OK).

RESULTS AND DISCUSSION

Juvenile kale plants are rich in structurally different flavonol glycosides and hydroxycinnamic acid derivatives. In total 71 flavonol glycosides have previously been tentatively identified in kale.[9] A total of 7 of these 71 compounds have been further identified with NMR in a previous study (Tables 1−5).[10] The

Table 2. Influence of Ultraviolet-B (UV-B, kJ m^{-2} UV-B_{BE}) and Temperature (T, °C) on Kaempferol Glycosides (mg g^{-1} of dry matter) in Juvenile Kale Plants[a]

			non-acylated triglucoside		monoacylated diglucoside				monoacylated triglucoside			
			K-3-*O*-soph- 7-*O*-D-glc[b]		K-3-*O*-fer-soph[b]	K-3-*O*-hfer-soph[b]		K-3-*O*-sin-soph[b]	K-3-*O*-caf- soph-7-*O*-D-glc[b]		K-3-*O*-fer- soph-7-*O*-D-glc[c]	
UV-B			*		ns	***		*	***		ns	
T			***		ns	***		ns	***		***	
UV-B × T			***		*	*		**	*		ns	
main effect												
UV-B	0.25		0.50 ± 0.094		0.12 ± 0.022	0.06 ± 0.010		0.02 ± 0.029	2.57 ± 0.382		0.94 ± 0.105	
	0.5		0.49 ± 0.226		0.11 ± 0.023	0.08 ± 0.030		0.04 ± 0.033	3.92 ± 1.077		0.97 ± 0.223	
	0.75		0.42 ± 0.229		0.13 ± 0.037	0.12 ± 0.061		0.06 ± 0.021	4.92 ± 0.657		0.91 ± 0.213	
	1.0		0.58 ± 0.190		0.12 ± 0.028	0.09 ± 0.029		0.03 ± 0.012	5.99 ± 1.787		1.01 ± 0.244	
	1.25		0.50 ± 0.190		0.14 ± 0.066	0.10 ± 0.020		0.06 ± 0.039	5.09 ± 1.022		1.04 ± 0.376	
T	5		0.63 ± 0.112		0.13 ± 0.049	0.07 ± 0.020		0.03 ± 0.034	3.97 ± 1.238		1.14 ± 0.186	b
	15		0.36 ± 0.139		0.12 ± 0.023	0.11 ± 0.038		0.05 ± 0.024	5.02 ± 1.713		0.81 ± 0.148	a
T	UV-B											
5		0.25	0.45 ± 0.034	bcd	0.10 ± 0.009	0.06 ± 0.006	ab	0.01 ± 0.001	a	2.33 ± 0.333	a	0.99 ± 0.117
		0.5	0.69 ± 0.006	e	0.10 ± 0.030	0.05 ± 0.013	a	0.01 ± 0.010	a	2.97 ± 0.091	ab	1.10 ± 0.027
		0.75	0.62 ± 0.034	de	0.12 ± 0.053	0.07 ± 0.014	ab	0.05 ± 0.026	ab	4.49 ± 0.656	abc	1.03 ± 0.254
		1.0	0.74 ± 0.047	e	0.13 ± 0.027	0.07 ± 0.009	ab	0.04 ± 0.006	ab	4.64 ± 0.156	bc	1.22 ± 0.128
		1.25	0.66 ± 0.078	e	0.18 ± 0.070	0.09 ± 0.025	ab	0.08 ± 0.048	b	5.41 ± 0.658	cd	1.35 ± 0.157
15		0.25	0.55 ± 0.118	cde	0.13 ± 0.024	0.07 ± 0.005	ab	0.05 ± 0.030	ab	2.79 ± 0.307	ab	0.87 ± 0.061
		0.5	0.28 ± 0.044	ab	0.12 ± 0.004	0.10 ± 0.008	abc	0.07 ± 0.012	ab	4.87 ± 0.439	bc	0.84 ± 0.267
		0.75	0.22 ± 0.095	a	0.14 ± 0.016	0.16 ± 0.053	c	0.07 ± 0.008	ab	5.33 ± 0.346	cd	0.80 ± 0.085
		1.0	0.41 ± 0.089	abcd	0.10 ± 0.012	0.11 ± 0.019	bc	0.02 ± 0.010	ab	7.33 ± 1.584	d	0.80 ± 0.036
		1.25	0.34 ± 0.089	abc	0.10 ± 0.029	0.10 ± 0.020	abc	0.04 ± 0.019	ab	4.76 ± 1.364	bc	0.74 ± 0.231

[a]The concentration of the kaempferol glycosides was quantitated as kaempferol-3-*O*-glucoside equivalents. Values (means ± standard deviation) with the same letters are not significantly different (Tukey's HSD test (n = 3) is calculated at $p \leq 0.05$) for each kaempferol glycoside. Key: *, significant at $p \leq 0.05$; **, significant at $p \leq 0.01$; ***, significant at $p \leq 0.005$; ns, not significant. Abbreviations: K, kaempferol; soph, sophorose; glc, glucose; caf, caffeoyl; fer, feruloyl; hfer, hydroxyferuloyl; sin, sinapoyl. [b]The compound was tentatively identified by HPLC-DAD−MS^n as shown by Schmidt et al.[9] [c]The compound was identified with NMR as shown by Fiol et al.[10]

main hydroxycinnamic acid derivatives in kale are caffeoylquinic acid, disinapoyl-gentiobiose, and sinapoyl-feruloyl-gentiobiose and have been further identified with NMR in a previous study.[10] Kale seems to be an ideal model crop plant to investigate the interaction of moderate UV-B and temperature due to the high number of structurally different flavonoid glycosides and hydroxycinnamic acid derivatives. In this study, 20 compounds were investigated, revealing a structure-specific response of the main flavonol glycosides (10 compounds) and structurally related minor flavonol glycosides (7 compounds) and hydroxycinnamic acid derivatives (3 compounds) to moderate UV-B radiation at daily mean temperatures of 5 and 15 °C. The flavonol glycosides were classified by the type of aglycon, the number of sugar moieties, the acylation pattern (non-acylated and acylated flavonol glycosides), and the type of hydroxycinnamic acid acylated. The results point to a structure-dependent response of flavonol glycosides to UV-B radiation and temperature. Of the 20 investigated compounds, 12 and 11 were influenced by UV-B radiation and temperature, respectively (Tables 1−4). An interaction of both these factors was obtained for monoacylated quercetin glycosides and 6 of 11 kaempferol glycosides (the monoacylated kaempferol diglycosides and the non-acylated and the caffeic and hydroxyferulic acid monoacylated kaempferol triglycosides). All investigated quercetin glycosides and the non-acylated as well as the monoacylated kaempferol glycosides that have a catechol structure in the hydroxycinnamic acid residue were affected by UV-B radiation. With regard to temperature, the monoacylated quercetin glycosides and 6 of 11 kaempferol glycosides (mainly the non-acylated and monoacylated kaempferol triglycosides) were influenced. For the expression of genes coding for key enzymes involved in flavonol biosynthesis, an effect of moderate UV-B radiation and an interaction of UV-B radiation and temperature was determined (Table 5).

All *quercetin glycosides* were affected by UV-B radiation (Table 1). Temperature was observed to influence only the concentration of the four monoacylated quercetin glycosides, and an interaction of UV-B radiation and temperature was found for these compounds. The concentration of the non-acylated quercetin-3-*O*-sophoroside-7-*O*-D-glucoside increased with increased radiation from 0.25 to 1.0 kJ m^{-2} UV-B_{BE}, while the temperature had no effect. The highest concentrations of the monoacylated quercetin-3-*O*-feruloyl-sophoroside-7-*O*-D-glucoside and quercetin-3-*O*-sinapoyl-sophoroside-7-*O*-D-glucoside/quercetin-3-*O*-sophoroside-7-*O*-sianpoyl-diglucoside were observed at 1.25 kJ m^{-2} UV-B_{BE} and at 15 °C. In contrast, the concentrations of quercetin-3-*O*-hydroxyferuloyl-sophoroside-7-*O*-D-glucoside increased at a high UV-B radiation level of 1.25 kJ m^{-2} UV-B_{BE} at 5 °C. However, at 15 °C and for all UV-B radiation levels the concentrations of this compound were even higher. The concentrations of the complex diacylated quercetin-3-*O*-disinapoyl-triglucoside-7-*O*-D-glucoside rose with increasing UV-B radiation from 0.25 to 0.75 kJ m^{-2} UV-B_{BE}, and this was independent of temperature. Our study underlines the importance of investigating the *acylation pattern* (non-acylated, mono- and diacyalted), since the profiles and concentrations of these compounds are affected by the

Table 3. Influence of Ultraviolet-B (UV-B, kJ m^{-2} UV-B_{BE}) and Temperature (T, °C) on Kaempferol Glycosides (mg g^{-1} of dry matter) in Juvenile Kale Plants[a]

			monoacylated triglucoside		monoacylated tetraglucoside		diacylated tetraglucoside
			K-3-*O*-hfer-soph-7-*O*-D-glc[c]	K-3-*O*-sin-soph-7-*O*-D-glc[c]	K-3-*O*-hfer-soph-7-*O*-diglc[b]	K-3-*O*-sin-soph-7-*O*-diglc[c]	K-3-*O*-Disin- triglc-7-*O*-D-glc[c]
UV-B			***	ns	**	ns	ns
T			ns	***	ns	*	ns
UV-B × *T*			**	ns	ns	ns	ns
main effect							
UV-B	0.25		3.00 ± 0.551	1.79 ± 0.348	1.24 ± 0.279 ab	1.68 ± 0.122	0.20 ± 0.015
	0.5		3.69 ± 0.596	1.83 ± 0.404	1.28 ± 0.274 ab	1.77 ± 0.180	0.21 ± 0.027
	0.75		4.42 ± 0.371	1.72 ± 0.478	1.55 ± 0.420 b	1.84 ± 0.209	0.23 ± 0.020
	1.0		4.51 ± 0.838	1.82 ± 0.544	0.83 ± 0.190 a	1.61 ± 0.252	0.20 ± 0.030
	1.25		4.09 ± 1.132	1.82 ± 0.777	0.85 ± 0.354 a	1.65 ± 0.413	0.20 ± 0.052
T	5		4.01 ± 0.744	2.20 ± 0.260 b	1.24 ± 0.399	1.82 ± 0.191 b	0.21 ± 0.020
	15		3.86 ± 1.040	1.39 ± 0.298 a	1.06 ± 0.400	1.60 ± 0.258 a	0.20 ± 0.038
T	UV-B						
5		0.25	3.38 ± 0.525 ab	2.07 ± 0.157	1.40 ± 0.222	1.74 ± 0.128	0.20 ± 0.012
		0.5	3.26 ± 0.171 ab	2.09 ± 0.079	1.18 ± 0.227	1.82 ± 0.155	0.20 ± 0.019
		0.75	4.47 ± 0.577 b	2.13 ± 0.269	1.74 ± 0.484	1.89 ± 0.276	0.23 ± 0.023
		1.0	4.09 ± 0.326 ab	2.24 ± 0.408	0.93 ± 0.099	1.78 ± 0.199	0.21 ± 0.032
		1.25	4.87 ± 0.501 b	2.49 ± 0.168	0.95 ± 0.287	1.88 ± 0.275	0.22 ± 0.007
15		0.25	2.61 ± 0.202 a	1.51 ± 0.197	1.09 ± 0.265	1.61 ± 0.088	0.19 ± 0.019
		0.5	4.11 ± 0.565 ab	1.58 ± 0.456	1.38 ± 0.327	1.71 ± 0.218	0.22 ± 0.034
		0.75	4.37 ± 0.068 b	1.32 ± 0.101	1.36 ± 0.310	1.79 ± 0.160	0.21 ± 0.019
		1.0	4.92 ± 1.062 b	1.41 ± 0.229	0.78 ± 0.250	1.45 ± 0.200	0.19 ± 0.032
		1.25	3.30 ± 1.046 ab	1.15 ± 0.379	0.70 ± 0.430	1.42 ± 0.440	0.17 ± 0.070

[a]The concentration of the kaempferol glycosides was quantitated as kaempferol-3-*O*-glucoside equivalents. Values (means ± standard deviation) with the same letters are not significantly different (Tukey's HSD test (n = 3) is calculated at $p \leq 0.05$) for each kaempferol glycoside. Key: *, significant at $p \leq 0.05$; **, significant at $p \leq 0.01$; ***, significant at $p \leq 0.005$; ns, not significant. Abbreviations: K, kaempferol; soph, sophorose; glc, glucose; diglc, diglucoside; triglc, triglucoside; hfer, hydroxyferuloyl; sin, sinapoyl; disin, disinapoyl. [b]The compound was tentatively identified by HPLC-DAD−MS^n as shown by Schmidt et al.[9] [c]The compound was identified with NMR as shown by Fiol et al.[10]

interaction of UV-B radiation and temperature. Monoacylated quercetin glycosides were affected by UV-B radiation dependent on the temperature. To account for this, we assume that a higher antioxidant activity in the plant is due to the hydroxycinnamic acid residue compared to the non-acylated quercetin glycoside. Interestingly, the non-acylated and the diacylated quercetin glycosides were affected by UV-B radiation only. The effect of the *aglycon* was confirmed as quercetin glycosides increased with higher UV-B radiation, which we assumed to be an adaptation of the plant and which has previously led to an assumption that the catechol structure of the B-ring enhances the antioxidant activity against ROS in kale.[5] In contrast, another study on kale showed that a single dose of moderate UV-B radiation (0.44 kJ m^{-2} d^{-1} UV-B_{BE}) mainly resulted in a decrease of quercetin glycosides.[20] An increase of quercetin glycosides has also been shown for several plant species with UV-B radiation levels of approximately 5 kJ m^{-2} d^{-1} UV-B_{BE} and higher for several weeks.[2] In silver birch (*Betula pendula*) leaves, quercetin glycosides increased at 3.74−4.48 kJ m^{-2} d^{-1} UV-B_{BE} for 30 days comparable to our results.[17] In canola (*Brassica napus*) leaves, the non-acylated quercetin-3-*O*-sophoroside-7-*O*-D-glucoside and the corresponding kaempferol triglycoside as well as the sinapic acid monoacylated quercetin glycoside were enhanced by 13 kJ m^{-2} d^{-1} UV-B_{BE} for 16 days, while the sinapic acid monoacylated kaempferol glycoside concentration was not affected.[29] Our study showed that even moderate UV-B radiation applied in subsequent daily doses can modify the flavonoid profile by increasing polyhydroxylated compounds, namely, quercetin glycosides. This finding is underlined by a study of Gotz et al.,[16] where quercetin glycosides increased at 0.54 kJ m^{-2} d^{-1} UV-B_{BE} for several days in *Arabidopsis*. A decrease in temperature (ambient temperature (14−28 °C) compared to 2 °C higher than ambient (16−30 °C)) and an increase of UV-B radiation (32% higher than ambient (0.04−0.11 kJ m^{-2} d^{-1} UV-B_{BE} on a summer day)) for several weeks led to higher concentrations of quercetin glycosides in willow;[22] however, interactions between UV-B radiation and temperature were not reported. In a study on arnica, quercetin-3-*O*-β-D-glucoside and kaempferol-3-*O*-β-D-glucoside were not affected by UV-B radiation, comparing ambient UV-B radiation (8.0 kJ m^{-2} d^{-1} UV-B_{BE}) to zero UV-B radiation for one month.[23] However, the overall quercetin to kaempferol ratio was enhanced at lower temperatures of 20 °C compared to 25 °C. As a mountain plant, arnica might be adapted to higher UV-B radiation levels. The enhancement of acylated quercetin glycosides in field-grown kale was caused by a decrease in temperature from 12 to 0 °C rather than a decrease of photosynthetic active radiation (PAR) from 20 to 4 mol m^{-2} d^{-1}.[30] However, non-acylated and monoacylated quercetin glycosides increased at moderate PAR compared to low PAR at 5 and 10 °C under defined conditions in climate chambers.[27] In the present experiment moderate UV-B radiation given in subsequent daily doses led to a higher increase of monoacylated quercetin glycosides. We therefore hypothesize that a higher ROS level results from UV-B radiation rather than PAR. In *Arabidopsis*, not only structurally different quercetin glycosides, including quercetin-3-*O*-glucoside-7-*O*-rhamnoside, quercetin-3-*O*-rhamnoside-7-*O*-rhamno-

Table 4. Influence of Ultraviolet-B (UV-B, kJ m^{-2} UV-B_{BE}) and Temperature (T, °C) on Hydroxycinnamic Acid Derivatives (mg g^{-1} of dry matter) in Juvenile Kale Plants[a]

			caffeoylquinic acid[b]	disinapoyl-gentiobiose[b]		sinapoyl-feruloyl- gentiobiose[b]
UV-B			ns	ns		ns
T			ns	*		ns
UV-B × T			*	ns		ns
	main effect					
UV-B	0.25		0.59 ± 0.026	0.10 ± 0.014		0.16 ± 0.017
	0.5		0.58 ± 0.060	0.10 ± 0.019		0.17 ± 0.021
	0.75		0.62 ± 0.106	0.10 ± 0.014		0.18 ± 0.033
	1.0		0.58 ± 0.068	0.09 ± 0.020		0.17 ± 0.024
	1.25		0.60 ± 0.095	0.09 ± 0.034		0.19 ± 0.040
T	5		0.61 ± 0.081	0.09 ± 0.012	a	0.17 ± 0.027
	15		0.58 ± 0.061	0.11 ± 0.022	b	0.18 ± 0.029
T	UV-B					
5		0.25	0.58 ± 0.029	0.09 ± 0.008		0.15 ± 0.013
		0.5	0.53 ± 0.023	0.09 ± 0.015		0.17 ± 0.024
		0.75	0.63 ± 0.150	0.09 ± 0.011		0.18 ± 0.046
		1.0	0.64 ± 0.022	0.09 ± 0.021		0.17 ± 0.015
		1.25	0.67 ± 0.038	0.08 ± 0.002		0.20 ± 0.015
15		0.25	0.60 ± 0.021	0.11 ± 0.009		0.18 ± 0.007
		0.5	0.63 ± 0.018	0.12 ± 0.008		0.18 ± 0.017
		0.75	0.60 ± 0.072	0.11 ± 0.015		0.19 ± 0.026
		1.0	0.53 ± 0.035	0.10 ± 0.022		0.18 ± 0.034
		1.25	0.53 ± 0.075	0.11 ± 0.049		0.18 ± 0.061

[a]The concentration of the hydroxycinnamic acid derivatives was quantitated as caffeoylquinic acid equivalents. Values (means ± standard deviation) with the same letters are not significantly different (Tukey's HSD test (n = 3) is calculated at $p \leq 0.05$) for each hydroxycinnamic acid derivative. Key: *, significant at $p \leq 0.05$; **, significant at $p \leq 0.01$; ***, significant at $p \leq 0.005$; ns, not significant. [b]The compound was identified with NMR as shown by Fiol et al.[10]

side, and quercetin-3-*O*-rhamnoside-glucoside-7-*O*-rhamnoside, but also the corresponding kaempferol glycosides were observed to increase at 0.627 kJ m^{-2} d^{-1} UV-B_{BE} for 12 days.[31] In contrast, in kale, several kaempferol glycosides were enhanced (Tables 2 and 3), while others were not affected, thereby suggesting a different role of kaempferol glycosides in the plant's response to UV-B radiation at different temperatures.

Of 11 investigated *kaempferol glycosides*, 6 responded to different interactions of UV-B radiation and temperature (Tables 2 and 3). At 5 °C, the non-acylated kaempferol glycoside had the highest concentration combined with UV-B radiation levels of 0.5−1.25 kJ m^{-2} UV-B_{BE}, whereas at 15 °C a UV-B radiation level of 0.25 kJ m^{-2} UV-B_{BE} was adequate to produce the highest concentration. Moreover, the concentration levels of the monoacylated kaempferol diglycosides show a response to an interaction of UV-B radiation and temperature. Kaempferol-3-O-feruloyl-sophoroside was not affected by UV-B radiation or temperature. The corresponding hydroxyferulic acid monoacylated kaempferol diglycoside was also not affected at 5 °C under different UV-B radiation conditions, whereas, at 15 °C, its highest concentration was determined at 0.75 kJ m^{-2} UV-B_{BE}. In contrast, the sinapic acid monoacylated kaempferol diglycoside increased at 5 °C with increasing UV-B radiation levels of up to 1.25 kJ m^{-2} UV-B_{BE}, whereas, at 15 °C, the doses of UV-B radiation had no effect. For kaempferol triglycosides, the results showed that kaempferol-3-*O*-caffeoyl-sophoroside-7-*O*-D-glucoside strongly increased with UV-B radiation levels from 0.25 up to 1.25 kJ m^{-2} UV-B_{BE} at 5 °C, and at 15 °C, an increase was determined from 0.25 up to 1.0 kJ m^{-2} UV-B_{BE}, thereby showing a clear response to an interaction of UV-B radiation and temperature for this compound. The hydroxyferulic acid monoacylated kaempferol triglycoside was also influenced by interacting UV-B radiation and temperature. The lowest concentration for this compound was found at 0.25 kJ m^{-2} UV-B_{BE} and 15 °C. The ferulic acid and sinapic acid monoacylated kaempferol triglycosides were not affected by an interaction of UV-B radiation and temperature, but were strongly affected by temperature alone, which resulted in higher concentrations at 5 °C compared to 15 °C. Kaempferol tetraglycosides acylated with hydroxyferulic acid (kaempferol-3-*O*-hydroxyferuloyl-sophoroside-7-*O*-diglucoside) and sinapic acid (kaempferol-3-*O*-sinapoyl-sophoroside-7-*O*-diglucoside) were not affected by an interaction of UV-B radiation and temperature. The level of the hydroxyferulic acid monoacylated kaempferol tetraglycoside decreased when the compound was exposed to 0.75−1.0 kJ m^{-2} UV-B_{BE}, and this reaction was found to be independent of temperature. In contrast, the sinapic acid monoacylated kaempferol tetraglucoside was present at higher concentrations at 5 °C, and this was independent of the UV-B intensities. To summarize, the *hydroxycinnamic acid residue* influenced the response of flavonol glycosides to UV-B radiation and temperature; e.g., the caffeic acid and hydroxyferulic acid monoacylated kaempferol triglycosides (containing a catechol structure) were affected by UV-B radiation and showed an interaction of UV-B radiation and temperature. Of note is that the ferulic and sinapic acid monoacylated kaempferol triglycosides (no catechol structure) were affected by temperature alone. Similarly, as in kale, the ferulic acid and sinapic acid monoacylated kaempferol triglycosides were not affected by the UV-B treatment in leafy *Brassica* pak choi irradiated with high dosages of 20−24 kJ m^{-2} d^{-1} UV-B_{BE} for 7 days.[21] Furthermore, in pak choi at 9 °C, the concentration of the

dx.doi.org/10.1021/jf4054066 | J. Agric. Food Chem. 2014, 62, 4054−4062

Table 5. Influence of Ultraviolet-B (UV-B, kJ m^{-2} UV-B_{BE}) and Temperature (T, °C) on the Relative Expression of Genes Presumably Coding for Flavanone 3β-Hydroxylase (*F3H*), Flavonol Synthase (*FLS*), and Flavonol 3′-Hydroxylase (*F3′H*)[a]

			flavanone 3β-hydroxylase		flavonol synthase		flavonol 3′-hydroxylase	
UV-B			***		***		***	
T			ns		***		***	
UV-B × T			***		***		***	
	main effect							
UV-B		0.25	1.17 ± 0.5679		0.004 ± 0.0013		0.02 ± 0.0122	
		0.5	3.13 ± 0.7195		0.011 ± 0.0102		0.06 ± 0.0239	
		0.75	0.72 ± 0.4370		0.004 ± 0.0020		0.07 ± 0.0580	
		1.0	0.35 ± 0.1641		0.001 ± 0.0005		0.03 ± 0.0265	
		1.25	0.44 ± 0.2250		0.003 ± 0.0018		0.05 ± 0.0207	
T		5	1.23 ± 1.3505		0.007 ± 0.0072		0.02 ± 0.0148	
		15	1.10 ± 0.8930		0.003 ± 0.0017		0.07 ± 0.0355	
T		UV-B						
5		0.25	0.68 ± 0.0390	ab	0.003 ± 0.0002	abc	0.01 ± 0.0032	a
		0.5	3.72 ± 0.1942	e	0.020 ± 0.0032	d	0.04 ± 0.0063	abcd
		0.75	1.00 ± 0.4624	bc	0.006 ± 0.0005	c	0.02 ± 0.0073	abc
		1.0	0.26 ± 0.0750	a	0.002 ± 0.0002	ab	0.01 ± 0.0034	ab
		1.25	0.46 ± 0.3144	ab	0.004 ± 0.0018	abc	0.03 ± 0.0218	abcd
15		0.25	1.65 ± 0.3251	c	0.005 ± 0.0004	bc	0.03 ± 0.0075	abc
		0.5	2.50 ± 0.2625	d	0.002 ± 0.0009	abc	0.08 ± 0.0158	d
		0.75	1.16 ± 0.4135	bc	0.002 ± 0.0009	abc	0.12 ± 0.0300	e
		1.0	0.45 ± 0.1831	ab	0.001 ± 0.0004	a	0.05 ± 0.0185	bcd
		1.25	0.44 ± 0.1660	ab	0.002 ± 0.0013	abc	0.06 ± 0.0140	cd

[a]Relative transcript levels (means ± standard deviation) in juvenile kale plants were normalized on the basis of expression of actin. Values with the same letters are not significantly different (Tukey's HSD test (n = 3) is calculated at $p \leq 0.05$). Key: *, significant at $p \leq 0.05$; **, significant at $p \leq 0.01$; ***, significant at $p \leq 0.005$; ns, not significant.

caffeic acid monoacylated kaempferol triglycoside decreased, but it was not affected at 22 °C.[21] In contrast, in kale, the kaempferol-3-*O*-caffeoyl-sophoroside-7-*O*-glucoside increased after five subsequent daily doses of moderate UV-B radiation with an interaction of UV-B radiation and temperature. The influence of temperature on the effect of UV-B radiation was less evident in pak choi[21] than in our study despite a higher dose (20−24 kJ m^{-2} d^{-1} UV-B_{BE} for 7 days)[21] compared to the moderate dose of UV-B radiation (0.25−1.25 kJ m^{-2} UV-B_{BE} for 5 d) used here in kale that elicited a higher impact in terms of affecting the concentrations of flavonol glycosides. A characteristic structure prevalent in kale's flavonoid glycosides was the *number of glucose moieties*. However, in silver birch seedlings, the flavonol glycosides quercetin-3-galactoside, quercetin-3-rhamnoside, and kaempferol-3-rhamnoside were enhanced after UV-B radiation (7.3−8.5 kJ m^{-2} d^{-1} UV-B_{BE} for 10 d), whereas several other quercetin and kaempferol glycosides remained unaffected.[32] Although we found only glucose as the sugar moiety in kale,[10] there is a substitution effect of the 7-*O* position for diglycosides (no glucose moiety in the 7-*O* position) and tri- and tetraglycosides (one and two glucose moieties in the 7-*O* position, respectively). In summary, the monoacylated kaempferol diglycosides showed interactions of UV-B radiation and temperature independent of the acylated hydroxycinnamic acid residue. For monoacylated kaempferol triglucosides, interactions of UV-B radiation and temperature were observed only if the acylated hydroxycinnamic acid included a catechol structure. In contrast, the monoacylated kaempferol tetraglycosides were not influenced by the interaction of UV-B radiation and temperature. One possible reason for this is that the molecule size influences the activity and the synthesis in response to ROS-induced stress. The complex diacylated kaempferol-3-*O*-disinapoyl-triglucoside-7-*O*-D-glucoside was affected by neither UV-B radiation nor temperature. The effect of the *acylation pattern* has been discussed for the quercetin glycosides. However, the acylated hydroxycinnamic acid and the number of glucose moieties seem to have a higher impact.

The *hydroxycinnamic acid derivatives* were hardly affected by UV-B radiation or temperature in kale (Table 4). Hydroxycinnamic acids were previously shown to act as scavengers to ROS induced by UV-B radiation.[3] In pak choi irradiated with 20−24 kJ m^{-2} d^{-1} UV-B_{BE} for 7 d, the malate esters of coumaric, caffeic, ferulic, hydroxyferulic, and sinapic acid increased at 9 °C due to the applied UV-B radiation, but were not affected at 22 °C.[21] The opposite phenomenon was observed in kale where concentrations of disinapoyl-gentiobiose and sinapoyl-feruloyl-gentiobiose did not change in response to UV-B radiation and temperature interactions. However, the concentration of disinapoyl-gentiobiose generally increased at 15 °C compared to 5 °C, while for sinapoyl-feruloyl-gentiobiose no effect of UV-B radiation or temperature was found. The biosynthesis of hydroxycinnamic acids is probably reduced in favor of flavonoid biosynthesis at the moderate UV-B we used in this experiment compared to ambient and higher UV-B levels as demonstrated in pak choi. To add to this notion, in willow and in arnica only a decrease in temperature resulted in higher concentrations of caffeoylquinic acid and its derivatives, but an increased UV-B radiation had no effect.[22,23] In addition, neither Morales et al.[17] nor Anttila et al.[33] found any influence of UV-B radiation (3.74−4.48 kJ m^{-2} d^{-1} UV-B_{BE} for 30 d and 2.75−5.23 kJ m^{-2} d^{-1} UV-B_{BE} for several weeks, respectively) on caffeoylquinic acid in silver birch, underlining the findings in kale where caffeoylquinic acid was influenced by an interaction of UV-B radiation and temperature but neither UV-B radiation nor temperature had a significant effect on this compound.

Moreover, 5-caffeoylquinic acid increased at 7.3−8.5 kJ m^{-2} d^{-1} UV-B_{BE} for 10 d in silver birch, but 3-caffoeylquinic acid was not affected.[32] This finding supports the conclusion that the hydroxycinnamic acid response is structure-specific.

qRT-PCR expression analysis was performed for *key genes involved in the flavonol biosynthesis* pathway in *B. oleracea*. For this purpose, primer pairs were developed to specifically analyze the expression differences of genes presumably coding for flavanone 3*β*-hydoxylase (*F3H*; formation of dihydroflavonols from flavanones), flavonol synthase (*FLS*; formation of flavonols from dihydroflavonols), and flavonol 3′-hydroxylase (*F3′H*; hydroxylation of the B-ring of flavonoids) (Table 5). Kilian et al.[25] demonstrated that, due to UV-B stress, genes were up- or downregulated in a time-dependent manner with a maximum expression 6 h after the treatment. In the present study, the kale plants were harvested after an adaptation time of 24 h, suggesting that the mRNA expression was adjusted during the adaptation time. The expression of the genes of the key enzymes involved in flavonol biosynthesis increased with maximum expression at 0.5 kJ m^{-2} UV-B_{BE} (*F3H*, *FLS*) or 0.75 kJ m^{-2} UV-B_{BE} (*F3′H*). This observation suggests that the kale plants were still affected by ROS due to the applied moderate UV-B radiation as also reported for several species at higher UV-B radiation doses.[2] For all three investigated genes, their expression patterns were influenced by an interaction of UV-B radiation and temperature. UV-B radiation affected the expression of all three genes, while temperature affected the expression of *FLS* and *F3′H*, but not of *F3H*. The expression of the *F3H* gene was highest at 0.5 kJ m^{-2} UV-B_{BE} and was independent of temperature. This expression was observed to correspond to the higher concentrations of the non-acylated kaempferol triglycoside—a precursor of the monoacylated kaempferol triglycosides that occur in high concentrations. Consistent with a study of purple kale,[24] a cold-induced induction of *F3H* was reported and is supported by our data where at 5 °C (0.5 kJ m^{-2} UV-B_{BE}) the expression of *F3H* was higher than at 15 °C. Furthermore, the expression of the *FLS* gene was also highest at 0.5 kJ m^{-2} UV-B_{BE} at 5 °C, but hardly affected under different levels of UV-B radiation at 15 °C. This could be responsible for the increased concentrations of the hydroxyferulic acid monoacylated kaempferol triglycoside at 5 °C compared to 15 °C, since the catechol structure of the acylated hydroxyferulic acid seems to be important in the plant's response to UV-B radiation. In soybean (*Glycine max*), a single dose of UV-B radiation (not specified) led to a higher activity of the enzymes flavanone 3*β*-hydroxylase and flavonol synthase.[34] Both of these enzymes are important for the biosynthesis of kaempferol—a finding that adds further support to our study. In contrast, the expression of the *F3′H* gene was high at 0.75 kJ m^{-2} UV-B_{BE} at 15 °C, but not affected under different levels of UV-B radiation at 5 °C. The high mRNA expression of *F3′H* resulted in higher concentrations of monoacylated quercetin glycosides compared to those at 5 °C. We assume that this is due to an increased response to the UV-B-induced ROS in kale.[35]

In summary, the present study in kale underlines the structure-dependent response of flavonol glycosides. Additionally, the response of flavonol glycosides and hydroxycinnamic acid derivatives was clearly dependent on the interaction of UV-B radiation and temperature. All quercetin glycosides increased by higher UV-B radiation. Nevertheless, high concentrations of monoacylated quercetin glycosides were determined at 15 °C compared to 5 °C. In contrast to quercetin glycosides, kaempferol glycosides showed a more diverse response to UV-B radiation and temperature. A catechol structure in quercetin glycosides and in the acylated hydroxycinnamic acid residues seems to be important for the response to UV-B radiation. Moreover, the expression of genes coding for key enzymes involved in flavonol biosynthesis was increased by UV-B exposure. As the potential beneficial health effects of kale are directly related to the profile and concentration of flavonol glycosides and hydroxycinnamic acid derivatives,[11] moderate UV-B doses combined with pointed temperature treatment might be a suitable application for enhancing the phenolic profile in the plant.

AUTHOR INFORMATION

Corresponding Author

*Phone: +49 0 33701-78307. Fax: +49 0 33701-55391. E-mail: neugart@igzev.de.

Funding

We sincerely thank the DFG (Deutsche Forschungsgemeinschaft) for funding (Projects KR-2066/3-1 and KR-1452/12-1).

Notes

The authors declare no competing financial interest.

ACKNOWLEDGMENTS

We thank Peter Klaering for support with the statistical analyses.

ABBREVIATIONS USED

UV-B, ultraviolet-B; UV-BBE, biologically effective UV-B; ROS, reactive oxygen species; PAR, photosynthetic active radiation; HPLC, high-pressure liquid chromatography; DAD, diode array detector; ESI, electrospray ionization; MS, mass spectrometry; NMR, nuclear magnetic resonance

REFERENCES

(1) Jansen, M. A. K. Ultraviolet-B radiation effects on plants: induction of morphogenic responses. *Physiol. Plant.* **2002**, *116*, 423−429.

(2) Jansen, M. A. K.; Hectors, K.; O'Brien, N. M.; Guisez, Y.; Potters, G. Plant stress and human health: do human consumers benefit from UV-B acclimated crops? *Plant Sci.* **2008**, *175*, 449−458.

(3) Edreva, A. The importance of non-photosynthetic pigments and cinnamic acid derivatives in photoprotection. *Agric., Ecosyst. Environ.* **2005**, *106*, 135−146.

(4) Agati, G.; Tattini, M. Multiple functional roles of flavonoids in photoprotection. *New Phytol.* **2010**, *186*, 786−793.

(5) Zietz, M.; Weckmuller, A.; Schmidt, S.; Rohn, S.; Schreiner, M.; Krumbein, A.; Kroh, L. W. Genotypic and climatic influence on the antioxidant activity of flavonoids in kale (*Brassica oleracea* var. *sabellica*). *J. Agric. Food Chem.* **2010**, *58*, 2123−2130.

(6) Ferreres, F.; Fernandes, F.; Oliveira, J. M. A.; Valentão, P.; Pereira, J. A.; Andrade, P. B. Metabolic profiling and biological capacity of *Pieris brassicae* fed with kale (*Brassica oleracea* L. var. *acephala*). *Food Chem. Toxicol.* **2009**, *47*, 1209−1220.

(7) Lin, L.-Z.; Harnly, J. M. Identification of the phenolic components of collard greens, kale, and Chinese broccoli. *J. Agric. Food Chem.* **2009**, *57*, 7401−7408.

(8) Olsen, H.; Aaby, K.; Borge, G. I. A. Characterization and quantification of flavonoids and hydroxycinnamic acids in curly kale (*Brassica oleracea* L. Convar. *acephala* Var. *sabellica*) by HPLC-DAD-ESI-MS^n. *J. Agric. Food Chem.* **2009**, *57*, 2816−2825.

(9) Schmidt, S.; Zietz, M.; Schreiner, M.; Rohn, S.; Kroh, L. W.; Krumbein, A. Identification of complex, naturally occurring flavonoid glycosides in kale (*Brassica oleracea* var. *sabellica*) by high-performance liquid chromatography diode-array detection/electrospray ionization

multi-stage mass spectrometry. *Rapid Commun. Mass Spectrom.* **2010**, *24*, 2009−2022.
(10) Fiol, M.; Adermann, S.; Neugart, S.; Rohn, S.; Mügge, C.; Schreiner, M.; Krumbein, A.; Kroh, L. W. Highly glycosylated and acylated flavonols isolated from kale (*Brassica oleracea* var. *sabellica*)—structure−antioxidant activity relationship. *Food Res. Int.* **2012**, *47*, 80−89.
(11) Stochmal, A.; Oleszek, W. Effect of acylation of flavones with hydroxycinnamic acids on their spectral characteristics. *Nat. Prod. Commun.* **2007**, *2*, 571−574.
(12) Ryan, K. G.; Markham, K. R.; Bloor, S. J.; Bradley, J. M.; Mitchell, K. A.; Jordan, B. R. UVB radiation induced increase in quercetin: kaempferol ratio in wild-type and transgenic lines of petunia. *Photochem. Photobiol.* **1998**, *68*, 323−330.
(13) Reifenrath, K.; Mueller, C. Species-specific and leaf-age dependent effects of ultraviolet radiation on two Brassicaceae. *Phytochemistry* **2007**, *68*, 875−885.
(14) Winter, T. R.; Rostas, M. Ambient ultraviolet radiation induces protective responses in soybean but does not attenuate indirect defense. *Environ. Pollut.* **2008**, *155*, 290−297.
(15) Zhang, J. M.; Satterfield, M. B.; Brodbelt, J. S.; Britz, S. J.; Clevidence, B.; Novotny, J. A. Structural characterization and detection of kale flavonoids by electrospray ionization mass spectrometry. *Anal. Chem.* **2003**, *75*, 6401−6407.
(16) Goetz, M.; Albert, A.; Stich, S.; Heller, W.; Scherb, H.; Krins, A.; Langebartels, C.; Seidlitz, H. K.; Ernst, D. PAR modulation of the UV-dependent levels of flavonoid metabolites in *Arabidopsis thaliana* (L.) Heynh. leaf rosettes: cumulative effects after a whole vegetative growth period. *Protoplasma* **2010**, *243*, 95−103.
(17) Morales, L. O.; Tegelberg, R.; Brosche, M.; Keinanen, M.; Lindfors, A.; Aphalo, P. J. Effects of solar UV-A and UV-B radiation on gene expression and phenolic accumulation in *Betula pendula* leaves. *Tree Physiol.* **2010**, *30*, 923−934.
(18) Schreiner, M.; Mewis, I.; Huyskens-Keil, S.; Jansen, M. A. K.; Zrenner, R.; Winkler, J. B.; O'Brien, N.; Krumbein, A. UV-B-induced secondary plant metabolites—potential benefits for plant and human health. *Crit. Rev. Plant Sci.* **2012**, *31*, 229−240.
(19) Sangtarash, M. H.; Qaderi, M. M.; Chinnappa, C. C.; Reid, D. M. Differential sensitivity of canola (*Brassica napus*) seedlings to ultraviolet-B radiation, water stress and abscisic acid. *Environ. Exp. Bot.* **2009**, *66*, 212−219.
(20) Neugart, S.; Zietz, M.; Schreiner, M.; Rohn, S.; Kroh, L. W.; Krumbein, A. Structurally different flavonol glycosides and hydroxycinnamic acid derivatives respond differently to moderate UV-B radiation exposure. *Physiol. Plant.* **2012**, *145*, 582−593.
(21) Harbaum-Piayda, B.; Walter, B.; Bengtsson, G. B.; Hubbermann, E. M.; Bilger, W.; Schwarz, K. Influence of pre-harvest UV-B irradiation and normal or controlled atmosphere storage on flavonoid and hydroxycinnamic acid contents of pak choi (*Brassica campestris* L. ssp. *chinensis* var. *communis*). *Postharvest Biol. Technol.* **2010**, *56*, 202−208.
(22) Nybakken, L.; Horkka, R.; Julkunen-Tiitto, R. Combined enhancements of temperature and UVB influence growth and phenolics in clones of the sexually dimorphic *Salix myrsinifolia*. *Physiol. Plant.* **2012**, *145*, 551−564.
(23) Albert, A.; Sareedenchai, V.; Heller, W.; Seidlitz, H. K.; Zidorn, C. Temperature is the key to altitudinal variation of phenolics in *Arnica montana* L. cv. ARBO. *Oecologia* **2009**, *160*, 1−8.
(24) Zhang, B.; Hu, Z.; Zhang, Y.; Li, Y.; Zhou, S.; Chen, G. A putative functional MYB transcription factor induced by low temperature regulates anthocyanin biosynthesis in purple kale (*Brassica oleracea* var. *acephala* f. tricolor). *Plant Cell Rep.* **2012**, *31*, 281−289.
(25) Kilian, J.; Whitehead, D.; Horak, J.; Wanke, D.; Weinl, S.; Batistic, O.; D'Angelo, C.; Bornberg-Bauer, E.; Kudla, J.; Harter, K. The AtGenExpress global stress expression data set: protocols, evaluation and model data analysis of UV-B light, drought and cold stress responses. *Plant J.* **2007**, *50*, 347−363.
(26) Caldwell, M. M. Solar UV irradiation and the growth and development of higher plants. In *Photophysiology*; Giese, A. C., Ed.; Academic Press: New York, 1971; Vol. *6*, pp 131−177.
(27) Neugart, S.; Fiol, M.; Schreiner, M.; Rohn, S.; Zrenner, R.; Kroh, L. W.; Krumbein, A. Low and moderate photosynthetically active radiation affects the flavonol glycosides and hydroxycinnamic acid derivatives in kale (*Brassica oleracea* var. *sabellica*) dependent on two low temperatures. *Plant Physiol. Biochem.* **2013**, *72*, 161−168.
(28) Ruijter, J. M.; Ramakers, C.; Hoogaars, W. M. H.; Karlen, Y.; Bakker, O.; van den Hoff, M. J. B.; Moorman, A. F. M. Amplification efficiency: linking baseline and bias in the analysis of quantitative PCR data. *Nucleic Acids Res.* **2009**, *37*, e45.
(29) Olsson, L. C.; Veit, M.; Weissenbock, G.; Bornman, J. F. Differential flavonoid response to enhanced UV-B radiation in *Brassica napus*. *Phytochemistry* **1998**, *49*, 1021−1028.
(30) Neugart, S.; Kläring, H.-P.; Zietz, M.; Schreiner, M.; Rohn, S.; Kroh, L. W.; Krumbein, A. The effect of temperature and radiation on flavonol aglycones and flavonol glycosides of kale (*Brassica oleracea* var. *sabellica*). *Food Chem.* **2012**, *133*, 1456−1465.
(31) Hectors, K.; van Oevelen, S.; Guisez, Y.; Prinsen, E.; Jansen, M. A. K. The phytohormone auxin is a component of the regulatory system that controls UV-mediated accumulation of flavonoids and UV-induced morphogenesis. *Physiol. Plant.* **2012**, *145*, 594−603.
(32) Tegelberg, R.; Julkunen-Tiitto, R. J.; Aphalo, P. J. Red:far-red light ratio and UV-B radiation: their effects on leaf phenolics and growth of silver birch seedlings. *Plant, Cell Environ.* **2004**, *27*, 1005−1013.
(33) Anttila, U.; Julkunen-Tiitto, R.; Rousi, M.; Yang, S.; Rantala, M. J.; Ruuhola, T. Effects of elevated ultraviolet-B radiation on a plant-herbivore interaction. *Oecologia* **2010**, *164*, 163−175.
(34) Kim, B. G.; Kim, J. H.; Kim, J.; Lee, C.; Ahn, J.-H. Accumulation of flavonols in response to ultraviolet-B irradiation in soybean is related to induction of flavanone 3-beta-hydroxylase and flavonol synthase. *Mol. Cells* **2008**, *25*, 247−252.
(35) Agati, G.; Cerovic, Z. G.; Pinelli, P.; Tattini, M. Light-induced accumulation of ortho-dihydroxylated flavonoids as non-destructively monitored by chlorophyll fluorescence excitation techniques. *Environ. Exp. Bot.* **2011**, *73*, 3−9.

JOURNAL OF AGRICULTURAL AND FOOD CHEMISTRY

Article

pubs.acs.org/JAFC

Synthesis and Antifungal Activity of Nicotinamide Derivatives as Succinate Dehydrogenase Inhibitors

Yong-Hao Ye,*[,†,‡,∥] Liang Ma,[†,‡,∥] Zhi-Cheng Dai,[†,‡] Yu Xiao,[†,‡] Ying-Ying Zhang,[†,‡] Dong-Dong Li,[§] Jian-Xin Wang,[†,‡] and Hai-Liang Zhu[§]

[†]College of Plant Protection, Jiangsu Key Laboratory of Pesticide Science, Nanjing Agricultural University, Nanjing 210095, People's Republic of China

[‡]Key Laboratory of Integrated Management of Crop Diseases and Pests, Ministry of Education, Nanjing 210095, People's Republic of China

[§]State Key Laboratory of Pharmaceutical Biotechnology, School of Life Sciences, Nanjing University, Nanjing 210093, People's Republic of China

ABSTRACT: Thirty-eight nicotinamide derivatives were designed and synthesized as potential succinate dehydrogenase inhibitors (SDHI) and precisely characterized by ^{1}H NMR, ESI-MS, and elemental analysis. The compounds were evaluated against two phytopathogenic fungi, *Rhizoctonia solani* and *Sclerotinia sclerotiorum*, by mycelia growth inhibition assay in vitro. Most of the compounds displayed moderate activity, in which, **3a-17** exhibited the most potent antifungal activity against *R. solani* and *S. sclerotiorum* with IC_{50} values of 15.8 and 20.3 μM, respectively, comparable to those of the commonly used fungicides boscalid and carbendazim. The structure−activity relationship (SAR) of nicotinamide derivatives demonstrated that the meta-position of aniline was a key position contributing to the antifungal activity. Inhibition activities against two fungal SDHs were tested and achieved the same tendency with the data acquired from in vitro antifungal assay. Significantly, **3a-17** was demonstrated to successfully suppress disease development in *S. sclerotiorum* infected cole in vivo. In the molecular docking simulation, sulfur and chlorine of **3a-17** were bound with PHE291 and PRO150 of the SDH homology model, respectively, which could explain the probable mechanism of action between the inhibitory and target protein.

KEYWORDS: *nicotinamide, antifungal activity, succinate dehydrogenase inhibitors*

INTRODUCTION

As one of the most important categories of agrochemicals,[1,2] carboxamide fungicides have been intensively employed throughout the world to fight against highly destructive plant pathogens, such as *Botrytis cinerea*, *Sclerotinia* spp., *Leveillula taurica*, and *Spherotheca macularis*.[3−5] From the first carboxamide fungicide carboxin for crop protection to those newly discovered, these molecules cover boscalid (BASF), bixafen (Bayer), fluopyram (Bayer), and isopyrazam (Syngenta) (Figure 1). The initial narrow biological spectrum was broadened with progress of the chemical structure modification. These pyridine carboxamide group of pesticides have a common target receptor, succinate dehydrogenase (SDH, EC 1.3.5.1).[6] They act as SDH inhibitors (SDHIs) and disrupt the mitochondrial tricarboxylic acid cycle and respiration chain.

On the basis of the molecular structure of boscalid, a new series of nicotinamide compounds containing an active skeleton, ortho-replaced pyridine amide, have been synthsized. As shown in Figure 2, the *p*-chloride phenyl ring of boscalid was removed, and the chloride atom on the ortho position of pyridine was replaced by sulfur methyl or sulfur benzyl. This modification kept the nicotinamide moiety, which is important to the fungicide activity, and ensured molecular weight and pharmacological properties such as solubility similar to those of boscalid.

In this study, structure-based drug design strategies and homology modeling in the development of novel SDH inhibitors are presented using Discovery Studio 3.1 (Accelrys Inc.).[7,8] To explore the advantage of different substituents at the ortho position of pyridine, we calculated the interaction energy (Table 1) by docking these ligands to the binding site of porcine SDH. On the basis of scores of binding energy, we revealed that sulfur methyl was more suitable than sulfur benzyl for introduction into the ortho position of pyridine. Thus, we focused on sulfur methyl substituted target compounds while synthesizing some sulfur benzyl substituted target compounds to verify our virtual screening.

MATERIALS AND METHODS

Chemicals and Instruments. *Instruments.* All chemicals and reagents used in the current study were of analytical grade (provided by Nanjing Chemical Regent Co., Ltd.). The reactions were monitored by thin layer chromatography (TLC) using precoated silica gel GF_{254} plates from Qingdao Haiyang Chemical, China. Melting points (uncorrected) were determined on an SPSIC WRS-1B digital melting-point apparatus (Shanghai, China). ESI mass spectra were obtained on a Mariner System 5304 mass spectrometer. ^{1}H NMR spectra were collected on a Bruker Avance III 400 NMR spectrometer with $CDCl_3$ as solvent at room temperature. The chemical shifts (δ) are reported in parts per million with reference to internal TMS, and coupling constants (J) are given in hertz. Elemental analyses were performed on a CHN-O-Rapid instrument and were within ±0.4% of the theoretical values.

Received: December 3, 2013
Revised: March 31, 2014
Accepted: April 10, 2014
Published: April 10, 2014

ACS Publications © 2014 American Chemical Society

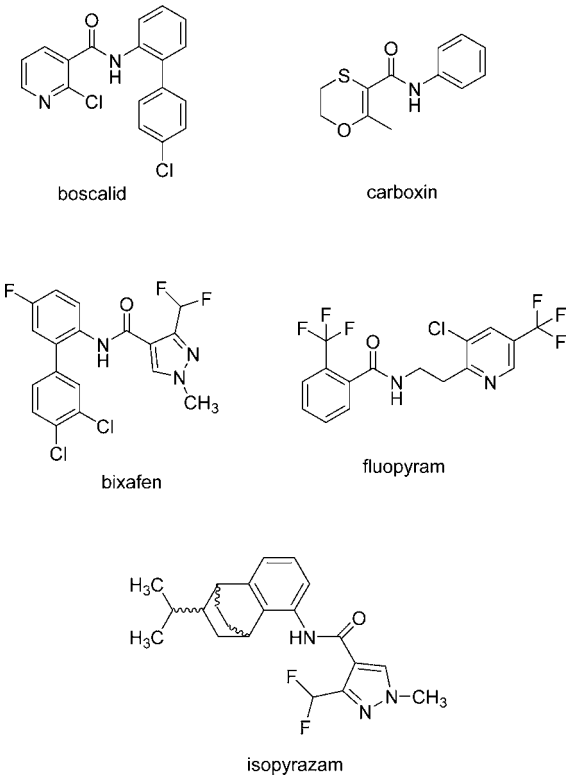

Figure 1. Structural formulas of the studied succinate dehydrogenase inhibitor (SDHI) fungicides.

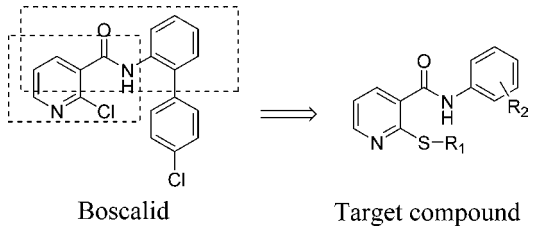

Figure 2. Design of target compounds.

Table 1. Scores of -cdock_interaction_energy for Virtual Screening in Synthesis Design[a]

Compounds		Scores of -cdock_ interaction_engry	Average engry
R_1	R_2		
		38.61	
CH_3-		38.96	38.99
		39.40	
		35.18	
		35.10	35.01
		34.77	
		34.08	
		34.52	34.24
		34.11	

[a]The higher the scores of -cdock_interaction_energy, the easier the bonding between chemical ligands and receptor.

*2-(Methylthio)nicotinic acid (**2a**).* 2-Mercaptonicotinic acid (1.55 g, 10 mmol) was dissolved in *N*,*N*-dimethylformamide (DMF, 40 mL), and K_2CO_3 (4.14 g, 30 mmol) was added. Iodomethane (685 μL, 11 mmol) was added dropwise, and the mixture was stirred for 1 h at room temperature. With stirring, the pH of the solution was adjusted to 2−3 with 5% HCl solution. The precipitated solid was filtered, washed with cold water, and allowed to air-dry overnight to afford 1.61 g of the acid **2a** (9.5 mmol, 95%) as a white solid: mp 171−172 °C; ^{1}H NMR (400 MHz, DMSO-d_6) δ 2.59 (s, 3H, CH_3), 7.12 (dd, 1H, J = 7.7, 4.8 Hz, Py−H), 8.34 (dd, 1H, J = 7.8, 1.6 Hz, Py−H), 8.67 (dd, 1H, J = 4.6, 1.6 Hz, Py−H); MS (ESI), 170.02 ($C_7H_7NO_2S$, $[M + H]^+$). Anal. Calcd for $C_7H_7NO_2S$: C, 49.69; H, 4.17; N, 8.28. Found: C, 49.88; H, 4.11; N, 8.32.

*2-((2-Fluorobenzyl)thio)nicotinic Acid (**2b**) and 2-((4-Nitrobenzyl)-thio)nicotinic Acid (**2c**).* 2-Mercaptonicotinic acid (32 mmol, 5.0 g) was dissolved together with potassium hydroxide (20 mol, 1.2 g) in 30 mL of ethanol. Benzyl bromide (1-(bromomethyl)-2-fluorobenzene or 1-(bromomethyl)-4-nitrobenzene) was added dropwise, and the mixture was refluxed for 30 min. After cooling, the reaction mixture was concentrated to approximately 15 mL. The residue was treated with 20 mL of water and slightly acidified with 5% HCl solution. The precipitate was filtered, washed with water, and recrystallized from ethanol to give white crystals of **2b** or **2c** as a white or yellow solid, respectively.

Data for **2b**: yield, 72.5%; mp, 184−185 °C; ^{1}H NMR (400 MHz, DMSO-d_6) δ 4.40 (s, 2H, S−CH_2−Ar), 7.12−7.16 (m, 2H, Py−H, Ar), 7.26−7.28 (m, 1H, Ph−H), 7.29−7.23 (m, 1H, Ph−H), 7.52 (dt, 1H, J = 7.7, 1.4 Hz, Ph−H), 8.23 (dd, 1H, J = 3.8, 1.8 Hz, Py−H), 8.52 (dd, 1H, J = 7.6, 3.8 Hz, Py−H); MS (ESI), 264.04 ($C_{13}H_{10}FNO_2S$, $[M + H]^+$). Anal. Calcd for $C_{13}H_{10}FNO_2S$: C, 59.31; H, 3.83; N, 5.32. Found: C, 59.48; H, 3.61; N, 5.42.

Data for **2c**: yield, 71.9%; mp, 163−164 °C; ^{1}H NMR (400 MHz, DMSO-d_6) δ 4.42 (s, 2H, S−CH_2−Ar), 7.14−7.15 (m, H, Py−H), 7.56 (dd, 2H, J = 8.8 Hz, Ph−H), 8.14 (d, 2H, J = 8.0 Hz, Ph−H), 8.24 (dd, 1H, J = 4.2, 1.7 Hz, Py−H), 8.50 (dd, 1H, J = 7.8, 2.9 Hz, Py−H); MS (ESI), 291.04 ($C_{13}H_{10}N_2O_4S$, $[M + H]^+$). Anal. Calcd for $C_7H_7NO_2S$: C, 53.79; H, 3.47; N, 9.65. Found: C, 53.52; H, 3.50; N, 9.49.

*General Procedure for the Synthesis of Compounds **3**.* A mixture of compound **2** (1 mmol) and $SOCl_2$ (15 mL, acted as both reactant and solvent) was stirred and refluxed at 75 °C for 2 h. Remaining $SOCl_2$ was removed by distillation under reduced pressure. After $SOCl_2$ was completely removed, the solid residue was then directly dissolved in anhydrous CH_2Cl_2 (20−30 mL). Appropriate substituted aniline or alkylamine (1 mmol) was added slowly (finished in 1 min), and the mixture was stirred at room temperature for 2−3 h.

The reaction mixture was washed with HCl solution (5%, 50 mL) and NaOH solution (5%, 50 mL) several times. The CH_2Cl_2 solution was collected and dried by anhydrous Na_2SO_4. Further purification was carried out by silica gel column chromatography with petroleum ether/EtOAc (5:1) as eluent. After recrystallization from EtOAc, final compounds **3a-01**−**3a-27**, **3b-01**−**3b-06**, and **3c-01**−**3c-05** were obtained.

*2-(Methylthio)-N-phenylnicotinamide **3a-01**:* white powder; yield, 80.3%; mp, 151−152 °C; ^{1}H NMR (400 MHz, DMSO-d_6) δ 2.47 (s, 3H, S−CH_3), 7.12 (t, 1H, J = 7.4 Hz, Ph−H), 7.26 (dd, 1H, J = 7.5, 4.9 Hz, Py−H), 7.36 (t, 2H, J = 7.7 Hz, Ph−H), 7.70−7.72 (m, 2H, Ph−H), 7.91 (dd, 1H, J = 7.6, 1.6 Hz, Py−H), 8.59 (dd, 1H, J = 4.8, 1.6 Hz, Py−H), 10.46 (s, 1H, CONH); MS (ESI), 245.07 ($C_{13}H_{12}N_2OS$, $[M + H]^+$). Anal. Calcd for $C_{13}H_{12}N_2OS$: C, 63.91; H, 4.95; N, 11.47. Found: C, 63.63; H, 4.54; N, 11.46.

*N-(2-Fluorophenyl)-2-(methylthio)nicotinamide **3a-02**.* white powder; yield, 57.0%; mp, 163−164 °C; ^{1}H NMR (400 MHz, DMSO-d_6) δ 2.48 (s, 3H, S−CH_3), 7.14 (dd, 1H, J = 8.4, 1.6 Hz, Ph−H), 7.29 (dd, 1H, J = 7.6, 4.3 Hz, Py−H), 7.41−7.44 (m, 1H, Ph−H), 7.47 (d, 1H, J = 8.0 Hz, Ph−H), 7.70 (dd, 1H, J = 9.4, 1.8 Hz, Ph−H), 8.02 (dd, 1H, J = 7.5, 1.9 Hz, Py−H), 8.71 (dd, 1H, J = 6.2, 1.7 Hz, Py−H), 10.56 (s, 1H, CONH); MS (ESI), 263.06 ($C_{13}H_{11}FN_2OS$, $[M + H]^+$). Anal. Calcd for $C_{13}H_{11}FN_2OS$: C, 59.53; H, 4.23; N, 10.68. Found: C, 59.37; H, 4.45; N, 10.96.

*N-(2-Chlorophenyl)-2-(methylthio)nicotinamide **3a-03**:* white crystal; yield, 85.2%; mp, 196−197 °C; ^{1}H NMR (400 MHz, DMSO-

d_6) δ 2.48 (s, 3H, S−CH_3), 7.26−7.33 (m, 2H, Ph−H, Py−H), 7.41 (dt, 1H, J = 7.6, 1.4 Hz, Ph−H), 7.57 (dd, 1H, J = 8.0, 1.4 Hz, Ph−H), 7.63 (dd, 1H, J = 7.9, 1.3 Hz, Ph−H), 8.00 (dd, 1H, J = 7.1, 1.6 Hz, Py−H), 8.62 (dd, 1H, J = 4.8, 1.7 Hz, Py−H), 10.22 (s, 1H, CONH); MS (ESI), 278.03 ($C_{13}H_{11}ClN_2OS$, $[M + H]^+$). Anal. Calcd for $C_{13}H_{11}ClN_2OS$: C, 56.01; H, 3.98; N, 10.05. Found: C, 55.73; H, 3.75; N, 10.26.

N-(2-Bromophenyl)-2-(methylthio)nicotinamide ***3a-04:*** yellow powder; yield, 88.7%; mp, 142−143 °C; ^{1}H NMR (400 MHz, DMSO-d_6) δ 2.51 (s, 3H, S−CH_3), 7.23−7.30 (m, 2H, Ph−H, Py−H), 7.41 (dt, 1H, J = 7.6, 1.3 Hz, Ph−H), 7.57 (dd, 1H, J = 7.9, 1.3 Hz, Ph−H), 7.73 (dd, 1H, J = 8.0, 1.3 Hz, Ph−H), 8.01 (dd, 1H, J = 7.6, 1.4 Hz, Py−H), 8.62 (dd, 1H, J = 4.8, 1.7 Hz, Py−H), 10.19 (s, 1H, CONH); MS (ESI), 322.98 ($C_{13}H_{11}BrN_2OS$, $[M + H]^+$). Anal. Calcd for $C_{13}H_{11}BrN_2OS$: C, 48.31; H, 3.43; N, 8.67. Found: C, 48.36; H, 3.75; N, 8.30.

2-(Methylthio)-N-(o-tolyl)nicotinamide ***3a-05:*** white powder; yield, 42.1%; mp, 197−198 °C; ^{1}H NMR (400 MHz, DMSO-d_6) δ 2.29 (s, 3H, Ar−CH_3), 2.49 (s, 3H, S−CH_3), 7.16−7.28 (m, 4H, 3Ph−H, Py−H), 7.39 (d, 1H, J = 7.3 Hz, Ph−H), 7.95 (d, 1H, J = 7.1 Hz, Py−H), 8.60 (dd, 1H, J = 4.8, 1.6 Hz, Py−H), 9.99 (s, 1H, CONH); MS (ESI), 259.08 ($C_{14}H_{14}N_2OS$, $[M + H]^+$). Anal. Calcd for $C_{14}H_{14}N_2OS$: C, 65.09; H, 5.46; N, 10.84. Found: C, 65.18; H, 5.93; N, 10.47.

2-(Methylthio)-N-(2-(trifluoromethyl)phenyl)nicotinamide ***3a-06:*** white crystal; yield, 60.3%; mp, 164−165 °C; ^{1}H NMR (400 MHz, DMSO-d_6) δ 2.48 (s, 3H, S−CH_3), 7.30 (dd, 1H, J = 7.6, 4.8 Hz, Py−H), 7.55−7.59 (m, 2H, Ph−H), 7.76−7.79 (m, 1H, Ph−H), 7.82 (d, 1H, J = 7.9 Hz, Ph−H), 7.92 (dd, 1H, J = 7.6, 1.6 Hz, Py−H), 8.62 (dd, 1H, J = 4.8, 1.7 Hz, Py−H), 10.31 (s, 1H, CONH); MS (ESI), 313.05 ($C_{14}H_{11}F_3N_2OS$, $[M + H]^+$). Anal. Calcd for $C_{14}H_{11}F_3N_2OS$: C, 53.84; H, 3.55; N, 8.97. Found: C, 53.51; H, 3.24; N, 8.64.

N-(2,4-Dichlorophenyl)-2-(methylthio)nicotinamide ***3a-07:*** light yellow powder; yield, 51.7%; mp, 183−184 °C; ^{1}H NMR (400 MHz, DMSO-d_6) δ 2.48 (s, 3H, S−CH_3), 7.20−7.24 (m, 1H, Ph−H), 7.28 (dd, 1H, J = 7.6, 4.8 Hz, Py−H), 7.43 (dd, 1H, J = 8.6, 1.9 Hz, Ph−H), 7.63−7.73 (m, 1H, Ph−H), 8.00 (d, 1H, J = 7.6 Hz, Py−H), 8.63 (dd, 1H, J = 4.8, 1.7 Hz, Py−H), 10.31 (s, 1H, CONH); MS (ESI), 312.99 ($C_{13}H_{10}Cl_2N_2OS$, $[M + H]^+$). Anal. Calcd for $C_{13}H_{10}Cl_2N_2OS$: C, 49.85; H, 3.22; N, 8.94. Found: C, 49.33; H, 3.10; N, 8.54.

N-(2,6-Difluorophenyl)-2-(methylthio)nicotinamide ***3a-08:*** white powder; yield, 56.1%; mp, 191−192 °C; ^{1}H NMR (400 MHz, DMSO-d_6) δ 2.47 (s, 3H, S−CH_3), 7.28 (dd, 1H, J = 7.6, 4.8 Hz, Py−H), 7.50 (dd, 1H, J = 8.6, 2.3 Hz, Ph−H), 7.66 (d, 1H, J = 8.6 Hz, Ph−H), 7.75 (d, 1H, J = 2.4 Hz, Ph−H), 8.00 (dd, 1H, J = 7.6, 1.6 Hz, Py−H), 8.62 (dd, 1H, J = 4.8, 1.6 Hz, Py−H), 10.29 (s, 1H, CONH); MS (ESI), 281.05 ($C_{13}H_{10}F_2N_2OS$, $[M + H]^+$). Anal. Calcd for $C_{13}H_{10}F_2N_2OS$: C, 55.71; H, 3.60; N, 9.99. Found: C, 55.03; H, 3.38; N, 9.62.

2-(Methylthio)-N-(2,4,5-trichlorophenyl)nicotinamide ***3a-09:*** white powder; yield, 72.8%; mp, 183−184 °C; ^{1}H NMR (400 MHz, DMSO-d_6) δ 2.43 (s, 3H, S−CH_3), 7.24 (dd, 1H, J = 7.8, 4.8 Hz, Py−H), 7.67 (dd, 1H, J = 8.2, 3.6 Hz, Ph−H), 8.21−8.23 (m, 2H, Ph−H, Py−H), 8.66 (dd, 1H, J = 4.8, 1.8 Hz, Py−H); MS (ESI), 346.95 ($C_{13}H_9Cl_3N_2OS$, $[M + H]^+$). Anal. Calcd for $C_{13}H_{10}F_2N_2OS$: C, 44.92; H, 2.61; N, 8.06. Found: C, 45.02; H, 2.41; N, 8.07.

N-(2,5-Dimethoxyphenyl)-2-(methylthio)nicotinamide ***3a-10:*** white−gray powder; yield, 58.2%; mp, 189−190 °C; ^{1}H NMR (400 MHz, DMSO-d_6) δ 2.48 (s, 3H, S−CH_3), 3.73 (s, 3H, Ar−OCH_3), 3.78 (s, 3H, Ar−OCH_3), 6.74 (dd, 1H, J = 9.0, 3.0 Hz, Ph−H), 7.01 (d, 1H, J = 9.0 Hz, Ph−H), 7.24 (dd, 1H, J = 7.5, 4.9 Hz, Py−H), 7.60 (s, 1H, Ph−H), 7.91 (d, 1H, J = 7.1 Hz, Py−H), 8.58 (dd, 1H, J = 4.8, 1.6 Hz, Py−H), 9.59 (s, 1H, CONH); MS (ESI), 305.09 ($C_{15}H_{16}N_2O_3S$, $[M + H]^+$). Anal. Calcd for $C_{15}H_{16}N_2O_3S$: C, 59.19; H, 5.30; N, 9.20. Found: C, 59.69; H, 5.70; N, 9.01.

N-(3-Fluorophenyl)-2-(methylthio)nicotinamide ***3a-11:*** white powder; yield, 83.2%; mp, 171−172 °C; ^{1}H NMR (400 MHz, DMSO-d_6) δ 2.49 (s, 3H, S−CH_3), 7.12 (dt, 1H, J = 9.0, 2.5 Hz, Ph−H), 7.28 (dd, 1H, J = 7.6, 4.9 Hz, Py−H), 7.38−7.42 (m, 1H, Ph−H), 7.46−7.48 (m, 1H, Py−H), 7.69 (td, 1H, J = 11.6, 2.0 Hz, Ph−H), 7.94 (dd, 1H, J = 7.6, 1.7 Hz, Ph−H), 8.60 (dd, 1H, J = 4.9, 1.7 Hz, Py−H), 10.68 (s, 1H, CONH); MS (ESI), 263.06 ($C_{13}H_{11}FN_2OS$, $[M + H]^+$). Anal. Calcd for $C_{13}H_{11}FN_2OS$: C, 59.53; H, 4.23; N, 10.68. Found: C, 59.41; H, 4.29; N, 10.10.

N-(3-Bromophenyl)-2-(methylthio)nicotinamide ***3a-12:*** light yellow powder; yield, 82.0%; mp, 168−169 °C; ^{1}H NMR (400 MHz, DMSO-d_6) δ 2.49 (s, 3H, S−CH_3), 7.28 (dd, 1H, J = 7.5, 4.8 Hz, Py−H), 7.33−7.35 (m, 2H, Ph−H), 7.63−7.66 (m, 1H, Ph−H), 7.94 (dd, 1H, J = 7.6, 1.7 Hz, Ph−H), 8.05−8.06 (m, 1H, Py−H), 8.61 (dd, 1H, J = 4.9, 1.7 Hz, Py−H), 10.63 (s, 1H, CONH); MS (ESI), 322.98 ($C_{13}H_{11}BrN_2OS$, $[M + H]^+$). Anal. Calcd for $C_{13}H_{11}BrN_2OS$: C, 48.31; H, 3.43; N, 8.67. Found: C, 48.26; H, 3.71; N, 8.60.

2-(Methylthio)-N-(3-(trifluoromethyl)phenyl)nicotinamide ***3a-13:*** white powder; yield, 82.0%; mp, 168−169 °C; ^{1}H NMR (400 MHz, DMSO-d_6) δ 2.49 (s, 3H, S−CH_3), 7.31 (dd, 1H, J = 7.0, 4.0 Hz, Py−H), 7.36−7.38 (m, H, Ph−H), 7.74 (dd, 1H, J = 8.4, 2.0 Hz, Ph−H), 7.79 (dd, 1H, J = 8.2, 2.0 Hz, Ph−H), 7.91 (dd, 1H, J = 7.6, 1.8 Hz, Ph−H), 8.12 (dd, 1H, J = 8.6, 3.4 Hz, Py−H), 8.61 (dd, 1H, J = 6.0, 1.6 Hz, Py−H), 10.38 (s, 1H, CONH); MS (ESI), 313.05 ($C_{14}H_{11}F_3N_2OS$, $[M + H]^+$). Anal. Calcd for $C_{14}H_{11}F_3N_2OS$: C, 53.84; H, 3.55; N, 8.97. Found: C, 53.91; H, 3.67; N, 9.01.

2-(Methylthio)-N-(3-nitrophenyl)nicotinamide ***3a-14:*** yellow powder; yield, 75.2%; mp, 198−199 °C; ^{1}H NMR (400 MHz, DMSO-d_6) δ 2.49 (s, 3H, S−CH_3), 7.31 (dd, 1H, J = 7.6, 4.8 Hz, Py−H), 7.68 (t, 1H, J = 8.2 Hz, Ph−H), 8.00−8.02 (m, 2H, Ph−H), 8.06 (dd, 1H, J = 8.2, 1.0 Hz, Ph−H), 8.64 (dd, 1H, J = 4.9, 1.7 Hz, Py−H), 8.75 (t, 1H, J = 2.0 Hz, Py−H), 10.95 (s, 1H, CONH); MS (ESI), 290.05 ($C_{14}H_{11}F_3N_2OS$, $[M + H]^+$). Anal. Calcd for $C_{13}H_{11}N_3O_3S$: C, 53.97; H, 3.83; N, 14.52. Found: C, 53.99; H, 3.50; N, 14.65.

N-(3-Methoxyphenyl)-2-(methylthio)nicotinamide ***3a-15:*** white powder; yield, 90.1%; mp, 165−166 °C; ^{1}H NMR (400 MHz, DMSO-d_6) δ 2.48 (s, 3H, S−CH_3), 3.76 (s, 3H, Ar−OCH_3), 6.70−6.73 (m, H, Ph−H), 7.25−7.28 (m, 3H, 2Ph−H, Py−H), 7.40 (s, H, Ph−H), 7.90 (dd, 1H, J = 7.6, 1.7 Hz, Py−H), 8.06 (dd, 1H, J = 8.2, 1.0 Hz, Py−H), 8.60 (dd, 1H, J = 4.9, 1.7 Hz, Py−H), 10.45 (s, 1H, CONH); MS (ESI), 290.05 ($C_{14}H_{14}N_2O_2S$, $[M + H]^+$). Anal. Calcd for $C_{14}H_{14}N_2O_2S$: C, 53.97; H, 3.83; N, 14.52. Found: C, 53.99; H, 3.50; N, 14.65.

N-(3,4-Dichlorophenyl)-2-(methylthio)nicotinamide ***3a-16:*** white crystal; yield, 88.4%; mp, 151−152 °C; ^{1}H NMR (400 MHz, DMSO-d_6) δ 2.49 (s, 3H, S−CH_3), 7.29 (dd, 1H, J = 7.6, 4.9 Hz, Py−H), 7.64 (s, 2H, Ph−H), 7.96 (dd, 1H, J = 7.6, 1.7 Hz, Ph−H), 8.09 (s, 2H, Py−H), 8.62 (dd, 1H, J = 4.9, 1.5 Hz, Py−H), 10.75 (s, 1H, CONH); MS (ESI), 290.05 ($C_{13}H_{10}Cl_2N_2OS$, $[M + H]^+$). Anal. Calcd for $C_{13}H_{10}Cl_2N_2OS$: C, 53.97; H, 3.83; N, 14.52. Found: C, 53.99; H, 3.50; N, 14.65.

N-(3-Chloro-4-fluorophenyl)-2-(methylthio)nicotinamide ***3a-17:*** white powder; yield, 82.0%; mp, 160−161 °C; ^{1}H NMR (400 MHz, DMSO-d_6) δ 2.49 (s, 3H, S−CH_3), 7.28 (dd, 1H, J = 7.6, 4.8 Hz, Py−H), 7.45 (t, 1H, J = 9.1 Hz, Ph−H), 7.60−7.65 (m, 1H, Ph−H), 7.94 (dd, 1H, J = 7.6, 1.7 Hz, Ph−H), 8.02 (dd, 1H, J = 6.9, 2.5 Hz, Py−H), 8.62 (dd, 1H, J = 4.8, 1.7 Hz, Py−H), 10.68 (s, 1H, CONH); MS (ESI), 297.02 ($C_{13}H_{10}ClFN_2OS$, $[M + H]^+$). Anal. Calcd for $C_{13}H_{10}ClFN_2OS$: C, 52.62; H, 3.40; N, 9.44. Found: C, 52.87; H, 3.53; N, 9.65.

N-(4-Chloro-3-fluorophenyl)-2-(methylthio)nicotinamide ***3a-18:*** white powder; yield, 82.7%; mp, 150−151 °C; ^{1}H NMR (400 MHz, $CDCl_3$) δ 2.48 (s, 3H, S−CH_3), 7.28 (dd, 1H, J = 7.6, 4.9 Hz, Py−H), 7.49 (dd, 1H, J = 8.9, 1.8 Hz, Ph−H), 7.58 (t, 1H, J = 8.6 Hz, Ph−H), 7.86 (dd, 1H, J = 11.9, 2.3 Hz, Ph−H), 7.94 (dd, 1H, J = 7.6, 1.6 Hz, Py−H), 8.62 (dd, 1H, J = 4.8, 0.9 Hz, Py−H), 10.78 (s, 1H, CONH); MS (ESI), 397.02 ($C_{23}H_{40}N_2OS$, $[M + H]^+$). Anal. Calcd for $C_{23}H_{40}N_2OS$: C, 54.62; H, 3.40; N, 9.44. Found: C, 57.47; H, 3.62; N, 9.48.

N-(3,5-Bis(trifluoromethyl)phenyl)-2-(methylthio)nicotinamide ***3a-19:*** white powder; yield, 74.8%; mp, 153−154 °C; ^{1}H NMR (400 MHz, DMSO-d_6) δ 2.50 (s, 3H, S−CH_3), 7.32 (dd, 1H, J = 6.5, 4.8 Hz, Py−H), 7.87 (s, 1H, Ph−H), 8.05 (dd, 1H, J = 7.6, 1.7 Hz, Py−H), 8.41 (s, 2H, Ph−H), 8.65 (dd, 1H, J = 4.8, 1.6 Hz, Py−H), 11.09 (s, 1H, CONH); MS (ESI), 281.04 ($C_{15}H_{10}F_6N_2OS$, $[M + H]^+$). Anal. Calcd for $C_{15}H_{10}F_6N_2OS$: C, 47.37; H, 2.65; N, 7.37. Found: C, 47.35; H, 2.99; N, 7.15.

2-(Methylthio)-N-(3,4,5-trifluorophenyl)nicotinamide ***3a-20:*** white powder; yield, 60.3%; mp, 146−147 °C; ^{1}H NMR (400 MHz, DMSO-d_6) δ 2.49 (s, 3H, S−CH_3), 7.30 (dd, 1H, J = 7.6, 4.9 Hz, Py−H),

7.63 (dd, 2H, J = 10.2, 6.5 Hz, Ph−H), 7.95 (dd, 1H, J = 7.6, 1.7 Hz, Py−H), 8.63 (dd, 1H, J = 4.9, 1.7 Hz, Py−H), 10.82 (s, 1H, CONH); MS (ESI), 299.04 ($C_{13}H_9F_3N_2OS$, $[M + H]^+$). Anal. Calcd for $C_{13}H_9F_3N_2OS$: C, 52.35; H, 3.04; N, 9.39. Found: C, 52.12; H, 3.01; N, 9.67.

N-(4-Fluorophenyl)-2-(methylthio)nicotinamide ***3a-21:*** white powder; yield, 51.9%; mp, 153−154 °C; ^{1}H NMR (400 MHz, DMSO-d_6) δ 2.48 (s, 3H, S−CH_3), 7.19−7.28 (m, 3H, 2Ph−H, Py−H), 7.73 (dd, 2H, J = 9.2, 5.0 Hz, Ph−H), 7.92 (dd, 1H, J = 7.6, 1.7 Hz, Py−H), 8.60 (dd, 1H, J = 4.9, 1.7 Hz, Py−H), 10.52 (s, 1H, CONH); MS (ESI), 262.06 ($C_{13}H_{11}FN_2OS$, $[M + H]^+$). Anal. Calcd for $C_{13}H_{11}FN_2OS$: C, 59.53; H, 4.23; N, 7.24. Found: C, 59.71; H, 4.65; N, 7.61.

N-(4-Chlorophenyl)-2-(methylthio)nicotinamide ***3a-22:*** white powder; yield, 68.9%; mp, 169−170 °C; ^{1}H NMR (400 MHz, DMSO-d_6) δ 2.49 (s, 3H, S−CH_3), 7.27 (dd, 1H, J = 7.6, 4.9 Hz, Py−H), 7.43 (d, 2H, J = 8.9 Hz, Ph−H), 7.75 (d, 2H, J = 8.8 Hz, Ph−H), 7.93 (dd, 1H, J = 7.6, 1.7 Hz, Py−H), 8.60 (dd, 1H, J = 4.8, 1.7 Hz, Py−H), 10.59 (s, 1H, CONH); MS (ESI), 279.03 ($C_{13}H_{11}ClN_2OS$, $[M + H]^+$). Anal. Calcd for $C_{13}H_{11}ClN_2OS$: C, 56.01; H, 3.98; N, 10.05. Found: C, 55.63; H, 4.09; N, 10.15.

2-(Methylthio)-N-(p-tolyl)nicotinamide ***3a-23:*** white crystal; yield, 86.9%; mp, 161−162 °C; ^{1}H NMR (400 MHz, DMSO-d_6) δ 2.29 (s, 3H, Ar−CH_3), 2.48 (s, 3H, S−CH_3), 7.17 (d, 2H, J = 8.3 Hz, Ph−H), 7.26 (dd, 1H, J = 7.6, 4.8 Hz, Py−H), 7.59 (d, 2H, J = 8.3 Hz, Ph−H), 7.89 (dd, 1H, J = 7.6, 1.6 Hz, Py−H), 8.59 (dd, 1H, J = 4.9, 1.7 Hz, Py−H), 10.37 (s, 1H, CONH); MS (ESI), 259.08 ($C_{14}H_{14}N_2OS$, $[M + H]^+$). Anal. Calcd for $C_{14}H_{14}N_2OS$: C, 65.09; H, 5.46; N, 10.84. Found: C, 65.03; H, 5.26; N, 11.01.

N-(4-Methoxyphenyl)-2-(methylthio)nicotinamide ***3a-24:*** white powder; yield, 67.2%; mp, 175−176 °C; ^{1}H NMR (400 MHz, DMSO-d_6) δ 2.48 (s, 3H, Ar−CH_3), 3.75 (s, 3H, S−CH_3), 6.93 (d, 2H, J = 9.0 Hz, Ph−H), 7.25 (dd, 1H, J = 7.5, 4.9 Hz, Py−H), 7.63 (d, 2H, J = 8.9 Hz, Ph−H), 7.91 (dd, 1H, J = 7.5, 1.4 Hz, Py−H), 8.58 (dd, 1H, J = 4.8, 1.6 Hz, Py−H), 10.37 (s, 1H, CONH); MS (ESI), 275.08 ($C_{14}H_{14}N_2O_2S$, $[M + H]^+$). Anal. Calcd for $C_{14}H_{14}N_2O_2S$: C, 61.29; H, 5.14; N, 10.21. Found: C, 61.12; H, 5.32; N, 10.60.

2-(Methylthio)-N-(4-nitrophenyl)nicotinamide ***3a-25:*** yellow powder; yield, 43.1%; mp, 182−183 °C; ^{1}H NMR (400 MHz, DMSO-d_6) δ 2.50 (s, 3H, Ar−CH_3), 7.30 (dd, 1H, J = 7.6, 4.9 Hz, Py−H), 7.96−8.01 (m, 3H, 2 Ph−H, 1 Py−H), 8.29 (d, 2H, J = 9.2 Hz, Ph−H), 8.63 (dd, 1H, J = 4.8, 1.6 Hz, Py−H), 11.05 (s, 1H, CONH); MS (ESI), 290.05 ($C_{13}H_{11}N_3O_3S$, $[M + H]^+$). Anal. Calcd for $C_{13}H_{11}N_3O_3S$: C, 53.97; H, 3.83; N, 14.52. Found: C, 54.09; H, 3.99; N, 14.41.

N-Cyclohexyl-2-(methylthio)nicotinamide ***3a-26:*** white powder; yield, 88.4%; mp, 141−142 °C; ^{1}H NMR (400 MHz, $CDCl_3$) δ 1.19−1.79 (m, 10H, cyclohexane), 2.50 (s, 3H, S−CH_3), 3.59−3.62 (m, 1H, N−CH_2-cyclohexane), 7.33 (dd, 1H, J = 7.7, 4.6 Hz, Py−H), 8.02 (dd, 1H, J = 8.0, 1.7 Hz, Py−H), 8.68 (dd, 1H, J = 4.8, 1.6 Hz, Py−H); MS (ESI), 251.11 ($C_{13}H_{18}N_2OS$, $[M + H]^+$). Anal. Calcd for $C_{13}H_{18}N_2OS$: C, 62.37; H, 7.25; N, 11.19. Found: C, 62.47; H, 7.14; N, 11.03.

N-Hexadecyl-2-(methylthio)nicotinamide ***3a-27:*** white powder; yield, 94.1%; mp, 137−138 °C; ^{1}H NMR (400 MHz, $CDCl_3$) δ 0.93 (s, 3H, $(CH_2)_{14}C\underline{H}_3$), 1.34 (s, 28H, $(C\underline{H}_2)_{14}CH_3$), 1.67 (s, 2H, N−$C\underline{H}_2$−$(CH_2)_{14}CH_3$), 2.49 (s, 3H, S−$CH_3$), 7.23 (dd, 1H, J = 7.7, 4.8 Hz, Py−H), 8.21 (dd, 1H, J = 7.8, 1.8 Hz, Py−H), 8.65 (dd, 1H, J = 4.8, 1.9 Hz, Py−H); MS (ESI), 393.29 ($C_{23}H_{40}N_2OS$, $[M + H]^+$). Anal. Calcd for $C_{23}H_{40}N_2OS$: C, 70.36; H, 10.27; N, 7.13. Found: C, 70.57; H, 10.40; N, 7.16.

2-((2-Fluorobenzyl)thio)-N-phenylnicotinamide ***3b-01:*** white powder; yield, 54.8%; mp, 181−182 °C; ^{1}H NMR (400 MHz, DMSO-d_6) δ 4.46 (s, 2H, S−CH_2−Ar), 7.03 (t, 1H, J = 7.5 Hz, Ph−H), 7.12−7.21 (m, 2H, Ph−H), 7.30−7.35 (m, 3H, 2Ph−H, 1 Py−H), 7.52−7.58 (m, 2H, Ph−H), 7.58 (d, 1H, J = 7.8 Hz, Ph−H), 7.99 (d, 1H, J = 7.4 Hz, Py−H), 8.69 (dd, 1H, J = 8.8, 3.2 Hz, Py−H), 10.25 (s, 1H, CONH); MS (ESI), 339.09 ($C_{19}H_{15}FN_2OS$, $[M + H]^+$). Anal. Calcd for $C_{19}H_{15}FN_2OS$: C, 67.44; H, 4.47; N, 8.28. Found: C, 67.01; H, 4.72; N, 8.39.

2-((2-Fluorobenzyl)thio)-N-(2-fluorophenyl)nicotinamide ***3b-02:*** white powder; yield, 75.1%; mp, 188−189 °C; ^{1}H NMR (400 MHz, DMSO-d_6) δ 4.45 (s, 2H, S−CH_2−Ar), 7.11−7.24 (m, 2H, Ph−H), 7.26−7.30 (m, 3H, 2Ph−H, 1 Py−H), 7.40 (t, 1H, J = 8.0 Hz, Ph−H), 7.56−7.61 (m, 2H, Ph−H), 7.63 (d, 1H, J = 8.0 Hz, Ph−H), 8.00 (d, 1H, J = 7.7 Hz, Py−H), 8.67 (dd, 1H, J = 7.9, 1.7 Hz, Py−H), 10.24 (s, 1H, CONH); MS (ESI), 366.08 ($C_{19}H_{14}ClFN_2OS$, $[M + H]^+$). Anal. Calcd for $C_{19}H_{14}F_2N_2OS$: C, 64.03; H, 3.96; N, 7.86. Found: C, 64.19; H, 4.30; N, 7.44.

N-(2-Chlorophenyl)-2-((2-fluorobenzyl)thio)nicotinamide ***3b-03:*** white powder; yield, 67.1%; mp, 174−175 °C; ^{1}H NMR (400 MHz, DMSO-d_6) δ 4.45 (s, 2H, S−CH_2−Ar), 7.12−7.21 (m, 2H, Ph−H), 7.28−7.33 (m, 3H, 2Ph−H, 1 Py−H), 7.40 (t, 1H, J = 8.1 Hz, Ph−H), 7.51−7.56 (m, 2H, Ph−H), 7.61 (d, 1H, J = 7.8 Hz, Py−H), 8.04 (d, 1H, J = 7.5 Hz, Py−H), 8.63 (dd, 1H, J = 7.8, 1.7 Hz, Py−H), 10.23 (s, 1H, CONH); MS (ESI), 373.05 ($C_{19}H_{14}ClFN_2OS$, $[M + H]^+$). Anal. Calcd for $C_{19}H_{14}ClFN_2OS$: C, 61.21; H, 3.78; N, 7.51. Found: C, 61.28; H, 3.70; N, 7.39.

N-(3-Bromophenyl)-2-((2-fluorobenzyl)thio)nicotinamide ***3b-04:*** light yellow powder; yield, 70.4%; mp, 179−180 °C; ^{1}H NMR (400 MHz, DMSO-d_6) δ 4.45 (s, 2H, S−CH_2−Ar), 7.12−7.21 (m, 2H, Ph−H), 7.28−7.33 (m, 3H, 2Ph−H, 1 Py−H), 7.40 (t, 1H, J = 8.1 Hz, Ph−H), 7.51−7.56 (m, 2H, Ph−H), 7.61 (d, 1H, J = 7.8 Hz, Py−H), 8.04 (d, 1H, J = 7.5 Hz, Py−H), 8.63 (dd, 1H, J = 4.8, 1.6 Hz, Py−H), 10.67 (s, 1H, CONH); MS (ESI), 373.05 ($C_{19}H_{14}ClFN_2OS$, $[M + H]^+$). Anal. Calcd for $C_{19}H_{14}ClFN_2OS$: C, 61.21; H, 3.78; N, 7.51. Found: C, 61.28; H, 3.70; N, 7.39.

2-((2-Fluorobenzyl)thio)-N-(3-methoxyphenyl)nicotinamide ***3b-05:*** white powder; yield, 89.3%; mp, 184−185 °C; ^{1}H NMR (400 MHz, DMSO-d_6) δ 3.74 (s, 3H, O−CH_3), 4.44 (s, 2H, S−CH_2−Ar), 6.68−6.71 (m, 1H, Ph−H), 7.12 (td, 1H, J = 7.5, 1.0 Hz, Ph−H), 7.24 (d, 2H, J = 5.0 Hz, Ph−H), 7.28−7.35 (m, 2H, 1 Ph−H, 1 Py−H), 7.38 (s, 1H, Ph−H), 7.50 (td, 1H, J = 7.7, 1.5 Hz, Ph−H), 7.95 (dd, 1H, J = 7.6, 1.6 Hz, Py−H), 8.62 (dd, 1H, J = 4.8, 1.6 Hz, Py−H), 10.43 (s, 1H, CONH); MS (ESI), 369.10 ($C_{20}H_{17}FN_2O_2S$, $[M + H]^+$). Anal. Calcd for $C_{20}H_{17}FN_2O_2S$: C, 65.20; H, 4.65; N, 7.60. Found: C, 65.31; H, 4.96; N, 7.14.

2-((2-Fluorobenzyl)thio)-N-(4-fluorophenyl)nicotinamide ***3b-06:*** white powder; yield, 81.0%; mp, 163−164 °C; ^{1}H NMR (400 MHz, DMSO-d_6) δ 4.45 (s, 2H, S−CH_2−Ar), 7.13 (t, 1H, J = 9.3 Hz, Ph−H), 7.18 (t, H, J = 7.5 Hz, Ph−H), 7.29−7.33 (m, 2H, 1 Ph−H, 1 Py−H), 7.42 (d, 1H, J = 8.9 Hz, Ph−H), 7.51 (td, 1H, J = 7.7, 1.4 Hz, Ph−H), 7.72 (d, 1H, J = 8.8 Hz, Ph−H), 7.98 (dd, 1H, J = 7.6, 1.6 Hz, Py−H), 8.64 (dd, 1H, J = 4.8, 1.6 Hz, Py−H), 10.60 (s, 1H, CONH); MS (ESI), 357.08 ($C_{19}H_{14}F_2N_2OS$, $[M + H]^+$). Anal. Calcd for $C_{19}H_{14}F_2N_2OS$: C, 64.03; H, 3.96; N, 7.86. Found: C, 64.25; H, 3.69; N, 7.54.

2-((4-Nitrobenzyl)thio)-N-phenylnicotinamide ***3c-01:*** light yellow powder; yield, 75.9%; mp, 176−177 °C; ^{1}H NMR (400 MHz, DMSO-d_6) δ 4.55 (s, 2H, S−CH_2−Ar), 7.11 (t, 1H, J = 7.8 Hz, Ph−H), 7.26 (d, 2H, J = 8.6 Hz, Ph−H), 7.31 (dd, 1H, J = 7.6, 4.8 Hz, Py−H), 7.69 (d, 2H, J = 8.7 Hz, Ph−H), 7.75 (d, 2H, J = 8.8 Hz, Ph−H), 7.98 (dd, 1H, J = 7.6, 1.6 Hz, Py−H), 8.15 (d, 2H, J = 8.8 Hz, Ph−H), 8.61 (dd, 1H, J = 4.8, 1.6 Hz, Py−H), 10.63 (s, 1H, CONH); MS (ESI), 366.08 ($C_{19}H_{15}N_3O_3S$, $[M + H]^+$). Anal. Calcd for $C_{19}H_{14}BrN_3O_3S$: C, 62.46; H, 4.14; N, 11.50. Found: C, 62.31; H, 4.09; N, 11.74.

N-(3-Bromophenyl)-2-((4-nitrobenzyl)thio)nicotinamide ***3c-02:*** yellow powder; yield, 88.0%; mp, 187−188 °C; ^{1}H NMR (400 MHz, DMSO-d_6) δ 4.56 (s, 2H, S−CH_2−Ar), 7.20 (dd, 1H, J = 7.6, 1.8 Hz, Ph−H), 7.32 (dd, 1H, J = 7.6, 4.8 Hz, Py−H), 7.40 (t, 1H, J = 8.1 Hz, Ph−H), 7.59 (d, 1H, J = 9.0 Hz, Ph−H), 7.69 (d, 2H, J = 8.7 Hz, Ph−H), 7.89 (s, 1H, Ph−H), 8.00 (dd, 1H, J = 7.6, 1.6 Hz, Py−H), 8.15 (d, 2H, J = 8.8 Hz, Ph−H), 8.61 (dd, 1H, J = 4.8, 1.6 Hz, Py−H), 10.65 (s, 1H, CONH); MS (ESI), 443.99 ($C_{19}H_{14}BrN_3O_3S$, $[M + H]^+$). Anal. Calcd for $C_{19}H_{14}BrN_3O_3S$: C, 51.36; H, 3.18; N, 9.46. Found: C, 51.74; H, 3.25; N, 9.81.

N-(4-Bromophenyl)-2-((4-nitrobenzyl)thio)nicotinamide ***3c-03:*** yellow powder; yield, 72.9%; mp, 197−198 °C; ^{1}H NMR (400 MHz, DMSO-d_6) δ 4.55 (s, 2H, S−CH_2−Ar), 7.32 (dd, 1H, J = 7.8, 4.4 Hz, Py−H), 7.38−7.43 (m, 2H, Ph−H), 7.58 (d, 2H, J = 8.2 Hz, Ph−H), 7.72 (d, 2H, J = 9.2 Hz, Ph−H), 7.99 (dd, 1H, J = 7.6, 1.8 Hz, Py−H), 8.14 (d, 2H, J = 8.4 Hz, Ph−H), 8.63 (dd, 1H, J = 4.8, 1.7 Hz, Py−H), 10.66 (s, 1H, CONH); MS (ESI), 443.99 ($C_{19}H_{14}BrN_3O_3S$, $[M + H]^+$).

Table 2. Structures and IC_{50} Values against *R. solani* and *S. sclerotiorum* of 3a, 3b, and 3c

			IC_{50}[a] (μM)	
compd no.	R_1	R_2	*R. solani*	*S. sclerotiorum*
3a-01	CH_3-	C_6H_5-	42.7 ± 1.1	76.2 ± 1.3
3a-02[b]	CH_3-	$2F-C_6H_4-$	201.7 ± 2.9	238.5 ± 2.9
3a-03	CH_3-	$2Cl-C_6H_4-$	105.2 ± 2.1	179.8 ± 1.9
3a-04[b]	CH_3-	$2Br-C_6H_4-$	102.2 ± 1.9	77.7 ± 1.3
3a-05	CH_3-	$2CH_3-C_6H_4-$	124.7 ± 2.0	70.8 ± 1.3
3a-06[b]	CH_3-	$2CF_3-C_6H_4-$	210.8 ± 2.8	205.4 ± 2.0
3a-07[b]	CH_3-	$2,4\text{-}2Cl-C_6H_3-$	147.4 ± 1.5	112.5 ± 1.5
3a-08[b]	CH_3-	$2,6\text{-}2F-C_6H_3-$	164.8 ± 1.5	200.9 ± 2.0
3a-09[b]	CH_3-	$2,4,5\text{-}3Cl-C_6H_2-$	190.2 ± 1.9	122.9 ± 1.7
3a-10[b]	CH_3-	$2,5\text{-}2CH_3O-C_6H_3-$	234.2 ± 2.8	226.4 ± 3.0
3a-11[b]	CH_3-	$3F-C_6H_4-$	85.5 ± 1.2	79.5 ± 1.0
3a-12[b]	CH_3-	$3Br-C_6H_4-$	35.5 ± 1.1	21.4 ± 0.9
3a-13	CH_3-	$3CF_3-C_6H_4-$	195.5 ± 2.0	195.5 ± 1.9
3a-14[b]	CH_3-	$3NO_2-C_6H_4-$	149.9 ± 1.6	114.2 ± 1.4
3a-15	CH_3-	$3CH_3O-C_6H_4-$	38.4 ± 1.0	67.5 ± 1.0
3a-16[b]	CH_3-	$3,4\text{-}2Cl-C_6H_3-$	88.7 ± 1.2	36.0 ± 0.9
3a-17[b]	CH_3-	$3Cl-4F-C_6H_3-$	15.8 ± 0.9	20.3 ± 0.8
3a-18[b]	CH_3-	$3Cl-4F-C_6H_3-$	130.4 ± 2.6	72.5 ± 0.5
3a-19[b]	CH_3-	$3,5\text{-}2CF_3-C_6H_3-$	95.7 ± 1.7	68.6 ± 1.0
3a-20[b]	CH_3-	$3,4,5\text{-}3F-C_6H_2-$	242.7 ± 2.6	249.3 ± 2.8
3a-21	CH_3-	$4F-C_6H_4-$	165.7 ± 1.7	121.5 ± 1.2
3a-22	CH_3-	$4Cl-C_6H_4-$	162.1 ± 1.7	115.5 ± 1.3
3a-23	CH_3-	$4CH_3-C_6H_4-$	101.7 ± 1.1	90.5 ± 1.0
3a-24	CH_3-	$4CH_3O-C_6H_4-$	136.5 ± 1.2	>250
3a-25	CH_3--	$4NO_2-C_6H_4-$	135.0 ± 1.2	>250
3a-26	CH_3-	$C_6H_{11}-$	>500	>500
3a-27	CH_3-	$CH_3\ (CH_2)_{15}-$	>500	>500
3b-01[b]	$2F-C_6H_5-CH_2-$	C_6H_5-	>250	>250
3b-02[b]	$2F-C_6H_5-CH_2-$	$2F-C_6H_4-$	>250	>250
3b-03[b]	$2F-C_6H_5-CH_2-$	$2Cl-C_6H_4-$	199.4 ± 1.8	>250
3b-04[b]	$2F-C_6H_5-CH_2-$	$3Br-C_6H_4-$	146.9 ± 1.5	>250
3b-05[b]	$2F-C_6H_5-CH_2-$	$3CH_3O-C_6H_4-$	135.6 ± 1.4	>250
3b-06[b]	$2F-C_6H_5-CH_2-$	$4F-C_6H_4-$	>250	>250
3c-01[b]	$4NO_2-C_6H_5-CH_2-$	C_6H_5-	187.7 ± 1.5	>250
3c-02[b]	$4NO_2-C_6H_5-CH_2-$	$3Br-C_6H_4-$	171.3 ± 1.6	157.7 ± 1.4
3c-03[b]	$4NO_2-C_6H_5-CH_2-$	$4Br-C_6H_4-$	>250	>250
3c-04[b]	$4NO_2-C_6H_5-CH_2-$	$4F-C_6H_4-$	>250	>250
3c-05[b]	$4NO_2-C_6H_5-CH_2-$	$3CH_3O-C_6H_4-$	158.8 ± 1.4	166.9 ± 1.7
boscalid			3.1 ± 0.5	0.3 ± 0.1
carbendazim			8.4 ± 0.6	1.1 ± 0.1

[a]Values are the mean ± standard deviation (SD) of three replicates. [b]Compounds first reported.

Anal. Calcd for $C_{19}H_{14}BrN_3O_3S$: C, 51.36; H, 3.18; N, 9.46. Found: C, 51.76; H, 3.24; N, 9.30.

N-(4-Fluorophenyl)-2-((4-nitrobenzyl)thio)nicotinamide ***3c-04****:* yellow powder; yield, 61.3%; mp, 174−175 °C; ^{1}H NMR (400 MHz, DMSO-d_6) δ 4.56 (s, 2H, S−CH_2−Ar), 7.13 (td, 1H, J = 7.5, 0.2 Hz, Ph−H), 7.18 (t, 1H, J = 10.3 Hz, Ph−H), 7.28−7.35 (m, 4H, 3 Ph−H, 1 Py−H), 7.51 (td, 1H, J = 7.7, 1.5 Hz, Ph−H), 7.62−7.65 (m, 1H, Ph−H), 8.01 (dd, 1H, J = 7.6, 1.6 Hz, Py−H), 8.04 (s, 1H, Ph−H), 8.64 (dd, 1H, J = 4.8, 1.6 Hz, Py−H), 10.67 (s, 1H, CONH); MS (ESI), 417.00 ($C_{19}H_{14}BrFN_2OS$, $[M + H]^+$). Anal. Calcd for $C_{19}H_{14}BrFN_2OS$: C, 54.69; H, 3.38; N, 6.71. Found: C, 54.47; H, 3.39; N, 6.34.

N-(3-Methoxyphenyl)-2-((4-nitrobenzyl)thio)nicotinamide ***3c-05****:* white crystal; yield, 58.3%; mp, 180−181 °C; ^{1}H NMR (400 MHz, DMSO-d_6) δ 4.55 (s, 2H, S−CH_2−Ar), 6.69−6.72 (m, 1H, Ar), 7.26 (d, 2H, J = 5.0 Hz, Ph−H), 7.30 (dd, 1H, J = 7.6, 4.9 Hz, Py−H), 7.39 (s, 1H, Ph−H), 7.69 (d, 2H, J = 8.6 Hz, Ph−H), 7.96 (dd, 1H, J = 7.6, 1.4 Hz, Py−H), 8.15 (d, 2H, J = 8.7 Hz, Ph−H), 8.61 (dd, 1H, J = 4.8, 1.5 Hz, Py−H), 10.44 (s, 1H, CONH); MS (ESI), 396.09 ($C_{20}H_{17}N_3O_4S$, $[M + H]^+$). Anal. Calcd for $C_{20}H_{17}N_3O_4S$: C, 60.75; H, 4.33; N, 10.63. Found: C, 60.22; H, 4.31; N, 10.91.

Biological Testing. *Plant Pathogenic Fungi.* The test fungi, *Rhizoctonia solani* and *Sclerotinia sclerotiorum*, were provided by the Laboratory of Plant Disease Control, Nanjing Agricultural University. After retrieval from the storage tube, the strains were incubated in PDA at 25 °C for a week to get new mycelia for the antifungal assay.

Antifungal Bioassay. The fungicidal activity of the synthetic compounds was tested in vitro against two plant pathogenic fungi using a mycelia growth inhibition method.[9] The synthesized compounds were dissolved in DMSO to prepare the 10 mg/mL stock solution before mixing with molten agar below 60 °C. The media containing compounds at a concentration of 25 mg/mL for the initial screening were then poured into sterilized Petri dishes. After appropriate days at 25 °C, the colony diameter of each strain was measured with the original mycelial disk diameter (5 mm) subtracted from this measurement. Percentage inhibition was calculated as $(1 - a/b) \times 100\%$, where a is the colony diameter in Petri dishes with compounds and b is the mean colony diameter in Petri dishes without tested

dx.doi.org/10.1021/jf405437k | J. Agric. Food Chem. 2014, 62, 4063−4071

compounds. DMSO served as negative control, whereas commercially available agricultural fungicides carbendazim and boscalid were used as positive controls. Each measurement consisted of at least three replicates. The concentration-dependent curve was the values of inhibition rates for the *Y* axis against the test sample concentrations (mg/mL) for the *X* axis. The IC_{50} value (Table 2) was defined as the concentration required for 50% inhibition of mycelial growth.

In Vivo Testing on Cole Leaves Infected by S. sclerotiorum. Strain *S. sclerotiorum* and susceptible cole leaves collected from Pailou Experimental Centre of Nanjing Agricultural University were used to measure the efficacy of compounds in vivo.[10] Healthy cole leaves were sprayed with compounds (0.5 mg/mL) and subsequently cultivated at 20 °C for 24 h before artificial inoculation with strain *S. sclerotiorum*. Results were observed as diameters of symptoms after cultivation at 20 °C for 36 h. Carbendazim (50% WP, Jiangsu Rotam Lanfeng Biochemical Co., Ltd., China) was coassayed as the positive control. The efficacy of disease control was calculated as $(1 - c/d) \times 100$, where c is the diameter of the treatment and d is the diameter of the negative control. The disease control picture is shown in Figure 3.

Figure 3. Effects of compound **3a-17** against *S. sclerotiorum* infected cole leaves.

Enzyme Assay in Vitro. *Isolation of R. solani and S. sclerotiorum.* Fungus mitochondrial was isolated according to a previously reported method.[11] Cultures were inoculated at 0.05 $OD_{600\ nm}$ and grown on a reciprocal shaker (180 rpm, 25 °C) for 5 days in Sabouraud maltose broth (SMB) medium. Cells were harvested by vacuum filtration and disrupted in liquid nitrogen using a mortar and pestle. The resultant powder was resuspended to 10% w/v in mitochondrial extraction buffer (10 mM KH_2PO_4, pH 7.2, 10 mM KCl, 10 mM $MgCl_2$, 0.5 M sucrose, 0.2 mM EDTA, 2 mM PMSF). The extract was clarified by centrifugation (5000*g*, 4 °C for 10 min, 2 times), and intact mitochondria were then pelleted at 10000*g* for 20 min at 4 °C and resuspended in the same buffer. Mitochondrial suspensions were brought to a concentration of 10 mg/mL and stored at −80 °C until use. SDH activity was found to remain stable for months.

Succinate:Ubiquinone/DCPIP Activity Inhibition. Mitochondrial suspensions were diluted 1/20 in extraction buffer and preactivated at 30 °C for 30 min in the presence of 10 mM succinate. Succinate:ubiquinone/DCPIP activity inhibition measurements were performed by adding 10 μL of preactivated mitochondria to 200 μL of assay buffer (50 mM phosphate-sodium, pH 7.2, 250 mM sucrose, 3 mM NaN_3, 10 mM succinate) supplemented with 140 μM dichlorophenolindophenol (DCIP) and 1 mM 2,3-dimethoxy-5-methyl-1,4-benzoquinone (Q_0). Inhibitor concentrations ranged between 4.4 and 150 μM, with uniform 2× dilution factor steps (six inhibitor concentrations + DMSO control). A total of 96 well plates were pre-equilibrated at reaction temperature (30 °C) for 10 min before the reactions were started by the addition of 10 μL of preactivated *R. solani* mitochondrial suspension. DCPIP reduction was conducted at 30 °C and monitored at 595 nm. Calculated absorbance slopes (OD/h) were used for half-inhibitory concentration (IC_{50}) calculations using GraphPad Prism 5.0 software.

Molecular Docking. *Homology Modeling.* The NCBI protein database (http://www.ncbi.nlm.nih.gov/sites/entrez) was used to search the SDH amino acid sequence of *S. sclerotiorum*. The employed hypothetical protein sequences were XP_001591238, XP_001594577, XP_001597467, and XP_001593251, reported by Birren. The BLAST server (http://blast.ncbi.nlm.nih.gov) was used to search the templates for these four chains. We applied succinate dehydrogenase from porcine heart (PDB code 1ZOY) and avian (PDB code 1YQ3) as two templates, and the homologies of amino acid sequences were aligned. Homology modeling of SDH from *S. sclerotiorum* was carried out using DS MODELER, which is a module integrated in Discovery Studio (version 3.1). The obtained models were evaluated by Ramachandran plots using Discovery Studio software. All of the algorithms and parameters were set as default.

Molecular Docking. The automated docking was performed with DS-CDocker implemented in Discovery Studio (version 3.1).[12] The three-dimensional structures of picked compounds were constructed using Chem. 3D ultra 11.0 software [Chemical Structure Drawing Standard; Cambridge Soft Corp., USA (2009)]. Then they were energetically minimized by using MOPAC with 100 iterations and minimum RMS gradient of 0.10. The Gasteiger−Hückel charges of ligands were assigned. All bound water and ligands were eliminated from the protein, and the polar hydrogens and the Kollman-united charges were added to the proteins.

RESULTS AND DISCUSSION

Chemical Synthesis. Scheme 1 and Table 2 describe the synthesis and chemical structures of these nicotinamide

Scheme 1. General Synthesis of Compound 3a, 3b, and 3c[a]

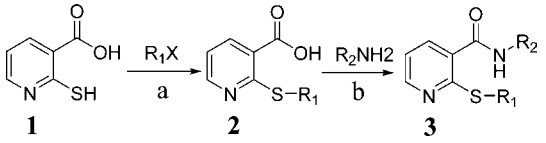

1 2 3

[a]Reagents and conditions: if $R_1X = CH_3I$, (a) DMF, pH 8−9, rt, 16−24 h; 5% $HCl_{(aq)}$, pH 2−3; if R_1X = BnBr, (a) ethanol, K_2CO_3, rt, 1−2 h; 5% $HCl_{(aq)}$, pH 2−3; (b) $SOCl_2$, 75 °C, reflux, 3−4 h; CH_2Cl_2, rt, 3 h.

derivatives. Compound **1** is reacted with RX (iodomethane or benzyl bromide) to afford corresponding compound **2**. Compounds **2** were first transformed into nicotinyl chloride in the presence of $SOCl_2$ and then reacted with appropriate substituted aniline or alkylamine to afford the target compounds **3a**, **3b**, and **3c**. All of the synthetic compounds gave satisfactory analytical and spectroscopic data, which were in full accordance with their depicted structures.

Among them, **2b**, **2c** and 26 compounds of **3a**, **3b**, and **3c** series are first reported and others were reported with antifungal activities for the first time (Table 2).

Fungicidal Activities. The antifungal activities of the synthetic molecules, which are expressed as IC_{50} (median inhibitory concentration) values, were determined using a mycelia growth inhibitory rate method. All of the synthetic compounds exhibited antifungal effects to *R. solani* and *S. sclerotiorum*. The results are shown in Table 2.

Compared to **3a**, most compounds of the **3b** and **3c** series showed weak antifungal activity with IC_{50} values >150 μM. However, when other groups replacing sulfur methyl are introduced at the R_1 position, the IC_{50} values of series **3a** compounds decreased at least 4−5-fold, which were observed by comparing the data **3a-01** (IC_{50} = 42.7 μM) and **3b-01** (IC_{50} > 250 μM), **3c-01** (IC_{50} = 187.7 μM); **3a-12** (IC_{50} = 35.5 μM) and **3c-02** (IC_{50} = 171.3 μM); **3a-15** (IC_{50} = 28.4 μM) and **3c-05** (IC_{50} = 185.8 μM) for *R. solani* inhibition activity. The result verified the previous design idea that sulfur methyl had more advantages in antifungal activity than sulfur benzyl at the R_1 position. It seems a small steric hindrance at R_1 position is conducive to combining the nicotinamide ligands and the SDH

dx.doi.org/10.1021/jf405437k | J. Agric. Food Chem. 2014, 62, 4063−4071

active domain. Therefore, it is more reasonable that we mainly synthesized **3a** series compounds, which were more likely to be developed as potential fungicides.

Most **3a** derivatives exhibited antifungal effects with IC_{50} of <250 μM except **3a-26** and **3a-27**. With the alkane and cyclohexane substitution at the R_2 position, these two compounds show IC_{50} values of >500 μM to both *R. solani* and *S. sclerotiorum*, far larger than the expected activity, indicating that the presence of a nonaromatic group at the R_2 position may cause significant loss of fungicidal activity of **3a** derivatives.

In total, 7 compounds (**3a-01**, **3a-11**, **3a-12**, **3a-15**, **3a-16**, **3a-17**, and **3a-19**) and 11 compounds (**3a-01**, **3a-04**, **3a-05**, **3a-11**, **3a-12**, **3a-15**, **3a-16**, **3a-17**, **3a-18**, **3a-19**, and **3a-23**) displayed IC_{50} values of <100 μM against *R. solani* and *S. sclerotiorum*, respectively. Among them, **3a-17** exhibited the highest activity against *R. solani* with an IC_{50} value of 15.8 μM, which was half-fold that of the positive control carbendazim. Besides, **3a-12** exhibited the second highest activity against the two pathogens. Other compounds exhibited moderate to weak antifungal activities with IC_{50} values ranging from 100 to 250 μM. The best four compounds against two fungi were all substituted in the meta-position, demonstrating that the presence of substitution in the meta-position of the side phenyl ring was favorable for antifungal activity. This finding was similar to the previous Masatsugu ODA's study.[15]

The structure−activity relationships of these compounds can be summarized: (1) Sulfur methyl has more advantages for antifungal activity than sulfur benzyl at the R_1 position. (2) The presence of an aromatic ring at the R_2 position plays an important role in the antifungal activity. (3) Substitution in the meta-position of the side phenyl ring (R_2) may be essential for enhancing antifungal activity.

In Vivo Testing on Cole Leaves Infected by *S. sclerotiorum*. Among the compounds tested for antifungal activity in vitro, **3a-17** was found to be potent against *S. sclerotiorum*. Therefore, it was further evaluated in the greenhouse for the control of *S. sclerotiorum* infected cole. The efficacy of the treatment is shown in Figure 3. The untreated negative control (pathogen only) resulted in 100% disease incidence (0% healthy plant standard) 24 h after transplantation. Treatment with 0.5 mg/mL **3a-17** resulted in 43.9% healthy plant standard after 36 h of treatment (Table 3). In contrast, leaves treated with carbendazim at the same concentration resulted in 64.2% healthy plant standard. Thus, significant differences existed among the treated and untreated groups for disease control experiments in the greenhouse cole leaves.

Table 3. In Vivo Efficacy of 500 μg/mL Compounds on Cole Leaves Infected by *Sclerotinia sclerotiorum*[a]

	diameter of lesions (mm)	protection efficacy (%)
3a-17	8.3 ± 0.8	43.92
carbendazim	5.3 ± 0.4	64.19
negative control	14.8 ± 0.9	

[a]Statistical analysis of the data was performed by analysis of variance (one-way ANOVA). A probability value of $p \leq 0.05$ was considered to denote a statistically significance difference.

Fungal SDH Inhibition Activities. Seven compounds with IC_{50} values of <100 μM were selected and tested against SDH enzymes in vitro. As demonstrated in Table 4, **3a-17** showed the best activity and inhibitory abilities against SDH enzymes of the tested compounds with IC_{50} values from 20 to 50 μM and exhibited the same tendency as the data acquired by using the mycelia growth inhibition assay in vitro. It fully proved that the nicotinamides designed in this paper displayed as good inhibitory effects on SDH enzymes as other successfully developed carboxamide fungicides.

Table 4. IC_{50} Values of Fungal SDH Inhibition Activity (in Vitro)

	IC_{50} (μM)	
compd no.	*R. solani*	*S. sclerotiorum*
3a-01	24.0 ± 0.1	30.7 ± 0.2
3a-11	30.8 ± 0.2	36.3 ± 0.1
3a-12	21.1 ± 0.2	30.0 ± 0.2
3a-15	28.5 ± 0.3	36.8 ± 0.2
3a-16	40.8 ± 0.2	35.7 ± 0.3
3a-17	19.6 ± 0.2	23.9 ± 0.2
3a-19	40.1 ± 0.2	32.6 ± 0.2

Interactions with SDH. *Homology Modeling.* The trace, the templates, and the homology model and the secondary and tertiary structures of the protein are quite similar, all of which is shown in Figure 4A,B). A Ramachandran plot of this minimized model showed that 95.41% of the residues were located in the allowed regions (91.16% most favored) and only 4.59% (54 residues) were outside the allowed regions for the model. As these disallowed residues were far from the succinate dehydrogenase active site, they did not significantly contribute to the function of protein acceptor. Evaluated by the plot, the quality of the homology model is suitable as a molecular docking receptor.

Binding Mode Analysis. In an effort to elucidate the possible mechanism of inducing fungicidal activity by these nicotinamide compounds and explain the previous assumption, molecular docking of **3c-17** and another 10 selected compounds into the homology model according to the binding site of ubiquinone on reported SDH complex structure (1ZOY and 1YQ3, pdb) was performed, respectively. Boscalid was docked as contrast at the same time. The CDOCKER scores are provided in Table 5, in which, compounds got the same tendency with their antifungal and SDH inhibitory activities. Boscalid and **3c-17** showed the best two −cdock_interaction_energy scores of 34.27 and 27.93, respectively. Three-dimensional schematic diagrams clearly explained the possible optimal combination between the ligands and receptor protein. Boscalid is well bound to the receptor protein with its amino hydrogen toward the carboxyl oxygen of GLU171 of chain B, and its amide oxygen interacted with the indole hydrogen of TRP167. Besides, two rings of indole both had pi−pi interactions with 3.8 Å distance to reinforce molecular boscalid near TPR167 (Figure 5A), and the amide group of boscalid interacted well with residues around the binding site. As shown in Figure 5B, sulfur and chlorine of **3a-17** are well bound with the amino hydrogen of PHE291 and the pyrrolidine hydrogen of PRO150, respectively. Two-dimensional diagrams are also displayed as Figure 6, in which all of the amino acid residues interacted with the ligand, including weak interaction such as van der Waals interactions and polar interactions. Thus, a stable complex based on these interactions was formed. Associated with the virtual screening results (Table 1), this binding model indicated that the introduction of a sulfur methyl moiety allowed the ligand to more easily combine with SDH.

The docked compounds mainly interacted by H-bond with B, C, and D chains of receptor protein, which is consistent with previous studies on boscalid and other SDHIs (such as carboxin,

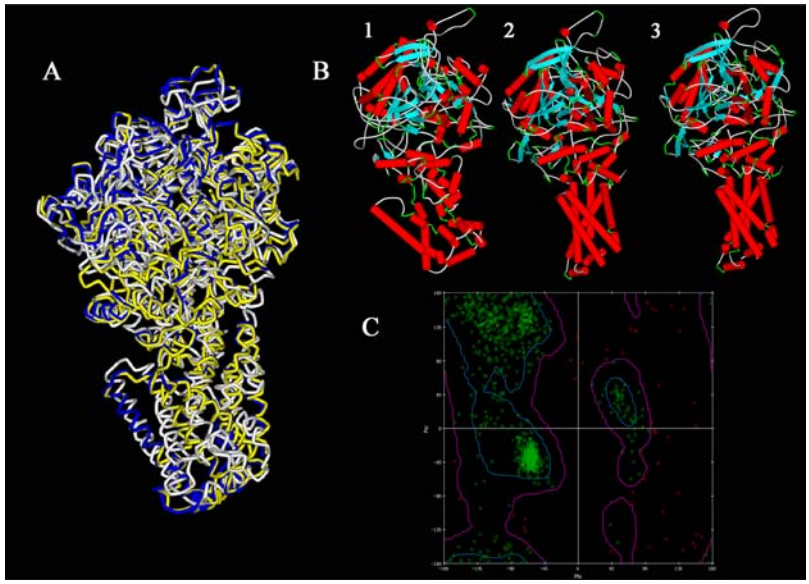

Figure 4. Three-dimensional schematic and Ramachandran plot of *S. sclerotiorum* SDH homology model and templates (1ZOY and 1YQ3): (A) tube trace of the two templates and the model (white color shows model, yellow color shows the template 1YQ3, and blue color shows the template 1ZOY); (B) secondary structures model (1) and templates 1YQ3 (2) and 1ZOY (3); (C) Ramachandran plot of the model (residues distribution plot).

Table 5. -cdock_interaction_energy of Compounds and *S. sclerotiorum* SDH (Homology Model)

compd no.	-cdock_interaction_energy ΔGb (kcal/mol)	compd no.	-cdock_interaction_energy ΔGb (kcal/mol)
3a-01	23.07	**3a-17***	27.93
3a-11*	23.17	**3a-18***	21.63
3a-12*	25.44	**3a-19***	24.59
3a-14*	20.71	**3b-02***	19.54
3a-15	24.09	**3c-02***	20.61
3a-16*	24.93	boscalid	34.27

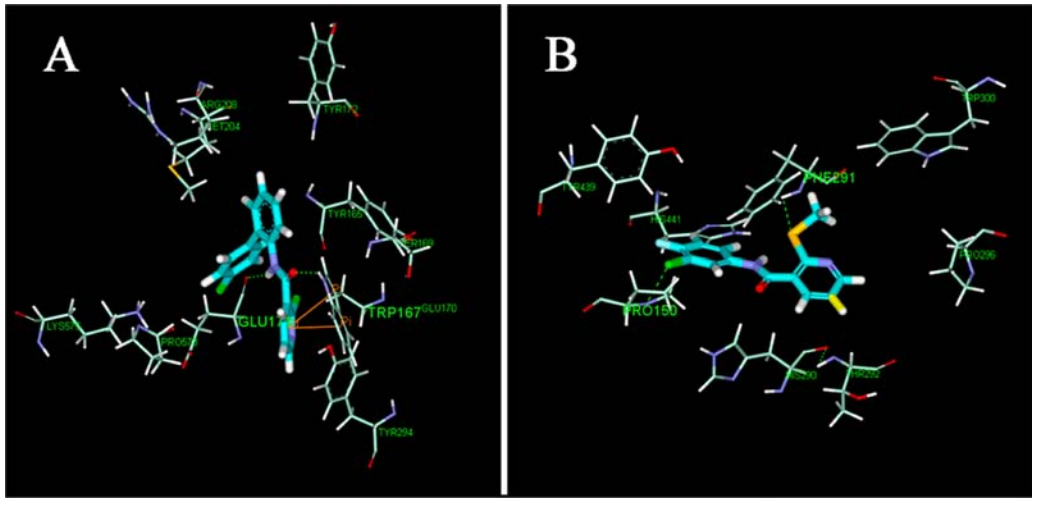

Figure 5. Interaction of boscalid, **3a-17**, and amino acid residues near the ligands (3D diagram).

fluopyram, bixafen, and isopyrazam).[13] Docking studies predicted the activity level and even possibly resistance site through identifying the key amino acid residues that were important for binding of different SDHIs. Resistant fungal genotype analysis verified that most of those key residues involved in forming the binding cavity were related to resistance formation.[14,15]

In conclusion, a series of nicotinamide derivatives as SDHIs were designed, prepared, and evaluated for their antifungal activity against *R. solani* and *S. sclerotiorum*. Some synthetic compounds displayed potent antifungal inhibitory activities with compound **3a-17** being the most effective. In vivo testing demonstrated that **3a-17** could effectively control the disease on *S. sclerotiorum* infected cole leaves. Meanwhile, the structure–activity relationships and molecular modeling study offered further insight into interactions between the receptor and ligand. The binding model of **3a-17** implied that the introduction of a

dx.doi.org/10.1021/jf405437k | *J. Agric. Food Chem.* 2014, 62, 4063–4071

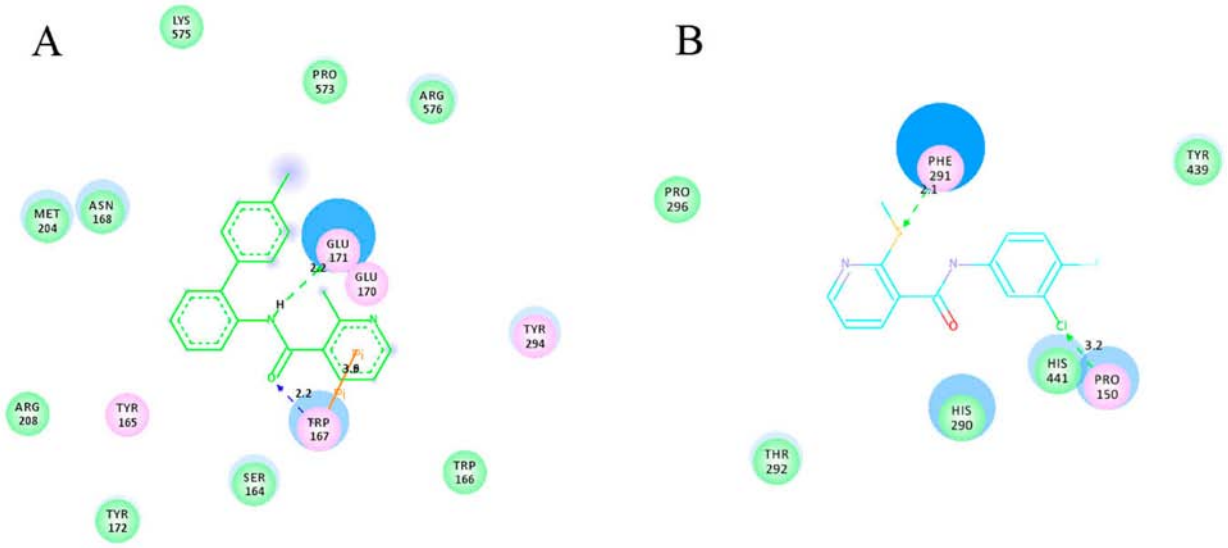

Figure 6. Interaction of boscalid, **3a-17**, and amino acid residues near the ligands (2D diagram). The purple circles show the amino acids that participated in hydrogen bonding or polar interactions. The green circles show the amino acids that participated in the van der Waals interactions. The p-cation interactions are shown as orange lines, and hydrogen bond interactions are represented by a blue or green dashed arrow directed toward the electron donor.

sulfur methyl moiety made the ligand easier to combine with SDH.

AUTHOR INFORMATION

Corresponding Author

*(Y.-H.Y.) Phone: +86-25-84395479. Fax: +86-25-84395479. E-mail: yeyh@njau.edu.cn.

Author Contributions

‖Y.-H.Y. and L.M. contributed equally to this paper.

Funding

This work was cosupported by the National Basic Research Program of China (2010CB126100), National Natural Science Foundation of China (30901854), Fundamental Research Funds for the Central Universities (KYZ201107), and Special Fund for Agro-scientific Research in the Public Interest (201303023).

Notes

The authors declare no competing financial interest.

REFERENCES

(1) Schmeling, B. V.; Kulka, M. Systemic fungicidal activity of 1,4-oxathiin derivatives. *Science* **1996**, *3722*, 659−660.

(2) Yang, J. C.; Zhang, J. B.; Chai, B. S.; Liu, C. L. Progress of the development on the novel amides fungicides. *Agrochemicals* **2008**, *1*, 6−9.

(3) Xiao, Y. S.; Yan, X. J.; Xu, Y. J.; Huang, J. X.; Yuan, H. Z.; Liang, X. M.; Zhang, J. J.; Wang, D. Q. Design, synthesis and fungicidal activity of 11-alkoxyimino-5,6-dihydro-dibenzo[*b*,*e*]azepine-6-one derivatives. *Pest Manag. Sci.* **2013**, *69*, 814−826.

(4) Zhou, S. F.; Li, F. B.; Zhang, P. Z.; Jiang, L. Synthesis and antifungal activity of novel 1-(1*H*-benzoimidazol-1-yl)propan-2-one oxime-ethers containing the morpholine moiety. *Res. Chem. Intermediat.* **2013**, *39* (4), 1735−1743.

(5) Wu, Z. B.; Hu, D. Y.; Kuang, J. Q.; Cai, H.; Wu, S. X.; Xue, W. Synthesis and antifungal activity of *N*-(substituted pyridinyl)-1-methyl(phenyl)-3-(trifluoromethyl)-1*H*-pyrazole-4-carboxamide derivatives. *Molecules* **2012**, *17*, 14205−14218.

(6) Scalliet, G.; Bowler, J.; Luksch, T.; Kirchhofer, A. L.; Steinhauer, D.; Ward, K.; Niklaus, M.; Verras, A.; Csukai, M.; Daina, A.; Fonne-Pfister, R. Mutagenesis and functional studies with succinate dehydrogenase inhibitors in the wheat pathogen *Mycosphaerella graminicola*. *PLoS One* **2012**, *7*, e35429.

(7) Oyedotun, K. S.; Lemire, B. D. The quaternary structure of the *Saccharomyces cerevisiae* succinate dehydrogenase homology modeling, cofactor docking, and molecular dynamics simulation studies. *J. Biol. Chem.* **2004**, *279*, 9424−9431.

(8) Liao, C. Z.; Sitzmann, M.; Pugliese, A.; Nicklaus, M. C. Software and resources for computational medicinal chemistry. *Future Med. Chem.* **2011**, *3*, 1057−1085.

(9) Xiao, Y.; Li, H. X.; Li, C.; Wang, J. X.; Li, J.; Wang, M. H.; Ye, Y. H. Antifungal screening of endophytic fungi from *Ginkgo biloba* for discovery of potent anti-phytopathogenic fungicides. *FEMS Microbiol. Lett.* **2013**, *339*, 130−136.

(10) Wang, L. L.; Li, C.; Zhang, Y.; Qiao, C.; Ye, Y. H. Synthesis and biological evaluation of benzofuroxan derivatives as fungicides against phytopathogenic fungi. *J. Agric. Food Chem.* **2013**, *61*, 8632−8640.

(11) Zeun, R.; Scalliet, G.; Oostendorp, M. Biological activity of sedaxane a novel broad-spectrum fungicide for seed treatment. *Pest Manag. Sci.* **2013**, *69*, 527−534.

(12) Du, Q. R.; Li, D. D.; Pi, Y. Z.; Li, J. R.; Sun, J.; Fang, F.; Zhong, W. Q.; Gong, H. B.; Zhu, H. L. Novel 1,3,4-oxadiazole thioether derivatives targeting thymidylate synthase as dual anticancer/antimicrobial agents. *Bioorg. Med. Chem.* **2013**, *21*, 2286−2297.

(13) Oda, M.; Sakaki, T.; Sasaki, N.; Nonaka, H.; Yamagishi, K.; Tomita, H. Quantitative structure-activity-relationships of 2-chloropyridine-3-carboxamide fungicides. *J. Pestic. Sci.* **1993**, *18*, 49−57.

(14) Avenot, H. F.; Michailides, T. J. Progress in understanding molecular mechanisms and evolution of resistance to succinate dehydrogenase inhibiting (SDHI) fungicides in phytopathogenic fungi. *Crop Prot.* **2010**, *29*, 643−651.

(15) Fraaije, B. A.; Bayon, C.; Atkins, S.; Cools, H. J.; Lucas, J. A.; Fraaije, M. W. Risk assessment studies on succinate dehydrogenase inhibitors, the new weapons in the battle to control Septoria leaf blotch in wheat. *Mol. Plant Pathol.* **2012**, *13*, 263−275.

JOURNAL OF AGRICULTURAL AND FOOD CHEMISTRY

Article

pubs.acs.org/JAFC

Occurrence of Sudan I in Paprika Fruits Caused by Agricultural Environmental Contamination

Yunhe Lian,[†] Wei Gao,*[,‡] Li Zhou,[†] Naiying Wu,[§] Qingguo Lu,[‡] Wenjie Han,[‡] and Xiaowei Tie[#]

[†]Hebei Engineering Technology Research Center of Natural Pigments, Handan 057250, Hebei, People's Republic of China

[‡]Chenguang Biotech Group Limited Corporation, Handan 057250, Hebei, People's Republic of China

[§]School of Science, Hebei University of Engineering, Handan 056038, Hebei, People's Republic of China

[#]Eurofins Scientific Group, Suzhou 215000, Jiangsu, People's Republic of China

Supporting Information

ABSTRACT: Current research has demonstrated the presence of sub parts per billion levels of Sudan dye in paprika fruits during the vegetation process, which is difficult to understand on the basis of the conventional concept of cross-contamination or malicious addition. Detailed surveys on Sudan dyes I–IV in paprika fruits, soils, and agronomic materials used from seven fields of Xinjiang (China) were conducted to investigate the natural contamination. Results revealed that Sudan dyes II–IV were never detected and that Sudan I existed in almost all samples except for the mulching film and irrigation water. The higher total amount of Sudan I in soils, pesticides, and fertilizers compared to coated seeds indicated the combination of Sudan I-contaminated soils and application of Sudan I-containing agronomic materials constitutes a major source of 0.18–2.52 μg/kg levels of Sudan I in fruits during the growth period. The study offers a more reasonable explanation for the previously observed Sudan I in paprika fruits.

KEYWORDS: *paprika fruit, Sudan I, agricultural environment, agronomic materials, UPLC-MS/MS, GPC*

INTRODUCTION

Sudan dyes I–IV are attractive as coloring additives in foodstuffs due to their intense red-orange color (Figure 1).[1]

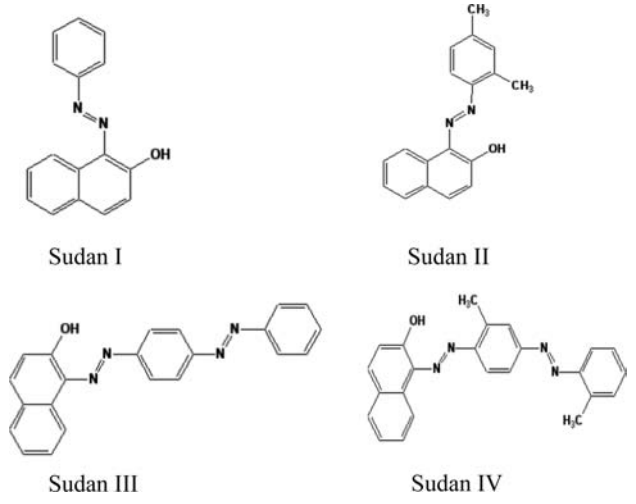

Figure 1. Chemical structures of Sudan dyes I–IV.

However, Sudan dyes have been classified as category 3 carcinogens by the International Agency for Research on Cancer,[2] and thus Sudan dyes are not allowed as food additives in most countries, including the European Union and China.[3−6] Consequently, monitoring and controlling the abuse of Sudan dyes in foodstuffs is of great importance for guaranteeing the safety of consumers.

Various analytical methods for the determination of Sudan dyes have been developed, including high-performance liquid chromatography (HPLC) with different detectors,[7−11] liquid chromatography–mass spectrometry (LC-MS),[12−14] enzyme immunoanalysis,[15−17] voltammetric techniques,[18] and chemiluminescence flow injection analysis.[19] Among them, LC-MS/MS displays outstanding advantages in both rapidly identifying Sudan dyes and accurately quantitating the amount at ultratrace levels. As the detection level was lowered through innovative techniques, more and more incidents involving Sudan dyes at sub parts per million levels were documented in recent years. For example, the 2011 RASFF (Rapid Alert System for Food and Feed) annual report showed that, of 18 entries with detections of Sudan dye (mainly Sudan dyes I and IV) in different foodstuffs, 13 samples measured showed only low-level ranges of 0.1–3.8 mg/kg.[20] Among a total of 21 samples of various spices and foodstuffs analyzed, 15 of them were found to contain Sudan dye I, III, or IV at low concentrations in the range of 0.0033–0.87 mg/kg.[21]

With the increasing presence of Sudan dyes at milligram per kilograms levels, it is inevitable for researchers to be focused on the contamination source in the context of reducing the levels where possible. Until now, their presence is ascribed to two possible explanations: either illegal addition or cross-contamination. Generally, levels of several 100–1000 mg/kg of Sudan dyes are needed to enhance the color of paprika and paprika

Received: December 12, 2013
Revised: April 12, 2014
Accepted: April 15, 2014
Published: April 15, 2014

ACS Publications © 2014 American Chemical Society

Table 1. Major Analytical Performance of the Method for Paprika Fruit

analyte	matrix-matched regression eq[a]	R^2	linear range (μg/kg)	LOD (μg/kg)	LOQ (μg/kg)	RSD[b] (%)	recovery[c] (%)
Sudan I	$Y = 647.19X + 6.99$	0.9991	0.1−20	0.06	0.09	7.25	84.0 ± 4.72 (0.4), 87.2 ± 6.85 (4.0), 89.6 ± 2.83 (10.0)
Sudan II	$Y = 352.16X + 1.74$	0.9994	0.1−20	0.05	0.15	9.58	85.7 ± 7.18 (0.4), 84.3 ± 5.13 (4.0), 91.5 ± 6.08 (10.0)
Sudan III	$Y = 616.15X + 15.15$	0.9990	0.1−20	0.08	0.22	12.38	81.6 ± 3.15 (0.4), 70.4 ± 5.32 (4.0), 82.3 ± 4.97 (10.0)
Sudan IV	$Y = 44.64X + 32.71$	0.9996	0.1−20	0.12	0.31	10.21	80.0 ± 5.32 (0.4), 82.5 ± 3.17 (4.0), 84.8 ± 3.45 (10.0)

[a]Where X is the mass concentration (μg/kg) and Y is the peak area. [b]Relative standard deviation, $n = 5$, $c = 5$ μg/kg. [c]Mean ± SE, $n = 3$.

Table 2. Mean Concentrations of Sudan I in Paprika Stem and Fruit Samples Prepared Independently from Different Fields (Mean ± SE, $n = 3$)

				paprika fruit/maturation stage		
field	paprika type	paprika species	stem (μg/kg)	green (80 days)[a] (μg/kg)	orange (86 days) (μg/kg)	red (95 days) (μg/kg)
1	urn	*C. frutescens*	1.49 ± 0.07[b]	0.76 ± 0.04	1.10 ± 0.07	0.68 ± 0.09
2	urn	*C. frutescens*	0.84 ± 0.05	0.28 ± 0.01	0.10 ± 0.04	0.26 ± 0.03
3	bell	*C. annuum*	—[c]	0.51 ± 0.02	0.22 ± 0.01	0.18 ± 0.02
4	urn	*C. frutescens*	—	—	2.06 ± 0.14	0.63 ± 0.06
5	urn	*C. frutescens*	1.32 ± 0.02	—	0.63 ± 0.03	1.08 ± 0.13
6	line	*C. frutescens*	1.04 ± 0.02	—	0.33 ± 0.02	1.00 ± 0.15
7	urn	*C. frutescens*	2.49 ± 0.03	1.59 ± 0.10	2.52 ± 0.21	0.53 ± 0.05

[a]Maturation stage was expressed by the fruit color and days after sowing. [b]Concentrations are expressed on a dry matter basis. [c]—, means lack of sample.

products.[22] For this reason, the European Union set 500 μg/kg as an action limit for Sudan dyes in foodstuffs to differentiate between adulterations and cross-contaminations.[23] The explanation of cross-contamination can be supported by several observations. Hoenicke reported that Sudan dyes I and IV at milligram per kilogram level were detected in red bags used for drying, transportation, and storage of the paprika pods and in lubricants used for greasing of the extraction plants and, thus, suggested that Sudan dyes detected may result from cross-contamination caused by some materials containing Sudan dyes.[24] Similar conclusions of cross-contamination have been reported by RASFF[20] and Schummer et al.[21]

The aim of the present study was to identify the source of the natural contamination of Sudan dyes in paprika fruits by investigating the potential presence of Sudan dyes I−IV and their contents in agricultural materials used. Our results showed that only Sudan I was present and, therefore, we have studied the distribution of Sudan I within the paprika as well as its contamination in some agronomic materials and the soils. This study provides a new insight into re-evaluating the origin of Sudan dyes in paprika fruits and paprika products.

MATERIALS AND METHODS

Reagents and Materials. Sudan dyes I−IV were obtained from Dr. Ehrenstorfer GmbH (Augsburg, Germany). Acetonitrile was purchased from Fisher Scientific (Waltham, MA, USA). All other chemicals and solvents such as HPLC grade isopropyl alcohol and formic acid were purchased from Kermel Chemical Co. Ltd. (Tianjin, China). Ultrapure water was produced by using a Master-S UVF ultrapure water system (Shanghai, China). Stock standard solutions of Sudan dyes I−IV (100 mg/kg) were prepared with acetonitrile in a volumetric flask and stored at 4 °C in the dark. Intermediate working mix solutions at 1 mg/kg were obtained by appropriate dilution of the stock solution with acetonitrile.

Apparatus. All analyses were performed on an Acquity TQD ultraperformance liquid chromatography (UPLC) system equipped with an autosampler system (Waters, Milford, MA, USA), coupled to tandem mass spectrometry operated in positive electrospray ionization (ESI+) mode and multiple reactions monitoring (MRM) mode. The data measured were processed with MassLynx V4.1 software.

Sample Collection and Preparation. Sample collection was undertaken in seven planting areas (30−50 km apart from each other) in the Xinjiang Uygur Autonomous Region (China). These fields were away from industry and roads and were amended with commercial pesticide (imidacloprid) and fertilizer (chili special-purpose fertilizer) after growth for 7, 30, and 60 days. For each field, paprika samples at three different stages of ripening including green, orange, and red fruits were collected from the same plant at the 80th, 86th, and 95th days after seeding, respectively. Each batch of samples in the same maturation degree comprised three replicates of subsamples from different paprika plants. All of the corresponding paprika stems and soils adhering to the root system (rhizosphere soils) were sampled 95 days after sowing. The sample type and amount are listed in Table 1. In addition, samples of the pesticide, fertilizer, mulching film, coated seed, and irrigation water were collected from farmers in the planting areas.

Paprika fruit and stem samples were dried at 80 °C in an oven and then ground using an FW135 universal grinder (Taisite Instrument Co., Ltd., Tianjin, China). Air-dried soils and chemical fertilizers were pulverized and sieved through an 80-mesh stainless steel sieve. All of the dry powdered samples were homogenized and stored in glass bottles at room temperature prior to extraction and analysis. Mulching films were cut finely into 0.4 cm^2 fragments using scissors and homogenized awaiting extraction. All samples were stored at room temperature prior to extraction and analysis.

Extraction Procedure. Extraction and analysis were conducted using a modification of the method of the European Commission.[25] A 5.0 g (fertilizer), 20.0 g (soil, coated seed, and mulching film), 1.0 g (stem and fruit), or 10 mL (irrigation water) aliquot of the sample was transferred into a 250 mL volumetric flask and diluted with 10 mL (60 mL for 20 g samples) of acetonitrile. Thereafter, samples were shaken for 2 min by an XW-80A model vortex apparatus (Jingke Co., Ltd., Shanghai, China) and then extracted in an ultrasonic bath (TH-300B model ultrasound cleaner, Tianhua Ultrasound Instrument Co., Ltd., Jining, China) for 10 min (30 min for 20 g samples). After

dx.doi.org/10.1021/jf5013067 | J. Agric. Food Chem. 2014, 62, 4072−4076

centrifugation (H-2050R model freezing centrifuge, Changsha Xiangyi centrifuge equipment Co., Ltd., Changsha, China) at 10000 rpm for 5 min at 5 °C, supernatants of samples were filtered through a 0.22 μm syringe filter into a 2 mL screw-cap vial. Then, 10 μL of this solution were injected into UPLC-MS/MS for analysis.

The pesticide samples were 0.5 mL and dissolved in 10 mL of cyclohexane/ethyl acetate (50:50, v/v), then purified through a PrepLinc gel permeation chromatography (GPC) system (J2 Scientific, Columbia, MD, USA) and eluted with cyclohexane/ethyl acetate (50:50, v/v) at a flow rate of 5 mL/min using a modification of the method of Song et al.[26] Finally, the eluates were evaporated and redissolved with acetonitrile, followed by filtering through a 0.22 μm syringe filter into a 2 mL screw-cap vial awaiting UPLC-MS/MS analysis.

UPLC-MS/MS Conditions. A 50 mm × 2.1 mm × 5 μm reversed phase C18 Waters Acquity BEH column, heated at 35 °C, was eluted using a mixture of acetonitrile (A) and 0.1% formic acid water solution (B) at a flow rate of 0.35 mL/min. The gradient elution was realized as follows: 0−0.5 min, 70% A; 0.5−3.0 min, 70−95% A; 3.0−4.0 min, 95% A; 4.0−5.0 min, 95−70% A.

The optimized experimental design parameters for ESI were as follows: capillary voltage, 1.0 kV; extractor cone voltage, 3.0 V; RF lens, 0.0 V; source temperature, 120 °C; desolvation temperature, 420 °C; desolvation gas flow, 700 L/h; cone gas flow, 50 L/h. The qualitative ion pairs of Sudan dyes I−IV as well as the cone voltage and the collision energy are shown in Table 2.

Data Analysis. Qualitative analysis was performed by comparing the retention times of qualitative ion pair peaks of the samples with those of standard chromatograms. Quantification was based on the external standard method. The matrix-matched standard curve of paprika fruit was done with blank samples spiked with 10 gradient concentrations of Sudan dyes I−IV immediately prior to UPLC-MS/MS analysis. The concentrations of Sudan dyes were then quantified by comparing the peak area of the particular compound in sample extracts with the corresponding external standard after replicate analysis.

Quality Assurance. Standard solutions of Sudan dyes I−IV were run at the beginning of the sample analysis to determine the relative response factors and evaluate peak resolution. A solvent blank was processed through the entire procedure and analyzed prior to and after each set of eight samples.

Each sample analysis was set up in duplicate. Results were considered invalid when the difference between duplicate analyses was >10% of the mean value of three values. Any sample showing no response or less than the limit of quantitation (LOQ) was concentrated to recheck or else reported as nondetected (ND).

RESULTS AND DISCUSSION

Analytical Performance of UPLC-MS/MS for Sudan Dyes. UPLC-MS/MS displays outstanding advantages in both rapidly identifying Sudan dyes and accurately quantitating the amount at ultratrace levels and, thus, was selected to determine the Sudan dye contamination in this study.

The major analytical performances of the method for Sudan dyes I−IV were investigated. As shown in Table 1, the limit of detection (LOD) and the limit of quantitation (LOQ) of 0.05−0.12 and 0.09−0.31 μg/kg were estimated on the basis of 3 and 10 times the signal-to-noise ratio (S/N), respectively. Recovery experiments were carried out by spiking three different concentrations (0.4, 4.0, 10.0 μg/kg) of standard solutions into a selected sample. The mean recovery was in the range of 70.4−91.5%. The precision of the analytical method was evaluated by repeatedly analyzing the spiked samples five times, yielding reproducible responses with the relative standard deviation of 7.3−12.4%. Sudan dyes I−IV exhibited good linearity ($R^2 \geq 0.9990$), indicating this method offered improved sensitivity.

Confirmation of Sudan I Contamination in Paprika Fruit. Figures 1 and 2 depict the UPLC-MS/MS chromatographic separation of Sudan dyes I, II, III, and IV in a standard solution (0.5 μg/kg) and a random paprika fruit sample. The retention times of standard solution are 1.44 min for Sudan I, 2.18 min for Sudan II, 2.91 min for Sudan III, and 4.90 min for Sudan IV, whereas for the paprika sample, only a Sudan I peak is observed at 1.47 min; Sudan dyes II, III, and IV were not detected, suggesting that Sudan dyes II, III, and IV did not exist in the paprika sample. Further analysis showed that the abundance ratio of Sudan I between the two ions of m/z 249.3 → 156.1 and 249.3 → 93.1 (qualitative ion pair) in paprika sample was 0.48 and 2.1% higher than that of the standard (0.47), which was within the acceptable deviations (±20%).[27] Therefore, it was concluded that only Sudan I contamination occurred in the paprika fruit.

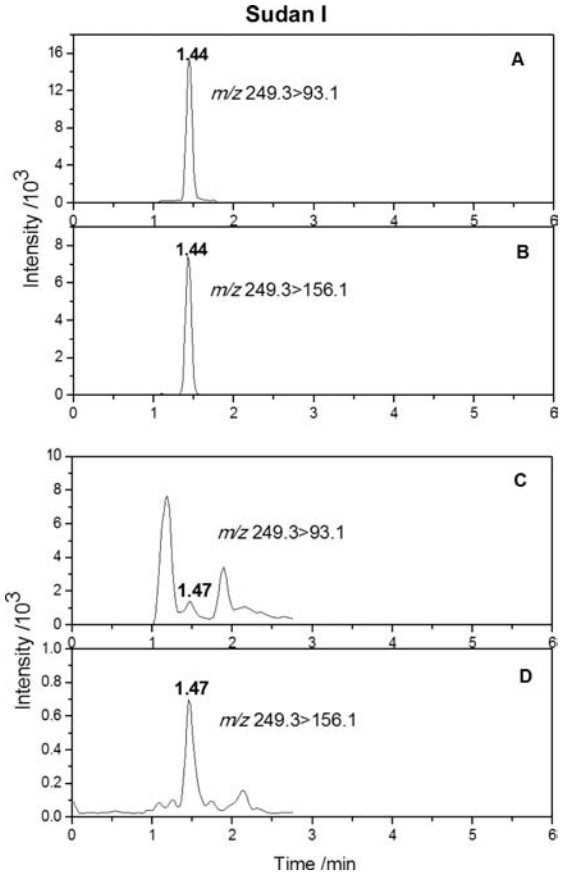

Figure 2. UPLC-MS/MS MRM trace obtained from standard solution (0.5 μg/kg) of Sudan I (A, B) and paprika sample of Sudan I (C, D).

Level of Sudan I Contamination in Paprika Fruit. Sudan I levels in paprika fruits and paprika stems from seven fields in Xinjiang (China) were investigated in triplicate (three aliquots of the same sample individually extracted and injected). As shown in Table 2, ultratrace levels of Sudan I contamination occurred in not only all paprika fruits but also the corresponding paprika stems. Considering all samples were directly collected by researchers from the field, neither addition nor cross-contamination occurred during the sample preparation and analysis processes, indicating that Sudan I contamination in paprika had really occurred over its growth period and was a universal phenomenon in the surveyed regions.

Table 3. Concentrations of Sudan I in Different Agronomic Materials (Soil, Pesticide, Fertilizer, Mulching Film, Coated Seed, and Irrigation Water) from Different Fields (Mean ± SE, n = 3)

field	soil (μg/kg)	pesticide (μg/kg)	fertilizer (μg/kg)	mulching film (μg/kg)	coated seed (μg/kg)	irrigation water (μg/kg)
1	0.0180 ± 0.0005	0.75 ± 0.04	0.03 ± 0.02	ND[a]	0.03 ± 0.02	ND
2	0.0090 ± 0.0004	0.50 ± 0.03	0.02 ± 0.01	ND	0.04 ± 0.01	ND
3	0.0120 ± 0.0005	0.62 ± 0.02	0.04 ± 0.02	ND	0.07 ± 0.03	ND
mean	0.013	0.62	0.03	ND	0.05 ± 0.02	ND

[a]Not detected. All samples were prepared independently.

The spatial variability of Sudan I was investigated by comparing the concentrations of Sudan I in five mature urn samples from different fields. As seen from Table 2, variability of the Sudan I levels of the same type changed with fields, with the maximum value of 1.08 μg/kg in field 5 and the minimum value of 0.26 μg/kg in field 2. Conversations with farmers revealed that such a large difference among fields ($p < 0.05$) was possibly attributable to the different operating conditions among different farmers.

To assess the evolution of Sudan I level over different stages of maturation, green paprika, orange paprika, and red paprika samples were collected from four fields (fields 1, 2, 3, and 6) for analysis. As shown in Table 2, no clear variation tendency of Sudan I level was observed with respect to paprika colors; four values at the same maturity stage were averaged, and the mean concentrations were 0.53 μg/kg for green paprika, 0.44 μg/kg for orange paprika, and 0.50 μg/kg for red paprika. These findings suggested that the Sudan I level remained almost unchanged with various maturation periods, and there may be no enrichment or degradation of Sudan I during the maturation process of paprika fruit.

Source of Sudan I Contamination in Paprika Fruits. To trace the source of Sudan dye contamination in paprika fruits, Sudan dye concentrations in reagents used in experiments, soils, and several agronomic materials, including pesticide, fertilizer, mulching film, coated seed, and irrigation water, were determined.

No Sudan dyes were detected in any of the reagents used. Sudan dyes II, III, and IV were never detected in any samples, and Sudan I was detected only in soils, pesticides, fertilizers, and coated seeds (Table 3). Generally, about 10.00 g of fertilizer, 0.03 g of pesticide, and 60.00 g of rhizosphere soil are applied in the process from sowing to maturity for a paprika fruit; however, only 0.008 g of coated seed is used. With this planting mode taken into account, the total amount of Sudan I in soils, pesticides, and fertilizers seems to correlate well with Sudan I concentration in paprika fruits (Table 4). Moreover, the mean Sudan I contents in soils, pesticides, and fertilizers were at least 2 orders of magnitude higher than that in coated seeds. These all together provide evidence for the major contribution of pesticide, fertilizer, and soil to Sudan I contamination in paprika fruit during its vegetation period.

Table 4. Total Amounts of Fruit, Soil, Pesticide, Fertilizer, Coated Seed per Fruit, and Total Amount of Sudan I in These Materials per Fruit

sample	total amount (μg) used per fruit	total amount (μg) of Sudan I in materials[a]
fruit	5.0×10^6	9.0×10^{-4}–5.4×10^{-3}
soil	6.0×10^7	6.0×10^{-4}–1.2×10^{-3}[b]
pesticide	9.0×10^4	$(4.5–6.9) \times 10^{-5}$
fertilizer	1.0×10^7	$(2.0–4.0) \times 10^{-4}$
coated seed	8.0×10^3	$(2.4–5.6) \times 10^{-7}$

[a]The amount range represented the different values for different species. [b]The data were calculated by using the rhizosphere soil.

During paprika cropping, Sudan I from the fertilizer may be absorbed by the root and transported to other parts of the plant including the stem and fruit. When pesticides are sprayed, Sudan I from the pesticide may be absorbed by the fruit or absorbed by the soil and then transported to the fruit. Soil contamination of planting areas may come from cumulative agriculture practices for many years due to application of Sudan I-containing pesticide and fertilizer, and when paprika was planted in the Sudan I-contaminated soil, Sudan I may migrate from the soil to different parts of the plant including the fruit.

As for the source of Sudan I in the pesticide and fertilizer, it can be traced to usage of Sudan dyes in chemical industry. Sudan dyes I–IV are widely used for different industrial and scientific applications such as oils, fats, plastics, printing inks, waxes, and spirit varnishing, among others,[28] which were often used as raw and auxiliary materials in manufacturing agronomic materials or in their packaging due to great access. Therefore, the most effective way of controlling Sudan I contamination in paprika is to eliminate the abuse of Sudan dyes in the manufacture of agronomic materials and packages.

To our knowledge, the present study is the first to report the occurrence of sub parts per billion levels of Sudan I contamination in paprika fruits in the process of growth. The Sudan I-contaminated soil combined with application of Sudan I-containing agronomic materials contributes to paprika fruit contamination. Due to the widespread use of Sudan I-containing agronomic materials during agricultural production, soils are contaminated with Sudan I to some extent, which results in the Sudan I contamination in paprika in conjunction with the effect of agronomic materials during the growth period. This discovery has significant implication for re-evaluating the origin of Sudan I in paprika fruits and paprika products.

■ ASSOCIATED CONTENT

Supporting Information

Type and amount of samples collected from different fields, compound-specific UPLC-ESI-MS/MS parameters for Sudan dyes I–IV, analytical method validation for other sample matrices (soil, pesticide, fertilizer, mulching film, coated seed, and irrigation water), and UPLC-MS/MS MRM trace obtained from standard solution (0.5 μg/kg) and paprika sample of Sudan II, Sudan III, and Sudan IV. This material is available free of charge via the Internet at http://pubs.acs.org.

AUTHOR INFORMATION

Corresponding Author

*(W.G.) Phone: +86 310 885 9305. Fax: +86 310 885 9306. E-mail: gaowei2003425@163.com.

Funding

The present work was supported by the National International S&T Cooperation Project (No. 2014DFA31220).

Notes

The authors declare no competing financial interest.

REFERENCES

(1) Capitán, F.; Capitán-Vallvey, L. F.; Fernández, M. D.; de Orbe, I.; Avidad, R. Determination of colorant matters mixtures in foods by solid-phase spectrophotometry. *Anal. Chim. Acta* **1996**, *331*, 141−148.

(2) IARC, International Agency for Research on Cancer. *Monographs on the evaluation of carcinogenic risks to humans*, Vol. 99. 1975; http://monographs.iarc.fr/ENG/Monographs /vol99/mono99.pdf (accessed March 31, 2014).

(3) Commission Decision. . Commission decision 2003/460/EC on emergency measures regarding hot chilli and hot chilli products. *Off. J. Eur. Communities* **2003**, *L154*, 114−115.

(4) Commission Decision. . Commission decision 2004/92/EC on emergency measures regarding hot chilli and hot chilli product. *Off. J. Eur. Communities* **2004**, *L27*, 52−53.

(5) Commission Decision. . Commission decision 2005/402/EC on emergency measures regarding chilli products, curcuma and palm oil. *Off. J. Eur. Communities* **2005**, *L135*, 34−36.

(6) *Ministry of Health of the People's Republic of China, 2005 No. 05*; http://www.moh.gov.cn/publicfiles/business/htmlfiles/mohbgt/pw10505/200804/27332.htm (in Chinese, accessed Dec 12, 2008).

(7) *News Notification: 03/99, Subject: Corrected Method for the Detection of Sudan*; European Commission: Brussels, Belgium, 1999; http://img1.chem17.com/5/2008/ar005325161002.pdf.

(8) *National Standard of the People's Republic of China*, GB/T 19681-2005: The method for the determination of Sudan dyes in foods: High performance liquid chromatography; China Standard Press: Beijing, China, 2005.

(9) Cornet, V.; Govaert, Y.; Moens, G.; Loco, J. V.; Degroodt, J. M. Development of a fast analytical method for the determination of Sudan dyes in chili- and curry-containing foodstuffs by high-performance liquid chromatography−photodiode array detection. *J. Agric. Food Chem.* **2006**, *54*, 639−644.

(10) He, L. M.; Su, Y. J.; Fang, B. H.; Shen, X. G.; Zeng, Z. L.; Liu, Y. H. Determination of Sudan dye residues in eggs by liquid chromatography and gas chromatography−mass spectrometry. *Anal. Chim. Acta* **2007**, *594*, 139−146.

(11) Long, C. Y.; Mai, Z. B.; Yang, X. F.; Zhu, B. H.; Xu, X. M.; Huang, X. D.; Zou, X. Y. A new liquid−liquid extraction method for determination of 6 azo-dyes in chilli products by high-performance liquid chromatography. *Food Chem.* **2011**, *126*, 1324−1329.

(12) Calbiani, F.; Careri, M.; Elviri, L.; Mangia, A.; Pistarà, L.; Zagnoni, I. Development and in-house validation of a liquid chromatography−electrospray−tandem mass spectrometry method for the simultaneous determination of Sudan I, Sudan II, Sudan III and Sudan IV in hot chilli products. *J. Chromatogr., A* **2004**, *1042*, 123−130.

(13) Murty, M. R. V. S.; Sridhara Chary, N.; Prabhakar, S.; Prasada Raju, N.; Vairamani, M. Simultaneous quantitative determination of Sudan dyes using liquid chromatography−atmospheric pressure photoionization−tandem mass spectrometry. *Food Chem.* **2009**, *115*, 1556−1562.

(14) Pardo, O.; Yusà, V.; León, N.; Pastor, A. Development of a method for the analysis of seven banned azo-dyes in chilli and hot chilli food samples by pressurised liquid extraction and liquid chromatography with electrospray ionization-tandem mass spectrometry. *Talanta* **2009**, *78*, 178−186.

(15) Han, D.; Yu, M.; Knopp, D.; Niessner, R.; Wu, M.; Deng, A. P. Development of a highly sensitive and specific enzyme-linked immunosorbent assay for detection of Sudan I in food samples. *J. Agric. Food Chem.* **2007**, *55*, 6424−6430.

(16) Wang, Y. Z.; Wei, D. P.; Yang, H.; Yang, Y.; Xing, W. W.; Li, Y.; Deng, A. P. Development of a highly sensitive and specific monoclonal antibody-based enzyme-linked immunosorbent assay (ELISA) for detection of Sudan I in food samples. *Talanta* **2009**, *77*, 1783−1789.

(17) Xu, T.; Wei, K. Y.; Wang, J.; Eremin, S. A.; Liu, S. Z.; Li, Q. X.; Li, J. Development of an enzyme-linked immunosorbent assay specific to Sudan red I. *Anal. Biochem.* **2010**, *405*, 41−49.

(18) Du, M. J.; Han, X. G.; Zhou, Z. H.; Wu, S. G. Determination of Sudan I in hot chili powder by using an activated glassy carbon electrode. *Food Chem.* **2007**, *105*, 883−888.

(19) Liu, Y. H.; Song, Z. H.; Dong, F. X.; Zhang, L. Flow injection chemiluminescence determination of Sudan I in hot chilli sauce. *J. Agric. Food Chem.* **2007**, *55*, 614−617.

(20) RASFF. *Rapid Alert System for Food and Feed*; available at http://ec.europa.eu/food/food/rapidalert/indexen.htm/ (accessed Sept 13, 2012).

(21) Schummer, C.; Sassel, J.; Bonenberger, P.; Moris, G. Low-level detections of Sudan I, II, III and IV in spices and chili-containing foodstuffs using UPLC-ESI-MS/MS. *J. Agric. Food Chem.* **2013**, *61*, 2284−2289.

(22) American Spice Trade Association (ASTA). *Sudan red and related dyes − white paper [EB/OL]*; http://www.astaspice.org/files/public/SudanWhitePaper.pdf, 2005 (accessed Dec 12, 2013).

(23) Summary record of the standing committee on the food chain and animal health held in Brussels on 14 December 2006; SANCO-D1(06)D/413447; European Commission: Brussels, Belgium, 2006; http://ec.europa.eu/food/committees/regulatory/scfcah/toxic/summary 23_en. pdf (accessed Nov 29, 2013).

(24) Hoenicke, K. *Detection of low amounts of Sudan dyed and other illegal dyes in food and oleoresins. Analytical Artefact or Cross-Contamination?* Europe Section of AOAC International Limassol, Cyprus; Nov 6−7, 2006; http://www.aoaceurope.com/katrinhoenicke.pdf (accessed Sept 13, 2012).

(25) European Commission, Health and Consumer Protection Directorate General, Committee IV − Food Safety in Production and Currency, Part III − Physical and Chemical Substances Surveillance. *New Method Declaration*, March 1999.

(26) Song, H.; Lian, G. Y.; Du, L. J.; Li, H. P.; Xue, P.; Yuan, L.; Song, J.; Li, B. P. Determination of Para Red and Sudan red dyes in *Capsicum* and *Capsicum* products by high performance liquid chromatography with GPC. *Food Sci.* **2006**, *27*, 611−613.

(27) Commission of the European Communities. *Off. J. Eur. Communities* **2002**, *L221*, 8−36 (2002/657/EC).

(28) Ertaş, E.; Özer, H.; Alasalvar, C. A rapid HPLC method for determination of Sudan dyes and Para Red in red chilli pepper. *Food Chem.* **2007**, *105*, 756−760.

JOURNAL OF AGRICULTURAL AND FOOD CHEMISTRY

Article

pubs.acs.org/JAFC

Diamide Insecticide Target Site Specificity in the *Heliothis* and *Musca* Ryanodine Receptors Relative to Toxicity

Suzhen Qi,[†,#,⊥] Peter Lümmen,[§] Ralf Nauen,[§] and John E. Casida*[,†]

[†]Environmental Chemistry and Toxicology Laboratory, Department of Environmental Science, Policy and Management, University of California, Berkeley, California 94720-3112, United States

[§]Small Molecules Research, Pest Control, Bayer CropScience AG, Alfred Nobel Strasse 50, Monheim, Germany 40789

[#]Department of Applied Chemistry, College of Science, China Agricultural University, Beijing, China 100193

Supporting Information

ABSTRACT: Anthranilic and phthalic diamides act on the ryanodine receptor (RyR), which constitutes the Ca^{2+}-activated Ca^{2+} channel and can be assayed as shown here in *Heliothis* thoracic muscle tissue with anthranilic diamide [^{3}H]chlorantraniliprole ([^{3}H]Chlo), phthalic diamide [^{3}H]flubendiamide ([^{3}H]Flu), and [^{3}H]ryanodine ([^{3}H]Ry). Using *Heliothis* with [^{3}H]Chlo or [^{3}H]Flu gives very similar anthranilic and phthalic diamide binding site structure−activity correlations, indicating a common binding site. The anthranilic and phthalic diamide stimulation of [^{3}H]Ry binding in *Heliothis* generally parallels their inhibition of [^{3}H]Chlo and [^{3}H]Flu binding. In *Musca* adults [^{3}H]Ry binding site stimulation is a good predictor of in vivo activity for anthranilic but not phthalic diamides, and no high-affinity [^{3}H]Flu specific binding site is observed. These relationships establish species differences in diamide target site specificity important in structure optimization and target site-based resistance mechanisms.

KEYWORDS: *ryanodine receptor, anthranilic diamides, phthalic diamides, structure−activity relationship, toxicity*

INTRODUCTION

Diamides are the newest major class of insecticides.[1−6] They combine outstanding potency on many major agricultural pests with low mammalian toxicity. The current diamides are of two chemotypes. Anthranilic diamides are exemplified by chlorantraniliprole (Chlo) and cyantraniliprole (Cyan)[3−6] and phthalic diamides by flubendiamide (Flu).[1,2] Their mode of action is different from that of all other insecticides so target site cross resistance is not a problem.[7] Both chemotypes are Ca^{2+} channel modulators and ryanodine (Ry) receptor (RyR) activators in essentially the same way; that is, no differences are apparent in their electrophysiological effects on insect muscle preparations.[1−6] Cross resistance between Chlo and Flu in control of *Plutella xylostella*[8−10] further suggests a common mode of action.

The molecular targets of Ry and the diamides in insects are partially characterized with appropriate radioligands, that is, [^{3}H]Ry,[11,12] [^{3}H]Chlo,[13] and [^{3}H]Flu[2,14] (Figure 1). Species differences are apparent in these binding sites. The [^{3}H]Flu, [^{3}H]Chlo, and [^{3}H]Ry sites have been studied in muscle tissues of *Musca*, *Apis*, *Heliothis*, and *Agrotis*[15] with major differences between species: [^{3}H]Ry binding and [^{3}H]Chlo binding have common characteristics in all of these insects based on Ca^{2+} and ATP effects and interactions with unlabeled Ry, Chlo, Cyan, and Flu, but no high affinity [^{3}H]Flu binding site was evident in *Musca* and *Apis* under our test conditions.[15] The goal of this investigation is to establish if the anthranilic and phthalic diamides have a common target site in some species but not others (e.g., *Heliothis* versus *Musca*) and if radioligand binding studies reflect the in vivo actions and toxic effects. These relationships are important in insecticide design, species specificity, and resistance management.

MATERIALS AND METHODS

Chemicals. [^{3}H]Ry (95 Ci/mmol) was purchased from PerkinElmer Life Sciences (Boston, MA, USA). [^{3}H]Chlo was synthesized in house.[13] Twenty-six anthranilic and phthalic diamides with generic structures shown in Figure 2 were used to compare the chemotype−activity relationships of binding assays with toxicity. Although the structures of individual compounds were not revealed for reasons of patenting status, their classification into two distinct chemotypes provided the opportunity to establish the relevance of the binding site assay results to toxicity in both the anthranilic and phthalic diamide series. [^{3}H]Flu and 11 analogues of Chlo were provided by Bayer CropScience (Monheim, Germany), and 12 analogues of Flu were supplied by Nihon Nohyaku (Tokyo, Japan). The compounds are numbered on the general basis of potency from the most to the least in the *Heliothis* thoracic muscle binding assay with [^{3}H]Chlo for the anthranilic diamide set and [^{3}H]Flu for the phthalic diamides as described later.

[^{3}H]Chlo, [^{3}H]Flu, and [^{3}H]Ry Binding Assays in Vitro. Membranes with associated RyR from *Heliothis* and *Musca* thoracic flight muscle were prepared as described and stored at −80 °C.[15] Each reaction mixture contained 1 nM [^{3}H]Chlo, [^{3}H]Flu, or [^{3}H]Ry, 200 μg of membrane protein,[13,15] and 30 nM test compound (in 2 μL of dimethyl sulfoxide) in binding buffer (0.8 mM $CaCl_2$, 2 mM ATP-Mg^{2+} salt, and 1.5 M KCl in 10 mM Hepes, pH 7.4) with a final volume of 412 μL. Incubations were for 120 min at 37 °C. Nonspecific binding was determined with 10 μM Chlo for [^{3}H]Chlo, 10 μM Flu for [^{3}H]Flu, and 10 μM Ry for [^{3}H]Ry binding. Bound radioligand

Received: December 20, 2013
Accepted: April 18, 2014
Published: April 18, 2014

 © 2014 American Chemical Society

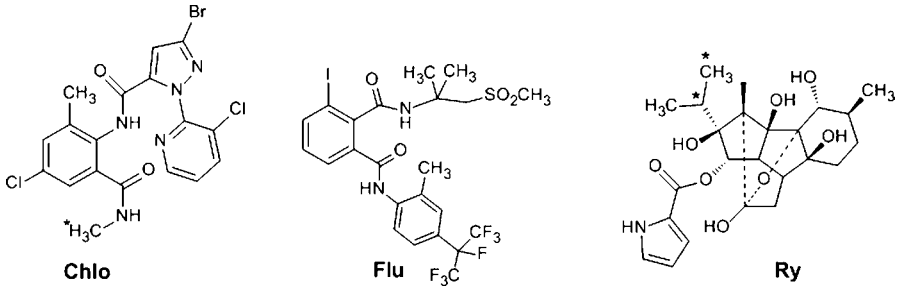

Figure 1. Diamide and ryanodine radioligands showing ^{3}H-labeling positions for [^{3}H]Chlo and [^{3}H]Ry (labeling site for [^{3}H]Flu not disclosed).

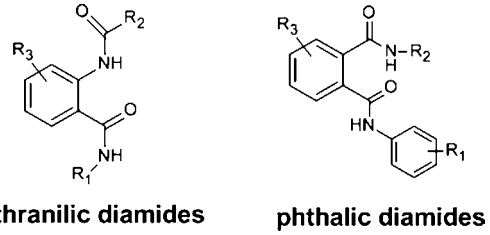

Figure 2. Diamides with various substituents (R_1, R_2, and R_3). The phthalic diamides are also referred to as 1,2-benzenedicarboxamides (BDCAs).

was harvested by filtration and quantitated according to earlier studies, and the percentage inhibition or stimulation versus control was determined.[13,15]

Heliothis and Spodoptera Bioassays. The efficacy of diamides against insecticide-susceptible strains of *Heliothis virescens* and *Spodoptera frugiperda* was tested using an artificial diet-based bioassay as described elsewhere.[16] Briefly, cylinders of artificial diet (height, 0.6 cm; diameter, 1.5 cm) were placed in 24-well tissue culture plates. Insecticide stock solutions were prepared by dissolving active ingredient in a 3:1 (v/v) mixture of dimethylformamide and emulsifier W. Subsequently, the stock solution was diluted with water. Twelve diet cylinders were each applied with 100 μL per concentration and represented one replicate. The experiment was repeated three times with two replicates per concentration. One second-instar larva was transferred to each treated cylinder. The plates were covered with tissue paper, sealed with a ventilated lid, and stored at room temperature in the dark. Percentage efficacy was assessed after 7 days. The toxicity ratings were generated by summing the assessed percentage efficacy (larvae dead or showing irreversible symptoms of poisoning) for each individual concentration tested; for example, in tests at 1000, 200, 40, 8, 1.6, 0.32, 0.064, and 0.0128 ppm and corresponding efficacy values of 100, 100, 100, 100, 100, 70, 20, and 0%, the toxicity index is 590.

***Musca* Poisoning Signs and [^{3}H]Chlo and [^{3}H]Ry Binding Assays in Vivo.** Twenty adult *Musca* anesthetized with carbon dioxide for 10 min were individually injected with a discriminating dose of each compound of 0.1 μg/fly (about 5 μg/g) into either the thorax or the abdomen (two sets of flies). Two hours after treatment, poisoning signs were observed for each fly to obtain a total rating for the set of 20 flies using the following system: 0 for normal, 1 for impaired movement, and 2 for dead. The final poisoning signs were equal to the number of impaired flies plus twice the number of dead flies multiplied by 2.5, that is, 100% impaired movement = 50 and 100% mortality = 100 poisoning rating. Thoraces were recovered 2 h after injection to determine ex vivo inhibition or stimulation of binding. Ten thoraces were homogenized by a Polytron (Brinkmann Instruments) in 1 mL of membrane preparation buffer (10 μM phenylmethanesulfonyl floride, 0.8% bovine serum albumin, and 303 mM sucrose in 20 mM Tris-maleate, pH 7.0) for 40 s.[15] Each homogenate was filtered through four layers of 64 μm mesh nylon screen after centrifuging at 700*g* for 30 min, and then 200 μL was used for radioligand binding assay as described above for binding in vitro.[15]

Statistical Analysis. Linear regression was performed to calculate the correlation among [^{3}H]Chlo, [^{3}H]Flu, and [^{3}H]Ry binding or versus toxicity for each compound with *Heliothis* or [^{3}H]Chlo and [^{3}H]Ry binding in vitro versus in vivo and binding in vitro/in vivo versus toxicity for each compound with *Musca*. GraphPad Prism 5.0 software was used to plot and analyze data.

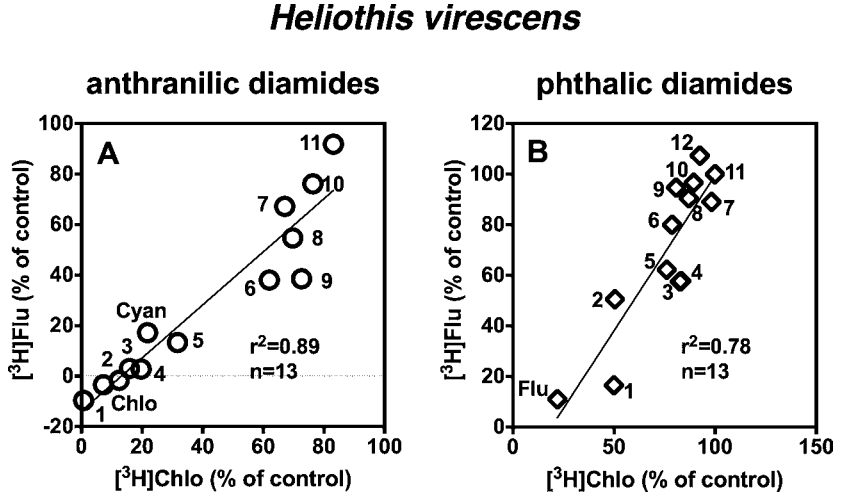

Figure 3. *Heliothis* toxicological profiles for anthranilic (A) and phthalic (B) diamide inhibition of [^{3}H]Chlo and [^{3}H]Flu binding assayed at 30 nM test compound.

dx.doi.org/10.1021/jf501236h | J. Agric. Food Chem. 2014, 62, 4077−4082

RESULTS

Heliothis RyR. *Diamide Toxicological Profiles for [^{3}H]Chlo and [^{3}H]Flu Binding Sites.* The 11 anthranilic analogues plus Chlo and Cyan were tested at a discriminating concentration (30 nM) for inhibition of [^{3}H]Chlo and [^{3}H]Flu binding (Figure 3A), and the same experiment was made with the 12 phthalic analogues plus Flu at 30 nM (Figure 3B). The anthranilic and phthalic diamides have the same efficacy for inhibiting binding at the Chlo site as for the Flu site (Figure 4).

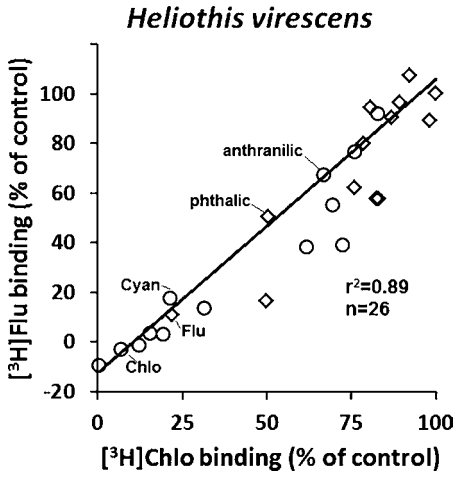

Figure 4. *Heliothis* toxicological profiles for anthranilic and phthalic diamide inhibition of [^{3}H]Chlo and [^{3}H]Flu binding assayed at 30 nM test compound. Individual compounds are identified in Figure 3.

Diamide Toxicological Profiles Relative to Insecticidal Activity. The binding site profiles were compared with the insecticidal activities for the anthranilic diamides with [^{3}H]Chlo (Figure 5A) and [^{3}H]Flu (Figure 5B). The potency of the anthranilic diamides to inhibit [^{3}H]Chlo and [^{3}H]Flu binding is consistent with their insecticidal activity. Because [^{3}H]Chlo and [^{3}H]Flu binding data are very similar, this also means that with *Heliothis* the use of either radioligand predicts toxicity in both diamide chemotypes.

Diamides Increase [^{3}H]Ry Binding. The two sets of diamides inhibitory to [^{3}H]Chlo and [^{3}H]Flu binding (Figure 5A, B) were assayed for effect on [^{3}H]Ry binding (Figure 5C) with a much lower correlation to toxicity (r^2 = 0.08). Inhibition at the diamide binding site assayed with [^{3}H]Chlo and [^{3}H]Flu is generally associated with increased binding at the [^{3}H]Ry site, that is, they are negatively correlated (Figure 6).

Musca RyR. *Diamide Toxicological Profiles for [^{3}H]Chlo and [^{3}H]Ry Binding Sites.* The experiments for in vitro inhibition of [^{3}H]Chlo and [^{3}H]Ry binding by 13 anthranilic diamides and 13 phthalic diamides described above with *Heliothis* RyR were also performed with *Musca* RyR under the same conditions. The toxicological profile was defined for the [^{3}H]Chlo binding site but not for the [^{3}H]Flu site because the latter radioligand does not undergo sufficient specific binding for meaningful determinations. Some anthranilic diamides inhibit [^{3}H]Chlo binding and can greatly stimulate [^{3}H]Ry binding (Figure 7A), whereas phthalic diamides can double [^{3}H]Chlo binding with less effect on [^{3}H]Ry binding (Figure 7B,A+B). The diamides were assayed both in vitro and in vivo, giving a good correlation between the findings for [^{3}H]Chlo binding with anthranilic diamides but a poor correlation with phthalic diamides (Supporting Information Figure 1) and the same trend for [^{3}H]Ry binding assays (Supporting Information Figure 2).

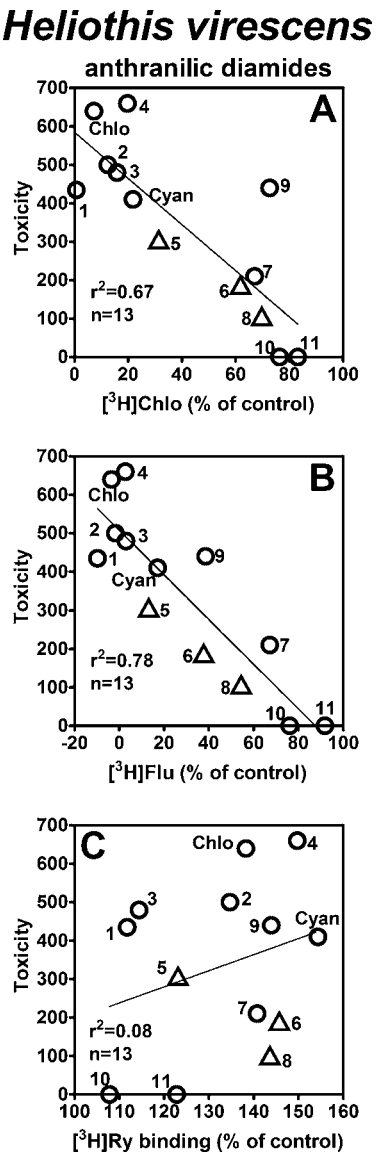

Figure 5. *Heliothis* and *Spodoptera* insecticidal activity of anthranilic diamides relative to potency for inhibition of *Heliothis* [^{3}H]Chlo (A) and [^{3}H]Flu (B) binding and stimulation of [^{3}H]Ry (C) binding assayed at 30 nM test compound. Toxicity data for *Heliothis* are used for eight compounds (○) and for *Spodoptera* with the other three compounds (**5**, **6**, and **8**) (△) where *Heliothis* data were not available. The *Heliothis* value averaged 90 ± 30% of the *Spodoptera* value for the eight compounds assayed with both species (see Supporting Information Table 1).

Diamide Toxicological Profiles for [^{3}H]Chlo and [^{3}H]Ry Binding Relative to Insecticidal Activity. [^{3}H]Chlo (Figure 8A,B) and [^{3}H]Ry (Figure 8C,D) binding site profiles were compared with the insecticidal activities for the anthranilic and phthalic diamide sets. The insecticidal activity of the anthranilic and phthalic diamides is poorly related to their inhibition of [^{3}H]Chlo binding but better correlated with their stimulation of [^{3}H]Ry binding. Generally similar results were observed with in vivo binding studies (Supporting Information Figures 1 and 2).

Species Differences in Binding Sites for [^{3}H]Chlo and [^{3}H]Ry. In the binding studies with *Heliothis* and *Musca*,

dx.doi.org/10.1021/jf501236h | J. Agric. Food Chem. 2014, 62, 4077−4082

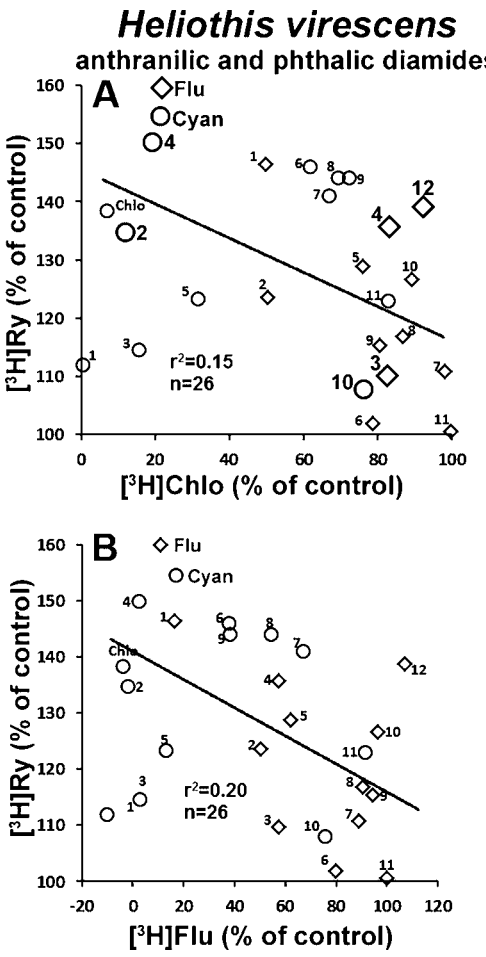

Figure 6. *Heliothis* toxicological profiles for anthranilic diamide and phthalic diamide inhibition of [^{3}H]Chlo (A) and [^{3}H]Flu (B) binding versus stimulation of [^{3}H]Ry binding assayed at 30 nM test compound.

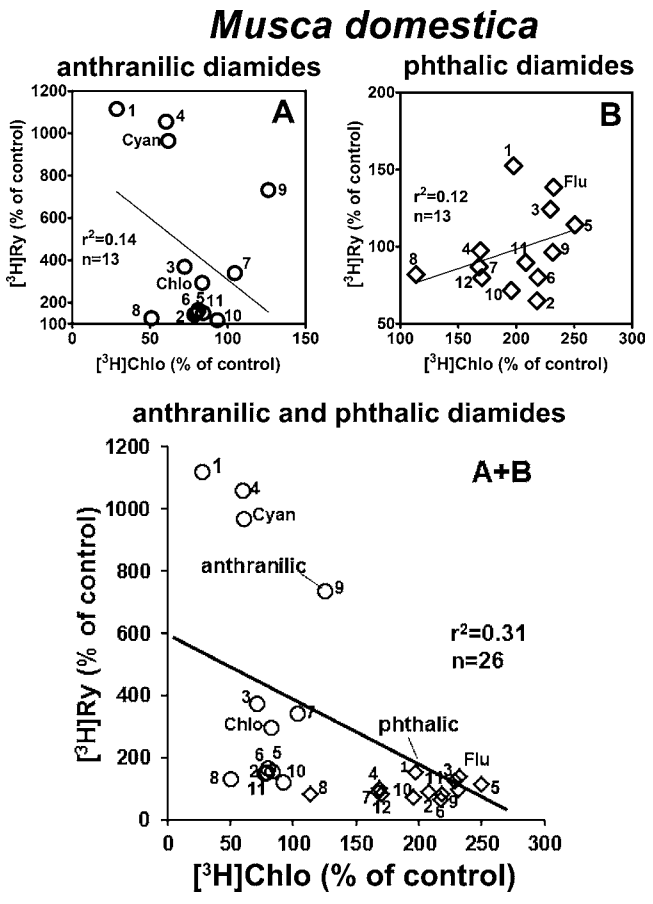

Figure 7. *Musca* toxicological profiles for anthranilic (A) and phthalic (B) diamides or both (A+B) relative to effects on [^{3}H]Chlo and [^{3}H]Ry binding assayed at 30 nM test compound.

anthranilic diamides generally inhibit [^{3}H]Chlo binding (Supporting Information Figure 3A) and stimulate [^{3}H]Ry binding (Supporting Information Figure 3B). In contrast, phthalic diamides generally inhibit [^{3}H]Chlo binding in *Heliothis* but stimulate binding in *Musca* (Supporting Information Figure 3A). The stimulation of [^{3}H]Ry binding by anthranilic diamides is much greater in *Musca* than in *Heliothis* (Supporting Information Figure 3B).

DISCUSSION

The RyR is recognized as a major target for insecticide action, and now more and more genomic analysis information is available on target and nontarget insect species.[17,18] The present study is an early step in evaluating species variations in insect RyR toxicology. There appears to be more than one type of diamide site in insects. In *Musca* the [^{3}H]Chlo, [^{3}H]Ry, and [^{3}H]Flu binding sites are conformationally different, but in *Heliothis* RyR, anthranilic and phthalic diamide insecticides displace each other when determined as either [^{3}H]Chlo or [^{3}H]Flu binding and therefore probably bind at the same or closely coupled sites.

Mammalian genomes express three different isoforms of the RyR, whereas insect genomes encode only a single RyR gene, and the low amino acid identity between mammal and insect RyRs probably contributes to the high selectivity of diamides.[19,20] To date, neither Chlo[21] nor Flu[22] has been found to exhibit cross resistance with other commercial insecticides. All field-evolved resistant lepidoptera populations that have been tested against the two diamides have shown cross-resistance between Chlo and Flu, which appears to be due to a single amino acid mutation in the RyR C-terminal transmembrane domain, which encodes the proposed binding site of diamides.[10] There is high homology between lepidoptera RyR genes; thus, the conserved transmembrane region might contribute to the same binding sites for Chlo and Flu.

A set of anthranilic diamides and another of phthalic diamides were evaluated with [^{3}H]Chlo and [^{3}H]Flu binding assays as predictors of toxicity using data from ingestion of the anthranilic diamides by lepidoptera larvae in the Bayer laboratory and injection of both diamide chemotypes into *Musca* in the Berkeley laboratory. In *Heliothis*, the [^{3}H]Chlo and [^{3}H]Flu binding assays were good predictors of toxicity for both the anthranilic and phthalic diamides. In *Musca*, the binding site−toxicity correlations were less favorable or absent, possibly due in part to diamide detoxification. Although the data are not shown, the in vivo RyR inhibition in *Musca* was nearly the same for injections into either the thorax or the abdomen, indicating that thoracic muscle RyR binding occurred mostly in vivo rather than during the binding assay.

The potency of diamides as inhibitors of [^{3}H]Chlo and [^{3}H]Flu binding is generally correlated with their effectiveness in stimulating [^{3}H]Ry binding; that is, binding at the Chlo/Flu site opens or increases the open time of the Ca^{2+} channel. A

dx.doi.org/10.1021/jf501236h | J. Agric. Food Chem. 2014, 62, 4077−4082

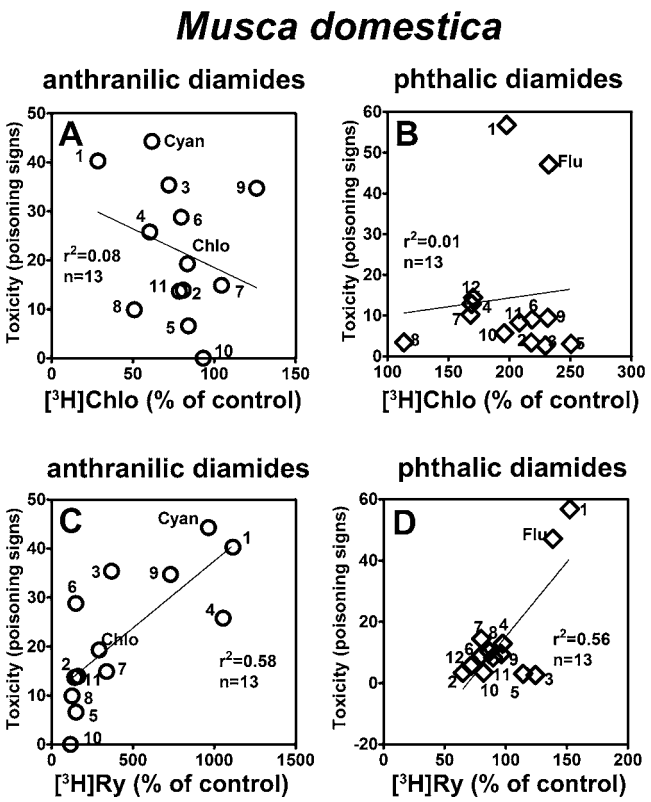

Figure 8. *Musca* insecticidal activity of anthranilic (A) and phthalic (B) diamides relative to potency for inhibition of [^{3}H]Chlo binding (A, B) and stimulation of [^{3}H]Ry (C, D) binding assayed at 30 nM test compound.

series of Chlo analogues was tested with *Musca* RyR both in vitro and in vivo for effects on [^{3}H]Ry binding with stimulation in most cases, a relationship also observed with a number of Flu analogues, further generalizing the diamide activity as a stimulator of the [^{3}H]Ry site. Thus, the observation of enhanced [^{3}H]Ry binding seems to be a reliable indicator of diamide action at the Ca^{2+}-modulated Ca^{2+} channel.

The stimulation of [^{3}H]Chlo binding to *Musca* membranes by phthalic diamides may be due to the fact that their affinity for the *Musca* RyR is much lower (our estimate of the apparent K_d of Flu is about 185 nM) than for the *Heliothis* RyR. Therefore, the phthalic diamide concentrations used in this study may not be sufficient to provide effective competition with the high-affinity radioligand [^{3}H]Chlo, as is the case with the *Heliothis* receptor having a higher affinity for phthalic diamides. An increase in the open probability of the *Musca* RyR induced by phthalic diamides could plausibly explain the stimulatory effect on [^{3}H]Chlo binding by increasing the number of radioligand binding sites. The underlying assumption is that diamides are conformation-sensitive ligands which preferentially bind to the open channel as shown for [^{3}H]Flu.[23]

Continuing progress in defining insect RyR regions critical to both anthranilic and phthalic diamide sensitivity is helping to define the basis for diamide selectivity among insect species and between insects and mammals.[24]

■ ASSOCIATED CONTENT

Ⓢ Supporting Information

Table of the diamides studied and effects on [^{3}H]Chlo and [^{3}H]Flu binding. Three supplemental figures, two for *Musca* toxicological profiles and the third comparing [^{3}H]Chlo and [^{3}H]Flu toxicological profiles between *Heliothis* and *Musca*. This material is available free of charge via the Internet at http://pubs.acs.org.

■ AUTHOR INFORMATION

Corresponding Author

*(J.E.C.) Phone: (510) 642-4524. Fax: (510) 642-6497. E-mail: ectl@berkeley.edu.

Present Address

⊥(S.Q.) College of Science, China Agricultural University, Beijing, China 100193.

Funding

S.Q. was supported in part by State Scholarship Fund No. 2011635138 provided by the Chinese Scholarship Council.

Notes

The authors declare no competing financial interest.

■ ACKNOWLEDGMENTS

We thank Masanori Tohnishi and colleagues at Nihon Nohyaku as well as Rüdiger Fischer at Bayer CropScience for kindly supplying phthalic diamides and anthranilic diamides, respectively. S.Q. thanks Professor Chengju Wang of China Agricultural University for academic counsel. Helpful advice and assistance were provided by Chunqing Zhao, Xusheng Shao, and Breanna Ford of the Berkeley Laboratory.

■ ABBREVIATIONS USED

Chlo, chlorantraniliprole; Cyan, cyantraniliprole; Flu, flubendiamide; Ry, ryanodine; RyR, ryanodine receptor

■ REFERENCES

(1) Tohnishi, M.; Nakao, H.; Furuya, T.; Seo, A.; Kodama, H.; Tsubata, K.; Fujioka, S.; Kodama, H.; Hirooka, T.; Nishimatsu, T. Flubendiamide, a novel insecticide highly active against lepidopterous insect pests. *J. Pestic. Sci.* **2005**, *30*, 354−360.

(2) Ebbinghaus-Kintscher, U.; Luemmen, P.; Lobitz, N.; Schulte, T.; Funke, C.; Fischer, R.; Masaki, T.; Yasokawa, N.; Tohnishi, M. Phthalic acid diamides activate ryanodine-sensitive Ca^{2+} release channels in insects. *Cell Calcium* **2006**, *39*, 21−33.

(3) Cordova, D.; Benner, E. A.; Sacher, M. D.; Rauh, J. J.; Sopa, J. S.; Lahm, G. P.; Selby, T. P.; Stevenson, T. M.; Flexner, L.; Gutteridge, S.; Rhoades, D. F.; Wu, L.; Smith, R. M.; Tao, Y. Anthranilic diamides: a new class of insecticides with a novel mode of action, ryanodine receptor activation. *Pestic. Biochem. Physiol.* **2006**, *84*, 196−214.

(4) Sattelle, D. B.; Cordova, D.; Cheek, T. R. Insect ryanodine receptors: molecular targets for novel pest control chemicals. *Invert. Neurosci.* **2008**, *8*, 107−119.

(5) Hamaguchi, H.; Hirooka, T.; Masaki, T. Insecticides affecting calcium homeostasis. In *Modern Crop Protection Compounds*, 2nd ed.; Kramer, W., Schirmer, U., Jeschke, P., Witschel, M., Eds.; Wiley: Weinheim, Germany, 2012; pp 1389−1425.

(6) Jeanguenat, A. The story of a new insecticidal chemistry class: the diamides. *Pest Manage. Sci.* **2013**, *69*, 7−14.

(7) Nauen, R.; Elbert, A.; McCaffery, A.; Slater, R.; Sparks, T. C. IRAC: Insecticide resistance, and mode of action classification of insecticides. In *Modern Crop Protection Compounds*, 2nd ed.; Kramer, W., Schirmer, U., Jeschke, P., Witschel, M., Eds.; Wiley: Weinheim, Germany, 2012; pp 935−954.

(8) Troczka, B.; Zimmer, C. T.; Elias, J.; Schorn, C.; Bass, C.; Davies, T. G. E.; Field, L. M.; Williamson, M. S.; Slater, R.; Nauen, R. Resistance to diamide insecticides in diamondback moth, *Plutella xylostella* (Lepidoptera: *Plutellidae*) is associated with a mutation in the membrane-spanning domain of the ryanodine receptor. *Insect Biochem. Mol. Biol.* **2012**, *42*, 873−880.
(9) Wang, X.; Khakame, S. K.; Ye, C.; Yang, Y.; Wu, Y. Characterisation of field-evolved resistance to chlorantraniliprole in the diamondback moth, *Plutella xylostella*, from China. *Pest Manage. Sci.* **2013**, *69*, 661−665.
(10) Teixeira, L. A.; Andaloro, J. T. Diamide insecticides: global efforts to address insect resistance stewardship challenges. *Pestic. Biochem. Physiol.* **2013**, *106*, 76−78.
(11) Pessah, I. N.; Francini, A. O.; Scales, D. J.; Waterhouse, A. L.; Casida, J. E. Calcium-ryanodine receptor complex. Solubilization and partial characterization from skeletal muscle junctional sarcoplasmic reticulum vesicles. *J. Biol. Chem.* **1986**, *261*, 8643−8648.
(12) Lehmberg, E.; Casida, J. E. Similarity of insect and mammalian RyR binding site. *Pestic. Biochem. Physiol.* **1994**, *48*, 145−152.
(13) Isaacs, A. K.; Qi, S.; Sarpong, R.; Casida, J. E. Insect ryanodine receptor: distinct but coupled insecticide binding sites for [*N*-C^3H_3]chlorantraniliprole, flubendiamide, and [^{3}H]ryanodine. *Chem. Res. Toxicol.* **2012**, *25*, 1571−1573.
(14) Kato, K.; Kiyonaka, S.; Sawaguchi, Y.; Tohnishi, M.; Masaki, T.; Yasokawa, N.; Mizuno, Y.; Mori, E.; Inoue, K.; Hamachi, I.; Takeshima, H.; Mori, Y. Molecular characterization of flubendiamide sensitivity in the lepidopterous ryanodine receptor Ca^{2+} release channel. *Biochemistry* **2009**, *48*, 10342−10352.
(15) Qi, S.; Casida, J. E. Species differences in chlorantraniliprole and flubendiamide insecticide binding sites in the ryanodine receptor. *Pestic. Biochem. Physiol.* **2013**, *107*, 321−326.
(16) Nauen, R.; Konanz, S.; Hirooka, T.; Nishimatsu, T.; Kodama, H. Flubendiamide: a unique tool in resistance management tactics for pest lepidoptera difficult to control. *Pflanzenschutz−Nachr. Bayer* **2007**, *60*, 247−262.
(17) Puente, E.; Suner, M.; Evans, A. D.; McCaffery, A. R.; Windass, J. D. Identification of a polymorphic ryanodine receptor gene from *Heliothis virescens* (Lepidoptera: Noctuidae). *Insect Biochem. Mol. Biol.* **2000**, *30*, 335−347.
(18) Lanner, J. T.; Georgiou, D. K.; Joshi, A. D.; Hamilton, S. L. Ryanodine receptors: structure, expression, molecular details, and function in calcium release. In *Calcium Signaling: a Subject Collection from Cold Spring Harbor Perspectives in Biology*; Cold Spring Harbor Perspectives in Biology 2; Bootman, M. D., Berridge, M. J., Putney, J. W., Roderick, H. L., Eds.; Cold Spring Harbor Laboratory: Cold Spring Harbor, NY, USA, **2010**; a003996.
(19) Rossi, D.; Sorrentino, V. Molecular genetics of ryanodine receptors Ca^{2+} release channels. *Cell Calcium* **2002**, *32*, 307−319.
(20) Vazquez-Martinez, O.; Canedo-Merino, R.; Diaz-Munoz, M.; Riesgo-Escovar, J. R. Biochemical characterization, distribution and phylogenetic analysis of *Drosophila melanogaster* ryanodine and IP3 receptors, and thapsigargin sensitive Ca^{2+} ATPase. *J. Cell. Sci.* **2003**, *116*, 2483−2494.
(21) Lahm, G. P.; Selby, T. P.; Freudenberger, J. H.; Stevenson, T. M.; Myers, B. J.; Seburyamo, G.; Smith, B. K.; Flexner, L.; Clark, C. E.; Cordova, D. Insecticidal anthranilic diamides: a new class of potent ryanodine receptor activators. *Bioorg. Med. Chem. Lett.* **2005**, *15*, 4898−4906.
(22) Ebbinghaus-Kintscher, U.; Luemmen, P.; Raming, K.; Masaki, T.; Yasokawa, N. Flubendiamide, the first insecticide with a novel mode of action on insect ryanodine receptors. *Pflanzenschutz−Nachr. Bayer* **2007**, *60*, 117−140.
(23) Lümmen, P.; Ebbinghaus-Kintscher, U.; Funke, C.; Fischer, R.; Masaki, T.; Yasokawa, N.; Tohnishi, M. Phthalic acid diamides activate insect ryanodine receptors. *ACS Symp. Ser.* **2007**, *No. 948*, 235−248.
(24) Tao, Y.; Gutteridge, S.; Benner, E. A.; Wu, L.; Rhoades, D. F.; Sacher, M. D.; Rivera, M. A.; Desaeger, J.; Cordova, D. Identification of a critical region in the *Drosophila* ryanodine receptor that confers sensitivity to diamide insecticides. *Insect Biochem. Mol. Biol.* **2013**, *43*, 820−828.

JOURNAL OF AGRICULTURAL AND FOOD CHEMISTRY

Article

pubs.acs.org/JAFC

PGR5 and NDH Pathways in Photosynthetic Cyclic Electron Transfer Respond Differently to Sublethal Treatment with Photosystem-Interfering Herbicides

Haifeng Qian,*[,†,‡,§] Takuma Tsuji,[§] Tsuyoshi Endo,*[,§] and Fumihiko Sato*[,§]

[†]Department of Food Science and Technology, Zhejiang University of Technology, Hangzhou, 310032 China

[‡]College of Biological and Environmental Engineering, Zhejiang University of Technology, Hangzhou, 310032 China

[§]Graduate School of Biostudies, Kyoto University, Oiwakecho, Kitashirakawa, Sakyo, Kyoto, 606-8502 Japan

Supporting Information

ABSTRACT: Effects of sublethal levels of the photosystem-interfering herbicides atrazine (Atr) and methyl viologen (MV) on photosynthetic electron transport were investigated in *Arabidopsis thaliana* mutants with defects in cyclic electron transfer (CET) activity. Analysis based on chlorophyll fluorescence parameters showed that *pgr*5 mutant (a defect in the PGR5 pathway) was more sensitive to both Atr and MV than wild type (Wt) and *pnsB*3 mutant (a defect in the NDH pathway). Real-time PCR (polymerase chain reaction) analysis of transcripts indicated that Wt plants showed marked increases in transcripts in the PRG5 and NDH pathways under treatment with either Atr or MV. In contrast, Atr increased the gene transcripts in CET, but MV decreased them in *pnsB*3 mutant plants. Atr did not increase the transcripts, while MV down-regulated them in *pgr*5 mutant. Immunoblot analysis partially supported the changes in the transcripts; that is, the protein levels of PGRL1 and PGR5 were increased in *pnsB*3 mutant, while no protein level was increased in *pgr*5 mutant after the herbicide treatment. The present results suggest that cyclic electron transport is very sensitive to photosystem-interference induced by chemicals and that the PGR5 pathway is very critical for regulation. Thus, *pgr*5 mutants may be useful plants for monitoring photosystem-interfering herbicides.

KEYWORDS: *Arabidopsis thaliana, cyclic electron transport, pgr5, pnsB3, herbicide*

INTRODUCTION

Increasing amounts of herbicides are being used to control weed growth, and these now account for up to 50%−60% of total nonfertilizer chemicals in agriculture.[1] Although herbicides do effectively control weed growth, almost 99.9% of them enter the environment, where they affect nontarget organisms.[2,3] Among herbicides, the inhibition of photosynthesis is the most common and effective mechanism of action, since photosynthesis is ubiquitous in plants. Atrazine (Atr) and methyl viologen (MV) are commonly used herbicides. Atr displaces plastoquinone from its binding site (the Q_B site) in the D1 protein[4] and inhibits chloroplast electron flow from plastoquinone A to Q_B, and reduces ATP and NADPH production and CO_2 fixation.[5] MV accepts electrons from the Fe-SA/Fe-SB iron−sulfur cluster of photosystem I (PSI) and reduces NADPH generation and CO_2 fixation.[6] MV reduced by PSI, in turn, reduces molecular oxygen to a superoxide radical and then induces the peroxidation of lipids and other cellular components, leading to a rapid loss of membrane integrity, photooxidation, desiccation, and plant death.[7]

Although their primary targets have been well-characterized, the effects of sublethal doses of these chemicals diffused into the environment, as mentioned above, are not yet clear. The application of sublethal concentrations of these chemicals may disrupt linear photosynthetic electron transfer (LET) and decrease the production of the energy-rich compounds NADPH and ATP. Plants may cope with this stress by adjusting photosynthetic electron transfer in various ways, such as by intensifying electron transfer through a process known as cyclic electron transfer (CET) to produce more ATP to drive protein repair.[8−11] The additional ATP arising from CET may compensate for the insufficient production of ATP from LET, thus supporting CO_2 fixation, since LET alone cannot produce sufficient ATP to satisfy the required stoichiometry.[12] In fact, CET is an essential physiological process for efficient photosynthesis.[13] CET can balance the ATP/NADPH production ratio to protect photosystems[14−16] by inducing nonphotochemical quenching (qN) to dissipate excessive absorbed light energy.[17] CET generally occurs through two routes in higher plants: the PGR5 and chloroplast NAD(P)H dehydrogenase (NDH) pathways. In the PGR 5 pathway, electron transfer is mediated by the proton gradient regulation 5 (PGR 5) and pgr5-like 1 (PGRL1) proteins. In the NDH pathway, electrons are cycled around PSI by the thylakoid-embedded NDH complex.[11,14]

To verify the effects of sublethal levels of photosystem-interfering herbicides on CET, we measured photosynthetic electron transfer activity based on chlorophyll fluorescence parameters, gene expression, and protein accumulation of components in the LET and CET pathways using two *A. thaliana* mutants, which have defects in either the LET or CET

Received: January 11, 2014
Revised: April 14, 2014
Accepted: April 15, 2014
Published: April 15, 2014

ACS Publications © 2014 American Chemical Society

pathway: i.e., a *pgr*5 mutant, which is deficient in antimycin A-sensitive cyclic flow from ferredoxin to plastoquinone,[18] and a *pnsB*3 mutant, which is deficient in NDH-dependent cyclic flow from NADPH to plastoquinone.[19] Our experimental results revealed that cyclic electron transport is very sensitive to photosystem-interference induced by chemicals and the PGR5 pathway is very critical for regulation.

MATERIALS AND METHODS

***Arabidopsis thaliana* Culture.** Seeds of *A. thaliana* (ecotype Columbia; Wt and *pgr*5 and *pnsB*3 (formerly *ndf*4) were sterilized and germinated on Murashige-Skoog (MS) medium containing 0.8% w/v agar and 1% w/v sucrose for 2 weeks before transfer to a 6 cm pot containing compost with vermiculite (1:1). After 2 weeks in soil, the seedlings were transferred to 1/2 MS liquid medium to adapt to the culture conditions. The seedlings were exposed to 0.2 μM Atr or 0.8 μM MV for 6 days. These herbicide concentrations, which were selected based on a previous report by Sato et al.,[23] did not cause growth inhibition of *A. thaliana* phenotype after 6 days of growth. The plants were grown in an air-conditioned room at 23 °C under a 10 h light/14 h dark cycle at a light intensity of 40 μmol photons m^{-2} s^{-1}. Four to eight replicates were prepared for each treatment. Samples were collected after 3 and 6 days of herbicide treatment for photosynthetic chlorophyll fluorescence and gene expression analyses.

Chlorophyll Fluorescence Analysis. One seedling in the herbicide-treated or control group was collected and immersed in *N*,*N*-dimethylformamide to extract chlorophyll according to the method of Inskeep and Bloom.[24] The chlorophyll-extracted liquids were measured for absorbance values at 647 and 664.5 nm using a spectrophotometer, and chlorophyll a (chl a) and chlorophyll b (chl b) contents were calculated according to the formula reported in Inskeep and Bloom.[24] Chlorophyll fluorescence parameters were measured using a MINI-PAM (pulse-amplitude modulation) portable chlorophyll fluorometer (Walz, Germany). The maximum quantum yield [F_v/F_m], the quantum yield of photochemistry in PSII [$\Phi_{II} = (F_m' - F_s)/F_m'$], photochemical quenching [$qP = (F_m' - F_s)/(F_m' - F_o')$], and nonphotochemical quenching [$qN = 1 - (F_m' - F_o')/(F_m - F_o)$] were calculated based on the measured chlorophyll fluorescence. The leaves were exposed to both low light (270 μmol photons m^{-2} s^{-1}, LL) and high light (1410 μmol photons m^{-2} s^{-1}, HL) for the measurement of all chlorophyll fluorescence parameters. For detailed explanations of each chlorophyll fluorescence parameter, see van Kooten and Snel.[25]

Real-Time Quantitative PCR (polymerase chain reaction). Total RNA was extracted from control and herbicide-treated seedlings using the RNeasy PlantMini Kit (Qiagen, CA, USA). RNA concentrations were measured spectrophotometrically at 260 nm. The 260/280 nm ratios were determined and closed to 2.0, which showed the purity of the total RNA was high. The integrity of RNA was verified by visualizing the samples on ethidium bromide-stained agarose gels (Figure S1 of the Supporting Information); no significant degradation was observed. A 1-μg sample of the total RNA was used as a template for cDNA synthesis using SuperScript III reverse transcriptase (Invitrogen) with random primers. Real-time PCR was performed using iQ SYBR Green Supermix (Bio-Rad) in the CFX96 real-time PCR detection system (Bio-Rad). The cycle parameters consisted of one cycle of 3 min s at 95 °C and then 39 cycles of 10 s at 95 °C followed by 10 s at 55 °C and 30 s at 72 °C. The obtained data were analyzed using CFX manager software (Bio-Rad). Sixteen genes involved in the LET and CET pathways were selected for analysis; the primer pairs for each of these genes are listed in Table S1 of the Supporting Information. Expression of the housekeeping gene Actin 2 was used to normalize the expression profiles of the analyzed genes. Relative quantification of gene expression among the treatment groups was performed using the $2^{-\Delta\Delta Ct}$ method.[26]

Extraction of Crude Thylakoid Membrane Fraction, Protein Electrophoresis, and Western Blot Analysis. Rosette leaves from herbicide-treated plants and control plants were collected for extraction of the thylakoid membrane fraction on ice. As described by Takabayashi et al.,[19] rosette leaves were homogenized with protein extraction buffer (0.3 M sorbitol, 50 mM HEPES-KOH (pH 7.6), 1 mM $MgCl_2$, 1 mM $MnCl_2$, 2 mM EDTA, 30 mM KCl, 0.25 mM KH_2PO_4). The pellet obtained after centrifugation at 3000*g* for 5 min was then washed twice with 1× HEPES buffer without sorbitol. The isolated thylakoid fraction was finally treated in SDS−PAGE sample buffer (10 mM EDTA, 0.2 M DTT, 4% SDS, 0.2% Bromephenol blue, 20% glycerol, 100 mM Tris−HCl, pH 6.8) at 37 °C for 1 h. Protein corresponding to 0.5 g of chlorophyll was subjected to SDS−PAGE with a 12.5% polyacrylamide−SDS gel. The proteins in the gel were then blotted onto a polyvinylidene difluoride (PVDF) membrane (Millipore Corporation) using a transblot apparatus (Bio-Rad). A Western blot analysis was performed with rabbit antibodies against PNSB1, PNSB3, NDHH, PGRL1, PGR5, PsaB, Cytf, and RbcL. The blotted bands were detected using Western Lightning Chemiluminescence Reagent Plus (PerkinElmer Inc.) together with anti-rabbit IgG (Amersham). The amounts of protein in each sample were qualitatively compared using Coomassie Brilliant Blue (CBB) dye to stain the SDS-polyacrylamide gels, and normalized before the samples were subjected to Western blot analysis.

Data Analysis. The data are presented as the mean ± standard error of the mean (SEM). Statistical significance was tested via one-way ANOVA. Values were considered significantly different at a p value of less than 0.05.

RESULTS

Effects of Atr and MV on Chlorophyll Content and Photosynthetic Activities. Treatment with Atr and MV did not cause severe growth defects in Wt *Arabidopsis* seedlings, as noted in the Materials and Methods. However, the measurement of chlorophyll content, a biomarker that reflects the status of photosynthesis in plants, revealed that there were different effects in mutants (Table 1). Whereas untreated and Atr-treated Wt, *pnsB*3, and *pgr*5 seedlings, as well as MV-treated Wt and *pnsB*3 seedlings, showed no effects on Chl a and Chl b content, MV-treated *pgr*5 significantly decreased the Chl a and Chl b contents to 65% and 50% of the control levels, respectively.

The measurement of chlorophyll fluorescence parameters, i.e., the maximal quantum yield (F_v/F_m), the quantum yield of PSII (ΦII), photochemical quenching (qP), and nonphotochemical quenching (qN) under low light (LL) and high light (HL), revealed more differences in mutants, whereas the concentrations of the herbicides used did not significantly alter the fluorescence parameters in Wt plants (see Figure 1, 3 days treatment). First, we compared F_v/F_m in nontreated seedlings of Wt and mutants, and we found that F_v/F_m was almost the same in the Wt, *pgr*5, and *pnsB*3 plants. Treatment with herbicides for 3 days also did not cause severe changes in F_v/F_m, and the value was approximately 0.75 (Figure 1A). Treatment with Atr or MV for 6 days also did not cause a statistically significant decrease in F_v/F_m in both Wt and the *pnsB*3 mutant. In the *pgr*5 mutant, however, F_v/F_m significantly decreased, in comparison with the control (*pgr*5-Con), after 6 days of treatment with Atr or MV.

The quantum yield of PSII (Φ_{II}) showed similar but much greater changes than F_v/F_m, especially under HL (Figure 1B and C). The control without chemical treatment for 3 days showed no significant differences in Φ_{II} between Wt and the two mutants under both LL and HL conditions. In the *pgr*5 mutant, however, Φ_{II} was significantly lower than those in the Wt and *pnsB*3 mutant after culture for 6 days even under control conditions without chemical treatment, especially under HL, as reported previously.[18] Treatment with Atr for 3 days also did not induce significant changes in the Φ_{II} level under LL or HL conditions, whereas treatment for 6 days clearly

Table 1. Changes in Chlorophyll Contents after 6 days of Treatment with Atr or MV[a,b]

	control group			Atr-treated group			MV-treated group		
	Wt	*pgr*5 mutant	*pnsB*3 mutant	Wt	*pgr*5 mutant	*pnsB*3 mutant	Wt	*pgr*5 mutant	*pnsB*3 mutant
Chl a (mg/g FW)	1.34 ± 0.08 ab	1.08 ± 0.18 bc	1.31 ± 0.08 ab	1.13 ± 0.19 ab	0.92 ± 0.08 b	1.28 ± 0.19 ab	1.18 ± 0.15 ab	0.70 ± 0.02 c	1.59 ± 0.24 a
Chl b (mg/g FW)	0.29 ± 0.07 a	0.18 ± 0.02 abc	0.28 ± 0.03 a	0.16 ± 0.03 abc	0.13 ± 0.02 bc	0.26 ± 0.08 ab	0.25 ± 0.04 ab	0.09 ± 0.02 c	0.30 ± 0.06 a

[a]Data are expressed as the mean ± SEM. [b]Different letters represent statistically significant differences at $p < 0.05$ based on one-way ANOVA.

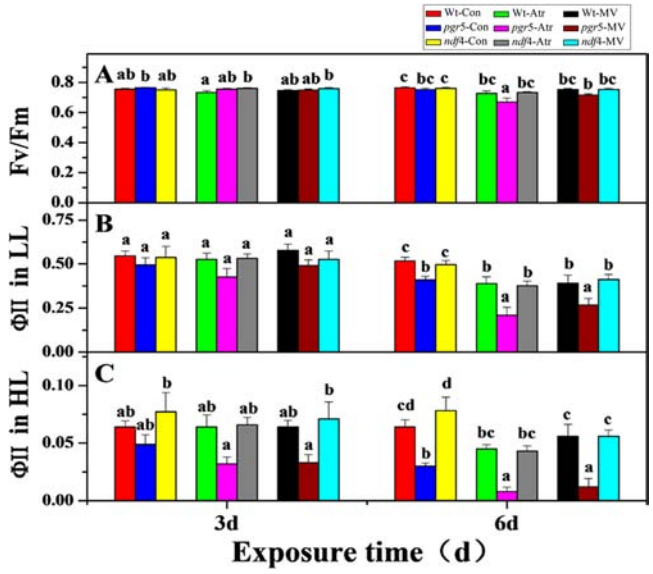

Figure 1. PSII fluorescence parameters: maximum quantum yield of PSII (F_v/F_m) and the quantum yield of photochemistry in PSII (ΦII) under LL and HL conditions. Different letters represent statistically significant differences at $p < 0.05$ based on one-way ANOVA.

decreased the Φ_{II} level in all seedlings in comparison with the levels in untreated seedlings (Figure 1B), and the reduction induced by Atr was more evident under HL conditions (Figure 1C). The changes in Φ_{II} under the treatment with MV were similar to those under treatment with Atr. Under all treatment conditions, the *pgr*5 showed the lowest Φ_{II} among the three genotypes, and this difference was more pronounced under HL conditions.

The *pgr*5 mutant showed a clear decrease in photochemical quenching (qP) in comparison with the Wt and *pnsB*3 plants after 3 days of culture even under control conditions (Figure 2A). Treatment with either Atr or MV, especially under HL conditions, produced an even greater decrease in qP in the *pgr*5 mutant, and this reduction was more enhanced after culture for 6 days (Figure 2B). While both the Wt and *pnsB*3 mutant also showed decreases in qP under treatment with Atr or MV after 6 days of culture, the reduction in the *pgr*5 mutant was extreme. Since a low qP reflects a reduced plastoquinone pool, these results support the importance of the PGR5 pathway for the maintenance of electron transfer.

The *pgr*5 mutant also showed lower nonphotochemical quenching (qN) than the Wt and the *pnsB*3 mutant even under control untreated conditions (Figure 2C and D), indicating the importance of the PGR5 pathway for qN formation. On the other hand, treatment with Atr and MV did not affect qN in Wt and *psnB*3 under either LL or HL conditions. While the *pgr*5 mutant showed a reduced qN under all conditions, the differences among the genotypes were much smaller than those for qP (Figure 2C).

Treatment with Atr and MV and Photosynthesis-Related Gene Transcription in Mutants. Given that Atr and MV affected chlorophyll fluorescence parameters in both Wt and mutants significantly until 6 days of exposure, we collected 6-day-treated samples to analyze gene transcripts. The expression of genes related to PSI (*psa*D1), PSII (*psb*A), Fd (*fd*1 and *fd*2), FNR (*fnr*1 and *fnr*2), CET (*pnsB*3, *lhca*5, *ndh*H, *pnsB*1, *ppl*2, *ndh*N, *pgr*5, *pgrl*1A, and *pgr*1B), and the Calvin cycle (*rbc*L) was analyzed in Wt, *pnsB*3, and *pgr*5 plants under

dx.doi.org/10.1021/jf500143f | J. Agric. Food Chem. 2014, 62, 4083−4089

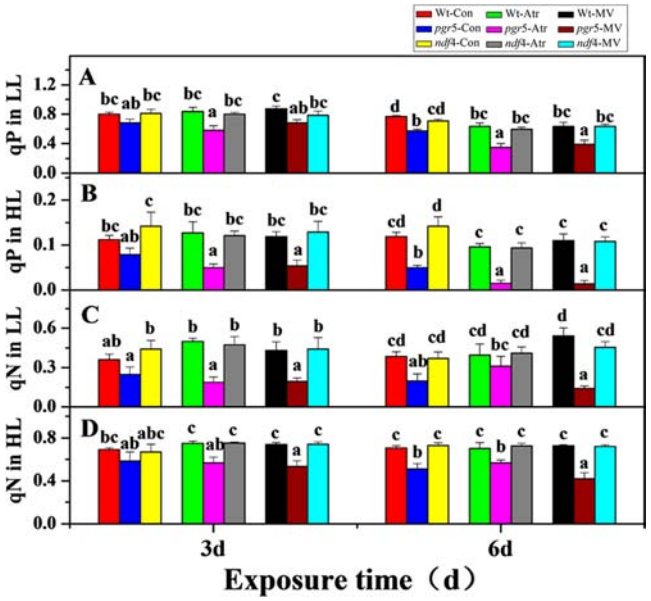

Figure 2. Effects of Atr and MV on the chlorophyll fluorescence parameters photochemical quenching (qP) and nonphotochemical quenching (qN) under LL and HL conditions. Different letters represent statistically significant differences at $p < 0.05$ based on one-way ANOVA.

control conditions after 6 days of culture without herbicide treatment (Figure 3). While there were no significant

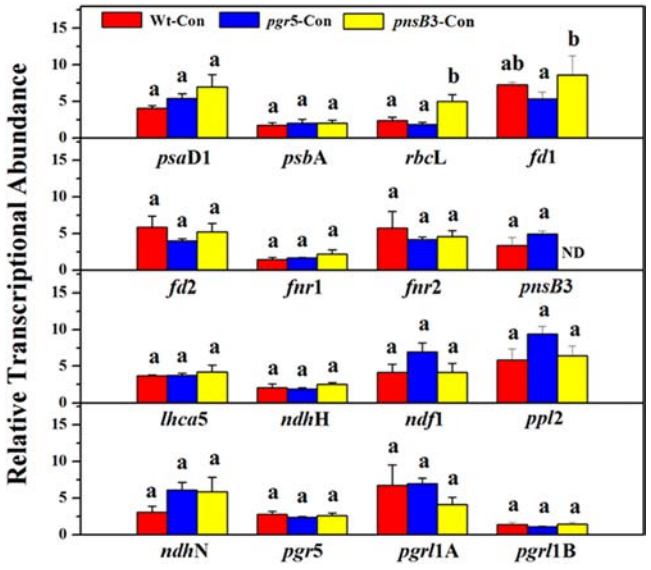

Figure 3. Differences in photosynthesis-related gene transcription between Wt plants and the two mutants. The mRNA levels of all of the examined genes are normalized to that of Actin 2. Different letters represent statistically significant differences at $p < 0.05$ based on one-way ANOVA.

differences in the transcript levels of many of these genes among the three genotypes, the *rbc*L transcript level in the *pnsB*3 mutant was higher than those in the Wt and *pgr*5 mutant and the transcript level of *fd*1 in the *pgr*5 mutant was lower than that in the *pnsB*3 mutant. Naturally, there was no transcription of the *pnsB*3 gene in the *pnsB*3 mutant.

When gene expression in seedlings that were treated with Atr or MV was compared with that in a control culture without treatment, the three genotypes showed considerably different responses. In the Wt plants, Atr and MV up-regulated the transcriptions of several photosynthesis-related genes (Figure 4A and B). In fact, the levels of 12 and 6 gene transcripts involved in the CET and LET pathways were up-regulated in Atr- and MV-treated samples, respectively, compared to the control. Interestingly, both Atr- and MV-treatment significantly increased transcript levels of *fnr*1, *pgrl*1A, and *pgrl*1B. On the other hand, the *pgr*5 and *pnsB*3 mutants showed much smaller increases than the Wt (Figure 4D−F). Only several genes were significantly increased in both *pgr*5/*pnsB*3 mutants treated with Atr and MV, although the genes that were increased differed between the *pgr*5 and *pnsB*3 mutants; e.g., none of the transcripts examined in the NDH pathway were increased in *pgr*5, whereas some showed an increase in the *pnsB*3 mutant (Figure 4C and E). The levels of the *fd*2, *pgr1*lA, and *psb*A transcripts were increased approximately 2-fold in Atr-treated *pnsB*3 mutant, whereas more than a 2-fold increase was observed for *fnr*1 and *pgr1*lB in Atr-treated *pgr*5 mutant.

Treatment with MV considerably decreased the transcript levels of most of the genes examined in both the *pgr*5 and *pnsB*3 mutants in comparison with those in the Wt (Figure 4D and F). The electrophoresis of the extracted RNAs confirmed that the mRNA of all samples was high quality (Figure S1 of the Supporting Information), indicating that the decrease of photosynthesis-related gene transcripts examined in CEF mutants was caused by herbicides treatment, not by RNA degradation in the extracted process, and that MV showed stronger inhibitory effect on gene transcript than Atr. These stronger effects of MV on gene expression were in contrast to its modest effects on photosynthetic activities as measured by chlorophyll fluorescence analysis.

Treatment with Atr and MV and the Accumulation of Chloroplast Proteins in Mutants. To confirm the effects of herbicides on protein accumulation in mutants, immunoblot analysis was conducted. While the accumulation of NDH complex proteins in the *pnsB*3 mutant or of proteins (PGR1 and PGRL1) in the PGR5 pathway in the *pgr*5 mutant was considerably reduced due to their respective mutations, the levels of other proteins were almost constant among the Wt and mutants under control growth conditions without herbicide treatment (Figure 5). Whereas treatment with Atr or MV increased the expression of many photosynthetic genes in Wt plants, these herbicides had only marginal effects on the accumulation of the corresponding proteins; e.g., while treatment with either Atr or MV increased the accumulation of PNSB3, Atr reduced, and PG increased, the accumulation of NDHH. The accumulation of PNSB1 was not significantly affected by herbicide treatment. Similarly, the effects of herbicides in both the *pgr*5 and *pns*B3 mutants were not as dramatic as the changes in transcript levels; while treatment with Atr decreased the accumulation of NDHH in *pgr*5 mutant, the accumulation of other NDH subunit proteins was unaffected by treatment with Atr or MV. There was a dramatic change in the accumulation of RbcL; while treatment with Atr reduced the accumulation of RbcL in Wt, it increased the accumulation of RbcL in both the *pgr*5 and *pns*B3 mutants, and treatment with MV did not affect the accumulation of RbcL in the Wt or mutants.

dx.doi.org/10.1021/jf500143f | J. Agric. Food Chem. 2014, 62, 4083−4089

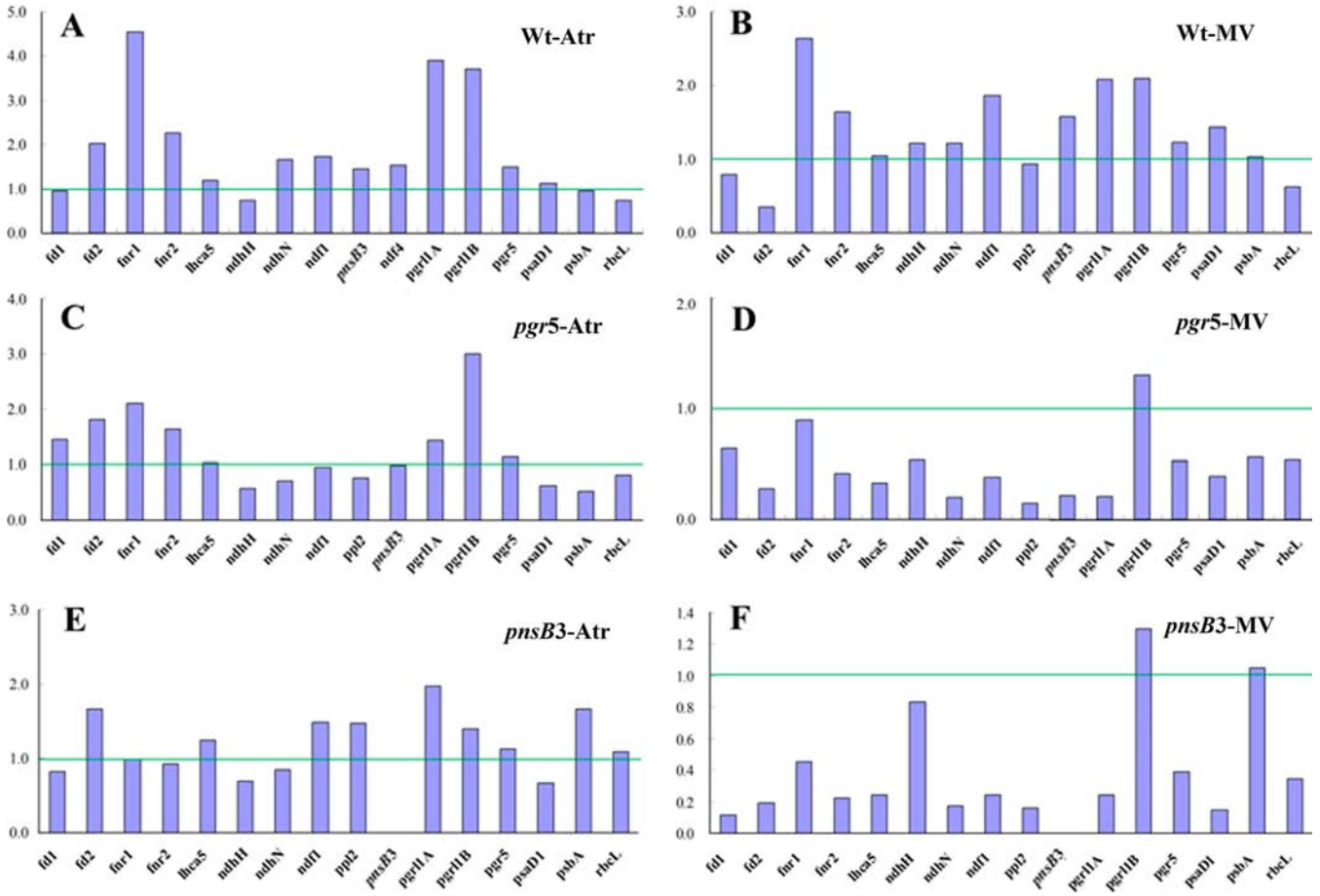

Figure 4. Relative transcript levels in Atr- and MV-treated plants compared to the corresponding controls. The columns indicate the relative transcript levels in treated plants compared to the corresponding controls. Transcript levels were measured using real-time PCR and normalized to the expression of the reference gene Actin 2. One indicates no change in transcript levels; <1 indicates a decrease in transcript levels; and >1 indicates an increase in transcript levels under drought stress compared to the control.

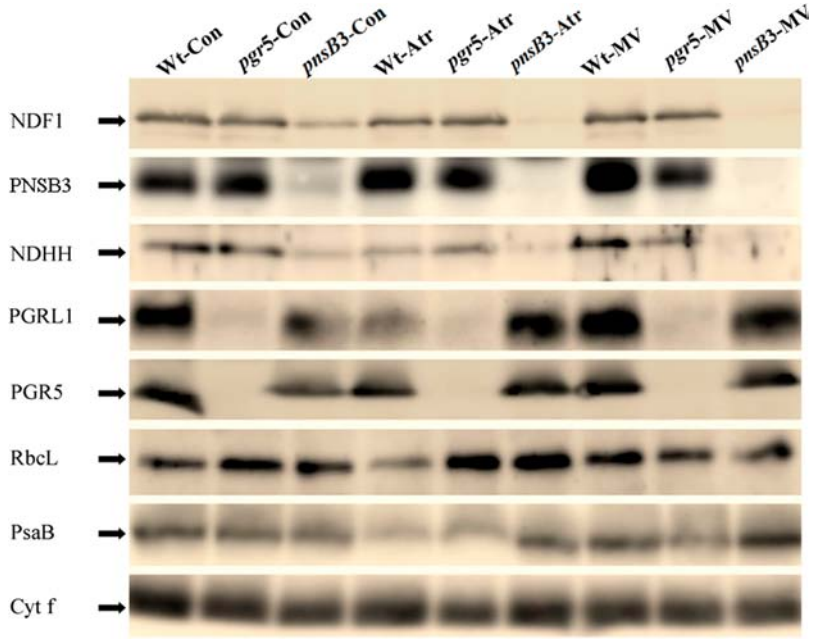

Figure 5. Effects of Atr and MV on translation of the following proteins: PNSB1, PNSB3, NDHH, PGRL1, PGR5, RbcL, PsaB, and Cyt f. Equal amounts of protein were extracted from the stroma and thylakoid membrane fractions, and the lanes were loaded with protein samples corresponding to 0.5 mg of Chl. All eight tested proteins were immunodetected using specific antibodies.

dx.doi.org/10.1021/jf500143f | J. Agric. Food Chem. 2014, 62, 4083−4089

DISCUSSION

We examined the effects of sublethal concentrations of Atr and MV, both of which are well-known photosystem-interfering herbicides that are widely used in agriculture,[20] on photosynthetic activity, gene expression, and protein accumulation in plants, since residual Atr and MV from farms contaminate soil, groundwater, rivers, and ponds and are frequently detected in the environment. The concentration of Atr has been shown to reach 120 μg/L in agricultural basins, 14 μg/L in urban basins, and 22 μg/L in river basins,[21] while the levels of MV in soil are as high as 8.1−35.02 ppm.[22] We used concentrations of Atr (0.2 μM, 51.2 μg/L) and MV (0.8 μM, 103 μg/L) that were close to the concentrations observed in the environment. We also used two CET mutants (*pgr*5 and *pnsB*3), which have mutations in the PGR5 and NDH pathways, since we expected that both Atr and MV would affect photosynthetic electron transport and, consequently, CEF. In fact, these two mutants grew well as Wt plants under herbicide-free conditions,[13,19] and they should be suitable for monitoring the effects of sublethal concentrations of herbicides.

Chlorophyll fluorescence was more sensitive to the herbicide treatment than chlorophyll content and other growth parameters, implicating that even if phenotypic symptoms are not detected, electron transfer may be disturbed before photodamage emerges, as reflected by F_v/F_m. Results from the chlorophyll fluorescence demonstrated that *pgr*5 mutant was more sensitive to the herbicide treatment than *pns*B3 mutant, implicating that the PGR5 pathway plays a crucial role in the regulation of electron transfer, and *pgr*5 mutants should be suitable plants for monitoring herbicides, especially photosystem-interfering herbicides. An interesting question raised by our results is how Atr and MV, which have different primary targets in electron transfer, induce similar effects in photosynthetic electron transfer, as reflected by chlorophyll fluorescence parameters. For example, the reduction of Φ_{II} and qP in Wt by MV (see Figure 2A and B), and the increase in qN in *pgr*5 by Atr (see Figure 2C) cannot be explained simply by inhibition of the primary targets of these chemicals. Furthermore, treatment with Atr and MV similarly enhanced transcripts of photosynthetic genes in Wt plants. One of the possible reason might be that both Atr and MV may form reactive oxygen species (ROS), which in turn may decrease the efficiency of electron transport, i.e., ΦII (Figure 1B and C) and qP (Figure 2A and B). Another possibility is the limitation of electron transfer through the cytochrome b6/f complex induced by the inhibition of PSII or by electron leakage through MV in PSI. This limited impairment of electron flow in cytochrome b6/f would be enhanced in *pgr*5 mutants, which should limit the transfer of electrons from PSI.

Another interesting finding is a discrepancy in the effects of these herbicides on gene transcript and protein translation. Two possibilities may exist for explaining this discrepancy. One was that sublethal concentrations of Atr and MV have very limited effects on photoinhibition, as reflected by the small changes in F_v/F_m. Thus, even if transcription is disturbed by these chemicals, their effects on protein accumulation are rather marginal. Another possibility is that *Arabidopsis* is a eukaryotic species and that it is uncoupling between gene transcription and translation; the dynamics of protein accumulation is different from that of transcription. Therefore, the differences at the protein level are probably not detectable at the same time points as transcription. While Atr and MV had similar effects on parameters of chlorophyll fluorescence, they showed considerably different effects on the transcription of several photosynthetic genes. Whereas the transcripts of many photosynthetic genes in Wt were induced by both chemicals, most of their transcripts decreased in CET mutants, especially by treatment with MV. This difference in their effects may be helpful for understanding the molecular responses of plants induced by low concentration of these two herbicides.

In conclusion, CET plays a crucial role in the regulation of photosynthetic electron transfer, and *pgr*5 mutant is more sensitive to photosystem-interfering chemicals. The *pgr*5 mutant should be a suitable plant for monitoring pollution by these chemicals. Chlorophyll fluorescence and transcript analysis are sensitive for detecting disturbance, and they can be given priority to analyze herbicide toxicity as biological parameters in sublethal concentrations.

ASSOCIATED CONTENT

Supporting Information

Sequences of the primer pairs used for real-time PCR; and detection of total RNA extracted from *Arabidopsis thaliana* with the RNeasy PlantMini Kit via agarose gel electrophoresis. This material is available free of charge via the Internet at http://pubs.acs.org.

AUTHOR INFORMATION

Corresponding Author

*. Haifeng Qian: hfqian@zjut.edu.cn (email), 86-571-88320742 (Tel), 86-571-88320599 (Fax). Tsuyoshi Endo: tuendo@kais.kyoto-u.ac.jp (email), 81-75-753-6381 (Tel), 81-75-753-6398 (Fax); Fumihiko Sato: fsato@lif.kyoto-u.ac.jp (email), 81-75-753-6381 (Tel), 81-75-753-6398 (Fax).

Funding

This work was supported in part by a Grant-in-Aid for a JSPS Fellowship (H.Q.).

Notes

The authors declare no competing financial interest.

ACKNOWLEDGMENTS

We would like to thank Shouko Kusama, Yasuyuki Yamada, Masahiro Ikeuchi, and Noriko Ishikawa for their help with some of the experiments.

REFERENCES

(1) Carter, A. D. Herbicide movement in soils: principles, pathways and processes. *Weed Res.* **2000**, *40*, 113−122.

(2) Pimentel, D. Amounts of pesticides reaching target pests: Environmental impacts and ethics. *J. Agric. Environ. Ethic.* **1995**, *8*, 17−29.

(3) Gavrilescu, M. Fate of pesticides in the environment and its bioremediation. *Eng. Life Sci.* **2005**, *5*, 497−525.

(4) Oettmeier, W. Herbicides of photosystem II. In *The Photosystems: Structure, Function and Molecular Biology*; Barber, J., Ed.; Elsevier Science Publishers: Amsterdam, 1992; pp 349−408.

(5) Hess, D. F. Light-dependent herbicides: An overview. *Weed. Sci.* **2000**, *48*, 160−170.

(6) Holt, J. S. Mechanisms and agronomic aspects of herbicide resistance. *Annu. Rev. Plant Physiol. Plant Mol. Biol.* **1993**, *44*, 203−229.

(7) Dodge, A. D. Herbicides interacting with photosystem I. In *Herbicides and Plant Metabolism*; Dodge, A. D., Ed.; Cambridge University Press: Cambridge, 1989; pp 37−50.

(8) Joliot, P.; Joliot, A. Cyclic electron transfer in plant leaf. *Proc. Natl. Acad. Sci. U.S.A.* **2002**, *99*, 10209−10214.

(9) Kramer, D. M.; Avenson, T. J.; Edwards, G. E. Dynamic flexibility in the light reactions of photosynthesis governed by both electron and proton transfer reactions. *Trends. Plant. Sci.* **2004**, *9*, 349−357.
(10) Miyake, C.; Horiguchi, S.; Makino, A.; Shinzaki, Y.; Yamamoto, H.; Tomizawa, K. Effects of light intensity on cyclic electron flow around PSI and its relationship to non-photochemical quenching of chl fluorescence in tobacco leaves. *Plant. Cell. Physiol.* **2005**, *46*, 1819−1830.
(11) Lehtimäki, N.; Lintala, M.; Allahverdiyeva, Y.; Aro, E. M.; Mulo, P. Drought stress-induced upregulation of components involved in ferredoxin-dependent cyclic electron transfer. *J. Plant. Physiol.* **2010**, *167*, 1018−1022.
(12) Endo, T.; Ishida, S.; Ishikawa, N.; Sato, F. Chloroplastic NAD(P)H dehydrogenase complex and cyclic electron transport around photosystem I. *Mol. Cells* **2008**, *25*, 158−162.
(13) Munekage, Y.; Hashimoto, M.; Miyake, C.; Tomizawa, K. I.; Endo, T.; Tasaka, M.; Shikanai, T. Cyclic electron flow around photosystem I is essential for photosynthesis. *Nature* **2004**, *429*, 579−582.
(14) Shikanai, T. Cyclic electron transport around photosystem I: Genetic approaches. *Annu. Rev. Plant. Biol.* **2007**, *58*, 199−217.
(15) Miyake, C. Alternative electron flows (water−water cycle and cyclic electron flow around PSI) in photosynthesis: molecular mechanisms and physiological functions. *Plant Cell Physiol.* **2010**, *51*, 1951−1963.
(16) Takahashi, S.; Badger, M. R. Photoprotection in plants: a new light on photosystem II damage. *Trends Plant Sci.* **2011**, *16*, 53−60.
(17) Niyogi, K. K. Photoprotection revisited: genetic and molecular approaches. *Annu. Rev. Plant. Physiol. Plant. Mol. Biol.* **1999**, *50*, 333−359.
(18) Munekage, Y.; Hojo, M.; Meurer, J.; Endo, T.; Tasaka, M.; Shikanai, T. PGR5 involved in cyclic electron flow around photosystem I and is essential for photoprotection in *Arabidopsis*. *Cell* **2002**, *110*, 361−371.
(19) Takabayashi, A.; Ishikawa, N.; Obayashi, T.; Ishida, S.; Obokata, J.; Endo, T.; Sato, F. Three novel subunits of *Arabidopsis* chloroplastic NAD(P)H dehydrogenase identified by bioinformatic and reverse genetic approaches. *Plant. J.* **2009**, *57*, 207−219.
(20) National Agricultural Statistics Service (NASS) [Internet]. Quick Stats; United States Department of Agriculture: 2011; http://www.quickstats.nass.usda.gov/.
(21) Cox, C. Atrazine: environmental contamination and ecological effects. *J. Pest. Reform.* **2001**, *21*, 12−20.
(22) Roberts, T. R.; Dyson, M. C. G.; Lane, J. S. Deactivation of the biological activity of paraquat in the soil environment: a review of long-term environmental fate. *J. Agric. Food. Chem.* **2002**, *50*, 3623−3631.
(23) Sato, F.; Takeda, S.; Yamada, Y. A comparison of effects of several herbicides on photoautotrophic, photomixotrophic and heterotrophic cultured tobacco cells and seedlings. *Plant. Cell. Rep.* **1987**, *6*, 401−404.
(24) Inskeep, W. P.; Bloom, P. R. Extinction Coefficients of Chlorophyll a and b in N, N-Dimethylformamide and 80% Acetone. *Plant Physiol.* **1985**, *77* (2), 483−485.
(25) van Kooten, O.; Snel, J. F. H. The use of chlorophyll fluorescence nomenclature in plant stress physiology. *Photosynth. Res.* **1990**, *25*, 147−150.
(26) Livak, K. J.; Schmittgen, T. D. Analysis of relative gene expression data using real-time quantitative PCR and the $2^{-\Delta\Delta Ct}$ method. *Methods* **2001**, *25*, 402−408.

JOURNAL OF AGRICULTURAL AND FOOD CHEMISTRY

Article

pubs.acs.org/JAFC

Improvement in Day Zero Recoveries in Field Soil Dissipation Studies Using Larger Diameter Soil Samples

Ashok K. Sharma,* Harry J. Strek,† and Aldos C. Barefoot

Stine Haskell Research Center, E. I. DuPont de Nemours and Co., Newark, Delaware 19711, United States

ABSTRACT: Obtaining acceptable recovery of the applied test substance at zero time in field soil dissipation studies has been a subject of considerable interest among scientists conducting regulatory field studies. In particular, achieving recoveries of ≥90% in soil samples collected immediately after applications in most studies has been elusive. This study investigated a modified soil sampling method, which could be used not only on day zero but for the entire study duration, to see if the recoveries in soil samples, especially in the early stages, can be improved. The modified sampling system has demonstrated that recoveries averaging 90% are possible and can be routinely obtained on day zero. Description of this modified sampling procedure and statistical analysis of the data collected for day zero samples are discussed.

KEYWORDS: *day zero recoveries, field dissipation studies, large diameter soil cores*

INTRODUCTION

Field dissipation studies for crop protection chemicals are an important and expensive portion of the environmental fate studies required for registration of new agrochemicals. Typically, a test substance is applied to a leveled bare soil plot of suitable size, and then soil samples are collected in 6 in. depth segments to a depth of 36 in.[1,2] or more. Soil sampling is typically initiated immediately after application (zero time samples) and continued until substantial dissipation of the applied chemical and its metabolites has been demonstrated. To meet the study objectives, it is essential to achieve a nearly quantitative recovery of the applied chemical in zero time samples, commonly referred to as day zero samples. As noted in the EPA's guideline[1] "time zero concentration lays the foundation for all subsequent sampling and is used to build confidence that the pesticide was applied uniformly and accurately".

Using the commonly employed soil sampling procedures, in which soil cores of approximately 2 in. diameter are collected in 6 in. depth segments, the uppermost 6 in. deep sample should have 100% of the applied chemical at time zero. However, such day zero samples frequently fail to show acceptable recovery. Zero time recoveries are often below 75−80% and display high levels of variability. This shortcoming has been a subject of several symposia at agrochemical scientific conferences[4] and the EPA's rejection rate analysis,[3] as well as several presentations at scientific conferences.[5,6]

Low recoveries at day zero have been considered a significant deficiency in the conduct of field dissipation studies, because they imply either gross errors in the chemicals' application process, poor sampling technique, or deficient analytical methods. Although all of these factors can cause poor recoveries in theory, application methods and analytical methods were set aside as major causes because the test substance applications are typically conducted by skilled field and laboratory personnel and always initiated under favorable weather conditions. Analytical methods employed are usually robust and typically deliver 80−110% recoveries in concurrent analysis with 10−15% standard deviation; otherwise, the methods would be unacceptable for regulatory authorities. On the basis of the analytical methods' capabilities averaging 90% recovery, day zero soil sample recoveries of equal magnitude should be achievable.

Before embarking on attempts to improve the recoveries, we analyzed the data available from a large number of our own field studies as well as information from recent symposia. Data compiled in appendices of ref 4 provided a good starting point to formulate a working hypothesis. The hypothesis was that better recoveries in soil cores could be achieved if the amount of treated soil, as a percentage of the total sample collected, could be increased substantially by not only increasing the sampled area but reducing the sample depth at the same time. Our statistical analysis of data in ref 4 indicated that day zero recoveries based on the secondary sample type (Figure 1), such

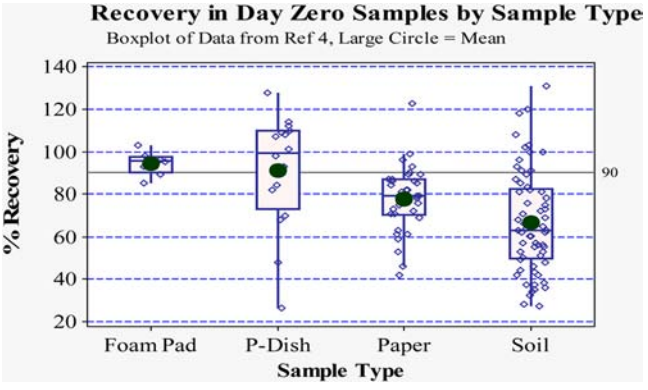

Figure 1. Recovery in day zero samples by sample type box plot of data from ref 4. Large circle = mean.

Received: February 4, 2014
Revised: April 13, 2014
Accepted: April 15, 2014
Published: April 15, 2014

 © 2014 American Chemical Society

as Petri dishes and foam pads, were consistently good but soil samples collected to 6 in. depth were frequently quite deficient. A different perspective of the same data, illustrated in Figure 2,

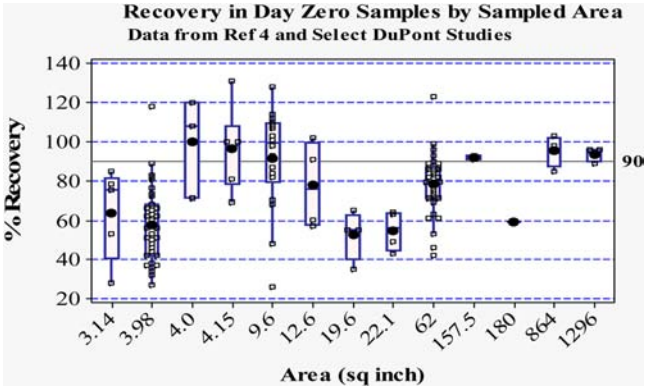

Figure 2. Recovery in day zero samples by sampled area [data from ref 4 and select DuPont studies].

focused on the surface area sampled without regard to the device used. It also suggested that samples with larger surface area had a higher probability of achieving good recovery. In our opinion, secondary devices frequently achieved good recoveries primarily because they have a larger surface area than soil cores. In our own experience also, secondary devices such as Petri dishes or papers, which had a larger surface area, and in which the applied test substance could be analyzed without the encumbrances associated with the soil homogenization and matrix extractions, were generally successful in obtaining good day zero recoveries. However, 2 in. diameter soil cores collected to 6 in. depth, a method used consistently at all sampling intervals, invariably showed day zero recoveries that seldom exceeded 75−80%.

Our objective, therefore, was to determine if the soil sampling method or sampling device could be modified so that the day zero recoveries in soil cores collected could be improved substantially. This was important not only because the degradation kinetics always employ the soil core data but also because it is the only device used over the entire study duration. If day zero recoveries in soil cores are unreliable, one cannot be certain at which later sampling intervals the recoveries begin to be reliable. The secondary devices can verify application rates; however, they can be used only at day zero but not for later sampling intervals. We postulated that if a chemical can be applied accurately as often supported by the recoveries in secondary monitoring devices, then for a vast majority of the agrochemicals, and for most of the formulations employed, recoveries equivalent to the average recovery delivered by the analytical method should be achievable in soil samples.

MATERIALS AND METHODS

We assumed that low recoveries in 6 in. deep soil cores having a 2 in. diameter were possibly due to two shortcomings of these soil samples. First, the portion of soil in a 6 in. deep sample carrying the applied test chemical on day zero was miniscule (approximately 1%) as compared with the total amount of soil sampled. Unless homogenization procedures capture this entire residue and mixe it uniformly in the entire sample, lower recoveries would be encountered. One possible solution was to collect the uppermost soil sample to depth of 2 in., instead of the traditional 6 in. depth. Second, a 2 in. surface area for sampling the uppermost soil sample appeared inadequate because the small surface area in a field study was vulnerable to spot-to-spot variability of the residue present on soil surface. Therefore, we decided to collect a larger surface area of at least 4 in. or possibly 6 in. diameter to a depth of only 2 in. for the uppermost sample.

Although soil cores of larger than 2 in. diameter have been attempted by many working in this area, sampling has generally been to a typical 6 in. depth. Perhaps for that reason, we are not aware of any published studies that have demonstrated consistently high recoveries in large-diameter soil samples. In particular, increasing the collection of treated soil as a percentage of total sample by collecting a shallower depth was considered an essential element of sampling the uppermost soil core. To our knowledge a systematic study that utilized a combination of larger surface area and shallow depth for sampling the uppermost soil sample has not been reported in peer-reviewed literature. Initially, we decided to evaluate a comparison of a shallower uppermost depth of only 2 in. instead of 6 in. and a larger surface area

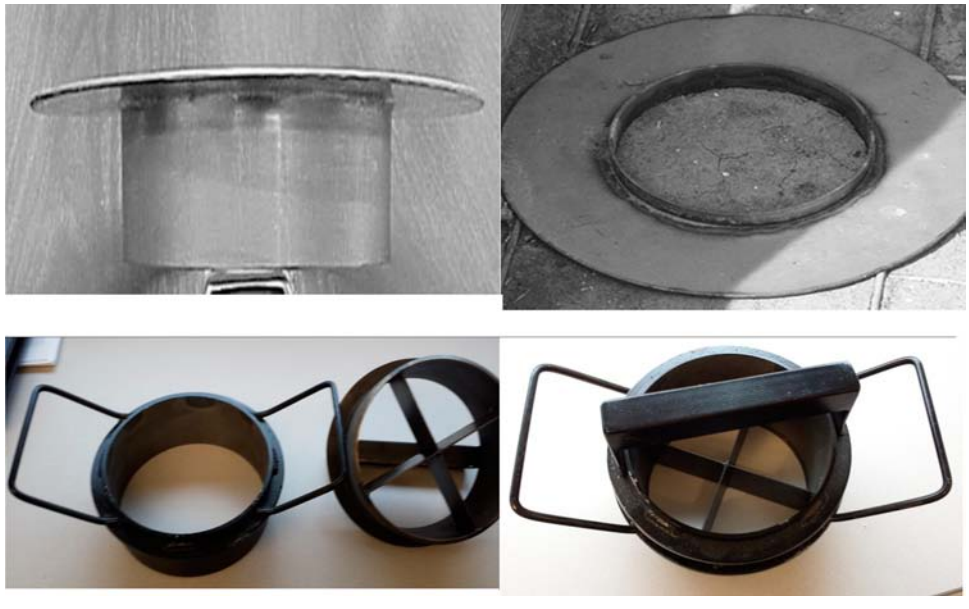

Figure 3. Large-diameter soil sampling devices.

dx.doi.org/10.1021/jf500607r | J. Agric. Food Chem. 2014, 62, 4090−4094

of 4−6 in. diameter in parallel with traditional 2 in. on day zero to determine if such sampling leads to better day zero recoveries.

To test this hypothesis, we conducted multiple types of soil sampling within the same studies at four sites each in the United States and European Union. In conformance with regulatory guidelines, three replicate samples, each composed of five cores sampled from randomly selected areas, were collected at each location and for each sample type. Within each study, at least two types of soil samples were collected for the uppermost soil horizon. One of the sample types was a set of traditional 2 in. (5 cm) cores with standard 6 in. (15 cm) depth; a second set was of either medium core (4 in. diameter) or large core (6 in. diameter), both to a 2 in. depth. Collection of the 2 in. depth soil samples was performed using the device displayed in Figure 3. Such devices, which had ca. 4 in. internal diameter in the European studies and ca. 6 in. diameter in the U.S. studies, were collected by pressing the device into the soil until the upper lip was in line with the soil surface. Soil inside this sampler was collected using a spoonlike implement by scraping soil to a 2 in. depth. The depth sampled was easily noted when soil up to the bottom of this device had been removed. After uppermost depth had been collected, the device remained in place until all lower depth soil sampling had been completed. In each case, lower depths were sampled as usual, namely, 2 in. diameter samples for all deeper soil samples, although the depth of these lower segments was changed slightly from the regular 6 in. (illustrated in Figure 4).

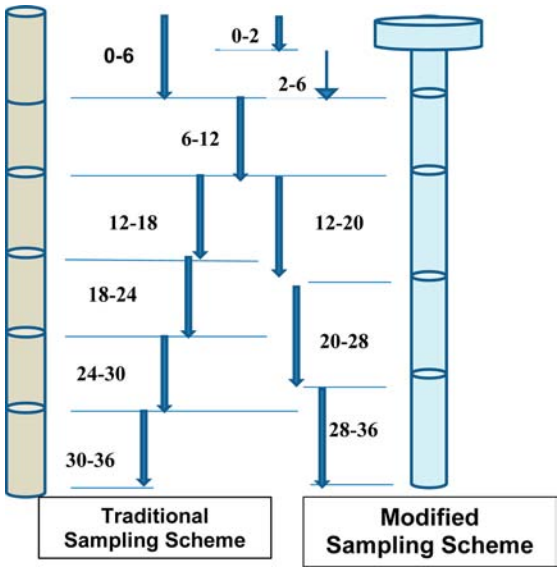

Figure 4. Traditional and modified soil sampling schemes (depth segments in inches).

All soil samples were five replicate cores combined to generate one sample. The combined sample, typically weighing 2−3 kg for 2 in. cores, 4−5 kg for 4 in. cores, and 7−8 kg for 6 in. cores, was homogenized using a mechanical soil mixer with added dry ice to prevent chemical changes during homogenization. After homogenization, a subsample weighing approximately 500 g was saved for analysis and stored in a freezer until the start of analysis. Typically, 10 g aliquots of homogenized soil were extracted and analyzed using analytical methods specific for the test substance applied. For the purpose of this paper, only the uppermost depth samples are reported because the test substance resides only in the uppermost samples on day zero. Remaining lower depth samples were also analyzed and submitted to various regulatory authorities. Because the depth segments using the two devices were different, a comparison of the data by these two methods was possible by converting the residues obtained in parts per billion into mass per unit area (g/ha or lb/acre) and were then calculated as percent of applied amounts. Equations for such calculations are shown below:

$$\text{residue}\left(\frac{\text{g}}{\text{ha}}\right) = \frac{\text{ppb in soil sample}\left(\frac{\text{ng}}{\text{g}}\right) \times \text{wt of 5 cores (g)} \times \text{area 1 ha (sq cm)}}{\text{surface area of 5 cores (sq cm)} \times \text{conversion factor}\left(\frac{\text{ng}}{\text{g}}\right)}$$

$$\text{recovery (\%)} = \frac{\left(\frac{\text{g}}{\text{ha}}\right)\text{found} \times 100}{\left(\frac{\text{g}}{\text{ha}}\right)\text{applied}}$$

One calculation for illustrative purposes is shown below:

ppb in soil = 209.10

soil weight of 5 cores (g) = 7146.9

inside diameter of 2 in. deep core = 15.3 cm (radius = 7.65cm)

surface area of 5 cores = 5 × pi × $(7.65\ \text{cm})^2$ = 919.269 sq cm

area of 1 ha in sq cm = 10^8 sq cm

Therefore

$$\text{g/ha in sample} = \frac{7146.9\ \text{g} \times 209.100\ \text{ppb} \times 10^8\ \text{sq cm/ha}}{(10^9\ \text{ng/g} \times 919.269\ \text{sq cm})} = 162.57\ \text{g/ha}$$

amount applied = 200 g/ha

recovery (%) = (162.57 × 100)/200 = 81.3%

Soils weights and areas used were for five cores because five replicate cores were collected and combined to obtain one sample for analysis as is customary in regulatory studies. When multiple samples of each type were collected in a study, the replicates were not averaged for statistical analysis and the residues were not corrected for fresh fortification recoveries. The analytical method employed in the initial investigation provided 92% recovery with 10% standard deviation. Recovery numbers obtained were rounded to one decimal place for use in statistics. All statistical analysis was conducted using Minitab software, version 16.1.

RESULTS AND DISCUSSION

Results from the initial trials (four in the United States and four in the European Union), where a small diameter (2.25 in. surface diameter) and an additional either 3.8 or 5.75 in. diameter sample had been collected for the uppermost depth, are displayed in Figure 5. These samples were collected concurrently from the same test sites and for the same chemical applied. Samples collected were analyzed by using the same method for comparison of recoveries on day zero (note 3.75 and 5.75 in. diameter samples are sometimes referred to as 4 or 6 in. samples for simplicity). Data summarized in Figure 5 (24 samples of each type) illustrated that larger diameter soil cores collected to a shallower depth were indeed more accurate in demonstrating the day zero residues. Whereas small-diameter samples found an average 80% recovery for all samples collected, the larger cores averaged >90%. Statistically the difference in recoveries was significant when small-core data were compared with medium (3.75 in.) or larger cores (5.75 in.). In the studies conducted in the United States, we even analyzed a separate set of 10 large-diameter samples as single replicates and compared them with their respective 5-sample composites (obtained by combining 5 large cores from one

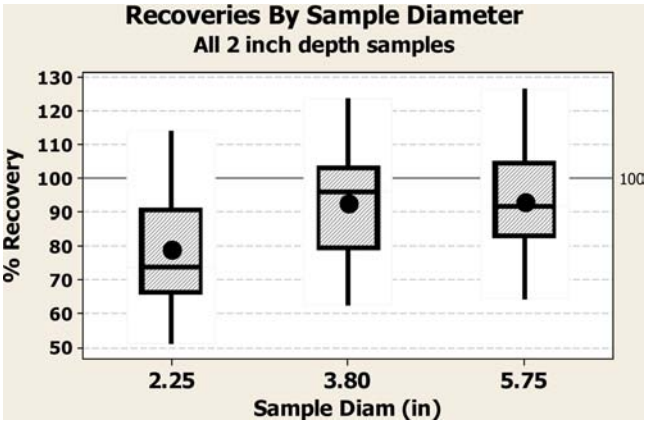

Figure 5. Day zero recoveries using small- and large-diameter devices.

subplot) to see if each individual sample also achieved the desired results of acceptable recovery. Even the single-replicate samples (Figure 6) showed an average recovery in the 90%

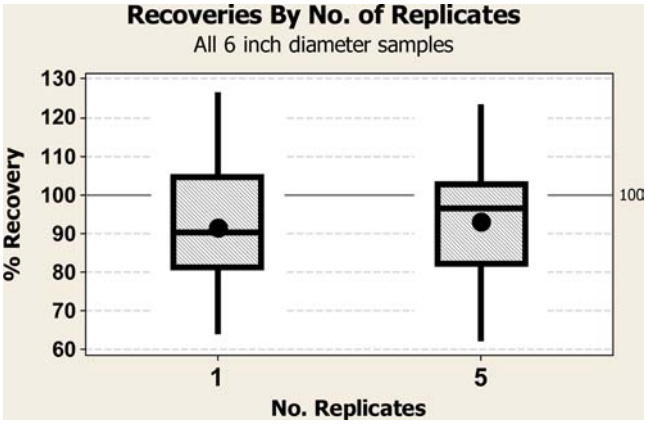

Figure 6. Large diameter sample recoveries by number of replicates.

range, even though sample-to-sample variability was somewhat higher as compared to the 5-sample composites. These results appeared to validate the hypothesis that acceptable recovery in day zero samples could be achieved if larger-diameter samples were collected to a shallow depth for the uppermost soil samples.

As a result of the encouraging data from trial experiments described above, we changed our sampling practice for subsequent field dissipation studies to collect the uppermost soil sample as a minimum 4 in. diameter and only to a 2 in. depth (modified sampling illustrated in Figure 4). For practical reasons, our European contract facilities have all adopted the medium (10 cm internal diameter) devices, whereas all U.S. cooperators have been using the larger (5.75 in. internal diameter) device, not only for day zero samples but for the entire study duration. The reason for extending this sampling practice beyond day zero was that we do not always know in advance when a test substance will have migrated into lower depths. Moreover, varying sampling practices within the same study could create bias among various intervals due to changing sampling methods. Once the uppermost sample is collected with a spoonlike implement, the large-diameter sampler is kept in place and all lower depth samples are collected from areas inside this device. Because these larger diameter devices have been adopted into practice, our day zero samples from most field studies have shown consistently improved recoveries (Figure 7). Results from more than 40 field studies (N = 161 is

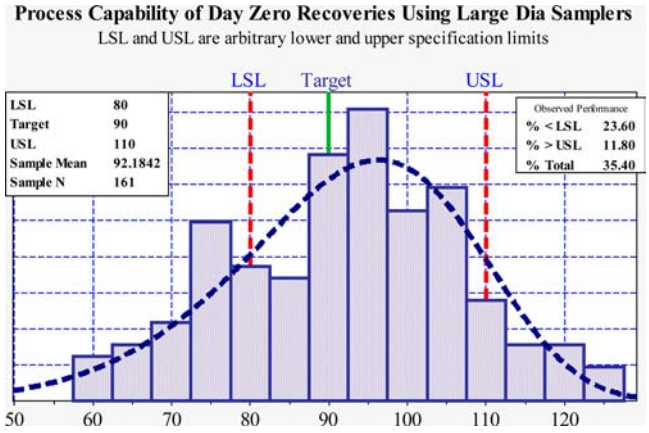

Figure 7. Day zero recoveries using larger diameter 2 in. deep cores.

the total number of day zero samples from all studies) conducted over 5 years and with four different test substances applied at different use rates are summarized in Figure 7. It should be noted that all four test substances were nonvolatile (chlorsulfuron, penthiopyrad, chlorantraniliprole, and cyantraniliprole) but had significantly different physicochemical properties. Even though water solubility, dissipation rates, or formulations used varied substantially among these compounds, we do not believe such properties have a significant impact on the capability of achieving good day zero recoveries.

For statistical analysis, 80 and 110% were arbitrarily chosen as the lower and upper specification limits (LSL and USL, respectively) because most of the analytical method recoveries were in the same range, and average analytical method recovery of about 90% for all four compounds was set as the target. In addition, choice of lower and upper specification limits for recoveries in the 80−110% range was based on the assumption that such results are considered acceptable by most regulatory authorities. Selection of a somewhat less strict specification of 70% for the LSL and 120% for the USL would also be acceptable, and Figure 7 shows essentially all results obtained are within the less strict range. We still encounter <80% recoveries in some individual samples, as is obvious from the illustration in Figure 7; however, such occurrences are less frequent with our modified sampling system. Undoubtedly, factors other than sampling methods (such as inadvertent errors in sample collection, homogenization, or analysis) continue to play a role. Nevertheless, results from nearly 45 field studies conducted within the past 5 years have shown that fewer than 23.6% samples displayed recoveries below 80%. Within this data set, we examined if the amount of test substance applied or the nature of chemical carried any statistical significance (Figure 8). Analysis of means (at 95% confidence) based on such groups did not display dependence of recoveries, either on the nature of the test substance or on the application rate for chemicals used. Instead, the variability simply reflected the variability observed in the analytical method for analysis of a large number of samples. A somewhat lower average recovery for one test compound (TM-1) was in line with slightly lower average recoveries in fresh fortifications for the analytical method employed for that compound and had nothing to do with the nature of this compound. In our view, this new sampling method may help improve day zero

dx.doi.org/10.1021/jf500607r | J. Agric. Food Chem. 2014, 62, 4090−4094

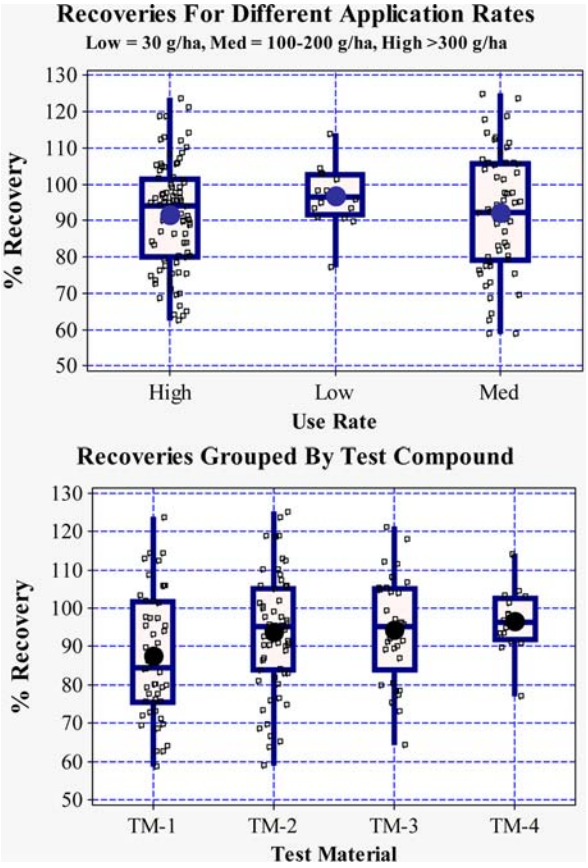

Figure 8. Recoveries based on test substance and application rates.

recoveries for all test compounds, regardless of the use rate, chemical structure, or formulation used.

Use of 6 in. diameter devices for sampling the uppermost 2 in. of soil as a standard practice is currently carried out using our most recent sampler[7] displayed in the bottom part of Figure 3. This sampler is a two-piece device, in which the inner piece with four quadrants is placed inside the outer casing, shown on the left side of the figure. The assembled device is pressed into soil with a hydraulic press. The lip at the top of the outer casing stops the device at a 2 in. depth. Technicians can grab the handle and rotate the inner piece of this sampler by approximately 30°, which cleanly separates the uppermost 2 in. of soil from the column below. The inner piece can be lifted and held above a bag into which soil is dislodged by gently hitting the device with a rubber hammer. The inside device quadrants assist in not only separating the uppermost 2 in. of soil but also help keep the soil in place while the inside portion is lifted. If a portion of the soil falls within the outer casing, it is recovered using a spoonlike implement.

An important point worth reiterating is that large-diameter samplers are effective in combination with a shallow (2 in.) depth only, and the 6 in. diameter is perhaps the upper limit beyond which any further increase in area sampled begins to create homogenization issues. Five replicate cores (6 in. diameter−2 in. depth] composited to obtain one sample generate soil samples that weigh 7−9 kg. The homogenization equipment in use at most facilities we work with can handle samples of 2−10 kg, but work best for 2−5 kg sample sizes. Larger diameter cores collected to 6 in. depths will lead to substantially large sample weights (around 20 kg), and homogenization issues will again negate the advantage offered by larger surface area. For this reason, we have not attempted using large-diameter cores for any lower depths or any >2 in. depth samples.

In conclusion, instead of collecting 2 in. diameter soil cores to a 6 in. depth for the uppermost soil sample (a standard practice), a larger diameter device and collection of a shallower depth for the uppermost soil core can be used to achieve a significant improvement in day zero recoveries.

AUTHOR INFORMATION

Present Address

[†](H.J.S.) Bayer Crop Sciences, Germany.

Notes

The authors declare no competing financial interest.

ACKNOWLEDGMENTS

We acknowledge contributions made by Fred Rice of ABC Laboratories, Columbia, MO, USA; Jeff Old of Charles River Laboratories, Scotland, UK; and Mick Qualls of Qualls Research, Ephrata, WA, USA.

REFERENCES

(1) U.S. EPA Office of Pesticide Programs. *Fate, Transport and Transformation Test Guidelines*; Washington, DC, USA, 2008; OPPTS 835.6100.

(2) European Union. *Council Directive 91/414/EEC, Rev 7.0, Annex 1, Fate and Behavior in the Environment*, 2007; 7.1.1.2.2, Field Studies.

(3) U.S. EPA. *Pesticide Reregistration Rejection Rate Analysis, Environmental Fate*; Washington, DC, USA, 1993; EPA 738-R-93-010.

(4) Graham, D. G.; Clay, V.; Jackson, S. H.; Jones, R. Field soil dissipation studies: the measurement of zero-time residues. In *Terrestrial Field Dissipation Studies*; ACS Symposium Series 842; Arthur, E. L., Barefoot, A. C., Clay, V. E., Eds.; American Chemical Society: Washington, DC, USA, 2003.

(5) Portions of this work presented at the following conferences: Sharma, A. K.; Strek, H. J.; Barefoot, A. C. ACS National Meeting, Washington, DC, 2005. Huber, A.; Strek, H. J.; Sharma, A. K. XIII Symposium. Pesticide Chemistry−Environmental Fate and Human Health, Univ. Sacre Cuore, Piacenza, Italy, 2007.

(6) U.S. Environmental Protection Agency and Pest Management Regulatory Agency (PMRA), Canada. ACS National Meeting, Anaheim, CA, USA, 2004.

(7) Device in Figure 8 was fabricated by Mick Qualls, Qualls Agricultural Laboratory, 3975 Dodson Road N., Ephrata, WA, USA. (e-mail: mqualls@qa-lab.com).

JOURNAL OF AGRICULTURAL AND FOOD CHEMISTRY

Article

pubs.acs.org/JAFC

Long-Term Experiment with Orchard Floor Management Systems: Influence on Apple Yield and Chemical Composition

Ana Slatnar,*[,†] Maria Licznar-Malanczuk,[‡] Maja Mikulic-Petkovsek,[†] Franci Stampar,[†] and Robert Veberic[†]

[†]Biotechnical Faculty, Agronomy Department, Chair for Fruit, Wine and Vegetable Growing, University of Ljubljana, Jamnikarjeva 101, SI-1000 Ljubljana, Slovenia

[‡]Faculty of Live Sciences and Technology, Department of Horticulture, University of Environmental and Life Sciences, , Grunwaldzki 24a, 50-363 Wroclaw, Poland

ABSTRACT: The study focuses on the response of apple primary and secondary metabolism and some important quality parameters to three living mulch treatments, classical herbicide fallow, and black polypropylene strip application in two apple cultivars. Primary and secondary metabolites were analyzed after 10 years of ground cover experiments. Soluble solids, firmness, and color measurements indicate differences among orchard floor management treatments. Significantly, lower levels of individual sugars have been measured in fruit of different living mulch treatments compared with fruit harvested from trees subjected to the herbicide strip treatment. Total sugar content was higher in fruit of the herbicide strip treatment in both cultivars analyzed. Significantly higher levels of total organic acids were only detected in 'Pinova' fruit of the *Festuca ovina* L. treatment. Long-term response of both cultivars to living mulch treatments indicated that apples increase the accumulation of almost all analyzed individual phenolic compounds.

KEYWORDS: *Malus domestica Borkh., living mulch, black polypropylene strip, sugars, organic acids, phenolics*

INTRODUCTION

Proper choice of orchard floor management system protects the soil from weed occurrence, reduces soil erodability, improves the supply of water and nutrients to the plants, and supports sustainable fruit production for many decades.[1] Among several weed control options applicable in organic fruit production, the introduction of living mulch (green cover plants) deserves particular consideration because of its potential benefits to orchard biodiversity and improvement of soil quality.[2] Moreover, living mulch protects the soil surface similar to sod during the vegetation periods of fruit trees.[3] The widespread adoption of this system is hindered by the fact that the covering plant competes with the fruit tree, which can potentially result in reduced growth and yield of the fruit crop.[2] An effective cropping system can be maintained with a living mulch strip to control water runoff and soil erosion. These plants can also produce suitable allelochemicals to control weed seed germination and possibly suppress established weeds without affecting growth and yield of the primary crop. The living mulch should be noncompetitive or easily suppressed to render it noncompetitive without losing its allopathic characteristics. This might be accomplished by gene transfer from an organism known to have allopathic characteristics, such as subterranean clover, into a compatible living mulch plant.[2]

The implementation of living mulch in the rows of apple trees was shown to delay the beginning of cropping[4−6] and often contributed to the reduction of cumulative yield in the years of fruit production peak.[1,7] Experiments monitoring fruit trees of various stages consistently determined significantly lower competition of annual cover crop species compared to perennials.[8,9] The application of living mulch affects both external and internal fruit quality parameters. Hornig and Bünemann[10] analyzed fruit from a young apple orchard and reported that white clover (*Trifolium repens* L.) living mulch led to a reduction of mean fruit weight compared to a herbicide treatment. On the contrary, Lipecki and Wieniarska[8] could not confirm any significant differences in fruit quality when comparing several annual species used as a green cover. It has additionally been determined that the introduction of living mulch, particularly grass species, contributes to an increase of red surface skin area of apple fruits.[10,11] This effect could also be observed in full cropping period of the trees.[9]

Apples are a rich source of different classes of phenolic compounds. They have been reported as a source of naturally occurring antioxidants, which contribute to prevention of oxidative damage caused by free radicals which lead to development of many chronic human diseases.[12] The content and profile of phenolics in fruit is influenced by several factors, including climate,[13] the effect of light,[14] cultivars,[15,16] temperature, mineral nutrition, water management, grafting, application of elicitors, stimulating agents, plant activators,[17] and exposure to various kind of stress.[18] Mikulic-Petkovsek et al.[15] established that organically grown apples exhibited a higher content of phenolic compounds in apple compared to apples cultivated according to integrated practices. This may be due to the absence of synthetic fertilizers, pesticides, and growth regulators, which are banned in organic production. Therefore, organically grown plants are more exposed to environmental

Received: February 18, 2014
Revised: April 15, 2014
Accepted: April 15, 2014
Published: April 15, 2014

ACS Publications © 2014 American Chemical Society

stress and form specific stress metabolites which can beneficially contribute to internal fruit quality.[18]

The present trial was conducted to evaluate the long-term effects of different living mulches on selected quality parameters and content and diversity of primary and secondary metabolites in comparison to traditional herbicide strip weed prevention. It is important to identify the production systems which stimulate the synthesis of important plant metabolites and simultaneously present a minimal negative impact on the environment. The aim of this study was to determine the influence of different ground cover management systems (many years of orchard floor treatment) on fruit quality parameters, and profiles of primary and secondary metabolites after a ten-year period of tree adaptation. Up to the present date, research has been limited to short-term experiments and did not focus on the effect of living mulches on primary and secondary metabolites.

MATERIALS AND METHODS

Field Experimental. Apple trees (*Malus domestica* Borkh.) of the 'Ligol' and 'Pinova' cv. grafted on a semidwarf rootstock P2 were planted in spring 2004 at the planting distance of 3.5 m × 1.2 m (2380 trees per ha) on the haplic luvisol derived from silty light loam. The trees were planted at the Fruit Experimental Station in Samotwor (51°06′12″N, 16°49′52″E) managed by the University of Environmental and Life Sciences in Wroclaw (Poland). The average annual temperature of this area is 8.6 °C and the total rainfall 586 mm per year. Five treatments (orchard floor management systems) were established, and 1 m wide strips were randomly assigned to each treatment located in the center of tree rows. Immediately after apple planting, three living mulch plants were sown: (1) annual French marigold (*Tagetes patula* L.), dwarf cultivars "Carmen" or "Columbina" (15 kg per ha), renewed in the subsequent years of experiment, (2) perennial colonial bent grass (*Agrostis vulgaris* With.), cultivar "Frasek" (34 kg per ha), and (3) perennial blue fescue (*Festuca ovina* L.), cultivar "Edolana"(30 kg per ha). The latter was sown in spring 2005 to replace the annual dwarf nasturtium (*Tropaeolum majus nanum* L.), which was only maintained in the first year of orchard establishment. The other two treatments consisted of the application of black polypropylene fabric or maintenance of herbicide strip in the row. Black polypropylene fabric (AGRO 84F-170 TKANINA PP, 94 g·m^{-2}) was applied in spring of 2004 and maintained during the course of the experimental trial. Herbicide treatment was maintained in accordance with current recommendations for commercial orchards. Following the second year after planting, two or three applications of a glyphosate and 2-methyl-4-chlorophenoxyacetic acid (MCPA) mixture were sprayed 4.0 + 2.0 L per ha.

Grassy strips were maintained between tree rows and mown several times per vegetation season. Slender spindles were formed, and trees were fertilized with nitrogen (ammonium nitrate or urea) each year at an average rate of 50 kg per ha. Apple tree protection was carried out in accordance with current recommendations of the Orchard Protection Program.

The experiment was established in a randomized block design in four replications. Within each replication, 4.8 m × 1 m plots were delimited for each orchard floor management system with four trees per plot. Each year (2010−2013), yield per plot was measured for each replication separately. Late spring frost (−2 °C, May 3, 2011) caused flower damage of apple trees in the full blooming period in the entire Lower Silesia area, and thus the 2011 yield was relevant.

Plant Material. Apple fruit of 'Ligol' and 'Pinova' cv. were harvested between September 18−19 and 25−27, depending on the cultivar. The optimal harvest time was established based on the average harvest time for both cultivars in the Lower Silesia area. Apples were delivered to the laboratory of the University of Ljubljana in Slovenia, Chair for Fruit, Wine and Vegetable Growing, where they were immediately analyzed.

Chemicals. Sucrose, glucose, fructose, sorbitol, citric, malic, shikimic, and fumaric acids from Sigma-Aldrich Chemie GmbH (Steinheim, Germany) were used for quantification of sugars and organic acids. The standards used to determine the phenolic compounds in samples were: chlorogenic acid (5-caffeoylquinic acid) and quercetin-3-*O*-rutinoside from Sigma-Aldrich, (−)-epicatechin, (+)-catechin, procyanidin B2, procyanidin B1, phloridzin dihydrate, cyanidin-3-*O*-galactoside, quercetin-3-*O*-rhamnoside, quercetin-3-*O*-galactoside, quercetin-3-*O*-glucoside, quercetin-3-*O*-arabinofuranoside, and quercetin-3-*O*-xyloside from Fluka Chemie (Buchs, Switzerland). Methanol for extraction of phenolics was acquired from Sigma-Aldrich. The chemicals for the mobile phases were HPLC-MS grade sulfuric acid, acetonitrile, and formic acid from Fluka. Water for mobile phase was double distilled and purified with the Milli-Q system (Millipore, Bedford, MA).

Fruit Quality Parameters. Fruit quality parameters were estimated in the tenth year after planting (2013). The firmness was measured on two peeled sides in the equatorial plane of the fruit with a penetrometer (TR, Turini, Italy) equipped with an 11 mm tip. The depth of tip penetration was 8 mm. To determine soluble solids content (SSC), the pulp from each fruit was crushed and the intact juice was immediately analyzed with a digital refractometer (model WM-7, Atago, Tokyo, Japan). Peel color was measured with a portable colorimeter (CR-200 b Chroma; Minolta, Osaka, Japan) with C illuminant and expressed with L^* parameter and hue angle. The colorimeter was calibrated with a white standard calibration plate before use. In the CIE Lab system of color representation, the L^* value corresponds to a dark−bright scale and represents the relative lightness of colors with a range from 0 to 100 (0 = black, 100 = white). The hue angle ($h°$) is expressed in degrees from 0 to 360 (0°, red; 90°, yellow; 180°, green; 270°, blue). Peel color was measured on sun-exposed sides in the middle of each fruit to ensure equal measurement conditions.

Analysis of Individual Carbohydrates and Organic Acids. Apple fruit harvested in 2013 were analyzed for the content of carbohydrates (sorbitol, sucrose, glucose, and fructose) and organic acids (malic, citric, shikimic, and fumaric acids). The stalk, sepal, and core were removed from the fruit, and 5 g of fresh weight (FW) were immersed into 25 mL of double-distilled water and homogenized with a homogenizer (T25 basic Ultra-Turrax, IKA Labortechnik, Janke and Kunkel GmbH, Staufen, Germany). Fruit samples were left for half an hour at room temperature with frequent stirring. Samples were centrifuged for 4 min at 10 000 rpm; the supernatants were filtered through a 0.25 μm cellulose filter produced by Macherey-Nagel (Düren, Germany), poured into vials, and analyzed using high performance liquid chromatography (HPLC; Thermo Scientific, San Jose, CA, USA). For the analysis of organic acids, a Rezex ROA Organic acid column (300 mm × 7.8 mm) (Phenomenex, Torrance, CA, USA), heated to 65 °C, with 4 mM sulfuric (VI) acid as the mobile phase and a UV detector set to 210 nm, was used.

For the determination of sugars, a Rezex RCM-monosaccharide column (300 mm × 7.8 mm) (Phenomenex, Torrance, CA, USA) heated to 65 °C, with double-distilled water as the mobile phase and a RI detector, were utilized. The concentrations were recalculated using the calibration curve of standards of known concentrations.

Analysis of Individual Phenolics. The apples were peeled with a mechanical peeler, and the peel was separated from the pulp. The extraction of fruit samples (peel and pulp separately) was done as described by Slatnar et al.,[19] with some modification. Fresh apple samples were ground to a fine powder in a mortar chilled with liquid nitrogen. The samples of 10 g of pulp or 3 g of peel were extracted with 10 mL of methanol containing 3% (v/v) formic acid in a cooled ultrasonic bath for 1 h. After extraction, the fruit extracts were centrifuged for 7 min at 10000 rpm. The supernatant was filtered through a Chromafil AO-45/25 polyamide filter produced by Macherey-Nagel and transferred to a vial prior into injection in the HPLC system.

Phenolic compounds were analyzed on a Thermo Scientific Dionex UltiMate 3000 series UHPLC+ focused (Thermo Scientific, San Jose, CA, USA) with a diode array detector at 280 nm (flavanols, cinnamic acid derivatives), 350 nm (flavonols), and 530 nm (anthocyanins). Spectra of the compounds were recorded between 200 and 600 nm.

Table 1. Effect of Different Orchard Floor Management Systems on Quality Parameters of Harvested 'Ligol' and 'Pinova' Fruit (means ± SE)

cultivar		*Agrostis*	*Festuca*	*Tagetes*	herbicide strip	black polypropylene fabric
'Ligol'	yield (kg tree^{-1})	12.31 ± 3.21 NS[a]	12.88 ± 3.31 NS	12.55 ± 2.47 NS	15.97 ± 1.39 NS	17.22 ± 2.04 NS
	soluble solids (%)	13.37 ± 0.25 b	12.49 ± 0.21 a	13.08 ± 0.32 ab	15.19 ± 0.30 c	13.28 ± 0.26 ab
	firmness (kg cm^{-2})	7.20 ± 0.08 NS	6.89 ± 0.12 NS	7.14 ± 0.11 NS	7.18 ± 0.09 NS	6.98 ± 0.10 NS
	L^*	39.13 ± 1.19 NS	35.16 ± 1.14 NS	39.15 ± 2.05 NS	41.98 ± 2.23 NS	38.35 ± 1.93 NS
	$h°$	36.52 ± 2.76 NS	23.02 ± 1.47 NS	35.71 ± 5.96 NS	36.79 ± 3.88 NS	31.34 ± 3.94 NS
'Pinova'	yield (kg tree^{-1})	6.51 ± 2.69 a	8.30 ± 2.41 a	8.71 ± 1.10 ab	12.19 ± 2.75 b	9.84 ± 0.66 ab
	soluble solids (%)	13.96 ± 0.23 NS	14.22 ± 0.22 NS	14.07 ± 0.27 NS	14.37 ± 0.20 NS	14.50 ± 0.23 NS
	firmness (kg cm^{-2})	8.33 ± 0.19 b	7.57 ± 0.13 a	8.23 ± 0.16 b	7.64 ± 0.12 a	7.76 ± 0.17 a
	L^*	45.96 ± 1.18 NS	47.49 ± 1.48 NS	45.88 ± 1.33 NS	49.51 ± 1.59 NS	48.39 ± 1.64 NS
	$h°$	40.05 ± 3.33 NS	43.07 ± 3.47 NS	38.61 ± 3.20 NS	51.27 ± 3.84 NS	40.89 ± 3.10 NS

[a]Different letters (a–c; NS, not significant) in rows represent statistically significant differences among treatments at $p < 0.05$ (Duncan test) for each cultivar separately.

The column was a Gemini C_{18} (150 mm × 4.6 mm 3 μm; Phenomenex, Torrance, CA, USA) operated at 25 °C. The elution solvents were aqueous 0.1% formic acid in twice-distilled water (A) and 0.1% formic acid in acetonitrile (B). Samples were eluted according to the linear gradient from 5% to 20% B in the first 15 min, followed by a linear gradient from 20% to 30% B for 5 min, then an isocratic mixture for 5 min, followed by a linear gradient from 30% to 90% B for 5 min, and then an isocratic mixture for 15 min before returning to the initial conditions.[20] The injection amount was 20 μL and flow rate 0.6 mL min^{-1}.

All phenolic compounds were identified by an HPLC-Finnigan MS detector and an LCQ Deca XP MAX (Thermo Finnigan, San Jose, CA, USA) instrument with electrospray interface (ESI) operating in positive (for anthocyanins) and negative (other phenolic groups) ion mode. The analyses were carried out using full scan data-dependent MS^n scanning from m/z 110 to 1500. Column and chromatographic conditions were identical to those used for the HPLC-DAD analyses. The injection volume was 10 μL, and the flow rate maintained at 0.6 mL min^{-1}. The capillary temperature was 250 °C, and the sheath gas and auxiliary gas were 60 and 15 arbitrary units, respectively; the source voltage was 3 kV for negative ionization and 4 kV for positive ionization and normalized collision energy was between 20–35%. Spectral data were elaborated using the Excalibur software (Thermo Scientific). The identification of compounds was confirmed by fragmentation, comparison of retention times and compound spectra as well as by adding the standard solution to the sample.

Statistical Evaluation. Results were statistically analyzed with a Statgraphics Plus program for Windows 4.0, using one-way analysis of variance (ANOVA). The difference in content levels were estimated with Duncan's Multiple Range Test. *P*-values of less than 0.05 were considered statistically significant. The data of yield quantity was analyzed using one-way analysis of variance for a randomized block design. The multiple comparisons were performed at the 5% significance level using Duncan's Multiple Range Test.

Multivariate statistical analysis (hierarchical cluster analysis) was conducted in order to interpret the differences in analyzed compounds among orchard floor management systems. Ward's method based on squared Euclidian distance was used to interpret the differences in all analyzed compounds.

RESULTS AND DISCUSSION

Yield, External Fruit Quality Parameters, and Primary Metabolites. The mean yield (2010–2013) at harvest differed among soil management treatments and ranged from 12.31 to 17.22 kg per tree in 'Ligol' and from 6.51 to 12.19 kg per tree in 'Pinova' cultivar (Table 1). No significant differences among treatments have been determined for 'Ligol' cultivar. However, in 'Pinova' cultivar, significant differences have been observed among treatments. Higher yields have been monitored in herbicide treatment in comparison with *Agrostis vulgaris* With. and *Festuca ovina* L. living mulches (Table 1). Similarly, lower yield has been reported in research by some authors,[2,4,5] who investigated the effect of living mulches in young apple orchards. Moreover, Yao et al.[7] determined that *Festuca rubra* L. caused lower yields during several years of monitoring in a full cropping orchard.

Soluble solids concentration was significantly higher in the herbicide treatment in comparison with all other orchard floor management systems in 'Ligol' cultivar. However, no significant changes in soluble solids have been noted among treatments in 'Pinova' cultivar (Table 1).

Firmness provides information on fruit freshness and is often considered a crucial parameter in a consumer's decision making for an apple purchase. In the present experiment, the firmness level at harvest ranged from 6.89 to 7.20 kg cm^{-2} in 'Ligol' and from 7.57 to 8.33 kg cm^{-2} in 'Pinova' cultivar (Table 1). Again, types of soil management exhibited different responses to treatments in this fruit parameter. No significant differences among treatments have been determined for firmness in 'Ligol'. However, significantly higher values have been measured for the 'Pinova' cultivar of the *Agrostis vulgaris* With. and *Tagetes patula* L. treatments.

In the study by Fausett and Rom,[21] black plastic fabric treatment caused an increase of average fruit firmness and a decrease of average soluble solids in "Gala" apples. Similarly, fruit sampled from trees subjected to black polypropylene fabric treatment also contained lower soluble solids in 'Ligol' cultivar.

To evaluate the potential of different ground cover management systems on color development, the changes in the colorimetric parameter L^* and hue angle ($h°$) were monitored. The hue angle ($h°$) is one of the most appropriate indicators of color changes during apple fruit growth.[22] Different orchard floor management systems did not exhibit any influence on hue value or colorimetric parameter measured on the sun-exposed side of apple fruit of both analyzed cultivars (Table 1). Several authors similarly report that fruit from organic and conventional practices do not differ in peel color,[23] which could be linked to the results of our study. Namely, organic production is mostly characterized by the implementation of weed control practices other than herbicides and a herbicide strip is frequently used in integrated orchard management. Kühn and Lindhard Pedersen[9] conversely reported that grass (*Festuca rubra* L. with *Poa pratensis* L.)

Table 2. Effect of Different Orchard Floor Management Systems on the Content of Organic Acids and Sugars in Harvested 'Pinova' Fruit (mean ± SE g kg^{-1} FW, n = 8)

	Agrostis	*Festuca*	*Tagetes*	herbicide strip	black polypropylene fabric
sucrose	14.57 ± 1.88 a[b]	24.64 ± 1.63 b	29.93 ± 2.87 b	25.49 ± 1.99 b	27.71 ± 3.97 b
glucose	16.03 ± 2.40 NS	12.62 ± 0.85 NS	9.66 ± 1.76 NS	15.36 ± 1.05 NS	11.92 ± 1.68 NS
fructose	72.97 ± 0.79 b	68.40 ± 0.98 a	70.90 ± 1.21 ab	77.46 ± 1.18 c	70.73 ± 2.20 ab
sorbitol	2.22 ± 0.15 NS	2.13 ± 0.09 NS	2.45 ± 0.16 NS	2.37 ± 0.17 NS	2.62 ± 0.12 NS
total sugars	**110.63 ± 1.79 a**	**108.93 ± 2.18 a**	**114.26 ± 1.52 ab**	**120.53 ± 2.49 c**	**117.57 ± 1.75 bc**
citric acid	0.33 ± 0.03 NS	0.34 ± 0.03 NS	0.28 ± 0.04 NS	0.29 ± 0.03 NS	0.28 ± 0.03 NS
malic acid	4.90 ± 0.49 NS	5.48 ± 0.26 NS	4.66 ± 0.41 NS	4.37 ± 0.34 NS	4.23 ± 0.29 NS
shikimic acid[a]	18.26 ± 1.43 b	12.50 ± 0.68 a	12.42 ± 1.34 a	12.50 ± 0.74 a	12.28 ± 1.14 a
fumaric acid[a]	0.57 ± 0.04 b	0.47 ± 0.04 a	0.42 ± 0.04 a	0.40 ± 0.02 a	0.41 ± 0.02 a
total organic acids	**4.88 ± 0.37 a**	**5.88 ± 0.23 b**	**5.05 ± 0.38 ab**	**4.68 ± 0.35 a**	**4.48 ± 0.29 a**

[a]mg kg^{-1} FW [b]Different letters (a–c; NS, not significant) in rows represent statistically significant differences among treatments at $p < 0.05$ (Duncan test).

Table 3. Effect of Different Orchard Floor Management Systems on the Content of Organic Acids and Sugars in Harvested 'Ligol' Fruit (mean ± SE g kg^{-1} FW, n = 8)

	Agrostis	*Festuca*	*Tagetes*	herbicide strip	black polypropylene fabric
sucrose	29.18 ± 2.02 ab[b]	29.03 ± 1.59 ab	25.64 ± 1.53 a	38.66 ± 2.41 c	32.95 ± 1.95 b
glucose	9.13 ± 0.76 NS	7.59 ± 0.79 NS	8.65 ± 0.75 NS	7.80 ± 0.85 NS	6.86 ± 0.57 NS
fructose	76.08 ± 1.20 b	70.90 ± 0.81 a	75.78 ± 1.54 b	80.49 ± 1.01 c	76.20 ± 1.22 b
sorbitol	1.58 ± 0.08 ab	1.37 ± 0.07 a	1.58 ± 0.09 ab	1.75 ± 0.06 b	1.45 ± 0.08 a
total sugars	**115.79 ± 2.24 b**	**106.66 ± 1.82 a**	**114.74 ± 2.79 b**	**128.91 ± 1.04 c**	**117.69 ± 1.18 b**
citric acid	0.23 ± 0.02 b	0.22 ± 0.02 b	0.17 ± 0.01 a	0.19 ± 0.02 ab	0.19 ± 0.01 ab
malic acid	4.43 ± 0.16 NS	4.04 ± 0.11 NS	3.80 ± 0.20 NS	4.09 ± 0.26 NS	4.38 ± 0.14 NS
shikimic acid[a]	5.17 ± 0.22 b	5.11 ± 0.20 b	4.29 ± 0.13 a	4.82 ± 0.29 ab	4.42 ± 0.20 a
fumaric acid[a]	0.22 ± 0.01 c	0.21 ± 0.01 bc	0.16 ± 0.01 a	0.17 ± 0.02 a	0.19 ± 0.01 ab
total organic acids	**4.66 ± 0.17 NS**	**4.27 ± 0.11 NS**	**3.98 ± 0.21 NS**	**4.30 ± 0.28 NS**	**4.60 ± 0.15 NS**

[a]mg kg^{-1} FW [b]Different letters (a–c; NS, not significant) in rows represent statistically significant differences among treatments at $p < 0.05$ (Duncan test).

decrease leaf N content level, shoot growth, and yield but increase the percentage of optimal colored fruit.

In addition to different aromatic compounds, sugars and organic acids play important roles defining the character and quality of flavor and organoleptic properties of apples. Sucrose, fructose, glucose, and sorbitol have been quantified in apple fruit harvested from trees subjected to different orchard floor management treatments (Tables 2 and 3). Hecke et al.[24] and Mikulic-Petkovsek et al.[25] obtained similar results for apple fruit sugar composion. Significantly lower levels of individual sugars (with the exception of glucose, where differences among treatments were not significant for both cultivars) have been measured more often in fruit of different living mulch treatments compared with fruit harvested from trees subjected to the herbicide strip treatment. Consequently, total sugar content was higher in fruit of the herbicide strip treatment in both cultivars analyzed (Tables 2 and 3).

Malic and citric acids were the prevalent components from the group of organic acids, and shikimic and fumaric acids were only quantified in minor amounts. Similar composition has previously been reported by Mikulic-Petkovsek et al.[25] The results on organic acid composition in apple fruit subjected to different orchard floor management treatments were less conclusive compared to the data on individual/total sugar content (Tables 2 and 3). Generally, the content of organic acids was similar in all treatments, however, in the case of citric acid in 'Ligol' and shikimic and fumaric acid in both cultivars, the content was significantly higher in fruit from different living mulch combinations (Tables 2 and 3). Subsequently, significantly higher levels of total organic acids were only detected in 'Pinova' fruit of the *Festuca ovina* L. strip treatment. Differences in sugar/organic acid composition among treatments could be explained by the competition for nutrients between fruit trees and green cover plants mostly affecting sugar synthesis. In a study by Nazrala,[26] titratable acidity increased and cell sap pH level decreased when vines were grown in combination with a cover crop compared to the control treatment where bare soil was left under the plants.

Phenolic Compounds in Pulp and Peel. Phenolic compounds are a class of secondary metabolites, i.e., compounds that are not essential for the survival of plants but are produced to enhance their ability to withstand various stress factors. Principally, due to their antioxidant properties, there is much interest in the potential health benefits of phenolic compounds in our diets.[27] These two reasons must be considered when new orchard management techniques with possible effects on fruit and leaf phenolic content are introduced. The analyzed phenolics in apple fruit were classified into five groups: hydroxycinnamic acids, dihydrochalcones, flavan-3-ols, flavonols, and anthocyanins.

The occurrence and content of different phenolic compounds has previously been reported in many apple cultivars[15,25] and confirmed also in our present study. However, the content of phenolic compounds in apple fruit is greatly

Table 4. Content of Individual Phenolic Compounds (mean ± SE, mg 100 g^{-1} FW, n = 8) in Pulp of 'Pinova' Apples from Different Orchard Floor Management Systems

	Agrostis	*Festuca*	*Tagetes*	herbicide strip	black polypropylene fabric
chlorogenic acid	5.59 ± 0.34 a[a]	5.80 ± 0.17 a	6.71 ± 0.36 b	6.20 ± 0.26 ab	5.69 ± 0.18 a
4-*O*-*p*-coumaroylquinic acid	0.15 ± 0.01 NS	0.13 ± 0.01 NS	0.12 ± 0.01 NS	0.13 ± 0.01 NS	0.11 ± 0.01 NS
total hydroxycinnamic acids	**6.09 ± 0.43 NS**	**5.96 ± 0.18 NS**	**6.89 ± 0.38 NS**	**6.35 ± 0.27 NS**	**5.83 ± 0.18 NS**
procyanidin B2	3.19 ± 0.32 NS	3.34 ± 0.38 NS	3.40 ± 0.37 NS	3.35 ± 0.31 NS	2.43 ± 0.28 NS
procyanidin B1	1.58 ± 0.18 NS	1.53 ± 0.19 NS	1.85 ± 0.20 NS	1.71 ± 0.14 NS	1.34 ± 0.13 NS
procyanidin trimer 1	1.29 ± 0.13 NS	1.14 ± 0.12 NS	1.03 ± 0.08 NS	1.18 ± 0.06 NS	0.93 ± 0.05 NS
procyanidin trimer 2	0.31 ± 0.06 b	0.16 ± 0.03 a	0.15 ± 0.04 a	0.20 ± 0.02 a	0.16 ± 0.03 a
epicatechin	2.58 ± 0.23 NS	2.41 ± 0.23 NS	2.85 ± 0.24 NS	2.36 ± 0.12 NS	2.33 ± 0.16 NS
catechin	0.02 ± 0.00 NS	0.02 ± 0.00 NS	0.03 ± 0.00 NS	0.02 ± 0.00 NS	0.03 ± 0.00 NS
total flavanols	**9.16 ± 0.91 NS**	**8.59 ± 0.92 NS**	**8.70 ± 0.71 NS**	**8.67 ± 0.62 NS**	**6.87 ± 0.56 NS**
phloretin-2-*O*-(2-xylosylglucoside)	0.58 ± 0.04 NS	0.51 ± 0.03 NS	0.55 ± 0.04 NS	0.62 ± 0.04 NS	0.54 ± 0.04 NS
phloridzin	0.38 ± 0.02 NS	0.35 ± 0.01 NS	0.38 ± 0.02 NS	0.41 ± 0.02 NS	0.36 ± 0.02 NS
total dihydrochalcones	**0.96 ± 0.06 NS**	**0.86 ± 0.04 NS**	**0.96 ± 0.06 NS**	**1.01 ± 0.06 NS**	**0.92 ± 0.05 NS**
Q.-3-*O*-galactoside[b]	0.01 ± 0.00 bc	0.00 ± 0.00 a	0.01 ± 0.00 ab	0.01 ± 0.00 c	0.01 ± 0.00 bc
Q.-3-*O*-glucoside	0.03 ± 0.00 ab	0.02 ± 0.00 a	0.03 ± 0.00 b	0.02 ± 0.00 a	0.02 ± 0.00 b
Q.-3-*O*-xyloside	0.02 ± 0.00 b	0.02 ± 0.00 a	0.02 ± 0.00 a	0.02 ± 0.00 a	0.02 ± 0.00 a
Q.-3-*O*-arabinopyranoside	0.01 ± 0.00 NS	0.01 ± 0.00 NS	0.01 ± 0.00 NS	0.01 ± 0.00 NS	0.01 ± 0.00 NS
Q.-3-*O*-arabinofuranoside	0.04 ± 0.00 b	0.03 ± 0.00 a	0.03 ± 0.00 a	0.03 ± 0.00 a	0.03 ± 0.00 a
Q.-3-*O*-rhamnoside	0.31 ± 0.02 NS	0.29 ± 0.01 NS	0.34 ± 0.03 NS	0.30 ± 0.01 NS	0.29 ± 0.01 NS
total flavonols	**0.39 ± 0.02 NS**	**0.37 ± 0.01 NS**	**0.40 ± 0.03 NS**	**0.39 ± 0.01 NS**	**0.37 ± 0.01 NS**

[a]Different letters (a−c; NS, not significant) in rows represent statistically significant differences among treatments at $p < 0.05$ (Duncan test). [b]Q.: quercetin.

Table 5. Content of Individual Phenolic Compounds (mean ± SE, mg 100 g^{-1} FW, n = 8) in Pulp of 'Ligol' Apples From Different Orchard Floor Management Systems

	Agrostis	*Festuca*	*Tagetes*	herbicide strip	black polypropylene fabric
chlorogenic acid	5.62 ± 0.08 c[a]	4.68 ± 0.24 a	5.71 ± 0.26 c	4.92 ± 0.25 ab	5.43 ± 0.24 bc
4-*O*-*p*-coumaroylquinic acid	0.11 ± 0.01 NS	0.10 ± 0.01 NS	0.10 ± 0.01 NS	0.09 ± 0.01 NS	0.10 ± 0.01 NS
total hydroxycinnamic acids	**5.78 ± 0.08 c**	**4.81 ± 0.25 a**	**5.85 ± 0.27 c**	**5.06 ± 0.26 ab**	**5.57 ± 0.25 bc**
procyanidin B2	3.73 ± 0.25 NS	3.00 ± 0.22 NS	3.32 ± 0.22 NS	3.06 ± 0.22 NS	3.06 ± 0.15 NS
procyanidin B1	1.14 ± 0.10 NS	0.91 ± 0.09 NS	1.00 ± 0.05 NS	0.98 ± 0.06 NS	0.98 ± 0.04 NS
procyanidin trimer 1	1.73 ± 0.12 NS	1.50 ± 0.13 NS	1.68 ± 0.14 NS	1.36 ± 0.12 NS	1.63 ± 0.08 NS
procyanidin trimer 2	0.08 ± 0.02 NS	0.07 ± 0.01 NS	0.08 ± 0.02 NS	0.05 ± 0.02 NS	0.04 ± 0.01 NS
epicatechin	2.20 ± 0.09 NS	1.97 ± 0.14 NS	2.30 ± 0.20 NS	1.80 ± 0.09 NS	2.07 ± 0.04 NS
catechin	0.03 ± 0.00 NS	0.03 ± 0.00 NS	0.04 ± 0.00 NS	0.04 ± 0.00 NS	0.03 ± 0.00 NS
total flavanols	**9.01 ± 0.53 NS**	**7.45 ± 0.55 NS**	**8.42 ± 0.59 NS**	**7.63 ± 0.34 NS**	**7.80 ± 0.33 NS**
phloretin-2-*O*-(2-xylosylglucoside)	0.02 ± 0.00 b	0.02 ± 0.00 b	0.01 ± 0.00 ab	0.01 ± 0.00 a	0.01 ± 0.00 a
phloridzin	0.31 ± 0.02 bc	0.29 ± 0.01 b	0.34 ± 0.01 c	0.30 ± 0.01 bc	0.23 ± 0.02 a
total dihydrochalcones	**0.34 ± 0.03 bc**	**0.31 ± 0.02 abc**	**0.36 ± 0.02 c**	**0.28 ± 0.01 ab**	**0.25 ± 0.03 a**
Q.-3-*O*-galactoside[b]	0.01 ± 0.00 NS	0.01 ± 0.00 NS	0.01 ± 0.00 NS	0.01 ± 0.00 NS	0.01 ± 0.00 NS
Q.-3-*O*-glucoside	0.02 ± 0.00 NS	0.01 ± 0.00 NS	0.02 ± 0.00 NS	0.02 ± 0.00 NS	0.02 ± 0.00 NS
Q.-3-*O*-xyloside	0.03 ± 0.00 b	0.03 ± 0.00 ab	0.04 ± 0.00 b	0.02 ± 0.01 a	0.02 ± 0.01 a
Q.-3-*O*-arabinopyranoside	0.01 ± 0.00 bc	0.01 ± 0.00 a	0.01 ± 0.00 c	0.01 ± 0.00 bc	0.01 ± 0.00 ab
Q.-3-*O*-arabinofuranoside	0.02 ± 0.00 NS	0.02 ± 0.00 NS	0.02 ± 0.00 NS	0.02 ± 0.00 NS	0.02 ± 0.00 NS
Q.-3-*O*-rhamnoside	0.16 ± 0.00 ab	0.15 ± 0.01 ab	0.20 ± 0.01 c	0.18 ± 0.01 bc	0.15 ± 0.00 a
total flavonols	**0.25 ± 0.01 a**	**0.23 ± 0.02 a**	**0.29 ± 0.01 b**	**0.24 ± 0.01 a**	**0.23 ± 0.01 a**

[a]Different letters (a−c; NS, not significant) in rows represent statistically significant differences among treatments at $p < 0.05$ (Duncan test). [b]Q.: quercetin.

affected by genetic variations among cultivars and environmental factors such as climatic conditions, stress, and implementation of different production measures.[15,25] Moreover, the phenolic profile also differs between apple peel and pulp, the latter being significantly less abundant in secondary metabolites.[15] The comparison of phenolic compounds among

dx.doi.org/10.1021/jf500846r | J. Agric. Food Chem. 2014, 62, 4095−4103

Table 6. Content of Individual Phenolic Compounds (mean ± SE, mg 100g^{-1} FW, n = 8) in Peel of 'Pinova' Apples from Different Orchard Floor Management Systems

	Agrostis	*Festuca*	*Tagetes*	herbicide strip	black polypropylene fabric
4-*O*-*p*-coumaroylquinic acid	1.00 ± 0.07 ab[a]	1.16 ± 0.09 b	1.19 ± 0.10 b	0.86 ± 0.03 a	0.91 ± 0.06 a
p-coumaric acid hexoside	13.98 ± 1.17 abc	16.33 ± 0.79 c	14.43 ± 0.97 bc	11.66 ± 1.12 a	11.79 ± 0.66 ab
chlorogenic acid	16.00 ± 1.53 NS	15.46 ± 1.12 NS	19.13 ± 1.38 NS	16.85 ± 1.67 NS	15.48 ± 0.97 NS
total hydroxycinnamic acids	**30.98 ± 2.67 NS**	**34.11 ± 2.14 NS**	**33.12 ± 1.86 NS**	**31.25 ± 2.20 NS**	**27.25 ± 0.98 NS**
epicatechin	42.39 ± 4.16 NS	47.68 ± 6.59 NS	48.32 ± 3.67 NS	37.56 ± 7.91 NS	35.97 ± 3.85 NS
procyanidin B1	7.51 ± 0.64 NS	8.45 ± 0.76 NS	10.30 ± 1.16 NS	8.28 ± 0.43 NS	7.41 ± 0.58 NS
procyanidin B2	53.50 ± 5.44 a	52.08 ± 3.21 a	64.56 ± 5.86 ab	73.92 ± 2.08 b	66.64 ± 4.46 b
procyanidin dimer	14.89 ± 0.69 NS	16.26 ± 1.17 NS	15.22 ± 1.85 NS	15.75 ± 1.46 NS	16.99 ± 0.78 NS
procyanidin trimer 1	17.24 ± 3.11 ab	44.96 ± 4.24 c	21.46 ± 5.91 b	8.11 ± 1.65 a	9.60 ± 2.16 a
procyanidin trimer 2	42.39 ± 4.16 ab	47.68 ± 6.59 b	48.32 ± 3.67 b	37.56 ± 7.91 a	35.97 ± 3.85 a
procyanidin trimer 3	8.67 ± 0.68 bc	9.68 ± 0.71 c	7.20 ± 0.84 ab	6.80 ± 0.37 a	7.59 ± 0.60 ab
procyanidin tetramer 1	8.42 ± 0.66 bc	9.32 ± 0.71 c	8.67 ± 0.92 bc	4.44 ± 1.18 a	6.29 ± 0.94 ab
procyanidin tetramer 2	7.83 ± 0.59 NS	8.36 ± 0.79 NS	8.99 ± 0.73 NS	6.77 ± 0.43 NS	6.33 ± 0.95 NS
procyanidin tetramer 3	31.82 ± 1.74 a	40.38 ± 3.36 b	35.67 ± 3.47 ab	28.29 ± 1.29 a	31.78 ± 2.29 a
procyanidin tetramer 4	7.04 ± 0.51 cd	8.55 ± 0.53 d	5.48 ± 0.48 bc	3.79 ± 0.41 a	5.35 ± 0.73 bc
total flavanols	**268.01 ± 16.11 NS**	**298.58 ± 20.40 NS**	**295.95 ± 19.49 NS**	**238.25 ± 11.97 NS**	**260.53 ± 13.62 NS**
phloretin-2-*O*-(2-xylosylglucoside)	10.84 ± 0.94 NS	12.59 ± 1.10 NS	13.93 ± 1.11 NS	10.52 ± 0.67 NS	11.02 ± 0.83 NS
phloridzin	17.85 ± 1.60 NS	19.16 ± 1.95 NS	16.42 ± 1.41 NS	13.33 ± 1.59 NS	14.71 ± 1.25 NS
total dihydrochalcones	**26.26 ± 2.90 NS**	**31.74 ± 2.99 NS**	**29.73 ± 2.48 NS**	**23.85 ± 2.22 NS**	**25.73 ± 2.02 NS**
Q.-3-*O*-rutinoside[b]	2.82 ± 0.42 NS	2.35 ± 0.40 NS	1.50 ± 0.44 NS	1.62 ± 0.34 NS	1.84 ± 0.50 NS
Q.-3-*O*-galactoside	100.26 ± 10.03 NS	93.20 ± 11.71 NS	68.51 ± 15.35 NS	59.57 ± 11.04 NS	58.98 ± 13.09 NS
Q.-3-*O*-glucoside	24.22 ± 2.33 b	23.40 ± 2.88 b	17.95 ± 2.84 ab	14.65 ± 2.22 a	14.00 ± 3.06 a
Q.-3-*O*-xyloside	23.35 ± 1.78 bc	24.92 ± 2.44 c	17.90 ± 2.54 ab	14.89 ± 2.04 a	16.77 ± 2.66 a
Q.-3-*O*-arabinopyranoside	2.83 ± 0.22 c	2.72 ± 0.21 bc	2.09 ± 0.32 abc	1.72 ± 0.24 a	2.03 ± 0.33 ab
Q.-3-*O*-arabinofuranoside	39.48 ± 1.90 NS	42.74 ± 3.87 NS	34.51 ± 5.10 NS	27.48 ± 3.77 NS	36.72 ± 2.46 NS
Q.-3-*O*-rhamnoside	54.95 ± 3.86 b	55.24 ± 4.79 b	35.25 ± 4.12 a	34.16 ± 4.46 a	35.86 ± 5.54 a
total flavonols	**251.31 ± 21.55 b**	**241.00 ± 25.00 b**	**182.72 ± 31.22 ab**	**154.08 ± 23.86 a**	**158.05 ± 29.87 a**
Cy.-3-*O*-galactoside[b]	4.49 ± 0.66 NS	6.09 ± 1.41 NS	6.15 ± 1.07 NS	3.90 ± 0.47 NS	4.51 ± 1.18 NS
Cy.-3-*O*-arabinoside	0.25 ± 0.02 NS	0.28 ± 0.06 NS	0.29 ± 0.02 NS	0.17 ± 0.02 NS	0.31 ± 0.05 NS
Cy.-7-*O*-arabinoside	0.06 ± 0.01 NS	0.10 ± 0.02 NS	0.07 ± 0.02 NS	0.03 ± 0.01 NS	0.08 ± 0.03 NS
total anthocyanins	**4.77 ± 0.69 NS**	**6.42 ± 1.48 NS**	**6.46 ± 1.13 NS**	**4.11 ± 0.50 NS**	**3.91 ± 1.06 NS**

[a]Different letters (a–c; NS, not significant) in rows represent statistically significant differences among treatments at $p < 0.05$ (Duncan test). [b]Q., quercetin; Cy., cyanidin.

treatments was thus performed in both outer (peel) and inner (pulp) fruit tissue and discussed separately.

The content of individual phenolic groups and compounds in apple pulp differed between cultivars and among treatments analyzed (Tables 4 and 5). However, different orchard floor management systems did not exhibit any influence on the content of analyzed phenolic groups in 'Pinova' apples although changes in individual phenolic compounds have been determined (Table 4). On the other hand, specific green cover systems: living mulches positively affected the content of hydroxycinnamic acids, dihydrochalcones, and flavonols in "Ligor" cultivar (Table 5). Individual phenolic compounds as well as their sum were often significantly higher in fruit harvested from trees of the *Tagetes patula* L. (Table 5) treatment.

This indistinct differences in pulp phenolic composition among treatments was expected because the pulp is less exposed to outer environmental stress if compared with peel. Apples of the 'Ligol' cultivar could intensively react to nutrient and water competition between green cover plants and trees and up-regulate the synthesis of phenolic compounds (induced stress response). On the other hand, 'Pinova' cultivar trees did not exhibit the same physiological behavior. Organic mulching can also modify many soil properties and, according to Janick,[28] apple trees form a network of fibrous fine roots in the top 15 cm soil, responsible for increased absorption of water and nutrients. This uppermost soil layer is the area where mulch type affects the biotic and abiotic properties of the underlying soil. Brady and Weil[29] suggest that temperature buffering, moisture conservation, and increased biological diversity could result from the application of organic mulches. These have the ability to moderate soil temperature, act as a source of organic carbon for soil organisms, reduce evaporation, and improve infiltration, and therefore mulching is a superior form of weed control to herbicide applications.

The qualitative composition of apple peel polyphenols was almost analogous to that determined for pulp, with the exception of cyanidin glycosides, which were detected in skin of both red-colored cultivars. Fruit of the 'Pinova' cultivar contained similar levels of analyzed phenolic groups (with the

dx.doi.org/10.1021/jf500846r | J. Agric. Food Chem. 2014, 62, 4095–4103

Table 7. Content of Individual Phenolic Compounds (mean ± SE, mg 100 g^{-1} FW, n = 8) in Peel of 'Ligol' Apples from Different Orchard Floor Management Systems

	Agrostis	*Festuca*	*Tagetes*	herbicide strip	black polypropylene fabric
4-*O*-*p*-coumaroylquinic acid	0.38 ± 0.03 c[a]	0.38 ± 0.04 c	0.35 ± 0.02 bc	0.22 ± 0.01 a	0.29 ± 0.01 ab
p-coumaric acid hexoside	3.15 ± 0.26 b	3.24 ± 0.21 b	3.38 ± 0.19 b	2.01 ± 0.11 a	2.85 ± 0.22 b
chlorogenic acid	4.87 ± 0.22 ab	4.77 ± 0.37 ab	5.67 ± 0.27 c	5.18 ± 0.21 bc	4.27 ± 0.24 a
total hydroxycinnamic acids	**8.69 ± 0.54 ab**	**8.16 ± 0.60 ab**	**9.64 ± 0.52 b**	**7.41 ± 0.28 a**	**7.72 ± 0.58 a**
catechin	2.71 ± 0.40 b	2.94 ± 0.10 b	2.50 ± 0.14 ab	1.91 ± 0.11 a	2.26 ± 0.14 ab
epicatechin	21.13 ± 2.00 bc	22.91 ± 1.55 c	19.11 ± 1.43 bc	12.08 ± 0.43 a	17.60 ± 0.64 b
procyanidin B1	6.99 ± 0.89 bc	7.92 ± 0.42 c	7.08 ± 0.66 bc	5.01 ± 0.27 a	5.92 ± 0.52 ab
procyanidin B2	15.71 ± 1.27 NS	16.67 ± 2.03 NS	18.47 ± 1.89 NS	20.56 ± 0.98 NS	20.99 ± 2.62 NS
procyanidin dimer	3.53 ± 0.19 c	3.20 ± 0.26 bc	2.97 ± 0.09 b	2.07 ± 0.15 a	2.39 ± 0.09 a
procyanidin trimer 1	8.01 ± 2.04 NS	8.88 ± 1.34 NS	7.84 ± 1.22 NS	4.46 ± 0.99 NS	5.52 ± 0.95 NS
procyanidin trimer 2	20.41 ± 1.50 c	20.25 ± 1.93 c	18.51 ± 1.26 bc	11.86 ± 0.58 a	15.17 ± 0.60 ab
procyanidin trimer 3	2.40 ± 0.15 c	2.15 ± 0.27 bc	2.37 ± 0.16 c	1.56 ± 0.10 a	1.83 ± 0.08 ab
procyanidin tetramer 1	0.95 ± 0.10 b	0.76 ± 0.10 b	0.85 ± 0.08 b	0.69 ± 0.05 ab	0.47 ± 0.10 a
procyanidin tetramer 2	4.32 ± 0.32 b	3.95 ± 0.44 ab	4.21 ± 0.26 b	3.31 ± 0.13 a	3.24 ± 0.19 a
procyanidin tetramer 3	9.81 ± 0.81 b	8.04 ± 1.08 b	8.87 ± 0.77 b	5.58 ± 0.35 a	5.81 ± 0.46 a
procyanidin tetramer 4	0.36 ± 0.04 NS	0.48 ± 0.04 NS	0.33 ± 0.07 NS	0.29 ± 0.04 NS	0.37 ± 0.03 NS
total flavanols	**101.23 ± 9.62 c**	**96.59 ± 6.26 bc**	**89.63 ± 3.72 bc**	**69.31 ± 2.45 a**	**82.68 ± 3.55 ab**
phloretin-2-*O*-(2-xylosylglucoside)	0.13 ± 0.01 b	0.14 ± 0.01 b	0.12 ± 0.01 ab	0.13 ± 0.01 b	0.10 ± 0.00 a
phloridzin	3.78 ± 0.31 b	3.92 ± 0.24 b	4.18 ± 0.34 b	2.36 ± 0.20 a	2.89 ± 0.21 a
total dihydrochalcones	**3.92 ± 0.32 b**	**4.07 ± 0.25 b**	**4.30 ± 0.34 b**	**2.49 ± 0.21 a**	**2.99 ± 0.21 a**
Q.-3-*O*-rutinoside[b]	1.04 ± 0.27 NS	1.43 ± 0.33 NS	1.30 ± 0.32 NS	0.62 ± 0.12 NS	0.62 ± 0.12 NS
Q.-3-*O*-galactoside	20.44 ± 5.04 NS	27.50 ± 5.57 NS	21.11 ± 4.63 NS	12.02 ± 2.32 NS	15.01 ± 3.16 NS
Q.-3-*O*-glucoside	5.48 ± 0.79 ab	6.45 ± 0.85 b	5.65 ± 0.97 b	3.17 ± 0.47 a	4.14 ± 0.72 ab
Q.-3-*O*-xyloside	6.35 ± 0.78 ab	7.31 ± 0.91 b	6.89 ± 1.08 b	3.95 ± 0.55 a	4.20 ± 0.59 a
Q.-3-*O*-arabinopyranoside	0.77 ± 0.15 abc	1.00 ± 0.17 c	0.83 ± 0.14 bc	0.44 ± 0.04 a	0.55 ± 0.06 ab
Q.-3-*O*-arabinofuranoside	11.47 ± 1.64 ab	13.07 ± 1.68 b	11.47 ± 1.96 ab	7.17 ± 1.09 a	7.46 ± 1.05 a
Q.-3-*O*-rhamnoside	23.07 ± 2.65 ab	26.12 ± 2.94 b	23.51 ± 3.71 ab	15.08 ± 2.38 a	16.86 ± 2.34 a
total flavonols	**68.63 ± 11.23 ab**	**82.87 ± 12.10 b**	**69.40 ± 12.57 ab**	**39.20 ± 5.80 a**	**44.35 ± 6.73 a**
Cy.-3-*O*-galactoside[b]	9.56 ± 2.45 ab	13.65 ± 1.92 b	11.41 ± 1.76 b	4.54 ± 0.82 a	9.83 ± 1.46 ab
Cy.-3-*O*-arabinoside	0.61 ± 0.16 ab	0.79 ± 0.10 b	0.75 ± 0.11 b	0.29 ± 0.05 a	0.58 ± 0.08 ab
Cy.-7-*O*-arabinoside	0.46 ± 0.12 b	0.57 ± 0.07 b	0.53 ± 0.08 b	0.17 ± 0.02 a	0.44 ± 0.06 b
Cy.-3-*O*-xyloside	0.04 ± 0.01 NS	0.05 ± 0.01 NS	0.05 ± 0.01 NS	0.03 ± 0.01 NS	0.06 ± 0.01 NS
total anthocyanins	**10.67 ± 2.73 ab**	**15.06 ± 2.07 b**	**12.67 ± 1.92 b**	**5.03 ± 0.89 a**	**10.91 ± 1.60 ab**

[a]Different letters (a−c; NS, not significant) in rows represent statistically significant differences among treatments at $p < 0.05$ (Duncan test). [b]Q., quercetin; Cy., cyanidin.

exception of flavanols) regardless of different orchard floor management systems used (Table 6). However, the content of some individual phenolic compounds from the groups of hydroxycinnamic acids and flavan-3-ols were significantly higher in the *Festuca ovina* L. or *Agrostis vulgaris* With. treatment. Interestingly, the application of herbicide or the use of black polypropylene fabric cover caused lower levels of specific individual phenolic compounds (Table 6). These results potentially indicate lesser environmental stress conditions of these trees compared with living mulches causing decreased synthesis of stress-induced phenolics. Similar studies on apple and stress-related phenolic compounds have been reported by different authors.[15,30,31]

Statistical comparison of orchard floor management systems in regard to the phenolic profile of 'Ligol' apples revealed significant differences in content levels of phenolic groups and individual compounds (Table 7). Similar to 'Pinova' cultivar, the synthesis of individual phenolic compounds increased/decreased as a response to different ground cover treatments. However, in 'Ligol' cultivar, significantly higher levels of phenolic groups have been analyzed in apples harvested from trees subjected to different living mulches. It is hard to determine the optimal green cover plant causing the highest phenolic content of most stress-induced phenolics (Table 7). The *Festuca ovina* L. and *Tagetes patula* L. effects on total and some individual anthocyanin content were significant, but all living mulches also affected the synthesis of individual phenolic from groups hydroxycinnamic acids, dihydrochalcones, flavan-3-ols, and flavonols (Table 7). Lee and Steenwerth[32] similarly reported that barley (*Hordeum vulgare* L.) green cover plant positively influenced the formation of grape anthocyanins.

Optimal orchard management systems includes maintenance of green cover plants under the tree canopy controlling water runoff and soil erosion. Moreover, some of these living mulches produce alleochemicals preventing weed germination or even suppress the established weeds without affecting the growth and yield of the main crop. The variation in primary and secondary metabolites observed in response to management

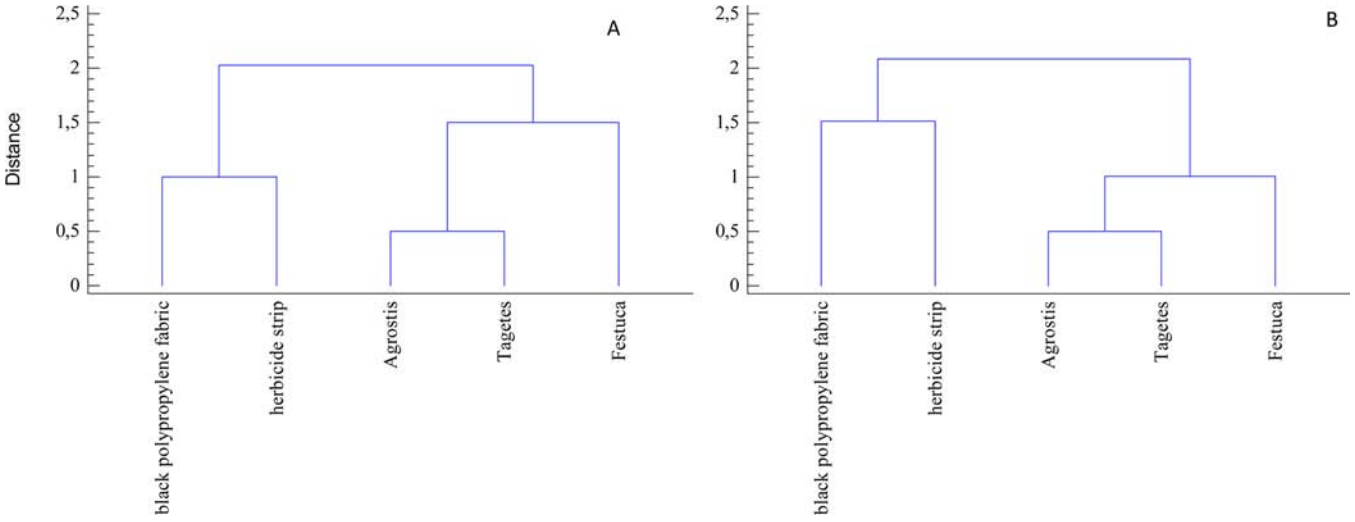

Figure 1. Dendrogram of 'Pinova' (A) and 'Ligol' (B) cultivars managed according to different orchard floor management systems, using Ward's method based on square Euclidian distance considering analyzed primary and secondary metabolites.

practices is not surprising considering the wide range of climatic, edaphic, cover crop, and other conditions affecting their synthesis. The effect of living mulches is immediately evident in fruit peel but less in apple pulp. This could be associated with the physiological role of skin in providing a physical and chemical barrier against environmental stress. Clustering the effects of different green cover plants on primary and secondary metabolites revealed similarities among *Agrostis vulgaris* With., *Tagetes patula* L., and *Festuca ovina* L. treatments in both cultivars analyzed (Figure 1). Average values were considered for the cluster analysis which revealed similarities among living mulch treatments. The reason for the formation of these groups can be found in similar patterns of primary and secondary metabolite composition of apple fruit subjected to living mulch treatments. The differences in phenolic compound levels among treatments were more distinct in 'Ligol' cultivar, but cluster analysis also revealed similarities among green cover treatments in 'Pinova' apples as they generally contained higher levels of individual phenolic compounds. On the other hand, total sugar levels of both cultivars were significantly lower in apples harvested from trees of all three living mulches (Tables 2 and 3).

Can the competing relationship between green cover plants and trees therefore be regarded as a positive measure? If we strive to produce apples with increased content level of phenolic compounds and enhanced defense of plants to stress (such as pathogen attack), the use of green cover plants should be promoted. Are apples harvested from trees subjected to increased stress also healthier? According to many studies describing health beneficial properties of apple phenolics,[27] the results confirm the positive effects of green cover plants under the tree canopy not just only on environmental levels (biodiversity, weed/erosion control) but at the same time providing healthy fruit for health-conscious consumers. The present research can represent a foundation for primary and secondary component profiling of apples managed according to different orchard floor management systems. Further studies are needed to fully encompass the impact of living mulches on apple fruit composition.

AUTHOR INFORMATION

Corresponding Author

*Phone: +386 1 320 31 44. Fax: +386 1 256 57 82. E-mail: ana.slatnar@bf.uni-lj.si.

Funding

This work is part of the program Horticulture P4-0013-0481 supported by the Slovenian Ministry of Higher Education, Science and Technology and the Polish Ministry of Science and Higher Education as the part of statutory activities of the Department of Horticulture, University of Environmental and Life Sciences in Wrocław.

Notes

The authors declare no competing financial interest.

REFERENCES

(1) Atucha, A.; Merwin, I. A.; Brown, M. G. Long-term Effects of Four Groundcover Management Systems in an Apple Orchard. *HortScience* **2011**, *46*, 1176−1183.

(2) Granatsteina, D.; Sánchez, B. Research Knowledge and Needs for Orchard Floor Management in Organic Tree Fruit Systems. *Int. J. Fruit. Sci.* **2009**, *9*, 257−281.

(3) Hartwig, N. L.; Ammon, H. U. 50th Anniversary—Invited Article—-Cover Crops and Living Mulches. *Weed Sci.* **2002**, *50*, 688−699.

(4) Merwin, I. A.; Stiles, W. C. Orchard groundcover management impacts on apple tree growth and yield, and nutrient availability and uptake. *J. Am. Soc. Hortic. Sci.* **1994**, *119*, 209−215.

(5) Mika, A.; Krzewińska, D.; Olszewski, T. Effect of mulches herbicides and cultivation as orchard ground cover management systems in young apple tree orchard. *J. Fruit Ornamental Plant Res.* **1998**, *6*, 1−13.

(6) Hartley, M. J.; Rahman, A.; K.C, H.; James, T. K. Assessing ground covers in a newly planted apple orchard. *N. Z. Plant Protect.* **2000**, *53*, 22−27.

(7) Yao, S.; Merwin, I. A.; Bird, G. W.; Abawi, G. S.; Thies, J. E. Orchard floor management practices that maintain vegetative or biomass groundcover stimulate soil microbial activity and alter soil microbial community composition. *Plant Soil* **2005**, *271*, 377−389.

(8) Lipecki, J.; Wieniarska, J. Living Mulches in the Apple Orchard—An Alternative for Herbicides? International Conference Fruit Production and Fruit Breeding, Tartu, Estonia, September 12−13, 2000, pp 104−106.

(9) Kuhn, B. F.; Pedersen Lindhard, H. Cover Crop and Mulching Effects on Yield and Fruit Quality in Unsprayed Organic Apple Production. *Eur. J. Hortic. Sci.* **2009**, *74*, 247−253.
(10) Hornig, R.; Bunemann, G. Ground covers and fertigation in apple orchards with integrated production 0.1. Growth, yield, and fruit quality. *Gartenbauwissenschaft* **1995**, *60*, 262−268.
(11) Granatstein, D.; Mullinix, K. Mulching options for northwest organic and conventional orchards. *HortScience* **2008**, *43*, 45−50.
(12) Lee, K. W.; Kim, Y. J.; Kim, D. O.; Lee, H. J.; Lee, C. Y. Major phenolics in apple and their contribution to the total antioxidant capacity. *J. Agric. Food Chem.* **2003**, *51*, 6516−6520.
(13) Stracke, B. A.; Rufer, C. E.; Weibel, F. P.; Bub, A.; Watzl, B. Three-Year Comparison of the Polyphenol Contents and Antioxidant Capacities in Organically and Conventionally Produced Apples (*Malus domestica* Bork. Cultivar 'Golden Delicious'). *J. Agric. Food Chem.* **2009**, *57*, 4598−4605.
(14) Jakopic, J.; Stampar, F.; Veberic, R. The influence of exposure to light on the phenolic content of 'Fuji' apple. *Sci. Hortic.* **2009**, *123*, 234−239.
(15) Mikulic-Petkovsek, M.; Slatnar, A.; Stampar, F.; Veberic, R. The influence of organic/integrated production on the content of phenolic compounds in apple leaves and fruits in four different varieties over a 2-year period. *J. Sci. Food Agric.* **2010**, *90*, 2366−2378.
(16) Mikulic-Petkovsek, M.; Stampar, F.; Veberic, R. Accumulation of phenolic compounds in apple in response to infection by the scab pathogen, *Venturia inaequalis*. *Physiol. Mol. Plant Pathol.* **2009**, *74*, 60−67.
(17) Treutter, D. Managing Phenol Contents in Crop Plants by Phytochemical Farming and Breeding—Visions and Constraints. *Int. J. Mol. Sci.* **2010**, *11*, 807−857.
(18) Treutter, D. Biosynthesis of phenolic compounds and its regulation in apple. *Plant Growth Regul.* **2001**, *34*, 71−89.
(19) Slatnar, A.; Stampar, F.; Veberic, R. Influence of bicarbonate salts, used against apple scab, on selected primary and secondary metabolites in apple fruit and leaves. *Sci. Hortic.* **2012**, *143*, 197−204.
(20) Wang, S. Y.; Zheng, W.; Galletta, G. J. Cultural system affects fruit quality and antioxidant capacity in strawberries. *J. Agric. Food Chem.* **2002**, *50*, 6534−6542.
(21) Fausett, J. B.; Rom, C. R. The effects of transitioning a mature high-density orchard from standard herbicide ground-cover management system to organic ground-cover management systems; *Horticultural Studies 2000*; Arkansas Agricultural Experiment Station Research Series; University of Arkansas Division of Agriculture: Fayetteville, AK, 2001; Vol. *483*, pp 33−36.
(22) Greer, D. H. Non-destructive chlorophyll fluorescence and colour measurements of 'Braeburn' and 'Royal Gala' apple (*Malus domestica*) fruit development throughout the growing season. *N. Z. J. Crop Hortic. Sci.* **2005**, *33*, 413−421.
(23) Peck, G. M.; Andrews, P. K.; Reganold, J. P.; Fellman, J. K. Apple orchard productivity and fruit quality under organic, conventional, and integrated management. *HortScience* **2006**, *41*, 99−107.
(24) Hecke, K.; Herbinger, K.; Veberic, R.; Trobec, M.; Toplak, H.; Stampar, F.; Keppel, H.; Grill, D. Sugar-, acid- and phenol contents in apple cultivars from organic and integrated fruit cultivation. *Eur. J. Clin. Nutr.* **2006**, *60*, 1136−1140.
(25) Mikulic-Petkovsek, M.; Stampar, F.; Veberic, R. Parameters of inner quality of the apple scab resistant and susceptible apple cultivars (*Malus domestica* Borkh.). *Sci. Hortic.* **2007**, *114*, 37−44.
(26) Nazrala, J. J. B. Influence of the management of the soil and covers in the canopy microclimate of vine, grape and wine composition. *Rev. Fac. Cienc. Agrar., Univ Nac. Cuyo* **2008**, *40*, 85−104.
(27) Boyer, J.; Liu, R. Apple phytochemicals and their health benefits. *Nutr. J.* **2004**, *3*, 1−15.
(28) Janick, J. *Horticulture Science*, 4th ed.; W.H. Freeman and Company: New York, 1986; 746 pp.
(29) Brady, N.; Weil, R. *The Nature and Properties of Soils*. 14th ed.; Prentice Hall: New York, 2008; p 992.
(30) Treutter, D. Significance of flavonoids in plant resistance: a review. *Environ. Chem. Lett.* **2006**, *4*, 147−157.
(31) Ruhmann, S.; Leser, C.; Bannert, M.; Treutter, D. Relationship between growth, secondary metabolism, and resistance of apple. *Plant Biol.* **2002**, *4*, 137−143.
(32) Lee, J.; Steenwerth, K. L. 'Cabernet Sauvignon' grape anthocyanin increased by soil conservation practices. *Sci. Hortic.* **2013**, *159*, 128−133.

JOURNAL OF AGRICULTURAL AND FOOD CHEMISTRY

Article

pubs.acs.org/JAFC

Combination of Running-Buffer-Mediated Extraction and Polyamidoamine-Dendrimer-Assisted Capillary Electrophoresis for Rapid and Sensitive Determination of Free Fatty Acids in Edible Oils

Jingqing Wu, Ying Ge, and Weidong Qin*

Key Laboratory of Theoretical and Computational Photochemistry, Ministry of Education, College of Chemistry, Beijing Normal University, Beijing 100875, China

Supporting Information

ABSTRACT: A method was developed for determining free fatty acids in edible plant oils by incorporation of running-buffer-mediated liquid−liquid extraction and polyamidoamine-dendrimer-assisted capillary electrophoresis−capacitively coupled contactless conductivity detection. The recoveries for the extraction were in the range of 90.1% and 110.3%. Addition of dendrimer to the running buffer improved the separation of fatty acids. Under the optimized buffer conditions, i.e., 3 mM pelargonic acid, 39 mM tris(hydroxymethyl)aminomethane, 30 mM polyoxyethylene 23 lauryl ether, 35% acetonitrile, 15% 2-propanol, 2.5% 1-octanol, and 300 μM polyamidoamine generation 2 at apparent pH 8.53, the 10 model fatty acids were separated in 18 min with detection limits ranging from 0.46 to 3.28 μM. The successful determination of fatty acids in real samples suggests that the method is simple, cost-effective, and easy to operate and is suitable for scanning free fatty acid in edible plant oils.

KEYWORDS: *capillary electrophoresis−capacitively coupled contactless conductivity detection, polyamidoamine dendrimer, free fatty acids, edible plant oil*

INTRODUCTION

Free fat acids (FFAs) in edible plant oils ordinarily originate from crude plant oils and hydrolysis of triacylglycerols (TAGs) during processing and storage. FFAs affect the flavor quality of the oil. Moreover, they are chemically unstable, and a high concentration of FFAs may lead to the rancidity of the oil and formation of peroxides that are toxic to humans. Therefore, FFA content is one of the most concerned indices of edible oils.

Total FFAs in edible plant oil can be determined by nonaqueous titrimetry recommended by the American Oil Chemists' Society (AOCS).[1] The method is simple but uses a large amount of organic solvents and cannot determine the contents of individual FFAs. The individual FFA concentration in edible oil can be obtained by chromatography methods.[2−4] In gas chromatography (GC), FFAs are derivatized to methyl or trimethylsilyl esters.[5,6] In high-performance liquid chromatography (HPLC), they can be directly detected[7] but are often derivatized for higher detection sensitivity.[8,9] Owing to its high separation efficiency, capillary electrophoresis (CE) has been considered as an alternative technique for fatty acid analysis.[10−13] Capacitively coupled contactless conductivity detection (C^4D) is based on conductivity differences between the sample zones and the background electrolyte (BGE); it is an ideal detection approach for analytes lacking chromophores. Moreover, C^4D overcomes the problem of short path length that is encountered by the on-column photometric detection. Despite the obvious advantages of CE−C^4D, only a few works applied this technique in FFA analysis.[14,15]

Another aspect should be considered for CE analysis of FFA is separation. Since fatty acids (FAs) possess carboxyl groups, they can be separated straightforwardly under normal polarity mode in neutral or basic running buffers, in which they migrate to the detector following the cathodic electroosmotic flow (EOF).[11] However, it was suggested that reversed EOF combined with a negative separation voltage is favorable, because in this case the solutes comigrate with EOF and better reproducibility of migration time could be achieved.[16,17] The commonly used strategy for reversing EOF is dynamic coating due to its versatility and simplicity;[18] for this application, cationic surfactants such as tetradecyltrimethylammonium bromide (TTAB)[19,20] and cetyltrimethylammonium bromide (CTAB) are often used. Usually cationic surfactants at millimolar levels are needed for EOF reversal in aqueous media, but the concentrations can be higher in nonaqueous solutions.[21] This is not favorable if C^4D is employed, because the baseline noise would markedly increase upon elevated buffer conductivity.

Polyamidoamine (PAMAM) dendrimers are highly branched, symmetrical macromolecules with high-density functional groups.[22] They possess three kinds of structural components: cores, interior repeating units, and terminal groups. PAMAMs terminated with primary amine groups are full-generation dendrimers (G*n*, where *n* is an integer), whereas those terminated with methyl ester groups are half-generation ones (G*n*.5). Due to protonation of the amino groups, the full-generation PAMAMs are positively charged at pH <10[23] and, therefore, can readily adsorb on the silica surface. This property

Received: December 13, 2013
Revised: March 22, 2014
Accepted: April 16, 2014
Published: April 16, 2014

ACS Publications © 2014 American Chemical Society

dx.doi.org/10.1021/jf4056105 | J. Agric. Food Chem. 2014, 62, 4104−4111

renders PAMAMs potentially ideal EOF reversers for C^4D analysis, because no anions were introduced into running buffers as the conventional surfactant salts do.

We herein investigate CE−C^4D analysis of FFAs of different chain lengths varying from C8 to C20, including saturated and unsaturated, *trans*- and *cis*-FFAs, using PAMAMs as additive to reverse EOF and to improve separation. We are also to demonstrate the highly effective liquid−liquid extraction of FFAs from the plant oils using the PAMAM-containing, alkaline running buffer as extraction solution. The advantages of the extraction are obvious: neither desorption as in solid-phase extraction[24] nor back-extraction or evaporation as in conventional liquid−liquid extraction[25] is required; indeed, the extract can be directly analyzed. The influences of PAMAM generation and concentration, buffer composition and pH, organic solvents, and C^4D parameters were investigated and optimized. Finally, the developed method was applied to analysis of FFAs in real edible oil samples.

MATERIALS AND METHODS

Chemicals and Solutions. All reagents were of analytical grade. Cetyltrimethylammonium bromide (CTAB), methanol (MeOH), acetonitrile (ACN), tris(hydroxymethyl)aminomethane (Tris), 1-octanol, 2-propanol, and *n*-hexane were purchased from Beijing Chemical Plant (Beijing, China). Polyoxyethylene 23 lauryl ether (Brij 35) and pelargonic (C9:0), palmitic (C16:0), linoleic (C18:2 *cis*-9, *cis*-12), oleic (C18:1 *cis*-9), and elaidic (C18:1 *trans*-9) acids were the products of Aladdin (Shanghai, China). Hexanoic (C6:0), octanoic (C8:0), capric (C10:0), lauric (C12:0), myristic (C14:0), and stearic (C18:0) acids were obtained from Labebuy Reagents (Hangzhou, Zhejiang, China). Individual fatty acid stock solutions, at 20.0 mM each, and working standard mixtures, typically at 0.02 mM each, were prepared in methanol and stored in a refrigerator until use.

Synthesis of PAMAM Dendrimers. PAMAMs of different generations were synthesized following the procedures described elsewhere.[22] Briefly, methyl acrylate was added dropwise to the methanolic solution of ethylenediamine, and the mixture was allowed for Michael addition at room temperature for 24 h. Afterward, the adduct was let for amidation with excessive ethylenediamine under room temperature for 64 h, yielding amine-terminated PAMAM. The first two steps produced PAMAM generation zero (G0). Synthesis of higher generation PAMAMs was accomplished by repeating progressively the Michael addition (for half-generations)/amidation (for entire generations) cycles. The product of each step was purified by washing with methanol, followed by drying under vacuum. The PAMAMs were tested by a Bruker Advance III-400 MHz NMR spectrometer (Rheinstetten, Germany). The ^1H NMR results of PAMAMs G0, G1, G2, G3, and G4 are given in section 1 of the Supporting Information.

Capillary Electrophoresis. A high-voltage supply HB-F303-1AC (Hengbo, Tianjin, China) was employed to offer potentials for electrophoretic separation. A VC2002 function generator (Shengli Cooperation, Shenzhen, Guangdong, China) delivered a sinusoidal wave at a frequency between 1 Hz and 2 MHz and amplitude between 0 and 20 $V_{p\text{-}p}$ (peak to peak) to the excitation electrode of a homemade C^4D instrument, which was described previously.[16] The data were collected by an IBM PC compatible computer via a CT22 data acquisition unit (Qianpu, Shanghai, China) and processed with a HW2000 chromatography station (Qianpu).

An uncoated fused-silica capillary (Yongnian Optical Fiber, Hebei, China) of 55 cm length (48 cm effective length) × 50 μm i.d. was used for separation. The fresh capillary was conditioned by pressure flushing, successively, with 0.5 mM NaOH (20 min), deionized water (20 min), and running buffer (10 min). Every day before use the capillary was rinsed with deionized water for 10 min, followed by running buffer for 10 min. All solutions were filtered through 0.45 μm filters (Jiu Ding High Tech., Beijing, China) before use. Samples were injected hydrostatically at a height difference of 35 cm for 20 s, corresponding to an injection volume of 19.5 nL, as estimated using CE Expert software (Beckman Coulter, Fullerton, CA). Separations were performed at 15 kV at ambient temperature. Between runs, the capillary was regenerated by flushing with running buffer for 5 min. If the running buffer changed, the capillary was rinsed with the new buffer for 20 min before experiment. The EOFs were determined using the method proposed by Williams et al.[26]

Orthogonal Design. The organic solvents acetonitrile, 2-propanol, and 1-octanol were commonly used agents in CE; in this experiment, they were added to running buffer to increase the solubility and separation of FAs. To obtain the best resolution in short analysis time, orthogonal design (OD) was employed to optimize the concentrations of the organic solvents. The boundaries of individual organic solvents were determined by preliminary experiments, based on which three-level three-factor OD was built, and a total of nine experimental conditions were tested, as shown in Table S1 of the Supporting Information. To rank the CE performance of each condition, chromatographic optimization functions (COFs) were adopted as criteria[27]

$$\mathrm{COF} = \sum_{i=1}^{n-1} A_i \ln\left(\frac{R_i}{R_{i\mathrm{D}}}\right) + B(t_\mathrm{D} - t_n) \quad (1)$$

where A_i and B are weighting parameters, which are both assigned to 1 in this experiment. R_i and $R_{i\mathrm{D}}$ (set to 1.5) are the determined and desired resolution values for the ith peak pair. The time terms t_D and t_n stand for a desired maximum analysis time (20 min in this experiment) and the time of the last peak, respectively. The higher COF value represents the better CE performance.

The R_i in eq 1 was defined as

$$R_i = \frac{2(t_2 - t_1)}{W_2 + W_1} \quad (2)$$

where t_1, t_2 and W_1, W_2 are the migration times and the peak widths of two successive peaks, peak 1 being the first one and peak 2 the next one adjacent to it.

Analysis of Edible Plant Oil Samples. *CE−C^4D Analysis.* Samples of soybean oil, sunflower seed oil, and maize oil were bought from a local supermarket. For simplicity and efficiency in sample preparation, the buffer-mediated liquid−liquid extraction was adopted. Briefly, a 0.25 mL oil sample was added to 0.5 mL of running buffer. The admixture was vortexed for 9 min (this is the optimal extraction time; see section 3 of the Supporting Information for details) and then centrifuged at 3500 rpm for 5 min. The aqueous phase was diluted 5−50 times with methanol and used directly for CE analysis.

Recoveries (R%) of FFAs from the plant oil samples were assessed on the basis of three spiking levels, using

$$R\% = \frac{S_2 - S_1}{S_0} \times 100 \quad (3)$$

where S_1 and S_2 are the peak areas of an FFA in unspiked and spiked samples, respectively; S_0 is the peak area of this FFA prepared in matched matrix at the spiking concentration.

GC−Mass Spectrometry (MS) Analysis. Extraction of FFAs from oil samples and the subsequent esterification of the FFAs were carried out following refs 24, 28, and 29, with slight modification. Briefly, 5.0 mL of vegetable oil sample was extracted three times with 10 mL of Na_2CO_3 solution (2 g/100 mL). The aqueous phase was titrated with 1 M HCl to pH 2 and extracted three times with 10 mL methylene chloride. The methylene chloride fractions were combined and evaporated to dryness. The residue was dissolved in 3 mL of methanol, added slowly with 0.15 mL of concentrated sulfuric acid, and refluxed at 80 °C for 2 h. To extract the fatty acid methyl esters, 5 mL of *n*-hexane was added, followed by 5 mL of aqueous NaCl solution (1%, w/w) to facilitate phase separation. The mixture was vortexed for 5 min, and then the supernatant was collected and diluted (typically 200 folds) with *n*-hexane before GC−MS analysis.

GC−MS analysis was performed on an Agilent 7890A gas chromatograph (Agilent Technologies, Santa Clara, CA) coupled to an Agilent HP 5975C quadrupole mass spectrometer (Agilent). The gas chromatograph was equipped with an Agilent HP-5 fused-silica capillary column (length, 30 m; i.d., 250 μm; film thickness, 0.25 μm). The flow rate of the helium carrier gas was 1 mL/min. The GC oven temperature program was as follows: initial oven temperature 30 °C, ramped to 230 °C at 20 °C/min, afterward to 270 °C at 5 °C/min, and then to 280 °C at 10 °C/min, and held for 7 min. The interface, injector, ion source, and quadrupole were kept at 280, 250, 230, and 150 °C, respectively. One microliter of the esterified FFAs prepared in *n*-hexane was injected in splitless mode using an autosampler (Agilent HP 7683B). The solvent delay time was set at 3 min. For each oil sample, the MS was first operated on the total ion current (TIC) mode, scanning from *m*/*z* 50 to 500, for identification purposes and then on selected ion monitoring (SIM) mode for quantification.

AOCS Nonaqueous Titrimetry. The total FFA contents in plant oil samples were determined according to the method recommended by the American Oil Chemists' Society (AOCS).[1] For calibration, a blank titration of the organic solvent was performed following the procedures in the literature.[30]

RESULTS AND DISCUSSION

Preliminary experiments suggested that higher-generation PAMAMs had stronger EOF-reversing ability (Figure S2 of the Supporting Information). However, PAMAM G2 could provide the best CE performance in terms of separation efficiency and analysis time. Therefore, it was chosen for the following method development.

Comparison of PAMAM and CTAB as EOF Reversers. Figure 1 indicates that, in the presence of 30 μM PAMAM G2, the EOFs reversed for the buffers of Tris and carboxylic acids (chain lengths from C6 to C12) prepared in 50% (v/v) methanol. With regard to CTAB as EOF reverser, however, the cathodic EOF mobility was only slightly reduced at 1 mM, reached nearly zero at 5 mM, reversed with further increase in CTAB concentration, and leveled off at 10 mM, with a maximum anodic EOF mobility of -0.5×10^{-4} cm^2 V^{-1} s^{-1}. This value was only about one-third of that generated by 30 μM PAMAM G2 in the same buffer, which is not favorable for quick analysis. Moreover, the baseline noise with a high concentration of CTAB increased dramatically and no peaks corresponding to FAs could be identified (Figure S3 of Supporting Information).

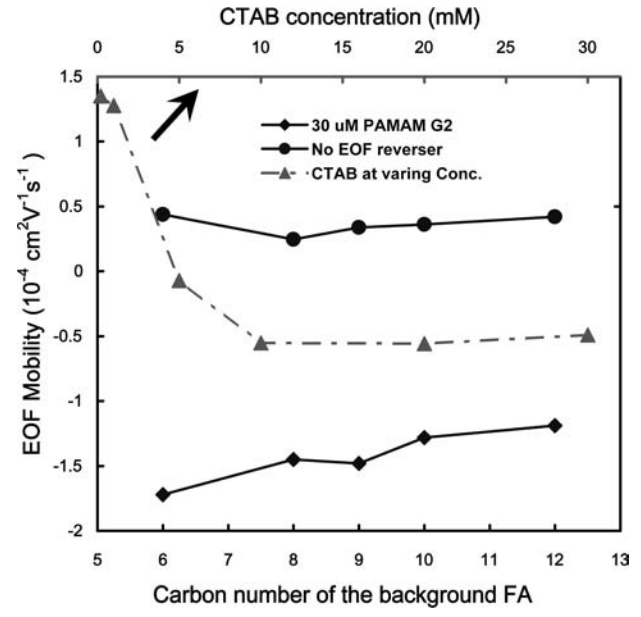

Figure 1. Comparison of EOF reversal ability of PAMAM G2 and CTAB. Testing buffers contained 10 mM Tris, 5 mM FAs (pelargonic acid for CTAB experiments), 50% (v/v), and EOF reversers as depicted in the figure legends.

The results suggested that PAMAM G2 was positively charged in the buffer containing high-concentration organic solvents, and was an effective EOF reverser, predominantly owing to its high densities of surface functional groups.[31] The slight cathodic increase in EOF as a function of chain length of the background fatty acids might be the consequence of the stronger wall adsorption of the longer hydrophobic chains.[21]

Effect of PAMAM on Separation. Figure 2A depicts that the analysis time decreased rapidly, from ca. 35 to ca. 21 min, when the PAMAM concentration increased from 30 to 100 μM. In the presence of 300 μM dendrimer, the FAs were

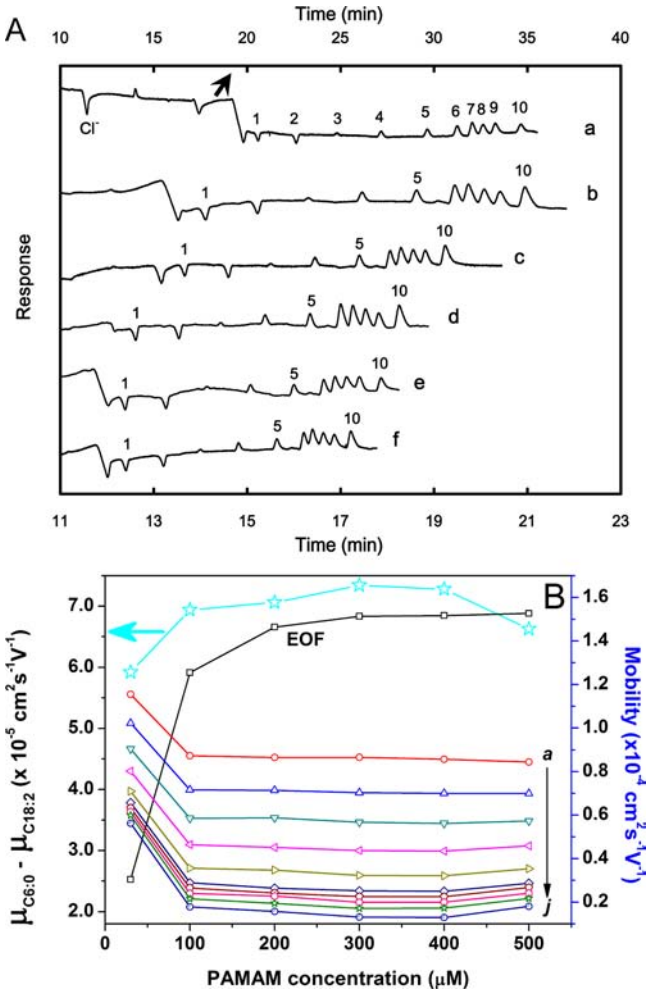

Figure 2. Influence of PAMAM concentration on electropherograms (A) and mobilities (B). Conditions in panel A: The buffers contained 39 mM Tris, 3 mM pelargonic acid (C9:0), 30 mM Brij 35, 20% 2-propanol, 30% acetonitrile, 2.5% 1-octanol. The PAMAM G2 concentrations were 30, 100, 200, 300, 400, and 500 μM for traces a, b, c, d, e, and f, respectively. All the contents of organic solvents in buffers were of volume percentages. Capillary: 55 cm × 50 μm. Separation voltage: 15 kV. C^4D: 20 $V_{p\text{-}p}$ × 100 kHz. Peak identities: 1, C6:0; 2, C8:0; 3, C10:0; 4, C12:0; 5, C14:0; 6, C18:2; 7, C16; 8, C18:1; 9, C18:1(t); 10, C18:0. Conditions in panel B: curves a−j corresponded to FAs 1−10 in panel A.

dx.doi.org/10.1021/jf4056105 | J. Agric. Food Chem. 2014, 62, 4104−4111

baseline separated within 18 min. Although the analysis time was further shortened with progressive addition, resolution between the FAs deteriorated.

Migration of the FAs in capillary is influenced by their interactions with capillary wall and with PAMAM. The former is adsorption, leading to low migration velocity and, usually, low separation efficiency; it is intensified by the increasing FA chain length.[21] The latter is based on electrostatic attraction. To understand in depth the effect of PAMAM, the EOF mobility and effective mobilities of the FAs were plotted versus dendrimer concentration (Figure 2B). The anodic EOF mobility increased rapidly with PAMAM concentration from 30 to 200 μM and leveled off at 300 μM. On the other hand, the FA mobilities significantly decreased with PAMAM concentration from 30 to 100 μM. In addition, variation of the mobility difference between the first and the last FAs, C6:0 and C18:2, as a function of dendrimer concentration shows a convex profile, with a maximum at 300 μM, under which condition high resolution could be realized. The results suggest that PAMAM dendrimer played an important role in separation time and resolution.

Selection of BGE Constituents. The C^4D response is theoretically determined by conductivities of analyte, BGE co-ion and counterion, and the transfer ratio as well.[32] BGE co-ion is empirically highly influential on peak intensity and shape and should be selected carefully. Increasing conductivity difference between analyte and BGE co-ion can improve detection sensitivity, but can also result in more fronting or tailing peaks, which are unfavorable for high resolution. Given the fact that the carbon numbers of the FFAs occurring naturally in plant oils are usually even, from 12 to 22,[33] and taking into consideration both the detection sensitivity and peak symmetry, we choose pelargonic acid (C9:0) as buffering acid in BGE.

Regarding background counterions, the following bases were investigated: tributylamine, methylamine, ethylamine, triethylamine, ammonia, and Tris. Although some fatty acids could be detected with tributylamine, they suffered from the drawbacks of long analysis time and low signal-to-noise ratio (trace a of Figure 3). The electropherograms with buffers containing methylamine, ethylamine, and triethylamine showed serious baseline noise such that the signal from fatty acid could be hardly identified (traces b–d). While all the fatty acids could be detected with the BGE buffered by ammonia, the palmitic acid, oleic acid, and elaidic acid were not baseline separated (trace e), and the resolution was not improved with further optimization. For Tris as the background cation (trace f), relatively low baseline noise was exhibited and all the fatty acids could be detected with high sensitivity in acceptable analysis time; moreover, the resolution among the peaks could be further optimized to realize baseline separation. Consequently, Tris was selected as background cation for subsequent method development.

Influence of Organic Solvents and Brij 35. Table 1 lists the COF values of each run as well as the sum of the COFs under investigating variables (K1–K3). According to the largest donating rule, the largest sum of COF corresponds to the optimum level of the factor. Therefore, the optimal organic solvent composition in the buffer should be 15% 2-propanol (A2), 35% acetonitrile (B2), and 2.5% 1-octanol (C3).

As an often-used organic additive, Brij 35 affected the separation performance. By investigating the dependence of resolution and analysis time on the Brij 35 concentration

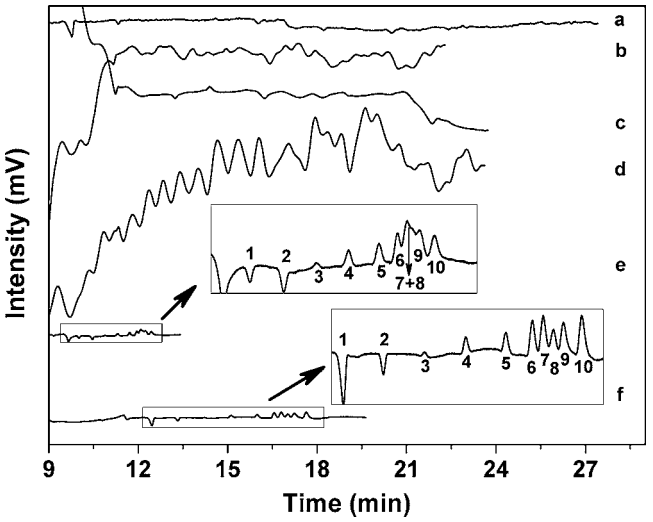

Figure 3. Influence of BGE cation buffers: 300 μM PAMAM G2, 30 mM Brij 35, 20% 2-propanol, 30% acetonitrile, 2.5% 1-octanol, 5 mM pelargonic acid (C9:0), and the following cations at 45 mM each: a, tributylamine; b, ethylamine; c, triethylamine d, methylamine; e, ammonia; f, Tris. All the other conditions were the same as Figure 2.

Table 1. Three-Level Orthogonal Array Design Used To Screen Significant Factors[a]

run	factor A $C_{2\text{-propanol}}$ (%)	factor B $C_{\text{acetonitrile}}$ (%)	factor C $C_{1\text{-octanol}}$ (%)	code	COF
1	10	30	1.5	A1B1C1	7.20
2	10	35	2.0	A1B2C2	8.82
3	10	40	2.5	A1B3C3	8.36
4	15	30	2.0	A2B1C2	4.06
5	15	35	2.5	A2B2C3	11.65
6	15	40	1.5	A2B3C1	9.03
7	20	30	2.5	A3B1C3	7.10
8	20	35	1.5	A3B2C1	8.74
9	20	40	2.0	A3B3C2	8.19
K1	24.38	18.35	24.96		
K2	24.74	29.2	21.07		
K3	24.02	25.58	27.1		
optimum	A2	B2	C3		

[a]Detailed information is listed in Table S1 of the Supporting Information.

(Figure S4 of the Supporting Information), we found that Brij 35 at 30 mM was optimal.

Influence of Buffer pH. The running buffers were prepared by mixing aqueous buffer solutions with organic solvents; therefore, the pH values of the aqueous phases and the apparent pH values (denoted by pH*) of the final mixtures were measured. The influence of buffer pH was investigated at a fixed buffer concentration of 42 mM, by altering the Tris/pelargonic acid ratio from 41/1 to 33/9, corresponding to pH* and pH values of 8.79–9.36 and 8.29–8.67, respectively. It was found that the migration times of the FAs decreased upon increasing buffer acidity; at pH* 8.53 (pH 9.18), all the FAs were well-separated with the highest detection sensitivity (Figure S5 of the Supporting Information).

Increasing buffer acidity was achieved by increasing the pelargonic acid/Tris ratio of the BGE. Theoretically, the

dx.doi.org/10.1021/jf4056105 | J. Agric. Food Chem. 2014, 62, 4104–4111

Table 2. CE−C^{4}D Performance

	C8:0	C10:0	C12:0	C14:0	C18:2	C16:0	C18:1	C18:1(*t*)	C18:0
linear range (μM)	7.5−75	10−300	5.0−150	3.0−90	1.5−45	1.5−38	2.0−38	2.5−63	1.5−45
intercept ($\times 10^3$)	−1.03	−0.73	−1.03	−0.69	0.68	−0.16	−0.29	−1.58	1.95
slope ($\times 10^5$)	1.98	1.19	4.06	6.40	9.19	11.64	9.14	10.27	12.33
r^2	0.9975	0.9991	0.9993	0.9988	0.9966	0.9996	0.9969	0.9998	0.9996
LOD (μM)	0.81	3.28	1.05	0.89	0.46	0.49	0.61	0.70	0.46
LOD (μg/mL)	0.12	0.57	0.21	0.20	0.13	0.13	0.17	0.20	0.13
	Intraday Precision (RSD%, n = 5 at 20 μM)								
migration time	0.12	0.15	0.24	0.31	0.39	0.40	0.42	0.45	0.49
peak area	8.54	9.33	7.31	9.46	7.51	9.28	5.11	9.91	7.90
	Interday Precision (RSD%, 3 days n = 3 × 5 = 15 at 20 μM)								
migration time	0.12	0.18	0.25	0.33	0.41	0.40	0.47	0.43	0.46
peak area	7.43	8.99	7.29	6.31	5.92	8.86	4.98	7.42	7.99

Table 3. Recoveries (%) of FFAs from the Oil Samples by Running-Buffer-Mediated Extraction

	concn spiked (μM)	sunflower seed oil	maize oil	soybean oil
C8:0	7.5/10.0/12.5	109.2/106.1/95.2	108.3/95.6/98.2	106.2/105.8/104.2
C10:0	10.0/20.0/40.0	106.4/102.6/103.1	110.1/110.3/103.7	102.7/101.4/100.7
C12:0	5.0/10.0/20.0	103.6/101.5/103.2	96.2/104.6/93.2	90.7/99.1/92.8
C14:0	3.0/6.0/12.0	96.4/92.1/94.1	95.4/108.6/106.3	101.2/93.5/90.1
C18:2	1.5/3.0/6.0	102.9/95.7/99.9	90.4/93.4/100.1	103.5/95.8/110.2
C16:0	1.5/3.0/6.0	95.3/97.1/100.1	98.1/103.9/100.3	103.6/91.8/102.5
C18:1	1.5/3.0/6.0	109.2/91.0/103.0	109.3/93.3/101.9	101.4/109.3/103.4
C18:1(*t*)	2.5/5.0/10.0	103.4/102.1/93.9	108.8/105.6/90.7	105.4/93.6/97.1
C18:0	1.5/3.0/6.0	92.8/94.2/101.5	108.4/99.2/90.7	100.6/91.9/106.6

effective mobilities of FAs in low pH* buffer would decrease, resulting in prolonged analysis time. Therefore, the phenomenon was not caused by protonation/deprotonation of FAs. We think two important factors should be considered in interpreting the migration of FAs. One is protonation of the terminal amino group of PAMAM molecules. Adsorption of these positively charged molecules on the inner wall of the capillary would enhance the anodic EOF, leading to high apparent mobilities of the FAs. However, in the running buffer, migration of FAs would be retarded by the interaction with the protonated PAMAMs. The second is the elution effect of pelargonic acid. It was reported that significant wall adsorption occurred for FAs at all chain lengths during separation, even in buffer prepared in pure organic solvent.[21] Increasing the background pelargonic acid concentration for higher buffer acidity would also promote the elution of FAs from the capillary wall, giving rise to two consequences that oppositely affect the CE performance: (a) suppressing peak tailing and hence providing better resolution and (b) enhancing the mobilities of the FAs and often unfavorably degrading the separation. As a compromise between analysis time and resolution, the BGE containing 39 mM Tris and 3 mM pelargonic acid at pH* 8.53 was adopted.

Optimization of C^{4}D Parameters. It was found that the peak intensity increased proportionally with growing excitation voltage; therefore, the maximum output of the functional generator, 20 $V_{p\text{-}p}$, was employed. The influence of the oscillation frequency was studied between 50 and 200 kHz (Figure S6 of the Supporting Information), and highest peak heights were achieved at 100 kHz. The decreasing response at higher frequency was likely attributed to the high stray capacitance between the electrodes.[34]

Analytical Performance and Application. The method was evaluated using the optimized buffer comprising 39 mM Tris, 3 mM pelargonic acid (C9:0), 30 mM Brij 35, 35% ACN, 15% 2-propanol, 2.5% 1-octanol, and 300 μM PAMAM G2 at pH* 8.53. The limits of detection (LODs, signal-to-noise ratio of 3) for most FAs were at sub-micromolar level, in the range of 0.46−3.28 μM, equivalent to mass concentrations of 0.12−0.57 μg/mL (Table 2). The higher LOD for capric acid might result from the utilization of pelargonic acid as background co-ion. The two FAs differ by only one carbon in chain lengths, and the small mobility difference between analyte and background co-ion theoretically accounts for the low detection sensitivity.[34] However, employing PAMAM rather than the conventional cationic surfactants with higher conductivity as EOF reverser significantly decreased the baseline noise, resulting in the higher sensitivity of the C^{4}D method. The overall detectability for fatty acids averaged 34-fold more sensitive than the commonly adopted CE−indirect UV method.[35] It is superior to the previous CE−C^{4}D results (35−319 μM[14]) and better than the recently reported 0.9−1.5 μg/mL,[15] which is the best detection sensitivity so far published on CE−C^{4}D. Indeed, it is even comparable to liquid chromatography−C^{4}D.[36]

The linearity of the detector response for each fatty acid was investigated on seven concentration levels, and calibration curves were constructed by plotting the peak areas of each fatty acid against the concentrations. Table 2 indicates that, in the concentration range studied, the squared correlation coefficients (r^2 values) for all the calibration graphs were higher than 0.996, suggesting the good linearity of the method. The precisions of migration times and peak areas were studied on the standard mixture at 20 μM each, using C6:0 as internal standard. Five consecutive injections were performed for intraday repeatability evaluation (n = 5), and interday reproducibility was estimated on three consecutive days (n = 3 × 5 = 15). It was found that the intraday and interday variabilities of the migration time, expressed in relative standard

dx.doi.org/10.1021/jf4056105 | J. Agric. Food Chem. 2014, 62, 4104−4111

deviations (RSDs), were no more than 0.49% and 0.47%, respectively. The corresponding values for peak areas were no more than 9.91% and 8.99%, respectively. The good precision of the migration time should partly originate from the utilization of dendrimer as EOF reverser. The precisions of migration time and peak area were in accordance with the requirements set by the US FDA guidelines.[37] The data of peak areas were statistically checked for random errors with *F*-test and systematic errors with *t*-test. No significant differences within the data were found, with $F \leq 5.71$ ($F_{(4,4)} = 6.39$, at 95% confidence limit) and $t \leq 2.57$ ($t_8 = 2.90$, at 98% confidence limit).

The running-buffer-mediated extraction process was optimized in terms of extraction time. The extracted FFA content increased with extraction time and leveled off at 9 min (Figure S1 of the Supporting Information). With an extraction time of 9 min, the recoveries of FFAs from the plant oils at three concentration levels were between 90.1% and 110.3% (Table 3), suggesting the effectiveness of the PAMAM-containing running buffer as extraction solution. The surface primary amino groups of the PAMAM G2 molecule have protonation constants (pKs) of ca. 9.0;[23] therefore, in the running buffer at pH* 8.53, the dendrimers were partly positively charged. On the other hand, the FFAs were negatively charged because the pK_a values of their carboxyl groups are around 5.[11] The PAMAM−FFA interaction, driven by acid−base chemistry and ion pairing, resulted in assembly of FFAs on the PAMAM surface,[38] facilitating the FFAs partitioning into the running buffer.

To demonstrate its applicability, the developed method was applied in determination of FFAs in plant oil samples (Figure 4). Due to the influence of sample matrices, the migration times

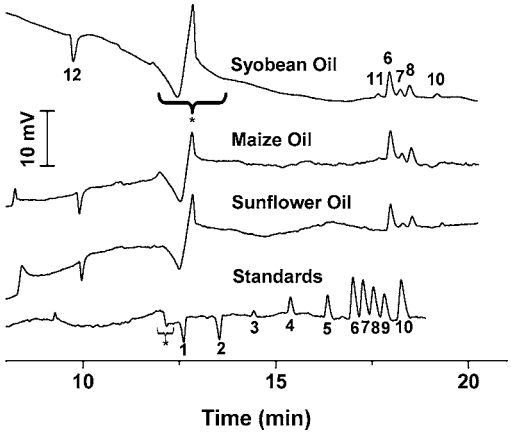

Figure 4. Electropherograms of the FFAs in real samples. Peak identities: 1−10 were the same as Figure 2; 11, unknown; 12, Cl^-; *, system peak. The concentration of PAMAM G2 was 300 μM. The extracts of soybean oil, maize oil, and sunflower seed oil were diluted 5-, 10-, and 50-fold, respectively, with methanol. The concentrations of FAs in standard solution were 0.02 mM each.

of the peaks in oils shifted, and the baseline noise increased for some samples (baseline noises for the traces in Figure 4 were 37, 23, 52, and 63 μV for standard solution, soybean, sunflower seed, and maize oils, respectively; the baseline noise of the detector was different during daytime and night—it was usually somewhat lower at night). However, the FFAs in real samples were separated with slightly better resolution yet much shorter analysis time than the previous report.[15] Moreover, treatments of oil samples were simple, efficient, and easy to operate, and the total analysis time is no more than 35 min. For comparison, the FFAs in the oil samples were also analyzed by AOCS nonaqueous titration and GC−MS (for chromatograms, refer to Figure S7 of the Supporting Information). Table 4 indicates

Table 4. Free Fatty Acids Contents (as Lauric Acid, %) Determined in Three Plant Oils

	soybean oil		sunflower seed oil		maize oil	
	this method	GC−MS	this method	GC−MS	this method	GC−MS
C18:2	0.0074	0.0080	0.0801	0.0977	0.0181	0.0170
C16:0	0.0012	0.0015	0.0087	0.0092	0.0029	0.0034
C18:1	0.0036	0.0044	0.0312	0.0281	0.0087	0.0109
C18:0	0.0002	0.0004	0.0054	0.0048	ND[a]	0.0001
total	0.0125	0.0143	0.126	0.139	0.0298	0.0315
			AOCS Method			
total	0.0138		0.121		0.0328	

[a]Under the LOD. According to the sample preparation procedure, the FFAs in maize oil sample were 20-fold diluted before injection.

that the results from the three methods agreed well. C16:0, C18:0, C18:1, and C18:2 were all detected in soybean oil and sunflower seed oil by CE−C^4D and GC−MS. Although a discrepancy is found between the two methods on the concentration of C18:0 in maize oil, we think this is mainly due to the overall 20-fold dilution of the FFAs for this oil during sample preparation, making the final concentration of C18:0 below the LOD. None of the edible oils studied contained trans fatty acid C18:1(*t*). The FFA concentrations (as lauric acid) were in the range of 0.0138%−0.121%, in compliance with the China national standards on maize, soybean, and sunflower seed oils.[39−41] The FFA contents determined in this work were higher than those reported by Wei et al.,[24] but the total FFA contents in our sample oils were lower than the previous reports (for maize oil,[30,42] soybean oil,[30] and sunflower seed oil[42,43]). In fact, contents of different FFAs in edible oils vary widely,[24] and some FFAs may occur at trace levels. Therefore, though only four FFAs were detected in the oil samples by CE−C^4D and GC−MS, other FFAs might also exist, but at extremely low concentrations, i.e., lower than the LOD of GC−MS, which was ca. 0.05 μg/mL (for C16:0; the value could be lower for shorter-chain FFAs) in TIC mode for oil samples in this experiment.

To evaluate this new strategy in depth, a previously reported CE−UV method[44] for determining fatty acids was carried out. Figure S8 of the Supporting Information indicates that the peaks of the FFAs in the real samples overlapped due to the tailing shapes. Moreover, the detection sensitivities were low, with LODs of 1.2−9.0 μg/mL for FA standards.

Summing up, the running-buffer-mediated liquid−liquid extraction approach enables quick and quantitative extraction of FFAs from the plant oils. Addition of PAMAM dendrimers to running buffer effectively shortens the analysis time and improves the separation of the analytes, and the CE−C^4D analysis based on the PAMAM-containing buffer provides higher detection sensitivity relative to those using conventional cationic surfactants as EOF reversers. The methodology is a promising alternative for determining FFAs in edible oils; importantly, it is fast, cost-effective, and easier to operate than the traditional chromatographic techniques.

■ ASSOCIATED CONTENT

Supporting Information

The ^{1}H NMR results (section 1), orthogonal design (Table S1), effect of extraction time (Figure S1), influence of PAMAM generation (Figure S2), influence of CTAB and PAMAM as EOF reverser (Figure S3), effect of Brij 35 concentration (Figure S4); influence of buffer pH* (Figure S5), influence of oscillation frequency (Figure S6), FFAs in real samples determined by GC−MS (Figure S7), FFAs in real samples determined by CE−UV (Figure S8). This material is available free of charge via the Internet at http://pubs.acs.org.

■ AUTHOR INFORMATION

Corresponding Author

*E-mail: qinwd@bnu.edu.cn. Tel: + 86-10-58802531. Fax: + 86-10-58802075.

Funding

This work was supported by the National Natural Science Foundation of China (20975014) and the Fundamental Research Funds for the Central Universities.

Notes

The authors declare no competing financial interest.

■ ABBREVIATIONS USED

FFA, free fatty acids; FA, fatty acids; PAMAM, polyamidoamine dendrimer; TAGs, hydrolysis of triacylglycerols; CE−C^{4}D, capillary electrophoresis−capacitively coupled contactless conductivity detection; EOF, electroosmotic flow; BGE, background electrolyte; TTAB, tetradecyltrimethylammonium bromide; CTAB, cetyltrimethylammonium bromide; Brij 35, polyoxyethylene 23 lauryl ether; Tris, tris(hydroxymethyl)-aminomethane; OD, orthogonal design; COF, chromatographic optimization function; GC−MS, gas chromatography−mass spectrometry.

■ REFERENCES

(1) AOCS. *Official Methods and Recommended Practices of the American Oil Chemists' Society*, 4th ed.; American Oil Chemists' Society: Champaign, IL, 1989; Ca 5a-40.

(2) Chen, Z. Y.; Kwan, K. Y.; Tong, K. K.; Ratnayake, W. M. N.; Li, H. Q.; Leung, S. S. F. Breast milk fatty acid composition: A comparative study between Hong Kong and Chongqing Chinese. *Lipids* **1997**, *32*, 1061−1067.

(3) Garcia, P.; Franco, P.; Alvarez, R.; de Lera, A. R. Separation of regioisomers and enantiomers of underivatized saturated and unsaturated fatty acid monoacylglycerols using enantioselective HPLC. *J. Sep. Sci.* **2011**, *34*, 999−1003.

(4) De Baere, S.; Eeckhaut, V.; Steppe, M.; De Maesschalck, C.; De Backer, P.; Van Immerseel, F.; Croubels, S. Development of a HPLC-UV method for the quantitative determination of four short-chain fatty acids and lactic acid produced by intestinal bacteria during in vitro fermentation. *J. Pharm. Biomed. Anal.* **2013**, *80*, 107−115.

(5) Brondz, I. Development of fatty acid analysis by high-performance liquid chromatography, gas chromatography, and related techniques. *Anal. Chim. Acta* **2002**, *465*, 1−37.

(6) Gutnikov, G. Fatty-acid profiles of lipid samples. *J. Chromatogr. B. Biomed. Appl.* **1995**, *671*, 71−89.

(7) Merlin, J. F.; Gresti, J.; Bellenger, S.; Narce, M. Fast high performance liquid chromatography analysis in lipidomics: Separation of radiolabelled fatty acids and phosphatidylcholine molecular species using a monolithic C-18 silica column. *Anal. Chim. Acta* **2006**, *565*, 163−167.

(8) Durst, H. D.; Milano, M.; Kikta, E. J.; Connelly, S. A.; Grushka, E. Phenacyl esters of fatty-acids via crown ether catalysts for enhanced ultraviolet detection in liquid-chromatography. *Anal. Chem.* **1975**, *47*, 1797−1801.

(9) Miwa, H.; Yamamoto, M.; Nishida, T.; Nunoi, K.; Kikuchi, M. High-performance liquid-chromatographic analysis of serum long-chain fatty-acids by direct derivatization method. *J. Chromatogr.-Biomed.* **1987**, *416*, 237−245.

(10) Simas Porto, B. L.; Nora de Souza, M. V.; Leal de Oliveira, M. A. Analysis of omega 3 fatty acid in natural and enriched chicken eggs by capillary zone electrophoresis. *Anal. Sci.* **2011**, *27*, 541−546.

(11) De Castro, P. M.; Barra, M. M.; Ribeiro, M. C. C.; Aued-Pimentel, S.; Da Silva, S. A.; De Oliveira, M. A. L. Total trans fatty acid analysis in spreadable cheese by capillary zone electrophoresis. *J. Agric. Food Chem.* **2010**, *58*, 1403−1409.

(12) Corradini, C.; Bianchi, F.; Matteuzzi, D.; Amoretti, A.; Rossi, M.; Zanoni, S. High-performance anion-exchange chromatography coupled with pulsed amperometric detection and capillary zone electrophoresis with indirect ultra violet detection as powerful tools to evaluate prebiotic properties of fructooligosaccharides and inulin. *J. Chromatogr. A* **2004**, *1054*, 165−173.

(13) Breadmore, M. C.; Henderson, R. D.; Fakhari, A. R.; Macka, M.; Haddad, P. R. Separation of Nile Blue-labelled fatty acids by CE with absorbance detection using a red light-emitting diode. *Electrophoresis* **2007**, *28*, 1252−1258.

(14) Oliveira, M. A. L.; do Lago, C. L.; Tavares, M. F. M.; da Silva, J. A. F. Analysis of fatty acids by capillary electrophoresis with contactless conductivity detection. *Quim. Nova* **2003**, *26*, 821−824.

(15) Wong, Y. F.; Saad, B.; Makahleh, A. Capillary electrophoresis with capacitively coupled contactless conductivity detection for the determination of cis/trans isomers of octadec-9-enoic acid and other long chain fatty acids. *J. Chromatogr. A* **2013**, *1290*, 82−90.

(16) Yang, Z. J.; Qin, W. D. Separation of fluoroquinolones in acidic buffer by capillary electrophoresis with contactless conductivity detection. *J. Chromatogr. A* **2009**, *1216*, 5327−5332.

(17) Fung, Y. S.; Lau, K. M. Analysis of organic acids and inorganic anions in beverage drinks by capillary electrophoresis. *Electrophoresis* **2003**, *24*, 3224−3232.

(18) Melanson, J. E.; Baryla, N. E.; Lucy, C. A. Double-chained surfactants for semipermanent wall coatings in capillary electrophoresis. *Anal. Chem.* **2000**, *72*, 4110−4114.

(19) Haddad, P. R.; Harakuwe, A. H.; Buchberger, W. Separation of inorganic and organic anionic components of bayer liquor by capillary zone electrophoresis. 1. Optimization of resolution with electrolyte-containing surfactant mixtures. *J. Chromatogr. A* **1995**, *706*, 571−578.

(20) Boden, J.; Darius, M.; Bachmann, K. Determination of inorganic and small organic-anions in pure boric-acid using capillary zone electrophoresis. *J. Chromatogr. A* **1995**, *716*, 311−317.

(21) Gallaher, D. L.; Johnson, M. E. Nonaqueous capillary electrophoresis of fatty acids derivatized with a near-infrared fluorophore. *Anal. Chem.* **2000**, *72*, 2080−2086.

(22) Tomalia, D. A.; Baker, H.; Dewald, J.; Hall, M.; Kallos, G.; Martin, S. A new class of polymers: Starburst-dendritic macromolecules. *Polym. J.* **1985**, *17*, 117−132.

(23) Cakara, D.; Kleimann, J.; Borkovec, M. Microscopic protonation equilibria of poly(amidoamine) dendrimers from macroscopic titrations. *Macromolecules* **2003**, *36*, 4201−4207.

(24) Wei, F.; Zhao, Q.; Lv, X.; Dong, X. Y.; Feng, Y. Q.; Chen, H. Rapid magnetic solid-phase extraction based on monodisperse magnetic single-crystal ferrite nanoparticles for the determination of free fatty acid content in edible oils. *J. Agric. Food Chem.* **2013**, *61*, 76−83.

(25) Liu, Q.; Han, F.; Xie, K.; Miao, H.; Wu, Y. N. Simultaneous determination of total fatty acid esters of chloropropanols in edible oils by gas chromatography−mass spectrometry with solid-supported liquid−liquid extraction. *J. Chromatogr. A* **2013**, *1314*, 208−215.

(26) Williams, B. A.; Vigh, C. Fast, accurate mobility determination method for capillary electrophoresis. *Anal. Chem.* **1996**, *68*, 1174−1180.

(27) Wang, Y.; Harrison, M.; Clark, B. J. Optimising reversed-phase liquid chromatographic separation of an acidic mixture on a monolithic

stationary phase with the aid of response surface methodology and experimental design. *J. Chromatogr. A* **2006**, *1105*, 199−207.
(28) Avery, S. V.; Howlett, N. G.; Radice, S. Copper toxicity towards *Saccharomyces cerevisiae*: Dependence on plasma membrane fatty acid composition. *Appl. Environ. Microbiol.* **1996**, *62*, 3960−3966.
(29) Allison, M. J.; Bryant, M. P.; Keeney, M.; Katz, I. Metabolic function of branched-chain volatile fatty acids, growth factors for ruminococci. 2. biosynthesis of higher branched-chain fatty acids and aldehydes. *J. Bacteriol.* **1962**, *83*, 1084−1093.
(30) Makahleh, A.; Saad, B. Flow injection determination of free fatty acids in vegetable oils using capacitively coupled contactless conductivity detection. *Anal. Chim. Acta* **2011**, *694*, 90−94.
(31) Tomalia, D. A.; Naylor, A. M.; Goddard, W. A. Starburst dendrimers—Molecular-level control of size, shape, surface-chemistry, topology, and flexibility from atoms to macroscopic matter. *Angew. Chem., Int. Ed. Engl.* **1990**, *29*, 138−175.
(32) Zemann, A. J. Conductivity detection in capillary electrophoresis. *TrAC-Trends Anal. Chem.* **2001**, *20*, 346−354.
(33) de Oliveira, M. A. L.; Micke, G. A.; Bruns, R. E.; Tavares, M. F. M. Factorial design of electrolyte systems for the separation of fatty acids by capillary electrophoresis. *J. Chromatogr. A* **2001**, *924*, 533−539.
(34) Brito-Neto, J. G. A.; da Silva, J. A. F.; Blanes, L.; do Lago, C. L. Understanding capacitively coupled contactless conductivity detection in capillary and microchip electrophoresis. Part 1. Fundamentals. *Electroanalysis* **2005**, *17*, 1198−1206.
(35) Vergara-Barberan, M.; Escrig-Domenech, A.; Lerma-Garcia, M. J.; Simo-Alfonso, E. F.; Herrero-Martinez, J. M. Capillary electrophoresis of free fatty acids by indirect ultraviolet detection: Application to the classification of vegetable oils according to their botanical origin. *J. Agric. Food Chem.* **2011**, *59*, 10775−10780.
(36) Makahleh, A.; Saad, B.; Siang, G. H.; Saleh, M. I.; Osman, H.; Salleh, B. Determination of underivatized long chain fatty acids using RP-HPLC with capacitively coupled contactless conductivity detection. *Talanta* **2010**, *81*, 20−24.
(37) U.S. Department of Health and Human Services, Food and Drug Administration, Center for Drug Evaluation and Research, Center for Veterinary Medicine. Guidance for Industry, Bioanalytical Method Validation, September, 2013. http://www.fda.gov/downloads/drugs/guidancecomplianceregulatoryinformation/guidances/UCM368107.pdf (date last accessed, March 20, 2014).
(38) Chechik, V.; Zhao, M. Q.; Crooks, R. M. Self-assembled inverted micelles prepared from a dendrimer template: Phase transfer of encapsulated guests. *J. Am. Chem. Soc.* **1999**, *121*, 4910−4911.
(39) China State Bureau of Quality and Technical Supervision. *National Standard of the People's Republic of China—Maize Oil (GB 10464-2003)*; 2003.
(40) China State Bureau of Quality and Technical Supervision. *National Standard of the People's Republic of China—Soybean Oil (GB 1535-2003)*; 2003.
(41) China State Bureau of Quality and Technical Supervision. *National Standard of the People's Republic of China—Sunflower Seed Oil (GB 10464-2003)*; 2003.
(42) Ayyildiz, H. F.; Kara, H.; Sherazi, S. T. H. A Novel approach for determination of free fatty acids in vegetable oils by a flow injection system with manual injection. *Lipids* **2011**, *46*, 1181−1190.
(43) Tasan, M.; Gecgel, U.; Demirci, M. Effects of storage and industrial oilseed extraction methods on the quality and stability characteristics of crude sunflower oil (*Helianthus annuus* L.). *Grasas Aceites (Sevilla, Spain)* **2011**, *62*, 389−398.
(44) Zuriguel, V.; Causse, E.; Bounery, J. D.; Nouadje, G.; Simeon, N.; Nertz, M.; Salvayre, R.; Couderc, F. Short chain fatty acids analysis by capillary electrophoresis and indirect UV detection or laser-induced fluorescence. *J. Chromatogr. A* **1997**, *781*, 233−238.

JOURNAL OF AGRICULTURAL AND FOOD CHEMISTRY

Article

pubs.acs.org/JAFC

Dopant-Assisted Atmospheric Pressure Photoionization of Patulin in Apple Juice and Apple-Based Food with Liquid Chromatography–Tandem Mass Spectrometry

Kai Zhang,*[,†] Jon W. Wong,[†] Huy Mai,[‡] and Mary W. Trucksess[†]

[†]Center for Food Safety and Applied Nutrition, Office of Regulatory Science, U.S. Food and Drug Administration, HFS-706, 5100 Paint Branch Parkway, College Park, Maryland 20740, United States

[‡]Office of Regulatory Affairs, Kansas City District Laboratory, U.S. Food and Drug Administration, 11630 West 80th Street, Lenexa, Kansas 66214, United States

Supporting Information

ABSTRACT: A dopant-assisted atmospheric pressure photoionization (APPI) with liquid chromatography tandem mass spectrometry (LC-MS/MS) method was developed to determine patulin in apple juice and apple-based food. Different dopants, dopant flow rates, and LC separation conditions were evaluated. Using toluene as the dopant, the LC-APPI-MS/MS method achieved a linear calibration from 12.5 to 2000 μg/L (r^2 > 0.99). Matrix-dependent limits of quantitation (LOQs) were from 8 μg/L (solvent) to 12 μg/L (apple juice). [^{13}C]-Patulin-fortified apple juice samples were directly analyzed by the LC-APPI-MS/MS method. Other apple-based food was fortified with [^{13}C]-patulin, diluted using water (1% formic acid), centrifuged, and filtered, followed by LC-APPI-MS/MS analysis. In clear apple juice, unfiltered apple cider, applesauce, and apple-based baby food, average recoveries were 101 ± 6% (50 μg/kg), 103 ± 5% (250 μg/kg), and 102 ± 5% (1000 μg/kg) (av ± SD, n = 16). Using the suggested method, patulin was detected in 3 of 30 collected market samples with concentrations ranging from <LOQ to 18 μg/L. The use of [^{13}C]-patulin allowed quantitation using solvent calibration standards with satisfactory precision and accuracy.

KEYWORDS: *patulin, apple juice, APPI, dopant-assisted, stable isotope dilution, LC-MS/MS*

INTRODUCTION

The United States has the largest consumer market of apple juice in the world. To meet the demands of the market, 1.3 billion pounds of apples was processed to produce apple juice and cider in 2010.[1] Interestingly, the United States is also the world's largest importer of apple juice and spent more than $400 million on this product between 2006 and 2007.[2]

The current apple juice production procedures of heating, filtration, and pasteurization cannot eliminate patulin,[3] a toxic mycotoxin excreted by fungal species of the genera *Penicillium* and *Aspergillus*, especially *Penicillium expansum*, which grow on fruits.[4−6] The presence of patulin in fruit juices and processed apple foods highlights the importance of regulatory controls to minimize dietary exposure to patulin. Many countries, including the United States, have established a tolerance or action level of patulin at 50 μg/L (ppb) in apple juice.[7,8] The European Union (EU) maximum levels of patulin in baby foods and fruit juices are 10 and 50 μg/L, respectively.[9]

Gas chromatography−mass spectrometry (GC-MS),[10−12] LC-UV,[13−15] and thin layer chromatography (TLC)[16] methods have been developed to determine patulin in fruit juices and enforce established regulatory limits of patulin. These testing methods require multiple, time-consuming sample preparation steps, involving extraction, partitioning, concentration, and derivatization, to achieve the sensitivity and specificity necessary for regulatory control. A fluorescence immunoassay was developed for the determination of patulin, but it required noncommercially available antibodies.[17]

In recent years, LC-MS/MS has been increasingly used for patulin analysis because of its superior sensitivity and specificity.[18−21] Most LC-MS/MS methods use an electrospray ionization (ESI) source operating in positive or negative mode. As an alternative to ESI, an atmospheric pressure photoionization (APPI) source can be coupled with LC for the analysis of polar and nonpolar chemical compounds.[22,23] In the APPI ionization source, target analytes can be directly ionized by photons or charge exchange reactions with the ion molecules of a primary reagent (dopant) if direct photoionization cannot provide sufficient sensitivity.[24,25] Because of its characteristic gas-phase ionization mechanism, APPI is less prone to matrix ion suppression than ESI,[26] which means that for certain compounds, APPI produces better sensitivity and eliminates the need to use matrix-matched calibration standards for quantitation. So far, only a few studies have explored whether APPI can be applied for the analysis of mycotoxins in foods,[27−29] and information regarding APPI analysis of patulin has not been well-documented.[30] The objective of this study was to develop an APPI method with a simple sample preparation procedure that can detect patulin in apple juice and processed apple foods. Important APPI parameters, such as candidate dopants, dopant flow rate, and LC flow rate, were

Received: February 10, 2014
Revised: April 16, 2014
Accepted: April 23, 2014
Published: April 23, 2014

ACS Publications This article not subject to U.S. Copyright. Published 2014 by the American Chemical Society

dx.doi.org/10.1021/jf5006726 | J. Agric. Food Chem. 2014, 62, 4112−4118

Table 1. Chemical Structures, Molecular Formulas/Weights, CAS Registry Numbers, and LC-MS Parameters of Patulin and [^{13}C]-Patulin[a]

Analyte	Chemical structure	CAS#	Molecular weight	Retention time (min)	MRM transitions	DP (eV)	EP (eV)	CE (eV)	CXP (eV)
Patulin ($C_7H_6O_4$)	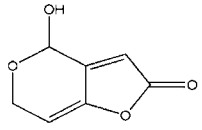	149-29-1	154.02	6.2	**153.0>108.9**	-55	-10	-12	-10
					153.0>81.0	-55	-10	-12	-10
[^{13}C]-Patulin ($^{13}C_7H_6O_4$)	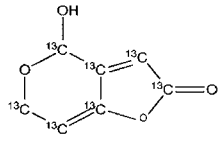	not available	161.05	6.2	**160.0>115.0**	-13	-10	-12	-10
					160.0>86.0	-18	-10	-12	-10

[a]Transitions in bold were used for quantitation.

evaluated and optimized to determine whether APPI is a viable tool for patulin analysis.

MATERIALS AND METHODS

Chemicals and Materials. LC grade acetonitrile, acetone, methanol, water, toluene (99.9%), MS grade formic acid, and ammonium formate were purchased from Fisher Scientific (Pittsburgh, PA, USA). Anisole (≥99%), bromobenzene (99.9%), and chlorobenzene (99.9%) were purchased from Sigma-Aldrich (St. Louis, MO, USA).

Standards. Stock solutions of patulin (100 μg/mL, in acetonitrile) and a stable isotope-labeled internal standard (IS), [^{13}C]-patulin (25 μg/mL, in acetonitrile) were purchased from Romer Laboratories, Inc. (Union, MO, USA). Structures, CAS Registry Numbers, and molecular weights of patulin and [^{13}C]-patulin can be found in Table 1. Spiking solutions of patulin at 1000, 5000, and 20000 μg/L were prepared by diluting the stock solution using acetonitrile and stored at −20 °C in the dark. A working solution of [^{13}C]-patulin at 2000 μg/L was prepared in the same fashion. Fresh solvent-only and matrix-matched (apple juice, applesauce, apple-based baby food, and apple cider) calibration solutions at 12.5, 25, 50, 100, 250, 500, 1000, and 2000 μg/L were prepared on the day of experiments by a series of dilutions of prepared spiking solutions using water with 1% formic acid or blank sample matrix extracts in volumetric flasks. Prior to LC-MS analysis, each calibration standard (1.0 mL) was pipetted into LC autosampler vials and fortified with 25 μL of the [^{13}C]-patulin working solution (2000 μg/L). The final concentration of [^{13}C]-patulin was 50 μg/L.

Sample Preparation. Clear and unfiltered apple juice samples (1.0 ± 0.05 mL) were pipetted into LC sample vials and spiked with 25 μL of the [^{13}C]-patulin working solution, followed by manual shaking for 1 min. Clear juice samples were analyzed by LC-APPI-MS/MS without any additional sample preparation. Unfiltered apple juice or apple cider samples were transferred into Amicon Ultra-4 centrifugal filters with Ultracel-3 membrane (EMD Millipore, Billerica, MA, USA) and centrifuged for 15 min at 4500 rpm (4200*g*). The collected filtrates were analyzed by LC-APPI-MS/MS. Other processed apple samples (1.0 ± 0.05 g of applesauce or apple-based baby food) were weighed out in 15 mL disposable glass vials, fortified with 25 μL of the [^{13}C]-patulin working solution, and homogenized by manual shaking for 2 min with 1 mL of water (1% formic acid). Homogenized samples were transferred into the same centrifugal filters and centrifuged (CR 4i, ThermoElectro Corp., Milford, MA, USA) for 15 min at 4500 rpm (4200*g*). The resulting filtrates were pipetted into autosampler vials for LC-APPI-MS/MS analysis.

Recovery Studies. Recovery studies were conducted in clear apple juice, unfiltered apple cider, applesauce, and apple-based baby food matrices at 50, 250, and 1000 μg/kg (Table 2). Blank samples (1.0 g) were fortified using 50 μL of the spiking solutions at 1000, 5000, and 20000 μg/L and 25 μL of the [^{13}C]-patulin working solution and prepared as described above. At each fortification level, samples were prepared in quadruplicates. Patulin was quantitated using solvent calibration standards with the IS, [^{13}C]-patulin. No patulin was detected in the blank samples used for recovery studies. Blank samples were collected from the Washington, DC, USA, metropolitan area.

Table 2. Recoveries in Fortified Matrices

	recovery (%, ±SD, n = 4)				
fortification (μg/L)	apple cider (unfiltered)	apple juice (clear)	apple sauce	apple-based baby food	av (n = 16)
50	110 ± 2	98 ± 3	100 ± 4	96 ± 2	101 ± 6
250	107 ± 3	96 ± 5	104 ± 2	103 ± 2	103 ± 5
1000	103 ± 3	96 ± 5	105 ± 3	103 ± 4	102 ± 5

Matrix-Dependent Instrument Limit of Detection. The matrix-dependent limits of detection and quantitation (LOD and LOQ, respectively) for patulin were obtained by following procedures from the U.S. Environmental Protection Agency's (EPA) protocol.[31] The matrix-dependent LOD was determined by analyzing eight replicates of patulin solvent and matrix-matched calibration standards at 12.5, 25, and 50 μg/L, respectively. Matrix-matched calibration standards were made by spiking a patulin working solution (1000 μg/L) into blank matrix extracts of clear apple juice, unfiltered apple cider, applesauce, and apple-based baby food. Blank matrix extracts were prepared as described above. The mean and standard deviation (SD) of patulin were obtained from the eight replicates. The matrix-dependent LOD was calculated using the formula LOD = 2.998 × SD (critical $t_{0.01}$ = 2.998 for degree of freedom (df) of 7). The corresponding matrix-dependent LOQ was calculated as 3 × LOD. At the LOQ the second transition (m/z 153.0 to 81.0) for patulin was measurable.

LC-APPI-MS/MS Analysis. All sample analyses were performed on a Shimadzu Prominence/20 series (Columbia, MD, USA) LC coupled with an Applied Biosystems 5500 quadruple linear ion trap mass spectrometer with an APPI interface source. A Phenomenex Kinetex XB-C18 LC column (100 mm × 2.1 mm i.d., 2.6 μm) and a 10 × 2.1 mm guard cartridge were used for LC separation (Torrance, CA, USA). The LC mobile phases consisted of 10 mM ammonium formate/0.1% formic acid/water (A) and 10 mM ammonium formate/0.1% formic acid/methanol (B). Gradient elution at 0.1 mL/min flow rate started at 5% B, ramped to 40% B in 3 min and then to 100% B by 3.5 min, held for 3 min, and changed to 5% B at 7 min. Total run time was 10 min, including 3 min of column conditioning time. The injection volume was 5 μL, and the column temperature was 40 °C.

The mass spectrometer was operated in negative ionization mode with scheduled multiple reaction monitoring scanning (sMRM). Scan time was 0.5 s, and the sMRM detection window was 60 s. The APPI

dx.doi.org/10.1021/jf5006726 | J. Agric. Food Chem. 2014, 62, 4112−4118

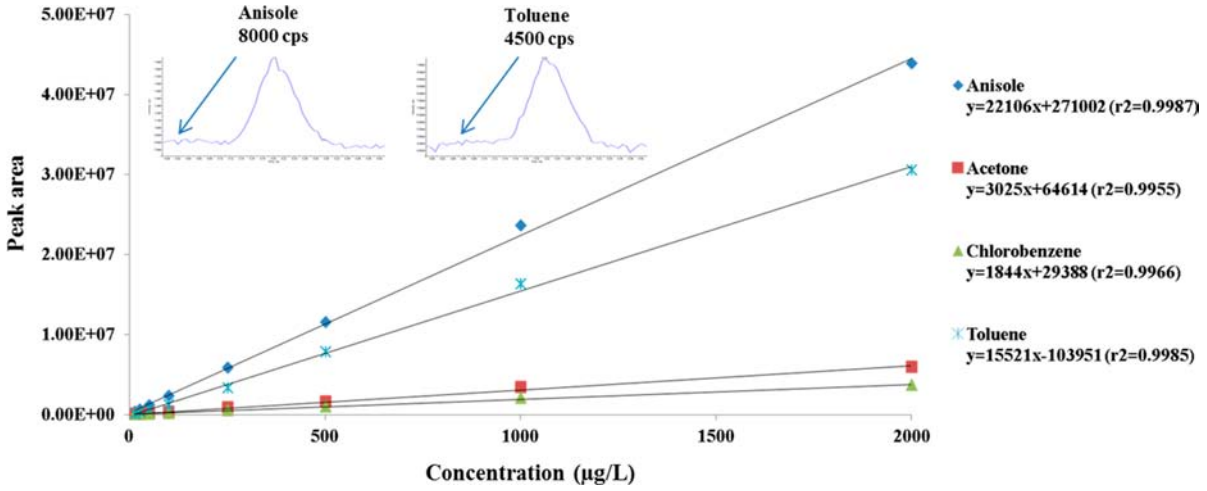

Figure 1. Matrix-matched calibration curve (12.5−2000 μg/L) associated with different dopants. (Inset) Base lines in extracted APPI ion chromatograms of patulin (153.0 → 108.9) at 12.5 μg/L associated with anisole and toluene.

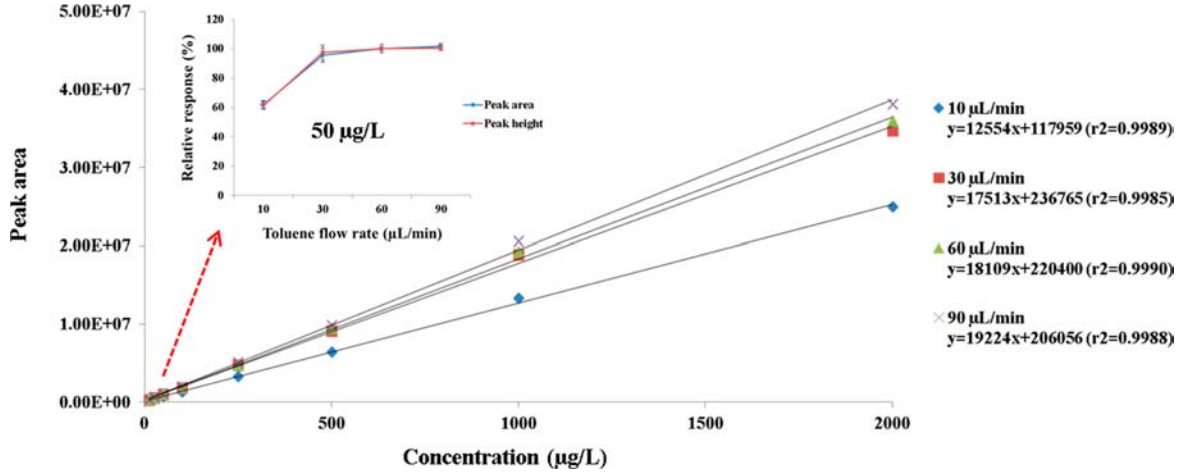

Figure 2. Effect of dopant flow rate. (Inset) Relative peak area/height (%) versus dopant flow rate (50 μg/L).

source was equipped with a krypton lamp that can emit photons with 10.0 eV. The MRM transitions of patulin and [^{13}C]-patulin were generated by directly infusing calibration standards into the APPI source (Table 1). Ionization source-dependent parameters were set by flow injection experiments as follows: curtain gas (CUR), 30 psi; ion spray voltage, − 800 V for the negative mode; nitrogen collision gas (CAD), medium; source temperature (TEM), 450 °C; and ion source gases 1 and 2 (GS1 and GS2), at 80 and 30 psi. Resolution at Q1 and Q3 was set to unit. Dopants were introduced into the ion source using a Harvard model 11 syringe pump (Harvard Apparatus, Holliston, MA, USA) at predefined rates. Analyst 1.6.1 was used to operate the instruments, and MultiQuan 2.0 was used to process data files (Applied Biosystems, Foster City, CA, USA).

RESULTS AND DISCUSSION

Unlike electrospray ionization, atmospheric pressure photoionization happens in the gas phase. In the course of LC-APPI-MS analysis, analytes, coeluted matrix components and LC mobile phases are first evaporated and then introduced into an APPI ion source, followed by reactions with dopant photoions. Dopant is added to the photoionization region via postcolumn infusion, reacting with photons emitted by a krypton discharge lamp. The selection of dopant, dopant flow rate, and LC flow rate can affect the sensitivity of target analytes, so these important parameters were evaluated and optimized as described below.[22]

Dopant-Assisted APPI (DA-APPI). When direct APPI cannot provide sufficient sensitivity, a dopant is often introduced into the APPI source, improving the photoionization efficiency of target analytes via charge exchange reactions, a procedure often referred to as DA-APPI. It is important to compare available candidate dopants when DA-APPI methods are developed.[24] Under identical LC and APPI conditions, the dopants, acetone, anisole, bromobenzene, chlorobenzene, and toluene[24] were introduced into the APPI source at 60 μL/min and were compared using the slope coefficient of an eight-point apple juice matrix-matched calibration curve (12.5−2000 μg/L), background noise, and the signal-to-noise ratio (S/N). Without using dopant or using bromobenzene as dopant, patulin could not be detected below 100 μg/L. To screen patulin at the FDA action level, 50 μg/L, one would prefer to use a method with a LOQ below the action level (e.g., LOQ ≤ 2/5 at a specified level as suggested by Codex).[32] Therefore, bromobenzene was not selected.

In general, a larger slope coefficient indicates better signal intensity. On the basis of the slop coefficients associated with anisole, acetone, chlorobenzene, and toluene (Figure 1), anisole and toluene should be more efficient dopants than acetone or

dx.doi.org/10.1021/jf5006726 | J. Agric. Food Chem. 2014, 62, 4112−4118

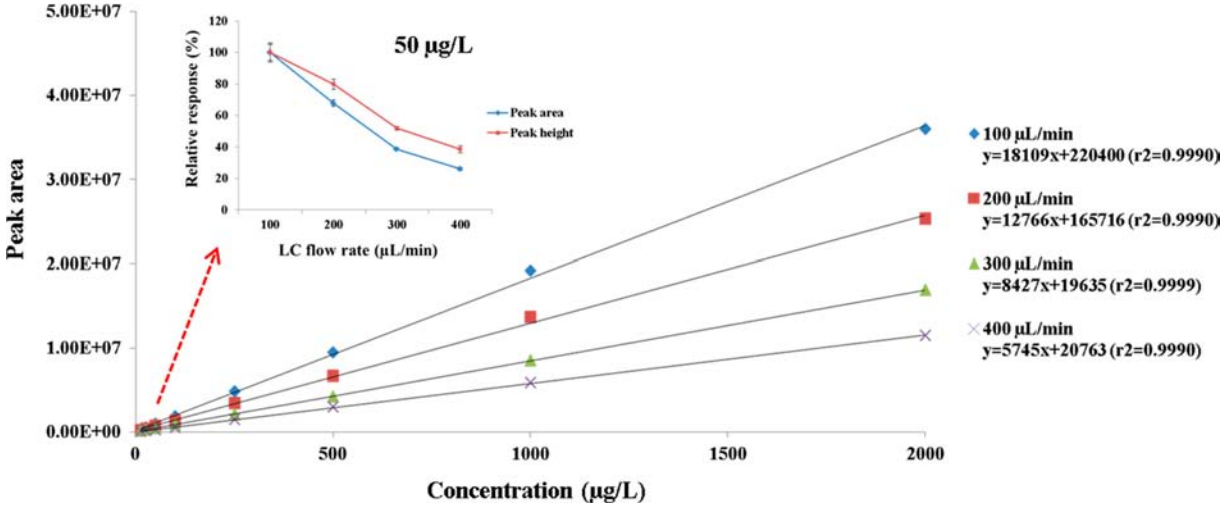

Figure 3. Effect of LC flow rates. (Inset) Relative peak/height (%) versus LC flow rate (50 μg/L).

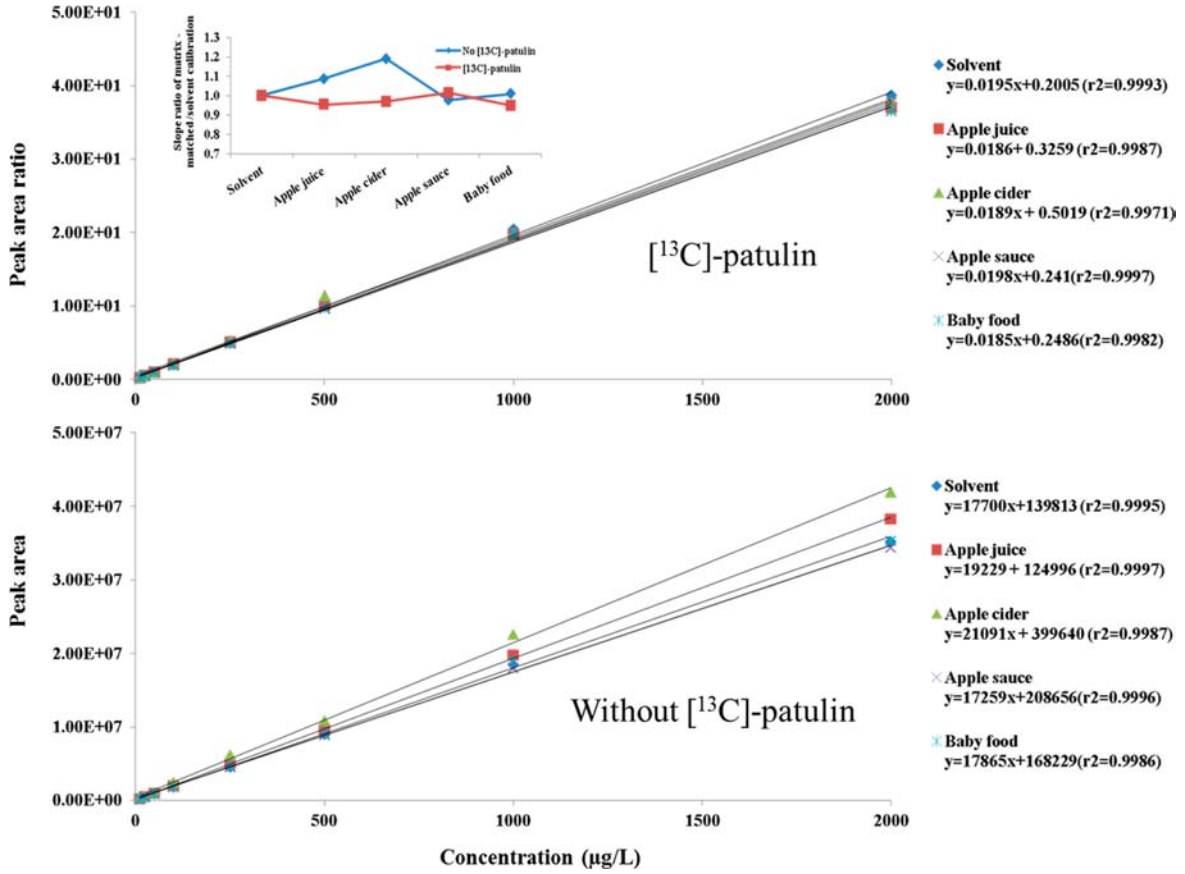

Figure 4. Solvent and matrix-matched calibration curves. (Inset) Slope ratio of matrix-matched and solvent calibration curves with/without [^{13}C]-patulin as IS.

chlorobenzene. Anisole has been reported to produce better photoionization efficiency than toluene,[24] but the better response (peak area/height) of target analytes could be accompanied by a higher background noise due to the fact that dopant photoions could not differentiate target analytes from ionizable matrix components or impurities in the source. Indicatively, the S/N of patulin (estimated using the S/N script in Analyst 1.6.1) at 12.5 μg/L for toluene (16), anisole (15), chlorobenzene (10), and acetone (5) suggested that comparable S/N ratios were achieved using toluene and anisole as dopant. The better signal intensity of patulin was offset by a higher background noise when using anisole as dopant. The background noise (intensity of baseline) associated with anisole was around 8000 cps, whereas it was 4500 cps with toluene (Figure 1, inset), so either anisole or toluene could be chosen as the final dopant for the study. As a more routinely used chemical reagent, toluene was chosen as the dopant for the following studies.

Effect of Dopant Flow Rate. The abundance of dopant photoions plays an important role in the ionization efficiency of

dx.doi.org/10.1021/jf5006726 | J. Agric. Food Chem. 2014, 62, 4112−4118

target analytes. Because of the consumption of dopant photoions by solvent, neutral species, and other matrix components, sufficient dopant photoions would lead to a complete reaction of analyte molecules in the APPI source, achieving good sensitivity. Under identical LC conditions, toluene was infused into the APPI source at 10, 30, 60, and 90 μL/min. The corresponding slope coefficients and peak areas/heights of patulin at 50 μg/L (average of four replicates) were monitored. Figure 2 clearly demonstrates that once the toluene flow rate reached 30 μL/min, the increase in the slope coefficient was just marginal at a higher dopant flow rate. When the dopant flow rate was changed from 10 to 30 μL/min, from 30 to 60 μL/min, and from 60 to 90 μL/min, the corresponding increases in the peak area/height were around 50, 10, and 2%, respectively, suggesting that a flow rate of 60 μL/min would be sufficient to have a majority of patulin molecules ionized in the ion source. Additionally, when toluene was infused into the APPI source at 30, 60, and 90 μL/min, the corresponding S/N of patulin was similar. On the basis of these findings, the final dopant flow rate was set at 60 μL/min.

Effect of LC Flow Rate. APPI is a mass-flow-dependent ionization source. A higher LC flow rate would introduce more LC mobile phase into the source, competing with analyte molecules for dopant photoions. The impact of the LC flow rate on the intensity of patulin was investigated using flow rates of 100, 200, 300, and 400 μL/min. The slope coefficient at 100 μL/min is 1.5, 2, and 3 times more than the slope coefficient at 200, 300, and 400 μL/min, respectively (Figure 3). The peak area/height of patulin at 50 μg/L (average of four replicates) decreased with increasing LC flow rates (Figure 3, inset). Similar observations were reported in previous studies.[29,33] When samples were eluted using 400 μL/min, the retention time of patulin was 1.8 min, whereas when samples were eluted using 100 μL/min, patulin was eluted from the column at 6.2 min. However, the faster LC separation caused a significant decrease in signal intensity. For example, the peak area/height of 50 μg/L patulin would shrink more than 70% when the LC flow rate was switched from 100 to 400 μL/min. Our observations demonstrate that the APPI source is more suited for lower LC flow rates; therefore, the LC flow rate was set at 100 μL/min.

Calibration Range and LOQs. Solvent and matrix-matched calibration curves were compared using calibration standards ranging from 12.5 to 2000 μg/L. Matrix-matched calibration curves were established in blank matrices of apple juice, apple cider, applesauce, and apple-based baby food. Although good linearity ($r^2 > 0.99$) is achieved in all matrices, the slopes of solvent and matrix-matched calibration curves vary to some extent (Figure 4). For example, when [^{13}C]-patulin is not used, the slope difference between the solvent and matrix for apple sauce is statistically different. Using [^{13}C]-patulin makes the slopes statistically identical between the solvent and matrix, suggesting that [^{13}C]-patulin enhances the quantitation. If a stable isotope uniformly labeled IS can be fortified into samples prior to sample preparation, quantitation with the IS would offset any variations caused by matrix effects, sample loss, or instrumental performance.[21,34,35]

Due to the 2 times dilution in the sample preparation procedures, an LOQ lower than 25 μg/L is desirable. This way we could quantitate samples containing patulin at 50 μg/L or higher concentrations. Following the EPA protocol, the LOQs in the solvent and in the four apple matrices were estimated in a statistical manner. The LOQs were from 8 μg/L (solvent) to 12 μg/L (apple juice). The LOQ for this method suggests it would be sensitive enough to monitor patulin.

Recovery Studies. Recovery studies were conducted in clear apple juice, unfiltered apple cider, applesauce, and apple-based baby food. Fortified samples were prepared using a few simple steps, fortification of [^{13}C]-patulin, dilution, centrifugation, and filtration. Individual recoveries at each fortification level ranged from 96% (50 μg/L, baby food) to 110% (50 μg/L, unfiltered apple cider) with a standard derivation (SD) of <6%. For the four tested matrices, the average recoveries were 101 ± 6% (50 μg/L), 103 ± 5% (250 μg/L), and 102 ± 5% (1000 μg/L) (av ± SD, n = 16).

Incurred Samples. Ten clear apple juice samples, 5 unfiltered apple cider samples, 10 applesauce samples, and 5 apple-based baby food samples were collected from local stores and analyzed using the LC-APPI-MS/MS method. In two of the apple juices samples, patulin was detected at 15 ± 1 and 18 ± 1 μg/L (n = 3), and in one of the applesauce samples, patulin was detected at <10 μg/L. The occurrence of patulin in fruit juices is unavoidable, but in the three incurred samples, detected concentrations were below the FDA action level. These samples were collected for method development and testing purposes but not for official surveys for risk assessment. The results of this study should not be interpreted as a representation of the local apple juice market.

Method Uncertainty. Uncertainty is a summarized statistic on the performance of an analytical method within a defined time period. Method uncertainty can be estimated using method detection limit, accuracy, and standard derivation of recovery of analyte in spiked samples because these factors reflect the performance of instrument and sample preparation.[36] Therefore, the performance of our method was evaluated using eight batches of apple juice samples analyzed within a 4 week time period. In each batch, 12 blank apple juice samples were fortified with patulin at 50, 250, or 1000 μg/L, with 4 replicates at each fortification concentration. The resulting recoveries of the 96 samples are plotted in Figure 5. The expanded uncertainties (k = 2) with 50, 250, and 1000 μg/L are 26, 11, and 9%, respectively (Supporting Information).

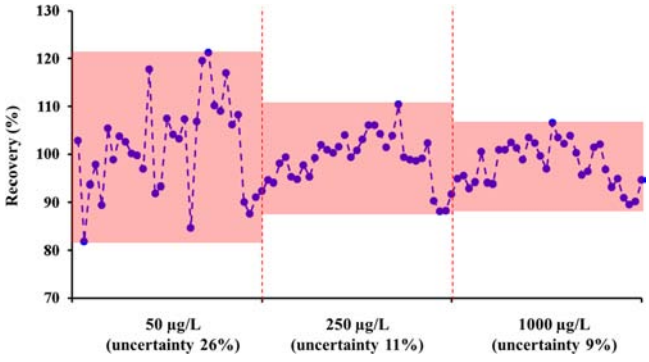

Figure 5. Method uncertainty (96 quality assurance recovery samples analyzed within 4 weeks).

Data quality in this study was ensured by the use of isotope dilution MS quantitation with satisfactory reproducibility in the four apple-based matrices tested. The sensitivity of the LC-APPI-MS/MS method is superior or comparable to those of existing methods but does not require time-consuming sample preparation or matrix-matched calibration standards. This

method would enhance the operation efficiency of routine surveillance activities and improve turnaround time.

■ ASSOCIATED CONTENT

Supporting Information

Estimated uncertainties. This material is available free of charge via the Internet at http://pubs.acs.org.

■ AUTHOR INFORMATION

Corresponding Author

*(K.Z.) Phone: (240) 402-2318. Fax: (301) 436-2332. E-mail: kai.zhang@fda.hhs.gov.

Notes

The authors declare no competing financial interest.

■ REFERENCES

(1) USDA Economics, Statistics and Market Information System. U.S. Apple Statistics; http://usda.mannlib.cornell.edu/MannUsda/viewDocumentInfo.do?documentID=1825 (accessed Aug 10, 2013).

(2) USDA Foreign Agricultural Service. World Markets and Trade. Apple Juice (June 2007); http://www.fas.usda.gov/htp/horticulture/Apple%20Juice/Apple_Juice_2006_07.pdf (accessed Aug 10, 2013).

(3) Trucksess, M. W.; Tang, Y. Solid phase extraction method for patulin in apple juice and unfiltered apple juice. *Mycotoxin Protocols*; Methods of Molecular Biology 157; Trucksess, M. W., Pohland, A. E., Eds.; Humana Press: Totowa, NJ, USA, 2001; pp 205−213.

(4) Jimenez, M.; Sanchis, V.; Mateo, R.; Hernandez, E. Detection and quantification of patulin and griseofulvin by high pressure liquid chromatography in different strains of *Penicillium griseofulvum* Dierckx. *Mycotoxin Res.* **1988**, *4*, 59−66.

(5) United Kingdom Committee on Toxicity. *Mutagenicity and Carcinogenicity of Chemicals in Food, Consumer Products and the Environment*, Annual Report; HMSO: London, UK, 1992.

(6) Food and Agricultural Organization, World Health Organization. *Evaluation of Certain Food Additives and Contaminants*, 44th Report of the Joint FAO/WHO Expert Committee on Food Additives, Technical Report Series 859; WHO: Geneva, Switzerland, 1995.

(7) Food and Agriculture Organization of the United Nations. *Worldwide Regulations for Mycotoxins, A Compendium*; FAO Food and Nutrition Paper 64; Rome, Italy, 1996.

(8) U.S. FDA. Compliance Program Guidance Manual. Chapter 07. Molecular Biology and Natural Toxins, 7307.001; 2007; www.fda.gov/downloads/Food/GuidanceComplianceRegulatoryInformation/ComplianceEnforcement/ucm073294.pdf (accessed Aug 10, 2013).

(9) Commission Regulation (EC) No. 1881/2006 of 19 December 2006 setting maximum levels for certain contaminants in foodstuffs. *Off. J. Eur. Union* **2006**; http://eur-lex.europa.eu/LexUriServ/LexUriServ.do?uri=CONSLEG:2006R1881:20100701:EN:PDF (accessed Aug 10, 2013).

(10) Tarter, E. J.; Scott, P. M. Determination of patulin by capillary gas chromatography of the heptafluorobutyrate derivative. *J. Chromatogr.* **1991**, *538*, 441−446.

(11) Roach, J. A.; White, K. D.; Trucksess, M. W.; Thomas, F. S. Capillary gas chromatography/mass spectrometry with chemical ionization and negative ion detection for confirmation of identity of patulin in apple juice. *J. AOAC. Int.* **2000**, *83*, 104−112.

(12) Kharandi, N.; Babri, M.; Azad, J. A novel method for determination of patulin in apple juices by GC-MS. *Food Chem.* **2013**, *141*, 1619−1623.

(13) AOAC International. Method 974.18 for patulin. *Official Methods of Analysis*, 16th ed.; Arlington, VA, USA, 1995; Chapter 49.

(14) Brause, A. R.; Trucksess, M. W.; Thomas, F. S.; Page, S. W. Determination of patulin in apple juice by liquid chromatography: collaborative study. *J. AOAC Int.* **1996**, *79*, 451−455.

(15) Trucksess, M. W.; Tang, Y. Solid phase extraction method for patulin in apple juice and unfiltered apple juice. *J. AOAC Int.* **1999**, *82*, 1109−1113.

(16) Welke, J. E.; Hoeltz, M.; Dottori, H. A.; Noll, I. B. Quantitative analysis of patulin in apple juice by thin-layer chromatography using a charge coupled device detector. *Food Addit. Contam. Part A* **2009**, *26*, 754−758.

(17) de Champdoré, M.; Bazzicalupo, P.; De Napoli, L.; Montesarchio, D.; Di Fabio, G.; Cocozza, I.; Parracino, A.; Rossi, M.; D'Auria, S. A new competitive fluorescence assay for the detection of patulin toxin. *Anal. Chem.* **2007**, *79*, 751−757.

(18) Malysheva, S. V.; Diana Di Mavungu, J.; Boonen, J.; De Spiegeleer, B.; Goryacheva, I. Y.; Vanhaecke, L.; De Saeger, S. Improved positive electrospray ionization of patulin by adduct formation: usefulness in liquid chromatography-tandem mass spectrometry multi-mycotoxin analysis. *J. Chromatogr., A* **2012**, *1270*, 334−339.

(19) Christensen, H. B.; Poulsen, M. E.; Rasmussen, P. H.; Christen, D. Development of an LC-MS/MS method for the determination of pesticides and patulin in apples. *Food Addit. Contam. Part A* **2009**, *26*, 1013−1023.

(20) Kataoka, H.; Itano, M.; Ishizaki, A.; Saito, K. Determination of patulin in fruit juice and dried fruit samples by in-tube solid-phase microextraction coupled with liquid chromatography-mass spectrometry. *J. Chromatogr., A* **2009**, *1216*, 3746−3750.

(21) Desmarchelier, A.; Mujahid, C.; Racault, L.; Perring, L.; Lancova, K. Analysis of patulin in pear- and apple-based foodstuffs by liquid chromatography electrospray ionization tandem mass spectrometry. *J. Agric. Food Chem.* **2011**, *59*, 7659−7665.

(22) Robb, D. B.; Covery, T. R.; Bruins, A. P. Atmospheric pressure photoionization: an ionization method for liquid chromatography-mass spectrometry. *Anal. Chem.* **2000**, *72*, 3653−3659.

(23) Cai, Y.; Kingery, D.; McConnell, O.; Bach, A. C., II. Advantages of atmospheric pressure photoionization mass spectrometry in support of drug discovery. *Rapid Commun. Mass Spectrom.* **2005**, *19*, 1717−1724.

(24) Smith, D. R.; Robb, D. B.; Blades, M. W. Comparison of dopants for charge exchange ionization of nonpolar polycyclic aromatic hydrocarbons with reversed-phase LC-APPI-MS. *J. Am. Soc. Mass Spectrom.* **2009**, *20*, 73−79.

(25) Robb, D. B.; Blades, M. W. State-of-the-art in atmospheric pressure photoionization for LC/MS. *Anal. Chim. Acta* **2008**, *627*, 34−49.

(26) Hanold, K. A.; Fischer, S. M.; Cormia, P. H.; Miller, C. E.; Syage, J. A. Atmospheric pressure photoionization. 1. General properties for LC/MS. *Anal. Chem.* **2004**, *76*, 2842−2851.

(27) Capriotti, A. L.; Foglia, P.; Gubbiotti, R.; Roccia, C.; Samperi, R.; Laganà, A. Development and validation of a liquid chromatography/atmospheric pressure photoionization-tandem mass spectrometric method for the analysis of mycotoxins subjected to commission regulation (EC) no. 1881/2006 in cereals. *J. Chromatogr., A* **2010**, *1217*, 6044−6051.

(28) Cavaliere, C.; Foglia, P.; Pastorini, E.; Samperi, R.; Laganà, A. Liquid chromatography/tandem mass spectrometric confirmatory method for determining aflatoxin M1 in cow milk: comparison between electrospray and atmospheric pressure photoionization sources. *J. Chromatogr., A* **2006**, *1101*, 69−78.

(29) Tanaka, H.; Takino, M.; Sugita-Konishi, Y.; Tanaka, T.; Toriba, A.; Hayakawa, K. Determination of nivalenol and deoxynivalenol by liquid chromatography/atmospheric pressure photoionization mass spectrometry. *Rapid Commun. Mass Spectrom.* **2009**, *23*, 3119−3124.

(30) Takino, M.; Daishima, S.; Nakahara, T. Liquid chromatography/mass spectrometric determination of patulin in apple juice using atmospheric pressure photoionization. *Rapid Commun. Mass Spectrom.* **2003**, *17*, 1965−1972.

(31) U.S. Environmental Protection Agency. Title 40−Protection of the Environment. Part 136; U.S. Government Printing Office: Washington, DC, USA, 2010; http://ecfr.gpoaccess.gov/cgi/t/text/text-idx?c=ecfr&tpl=/ecfrbrowse/Title40/40cfr136_main_02.tpl (accessed Aug 15, 2013).

(32) Codex Alimentarius Commission. *Procedural Manual*, 21st ed.; http://www.codexalimentarius.org/procedures-strategies/procedural-manual/en/ (accessed Jan 29, 2014).
(33) Yang, C.; Henion, J. Atmospheric pressure photoionization liquid chromatographic-mass spectrometric determination of idoxifene and its metabolites in human plasma. *J. Chromatogr., A* **2002**, *970*, 155−165.
(34) Rychlik, M.; Schieberle, P. Quantification of the mycotoxin patulin by a stable isotope dilution assay. *J. Agric. Food Chem.* **1999**, *47*, 3749−3755.
(35) Zhang, K.; Wong, J. W.; Hayward, D. G.; Vaclavikova, M.; Liao, C. D.; Trucksess, M. W. Determination of mycotoxins in milk-based products and infant formula using stable isotope dilution assay and liquid chromatography tandem mass spectrometry. *J. Agric. Food Chem.* **2013**, *61*, 6265−6273.
(36) Ellison, S. R. L., Williams, A., Eds. Chapter 8. STEP 4. Calculating the Combined Uncertainty. In *Eurachem/CITAC Guide: Quantifying Uncertainty in Analytical Measurement*, 3rd ed.; 2012; ISBN 978-0-948926-30-3.

JOURNAL OF AGRICULTURAL AND FOOD CHEMISTRY

Article

pubs.acs.org/JAFC

Release of Antioxidant Capacity from Five Plant Foods during a Multistep Enzymatic Digestion Protocol

Valentina Azzurra Papillo,[†] Paola Vitaglione,[†] Giulia Graziani,[†] Vural Gokmen,[‡] and Vincenzo Fogliano*[,§]

[†]Department of Agriculture and Food Science, University of Naples "Federico II", Naples, Italy

[‡]Food Engineering Department, Hacettepe University, 06800 Beytepe, Ankara, Turkey

[§]Food Quality and Design Group, Wageningen University and Research Centre, P.O. Box 8129, 6700 EV Wageningen, The Netherlands

ABSTRACT: This study aimed at elucidating the influence of food matrix on the release of antioxidant activity from five plant foods (apple, spinach, walnut, red bean, and whole wheat). To this purpose a protocol based on sequential enzymatic digestion was adopted. The total antioxidant capacity (TAC) of both solubilized and insoluble materials was measured at each step. Results showed that the overall TAC obtained by enzyme treatments was usually higher than that obtained by chemical extraction-based methods. In apple most of the TAC was released upon water washing and after pepsin treatment, whereas in spinach, beans, and whole wheat the TAC released by treatments with bacterial enzymes was prominent. Walnut had the highest TAC value, which was mainly released after pancreatin treatment. Therefore, the enzyme treatment is fundamental to estimate the overall potential TAC of foods having a high amount of polyphenols bound to dietary fiber or entrapped in the food matrix.

KEYWORDS: *in vitro digestion, foods, antioxidant capacity, phytochemicals, bioaccessibility*

INTRODUCTION

Epidemiological studies have associated the consumption of fruits, vegetables, whole grains, and legumes to a reduced risk of chronic diseases such cardiovascular diseases, diabetes, and some type of cancers, especially colorectal cancer.[1−4]

The amount and the type of dietary fiber and phytochemicals were recognized as major determinants responsible for the health benefits of these foods. Many phytochemicals are chemically reactive compounds that can counteract the action of reactive oxygen species, thus preventing the oxidation of biological substrates such as lipids, DNA, and proteins. During the past 20 years researchers' attention was focused on phytochemicals antioxidant properties and vast knowledge was built over time on specific food molecules, body metabolites, and cellular mechanisms acting in biological systems following their ingestion.[5,6]

It was well established that even for phytochemicals showing a high antioxidant capacity in vitro this property alone cannot explain the systemic health benefits. The extended biotransformation of many dietary phytochemicals once ingested and their low bioavailability led to tissue concentrations that are much below those showing antioxidant ability in vitro. Mounting evidence indicated that other biological properties including modulation of inflammation, detoxification, and immune response can play a major role in body defense at a systemic level.[7−10]

On the other hand, inside the gastrointestinal (GI) tract (stomach, small intestine, and lower gut) the antioxidant activity of dietary phytochemicals may have a central role: their concentration is mainly dependent on the amount in the ingested food, and their chemical form is usually the same present in the food. Phytochemicals can be found in food in either free or bound form. In the latter case they can be covalently linked to polysaccharides (as occurs to phenolic acids in cereal/nut/legume dietary fiber) or physically aggregated with chloroplast proteins (as occurs to carotenoids in tomatoes or spinach).[11−15] In nuts, fruits, and vegetables, phytochemicals are present mainly in free form that can be extracted in water or hydroalcoholic solutions. Contrarily, in whole cereals and legumes, bound antioxidants are the most dominant form that can be extracted only after chemical hydrolysis. Apples' main antioxidant molecules are soluble polyphenols such as chlorogenic acid, catechin, epicatechin, and phloridzin.[16] Spinach composition is similar to that of apple with many free phenolic compounds; however, they have a more consistent fiber structure that could limit the phytochemicals' extractability.[17] Walnut antioxidant capacity was principally attributed to ellagic and gallic acids that are present as polymers and bound to sugars, forming hydrolyzable tannins; their solubility depends on their degree of polymerization.[18] Polyphenol compounds are the major phytochemicals in red beans,[19,20] and many of them are bound to polysaccharides and proteins of cell wall with ester and ether links.[21,22] Whole wheat antioxidant capacity is due to phenolic acids, principally to ferulic acid and flavonoids: 90% of them are covalently bound to cell wall polysaccharides that are insoluble in organic solvents.[23,24]

After ingestion, the digestion processes modified foods' physical structure regulating the bioaccessibility (i.e., the possibility to be released in the lumen and eventually absorbed) as well as the antioxidant capacity (i.e., availability to react with oxidant species) of bound phytochemicals in the GI environment. We have previously demonstrated that an in vitro

Received: November 11, 2013
Revised: April 8, 2014
Accepted: April 10, 2014
Published: April 10, 2014

ACS Publications © 2014 American Chemical Society

dx.doi.org/10.1021/jf500695a | J. Agric. Food Chem. 2014, 62, 4119−4126

sequential enzyme digestion of the water-insoluble fraction of cocoa resulted in the release of antioxidant capacity (due to material solubilized by digestion) and in a contemporary increase of the antioxidant capacity of the remaining insoluble material.[25] Moreover, it has been recently reported that the antioxidant capacity of the insoluble wheat bran can be restored by treatment with an antioxidant-rich soluble beverage.[26]

In vitro digestion protocols have been widely used to study the digestibility, bioaccessibility, and structural changes of food macronutrients, particularly proteins and starch.[27]

Recently, also the effects of digestive process on the food antioxidant activity and on some phytochemicals were studied. Saura-Calixto et al.[28] studied the bioaccessibility of polyphenols from different foods after enzymatic hydrolysis and after colonic fermentation: results indicated that about 48% of polyphenols are bioaccessible in the small intestine, whereas 42% become bioaccessible in the large intestine. More recently, Pastoriza et al.[29] developed the global antioxidant response (GAR) measuring the total antioxidant capacity (TAC) of the soluble and insoluble fraction throughout an in vitro digestion. They found that after digestion TAC was higher than that obtained with the usual chemical extraction and the QUENCHER method. Finally, Gong et al.[30] studied the TAC of cereals after in vitro digestion. Also, these authors confirmed that TAC measured after enzymatic digestion is much higher than that observed on undigested foods.

This study aimed at (i) elucidating the influence of food matrix and phytochemical disposition on the potential food antioxidant activity, (ii) providing a complete picture of the contribution of different plant foods to keep a redox balance inside the GI environment, and (iii) giving useful data to design foods providing a controlled release of phytochemicals. To this purpose five plant foods (apple, spinach, walnut, red bean, and whole wheat) having different physical structures, as well as different macronutrient and phytochemical compositions and forms, were selected; a sequential multistep enzyme treatment-based protocol was developed; and the release of antioxidant activity as well as the antioxidant capacity of insoluble food material was measured at each step.[11]

MATERIALS AND METHODS

Chemicals and Reagents. 6-Hydroxy-2,5,7,8-tetramethylchroman-2-carboxylic acid (Trolox), 2,2-diphenyl-1-picrylhydrazyl (95%), sodium bicarbonate, and sodium hydroxide were purchased from Sigma-Aldrich (Milan, Italy). Cellulose (powder from spruce) was purchased from Fluka (Buchs, Switzerland).

All chemicals and solvents used were of HPLC grade; ethanol was purchased from Carlo Erba (Milan, Italy), whereas the other solvents were from Merck-Millipore (Darmstadt, Germany).

The enzymes pepsin (≥250 U/mg solid) from porcine gastric mucosa, pancreatin (4 × USP) from porcine pancreas, protease from *Streptomyces griseus*, called also Pronase E (≥3.5 U/mg solid), and Viscozyme L were purchased from Sigma-Aldrich (Milan, Italy).

Samples. The tested plant foods were apple (var. *annurca*) without skin, frozen spinach after microwave cooking, walnuts, canned red beans, and whole wheat breakfast cereals. As whole grain, Shredded Wheat (General Mills, Minneapolis, MN, USA) was used, whereas the other foods were purchased at a local market and immediately freeze-dried. The macronutrient composition of foods expressed as percentage of each nutrient class by total weight is shown in Table 1. After freeze-drying, all samples were ground by a mill (Grindomix-Retsch GM200 type), and the digestion protocols were run three times on each sample. The TAC of each sample was also measured in triplicate.

Table 1. Macronutrient Composition of the Studied Foods Expressed in Percentage by Dry Weight

	protein	fat	carbohydrate	dietary fiber	insoluble vs total DF (%)
apple	2	1	80	17	65
spinach	37	0	39	24	77
bean	23	2	56	19	77
whole wheat	12	2	73	13	84
walnut	15	73	5	7	87

Chemical Extractions. *Hydroalcoholic Extraction.* One gram of dry food was extracted with 10 mL of methanol/water (70:30 v/v) for 30 min in an ultrasonic bath. The solution was centrifuged at 2800*g* for 5 min at 4 °C, and the antioxidant activity of the supernatant was measured with the DPPH assay as described below.[28] The TAC of hydroalcoholic extract (HAE_TAC) was expressed as millimoles of Trolox equivalent (TE) per kilogram of dry matter.

Alkaline Hydrolysis. Alkaline hydrolysis was performed on the pellets obtained after hydroalcoholic extraction that were added with 20 mL of 4 M NaOH for 2 h under agitation.[12] At the end of the reaction, the pH was brought between 2 and 3 with 6 M HCl, and the sample was centrifuged at 2800*g* for 15 min at 4 °C. The supernatant was extracted three times with 50 mL of ethyl acetate, and the combined extracts were evaporated to dryness and subsequently dissolved in methanol/water (70:30 v/v). Ten milliliters of methanol/water (70:30 v/v) was added to the pellet, and the mixture was kept in agitation for 30 min; mixture centrifugation and supernatant collections followed. The antioxidant activity of individual extracts was measured by the DPPH assay as above-described and finally summed to obtain the total antioxidant activity of the chemical extraction (TPE_TAC).

In Vitro Digestion Procedure. Each food was digested using a protocol including water washing and a sequential multistep enzymatic treatment.[29] Samples were incubated with the enzymes in agitation to 120 oscillations/min at 37 °C using a shaking thermostatic bath. The digestion scheme is summarized in Figure 1: at the end of each digestion step the soluble and insoluble materials were separated by centrifugation (2800*g* for 3 min, 4 °C). The soluble part was used for the TAC measurement, whereas the insoluble part was further digested in the following step. The final insoluble material obtained

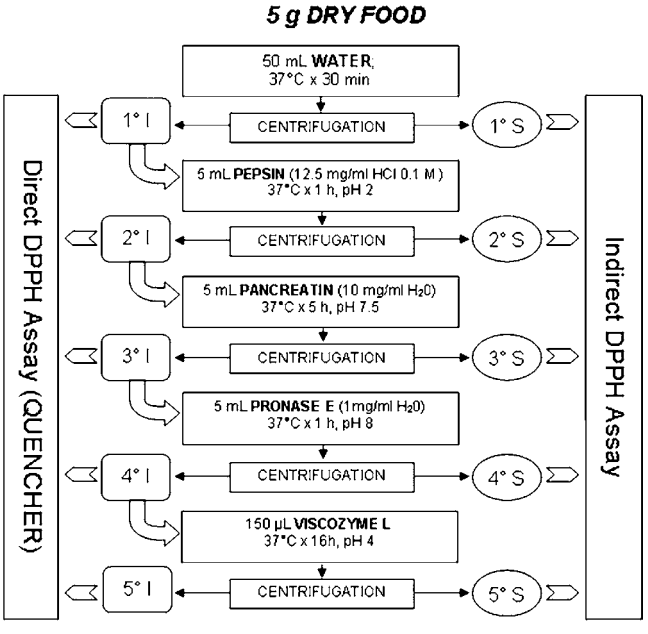

Figure 1. Protocol of the in vitro multistep enzymatic digestion.

dx.doi.org/10.1021/jf500695a | J. Agric. Food Chem. 2014, 62, 4119−4126

after the four enzymatic digestions (sample 5°I) and the soluble fractions were used to calculate the overall TAC.

Five grams of milled dry sample of each food was subjected to in vitro digestion. The first step was done by suspending the material in 50 mL of water to extract all of the water-soluble component. After 30 min at 37 °C under stirring, the samples were centrifuged, and the pellets obtained by centrifugation (1°I) were resuspended in acidified water (6 M HCl up to pH 2); 5 mL of pepsin solution (12.5 mg/mL 0.1 M HCl) was added, and the mixture was incubated for 1 h (gastric phase). The subsequent centrifugation of the mixture allowed the recovery of the insoluble material (2°I); after increase of the pH to 7.5 with $NaHCO_3$, 5 mL of a 10 mg/mL pancreatin solution was added, and the mixture was kept for 5 h in agitation (duodenal phase). Finally, the remaining insoluble materials were treated first (3°I) with 5 mL of 1 mg/mL Pronase E solution (pH 8, 1 h) and then (4°I) with 150 μL of Viscozyme L (16 h, pH 4), obtaining the final pellet (5°I). Pronase E could simulate bacterial protease activity and is particularly suitable to hydrolyze insoluble material, whereas Viscozyme L, containing a mix of enzymes hydrolyzing complex polysaccharides, was used to obtain a final disruption of the plant food matrix chemical structures.

At each step the antioxidant activities of both soluble and insoluble parts were measured. In particular after separation, both supernatants and the pellets were weighed; then an aliquot of the supernatant was used to calculate the dry weight of the supernatant, whereas the remaining part was stored at −40 °C to measure soluble antioxidant activity. A small aliquot (<5%) of the pellet was weighed, frozen, and lyophilized to measure the antioxidant activity of the insoluble fraction using the QUENCHER method,[11] whereas the rest was used for the successive enzymatic incubations.

The dry matter of each supernatant was subtracted from the dry weight of each pellet from the previous digestive step; therefore, the soluble and insoluble TAC values were calculated on the basis of the effective amount of each supernatant and pellet.

Measurement of Antioxidant Activity. *DPPH Assay on Soluble Material.* The DPPH assay was applied to measure TAC of digestion soluble fractions (supernatants) and hydroalcoholic and alkaline hydrolysis extracts. The DPPH scavenging capacity was evaluated by diluting DPPH in pure methanol by adjusting the absorbance of the DPPH radical solution to 0.9 ± 0.02 at 517 nm.[31] Two hundred microliters of sample was added to 1 mL of DPPH solution, and after 10 min, the absorbance was measured. Percentage of inhibition was calculated against a control and compared to a Trolox standard curve, 5−125 μM. TAC was expressed as millimoles of TE per kilogram of dry matter. Each extraction and alkaline hydrolysis was performed in duplicate.

It is relevant to mention that in a first set of experiments we also employed ABTS instead of DPPH as probe to measure the released TAC. However, we observed that using ABTS both the switches of pH and the enzyme solutions interfered with the measure of TAC, whereas when using DPPH this problem was overcome.

Direct DPPH Assay (QUENCHER). TAC values of freeze-dried whole foods (W_TAC) and insoluble fractions obtained at each step of digestion procedure were evaluated using the QUENCHER procedure adopting DPPH as colorimetric probe.[11] This method was based on the direct contact of the dry sample with the DPPH solution obtained after dilution of stock solution with methanol/water (50:50 v/v) until an absorbance of 0.9 ± 0.02 at 517 nm was obtained. The sample was incubated with DPPH radical in agitation for 2 h; subsequently, the mixture was centrifuged at 2800*g* for 3 min at 4 °C, and the supernatant absorbance was measured at a wavelength of 517 nm.

Calculation and Statistical Analysis. The overall soluble TAC was called potentially bioaccessible TAC (PB_TAC) and was calculated as the sum of TAC of soluble fractions at each digestion step (PB_TAC = Σ (1° → 5°) S_TAC).

The overall potential TAC (OP_TAC) was calculated as the sum of the potentially bioaccessible TAC and that of the last insoluble fraction (OP_TAC= PB_TAC + 5°I_TAC)

The food TAC due to free phytochemicals was measured on material derived from water washing of food (Free_TAC = 1°S) upon digestion protocol or on hydroalcoholic extracts upon chemical protocol (HAE_TAC).

The food TAC due to bound phytochemicals was calculated as the sum of TAC of soluble fractions after pepsin, pancreatin, Pronase E, and Viscozyme L treatment upon digestion protocol (Bound_TAC = Σ(2° → 5°)S_TAC) or was that obtained on alkaline hydrolysis extract upon chemical protocol (AHE_TAC).

Overall TAC (TPE_TAC) measured by the chemical method was calculated as the sum of HAE_TAC and AHE_TAC.

Data were reported as the mean ± standard error of three analyses for each type of extraction and parameter. The significance of differences was determined by ANOVA, Duncans' post hoc test, and bivariate correlation using SPSS 13.0. Significance level was set at p = 0.05.

RESULTS

Figure 2 shows TAC values of the five foods measured directly on the whole foods by using the QUENCHER method

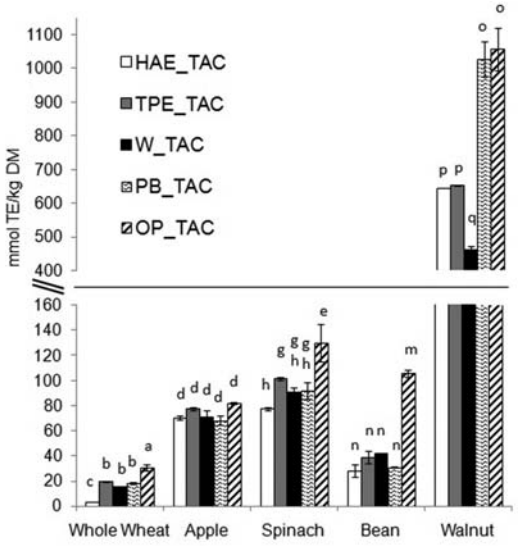

Figure 2. Comparison of TAC (mmol TE/kg dry matter ± SEM) obtained with hydroalcoholic extraction (HAE), alkaline hydrolysis after hydroalcoholic extraction (TPE), direct measure without extraction, QUENCHER (W), and enzymatic extraction. TAC of the latter is calculated both as only the sum of potentially bioaccessible antioxidant activity in the gastrointestinal tract (B) and as the sum of bioaccessible antioxidant activity with the last insoluble fraction (OP).

(W_TAC), on chemical extracts (only hydroalcoholic and total hydroalcoholic plus alkaline hydrolysis, HAE_TAC and TPE_TAC, respectively), on fractions solubilized upon in vitro GI digestion (potentially bioaccessible TAC; PB_TAC), and on all fractions solubilized plus the insoluble fraction collected after the last in vitro digestion step (overall potential TAC; OP_TAC). The values of TAC, expressed as millimoles of Trolox equivalent per kilogram of dry matter, ranged from 3.2 to 30.5, from 68.2 to 82.1, from 77.7 to 130.1, from 28.2 to 105.8, and from 462.0 to 1056.9 for whole wheat, apple, spinach, bean, and walnut, respectively.

Looking at the values obtained by chemical extraction methods (HAE_TAC and TPE_TAC), data confirmed that most of TPE_TAC in whole wheat was due to bound phytochemicals. With regard to the other foods, only in spinach did bound phytochemicals contribute to differentiate TPE_-TAC from HAE_TAC, there being no difference between these two measures in beans, apples, and walnuts. On the other hand,

dx.doi.org/10.1021/jf500695a | J. Agric. Food Chem. 2014, 62, 4119−4126

Table 2. Soluble TAC at Each Step of in Vitro Digestion for the Different Foods

		TAC[a] (mmol TE/kg DM ± SEM)			%	
food	treatment	soluble (S)	insoluble (I)	S + I	S	I
apple	water	26.6 ± 0.3a	12.5 ± 5.9a	39.1 ± 5.6	68	32
	pepsin	27.7 ± 5.8a	13.4 ± 2.3a	41.2 ± 8.1	67	33
	pancreatin	8.5 ± 0.3b	19.8 ± 1.1a	28.3 ± 1.5	30	70
	Pronase E	2.5 ± 0.1b	9.1 ± 2.6a	11.6 ± 2.6	21	79
	Viscozyme L	2.8 ± 0.9b	13.9 ± 4.4a	16.7 ± 5.3	17	83
spinach	water	38.1 ± 2.9a	107.1 ± 10.6a	145.3 ± 7.0	26	74
	pepsin	22.2 ± 0.2b	87.7 ± 4.3a	109.9 ± 4.0	20	80
	pancreatin	19.5 ± 2.9b	54.0 ± 5.2b	73.5 ± 2.4	26	74
	Pronase E	9.2 ± 2.1c	57.7 ± 8.4b	66.9 ± 6.2	14	86
	Viscozyme L	3.0 ± 0.0c	38.1 ± 6.3b	41.1 ± 6.3	8	92
bean	water	4.8 ± 0.3b	39.5 ± 0.8b	44.4 ± 1.2	11	89
	pepsin	11.3 ± 0.4a	40.6 ± 0.3b	51.9 ± 0.0	22	78
	pancreatin	10.3 ± 1.0a	44.9 ± 3.0b	55.0 ± 1.9	19	71
	Pronase E	3.6 ± 0.1b	46.3 ± 5.0b	50.0 ± 5.1	7	93
	Viscozyme L	0.8 ± 0.1c	74.9 ± 2.9a	75.7 ± 2.8	1	99
whole wheat	water	2.6 ± 0.1cd	10.7 ± 2.3ab	13.3 ± 2.2	20	80
	pepsin	3.1 ± 0.1bc	7.8 ± 0.4bc	10.9 ± 0.3	28	72
	pancreatin	6.8 ± 0.5a	3.8 ± 0.1c	10.6 ± 0.6	64	36
	Pronase E	3.9 ± 0.4b	6.2 ± 0.1c	10.1 ± 0.4	39	61
	Viscozyme L	1.6 ± 0.1d	12.5 ± 1.2a	14.1 ± 1.3	11	89
walnut	water	443.5 ± 17.2a	431.0 ± 24.3a	874.5 ± 41.5	51	49
	pepsin	134.7 ± 6.2c	225.6 ± 40.1b	360.3 ± 46.4	37	63
	pancreatin	302.2 ± 54.8b	104.1 ± 47.0c	406.3 ± 7.8	74	26
	Pronase E	105.5 ± 3.3c	16.7 ± 4.6c	122.2 ± 7.9	86	14
	Viscozyme L	40.7 ± 12.1c	30.2 ± 12.0c	70.9 ± 0.1	57	43

[a]Different letters within the same column indicate statistically significant differences ($P < 0.05$).

direct measure of TAC on the whole food by QUENCHER procedure gave results substantially in line with those achieved with multiple chemical extraction procedures, W_TAC being well in line or slightly higher in all cases, but in walnuts it was significantly lower.

Interestingly, looking at the TAC values of fractions obtained upon in vitro GI digestion, data showed that the last insoluble material collected at the end of the in vitro GI digestion (sample 5°I) did not contribute significantly to the OP_TAC in the case of apple and walnut (i.e., most of the antioxidant compounds were released during the first three digestion steps). On the contrary, the last insoluble fractions of wheat, spinach, and bean significantly contributed to the OP_TAC.

The results of soluble and insoluble TAC obtained for each sample after each digestion step by the various enzymes are summarized in Table 2. The values (mmol TE/kg) of soluble TAC at each digestion step ranged from 2.5 to 27.7, from 3.0 to 38.1, from 0.8 to 11.3, from 1.6 to 6.8, and from 40.7 to 443.5 for apple, spinach, bean, whole wheat, and walnut, respectively. The insoluble fractions have TACs (mM/kg) ranging from 9.1 to 19.8, from 38.1 to 107.1, from 39.5 to 74.9, from 3.8 to 12.5, and from 16.7 to 431.0 for apple, spinach, bean, whole wheat, and walnut, respectively.

It is worth noting that also the percentages of soluble and insoluble antioxidant activity of each step were completely different among the various foods; they varied for the soluble fraction from 1% after bean digestion by Viscozyme L to 86% after walnut treatment by Pronase E.

In apple the treatment with water and the following one with pepsin extracted most of the antioxidants having a water-soluble nature, leaving at each step about 30% of the TAC in the insoluble material. The following steps resulted in small but significant TAC release (between 17 and 30%). Interestingly, despite the release of soluble TAC, the TAC of insoluble moiety was not reduced and it remained more or less constant (ranging between 10 and 20 TE/kg).

Unlike the apple, in spinach a large percentage (74−92%) of antioxidant compounds remained in the insoluble material after treatment with water. In particular, the first pellet has the highest value of antioxidant activity. As expected, soluble antioxidant activity as well as insoluble antioxidant activity decreased progressively during the digestion.

Also for the beans, the insoluble TAC was very high (71−99%) at each digestion step, and it even increased (from 40 to 75 mmol TE/kg) upon digestion; the highest value was found after Viscozyme L treatment, thus suggesting that in beans many antioxidant compounds are buried in the tight polysaccharide/protein network typical of legumes and are released during this kind of enzymatic digestion process.

Whole wheat had the lowest absolute TAC values among the tested foods. However, similarly to the beans, it showed the highest value of insoluble TAC after the last enzymatic treatment. Interestingly, a significant percentage of antioxidant activity was also released by the action of pancreatin.

Walnut antioxidant activity values were by far the highest among the investigated foods. In the first step, about 50% of the

antioxidant activity was solubilized and the other 50% remained bound to the matrix; this soluble fraction was about half of the soluble TAC, whereas another 30% was released after pancreatin action.

DISCUSSION

The systemic effects of dietary phytochemicals could occur through powerful anti-inflammatory mechanisms that might be also triggered by the low concentration of their metabolites found in the blood and other tissues.[5,32,33] However, the control of oxidative stress operated by dietary antioxidants inside the GI environment, also resulting in modulation of GI permeability, is emerging as a physiologically relevant function.[34] Within this framework, the ability of a food to quench free radicals inside the GI tract may be fundamental to predict its health benefits in situ.

The values of TAC used to construct food antioxidant activity databases were mainly obtained on hydroalcoholic extracts of the foods,[12,35] thus taking into account only the activity of soluble phytochemicals and not considering those present in the insoluble polymerized form, covalently bound to food structures or physically entrapped in the food matrix.[35] Already in 1998, Saura Calixto and co-workers first pointed out the concept of antioxidant dietary fiber, highlighting the importance of this food component.[36] More recently, the possible physiological role of antioxidant bound to cereal dietary fiber and in general to the insoluble food material was proposed.[37,38]

Use of Enzymes Is Fundamental To Properly Assess Food TAC. The first finding of the present study was that the TAC measured taking into account the bound compounds which are released during the in vitro enzymatic digestion procedure is usually much higher ($p < 0.05$) than that calculated by the standard extraction methodology or even by the direct measure (QUENCHER) on undigested foods. In all foods but apples the value of OP_TAC was significantly higher than the TPE_TAC. The difference was about 20% in spinach, 40% in whole wheat and walnut and 60% in bean. The difference due to the enzymatic digestion becomes enormous in whole wheat if the TAC of the hydroalcoholic extract (HAE) instead of the alkaline hydrolysis extract (TPE) was considered, confirming the previous finding by Delgado et al.[39] It should be taken into account that alkaline hydrolysis is very efficient in releasing phenolic compounds from wheat bran; however, it has no physiological meaning.[40]

This evidence fully confirmed the findings by Pastoriza and co-workers,[29] who simulated the digestion of 27 foods and calculated the so-called GAR by adding soluble and insoluble antioxidant activities at the end of the digestion process. These authors did not measure the TAC at each step (as reported in the present paper); however, they clearly demonstrated that the total TAC after enzymatic digestion is much greater than that obtained by the chemical extraction as well as by the direct QUENCHER procedure for all of the tested foods. It is worth noting that these authors performed oral gastric and small intestine simulated digestion, whereas in the present study also a step simulating the protease and polysaccharidase activity of intestinal bacteria has been performed.

TAC Release during the Multistep Enzymatic Digestion Is Different for the Five Foods. The relevance of the detailed information that was obtained considering the TAC released for each food at the various digestion steps can be appreciated from the data presentation reported in Figure 3. In this figure the TAC values were split into free TAC, that obtained with water extraction, and bound TAC, which is further subdivided in pepsin, pancreatin, and Pronase E plus Viscozyme L.

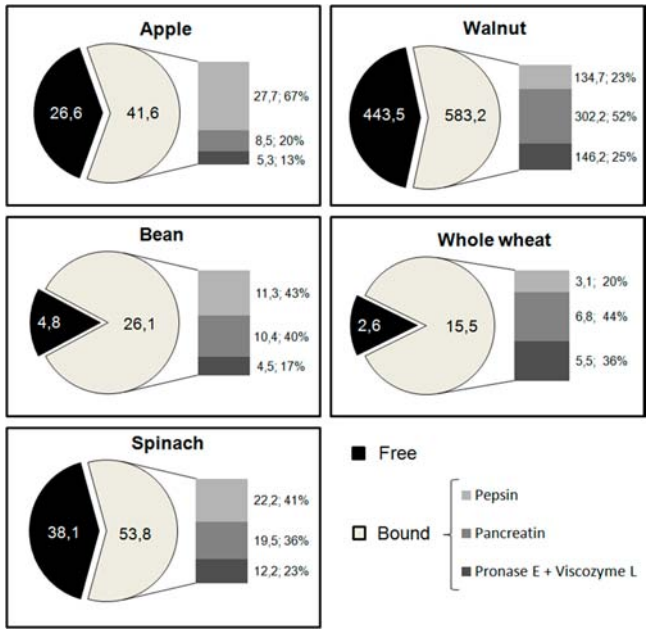

Figure 3. Release of TAC (expressed in mmol TE/kg DM) during the multistep enzymatic digestion illustrated in Figure 1. "Free" TAC is the value measured on the fraction after water extraction, whereas "bound" TAC is that after pepsin, pancreatin, pronase E, and Viscozyme L actions.

Among the tested foods whole wheat had by far the largest proportion of insoluble TAC when the chemical procedure was applied. This is related to the presence of phenolic acids covalently bound to the insoluble polysaccharides.[23] Digestion data were not different regarding the absolute TAC value; however, they demonstrated that the insoluble material is not significantly solubilized with the pepsin, whereas the action of pancreatin is able to release part of the TAC. This is in agreement with a previous hypothesis highlighting the role of cereal dietary fiber in transporting the antioxidants through the gut, allowing a slow release during digestion and intestinal microbiota fermentation.[41]

Looking at the TAC data from the chemical extractions, apple and walnut behaved opposite to whole grain: in these foods the large majority of TAC is extracted with hydroalcoholic solution, and a limited fraction can be released after alkaline hydrolysis. Interestingly, looking at the enzymatic procedure for apples, the OP_TAC and TPE_TAC values are similar and the antioxidant activity is mostly released after gastric digestion. On the other hand, when the enzymatic procedure was applied on walnut, the contribution to the TAC of the insoluble part is much larger than expected and a very significant part of TAC is released only after pancreatin and Pronase E actions. This is well in line with the claimed potential effects raised by the metabolites produced by the microbiota action on nut polyphenols.[42,43]

The pattern of TAC solubilized with the enzyme treatment from bean and spinach showed many similarities, although spinach has absolute values about 3 times higher than bean. In both foods, about 30% of the TAC measured by chemical extraction was obtained using alkaline hydrolysis. Also, the

patterns of the release during the various digestive steps were quite similar. On the other hand, looking at the PB_TAC, the amount of TAC present in the insoluble material is much higher in bean (showing a picture similar to that of whole grain) than in spinach (which is similar to apple). This is probably related to the high content of dietary fiber in beans that is presumably bound to many antioxidant compounds.[44] This is confirmed by the experimental finding that a very significant amount of TAC is released from beans after Viscozyme L addition.

Release of Antioxidant Activity Is Dependent on the Nature of the Food Matrix. The overall findings of this paper were consistent with the chemical and physical nature of the food investigated and with the amount of insoluble total dietary fiber in walnut (~87%) > whole wheat (~84%) > beans = spinach (about 77%) > apple (about 65%).[45,46] In this study the contribution of phytochemicals bound to the fiber was considered in the calculation of the OP_TAC, using a multienzyme complex (Viscozyme L) containing a wide range of carbohydrases (including arabanase, cellulase, β-glucanase, hemicellulase, and xylanase). Moreover also Pronase E, a preparation containing a mixture of bacterial protease particularly suitable for insoluble material, was adopted.

This difference in the experimental approach with respect to the works previously performed was of utmost importance. In fact, data clearly showed that in foods having a high amount of insoluble dietary fiber and/or phytochemicals bound to dietary fiber or entrapped in the food structures (as in whole wheat, spinach, and bean), the action of bacterial enzymes might dramatically increase the antioxidant potential of the food residues in the lower GI tract. We have previously highlighted the physiological importance of this phenomenon for cereal dietary fiber and whole grains.[41] Here this relevance was extended to all foods having a strong fiber structure, such as spinach,[47] as well as to other polyphenol-rich foods having a significant amount of insoluble component made up of polysaccharides and proteins bound with phenolic acids, flavonols, anthocyanins, and proanthocyanidins.[19−22] It is worth remembering that this in vitro approach does not take into account the bacterial biotransformation, being focused only on the relationship between disruption of food structure and release of TAC from chemical and enzyme points of view.

Have These Findings Any Possible Health Implications? Epidemiological studies indicated that dietary fiber content in plant foods may majorly contribute to the negative associations between their intake and colorectal cancer risk.[48−50] Looking at the results of this paper with a wider physiological prospective, they suggested that the TAC of the insoluble material produced at each step of the digestion, more than the simple amount of dietary fiber, might be considered for a more reliable evaluation of the potential benefits of some foods inside the GI tract. It has been recently reported that individuals with a low bacterial richness harbored a more pronounced inflammation-associated microbiota when compared with high bacterial richness individuals.[51] The insoluble material present in the colon after the whole digestion, through a chemical action in the gut environment, may play a major role in reducing local oxidative stress and in modifying microbiota composition, consequently ameliorating gut permeability and boosting anti-inflammatory mechanisms and immunity.

The data demonstrated that for those foods having a high amount of polyphenols bound to dietary fiber or entrapped in the food matrix, the action of bacterial enzyme is fundamental to predict the overall potential TAC. Moreover, they highlighted the amount of TAC bound to the insoluble material for five main representative plant foods. In this way a measure of the overall antioxidant potential of a food against oxidative stress was provided. These findings clarified the physiological relevance of the antioxidant activity of the insoluble components that can be also restored by the presence of soluble antioxidant as recently proposed by Gökmen and coworkers.[26]

This finding pointed out the need to reconsider the correlations performed between TAC dietary intake and health outcomes. In fact, for many foods the TAC reported in the available food antioxidant database were determined with conventional extraction methods, and for many foods they gave poor indications.[35,52] In the future, it would be advisable to use the TAC measured after enzymatic digestion procedure, including microbiota-like bacterial enzymes, to obtain a more reliable picture, particularly when the health effects of the foods within the gastrointestinal tract are considered.

AUTHOR INFORMATION

Corresponding Author

*(V.F.) Phone:+31 (0)317485171. Fax: +31 (0)317485171. E-mail: vincenzo.fogliano@wur.nl.

Notes

The authors declare no competing financial interest.

ABBREVIATIONS USED

AHE_TAC, TAC of alkaline hydrolysis extract; PB_TAC, TAC potentially bioaccessible (sum of the five digestion soluble fractions); BOUND_TAC, bound TAC (PB_TAC − FREE_TAC); HAE_TAC, TAC of hydroalcoholic extract; FREE_TAC, free TAC (1°S of digestion); OP_TAC, overall potential TAC (PB_TAC + 5°I_TAC); TAC, total antioxidant capacity; TPE_TAC, AHE_TAC + HAE_TAC; W_TAC, TAC of whole food measured with QUENCHER

REFERENCES

(1) Bouchenak, M.; Lamri-Senhadji, M. Nutritional quality of legumes, and their role in cardiometabolic risk prevention: a review. *J. Med. Food* **2013**, *16*, 185−198.

(2) Arts, I. C.; Hollman, P. C. Polyphenols and disease risk in epidemiologic studies. *Am. J. Clin. Nutr.* **2005**, *81*, 317S−325S.

(3) Liu, S.; Manson, J. E.; Stampfer, M. J.; Hu, F. B.; Giovannucci, E.; Colditz, G. A.; Hennekens, C. H.; Willett, W. C. A prospective study of whole-grain intake and risk of type 2 diabetes mellitus in US women. *Am. J. Public Health* **2000**, *90*, 1409−1415.

(4) Banel, D. K.; Hu, F. B. Effects of walnut consumption on blood lipids and other cardiovascular risk factors: a meta-analysis and systematic review. *Am. J. Clin. Nutr.* **2009**, *90*, 56−63.

(5) Del Rio, D.; Rodriguez-Mateos, A.; Spencer, J. P.; Tognolini, M.; Borges, G.; Crozier, A. Dietary (poly)phenolics in human health: structures, bioavailability, and evidence of protective effects against chronic diseases. *Antioxid. Redox Signal.* **2013**, *18*, 1818−1892.

(6) Manach, C.; Hubert, J.; Llorach, R.; Scalbert, A. The complex links between dietary phytochemicals and human health deciphered by metabolomics. *Mol. Nutr. Food Res.* **2009**, *53*, 1303−1315.

(7) Valtuena, S.; Pellegrini, N.; Franzini, L.; Bianchi, M. A.; Ardigo, D.; Del Rio, D.; Piatti, P.; Scazzina, F.; Zavaroni, I.; Brighenti, F. Food selection based on total antioxidant capacity can modify antioxidant intake, systemic inflammation, and liver function without altering markers of oxidative stress. *Am. J. Clin. Nutr.* **2008**, *87*, 1290−1297.

(8) Halliwell, B.; Rafter, J.; Jenner, A. Health promotion by flavonoids, tocopherols, tocotrienols, and other phenols: direct or

indirect effects? Antioxidant or not? *Am. J. Clin. Nutr.* **2005**, *81*, 268S−276S.
(9) Peluso, I.; Miglio, C.; Morabito, G.; Ioannone, F.; Serafini, M. Flavonoids and immune function in human: a systematic review. *Crit. Rev. Food Sci. Nutr.* **2013**, *53* (7), 706−721.
(10) Lampe, J. W. Health effects of vegetables and fruit: assessing mechanisms of action in human experimental studies. *Am. J. Clin. Nutr.* **1999**, *70*, 475S−490S.
(11) Gokmen, V.; Serpen, A.; Fogliano, V. Direct measurement of the total antioxidant capacity of foods: the 'QUENCHER' approach. *Trends Food Sci. Technol.* **2009**, *20*, 278−288.
(12) Pellegrini, N.; Serafini, M.; Salvatore, S.; Del Rio, D.; Bianchi, M.; Brighenti, F. Total antioxidant capacity of spices, dried fruits, nuts, pulses, cereals and sweets consumed in Italy assessed by three different in vitro assays. *Mol. Nutr. Food Res.* **2006**, *50*, 1030−1038.
(13) Hernandez, I.; Alegre, L.; Van Breusegem, F.; Munne-Bosch, S. How relevant are flavonoids as antioxidants in plants? *Trends Plant Sci.* **2009**, *14*, 125−132.
(14) Faulks, R.; Southon, S. Carotenoids, metabolism and disease. In *Handbook of Nutraceuticals and Functional Foods*; CRC Press: Boca Raton, FL, USA, 2001; Vol. 9.
(15) Bernhardt, S.; Schlich, E. Impact of different cooking methods on food quality: retention of lipophilic vitamins in fresh and frozen vegetables. *J. Food Eng.* **2006**, *77*, 327−333.
(16) Napolitano, A.; Cascone, A.; Graziani, G.; Ferracane, R.; Scalfi, L.; Di Vaio, C.; Ritieni, A.; Fogliano, V. Influence of variety and storage on the polyphenol composition of apple flesh. *J. Agric. Food Chem.* **2004**, *52*, 6526−6531.
(17) Bottino, A.; Degl'Innocenti, E.; Guidi, L.; Graziani, G.; Fogliano, V. Bioactive compounds during storage of fresh-cut spinach: the role of endogenous ascorbic acid in the improvement of product quality. *J. Agric. Food Chem.* **2009**, *57*, 2925−2931.
(18) Fukuda, T.; Ito, H.; Yoshida, T. Antioxidative polyphenols from walnuts (*Juglans regia* L.). *Phytochemistry* **2003**, *63*, 795−801.
(19) Beninger, C. W.; Hosfield, G. L. Flavonol glycosides from Montcalm dark red kidney bean: implications for the genetics of seed coat color in *Phaseolus vulgaris* L. *J. Agric. Food Chem.* **1999**, *47*, 4079−4082.
(20) Díaz, A. M.; Caldas, G. V.; Blair, M. W. Concentrations of condensed tannins and anthocyanins in common bean seed coats. *Food Res. Int.* **2010**, *43*, 595−601.
(21) Luthria, D. L.; Pastor-Corrales, M. A. Phenolic acids content of fifteen dry edible bean (*Phaseolus vulgaris* L.) varieties. *J. Food Compos. Anal.* **2006**, *19*, 205−211.
(22) Garcia, E.; Filisetti, T. M. C. C.; Udaeta, J. E. M.; Lajolo, F. M. Hard-to-cook beans (*Phaseolus vulgaris*): involvement of phenolic compounds and pectates. *J. Agric. Food Chem.* **1998**, *46*, 2110−2116.
(23) Adom, K. K.; Liu, R. H. Antioxidant activity of grains. *J. Agric. Food Chem.* **2002**, *50*, 6182−6187.
(24) Liu, R. H. Whole grain phytochemicals and health. *J. Cereal Sci.* **2007**, *46*, 207−219.
(25) Fogliano, V.; Corollaro, M. L.; Vitaglione, P.; Napolitano, A.; Ferracane, R.; Travaglia, F.; Arlorio, M.; Costabile, A.; Klinder, A.; Gibson, G. In vitro bioaccessibility and gut biotransformation of polyphenols present in the water-insoluble cocoa fraction. *Mol. Nutr. Food Res.* **2011**, *55* (Suppl. 1), 44−55.
(26) Celik, E. E.; Gokmen, V.; Fogliano, V. Soluble antioxidant compounds regenerate the antioxidants bound to insoluble parts of foods. *J. Agric. Food Chem.* **2013**, *61*, 10329−10334.
(27) Hollebeeck, S.; Borlon, F.; Schneider, Y. J.; Larondelle, Y.; Rogez, H. Development of a standardised human in vitro digestion protocol based on macronutrient digestion using response surface methodology. *Food Chem.* **2013**, *138*, 1936−1944.
(28) Saura-Calixto, F.; Serrano, J.; Goni, I. Intake and bioaccessibility of total polyphenols in a whole diet. *Food Chem.* **2007**, *101*, 492−501.
(29) Pastoriza, S.; Delgado-Andrade, C.; Haro, A.; Rufián-Henares, J. A. A physiologic approach to test the global antioxidant response of foods. The GAR method. *Food Chem.* **2011**, *129*, 1926−1932.
(30) Gong, L.; Jin, C.; Wu, X.; Zhang, Y. Relationship between total antioxidant capacities of cereals measured before and after in vitro digestion. *Int. J. Food Sci. Nutr.* **2013**, *64*, 850−856.
(31) Brand-Williams, W.; Cuvelier, M. E.; Berset, C. Use of a free radical method to evaluate antioxidant activity. *LWT−Food Sci. Technol.* **1995**, *28*, 25−30.
(32) Jensen, G. S.; Wu, X. L.; Patterson, K. M.; Barnes, J.; Carter, S. G.; Scherwitz, L.; Beaman, R.; Endres, J. R.; Schauss, A. G. In vitro and in vivo antioxidant and anti-inflammatory capacities of an antioxidant-rich fruit and berry juice blend. Results of a pilot and randomized, double-blinded, placebo-controlled, crossover study. *J. Agr Food Chem.* **2008**, *56*, 8326−8333.
(33) Holst, B.; Williamson, G. Nutrients and phytochemicals: from bioavailability to bioefficacy beyond antioxidants. *Curr. Opin. Biotechnol.* **2008**, *19*, 73−82.
(34) Maeda, T.; Miyazono, Y.; Ito, K.; Hamada, K.; Sekine, S.; Horie, T. Oxidative stress and enhanced paracellular permeability in the small intestine of methotrexate-treated rats. *Cancer Chemother. Pharmacol.* **2010**, *65*, 1117−1123.
(35) Pellegrini, N.; Serafini, M.; Colombi, B.; Del Rio, D.; Salvatore, S.; Bianchi, M.; Brighenti, F. Total antioxidant capacity of plant foods, beverages and oils consumed in Italy assessed by three different in vitro assays. *J. Nutr.* **2003**, *133*, 2812−2829.
(36) Saura-Calixto, F. Antioxidant dietary fiber product: a new concept and a potential food ingredient. *J. Agric. Food Chem.* **1998**, *46*, 4303−4306.
(37) Vitaglione, P.; Napolitano, A.; Fogliano, V. Cereal dietary fibre: a natural functional ingredient to deliver phenolic compounds into the gut. *Trends Food Sci. Technol.* **2008**, *19*, 451−463.
(38) Serpen, A.; Capuano, E.; Fogliano, V.; Gokmen, V. A new procedure to measure the antioxidant activity of insoluble food components. *J. Agric. Food Chem.* **2007**, *55*, 7676−7681.
(39) Delgado-Andrade, C.; Conde-Aguilera, J. A.; Haro, A.; de la Cueva, S. P.; Rufian-Henares, J. A. A combined procedure to evaluate the global antioxidant response of bread. *J. Cereal Sci.* **2010**, *52*, 239−246.
(40) Liyana-Pathirana, C. M.; Shahidi, F. Importance of insoluble-bound phenolics to antioxidant properties of wheat. *J. Agric. Food Chem.* **2006**, *54*, 1256−1264.
(41) Napolitano, A.; Costabile, A.; Martin-Pelaez, S.; Vitaglione, P.; Klinder, A.; Gibson, G. R.; Fogliano, V. Potential prebiotic activity of oligosaccharides obtained by enzymatic conversion of durum wheat insoluble dietary fibre into soluble dietary fibre. *Nutr. Metab. Cardiovasc. Dis: NMCD* **2008**, *19*, 283−290.
(42) Landete, J. M. Ellagitannins, ellagic acid and their derived metabolites: a review about source, metabolism, functions and health. *Food Res. Int.* **2011**, *44*, 1150−1160.
(43) Larrosa, M.; García-Conesa, M. T.; Espín, J. C.; Tomás-Barberán, F. A. Bioavailability and metabolism of ellagic acid and ellagitannins. In *Flavonoids and Related Compounds*; CRC Press: Boca Raton, FL, USA, 2012.
(44) Bravo, L. Polyphenols: chemistry, dietary sources, metabolism, and nutritional significance. *Nutr. Rev.* **1998**, *56*, 317−333.
(45) Sabaté, J.; Wien, M. Consumption of nuts in the prevention of cardiovascular disease. *Cardiovasc. Dis.* **2013**, *2*, 258−266.
(46) Anderson, J. W.; Bridges, S. R. Dietary fiber content of selected foods. *Am. J. Clin. Nutr.* **1988**, *47*, 440−447.
(47) Castenmiller, J. J.; West, C. E.; Linssen, J. P.; van het Hof, K. H.; Voragen, A. G. The food matrix of spinach is a limiting factor in determining the bioavailability of β-carotene and to a lesser extent of lutein in humans. *J. Nutr.* **1999**, *129*, 349−355.
(48) Aune, D.; Chan, D. S.; Lau, R.; Vieira, R.; Greenwood, D. C.; Kampman, E.; Norat, T. Dietary fibre, whole grains, and risk of colorectal cancer: systematic review and dose-response meta-analysis of prospective studies. *BMJ* **2011**, *343*, d6617.
(49) Murphy, N.; Norat, T.; Ferrari, P.; Jenab, M.; Bueno-de-Mesquita, B.; Skeie, G.; Dahm, C. C.; Overvad, K.; Olsen, A.; Tjonneland, A.; Clavel-Chapelon, F.; Boutron-Ruault, M. C.; Racine, A.; Kaaks, R.; Teucher, B.; Boeing, H.; Bergmann, M. M.;

Trichopoulou, A.; Trichopoulos, D.; Lagiou, P.; Palli, D.; Pala, V.; Panico, S.; Tumino, R.; Vineis, P.; Siersema, P.; van Duijnhoven, F.; Peeters, P. H.; Hjartaker, A.; Engeset, D.; Gonzalez, C. A.; Sanchez, M. J.; Dorronsoro, M.; Navarro, C.; Ardanaz, E.; Quiros, J. R.; Sonestedt, E.; Ericson, U.; Nilsson, L.; Palmqvist, R.; Khaw, K. T.; Wareham, N.; Key, T. J.; Crowe, F. L.; Fedirko, V.; Wark, P. A.; Chuang, S. C.; Riboli, E. Dietary fibre intake and risks of cancers of the colon and rectum in the European prospective investigation into cancer and nutrition (EPIC). *PLoS One* **2012**, *7*, e39361.

(50) Cho, S. S.; Qi, L.; Fahey, G. C., Jr.; Klurfeld, D. M. Consumption of cereal fiber, mixtures of whole grains and bran, and whole grains and risk reduction in type 2 diabetes, obesity, and cardiovascular disease. *Am. J. Clin. Nutr.* **2013**, *98*, 594−619.

(51) Le Chatelier, E.; Nielsen, T.; Qin, J.; Prifti, E.; Hildebrand, F.; Falony, G.; Almeida, M.; Arumugam, M.; Batto, J. M.; Kennedy, S.; Leonard, P.; Li, J.; Burgdorf, K.; Grarup, N.; Jorgensen, T.; Brandslund, I.; Nielsen, H. B.; Juncker, A. S.; Bertalan, M.; Levenez, F.; Pons, N.; Rasmussen, S.; Sunagawa, S.; Tap, J.; Tims, S.; Zoetendal, E. G.; Brunak, S.; Clement, K.; Dore, J.; Kleerebezem, M.; Kristiansen, K.; Renault, P.; Sicheritz-Ponten, T.; de Vos, W. M.; Zucker, J. D.; Raes, J.; Hansen, T.; Meta, H. I. T. C.; Bork, P.; Wang, J.; Ehrlich, S. D.; Pedersen, O.; Guedon, E.; Delorme, C.; Layec, S.; Khaci, G.; van de Guchte, M.; Vandemeulebrouck, G.; Jamet, A.; Dervyn, R.; Sanchez, N.; Maguin, E.; Haimet, F.; Winogradski, Y.; Cultrone, A.; Leclerc, M.; Juste, C.; Blottiere, H.; Pelletier, E.; LePaslier, D.; Artiguenave, F.; Bruls, T.; Weissenbach, J.; Turner, K.; Parkhill, J.; Antolin, M.; Manichanh, C.; Casellas, F.; Boruel, N.; Varela, E.; Torrejon, A.; Guarner, F.; Denariaz, G.; Derrien, M.; van Hylckama Vlieg, J. E.; Veiga, P.; Oozeer, R.; Knol, J.; Rescigno, M.; Brechot, C.; M'Rini, C.; Merieux, A.; Yamada, T. Richness of human gut microbiome correlates with metabolic markers. *Nature* **2013**, *500*, 541−546.

(52) Pryor, W. A.; Cornicelli, J. A.; Devall, L. J.; Tait, B.; Trivedi, B. K.; Witiak, D. T.; Wut, M. A rapid screening test to determine the antioxidant potencies of natural and synthetic antioxidants. *J. Org. Chem.* **1993**, *58*, 3521−3532.

JOURNAL OF AGRICULTURAL AND FOOD CHEMISTRY

Article

pubs.acs.org/JAFC

Immune Regulation and Anti-inflammatory Effects of Isogarcinol Extracted from *Garcinia mangostana* L. against Collagen-Induced Arthritis

Yanxia Fu,[†,∥] Hailing Zhou,[†,∥] Mengqi Wang,[†] Juren Cen,[†,‡] and Qun Wei*[,†]

[†]Department of Biochemistry and Molecular Biology, Beijing Normal University, Gene Engineering and Biotechnology Beijing Key Laboratory, Beijing 100875, People's Republic of China

[‡]Key Laboratory of Protection and Development Utilization of Tropical Crop Germplasm Resources, Ministry of Education, College of Landscape and Horticulture, Hainan University, Haikou 570228, People's Republic of China

ABSTRACT: Isogarcinol is a natural compound that we extracted from *Garcinia mangostana* L., and we were the first to report that it is a new immunosuppressant. In the present study, we investigated the immune regulation and anti-inflammatory effects of isogarcinol on collagen-induced arthritis (CIA) and explored its potential mechanism in the treatment of rheumatoid arthritis. The oral administration of isogarcinol significantly reduced clinical scores, alleviated cartilage and bone erosion, and reduced the levels of serum inflammatory cytokines in CIA mice. Isogarcinol inhibited xylene-induced mouse ear edema in vivo. In vitro, isogarcinol decreased iNOS and COX-2 mRNA expression and NO content by inhibiting NF-κB expression. Furthermore, isogarcinol decreased the activity of NFAT and inhibited IL-2 expression. The mechanism of action of isogarcinol is associated with down-regulation of both autoimmune and inflammatory reactions.

KEYWORDS: *Garcinia mangostana Linn., isogarcinol, collagen-induced arthritis, inflammation, immunity*

INTRODUCTION

It is well-known that the consumption of fruits can reduce the incidence of cancer, arthritis, inflammation, heart disease, and brain dysfunction.[1] Mangosteen (*Garcinia mangostana* L.) is a slow-growing tropical evergreen tree with leathery, glabrous leaves. The edible portion of the mangosteen fruit is milky white, whereas the pericarp of mangosteen is dark-purple to red-purple. The pericarp, which accounts for approximately two-thirds of the entire fruit weight, is agricultural waste. People in Southeast Asia have used this waste pericarp in folk medicine for the treatment of abdominal pain, diarrhea, dysentery, infected wounds, suppuration, and chronic ulcers;[2] furthermore, the consumption of mangosteen products has increased as a dietary supplement in the United States because of their potent antioxidant properties.[3] Experimental studies have demonstrated that extracts of mangosteen have antitumor, antioxidant, and antibacterial activities,[4] and using mangosteen extracts for the prevention of chronic diseases is very popular.[2]

Rheumatoid arthritis (RA) is an autoimmune disease that is characterized by chronic inflammatory symptoms such as pain, swelling, and progressive destruction of joints and results in disability.[5] The prevalence of arthritis has increased over the past decade because of the world's aging population; approximately 1−2% of the world's population is thought to be affected by RA, and one in three patients is likely to become severely disabled within 20 years.[6] To date, the exact etiology of RA remains unknown, and a cure has not yet been developed.[7]

Because RA is characterized by overactive immune responses, most current treatment options involve the administration of immune suppressants alone or in conjunction with disease-modifying antirheumatic drugs (DMARDs) or destruction of autoreactive lymphocytes with antibodies.[8] Unfortunately, these drugs are not suitable for long-term treatment due to their side effects and toxicity.[9] DMARDs can retard joint destruction, but many patients cannot tolerate the side effects of these drugs.[5] Calcineurin (CN) inhibitors such as cyclosporin A (CsA) and tacrolimus (also called FK-506) have potent immunosuppressive and anti-inflammatory effects and have been shown to be beneficial in the treatment of inflammatory and autoimmune diseases such as RA.[10] However, the use of these drugs is associated with severe hepatotoxicity and nephrotoxicity.[11] Cytokine antagonists decrease inflammation and joint destruction, but they interfere with immune defense; in addition, they must be administered by injection, which increases the risk of infections.[12] The future treatment for RA should provide more effective relief with fewer side effects and lower cost. Due to the long-term use and side effects of antiarthritis drugs, dietary supplements are widely used to treat arthritis. According to the 2007 National Health Interview Survey (NHIS) in the United States, the use of natural products (17.7%) is an important part of alternative medicine. The frequency of adults who use alternative medicine to treat arthritis reached 8.7%, indicating that the treatment of arthritis with natural products is popular in the United States.[13]

Our group has focused on screening immunosuppressants from natural products with CN as the target enzyme and docking the binding domain between CN and CN inhibitors.[14,15] Isogarcinol (Figure1) is a natural compound that we screened from *Garcinia mangostana* L. with CN as the target enzyme. It was reported that isogarcinol is a new powerful, low-toxicity

Received: December 30, 2013
Revised: March 27, 2014
Accepted: April 16, 2014
Published: April 16, 2014

ACS Publications © 2014 American Chemical Society

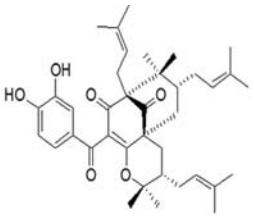

Figure 1. Chemical structure of isogarcinol.

immunosuppressant because it significantly inhibits the proliferation of spleen T-lymphocytes induced by concanavalin A (ConA) and the mixed lymphocyte reaction (MLR); the oral administration of isogarcinol in mice resulted in a dose-dependent decrease in delayed type hypersensitivity (DTH) and prolonged graft survival in allogeneic skin transplantation. More importantly, isogarcinol had lower toxicity on liver and kidney function than CsA in experimental animals.[16]

CN plays a crucial role in the autoimmune and inflammation responses and involves a variety of physiological and pathological processes.[17] The clinical interest in CN is mainly focused on T cells and other cells of the immune system and particularly involves CN and nuclear factor of activated T cells (NFAT) signaling, which is the principal target of widely prescribed immunosuppressive drugs, such as CsA and FK506.[13] It was reported that nuclear transcription factor kappa B (NF-κB) was also controlled by CN in immune cells.[18] Both isogarcinol and CsA are CN inhibitors, and because of the efficacy but high

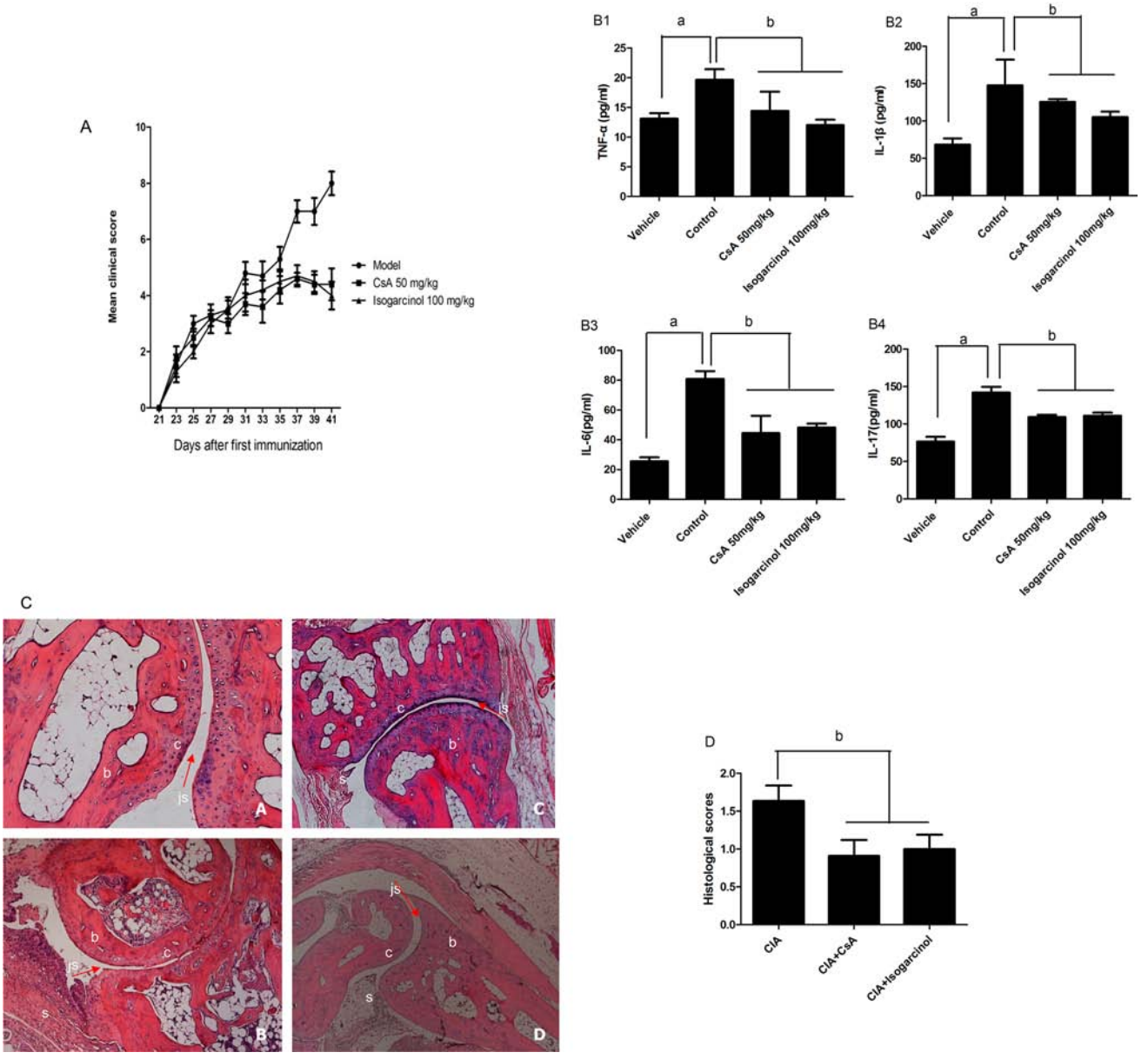

Figure 2. Isogarcinol attenuates collagen-induced arthritis: (A) mean of clinical scores; (B1) isogarcinol reduced the content of TNF-α in the serum of CIA; (B2) isogarcinol reduced the content of IL-1β in the serum; (B3) isogarcinol reduced the content of IL-6 in the serum; (B4) isogarcinol reduced the content of IL-17 in the serum; (C) representative histological changes of joint tissues stained with H&E (×100 original magnification). The upper case A represents vehicle mice; B, CIA mice; C and D, CIA mice treated with CsA or isogarcinol, respectively. The lower case b denotes the bone; c, the cartilage; s, the synovium; and js, the joint space. (D) Histological scores of isogarcinol are expressed as the mean ± SD (n = 7). Different letters above bars designate significant difference between groups, $P < 0.05$.

dx.doi.org/10.1021/jf405790q | J. Agric. Food Chem. 2014, 62, 4127−4134

liver and kidney toxicity of CsA, we wanted to determine whether orally administered isogarcinol could be a novel and effective agent for the treatment of rheumatoid arthritis and to elucidate the potential underlying mechanisms.

MATERIALS AND METHODS

Materials. Bovine type II collagen and complete Freund's adjuvant that induced collagen-induced arthritis (CIA) were purchased from Chondrex (USA). RAW 264.7 murine macrophages were obtained from the American Type Culture Collection. Specific pathogen-free male DBA/1J mice were acquired from the National Resource Center for Mutant Mice Model Animal Research Center of Nanjing University. Specific pathogen-free male ICR mice (6−8 weeks) were purchased from the Vital River Laboratories (Beijing, China). All mice were set aside under standard conditions with a 12 h light/dark cycle after initial acclimatization for approximately 1 week with ad libitum access to standard mouse chow and water. All animal experimental procedures were approved by the Animal Ethics Committee of Beijing Normal University and were carried out in strict accordance with institutional guidelines. All efforts were made to minimize the number of animals used and their suffering.

Induction of CIA. CIA was induced as previously described.[19] Briefly, DBA/1J mice were intradermally injected at the base of the tail with 100 μg of bovine type II collagen emulsified with an equal volume of Freund's complete adjuvant. The day of the first immunization was defined as day 0. Three weeks after the primary immunization, the mice were boosted with 100 μg of CII in Freund's incomplete adjuvant via the same route. After the secondary immunization, the mice were randomly divided into four groups (seven per group): (1) normal nonimmunized group, (2) CIA group, (3) CIA plus CsA group (50 mg per kg), and (4) CIA plus isogarcinol group (100 mg per kg). Mice in the normal group received an oral gavage of 0.2 mL of peanut oil containing 1% DMSO daily from day 21 to 42; mice in the isogarcinol or CsA group received an oral gavage of the same volume containing 100 mg/kg isogarcinol or 50 mg/kg CsA daily from day 21 to 42. On day 42, after anesthetization with pentobarbital, blood samples were collected from all mice via cardiac punctures. The levels of IL-1β, TNF-α, IL-6, and IL-17 in serum were measured using ELISA kits according to the manufacturer's instructions.

Clinical Assessment and Histopathological Analysis of Arthritis. The clinical severity of arthritis in the paws was evaluated in a double-blind manner using a semiquantitative scoring system as described previously:[20] 0 = no evidence of erythema and swelling, 1 = swelling and erythema of the digit, 2 = mild erythema of the limb, 3 = gross erythema and swelling of the digit, and 4 = ankylosis of the limb or gross swelling deformity and the inability to use the limb. On the final day of the experiments, the hind paws were harvested, fixed, decalcified, and then embedded in paraffin. The tissues were longitudinally cut into 5 μm serial sections and stained with hematoxylin and eosin (H&E). Histopathological changes in the joints were examined under light microscopy and scored in a range from 0 to 3, where 0 = normal, 1 = mild synovitis or slight cartilage erosion, 2 = moderate synovitis and cartilage erosion, and 3 = erosion of the cartilage or bone destruction.

Xylene-Induced Mouse Ear Edema. The ear edema model was employed to evaluate anti-inflammatory activity. For this model, 30 min after drug administration, inflammation was induced by the topical application of xylene (30 μL) on the inner and outer surfaces of the right ear of each ICR mouse. The left ear was kept as the control. At 30 min after xylene application, the animals were killed by cervical dislocation. Disck sections of 8 mm in diameter were punched from each ear and then weighed. The inflammation was assessed on the basis of the difference in weight between the punches from the right and left ears.[21]

Real-Time Quantitative PCR for iNOS, COX-2, and IL-2. RNA was extracted using TRIZOL (BioTeke, China) as described by the manufacturer. Real-time quantitative PCR was performed to detect the mRNA expression of iNOS, COX-2, and IL-2 in RAW 264.7 cells. The primer sequences for the reference genes were as follows: for β-actin, AGAGGGAAATCGTGCGTGAC (forward) and CAATAGTGATGACCTGGCCGT (reverse); for IL-2, CCTGAGCAGGATGGAGAATTACA (forward) and TCCAGAACATGCCGCAGAG (reverse); for iNOS, GGCAGCCTGTGAGACCTTTG (forward) and GCATTGGAAGTGAAGCGTTTC (reverse); and for COX-2, TGAGTACCGCAAACGCTTCTC (forward) and TGGACGAGGTTTTTCCACCAG (reverse). Real-time quantitative PCR was performed on an Applied Biosystems 7500. The relative quantification of target mRNA was calculated using the comparative $2^{-\Delta\Delta CT}$ method after normalization with the internal control. Reactions were performed in triplicate. The results are shown as the mean ± SD.

Nitrite Determinations. Measurement of nitrite accumulation into the culture medium was used to determine NO production. RAW 264.7 cells were induced with LPS (10 μg/mL) or a combination of LPS (10 μg/mL) and isogarcinol or CsA in 6-well plates for 24 h, the culture medium was collected, and nitrite was measured using Griess reagent (Applygen, China) according to the manufacturer's instructions.

Western Blot Analysis for IκB-α. The secretion of IκB-α was induced by incubating Jurkat cells with 100 ng/mL phorbol 12-myristate 13-acetate (PMA) and 1 μM ionomycin (Ion). Cells were treated with PMA and Ion or a combination of CsA or different doses of isogarcinol and PMA and Ion. The cells were harvested by centrifugation after 24 h and washed twice with PBS. Then, the cells were lysed on ice for 20 min. The cell-free supernatant was collected for Western blot analysis. Protein quantitation was performed with a bicinchoninic acid (BCA) protein quantitation kit. The samples were separated using discontinuous SDS-PAGE and transferred to PVDF membranes, which were blotted with primary antibody and secondary antibodies, and specific bands were visualized using an electrochemiluminescene (ECL) kit.

Dual-Luciferase Reporter Gene Assay. NFAT transcription activity was investigated using two reporter gene assay systems. RAW 264.7 macrophage cells plated in 24-well plates were cotransfected with the p-firefly luciferase (FL)-NFAT plasmid and the p-renilla luciferase (RL)-SV40 endogenous control plasmid. Twenty-four hours after transfection, cells were incubated with PMA + Ion or a combination of different doses of isogarcinol and PMA + Ion for 24 h. NFAT activity was measured using a Dual-Luciferase Reporter Kit (Promega) according to the manufacturer's protocol.

Statistics. All data presented were obtained from three independent experiments and are presented as mean ± standard deviation (SD). One-way analysis of variation (ANOVA) followed by Bonferroni's Multiple Comparison Test was used to compare experimental groups with the control groups using GraphPad Prism 5.0 software. The mean values were compared using Student ' s t test. Values of $P \leq 0.05$ were considered to be significant.

RESULTS

Isogarcinol Inhibited Collagen-Induced Arthritis. The experimental results showed that isogarcinol treatment reduced

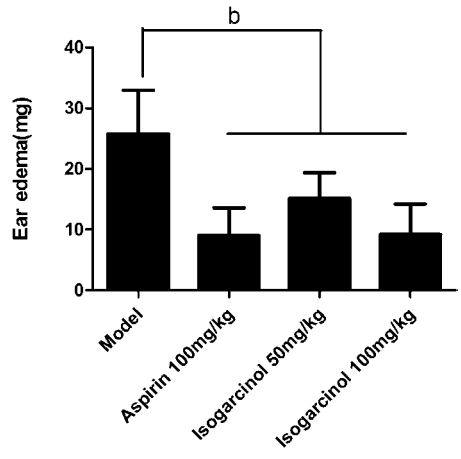

Figure 3. Isogarcinol inhibited xylene-induced mouse ear edema. All values are expressed as the mean ± SD (n = 7). Different letters above bars designate significant difference between groups, $P < 0.05$.

the mean arthritis scores (Figure 2A) and reduced the levels of IL-1β,TNF-α, IL-6, and IL-17 (Figure 2B) in the serum based on measurements with ELISA kits. The histopathological change in the joints was examined under light microscopy and scored from 0 to 3, based on the synovitis and cartilage or bone destruction scales. We can see from Figure 2C,D that there was obvious evidence of synovial hyperplasia, joint space narrowing, and bone and cartilage erosion in the joints of the CIA group mice, whereas in the isogarcinol-treated group these changes were scarcely observed.

Effects of Isogarcinol on Acute Inflammatory Animal Models in Vivo. Xylene-induced mouse ear edema was used to inspect the action of isogarcinol on inflammatory experiments in vivo. Figure 3 shows that isogarcinol reduced the ear edema induced by xylene. Oral administration of 100 mg/kg isogarcinol has a similar effect to that of aspirin on xylene-induced ear edema.

Effect of Isogarcinol on Anti-inflammation in Vitro. RAW 264.7 cells were cultured in 6-well plates at a density of 1×10^6/mL and treated with LPS (10 μg/mL) or a combination of LPS (10 μg/mL) and isogarcinol for 24 h. Then the supernatant was collect to test NO by Griess assay, and the cells were collected to test iNOS and COX-2 mRNA expression by real-time quantitative PCR. Panels A and C of Figure 4 show that isogarcinol significantly inhibited iNOS and COX-2 mRNA expression. Furthermore, isogarcinol suppressed NO production in the supernatant of RAW 264.7 cells (Figure4B). In this study, we tested the expression of IκB-α by Western blot in

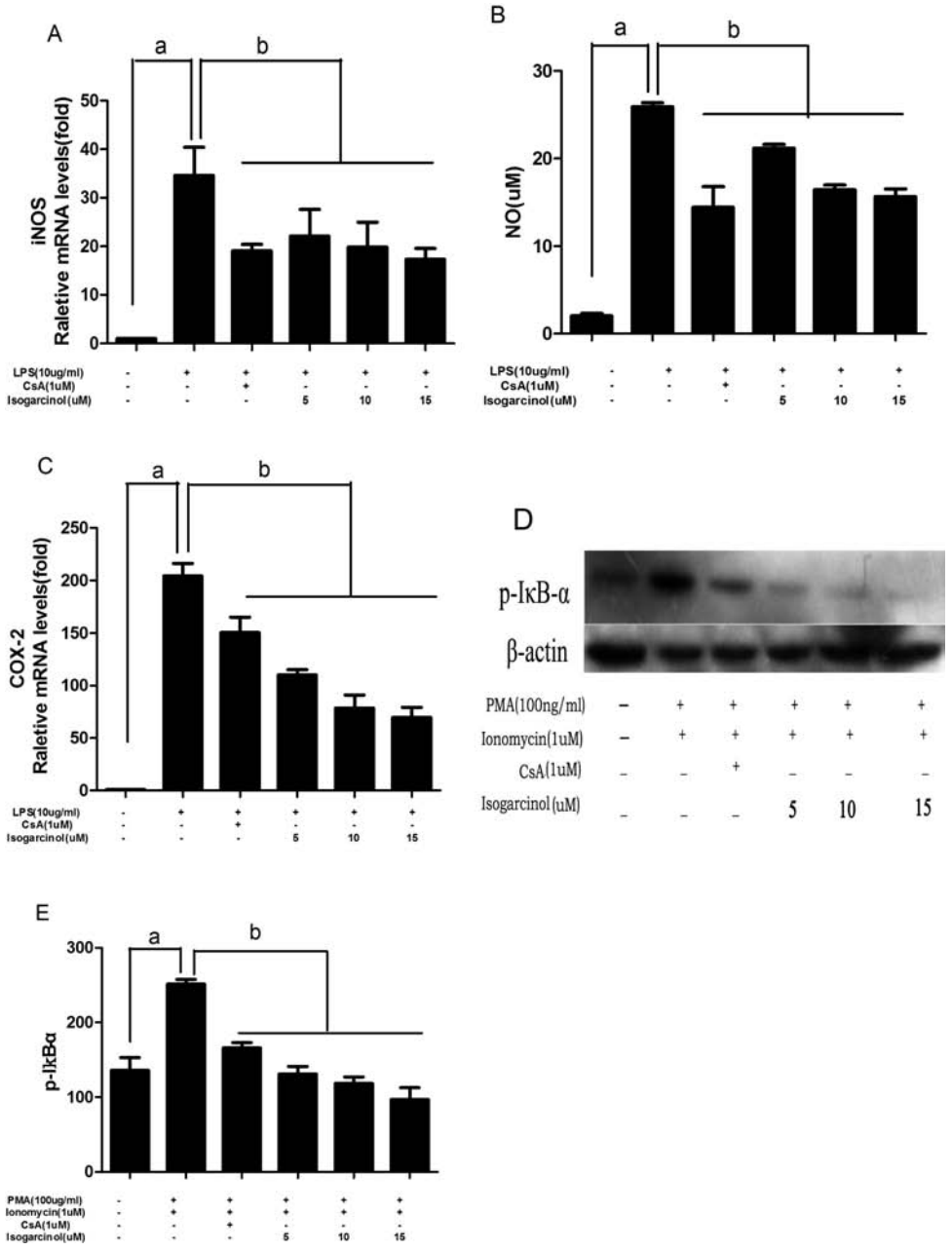

Figure 4. Anti-inflammatory mechanism of isogarcinol: (A) isogarcinol inhibited iNOS mRNA expression in RAW 264.7 cells; (B) isogarcinol inhibited the production of NO in RAW 264.7 cells; (C) isogarcinol inhibited COX-2 mRNA expression in RAW 264.7 cells; (D) effects of isogarcinol on the expression of p-iκb-α; (E) quantification of Western blot. All values are expressed as the mean ± SD of three independent experiments performed in triplicate (n = 3). Different letters above bars designate significant difference between groups, $P < 0.05$.

dx.doi.org/10.1021/jf405790q | J. Agric. Food Chem. 2014, 62, 4127−4134

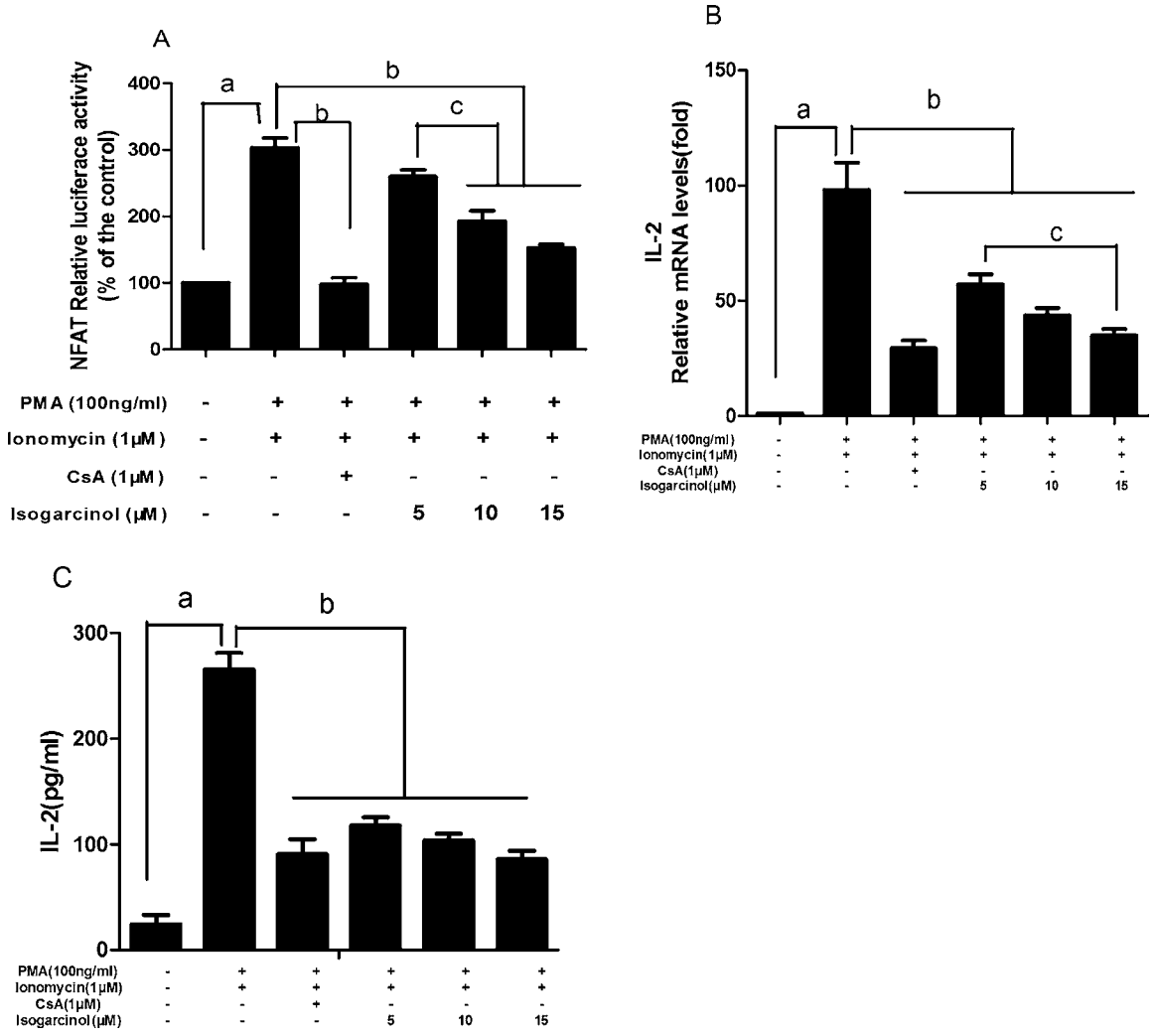

Figure 5. Immune regulation mechanism of isogarcinol: (A) isogarcinol suppressed NFAT activity; (B) inhibitory effect of isogarcinol on IL-2 activity; (C) inhibitory effect of isogarcinol on IL-2 expression. Results are mean values ± SD of three independent experiments performed in triplicate (n = 3). Different letters above bars designate significant difference between groups, $P < 0.05$.

Jurkat cells to determine whether isogarcinol affected NF-κB. As shown in Figure4D, the content of p-iκB increased with PMA and Ion stimulation and then decreased when treated with isogarcinol.

Effect of Isogarcinol on Immune Regulation in Vitro. CsA displays its immunosuppressive effect by inhibiting the NFAT/IL-2 signaling pathway. To determine whether isogarcinol influenced the NFAT/IL-2 signaling pathway, RAW 264.7 cells were treated with PMA + Ion or a combination of isogarcinol and PMA + Ion for 24 h. Then the supernatant was collect to test IL-2 by ELISA assay; the cells were collected to test NFAT and IL-2 mRNA expression using the dual-luciferase reporter gene assay and real-time quantitative PCR, respectively. The data in Figure5A suggest isogarcinol inhibition of NFAT and IL-2 mRNA expression (Figure 5B) and IL-2 content (Figure 5C).

■ DISCUSSION

In this study, we find that the immunosuppressant isogarcinol markedly inhibited joint swelling; significantly decreased clinical and pathological scores; reduced IL-1β, TNF-α, IL-17, and IL-6 levels in the serum; and prevented joint damage caused by collagen in DBA/1J mice. Pro-inflammatory cytokines such as IL-1β, TNF-α, and IL-6 are highly expressed in the rheumatoid joint and play key roles in the pathogenesis of RA.[22] IL-17 is a T cell-derived cytokine, which leads to angiogenesis, joint inflammation, cartilage destruction, and bone erosion; the inhibition of IL-17 limits inflammation and joint erosion in several animal models of arthritis.[23,24] Inhibition of the production of IL-17 may be one factor in the cartilage protection by isogarcinol.

Isogarcinol significantly decreased NO production and iNOS mRNA expression in the LPS-stimulated RAW 264.7 macrophages. NO is an essential messenger molecule produced during the inflammatory response by activated macrophages,[25] but overproduction of NO is associated with the initiation of apoptosis of chondrocytes.[26] The inhibition of excessive NO by the suppression of iNOS mRNA expression may be another factor in the cartilage protection of isogarcinol. It was reported that CN is necessary for iNOS expression,[27] and compounds that inhibit the iNOS enzymatic level have anti-inflammatory effects.[28] COX-2, which is an inducible isoform and catalyzes the rate-limiting step in the oxidation of arachidonic acid to prostaglandins, plays a major role in inflammatory reactions and is responsible for the characteristic inflammatory symptoms.[29] COX-2 and iNOS are important inducible enzymes that mediate inflammatory processes; isogarcinol significantly

dx.doi.org/10.1021/jf405790q | J. Agric. Food Chem. 2014, 62, 4127−4134

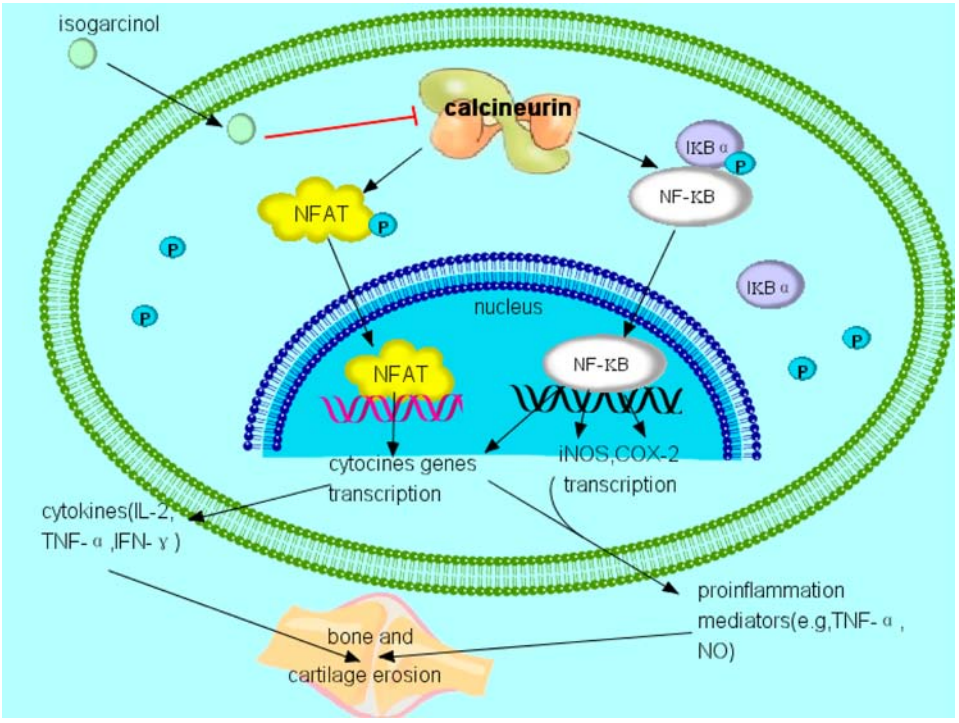

Figure 6. Mechanism of action of isogarcinol. The green, round cell membrane represents the membrane of the immune cell, and the semicircular blue membrane represents the nuclear membrane. CN activates the transcription factors, NFAT and NF-κB, which transcribe cytokines and inflammatory inducible enzyme (iNOS, COX2) genes, respectively, and then the expression of inflammatory factors, such as IL-1β, TNF-α, IL-6, and NO, which lead to articular bone and cartilage erosion. Isogarcinol is an inhibitor of CN; it inhibits CN activity and then inhibits NFAT and NF-κB transcription inflammatory factors and thus exerts its immune regulation and anti-inflammatory effects.

inhibited iNOS and COX-2 levels, decreased NO production, and reduced ear edema induced by xylene. Therefore, isogarcinol is an effective anti-inflammatory agent, and these findings may explain why isogarcinol inhibits chronic inflammatory arthritis.

NF-κB plays an important role in the inflammatory response, and it regulates the expression of numerous components in the immune system, including IL-2, pro-inflammatory cytokines (IL-6, IL-1β, and TNF-α), and inducible enzymes (iNOS and COX2).[30] In rest cells, NF-κB is constitutively localized in the cytosol with an inhibitory protein called inhibitor κB (IκB). The degradation and phosphorylation of IκB-α is necessary to release NF-κB from the cytoplasmic NF-κB/IκB-α complex and allow its subsequent translocation to the cell nucleus.[31] Nuclear factor-κB acts at the crossroads of many signaling pathways; the excessive activation of NF-κB can lead to inflammatory and autoimmune diseases or cancers.[32] NF-κB plays an important role in the pathogenesis of RA, its mainly pro-inflammatory regulators TNF-α, IL-1β, and IL-6, linked directly to cartilage degradation and bone erosion in RA.[33,34] It was reported that oral administration of NF-κB inhibitors could attenuate CIA.[35] In recent years, there has been extensive research on the connection between inflammation and cancer; inhibition of NF-κB could inhibit inflammation and reduce the incidence of cancer.[36,37] It was reported that garcinol possesses anti-inflammatory and anticancer activities.[38,39] In this study, we found that isogarcinol significantly inhibited inflammatory cytokines, COX-2 ,iNOS, and NF-κB expression, and it may be effective as an anticancer agent, but this requires further study.

The NF-κB pathway is a key regulator in the development of regulatory T cell (Tregs).[40] Tregs are crucial for restoring immune tolerance, and they are likely to play a regulatory role in RA.[41] Isogarcinol inhibited $CD4^+$ and $CD4^+$ $CD25^+$ in spleen cells stimulated by ConA (data not shown here). It was reported that NF-κB can be activated by CN and that the activity of CN was strongly correlated with the severity of arthritis in an RA animal model.[42] We find that isogarcinol inhibited CN activity but did not influence CN content in Jurkat cells (data not shown here). Glycyrol, another immunosuppressant screened by our group with CN as its target enzyme, has an action similar to that of isogarcinol on RA. It was reported that immunosuppressive and anti-inflammatory effects of curcumin were achieved by inhibiting NFAT and NF-κB signal pathways through blocking Ca^{2+} mobilization.[43]

NF-κB is only one of many CN substrates; NFAT is the main substrate of CN in immune cells. CN and NFAT regulate the expression of a large number of cytokines and cell-surface receptors that are essential for a productive immune response.[44,45] Despite the lack of structural similarity between FK506 and CsA, the mechanisms of action of these two drugs are very similar as they both inhibit CN and NFAT to exert their immune-suppressive effects. We found that isogarcinol inhibits NFAT activity and IL-2 expression. To summarize our experimental data and referenced studies mentioned above, we draw a possible mechanism of action of isogarcinol in RA (Figure 6). CN activates the transcription factors, NFAT and NF-κB, which transcribe cytokines and inflammatory inducible enzyme (such as iNOS and COX-2) genes, respectively, and then the expression of inflammatory factors, such as IL-1β, TNF-α, IL-6, and NO, which lead to articular bone and cartilage erosion. As an inhibitor of CN, isogarcinol inhibits CN activity and then inhibits NFAT and NF-κB transcription inflammatory factors and thus plays its immune regulation and anti-inflammatory roles.

RA is a Th1-mediated autoimmune disease that is characterized by chronic inflammatory symptoms, so we wanted to

ensure anti-inflammation or immunosuppression, which are the major mechanisms of action of isogarcinol in RA. To date, the actual mechanism is not clear because inflammation and immunity are inseparable at the cellular and molecular levels of many chronic inflammatory diseases; inflammation and immunity are two aspects of one issue, and they overlap but are inseparable. However, what is clear is that the use of anti-inflammatory drugs or immunosuppressive drugs alone is not effective. The development and application of drugs that combine anti-inflammatory activity and immune regulatory activity will be main research aims. In this study, we found both immunosuppression and anti-inflammatory effects of isogarcinol extracted from mangosteen fruit; therefore, we expect that this compound will become a potential drug candidate for RA.

Overall, isogarcinol is a low toxicity, peroral compound that we extracted from mangosteen fruit; the experimental data in this study showed that it is effective as an antiarthritis agent, and the therapeutic effect was associated with the down-regulation of both the inflammatory and autoimmune reactions.

AUTHOR INFORMATION

Corresponding Author

*(Q.W.) Phone: 86-010-58807365. Fax: 86-010-58807365. E-mail: weiq@bnu.edu.cn.

Author Contributions

‖Y.F. and H.Z. contributed equally to this work.

Funding

The work was supported by the National Natural Science Foundation of China, the National Important Novel Medicine Research Project, and the Fundamental Research Funds for the Central Universities.

Notes

The authors declare no competing financial interest.

ABBREVIATIONS USED

CIA, collagen-induced arthritis; CN, calcineurin; CsA, cyclosporine A; FK-506, tacrolimus; iNOS, inducible nitric oxidase synthase; Ion, Ionomycin; LPS, lipopolysaccharide; NFAT, nuclear factor of activated T cells; NF-κB, nuclear transcription factor kappa B; RA, rheumatoid arthritis

REFERENCES

(1) Feskanich, D.; Ziegler, R. G.; Michaud, D. S.; et al. Prospective study of fruit and vegetable consumption and risk of lung cancer among men and women. *J. Natl. Cancer Inst.* **2000**, *92*, 1812−1823.

(2) Kondo, M.; Zhang, L.; et al. Bioavailability and antioxidant effects of a xanthone-rich mangosteen (*Garcinia mangostana*) product in humans. *J. Agric. Food Chem.* **2009**, *57*, 8788−8792.

(3) Jung, H. A.; Su, B. N.; Keller, W. J.; Mehta, R. G.; Kinghorn, A. D. Antioxidant xanthones from the pericarp of *Garcinia mangostana* (mangosteen). *J. Agric. Food Chem.* **2006**, *54*, 2077−2082.

(4) Pedraza-Chaverri, J.; Cárdenas-Rodríguez, N.; Orozco-Ibarra, M.; Pérez-Rojas, J. M. Medicinal properties of mangosteen (*Garcinia mangostana*). *Food Chem Toxicol.* **2008**, *46*, 3227−3239.

(5) Smolen, J. S.; et al. New therapies for the treatment of rheumatoid arthritis. *Lancet* **2007**, *370*, 1861−1874.

(6) Mount, C.; Featherstone, J. Rheumatoid arthritis market. *Nat. Rev. Drug Discovery* **2005**, *4*, 11−12.

(7) Sadiq, U.; Asif, M.; Mir, S.; et al. Anti-inflammatory and antioxidant activity of Trachyspermumammi seeds in collagen induced arthritis in rats. *Int. J. Drug, Dev. Res.* **2012**, *4* (1), 210−219.

(8) Dass, S. V.; Byoung, S. K. Targeting TNF superfamily members for therapeutic intervention in rheumatoid arthritis. *Cytokine* **2012**, *57*, 305−312.

(9) Smolen, J. S.; Steiner, G. Therapeutic strategies for rheumatoid arthritis. *Nat. Rev. Drug Discovery* **2003**, *2*, 473−488.

(10) Bornadata, B.; Brazil, M. Adalimumab. *Nat. Rev. Drug Discovery* **2003**, *2*, 693−694.

(11) Scott, L. J.; McKeage, K.; et al. Tacrolimus: a further update of its use in the management of organ transplantation. *Drugs* **2003**, *63*, 1247.

(12) McInnes, I. B.; Schett, G. Cytokines in the pathogenesis of rheumatoid arthritis. *Nat. Rev. Immunol.* **2007**, *7*, 429−442.

(13) Wang, K.; Chen, L.; Tseng, S.; et al. Anti-inflammatory effects of resveratrol and oligostilbenes from *Vitis thunbergii* var. *taiwaniana* against lipopolysaccharide-induced arthritis. *J. Agric. Food Chem.* **2011**, *59*, 3649−3656.

(14) Lei, H.; Luo, J.; Tong, L.; et al. Quercetin binds to calcineurin at a similar region to cyclosporin A and tacrolimus. *Food Chem.* **2011**, *127*, 1169−1174.

(15) Peng, L.; Qi, Y.; Wu, H.; Wei, Q. Interaction of glycyrol with calcineurin A studied by spectroscopic methods and docking. *IUBMB Life* **2011**, *63* (1), 14−20.

(16) Cen, J.; Shi, M.; Yang, Y.; Fu, Y.; et al. Isogarcinol is a new immuno-suppressant. *PLoS One* **2013**, DOI: 10.1371/journal.-pone.0066503.

(17) Rusnak, F.; Mertz, P. Calcineurin: form and function. *Physiol Rev.* **2000**, *80*, 1483−1521.

(18) Baksh, S.; Burakoff, S. J. The role of calcineurin in lymphocyte activation. *Semin. Immunol.* **2000**, *12*, 405−415.

(19) Brand, D. D.; Latham, K. A.; Rosloniec, F. Collagen-induced arthritis. *Nat. Protoc.* **2007**, *2*, 1269−1275.

(20) Seung-A, Y.; et al. Calcineurin is expressed and plays a critical role in inflammatory arthritis. *J. Immunol.* **2006**, *177*, 2681−2690.

(21) Man, S.; Wang, J.; Gao, W.; Guo, L. Y; et al. Chemical analysis and anti-inflammatory comparison of the cell culture of *Glycyrrhiza* ith its field cultivated variety. *Food Chem.* **2013**, *136*, 513−517.

(22) Kim, H. S.; Kim, A. R.; Park, H. J.; Park, D. K.; Kim do, K.; et al. *Morus bombycis* Koidzumi extract suppresses collagen-induced arthritis by inhibiting the activation of nuclear factor-κB and activator protein-1 in mice. *J. Ethnopharmacol.* **2011**, *136*, 392−398.

(23) Lubberts, E.; van den Bersselaar, L.; et al. IL-17 promotes bone erosion in murine collagen-induced arthritis through loss of the receptor activator of NF-κB ligand/osteoprotegerin balance. *J. Immunol.* **2003**, *170*, 2655−2662.

(24) van den Berg, W. B.; Moissec, P. IL-17 as a future therapeutic target for rheumatoid arthritis. *Nat. Rev. Rheumatol.* **2009**, *5*, 549−553.

(25) Jacobs, A. T.; Ignarro, L. J. LPS-induced expression of IFN-β mediates the timing of iNOS induction in RAW264.7 macrophages. *J. Biol. Chem.* **2001**, *276* (57), 47950−47957.

(26) Bogdan, C. Nitric oxide and the immune response. *Nat. Immunol.* **2001**, *2*, 907−916.

(27) Eun, M. S.; Zhou, H. Y.; et al. Anti-inflammatory effects of glycyrol isolated from *Glycyrrhiza uralensis* in LPS-stimulated RAW264.7 macrophages. *Int. Immunopharmacol.* **2008**, *8*, 1524−1532.

(28) Vallance, P.; Leiper, J. Blocking NO synthesis: how, where and why? *Nat. Rev. Drug Discovery* **2002**, *1*, 939−950.

(29) Liao, C. H.; Liang, Y. C.; Lin, J. K. Suppression of inducible nitric oxide synthase and cyclooxygenase-2 in downregulating nuclear factor-κB pathway by garcinol. *Mol. Carcinog.* **2004**, *41*, 140−149.

(30) Li, Q.; Verma, I. M. NF-κB regulation in the immune system. *Nat. Rev. Immunol.* **2002**, *2*, 725−734.

(31) Hyuck, S.; et al. Licochalcone A isolated from licorice suppresses lipopolysaccharide-stimulated inflammatory reactions in RAW264.7 cells and endotoxin shock in mice. *J. Mol. Med.* **2008**, *86*, 1287−1295.

(32) Moynagh, P. N. The NF-κB pathway. *J. Cell Sci.* **2005**, *118*, 4389−4392.

(33) Karmakar, S.; Kay, J.; Gravallese, E. M. Bone damage in rheumatoid arthritis: mechanistic insights and approaches to prevention. *Rheum. Dis. Clin. North Am.* **2010**, *36*, 385.

(34) Goldring, S. R. Bone and joint destruction in rheumatoid arthritis: what is really happening? *J. Rheumatol. Suppl.* **2002**, *65*, 44.

(35) Lansdell, T. A.; O'Reilly, S.; Woolliscroft, T.; et al. Attenuation of collagen-induced arthritis by orally available imidazoline-based NF-κB inhibitors. *Bioorg. Med. Chem. Lett.* **2012**, *3*, 1−4.
(36) Balkwill, F.; Mantovani, A. Inflammation and cancer: back to Virchow? *Lancet* **2001**, *357*, 539−545.
(37) Baud, V.; Karin, M. Is NF-κB a good target for cancer therapy? Hopes and pitfalls. *Nat. Rev. Drug Discovery* **2009**, *8* (1), 33−40.
(38) Hong, L.; et al. Mechanisms of growth arrest by zinc ribbon domain-containing 1 in gastric cancer cells. *Carcinogenesis* **2007**, *28* (8), 1622−1628.
(39) Yu, S. Y.; Liao, C. H.; Chien, M. H.; et al. Induction of $p21^{Waf1/Cip1}$ by garcinol via downregulation of p38-MAPK signaling in p53-independent H1299 lung cancer. *J. Agric. Food Chem.* **2014**, *62*, 2085−2095.
(40) Long, M.; Park, S.-G.; Strickland, I.; Hayden, M. S.; Ghosh, S. Nuclear factor-κB modulates regulatory T cell development by directly regulating expression of Foxp3 transcription factor. *Immunity* **2009**, *31*, 921−931.
(41) Prakken, B.; Wehrens, E.; van Wijk, F. Quality or quantity? Unraveling the role of Treg cells in rheumatoid arthritis. *Arthritis Rheum.* **2013**, *3*, 552−554.
(42) Gopa, B.; Hindupur, K. A.; Mone, Z.; et al. Mitochondria to nucleus stress signaling: a distinctive mechanism of NF-κB/Rel activation through calcineurin-mediated inactivation of IκB. *J. Cell Biol.* **2003**, *161*, 507−519.
(43) Kliem, C.; Merling, A.; Giaisi, M.; et al. Curcumin suppresses T cell activation by blocking Ca^{2+} mobilization and nuclear factor of activated T cells (NFAT) activation. *J. Biol. Chem.* **2012**, *287*, 10200−10209.
(44) Clipstone, N. A.; Crabtree, G. R. Calcineurin is a key signaling enzyme in T lymphocyte activation and the target of the immunosuppressive drugs cyclosporin A and FK506. *Ann. N. Y. Acad. Sci.* **1993**, *696*, 20−30.
(45) Kiani, A.; Rao, A.; Aramburu, J. Manipulating immune responses with immunosuppressive agents that target NFAT. *Immunity* **2000**, *12*, 359−372.

JOURNAL OF AGRICULTURAL AND FOOD CHEMISTRY

Article

pubs.acs.org/JAFC

Kinetics and Molecular Docking Studies of the Inhibitions of Angiotensin Converting Enzyme and Renin Activities by Hemp Seed (*Cannabis sativa* L.) Peptides

Abraham T. Girgih,[†] Rong He,[†,‡] and Rotimi E. Aluko*[,†]

[†]Department of Human Nutritional Sciences and The Richardson Centre for Functional Foods and Nutraceuticals, University of Manitoba, Winnipeg, Manitoba R3T2N2, Canada

[‡]College of Food Science and Engineering, Nanjing University of Finance and Economics, Nanjing 210046, People's Republic of China

ABSTRACT: Four novel peptide sequences (WVYY, WYT, SVYT, and IPAGV) identified from an enzymatic digest of hemp seed proteins were used for enzyme inhibition kinetics and molecular docking studies. Results showed that WVYY (IC_{50} = 0.027 mM) was a more potent ($p < 0.05$) ACE-inhibitory peptide than WYT (IC_{50} = 0.574 mM). However, WYT (IC_{50} = 0.054 mM) and SVYT (IC_{50} = 0.063 mM) had similar renin-inhibitory activity, which was significantly better than that of IPAGV (IC_{50} = 0.093 mM). Kinetics studies showed that WVYY had a lower inhibition constant (K_i) of 0.06 mM and hence greater affinity for ACE when compared to the 1.83 mM obtained for WYT. SVYT had lowest K_i value of 0.89 mM against renin, when compared to the values obtained for WYT and IPAGV. Molecular docking results showed that the higher inhibitory activities of WVYY and SVYT were due to the greater degree of noncovalent bond-based interactions with the enzyme protein, especially formation of higher numbers of hydrogen bonds with active site residues.

KEYWORDS: *hemp seed, antihypertensive peptides, angiotensin-converting enzyme, renin, enzyme inhibition kinetics, molecular docking*

INTRODUCTION

Food-protein-derived peptides have been shown to exert a variety of bioactivities during in vitro and in vivo testing as antioxidant,[1−3] antihypertensive,[4−6] and immunomodulatory[7,8] agents. Other works have also produced food-protein-derived peptides with antibacterial,[9−11] anticancer,[12−14] antidiabetic,[15−17] and anti-inflammatory[18−20] properties. These bioactive peptides could be generated from animal and plant sources through enzymatic hydrolysis of the isolated proteins with single or a combination of proteases. In this respect, several studies have produced natural antihypertensive peptides that may be used to prevent or manage hypertension.[5,21−24] The use of natural peptide sequences as antihypertensive agents is attractive because in some patients pharmaceutical drugs have been reported to cause undesirable side effects and health complications, such as dry cough, edema, skin rashes, and diarrhea during prolonged administration.[25−27] Hypertension in human beings is regulated by the renin−angiotensin systems (RAS), which also ensures fluid homeostasis; a malfunctioning of this system could result in the development of chronic diseases such as hypertension, kidney failure, liver malfunction, diabetes, and cancer.[28] Three enzymes, namely, renin, angiotensin I converting enzyme (ACE), and chymase, are the key catalysts involved in the operation of RAS. The RAS operates as follows: renin, an aspartyl protease produced from the kidney, converts angiotensinogen (a product of the liver) into an inactive angiotensin I (AT-I).[29] Subsequently, ACE catalyzes the conversion of AT-I into a pro-hypertensive octapeptide and potent vasoconstrictor angiotensin II (AT-II). ACE also inactivates a vasodilator named bradykinin, which leads to increased vasopressive effects and contributes to blood pressure (BP) elevation.[29] Studies have shown that prolonged therapy with ACE-inhibitory antihypertensive drugs leads to AT-I accumulation and could activate an alternate pathway involving chymase, which is also capable of converting AT-I to AT-II independent of ACE; such a reaction can result in the failure of the antihypertensive drug therapy.[30] In contrast, there is growing evidence that direct inhibition of renin could offer a better control of elevated BP than ACE because accumulation of AT-I in substantial amounts that could be converted to AT-II in some organs via an ACE-independent pathway catalyzed by chymase is prevented. However, sole inhibition of renin may not prevent ACE-catalyzed bradykinin degradation; therefore, a dual strategy for inhibition of renin and ACE simultaneously is suggested to be the more effective therapy for BP control when compared to single ACE therapy approach.[31]

Currently, our main research focus is to purify and identify food-based antihypertensive or bioactive substances that would possess dual ability to inhibit renin and ACE activities. Recently, a number of antihypertensive peptides with multifunctional properties capable of inhibiting ACE and renin enzymes in vitro and in vivo conditions have been produced from various plant and animal food sources. Peptides with dual ability to inhibit ACE and renin have through enzymatic hydrolysis been identified from seaweeds,[32] yellow field pea

Received: January 15, 2014
Revised: April 2, 2014
Accepted: April 15, 2014
Published: April 15, 2014

ACS Publications © 2014 American Chemical Society

seeds,[33] flaxseed,[34] rapeseed,[21] and hemp seed.[35,36] Previous work also showed that a pea protein hydrolysate reduced renal renin mRNA production in a chronic kidney disease rat model after 8 weeks of oral diet intake.[37] Our previous work has shown that dietary inclusion of a multifunctional hemp seed protein hydrolysate was effective in the prevention and management of hypertension in spontaneously hypertensive rats.[38] We have also determined the amino acid sequence of peptides that may be responsible for the antihypertensive effect of hemp seed protein hydrolysate and confirmed BP-reducing effects of the peptides in spontaneously hypertensive rats (SHR).[36] Despite the potential bioactive properties as well as health benefits of hemp seed peptides, there is paucity of information in the area of structure−function of blood-pressure-lowering peptides as well as enzyme inhibition kinetics studies. Structure−function studies will provide new information on the relationships of amino acid composition and sequence with antihypertensive activity, which could enhance method development to produce potent peptides from food proteins. Information from structure−function studies could also enhance development of novel and potent peptidomimetics using known peptide sequences as templates. Kinetic studies will provide useful information to decide the optimal dose of the peptide needed to achieve maximal preventive effects. In addition, the mode of inhibition of ACE and renin activities when determined by kinetics and molecular docking studies will provide additional information for structure−function studies of antihypertensive peptides. Therefore, the objective of this study was to determine the kinetics of ACE and renin inhibitions as well as potential enzyme−ligand binding configurations by four hemp seed peptides that have been shown to reduce systolic BP in SHR.

MATERIALS AND METHODS

Materials. *N*-[3-(2-Furyl)acryloyl]phenylalanylglycylglycine (FAPGG) and ACE from rabbit lung (EC 3.4.15.1) were purchased from Sigma-Aldrich (St. Louis, MO). Human recombinant Renin Inhibitor Screening Assay Kit was purchased from Cayman Chemicals (Ann Arbor, MI). Hemp seed protein-derived peptide sequences (WYT, WVYY, SVYT, and IPAGV) with demonstrated antihypertensive effects in SHR[36] were synthesized (>95% purity) by GenWay Biotech (GenWay Biotech Inc., San Diego, CA).

Kinetics of ACE Inhibition. The ability of WYT and WVYY to inhibit in vitro activity of ACE was measured in triplicates as previously reported.[34] Briefly, 1 mL of 0.5 mM FAPGG (dissolved in 50 mM Tris−HCl buffer containing 0.3 M NaCl, pH 7.5) was mixed with 20 μL of ACE (final activity of 20 mU) and 200 μL of peptide in 50 mM Tris−HCl buffer. The rate of decrease in absorbance at 345 nm was recorded for 2 min at room temperature. Tris−HCl buffer was used instead of peptide solutions in the blank experiment. ACE activity was expressed as a rate of reaction (ΔA/min) and inhibitory activity was calculated using the equation below

$$\text{ACE inhibition (\%)} = [[(\Delta A/\text{min})_{\text{blank}} - (\Delta A/\text{min})_{\text{sample}}] / (\Delta A/\text{min})_{\text{blank}}] \times 100$$

where $(\Delta A/\text{min})_{\text{sample}}$ and $(\Delta A/\text{min})_{\text{blank}}$ are the ACE activity in the presence and absence of peptides, respectively. The concentration of each peptide that inhibited ACE activity by 50% (IC_{50}) was calculated using nonlinear regression from a plot of percentage ACE inhibition versus peptide concentration. The kinetics of ACE inhibition was studied with 0.0625, 0.125, 0.25, and 0.5 mM FAPGG. The mode of ACE inhibition was determined from the Lineweaver−Burk plots, while inhibition constant (K_i) was calculated as the *X*-axis intercept from a plot of the slope of the Lineweaver−Burk lines against peptide concentration.[39]

Kinetics of Renin Inhibition. In vitro inhibition of human recombinant renin activity was conducted according to the previously described method,[33] using the Renin Inhibitor Screening Assay Kit. Prior to the assay, renin buffer was diluted with 50 mM Tris-HCl, pH 8.0, containing 100 mM NaCl. The renin protein solution was diluted 20 times with assay buffer before use, and the assay buffer was prewarmed to 37 °C before the reaction was initiated in a fluorometric microplate reader (Spectra MAX Gemini, Molecular Devices, Sunnyvale, CA) maintained at 37 °C. Before the reaction, (1) 20 μL of substrate, 160 μL of assay buffer, and 10 μL of Milli-Q water were added to the background wells; (2) 20 μL of substrate, 150 μL of assay buffer, and 10 μL of Milli-Q water were added to the control wells; and (3) 20 μL of substrate, 150 μL of assay buffer, and 10 μL of peptide samples (WYT, SVYT, or IPAGV) were added to the inhibitor wells. The reaction was initiated by adding 10 μL of renin to the control and sample wells. The microplate was shaken for 10 s to mix followed by incubation at 37 °C for 15 min; fluorescence intensity (FI) was recorded using excitation and emission wavelengths of 340 and 490 nm, respectively. The percentage inhibition was calculated as follows:

$$\text{inhibition\%} = \{[(\text{FI of control well}) - (\text{FI of sample well})] / (\text{FI of control well})\} \times 100$$

The peptide concentration that inhibited 50% of renin activity was determined and defined as the IC_{50} value and was calculated by nonlinear regression as performed for ACE. The renin inhibition kinetics studies were conducted using 0.625, 1.25, 2.5, 5, and 10 μM of substrate in the absence and presence of peptides. Lineweaver−Burk plots were used to calculate inhibition constant as described above for ACE.

Molecular Docking Studies. Molecular docking was performed using Accelrys Discovery Studio software 2.5 (DS 2.5) as previously described.[40] The structures of WYT, WVYY, SVYT, and IPAGV were generated with DS 2.5, and the energy was minimized with the CHARMm program. For ACE docking, a crystal structure of human ACE bound with lisinopril (an ACE-inhibitory drug) (PDB ID 1O8A) was used as ACE molecule. A binding site was created by the digital removal of lisinopril with the radius of 15 Å, and coordinates x = 41.268, y = 34.559, z = 45.393. Automated molecular docking was performed using the partial flexibility CDOCKER tool of the DS 2.5 software in the presence of cofactors (zinc and chloride ions). For renin docking, a crystal structure of human renin bound with aliskiren (a renin-inhibitory drug) (PDB ID 2V0Z) was used. All the water molecules present in the protein except two water molecules (H_2O184 and H_2O250) and aliskiren were digitally removed and hydrogen atoms were added to the protein structure. A binding site was created using a radius of 10 Å around the ligand and with coordinates x = 7.568, y = 46.092, z = 68.842.[41] Evaluation of the molecular docking was performed according to the scores and binding-energy value in order to obtain the best poses for peptides. DS 2.5 software was also used to identify the hydrogen bonds as well as the hydrophobic, hydrophilic, electrostatic, and coordination interactions between residues located at the ACE and renin active sites.

Statistical Analysis. Enzyme inhibition assays were conducted in triplicates and analyzed by one-way analysis of variance. Data are reported as mean ± standard deviation. Statistical significance of differences was evaluated by Duncan's multiple range test ($p < 0.05$) using the Statistical Analysis Systems software version 9.2 (SAS, Cary, NC).

RESULTS AND DISCUSSION

ACE- and Renin-Inhibitory Activities of Hemp Seed Peptides. Figure 1A shows that the ACE-inhibitory IC_{50} values for WVYY and WYT were 0.027 and 0.574 mM, respectively ($p < 0.05$). These IC_{50} values are lower than the values previously reported for pea dipeptides IR (2.25 mM), KF (7.23 mM), and EF (2.98 mM).[33] The IC_{50} value for WYT is similar to 0.3−0.7 mM but higher than the 0.115−0.129 mM values reported for various mushroom peptides.[42] However, the IC_{50} value for WVYY shows

dx.doi.org/10.1021/jf5002606 | J. Agric. Food Chem. 2014, 62, 4135−4144

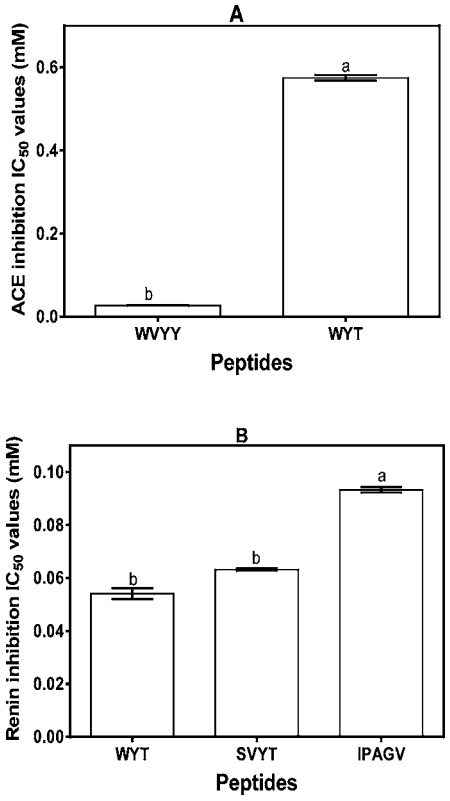

Figure 1. Inhibitory concentration of synthesized hemp seed peptides that reduced 50% (IC_{50}) in vitro activity of (A) ACE and (B) renin. Bars with different letters have mean values that are significantly different at $p < 0.05$. Values are means ± SD ($n = 3$).

that this peptide is a better ACE inhibitor than the mushroom peptides. The strong ACE-inhibitory activities exhibited by WVYY are consistent with earlier reported results, which showed that the presence of hydrophobic or aromatic amino acid residues such as phenylalanine, tyrosine, and proline at the C-terminal of peptides positively contributed toward the enhancement of ACE-inhibitory activities.[43,44] Hayes et al.[45] reported the identification of a range of novel propeptide angiotensin converting enzyme inhibitors in a casein fermentate produced by the action *Lactobacillus animalis* DPC6134. The casein fermentate peptides showed showed a correlation between the C-terminal tripeptide sequences and degree of ACE inhibition. In particular, binding of casein fermentate peptides to ACE active sites was shown to be influenced by the hydrophobicity of the three C-terminal amino acid residues, with aromatic or branched side chain amino acid residues being preferred. Thus, the presence of valine (V) in the tripeptide C-terminal sequence of WVYY may have contributed to the strong ACE-inhibitory properties of this peptide. The availability of two bulky tyrosine (Y) groups at the C-terminal may also have potentiated stronger inhibition of ACE activities when compared to WYT that has a hydrophilic amino acid threonine (T) at the C-terminal. Moreover, on the basis of other studies,[46−48] the presence of a branched-chain aliphatic amino acid such as valine at the N-terminal as well as the availability of an ionizable functional group (e.g, in tryptophan, W) may have also contributed to making WVYY a better ACE inhibitor than WYT.

Renin catalyzes the first and rate-limiting step that initiates production of vasoconstricting peptides responsible for BP elevation; therefore, down-regulation of renin's activity may enhance vasodilation. To the best of our knowledge, there is scanty information about the properties and occurrence of renin-inhibitory peptides from natural sources. Currently, there is only one known commercially available potent nonpeptidic renin inhibitor (aliskerin, IC_{50} = 0.6 nM), thus justifying the ongoing research for renin inhibitors from naturally occurring food sources. The IC_{50} values of the synthesized hemp seed peptides identified in this study with potent renin inhibitory properties are shown in Figure 1B. The tripeptide WYT exhibited the strongest inhibitory capacity with the lowest IC_{50} value of 0.054 mM when compared to the tetrapeptide (SVYT = 0.063 mM) and the pentapeptide (IPAGV = 0.093 mM). Renin-inhibitory IC_{50} values of the hemp seed peptides are very low when compared to the 9.20, 17.78, and 22.66 mM values for pea peptides IR, KF, and EF, respectively. Similarly, higher renin-inhibitory IC_{50} values were reported for rapeseed peptides RALP (0.968 mM), LY (1.868 mM), and TF (3.061 mM).[21] The potent renin-inhibitory data obtained in this study is in agreement with results from previous works that have suggested the presence of all or at least some of the following characteristics for good renin inhibition: one hydrophobic side chain at the N-terminal, bulky chains at the C-terminal, one

Table 1. Kinetics Constants of Enzyme-Catalyzed Reactions at Different Peptide Concentrations[a]

(A) Angiotensin-Converting Enzyme					
		WVYY		WYT	
catalytic parameter	control	0.04 mM	0.08 mM	0.21 mM	0.85 mM
V_{max} (ΔA/min)	0.014 ± 0.000	0.002 ± 0.000	0.006 ± 0.000	0.012 ± 0.000	0.008 ± 0.000
K_m (mM)	0.543 ± 0.004	0.841 ± 0.003	0.744 ± 0.003	0.870 ± 0.003	0.767 ± 0.001
CE	0.026 ± 0.000	0.002 ± 0.000	0.008 ± 0.000	0.014 ± 0.000	0.011 ± 0.000
K_i (mM)			0.06 ± 0.00 b		1.83 ± 0.03 a
(B) Renin					
		WY		SVYT		IPAGV	
catalytic parameter	control	0.43 mM	1.07 mM	0.43 mM	1.07 mM	0.43 mM	1.07 mM
V_{max} (FI/min)	87.56 ± 0.97	36.87 ± 0.14	16.42 ± 0.05	25.73 ± 0.26	16.57 ± 0.07	29.94 ± 0.03	17.84 ± 0.01
K_m (μM)	5.62 ± 0.28	4.63 ± 0.01	2.62 ± 0.01	4.90 ± 0.07	3.90 ± 0.04	4.86 ± 0.02	3.42 ± 0.04
CE	15.58 ± 0.82	7.96 ± 0.01	6.26 ± 0.01	5.25 ± 0.03	4.25 ± 0.02	6.15 ± 0.02	5.22 ± 0.06
K_i (mM)		1.93 ± 0.02 b			0.89 ± 0.01 c		6.17 ± 0.02 a

[a] K_m is the Michaelis constant, V_{max} is maximum reaction velocity, CE is the catalytic efficiency (V_{max}/K_m), and K_i is the enzyme−inhibitor dissociation constant.

dx.doi.org/10.1021/jf5002606 | J. Agric. Food Chem. 2014, 62, 4135−4144

hydrogen bond donor, and two hydrogen bond acceptors.[41,49,50] This is because the hemp seed peptides had most of these qualities as a result of the presence of P, L, Y, W, I, and V amino acid residues.

Kinetics of ACE Inhibition. A Lineweaver–Burk plot was used for the estimation of the modes of ACE inhibition by the hemp seed peptides, and results are shown in Figure 2 for

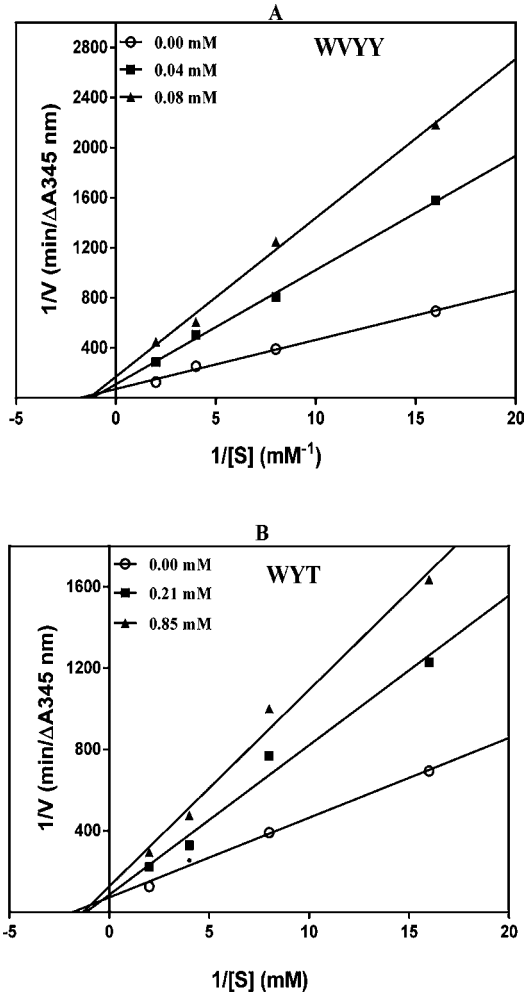

Figure 2. Lineweaver–Burk plots of angiotensin I-converting enzyme (ACE) inhibition by different concentrations of synthesized hemp seed peptides at varying substrate concentrations (0.0625–0.5 mM). V = the initial rate of reaction [ΔA_{345} (nm)/min].

WVYY (A) and WYT (B). From the linear regression fit of the kinetics data, the K_m value of ACE activity in the absence of the inhibiting peptide was estimated to be 0.543 mM (Table 1A). The K_m value was higher in the presence of peptides, which is an indication that more substrate was required for enzyme catalysis, and hence, the enzyme was less efficient. However, the K_m value reduced when peptide concentration was increased, which suggests that, at higher peptide levels, more peptides become bound to the enzyme active site to prevent formation of an enzyme–substrate complex. The V_{max} for uninhibited ACE reaction was 0.014 A min^{-1}, and this velocity decreased dose-dependently in the presence of peptides (WVYY and WYT), though WVYY appeared to be more effective (Table 1A). The lower V_{max} in the presence of WVYY is consistent with the higher potency (lower IC_{50} value) when compared to WYT as

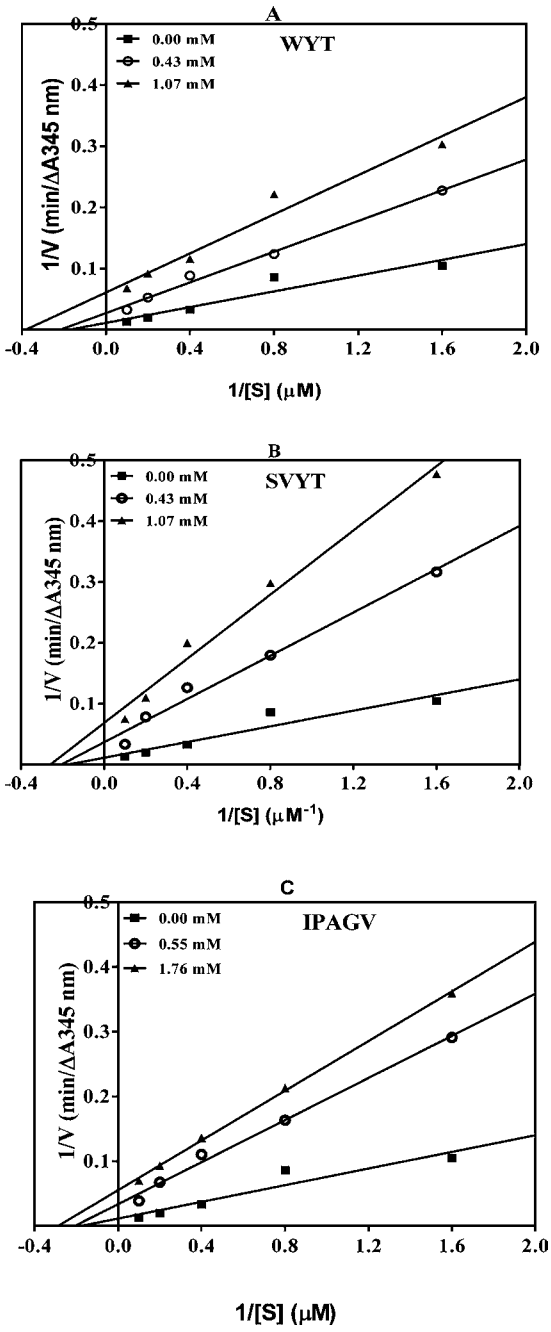

Figure 3. Lineweaver–Burk plots of the inhibition of human recombinant renin by different concentrations of synthesized hemp seed peptides at varying substrate concentrations (0.625–10 μM); V = initial rate of reaction (change in fluorescence intensity/min).

ACE inhibitors. Thus, the results indicate that the activation energy of the catalytic reaction was increased in the presence of WVYY and WYT because the rate of enzyme reaction was slowed down. The K_m and V_{max} values obtained in this study are slightly higher than those previously reported for hemp seed protein hydrolysate and its ultrafiltration membrane fractions.[35] The catalytic efficiency (CE) of the uninhibited ACE-catalyzed reaction was 0.026, which decreased in a dose-dependent manner in the presence of WVYY and WYT. The reduced CE is directly related to lower V_{max} and IC_{50} values, suggesting that the peptides had some binding affinity to the enzyme, which led to reduced catalytic ability. WVYY and WYT exhibited a

dx.doi.org/10.1021/jf5002606 | J. Agric. Food Chem. 2014, 62, 4135–4144

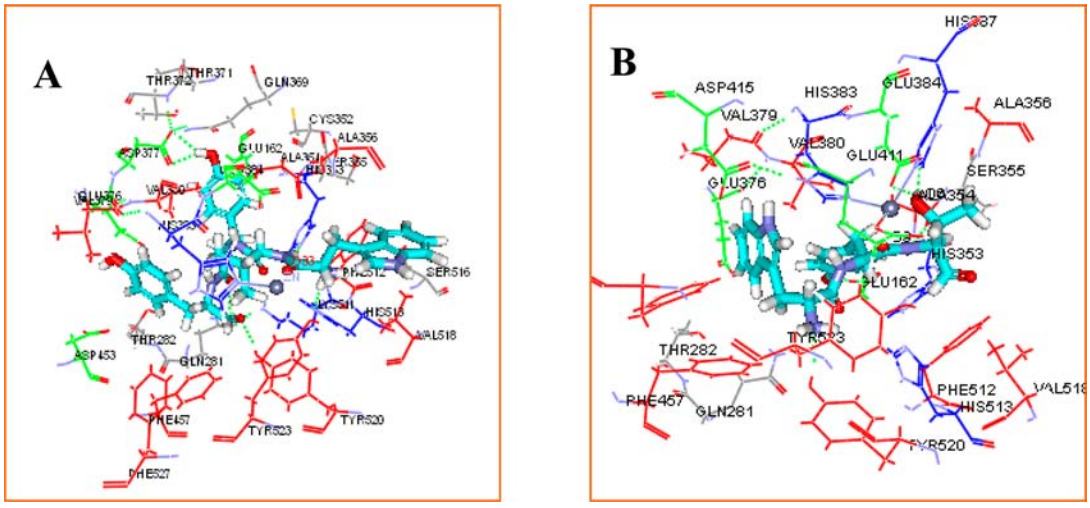

Figure 4. Automated molecular docking of WVYY (A) and WYT (B) at the angiotensin-converting enzyme (ACE) active site. ACE hydrophobic residues are represented in red, positively charged residues in blue, and negatively charged residues and hydrogen bonds in green, while other residues and the zinc atom are represented automatically. Image obtained with Accelrys DS Visualizer software.

Table 2. Residues of tACE Having at Least One Atom at a Distance of 3.5 Å around the Docked Peptide[a]

tACE residues	WVYY	WYT	lisinopril
Glu162	√	√	√
Gln281	√	√	√
Thr282	√	√	–
Cys352	√	–	–
His353	√	√	√
Ala354	√	√	√
Ser355	√	√	√
Ala356	√	√	√
Gln369	√	–	√
Thr371	√	–	–
Thr372	√	–	–
Glu376	√	√	–
Asp377	√	–	–
Val379	√	√	–
Val380	√	√	√
His383	√	√	√
Glu384	√	√	√
His387	–	√	√
Glu411	–	√	√
Asp415	–	√	–
Asp453	√	–	–
Phe457	√	√	√
Lys511	√	–	√
Phe512	√	√	√
His513	√	√	√
Val518	√	√	√
Tyr520	√	√	√
Tyr523	√	√	√
Phe527	√	√	√
total	26	22	20

[a]The residues around lisinopril in the tACE (PDB ID 1O86) are also shown.

Table 3. Hydrogen Bonds Observed between the Docked Top Ranked Pose of Peptides and tACE[a]

	no. of H-bonds and corresponding distance (Å)		
tACE residues involved in H-bonding[b]	WVYY	WYT	lisinopril
Glu162:OE1	–	–	1 (2.23)
Glu162:OE2	–	1 (2.18)	–
Gln281:HE22	2 (2.12, 2.21)	–	2 (2.18, 2.41)
His353:NE22	1 (2.21)	–	–
Ala354:O	–	1 (2.35)	1 (2.04)
Ala354:HN	–	–	1 (2.01)
Asp377:OD1	1 (2.09)	–	–
Asp377:OD2	1 (2.22)	–	–
Glu384:OE1	–	1 (2.31)	–
Glu384:OE2	–	1 (2.11)	1 (2.48)
Lys511:HZ1	–	–	1 (1.93)
His513:NE2	1 (2.192)	–	–
Tyr520:HH	1 (1.93)	1 (1.97)	1 (2.06)
Tyr522:OH	–	–	1 (2.42)
total	7	5	9

[a]The residue numbers belong to tACE (PDB ID 1O86). [b]H-bond position:donor or acceptor atoms. Repeated residues indicate formation of two separate H-bonds by the same amino acid. "E", "D", and "Z" represent the presence of other residues near the donor or acceptor atom.

mixed-type mode of enzyme inhibition, implying that the peptides bind to the ACE enzyme at positions that include both the active and nonactive sites in order to reduce catalytic activity. Binding to either the active or nonactive site would have, respectively, blocked substrate binding or produce enzyme conformations that reduced substrate affinity for the active site. The K_i of WVYY and WYT for ACE inhibition were calculated to be 0.039 mg/mL (0.06 mM) and 0.858 mg/mL (1.83 mM), respectively, which are lower than the 2.55−4.74 mg/mL (3.92−7.31 mM) values reported for the hemp seed protein hydrolysate and its membrane fractions,[35] indicating a stronger inhibitory capacity of the pure peptides in comparison to the peptide mixture. The lower K_i value for WVYY is consistent with the observed greater reductions in V_{max} and CE when compared to the reductions produced by WYT.

Renin-Inhibitory Kinetics. Parts A, B, and C of Figure 3 illustrate the double-reciprocal plots of the renin-catalyzed reaction in the absence or presence of WYT, SVYT, and IPAGV, respectively. These three peptide sequences were

dx.doi.org/10.1021/jf5002606 | J. Agric. Food Chem. 2014, 62, 4135−4144

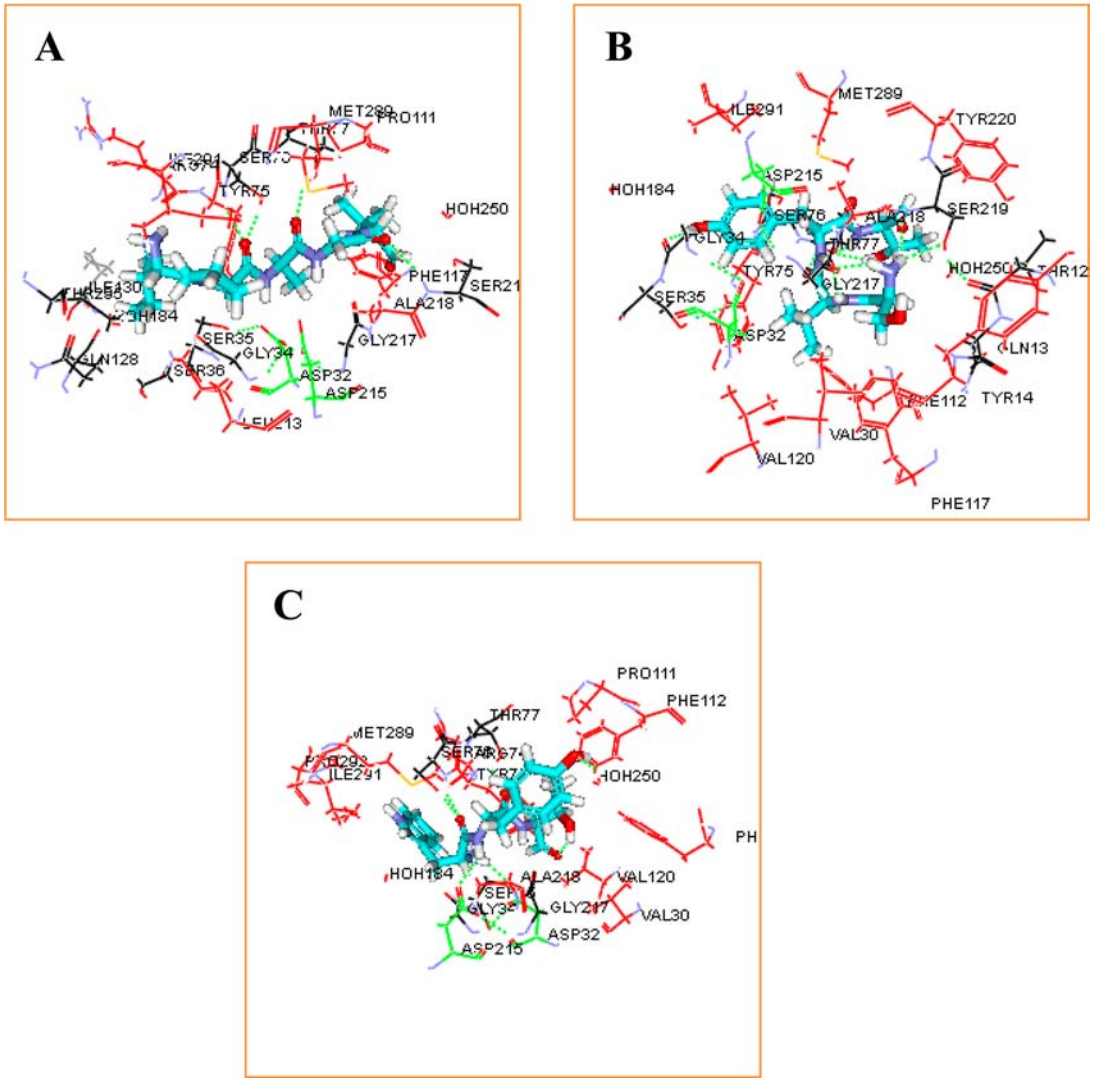

Figure 5. Automated molecular docking of IPAGV (A), SVYT (B), and WYT (C) at the renin active site. Renin hydrophobic residues are represented in red, hydrophilic residues are represented in black, and negatively charged residues and hydrogen bonds are represented in green, while other residues are represented automatically. Image obtained with Accelrys DS Visualizer software.

found to display mostly uncompetitive mode of renin inhibition. For example, the K_m of WYT showed a greater reduction from 4.631 to 2.623 μM when compared to the decrease in K_m observed for SVYT and IPAGV (Table 1B). SVYT, however, exhibited the lowest ranges of V_{max} (25.73−16.57 FI/min) and CE (5.249−4.247) values, which is an indication of reduced enzyme velocity in the presence of the peptide. The uncompetitive mode results suggest that the peptide bind mostly to the renin−substrate complex to cause reductions in the reaction velocity as well as the catalytic efficiency. It is presumed that the binding of the peptide to the renin−substrate complex is responsible for the simultaneous decreases in V_{max} and K_m values (Table 1). This is because the reduced effectiveness of the renin−substrate complex (reduced V_{max}) will lead to increased affinity of renin for the substrate and hence reduction in the K_m value. Renin inhibition by the peptides, which was reflected in the reduced CE as peptide level was increased, indicated the lower ability of the enzyme to convert the substrate into products. The lower K_i of SVYT indicated that this peptide may be able to more strongly bind to the renin−substrate complex (resistant to substrate-dependent dislodgement) when compared to WYT and IPAGV. The K_m for renin substrate in the absence of the inhibitor was determined to be 5.621 μM, which is higher than those from other studies, such as 1.3,[51] 4.416,[34] and 4.01 μM,[52] but is, however, lower than the 6.4 μM value reported by Yuan et al.[53] The difference in K_m values could be attributed to the different sources from which renin enzyme was procured for these studies and/or the variations in experimental conditions/approaches that may have been used.

Molecular Docking Studies. Figure 4 shows the best poses for the WVYY and WYT when present within the ACE catalytic site and in the presence of Zn^{2+}. The best pose for each peptide was stabilized mainly by electrostatic interactions and hydrophobic interactions that exist between amino acid residues of ACE and those of each peptide within a distance of 3.5 Å (Table 2). The poses were also stabilized by hydrogen bond formation with ACE amino acid residues (Table 3). WVYY had a higher number of total interactions (26) with ACE residues, which could have contributed to the higher inhibitory activity (lower IC_{50} value) when compared to WYT, which showed 22 interactions. This was confirmed by the lowest binding electrostatic energy value of −114.06 kJ/mol for WVYY when compared to −92.91 kJ/mol for WYT. Similarly,

dx.doi.org/10.1021/jf5002606 | J. Agric. Food Chem. 2014, 62, 4135−4144

the van der Waals energy of −5.23 kJ/mol was lower for WVYY when compared to −0.67 kJ/mol for WYT. The binding energy data agree with the fact that WVYY had higher ACE-binding affinity (lower K_i value) when compared to WYT, as shown in Table 1. The higher activity of WVYY may also be due to a higher degree of interactions with S1 (Ala354, Glu384, Tyr523 residues) and S2′ (Gln281, Tyr520, Lys511, His513, His353) subsites of the active site of ACE (Table 2). WVYY interacted with these S1 and S2′ subsites residues in a similar manner to the observed interactions between lisinopril and ACE.[54] In contrast, the weaker WYT interacted with all the ACE S1 and S2′ subsites residues with the exception of Lys511 (Table 2). As shown in Table 3, the ability of peptides to form multiple H-bond interactions with ACE could have contributed to peptide-induced inhibition of enzyme activity by stabilizing the noncatalytic enzyme−peptide complex structure. Similar results showing multiple H-bond formation between ACE-inhibitory peptides VPP or IPP and ACE residues have also been reported.[55] Also important is that the inhibitory capacity seem to be directly correlated to the number of H-bonds formed; lisinopril has the highest ACE-inhibitory activity and formed nine H-bonds, followed by WVYY (seven bonds) and WYT (five bonds). It is not only the number of H-bonds that seems to contribute to ACE-inhibitory potency of the peptides but also the ACE residues involved. This is because the more potent WVYY formed two H-bonds with Gln281 as well one H-bond each with His353 and His513 (Table 3), all amino acid residues that are critical components of the ACE active site. The weaker-acting WYT does not form any H-bond with Gln281, His353, and His513. The docking results also showed that the interactions between ACE-inhibitory pepitdes and Zn^{2+} at the enzyme active site also play a significant role in modulating catalysis, as previously suggested.[56] Figure 4 shows that WVYY and WYT were well-positioned to interact with the active site Zn^{2+} atom. Since the distance between the peptide C-terminal residue carbonyl oxygen and Zn^{2+} has been shown to account for the varied degrees of inhibition by peptides, then the shorter the Zn^{2+} distance to the carbonyl oxygen of the peptide, the greater the degree of inhibition.[57] The average distance between the WVYY peptide bond carbonyl oxygen and Zn^{2+} was 2.28 Å in comparison to 2.38 Å for WYT, hence the higher ACE-inhibitory activity (lower IC_{50} value, Table 1) observed for WVYY. A previous work has also shown that arachin-derived peptides IKP and IEP with 2.73 and 3.036 Å Zn^{2+} coordination distances had 7 and 18 μM IC_{50} values, respectively, for ACE inhibition.[57]

Figure 5A−C shows the docking of peptides with the active site of renin. SVYT had the lowest electrostatic binding energy value of −113.08 kJ/mol when compared to −83.96 kJ/mol for IPAGV and −92.91 kJ/mol for WYT. The results are consistent with the kinetics data (Table 1), which showed that SVYT had the highest binding affinity (lowest K_i value) followed by WYT and then IPAGV. Potential binding energy was also lowest for SVYT (−106.16 kJ/mol) when compared to IPAGV (−70.37 kJ/mol) and WYT (−80.74 kJ/mol). In contrast, the van der Waals energy values were −13.51, −8.36, and −0.67 kJ/mol for IPAGV, SVYT, and WYT, respectively. The results suggest that SVYT had better affinity toward renin followed by WYT and IPAGV in that order. The total number of interactions between each peptide and renin active site residues is very similar; in contrast, aliskiren had a greater number of interactions (Table 4). A previous report had shown that binding to the unique S3 subpocket ($S3^{sp}$) (Gln13, Tyr14, Val30, Tyr155, Ala218, Ser219, Ala303) of renin is necessary for high-affinity inhibition of enzyme activity.[58] In this respect, SVYT showed interactions with five of these residues (Gln13, Tyr14, Val30, Ala218, and Ser219), while WYT (Val30 and Ala218) and IPAGV (Ala218 and Ser219) interacted with two residues each (Table 4). In contrast, the powerful drug aliskiren formed interactions with all the $S3^{sp}$ residues. The lower peptide binding capacity to $S3^{sp}$ residues may be responsible for lower renin-inhibitory activity when compared to aliskiren. The results are in agreement with a previous work that had suggested peptide modification to improve lipophilic character as a means of enhancing binding to $S3^{sp}$ residues and increase renin-inhibitory capacity.[58] However, the fact that the three peptides still showed high renin-inhibitory capacity (low IC_{50} values) may be due to their ability to form electrostatic and hydrophobic interactions with the aspartate residues Asp32 and Asp215 (Table 4); these two residues are critical participants during renin catalysis.[59] The inhibitory activity of the three peptides may also be correlated to their ability to form multiple H-bonds with renin residues, as shown in Table 5. While the high renin-inhibitory activity of SVYT may be due to the higher

Table 4. Residues of Renin Having at Least One Atom at a Distance of 3.5 Å around the Docked Peptide[a]

tACE residues	IPAGV	SVYT	WYT	aliskiren
Thr12	–	√	–	√
Gln13	–	√	–	√
Tyr14	–	√	–	√
Val30	–	√	√	√
Asp32	√	√	√	√
Gly34	√	√	√	√
Ser35	√	√	√	√
Ser36	√	–	–	–
Trp39	–	–	–	√
Arg74	√	–	√	√
Tyr75	√	√	√	√
Ser76	√	√	√	√
Thr77	√	√	√	√
Pro111	√	–	√	√
Phe112	–	√	√	√
Leu114	–	–	–	√
Ala115	–	–	–	√
Phe117	√	√	√	√
Val120	–	√	√	√
Gln128	√	–	–	√
Ile130	√	–	–	√
Tyr155	–	–	–	√
Leu213	√	–	–	√
Asp215	√	√	√	√
Thr216	–	–	–	√
Gly217	√	√	√	√
Ala218	√	√	√	√
Ser219	√	√	–	√
Tyr220	–	√	–	–
Met289	√	√	√	–
Ile291	√	√	√	√
Pro292	–	–	√	–
Thr295	√	–	–	√
Ala303	–	–	–	√
total	20	20	18	30

[a]The residues around aliskiren in the renin (PDB ID 2V0Z) are also shown.

dx.doi.org/10.1021/jf5002606 | J. Agric. Food Chem. 2014, 62, 4135−4144

Table 5. Hydrogen Bonds Observed between the Docked Top Ranked Pose of Peptides and Renin[a]

renin residues involved in H-bonding[b]	no. of H-bonds and corresponding distance (Å)			
	IPAGV	SVYT	WYT	aliskiren
Tyr14:O	–	–	–	1 (2.25)
Asp32:OD1	–	–	–	1 (2.04)
Asp32:OD2	–	–	1 (2.47)	1 (2.16)
Gly34:O	–	1 (1.97)	–	1 (1.99)
Arg74:O	–	–	–	1 (1.99)
Ser76:HN	1 (2.11)	–	1 (2.23)	1 (2.11)
Ser76:HG	1 (1.88)	–	1 (1.97)	–
Thr77:OG1	–	2 (2.07, 2.34)	–	–
Thr77:HG1	1 (1.92)	1 (2.30)	1 (2.10)	–
Asp215:OD1	–	–	1 (2.33)	1 (2.11)
Gly217:O	–	3 (2.07, 2.07, 2.15)	–	–
Ser219:HN	1 (2.66)	1 (1.92)	–	–
Ser219:OG	–	1 (2.35)	–	–
water:HOH184:H2	–	–	–	1 (2.02)
water:HOH250:H2	–	–	1 (2.20)	–
total	4	9	6	8

[a]The residue numbers belong to renin (PDB ID 2V0Z). [b]H-bond position:donor or acceptor atoms. Repeated residues indicate formation of two separate H-bonds by the same amino acid. "D", "G", and "N" represent the presence of other residues near the donor or acceptor atom.

number (nine) of H-bond formation, only WYT formed H-bonds with the critical catalytic residues Asp32 and Asp215 (Table 5). Aliskiren also formed H-bonds with Asp32 and Asp215. In contrast, IPAGV formed the lowest number of H-bonds (four) and none of the bonds involved Asp32 and Asp215; the lower number and absence of interaction with active site residues may be responsible for this peptide having the lowest renin-inhibitory activity (higher IC_{50} value). It is important to note that though both WYT and aliskiren formed H-bonds with Asp32 and Asp215 residues, the bond length was shorter for the drug (2.16 and 2.11 Å) when compared to the peptide (2.47 and 2.33 Å), hence the higher drug renin-inhibitory activity. These results suggest that the renin or ACE-inhibitory properties of peptides depend not only on the number of interactions with active site residues but the quality of such interactions such as type of residue (catalytic versus noncatalytic) and length of the bond.

AUTHOR INFORMATION

Corresponding Author

*Telephone +1(204) 474-9555. Fax +1(204) 474-7593. E-mail: rotimi.aluko@umanitoba.ca.

Funding

This work was funded through an operating grant from the Manitoba Agri-Food Research and Development Initiative (ARDI) and a Discovery grant from the Natural Sciences and Engineering Research Council of Canada (NSERC) to R.E.A.

Notes

The authors declare no competing financial interest.

REFERENCES

(1) Chen, G. T.; Zhao, L.; Zhao, L. Y.; Cong, T.; Bao, S. F. In vitro study on antioxidant activities of peanut protein hydrolysate. *J. Sci. Food Agric.* **2007**, *87*, 357−362.

(2) Girgih, A. T.; Udenigwe, C. C.; Hasan, F. M.; Gill, T. A.; Aluko, R. E. Antioxidant properties of salmon (*Salmo salar*) protein hydrolysate and peptide fractions isolated by reverse-phase HPLC. *Food Res. Int.* **2013**, *52*, 315−322.

(3) Xie, Z.; Huang, J.; Xu, X.; Jin, Z. Antioxidant activity of peptides isolated from alfalfa leaf protein hydrolysate. *Food Chem.* **2008**, *111*, 370−376.

(4) Martínez-Maqueda, D.; Miralles, B.; Recio, I.; Hernández-Ledesma, B. Antihypertensive peptides from food proteins: A review. *Food Funct.* **2012**, *3*, 350−361.

(5) He, R.; Malomo, S. A.; Girgih, A. T.; Ju, X.; Aluko, R. E. Glycinyl-histidinyl-serine (GHS), a novel rapeseed protein-derived peptide has blood pressure-lowering effect in spontaneously hypertensive rats. *J. Agric. Food Chem.* **2013**, *61*, 8396−8402.

(6) Escudero, E.; Mora, L.; Fraser, P. D.; Aristoy, M.-C.; Arihara, K.; Toldra, F. Purification and identification of antihypertensive peptides in Spanish dry-cured ham. *J. Proteomics* **2013**, *78*, 499−507.

(7) Regazzo, D.; Da Dalt, L.; Lombardi, A.; Andrighetto, C.; Negro, A.; Gabai, G. Fermented milks from *Enterococcus faecalis* TH563 and *Lactobacillus delbrueckii* subsp. *bulgaricus* LA2 manifest different degrees of ACE-inhibitory and immunomodulatory activities. *Dairy Sci. Technol.* **2010**, *90*, 469−476.

(8) Ndiaye, F.; Vuong, T.; Duarte, J.; Aluko, R. E.; Matar, C. Anti-oxidant, anti-inflammatory and immunomodulating properties of an enzymatic protein hydrolysate from yellow field pea seeds. *Eur. J. Nutr.* **2012**, *51*, 29−37.

(9) Hartmann, R.; Meisel, H. Food-derived peptides with biological activity: From research to food applications. *Curr. Opin. Biotechnol.* **2007**, *18*, 163−169.

(10) Korhonen, H.; Pihlanto, A. Bioactive peptides: Production and functionality. *Int. Dairy J.* **2006**, *16*, 945−960.

(11) Madureira, A. R.; Tavares, T.; Gomes, A. M. P.; Pintado, M. E.; Malcata, F. X. Invited review: Physiological properties of bioactive peptides obtained from whey proteins. *J. Dairy Sci.* **2010**, *93*, 437−455.

(12) Bhutia, S. K.; Maiti, T. K. Targeting tumors with peptides from natural sources. *Trends Biotechnol.* **2008**, *26*, 210−217.

(13) Hoskin, D. W.; Ramamoorthy, A. Studies on anticancer activities of antimicrobial peptides. *Biochim. Biophys. Acta−Biomembr.* **2008**, *1778*, 357−375.

(14) Wu, J. M.; Jan, P. S.; Yu, H. C.; Haung, H. Y.; Fang, H. J.; Chang, Y. I.; Cheng, J. W.; Chen, H. M. Structure and function of a custom anticancer peptide, CB1a. *Peptides* **2009**, *30*, 839−848.

(15) Billyard, T.; McTernan, P.; Kumar, S. Potential therapies based on antidiabetic peptides. *Best Pract. Res.: Clin. Endocrinol. Metabol.* **2007**, *21*, 641−655.

(16) Huang, F. J.; Wu, W. T. Purification and characterization of a new peptide (S-8300) from shark liver. *J. Food Biochem.* **2010**, *34*, 962−970.

(17) Zhu, C. F.; Li, G. Z.; Peng, H. B.; Zhang, F.; Chen, Y.; Li, Y. Effect of marine collagen peptides on markers of metabolic nuclear receptors in type 2 diabetic patients with/without hypertension. *Biomed. Environ. Sci.* **2010**, *23*, 113−120.
(18) Cifarelli, V.; Trucco, M.; Luppi, P. Anti-inflammatory effects of C-peptide prevent endothelial dysfunction in type 1 diabetes. *Immunol. Endocr. Metab. Agents Med. Chem.* **2011**, *11*, 59−70.
(19) Haidet, J.; Cifarelli, V.; Trucco, M.; Luppi, P. Anti-inflammatory properties of C-peptide. *Rev. Diabetic Stud.* **2009**, *6*, 168−179.
(20) Young, D.; Fan, M. Z.; Mine, Y. Egg yolk peptides up-regulate glutathione synthesis and antioxidant enzyme activities in a porcine model of intestinal oxidative stress. *J. Agric. Food Chem.* **2010**, *58*, 7624−7633.
(21) He, R.; Malomo, S. A.; Alashi, A.; Girgih, A. T.; Ju, X.; Aluko, R. E. Purification and hypotensive activity of rapeseed protein-derived renin and angiotensin converting enzyme inhibitory peptides. *J. Funct. Foods* **2013**, *5*, 781−789.
(22) Majumder, K.; Chakrabarti, S.; Morton, J. S.; Panahi, S.; Kaufman, S.; Davidge, S. T.; Wu, J. Egg-derived tripeptide IRW exerts antihypertensive effects in spontaneously hypertensive rats. *PLoS One* **2013**, *8*, e82829.
(23) Chen, J.; Liu, S.; Ye, R.; Cai, G.; Ji, B.; Wu, Y. Angiotensin-I converrting enzyme (ACE) inhibitory tripeptides from rice protein hydrolysate: purification and characterization. *J. Funct. Foods* **2013**, *5*, 1684−1692.
(24) Liu, L.; Liu, L.; Lu, B.; Chen, M.; Zhang, Y. Evaluation of bamboo shoot peptide preparation with angiotensin converting enzyme inhibitory and antioxidant abilities from byproducts of canned bamboo shoots. *J. Agric. Food Chem.* **2013**, *61*, 5526−5533.
(25) Tenenbaum, A.; Grossman, E.; Shemesh, J.; Fisman, E. Z.; Nosrati, I.; Motro, M. Intermediate but not low doses of aspirin can suppress angiotensin-converting enzyme inhibitor-induced cough. *Am. J. Hypertens.* **2000**, *13*, 776−782.
(26) Abassi, Z.; Winaver, J.; Feuerstein, G. Z. The biochemical pharmacology of renin inhibitors: Implications for translational medicine in hypertension, diabetic nephropathy and heart failure: Expectations and reality. *Biochem. Pharmacol.* **2009**, *78*, 933−940.
(27) Gunkel, A.R.; Thurner, K. H; Kanonier, G.; Sprinzl, G. M.; Thumfart, W. F. Angioneurotic edema as a reaction to angiotensin-converting enzyme inhibitors. *Am. J. Otolaryngol.* **1996**, *17*, 87−91.
(28) Crowley, S. D.; Coffman, T. M. Recent advances involving the renin−angiotensin system. *Exp. Cell Res.* **2012**, *318*, 1049−1056.
(29) Peach, M. J. Renin−angiotensin system; biochemistry and mechanisms of action. *Physiol. Rev.* **1997**, *57*, 313−370.
(30) Borer, J. S. Angiotensin-converting enzyme inhibition: A landmark advance in treatment for cardiovascular diseases. *Eur. Heart J.* **2007**, No. Supplement 9(E), E2−E9.
(31) Harel, Z.; Gilbert, C.; Wald, R.; Bell, C.; Perl, J.; Juurlink, D.; Beyene, J.; Shah, P. S. The effect of combination treatment with aliskiren and blockers of the renin−angiotensin system on hyperkalaemia and acute kidney injury: Systematic review and meta-analysis. *Br. Med. J.* **2012**, *344*, e42.
(32) Fitzgerald, C.; Mora-Soler, L.; Gallagher, E.; O'Connor, P.; Prieto, J.; Soler-Vila, A.; Hayes, M. Isolation and characterization of bioactive pro-peptides with in vitro renin inhibitory activities from the macroalga *Palmaria palmata*. *J. Agric. Food Chem.* **2012**, *60*, 7421−7427.
(33) Li, H.; Aluko, R. E. Identification and inhibitory properties of multifunctional peptides from pea protein hydrolysate. *J. Agric. Food Chem.* **2010**, *58*, 11471−11476.
(34) Udenigwe, C. C.; Lin, Y. S.; Hou, W. C.; Aluko, R. E. Kinetics of the inhibition of renin and angiotensin I-converting enzyme by flaxseed protein hydrolysate fractions. *J. Funct. Foods* **2009**, *1*, 199−207.
(35) Girgih, A. T.; Udenigwe, C. C.; Li, H.; Adebiyi, A. P.; Aluko, R. E. Kinetics of enzyme inhibition and antihypertensive effects of hemp seed (*Cannabis sativa* L.) protein hydrolysates. *J. Am. Oil Chem. Soc.* **2011**, *88*, 1767−1774.
(36) Girgih, A. T.; He, R.; Malomo, S. A.; Offengenden, M.; Wu, J.; Aluko, R. E. Structural and functional characterization of hemp seed (*Cannabis sativa* L.) protein-derived antioxidant and antihypertensive peptides. *J. Funct. Foods* **2014**, *6*, 384−394.
(37) Li, H.; Prairie, N.; Udenigwe, C. C.; Adebiyi, A. P.; Tappia, P.; Aukema, H. M.; Jones, P. J. H.; Aluko, R. E. Blood pressure lowering effect of a pea protein hydrolysate in hypertensive rats and humans. *J. Agric. Food Chem.* **2011**, *59*, 9854−9860.
(38) Girgih, A. T.; Alashi, A. M.; He, R.; Malomo, S. A.; Aluko, R. E. Preventive and treatment effects of hemp seed (*Cannabis sativa* L.) meal protein hydrolysate against high blood pressure in spontaneously hypertensive rats. *Eur. J. Nutr.* **2014**, DOI: 10.1007/s00394-013-0625-4.
(39) Li, H.; Aluko, R. E. Kinetics of the inhibition of calcium/calmodulin-dependent protein kinase II by pea protein-derived peptides. *J. Nutr. Biochem.* **2005**, *16*, 656−662.
(40) Pan, D.; Cao, J.; Guo, H.; Zhao, B. Studies on purification and the molecular mechanism of a novel ACE inhibitory peptide from whey protein hydrolysate. *Food Chem.* **2012**, *130*, 121−126.
(41) Thangapandian, S.; John, S.; Sakkiah, S.; Lee, K. W. Potential virtual lead identification in the discovery of renin inhibitors: Application of ligand and structure-based pharmacophore modeling approaches. *Eur. J. Med. Chem.* **2011**, *46*, 2469−2476.
(42) Lau, C. C.; Abdullah, N.; Shuib, A. S.; Aminudin, N. Novel angiotensin I-converting enzyme inhibitory peptides derived from edible mushroom *Agaricus bisporus* (J.E. Lange) Imbach identified by LC−MS/MS. *Food Chem.* **2014**, *148*, 396−401.
(43) Kobayashi, Y.; Yamauchi, T.; Katsuda, T.; Yamaji, H.; Katoh, S. Angiotensin-I converting enzyme (ACE) inhibitory mechanism of tripeptides containing aromatic residues. *J. Biosci. Bioeng.* **2008**, *106*, 310−312.
(44) Wu, J.; Aluko, R. E.; Nakai, S. Structural requirements of angiotensin I-converting enzyme inhibitory peptides: Quantitative structure−activity relationship study of di- and tripeptides. *J. Agric. Food Chem.* **2006**, *54*, 732−738.
(45) Hayes, M.; Stanton, C.; Slattery, H.; O'Sullivan, O.; Hill, C.; Fitzgerald, G. F.; Ross, R. P. Casein fermentate of *Lactobacillus animalis* DPC6134 contains a range of novel propeptide angiotensin-converting enzyme inhibitors. *Appl. Environ. Microbiol.* **2007**, *73*, 4658−4667.
(46) Shu, M.; Cheng, X.; Zhang, Y.; Wang, Y.; Lin, Y.; Wang, L.; Lin, Z. Predicting the activity of ACE inhibitory peptides with a novel mode of pseudo amino acid composition. *Protein Pept. Lett.* **2011**, *18*, 1233−1243.
(47) Wang, X. Y.; Wang, J.; Hu, Y.; Lin, Y.; Shu, M.; Wang, L.; Cheng, X. M.; Lin, Z. H. Predicting the activity of peptides based on amino acid information. *J. Chin. Chem. Soc.* **2011**, *58*, 877−883.
(48) Wang, Z.; Zhang, S.; Jin, H.; Wang, W.; Huo, J.; Zhou, L.; Wang, Y.; Feng, F.; Zhang, L. Angiotensin-I-converting enzyme inhibitory peptides: Chemical feature based pharmacophore generation. *Eur. J. Med. Chem.* **2011**, *46*, 3428−3433.
(49) John, S.; Thangapandian, S.; Arooj, M.; Hong, J. C.; Kim, K. D.; Lee, K. W. Development, evaluation and application of 3D QSAR pharmacophore model in the discovery of potential human renin inhibitors. *BMC Bioinf.* **2011**, *12* (Suppl 14), S4.
(50) Udenigwe, C. C.; Li, H.; Aluko, R. E. Quantitative structure−activity relationship modeling of renin-inhibiting dipeptides. *Amino Acids* **2012**, *42*, 1379−1386.
(51) Wang, G. T.; Chung, C. C.; Holzman, T. F.; Krafft, G. A. A continuous fluorescence assay of renin activity. *Anal. Biochem.* **1993**, *210*, 351−359.
(52) Ajibola, C. F.; Eleyinmi, A. F.; Aluko, R. E. Kinetics of the inhibition of renin and angiotensin I converting enzyme by polar and non-polar polyphenolic extracts of *Vernonia amygdalina* and *Gongronema latifolium* leaves. *Plant Foods Hum. Nutr.* **2011**, *66*, 320−327.
(53) Yuan, L.; Wu, J.; Aluko, R. E.; Ye, X. Kinetics of renin inhibition by sodium houttuyfonate analogs. *Biosci., Biotechnol. Biochem.* **2006**, *70*, 2275−2280.

(54) Natesh, R.; Schwager, S. L. U.; Evans, H. R.; Sturrock, E. D.; Acharya, K. R. Structural details on the binding of antihypertensive drugs captopril and enalaprilat to human testicular angiotensin I-converting enzyme. *Biochemistry* **2004**, *43*, 8718−8724.
(55) Pina, A. S.; Roque, A. C. A. Studies on the molecular recognition between bioactive peptides and angiotensin-converting enzyme. *J. Mol. Recognit.* **2009**, *22*, 162−168.
(56) Natesh, R.; Schwager, S. L.; Sturrock, E. D.; Acharya, K. R. Crystal structure of the human angiotensin-converting enzyme−lisinopril complex. *Nature* **2003**, *421*, 551−554.
(57) Jimsheena, V.; Gowda, L. R. Arachin derived peptides as selective angiotensin I-converting enzyme (ACE) inhibitors: Structure−activity relationship. *Peptides* **2010**, *31*, 1165−1176.
(58) Rahuel, J.; Rasetti, V.; Maibaum, J.; Rueger, H.; Goschke, R.; Cohen, N. C.; Stutz, S.; Cumin, F.; Fuhrer, W.; Wood, J. M.; Grutter, M. G. Structure-based drug design: The discovery of novel nonpeptide orally active inhibitors of human renin. *Chem. Biol.* **2000**, *7*, 493−504.
(59) Sielecki, A. R.; Hayakawa, K.; Fujinaga, M.; Murphy, M.; Fraser, M.; Muir, A. K.; Carilli, C. T.; Lewicki, J. A.; Baxter, J. D.; James, M. Structure of recombinant human renin, a target for cardiovascular-active drugs, at 2.5 Å resolution. *Science* **1989**, *243*, 1346−1351.

JOURNAL OF AGRICULTURAL AND FOOD CHEMISTRY

Article

pubs.acs.org/JAFC

Hepatoprotective Sesquiterpenes and Rutinosides from *Murraya koenigii* (L.) Spreng

Qin-Ge Ma,[†] Yan-Gai Wang,[‡] Wen-Min Liu,[†] Rong-Rui Wei,[†] Jian-Bo Yang,[§] Ai-Guo Wang,[§] Teng-Fei Ji,[§] Jin Tian,[∥] and Ya-Lun Su*[,§]

[†]College of Chemistry and Pharmaceutical Engineering, Nanyang Normal University, Nanyan 473061, People's Republic of China

[‡]Department of Pharmacy, Xuanwu Hospital of Capital Medical University, Beijing 100053, People's Republic of China

[§]State Key Laboratory of Bioactive Substance and Function of Natural Medicines, Institute of Materia Medica, Chinese Academy of Medical Sciences and Peking Union Medical College, Beijing 100050, People's Republic of China

[∥]College of Agriculture and Biotechnology, China Agricultural University, Beijing 100193, People's Republic of China

Supporting Information

ABSTRACT: Three new sesquiterpenes (**1**−**3**) and two new rutinosides (**4** and **5**) along with 17 known compounds (**6**−**22**) were isolated from the leaves of *Murraya koenigii* (L.) Spreng. The new compounds were elucidated as (3*R*,5*S*,6*R*)-3,5,6-trihydroxy-1,1,5-trimethylcyclohexyl-8-butyn-9-one (**1**), (8*E*,9*R*)-ethyl-7-(3*S*,5*R*,6*S*)-3,6-dihydroxy-1,1,5-trimethylcyclohexyl-9-hydroxybut-8-enoate (**2**), (3*R*)-3-*O*-*β*-D-glucoside-6′-D-apiose-*β*-ionone (**3**), 4-*O*-*β*-D-rutinosyl-3-methoxyphenyl-1-propanone (**4**), and 1-*O*-*β*-D-rutinosyl-2(*R*)-ethyl-1-pentanol (**5**) based on their spectroscopic data. Compounds **1**, **4**, **5**, **18**, and **21** (10 *μ*M) exhibited moderate hepatoprotective activities.

KEYWORDS: *Murraya koenigii, sesquiterpene, rutinoside, hepatoprotective activity*

INTRODUCTION

Murraya koenigii L. (Rutaceae) is well-known as curry leaf, which has been widely cultivated as a spice in tropical and subtropical countries. The leaf of *M. koenigii* has been used for hundreds of years in southeast Asia as a traditional medicine and functional food to prevent and treat various diseases.[1]

Different kinds of compounds, including carbazole alkaloids,[2] volatile oils,[3] and other compounds, had been isolated from the leaves of *M. koenigii*.[4] These compounds exhibited various bioactivities, such as hypoglycemic and hypolipemic,[5] antidiarrheal,[6] antioxidant and radical-scavenging,[7] and antimicrobial activities.[8]

A preliminary screening assay exhibited that the *n*-butanol-soluble fraction from the leaves of *M. koenigii* inhibited hepatoprotective activities, which prompted us to further investigate its constituents. As a result, 22 compounds (Figure 1), including three new sesquiterpenes (**1**−**3**) and two new rutinosides (**4** and **5**) along with 17 known compounds (**6**−**22**), were isolated from the active fraction of *M. koenigii*. Their structures (Figure 1) were elucidated by extensive analysis of their spectroscopic data. Meanwhile, we evaluated their hepatoprotective activities against D-galactosamine-induced WB-F344 cell damage and found that compounds **1**, **4**, **5**, **18**, and **21** (10 *μ*M) showed moderate hepatoprotective activities.

MATERIALS AND METHODS

General Experimental Procedures. The optical rotations were measured on a PerkinElmer 241 polarimeter at 20 °C.[9] Melting points were recorded on a XT5B microscopic melting point apparatus (Beijing Tech Electro-Optical Instrument Factory, China), which was uncorrected.[10] The circular dichroism (CD), infrared (IR), and ultraviolet (UV) spectra were measured with a JASCO J-815 CD spectrometer, a Nicolet 5700 FTIR microscope spectrometer, and a Hitachi UV-240 spectrophotometer, respectively.[11] Nuclear magnetic resonance (NMR) spectra were recorded on Varian Mercury-300 and Inova-500 spectrometers, with tetramethylsilane (TMS) as an internal standard. The high-resolution electrospray ionization mass spectrometry (HRESIMS) data were acquired on an Agilent 1100 series LC/MSD Trap SL mass spectrometer. Reversed-phase high-performance liquid chromatography (HPLC) was performed on a Shimadzu LC-6AD instrument using a SPD-20A detector and a YMC-Pack ODS-A column (250 × 20 mm, 5 *μ*m). Column chromatography was carried out on Sephadex LH-20 (Amersham Pharmacia, Sweden), silica gel H, 100−200 and 200−300 mesh (Qingdao Marine Chemical, Inc., Qingdao, China). Thin-layer chromatography (TLC) was performed on pre-coated silica gel GF254 plates, and the spots were visualized under UV light (254 or 356 nm) or spraying with 10% H_2SO_4 in 95% EtOH, followed by heating.[12]

Plant Material. The leaves of *M. koenigii*, family Rutaceae, were collected from Xishuangbanna, Yunnan, China, in August 2010[10] and authenticated by Prof. Lin Ma (Institute of Materia Medica, Beijing, China). A voucher specimen (ID-S-2436) has been deposited in the Herbarium of Institute of Materia Medica, Beijing, China.

Extraction and Isolation. The air-dried leaves of *M. koenigii* (22.50 kg) were extracted 3 times with 95% EtOH (3 × 20 L) heating under reflux to give 2.10 g of crude extract. The combined extracts were successively partitioned with $CHCl_3$, EtOAc, and *n*-butanol to yield three fractions: $CHCl_3$-soluble fraction (33.50 g), EtOAc-soluble fraction (24.90 g), and *n*-butanol-soluble fraction (221.20 g).

The *n*-butanol-soluble fraction was subjected to the macroporous adsorbent resin (Diaion-101) column, which were eluted with 20, 40, 60, and 95% ethanol to obtain four fractions: A (25.50 g), B (30.60 g),

Received: January 29, 2014
Revised: April 21, 2014
Accepted: April 21, 2014
Published: April 21, 2014

ACS Publications © 2014 American Chemical Society

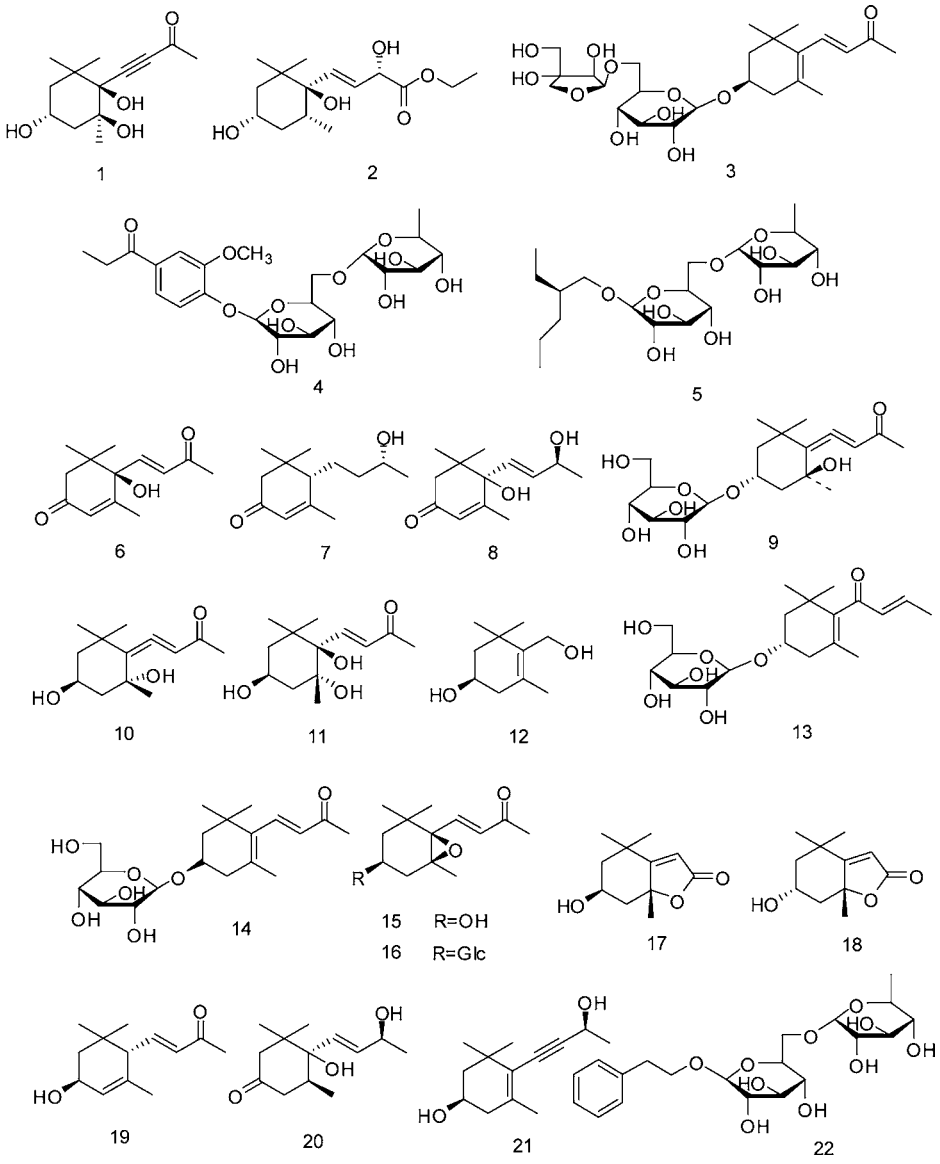

Figure 1. Structures of compounds **1**−**22**.

C (12.80 g), and D (5.40 g). The A part was purified on a Sephadex LH-20 column with a gradient system of MeOH/H_2O to give two sub-fractions: A-a and A-b. The separation of A-b (6.40 g) by medium-pressure liquid chromatography (MPLC) (10−30% MeOH−H_2O) and preparative HPLC (detection at 205 nm, 7 mL/min),[9] successively, yielded compounds **4** (9.00 mg), **5** (7.00 mg), and **22** (7.00 mg). Similarly, the B part was chromatographed over Sephadex LH-20 eluted with MeOH to give two sub-fractions: B-a and B-b. The separation of B-a (3.65 g) by MPLC (15−40% MeOH−H_2O) and preparative HPLC (detection at 205 nm, 7 mL/min), successively, yielded compounds **3** (10.00 mg), **13** (4.00 mg), **14** (10.31 mg), and **16** (11.76 mg). The separation of B-b (12.50 g) by MPLC (20−50% MeOH−H_2O) and preparative HPLC (detection at 205 nm, 7 mL/min), successively, yielded compounds **1** (6.51 mg), **2** (7.40 mg), **6** (3.10 mg), **7** (3.30 mg), **8** (4.70 mg), **9** (9.53 mg), **10** (12.30 mg), **11** (3.44 mg), **12** (6.63 mg), **15** (16.23 mg), **17** (18.43 mg), **18** (10.60 mg), **19** (5.43 mg), **20** (6.10 mg), and **21** (12.31 mg).

(3R,5S,6R)-3,5,6-Trihydroxy-1,1,5-trimethylcyclohexyl-8-butyn-9-one (1). White amorphous power. $[\alpha]_D^{20}$ −2.48 (*c* 0.08, MeOH). Melting point (mp): 153.4−154.9 °C. HRESIMS: *m*/*z* 263.1264 (calcd for $C_{13}H_{20}O_4Na$, 263.1254). UV (MeOH) λ_{max}: 201, 264 nm. CD (MeOH): 314 ($\Delta\varepsilon$, +0.33), 263 ($\Delta\varepsilon$, −2.04) nm. IR ν_{max}: 3454.9, 2932.7, 1670.8, 1381.7, 1044.6 cm^{-1}. ^1H NMR (CD_3COCD_3, 300 MHz) and ^{13}C NMR (CD_3COCD_3, 125 MHz) data: see Table 1.

(8E,9R)-Ethyl-7-(3S,5R,6S)-3,6-dihydroxy-1,1,5-trimethylcyclohexyl-9-hydroxybut-8-enoate (2). White amorphous power. $[\alpha]_D^{20}$ −5.49 (*c* 0.30, MeOH). mp: 157.4−156.9 °C. HRESIMS: *m*/*z* 309.1648 (calcd for $C_{15}H_{26}O_5Na$, 309.1672). UV (MeOH) λ_{max}: 203 nm. CD (MeOH): 222 ($\Delta\varepsilon$, −7.50) nm; IR ν_{max}: 3392.5, 2967.2, 2933.0, 1737.5, 1368.3, 1045.2 cm^{-1}. ^1H NMR (CD_3COCD_3, 300 MHz) and ^{13}C NMR (CD_3COCD_3, 125 MHz) data: see Table 1.

(3R)-3-O-β-D-Glucoside-6′-D-apiose-β-ionone (3). White amorphous power. $[\alpha]_D^{20}$ +1.50 (*c* 0.67, MeOH). mp: 187.7−188.5 °C. HRESIMS: *m*/*z* 525.2323 (calcd for $C_{24}H_{38}O_{11}Na$, 525.2306). UV (MeOH) λ_{max}: 203, 221, 291 nm. CD (MeOH): 276 ($\Delta\varepsilon$, +0.64), 322 ($\Delta\varepsilon$, −0.49) nm. IR ν_{max}: 3318.6, 2925.0, 1667.0, 1373.2, 1072.3 cm^{-1}. ^1H NMR (CD_3OD, 300 MHz) and ^{13}C NMR (CD_3OD, 125 MHz) data: see Table 2.

4-O-β-D-Rutinosyl-3-methoxyphenyl-1-propanone (4). White amorphous power. $[\alpha]_D^{20}$ −2.45 (*c* 0.50, MeOH). mp: 194.1−195.5 °C. HRESIMS: *m*/*z* 511.1797 (calcd for $C_{22}H_{32}O_{12}Na$, 511.1786). UV (MeOH) λ_{max}: 203, 222, 266, 301 nm. IR ν_{max}: 3399.3, 1671.8, 1592.9, 1512.1 cm^{-1}. ^1H NMR (CD_3OD, 300 MHz) and ^{13}C NMR (CD_3OD, 125 MHz) data: see Table 3.

dx.doi.org/10.1021/jf5005034 | J. Agric. Food Chem. 2014, 62, 4145−4151

Table 1. ^{1}H NMR (300 MHz, CD_3COCD_3), ^{13}C NMR (125 MHz, CD_3COCD_3), and HMBC Correlations of Compounds 1 and 2

	1			2		
	δ_H	δ_C	HMBC ($^{1}H-^{13}C$)	δ_H	δ_C	HMBC ($^{1}H-^{13}C$)
1		39.5			40.2	
2eq	1.56 (m)	46.8	C-1, C-3, C-4, C-6	1.66 (m)	46.1	C-1, C-3, C-4, C-6
2ax	1.53 (m)	46.8	C-1, C-3, C-4, C-6	1.22 (m)	46.1	C-1, C-3, C-4, C-6
3	4.08 (m)	63.6		3.77 (m)	66.5	
4eq	1.91 (m)	45.8	C-2, C-3, C-6	1.66 (m)	40.1	C-2, C-3, C-5, C-6
4ax	1.47 (m)	45.8	C-2, C-3, C-6	1.22 (m)	40.1	C-2, C-3, C-5, C-6
5		57.7		1.95 (m)	34.9	C-1, 15-CH_3
6		93.0			77.6	
7		75.8		5.83 (d, 16.5)	137.7	C-6, C-8, C-9
8		107.6		5.81 (dd, 16.5, 4.8)	128.2	C-7, C-9, C-10
9		191.6		4.68 (d, 4.8)	72.5	C-10
10	2.32 (s)	16.4	C-8		173.8	
11	1.31 (s)	22.5		4.16 (dd, 14.1, 6.6)	61.4	C-10
12	0.79 (s)	26.7		1.22 (t, 14.1, 6.6)	14.5	
13	0.96 (s)	26.3		0.97 (s)	25.7	
14				0.84 (s)	24.9	
15				0.79 (d, 6.9)	16.4	

Table 2. ^{1}H NMR (300 MHz, CD_3OD), ^{13}C NMR (125 MHz, CD_3OD), and HMBC Correlations of Compound 3

	3				3		
	δ_H	δ_C	HMBC ($^{1}H-^{13}C$)		δ_H	δ_C	HMBC ($^{1}H-^{13}C$)
1		37.8		13	1.82 (s)	21.8	C-5
2eq	2.00 (m)	47.4	C-1, C-3, C-4, C-6	1′	4.46 (d, 7.8)	102.7	C-3, C-2′
2ax	1.58 (m)	47.4	C-1, C-3, C-4, C-6	2′	3.43 (m)	76.8	C-4′
3	4.11 (m)	72.9	C-1′	3′	3.18 (m)	75.1	C-4′, C-5′
4eq	2.58 (m)	40.5	C-2, C-3, C-6	4′	3.37 (m)	78.0	C-3′, C-5′
4ax	2.20 (m)	40.5	C-2, C-3, C-6	5′	3.32 (m)	71.7	C-2′, C-3′
5		134.0		6′a	4.00 (m)	68.6	C-5′
6		137.1		6′b	3.63 (m)	68.6	C-5′
7	7.37 (d, 16.2)	144.4	C-1, C-5, C-8, C-9	1″	5.02 (d, 39)	110.8	C-2″, C-3″, C-6′
8	6.18 (d, 16.2)	133.1	C-6, C-9, C-10	2″	3.79 (m)	75.0	C-3″, C-4″, C-5″
9		201.2		3″	3.26 (m)	80.5	C-4″
10	2.33 (s)	27.2	C-9	4″a	3.97 (m)	78.0	C-2″, C-5″
11	1.17 (s)	28.8	C-1	4″b	3.91 (m)	78.0	C-2″, C-5″
12	1.14 (s)	30.5	C-1	5″	3.59 (s)	65.7	C-2″, C-3″, C-4″

*1-O-β-D-Rutinosyl-2(R)-ethyl-1-pentanol (**5**).* White amorphous power. $[\alpha]_D^{20}$ −1.55 (*c* 0.50, MeOH). mp: 143.3−145.6 °C. HRESIMS: *m*/*z* 447.2214 (calcd for $C_{19}H_{36}O_{10}Na$, 447.2201). UV (MeOH) λ_{max}: 203 nm. CD (MeOH): 242 ($\Delta\varepsilon$, −0.04) nm. IR ν_{max}: 3384.6, 2928.8, 1362.8 cm^{-1}. ^{1}H NMR (CD_3OD, 300 MHz) and ^{13}C NMR (CD_3OD, 125 MHz) data: see Table 3.

Hepatoprotective Assay. We evaluated the hepatoprotective activities of compounds **1**−**22** (Figure 1), which were tested against D-galactosamine-induced toxicity in WB-F344 cells using a 3-(4,5-dimethylthiazol-2-yl)-2,5-diphenyltetrazolium bromide (MTT) colorimetric method.[8] The WB-F344 cell lines were cultured in Dulbecco's modified Eagle's medium (DMEM) supplemented with 3% fetal calf serum, 100 units/mL penicillin, and 100 units/mL streptomycin in 5% CO_2 and incubated at 37 °C, which were placed in a 96-well microplate and precultured for 24 h.[13]

After this, the cultured cells were measured for cytotoxic effects, which were exposed to 40 mM D-galactosamine after 24 h. At last, the medium was replaced with the surum-free medium (0.5 mg/mL MTT) for 3.5 h of incubation. After removal of the medium and the addition of DMSO (150 μL/well) into the microplate, the formazan crystals were redissolved.[13] The optical density (OD) was measured by a microplate reader at a wavelength of 492 nm, and the inhibition was calculated as inhibition (%) = $[(OD_{(sample)} - OD_{(control)})/(OD_{(normal)} - OD_{(control)})] \times 100$.[16]

Statistical Analysis. Compounds **1**−**22** were bioassayed with the bicyclol (hepatoprotective activity drug) as the positive control for their hepatoprotective activities against D-galactosamine-induced toxicity in WB-F344 cells.[14] The results of pharmacological activities are shown in Table 4, with the inhibition (%) of compounds **1**, **4**, **5**, **18**, and **21** based on the computing formula with values of 43.7, 54.3, 45.1, 27.0, and 49.5, respectively. Furthermore, all of the values were expressed as means ± standard deviation (SD) of three experiments. The significance of unpaired observations between normal or control and tested samples was determined by Student's *t* test.[16] Differences were considered significant at $p < 0.05$.[15] Therefore, compounds **1**, **4**, **5**, **18**, and **21** exhibited moderate hepatoprotective activities.

RESULTS AND DISCUSSION

Structure Elucidation of New Compounds. Compound **1** was obtained as a white amorphous power. Its molecular formula was deduced as $C_{13}H_{20}O_4$ from the analysis of its HRESIMS at *m*/*z* 263.1264 (calcd for $C_{13}H_{20}O_4Na$, 263.1254) corresponding to four degrees of unsaturation. The UV spectrum showed the adamantane-type sesquiterpene absorp-

dx.doi.org/10.1021/jf5005034 | J. Agric. Food Chem. 2014, 62, 4145−4151

Table 3. ^{1}H NMR (300 MHz, CD_3OD), ^{13}C NMR (125 MHz, CD_3OD), and HMBC Correlations of Compounds 4 and 5

	4			5		
	δ_H	δ_C	HMBC (^{1}H−^{13}C)	δ_H	δ_C	HMBC (^{1}H−^{13}C)
1		131.4		4.06 (d, 2.1)	83.8	C-1′
2	7.61 (d, 1.8)	114.9	C-4, C-6, C-7	1.60 (m)	45.8	C-4
3a		149.3		2.18 (m)	36.7	C-2, C-6
3b		149.3		1.16 (m)	36.7	C-2, C-6
4a		150.7		2.09 (m)	27.3	
4b		150.7		1.17 (m)	27.3	
5	7.22 (d, 8.4)	110.9	C-1, C-3, C-4	0.87 (s)	19.3	
6a	7.70 (dd, 8.4, 1.8)	122.3	C-4, C-5, C-7	1.70 (m)	28.7	C-2, C-3
6b	7.70 (dd, 8.4, 1.8)	122.3	C-4, C-5, C-7	1.19 (m)	28.7	C-2, C-3
7		200.6		0.89 (s)	13.9	
8	3.07 (dd, 14.4, 7.2)	30.9	C-7, C-9			
9	1.20 (t, 7.2, 3.6)	7.4				
3-$OCHH_3$	3.93 (s)	55.2				
1′	5.03 (d, 7.2)	100.4	C-3′, C-4, C-5′	4.25 (d, 7.5)	102.9	C-1, C-3′, C-5′
2′	3.52 (m)	73.3		3.40 (s)	76.6	
3′	3.49 (m)	76.5		3.37 (m)	78.1	
4′	3.39 (m)	70.0		3.60 (m)	71.0	
5′	3.61 (m)	75.7		3.83 (m)	77.6	
6′a	4.04 (m)	66.4		3.95 (m)	67.9	
6′b	3.62 (m)	66.4		3.54 (m)	67.9	
1″	4.69 (d, 1.8)	100.7	C-2″, C-3″, C-6′	5.02 (d, 1.8)	110.4	C-3″, C-6′
2″	3.83 (m)	70.8		3.30 (m)	71.7	
3″	3.71 (m)	70.9		3.93 (m)	74.7	
4″	3.39 (m)	72.6		3.13 (m)	74.9	
5″	3.69 (m)	68.4		3.58 (m)	65.8	
6″	1.19 (d, 7.2)	16.5		0.85 (m)	20.2	

Table 4. Hepatoprotective Effects of Selective Compounds (10 μM) against D-Galactosamine-Induced Toxicity in WB-F344 Cells[a]

compound	cell survival rate (percentage of normal)	inhibition (percentage of control)
normal	100.0 ± 3.4	
control	45.5 ± 6.9	
bicyclol	59.6 ± 7.1[b]	25.9
1	69.3 ± 7.1[b]	43.7
4	75.1 ± 9.0[b]	54.3
5	70.1 ± 7.2[b]	45.1
18	60.2 ± 0.2[b]	27.0
21	72.5 ± 8.5[b]	49.5

[a]Results were expressed as means ± SD (n = 3; for normal and control, n = 6). Bicyclol was used as a positive control (10 μM). [b]p < 0.05.

tions at λ_{max} 201 and 264 nm.[17] Its IR spectrum indicated the presence of hydroxy (3454.9 cm^{-1}), carbonyl (1670.8 cm^{-1}), and methyl (1381.7 cm^{-1}) functionalities.

The ^{1}H NMR spectrum of compound **1** showed the presence of a multiplet at δ_H 4.08 (1H, m, H-3) and three methyl group singlets at δ_H 1.31 (3H, s), 0.96 (3H, s), and 0.79 (3H, s) (Table 1). These spectral characteristics coupled with the biosynthetic pathway (biogenetic isoprene rule) indicated the presence of the adamantane-type sesquiterpene[18] skeleton in compound **1**. The ^{13}C NMR spectrum (Table 1) showed 13 carbon signals. Besides one carbonyl (δ_C 191.6), four methyl carbons, and two sp-hybridized carbons, the remaining six sp^3-hybridized carbons were attributed to the cyclohexane. The planar structure of compound **1** was established on the basis of the correlations of H-2/C-1, C-3, C-4, and C-6; H-4/C-2, C-3, and C-6; and 10-CH_3/C-8 (Figure 2) in the heteronuclear multiple-bond correlation (HMBC) spectrum, and its relative configuration was determined by the correlations of H-3/5-OH and 3-OH/13-CH_3 (Figure 2) in the nuclear Overhauser effect spectrometry (NOESY) spectrum.

The absolute configuration of compound **1** was determined by the CD method. Because the $Mo_2(OAc)_4$-induced CD method has been successfully used to determine the absolute configuration of dozens of organic compounds with a 1,2-diol substructure,[19] we study the $Mo_2(OAc)_4$-induced CD spectrum of compound **1**, which contained a 5,6-diol unit. A positive Cotton effect was observed at 314 nm in the CD spectrum, and the absolute configurations of C-5 and C-6 were determined as 5*S* and 6*R*, respectively, by applying the spiral rule.[19] In addition, according to the correlations of the NOESY spectrum, the absolute configuration of C-3 was deduced as 3*R*. Thus, compound **1** was identified as (3*R*,5*S*,6*R*)-3,5,6-trihydroxy-1,1,5-trimethylcyclohexyl-8-butyn-9-one.

Compound **2** was isolated as a white amorphous power. The molecular formula was deduced as $C_{15}H_{26}O_5$ from HRESIMS at m/z 309.1648 (calcd for $C_{15}H_{26}O_5Na$, 309.1672), indicating three degrees of unsaturation. Its UV spectrum showed absorbance at λ_{max} 203 nm, and the IR spectrum indicated the presence of hydroxy (3392.5 cm^{-1}), carbonyl (1737.5 cm^{-1}), and methyl (1368.3 cm^{-1}) functionalities. The UV and IR spectrum data of compound **2** were similar to those of compound **1**. Therefore, compound **2** was concluded to be an adamantane-type sesquiterpene.[17]

The ^{1}H NMR spectrum of compound **2** showed the presence of a multiplet at δ_H 3.77 (1H, m, H-3) and three methyl group singlets at δ_H 0.97 (3H, s), 0.84 (3H, s), and 0.79 (3H, s)

dx.doi.org/10.1021/jf5005034 | J. Agric. Food Chem. 2014, 62, 4145−4151

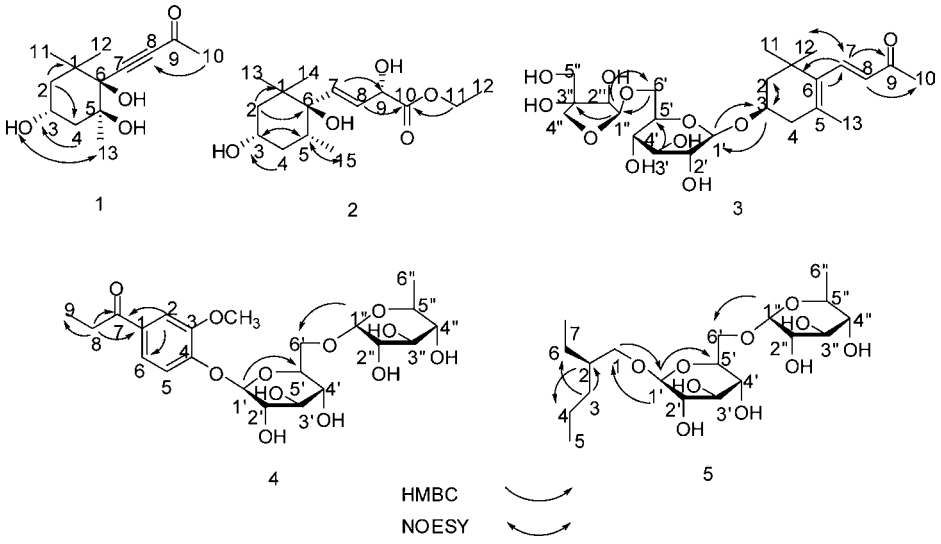

Figure 2. Key HMBC (H → C) and NOESY correlations of compounds **1**−**5**.

(Table 1). The above data suggested that compound **2** possessed the adamantane-type sesquiterpene skeleton.[20] A trans-double bond at δ_H 5.83 (1H, d, J = 16.5 Hz, H-7) and 5.81 (1H, d, J = 16.5 Hz, H-8) and a $-CH_2CH_3$ fragment at δ_H 4.16 (2H, dd, J = 14.1 and 6.6 Hz) and 1.22 (3H, t, J = 14.1 and 6.6 Hz) were observed in the ^{1}H NMR spectrum of compound **2**. The ^{13}C NMR spectrum (Table 1) showed 15 carbon signals consisting of one carbonyl (δ_C 173.8), two trans-double bond carbons, six saturated carbons of the cyclohexane, etc. Moreover, the structure of compound **2** was determined by the HMBC correlations of H-2/C-1, C-3, C-4, and C-6; H-4/C-2, C-3, C-5, and C-6; H-5/C-1 and 15-CH_3; H-7/C-6, C-8, and C-9; H-8/C-7, C-9, and C-10; and H-9/C-10 (Figure 2) and the NOESY correlations of H-3/H-5 and H-5/15-CH_3.

The absolute configurations of C-3, C-5, and C-6 were determined as 3*S*, 5*R*, and 6*S*, respectively, by biosynthetic considerations and the literature.[20] In addition, the absolute configuration of C-9 was determined as 9*R* on the basis of a negative Cotton effect at 222 nm in the CD spectrum.[20] Hence, compound **2** was identified as (8*E*,9*R*)-ethyl-7-(3*S*,5*R*,6*S*)-3,6-dihydroxy-1,1,5-trimethylcyclohexyl-9-hydroxybut-8-enoate.

Compound **3** was obtained as a white amorphous power. Its molecular formula was deduced as $C_{24}H_{38}O_{11}$ based on HRESIMS at m/z 525.2323 (calcd for $C_{24}H_{38}O_{11}Na$, 525.2306), indicating six degrees of unsaturation. The UV spectrum showed absorptions at λ_{max} 203, 221, and 291 nm. Its IR spectrum displayed absorptions of hydroxy (3318.6 cm^{-1}), carbonyl (1667.0 cm^{-1}), and methyl (1373.2 cm^{-1}) functionalities.

The ^{1}H NMR spectrum of compound **3** showed a multiplet at δ_H 4.11 (1H, m, H-3) and three methyl groups singlet at δ_H 1.17 (3H, s), 1.14 (3H, s), and 1.82 (3H, s), which revealed the typical characteristic of the adamantane-type sesquiterpene skeleton.[20] In the aromatic field, the signals at δ_H 7.37 (1H, d, J = 16.2 Hz, H-7) and 6.18 (1H, d, J = 16.2 Hz, H-8) suggested the existence of a trans-double bond. Moreover, two anomeric protons resonated at δ_H 4.46 (1H, d, J = 7.8 Hz, H-1′) and 5.02 (1H, d, J = 3.9 Hz, H-1″) indicated the presence of glucosyl and apiosyl moieties[21] in compound **3** according to the data of ^{1}H and ^{13}C NMR spectra (Table 2). The structure of compound **3** was established on the HMBC correlations of H-2/C-1, C-3, C-4, and C-6; H-3/C-1′; H-4/C-2, C-3, and C-6; H-7/C-1, C-5, C-8, and C-9; H-8/C-6, C-9, and C-10; 10-CH_3/C-9; H-1′/C-3; and H-1″/C-6′ (Figure 2) and the NOESY correlations of H-2/H-3 and H-3/H-4.

The absolute configuration of C-3 was determined by the CD method. First, compound **3** was hydrolyzed[22] to afford the aglycone **3a**. The positive Cotton effect at 276 nm and the negative Cotton effect at 322 nm were observed in the CD spectrum of compound **3a**. According to the spiral rule and the literature,[23] the absolute configuration of C-3 was determined as 3*R*. Therefore, compound **3** was identified as (3*R*)-3-*O*-*β*-D-glucoside-6′-D-apiose-*β*-ionone.

Compound **4** was obtained as a white amorphous power. Its molecular formula was established as $C_{22}H_{32}O_{12}$ on the basis of HRESIMS at m/z 511.1797 (calcd for $C_{22}H_{32}O_{12}Na$, 511.1786) corresponding to four degrees of unsaturation. The UV spectrum showed absorptions at λ_{max} 203, 222, 266, and 301 nm. Its IR spectrum displayed the presence of hydroxy (3399.3 cm^{-1}) and benzene ring (1671.8, 1592.9, and 1512.1 cm^{-1}) functionalities.

In the ^{1}H NMR spectrum of compound **4**, an ABX system was shown at δ_H 7.61 (1H, d, J = 1.8 Hz, H-2), 7.22 (1H, d, J = 8.4 Hz, H-5), and 7.70 (1H, dd, J = 8.4, 1.8 Hz, H-6) in the aromatic field. The anomeric signals at δ_H 5.03 (1H, d, J = 7.2 Hz, H-1′) and 4.69 (1H, d, J = 1.8 Hz, H-1″) suggested the existence of a rutinosyl moiety[24] in compound **4** according to the ^{1}H and ^{13}C NMR spectra (Table 3). Additionally, a quartet at δ_H 3.07 (2H, dd, J = 14.4 and 7.2 Hz, H-8) and a triplet at δ_H 1.20 (1H, t, J = 7.2 and 3.6 Hz, H-9) were displayed in the ^{1}H NMR spectrum, which suggested the presence of the $-CH_2CH_3$ fragment in compound **4**. The structure of compound **4** was determined by the HMBC correlations of H-2/C-4, C-6, and C-7; H-5/C-1, C-3, and C-4; H-6/C-4, C-5, and C-7; H-8/C-7 and C-9; H-1′/C-3′, C-4, and C-5′; and H-1″/C-2″ and C-6′ (Figure 2). Consequently, compound **4** was identified as 4-*O*-*β*-D-rutinosyl-3-methoxyphenyl-1-propanone.

Compound **5** was isolated as a white amorphous power. Its molecular formula was deduced as $C_{19}H_{36}O_{10}$ from HRESIMS data at m/z 447.2214 (calcd for $C_{19}H_{36}O_{10}Na$, 447.2201), implying two degrees of unsaturation. The UV spectrum showed absorption at λ_{max} 203 nm, and the IR spectrum indicated the presence of hydroxy (3384.6 cm^{-1}) and methyl (2928.8 and 1362.8 cm^{-1}) functionalities.

dx.doi.org/10.1021/jf5005034 | J. Agric. Food Chem. 2014, 62, 4145−4151

In comparison of the ^{1}H NMR data of compounds **5** and **4**, compound **5** also had two typical doublets at δ_H 4.25 (1H, d, J = 7.5 Hz, H-1′) and 5.02 (1H, d, J = 1.8 Hz, H-1″) in the ^{1}H NMR spectrum and a rutinosyl[24] was concluded in compound **5** by the ^{1}H and ^{13}C NMR spectra (Table 3). Moreover, some typical signals at δ_H 4.06 (2H, d, J = 2.1 Hz, H-1), 1.60 (1H, m, H-2), 0.87 (3H, s, 5-CH_3), and 0.89 (3H, s, 7-CH_3) were observed in the ^{1}H NMR spectrum, which concluded the 2-ethyl-2-pentanol fragment in compound **5** according to correlations of H-2/C-4; H-3/C-2 and C-6; and H-6/C-2 and C-3 in the HMBC spectrum. Finally, the planar configuration of compound **5** was determined by the HMBC correlations of H-1/C-1′; H-1′/C-1, C-3′, and C-5′; and H-1″/C-3″ and C-6′ (Figure 2).

Acid hydrolysis of compound **5** afforded the aglycone **5a**,[25] and the 2*R* chirality of **5a** was deduced from the optical value $[\alpha]_D^{20}$ −3.20 (*c* 0.10, MeOH) by comparing to ref 26. Therefore, compound **5** was identified as 1-*O*-*β*-D-rutinosyl-2(*R*)-ethyl-1-pentanol.

In addition, 17 known compounds were isolated and identified as (*R*)-(−)-dehydrovomifoliol (**6**),[27] blumenol C (**7**),[28] blumenol A (**8**),[29] icariside B1(**9**),[30] icariside B1 aglycone (**10**),[31] (3*S*,5*R*,6*R*,8*E*)-3,5,6-trihydroxy-1,1,5-trimethylcyclohexyl-8-buten-9-one (**11**),[32] (4*R*)-4-hydroxy-2,6,6-trimethyl-1-cyclohexene-1-methanol (**12**),[33] (8*E*)-3(*R*)-*O*-*β*-D-glucopyranosyloxy-1,5,5-trimethyl-7-cyclohexen-8-buten-7-one (**13**),[34] 3*β*-glucopyranosyloxy-*β*-ionone (**14**),[35] 3*β*-hydroxy-5*α*,6*α*-epoxy-7-megastigmen-9-one (**15**),[36] 3-*O*-*β*-D-glucopyranosyloxy-5*α*,6*α*-epoxy-7-megastigmen-9-one (**16**),[37] loliolide (**17**),[38] (−)-epiloliolide (**18**),[39] (3*R*,6*R*,7*E*)-3-hydroxy-*α*-ionone (**19**),[38] 5,6-dihydrovomifoliol (**20**),[40] (3*S*,9*R*)-9-hydroxy-7-butynyl-1,1,5-trimethyl-5-cyclohexen-3-ol (**21**),[41] and 8-phenylethyl-*O*-*β*-D-rutinoside (**22**)[24] by comparison of their physical and spectroscopic data to those reported in the references. Among them, compounds **6**−**21** belonged to sesquiterpenes and compound **22** belonged to rutinosides.

Acid Hydrolysis of Compounds 3−5. Compounds **3**−**5** (4 mg) were each treated in 5% HCl (0.5 mL) and heated at 90 °C for 2 h.[42] After cooling, each reaction mixture was extracted with EtOAc, and the aqueous layer was neutralized with 0.1 M NaOH. Therefore, glucose and apiose were obtained from compound **3**, which was detected by TLC with authentic sugars. Similarly, we obtained glucose and rhamnose from compounds **4** and **5**. The types of these sugars were identified by the TLC method.[43] Under the condition of 14:6:1 $CHCl_3$/MeOH/H_2O (Kieselgel 60 F_{254} plate), the R_f values of glucose, apiose, and rhamnose were 0.13, 0.31, and 0.24, respectively. Meanwhile, the R_f values (6:4:3 *n*-BuOH/pyridine/H_2O, Cellulose 60 F plate) of glucose, apiose, and rhamnose were 0.37, 0.55, and 0.47, respectively.

Hepatoprotective Activities. Compounds **1**−**22** were evaluated for their hepatoprotective activities against D-galactosamine-induced WB-F344 cell damage. Among of them, compounds **1**, **4**, **5**, **18**, and **21** (10 μM) exhibited moderate hepatoprotective activities (Table 4).

■ ASSOCIATED CONTENT

Supporting Information

Additional spectra of compounds **1**−**5**. This material is available free of charge via the Internet at http://pubs.acs.org.

■ AUTHOR INFORMATION

Corresponding Author

*Telephone/Fax: +86-10-6316-5327. E-mail: suyalun@imm.ac.cn.

Funding

This project was supported by the National Science and Technology Project of China (2012ZX09301002-002)-PCSIRT (IRT1007).[10]

Notes

The authors declare no competing financial interest.

■ ACKNOWLEDGMENTS

The authors express their appreciation to the Department of Instrumental Analysis of Peking Union Medical College and Chinese Academy of Medical Sciences for the NMR, IR, UV, HRESIMS, and CD measurements.

■ REFERENCES

(1) Zhou, L. X.; Zheng, H. C.; Yang, C. R. The research progress on plants of *Murraya*. *J. Pharm. Pract.* **1997**, *15*, 214−219.

(2) Anupam, N.; Suvra, M.; Avijit, B.; Julie, B. Review on chemistry and pharmacology of *Murraya koenigii* Spreng (Rutaceae). *J. Chem. Pharm. Res.* **2010**, *2*, 286−299.

(3) Rana, V. S.; Juyal, J. P.; Rashmi; Amparo Blazquez, M. Chemical constituents of the volatile oil of *Murraya koenigii* leaves. *Int. J. Aromather.* **2004**, *14*, 23−25.

(4) Luo, Q.; Wang, S. M.; Lu, Q.; Luo, J.; Cheng, Y. X. Identification of compounds from the water soluble extract of *Cinnamomum cassia* barks and their inhibitory effects against high-glucose-induced mesangial cells. *Molecules* **2013**, *18*, 10930−10943.

(5) Dineshkumar, B.; Analava, M.; Manjunatha, M. Antidiabetic and hypolipidemic effects of mahanimbine (carbazole alkaloid) from *Murraya koenigii* (rutaceae) leaves. *Int. J. Phytomed.* **2010**, *2*, 22−30.

(6) Suvra, M.; Anupam, N.; Manoj, K.; Samir, K. B.; Ashes, D.; Upadhyay, S. N.; Singh, R. K.; Avijit, B.; Julie, B. Antidiarhoeal activity of carbazole alkaloids from *Murraya koenigii* Spreng (Rutaceae) seeds. *Fitoterapia* **2010**, *81*, 72−74.

(7) Jagan Mohan Rao, L.; Ramalakshmi, K.; Borse, B. B.; Baghavan, B. Antioxidant and radical-scavenging carbazole alkaloids from the oleoresin of curry leaf (*Murraya koenigii* Spreng). *Food Chem.* **2007**, *100*, 742−747.

(8) Rahman, M. M.; Gray, A. I. A benzoisofuranone derivative and carbazole alkaloids from *Murraya koenigii* and their antimicrobial activities. *Phytochemistry* **2005**, *66*, 1601−1606.

(9) Liu, H.; Li, C. J.; Yang, J. Z.; Ning, N.; Si, Y. K.; Li, L.; Chen, N. H.; Zhao, Q.; Zhang, D. M. Carbazole alkaloids from the stems of *Clausena lansium*. *J. Nat. Prod.* **2012**, *75*, 677−682.

(10) Ma, Q. G.; Tian, J.; Yang, J. B.; Wang, A. G.; Ji, T. F.; Wang, Y. G.; Su, Y. L. Bioactive carbazole alkaloids from *Murraya koenigii* (L.) Spreng. *Fitoterapia* **2013**, *87*, 1−6.

(11) Wu, X. F.; Hu, Y. C.; Gao, S.; Yu, S. S.; Pei, Y. H.; Tang, W. Z.; Huang, X. Z. Two new compounds from the roots of *Lysidice rhodostegia*. *J. Asian Nat. Prod. Res.* **2007**, *9*, 471−477.

(12) Yu, L.; Yang, J. Z.; Chen, X. G.; Shi, J. G.; Zhang, D. M. Cytotoxic triterpenoid glycosides from the roots of *Gordonia chrysandra*. *J. Nat. Prod.* **2009**, *72*, 866−870.

(13) Hsiao, P. C.; Liaw, C. C.; Hwang, S. Y.; Cheng, H. L.; Zhang, L. J.; Shen, C. C.; Hsu, F. L.; Kuo, Y. H. Antiproliferative and hypoglycemic cucurbitane-type glycosides from the fruits of *Momordica charantia*. *J. Agric. Food Chem.* **2013**, *61*, 2979−2986.

(14) Liu, Y. F.; Liang, D.; Luo, H.; Hao, Z. Y.; Wang, Y.; Zhang, C. L.; Zhang, Q. J.; Chen, R. Y.; Yu, D. Q. Hepatoprotective iridoid glycosides from the roots of *Rehmannia glutinosa*. *J. Nat. Prod.* **2012**, *75*, 1625−1631.

(15) Lin, M. H.; Liu, H. K.; Huang, W. J.; Huang, C. C.; Wu, T. H.; Hsu, F. L. Evaluation of the potential hypoglycemic and *β*-cell

protective constituents isolated from corni fructus to tackle insulin-dependent diabetes mellitus. *J. Agric. Food Chem.* **2011**, *59*, 7743−7751.
(16) Li, Y.; Zhang, D. M.; Li, J. B.; Yu, S. S.; Li, Y.; Luo, Y. M. Hepatoprotective sesquiterpene glycosides from *Sarcandra glabra*. *J. Nat. Prod.* **2006**, *69*, 616−620.
(17) Park, J. H.; Lee, D. G.; Yeon, S. W.; Kwon, H. S.; Shin, D. J.; Park, H. S.; Kim, Y. S.; Bang, M. H.; Baek, N. I. Isolation of megastigmane sesquiterpenes from the silkworm (*Bombyx mori* L.) droppings and their promotion activity on HO-1 and SIRT1. *Arch. Pharm. Res.* **2011**, *34*, 533−542.
(18) Zhang, Z.; Zhang, W.; Ji, Y. P.; Zhao, Y.; Wang, C. G.; Hu, J. F. Gynostemosides A−E, megastigmane glycosides from *Gynostemma pentaphyllum*. *Phytochemistry* **2010**, *71*, 693−700.
(19) Liu, J.; Du, D.; Si, Y. K.; Lv, H. J.; Wu, X. F.; Li, Y.; Liu, Y. Y.; Yu, S. S. Application of dimolybdenum reagent $Mo_2(OAc)_4$ for determination of the absolute configurations of *vic*-diols. *Chin. J. Org. Chem.* **2010**, *30*, 1270−1278.
(20) Cirilo, P.; Juan, T. Absolute structures of two new C_{13}-norisoprenoids from *Apollonias barbujana*. *J. Nat. Prod.* **1996**, *59*, 69−72.
(21) Jun, C.; Ryan, C. Phenolic glycosides and ionone glycoside from the stem of *Sargentodoxa cuneata*. *Phytochemistry* **2005**, *66*, 2752−2758.
(22) Liu, C. M.; Li, B.; Shen, Y. H.; Zhang, W. D. Heterocyclic compounds and aromatic diglycosides from *Bretschneidera sinensis*. *J. Nat. Prod.* **2010**, *73*, 1582−1585.
(23) Frederick, K.; Chang, A. N. Synthesis of (3*S*)-and (3*R*)-3-hydroxy-bionone and their transformation into (3*S*)-and (3*R*)-*β*-cryptoxanthin. *Synthesis* **2011**, *3*, 509−516.
(24) Umehara, K.; Hattori, I.; Miyase, T.; Ueno, A.; Hara, S.; Kageyama, C. Studies on the constituents of leaves of *Citrus unshiu* Marcov. *Chem. Pharm. Bull.* **1988**, *36*, 5004−5008.
(25) Erika, M.; Koichi, M.; Masao, K. Chemical constituents of *Hypericum erectum* Thunb. *J. Nat. Med.* **2008**, *62*, 467−469.
(26) Herbert, C. B.; Ramachandra, G. N.; Raman, K. B.; Chongsuh, P.; Bakthan, S. Chiral synthesis via organoboranes. 4. Synthetic utility of boronic esters of essentially 100% optical purity, synthesis of homologated boronicacids and esters of very high enantiomeric purities. *J. Org. Chem.* **1985**, *50*, 5586−5592.
(27) Mori, K. Synthesis of the optically active dehydrovomifoliol, synthetic proof of the absolute configuration of (+)-abscisic acid. *Tetrahedron Lett.* **1973**, *28*, 2635−2638.
(28) Matsunami, K.; Otsuka, H.; Takeda, Y. Structural revisions of blumenol C glucoside and byzantionoside B. *Chem. Pharm. Bull.* **2010**, *58*, 438−441.
(29) Kuo, P. C.; Yang, M. L.; Hwang, T. L.; Lai, Y. Y.; Li, Y. C.; Thang, T. D.; Wu, T. S. Anti-inflammatory diterpenoids from *Croton tonkinensis*. *J. Nat. Prod.* **2013**, *76*, 230−236.
(30) Luecha, P.; Umehara, K.; Miyase, T.; Noguchi, H. Antiestrogenic constituents of the thai medicinal plants *Capparis flavicans* and *Vitex glabrata*. *J. Nat. Prod.* **2009**, *72*, 1954−1959.
(31) Li, S. M.; Yang, X. W.; Shen, Y. H.; Feng, L.; Wang, Y. H.; Zeng, H. W.; Liu, X. H.; Tian, J. M.; Shi, Y. N.; Long, C. L.; Zhang, W. D. Chemical constituents of *Aeschynanthus bracteatus* and their weak anti-inflammatory activities. *Phytochemistry* **2008**, *69*, 2200−2204.
(32) Tan, S. T.; Wilkins, A. L.; Holland, P. T.; Mcghie, T. K. Extractives from New Zealand honeys. 3. Unifloral thyme and willow honey constituents. *J. Agric. Food Chem.* **1990**, *38*, 1833−1838.
(33) Ruettimann, A.; Mayer, H. Synthesis of optically active natural carotenoids and structurally related natural products, v. synthesis of (3*R*,3′*R*)-, (3*S*,3′*S*)- and (3*R*,3′*S*;meso)-zeaxanthin by asymmetric hydroboration, a new approach to optically active carotenoid building units. *Helv. Chim. Acta* **1980**, *63*, 1456−1462.
(34) Baumes, R. L.; Aubert, C. C.; Gunata, Z. Y.; Moor, W. D.; Bayonove, C. L. Structures of two C_{13}-norisoprenoid glucosidic precursors of wine flavor. *J. Essent. Oil Res.* **1994**, *6*, 587−599.
(35) Fiorentino, A.; Dabrosca, B.; Pacifico, S.; Mastellone, C.; Piscopo, V.; Monaco, P. Spectroscopic identification and antioxidant activity of glucosylated carotenoid metabolites from *Cydonia vulgaris* fruits. *J. Agric. Food Chem.* **2006**, *54*, 9592−9597.
(36) Cheng, J. T.; He, J.; Li, X. Y.; Wu, X. D.; Shao, L. D.; Dong, L. B.; Deng, X.; Gao, X.; Peng, L. Y.; Cheng, X.; Li, Y.; Zhao, Q. S. Three new sucrose fatty acid esters from *Equisetum hiemale* L. *Helv. Chim. Acta* **2012**, *95*, 1158−1163.
(37) Yamamoto, M.; Akita, T.; Koyama, Y.; Sueyoshi, E.; Matsunami, K.; Otsuka, H.; Shinzato, T.; Takashima, A.; Aramoto, M.; Takeda, Y. Euodionosides A−G: Megastigmane glucosides from leaves of *Euodia meliaefolia*. *Phytochemistry* **2008**, *69*, 1586−1596.
(38) Machida, K.; Kikuchi, M. Norisoprenoids from *Viburnum dilatatum*. *Phytochemistry* **1996**, *41*, 1333−1336.
(39) Borkosky, S.; Valdes, D. A.; Bardon, A.; Diaz, J. G.; Herz, W. Sesquiterpene lactones and other constituents of *Eirmocephala megaphylla* and *Cyrtocymura cincta*. *Phytochemistry* **1996**, *42*, 1637−1639.
(40) Gonzalez, A. G.; Guillermo, J. A.; Ravelo, A. G.; Jimenez, I. A.; Gupta, M. P. 4,5-Dihydroblumenol A, a new nor-isoprenoid from *Perrottetia multiflora*. *J. Nat. Prod.* **1994**, *57*, 400−402.
(41) Skouroumounis, G. K.; Sefton, M. A. Acid-catalyzed hydrolysis of alcohols and their *β*-D-glucopyranosides. *J. Agric. Food Chem.* **2000**, *48*, 2033−2039.
(42) Chang, J.; Case, R. Phenolic glycosides and ionone glycoside from the stem of *Sargentodoxa cuneata*. *Phytochemistry* **2005**, *66*, 2752−2758.
(43) He, J.; Shen, Y.; Jiang, J. S.; Yang, Y. N.; Feng, Z. M.; Zhang, P. C.; Yuan, S. P.; Hou, Q. New polyacetylene glucosides from the florets of *Carthamus tinctorius* and their weak anti-inflammatory activities. *Carbohydr. Res.* **2011**, *346*, 1903−1908.

JOURNAL OF AGRICULTURAL AND FOOD CHEMISTRY

Article

pubs.acs.org/JAFC

Docosahexaenoic Acid Inhibits Vascular Endothelial Growth Factor (VEGF)-Induced Cell Migration via the GPR120/PP2A/ERK1/2/eNOS Signaling Pathway in Human Umbilical Vein Endothelial Cells

Che-Yi Chao,[†,∥] Chong-Kuei Lii,[†,‡,∥] Siou-Yu Ye,[‡] Chien-Chun Li,[#,⊥] Chia-Yang Lu,[‡] Ai-Hsuan Lin,[‡] Kai-Li Liu,*[,#,⊥] and Haw-Wen Chen*[,‡]

[†]Department of Health and Nutrition Biotechnology, Asia University, Taichung, Taiwan

[‡]Department of Nutrition, China Medical University, Taichung, Taiwan

[#]School of Nutrition, Chung Shan Medical University, Taichung, Taiwan

[⊥]Department of Nutrition, Chung Shan Medical University Hospital, Taichung, Taiwan

ABSTRACT: Cell migration plays an important role in angiogenesis and wound repair. Vascular endothelial growth factor (VEGF) is an endothelial cell-specific mitogen that is essential for endothelial cell survival, proliferation, and migration. Docosahexaenoic acid (DHA), an n-3 polyunsaturated fatty acid, shows both anti-inflammatory and antioxidant activities in vitro and in vivo. This study investigated the molecular mechanism by which DHA down-regulates VEGF-induced cell migration. HUVECs were used as the study model, and the MTT assay, Western blot, wound-healing assay, and phosphatase activity assay were used to explore the effects of DHA on cell migration. GPR120 is the putative receptor for DHA action. The results showed that DHA, PD98059 (an ERK1/2 inhibitor), and GW9508 (a GPR120 agonist) inhibited VEGF-induced cell migration. In contrast, pretreatment with okadaic acid (OA, a PP2A inhibitor) and *S*-nitroso-*N*-acetyl-DL-penicillamine (an NO donor) reversed the inhibition of cell migration by DHA. VEGF-induced cell migration was accompanied by phosphorylation of ERK1/2 and eNOS. Treatment of HUVECs with DHA increased PP2A enzyme activity and decreased VEGF-induced phosphorylation of ERK1/2 and eNOS. However, pretreatment with OA significantly decreased DHA-induced PP2A enzyme activity and reversed the DHA inhibition of VEGF-induced ERK1/2 and eNOS phosphorylation. These results suggest that stimulation of PP2A activity and inhibition of the VEGF-induced ERK1/2/eNOS signaling pathway may be involved in the DHA suppression of VEGF-induced cell migration. Thus, the effect of DHA on angiogenesis and wound repair is at least partly by virtue of its attenuation of cell migration.

KEYWORDS: *cell migration, docosahexaenoic acid (DHA), human umbilical vein endothelial cells (HUVECs), nitric oxide (NO), vascular endothelial growth factor (VEGF)*

INTRODUCTION

Docosahexaenoic acid (DHA, 22:6, n-3) is enriched in fatty fish and fish oil supplements and is well-known for its anti-inflammatory,[1] immunomodulatory,[2] and anticancer[3] properties. Cancer is among the leading causes of death in both economically developed countries and developing countries.[4] Epidemiological studies show that a diet rich in n-3 polyunsaturated fatty acids (PUFAs) is correlated with reduced risk of angiogenic diseases such as cancers.[5,6] DHA has been shown to inhibit vascular sprout formation in retinal microvascular endothelial cells.[7] However, the mechanism underlying the inhibition of cell migration by DHA, which is critical for angiogenesis and wound repair, is not fully understood.

G protein-coupled receptors (GPRs) are important signaling molecules involved in many cellular functions. Specific ligand binding to GPRs stimulates and induces a variety of cellular responses via several second messenger pathways, for example, regulation of cAMP generation, the phospholipase C pathway, ion channels, and mitogen-activated protein kinases.[8−10] In a previous study, Oh et al.[11] found that DHA exerted potent anti-inflammatory effects through GPR120.

Angiogenesis, the process of the formation of new blood vessels by sprouting of the preexisting microvascular network, is involved in numerous physiological processes including embryogenesis, tissue remodeling, wound healing,[12] and disease development such as diabetic retinopathy, rheumatoid arthritis, tumor growth, and growth of atherosclerotic plaques.[13] Angiogenesis is controlled by vascular endothelial growth factor (VEGF), a pro-angiogenic factor.[14] VEGF-induced signal transduction involves binding to tyrosine kinase receptors, which leads to endothelial cell proliferation, migration, and new vessel formation.[15] VEGF was reported to induce a wide variety of signaling pathways, including protein kinase C, phospholipase C-γ, extracellular signal-regulated kinase (ERK), p38 MAPK, phospholipase C, and phosphatidyl inositol 3-kinase (PI3K)/Akt.[16] Hence, it is critical to understand the VEGF-activated signaling pathways that play an important role in VEGF-mediated cell processes.

Nitric oxide (NO), which is synthesized from the amino acid L-arginine by the NOS family of enzymes, is a gaseous molecule

Received: February 12, 2014
Revised: April 1, 2014
Accepted: April 15, 2014
Published: April 15, 2014

ACS Publications © 2014 American Chemical Society

with a wide range of physiological and pathophysiological activities, including the regulation of angiogenesis.[17] The NOS family is composed of three members: neuronal NOS (nNOS), endothelial NOS (eNOS), and inducible NOS (iNOS). eNOS is constitutively expressed in endothelial cells, but various physical and chemical stimuli affect eNOS levels in vivo and in vitro.[18] Moreover, eNOS is activated upon exposure to fluid shear stress and numerous agonists via cellular events such as protein phosphorylation.

Protein phosphatase 2A (PP2A) is a heterotrimeric complex composed of three subunits including a structural subunit (PP2A-A), a regulatory subunit (PP2A-B), and a catalytic subunit (PP2A-C).[19] PP2A is a crucial intracellular serine/threonine phosphatase.[20] In addition, PP2A plays a significant role in the regulation of specific signal transduction cascades including ERK1/2,[21] JNK,[22] and p38 MAPK.[23] In recent years, PP2A was shown to have tumor suppressor activity in myeloid CML-BC patient-derived mononuclear marrow cells.[24] Thus, enhancement of PP2A tumor suppressor activity may represent a potential therapeutic strategy for malignancy.

The antitumor effect of DHA has been studied in MCF-7 human breast cancer cells by induction of heme oxygenase 1 and inhibition of TPA-induced matrix metalloproteinase 9 (MMP-9) expression.[3] Moreover, DHA was reported to have a potent anti-angiogenic effect.[25] The pro-angiogenic effect of VEGF and NO has also been demonstrated.[15] In this study, therefore, we investigated whether DHA has an opposing effect on cell migration that is associated with angiogenesis and wound repair and the possible mechanisms involved.

MATERIALS AND METHODS

Reagents. Medium 199 (M199), Dulbecco's modified Eagle's medium, 0.25% trypsin−EDTA, and penicillin−streptomycin−amphotericin solution were from GIBCO-BRL (Grand Island, NY, USA); endothelial cell growth supplement (ECGS) was from Upstate Biotechnology (Lake Placid, NY, USA); fetal bovine serum (FBS) was from HyClone (Logan, UT, USA); DHA was from Cayman Chemical (Ann Arbor, MI); 3-(4,5-dimethylthiazol-2-yl)-2,5-diphenyltetrazolium bromide, sodium bicarbonate, heparin, gelatin, *S*-nitroso-*N*-acetyl-DL-penicillamine (SNAP, NO donor), LY294002 (PI3K kinase inhibitor), GW9508 (GPR120 agonist), and antibody against β-actin were from Sigma-Aldrich (St. Louis, MO, USA); VEGF was from Peprotech (Rocky Hill, NJ, USA); okadaic acid (OA) was from Millipore (Darmstadt, Germany); PD98059 (ERK1/2 inhibitor) was from TOCRIS (Ellisville, MO, USA); and antibodies against ERK1/2, phospho-ERK1/2, eNOS, and phospho-eNOS were from Cell Signaling Technology (Danvers, MA, USA).

Cell Cultures. The human umbilical vein endothelial cell line (HUVEC; CC-2517) was obtained from Clonetics (San Diego, CA, USA) and was cultured on gelatin-coated cell culture dishes in M199 supplemented with 2.2 g/L sodium bicarbonate ($NaHCO_3$), 0.1 g/L heparin, 37.5 mg/L ECGS, 20% FBS, 100,000 units/L penicillin, 0.25 mg/mL amphotericin, and 100 mg/L streptomycin at 37 °C in a 5% CO_2 humidified incubator.

DHA Preparation. DHA samples were prepared as described previously.[1]

Cell Viability Assay. Cell viability was assessed by the MTT assay. The MTT assay measures the ability of viable cells to reduce a yellow 3-(4,5-dimethylthiazol-2-yl)-2,5-diphenyltetrazolium bromide to a purple formazan by mitochondrial succinate dehydrogenase. HUVECs were grown to 80−90% confluence and then treated with various concentrations of DHA (0−200 μM) and GW9508 (1−10 μM) with or without VEGF (50 ng/mL) for 8 h in M199 containing 2% FBS. Finally, the medium was removed, and the cells were washed with phosphate-buffered saline (PBS). The cells were then incubated with MTT (0.5 mg/mL) in M199 medium at 37 °C for an additional 3 h. The medium was removed, and 2-propanol was added to dissolve the formazan. After centrifugation at 10000*g* for 5 min, the supernatant of each sample was transferred to 96-well plates, and absorbance was read at 595 nm in an ELISA reader. The absorbance in the control group was regarded as 100% cell viability.

Western Blotting Analysis. After each experiment, cells were washed twice with PBS and were harvested with 150 μL of lysis buffer (10 mM Tris-HCl, pH 8.0, 0.1% Triton X-100, 320 mM sucrose, 5 mM EDTA, 1 mM PMSF, 1 mg/L leupeptin, 1 mg/L aprotinin, and 2 mM DTT). Cell homogenates were centrifuged at 14000*g* for 20 min at 4 °C. The resulting supernatant was used as a cellular protein for Western blotting analysis. The total protein was analyzed by use of the Coomassie Plus protein assay reagent kit (Pierce Biotechnology Inc., Rockford, IL, USA). Equal amounts of cellular proteins were electrophoresed in a sodium dodecyl sulfate (SDS)−polyacrylamide gel, and proteins were then transferred to polyvinylidene fluoride membranes (Millipore Corp., Bedford, MA, USA). Nonspecific binding sites on the membranes were blocked with 5% nonfat milk in 15 mM Tris/150 mM NaCl buffer (pH 7.4) at room temperature for 2 h. Membranes were probed with anti-ERK1/2, antiphospho-ERK1/2, anti-eNOS, antiphospho-eNOS, and anti-β-actin. The membranes were then probed with the secondary antibody labeled with horseradish peroxidase. The bands were visualized by using an enhanced chemiluminescence kit (PerkinElmer Life Science, Boston, MA, USA) and were scanned by use of a luminescence image analyzer (LAS-4000, FUJIFILM, Japan). The bands were quantitated with ImageGauge software (FUJIFILM).

Cell Migration Assay. An in vitro wound-healing assay was used to measure directional endothelial cell migration. HUVECs were seeded onto gelatin-coated 6-well plates and allowed to form a confluent monolayer. Monolayers were wounded by using a sterile 200 μL pipet tip, washed with PBS to remove floating cells, and photographed (time 0). Cells were then cultured in M199 medium containing 2% FBS and 50 ng/mL VEGF. Meanwhile, the cells were treated with various concentrations of DHA (0−100 μM) with or without SNAP (20 μM) or OA (10 nM) for 8 h. In addition, the cells were treated with GW9508 (10 μM) for 8 h. Cells were then photographed (100× magnification) to monitor cell migration into the wounded area, and the width of the cell-free zone (distance between the edges of the injured monolayer) was calculated.

PP2A Activity Assay. PP2A activity was determined by use of a Ser/Thr phosphatase assay kit according to the instructions of the manufacturer (Upstate, Darmstadt, Germany). After treatment, cells were scraped with lysis buffer (10 mM tris/Triton X-100, 0.32 M sucrose, 5 mM EDTA) and protease inhibitors, sonicated for 10 s, and centrifuged at 2000*g* for 5 min. Thereafter, phosphopeptide (K-R-pT-I-R-R) was added to the cell lysate, followed by incubation at room temperature for 15 min, and then Malachite Green phosphate was added and the reaction was allowed to proceed at room temperature for another 15 min for color development. The relative absorbance was measured at 650 nm in a microplate reader (Bio-Rad).

Statistical Analysis. Data were analyzed by using analysis of variance (SAS Institute, Cary, NC, USA). The significance of the difference between mean values was determined by one-way analysis of variance followed by Tukey's test. p values <0.05 were taken to be statistically significant.

RESULTS

Effect of DHA and GW9508 on Cell Viability in the Presence or Absence of VEGF. As measured by the MTT assay, the cell viabilities of HUVECs treated with VEGF alone; 50, 100, or 200 μM DHA; or VEGF and 50, 100, or 200 μM DHA were 110.5 ± 6.6, 92.9 ± 1.2, 92.4 ± 2.7, 12.1 ± 2.5, 103.6 ± 7.4, 98.5 ± 7.8, and 11.8 ± 0.8%, respectively, compared with the unstimulated controls (100%). Thus, there were no adverse effects on the growth of cells up to a concentration of 100 μM DHA in the presence or absence of 50 ng/mL VEGF, which was used to induce cell migration. The

highest concentration of DHA used in the present study was 100 μM.

The cell viabilities of HUVECs treated with VEGF alone, 1 or 10 μM GW9508, or VEGF and 1 or 10 μM GW9508 were 116.3 ± 5.8, 97.6 ± 3.5, 99.1 ± 2.5, 107.6 ± 4.5, and 107.0 ± 7.3%, respectively, compared with the unstimulated controls (100%). Thus, there were no adverse effects on the growth of cells up to a concentration of 10 μM GW9508 in the presence or absence of 50 ng/mL VEGF.

DHA Inhibits VEGF-Induced Cell Migration of HUVECs. Endothelial cell migration is necessary to angiogenesis and wound repair. In addition to activation by chemotactic, hepatotactic, and mechanotactic stimuli, angiogenesis involves degradation of the extracellular matrix by matrix metalloproteinases (MMPs) to enable progression of the migrating cells.[26] Moreover, at least 10 MMPs are up-regulated during wound healing by epidermal, dermal, fibroblast, and blood cells in mammals.[27] To determine the effect of DHA on endothelial cell migration in vitro, confluent monolayers of HUVECs were scratched and cultured with M199 medium containing 2% FBS plus 50 ng/mL VEGF alone or in addition to 100 μM DHA. As shown in Figure 1, VEGF significantly induced cell migration, whereas coculture with DHA inhibited the VEGF-induced cell migration ($p < 0.05$).

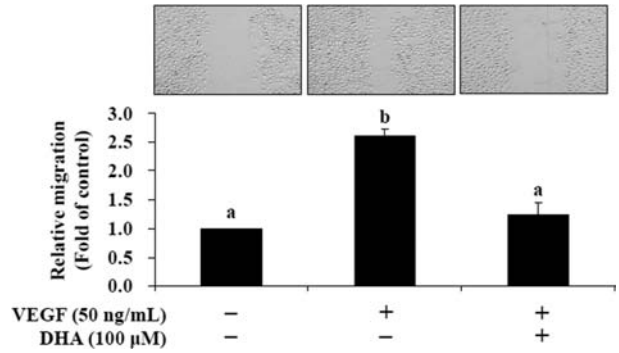

Figure 1. DHA inhibits VEGF-induced migration of HUVECs. Cells were scratched and then stimulated with 50 ng/mL VEGF in the presence or absence of 100 μM DHA for 8 h. Migration was observed by using a phase-contrast microscope, at 100× magnification. Values are the mean ± SD, $n = 3$. Values not sharing the same letter are significantly different ($p < 0.05$).

Phosphorylation of ERK1/2 and eNOS Is Involved in VEGF-Induced Cell Migration. VEGF has been shown to induce a wide variety of signaling pathways that transduce the physiological or pathophysiological activities of VEGF. ERK1/2 is one such pathway. It has been shown that there is a relationship between ERK1/2 phosphorylation and eNOS activation in rat sinusoidal endothelial cells.[28] Thus, we determined the effect of VEGF on both ERK1/2 and eNOS phosphorylation. As shown in Figure 2A, VEGF stimulated the phosphorylation of ERK1/2 and eNOS, and this activation was abolished by the ERK1/2 inhibitor PD98059. However, VEGF showed no effect on Akt phosphorylation (data not shown). VEGF stimulated cell migration, and this effect was dependent on ERK1/2 (Figure 2B). These results suggested that VEGF stimulation of cell migration is mediated by the ERK1/2/eNOS pathway.

Inhibition of VEGF-Induced Cell Migration by DHA Is Associated with the Induction of PP2A Enzyme Activity and the Inhibition of ERK1/2 and eNOS Phosphorylation. Tumor metastasis, the spreading of the primary tumor to distant organs, is recognized to be one of the major causes of failure in the treatment of cancer.[29] Thus, intervention in a key step in the metastatic process, such as angiogenesis, is an effective mechanism for cancer therapy. VEGF plays a critical role in tumor angiogenesis and has been shown to phosphorylate eNOS on Ser1177 in glomerular endothelial cells.[30] NO produced by activation of eNOS regulates angiogenesis. Dephosphorylation of phosphorylated eNOS is mediated by protein phosphatase 2A (PP2A).[31] In the present study, the role of DHA in VEGF-induced cell migration was studied by using a wound-healing assay. As shown in Figure 3A, DHA inhibited VEGF-induced cell migration, and this inhibition was abolished by treatment with the PP2A inhibitor, OA. These results suggested that DHA inhibition of VEGF-induced cell migration is likely associated with activation of PP2A enzyme activity.

Recently, it was shown that PP2A has tumor suppressor activity in myeloid CML-BC patient-derived mononuclear marrow cells.[24] We used the Ser/Thr phosphatase assay to measure PP2A enzyme activity. As shown in Figure 3B, DHA significantly stimulated PP2A enzyme activity compared with that in the control group, and this activation was attenuated by treatment with OA. We next examined whether OA reversed the DHA inhibition of VEGF-induced ERK1/2 and eNOS phosphorylation. As shown in Figure 3C, VEGF induced phosphorylation of ERK1/2 and eNOS, and pretreatment with DHA attenuated this induction. Nevertheless, pretreatment with OA reversed the inhibition of eNOS phosphorylation by DHA. OA also reversed the attenuation of VEGF-induced ERK1/2 phosphorylation by DHA, although this effect was not significant.

Effect of GPR120 Agonist on VEGF-Induced Phosphorylation of ERK1/2 and eNOS as well as Cell Migration. GPR120 is a physiological receptor for long-chain fatty acids, in particular n-3 fatty acids, such as α-linolenic acid, eicosapentaenoic acid (EPA), and DHA.[11,32] To determine the role of GPR120 in DHA's inhibition of cell migration, we used the GPR120 agonist GW9508. As shown in Figure 4A, GW9508 had an effect similar to that of DHA on the VEGF-induced phosphorylation of ERK1/2 and eNOS. Moreover, the inhibitory effect of DHA on VEGF-induced cell migration was replicated by GW9508 (Figure 4B). These results suggested that the effects of DHA were highly associated with binding to GPR120.

SNAP Reverses DHA Inhibition of VEGF-Induced Cell Migration. VEGF activates eNOS and stimulates the release of NO from HUVECs.[33] Endothelium-derived NO is critical regulator of endothelial cell migration, survival, and angiogenesis.[34] To determine the effect of the NO donor SNAP on endothelial cell migration in vitro, confluent monolayers of HUVECs were scratched and cultured in M199 medium containing 2% FBS plus vehicle, 50 ng/mL VEGF, 100 μM DHA and 50 ng/mL VEGF, or 100 μM DHA, 20 μM SNAP, and 50 ng/mL VEGF, respectively. As shown in Figure 5, SNAP reversed DHA inhibition of VEGF-induced cell migration.

■ DISCUSSION

Cancer has attracted considerable attention in the past decades because it is among the leading causes of death globally.[4] Protection against cancer by DHA is attributed to the anti-

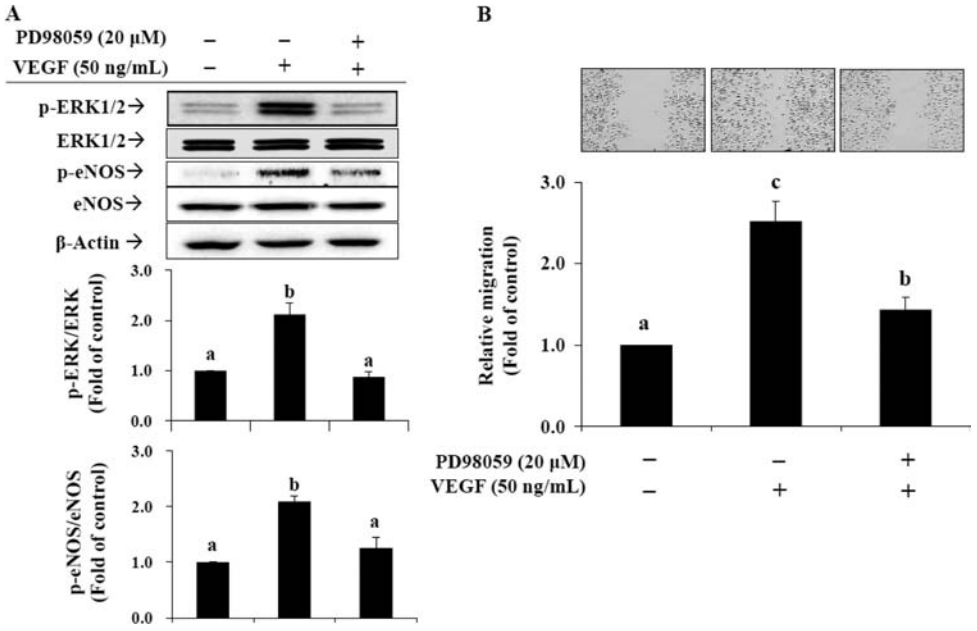

Figure 2. Phosphorylation of ERK1/2 and eNOS is involved in VEGF-induced migration of HUVECs. (A) Cells were starved in M199 containing 2% FBS for 7 h and then pretreated with 20 μM of the ERK1/2 inhibitor PD98059 for 1 h followed by incubation with 50 ng/mL VEGF for another 15 min. (B) Cells were scratched and were cotreated with 20 μM PD98059 and 50 ng/mL VEGF or treated with 50 ng/mL VEGF for 8 h. Values are the mean ± SD, n = 3. Values not sharing the same letter are significantly different (p < 0.05).

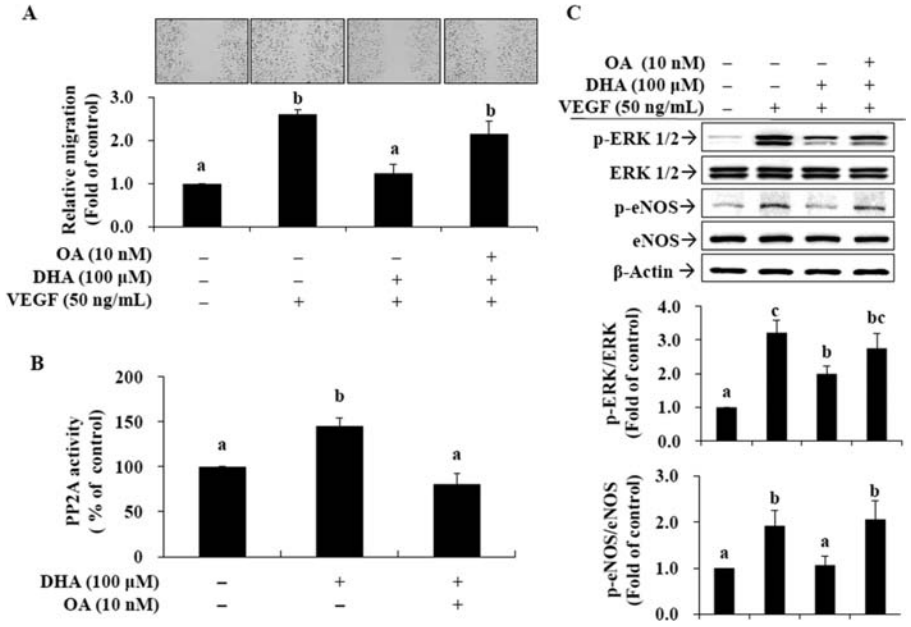

Figure 3. Protein phosphatase 2A (PP2A) is involved in DHA inhibition of VEGF-induced phosphorylation of ERK1/2 and eNOS and cell migration. (A) HUVECs were scratched and pretreated with or without 10 nM of the PP2A inhibitor okadaic acid (OA) for 1 h and were then treated with 100 μM DHA along with 50 ng/mL VEGF or with 50 ng/mL VEGF for another 8 h. (B) HUVECs were pretreated with or without 10 nM OA for 1 h and were then treated with 100 μM DHA for another 4 h. (C) HUVECs were pretreated with 10 nM OA for 1 h and were then treated with 100 μM DHA for 8 h before being challenged with 50 ng/mL VEGF for another 15 min. Values are the mean ± SD, n = 3. Values not sharing the same letter are significantly different (p < 0.05).

angiogenic activity of DHA.[35] However, the mechanisms by which DHA inhibits angiogenesis are still not fully clarified. In this study, we explored the inhibition of HUVEC cell migration by DHA and the possible mechanisms involved. We demonstrated that DHA inhibits VEGF-induced HUVEC cell migration and that this suppression is likely associated with binding to GPR120, activation of PP2A enzyme activity, and inhibition of the ERK1/2/eNOS signaling pathway.

Several mechanisms have been proposed to demonstrate the inhibitory role of DHA in angiogenesis, including induction of apoptosis and reduction of cell proliferation.[36−38] Rose and Connolly[36] proposed that the inhibition of breast cancer cell proliferation by DHA was related to the reduced production of series 2 eicosanoids. Although DHA may prevent the occurrence of angiogenic diseases, it has potential side effects on subjects receiving revascularization therapy because of its

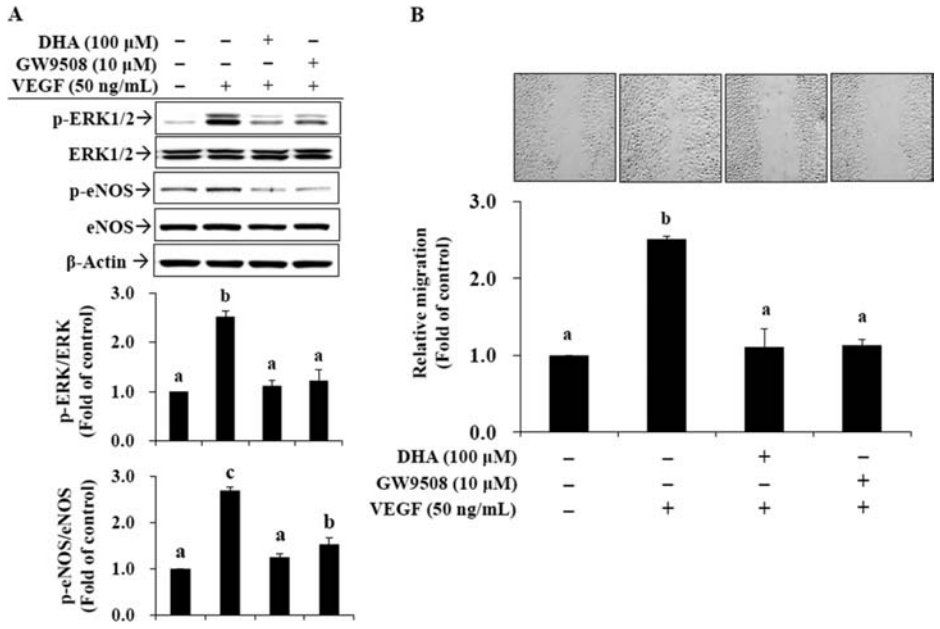

Figure 4. Effect of GPR120 agonist on phosphorylation of ERK1/2 and eNOS and cell migration induced by VEGF in HUVECs. (A) Cells were pretreated with 100 μM DHA or 10 μM GW9508 for 8 h followed by incubation with 50 ng/mL VEGF for another 15 min. (B) Cells were scratched and were cotreated with 100 μM DHA or 10 μM GW9508 along with 50 ng/mL VEGF for 8 h. Values are the mean ± SD, n = 3. Values not sharing the same letter are significantly different ($p < 0.05$).

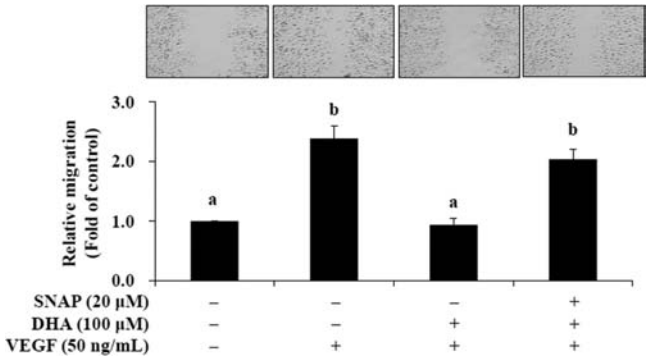

Figure 5. SNAP reverses DHA inhibition of VEGF-induced migration in HUVECs. Cells were scratched and were treated with 50 ng/mL VEGF alone, cotreated with 100 μM DHA and 50 ng/mL VEGF, or cotreated with 20 μM SNAP, 100 μM DHA, and 50 ng/mL VEGF for 8 h. Values are the mean ± SD, n = 3. Values not sharing the same letter are significantly different ($p < 0.05$).

inhibition of cell migration.[39] In recent years, EPA and DHA have been shown to inhibit angiogenesis, possibly by regulating the production or activation of various pro-angiogenic factors such as eNOS, VEGF, cyclooxygenase 2 (COX-2)-derived prostanoids, and MMP-9.[7,40,41] Moreover, EPA and DHA dose-dependently inhibit ERK1/2 phosphorylation, and this is likely associated with reduced PGE_2 and VEGF production by EPA and DHA in HT-29 human colorectal cells.[40]

VEGF has been shown to induce eNOS phosphorylation and cell migration in HUVECs, and this activation is abolished by DHA.[42] Moreover, DHA has been demonstrated to inhibit TPA-induced MMP-9 expression and cell migration and invasion in MCF-7 breast cancer cells.[3] Consistent with the results of these previous studies, our data showed that DHA exerted an inhibitory effect on VEGF-induced cell migration in HUVECs (Figure 1). Cell migration is essential for angiogenesis. Thus, the results of the present study suggest that DHA is a potential anti-angiogenic agent.

ERK1/2 is known to play an important role in cell proliferation, and protein phosphatases are generally identified as inhibitors of cell proliferation via dephosphorylation of ERK1/2.[21] Activation of the Akt/eNOS[43] or ERK1/2/eNOS[30] pathways is reported to be involved in VEGF-induced NO release. In the present study, VEGF activated phosphorylation of ERK1/2 but not of Akt (data not shown). Pretreatment with the ERK1/2 inhibitor PD98059 abolished VEGF-induced phosphorylation of ERK1/2 and eNOS in HUVECs (Figure 2A). These results suggest that eNOS is the downstream target of ERK1/2. Moreover, DHA was shown to inhibit VEGF-induced cell migration via suppression of the ERK1/2/eNOS signaling pathway (Figure 3A,C). Similar to DHA treatment, the ERK1/2 inhibitor PD98059 abolished cell migration (Figure 2B). Furthermore, as shown in Figure 5, SNAP reversed the DHA inhibition of VEGF-induced cell migration. These results strongly suggest that the DHA inhibition of VEGF-induced cell migration is through the ERK1/2/eNOS-mediated signaling pathway.

Reversible protein phosphorylation plays an important role in many cellular processes.[20] In general, cells use protein phosphorylation to alter enzyme properties such as activity and cell distribution of key regulatory proteins involved in specific pathways. Through the use of specific PP2A inhibitors and gene silencing technique, PP2A has been shown to play a key role in the regulation of cell cycle, cell morphology, and development. In addition, PP2A was demonstrated to be a tumor suppressor and can be a target for cancer therapy.[44] For example, it is reported that conjugated linoleic acid inhibits the proliferation of MCF-7 human breast cancer cells and that the working mechanisms include activation of PP2A and inhibition of ERK1/2 activation.[21] Pretreatment with the PP2A inhibitor OA reverses the effect of conjugated linoleic acid on both increased PP2A expression level and dephosphorylation of ERK1/2. This

result strongly suggests that dephosphorylation of ERK1/2 is mediated by PP2A.

Phosphorylated eNOS is also a substrate of PP2A.[31] It is reported that endostatin inhibits endothelial cell migration and angiogenesis by down-regulating the phosphorylation of eNOS at Ser1177 via PP2A, which results in a decrease in NO synthesis.[45,46] In the present study, we demonstrated that DHA activated PP2A enzyme activity, which was inhibited by OA pretreatment (Figure 3B). Pretreatment with OA reversed the inhibitory effect of DHA on VEGF-induced cell migration and phosphorylation of ERK1/2 and eNOS (Figure 3A,C). These results indicate that PP2A participates in the DHA inhibition of VEGF-induced ERK1/2/eNOS phosphorylation and cell migration. Activation of PP2A by DHA is by an as yet unidentified signaling pathway.

DHA exerts anti-inflammatory effects, but the mechanisms of these effects are not fully understood. It has been shown that GPR120 functions as an n-3 PUFA receptor.[11] In an in vitro study using RAW 264.7 cells and primary intraperitoneal macrophages, stimulation of GPR120 with n-3 PUFAs or the chemical agonist GW9508 causes a wide range of anti-inflammatory effects. All of these effects are abolished by GPR120 knockdown. Therefore, we hypothesize that DHA inhibits VEGF-induced cell migration through binding with GPR120. We used the GPR120 agonist GW9508 to simulate the activation of GPR120 by DHA in the suppression of VEGF-induced cell migration. The results showed that GW9508 significantly inhibited VEGF-induced cell migration, and the inhibitory effect was similar to that of DHA (Figure 4B). In addition, GW9508 significantly suppressed VEGF-induced phosphorylation of ERK1/2 and eNOS (Figure 4A), which is critical to cell migration.

Our findings in the present study are presented schematically in Figure 6. In conclusion, DHA significantly inhibits VEGF-induced phosphorylation of ERK1/2 and eNOS and cell migration via binding to GPR120 and induction of PP2A enzyme activity in HUVECs. Treatment with the NO donor SNAP reverses the DHA inhibition of VEGF-induced cell migration. Taken together, these results support an opposing role of DHA in cell migration, which is implicated in its anticancer and anti-wound-repair properties.

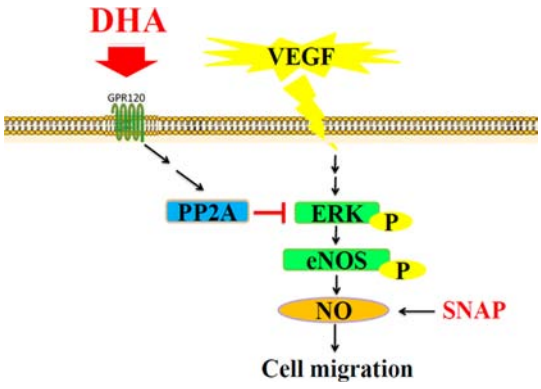

Figure 6. Model showing the pathways that mediate DHA inhibition of VEGF-induced cell migration in HUVECs. DHA inhibits VEGF-induced cell migration via binding to GPR120, activation of PP2A, and inhibition of ERK1/2 and eNOS phosphorylation.

AUTHOR INFORMATION

Corresponding Authors

*(H.-W.C.) Mail: Department of Nutrition, China Medical University, Taichung 404, Taiwan. Phone: +886 4 22053366, ext. 7520. Fax: +886 4 2206 2891. E-mail: chenhw@mail.cmu.edu.tw.

*(K.-L.L.) Mail: School of Nutrition, Chung Shan Medical University, Taichung 402, Taiwan. Phone: +886 4 24730022, ext. 12136. Fax: +886 4 2324 8175. E-mail: kaililiu@csmu.edu.tw.

Author Contributions

‖C.-Y.C. and C.-K.L. contributed equally to this study.

Funding

This study was supported by Grants NSC-101-2313-B-039-007-MY3 and CMU101-ASIA-11.

Notes

The authors declare no competing financial interest.

ABBREVIATIONS USED

COX-2, cyclooxygenase 2; DHA, docosahexaenoic acid; ECGS, endothelial cell growth supplement; eNOS, endothelial NOS; EPA, eicosapentaenoic acid; ERK, extracellular signal-regulated kinase; FBS, fetal bovine serum; GPRs, G protein-coupled receptors; HUVECs, human umbilical vein endothelial cells; MAPK, mitogen-activated protein kinase; MMP-9, matrix metalloproteinase 9; nNOS, neuronal NOS; NO, nitric oxide; OA, okadaic acid; PBS, phosphate-buffered saline; PGE_2, prostaglandin E_2; PI3K, phosphatidyl inositol 3-kinase; PP2A, protein phosphatase 2A; PUFAs, polyunsaturated fatty acids; SNAP, *S*-nitroso-*N*-acetyl-DL-penicillamine; VEGF, vascular endothelial growth factor

REFERENCES

(1) Yang, Y. C.; Lii, C. K.; Wei, Y. L.; Li, C. C.; Lu, C. Y.; Liu, K. L.; Chen, H. W. Docosahexaenoic acid inhibition of inflammation is partially via cross-talk between Nrf2/heme oxygenase 1 and IKK/NF-κB pathways. *J. Nutr. Biochem.* **2013**, *24*, 204−212.

(2) Simopoulos, A. P. Omega-3 fatty acids in inflammation and autoimmune diseases. *J. Am. Coll. Nutr.* **2002**, *21*, 495−505.

(3) Chen, H. W.; Chao, C. Y.; Lin, L. L.; Lu, C. Y.; Liu, K. L.; Lii, C. K.; Li, C. C. Inhibition of matrix metalloproteinase-9 expression by docosahexaenoic acid mediated by heme oxygenase 1 in 12-*O*-tetradecanoylphorbol-13-acetate-induced MCF-7 human breast cancer cells. *Arch. Toxicol.* **2013**, *87*, 857−869.

(4) American Cancer Society. *Cancer Facts & Figures 2007*; American Cancer Society: Atlanta, GA, USA, 2007.

(5) Brasky, T. M.; Lampe, J. W.; Potter, J. D.; Patterson, R. E.; White, E. Specialty supplements and breast cancer risk in the VITamins And Lifestyle (VITAL) Cohort. Cancer epidemiology, biomarkers and prevention: a publication of the American Association for Cancer Research, cosponsored by the American Society of Preventive. *Oncology* **2010**, *19*, 1696−1708.

(6) Wolk, A.; Larsson, S. C.; Johansson, J. E.; Ekman, P. Long-term fatty fish consumption and renal cell carcinoma incidence in women. *JAMA, J. Am. Med. Assoc.* **2006**, *296*, 1371−1376.

(7) Matesanz, N.; Park, G.; McAllister, H.; Leahey, W.; Devine, A.; McVeigh, G. E.; Gardiner, T. A.; McDonald, D. M. Docosahexaenoic acid improves the nitroso-redox balance and reduces VEGF-mediated angiogenic signaling in microvascular endothelial cells. *Invest. Ophthalmol. Vis. Sci.* **2010**, *51*, 6815−6825.

(8) Ulloa-Aguirre, A.; Stanislaus, D.; Janovick, J. A.; Conn, P. M. Structure-activity relationships of G protein-coupled receptors. *Arch. Med. Res.* **1999**, *30*, 420−435.

(9) Gether, U. Uncovering molecular mechanisms involved in activation of G protein-coupled receptors. *Endocr. Rev.* **2000**, *21*, 90−113.
(10) Schulte, G.; Fredholm, B. B. Signaling from adenosine receptors to mitogen-activated protein kinases. *Cell. Signal.* **2003**, *15*, 813−827.
(11) Oh, D. Y.; Talukdar, S.; Bae, E. J.; Imamura, T.; Morinaga, H.; Fan, W.; Li, P.; Lu, W. J.; Watkins, S. M.; Olefsky, J. M. GPR120 is an omega-3 fatty acid receptor mediating potent anti-inflammatory and insulin-sensitizing effects. *Cell* **2010**, *142*, 687−698.
(12) Fischer, C.; Schneider, M.; Carmeliet, P. Principles and therapeutic implications of angiogenesis, vasculogenesis and arteriogenesis. *Handb. Exp. Pharmacol.* **2006**, 157−212.
(13) Griffioen, A. W.; Molema, G. Angiogenesis: potentials for pharmacologic intervention in the treatment of cancer, cardiovascular diseases, and chronic inflammation. *Pharmacol. Rev.* **2000**, *52*, 237−268.
(14) Nakagawa, K.; Shibata, A.; Saito, T.; Sookwong, P.; Kato, S.; Tsuduki, T.; Matsubara, K.; Miyazawa, T. Phosphatidylcholine hydroperoxide promotes VEGF-induced angiogenesis in endothelial cells and rat aorta ring cultures. *Biochim. Biophys. Acta* **2011**, *1810*, 1205−1211.
(15) Hoeben, A.; Landuyt, B.; Highley, M. S.; Wildiers, H.; Van Oosterom, A. T.; De Bruijn, E. A. Vascular endothelial growth factor and angiogenesis. *Pharmacol. Rev.* **2004**, *56*, 549−580.
(16) Giles, F. J. The vascular endothelial growth factor (VEGF) signaling pathway: a therapeutic target in patients with hematologic malignancies. *Oncologist* **2001**, *6* (Suppl.5), 32−39.
(17) Duda, D. G.; Fukumura, D.; Jain, R. K. Role of eNOS in neovascularization: NO for endothelial progenitor cells. *Trends Mol. Med.* **2004**, *10*, 143−145.
(18) Fleming, I. Molecular mechanisms underlying the activation of eNOS. *Pflugers Archiv.* **2010**, *459*, 793−806.
(19) Shi, Y. Assembly and structure of protein phosphatase 2A. *Sci. China Ser. C, Life Sci./Chinese Acad. Sci.* **2009**, *52*, 135−146.
(20) Janssens, V.; Goris, J. Protein phosphatase 2A: a highly regulated family of serine/threonine phosphatases implicated in cell growth and signalling. *Biochem. J.* **2001**, *353*, 417−439.
(21) Miglietta, A.; Bozzo, F.; Gabriel, L.; Bocca, C.; Canuto, R. A. Extracellular signal-regulated kinase 1/2 and protein phosphatase 2A are involved in the antiproliferative activity of conjugated linoleic acid in MCF-7 cells. *Br. J. Nutr.* **2006**, *96*, 22−27.
(22) Zhao, B.; Sun, L.; Haas, M.; Denenberg, A. G.; Wong, H. R.; Shanley, T. P. PP2A regulates upstream members of the c-jun N-terminal kinase mitogen-activated protein kinase signaling pathway. *Shock* **2008**, *29*, 181−188.
(23) Lee, T.; Kim, S. J.; Sumpio, B. E. Role of PP2A in the regulation of p38 MAPK activation in bovine aortic endothelial cells exposed to cyclic strain. *J. Cell. Physiol.* **2003**, *194*, 349−355.
(24) Neviani, P.; Santhanam, R.; Trotta, R.; Notari, M.; Blaser, B. W.; Liu, S.; Mao, H.; Chang, J. S.; Galietta, A.; Uttam, A.; Roy, D. C.; Valtieri, M.; Bruner-Klisovic, R.; Caligiuri, M. A.; Bloomfield, C. D.; Marcucci, G.; Perrotti, D. The tumor suppressor PP2A is functionally inactivated in blast crisis CML through the inhibitory activity of the BCR/ABL-regulated SET protein. *Cancer Cell* **2005**, *8*, 355−368.
(25) Spencer, L.; Mann, C.; Metcalfe, M.; Webb, M.; Pollard, C.; Spencer, D.; Berry, D.; Steward, W.; Dennison, A. The effect of omega-3 FAs on tumour angiogenesis and their therapeutic potential. *Eur. J. Cancer* **2009**, *45*, 2077−2086.
(26) Lamalice, L.; Le Boeuf, F.; Huot, J. Endothelial cell migration during angiogenesis. *Circ. Res.* **2007**, *100*, 782−794.
(27) Gill, S. E.; Parks, W. C. Metalloproteinases and their inhibitors: regulators of wound healing. *Int. J. Biochem. Cell Biol.* **2008**, *40*, 1334−1347.
(28) Liu, S.; Rockey, D. C. Cicletanine stimulates eNOS phosphorylation and NO production via Akt and MAP kinase/Erk signaling in sinusoidal endothelial cells. *Am. J. Physiol. Gastrointest. Liver Physiol.* **2013**, *305*, G163−G171.
(29) Zhang, J.; Lu, A.; Beech, D.; Jiang, B.; Lu, Y. Suppression of breast cancer metastasis through the inhbition of VEGF-mediated tumor angiogenesis. *Cancer Ther.* **2007**, *5*, 273−286.
(30) Feliers, D.; Chen, X.; Akis, N.; Choudhury, G. G.; Madaio, M.; Kasinath, B. S. VEGF regulation of endothelial nitric oxide synthase in glomerular endothelial cells. *Kidney Int.* **2005**, *68*, 1648−1659.
(31) Greif, D. M.; Kou, R.; Michel, T. Site-specific dephosphorylation of endothelial nitric oxide synthase by protein phosphatase 2A: evidence for crosstalk between phosphorylation sites. *Biochemistry* **2002**, *41*, 15845−15853.
(32) Hirasawa, A.; Tsumaya, K.; Awaji, T.; Katsuma, S.; Adachi, T.; Yamada, M.; Sugimoto, Y.; Miyazaki, S.; Tsujimoto, G. Free fatty acids regulate gut incretin glucagon-like peptide-1 secretion through GPR120. *Nat. Med.* **2005**, *11*, 90−94.
(33) Hsu, Y. H.; Chen, Y. C.; Chen, T. H.; Sue, Y. M.; Cheng, T. H.; Chen, J. R.; Chen, C. H. Far-infrared therapy induces the nuclear translocation of PLZF which inhibits VEGF-induced proliferation in human umbilical vein endothelial cells. *PLoS One* **2012**, *7*, e30674.
(34) Cooke, J. P.; Losordo, D. W. Nitric oxide and angiogenesis. *Circulation* **2002**, *105*, 2133−2135.
(35) Kim, H. J.; Vosseler, C. A.; Weber, P. C.; Erl, W. Docosahexaenoic acid induces apoptosis in proliferating human endothelial cells. *J. Cell. Physiol.* **2005**, *204*, 881−888.
(36) Rose, D. P.; Connolly, J. M. Antiangiogenicity of docosahexaenoic acid and its role in the suppression of breast cancer cell growth in nude mice. *Int. J. Oncol.* **1999**, *15*, 1011−1015.
(37) Tsuzuki, T.; Shibata, A.; Kawakami, Y.; Nakagaya, K.; Miyazawa, T. Anti-angiogenic effects of conjugated docosahexaenoic acid in vitro and in vivo. *Biosci., Biotechnol., Biochem.* **2007**, *71*, 1902−1910.
(38) Zajdel, A.; Wilczok, A.; Chodurek, E.; Gruchlik, A.; Dzierzewicz, Z. Polyunsaturated fatty acids inhibit melanoma cell growth in vitro. *Acta Polym. Pharm.* **2013**, *70*, 365−369.
(39) Zhuang, W.; Wang, G.; Li, L.; Lin, G.; Deng, Z. Omega-3 polyunsaturated fatty acids reduce vascular endothelial growth factor production and suppress endothelial wound repair. *J. Cardiovasc. Transl. Res.* **2013**, *6*, 287−293.
(40) Calviello, G.; Di Nicuolo, F.; Gragnoli, S.; Piccioni, E.; Serini, S.; Maggiano, N.; Tringali, G.; Navarra, P.; Ranelletti, F. O.; Palozza, P. n-3 PUFAs reduce VEGF expression in human colon cancer cells modulating the COX-2/PGE2 induced ERK-1 and -2 and HIF-1α induction pathway. *Carcinogenesis* **2004**, *25*, 2303−2310.
(41) Szymczak, M.; Murray, M.; Petrovic, N. Modulation of angiogenesis by omega-3 polyunsaturated fatty acids is mediated by cyclooxygenases. *Blood* **2008**, *111*, 3514−3521.
(42) Kornfeld, S.; Goupille, C.; Vibet, S.; Chevalier, S.; Pinet, A.; Lebeau, J.; Tranquart, F.; Bougnoux, P.; Martel, E.; Maurin, A.; Richard, S.; Champeroux, P.; Mahéo, K. Reducing endothelial NOS activation and interstitial fluid pressure with n-3 PUFA offset tumor chemoresistance. *Carcinogenesis* **2012**, *33*, 260−267.
(43) Michaud, S. E.; Dussault, S.; Groleau, J.; Haddad, P.; Rivard, A. Cigarette smoke exposure impairs VEGF-induced endothelial cell migration: role of NO and reactive oxygen species. *J. Mol. Cell. Cardiol.* **2006**, *41*, 275−284.
(44) Janssens, V.; Goris, J.; Van Hoof, C. PP2A: the expected tumor suppressor. *Curr. Opin. Genet. Dev.* **2005**, *15*, 34−41.
(45) Schmidt, A.; Wenzel, D.; Thorey, I.; Werner, S.; Fleischmann, B. K.; Bloch, W. Endostatin down-regulates soluble guanylate cyclase (sGC) in endothelial cells in vivo: influence of endostatin on vascular endothelial growth factor (VEGF) signaling. *Endothelium* **2005**, *12*, 251−257.
(46) Urbich, C.; Reissner, A.; Chavakis, E.; Dernbach, E.; Haendeler, J.; Fleming, I.; Zeiher, A. M.; Kaszkin, M.; Dimmeler, S. Dephosphorylation of endothelial nitric oxide synthase contributes to the anti-angiogenic effects of endostatin. *FASEB J.* **2002**, *16*, 706−708.

JOURNAL OF AGRICULTURAL AND FOOD CHEMISTRY

Article

pubs.acs.org/JAFC

Antioxidant Activity and Delayed Aging Effects of Hot Water Extract from *Chamaecyparis obtusa* var. *formosana* Leaves

Szu-Chin Cheng,[†] Wen-Hsuan Li,[§] Yeu-Ching Shi,[§] Pei-Ling Yen,[†] Huan-You Lin,[†] Vivian Hsiu-Chuan Liao,*[,§] and Shang-Tzen Chang*[,†]

[†]School of Forest and Resource Conservation, National Taiwan University, Taipei 10617, Taiwan

[§]Department of Bioenvironmental Systems Engineering, National Taiwan University, Tapei 10617, Taiwan

Supporting Information

ABSTRACT: The antioxidant activity and delayed aging effects of hot water extracts from leaves of *Chamaecyparis obtusa* var. *formosana* were investigated. Free radical, superoxide radical scavenging, and total phenolic content assays were employed to evaluate the *in vitro* activities of the extracts. In addition, *in vivo* assays using the nematode *Caenorhabditis elegans* were also performed in this study. The results showed that among all soluble fractions obtained from the extracts, the ethyl acetate-soluble fraction has the best *in vitro* and *in vivo* antioxidant activities. Moreover, it decreased significantly the deposition of lipofuscin (aging pigment) and extended the lifespan of *C. elegans*. Bioactivity-guided fractionation yielded six potent antioxidant constituents from the ethyl acetate-soluble fraction, namely, catechin, quercetin, quercetin-3-*O*-α-rhamnoyranoside, myricetin-3-*O*-α-rhamnoyranoside, vanillic acid, and 4-hydroxybenzoic acid. Quercetin-3-*O*-α-rhamnoyranoside pretreatment showed the highest survival of *C. elegans* upon juglone exposure. Taken together, the results revealed that hot water extracts from *C. obtusa* var. *formosana* leaves have the potential to be used as a source for antioxidant or delayed aging health food.

KEYWORDS: *antioxidant activity, Chamaecyparis obtusa var. formosana, delayed aging effect, Caenorhabditis elegans*

INTRODUCTION

Chamaecyparis obtusa var. *formosana* is a conifer species indigenous to Taiwan and is commonly called "Taiwan Hinoki". It can be found in mountains at elevations from 1800 to 2600 m. Several studies have revealed that *C. obtusa* var. *formosana* exerts various biological activities, including cytotoxic, allopathic, antioxidant, and antitermite activities.[1−5] However, to the best of our knowledge there is no prior report on the antioxidant activities of hot water extracts from *C. obtusa* var. *formosana* leaves. Thus, this study was the first to investigate the antioxidant compounds of *C. obtusa* var. *formosana* leaves.

Oxidative stress has been linked to the development of various diseases, including inflammation, diabetes, cancers, aging, and Alzheimer's disease.[6−9] Oxidative stress reflects an imbalance between the production of free radicals and reactive metabolites, also known as oxidants or reactive oxygen species (ROS) in organisms. Intracellular ROS are considered harmful because they react with proteins, lipids, DNA, and other important biomolecules, thus leading to progressive loss of cellular integrity and functionality.[10] In particular, an increase in intracellular oxidative stress has been linked to play a vital role in aging and age-related diseases.[11,12]

The soil nematode *Caenorhabditis elegans* has become a prominent model for studying stress resistance, aging, and age-related diseases[13] due to its relatively short lifespan and developmental cycle and the existence of mutants and genetic and environmental manipulations that influence its lifespan.[13,14]

This study evaluated the antioxidant activities of hot water extracts and their constituents from leaves of *C. obtusa* var. *formosana* both *in vitro* and *in vivo*. The nematode *C. elegans* was used as an *in vivo* model to examine their protective potential including oxidative stress resistance and longevity. Our findings showed that a hot water extract of *C. obtusa* var. *formosana* leaves provides resistance against oxidative stress and delayed aging effects in an intact organism.

MATERIALS AND METHODS

Plant Materials. The fresh, mature leaves of *Chamaecyparis obtusa* var. *formosana* were sampled from Mt. Chilan in Ilan County, Taiwan. The species was identified by Yen-Ray Hsui at the Taiwan Forestry Research Institute, and a voucher specimen (ChObvFoL31) was deposited in the laboratory of wood chemistry, School of Forestry and Resource Conservation, National Taiwan University. The materials were air-dried at ambient temperature (25 °C).

Chemicals. 1,1-Diphenyl-2-picrylhydrazyl (DPPH), Folin−Ciocalteu reagent, quercetin, nitroblue tetrazolium chloride (NBT), xanthine oxidase, and (+)-catechin were purchased from Sigma Chemical Co. (MO, USA). HPLC grade methanol, Na_2CO_3, and KH_2PO_4 were purchased from Merck (Darmstadt, Germany). Ethyl acetate and *n*-butanol were purchased from ECHO Chemical Co. (Miaoli, Taiwan). Ethanol was purchased from Shimakyu Co. (Osaka, Japan). Gallic acid, Na_2EDTA, KOH, and NMR solvent were purchased from Acros (Geel, Belgium).

Extraction and Identification of Compounds. Fresh leaves were added to boiling double-distilled water and allowed to infuse for 6 h. The extract was decanted, filtered under vacuum, concentrated in a rotary evaporator, and then lyophilized. The resulting crude extract (579 g) was fractionated successively with ethyl acetate, *n*-butanol, and

Received: February 17, 2014
Revised: April 9, 2014
Accepted: April 15, 2014
Published: April 28, 2014

ACS Publications © 2014 American Chemical Society

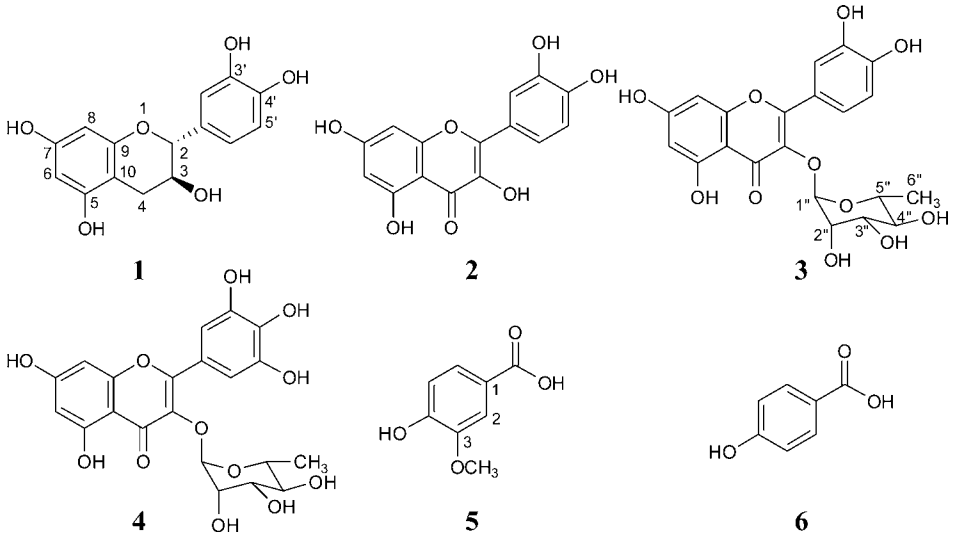

Figure 1. Structures of six phytochemicals in the ethyl acetate-soluble fraction of a hot water extract from *C. obtusa* var. *formosana* leaves: catechin (**1**); quercetin (**2**); quercetin-3-*O*-α-rhamnopyranoside (**3**); myricetin-3-*O*-α-rhamnopyranoside (**4**); vanillic acid (**5**); 4-hydroxybenzoic acid (**6**).

water to yield soluble fractions of ethyl acetate (46.7 g), *n*-butanol (138.5 g), and water (377.3 g). The phytochemicals from the ethyl acetate-soluble fraction were separated and purified by semipreparative HPLC on a Agilent model 1100 pump equipped with a UV detector (Agilent 1100) and a 250 mm × 10.0 mm i.d., 5 μm Luna RP-18 column (Phenomenex, CA, USA). The mobile phase used was solvent A (100% methanol) and solvent B (ultrapure water). Elution conditions were 0−40 min of 25−60% A to B (linear gradient); 40−60 min of 60−100% A to B (linear gradient). ESI-MS data were collected using a Finnigan MAT-95S mass spectrometer, and NMR spectra were recorded by a Bruker Avance 500 MHz FT-NMR spectrometer. The structures of chemical compounds **1**−**6** (as shown in Figure 1) were identified by ESI-MS and NMR, and all spectral data were consistent with those reported in the literature.[15−19]

1,1-Diphenyl-2-picrylhydrazyl Assay. The DPPH radical scavenging activity of the test extracts or compounds from *C. obtusa* var. *formosana* leaves was examined according to the method previously reported.[20] Briefly, 10 μL of test samples in dimethyl sulfoxide (DMSO) were mixed with 90 μL of 50 mM Tris-HCl buffer (pH 7.4) and 200 μL of 0.1 mM DPPH−ethanol solution. After 30 min of incubation at ambient temperature, the reduction of the DPPH radical was measured by reading the absorbance at 517 nm using an ELISA reader (SpectraMax 190, Molecular Devices, CA, USA). (+)-Catechin was used as a positive control. Three replicates were made for each test sample. The inhibition percentage was calculated according to the following equation:

$$\%\ \text{inhibition} = [(\text{absorbance of control} - \text{absorbance of sample})/\text{absorbance of control}] \times 100$$

Superoxide Radical Scavenging Assay (NBT Assay). Measurement of superoxide radical scavenging activity was carried out according to the method of Chang et al.[20] Briefly, 20 μL of 15 mM Na_2EDTA in buffer (50 mM KH_2PO_4/KOH, pH 7.4), 50 μL of 0.6 mM nitroblue tetrazolium chloride in buffer, 30 μL of 3 mM hypoxanthine in 50 mM KOH, 5 μL of the test extracts or compounds in methanol, and 145 μL of buffer were mixed in 96-well microplates. The reaction was started by adding 50 μL of xanthine oxidase in buffer (1 unit in 10 mL of buffer) to the mixture. The reaction mixture was incubated at ambient temperature, and the absorbance at 570 nm was determined every 1 min up to 8 min using the ELISA reader. (+)-Catechin and quercetin, well-known antioxidants, were used as positive controls. Three replicates were made for each test sample. The percent inhibition ratio was calculated according to the following equation:

$$\%\ \text{inhibition} = [1 - (\text{rate of sample reaction}/\text{rate of control reaction})] \times 100$$

Total Phenolic Content Measurement. The amount of total phenolics was measured by the Folin−Ciocalteu method according to Chang et al.,[20] using gallic acid as a standard, and a calibration curve was obtained with solutions of 0.08, 0.04, 0.02, 0.01, and 0.005 mg/mL of this compound. A 0.4 mL aliquot of diluted extract (all fractions were diluted with methanol to adjust the absorbance within the calibration limits), 0.4 mL of 1 mol/L Folin−Ciocalteu reagent, and 0.8 mL of Na_2CO_3 (20%, w/v) were mixed. After 8 min, the mixture was centrifuged at 15300*g* for 10 min. Then the absorbance of the supernatant solution was measured at 730 nm by using ELISA and against a blank prepared similarly but containing distilled water instead of extract. The concentration of phenolics thus obtained was multiplied by the dilution factor, and the results were expressed as the equivalent to milligrams of gallic acid per gram of extract (mg GAE/g).

***C. elegans* Handling.** The strain used in this study was Bristol N2 (wild-type), which was obtained from the *Caenorhabditis* Genetics Center (CGC; University of Minnesota). *C. elegans* was maintained and assayed at 20 °C on nematode growth medium (NGM) agar plates carrying a lawn of *Escherichia coli* (*E. coli.*) OP50. Synchronization of nematode cultures was performed by hypochlorite treatment of gravid hermaphrodites.[21]

***C. elegans* Oxidative Stress Resistance Assays.** Synchronized wild-type L1 larvae were incubated in liquid S-basal medium containing *E. coli* OP50 bacteria at 10^9 cells/mL with extract or 0.1% DMSO (Wako, Saitama, Japan) as the solvent control for 72 h. Subsequently, adult nematodes were immediately subjected to the oxidative stress assay. For this assay, juglone (5-hydroxy-1,4-naphthoquinone) (Sigma, MO, USA), an ROS-generating compound, was employed to induce oxidative stress in *C. elegans*. Extract-treated and control adult nematodes were transferred to S-basal medium containing 250 μM juglone for 2.5 h[22,23] and then scored for viability. The survival of *C. elegans* was determined by touch-provoked movement.[24] Nematodes were scored as dead when they failed to respond to repeated touching with a platinum wire pick. The test was performed independently at least three times.

***C. elegans* Intracellular Reactive Oxygen Species Measurement.** Wild-type nematodes were raised from L1 larvae as described in the oxidative stress resistance assays. Subsequently, intracellular ROS in *C. elegans* were measured using 2′,7′-dichlorodihydrofluorescein diacetate (H_2DCFDA) (Sigma, MO, USA). Approximately 100 nematodes were sonicated after extract treatment, and the lysates were

then collected for ROS measurement.[23,25,26] Worm samples were incubated with H_2DCFDA (at a final concentration of 50 μM in phosphate-buffered saline) in an FLx800 microplate fluorescent reader (Bio-Tek Instruments, VT, USA) for quantification of fluorescence with excitation at 485 nm and emission at 530 nm. Samples were read after 3 h.

C. elegans Lifespan Assays. *C. elegans* lifespan analyses were performed in the same manner for all treatments at 20 °C. Synchronized L1 larvae were transferred to NGM plates in the absence or presence of 2 or 20 μg/mL ethyl acetate-soluble fraction, and *C. elegans* was allowed to develop to adulthood. Surviving and dead animals were counted daily (starting on the first day of adulthood) until all nematodes died. Animals that did not move when gently prodded (with a platinum wire) were scored as dead. Nematodes suffering from internal hatch (a defect in egg laying) and those that crawled off the NGM plate were not included in the lifespan counts. During the reproductive period, adult nematodes were transferred to fresh NGM plates every day during the progeny production period and then every other day thereafter. To avoid antibacterial effects of extract, lifespan assays were conducted with UV-killed *E. coli* OP50 according to Gruber et al.[27] The lifespan assays were performed at least three times.

C. elegans Intracellular Lipofuscin Assays. Wild-type animals were raised from L1 larvae as in the lifespan assays. On the fourth and eighth days of adulthood, the intestinal autofluorescence of lipofuscin was analyzed according to Liao et al.[28] Randomly selected worms from each set of experiments were mounted onto microscope slides coated with 3% agarose, anesthetized with 2% sodium azide, and capped with coverslips. The autofluorescence of lipofuscin was captured with a Leica epifluorescence microscope (Leica, Wetzlar, Germany) using the DAPI filter set (with excitation at 340−380 nm and emission at 435−485 nm) and a cooled charge-coupled device camera. The lipofuscin level for each worm was quantified by determining the average pixel intensity in each animal's intestine using Image-Pro Plus software (Media Cybernetics, MD, USA).

Statistical Analyses. For the lifespan assays, survival of *C. elegans* was plotted using Kaplan−Meier survival curves and analyzed by the log-rank test using GraphPad Prism (GraphPad Software, Inc., CA, USA). Other data were expressed as mean ± SE (n = 3). The significance of difference was calculated by Scheffe's test, and values of $p < 0.05$ were considered significant.

RESULTS AND DISCUSSION

***In Vitro* Antioxidant Activities of a Hot Water Extract from *C. obtusa* var. *formosana* Leaves.** Strong activity in scavenging DPPH and superoxide radical of hot water extracts is shown in Table 1. The DPPH free radical inhibitory (IC_{50}) ability of the hot water extract is 8.5 ± 0.2 μg/mL, and the IC_{50} values of three fractions increased as follows: ethyl acetate (6.3 ± 0.2 μg/mL), *n*-butanol (7.2 ± 0.1 μg/mL), and water (30.2 ± 3.1 μg/mL). In addition, the scavenging ability of superoxide, the most common radical in our organisms, was also tested. Their IC_{50} values decreased in the order ethyl acetate-soluble fraction (1.6 ± 0.0 μg/mL), crude extract (2.6 ± 0.2 μg/mL), *n*-butanol-soluble fraction (3.1 ± 0.1 μg/mL), and water-soluble fraction (8.4 ± 0.1 μg/mL). These results demonstrated that the hot water extract has potential as an antioxidant source. Among all soluble fractions, the ethyl acetate-soluble fraction has the best inhibitory effect on free radical scavenging ability.

Table 1. DPPH Radical and Superoxide Radical Scavenging Activity and Total Phenolic Contents of a Hot Water Extract from *C. obtusa* var. *formosana* Leaves and Its Soluble Fractions[a]

	DPPH	NBT	TPC
specimen	IC_{50} (μg/mL)	IC_{50} (μg/mL)	(mg GAE/g)
HWE	8.5 ± 0.2 b	2.6 ± 0.2 b	282.4 ± 7.3 c
EAF	6.3 ± 0.2 c	1.6 ± 0.0 c	649.8 ± 9.6 a
BF	7.2 ± 0.1 c	3.1 ± 0.1 b	368.2 ± 12.1 b
WF	30.2 ± 3.1 a	8.4 ± 0.1 a	147.7 ± 5.2 d

[a]HWE: hot water extract; EAF: ethyl acetate-soluble fraction; BF: *n*-butanol-soluble fraction; WF: water-soluble fraction. DPPH: DPPH free radical scavenging effect; NBT: superoxide radical scavenging assay; TPC: total phenolic content. Different letters (a−d) are significantly different at $p < 0.05$ according to Scheffe's test (mean ± SE, n = 3). The IC_{50} value of catechin is 2.9 μg/mL (DPPH) and 2.7 μg/mL (NBT), respectively.

Total Phenolic Contents of a Hot Water Extract from *C. obtusa* var. *formosana* Leaves and Its Soluble Fractions. Phenolic compounds are well-known radical scavengers in the plant kingdom, and they have been proved to have various biological effects.[29−32] Table 1 shows the total phenolic content of the crude extract and its derived fractions calculated as gallic acid equivalent (GAE) in milligrams per gram of sample. Accordingly, the total phenolic content of the ethyl acetate-soluble fraction (649.8 ± 9.6 mg GAE/g) was significantly higher than that of the *n*-butanol-soluble fraction (368.2 ± 12.1 mg GAE/g), crude extracts (282.4 ± 7.3 mg GAE/g), and water fraction (147.7 ± 5.2 mg GAE/g). These results indicated that the total phenolic content of the hot water extract from *C. obtusa* var. *formosana* leaves could be effectively enriched in the ethyl acetate-soluble fraction.

Enhanced Oxidative Stress Resistance of Wild-Type *C. elegans* by a Hot Water Extract from *C. obtusa* var. *formosana* Leaves. According to the above-mentioned results, the hot water extract of *C. obtusa* var. *formosana* leaves, especially the ethyl acetate-soluble fraction, has an excellent *in vitro* antioxidant activity. To further investigate the antioxidant activity of the hot water extract and different fractions in living organisms, the *C. elegans* model was employed. Wild-type L1 larvae were pretreated with the hot water extracts (2 and 20 μg/mL) and 0.1% DMSO as the solvent control for 72 h before immediate exposure to juglone (250 μM), a redox cycler that generates intracellular oxidative stress, and then incubated for 2.5 h.[22,23]

During pretreatment with the extracts, no adverse effects on the worms including survival, growth rate, and morphological changes were observed (data not shown). Pretreatment with 2 and 20 μg/mL extracts enhanced the worms' resistance to juglone-induced oxidative stress (survival of 2 μg/mL- and 20 μg/mL-treated worms was 69.3 ± 6.0% and 88.1 ± 3.2%, respectively). Since as low as 2 μg/mL extract was able to significantly defend against the juglone-induced oxidative stress, 2 μg/mL extract was chosen as the working concentration for further experiments.

Different soluble fractions derived from hot water extracts were further examined. As shown in Figure 2, both the hot water crude extract and ethyl acetate-soluble fraction increased significantly the survival of *C. elegans* compared with the control (0.1% DMSO). In addition, the ethyl acetate-soluble fraction exhibited higher survival against juglone-induced oxidative stress (Figure 2). The increase in the worms' survival may be attributed to the chemical components in extracts with abilities for scavenging free radicals to reduce the juglone-induced oxidative stress in *C. elegans*, which was in good agreement with the *in vitro* antioxidant data (Table 1).

Influence of Hot Water Extracts from *C. obtusa* var. *formosana* Leaves on Intracellular ROS Levels in *C.*

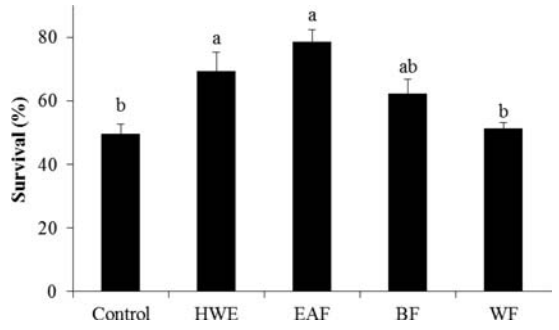

Figure 2. Survival of *C. elegans* (wild-type) treated with 2 μg/mL hot water extract of *C. obtusa* var. *formosana* leaves and its soluble fractions under oxidative stress induced by juglone. HWE: hot water extract; EAF: ethyl acetate-soluble fraction; BF: *n*-butanol-soluble fraction; WF: water-soluble fraction. Different letters (a, b) are significantly different at $\alpha = 0.05$ according to Scheffe's test (mean ± SE, $n = 3$).

***elegans*.** After pretreatment with extracts, the intracellular ROS levels in *C. elegans* were then examined. Nonfluorescent DCF-DA is a freely cell-permeable dye, which is readily converted to the fluorescent 2′,7′-dichlorofluorescein (DCF) due to an interaction with intracellular H_2O_2. As shown in Figure 3, the fluorescence intensities of the control and hot

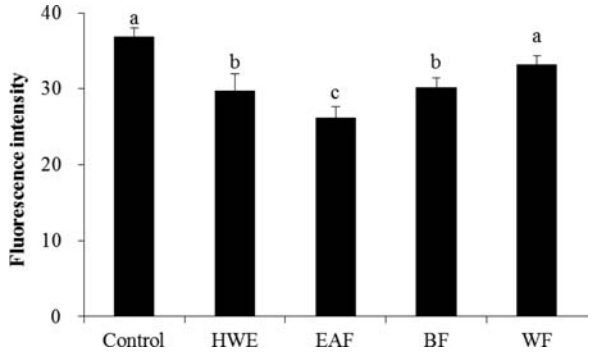

Figure 3. Effects of 2 μg/mL hot water extract from *C. obtusa* var. *formosana* leaves and its soluble fractions on ROS accumulation. Results are expressed as relative fluorescence units (RFU), fluorescence relative to total proteins in worm lysates. HWE: hot water extract; EAF: ethyl acetate-soluble fraction; BF: *n*-butanol-soluble fraction; WF: water-soluble fraction. Different letters (a–c) are significantly different at $\alpha = 0.05$ according to Scheffe's test (mean ± SE, $n = 3$).

water crude extract were 36.9 ± 1.1 and 29.7 ± 2.3 units, respectively, revealing that the hot water crude extract significantly decreased the intracellular ROS in wild-type L1 larvae pretreated at 2 μg/mL. Among three subfractions of crude extract, the ethyl acetate-soluble fraction showed a significant decrease in the fluorescence intensity (26.2 ± 1.5 units) compared with the control and hot water crude extract. These results demonstrated that the crude extract and its ethyl acetate-soluble fraction may act against oxidative stress due to its ROS-scavenging ability.

Effects of Ethyl Acetate-Soluble Fraction of a Hot Water Extract from *C. obtusa* var. *formosana* Leaves on Lifespan Extension of *C. elegans*. The ethyl acetate-soluble fraction of a hot water extract from *C. obtusa* var. *formosana* leaves not only had the highest phenolic contents but also exhibited the best antioxidant activity in both *in vitro* and *in vivo* antioxidant tests (Table 1, Figure 2). Accordingly, the ethyl acetate-soluble fraction was selected to evaluate the ability of lifespan extension using the *C. elegans* model. Adult wild-type worms grown under our standard laboratory conditions at 20 °C (feeding with UV-killed bacteria) have a mean lifespan of 20.0 ± 0.5 days with a maximum lifespan of 35.0 ± 0.9 days (the age at death of the oldest animals) (Figure 4). Ethyl

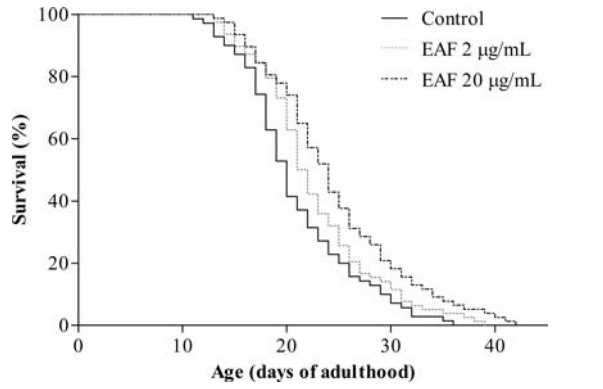

Figure 4. Effects of the ethyl acetate-soluble fraction of a hot water extract from *C. obtusa* var. *formosana* leaves on *C. elegans* (wild-type) lifespan. Survival curve's *p* value (compared with the control by log-rank test) of EAF 2 and 20 μg/mL are 0.0035 and 0.0008, respectively. EAF: ethyl acetate-soluble fraction.

acetate soluble fraction-treated worms had a statistically significant increased lifespan compared with untreated ones (log-rank test $p = 0.0035$ and 0.0008 for 2 and 20 μg/mL, respectively, untreated vs treated) (Figure 4, Table 2). This result suggests that the ethyl acetate-soluble fraction of a hot water extract from *C. obtusa* var. *formosana* has a beneficial effect against aging for organisms.

Table 2. Effects of Ethyl Acetate Soluble Fraction of a Hot Water Extract from *C. obtusa* var. *formosana* Leaves on *C. elegans* (Wild-Type) Lifespan Values[a]

		conc (μg/mL)	
lifespan	control	2	20
mean	20.0 ± 0.5	21.5 ± 0.4	24.0 ± 0.6
maximum	35.0 ± 0.9	38.0 ± 0.6	41.0 ± 1.1
log-rank test		$p = 0.0035$**	$p = 0.0008$***

[a]Results are expressed as relative fluorescence units (RFU), fluorescence relative to total proteins in worm lysates.

Effects of Ethyl Acetate-Soluble Fraction of a Hot Water Extract from *C. obtusa* var. *formosana* Leaves on Lipofuscin Levels in *C. elegans*. Lipofuscin (aging pigments) levels in the intestines of the *C. elegans* were examined, as lipofuscin is an endogenous intestinal autofluorescent material that accumulates in aged *C. elegans*. The lipofuscin levels in the intestines of control and ethyl acetate soluble fraction-treated worms on the fourth and eighth days of adulthood were measured. On the fourth day of adulthood, the intestinal lipofuscin levels of ethyl acetate soluble fraction-treated worms were similar to those of the control (Figure 5). On the eighth day of adulthood, there was a significant decrease in intestinal lipofuscin level between the control (12.4 ± 0.6 unit) and ethyl acetate soluble fraction-treated worms (2 and 20 μg/mL: 9.7 ± 0.2 units and 9.1 ± 0.6 units). The results suggest that the ethyl acetate-soluble fraction of the hot water extract from *C. obtusa*

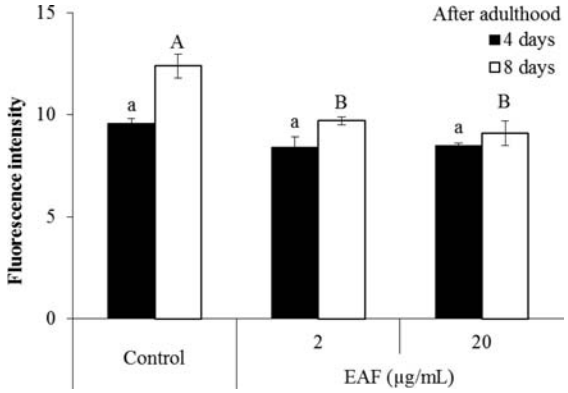

Figure 5. Effects of the ethyl acetate-soluble fraction of a hot water extract from *C. obtusa* var. *formosana* leaves on the lipofuscin accumulation of *C. elegans* (wild-type). Results are expressed as relative fluorescence units (RFU), fluorescence relative to total proteins in worm lysates. Different letters (a, A, B) are significantly different at $\alpha = 0.05$ according to Scheffe's test (mean ± SE, $n = 3$). EAF: ethyl acetate-soluble fraction.

var. *formosana* leaves could delay aging in *C. elegans* by inhibiting lipofuscin accumulation.

Constituents of Ethyl Acetate-Soluble Fraction of a Hot Water Extract from *C. obtusa* var. *formosana* Leaves and Their Antioxidant Activities. Constituents from the ethyl acetate-soluble fraction that might contribute to the observed oxidative stress resistance were then determined. By following the bioactivity-guided fractionation procedure, phytochemicals in the ethyl acetate-soluble fraction of a hot water extract from *C. obtusa* var. *formosana* leaves were isolated using semipreparative high-performance liquid chromatography (HPLC). NMR spectra and mass spectroscopy were employed to identify six constituents (Figure 1): catechin (**1**), quercetin (**2**), quercetin-3-*O*-α-rhamnopyranoside (**3**), myricetin-3-*O*-α-rhamnopyranoside (**4**), vanillic acid (**5**), and 4-hydroxybenzoic acid (**6**). The highest content of phytochemicals in *C. obtusa* var. *formosana* leaves was **3** (17.70 ± 0.6 mg/g of crude extracts), followed by **4** (6.79 ± 0.2 mg/g of crude extracts) > **1** (5.89 ± 0.1 mg/g of crude extracts) > **2** (4.17 ± 0.1 mg/g of crude extracts) > **5** (2.34 ± 0.3 mg/g of crude extracts) > **6** (1.21 ± 0.0 mg/g of crude extracts).

In vitro and *in vivo* antioxidant activities of each chemical were investigated. In the DPPH free radical scavenging assay, **2** had the lowest IC_{50} value (6.6 ± 0.4 μM), followed by **4** < **3** < **1**, with IC_{50} values of 7.2 ± 0.2, 8.5 ± 0.1, and 10.6 ± 0.2 μM, respectively. Compounds **5** and **6** did not have significant inhibitory effects on scavenging DPPH free radicals, and their IC_{50} values were higher than 50 μM (Table 3). Furthermore, in the *C. elegans* oxidative stress resistance assay, the antioxidant activities of phytochemicals can be ranked as **3** > **2** > **4** > **1** > **5** = **6** (Table 3). All compounds exhibited higher survival than that of the control (48.3 ± 0.5%). Previous studies had reported that **1** and **2** were excellent antioxidant agents in *C. elegans*.[33,34] It is interesting to note that **5** and **6** did not show significant *in vitro* antioxidant activity, whereas they showed a beneficial antioxidant effect in the *C. elegans* model.

Among the six compounds derived from *C. obtusa* var. *formosana* leaves, quercetin-3-*O*-α-rhamnopyranoside (**3**) has the highest content and was the most effective antioxidant in the *C. elegans* model. This finding suggests that quercetin-3-*O*-α-rhamnopyranoside (**3**) from the ethyl acetate-soluble fraction of *C. obtusa* var. *formosana* leaves might play a key role in the observed oxidative stress resistance. Additionally, quercetin (**2**) is a well-known antioxidant in both the *in vitro* assay and the *C. elegans* model.[35,36] It is noted that compound **3** is quercetin with a rhamnopyranoside group at the 3-position. This study found that the antioxidant activity in the *C. elegans* model was enhanced when quercetin contains a sugar. The antioxidant effect may be attributed to the moiety promoted by the rhamnopyranoside that can facilitate flavonoid absorption as described in the animal model.[37]

Table 3. Contents and Antioxidant Activities of Six Phytochemicals from the Ethyl Acetate-Soluble Fraction of Hot Water Extracts from *C. obtusa* var. *formosana* Leaves[a]

phytochemical	contents (mg/g of crude)	IC_{50} (μM) DPPH radical	*C. elegans*[b] survival (%)
catechin (**1**)	5.89 ± 0.1	10.6 ± 0.2 a	61.7 ± 1.0 d
quercetin (**2**)	4.17 ± 0.1	6.6 ± 0.4 d	77.3 ± 0.8 b
quercetin-3-*O*-α-rhamnopyranoside (**3**)	17.70 ± 0.6	8.5 ± 0.1 b	90.5 ± 0.5 a
myricetin-3-*O*-α-rhamnopyranoside (**4**)	6.79 ± 0.2	7.2 ± 0.2 c	70.1 ± 0.7 c
vanillic acid (**5**)	2.34 ± 0.3	>50	53.4 ± 0.7 e
4-hydroxybenzoic acid (**6**)	1.21 ± 0.0	>50	54.3 ± 0.6 e
control (0.1% DMSO)			48.3 ± 0.5 f

[a]Different letters (a–f) are significantly different at $\alpha = 0.05$ according to Scheffe's test (mean ± SE, $n = 3$). [b]Concentration of sample is 10 μM and observed after 2.5 h of 250 μM juglone exposure.

In conclusion, results obtained from this study revealed that hot water extracts from *C. obtusa* var. *formosana* leaves had excellent *in vitro* antioxidant activities via free radical and superoxide radical scavenging and total phenolic content assays. Furthermore, the hot water extracts promoted the resistance of oxidative stress in *C. elegans*. Among all soluble fractions obtained from hot water extracts, the ethyl acetate-soluble fraction exhibited the best antioxidant activities in both *in vitro* and *C. elegans* models. Moreover, it delayed the aging phenomenon (reduction of lipofuscin deposition and lifespan extension). Moreover, six potent antioxidant constituents, namely, catechin, quercetin, quercetin-3-*O*-α-rhamnopyranoside, myricetin-3-*O*-α-rhamnopyranoside, vanillic acid, and 4-hydroxybenzoic acid, were identified from the ethyl acetate-soluble fraction by bioactivity-guided fractionation. Among them, quercetin-3-*O*-α-rhamnopyranoside exhibited the best *in vivo* antioxidant activity and was of the highest content in hot water extracts, suggesting that it might play the key role in the observed antioxidant activity of extracts. The results in the present study indicated that hot water extracts from *C. obtusa* var. *formosana* leaves have the potential to be used as a source for an antioxidant or delayed aging health food and warrants further investigations.

■ ASSOCIATED CONTENT

Ⓢ Supporting Information

This material is available free of charge via the Internet at http://pubs.acs.org.

■ AUTHOR INFORMATION

Corresponding Authors

*(V. H.-C. Liao) Phone: +886-2-33665239. Fax: +886-2-33663462. E-mail: vivianliao@ntu.edu.tw.

*(S.-T. Chang) Phone: +886-2-33664626. Fax: +886-2-23654520. E-mail: peter@ntu.edu.tw.

Notes

The authors declare no competing financial interest.

■ ACKNOWLEDGMENTS

We gratefully acknowledge Prof. B. T. Guan and Prof. S. T. Lin for providing samples and all members of the CHEMTREE laboratory for technical assistance. We also thank Shou-Ling Huang (Department of Chemistry, National Taiwan University) for NMR spectral analyses and Dr. T. F. Yeh for his constructive and valuable comments.

■ REFERENCES

(1) Cheng, S. S.; Chang, H. T.; Wu, C. L.; Chang, S. T. Anti-termitic activities of essential oils from coniferous trees against *Coptotermes formosanus*. *Bioresour. Technol.* **2007**, *98*, 456−459.

(2) Chien, S. C.; Chang, J. Y.; Kuo, C. C.; Hsieh, C. C.; Yang, N. S.; Kuo, Y. H. Cytotoxic and novel skeleton compounds from the heartwood of *Chamaecyparis obtusa* var. *formosana*. *Tetrahedron Lett.* **2007**, *48*, 1567−1569.

(3) Kuo, P. M.; Chu, F. H.; Chang, S. T.; Hsiao, W. F.; Wang, S. Y. Insecticidal activity of essential oil from *Chamaecyparis formosensis* Matsum. *Holzforschung* **2007**, *61*, 595−599.

(4) Marimuthu, P.; Wu, C. L.; Chang, H. T.; Chang, S. T. Antioxidant activity of the ethanolic extract from the bark of *Chamaecyparis obtusa* var. *formosana*. *J. Sci. Food Agric.* **2008**, *88*, 1400−1405.

(5) Tseng, M. H.; Lai, W. R.; Hsieh, C. L.; Kuo, Y. H. Allelopathy on bark of downed logs of *Chamaecyparis obtusa* sieb. and Zucc. var. *formosana* (Hayata) Rehder. *J. Chem. Ecol.* **2007**, *33*, 1283−1296.

(6) Forsberg, L.; de Faire, U.; Morgenstern, R. Oxidative stress, human genetic variation, and disease. *Arch. Biochem. Biophys.* **2001**, *389*, 84−93.

(7) Griffiths, H. R. ROS as signalling molecules in T cells−evidence for abnormal redox signalling in the autoimmune disease, rheumatoid arthritis. *Redox Rep.* **2005**, *10*, 273−280.

(8) Kovacic, P.; Jacintho, J. D. Mechanisms of carcinogenesis: focus on oxidative stress and electron transfer. *Curr. Med. Chem.* **2001**, *8*, 773−796.

(9) Valko, M.; Rhodes, C. J.; Moncol, J.; Izakovic, M.; Mazur, M. Free radicals, metals and antioxidants in oxidative stress-induced cancer. *Chem.-Biol. Interact.* **2006**, *160*, 1−40.

(10) Finkel, T.; Holbrook, N. J. Oxidants, oxidative stress and the biology of ageing. *Nature* **2000**, *408*, 239−247.

(11) Bokov, A.; Chaudhuri, A.; Richardson, A. The role of oxidative damage and stress in aging. *Mech. Ageing Dev.* **2004**, *125*, 811−826.

(12) Cencioni, C.; Spallotta, F.; Martelli, F.; Valente, S.; Mai, A.; Zeiher, A. M.; Gaetano, C. Oxidative stress and epigenetic regulation in ageing and age-related diseases. *Int. J. Mol. Sci.* **2013**, *14*, 17643−17663.

(13) Olsen, A.; Vantipalli, M. C.; Lithgow, G. J. Using *Caenorhabditis elegans* as a model for aging and age-related diseases. *Ann. N.Y. Acad. Sci.* **2006**, *1067*, 120−128.

(14) Honda, Y.; Honda, S. Oxidative stress and life span determination in the nematode *Caenorhabditis elegans*. *Ann. N.Y. Acad. Sci.* **2002**, *959*, 466−474.

(15) Tan, J. W.; Bednarek, P.; Liu, H. K.; Schneider, B.; Svatoš, A.; Hahlbrock, K. Universally occurring phenylpropanoid and species-specific indolic metabolites in infected and uninfected *Arabidopsis thaliana* roots and leaves. *Phytochemistry* **2004**, *65*, 691−699.

(16) Chung, S. K.; Kim, Y. C.; Takaya, Y.; Terashima, K.; Niwa, M. Novel flavonol glycoside, 7-*O*-methyl mearnsitrin, from *Sageretia theezans* and its antioxidant effect. *J. Agric. Food Chem.* **2004**, *52*, 4664−4668.

(17) Ma, X. F.; Tian, W. X.; Wu, L. H.; Cao, X. L.; Ito, Y. Isolation of quercetin-3-*O*-L-rhamnoside from *Acer truncatum* Bunge by high-speed counter-current chromatography. *J. Chromatogr. A* **2005**, *1070*, 211−214.

(18) Lallemand, J. Y.; Duteil, M. ^{13}C NMR spectra of quercetin and rutin. *Org. Magn. Reson.* **1977**, *9*, 179−180.

(19) Benavides, A.; Montoro, P.; Bassarello, C.; Piacente, S.; Pizza, C. Catechin derivatives in *Jatropha macrantha* stems: characterisation and LC/ESI/MS/MS quali-quantitative analysis. *J. Pharm. Biomed. Anal.* **2006**, *40*, 639−647.

(20) Chang, S. T.; Wu, J. H.; Wang, S. Y.; Kang, P. L.; Yang, N. S.; Shyur, L. F. Antioxidant activity of extracts from *Acacia confusa* bark and heartwood. *J. Agric. Food Chem.* **2001**, *49*, 3420−3424.

(21) Sulston, J.; Hodgkin, J. Methods. In *The Nematode Caenorhabditis elegans*; Wood, W. B., Ed.; Cold Spring Harbor Laboratory Press: New York, NY, USA, 1998; pp 587−606.

(22) Hsu, F. L.; Li, W. H.; Yu, C. W.; Hsieh, Y. C.; Yang, Y. F.; Liu, J. T.; Shih, J.; Chu, Y. J.; Yen, P. L.; Chang, S. T.; Liao, V. H. *In vivo* antioxidant activities of essential oils and their constituents from leaves of the Taiwanese *Cinnamomum osmophloeum*. *J. Agric. Food Chem.* **2012**, *60*, 3092−3097.

(23) Li, W. H.; Shi, Y. C.; Tseng, I. L.; Liao, V. H. Protective efficacy of selenite against lead-induced neurotoxicity in *Caenorhabditis elegans*. *PLoS One* **2013**, *8*, e62387.

(24) Lithgow, G. J.; White, T. M.; Melov, S.; Johnson, T. E. Thermotolerance and extended life-span conferred by single-gene mutations and induced by thermal stress. *Proc. Natl. Acad. Sci. U.S.A.* **1995**, *92*, 7540−7544.

(25) Smith, J. V.; Luo, Y. Elevation of oxidative free radicals in Alzheimer's disease models can be attenuated by *Ginkgo biloba* extract EGb 761. *J. Alzheimers Dis.* **2003**, *5*, 287−300.

(26) Zhang, L.; Jie, G.; Zhang, J.; Zhao, B. Significant longevity-extending effects of EGCG on *Caenorhabditis elegans* under stress. *Free Radical Biol. Med.* **2009**, *46*, 414−421.

(27) Gruber, J.; Tang, S. Y.; Halliwell, B. Evidence for a trade-off between survival and fitness caused by resveratrol treatment of *Caenorhabditis elegans*. *Ann. N.Y. Acad. Sci.* **2007**, *1100*, 530−542.

(28) Liao, V. H.; Yu, C. W.; Chu, Y. J.; Li, W. H.; Hsieh, Y. C.; Wang, T. T. Curcumin-mediated lifespan extension in *Caenorhabditis elegans*. *Mech. Ageing Dev.* **2011**, *132*, 480−487.

(29) Cao, Z. M.; Wu, Y. J.; Curry, K.; Wu, Z. X.; Christen, Y.; Luo, Y. *Ginkgo biloba* extract EGb 761 and Wisconsin ginseng delay sarcopenia in *Caenorhabditis elegans*. *J. Gerontol. Ser. A Biol. Sci. Med. Sci.* **2007**, *62*, 1337−1345.

(30) Suárez, B.; Álvarez, Á. L.; García, Y. D.; del Barrio, G.; Lobo, A. P.; Parra, F. Phenolic profiles, antioxidant activity and *in vitro* antiviral properties of apple pomace. *Food Chem.* **2010**, *120*, 339−342.

(31) Vaquero, M. J. R.; Serravalle, L. R. T.; de Nadra, M. C. M.; de Saad, A. M. S. Antioxidant capacity and antibacterial activity of phenolic compounds from argentinean herbs infusions. *Food Control* **2010**, *21*, 779−785.

(32) Yang, C. S.; Prabhu, S.; Landau, J. Prevention of carcinogenesis by tea polyphenols. *Drug Metab. Rev.* **2001**, *33*, 237−253.

(33) Pietsch, K.; Saul, N.; Menzel, R.; Stürzenbaum, S. R.; Steinberg, C. E. W. Quercetin mediated lifespan extension in *Caenorhabditis elegans* is modulated by *age-1*, *daf-2*, *sek-1* and *unc-43*. *Biogerontology* **2009**, *10*, 565−578.

(34) Saul, N.; Pietsch, K.; Menzel, R.; Stürzenbaum, S. R.; Steinberg, C. E. W. Catechin induced longevity in *C. elegans*: from key regulator genes to disposable soma. *Mech. Ageing Dev.* **2009**, *130*, 477−486.

(35) Coskun, O.; Kanter, M.; Korkmaz, A.; Oter, S. Quercetin, a flavonoid antioxidant, prevents and protects streptozotocin-induced oxidative stress and beta-cell damage in rat pancreas. *Pharmacol. Res.* **2005**, *51*, 117−123.

(36) Jara-Palacios, M. J.; González-Manzano, S.; Escudero-Gilete, M. L.; Hernanz, D.; Dueñas, M.; González-Paramás, A. M.; Heredia, F. J.; Santos-Buelga, C. Study of zalema grape pomace: phenolic composition and biological effects in *Caenorhabditis elegans*. *J. Agric. Food Chem.* **2013**, *61*, 5114−5121.

(37) Heim, K. E.; Tagliaferro, A. R.; Bobilya, D. J. Flavonoid antioxidants: chemistry, metabolism and structure-activity relationships. *J. Nutr. Biochem.* **2002**, *13*, 572−584.

JOURNAL OF AGRICULTURAL AND FOOD CHEMISTRY

Article

pubs.acs.org/JAFC

Savinase, the Most Suitable Enzyme for Releasing Peptides from Lentil (*Lens culinaris* var. Castellana) Protein Concentrates with Multifunctional Properties

Patricia Garcia-Mora, Elena Peñas, Juana Frias, and Cristina Martínez-Villaluenga*

Department of Food Characterization, Quality and Safety, Institute of Food Science, Technology and Nutrition, Juan de la Cierva 3, 28006 Madrid, Spain

ABSTRACT: The aim of this study was to produce multifunctional hydrolysates from lentil protein concentrates. Four different proteases (Alcalase, Savinase, Protamex, and Corolase 7089) and different hydrolysis times were evaluated for their degree and pattern of proteolysis and their angiotensin I-converting enzyme (ACE) inhibitory and antioxidant activities. Alcalase and Savinase showed the highest proteolytic effectiveness ($P \leq 0.05$), which resulted in higher yield of peptides. The hydrolysate produced by Savinase after 2 h of hydrolysis (S2) displayed the highest ACE-inhibitory (IC_{50} = 0.18 mg/mL) and antioxidant activity (1.22 μmol of Trolox equiv/mg of protein). Subsequent reverse-phase HPLC−tandem mass spectrometric analysis of 3 kDa permeates of S2 showed 32 peptides, mainly derived from convicilin, vicilin, and legumin containing bioactive amino acid sequences, which makes them potential contributors to ACE-inhibitory and antioxidant activities detected. The ACE-inhibitory and antioxidant activities of S2 were significantly improved after in vitro gastrointestinal digestion ($P \leq 0.05$). Multifunctional hydrolysates could encourage value-added utilization of lentil proteins for the formulation of functional foods and nutraceuticals.

KEYWORDS: *lentil protein hydrolysates, alkaline proteases, antioxidant peptides, ACE-inhibitory peptides*

INTRODUCTION

Hypertension is a public health problem associated with cardiovascular complications affecting 25% adult population worldwide.[1] Moreover, the increasing number of individuals with metabolic syndrome is contributing to the rising prevalence of hypertension. In view of its high prevalence, pharmacotherapy and diet and lifestyle modifications are applied for treatment of hypertension. Inhibition of angiotensin I-converting enzyme (ACE; EC 3.4.15.1) has been used as a target therapy for treatment of hypertension.[2] This enzyme plays a crucial role in the renin−angiotensin and kinin−kallikrein systems regulating blood pressure.[3] Inhibition of ACE reduces the concentration of angiotensin II, a vasoconstrictor octapeptide, while it increases levels of the vasodilator peptide bradykinin, which results in the lowering of blood pressure.[2]

A recent study has shown increased participation of reactive oxygen species and reduced antioxidant enzymatic defense in the pathogenesis of hypertension.[4] Oxidative stress affects several cellular signaling cascades and cellular functions,[5] reducing the bioavailability of nitric oxide, a vasodilatory molecule involved in smooth muscle relaxation in the cardiovascular system.[6] In addition, oxidation of membrane lipids brings about lipid peroxidation products, which damage proteins in the cardiovascular system.[7] Therefore, amelioration of oxidative stress in addition to inhibition of ACE provides a multitarget therapy that may improve the clinical efficacy of pharmacological treatments for management of hypertension and other cardiovascular disorders.

Because of the adverse side effects of synthetic drugs, functional foods containing natural compounds are alternative strategies to drug therapy.[8] Food-derived bioactive peptides with more than one bioactivity have multifunctional properties that can potentially be useful in targeting the multiple pathophysiological conditions underlying hypertension.[9] Much research has been focused on the generation of peptides derived from animal and plant food proteins for the management of hypertension.[10] To date, milk is the main source of ACE-inhibitory peptides, in addition to egg, meat, and fish.[11] However, plant sources have gained less attention in this respect.

Lentil is a traditional pulse crop providing economic benefits in addition to the benefits derived from crop rotation, nitrogen fixation, and sustainable agriculture.[12] Lentils are a staple food in many countries, providing an inexpensive source of protein in the diet (20−30%); however, they are largely underexploited for new emerging applications in the functional foods and nutraceutical areas. Previous studies have shown the potential of lentil proteins as source of ACE-inhibitory peptides.[13,14] In contrast, no studies have been conducted to produce multifunctional hydrolysates from lentil proteins exhibiting both ACE-inhibitory and antioxidant activities so far, which would open up new possibilities for value-added applications of lentil.

Bioactive peptides may be produced by enzymatic hydrolysis of food proteins with enzymes of microbial, plant, or gastrointestinal origin. Several enzymes have been used to produce lentil hydrolysates with bioactive properties such as Alcalase + Flavourzyme, bromelain, papain, and gastrointestinal enzymes.[13,14] These studies have shown that ACE-inhibitory activity of lentil hydrolysates strongly depends on protease specificity. Moreover, the release of bioactive peptides and,

Received: February 18, 2014
Revised: April 15, 2014
Accepted: April 16, 2014
Published: April 16, 2014

ACS Publications © 2014 American Chemical Society

consequently, the biological activity of protein hydrolysates can be affected by operational conditions such as hydrolysis time.[15] The objective of this work was to produce multifunctional lentil hydrolysates with ACE-inhibitory and antioxidant peptides. The effect of protease type and hydrolysis time on the proteolytic pattern and ACE-inhibitory and antioxidant activities of lentil hydrolysates was also studied. This information is critical for the development of value-added products, particularly as ingredients for the functional food and nutraceutical markets.

MATERIALS AND METHODS

Materials. Lentil seeds (*Lens culinaris* var. Castellana) were provided by Semillas Iglesias S.A. (Salamanca, Spain) and stored in polyethylene bins at 4 °C. Commercial food-grade enzymes Alcalase 2.4L FG, Savinase, and Protamex were kindly provided by Novozymes (Bagsvaerd, Denmark). Alcalase and Savinase are alkaline serine proteases from *Bacillus licheniformis* and *Bacillus* sp., respectively. Protamex is a *Bacillus* protease complex consisting of subtilisin and neutral protease (EC 3.4.24.28). Corolase 7089 is a fungal neutral protease provided by AB Enzymes GmbH (Darmstadt, Germany). Tripeptide Abz-Gly-Phe(NO_2)-Pro was purchased from Cymit-Quimica (Barcelona, Spain). All other chemicals were purchased from Sigma–Aldrich Quimica (Madrid, Spain) unless otherwise specified.

Preparation of Lentil Protein Concentrates. Whole lentil seeds were ground in a coffee mill (Moulinex, Allençon, France) and passed through a 60-mesh sieve and 0.5 mm pore size. The lentil powders were stored at −20 °C before use. Total protein concentration in lentil flour was determined as total nitrogen multiplied by 6.25. Total nitrogen of lentil flours was analyzed in duplicate on a Leco Trumac apparatus (Leco Corp., St. Joseph, MI).

Lentil protein concentrates were prepared by alkaline extraction. Briefly, lentil flour was suspended in water (solid-to-solvent ratio 1:10 w/v) and the pH value was adjusted to 8. The suspension was stirred in an orbital shaker (Infors, Switzerland) at 20 °C for 1 h and then vacuum-filtered through a filter funnel (100–160 μm nominal pore size) to remove solids. Finally, filtrates were freeze-dried and stored under vacuum and dark conditions in plastic bags at −20 °C until further analysis. The soluble protein concentration in the filtrates was determined by the DC protein assay (Bio-Rad Laboratories, Hercules, CA) following the manufacturer's protocol. Bovine serum albumin (BSA) was used as standard at a concentration range from 0 to 1 mg/mL.

Enzymatic Proteolysis. Freeze-dried lentil protein concentrates were suspended in deionized water (2% w/v) and equilibrated at 40 °C, and the pH value was adjusted to 8 with 0.1 M NaOH. Enzymatic proteolysis was carried out at an enzyme to substrate ratio (E/S) of 0.1 AU/mg of soluble protein at 40 °C and pH 8. Aliquots were withdrawn at 0, 1, 2, 3, 4, 5, and 6 h from reaction mixtures and heated at 80 °C for 15 min for enzyme inactivation. Finally, hydrolysates were centrifuged at 23430*g* at 10 °C for 10 min, freeze-dried, and stored at −20 °C until use. Protein concentration was determined by the DC protein assay (Bio-Rad). Samples were coded for protease type (A = Alcalase, S = Savinase, P = Protamex, and C = Corolase 7089) followed by hydrolysis time (1, 2, 3, 4, 5, and 6). For example, S2 hydrolysates are those produced from lentil concentrate hydrolyzed by Savinase for 2 h. Hydrolysis were performed at least in triplicate for each enzyme.

Degree of Hydrolysis. The degree of hydrolysis (DH) was calculated by determination of free amino groups by reaction with 2,4,6-trinitrobenzenesulfonic acid according to Adler-Nissen.[16] Total number of amino groups in lentil protein concentrate was determined after acid hydrolysis in 6 N HCl at 110 °C for 24 h in vials sealed under nitrogen. Analyses were performed in duplicate. Degree of hydrolysis (percentage) was calculated from the following equation:

$$DH = 100 \times [(AN_2 - AN_1)/N_{pb}]$$

where AN_1 is amino nitrogen content in the protein substrate before hydrolysis, AN_2 is amino nitrogen content in the free protein after hydrolysis, and N_{pb} is the total amino groups in the protein substrate (all expressed as milligrams of tyrosine equivalents/gram of protein) as determined with 6 N HCl at 110 °C for 24 h.

Sodium Dodecyl Sulfate–Polyacrylamide Gel Electrophoresis. SDS–PAGE analysis of the protein hydrolysates was performed on NuPAGE Novex 4–12% Bis-Tris gels in the XCell-sure lock mini-cell system (Invitrogen, Madrid, Spain). Electrophoresis was carried out at 200 V. NuPAGE MES-SDS and NuPAGE LDS were used as running and sample buffers (Invitrogen), respectively. Runs were carried out under nonreducing conditions in which 2-mercaptoethanol was omitted in the denaturing buffer. Electrophoretic bands were stained with SimplyBlue SafeStain (Invitrogen), followed by destaining in deionized water. The molecular weights of poly- and oligopeptides were determined by comparison with the molecular weight marker solution Mark 12 (Invitrogen).

ACE-Inhibitory Activity. ACE-inhibitory activity of samples was measured in duplicate following the fluorescence-based protocol of Sentandreu and Toldrá.[17] The generated fluorescence was read every minute for 30 min at emission and excitation wavelengths of 355 and 405 nm, respectively, in a microplate fluorometer, Synergy HT (Biotek, Winooski, VT). IC_{50} values, expressed in protein concentration (milligrams per milliliter), were calculated for the most active hydrolysates. IC_{50} was determined by dose–response curves in which the range of protein concentration (0–0.5 mg/mL) was distributed in a logarithmic scale and by use of the nonlinear regression sigmoidal curve-fit function in GraphPad Prism 4.00 (Graphpad Software Inc., San Diego, CA). Protein concentration of 3 kDa permeates was measured by DC protein assay (Bio-Rad).

Oxygen Radical Absorbance Capacity. ORAC of samples was measured in duplicate by fluorescence as described previously.[18] Results were expressed as micromoles of Trolox equivalents (TE) per milligram of protein.

Proteomic Analyses. Matrix-assisted laser desorption/ionization time-of-flight (MALDI-TOF) analysis was performed for the most active hydrolysates. Peptide mass fingerprint was performed on a Voyager-DE Pro mass spectrometer (Applied Biosystems, Foster City, CA) equipped with a pulsed 337 nm nitrogen laser (1 ns pulse width and 3 Hz frequency), which was operated in the reflector mode for positive ions. Parameters of the instrument were as follows: acceleration voltage of 20 kV, an extraction voltage of ions generated by laser desorption was introduced into a time-of-flight analyzer (1.3 m flight path) with an acceleration voltage of 20 kV, 76% grid voltage, 0.001% ion guide wire voltage, and delayed extraction time of 400 ns. The samples were mixed with the matrix at a ratio of 1:5 (v/v), and 1 μL of this solution was spotted onto a flat stainless-steel sample plate and dried in air. Mass spectra were obtained over the m/z range 500–4000. External mass calibration was applied by use of the monoisotopic $[M + H]^+$ values of des-Arg^1-bradykinin, angiotensin I, insulin, Glu^1-fibrinopeptide B, and adrenocorticotropic hormone fragments 1–17, 18–39, and 7–38.

For peptide identification, 10 μg of the most active hydrolysate was desalted by reverse-phase (PorosR2) chromatography with 80% acetonitrile (ACN)/0.1% trifluoroacetic acid (TFA). Later, the peptides were dried and resuspended in 10 μL of 0.1% TFA. An aliquot of 5 μL of resuspended sample was injected into the linear trap quadrupole (LTQ) Orbitrap Velos (Thermo Scientific). Peptides were loaded onto a C18-A1 ASY-column 2 cm precolumn (Thermo Scientific) and then eluted onto a Biosphere C18 column (C18, inner diameter 75 μm, 15 cm long, 3 μm particle size) (NanoSeparations) at a flow rate of 250 nL/min on a nanoEasy high-performance liquid chromatography (HPLC) instrument (Proxeon) coupled to a nanoelectropray ion source (Proxeon).

The mobile phases used consisted of 0.1% formic acid/2% ACN (solvent A) and 0.1% formic acid in 100% ACN (solvent B). The solvent gradient was from 100% A to 35% B in 140 min. Mass spectra were acquired in the positive-ion mode. Full-scan MS spectra (m/z 400–1800) were acquired with a target value of 1 000 000 at a resolution of 30 000 at m/z 400, and the 15 most intense ions were

selected for collision-induced dissociation fragmentation in the LTQ with a target value of 10 000 and normalized collision energy of 38%. Precursor ion charge-state screening and monoisotopic precursor selection were enabled. Singly charged ions and unassigned charge states were rejected. Dynamic exclusion was enabled with a repeat count of 1 and exclusion duration of 30 s.

Proteome Discoverer 1.4.288 (Thermo) with MASCOT 2.3 was used to search in NCBI database, taxonomy Viridiplantae (1 530 236 sequences) and a homemade database with the *Lens culinaris* entries in UniProt (336 sequences, 75 114 residues). Database search parameters used were the following: peptide tolerance, 10 ppm; fragment ion tolerance, 0.8 Da; no enzyme and variable modification, methionine oxidation. In all peptide identification, the probability scores were greater than the score fixed by Mascot as significant with a *p*-value minor than 0.05. The automatic decoy database search function of Protein Discover was enabled to allow estimation of false discovery rate (FDR). Sequence identification with reported biological activity was compared with bioactive peptide sequences submitted to the BIOPEP database (http://www.uwm.edu.pl/biochemia/index.php/pl/biopep).

In Vitro Gastrointestinal Digestion. Lentil hydrolysates produced by selected protease type and hydrolysis time were further subjected to simulated gastrointestinal digestion by sequential hydrolysis with pepsin and pancreatin.[19] Digestions were stopped by heating samples in boiling water for 10 min. Samples were stored at −20 °C and then freeze-dried. Protein content was determined for each sample by the DC protein assay (Bio-Rad).

Statistical Analysis. Data were subjected to one-way analysis of variance (ANOVA) by Statgraphics Centurion XVI software, version 16.1.17 (Statistical Graphics Corporation, Rockville, MD). Differences between samples were compared by Duncan's multiple-range test at $P \leq 0.05$ probability levels.

RESULTS AND DISCUSSION

Protein content of lentil flour (27.4% ± 0.1% on dry basis) was within the range of reported values for lentil flours.[20] Alkaline extraction at pH 8 led to 80% extraction of total protein. Thus, protein content of lentil var. Castellana protein concentrate was 75.54% ± 0.2% on dry basis, which was comparable to previous data for red and green lentil protein concentrates (78.2% ± 0.2% and 79.1% ± 0.3%).[21] The obtained lentil protein concentrate was hydrolyzed by different enzymes (Alcalase, Savinase, Protamex, and Corolase 7089) to determine the most effective one for hydrolyzing lentil proteins and releasing ACE-inhibitory and antioxidant peptides.

Proteolytic Pattern of Hydrolysis. To evaluate hydrolysis efficiency, the degree of hydrolysis (DH) value is a widely used criterion, as it is highly related to the hydrolytic process yield. Figure 1 shows the effect of protease type and hydrolysis time in the DH of lentil proteins. DH values increased gradually, reaching a plateau at 5 h for Alcalase, Savinase, and Protamex (23%, 15%, and 11%) and at 4 h for Corolase 7089 (10%). The significant differences ($P \leq 0.05$) found among DH values of lentil hydrolysates may be attributed to different enzyme specificity.[22] Subtilisins have a broad specificity, which explains the higher proteolytic efficiency of Alcalase and Savinase compared to Protamex and Corolase 7089. Our results agree with previous studies showing the ability of Alcalase to produce protein hydrolysates with higher DH than other enzymes.[23] Maximum DH observed in the present study for Alcalase hydrolysates (23%) is comparable to values reported in earlier studies for other legume proteins.[24,25] In contrast, the degree of hydrolysis of cowpea and bean proteins by Alcalase was found to be significantly different from that of lentil proteins (35.7% and 14%, respectively) .[26,27] These differences in the susceptibility of lentil proteins to hydrolysis might be attributed

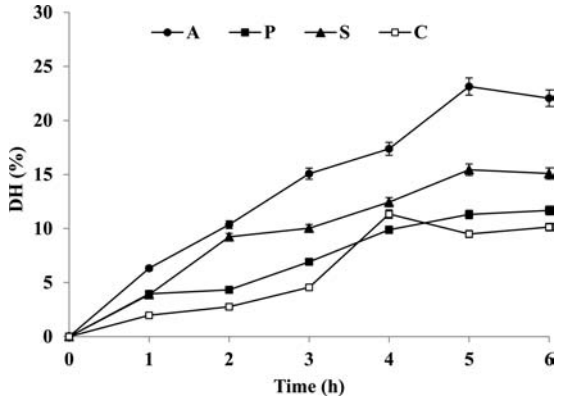

Figure 1. Degree of hydrolysis (DH) of lentil proteins for different proteases and hydrolysis times. The experiments were performed in duplicate. Bars indicate standard deviation. A, Alcalase; S, Savinase; P, Protamex; C, Corolase 7089.

to their particular structure.[28] Enzymatic treatments with sequential addition of Alcalase (1 h) and Flavourzyme (1.5 h) have also been used to increase proteolytic efficiency in the production of lentil hydrolysates.[29] In this case, high DH values were obtained (58% and 64% for red and green lentil proteins, respectively); however, extensive proteolysis is not recommended because peptides generated may produce bitterness and worsen important technological properties required for particular food industry applications.

Figure 2 shows the electrophoretic profiles of lentil hydrolysates produced by (A) Alcalase, (B) Savinase, (C) Protamex, and (D) Corolase 7089. Nonhydrolyzed protein concentrate (Figure 2, lanes 2) showed nine intense bands with apparent molecular masses (MM) from 14.4 to 95 kDa. The major bands found in lentil concentrate had estimated MM of 50 and 65 kDa, which probably correspond to subunits of vicilin (48 kDa) and convicilin (63 kDa), respectively.[30] Other bands with lower MM of 40, 20, and <15 kDa were considered to belong to 11S acidic subunit, 11S basic subunit, and a mixture of γ-vicilin and albumin polypeptides, respectively.[31] The electrophoretic profile of protein concentrates from lentil var. Castellana was similar to that reported for green and red lentil concentrates.[13] Major polypeptides found in lentil protein concentrate were readily hydrolyzed by Alcalase to small peptides <10 kDa after 1 h (Figure 2A, lane 3). Longer hydrolysis times from 4 to 6 h induced further breakdown of peptide bonds and formation of much smaller fractions at MM < 6 kDa (Figure 2A, lanes 6−8). Our results agree with previous studies in which Alcalase digestion was efficient in producing small peptides with MM below 10 kDa from chickpea[24] and bean[26,31] proteins. In addition, sequential use of Alcalase and Flavorzyme to produce peptides from lentil proteins has been proven more effective than the use of gastrointestinal enzymes, papain, and bromelain.[13] Similarly to Alcalase, protein digestion by Savinase was also efficient. A sharp reduction of most polypeptides (30, 40, 50, 55, and 65 kDa) present in lentil protein concentrate was observed after 1 h of hydrolysis, appearing as new bands under 14 kDa (Figure 2B, lane 3). As hydrolysis progressed, polypeptides with estimated MM of 50, 55, and 65 kDa were completely degraded (Figure 2B, lanes 4−8). In addition, the reduction of intensity of bands with MM <14 kDa suggested further degradation of the peptides into much smaller fragments. In contrast, Protamex and Corolase 7089 digestions were not as

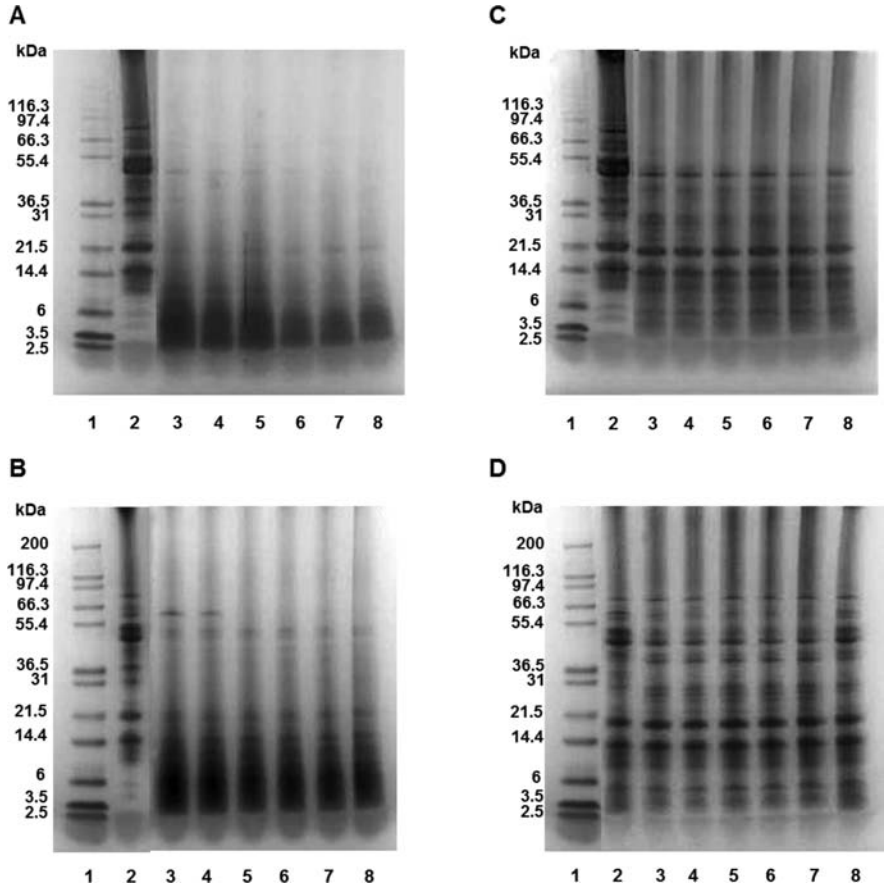

Figure 2. Sodium dodecyl sulfate−polyacrylamide gel electrophoresis (SDS−PAGE) profiles of lentil hydrolysates obtained for different proteases and hydrolysis times. (A) Alcalase; (B) Savinase; (C) Protamex; (D) Corolase 7089 hydrolysates. Lane 1, molecular weight marker Mark 12; lanes 2−8, respectively 0, 1, 2, 3, 4, 5, and 6 h of hydrolysis.

efficient as Alcalase and Savinase digestions, consistent with DH values (Figure 2C,D). Protamex digestion completely degraded high- and medium-molecular weight polypeptides (estimated MM 30, 37, 60, 67, and 90 kDa) within 1 h (Figure 2C, lane 3). As a consequence, the appearance of some bands between 30 and 20 kDa and <10 kDa was observed. Further treatment with Protamex resulted in slight changes in the digest profile, such as the disappearance of some bands with apparent MM between 30 and 20 kDa, and increased intensity of the fraction <10 kDa (Figure 2C, lanes 4−8). Finally, Corolase 7089 treatment decreased the intensity of bands with MM 50, 55, 67 kDa, while the appearance of lower MM bands at 25 and 28 kDa and under 6 kDa were observed after 1 h (Figure 2D, lane 3). Longer digestion time had little impact on the SDS−PAGE profiles, in which only the increased intensity in the fraction under 6 kDa was observed (Figure 2D, lanes 4−8). Resistance of lentil and other legume proteins to proteases such as Protamex and Corolase 7089 has not been reported previously.

ACE Inhibitory Activity of Lentil Protein Hydrolysates. ACE-inhibitory peptides are generally short amino acid sequences, since the active site of ACE cannot accommodate large peptide molecules.[32] Therefore, samples were ultrafiltered through a 3 kDa cutoff membrane and the permeate was used for ACE-inhibitory analysis. Nonhydrolyzed lentil protein concentrate showed weak ACE-inhibitory activity (20% inhibition). ACE-inhibitory activity of hydrolysates was significantly affected by the protease used and the hydrolysis time (Table 1). Alcalase and Savinase hydrolysates exhibited higher ACE inhibition (64−71% and 56−63%, respectively) than Protamex (31−46%) and Corolase 7089 (28−50%)

Table 1. Effect of Hydrolysis Time and Protease Type on ACE-Inhibitory Activity of Lentil Hydrolysates[a]

time (h)	ACE inhibition (%)			
	A	S	P	C
0	20.34 ± 1.48 A a	20.49 ± 0.53 A a	21.20 ± 4.02 A a	20.17 ± 0.1 A a
1	64.37 ± 1.57 B c	56.73 ± 1.54 B b	46.52 ± 3.84 D a	41.51 ± 0.12 D a
2	64.37 ± 0.25 B c	63.35 ± 2.41 C c	41.04 ± 1.17 CD a	50.57 ± 5.45 E b
3	71.65 ± 0.74 D c	59.08 ± 0.42 B b	38.10 ± 1.90 C a	36.79 ± 2.28 CD a
4	70.37 ± 2.93 D c	59.08 ± 1.61 B b	40.50 ± 1.42 C a	36.23 ± 4.42 CD a
5	68.00 ± 2.36 CD c	57.41 ± 2.08 B b	31.86 ± 1.11 B a	33.19 ± 3.46 BC a
6	67.74 ± 1.98 BC c	56.33 ± 2.23 B b	31.23 ± 0.04 B a	28.37 ± 1.19 B a

[a]Data indicate mean value ± standard deviation of two independent experiments. Different uppercase letters within a column are significantly different ($P < 0.05$, Duncan's test). Different lowercase letters within a row are significantly different ($P < 0.05$, Duncan's test). A, Alcalase; S, Savinase; P, Protamex; C, Corolase 7089. Protein concentration of samples in the ACE inhibition assay was 0.5 mg/mL.

dx.doi.org/10.1021/jf500849u | J. Agric. Food Chem. 2014, 62, 4166−4174

digests, regardless of hydrolysis time. ACE-inhibitory efficacy is directly associated with chain length and peptide sequence. Short peptide chains containing between 3 and 12 amino acid residues and Tyr, Phe and Pro or hydrophobic amino acids are reported to be the most favorable sequences for ACE inhibition.[10] Alcalase and Savinase produced hydrolysates with a higher yield of shorter peptide sequences (Figure 2A,B) that, in conjunction with their specificity for aromatic or hydrophobic residues at position P1[22], is consistent with their higher ACE-inhibitory efficacy. ACE-inhibitory activity of hydrolysates gradually increased ($P \leq 0.05$), reaching maximum values after 1−3 h depending on the enzyme, while this activity decreased with extended hydrolysis time ($P \leq 0.05$) likely due to active amino acid sequences were cleaved by protease. IC_{50} values were calculated for A3 and S2 hydrolysates, selected for their highest ACE-inhibitory activities. The selected hydrolysis time (3 h for Alcalase and 2 h for Savinase) was chosen because no significant improvements were found with further digestion times ($P \geq 0.05$). The A3 and S2 hydrolysates exhibited significantly different ($P \leq 0.05$) IC_{50} values of 0.25 ± 0.02 and 0.18 ± 0.02 mg of protein/mL, respectively. It is worth noting the considerably higher ACE-inhibitory activity of S2 hydrolysates compared to A3 hydrolysates ($P \leq 0.05$). These results suggest that Savinase should generate peptides with more favorable amino acid sequences than Alcalase. As far as we know, this is the first evidence showing the effectiveness of Savinase in releasing ACE-inhibitory peptides from legume proteins. IC_{50} values of ACE-inhibitory peptides in A3 and S2 hydrolysates are higher when compared to activities of peptides released from lentil proteins by gastrointestinal enzymes (0.43−0.89 mg/mL).[14,33,34] Moreover, the ACE-inhibitory activity of S2 hydrolysates found in this work is within the range of reported IC_{50} values for red and green lentil concentrates hydrolyzed by Alcalase/Flavourzyme, bromelain, and papain (0.19−0.08 mg/mL), although it is noteworthy that much longer hydrolysis time (8 h) were used in the case of both plant proteases.[13] The ACE-inhibitory activity of A3 and S2 hydrolysates is quite promising in comparison to activities reported for Alcalase hydrolysates from different legumes such as cowpea, chickpea, mung bean, and soybean, exhibiting IC_{50} values ranging from 2.5 to 0.13 mg/mL.[23,25,27,35]

Antioxidant Activity of Lentil Protein Hydrolysates. The effect of hydrolysis time and protease type on the potential antioxidant activity of lentil hydrolysates was determined by the ORAC-FL method, which reflects peroxyl radical scavenging activity.[36] Antioxidant mechanism assayed with ORAC method is based on a hydrogen atom transfer mechanism. A radical initiator is used to generate peroxyl radical $ROO^{\bullet}$ that abstracts a hydrogen atom from antioxidant molecules present in the sample. Results in Table 2 indicate that ORAC values of nonhydrolyzed lentil proteins were significantly lower compared to those of lentil hydrolysates ($P \leq 0.05$). Hydrolysis time and protease used greatly affected the radical scavenging activity of lentil protein hydrolysates. Hydrolysates produced with Alcalase, Savinase, and Corolase 7089 displayed a gradual increase in peroxyl scavenging activity, reaching the highest values after 4, 2, and 3 h, respectively ($P \leq 0.05$). In contrast, Protamex hydrolysates showed the highest activity ($P \leq 0.05$) at the shortest time (1 h), after which a gradual decrease was observed ($P \leq 0.05$). The differences in antioxidant activity observed at different hydrolysis times could be attributable to the different peptides and amino acid sequences released during hydrolysis. This leads to a difference in their ability to act as donors of hydrogen atoms that may inhibit oxidative chain reactions or prevent their initiation. Higher antioxidant activity potential of A4 and S2 hydrolysates may be explained by the higher efficiency of Alcalase and Savinase in producing smaller peptides (Figure 2A,B). The molecular weight of peptides is believed to play a key role in scavenging oxygen radicals. Recent studies pointed out that the radical scavenging activity of cowpea and bean protein hydrolysates increased with decreasing molecular weight.[27,37] In fact, identified antioxidant peptides derived from food proteins are composed of 2−16 amino acid residues.[38] The higher efficiency of subtilases in releasing peroxyl scavenging peptides observed in the present study is consistent with their preferential specificity to cleave hydrophobic amino acids, which have been shown to act as proton donors.[39] Comparison of the ORAC values showed that S2 hydrolysate exhibited the highest peroxyl scavenging activity (0.8 μmol of TE/mg of protein), followed by A4 hydrolysate (0.7 μmol of TE/mg of protein). These results indicate that Savinase released antioxidant peptides with more favorable amino acid sequences than Alcalase. The ORAC values of permeates <3 kDa from S2 and A4 hydrolysates were also analyzed. Radical scavenging activity was 2-fold higher in these fractions compared to whole hydrolysates. A4 permeates exhibited 0.91 ± 0.05 μmol of TE/mg of protein and S2 permeates exhibited 1.22 ± 0.06 μmol of TE/mg of protein, suggesting that short peptides may be responsible for the potential antioxidant activity of protein hydrolysates, in agreement with previous studies.[27,37] To our knowledge, this is the first study on the production of hydrolysates with antioxidant activity from lentil proteins. The antioxidant activity of A4 and S2 hydrolysates, measured by the ORAC-FL method, was more than 2 times higher compared to that of Alcalase hydrolysates from different soybean cultivars.[40] In addition, lentil hydrolysates produced by subtilases in the present study exhibited ORAC values within the range of reported values for common vegetables (green pepper, spinach, purple onion, broccoli, beet, and cauliflower) considered as leading sources of antioxidant activity against peroxyl radicals (0.023−0.3 μmol of TE/mg dry weight).[36]

Table 2. Effect of Hydrolysis Time and Protease Type on Antioxidant Activity of Lentil Hydrolysates[a]

time (h)	ORAC (μmol of Trolox/mg of protein)			
	A	S	P	C
0	0.43 ± 0.02 A a	0.43 ± 0.02 A a	0.44 ± 0.02 A a	0.44 ± 0.03 A a
1	0.57 ± 0.03 B bc	0.52 ± 0.03 BC a	0.58 ± 0.03 E c	0.53 ± 0.04 BC ab
2	0.64 ± 0.2 C c	0.81 ± 0.02 F d	0.56 ± 0.03 CD b	0.50 ± 0.04 B a
3	0.62 ± 0.03 C b	0.75 ± 0.07 E c	0.55 ± 0.04 BCD a	0.54 ± 0.04 CD a
4	0.70 ± 0.05 D c	0.62 ± 0.05 D b	0.49 ± 0.02 B a	0.59 ± 0.02 D b
5	0.70 ± 0.04 D b	0.56 ± 0.05 C a	0.53 ± 0.03 BC a	0.55 ± 0.03 CD a
6	0.57 ± 0.03 B c	0.49 ± 0.05 B a	0.51 ± 0.04 AB ab	0.53 ± 0.02 BC bc

[a]Data indicate mean value ± standard deviation of two independent experiments. Different uppercase letters within a column are significantly different ($P < 0.05$, Duncan's test). Different lowercase letters within a row are significantly different ($P < 0.05$, Duncan's test). A, Alcalase; S, Savinase; P, Protamex; C, Corolase 7089.

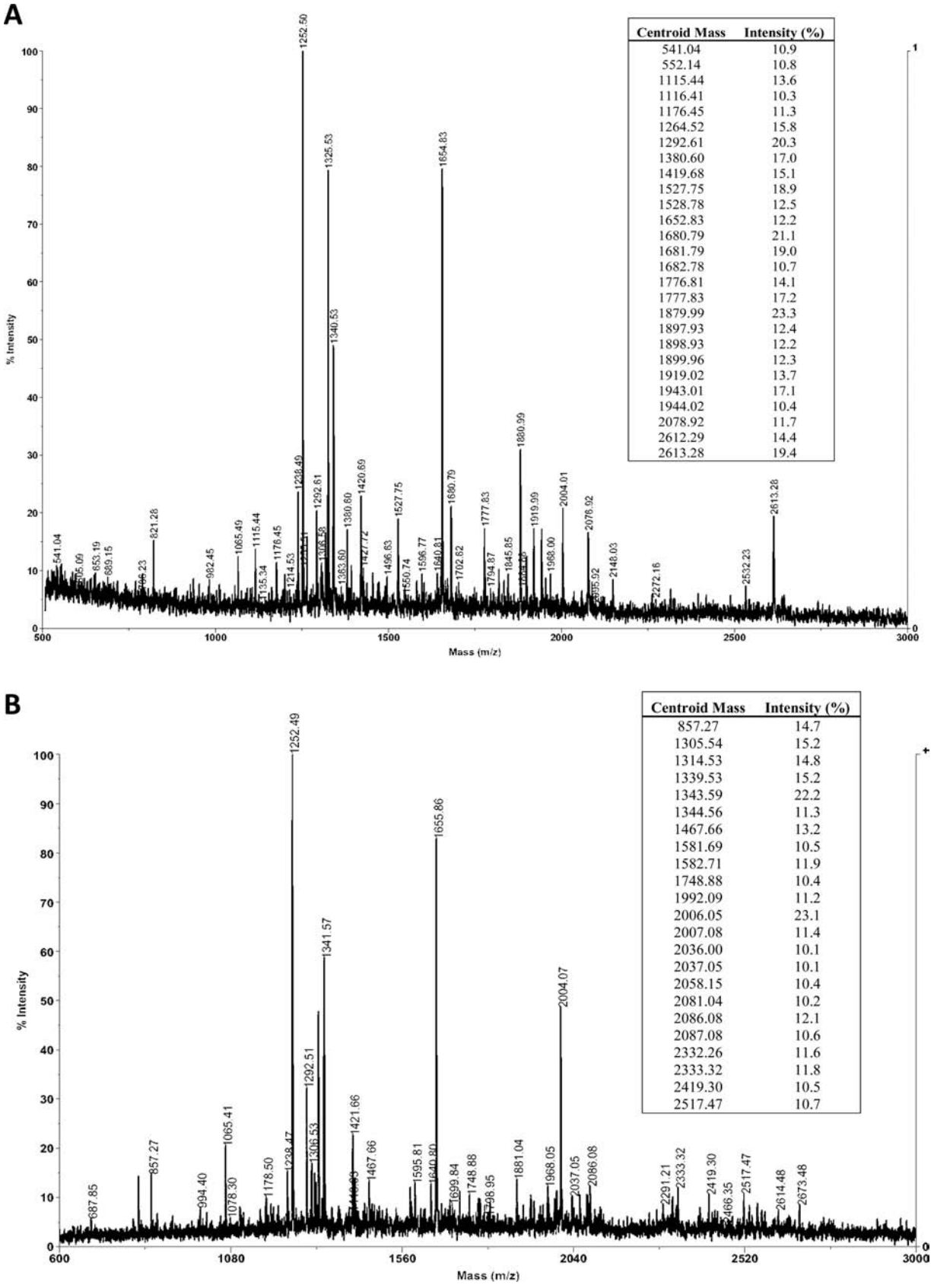

Figure 3. Peptide mass fingerprint of 3 kDa permeates of lentil hydrolysates: (A) A4 hydrolysate; (B) S2 hydrolysate. Mass spectra were obtained by MALDI-TOF in the reflector mode for positive ions. The respective table insets show differential peptide masses observed for each hydrolysate.

Peptide Mass Fingerprint of Selected Lentil Hydrolysates. A4 and S2 hydrolysates were selected for MALDI-TOF analysis on the basis of their highest biological activities. Figure 3 shows mass spectra of the 3 kDa permeates of A4 and

dx.doi.org/10.1021/jf500849u | J. Agric. Food Chem. 2014, 62, 4166−4174

S2 hydrolysates. Comparison of the spectra showed similarities between A4 and S2 hydrolysates such as the presence of high-intensity signals (m/z 1251.1−1255.5, 1325.5−1327.5, 1340.5−1342.5, 1652.8−1657.8, and 2004.0−2007.1) referred to either matrix-related clusters or peptides that could represent concomitants including nonspecific digestion products.[41,42] It is worth noting that A4 and S2 hydrolysates showed differential peptide masses with reduced intensity (see the inset mass peptide list in Figure 3). The different peptide profiles observed for A4 and S2 hydrolysates indicates that Alcalase and Savinase have different enzyme specificities, which is consistent with the above-mentioned results.

Identification of Bioactive Multifunctional Peptides. S2 hydrolysate was selected for peptide identification on the basis of its higher ACE-inhibitory and antioxidant activities, and the 3 kDa permeate was analyzed by reverse-phase (RP) HPLC−tandem mass spectrometry (MS/MS). Table 3 shows the list of peptides identified that contain, within their amino acid sequences, reported ACE-inhibitory (boldface) and antioxidant activity (underlined) sequences according to BIOPEP database. Identified peptides were fragments derived from lentil storage proteins (convicilin, vicilin, legumin, and albumin), allergen Len c 1, and lectin having at the C-terminus residues such as alanine (A), valine (V), leucine (L), tyrosine (Y), phenylalanine (F), and tryptophan (W). The presence of some of these amino acids in the ultimate position fulfils the rule proposed by Cheung et al.[43] about residues being preferred for ACE inhibitors and substrates. Moreover, peptides identified were characterized by the presence of several hydrophobic amino acids such as Ala (A), Pro (P), Val (V), Ile (I), Leu (L), Phe (F), Trp (W), Tyr (Y), and Met (M), which may act as proton donors .[39] Specifically, Tyr (Y) and Trp (W) have been reported as mainly responsible for the antioxidant activity of peptides in the ORAC-FL model.[44,45] In some peptides His (H) was also found, which has been commonly associated with antioxidant activity due to its hydrogen-donating and radical-trapping imidazole ring.[39] Taken all together, identification of the amino acid sequence of peptides in Savinase lentil hydrolysates has demonstrated their multifunctional properties that could make an important contribution in dietary interventions for prevention/therapy of hypertension. This is the first study showing an exhaustive characterization of the peptide fraction of lentil protein hydrolysates. So far, only three ACE-inhibitory peptides (KLRT, TLHGMV, and VNRLM) released by sequential pepsin−pancreatin hydrolysis from lentil proteins have been identified,[33] and none of them were identified in the present work.

Stability of ACE-Inhibitory and Antioxidant Peptides in Selected Lentil Hydrolysate to Gastrointestinal Digestion. There are numerous in vivo studies in animal models of hypertension and human clinical studies in hypertensive patients showing that oral administration of bioactive peptides from food proteins with ACE-inhibitory activity or foods containing these peptides results in the reduction of hypertension.[46] This body of evidence demonstrates that ACE-inhibitory peptides can resist gastrointestinal digestion to be absorbed in the intestine and ultimately reach the target molecule. Nevertheless, gastrointestinal enzymes may cause structural degradation of bioactive peptides and loss of their bioactivity. Therefore, it is important to determine their stability to gastrointestinal digestion. For this purpose, the most potent peptide fraction (3 kDa permeate of S2 hydrolysate) was further sequentially digested with pepsin and pancreatin to simulate gastrointestinal digestion. Some studies have reported a relationship between peptide structure and bioavailability; thus, small hydrophobic peptides tend to be resistant to gastrointestinal digestion and, therefore, are generally absorbed.[48] Accordingly, based on the cleavage mechanism of

Table 3. Amino Acid Sequences Found in 3 kDa Permeates of S2 Lentil Hydrolysates

MH^+ (Da)	peptide sequence[a]	protein	accession nos.
1252.78	**DLP**VL**RWL**	legumin A	388256; 483449; 126161
1252.78	**DLP**VL**RWLKL**	legumin A	388256; 483449; 126161
1927.07	DRRQEINKENVI**VKV**S	allergen Len c 1.0102	Q84UI0
835.47	EGGL**LLPH**	convicilin	Q9M3X8
1982.11	EGSL**LLPHY**NSRAIVIVT	vicilin	137582; 1297072
1876.87	FEGT**VF**ENGIDA**AY**RST	albumin-2	113570
977.57	INDK**YVL**L	albumin-2	P86782
1237.72	**LF**INDK**YVL**L	albumin-2	P86782
1002.55	NEDVI**VKV**S	allergen Len c 1.0101	Q84UI1
1831.99	NLERGDT**IKL**PAGTI**AY**	allergen Len c 1.0101	Q84UI1; Q84UI0
1945.07	NLERGDT**IKL**PAGTI**AYL**	allergen Len c 1.0101	Q84UI1; Q84UI0
2245.15	N**RF**QT**LY**ENENG**HIRL**LQ	allergen Len c 1.0101	42414629; 29539109; 29539111
1499.84	QEINKENVI**VKV**S	allergen Len c 1.0102	Q84UI0
2131.10	**RF**QT**LY**ENENG**HIRL**LQ	allergen Len c 1.0101	42414629; 29539109; 29539111
1269.69	RLSAEY**VRLY**	legumin type B	126164; 126166; 126170
1725.01	RRQEINKENVI**VKV**	allergen Len c 1.0102	Q84UI0
1927.07	RRQEINKENVI**VKV**S	allergen Len c 1.0102	Q84UI0
1098.63	SL**DLP**VL**RW**	legumin A	483449; 126161
1212.72	SL**DLP**VL**RWL**	legumin A	483449; 126162
1421.80	SVEIKEGSL**LLPH**	vicilin	137582; 1297072
1698.91	SVEIKEGSL**LLPHY**N	vicilin	137582; 1297072
1785.94	SVEIKEGSL**LLPHY**NS	vicilin	137582; 1297072
1377.74	SVEINEGGL**LLPH**	convicilin	7688242
1540.80	SVEINEGGL**LLPHY**	convicilin	Q9M3X8
1897.98	SVEINEGGL**LLPHY**NSR	convicilin	Q9M3X8
1817.93	**SWN**LQNGERANVV**IA**F	lectin	Q93WH6; Q93X49
1312.76	TSL**DLP**VL**RWL**	legumin A	483449; 126161
1512.88	TVTSL**DLP**VL**RWL**	legumin A	483449; 126161
2538.43	VEIKEGSL**LLPHY**NSR	vicilin	137582; 1297072
1290.70	VEINEGGL**LLPH**	convicilin	7688242
1634.91	VNSVEIKEGSL**LLPH**	vicilin	137582; 1297072
2155.15	VNSVEIKEGSL**LLPHY**NSR	vicilin	137582; 1297072

[a]Boldface and underlined sequence regions correspond to reported ACE-inhibitory and antioxidant activity, respectively, in BIOPEP (http://www.uwm.edu.pl/biochemia/index.php/pl/biopep) and Wu et al.[47]

Savinase, lentil hydrolysates produced in the present study were hydrophobic and with molecular masses below 3 kDa, which supports the potential bioavailability of such hydrolysates. Figure 4 shows ACE-inhibitory and antioxidant activities of 3

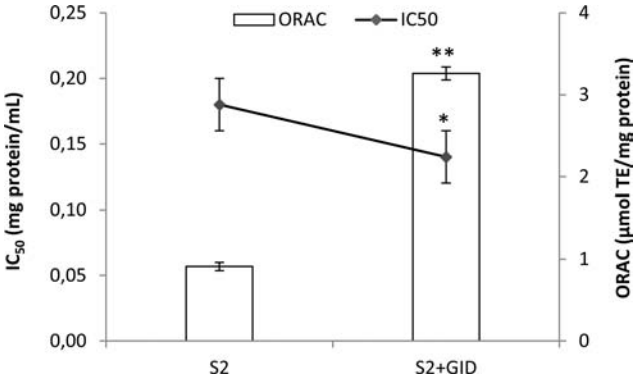

Figure 4. Stability to gastrointestinal digestion of ACE-inhibitory and antioxidant activity of 3 kDa permeates of A3 and S2 hydrolysates. Lines represent ACE-inhibitory activity, and bars show antioxidant activity before and after in vitro gastrointestinal digestion. *Statistical difference at $P < 0.05$; **Statistical difference at $P < 0.001$ (Duncan's test).

kDa permeate of S2 hydrolysate before and after in vitro gastrointestinal digestion. When peptides were subjected to in vitro gastrointestinal digestion, IC_{50} was slightly lower (0.14 mg of protein/mL) compared to that before digestion (0.18 mg of protein/mL), which indicates a higher ACE-inhibitory potency ($P \leq 0.05$). In addition, antioxidant activity of peptides in the 3 kDa fraction increased 3 times after gastrointestinal digestion ($P \leq 0.05$). These results suggest that peptides in S2 hydrolysates were either resistant or liberated new fragments with ACE-inhibitory and antioxidant activity after simulated gastrointestinal digestion. As consequence, peptides in S2 hydrolysate could preserve or improve its multifunctionality in the gastrointestinal tract.

In conclusion, this study reveals that subtilisins are the most suitable enzymes for lentil proteolysis and production of hydrolysates with ACE-inhibitory and antioxidant activities. The highest ACE-inhibitory and antioxidant activities were found in lentil hydrolysates treated with Savinase for 2 h at 40 °C. Therefore, Savinase is the best choice for cost-effective production of lentil multifunctional hydrolysates. Several peptides with amino acid sequences rich in hydrophobic amino acids were identified in these hydrolysates, which make them potential contributors to the dual bioactivity detected. Multifunctional hydrolysates could encourage value-added utilization of lentil proteins as functional ingredients of nutraceuticals for prevention of hypertension and cardiovascular diseases.

AUTHOR INFORMATION

Corresponding Author

*E-mail c.m.villaluenga@csic.es; tel +34 912587601; fax +34 915644853

Funding

This work was funded by the AGL2010-16310 project from the MINECO (Ministerio de Economía y Competitividad from Spain).

Notes

The authors declare no competing financial interest.

ACKNOWLEDGMENTS

We thank MINECO for granting P.G.-M. a predoctoral fellowship

ABBREVIATIONS

ACE, angiotensin I-converting enzyme; ACN, acetonitrile; DH, degree of hydrolysis; HPLC, high-performance liquid chromatography with photodiode array detection; LTQ, linear trap quadrupole; MALDI-TOF, matrix-assisted laser desorption/ionization time-of-flight; MM, molecular mass; ORAC, oxygen radical absorbance capacity; SDS−PAGE, sodium dodecyl sulfate−polyacrylamide gel electrophoresis; TE, Trolox equivalents; TFA, trifluoroacetic acid

REFERENCES

(1) World Health Organization (WHO). Cardiovascular diseases (CVDs), 2009 (Access date: 03 September 2013).

(2) Hong, F.; Ming, L.; Yi, S.; Zhanxia, L.; Yongquan, W.; Chi, L. The antihypertensive effect of peptides: A novel alternative to drugs? *Peptides* **2008**, *29*, 1062−1071.

(3) Skeggs, L. T.; Dorer, F. E.; Levine, M.; Lentz, K. E.; Kahn, J. R. The biochemistry of the renin-angiotensin system. *Adv. Exp. Med. Biol.* **1980**, *130*, 1−27.

(4) Bagatini, M. D.; Martins, C. C.; Battisti, V.; Gasparetto, D.; da Rosa, C. S.; Spanevello, R. M.; Ahmed, M.; Schmatz, R.; Chitolina Schetinger, M. R.; Morsch, V. M. Oxidative stress versus antioxidant defenses in patients with acute myocardial infarction. *Heart Vessels* **2011**, *26*, 55−63.

(5) Ray, P. D.; Huang, B.-W.; Tsuji, Y. Reactive oxygen species (ROS) homeostasis and redox regulation in cellular signaling. *Cell Signal* **2012**, *24*, 981−990.

(6) Toeroek, J. Participation of nitric oxide in different models of experimental hypertension. *Physiol. Res.* **2008**, *57*, 813−825.

(7) Mattson, M. P. Roles of the lipid peroxidation product 4-hydroxynonenal in obesity, the metabolic syndrome, and associated vascular and neurodegenerative disorders. *Exp. Gerontol.* **2009**, *44*, 625−633.

(8) Agyei, D.; Danquah, M. K. Industrial-scale manufacturing of pharmaceutical-grade bioactive peptides. *Biotechnol. Adv.* **2011**, *29*, 272−277.

(9) Udenigwe, C. C.; Aluko, R. E. Multifunctional cationic peptide fractions from flaxseed protein hydrolysates. *Plant Foods Hum. Nutr.* **2012**, *67*, 1−9.

(10) Erdmann, K.; Cheung, B. W. Y.; Schroeder, H. The possible roles of food-derived bioactive peptides in reducing the risk of cardiovascular disease. *J. Nutr. Biochem.* **2008**, *19*, 643−654.

(11) Hernandez-Ledesma, B.; del Mar Contreras, M.; Recio, I. Antihypertensive peptides: Production, bioavailability and incorporation into foods. *Adv. Colloid Interface Sci.* **2011**, *165*, 23−35.

(12) Northern Pulse Growers Association. http://www.northernpulse.com/growers/ (Access date: 19 September 2013).

(13) Barbana, C.; Boye, J. I. Angiotensin I-converting enzyme inhibitory properties of lentil protein hydrolysates: Determination of the kinetics of inhibition. *Food Chem.* **2011**, *127*, 94−101.

(14) Boye, J. I.; Roufik, S.; Pesta, N.; Barbana, C. Angiotensin I-converting enzyme inhibitory properties and SDS-PAGE of red lentil protein hydrolysates. *Food Sci. Technol.* **2010**, *43*, 987−991.

(15) Contreras, M. M.; Hernandez-Ledesma, B.; Amigo, L.; Martin-Alvarez, P. J.; Recio, I. Production of antioxidant hydrolysates from a whey protein concentrate with thermolysin: Optimization by response surface methodology. *Food Sci. Technol.* **2011**, *44*, 9−15.

(16) Adler-Nissen, J. Determination of the degree of hydrolysis of food protein hydrolysates by trinitrobenzenesulfonic acid. *J. Agric. Food Chem.* **1979**, *27*, 1256−1262.

(17) Sentandreu, M. Á.; Toldrá, F. A fluorescence-based protocol for quantifying angiotensin-converting enzyme activity. *Nat. Protoc.* **2006**, *1*, 2423−2427.
(18) Torino, M. I.; Limon, R. I.; Martinez-Villaluenga, C.; Makinen, S.; Pihlanto, A.; Vidal-Valverde, C.; Frias, J. Antioxidant and antihypertensive properties of liquid and solid state fermented lentils. *Food Chem.* **2013**, *136*, 1030−1037.
(19) Moreno, F. J.; Mellon, F. A.; Wickham, M. S. J.; Bottrill, A. R.; Mills, E. N. C. Stability of the major allergen Brazil nut 2S albumin (Ber e 1) to physiologically relevant in vitro gastrointestinal digestion. *FEBS J.* **2005**, *272*, 341−352.
(20) Roy, F.; Boye, J. I.; Simpson, B. K. Bioactive proteins and peptides in pulse crops: Pea, chickpea and lentil. *Food Res. Int.* **2010**, *43*, 432−442.
(21) Barbana, C.; Boucher, A. C.; Boye, J. I. In vitro binding of bile salts by lentil flours, lentil protein concentrates and lentil protein hydrolysates. *Food Res. Int.* **2011**, *44*, 174−180.
(22) Gupta, R.; Beg, Q. K.; Lorenz, P. Bacterial alkaline proteases: molecular approaches and industrial applications. *Appl. Microbiol. Biotechnol.* **2002**, *59*, 15−32.
(23) Medina-Godoy, S.; Ambriz-Perez, D. L.; Fuentes-Gutierrez, C. I.; German-Baez, L. J.; Gutierrez-Dorado, R.; Reyes-Moreno, C.; Valdez-Ortiz, A. Angiotensin-converting enzyme inhibitory and antioxidative activities and functional characterization of protein hydrolysates of hard-to-cook chickpeas. *J. Sci. Food Agric.* **2012**, *92*, 1974−1981.
(24) Yust, M. M.; Pedroche, J.; Giron-Calle, J.; Alaiz, M.; Millan, F.; Vioque, J. Production of ACE inhibitory peptides by digestion of chickpea legumin with alcalase. *Food Chem.* **2003**, *81*, 363−369.
(25) Li, G. H.; Le, G. W.; Liu, H.; Shi, Y. H. Mung-bean protein hydrolysates obtained with alcalase exhibit angiotensin I-converting enzyme inhibitory activity. *Food Sci. Technol. Int.* **2005**, *11*, 281−287.
(26) Rui, X.; Boye, J. I.; Simpson, B. K.; Prasher, S. O. Angiotensin I-converting enzyme inhibitory properties of Phaseolus vulgaris bean hydrolysates: Effects of different thermal and enzymatic digestion treatments. *Food Res. Int.* **2012**, *49*, 739−746.
(27) Segura Campos, M. R.; Chel Guerrero, L. A.; Betancur Ancona, D. A. Angiotensin-I converting enzyme inhibitory and antioxidant activities of peptide fractions extracted by ultrafiltration of cowpea Vigna unguiculata hydrolysates. *J. Sci. Food Agric.* **2010**, *90*, 2512−2518.
(28) Durak, A.; Baraniak, B.; Jakubczyk, A.; Swieca, M. Biologically active peptides obtained by enzymatic hydrolysis of Adzuki bean seeds. *Food Chem.* **2013**, *141*, 2177−2183.
(29) van der Ven, C.; Gruppen, H.; de Bont, D. B. A.; Voragen, A. G. J. Reversed phase and size exclusion chromatography of milk protein hydrolysates: relation between elution from reversed phase column and apparent molecular weight distribution. *Int. Dairy J.* **2001**, *11*, 83−92.
(30) ExPASy: Bioinformatic resource portal. (www.expasy.org) (Accesed date: 13 July 2013).
(31) Hernandez-Alvarez, J. A.; Carrasco-Castilla, J.; Davila-Ortiz, G.; Alaiz, M.; Giron-Calle, J.; Vioque-Pena, J.; Jacinto-Hernandez, C.; Jimenez-Martinez, C. Angiotensin-converting enzyme-inhibitory activity in protein hydrolysates from normal and anthracnose disease-damaged Phaseolus vulgaris seeds. *J. Sci. Food Agric.* **2013**, *93*, 961−966.
(32) Sirtori, C. R.; Galli, C.; Anderson, J. W.; Sirtori, E.; Arnoldi, A. Functional foods for dyslipidaemia and cardiovascular risk prevention. *Nutr. Res. Rev.* **2009**, *22*, 244−261.
(33) Akillioglu, H. G.; Karakaya, S. Effects of heat treatment and in vitro digestion on the angiotensin converting enzyme inhibitory activity of some legume species. *Eur. Food Res. Technol.* **2009**, *229*, 915−921.
(34) Jakubczyk, A.; Baraniak, B. Activities and sequences of the angiotensin I-converting enzyme (ACE) inhibitory peptides obtained from the digested lentil (*Lens culinaris*) globulins. *Int. J. Food Sci. Technol.* **2013**, *48*, 2363−2369.
(35) Kuba, M.; Tana, C.; Tawata, S.; Yasuda, M. Production of angiotensin I-converting enzyme inhibitory peptides from soybean protein with Monascus purpureus acid proteinase. *Process Biochem.* **2005**, *40*, 2191−2196.
(36) Ou, B. X.; Huang, D. J.; Hampsch-Woodill, M.; Flanagan, J. A.; Deemer, E. K. Analysis of antioxidant activities of common vegetables employing oxygen radical absorbance capacity (ORAC) and ferric reducing antioxidant power (FRAP) assays: A comparative study. *J. Agric. Food Chem.* **2002**, *50*, 3122−3128.
(37) Carrasco-Castilla, J.; Javier Hernandez-Alvarez, A.; Jimenez-Martinez, C.; Jacinto-Hernandez, C.; Alaiz, M.; Giron-Calle, J.; Vioque, J.; Davila-Ortiz, G. Antioxidant and metal chelating activities of peptide fractions from phaseolin and bean protein hydrolysates. *Food Chem.* **2012**, *135*, 1789−1795.
(38) Sarmadi, B. H.; Ismail, A. Antioxidative peptides from food proteins: A review. *Peptides* **2010**, *31*, 1949−1956.
(39) Elias, R. J.; Kellerby, S. S.; Decker, E. A. Antioxidant activity of proteins and peptides. *Crit. Rev. Food Sci. Nutr.* **2008**, *48*, 430−441.
(40) Darmawan, R.; Bringe, N. A.; de Mejia, E. G. Antioxidant capacity of alcalase hydrolysates and protein profiles of two conventional and seven low glycinin soybean cultivars. *Plant Foods Hum. Nutr.* **2010**, *65*, 233−240.
(41) Keller, B. O.; Li, L. Discerning matrix-cluster peaks in matrix-assisted laser desorption/ionization time-of-flight mass spectra of dilute peptide mixtures. *J. Am. Soc. Mass Spectrom.* **2000**, *11*, 88−93.
(42) Harris, W. A.; Janecki, D. J.; Reilly, J. P. Use of matrix clusters and trypsin autolysis fragments as mass calibrants in matrix-assisted laser desorption/ionization time-of-flight mass spectrometry. *Rapid Commun. Mass Spectrom.* **2002**, *16*, 1714−1722.
(43) Cheung, H. S.; Wang, F. L.; Ondetti, M. A.; Sabo, E. F.; Cushman, D. W. Binding of peptide substrates and inhibitors of angiotensin-converting enzyme. Importance of the COOH-terminal dipeptide sequence. *J. Biol. Chem.* **1980**, *255*, 401−407.
(44) Elias, R. J.; Bridgewater, J. D.; Vachet, R. W.; Waraho, T.; McClements, D. J.; Decker, E. A. Antioxidant mechanisms of enzymatic hydrolysates of β-lactoglobulin in food lipid dispersions. *J. Agric. Food Chem.* **2006**, *54*, 9565−9572.
(45) Hernández-Ledesma, B.; Dávalos, A.; Bartolomé, B.; Amigo, L. Preparation of antioxidant enzymatic hydrolysates from α-lactalbumin and β-lactoglobulin. Identification of active peptides by HPLC-MS/MS. *J. Agric. Food Chem.* **2005**, *53*, 588−593.
(46) Foltz, M.; van Buren, L.; Klaffke, W.; Duchateau, G. S. M. J. E. Modeling of the relationship between dipeptide structure and dipeptide stability, permeability, and ACE inhibitory activity. *J. Food Sci.* **2009**, *74*, H243−H251.
(47) Wu, J.; Yuan, L.; Aluko, R. E. Restriction of the in vitro formation of angiotensin II by leucinyl-arginyl-tryptophan, a novel peptide with potent angiotensin I-converting enzyme inhibitory activity. *Biosci. Biotechnol. Biochem.* **2006**, *70*, 1277−1280.
(48) Martinez-Maqueda, D.; Miralles, B.; Recio, I.; Hernadez-Ledesma, B. Antihypertensive peptides from food proteins: a review. *Food Funct.* **2012**, *3*, 350−361.

JOURNAL OF AGRICULTURAL AND FOOD CHEMISTRY

Article

pubs.acs.org/JAFC

Effects of Different Industrial Heating Processes of Milk on Site-Specific Protein Modifications and Their Relationship to in Vitro and in Vivo Digestibility

Yasuaki Wada[†,‡] and Bo Lönnerdal*[,†]

[†]Department of Nutrition, University of California, Davis, One Shields Avenue, Davis, California 95616, United States

[‡]Nutritional Science Institute, Morinaga Milk Industry Co., Ltd., 5-1-83 Higashihara, Zama 252-8583, Japan

ABSTRACT: Heating processes are applied to milk and dairy products to ensure their microbiological safety and shelf lives. However, how differences in "industrial" thermal treatments affect protein digestibility is still equivocal. In this study, raw milk was subjected to pasteurization, three kinds of ultra-high-temperature (UHT) treatment, and in-can sterilization and was investigated by in vitro and in vivo digestion and proteomic methods. In-can sterilized milk, followed by UHT milk samples, showed a rapid decrease in protein bands during the course of digestion. However, protein digestibility determined by a Kjeldahl procedure showed insignificant differences. Proteomic analysis revealed that lactulosyllysine, which reflects a decrease in protein digestibility, in α-lactalbumin, β-lactoglobulin, and caseins was higher in in-can sterilized milk, followed by UHT milk samples. Thus, industrial heating may improve the digestibility of milk proteins by denaturation, but the improvement is likely to be offset by heat-derived modifications involved in decreased protein digestibility.

KEYWORDS: *heating processes, milk proteins, protein digestibility, Maillard reaction, mass spectrometry*

INTRODUCTION

Milk is heat-treated in the dairy industry to ensure microbiological safety and to prolong shelf life. Pasteurization is the most common way to heat milk, typically at 72 °C for 15 s, which allows storage at 4 °C for a few weeks. Milk is also sterilized by ultra-high-temperature (UHT; 135−150 °C for 2−6 s) treatment, and the combination with aseptic packaging makes it distributable at ambient temperature for months. Similar to milk, ready-to-use (liquid) infant/enteral formulas are sterilized for the purpose of distribution at ambient temperature, and UHT treatment and in-can sterilization (>110 °C for 20−30 min) are commonly used. These types of heat treatment can affect their sensory, physicochemical, and nutritional qualities. The nutritional value of milk protein, which is generally recognized as excellent, is influenced by heating processes.[1]

Unfolding of tertiary and secondary structures (denaturation) is the principal change caused by heat treatment, and this generally increases protein digestibility, as is commonly known for legume proteins.[2] However, nonenzymatic posttranslational modifications also occur in milk proteins, which influence their nutritional properties negatively. The so-called Maillard reaction modifies the side chain of the protein; ε-amino groups of lysine (Lys) residues represent the primary target for an attack by reducing sugars such as lactose to form the Amadori product lactulosyllysine (Figure 1a), which can subsequently undergo a series of advanced reactions leading to a variety of modified structures such as N^{ε}-carboxymethyllysine (CML; Figure 1b).[3] Blocking of the ε-amino groups of Lys residues hinders tryptic digestion as well as the action of other digestive enzymes and, as a consequence, reduces protein digestibility.[4−6] The blocked Lys is no longer bioavailable, leading to a reduction in the biological value of milk protein.[7] Furthermore,

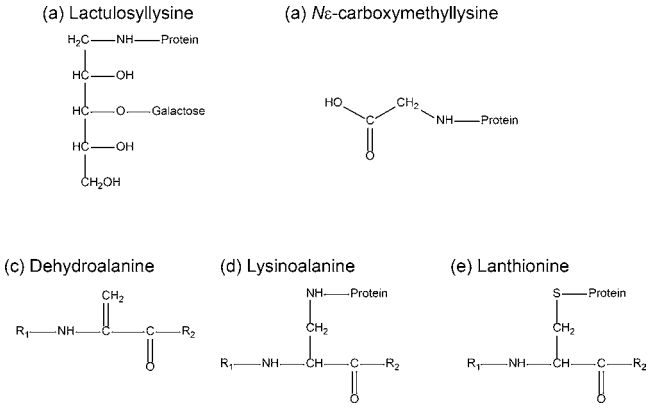

Figure 1. Chemical structures of heat-derived protein modifications. Lactulosyllysine (a) and N^{ε}-carboxymethyllysine (CML; b) are early/advanced Maillard reaction products, respectively. Dehydroalanine (c) is the precursor of cross-linked products lysinoalanine (d) and lanthionine (e).

β-elimination reactions occur to phosphoserine and cystine/cysteine (Cys) residues to form dehydroalanine (Figure 1c), which subsequently reacts with Lys and Cys residues to give cross-linked products such as lysinoalanine and lanthionine (Figure 1d,e)[8,9] They also reduce protein digestibility by inhibiting enzymatic proteolysis.[10] In addition, heating causes disulfide bond interchanges between proteins,[11] and some of the non-native complexes are resistant to digestion.[12] It is therefore important to identify and quantify these chemical

Received: December 16, 2013
Accepted: April 10, 2014
Published: April 10, 2014

ACS Publications © 2014 American Chemical Society

modifications from the standpoint of nutritional quality control of milk and dairy products. The recent advent of highly sensitive mass spectrometry (MS) technology has enabled direct determination of modifications in milk proteins, and the combination with enzymatic digestion prior to MS analysis has further allowed site-specific identification and semiquantification.[13−15]

The aim of this study was to use proteomic techniques to compare protein modifications of milk proteins exposed to different industrial heat processes. The same reference raw milk was subjected to pasteurization, three kinds of UHT (plate heat exchange, steam infusion, and steam injection) treatment, and in-can sterilization. Protein digestibility of milk samples was characterized in both in vitro and in vivo experiments. Milk samples were also applied to in-gel tryptic digestion followed by liquid chromatography (LC)-MS/MS analysis for simultaneous identification and semiquantification of modifications such as formation of lactulosyllysine, CML, and dehydroalanine. Lactulosyllysine and CML are early/advanced Maillard reaction products, respectively, and serve as markers of the thermal history. Dehydroalanine was selected instead of lysinoalanine and lanthionine because it is compatible with the analysis of lactulosyllysine and CML, whereas lysinoalanine and lanthionine are not. Formation of dehydroalanine has also been reported to reflect the thermal history, similar to lysinoalanine and lanthionine.[16]

MATERIALS AND METHODS

Milk Samples. Raw milk was heat-processed at the pilot plant of Morinaga Milk Industry Co., Ltd. (Zama, Japan), and the heating conditions were set by reference to those of the manufacturer's commercial products (Table 1). The heated milk samples were homogenized at 30 MPa, followed by lyophilization. The reference raw milk was lyophilized without homogenization. The lyophilized milk powders were stored at 4 °C until use. Indices of thermal history such as whey protein nitrogen index (WPNI) and lactulose contents were determined in all of the lyophilized milk samples by the Analytic Center of Morinaga Milk Industry,[17,18] and the results are shown in Table 2. On the basis of the results that in-can sterilized milk showed the highest lactulose and the lowest WPNI values, compositions such as protein, fat, carbohydrate, water, and ash were compared for lyophilized raw milk and in-can sterilized milk with standard methods in Morinaga Milk Industry, confirming that no notable change occurred after heat treatment (Table 3).

Table 1. Heat Treatment of Milk Samples

treatment	holding temp/time	F_0	reference product[a]
pasteurization	73 °C for 15 s	0	milk
plate UHT	140 °C for 2 s	2.6	milk
steam infusion	135 °C for 2 s	0.8	milk
steam injection	151 °C for 4 s	65	liquid enteral formula
in-can sterilization	121 °C for 20 min	20	liquid enteral formula

[a]Heating conditions were set by reference to those of the manufacturer's commercial products.

Sodium Dodecyl Sulfate−Polyacrylamide Gel Electrophoresis (SDS-PAGE) of Milk Samples. Milk powder samples were reconstituted with Milli-Q water (Millipore, Billerica, MA, USA) and subjected to centrifugation at 8500*g* for 30 min twice, and the upper fat layer was removed. The tiny pellet, formed after centrifugation, was thoroughly mixed with the skimmed milk fraction. Protein concentrations of skimmed milk were determined by using the Bradford method,[19] and they were adjusted to be the same among samples by dilution with deionized water. SDS-PAGE was performed under reducing/nonreducing conditions to separate the proteins (Bio-Rad, Hercules, CA, USA). Protein concentrations were determined by using the Bradford method, and 50 μg of protein was loaded for each sample onto 15% acrylamide resolving gel (pH 8.8) and 6% acrylamide stacking gel (pH 6.8). Electrophoresis was run at 150 V for 90 min, and gels were stained with Coomassie Brilliant Blue R-250 (Sigma-Aldrich, St. Louis, MO, USA).

Table 3. Nutrient Composition of Lyophilized Raw and In-Can Sterilized Milk

component (g/100 g)	raw	in-can sterilized
protein	25.5	25.5
fat	28.7	28.3
carbohydrate	38.2	38.2
ash	5.5	5.6
water	2.1	2.4

Proteomic Analysis. Proteomic analysis was conducted at the Proteomic Core Facility at the University of California, Davis, to site-specifically semiquantify lactulosyllysine, CML, phosphorylation on serine (Ser), threonine (Thr), and tyrosine (Tyr), and dehydroalanine formed from phosphoserine and Cys residues.

In-Gel Digestion. In-gel reduction, alkylation, and tryptic digestion were done as published previously.[20,21] Briefly, milk samples were reconstituted with deionized water and applied to electrophoresis to excise the fraction containing the entire protein band. The gel piece was dehydrated using acetonitrile (ACN), reduced with dithiothreitol, and alkylated using 55 mM iodoacetamide. Following further dehydration, sequencing grade modified trypsin (Promega, Madison, WI, USA; in 50 mM ammonium bicarbonate) was added in a 1:30 ratio (trypsin/protein), and the gel was incubated overnight at 37 °C. While the supernatant was collected into a new tube, 60% ACN (in 0.1% trifluoroacetic acid) was added to the remaining gel piece, which was then sonicated and centrifuged for collecting another supernatant. The supernatants were then dried by vacuum centrifugation.

Protein Identification. Digested peptides were analyzed by a Thermo Scientific Q Exactive Orbitrap mass spectrometer in conjunction with a Paradigm MG4 HPLC (Michrom Bio Resources, Auburn, CA, USA). The digested peptides were loaded onto a Michrom C18 trap and desalted before they were separated using a Michrom 200 μm × 150 mm Magic C18 AQ reverse phase column. A flow rate of 2 μL/min was used. Peptides were eluted using a 90 min gradient composed of buffers A (0.1% formic acid) and B (100% ACN), with 2−35% B over 70 min, 35−80% B for 5 min, 80% B for 2 min, then a decrease from 80 to 2% B in 1 min, and held at 2% B for 12 min. A spray voltage of 2.2 kV was used with a transfer capillary temperature of 200 °C. A MS survey scan was obtained for the m/z range of 300−1600. MS/MS spectra were acquired using a top 15 method, where the top 15 ions in the MS spectra were subjected to high-energy collisional dissociation. An isolation mass window of 2.0 m/z was used for the precursor ion selection, and a normalized collision energy of 27% was used for fragmentation. A 5 s duration was used for the dynamic exclusion.

Database Searching. Tandem mass spectra were extracted and charge states deconvoluted and deisotoped. All MS/MS samples were analyzed using X! Tandem (The GPM, thegpm.org; version TORNADO (2010.01.01.4)). X! Tandem was set up to search the

Table 2. Indices of Thermal History for Lyophilized Milk Samples

component	raw	pasteurized	plate UHT	steam infused	steam injected	in-can sterilized
WPNI (mg/g)	7.51	6.91	1.75	4.29	2.22	1.33
lactulose (mg/100 g)	20.2	19.6	204	42.0	241	1490

digestion enzyme trypsin. X! Tandem was searched with a fragment ion mass tolerance of 20 ppm and a parent ion tolerance of 20 ppm. Iodoacetamide derivative of Cys was specified in X! Tandem as a fixed modification. One of the targeted modifications [lactulosyllysine on Lys (+324.105647), CML on Lys (+58.005479), phosphorylation on Ser, Thr, and Tyr (+79.966331), dehydration of Ser (−18.010565), or dehydroalanine on Cys (−33.987721)], as well as acetylation of the N-terminus, ammonia loss of the N-terminus, *pyro*-glutamination of the N-terminus, and oxidation of methionine and tryptophan, were specified in X! Tandem as variable modifications.

Criteria for Protein Identification. Scaffold (version Scaffold_4.1.1, Proteome Software Inc., Portland, OR, USA) was used to validate MS/MS-based peptide and protein identifications, taking into consideration the Peptide Prophet algorithm, Protein Prophet algorithm, and false-discovery rates.[22−24] Proteins that contained similar peptides and could not be differentiated on the basis of MS/MS analysis alone were grouped to satisfy the principles of parsimony.

Peptide Semiquantification. Scaffold data were imported into Skyline (version 1.4.0.4421, MacCoss Lab, Department of Genome Science, University of Washington) to determine retention time and peak areas of peptides with targeted modifications. On the basis of the retention time, three different monoisotopic peak areas (M, M + 1, M + 2) were integrated for each specified peptide with Xcalibur (version 2.2 SP1.48, Thermo Scientific, Waltham, MA, USA), and they were summed to obtain higher confidence. For normalization between samples, the summed peak area was divided by the exclusive spectrum counts of all modified and nonmodified peptides derived from the parental protein, in Scaffold.

In Vitro Digestion. Milk powder samples were reconstituted and defatted as above and subjected to in vitro digestion.[25] Simulated gastric digestion was started with adjusting the pH to 2.0 (adult model) or 4.0 (infant model) with 1 M HCl. Porcine pepsin (Sigma-Aldrich; 2% in 1 mM HCl) was added to the sample in a 1:12.5 ratio (pepsin/protein). Samples were placed in an incubating shaker (New Brunswick Scientific, Edison, NJ, USA) at 140 rpm at 37 °C for 5, 10, 15, or 30 min. After this incubation, the pH of the samples was adjusted to 7.0 with 0.1 mol/L $NaHCO_3$.

Simulated intestinal digestion was performed following the gastric digestion (at pH 2.0 or 4.0). After the pH was adjusted to 7.0, pancreatin (Sigma-Aldrich; 0.4% in 0.1 mol/L $NaHCO_3$) was added to the samples in a 1:62.5 ratio (pancreatin/protein). Samples were placed in an incubator shaker at 140 rpm at 37 °C for 5, 10, 30, or 60 min. After the incubation, the enzymes were inactivated in a water bath at 85 °C for 3 min.

The digested samples were applied to reducing SDS-PAGE as described above, and each lane was loaded with the equivalent of 50 μg of protein before digestion. Protein digestibility of the samples subjected to gastric/intestinal digestion was determined using a Kjeldahl procedure as described previously.[26,27] Briefly, total nitrogen (N), and nonprotein N [NPN; soluble fraction after trichloroacetic acid (TCA; 12% final concentration) precipitation] were measured in milk samples before/after the digestion. Protein digestibility was defined as the ratio of $(NPN_{\text{after digestion}} - NPN_{\text{before digestion}})/(\text{total } N_{\text{before digestion}} - NPN_{\text{before digestion}})$. Protein digestibility was analyzed six times for each pH condition/time period tested.

In Vivo Digestion. A suckling rat pup model was used to investigate in vivo digestion of milk samples.[25,28−30] The study was approved by the International Animal Care and Use Committee of the University of California, Davis (protocol 17128), which is accredited by the American Association for the Accreditation of Laboratory Animal Care. Sprague−Dawley rats with litters of 12 pups (6 males + 6 females) were obtained commercially (Charles River, Wilmington, MA, USA), maintained in polycarbonate cages with wood shavings in a temperature-, humidity-, and light-controlled facility (22 °C, humidity 60%, and 12 h light/dark cycle), and allowed to consume deionized water and standard rat chow diet (Ralston Purina, St. Louis, MO, USA) ad libitum. Pups were randomly assigned as 3 males + 3 females/milk sample/time point. After acclimation to facility conditions, on day 14 postpartum, pups were separated from their dams for 6 h and then intubated with one of six types of milk (reconstituted, defatted, and adjusted to 30 g/L of protein), in a 1:36 v/w ratio [milk (mL)/body weight (g)]. Pups were euthanized with CO_2 asphyxiation at 0.5, 1, or 2 h after intubation. Stomach contents were collected and weighed. The small intestine was cut into upper and lower parts, and each part was perfused twice with 0.2 mL of phosphate-buffered saline (PBS) containing protease inhibitor cocktail (P2714, Sigma-Aldrich). Collected perfusates were stored at −80 °C until analysis.

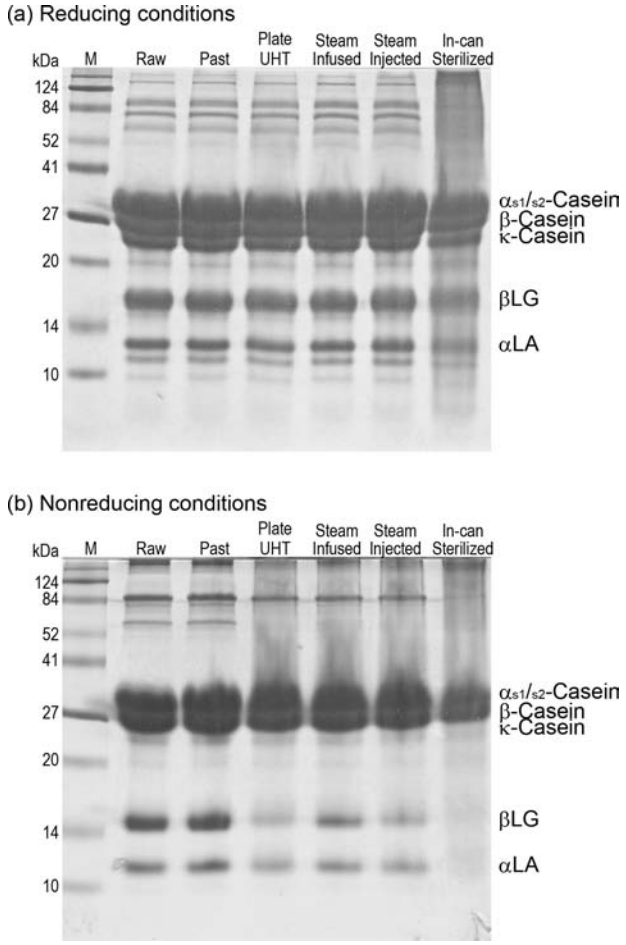

Figure 2. Electrophoresis of milk proteins. Milk samples were applied to SDS-PAGE analysis under (a) reducing and (b) nonreducing conditions. Fifty micrograms of protein was loaded onto a 15% gel, and the gel was stained with Coomassie Brilliant Blue R-250.

The perfusates underwent Western blotting. On the basis of the results obtained in the in vitro study, β-lactoglobulin (β-LG) was used as a marker protein of in vivo digestibility. The perfusates (5 μg of protein) were applied to reducing SDS-PAGE, and proteins were transferred to a Hybond ECL nitrocellulose membrane (GE Healthcare, Pewaukee, WI, USA). The membrane was blocked with 2% bovine serum albumin [in PBS containing 0.05% Tween-20 (PBST)] for 45 min at room temperature. After the membrane was washed three times with PBST, it was probed with rabbit anti-bovine β-LG antibody (Bethyl Laboratories Inc., Montogomery, TX, USA) in a 1:20000 dilution (antibody/blocking buffer) at room temperature for 45 min. After three washings with PBST, the membrane was probed with donkey anti-rabbit IgG antibody conjugated with horseradish peroxidase (GE Healthcare) in a 1:20000 dilution (antibody/blocking buffer) at room temperature for 45 min. After three washings with PBST, β-LG was detected by Pierce ECL Western Blotting Substrate (Thermo Scientific).

Statistical Analysis. Data on protein digestibility (Kjeldahl procedure) and stomach contents resulting from in vivo digestion were analyzed by one-way ANOVA and post-tested by the Tukey test

Table 4. Lactulosyllysine Derivatives of Lys in Milk Proteins[a]

protein	residue	amino acid	charge	raw[b]	pasteurized	plate UHT	steam infused	steam injected	in-can sterilized
α-LA	41−60	Lys98	[3+]	1.0	1.1	3.0	2.4	3.7	9.8
			[4+]	1.0	0.9	2.1	1.4	2.4	6.0
β-LG	41−60	Lys47	[3+]	1.0	1.0	1.6	2.1	2.5	3.6
	76−83	Lys77	[2+]	1.0	1.4	4.4	2.0	5.5	16.5
	76−101	Lys83 or 91	[4+]	1.0	1.2	4.5	1.6	2.1	10.2
	84−101	Lys91	[3+]	1.0	1.1	1.7	1.6	2.0	2.4
	125−138	Lys135	[2+]	1.0	1.0	3.0	2.3	4.0	6.2
			[3+]	1.0	1.1	2.8	2.1	4.0	4.8
α_{S1}-CN	4−22	Lys7	[3+]	1.0	0.8	2.6	2.0	3.0	6.3
			[4+]	1.0	1.1	3.1	1.8	3.3	6.1
	35−42	Lys36	[2+]	1.0	1.2	2.7	2.4	3.8	13.7
	80−90	Lys83	[2+]	1.0	1.0	1.8	1.5	4.6	12.4
			[3+]	1.0	1.9	4.1	1.9	4.9	9.7
	104−119	Lys105	[2+]	1.0	1.8	26.9	5.6	46.2	505.3
			[3+]	1.0	2.6	5.6	2.0	7.7	62.3
	120−132	Lys124	[2+]	1.0	3.7	11.9	2.8	9.4	101.6
	125−151	Lys132	[2+]	1.0	1.5	3.9	1.6	4.9	19.8
			[3+]	1.0	2.1	5.4	2.3	5.3	24.0
α_{S2}-CN	25−41	Lys32	[2+]	1.0	0.5	3.1	1.5	3.2	17.1
			[3+]	1.0	0.6	2.4	1.3	3.1	21.2
	71−91	Lys76 or 80	[3+]	1.0	1.1	4.1	1.7	4.3	10.1
			[4+]	1.0	1.2	3.5	1.7	3.6	8.5
	171−181	Lys173	[2+]	1.0	1.5	2.8	1.7	3.3	6.2
			[3+]	1.0	1.6	2.4	1.8	3.1	5.4
	174−188	Lys181	[2+]	1.0	1.6	3.9	2.4	3.3	8.0
			[3+]	1.0	1.2	2.5	1.6	2.9	4.9
			[4+]	1.0	1.5	2.3	1.6	2.5	4.0
	198−205	Lys199	[2+]	1.0	1.1	1.8	0.8	2.1	4.2
			[3+]	1.0	1.2	1.5	0.8	2.3	4.1
β-CN	170−183	Lys176	[2+]	1.0	0.9	1.4	1.1	1.5	5.8
			[3+]	1.0	1.1	1.5	1.0	2.1	4.5
κ-CN	22−34	Lys24	[2+]	1.0	1.9	5.6	4.1	6.1	12.1
			[3+]	1.0	2.0	4.9	3.5	5.2	11.3
	35−68	Lys46	[4+]	1.0	1.9	6.4	2.6	6.2	20.1
	69−97	Lys86	[3+]	1.0	1.0	4.1	3.3	4.7	34.7
			[4+]	1.0	1.6	4.7	2.3	3.8	31.1

[a]Milk samples were treated with trypsin, followed by LC-MS/MS analysis for identifying and semiquantifying trypic peptides containing lactullosyllysine in milk proteins. [b]Peak areas of the specific peptides are expressed as mean values (n = 2); normalized to raw milk.

using Prism 4 (version 4.03 GraphPad Software Inc., San Diego, CA, USA), and significance was demonstrated at $p < 0.05$.

RESULTS

Electrophoresis of Milk Proteins. Milk samples were applied to SDS-PAGE, and the band patterns were compared (Figure 2). A notable difference was observed for in-can sterilized milk; proteins smeared in a wide range of molecular weights, and the bands of intact milk proteins decreased under reducing/nonreducing conditions. This trend, although to a lesser extent, was also observed for the three UHT-treated milk samples under nonreducing condition, where disulfide bonds are kept intact. These results suggest that pasteurization essentially does not induce any protein associations; the three kinds of UHT treatments caused new disulfide bond formation between proteins, facilitating protein aggregation, and in-can sterilization modified the proteins to a greater extent by forming new disulfide bonds and possibly other noncovalent interactions.

Proteomic Analysis. Milk samples were applied to LC-MS/MS analysis following in-gel tryptic digestion for identifying and semiquantifying modifications involved in protein digestibility, such as lactulosyllysine, CML, and dehydroalanine on Ser and Cys residues, in major milk proteins. Relative amounts of quantified peptides with the above modifications are shown in Tables 4−6. It should be noted that some of the peptides containing the specified modifications were identified but could not be quantified probably because of low abundance. In-can sterilized milk had the highest signal intensity for lactulosyllysine at all of the modified sites in α-LA, β-LG, and CNs, followed by plate UHT and steam-injected milk. A similar trend was observed for CML; the highest signals were observed at Lys77

Table 5. Carboxymethyllysine in Milk Proteins[a]

protein	residue	amino acid	charge	raw[b]	pasteurized	plate UHT	steam infused	steam injected	in-can sterilized
β-LG	41−70	Lys47, 69, or 70	[3+]	1.0	0.3	0.2	0.3	0.2	0.1
	76−83	Lys77	[2+]	1.0	0.9	1.2	0.1	2.7	3.9
			[3+]	1.0	2.2	3.0	0.4	6.9	11.2
	125−138	Lys135	[3+]	1.0	0.6	0.6	0.8	1.1	0.8
α_{S1}-CN	4−22	Lys7	[3+]	nd	1.0[c]	1.7	1.0	1.7	4.9
			[4+]	nd	1.0[c]	1.5	1.0	1.6	3.8
	23−36	Lys34 or 36	[3+]	1.0	22.1	68.7	18.9	63.8	552.0
	80−90	Lys83	[2+]	1.0	3.4	20.9	3.7	20.1	142.5
			[3+]	1.0	3.4	4.6	0.9	4.9	16.2
α_{S2}-CN	71−80	Lys76	[2+]	1.0	2.9	10.1	1.5	18.2	28.6
	151−160	Lys152	[2+]	1.0	1.2	0.8	1.2	2.1	8.2
	171−181	Lys173	[2+]	1.0	6.7	11.3	2.4	11.5	54.8
			[3+]	1.0	26.5	35.1	13.6	20.5	115.6
	198−205	Lys199	[2+]	1.0	2.7	9.0	1.1	3.4	55.0
β-CN	98−107	Lys105	[2+]	nd	nd	nd	nd	nd	1.0[c]
	170−183	Lys176	[2+]	1.0	4.3	10.8	2.9	6.6	77.6
			[3+]	1.0	2.3	3.4	1.8	2.9	15.6
κ-CN	22−34	Lys24	[2+]	1.0	0.9	1.8	2.6	4.1	20.0
			[3+]	1.0	0.8	1.2	1.3	3.2	8.7

[a]Milk samples were treated with trypsin, followed by LC-MS/MS analysis for identifying and semiquantifying trypic peptides containing carboxymethyllysine in milk proteins. [b]Peak areas of the specific peptides are expressed as mean values (n = 2); normalized to raw milk. [c]Peak areas of the specific peptides are expressed as mean values (n = 2); normalized to other milk samples when the peak areas from raw milk were below the detection limit.

Table 6. Dehydroalanine Derivatives of Ser in Milk Proteins[a]

protein	residue	amino acid	charge	raw[b]	pasteurized	plate UHT	steam infused	steam injected	in-can sterilized
α_{S1}-CN	104−119	Ser115	[2+]	1.0	0.6	1.7	0.7	1.4	1.2
			[3+]	1.0	0.4	1.0	0.5	0.8	0.6
	106−119	Ser115	[2+]	1.0	0.4	0.8	0.5	1.4	1.1
β-CN	33−48	Ser35	[2+]	1.0	0.3	0.6	0.3	0.3	0.3

[a]Milk samples were treated with trypsin, followed by LC-MS/MS analysis for identifying and semiquantifying trypic peptides containing dehydroalanine on Ser in milk proteins. [b]Measured values of peak areas are shown (n = 1); normalized to raw milk.

in β-LG and all of the modified sites in CNs for in-can sterilized milk, which was followed by plate UHT and steam-injected milk. Some of the lactulosyllysine/CML sites could not be solely assigned, such as lactulosyllysine of Lys83/91 in β-LG, lactulosyllysine of Lys76/80 in α_{S2}-CN, CML of Lys47/69/70 in β-LG, and CML of Lys34/36 in α_{S1}-CN. However, by taking into consideration the fact that CML should be converted from lactulosyllysine and that trypsin can never recognize lactulosyllysine as a cleavage site,[3,5] it can be assumed that lactulosyllysine of Lys76/80 in α_{S2}-CN would be Lys76, CML of Lys47/69/70 in β-LG would be Lys47, and CML of Lys34/36 in α_{S1}-CN would be Lys 36. If this is true, all of the quantified CML sites would overlap the quantified lactulosyllysine sites except Lys152 in α_{s2}-CN and Lys105 in β_{s2}-CN. It should be noted that lactulosyllysine was also identified (but not quantifiable) at these sites (data not shown). In contrast with lactulosyllysine/CML, dehydroalanine could be quantified only at three sites in all of the major proteins. These signals were weak, and no clear trend was observed among the milk samples, indicating that dehydroalanine formation in the milk samples is very limited.

In addition to the above-mentioned modifications, phosphorylation on Ser, Thr, and Tyr was also semiquantified as it may provide further information in the context of heat treatment and proteins; milk proteins have generally been considered to be dephosphorylated after heat treatment of milk,[31] whereas proteins can be phosphorylated in the presence of phosphate after dry heating.[32,33] In this study, phosphorylation could be quantified at three Ser residues in α_{S1}-CN, α_{S2}-CN, and β-CN (Table 7). In general, they appear to be dephosphorylated after heating, but to a very limited extent, although phosphorylation of Ser46 increased in in-can sterilized milk.

In Vitro Digestion of Milk Samples. SDS-PAGE analysis of milk samples after in vitro digestion is shown in Figure 3. A rapid decrease in α-LA, β-LG, and CN bands was observed during the course of digestion in in-can sterilized milk, indicating that in-can sterilization facilitated enzymatic digestion of these proteins. The bands for α-LA and β-LG, but not CN, decreased over time in the three UHT-treated milk samples, but this did not occur as rapidly as in in-can sterilized milk. The digestibility appeared to be plate UHT > steam injected > steam-infused milk, according to the remaining band

Table 7. Phosphorylation of Ser in Milk Proteins[a]

protein	residue	amino acid	charge	raw[b]	pasteurized	plate UHT	steam infused	steam injected	in-can sterilized
α_{S1}-CN	119−134	Ser130	[2+]	1.0	0.7	1.0	0.9	0.7	0.5
			[3+]	1.0	0.8	0.7	0.7	0.8	0.5
α_{S2}-CN	40−56	Ser46	[2+]	1.0	2.1	0.9	1.8	0.7	4.0
			[3+]	1.0	2.1	0.6	1.4	0.4	4.3
β-CN	45−63	Ser50	[2+]	1.0	0.9	0.7	1.0	0.8	0.7
			[3+]	1.0	0.8	0.6	1.1	0.7	0.6

[a]Milk samples were treated with trypsin, followed by LC-MS/MS analysis for identifying and semiquantifying trypic peptides containing phosphorylation on Ser in milk proteins. [b]Peak areas of the specific peptides are expressed as mean values (n = 2); normalized to raw milk.

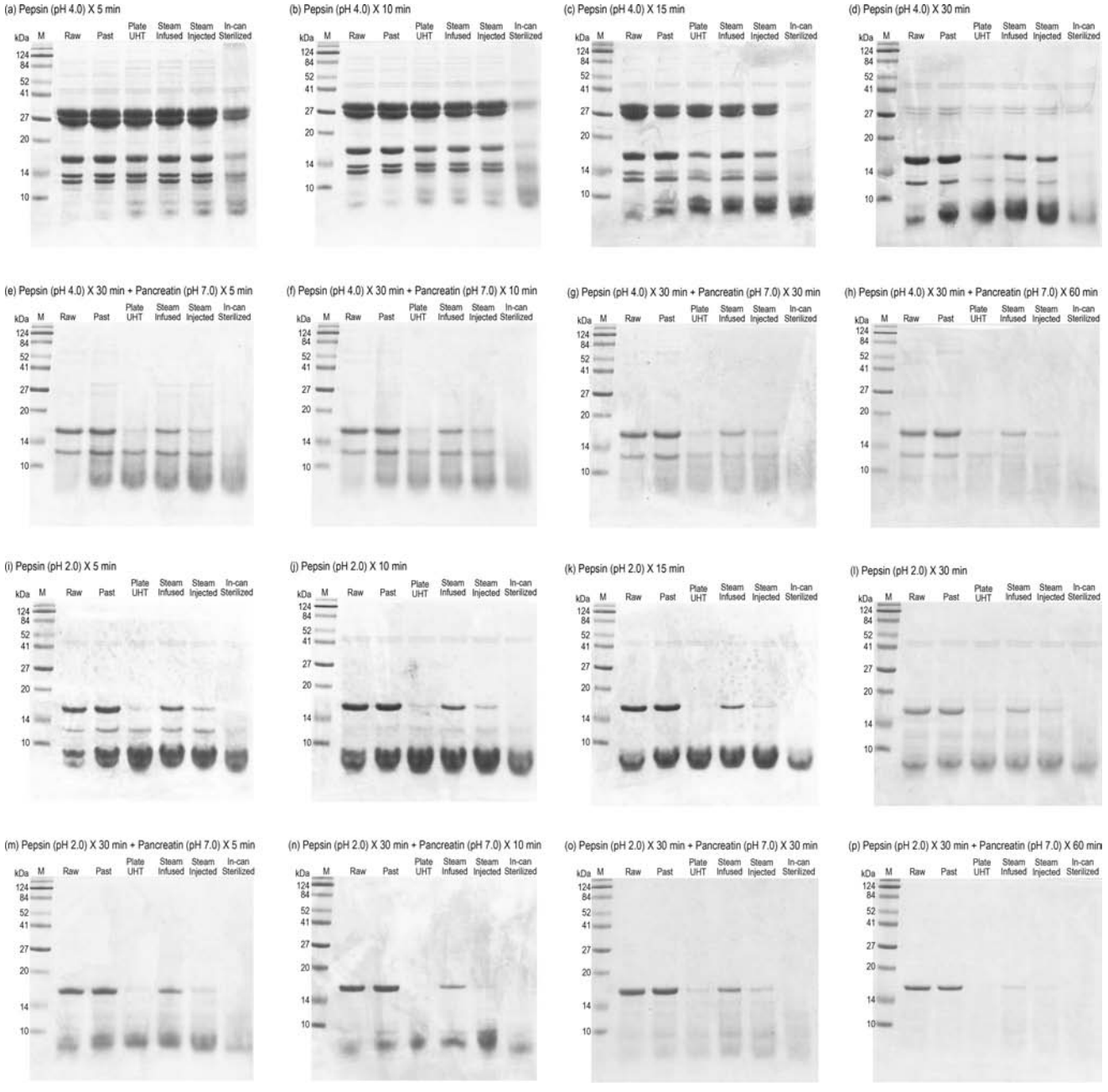

Figure 3. Electrophoresis of milk proteins after in vitro digestion. Milk samples were subjected to in vitro digestion using pepsin and pancreatin for different time periods. Both infant (a-h) and adult (i-p) digestion conditions were simulated by adopting different pH values during the peptic digestion. Fifty micrograms of protein (before digestion) was loaded onto a 15% gel, and the gel was stained with Coomassie Brilliant Blue R-250.

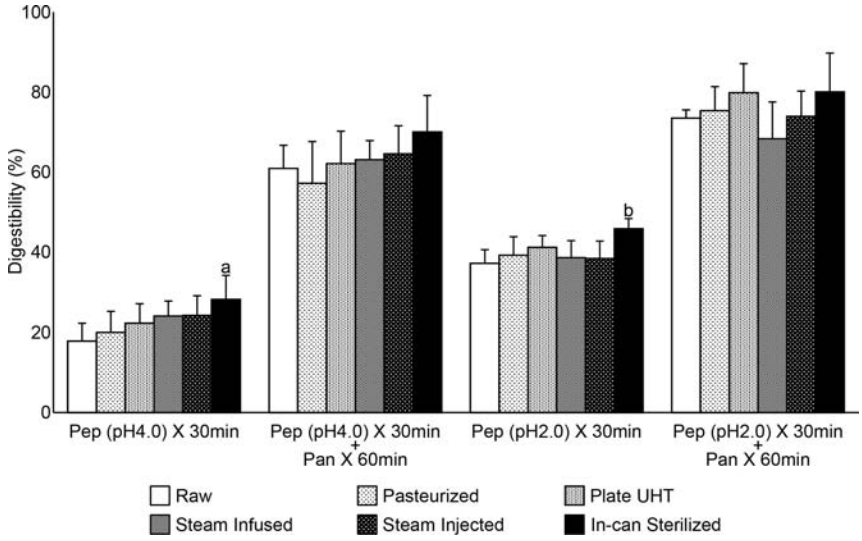

Figure 4. Protein digestibility of milk proteins after in vitro digestion. Protein digestibility was defined as the increase in NPN after in vitro digestion, which was determined by the combination of TCA precipitation and a Kjeldahl procedure. Each digestion and the subsequent procedures were conducted six times, and data are expressed as means ± SD. "a", $p < 0.05$ (in-can sterilized vs raw milk); "b", $p < 0.05$ (in-can sterilized vs raw or steam-injected milk).

intensities for α-LA and β-LG. In contrast to in-can sterilized milk and the three UHT-treated milk samples, pasteurized milk showed the same band patterns as raw milk throughout the digestion experiments, suggesting that pasteurization does not affect the digestibility of the milk proteins to any significant extent.

At the final time points of each peptic/pancreatic digestion, the digestibility of total milk protein was determined using a Kjeldahl procedure (Figure 4). In-can sterilized milk showed the highest digestibility of all the digestion conditions. However, the differences in total protein digestibility among the samples seem equivocal compared with the observations for the above SDS-PAGE.

In Vivo Digestion of Milk Samples. White coagulates, which are likely acid-precipitated CNs, were observed in the stomachs of rat pups after intubation with the milk samples (Figure 5a). Pups fed in-can sterilized milk had the smallest contents at 0.5 and 1 h, which was statistically lower at 1 h compared with the plate UHT milk-fed group ($p < 0.05$). At 2 h, there were no notable differences in stomach contents among the milk samples. This indicates that extensive heat treatment such as in-can sterilization can affect coagulation of CN negatively as previously reported for pasteurized milk.[34] Furthermore, a notable decrease in the pH of the stomach content was observed in the in-can sterilized milk-fed group at 2 h (Figure 5b), which may also corroborate damaged casein coagulation potential, manifested as impaired buffering activity.

Perfusates from the upper small intestine showed complex protein band patterns by SDS-PAGE (data not shown). Because β-LG exhibited a prominent difference in in vitro digestion among the milk samples, this protein was chosen to assess in vivo digestibility and was analyzed by Western blotting (Figure 6). At 0.5 h, strong β-LG bands were observed for raw milk and pasteurized milk in its intact form as well as partially fragmented forms, whereas intact bands were barely detected in the three UHT-treated milk samples and in-can sterilized milk. At 1 h, β-LG was still visible in raw milk, but the bands were barely detectable or invisible for the remaining five milk samples. At 2 h, no β-LG band was detectable for any of the milk samples. Western blotting of β-LG was also conducted for the lower intestine perfusates, but the bands were very faint and no clear differences were observed among the milk samples (data not shown).

DISCUSSION

MS techniques have extensively been utilized to characterize chemical modifications of milk proteins. However, the link between chemical characterization of the proteins and their nutritional consequences has rarely been discussed. In this study, heated milk samples were manufactured from the same reference raw milk and they were investigated in terms of both protein digestibility and proteomic characterization.

Sites of protein modifications have been a major interest in proteomic studies of milk proteins, and lactulosyllysine sites are often identified. In this study, α-LA had only one lactulosylation site at Lys98, which is the main lactulosylation site in this protein. This modification has been identified in UHT milk and powdered infant formulas.[35−37] As for β-LG, all five lactulosylation sites have previously been identified in pasteurized milk, UHT milk, and/or powdered infant formulas.[5,35,37] Among them, Lys47 is the best studied site because of its high reactivity.[38,39] Semiquantification has also been conducted using various kinds of dairy products.[15] All of the lactulosyllysine sites in CNs, except Lys199 in α_{S2}-CN, agree with previous studies.[5,37] Thus, the general agreement of the lactulosyllysine sites substantiates the validity of this study, and the new lactulosyllysine site (Lys199 in α_{S2}-CN) could be found probably due to methodological differences. With regard to semiquantification of protein modifications, our results look controversial at first glance in that both lactulosyllysine and CML were quantifiable in all heat-treated milk samples as well as raw milk (despite the absence of heat treatment). However, this observation is reasonable because some studies could quantify furosine, an indirectly measured product from Amadori compounds, and CML in raw milk samples.[40,41] The highest signals for lactulosyllysine and CML were observed at almost all of the sites in in-can sterilized milk, reflecting the severe thermal history resulting from slow rates of temperature rise/fall and the longest holding time at high temperature. To a lesser extent, the signals for the three UHT-treated milk

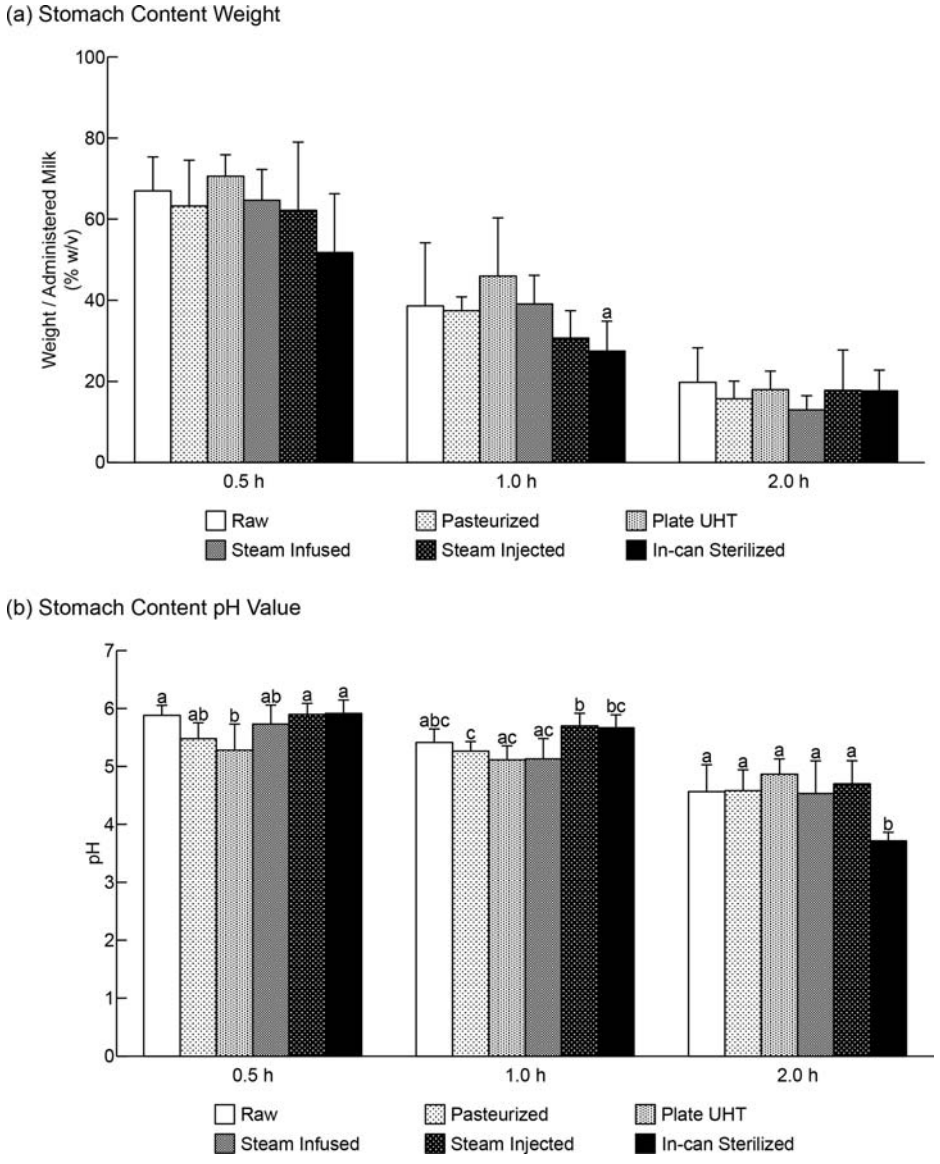

Figure 5. Stomach contents of suckling rat pups. Rat pups fed different milk samples were euthanized at 0.5, 1, and 2 h after intubation, and the stomach contents were obtained. Weight (a) and pH values (b) were measured, and data are expressed as means ± SD (n = 3 males + 3 females). "a", $p < 0.05$ (in-can sterilized vs plate UHT milk).

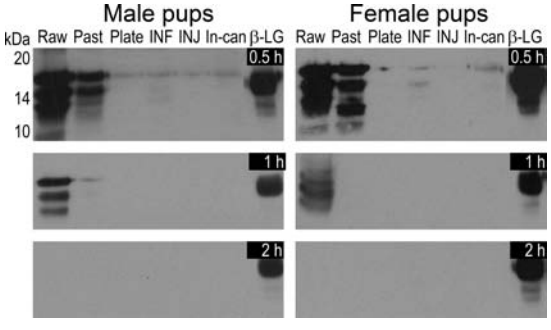

Figure 6. Western blotting of β-LG in upper intestine perfusates from suckling rat pups. Rat pups fed different milk samples were euthanized at 0.5, 1, and 2 h after intubation, and the upper intestines were perfused with PBS containing protease inhibitor. Five micrograms of protein was loaded, and β-LG was detected by Western blotting as an index of in vivo protein digestibility.

samples were also higher, probably because of the high holding temperature. However, steam-infused milk tended to show the lowest signals among the UHT-treated milk samples. The lowest heat damage of steam-infused milk among the three UHT-treated milk samples could arise not just from the lowest holding temperature but also from the dilution effect derived from the steam infusion.[42] No CML was identified in α-LA, and there were no distinct differences in CML amounts among the milk samples at the sites of β-LG compared with those of CNs. This possibly implies that CNs, the dominant proteins in cow's milk, might be competitive with whey proteins for progress of the Maillard reaction.

Both of the electrophoretic analyses in the in vitro and in vivo digestion assays demonstrated that in-can sterilization, followed by the three UHT treatments, facilitated enzymatic digestion of the major milk proteins, especially of β-LG. Facilitated digestion of intact milk proteins has also been observed in a study similar to ours; raw milk, pasteurized milk,

and sterilized milk were applied to in vitro digestion, and proteins in sterilized milk but not pasteurized milk exhibited better digestion.[43] With regard to β-LG, it has been shown in several studies that heat treatment promotes its digestion.[12,34,44,45] These positive effects of heat treatment on protein digestion can be attributed to protein denaturation, accelerating exposure of peptide bonds to digestive enzymes. Denaturation of milk proteins was apparent as WPNI values decreased for in-can sterilized milk followed by the three UHT-treated milk samples, and a faster gastric emptying rate/impaired gastric buffering activity of in-can sterilized milk was observed for in vivo digestion.

In contrast to the facilitated protein digestion discussed above, protein digestibility of milk samples, determined by a combination of in vitro digestion and a Kjeldahl procedure, showed insignificant differences among the milk samples. Similar results have been reported previously,[46,47] with some of the studies reporting positive effects accompanied by adverse consequences; some amino acids were not digestible, and small fragments resistant to digestion were formed.[43,44] Plausible explanations for these negative outcomes would be the fact that heating facilitates the formation of lactulosyllysine, the aggregation of proteins via cross-linked products such as lysinoalanine and lanthionine, and some newly formed disulfide bonds; these chemical structures inhibit the action of trypsin as well as other digestive enzymes, leading to a decrease in protein digestibility. In this study, in-can sterilized milk manifested the greatest formation of lactulosyllysine at many Lys residues in major milk proteins, such as α-LA, β-LG, and CNs, to an extent followed by plate UHT and steam-injected milk. With regard to protein aggregation, whereas proteomic analysis indicated that formation of lysinoalanine in all of the milk samples seems quantitatively limited, the results of SDS-PAGE suggest that the three kinds of UHT treatment caused new disulfide bond formation and that in-can sterilization modified the proteins to a greater extent by forming new disulfide bonds and possibly other noncovalent interactions. Thus, it can be speculated that a denaturation-mediated improvement in protein digestibility might be "offset" by the concomitant lactulosyllysine formation and protein aggregation involved in reducing protein digestibility. It should be added that the surface hydrophobicity of milk proteins, determined by a SDS-binding method,[48] showed only insignificant differences among milk samples (data not shown). Heating decreases surface hydrophobicity of caseins (the majority of total milk protein), whereas progress of the Maillard reaction increases surface hydrophobicity of total milk proteins. This observation may therefore reflect another "offset" chemistry in milk proteins. However, the possibility should be taken into consideration that total milk protein digestibility was practically the same because the heat treatment facilitates protein digestion but the resulting peptides might still be too large to be TCA-soluble.

Whereas no adverse effects on protein digestibility of heated raw milk were observed in this study even after in-can sterilization (despite the greatest formation of Amadori product on Lys residue causing inhibition of digestive enzymes such as trypsin), it seems that a decrease in protein digestibility has mostly been reported for milk-based infant/enteral formulas.[27,49−51] In general, the thermal history of milk-based formulas is more extensive than that for cow's milk because milk proteins are heat-treated as both "ingredients" and as "products (i.e., formulas)", which would promote the formation of Amadori products and cross-links (whereas our data of dehydroalanine suggested formation of cross-links may be limited after heating raw milk). In the context of ingredient manufacturing, industrial CN isolation involves isoelectric precipitation followed by neutralization at alkaline pH, and the alkaline treatment would facilitate the formation of cross-links such as lysinoalanine and lanthionine.[9] Furthermore, some of the above modifications proceed during long storage of ingredients/products at ambient temperature, possibly augmenting the modifications.[52]

In conclusion, industrial heating may improve the digestibility of proteins in raw milk by denaturation, but the improvement is likely to be offset by heat-derived modifications involved in the decrease in protein digestibility. However, this phenomenon may not hold true for dairy products such as infant/enteral formulas. Continuing studies are in progress to verify how protein modifications and consequential protein digestibility would differ between cow's milk samples and infant formulas.

AUTHOR INFORMATION

Corresponding Author

*(B.L.) Phone: (530) 752-8347. Fax: (530) 752-3564. E-mail: bllonnerdal@ucdavis.edu.

Notes

The authors declare no competing financial interest.

ACKNOWLEDGMENTS

We are grateful to Keisuke Miyazaki, Junichi Hashimoto, Hiroyoshi Yabuki, and Yuki Hayakawa, Morinaga Milk Industry, for preparing for the milk samples. We thank Dr. Brett Phinney and Darren Weber, University of California, Davis, for performing the proteomic analysis.

ABBREVIATIONS USED

UHT, ultra-high-temperature; Lys, lysine; CML, N^{ε}-carboxymethyllysine; Cys, cysteine; MS, mass spectrometry; LC, liquid chromatography; WPNI, whey protein nitrogen index; SDS-PAGE, sodium dodecyl sulfate−polyacrylamide gel electrophoresis; N, nitrogen; NPN, nonprotein N; TCA, trichloroacetic acid; β-LG, β-lactoglobulin; PBS, phosphate-buffered saline; PBST, PBS containing 0.05% Tween-20; ACN, acetonitrile; Ser, serine; α-LA, α-lactalbumin; CN, casein

REFERENCES

(1) Mauron, J. Influence of processing on protein quality. *J. Nutr. Sci. Vitaminol. (Tokyo)* **1990**, *36* (Suppl. 1), S57−S69.

(2) Kakade, M. L.; Evans, R. J. Chemical and enzymatic determinations of available lysine in raw and heated navy beans (*Phaseolus vulgaris*). *Can. J. Biochem.* **1966**, *44*, 648−650.

(3) van Boekel, M. A. J. S. Effect of heating on Maillard reactions in milk. *Food Chem.* **1998**, *62*, 403−414.

(4) Mauron, J.; Mottu, F.; Bujard, E.; Egli, R. H. The availability of lysine, methionine and tryptophan in condensed milk and milk powder. *In vitro* digestion studies. *Arch. Biochem. Biophys.* **1955**, *59*, 433−451.

(5) Marvin, L. F.; Parisod, V.; Fay, L. B.; Guy, P. A. Characterization of lactosylated proteins of infant formula powders using two-dimensional gel electrophoresis and nanoelectrospray mass spectrometry. *Electrophoresis* **2002**, *23*, 2505−2512.

(6) Rerat, A.; Calmes, R.; Vaissade, P.; Finot, P. A. Nutritional and metabolic consequences of the early Maillard reaction of heat treated milk in the pig. Significance for man. *Eur. J. Nutr.* **2002**, *41*, 1−11.

(7) Finot, P. A.; Magnenat, E. Metabolic transit of early and advanced Maillard products. *Prog. Food Nutr. Sci.* **1981**, *5*, 193−207.

(8) Swaisgood, H. E.; Catignani, G. L. Digestibility of modified milk proteins: nutritional implications. *J. Dairy Sci.* **1985**, *68*, 2782−2790.
(9) Friedman, M. Chemistry, biochemistry, nutrition, and microbiology of lysinoalanine, lanthionine, and histidinoalanine in food and other proteins. *J. Agric. Food Chem.* **1999**, *47*, 1295−1319.
(10) Robbins, K. R.; Baker, D. H.; Finley, J. W. Studies on the utilization of lysinoalanine and lanthionine. *J. Nutr.* **1980**, *110*, 907−915.
(11) Patel, H. A.; Singh, H.; Anema, S. G.; Creamer, L. K. Effects of heat and high hydrostatic pressure treatments on disulfide bonding interchanges among the proteins in skim milk. *J. Agric. Food Chem.* **2006**, *54*, 3409−3420.
(12) Peram, M. R.; Loveday, S. M.; Ye, A.; Singh, H. In vitro gastric digestion of heat-induced aggregates of β-lactoglobulin. *J. Dairy Sci.* **2013**, *96*, 63−74.
(13) Fenaille, F.; Morgan, F.; Parisod, V.; Tabet, J. C.; Guy, P. A. Solid-state glycation of β-lactoglobulin monitored by electrospray ionisation mass spectrometry and gel electrophoresis techniques. *Rapid Commun. Mass Spectrom.* **2003**, *17*, 1483−1492.
(14) Meltretter, J.; Seeber, S.; Humeny, A.; Becker, C. M.; Pischetsrieder, M. Site-specific formation of Maillard, oxidation, and condensation products from whey proteins during reaction with lactose. *J. Agric. Food Chem.* **2007**, *55*, 6096−6103.
(15) Meltretter, J.; Becker, C. M.; Pischetsrieder, M. Identification and site-specific relative quantification of β-lactoglobulin modifications in heated milk and dairy products. *J. Agric. Food Chem.* **2008**, *56*, 5165−5171.
(16) van Boekel, M. A. J. S. Heat-induced deamidation, dephosphorylation and breakdown of caseinate. *Int. Dairy J.* **1999**, *9*, 237−241.
(17) Harland, H. A.; Ashworth, U. S. A rapid method for estimation of whey proteins as an indication of baking quality of nonfat dry-milk solids. *Food Res.* **1947**, *12*, 247−251.
(18) Mikami, H.; Ishida, Y. Post-column fluorometric detection of reducing sugars in high performance liquid chromatography using arginine. *Bunseki Kagaku* **1983**, *1*, E207−E210.
(19) Bradford, M. M. A rapid and sensitive method for the quantitation of microgram quantities of protein utilizing the principle of protein-dye binding. *Anal. Biochem.* **1976**, *72*, 248−254.
(20) Shevchenko, A.; Wilm, M.; Vorm, O.; Mann, M. Mass spectrometric sequencing of proteins silver-stained polyacrylamide gels. *Anal. Chem.* **1996**, *68*, 850−858.
(21) Alvarado, R.; Tran, D.; Ching, B.; Phinney, B. S. A comparative study of in-gel digestions using microwave and pressure-accelerated technologies. *J. Biomol. Technol.* **2010**, *21*, 148−155.
(22) Keller, A.; Nesvizhskii, A. I.; Kolker, E.; Aebersold, R. Empirical statistical model to estimate the accuracy of peptide identifications made by MS/MS and database search. *Anal. Chem.* **2002**, *74*, 5383−5392.
(23) Nesvizhskii, A. I.; Keller, A.; Kolker, E.; Aebersold, R. A statistical model for identifying proteins by tandem mass spectrometry. *Anal. Chem.* **2003**, *75*, 4646−4658.
(24) Elias, J. E.; Gygi, S. P. Target-decoy search strategy for mass spectrometry-based proteomics. *Methods Mol. Biol.* **2010**, *604*, 55−71.
(25) Jou, M. Y.; Du, X.; Hotz, C.; Lönnerdal, B. Biofortification of rice with zinc: assessment of the relative bioavailability of zinc in a Caco-2 cell model and suckling rat pups. *J. Agric. Food Chem.* **2012**, *60*, 3650−3657.
(26) Hambraeus, L.; Forsum, E.; Abrahamsson, L.; Lönnerdal, B. Automatic total nitrogen analysis in nutritional evaluations using a block digestor. *Anal. Biochem.* **1976**, *72*, 78−85.
(27) Rudloff, S.; Lönnerdal, B. Solubility and digestibility of milk proteins in infant formulas exposed to different heat treatments. *J. Pediatr. Gastroenterol. Nutr.* **1992**, *15*, 25−33.
(28) Sandström, B.; Keen, C. L.; Lönnerdal, B. An experimental model for studies of zinc bioavailability from milk and infant formulas using extrinsic labeling. *Am. J. Clin. Nutr.* **1983**, *38*, 420−428.
(29) Lönnerdal, B.; Du, X.; Morris, K.; Rai, G.; Waworuntu, R. TGF β2 in human milk and infant formula resists digestion ain a suckling rat pup model. *J. Pediatr. Gastroenterol. Nutr.* **2010**, *50*, E199.
(30) Lönnerdal, B.; Mendoza, C.; Brown, K. H.; Rutger, J. N.; Raboy, V. Zinc absorption from low phytic acid genotypes of maize (*Zea mays* L.), barley (*Hordeum vulgare* L.), and rice (*Oryza sativa* L.) assessed in a suckling rat pup model. *J. Agric. Food Chem.* **2011**, *59*, 4755−4762.
(31) Singh, H. Heat stability of milk. *Int. J. Dairy Technol.* **2004**, *57*, 111−119.
(32) Li, C. P.; Salvador, A. S.; Ibrahim, H. R.; Sugimoto, Y.; Aoki, T. Phosphorylation of egg white proteins by dry-heating in the presence of phosphate. *J. Agric. Food Chem.* **2003**, *51*, 6808−6815.
(33) Li, C. P.; Hayashi, Y.; Enomoto, H.; Hu, F.; Sawano, Y.; Tanokura, M.; Aoki, T. Phosphorylation of proteins by dry-heating in the presence of pyrophosphate and some characteristics of introduced phosphate groups. *Food Chem.* **2009**, *114*, 1036−1041.
(34) Scanff, P.; Savalle, B.; Miranda, G.; Pelissier, J. P.; Guilloteau, P.; Toullec, R. In vivo gastric digestion of milk proteins. Effect of technological treatments. *J. Agric. Food Chem.* **1990**, *38*, 1623−1629.
(35) Siciliano, R.; Rega, B.; Amoresano, A.; Pucci, P. Modern mass spectrometric methodologies in monitoring milk quality. *Anal. Chem.* **2000**, *72*, 408−415.
(36) Lund, M. N.; Olsen, K.; Sørensen, J.; Skibsted, L. H. Kinetics and mechanism of lactosylation of α-lactalbumin. *J. Agric. Food Chem.* **2005**, *53*, 2095−2102.
(37) Arena, S.; Renzone, G.; Novi, G.; Paffetti, A.; Bernardini, G.; Santucci, A.; Scaloni, A. Modern proteomic methodologies for the characterization of lactosylation protein targets in milk. *Proteomics* **2010**, *10*, 3414−3434.
(38) Fogliano, V.; Monti, S. M.; Visconti, A.; Randazzo, G.; Facchiano, A. M.; Colonna, G.; Ritieni, A. Identification of a β-lactoglobulin lactosylation site. *Biochim. Biophys. Acta* **1998**, *1388*, 295−304.
(39) Leonil, J.; Molle, D.; Fauquant, J.; Maubois, J. L.; Pearce, R. J.; Bouhallab, S. Characterization by ionization mass spectrometry of lactosyl β-lactoglobulin conjugates formed during heat treatment of milk and whey and identification of one lactose-binding site. *J. Dairy Sci.* **1997**, *80*, 2270−2281.
(40) Ahmed, N.; Mirshekar-Syahkal, B.; Kennish, L.; Karachalias, N.; Babaei-Jadidi, R.; Thornalley, P. J. Assay of advanced glycation endproducts in selected beverages and food by liquid chromatography with tandem mass spectrometric detection. *Mol. Nutr. Food Res.* **2005**, *49*, 691−699.
(41) Pereda, J.; Ferragut, V.; Quevedo, J. M.; Guamis, B.; Trujillo, A. J. Heat damage evaluation in ultra-high pressure homogenized milk. *Food Hydrocolloids* **2009**, *23*, 1974−1979.
(42) Nangpal, A.; Reuter, H. Reference diagram for furosine content in UHT milk. *Kieler Milchw. Forsch.* **1990**, *42*, 77−86.
(43) Dupont, D.; Mandalari, G.; Mollé, D.; Jardin, J.; Rolet-Répécaud, O.; Duboz, G.; Léonil, J.; Mills, C. E.; Mackie, A. R. Food processing increases casein resistance to simulated infant digestion. *Mol. Nutr. Food Res.* **2010**, *54*, 1677−1689.
(44) Desrosiers, T.; Bergeron, G.; Savoie, L. Effect of heat treatments on in vitro digestibility of delactosed whey protein as determined by the digestion cell technique. *J. Food Sci.* **1987**, *52*, 1525−1528.
(45) Kitabatake, N.; Kinekawa, Y. Digestibility of bovine milk whey protein and β-lactoglobulin in vitro and in vivo. *J. Agric. Food Chem.* **1998**, *46*, 4917−4923.
(46) alKanhal, H. A.; al-Othman, A. A.; Hewedi, F. M. Changes in protein nutritional quality in fresh and recombined ultra high temperature treated milk during storage. *Int. J. Food Sci. Nutr.* **2001**, *52*, 509−514.
(47) Lacroix, M.; Léonil, J.; Bos, C.; Henry, G.; Airinei, G.; Fauquant, J.; Tomé, D.; Gaudichon, C. Heat markers and quality indexes of industrially heat-treated [^{15}N] milk protein measured in rats. *J. Agric. Food Chem.* **2006**, *54*, 1508−1517.
(48) Hiller, B.; Lorenzen, P. C. Surface hydrophobicity of physicochemically and enzymatically treated milk proteins in relation

to techno-functional properties. *J. Agric. Food Chem.* **2008**, *56*, 461−468.
(49) Sarwar, G.; Peace, R. W.; Botting, H. G. Differences in protein digestibility and quality of liquid concentrate and powder forms of milk-based infant formulas fed to rats. *Am. J. Clin. Nutr.* **1989**, *49*, 806−813.
(50) Sarwar, G.; Peace, R. W. The protein quality of some enteral products is inferior to that of casein as assessed by rat growth methods and digestibility-corrected amino acid scores. *J. Nutr.* **1994**, *124*, 2223−2232.
(51) Rutherfurd, S. M.; Moughan, P. J. Digestible reactive lysine in selected milk-based products. *J. Dairy Sci.* **2005**, *88*, 40−48.
(52) Ford, J. E.; Hurrell, R. F.; Finot, P. A. Storage of milk powders under adverse conditions. 2. Influence on the content of water-soluble vitamins. *Br. J. Nutr.* **1983**, *49*, 355−364.

JOURNAL OF AGRICULTURAL AND FOOD CHEMISTRY

Article

pubs.acs.org/JAFC

Structural Changes from Native Waxy Maize Starch Granules to Cold-Water-Soluble Pyrodextrin during Thermal Treatment

Yanjie Bai,[†] Liming Cai,[†] James Doutch,[‡,§] Elliot P. Gilbert,[‡] and Yong-Cheng Shi*[,†]

[†]Department of Grain Science and Industry, Kansas State University, Manhattan, Kansas 66506, United States

[‡]Bragg Institute, Australian Nuclear Science and Technology Organisation, Locked Bag 2001, Kirrawee DC, NSW 2232, Australia

ABSTRACT: The structural changes occurring during the thermal conversion of insoluble native waxy maize starch granules to cold-water-soluble pyrodextrin under acidic conditions have been investigated by multiple techniques, including synchrotron small-angle X-ray scattering (SAXS), wide-angle X-ray scattering, differential scanning calorimetry, and gel permeation chromatography. In a mixture of water/glycerol (20/80, w/w), the SAXS characteristic peak at ca. 0.6 nm^{-1} decreased in intensity as pyrodextrin solubility increased. The peak disappeared as pyrodextrin solubility reached 100%. Starch crystal size, its associated melting enthalpy, and pyrodextrin molecular size decreased as solubility increased. Although starch structure changed during thermal conversion, the pyrodextrins appeared identical to the native starch when observed in glycerol under a normal and polarized light microscope. It is proposed that the starch backbone is hydrolyzed by acid in the amorphous region and the crystalline region with starch molecules being hydrolyzed into small molecular fractions but persisting in a radial arrangement.

KEYWORDS: *pyrodextrin, dextrin, thermal treatment, small-angle X-ray scattering, starch structure*

1. INTRODUCTION

Thermal treatment of dry starch usually causes depolymerization at temperatures below 300 °C.[1] A degraded starch product prepared in the dry state by heating, or through a combination of heat and acid, is commonly called a "pyrodextrin".[2] The closely related term "dextrin" broadly refers to all degraded starch products regardless of the method used in the process. Dextrins may be produced by hydrolysis of starch with enzymes or acids in water, as well as by dextrinization or pyroconversion, or heating starch in its dry form.[2] Depending on the temperature, time, and level of acid used, pyrodextrins are generally classified into three categories: white dextrin, yellow or canary dextrin, and British gum;[2,3] however, these broad classifications are arbitrary, and classifying a given pyrodextrin product is not always easy. The properties of the products cover a wide range depending on pretreatment, level of acid used, and process conditions (e.g., temperature and time).[2] Yellow dextrin and more degraded British gum are soluble in cold water and become a viscous liquid with gummy and adhesive properties.[2] Traditionally, pyrodextrins have wide application in industry as adhesives, coatings, binders, and encapsulating agents.[1,2,4] The various applications and biological activities of pyrodextrins have been reviewed.[1] Pyrodextrin is suggested to be resistant to α-amylolysis and is considered as soluble dietary fiber,[4−10] which has many applications in the food industry. Preparation of indigestible dextrins by pyroconversion has been described.[11,12]

Changes in molecular structure during the dextrinization process have been suggested to involve hydrolysis, transglycosidation, and repolymerization of the glucans.[2,13] Starch molecules are significantly degraded by heat and acid, as reflected in a continual decrease in starch molecular weight, a progressive increase in solubility in water, decreased viscosity in water, and increased reducing value.[2,4,14] Transglycosidation results from the hydrolysis of the α-1,4 glucosidic linkages followed by a recombination of the fragments with nearby free hydroxyl groups to produce branched structures.[2] Transglycosidation and the branched structure of pyrodextrin have been proposed from the evidence of methylation[15,16] and reduced degree of β-amylolysis.[17] In addition, repolymerization has additionally been proposed due to the slight increase in viscosity and the decrease in reducing sugar content observed on dextrinization.[2]

Compared with extensive studies in molecular structure, few attempts have been made to understand the precise long-range structural changes during dextrinization. Pyrodextrins look identical to native granular starch when viewed in glycerol under both normal and polarized light microscopes,[2,4,18] and pyrodextrins have a wide-angle X-ray scattering (WAXS) pattern similar to native starch but with broader and weaker peaks.[5] However, the molecular arrangement in the pyrodextrin granules has not been thoroughly investigated; furthermore, it is not well understood why pyrodextrin is partially crystalline and retains its granular shape yet is readily soluble in water.

Small-angle X-ray scattering (SAXS), which probes larger length scales than WAXS, has been used to characterize the structure of native and modified starches.[19−29] Blazek and Gilbert[30] reviewed the application of SAXS to investigate starch structure. Native starch molecules are suggested to be arranged in a lamellar structure with a repeat spacing of ca. 9 nm, which corresponded to a SAXS peak at 0.6−0.7 nm^{-1}.[31] This SAXS peak disappears due to the loss of lamellar order in the case of starch gelatinization[22,32] and acid hydrolysis.[20,27] In this study, SAXS and WAXS were used to investigate the granular structure of pyrodextrin. We propose a model of starch

Received: January 6, 2014
Revised: March 29, 2014
Accepted: April 15, 2014
Published: April 29, 2014

ACS Publications © 2014 American Chemical Society

structural changes during thermal decomposition based on scattering, microscopy, gel permeation chromatography (GPC), and differential scanning calorimetry (DSC). These findings enable a greater understanding of the granular structure of pyrodextrin and the implications to its functionality.

2. EXPERIMENTAL SECTION

Materials. Waxy maize (WM) starch (Amoica TF) was obtained from National Starch LLC (Bridgewater, NJ, USA). Other chemicals used in the study were analytical grade.

Methods. *Preparation of Pyrodextrins.* Waxy maize starch (100 g dry weight) was suspended in water (150 mL), and the pH of the slurry was adjusted to 3.0 by 0.5 M HCl and stirred for 30 min. Starch was filtered to a cake with moisture content at approximately 50%. The starch cake was broken and dried in an oven at 40 °C for 24 h to a moisture content of 10−15%. The pH of the air-dried starch was approximately 4.0 at 10% solids in water. The dried starch was ground, passed through a screen (100 mesh), and heated in a forced-air oven at 170 °C. Samples were collected at 0.5, 1, 2, 3, and 4 h during heating and were kept at ambient temperature overnight. The resulting moisture content of the pyrodextrin samples was about 7%. In a separate experiment, the pH was adjusted to 2.5, and pyrodextrin was prepared as described above.

Light Microscopy. Starch granules were observed in glycerol or a mixture of glycerol and water using an optical microscope with a digital camera (model BX51, Olympus Co., Japan) under normal visible and polarized light.

Solubility. Starch (0.100 g) was dissolved in distilled water (0.9 mL) and centrifuged at 6708*g* for 3 min. Starch concentration in the supernatant (solubility) was determined by a hand-held refractometer (Fisher Scientific, Pittsburgh, PA, USA).

Gel Permeation Chromatography. GPC analysis was performed as previously described.[33] Starch hydrolysates (4 to 16 mg) were dissolved in DMSO (4 mL) by stirring at room temperature for 12 h. The solutions were filtering through a 2 μm filter (Millex-AP, Millipore, Billerica, MA, USA) and injected by an autosampler into a PL-GPC 220 system (Polymer Laboratories Inc., Amherst, MA, USA) with three Phenogel columns (00H-0642-K0; 00H-0644-K0; 00H-0646-K0; Phenomenex Inc., Torrance, CA, USA), one guard column (03B-0290-K0, Phenomenex Inc.), and a differential refractive index detector. The eluting solvent was DMSO containing 0.5 mM $NaNO_3$, and the flow rate was 0.8 mL/min. The column oven temperature was controlled at 80 °C. Standard dextrans (American Polymer Standards Co., Mentor, OH, USA) with different MWs were used for MW calibration. GPC results were analyzed using Cirrus GPC software version 3.0 (Agilent Technologies, Santa Clara, CA, USA).

Differential Scanning Calorimetry. Thermal properties of native starch and pyrodextrin products were determined by a Pyris-1 DSC (PerkinElmer, Norwalk, CT, USA). Samples were mixed with solvents of distilled water, water/glycerol mixture (20/80, w/w), or glycerol at a ratio of 1:3 (starch:solvent, w/w) and were lightly stirred with a spatula. Pyrodextrin pastes were sealed in a centrifuge vial and allowed to stand for 12 h at 25 °C for hydration. Pyrodextrin pastes (40−55 mg) were accurately weighed with a microbalance and placed into large DSC stainless steel pans. The DSC pans were sealed and held at 10 °C for 1 min and heated to 160 °C at 10 °C/min. Onset (T_o), peak (T_p), and conclusion (T_c) temperatures as well as enthalpy (ΔH) were determined. An empty pan was used as a reference. Native waxy maize starch was included as a control. Samples were analyzed in duplicate.

SAXS and WAXS. Pyrodextrin paste in water, water/glycerol mixture of 20/80 and 40/60 (w/w), or glycerol at a ratio of 1:1 (w/w) was prepared by manually mixing with a spatula followed by equilibrating at room temperature for 15 min.

Native starch and pyrodextrin pastes were examined by SAXS and WAXS at the X27C beamline at the National Synchrotron Light Source, Brookhaven National Laboratory. The details of the experimental setup at the X27C beamline have been reported elsewhere.[34−37] The wavelength of the X-ray was 1.371 Å. Two-dimensional WAXS and SAXS images were collected with an X-ray CCD detector (MarUSA) with resolution times of 30 and 60 s, respectively. The sample-to-detector distance was 155.6 mm for WAXS and 2018.5 mm for SAXS, respectively. The scattering angle in WAXS was calibrated using a polypropylene standard and an Al_2O_3 standard from the National Institute of Standards and Technology (Gaithersburg, MD, USA). The scattering angle in SAXS was calibrated by a AgBe standard. Pyrodextrin samples were sealed in a sample holder and placed on the hot stage (Instec Inc., Boulder, CO, USA).[33] The WAXS and SAXS spectra were background-subtracted by using an empty sample holder covered with two layers of Kapton film. Data are displayed in terms of arbitrary intensity versus q for SAXS where q is the magnitude of the scattering vector and is equal to $(4\pi \sin \theta)/\lambda$, where λ (nm) is the wavelength of the X-ray source and 2θ is the scattering angle. WAXS data are plotted as arbitrary intensity versus scattering angle.

Starch crystallinity was calculated as described elsewhere.[38] The approximate average size (D) in nm of crystallites in the samples was calculated from the Scherrer formula:

$$D = \frac{0.89 \times \lambda}{\beta \times \cos \theta}$$

where β is the angular width in radians at the half-maximum intensity corrected for instrumental line broadening and θ is half of the angular position of the peak in radians. In the present case, such broadening has a negligible influence compared to the width of the peaks observed.

Statistical Analysis. Each experiment was performed in duplicate. One-way analysis of variance was performed with the Minitab software (version 16.1.0, Minitab Inc., State College, PA, USA). Least significant differences for comparison of means were computed at $p < 0.05$.

3. RESULTS AND DISCUSSION

3.1. Solubility and Molecular Weight Distribution. The solubility of pyrodextrin was affected by process parameters including pH, temperature, and heating time. At a pH of 2.5 and 170 °C, starch became 100% soluble after heating for 0.5 h. At pH 3 and 170 °C, pyrodextrins with a solubility from 21% to 100% were produced by heating from 0.5 to 4 h (Table 1).

Table 1. Solubility of Pyrodextrin in Water Prepared at Different pH, Heating Temperature, and Heating Time

pH	temperature (°C)	time (h)	solubility (%)
2.5	170	0.5	100.0 a
3.0	160	4.0	42.0 b
3.0	170	0.5	21.2 c
		1.0	22.1 c
		2.0	97.1 a
		3.0	100.0 a
		4.0	100.0 a

Starch solubility increased rapidly during the first 2 h of the conversion. As the conversion continued, relatively little change occurred in the solubility. In contrast, at pH 3 and 160 °C, starch was only 42.0% soluble after being heated for 4 h (Table 1).

Molecular breakdown was indicated by a shift in molecular size distribution profile (Figure 1). The molecular weight of the waxy maize starch decreased rapidly at the beginning (0.5 to 1 h) of the conversion and slowed after 2 h. At the latter stage of dextrinization, starch molecular size remained in the range of 4.3×10^4 to 3.6×10^5 (Figure 1). These results suggest that starch molecules were hydrolyzed by acid and heat during dextrinization. Molecular scission was promoted by low pH, high temperature, and long reaction time, which is in agreement

dx.doi.org/10.1021/jf5000858 | J. Agric. Food Chem. 2014, 62, 4186−4194

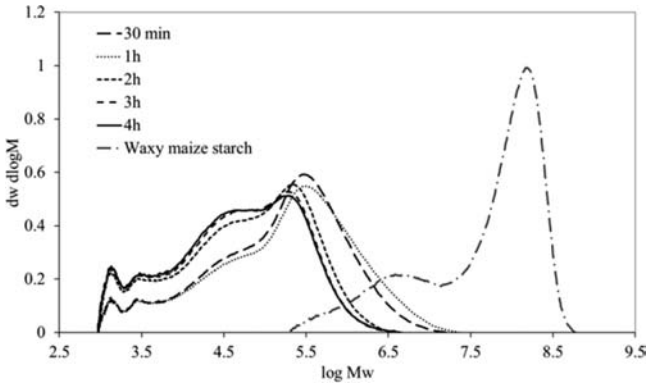

Figure 1. Molecular weight (M_w) distribution of native waxy maize starch and pyrodextrins prepared from heating at pH 3 and 170 °C for 0.5 to 4 h. The M_w is relative to dextran standards.

with previous studies.[2,5,14] To investigate the structural changes of starch from insoluble granules to water-soluble pyrodextrin, samples prepared by heating at pH 3 and 170 °C from 0.5 to 4 h were selected because their solubility ranged from 21% to 100%.

3.2. Birefringence of Pyrodextrin. After dextrinization, starch granules remained and products had a characteristic yellow color. When examined under a microscope, pyrodextrins in glycerol appeared identical to native starch and, under polarized light, showed strong birefringence (Figure 2), indicating a radial orientation of molecules. However, when the pyrodextrin was suspended in water, the starch granules ruptured quickly. Starch granules disappeared as starch molecules dissolved. Similar results have been reported in other studies.[2,39] It has been suggested that the crystallites of starch granules are oriented together in a parallel arrangement and undergo significant changes upon dextrinization.[17] To fully understand these changes in granular structure, SAXS and WAXS were employed to characterize the crystalline and amorphous regions and lamellar structure of pyrodextrins.

3.3. Small-Angle X-ray Scattering. The SAXS lamellar peak of native starch evolves only upon sufficient hydration,[28,40] but the solubility of pyrodextrins in water increases after dextrinization (Table 1), and starch granules of pyrodextrins with high solubility disintegrate in water and lose their structural information. To effectively probe the structural changes of starch granules during dextrinization by SAXS and WAXS, different ratios of glycerol to water were used to deliberately modulate the degree of plasticization. Glycerol is a less effective plasticizer than water, and pyrodextrins retain their granular shape in glycerol (Figure 2). Thus, using this approach, it becomes possible to elucidate the structure of pyrodextrins with different water solubility.

Native waxy maize starch and pyrodextrins showed no SAXS characteristic peak in glycerol at room temperature (Figure 3); however, a well-defined SAXS peak at 0.62 nm^{-1} was observed for the native starch in a mixture of water and glycerol (20/80 or 40/60, w/w) (Figures 3 and 4), which was attributed to the periodic lamellar arrangement of semicrystalline starch with a repeat distance of ca. 9 nm.[31] Compared with the native starch, pyrodextrins showed significantly different SAXS patterns in water/glycerol (20/80, w/w) (Figure 4). A characteristic SAXS peak was observed for starch heated for 0.5 and 1 h, but the scattering intensity at ca. 0.6 nm^{-1} was both lower and less resolved than for native starch, suggesting a partial reduction in lamellar periodicity. There also appears to be a slight shift in peak position to higher q (from 0.62 to 0.65 nm^{-1}), indicating a possible decrease in the repeat distance of the alternating crystalline and amorphous lamellae. Such a decrease in lamellar spacing may result from the hydrolysis of amorphous lamellae and a partial disruption in the crystalline lamellae, resulting in a closer periodic arrangement. However, since the peak width is also broader, this rearrangement is not uniform. The 9 nm scattering peak becomes less prominent after 2 h of dextrinization (Figure 4); this indicates that the lamellar structure of granular starch is significantly disrupted during the dextrinization process with a corresponding reduction in long-range order.

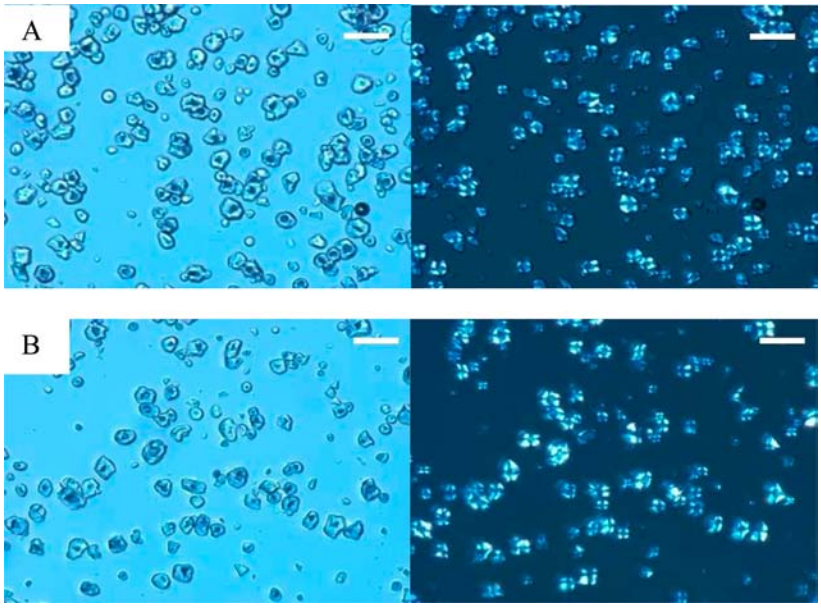

Figure 2. Microscopy images of (A) native waxy maize starch and (B) soluble pyrodextrin (100% solubility) in glycerol. Pyrodextrin was prepared at pH 3 and heated at 170 °C for 4 h. Scale bar in each graph represents 30 μm. Left images: unpolarized; right images: polarized.

dx.doi.org/10.1021/jf5000858 | J. Agric. Food Chem. 2014, 62, 4186−4194

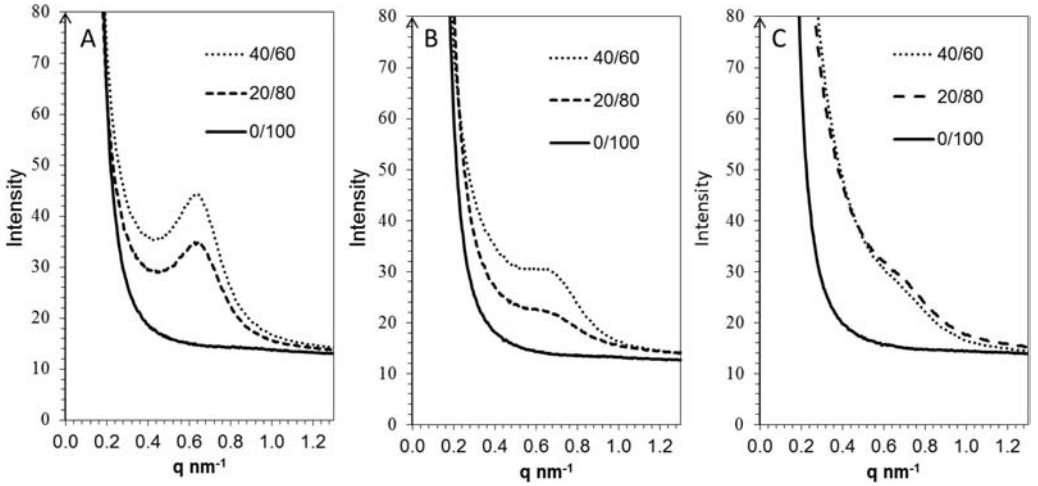

Figure 3. SAXS patterns of (A) native starch, (B) pyrodextrin after 0.5 h, and (C) pyrodextrin after 4 h in a solvent of water/glycerol with ratios of 40/60, 20/80, and 0/100.

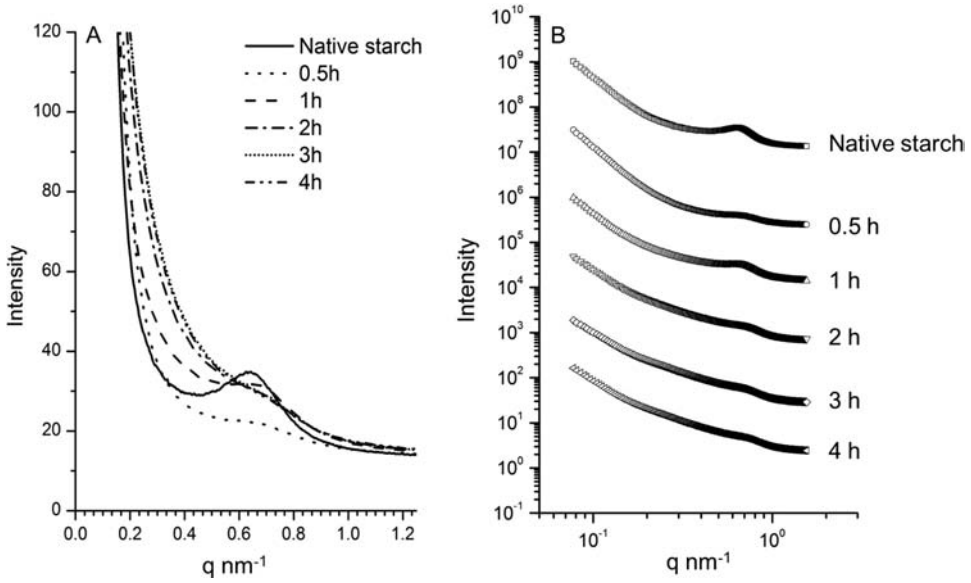

Figure 4. (A) Linear and (B) double-log scale SAXS plot of native starch and pyrodextrins in a solvent of water/glycerol (20/80, w/w). Data shown in log−log plot have been shifted vertically for clarity.

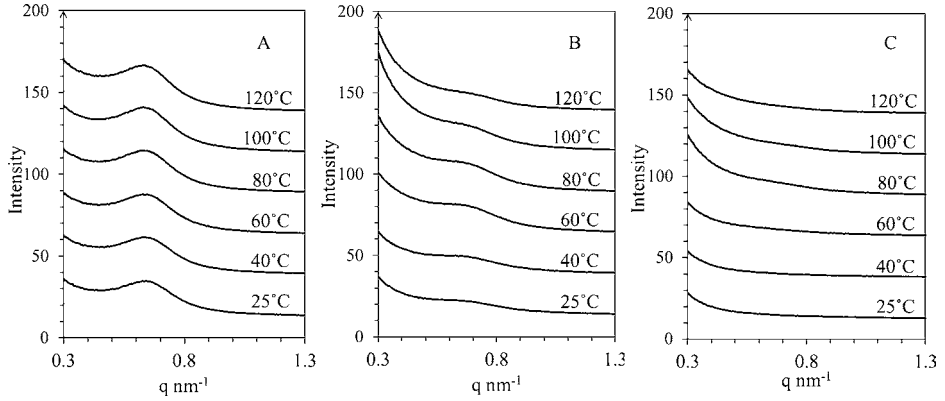

Figure 5. Small-angle X-ray scattering (SAXS) curves of native waxy maize starch (A), dextrin (pH 3, 170 °C, 0.5 h) (B), and dextrin (pH 3, 170 °C, 4 h) (C) in a mixture of water/glycerol (20/80, w/w). Data have been vertically offset for clarity.

The ratio of water to glycerol from 20/80 (w/w) to 40/60 (w/w) reveals interesting differences (Figure 3). For native starch, the size and position of the peak at ca. 0.62 nm^{-1} were little changed, but the peak for the 0.5 h pyrodextrin sample

dx.doi.org/10.1021/jf5000858 | J. Agric. Food Chem. 2014, 62, 4186−4194

became slightly more prominent. However, there appears to be an absence of a peak for the 4 h pyrodextrin sample, indicating a substantial loss of periodic lamellar order.

In addition to changing the ratio of water to glycerol (i.e., the degree of plasticization), both the native starch and pyrodextrin were heated in a mixture of water and glycerol (20/80, w/w), and their changes were examined by SAXS (Figure 5). The peak at ca. 0.62 nm^{-1} was little changed when the native waxy maize starch was heated from 25 to 100 °C.[33] For the 0.5 h pyrodextrin sample, the intensity of the peak at ca. 0.62 nm^{-1} became more pronounced from 25 to 60 °C but decreased after 60 °C, and the peak almost disappeared at 100 °C. These changes indicate that heating initially provides mobility and promotes the alignment of the periodic lamellar structure but destabilizes that structure at high temperatures.

Water plays dual roles when added to the pyrodextrins, functioning as either a plasticizer or solvent depending on the level of water used and the structure of the pyrodextrin. Glycerol alone is not able to solvate starch granules, and no SAXS peak is observed due to insufficient plasticization; thus they lack long-range order.[40,41] When water is added, hydration enables sufficient chain mobility to occur such that a proportion of the amylopectin branches are able to align (Figure 3). Conversely, in the absence of water, the branches maintain greater disorder and lamellar scattering is reduced. This is often considered within the formalism of nematic and smectic behavior; in the smectic state, helices are aligned into lamellae, with this breaking down into a laterally nonaligned, smectic, state in the absence of water. A water to glycerol ratio of 20/80 (w/w) is sufficient to allow the evolution of the 9 nm lamellar peak for starch granules at room temperature.[40] In this study, for the 0.5 h pyrodextrin, the SAXS peak at ca. 0.62 nm^{-1} increased as the ratio of water to glycerol increased from 0/100 to 40/60 (w/w) (Figure 3); however, for the 4 h pyrodextrin, no SAXS peak was observed by increasing the level of water (Figure 3) or heating (Figure 5), indicating permanent loss of any significant long-range order of the alternating lamellar structure. The 4 h pyrodextrin retained its granular shape and was birefringent in glycerol (Figure 2), but in the mixture of water and glycerol (40/60, w/w), it lost both its birefringence and granular shape (data not shown), indicating that its granular structure was so weak that it was disrupted by the mixture of water and glycerol. Water, acting as a solvent, was able to completely dissolve the 4 h pyrodextrin sample (Table 1).

It is proposed here that the loss of the periodic lamellar structure is due to the hydrolysis of the amorphous regions of starch and partial disruption of crystalline lamellae by heat. Acid primarily hydrolyzed the amorphous regions of the starch granule.[2] After a significant number of glycosidic bonds are cleaved and crystalline lamellae are disrupted, it is likely that it is no longer possible to form a periodic lamellar structure.

Comparing the SAXS results in this study (heating starch in dry form with acid) with the findings on the acid hydrolysis of starches in water is revealing.[20,27] When hydrolyzed by acid in water, the lamellar peak intensity increased during the early stages of acid hydrolysis followed by a decrease in the latter stages of hydrolysis. In studying the acid hydrolysis of pea starch in water, Wang et al.[27] also reported that the position of the lamellar peak was essentially constant within the first 6−12 days of hydrolysis but shifted to higher q after 35 days of hydrolysis. Relative crystallinity increased after the amorphous regions were selectively hydrolyzed in water and removed during filtration. In contrast, hydrolyzed products remained inside starch granules in this study, and the crystallinity decreased during dextrinization (Figure 6) as discussed in the next section.

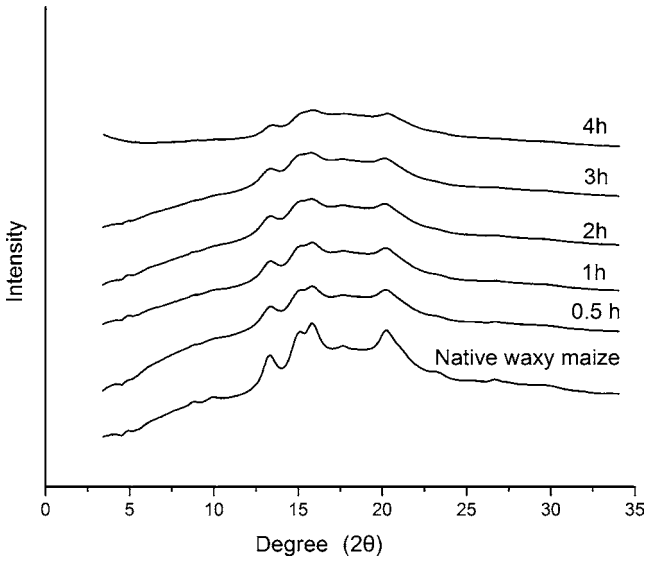

Figure 6. WAXS patterns of pyrodextrins (50%, w/w) in water/glycerol (20/80, w/w) mixture. Native waxy maize is shown as a reference. Pyrodextrins were prepared by heating waxy maize starch (pH 3.0) at 170 °C for 0.5, 1, 2, 3, and 4 h.

The SAXS data from the dextrinization were fitted using the unified method,[42] which has previously been shown to elucidate useful structural information on starch samples.[43] The results are shown in Table 2. Here two levels of fitting were used, a terminal power law for the low-q region, combined with a high-q power law/Guinier region and interference peak as described by Doutch and Gilbert.[43] The final data set at 4 h was fitted with a single power law and background.

The unified approach here is challenged by limited spatial dimension probed because of the limited q range used. However, the fitted parameters appear to indicate progressive loss of an ordered, periodic structure within the granules. This is shown most spectacularly at 4 h, with a loss of interference peak. The intensity of the lamellar peak shows a general decreasing trend through the time course of the experiment, followed by sudden loss between the measurements taken at 3−4 h. There is some variation in the Guinier region fitted, which may imply changes in the overall lamellar structure.[43] The changes in terminal power law also point to disruption in larger scale structures within the granules.

3.4. Wide-Angle X-ray Scattering. Native starch and pyrodextrins showed an A-type crystalline WAXS pattern[33] in the water/glycerol (20/80, w/w) mixture (Figure 6). It should be noted that the Bragg angle values for the peaks in this study were slightly different compared with an A-type crystalline pattern as measured by a conventional X-ray diffraction instrument[5] because the synchrotron X-ray wavelength used in this study was different.[33] Pyrodextrins showed broadened peaks with reduced intensity at 13, 16, and 21 degrees 2θ compared with the native starch (Figure 6). Similar results have been reported previously.[5] Crystallinity and crystal size were estimated[44] and are shown in Table 3. Crystallinity of the native waxy maize starch was approximately 43%, which is close to

Table 2. Unified Fitting Parameters for Pyrodextrins Prepared at pH 3 and 170 °C in a Mixture of Water and Glycerol (20/80, w/w)[a]

time (h)	B1 (cm^{-1} sr^{-1})	power law level 1	G2 (cm^{-1} sr^{-1})	radius of gyration (nm)	B2 (cm^{-1} sr^{-1})	power law level 2	peak intensity	peak position (nm^{-1})	peak hwhm (nm^{-1})	background (nm^{-1})
0	0.00013(6)	3.27(9)	75(7)	8.6(3)	0.0002(1)	3.5(1.6)	19(2)	0.64(1)	0.14(2)	12.7(4)
0.5	0.000500(6)	3.13(3)	261.160(4)	12.4(1)	0.0006(5)	3.03(2)	6.6(7)	0.64(3)	0.21(5)	13.2(4)
1	0.000056(1)	3.4(2)	87(6)	7.0(3)	0.003(8)	3.4(1.6)	11(3)	0.68(3)	0.14(6)	13(1)
2	0.0003(2)	3.1(1)	292(16)	11.7(4)	0.004(9)	2.7(7)	10(4)	0.63(4)	0.21(7)	13.1(6)
3	0.0010(7)	2.8(1)	336(16)	12.1(3)	0.005(1)	2.70(9)	9.9(9)	0.62(2)	0.21(4)	12.9(5)
4	0.000055(2)	3.4(2)	347(7)	11.7(1)	0.0041(1)	2.77(1)	9.4(6)	0.63(2)	0.22(2)	13(2)

[a]Values in parentheses indicate one standard deviation.

Table 3. Estimated Crystallinity (%), Crystal Size (D), and Full Width at Half-Maximum (fwhm) at 13.3 degree 2θ (q = 10.6 nm^{-1}) of Pyrodextrins Prepared at pH 3 and 170 °C in Water/Glycerol (20/80, w/w) Mixture

sample	time (h)	crystallinity (%)	fwhm (deg)	D (nm)
native starch	n.a.	43.3	0.78	9.6
dextrin	0.5	31.4	0.96	7.8
	1.0	31.7	1.06	7.0
	2.0	24.4	1.07	7.0
	3.0	20.3	1.08	7.0
	4.0	17.4	1.07	7.0

previous literature values.[44] Heating at 170 °C for 0.5 and 4.0 h reduced crystallinity to 31.4% and 14.0%, respectively. In addition, crystal size was reduced from 9.6 nm of native starch to 7.8 and 7.0 nm of pyrodextrins. These results indicate a loss of structural organization in a direction lateral to the semicrystalline lamellae due to the dextrinization process; however, for the 4 h pyrodextrin, WAXS still showed an A-type crystalline pattern in a mixture of water and glycerol (20/80, w/w), indicating the existence of a crystalline structure. Therefore, the crystalline region of starch was not completely destroyed, but crystallites became smaller during the dextrinization process. Weak crystallites after dextrinization also were noted when the starch and pyrodextrin samples were heated in the mixture of water and glycerol (20/80, w/w) (Figure 7). Crystallinity of native waxy maize starch changed little when it was heated from 26 to 80 °C. In contrast, the crystallinity of the 0.5 h pyrodextrin was significantly reduced at 80 °C, and 4 h pyrodextrin became essentially amorphous at 80 °C.

3.5. Thermal Properties. A reduction in the crystallinity of pyrodextrins from native starch (Table 3 and Figure 7) is also reflected in the DSC data (Figure 8 and Table 4). Once again, to effectively probe the structure and properties of pyrodextrins, different ratios of water to glycerol were used to deliberately modulate the degree of plasticization. In water, 0.5 h pyrodextrin showed a lower onset temperature and reduced enthalpy of melting endotherm compared with native starch. Pyrodextrins with higher solubility (2.0 h and 4.0 h samples) did not have an endothermic peak, indicating the loss of starch crystallinity in water at room temperature. In 80% glycerol, the gelatinization endotherm for the native starch was shifted to higher temperatures relative to water. Similar results were reported by other studies.[40,45−48] The enthalpy values of pyrodextrins (Table 4) decreased with increasing dextrinization time and are correlated with their degree of crystallinity (Table 3). Higher gelatinization enthalpy suggests higher crystallinity.[44,49]

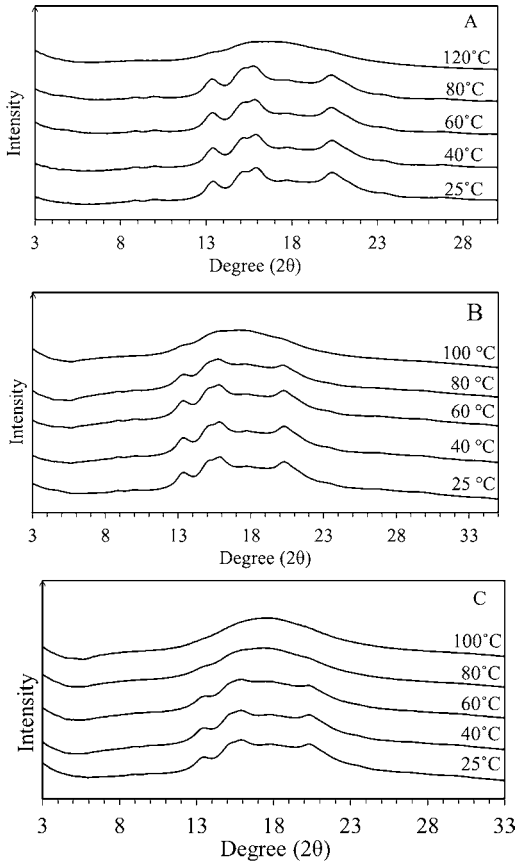

Figure 7. WAXS patterns of (A) waxy maize starch, (B) dextrin (solubility 21%), and (C) dextrin (solubility 100%) in a mixture of water/glycerol (20/80). Data have been offset vertically for clarity.

Comparing thermal properties of pyrodextrins in water and 80% glycerol reveals interesting results. For the 0.5 h pyrodextrin in 80% glycerol, the gelatinization peak was much broader and the enthalpy was much greater than that in water, suggesting that a portion of crystallites was sufficiently weak that they dissolved in water at room temperature but not in 80% glycerol. Glycerol has a large molecular weight and is not as effective as water as a plasticizer.[21] A broad melting peak also was observed for pyrodextrins of 2.0 and 4.0 h in the glycerol/water mixture (Figure 8), which supports this reasoning. The DSC results in 80% glycerol suggest that the crystalline region existed for all the pyrodextrin samples. Dextrinization affected the crystalline region and reduced the crystallinity and crystal size. The less perfect crystallites with short double helices exhibit sufficiently weakened interchain

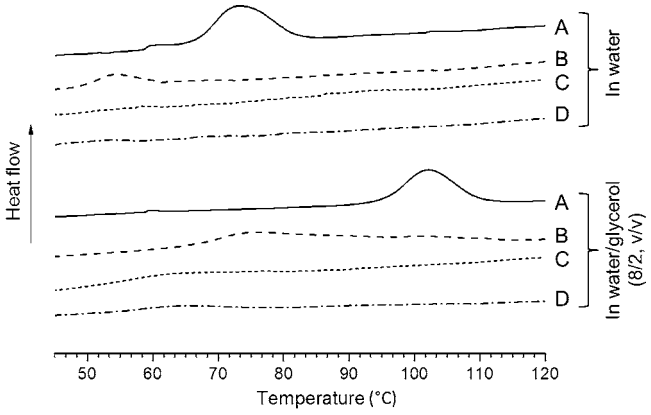

Figure 8. DSC profiles of (A) native starch and (B–D) pyrodextrins prepared at pH 3 and 170 °C for (B) 0.5 h, (C) 2 h, and (D) 4 h.

Table 4. Thermal Properties of Native Starch and Pyrodextrins Prepared at pH 3 and 170 °C for 0.5, 2, and 4 h As Determined by Differential Scanning Calorimetry[a]

solvent	time (h)	T_o (°C)	T_p (°C)	T_c (°C)	ΔH (J/g)
water	native	65.2 a	72.1 a	81.4 a	20.0 a
	0.5	49.3 b	53.2 b	58.2 b	6.9 b
	2.0	no endothermic peak			
	4.0				
water/glycerol mixture (20/80, w/w)	native	93.7 a	100.7 a	109.0 a	17.5 a
	0.5	63.8 b	74.2 b	103.1 ab	14.7 ab
	1.0	63.1 b	74.9 b	98.7 b	13.4 b
	2.0	47.1 d	61.9 c	86.3 c	10.1 c
	3.0	52.4 c	63.3 c	79.7 de	6.0 d
	4.0	52.6 c	63.2 c	77.4 e	4.6 e

[a]Values that do not share the same letter are significantly different ($p < 0.05$).

interactions that they disassociated in water at room temperature.

Native starch and pyrodextrins were also analyzed in 100% glycerol (Figure 9). The melting endotherm of each sample shifted to higher temperatures as expected. In addition, an exothermic peak was observed for all analyzed samples. The exothermic peak has been suggested to result from a starch–glycerol "interaction", including the plasticization of amorphous lamellar regions that enable the crystalline lamellae to form a periodic lamellar structure and thus enhance crystallization.[40] On the basis of the model proposed by Perry and Donald,[40] the DSC results therefore suggest that the starch–glycerol interaction exists for pyrodextrin samples of different solubility. The process of rearranging crystalline lamellae to form a periodic lamellar structure upon plasticization, as well as crystallization, exists for all the pyrodextrins in glycerol during heating. It is also worthy of note that when the native starch was heated by two heating–cooling cycles of 10–110–10–150 °C, the exothermic peak was observed in the first heating cycle but disappeared in the second heating cycle (Figure 9). In addition, little difference was observed for the endothermic peak between the two heating steps (Figure 9). The results suggest that the starch–glycerol interaction is irreversible and occurs prior to the melting of crystallites.

On the basis of WAXS and DSC results, in addition to the effect of hydrolysis of the amorphous region, it is proposed that changes in crystalline regions also affected the SAXS peak. For the 0.5 h pyrodextrin, although the crystalline region was affected by the dextrinization process, it still showed sufficient contrast, with respect to the hydrated amorphous region, to exhibit a SAXS peak. However, in highly soluble pyrodextrins, the overall crystalline region was significantly altered by the process, and the contrast between crystalline and amorphous areas was significantly reduced. The radial arrangement of the starch molecules was not altered during the dextrinization process however.

In conclusion, structural changes from native starch to pyrodextrin have been proposed in the literature[50] and are shown in Figure 10A. In this traditional model, starch was converted by acid hydrolysis in combination with heat into smaller fragments. Starch molecules repolymerized into a branched structure; however, native starch granules are partially crystalline, which is not reflected in the model.

A new model describing long-range structural changes of starch during dextrinization is proposed based on a complementary arsenal of characterization methods, namely, microscopy, GPC, SAXS, WAXS, and DSC (Figure 10B). As starch is heated at 170 °C for 0.5 h, the starch backbone is hydrolyzed by acid in the amorphous region and the crystallite size decreases. Starch molecules are hydrolyzed into small molecule fractions but remain in a radial arrangement. The semicrystalline lamellar structure still persists in the early stage of dextrinization. Upon proper plasticization, double helices tend to arrange in a periodic order; however, the periodicity is not as perfect as in native starch due to the hydrolyzed starch backbone and disrupted crystalline region.

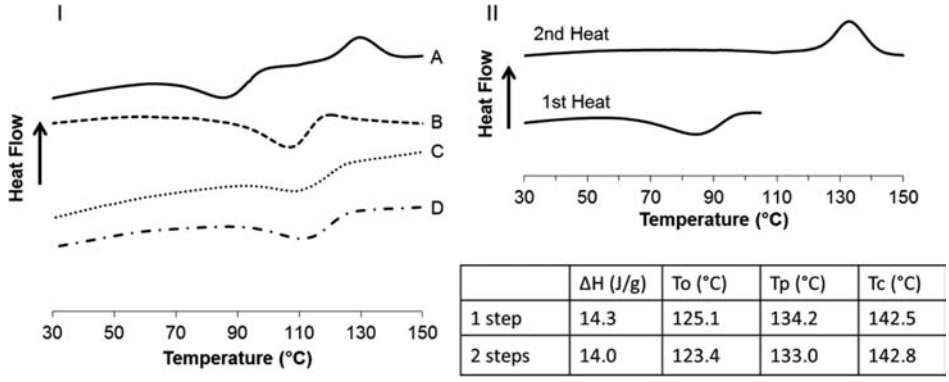

	ΔH (J/g)	To (°C)	Tp (°C)	Tc (°C)
1 step	14.3	125.1	134.2	142.5
2 steps	14.0	123.4	133.0	142.8

Figure 9. DSC traces of (A) native starch and (B–D) pyrodextrins prepared at pH 3 and 170 °C for (B) 0.5 h, (C) 2 h, and (D) 4 h in glycerol in one heating cycle (I) and native starch in glycerol in two heating cycles (heating from 10 to 108 °C, cooling to 10 °C, and reheating to 150 °C) (II).

dx.doi.org/10.1021/jf5000858 | J. Agric. Food Chem. 2014, 62, 4186–4194

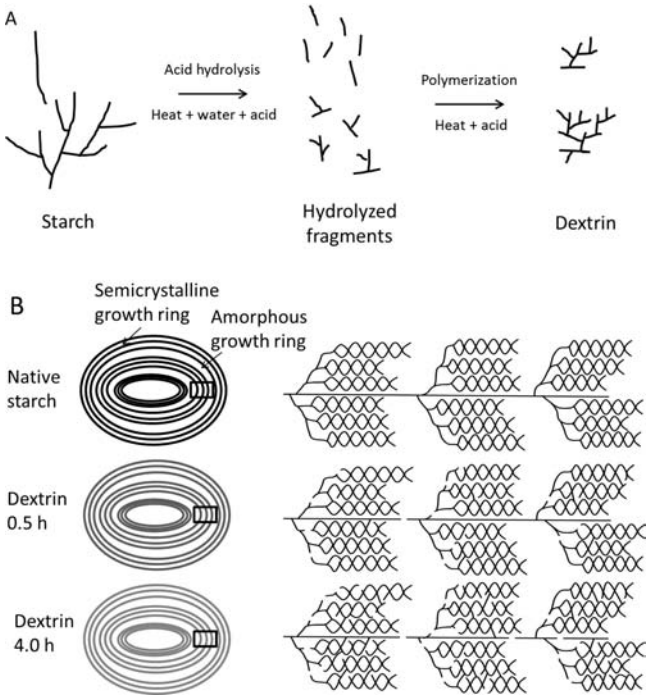

Figure 10. Structure changes from native starch to pyrodextrin. Part A is adapted from Rutenberg.[50] The new model (B) incorporates the concept of cluster model and reflects that native starch is partially crystalline.

As the dextrinization process continues, the starch backbone in the amorphous region is further hydrolyzed along with the crystalline region. Crystallinity decreases, crystallite size is reduced, and starch molecules are hydrolyzed to a smaller molecular weight. While a crystalline arrangement may still exist upon plasticization, due to the significant hydrolysis of the crystalline and amorphous region, a periodic structure of crystalline and amorphous lamellae can no longer be formed. Starch molecules still exist in a radial arrangement, however, and result in birefringence being maintained.

AUTHOR INFORMATION

Corresponding Author

*Tel: +1 785-532-6771. Fax: +1 785-532-7010. E-mail: ycshi@ksu.edu.

Present Address

[§]Diamond Light Source Ltd., Diamond House, Harwell Science and Innovation Campus, Didcot, Oxfordshire, OX11 0DE, United Kingdom.

Funding

Use of the National Synchrotron Light Source, Brookhaven National Laboratory, was supported by the U.S. Department of Energy, Office of Science, Office of Basic Energy Sciences, under Contract No. DE-AC02-98CH10886.

Notes

The authors declare no competing financial interest.

ACKNOWLEDGMENTS

We are grateful to Drs. Lixia Rong, Jie Zhu, Benjamin S. Hsiao, and Jun Wang for their help with the synchrotron X-ray scattering. We also thank Drs. Susan Sun, Jeff Wilson, and Rhett Kaufman for the use of the DSC. This is contribution number 13-221-J from the Kansas Agricultural Experiment Station.

REFERENCES

(1) Tomasik, P.; Wiejak, S.; Palasinski, M. The thermal decomposition of carbohydrates. Part II. The decomposition of starch. In *Advances in Carbohydrate Chemistry and Biochemistry*; Tipson, R. S.; Derek, H., Eds.; Academic Press: Orlando, FL, 1989; Vol. *47*, pp 279−343.

(2) Wurzburg, O. B. Converted Starches. In *Modified Starches: Properties and Uses*; Wurzburg, O. B., Ed.; CRC Press: Boca Raton, FL, 1986; pp 17−40.

(3) Kennedy, H. M.; Fischer, A. C. J. Starch and dextrins in prepared adhesives. In *Starch*, 2nd ed.; Whistler, R. L. B., James, N.; Paschall, E. F., Eds.; Academic Press: Orlando, FL, 1984; pp 593−610.

(4) Laurentin, A.; Cardenas, M.; Ruales, J.; Perez, E.; Tovar, J. Preparation of indigestible pyrodextrins from different starch sources. *J. Agric. Food Chem.* **2003**, *51*, 5510−5515.

(5) Kwon, S. K.; Chung, K. M.; Shin, S. I.; Moon, T. W. Contents of indigestible fraction, water solubility, and color of pyrodextrins made from waxy sorghum starch. *Cereal Chem.* **2005**, *82*, 101−104.

(6) Laurentin, A.; Edwards, C. A. Differential fermentation of glucose-based carbohydrates in vitro by human faecal bacteria - A study of pyrodextrinised starches from different sources. *Eur. J. Nutr.* **2004**, *43*, 183−189.

(7) Wang, Y. J.; Kozlowski, R.; Delgado, G. A. Enzyme resistant dextrins from high amylose corn mutant starches. *Starch/Starke* **2001**, *53*, 21−26.

(8) Wolf, B. W.; Bauer, L. L.; Fahey, G. C. Effects of chemical modification on in vitro rate and extent of food starch digestion: An attempt to discover a slowly digested starch. *J. Agric. Food Chem.* **1999**, *47*, 4178−4183.

(9) Sajilata, M. G.; Singhal, R. S.; Kulkarni, P. R. Resistant starch - A review. *Compr. Rev. Food Sci. Food Saf.* **2006**, *5*, 1−17.

(10) Barczynska, R.; Jochym, K.; Slizewska, K.; Kapusniak, J.; Libudzisz, Z. The effect of citric acid-modified enzyme-resistant dextrin on growth and metabolism of selected strains of probiotic and other intestinal bacteria. *J. Funct. Food* **2010**, *2*, 126−133.

(11) Ohkuma, K.; Matsuda, I.; Nogami, Y. Indigestible dextrin. U.S. Patent 5,358,729, 1994.

(12) Ohkuma, K.; Hanno, Y.; Inada, K.; Matsuda, I.; Katta, Y. Indigestible dextrin. U.S. Patent 5,472,732, 1995.

(13) Huber, K. C.; BeMiller, J. N., Modified starch: chemistry and properties. In *Starches: Characterization, Properties and Applications*; Bertolini, A., Ed.; CRC Press: Boca Raton, FL, 2009; pp 145−203.

(14) Terpstra, K. R.; Woortman, A. J. J.; Hopman, J. C. P. Yellow dextrins: Evaluating changes in structure and colour during processing. *Starch/Starke* **2010**, *62*, 449−457.

(15) Geerdes, J. D.; Lewis, B. A.; Smith, F. The constitution of corn starch dextrin. *J. Am. Chem. Soc.* **1957**, *79*, 4209−4212.

(16) Christensen, G. M.; Smith, F. The constitution of a sheat starch dextrin. *J. Am. Chem. Soc.* **1957**, *79*, 4492−4495.

(17) Brimhall, B. Structure of pyrodextrins. *Ind. Eng. Chem.* **1944**, *36*, 72−75.

(18) Stasiak, M.; Rusinek, R.; Molenda, M.; Fornal, J.; Blaszczak, W. Effect of potato starch modification on mechanical parameters and granules morphology. *J. Food Eng.* **2011**, *102*, 154−162.

(19) Gomand, S. V.; Lamberts, L.; Gommes, C. J.; Visser, R. G. F.; Delcour, J. A.; Goderis, B. Molecular and morphological aspects of annealing-induced stabilization of starch crystallites. *Biomacromolecules* **2012**, *13*, 1361−1370.

(20) Jenkins, P. J.; Donald, A. M. The effect of acid hydrolysis on native starch granule structure. *Starch/Starke* **1997**, *49*, 262−267.

(21) Donald, A. M. Plasticization and self assembly in the starch granule. *Cereal Chem.* **2001**, *78*, 307−314.

(22) Vermeylen, R.; Derycke, V.; Delcour, J. A.; Goderis, B.; Reynaers, H.; Koch, M. H. J. Structural transformations during gelatinization of starches in limited water: Combined wide- and small-angle X-ray scattering study. *Biomacromolecules* **2006**, *7*, 1231−1238.

(23) Vermeylen, R.; Derycke, V.; Delcour, J. A.; Goderis, B.; Reynaers, H.; Koch, M. H. J. Gelatinization of starch in excess water: Beyond the melting of lamellar crystallites. A combined wide- and small-angle X-ray scattering study. *Biomacromolecules* **2006**, *7*, 2624−2630.
(24) Cagiao, M. E.; Rueda, D. R.; Bayer, R. K.; Calleja, F. J. B. Structural changes of injection molded starch during heat treatment in water atmosphere: Simultaneous wide and small-angle X-ray scattering study. *J. Appl. Polym. Sci.* **2004**, *93*, 301−309.
(25) Vermeylen, R.; Goderis, B.; Delcour, J. A. An X-ray study of hydrothermally treated potato starch. *Carbohydr. Polym.* **2006**, *64*, 364−375.
(26) Blazek, J.; Gilbert, E. P. Effect of enzymatic hydrolysis on native starch granule structure. *Biomacromolecules* **2010**, *11*, 3275−3289.
(27) Wang, S. J.; Blazek, J.; Gilbert, E.; Copeland, L. New insights on the mechanism of acid degradation of pea starch. *Carbohydr. Polym.* **2012**, *87*, 1941−1949.
(28) Doutch, J.; Gilbert, E. P. Characterisation of large scale structures in starch granules via small-angle neutron and X-ray scattering. *Carbohydr. Polym.* **2013**, *91*, 444−451.
(29) Zhang, B. J.; Li, X. X.; Liu, J.; Xie, F. W.; Chen, L. Supramolecular structure of A- and B-type granules of wheat starch. *Food Hydrocolloids* **2013**, *31*, 68−73.
(30) Blazek, J.; Gilbert, E. P. Application of small-angle X-ray and neutron scattering techniques to the characterisation of starch structure: A review. *Carbohydr. Polym.* **2011**, *85*, 281−293.
(31) Cameron, R. E.; Donald, A. M. A small-angle X-ray-scattering study of the annealing and gelatinization of starch. *Polymer* **1992**, *33*, 2628−2636.
(32) Jenkins, P. J.; Donald, A. M. Geratinisation of starch: a combined SAXS/WAXS/DSC and SANS study. *Carbohydr. Res.* **1998**, *308*, 133−147.
(33) Cai, L.; Bai, Y.; Shi, Y.-C. Study on melting and crystallization of short-linear chains from debranched waxy starches by in situ synchrotron wide-angle X-ray diffraction. *J. Cereal Sci.* **2012**, *55*, 373−379.
(34) Chen, X.; Burger, C.; Fang, D.; Ruan, D.; Zhang, L.; Hsiao, B. S.; Chu, B. X-ray studies of regenerated cellulose fibers wet spun from cotton linter pulp in NaOH/thiourea aqueous solutions. *Polymer* **2006**, *47*, 2839−2848.
(35) Chen, X.; Burger, C.; Wan, F.; Zhang, J.; Rong, L.; Hsiao, B. S.; Chu, B.; Cai, J.; Zhang, L. Structure study of cellulose fibers wet-spun from environmentally friendly NaOH/urea aqueous solutions. *Biomacromolecules* **2007**, *8*, 1918−1926.
(36) Chu, B.; Hsiao, B. S. Small-angle X-ray scattering of polymers. *Chem. Rev.* **2001**, *101*, 1727−1762.
(37) Cai, L.; Shi, Y.-C.; Rong, L. X.; Hsiao, B. S. Debranching and crystallization of waxy maize starch in relation to enzyme digestibility. *Carbohydr. Polym.* **2010**, *81*, 385−393.
(38) Lopez-Rubio, A.; Flanagan, B. M.; Shrestha, A. K.; Gidley, M. J.; Gilbert, E. P. Molecular rearrangement of starch during in vitro digestion: Toward a better understanding of enzyme resistant starch formation in processed starches. *Biomacromolecules* **2008**, *9*, 1951−1958.
(39) Sjostrom, O. A. Microscopy of starches and their modifications. *Ind. Eng. Chem.* **1936**, *28*, 63−74.
(40) Perry, P. A.; Donald, A. M. The role of plasticization in starch granule assembly. *Biomacromolecules* **2000**, *1*, 424−432.
(41) Waigh, T. A.; Gidley, M. J.; Komanshek, B. U.; Donald, A. M. The phase transformations in starch during gelatinisation: a liquid crystalline approach. *Carbohydr. Res.* **2000**, *328*, 165−176.
(42) Gueneau, C.; Servant, C. Quantitative Determination of Low-Phase Volume Fraction in Ferro-Silicon Alloys by the Rietveld Profile-Refinement Method. Neutron Diffraction Data Compared with Other Methods. *J. Appl. Crystallogr.* **1995**, *28*, 707−716.
(43) Doutch, J.; Bason, M.; Franceschini, F.; James, K.; Clowes, D.; Gilbert, E. P. Structural changes during starch pasting using simultaneous rapid visco Analysis and small-angle neutron scattering. *Carbohydr. Polym.* **2012**, *88*, 1061−1071.
(44) Lopez-Rubio, A.; Flanagan, B. M.; Gilbert, E. P.; Gidley, M. J. A novel approach for calculating starch crystallinity and its correlation with double helix content: A combined XRD and NMR study. *Biopolymers* **2008**, *89*, 761−768.
(45) Liu, P.; Xie, F. W.; Li, M.; Liu, X. X.; Yu, L.; Halley, P. J.; Chen, L. Phase transitions of maize starches with different amylose contents in glycerol-water systems. *Carbohydr. Polym.* **2011**, *85*, 180−187.
(46) Habitante, A. M. B. Q.; Sobral, P. J. A.; Carvalho, R. A.; Solorza-Feria, J.; Bergo, P. V. A. Phase transitions of cassava starch dispersions prepared with glycerol solutions. *J. Therm. Anal. Calorim.* **2008**, *93*, 599−604.
(47) van Soest, J. J. G.; Bezemer, R. C.; deWit, D.; Vliegenthart, J. F. G. Influence of glycerol on the melting of potato starch. *Ind. Crop Prod.* **1996**, *5*, 1−9.
(48) Rajagopalan, S.; Seib, P. A. Granular cold-water-soluble starches prepared at atmospheric pressure. *J. Cereal Sci.* **1992**, *16*, 13−28.
(49) Cooke, D.; Gidley, M. J. Loss of crystalline and molecular order during starch gelatinization - origin of the enthalpic transition. *Carbohydr. Res.* **1992**, *227*, 103−112.
(50) Rutenberg, M. W. Starch and its modifications. In *Handbook of Water Soluble Gums and Resins*; Davidson, R. L., Ed.; McGraw-Hill: New York, NY, 1980.

JOURNAL OF AGRICULTURAL AND FOOD CHEMISTRY

Article

pubs.acs.org/JAFC

Identification of Potent Odorants in a Novel Nonalcoholic Beverage Produced by Fermentation of Wort with Shiitake (*Lentinula edodes*)

Yanyan Zhang,[†] Marco Alexander Fraatz,[†] Felix Horlamus,[†] Hendrich Quitmann,[‡] and Holger Zorn*[,†]

[†]Institute of Food Chemistry and Food Biotechnology, Justus Liebig University Giessen, Heinrich-Buff-Ring 58, 35392 Giessen, Germany

[‡]Institute of Bioprocess Engineering and Pharmaceutical Technology, Technische Hochschule Mittelhessen - University of Applied Sciences, Wiesenstrasse 14, 35390 Giessen, Germany

Supporting Information

ABSTRACT: Novel refreshments with pleasant flavors were developed by fermentation of wort with basidiomycetes. Among 31 screened fungi, shiitake (*Lentinula edodes*) produced the most pleasant flavor. It was perceived as fruity, slightly sour, and plum-like. Flavor compounds were isolated by liquid−liquid extraction (LLE) and by headspace solid phase microextraction (HS-SPME). The key odor-active compounds were analyzed by a gas chromatography system equipped with a tandem mass spectrometry detector and an olfactory detection port (GC-MS/MS-O) and aroma extract dilution analysis (AEDA). For HS-SPME, a revised method of increasing the GC inlet split ratio was used. Most of the key odor-active compounds (e.g., 2-acetylpyrrole, β-damascenone, (*E*)-2-nonenal, and 2-phenylethanol) were detected with both extraction techniques. However, distinct differences between these two methods were observed.

KEYWORDS: *shiitake, beverage, fermentation, olfactometry, headspace solid phase microextraction, liquid−liquid extraction, wort*

INTRODUCTION

Basidiomycetes are able to synthesize pharmacologically relevant secondary metabolites, natural flavor compounds, and highly sought after enzymes.[1] Because of their unique biochemical potential, basidiomycetes are ideal tools for the food industry. In addition to their nutritional value, therapeutic applications of basidiomycetes, based on their antibiotic, antioxidative, and anticarcinogenic properties, have been discussed.

Because of their high nutritional value and good microbial stability, fermented beverages are becoming increasingly popular all over the world.[2] They are produced by various manufacturing techniques, raw materials, and microorganisms.[3] The most common microorganisms used in traditional fermented beverages such as beer, wine, kwass, kombucha, and Chinese liquor are yeasts, lactic acid bacteria, acetobacter species, and lower fungi.

Only a few studies on beverage production using basidiomycetes have been published. Hill produced a soluble tea product with champagne-like properties in combination with Manchurian mushroom.[4] Lin et al. developed a novel beverage by *Saccharomyces* using shiitake stipe extract as a nitrogen source.[5] Hou and co-workers prepared a novel beverage by mixing polysaccharides extracted from BaChu mushroom with hawthorn juice and apple juice.[6] Okamura et al. reported on beer-like fermented drinks using *Pleurotus ostreatus*, *Tricholoma matsutake*, or *Agaricus subrufescens* instead of *Saccharomyces cerevisiae* as all of these fungi possess an alcohol dehydrogenase activity.[7,8] However, the unique capabilities of basidiomycetes in producing a wide range of natural flavors in beverages have been ignored for submerged cultivations so far. Because of consumers' demand for natural food, basidiomycetes producing natural flavor compounds are ideal candidates for developing novel fermentation systems. With the recent worldwide declining consumption of beer,[9] breweries are eagerly searching for innovative nonalcoholic alternatives to compensate for this negative trend. In a previous study, complex and pleasant flavor mixtures were formed by fermentation of byproducts of the food industry with basidiomycetes.[10] This approach was adopted and transferred to the development of novel beverages by utilizing basidiomycetes for the fermentation of wort.

Traditional liquid−liquid extraction (LLE) and headspace solid phase microextraction (HS-SPME) are commonly used in flavor analysis. HS-SPME is a rapid and solvent-free method with low detection limits, which has been used for the analysis of a wide variety of compounds. Key odor-active compounds may be determined by aroma extract dilution analysis (AEDA).[11] In contrast to LLE, no dilutable organic flavor extract is obtained by using HS-SPME. Therefore, successively diluted original samples were analyzed by SPME in previous studies.[12−16] A different approach, namely, increasing gas chromatograph (GC) inlet split ratios, has only been reported by Kim et al.[17]

In this study, novel refreshments with pleasant flavors were developed by fermentation of wort with basidiomycetes. The cultures were extracted using two different extractions techniques (LLE and HS-SPME). The key odor-active compounds were determined and compared using a GC equipped with a tandem mass spectrometry detector and an olfactory detection port (GC-MS/MS-O) and AEDA. For

Received: February 3, 2014
Revised: April 8, 2014
Accepted: April 9, 2014
Published: April 9, 2014

ACS Publications © 2014 American Chemical Society

Table 1. Odor Impression, Intensity, and Color of Wort after Fermentation with Basidiomycetes

no.	species	odor impression	fermentation time (h)	intensity[a]	color
1	*Agaricus arvensis*	metallic	6	4	reddish-brown
2	*Agrocybe aegerita*	toasted, cereals, sweetish	22	3	dark yellow
3	*Clitocybe geotropa*	odorless	24	1	yellow
4	*Fistulina hepatica*	metallic	4	2	yellow
5	*Flammula alnicola*	moldy	24	4	yellow
6	*Flammulina velutipes*	sweetish	18	2	dark yellow
7	*Fomes fomentarius*	wort (weak), less sweetish	40	2	reddish-brown
8	*Ganoderma applanatum*	playdough, medicinal	16	3	yellow
9	*Hericium erinaceus*	odorless	24	1	reddish-brown
10	*Hypsizygus tesselatus*	stale beer	23	4	yellow
11	*Kuehneromyces mutabilis*	grassy	16	4	reddish-brown
12	*Lactarius deliciosus*	wort (weak)	40	3	yellow
13	*Laetiporus sulphureus*	grassy, smoky	16	4	reddish-brown
14	*Lentinula edodes*	sweetish, fruity, plum-like, sourish	48	3	reddish-brown
15	*Lentinus squarrosulus*	sweetish, banana peel	22	3	yellow
16	*Lepiota procera*	soapy	16	2	yellow
17	*Lepista nuda*	cereal, popcorn, sweetish	8	3	yellow
18	*Meripilus giganteus*	wort (weak)	44	2	reddish-brown
19	*Panellus serotinus*	fresh, honey, sweetish	24	2	reddish-brown
20	*Pholiota aurivella*	earthy, medicinal	18	3	dark yellow
21	*Pholiota nameko*	chlorine	20	3	reddish-brown
22	*Pleurotus cornucopiae*	fruity, floral	14	3	yellow
23	*Pleurotus eous*	wort (weak)	16	2	reddish-brown
24	*Pleurotus flabellatus*	wort (weak)	21	2	reddish-brown
25	*Pleurotus floridanus*	fruity, moldy (weak)	22	2	reddish-brown
26	*Pleurotus ostreatus*	chemical	24	4	reddish-brown
27	*Pleurotus pulmonarius*	odorless	20	1	reddish-brown
28	*Polyporus squamosus*	malty, fruity (weak), sweetish	32	3	reddish-brown
29	*Polyporus umbellatus*	raspberry, kiwi, sourish	42	4	pale yellow
30	*Termitomyces albuminosus*	creamy, sourish	9	2	yellow
31	*Trametes versicolor*	honey, fermented fruit, tea, fresh	38	3	reddish-brown

[a] 1, odorless; 2, weak; 3, moderately intense; 4, strong; 5, very intense; the odor of unfermented wort was perceived as malty, sweetish, and aromatic (intensity 4).

aroma dilution analysis (ADA) by HS-SPME, increasing GC inlet split ratios were used.

MATERIALS AND METHODS

Chemicals and Materials. Thirty-one different basidiomycetes were obtained from the Centraalbureau voor Schimmelcultures (CBS, Utrecht, The Netherlands), the German Collection of Microorganisms and Cell Cultures (DSMZ, Braunschweig, Germany), and the Department of Molecular Wood Biotechnology and Technical Mycology (WBTM, Göttingen, Germany).

Authentic flavor standards were purchased from Alfa Aesar (Karlsruhe, Germany), Fisher Scientific (Schwerte, Germany), Sigma-Aldrich (Steinheim, Germany), TCI Deutschland (Eschborn, Germany), Th. Geyer (Hamburg, Germany), and VWR (Darmstadt, Germany). The chemicals were of analytical grade. For GC helium 5.0 and nitrogen 5.0 were used.

Wort Preparation. Wort (Kölsch type, 13 °Plato) was provided by the University of Applied Sciences (Giessen, Germany). Pilsner (80%, w/w), Munich (13%, w/w), and wheat (7%, w/w) malts were used for the production of the wort with a KB50 pilot-scale brewing device (Alfred Gruber GmbH, Eugendorf, Austria). After cooking, the wort was filtered (0.2 μm), filled into aluminum bottles, and pasteurized at 80 °C for 30 min. The wort was stored at −20 °C prior to usage.

Precultures and Fermentation of Wort. Culture flasks containing standard nutrition solution (100 mL/250 mL, medium volume/flask volume) were inoculated with fungal mycelium as published previously.[18] This preculture was incubated on a rotary shaker (24 °C, 150 rpm, 25 mm shaking diameter) in the dark until sufficient growth was obtained. Mycelia of 10 mL preculture broth were precipitated by means of centrifugation (4000 rpm, 2150*g*, 10 min, 20 °C) and washed three times with sterile water. The fungal pellets were resuspended in 10 mL of heat sterilized wort. This suspension was added into an Erlenmeyer flask (250 mL) containing 100 mL of wort. The fermentation was carried out at 24 °C for up to 48 h under aerobic conditions in a rotary shaker (150 rpm). During the fermentation, samples were taken every 2−4 h and were subsequently analyzed by sensory evaluation.

Sensory Evaluation of Cultures. The mycelium was removed by centrifugation (4000 rpm, 2150*g*, 5 min, 4 °C), and the supernatant was transferred to odorless snap-cap vials (20 mL). After storage for 15 min at 4 °C, the odor of the supernatant was assessed by at least three experienced sensory assessors. The odor intensity was rated on a scale of 1−5 (1, low intensity; 5, intense, strong odor). Samples with a distinctive and potent odor were additionally evaluated by tasting. Promising fermentations were repeated at least three times. In the final analysis the flavor was described by 10 panelists.

Headspace Solid Phase Microextraction. For HS-SPME, PDMS fibers (polydimethylsiloxane, film thickness = 100 μm, fiber length = 1 cm) (Supelco, Steinheim, Germany), PDMS/DVB fibers (polydimethylsiloxane/divinylbenzene, 65 μm, 1 cm), CAR/PDMS fibers (carboxen/polydimethylsiloxane, 75 μm, 1 cm), and DVB/CAR/PDMS fibers (divinylbenzene/carboxen/polydimethylsiloxane, 50/30 μm, 1 cm) in combination with an MPS 2XL multipurpose sampler (GERSTEL, Mülheim an der Ruhr, Germany) were used. Ten milliliters of the culture broth was transferred into a headspace vial (20 mL). The samples were agitated for 20 min (250 rpm) at 50, 55, or 60 °C, followed by headspace extraction, at the same temperature as

during the incubation, for 40, 45, or 50 min. Afterward, the analytes were directly desorbed in the split/splitless inlet at 250 °C using a SPME liner with 0.75 mm i.d. (Supelco) of the GC-MS/MS-O system for 1 min. After desorption, the fiber was heated at the respective recommended conditioning temperature in the SPME fiber conditioning station for 20 min.

Liquid−Liquid Extraction. The mycelium was removed from the fermentation broth by centrifugation (4000 rpm, 2150*g*, 5 min, 4 °C), and the culture supernatant was extracted three times with equal amounts of pentane/diethyl ether (1:1.12, v/v). The organic phases were combined, dried over anhydrous Na_2SO_4, and concentrated by means of a Vigreux column (water bath temperature = 45 °C) to a final volume of approximately 1 mL. Afterward, 100 μL of thymol (300 mg/L in pentane/diethyl ether) was added as internal standard (IS). The sample was used for AEDA in combination with GC-MS/MS-O analysis.

Aroma (Extract) Dilution Analysis. For LLE the flavor dilution (FD) factors were determined by AEDA. The organic extracts of the cultures were diluted with pentane/diethyl ether (1:1.12, v/v) in a series of 1:1 dilutions, and each dilution was sniffed twice until no odorants were perceived at the ODP 3 olfactory detection port (GERSTEL) of the GC-MS/MS-O system.

For HS-SPME, aroma dilution analysis was performed by increasing GC inlet split ratios.[17] Prior to sample analysis, the method was validated using six authentic flavor standards. Ten milliliters of the standard solution [43.9 mg of 2-acetylpyrrole (**37**/**2**), 24.6 mg of β-damascenone (**32**/**2**), 46.1 mg of methyl 2-methylbutanoate, 39.1 mg of 2-phenylacetaldehyde, 44.5 mg of 2-phenylethanol, and 46.5 mg of 3-phenylpropanol dissolved in 50 mL of ethanol and subsequently diluted 1:1000 with distilled water] was transferred into a HS vial (20 mL) and sealed with a Teflon screw cap. The standard solution was incubated at 60 °C for 20 min and extracted at the same temperature by means of HS-SPME with a CAR/PDMS fiber for 45 min. The volatiles were diluted stepwise by controlling the split ratio as follows: splitless (splitless time = 2 min), 2:1, 4:1, 8:1, 16:1, 32:1, 64:1, 128:1, and 256:1. The same procedure was applied for the samples.

Gas Chromatography. Gas chromatography was carried out using an Agilent 7890A gas chromatograph (Agilent Technologies, Waldbronn, Germany) equipped with an Agilent 7000B triple-quadrupole mass spectrometry (MS/MS) detector (Agilent Technologies). The column used was a polar 30 m × 0.25 mm i.d., 0.25 μm Agilent J&W VF-WAXms unless stated otherwise. Helium was used at a constant flow rate of 1.56 mL/min as the carrier gas. At the end of the capillary column, the carrier gas was split 1:1 into the Agilent 7000B detector and into the ODP 3. The oven temperature was programmed from 40 to 240 °C at 5 °C/min, with initial and final hold times of 3 and 12 min, respectively. Other conditions were as follows: inlet temperature, 250 °C; septum purge flow rate, 3 mL/min; scan mode, total ion current (TIC) in Q1; scan range, *m*/*z* 33−330; electron ionization energy, 70 eV; source temperature, 230 °C; quadrupole temperature, 150 °C; MS/MS transfer line temperature, 250 °C; He quench gas, 2.25 mL/min; N_2 collision gas, 1.5 mL/min; ODP 3 transfer line temperature, 250 °C; ODP 3 mixing chamber temperature, 150 °C; ODP 3 makeup gas, N_2.

GC-MS analyses were performed using an Agilent 7890A gas chromatograph (Agilent Technologies) equipped with a model 5975C mass spectrometry detector (Agilent Technologies), under the following conditions: carrier gas, helium; constant flow rate, 1.2 mL/min; inlet temperature, 250 °C; split ratio, 10:1; septum purge flow rate, 3 mL/min; 30 m × 0.25 mm i.d., 0.25 μm Agilent J&W DB-5MS column; temperature program, 40 °C (3 min), 5 °C/min to 300 °C (12 min); scan mode, TIC; scan range, *m*/*z* 33−330; electron ionization energy, 70 eV; source temperature, 230 °C; quadrupole temperature, 150 °C; transfer line temperature, 250 °C.

Compound Identification. For the identification of the flavor compounds, the odor impressions, the retention indices (RI), and the mass spectra of each compound were compared to authentic standards on two columns of different polarities (VF-WAXms and DB-5MS columns), published data, and the NIST 2011 MS library.

RESULTS AND DISCUSSION

Sensory Evaluation. Thirty-one different basidiomycetes were screened for the fermentation of wort. With most of the fungi significant changes of the aroma were observed. During the fermentation process the odor varied in quality and intensity. The most characteristic and intense odor impressions of the fermentations are listed in Table 1.

The odor of the cultures may be classified into three groups: pleasant, unpleasant, and odorless. The main pleasant odors included fruity (e.g., *Lentinula edodes*, *Polyporus umbellatus*, and *Trametes versicolor*), toasted (e.g., *Agrocybe aegerita* and *Pleurotus cornucopiae*), and honey-like (e.g., *Trametes versicolor* and *Panellus serotinus*) notes. Unpleasant odors, such as chlorine, medicinal, metallic, moldy, and smoky, were produced by a few basidiomycetes (e.g., *Agaricus arvensis*, *Flammula alnicola*, *Ganoderma applanatum*, *Laetiporus sulphureus*, and *Pholiota nameko*). Some basidiomycetes (e.g., *Meripilus giganteus*, *Pleurotus eous*, and *Pleurotus flabellatus*) diminished the typical odor of wort, some of them to completely odorless (e.g., *Clitocybe geotropa* and *Hericium erinaceus*). The cultures produced this variety of different odor impressions within the short fermentation time of up to 48 h. This phenomenon is remarkably different from previous investigations. Gallois et al. studied the capability of 29 different ligninolytic basidiomycetes to produce odors in 6 different media.[19] Flavors were perceived after an incubation period of 7−10 days. Kawabe and Morita reported that *Polyporus tuberaster* K 2606 produced a fruity and floral odor on day 13 in peptone−glucose−yeast medium.[20] The fast formation of flavor compounds in this study might be related to the available nutrients and flavor precursors in the wort. Wort represents a complex mixture of fermentable carbohydrates, peptides, proteins, lipids, metal and nonmetal ions, and polyphenols.[21] Therefore, it provides all essential nutrients and a proper environment for the growth of basidiomycetes. Furthermore, various potential flavor precursors such as phenolic acids, fatty acids, and amino acids were found in wort.[22−24] Hence, transformation time and transformation products strongly depend on the composition of medium used.

The generation of flavor compounds was often accompanied by a change of the color of the fermentation broth. Compared to the substrate wort, the color of most culture supernatants turned darker and reddish-brown (Table 1). The simultaneous production of aroma compounds and pigments by macrofungi was already reported by Badcock.[25] However, in the current study, the synthesis of odor and pigments was not correlated in all cases. *P. umbellatus* generated a strong and interesting fruity odor reminiscent of cherry and kiwi, but the color of the culture supernatant became lighter and more transparent.

After sensory evaluation by 10 panelists, wort fermented by shiitake was classified as the most interesting one. Shiitake produced a fresh, fruity, plum-like, sweet, and slightly sour flavor. During the fermentation the broth turned reddish-brown in color.

Shiitake represents an ideal candidate to develop a novel fermentation system. Due to its flavor, nutritional value, and presumed medicinal properties, shiitake has attracted high interest in recent years.[26] To the best of our knowledge, no studies on the volatile compounds of submerged-grown shiitake cultures in wort have been published so far. Shiitake is the second most popular edible mushroom in the global market and was the first medicinal macrofungus to enter the realm of

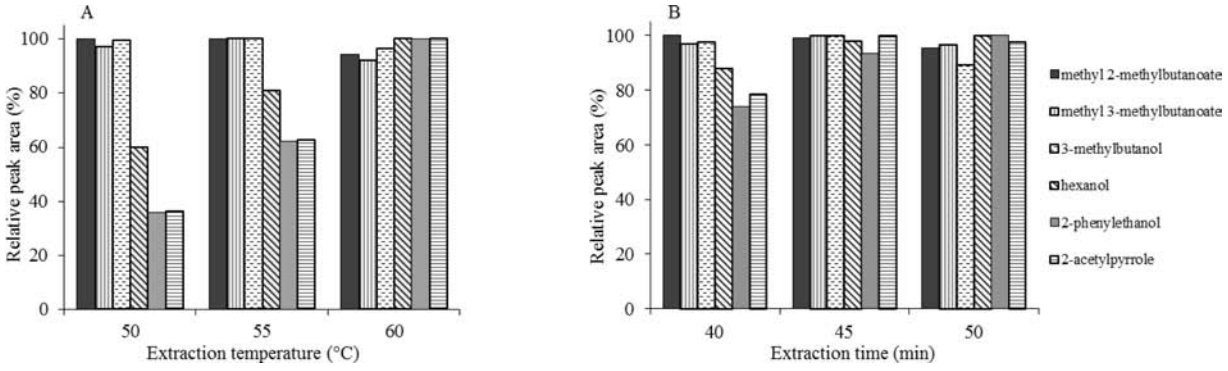

Figure 1. Influence of the extraction temperature (A) (CAR/PDMS fiber, 45 min extraction time) and extraction time (B) (CAR/PDMS fiber, 60 °C extraction temperature) on the extraction efficiency of selected odor compounds, expressed in percent of the maximum area.

modern biotechnology.[27] Therefore, high consumer acceptance and high market potential for the novel fermented beverage are expected.

Optimization of HS-SPME Parameters. SPME was invented by Pawliszyn in 1989.[28] This solvent-free extraction technique simplifies the sample preparation procedure considerably and has been widely used for food analysis. For the optimization of the HS-SPME method, six previously identified flavor compounds from the fermented wort were chosen. All of them matched the following criteria: baseline separation; distributed over the chromatographic run; and different chemical families.[15] In our study, common SPME parameters, including extraction temperature, extraction time, and fiber type, were found to greatly affect the number and intensity of perceived aroma compounds.

Extraction Temperature. The influence of different extraction temperatures (50, 55, and 60 °C) on the extraction efficiency was evaluated with a CAR/PDMS fiber. The peak areas of methyl 2-methylbutanoate, methyl 3-methylbutanoate, and 3-methylbutanol changed only slightly with elevated temperatures. The extraction efficiencies for 2-phenylethanol, 2-acetylpyrrole (**37/2**), and hexanol were enhanced significantly at increased temperatures (Figure 1A). With increased extraction temperature, the extraction efficiency for compounds with higher boiling points improved. This was in good agreement with a previous study.[29] Maximum relative peak areas were observed at 60 °C. Higher temperatures were not considered to avoid the formation of artifacts (e.g., Maillard reaction products) in the complex matrix wort. Therefore, 60 °C was selected as the optimum extraction temperature for further studies.

Extraction Time. For most compounds the extraction efficiency increased with extraction time, until equilibrium was reached after 45 min (Figure 1B). A prolonged extraction time led to a slight decrease of the areas of methyl 2-methylbutanoate, methyl 3-methylbutanoate, and 3-methylbutanol. Therefore, further experiments were carried out with an extraction time of 45 min.

Fiber Type. The extraction efficiencies of different SPME fiber types (CAR/PDMS, DVB/CAR/PDMS, PDMS/DVB, and PDMS) were evaluated by analyzing fermented wort samples by means of HS-SPME-GC-MS/MS-O. The coating material of the SPME fibers strongly influenced the extraction efficiency of odor-active compounds.

The number of odor-active compounds perceived at the ODP after extraction with the CAR/PDMS, DVB/CAR/PDMS, PDMS/DVB, and PDMS fibers were 30, 23, 19, and 8, respectively. The CAR/PDMS fiber was the most sensitive one, although two odors (octanal and an unidentified compound) could not be perceived. With the DVB/CAR/PDMS fiber a slightly reduced number of flavor compounds were detected during the first 15 min of the GC run (RI ≤ 1329). Seven of 32 flavor compounds [2-phenylacetaldehyde, 2-acetylthiazole, 2-phenylethanol acetate, β-damascenone (**32/2**), 2-phenylethanol, γ-nonalactone, and *o*-aminoacetophenone] were identified with all four fibers tested. DVB/CAR/PDMS fibers are widely used for flavor analysis, as the combination of three different materials can catch a wider range of polarities and volatilities.[30] However, for the analysis of fermented wort, a CAR/PDMS fiber was most efficient. This also indicates that the selection of the SPME fiber used for analysis depends strongly on the characteristics of the flavor compounds of the respective matrix. Due to its overall better performance, the CAR/PDMS fiber was chosen for further analysis of odor-active compounds.

Aroma (Extract) Dilution Analysis by LLE and HS-SPME. To evaluate the aroma profile of the fermented beverage, changes of the main odor-active compounds during the fermentation of wort were analyzed by two different extraction methods (LLE and HS-SPME) followed by an aroma (extract) dilution analysis. Different from LLE, no liquid dilutable aroma extract is obtained by SPME. For dilution analysis the original sample may be diluted. However, this might influence phase equilibrium due to a modified matrix composition. Therefore, ADA was performed after microextraction by applying different split inlet ratios. In preparation, the linear relationship between the peak area of the respective analyte and the split ratio of GC-MS/MS-O system was investigated by using a standard solution comprising six different flavor compounds. The regression plots showed a linear relationship with R^2 >0.989. Slopes of the respective equations ranged from −1.0 to −1.3. Kim et al. reported insufficient linearity for low and high split ratios due to an unstable carrier gas flow.[17] In our study, linear responses for all tested substances were obtained for a wide range of split ratios from splitless up to 256. Thus, increasing GC inlet split ratios was a fast and reliable tool for determining key odor-active compounds. Although the maximum split ratio of the GC was limited by the pneumatic controller, changing GC inlet split ratios combined with successive dilution of the original sample makes this method suitable even for very concentrated samples. The odor-active compounds identified by means of GC-MS/MS-O after LLE and HS-SPME of unfermented wort and wort fermented by shiitake are summarized in Table 2. A selection of

Table 2. Odor-Active Compounds Identified by Means of GC-MS/MS-O after LLE and HS-SPME of Unfermented Wort and Wort Fermented by Shiitake

	RI[a]					FD factor[b]			
						wort		fermented wort	
no.	VF-WAXms	DB-5MS	compound	odor impression	identification	LLE	HS-SPME	LLE	HS-SPME
1	931	<800	3-methylbutanal	green	MS, RI, odor	–[i]	1	–	1
2	996	<800	2,3-butanedione	buttery	MS, RI, odor	–	32	–	4
3	1018	<800	methyl 2-methylbutanoate[d]	fruity	MS, RI, odor	–	–	–	64
4	1026	<800	methyl 3-methylbutanoate	fruity	MS, RI	–	–	–	–
5	1074	<800	2,3-pentanedione	caramel	MS, RI, odor	–	2	–	–
6	1091	<800	hexanal	green	MS, RI, odor	–	1	–	–
7	1102	<800	(*E*)-2-methyl-2-butenal[d]	toasted, sweetish	MS, RI, odor	–	–	–	2
8	1126	877	3-methylbutyl acetate	fruity, sweetish	MS, RI, odor	–	–	–	2
9	1218	<800	3-methylbutanol	fresh, sourish	MS, RI, odor	–	–	1	1
10	1271	<800	thiazole (**10**)	rubber	MS, RI, odor	–	2	–	–
11	1291	nd[h]	unknown	caramel		2	–	1	–
12	1294	nd	1-octen-3-one[g]	mushroom	RI, odor	–	4	–	4
13	1348	910	2,5-dimethylpyrazine	baked, nutty	MS, RI, odor	2	64	2	32
14	1367	873	hexanol	green	MS, RI	–	–	–	–
15	1454	1051	(*E*)-2-octenal	toasted	MS, RI, odor	2	–	2	–
16	1464	907	methional	boiled potato	MS, RI, odor	–	256	–	64
17	1468	<800	acetic acid	sourish, vinegar	MS, RI, odor	2	1	4	1
18	1474	883	furfural	woody	MS, RI	–	–	–	–
19	1493	1029	2-ethylhexanol	green	MS, RI, odor	–	–	–	1
20	1522	1163	(*E*)-2-nonenal	green	MS, RI, odor	128	4	16	4
21	1528	964	benzaldehyde	almond, cereal	MS, RI, odor	–	4	–	2
22	1551	1099	linalool (**22**)	floral	MS, RI, odor	–	4	–	–
23	1563	1074	1-octanol	herbal, green	MS, RI	–	–	–	–
24	1583	<800	2-methylpropanoic acid	cheesy, sourish	MS, RI, odor	–	–	1	–
25	1593	nd	5-methylfurfural	caramel	MS, RI, odor	–	1	–	–
26	1655	1046	2-phenylacetaldehyde	floral	MS, RI, odor	16	4	4	–
27	1658	1020	2-acetylthiazole	toasted, sweetish	MS, RI, odor	16	128	1	8
28[c]	1684	867	2-methylbutanoic acid	cheesy, stinky,	MS, RI, odor	256	4	1	1
		860	3-methylbutanoic acid[e]	sourish					
29	1717	1154	(*Z*)-3-nonen-1-ol[d]	green	MS, RI, odor	–	–	–	16
30	1727	1184	naphthalene	medicinal	MS, RI, odor	–	16	–	–
31	1750	nd	unknown	burnt		64	32	32	16
32[c]	1827	1256	2-phenylethanol acetate	fruity, like pear	MS, RI, odor	16	64	4	64
		1380	*β*-damascenone (**32/2**)						
33	1872	993	hexanoic acid	floral	MS, RI, odor	8	4	–	–
34	1881	1086	2-methoxyphenol	floral, sweetish	MS, RI, odor	64	16	32	1
35	1892	1036	benzyl alcohol	leaf, floral	MS, RI, odor	–	–	–	1
36	1926	1113	2-phenylethanol	rose	MS, RI, odor	16	4	256	64
37[c]	1983	1109	maltol[f] (**37/1**)	burnt, sweetish	MS, RI, odor	256	32	32	4
		1064	2-acetylpyrrole (**37/2**)						
38	2040	1362	*γ*-nonalactone	caramel	MS, RI, odor	256	16	1	2
39	2046	1232	3-phenylpropanol	floral	MS, RI	–	–	–	–
40	2083	1383	(*E*)-methyl cinnamate[d] (**40**)	fruity	MS, RI, odor	–	–	–	16
41	2149	1817	hexadecanal	cardboard	MS, RI, odor	–	8	–	4
42	2179	nd	unknown	toasted		4	–	1	–
43	2202	1314	2-methoxy-4-vinylphenol (**43**)	sweetish	MS, RI, odor	2	2	–	–
44	2230	1920	methyl hexadecanoate	toasty, sweetish	MS, RI, odor	–	256	–	64
45	2241	1301	*o*-aminoacetophenone	grape	MS, RI, odor	–	16	–	16
46	2395	nd	*γ*-dodecalactone	sweetish	MS, RI, odor	–	16	–	2
47	2450	1173	benzoic acid	balsamic	MS, RI, odor	1	–	–	–
48	2529	1562	dodecanoic acid	fatty	MS, RI, odor	–	1	–	1
49	2575	1252	2-phenylacetic acid	toasted, pungent, sweetish	MS, RI, odor	128	–	64	–
50	2828	1430	cinnamic acid	honey	MS, RI	–	–	–	–
51	2864	1962	palmitic acid	oily	MS, RI	–	–	–	–

[a]Mean of RI values from LLE and HS-SPME. [b]Flavor dilution (FD) factor of the corresponding compound. [c]Odor corresponded to coeluting compounds. [d]Compound was detected only in the fermented beverage. [e]Compound was detected only in the unfermented wort. [f]Compound was

dx.doi.org/10.1021/jf5005463 | J. Agric. Food Chem. 2014, 62, 4195−4203

Table 2. continued

detected only in LLE. [g]MS spectrum was ambiguous; the compound was tentatively identified on the basis of RI, odor, and literature data,[33] [h]nd, no distinct MS spectrum on DB-5MS column. [i]−, odor was not perceived.

identified structures of aroma compounds with FD factors >1 are shown in Figure 2.

Main Odor-Active Compounds Identified after LLE. In total, 18 odor impressions were perceived in the liquid−liquid extracts of wort fermented with shiitake at the ODP during GC-MS/MS-O analysis (Table 2). The corresponding odor-active compounds were identified by comparison of the Kovats indices and mass spectra with those of the database and literature data and were confirmed by authentic standards on both polar and nonpolar GC columns. On the basis of the determined FD factors, 2-phenylethanol was the most important flavor compound in the fermented wort (FD 256). The compound with its typical rose odor was biosynthesized by shiitake during fermentation, possibly by biotransformation of L-phenylalanine. It has been shown that this metabolic pathway exists in basidiomycetes such as *Ischnoderma benzoinum*.[31] Other key odor compounds were 2-phenylacetic acid (FD 64), 2-methoxyphenol (FD 32), maltol (**37**/**1**) coeluting with 2-acetylpyrrole (**37**/**2**) (FD 32), a yet unknown compound with a burnt odor (FD 32), and (*E*)-2-nonenal (FD 16). The unknown compound was present in such low concentrations that a distinct mass spectrum could not be obtained. Further investigations are needed for a reliable identification.

All major odor-active compounds identified in the organic extract of the fermented wort after LLE (FD ≥ 16) were also present in the unfermented wort, but in different concentrations. The aroma compounds of wort with the highest FD factors were 2-methylbutanoic acid coeluting with 3-methylbutanoic acid (FD 256), maltol (**37**/**1**) coeluting with 2-acetylpyrrole (**37**/**2**) (FD 256), and γ-nonalactone (FD 256). γ-Nonalactone, maltol (**37**/**1**), and 2-acetylpyrrole (**37**/**2**) exhibited odor impressions typical for wort, such as malty, caramel, and toasted. After fermentation these predominant odors became less important (1 ≤ FD ≤ 32). 2-Methylbutanoic acid and γ-nonalactone could be perceived only in the undiluted fermented wort extract (FD 1).

Besides 2-phenylethanol, shiitake produced 3-phenylpropanol (39) (Figure 3), which was detected in the fermented beverage by mass spectrometry but not perceived at the ODP. Shiitake also produced 3-methylbutanol and 2-methylpropanoic acid. On the other hand, the peak areas of 3-methylbutanoic acid, hexanoic acid, cinnamic acid (50) (Figure 3), and palmitic acid (51) (Figure 3) decreased significantly during the fermentation. None of these compounds had a high impact on the overall flavor of fermented wort. Certain compounds (e.g., 3-methylbutanoic acid and cinnamic acid) were even below their limit of detection after fermentation. This implies that a wide variety of extracellular fungal enzymes, including laccases, lipoxygenases, and hydroperoxide lyases, might have catalyzed the degradation of these carboxylic acids, which can serve as an immediate carbon source for fungal growth.[18] However, these carboxylic acids might also have been precursors of some of the odor compounds, as shiitake produced aroma compounds such as 3-methylbutanol, 2-methylpropanoic acid, and 3-phenylpropanol. Krings et al. observed that 3-phenylpropanol was produced from cinnamic acid and L-phenylalanine.[31] The observed increase of the concentration of 3-methylbutanol might be associated with the simultaneous decrease of 3-methylbutanoic acid concentration.

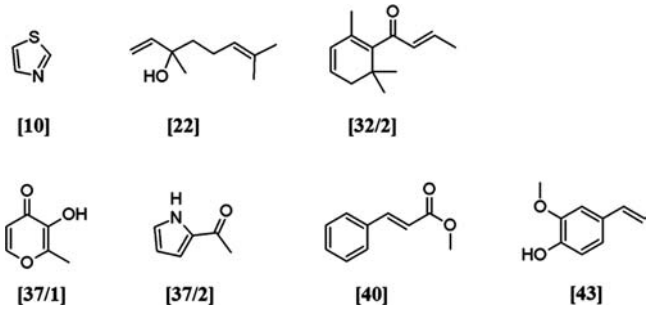

Figure 2. Selection of identified aroma compounds.

Although most of the odor impressions were caused by a single compound, two impressions (28 and 37) (Figure 3) originated from a mixture of compounds in both extracts. 2-Methylbutanoic acid and 3-methylbutanoic acid coeluted and represented a potent odor of wort (FD 256). They imparted a cheesy and sourish odor impression (28). During fermentation the FD factor was reduced to 1. Impression 37 (sweetish, burnt) was identified as a mixture of maltol (**37**/**1**) and 2-acetylpyrrole (**37**/**2**), which both impart a typical sweetish and burnt odor (Table 2).

The dominant odor impression of wort fermented with shiitake was fresh and fruity and thereby strikingly different from that of nonfermented wort. However, a single representative fruity flavor compound was not perceived by GC-MS/MS-O experiments after LLE. One possibility was that the fruity aroma did not result from the biosynthesis of new compounds, but from quantitative changes of several compounds. All of the most potent odor-active compounds of the culture were found in the wort extract as well, only the intensity of the aroma compounds changed remarkably. The intensity of typical aroma compounds of wort such as γ-nonalactone, maltol (**37**/**1**), 2-acetylpyrrole (**37**/**2**), and 2-acetylthiazole was very low in the fermented beverage.[32−34] The other possibility was that the compounds responsible for the fruity aroma were lost during either the extraction process or the GC-MS/MS-O analysis.[35] Hence, another extraction method was chosen for analyzing the fermentation system.

Main Odor-Active Compounds Identified by HS-SPME. By means of HS-SPME, 30 odor impressions were perceived for the unfermented wort and 29 from the fermented wort (Table 2). Methional (FD 256), methyl hexadecanoate (FD 256), 2-acetylthiazole (FD 128), β-damascenone (**32**/**2**) (FD 64), and 2,5-dimethylpyrazine (FD 64) were determined as the most potent odor-active compounds in wort. After fermentation by shiitake, the most important odorants (FD 64) were methional, methyl 2-methylbutanoate, methyl hexadecanoate, 2-phenylethanol acetate coeluting with β-damascenone (**32**/**2**), and 2-phenylethanol. Among them, methyl 2-methylbutanoate was detected only in the fermented beverage. The FD factor of 2-phenylethanol increased from 4 to 64 during the fermentation. It is noteworthy that especially the FD factors of the well-known typical wort flavors methional (FD 256), methyl hexadecanoate (FD 256), and 2-acetylthiazole (FD 128) decreased significantly during the fermentation (FD 64, 64,

dx.doi.org/10.1021/jf5005463 | J. Agric. Food Chem. 2014, 62, 4195−4203

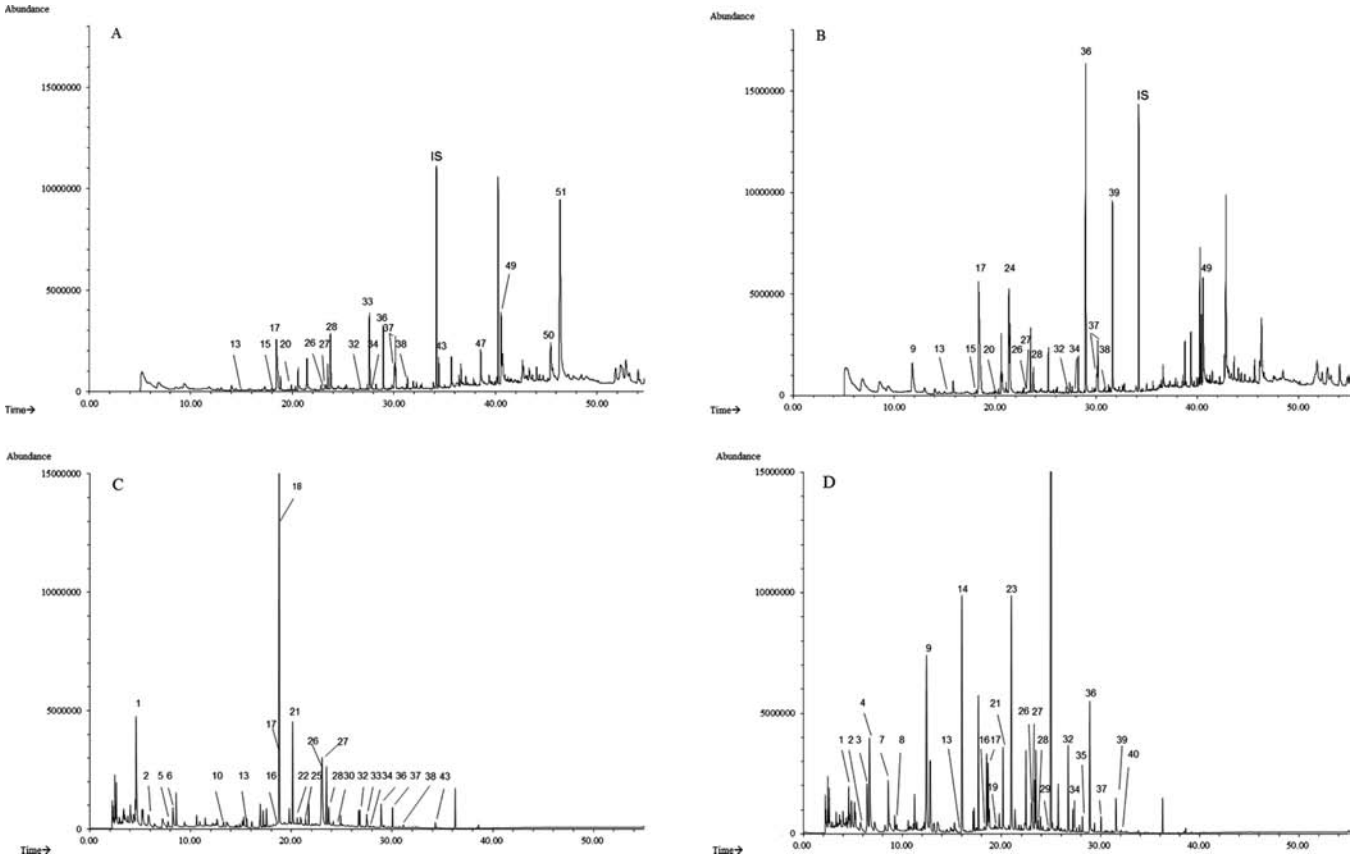

Figure 3. GC-MS/MS-O total ion current chromatograms of organic extracts of unfermented wort (A), of wort fermented by shiitake (B), after HS-SPME of unfermented wort (C), and of wort fermented by shiitake (D).

and 8, respectively). In addition, (*Z*)-3-nonen-1-ol (green), a yet unknown compound (burnt), (*E*)-methyl cinnamate (**40**) (fruity), and *o*-aminoacetophenone (grape) were also identified as potent odors in fermented wort (FD 16).

Despite not being perceivable at the ODP, shiitake produced methyl 3-methylbutanoate (4) (Figure 3), hexanol (14) (Figure 3), and 1-octanol (23) (Figure 3) de novo, whereas the peak area of furfural (18) (Figure 3) decreased significantly during the fermentation.

Analysis of the key odor-active compounds revealed the formation of methyl 2-methylbutanoate and (*E*)-methyl cinnamate (**40**) by shiitake. Both compounds have a typical fruity flavor and could not be detected in unfermented wort. In contrast to LLE, it was thus possible to identify the flavor compounds imparting the fruity aroma by means of HS-SPME. This is the first time that the formation of these compounds by shiitake is reported. As 2-methylbutanoic acid and cinnamic acid were detected in the LLE of wort, shiitake might transform these organic acids into their corresponding esters. Branched carboxylic acid and phenolic acids are known as flavor precursors in microbial cultures.[36]

Comparison of Potent Odor-Active Compounds Identified by LLE and HS-SPME. The extraction method may strongly influence the results of olfactometric analyses.[37] Depending on the extraction technique, an aroma compound might be detected or not during olfactometric analysis.[14] In our study, most of the determined key odor-active compounds of the fermented beverage were similar after LLE and HS-SPME. However, the FD factors of the individual compounds differed and some distinct differences were observed. LLE allowed the recovery of some key aroma compounds, such as 2-phenylacetic acid, a polar compound with a high boiling point (266 °C), which was hardly extracted by HS-SPME. This implied that HS-SPME was less sensitive for trapping low volatile and polar acids. This is in good agreement with a study of Yang and Peppard, who reported the adsorption of fatty acids on SPME fibers with low affinity.[38] On the other hand, HS-SPME was more appropriate for other main aroma compounds of the fermented beverage (e.g., methyl 2-methylbutanoate, methional, methyl hexadecanoate, and *o*-aminoacetophenone), which were not perceived in olfactometric analysis after LLE. The ester methyl 2-methylbutanoate is highly volatile as indicated by a RI of 1018. *o*-Aminoacetophenone and methional have low odor thresholds.[39,40] In the case of methional, panelists could recognize the potato-like smell above an olfactory threshold of 0.2 ppb in water.[40] These results suggest that HS-SPME has a better capacity for extracting highly volatile and trace compounds, which are easily lost during the extraction or concentration process of LLE, as already observed by Mebazaa et al.[41] The high sensitivity of SPME enabled trapping and identification of flavor compounds with low odor thresholds present in low concentrations with potentially high impact on the overall aroma of the sample.

In conclusion, all of the selected basidiomycetes grew well in wort, and many interesting odors were produced. Among them, shiitake was rated as the most promising species for producing a novel fermented beverage, exhibiting an interesting plum-like aroma. Odor-active compounds of the fermented beverage were identified using a combination of two different extraction methods. Odor-active compounds produced by shiitake, such as

dx.doi.org/10.1021/jf5005463 | *J. Agric. Food Chem.* 2014, 62, 4195−4203

2-phenylethanol, methyl 2-methylbutanoate, 2-phenylethanol acetate, and (*E*)-methyl cinnamate (**40**), were responsible for the overall flavor.

■ ASSOCIATED CONTENT

Supporting Information

Tables S1 and S2; Figures S1 and S2. This material is available free of charge via the Internet at http://pubs.acs.org.

■ AUTHOR INFORMATION

Corresponding Author

*(H.Z.) Phone: +49 641 99-34900. Fax: +49 641 99-34909. E-mail: holger.zorn@uni-giessen.de.

Funding

Y.Z. is grateful to the China Scholarship Council for financial support. We thank the DFG and the State of Hesse for funding the major instrumentation (INST 162/381-1 FUGG). This project (HA Project 305/11-50) is funded within the framework of Hessen ModellProjekte, financed with funds of LOEWE − Landes-Offensive zur Entwicklung Wissenschaftlich-ökonomischer Exzellenz, Förderlinie 3: KMU-Verbundvorhaben (State Offensive for the Development of Scientific and Economic Excellence).

Notes

The authors declare no competing financial interest.

■ REFERENCES

(1) Lomascolo, A.; Stentelaire, C.; Asther, M.; Lesage-Meessen, L. Basidiomycetes as new biotechnological tools to generate natural aromatic flavours for the food industry. *Trends Biotechnol.* **1999**, *17*, 282−289.

(2) McGovern, P. E.; Zhang, J.; Tang, J.; Zhang, Z.; Hall, G. R.; Moreau, R. A.; Nuñez, A.; Butrym, E. D.; Richards, M. P.; Wang, C. S.; Cheng, G.; Zhao, Z.; Wang, C. Fermented beverages of pre- and proto-historic China. *Proc. Natl. Acad. Sci. U.S.A.* **2004**, *101*, 17593−17598.

(3) Blandino, A.; Al-Aseeri, M. E.; Pandiella, S. S.; Cantero, D.; Webb, C. Cereal-based fermented foods and beverages. *Food Res. Int.* **2003**, *36*, 527−543.

(4) Hill, J. B. Process of making a soluble tea product with champagne-like properties. *Biotechnol. Adv.* **1997**, *15*, 535−535.

(5) Lin, P. H.; Huang, S. Y.; Mau, J. L.; Liou, B. K.; Fang, T. J. A novel alcoholic beverage developed from shiitake stipe extract and cane sugar with various *Saccharomyces* strains. *LWT−Food Sci. Technol.* **2010**, *43*, 971−976.

(6) Hou, X.; Zhang, N.; Xiong, S.; Li, S.; Yang, B. Extraction of BaChu mushroom polysaccharides and preparation of a compound beverage. *Carbohydr. Polym.* **2008**, *73*, 289−294.

(7) Okamura, T.; Ogata, T.; Minamimoto, N.; Takeno, T.; Noda, H.; Fukuda, S.; Ohsugi, M. Characteristics of beer-like drink produced by mushroom fermentation. *Food Sci. Technol. Res.* **2001**, *7*, 88−90.

(8) Okamura-Matsui, T.; Tomoda, T.; Fukuda, S.; Ohsugi, M. Discovery of alcohol dehydrogenase from mushrooms and application to alcoholic beverages. *J. Mol. Catal. B: Enzym.* **2003**, *23*, 133−144.

(9) Colen, L.; Swinnen, J. F. M. Beer drinking nations. The determinants of global beer consumption. LICOS Discussion Paper Series No. 270/2010, 2010; DOI:10.2139/ssrn.1752829.

(10) Bosse, A. K.; Fraatz, M. A.; Zorn, H. Formation of complex natural flavours by biotransformation of apple pomace with basidiomycetes. *Food Chem.* **2013**, *141*, 2952−2959.

(11) Grosch, W. Evaluation of the key odorants of foods by dilution experiments, aroma models and omission. *Chem. Senses* **2001**, *26*, 533−545.

(12) Akiyama, M.; Murakami, K.; Ohtani, N.; Iwatsuki, K.; Sotoyama, K.; Wada, A.; Tokuno, K.; Iwabuchi, H.; Tanaka, K. Analysis of volatile compounds released during the grinding of roasted coffee beans using solid-phase microextraction. *J. Agric. Food Chem.* **2003**, *51*, 1961−1969.

(13) Deibler, K. D.; Acree, T. E.; Lavin, E. H. Solid phase microextraction application in gas chromatography/olfactometry dilution analysis. *J. Agric. Food Chem.* **1999**, *47*, 1616−1618.

(14) Martí, M. P.; Mestres, M.; Sala, C.; Busto, O.; Guasch, J. Solid-phase microextraction and gas chromatography olfactometry analysis of successively diluted samples. A new approach of the aroma extract dilution analysis applied to the characterization of wine aroma. *J. Agric. Food Chem.* **2003**, *51*, 7861−7865.

(15) Aceña, L.; Vera, L.; Guasch, J.; Busto, O.; Mestres, M. Comparative study of two extraction techniques to obtain representative aroma extracts for being analysed by gas chromatography-olfactometry: application to roasted pistachio aroma. *J. Chromatogr., A* **2010**, *1217*, 7781−7787.

(16) Fan, W.; Qian, M. C. Identification of aroma compounds in Chinese "Yanghe Daqu" liquor by normal phase chromatography fractionation followed by gas chromatography/olfactometry. *Flavour Fragrance J.* **2006**, *21*, 333−342.

(17) Kim, T. H.; Lee, S. M.; Kim, Y. S.; Kim, K. H.; Oh, S.; Lee, H. J. Aroma dilution method using GC injector split ratio for volatile compounds extracted by headspace solid phase microextraction. *Food Chem.* **2003**, *83*, 151−158.

(18) Wu, S.; Zorn, H.; Krings, U.; Berger, R. G. Volatiles from submerged and surface-cultured beefsteak fungus, *Fistulina hepatica*. *Flavour Fragrance J.* **2007**, *22*, 53−60.

(19) Gallois, A.; Gross, B.; Langlois, D.; Spinnler, H. E.; Brunerie, P. Influence of culture conditions on production of flavour compounds by 29 ligninolytic basidiomycetes. *Mycol. Res.* **1990**, *94*, 494−504.

(20) Kawabe, T.; Morita, H. Volatile components in culture fluid of *Polyporus tuberaster*. *J. Agric. Food Chem.* **1993**, *41*, 637−640.

(21) Fantozzi, P.; Montanari, L.; Mancini, F.; Gasbarrini, A.; Addolorato, G.; Simoncini, M.; Nardini, M.; Ghiselli, A.; Scaccini, C. In *vitro* antioxidant capacity from wort to beer. *LWT−Food Sci. Technol.* **1998**, *31*, 221−227.

(22) Floridi, S.; Montanari, L.; Marconi, O.; Fantozzi, P. Determination of free phenolic acids in wort and beer by coulometric array detection. *J. Agric. Food Chem.* **2003**, *51*, 1548−1554.

(23) Kobayashi, N.; Kaneda, H.; Kano, Y.; Koshino, S. Determination of fatty acid hydroperoxides produced during the production of wort. *J. Inst. Brew.* **1993**, *99*, 143−146.

(24) Kennedy, A. I.; Taidi, B.; Dolan, J. L.; Hodgson, J. A. Optimisation of a fully defined medium for yeast fermentation studies. *Food Technol. Biotechnol.* **1997**, *35*, 261−265.

(25) Badcock, E. C. Preliminary account of the odour of wood-destroying fungi in culture. *Trans. Br. Mycol. Soc.* **1939**, *23*, 188−198.

(26) Silva, É. S.; Cavallazzi, J. R. P.; Muller, G.; Souza, J. V. B. Biotechnological applications of *Lentinus edodes*. *J. Food Agric. Environ.* **2007**, *5*, 403−407.

(27) Bisen, P. S.; Baghel, R. K.; Sanodiya, B. S.; Thakur, G. S.; Prasad, G. B. K. S. *Lentinus edodes*: a macrofungus with pharmacological activities. *Curr. Med. Chem.* **2010**, *17*, 2419−2430.

(28) Berladi, R. P.; Pawliszyn, J. The application of chemically modified fused silica fibers in the extraction of organics from water matrix samples and their rapid transfer to capillary columns. *J. Water Pollut. Res. J. Can.* **1989**, *24*, 179−191.

(29) Constant, M.; Collier, J. Headspace gas chromatography profiles of fruit-flavored malt beverages using solid-phase microextraction. *J. Am. Soc. Brew. Chem.* **1997**, *55*, 112−118.

(30) De Schutter, D. P.; Saison, D.; Delvaux, F.; Derdelinckx, G.; Rock, J. M.; Neven, H.; Delvaux, F. R. Optimisation of wort volatile analysis by headspace solid-phase microextraction in combination with gas chromatography and mass spectrometry. *J. Chromatogr., A* **2008**, *1179*, 75−80.

(31) Krings, U.; Hinz, M.; Berger, R. G. Degradation of [^{2}H]phenylalanine by the basidiomycete *Ischnoderma benzoinum*. *J. Biotechnol.* **1996**, *51*, 123−129.

(32) Beal, A. D.; Mottram, D. S. Compounds contributing to the characteristic aroma of malted barley. *J. Agric. Food Chem.* **1994**, *42*, 2880−2884.
(33) Fickert, B.; Schieberle, P. Identification of the key odorants in barley malt (caramalt) using GC/MS techniques and odour dilution analyses. *Nahrung* **1998**, *42*, 371−375.
(34) Vandecan, S. M. G.; Saison, D.; Schouppe, N.; Delvaux, F.; Delvaux, F. R. Optimisation of specialty malt volatile analysis by headspace solid-phase microextraction in combination with gas chromatography and mass spectrometry. *Anal. Chim. Acta* **2010**, *671*, 55−60.
(35) Chisholm, M. G.; Guiher, L. A.; Zaczkiewicz, S. M. Aroma characteristics of aged vidal blanc wine. *Am. J. Enol. Vitic.* **1995**, *46*, 56−62.
(36) Wu, S.; Zorn, H.; Krings, U.; Berger, R. G. Characteristic volatiles from young and aged fruiting bodies of wild *Polyporus sulfureus* (Bull.:Fr.) Fr. *J. Agric. Food Chem.* **2005**, *53*, 4524−4528.
(37) Ebeler, S. E.; Terrien, M. B.; Butzke, C. E. Analysis of brandy aroma by solid-phase microextraction and liquid-liquid extraction. *J. Sci. Food Agric.* **2000**, *80*, 625−630.
(38) Yang, X.; Peppard, T. Solid-phase microextraction for flavor analysis. *J. Agric. Food Chem.* **1994**, *42*, 1925−1930.
(39) Buttery, R. G.; Ling, L. C. Importance of 2-aminoacetophenone to the flavor of masa corn flour products. *J. Agric. Food Chem.* **1994**, *42*, 1−2.
(40) Guadagni, D. G.; Buttery, R. G.; Turnbaugh, J. G. Odour thresholds and similarity ratings of some potato chip components. *J. Sci. Food Agric.* **1972**, *23*, 1435−1444.
(41) Mebazaa, R.; Mahmoudi, A.; Rega, B.; Cheikh, R. B.; Camel, V. Analysis of human male armpit sweat after fenugreek ingestion: Instrumental and sensory optimization of the extraction method. *Food Chem.* **2010**, *120*, 771−782.

JOURNAL OF AGRICULTURAL AND FOOD CHEMISTRY

Article

pubs.acs.org/JAFC

A Comparison of Two Milling Strategies To Reduce the Mycotoxin Deoxynivalenol in Barley

Piyum A. Khatibi,[†] Greg Berger,[‡] Jhanel Wilson,[§] Wynse S. Brooks,[∥] Nicole McMaster,[†] Carl A. Griffey,[∥] Kevin B. Hicks,[‡] Nhuan P. Nghiem,[‡] and David G. Schmale, III*,[†]

[†]Department of Plant Pathology, Physiology, and Weed Science, Virginia Tech, Blacksburg, Virginia 24061, United States

[‡]Department of Crop, Soil, and Environmental Sciences, Rice Research and Extension Center, University of Arkansas, Stuttgart, Arkansas 72160, United States

[§]Sustainable Biofuels and Co-Products Research Unit, USDA, ARS, Eastern Regional Research Center, Wyndmoor, Pennsylvania 19038, United States

[∥]Department of Crop and Soil Environmental Sciences, Virginia Tech, Blacksburg, Virginia 24061, United States

Supporting Information

ABSTRACT: Winter barley (*Hordeum vulgare* L.), a potential feedstock for fuel ethanol production, may be contaminated with the trichothecene mycotoxin deoxynivalenol (DON). DON is a threat to feed and food safety in the United States and may become concentrated during the production of distillers dried grains with solubles (DDGS). DDGS is a coproduct of fuel ethanol production and is increasingly being used as feed for domestic animals. Therefore, new strategies to reduce the threat of DON in DDGS need to be developed and implemented for grain destined for fuel ethanol production. It is known that large concentrations of DON accumulate in the hulls of wheat and barley. Consequently, improved methods are needed to carefully remove the hull from the grain and preserve the starchy endosperm. Whole kernels from five Virginia winter barley genotypes were used to evaluate the abilities of two different milling strategies (roller milling and precision milling (FitzMill)) for their ability to remove the hull-enriched tissue from the kernel while maintaining starch levels and reducing DON levels in the endosperm-enriched tissue. After whole kernels were milled, DON and starch levels were quantified in the hull-enriched fractions and endosperm-enriched fractions. Initial milling experiments demonstrated that the precision mill system (6 min run time) is able to reduce more DON than the roller mill but with higher starch losses. The average percent DON removed from the kernel with the roller mill was 36.7% ± 5.5 and the average percent DON removed from the dehulled kernel with the precision mill was 85.1% ± 9.0. Endosperm-enriched fractions collected from the roller mill and precision mill contained starch levels ranging from 49.0% ± 12.1 to 59.1% ± 0.5 and 58.5% ± 1.6 to 65.3% ± 3.9, respectively. On average, the precision mill removed a mass of 23.1% ± 6.8 and resulted in starch losses of 9.6% ± 6.3, but produced an endosperm-enriched fraction with relatively very little average DON (5.5 ± 2.7 $\mu g\ g^{-1}$). In contrast, on average, the roller mill removed a mass of 12.2% ± 1.6 and resulted in starch losses of 2.1% ± 0.5, but produced an endosperm-enriched fraction with high average DON (20.7 ± 13.5 $\mu g\ g^{-1}$). In a time course precision milling experiment, we tested barley genotypes Nomini, Atlantic, and VA96-44-304 and attempted to reduce the starch loss seen in the first experiment while maintaining low DON concentrations. Decreasing the run time of the precision mill from 5 to 2 min, reduced starch loss at the expense of higher DON concentrations. Aspirated fractions revealed that the precision milled hull-enriched fraction contained endosperm-enriched components that were highly contaminated with DON. This work has important implications for the reduction of mycotoxins such as DON in barley fuel ethanol coproducts and barley enriched animal feeds and human foods.

KEYWORDS: *barley, hull, dehulling, milling, mycotoxin reduction, deoxynivalenol, starch retention, fermentation, distillers dried grains with solubles (DDGS)*

INTRODUCTION

Fusarium head blight (FHB), caused by the fungal plant pathogen *Fusarium graminearum* Schwabe (teleomorph *Gibberella zeae*), can be a devastating disease of grains such as wheat and barley.[1] During infection, the fungus produces a mycotoxin called deoxynivalenol (DON).[2] DON is a protein synthesis inhibitor[4] and ingestion of DON may lead to vomiting, feed refusal, and a compromised immune system.[5] Grain contaminated with DON may be rendered unusable for feed and food products.[3]

Distillers dried grains with solubles (DDGS), a coproduct of fuel ethanol production, is increasingly being used as feed for domestic animals. When grain, such as winter barley,[6] containing DON is used as feedstock to produce fuel ethanol, DON becomes concentrated in the DDGS.[7,8] The fuel ethanol industry relies on the sale of DDGS as feed for domestic animals for generating profits[9] and DDGS contaminated with mycotoxins such as DON are unmarketable.

Current methods to reduce or alleviate mycotoxin contamination in grain include blending clean grain with

Received: December 10, 2013
Accepted: April 15, 2014
Published: April 15, 2014

ACS Publications © 2014 American Chemical Society

contaminated grain (prohibited in Europe and not approved by the U.S Federal Drug Administration (FDA)), washing grain with water, and using adsorbents to bind mycotoxins.[10,11] Strategies to prevent DON production during storage include electron beam irradiation[12] and fungistats to prevent fungal growth.[13] These strategies may be effective, but are likely to require high equipment and labor costs. New cost-effective and commercially viable methods need to be developed and implemented to reduce DON contamination in barley destined for food and feed products.

Planting resistant barley cultivars can be one of the most effective ways to reduce FHB and DON accumulation; however, resistance conferring complete immunity to FHB has not been identified to date. In Virginia, new hulled and hulless barley cultivars that are resistant to FHB and DON accumulation are being developed.[14,15] With hulled barley, the hull is tightly fixed to the pericarp epidermis, while with hulless barley the hull loosely covers the caryopses.[16] Previous work has demonstrated that mycotoxins such as DON accumulate in the hull and outer regions of the kernel.[17−20] Thus, an alternative to hulled barley would be to plant hulless genotypes whose hull can be easily removed and that have higher starch content.[6] However, higher yields and higher revenues with hulled barley (bushels per acre) do not make hulless barley an attractive alternative for growers.[6] Past attempts at milling or pearling hulled grain to reduce mycotoxin levels were proven effective and showed reductions that ranged from 30% to 66%.[19−25] Inevitably, grain mass losses (i.e., starch, protein) occur and have ranged from 10% to 32%.[22,25−27] Recent advances in hull removal have led to a more effective and simpler dehulling strategy that may be more cost-effective and may minimize losses in grain mass.[28] The Fitzpatrick Comminuting Machine (precision mill) was shown to dehull kernels and produce fractions with much higher starch content than that of the original hulled kernel (71% vs 60% starch, respectively). Moreover, the process minimized starch loss to less than 1.5%.[28]

In this study, we evaluated the abilities of a FitzMill precision mill and a roller mill to remove the hulls and reduce DON in Virginia hulled barley samples without causing major starch losses. We hypothesized that the precision mill (compared to the roller mill) would more effectively remove hull-enriched tissue from hulled barley, thereby resulting in larger reductions of DON, higher starch concentrations, and smaller starch loss. Our work has important implications for the reduction of mycotoxins in barley fuel ethanol coproducts and barley enriched animal feeds and human foods.

MATERIALS AND METHODS

Barley Genotypes and Infection. Five Virginia winter hulled barley genotypes (Callao, Nomini, Atlantic, VA06B-32, VA96-44-304) were planted in 2009 in a randomized complete block with two replications in mist-irrigated nurseries at Mt. Holly, VA.[14] Research plots had dimensions of 1.5 m × 13.4 m and *Fusarium graminearum* colonized corn (*Zea mays*) kernels were applied to the plots at the boot stage to encourage infection and DON contamination in the harvested grain.[7,15] Grain was harvested in summer 2010 using a small plot research combine.

Roller Milling and Precision Milling. Ten hulled barley samples (five genotypes) from Virginia winter barley genotypes Callao, Nomini, Atlantic, VA06B-32, and VA96-44-304 were used to evaluate the abilities of two different milling strategies (roller milling and precision milling (FitzMill)) for their ability to remove the hull-enriched tissue from the kernel while maintaining starch levels and reducing DON levels in the endosperm-enriched tissue. The samples were first cleaned using a dockage tester (Carter Day International, Minneapolis, MN). For each barley genotype, two 500 g samples were roller milled, and two 500 g samples were precision milled. The roller mill flow consisted of one pass through 16 corrugations per 25.4 mm (mm) rolls with a 0.127 mm gap. After roller milling, the material was sifted with a SWECO sifter (SWECO, Florence, KY) containing a 24SSBC sieve. The milled kernel fraction (endosperm-enriched fraction) passed through the sieve while the hull-enriched fraction remained on top of the sieve screen. The precision milling was carried out similarly to that described by Hicks et al.[28] using a Fitzpatrick Comminuting Machine (Model D, W.J. Fitzpatrick Company, Chicago IL) also referred to as a FitzMill. Each 500 g sample was milled for 6 min using a 2AA sieve (1.9 mm) with the sharp blades rotating forward at 1750 rpm. Tests were run batch-wise in duplicate. Samples were loaded in the FitzMill chamber and during milling, the hull-enriched fractions were collected beneath the mill and the dehulled kernel fractions (endosperm-enriched fraction) were retained in the milling chamber. A comparison of hull removal efficiency was determined by measuring the mass fraction (% dry weight basis, (% d.w.b)) of the barley hull and dehulled kernel remaining after processing through the roller mill or precision mill.

Time Course Precision Milling. Three hulled barley genotypes (Nomini, Atlantic, and VA96-44-304) were chosen to determine the optimum run time for the FitzMill necessary to efficiently remove tissue enriched in hull from the kernel while minimizing starch loss. The grains used for these experiments were harvested in 2011 from barley genotypes that were planted in 2010 in a randomized complete block in mist-irrigated nurseries at Mt. Holly, VA and treated with *Fusarium graminearum* as described above. For each barley genotype, whole kernel subsamples of 500 g were dehulled using the FitzMill as described above except that samples were milled for only 2, 3, 4, or 5 min rather than the 6 min in the original experiment. A logarithmic trend line was applied to % mass fraction data derived from grain processed in the time course precision milling experiment.[28] Additionally, some of the individual hull and kernel fractions from these experiments were aspirated using a Grainman model 63-115-60VS Grain Cleaner Laboratory Aspirator (Grain Machinery Mfg. Corp., Miami, Florida, U.S.A.). The speed setting was 7, the feeder was set at 5, and the air control was set at 0.2. Two fractions were collected: the heavy fraction that was composed primarily of starch-enriched fractions (endosperm) and the light fraction composed primarily of fibrous hull.

Extraction of Deoxynivalenol. Samples containing approximately 10 g of whole kernels, hulls, and dehulled kernel fraction were ground in a coffee grinder (Hamilton Beach, model 80365, Southern Pines, NC) positioned at the expresso and 12 cup setting (Figure S1 in the Supporting Information [SI]). Mycotoxin extractions were performed following standard protocols on 1 g subsamples of the ground whole kernel, ground hull, and ground kernel (Figure S1).[29−31] Each subsample was combined with 10 mL extraction solvent (86% (v/v) acetonitrile in DI water) in a capped polypropylene tube. The solvent−sample mixture was placed on a shaker at 200 rpm for 1 h at room temperature and then passed through a cleanup column composed of a 1 g mixture of Bakerbond C18 (VWR, Radnor, PA) and aluminum oxide (active, neutral) (Sigma-Aldrich, St. Louis, MO) at a 1:3 ratio.

All samples were extracted for DON so the final concentration in isooctane was diluted ×20. If the sample was quantified to have a DON concentration of 0.5 $\mu g\ g^{-1}$ or less on the GC−MS, then the sample extract was quantified at a smaller dilution of ×2.5. This was done to ensure that DON levels fell within the standard curve.

For 1:20 dilutions, a 1 mL aliquot of eluent was transferred to a glass test tube and evaporated to dryness using a nitrogen evaporator set at 55 °C. Dried samples were then silylated with a 100 μL mixture of *N*-trimethylsilylimidazole (TMSI) and trimethylchlorosilane (TMCS) at a 100:1 ratio. Samples were then resuspended in 2 mL of isooctane containing 0.5 $\mu g\ g^{-1}$ mirex, followed by 2 mL of water to quench the reaction. Samples were vortexed for 10 s, and 100 μL of the isooctane−mirex supernatant was removed and transferred to

chromatography vials for gas chromatography−mass spectrometry (GC−MS) analysis. For 1:2.5 dilutions, the same method was followed, except that a 2 mL aliquot was dried down and resuspended in 0.5 mL of isooctane−mirex mixture.

GC−MS Analysis for Deoxynivalenol Quantification. GC−MS analysis was conducted using an Agilent 6890/5975 system operating in selected ion monitoring (SIM) mode. A 1 μL volume of each sample or known standard was injected by an autosampler in splitless mode onto an Agilent HP-5MS column, 0.25 mm inner-diameter by 0.25 μm film thickness by 30 m length. The inlet temperature was set to 250 °C with a constant column flow rate of 1.2 mL/min. The initial column temperature was held at 150 °C for 1 min, increased to 280 °C at a rate of 30 °C/min, and held constant for 3.5 min. A postrun method ramped the oven temperature to 325 °C and was held for 2.5 min. Mirex (Sigma-Aldrich, St. Louis, MO) was used as an internal control at 0.5 μg g^{-1}. SIM mode detected DON target ions at a mass:charge ratio of 512, with reference ions at 422 and 497.[32] SIM mode detected mirex target ions at mass:charge ratio of 272 with reference ions at 276 and 237. DON was quantified using a standard curve of ratios of DON area to mirex area versus DON standard concentration and fit to a linear regression model. DON standards (Romer Laboratories, Austria) were prepared in a DON-free wheat matrix[29] at concentrations of 0.05, 0.1, 0.25, 0.5, 1.0, 2.5, 5.0, 10, and 15 μg g^{-1}. The limit of quantitation (LOQ) for this method was determined to be 0.1 μg g^{-1}. Sample results were initially quantified using a standard curve with the first five standards (0.05 to 1 μg g^{-1}). If raw DON values were quantified as greater than 1 μg g^{-1}, calculations were performed using a standard curve containing all points. For quality assurance, samples of barley and wheat containing known levels of DON were concurrently prepared and interspersed among test samples for each GC−MS run. Quality assurance samples were considered acceptable if the quantified DON concentration did not deviate more than 20% of the expected concentration. DON recovery for barley using the DON extraction method described above has been reported to range between 100% and 105%.[30] The percentage of DON removed by milling an individual kernel was determined by adjusting the DON values of each fraction by multiplying by the appropriate mass fraction (% d.w.b) (Figure 1 or Figure 2) and then calculating the proportion of DON in the hull-enriched tissue that was removed relative to the total DON (the DON concentration in the kernel's hull-enriched tissue plus the DON concentration in the kernel's endosperm-enriched tissue). A logarithmic trend line was determined to be the best fit and was applied to the % DON removed from dehulling whole kernels processed in the time course precision milling experiment.

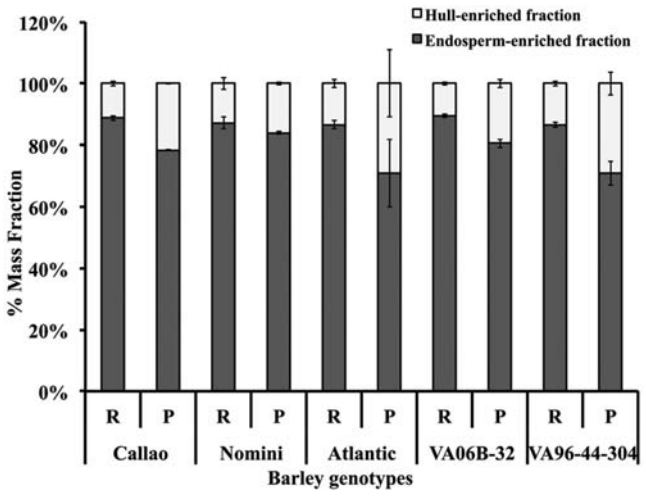

Figure 1. Percent mass fractions (% d.w.b.) of endosperm-enriched fractions and hull-enriched fractions from whole kernels processed in the roller mill (R) and precision mill (P). Five barley genotypes were used and run in duplicate and values given are mean ± standard deviation.

Statistical Analyses. A two-way analysis of variance (ANOVA) was performed to test for significant differences among genotypes, mill type, and time points during precision milling using PROC GLIMMIX in SAS (version 9.2; SAS Institute, Cary, NC). A Tukey−Kramer's honestly significant difference (HSD) posthoc test was performed for variables that differed at $P \leq 0.05$. A correlation analysis was performed between DON levels in the whole kernels and % hull mass fraction using JMP (version 9.0.0; SAS Institute Inc., Cary, NC). For the time course precision mill experiment, an analysis was performed to determine if % DON reduction and % hull mass fraction were correlated and if % starch loss and % hull mass fraction were correlated using JMP (version 9.0.0; SAS Institute Inc., Cary, NC).

Starch Analysis. Starch content was determined through chemical analysis of the hull-enriched and endosperm-enriched fractions remaining after precision milling and roller milling. A logarithmic trend line was applied to starch content data derived from grain processed in the time course precision milling experiment.[28] Fractions with high starch content were considered to be endosperm-enriched fractions, and fractions with low starch were considered hull-enriched fractions. Starch content of hull and kernel samples was determined by analyzing approximately 100 mg of sample using a starch determination kit (Megazyme International Ireland Ltd., Bray Business Park, Bray, Co. Wicklow, Ireland.[33] Enzyme digestions were conducted following the Megazyme protocol,and the hydrolyzed starch solutions were diluted to 50 mL with water. This method was modified by use of an YSI 2700 Analyzer (YSI Incorporated, Yellow Springs, Ohio) fitted with an YSI 2710 turntable for automated glucose determination. The percentage of starch lost by milling an individual kernel was determined by adjusting the starch compositional values of each fraction by multiplying by the appropriate mass fraction (% d.w.b.) (Figure 1 or Figure 2) and then calculating the proportion of starch in the hull-enriched tissue that was removed relative to the total starch composition (the starch in the kernel's hull-enriched tissue plus the starch in the kernel's endosperm-enriched tissue).

RESULTS

Mass Fractions from the Roller Mill and Precision Mill. After milling whole kernels in the roller mill and precision mill, components were separated into endosperm-enriched fractions and hulled-enriched fractions. Under the conditions tested, the precision mill system resulted in larger hull-enriched mass fractions and smaller endosperm-enriched mass fractions than the roller mill system. An ANOVA confirmed an effect of milling strategy on hull-enriched and endosperm-enriched mass fractions ($P \leq 0.05$) (Table S1). The roller mill resulted in endosperm-enriched percent mass fractions that ranged from 86.6% ± 1.3 to 89.6% ± 0.5 and hull-enriched percent mass fractions that ranged from 10.5% ± 0.5 to 13.4% ± 1.3 (Figure 1). The precision mill resulted in endosperm-enriched percent mass fractions that ranged from 70.8% ± 10.9 to 84.1% ± 0.4 and hull-enriched percent mass fractions that ranged from 16.0% ± 0.4 to 29.2% ± 10.9 (Figure 1). On average, the roller mill yielded endosperm-enriched and hull-enriched fractions of 87.8% ± 1.5 and 12.2% ± 1.6, while the precision mill yielded an average percent mass fraction of endosperm-enriched and hull-enriched fractions of 76.9% ± 6.8 and 23.1% ± 6.8, respectively (Figure 1). Average mass recovery was 97.3% and 99.8% for the roller mill and precision mill, respectively (not shown).

Deoxynivalenol Levels in Barley Fractions. DON levels in whole kernels ranged from 14.3 ± 4.6 μg g^{-1} (Nomini) to 38.8 ± 14.6 μg g^{-1} (Atlantic) (Table 1). Whole kernels that were processed in the roller mill resulted in endosperm-enriched fractions containing DON concentrations that ranged

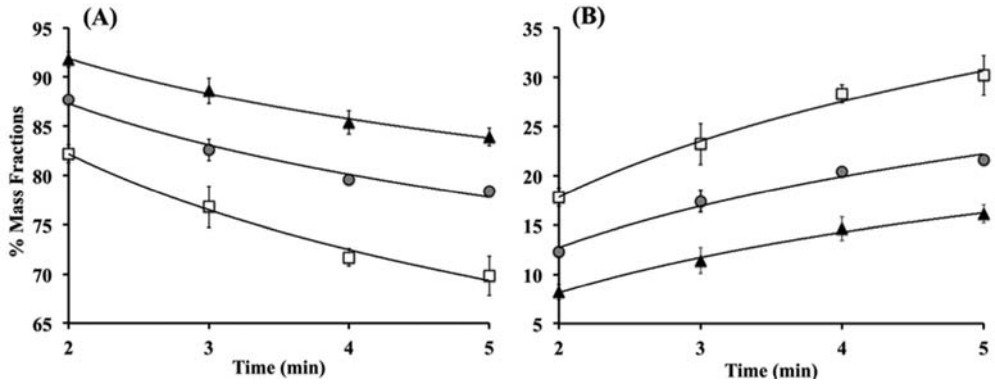

Figure 2. Time course precision mill percent mass fractions (% d.w.b.) of (A) hull-enriched fractions from whole kernels of barley genotypes Nomini (**triangle**, $y = -8.85 \ln(x) + 98.02$, $R^2 = 0.99$), Atlantic (**circle**, $y = -10.37 \ln(x) + 94.49$, $R^2 = 0.98$), and VA96-44-304 (**square**, $y = -14.00 \ln(x) + 91.88$, $R^2 = 0.99$) and (B) endosperm-enriched fractions from whole kernels of barley genotypes Nomini (**triangle**, $y = 8.85 \ln(x) + 1.98$, $R^2 = 0.99$), Atlantic (**circle**, $y = 10.37 \ln(x) + 5.51$, $R^2 = 0.98$), and VA96-44-304 (**square**, $y = 14.00 \ln(x) + 8.12$, $R^2 = 0.99$). Each time point for a given genotype was run in duplicate, and values given are mean ± standard deviation.

Table 1. Concentration of DON (μg g^{-1}) in the Endosperm-Enriched Fractions and Hull-Enriched Fractions from Whole Kernels Processed in the Roller Mill and the Precision Mill; Five Barley Genotypes Were Used and Run in Duplicate

		roller mill[a]			precision mill[a]		
genotype	whole kernel[a]	endosperm-enriched fractions	hull-enriched fractions	% DON removed[b]	endosperm-enriched fractions	hull-enriched fractions	% DON removed[b]
Callao	18.3 ± 2.3	12.9 ± 3.0	71.3 ± 11.2	41.4 ± 3.8	3.0 ± 2.1	107.3 ± 8.2	91.1 ± 5.3
Nomini	14.3 ± 4.6	9.4 ± 3.8	46.1 ± 11.1	42.5 ± 0.0	5.6 ± 1.8	69.4 ± 26.7	69.8 ± 1.0
Atlantic	38.8 ± 14.6	35.5 ± 18.1	109.0 ± 4.5	34.0 ± 8.4	8.9 ± 2.6	179.8 ± 14.4	87.6 ± 9.0
VA06B-32	16.2 ± 3.4	12.1 ± 2.0	51.6 ± 8.8	33.3 ± 1.0	3.4 ± 1.1	82.2 ± 3.3	85.9 ± 2.5
VA96-44-304	31.7 ± 2.8	33.6 ± 5.8	102.6 ± 8.6	32.3 ± 0.3	6.4 ± 1.3	155.0 ± 2.8	90.9 ± 0.2
grand mean	23.9 ± 11.9	20.7 ± 13.7	76.1 ± 28.0	36.7 ± 5.5	5.5 ± 2.7	118.7 ± 45.8	85.1 ± 9.1

[a]Values given are mean ± standard deviation. [b]The percentage of DON removed by milling an individual kernel was determined by adjusting the DON values of each fraction by multiplying by the appropriate mass fraction (Figure 1) and then calculating the proportion of DON in the hull-enriched tissue that was removed relative to the total DON (the kernel's hull-enriched tissue plus the kernel's endosperm-enriched tissue).

Table 2. Percent Starch (% d.w.b.) Analysis of Endosperm-Enriched Fractions and Hull-Enriched Fractions from the Roller Mill and the Precision Mill Derived from Five Hulled Barley Genotypes; Five Barley Genotypes Were Used and Run in Duplicate

	roller mill[a]			precision mill[a]		
barley genotype	endosperm-enriched fractions	hull-enriched fractions	% starch loss[b]	endosperm-enriched fractions	hull-enriched fractions	% starch loss[b]
Callao	57.4 ± 3.7	11.1 ± 0.1	2.4 ± 0.1	59.9 ± 3.5	19.5 ± 0.0	8.2 ± 0.5
Nomini	57.4 ± 1.3	7.2 ± 0.8	1.8 ± 0.5	58.5 ± 1.6	13.5 ± 3.2	4.2 ± 1.0
Atlantic	59.1 ± 0.5	7.5 ± 1.1	1.9 ± 0.1	65.3 ± 3.9	30.0 ± 9.5	16.7 ± 10.5
VA06B-32	59.0 ± 0.1	8.5 ± 1.5	1.7 ± 0.4	61.5 ± 0.6	13.5 ± 0.2	5.0 ± 0.4
VA96-44-304	49.0 ± 12.1	7.7 ± 1.3	2.5 ± 0.8	60.8 ± 0.2	23.5 ± 0.9	13.7 ± 1.7
grand mean	56.4 ± 5.8	8.4 ± 1.7	2.1 ± 0.5	61.2 ± 3.0	20.0 ± 7.4	9.6 ± 6.3

[a]Values given are mean ± standard deviation. [b]The percentage of starch lost by milling an individual kernel was determined by adjusting the starch compositional values of each fraction by multiplying by the appropriate mass fraction (Figure 1) and then calculating the proportion of starch in the hull-enriched tissue that was removed relative to the total starch percentage (the kernel's hull-enriched tissue plus the kernel's endosperm-enriched tissue).

from 9.4 ± 3.8 μg g^{-1} to 35.5 ± 18.1 μg g^{-1} and DON levels in the hull-enriched fractions that ranged from 46.1 ± 11.1 μg g^{-1} to 109.0 ± 4.5 μg g^{-1} (Table 1). Conversely, whole kernels processed in the precision mill resulted in endosperm-enriched fractions containing DON concentrations that ranged from 3.0 ± 2.1 μg g^{-1} to 8.9 ± 2.6 μg g^{-1} and DON levels in the hull-enriched fractions that ranged from 69.4 ± 26.7 μg g^{-1} to 179.8 ± 14.4 μg g^{-1} (Table 1). For the five barley genotypes analyzed, the grand mean DON concentration of the endosperm-enriched fractions and hull-enriched fractions from the roller mill was 20.7 ± 13.7 μg g^{-1} and 76.1 ± 28.0 μg g^{-1}, while the grand mean DON concentration from the precision mill fractions yielded 5.5 ± 2.7 μg g^{-1} and 118.7 ± 44.9 μg g^{-1}, respectively (Table 1). An ANOVA demonstrated a significant ($P \leq 0.05$) effect of genotype and milling strategy on DON levels in the endosperm-enriched and hull-enriched fractions (Table S1). DON removed from the milled kernel using the precision mill ranged from 69.8% ± 1.0 to 91.1% ± 5.3 versus 32.3% ± 0.3 to 42.5% ± 0.0 using the roller mill (Table 1). Significant differences ($P \leq 0.05$) in the % DON removed was observed between the mill used and genotype * mill interactions (Table S1 in the SI).

dx.doi.org/10.1021/jf501208x | J. Agric. Food Chem. 2014, 62, 4204−4213

Table 3. Precision Milled Aspirated Hull-Enriched Fraction and Endosperm-Enriched Fraction Analysis Showing % Mass Fraction, DON Concentration ($\mu g\ g^{-1}$), and % Starch That Resulted in Clarified Hull-Enriched Fractions (H) and Endosperm-Enriched Fractions (E)

		precision milled aspirated samples[a]							
		aspirated hull-enriched fractions				aspirated endosperm-enriched fractions			
genotype	time (min)		% mass fraction	DON ($\mu g\ g^{-1}$)	% starch		% mass fraction	DON ($\mu g\ g^{-1}$)	% starch
Nomini	2					H	7.6	4.5	0.9
						E	92.4	2.8	60.2
	3					H	10.0	4.1	0.8
						E	90.0	2.1	61.8
	4								
	5	H	81.5	4.8	4.7				
		E	18.5	98.6	52.0				
Atlantic	2					H	4.9	3.8	3.2
						E	95.1	3.5	62.2
	3					H	4.0	2.6	1.3
						E	96.0	1.8	66.1
	4								
	5	H	75.8	5.4	11.2				
		E	24.2	131.0	65.6				
VA96-44-304	2					H	5.3	7.7	1.6
						E	94.7	6.5	55.6
	3					H	3.3	5.6	1.4
						E	96.7	4.0	59.9
	4	H	72.4	9.1	8.6				
		E	27.7	131.4	59.3				
	5	H	69.9	9.2	9.9				
		E	30.1	109.4	60.9				

[a]Aspirated samples were single runs.

Starch Composition of Endosperm-Enriched and Hull-Enriched Fractions. Whole kernels processed in the roller mill resulted in starch levels in the endosperm-enriched fractions that ranged from 49.0% ± 12.1 to 59.1% ± 0.5 and starch levels in the hull-enriched fractions that ranged from and 7.2% ± 0.8 to 11.1% ± 0.1 (Table 2). Conversely, the precision mill resulted in starch composition in the endosperm-enriched fractions that ranged from 58.5% ± 1.6 to 65.3% ± 3.9 and starch levels in the hull-enriched fractions that ranged from 13.5% ± 3.2 to 30.0% ± 9.5 (Table 2). For the 5 barley genotypes analyzed, the grand mean starch concentration of the endosperm-enriched fractions and hull-enriched fractions from the roller mill was 56.4% ± 5.8 and 8.4% ± 1.7, while the average for the precision mill fractions was 61.2% ± 3.0 and 20.0% ± 7.4, respectively (Table 2). Starch lost from the milled kernel using the roller mill and precision mill ranged from 1.8% ± 0.5 to 2.5% ± 0.8 and 4.2% ± 1.0 to 16.7% ± 10.5, respectively (Table 2). Average starch loss from the roller mill was 2.1% ± 0.5 and average starch loss from the precision mill was 9.6% ± 6.3 (Table 2). An ANOVA demonstrated a significant ($P \leq 0.05$) effect of milling strategy on starch levels in the endosperm-enriched fractions and an effect of genotype, milling strategy, and genotype * mill interactions on starch levels in the hull-enriched fractions (Table S1).

Time Course Precision Milling-Percent Mass Fraction. Three of the barley genotypes that were analyzed in the first analysis (Nomini, Atlantic, and VA96-44-304) were subject to time course precision milling to locate a milling time that resulted in lower starch loss. Longer precision milling times resulted in larger amounts of hull-enriched fractions and smaller amounts of endosperm-enriched fractions (Figure 2). Time course precision milling generated hull-enriched mass fractions ranging from 8.2% ± 0.8 (2 min, Nomini) to 30.2% ± 2.0 (5 min, VA96-44-304) and endosperm-enriched mass fractions ranging from 69.8% ± 2.0 (5 min, VA96-44-304) to 91.8% ± 0.8 (2 min, Nomini) (Figure 2). Significant differences ($P \leq 0.05$) for genotype, time, and genotype * time interactions were observed for endosperm-enriched and hull-enriched % mass fractions in the time course precision mill experiment (Table S2). Aspirated samples revealed that hull-enriched fractions were contaminated with small amounts of components enriched in endosperm (which were separated by aspiration) and endosperm-enriched fractions that were contaminated with small amounts of components enriched in hulls (which were also separated by aspiration) (Table 3). Endosperm-enriched fractions that were contaminating the hull-enriched fraction ranged from 18.5% (Nomini, 5 min) to 30.1% (VA96-44-304, 5 min) and hull-enriched fractions that were contaminating the endosperm-enriched fraction ranged from 3.3% (VA96-44-304, 3 min) to 10% (Nomini, 3 min) (Table 3).

Time Course Precision Milling-DON and Starch Levels. From 2 to 5 min, barley genotypes Nomini, Atlantic, and VA96-44-304 had increases in the proportion of DON that was removed from the dehulled kernel, with percentages ranging from 45.0% ± 7.1 to 68.8% ± 8.5, 68.9% ± 7.2 to 90.5% ± 1.1, and 66.1% ± 4.3 to 92.7% ± 1.7, respectively (Figure 3). Thus, DON levels increased in the hull-enriched fractions and decreased in the endosperm-enriched fractions as precision milling time increased. For example, the endosperm-enriched fraction of Nomini, Atlantic, and VA96-44-304 had DON concentrations that decreased from 12.2 ± 2.9 to 8.1 ± 3.8, from 9.9 ± 4.0 to 3.1 ± 0.1, and from 19.8 $\mu g\ g^{-1}$ ± 1.9 (2 min)

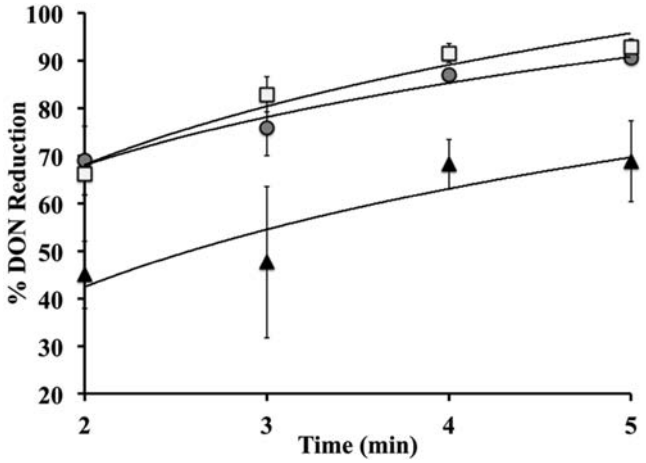

Figure 3. Percentage of DON removed by dehulling barley genotypes Nomini (**triangle**, $y = 29.73 \ln(x) + 21.82$, $R^2 = 0.84$), Atlantic (**circle**, $y = 24.82 \ln(x) + 50.79$, $R^2 = 0.97$), and VA96-44-304 (**square**, $y = 30.13 \ln(x) + 47.22$, $R^2 = 0.94$) in the precision mill from 2 to 5 min. Each time point for a given genotype was run in duplicate, and values given are mean ± standard deviation. The percentage of DON removed by milling an individual kernel was determined by multiplying the DON values ($\mu g\ g^{-1}$) of each fraction by the appropriate mass fraction value (Figure 2A, B) and then calculating the proportion of DON in the hull-enriched tissue that was removed relative to the total DON.

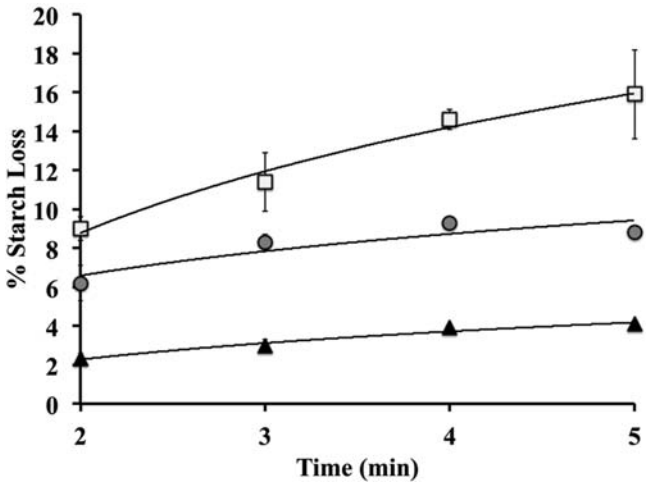

Figure 4. Percent starch lost (% d.w.b.) from dehulling kernels of barley genotypes Nomini (**triangle**, $y = 2.08 \ln(x) + 0.83$, $R^2 = 0.97$), Atlantic (**circle**, $y = 3.10 \ln(x) + 4.44$, $R^2 = 0.81$), and VA96-44-304 (**square**, $y = 7.82 \ln(x) + 3.36$, $R^2 = 0.98$) in the time course precision milling experiment. Each time point for a given genotype was run in duplicate, and values given are mean ± standard deviation. The percentage of starch lost by milling an individual kernel was determined by multiplying the starch compositional values (%) of each fraction by the appropriate mass fraction (Figure 2A, B) and then calculating the proportion of starch in the hull-enriched tissue that was removed relative to the total starch percentage.

to 5.1 $\mu g\ g^{-1}$ ± 0.4 (5 min), respectively (data not shown). Correspondingly, the hull-enriched fraction had DON concentrations that went from 110.6 ± 6.8 to 88.9 ± 2.1, from 150.8 ± 10.5 to 108.2 ± 10.5, and from 178.7 $\mu g\ g^{-1}$ ± 6.4 (2 min) to 152.0 $\mu g\ g^{-1}$ ± 10.2 (5 min), respectively (data not shown). There were significant differences ($P \leq 0.05$) in DON concentration between time points in the endosperm-enriched fractions and significant differences ($P \leq 0.05$) between genotypes and between time points in the hull-enriched fractions (Table S2).

When precision milling time increased (2 to 5 min), so did the proportion of starch lost when the hull-enriched tissue was removed likely due to simultaneous removal of small amounts of endosperm (Figure 4). As more and more hull was removed, eventually the precision mill blades struck the dehulled kernel and removed more endosperm.[28] Significant differences ($P \leq 0.05$) were observed for % starch loss between time points and genotypes (Table S2 in the SI). Starch loss ranged from 2.3% ± 0.3 to 4.1% ± 0.1 for Nomini, 6.2% ± 0.9 to 8.8% ± 0.1 for Atlantic, and 9.0% ± 0.6 to 15.9% ± 2.3 for VA96-44-304 (Figure 4). Barley genotype VA96-44-304 had the largest loss of starch during dehulling in the precision mill. Although starch loss increased from 2 to 5 min, precision milling led to increases in the starch concentration for the endosperm-enriched fractions. The starch composition (increasing in milling time) for the endosperm-enriched fractions of Nomini, Atlantic, and VA96-44-304 increased from 55.6% ± 0.3 to 60.0% ± 1.5, 57.6% ± 3.1 to 61.5% ± 1.0, and 55.9% ± 0.5 (2 min) to 61.2% ± 0.0 (5 min), respectively (data not shown). The starch composition (increasing in milling time) for the hulled-enriched fractions ranged from 14.8% ± 0.1 to 13.4% ± 0.3, 26.9% ± 2.4 to 21.4% ± 0.4, and 25.6% ± 0.1 (2 min) to 26.7% ± 2.2 (5 min), respectively (data not shown). There were significant differences ($P \leq 0.05$) in % starch between time points in the endosperm-enriched fractions and significant differences between genotypes and genotype ∗ time interactions in the hull-enriched fractions (Table S2).

The percent starch lost by dehulling and the percent DON removed in the precision mill was significantly correlated with the % hull mass fraction ($r = 0.95$, $P < 0.0001$ and $r = 0.87$, $P < 0.0001$, respectively) (Figure 5). When a linear model was fit to the trend lines, the slope (rate) of starch loss and DON removal were 0.63 and 2.26, respectively (Figure 5). However, the logarithmic model was a better fit for the DON removal (R^2 of 0.81, Figure 5).

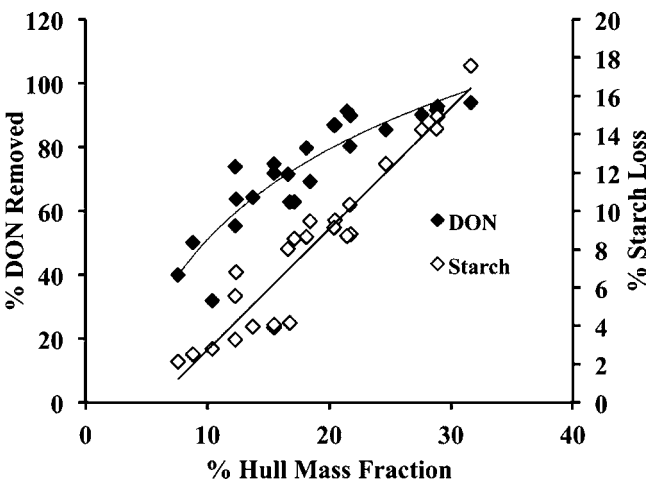

Figure 5. Percent DON removed ($y = 40.84 \ln(x) - 43.05$, $R^2 = 0.81$) and % starch loss ($y = 0.63x - 3.59$, $R^2 = 0.91$) as a function of the % hull mass fraction during time course precision milling. The amount of DON removed and the amount of starch lost increased as the mass of the hull fraction increased.

dx.doi.org/10.1021/jf501208x | J. Agric. Food Chem. 2014, 62, 4204−4213

Time Course Precision Milling-Aspirated Samples. The aspirated hull-enriched fractions possessed components enriched in endosperm that contained DON levels ranging from 98.6 $\mu g\ g^{-1}$ (Nomini, 5 min) to 131.4 $\mu g\ g^{-1}$ (VA96-44-304, 4 min) and components enriched in hulls that contained DON ranging from 4.8 $\mu g\ g^{-1}$ (Nomini, 5 min) to 9.2 $\mu g\ g^{-1}$ (VA96-44-304, 5 min) (Table 3). The aspirated endosperm-enriched fractions possessed components enriched in hulls that contained DON levels that ranged from 2.6 $\mu g\ g^{-1}$ (Atlantic, 3 min) to 7.7 $\mu g\ g^{-1}$ (VA96-44-304, 2 min) and components enriched in endosperm that contained DON ranging from 1.8 $\mu g\ g^{-1}$ (Atlantic, 3 min) to 6.5 $\mu g\ g^{-1}$ (VA96-44-304, 2 min) (Table 3).

The hull-enriched fractions contained endosperm-enriched components that could be removed by aspiration, and these isolated subfractions had starch levels that ranged from 52.0% (Nomini, 5 min) to 65.6% (Atlantic, 5 min) and the hull-enriched components remaining after aspiration had starch composition that ranged from 4.7% (Nomini, 5 min) to 11.2% (Atlantic, 5 min) (Table 3). The endosperm-enriched fractions contained hull-enriched components that were isolated by aspiration and these isolated subfractions had starch levels that ranged from 0.8% (Nomini, 3 min) to 3.2% (Atlantic, 2 min). The endosperm-enriched components remaining after aspiration had starch levels that ranged from 55.6% (VA96-44-304, 2 min) to 66.1% (Atlantic, 3 min) (Table 3).

DISCUSSION

Previous interest in using barley as a potential feedstock for fuel ethanol production[6] led to the development of methods to create more efficient, high-starch ethanol feedstocks from hulled barley using a precision dehulling process.[28] Occasionally, barley kernels may contain high levels of the mycotoxin DON, and while such kernels can be used to make fuel ethanol, the DON concentrates in the ethanol coproduct DDGS, making it unmarketable. DDGS sales are critical for an ethanol plant's economic viability. In this report, we compared the abilities of two milling strategies (roller mill and FitzMill precision mill) to remove DON-contaminated hull-enriched tissue from winter barley, while preserving starch levels in the kernel. This work was based on the report that the FitzMill offers a simple process for dehulling hulled barley to produce a dehulled kernel with higher starch content[28] and other reports that have shown DON accumulating in the hull and peripheral regions of the kernel.[17−20]

Roller Mill vs Precision Mill. In our study, the roller mill removed a smaller mass of hull-enriched tissue from the kernel (Figure 1) and yielded endosperm-enriched fractions with larger concentrations of DON than the precision mill (Table 2). This result can be explained by the mechanics of the roller mill and precision mill systems. The roller mill is a common milling technique[27,34] that involves running kernels between multiple corrugated rolls and does not result in localized hull tissue removal, resulting in ground grain (Figure S1a, in the SI) that requires multiple flows and/or sieving steps[27] to separate hull from endosperm. In contrast, the precision mill system uses sharp blades that shear the barley, swiping the kernels parallel to the central axis and lifting the hull from the kernel resulting in an intact, dehulled kernel (Figure S1d and e [SI], kernel and hull processed in the precision mill, respectively).[28]

The precision mill had a 2-fold effect of reducing DON (Table 1) and increasing the starch concentration in the endosperm-enriched fractions relative to the results with the roller mill (Table 2), which is important for fuel ethanol production. Hicks et al.[28] reported that Thoroughbred, a hulled barley cultivar, processed in the precision mill resulted in hull mass fractions of ∼14% that were composed of less than 6% starch, which corresponded to less than 1.5% starch loss from the original kernel. However, in our study with five other barley genotypes, the precision mill removed much more mass than seen with Thoroughbred. On average, the precision mill removed a mass of 23.1% (hull-enriched fraction) while the roller mill resulted in only a 12.2% mass removal (Figure 1). Therefore, while the precision mill resulted in much lower DON levels in the endosperm-enriched fractions by removing more hull-enriched tissue (Table 1), the precision mill resulted in higher starch losses (Table 2). Hull-enriched fractions collected from the roller mill and precision mill, contained starch levels that ranged from 7.2% to 11.1% and 13.5% to 30.0% (Table 2), respectively. To calculate the amount of starch lost when the hull is removed, the starch contents in the hull-enriched fraction and endosperm-enriched fraction were adjusted on the basis of their respective percent mass fraction, and then the proportion of starch in the hull (i.e., the adjusted starch value in the hull-enriched fraction) relative to total starch was calculated. An evaluation of starch levels adjusted on the basis of the mass fraction showed that grain processed in the roller mill yielded an average of 49.5 g of starch per 100 g of kernel versus 47.1 g of starch per 100 g of kernel for grain processed in the precision mill. The average starch lost to the hull was 2.1% from grain processed in the roller mill and an average of 9.6% starch loss from grain processed in the precision mill (Table 2). This level of starch loss was larger than the previously reported starch loss of 1.5%.[28] Thus, comparison of the two milling strategies certainly demonstrated that the precision mill system is able to remove more DON (Table 1) than the roller mill (Table 1), but at the expense of starch loss (Table 2) for these genotypes. Consequently, to make up for starch loss, additional grain may have to be processed; however, using grain containing little DON would improve the quality of the DDGS and obviously be favored over starch losses observed when using the precision mill system.

Time Course Precision Milling. Since more endosperm-enriched tissue and starch were removed from the kernel during precision milling (Figure 1 and Table 2) than expected, a time course experiment was conducted by running the precision mill at increments of one min (2, 3, 4, or 5 min) using whole kernels from three of the five barley genotypes tested in the first experiment (Nomini, Atlantic, and VA96-44-304). Time course precision milling conducted at shorter run times provided fractions with improved percent mass values for which mass loss was reduced from the endosperm-enriched fraction into the hull-enriched fraction (Figure 2). A 2 min run time produced hull-enriched mass fractions that were closest to those reported in Hicks et al.[28] In the first precision mill experiment (Figure 1), the hull-enriched percent mass fraction for Nomini (16.0%), Atlantic (29.2%), and VA96-44-304 (29.2%) were reduced to 8.2%, 12.3%, and 17.8% at 2 min, respectively (Figure 2). Other examples of using milling to reduce DON include work using a semi-industrial semolina mill, which demonstrated a 45% loss of DON when 10% of the grain tissue was removed[22] and 66% DON reduction after 15 s of pearling using an abrasive type dehulling procedure when 15% of the grain mass was removed.[25] In our study, hull-enriched mass fractions of 10% and 15% corresponded to a

51% and 68% reduction of DON, respectively (Figure 5). Although we were able to reduce the mass lost during milling by reducing the run time, DON levels correspondingly increased, and the starch concentration decreased. DON levels in the endosperm-enriched fractions were as much as 4-fold higher (5.1 μg g^{-1} (5 min) vs 19.8 μg g^{-1} (2 min) for VA96-44-304) (data not shown) and starch concentrations were as much as 8.7% lower at 2 min (55.9%) versus 5 min (61.2% for VA96-44-304) (data not shown). Starch lost during milling was reduced with lower run times; however, even at 2 min the percent starch lost was still higher than 1.5%, with values of 2.3%, 6.2%, and 9.0% for barley genotypes Nomini, Atlantic, and VA96-44-304, respectively (Figure 4).

The results of this work were unexpected as we were not able to produce endosperm-enriched fractions from the precision mill with reduced losses in grain mass and reduced starch loss as those reported previously.[28] Hicks' group conducted their analysis using the Virginia winter barley genotype Thoroughbred, which was harvested in 2005, and may explain some of the differences between studies. Phenotypic differences between genotypes,[14,15] seasonal differences in FHB disease levels,[15] and grain quality and composition[6] may also impact kernel characteristics such as starch content and hull removal potential. Years with low FHB may yield unadulterated kernels with unaltered starch concentrations. In contrast, years with high FHB may yield kernels with reduced starch and brittle hulls that may fall off easily in the mill, leading to unintended removal of endosperm tissue.[3] These reasons, as well as differences in disease levels that may occur between plots of the same genotype in a given year, may help explain any high standard deviations seen with some of the data, such as the observations for the Atlantic genotype in the first milling experiment. A correlation analysis of data in this study revealed that concentrations of DON in the whole kernels were significantly correlated with the hull percent mass fractions (roller mill: $r = 0.81$, $P < 0.0001$; precision mill: $r = 0.86$, $P < 0.0001$). We also wanted to test the hypothesis that during precision milling some components of the endosperm-enriched tissue were included in the hull-enriched fraction and that some hull-enriched components were included in the endosperm-enriched fraction. Therefore, we aspirated these samples in an attempt to improve fraction purity. Following aspiration of time course, precision-milled samples, hull-enriched fractions were found to contain endosperm-enriched components at percent mass fractions that ranged from 18.5% (Nomini, 5 min) to 30.1% (VA96-44-304, 5 min) and endosperm-enriched fractions were found to contain hull-enriched components at percent mass fractions that ranged from 3.3% (VA96-44-304, 3 min) to 10.0% (Nomini, 3 min) (Table 3). This confirmed that cross contamination of milling fractions occurs when the precision mill is abrading the surface of the kernel to remove the hull, it is also removing some endosperm.

The hypothesis that milling will reduce DON levels was demonstrated with the removal of the hull-enriched tissue in the first experiment (Table 1, Figure 3), and we were able to further reduce the concentration of DON by aspirating the endosperm-enriched fractions to remove contaminating hull-enriched tissue. At the 2 min mark, DON was reduced in aspirated samples from 12.2 μg g^{-1} to 2.8 μg g^{-1} (Nomini), 9.9 μg g^{-1} to 3.5 μg g^{-1} (Atlantic), and 19.8 μg g^{-1} to 6.5 μg g^{-1} (VA96-44-304) (Table 3). Aspiration of the hull-enriched fractions from the time course, precision mill experiment revealed that the endosperm-enriched components in the hull-enriched fraction are highly contaminated with DON, while the purified hulls contained DON at relatively low levels (Table 3). This was in contrast to our initial understanding that DON accumulates in the barley hull, which was based on our first set of dehulling experiments and previous work[17,18] but is consistent with the results from Rios et al.[35] This group reported that the finest particles of semolina from durum wheat have a 3−5-fold increase in DON concentration and may indicate the need to control the distribution of these fine particles during milling.[35] Thus, while aspiration of endosperm-enriched tissue yielded a more pure endosperm-enriched fraction with reduced DON, it is unlikely that the aspiration process will be used in a dry grind ethanol plant to salvage starch lost to the hull-enriched fractions, which we found to be highly contaminated with DON. A more likely scenario is dehulling for roughly 6 min in the precision mill, using the more than 75% mass of endosperm for ethanol production (Figure 1), and burning the remaining DON contaminated hull-enriched fraction to generate energy for the plant. This process would improve the resultant DDGS by generating a coproduct with little DON and would improve the economics of fuel ethanol production. Also relevant to DDGS production is protein content in the milled grain. Prior work, reported that after 10 min using the precision mill system, the amount of protein in the processed kernel stayed relatively constant at about 8%.[28] Similarly, the protein content in our time course experiment stayed relatively even from two to 5 min with endosperm-enriched fractions containing protein on average of about 9.5% (data not shown). Future research efforts should focus on elucidating the distribution of DON in barley and methods to isolate and remove the highly contaminated endosperm-enriched tissue, while maximizing starch retention in barley and other cereal grains.

Commercial mills may be able to leverage the milling strategies described here for mitigating DON. When DON levels are of concern or exceed acceptable limits, millers could follow the milling guidelines presented in this study and modify their mill settings or separate products from different mill streams to minimize DON content in their finished products. Such strategies, however, may be linked in part to knowledge of the genotype/variety of barley that will be processed. If mills are primarily interested in using barley as a feedstock that is high in starch (e.g., for fuel ethanol production), then the comparative information presented here should be of value for maximizing the amount of desired product (flour or dehulled grain) versus byproducts (hulls), regardless of DON.

■ ASSOCIATED CONTENT

Ⓢ Supporting Information

This material is available free of charge via the Internet at http://pubs.acs.org.

■ AUTHOR INFORMATION

Corresponding Author

*Email: dschmale@vt.edu. Telephone: (540) 231-6943. Fax: (540) 231-7477.

Author Contributions

For correspondence about DON analyses conducted in this work, please contact D.G.S. For correspondence about milling methods used in this work, please contact K.B.H. For correspondence about specific barley genotypes used in this work, please contact C.A.G.

Funding

This work was supported primarily by a grant to David G. Schmale (D.G.S.), Carl A. Griffey (C.A.G.), and Kevin B. Hicks (K.B.H.) from the Biodesign and Bioprocessing Research Center at Virginia Tech (Project #208-11-110A-012-331-1). Grants to D.G.S. by the Maryland Grains Producers Utilization Board (Proposal #10121612), the Virginia Agricultural Council (Proposal #10183402), the Virginia Small Grains Board (Proposal #10278306) and the United States Wheat and Barley Scab Initiative (Proposal #07185403) also provided support for the work. The conclusions presented here are those of the authors and do not necessarily reflect the views of the United States Department of Agriculture. Mention of trade names or commercial products in this article is solely for the purpose of providing specific information and does not imply recommendation or endorsement by the USDA.

Notes

The authors declare no competing financial interest.

■ ACKNOWLEDGMENTS

The authors thank Michael Kurantz and Robyn Moten for conducting the compositional analysis of the barley fractions.

■ ABBREVIATIONS

ANOVA: analysis of variance; DDGS: distillers dried grains with solubles; DON: deoxynivalenol; DWB: dried weight basis; FHB: fusarium head blight; GC-MS: gas chromatography–mass spectrometry; LOQ: limit of quantitation; SIM: selected ion monitoring; TMCS: trimethylchlorosilane; TMSI: *N*-trimethylsilylimidazole

■ REFERENCES

(1) Goswami, R. S.; Kistler, H. C. Heading for disaster: *Fusarium graminearum* on cereal crops. *Molecular Plant Pathology* **2004**, *5*, 515–525.

(2) Jansen, C.; von Wettstein, D.; Schafer, W.; Kogel, K. H.; Felk, A.; Maier, F. J. Infection patterns in barley and wheat spikes inoculated with wild-type and trichodiene synthase gene disrupted Fusarium graminearum. *Proc. Natl. Acad. Sci. U.S.A.* **2005**, *102*, 16892–7.

(3) McMullen, M.; Jones, R.; Gallenberg, D., Scab of Wheat and Barley: A Re-emerging Disease of Devastating Impact. *Plant Disease* **1997**, *81*.

(4) McLaughlin, C. S.; Vaughn, M. H.; Campbell, J. M.; Wei, C. M.; Stafford, M. E.; Hansin, B. S. Inhibition of protein synthesis by trichothecenes. *Mycotoxins Hum. Anim. Health, Proc. Conf.* **1977**, *19*, 263–273.

(5) Peska, J. J. Deoxynivalenol: toxicity, mechanisms and animal health risks. *Animal Feed Sci. Technol.* **2007**, *137*, 283–298.

(6) Griffey, C.; Brooks, W.; Kurantz, M.; Thomason, W.; Taylor, F.; Obert, D.; Moreau, R.; Flores, R.; Sohn, M.; Hicks, K. Grain Composition of Virginia winter barley and implications for use in feed, food, and biofuels production. *J. Cereal Sci.* **2010**, *51*, 41–49.

(7) Khatibi, P. A.; Montanti, J.; Nghiem, N. P.; Hicks, K. B.; Berger, G.; Brooks, W. S.; Griffey, C. A.; Schmale, D. G., III. Conversion of deoxynivalenol to 3-acetyldeoxynivalenol in barley-derived fuel ethanol co-products with yeast expressing trichothecene 3-O-acetyltransferases. *Biotechnol. Biofuels* **2011**, *4*, 26.

(8) Schaafsma, A. W.; Limay-Rios, V.; Paul, D. E.; Miller, J. D. Mycotoxins in fuel ethanol co-products derived from maize: a mass balance for deoxynivalenol. *J. Sci Food Agric.* **2009**, *89*, 1574–80.

(9) Madson, P. W.; Monceaux, D. A. *Fuel Ethanol Production*; KATZEN International Inc: Cincinnati, OH, 1995.

(10) Binder, E. M. Managing the risk of mycotoxins inmodern feed production. *Anim. Feed Sci. Technol.* **2007**, *133*, 149–166.

(11) Diaz-Llano, G.; Smith, T. K. Effects of feeding grains naturally contaminated with Fusarium mycotoxins with and without a polymeric glucomannan mycotoxin adsorbent on reproductive performance and serum chemistry of pregnant gilts. *J. Anim Sci.* **2006**, *84*, 2361–6.

(12) Stepanik, T.; Kost, D.; Nowicki, T.; Gaba, D. Effects of electron beam irradiation on deoxynivalenol levels in distillers dried grain and solubles and in production intermediates. *Food Addit. Contam.* **2007**, *24*, 1001–6.

(13) Magan, N.; Aldred, D. Post-harvest control strategies: minimizing mycotoxins in the food chain. *Int. J. Food Microbiol.* **2007**, *119*, 131–9.

(14) Khatibi, P. A.; Berger, G.; Liu, S.; Brooks, W. S.; Griffey, C. A.; Schmale, D. G. Resistance to Fusarium head blight and deoxynivalenol accumulation in Virginia barley. *Plant Dis.* **2011**, *96*, 279–284.

(15) Berger, G.; Green, A.; Khatibi, P.; Brooks, W.; Rosso, L.; Liu, S.; Griffey, C.; Schmale, D. Characterization of Fusarium head blight (FHB) resistance and deoxynivalenol accumulation in hulled and hulless winter barley. *Plant Dis.* **2014**, *98*, 599–606.

(16) Taketa, S.; Amano, S.; Tsujino, Y.; Sato, T.; Saisho, D.; Kakeda, K.; Nomura, M.; Suzuki, T.; Matsumoto, T.; Sato, K.; Kanamori, H.; Kawasaki, S.; Takeda, K. Barley grain with adhering hulls is controlled by an ERF family transcription factor gene regulating a lipid biosynthesis pathway. *Proc. Natl. Acad. Sci. U.S.A.* **2008**, *105*, 4062–7.

(17) Clear, R. M.; Patrick, S. K.; Nowicki, T.; Gaba, D.; Edney, M.; Babb, J. C. The effect of hull removal and pearling on *Fusarium* species and trichothecenes in hulless barley. *Can. J. Plant Sci.* **1997**, *77*, 161–166.

(18) Legzdina, L.; Buerstmayr, H. Comparison of infection with *Fusarium* head blight and accumulation of mycotoxins in grain of hulless and covered barley. *Cereal Sci.* **2004**, *40*, 61–67.

(19) Lee, U.-S.; Jang, H.-S.; Tanaka, T.; Oh, Y.-J.; Cho, C.-M.; Ueno, Y. Effect of milling on decontamination of *Fusarium* mycotoxins nivalenol, deoxynivalenol, and zearalenone in Korean wheat. *J. Agric. Food Chem.* **1987**, *35*, 126–129.

(20) Trigo-Stockli, D. M.; Deyoe, C. W.; Satumbaga, R. F.; Pedersen, J. R. Distribution of deoxynivalenol and zearalenone in milled fractions of wheat. *Cereal Chem.* **1996**, *73*, 388–391.

(21) Fandohan, P.; Ahouansou, R.; Houssou, P.; Hell, K.; Marasas, W. F.; Wingfield, M. J. Impact of mechanical shelling and dehulling on Fusarium infection and fumonisin contamination in maize. *Food addit. contam.* **2006**, *23*, 415–21.

(22) Rios, G.; Pinson-Gadais, L.; Abecassis, J.; Zakhia-Rozis, N.; Lullien-Pellerin, V. Assessment of dehulling efficiency to reduce deoxynivalenol and *Fusarium* level in durum wheat grains. *J. Cereal Sci.* **2009**, *49*, 387–392.

(23) Dexter, J. E.; Marchylo, B. A.; Clear, R. M.; Clarke, J. M. Effect of Fusarium head blight on semolina milling and pasta-making quality of durum wheat. *Cereal Chem.* **1997**, *74*, 519–525.

(24) Dexter, J. E.; Clear, R. M.; Preston, K. R. Fusarium head blight: effect on the milling and baking of some Canadian wheats. *Cereal Chem.* **1996**, *73*, 695–701.

(25) House, J. D.; Nyachoti, C. M.; Abramson, D. Deoxynivalenol removal from barley intended as swine feed through the use of an abrasive pearling procedure. *J. Agric. Food Chem.* **2003**, *51*, 5172–5175.

(26) Trenholm, H. L.; Charmley, L. L.; Prelusky, D. B.; Warner, R. M. Two physical methods for the decontamination of four cereals contaminated with deoxynivalenol and zearalenone. *J. Agric. Food Chem.* **1991**, *39*, 356–360.

(27) Flores, R. A.; Hicks, K. B.; Eustace, D. W.; Phillips, J. High-starch and high-β-glucan barley fractions milled with experimental mills. *Cereal Chem.* **2005**, *82*, 727–733.

(28) Hicks, K. B.; Wilson, J.; Flores, R. A., Progressive hull removal from barley using the Fitzpatrick comminuting mill. *Appl. Eng. Agric.* **2011**, *27*.

(29) Mirocha, C. J.; Kolaczkowski, E.; Xie, W.; Yu, H.; Jelen, H. Analysis of deoxynivalenol and its derivatives (batch and single kernel) using gas chromatography/mass spectrometry. *J. Agric. Food Chem.* **1998**, *46*, 1414–1418.

(30) Tacke, B. K.; Casper, H. H. Determination of deoxynivalenol in wheat, barley, and malt by column cleanup and gas chromatography with electron capture detection. *J. AOAC Int.* **1996**, *79*, 472−5.
(31) Lagana, A.; Curini, R.; D'Ascenzo, G.; De Leva, I.; Faberi, A.; Pastorini, E. Liquid chromatography/tandem mass spectrometry for the identification and determination of trichothecenes in maize. *Rapid Commun. Mass Spectrom.* **2003**, *17*, 1037−43.
(32) Rodrigues-Fo, E.; Mirocha, C. J.; Xie, W.; Krick, T. P.; Martinelli, J. A. Electron ionization mass spectral fragmentation of deoxynivalenol and related tricothecenes. *Rapid Commun. Mass Spectrom.* **2002**, *16*, 1827−35.
(33) AACC, Approved method 76-13. In *Total Starch Assay Procedure (Megazyme Amyloglucosidase/alpha/Amylase Method)*, AACC International: 10th ed. St. Paul, MN, 2000.
(34) Izydorczyk, M. S.; Dexter, J. E.; Desjardins, R. G.; Rossnagel, B. G.; Lagasse, S. L.; Hatcher, D. W. Roller milling of Canadian hull-less barley: Optimization of roller milling conditions and composition of mill streams. *Cereal Chem.* **2003**, *80*, 637−644.
(35) Rios, G.; Zakhia-Rozis, N.; Chaurand, M.; Richard-Forget, F.; Samson, M. F.; Abecassis, J.; Lullien-Pellerin, V. Impact of durum wheat milling on deoxynivalenol distribution in the outcoming fractions. *Food Addit. Contam.* **2008**, *26*, 487−496.

JOURNAL OF AGRICULTURAL AND FOOD CHEMISTRY

Article

pubs.acs.org/JAFC

Enhanced Biocontrol Activity of *Rhodotorula mucilaginosa* Cultured in Media Containing Chitosan against Postharvest Diseases in Strawberries: Possible Mechanisms Underlying the Effect

Hongyin Zhang,*[,†] Lingling Ge,[‡] Keping Chen,[‡] Lina Zhao,[†] and Xiaoyun Zhang[†]

[†]College of Food and Biological Engineering, Jiangsu University, Zhenjiang 212013, Jiangsu People's Republic of China

[‡]Institute of Life Sciences, Jiangsu University, Zhenjiang 212013, Jiangsu People's Republic of China

ABSTRACT: The effect of *Rhodotorula mucilaginosa* cultured in media containing chitosan on its antogonistic activity against postharvest diseases of strawberries and the possible mechanisms involved are discussed. Two-dimensional gel electrophoresis were applied in the analysis of the proteins of *R. mucilaginosa* in response to chitosan. Compared with the application of *R. mucilaginosa* alone, the biocontrol efficacy of the yeast combined with 0.5% chitosan was enhanced greatly, with significant increase in chitinase activity of antagonistic yeast, polyphenoloxidase, peroxidase, phenylalanine ammonia lyase, chitinase and β-1,3-glucanase activity, and with an inhibition of lipid peroxidation of strawberries. The population of *R. mucilaginosa* harvested from NYDB amended with chitosan at 0.5% increased rapidly in strawberry wounds compared with those harvested from NYDB without chitosan. In the cellular proteome, several differentially expressed proteins were identified, most of which were related to basic metabolism.

KEYWORDS: *chitosan, Rhodotorula mucilaginosa, antagonistic activity, strawberries, differentially expressed proteins*

INTRODUCTION

Rhizopus stolonifer and *Botrytis cinerea* are two of the most destructive fungi of strawberries which can cause *Rhizopus* decay and gray mold separately.[1] Due to these diseases, tremendous economic losses are caused. Traditionally, *R. stolonifer* and *B. cinerea* are controlled mainly by treatment with synthetic fungicides. However, with deeper research, gradually developed fungicide resistance in pathogens were detected and potential harmful effects on human health and the environment were perceived, which leads to an urgent demand for alternative control approaches with good efficacy, low residues, and ensured safety.[2]

Biological control with antagonistic yeasts has emerged as a potential method to reduce synthetic fungicide usage.[2,3] Phylloplane yeast *Rhodotorula mucilaginosa* combined with fungicides has been reported to effectively control *Botrytis cinerea* on geranium seedlings.[4] Our research team found that *Rhodotorula mucilaginosa* showed biocontrol efficacy against blue mold and gray mold of apples caused by *Penicillium expansum* and *B. cinerea*, respectively.[5] However, making biological control a practical way requires the enhancement of the consistency and efficacy of antagonistic yeasts (including *R. mucilaginosa*) in controlling postharvest diseases.[2,6]

Many attempts have been proposed to improve the performance of postharvest biocontrol yeasts. Besides combining antagonists with some exogenous substances (organic and inorganic additives),[2,6−9] combination with some physiological manipulation may also be an effective way.[2] For example, Teixido et al. (1998) found that the cultivation of the yeast in a low water activity modified liquid media can improve the biocontrol efficacy of *Candida sake*.[10] According to Li and Tian (2006), induced accumulation of internal trehalose could improve both the viability and biocontrol activity of *Cryptococcus laurentii* under stresses of low temperature and controlled atmosphere.[11] Recently, it has reported that the combination with chitin in the culture media may increase the bicontrol activity of *C. laurentii* significantly.[12]

Chitosan, a high molecular weight β-(1,4)-glucosamine polymer, produced from the chitin components by deacetylation, which is the second most abundant polysaccharide found in nature, is an important structural component of the cell wall of some plant-pathogenic fungi.[13] It has been demonstrated to be nontoxic and safe to animals and hold great potential for food applications with its unique physiological and biological properties.[14−16] Chitosan has been shown to form an ideal coating on fruit and also have antifungal activity against a wide range of fungal pathogens.[17] Li and Yu (2001) found that chitosan could reduce the incidence of brown rot caused by *Monilinia fructicola* significantly and delay the development of disease compared with the control.[18] Moreover, Yu et al. (2007) reported that combination of chitosan and antagonistic yeast *C. laurentii* resulted in a synergistic inhibition of the blue mold rot.[19] However, to our knowledge, there is no report referring to enhancing the biocontrol efficacy of antagonistic yeast against postharvest disease by addition of chitosan to the growth media and the mode of action involved.

The objective of this study was to determine the impact of adding chitosan in the culture media on the efficacy of the *R. mucilaginosa* against *Rhizopus* decay, gray mold decay, and natural decay of strawberries and discuss the possible physiological and molecular mechanisms involved.

Received: January 7, 2014
Revised: April 13, 2014
Accepted: April 13, 2014
Published: April 14, 2014

ACS Publications © 2014 American Chemical Society

dx.doi.org/10.1021/jf500065n | *J. Agric. Food Chem.* 2014, 62, 4214−4224

MATERIALS AND METHODS

Fruits Material. Strawberries (*Fragaria ananassa* Duch.) cultivars "fengxiang" were harvested early in the morning and rapidly transferred to the laboratory. Berries were sorted on the basis of size, ripeness, and blemishes such as injuries or infections.

Chitosan. Chitosan with 90% deacetylation was bought from Sangon Company (shanghai, China) .

Antagonist and Growth Conditions. The yeast antagonist *Rhodotorula mucilaginosa* was isolated from the surfaces of peach blossom which was picked in unsprayed orchards. The yeast was first identified by a VITEK 32 Automicrobic system (BioMérieux Company, Marcy l'Etoile, France). To identify the yeast, sequence analysis of the 5.8S internal transcribed spacer (ITS) rDNA (rDNA) region was used.[20] In animal tests, including physiology experiments, acute toxicity studies, and the Ames test, *R. mucilaginosa* was demonstrated to be safe (our unpublished data). *R. mucilaginosa* isolates were maintained at 4 °C on nutrient yeast dextrose agar (NYDA) medium (8 g og nutrient broth, 5 g of yeast extract, 10 g of glucose, and 20 g of agar in 1 L of distilled water). Liquid cultures of the yeast were grown in 250 mL Erlenmeyer flasks containing 50 mL of nutrient yeast dextrose broth (NYDB) which had been inoculated with a loop of the culture. Flasks were incubated on a QYC-200 rotary shaker (FuMa, China) at 28 °C for 20 h. After incubation, cells were harvested by centrifugation at 7000*g* for 10 min by using a TGL-16 M centrifuge (XiangYi, China) and washed twice with sterile distilled water in order to remove the residual medium. Then the yeast cell pellets were resuspended in sterile distilled water, counted using a JSQA hemocytometer (HongTai, China), and adjusted to an initial concentration of 5×10^8 cells mL^{-1}. Then 1 mL of the above-mentioned yeast suspensions were added to nutrient yeast dextrose broth (NYDB) or NYDB amended with chitosan at different concentrations (0.01%, 0.1%, 0.25%, 0.5%, 1%) (NYDB + chitosan) on a rotary shaker at 200 rpm at 28 °C for 24 h. After incubation, centrifuged the yeast cells at 7000*g* for 10 min and washed twice with sterile distilled water. Cell pellets were resuspended and counted as described above and adjusted to a concentration of 1×10^8 cells mL^{-1}. Besides, the growth media was filtered through a Millipore membrane (0.45 μm) and the supernatant was used for biocontrol and chitinase activity assay.

Fungal Pathogen and Growth Conditions. The pathogen *Rhizopus stolonifer* (Ehrenb.: Fr) Vuill. and *Botrytis cinerea* (Pers.: Fr.) were isolated from infected strawberries. The organisms were identified according to their cultural and micro- and macroscopic morphological characteristics. These cultures were maintained on potato dextrose agar (PDA) media (containing the extract from 200 g of boiled potato, 20 g of glucose, and 20 g of agar in 1 L of distilled water) at 4 °C. Before use, the mold should be activated on PDA at 25 °C. Spore suspensions were prepared by removing the spores from the sporulating edges of a 7 day old culture with a bacteriological loop and suspending them in sterile distilled water. After counting with a hemocytometer, the spore concentration was adjusted to a required concentration.

Effects of Chitosan on Biocontrol of *R. mucilaginosa* to *Rhizopus* Decay and Gray Mold Decay of Strawberries. The surface of strawberries was wounded using a sterile cork borer (approximately 3 mm diameter and 3 mm deep) and treated with 30 μL of following solution: (1) the cell suspensions of *R. mucilaginosa* (1×10^8 cells mL^{-1}) which were harvested either from the media of NYDB or NYDB + chitosan at different concentrations (0.01%, 0.1%, 0.25%, 0.5%, 1%); (2) sterile distilled water as the control. Two hours later, 30 μL of *R. stolonifer* suspensions (1×10^4 spores mL^{-1}) or *B. cinerea* suspensions (1×10^5 cells mL^{-1}) were added into each wound of strawberries. After air-drying, the samples were put in trays sealed with plastic film. Then the samples in the trays were incubated at 20 °C and a high relative humidity (about 95%). The number of the infected fruits and their lesion diameters were observed after 3 d inoculation. There were three replicates per treatment and 18 fruits in each replicate. All treatments were arranged in a randomized complete block design, and the experiment was conducted twice.

Efficacy of Cell-Free Culture Filtrate of *R. mucilaginosa* Incubated in Different Media in Controlling *Rhizopus* Decay and Gray Mold Decay of Strawberries. Fresh fruits were treated as described above to evaluate the efficacy of *R. mucilaginosa* harvested from different media in the control of the *Rhizopus* decay and gray mold decay of strawberries. Then 30 μL of following solution were added in each wound of fruits: (1) a solution of cell-free filtered supernatant through a Millipore membrane (0.45 μm) from the media of NYDB or NYDB + chitosan at different concentrations (0.01%, 0.1%, 0.25%, 0.5%, 1%), (2) sterile distilled water as the control. Two hours later, 30 μL of *R. stolonifer* suspensions (1×10^4 spores mL^{-1}) or *B. cinerea* suspensions (1×10^5 cells mL^{-1}) were added into each wound. After air-drying, the samples were put in trays sealed with plastic film. Then the samples in the trays were incubated at 20 °C and a high relative humidity (about 95%). The number of the infected fruits and their lesion diameters were examined after 3 d inoculation. There were three replicates per treatment and 18 fruits in each replicate. All treatments were arranged in a randomized complete block design, and the experiment was conducted twice.

Effects of Chitosan on Biocontrol Efficacy of *R. mucilaginosa* to Natural Decay Development of Strawberries. To inoculate yeast on fruits, dipping them in the cell suspensions of (1) *R. mucilaginosa* (1×10^8 cells mL^{-1}) harvested from the media of NYDB, (2) *R. mucilaginosa* (1×10^8 cells mL^{-1}) harvested from the media of NYDB + chitosan at different concentrations (0.01%, 0.1%, 0.25%, 0.5%, 1%), and (3) sterile distilled water as the control respectively for 30 s, then air-dried. The treated fruits were sealed separately in polyethylene-lined plastic boxes to retain high humidity. Fruits were stored at 4 °C for 20 d, after that, transferred them to the condition at 20 °C for 7 d, which can determine the disease development under normal shelf life conditions. After observation, infection severity was recorded. There were three replicate trials of 20 fruits with a complete randomization in each test, and experiments were repeated twice.

Effects of Chitosan on Population Growth of *R. mucilaginosa* in Strawberry Wounds. Fruits were wounded as described above to evaluate the biocontrol efficacy against *Rhizopus* decay and gray mold decay of strawberries. Then 30 μL of 1×10^8 cells mL^{-1} *R. mucilaginosa* solution harvested either from NYDB or NYDB + 0.5% chitosan were added in each wound. At different times (0, 12, 24, 48, and 72 h) at 20 °C after the treatment, the samples were harvested. The tissue was removed with a sterile cork borer (9 mm diameter and 10 mm deep) and ground with a 150 mL Erlenmeyer flasks, grinding the sample pieces by a glass rod in 10 mL of sterile 0.85% sodium chloride solution. After that, serial 10-fold suitable dilutions were made and 0.1 mL of suitable dilution was spread in NYDA plates. The plates were incubated at 28 °C for 2 d, and the colonies were counted afterward. Population densities of *R. mucilaginosa* were expressed as log 10 CFU (colony-forming units) per wound. There were two replicates per treatment and 5 fruits per replicate, and the experiments were repeated twice.

Assay for Chitinase Activity of the Cell-Free Culture Filtrate of *R. mucilaginosa* Incubated in Different Growth Media. To determine the chitinase activity, a reaction mixture was prepared by adding 0.5 mL of 5 mg mL^{-1} colloidal chitosan containing 1.2 μmol sodiumazide and 56 μmol sodium acetate to 0.5 mL of enzyme supernatant.[21] The enzyme−substrate mixture was incubated at 37 °C for 2 h with constant shaking. After that, centrifuging at 7680*g* for 10 min was used to stop the reaction. Following the centrifuging, 0.5 mL of enzyme supernatant was incubated at 37 °C for 2 h with 0.1 mL of 3% (w/v) desalted snail gut enzyme (Sigma) and 0.1 mL of 1 mol L^{-1} potassium phosphate buffer (pH 7.1) to hydrolyze the chitosan oligomers.[22] The resulting *N*-acetyl-D-glucosamine(GlcNAc) was determined following the method described by Reissig et al. (1955) using internal standards of GlcNAc.[23] For the sample, substrate blanks and standard, each contained in a volume of 0.5 mL in a test tube, 0.1 mL of potassium tetraborate was added. The tubes were heated in a vigorously boiling water bath for exactly 3 min, and then the tubes were cooled in tap water. *p*-Dimethylaminobenzaldehyde (DMAB) reagent of 3 mL was added afterward, then they were mixed and placed in a bath at 37 °C. After precisely 20 min, the tubes were cooled

in tap water and read without delay at 585 nm. The specific activity was expressed as microgram of GlcNAc per milliliter. There were three replicates in each experiment. The experiment was conducted twice.

Effects of *R. mucilaginosa* Incubated in Different Growth Media on Strawberry Enzyme Activities and Lipid Peroxidation. Fruits were wounded as described above to evaluate the yeast biocontrol activity against *Rhizopus* decay and gray mold decay of strawberries. Then 30 μL of a cell suspension of *R. mucilaginosa* at 1×10^8 cells mL^{-1} harvested either from the media of NYDB or NYDB + 0.5% chitosan after the incubation for 24 h were added in each wound. Treatment with sterile distilled water was served as the control. After air-drying, the strawberries were put in trays sealed with plastic film. Then the samples in the trays were incubated at 20 °C and a high relative humidity (about 95%). At 0, 24, 48, and 72 h after treatment, samples were harvested. After removing the wound tissue with a sterile borer (6 mm diameter and 5 mm deep), the fresh tissue around the wound was picked up by another sterile borer (9 mm diameter and 10 mm deep). Two grams of the fresh tissue from six fruits was grounded with 10 mL of cold (4 °C) 50 mM different buffers containing 1.33 mmol per liter EDTA and 1% polyvinyl pyrolidone (PVPP) in a mortar and pestle to assay different enzymes: sodium acetate buffer (pH 5.0) for chitosanase and β-1,3-glucanase, sodium phosphate buffer (pH 6.4) for polyphenoloxidase (PPO), peroxidase (POD), and malondialdehyde (MDA) and borate buffer (pH 8.8) for phenylalanine ammonia lyase (PAL). The homogenates were centrifuged (4 °C) for 15 min at 12000*g*, and the supernatants were kept for the assay. There were three replicates per treatment. The experiment was conducted twice. The testing methods of enzyme activities were described as below.

The PPO activity was measured following the method described by Waite (1976) with some modifications.[24] First 0.1 mL of crude enzyme extract (supernatant extract) was added to 2.9 mL of catechol (50 mM sodium phosphate, pH 6.4, and 0.1 M catechol, incubated at 30 °C for 5 min) as a substrate. Then the change in absorbance at 398 nm was recorded once every 30 s for 3 min. The amount of the enzyme extract producing an increase of A_{398} by 0.01 in 1 min was defined as one unit of the PPO activity. The PPO enzyme activity was expressed as U per gram fresh weight (FW).

The POD activity was measured as the method described by Lurie et al. (1997) with some modifications, using guaiacol as a substrate.[25] The reaction mixture should be inoculated for 5 min at 30 °C, which containing 0.2 mL of crude enzyme extract, 2.2 mL of 0.3% guaiacol (prepared by 50 mM sodium phosphate buffer, pH 6.4, incubated at 30 °C for 5 min). Then 0.6 mL of 0.3% H_2O_2 (prepared by 50 mM sodium phosphate, pH 6.4, and incubated at 30 °C for 5 min) was added to initiate the reaction. The POD activity was determined by measuring at A_{470} once every 30 s for 3 min. A cuvette containing all components except added 0.6 mL of distilled water was used as a control. The POD activity was expressed as U per gram FW. One unit was defined as ΔA_{470} of 0.01 per min.

The PAL activity was assayed as the method described by Assis et al. (2001) with some modifications.[26] Simply, after preincubation of 3 mL of borate buffer (50 mM, pH 8.8) containing 10 mM L^{-1} phenylalanine for 10 min at 37 °C, 1 mL of crude enzyme extract was added. After mixing, the initial absorbance of the reaction mixture was immediately recorded at 290 nm. Then the reaction mixture was incubated at 37 °C. After 60 min, A_{290} was measured and recorded again. Calculating the difference value between the pre- and postabsorbance. The blank was a cuvette containing all components except 1 mL of distilled water was added. One unit of the PAL was defined as the formation of 1 μg of cinnamic acid equivalents per hour, and the specific activity was expressed as the U per gram FW.

The lipid peroxidation was determined in terms of MDA content by thiobarbituric acid (TBA) reaction as described by Du and Bramlage.[27] Briefly, 2 mL of 0.6% TBA in 20% trichloroacetic acid was added into 2 mL of crude enzyme sample. The solution was heated at 100 °C for 10 min, then quickly cooled in an ice-bath and centrifuged (4 °C) for 15 min at 10000*g*, and afterward the supernatants were harvested and assayed. The absorbance of supernatants was recorded at 532, 600, and 450 nm. MDA content was calculated according to the formula C_{MDA} (μmol L^{-1}) = $6.45 \times (A_{532} - A_{600}) - 0.56 \times A_{450}$ and expressed as μmol MDA g^{-1} FW.

Assay of chitinase activity of strawberries was determined as described above to evaluate the chitinase activity of different growth media, and the specific activity was expressed as the U per gram FW, one unit was defined as microgram of GlcNAc per hour.

β-1,3-Glucanase was assayed by measuring the amount of reducing sugar released from the substrate by the method reported by Ippolito et al., with some modifications.[28] A crude enzyme sample of 250 μL was routinely added to 250 μL of 0.2% laminarin (w/v) in 50 mM, pH 5.0, potassium acetate buffer, and incubated at 37 °C for 1 h. For the control, the same mixture was similarly diluted at zero incubation time. Then 1.5 mL of 3,5-dinitrosalicylate was added and boiled for 5 min on a water bath to stop the reaction, and the amount of reducing sugars was measured spectrophotometrically at 500 nm using a UV-1601 spectrophotometer (Shimadzu, Japan). The formation of 1 mg glucose equivalents per hour was defined as one unit of the β-1,3-glucanase activity, and the specific activity was expressed as the U per gram FW.

Protein Sample Preparation. Liquid cultures of the yeast were grown in NYDB or NYDB + 0.5% chitosan, respectively, as described above (Antagonist and Growth Conditions). The yeast cells were harvested from NYDB or NYDB + 0.5% chitosan by centrifuging at 10000*g* for 10 min (4 °C) and washed three times with cold double-distilled water to remove residual medium. The protein sample preparation for 2-DE, and image analysis were performed as described by Zhao et al.[29] Protein samples were kept at −70 °C until use. The protein concentration was determined according to Bradford's method using bovine serum albumin as standard.[30]

2-DE and Image Analysis. Two-dimensional electrophoresis (2-DE) and image analysis were performed as described by Wang et al.[31]

Protein In-Gel Digestion. Protein in-gel digestion was performed as described by Zhang et al.[32]

Protein Identification by MALDI-TOF/TOF and Database Query. Protein identification by MALDI-TOF/TOF and database query were performed as described by Wang et al.[31]

Statistical Analysis. The data were analyzed by the analysis of variance (ANOVA) using the statistical program SPSS/PC version II.x (SPSS Inc. Chicago, Illinois, USA). The Duncan's multiple range test was used for means separation. In addition, when the group of the data was two, the independent samples *t* test was applied for means separation. The statistical significance was assessed at the level $P = 0.05$.

RESULTS

Effect of Chitosan on Biocontrol of *R. mucilaginosa* to *Rhizopus* Decay and Gray Mold Decay of Strawberries. Compared with the control after 3 d storage at 20 °C, treatments of *R. mucilaginosa* at 1×10^8 cells mL^{-1} effectively controlled *Rhizopus* decay of strawberries (Figure 1, $P < 0.05$), and the application of chitosan at the concentration 0.5% during cultivation significantly improved the biocontrol efficacy of *R. mucilaginosa* compared with the cultivation without chitosan ($P < 0.05$).

Compared with the control after 3 d storage at 20 °C, *R. mucilaginosa* at 1×10^8 cells mL^{-1} cultivation in the NYDB had no impact on the disease incidence of gray mold decay (Figure 1, $P < 0.05$). However, treatments with application of *R. mucilaginosa* cultivation in the NYDB media amended with chitosan at all tested concentrations except 1% could reduce the disease incidence of gray mold decay of strawberries. The antagonistic activity of *R. mucilaginosa* was shown to be greatly enhanced through cultivation in the NYDB media amended with chitosan at the optimal concentration (0.5%) compared with that cultivated in NYDB without chitosan ($P < 0.05$).

Efficacy of Cell-Free Culture Filtrate of *R. mucilaginosa* Incubated in Different Media in Controlling *Rhizopus*

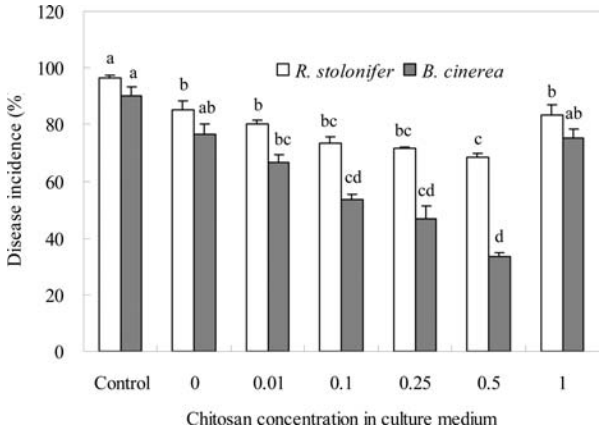

Figure 1. Effect of chitosan on biocontrol of *R. mucilaginosa* to *Rhizopus* decay and gray mold of strawberries. Fruit treatments are as follows: Control = sterile distilled water, 0 = *R. mucilaginosa* which were harvested from the media of NYDB (0.01%, 0.1%, 0.25%, 0.5%, 1%) = *R. mucilaginosa* which were harvested from the media of NYDB + chitosan at different concentrations (0.01%, 0.1%, 0.25%, 0.5%, 1%). Each value is the mean of two experiments. Bars represent standard deviations. Different letter indicates significant differences (P = 0.05) according to the Duncan's multiple range test.

Decay and Gray Mold Decay of Strawberries. The cell-free culture filtrates of *R. mucilaginosa* incubated in NYDB had no significant control efficacy on the *Rhizopus* decay and gray mold decay of strawberries after 3 d storage at 20 °C. However, compared with the control, the cell-free culture filtrates of NYDB media amended with 0.25% 0.5%, and 1% chitosan in which *R. mucilaginosa* was incubated for 24 h exhibited a significant control activity against *Rhizopus* decay in strawberry wounds after 3 d incubation at 20 °C (Figure 2). Similarly, the cell-free culture filtrates of NYDB media added with 0.5% chitosan significantly controlled the gray mold decay in strawberry wounds (Figure 2).

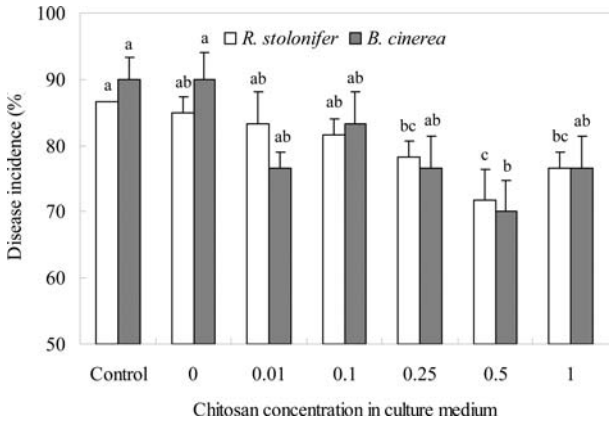

Figure 2. Effect of cell-free culture filtrate of *R. mucilaginosa* incubated in different media in controlling *Rhizopus* decay and gray mold decay of strawberries. Fruit treatments are as follows: Control = sterile distilled water, 0 = a solution of cell-free filtered supernatant from the media of NYDB (0.01%, 0.1%, 0.25%, 0.5%, 1%) = a solution of cell-free filtered supernatant from the media of NYDB + chitosan at different concentrations (0.01%, 0.1%, 0.25%, 0.5%, 1%). Each value is the mean of two experiments. Bars represent standard deviations. Different letter indicates significant differences (P = 0.05) according to the Duncan's multiple range test.

Effects of Chitosan on Biocontrol Efficacy of *R. mucilaginosa* to Natural Decay Development of Strawberries. Compared with the control after 20 d at 4 °C followed by 7 d at 20 °C, *R. mucilaginosa* at 1×10^8 cells mL^{-1} cultivated in the NYDB media had no impact on the natural decay incidence of strawberries (Figure 3). However, treatments with application of *R. mucilaginosa* cultivation in the NYDB media added with chitosan at all tested concentrations except 1% had a significantly biocontrol efficacy on the natural decay incidence of strawberries ($P < 0.05$). *R. mucilaginosa* cultivation in the NYDB media amended with 0.5% chitosan was the most effective in preventing natural decay development, which decreased the decay incidence of the fruit to 33.3% compared to 71.7% for the control and 58.9% for the *R. mucilaginosa* cultivation in the NYDB.

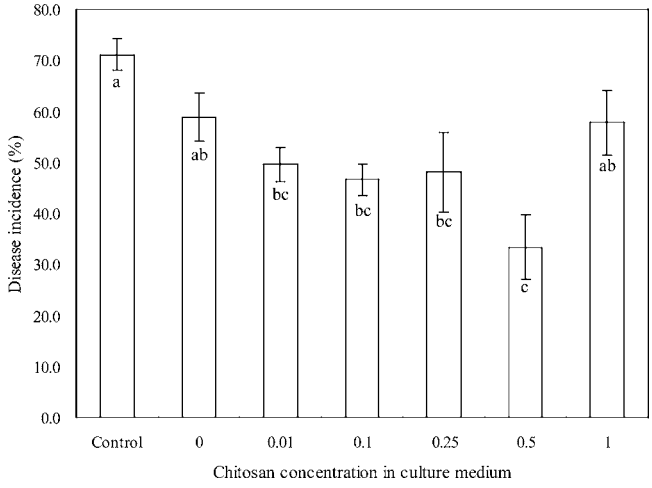

Figure 3. Effect of chitosan on biocontrol of *R. mucilaginosa* to natural decay of strawberries. Fruit treatments are as follows: Control = sterile distilled water, 0 = *R. mucilaginosa* which were harvested from the media of NYDB (0.01%, 0.1%, 0.25%, 0.5%, 1%) = *R. mucilaginosa* which were harvested from the media of NYDB + chitosan at different concentrations (0.01%, 0.1%, 0.25%, 0.5%, 1%). Each value is the mean of two experiments. Bars represent standard deviations. Different letter indicates significant differences (P = 0.05) according to the Duncan's multiple range test.

Effects of Chitosan on Population Growth of *R. mucilaginosa* in Strawberry Wounds. The antagonistic yeast *R. mucilaginosa*, whether cultivated in the NYDB or NYDB media amended with 0.5% chitosan, proliferated rapidly in strawberry wounds, especially during the first 24 h, and stabilized relatively thereafter (Figure 4). However, the population of *R. mucilaginosa* cultivated in NYDB amended with chitosan at 0.5% in strawberry wounds was higher than that of *R. mucilaginosa* cultivated in NYDB over the whole storage time except at 72 h ($P < 0.05$). Particularly, after 24 h of incubation in the wounds, the amount of *R. mucilaginosa* grown in chitosan-supplemented NYDB media was more than 3-fold higher than that of *R. mucilaginosa* grown in NYDB without chitosan.

Assay for Chitinase Activity of the Cell-Free Culture Filtrate of *R. mucilaginosa* Incubated in Different Growth Media. After 24 h incubation, the chitinase activity of the cell-free culture filtrates of *R. mucilaginosa* incubated in NYDB added with chitosan at 0.01, 0.5, and 1% had a higher level than that of *R. mucilaginosa* grown in NYDB. Especially

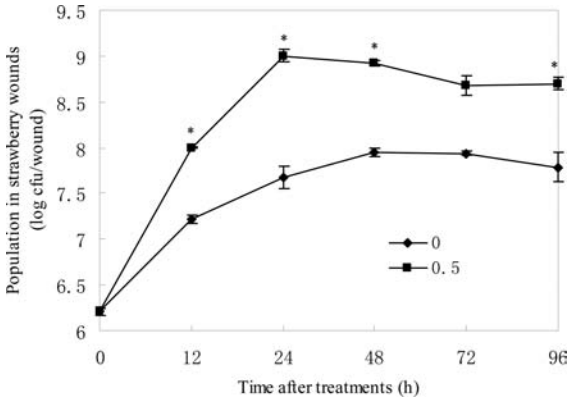

Figure 4. Effects of chitosan on population growth of *R. mucilaginosa* in strawberry wounds. 0 = *R. mucilaginosa* which were harvested from the media of NYDB 0.5% = *R. mucilaginosa* which were harvested from the media of NYDB + chitosan at the concentration of 0.5%. Bars represent standard errors. An asterisk (*) indicates significant differences ($P = 0.05$) according to the independent samples t test.

the chitinase activity of the cell-free culture filtrates incubated in NYDB with 0.5% chitosan had a higher level than that of the cell-free culture filtrates grown in NYDB amended with chitosan at other concentrations (Figure 5, $P < 0.05$). However,

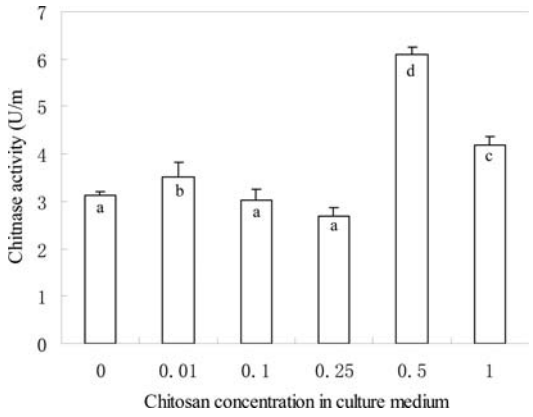

Figure 5. Chitinase activity of the cell-free culture filtrate of *R. mucilaginosa* incubated in media containing chitosan. Each value is the mean of two experiments. Bars represent standard deviations. Data in columns with different letters are statistically different according to Duncan's multiple range test at $P = 0.05$.

there was no significant difference of the chitinase activity between the cell-free culture filtrates of *R. mucilaginosa* grown in NYDB and the media added with 0.1 or 0.25% chitosan.

Effects of *R. mucilaginosa* Harvested from Different Media on PPO Activity of Strawberries. A peak of PPO activity of strawberries was exhibited in the treatment with *R. mucilaginosa* cultivated in the NYDB media amended with chitosan (0.5%) at 24 h after inoculation. However, after the decrease of the PPO activity at 24 h, it showed a following significant increase again after 48 h (Figure 6). On the other hand, no evident induction of PPO activity was observed in treatment with water or *R. mucilaginosa* cultivated in the NYDB throughout the whole storage period except at 72 h. It was obvious that the PPO activity of strawberries treated with *R. mucilaginosa* cultivated in the chitosan-supplemented media (0.5%) was higher than that of the control and that of strawberries treated with *R. mucilaginosa* cultivated in the

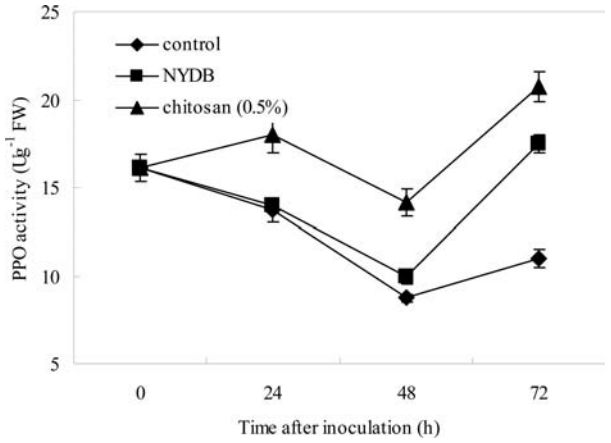

Figure 6. Effects of *R. mucilaginosa* harvested from different media on PPO activity of strawberries. Control = sterile distilled water, NYDB = *R. mucilaginosa* which were harvested from the media of NYDB, chitosan (0.5%) = *R. mucilaginosa* which were harvested from the media of NYDB + chitosan at the concentration of 0.5%. Each value is the mean of two experiments. Bars represent standard deviations.

NYDB without chitosan throughout the whole storage period (24, 48, and 72 h after inoculation).

Effects of *R. mucilaginosa* Harvested from Different Media on POD Activity of Strawberries. POD activity of strawberries treated with *R. mucilaginosa* cultivated in the chitosan-supplemented media (0.5%) and in the media of NYDB showed an uptrend within 48 h after inoculation, and, in the former, POD activity reached the highest peak at 72 h, while in the latter, almost no increase was observed after 48 h (Figure 7). The POD activity of the strawberries treated with *R.*

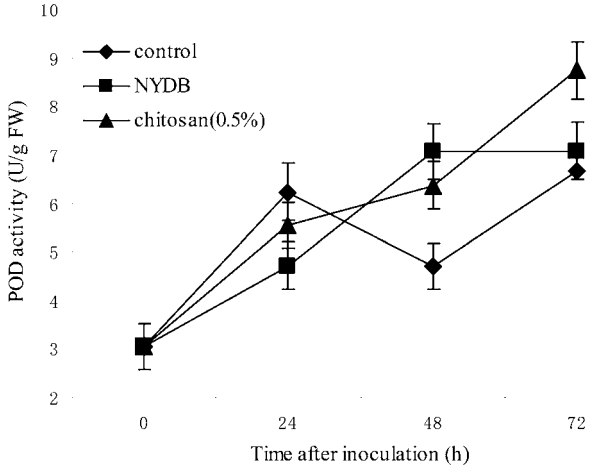

Figure 7. Effects of *R. mucilaginosa* harvested from different media on POD activity of strawberries. Control = sterile distilled water, NYDB = *R. mucilaginosa* which were harvested from the media of NYDB chitosan (0.5%) = *R. mucilaginosa* which were harvested from the media of NYDB + chitosan at the concentration of 0.5%. Each value is the mean of two experiments. Bars represent standard deviations.

mucilaginosa cultivated in the NYDB amended with chitosan (0.5%) was significantly higher than that of the control strawberries at 48 and 72 h.

Effects of *R. mucilaginosa* Harvested from Different Media on PAL Activity of Strawberries. Treatment with *R. mucilaginosa* cultivated in NYDB containing chitosan at 0.5% induced a peak of PAL activity of strawberries within 48 h after

inoculation and then decreased (Figure 8). Nevertheless, in the treatment with water or *R. mucilaginosa* cultivated in NYDB, no

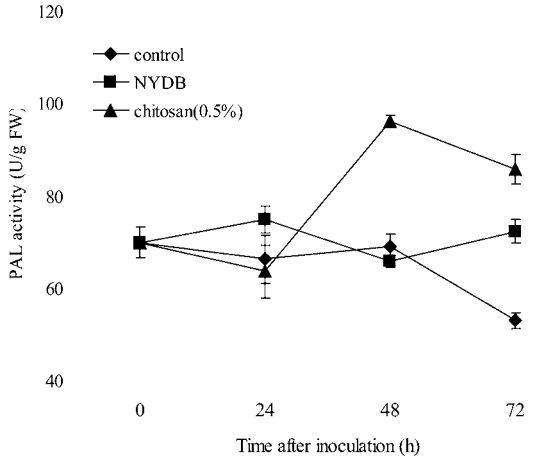

Figure 8. Effects of *R. mucilaginosa* harvested from different media on PAL activity of strawberries. Control = sterile distilled water, NYDB = *R. mucilaginosa* which were harvested from the media of NYDB, chitosan (0.5%) = *R. mucilaginosa* which were harvested from the media of NYDB + chitosan at the concentration of 0.5%. Each value is the mean of two experiments. Bars represent standard deviations.

evident peak of PAL activity was induced during the whole storage period. The PAL activity of strawberries treated with *R. mucilaginosa* incubated in chitosan-supplemented (0.5%) NYDB was significantly higher than that of strawberries treated with *R. mucilaginosa* incubated in NYDB and the control ($P < 0.05$) at 48 and 72 h after storage.

Effects of *R. mucilaginosa* Harvested from Different Media on MDA Content of Strawberries. The MDA contents of strawberries treated with *R. mucilaginosa* and water were demonstrated to have gradual linear ascending tendency during the storage period (Figure 9). The MDA content of strawberries treated with *R. mucilaginosa* cultivated in the NYDB amended with chitosan (0.5%) was obviously lower than that of the control ($P < 0.05$) at the whole storage period. What's more, it was obviously lower than that of strawberries

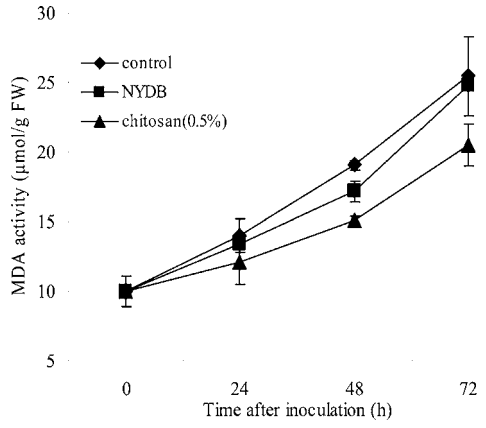

Figure 9. Effects of *R. mucilaginosa* harvested from different media on MDA content of strawberries. Control = sterile distilled water, NYDB = *R. mucilaginosa* which were harvested from the media of NYDB, chitosan (0.5%) = *R. mucilaginosa* which were harvested from the media of NYDB + chitosan at the concentration of 0.5%. Each value is the mean of two experiments. Bars represent standard deviations.

treated with *R. mucilaginosa* cultivated in the NYDB at 48 h after inoculation.

Effects of *R. mucilaginosa* Harvested from Different Media on Chitinase Activity of Strawberries. Throughout the whole storage period, the chitinase activity of strawberries treated with *R. mucilaginosa* cultivated both in the chitosan-supplemented media and in NYDB showed the similar tendency for change, moreover, the chitinase activity in the former treatment was slightly higher than that of the latter (Figure 10). However, in the control strawberries, the chitinase

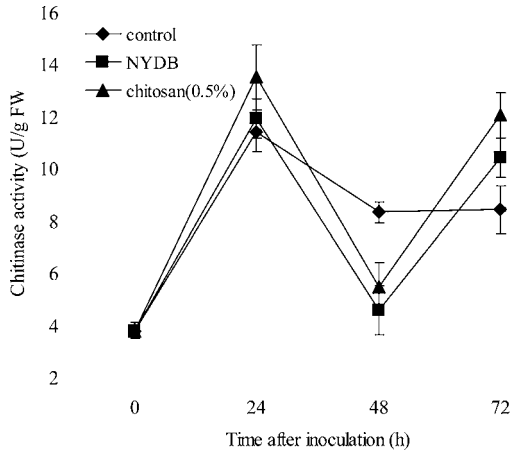

Figure 10. Effects of *R. mucilaginosa* harvested from different media on chitinase activity of strawberries. Control = sterile distilled water, NYDB = *R. mucilaginosa* which were harvested from the media of NYDB, chitosan (0.5%) = *R. mucilaginosa* which were harvested from the media of NYDB + chitosan at the concentration of 0.5%. Each value is the mean of two experiments. Bars represent standard deviations.

activity increased and reached the peak at 24 h, then decreased at 48 h, and then changed to be steady after 48 h. The chitinase activity of the control strawberries was significantly lower than those of the *R. mucilaginosa* cultivated in the chitosan-supplemented media treated strawberries at 24 and 72 h.

Effects of *R. mucilaginosa* Harvested from Different Media on β-1,3-Glucanase Activity of Strawberries. In the control strawberries, β-1,3-glucanase activity showed the down trend generally and only increased slightly at 48 h. A peak of β-1,3-glucanase activity at 48 h after inoculation and followed by an indistinctive decrease was observed in the treatment with *R. mucilaginosa* cultivated in the media of NYDB induced. However, compared with *R. mucilaginosa* cultivated in NYDB without chitosan and the control, the treatment with *R. mucilaginosa* cultivated in the NYDB media amended with chitosan (0.5%) can improve the β-1,3-glucanase activity of strawberries during the whole storage period, especially after 72 h incubation (Figure 11, $P < 0.05$).

Identification of Differentially Expressed Proteins. For protein identification by means of peptide mass fingerprints (PMF), MASCOT was applied to search protein database of Viridiplantae. In this study, ignoring very faint spots and spots with undefined shapes and areas, more than 480 protein spots were detected in each gel with Image Master 2D Elite software (Figure 12). A total of 52 proteins were differentially expressed when the yeast antagonist *R. mucilaginosa* were harvested from the NYDB amended with chitosan. Among the 52 proteins, there are 26 up-regulated proteins and 26 down-regulated

dx.doi.org/10.1021/jf500065n | J. Agric. Food Chem. 2014, 62, 4214−4224

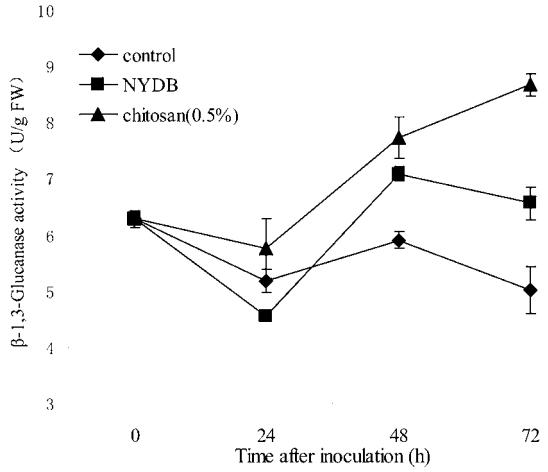

Figure 11. Effects of *R. mucilaginosa* harvested from different media on *β*-1,3-glucanase activity of strawberries. Control = sterile distilled water, NYDB = *R. mucilaginosa* which were harvested from the media of NYDB, chitosan (0.5%) = *R. mucilaginosa* which were harvested from the media of NYDB + chitosan at the concentration of 0.5%. Each value is the mean of two experiments. Bars represent standard deviations.

proteins. Due to the under-representation of yeast proteins in the protein database, only 16 protein spots were unambiguously identified by protein database analysis (Table 1). Of all the differentially expressed proteins identified, most of them were about the basic cell metabolism, including: N-6 DNA methylase (K-6), threonine synthase (K-14), glutaminase (K-4), phosphopantetheine-binding (K-15), amidohydrolase 3 (K-11), and actin (K-13), which can maintain cells normal morphology, protein kinase Cdc7 (K-10), which is involved in regulating complex cellular functions, while two-component system sensor protein (K-5) is concerned about osmotic stress on cells. In addition, we also identified sulfatase (K-3), bifunctional proline dehydrogenase/pyrroline-5-carboxylate dehydrogenase (K-16), putative peptidoglycan-binding protein, lysm containing domain (K-7), and several hypothetical proteins (K-1, -2, -8, -9, -12).

DISCUSSION

The results from this study showed that when *R. mucilaginosa* was cultivated in the media of NYDB amended with 0.5% chitosan, its antogonistic efficacy against the *Rhizopus* decay, gray mold decay, and natural decay of strawberries was greatly improved. Considering that the widely available natural component, chitosan, is cheap and safe to humans and the environment, it might be an effective, safe, and economical approach to enhance the biocontrol efficacy of *R. mucilaginosa* to postharvest decay of fruits. In our results, treatments with application of *R. mucilaginosa* cultivation in the NYDB media amended with chitosan at concentrations of 1% could not reduce the disease incidence of gray mold decay of strawberries compared with the control. This should be further studied to test the reason.

For harvested fruits, the diseases caused by fungi usually begin as a result of latent infections established in the field or wound infections.[2,33] The wounds, which inevitably occur during harvest, transport, and handling, not only damage the quality of harvested fruit[34] but also provide pathways for pathogen invasion, especially for the wound invading necrotrophic fungi such as *R. stolonifer*.[2,35] It has reported

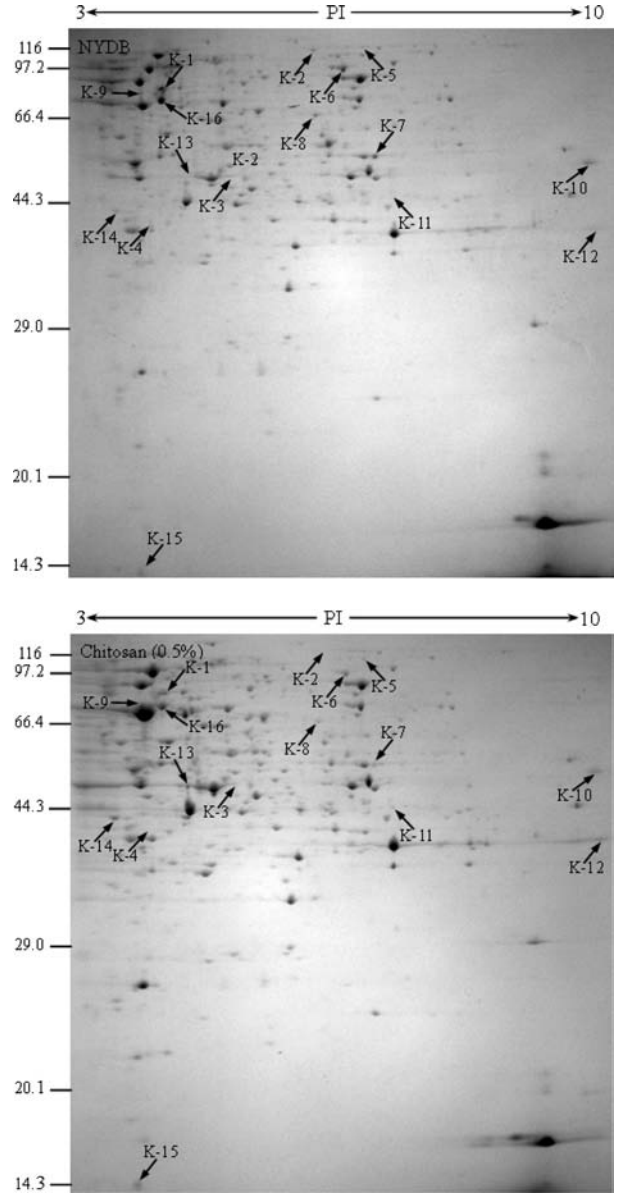

Figure 12. Two-dimensional pattern of intracellular proteins of *R. mucilaginosa* after cultivation in NYDB or NYDB amended with 0.5% chitosan powder.

that yeasts are capable of rapidly colonizing and growing in the wounds, which can provide an advantage over pathogen growth. Due to this property, antogonistic yeasts were chosen for biocontrol.[36] This study showed that *R. mucilaginosa* harvested from the chitosan-supplemented (0.5%) media proliferated more rapidly in strawberry wounds compared with those grown in NYDB without chitosan. Competition for nutrients and space is proposed to be the principal modes of action of *R. mucilaginosa* in antagonism with pathogens and the better biocontrol activity of the antagonists can be obtained with a higher the concentration of *R. mucilaginosa*,[5] we assume that the enhanced growth of the antagonistic yeast might be a major reason for adding chitosan in culture media, leading to the increased biocontrol efficacy of *R. mucilaginosa* against the *Rhizopus* decay, gray mold decay, and natural decay of strawberries.

In our test, chitinase activity was detected in different cell-free culture filtrate of *R. mucilaginosa* cultivated in different

Table 1. Identification of Cellular Proteins of *R. mucilaginosa* Showing Differential Expression under Chitosan Cultivation Using MS/MS Analysis

spot	protein name	NCBI accession	mass	PI	species	score	NP/PD
K-1	hypothetical protein FNP_2207	gil254302157	109274	5.07	*Fusobacterium nucleatum* subsp.	71	7/29
K-2	hypothetical protein	gil169777975	99456	6.18	*Aspergillus oryzae* RIB40	88	6/22
K-3	sulfatase	gil134101323	55546	6.43	*Saccharopolyspora erythraea* NRRL 2338	45	3/8
K-4	glutaminase	gil51596263	35967	5.01	*Yersinia pseudotuberculosis* IP 32 953	68	3/22
K-5	two-component system sensor protein	gil21229958	83320	6.06	*Xanthomonas campestris* pv campestris str. ATCC 33 913	82	7/15
K-6	N-6 DNA methylase	gil92109757	188696	5.79	*Nitrobacter hamburgensis* X14	88	11/29
K-7	putative peptidoglycan- binding protein, lysm containing domain	gil285019619	41099	8.98	*Xanthomonas albilineans*	84	7/21
K-8	hypothetical protein UM01172.1	gil71005306	71955	6.35	*Ustilago maydis* 521	80	7/13
K-9	hypothetical protein MGL_0058	gil164662323	70112	5.01	*Malassezia globosa* CBS 7966	97	9/23
K-10	protein kinase Cdc7	gil148228724	54289	9.04	*Xenopus laevis*	58	4/6
K-11	amidohydrolase 3	gil163941091	59770	5.61	*Bacillus weihenstephanensis* KBAB4	79	7/18
K-12	hypothetical protein ANHYDRO_00219	gil212695699	36793	9.18	*Anaerococcus hydrogenalis* DSM 7454	67	5/11
K-13	actin	gil57157304	41945	5.29	*Candida boidinii*	91	8/19
K-14	threonine synthase	gil242398391	39150	6.81	*Thermococcus sibiricus* MM 739	47	3/8
K-15	phosphopantetheine- binding	gil242261690	8997	4.76	*Clostridium cellulovorans* 743B	53	3/6
K-16	bifunctional proline dehydrogenase/pyrroline-5-carboxylate dehydrogenase	gil58584796	116883	5.94	*Wolbachia endosymbiont* strain TRS of *Brugia malayi*	75	10/28

media, so *R. mucilaginosa* can produce chitinase in all kinds of growth media, this was similar to some other strains of postharvest biocontrol yeasts such as *C. laurentii* and *Candida oleophila*, which were reported to be able to produce chitinase.[12,37,38] Besides, compared with the chitinase activity of the cell-free culture filtrates grown in NYDB media and NYDB plus chitosan at other concentrations, the activity of the cell-free culture filtrates of *R. mucilaginosa* grown in NYDB amended with 0.5% chitosan showed a higher level. On the test of efficacy of cell-free culture filtrate of *R. mucilaginosa* incubated in different media in controlling of *Rhizopus* decay and gray mold decay of strawberries, the filtrates incubated in NYDB had no significant control efficacy on the *Rhizopus* decay and gray mold decay of strawberries after 3 d storage at 20 °C. However, the cell-free culture filtrates of NYDB media added with 0.5% chitosan could effictively control the *Rhizopus* decay and gray mold decay in strawberry wounds compared to the control. The chitinase activity may have diverse biological roles including the antifungal activity, which is usually induced in the presence of the chitin.[39] Carstens et al. (2003) demonstrated that the chitinase produced by *Sacharomyces cerevisiae* could inhibit spore germination and hyphal growth of *B. cinerea* in vitro.[40] Yu et al. (2008) reported the antagonistic activity of *C. laurentii* combined with chitinase treatment showed a increased inhibition against blue mold decay caused by *Penicillium expansum* of pear fruit associated with the higher chitinase activities.[12] So we propose that the enhanced chitinase activity of antagonistic yeast is one of the determining factors to improve antagonistic activity of *R. mucilaginosa* against postharvest decay of strawberries.

In nature, plants survive the attack of many microorganisms by employing several layers of defense responses.[41] Besides constitutively expressed barriers, plants can recognize the presence of pathogens and respond by activating defense reactions.[42] The success of this defense response depends on some key factors, including the speed by which the plant recognizes the attacking pathogen and the intensity by which the appropriate defense mechanism is activated. According to the research, the effectiveness of this basal resistance can be improved by elicitors including specific biotic and abiotic stimuli experienced by the plant before contact with the pathogen.[43] Recent studies have revealed that the induction of disease resistance by elicitors is a sensitization process that primes the plant for more rapid deployment of the defenses.[44−46]

PPO catalyzes the oxidation of phenolics to quinones, which are more toxic to pathogens than the former.[47] Increased PPO activity is correlated with disease resistance in plants.[48,49] POD is bifunctional enzymes that can oxidize various substrates in the presence of H_2O_2, but it also produce reactive oxygen species (ROSs). POD catalyzes the last step of lignin biosynthesis. High POD activities are associated with the onset of induced resistance which involves several important plant defense mechanisms such as lignification and suberization.[25,28,33] So enhancement of lignification and suberization related to maintenance of integrity and vital functions of the cell and increased the levels of antimicrobial phenolic compounds in plant cells attacked by phytopathogens resulted in improvement of disease resistance. PAL is the first committed enzyme of the phenylpropanoid pathway which is directly involved in the synthesis of phenolics, phytoalexins, and lignins that are associated with the localized resistance processes.[50] It also has been reported that PAL is transcriptionally induced in response to development and ripening.[51] In addition, previous study reported that higher disease resistance and lower decay index accompanied by significantly increased PAL activity in MeJA-treated vegetable soybean pods, sweet cherry, and peach fruit.[52−54] Our results showed that PPO, POD, and PAL activity were enhanced in strawberry fruit while treated with *R. mucilaginosa* incubated in the NYDB media

amended with 0.5% chitosan compared with the case that without chitosan. On the basis of these, we assume that enhancement the activity of *R. mucilaginosa* to induce more defense enzymes such as PPO, POD, and PAL so as to enhance the resistance of strawberries may be another mechanism that chitosan enhances the antagonistic activity of *R. mucilaginosa* against postharvest decay of strawberries. *R. mucilaginosa* incubated in the NYDB media amended with 0.5% chitosan acted as biotic stimuli, which primed the strawberries for more rapid deployment of the defenses to pathogens.

MDA, a decomposition product of polyunsaturated fatty acids hydroperoxides, has been utilized very often as a suitable biomarker for lipid peroxidation, which is an effect of oxidative damage.[55] Increased lipid peroxidation has been regarded as a major characteristic of harvested fruits undergoing senescence and membrane injury.[56] In this study, MDA contents of strawberries treated with *R. mucilaginosa* cultivated in the culture media of the chitosan-supplement (0.5%) showed a lower level than that of both the control during the whole storage period and the treatment with *R. mucilaginosa* cultivated in NYDB at some storage time. This suggests that enhancing the activity of antagonistic yeast to inhibit the ripening and senescence of fruits may be one of the action modes by adding chitosan to improve antogonistic activity of *R. mucilaginosa* against postharvest decay of strawberries.

Our study displayed that *R. mucilaginosa* cultivated in the NYDB media amended with 0.5% chitosan induced more chitinase and a higher level of β-1,3-glucanase activity of strawberries compared with both the control and the *R. mucilaginosa* cultivated in NYDB. Previous study indicates that in plants, pathogenesis-related (PR) proteins are induced by a pathogen invasion, such as chitinases and β-1,3-glucanases, which are related to their capacity to degrade fungal cell wall in desease resistance process.[57] This induction can be enhanced by some elicitors with the improvement of resistance to pathogens in plants.[58,59] Therefore, we infer that improving the activity of antagonistic yeast to induce the production of pathogenesis-related (PR) proteins of strawberries may be another reason that a more remarkable upward trend was seen in the efficacy of *R. mucilaginosa* cultivated in the NYDB media amended with 0.5% chitosan in controlling postharvest decay of strawberries than the case in NYDB.

Furthermore, the identification of differentially expressed proteins showed that, compared with *R. mucilaginosa* harvested from the NYDB, there are a total of 52 proteins that were differentially expressed when the yeast antagonists were harvested from the NYDB amended with chitosan. Among the 52 proteins, there are 26 up-regulated proteins and 26 down-regulated proteins, and most of them are related to basic metabolism. This indicated that the basic metabolism of *R. mucilaginosa* was improved by chitosan induced incubation, so as to improve it's biocontrol efficacy to postharvest diseases of strawberries. Response patterns of *R. mucilaginosa* to chitosan induced incubation are complex, as the differentially abundant proteins are involved in multiple metabolic pathways.

In short, our results showed that chitosan induced incubation can improve the antagonistic activity of *R. mucilaginosa*, which may offer great practical potential in reducing the postharvest diseases of strawberry fruit. The mode of actions may include its ability to enhance competitiveness of yeast antagonist for nutrients and space with pathogens, to enhance chitinase activity of antagonistic yeast, to induce more defense enzymes such as PPO, POD, and PAL, to induce the production of pothogenesis-related (PR) proteins such as chitinase, β-1,3-glucanase of fruits, and to reduce lipid peroxidation, so as to enhance the resistance and delay the senescence of fruits. The proteomic analysis and comparison of *R. mucilaginosa* in response to chitosan suggested that 0.5% chitosan improved the basic metabolism of *R. mucilaginosa*, and this may be one of the molecular mechanisms by which enhancement the efficacy of *R. mucilaginosa* by adding chitosan in the culture media. All these should be further studied.

AUTHOR INFORMATION

Corresponding Author

*Phone: +86-511-88780201. Fax: +86-511-88780201. E-mail: zhanghongyin126@126.com (Hy Zhang).

Funding

This research was supported by the National Natural Science Foundation of China (31271967), the Research Fund for the Doctoral Program of Higher Education of China (20123227110015), and the Technology Support Plan of Zhenjiang (NY2013020).

Notes

The authors declare no competing financial interest.

REFERENCES

(1) Romanazzi, G.; Nigro, F.; Ippolito, A.; Salerno, M. Effect of short hypobaric treatments on postharvest rots of sweet cherries, strawberries and table grapes. *Postharvest Biol. Technol.* **2001**, *22*, 1−6.

(2) Janisiewicz, W. J.; Korsten, L. Biological control of postharvest diseases of fruits. *Annu. Rev. Phytopathol.* **2002**, *40*, 411−441.

(3) Leverentz, B.; Conway, W. S.; Janisiewicz, W.; Abadias, M.; Kurtzman, C. P.; Camp, M. J. Biocontrol of the food-borne pathogens *Listeria monocytogenes* and *Salmonella enterica* serovar poona on fresh-cut apples with naturally occurring bacterial and yeast antagonists. *Appl. Environ. Microbiol.* **2006**, *72*, 1135−1140.

(4) Buck, J. W. Combinations of fungicides with phylloplane yeasts for improved control of *Botrytis cinerea* on geranium seedlings. *Phytopathology* **2004**, *94*, 196−202.

(5) Li, R. P.; Zhang, H. Y.; Liu, W. M.; Zheng, X. D. Biocontrol of postharvest gray and blue mold decay of apples with *Rhodotorula mucilaginosa* and possible mechanisms of action. *Int. J. Food Microbiol.* **2011**, *146*, 151−156.

(6) Droby, S.; Wsiniewski, M.; Ei-Ghaouth, A.; Wilson, C. Biological control of postharvest diseases of fruit and vegetables: current achievements and future challenges. *Acta Hortic.* **2003**, *628*, 703−713.

(7) Droby, S. Improving quality and safety of fresh fruits and vegetables after harvest by the use of biocontrol agents and natural materials. *Acta Hortic.* **2006**, *709*, 45−51.

(8) Ippolito, A.; Nigro, F. Impact of preharvest application of biological control agents on postharvest diseases of fresh fruits and vegetables. *Crop Prot.* **2000**, *19*, 715−723.

(9) Sharma, R. R.; Singh, D.; Singh, R. Biological control of postharvest diseases of fruits and vegetables by microbial antagonists: a review. *Biol. Control* **2009**, *50*, 205−221.

(10) Teixido, N.; Vinas, I.; Usall, J.; Magan, N. Control of blue mold of apples by preharvest application of *Candida sake* grown in media with different water activity. *Phytopathology* **1998**, *88*, 960−964.

(11) Li, B. Q.; Tian, S. P. Effects of trehalose on stress tolerance and biocontrol efficacy of *Cryptococcus laurentii*. *J. Appl. Microbiol.* **2006**, *100*, 854−861.

(12) Yu, T.; Wang, L. P.; Yin, Y.; Wang, Y. X.; Zheng, X. D. Effect of chitin on the antagonistic activity of *Cryptococcus laurentii* against *Penicillium expansum* in pear fruit. *Int. J. Food Microbiol.* **2008**, *122*, 44−48.

(13) Bartnicki-Garcia, S. Cell wall composition and other biochemical markers in fungal phylogeny. In *Phytochemical Phylogeny*; Harbone, J. B., Ed.; Academic Press: London, 1970; pp 81−103.

(14) Bautista-Baños, S.; Hernández-Lauzardo, A. N.; Velázquez-del Valle, M. G.; Hernández-López, M.; Ait Barka, E.; Bosquez-Molina, E.; Wilson, C. L. Chitosan as a potential natural compound to control pre and postharvest diseases of horticultural commodities. *Crop Prot.* **2006**, *25*, 108−118.
(15) Dutta, P. K.; Tripathi, S.; Mehrotra, G. K.; Dutta, J. Perspectives for chitosan based antimicrobial films in food applications. *Food Chem.* **2009**, *114*, 1173−1182.
(16) Rabea, E.; Badawy, M. T.; Stevens, C.; Smagghe, G.; Steurbaut, W. Chitosan as antimicrobial agent: applications and mode of action. *Biomacromolecules* **2003**, *4*, 1457−1465.
(17) Bhaskara Reddy, M. V.; Belkacemi, K.; Corcuff, R.; Castaigne, F.; Arul, J. Effect of pre-harvest chitosan sprays on post-harvest infection by *Botrytis cinerea* and quality of strawberry fruit. *Postharvest Biol. Technol.* **2000**, *20*, 39−51.
(18) Li, H.; Yu, T. Effect of chitosan on incidence of brown rot, quality and physiological attributes of postharvest peach fruit. *J. Sci. Food Agr.* **2001**, *81*, 269−274.
(19) Yu, T.; Li, H. Y.; Zheng, X. D. Synergistic effect of chitosan and *Cryptococcus laurentii* on inhibition of *Penicillium expansum* infections. *Int. J. Food Microbiol.* **2007**, *114*, 261−266.
(20) Li, S. S.; Cheng, C.; Li, Z.; Chen, J. Y.; Yan, B.; Han, B. Z.; Reeves, M. Yeast species associated with wine grapes in China. *Int. J. Food Microbiol.* **2010**, *138*, 85−90.
(21) Abeles, F. B.; Bosshart, R. P.; Forrence, L. E.; Habig, W. H. Preparation and purification of glucanase and chitinase from bean leaves. *Plant Physiol.* **1971**, *47*, 129−134.
(22) Cabib, E.; Bowers, B. Chitin and yeast budding. Localization of chitin in yeast bud scars. *J. Biol. Chem.* **1971**, *246*, 152−159.
(23) Reissig, J. L.; Storminger, J. L.; Leloir, L. F. A modified colorimetric method for the estimation of *N*-acetylamino sugars. *J. Biol. Chem.* **1955**, *217*, 959−966.
(24) Waite, J. H. Calculating extinction coefficients for enzymatically produced *o*-quinones. *Anal. Biochem.* **1976**, *75*, 211−218.
(25) Lurie, S.; Fallik, E.; Handros, A.; Shapira, R. The possible involvement of peroxidase in resistance to *Botrytis cinereain* heat treated tomato fruit. *Physiol. Mol. Plant Pathol.* **1997**, *50*, 141−149.
(26) Assis, J.; Munoz, T.; Escribano, M.; Merodio, C. Effect of high carbon dioxide concentration on PAL activity and phenolic contents in ripening cherimoya fruit. *Postharvest Biol. Technol.* **2001**, *23*, 33−39.
(27) Du, D.; Bramlage, W. J. Modified thiobarbituric acid assay for measuring lipid oxidation in sugar-rich plant tissue extracts. *J. Agric. Food Chem.* **1992**, *40*, 1566−1570.
(28) Ippolito, A.; EI-Ghaouth, A.; Wilson, C. L.; Wisniewski, M. Control of postharvest decay of apple fruit by *Aureobasidium pullulans* and induction of defense responses. *Postharvest Biol. Technol.* **2000**, *19*, 265−272.
(29) Zhao, L. N.; Zhang, H. Y.; Lin, H. T.; Zhang, X. Y.; Ren, X. F. Effect of trehalose on the biocontrol efficacy of *Pichia caribbica* against postharvest gray mold and blue mold decay of apples. *Pest Manage. Sci.* **2013**, *69*, 983−989.
(30) Bradford, M. M. A rapid and sensitive method for the quantitation of microgram quantities of protein utilizing the principle of protein−dye binding. *Anal. Biochem.* **1976**, *72*, 248−254.
(31) Wang, Y.; Yang, L. M.; Xu, H. B.; Li, Q. F.; Ma, Z. Q.; Chu, C. G. Differential proteomic analysis of proteins in wheat spikes induced by *Fusarium graminearum*. *Proteomics* **2005**, *5*, 4496−4503.
(32) Zhang, L.; Yu, Z. F.; Jiang, L.; Jiang, J.; Luo, H. B.; Fu, L. R. Effect of post-harvest heat treatment on proteome change of peach fruit during ripening. *J. Proteomics* **2011**, *74*, 1135−1149.
(33) Prusky, D. Mechanism of resistance of fruits and vegetables to postharvest diseases. In *Postharvest Physiology and Pathology of Vegetables*; Bartz, J., Brecht, J., Eds.; Marcel Dekker Press: New York, 2003; pp 581−598.
(34) Miller, A. R. Harvest and handing injury: physiology, biochemistry, and deletion. In *Postharvest Physiology and Pathology of Vegetables*; Bartz, J., Brecht, J., Eds.; Marcel Dekker Press: New York, 2003; pp 177−208.
(35) Xu, X. M.; Bertone, C.; Berrie, A. Effects of wounding, fruit age and wetness duration on the development of cherry brown rot in the UK. *Plant Pathol.* **2007**, *56*, 114−119.
(36) Filonow, A. B. Role of competition for sugars by yeasts in the biocontrol of gray mold of apple. *Biocontrol Sci. Technol.* **1998**, *8*, 243−256.
(37) Bar-Shimon, M.; Yehuda, H.; Cohen, L.; Weiss, B.; Kobeshnikov, A.; Daus, A.; Goldway, M.; Wisniewski, M.; Droby, S. Characterization of extracellular lytic enzymes produced by the yeast biocontrol agent *Candida oleophila*. *Curr. Genet.* **2004**, *45*, 140−148.
(38) Chan, Z. L.; Tian, S. P. Interaction of antagonistic yeasts against postharvest pathogens of apple fruit and possible mode of action. *Postharvest Biol. Technol.* **2005**, *36*, 215−223.
(39) Dahiya, N.; Tewari, R.; Hoondal, G. S. Biotechnological aspects of chitinolytic enzymes: a review. *Appl. Microbiol. Biotechnol.* **2006**, *71*, 773−782.
(40) Carstens, M.; Vivier, M. A.; Van Rensburg, P.; Pretorius, I. S. Overexpression, secretion and antifungal activity of the *Saccharomyces cerevisiae* Chitinase. *Ann. Microbiol.* **2003**, *53*, 15−28.
(41) Schilmiller, A. L.; Howe, G. A. Systemic signaling in the wound response. *Curr. Opin. Plant Biol.* **2005**, *8*, 369−377.
(42) Yu, T.; Wu, P. G.; Qi, J. J.; Zheng, X. D.; Jiang, F.; Zhan, X. Improved control of postharvest blue mold rot in pear fruit by a combination of *Cryptococcus laurentii* and gibberellic acid. *Biol. Control* **2006**, *39*, 128−134.
(43) Ton, J.; Jakab, G.; Toquin, V.; Flors, V.; Iavicoli, A.; Maeder, M. N.; Métraux, J. P.; Mauch-Mani, B. Dissecting the {beta}-aminobutyric acid-induced priming phenomenon in arabidopsis. *Plant Cell* **2005**, *17*, 987−999.
(44) Molloy, C.; Cheah, L. H.; Koolaard, J. P. Induced resistance against *Sclerotinia sclerotiorum* in carrots treated with enzymatically hydrolysed chitosan. *Postharvest Biol. Technol.* **2004**, *33*, 61−65.
(45) Pieterse, C. M. J.; Van Loon, L. C. NPR1: the spider in the web of induced resistance signaling pathways. *Curr. Opin. Plant Biol.* **2004**, *7*, 456−464.
(46) Wang, F.; Feng, G.; Chen, K. Defense responses of harvested tomato fruit to burdock fructooligosaccharide, a novel potential elicitor. *Postharvest Biol. Technol.* **2009**, *52*, 110−116.
(47) Mayer, A. M.; Harel, E. Polyphenol oxidases in plants. *Phytochemistry* **1979**, *18*, 193−215.
(48) Jung, W. J.; Jin, Y. L.; Kim, Y. C.; Kim, K. Y.; Park, R. D.; Kim, T. H. Inoculation of *Paenibacillus illinoisensis* alleviates root mortality, activates of lignification-related enzymes, and induction of the isozymes in pepper plants infected by *Phytophthora capsici*. *Biol. Control* **2004**, *30*, 645−652.
(49) Mohammadi, M.; Kazemi, H. Changes in peroxidase and polyphenol oxidase activities in susceptible and resistant wheat heads inoculated with *Fusarium graminearum* and induced resistance. *Plant Sci.* **2002**, *162*, 491−498.
(50) Ryals, J. A.; Neuenschwander, U. H.; Willits, M. G.; Molina, A.; Steiner, H. Y.; Hunt, M. D. Systemic acquired resistance. *Plant Cell* **1996**, *8*, 1809−1819.
(51) George, D.; Angelos, K. K. A phenylalanine ammonia-lyase gene from melon fruit: cDNA cloning, sequence and expression in response to development and wounding. *Plant Mol. Biol.* **1994**, *26*, 473−479.
(52) Su, X. G.; Zheng, Y. H.; Feng, L.; Zhang, L.; Wang, F. Effects of exogenous MeJA on postharvest senescence and decay of vegetable soybean pods. *Plant Physiol. Mol. Biol.* **2003**, *29*, 52−58.
(53) Yao, H. J.; Tian, S. P. Effects of pre- and post-harvest application of salicylic acid or methyl jasmonate on inducing disease resistance of sweet cherry fruit in storage. *Postharvest Biol. Technol.* **2005a**, *35*, 253−262.
(54) Yao, H. J.; Tian, S. P. Effects of a biocontrol agent and methyl jasmonate on postharvest diseases of peach fruit and the possible mechanisms involved. *J. Appl. Microbiol.* **2005b**, *98*, 941−950.
(55) Bailly, C.; Benamar, A.; Corbineau, F.; Come, D. Changes in malondialdehyde content and in superoxide dismutase, catalase and glutathione reductase activities in sunflower seeds as related to

deterioration during accelerated aging. *Physiol. Plant.* **1996**, *97*, 104−110.
(56) Deighton, N.; Muckenschnabel, I.; Goodman, B. A.; Williamson, B. Lipid peroxidation and the oxidative burst associated with infection of *Capsicum annuum* by *Botrytis cinerea*. *Plant J.* **1999**, *20*, 485−492.
(57) Joosten, M. H. A. J.; Verbakel, H. M.; Nettekoven, M. E.; van Leeuwen, J.; van der Vossen, R. T. M.; de Wit, P. J. G. M. The phytopathogenic fungus *Cladosporium fulvum* is not sensitive to the chitinase and *β*-1,3-glucanase defence proteins of its host, tomato. *Physiol. Mol. Plant Pathol.* **1995**, *46*, 45−59.
(58) Charles, M. T.; Tano, K.; Asselin, A.; Arul, J. Physiological basis of UV-C induced resistance to *Botrytis cinerea* in tomato fruit. V. Constitutive defence enzymes and inducible pathogenesis-related proteins. *Postharvest Biol. Technol.* **2009**, *51*, 414−424.
(59) Qin, G. Z.; Tian, S. P.; Xu, Y.; Wan, Y. K. Enhancement of biocontrol efficacy of antagonistic yeasts by salicylic acid in sweet cherry fruit. *Physiol. Mol. Plant Pathol.* **2003**, *62*, 147−154.

JOURNAL OF AGRICULTURAL AND FOOD CHEMISTRY

Addition/Correction

pubs.acs.org/JAFC

Correction to Interfacial Structural Role of pH-Shifting Processed Pea Protein in the Oxidative Stability of Oil/Water Emulsions

Jiang Jiang, Bo Zhu, Yuanfa Liu,* and Youling L. Xiong*

J. Agric. Food Chem. **2014**, *62* (7), 1683−1691. DOI: 10.1021/jf405190h

An error was made in the Acknowledgments section by mistakenly citing an unrelated grant and the entire paragraph should have been presented as a Funding statement. The correct presentation is given below.

AUTHOR INFORMATION

Funding

The study was supported by the Ministry of Science and Technology, China (Grants 2012BAD28B04 and 2013AA102103), the National Natural Science Foundation, China (Grant 31301497), and the USDA Agriculture and Food Research Initiative, USA (Grant 2008-35503-18790).

Published: April 25, 2014

ACS Publications © 2014 American Chemical Society

JOURNAL OF AGRICULTURAL AND FOOD CHEMISTRY

Perspective

pubs.acs.org/JAFC

Terms of Use

Nanopesticides: Guiding Principles for Regulatory Evaluation of Environmental Risks

Rai S. Kookana,*[,†,‡] Alistair B. A. Boxall,[§] Philip T. Reeves,[∥] Roman Ashauer,[§] Sabine Beulke,[⊥] Qasim Chaudhry,[⊥] Geert Cornelis,[#] Teresa F. Fernandes,[□] Jay Gan,[●] Melanie Kah,[△] Iseult Lynch,[▼] James Ranville,[⬡] Chris Sinclair,[⊥] David Spurgeon,[■] Karen Tiede,[⊥] and Paul J. Van den Brink[○,▲]

[†]Commonwealth Scientific and Industrial Research Organisation (CSIRO), PMB 2, Glen Osmond, SA 5064, Australia

[‡]University of Adelaide, Waite Campus, Glen Osmond, SA 5064, Australia

[§]University of York, Heslington, York YO10 5DD, United Kingdom

[∥]Australian Pesticides and Veterinary Medicines Authority (APVMA), Canberra, ACT 2604, Australia

[⊥]The Food and Environment Research Agency (Fera), Sand Hutton, York YO41 1LZ, United Kingdom

[#]University of Gothenburg, Gothenburg, Sweden

[□]Heriot Watt University, Edinburgh, EH14 4AS, United Kingdom

[●]University of California, Riverside, California 92521, United States

[△]Department of Environmental Geosciences, University of Vienna, Vienna, Austria

[▼]School of Geography, Earth and Environmental Sciences, University of Birmingham, Edgbaston, Birmingham B15 2TT, United Kingdom

[⬡]Colorado School of Mines, Golden, Colorado 80401, United States

[■]Centre for Ecology and Hydrology, Maclean Building, Benson Lane, Wallingford, Oxfordshire OX10 8BB, United Kingdom

[○]Wageningen University, Wageningen, The Netherlands

[▲]Alterra, Wageningen, The Netherlands

ABSTRACT: Nanopesticides or nano plant protection products represent an emerging technological development that, in relation to pesticide use, could offer a range of benefits including increased efficacy, durability, and a reduction in the amounts of active ingredients that need to be used. A number of formulation types have been suggested including emulsions (e.g., nanoemulsions), nanocapsules (e.g., with polymers), and products containing pristine engineered nanoparticles, such as metals, metal oxides, and nanoclays. The increasing interest in the use of nanopesticides raises questions as to how to assess the environmental risk of these materials for regulatory purposes. Here, the current approaches for environmental risk assessment of pesticides are reviewed and the question of whether these approaches are fit for purpose for use on nanopesticides is addressed. Potential adaptations to existing environmental risk assessment tests and procedures for use with nanopesticides are discussed, addressing aspects such as analysis and characterization, environmental fate and exposure assessment, uptake by biota, ecotoxicity, and risk assessment of nanopesticides in aquatic and terrestrial ecosystems. Throughout, the main focus is on assessing whether the presence of the nanoformulation introduces potential differences relative to the conventional active ingredients. The proposed changes in the test methodology, research priorities, and recommendations would facilitate the development of regulatory approaches and a regulatory framework for nanopesticides.

KEYWORDS: *nanopesticides, environmental risk, ecotoxicity, environmental fate*

INTRODUCTION

Engineered nanoparticles (ENPs) are being, or have the potential to be, used in many industrial sectors including defense, energy generation and storage, agriculture, and environmental remediation.[1] One sector where the use of ENPs is receiving increasing interest is the pesticide sector with the development of a range of plant protection products that are termed "nanopesticides".[2−5] Nanopesticides "involve either very small particles of a pesticide active ingredient (ai) or other small engineered structures with useful pesticidal properties".[6] For the purpose of this paper, we regard a nanopesticide as a plant protection product in which nanotechnology (e.g., use of materials that have a physical form with at least one size dimension in the range of 1−100 nm) is employed to enhance the efficacy or reduce the environmental footprint of a pesticide ai. It is noteworthy, however, that so-called "nano" formulations of patented pesticides often contain size fractions beyond the 100 nm conventional "nanorange".[7]

Nanopesticides represent an emerging technological development that, in relation to pesticide use, could offer a range of

Received: January 14, 2014
Revised: April 19, 2014
Accepted: April 22, 2014
Published: April 22, 2014

 © 2014 American Chemical Society

Table 1. Potential Applications of Nanotechnology in the Pesticides Sector

function	how this can be achieved	current examples
enhanced apparent solubility	nano- and microemulsions	emulsion-based registered pesticides, Banner MAXX of Syngenta[64]
faster decomposition in soil and/or plant	nanocatalyst-conjugated ai in microcapsules	SDS-modified TiO_2/Ag conjugated with ai such as dimethomorph;[65] imidacloprid and avermectin[66]
controlled release	nanocapsules, nanospheres	polymeric stabilized bifenthrin;[67] nanocomposite 2,4-D;[68] porous hollow Si-encaged validamycin[69]
targeted delivery	nanocapsules	nanoenapcsulated glyphosate or sulfonylurea herbicide[2]
protection against premature degradation	nanocapsules with catalyst ai conjugate	TiO_2-M262 polymer metaflumizone;[70] porous hollow Si-encaged validamycin[69]
enhanced uptake/efficacy	nano- and microemulsions, nanospheres	nanopermethrin;[71] nanosphere insecticides[72]
enhanced toxicity to target organism (lower dose)	nanodispersions; nanosuspensions	nanodispersed triclosan[73]
nanoparticle as ai	nanometals and nanoclays	registered Nano-Ag biocide;[74] Nano-Si[75,76]

benefits including increased efficacy, durability, and a reduction in the amounts of active ingredients that need to be used.[2] A range of formulation types have been suggested including emulsions (e.g., nanoemulsions), nanocapsules (e.g., with polymers), and inorganic ENPs, such as metals, metal oxides, and nanoclays.[3−5] These products, which are at different stages in the product development cycle, can be used to improve the efficacy of existing pesticide active ingredients or to enhance their environmental safety profiles, or both (Table 1). In some cases, the ENP itself (or a solubilized form of the ENP) may "drive" the biological effect (e.g., nanosilver when used as a pesticide where the active component is the ionic silver that is released from the ENP), whereas in other cases nanotechnology is used to protect an ai or enhance its delivery to the site of action. In the future, nanotechnology may also provide benefits for precision farming through "smart field systems"; for example, wireless sensors could be linked via satellite to a laptop computer to detect and locate crop infestation with pathogens and to trigger application of pesticide as needed.[5] These systems have the potential to overcome the need to apply a pesticide to the entire crop, thereby protecting the environment through the use of reduced quantities and targeted application of the pesticide ai.

The increasing interest in the use of nanopesticides raises questions over how the environmental risk of these materials should be assessed for regulatory purposes. There is an increasing body of evidence (including from other applications of ENPs) that the factors and processes affecting the environmental behavior and effects of ENPs may differ from "conventional" substances that do not contain ENPs and, consequently, that methods used in current risk assessment approaches may need refining or replacing to deal with these differences. For example, the REACH framework for assessment of chemicals is considering amendments to its Annexes to account for some of the unique factors associated with ENPs. With respect to pesticides, the Scientific Advisory Panel of the Federal Insecticide, Fungicide, and Rodenticide Act (FIFRA) of the United States[8] discussed the adequacy of current procedures of hazard and exposure evaluation and concluded that (i) the potential risks of pesticides containing ENPs to humans and the environment may be different from those of conventional pesticides; (ii) the existing environmental fate and effects models are generally inadequate for predicting the behavior of nanopesticides; and (iii) additional metrics and parameters are needed for improved understanding of the environmental fate and effects processes associated with nanopesticides. European Union (EU) Regulation 1107/2009 for marketing authorization of plant protection products in Europe also requires the novel characteristics of a nanopesticide to be considered in the assessment process as it calls for due consideration of the interactions between the ai, safener (chemical substances used in combination with pesticides to make them "safer" and more targeted), synergists, and coformulants during the evaluation of a plant protection product.

In this paper, the current approaches for environmental risk assessment (ERA) of conventional pesticides are reviewed and their fitness for assessment of nanopesticides is analyzed (Table 2). In light of the insights generated, potential adaptations to existing ERA tests, as well as suitable alternative procedures for use with nanopesticides, are discussed. For the purpose of this review we consider three broad categories of nanopesticides: (i) where the nanoformulation is simply used to increase the apparent solubility/dispersion of the pesticide or to protect it from degradation in the formulation, but upon spraying is no longer associated with the ai; (ii) where the ENP is utilized to alter either the toxicokinetics or toxicodynamics of the pesticide, and as such is associated with the ai at least until it reaches the site of action; and (iii) where either the ENP itself or the nanopesticide complex is itself the active ingredient. It is the last category that presents the most complex scenario from a regulatory perspective. In all cases there exists also the potential for mixtures of "free" and nanoparticle-associated ai to coexist in the environment, the ratio of which may not be constant but change over time or as a function of the formulation and environmental conditions, thereby confounding measurements of efficacy and toxicity. Therefore, a key criterion for risk assessment purposes is the "durability" of the nano−ai complex following application of the nanopesticide.

CURRENT APPROACHES TO ENVIRONMENTAL RISK ASSESSMENT

Environmental risk assessments of pesticides are required in many regions of the world before a product can be placed on the market.[8,9] To limit the time, costs, and logistics needed for these risk assessments, a tiered approach focusing on key drivers of impact (e.g., Figure 1) is typically used. A tier is defined as a complete effect and exposure assessment resulting in an appropriate assessment end point. Each tier will involve the estimation of a predicted environmental concentration (PEC), which is the estimated concentration of an active substance in key environmental compartments including surface water, groundwater, and soil. The PECs are then compared to an effect end point such as a predicted no effect concentration (PNEC), the median effective concentration (EC_{50}), or no observed effect

Table 2. Different Environmental Fate Parameters Used for Conventional Pesticides and Their Relevance for Nanopesticides

characteristic	parameter/test currently used	is the characteristic relevant for NPs?	comments
distribution between soil, water, and air	K_{oc}/K_d	not appropriate	colloidal characteristics (aggregation, settlement, interaction with surfaces, matrix effects) drive the distribution, so other parameters may be needed; behavior will be concentration dependent, so studies should reflect likely environmental exposures; environmental parameters will affect particle behavior, so studies should cover environmentally relevant concentration ranges
	K_H	not appropriate	
	VP	not appropriate	
stability in soil, water, and sediment	DT_{50} soil	yes	half-lives of ENPs in different environmental matrices are relevant; the challenge is how to measure the ENPs; characteristics of the test matrices could be important in determining persistence, so a range of matrices should be tested
	DT_{50} water	yes	
	DT_{50} sediment	yes	
bioaccumulation	K_{ow} BCF	not appropriate	other parameters may emerge as understanding develops; rate constants for uptake and depuration may be a more suitable descriptor of potential accumulation; uptake is likely to be concentration dependent, so studies should reflect likely environmental exposures
		not appropriate	
environmental concentrations	PEC_{soil}	yes	mass concentration may not be the best metric for ENP risk, so it may be necessary to express exposure concentrations in other units such as particle number concentration or surface area concentration; exposure models may need refining to account for the processes important in transport of particles
	PEW_{sw}	yes	
	PEC_{sed}	yes	
	PEC_{gw}	yes	
	PEC_{air}	yes	
ecotoxicity	EC50, EC10	yes	maintenance of constant exposure conditions may be particularly challenging for nanopesticides; analytical characterization to support the tests may need to be considered; other units for effects concentration (e.g., particle size concentration) may be needed

dx.doi.org/10.1021/jf500232f | J. Agric. Food Chem. 2014, 62, 4227−4240

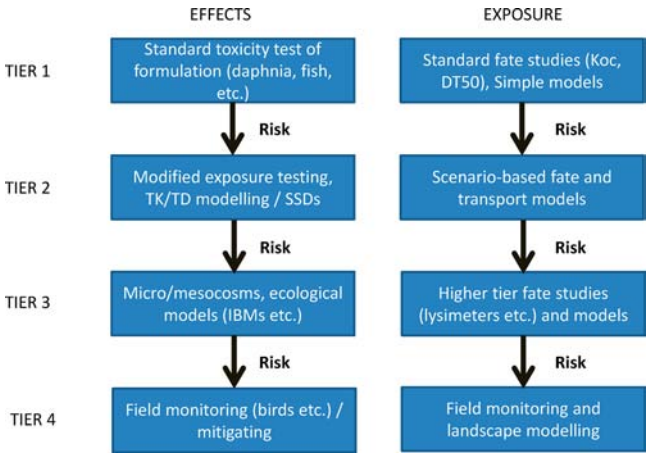

Figure 1. Tiered approach to environmental risk assessment of a pesticide.

concentration (NOEC) to derive a risk characterization ratio, which is compared with a regulatory trigger value. Uncertainty factors are incorporated into the process to account for the many uncertainties associated with extrapolating from regulatory fate and effect studies to impacts in the real environment.[10]

Under current regulations, PECs in soil, surface water, and groundwater need to be calculated for ERA purposes (e.g., FOCUS).[11] These concentrations are dependent on the use patterns of the product and the persistence and phase partitioning (e.g., sorption) of the ai in/between environmental compartments (e.g., soil, sediment, pore water). The movement of pesticide through the soil profile and ultimately to drainage systems or groundwater is described by models based on the convection−dispersion processes, whereas macropore transport is considered in some circumstances, for example, in the pesticide leaching model MACRO.[12] Pesticide runoff to surface streams is governed by off-site transport of pesticides in the solution phase, although erosion of the surface soil may also contribute to surface water contamination. Additional exposure pathways include off-target drifts during application, movement through subsurface drainage channels, and volatilization to, and deposition from, the atmosphere. Once in a water body, processes such as sorption, transformations, and flow dynamics influence the fate and risk of pesticides. These processes are characterized using the key parameters summarized in the following paragraphs.

Phase partitioning of the ai is often quantified with the sorption coefficients K_d or K_{oc}, (Table 2) and to characterize the nonlinear sorption behavior, the Freundlich isotherm is often measured. These measurements are usually carried out using the batch equilibration approach, where the soil and water phases are mixed to reach phase equilibrium.[13] Half-life ($t_{1/2}$) or half-dissipation time (DT_{50}) is used to indicate a pesticide's persistence in soil and can be measured in a laboratory incubation experiment or a field dissipation study.[14] The decrease of pesticide concentration in soil measured over time is used to fit kinetics models to derive $t_{1/2}$ or DT_{50}. Similarly, persistence is measured in water and sediment systems, and vapor pressure and Henry's law constant are required to estimate the potential for volatilization from soil or water.

The bioconcentration factor (BCF) is required to assess potential risks to high trophic levels and to classify compounds in terms of their persistence, bioaccumulation potential, or toxicity (PBT). Hydrophobicity (i.e., high K_{ow}) may trigger bioaccumulation tests that are conducted in accordance with relevant guidelines.[15] A BCF value for an ai can be derived in one of two ways. If bioaccumulation into nontarget organisms, such as fish, is viewed as a phase partitioning process, BCF can be calculated as the ratio of the uptake rate constant (K_{in}) to the depuration rate constant K_{out} measured in an exposure test that does not need to reach equilibrium. Alternatively, BCF can be calculated as the ratio of body residue to the concentration in water at the steady state.

The first tier of the assessment process typically uses simple exposure models with defined scenarios. For aquatic organisms, tests include studies with pelagic microalgae (green algae, blue-green algae, diatoms), aquatic plants (a monocotyledon and a dicotyledon), invertebrates (the crustaceans *Daphnia magna*, *Americamysis bahia*, the insect *Chironomus riparius*, oligochaeta *Lumbriculus variegatus*), and fish. For the terrestrial compartment, tests with earthworms (*Eisenia* sp., *Enchytraeus* sp.) and springtails (*Folsomia candida*) and studies into the effects on microbial community functions are most commonly conducted.

In the second tier, more complex exposure modeling may be used and more complex laboratory effect studies are likely to be employed such as modified exposure studies and/or toxicokinetic−toxicodynamic experiments and modeling or the development of species sensitivity distributions using additional nonstandard test species, preferably from taxa not included in the initial set of studies.

The third tier is used to assess processes such as biomagnification, recovery, and indirect effects using semirealistic exposure regimes and biological communities through the use of semifield experiments (i.e., microcosms, mesocosms) and ecological models. The last tier can include field monitoring of concentrations and effects of pesticide, although it is often difficult to get a clear view of the effects of a single pesticide given the presence of multiple stressors in agro-ecosystems. A diagrammatic representation of the tiered risk assessment approach currently used for pesticides is presented in Figure 1.

WHY MIGHT NANOPESTICIDES NEED A DIFFERENT APPROACH?

Over the past few years, understanding of the factors affecting the risks posed by ENPs to the environment has developed significantly. It is now recognized that many of the approaches and assumptions used to assess the risks of conventional chemicals may not be appropriate for ENPs and that some modifications may be required to risk assessment guidelines.[16,17] The OECD has a large work program that is considering how test guidelines may need to be adapted to assess the hazard of ENPs. In the following section we draw on some of this work, as well as the wider literature and the authors' expertise, to highlight how nanopesticides may differ from conventional pesticides in terms of their fate and effects and the implications of these differences for the ERA process.

For a conventional pesticide, it is usually assumed that ecotoxicity is related to ai mass concentration, and risk is therefore characterized using exposure and effects data expressed in terms of mass per volume or mass per mass of ai. However, for nanopesticides, other parameters such as particle number concentration and particle size distribution (PSD), as well as the ratio of "free" and nanoparticle-bound ai, may be important in determining the pesticide bioavailability and toxicity.[18−20] Analytical methodologies used to characterize the levels of available pesticides over time in regulatory fate and effect studies may therefore need to be supplemented with additional

methodologies that provide an understanding of the particle number concentration and particle size distribution over time. Approaches could include scattering methods (e.g., DLS), particle tracking methods (e.g., NTA), centrifugal methods (e.g., DCS), or fractionation methods (e.g., FFF), the latter method allowing for determination of ai size when coupled with appropriate chemical selective detectors. However, as these methods are not routine in pesticide analysis laboratories, this represents a significant change in approach. It is also important to note that nanopesticides will often undergo changes in their degree of dispersion or agglomeration over time, depending on the concentration of the nanopesticide and environmental factors such as pH, ionic strength, dissolved molecules of the test media, and as such are not equilibrium systems. Thus, characterization of a nanopesticide at different stages in its environmental life cycle and throughout fate and effect studies may be very important.

In standardized ecotoxicity studies, it is recommended that the test concentration should be kept within ±20% of the nominal test concentrations.[21] This is an important issue when considering products containing ENPs and so is also an issue for nanopesticides. For products containing ENPs, there is the question whether it is the mass concentration or the particle number concentration (and mean size) that should be maintained. It is clear that agglomerate/aggregate size and type will change throughout exposures. Furthermore, particle number varies markedly for ENPs of different sizes at a constant mass: for example, a particle mass of 100 ng corresponds to only 2.4×10^4 particles (spheres of unit density) of 2 μm in diameter, but to 2.4×10^{10} particles of 20 nm, or to 2.4×10^{13} particles of 2 nm.[22] Although the maintenance of a particle concentration to within ±20% of a starting concentration for a test is likely to be extremely challenging, it could be highly informative in understanding the risks of a nanopesticide to the natural environment.

The behavior of ENPs is similar to that of colloids, and therefore phase partitioning between environmental matrices cannot be assumed. For example, sorption and uptake into organisms are unlikely to be partitioning processes but rather involve active and receptor-mediated processes for uptake and aggregation and deposition processes for association with suspended matter, soil, or sediment. These processes will be dynamic,[23] whereas the phase partitioning driven process that occurs for conventional pesticides can to a large extent be modeled by equilibrium processes. Consequently, the use of soil sorption coefficients such as K_d or K_{oc} may not be relevant for modeling the movement of a nanopesticide within the environment (Table 2). Other factors such as the aggregation rate, sedimentation rate, and interaction of an ENP with surface receptors may need to be considered. The release rate of the ai from the ENP complex will also need to be characterized, as well as the ratio of free versus ENP-bound ai. Furthermore, transport of nanopesticides in air could be very different; for a conventional pesticide volatilization will be the process whereby the pesticide molecules transfer from soil and plant surfaces to the air, whereas for a nanopesticide the release of particles is likely to be important.

For aquatic and soil-dwelling organisms, dermal and respiratory surfaces represent a significant (often dominant) route of pesticide exposure. Partitioning principles govern the rate of entry across biological membranes such that the extent of absorption is driven by the chemical properties of the molecule (e.g., hydrophobicity) and the physiological structure (e.g., surface area, extent of sclerotization) of the biological surface. Upon entering the body, fugacity-driven distribution of the pesticide across different organs and tissues occurs, with fate in tissues determined by the organism's potential to biotransform molecules as a step toward elimination and by the potential to interact with the relevant cellular receptors. The primary (e.g., cytochrome P450), secondary (e.g., glutathione-s-transferase), and tertiary (e.g., ABC transporter) systems governing this metabolism and excretion are among the best studied biological pathways, whereas key uptake receptors are known as a function of the known mode(s) of action.

The diffusion and equilibrium partitioning that often dominate the cellular uptake of pesticides may not always be relevant for nanopesticides where the ai is bound to the ENP or is itself the ENP. As intact particles, there are a number of general mechanisms, such as passive and facilitated diffusion for direct transfer across biological membranes without enclosure[26] and active transport and endocytosis through membrane carrier proteins and channels,[27] that can result in the internalization of ENPs.[23,25]However, it is the mechanisms of endocytosis pathways that have received most attention through the use of pharmacological inhibitors[28] and gene activity disruption[29] to tease out the mechanisms and fluorescent labeled ENPs and antibody colocalization[30] studies to understand uptake kinetics and subcellular localization. Such studies have revealed that the size of ENPs taken up depends on the type of endocytosis and the corresponding vesicle sizes associated with their transport. Macropinosomes are generally 1−5 μm in diameter; calveolin-coated vesicles in the 50−80 nm range[31] and clathrin-mediated endocytosis structures are typically 120 nm in size. Most ENP have been found to localize in lysosomes following uptake,[32,33] which are sites of destruction for foreign or no longer useful materials, and there is thus the potential for release of locally high concentrations of pesticide from the lysosomes via the so-called "Trojan-horse" mechanism. The uptake pathway of a nanopesticide into organisms could therefore be very different from that of a conventional pesticide.

For conventional pesticides, the octanol/water partition coefficient (K_{ow}) is an important characteristic that indicates the affinity for lipid-rich tissues of nontarget organisms. Determining the K_{ow} values of ENPs is generally difficult because ENPs do not partition into either phase (Table 2). Rather, ENPs accumulate at the octanol/water interface because of their high surface energy.[34,35] Whereas the phase partitioning of organic molecules is driven partly by thermodynamics associated with water molecules versus the energy associated with partitioning to a surface, colloidal interactions are dependent on the net energy of attraction/repulsion with a surface.[36]

For pesticides it is usually assumed that dissipation, uptake, and distribution behavior is independent of the concentration. For nanopesticides it can be expected that phase partitioning, the relationship of mass concentration to particle concentration, uptake into biota, and distribution within organisms are all highly concentration dependent. It is likely that phase partitioning across membranes depends on the agglomeration status, size, and surface charge of ENPs; these parameters in turn depend on the concentration. For example, Handy et al.[37] in their idealized scenario of uptake of chemicals and ENPs by gills of freshwater fish, highlighted the key differences between lipophilic organic chemicals and ENPs. Prior to transfer across the gill epithelium, the substances must diffuse into the so-called unstirred layer (USL) made of water/mucous secretions. They observed that while small lipophilic organic molecules can easily diffuse into the USL and then through or between the

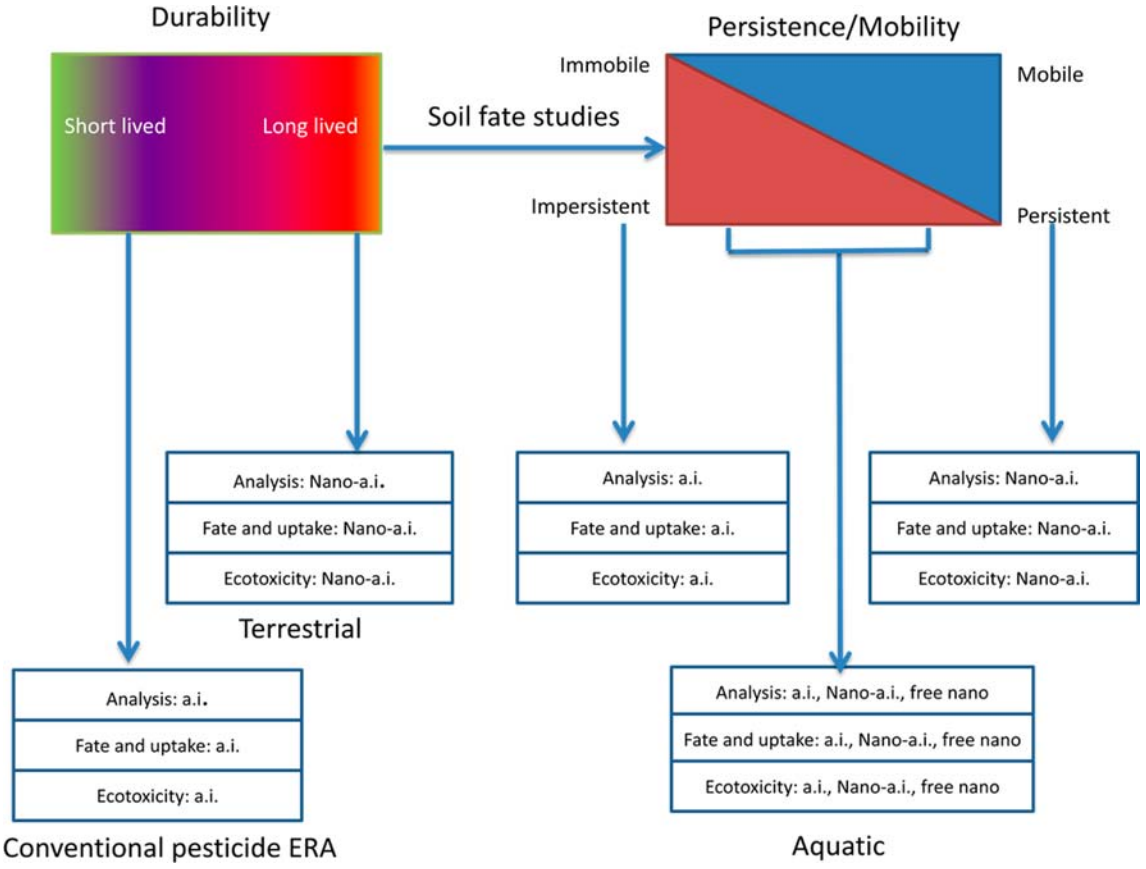

Figure 2. Conceptual strategy for assessing the environmental risks of a nanopesticide.

cells, ENPs are expected to diffuse at a slower rate that is influenced by humic substances and mucoproteins. In addition, ENPs may get entangled with mucoproteins, leading to prevention/retardation of their uptake. The size of ENPs precludes their uptake via ion or other transporters on the cell membranes. Furthermore, the Ca^{2+}- and Mg^{2+}-rich environment in the tight junctions between cells may trigger the aggregation of ENPs, thereby reducing their diffusion. Such processes at biological surfaces have the potential to alter the absorption and distribution of nanopesticides in comparison to traditional forms, with resultant effects on tissue distributions and biomagnification potential.

Quantifying internal exposure to ENPs may be required to understand the relationship between ENP properties and toxicity. For example, the rate of release of the ai will likely differ in different matrices. A consequence may be different exposure dynamics at target sites versus in the environment (e.g., fast release of ai in cellular compartments and slow release of ai in soil pore water due to different pH regimens and cellular enzymatic action). Quantitative property−toxicity relationships would help in the decision of how toxicity testing for ENPs should be standardized, but are not yet sufficiently developed or validated.

HOW COULD THE POTENTIAL RISK POSED BY A NANOPESTICIDE TO THE ENVIRONMENT BE ASSESSED?

It is clear from the above discussion that nanopesticides are likely to behave differently from conventional pesticides and that some of the traditional metrics used in ERA may be inappropriate for nanopesticides. Therefore, to adequately assess the environmental risk of a nanopesticide, alternative test methods and metrics may be required. Although in the future it may be possible to develop highly complex test methods and modeling approaches that accurately estimate the exposure and effects of a nanopesticide in a particular situation, we do not believe that the current knowledge allows us to do this at this time. It is also important to recognize that current approaches for conventional pesticide risk assessment employ many assumptions to address uncertainties and are by no means perfect themselves. To move forward in a pragmatic and implementable manner, we therefore propose a rational framework that accounts for the key differences between nanopesticides and conventional pesticides and where additional information may be required for their regulation. This aspect is further expanded in the sections below and illustrated schematically in Figure 2.

The proposed approach uses information on the durability of a nanopesticide product and the fate of the product in soil to make decisions on what component or mixture of components (e.g., conventional ai, nano−ai complex, or the free ENP acting as ai) should be tested and analyzed in aquatic fate studies and in aquatic and terrestrial ecotoxicity studies (Figure 2). The scientific rationale for this approach is that nanoformulation of a pesticide could be utilized to alter the toxicokinetics (i.e., the (rate of) uptake, biotransformation, distribution, and elimination) or the toxicodynamics (i.e., the mechanism or mode of toxic action of the ai), and by knowing which of these (or both) may be affected, rational decisions regarding modifications to existing tests or introduction of new tests could be made.

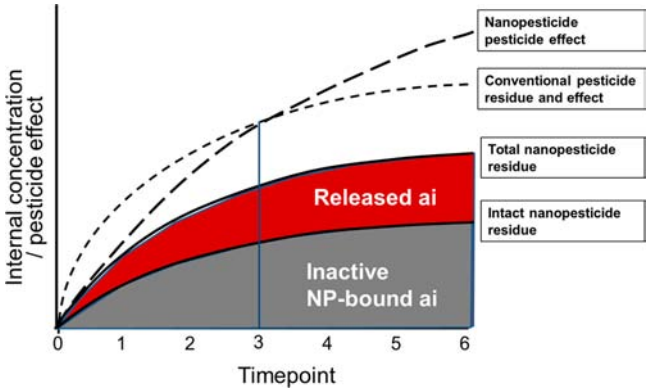

Figure 3. Schematic illustration of potential time-dependent (*x*-axis) effects on pesticide internal concentration and toxicity (*y*-axis) of nanoformulation pesticide preparations as compared to conventional forms. On the basis of the assumption that the ai is only active when released from the nanoformulation (which occurs over time), internal concentrations of released ai derived from the nanoformulation will increase over time as the pesticide is released from the nanocarrier. As a result, when exposure times are short in a test bioassay (e.g., up to timepoint 3), then the relatively small amount of ai that has been released may result in an observed toxicity that is lower than for the conventional ai formulation. In contrast, for longer term exposures (timepoints 4−6), the greater time allowed for ai release may result in higher internalized concentrations that can be associated with potential receptors to cause toxic effects that can be greater than for the conventional formulation.

Figure 3 provides an illustration of one scenario whereby the rate of release of ai from nanoformulation affects the duration of assessment required, assuming that the ai is only active in the free form. Other scenarios are also possible, such as the ai being active in the bound form also or even more active in the bound form, which would result in further alterations to the toxicokinetics diagram, but again an understanding of these effects would facilitate decision-making regarding appropriate testing durations and approaches. There is also potential for so-called Trojan-horse effects, whereby the uptake is of the nano−ai complex and the release of the ai occurs inside the plant cells; depending on the local environment, the release rate may be more dramatic, leading to extreme concentrations of ai that not occur via uptake of the free ai or to accumulation of NPs containing nonreleased ai. Such scenarios are not shown in Figure 3. Additionally, there is the potential that the ai may be more active in the bound state (nano−ai complex), in which case the nanoformulation would lead to higher local concentrations even at shorter time points.

If the nano component of a nanopesticide simply protects the ai from degradation in the formulation, then the fate and behavior of the ai will remain the same as in a conventional pesticide formulation and the nanocomponent will likely degrade during the application. Emulsions are a case in point. If the nanoformulation itself is the ai, or if the pesticide is more active when bound to the nanoparticle (e.g., as a result of increased local concentration, avidity effects, or optimal presentation of active site), then information about the conventional formulation will make only a minor contribution to understanding the nanoformulation. Thus, an understanding of where and how the nanoformulation is likely to affect the action of the ai will guide additional studies into characterization (e.g., particle number, ratio of free and nanoparticle-bound ai as a function of time/suspension conditions), fate and behavior, and efficacy, which may be required to gain regulatory approval. In the following sections we describe the different components of the scheme and the test approaches that could be employed. We start by considering the important elements of ENP characterization and quantification that are prerequisite to sound fate and effect assessment of nanopesticides.

CONSIDERATIONS FOR THE CHARACTERIZATION AND QUANTIFICATION OF NANOPESTICIDES

Similar considerations regarding the applicability of risk assessment approaches utilized for conventional chemicals to nanopesticides arise in terms of characterization, due to the challenges in analysis and characterization of nanobased materials in complex matrices.[38] Analysis of even conventional pesticides can be challenging at times.[39,40] Coupling this with the fact that techniques suitable for the detection, quantification, and characterization of nanopesticides (and indeed ENPs in general) in water, soil, and biota have not yet been validated or even developed in many cases leads to the conclusion that we are currently unable to adequately characterize these materials to support their risk assessment. Challenges are encountered due to the wide variety of nanopesticides and their presence as particle-bound forms making additional analysis (such as PSD, particle mass or number concentration, or surface charge) necessary. Expected environmental concentrations of nanopesticides will be low, and thus method sensitivity also becomes a challenge in the performance of fate and effect studies at environmentally relevant concentrations.

Techniques potentially suitable for the analysis of ENPs in environmental or food matrices have been extensively discussed in many reviews (e.g., Tiede et al.[41] and Hassellöv et al.[42]). To our knowledge no studies to date have examined the applicability of these methods of analysis to nanopesticides. Despite this, adequate analysis and characterization of nanopesticides are crucial for meaningful durability, fate, and ecotoxicity studies. This is indeed challenging, for not only the ai (conventional or ENP based) needs to be considered but the nano component (e.g., porous silica, metal oxide) also has to be characterized. Therefore, new methodologies will be required for nanopesticides, because extraction methods may alter the form of the nanopesticide, precluding any meaningful information on particle size distribution. Given the relatively high hydrophobicity of most pesticides,[43] strong nonpolar solvents under enhanced temperature and pressure conditions are often used to extract the residues.[39] However, such extraction procedures may affect the stability of the nano−ai complex.

On the basis of the assumption that various physical forms of the ai will display differences in mobility and toxicity, we propose a characterization scheme that employs the fractionation of the nanopesticides into three components: particulate (homo- and heteroaggregates incorporating ai), nanobound ai, and free ai. Size fractionation procedures (e.g., filtration, centrifugation) leading to operationally defined size classes are common in environmental analyses where size is relevant.[38,44] In particular, size fractionation, coupled to conventional pesticide analysis, could be used to determine the portion of the ai that remains associated with the nanocarrier and the agglomeration state of a nanocarrier, which will also influence ai fate and behavior. Although we propose that in principle this approach would in many cases provide an adequate level of characterization for risk assessment, current centrifugation and filtration methodologies require validation, and it is likely that further method development would be required to allow quantitative application.

dx.doi.org/10.1021/jf500232f | J. Agric. Food Chem. 2014, 62, 4227−4240

In some cases further characterization of the sample, or its size fractions, might be required. Physicochemical properties such as ENP size or shape could be characterized using the techniques outlined below and discussed in the literature. However, many conventional nanocharacterization methods (e.g., DLS, TEM) will lack the specificity needed to distinguish the nanopesticide from background particles as well as the sensitivity (limit of detection in terms of particle numbers) required for realistic environmental exposure concentrations.

Binary size separations (e.g., ultrafiltration, centrifugation), combined with appropriate physicochemical analysis of the fractions, can give information on the state of the ai as well as characteristics of the nanocarrier. Currently, two high-resolution size fractionation methods appear promising for application to nanopesticides. These are hydrodynamic chromatography (HDC),[45] which is somewhat analogous to the more commonly used size exclusion chromatography, and field flow fractionation (FFF). These approaches might find utility in cases when artifacts from filtration or centrifugation might be problematic or when a higher level of nanocharacterization (e.g., PSD of ai or nanocarrier) is desired. For some nonmetal based nanocomponents (e.g., polymers), detection, size characterization, and mass and/or particle number concentration analysis in environmental matrices could be particularly challenging.

For a nanopesticide consisting solely of a metal or metal oxide based ENP (i.e., where the ENP itself/dissolution of the ENP is the pesticide), conventional pesticide analysis is not required; however, chemical analysis for the element of interest (e.g., Ag, Si) using ICPMS will likely be possible. Element-specific size analysis is possible with specialized ICPMS techniques including FFF-ICPMS, HDC-ICPMS, and single particle ICPMS (spICP-MS) or even a combination of HDC-spICP-MS.[46−49] However, the use of complementary techniques such as TEM, NTA, and DLS is recommended to validate the measurements.

Recommended Approach for Characterization. Here we suggest a tiered analytical approach analogous to the tiered approach used in fate and ecotoxicology assessments. The degree to which one applies the methodology depends on the durability, mobility, and persistence of the respective nanopesticide. The tiered approach is detailed in Figure 4. At the simplest level (tier 1) the analytical approach is identical to what is currently performed for a pesticide ERA, namely, exhaustive extraction followed by analysis to quantify ai present in the samples. This is the most likely level needed for analysis of emulsions and short-lived, nonpersistent nanopesticides. However, if differences between nanoformulation and non-nanoformulation are seen in terms of durability, transport, and uptake, then additional "nano-analysis" of ai and carrier is required. This approach would likely be applied to polymer and "hard" ENPs (porous silica, metals, metal oxides). Although the approach involves methods that fractionate the nanocarrier, given the likely much higher toxicity of the ai over the nanocarrier, the chemical analysis of the fractions, or the online analysis in the case of HDC and FFF, is focused on quantification of the ai in each associated size fraction and on determination of whether the ai is free or nanobound. The exception is where the ai is the nanopesticide, for example, nano-Ag, in which case the additional physical characterization obtained by these methods (e.g., PSD of Ag) may prove valuable in the risk assessment.

EXPOSURE ASSESSMENT

Durability of the Product. The durability of the product will determine the extent to which the environment will be exposed to the nanopesticide. For some product types, for example, nanoemulsions or nanodispersions, that are used to enhance the apparent solubility, it is likely that following application the "nano" properties of the pesticide will be lost. In these cases we would recommend that the product be treated as a conventional pesticide in the risk assessment process. Information should be available from the product development studies that assist in assessing the likely durability of the nanopesticide following application. If the product is long-lived, we recommend that the terrestrial component of the risk assessment is carried out with the nano−ai complex. If available, persistence studies undertaken during product development would allow quantification of the release rates of the ai from the ai−nano complex as well as the ai and ENP degradation rates. Such measurements can be performed using the separation techniques described above.

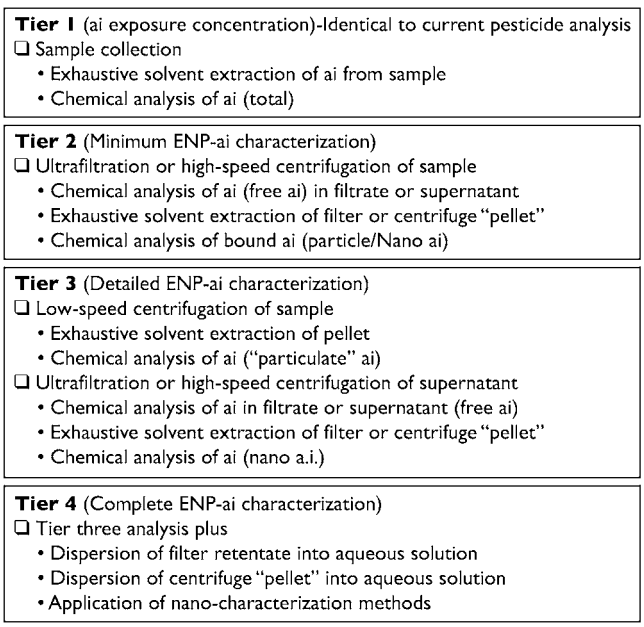

Figure 4. Tiered approach for analysis and characterization of nanopesticides.

Persistence. Using soil fate studies (e.g., column experiments, see Exposure Assessment below) nanopesticides can be characterized as persistent versus nonpersistent and mobile versus immobile. The outcome triggers how to continue the aquatic component of the risk assessment. If the nanopesticide (i.e., its nanoform) is nonpersistent, then the aquatic risk assessment may be conducted using only the ai. By contrast, if the nanopesticide is persistent, then the aquatic risk assessment has to be conducted using the nano−ai complex as well. If the persistence of the nano−ai complex is unclear or between those two clear-cut cases and threshold or trigger values need to be derived, then the aquatic risk assessment also needs to be carried out twice, that is, with the nano−ai complex and with the ai alone to cover possible worst case scenarios.

Persistence ($t_{1/2}$ or DT_{50}) of an ai may be influenced by its release from the carrier material. The release rate of the ai from the carrier and the degradation rate of the ai need to be quantified as both are key parameters in the transport models. We recommend incubation experiments with the ai as well as with the formulated product (i.e., the ENP−ai complex), where

the total concentration of the ai is measured. The difference between the experiment with the ai alone and with the ENP−ai complex would allow parametrization of the fate model by allowing estimates of release rate and degradation rate to be derived. However, it should be noted that this approach requires assumptions about the bioavailability of the ai when in the nano−ai complex. Two limit cases are possible: the ai in the nano−ai complex is equally accessible (bioavailable) for degradation as the ai without the nanocomplex, or the ai in the nano−ai complex is not degradable at all. An independent estimation of both the release rate and the degradation in the nano−ai complex is not possible from incubation experiments alone. However, an approach such as limited enzymolysis/proteolysis applied to the nano−ai complex and compared to the conventional ai would provide insights regarding the impact of the nanoformulation on the degradation/metabolism of the ai. This approach has been successfully applied to assess the impact of ENP on protein confirmation and degradation but has yet to be confirmed for environmental degradation. This approach could be a promising direction for initial testing.[50,51]

Mobility. The batch adsorption approach is not suitable for ENPs that are determined to undergo nonequilibrium processes. We suggest the use of column breakthrough experiments to derive nanopesticide mobility parameters as transport model inputs to estimate leaching or runoff/erosion movement. The experiments should not use excessive porewater velocity, as this may diminish the environmental relevance as velocity influences ENP fate.[52] These experiments should be undertaken with both the ai and the nanoformulation. In both cases, the concentration of ai in the leachate is measured and the fraction associated with the ENP−ai complex could be quantified using separation techniques, possibly in combination with advanced separation equipment such as FFF or HDC (as discussed in the characterization section above) to ensure robust quantification without interference from naturally occurring particles in the leachate. The fraction associated with soil colloids can be estimated from the difference in supernatant concentrations in the treatments (ai alone vs ENP−complex). Modeling techniques should be employed to derive the retardation (as opposed to sorption) parameters, which are based on the difference between the treatments using the release and degradation rates from durability studies, as described above.

Soils and Sediment−Water Test Systems for Sorption and Degradation Studies. The characteristics of soils for regulatory degradation and sorption studies are described in OECD guidelines.[13] Commonly used test soils are, in principle, suitable for studies with nanopesticides. However, additional criteria may be needed to ensure that soils with contrasting influences on ENP behavior are included in the studies. Important factors include pH, pore size distribution, ionic strength, dissolved organic carbon concentration, and clay content.[24] Characterization of persistence and sorption in sediment−water systems would follow the same principles as for soil, testing both the ai and the ENP−ai complex.

Fate and Exposure Modeling. The fate model would generally quantify free ai as well as the fraction of ai bound within the ENP−ai complex in different media. Existing fate models for pesticides could not be used without substantial revision and adaption to accommodate nanopesticide specific processes that are different from conventional pesticides. These differences include release of ai from nanopesticide complex, phase partitioning, agglomeration and changes in the ENP size distribution, possible interdependencies of particle size distribution, phase partitioning and degradation, as well as concentration dependence of all the above parameters.[36] The development of appropriate fate models for nanopesticides represents a significant challenge that will require substantial quantitative data from laboratory and field studies on nanopesticide behavior under various environmental conditions for model testing.

Uptake into Biota. Similarly to other ENPs, bioaccumulation cannot be viewed as a straight phase partitioning process, and K_{ow} is unlikely to be a good indicator for bioaccumulation potential of nanopesticides.[35] Therefore, BCF may not be estimated as the ratio of K_{in} and K_{out} in a short exposure tests and has been found to be not a relevant parameter to describe the bioaccumulation of ENPs.[53] It is generally considered that current standard protocols for bioaccumulation (e.g., fugacity-driven biomagnification) do not apply to ENPs (see below for more information; this has been reviewed previously[16,17]). As uptake processes for nanopesticides differ from those of conventional pesticides, the choice of test organisms may also have to be reconsidered. For example, filter feeders in aquatic environments (e.g., daphnids, bivalves) may be potentially vulnerable to elevated exposure due to their ability to process a large volume of media. For terrestrial systems, traditional test species such as earthworms that have a known potential for metal and organic chemical biomagnification are likely to be most relevant as they may accumulate larger amounts of nanopesticides. In the absence of a good predictor, such as K_{ow} for conventional pesticides, one has to rely on the testing of individual products. A test that reaches steady state may still yield the necessary information for assessing bioaccumulation potential, where bioaccumulation is calculated as the ratio of body residue over aqueous phase concentration at steady state. The experimental uptake test methods that explore uptake and depuration over time may be appropriate, but they need to (a) be designed using relevant dosing levels, (b) monitor steady state ENP concentrations in the media, (c) be representative of species likely to be exposed, and (d) be interpreted differently so as to reflect the uptake/depuration rates rather than the conventional BCFs. Whereas the need for global descriptors and predictive modeling frameworks for bioaccumulation assessment of ENPs is clear, considerable challenges remain in developing new or adapting existing protocols and approaches.[53] Time series based bioaccumulation studies to determine toxicokinetic parameters for nanopesticides are needed so the accumulation patterns of conventional pesticides and nanopesticides can be compared. These studies need to consider the form of the accumulated material (free versus nanobound ai) because this may have implications for the progression of toxicity over time (Figure 3).

EFFECTS ASSESSMENT

Are Current Standard Regulatory Approaches Applicable to Nanopesticides? As described above, there are standard regulatory approaches and tests that will need to be followed when the risks of conventional pesticides are assessed. A key question, therefore, is "are these standard ecotoxicity testing approaches appropriate for use on nanopesticides and are any modifications needed to these approaches?". The regulatory protection goals for a nanopesticide will be no different from those of a traditional pesticide, so the typical testing paradigm where acute and chronic effects data are generated for a range of trophic levels in different environmental compartments will be equally applicable to a nanopesticide. Questions

do, however, arise over which species should be tested and over whether specific test protocols need adaptation to cope with nanopesticides. The suitability of current standard test protocols for the assessment of hazard of products containing ENPs has been subject to much research and discussion. A technical workshop on the suitability of standard test methods for nanotoxicology[17] concluded recently that the standardized methods available for aquatic, sediment, and soil samples and mammalian and avian species provide a useful basis from which to develop appropriate effects studies for use with ENPs but that some modifications may be required. Some of these are discussed below.

Which Species Should Be Tested? Although the broad approach to testing may be relevant for effect assessment based on the range of currently utilized test organisms, the fate and form of a nanopesticide in an environment such as a surface water body could mean that certain organism types will have a higher degree of exposure than others. The requirement to include particle feeding organisms (e.g., filter or suspension feeders) in the test battery, as well as "conveyor-belt" feeders and benthic organisms, has already been proposed for general hazard assessment of ENPs, and these proposals should also apply to nanopesticides.

What Technical Modifications to Standard Test Protocols Could Be Needed? A wide range of technical modifications to standard test protocols have been proposed for ENPs,[16,17] which are likely to be equally required for nanopesticides. For example, appropriate references and controls (e.g., metal salts for metallic ENPs, larger scale (non-nanoscale) "bulk" materials, solvent controls) may be needed for comparative assessments; new dosing methods may be required to ensure homogeneous distributions of the material in the test systems; there may be a need for increased stirring/mixing of the water, or water changes, to maintain exposure concentrations in aquatic tests throughout a study; the duration of studies may need to be refined to reflect differences in the uptake kinetics of nanopesticides compared to conventional pesticides; and new characterization methods to track the dynamic behavior and fate of an ENP during an ecotoxicity study are likely to be needed and characterization may need to be done more frequently during a study than for a traditional pesticide. Some of the analytical approaches described under Recommended Approach for Characterization may be appropriate here. Two additional challenges associated with the application of standard test protocols for nanoformulations are (1) identification of the most appropriate dose metric and (2) accounting for nanoformulation agglomeration or aggregation, which also affects the available "nano" dose. As discussed earlier, mass is the metric utilized for ai and, indeed, for ENP to date, although there is considerable debate in the literature as to whether particle number, particle surface area, or reactive particle surface area would be more appropriate dose metrics for ENP[54] for dose–hazard and dose–exposure correlations. Aside from this, there is the unresolved question of how to compare the dose of conventional ai (free) versus nanoparticle-encapsulated/nanoparticle bound ai, which, as indicated in earlier sections, may be active in the bound form only or upon "release" only. Similar considerations apply to certain nanopharmaceuticals, and perhaps the approaches taken by medical regulators might be instructive in this respect. Considerations could include mass ai/ENP or mass ai/mass ENP while still reflecting the issue of durability of the nano–ai complex, as per Figure 2. Finally, the agglomeration potential of the nano–ai complex under actual exposure conditions would need to be factored into the assessment to correlate dose with response.

Role of Higher Tier Laboratory Ecotoxicity Testing Approaches. One of the main challenges in the risk assessment of nanopesticides will be how to combine the results from the standard effects studies and the exposure predictions. The use of higher tier laboratory ecotoxicity studies using, for example, natural waters rather than standard media or sediment–water test systems may overcome these issues. These approaches have been proposed for use in pesticide environmental risk assessment for some time now.[55] If designed correctly, the advantage of the approaches is that the test integrates the fate and effects processes that are likely to occur in the natural environment. Such approaches could be useful for assessing risk of nanopesticides until more mechanistic approaches are developed.

How Could Nanopesticides Interact with Other Environmental Contaminants? Whereas pesticides are assessed on a product by product basis, just like any other contaminant, in the real environment, they will co-occur with other substances, so mixture interactions are possible. Although risk assessment of environmental mixtures is not usually required for product risk assessment, it is possible that a nanopesticide will interact synergistically with other contaminants through the Trojan-horse effect.[56] This effect occurs when an ENP interacts with another substance and carries the substance into an organism or an organism tissue type. The effect can result in increased internal exposure to contaminants, which might not usually be accumulated. As our knowledge of these interactions increases, it may be necessary to incorporate these types of interactions into regulatory risk assessment schemes.

THE WAY FORWARD

Nanopesticides represent an attractive technological advancement from the standpoint of increased efficacy and protection of the environment and human health. The discussion in the preceding sections demonstrates that the factors and processes affecting the environmental behavior and effects of nanopesticides may differ from "conventional" pesticides, and therefore new or refined risk assessment approaches are needed. Unlike conventional pesticides, the uptake, bioavailability, and toxicity of nanopesticides are dependent on the particle number concentration and particle size distribution, as well as ratio of "free" and ENP-bound ai. Therefore, adaptation of existing methodologies and additional methodologies for analysis, characterization, environmental fate, and effect assessment are needed. However, considerable challenges exist, including maintenance of constant (±20%) particle concentration during the ecotoxicological tests, adequate characterization of the ENPs, identification and measurement of appropriate phase partitioning parameters (as conventional parameters may not apply), standardization of fate and toxicity testing protocols, and development of models (e.g., using quantitative structure–activity and property–toxicity relationships). Because current knowledge does not allow the accurate estimation of the exposure and effects of a nanopesticide in a particular situation, a pragmatic approach such as the one proposed here (Figure 2), coupled with a theoretical understanding of how nanoformulation might affect the toxicokinetics and/or toxicodynamics of the pesticide (Figure 3), is needed to move forward.

To implement this approach, a crucial decision-making step relates to the durability of a nanoformulated pesticide product and the fate of the product in soil. This allows identification of

whether the new product could be treated as a conventional pesticide or differently as a nanopesticide that demonstrates more activity as the ENP−ai complex. This step also guides the additional requirements in terms of ENP characterization and residue analysis as well as the fate and effect assessment. As discussed above, in several circumstances existing approaches can be used with some modifications and adaptations. Overall, the existing tiered risk assessment approach, such as that used in the EU, remains a useful framework for the risk assessment of nanopesticides, although with adaptions as presented above to account for potential alterations in the fate and behavior resulting from the nanoformulation. As the science of ENPs advances and new tools and techniques become available, the quality of data underpinning risk assessment will improve and further inform the regulatory requirements. In this regard, the collaborative efforts of the OECD Working Party on Manufactured Nanomaterials, the U.S. EPA, the APVMA, and other agencies may provide future guidance.

FUTURE NEEDS AND RECOMMENDATIONS

- Recent reviews on nanopesticides and ENPs used in crop protection and agricultural production[3−5] have discussed research priorities[57] and needs regarding nanospecific regulations.[58,59] Building on these, and including considerations of exactly where and how the nanoformulation might affect the environmental fate, behavior, and effects of a pesticide ai, we make the following recommendations relating to the development of a regulatory framework for nanopesticides. These are by no means exhaustive but merely indicative of different elements of an ERA (e.g., characterization, environmental fate and exposure, effect) required for an appropriate regulatory response for nanopesticides.
- A clear definition of what is/what is not a nanopesticide is needed for regulatory purposes. Definitions developed recently for nanomaterials in general may help, but these typically consider the size dimensions ranging between 1 and 100 nm and are only partially applicable to nanopesticides. Emerging pesticide nanoformulations are not only increasingly complex and biologically active but may also exhibit a potential change in the physicochemical properties and/or biological effects at a size range that is larger than the nanoscale (>100 nm). The need for inclusion of additional parameters[60] and larger size limits, for example, up to 1000 nm, has also been proposed for some nanomaterials.[61,62]
- Tools and techniques to characterize properties (such as primary particle shape, size range, surface properties) of complex formulations of nanopesticides are lacking. Without adequate analytical tools, regulatory requirements for robust data for risk assessment cannot be generated. Current ecotoxicological assessments have limited relevance due to a poor ability to characterize ENPs in complex environmental compartments at present, although this area is developing quickly. Despite greater attention to inorganic ENPs (compared to organic), detection and quantification of nanometal and metal oxides in complex matrices (e.g., formulations, environmental media) at environmentally realistic concentrations remain challenging. Nanopesticides are more complex products by design (Table 1) and therefore pose greater challenges to analysts. However, experience gained in the field of nanomedicine may be helpful for characterizing nanopesticides and should be integrated into the nanopesticide regulatory framework.
- Little advancement in exposure and effect modeling has so far occurred on ENPs and especially nanopesticides. Current models fail to take into consideration material sizes, shapes, functionalization, and surface properties and alterations in both ENPs and environmental matrices during exposure assessment.[63] Exposure models that differentiate the free and nanocomplex and the ENP size distribution and other toxicologically/fate relevant properties over time need to be developed as a matter of priority. Until we better understand the relationship between ENP properties and toxicity, we can only resort to toxicity testing case by case under conditions similar to those in the environment. As this may quickly become infeasible, sound ERA requires first the establishment of property−toxicity relationships based on comprehensive empirical data.
- Given the added uncertainty in risk assessment (such as that associated with detection and quantification, characterization, and exposure assessment) compared to "conventional" pesticides, the definition as well as the regulatory framework should consciously be made more adaptive and responsive to advancements in science and knowledge on nanopesticides. A pragmatic approach is to focus on understanding the persistence of the nano−ai complex and whether the nano−ai complex alters the activity of the ai relative to the conventional formulation as described here for reformulated pesticides. However, where the ENP itself is the ai, additional challenges remain.

Evidence-based decision-making is an expectation of contemporary regulators and demands that decisions are supported by science, and precaution is used where evidence is incomplete. To this end, regulators are warranted in erring on the side of caution until such time as the properties and behavior of nanopesticides are better understood. This may curtail the realization of full potential economic and environmental benefits of this rapidly expanding technology. It is also important that the product developer is aware that the nanoformulation of an already approved pesticide will require a separate ERA.

AUTHOR INFORMATION

Corresponding Author

Phone: +61 - 8- 83038450 email: Rai.Kookana@csiro.au.

Notes

The authors declare no competing financial interest.

ACKNOWLEDGMENTS

This paper was developed during a workshop (York, May 17−18, 2013) as a part of an IUPAC project on "Guiding principles to facilitate a harmonized ecological risk assessment framework for nanopesticides in the environment". Financial support to the project by IUPAC and the Australian Pesticides and Veterinary Medicines Authority (APVMA) is gratefully acknowledged. We thank the University of York for hosting the workshop.

ABBREVIATIONS USED

ai	active ingredient
APVMA	Australian Pesticides and Veterinary Medicines Authority

BCF	bioconcentration factor
DCS	differential centrifugal sedimentation
DLS	dynamic light scattering
DT_{50}	dissipation half-life
EC	European Commission
EC50	half-maximal effective concentration
EFSA	European Food Safety Authority
ENP	engineered nanoparticle
ERA	Environmental Risk Assessment
EU	European Union
FDA	U.S. Food and Drug Administration
FIFRA-SAP	Federal Insecticide, Fungicide, and Rodenticide Act−Scientific Advisory Panel (USA)
FFF	field flow fractionation
FOCUS	forum for the co-ordination of pesticide fate models and their use
HDC	hydrodynamic chromatography
IBMs	individual-based models
ICPMS	inductive coupled plasma mass spectrometry
IUPAC	International Union of Pure and Applied Chemistry
K_d	soil/water partitioning coefficient; sorption coefficient
K_{oc}	soil organic carbon:water partitioning coefficient
K_{ow}	octanol/water partition coefficient
NOEC	no observed effect concentration
NTA	nanoparticle tracking analysis
MACRO	model designed to incorporate preferential flow
OECD	Organisation for Economic Co-operation and Development
PBT	persistent, bioaccumulative and toxic
PEC	predicted environmental concentration
PSD	particle size distribution
SEM	scanning electron microscopy
spICPMS	single-particle inductive coupled plasma mass spectrometry
SSD	species sensitivity distribution
$t_{1/2}$	decay half-life
TK/TD	toxicokinetics/toxicodynamics
TEM	transmission electron microscopy
USL	unstirred layer

REFERENCES

(1) Aitken, R. J.; Chaudhry, M. Q.; Boxall, A. B. A.; Hull, M. Manufacture and use of nanomaterials: current status in the UK and global trends. *Occup. Med.* **2006**, *56*, 300−306.

(2) Pérez-de-Luque, A.; Rubiales, D. Nanotechnology for parasitic plant control. *Pest Manage. Sci.* **2009**, *65*, 540−545.

(3) Kah, M.; Beulke, S.; Tiede, K.; Hofmann, T. Nano-pesticides: state of knowledge, environmental fate and exposure modelling. *Crit. Rev. Environ. Sci. Technol.* **2013**, *43*, 1823−1867.

(4) Gogos, A.; Knauer, K.; Bucheli, T. Nanomaterials in plant protection and fertilization: current state, foreseen applications, and research priorities. *J. Agric. Food Chem.* **2012**, *60*, 9781−9792.

(5) Khot, L. R.; Sankaran, S.; Maja, J. M.; Ehsani, R.; Schuster, E. Application of nanomaterials in agricultural production and crop protection: a review. *Crop Prot.* **2012**, *35*, 64−70.

(6) Bergeson, L. L. Nanosilver: US EPA's pesticide office considers how best to proceed? *Environ. Qual. Manage.* **2010**, *19* (3), 79−85.

(7) EC. European Commission Recommendation on the definition of nanomaterial; http://osha.europa..eu/en/news/eu-euopean-commission-recommendation-on-the-definition-of-nanomaterial (Feb 28, 2012).

(8) FIFRA-SAP, 2009. Evaluation of the hazard and exposure associated with nanosilver and other nanometal pesticide products. U.S. Federal Insecticide, Fungicide, and Rodenticide Act (FIFRA) Scientific Advisory Panel (SAP); http://www.epa.gov/scipoly/sap/meetings/2009/november/110309ameetingminutes.pdf.

(9) EC (2009) Regulation (EC) No. 1107/2009 of the European parliament and the council of 21 October 2009 concerning the placing of plant protection products on the market and repealing Council Directives 79/117/EEC and 91/414/EEC. *Off. J. Eur. Union* **2009**, *309*, 1−50.

(10) EFSA. European Food Safety Authority, Panel on Plant Protection Products and their Residues). DRAFT Guidance Document on tiered risk assessment for plant protection products for aquatic organisms in edge-of-field surface waters. *EFSA J.* **2013**, *11* (7), 3290; DOI: 10.2903/j.efsa.2013.3290.

(11) FOCUS. FOCUS Surface Water Scenarios in the EU Evaluation Process under 91/414/EEC. Report, EC Document Reference SANCO/4802/2001-rev.1. Report of the FOCUS Working Group on Surface Water Scenarios, Brussels, Belgium, 2001.

(12) Jarvis, N. J.; Larsbo, M. MACRO (V5.2): Model use, calibration and validation. *Trans. ASABE* **2012**, *55*, 1413−1423.

(13) OECD TG 106. Adsorption−desorption using a batch equilibration method, Test Guideline 106, 2000.

(14) OECD TG 307. Aerobic and anaerobic transformation in soil, Test Guideline 307, 2002.

(15) OECD TG 305. Bioaccumulation in fish: aqueous and dietary exposure, Test Guideline 305, 2012.

(16) Handy, R. D.; Van den Brink, N.; Chappell, M.; Muhling, M.; Behra, R.; Dusinska, M.; Simpson, P.; Ahtiainen, J.; Jha, A. N.; Seiter, J.; Bednar, A.; Kennedy, A.; Fernandes, T. F.; Riediker, M. Practical considerations for conducting ecotoxicity test methods with manufactured nanomaterials: what have we learned so far? *Ecotoxicology* **2012**, *21* (4), 933−972.

(17) Handy, R. D.; Cornelis, G.; Fernandes, T. F.; Tsyusko, O.; Decho, A.; Sabo-Attwood, T.; Metcalfe, C.; Steevens, J.; Klaine, S. J.; Koelmans, A. A.; Horne, N. Ecotoxicity test methods for engineered nanomaterials: practical experiences and recommendations from the bench. *Environ. Toxicol. Chem.* **2012**, *31* (1), 15−31.

(18) French, R. A.; Jacobson, A. R.; Kim, B.; Isley, S. L.; Penn, R. N.; Baveye, P. C. Influence of ionic strength, pH, and cation valence on aggregation kinetics of titanium dioxide nanoparticles. *Environ. Sci. Technol.* **2009**, *43* (5), 1354−1359.

(19) Kümmerer, K.; Menz, J.; Schubert, T.; Thielemans, W. Biodegradability of organic nanoparticles in the aqueous environment. *Chemosphere* **2010**, *82* (10), 1387−1392.

(20) Sharma, V. K. Aggregation and toxicity of titanium dioxide nanoparticles in aquatic environment − a review. *J. Environ. Sci. Health, A* **2009**, *44* (14), 1485−1495.

(21) OECD TG 203. Fish, acute toxicity test, Test Guideline 203, 1992.

(22) Geiser, M.; Kreyling, W. G. Deposition and biokinetics of inhaled nanoparticles. *Particle Fibre Toxicol.* **2010**, *7* (2), DOI: 10.1186/1743-8977-7-2.

(23) Cornelis, G.; Hund-Rinke, K. M.; Kuhlbusch, T.; Van den Brink, N.; Nickel, C. Fate and bioavailability of engineered nanoparticles in soils: a review. *Crit. Rev. Environ. Sci. Technol.* **2013**, DOI: 10.1080/10643389.2013.829767.

(24) Salvati, A.; Aberg, C.; dos Santos, T.; Varela, J.; Pinto, P.; Lynch, I.; Dawson, K. A. Experimental and theoretical comparison of intracellular import of polymeric nanoparticles and small molecules: toward models of uptake kinetics. *Nanomedicine* **2011**, *7* (6), 818−826.

(25) Stone, V.; Johnston, H.; Schins, R. P. F. Development of in vitro systems for nanotoxicology: methodological considerations. *Crit. Rev. Toxicol.* **2009**, *39* (7), 613−626.

(26) Geiser, M.; Rothen-Rutishauser, B.; Kapp, N.; Schurch, S.; Kreyling, W.; Schulz, H.; Semmler, M.; Hof, V. I.; Heyder, J.; Gehr, P. Ultrafine particles cross cellular membranes by nonphagocytic mechanisms in lungs and in cultured cells. *Environ. Health Perspect.* **2005**, *113* (11), 1555−1560.

(27) Lee, K. J.; Nallathamby, P. D.; Browning, L. M.; Osgood, C. J.; Xu, X.-H. N. In vivo imaging of transport and biocompatibility of

single silver nanoparticles in early development of zebra fish embryos. *ACS Nano* **2007**, *1* (2), 133−143.
(28) dos Santos, T.; Varela, J.; Lynch, I.; Salvati, A.; Dawson, K. A. Effects of transport inhibitors on the cellular uptake of carboxylated polystyrene nanoparticles in different cell lines. *PLoS One* **2011**, *6* (9), DOI: 10.1371/journal.pone.0024438
(29) Unrine, J. M.; Shoults-Wilson, W. A.; Zhurbich, O.; Bertsch, P. M.; Tsyusko, O. V. Trophic transfer of Au nanoparticles from soil along a simulated terrestrial food chain. *Environ. Sci. Technol.* **2012**, *46* (17), 9753−9760.
(30) Shapero, K.; Fenaroli, F.; Lynch, I.; Cottell, D. C.; Salvati, A.; Dawson, K. A. Time and space resolved uptake study of silica nanoparticles by human cells. *Mol. Biosyst.* **2011**, *7* (2), 371−378.
(31) Patel, L.; Zaro, J.; Shen, W.-C. Cell penetrating peptides: Intracellular pathways and pharmaceutical perspectives. *Pharm. Res.* **2007**, *24* (11), 1977−1992.
(32) Stern, S. T.; Adiseshaiah, P. P.; Crist, R. M. Autophagy and lysosomal dysfunction as emerging mechanisms of nanomaterial toxicity. *Particle Fibre Toxicol.* **2012**, *9* (20), DOI: 10.1186/1743-8977-9-20.
(33) Sandin, P.; Fitzpatrick, L. W.; Simpson, J. C.; Dawson, K. A. High-speed imaging of Rab family small GTPases reveals rare events in nanoparticle trafficking in living cells. *ACS Nano* **2012**, *6* (2), 1513−1521, DOI: 10.1021/nn204448x.
(34) Hristovski, K.; Westerhoff, P.; Posner, J. Octanol-water partitioning of engineered nanomaterials. *J. Environ. Sci. Health, Part A* **2011**, *46*, 636−647.
(35) Petersen, E. J.; Huang, Q. G.; Weber, W. J. Relevance of octanol-water distribution measurements to the potential ecological uptake of multi-walled carbon nanotubes. *Environ. Toxicol. Chem.* **2010**, *29*, 1106−1112.
(36) Westerhoff, P.; Nowack, B. Searching for global descriptors of engineered nanomaterial fate and transport in the environment. *Acc. Chem. Res.* **2013**, *46*, 844−853.
(37) Handy, R. D.; Henry, T. B.; Scown, T. M.; Johnson, B. D.; Tyler, C. R. Manufactured nanoparticles: their uptake and effects on fish−a mechanistic analysis. *Ecotoxicology* **2008**, *17*, 396−409.
(38) von der Kammer, F.; Ferguson, P. L.; Holden, P. A.; Masion, A.; Rogers, K. R.; Klaine, S. J.; Koelmans, A. A. Analysis of engineered nanomaterials in complex matrices (environment and biota): general considerations and conceptual case studies. *Environ. Toxicol. Chem.* **2012**, *31* (1), 32−49.
(39) Hladik, M. L.; McWayne, M. M. Methods of analysis − determination of pesticides in sediment using gas chromatography/mass spectrometry. *Techniques Methods 5−C3*; USGS: Washington, DC, USA, 2012
(40) Britt, J. K.; McDowell, T. C.; Dwinell, S. E. Matrix decision procedure to assess new pesticides based on relative groundwater leaching potential and chronic toxicity. *Environ. Toxicol. Chem.* **1992**, *11*, 721−728.
(41) Tiede, K.; Hassellöv, M.; Breitbarth, E.; Chaudhry, Q.; Boxall, A. B. A. Considerations for environmental fate and ecotoxicity testing to support environmental risk assessments for engineered nanoparticles. *J. Chromatogr., A* **2009**, *1216* (3), 503−509.
(42) Hassellöv, M.; Readman, J. W.; Ranville, J. F.; Tiede, K. Nanoparticle analysis and characterization methodologies in environmental risk assessment of engineered nanoparticles. *Ecotoxicology* **2008**, *17* (5), 344−361.
(43) Noble, A. Partition coefficients (n-octanol−water) for pesticides. *J. Chromatogr., A* **1993**, *642* (1−2), 3−14.
(44) Lead, J. R.; Wilkinson, K. J. Aquatic colloids and nanoparticles: current knowledge and future trends. *Environ. Chem.* **2006**, *3* (3), 159−171.
(45) Tiede, K.; Boxall, A. B. A.; Wang, X.; Gore, D.; Tiede, D.; Baxter, M.; David, H.; Tear, S. P.; Lewis, J. Application of hydrodynamic chromatography-ICP-MS to investigate the fate of silver nanoparticles in activated sludge. *J. Anal. At. Spectrom.* **2010**, *25*, 1149−1154.
(46) Tuoriniemi, J.; Cornelis, G.; Hassellöv, M. Size discrimination and detection capabilities of single-particle ICPMS for environmental analysis of silver nanoparticles. *Anal. Chem.* **2012**, *84* (9), 3965−3972.
(47) Pace, H. E.; Rogers, N. J.; Jarolimek, C.; Coleman, V. A.; Higgins, C. P.; Ranville, J. F. Determining transport efficiency for the purpose of counting and sizing nanoparticles via single particle inductively coupled plasma mass spectrometry. *Anal. Chem.* **2011**, *83* (24), 9361−9369.
(48) Pergantis, S. A.; Jones-Lepp, T. L.; Heithmar, E. M. Hydrodynamic chromatography online with single particle-inductively coupled plasma mass spectrometry for ultratrace detection of metal-containing nanoparticles. *Anal. Chem.* **2012**, *84* (15), 6454−6462.
(49) Gray, E. P.; Bruton, T. A.; Higgins, C. P.; Halden, R. U.; Westerhoff, P. W.; Ranville, J. F. Analysis of gold nanoparticle mixtures: a comparison of hydrodynamic chromatography (HDC) and asymmetrical flow field-flow fractionation (AF4) coupled to ICP-MS. *J. Anal. At. Spectrom.* **2012**, *27*, 1532−1539.
(50) Cukalevski, R.; Lundqvist, M.; Oslakovic, C.; Dahlbäck, B.; Linse, S.; Cedervall, T. Structural changes in apolipoproteins bound to nanoparticles. *Langmuir* **2011**, *27* (23), 14360−14369.
(51) Yang, J. A.; Johnson, B. J.; Wu, S.; Woods, W. S.; George, J. M.; Murphy, C. J. Study of wild-type α-synuclein binding and orientation on gold nanoparticles. *Langmuir* **2013**, *29* (14), 4603−4615.
(52) Ben-Moshe, T.; Dror, I.; Berkowitz, B. Transport of metal oxide nanoparticles in saturated porous media. *Chemosphere* **2010**, *81*, 387−393.
(53) Hou, W. C.; Westerhoff, P.; Posner, J. D. Biological accumulation of engineered nanomaterials: a review of current knowledge. *Environ. Sci.−Processes Impacts* **2013**, *15*, 103−122.
(54) Oberdorster, G. Safety assessment for nanotechnology and nanomedicine: concepts of nanotoxicology. *J. Intern. Med.* **2009**, *267*, 89−105.
(55) Boxall, A. B. A.; Brown, C. D.; Barrett, K. Higher-tier laboratory methods for assessing the aquatic toxicity of pesticides. *Pest Manage. Sci.* **2002**, *58*, 637−648.
(56) Park, E. J.; Yi, J.; Kim, Y.; Choi, K.; Park, K. Silver nanoparticles induce cytotoxicity by a Trojan-horse type mechanism. *Toxicol. In Vitro* **2010**, *24* (3), 872−878.
(57) Kah, M.; Hofmann, T. Nanopesticides research: current trends and future priorities. *Environ. Int.* **2014**, *63*, 224−235.
(58) Stone, D.; Harper, B. J.; Lynch, I.; Dawson, K.; Harper, S. L. Exposure assessment: recommendations for nanotechnology-based pesticides. *Int. J. Occup. Environ. Health* **2010**, *16* (4), 467−474.
(59) Park, S.; Woodhall, J.; Ma, G.; Veinot, J. G. C.; Cresser, M. S.; Boxall, A. B. A. Regulatory ecotoxicity testing of engineered nanoparticles: are the results relevant to the natural environment? *Nanotoxicology* **2013**, DOI: 10.3109/17435390.2013.818173.
(60) SCENIHR 2010. Opinion on: Scientific Basis for the Definition of the Term "nanomaterial". Scientific Committee on Emerging and Newly Identified Health Risks (SCENIHR) 2010; available at http://ec.europa.eu/health/scientific_committees/emerging/docs/scenihr_o_032.pdf (accessed Sept 2013).
(61) House of Lords Science and Technology Committee Report on Nanotechnologies and Food. HL Paper 22-I, 2010; http://www.publications.parliament.uk/pa/ld200910/ldselect/ldsctech/22/22i.pdf (accessed Sept 2013).
(62) Health Canada. Interim policy statement on Health Canada's Working Definition for Nanomaterials, 2010; available at http://www.hc-sc.gc.ca/sr-sr/consult/_2010/nanomater/draft-ebauche-eng.php (accessed Sept 2013).
(63) Gottschalk, F.; Kost, E.; Nowack, B. Engineered nanomaterials in water and soils: a risk quantification based on approach on probabilistic exposure and effects modelling. *Environ. Toxicol. Chem.* **2013**, *32*, 1278−1287.
(64) ObservatoryNano. Nanotechnologies for nutrient and biocide delivery in agricultural production. Working Paper April 2010; available at http://www.observatorynano.eu/project/filesystem/files/Controlled%20delivery.pdf.

(65) Jianhui, Y.; Kelong, H.; Yuelong, W.; Suquin, L. Study on anti-pollution nano-preparation of dimethomorph and its performance. *Chin. Sci. Bull.* **2005**, *50*, 108−112.
(66) Guan, H.; Chi, D.; Yu, J.; Li, H. Dynamics of residues from a novel nano-imidacloprid formulation in soybean fields. *Crop Prot.* **2010**, *29*, 942−946.
(67) Liu, Y.; Tong, Z.; Prud'homme, R. K. Stabilized polymeric nanoparticles for controlled and efficient release of bifenthrin. *Pest Manage. Sci.* **2008**, *64*, 808−812.
(68) Hussein, M. Z. B.; Yahya, A. H.; Zainal, Z.; Kian, L. H. Nanocomposite-based controlled release formulation of a herbicide, 2,4-dichlorophenoxyacetate encapsulated in zinc-aluminium-layered double hydroxide. *Sci. Technol. Adv. Mater.* **2005**, *6*, 956−962.
(69) Liu, F.; Wen, L.-X.; Li, Z.-Z.; Yu, W.; Sun, H.-Y.; Chen, J.-F. Porous hollow silica nanoparticles as controlled delivery system for water soluble pesticide. *Mater. Res. Bull.* **2006**, *41*, 2268−2275.
(70) Ishaque, M.; Schnable, G.; Anspaugh, D. Agrochemical formulations comprising a pesticide, an organic UV-photoprotective filter and coated metal-oxide nanoparticles. WO/2009/153231, 2009.
(71) Anjali, C. H.; Khan, S. S.; Margulis-Goshen, K.; Magdassi, S.; Mukherjee, A.; Chandrasekaran, N. Formulation of water-dispersible nanopermethrin for larvicidal applications. *Ecotoxicol. Environ. Saf.* **2010**, *73*, 1932−1936.
(72) Boehm, A. L.; Martinon, I.; Zerrouk, R.; Rump, E.; Fessi, H. Nanoprecipiation technique for the encapsulation of agrochemical active ingredients. *J. Microencapsulation* **2003**, *20*, 433−441.
(73) Zhang, H. F.; Wang, D.; Butler, R.; Campbell, N. L.; Long, J.; Tan, B. E.; Duncalf, D. J.; Foster, A. J.; Hopkinson, A.; Taylor, D.; Angus, D.; Cooper, A. I.; Rannard, S. P. Formation and enhanced biocidal activity of water-dispersible organic nanoparticles. *Nat. Nanotechnol.* **2008**, *3*, 506−511.
(74) Costanza, J.; El Bawawy, A. M.; Tolaymot, T. M. Comment on "120 years of nanosilver history: implications for policy makers. *Environ. Sci. Technol.* **2011**, *45*, 7591−7592.
(75) Debnath, N.; Das, S.; Seth, D.; Chandra, R.; Bhattacharya, S.; Goswami, A. Entomotoxic effects of silica nanoparticles against *Sitophilus oryzae* (L.). *J. Pestic. Sci.* **2010**, *84*, 99−105.
(76) Nair, R.; Varghese, S. H.; Nair, B. G.; Maekewa, T.; Yoshida, Y.; Kumar, D. S. Nanoparticulate material delivery to plants. *Plant Sci.* **2010**, *179*, 154−163.

JOURNAL OF AGRICULTURAL AND FOOD CHEMISTRY

Article

pubs.acs.org/JAFC

Rapid HPLC-MS Method for the Simultaneous Determination of Tea Catechins and Folates

Monica Araya-Farias,[†,‡,§] Alain Gaudreau,[†,‡] Elodie Rozoy,[†,‡] and Laurent Bazinet*[,†,‡]

[†]Institute of Nutrition and Functional Foods (INAF) and [‡]Department of Food Sciences and Nutrition, Laval University, Quebec, QC, Canada G1V 0A6

ABSTRACT: An effective and rapid HPLC-MS method for the simultaneous separation of the eight most abundant tea catechins, gallic acid, and caffeine was developed. These compounds were rapidly separated within 9 min by a linear gradient elution using a Zorbax SB-C_{18} packed with sub 2 μm particles. This methodology did not require preparative and semipreparative HPLC steps. In fact, diluted tea samples can be easily analyzed using HPLC-MS as described in this study. The use of mass spectrometry detection for quantification of catechins ensured a higher specificity of the method. The percent relative standard deviation was generally lower than 4 and 7% for most of the compounds tested in tea drinks and tea extracts, respectively. Furthermore, the method provided excellent resolution for folate determination alone or in combination with catechins. To date, no HPLC method able to discriminate catechins and folates in a quick analysis has been reported in the literature.

KEYWORDS: *green tea, catechins, folates, HPLC, mass spectrometry*

INTRODUCTION

Green tea, a nonfermented tea, has become one of the most widely consumed beverages in the world. The increasing consumption of green tea can be explained by the health effects of some of its constituents. Indeed, green tea is rich in flavonoids (300−400 mg/g) and an excellent source of catechins, up to 20−30% of the green tea dry weight.[1,2] The eight most abundant catechins in tea are (−)-gallocatechin, (−)-epigallocatechin, (+)-catechin, (−)-epicatechin, (−)-epigallocatechin gallate, (−)-gallocatechin gallate, (−)-epicatechin gallate, and (−)-catechin gallate. The principal tea catechins are known for their strong antioxidant activity and their health benefits, including antiviral, antiallergic, anti-inflammatory, and anticariogenic properties.[3,4] In addition to tea catechins, green tea contains other polyphenols such as gallic acid, the main tea polyphenolic acid, and certain amounts of alkaloids such as caffeine. Although caffeine is well-known for its stimulatory effect, it has been reported that caffeine also exerts beneficial effects on human health including cardiovascular, gastrointestinal, and respiratory effects.[5] Caffeine affects also the taste of tea.[6] The composition of green tea catechins, phenolic acids, and caffeine varies according to variety, climate, horticultural conditions, and mainly in technologies applied during extraction, concentration, and storage.

Folates play a critical role in the reduction of neural tube defects in newborns and the risk of cardiovascular diseases.[7] Folic acid (FA) is not a significant natural form of folate. However, FA is synthetically produced and used as a dietary supplement because it is the most stable form of this vitamin. L-5-Methyltetrahydrofolic acid (L-5-MTHF) is a natural form of folate, and it is more bioactive than folic acid. However, it has limited stability especially when exposed to oxygen, light, or high temperatures.[8] Recently, research was focused on finding ways to stabilize this molecule in food matrices to reduce or replace the use of synthetic FA in fortified foods.[9,10] Rozoy et al.[10] showed that degradation of L-5-MTHF could be controlled by the addition of ascorbic acid. Some studies have proven that the antioxidant capacity of (−)-epigallocatechin gallate exceeds the effect of ascorbic acid at least 100 times.[11] Thus, the use of molecules with strong antioxidant activity such as catechins could be an interesting alternative to protect L-5-MTHF against oxidation.

To date, high-performance liquid chromatography (HPLC) remains the most used technique for the determination of catechins. Traditional HPLC coupled with ultraviolet (UV), photodiode array (DAD), electrochemical detection, and mass spectrometry (MS) are among the most employed methods in the identification of catechins.[12−20] In general, the analysis time is relatively long, 40−105 min, and between 5 and 10 compounds of interest can be simultaneously separated. From a quantitative point of view, fast HPLC approaches have not been extensively investigated, and only a few works have reported a simultaneous separation of all tea catechins in a relatively short time (within 25 min).[21−24] Most recently, ultrahigh-pressure liquid chromatography (UHPLC) has shown a considerable potential in terms of speed and separation efficiency.[25,26] However, UHPLC is still relatively new and requires specialized equipment able to withstand pressures of 1000 bar. Up to now, only a few applications of UHPLC have been reported for the analysis of catechins in tea samples.[27−30]

To enhance chromatographic performances in terms of efficiency and rapidity, several strategies can be implemented. An interesting approach would be to evaluate the use of columns packed with sub 2 μm particles. As described 30 years ago by Knox, Martin, and other authors, the use of short columns packed with small particles induces an increase in efficiency, optimal velocity, and mass transfer.[31−34]

Received: November 28, 2013
Revised: March 31, 2014
Accepted: April 15, 2014
Published: April 15, 2014

ACS Publications © 2014 American Chemical Society

The aim of this study was to develop an efficient and rapid HPLC method for the simultaneous separation of catechins, gallic acid, and caffeine in tea samples. To evaluate the resolution in other complex matrices, the method was applied to the determination of folates. Chromatographic analyses of L-5-MTHF in combination with green tea enriched extracts were also performed to evaluate the analytic performance of the method proposed in a complex solution. To perform faster analysis, a conventional HPLC system was equipped with a Zorbax Stable Bond (SB) C_{18} analytical column (4.6 × 50 mm) packed with 1.8 μm particles. HPLC was coupled with MS to attain sufficient sensitivity and selectivity for the identification of catechins, folates, and other constituents of tea samples. To the best of our knowledge, there is no method published yet on the simultaneous separation of catechins and folates.

MATERIALS AND METHODS

Chemical and Standards Preparation. Standards were purchased from Sigma Chemical Co. (St. Louis, MO, USA): gallic acid (GA, 98%), (−)-gallocatechin (GC, 98%), (−)-epigallocatechin (EGC, 98%), (+)-catechin (C, 98%), (−)-epicatechin (EC, 98%), (−)-epigallocatechin-3-gallate (EGCG, 95%), (−)-gallocatechin gallate (GCG, 98%), (−)-epicatechin gallate (ECG, 98%), (−)-catechin gallate (CG, 98%), and caffeine (CAF, 99%). HPLC grade water was obtained using a Siemens Purelab Ultra Water-Purification System (Siemens, USA). HPLC grade acetonitrile and formic acid were purchased from VWR International (Mississauga, ON, Canada) and Sigma-Aldrich (St. Louis, MO, USA) respectively.

The stock solutions were prepared by dissolving 5−10 mg of each standard compound in 10 mL of HPLC grade water/formic acid (99.9:0.1 v/v). Each stock solution was then used for the preparation of a mix of standards. Serial dilutions were then prepared with formic acid solution to produce calibration curves at different concentrations ranging between 3 and 50 μg/mL. All standard solutions were filtered through 0.2 μm PVDF syringe filters. A 10 μL aliquot of solutions was injected onto HPLC.

HPLC-MS Analysis. The HPLC UV-MS analyses were performed on an Agilent 1100 series (Santa Clara, CA, USA) HPLC system equipped with an Agilent diode array UV−vis detector (Agilent G1315 DAD), a vacuum degasser, a binary pump delivery (Agilent G1312A), a refrigerated autosampler (Agilent G1329A), and an HP mass spectrometer detector (MSD, model G1948B). Integration and data processing were performed by Chemstation software (LC/MSD Chemstation B.01.03 SR1). An Agilent Zorbax SB-C_{18} (4.6 mm id × 50 mm, 1.8 μm) column with a precolumn filter was used. HPLC UV-MS analyses were carried out using mobile phases consisting of 0.2% formic acid in water (A) and 0.1% formic acid in acetonitrile (B) (HPLC grade, EMD Chemicals Inc., Gibbstown, NJ, USA). The linear gradient elution system was as follows: 0−8 min, 0−5% (v/v) of B; 8−10 min, 5−25% (v/v) of B; 10−17 min, 25−100% (v/v) of B; and 17−23 min, 100−5% (v/v) of B, at a flow rate of 1 mL/min. The quantification of catechins by UV-DAD was performed at 230 nm. The column temperature was maintained at 25 °C, and the injection volume was 10 μL.

The same column of HPLC-DAD was used for analyses by MS. Mass spectra of catechins were recorded in the positive ionization mode using an electrospray (API-ES) ionizing source with nitrogen as drying gas. Spray chamber parameters were as follows: capillary potential, 3000 V; gas temperature, 350 °C; drying gas flow, 13 L/min; nebulizer pressure, 60 psi. Quantitative analysis by MS was carried out in the scanning mode, scan range being m/z 150−1000, setting the fragmentor value at 70 V with a molecular ion $[M+H]^+$ for each catechin chosen as the most abundant and representative signal.

Identification of compounds by HPLC-MS analysis was carried out by comparing retention times and mass spectra of the unknown peaks to those of the standards.

Preparation of Green Tea Samples. *Enriched Green Tea Drink.* An EGCG-enriched tea drink was prepared in our laboratory according to the procedure developed by Bazinet et al.[35] The green tea used in this experiment was a commercially available and Japanese green tea obtained from local retailer. Before being used, the green tea was stored in vacuum bags at room temperature in a dark and dry space. The EGCG-enriched tea drink was produced at a volume of 100 L, in conditions and with unit operations similar to the ones met in the food industry for the production of low-acid beverages. Dry leaves (3.5 kg) were brewed twice in 100 L of water. The first brewing step was carried out at 30 ± 2 °C for 10 min using a stainless steel double-jacket heated reservoir. The infusion was filtered to separate the leaves and to collect the filtrate. The filtered tea leaves were brewed again in 100 L of water at 80 ± 2 °C for1 h. The green tea leaves were squeezed and discarded. The second filtrate was adjusted to a pH value of 3.5 by lemon juice addition. The ECGC-enriched green tea was then pasteurized and aseptically bottled and stored at 4 °C.

Enriched Green Tea Extract. An enriched freeze-dried tea extract was prepared in our laboratory using the second filtrate, which was prepared according to the procedure previously cited. This extract was not adjusted to pH 3.5. The extracts were frozen at −30 °C for 48 h and lyophilized at 25 °C for 72 h (Virtis, Gardiner, NY, USA). For the analyses, 400 mg of extract was diluted to 25 mL with HPLC grade water. All prepared tea samples were filtered through 0.2 μm PVDF syringe filters. A 10 μL aliquot of this tea sample was injected onto HPLC. All tea samples were prepared and analyzed in triplicate for a total of nine analyses per sample.

Preparation of Folates. Solutions of folic acid and L-5-MTHF were prepared separately in CHES−HEPES buffer at a concentration of 227 μM. On the other hand, solutions of 1 mM L-5-MTHF with an enriched green extract (at 400 mg/L) were prepared in Britton−Robinson buffer[10] and analyzed by HPLC-MS.

Data Analysis. Calibration curves were done using standard solutions, and linearity was evaluated over six calibration points with three measurements for each calibration point. Detection limits (LOD) and quantitation limits (LOQ) were determined according to the ICH Harmonized Tripartite Guideline (Validation of Analytical Procedures: Text and Methodology Q_2 (R_1)).[36]

Repeatability of the method was calculated in terms of percent relative standard deviation (% RSD) by performing HPLC analysis on aliquots of each sample in triplicate on three consecutive days. Relative standard deviation (RSD) was defined as sample standard deviation divided by sample mean, multiplied by 100%.

RESULTS AND DISCUSSION

Description of Developing Steps To Improve the Methodology. A reversed-phase HPLC method coupled with mass spectrometry was developed. Two mobile phases, one containing HPLC grade water and the other containing acetonitrile, were tested. The formic acid was added to both mobile phases. The presence of acid in the mobile phases is essential to attain a complete separation of catechins.[17] Moreover, it was reported that catechins are most stable in acidic conditions.[37] Two different concentrations of formic acid (0.1 and 0.2%) were tested in the present study. Although a good separation was achieved with 0.1% formic acid in both mobile phases, improved peak shapes were obtained with the inclusion of 2% formic acid in the water mobile phase. Another reason for the use of the formic acid was its compatibility with mass spectrometry. The elution gradient program was described earlier.

Different absorption wavelengths have been reported in the literature for the determination of tea catechins, varying from 210 to 280 nm.[12−20] In our study, all catechins, gallic acid, and caffeine exhibited maximun absorbance at 210 and 230 nm. The absorbances at 210 nm were slightly larger than those at 230 nm, but the baseline shifts of chromatograms were also increased. Folates were found to have maximum absorbances at 280−290 nm, as was already mentioned in the literature.[38,39]

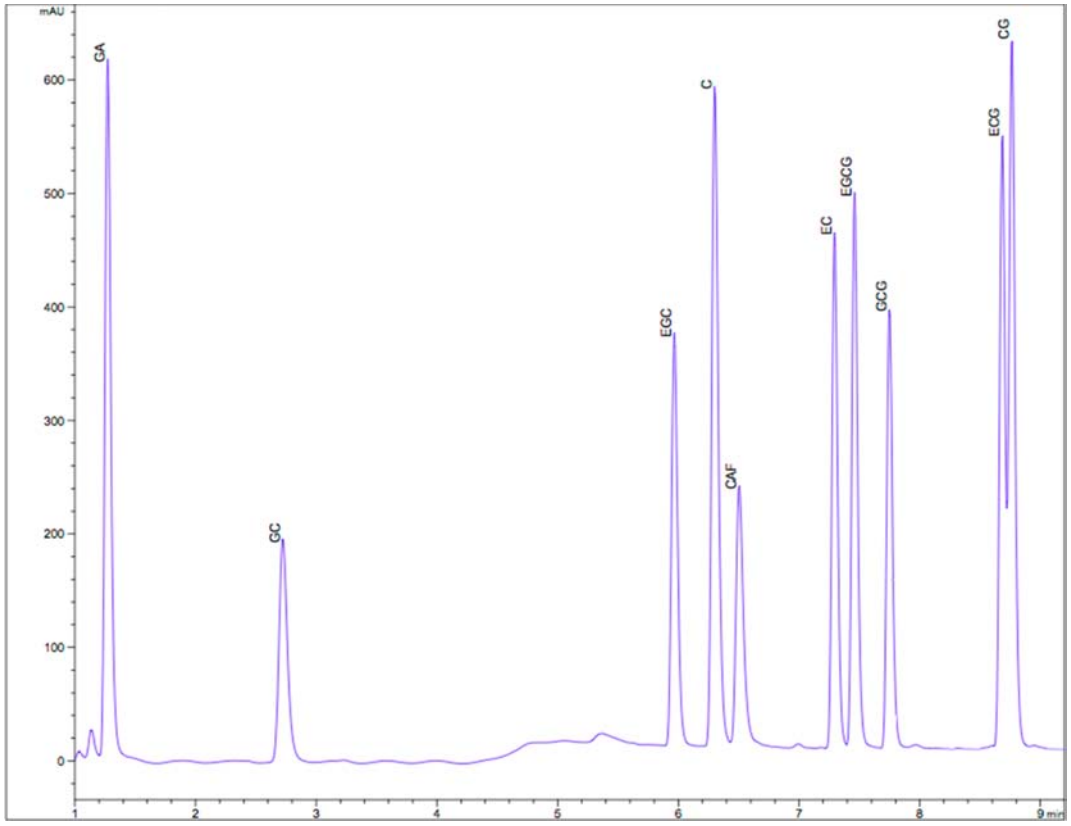

Figure 1. Chromatogram of mixed standards of GA, catechins, and CAF recorded by UV-DAD at 230 nm. GA, gallic acid; GC, gallocatechin; EGC, epigallocatechin; C, catechin; CAF, caffeine; EC, epicatechin; EGCG, epigallocatechin gallate; GCG, gallocatechin gallate; ECG, epicatechin gallate; CG, catechin gallate.

However, a strong absorption was also observed at the shortest wavelength (230 nm). The detector wavelength was then set at 230 nm as the best compromise to reach maximun absorbance for all compounds of interest.

To increase separation efficiency and speed of analysis, the HPLC system was equipped with a Zorbax SB-C_{18} column (4.6 mm id × 50 mm) packed with 1.8 μm silica-based particles. The use of small particles is one of the best solutions to improve chromatographic performances.[31−34] Moreover, good efficiency can be maintained with a short column and a high flow rate. On the other hand, the special and ultrapure silica support of the Zorbax SB-C_{18} column is designed to reduce or eliminate undesirable interactions between analytes and the silica surface, thereby providing best separation of all compounds. It is especially suited in applications that use high-sensitivity detectors such as mass spectrometers. That was another reason for the use of this specific column.

The performance of the Zorbax SB-C_{18} 1.8 μm column was compared to that of a YMC-Pack ODS-AM C_{18} 5 μm column, which has already been used for the determination of catechins. Both columns were tested under the same conditions. The Zorbax column gave good separation for all of the analytes within 9 min (Figure 1). However, the YMC-Pack ODS-AM column did not achieve a satisfactory resolution of EC, EGCG, ECG, and CG in the water/acetonitrile/formic acid system, and the separation time was generally long (47 min) (data not shown). In this context, the analysis time and solvent consumption were decreased by 5.2 times using the Zorbax SB-C_{18} column. The performance of the YMC-Pack ODS-AM column was better when the trifluoroacetic acid was added to the mobile phases as reported in our previous work.[19]

The critical step in the quantification of catechins, phenolic acids, and caffeine in tea by HPLC methods is the sample extraction. The extraction method must enable complete extraction of the compounds of interest without chemical modification or degradation. At present, a single extraction step with acetonitrile and methanol has been widely used to quantify polyphenols in tea.[14,16,24,40] However, our method allows the quantification of catechins in tea without any extraction with solvents. In fact, after the preparation of tea samples in boiling water, the samples needed only to be diluted and filtered prior to the HPLC analysis. Hu et al.[24] also analyzed catechins in tea after hot water brewing, but their method needed a semipreparative/preparative HPLC step prior to the identification of catechins by analytical HPLC.

Mass spectra of tea catechins was recorded in the 40−120 V fragmentor range to determine the highest sensitivity for each molecule. A fragmentor value of 70 V was chosen as the best compromise among all ions detected and applied to the tea samples. The method was tested in negative and positive ionization modes, but a better sensitivity and a significant improvement in signal-to-noise response were achieved when the mass spectrometer was operated in positive ionization mode. Pelillo et al.[22] also reported a better signal response when HPLC-MS analysis of green tea extracts was obtained with positive ion detection.

HPLC-MS Analysis and Peak Identification. The typical chromatogram of mixed standards of GA, catechins, and CAF is shown in Figure 1. For this separation, the generated back

Table 1. Retention Times and MS Spectral Data of Gallic Acid, Caffeine, and Catechin Standards

					retention time (min)			
compd[a]	regression eq	R^2	LOD (μg)	LOQ (μg)	UV[b]	MS	MW (g/mol)	M $[+H]^+$ (m/z)
GA	$y = 40.302x + 45.137$	0.9998	1.279	4.265	1.275	1.290	170.12	171.03
GC	$y = 19.293x - 13.746$	0.9999	0.509	1.696	2.690	2.704	306.27	307.08
EGC	$y = 27.426x - 20.407$	0.9999	0.972	3.241	5.966	6.001	306.03	307.08
C	$y = 44.752x + 15.259$	1.0000	0.450	1.501	6.324	6.338	290.03	291.10
CAF	$y = 13.534x - 3.347$	0.9999	1.014	3.380	6.534	6.548	194.14	195.10
EC	$y = 33.639x + 7.819$	1.0000	0.495	1.652	7.353	7.365	290.20	291.12
EGCG	$y = 33.756x - 11.891$	0.9998	1.328	4.427	7.518	7.534	458.40	459.10
GCG	$y = 16.302x - 8.936$	0.9999	0.717	2.392	7.819	7.830	458.40	459.07
ECG	$y = 23.987x - 1.002$	0.9999	0.515	1.716	8.770	8.863	442.40	443.08
CG	$y = 43.903x + 15.146$	0.9998	1.342	4.475	8.853	8.863	442.37	443.08

[a]GA, gallic acid; GC, gallocatechin; EGC, epigallocatechin; C, catechin; CAF, caffeine; EC, epicatechin; EGCG, epigallocatechin gallate; GCG, gallocatechin gallate; ECG, epicatechin gallate; CG, catechin gallate. [b]UV, detection at 230 nm.

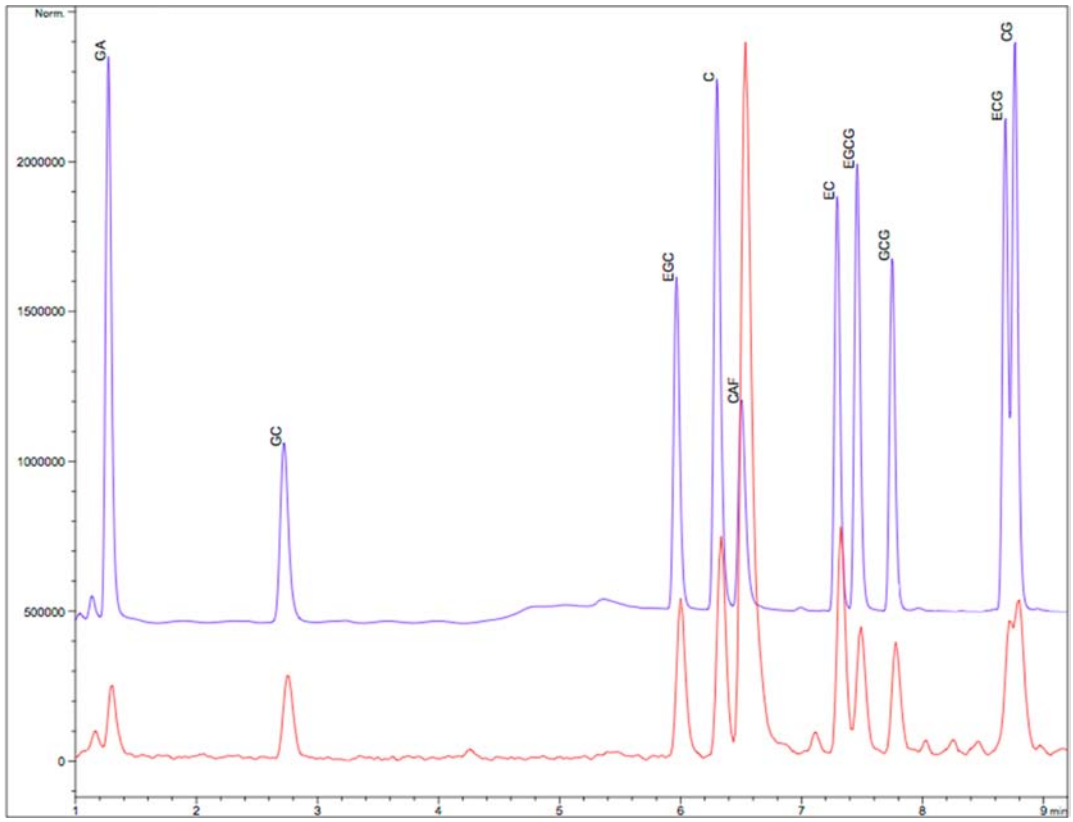

Figure 2. Chromatograms of catechin standards recorded by both UV-DAD (blue line) and MSD (red line) detectors at 230 nm. GA, gallic acid; GC, gallocatechin; EGC, epigallocatechin; C, catechin; CAF, caffeine; EC, epicatechin; EGCG, epigallocatechin gallate; GCG, gallocatechin gallate; ECG, epicatechin gallate; CG, catechin gallate.

pressure was around 220 MPa, which is very compatible with conventional HPLC system (HPLC standard pressure, up to 400 bar, 40 MPa).

The principal advantage of the here-developed HPLC-MS method is the high baseline resolution of 10 compounds in a very short time with an excellent separation quality for GA and CAF. The elution order was GA, GC, ECG, C, CAF, EC, EGCG, CGC, ECG, and CG. These 10 compounds were successfully separated within 9 min by linear gradient elution of formic acid solution and acetonitrile (Figure 1). Most HPLC methods for the separation of tea catechins are carried out on C_{18} 5 μm columns (4.6 mm id × 250 mm or 4.6 mm id × 150 mm), and 5−10 compounds can be simultaneously separated in 40−105 min.[12−20] Using a Zorbax SB-C_{18} sub 2 μm column, the HPLC analyses could be performed 4.4−12 times faster than those reported for a C_{18} 5 μm column, and because the pressure was only 220 MPa and solvent consumption 9 mL by analysis, this method is an excellent option for the determination of catechins.

Catechin detection was linear over the ranges tested (3−50 μg/mL) with coefficients of determination (R^2) between 0.9998 and 1.0000. LODs and LOQs for most standards were in the range of 0.5−1.0 and 1.0−4.0 μg, respectively. CG had the highest LOD at 1.342 μg, and C had the lowest LOD at 0.450 μg. The results are summarized in Table 1.

dx.doi.org/10.1021/jf4053258 | J. Agric. Food Chem. 2014, 62, 4241−4250

The retention time and MS spectral data of standards are shown in Table 1. The results are in agreement with the values reported in the literature.[22−24,40] In Figure 2 chromatograms of standards recorded by both UV and MSD detectors are compared. As shown in Figure 2, EGC and CG exhibited different retention times, and two peaks can be easily differentiated in UV spectra. However, EGC and CG had identical $[M+H]^+$ ions at 443.08, and only one peak (with a shoulder) can be observed in MS spectra. A typical mass spectrum of EGCG is shown in Figure 3. The mass spectra

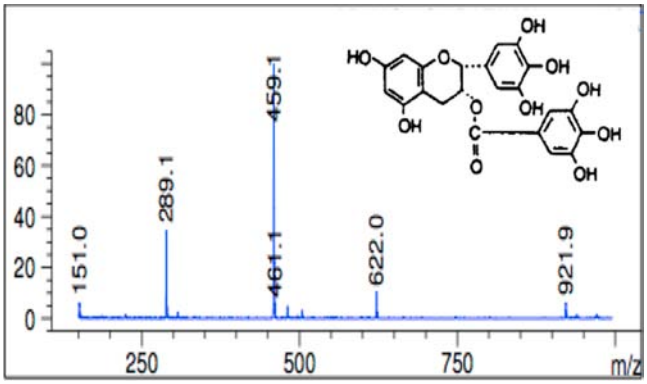

Figure 3. Mass spectrum of EGCG recorded by API-ES+ with the fragmentor set at 70 V.

showed a characteristic product ion of EGCG (m/z 459.1 is the $[M+H]^+$ion). Similar mass spectra were reported in the literature.[22] The mass spectrum contains several extra signals at m/z 151.1, 289.1, 622, 0 and 921.1. The m/z signal at 289.1 would be a typical fragment ion detected in the mass spectrum of catechins.[40]

To summarize the information given above, separation and identification of green tea compounds by HPLC are typically slow, requiring complex and time-consuming gradients.[12−20,41−,43] To date, only a few methods have allowed the simultaneous determination of the main catechins, gallic acid, and caffeine in <25 min. In the first study, four major catechins (ECGC, EGC, ECG, and EC), GA, and CAF were successfully separated within 20 min.[14] However, this study needed multiple extractions with aqueous methanol solutions. In the second study, 14 tea compounds including 8 catechins, GA, and CAF were separated within 15 min by a linear gradient elution of formic acid and methanol.[24] However, the method was focused principally on the preparation and purification of methylated catechins; thus, several steps of isolation and semipreparative HPLC were required. Furthermore, the time for cleaning and column conditioning was not mentioned. Although those methods are rapid, the preparation of samples may become a difficult task due to the numerous steps.

To our knowledge, only one chromatographic method based on the utilization of a Zorbax SB-C_{18} sub 2 μm column was developed for the analysis of phenolic compounds including tea catechins.[30] The analysis time was 12 min, and 6 standards (GC, EGCG, EC, GC, EC, CG) were separated with satisfactory resolution. However, there was no resolution for standards EGC and C. In the matrix of green tea infusion, the resolution was more critical, and only the peaks of GCG and ECG had good response and were sufficiently separated.

Separation and Identification of Catechins in Tea Samples. Identification of peaks of tea samples was carried out by comparing retention times and mass spectra of the standards and data in the literature (Tables 2 and 3). These results are in good agreement with catechin standards. The typical HPLC-UV profiles of enriched tea drink and green tea extracts are shown in Figures 4 and 5, respectively. In both tea samples we also observed a peak eluting at 8.4 min (not identified on the chromatogram) that could correspond to a second peak of GC.

The catechin contents in enriched green tea drink are shown in Table 2. The results obtained indicate that EGCG was in highest concentration (660.9 mg/L) in green tea drinks, whereas GA (3.0 mg/L) was the lowest. CG was not quantified due to its low level. As expected, calculated amounts of EGCG (the most interesting catechin compound) were higher than those of similar tea infusions or beverages[15] because we produced an EGCG-enriched green tea drink. Chen et al.[44] reported that one canned or bottled tea drink (250 mL) contained less green tea catechins (3−60 mg) than one cup of conventional brewed green tea drink (400−500 mg). The content of catechins in tea samples can vary depending on the conditions and technology used for the extraction and storage.[22] In terms of quantification, % RSD values obtained were quite low, ranging from 0.8 to 3.5%. The relatively low % RSD for GA, most catechins, and CAF indicated that this

Table 2. Retention Times and Contents of Gallic Acid, Caffeine, and Catechins in EGCG-Enriched Green Tea Drink

compd[a]	M $[+H]^+$ (m/z)	retention time, UV (min)	content (mg/L)	% RSD quantification	% RSD retention Time
GA		1.28 ± 0.02	3.02 ± 0.04	1.40	1.33
GC	307.06	2.71 ± 0.01	135.86 ± 4.75	3.50	0.55
EGC	307.09	5.99 ± 0.01	507.23 ± 4.00	0.79	0.13
CAT	291.12	6.29 ± 0.06	16.05 ± 0.24	1.50	0.97
CAF	195.09	6.54 ± 0.01	463.74 ± 4.59	0.99	0.09
EC	291.11	7.36 ± 0.00	118.00 ± 0.98	0.83	0.06
EGCG	459.09	7.52 ± 0.01	660.88 ± 15.94	2.41	0.06
GCG	459.10	7.82 ± 0.00	138.74 ± 1.48	1.07	0.05
ECG	443.11	8.69 ± 0.00	101.45 ± 2.66	2.62	0.00
CG		nd[c]	nd		
total catechins[b]			1660.69 ± 33.06		

[a]GA, gallic acid; GC, gallocatechin; EGC, epigallocatechin; C, catechin; CAF, caffeine; EC, epicatechin; EGCG, epigallocatechin gallate; GCG, gallocatechin gallate; ECG, epicatechin gallate; CG, catechin gallate. [b]Total catechins does not include GA and CAF. [c]nd, not detected due to very low concentration.

dx.doi.org/10.1021/jf4053258 | J. Agric. Food Chem. 2014, 62, 4241−4250

Table 3. Retention Times and Contents of Gallic Acid, Caffeine, and Catechins in Green Tea Extract

compd[a]	M [+H]$^+$ (m/z)	retention time, UV (min)	content (mg/g extract)	% RSD quantification	% RSD retention time
GA		1.29 ± 0.00	2.68 ± 0.49	18.35	0.11
GC	307.06	2.79 ± 0.14	50.48 ± 3.68	7.28	5.08
EGC	307.06	5.94 ± 0.00	205.88 ± 0.99	0.48	0.06
CAT	291.12	6.28 ± 0.00	6.85 ± 0.21	3.10	0.02
CAFF	195.10	6.48 ± 0.00	180.46 ± 4.05	2.24	0.03
EC	291.08	7.27 ± 0.00	2.35 ± 1.38	2.63	0.01
EGCG	459.06	7.43 ± 0.01	263.88 ± 0.71	0.27	0.02
GCG	459.10	7.73 ± 0.00	1.85 ± 1.73	3.34	0.02
ECG	443.05	8.66 ± 0.00	7.75 ± 9.63	12.69	0.02
CG		nd[c]	nd		
total catechins[b]			709.03 ± 7.39		

[a]GA, gallic acid; GC, gallocatechin; EGC, epigallocatechin; C, catechin; CAF, caffeine; EC, epicatechin; EGC, epigallocatechin; C, catechin; CAF, caffeine; EC, epicatechin; EGCG, epigallocatechin gallate; GCG, gallocatechin gallate; EGC, epicatechin gallate;CG, catechin gallate. [b]Total catechins does not include GA and CAF. [c]nd, not detected due to very low concentration.

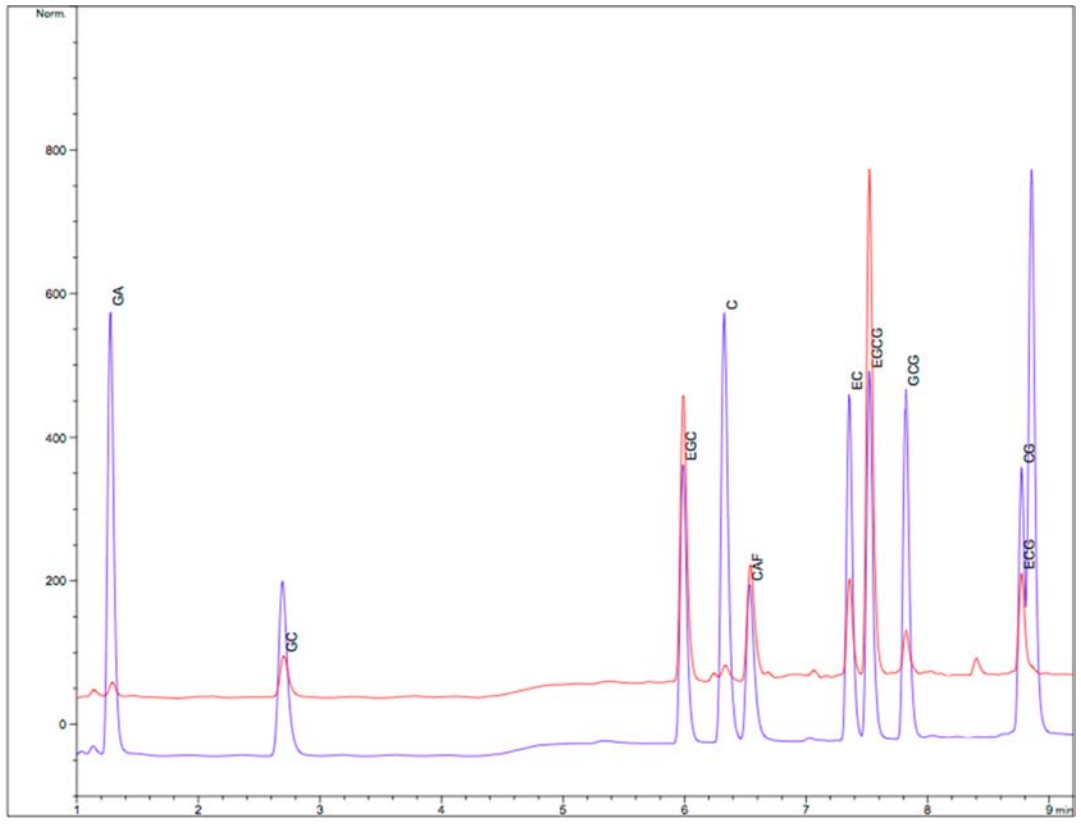

Figure 4. Chromatogram of enriched tea drink (red line) and catechin standards (blue line) recorded by UV-DAD detector at 230 nm. GA, gallic acid; GC, gallocatechin; EGC, epigallocatechin; C, catechin; CAF, caffeine; EC, epicatechin; EGCG, epigallocatechin gallate; GCG, gallocatechin gallate; ECG, epicatechin gallate; CG, catechin gallate.

method is repeatable and reproducible. Moreover, % RSD of HPLC retention time ranged from 0.0 to 1.3%.

The catechin contents of green tea extracts were 2−6 times higher than those of green tea drink (Table 3) (if compared on a dry basis). However, the % RSDs were slightly higher than those obtained in green tea drink samples. Generally, compounds with lower response (except ECG) had higher % RSD.

Recently, UHPLC-UV has shown considerable potential for the determination of tea compounds. One of the main advantages of UHPLC is related to the possibility of attaining either ultrafast or high resolving power separations.[27] In that study, they obtained an ultrafast and high-resolution UHPLC separation of a mixture of eight standards within 3−23 min depending on column length. However, when real tea samples are used, the identification of catechins is critical and the proposed method does not present enough resolving power to easily discriminate catechins contained in tea extracts. In this context, our method provides an excellent selectivity and resolution for catechins determination and quantification in real tea samples as shown in Figure 4 for enriched drink tea and in Figure 5 for green tea extract.

Application to Folate Determination. As demonstrated above, the method provides excellent separation and resolution

dx.doi.org/10.1021/jf4053258 | J. Agric. Food Chem. 2014, 62, 4241−4250

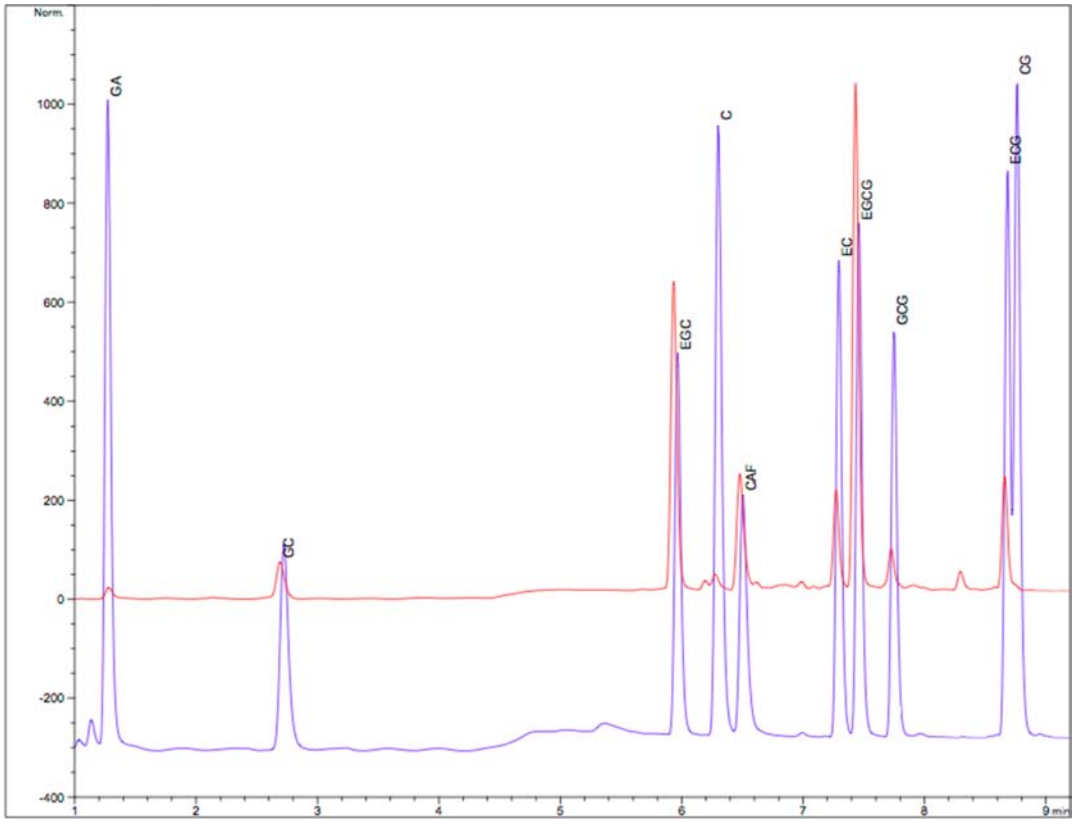

Figure 5. Chromatogram of green tea extracts (red line) and catechin standards (blue line) recorded by UV-DAD detector at 230 nm. GA, gallic acid; GC, gallocatechin; EGC, epigallocatechin; C, catechin; CAF, caffeine; EC, epicatechin; EGCG, epigallocatechin gallate; GCG, gallocatechin gallate; ECG, epicatechin gallate; CG, catechin gallate.

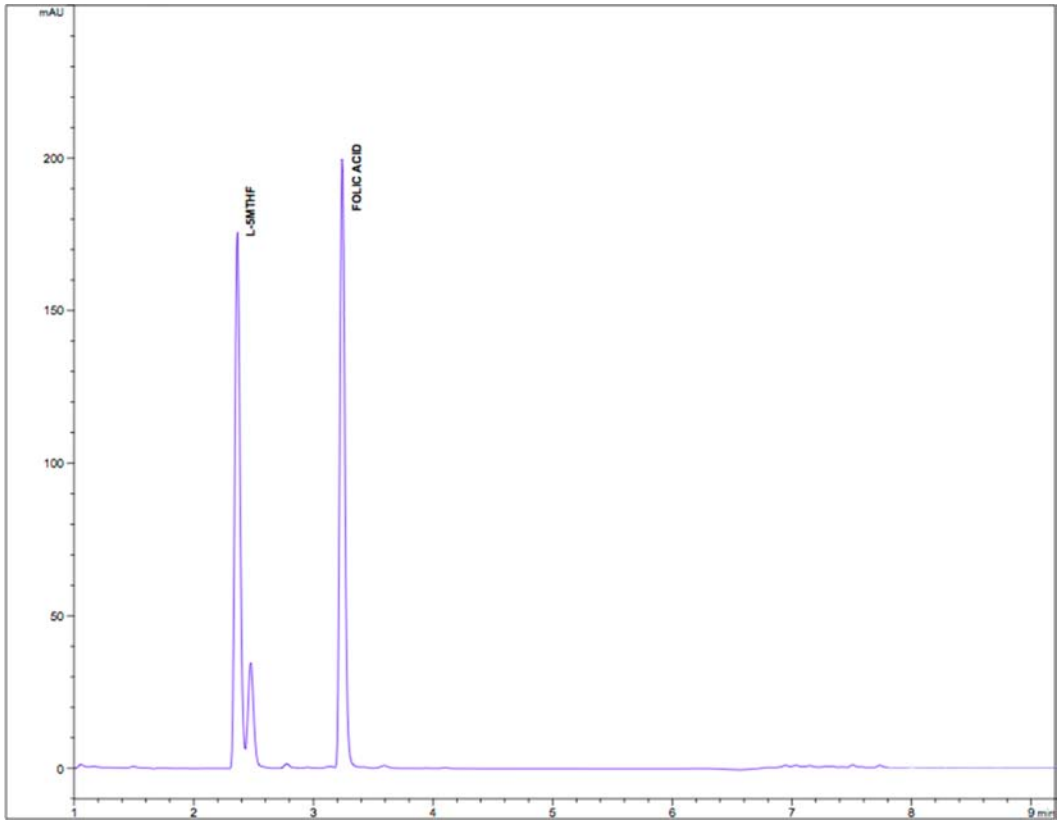

Figure 6. Chromatograms of folic acid and L-5MTHF recorded by UV-DAD detector at 230 nm.

dx.doi.org/10.1021/jf4053258 | *J. Agric. Food Chem.* 2014, 62, 4241−4250

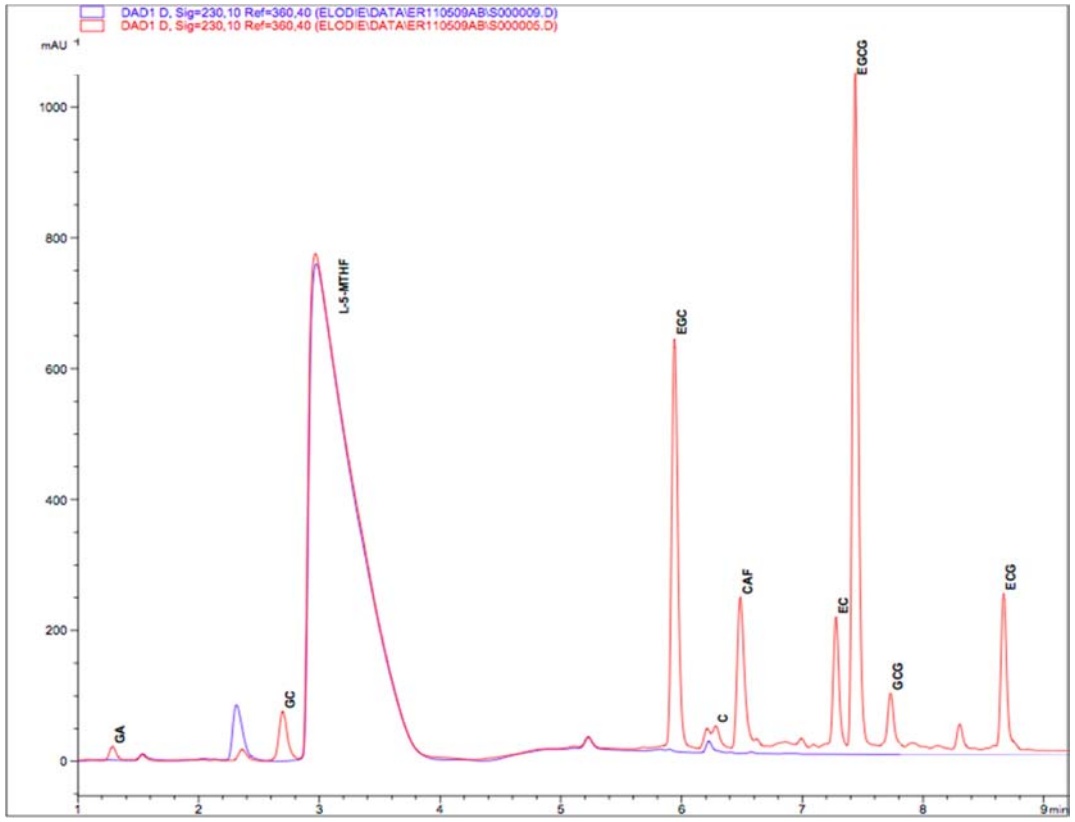

Figure 7. Chromatograms of L-5MTHF alone (blue line) or in combination with a green tea extract (red line) recorded by UV-DAD detector at 230 nm. GA, gallic acid; GC, gallocatechin; EGC, epigallocatechin; C, catechin; CAF, caffeine; EC, epicatechin; EGCG, epigallocatechin gallate; GCG, gallocatechin gallate; ECG, epicatechin gallate; CG, catechin gallate.

when applied in tea samples. To evaluate the resolution in other complex matrices, the method was thus applied to the determination of folates either alone or in combination with catechins. A typical chromatogram of folic acid and its natural form L-5MTHF is shown in Figure 6. The retention times were 2.36 and 3.44 min for L-5-MTHF (nonoxidized form) and folic acid, respectively. The small peak eluting at 2.48 min would correspond to an oxidation peak of L-5MTHF.[9] To illustrate the complexity of the matrix, L-5MTHF was mixed with green tea extract in Britton–Robinson buffer. The corresponding profiles are presented in Figure 7. The difference in the retention time for L-5MTHF after being mixed with catechins would be due to different buffers used during the analysis (CHES–HEPES vs Britton–Robinson). It appears from these figures that our method presents enough resolving power to discriminate folates from catechins in a very short time. Thus, it clearly demonstrated the potential of our HPLC-MS to provide qualitative and quantitative determinations when dealing with complex matrices.

Some important conclusions can be drawn from this study. First, we have developed a fast and simple method to determine catechins and catechin derivatives in tea samples. The chromatographic performances in terms of efficiency and rapidity were improved using a sub 2 μm column. In fact, 10 compounds from green tea were rapidly separated within 9 min with an excellent resolution. It represented roughly a 4.4–12-fold reduction in total analysis time (9 versus 40–105 min) from existing analytical methods for the analysis of catechins. Considering the lower solvent consumption (9 mL by analysis), our method was not only faster but also more ecological. The efficiency of the method was confirmed by analyzing complex matrices such as tea extracts. This represents one of the main advantages of this method because existing analytical methods do not present enough resolving power when dealing with real tea samples. Calibration data and % RSD demonstrate that this method is repeatable and reproducible. Finally, the proposed method was applied to the determination of folates maintaining excellent selectivity and sensitivity. Furthermore, the method provided excellent resolution even when the folates were mixed with the catechins. To our knowledge, no HPLC-MS method able to realize the simultaneous separation of antioxidants and a nutrient susceptible to oxidation has been yet published in the literature.

AUTHOR INFORMATION

Corresponding Author

*(L.B.) Mail: Institute of Nutrition and Functional Foods (INAF), Department of Food Sciences and Nutrition, Pavillon Paul-Comtois, 2425 rue de l'Agriculture, Laval University, Quebec (QC), Canada G1V 0A6. Phone: (418) 656-2131, ext. 7445. Fax: (418) 656-3353. E-mail: laurent.bazinet@fsaa.ulaval.ca.

Present Address

§(M.A.-F.) Institut Galien Paris-Sud, UMR CNRS 8612, Faculté de Pharmacie, Université Paris Sud, 5, rue JB Clément, 92290 Châtenay-Malabry Cedex, France.

Funding

We are grateful for the funding provided for the project by Agriculture and Agri-Food Canada, le Fonds Québécois de la Recherche sur la Nature et les Technologies, and Novalait Inc.

Notes

The authors declare no competing financial interest.

■ ABBREVIATIONS USED

UHPLC, ultrahigh-pressure liquid chromatography; HPLC, high-performance liquid chromatography; MS, mass spectrometry; UV−vis, ultraviolet−visible; DAD, diode array; RSD, relative standard deviation; GA, gallic acid; GC, gallocatechin; EGC, epigallocatechin; C, catechin; CAF, caffeine; EC, epicatechin; EGCG, epigallocatechin gallate; GCG, gallocatechin gallate; ECG, epicatechin gallate; CG, catechin gallate; L-5-MTHF, L-5-methyltetrahydrofolic acid

■ REFERENCES

(1) Dufresne, C.; Farnworth, E. R. A review of latest research findings on the health promotion properties of tea. *J. Nutr. Biochem.* **2001**, *12*, 404−421.

(2) Price, W. E.; Spitzer, J. C. Variations in the mounts of individual flavanols in a range of green teas. *Food Chem.* **1993**, *47*, 271−276.

(3) Khan, N.; Mukhtar, H. Tea polyphenols for health promotion. *Life Sci.* **2009**, *81*, 519−523.

(4) Zaveri, N. T. Green tea and its polyphenolic catechins: medicinal uses in cancer and noncancer applications. *Life Sci.* **2006**, *78*, 2073−2080.

(5) Butt, M. S.; Sultan, M. T. Coffee and its consumption: benefits and risks. *Crit. Rev. Food Sci. Nutr.* **2011**, *51*, 363−373.

(6) Thorngate, J. H.; Noble, A. C. Sensory evaluation of bitterness and astringency of 3*R*(−)-epicatechin and 3*S*(+)-catechin. *J. Sci. Food Agric.* **1995**, *67*, 531−535.

(7) Stanger, O. Physiology of folic acid in health and disease. *Curr. Drug Metab.* **2002**, *3*, 211−223.

(8) Jones, M. L.; Nixon, P. F. Tetrahydrofolates are greatly stabilized by binding to bovine milk folate-binding protein. *J. Nutr.* **2002**, *132*, 2690−2694.

(9) Liu, Y.; Tomiuk, S.; Rozoy, E.; Bazinet, L.; Green, T.; Kitts, D. Thermal oxidation studies on reduced folate, L-5-methyltetrahydrofolate (L-5-MTHF) and strategies for stabilization using food matrices. *J. Food Sci.* **2012**, *77*, C236−C243.

(10) Rozoy, E.; Simard, S.; Liu, Y.; Kitts, D.; Lessard, J.; Bazinet, L. The use of cyclic voltammetry to study the oxidation of L-5-methyltetrahydrofolate and its preservation by ascorbic acid. *Food Chem.* **2012**, *132*, 1429−1435.

(11) Hu, C.; Kitts, D. D. Evaluation of antioxidant activity of epigallocatechin gallate in biphasic model systems in vitro. *Mol. Cell. Biochem.* **2001**, *218*, 147−155.

(12) Ananingsih, V.; Sharma, A.; Zhou, W. Green tea catechins during food processing and storage: a review on stability and detection. *Food Res. Int.* **2013**, *2*, 469−479.

(13) Wang, H.; Helliwell, K.; You, X. Isocratic elution system for the determination of catechins, caffeine and gallic acid in green tea using HPLC. *Food Chem.* **2000**, *68*, 115−121.

(14) Zuo, Y.; Chen, H.; Deng, Y. Simultaneous determination of catechins, caffeine and gallic acids in green, oolong, black and pu-erh teas using HPLC with a photodiode array detector. *Talanta* **2002**, *57*, 307−316.

(15) Bronner, W. E.; Beecher, G. R. Method for determining the content of catechins in tea infusions by high-performance liquid chromatography. *J. Chromatogr., A* **1998**, *805*, 137−142.

(16) Nishitani, E.; Sagesaka, Y. M. Simultaneous determination of catechins, caffeine and other phenolic compounds in tea using new HPLC method. *J. Food Compos. Anal.* **2004**, *17*, 675−685.

(17) Dalluge, J. J.; Nelson, B. C. Determination of tea catechins. *J. Chromatogr., A* **2000**, *881*, 411−424.

(18) Del Rio, D.; Stewart, A. J.; Mullen, W.; Burns, J.; Lean, M. E.; Brighenti, F. HPLC-MS^n analysis of phenolic compounds and purine alkaloids in green and black tea. *J. Agric. Food Chem.* **2004**, *52*, 2807−2815.

(19) Labbé, D.; Araya-Farias, M.; Tremblay, A.; Bazinet, L. Electromigration feasibility of green tea catechins. *J. Membr. Sci.* **2005**, *254* (1−2), 101−109.

(20) Sano, M.; Tabata, M.; Suzuki, M.; Degawa, M.; Miyase, T.; Yamamoto, M. M. Simultaneous determination of twelve tea catechins by high-performance liquid chromatography with electrochemical detection. *Analyst* **2001**, *126*, 816−820.

(21) Goto, T.; Yoshida, Y.; Kiso, M.; Nagashima, H. Simultaneous analysis of individual catechins and caffeine in green tea. *J. Chromatogr., A* **1996**, *749*, 295−299.

(22) Pelillo, M.; Biguzzi, B.; Bendini, A.; Toschi, T. G.; Vanzani, M.; Lercker, G. Preliminary investigation into development of HPLC with UV and MS-electrospray detection for the analysis of tea catechins. *Food Chem.* **2002**, *78*, 369−374.

(23) Pelillo, M.; Biguzzi, B.; Bendini, A.; Toschi, T. G.; Vanzani, M.; Lercker, G. An investigation in theuse of HPLC with UV and MS-electrospray detection for quqntification of tea catechins. *Food Chem.* **2004**, *87*, 465−470.

(24) Hu, B.; Wang, L.; Zhou, B.; Zhang, X.; Sun, Y.; Ye, H.; Zhao, L.; Hu, Q.; Wang, G.; Zeng, X. Efficient procedure for isolating methylated catechins from green tea and effective simultaneous analysis of ten catechins, three purine alkaloids, and gallic acid in tea by high-performance liquid chromatography with diode array detection. *J. Chromatogr., A* **2009**, *1216*, 3223−3231.

(25) Nguyen, D. T.; Guillarme, D.; Rudaz, S.; Veuthey, J. L. Fast analysis in liquid chromatography using small particle size and high pressure. *J. Sep. Sci.* **2006**, *29*, 1836−1848.

(26) Wu, N.; Clausen, A. M. Fundamental and practical aspects of ultrahigh pressure liquid chromatography for fast separations. *J. Sep. Sci.* **2007**, *30*, 1167−1182.

(27) Guillarme, D.; Casetta, C.; Bicchi, C.; Veuthey, J. C. High throughput qualitative analysis of polyphenols in tea samples by ultra-high pressure liquid chromatography coupled to UV and mass spectrometry detectors. *J. Chromatogr., A* **2010**, *1217*, 6882−6890.

(28) Cooper, K. A.; Campos-Gimenez, E.; Jimenez-Alvarez, D.; Nagy, K. L.; Donovan, J. L.; Williamson, G. Rapid reversed phase ultra-performance liquid chromatography analysis of the major cocoa polyphenols and inter-relationships of their concentrations in chocolate. *J. Agric. Food Chem.* **2007**, *55*, 2841−2847.

(29) Novakova, L.; Zdenek, S.; Seifrtova, M.; Opletal, L.; Solich, P. Rapid qualitative and quantitative ultra high performance liquid chromatography method for simultaneous analysis of twenty nine common phenolic compounds of various structures. *Talanta* **2010**, *30*, 1970−1979.

(30) Zdenek, S.; Novakova, L.; Solich, P. Analysis of phenolic compounds by high performance liquid chromatography and ultra performance liquid chromatography. *Talanta* **2008**, *76*, 189−199.

(31) Knox, J. H. Practical aspect of LC theory. *J. Chromatogr. Sci.* **1977**, *15* (9), 352−364.

(32) Martin, M.; Eon, C.; Guichon, G. Study of pertinency of pressure in liquid chromatography. I. Theoretical analysis. *J. Chromatogr.* **1974**, *99*, 357−376.

(33) Giddings, J. C. Comparison of theoretical limit of separating speed in gas and liquid chromatography. *Anal. Chem.* **1965**, *37* (1), 60−63.

(34) Poppe, H. Some reflections on speed and efficiency of modem chromatographic methods. *J. Chromatogr., A* **1997**, *778*, 3−21.

(35) Bazinet, L.; Araya-Farias, M.; Doyen, A.; Trudel, D.; Tetu, B. Effect of process unit operations and long-term storage on catechin contents in EGCG-enriched tea drink. *Food Chem.* **2010**, *43*, 1692−1701.

(36) ICH Steering Comiteee. *Validation of Analytical Procedures: Text and Methodoly* Q_2 *(*R_1*). ICH Harmonised Tripatite Guideline*; 2005; pp 1−13.

(37) Zhu, Q. Y.; Zhang, A.; Tsang, D.; Huang, Y.; Chen, Z. Y. Stability of green tea catechin. *J. Agric. Food Chem.* **1997**, *45*, 4624−4628.

(38) Chladek, J.; Sispera, L.; Martınkova, J. High-performance liquid chromatographic assay for the determination of 5-methyltetrahydrofolate in human plasma. *J. Chromatogr., B* **2000**, *74*, 307−313.
(39) Opladen, T.; Ramaekers, T.; Heimann, G.; Blau, N. Analysis of 5-methyltetrahydrofolate in serum of healthy children. *Mol. Genet. Metab.* **2006**, *87*, 61−65.
(40) Poon, G. K. Analysis of catechins in tea extracts by liquid chromatography−electrospray ionization mass spectrometry. *J. Chromatogr., A* **1998**, *794*, 63−74.
(41) Bonoli, M.; Pelillo, M.; Toschi, T. T.; Lercker, G. Analysis of green tea catechins: comparative study between HPLC and HPCE. *Food Chem.* **2003**, *81*, 631−638.
(42) Chen, Q.; Zhao, J.; Gou, Z.; Wang, X. Determination of caffeine content and main catechins contents in green tea (*Camellia sinensis* L.) using taste sensor technique and multivariate calibration. *J. Food Compos. Anal.* **2010**, *23*, 353−358.
(43) Wang, R.; Zhou, W.; Jiang, X. Reaction kinetics of degradation and epimerization of epigallocatechin gallate (EGCG) in aqueous system over a wide temperature range. *J. Agric. Food Chem.* **2008**, *56*, 2694−2701.
(44) Chen, Z. Y.; Zhu, Q. Y.; Tsang, D.; Huang, Y. Degradation of green tea catechins in tea drinks. *J. Agric. Food Chem.* **2001**, *49*, 477−482.

JOURNAL OF AGRICULTURAL AND FOOD CHEMISTRY

Article

pubs.acs.org/JAFC

Re-evaluation of the 2,2-Diphenyl-1-picrylhydrazyl Free Radical (DPPH) Assay for Antioxidant Activity

J. Xie and K. M. Schaich*

Department of Food Science, Rutgers University, 65 Dudley Road, New Brunswick, New Jersey 08901, United States

ABSTRACT: Kinetics and stoichiometry of reactions between the 2,2-diphenyl-1-picrylhydrazyl (DPPH) stable radical and 25 antioxidant compounds with different structure, molecular weight, number of −OH groups, and redox potential were investigated by recording the loss of DPPH$^{\bullet}$ absorbance at 515 nm continuously for 10 min. A series of antioxidant concentrations was tested to determine linear response ranges and reaction saturation points. The primary feature distinguishing antioxidant activity—rate of initial reaction (<30 s)—was controlled by whether the dominant antioxidant mechanism was electron (very fast) or hydrogen atom (slow) transfer and by impairment of steric accessibility to the DPPH radical site by bulky ring adducts and multiple phenolic rings. Results raise serious questions regarding application of the DPPH assay for ranking antioxidants and natural extracts and suggest possible redirection of this assay to distinguish active reaction mechanisms by comparing reactions rates and patterns in different solvents and in 50% water/methanol mixtures at different pH values.

KEYWORDS: *antiradical activity, phenolic compounds, hydrogen atom transfer (HAT), single electron transfer (SET), DPPH, radical quenching kinetics, radical quenching capacity*

INTRODUCTION

The stable radical 2,2-diphenyl-1-picrylhydrazyl (DPPH$^{\bullet}$) (Figure 1) was first proposed for quantitating antioxidant (mostly phenol) content more than 50 years ago.[1,2] (Throughout this paper, DPPH denotes the stable radical DPPH$^{\bullet}$.) Reaction with DPPH was soon adapted for measuring radical quenching kinetics,[3,4] and since then, numerous variations in methods and time for following the reaction as well as for calculating relative antioxidant action by reaction stoichiometry have evolved.[5−10] The DPPH assay is simple and can be run in the most rudimentary laboratories; hence, it has seen extensive applications. Nevertheless, lack of standardization in sample preparation, reaction conditions, analytical protocols, and expression of antioxidant action make it difficult to compare results between laboratories.[11,12] To address this problem, assay protocols are currently being standardized by international bodies,[13] yet questions about which procedures should be standardized remain.

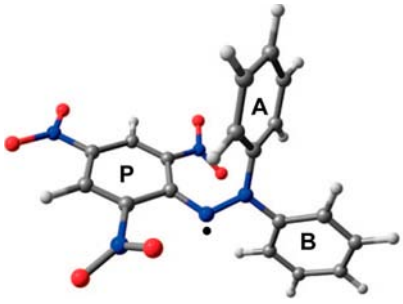

Figure 1. Three-dimensional structure of DPPH. Adapted from ref 14. Copyright 2008. American Chemical Society. Constituent atoms: oxygen (red), nitrogen (blue), carbon (gray), and hydrogen (white). The view is approximately perpendicular to the plane defined by the hydrazyl group N atoms and C-1 of the picryl ring (P). The radical site (N$^{\bullet}$) is protected by nitro groups oriented above and below it, by an *ortho* H atom on each of the phenyl rings (A and B), and by twisting of the rings to create a cage around N$^{\bullet}$.[14,15]

Largely ignored studies of DPPH reaction chemistry have shown that absolute and relative concentrations of DPPH and test antioxidants,[8] solvent polarity and hydrogen bonding strength,[2,16−19] pH,[11] temperature,[3] and oxygen all affect the rate and pathways of DPPH reaction with antioxidants. DPPH can be quenched by both electron[3] and hydrogen atom transfer[4] in at least four different sequences.[14] Solvent and pH, in particular, strongly influence the dominant mechanism and can screen for compounds acting by one specific mechanism or both. For example, hydrogen bonding solvents repress hydrogen atom transfer and favor electron transfer,[17−19] so compounds that are strongly active in hydrogen atom transfer appear to be slower reacting in the methanol and ethanol commonly used for the assay. Similarly, activity of compounds that quench primarily by electron transfer is strongly pH-dependent, being slowest in acid and increasing with pH as ionization of the phenolic group is facilitated.[20] Apparent reactivity of compounds with the capability of mixed quenching mechanisms thus can change markedly with reaction conditions.

Time and method of recording the reaction, as well as the reporting mode, determine which aspects of the reaction are observed and interpreted. Reporting mode is particularly problematic because many methods currently used for rating radical quenching activity yield numbers that allow comparison but provide little or no chemical information about the test antioxidants. Reporting methods such as IC_{50}[21] or EC_{50}

Received: January 14, 2014
Revised: April 16, 2014
Accepted: April 16, 2014
Published: April 16, 2014

 © 2014 American Chemical Society

(antioxidant concentration required to reduce 50% of the DPPH present),[5,10] antioxidant efficiency (AE = $1/EC_{50}\cdot T_{EC50}$)[22,23] (where T_{EC50} is the time needed to reach the steady state at EC_{50} concentration), and % DPPH reduction[24,25] provide values from which stoichiometry can be derived (moles of DPPH reduced per mole antioxidant) but ignore reaction kinetics. Expression of antioxidant activity as μmol equivalents of standards such as vitamin C[26] or Trolox[23] ignores chemistry altogether and just ranks compounds, assuming all act by the same mechanisms.

There is a major flaw in stoichiometric approaches if results are to be used to predict antioxidant activity in living tissues or in foods. DPPH is a stable radical that persists for hours in solution, while the radicals most active in real materials—hydroxyl radicals ($HO^{\bullet}$), superoxide anion ($O_2^{-\bullet}$), nitric oxide ($NO^{\bullet}$), and lipid peroxyl ($LOO^{\bullet}$) and alkoxyl ($LO^{\bullet}$) radicals—have lifetimes on the order of milliseconds to seconds (Table 1). With such short radical lifetimes, the number of reactive groups per antioxidant is less important than how fast each group can quench the radicals present.

Table 1. Lifetimes of Radicals Commonly Active in Living Tissues and in Foods[a]

radical (10^{-3} M, 37 °C)	lifetime
$HO^{\bullet}$	10^{-9} s
$L^{\bullet}$ (lipid alkyl)	10^{-8} s
$RO^{\bullet}$	10^{-6} s
$AnOO^{\bullet}$ (arachidonic acid)	10^{-5} s
$ROO^{\bullet}$	10 s

[a]Data are excerpted from ref 27. Adapted with permission from ref 27. Copyright 1986 Annual Reviews.

As will be emphasized in this article, many compounds have a very fast initial reaction with DPPH that is missed in the conventional practice of monitoring absorbance only after reaching steady-state (many minutes to hours). Papariello et al.[2] proposed that this initial reaction is the only relevant period for reactivity comparison since the reaction is second order, dependent on concentrations of DPPH as well as a phenolic compound, and the reaction product, $DPPH_2$, inhibits the phenol reaction. Some DPPH studies have measured reaction kinetics but not connected the data to antioxidant structure or other characteristics. In a key paper that has provided the basis for many current assays, Brand-Williams et al.[5] generated reaction response curves by recording DPPH absorbance at 0 and 1 min, then every 15 min until a steady-state was reached, testing a range of antioxidant concentrations. These authors actually recorded differences in reaction rates, yet ignored the important kinetic information and reported only values that express stoichiometry. Allowing the reaction to run to "completion" (i.e., plateau), as commonly recommended to track slow reacting compounds,[28] regardless of the time required, virtually guarantees that the assay will reflect stoichiometry rather than kinetics and will report radical quenching proportional to the number of phenoxyl groups, i.e., two electrons or two DPPH radicals reduced per OH.

Other studies have recorded full reaction curves, calculated some kinetic value, and shown distinctively different patterns in reaction kinetics for different phenolic compounds yet also failed to apply and utilize the kinetic information. Sanchez-Moreno[29] observed that initial fast reactions were complete in <30 s and that the main part of moderate rate reactions were complete in <2 min for many phenolic compounds, yet ignored this information and instead determined kinetics as the time required to reduce DPPH by 50% (TEC_{50}). Villano et al.[9] combined EC_{50} values and kinetics into an antioxidant efficiency term for reactions of polyphenols with DPPH. However, their results were compromised by ignoring the initial rapid reaction occurring within seconds (obvious in reaction curves) and, instead, calculating rates from the slow reaction extending over 60 to 180 min. Both studies emphasized stoichiometric analyses in comparing antioxidants.

In contrast, Ingold and colleagues[14,17,18,30−35] have compiled an impressive body of work specifically utilizing DPPH kinetics in initial fast reactions to distinguish radical quenching mechanisms of various antioxidants, i.e., hydrogen atom transfer, electron transfer, combinations of the two, and sequences of action, and to determine solvent effects on reaction mechanisms and kinetics.

As part of a larger project studying mechanisms and standardizing procedures in antioxidant activity assays, this research reinvestigated the chemistry and reaction conditions of the DPPH assay to elucidate active reaction mechanisms, identify factors that control reactions and distinguish antioxidants, optimize methodology, provide a basis for standardization, and determine appropriate applications. Our investigations showed that most antioxidant reactions were much faster than the time scale monitored by Brand-Williams et al.[5] and that in addition, there were distinct differences between phenolic compounds in the kinetics of the reactions. Thus, a major focus of this study was to determine reaction kinetics, evaluate relationships between kinetics and chemical properties and structure, and compare kinetics to conventional stoichiometry calculations for accurately measuring antiradical activity.

MATERIALS AND METHODS

Reagents. Antioxidants tested in this study were of the highest purity available, typically >99%. High purity 2,2-diphenyl-1-picrylhydrazyl (DPPH) and gallic acid were purchased from Eastman Organic Chemical (Rochester, NY). *n*-Propyl gallate, ferulic acid, benzoic acid, quercetin dihydrate, catechin gallate, uric acid, catechol, and *p*-coumaric acid were purchased from Sigma (St. Louis, MO). Pyrogallol, caffeic acid, 3-methyl catechol, Trolox, α-D-glucose, and epicatechin were purchased from Aldrich (Milwaukee, WI). L-Ascorbic acid and hydrochloric acid were purchased from Fisher (Fair Lawn, NJ). α-Tocopherol was from Cargill (Eddyville, IA). Hydroquinone was from Allied Chemical (New York, NY). Resorcinol and glutathione were purchased from Nutritional Biochemicals (Cleveland, OH). Chlorogenic acid was from Indofine (Hillsborough, NJ). DL-Lysine was from California Corp. for Biochemical Research (Los Angeles, CA). Phenol was from Mallinckrodt (St. Louis, MO). Vanillic acid, protocatechuic acid, sodium hydroxide, and HPLC-grade solvents (methanol, ethanol, acetone) were purchased from Sigma-Aldrich (St. Louis, MO). Water purified to 18 MΩ resistivity in a Milli-Q water purification system (Model 13681, Millipore, Bedford, MA) was used whenever water was required.

Reagent Preparation. DPPH reagent standard solution: 0.0036 g of DPPH was dissolved in 100 mL of methanol to generate a 0.0913 mM DPPH stock solution; working solutions were prepared fresh daily by diluting the stock solution with solvent sufficiently to reduce the absorbance at 515 nm to 1.00 (±0.02). This provided a starting DPPH concentration of 9.17×10^{-5} M, assuming an extinction coefficient of 10,900 $M^{-1}cm^{-1}$.[36] Methanol was used because DPPH stability in this solvent was greater than that in ethanol[37,38] or acetone,[39] which have also been reported in the literature as DPPH assay solvents.

Table 2. Molecular Properties and DPPH Reaction Characteristics of Antioxidants

			kinetics						stoichiometry mols DPPH/mol AOX[a]				ratio (AOX=100 μM)[b]
group	compd	M_w	# −OH[c]	E_7 (V)[d]	R_i[e]	/nmol AOX	/ −OH	k_2 ($M^{-1}S^{-1}$)	AOX linear range (μM)	10 μM	e/−OH	100 μM	EC_{50} (μM)	$\Delta DPPH_f/\Delta DPPH_i$
1	*n*-propyl gallate	212.20	3	0.41	34.64 ± 0.90	0.1143	0.0381	950.41 ± 28.78	1−250	5.81	1.94	0.81	7.5	1.00
	ascorbic acid	176.12	2	0.33	28.51 ± 0.77	0.1351	0.0676	2739.3 ± 55.23	1−25	1.99	1.00	0.89	19	1.05
	pyrogallol	126.11	3	0.51	21.02 ± 1.24	0.0809	0.0270	841.24 ± 3.65	1−250	3.02	1.01	0.78	15	1.16
2	3-methylcatechol	124.14	2	0.52	9.17 ± 0.18	0.0348	0.0174	337.12 ± 3.33	2.5−100	1.77	0.89	0.80	26	1.01
	quercetin	302.24	4	0.33	8.77 ± 0.02	0.0289	0.0072	274.16 ± 6.75	1−100	3.63	0.91	0.86	26.5	1.01
	catechol	110.11	2	0.53	6.18 ± 0.44	0.0204	0.0102	217.50 ± 10.23	1−100	3.94	1.97	0.79	19	1.29
	α-tocopherol	430.71	1	0.48	6.27 ± 0.28	0.0244	0.0244	264.61 ± 7.25	1−100	2.06	2.06	1.83	22.5	1.32
	caffeic acid	180.16	2	0.54	5.43 ± 0.11	0.0179	0.0090	283.46 ± 11.63	1−100	2.31	1.16	0.82	21	1.51
	epicatechin	290.27	4	0.44	5.00 ± 0.65	0.0153	0.0038	165.21 ± 5.14	1−100	2.58	0.65	0.79	19.5	1.60
	gallic acid	170.12	3	0.55	4.54 ± 0.12	0.0150	0.0050	129.48 ± 4.33	1−100	4.72	1.57	0.79	9.5	1.76
3	protocatechuic acid	154.12	2	0.68 b	2.17 ± 0.12	0.0072	0.0036	380.90 ± 6.33	1−10	1.46	0.73	0.54	56	2.89
	rosmarinic acid	360.31	4	0.54 a	1.32 ± 0.04	0.0044	0.0011	315.82 ± 7.07	1−10	3.02	0.76	0.76	16.5	5.88
	hydroquinone	110.11	2	0.46	1.26 ± 0.03	0.0041	0.0021	69.13 ± 3.62	1−50	1.38	0.69	0.56	47	4.54
	trolox	250.29	1	0.48	1.24 ± 0.07	0.0041	0.0041	45.23 ± 2.94	10−100	1.44	1.44	0.87	218	1.59
	ferulic acid	194.18	1	0.60	0.96 ± 0.04	0.0032	0.0032	34.44 ± 1.28	1−50	1.07	1.07	0.50	84	5.25
	chlorogenic acid	354.31	2	0.55	0.73 ± 0.10	0.0024	0.0012	270.16 ± 5.63	1−10	1.69	0.85	0.62	35	8.60
4	glutathione	307.32	0	0.24	0.18 ± 0.006	0.0006	(-)[f]	NLR[f]	NLR	nd[f]		0.06	nd	3.67
	resorcinol	110.11	2	0.81	0.13 ± 0.006	0.0004	0.0002	NLR	NLR	nd		0.05	nd	3.69
	vanillic acid	168.15	1		0.12 ± 0.008	0.0004	0.0004	NLR	NLR	nd		0.03	nd	3.27
5	phenol	94.11	1	0.90	no reaction									
	benzoic acid	122.12	1		no reaction									
	p-coumaric acid	164.16	1	0.59	no reaction									
	glucose	180.16	5		no reaction									
	uric acid	168.11	0		no reaction									
	lysine	146.19	0		no reaction									

[a]Stoichiometry determined at AOX concentrations of 10 and 100 μM. [b]Ratio of DPPH consumption measured at end of total reaction (final, f; $\Delta DPPH_f$) vs initial rapid reaction (initial, i, $\Delta DPPH_i$) for 100 μM antioxidant. [c]Number of reactive −OH groups. [d]Redox potential at pH 7. [e]R_i determined for AOX=100 μM is presented as nmol DPPH/sec, then this value is normalized to antioxidant amount (/nmol AOX) and to number of reactive -OH groups present (/−OH). [f](-), no −OH group; NLR, no linear response range; nd, response too low to determine stoichiometry accurately.

dx.doi.org/10.1021/jf500180u | J. Agric. Food Chem. 2014, 62, 4251−4260

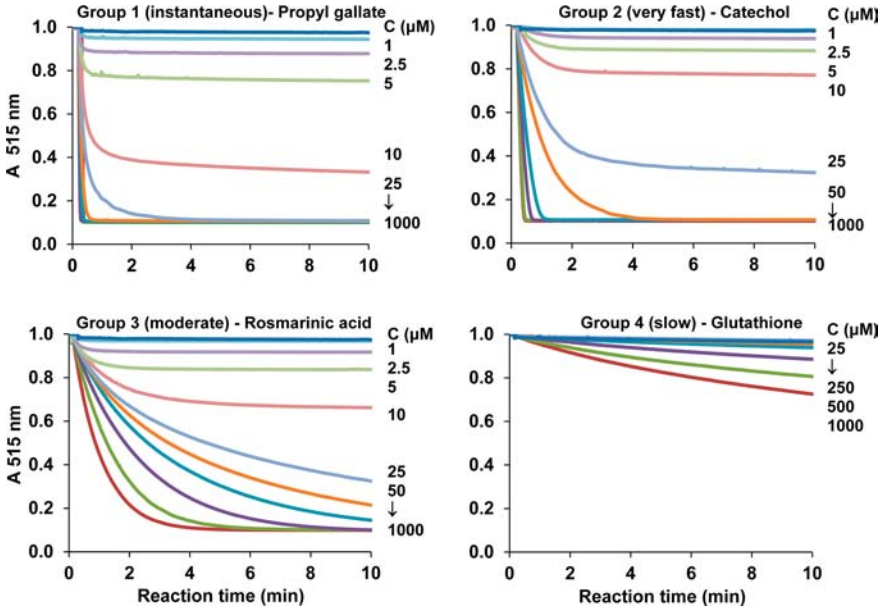

Figure 2. DPPH• reaction response curves for tested antioxidants fall into five classes: reactive Groups 1−4 are shown, Group 5 (no reaction) is not shown.

Antioxidant Preparation. Stock solutions (100 mM) of test antioxidants were prepared in methanol, then serially diluted to progressively lower concentrations for testing (typically 50, 25, 10, 5, 2.5, 1, 0.1, 0.05, 0.025, and 0.01 mM or until no reaction with DPPH was detectable). Antioxidant concentrations after the addition to DPPH (1000, 500, 250, 100, 50, 25, 10 μM, etc.) covered a range from well above [DPPH] to eliminate possible diffusion effects to well below the DPPH concentration to allow full reaction. From this point forward, all antioxidant concentrations noted are final reaction concentrations.

DPPH Quenching by Antioxidants. A Varian Cary 50 Bio Spectrometer system (Agilent, Santa Clara, CA) with Cary WinUV software was used to obtain all the data in this research. Three milliliters of diluted DPPH were pipetted into a quartz cuvette, and the absorbance at 515 nm was recorded to determine starting concentration. Thirty microliters of antioxidant solution were added and mixed rapidly by aspiration in the pipet, and recording of absorbance was initiated immediately. Adding microvolumes of antioxidant to a large volume of DPPH minimized dilution effects on the initial absorbance drop during reaction and facilitated accurate determination of reaction rates. Absorbance was recorded every 0.1 s for 10 min to generate reaction curves.

Solvent Effects. Catechol, hydroquinone, and resorcinol were selected as representative compounds from Groups 1−3 to test effects of solvent on reactivity with DPPH because they are isomers with great difference in reactivity but the same number of phenolic −OH groups and the same fundamental structure except for −OH position; they also have comparable solubility in the test solvents. Comparing phenolic compounds with different ring adducts would have made it difficult to distinguish solvation effects from shifts in radical quenching processes in the different test solvents. Glutathione was selected from Group 4 because it is a strong H donor, whereas reaction mechanisms of resorcinol and vanillic acid are unknown. To test the effect of solvent, 0.0913 mM DPPH stock solutions were prepared in ethanol, acetone, and 50% methanol as well as the standard methanol, and reactions were run with test antioxidants using the protocol described in the preceding paragraph. Initial reaction rates and final reaction stoichiometry were calculated as described under Data Analysis below.

pH Effects. Catechol, hydroquinone, resorcinol, and glutathione (representative samples from each group) were reacted with DPPH dissolved in 50% aqueous methanol as described above, with the addition of some samples for which the water phase was adjusted to pH 5 with HCl or to pH 9 with NaOH. Increases in reactivity with pH were used to identify electron transfer; H atom transfer is independent of pH.

Data Analysis. Initial reaction rates (R_i) were calculated from the initial absorbance drop (ΔA_i) in the linear reaction regions, determined by completion of reaction or regression equations with $R^2 > 0.9$. This region varied with antioxidant and concentration and so had to be determined separately for each compound; reaction times used for the calculations typically varied from 10 to 30 s. For compounds with incomplete reaction, the A at 30 s was used for R_i calculations. ΔA_i was converted to $\Delta[\text{DPPH}]_i$, and the initial rate (R_i) was reported directly as nmols DPPH quenched/s. Initial rates were also normalized to the amount of antioxidant (nmol DPPH/s/nmol AOX) and to the number of −OH groups (nmol DPPH/s/nmol AOX/number of −OH) to gain more insight into factors that may be controlling the DPPH reaction and antioxidant reactivity. Normalization to antioxidant concentration tracks how concentration affects the reaction and is important for elucidating the basic chemistry of the DPPH reaction, validating its use for rating antioxidants, and for determining protocols to be standardized. Rates were normalized to −OH groups because antioxidant reactivity in *in vitro* antioxidant capacity assays has so frequently been associated with this structural feature in test compounds. We wanted to investigate whether the relationships held also in rapid reactions that are most important for quenching short-lived radicals. R_i values were then plotted as a function of antioxidant concentration, and second order rate constants (k_2) revealing the concentration dependence of each antioxidant were determined from slopes of these curves.

Stoichiometry of the reaction (mols DPPH consumed/mol test antioxidant) was calculated from the absorbance drop after 10 min of reaction (ΔA_f) for 10 and 100 μM solutions. At the low antioxidant concentration (10 μM), interference with diffusion to DPPH was expected to be minimal; at 100 μM, the antioxidant concentration nearly equaled that of DPPH; hence, innate reactivity rather than diffusion should have controlled the reaction. Pearson correlation coefficients between various antioxidant properties and their reactions responses were calculated using the statistical functions in Excel software.

All glassware used was subjected to washes in denatured alcohol saturated with potassium hydroxide and in 1 N hydrochloric acid, with Milli-Q water rinses to remove potentially reactive contaminants. All analyses were performed at least in triplicate.

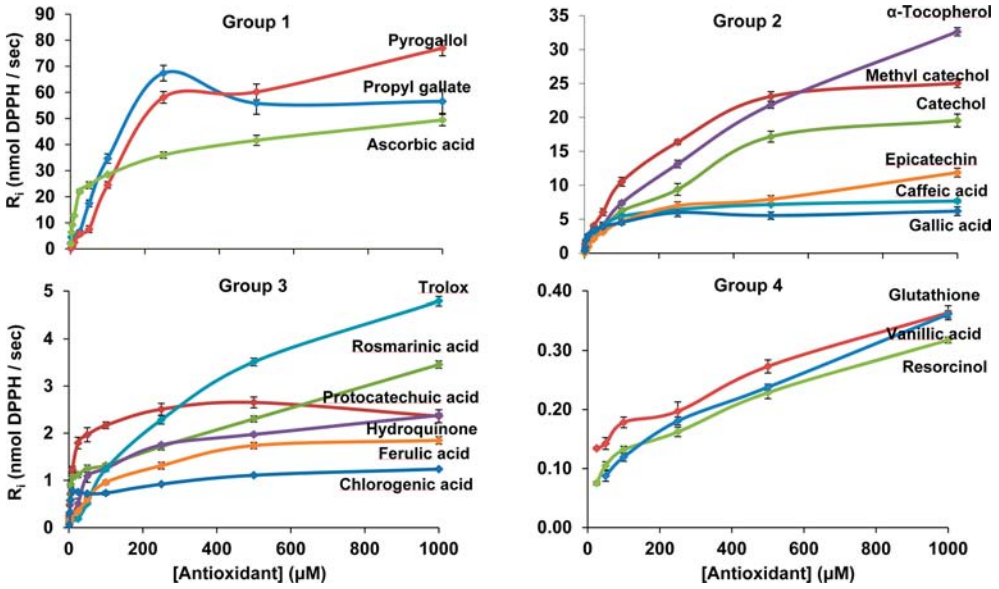

Figure 3. Effect of antioxidant concentrations on rates of initial reaction with DPPH.

■ RESULTS AND DISCUSSION

Preliminary studies in this laboratory recording DPPH loss continuously revealed a marked difference in the shapes of reaction curves for different antioxidants. Some antioxidants showed an immediate very fast reaction that was complete within seconds, while others showed a combination of fast and slower stages, and some showed only slow sustained reactions. To further investigate the reasons for these differences, determine best protocols for standardization of the DPPH antioxidant assays, and identify what useful chemical information can be derived from full reaction curves, reactions of 28 phenolic and nonphenolic compounds were studied in detail. Visual patterns of reaction curves were used for initial categorization, then initial reaction rates, antioxidant concentration dependence and linear reaction ranges, reaction stoichiometry, and degree of early reaction completion were calculated and compared with standard EC_{50} values, number of phenolic −OH (or other H donating) groups, and antioxidant redox potentials to learn more about factors controlling antioxidant reactions with DPPH.

Table 2 compiles these chemical properties and calculated reaction characteristics of tested antioxidants.

Kinetic Reaction Patterns and Initial Reaction Rates. Response curves of antioxidant reactions with DPPH revealed at least five distinctly different groups of reactivity (Figure 2) based on their reaction curve patterns and initial rates (R_i) at 100 μM (where antioxidant and DPPH concentrations are nearly equal, 0.1 mM AOX/0.0917 mM DPPH). (1) Extremely fast: instantaneous initial absorbance drop, R_i >20.0 nmol DPPH/s, the reaction is complete in less than 10 s, and $\Delta A_f/\Delta A_i = 1$; e.g., *n*-propyl gallate, pyrogallol, and ascorbic acid. (2) Fast: rapid initial absorbance drop, then the reaction continues more slowly, R_i = 4.0−10.0 nmol DPPH/s, and $\Delta A_f/\Delta A_i$ = 1−1.76; e.g., 3-methylcatechol, quercetin, catechol, α-tocopherol, caffeic acid, epicatechin, and gallic acid. (3) Medium: absorbance drop slow and continual over the reaction period, R_i = 0.5−4.0 nmol DPPH/s, and $\Delta A_f/\Delta A_i$ = 1.6−8.6; e.g., protocatechuic acid, rosmarinic acid, hydroquinone, Trolox, ferulic acid, and chlorogenic acid. (4) Slow: absorbance drop very slow and almost linear over time, R_i = 0.0−0.5 nmol DPPH/s, and $\Delta A_f/\Delta A_i$ = 3.3−3.7; e.g., glutathione, resorcinol, and vanillic acid. (5) Nonreactive: little or no drop of absorbance over the entire reaction time; e.g., phenol, benzoic acid, and *p*-coumaric acid.

As noted previously, antioxidants can quench DPPH by both electron and hydrogen atom transfer. Electron transfer is very fast (femtoseconds) and not diffusion-controlled, whereas hydrogen atom is slower and clearly diffusion-controlled.[40] Thus, compounds that reduce DPPH completely in less than 30 s (Group 1) act mostly, if not exclusively, by electron transfer in methanol. Compounds that reduce DPPH more slowly and require extended time for full reaction (Groups 2−4, $\Delta DPPH_f/\Delta DPPH_i$ > 1) act increasingly by hydrogen atom transfer, have reaction impeded by steric hindrance, or both.

Effects of Antioxidant Concentration on Reactivity with DPPH. Results of this study revealed significant variation among concentration−response patterns (Figure 3), k_2 and linear response range (Table 2), and saturation concentration (Figure 3) from the different reactivity groups.

For Group 1 (compounds with instantaneous reaction), k_2 values were the highest, and increase of initial reaction rates (R_i) was close to linear with antioxidant concentrations up to about 250 μM (final reaction concentration), then the reaction slowed. The one exception to this pattern was ascorbic acid, which was very reactive at the lowest concentrations, and small increases in concentration made dramatic differences in reaction rates, reflected in k_2 orders of magnitude larger than those of other antioxidants. This high reactivity is probably due to a combination of better accessibility to DPPH and low redox potential. At the same time, ascorbic acid reaction with DPPH also saturated rapidly with concentration (see linear range, Table 2) due to its propensity for secondary reactions at higher concentrations, and this was not reflected in k_2.

The k_2 values dropped as reactivity slowed progressively in Groups 1 through 4 (Table 2), indicating that increasing antioxidant concentrations had less effect on response. Indeed, for many compounds in Groups 2 and 3, reaction rates increased linearly with antioxidant only at the very low concentrations (100 and 10−50 μM, respectively), above which the response curves flattened, exhibiting more

dx.doi.org/10.1021/jf500180u | J. Agric. Food Chem. 2014, 62, 4251−4260

pronounced saturation with each group. There was no range of linear response in Group 4. That none of the antioxidants exhibited a perfectly linear response range and all exhibited some saturation demonstrate that factors other than antioxidant concentration also have important influences on reactivity. This poses a severe problem for quantitation of activity, especially in mixed extracts, since quantitative assays require that (1) the response is continually linear with reactant concentration or the assay must be conducted in a concentration range with linear response and that (2) analytes have comparable concentration dependence, as reflected in the second order rate constant (k_2), or a range of concentrations must be tested for each material.

The variability of k_2 within all groups warrants additional comment. As more antioxidant is added to the system, crowding of antioxidant molecules around the DPPH increases. This has two possible consequences, depending on antioxidant structure: (1) forcing reactive phenolic −OH groups into closer proximity to the DPPH radical site, thus facilitating reaction and (2) creating random molecular packing that impedes access to the DPPH radical. For compounds with lower k_2 values (e.g., hydroquinone, Trolox, and ferulic acid in Group 3), reaction curves were consistent with increased packing interference at higher antioxidant concentrations, while the curves of protocatechuic acid, rosmarinic acid, and chlorogenic acid showed greater reaction rate increase with added antioxidant (higher k_2), consistent with forced DPPH access by the increased packing.

Stoichiometry of Antioxidant Reactions. At 10 μM antioxidant concentrations (DPPH/AOX ∼10, conditions where multiple DPPH molecules should be sufficiently close to each antioxidant molecule that diffusion limitations on reaction are minimal), *n*-propyl gallate, tocopherol, and catechol were the only compounds to donate the expected two electrons per phenolic−OH group (Table 2). Ascorbic acid reacted one electron per OH group and other monophenols donated slightly less than one electron, while stoichiometry with compounds having more complex structure (epicatechin, rosmarinic acid, and quercetin) dropped still further. At antioxidant concentrations (100 μM) comparable to those of DPPH, stoichiometry dropped dramatically to fractions of an electron per OH group for every compound except tocopherol. Plots of stoichiometry over the entire antioxidant concentration range confirmed that stoichiometry was not constant but decreased with antioxidant concentration (Figure 4). The greatest stoichiometry change with concentration occurred at the lowest concentrations of the most reactive phenolic compounds. Differences in stoichiometry were obscured at high antioxidant concentrations, showing once again that reaction conditions markedly affected the picture given for both relative and absolute reactivity. Such nonconstant stoichiometry creates distinct problems for use of the DPPH assay in quantitating and comparing the antioxidant action of extracts with unknown composition and concentration.

As with initial rate, stoichiometry showed negligible correlation to the number of phenolic −OH groups per antioxidant molecule or to redox potential (Table 3). There was also little correlation between stoichiometry and initial reaction rate (0.52 and 0.14 for 10 and 100 μM antioxidant, respectively), so evaluations of antioxidant activity based on stoichiometric measures alone will miss differences between antioxidants at high concentrations and misrepresent the actual reactivity of many antioxidants at low concentrations.

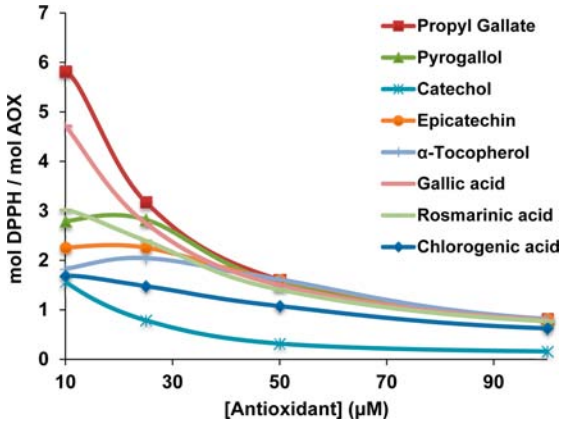

Figure 4. Inverse relationship between stoichiometry and antioxidant concentration for representative antioxidants from each reactivity group.

EC_{50}. As expected, antioxidant concentrations necessary to reduce DPPH by 50% appeared in reverse order to reactivity (Table 2, EC_{50} column). Less than 20 μM final concentrations were required by very fast reacting compounds (Group 1), and this value increased progressively in Groups 2 and 3. Compounds in Group 4 were unable to reduce DPPH by 50%. There was considerable variability within reactivity groups, which probably accounts for the lack of correlations between EC_{50} and M_w or redox potentials, and only a weak negative relationship to the number of phenolic −OH groups (−0.52), initial reaction rate (−0.36), and stoichiometry (−0.40) (Table 3). Thus, as with stoichiometry, the use of EC_{50} alone will give a distorted and inaccurate measure of actual antioxidant reaction with DPPH when comparing antioxidants from different structural classes.

Molecular Properties Controlling Antioxidant Reactivity with DPPH. Although previous studies have associated antioxidant activity within structural classes of phenolic compounds with redox potential[41] and number of phenolic −OH groups,[9] low Pearson correlation coefficients indicated that these factors could not explain the differences in reactivity between structural classes in this study (Table 3). Thus, alternate explanations must be sought.

Steric accessibility must be recognized as a key problem in reaction with DPPH since the radical site is protected inside a reaction cage formed by the two phenyl rings orthogonal to each other, and the picryl ring angled about 30° with its two nitro groups oriented above and below the radical site[14,15] (Figure 1). Most phenolic compounds in Groups 2−4 have more complex ring adducts or multiple rings that can impede the access of phenolic −OH groups to the hindered radical site of DPPH and reduce observed reactivity. Comparing $\Delta DPPH_f/\Delta DPPH_i$ provides support for steric accessibility to the DPPH radical site as a major controller of reactivity (last column, Table 2). Small monophenols with only −OH ring adducts showed a $\Delta DPPHf_f/\Delta DPPH_i$ ratio of ∼1, indicating that the reaction was complete within seconds. This ratio increased with the number and complexity of ring adducts, reflecting a slowing of reaction as molecules had to rotate to orient reactive groups toward the DPPH radical site and as bulky ring adducts or multiple rings interfered with free diffusion to DPPH. The pronounced saturation of DPPH reaction rates with increasing antioxidant concentration shown in slower reacting Groups 2−4 (Figure 3) as well as inhibition of reactions in mixtures of

Table 3. Pearson Coefficients for Relationships of Antioxidant Properties to Reactivity with DPPH

	rates				stoichiometry		
	ΔA_i	ΔA_F	R_i/s	k_2	10 μM	100 μM	EC_{50}
mol wt.	−0.06	0.11	−0.16	−0.13	−0.04	0.43	0.02
phenol −OH	0.44	0.63	0.30	0.31	0.57	0.22	−0.52
E_7 (V)	−0.48	−0.44	−0.34	−0.09	−0.23	−0.17	0.13

Table 4. Comparison of Solvent Effects on DPPH Quenching Rate (R_i) and Total DPPH Consumption after 10 min of Reaction by Selected Antioxidants (100 μM Final Concentration)

	Solvent			
antioxidants	methanol	50% aq. methanol	ethanol	acetone
	Initial Rate, R_i (nmol DPPH/s)			
pyrogallol	21.02 ± 1.24	30.56 ± 1.32	1.56 ± 0.05	0.30 ± 0.01
catechol	6.18 ± 0.44	11.92 ± 0.54	0.47 ± 0.02	0.18 ± 0.01
hydroquinone	1.26 ± 0.03	6.84 ± 0.46	0.48 ± 0.03	0.12 ± 0.02
resorcinol	0.13 ± 0.01	0.35 ± 0.02	no reaction	no reaction
glutathione	0.18 ± 0.01	1.30 ± 0.09	0.10 ± 0.01	no reaction
	Total DPPH Consumption (μmol)			
pyrogallol	0.25 ± 0.02	0.24 ± 0.02	0.21 ± 0.01	0.015 ± 0.000
catechol	0.24 ± 0.01	0.24 ± 0.02	0.20 ± 0.01	0.003 ± 0.000
hydroquinone	0.17 ± 0.01	0.23 ± 0.02	0.13 ± 0.01	0.044 ± 0.001
resorcinol	0.01 ± 0.00	0.07 ± 0.00	no reaction	no reaction
glutathione	0.02 ± 0.00	0.14 ± 0.01	0.005 ± 0.000	no reaction

phenolic compounds (manuscript in preparation) are similarly consistent with steric interference imposed by molecules blocking access to the radical site, rather than accumulation of $DPPH_2$ that reportedly inhibits the reaction.[4] These results suggest that steric hindrance may be the most important factor limiting the reaction of phenolic compounds with DPPH and thus raise questions about the validity of the DPPH assay for rating the activity of antioxidants with different structures. Computer analysis of molecular docking of antioxidants with DPPH should clarify the role of steric accessibility in this assay.

Inductive effects of ring substituents on reactivity with DPPH must also be considered. Slower reacting phenolic compounds tended to have more electron-withdrawing ring substituents (COOH, C═C, and COOR) or multiple rings which deactivate phenolic −OH groups to ionization or H atom transfer. However, there was little direct correlation between reaction rates and estimated Hammett sigma constants, measures of how strongly ring substituents at meta and para positions donate or withdraw electrons from reactive groups (data not shown). Thus, other factors have a stronger influence than inductive effects on DPPH reaction rates.

Finally, DPPH is a mixed mode reagent, so the balance between electron and hydrogen atom transfer for individual compounds and in different reaction environments must contribute to the control of reaction rates with DPPH. As shown above, compounds capable of electron transfer react more rapidly with DPPH, while hydrogen atom donors react more slowly. Some insights into the relationship between the dominant mechanism and reaction rate are provided by the solvent effects on reactions discussed below.

Effects of Solvent on Antioxidant Reactivity with DPPH. To determine the optimum solvent for standardization and to explore whether these solvent effects could be further used to advantage to investigate reaction processes, we reacted DPPH with glutathione (a strong H donor) and phenols (pyrogallol, catechol, hydroquinone, and resorcinol) having closely related structure from each of the reactivity groups in methanol, ethanol, acetone, and 50% aqueous methanol, solvents most often in assays of antioxidant activity. For the phenolic compounds, reactions were fastest in methanol and slowed dramatically in ethanol or acetone (Table 4).

A number of papers have documented that hydrogen bonding solvents generally decrease hydrogen atom transfers because they complex with both DPPH[4,14] and phenolic compounds,[16,19,31] thus blocking reaction. Consistent with these observations, the relative rates for solvents in this study are in the reverse order of hydrogen bond accepting ability of the three solvents, i.e., hydrogen bond parameters β_2^H are 0.41, 0.44, and 0.50 for methanol, ethanol, and acetone, respectively.[42] Litwinienko and Ingold have shown that HAT cannot occur from hydrogen bonded complexes between solvent and hydrogen atom donor, XH···S, so the most simplistic explanation for the solvent effects is differences in the strength of hydrogen bonding of the solvent to phenolic −OH groups and/or to DPPH that interferes with the release of H atoms.[17,18,43]

Slowing of reactions in ethanol may also be attributed to increased viscosity slowing the diffusion of antioxidants to the DPPH radicals or to increased steric interference with phenol access to the DPPH radical site. Acetone is particularly effective in inhibiting hydrogen transfer from vicinal diphenols because it hydrogen bonds very strongly to both phenolic −OH groups, completely blocking both electron and hydrogen transfer.[16] In addition, DPPH reacts with phenolic compounds via rapid sequential proton loss electron transfer (SPLET) in ionizing solvents and by slower hydrogen atom transfer (HAT) in nonionizing solvents or in the presence of acid.[18] Both methanol and ethanol partially ionize, allowing both electron and hydrogen transfer, but acetone is nonionizing. Thus, DPPH radical quenching is minimal in acetone because both electron and hydrogen atom transfers are strongly inhibited.

Diluting methanol to 50% with water greatly increased the reaction rate by about 50% for pyrogallol, which is a strong electron transfer compound, but considerably more for

antioxidants that acted preferentially by hydrogen atom transfer. Glutathione, a strong hydrogen donor, increased more than seven times in rate. Water is a known proton transfer medium; it supports ionization of solutes, has lower hydrogen bonding strength (β_2^H = 0.38[42]) than the organic solvents tested, and stabilizes the polar transition states necessary for hydrogen atom abstraction.[41] All of these actions markedly facilitate hydrogen atom transfer.

Solvent effects extended variably to reaction stoichiometry. Fifty percent methanol did not alter the reactivity of pyrogallol and catechol (strong electron transfer antioxidants) relative to methanol but increased the total reaction of hydroquinone by 50% and of resorcinol and glutathione by 7 times.

In terms of DPPH assay standardization, these results indicate that of the solvents studied here, methanol is the solvent of choice. That it selects for antioxidants acting predominantly or exclusively by SET does present the disadvantage that strong electron transfer agents appear to be the most active antioxidants[17] while known physiological antioxidants such as glutathione and uric acid that act almost exclusively by HAT are tremendously underrated. Nevertheless, running DPPH assays in 50% aqueous methanol in parallel with neat methanol offers opportunities to distinguish compounds that act by HAT, elucidate dominant reaction mechanisms of individual antioxidants and of mixed composition extracts, and provide important insights into behaviors that may be expected in multiphase systems such as cells and foods where lipid phases would favor electron transfers and aqueous phases would favor hydrogen atom transfers.

Effects of pH on Kinetics and Reaction. Antioxidants from the solvent tests were further evaluated in 50% aqueous methanol in which the water portion was varied in pH (5, 7, and 9) by the addition of high purity HCl or NaOH. Initial rates for known electron transfer agents pyrogallol and catechol increased notably with pH, while hydrogen atom donors glutathione and resorcinol showed negligible change (Figure 5).

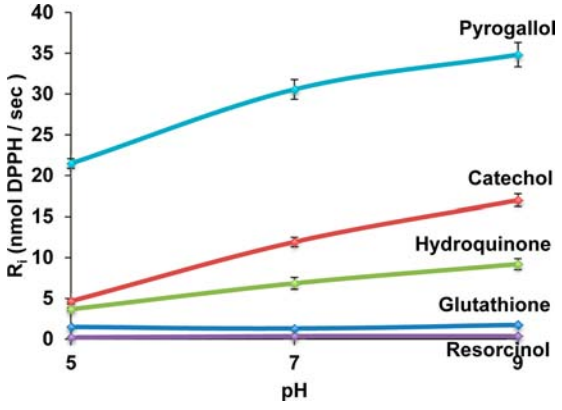

Figure 5. Effect of pH on initial rates of antioxidant reactions with DPPH. [AOX] = 100 μM (final); solvent = 50% aqueous methanol. pH effects on final stoichiometry in the same reactions were negligible.

Hydroquinone, which acts by both electron and hydrogen transfers, exhibited intermediate rate increases. Thus, pH effects on rates of antioxidant reaction with DPPH in 50% methanol can be advantageously combined with solvent effects to distinguish between electron and hydrogen atom transfers as dominant reaction mechanisms. Differences were only seen with reaction rates; essentially, no change occurred with reaction stoichiometry as pH was varied (data not shown).

Recommendations for the Use of DPPH Reactions in the Evaluation of the Radical Quenching Activity of Antioxidants. The DPPH reaction has been used extensively to compare and rank the antioxidant effectiveness of a wide range of natural extracts in now thousands of studies. Nonetheless, results reported here raise serious questions about its validity for quantitating and comparing the activity of antioxidants with different sizes and structures, and especially for ranking their relative reactivity due to the following significant limitations of the DPPH reaction: (1) Absorbance measurements only after long reaction periods are inadequate for quantitating antioxidant reaction with DPPH because they miss important initial reactions that provide critical distinction between the reactivity of antioxidants with different structures and do not determine reaction rates. Final stoichiometry determined from total absorbance drops reflects the numbers of hydrogen atom donating groups almost exclusively and thus overestimates the activity of polyphenols and underestimates activity of monophenols. These conventional analyses also ignore antioxidant concentration effects and reaction saturation.

(2) Full and accurate evaluation of antioxidant reactivity rather than capacity requires recording DPPH loss continuously over the full reaction time, with calculation of reaction kinetics from early response (immediate to 30 s). However, accurate measurements of the initial very rapid reaction rates requires fast kinetic techniques such as continuous or stopped flow mixing because the initial electron transfer from antioxidant to DPPH is too fast to quantitate using manual mixing and conventional spectrophotometers.

(3) Accurate information cannot be gained from single antioxidant concentrations, particularly in extracts not normalized to the concentration of phenolic compounds. Rather, reactions must be run over a range of antioxidant concentrations from dilute (diffusion controlled) to approximately equal to DPPH. Concentrations greater than DPPH as conventionally used to determine second order rate constants are not valid due to reaction saturation and interference with steric accessibility to DPPH. Determining reaction response as a function of antioxidant concentration clearly identifies valid linear response ranges and saturation levels, and differentiates reactivity patterns.

(4) Allowing reactions to run to completion over many minutes to hours is warranted for the quantitation of phenols, as described in early applications of DPPH,[2] and reflects potential antioxidant capacity but is irrelevant for determining the important initial rates of antioxidant reaction with DPPH. Analyses of immediate (0−2 min) rather than long reactions should be stressed when determining antioxidant reactivity.

(5) Steric accessibility to the DPPH radical site appears to control the reaction more than specific identifiable chemical properties of the antioxidants. Initial reaction rates are most rapid with the simplest phenolic compounds and decrease with the addition of bulky ring adducts and multiple rings. These differences are largely obscured and may even be reversed when reactions are monitored only after the long periods allowed for reaching equilibrium. Furthermore, compounds known to have strong antioxidant activity, e.g., glutathione and BHT,[11] show only slow reactivity with DPPH at least in part due to strongly steric limitations.

Because structure rather than chemistry appears to dominate the reaction rate, it is our scientific judgment that reaction with DPPH should not be used to compare or infer the potential antioxidant activity of antioxidant mixtures, prepared or in

extracts, where different structural classes are present and may not even be known. Ascorbic acid contents, in particular, will enhance reactivity disproportionately, so its concentrations in extracts must be determined to accurately interpret results.

A potential alternative application of the DPPH reaction may be distinction of electron transfer versus hydrogen atom transfer as dominant reaction mechanisms of individual antioxidant compounds. Even here, though, qualitative information about reaction mechanisms of mixtures and extracts can be derived from reaction response patterns and kinetic solvent effects, but rates of general radical reactivity for mixtures cannot be quantified accurately due to limitations in steric accessibility to the DPPH radical site.

AUTHOR INFORMATION

Corresponding Author

*Phone: 848-932-5454. Fax: 732-932-6776. E-mail: schaich@aesop.rutgers.edu.

Notes

The authors declare no competing financial interest.

REFERENCES

(1) Blois, M. S. Antioxidant determination by use of a stable free radical. *Nature* **1958**, *181*, 1199−1200.

(2) Papariello, G. J.; Janish, M. A. M. Diphenylpicrylhydrazyl as an organic analytical reagent in the spectrophotometric analysis of phenols. *Anal. Chem.* **1966**, *38* (2), 211−214.

(3) McGowan, J. C.; Powell, T.; Raw, R. The rates of reaction of α,α-diphenyl-β-picrylhydrazyl with certain amines and phenols. *J. Chem. Soc.* **1959**, 3103−3110.

(4) Hogg, J. S.; Lohmann, D. H.; Russell, K. S. The kinetics of reaction of 2,2-diphenyl-1-picrylhydrazyl with phenols. *Can. J. Chem.* **1961**, *39*, 1588−1594.

(5) Brand-Williams, W.; Cuvelier, M. E.; Berset, C. Use of a free radical method to evaluate antioxidant activity. *LWT Food Sci. Technol.* **1995**, *28* (1), 25−30.

(6) Apak, R.; Gorinstein, S.; Böhm, V.; Schaich, K. M.; Özyürek, M.; Güçlü, K. Methods of measurement and evaluation of natural antioxidant capacity/activity (IUPAC Technical Report). *Pure Appl. Chem.* **2013**, *85* (5), 957−998.

(7) Kedare, S. B.; Singh, R. P. Genesis and development of DPPH method of antioxidant assay. *J. Food Sci. Technol.* **2011**, *48* (4), 412−422.

(8) Mishra, K.; Ojha, H.; Chaudhury, N. K. Estimation of antiradical properties of antioxidants using DPPH assay: A critical review and results. *Food Chem.* **2012**, *130* (4), 1036−1043.

(9) Villaño, D.; Fernandez-Pachon, M. S.; Moya, M. L.; Troncoso, A. M.; Garcia-Parrilla, M. C. Radical scavenging ability of polyphenolic compounds towards DPPH free radical. *Talanta* **2007**, *71* (1), 230−235.

(10) Bondet, V.; Brand-Williams, W.; Berset, C. Kinetics and mechanisms of antioxidant activity using the DPPH free radical method. *Lebensm. Wiss. Technol.* **1997**, *30*, 609−615.

(11) Dawidowicz, A. L.; Wianowska, D.; Olszowy, M. On practical problems in estimation of antioxidant activity of compounds by DPPH method. *Food Chem.* **2012**, *131* (3), 1037−1043.

(12) Prior, R. L.; Wu, X.; Schaich, K. M. Standardized methods for the determination of antioxidant capacity and phenolics in foods and dietary supplements. *J. Agric. Food Chem.* **2005**, *53* (10), 4290−4302.

(13) Plank, D. W.; Szpylka, J.; Sapirstein, H.; Woollard, D.; Zapf, C. M.; Lee, V.; Chen, C. Y.; Liu, R. H.; Tsao, R.; Düsterloh, A.; Baugh, S. Determination of antioxidant activity in foods and beverages by reaction with 2,2′-diphenyl-1-picrylhydrazyl (DPPH): collaborative study First Action 2012.04. *J. AOAC Int.* **2012**, *95* (6), 1562−1569.

(14) Foti, M. C.; Daquino, C.; Mackie, I. D.; DiLabio, G. A.; Ingold, K. U. Reaction of phenols with the 2,2-diphenyl-1-picrylhydrazyl radical. Kinetics and DFT calculations applied to determine ArO-H bond dissociation enthalpies and reaction mechanism. *J. Org. Chem.* **2008**, *73*, 9270−9282.

(15) Williams, D. E. Structure of 2,2-diphenyl-1-picrylhydrazyl free radical. *J. Am. Chem. Soc.* **1966**, *88* (23), 5665−5666.

(16) Barclay, L. R. C.; Edwards, C. E.; Vinqvist, M. R. Media effects on antioxidant activities of phenols and catechols. *J. Am. Chem. Soc.* **1999**, *121* (26), 6226−6231.

(17) Litwinienko, G.; Ingold, K. U. Abnormal effects on hydrogen atom abstractions. 1. The reactions of phenols with 2,2-diphenyl-1-picrylhydrazyl (DPPH•) in alcohols. *J. Org, Chem.* **2003**, *68*, 3433−3438.

(18) Litwinienko, G.; Ingold, K. U. Abnormal solvent effects on hydrogen atom abstraction. 3. Novel kinetics in sequential proton loss electron transfer chemistry. *J. Org, Chem.* **2005**, *70*, 8982−8990.

(19) Foti, M. C.; Ruberto, G. Kinetic solvent effects on phenolic antioxidants determined by spectrophotometric measurements. *J. Agric. Food Chem.* **2000**, *49* (1), 342−348.

(20) Nanjo, F.; Goto, K.; Seto, R.; Suzuki, M.; Sakai, M.; Hara, Y. Scavenging effects of tea catechins and their derivatives on 1,1-diphenyl-2-picrylhydrazyl radical. *Free Radical Biol. Med.* **1996**, *21* (6), 895−902.

(21) Gamez, E. J. C.; Luyengi, L.; Lee, S. K.; Zhu, L.-F.; Zhou, B.-N.; Fong, H. H. S.; Pezzuto, J. M.; Kinghorn, A. D. Antioxidant flavonoid glycosides from Daphniphyllum calycinum. *J. Nat. Prod.* **1998**, *61* (5), 706−708.

(22) Butkovic, V.; Klasinc, L.; Bors, W. Kinetic study of flavonoid reactions with stable radicals. *J. Agric. Food Chem.* **2004**, *52*, 2816−2820.

(23) Awika, J. M.; Rooney, L. W.; Wu, X.; Prior, R. L.; Cisneros-Zevallos, L. Screening methods to measure antioxidant activity of sorghum (Sorghum bicolor) and sorghum products. *J. Agric. Food Chem.* **2003**, *51*, 6657−6662.

(24) Burda, S.; Oleszek, W. Antioxidant and antiradical activities of flavonoids. *J. Agric. Food Chem.* **2001**, *49*, 2774−2779.

(25) Stratil, P.; Klejdus, B.; Kuban, V. Determination of total content of phenolic compounds and their antioxidant activity in vegetables: evaluation of spectrophotometric methods. *J. Agric. Food Chem.* **2006**, *54*, 607−616.

(26) Kim, D.-O.; Lee, K. W.; Lee, H. J.; Lee, C. Y. Vitamin C equivalent antioxidant capacity (VCEAC) of phenolic phytochemicals. *J. Agric. Food Chem.* **2002**, *50*, 3713−3717.

(27) Pryor, W. A. Oxy-radicals and related species: their formation, lifetimes and reactions. *Annu. Rev. Physiol.* **1986**, *48*, 657−667.

(28) Molyneux, P. The use of the stable free radical diphenylpicrylhydrazyl (DPPH) for estimating antioxidant activity. *Songklanakarin J. Sci. Technol.* **2004**, *26* (2), 211−219.

(29) Sánchez-Moreno, C.; Larrauri, J. A.; Saura-Calixto, F. A procedure to measure the antiradical efficiency of polyphenols. *J. Sci. Food Agric.* **1998**, *76* (2), 270−276.

(30) Bowry, V. W.; Ingold, K. U. Extraordinary kinetic behavior of the α-tocopheroxyl (Vitamin E) radical. *J. Org. Chem.* **1995**, *60*, 5456−5467.

(31) MacFaul, P. A.; Ingold, K. U.; Lusztyk, J. Kinetic solvent effects on hydrogen atom abstraction from phenol, aniline, and diphenylamine. The importance of hydrogen bonding on their radical-trapping (antioxidant) activities. *J. Org, Chem.* **1996**, *61*, 1316−1321.

(32) Valgimigli, L.; Banks, J. T.; Ingold, K. U.; Lusztyk, J. Kinetic solvent effects on hydroxylic hydrogen atom abstractions are independent of the nature of the abstracting radical. Two extreme tests using Vitamin E and phenol. *J. Am. Chem. Soc.* **2000**, *117* (40), 9966−9971.

(33) Valgimigli, L.; Ingold, K. U.; Lusztyk, J. Solvent effects on the reactivity and free spin distribution of 2,2-diphenyl-1-picrylhydrazyl radicals. 1. *J. Org, Chem.* **1996**, *61* (22), 7947−7950.

(34) Foti, M. C.; Amorati, R.; Pedulli, G. F.; Daquino, C.; Pratt, D. A.; Ingold, K. U. Influence of "remote" intramolecular hydrogen bonds on the stabilities of phenoxyl radicals and benzyl cations. *J. Org, Chem.* **2010**, *75* (13), 4434−4440.

(35) Foti, M. C.; Daquino, C.; DiLabio, G. A.; Ingold, K. U. Kinetics of the oxidation of quercetin by 2,2-diphenyl-1-picrylhydrazyl (DPPH$^{\bullet}$). *Org. Lett.* **2011**, *13* (18), 4826−4829.
(36) Lebeau, J.; Furman, C.; Bernier, J.-L.; Duriez, P.; Teissier, E.; Cotelle, N. Antioxidant properties of di-tert-butylhydroxylated flavonoids. *Free Radical Biol. Med.* **2000**, *29* (9), 900−912.
(37) Cos, P.; Hermans, N.; Calomme, M.; Maes, L.; De, B. T.; Pieters, L.; Vlietinck, A. J.; Vanden, B. D. Comparative study of eight well-known polyphenolic antioxidants. *J. Pharm. Pharmacol.* **2003**, *55*, 1291−1297.
(38) Nishizawa, M.; Kohno, M.; Nishimura, M.; Kitagawa, A.; Niwano, Y. Non-reductive scavenging of 1,1-diphenyl-2-picrylhydrazyl (DPPH) by peroxy radical: A useful method for quantitative analysis of peroxy radical. *Chem. Pharm. Bull.* **2005**, *53*, 714−716.
(39) Sawai, Y.; Moon, J.-H. NMR analytical approach to clarify the molecular mechanisms of the antioxidative and radical scavenging activities of antioxidants in tea using 1,1-diphenyl-2-picrylhydrazyl. *J. Agric. Food Chem.* **2000**, *48*, 6247−6253.
(40) Ganapathi, M. R.; Hermann, R.; Naumov, S.; Brede, O. Free electron transfer from several phenols to radical cations of non-polar solvents. *Phys. Chem. Chem. Phys.* **2000**, *2* (21), 4947−4955.
(41) Butkovic, V.; Klasinc, L.; Bors, W. Kinetic study of flavonoid reactions with stable radicals. *J. Agric. Food Chem.* **2004**, *52*, 2816−2820.
(42) Abraham, M. H.; Grellier, P. L.; Prior, D. V.; Morris, J. J.; Taylor, P. J. Hydrogen bonding. Part 10. A scale of solute hydrogen-bond basicity using log K values for complexation in tetrachloromethane. *J. Chem. Soc., Perkin Trans. 2* **1990**, No. 4, 521−529.
(43) Litwinienko, G.; Ingold, K. U. Solvent effects on the rates and mechanisms of reaction of phenols with free radicals. *Acc. Chem. Res.* **2007**, *40* (3), 222−230.

JOURNAL OF AGRICULTURAL AND FOOD CHEMISTRY

Article

pubs.acs.org/JAFC

Extraction of Aflatoxins from Liquid Foodstuff Samples with Polydopamine-Coated Superparamagnetic Nanoparticles for HPLC-MS/MS Analysis

Cassandra McCullum,[†] Paul Tchounwou,[‡] Li-Sheng Ding,[§] Xun Liao,*[,§] and Yi-Ming Liu*[,†,§]

[†]Department of Chemistry and Biochemistry, Jackson State University, 1400 Lynch Street, Jackson, Mississippi 39217, United States

[‡]Department of Biology, Jackson State University, 1400 Lynch Street, Jackson, Mississippi 39217, United States

[§]Chengdu Institute of Biology, Chinese Academy of Sciences, South Renmin Nan Road, Chengdu 610041, China

ABSTRACT: A facile magnetic solid phase extraction (MSPE) of aflatoxins (AFs) from liquid samples was developed using polydopamine-coated magnetic nanoparticles (PD-MNPs) as the adsorbent. PD-MNPs were prepared from amine-terminated MNPs and dopamine via an in situ oxidative self-polymerization approach. Under the selected MSPE conditions, extraction yields ranging from 59.3% for AF G_2 to 89.0% for AF B_1 were obtained with good repeatability. Coupled with HPLC-MS/MS quantification, the MSPE procedure serves not only for sample cleanup but also for AFs enrichment that is highly desired for trace analysis. The proposed MSPE-HPLC-MS/MS method had a linear calibration curve in the concentration range from 0.00600 to 3.00 ng/mL aflatoxin and limits of detection of 0.0012 ng/mL for AF B_1, AF B_2, and AF G_1, and 0.0031 ng/mL for AF G_2.

KEYWORDS: *aflatoxin quantification, HPLC-MS/MS, sample pretreatment, magnetic solid phase extraction, polydopamine coated magnetic nanoparticles, wine analysis*

INTRODUCTION

Mycotoxins are toxic secondary metabolites produced by organisms of the fungi kingdom, commonly known as molds.[1,2] Aflatoxins (AFs) are mycotoxins derived by *Aspergillus flavus* (*A. flavus*) and *Aspergillus parasiticus* (*A. parasiticus*) and are listed as Group I carcinogens by the International Agency for Research on Cancer (IARC), a body of the World Health Organization (WHO). There are four major natural aflatoxins (i.e., AF B_1, AF B_2, AF G_1, and AF G_2). AF B_1 and AF B_2 are produced by *A. flavus*, whereas AF G_1 and AF G_2 are produced by both *A. flavus* and *A. parasiticus*. AF B_1 is the molecule with the highest toxic significance. The hierarchy of toxicity, carcinogenicity, and mutagenicity of different aflatoxins is in the order AF B_1 > AF G_1 > AF B_2 > AF G_2.[3,4] The occurrence of aflatoxins is influenced by certain environmental factors. Hence, the extent of contamination will vary with geographic location, agricultural and agronomic practices, and the susceptibility of commodities to fungal invasion during preharvest, storage, and/or processing periods. On a worldwide scale, aflatoxins are found in stored food commodities and oil seeds such as corn, peanuts, and so forth.[5,6]

To achieve quantitative analysis of aflatoxins, analytical methods based on various instrumental techniques have been developed.[7,8] High-performance liquid chromatography−mass spectrometric (HPLC−MS) methods have drawn the most interest due to their excelling selectivity. However, HPLC−MS analysis is prone to matrix effects, which are dependent on analytes, sample matrices, LC−MS conditions, and sample preparation.[9,10] To some degree, use of internal standards, especially stable isotope dilution, alleviates the problems associated with matrix effects.[11,12] A major disadvantage of HPLC-MS stable isotope dilution analysis is the need for expensive isotope-labeled analogues of the analytes. In addition, when analyte concentrations in a sample solution are below the limit of quantitation (LOQ) of the method, enrichment of the analytes must be carried out prior to analysis. Many procedures for sample cleanup and/or analyte enrichment have been reported. Immunoaffinity columns have been used for long to extract aflatoxins from various sample matrices.[13,14] The advantages of these affinity extraction procedures are that they are selective and sensitive. However, the immunoaffinity columns are normally costly. To reduce the cost of analysis, chemical mini-columns, particularly florisil-packed columns were proposed and proven effective for sample cleanup in aflatoxin analysis.[15−17] Major drawbacks of these column-based procedures include a time-consuming elution of the retained analytes and use of significant quantities of toxic organic solvents. Solid-phase extraction (SPE) of aflatoxins with C_{18} cartridges has been successfully developed.[18−20]

Magnetic solid-phase extraction (MSPE) is a new version of SPE. It is based on the use of superparamagnetic nanoparticles as adsorbent.[21−23] In MSPE, the adsorbent needs not to be packed into a cartridge as in traditional SPE. Instead, a suspension of the nanometer-sized adsorbent is added and mixed well with the sample solution to extract analytes. After extraction, the adsorbent can be easily separated from the solution and collected through magnetic decantation by means of an external magnet. There is no need for tedious centrifugation or filtration in MSPE. Therefore, MSPE is

Received: February 13, 2014
Revised: April 25, 2014
Accepted: April 28, 2014
Published: April 28, 2014

ACS Publications © 2014 American Chemical Society

dx.doi.org/10.1021/jf501659m | J. Agric. Food Chem. 2014, 62, 4261−4267

quick, easy to perform, and importantly, well-suited to handle liter volumes of samples, which means a large enrichment factor can be conveniently obtained. Use of MSPE in quantitative analysis of estrogens[24] and isoflavones[25] in milk samples has been reported.

The aim of the present research was to develop a rapid, cost-effective, and efficient MSPE procedure for HPLC−MS/MS quantification of aflatoxins in liquid foodstuff samples. This procedure serves not only for sample cleanup, eliminating any potential matrix effects on the subsequent HPLC−MS/MS analysis, but also for AF enrichment, allowing the quantification at very low levels. To achieve high extraction efficiency, superparamagnetic Fe_3O_4 nanoparticles with different surface modifications were synthesized, characterized by using TEM and FTIR and evaluated as the MSPE adsorbent. MSPE parameters affecting the extraction efficiency, including extraction time, eluting solvent, and so forth were investigated. Finally, rapid analysis of low levels of aflatoxins in red wine samples by using the proposed MSPE−HPLC−MS/MS method was demonstrated.

MATERIALS AND METHODS

Reagents and Chemicals. Aflatoxin standards, dopamine (structures are shown in Figure 1), 1,6-hexamethylenediamine, anhydrous sodium acetate, iron(III) chloride hexahydrate ($FeCl_3·6H_2O$), ethylene glycol, HPLC grade acetonitrile, methanol, and formic acid were purchased from Sigma-Aldrich Chemicals (St. Louis, MO). Other chemicals and solvents were of analytical grade. Milli-Q water (Millipore, Bedford, MA) was used throughout the work.

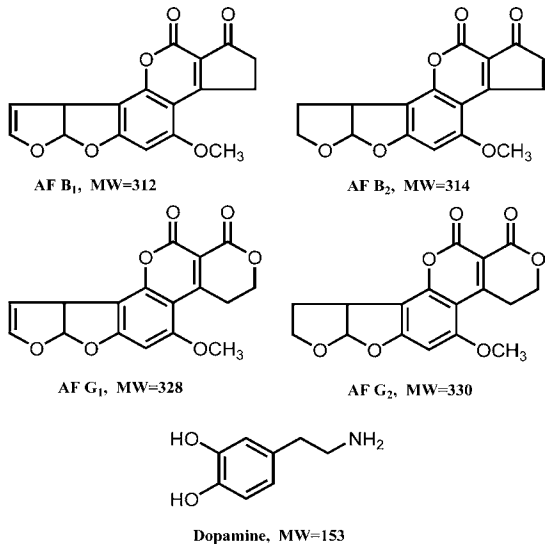

Figure 1. Chemical structures of the compounds involved in this work: AF B_1, AF B_2, AF G_1, AF G_2, and dopamine.

Preparation of Polydopamine-MNPs. Amine-terminated Fe_3O_4 magnetic nanoparticles (AMNPs) were prepared by a one-pot hydrothermal procedure previously reported (illustrated in Figure 2).[26] Briefly, 4.33 g of 1,6-hexanediamine, 1.33 g of anhydrous sodium acetate, and 0.66 g of $FeCl_3·6H_2O$ were dissolved in 25 mL of ethylene glycol by vigorously stirring at 50 °C to obtain a clear solution. It was then transferred to a Teflon-lined autoclave for 6 h at 198 °C to obtain AMNPs. The AMNPs were rinsed with water and ethanol twice. After each rinse step, the AMNPs were separated from the supernatant by using an external magnet. AMNPs were dried at 50 °C under N_2 overnight. To prepare polydopamine coated MNPs (PD-MNPs), an in situ oxidative self-polymerization procedure was used.[27−29] A suspension of AMNPs was prepared by dispersing 220 mg of AMNPs in 10 mL of 10 mM Tris-HCl buffer solution (pH 8.5) through sonication for 15 min. Dopamine HCl (2.5 mg/mL) was added to the AMNPs suspension with vigorous stirring, and the pH of the mixture was adjusted to 8.5 by addition of 10 mM sodium hydroxide. The solution was placed on a shaker for 12 h after which PD-MNPs were collected by magnetic decantation, washed three times with water, and finally redispersed in 5.0 mL water by sonication for 15 min.

Characterization of PD-MNPs. Transmission electron microscopic (TEM) images were acquired on a JEOL, JEM-1011 with a resolution of 0.2 nm lattice. FT-IR spectra were obtained by a Nexus 670 E.S.P. Fourier transform-infrared spectrometer.

Aflatoxin Standard Solutions. Aflatoxin standard mixture containing 1000 ng/mL AF B_1, AF G_1 and 300 ng/mL AF B_2, AF G_2 (Sigma-Aldrich, St. Louis, MO) was allotted at 100 uL per centrifuge tube and stored at −20 °C until use. The work standard solutions were prepared daily by appropriate dilution with methanol/water (50:50, v/v).

Magnetic Solid Phase Extraction of Aflatoxins. To an Erlenmeyer flask containing 50 mL of sample, 100 μL of the PD-MNPs suspension prepared above was added. The mixture was shaken for 10 min on an oscillator. The flask was placed on a magnet for 30 s to let PD-MNPs settle down. The supernatant was discarded. After washing twice with 500 μL of water, aflatoxins were eluted from the PD-MNPs with 250 μL of warm acetonitrile/methanol (1:1) at about 60 °C for 3 min. After magnetic separation, 100 μL of supernatant was transferred to a centrifuge vial and mixed with 100 μL of water. After being filtered through a 0.22 μm filtration membrane, portions (5 μL) were injected into the HPLC−ESI−MS/MS

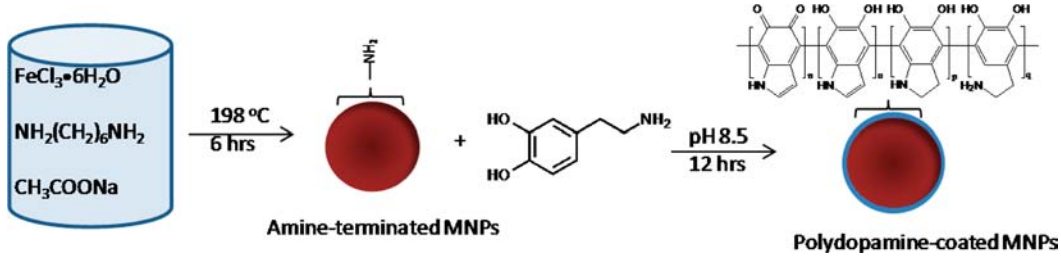

Figure 2. Illustration of PD-MNPs preparation involving two steps: (1) one-pot synthesis of amine-terminated magnetic nanoparticles (AMNPs) from $FeCl_3$ and hexanediamine and (2) coating AMNPs with polydopamine via in situ oxidative self-polymerization of dopamine.

system for analysis without further purification. The MSPE procedure is illustrated in Figure 3.

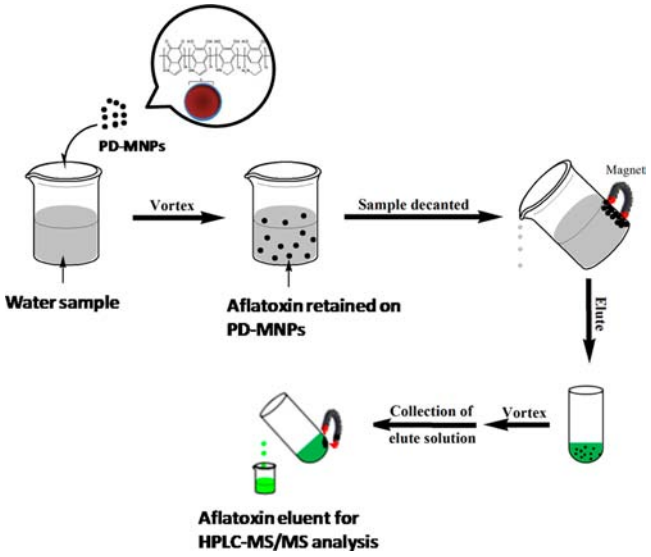

Figure 3. Illustration of the proposed MSPE procedure for facile extraction of aflatoxins followed by HPLC–MS/MS quantification.

HPLC–MS/MS Analysis of Aflatoxins. The system consisted of two pumps (LC-10ADvp, Shimadzu, Toyoto, Japan), an online degasser (DGU-12A, Shimadzu), and a triple quadrupole mass spectrometer equipped with a heated ESI source (TSQ Quantum, Thermo Scientific, San Jose, CA). Both the LC and mass spectrometer were controlled by Xcalibur software (Thermo Finnigan). A C_{18} reversed-phase column (Ascentis, 3 μm particle size, 10 cm × 2.1 mm, Sigma-Aldrich, St. Louis, MO) was used for separation. MeOH/water mixture (60/40, v/v) containing 5 mM ammonium acetate was used as the mobile phase at a flow rate of 0.150 mL/min. Sample injection volume was 5 μL. Data were acquired in full scan and SRM mode. The MS detector was operated in the positive ion mode with the following settings: spray voltage of 3 kV, vaporization temperature of 270 °C, capillary temperature of 300 °C, sheath gas pressure of 35 (arb), auxiliary gas pressure of 10 (arb), tube lens voltage of 150 V, and capillary voltage of 35 V. SRM parameters for MS detection of aflatoxins are summarized in Table 1.

Table 1. SRM Data Acquisition Parameters for Aflatoxins

aflatoxin	molecular weight	precursor ion (m/z)	product ion (m/z)	collision energy
AF B_1	312	313	285	28
AF B_2	314	315	259	28
AF G_1	328	329	243	28
AF G_2	330	331	245	28

RESULTS AND DISCUSSION

Synthesis and Characterization of PD-MNPs. MSPE is gaining attention because it is quick, easy to perform, inexpensive, and suitable for working with large volume samples.[21−23] The success of a MSPE procedure depends largely on the surface chemistry of the superparamagnetic nanometer-sized adsorbent particles. Polydopamine-coated nanoparticles have been widely used in biological and pharmaceutical technology arenas.[27−30] In this study, it was found that a highly stable polydopamine coating could be formed on the surface of amine-terminated Fe_3O_4 superparamagnetic nanoparticles via oxidative self-polymerization of dopamine. Because the polydopamine coating thus formed is composed of dihydroxyindole, indoledione, and dopamine units (as illustrated by Figure 2),[31,32] PD-MNPs are expected to have a high affinity for aflatoxins through a combination of charge transfer, π-stacking, and hydrogen-bonding interactions, and therefore, they are expected to serve as a highly effective MSPE adsorbent for extracting these compounds from solutions.

One-pot synthesis of amine-terminated MNPs (AMNPs) was achieved by following a procedure previously reported[26] using $FeCl_3{\cdot}6H_2O$ as the precursor of magnetic particles and hexamethylenediamine as an amino group source. From the TEM results, AMNPs prepared were ∼30 nm in diameter in average and had a circular shape. The FT-IR spectrum (Figure 4A) shows strong absorptions at 575 cm^{-1} arising from the vibration of the Fe−O bond and at 3133.5 and 3420.9 cm^{-1} from N−H $_{bond}$ in the amine group. PD-MNPs were easily prepared by incubating AMNPs with dopamine in a Tris buffer at pH 8.5 for 3 h. TEM analysis showed that PD-MNPs obtained had an average diameter of ∼40 nm. In the FT-IR spectrum of PD-MNPs (Figure 4B), a strong absorption band at 1400 cm^{-1} and a moderate band at 1600 cm^{-1} are observed, clearly indicating the presence of polymerized aromatic structures. In addition, an absorption band at 3100−3450 cm^{-1} is much stronger than that in AMNPs spectrum, which is due to the overlapping of hydroxyls and amines in polydopamine. These results suggest that PD coating of AMNPs was successful. It was also noted that the suspendability of PD-MNPs was much improved from that of the precursor AMNPs or bare Fe_3O_4 nanoparticles. A diluted suspension of PD-MNPs was stable for several days in terms of its appearance. UV−vis monitoring of the suspension for 1 week did not detect any leaching of polydopamine or its components from the nanoparticles.

MSPE of Aflatoxins with PD-MNPs. In the MSPE study, alflatoxin standard solutions prepared in water were used. PD-MNPs were added to 50 mL of a standard solution in each extraction test. Aflatoxins extracted from the solution were subsequently retrieved from the PD-MNPs and quantified by HPLC–MS/MS. Several HPLC–MS methods have been reported for aflatoxin quantification.[11,12,18,20,33] In the present study, several mobile phases, including MeOH/H_2O (60:40) containing 5 mM ammonium acetate, MeOH/H_2O (60:40) containing 0.1% formic acid, ACN/H_2O (60:40) containing 5 mM ammonium acetate, and MeOH/ACN/H_2O (60:20:20), were tested for the separation on a C_{18} column. It was found that isocratic elution with MeOH/H_2O (60:40) containing 5 mM ammonium acetate resulted in the best analytical results in terms of separation efficiency and detection sensitivity. The aflatoxins tested were separated within 4.5 min. Intriguingly, introducing ammonium acetate to the mobile phase significantly improved the detection sensitivity. However, no similar effects were observed with formic acid (0.1% v/v), a commonly used additive to enhance ionization efficiency in HPLC–MS analysis.

Effects of PD-MNPs amount on extraction efficiency were investigated. In a set of extraction tests, 10, 25, 50, 75, 100, 150, 200, and 500 μL of PD-MNPs suspension were added to different 50.0 mL portions of a standard solution containing 0.100 ng/mL AF B_1, respectively. On the basis of the peak areas

dx.doi.org/10.1021/jf501659m | J. Agric. Food Chem. 2014, 62, 4261−4267

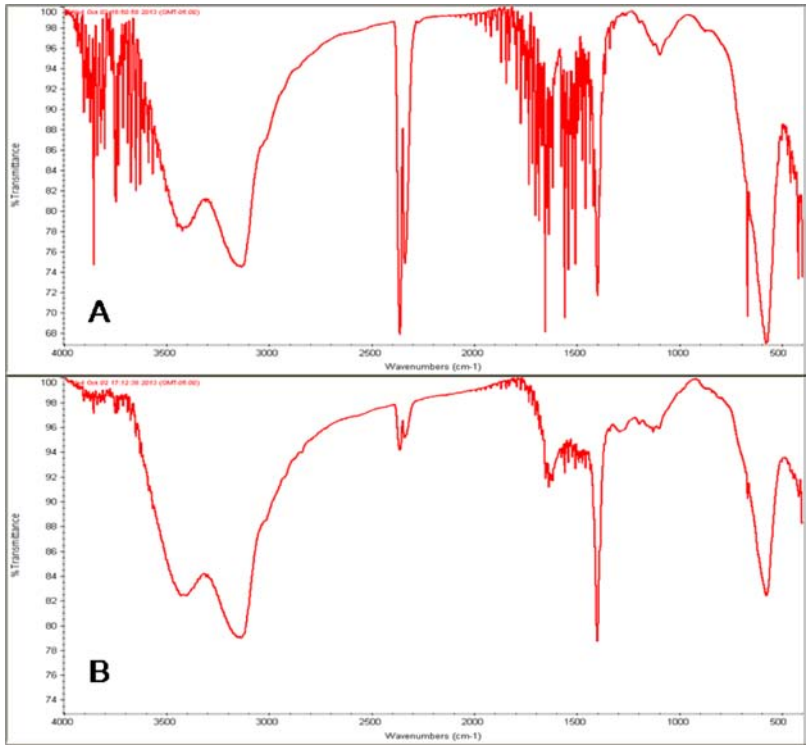

Figure 4. FT-IR spectra of AMNPs (A) and PD-AMNPs (B).

obtained from the HPLC–MS/MS analysis of the eluent from each test, the extraction efficiency of AF B1 was assessed. It was found that extraction efficiency increased [from 33.1 ± 7.2% to 89.2 ± 2.6% (n = 3)] with the increase in PD-MNPs amount and remained nearly constant when >75 μL of PD-MNPs suspension was used. For further studies, 100 μL of PD-MNPs suspension was added to 50 mL of sample to extract aflatoxins. Extraction times of 5, 10, and 20 min were tested. The extraction efficiency of AF B1 obtained were 86.7 ± 2.2%, 89.7 ± 1.7%, and 89.5 ± 0.3% (n = 3), respectively. Desorption of aflatoxins retained on PD-MNPs is also critical to the success of the MSPE development. Elution conditions, including eluting solvent, elution time (1, 2, 3, 5, and 10 min), and elution temperature (30, 45, 60, 80 °C) were investigated to achieve a high retrieval efficiency. Several eluting solvents were tested. Results of retrieval efficiency for AF B_1 are summarized in Figure 5. Elution with water produced an eluent solution containing nondetectable aflatoxins. Methanol/acetonitrile (1:1) was found most effective to retrieve aflatoxins from PD-MNPs. On the basis of these studies, methanol/acetonitrile (1:1) as the eluting solvent and an elution time of 3 min at 60 °C were selected for desorption of aflatoxin from PD-MNPs. An equal amount of water was added to the elution solution prior to HPLC–MS/MS analysis in order to minimize the solvent effects on the separation. Interestingly, when using AMNPs or bare Fe_3O_4 MNPs for MSPE of aflatoxin, the extraction efficiency was found to be significantly lower. This may be due to either a low affinity of aflatoxins to these adsorbents or poor desorption of aflatoxins from them under the selected elution conditions. PD-MNPs exhibit a very high affinity for aflatoxins because of combined interactions arising from charge transfer, π-stacking, and hydrogen bonding, most of which do not exist in the case of AMNPs or bare Fe_3O_4 MNPs.

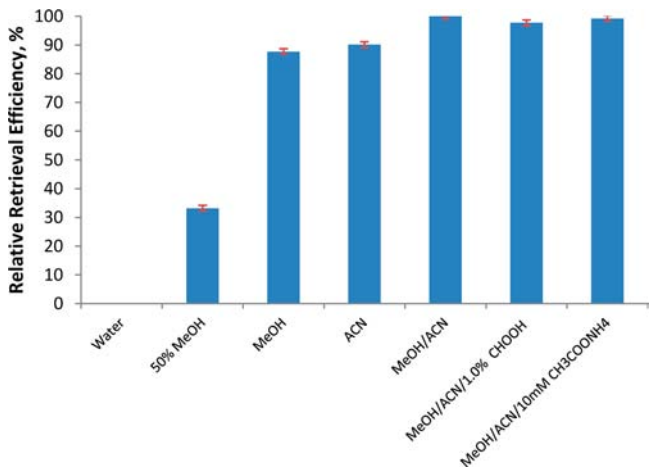

Figure 5. Comparing the effectiveness of retrieving AF B_1 retained on PD-MNPs with different eluting solvents.

Under the selected MSPE conditions, two standard solutions of aflatoxins at concentrations ranging from 0.0100–0.300 ng/mL were extracted to determine the extraction recovery for all the four aflatoxins tested. Aflatoxins extracted were quantified by using a calibration curve prepared from standard water solutions of aflatoxins. The recovery for the four aflatoxins ranged from 58.6 to 91.0% (Table 2). The difference in recovery is likely because of the fact that AF B_1 and AF B_2 are more hydrophobic than AF G_1 and AF G_2. These recovery values are significantly higher than many of those obtained from SPE procedures. It should be pointed out that the proposed MSPE offers an enrichment factor of 100, which is attractive for analysis of samples containing aflatoxins at very low levels.

dx.doi.org/10.1021/jf501659m | J. Agric. Food Chem. 2014, 62, 4261–4267

Table 2. Extraction Efficiency of the Proposed MSPE for Aflatoxins from Water

sample	aflatoxin	conc added (ng/mL)	conc found[a] (ng/mL)	SD (n = 3)	recovery (%)
std solution no. 1	AF B1	0.0300	0.0261	0.0012	87.0
	AF B2	0.0100	0.0074	0.0004	74.0
	AF G1	0.0300	0.0194	0.0012	64.6
	AF G2	0.0100	0.0060	0.0005	60.0
std solution no. 2	AF B1	0.300	0.2731	0.0119	91.0
	AF B2	0.100	0.0732	0.0056	73.2
	AF G1	0.300	0.1981	0.0077	66.0
	AF G2	0.100	0.0586	0.0021	58.6

[a]Means of three replicates.

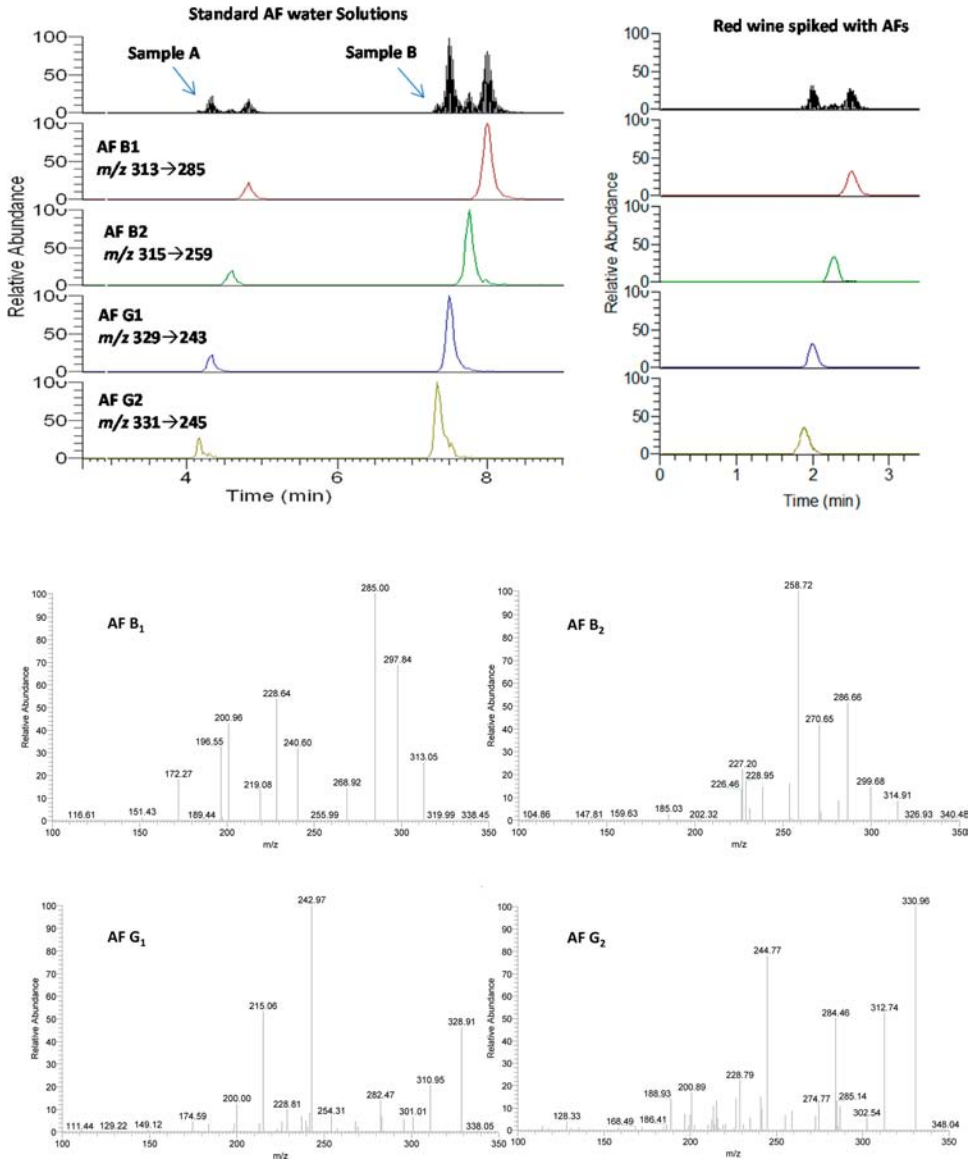

Figure 6. MSPE−HPLC−MS/MS determination of aflatoxins in water and red wine: chromatograms and MS^2 spectra for each aflatoxin involved. Sample A: water spiked with 0.0300 ng/mL of AF B_1 and G_1 and 0.0100 ng/mL of AF B_2 and G_2. Sample B: water spiked with 0.150 ng/mL of AF B_1 and G_1 and 0.0500 ng/mL of AF B_2 and G_2. Red wine: sample spiked with 0.0600 ng/mL of AF B_1 and G_1 and 0.0200 ng/mL of AF B_2 and G_2.

Quantification of Trace Aflatoxins in Red Wine Samples. Monitoring aflatoxin levels in foodstuff is highly important. In this work, quick, selective, and sensitive quantification of trace aflatoxins in red wines by coupling the proposed MSPE with HPLC−MS/MS analysis is demonstrated. To obtain the analytical figures of merit for the MSPE−HPLC−MS/MS method, simultaneous quantification of authentic AF B_1, AF B_2, AF G_1, and AF G_2 solutions was performed. The behaviors of chromatographic retention and product ion spectra of these four aflatoxins are shown in Figure 6. Under the selected HPLC−MS analytical conditions, the four aflatoxins were well-separated from each other. For each

dx.doi.org/10.1021/jf501659m | J. Agric. Food Chem. 2014, 62, 4261−4267

Table 3. Analytical Results of Red Wine Samples

	AF found (ng/mL)	AF added (ng/mL)	total AF found (ng/mL)	RSD (%, n = 3)	recovery (%)
sample no. 1					
AF B_1	ND	0.0100	0.0108	6.7	108.0
AF B_2	ND	0.0033	0.0030	7.1	90.9
AF G_1	ND	0.0100	0.0099	3.5	99.0
AF G_2	ND	0.0033	0.0033	5.2	100.0
sample no. 2					
AF B_1	ND	0.0600	0.0607	2.3	101.2
AF B_2	ND	0.0200	0.0194	1.8	97.0
AF G_1	ND	0.0600	0.0614	3.9	102.3
AF G_2	ND	0.0200	0.0197	3.6	98.5

ND: not detected.

aflatoxin tested, a characteristic product ion was obtained. Ion transitions (i.e., m/z 313 → 285 for AF B_1, m/z 315 → 259 for AF B_2, m/z 329 → 243 for AF G_1, and m/z 331 → 245 for AF G_2) were monitored using the SRM detection mode. Five-point calibration curves were prepared with authentic aflatoxin solutions at concentrations ranging from 0.00600 to 3.00 ng/mL in water. These solutions were submitted to the proposed MSPE procedure and injected into the HPLC−MS system for quantification. Peak areas were used for the calculation. Regression analysis of the results yielded linear calibration equations for all four aflatoxins tested with r^2 values >0.995. Interday (5 days) precisions of the slope and intercept of the calibration curves were found to be in the range between 3.5% and 5.6% (RSD, n = 5). From the calibration curves, the limits of detection were estimated to be in the range from 0.0012 ng/mL for AF B_1, AF B_2, and AF G_1 to 0.0031 ng/mL for AF G_2 (signal/noise = 3). These results indicate that the present method is very sensitive for the analysis of aflatoxins. It should be pointed out that these LODs are so low because the MSPE extraction provides a 100-fold enrichment factor (i.e., the sample is preconcentrated by a factor of 100 through the extraction), which is a significant gain of using the proposed MSPE procedure.

The proposed MSPE−HPLC−MS/MS method was applied to quantification of aflatoxins in liquid foodstuff samples, taking red wine as a model system. Two red wine samples were purchased from a local store and analyzed to determine the four aflatoxins. To verify the analytical results these samples were spiked with authentic aflatoxins and analyzed again. A typical chromatogram obtained from these analyses is shown in Figure 6. Peaks corresponding to AFs were well-identified. No unknown peaks appeared in the chromatogram, indicating that the method was specific for the determination of aflatoxins. The analytical results are summarized in Table 3. As can be seen, both the accuracy and the repeatability of the present MSPE−HPLC−MS method are good, because all recovery values are >90% and RSDs are <8%. These results suggest that the proposed method is useful for rapid quantification of aflatoxins in red wines. As shown in Table 3, aflatoxins were not detected in the wine samples tested. These results are in agreement with those reported previously.[12] Unlike some other mycotoxins such as ochratoxin A, aflatoxins in wine do not present a problem. Red wine samples are analyzed in this work as a model to demonstrate the usefulness of the proposed MSPE procedure. It is expected that the proposed method can be applied to analysis of other liquid foodstuff samples such as beer, vegetable fluids, among others. It is worth noting that because AF contents in these samples are normally below the LODs of HPLC−MS methods, enrichment of the analytes is needed prior to the analysis. The present MSPE procedure offers an enrichment factor of 100 for aflatoxins, which is attractive in analysis of these liquid foodstuff samples.

In conclusion, polydopamine-coated Fe_3O_4 core−shell superparamagnetic nanoparticles (PD-MNPs) can be easily prepared from amine-terminated Fe_3O_4 MNPs and dopamine via an in situ oxidative self-polymerization approach. The resultant PD-MNPs are of high stability and suspensibility. More importantly, they exhibit a high affinity to aflatoxins, thus enabling a facile and effective magnetic solid phase extraction (MSPE) of these toxins from large volume liquid samples. Using PD-MNPs as the adsorbent, MSPE of aflatoxins from liquid foodstuff samples proves effective for subsequent HPLC−MS/MS analysis and offers a considerable enrichment factor that is highly desired for quantification of trace aflatoxins. To the best of our knowledge, this is the first report on MSPE of this important group of toxins from foodstuff samples. As demonstrated in this work, the proposed MSPE−HPLC−MS/MS method is fast, very sensitive, and applicable to fast quantification of aflatoxins in water, red wine, and likely other liquid foodstuff samples.

AUTHOR INFORMATION

Corresponding Authors

*E-mail: (Y.-M.L.) yiming.liu@jsums.edu. Tel.: 1-601-979-3491.

*E-mail: (X.L.) liaoxun@cib.ac.cn. Tel./Fax: +86 28 85229227.

Funding

Financial support from National Institutes of Health (GM 089557 to Y.-M.L and G12MD007581 to P.B.T.) and National Natural Science Foundation of China (no. 81173536 and 21202161 to X.L.) are gratefully acknowledged. C.M. is a scholar of U.S. Department of Education/Title III Graduate Education Program at Jackson State University (grant no. P031B090212-13).

Notes

The authors declare no competing financial interest.

ABBREVIATIONS USED

AF, aflatoxin; AF B_1, aflatoxin B_1; AF B_2, aflatoxin B_2; AF G_1, aflatoxin G_1; AF G_2, aflatoxin G_2; MNPs, magnetic nanoparticles; AMNPS, amine-terminated magnetic nanoparticles; PD-MNPs, polydopamine coated magnetic nanoparticles; MSPE, magnetic solid phase extraction

REFERENCES

(1) Richard, J. L. Some major mycotoxins and their mycotoxicoses an overview. *Int. J. Food Microbiol.* **2007**, *119*, 3−10.

(2) Wild, C. P.; Gong, Y. Y. Mycotoxins and human disease: a largely ignored global health issue. *Carcinogenesis* **2011**, *31*, 71−82.

(3) Kensler, T. W.; Roebuck, B. D.; Wogan, G. N.; Groopman, J. D. Aflatoxin: a 50-year odyssey of mechanistic and translational toxicology. *Toxicol. Sci.* **2011**, *120*, S28−S48.

(4) Fernández-Cruz, M. L.; Mansilla, M. L.; Tadeo, J. L. Mycotoxins in fruits and their processed products: analysis, occurrence and health implications. *J. Adv. Res.* **2010**, *1*, 113−122.

(5) Bryden, W. L. Mycotoxins in the food chain: human health implications. *Asia Pac. J. Clin. Nutr.* **2007**, *16*, 95−101.

(6) Li, F. Q.; Li, Y. W.; Wang, Y. R.; Luo, X. Y. Natural occurrence of aflatoxins in chinese peanut butter and sesame paste. *J. Agric. Food Chem.* **2009**, *57*, 3519−3524.

(7) Turner, N. W.; Subrahmanyam, S.; Piletsky, S. A. Analytical methods for determination of mycotoxins: a review. *Anal. Chim. Acta* **2009**, *632*, 168−180.

(8) Köppen, R.; Koch, M.; Siegel, D.; Merkel, S.; Maul, R.; Nehls, I. Determination of mycotoxins in foods: current state of analytical methods and limitations. *Appl. Microbiol. Biotechnol.* **2010**, *86*, 1595−1612.

(9) Souverain, S.; Rudaz, S.; Veuthey, J. L. Matrix effect in LC-ESIMS and LC-APCI-MS with off-line and on-line extraction procedures. *J. Chromatogr. A* **2004**, *1058*, 61−66.

(10) Trufelli, H.; Palma, P.; Famiglini, G.; Cappiello, A. An overview of matrix effects in liquid chromatography−mass spectrometry. *Mass Spectrom. Rev.* **2011**, *30*, 491−509.

(11) Cervino, C.; Asam, S.; Knopp, D.; Rychlik, M.; Niessner, R. Use of isotope-labeled aflatoxins for LC-MS/MS stable isotope dilution analysis of foods. *J. Agric. Food Chem.* **2008**, *56*, 1873−1879.

(12) Al-Taher, F.; Banaszewski, K.; Jackson, L.; Zweigenbaum, J.; Ryu, D.; Cappozzo, J. Rapid method for the determination of multiple mycotoxins in wines and beers by LC-MS/MS using a stable isotope dilution assay. *J. Agric. Food Chem.* **2013**, *61*, 2378−2384.

(13) Garcia-Villanova, R. J.; Cordón, C.; González Paramás, A. M.; Aparicio, P.; Garcia Rosales, M. E. simultaneous immunoaffinity column cleanup and HPLC analysis of aflatoxins and ochratoxin A in Spanish bee pollen. *J. Agric. Food Chem.* **2004**, *52*, 7235−7239.

(14) Stroka, J.; Anklam, E. Immunoaffinity column cleanup with liquid chromatography using post-column bromination for determination of aflatoxins in peanut butter, pistachio paste, fig paste, and paprika powder: collaborative study. *J. AOAC Int.* **2000**, *83*, 320−340.

(15) Wilson, T. J.; Romer, T. R. Use of the Mycosep multifunctional cleanup column for liquid chromatographic determination of aflatoxins in agricultural products. *J. − Assoc. Off. Anal. Chem.* **1991**, *74*, 951−956.

(16) Sobolev, V. S.; Dorner, J. W. Cleanup procedure for determination of aflatoxins in major agricultural commodities by liquid chromatography. *J. AOAC Int.* **2002**, *285*, 642−645.

(17) Holaday, C. E. Minicolumn chromatography: state of the art. *J. Am. Oil Chem. Soc.* **1981**, *58*, 931A−934A.

(18) Bacaloni, A.; Cavaliere, C.; Faberi, A.; Pastorini, E.; Samperi, R.; Lagana, A. Automated on-line solid phase extraction-liquid chromatography−electrospray tandem mass spectrometry method for the determination of ochratoxin A in wine and beer. *J. Agric. Food Chem.* **2005**, *53*, 5518−5525.

(19) Sobolev, V. S. Simple, rapid, and inexpensive cleanup method for quantitation of aflatoxins in important agricultural products by HPLC. *J. Agric. Food Chem.* **2007**, *55*, 2136−2141.

(20) Romero-Gonzalez, R.; Martinez Vidal, J. L.; Aguilera-Luiz, M. M.; Frenich, A. G. Application of conventional solid-phase extraction for multimycotoxin analysis in beers by ultrahigh-performance liquid chromatography-tandem mass spectrometry. *J. Agric. Food Chem.* **2009**, *57*, 9385−9392.

(21) Safarikova, M.; Safarik, I. Magnetic solid-phase extraction. *J. Magn. Magn. Mater.* **1999**, *194*, 108−112.

(22) Lin, P. C.; Tseng, M. C.; Su, A. K.; Chen, Y. J.; Lin, C. C. Functionalized magnetic nanoparticles for small-molecule isolation, identification, and quantification. *Anal. Chem.* **2007**, *79*, 3401−3408.

(23) Song, Y.; Zhao, S.; Tchounwou, P.; Liu, Y. M. A nanoparticle-based solid-phase extraction method for liquid chromatography-electrospray ionization-tandem mass spectrometric analysis. *J. Chromatogr. A* **2007**, *1166*, 79−84.

(24) Gao, Q.; Luo, D.; Bai, M.; Chen, Z. W.; Feng, Y. Q. Rapid determination of estrogens in milk samples based on magnetite nanoparticles/polypyrrole magnetic solid-phase extraction coupled with liquid chromatography−tandem mass spectrometry. *J. Agric. Food Chem.* **2011**, *59*, 8543−8549.

(25) Qing, L. S.; Xue, Y.; Liu, Y. M.; Liang, J.; Xie, J.; Liao, X. Rapid magnetic solid-phase extraction for the selective determination of isoflavones in soymilk using baicalin-functionalized magnetic nanoparticles. *J. Agric. Food Chem.* **2013**, *61*, 8072−8078.

(26) Wang, L.; Bao, J.; Wang, L.; Zhang, F.; Li, Y. One-pot synthesis and bioapplication of amine-functionalized magnetite nanoparticles and hollow nanospheres. *Chem.—Eur. J.* **2006**, *12*, 6341−6347.

(27) Xu, C.; Xu, K.; Gu, H.; Zheng, R.; Liu, H.; Zhang, X.; Guo, Z.; Xu, B. Dopamine as a robust anchor to immobilize functional molecules on the iron oxide shell of magnetic nanoparticles. *J. Am. Chem. Soc.* **2004**, *126*, 9938−9939.

(28) Amstad, E.; Gillich, T.; Bilecka, I.; Textor, M.; Reimhult, E. Ultrastable iron oxide nanoparticle colloidal suspensions using dispersants with catechol-derived anchor groups. *Nano Lett.* **2009**, *9*, 4042−4048.

(29) Ren, Y.; Rivera, J. G.; He, L.; Kulkarni, H.; Lee, D. K.; Messersmith, P. B. Facile, high efficiency immobilization of lipase enzyme on magnetic iron oxide nanoparticles via a biomimetic coating. *BMC Biotechnol.* **2011**, *11*, 63−70.

(30) Lee, H.; Dellatore, S. M.; Miller, W. M.; Messersmith, P. B. Mussel-inspired surface chemistry for multifunctional coatings. *Science* **2007**, *318*, 426−430.

(31) Liebscher, J.; Mrówczyński, R.; Scheidt, H. A.; Filip, C.; Hădade, N. D.; Turcu, R.; Bende, A.; Beck, S. Structure of polydopamine: a never-ending story? *Langmuir* **2013**, *29*, 10539−10548.

(32) Dreyer, D. R.; Miller, D. J.; Freeman, B. D.; Paul, D. R.; Bielawski, C. W. Perspectives on poly (dopamine). *Chem. Sci.* **2013**, *4*, 3796−3802.

(33) Huang, B.; Han, Z.; Cai, Z.; Wu, Y.; Ren, Y. Simultaneous determination of aflatoxins B1, B2, G1, G2, M1 and M2 in peanuts and their derivative products by ultra-high-performance liquid chromatography−tandem mass spectrometry. *Anal. Chim. Acta* **2010**, *662*, 62−68.

JOURNAL OF AGRICULTURAL AND FOOD CHEMISTRY

Article

pubs.acs.org/JAFC

Analysis of Phytostanyl Fatty Acid Esters in Enriched Foods via UHPLC-APCI-MS

Birgit Scholz,[†] Andreas Barnsteiner,[†] Katharina Feist,[†] Wolfgang Schmid,[‡] and Karl-Heinz Engel*[,†]

[†]Lehrstuhl für Allgemeine Lebensmitteltechnologie, Technische Universität München, Maximus-von-Imhof-Forum 2, D-85350 Freising, Germany

[‡]Bayerisches Landesamt für Gesundheit und Lebensmittelsicherheit, Veterinärstrasse 2, D-85764 Oberschleissheim, Germany

ABSTRACT: A method for the analysis of phytostanyl fatty acid esters, the functional ingredients of cholesterol-lowering enriched foods, was developed. The procedure is based on (i) separation of the intact esters via reversed-phase ultrahigh-performance liquid chromatography; (ii) detection by atmospheric pressure chemical ionization−mass spectrometry; and (iii) quantitation using selected ion monitoring (SIM) mode. Employing a C8 column, phytostanyl fatty acid esters sharing the same stanol nucleus could be separated according to the esterified fatty acids while esters with different stanol moieties could be distinguished via SIM based on the formation of an intense fragment ion $[M - \text{fatty acid} + H]^+$. The suitability of the approach was demonstrated using different types of enriched foods reflecting the diversity in potential matrices (skimmed milk drinking yogurt, margarine, and soft-cheese-style spread). The developed methodology extends the analytical basis for authenticity and quality assessments of functional foods enriched with phytostanyl fatty acid esters.

KEYWORDS: *phytostanyl fatty acid ester, enriched foods, RP-UHPLC-APCI-MS*

INTRODUCTION

An increased plasma cholesterol level is an acknowledged risk factor for the development of cardiovascular diseases.[1−4] By the 1950s phytosterols have been used to achieve cholesterol-lowering effects in humans.[2] There has been increasing scientific evidence for a negative correlation between dietary intake of phytosterols/-stanols and plasma and low-density lipoprotein cholesterol levels.[3,4] Therefore, phytosterols are incorporated into a broad spectrum of various food categories. For technological reasons, the plant sterols/stanols are commonly esterified with fatty acids (FA). In the course of their safety assessment, in the European Union the profiles of both the sterols/stanols and the fatty acids have been specified by the Scientific Committee on Food (SCF); sterols/stanols are to be obtained from vegetable oils or tall oil, and the fatty acids used for esterification have to be derived from vegetable oils.[5−7] In this context, the development of suitable analytical methods allowing the elucidation of the qualitative and quantitative compositions of the esters has received increasing scientific interest. They are the essential basis for authenticity assessments as required according to the aforementioned regulations. An additional aspect reinforcing the importance of knowledge on the detailed compositions of the intact esters is a potential difference between individual phytosteryl/-stanyl fatty acid esters concerning their cholesterol-lowering efficacies. *In vitro* and *in vivo* observations of intestinal hydrolysis rates, the decisive step for the release of the phytosterols/-stanols to exert their mechanism of action showed dependencies on both the phytosterol/-stanol structures and the fatty acid moieties of distinct esters.[8−10]

However, qualitative and quantitative chromatographic analysis of phytosteryl/-stanyl fatty acid esters in their intact form is not trivial. The ester preparations used for food fortification vary regarding sterol/stanol as well as fatty acid moieties; the resulting multitude of high molecular weight compounds with a high degree of structural similarities constitutes a challenge for chromatographic separations. Recent publications showed a medium polar and temperature-stable trifluoropropylmethyl polysiloxane column to be the best choice for the gas chromatography (GC)-based separation of plant stanyl and steryl fatty acid esters, with only the esters of saturated and monounsaturated fatty acid esters of the same chain length eluting at the same time.[11,12] A detailed compositional analysis of individual plant steryl/stanyl fatty acid esters contained in functional foods could thus be performed for the first time. Yet, due to the high boiling points of these constituents and due to the presence of reactive double bonds in the fatty acid moieties, thermal degradations during high-temperature GC are a critical disadvantage of this chromatographic technique. This drawback could be successfully compensated for by the use of respective correction factors.[11]

Nevertheless, liquid chromatography (LC)-based approaches seem to be more appropriate for the analysis of intact phytosterol/-stanol fatty acid esters. Billheimer et al.[13] were the first to report a reversed-phase (RP) liquid chromatography-based separation of molecular species of steryl fatty acid esters utilizing a C18 column, but resolution was not satisfactory and, owing to the UV-detector employed, the sensitivity of the method was low. Meanwhile, further efforts have been made regarding liquid chromatographic analysis; however, all of them suffer from either insufficient resolutions of the single esters, long analysis times, lack of sensitivity, or

Received: February 24, 2014
Revised: April 24, 2014
Accepted: April 25, 2014
Published: April 25, 2014

ACS Publications © 2014 American Chemical Society

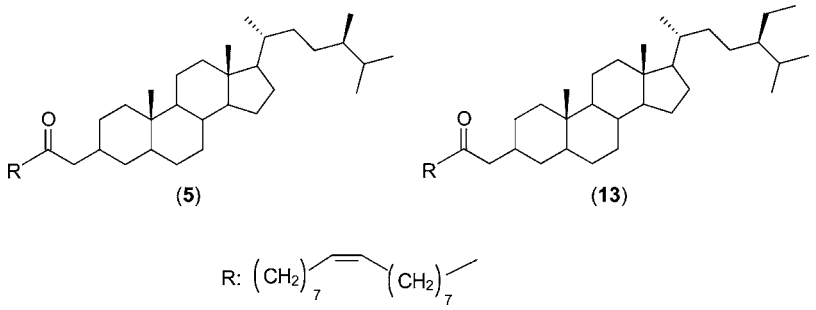

Figure 1. Structures of representative phytostanyl fatty acid esters: campestanyl-18:1, **5**; sitostanyl-18:1, **13**. The numbers correspond to those shown in Table 1 and Figure 2.

combinations of these chromatographic issues.[14−16] In addition to the application of electrospray ionization (ESI) as reported by Caboni et al.,[17] the work by Mezine et al.[18] described a promising approach using positive atmospheric pressure chemical ionization (APCI)−mass spectrometry (MS) detection, and differentiating steryl/stanyl esters that were incompletely separated or coeluting via ion extraction. Nevertheless, in addition to an unsatisfactory resolution, detailed qualitative and quantitative data on the individual esters analyzed in fortified foods were lacking.

Therefore, the objective of the present study was to develop a thermally nondestructive, rapid, and sensitive chromatographic method based on ultrahigh-performance liquid chromatography (UHPLC)-separation in combination with MS-detection for the quantitation of intact phytostanyl fatty acid esters. The suitability of the approach should be demonstrated using different types of enriched foods reflecting the diversity in potential matrices (skimmed milk drinking yogurt, margarine, and soft-cheese-style spread). Representative structures of the analyzed campestanyl and sitostanyl fatty acid esters are shown in Figure 1.

MATERIALS AND METHODS

Sample Material. Skimmed milk drinking yogurt "Emmi Benecol strawberry" enriched with phytostanyl esters (Emmi, Luzern, Switzerland) was purchased in a local supermarket (Munich, Germany). In the list of ingredients, the following information was included: 3.0 g of phytostanols, 2.1 g of fat (without stanol), and 3.0 g of protein/(100 g).

Margarine "Benecol—Margaryna roślinna o zwartości trzech czwartych tłuszczu" enriched with phytostanyl esters (Bunge Polska Sp. Z.o.o. Karczew, Poland) was purchased in a supermarket in Poland. In the list of ingredients, the following information was included: 8.0 g of phytostanols and 60 g of fat/(100 g).

Soft-cheese-style spread "Benecol—Soft Cheese style spread light" enriched with phytostanyl esters (McNeill Nutritionals Ltd., Wokingham, U.K.) was purchased in a supermarket in the U.K. In the list of ingredients, the following information was included: 4.0 g of phytostanols, 13.9 g of fat, and 8.1 g of protein/(100 g).

Chemicals. Cholesteryl linolenate (≥85%), diethyl ether (Et_2O; extra pure), ethyl acetate (EtOAc; CHROMASOLV, for HPLC), and hydrochloric acid (25%) were obtained from Sigma-Aldrich (Steinheim, Germany). Methanol (MeOH) (ROTISOLV, Ultra LC-MS) was purchased from Carl Roth (Karlsruhe, Germany). *n*-Hexane (AnalR NORMAPUR) and sodium sulfate (anhydrous) were purchased from VWR International (Darmstadt, Germany). Methyl *tert*-butyl ether (MTBE) was supplied by Evonik Industries AG (Essen, Germany) and was distilled prior to use. A mixture of phytostanyl fatty acid esters ("plant stanol ester", STAEST-115; 96.8% phytostanyl esters with an ester profile of 55.9% sitostanyl-18:1, 18.4% sitostanyl-18:2, 8.1% sitostanyl-18:3, 5.7% campestanyl-18:1, 4.1% sitostanyl-16:0, 1.9% campestanyl-18:2, 1.5% sitostanyl-18:0, 1.3% sitostanyl-20:1, 0.8% campestanyl-18:3, 0.5% sitostanyl-20:0, 0.4% sitostanyl-22:1, 0.4% campestanyl-16:0, 0.3% sitostanyl-22:0, 0.2% sitostanyl-16:1, 0.2% campestanyl-18:0, 0.1% campestanyl-20:1, 0.1% campestanyl-20:0, 0.04% campestanyl-22:1, 0.03% campestanyl-22:0, and 0.03% campestanyl-16:1) was provided by Raisio Group (Raisio, Finland). Reference compounds for stanyl fatty acid esters were synthesized according to previously described procedures.[12,19]

Lipid Extraction. The extraction of lipids from skimmed milk drinking yoghurts as well as from the soft-cheese-style spread was performed according to a previously described method.[11,20] First, the drinking yoghurt was homogenized by vigorous shaking and the soft-cheese-style spread by using an electric blender. A 300 μL aliquot of the internal standard (IS) cholesteryl linolenate [2.5 mg/mL in *n*-hexane/MTBE (3:2, v/v)] was put into a reaction vessel, and the solvent was removed by a gentle stream of nitrogen. A 100 mg amount of drinking yoghurt or 75 mg of soft-cheese spread, a magnetic stir bar, 400 μL of bidistilled water, and 1 mL of hydrochloric acid (25%) were added, and the sealed vessel was sonicated until the internal standard was dispersed; the completeness of the dispersion was examined visually. The digestion was performed at 130 °C for 45 min. After cooling to room temperature, 1 mL of bidistilled water was added, and the solution was filtered using a 0.45 μm membrane filter. The vial and the filter were washed three times with 5 mL of bidistilled water until the pH of the filtrate was neutral. The lipids were extracted three times with 5 mL of *n*-hexane/MTBE (3:2, v/v), and the combined extracts were dried with sodium sulfate. An aliquot of the drinking yoghurt extract was dried under nitrogen, re-dissolved in the same volume of EtOAc, and directly used for UHPLC-MS analysis. The soft-cheese-style spread extract was further subjected to solid-phase extraction (SPE).

For lipid extraction from the margarine sample, a previously published method was used.[11] A 30 mg amount of the sample was weighed into a vessel; 300 μL of the internal standard cholesteryl linolenate [2.5 mg/mL in *n*-hexane/MTBE (3:2, v/v)], 5 mL of *n*-hexane/MTBE (3:2, v/v), and sodium sulfate were added and sonicated for 1 min. The solution was filtered through a 0.45 μm membrane filter. The vessel and the filter were washed twice with 5 mL of *n*-hexane/MTBE (3:2, v/v), and the combined extracts were used for solid-phase extraction.

Solid-Phase Extraction. A 500 μL aliquot of the lipid extracts of the margarine and the soft-cheese-style spread was dried via a gentle stream of nitrogen and re-dissolved in the same volume of *n*-hexane. Aliquots of 120 μL of the lipid extract were loaded onto a Strata NH_2, 55 μm, 70 Å, 400 mg/(3 mL) SPE cartridge (Phenomenex, Aschaffenburg, Germany) previously conditioned with 2 × 3 mL of *n*-hexane, and the stanyl/steryl fatty acid esters were eluted with 2 × 3 mL of *n*-hexane/Et_2O (99:1, v/v). After evaporation of the solvent by a gentle stream of nitrogen, the residue was dissolved in 150 μL of EtOAc, filtered through a 0.45 μm membrane filter, and subjected to UHPLC-MS analysis.

Analysis by UHPLC-APCI-MS. Samples were analyzed by injecting 0.8 μL into a 1290 Infinity Series UHPLC system (Agilent Technologies, Waldbronn, Germany) coupled to a Surveyor MSQ Plus single quadrupole mass-selective detector, using an APCI source

dx.doi.org/10.1021/jf500957a | J. Agric. Food Chem. 2014, 62, 4268−4275

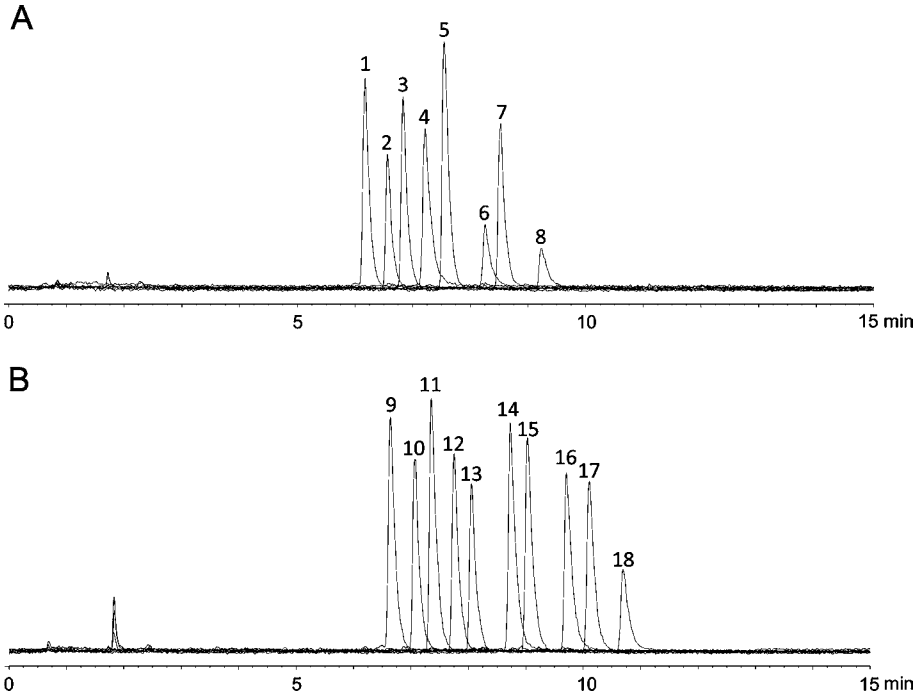

Figure 2. RP-UPLC-APCI-MS-based separation of synthesized phytostanyl fatty acid esters on a C8 column. Overlay of (A) SIM chromatograms of campestanyl fatty acid esters at m/z 385.3; (B) SIM chromatograms of sitostanyl fatty acid esters at m/z 399.3. The peak numbering corresponds to that in Table 1.

(Dionex Softron GmbH, Germering, Germany). UHPLC separation was carried out on a 150 mm × 2.10 mm i.d., 1.7 μm, 100 Å, Kinetex C8 column (Phenomenex, Aschaffenburg, Germany) at 50 °C and a flow rate of 0.58 mL/min. The mobile phase was composed of MeOH and water with the following gradient: from 90% to 95% MeOH within 1.20 min and holding until 3 min; from 95% to 100% MeOH between 3 and 12 min, and back to the initial 90% from 12 to 15 min. The MS parameters were set as follows: ionization mode, APCI (positive); probe temperature, 400 °C; N_2 nebulizer pressure, 45 psi; cone voltage, 80 V; coronal discharge, 8 μA. Instrument control and data acquisition were performed by Xcalibur software 2.0.7, Thermo MSQ 2.0 (Thermo Scientific, Austin, TX, USA), Chromeleon software 6.80 (Dionex Corp., Sunnyvale, CA, USA) in combination with Agilent Instrument Control Framework (Agilent Technologies, Waldbronn, Germany). Mass spectra of synthesized reference compounds were recorded in full scan mode at a mass range of m/z 100−750. For quantitative analyses the MS detector was adjusted to monitor positive ions in the selected ion monitoring (SIM) mode with a mass window of 0.2 at m/z 369.3, 385.3, and 399.3, respectively.

Identification and Quantitation by UHPLC-APCI-MS. The identities of the phytostanyl fatty acid esters extracted from enriched foods were confirmed via comparison of relative retention times to those of synthesized standard compounds in the respective SIM mode. Stanyl fatty acid esters were quantitated by generating five-point calibration functions with 0.1, 0.26, 0.43, 0.6, and 0.76 mg of total esters (STAEST-115)/mL, except for campestanyl-20:0, campestanyl-20:1, and campestanyl-18:0 which were quantitated via three-point calibration functions with 0.43, 0.6, and 0.76 mg of total esters (STAEST-115)/mL. Each calibration point was analyzed in triplicate. Linear regression was confirmed in ratio of areas (area of stanyl ester/area of IS) and amounts (amount of stanyl ester/amount of IS).

Validation of the UHPLC-APCI-MS-Based Approach. Recovery rates were determined by spiking nonenriched products with known amounts of the plant stanyl ester mixture STAEST-115. To 100 mg of skimmed milk yogurt (0.1% fat), 30 mg of margarine (45% fat), and 75 mg of cream cheese (13% fat) were added 5, 4.5, and 4.9 mg of the phytostanyl ester mixture, respectively. Subsequently, the spiked samples were subjected to the extraction procedures as described previously. The limits of detection (LOD) and the limits of quantitation (LOQ) were determined according to the method of Vogelgesang and Hädrich.[21] As quality control measures, the performance of the instrument was regularly confirmed by assessing the responses obtained for the calibration solutions and by analyzing and quantitating the same skimmed milk drinking yogurt extract each time a new batch of samples was subjected to LC-MS analysis.

■ RESULTS AND DISCUSSION

Optimization of RP-UHPLC-Separation. Using positive-ion APCI-MS, an intense formation of the fragment ion $[M - FA + H]^+$ has been described for phytosteryl and phytostanyl fatty acid esters.[18,22] Therefore, in order to establish suitable UHPLC conditions for the separation of synthesized reference compounds, the MS detector was operated in the positive-ion APCI SIM mode, at m/z 385.3 for campestanyl fatty acid esters and at m/z 399.3 for sitostanyl fatty acid esters; this resulted in a highly specific and sensitive detection of the analytes. The UHPLC separation was optimized for the stanyl esters of fatty acids occurring in the vegetable oils authorized as sources.[5−7] In addition, GC-FID data previously published for evaluating the composition of intact phytostanyl fatty acid esters in enriched foods were taken into account.[11] Former efforts to establish RP-LC-based analyses of individual plant steryl/stanyl fatty acid esters used C18 columns.[13−17,23] A more recent study employed a hexyl phenyl column; however, this column also did not yield sufficient separations.[18] In the present study a C8 (1.7 μm) column was shown to enable a separation of all stanyl fatty acid esters consisting of the same stanol nucleus within a rather short analysis time (12 min). The achieved resolution factors were all higher than 1. Preliminary studies confirmed that the particle size of the employed column significantly contributed to the achieved separation (data not shown). Those esters exhibiting different stanol nuclei were further distinguished via the selection of masses corresponding to the fragment ions $[M - FA + H]^+$ in the SIM mode. Overlays of

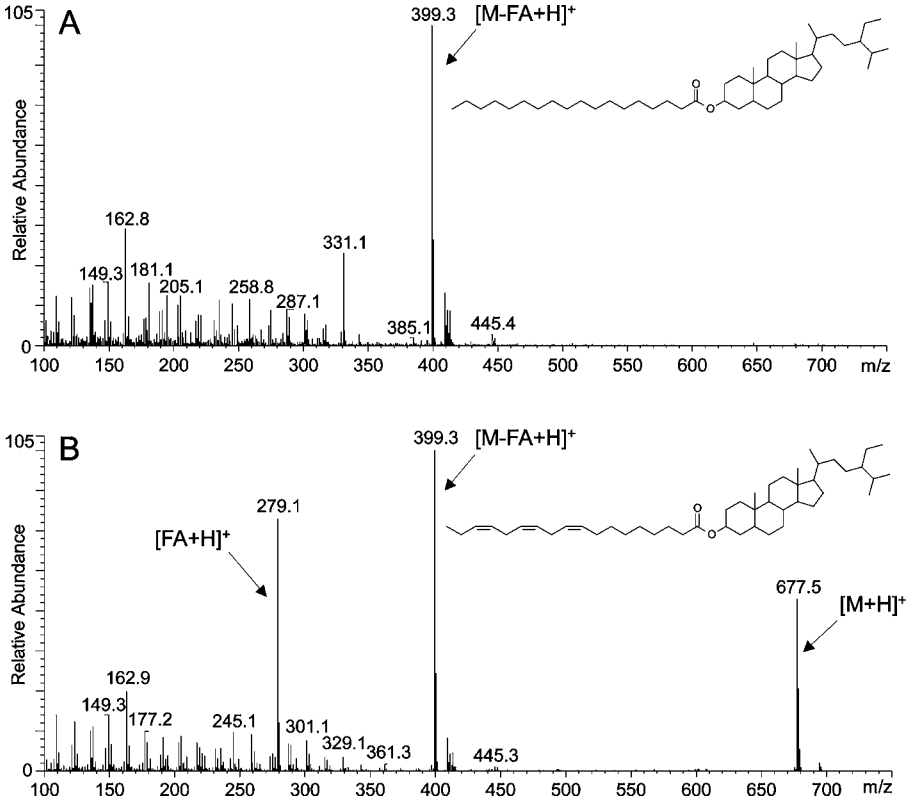

Figure 3. APCI-MS spectra of (A) sitostanyl stearate and (B) sitostanyl linolenate: $[M + H]^+$, protonated molecular ion; [FA], fatty acid.

Table 1. Relative Retention Times, Selected Ions, Limits of Detection, and Limits of Quantitation of Individual Phytostanyl Fatty Acid Esters

		RRT[a,b]	$[M - FA + H]^+$ m/z[b]	LOD[c] (μg/mL)	LOQ[c] (μg/mL)
1	campestanyl-18:3	1.165	385	0.09	0.28
2	campestanyl-16:1	1.240	385	n.d.[d]	n.d.
3	campestanyl-18:2	1.291	385	0.10	0.30
4	campestanyl-16:0	1.362	385	0.06	0.17
5	campestanyl-18:1	1.421	385	0.11	0.32
6	campestanyl-18:0	1.553	385	0.10	0.28
7	campestanyl-20:1	1.613	385	0.07	0.21
8	campestanyl-20:0	1.742	385	0.10	0.25
9	sitostanyl-18:3	1.252	399	0.05	0.16
10	sitostanyl-16:1	1.334	399	n.d.	n.d.
11	sitostanyl-18:2	1.376	399	0.09	0.26
12	sitostanyl-16:0	1.459	399	0.04	0.13
13	sitostanyl-18:1	1.505	399	0.07	0.21
14	sitostanyl-18:0	1.651	399	0.06	0.17
15	sitostanyl-20:1	1.707	399	0.08	0.25
16	sitostanyl-20:0	1.836	399	0.04	0.10
17	sitostanyl-22:1	1.893	399	0.05	0.15
18	sitostanyl-22:0	2.019	399	0.03	0.09

[a]Retention times relative to cholesteryl linolenate (Kinetex C8, 1.7 μ). [b]Relative retention times and mass spectra were determined using synthesized reference compounds. [c]Limits of detection (LOD) and limits of quantitation (LOQ) were determined using the plant stanyl fatty acid mixture STAEST-115 according to ref 21 and are expressed as μg of plant stanyl fatty acid ester/(mL of injection volume). [d]LODs and LOQs were not determined (n.d.) for campestanyl-16:1 and sitostanyl-16:1, as these compounds could not be detected in any of the samples analyzed.

the chromatograms obtained for the synthesized sitostanyl and campestanyl fatty acid esters are shown in Figure 2. The order of elution was impacted by both the chain length and the degree of saturation of the esterified fatty acids: the lower the carbon number and the higher the number of double bonds, the shorter was the retention time. Additionally, campestanyl fatty acid esters eluted earlier than the corresponding sitostanyl fatty acid esters. The observed retention behavior is similar to elution profiles described for phytosteryl/-stanyl as well as cholesteryl fatty acid esters on reversed phases.[13,14,17,18,24,25] In contrast to the approach chosen by Mezine et al.,[18] a step $MeOH/H_2O$ gradient was used instead of a linear gradient of acetonitrile in water, as on the one hand gradient elution improved the chromatographic separation and on the other

dx.doi.org/10.1021/jf500957a | J. Agric. Food Chem. 2014, 62, 4268−4275

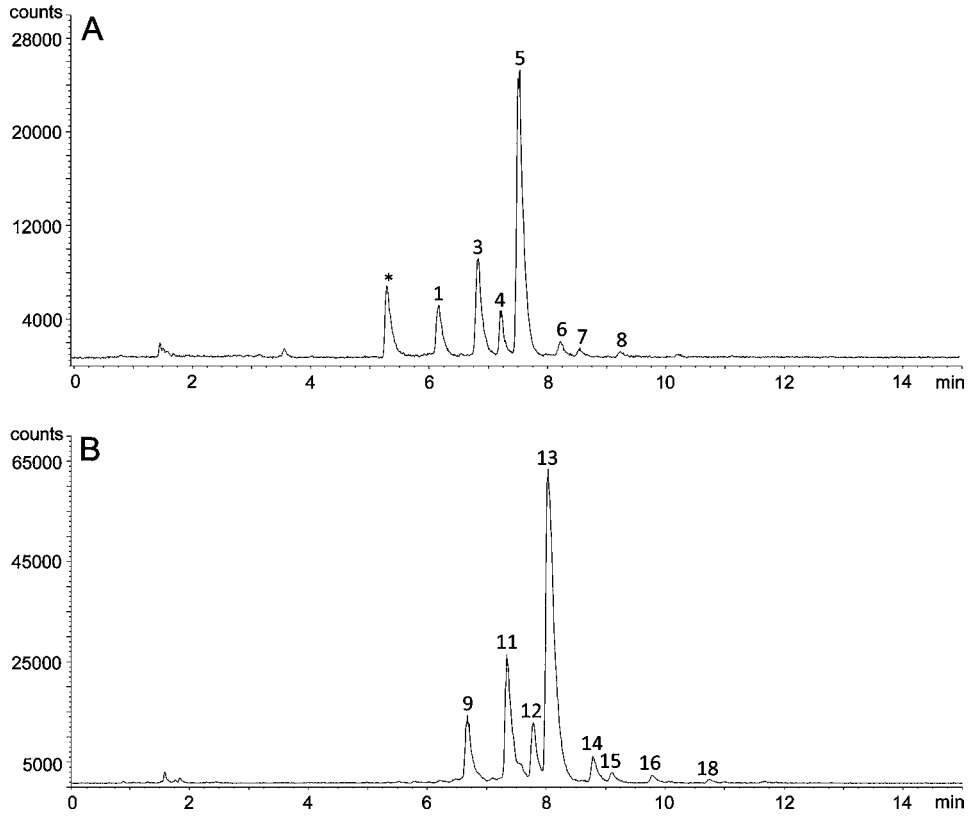

Figure 4. LC-APCI-MS analysis of phytostanyl fatty acid esters extracted from enriched skimmed milk drinking yogurt. (A) SIM chromatogram of campestanyl fatty acid esters at m/z 385.3. (B) SIM chromatogram of sitostanyl fatty acid esters at m/z 399.3. The peak numbering is in accordance with those of Figure 1 and Table 1. The asterisk in panel A is derived from the internal standard cholesteryl linolenate. For conditions, see Materials and Methods.

hand the use of methanol also provided a much better resolution and peak shape. In addition, an enhanced ionization efficiency has been ascribed to methanol as solvent in LC-APCI-MS applications due to a reduced proton affinity when compared to acetonitrile.[26]

LC-MS-APCI Data. Full scan APCI mass spectra of the synthesized reference compounds were recorded under the established LC conditions; as examples, the positive full scan mass spectra of sitostanyl stearate and sitostanyl linolenate are shown in Figure 3. The fragment ion $[M - FA + H]^+$ used for detection of the standard compounds was shown to constitute the base peak of all stanyl fatty acid ester spectra; a cone voltage of 80 V turned out to be optimum for the formation of this ion. Protonated molecular ions $[M + H]^+$ were only observed in spectra of stanols esterified to unsaturated fatty acids; however, intensities were low for stanyl esters of monounsaturated fatty acids, whereas poly-unsaturation favored the formation of molecular ions. Likewise, the extent of the formation of a characteristic fragment ion $[FA + H]^+$ correlated with the number of double bonds in the fatty acid moiety. When using ESI-MS, the addition of salts to the mobile phase was required to achieve sufficient ionizability of plant steryl fatty acid esters; however, this resulted in longer retention times and broader peak shapes.[17] This drawback could be avoided with the developed APCI-based approach.

LC-MS-APCI Quantitation. As the fragment $[M - FA + H]^+$ occurred in high abundance in the mass spectra of all esters, quantitation of campestanyl fatty acid esters (m/z 385.3) and sitostanyl fatty acid esters (m/z 399.3) in SIM mode was based on this ion. Chromatographic data and selected ions for individual phytostanyl fatty acid esters are shown in Table 1. The employed internal standard cholesteryl linolenate showed a fragmentation pattern similar to the plant stanyl fatty acid esters, thus enabling detection in SIM mode at m/z 369.3, the mass corresponding to the fragment ion $[M - FA + H]^+$. The chromatographic usefulness of cholesteryl linolenate as internal standard was confirmed via injection and subsequent selected ion monitoring at m/z 385.3 and m/z 399.3. The compound exhibited a fragment ion at m/z 385, indicating a cleavage of the acyl moiety. Owing to the shorter retention time of the internal standard, this fragment ion did not impair campestanyl ester quantitation, and therefore its concentration dependency was not further pursued.

The determined limits of detection and limits of quantitation of the individual plant stanyl fatty acid esters as occurring in the mixture STAEST-115 are also given in Table 1. For campestanyl fatty acid esters, they were in the same order of magnitude as those achieved for the previously described GC-based approach.[11] In contrast, for sitostanyl esters (except for palmitate), the LODs and LOQs obtained via the UHPLC analysis were considerably lower; this reflects the increased thermal degradation of these later eluting compounds in the course of high-temperature GC. The impact of the matrices and the different work-up procedures has been taken into account by the determination of individual recovery rates for each of the analyzed products.

In order to compensate for varying detector responses of distinct stanyl fatty acid esters, external five-point-calibration functions were generated, calibrating the response ratio of each individual stanyl fatty acid ester and the internal standard. Only

Table 2. Repeatability and Reproducibility Data for the Analysis of Phytostanyl Fatty Acid Esters in Enriched Skimmed Milk Drinking Yogurts

	sample I				sample II			
	operator 1	operator 1	operator 1	operator 2	operator 1	operator 1	operator 1	operator 2
stanyl fatty acid esters [g/(100 g)]	day 1	day 2	day 3	day 1	day 1	day 2	day 3	day 1
campestanyl-18:3	0.09 ± 0.00[a]	0.09 ± 0.00	0.09 ± 0.00	0.09 ± 0.00	0.08 ± 0.01	0.08 ± 0.00	0.09 ± 0.00	0.09 ± 0.01
campestanyl-18:2	0.21 ± 0.00	0.21 ± 0.01	0.21 ± 0.00	0.21 ± 0.00	0.21 ± 0.01	0.21 ± 0.01	0.21 ± 0.00	0.20 ± 0.00
campestanyl-16:0	0.05 ± 0.00	0.05 ± 0.00	0.05 ± 0.01	0.05 ± 0.00	0.05 ± 0.00	0.05 ± 0.00	0.05 ± 0.01	0.05 ± 0.00
campestanyl-18:1	0.65 ± 0.01	0.68 ± 0.00	0.65 ± 0.00	0.67 ± 0.01	0.66 ± 0.01	0.66 ± 0.01	0.68 ± 0.01	0.67 ± 0.01
campestanyl-18:0	0.02 ± 0.00	0.02 ± 0.00	0.02 ± 0.00	0.02 ± 0.00	0.02 ± 0.00	0.02 ± 0.00	0.02 ± 0.00	0.02 ± 0.00
campestanyl-20:1	0.01 ± 0.00	0.01 ± 0.00	0.01 ± 0.00	0.01 ± 0.00	0.01 ± 0.00	0.01 ± 0.00	0.01 ± 0.00	0.01 ± 0.00
campestanyl-20:0	0.01 ± 0.00	0.01 ± 0.00	0.01 ± 0.01	0.01 ± 0.00	0.01 ± 0.00	0.01 ± 0.00	0.01 ± 0.00	0.01 ± 0.00
sitostanyl-18:3	0.32 ± 0.02	0.32 ± 0.01	0.33 ± 0.02	0.33 ± 0.01	0.32 ± 0.00	0.33 ± 0.01	0.33 ± 0.01	0.32 ± 0.00
sitostanyl-18:2	0.79 ± 0.01	0.79 ± 0.01	0.79 ± 0.02	0.78 ± 0.01	0.79 ± 0.02	0.80 ± 0.01	0.81 ± 0.01	0.79 ± 0.01
sitostanyl-16:0	0.17 ± 0.00	0.17 ± 0.00	0.19 ± 0.04	0.18 ± 0.01	0.18 ± 0.01	0.19 ± 0.00	0.17 ± 0.01	0.18 ± 0.00
sitostanyl-18:1	2.59 ± 0.04	2.60 ± 0.03	2.60 ± 0.01	2.61 ± 0.02	2.64 ± 0.03	2.64 ± 0.04	2.68 ± 0.06	2.69 ± 0.07
sitostanyl-18:0	0.08 ± 0.00	0.08 ± 0.00	0.08 ± 0.00	0.07 ± 0.00	0.07 ± 0.00	0.07 ± 0.00	0.07 ± 0.00	0.08 ± 0.00
sitostanyl-20:1	0.04 ± 0.00	0.04 ± 0.00	0.04 ± 0.00	0.05 ± 0.00	0.05 ± 0.01	0.04 ± 0.00	0.03 ± 0.00	0.05 ± 0.00
sitostanyl-20:0	0.02 ± 0.00	0.02 ± 0.00	0.02 ± 0.00	0.02 ± 0.00	0.02 ± 0.00	0.02 ± 0.00	0.02 ± 0.00	0.02 ± 0.00
sitostanyl-22:0	0.01 ± 0.00	0.01 ± 0.00	0.01 ± 0.02	0.01 ± 0.00	0.01 ± 0.00	0.01 ± 0.00	0.01 ± 0.00	0.01 ± 0.00
total phytostanyl esters	5.06 ± 0.08	5.10 ± 0.01	5.08 ± 0.01	5.10 ± 0.02	5.12 ± 0.06	5.15 ± 0.06	5.20 ± 0.08	5.18 ± 0.08
esterified stanols[b]	3.10 ± 0.05	3.13 ± 0.01	3.12 ± 0.00	3.13 ± 0.01	3.14 ± 0.04	3.16 ± 0.04	3.19 ± 0.05	3.18 ± 0.05

[a]Values represent the mean ± standard deviation (n = 3). [b]Calculated on the basis of stanyl esters.

Table 3. Repeatability and Reproducibility Data for the Analysis of Phytostanyl Fatty Acid Esters in Enriched Margarine

	operator 1	operator 1	operator 1	operator 2
stanyl fatty acid esters [g/(100 g)]	day 1	day 2	day 3	day 1
campestanyl-18:3	0.25 ± 0.00[a]	0.24 ± 0.00	0.27 ± 0.00	0.27 ± 0.01
campestanyl-18:2	0.81 ± 0.02	0.80 ± 0.04	0.81 ± 0.00	0.85 ± 0.00
campestanyl-16:0	0.21 ± 0.01	0.21 ± 0.02	0.21 ± 0.01	0.22 ± 0.00
campestanyl-18:1	2.71 ± 0.03	2.75 ± 0.08	2.77 ± 0.03	2.71 ± 0.04
campestanyl-18:0	0.07 ± 0.01	0.07 ± 0.01	0.07 ± 0.00	0.07 ± 0.01
campestanyl-20:1	0.06 ± 0.01	0.05 ± 0.02	0.06 ± 0.00	0.06 ± 0.00
campestanyl-20:0	0.03 ± 0.01	0.02 ± 0.01	0.03 ± 0.00	0.03 ± 0.00
sitostanyl-18:3	0.58 ± 0.02	0.53 ± 0.02	0.56 ± 0.01	0.53 ± 0.02
sitostanyl-18:2	1.88 ± 0.02	1.86 ± 0.03	1.83 ± 0.03	1.90 ± 0.05
sitostanyl-16:0	0.47 ± 0.01	0.51 ± 0.06	0.51 ± 0.02	0.52 ± 0.02
sitostanyl-18:1	6.65 ± 0.11	6.81 ± 0.12	6.85 ± 0.12	6.65 ± 0.04
sitostanyl-18:0	0.19 ± 0.01	0.18 ± 0.02	0.19 ± 0.01	0.17 ± 0.01
sitostanyl-20:1	0.13 ± 0.06	0.12 ± 0.01	0.11 ± 0.01	0.11 ± 0.01
sitostanyl-20:0	0.05 ± 0.01	0.05 ± 0.01	0.05 ± 0.00	0.05 ± 0.00
sitostanyl-22:1	0.06 ± 0.03	0.04 ± 0.01	0.04 ± 0.01	0.05 ± 0.01
sitostanyl-22:0	0.02 ± 0.01	0.02 ± 0.01	0.03 ± 0.00	0.03 ± 0.01
total phytostanyl esters	14.17 ± 0.20	14.26 ± 0.31	14.39 ± 0.14	14.23 ± 0.07
esterified stanols[b]	8.92 ± 0.12	8.75 ± 0.19	8.83 ± 0.08	8.73 ± 0.04

[a]Values represent the mean ± standard deviation (n = 3). [b]Calculated on the basis of stanyl esters.

for campestanyl-18:0, -20:0, and -20:1 three-point-calibration functions were used, because of the lack of responses for these components in the calibration mixtures at the lowest concentrations. The coefficients of determination (R^2) were in the range of 0.9914−0.9997, confirming a linear relationship of each plant stanyl fatty acid ester within the respective concentration range in comparison to the internal standard. Area ratios and amount ratios of the investigated plant stanyl esters were consistently within the range of the calibration.

Plant Stanyl Fatty Acid Esters in Skimmed Milk Drinking Yogurts. Skimmed milk drinking yogurts were selected to test the suitability of the developed UHPLC-APCI-MS methodology because they are examples for protein-based, low-fat enriched dairy products. For this food category a method allowing the fast extraction of intact fatty acid stanyl esters has been described, based on acid digestion of the protein matrix.[11] No degradation or hydrolysis of the esters has been observed during this work-up step.[11,20] Due to the fat content of only 2.1% in this type of product, no interferences with lipid matrix constituents during chromatographic analysis were expected. Preliminary LC-MS experiments revealed a pronounced signal suppression caused by coeluting triglycerides only if the ratio of triglycerides and plant stanyl fatty acid esters in the injection solutions was higher than 1. EtOAc was chosen as injection solvent as the stanyl ester extracts could not be completely dissolved in more polar media. The SIM

Table 4. Repeatability and Reproducibility Data for the Analysis of Phytostanyl Fatty Acid Esters in Enriched Soft-Cheese-Style Spread

	sample I				sample II			
	operator 1	operator 1	operator 1	operator 2	operator 1	operator 1	operator 1	operator 2
stanyl fatty acid esters [g/(100 g)]	day 1	day 2	day 3	day 1	day 1	day 2	day 3	day 1
campestanyl-18:3	0.12 ± 0.00[a]	0.12 ± 0.00	0.11 ± 0.00	0.12 ± 0.00	0.13 ± 0.01	0.12 ± 0.00	0.11 ± 0.01	0.12 ± 0.01
campestanyl-18:2	0.27 ± 0.01	0.27 ± 0.01	0.25 ± 0.01	0.27 ± 0.01	0.28 ± 0.02	0.28 ± 0.01	0.27 ± 0.01	0.28 ± 0.01
campestanyl-16:0	0.07 ± 0.00	0.06 ± 0.01	0.05 ± 0.00	0.06 ± 0.01	0.06 ± 0.02	0.07 ± 0.00	0.07 ± 0.01	0.06 ± 0.00
campestanyl-18:1	0.84 ± 0.01	0.82 ± 0.02	0.84 ± 0.02	0.84 ± 0.00	0.83 ± 0.01	0.82 ± 0.00	0.87 ± 0.02	0.85 ± 0.01
campestanyl-18:0	0.02 ± 0.00	0.03 ± 0.00	0.03 ± 0.00	0.04 ± 0.00	0.03 ± 0.01	0.03 ± 0.00	0.04 ± 0.00	0.03 ± 0.00
campestanyl-20:1	0.02 ± 0.00	0.02 ± 0.00	0.02 ± 0.00	0.02 ± 0.00	0.02 ± 0.00	0.02 ± 0.00	0.02 ± 0.00	0.02 ± 0.00
campestanyl-20:0	0.01 ± 0.00	0.01 ± 0.00	0.01 ± 0.00	0.01 ± 0.00	0.01 ± 0.00	0.01 ± 0.00	0.01 ± 0.00	0.01 ± 0.00
sitostanyl-18:3	0.45 ± 0.00	0.45 ± 0.00	0.46 ± 0.01	0.45 ± 0.00	0.51 ± 0.02	0.47 ± 0.01	0.45 ± 0.00	0.48 ± 0.01
sitostanyl-18:2	1.10 ± 0.00	1.09 ± 0.00	1.09 ± 0.04	1.11 ± 0.01	1.13 ± 0.00	1.11 ± 0.00	1.13 ± 0.02	1.13 ± 0.01
sitostanyl-16:0	0.26 ± 0.01	0.26 ± 0.00	0.24 ± 0.01	0.26 ± 0.01	0.24 ± 0.01	0.26 ± 0.01	0.25 ± 0.01	0.26 ± 0.02
sitostanyl-18:1	3.62 ± 0.03	3.60 ± 0.03	3.75 ± 0.05	3.61 ± 0.05	3.68 ± 0.06	3.61 ± 0.02	3.76 ± 0.04	3.65 ± 0.02
sitostanyl-18:0	0.11 ± 0.00	0.11 ± 0.00	0.10 ± 0.00	0.11 ± 0.01	0.11 ± 0.00	0.11 ± 0.00	0.11 ± 0.01	0.10 ± 0.01
sitostanyl-20:1	0.07 ± 0.01	0.07 ± 0.00	0.06 ± 0.01	0.07 ± 0.01	0.06 ± 0.01	0.07 ± 0.00	0.05 ± 0.01	0.07 ± 0.00
sitostanyl-20:0	0.04 ± 0.01	0.04 ± 0.00	0.03 ± 0.00	0.04 ± 0.00	0.03 ± 0.00	0.03 ± 0.00	0.03 ± 0.00	0.03 ± 0.00
sitostanyl-22:0	0.01 ± 0.00	0.02 ± 0.00	0.01 ± 0.00	0.01 ± 0.00	0.02 ± 0.00	0.01 ± 0.00	0.01 ± 0.00	0.01 ± 0.00
total phytostanyl esters	6.99 ± 0.03	6.96 ± 0.03	7.05 ± 0.12	7.01 ± 0.04	7.13 ± 0.03	7.01 ± 0.02	7.18 ± 0.04	7.09 ± 0.04
esterified stanols[b]	4.29 ± 0.02	4.27 ± 0.02	4.33 ± 0.07	4.30 ± 0.02	4.37 ± 0.02	4.30 ± 0.01	4.41 ± 0.02	4.35 ± 0.02

[a]Values represent the mean ± standard deviation (n = 3). [b]Calculated on the basis of stanyl esters.

chromatograms for campestanyl and sitostanyl fatty acid esters extracted from skimmed milk drinking yogurts are shown in Figure 4. The detailed compositions of phytostanyl fatty acid esters and the total contents of phytostanyl esters determined in skimmed milk drinking yogurts are given in Table 2. Oleic acid esters dominated the chromatogram followed by esters of linoleic, linolenic, and palmitic acid, whereas the fatty acids consisting of 20 and 22 carbon atoms were only esterified to a minor extent; this pattern indicated rapeseed oil as the fatty acid source for esterification.[27] The calculated amounts of total phytostanols were in good agreement with the labeling ("plant stanol 3.0%"). In addition, both the individual ester contents and percentage distributions determined via the presented approach are corresponding to data obtained via GC/FID on intact plant stanyl fatty acid esters in yogurt drinks of the same type and brand.[11] Phytostanyl esters of palmitoleic acid could not be identified, and sitostanyl-22:1 was also not detectable in the present work; however, a direct comparison of the two approaches, in that respect, is not possible due to coelution of esters of saturated and monounsaturated fatty acids in the GC-based method. Two bottles from different batches were analyzed in triplicate on 3 days by one operator, revealing excellent repeatability of the method. A quantitation of comparable ester contents after analysis of the samples by a second operator demonstrated the reproducibility of the method. Recovery rates of the analytical approach were calculated to be 97.70 ± 0.5%; they further confirm the stability of the analytes during acid digestion of the protein matrix.

Plant Stanyl Fatty Acid Esters in Enriched Margarines. Margarines enriched with plant stanyl fatty acid esters were selected as an example for fat-based food matrices. In this case, prior removal of interfering lipid matrix constituents was required. Recently, aminopropyl-based solid-phase extraction was shown to be a suitable tool for the selective separation of plant stanyl fatty acid esters from other lipids.[19,28] Hence, a rapid and efficient SPE-based preseparation was established, using aminopropyl-modified silica cartridges and a mixture of *n*-hexane/diethyl ether (99:1, v/v) for the elution of phytostanyl fatty acid esters. The recovery of the stanyl ester mixture STAEST-115 spiked to a nonenriched margarine was very good (97.19 ± 1.44%). Table 3 shows the quantitative data obtained after investigation of a commercial margarine on three different days and additionally by a second operator; the results were excellent regarding both repeatability and reproducibility. The calculated contents of total phytostanols were in very good agreement with the amounts declared on the label. Being similar to the pattern of the esters detected in skimmed milk drinking yogurts, the distribution of the plant stanyl fatty acid esters determined in margarine suggested rapeseed fatty acids having been used for esterification. In addition to the compounds determined in skimmed milk drinking yogurts, sitostanyl-22:1 could also be detected and quantitated, accounting for approximately 0.3% of total esters in the margarine sample.

Plant Stanyl Fatty Acid Esters in Soft-Cheese-Style Spread. The soft-cheese-style spread was selected because it consists of both considerable amounts of protein and fat. Consequently, a combination of the acid digestion applied to the skimmed milk drinking yogurts and the solid-phase extraction employed for removal of triglycerides in the margarine sample was used for this type of product. This allowed such a complex food matrix also to be analyzed quickly and without further methodological modifications. The approach showed good recovery rates of 96.39 ± 0.26% determined via the addition of the plant stanyl ester mixture STAEST-115 to a nonenriched cream cheese. The distributions of the plant stanyl fatty acid esters analyzed in two packages of soft-cheese-style spread resembled those determined in drinking yogurts and margarine, once more indicating rapeseed oil as the fatty acid source and at the same time confirming the reliability of the established analytical approach. Table 4 presents the quantitative data for two packages of cheese spread obtained by triplicate analyses on 3 days and by an

additional second operator, their low deviations proving excellent repeatability and good reproducibility. The calculated amounts of total phytostanol contents matched the declared amounts.

In conclusion, an RP-UHPLC-APCI-MS-based analytical approach enabling a simple, robust, and fast detection of plant stanyl fatty acid esters extracted from different types of enriched foods was established. Plant stanyl fatty acid esters consisting of the same stanol moiety could be resolved on a C8 column and analyzed in SIM mode for highly sensitive detection that differentiates esters depending on the esterified stanol moiety. Thus, an excellent separation was accomplished without having to manage the issue of thermal degradation of unsaturated long-chain fatty acid esters, the major drawback of GC-based approaches. Fast and facile sample preparation was used and extensively validated for three different types of enriched foods available on the European market, providing a range of extraction methods being suitable for either protein-based matrices, lipid-based matrices, or a combination of both. The aquired detailed qualitative and quantitative data on plant stanyl fatty acid esters will extend the analytical portfolio for the assessment of functional foods in terms of authenticity and in terms of the contribution of intact esters to the cholesterol lowering effects.

AUTHOR INFORMATION

Corresponding Author

*Phone: +49 (0)8161 71 4250. Fax: +49 (0)8161 71 4259. E-mail: k.h.engel@wzw.tum.de.

Notes

The authors declare no competing financial interest.

REFERENCES

(1) Calpe-Berdiel, L.; Escolà-Gil, J. C.; Blanco-Vaca, F. New insights into the molecular actions of plant sterols and stanols in cholesterol metabolism. *Atherosclerosis* **2009**, *203*, 18−31.

(2) Piironen, V.; Lindsay, D. G.; Miettinen, T. A.; Toivo, J.; Lampi, A.-M. Plant sterols: biosynthesis, biological function and their importance to human nutrition. *J. Sci. Food Agric.* **2000**, *80*, 939−966.

(3) Demonty, I.; Ras, R. T.; van der Knaap, H. C. M.; Duchateau, G. S. M. J. E.; Meijer, L.; Zock, P. L.; Geleijnse, J. M.; Trautwein, E. A. Continuous dose-response relationship of the LDL-cholesterol-lowering effect of phytosterol intake. *J. Nutr.* **2008**, *139*, 271−284.

(4) Plat, J.; Mensink, R. P. Plant stanol and sterol esters in the control of blood cholesterol levels: Mechanism and safety aspects. *Am. J. Cardiol.* **2005**, *96*, 15−22.

(5) SCF (Scientific Committee on Food). Opinion of the scientific commitee on food on a request for the safety assessment of the use of phytosterol esters in yellow fat spreads, 2000; http://ec.europa.eu/food/fs/sc/scf/out56_en.pdf (last accessed: Apr. 22, 2014).

(6) SCF (Scientific Committee on Food). Opinion of the scientific committee on food on the application from ADM for the approval of plant sterol-enriched foods, 2003; http://ec.europa.eu/food/fs/sc/scf/out192_en.pdf (last accessed: Apr. 22, 2014).

(7) SCF (Scientific Committee on Food). Opinion of the scientific committee on food on the applications for approval of a variety of plant-sterol enriched food, 2003; http://ec.europa.eu/food/fs/sc/scf/out174_en.pdf (last accessed: Apr. 22, 2014).

(8) Ash, M.; Hang, J.; Dussault, P.; Carr, T. Phytosterol stearate esters elicit similar responses on plasma lipids and cholesterol absorption but different responses on fecal neutral sterol excretion and hepatic free cholesterol in male syrian hamsters. *Nutr. Res. (N. Y., NY, U. S.)* **2011**, *31*, 537−543.

(9) Brown, A. W.; Hang, J.; Dussault, P. H.; Carr, T. P. Plant sterol and stanol substrate specificity of pancreatic cholesterol esterase. *J. Nutr. Biochem.* **2010**, *21*, 736−740.

(10) Lubinus, T.; Barnsteiner, A.; Skurk, T.; Hauner, H.; Engel, K.-H. Fate of dietary phytosteryl/-stanyl esters: analysis of individual intact esters in human feces. *Eur. J. Nutr.* **2013**, *52*, 997−1013.

(11) Barnsteiner, A.; Lubinus, T.; Di Gianvito, A.; Schmid, W.; Engel, K.-H. GC-based analysis of plant stanyl fatty acid esters in enriched foods. *J. Agric. Food Chem.* **2011**, *59*, 5204−5214.

(12) Barnsteiner, A.; Esche, R.; Di Gianvito, A.; Chiavaro, E.; Schmid, W.; Engel, K.-H. Capillary gas chromatographic analysis of complex phytosteryl/-stanyl ester mixtures in enriched skimmed milk-drinking yoghurts. *Food Control* **2012**, *27*, 275−283.

(13) Billheimer, J. T.; Avart, S.; Milani, B. Separation of steryl esters by reversed-phase liquid chromatography. *J. Lipid Res.* **1983**, *24*, 1646−1651.

(14) Evershed, R. P.; Male, V. L.; Goad, L. Strategy for the analysis of steryl esters from plant and animal tissues. *J. Chromatogr. A* **1987**, *400*, 187−205.

(15) Gordon, M. H.; Griffith, R. E. Steryl ester analysis as an aid to the identification of oils in blends. *Food Chem.* **1992**, *43*, 71−78.

(16) Kuksis, A.; Myher, J. J.; Marai, L.; Little, J. A.; McArthur, R. G.; Roncari, D. A. K. Fatty acid composition of individual plasma steryl esters in phytosterolemia and xanthomatosis. *Lipids* **1986**, *21*, 371−377.

(17) Caboni, M. F.; Iafelice, G.; Pelillo, M.; Marconi, E. Analysis of fatty acid steryl esters in tetraploid and hexaploid wheats: Identification and comparison between chromatographic methods. *J. Agric. Food Chem.* **2005**, *53*, 7465−7472.

(18) Mezine, I.; Zhang, H.; Macku, C.; Lijana, R. Analysis of plant sterol and stanol esters in cholesterol-lowering spreads and beverages using high-performance liquid chromatography−atmospheric pressure chemical ionization−mass spectroscopy. *J. Agric. Food Chem.* **2003**, *51*, 5639−5646.

(19) Esche, R.; Barnsteiner, A.; Scholz, B.; Engel, K.-H. Simultaneous analysis of free phytosterols/phytostanols and intact phytosteryl/phytostanyl fatty acid and phenolic acid esters in cereals. *J. Agric. Food Chem.* **2012**, *60*, 5330−5339.

(20) Esche, R.; Carcelli, A.; Barnsteiner, A.; Sforza, S.; Engel, K.-H. Analysis of phytosteryl and phytostanyl fatty acid esters in enriched dairy foods: A combination of acid digestion, lipid extraction, and on-line LC-GC. *Eur. Food Res. Technol.* **2013**, *236*, 999−1007.

(21) Vogelgesang, J.; Hädrich, J. Limits of detection, identification and determination: A statistical approach for practitioners. *Accredit. Qual. Assur.* **1998**, *3*, 242−255.

(22) Rudell, D. R.; Buchanan, D. A.; Leisso, R. S.; Whitaker, B. D.; Mattheis, J. P.; Zhu, Y.; Varanasi, V. Ripening, storage temperature, ethylene action, and oxidative stress alter apple peel phytosterol metabolism. *Phytochemistry* **2011**, *72*, 1328−1340.

(23) Gordon, M. H.; Griffith, R. E. A comparison of the steryl esters of coconut and palm kernel oils. *Fett Wiss. Technol.* **1992**, *94*, 218−221.

(24) Cheng, B.; Kowal, J. Analysis of adrenal cholesteryl esters by reversed phase high performance liquid chromatography. *J. Lipid Res.* **1994**, *35*, 1115−1121.

(25) Rozenberg, R.; Ruibal-Mendieta, N. L.; Petitjean, G.; Cani, P.; Delacroix, D. L.; Delzenne, N. M.; Meurens, M.; Quetin-Leclercq, J.; Habib-Jiwan, J.-L. Phytosterol analysis and characterization in spelt (*Triticum aestivum* ssp. *spelta* L.) and wheat (*T. aestivum* L.) lipids by LC/APCI-MS. *J. Cereal Sci.* **2003**, *38*, 189−197.

(26) Kostiainen, R.; Kauppila, T. J. Effect of eluent on the ionization process in liquid chromatography−mass spectrometry. *J. Chromatogr. A* **2009**, *1216*, 685−699.

(27) *CODEX Standard For Named Vegetable Oils*, Codex Standard 210-1999, 1999.

(28) Oelschlägel, S.; Menzel, C.; Speer, K. Phytosterols and steryl esters in diverse *Cucurbita*, *Cucumis* and *Citrullus* seed oils. *Lipid Technol.* **2012**, *24*, 181−184.

JOURNAL OF AGRICULTURAL AND FOOD CHEMISTRY

Article

pubs.acs.org/JAFC

Sensitive Quantitation of Polyamines in Plant Foods by Ultrasound-Assisted Benzoylation and Dispersive Liquid−Liquid Microextraction with the Aid of Experimental Designs

Edgar Pinto, Armindo Melo, and Isabel M. P. L. V. O. Ferreira*

REQUIMTE/Departamento de Ciências Químicas, Laboratório de Bromatologia e Hidrologia, Faculdade de Farmácia, Universidade do Porto. Rua de Jorge Viterbo Ferreira 228, 4050-313 Porto, Portugal

Supporting Information

ABSTRACT: A new method involving ultrasound-assisted benzoylation and dispersive liquid−liquid microextraction was optimized with the aid of chemometrics for the extraction, cleanup, and determination of polyamines in plant foods. Putrescine, cadaverine, spermidine, and spermine were derivatized with 3,5-dinitrobenzoyl chloride and extracted by dispersive liquid−liquid microextraction using acetonitrile and carbon tetrachloride as dispersive and extraction solvents, respectively. Two-level full factorial design and central composite design were applied to select the most appropriate derivatization and extraction conditions. The developed method was linear in the 0.5−10.0 mg/L range, with a $R^2 \geq 0.9989$. Intra- and interday precisions ranged from 0.8 to 6.9% and from 3.0 to 10.3%, respectively, and the limit of detection ranged between 0.018 and 0.042 μg/g of fresh weight. This method was applied to the analyses of six different types of plant foods, presenting recoveries between 81.7 and 114.2%. The method is inexpensive, versatile, simple, and sensitive.

KEYWORDS: *plant foods, putrescine, cadaverine, spermidine, spermine, response surface methodology, HPLC−DAD*

INTRODUCTION

The polyamines putrescine, cadaverine, spermidine, and spermine are low-molecular-weight organic amines with aliphatic structure, which have been implicated in several biological processes, such as plant growth and development.[1] These compounds are naturally found in many plant foods and are involved in the regulation of a diverse range of vital cellular processes in eukaryotic cells. In plants, the most common polyamines are putrescine, spermidine, and spermine and are usually localized in the cytoplasm and organelles (e.g., vacuoles, mitochondria, and chloroplasts) of plant cells.[2,3]

The dietary intake of polyamines influences human health. Their biological role in humans includes participation in cell growth and proliferation, pain sensitization, stabilization of DNA, gene transcription, apoptosis, regulation of the immune response, maintenance of intestinal function, and protein synthesis.[4,5] It has been suggested that increasing polyamine intake has several health benefits, such as decreasing age-associated pathologies and increasing longevity.[6] However, a polyamine-deficient diet has also been proposed as an efficient nutritional strategy for several human conditions.[7]

Plant foods have very low levels of polyamines, ranging from a few milligrams to less than a 100 mg/kg. Thus, methods to perform polyamine quantitation in plant foods frequently report results as non-detectable or below the limit of detection (LOD)/limit of quantitation (LOQ) because of the high sensitivity required.[8−10] Plant foods are a very complex and variable matrix;[2,3] thus, efficient cleanup and pre-concentration techniques are needed to obtain sensitive and accurate quantitation of polyamines. Because plant foods are solid matrixes, an extraction/deproteinization is also required. The deproteinization process is usually performed with diluted strong acids, such as perchloric, hydrochloric, and trichloroacetic acids.[11−13]

Chemical derivatization has become widely accepted in polyamine analysis, enabling great sensitivity and selectivity to be achieved. Nowadays, there are several derivatization reagents that can be used for ultraviolet (UV) and/or fluorescence detection, including *o*-phthaldialdehyde, dansyl chloride, 6-aminoquinolyl-*N*-hydroxysuccinimidyl carbamate, dabsyl chloride, 3,5-dinitrobenzoyl chloride, 1,2-naphthoquinone-4-sulfonate, benzoyl chloride, 4-chloro-3,5-dinitrobenzotrifluoride, diethyl ethoxymethylenemalonate, and others.[14,15] Among them, 3,5-dinitrobenzoyl chloride shows several advantages, such as its low price, commercial availability, and fast reaction times, at room temperature.[16]

Many sample preparation techniques have been developed for cleanup purposes. Liquid−liquid extraction (LLE) and solid-phase extraction (SPE) are some of the most widely used techniques; however, they require large quantities of organic solvents and are time-consuming.[12,13] Solid-phase microextraction (SPME) and single-drop microextraction (SDME) have been increasingly used in the last few years because of their eco-friendly nature.[17,18] However, these procedures also had some drawbacks, such as high price, short durability of the extraction fibers, and sample carryover.[19] Dispersive liquid−liquid microextraction (DLLME) is a novel sample preparation technique based on a ternary component mixture consisting of an aqueous sample, a dispersive solvent, and an extraction

Received: February 24, 2014
Revised: April 28, 2014
Accepted: April 28, 2014
Published: April 28, 2014

ACS Publications © 2014 American Chemical Society

dx.doi.org/10.1021/jf500959g | J. Agric. Food Chem. 2014, 62, 4276−4284

solvent. It presents several advantages, such as simplicity, high recovery, quickness, and low cost.[20]

Several methods have been developed for the analysis of polyamines, including micellar electrokinetic chromatography,[21] gas chromatography (GC),[17] thin-layer chromatography,[22] ion chromatography,[23] and liquid chromatography (LC).[24] Overall, LC is the most widely used technique in the determination of polyamines in different kinds of food because of its high selectivity, sensitivity, and applicability.

Growing interest arises in coupling derivatization and DLLME, followed by chromatographic separation (i.e., LC or GC) for the analysis of different kinds of compounds.[25,26] The potentiality of these methods to simplify experimental procedures, decrease sample loss, increase method sensitivity, and remove interferences is seen as a great improvement in the analytical chemistry field.[27] The development of a derivatization and DLLME method requires selection of several variables (concentration of derivatization reagent, reaction time, reaction temperature, dispersive solvent volume, extraction solvent volume, and ionic strength) to establish optimum conditions. The optimization of a multivariable system through a one-variable-at-a-time procedure can be time-consuming and neglect potential interactions between variables. The two-level full factorial design is a useful tool for preliminary screening of experimental factors that needed to be optimized, whereas response surface methodology (RSM) aids to understand interactions among the parameters that should be optimized to determine the optimum operational conditions for the system or to determine a specific region that satisfies the operating specifications.[28] Consequently, these chemometric methods, when applied to derivatization and miniaturized extraction procedures, improve the quality of analytical data. However, until now, few studies apply these procedures.

A new method is presented for the detection and quantitation of putrescine, cadaverine, spermidine, and spermine using ultrasound-assisted benzoylation followed by DLLME and high-performance liquid chromatography−diode array detection (HPLC−DAD). The benzoylation procedure and extraction conditions were optimized with the aid of two-level full factorial designs and central composite design (CCD). The developed method was applied to several plant food samples.

MATERIALS AND METHODS

Chemicals and Standard Solutions. Putrescine dihydrochloride, cadaverine dihydrochloride, spermidine trihydrochloride, 1,7-diaminoheptane [internal standard (IS)], spermine tetrahydrochloride, hydrochloric acid, acetonitrile, methanol, acetone, and 3,5-dinitrobenzoyl chloride were purchased from Sigma-Aldrich (St. Louis, MO). Boric acid, sodium hydroxide, potassium chloride, and sodium chloride were from VWR (Radnor, PA). Perchloric acid ($HClO_4$), carbon tetrachloride, chlorobenzene, chloroform, dichloromethane, tetrachloroethylene, and trichloroethylene were obtained from Merck (Darmstadt, Germany).

Standard stock solutions were prepared by dissolving each compound in 0.1 M HCl at a final concentration of 1000 mg/L. Working standard solutions were prepared daily from the stock solutions by adequate dilution with 0.1 M HCl. Sodium borate buffer was prepared from dilution of H_3BO_3 and KCl in water (0.5 M each), followed by titration with NaOH (0.5 M) to pH 10. 3,5-Dinitrobenzoyl chloride (56 mM) was prepared by dissolving a proper amount of the solid compound in acetonitrile.

Instrumentation and Chromatographic Conditions. Chromatographic analysis was performed with an analytical HPLC unit (Jasco, Tokyo, Japan) equipped with Jasco PU-2080 HPLC pumps, Jasco MD-2010 Plus multiwavelength detector, and a column oven model 7981 (Jones Chromatography, Hengoed, U.K.). The column used was a 250 × 4.6 mm inner diameter, 5 μm, Ultracarb 30-ODS RP-18 (Phenomenex, Milford, MA). The Borwin PDA controller software (JMBS Developments, Le Fontanil, France) was used for system control and data acquisition. The column temperature was set at 35 °C, and the chromatographic separation was carried out by gradient elution with two solvent mixtures at a 1 mL/min flow rate. Solvent A consisted of 10 mM aqueous sodium formate/formic acid buffer at pH 3, and solvent B consisted of acetonitrile. The linear gradient program was as follow: 0−5 min, 40% B; 5−11 min, 58% B; 11−15 min, 58% B; 15−20 min, 65% B; 20−23 min, 65% B; 23−28 min, 95% B; 28−30 min, 95% B; and 30−40 min, column rinse and re-equilibration. The total run time, including polyamine separation, column rinse, and re-equilibration, was of 40 min. Diode array detection was carried out at the wavelength of 250 nm.

Sample Preparation. Plant food samples (lettuce, carrot, onion, cabbage, tomato, and apple) were purchased at local supermarkets. Samples were washed with ultrapure water, frozen at −80 °C, and freeze-dried. The lyophilized samples were homogenized by grinding in a blender and sieved through a nylon sieve of 150 μm mesh size. Free polyamines were determined according to Zhou and Yu,[11] with minor modifications. Lyophilized samples (100 mg) were homogenized in 2.5 mL of 5% (v/v) cold $HClO_4$ and incubated at 4 °C for 1 h. After centrifugation at 17000*g* for 30 min, the supernatant was collected and used as a sample extract to determine the content of polyamines.

Derivatization, Cleanup, and Pre-concentration. A 2 mL volume of standard solution or sample extract was placed in a 10 mL tube, and 0.5 M borate buffer (pH 10.0) and 2 M NaOH were added to adjust pH to 10. After that, 680 μL of 3,5-dinitrobenzoyl chloride in acetonitrile (56 mM) was added to the previous solution, which was subjected to vortexing. Afterward, the mixture was ultrasonicated for 15 min at room temperature. Benzoylated polyamines were extracted by the DLLME method by adding 500 mg of NaCl and 205 μL of carbon tetrachloride (extraction solvent) into the sample solution to form a cloudy solution. After vortexing for 1 min, the mixture was centrifuged for 5 min at 5000 rpm, and the organic phase was aspirated into a microsyringe and collected into a 2 mL glass vial. The organic phase was evaporated in a gentle stream of N_2 and reconstituted in 100 μL of acetonitrile. Finally, 20 μL was injected into the HPLC system for analysis.

Experimental Design. Several trials were conducted to optimize the benzoylation and DLLME conditions for the quantitative analyses of polyamines in plant foods using RSM. A two-level (2^k) factorial design was created to screen the main variables affecting the derivatization and extraction procedures. This technique is a powerful tool for screening the key variables in a multivariable system. Two different full factorial designs were created for trials at low (−1) and high (+1) concentration levels with five central points. The experiments were performed to evaluate the significance of seven variables (3,5-dinitrobenzoyl chloride concentration, 3,5-dinitrobenzoyl chloride volume, derivatization time, derivatization temperature, dispersive solvent volume, extraction solvent volume, and amount of NaCl) under study. In the first full factorial design, the evaluated variables were 3,5-dinitrobenzoyl chloride concentration (35−65 mM), 3,5-dinitrobenzoyl chloride volume (400−800 μL), derivatization time (15−40 min), and derivatization temperature (20−50 °C). The screening of the main variables affecting the derivatization procedure was performed without performing the extraction procedure to exclude potential effects arising from it. In the second full factorial design, the variables dispersive solvent volume (400−800 μL), extraction solvent volume (50−250 μL), and amount of NaCl (500−800 mg) were evaluated. The DLLME procedure was carried out after fixing the most suitable derivatization conditions. Afterward, the significant variables were optimized using a CCD.

Experiments with three independent variables, 3,5-dinitrobenzoyl chloride concentration (X_1), dispersive solvent volume (X_2), and extraction solvent volume (X_3), were conducted by applying a CCD consisting of a complete 20-factorial design with six center points and

two axial points on the axis of each design variable at a distance of α = 1.682 from the design center. The response was the sum of all polyamine peak areas. Experiments were carried out as follows: 3,5-dinitrobenzoyl chloride concentration (35−65 mM), dispersive solvent volume (400−800 μL), and extraction solvent volume (100−250 μL). The complete experimental design (see the Supporting Information) was performed using the Design Expert Trial Version 7 (Stat-Ease, Inc., Minneapolis, MN) software.

Method Validation. Mixed standard solutions (ranging from 0.5 to 10 mg/L) containing putrescine, cadaverine, spermidine, and spermine were subjected to the derivatization, cleanup, and preconcentration procedures described above. Calibration curves were constructed by the least-squares linear regression model, using the ratio between the peak area of each polyamine and the peak area of IS. The deviation from linearity was evaluated by applying the lack-of-fit test to the calibration curves of each polyamine. The intraday precision was calculated from the results of five replicate analyses in a single day of standards prepared at three concentration levels (0.5, 2.5, and 10 mg/L), whereas the interday precision was calculated from results obtained in five consecutive days. The LOD and LOQ were calculated on the basis of the calibration curve parameters according to Miller and Miller.[29]

Accuracy, on the basis of the recovery percentage {R, % = [(concentration of the spiked sample − concentration of the unspiked sample)/added concentration] × 100}, was estimated from triplicate experiments performed with lettuce, carrot, onion, cabbage, tomato, and apple samples (ca. 100 mg) spiked with 0.1 mL volume of a mixed standard solution (2.5 mg/L of each polyamine) to obtain a content of 2.5 μg/g in each plant food. Results of polyamine contents in plant foods were expressed as micrograms per gram of fresh weight.

The stability of the extracts was tested by analyzing the extract of 5 mg/L standard solution at 0, 1, 2, 6, and 24 h after the derivatization and extraction procedure. During this time period, extracts were stored at 4 °C.

RESULTS AND DISCUSSION

Experimental Parameter Selection. Working standard solutions containing putrescine, cadaverine, spermidine, and spermine (see chemical structures in Figure 1) at a fixed concentration (5 mg/L) were used to study the buffer capacity of the derivatization procedure and the performance of different dispersive and extraction solvents on the DLLME procedure. To evaluate the buffer capacity, standard solutions were diluted in 5% (v/v) $HClO_4$ solution to replicate the extraction conditions used in real plant food sample extraction. The obtained extracts presented a pH value around 1. Because the benzoylation reaction requires pH around 10, borate buffer (0.5 M) with 2 M NaOH provided a pH of 10 and was used in further experiments.

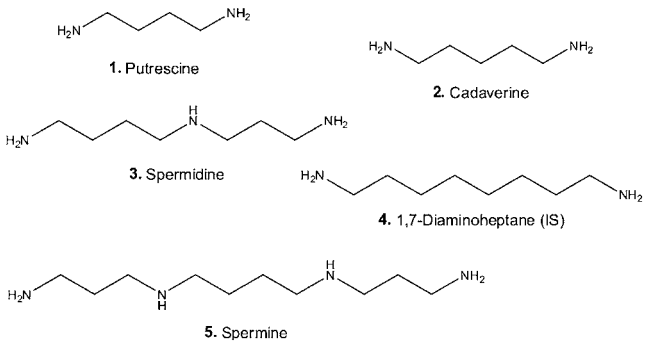

Figure 1. Chemical structure of (1) putrescine, (2) cadaverine, (3) spermidine, (4) IS, and (5) spermine.

Choosing the most suitable dispersive and extraction solvents is a crucial step to obtain the maximum extraction efficiency. The dispersive solvent should be miscible with both aqueous and organic phases, while the extraction solvent must have higher density than water, low water solubility, and high extraction efficiency for the target compounds.[20] Three dispersive solvents (methanol, acetonitrile, and acetone) and six extraction solvents (carbon tetrachloride, chloroform, chlorobenzene, dichloromethane, trichloroethylene, and tetrachloroethylene) were evaluated. The 5 mg/L standard solution was diluted in 5% (v/v) $HClO_4$ solution, derivatized, and subjected to the DLLME procedure. Triplicate measurements were performed for each tested solvent. The use of acetonitrile as a dispersive solvent led to higher peak areas for all of the tested polyamines (Figure 2A), indicating that higher sensitivity could be obtained with this solvent. Carbon tetrachloride presented higher extraction efficiency for all of the target compounds (Figure 2B); thus, it was selected as an extraction solvent.

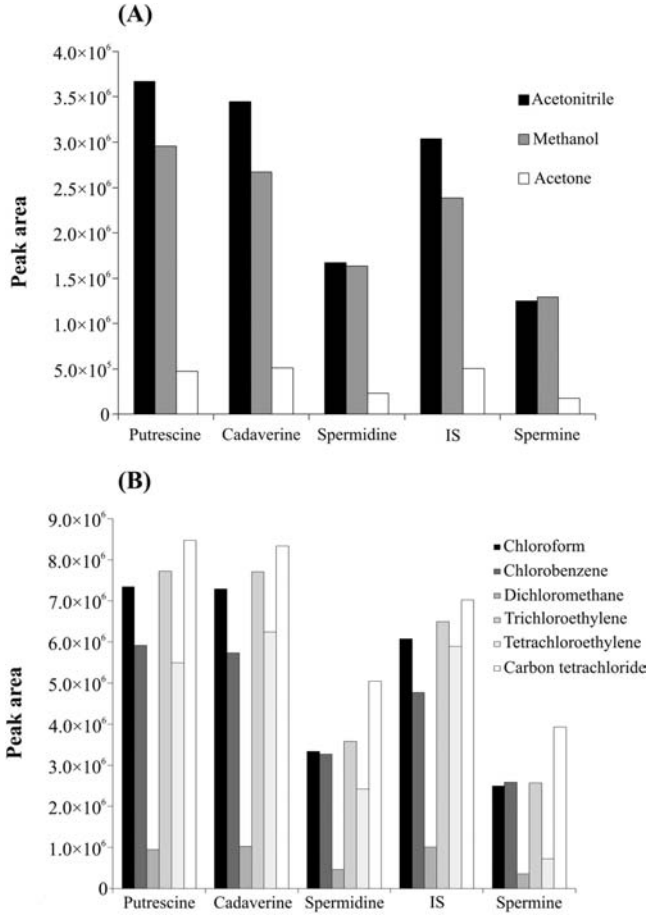

Figure 2. Selection of (A) dispersive and (B) extraction solvents.

Two-Level Full Factorial Design. The main effects of the seven studied variables in the screening experiments are presented in Figure 3 in the form of a Pareto chart. The same standard solution used to perform the selection of the dispersive and extraction solvents was used in the two-step experimental design (two-level full factorial design for screening and CCD for optimization). The magnitude of the effects is highlighted in an ordered bar chart, where the bar length of the vertical axis is proportional to the significance of the variables.

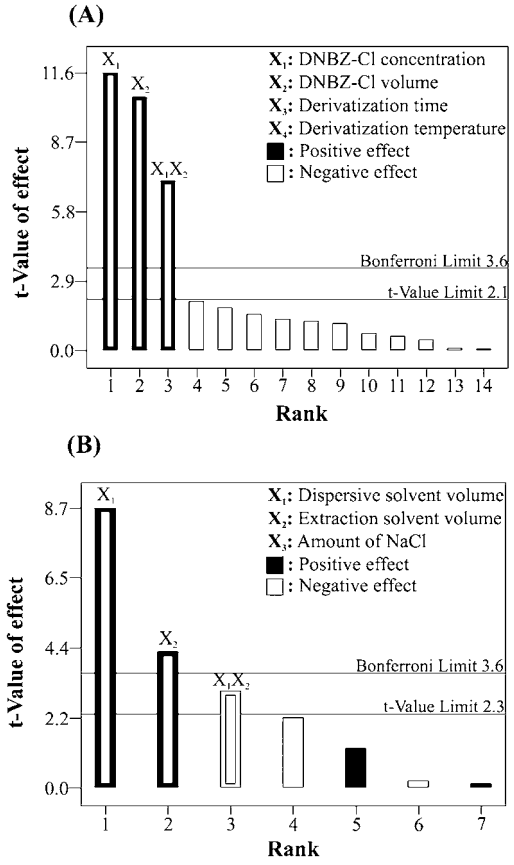

Figure 3. Main effect Pareto chart for the two-level full factorial design of the screening experiments of (A) derivatization and (B) extraction.

With regard to the derivatization procedure, the significance of the variables 3,5-dinitrobenzoyl chloride concentration, 3,5-dinitrobenzoyl chloride volume, derivatization time, and derivatization temperature was evaluated. The variables 3,5-dinitrobenzoyl chloride concentration and 3,5-dinitrobenzoyl chloride volume as well as the interaction between them were statistically significant ($p < 0.05$), with a positive effect on the response. Thus, these variables were selected for further assessment in the CCD. For the extraction procedure, the significance of the variables dispersive solvent volume, extraction solvent volume, and amount of NaCl was assessed. The variables dispersive solvent volume and extraction solvent volume as well as the interaction between them were statistically significant ($p < 0.05$) and, thus, were considered for optimization. Because the variables "3,5-dinitrobenzoyl chloride volume" and "dispersive solvent volume" tested in the first and second full factorial designs, respectively, rely on the use of acetonitrile, the two variables were designated throughout the optimization procedure as just "dispersive solvent volume". The variables derivatization time, derivatization temperature, and amount of NaCl showed no significant effect on the peak area of polyamines and, thus, were fixed for further experiments at 15 min, room temperature, and 500 mg, respectively. Faster reaction times, without the need for heating and with a lower amount of reagents involved, were achieved without compromising method sensitivity.

CCD. For CCD, 20 experiments were carried out with randomly selected different combinations of the 3,5-dinitrobenzoyl chloride concentration (X_1), dispersive solvent volume (X_2), and extraction solvent volume (X_3) parameters using statistically designed experiments. The sum of all polyamine peak areas as a function of X_1, X_2, and X_3 was used as a response for the CCD design. Models were validated by two diagnostic residuals, the R^2 and Q^2 values. Typical values indicating good models are $R^2 > 0.75$ and $Q^2 > 0.60$.[30,31] In our study, the values of R^2 predicted and R^2 adjusted were 0.92 and 0.97, respectively, and the Q^2 value was 0.92, indicating the goodness of the model. Adequate precision, measured as a signal-to-noise ratio, was 26.54 (greater than 4 as desirable), which also indicates the adequacy of the present model. As shown in Table 1, the F value was 66.1, which indicates that the regression model is statistically significant ($p < 0.01$) at the 99% confidence level. Values of probability > F for X_1, X_2, X_3, X_1X_2, X_2X_3, X_1^2, X_2^2, and X_3^2 were lower than 0.05, which indicates that they are significant model terms. Despite its non-significance, the interaction X_1X_3 was considered in the model. Thus, a hierarchical model was applied. The lack-of-fit was 1.29, non-significant as desired, and the quadratic model was valid.[32]

Three-dimensional surface and contour plots were drawn to investigate the interactive effect of two factors on the sum of polyamine peak areas (Figure 4). Figure 4A shows the combined effect of the 3,5-dinitrobenzoyl chloride concentration and dispersive solvent volume. Figure 4B shows the

Table 1. Analysis of Variance (ANOVA) for the Response Surface Model for the Sum of Polyamine Peak Areas

source	coefficient estimate	standard error	sum of squares	degrees of freedom	mean square	F value	probability > F	remarks
model			2.54×10^{15}	9	2.83×10^{14}	66.1	<0.0001	significant
intercept	3.62×10^{7}	8.43×10^{5}		1				
X_1	4.41×10^{6}	5.59×10^{5}	2.66×10^{14}	1	2.66×10^{14}	62.2	<0.0001	significant
X_2	1.08×10^{7}	5.59×10^{5}	1.60×10^{15}	1	1.60×10^{15}	375	<0.0001	significant
X_3	3.06×10^{6}	5.59×10^{5}	1.28×10^{14}	1	1.28×10^{14}	29.9	0.0003	significant
X_1X_2	-3.56×10^{6}	7.31×10^{5}	1.02×10^{14}	1	1.02×10^{14}	23.8	0.0006	significant
X_1X_3	9.77×10^{4}	7.31×10^{5}	7.64×10^{10}	1	7.64×10^{10}	0.018	0.8963	not significant
X_2X_3	-3.42×10^{6}	7.31×10^{5}	9.36×10^{13}	1	9.36×10^{13}	21.9	0.0009	significant
X_1^2	-2.09×10^{6}	5.45×10^{5}	6.28×10^{13}	1	6.28×10^{13}	14.7	0.0033	significant
X_2^2	-4.52×10^{6}	5.45×10^{5}	2.94×10^{14}	1	2.94×10^{14}	68.8	<0.0001	significant
X_3^2	-1.70×10^{6}	5.45×10^{5}	4.18×10^{13}	1	4.18×10^{13}	9.79	0.0107	significant
residual			4.27×10^{13}	10	4.27×10^{13}			
lack-of-fit			2.40×10^{13}	5	4.81×10^{12}	1.29	0.3949	not significant
pure error			1.87×10^{13}	5	3.74×10^{12}			
total			2.59×10^{15}	19				

dx.doi.org/10.1021/jf500959g | J. Agric. Food Chem. 2014, 62, 4276−4284

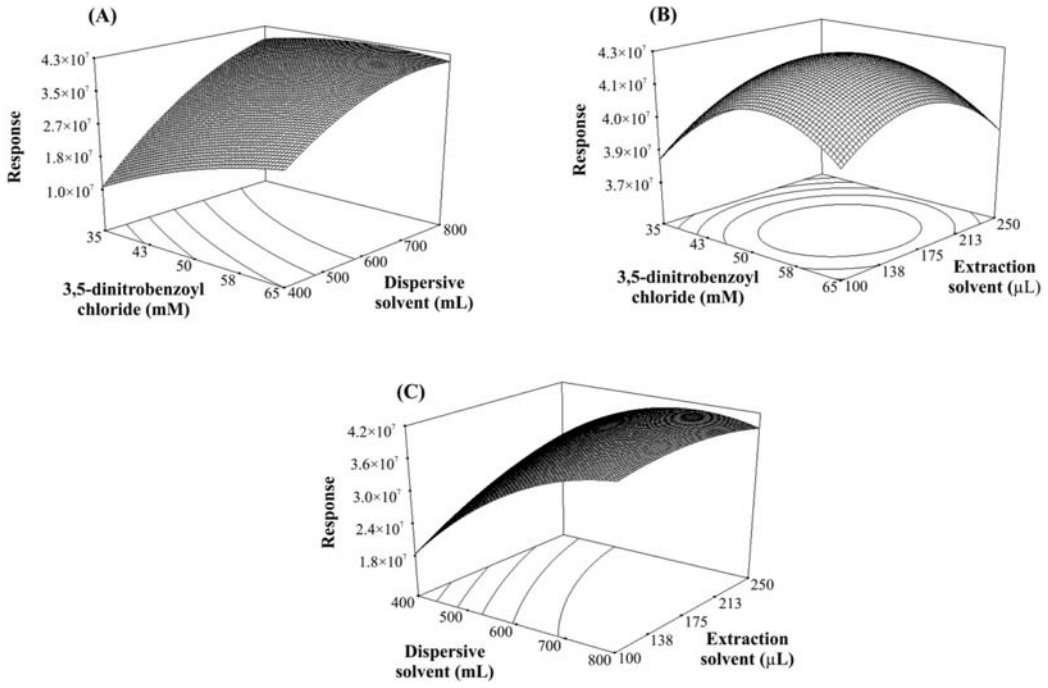

Figure 4. Response surface plots for the CCD: (A) concentration of 3,5-dinitrobenzoyl chloride and dispersive solvent volume, (B) concentration of 3,5-dinitrobenzoyl chloride and extraction solvent volume, and (C) dispersive solvent volume and extraction solvent volume.

combined effect of the 3,5-dinitrobenzoyl chloride concentration and extraction solvent volume, while Figure 4C shows the combined effect of the dispersive solvent and extraction solvent volumes.

An evaluation of the optimum combination of the three studied parameters was performed to maximize the response while reducing the extraction time. Desirability indices were achieved to maximize the response, and the following optimum conditions were selected: 56 mM 3,5-dinitrobenzoyl chloride, 680 μL of dispersive solvent, and 205 μL of carbon tetrachloride. Confirmatory experiments were conducted with the parameters selected by the experimental model. The obtained response of 3.82×10^6 was within the 95% prediction response interval (from 3.5×10^6 to 4.1×10^7), which indicates the adequacy of the obtained model given by the RSM. The optimization procedure enabled an enrichment of all polyamines in the aqueous extracts, resulting in a higher sensitivity, as shown in the chromatograms of Figure 5.

The use of the optimized 3,5-dinitrobenzoyl chloride concentration (56 mM) ensured a fast and efficient reaction. However, it also yielded some unwanted byproducts, which undesirably affected the analysis. To overcome this problem, the use of ultrasonication during the derivatization reaction was tested, and it proved to be effective in lowering the amount of byproducts, as also observed by Jia et al.[26] Thus, this procedure was adopted for further polyamine analyses.

Method Validation. Linearity, precision, intercept, and slope errors, LOQ, and LOD of the optimized analytical method were evaluated. Results are shown in Tables 2−4. Method validation was performed with standard solutions. The non-significant lack-of-fit obtained (calculated F values were lower than the tabulated value) for putrescine, cadaverine, spermidine, and spermine calibration curves proved their linearity in the 0.5−10.0 mg/L range. Moreover, correlation coefficients (R^2) of 0.9989 or higher were obtained (Table 2). Intra- and interday precisions for peak areas, expressed as

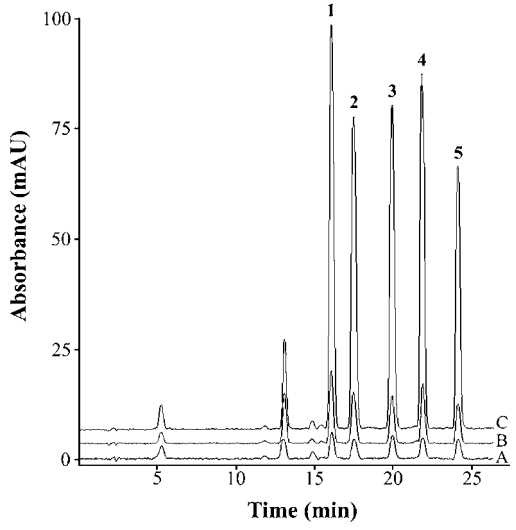

Figure 5. Chromatograms of method optimization for the standard concentration at 5 mg/L. (A) Before the optimization procedure. (B) After the derivatization optimization. (C) After the derivatization and DLLME optimization. Peaks: (1) putrescine, (2) cadaverine, (3) spermidine, (4) IS, and (5) spermine.

percent relative standard deviation (% RSD), ranged from 0.8 to 6.9% and from 3.0 to 10.3%, respectively (Table 3).

LOQ and LOD were expressed as micrograms per gram of plant food fresh weight considering a moisture content of 95, 87, 86, 91, 83, and 94% for lettuce, carrot, onion, cabbage, apple, and tomato, respectively. For all of the analyzed plant foods, the LOQs of putrescine, cadaverine, spermidine, and spermine ranged between 0.054 and 0.062, between 0.095 and 0.109, between 0.100 and 0.115, and between 0.123 and 0.141 μg/g, respectively. Similarly, the LODs of putrescine, cadaverine, spermidine, and spermine ranged between 0.016 and 0.018, between 0.029 and 0.033, between 0.030 and 0.034,

Table 2. Linear Range, Regression Equations, Correlation Coefficient (R^2), Intercept, and Slope Errors of the Optimized Method

compound	linear range (mg/L)	regression equation	R^2	intercept errors	slope errors
putrescine	0.5−10	$y = 0.2701x + 0.0216$	0.9997	0.0216−0.0514	0.270−0.276
cadaverine	0.5−10	$y = 0.2524x + 0.0196$	0.9993	0.0196−0.0689	0.252−0.262
spermidine	0.5−10	$y = 0.2601x + 0.0062$	0.9992	0.0062−0.0598	0.260−0.270
spermine	0.5−10	$y = 0.203x + 0.0297$	0.9989	0.0297−0.0810	0.203−0.213

Table 3. Intra- and Interday Precisions for Peak Areas Evaluated at Three Concentrations[a]

	intraday (n = 3)			interday (n = 3 × 5 days)		
compound	0.5 mg/L	2.5 mg/L	10 mg/L	0.5 mg/L	2.5 mg/L	10 mg/L
putrescine	4.1	3.1	1.6	5.1	4.0	3.5
cadaverine	3.9	2.2	0.8	4.6	3.9	3.0
spermidine	5.7	5.5	4.1	7.8	6.7	4.1
spermine	6.9	6.8	5.3	10.3	8.2	6.6

[a]Data are presented as % RSD.

Table 4. Unspiked Concentration, Spiked Concentration, Relative Standard Deviation (RSD, %), and Recovery Percentage (R, %) of Plant Food Samples[a]

		putrescine			cadaverine			spermidine			spermine		
plant food sample	spiking (μg/g)	found (μg/g)	RSD (%)	R (%)	found (μg/g)	RSD (%)	R (%)	found (μg/g)	RSD (%)	R (%)	found (μg/g)	RSD (%)	R (%)
lettuce	0	3.66	3.83	107.4	0.16	6.25	102.6	0.76	3.95	95.2	1.31	5.34	91.8
	2.5	6.35	3.46		2.72	4.41		3.14	5.10		3.61	4.99	
carrot	0	29.0	1.38	88.6	0.23	4.35	95.4	1.17	4.27	100.2	5.85	5.47	109.2
	2.5	31.2	2.88		2.61	4.21		3.68	4.89		8.58	6.64	
onion	0	6.39	3.91	104.4	1.86	5.38	93.8	0.24	4.17	110.5	6.29	5.56	88.8
	2.5	9.00	5.67		4.21	2.14		3.00	6.67		8.51	5.76	
cabbage	0	4.29	3.03	96.2	0.20	5.00	101.8	0.65	6.15	95.4	5.52	5.62	89.6
	2.5	6.70	3.43		2.75	2.55		3.04	3.95		7.76	5.67	
apple	0	3.52	1.14	86.4	0.42	7.14	97.0	0.58	8.62	90.2	1.87	6.95	81.7
	2.5	5.68	3.52		2.84	3.52		2.83	7.42		3.91	9.97	
tomato	0	34.5	3.19	114.2	0.18	5.56	103.3	0.90	6.67	94.2	1.23	8.13	91.2
	2.5	37.4	3.48		2.76	2.90		3.25	4.62		3.51	6.55	

[a]Data are presented as the mean (n = 3).

and between 0.037 and 0.042 μg/g, respectively. The LOD achievable with our method was significantly lower when compared to other methodologies[9,12,23,24,33−41] because of the efficiency of cleanup and pre-concentration procedures. It was 28−111-fold lower than the micellar electrokinetic capillary chromatography (MECK)−UV method employing derivatization with benzoyl chloride applied to plant foods.[8,33] In fact, our method was 6-fold more sensitive for the quantitation of putrescine and spermine than one of the most sensitive methods described, which relies on the use of SPE and tandem mass spectrometry for the quantitation of polyamines in fish[34] and lower than the LOD reported in plant analysis.[9,35] The stability of the derivatized and extracted polyamines was very good over the 24 h, with a mean RSD of only 2.2%. This is a clear advantage over *o*-phthaldialdehyde and dabsyl derivatization procedures.

Plant Food Sample Analysis. To assess the applicability of the proposed method, putrescine, cadaverine, spermidine, and spermine were determined in six plant food samples (lettuce, carrot, onion, cabbage, tomato, and apple) (Figure 6). All four polyamines, including cadaverine, which is not usually detected in plant foods, were quantified in the analyzed plant food samples (Table 4). Generally, putrescine was the most abundant polyamine, with values ranging between 3.52 and 34.5 μg/g. Spermine was the second most abundant polyamine, with mean contents of 1.31, 5.85, 6.29, 5.52, 1.87, and 1.23 μg/g in lettuce, carrot, onion, cabbage, apple, and tomato, respectively. The mean content of spermidine in the analyzed plant food samples ranged between 0.24 and 1.17 μg/g, whereas mean contents for cadaverine were 0.16, 0.23, 1.86, 0.20, 0.42, and 0.18 μg/g in lettuce, carrot, onion, cabbage, apple, and tomato, respectively. The recovery percentage of polyamines, evaluated in lettuce, carrot, onion, cabbage, tomato, and apple, was between 81.7 and 114.2% (Table 4). For each concentration, a Student's t test was performed for each type of plant food, and the comparison between the expected and experimental concentrations presented no statistical difference ($p > 0.05$), which confirmed the accuracy of the method in these different types of matrixes. The RSD from three independent extractions with or without polyamine fortification ranged from 1.14 to 9.97%, indicating that reproducible results were obtained.

Moreover, this method is also inexpensive and easy to perform, and the derivatized polyamines dissolved in acetonitrile could be stored for 24 h at 4 °C without significant decomposition. The present method was successfully applied to analyze polyamines in six different types of plant foods with a wide range of polyamine contents (from 0.16 to 34.5 μg/g).

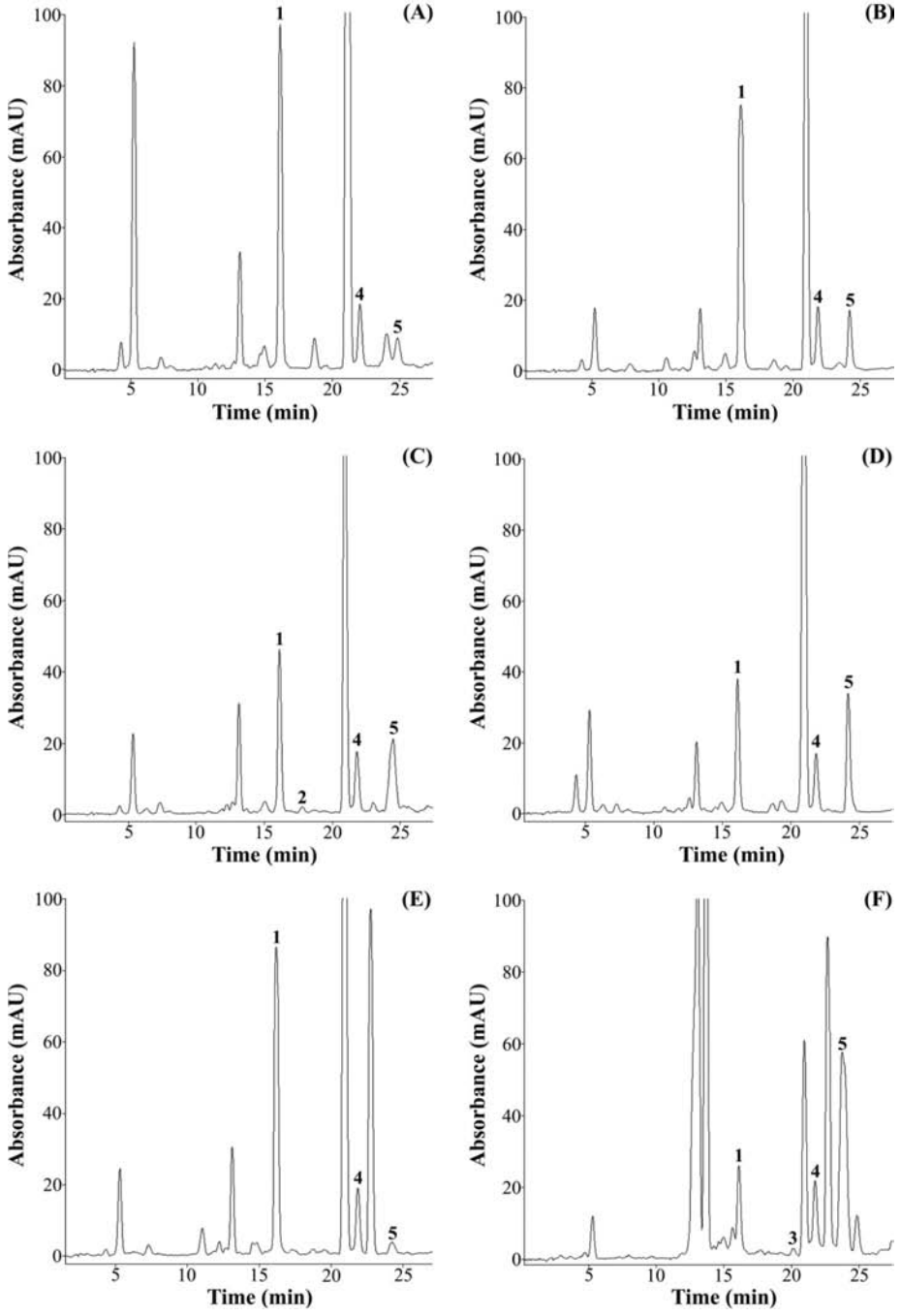

Figure 6. Representative chromatograms of plant food samples: (A) lettuce, (B) carrot, (C) onion, (D) cabbage, (E) tomato, and (F) apple. Peaks: (1) putrescine, (2) cadaverine, (3) spermidine, (4) IS, and (5) spermine.

The good recoveries of polyamines obtained in the analyses of plant food samples (81.7−114.2%) shown that the developed method has wide applicability and uses equipment easily available in quality control laboratories. Great precision was obtained, as observed from the low RSDs obtained in the six different plant foods.

■ ASSOCIATED CONTENT

Supporting Information

Coded and uncoded values of the independent variables of the CCD for the method optimization (Table S1) and LOD and LOQ (μg/g of fresh weight) of the optimized method for each plant food (Table S2). This material is available free of charge via the Internet at http://pubs.acs.org.

■ AUTHOR INFORMATION

Corresponding Author

*Telephone: +351-220428642. Fax: +351-226-093-390. E-mail: isabel.ferreira@ff.up.pt.

Funding

Edgar Pinto and Armindo Melo thank the Portuguese Foundation for Science and Technology (FCT) for their Grants SFRH/BD/67042/2009 and SFRH/BPD/86898/2012, respectively. This work received financial support from the European Union (FEDER funds through COMPETE) and

National Funds (FCT) through Project Pest-C/EQB/LA0006/2013. The work also received financial support from the European Union (FEDER funds) under the framework of QREN through Project NORTE-07-0124-FEDER-000069. To all financing sources, the authors are greatly indebted.

Notes

The authors declare no competing financial interest.

REFERENCES

(1) Fuell, C.; Elliott, K. A.; Hanfrey, C. C.; Franceschetti, M.; Michael, A. J. Polyamine biosynthetic diversity in plants and algae. *Plant Physiol. Biochem.* **2010**, *48*, 513−520.

(2) Kalač, P.; Krausová, P. A review of dietary polyamines: Formation, implications for growth and health and occurrence in foods. *Food Chem.* **2005**, *90*, 219−230.

(3) Kusano, T.; Berberich, T.; Tateda, C.; Takahashi, Y. Polyamines: Essential factors for growth and survival. *Planta* **2008**, *228*, 367−381.

(4) Larque, E.; Sabater-Molina, M.; Zamora, S. Biological significance of dietary polyamines. *Nutrition* **2007**, *23*, 87−95.

(5) Moinard, C.; Cynober, L.; de Bandt, J. P. Polyamines: Metabolism and implications in human diseases. *Clin. Nutr.* **2005**, *24*, 184−197.

(6) Soda, K. Polyamine intake, dietary pattern, and cardiovascular disease. *Med. Hypotheses* **2010**, *75*, 299−301.

(7) Bell, R. F.; Borzan, J.; Kalso, E.; Simonnet, G. Food, pain, and drugs: Does it matter what pain patients eat? *Pain* **2012**, *153*, 1993−1996.

(8) Kalač, P.; Křížek, M.; Pelikánová, T.; Langová, M.; Veškrna, O. Contents of polyamines in selected foods. *Food Chem.* **2005**, *90*, 561−564.

(9) Lavizzari, T.; Teresa Veciana-Nogués, M.; Bover-Cid, S.; Mariné-Font, A.; Carmen Vidal-Carou, M. Improved method for the determination of biogenic amines and polyamines in vegetable products by ion-pair high-performance liquid chromatography. *J. Chromatogr. A* **2006**, *1129*, 67−72.

(10) Lavizzari, T.; Veciana-Nogues, M. T.; Weingart, O.; Bover-Cid, S.; Marine-Font, A.; Vidal-Carou, M. C. Occurrence of biogenic amines and polyamines in spinach and changes during storage under refrigerator. *J. Agric. Food Chem.* **2007**, *55*, 9514−9519.

(11) Zhou, Q.; Yu, B. Changes in content of free, conjugated and bound polyamines and osmotic adjustment in adaptation of vetiver grass to water deficit. *Plant Physiol. Biochem.* **2010**, *48*, 417−425.

(12) Restuccia, D.; Spizzirri, U. G.; Puoci, F.; Cirillo, G.; Curcio, M.; Parisi, O. I.; Iemma, F.; Picci, N. A new method for the determination of biogenic amines in cheese by LC with evaporative light scattering detector. *Talanta* **2011**, *85*, 363−369.

(13) Mayr, C. M.; Schieberle, P. Development of stable isotope dilution assays for the simultaneous quantitation of biogenic amines and polyamines in foods by LC−MS/MS. *J. Agric. Food Chem.* **2012**, *60*, 3026−3032.

(14) Önal, A.; Tekkeli, S. E. K.; Önal, C. A review of the liquid chromatographic methods for the determination of biogenic amines in foods. *Food Chem.* **2013**, *138*, 509−515.

(15) Gomez-Alonso, S.; Hermosin-Gutierrez, I.; Garcia-Romero, E. Simultaneous HPLC analysis of biogenic amines, amino acids, and ammonium ion as aminoenone derivatives in wine and beer samples. *J. Agric. Food Chem.* **2007**, *55*, 608−613.

(16) Kirschbaum, J.; Rebscher, K.; Brückner, H. Liquid chromatographic determination of biogenic amines in fermented foods after derivatization with 3,5-dinitrobenzoyl chloride. *J. Chromatogr. A* **2000**, *881*, 517−530.

(17) Ali Awan, M.; Fleet, I.; Paul Thomas, C. L. Determination of biogenic diamines with a vaporisation derivatisation approach using solid-phase microextraction gas chromatography−mass spectrometry. *Food Chem.* **2008**, *111*, 462−468.

(18) Asensio-Ramos, M.; Ravelo-Pérez, L. M.; González-Curbelo, M. Á.; Hernández-Borges, J. Liquid phase microextraction applications in food analysis. *J. Chromatogr. A* **2011**, *1218*, 7415−7437.

(19) Rezaee, M.; Yamini, Y.; Faraji, M. Evolution of dispersive liquid−liquid microextraction method. *J. Chromatogr. A* **2010**, *1217*, 2342−2357.

(20) Zgoła-Grześkowiak, A.; Grześkowiak, T. Dispersive liquid−liquid microextraction. *TrAC, Trends Anal. Chem.* **2011**, *30*, 1382−1399.

(21) Zhang, N.; Wang, H.; Zhang, Z.-X.; Deng, Y.-H.; Zhang, H.-S. Sensitive determination of biogenic amines by capillary electrophoresis with a new fluorogenic reagent 3-(4-fluorobenzoyl)-2-quinolinecarboxaldehyde. *Talanta* **2008**, *76*, 791−797.

(22) Naguib, K.; Ayesh, A. M.; Shalaby, A. R. Studies on the determination of biogenic amines in foods. 1. Development of a TLC method for the determination of eight biogenic amines in fish. *J. Agric. Food Chem.* **1995**, *43*, 134−139.

(23) Cinquina, A. L.; Calí, A.; Longo, F.; Santis, L. D.; Severoni, A.; Abballe, F. Determination of biogenic amines in fish tissues by ion-exchange chromatography with conductivity detection. *J. Chromatogr. A* **2004**, *1032*, 73−77.

(24) Tahmouzi, S.; Khaksar, R.; Ghasemlou, M. Development and validation of an HPLC−FLD method for rapid determination of histamine in skipjack tuna fish (*Katsuwonus pelamis*). *Food Chem.* **2011**, *126*, 756−761.

(25) Melo, A.; Cunha, S. C.; Mansilha, C.; Aguiar, A.; Pinho, O.; Ferreira, I. M. P. L. V. O. Monitoring pesticide residues in greenhouse tomato by combining acetonitrile-based extraction with dispersive liquid−liquid microextraction followed by gas chromatography−mass spectrometry. *Food Chem.* **2012**, *135*, 1071−1077.

(26) Jia, S.; Ryu, Y.; Kwon, S. W.; Lee, J. An in situ benzoylation-dispersive liquid−liquid microextraction method based on solidification of floating organic droplets for determination of biogenic amines by liquid chromatography−ultraviolet analysis. *J. Chromatogr. A* **2013**, *1282*, 1−10.

(27) Huang, K.-J.; Wei, C.-Y.; Liu, W.-L.; Xie, W.-Z.; Zhang, J.-F.; Wang, W. Ultrasound-assisted dispersive liquid−liquid microextraction combined with high-performance liquid chromatography−fluorescence detection for sensitive determination of biogenic amines in rice wine samples. *J. Chromatogr. A* **2009**, *1216*, 6636−6641.

(28) Melo, A.; Aguiar, A.; Mansilha, C.; Pinho, O.; Ferreira, I. M. P. L. V. O. Optimisation of a solid-phase microextraction/HPLC/diode array method for multiple pesticide screening in lettuce. *Food Chem.* **2012**, *130*, 1090−1097.

(29) Miller, J. N.; Miller, J. C. *Statistics and Chemometrics for Analytical Chemistry*, 5th ed.; Pearson Education, Ltd.: Upper Saddle River, NJ, 2005.

(30) Consonni, V.; Ballabio, D.; Todeschini, R. Evaluation of model predictive ability by external validation techniques. *J. Chemom.* **2010**, *24*, 194−201.

(31) Mandenius, C. F.; Brundin, A. Bioprocess optimization using design-of-experiments methodology. *Biotechnol. Prog.* **2008**, *24*, 1191−1203.

(32) Khodadoust, S.; Hadjmohammadi, M. Determination of *N*-methylcarbamate insecticides in water samples using dispersive liquid−liquid microextraction and HPLC with the aid of experimental design and desirability function. *Anal. Chim. Acta* **2011**, *699*, 113−119.

(33) Křížek, M.; Pelikánová, T. Determination of seven biogenic amines in foods by micellar electrokinetic capillary chromatography. *J. Chromatogr. A* **1998**, *815*, 243−250.

(34) Sagratini, G.; Fernández-Franzón, M.; De Berardinis, F.; Font, G.; Vittori, S.; Mañes, J. Simultaneous determination of eight underivatised biogenic amines in fish by solid phase extraction and liquid chromatography−tandem mass spectrometry. *Food Chem.* **2012**, *132*, 537−543.

(35) Chiacchierini, E.; Restuccia, D.; Vinci, G. Evaluation of two different extraction methods for chromatographic determination of bioactive amines in tomato products. *Talanta* **2006**, *69*, 548−555.

(36) Gloria, M. B. A.; Tavares-Neto, J.; Labanca, R. A.; Carvalho, M. S. Influence of cultivar and germination on bioactive amines in soybeans (*Glycine max* L. Merril). *J. Agric. Food Chem.* **2005**, *53*, 7480−7485.

(37) Hernández-Jover, T.; Izquierdo-Pulido, M.; Veciana-Nogués, M. T.; Vidal-Carou, M. C. Ion-pair high-performance liquid chromatographic determination of biogenic amines in meat and meat products. *J. Agric. Food Chem.* **1996**, *44*, 2710−2715.
(38) Fiechter, G.; Sivec, G.; Mayer, H. K. Application of UHPLC for the simultaneous analysis of free amino acids and biogenic amines in ripened acid-curd cheeses. *J. Chromatogr. B: Anal. Technol. Biomed. Life Sci.* **2013**, *927*, 191−200.
(39) Mayer, H. K.; Fiechter, G.; Fischer, E. A new ultra-pressure liquid chromatography method for the determination of biogenic amines in cheese. *J. Chromatogr. A* **2010**, *1217*, 3251−3257.
(40) Dadáková, E.; Křížek, M.; Pelikánová, T. Determination of biogenic amines in foods using ultra-performance liquid chromatography (UPLC). *Food Chem.* **2009**, *116*, 365−370.
(41) De Mey, E.; Drabik-Markiewicz, G.; De Maere, H.; Peeters, M. C.; Derdelinckx, G.; Paelinck, H.; Kowalska, T. Dabsyl derivatisation as an alternative for dansylation in the detection of biogenic amines in fermented meat products by reversed phase high performance liquid chromatography. *Food Chem.* **2012**, *130*, 1017−1023.

JOURNAL OF AGRICULTURAL AND FOOD CHEMISTRY

Article

pubs.acs.org/JAFC

Intestinal Anti-inflammatory Effects of Oligosaccharides Derived from Lactulose in the Trinitrobenzenesulfonic Acid Model of Rat Colitis

Francesca Algieri,[†,∥] Alba Rodríguez-Nogales,[†,∥] Natividad Garrido-Mesa,[†] Teresa Vezza,[†] José Garrido-Mesa,[†] M. Pilar Utrilla,[†] Antonia Montilla,[§] Alejandra Cardelle-Cobas,[§] Agustín Olano,[§] Nieves Corzo,[§] Eduardo Guerra-Hernández,[‡] Antonio Zarzuelo,[†] M. Elena Rodriguez-Cabezas,[†] and Julio Galvez*[,†]

[†]CIBER-EHD, Department of Pharmacology, ibs.GRANADA, Center for Biomedical Research (CIBM), University of Granada, Granada, Spain

[§]Departamento de Bioactividad y Análisis de Alimentos, Instituto de Investigación en Ciencias de la Alimentación CIAL (CSIC-UAM), Madrid, Spain

[‡]Department of Nutrition and Bromatology, University of Granada, Granada, Spain

Supporting Information

ABSTRACT: Intestinal microbiota modulation is becoming an interesting approach to manage inflammatory bowel disease and can be achieved by the administration of prebiotics. Previous studies showed the intestinal anti-inflammatory effects of the prebiotic lactulose. The aim of the present study was to test the preventative effects of oligosaccharides derived from lactulose with prebiotic properties (OsLu) in the trinitrobenzenesulfonic acid model of rat colitis and compare them with those of lactulose. Both treatments modified bacterial profile in intestinal contents, increasing the bifidobacteria and lactobacilli counts and up-regulating the production of short-chain fatty acids, although OsLu generated a larger amount. OsLu also inhibited to a greater extent different pro-inflammatory markers such as interleukins (IL) 1, 6, 12, and 23 and chemokines (MCP-1 and CINC-1). However, both prebiotics equally restored colonic epithelial integrity, evaluated both with a histological score (OsLu, 9.8 ± 2.2; and lactulose, 12.1 ± 2.1, vs colitic control, 27.3 ± 3.3) and by measuring several key proteins of the mucosal barrier (MUC-2, MUC-3, and TTF-3). OsLu effect was also associated with an inhibition of iNOS expression and a reduction of Th17 cell activity in the inflamed tissue that facilitated the intestinal mucosa barrier recovery. In conclusion, OsLu showed a better anti-inflammatory profile than lactulose in this model of experimental colitis.

KEYWORDS: *intestinal anti-inflammatory effect, lactulose-derived oligosaccharides, prebiotic, TNBS rat colitis*

INTRODUCTION

Inflammatory bowel disease (IBD) usually refers to two related conditions, ulcerative colitis (UC) and Crohn's disease, characterized by chronic and spontaneously relapsing inflammation. Among the clinical symptoms of IBD are abdominal pain, diarrhea, rectal bleeding, malaise, and weight loss. Although the exact etiology of IBD remains unknown, both inflammatory conditions have similar pathophysiology background, and several studies indicate that a combination of factors such as genetic susceptibility, intestinal microbiota, dietary factors, intestinal barrier dysfunction, and an abnormal immune response to intestinal bacteria leads to chronic intestinal inflammation.[1] In fact, IBD may be considered as a maladaptation of host commensal mutualism that promotes intestinal microbiota imbalance, termed dysbiosis. It is typically characterized by a decline in bacterial diversity, with a relative predominance of potential pathogenic bacteria and an insufficient amount of protective species, which leads to chronic intestinal inflammation.[2] As a consequence, an interesting approach to IBD management could be a change of the microbiota, in a preventative and/or therapeutic manner, to protect the intestine against inflammation, stimulate tissue repair, and restore the homeostasis in genetically susceptible hosts. This could explain, at least partially, the remission that sometimes is achieved in intestinal inflammation after treatment with antibiotics such as metronidazole or ciprofloxacin.[3] Unfortunately, the prolonged use of antibiotics in the management of these intestinal conditions is limited due to the risk of severe adverse effects. For this reason, it is very important to find other effective strategies focused on microbiota balance restoration, with a better safety profile. This could be the case of prebiotics, which are defined as selectively fermented ingredients that allow specific changes, in both the composition and/or activity in the gastrointestinal microbiota, that confers benefits upon host well being and health.[4]

The efficacy of the prebiotics on intestinal inflammation has been most extensively studied in experimental colitis models, which, in addition, have provided insight into possible

Received: June 19, 2013
Revised: April 15, 2014
Accepted: April 27, 2014
Published: April 27, 2014

ACS Publications © 2014 American Chemical Society

mechanisms involved in their intestine anti-inflammatory properties.[5] One of these consists in the modification of the intestinal microbial composition by stimulating the growth of commensal protective bacteria and therefore enhancing resistance to disease-inducing bacteria colonization and contributing to colitis improvement. Besides, the promotion of protective bacteria growth can result in up-regulation of epithelial defense mechanisms that protect against intestinal inflammation. Prebiotics are fermented by anaerobic colonic microbiota, and there is an increase of short-chain fatty acids (SCFA), mainly acetate, butyrate, and propionate, that may also improve colitis condition; thus, butyrate is the major energy source for colonocytes and has an essential role in the maturation of colonic epithelium, regeneration of mucosa, and induction of cell differentiation.[6] Moreover, the impact of prebiotics on the host immune system can also contribute to their beneficial effects. In this regard, it has been described that prebiotics have the ability to modulate the production of pro- and anti-inflammatory cytokines and, thus, lessen the intestinal inflammation.

Many different substances are claimed to be prebiotics, but mainly carbohydrates have proven to display prebiotic properties in humans.[4,7] Lactulose is a synthetic disaccharide composed of fructose and galactose primarily used as a laxative and for the treatment of portal-systemic encephalopathy.[8−10] Following oral administration, intact lactulose reaches the colon, where it is split by bacteria in the distal small intestine and colon, lowering fecal pH, promoting beneficial microbiota growth such as bifidobacteria and lactobacilli, and inhibiting pathogenic bacteria expansion like *Salmonella*.[11]

In fact, preclinical studies have demonstrated a protective effect of lactulose in rodent models of colitis.[11−13] To date, there is only one pilot study reported in humans, in which oral lactulose was administered as adjuvant therapy to standard medication. The study concluded that prebiotic consumption did not ameliorate clinical activity, endoscopic score, or immunohistochemical parameters, although it improved the quality of life of UC patients receiving the prebiotic.[14] Furthermore, and although generally considered safe and innocuous, lactulose may be associated with several adverse events, including abdominal discomfort, abdominal distension, increased intestinal gas production, and flatulence, due to the fact that it is mainly consumed by the bacteria in the proximal colon.[15] All of these facts could justify the search for alternatives to lactulose with modified prebiotic properties, thus achieving a higher efficacy in intestinal inflammation with fewer side effects.

Oligosaccharides derived from lactulose (OsLu) are new bioactive carbohydrates synthesized with the aim of obtaining more slowly fermenting prebiotics able to reach the distal colon unhydrolyzed.[16−18] Different in vitro fermentation assays using pure cultures as well as fecal inoculums have demonstrated that when these oligosaccharides were used as sole carbon source, there was a stimulation of bifidobacteria and lactobacilli growth. Thus, when long incubation periods were used in fermentative assays, OsLu showed higher prebiotic index values than the native disaccharide.[19,20] These investigations proved that OsLu improved lactulose prebiotic properties and, therefore, it is reasonable to suppose that OsLu could present a higher efficacy in intestinal inflammation. More recently, the modulatory effects of OsLu on microbial composition in the cecum and colon of growing rats have been evaluated, with particular emphasis on their bifidogenic effect, showing that OsLu produced a significant and selective increase of *Bifidobacterium animalis* in these intestine locations.[21] All of these findings support a prebiotic role of galactosyl-fructoses in functional foods.

The aim of the present study was to test the preventative effects of OsLu in the trinitrobenzenesulfonic acid (TNBS) model of rat colitis, a well-established model of intestinal inflammation with some resemblance to human IBD,[22] and compare its efficacy with that of its parent compound, lactulose. Special attention was paid to their effects on the expression of some of the inflammatory mediators, such as pro-inflammatory cytokines (interleukins (IL)-1β, IL-6, IL-12, IL-17, and IL-23), chemokines (cytokine-induced neutrophil chemoattractant (CINC)-1 and monocyte chemotactic protein (MCP)-1), and an inducible enzyme (inducible nitric oxide synthase (iNOS)), as well as different markers of epithelial integrity in the mucosa, such as the mucins MUC-2 and MUC-3 and the protein trefoil factor (TFF)-3. The prebiotic capacity was assessed by measuring the production of SCFA and the effects on the microbiota composition. In summary, OsLu therapeutic efficacy was greater than that of lactulose, maybe due to its better immunomodulatory properties together with a superior capacity of SCFA production.

MATERIALS AND METHODS

This study was carried out in accordance with the *Guide for the Care and Use of Laboratory Animals* as promulgated by the National Institutes of Health. The experimental protocol was approved by the Commission of Ethics in Animal Experimentation (Protocol CEEA 2010-286) of the University of Granada (Spain).

Reagents and Synthesis of Oligosaccharides Derived from Lactulose (OsLu). All chemicals were obtained from Sigma Chemical (Madrid, Spain), unless otherwise stated. Glutathione reductase was provided by Boehringer Mannheim (Barcelona, Spain). A commercial preparation Duphalac (Abbott Healthcare, Barcelona, Spain), which contains 670 g/L lactulose, was used as control and to synthesize OsLu. Enzymatic reactions have been performed at 50 °C and pH 6.5 using a β-galactosidase from *Aspergillus oryzae* (16 Ud/mL) in an orbital shaker at 300 rpm for 24 h. Afterward, samples were immediately immersed in boiling water for 10 min to inactivate the enzyme. Then, the mixture of oligosaccharides was treated with yeasts to eliminate monosaccharides following the method of Sanz et al.,[23] with some modifications. Briefly, the oligosaccharide reaction mixture 20% (w/v) was treated with fresh *Saccharomyces cerevisiae* 1.5% (w/v) (Levital, Panibérica de Levadura, Valladolid, Spain) at 30 °C for 48 h in an orbital shaker (300 rpm) and submitted to vacuum filtration to remove the yeasts. Sample was concentrated at 38−40 °C in a rotary evaporator (Büchi Labortechnik AG, Flawil, Switzerland). Mono- and disaccharides as well as OsLu were analyzed by GC-FID.[24] Degree of polymerization (DP) of the oligosaccharides found in the purified fraction from the synthesis mixture was also determined by matrix-assisted laser desorption ionization time-of-flight mass spectrometry (MALDI-TOF-MS). Before yeast treatment, the transglycosylation mixtures contained 76% sugars, which corresponded to 40% monosaccharides, 6% lactulose, and 30% OsLu. After yeast treatment, the composition of mixtures was 28% of monosaccharides, 12% lactulose, and 36% OsLu (17% disaccharides, 13% trisaccharides, 5% tetrasaccharides, and 1% pentasaccharides. MALDI-TOF-MS analysis allowed detection of oligosaccharides with a higher DP of 6, 7, or 8, which could not be quantified by gas chromatography. Also, another analysis of OsLu showed the presence 5% salts and 1% nitrogen with a dry matter of 82%.

Experimental Design. Female Wistar rats (180−200 g) obtained from Janvier (St Berthevin Cedex, France) were housed individually in Makrolon cages, maintained in an air-conditioned atmosphere with a 12 h light−dark cycle, and provided with free access to tap water and food. The rats were randomly assigned to four groups (n = 10); two of

them (noncolitic and control groups) received tap water, and the others (treated groups) were given lactulose or OsLu in the drinking water, daily prepared, at the concentration of 2.5% (w/v) for 3 weeks. The average rat intake was approximately of 0.25 g/day (the mean water intake was 10.2 ± 0.9 mL/rat and day, without showing differences among groups). This dose was equivalent to that used in a previous study with lactulose in the same experimental model of rat colitis.[12]

Two weeks after the start of the experiment, the rats were fasted overnight and rendered colitic as previously described.[12] Briefly, they were anaesthetized with isofluorane and given 10 mg of TNBS dissolved in 0.25 mL of 50% ethanol (v/v) by means of a Teflon cannula inserted 8 cm through the anus. During and after TNBS administration, the rats were kept in a head-down position until they recovered from the anesthetic and were then returned to their cages. Rats from the noncolitic group were administered intracolonically 0.25 mL of phosphate-buffered saline instead of TNBS. All rats were killed with an overdose of halothane 1 week after colitis induction.

In another set of experiments, the efficacy of both lactulose and OsLu was evaluated in the same experimental model for a longer period of time, 3 weeks. In this assay, a second dose of 10 mg of TNBS dissolved in 50% ethanol was administered 2 weeks after the initial TNBS colonic instillation, in an attempt to mimic the relapses common in human IBD. Ten animals from each colitic group (control and prebiotic treated) and five from the noncolitic group were sacrificed after 1, 2, and 3 weeks of colitis induction, so the efficacy of OsLu after 1 week was performed twice.

Assessment of Colonic Damage. The body weight and water and food intakes were recorded daily throughout the experiment. Once the rats were sacrificed, the colon was removed aseptically and placed on an ice-cold plate and longitudinally opened, and luminal contents were collected for the microbiological studies (see below). Afterward, the colonic segment was cleaned of fat and mesentery and blotted on filter paper; each specimen was weighed and its length measured under a constant load (2 g). The colon was scored for macroscopically visible damage on a 0−10 scale by two observers unaware of the treatment, according to the criteria previously reported,[12] which take into account the extent as well as the severity of colonic damage. Representative whole gut specimens (0.5 cm^2) were taken from a region of the inflamed colon corresponding to the adjacent segment to the gross macroscopic damage and were fixed in 4% buffered formaldehyde for the histological studies. Equivalent colonic segments were also obtained from the noncolitic group. The colon was subsequently minced, aliquoted, and kept frozen at −80 °C until biochemical determinations and RNA extraction were performed.

For the histological studies, cross sections were selected and embedded in paraffin. Full-thickness sections of 5 μm were obtained at different levels and stained with hematoxylin and eosin. The histological damage was evaluated by a pathologist observer, who was blinded to the experimental groups, according to the criteria previously described by Arribas et al.[25]

Myeloperoxidase activity (MPO) was measured according to the technique previously described,[26] and the results were expressed as MPO units per gram of wet tissue; one unit of MPO activity was defined as that degrading 1 μmol of hydrogen peroxide per minute at 25 °C. Total glutathione content (GSH) was quantified with the recycling assay,[27] and the results were expressed as nanomoles per gram of wet tissue.

The analysis of gene expression in the colonic samples was performed by real-time quantitative PCR (RT-qPCR). For this purpose total RNA from colonic samples was isolated using Trizol following the manufacturer's protocol. All RNA samples were quantified with the Thermo Scientific NanoDrop 2000 spectrophotometer, and 2 μg of RNA was reverse transcribed using oligo(dT) primers (Promega, Southampton, UK). RT-qPCR amplification and detection were performed on optical grade 48-well plates in an Eco Real-Time PCR System (Illumina, San Diego, CA, USA) with 20 ng of cDNA, the KAPA SYBR FAST qPCR Master Mix (Kapa Biosystems, Inc., Wilmington, MA, USA), and specific primers at their annealing temperature (T_a) (Table 1). To normalize mRNA expression, the expression of the housekeeping gene, glyceraldehyde-3-phosphate dehydrogenase (GAPDH), was measured. The mRNA relative quantitation was calculated using the ΔΔCt method.

Table 1. Primer Sequences Used in Real-Time PCR (RT-qPCR) Assays in Colonic Tissue

gene	sequence (3′−5′)	annealing temperature (°C)
GAPDH	FW: CCATCACCATCTTCCAGGAG RV: CCTGCTTCACCACCTTCTTG	60
IL-1β	FW: GATCTTTGAAGAAGAGCCCG RV: AACTATGTCCCGACCATTGC	59
IL-6	FW: CTTCCAGCCAGTTGCCTTCTTG RV: TGGTCTGTTGTGGGTGGTATCC	60
IL-12	FW: ATCCAGTGTGGTGATGGTTGTG RV: TGTCCGAGTCCAGCAGGTG	60
IL-17	FW: TGGACTCTGAGCCGCAATGAGG RV: GACGCATGGCGGACAATAGAGG	60
IL-23	FW: ATCCAGTGTGGTGATGGTTGTG RV: TGTCCGAGTCCAGCAGGTG	60
iNOS	FW: AAGAGACGCACAGGCAGAGG RV: AGCAGGCACACGCAATGATG	60
CINC-1	FW: CCGAAGTCATAGCCACACTCAAG RV: TCACCAGACAGACGCCATCG	60
MCP-1	FW: TCTTCCTCCACCACTATGC RV: TCTCCAGCCGACTCFATTG	60
TFF-3	FW: ATGGAGACCAGAGCCTTCTG RV: ACAGCCTTGTGCTGACTGTA	59
MUC-2	FW: ACCACCATTACCACCACCTCAG RV: CGATCACCACCATTGCCACTG	60
MUC-3	FW: CACAAAGGCAAGAGTCCAGA RV: ACTGTCCTTGGTGCTGCTGAATG	60

Microbial Analysis of the Colonic Contents. For DNA extraction, samples from colonic contents were diluted 1:12 (w/v) in the lysis buffer ASL provided by the QIAamp DNA stool mini kit (Qiagen, Hilden, Germany), according to the manufacturer's instructions. The suspensions were transferred to a Lysing Matrix E tube that contained a mixture of ceramic and silica particles designed to efficiently lyse microorganisms (Qiagen). Tubes were shaken in a Precellys apparatus (VWR, Villeurbanne, France) at 5.5 rpm for 30 s twice. DNA was then extracted by using a QIAamp DNA stool minikit from Qiagen, as recommended by the manufacturer (protocol for isolation of DNA for pathogen detection), except that a supplemental mixture of enzymes (mutanolysin at 90 U and lysozyme at 9 mg/mL) was added to the lysis buffer. RT-qPCR was used to characterize the bacterial DNA present in the colonic content samples as reported previously.[28] For this purpose, a series of genus-specific primer pairs

was used (Table 2). PCR amplification and detection were performed on optical grade 48-well plates in an Eco Real-Time PCR System (Illumina). In this case, each reaction mixture (10 μL) was composed of 5 μL of KAPA SYBR FAST qPCR Master Mix (Kapa Biosystems, Inc.), 0.25 μL of each specific primer at a concentration of 10 μM, and 2 μL of DNA template. Standard curves were created using serial 10-fold dilutions of bacterial DNA extracted from pure cultures with a bacterial population ranging from 2 to 9 log colony-forming units (CFUs), as determined by plate counts. One strain belonging to each of the bacterial genera or groups targeted in this study was used to construct the standard curve. More specifically, the strains from which the DNA was extracted were the following: *Bifidobacterium longum* CECT 4551, *Clostridium coccoides* DSMZ 935, *Bacteroides fragilis* DSMZ 2151, and *Lactobacillus salivarius* CECT 2197. All of them were obtained from the Spanish Collection of Type Cultures (CECT) or the German Collection of Microorganisms and Cell Cultures (DSMZ).

Table 2. Primer Sequences Used for Microbiological Analysis in Real-Time PCR (RT-qPCR) Assays in the Colonic Contents

target bacterial group	sequence (5′−3′)	annealing temperature (°C)
Bacteroides	g-Bfra-F: ATAGCCTTTCGAAAGRAAGAT	50
	g-Bfra-R: CCAGTATCAACTGCAATTTTA	
Clostridium cluster XIVa−XIVb	g-Ccoc-F: AAATGACGGTACCTGACTAA	50
	g-Ccoc-R: CTTTGAGTTTCATTCTTGCGAA	
Bifidobacterium	g-Bifid-F: CTCCTGGAAACGGGTGG	50
	g-Bifid-R: GGTGTTCTTCCCGATATCTACA	
Lactobacillus	Lab 159: GGAAACAG(A/G) TGCTAATACCG	61
	Lab 677: CACCGCTACACATGGAG	

Short-Chain Fatty Acid (SCFA) Determinations. To quantify the SCFA concentrations in the colonic luminal contents, the samples were homogenized with 150 mM $NaHCO_3$ (pH 7.8) (1:5 w/v) in an argon atmosphere. Samples were incubated for 24 h at 37 °C and stored at −80 °C until the extraction. To extract the SCFAs, 50 μL of the internal standard 2-methylvaleric acid (100 mM), 10 μL of sulfuric acid, and 0.3 mL of chloroform were added to 1 mL of the homogenate and, then, centrifuged at 10000*g* for 5 min at 4 °C. The organic layer was dehydrated with sodium anhydrous sulfate and centrifuged at 10000*g* for 5 min at 4 °C. One microliter of the supernatant was injected into a gas chromatograph (PerkinElmer Autosystem GC-FID, Waltham, MA, USA) equipped with a capillary column (CPWAX 52CB, 60 m × 0.25 mm, 0.25 μm, Varian, Middelburg, The Netherlands) and connected to a Star Chromatography WorkStation program (version 6, Varian) to quantify the samples. Operating conditions were as follows: injector, 275 °C; detector, 300 °C; initial column temperature, 90 °C for 0.1 min then increasing at 15 °C/min to 245 °C and held for 4 min at 245 °C. The flow of carrier gas (nitrogen) was 1 mL/min. The gas chromatography system had a split ratio 1:33. Acetate, propionate, and butyrate concentrations between 0.30 and 60 mM were used to make the standard curve. A linear relationship was found between the peak area ratio SCFA/IS using the same protocol as that for samples.

Statistics. All results are expressed as the mean ± SEM. Differences between means were tested for statistical significance using a one-way analysis of variance (ANOVA) with the Tukey post hoc test. Differences between proportions were analyzed with the chi-squared test. All statistical analyses were carried out with GraphPad Prism version 5.0 (La Jolla, CA, USA), with statistical significance set at $P < 0.05$.

RESULTS

Preventative Effects of Lactulose and OsLu on TNBS Rat Colitis. The administration of either lactulose or OsLu for 2 weeks did not induce any symptoms of diarrhea or significantly affect weight evolution. However, once the colitis was induced, both groups of treated rats showed an overall lower impact of TNBS-induced colonic damage compared to the TNBS control group. The anti-inflammatory effect was evidenced macroscopically by a significantly lower colonic damage score than that of control rats ($P < 0.05$), with a significant reduction in the extent of colonic necrosis and/or inflammation induced by the administration of TNBS/ethanol (Table 3). The weight/length ratio was increased significantly in colitic rats as a consequence of the inflammatory process when compared with noncolitic rats, and no significant differences were observed among the two treated groups and the corresponding colitic control (Table 3).

The histological evaluation of the colonic segments confirmed the intestinal anti-inflammatory effect of both lactulose and OsLu (Figure 1). The colonic samples from the untreated colitic control group showed extensive ulceration of the mucosa that typically affected >75% of the surface. Also, severe inflammation that involved all of the intestinal layers was observed, and it was associated with diffuse leukocyte infiltration, mainly composed of neutrophils in the mucosa layer and, to a lesser extent, lymphocytes in the submucosa. In addition, the inflammatory process was associated with severe goblet cell depletion (Figure 1B). In this group of rats, the grade of lesion was considered as severe, with a score value (mean ± SEM) of 27.3 ± 3.3 (Figure 1E). On the contrary, the histological assessment of the colonic specimens from rats treated with either lactulose (Figure 1C) or OsLu (Figure 1D) showed an evident recovery of the colonic tissue, displaying a significantly reduced score in comparison with untreated colitic rats. Thus, most of the samples revealed a restoration of the

Table 3. Effects of Lactulose and Oligosaccharides Derived from Lactulose (OsLu) on Colonic Macroscopic Damage Score, Weight/Length Ratio, Myeloperoxidase (MPO) Activity, and Glutathione (GSH) Content in TNBS Experimental Rat Colitis[a]

group (n = 10)	damage score (0−10)	weight/length (mg/cm)	MPO (mU/g tissue)	GSH (nmol/g tissue)
noncolitic	0	63.9 ± 1.9	14.5 ± 1.4	1878 ± 29
TNBS control	7.9 ± 0.2	175.8 ± 9.8	616.5 ± 67.6	603 ± 91
lactulose	7.1 ± 0.2*	211.9 ± 26.7	355.5 ± 78.1*	871 ± 96*
OsLu	6.3 ± 0.3*#	156.8 ± 8.9#	335.7 ± 55.6*	878 ± 99*

[a]Data are expressed as means ± SEM. *, $P < 0.05$ vs TNBS control group. #, $P < 0.05$ vs Lactulose-treated group. All colitic groups statistically differ from the noncolitic group ($P < 0.05$).

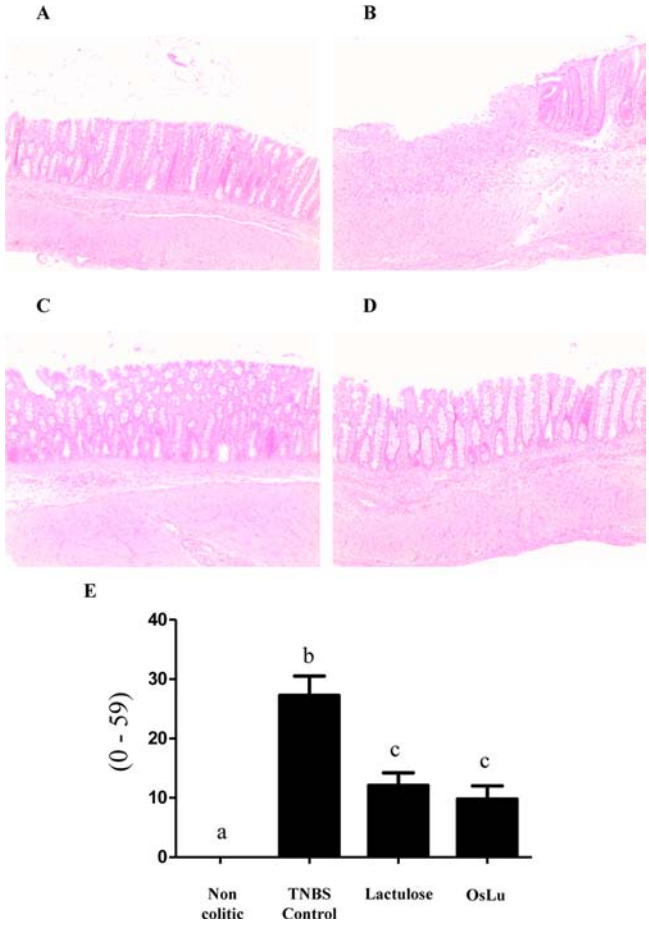

Figure 1. Histological sections of colonic tissue stained with hematoxylin and eosin showing the effects of lactulose and oligosaccharides derived from lactulose (OsLu) in TNBS rat colitis 1 week after damage induction: (A) noncolitic; (B) TNBS-control; (C) lactulose; (D) oligosaccharides derived from lactulose (OsLu); (E) microscopic score assigned according to the criteria previously described.[31] Data (n = 10 per group) are expressed as means ± SEM; groups with different letters statistically differ ($P < 0.05$).

epithelial cell layer, a maximum of only 25% of the epithelium being affected in contrast to the extensive ulceration observed in TNBS control group. In addition, goblet cells appeared replenished with their mucin content, and it a reduction in the inflammatory infiltrate was also observed, which was slight to moderate with a patchy distribution.

The intestinal anti-inflammatory effect was confirmed biochemically, because both treated groups showed significantly reduced colonic MPO activity (Table 3), which agrees with the reduction of neutrophil infiltration observed in the histological study and thus demonstrates the intestinal anti-inflammatory effect of the treatment.[29] In addition, the administration of lactulose or OsLu partially restored colonic glutathione content, a tripeptide with antioxidant properties, which was depleted in colitic rats as a consequence of the colonic oxidative stress induced by the inflammatory process, similar to that previously reported in this model of experimental colitis[12] (Table 3).

The colonic inflammatory status in control colitic rats was also characterized by an increased expression of the different pro-inflammatory markers evaluated, including the cytokines IL-1β, IL-6, IL-12, IL-17, and IL-23, the chemokines CINC-1 and MCP-1, and the inducible enzyme iNOS, in comparison with the noncolitic group. The evaluation of the cytokines revealed that the pretreatment of colitic rats with OsLu was able to significantly reduce the expression of all of them, whereas lactulose administration decreased the expression of only IL-6 in the colonic tissue, without showing statistical differences with the other cytokines assayed in comparison with untreated colitic rats (Figure 2). These results suggest that the amelioration of the altered immune response that characterizes the colonic inflammatory process is involved in the beneficial effect observed in both treated groups, but OsLu showed a higher efficacy than lactulose. Similarly, only the treatment of colitic rats with OsLu resulted in a significant reduction of the expression of colonic iNOS (Figure 2) and the chemokines CINC-1 and MCP-1 (Figure 3), which could support the lower infiltration of either neutrophils and macrophages in the inflamed tissue, that was evidenced both biochemically and histologically. Of note, both lactulose and OsLu managed to completely restore the expression of proteins involved in colonic epithelial integrity (MUC-2, MUC-3, and TFF-3), which were significantly reduced in colitic rats when compared to healthy ones (Figure 3) and could promote the recovery of the epithelial layer observed in the histological studies.

Effects of Lactulose and OsLu on TNBS-Reactivated Rat Colitis. In this assay the impact of a longer prebiotic treatment was evaluated. Also, and to simulate the "flare-ups" that occur in human IBD, a second intracolonic dose of 10 mg of TNBS in ethanol was administered 2 weeks after the first administration, which resulted in a reactivation of the colonic inflammatory process. The results confirmed the intestine anti-inflammatory effects exerted by lactulose or OsLu in this experimental model of colitis at the different time points evaluated. Thus, macroscopically, both compounds were able to significantly reduce the colonic score and weight/length ratio 1 and 2 weeks after the first colonic insult, as well as 1 week after the second TNBS administration (Table 4). These beneficial effects were confirmed biochemically by a reduction in the colonic MPO activity, thus reflecting a lower leukocyte infiltration, which was significant for all treated groups at the different time points evaluated, except for lactulose 1 week after reactivation of the inflammatory process (Figure 4). When the colonic oxidative status was assessed by glutathione content determination, both lactulose and OsLu were able to significantly reduce the depletion of this peptide 1 week after the first administration of TNBS, whereas only the lactulose derivative OsLu was able to significantly restore its colonic content after the reactivation of colonic damage (Figure 4).

The evaluation of the different biochemical markers by qPCR confirmed the results described above, for both lactulose and OsLu, when the inflammatory process was evaluated 1 week after the first administration of TNBS. The evaluation after 2 weeks revealed that the expression of the pro-inflammatory cytokines and chemokines was reduced in the control colitic group in comparison with the data observed in the same group at the first week, although most of them were still significantly higher than in healthy rats. However, the evaluation of the proteins related with the epithelial integrity (MUC-2, MUC-3, and TFF-3) revealed that only MUC-2 showed a significant reduced expression in comparison with noncolitic rats (Figures 5 and 6). Because the amelioration of the colonic inflammatory process took place at this time due to its normal resolution, the beneficial effects exerted by the treatments were less evident than in the first week of treatment. In fact, these were noticeable for both compounds when IL-6 or IL-17 was

dx.doi.org/10.1021/jf500678p | J. Agric. Food Chem. 2014, 62, 4285−4297

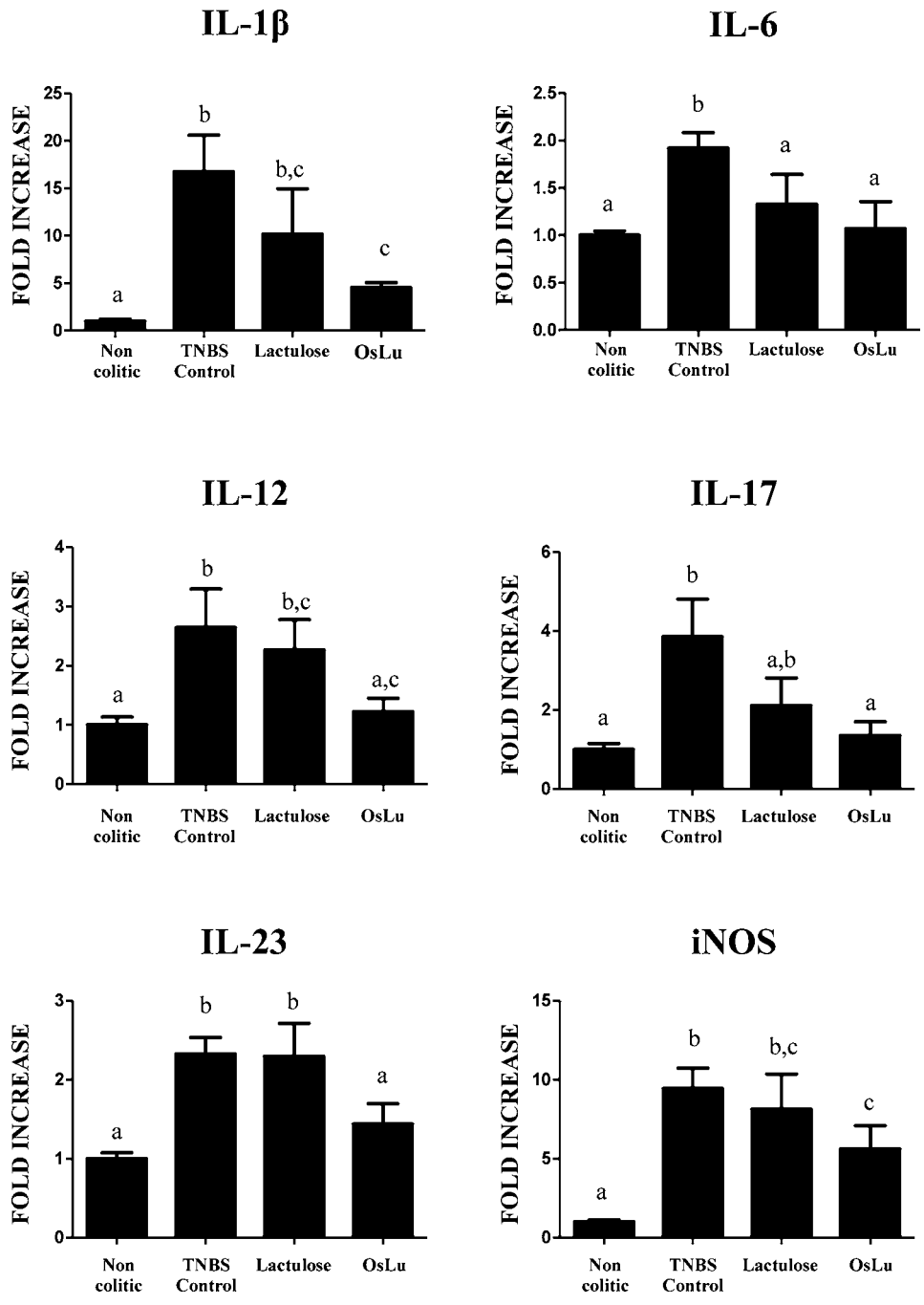

Figure 2. Effects of lactulose and oligosaccharides derived from lactulose (OsLu) on the colonic expression of the cytokines IL-1β, IL-6, IL-12, IL-17, and IL-23 and inducible nitric oxide synthase (iNOS) analyzed by RT-PCR in TNBS rat colitis 1 week after damage induction. Data (n = 10 per group) are expressed as means ± SEM; groups with different letters statistically differ (P < 0.05).

considered and only for OsLu when IL-12 or the chemokines MCP-1 and CINC-1 or the mucin MUC-2 was evaluated (Figures 5 and 6).

The reactivation of the inflammatory process typically resulted in a new increment of the expression of most of the pro-inflammatory cytokines, including IL-1β, IL-6, IL-12, and IL-23, as well as for iNOS, together with a reduction of the expression of the mucins and TFF-3. At this time, OsLu also showed a higher beneficial effect than lactulose, because the derivative reduced the expression of all the cytokines for which expression was up-regulated 1 week after the second administration of TNBS, whereas lactulose reduced only IL-6 (Figure 5). At this time, only MUC-2 expression was restored after the treatment with both lactulose and OsLu, without showing a significant effect in comparison with colitic control group, when MUC-3 or TFF-3 was considered (Figure 6).

Effects of Lactulose and OsLu on TNBS on Microbiota Composition and SCFA Production in Colitic Rats. The evaluation of the microbial content in the colonic lumen 1 week after the first administration of TNBS evidenced a significant decrease in the counts of both lactobacilli and bifidobacteria and, on the contrary, an increase in clostridia and bacteroides in TNBS colitic rats in comparison with the healthy ones (Figure 7). Treatment with lactulose or with OsLu resulted in a

dx.doi.org/10.1021/jf500678p | J. Agric. Food Chem. 2014, 62, 4285−4297

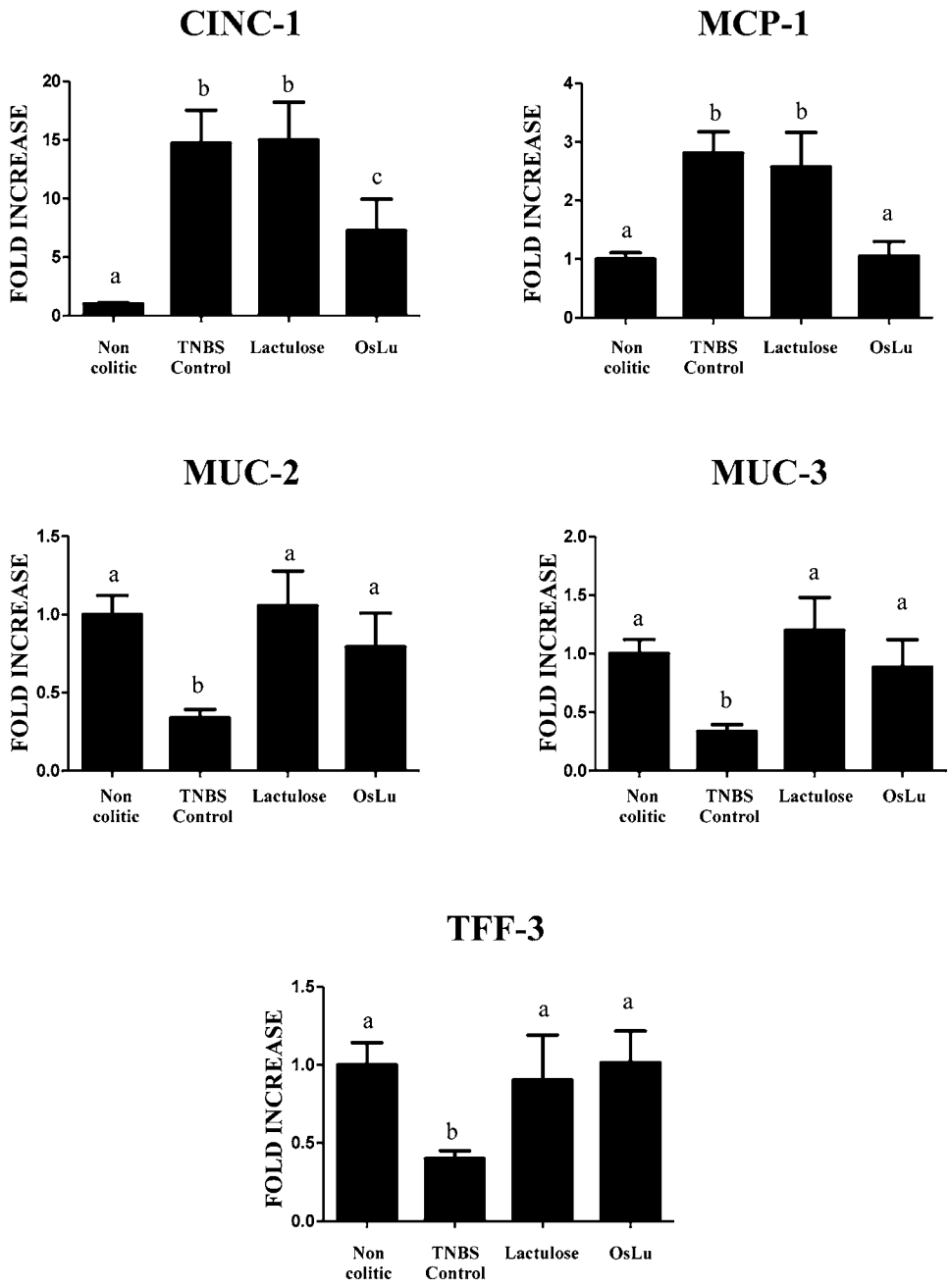

Figure 3. Effects of lactulose and oligosaccharides derived from lactulose (OsLu) on the colonic expression of the chemokines cytokine-induced neutrophil chemoattractant (CINC)-1 and monocyte chemotactic protein (MCP)-1, the mucins MUC-2 and MUC-3, and the trefoil factor (TFF)-3 analyzed by RT-PCR in TNBS rat colitis 1 week after damage induction. Data (n = 10 per group) are expressed as means ± SEM; groups with different letters statistically differ ($P < 0.05$).

Table 4. Effects of Lactulose and Oligosaccharides Derived from Lactulose (OsLu) on Colonic Macroscopic Damage Score and Weight/Length (W/L) Ratio in TNBS-Reactivated Experimental Rat Colitis[a]

	1 week		2 weeks		3 weeks	
group	score (0−10)	W/L (mg/cm)	score (0−10)	W/L (mg/cm)	score (0−10)	W/L (mg/cm)
noncolitic (n = 5)	0	68.7 ± 3.1	0	72.1 ± 2.9	0	75.7 ± 4.9
TNBS control (n = 10)	7.6 ± 0.5	148.4 ± 3.0	5.3 ± 0.3	155.5 ± 17.2	7.7 ± 0.2	161.3 ± 9.8
lactulose (n = 10)	5.7 ± 0.4*	124.1 ± 13.9	3.6 ± 0.6*	111.9 ± 23.1	5.5 ± 0.2*	96.7 ± 5.8*
OsLu (n = 10)	5.1 ± 0.8*	104.8 ± 9.1*	4.0 ± 0.4*	116.1 ± 13.8	5.4 ± 0.4*	105.7 ± 9.9*

[a]Data are expressed as means ± SEM. *, $P < 0.05$ vs TNBS control group. All colitic groups statistically differ from the noncolitic group ($P < 0.05$).

significant increase in both lactobacilli and bifidobacteria counts when compared with the control colitic group, although no significant modification was observed when clostridia or bacteroides counts were considered. When the microbial

dx.doi.org/10.1021/jf500678p | J. Agric. Food Chem. 2014, 62, 4285−4297

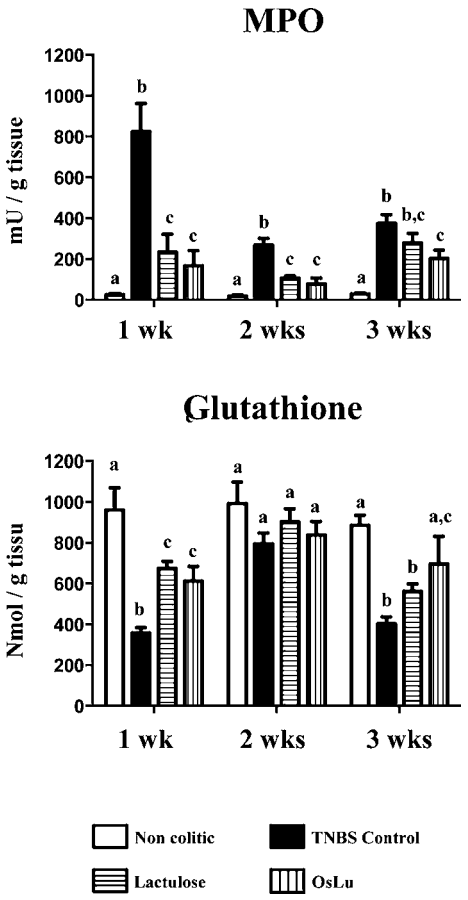

Figure 4. Effects of lactulose and oligosaccharides derived from lactulose (OsLu) on colonic myeloperoxidase (MPO) activity and glutathione content in reactivated TNBS-rat colitis. Data (n = 10 per group) are expressed as means ± SEM; groups with different letters statistically differ ($P < 0.05$).

content was evaluated after 2 weeks, a restoration in both lactobacilli and bifidobacteria counts was observed in the rats from the colitic control group, without showing statistical differences with the healthy group; however, increased counts of clostridia and bacteroides were obtained in colitic rats in comparison with noncolitic ones. No significant modification was obtained in any of the bacterial groups studied with either lactulose or OsLu when compared with the corresponding colitic control group (Figure 7).

The reactivation of the inflammatory process after the second dose of TNBS resulted in a new reduction of lactobacilli and bifidobacteria after 1 week, whereas the numbers of clostridia and bacteroides were increased. OsLu was again able to significantly increase the counts of lactobacilli and bifidobacteria in comparison with the control colitic rats, whereas lactulose was devoid of any significant effect. Also, no significant modifications were observed among colitic groups when clostridia or bacteroides were considered (Figure 7).

As a consequence, the colonic inflammatory process was associated, at weeks 1 and 3, with a significant reduction in the production of the different SCFA (acetate, propionate, and butyrate) evaluated (Figure 8), as it has been previously reported in the same model of experimental colitis.[25] The beneficial effects exerted by the treatments of lactulose and OsLu in colitic rats were associated with an increased production of all the SCFA 1 week after the first administration of TNBS. Moreover, OsLu was able to restore these levels without showing statistical differences with noncolitic rats (Figure 8). However, 1 week after colitis reactivation, only OsLu was able to raise the production of the SCFA in comparison with nontreated colitic rats (Figure 8).

DISCUSSION

A decrease in bacterial diversity has been reported to occur in IBD patients, characterized by reduced levels of protective species with relative predominance of pathobionts, thus promoting a deregulation of the immune response. As a consequence, an interesting approach to the treatment of intestinal inflammation would be the restoration of microbiota balance.[2]

In the present study we described the beneficial effects exerted by oligosaccharides derived from lactulose (OsLu) in the TNBS model of rat colitis, comparing them with those achieved by its precursor, lactulose. OsLu has been characterized by a slower fermentation by the colonic microbiota than lactulose, so the oligosacharides are able to reach the distal colon without great alterations.[19,20] Theoretically, these properties could be of great interest for the treatment of human IBD, because distal areas of the large intestine are typically affected in UC and very frequently in Crohn's disease. Furthermore, the delayed fermentation could account for a better patient tolerability than lactulose, because the effects derived from its fermentation in the proximal colon would be avoided. Actually, both lactulose and OsLu were able to reduce the colonic damage observed 1 week after colonic induction with TNBS. Previous studies carried out with different oligosaccharides also displayed an improvement in the macroscopic scores, indicating changes in the colitic rats receiving the pretreatment with oligosaccharides. Thus, for example, colitic rats pretreated with goat milk oligosaccharides[30] or FOS[31] showed significant amelioration of the intestinal inflammatory process in comparison with nontreated groups. It is interesting to note that this beneficial effect was also evidenced when the two prebiotics were administered for a longer period of time to colitic rats with a reactivation of the intestinal inflammation with a second instillation of TNBS, both prebiotics showing a similar efficacy. Unfortunately, a curative protocol with this type of product is not convenient because previous observations have shown a deleterious effect of lactulose or OsLu when the administration starts once the colitis is established. Other authors have reported similar observations with different treatments in experimental colitis in rodents.[32]

As expected, the treatments were able to modify intestinal bacteria composition that was altered due to the colitic process, mainly derived from their ability to increase the counts of either lactobacilli or bifidobacteria. In addition, the beneficial effect on microbiota composition exerted by both treatments was associated with an improvement of the defensive mechanisms of the intestinal epithelial barrier, the architecture of which appeared to be restored in the histological studies. The administration of lactulose or OsLu normalized the expression of the mucins MUC-2 and MUC-3, primary constituents of the mucus layer in the colon,[33] as well as of TFF-3, a bioactive peptide involved in epithelial protection and repair.[34] This could be one of the mechanisms for preserving the mucus-secreting layer that covers the epithelium and acts as a physical barrier protecting its integrity. This effect may be key for the intestinal anti-inflammatory capacity exerted by these pre-

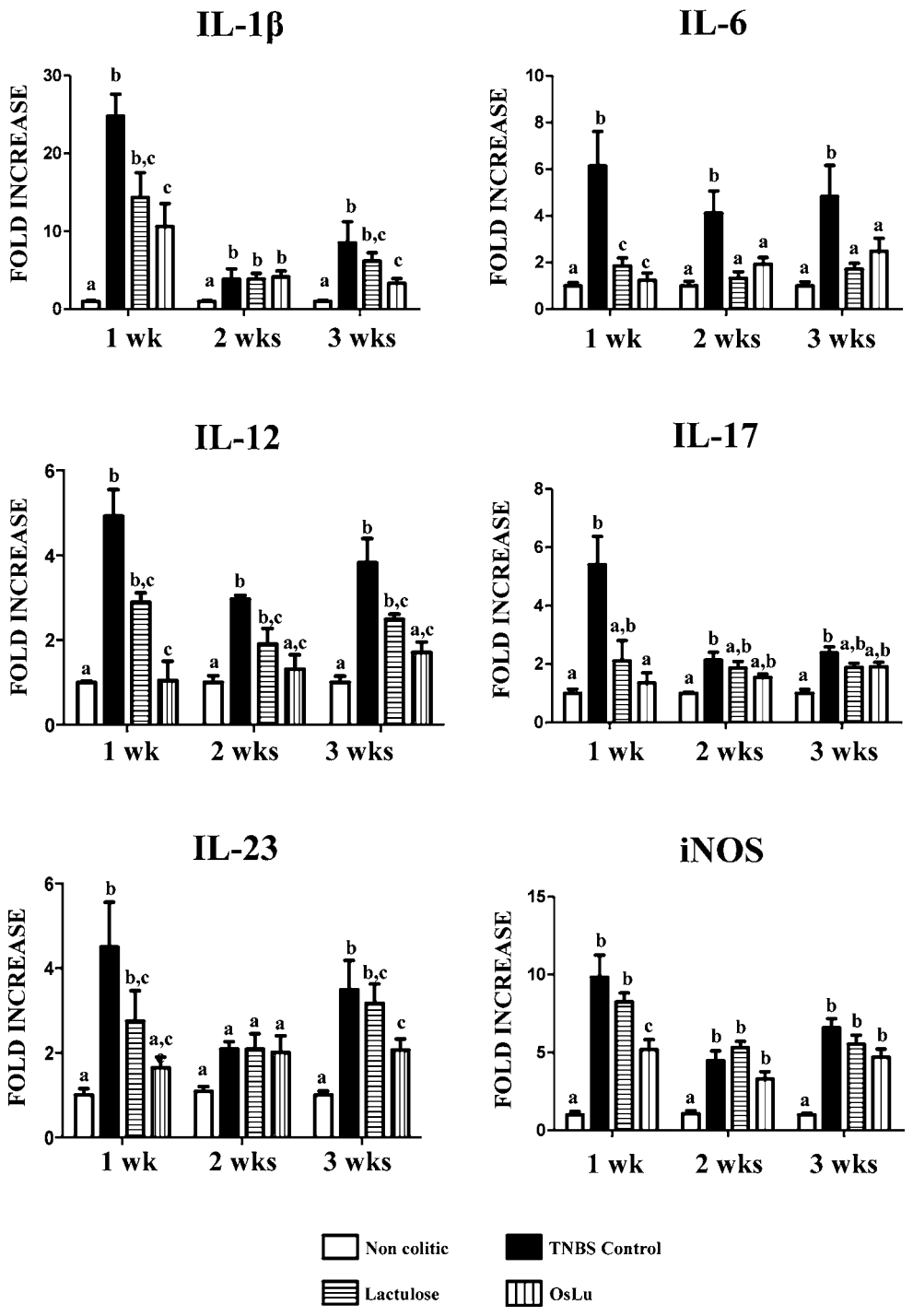

Figure 5. Effects of lactulose and oligosaccharides derived from lactulose (OsLu) on the colonic expression of the cytokines IL-1β, IL-6, IL-12, IL-17, and IL-23 and inducible nitric oxide synthase (iNOS) analyzed by RT-PCR in reactivated TNBS rat colitis. Data (n = 10 per group) are expressed as means ± SEM; groups with different letters statistically differ (P < 0.05).

biotics. Epithelial barrier function impairment is considered to be one of the initial steps in intestinal inflammation that facilitates the access of antigens from the intestinal lumen and, hence, generates an exacerbated immune response.[35,36] Moreover, human IBD has been associated with a defective colonic mucus layer and a reduced number of goblet cells.[37]

Furthermore, both lactulose and OsLu were able to increase the reduced production of SCFA observed in colitis rats, which may help with the regeneration of the inflamed mucosa, given the key role attributed to these acids in the intestine homeostasis and immune response.[38] This may be responsible for modifications in the biochemical markers of the immune response observed in the colonic tissue. It is interesting to note the differences observed between OsLu and lactulose on the Th17 pathway that could account for the higher anti-inflammatory efficacy of OsLu. The IL-17 pathway is crucial in the pathogenesis of IBD.[39] Thus, IL-17 contributes to neutrophil migration, expansion, and function and enhances dendritic cell maturation, T cell priming, and the production of inflammatory mediators from different cell types. Furthermore,

dx.doi.org/10.1021/jf500678p | J. Agric. Food Chem. 2014, 62, 4285−4297

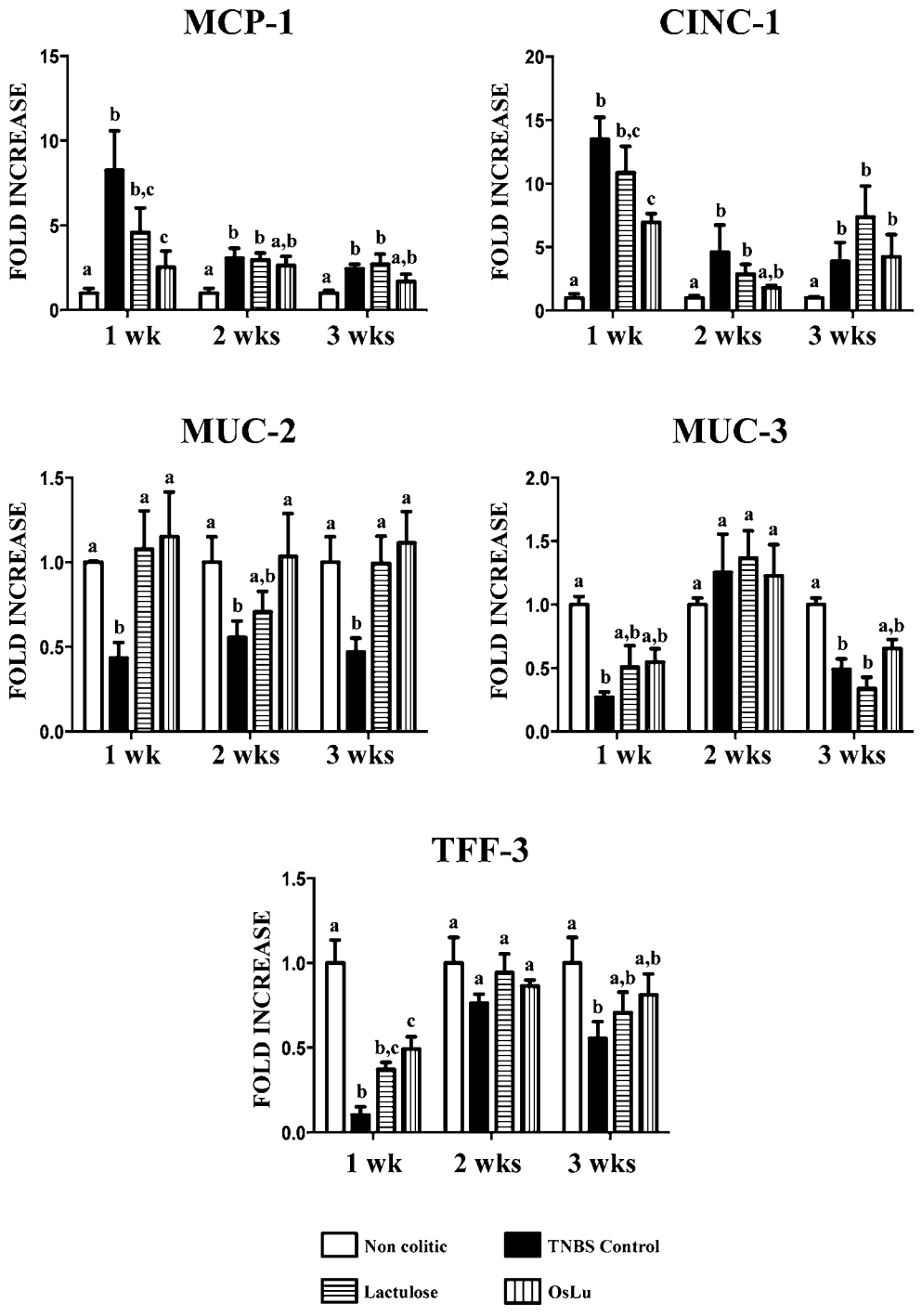

Figure 6. Effects of lactulose and oligosaccharides derived from lactulose (OsLu) on the colonic expression of the chemokines cytokine-induced neutrophil chemoattractant (CINC)-1 and monocyte chemotactic protein (MCP)-1, the mucins MUC-2 and MUC-3, and the trefoil factor (TFF)-3 analyzed by RT-PCR in reactivated TNBS rat colitis. Data (n = 10 per group) are expressed as means ± SEM; groups with different letters statistically differ ($P < 0.05$).

IL-17 can synergize with other cytokines to promote the release of additional pro-inflammatory cytokines, thus being essential for maintaining the inflammatory response in the intestine. As confirmed in the present study, experimental colitis has also been reported to be associated with an increased IL-17 production;[40] in fact, in TNBS colitis, the infiltration of CD4 lymphocytes and neutrophils, mostly driven by a Th1/Th17 cytokine response, is one of the predominant features in the initiation and perpetuation of the inflammatory process.[41] Furthermore, the inhibition in the expression of chemotactic mediators CINC-1 and MCP-1 in the inflamed tissue probably contributes to lowering the leukocyte infiltration and activation that could also account for the higher efficacy shown by OsLu because it is well described that, in the first steps of gut inflammation, margination and extravasation of circulating leukocytes probably result in the perpetuation of the inflammatory process.[42] Other mechanisms may also explain the differences displayed by both prebiotics, and one of these could be related to the ability of OsLu, but not lactulose, to significantly inhibit colonic iNOS expression in the inflamed

dx.doi.org/10.1021/jf500678p | J. Agric. Food Chem. 2014, 62, 4285−4297

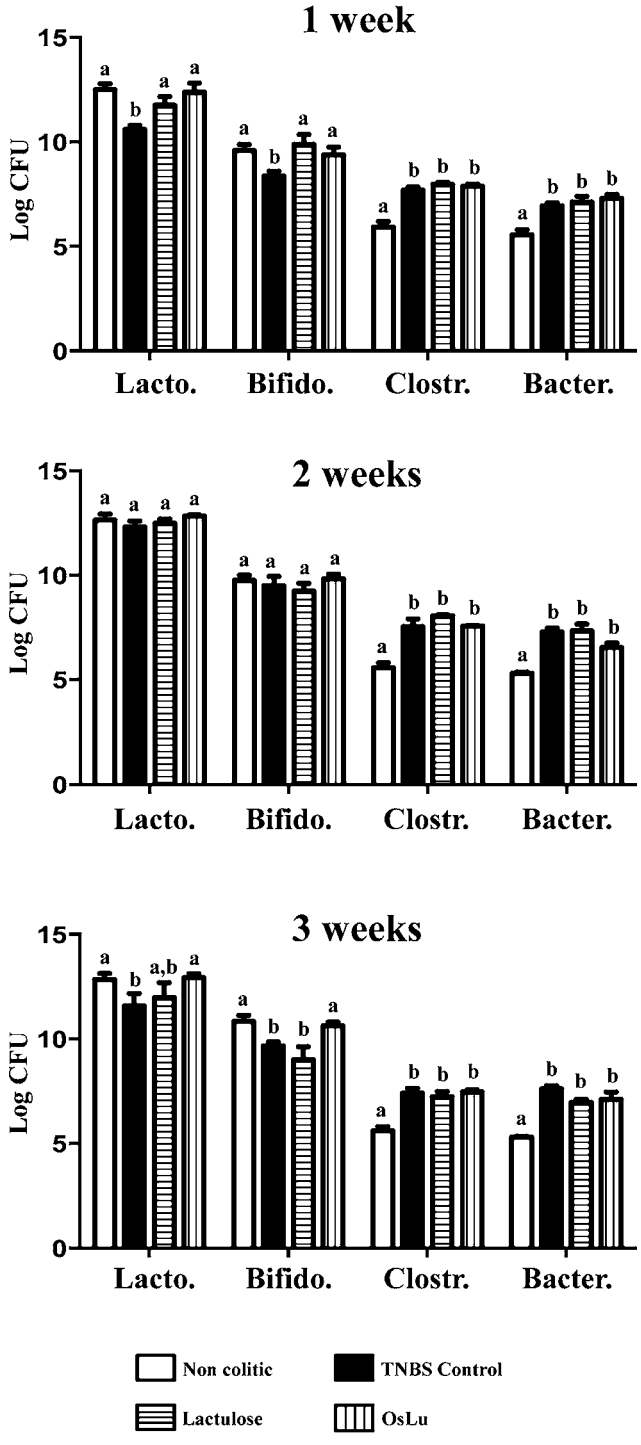

Figure 7. Effects of lactulose and oligosaccharides derived from lactulose (OsLu) on the bacterial profile in the colonic luminal contents in reactivated TNBS rat colitis. The counts of lactobacilli, bifidobacteria, clostridia, and bacteroides (expressed as log of colony forming units (CFU)) were analyzed by RT-PCR. Data (n = 10 per group) are expressed as means ± SEM; groups with different letters statistically differ (P < 0.05).

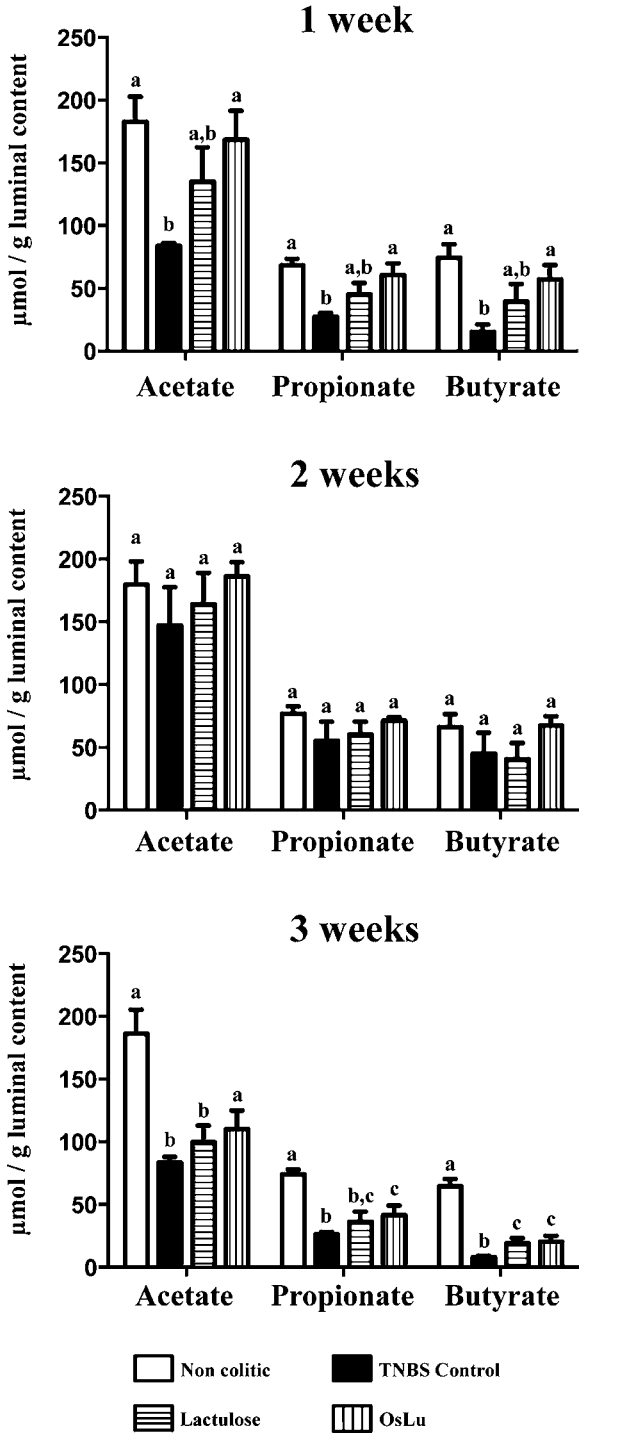

Figure 8. Effects of lactulose and oligosaccharides derived from lactulose (OsLu) on short-chain fatty acid (acetate, propionate, and butyrate) production in the colonic luminal contents in reactivated TNBS rat colitis. Data (n = 10 per group) are expressed as means ± SEM; groups with different letters statistically differ (P < 0.05).

intestine, thus avoiding the deleterious effect that NO overproduction may exert on the colonic tissue in these intestinal conditions.[43]

In conclusion, OsLu shows better anti-inflammatory properties than lactulose, probably derived from the improvement of the luminal microbiota balance and a greater SCFA production, which was associated with an inhibition of iNOS expression and a reduction of Th17 cell activity in the inflamed tissue that, in turn, promote intestinal membrane integrity and a faster recovery of the inflamed tissue. After this preclinical study of OsLu, these oligosaccharides could be considered for a clinical study to test its efficacy in maintenance of IBD remission and preventing relapses.

dx.doi.org/10.1021/jf500678p | J. Agric. Food Chem. 2014, 62, 4285−4297

■ ASSOCIATED CONTENT

Supporting Information

Figure S1. This material is available free of charge via the Internet at http://pubs.acs.org.

■ AUTHOR INFORMATION

Corresponding Author

*(J.G.) E-mail: jgalvez@ugr.es. Phone: 34-958-241793. Fax: 34-958-248964.

Author Contributions

‖F.A. and A.R.-N. contributed equally to this study.

Funding

This work was supported by the Spanish Ministry of Economy and Competitivity (SAF2011-29648), by Consolider-Ingenio 2010: FUNC-C-FOOD CSD 2007-00063, and by Junta de Andalucia (AGR-6826 and CTS 164) with funds from the European Union. F.A. is a predoctoral fellow of the Junta de Andalucia; J.G.-M. is a predoctoral fellow of the Spanish Ministry of Education and Science; N.G.-M. is a postdoctoral fellow of the Ramon Areces Foundation; M.E.R.-C. is a postdoctoral fellow of CIBEREHD. CIBEREHD is funded by the Instituto de Salud Carlos III.

Notes

The authors declare no competing financial interest.

■ ABBREVIATIONS USED

CINC-1, cytokine-induced neutrophil chemoattractant-1; FOS, fructo-oligosaccharides; GOS, galacto-oligosaccharides; GSH, glutathione; IBD, inflammatory bowel disease; iNOS, nitric oxide synthase; IL, interleukin; MCP-1, monocyte chemotactic protein-1; MPO, myeloperoxidase activity; OsLu, oligosaccharides derived from lactulose; SCFA, short-chain fatty acids; TNBS, trinitrobenzenesulfonic acid; UC, ulcerative colitis

■ REFERENCES

(1) Sartor, R. B. Mechanisms of disease: pathogenesis of Crohn's disease and ulcerative colitis. *Nat. Clin. Pract. Gastroenterol. Hepatol.* **2006**, *3*, 390−407.

(2) Frank, D. N.; St Amand, A. L.; Feldman, R. A.; Boedeker, E. C.; Harpaz, N.; Pace, N. R. Molecular-phylogenetic characterization of microbial community imbalances in human inflammatory bowel diseases. *Proc. Natl. Acad. Sci. U.S.A.* **2007**, *104*, 13780−13785.

(3) Khan, K. J.; Ullman, T. A.; Ford, A. C.; Abreu, M. T.; Abadir, A.; Marshall, J. K.; Talley, N. J.; Moayyedi, P. Antibiotic therapy in inflammatory bowel disease: a systematic review and meta-analysis. *Am. J. Gastroenterol.* **2011**, *106*, 661−673.

(4) Roberfroid, M.; Gibson, G. R.; Hoyles, L.; McCartney, A. L.; Rastall, R.; Rowland, I.; Wolvers, D.; Watzl, B.; Szajewska, H.; Stahl, B.; Guarner, F.; Respondek, F.; Whelan, K.; Coxam, V.; Davicco, M. J.; Léotoing, L.; Wittrant, Y.; Delzenne, N. M.; Cani, P. D.; Neyrinck, A. M.; Meheust, A. Prebiotic effects: metabolic and health benefits. *Br. J. Nutr.* **2010**, *104*, S1−S63.

(5) Looijer-van Langen, M. A.; Dieleman, L. A. Prebiotics in chronic intestinal inflammation. *Inflamm. Bowel Dis.* **2009**, *15*, 454−462.

(6) Wong, J. M.; de Souza, R.; Kendall, C. W.; Emam, A.; Jenkins, D. J. Colonic health: fermentation and short chain fatty acids. *J. Clin. Gasgroenterol.* **2006**, *40*, 235−2243.

(7) Swennen, K.; Courtin, C. M.; Delcour, J. A. Non-digestible oligosaccharides with prebiotic properties. *Crit. Rev. Food Sci. Nutr.* **2006**, *46*, 459−471.

(8) Schumann, C. Medical, nutritional and technological properties of lactulose. An update. *Eur. J. Nutr.* **2002**, *41* (Suppl. 1), I17−I25.

(9) Olano, A.; Corzo, N. Lactulose as a food ingredient. *J. Sci. Food Agric.* **2009**, *89*, 1987−1990.

(10) Panesar, P. S.; Kumari, S. Lactulose: production, purification and potential applications. *Biotechnol. Adv.* **2011**, *29*, 940−948.

(11) Rumi, G.; Tsubouchi, R.; Okayama, M.; Kato, S.; Mózsik, G.; Takeuchi, K. Protective effect of lactulose on dextran sulfate sodium-induced colonic inflammation in rats. *Dig. Dis. Sci.* **2004**, *49*, 1466−1472.

(12) Camuesco, D.; Peran, L.; Comalada, M.; Nieto, A.; Di Stasi, L. C.; Rodriguez-Cabezas, M. E.; Concha, A.; Zarzuelo, A.; Galvez, J. Preventative effects of lactulose in the trinitrobenzenesulphonic acid model of rat colitis. *Inflamm. Bowel Dis.* **2005**, *11*, 265−271.

(13) Chen, X.; Zhai, X.; Shi, J.; Liu, W. W.; Tao, H.; Sun, X.; Kang, Z. Lactulose mediates suppression of dextran sodium sulfate-induced colon inflammation by increasing hydrogen production. *Dig. Dis. Sci.* **2013**, *58*, 1560−1568.

(14) Hafer, A.; Krämer, S.; Duncker, S.; Krüger, M.; Manns, M. P.; Bischoff, S. C. Effect of oral lactulose on clinical and immunohistochemical parameters in patients with inflammatory bowel disease: a pilot study. *BMC Gastroenterol.* **2007**, *7*, 36.

(15) Munoz, S. J. Hepatic encephalopathy. *Med. Clin. North Am.* **2008**, *92*, 795−812.

(16) Cardelle-Cobas, A.; Martínez Villaluenga, C.; Villamiel, M.; Olano, A.; Corzo, N. Synthesis of oligosaccharides derived from lactulose and Pectinex Ultra SP-L. *J. Agric. Food Chem.* **2008**, *56*, 3328−3333.

(17) Cardelle-Cobas, A.; Villamiel, M.; Olano, A.; Corzo, N. Isomerization of lactose-derived oligosaccharides. A case study using sodium aluminate. *J. Agric. Food Chem.* **2008**, *56*, 10954−10959.

(18) Martínez-Villaluenga, C.; Cardelle-Cobas, A.; Olano, A.; Corzo, N.; Villamiel, M.; Jimeno, M. L. Enzymatic synthesis and identification of two trisaccharides produced from lactulose by transgalactosylation. *J. Agric. Food Chem.* **2008**, *56*, 557−563.

(19) Cardelle-Cobas, A.; Corzo, N.; Olano, A.; Pélaez, C.; Requena, T.; Ávila, M. Galactooligosaccharides derived from lactose and lactulose: influence of linkage and composition on *Streptococcus*, *Lactobacillus* and *Bifidobacterium* strains growth. *Int. J. Food Microbiol.* **2011**, *149*, 81−87.

(20) Cardelle-Cobas, A.; Olano, A.; Corzo, N.; Villamiel, M.; Collins, M.; Kolida, S.; Rastall, R. A. In vitro fermentation of lactulose-derived oligosaccharides by mixed fecal microbiota. *J. Agric. Food Chem.* **2012**, *60*, 2024−2032.

(21) Marín-Manzano, M. C.; Abecia, L.; Hernández-Hernández, O.; Sanz, M. L.; Montilla, A.; Olano, A.; Rubio, L. A.; Moreno, F. J.; Clemente, A. Galacto-oligosaccharides derived from lactulose exert a selective stimulation on the growth of *Bifidobacterium animalis* in the large intestine of growing rats. *J. Agric. Food Chem.* **2013**, *61*, 7560−7567.

(22) Elson, C. O.; Sartor, R. B.; Tennyson, G. S.; Riddell, R. H. Experimental models of inflammatory bowel disease. *Gastroenterology* **1995**, *109*, 1344−1367.

(23) Sanz, M. L.; Polemis, N.; Morales, V.; Corzo, N.; Drakoularakou, A.; Gibson, G. R.; Rastall, R. A. In vitro investigation into the potential prebiotic activity of honey oligosaccharides. *J. Agric. Food Chem.* **2005**, *53*, 2914−2921.

(24) Anadón, A.; Martínez, M. A.; Ares, I.; Castellano, V.; Martínez-Larrañaga, M. R.; Corzo, N.; Olano, A.; Montilla, A.; Recio, I.; Martínez-Maqueda, D.; Miralles, B.; Fornari, T.; García-Risco, M. R.; Gonzalez, M.; Reglero, G. Acute and repeated dose (28 days) oral safety studies of ALIBIRD in rats. *J. Food Prot.* **2013**, *76*, 1226−1239.

(25) Arribas, B.; Suárez-Pereira, E.; Ortiz Mellet, C.; García Fernández, J. M.; Buttersack, C.; Rodríguez-Cabezas, M. E.; Garrido-Mesa, N.; Bailon, E.; Guerra-Hernández, E.; Zarzuelo, A.; Gálvez, J. D-D-fructose dianhydride-enriched caramels: effect on colon microbiota, inflammation, and tissue damage in trinitrobenzenesulfonic acid-induced colitic rats. *J. Agric. Food Chem.* **2010**, *58*, 6476−6484.

(26) Krawisz, J. E.; Sharon, P.; Stenson, W. F. Quantitative assay for acute intestinal inflammation based on myeloperoxidase activity. Assessment of inflammation in rat and hamster models. *Gastroenterology* **1984**, *87*, 1344−1350.

(27) Anderson, M. E. Determination of glutathione and glutathione disulfide in biological samples. *Methods Enzymol.* **1985**, *113*, 548−555.
(28) Collado, M. C.; Delgado, S.; Maldonado, A.; Rodríguez, J. M. Assessment of the bacterial diversity of breast milk of healthy women by quantitative real-time PCR. *Lett. Appl. Microbiol.* **2009**, *48*, 523−528.
(29) Veljaca, M.; Lesch, C. A.; Pllana, R.; Sanchez, B.; Chan, K.; Guglietta, A. BPC-15 reduces trinitrobenzene sulfonic-induced colonic damage in rats. *J. Pharmacol. Exp. Ther.* **1995**, *272*, 417−422.
(30) Lara-Villoslada, F.; Debras, E.; Nieto, A.; Concha, A.; Gálvez, J.; López-Huertas, E.; Boza, J.; Obled, C.; Xaus, J. Oligosaccharides isolated from goat milk reduce intestinal inflammation in a rat model of dextran sodium sulfate-induced colitis. *Clin. Nutr.* **2006**, *25*, 477−488.
(31) Koleva, P. T.; Valcheva, R. S.; Sun, X.; Gänzle, M. G.; Dieleman, L. A. Inulin and fructo-oligosaccharides have divergent effects on colitis and commensal microbiota in HLA-B27 transgenic rats. *Br. J. Nutr.* **2012**, *108*, 1633−1643.
(32) Obermeier, F.; Dunger, N.; Deml, L.; Herfarth, H.; Schölmerich, J.; Falk, W. CpG motifs of bacterial DNA exacerbate colitis of dextran sulfate sodium-treated mice. *Eur. J. Immunol.* **2002**, *32*, 2084−2092.
(33) Tytgat, K. M.; Bovelander, F. J.; Opdam, F. J.; Einerhand, A. W.; Büller, H. A.; Dekker, J. Biosynthesis of rat MUC2 in colon and its analogy with human MUC2. *Biochem. J.* **1995**, *309*, 221−229.
(34) Mashimo, H.; Wu, D. C.; Podolsky, D. K.; Fishman, M. C. Impaired defense of intestinal mucosa in mice lacking intestinal trefoil factor. *Science* **1996**, *274*, 262−265.
(35) Mankertz, J.; Schulzke, J. D. Altered permeability in inflammatory bowel disease: pathophysiology and clinical implications. *Curr. Opin. Gastroenterol.* **2007**, *23*, 379−383.
(36) Su, L.; Shen, L.; Clayburgh, D. R.; Nalle, S. C.; Sullivan, E. A.; Meddings, J. B.; Abraham, C.; Turner, J. R. Targeted epithelial tight junction dysfunction causes immune activation and contributes to development of experimental colitis. *Gastroenterology* **2009**, *136*, 551−563.
(37) Gersemann, M.; Becker, S.; Kübler, I.; Koslowski, M.; Wang, G.; Herrlinger, K. R.; Griger, J.; Fritz, P.; Fellermann, K.; Schwab, M.; Wehkamp, J.; Stange, E. F. Differences in goblet cell differentiation between Crohn's disease and ulcerative colitis. *Differentiation* **2009**, *77*, 84−94.
(38) Arpaia, N.; Campbell, C.; Fan, X.; Dikiy, S.; van der Veeken, J.; deRoos, P.; Liu, H.; Cross, J. R.; Pfeffer, K.; Coffer, P. J.; Rudensky, A. Y. Metabolites produced by commensal bacteria promote peripheral regulatory T-cell generation. *Nature* **2013**, *504*, 451−455.
(39) Sarra, M.; Pallone, F.; Macdonald, T. T.; Monteleone, G. IL-23/IL-17 axis in IBD. *Inflamm. Bowel Dis.* **2010**, *16*, 1808−1813.
(40) Camuesco, D.; Rodríguez-Cabezas, M. E.; Garrido-Mesa, N.; Cueto-Sola, M.; Bailón, E.; Comalada, M.; Arribas, B.; Merlos, M.; Balsa, D.; Zarzuelo, A.; Janer, G.; Xaus, J.; Román, J.; Gálvez, J. The intestinal anti-inflammatory effect of dersalazine sodium is related to a down-regulation in IL-17 production in experimental models of rodent colitis. *Br. J. Pharmacol.* **2012**, *165*, 729−740.
(41) Zhang, Z.; Zheng, M.; Bindas, J.; Schwarzenberger, P.; Kolls, J. K. Critical role of IL-17 receptor signaling in acute TNBS-induced colitis. *Inflamm. Bowel Dis.* **2006**, *12*, 382−388.
(42) Garcia-Ramallo, E.; Marques, T.; Prats, N.; Beleta, J.; Kunkel, S. L.; Godessart, N. Resident cell chemokine expression serves as the major mechanism for leukocyte recruitment during local inflammation. *J. Immunol.* **2002**, *169*, 6467−6473.
(43) Pavlick, K. P.; Laroux, F. S.; Fuseler, J.; Wolf, R. E.; Gray, L.; Hoffman, J.; Grisham, M. B. Role of reactive metabolites of oxygen and nitrogen in inflammatory bowel disease. *Free Radical Biol. Med.* **2002**, *33*, 311−322.

JOURNAL OF AGRICULTURAL AND FOOD CHEMISTRY

Article

pubs.acs.org/JAFC

Coumestrol Induces Mitochondrial Biogenesis by Activating Sirt1 in Cultured Skeletal Muscle Cells

Dae-Bang Seo,[†,∥] Hyun Woo Jeong,[‡,∥] Sang-Jun Lee,[*,‡] and Sung-Joon Lee[*,†]

[†]College of Life and Environmental Sciences, Division of Food Science, Korea University, Seoul 136-713, Republic of Korea

[‡]Beauty Food Division, Amorepacific R&D Unit, Gyunggi-do 446-729, Republic of Korea

Supporting Information

ABSTRACT: The mitochondrion is a central organelle in cellular energy homeostasis; thus, reduced mitochondrial activity has been associated with aging and metabolic disorders. This paper provides biological evidence that coumestrol, which is a natural isoflavone, activates mitochondrial biogenesis. In cultured myocytes, coumestrol activated the silent information regulator two ortholog 1 (Sirt1) through the elevation of the intracellular NAD^+/NADH ratio. Coumestrol also increased the mitochondrial contents and induced the expression of key proteins in the mitochondrial electron transfer chain in cultured myocytes. A Sirt1 inhibitor and Sirt1-targeting siRNAs abolished the effect of coumestrol on mitochondrial biogenesis. Similar to an increase in mitochondrial content, coumestrol improved myocyte function with increased ATP concentration. Taken together, the data suggest that coumestrol is a novel inducer of mitochondrial biogenesis through the activation of Sirt1.

KEYWORDS: *coumestrol, mitochondrial biogenesis, Sirt1, myocyte*

INTRODUCTION

The mitochondrion produces most of the cellular ATP via aerobic respiration and regulates various cellular processes, including signaling pathways, growth, differentiation, cell cycle, and apoptosis.[1] Because the maintenance of mitochondrial functions is critical for maintaining energy homeostasis, mitochondrial biogenesis, which maintains cellular mitochondrial content, has been considered a critical biomarker to assess cellular longevity and functionality. Mitochondrial biogenesis is regulated by multiple factors, one of which is a nuclear-encoded transcription factor, nuclear respiratory factor 1 (NRF1), that induces the expression of transcription factor A mitochondria (tfam) and other mitochondria-related genes in nucleus DNA.[2] Tfam is a key mitochondrial transcription factor, which is responsible for the regulation of mitochondrial DNA (mtDNA)-encoded genes and the replication of mtDNA. Therefore, mitochondrial biogenesis is regarded as a complex process that is coordinated by nuclear (by NRF1) and mitochondrial (by tfam) genes.[1]

Although the molecular mechanism of mitochondrial biogenesis is not fully understood, it has been reported that peroxisome proliferator-activated receptor gamma coactivator 1 α (PGC1α) has been reported as a positive regulator that directly interacts with NRF1 to form a transcription complex.[3] PGC1α forms a transcription complex with NRF1 to increase the transcriptional activity of NRF1. In addition, PGC1α also regulates glucose and lipid homeostasis through interaction with various transcription factors, such as peroxisome proliferator-activated receptor γ, retinoid X receptor, and cAMP response element-binding protein.[4−6]

Silent information regulator two ortholog 1 (Sirt1), which is an NAD^+-dependent histone deacetylase, is a mammalian homologue of the silent mating-type information regulation 2 (Sir2) gene in *Saccharomyces cerevisiae*, which has been studied as a "longevity gene"; thus, Sir2 overexpression results in a lifespan extension in small-animal models, such as budding yeasts, nematodes, and fruit flies.[7−9] Calorie restriction has been known to exhibit a positive effect on lifespan extension,[10] whereas the deletion of Sir2 diminished the effect on lifespan extension.[11] These results imply that Sir2 activity mediates the effect of calorie restriction on longevity. Therefore, Sir2 is regarded as a central molecule in the network of energy metabolism and lifespan. In mammals, Sirt1 has been reported to regulate energy metabolism and response to calorie restriction.[12] For these reasons, small molecules that target Sirt1 are being developed to overcome metabolic disorders, including obesity, insulin resistance, and type 2 diabetes.

In addition to the roles in longevity, Sirt1 has been proposed to be one of the most important positive regulators for regulating cellular mitochondrial number.[13] Upon activation, Sirt1 facilitates the deacetylation and activation of PGC1α.[13] As above-mentioned, activated PGC1α can trigger mitochondrial biogenesis through interaction with NRF1. Thus, it is also feasible that mitochondrial biogenesis can be achieved by the activation of Sirt1.

Coumestrol, which is a daidzein-derived coumestan, is a natural organic compound that is found in some plants, including alfalfa, legumes, Brussels sprouts, spinach, clover, and soybeans.[14] Various biological activities of coumestrol have been reported, including antioxidant activity,[15] the inhibition of osteoclast differentiation,[16] the inhibition of adipocyte differentiation, and reduced lipid accumulation.[17] As a phytoestrogen, coumestrol also exerts an estrogenic effect, with strong binding affinities for estrogen receptors α and β,[14,18] and the positive effects of coumestrol on bone metabolism and uterine

Received: October 31, 2013
Revised: March 28, 2014
Accepted: April 8, 2014
Published: April 8, 2014

ACS Publications © 2014 American Chemical Society

growth are well-studied in ovariectomized animals.[19,20] Finally, coumestrol attenuated tumorigenesis.[21,22] However, the molecular target and mechanism of action of coumestrol have not been clearly understood.

Recently, it has been proposed that flavonoids and their derivatives induce mitochondrial biogenesis through the activation or expression of Sirt1 in proximal renal tubular cells.[23] Therefore, here we investigated whether coumestrol has positive effects on mitochondrial biogenesis and compared the activity of coumestrol with resveratrol, which is a compound that is known as a Sirt1 activator. Sirt1 activity was determined, and coumestrol-induced mitochondrial biogenesis was assessed by mitochondrial content and by the expression of mitochondria-related genes in differentiated myocytes. The effect of Sirt1 activation on the coumestrol-mediated induction of mitochondrial biogenesis was confirmed by utilizing a Sirt1 inhibitor and Sirt1-specific siRNAs. The effect of coumestrol-mediated mitochondrial biogenesis was confirmed by the measurement of cellular ATP concentrations.

MATERIALS AND METHODS

Reagents. Coumestrol and nicotinamide were purchased from Sigma (St. Louis, MO, USA). The antibodies for NADH dehydrogenase 1α subcomplex 9 (NDUFA9), succinate dehydrogenate complex subunit A (SDHA), ubiquinol cytochrome *c* reductase core protein 2 (UQCRC2), cytochrome oxidase subunit 1 (COX1), ATP synthase mitochondria F1 complex α subunit 1 (ATP5a), PGC1, and NRF1, as well as scrambled and Sirt1 siRNAs, were purchased from Santa Cruz Biotechnology (Dallas, TX, USA). The β-actin antibody was purchased from Cell Signaling Technology (Danvers, MA, USA), and horseradish peroxidase (HRP)-conjugated anti-mouse, anti-rabbit, and anti-goat secondary antibodies were purchased from Bio-Rad (Hercules, CA, USA).

Cell Culture. C2C12 mouse myocytes were purchased from the American Type Culture Collection (Manassas, VA, USA). Cells were grown in Dulbecco's modified Eagle medium (DMEM, Lonza), which was supplemented with 10% fetal bovine serum (FBS, HyClone, Logan, UT, USA). All media were supplemented with 100 units/mL penicillin and 100 mg/mL streptomycin (Sigma), and C2C12 cells were grown at 37 °C in a humidified atmosphere, which contained 5% CO_2. For differentiation, confluent C2C12 cells were maintained with DMEM, which was supplemented with 2% horse serum (HyClone) for 7 days. During differentiation, the medium was changed daily.

Sirt1 Activity Assay. Sirt1 activity was examined using a SIRT1 Fluorimetric Drug Discovery Kit (Enzo Life Sciences, Farmingdale, NY, USA) with minor modifications, as described previously.[24] Briefly, total protein (25 μg) was dissolved in the assay buffer and incubated in the presence of NAD^+ (100 μM) at 37 °C for 30 min. The acetylated substrate (Fluor-de-Lys-Sirt1 substrate) was then added, and the mixture was incubated at 37 °C for 45 min. After incubation, deacetylated substrates were detected on a TECAN M200 PRO fluorometric plate reader (Tecan, Männedorf, Switzerland).

Measurement of Cellular NAD^+/NADH Ratio. The NAD^+/NADH ratio was determined using an NAD/NADH assay kit (Biovision, Miltipas, CA, USA), following the manufacturer's protocol. Briefly, cells were lysed with extraction buffer (400 μL) by the freeze–thaw method. Extracts were vortexed for 10 s and centrifuged at 18000 rcf for 5 min. The supernatants were then equally divided into two microcentrifuge tubes. Half of the samples were incubated at 60 °C for 30 min to disrupt NAD^+ and remain NADH only. Unheated samples (NADt; NAD^+ plus NADH) and heated (NADH only) samples were incubated with a NAD cycling enzyme, which converts NAD^+ to NADH at room temperature for 5 min. Then, the mixtures were mixed with the NADH developing agent and incubated at room temperature for 1 h. NADH levels were determined by measuring the absorbance at 450 nm using a TECAN M200 PRO fluorometric plate reader. NAD^+ levels were calculated by subtracting NADH from NADt.

Measurement of Mitochondrial Density. Mitochondrial content was measured using the MitoTracker Green FM (Invitrogen, Carlsbad, CA, USA) reagent. Briefly, cells were rinsed with PBS and incubated with MitoTracker Green FM (50 nmol) for 30 min. Fluorescence was measured using a TECAN M200 PRO fluorometric plate reader to determine the density of mitochondria.

Western Blotting. An equal amount (60 μg) of protein per sample was separated on NuPAGE Novex Tris–acetate gels (Invitrogen) and transferred to membranes using an iBlot dry transfer device (Invitrogen). Membranes were blocked with 5% skim milk (Sigma) in Tris-buffered saline (Bio-Rad), which was supplemented with 0.1% Tween-20 (Sigma) (TBST) at room temperature for 30 min. After blocking, the membranes were incubated with primary antibodies, which were dissolved in TBST/5% bovine serum albumin (BSA, Sigma) with gentle shaking at 4 °C overnight. After three washings with TBST, the blots were hybridized with HRP-conjugated secondary antibodies in TBST/5% BSA at room temperature for 2 h and washed three times with TBST. After washing, the membranes were incubated with enhanced chemiluminescence reagents (Santa Cruz Biotechnology) and analyzed with an LAS-3000 imaging system (Fujifilm, Tokyo, Japan). Relative expression levels of proteins were measured using Multigauge software (Fujifilm).

siRNA Transfection. For the knockdown of Sirt1, differentiated C2C12 myocytes were transfected with scrambled or mouse Sirt1 siRNA using the Lipofectamine 2000 reagent (Invitrogen). After transfection, cells were incubated in Opti-MEM (Invitrogen) medium for 4 h. After transfection, the medium was replaced with fresh DMEM, which contained 10% FBS.

Measurement of ATP. ATP content was determined using an ATP determination kit (Invitrogen). Briefly, extracts were mixed with a reaction solution, which contained firefly luciferase and D-luciferin. ATP content was measured using a Wallac 1420 Victor^2 multilabel counter microplate reader (PerkinElmer, Waltham, MA, USA) and normalized with the protein concentration of each sample.

Glucose Uptake Assay. Glucose uptake was assessed by using a glucose uptake cell-based assay kit (Cayman Chemical Co., Ann Arbor, MI, USA), following the manufacturer's protocol with minor modifications. Briefly, cells in a 96-well black, clear-bottom plate were washed with PBS three times and the medium was changed into glucose-free DMEM (Lonza) containing 150 μg/mL 2-NBDG (fluorescent-labeled deoxyglucose analogue). Cells were incubated for a further 1 h, and the plate was centrifuged at 400 rcf for 5 min. After centrifugation, supernatant was discarded and cell-based assay buffer (200 μL) was added to each well. The plate was centrifuged at 400 rcf for 5 min, the supernatant was discarded, and cell-based assay buffer (100 μL) was added one more time. The amount of 2-NBDG taken up by the cells was immediately measured at the wavelength of 485/535 nm (excitation/emission) using a TECAN M200 PRO fluorometric plate reader.

Statistical Analyses. The results are representative of the data from three or more independent experiments. All data points represent the average of triplicate samples. Error bars represent the standard deviation (SD). The *p* values, which were calculated from a one-way ANOVA followed by Dunnett's procedure, that were <0.01 were interpreted as statistically significant.

RESULTS

Coumestrol Activates Sirt1. Coumestrol significantly and dose-dependently increased Sirt1 activity in differentiated C2C12 myocytes (Figure 1A). The effect of coumestrol (CMS; 1 and 10 μM) on Sirt1 activity was comparable with that of resveratrol (Res; 50 μM), which indicated that coumestrol is a potent inducer of Sirt1 activity. Sirt1 activity is directly regulated by the intracellular NAD^+/NADH ratio; thus, we measured the intracellular NAD^+/NADH ratio in cells that were stimulated with coumestrol. Corresponding with Sirt1 activity, coumestrol caused a dose-dependent induction of the intracellular NAD^+/NADH ratio, which demonstrated that

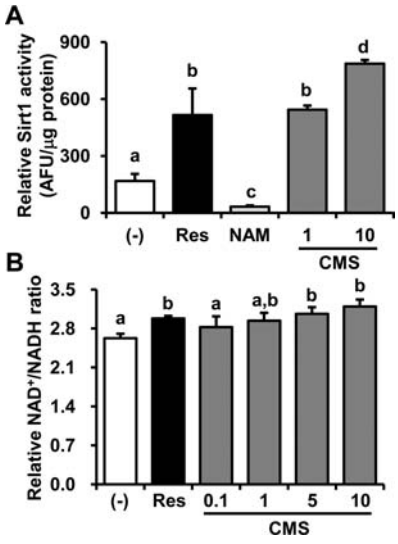

Figure 1. Coumestrol activates Sirt1. (A) Sirt1 activity assay. Differentiated C2C12 cells were treated with DMSO, resveratrol (Res; 50 μM), nicotinamide (NAM; 1 mM), or coumestrol (CMS; 1 or 10 μM, respectively) for 24 h, and Sirt1 activity assay was assessed as described under Materials and Methods. Relative Sirt1 activity is shown as a bar graph. AFU, arbitrary fluorescence unit. (B) Intracellular NAD^+/NADH ratio. C2C12 myocytes were treated with Res (25 μM) or CMS (0.1, 1, 5, and 10 μM, respectively) for 12 h. Cells were rinsed with PBS, and intracellular NAD^+/NADH ratio was measured. Values that do not share the same letter are significantly different ($p < 0.01$).

coumestrol activates Sirt1, at least in part, through the elevation of the intracellular NAD^+/NADH ratio (Figure 1B).

Coumestrol Induces Mitochondrial Biogenesis. We demonstrated that coumestrol activates Sirt1 (Figure 1), which induces mitochondrial biogenesis.[13] To determine whether coumestrol promotes mitochondrial biogenesis similar to other Sirt1 activators,[25,26] we quantified the mitochondrial density in differentiated C2C12 myocytes that were treated with coumestrol. Coumestrol increased the mitochondrial content in a dose-dependent manner (Figure 2A). Moreover, the protein expression of mitochondrial electron transfer chain (ETC) components, such as NDUFA9, SDHA, UQCRC2, COX1, and ATP5a, and transcriptional regulators that are responsible for mitochondrial biogenesis, such as PGC1 and NRF1, were augmented with coumestrol stimulation (Figure 2B,C). Corresponding with protein expression, the mRNA expression of mitochondria-related genes was also up-regulated by coumestrol (Supporting Information Figure S1), which suggested that coumestrol can induce mitochondrial biogenesis through the transcriptional regulation of the expression of mitochondrial biogenesis-related genes.

Chemical Inhibitor of Sirt1 Prevents Coumestrol-Mediated Mitochondrial Biogenesis. To establish whether Sirt1 plays an important role in mediating coumestrol-induced mitochondrial biogenesis, we examined the effects of the Sirt1 inhibitor nicotinamide. To inhibit Sirt1 activation, cells were stimulated with a high dose of nicotinamide (1 mM) before coumestrol stimulation. The results demonstrated that the mitochondriogenic effect of coumestrol was prevented by nicotinamide pretreatment, which was assessed with mitochondrial density (Figure 3A). Additionally, the expression of mitochondrial ETC-related genes was not increased upon coumestrol treatment in the presence of nicotinamide (Figure

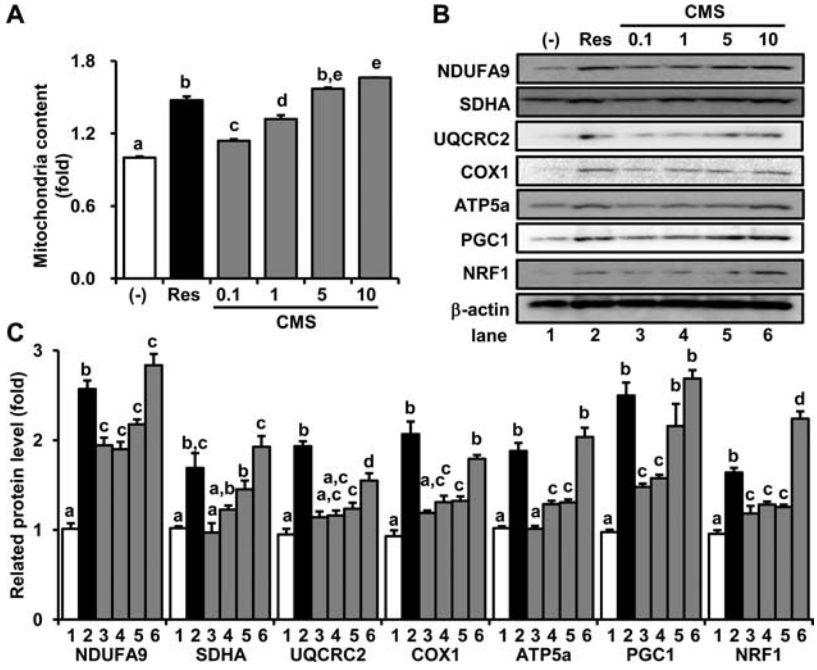

Figure 2. Coumestrol induces mitochondrial biogenesis. C2C12 myotubes were treated with resveratrol (Res; 25 μM) or coumestrol (CMS; 0.1, 1, 5, and 10 μM, respectively) for 24 h. (A) Mitochondrial density was measured using the Mitotracker Green FM reagent. Relative mitochondrial density is shown as a bar graph. (B) After rinsing with PBS, cells were harvested, and proteins were extracted and blotted with antibodies against specific proteins (NDUFA9, SDHA, UQCRC2, COX1, ATP5a, PGC1, and NRF1). β-Actin was used as a loading control. (C) Protein expression level of each protein shown in (B). Each number under the bar graph indicates the lane number in (B). Values that do not share the same letter are significantly different ($p < 0.01$).

dx.doi.org/10.1021/jf404882w | J. Agric. Food Chem. 2014, 62, 4298−4305

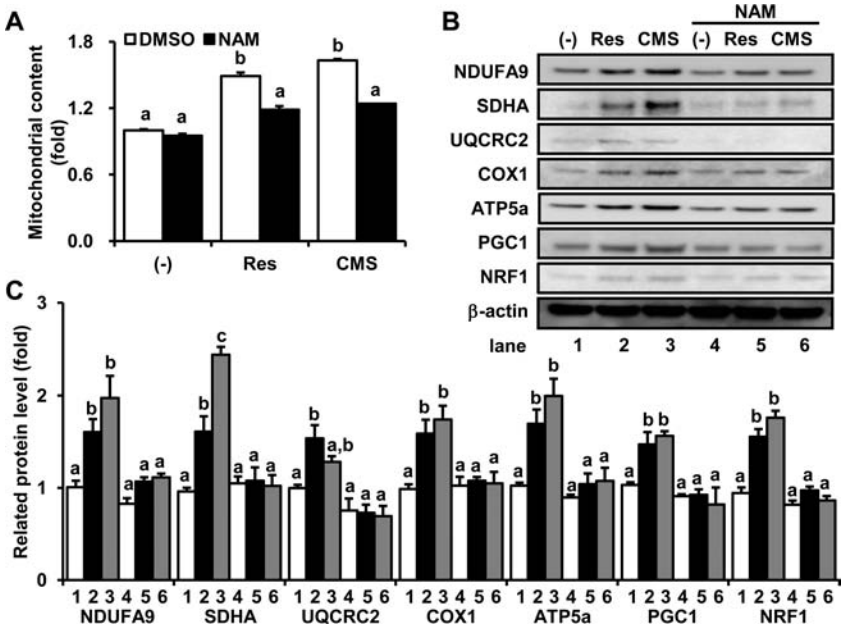

Figure 3. Nicotinamide prevents Sirt1-mediated mitochondrial biogenesis. C2C12 cells were pretreated with DMSO (control) or nicotinamide (NAM; 1 mM) for 2 h. Then, cells were treated with resveratrol (Res; 25 μM) or coumestrol (CMS; 10 μM) for an additional 24 h. (A) After incubation, mitochondrial density was determined. (B) After washing with PBS, cells were harvested, and proteins were blotted with specific antibodies. β-Actin was used as a loading control. (C) Densitometry of Western blots shown in (B). Values that do not share the same letter are significantly different ($p < 0.01$).

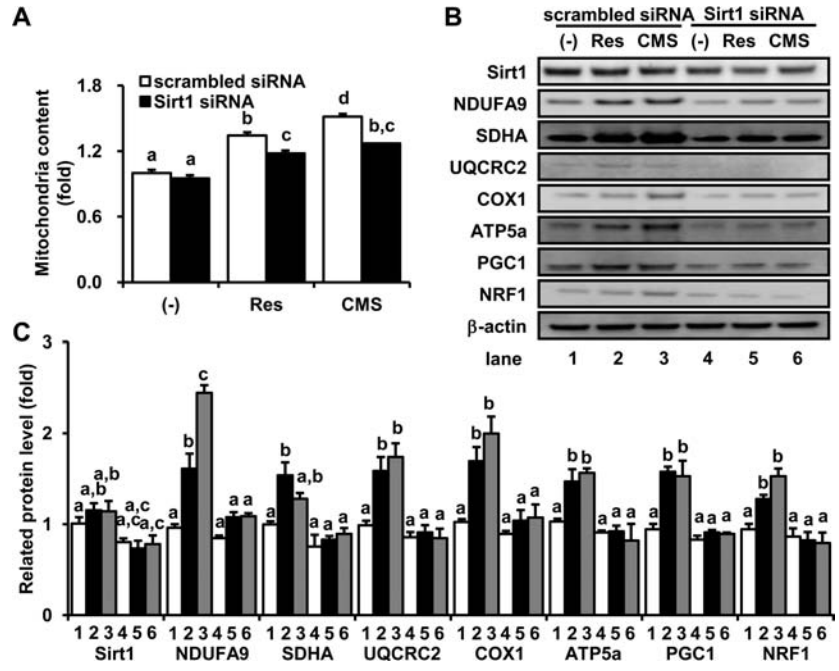

Figure 4. Sirt1 siRNA blunts the effect of coumestrol on mitochondrial biogenesis. C2C12 cells were transfected with scrambled or Sirt1 siRNA. After transfection, cells were treated with resveratrol (Res; 25 μM) or coumestrol (CMS; 10 μM) for 24 h. (A) Mitochondrial density was determined. (B) Proteins were blotted with antibodies that targeted mitochondrial proteins and their regulators. β-Actin was used as a loading control. The expression of each protein was normalized and shown as bar graphs (C). Values that do not share the same letter are significantly different ($p < 0.01$).

3B). These data suggest that Sirt1 mediates the mitochondriogenic effect of coumestrol in myocytes.

Knockdown of Sirt1 Lessens the Effect of Coumestrol on Mitochondrial Biogenesis. The nicotinamide treatment indicated that the inhibition of Sirt1 activity abolishes the effect of coumestrol on mitochondrial biogenesis (Figure 3). To confirm the Sirt1-dependent effect of coumestrol, the expression of Sirt1 was knocked down with Sirt1-specific siRNAs (Supporting Information Figure S2). Similar to the nicotinamide pretreatment, knockdown of the Sirt1 expression also abolished the effect of coumestrol on mitochondrial biogenesis (Figure 4A) and mitochondrial ETC protein

dx.doi.org/10.1021/jf404882w | J. Agric. Food Chem. 2014, 62, 4298−4305

expression (Figure 4B). Similar results were obtained with resveratrol. Taken together, these results demonstrate that both resveratrol and coumestrol induce mitochondrial biogenesis in a Sirt1-dependent manner.

Coumestrol Increases ATP Content in a Sirt1-Dependent Manner and Augments Glucose Uptake. To confirm whether coumestrol contributes to ATP production through the induction of mitochondrial content, we measured cellular ATP concentrations in cells that were stimulated with coumestrol. In agreement with increased mitochondrial content (Figure 2), coumestrol induced cellular ATP concentrations in C2C12 myocytes (Figure 5A); however, the blockade of Sirt1 activity with nicotinamide prevented coumestrol-mediated ATP production (Figure 5B). Collectively, these data indicate that coumestrol induces mitochondrial biogenesis and, consequently, increases cellular ATP level through the activation of Sirt1.

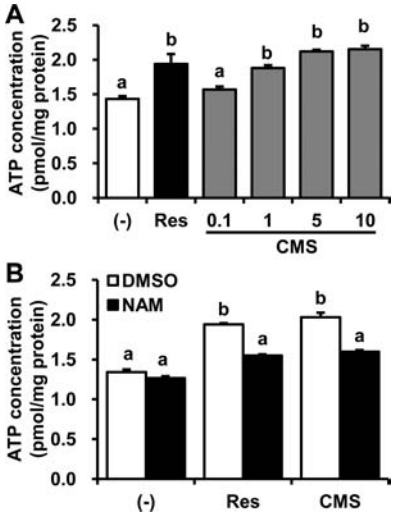

Figure 5. Coumestrol increases ATP content in cultured myocytes in a Sirt1-dependent manner. (A) Differentiated C2C12 cells were treated with resveratrol (Res; 50 μM) or coumestrol (CMS; 0.1, 1, 5, and 10 μM, respectively) for 24 h. After incubation, the ATP level was determined by using an ATP determination kit. (B) After differentiation, C2C12 myocytes were pretreated with DMSO (for control) or nicotinamide (NAM; 1 mM) for 2 h. Then, cells were treated with Res (50 μM) or CMS (10 μM) for 24 h. Cellular ATP content was measured as described under Materials and Methods. Values that do not share the same letter are significantly different ($p < 0.01$).

Glucose is the primary energy source for ATP production. Increased ATP content in coumestrol-treated myocytes (Figure 5) indicates that coumestrol might be associated with glucose uptake. To elucidate whether coumestrol enhances glucose uptake in skeletal muscle, we assessed the glucose uptake assay. As shown in Figure 6, coumestrol slightly but significantly increased glucose uptake, compared to control. These data suggest that coumestrol is able to enhance energy metabolism.

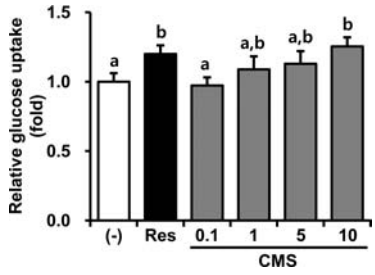

Figure 6. Coumestrol augments glucose uptake in differentiated myocytes. Differentiated C2C12 myocytes were treated with DMSO (for control), resveratrol (Res; 50 μM), or coumestrol (CMS; 0.1, 1, 5, and 10 μM, respectively) for 24 h. Cellular glucose uptake was measured as described under Materials and Methods and shown as a bar graph. Values that do not share the same letter are significantly different ($p < 0.01$).

DISCUSSION

As "power plants" of cells and regulators of diverse cellular activities, mitochondria play an important role in cellular energy balance and survival. Not surprisingly, mitochondrial dysfunction is associated with several cellular dysfunctions and diseases, including metabolic disorders. For example, mitochondrial dysfunction has been reported to be closely associated with β-cell failure.[27] Additionally, impaired mitochondrial bioenergetic capacity is observed in the skeletal muscle of type 2 diabetes patients.[28] In fat and muscle tissues from obese rodents, mitochondrial density, mitochondrial function, and ATP content are down-regulated.[29] Accordingly, it is likely that mitochondrial dysfunction can be observed in various organs or in tissues of metabolic syndromes. Therefore, maintaining mitochondrial function by inducing mitochondrial biogenesis is required to sustain a healthy life.

Here, we demonstrated that coumestrol is able to induce Sirt1 activity and mitochondrial biogenesis. By promoting mitochondrial content, coumestrol increased cellular ATP levels and glucose uptake, implying that coumestrol could improve energy metabolism. Interestingly, the expression and activity of Sirt1 gradually decline with aging, and mitochondrial content and function are also age-dependently decreased.[30−32] Considering the mitochondriogenic effect of Sirt1, it is feasible that decreased Sirt1 activity could be a causal factor of blunted mitochondrial biogenesis, which thereby diminishes mitochondrial density and causes aging-related dysfunctions in aged cells. As for other Sirt1 activators,[25,26,33] we demonstrated that coumestrol also increases mitochondrial content through the activation of Sirt1 in muscle cells. Therefore, it is feasible that coumestrol has the potential to attenuate aging-related mitochondrial dysfunction.

The benefit of Sirt1 activation is not limited to mitochondrial rejuvenation. For example, Sirt1 modulates glucose homeostasis by regulating PGC1α and forkhead box O1 activity in the liver.[34] The loss of function of Sirt1 in the pancreas is associated with decreased insulin secretion,[35] and Sirt1 is activated during glucose-stimulated insulin secretion.[36] These data imply that Sirt1 may be involved in the regulation of glucose homeostasis. Furthermore, Sirt1 is also able to control lipid metabolism. In fact, Sirt1 deacetylates and deactivates sterol regulatory element binding protein 1c (SREBP1c), which is a master transcriptional regulator of lipogenesis-related genes.[37] Conversely, Sirt1 enhances lipid catabolism through the activation of AMP-activated protein kinase (AMPK), which is a master regulator of energy metabolism.[38] Additionally, Sirt1 is implicated in the expression and secretion of adiponectin,[39,40] which is an adipocytokine that regulates glucose and lipid metabolism to promote insulin sensitivity. Therefore, it is feasible that Sirt1 activation can improve, or at least modify, glucose and lipid metabolism, which are closely related with metabolic disorders. Remarkably, we observed that coumestrol decreased the mRNA expression of lipogenic genes (e.g.,

SREBP1c and fatty acid synthase) in adipocytes and hepatocytes, whereas coumestrol increased fatty acid oxidation-related genes in myocytes (e.g., acyl-CoA oxidase and carnitine-palmitoyl transferase 1) (Supporting Information Figure S3), indicating that coumestrol could also modulate lipid metabolism to ameliorate metabolic disorders.

Although Sirt1 is beneficial to the regulation of energy metabolism, the effect of Sirt1 in cancer development is controversial. The ectopic expression of Sirt1 attenuated colon cancer progression in mice,[41] and an allelic loss or a mutation of Sirt1 is present in various tumor cells.[42] In contrast, Sirt1 expression level is up-regulated in some tumor cells, and Sirt1 enhances matrix metalloproteinase 2 expression and activity to promote cancer cell migration.[43,44] Furthermore, a specific Sirt1 activator has been reported to promote tumor cell migration and invasion in mice.[45] As an oncogene, Sirt1 activation could lead to tumorigenesis. However, coumestrol displayed anticancer activities by suppressing some tumor development with the modulation of estrogen receptor β and casein kinase II activities.[21,22] Thus, the collective effects of coumestrol appear beneficial without affecting cancer risk. The molecular mechanism of the coumestrol-mediated inhibition of tumor progression requires further study.

As the regulators of energy metabolism and mitochondrial biogenesis, it has been proposed that Sirt1 and AMPK activate each other. AMPK has been reported to increase NAD^+ to activate Sirt1.[46] In contrast, Sirt1 mediates the deacetylation of liver kinase B1,[47] which is an upstream regulator of AMPK. On the basis of these results, it is likely that Sirt1 and AMPK might assemble a positive feedback loop to enhance energy catabolism. According to the previous data, it might be possible that coumestrol could activate AMPK, which is a regulator of Sirt1. Although it remains unclear which one, Sirt1 or AMPK, is the upstream regulator of the other, we observed that coumestrol increased the phosphorylation level of the AMPKα catalytic subunit (Supporting Information Figure S4). Similar to Sirt1, AMPK is also reported to regulate mitochondrial biogenesis and catabolism.[38] On the basis of these data, it is likely that AMPK activation may boost the favorable effect of coumestrol on mitochondrial biogenesis and energy metabolism. Further studies, including in vivo experiments, will reveal the effect of coumestrol on energy metabolism and on the correlation between AMPK and Sirt1.

In conclusion, we demonstrated that coumestrol is an effective inducer of mitochondrial biogenesis. Coumestrol caused a small elevation in the intracellular NAD^+/NADH ratio, but a major induction of Sirt1 activation, which suggests that other factors in addition to NAD^+/NADH ratios are involved in this effect. The coumestrol-mediated mitochondrial biogenesis was abolished by the inhibition of Sirt1 activity. Increased mitochondrial content induced by coumestrol caused an elevation of cellular ATP levels and an increase of glucose uptake. Collectively, our data suggest that coumestrol is an effective Sirt1 activator and enhancer of mitochondrial number and function.

■ ASSOCIATED CONTENT

Supporting Information

Figures S1−S4. Figure S1. mRNA expression of mitochondria-related genes upon coumestrol treatment. C2C12 cells were treated with Res (50 μM) or CMS (0.1, 1, and 10 μM, respectively) for 24 h. After incubation, cells were rinsed with PBS. RNAs were isolated using the TRIzol reagent (Invitrogen), and cDNAs were synthesized using a RevertAid First Strand cDNA Synthesis Kit (Fermentas). The relative mRNA level of mitochondria-related genes was measured by qPCR (Rotor-Gene 3000, Corbett Research) and normalized to GAPDH. Values that do not share the same letter are significantly different ($p < 0.01$). Figure S2. Reduced Sirt1 mRNA expression by siRNA transfection. C2C12 myocytes were transfected with scrambled or Sirt1 siRNA, as described in Figure 4. After transfection, cells were rinsed with PBS. RNAs were isolated, and cDNAs were synthesized using the TRIzol reagent and a RevertAid First Strand cDNA Synthesis Kit as described in Figure S1. The relative mRNA expression of Sirt1 was determined by qPCR and normalized to GAPDH. Values that do not share the same letter are significantly different ($p < 0.01$). Figure S3. Coumestrol represses lipogenic gene expression and enhances fatty acid oxidation-related genes. For adipocyte differentiation, confluent 3T3-L1 cells were incubated with DMEM supplemented with 10% FBS, 0.39 μg/mL dexamethasone, 115 μg/mL isobutylmethylxanthine, and 10 μg/mL insulin (DMI) for 48 h. After DMI treatment, the medium was changed into DMEM supplemented with 10% FBS and 10 μg/mL of insulin every 2 days for 2 weeks to complete adipocyte differentiation. HepG2 human hepatoma cells were grown in DMEM supplemented with 10% FBS. All cells were grown at 37 °C in a humidified atmosphere, which contained 5% CO_2, and all media were supplemented with 100 units/mL penicillin and 100 mg/mL streptomycin. (A) Differentiated 3T3-L1 adipocytes, (B) HepG2 hepatoma cells, and (C) differentiated C2C12 myocytes were treated with Res (50 μM) or CMS (0.1, 1, and 10 μM, respectively) for 24 h. After incubation, cells were rinsed with PBS. RNAs were isolated and cDNAs were synthesized using the TRIzol reagent and a RevertAid First Strand cDNA Synthesis Kit, as described in Figure S1. The relative mRNA expression of indicated genes was determined by qPCR and normalized to GAPDH. Values that do not share the same letter are significantly different ($p < 0.01$). Figure S4. Coumestrol activates AMPK and increases glucose uptake. (A) C2C12 myotubes were treated with Res (50 μM) or CMS (0.1, 1, 5, and 10 μM, respectively) for 2 h. After incubation, cells were rinsed with PBS, and proteins were extracted. Proteins were blotted with antibodies that target AMPK and p-AMPK. β-Actin was used as a loading control. (B) p-AMPK/AMPK ratio is shown as a bar graph. (C) Differentiated C2C12 myocytes were starved with low-glucose DMEM supplemented with 0.1% BSA overnight. After starvation, cells were treated with DMSO (for control), Res (50 μM), or CMS (0.1, 1, 5, and 10 μM, respectively) for 2 h. Cellular glucose uptake was measured as described under Materials and Methods and shown as a bar graph. Values that do not share the same letter are significantly different ($p < 0.01$). This material is available free of charge via the Internet at http://pubs.acs.org.

■ AUTHOR INFORMATION

Corresponding Authors

*(Sung-Joon Lee) Mail: Department of Biotechnology, Graduate School of Life Sciences and Biotechnology, Korea University, Seoul 136-713, Republic of Korea. Phone: 82-2-3290-3029. E-mail: junelee@korea.ac.kr.

*(Sang-Jun Lee) Mail: Beauty Food Division, Amorepacific R&D Unit, Gyunggi-do 446-729, Republic of Korea. Phone: 82-31-280-5601. E-mail: leesjun@amorepacific.com.

Author Contributions

[‖]D.-B.S. and H.W.J. equally contributed to this work.

Notes

The authors declare no competing financial interest.

■ ACKNOWLEDGMENTS

We appreciate the valuable comments of Prof. Valter D. Longo (USC) during manuscript preparation. This work was supported by the R&D program of MOTIE/KIAT. (N0000697, Establishment of Infra Structure for Anti-aging Industry Support) and Cooperative Research Program for Agriculture Science & Technology Development (Project No. PJ01009003) of the Rural Development Administration, Republic of Korea.

■ ABBREVIATIONS USED

Sirt1, silent information regulator two ortholog 1; NRF1, nuclear respiratory factor 1; Tfam, transcription factor A mitochondria; mtDNA, mitochondrial DNA; PGC1α, peroxisome proliferator-activated receptor γ coactivator 1α; Sir2, silent mating-type information regulation 2; NDUFA9, NADH dehydrogenase 1α subcomplex 9; SDHA, succinate dehydrogenase complex subunit A; UQCRC2, ubiquinol cytochrome c reductase core protein 2; COX1, cytochrome oxidase subunit 1; ATP5a, ATP synthase mitochondria F1 complex α subunit 1; HRP, horseradish peroxidase; DMEM, Dulbecco's modified Eagle medium; FBS, fetal bovine serum; ETC, electron transfer chain; SREBP1c, sterol regulatory element binding protein 1c; AMPK, AMP-activated protein kinase

■ REFERENCES

(1) McBride, H. M.; Neuspiel, M.; Wasiak, S. Mitochondria: more than just a powerhouse. *Curr. Biol.* **2006**, *16*, R551−R560.

(2) Virbasius, J. V.; Scarpulla, R. C. Activation of the human mitochondrial transcription factor A gene by nuclear respiratory factors: a potential regulatory link between nuclear and mitochondrial gene expression in organelle biogenesis. *Proc. Natl. Acad. Sci. U.S.A.* **1994**, *91*, 1309−1313.

(3) Wu, Z.; Puigserver, P.; Andersson, U.; Zhang, C.; Adelmant, G.; Mootha, V.; Troy, A.; Cinti, S.; Lowell, B.; Scarpulla, R. C.; Spiegelman, B. M. Mechanisms controlling mitochondrial biogenesis and respiration through the thermogenic coactivator PGC-1. *Cell* **1999**, *98*, 115−124.

(4) Puigserver, P.; Adelmant, G.; Wu, Z.; Fan, M.; Xu, J.; O'Malley, B.; Spiegelman, B. M. Activation of PPARγ coactivator-1 through transcription factor docking. *Science* **1999**, *286*, 1368−1371.

(5) Delerive, P.; Wu, Y.; Burris, T. P.; Chin, W. W.; Suen, C. S. PGC-1 functions as a transcriptional coactivator for the retinoid X receptors. *J. Biol. Chem.* **2002**, *277*, 3913−3917.

(6) Wallberg, A. E.; Yamamura, S.; Malik, S.; Spiegelman, B. M.; Roeder, R. G. Coordination of p300-mediated chromatin remodeling and TRAP/mediator function through coactivator PGC-1α. *Mol. Cell* **2003**, *12*, 1137−1149.

(7) Tissenbaum, H. A.; Guarente, L. Increased dosage of a sir-2 gene extends lifespan in *Caenorhabditis elegans*. *Nature* **2001**, *410*, 227−230.

(8) Rogina, B.; Helfand, S. L. Sir2 mediates longevity in the fly through a pathway related to calorie restriction. *Proc. Natl. Acad. Sci. U.S.A.* **2004**, *101*, 15998−16003.

(9) Kaeberlein, M.; McVey, M.; Guarente, L. The SIR2/3/4 complex and SIR2 alone promote longevity in *Saccharomyces cerevisiae* by two different mechanisms. *Genes Dev.* **1999**, *13*, 2570−2580.

(10) Lin, S. J.; Kaeberlein, M.; Andalis, A. A.; Sturtz, L. A.; Defossez, P. A.; Culotta, V. C.; Fink, G. R.; Guarente, L. Calorie restriction extends *Saccharomyces cerevisiae* lifespan by increasing respiration. *Nature* **2002**, *418*, 344−348.

(11) Lin, S. J.; Defossez, P. A.; Guarente, L. Requirement of NAD and SIR2 for life-span extension by calorie restriction in *Saccharomyces cerevisiae*. *Science* **2000**, *289*, 2126−2128.

(12) Ho, C.; van der Veer, E.; Akawi, O.; Pickering, J. G. SIRT1 markedly extends replicative lifespan if the NAD^+ salvage pathway is enhanced. *FEBS Lett.* **2009**, *583*, 3081−3085.

(13) Gurd, B. J. Deacetylation of PGC-1α by SIRT1: importance for skeletal muscle function and exercise-induced mitochondrial biogenesis. *Appl. Physiol. Nutr. Metab.* **2011**, *36*, 589−597.

(14) Bickoff, E. M.; Booth, A. N.; Lyman, R. L.; Livingston, A. L.; Thompson, C. R.; Deeds, F. Coumestrol, a new estrogen isolated from forage crops. *Science* **1957**, *126*, 969−970.

(15) Jeon, H. Y.; Seo, D. B.; Shin, H. J.; Lee, S. J. Effect of *Aspergillus oryzae*-challenged germination on soybean isoflavone content and antioxidant activity. *J. Agric. Food Chem.* **2012**, *60*, 2807−2814.

(16) Kanno, S.; Hirano, S.; Kayama, F. Effects of the phytoestrogen coumestrol on RANK-ligand-induced differentiation of osteoclasts. *Toxicology* **2004**, *203*, 211−220.

(17) Taxvig, C.; Specht, I. O.; Boberg, J.; Vinggaard, A. M.; Nellemann, C. Dietary relevant mixtures of phytoestrogens inhibit adipocyte differentiation in vitro. *Food Chem. Toxicol.* **2013**, *55*, 265−271.

(18) Bickoff, E. M.; Livingston, A. L.; Booth, A. N. Estrogenic activity of coumestrol and related compounds. *Arch. Biochem. Biophys.* **1960**, *88*, 262−266.

(19) Ye, S. F.; Saga, I.; Ichimura, K.; Nagai, T.; Shinoda, M.; Matsuzaki, S. Coumestrol as well as isoflavones in soybean extract prevent bone resorption in ovariectomized rats. *Endocr. Regul.* **2003**, *37*, 145−152.

(20) Markaverich, B. M.; Webb, B.; Densmore, C. L.; Gregory, R. R. Effects of coumestrol on estrogen receptor function and uterine growth in ovariectomized rats. *Environ. Health Perspect.* **1995**, *103*, 574−581.

(21) Lee, Y. H.; Yuk, H. J.; Park, K. H.; Bae, Y. S. Coumestrol induces senescence through protein kinase CKII inhibition-mediated reactive oxygen species production in human breast cancer and colon cancer cells. *Food Chem.* **2013**, *141*, 381−388.

(22) Hedelin, M.; Lof, M.; Olsson, M.; Adlercreutz, H.; Sandin, S.; Weiderpass, E. Dietary phytoestrogens are not associated with risk of overall breast cancer but diets rich in coumestrol are inversely associated with risk of estrogen receptor and progesterone receptor negative breast tumors in Swedish women. *J. Nutr.* **2008**, *138*, 938−945.

(23) Rasbach, K. A.; Schnellmann, R. G. Isoflavones promote mitochondrial biogenesis. *J. Pharmacol. Exp. Ther.* **2008**, *325*, 536−543.

(24) Jeong, H. W.; Cho, S. Y.; Kim, S.; Shin, E. S.; Kim, J. M.; Song, M. J.; Park, P. J.; Sohn, J. H.; Park, H.; Seo, D. B.; Kim, W. G.; Lee, S. J. Chitooligosaccharide induces mitochondrial biogenesis and increases exercise endurance through the activation of Sirt1 and AMPK in rats. *PLoS One* **2013**, *7*, e40073.

(25) Gomes, A. P.; Duarte, F. V.; Nunes, P.; Hubbard, B. P.; Teodoro, J. S.; Varela, A. T.; Jones, J. G.; Sinclair, D. A.; Palmeira, C. M.; Rolo, A. P. Berberine protects against high fat diet-induced dysfunction in muscle mitochondria by inducing SIRT1-dependent mitochondrial biogenesis. *Biochim. Biophys. Acta* **2012**, *1822*, 185−195.

(26) Csiszar, A.; Labinskyy, N.; Pinto, J. T.; Ballabh, P.; Zhang, H.; Losonczy, G.; Pearson, K.; de Cabo, R.; Pacher, P.; Zhang, C.; Ungvari, Z. Resveratrol induces mitochondrial biogenesis in endothelial cells. *Am. J. Physiol. Heart Circ. Physiol.* **2009**, *297*, H13−H20.

(27) Ma, Z. A.; Zhao, Z.; Turk, J. Mitochondrial dysfunction and β-cell failure in type 2 diabetes mellitus. *Exp. Diabetes Res.* **2012**, *2012*, 703538.

(28) Kelley, D. E.; He, J.; Menshikova, E. V.; Ritov, V. B. Dysfunction of mitochondria in human skeletal muscle in type 2 diabetes. *Diabetes* **2002**, *51*, 2944−2950.

(29) Valerio, A.; Cardile, A.; Cozzi, V.; Bracale, R.; Tedesco, L.; Pisconti, A.; Palomba, L.; Cantoni, O.; Clementi, E.; Moncada, S.;

Carruba, M. O.; Nisoli, E. TNF-α downregulates eNOS expression and mitochondrial biogenesis in fat and muscle of obese rodents. *J. Clin Invest.* **2006**, *116*, 2791−2798.
(30) Huang, P. S.; Son, J. H.; Abbott, L. C.; Winzer-Serhan, U. H. Regulated expression of neuronal SIRT1 and related genes by aging and neuronal β2-containing nicotinic cholinergic receptors. *Neuroscience* **2011**, *196*, 189−202.
(31) Lambert, A. J.; Wang, B.; Yardley, J.; Edwards, J.; Merry, B. J. The effect of aging and caloric restriction on mitochondrial protein density and oxygen consumption. *Exp. Gerontol.* **2004**, *39*, 289−295.
(32) Masuyama, M.; Iida, R.; Takatsuka, H.; Yasuda, T.; Matsuki, T. Quantitative change in mitochondrial DNA content in various mouse tissues during aging. *Biochim. Biophys. Acta* **2005**, *1723*, 302−308.
(33) Funk, J. A.; Odejinmi, S.; Schnellmann, R. G. SRT1720 induces mitochondrial biogenesis and rescues mitochondrial function after oxidant injury in renal proximal tubule cells. *J. Pharmacol. Exp. Ther.* **2010**, *333*, 593−601.
(34) Rodgers, J. T.; Lerin, C.; Haas, W.; Gygi, S. P.; Spiegelman, B. M.; Puigserver, P. Nutrient control of glucose homeostasis through a complex of PGC-1α and SIRT1. *Nature* **2005**, *434*, 113−118.
(35) Ramsey, K. M.; Mills, K. F.; Satoh, A.; Imai, S. Age-associated loss of Sirt1-mediated enhancement of glucose-stimulated insulin secretion in β cell-specific Sirt1-overexpressing (BESTO) mice. *Aging Cell* **2008**, *7*, 78−88.
(36) Bordone, L.; Motta, M. C.; Picard, F.; Robinson, A.; Jhala, U. S.; Apfeld, J.; McDonagh, T.; Lemieux, M.; McBurney, M.; Szilvasi, A.; Easlon, E. J.; Lin, S. J.; Guarente, L. Sirt1 regulates insulin secretion by repressing UCP2 in pancreatic β cells. *PLoS Biol.* **2006**, *4*, e31.
(37) Ponugoti, B.; Kim, D. H.; Xiao, Z.; Smith, Z.; Miao, J.; Zang, M.; Wu, S. Y.; Chiang, C. M.; Veenstra, T. D.; Kemper, J. K. SIRT1 deacetylates and inhibits SREBP-1C activity in regulation of hepatic lipid metabolism. *J. Biol. Chem.* **2010**, *285*, 33959−33970.
(38) Hou, X.; Xu, S.; Maitland-Toolan, K. A.; Sato, K.; Jiang, B.; Ido, Y.; Lan, F.; Walsh, K.; Wierzbicki, M.; Verbeuren, T. J.; Cohen, R. A.; Zang, M. SIRT1 regulates hepatocyte lipid metabolism through activating AMP-activated protein kinase. *J. Biol. Chem.* **2008**, *283*, 20015−20026.
(39) Qiao, L.; Shao, J. SIRT1 regulates adiponectin gene expression through Foxo1-C/enhancer-binding protein alpha transcriptional complex. *J. Biol. Chem.* **2006**, *281*, 39915−39924.
(40) Qiang, L.; Wang, H.; Farmer, S. R. Adiponectin secretion is regulated by SIRT1 and the endoplasmic reticulum oxidoreductase Ero1-L α. *Mol. Cell. Biol.* **2007**, *27*, 4698−4707.
(41) Firestein, R.; Blander, G.; Michan, S.; Oberdoerffer, P.; Ogino, S.; Campbell, J.; Bhimavarapu, A.; Luikenhuis, S.; de Cabo, R.; Fuchs, C.; Hahn, W. C.; Guarente, L. P.; Sinclair, D. A. The SIRT1 deacetylase suppresses intestinal tumorigenesis and colon cancer growth. *PLoS One* **2008**, 3, e2020.
(42) Han, J.; Hubbard, B. P.; Lee, J.; Montagna, C.; Lee, H. W.; Sinclair, D. A.; Suh, Y. Analysis of 41 cancer cell lines reveals excessive allelic loss and novel mutations in the SIRT1 gene. *Cell Cycle* **2013**, *12*, 263−270.
(43) Lovaas, J. D.; Zhu, L.; Chiao, C. Y.; Byles, V.; Faller, D. V.; Dai, Y. SIRT1 enhances matrix metalloproteinase-2 expression and tumor cell invasion in prostate cancer cells. *Prostate* **2013**, *73*, 522−530.
(44) Jang, K. Y.; Noh, S. J.; Lehwald, N.; Tao, G. Z.; Bellovin, D. I.; Park, H. S.; Moon, W. S.; Felsher, D. W.; Sylvester, K. G. SIRT1 and c-Myc promote liver tumor cell survival and predict poor survival of human hepatocellular carcinomas. *PLoS One* **2012**, *7*, e45119.
(45) Suzuki, K.; Hayashi, R.; Ichikawa, T.; Imanishi, S.; Yamada, T.; Inomata, M.; Miwa, T.; Matsui, S.; Usui, I.; Urakaze, M.; Matsuya, Y.; Ogawa, H.; Sakurai, H.; Saiki, I.; Tobe, K. SRT1720, a SIRT1 activator, promotes tumor cell migration, and lung metastasis of breast cancer in mice. *Oncol. Rep.* **2012**, *27*, 1726−1732.
(46) Canto, C.; Gerhart-Hines, Z.; Feige, J. N.; Lagouge, M.; Noriega, L.; Milne, J. C.; Elliott, P. J.; Puigserver, P.; Auwerx, J. AMPK regulates energy expenditure by modulating NAD^+ metabolism and SIRT1 activity. *Nature* **2009**, *458*, 1056−1060.
(47) Lan, F.; Cacicedo, J. M.; Ruderman, N.; Ido, Y. SIRT1 modulation of the acetylation status, cytosolic localization, and activity of LKB1. Possible role in AMP-activated protein kinase activation. *J. Biol. Chem.* **2008**, *283*, 27628−27635.

JOURNAL OF AGRICULTURAL AND FOOD CHEMISTRY

Article

pubs.acs.org/JAFC

Caffeic Acid Phenethyl Ester, a Major Component of Propolis, Suppresses High Fat Diet-Induced Obesity through Inhibiting Adipogenesis at the Mitotic Clonal Expansion Stage

Seung Ho Shin,[†,#] Sang Gwon Seo,[†,‡,§,#] Soyun Min,[†] Hee Yang,[†] Eunjung Lee,[†,‡] Joe Eun Son,[†] Jung Yeon Kwon,[∥] Shuhua Yue,[⊥] Min-Yu Chung,[†] Kee-Hong Kim,[∥] Ji-Xin Cheng,[⊥,¶] Hyong Joo Lee,*[,√] and Ki Won Lee*[,‡,§,√]

[†]Department of Agricultural Biotechnology and Center for Agricultural Biomaterials, [‡]WCU Biomodulation Major, Department of Agricultural Biotechnology and Center for Food and Bioconvergence, Seoul National University, Seoul 151-921, Republic of Korea

[§]Advanced Institutes of Convergence Technology, Seoul National University, Suwon 443-270, Republic of Korea

[√]Research Institute of Bio Food Industry, Institute of Green Bio Science and Technology, Seoul National University, Pyeongchang 232-916, Republic of Korea

[∥]Department of Food Science, [⊥]Weldon School of Biomedical Engineering, [¶]Department of Chemistry, Purdue University, West Lafayette, Indiana 47907, United States

Supporting Information

ABSTRACT: In the present study, we aimed to investigate the antiobesity effect of CAPE in vivo, and the mechanism by which CAPE regulates body weight in vitro. To confirm the antiobesity effect of CAPE in vivo, mice were fed with a high fat diet (HFD) with different concentrations of CAPE for 5 weeks. CAPE significantly reduced body weight gain and epididymal fat mass in obese mice fed a HFD. In accordance with in vivo results, Oil red O staining results showed that CAPE significantly suppressed MDI-induced adipogenesis of 3T3-L1 preadipocytes. FACS analysis results showed that CAPE delayed MDI-stimulated cell cycle progression, thereby contributing to inhibit mitotic clonal expansion (MCE), which is a prerequisite step for adipogenesis. Also, CAPE regulated the expression of cyclin D1 and the phosphorylation of ERK and Akt, which are upstream of cyclin D1. These results suggest that CAPE exerts an antiobesity effect in vivo, presumably through inhibiting adipogenesis at an early stage of adipogenesis.

KEYWORDS: *caffeic acid phenethyl ester, diet-induced obesity, 3T3-L1 preadipocytes, adipogenesis, mitotic clonal expansion*

INTRODUCTION

Obesity is a major health problem worldwide that is associated with the increased risk of type 2 diabetes and other chronic diseases.[1,2] Obesity is characterized by an increase in adipose tissue mass, which is associated with an increased fat cell number (hyperplasia) and cell size (hypertrophy).[3] It is the murine 3T3-L1 cell line that can mimic in vivo fat cell hyperplasia and hypertrophy. The 3T3-L1 cell line is a well-established in vitro model for adipogenesis, a differentiation program of preadipocytes to adipocytes.[4−6] Adipogenesis of 3T3-L1 preadipocytes involves growth arrest, mitotic clonal expansion (MCE), and terminal differentiation.[6−8] In particular, MCE is a prerequisite step for transcriptional activation and terminal differentiation of adipocytes.[9] Thus, suppression of MCE could be an effective strategy for the prevention of adipogenesis during the development of obesity.

MCE is associated with elevated mRNA levels of adipogenic transcription factors, such as CCAAT/enhancer-binding protein (C/EBP) α, C/EBPβ, and peroxisome proliferator-activated receptor (PPAR) γ.[9] One of the major events that occur during MCE is increased levels of cell cycle regulators, including cyclins and cyclin-dependent kinases (CDKs).[10] During the G1 phase of cell cycling, activated cyclin D and E bind with their catalytic partners to form active kinase complexes. While cyclin D binds to CDK4 or CDK6 and cyclin E binds to CDK2, cyclin A and B interact with CDK2 and CDK1, leading to the initiation of cell cycle progression through S phase. These kinase complexes inactivate retinoblastoma (Rb) proteins and/or induce hyperphosphorylation of Rb,[11] resulting in transcriptional activation of the S phase-associated genes,[12] which allows the preadipocytes synchronously to pass through the G1/S checkpoint.[9] MCE is also associated with a decrease of p27, a CDK inhibitor,[13] which inhibits the phosphorylation of Rb through kinase complexes, such as CDK4/cyclin D1.[14] ERK and PI3K/Akt-mediated signaling pathways are also involved in the initiation of cell cycle progression, contributing to adipogenesis.[15,16] Therefore, blockade or a delay of the cell cycle progression by inactivating cell cycle regulators, upregulation of CDK inhibitors, and/or inhibiting MAPK and PI3K/Akt-mediated signaling pathways during MCE would effectively contribute to suppressing adipogenesis.

Received: November 19, 2013
Revised: March 9, 2014
Accepted: March 10, 2014
Published: March 10, 2014

ACS Publications © 2014 American Chemical Society

Caffeic acid phenethyl ester (CAPE) is a polyphenol abundantly found in propolis, a resinous mixture that honey bees collect from tree buds, sap flows, and other botanical sources. Approximately 12−17 mg/g of CAPE is obtained from propolis ethyl acetate extract.[17,18] So far, there has been no study about the antiobesity effect of CAPE in vivo. Although studies conducted by Juman et al.[19,20] demonstrated that CAPE reduced the production and secretion of adipokines as well as transcription factors associated with adipogenesis in 3T3-L1 preadipocytes, the molecular mechanism by which CAPE regulates adipogenesis is not studied. Hence, we investigated the antiobesity effect of CAPE in the diet-induced obesity (DIO) animal model and the mechanism by which CAPE regulates body weight using 3T3-L1 preadipocytes.

MATERIALS AND METHODS

Chemicals. CAPE (of which purity is 99.4%) was obtained from Chromadex Inc. (Santa Ana, CA, USA). Antibodies against p-Akt, Akt, and C/EBPα were purchased from Cell Signaling Biotechnology (Beverly, MA, USA), and antibodies against p-ERK, ERK, cyclin D1, cyclin A1, and PPARγ were purchased from Santa Cruz Biotechnology (Santa Cruz, CA, USA). Antibody against β-actin was purchased from Sigma (St. Louis, MO, USA). Dexamethasone, 3-isobutyl-1-methylxanthine (IBMX), and insulin were purchased from Sigma.

Animals and Diets. Male C57BL/6N mice (5-wk old) were purchased from Koatech (Pyeongtaek, Korea). After 1 week of acclimation, mice were housed in climate-controlled quarters (23 ± 3 °C at 50 ± 10% humidity) with a 12-h light/12-h dark cycle. All experimental procedures were approved by Hallym University (Gangwon-do, Korea). Mice were divided into five dietary groups (n = 10−11 per each group): a normal diet (10% fat from calorie), a high fat diet (HFD; 60% fat from calorie), and a HFD supplemented with 0.02, 0.1, or 0.5% CAPE (w/w). The standard diet and HFD were purchased from Research Diets, Inc. (New Brunswick; NJ, USA) and were given in the form of pellets for 5 weeks. Body weight was recorded every week, and food intake was monitored every two days. Food was removed 12 h before the animals were sacrificed. The mice were anesthetized, and adipose tissue, the liver, and kidney were removed, weighed, and stored at −70 °C until analysis.

Cell Culture and Adipocytes Differentiation. 3T3-L1 mouse preadipocyte cell line was kindly provided by Dr. J. B. Kim (Seoul National University, Seoul, Korea). 3T3-L1 preadipocytes were maintained in Dulbecco's modified Eagle's medium (DMEM) supplemented with 10% bovine calf serum (BCS) at 5% CO_2 and 37 °C until confluence. Confluent cells were incubated in DMEM supplemented with 10% fetal bovine serum (FBS) and MDI cocktail [1 μM dexamethasone, 0.5 mM IBMX, and 5 μg/mL insulin]. After 2 days, the medium was replaced with DMEM containing 10% FBS and insulin (5 μg/mL). Medium was then replaced every two days with DMEM containing 10% FBS.

Oil Red O Staining. 3T3-L1 preadipocytes were seeded in 24-well plates at a density of 2.5×10^4 cells/well and incubated until confluence. The cells were then incubated with 10% FBS DMEM supplemented with MDI cocktail with or without CAPE (10, 20, and 40 μM). The medium was then changed to 10% FBS DMEM supplemented with 5 μg/mL of insulin, and replaced every two days. After the induction of cell differentiation, the medium was removed, and the mature 3T3-L1 adipocytes were fixed in 10% formalin. After fixing with 10% formalin, the cells were washed with 1,2-propanediol (Sigma, St. Louis, MO, USA) and stained with Oil red O solution. Stained cells were then washed with phosphate buffered saline (PBS), and the lipid droplets stained with Oil red O were eluted with isopropyl alcohol and quantified by measuring the absorbance at 515 nm by spectrophotometer.

Multimodal Coherent Anti-Stokes Raman Scattering (CARS) Microscope. CARS and two-photon excitation fluorescence (TPEF) imaging analysis were performed as described previously.[21] For CARS/TPEF imaging of lipid droplets in adipocytes, the wavenumber difference between the pump laser and Stokes laser was tuned to 2840 cm^{-1}, which matches the Raman shift of the symmetric CH_2 stretch vibration in lipid molecules. The forward detected CARS signal was collected by an air condenser (numerical aperture = 0.55), transmitted through a 600/65-nm bandpass filter and detected by a photomultiplier tube (PMT, H7422-40, Hamamatsu, Japan). For TPEF imaging of intracellular fluorescent CAPE, the back-reflected signal was collected by the objective, spectrally separated from the excitation source, transmitted through a 520/40-nm bandpass filter and detected by a PMT (H7422-40, Hamamatsu, Japan) mounted at the back port of the microscope. Acquisition time for each image was 1.12 s. Images were analyzed using Fluo-View software (Olympus, PA, USA).

Western Blot Assay. Western blot analysis was performed as previously described.[22] In brief, 3T3-L1 preadipocytes were seeded in a 6 cm dish at a density of 1.5×10^5 cells per dish and cultured for two days with DMEM supplemented with 10% BCS. Confluent cells were subjected to adipogenesis with MDI in the presence or absence of CAPE (10, 20, and 40 μM). Cells were lysed, loaded onto 10% sodium dodecyl sulfate−polyacrylamide gel electrophoresis (SDS−PAGE), and transferred to nitrocellulose membranes (GE healthcare, Piscataway, NJ, USA). The membrane was blocked with 5% skim milk and incubated with the indicated primary antibodies. The membrane was then incubated with HRP-conjugated secondary antibodies. Protein bands were visualized by a chemiluminescence detection kit (Amersham Pharmacia Biotech; Piscataway, NJ, USA), and the density of the protein bands was quantified using the NIH Image J analysis program.

Trypan Blue Assay. 3T3-L1 preadipocytes were seeded in 24-well plates at a density of 2.5×10^4 cells per well and incubated in DMEM supplemented with 10% FBS with or without CAPE (10, 20, and 40 μM). Cells were trypsinized and stained with 0.4% trypan blue for 5 min. The stained cells were loaded onto a hematocytometer, and the viable cells were counted.

Flow Cytometry Using a Fluorescence-Activated Cell Sorter (FACS) Analysis. 3T3-L1 preadipocytes were seeded in a 6 cm dish at a density of 1.5×10^5 cells per dish. Confluent cells were differentiated with MDI cocktail in the presence or absence of CAPE (40 μM). After centrifugation (1,000 rpm for 3 min), cells were suspended in 70% ethanol (v/v) and fixed overnight at 4 °C. The fixed cells were then centrifuged (1,500 rpm for 3 min), resuspended in PBS containing propidium iodide (PI) solution (Sigma, St. Louis, MO, USA) and RNase (Amresco, Solon, OH, USA), and incubated at 37 °C in the dark (10 min). Cell fluorescence was measured using a FACS calibur flow cytometer (Becton-Kickinson; San Jose, CA, USA). Ten thousands cells in each sample were analyzed.

Real-Time Quantitative PCR. Messenger RNA (mRNA) was extracted from mouse epididymal fat tissue using RNA-Bee (TEL-TEST; Pearland, TX, USA) and reverse transcribed into cDNA using Promega product (Fitchburg, WI, USA). Real-time quantitative PCR was performed as described previously[23] using the SYBR Green RT-PCR kit from Fermentas (Glen Burnie, MD, USA). Each reaction yielded amplicons of 101 bp. Results are expressed relative to β-actin.

Statistical Analysis. In vitro data were expressed as the means ± SD, and Student's t test was used for comparisons. A probability value of $p < 0.05$ or $p < 0.01$ was used as the criterion for statistical significance. For in vivo study, data were expressed as the means ± SEM. One-way ANOVA with Newman−Keuls test was used to evaluate mean differences between groups. Data were analyzed using Graph Pad Prism (version 4.03; Graph Pad Software, Inc., San Diego, CA, USA). Means with superscripts of different letters were significantly different at $p < 0.05$.

RESULTS AND DISCUSSION

CAPE Suppresses HFD-Induced Body Weight Gain in C57BL/6N Mice. To investigate the antiobesity activity of CAPE in vivo, mice (5 wk old) were fed with a HFD supplemented with different concentrations of CAPE (0, 0.02, 0.1, or 0.5%) for 5 weeks. In regard to the antiobesity effect of CAPE in DIO animal model, Bezerra et al. reported that CAPE

improves glucose sensitivity and reduces hepatic steatosis without altering body weight.[24] However, in their study, they fed HFD to mice without CAPE for 8 weeks and started CAPE administration after the mice already became obese. Unlike the previous study, we started HFD and CAPE administration at the same time. The result shows that HFD-fed mice showed greater level of adiposity (Figure 1A). However, HFD-fed mice

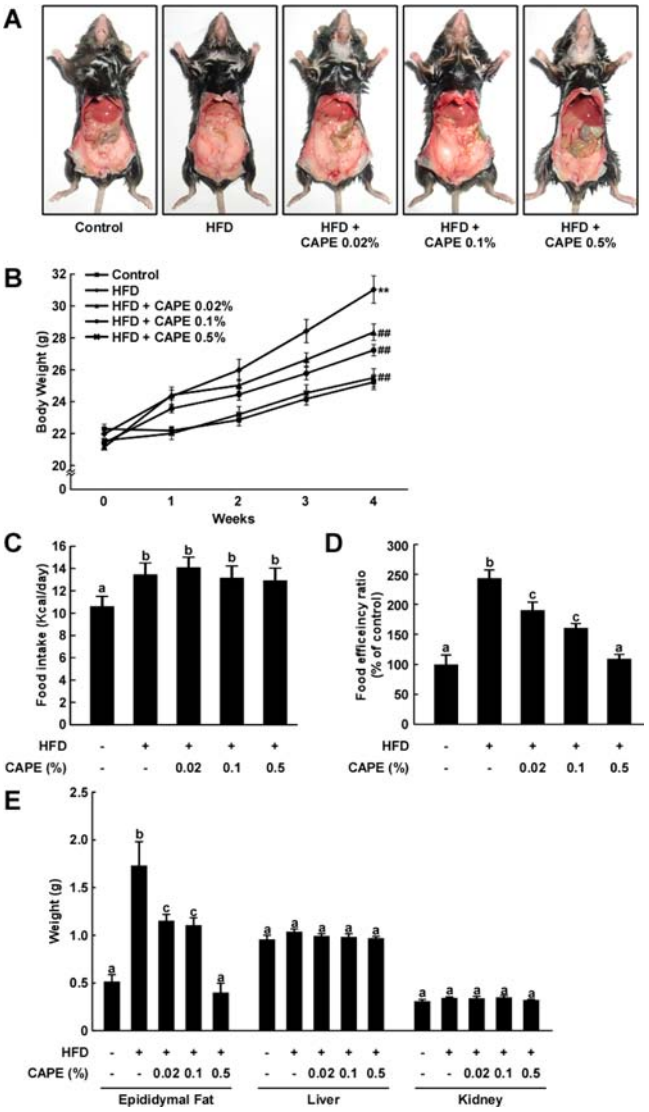

Figure 1. Effects of CAPE on HFD-induced obesity in C57BL/6N mice (n = 11). (A and B) CAPE treatment for 5 weeks alleviated HFD-induced weight gain in C57BL/6N mice. (C) Food intake was slightly reduced by CAPE (0.1 and 0.5%). (D) Food efficiency ratio was attenuated by CAPE treatment. (E) Epididymal fat tissue mass was significantly reduced by CAPE treatment, but liver and kidney tissue masses were unaffected by CAPE treatment. Values are expressed as the means ± SEM. The means marked with superscript letters are significantly different ($p < 0.05$).

supplemented with CAPE showed decreased level of adiposity in a dose-dependent manner (Figure 1A). Indeed, HFD-fed mice displayed significantly increased body weight ($p < 0.01$) (Figure 1B). CAPE decreased HFD-induced body weight gain completely to control levels at 0.5% ($p < 0.01$) (Figure 1B). Although food intake was affected slightly by HFD or CAPE as the same tendency as weight gain (Figure 1C), HFD or CAPE-induced body weight gain change was much more significant than food intake change. To normalize weight gain change to food intake, we estimated food efficiency ratio (FER) which was calculated by dividing the weight increase by the food intake. Compared to control mice, HFD-fed mice had 3.3 times greater FER, which was significantly decreased by the supplementation of CAPE at 0.02, 0.1, and 0.5% ($p < 0.05$) (Figure 1D). To investigate which organ was most affected by HFD, we weighed several organs including epididymal fat and liver. HFD increased epididymal fat mass by 3.5 times and CAPE significantly decreased epididymal fat mass ($p < 0.05$) without affecting the weights of other major organs, such as kidney and liver (Figure 1E). Indeed, dietary supplementation of CAPE at 0.5% decreased adipose tissue mass to control levels ($p < 0.05$) (Figure 1E). In particular, high concentration of CAPE (0.5%) nearly normalized it to the extent observed in the mice fed a control diet. We next examined the effect of CAPE on the expression of genes associated with adiposity. CAPE inhibited mRNA expression of adipogenic and lipogenic genes such as PPARγ, C/EBPα, and fatty acid synthase (FAS) (Figure S1, Supporting Information), and induced mRNA expression of lipolytic and thermogenic genes such as adipose triacylglycerol lipase (ATGL), peroxisome proliferator-activated receptor gamma coactivator 1α (PGC-1α), and long chain acyl CoA synthetase (ACSL) (Figure S2, Supporting Information). These data collectively suggest that the supplementation of CAPE attenuates HFD-induced body weight gain, which is attributable to fat mass reduction possibly by inhibiting adipogenesis and increasing energy expenditure.

CAPE Inhibits MDI-Induced Adipogenesis in 3T3-L1 Preadipocytes. To elucidate the underlying molecular mechanism of the antiobesity effect of CAPE, we used 3T3-L1 preadipocytes. Since Juman et al. reported that CAPE inhibits the differentiation of 3T3-L1 preadipocytes,[19,20] we confirmed the antiadipogenic activity of CAPE. Consistent with a previous report by Juman et al., CAPE dose-dependently inhibited the adipogenesis of 3T3-L1 preadipocytes (Figure 2A,B). We attempted to compare the antiadipogenic activity of CAPE with genistein, which is widely known as a suppressor of adipogenesis[25−27] during the differentiation of 3T3-L1 preadipocytes. Interestingly, a lower level of CAPE (40 μM) more effectively reduced cellular lipid contents than genistein (80 μM) (Figure 2B).

CARS/TPEF microscopy has recently been developed as a novel noninvasive and label-free imaging technique to visualize lipid-rich biological structures and naturally fluorescent intracellular molecules.[21] In an attempt to visualize lipid accumulation in differentiated adipocytes, CARS/TPEF microscopic analysis was performed. We observed that CAPE treatment dramatically reduces the number and size of lipid droplets of fully differentiated 3T3-L1 cells with a complete inhibition of adipogenesis at 40 μM (Figure 2C). Since CAPE is a naturally fluorescent molecule, CARS/TPEF microscopy also allowed us to visualize intracellular accumulation of CAPE, which is mostly found in the cytoplasm of differentiated 3T3-L1 preadipocytes (Figure 2C).

To confirm the antiadipogenic effect of CAPE at the molecular level, we checked the protein level of two well-known adipocyte marker genes, PPARγ and C/EBPα. Figure 2D showed that CAPE attenuated the protein level of PPARγ and C/EBPα (Figure 2D). We next performed the trypan blue assay to check whether these antiadipogenic activities of CAPE come from its cytotoxicity. The trypan blue assay showed that CAPE,

dx.doi.org/10.1021/jf405088f | J. Agric. Food Chem. 2014, 62, 4306−4312

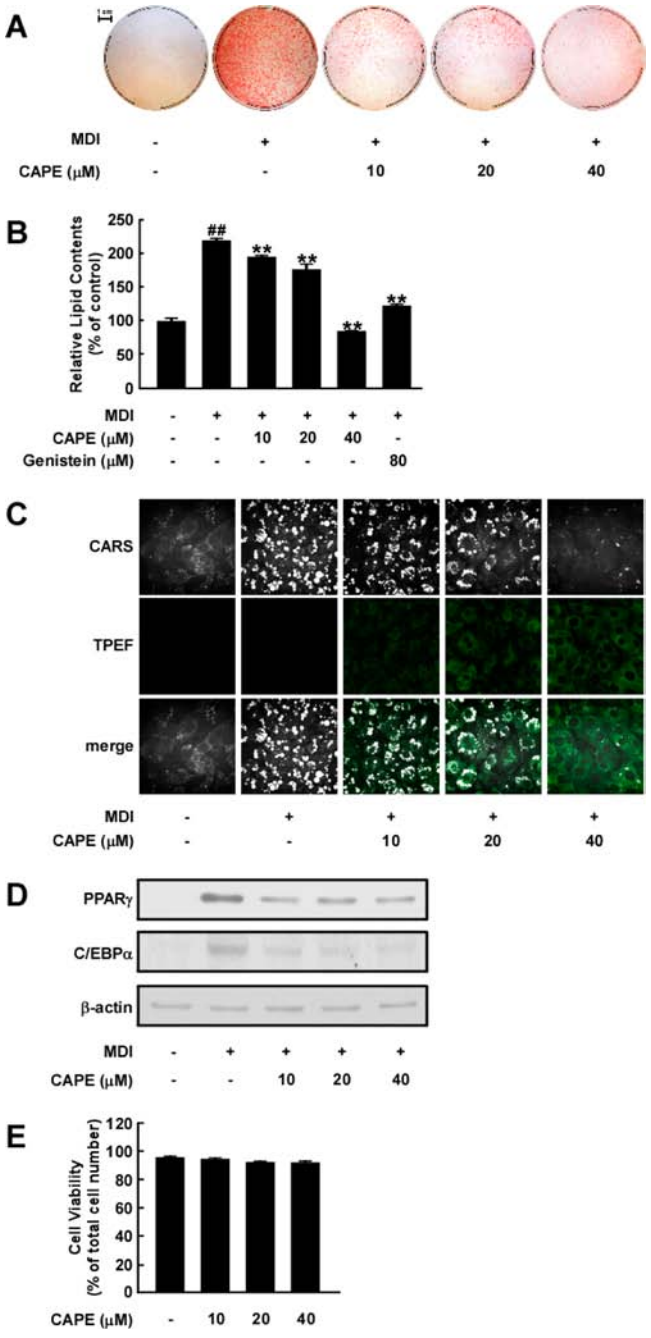

Figure 2. Effects of CAPE on MDI-induced adipogenesis in 3T3-L1 preadipocytes. (A,B) CAPE effectively inhibited MDI-induced adipogenesis of 3T3-L1 preadipocytes. Antiadipogenic effect of CAPE was better than that of genistein. Data are expressed as the means ± SEM from three separate experiments. (C) CAPE inhibited intracellular lipid accumulation of adipocytes, as evidenced by multimodal CARS/TPEF microscopy. (D) CAPE suppressed the protein expressions of MDI-induced PPARγ and C/EBPα. Data are representative of three independent experiments that showed the same tendency. (E) CAPE did not show cytotoxicity in 3T3-L1 preadipocytes up to 40 μM. Data are expressed as the means ± SEM from three separate experiments. ## indicate a significant difference between the control group and the group treated with MDI alone ($p < 0.01$), and ** indicate a significant difference between groups treated with MDI alone and treated with MDI plus CAPE ($p < 0.01$).

up to 40 μM, did not show any toxicity in 3T3-L1 preadipocytes (Figure 2E). Collectively, these findings indicate that CAPE suppresses MDI-induced adipogenesis of 3T3-L1 preadipocytes dose-dependently.

CAPE Exerts Its Antiadipogenic Activity at the Early Stage of Differentiation. A previous study conducted by Juman et al.[19] demonstrated that 50 μM CAPE significantly decreases total lipid contents of differentiated 3T3-L1 preadipocytes by ~17% compared to that of MDI-treated control cells.[19] However, our result showed that 40 μM CAPE completely inhibited adipogenesis of 3T3-L1 preadipocytes. We hypothesized that this discrepancy might be due to different CAPE-treated period, because they treated CAPE during days 3−7,[19] whereas we treated CAPE for the whole adipogenesis process. To clarify this discrepancy and to gain insight into the molecular mechanism underlying CAPE-inhibited adipogenesis, we examined the effect of CAPE (40 μM) on the adipogenesis of 3T3-L1 preadipocytes at different stages of cell differentiation (Figure 3A). Oil red O staining results showed that

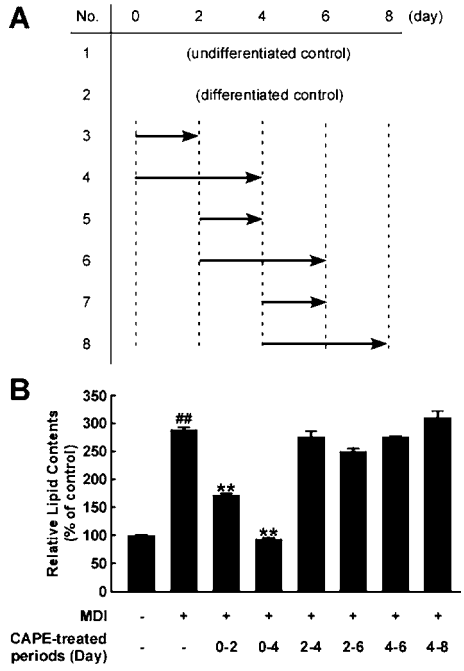

Figure 3. Effects of CAPE on 3T3-L1 preadipocytes during different stages of MDI-induced adipogenesis. (A) A time schedule for CAPE treatment during cellular differentiation. (B) CAPE reduced lipid accumulation when treated during days 0−2. Data are expressed as the mean ± SEM from three separate experiments. ## indicate a significant difference between the control group and the group treated with MDI alone ($p < 0.01$), and ** indicate a significant difference between groups treated with MDI alone and treated with MDI plus CAPE ($p < 0.01$).

CAPE treatment between days 0−2 and 0−4 significantly suppressed MDI-induced adipogenesis ($p < 0.01$) (Figure 3B). In particular, the treatment of CAPE at 40 μM during day 0−4 almost blocked lipid accumulation similar to the extent observed in undifferentiated control cells. Notably, CAPE exerted little effect on the adipogenesis of 3T3-L1 preadipocytes when it was treated at days 2−4, 2−6, 4−6, and 4−8. Since adipogenesis of 3T3-L1 preadipocytes consist of MCE in the early phase of differentiation and terminal differentiation,[6−8] these results indicate that CAPE inhibits adipogenesis by suppressing cellular differentiation during MCE, an early stage of adipogenesis. Also, CAPE treatment during days 2−4

dx.doi.org/10.1021/jf405088f | J. Agric. Food Chem. 2014, 62, 4306−4312

in our study showed antiadipogenic activity similar to the previous result by Juman et al. Since they treated CAPE after MDI treatment, their result corresponds to the CAPE treatment during days 2−4 in our study.

CAPE Delays Cell Cycle Progression during the Early Stage of Cellular Differentiation. We further attempted to elucidate the effect of CAPE on MCE during adipogenesis. The inhibitory effect of CAPE on cell cycle progression was examined (Figure 4). FACS analysis data showed that MDI-induced cell cycle progression was likely delayed by 40 μM of CAPE treatment (Figure 4A). The cell population in each stage of the cell cycle was quantified (Figure 4B). Untreated 3T3-L1 preadipocytes showed no remarkable changes in cell cycle progression during 36 h of culture, mostly staying in the G1/S checkpoint (basal state). However, cells passed the G1/S checkpoint at 16 h of MDI treatment and passed the S to G2/M phase at 20 h of MDI treatment. The cells exited the M phase and reentered into G1 phase from 24 to 36 h of MDI treatment. Meanwhile, cells treated with CAPE at 40 μM stayed at the G1/S checkpoint until 20 h of MDI treatment, but they entered S phase at 24 h. Moreover, we observed that cells treated with CAPE did not exit the G2/M phase and were arrested at the G2/M phase at 36 h (Figure 4B). These collectively indicate that CAPE delays cell cycle progression during MCE, thereby inhibiting adipogenesis of 3T3-L1 preadipocytes stimulated by MDI.

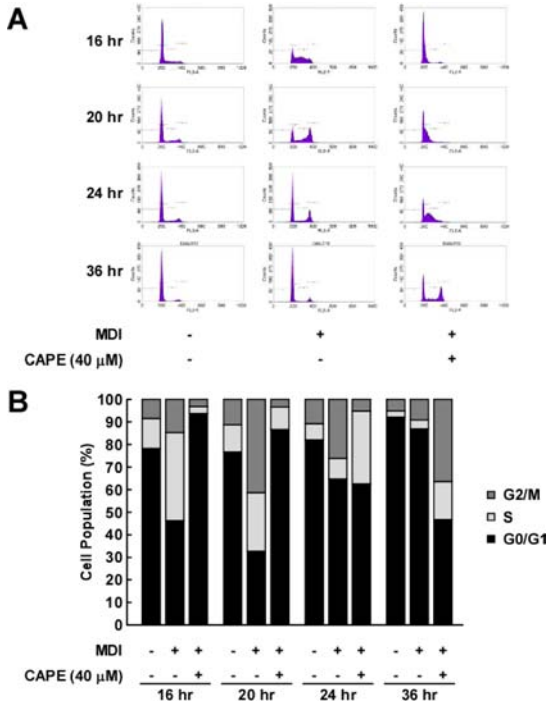

Figure 4. Effects of CAPE on MDI-induced cell cycle progression in 3T3-L1 preadipocytes. (A) CAPE inhibited the MDI-induced cell cycle progression of 3T3-L1 preadipocytes. Data are representative of three independent experiments that showed the same tendency. (B) The population of cells in each stage of the cell cycle was quantified.

CAPE Suppresses the Expression of Cyclin D1 during MCE. Since G1/S progression was significantly attenuated by CAPE treatment, we measured the protein expression level of cyclin D1, which has been reported to be implicated in G1/S transition. We found that the protein level of cyclin D1 was up-regulated in MDI-treated 3T3-L1 cells and that CAPE (40 μM) suppressed MDI-mediated upregulation of cyclin D1 (Figure 5A). We checked the mRNA expression level of cyclin D1 to investigate whether CAPE regulates cyclin D1 expression at the transcriptional level. We found that the mRNA level of cyclin D1 was also suppressed by 40 μM CAPE treatment (Figure 5B), indicating that CAPE inhibits cyclin D1 expression at the transcriptional level.

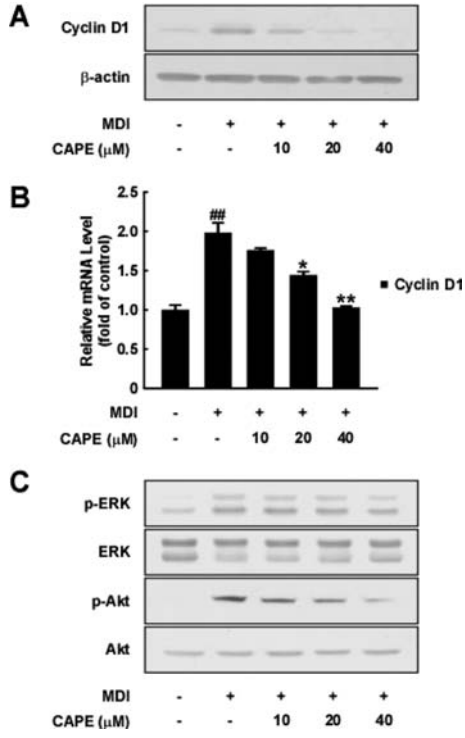

Figure 5. Effects of CAPE on cyclin D1 expression and its upstream signaling pathway in 3T3-L1 preadipocytes. (A) CAPE suppressed MDI-induced cyclin D1 protein expression. Data are representative of three independent experiments that showed the same tendency. (B) CAPE suppressed MDI-induced cyclin D1 mRNA expression. Data are expressed as the mean ± SEM from three separate experiments. ## indicate a significant difference between the control group and the group treated with MDI alone ($p < 0.01$), * indicates a significant difference between groups treated with MDI alone and treated with MDI plus CAPE ($p < 0.05$), and **, indicate a significant difference between groups treated with MDI alone and those treated with MDI plus CAPE ($p < 0.01$). (C) CAPE suppressed MDI-induced ERK and Akt phosphorylation. Data are representative of three independent experiments that showed the same tendency.

The result that CAPE decreased both the mRNA and protein levels of cyclin D1 prompted us to investigate the upstream signaling pathway of cyclin D1 expression. We estimated the effect of CAPE on MDI-induced ERK and Akt phosphorylation, which have been reported as upstream of cyclin D1. We found that MDI-induced phosphorylation of ERK and Akt was decreased by CAPE (40 μM) (Figure 5C). Collectively, CAPE suppressed mitotic clonal expansion of 3T3-L1 by down-regulating cyclin D1 by blocking MDI-mediated phosphorylation of ERK and Akt during MCE.

■ ASSOCIATED CONTENT

Supporting Information

Effects of CAPE on HFD-induced mRNA expression of adipogenic and lipogenic genes in C57BL/6N mice (N = 55); effects of CAPE on mRNA expression of lipolytic and thermogenic genes in C57BL/6N mice (N = 55). This material is available free of charge via the Internet at http://pubs.acs.org.

■ AUTHOR INFORMATION

Corresponding Authors

*(H.J.L.) Tel: 82-2-880-4853. Fax: 82-2-873-5095. E-mail: leehyjo@snu.ac.kr.

*(K.W.L.) Tel: 82-2-880-4661. Fax: 82-2-878-6178. E-mail: kiwon@snu.ac.kr.

Author Contributions

#S.H.S. and S.G.S. contributed equally to this work.

Funding

This research was supported by grant from National Research Foundation (NRF) of Korea (No. 2012M3A9C4048818) funded by the ministry of Science, ICT and Future Planning. This research was also supported by the grant from National Leap Research Program (No. 2010-0029233) through the National Research Foundation of Korea funded by the Ministry of Education, Science and Technology of Korea, Republic of Korea.

Notes

The authors declare no competing financial interest.

■ ACKNOWLEDGMENTS

We thank Kang, M. J., Suk, S. J., and Jung, E. S. for critical reading of this manuscript and Lee, D. E. and Song, N. R. for discussions.

■ ABBREVIATIONS USED

ACSL, long chain acyl CoA synthetase; ATGL, adipose triacylglycerol lipase; BCS, bovine calf serum; CAPE, caffeic acid phenethyl ester; CARS, coherent anti-Stokes Raman scattering; CDK, cyclin-dependent kinase; C/EBP, CCAAT-enhancer-binding protein; DIO, diet-induced obesity; ERK, extracellular signal-regulated kinase; FACS, fluorescence activated cell sorting; FAS, fatty acid synthase; FBS, fetal bovine serum; FER, food efficiency ratio; HFD, high fat diet; HRP, horseradish peroxidase; IBMX, isobutylmethylxanthine; MAPK, mitogen-activated protein kinase; MCE, mitotic clonal expansion; MDI, mixture of isobutylmethylxanthine, dexamethasone and insulin; PI, propidium iodide; PI3K, phosphatidylinositol 3-kinase; PGC-1α, peroxisome proliferator-activated receptor gamma coactivator 1α; PPAR, peroxisome proliferator-activated receptor; Rb, retinoblastoma; TPEF, two-photon excitation fluorescence

■ REFERENCES

(1) Hotamisligil, G. S. Inflammation and metabolic disorders. *Nature* **2006**, *444*, 860−867.

(2) Kopelman, P. G. Obesity as a medical problem. *Nature* **2000**, *404*, 635−643.

(3) Camp, H. S.; Ren, D.; Leff, T. Adipogenesis and fat-cell function in obesity and diabetes. *Trends Mol. Med.* **2002**, *8*, 442−447.

(4) Green, H.; Kehinde, O. An established preadipose cell line and its differentiation in culture. II. Factors affecting the adipose conversion. *Cell* **1975**, *5*, 19−27.

(5) Green, H.; Kehinde, O. Spontaneous heritable changes leading to increased adipose conversion in 3T3 cells. *Cell* **1976**, *7*, 105−113.

(6) Rosen, E. D.; Spiegelman, B. M. Molecular regulation of adipogenesis. *Annu. Rev. Cell Dev. Biol.* **2000**, *16*, 145−171.

(7) Otto, T. C.; Lane, M. D. Adipose development: from stem cell to adipocyte. *Crit. Rev. Biochem. Mol. Biol.* **2005**, *40*, 229−242.

(8) Rosen, E. D.; MacDougald, O. A. Adipocyte differentiation from the inside out. *Nat. Rev. Mol. Cell Biol.* **2006**, *7*, 885−896.

(9) Tang, Q. Q.; Otto, T. C.; Lane, M. D. Mitotic clonal expansion: a synchronous process required for adipogenesis. *Proc. Natl. Acad. Sci. U.S.A.* **2003**, *100*, 44−49.

(10) Nam, M.; Lee, W. H.; Bae, E. J.; Kim, S. G. Compound C inhibits clonal expansion of preadipocytes by increasing p21 level irrespectively of AMPK inhibition. *Arch. Biochem. Biophys.* **2008**, *479*, 74−81.

(11) Harbour, J. W.; Dean, D. C. The Rb/E2F pathway: expanding roles and emerging paradigms. *Genes Dev.* **2000**, *14*, 2393−2409.

(12) Coqueret, O. New targets for viral cyclins. *Cell Cycle* **2003**, *2*, 293−295.

(13) Zhang, J. W.; Tang, Q. Q.; Vinson, C.; Lane, M. D. Dominant-negative C/EBP disrupts mitotic clonal expansion and differentiation of 3T3-L1 preadipocytes. *Proc. Natl. Acad. Sci. U.S.A.* **2004**, *101*, 43−47.

(14) Sherr, C. J. Cancer cell cycles. *Science* **1996**, *274*, 1672−1677.

(15) Aguda, B. D.; Algar, C. K. A structural analysis of the qualitative networks regulating the cell cycle and apoptosis. *Cell Cycle* **2003**, *2*, 538−544.

(16) Gauthier, R.; Harnois, C.; Drolet, J. F.; Reed, J. C.; Vezina, A.; Vachon, P. H. Human intestinal epithelial cell survival: differentiation state-specific control mechanisms. *Am. J. Physiol. Cell Physiol.* **2001**, *280*, C1540−C1554.

(17) Izuta, H.; Shimazawa, M.; Tazawa, S.; Araki, Y.; Mishima, S.; Hara, H. Protective effects of Chinese propolis and its component, chrysin, against neuronal cell death via inhibition of mitochondrial apoptosis pathway in SH-SY5Y cells. *J. Agric. Food Chem.* **2008**, *56*, 8944−8953.

(18) Demestre, M.; Messerli, S. M.; Celli, N.; Shahhossini, M.; Kluwe, L.; Mautner, V.; Maruta, H. CAPE (caffeic acid phenethyl ester)-based propolis extract (Bio 30) suppresses the growth of human neurofibromatosis (NF) tumor xenografts in mice. *Phytother. Res,* **2009**, *23*, 226−230.

(19) Juman, S.; Yasui, N.; Okuda, H.; Ueda, A.; Negishi, H.; Miki, T.; Ikeda, K. Caffeic acid phenethyl ester inhibits differentiation to adipocytes in 3T3-L1 mouse fibroblasts. *Biol. Pharm. Bull.* **2010**, *33*, 1484−1488.

(20) Juman, S.; Yasui, N.; Okuda, H.; Ueda, A.; Negishi, H.; Miki, T.; Ikeda, K. Caffeic acid phenethyl ester suppresses the production of adipocytokines, leptin, tumor necrosis factor -alpha and resistin, during differentiation to adipocytes in 3T3-L1 cells. *Biol. Pharm. Bull.* **2011**, *34*, 490−494.

(21) Le, T. T.; Yue, S.; Cheng, J. X. Shedding new light on lipid biology with coherent anti-Stokes Raman scattering microscopy. *J. Lipid Res.* **2010**, *51*, 3091−3102.

(22) Kang, N. J.; Lee, K. W.; Lee, D. E.; Rogozin, E. A.; Bode, A. M.; Lee, H. J.; Dong, Z. Cocoa procyanidins suppress transformation by inhibiting mitogen-activated protein kinase kinase. *J. Biol. Chem.* **2008**, *283*, 20664−20673.

(23) Livak, K. J.; Schmittgen, T. D. Analysis of relative gene expression data using real-time quantitative PCR and the 2(-Delta Delta C(T)) method. *Methods* **2001**, *25*, 402−408.

(24) Bezerra, R. M.; Veiga, L. F.; Caetano, A. C.; Rosalen, P. L.; Amaral, M. E.; Palanch, A. C.; de Alencar, S. M. Caffeic acid phenethyl ester reduces the activation of the nuclear factor kappaB pathway by high-fat diet-induced obesity in mice. *Metab.: Clin. Exp.* **2012**, *61*, 1606−1614.

(25) Harmon, A. W.; Harp, J. B. Differential effects of flavonoids on 3T3-L1 adipogenesis and lipolysis. *Am. J. Physiol. Cell Physiol.* **2001**, *280*, C807−C813.

(26) Naaz, A.; Yellayi, S.; Zakroczymski, M. A.; Bunick, D.; Doerge, D. R.; Lubahn, D. B.; Helferich, W. G.; Cooke, P. S. The soy isoflavone genistein decreases adipose deposition in mice. *Endocrinology* **2003**, *144*, 3315−3320.
(27) Hsu, C. L.; Huang, S. L.; Yen, G. C. Inhibitory effect of phenolic acids on the proliferation of 3T3-L1 preadipocytes in relation to their antioxidant activity. *J. Agric. Food Chem.* **2006**, *54*, 4191−4197.

JOURNAL OF AGRICULTURAL AND FOOD CHEMISTRY

Article

pubs.acs.org/JAFC

Variability in the Antioxidant Activity of Dietary Supplements from Pomegranate, Milk Thistle, Green Tea, Grape Seed, Goji, and Acai: Effects of in Vitro Digestion

Susanne M. Henning,*[,†] Yanjun Zhang,[†] Victoria G. Rontoyanni,[†,‡] Jianjun Huang,[†] Ru-Po Lee,[†] Amy Trang,[†] Gloria Nuernberger,[†] and David Heber[†]

[†]Center for Human Nutrition, David Geffen School of Medicine, University of California, Los Angeles, California 90095, United States

[‡]Epidemiology Department, Office of the Chief Quality Officer, Baylor Scott & White Health, Dallas, Texas 75206, United States

ABSTRACT: The antioxidant activity (AA) of fruits and vegetables has been thoroughly investigated but less is known about the AA of dietary supplements (DS). We therefore assessed the AA of three to five DS each from pomegranate, milk thistle, green tea, grapes, goji, and acai using four widely used standard methods. The secondary objective was to determine the effects of in vitro digestion on their AA. The AA of the DS prior to digestion ranked as follows: pomegranate > resveratrol > green tea > grape seed > milk thistle and very low in goji and acai with significant group variability in AA. The AA after in vitro simulated digestion of the mouth, stomach, and small intestine compared to undigested supplement was decreased for green tea and grape seed but increased for pomegranate, resveratrol, milk thistle, goji, and acai to various extents. Although polyphenols provide the major antioxidant potency of the tested supplements, our observations indicate that digestion may alter antioxidant properties depending in part on the variations in polyphenol content.

KEYWORDS: *pomegranate, antioxidant activity, in vitro digestion, dietary supplements, green tea, milk thistle, acai, goji, resveratrol, grape seed*

INTRODUCTION

Over half of U.S. adults consume at least one dietary supplement (DS) per day as estimated by data from the National Health and Nutrition Examination Survey (NHANES) 1999−2002.[1] According to Yang et al.,[2] DS provide 25% of dietary total antioxidant capacity in U.S. adults. Polyphenolic phytochemicals are the most frequently occurring phytochemicals in DS with in vitro antioxidant properties.[3] On the basis of an evaluation of the NHANES 2001−2002 data, flavonoid and proanthocyanidin intake contributes 56% of total antioxidants in the diet.[2] Although polyphenols are principally ingested in the diet, commercially available polyphenolic supplements are numerous and commonly used and may contribute to the antioxidant intake. Typical DS that contain antioxidant polyphenols are derived from pomegranate fruit (*Punica granatum* L.), green tea (*Camellia sinensis*), and grapes (*Vitis vinifera*). Other DS such as milk thistle (*Silybum marianum*) extract, acai (*Euterpe oleracea*), and goji berries (*Lycium barbarum* L.) are commonly consumed for their antioxidant activity (AA) but contain very different phytochemical structures (e.g., stilbenes for resveratrol), all of which have some AA.

The main phytochemicals held responsible for AA vary considerably in these DS. Pomegranate fruit contains ellagitannins, gallotannins, ellagic acid, and smaller amounts of flavonoids and anthocyanins.[4−6] Green tea extracts contain polyphenols including (−)-epicatechin, (−)-epigallocatechin, and their gallate derivatives (−)-epicatechin-3-gallate and (−)-epigallocatechin-3-gallate, which are distinguished by their potent antioxidant and anti-inflammatory properties, offering cardiovascular and neural protection, and for their effects on fat oxidation.[7] Proanthocyanidins in grape seed extract are the main polyphenolic ingredients responsible for its antioxidant, anti-inflammatory, and antimicrobial effects.[7,8] Resveratrol (3,5,4′-trihydroxystilbene) is a stilbene polyphenol that exerts anti-inflammatory, antioxidant, and estrogenic effects and anticancer properties.[9] Although advertised as a grape extract, it is commonly extracted from the root of Japanese knotwood and occurs as a phytoalexin on the skin of grapes grown in humid conditions, where they are susceptible to fungal infection. The fruit of the milk thistle plant, with its active ingredient and flavonoid complex, silymarin, has been used to promote liver health. Silybin, a flavonolignan, represents about 50−70% of the silymarin extract, among other flavonolignans and flavonoids. Silybin and the rest of the silymarin constituents have demonstrated liver-protective properties under experimental conditions due to their antioxidant and anti-inflammatory properties.[10] In recent years, two berry species rich in polyphenolic phytochemicals, acai berry (Amazonian palm berry) and goji berry, have been widely promoted as having antioxidant properties attributed to their primary active ingredients, β-carotene, β-cryptoxanthin, zeaxanthin, and polysaccharides in goji berry fruit[11] and anthocyanins and other polyphenols in acai berry.[12−15]

Received: January 15, 2014
Revised: April 7, 2014
Accepted: April 18, 2014
Published: April 18, 2014

 © 2014 American Chemical Society

It was the objective of the present study to assess the variability of composition and AA of three to five commercially available DS from pomegranate, green tea, grape seed, milk thistle, resveratrol, acai, and goji berry using four antioxidant assays. The oxygen radical absorbing capacity (ORAC) hydrophilic and lipophilic, which measures a hydrogen atom transfer reaction, was used in addition to assays measuring electron transfer/reducing capacities such as the Trolox equivalent antioxidant capacity (TEAC), ferric reducing antioxidant power (FRAP), and free radical scavenging properties by the diphenyl-1-picrylhydrazyl (DPPH) radical.

In a second phase, we determined the effect of digestion on the AA of these popular DS because we were interested in whether antioxidant activity would survive the digestive processes. Although in vivo feeding or supplementation studies in animals or humans provide the ultimate tests, in vitro digestion models simulating digestive pH and enzymatic exposure provide a practical alternative for investigating the impact of digestion on DS antioxidant properties.[16] The DS were treated under in vitro simulated gastrointestinal conditions, and the AA was analyzed using the TEAC assay. The TEAC assay was chosen from among the four antioxidant assays used in the first phase of our studies because TEAC exhibited the highest correlation with the sum of all antioxidant assays. It was also the most reproducible among the methods used.

MATERIALS AND METHODS

Chemicals and Reagents. All solvents were purchased from Fisher Scientific Co. (Tustin, CA, USA). 2,2′-Azinobis(3-ethylbenzothiazoline-6-sulfonic acid) diammonium salt (ABTS), manganese dioxide, 6-hydroxy-2,5,7,8-tetramethylchroman-2-carboxylic acid (Trolox), ferrous chloride, fluorescein sodium salt, and (2,4,6-tris(2-pyridyl)-s-triazine, 1,1-dipenyl-2-picrylhydrazyl (DPPH) were purchased from Sigma-Aldrich Co. (St. Louis, MO, USA). Randomly methylated β-cyclodextrin was purchased from CTD Holdings (Alachua, FL, USA).

Dietary Supplements. A total of 25 antioxidant DS from 7 different categories, acai berry (n = 3, A1−A3), goji berry (n = 3, G1−G3), grape seed (n = 3, GS1−GS3), green tea (n = 4, GT1−GT4), milk thistle (n = 4, MT1−MT4), pomegranate (n = 5 samples, PM1−PM5), and resveratrol (n = 3, Res1−Res3), were obtained on the basis of accessibility to the average consumer (purchased from retail stores, chain pharmacies, Internet, or mail order). The DS were delivered in the form of encapsulated powder (n = 17 samples), soft gel (n = 4), tablet (n = 2), or liquid (n = 2). The antioxidant activity of all DS was determined prior to the expiration date as stated on their packages. The main information found on the packaging label of all tested DS is listed in Table 1. The pomegranate extract DS tested were PomX (POM Wonderful LLC, Los Angeles, CA, USA), Healthy Pomegranate (Nature's Bounty, Bohemia, NY, USA), Full-Spectrum Pomegranate (Life Extension, Ft. Lauderdale FL, USA), Pomegranate 40:40 Complex (All Solar, Henderson, NV, USA), and Pomella (+PLUS) (Phytosensia, Indianapolis, IN, USA; and Pomella, Noblesville, IN, USA). The green tea extract DS tested were Green Tea Extract (Radiance, Encinitas, CA, USA), Green Tea Complex (Safeway Inc., Pleasanton, CA, USA), Standardized Extract Green Tea (Nature's Bounty), and Green Tea Standardized (Nature's Way, Lehi, UT, USA). The milk thistle extract DS used were Milk Thistle XTRA (Sundown Naturals, Boca Raton, FL, USA), Standardized Extract Milk Thistle (Nature's Bounty), Super Maximum Milk Thistle Extract (Vitamin Shoppe, North Bergen, NJ, USA), and Milk Thistle (Safeway, Pleasanton, CA, USA). The grape seed extract DS used were Grapeseed Extract (Radiance, Ronkonkoma, NY, USA), Masquelier's Tru-OPCs (Nature's Way), and ActiVin Grape Seed Extract (Paradise, Huntington Beach, CA, USA). The acai extract DS were Acai (Nature's Bounty), Acai Extract (Vitamin Shoppe), and Acai with Green Tea (Radiance). Resveratrol extracts obtained were Resveratrol forte (Enzymatic Therapy, Green Bay, WI, USA), Reservie and Trans-Resveratrol (Vitamin Shoppe), and Resveratrol, Synergistic Formula (Nature's Way). Goji berry juice/extracts used were Goji Gold (Dynamic Health, Brooklyn, NY, USA), Goji 100 (Genesis Today, Austin, TX, USA), and Goji Berry (Ultra Laboratories, Carson, CA, USA).

Table 1. Labeling Information of All Dietary Supplements[a]

ID	main ingredients
	pomegranate
PM1	pomegranate extract
PM2	pomegranate extract (40% ellagic acid)
PM3	pomegranate extract [30% punicalagins (120 mg)]; plus pomegranate blend [22% (30 mg) punicic acid]
PM4	vitamin C; plus pomegranate extract (40% punicalagins/40% ellagic acid)
PM5	pomegranate extract [30% punicalagins (240 mg)]
	green tea extract
GT1	green tea extract (15% polyphenols, 95 mg in two capsules)
GT2	green tea extract (25% polyphenols, 8.5% EGCG, 5% caffeine), 790 mg; plus green tea powder (leaf, 210 mg)
GT3	green tea extract (15% polyphenols 95 mg in two capsules)
GT4	green tea extract (9% polyphenols) plus green tea (leaf)
	resveratrol
Res1	resveratrol, 100% *trans*-resveratrol, 175 mg; plus Japanese sophora flower bud extract, 74% rutin (quercetin rutinoside), 75 mg
Res2	250 mg of *trans*-resveratrol; plus quercetin (quercetin dihydrate, 100 mg)
Res3	red wine extract (30% polyphenols, 60 mg); plus red wine powder; plus Japanese knotweed (50% resveratrol 75 mg)
	grape seed extract (95% polyphenols 95 mg)
	grape seed extract
GS1	grapeseed extract (50% polyphenols 100 mg); plus citrus bioflavonoids 300 mg
GS2	grape seed extract (95% antioxidants; 65% oligomeric procyanidins (OPCs), 30% other active polyphenols
GS3	grape seed extract 100:1
	milk thistle
MT1	milk thistle extract (80% silymarin 192 mg)
MT2	milk thistle extract (80% silymarin 140 mg)
MT3	milk thistle extract (80% silymarin 240 mg)
MT4	milk thistle extract (80% silymarin 140 mg)
	acai
Acai1	acai extract
Acai2	acai berry 5:1 extract
Acai +GT	acai (20:1 extract equivalent to 1000 mg); plus green tea (4:1 extract equivalent to 500 mg)
	goji
Goji1	100% goji juice
Goji2	goji liquid concentrate
Goji3	goji berry extract (20% polysaccharides)

[a]DS, dietary supplements; PM, pomegranate; GT, green tea; EGCG, (−)-epigallocatechin gallate; GS, grape seed; Res, resveratrol; MT, milk thistle.

Digestive Enzymes. All digestive enzymes were purchased from Sigma-Aldrich. All enzyme solutions were freshly prepared for each experiment to avoid potential decreases over time in enzyme activities. α-Amylase from *Aspergillus oryzae* (∼30 units/mg) was dissolved in the phosphate buffer saline (PBS) solution (160 units/mL) that was preadjusted to pH 6.5. Porcine pepsin from gastric mucosa (≥250 units/mg solid) was dissolved at 40 mg/mL in 0.1 M HCl. Pancreatin from porcine pancreas was mixed with a porcine bile extract mixture at a constant ratio of 1:6 and dissolved in 0.1 M $NaHCO_3$. Pancreatin contains several enzymes, including amylase, trypsin, lipase, ribonuclease, and protease. Bile extract contains glycine and taurine conjugates of hyodeoxycholic acid and other bile salts.

In Vitro Digestion. The in vitro digestion was performed according to the methods described by Chohan et al.[17] and Werner and Böhm.[18] Each digestion step was optimized separately. The AA of the in vitro digestion treatment (enzyme and pH adjustment alone) was minimal (0.12 mmol TE/100 g).

Salivary Step. Two hundred and fifty milligrams of aqueous sample extracts were crushed lightly and dissolved for 2 min in 4 mL of α-amylase in PBS solution (160 units/mL; adjusted to pH 6.5) by using a preheated pestle and mortar at 37 °C.

Gastric Step. Immediately after the salivary step, the mixture was acidified to pH 3.0 (with 0.1 M HCl) and incubated with pepsin solution in 0.1 M HCl for 60 min at 37 °C at ∼190 strokes/min.

Duodenal Step. Following the gastric simulation step, the mixture was raised to pH 6.5−7 with 1 M $NaHCO_3$ and incubated with pancreatin and bile extract in 0.1 M $NaHCO_3$ for 120 min at 37 °C in a shaking water bath at 190 strokes/min. The in vitro digested mixture was centrifuged at 2060*g* for 5 min at 4 °C, filtered through filter paper (Whatman grade 1) and a 0.2 μm pore size nylon filter, and adjusted to pH 5.5−6.0 with 0.1 M HCl. Digested samples were stored at −20 °C until analysis for no longer than 1 week.

Preparation of Nondigested (Control) Sample Extracts. Nondigested controls were prepared by extracting 250 mg per sample in water to a concentration matching the concentration of the in vitro digested sample mixtures.

Antioxidant Assays. Except for the lipophilic ORAC assay, the 25 nondigested DS were extracted in a 10-fold volume of methanol to weight (250 mg DS/2.5 mL). Samples were vortexed (10 min), sonicated (10 min), and centrifuged (10 min at 2000*g*). Supernatants were diluted with aqueous buffers depending on the assay. Sonication had no significant effect on the AA. For the digested and nondigested (control) DS, extraction was performed with water as mentioned above.

Trolox Equivalent Antioxidative Capacity (TEAC). The TEAC was determined by measuring the ability to scavenge ABTS radical cations produced by oxidation of ABTS with manganese dioxide. The assay was performed as previously reported.[19] Briefly, ABTS radical cations were prepared by adding solid manganese dioxide (80 mg) to a 5 mM aqueous stock solution of $ABTS^+$ (20 mL using a 75 mM sodium/potassium (Na/K) buffer of pH 7). Trolox, a water-soluble analogue of vitamin E, was used as an antioxidant standard. A standard calibration curve was constructed for Trolox at 0−0.3 mM concentrations. DS extracts (250 mg/2.5 mL of MeOH) were diluted in Na/K buffer. Diluted samples were mixed with 200 μL of $ABTS^+$ radical cation solution in 96-well plates, and absorbance was read (at 750 nm) after 30 min in a VersaMax microplate reader (Molecular Devices, Sunnyvale, CA, USA). TEAC values were calculated from the Trolox standard curve and expressed as Trolox equivalents (mmol TE/100 g). All samples were extracted in duplicate, and the TEAC assay was performed in triplicate for each extract.

Total Oxygen Radical Absorbance Capacity (ORAC). The ORAC assay was conducted as previously described.[20] For the hydrophilic ORAC a mixture of 200 μL of fluorescein sodium salt (0.1 μM) was used as the target of free radical attack, and 75 μL of 2,2′-azobis(amidinopropane) dihydrochloride (AAPH) (63.4 mM) was used as a peroxyl radical generator at 37 °C combined with 20 μL of each sample extract. DS extracts (250 mg/2.5 mL of MeOH) were diluted in Na/K buffer. Trolox standards ranged from 5 to 100 μM. For the lipophilic ORAC DS were extracted twice using hexane. The hexane extracts were combined and evaporated. The dried hexane extract was dissolved in 250 μL of acetone and diluted with 750 μL of 7% randomly methylated β-cyclodextrin (RMCD) solution (50% acetone/50% water, v/v). Extracts were further diluted in 7% RMCD. Trolox standard was also diluted in 7% RMCD. AAPH concentration was adjusted to provide a decay curve with no more than 5% of antioxidant activity remaining at the end of the reaction. The decrease in fluorescence was determined at excitation of 535 nm and emission of 595 nm every 2 min for 60 min in a SpectraMax GeminiEM plate reader (Molecular Devices). The ORAC value was evaluated as the area under curve (AUC) and calculated by taking into account the Trolox reading using the following equation: $(AUC_{sample} - AUC_{buffer})/(AUC_{Trolox} - AUC_{buffer}) \times$ dilution factor of sample × initial Trolox concentration (mM). For each sample, four serial dilutions in phosphate buffer (pH 7.4) were measured. The optimum concentration was used for further analyses in four to six replicates.

Free Radical Scavenging Capacity. The free radical scavenging capacity was analyzed by the DPPH assay.[19] DPPH is a stable organic nitrogen radical with purple color. Upon reduction by an antioxidant, the solution color fades and the reaction can be monitored by a spectrophotometer at 517 nm. The decrease in absorbance is proportional to the antioxidant capacity and can be measured in comparison to Trolox as standard. All samples and standard were diluted in methanol. Twenty microliter aliquots from the test compounds were mixed with 200 μL of DPPH (0.6 mM) in methanol, and the change in optical density (517 nm) was monitored after 30 min using a VersaMax plate reader (Molecular Devices).

Ferric Reducing Antioxidant Power Assay. The FRAP assay was performed using an established standardized method described by Benzie and Strain.[21] Reaction mixtures were prepared by combining 10 mM 2,4,6-tri(2-pyridyl-*s*-triazine) (TPTZ), 20 mM ferric chloride, and 30 mM (pH 3.6) sodium acetate buffer in a 1:1:10 ratio. Trolox was used as standard in a range from 0 to 0.1 mM. Samples extracted in a 10-fold volume of methanol (w/v) were diluted in acetate buffer. A 200 μL reaction solution was warmed to 37 °C for 10 min prior to the addition of 20 μL of diluted sample extracts. Sample absorbance was read at 593 nm in a VersaMax plate reader (Molecular Devices). Results were compared to the Trolox standard curve and expressed as TE.

Chemical Analysis. Chemical markers were analyzed by high-performance liquid chromatography (HPLC) using a Waters Alliance 2690/2695 HPLC system (Waters, Milford, MA, USA) with a 996 PDA detector. GT chemical markers were extracted with a 75% MeOH/25% H_2O mixture and separated using a Phenomenex Synergi 4 μ Hydro-RP column (150 × 4.6 mm, 80A) (Phenomenex, Torrance, CA, USA) with a gradient mobile phase of 0.25% H_3PO_4 in water (solvent A) and 0.1% H_3PO_4 in acetonitrile/MeOH (1:1, v/v) + 1.0% THF (solvent B). Solvent composition starting at T = 0 min with 95% solvent A and 5% solvent B changed to 20% solvent A and 80% B at T = 50 min and back to the initial mixture at T = 51−60 min. All standards were purchased from Sigma-Aldrich Co. or ChromaDex (Irvine, CA, USA). The pomegranate DS were homogenized in dimethyl sulfoxide, sonicated, and vortexed for 20 min each, diluted with methanol/water (1:1, v/v), centrifuged for 5 min at 8000*g*, and separated on a Zorbax SB C_{18}, column (5 μm 4.6 × 250 mm) (Agilent, Santa Clara, CA, USA) using a gradient of 0.1% H_3PO_4 in water (solvent A) and acetonitrile (solvent B). Solvent mixture changed from T = 0 min at 95% solvent A and 5% solvent B to 60% solvent A and 40% solvent B at 30 min. Resveratrol was quantified in a methanol extract using an Agilent Poroshell120 SB-C18 column (2.7 μm 100 × 4.6 mm) with a gradient mobile phase of 0.4% H_3PO_4 in water (solvent A) and acetonitrile (solvent B). The solvent mixture was changed from T = 0 min at 80% solvent A and 20% solvent B to 40% solvent A and 60% solvent B at 8 min and returning to initial solvent mixture at 9−13 min.

Determination of Total Phenolics. The colorimetric method by Singleton et al.[22] was used to determine the total phenol content. Gallic acid was used to prepare a standard curve, and final values are expressed in gallic acid equivalents (GAE). Diluted DS extracts were incubated with Folin−Ciocalteu phenol reagent (Sigma-Aldrich Co.). The color was developed by adding sodium carbonate (20%) and absorbance measured at 755 nm.

Statistical Analysis. Values in the results are means (95% CI), unless otherwise specified. With regard to nondigested antioxidant activity of all 25 samples, data were analyzed separately for each antioxidant assay method using one-way ANOVA in IBM SPSS Statistics (version 21.0; IBM Corp., Armonk, NY, USA), with type of DS as a between-group factor. Multiple-comparisons testing was adjusted using Tukey's honestly significant difference test when there was a significant group effect. Pearson's correlation coefficient was used to investigate the pairwise associations between variables, unless

Table 2. Antioxidant Capacity of 25 Non-digested Antioxidant DS Available in the United States[a]

	TEAC[b] in MeOH[c] mmol TE/100 g	FRAP[b] in MeOH mmol TE/100 g	DPPH[b] in MeOH mmol TE/100 g	ORAC-hydro[b] mmol TE/100 g	ORAC-lipo mmol TE/100 g	sum of methods[b] mmol TE/100 g
PM1	803.9	578.8	536.2	452.6	0.103	2371.6
PM2	70.2	34.6	27.7	6.9	0.083	139.5
PM3	519.0	400.3	364.5	301.9	1.205	1586.9
PM4	843.0	633.3	693.1	417.2	1.152	2647.5
PM5	1141.7	853.2	780.6	471.3	0.108	3246.8
meanH[d] ± SD	826.9 ± 254.7d	616.4 ± 186.6d	593.6 ± 183.1d	410.8 ± 75.9	0.6 ± 0.6	2448.3 ± 684.3d
meanL[d] ± SD	675.6 ± 404.0	500.1 ± 306.3	480.4 ± 298.7	330.0 ± 192.2	0.5 ± 0.6	1986.5 ± 1190.5
GT1	207.7	106.8	119.5	159.2	0.214	593.4
GT2	381.2	168.4	204.5	242.7	0.032	996.9
GT3	274.6	128.9	166.7	240.0	0.226	810.4
GT4	1054.5	583.0	574.4	673.8	0.343	2886.0
mean ± SD	479.5 ± 389.9	246.8 ± 225.6e	266.3 ± 208.3e	328.9 ± 233.2	0.2 ± 0.1	1321.7 ± 1055.9
Res1	423.5	100.8	63.6	632.9	16.95	1237.8
Res2	916.6	254.1	159.6	1259.5	1.352	2591.2
Res3	435.5	155.3	148.2	486.7	1.094	1226.8
mean ± SD	591.9 ± 281.3	170.0 ± 77.7e	123.8 ± 52.4e	793.0 ± 410.5d	6,5 ± 9.1	1685.3 ± 784.6
GS1	156.2	76.0	112.2	167.0	1.827	513.2
GS2	204.6	101.0	131.2	285.8	0.176	722.7
GS3	592.3	335.3	402.7	333.4	0.009	1663.6
mean ± SD	317.7 ± 239.0	170.8 ± 143.0e	215.4 ± 162.5e	262.1 ± 85.7e	0.7 ± 1.0	966.5 ± 612.7
MT1	211.7	42.5	27.0	54.2	1.411	336.8
MT2	228.2	42.0	49.5	63.8	0.069	383.6
MT3	313.4	67.0	49.8	75.3	0.314	505.9
MT4	244.2	46.7	54.2	71.7	0.095	416.9
mean ± SD	249.4 ± 44.7e	49.6 ± 11.8e	45.1 ± 12.3e	66.3 ± 9.4	0.5 ± 0.6	410.8 ± 71.4e
Acai1	0.5	0.7	0.3	1.2	0.810	3.6
Acai2	4.4	2.3	n.d.	3.9	0.352	10.9
mean ± SD	2.5 ± 2.7e	1.5 ± 1.1e		2.6 ± 1.9e	0.6 ± 0.3	7.3 ± 5.2e
Acai+GT	181.0	94.0	117.9	209.5	14.3	616.7
Goji1	2.2	1.4	2.6	3.2	2.4	11.8
Goji2	0.4	0.1	0.2	0.8	0.008	1.6
Goji3	5.5	1.3	1.4	15.5	0.04	23.7
mean ± SD	2.7 ± 2.6e	0.9 ± 0.7e	1.4 ± 1.2e	6.5 ± 7.9e	0.8 ± 1.4	12.4 ± 11.1e

[a]DS, dietary supplements; TEAC, Trolox equivalent antioxidant capacity; DPPH, diphenyl-1-picrylhydrazyl; FRAP, ferric reducing antioxidant power; ORAC, oxygen radical absorbing capacity; TE, Trolox equivalents; PM, pomegranate; GT, green tea; Res, resveratrol; GS, grape seed; MT, milk thistle. Mean values within a column with unlike letters were significantly different ($P < 0.05$; Tukey's multiple-comparison test). [b]One-way ANOVA of the absolute values in antioxidant activity for DS category effect; $P < 0.01$. [c]Except for acai and goji, which do not mix well with MeOH and were extracted in water. [d]PM2 is excluded from meanH (higher mean) and is included in meanL (lower mean).

Spearman's rho was used where specified. Differences were considered significant at $P < 0.05$.

RESULTS

Antioxidant Activity of 25 Nondigested DS by Different Assays. A total of 25 of the most popular DS categories sold in the United States were tested for their antioxidant activity by TEAC, DPPH, ORAC, and FRAP assays; methanol was used as the extraction solvent except for the lipophilic ORAC, in which hexane was used (Table 2). One-way ANOVA of the absolute values in antioxidant activity demonstrated a significant DS type effect for TEAC ($P = 0.004$), FRAP ($P = 0.000$), DPPH ($P = 0.000$), OPAC-hydro ($P = 0.001$), sum of methods ($P = 0.001$), but not for ORAC-lipo (NS). The AA varied depending on the solubility in water or organic solvents.

TEAC. Pairwise testing showed significantly higher TEAC values for pomegranate versus milk thistle ($P < 0.05$), acai ($P < 0.025$), and goji ($P < 0.01$); no other differences between types of DS reached statistical significance.

FRAP. FRAP values were higher for pomegranate versus green tea ($P < 0.025$), grape seed ($P = 0.01$), milk thistle ($P < 0.001$), resveratrol ($P = 0.01$), acai ($P < 0.01$), and goji ($P <$

Table 3. Correlation Matrix of the Different Antioxidant Assays[a]

		TEAC	FRAP	DPPH	ORAC-hydro	ORAC-lipo
TEAC	Pearson correlation	1	**0.918**[b]	**0.879**[b]	**0.788**[b]	−0.055
	signif (2-tailed)		0.000	0.000	0.000	0.793
	N	25	25	24	25	25
FRAP	Pearson correlation	**0.918**[b]	1	**0.987**[b]	**0.545**[b]	−0.131
	signif (2-tailed)	0.000		0.000	0.005	0.533
	N	25	25	24	25	25
DPPH	Pearson correlation	**0.879**[b]	**0.987**[b]	1	**0.465**[c]	−0.163
	signif (2-tailed)	0.000	0.000		0.022	0.446
	N	24	24	24	24	24
ORAC-hydro	Pearson correlation	**0.788**[b]	**0.545**[b]	**0.465**[c]	1	0.198
	signif (2-tailed)	0.000	0.005	0.022		0.343
	N	25	25	24	25	25
ORAC-lipo	Pearson correlation	−0.055	−0.131	−0.163	0.198	1
	signif (2-tailed)	0.793	0.533	0.446	0.343	
	N	25	25	24	25	25

[a]TEAC, Trolox equivalent antioxidant capacity; DPPH, diphenyl-1-picrylhydrazyl; FRAP, ferric reducing antioxidant power; ORAC, oxygen radical absorbing capacity. [b]Correlation is significant at $P < 0.01$. [c]Correlation is significant at $P < 0.05$.

Table 4. Chemical Compositions (Percent) of Green Tea (GT), Pomegranate (PM), and Resveratrol (Res) DS[a]

(A) Green Tea				
content	GT1	GT2	GT3	GT4
theobromine	0.1 ± 0.002	0.08 ± 0.005	0.08 ± 0.001	0.11 ± 0.001
EGC	1.6 ± 0.05	2.4 ± 0.123	1.5 ± 0.023	2.4 ± 0.004
(±)-catechin	0.4 ± 0.03	0.2 ± 0.007	0.66 ± 0.01	0.88 ± 0.002
caffeine	2.7 ± 0.08	3.8 ± 0.05	3.1 ± 0.02	1.26 ± 0.05
EC	0.5 ± 0.02	0.67 ± 0.04	0.64 ± 0.02	2.25 ± 0.014
EGCG	3.35 ± 0.2	6.5 ± 0.38	3.98 ± 0.04	27.16 ± 0.18
ECG	2.05 ± 0.1	4.27 ± 0.25	3.78 ± 0.01	13.98 ± 0.006
sum of catechins	7.9	14.0	11.1	46.7
(B) Pomegranate				
content	PM1	PM2	PM3	PM4	PM5
punicalagins A and B	4.4 ± 0.04	0	11.9 ± 0.2	22.8 ± 0.2	28.2 ± 0.5
ellagic acid	4.3 ± 0.07	24.6 ± 0.20	0.9 ± 0	21.5 ± 0.14	1.7 ± 0.04
(C) Resveratrol				
content	Res1	Res2	Res3	
quercetin	0.15 ± 0.0	18.52 ± 0.12	0.03 ± 0.002	
resveratrol	18.2 ± 0.05	32.1 ± 0.3	10.9 ± 0.05	

[a]DS, dietary supplements; EGC, (−)-epigallocatechin; EC, (−)-epicatechin; EGCG, (−)-epigallocatechin gallate; ECG, (−)-epicatechin gallate.

0.001); no other differences between other DS types reached statistical significance.

DPPH. Pairwise testing demonstrated higher DPPH values for pomegranate versus green tea ($P < 0.05$), grape seed ($P < 0.05$), milk thistle ($P = 0.001$), resveratrol ($P < 0.01$), and goji ($P = 0.001$); no other differences between other DS types reached statistical significance (acai not included in the model due to lack of sample power).

ORAC-hydro. Contrary to the TEAC, FRAP, and DPPH, ORAC-hydro values were significantly higher only for resveratrol compared to grape seed ($P < 0.05$), acai ($P < 0.01$), goji ($P = 0.001$), and green tea ($P = 0.052$).

ORAC-lipo. The lipophilic ORAC evaluates the AA of the lipophilic antioxidants. The contribution of the AA measured by the lipophilic ORAC is minor in the supplements with high polyphenolic content. However, for goji juice (Goji1), the lipophilic ORAC contributed considerable AA to the total activity, whereas the goji extracts (Goji2 and Goji3) lost most of the lipophilic AA (Table 2).

Sum of Methods. For the sum of all methods that measure the AA, results were highly correlated to TEAC values; we found that the antioxidant capacity is highest in pomegranate and decreasing in the following order: pomegranate ≫ resveratrol > green tea > grape seed > milk thistle ≫ goji > acai, with significance reached for pomegranate versus milk thistle, acai, and goji ($P < 0.01$).

In addition, TEAC was highly correlated with FRAP, DPPH, and ORAC-hydro ($r = 0.79–0.92$, $P < 0.001$), and FRAP and DPPH were highly correlated with each other ($r = 0.99$, $P < 0.001$) and moderately correlated with ORAC-hydro ($r =$

dx.doi.org/10.1021/jf500106r | J. Agric. Food Chem. 2014, 62, 4313−4321

0.47−0.55, $P < 0.025$). The correlation matrix is depicted in Table 3.

Variation of AA in Each Category. Extensive differences in AA were observed among the DS in each category. For example, PM2 exhibited significantly lower AA compare to the other four pomgranate DS; GT4, Res2, and GS3 exhibited significantly higher AA compared to other DS in each category. This was closely correlated to the chemical composition of marker compounds.

Chemical Analyses and Associations with Antioxidant Activity. DS from pomegranate, green tea, and resveratrol/quercetin were analyzed using HPLC with PDA detection, and the concentration of known chemical markers was quantified before and after digestion (Tables 4 and 5). Total phenolic content was determined for the DS with high polyphenol content before and after digestion using the GAE assay (Table 6).

Table 5. Change in Content of Chemical Marker Compounds in Green Tea, Pomegranate, and Resveratrol DS during in Vitro Digestion[a]

dietary supplement	marker chemical	% of control
PM5	punicalagins A and B	88.5
	ellagic acid	208.7
GT4	theobromine	70.2
	EGC	51.0
	(±)-catechin	81.5
	caffeine	87.2
	EC	78.4
	EGCG	63.0
	ECG	73.3
	sum of catechins	66.5
Res2	resveratrol	239.8

[a]PM, pomegranate; GT, green tea; EGC, (−)-epigallocatechin; EC, (−)-epicatechin; EGCG, (−)-epigallocatechin gallate; ECG, (−)-epicatechin gallate; Res, resveratrol.

In pomegranate supplements, punicalagins A and B and ellagic acid were quantified. Pomegranate supplements with the highest content of punicalagins A and B (PM4 and PM5) showed high antioxidant activity, whereas pomegranate supplements with high ellagic acid showed the lowest antioxidant activity (PM2); a highly significant correlation coefficient was reported between pomegranate antioxidant activity by TEAC, FRAP, DPPH, or sum of methods and punicalagin A and B content (Spearman's rho = 0.90, $P < 0.05$). Although PM1 had low content of punicalagins A and B and ellagic acid, its antioxidant activity was relatively high. It appears that other polyphenols or ellagitannins of larger molecular weights may have contributed considerably to the AA of PM1, as indicated by the high content of total phenolics, expressed as GAE, in PM1. In fact, the AA was increased by 50% for PM1 after digestion compared to nondigested controls (PM1-digested, 667.1 ± 23.1 mmol TE/100 g; PM1-control, 420.6 ± 76.2 mmol TE/100 g).

Among the GT supplements, the ECG, EC, and EGCG contents were highly correlated ($r = >0.99$; $P < 0.01$) with the AA measured by TEAC, FRAP, DPPH, and ORAC-hydro, with the correlation coefficient between sum of catechins and sum of methods reaching $r = 1.0$ ($P < 0.001$). GT4 reported the highest catechin concentration and highest AA. However, after digestion, the catechin content of known chemical markers (ECG, EC, CG, EGC, EGCG, and GCG) was decreased by 90%, whereas the AA decreased by only 22%.

The resveratrol DS contained mixtures of resveratrol and quercetin, with quercetin highly correlating with TEAC ($r = 1.0$, $P < 0.025$) and sum of methods ($r = 1.0$, $P = 0.001$) and with resveratrol showing similar associations but without reaching significance due to the small sample size ($r > 0.93$, $P = 0.22$, $n = 3$). Within samples tested, Res2 showed the highest resveratrol/quercetin content and highest AA. Total phenolic content highly correlated with TEAC for both digested and nondigested (control) DS samples ($r = 0.9956$, $P < 0.01$).

Antioxidant Activity of Digested DS Samples. On the basis of the highest AA in the nondigested samples, one DS from each category was selected for in vitro digestion. The AA measured in the digested samples is summarized in Table 6. The order of antioxidant potency of the in vitro digested DS was as follows: PM5 > GT4 > GS3 ≫ Res2, MT3 > goji3, acai2 extracts. PM5 reported the highest TEAC values, 427 times higher than that of acai, the DS that exhibited the lowest TEAC values: 1109.4 ± 8.2 mmol TE/100 g compared to 2.6 ± 0.1 mmol TE/100 g, respectively. TEAC of in vitro digested GT4 and GS3 was 73 and 46.5% that of PM5 and 16.6 and 10.5 times greater than that of Res2, respectively.

Digested versus Nondigested (Control) DS Samples. The digestion was performed with water extracts of all DS and was compared to nondigested DS samples extracted in water (Table 6). Other than for GT4 and GS3, which showed 21.5 and 8.1% lower TEAC values after in vitro digestion compared to the nondigested samples extracted in H_2O, the other DS samples demonstrated either similar or higher TEAC values after in vitro digestion (Table 6). For resveratrol and milk thistle the AA was significantly lower in the digested sample compared to the nondigested sample extracted in methanol (Table 3) because their solubility is higher in methanol compared with water. For goji and acai the AA was very low in the digested and nondigested samples extracted in water or methanol.

DISCUSSION

To our knowledge, this is the first study to comprehensively evaluate and compare the antioxidant potency of commercially available polyphenol-rich antioxidant DS, including extracts from pomegranate, green tea, grape seed, resveratrol, milk thistle, and acai, and goji berry, utilizing different antioxidant assays before and after in vitro digestion. In the present study, pomegranate DS expressed the most potent antioxidant capacity, followed by resveratrol, green tea, grape seed, and milk thistle extracts, whereas acai and goji berry demonstrated negligible antioxidant properties across all four antioxidant assays and in the in vitro digestion model. The AA of resveratrol extract and milk thistle was influenced by the solvent used for extraction, with 10−20-fold greater values comparing the methanol to water extract. Hence, it appears that both resveratrol and milk thistle DS may efficiently express their AA when ingested in ethanol (alcoholic) solutions. There is earlier evidence showing that the solubility of *trans*-resveratrol in ethanol plus water mixtures increases with increasing mole fraction of ethanol,[23] which together with the present data might partly explain red wine's antioxidant properties. Previous studies on milk thistle evaluated its AA mainly in aqueous extracts[24,25] and have demonstrated even lower values for TEAC, with one study[25] reporting 133.4 μg TE/g of milk

Table 6. Gallic Acid Equivalents (GAE) and Antioxidant Activity by TEAC Method of in Vitro Digested and Nondigested (Control) DS[a]

	GAE (mg/L)	TEAC (mmol TE/100 g)	digested (% of control H_2O)
PM5			
digested (H_2O)	16924 ± 489	1109.4 ± 8.2	101.7
control (H_2O)	17419 ± 1027	1090.5 ± 24.6	
GT4			
digested (H_2O)	11075 ± 172	811.7 ± 39.1	78.5
control (H_2O)	14779 ± 959	1034.1 ± 15.8	
GS3			
digested (H_2O)		515.9 ± 12.7	91.9
control (H_2O)		561.2 ± 70.2	
Res2			
digested (H_2O)	771 ± 2	49.0 ± 6.2	124.8
control (H_2O)	552 ± 14	39.2 ± 4.0	
MT3			
digested (H_2O)		35.8 ± 0.8	720.1
control (H_2O)		5.0 ± 0.01	
Goji3			
digested (H_2O)		10.8 ± 0.5	175.6
control (H_2O)		6.1 ± 0.4	
Acai2			
digested (H_2O)		2.6 ± 0.05	124.5
control (H_2O)		2.1 ± 0.01	

[a]DS, dietary supplements; TEAC, Trolox equivalent antioxidant capacity; TE, Trolox equivalents; PM, pomegranate; GT, green tea; GS, grape seed; Res, resveratrol; MT, milk thistle.

thistle powder compared to 5 mmol TE/100 g = 12.5 mg TE/g of our aqueous milk thistle extract sample (Table 6). A similar ranking of the AA of beverages from previous research from our laboratory also showed the highest AA for pomegranate > red wine > grape juice.[19] Tea did not show considerable AA because bottled tea beverages were used.[19]

Significant variation in AA between DS from the same category corresponding to variation in the chemical composition was observed, although the DS, according to the label information, are supposed to provide the same health benefits. The AA of pomegranate DS was closely associated with the chemical composition. Except for PM2, all other pomegranate DS showed the highest AA. The AA of PM2 was very low compared to the other pomegranate supplements because it mainly contains ellagic acid and no punicalagins A and B. As previously described,[26] the official marker compound for pomegranate supplements is ellagic acid, whereas authentic pomegranate has only small amounts of ellagic acid. Whether ellagic acid from other sources is added to these supplements or the increase in ellagic acid occurred as the result of manufacturing was not determined. However, high amounts of ellagic acid only resulted in lower AA compared to supplements including punicalagins. Differential response of two pomegranate DS (PM1 and PM5) to in vitro digestion with α-amylase, pepsin, pancreatin, and bile salts was observed. Although PM5 showed no change of AA, the AA was increased by 50% for PM1 compared to nondigested controls. It appears that because PM1 contains relatively low concentrations of punicalagins A and B and ellagic acid, its AA is based on larger ellagitannins, which, during the in vitro digestion process, are further dissolved or converted to smaller compounds with higher antioxidant activity. Similar results have been found in another study where the AA of pomegranate juice increased significantly after in vitro digestion.[27] In vivo, the hydrolysis of pomegranate ellagitannins to ellagic acid and further metabolism by the gut microbiota to yield urolithins have been documented.[28−30] These metabolites in turn exhibit AA.[31]

In the current study, the antioxidant supplements with the lowest AA, and of minor significance, were acai and goji berries. Results from other published in vitro and in vivo studies testing the antioxidant effects of acai juice/pulp or goji berry fruit demonstrated strong variability in AA due to differences in sourcing and processing of the material. Freeze-dried acai pulp/skin powder demonstrated 1.03 mmol TE/g by the ORAC assay.[32] Enhanced AA in human plasma has been shown for acai pulp and acai juice after a single ingestion in one study utilizing the ORAC assay.[33] In vitro analyses of goji fruit extracts have captured its antioxidant properties, including inhibition of $DPPH^{-}$ radical-scavenging activity.[14,15,34] A study by Luo et al.[35] reported a stronger in vitro AA by TEAC and ORAC assays of goji fruit water, methanol extracts, and crude polysaccharide extracts compared to purified polysaccharide fractions. In the study by Luo, goji demonstrated levels of TEAC values of maximal 0.5 mmol TE/100 g, which are lower than the AA demonstrated by our goji samples.[35] Most likely the differences in antioxidant activity in the present study and earlier investigations of acai and goji berries are caused by losses of AA during processing of the berry pulp during manufacturing of the supplements. The main antioxidant compounds in acai and goji berries are anthocyanins, carotenoids, and polysaccharides, respectively. Anthocyanins are prone to degradation during processing and storage (pH, temperature, light, oxygen, enzymes, presence of ascorbic acid, sugars, sulfur dioxide or sulfite salts, metal ions, and copigments)[36] and were not likely to contribute to antioxidant activities, which were very small in any case. In the lipophilic ORAC test, the goji berries demonstrated high variability, with the goji juice (Goji1) exhibiting somewhat higher lipophilic AA compared to the goji extracts (Goji2 and Goji3), suggesting that the goji juice contained some carotenoids.

In the present study, in vitro simulation of gastrointestinal digestion did not adversely affect the antioxidant capacity of any of the DS extracts, other than for green tea, which lost 21.5% of AA during digestion. Similarly, earlier work on the impact of in vitro digestion on commercially available tea juices (longjing green tea, jasmine, and oolong) demonstrated a significant decrease of AA as well as total polyphenol content.[37] In the presented study the tea polyphenol content decreased by only 10%. Possibly the exposure to alkaline pH transformed EGCG and EGC to hetero- and homodimers such as theasinensin, which most likely retained the antioxidant activity.[39] A small decrease in AA was also observed for grape seed extracts (8.1%). However, a study by Janisch demonstrated an increase in release of flavans and procyanidins from grape seed extract with good scavenging potential against reactive oxygen species under conditions of in vitro digestion.[38] In addition to potential changes through the digestive process, possible interactions of food ingested concurrent with the DS have been reported[40] and more detailed future evaluations are warranted.

In agreement with our previous study on polyphenol-rich antioxidant beverages, the order of antioxidant capacity correlated well between the different methods with the exception of the ORAC method. The ORAC assay principle is based on a temperature-dependent free radical generator reaction and protection from oxidation over a 60 min period. Although the ORAC method is the most commonly used assay by food manufacturers,[19] our laboratory has reported poor reproducibility of this method due to temperature variation in commonly used plate readers (unpublished data). As we concluded in our earlier paper, it is important to run multiple antioxidant methods rather than just the ORAC method to get a better estimate of antioxidant capacity and to substantiate in vitro results with clinical studies. The TEAC assay correlated best to the sum of the assays and was the most reproducible. Using the DPPH assay all dilutions are performed using methanol instead of buffer, which lowers the reproducibility.

In conclusion, our results demonstrate that except for green tea and grape seed extracts no significant loss of antioxidant activity was observed during in vitro digestion.

AUTHOR INFORMATION

Corresponding Author

*(S.M.H.) Phone:(310) 825-9345. E-mail: shenning@mednet.ucla.edu.

Author Contributions

No one from Pom Wonderful, Inc., had any role in the conduct of the study, the analysis of the data, or the preparation of the manuscript. The authors alone are responsible for the content and writing of the manuscript.

Funding

The research was funded by unrestricted funds of the Department of Medicine of the David Geffen School of Medicine at UCLA. The chemical analyses were conducted with partial support from POM Wonderful Inc., Los Angeles, CA, USA.

Notes

The authors declare no competing financial interest.

ABBREVIATIONS USED

DPPH, diphenyl-1-picrylhydrazyl; DS, dietary supplements; EC, (−)-epicatechin; ECG, (−)-epicatechin gallate; EGC, (−)-epigallocatechin; EGCG, (−)-epigallocatechin gallate; GAE, gallic acid equivalents; FRAP, ferric reducing antioxidant power; NHANES, National Health and Nutrition Examination Survey; ORAC, oxygen radical absorbing capacity; PM, pomegranate; TE, Trolox equivalents; TEAC, Trolox equivalent antioxidant capacity

REFERENCES

(1) Chun, O. K.; Floegel, A.; Chung, S. J.; Chung, C. E.; Song, W. O.; Koo, S. I. Estimation of antioxidant intakes from diet and supplements in U.S. adults. *J. Nutr.* **2010**, *140*, 317−324.

(2) Yang, M.; Chung, S. J.; Chung, C. E.; Kim, D. O.; Song, W. O.; Koo, S. I.; Chun, O. K. Estimation of total antioxidant capacity from diet and supplements in US adults. *Br. J. Nutr.* **2011**, *106*, 254−263.

(3) Proteggente, A. R.; Pannala, A. S.; Paganga, G.; Van Buren, L.; Wagner, E.; Wiseman, S.; Van De Put, F.; Dacombe, C.; Rice-Evans, C. A. The antioxidant activity of regularly consumed fruit and vegetables reflects their phenolic and vitamin C composition. *Free Radical Res.* **2002**, *36*, 217−233.

(4) Heber, D.; Seeram, N. P.; Wyatt, H.; Henning, S. M.; Zhang, Y.; Ogden, L. G.; Dreher, M.; Hill, J. O. Safety and antioxidant activity of a pomegranate ellagitannin-enriched polyphenol dietary supplement in overweight individuals with increased waist size. *J. Agric. Food Chem.* **2007**, *55*, 10050−10054.

(5) Johanningsmeier, S. D.; Harris, G. K. Pomegranate as a functional food and nutraceutical source. *Annu. Rev. Food Sci. Technol.* **2011**, *2*, 181−201.

(6) Rosenblat, M.; Volkova, N.; Aviram, M. Pomegranate juice (PJ) consumption antioxidative properties on mouse macrophages, but not PJ beneficial effects on macrophage cholesterol and triglyceride metabolism, are mediated via PJ-induced stimulation of macrophage PON2. *Atherosclerosis* **2010**, *212*, 86−92.

(7) Kidd, P. M. Bioavailability and activity of phytosome complexes from botanical polyphenols: the silymarin, curcumin, green tea, and grape seed extracts. *Altern. Med. Rev.* **2009**, *14*, 226−246.

(8) Nassiri-Asl, M.; Hosseinzadeh, H. Review of the pharmacological effects of *Vitis vinifera* (grape) and its bioactive compounds. *Phytother. Res.* **2009**, *23*, 1197−1204.

(9) Wenzel, E.; Somoza, V. Metabolism and bioavailability of *trans*-resveratrol. *Mol. Nutr. Food Res.* **2005**, *49*, 472−481.

(10) Loguercio, C.; Festi, D. Silybin and the liver: from basic research to clinical practice. *World J. Gastroenterol.* **2011**, *17*, 2288−2301.

(11) Potterat, O. Goji (*Lycium barbarum* and *L. chinense*): phytochemistry, pharmacology and safety in the perspective of traditional uses and recent popularity. *Planta Med.* **2010**, *76*, 7−19.

(12) Poulose, S. M.; Fisher, D. R.; Larson, J.; Bielinski, D. F.; Rimando, A. M.; Carey, A. N.; Schauss, A. G.; Shukitt-Hale, B. Anthocyanin-rich acai (*Euterpe oleracea* Mart.) fruit pulp fractions attenuate inflammatory stress signaling in mouse brain BV-2 microglial cells. *J. Agric. Food Chem.* **2012**, *60*, 1084−1093.

(13) Schauss, A. G.; Wu, X.; Prior, R. L.; Ou, B.; Patel, D.; Huang, D.; Kababick, J. P. Phytochemical and nutrient composition of the freeze-dried Amazonian palm berry, *Euterpe oleraceae* Mart. (acai). *J. Agric. Food Chem.* **2006**, *54*, 8598−8603.

(14) Li, X. L.; Zhou, A. G. Evaluation of the antioxidant effects of polysaccharides extracted from *Lycium barbarum*. *Med. Chem. Res.* **2007**, *15*, 471−482.

(15) Li, X. M.; Li, X. L.; Zhou, A. G. Evaluation of antioxidant activity of the polysaccharides extracted from *Lycium barbarum* fruits in vitro. *Eur. Polym. J.* **2007**, *43*, 488−497.

(16) Hur, S. J.; Lim, B. O.; Decker, E. A.; McClements, D. J. In vitro human digestion models for food applications. *Food Chem.* **2011**, *125*, 1−12.

(17) Chohan, M.; Naughton, D. P.; Jones, L.; Opara, E. I. An investigation of the relationship between the anti-inflammatory activity, polyphenolic content, and antioxidant activities of cooked and in vitro digested culinary herbs. *Oxid. Med. Cell. Longev.* **2012**, DOI: 10.1155/2012/627843.

(18) Werner, S.; Bohm, V. Bioaccessibility of carotenoids and vitamin E from pasta: evaluation of an in vitro digestion model. *J. Agric. Food Chem.* **2011**, *59*, 1163−1170.
(19) Seeram, N. P.; Aviram, M.; Zhang, Y.; Henning, S. M.; Feng, L.; Dreher, M.; Heber, D. Comparison of antioxidant potency of commonly consumed polyphenol-rich beverages in the United States. *J. Agric. Food Chem.* **2008**, *56*, 1415−1422.
(20) Prior, R. L.; Hoang, H.; Gu, L.; Wu, X.; Bacchiocca, M.; Howard, L.; Hampsch-Woodill, M.; Huang, D.; Ou, B.; Jacob, R. Assays for hydrophilic and lipophilic antioxidant capacity (oxygen radical absorbance capacity (ORAC(FL))) of plasma and other biological and food samples. *J. Agric. Food Chem.* **2003**, *51*, 3273−3279.
(21) Benzie, I. F.; Strain, J. J. The ferric reducing ability of plasma (FRAP) as a measure of "antioxidant power": the FRAP assay. *Anal. Biochem.* **1996**, *239*, 70−76.
(22) Singleton, V. L.; Rossi, J. A. Colorimetry of total phenolics with phosphomolybdic-phosphotungstic acid reagents. *Am. J. Enol. Vitic.* **1965**, *16*, 144−158.
(23) Sun, X.; Shao, Y.; Yan, W. Measurement and correlation of solubilities of *trans*-resveratrol in ethanol + water and acetone + water mixed solvents at different temperatures. *J. Chem. Eng. Data* **2008**, *53*, 2562−2566.
(24) Pereira, C.; Calhelha, R. C.; Barros, L.; Ferreira, I. C. F. R. Antioxidant properties, anti-hepatocellular carcinoma activity and hepatotoxicity of artichoke, milk thistle and borututu. *Ind. Crops Prod.* **2013**, *49*, 61−65.
(25) Yang, C.-C.; Fang, J.-Y.; Hong, T.-L.; Wang, T.-C.; Zhou, Y.-E.; Lin, T.-C. Potential antioxidant properties and hepatoprotective effects of an aqueous extract formula derived from three Chinese medicinal herbs against CCl_4-induced liver injury in rats. *Int. Immunopharmacol.* **2013**, *15*, 106−113.
(26) Zhang, Y.; Wang, D.; Lee, R. P.; Henning, S. M.; Heber, D. Absence of pomegranate ellagitannins in the majority of commercial pomegranate extracts: implications for standardization and quality control. *J. Agric. Food Chem.* **2009**, *57*, 7395−7400.
(27) Ryan, L.; Prescott, S. L. Stability of the antioxidant capacity of twenty-five commercially available fruit juices subjected to an in vitro digestion. *Int. J. Food Sci. Technol.* **2010**, *45*, 1191−1197.
(28) Cerda, B.; Espin, J. C.; Parra, S.; Martinez, P.; Tomas-Barberan, F. A. The potent in vitro antioxidant ellagitannins from pomegranate juice are metabolised into bioavailable but poor antioxidant hydroxy-6*H*-dibenzopyran-6-one derivatives by the colonic microflora of healthy humans. *Eur. J. Nutr.* **2004**, *43*, 205−220.
(29) Cerda, B.; Periago, P.; Espin, J. C.; Tomas-Barberan, F. A. Identification of urolithin a as a metabolite produced by human colon microflora from ellagic acid and related compounds. *J. Agric. Food Chem.* **2005**, *53*, 5571−5576.
(30) Espin, J. C.; Gonzalez-Barrio, R.; Cerda, B.; Lopez-Bote, C.; Rey, A. I.; Tomas-Barberan, F. A. Iberian pig as a model to clarify obscure points in the bioavailability and metabolism of ellagitannins in humans. *J. Agric. Food Chem.* **2007**, *55*, 10476−10485.
(31) Bialonska, D.; Kasimsetty, S. G.; Khan, S. I.; Ferreira, D. Urolithins, intestinal microbial metabolites of pomegranate ellagitannins, exhibit potent antioxidant activity in a cell-based assay. *J. Agric. Food Chem.* **2009**, *57*, 10181−10186.
(32) Schauss, A. G.; Wu, X.; Prior, R. L.; Ou, B.; Huang, D.; Owens, J.; Agarwal, A.; Jensen, G. S.; Hart, A. N.; Shanbrom, E. Antioxidant capacity and other bioactivities of the freeze-dried Amazonian palm berry, *Euterpe oleraceae* Mart. (acai). *J. Agric. Food Chem.* **2006**, *54*, 8604−8610.
(33) Mertens-Talcott, S. U.; Rios, J.; Jilma-Stohlawetz, P.; Pacheco-Palencia, L. A.; Meibohm, B.; Talcott, S. T.; Derendorf, H. Pharmacokinetics of anthocyanins and antioxidant effects after the consumption of anthocyanin-rich acai juice and pulp (*Euterpe oleracea* Mart.) in human healthy volunteers. *J. Agric. Food Chem.* **2008**, *56*, 7796−7802.
(34) Zhang, Z.; Liu, X.; Zhang, X.; Liu, J.; Hao, Y.; Yang, X.; Wang, Y. Comparative evaluation of the antioxidant effects of the natural vitamin C analog 2-*O*-*β*-D-glucopyranosyl-L-ascorbic acid isolated from goji berry fruit. *Arch. Pharm. Res.* **2011**, *34*, 801−810.
(35) Luo, Q.; Cai, Y.; Yan, J.; Sun, M.; Corke, H. Hypoglycemic and hypolipidemic effects and antioxidant activity of fruit extracts from *Lycium barbarum*. *Life Sci.* **2004**, *76*, 137−149.
(36) Mena, P.; Martí, N.; García-Viguera, C. Varietal blends as a way of optimizing and preserving the anthocyanin content of pomegranate (*Punica granatum* L.) juices. *J. Agric. Food Chem.* **2014**, DOI: 10.1021/jf405129q.
(37) Chen, G.-L.; Hu, K.; Zhong, N.-J.; Guo, J.; Gong, Y.-S.; Deng, X.-T.; Huang, Y.-S.; Chu, D.-K.; Gao, Y.-Q. Antioxidant capacities and total polyphenol content of nine commercially available tea juices measured by an in vitro digestion model. *Eur. Food Res. Technol.* **2013**, *236*, 303−310.
(38) Janisch, K. M.; Olschlager, C.; Treutter, D.; Elstner, E. F. Simulated digestion of *Vitis vinifera* seed powder: polyphenolic content and antioxidant properties. *J. Agric. Food Chem.* **2006**, *54*, 4839−4848.
(39) Neilson, A. P.; Song, B. J.; Sapper, T. N.; Bomser, J. A.; Ferruzzi, M. G. Tea catechin auto-oxidation dimers are accumulated and retained by Caco-2 human intestinal cells. *Nutr. Res. (N.Y.)* **2010**, *30*, 327−340.
(40) Zhang, H.; Yu, D.; Sun, J.; Liu, X.; Jiang, L.; Guo, H.; Ren, F. Interaction of plant phenols with food macronutrients: characterisation and nutritional-physiological consequences. *Nutr. Res. Rev.* **2013**, 1−15.

JOURNAL OF AGRICULTURAL AND FOOD CHEMISTRY

Article

pubs.acs.org/JAFC

Oxidative Degradation of Quercetin with Hydrogen Peroxide Using Continuous-Flow Kinetic Electrospray–Ion Trap–Time-of-Flight Mass Spectrometry

Jeremy S. Barnes and Kevin A. Schug*

Department of Chemistry and Biochemistry, The University of Texas at Arlington, Arlington, Texas 76019-0065, United States

ABSTRACT: The time-dependent hydrogen peroxide-induced oxidative degradation of aqueous quercetin at pH 7.4 was measured using an in-house-built online continuous-flow device made of concentric capillary tubes, modified to fit a photodiode array (PDA) detector and the inlet of an electrospray ionization–ion trap–time-of-flight mass spectrometer (ESI-IT-TOF-MS). As the reaction time was increased, the deprotonated quercetin ion signal, $[Q - H]^-$, decreased, and the formation of degradation product ions was observed. Structures for degradation product ions were proposed using higher order tandem mass spectrometry (up to MS^3) and high mass accuracy. The determined degradation pathways included oxidation, hydroxylation, cyclic peroxylation, ring cleavage, and small molecule loss. The most intense degradation product observed was 2,4,6-trihydroxybenzoate, which was proposed to be the end point of the peroxylation pathway and the favored degradation pathway under these conditions. This pathway is believed to be the result of nucleophilic attack by hydrogen peroxide at the C2 position of quercetin. This was followed by a cross ring cyclic peroxylation event at C2–C4, which resulted in an intermediate depside that was defined by C-ring-opening due to loss of C3-OH and cleavage of the peroxy bond. Further cleavage of the depside resulted in the 2,4,6-trihydroxybenzoate. A sodiated pseudo adduct of the dimerized trihydroxybenzoate was believed to be induced under electrospray conditions. A computational study was performed to justify the position within the C-ring for both the attack by nucleophilic oxidants and the cyclic peroxylated intermediate structure.

KEYWORDS: *quercetin, oxidative degradation, hydrogen peroxide, reactive oxygen species, continuous-flow kinetics, higher order fragmentation, mass accuracy, electrospray ionization, ion trap–time-of-flight mass spectrometry*

INTRODUCTION

Quercetin is one of the most abundant dietary flavonols and can be found in significant quantities as a glycoside in teas, red wine, and onions.[1] In addition to its promising potential to reduce the risk of cancer, quercetin has been shown to be a natural histamine reducer and an effective anti-inflammatory agent.[2−4] Some theories suggest that the quercetin aglycone may be involved in several signal transduction pathways and has been shown to interact with key receptors involved with the development of cancers, inflammation, and carcinogenesis.[5] Quercetin has been shown to be highly effective at scavenging reactive oxygen species (ROS) in vitro.[6] Because of this antioxidant characteristic, it is no surprise that quercetin has drawn significant interest in the supplement market and food industry. A recent study of improving nutrients in vegetables has even shown organic tomatoes to have a 79% increase in quercetin compared to tomatoes grown conventionally.[7] The protective nature of the compound may be a primary reason behind some of the related therapeutic benefits of organic vegetables.

The antioxidant characteristics of quercetin can be correlated to the many pharmacophores of its chemical structure (Figure 1). The catechol-like structures that can be formed between the hydroxyl group at C5 and the C4 keto group and between the hydroxyl group at C3 and the C4 keto group, as well as the *o*-dihydroxy structure located on the B-ring, allows for free radical neutralization via hydrogen atom donation. Quercetin becomes a free radical during the process, but due to electron delocalization, a characteristic of phenoxy radicals, the species is too low in energy to react.[8,9] These attributes provide multiple facets for quercetin to contribute to the body's antioxidant shield, providing balance against the oxidative attack of ROS.

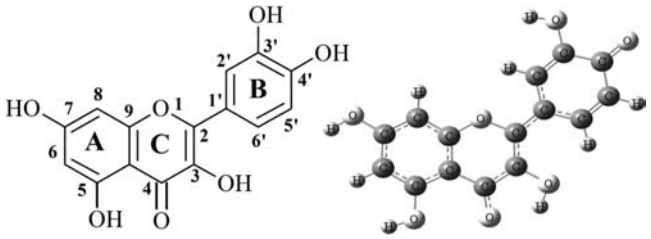

Figure 1. Generic resonance structure of quercetin and the deprotonated quercetin anion $[Q - H]^-$ in its lowest energy configuration (LEC) using Gaussian 03 and optimized with DFT/B3LYP and a 6-31G basis set.

One of the most common ROS in the body is hydrogen peroxide (H_2O_2). In addition to hydrogen peroxide being a nonradical ROS, decomposition of hydrogen peroxide in aqueous solution leads to the formation of hydroxyl and hydroperoxyl radicals.[10] Although it may have some protective function in the urinary system, H_2O_2 has been commonly

Received: February 5, 2014
Revised: April 14, 2014
Accepted: April 23, 2014
Published: April 23, 2014

 © 2014 American Chemical Society

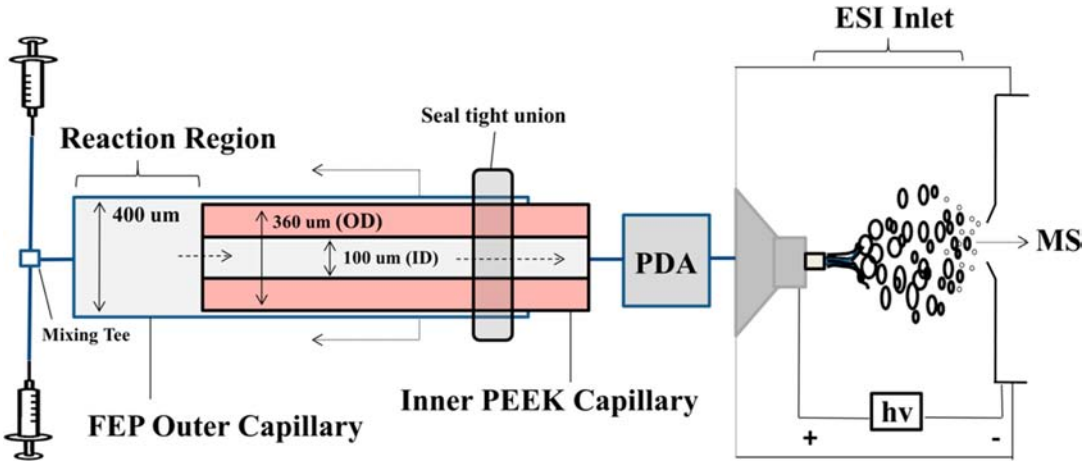

Figure 2. Online kinetic continuous-flow device constructed from two concentric capillary tubes that interfaces with UV and MS detection.

considered a cytotoxin.[11] Despite the fact it is commonly used around households to clean wounds, H_2O_2 may lead to further tissue injury.[12] This sterilizing agent is often used in aseptic packaging techniques and is commonly employed in wine production to oxidize sulfites, reducing allergic reactions. Hydrogen peroxide may also be used to decontaminate apples infected with *Escherichia coli*.[13]

Many studies have focused on quercetin's ability to shield against H_2O_2-induced DNA damage, even in trace amounts above 10 μM, by presumably scavenging the generated free radicals.[14−17] Lipid peroxidation may also be slowed by quercetin through scavenging of hydroxyl radicals spawned by UV photolysis of hydrogen peroxide.[18] In contrast, quercetin was suggested to combat lipid peroxidation by generation of hydrogen peroxide by donating protons from its hydroxyl groups to superoxide radicals.[19] This flavonol also plays a role in inhibiting platelet functions, such as platelet aggregation and platelet adhesion. These functions are believed to be driven by a signal pathway that includes a burst of hydrogen peroxide, which may explain the link between red wine consumption and reduced risk of cardiovascular disease.[20] To fully understand how quercetin may provide health benefits, the study of quercetin's interaction with hydrogen peroxide and the nature of the resultant oxidative degradation products should be considered a topic of substantial significance.

The polyphenolic structure of quercetin has strong absorption of UV-A (λ_{max} = 365 nm) and UV-C light (λ_{max} = 256 nm). Small changes to the skeletal structure could disrupt electron delocalization, so that by monitoring the UV spectrum, kinetic information on degradation reaction can be obtained. Some quercetin degradation pathways studied in this fashion have included UV-induced, electrochemical, free radical, enzymatic, metal-catalyzed, and autoxidation degradation.[21−24] Unfortunately, the multitude of species generated (up to 22 in studies by Zhou et al.[21]), combined with secondary oxidation events, can make the data convoluted and difficult to interpret. Without proper hyphenation, the results are limited to determining bulk antioxidant character and degradation rates and do not offer clues for elucidating degradative mechanisms or specific structural details of related reaction products.

Quercetin is also easily ionized, which makes electrospray ionization mass spectrometry and tandem mass spectrometry (ESI-MS^n) ideally suited to supplement UV data, allowing qualitative identification and structural characterization by fragmentation. A few studies have used this technique to characterize quercetin degradation pathways. Buchner et al. proposed thermal degradation of quercetin led to cross-ring cleavage and solvent adducts formed by nucleophilic attack at C2.[8] Along with solvent adducts, Hvattum et al. demonstrated degradation of quercetin by loss of CO at the C3 position when reacted with a free radical generator, 2,2-diphenyl-1-picrylhydrazyl (DPPH).[25] Zhou et al. completed an extensive comparative study of quercetin degradation by electrochemistry, air oxidation, enzymes, and the free radical generator azobis(isobutyronitrile) (AIBN).[21,26] They proposed that quercetin hydroxylated at the C2 position could lead to three separate pathways, one that follows the C-ring opening at the O1−C2 bond, one with C-ring opening at the C2−C3 bond, and one with C-ring opening at the C3−C4 bond.

Ion trap−time-of-flight (IT-TOF) mass detection provides the potential for definitive identification of polyphenolic compounds using higher order fragmentation and elemental formula determination with high mass accuracy.[27,28] Previously, the authors combined ESI-IT-TOF-MS with an in-house built capillary mixer with an adjustable reactor volume (motivated by Wilson and Konnermann[29]) to collect time-resolved mass spectral measurements of thermal degradation of quercetin in weakly acidic aqueous media and at physiological conditions.[30] In that study, it was proposed that thermally accelerated degradation followed a pathway that included a hydroxylation event at C2, which was proposed to lead to ring cleavage starting by C-ring opening at the O1−C2 bond. This led to a chalcan-trione intermediate structure. It was suggested that further nucleophilic attack of the chalcan-trione at the C2, C3, and C4 carbons resulted in A-type and B-type ions, of which the most preferred led to the A-type ions, 2,4,6-trihydroxy-2-oxo-2-phenylacetate and 2,4,6-trihydroxy-2-hydroxyl-2-phenylacetate ions.

Ab initio and semiempirical computational studies of quercetin's reactivity can provide insight into degradation pathways and solidify the understanding of how it neutralizes free radicals. Through the evaluation of bond dissociation energy (BDE) and reaction energies, it has been proposed that quercetin reacts with free radical ROS through hydrogen atom transfer (HAT) and that the activity is focused in the B- and C-rings.[31−35] In addition, interpretation of spin densities and charge distributions has consistently shown the C2 position in

dx.doi.org/10.1021/jf500619x | J. Agric. Food Chem. 2014, 62, 4322−4331

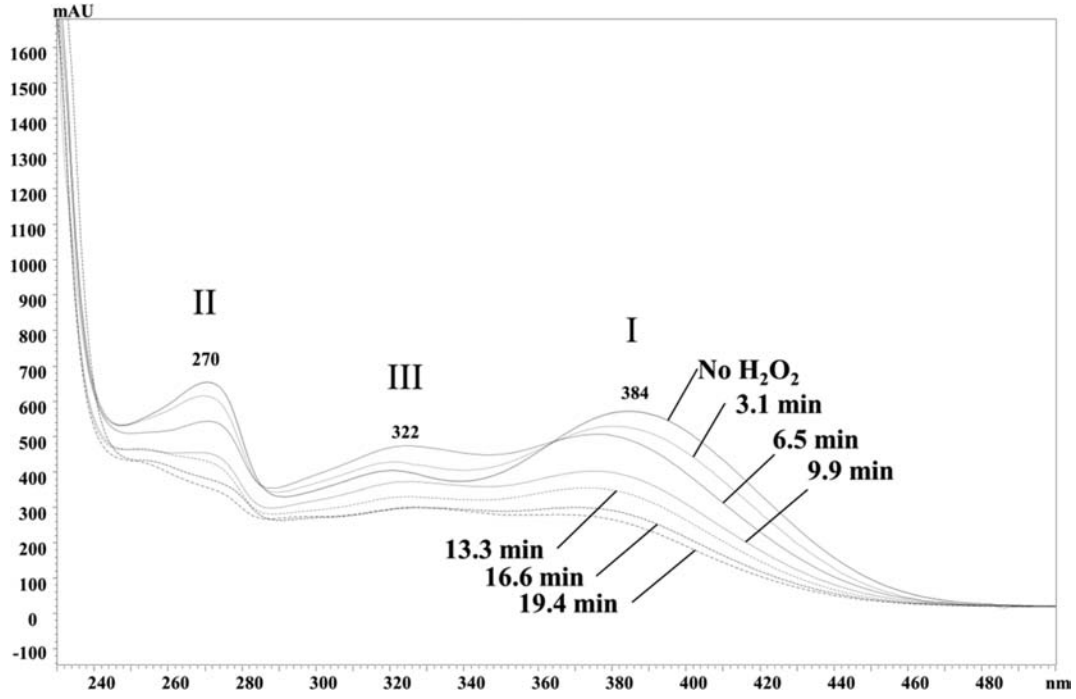

Figure 3. Changes to the UV−vis spectral profile with increasing reaction time after mixing 65 μM quercetin (pH 7.4) and 0.1% H_2O_2 at a ratio of 10:1.5 μL/min.

the C-ring to be the favored site for nucleophilic attack by single and double oxygen species.[23,32,35,36]

To witness the kinetic characteristics of the reactivity between aqueous quercetin and hydrogen peroxide, an in-house-built online capillary mixing device with an adjustable reactor volume was connected to a photodiode array detector. The eluent then was led into the electrospray inlet of an ion trap−time-of-flight (IT-TOF) MS system. The reaction time (3.1−19.4 min) could be controlled by making adjustments to the device. Incorporation of continuous-flow kinetic measurements with UV−vis, MS^n, and high mass accuracy allowed for a novel in-depth study of the interaction between quercetin and free radical species associated with hydrogen peroxide degradation. This embodiment and application of a combined online and mass spectrometry-based degradation study has not been previously conducted.

METHODS AND EQUIPMENT

Reagents and Solution. Aqueous solutions of quercetin (65 μM) were adjusted to pH 7.4 with sodium hydroxide (0.1 N) as described previously.[30] Fresh solutions were prepared at each measured time point. Hydrogen peroxide (0.1% v/v) was prepared by diluting hydrogen peroxide (3%; Walgreens, Deerfield, IL, USA) with LC-MS grade water (Burdick and Jackson, Muskegon, MI, USA).

Kinetic Device. Kinetic measurements were performed using a continuous-flow device, which was built in-house (Figure 2) and consisted of two concentric capillary tubes. Two 2.5 mL glass syringes (7.284 mm internal diameter (i.d.); Hamilton, Reno, NV, USA) were connected to a micromixing tee (IDEX, Lake Forest, IL, USA) via 1 ft lengths of polyetheretherketone (PEEK) tubing ($^1/_{16}$ in. outer diameter (o.d.); 0.005 in. i.d.). A 5 ft length of fluorinated ethylene propylene (FEP) tubing (400 μm i.d.; 1000 μm o.d.) was connected to the outlet end of the mixing tee. The downstream end of the FEP tubing was inserted over a 5 ft length of PEEK tubing (100 μm i.d.; 360 μm o.d.). A stainless steel union (0.052 in. thru-hole) was slid over the FEP tubing 2 in. from the downstream end of the outer capillary and tightened with a fitting and a ferrule to seal any leaks. The downstream outlet end of the PEEK tubing (outer capillary) was connected to a PDA, which in turn was connected to the inlet of the ESI. The syringes were driven by two syringe pumps (NE-1010, New Era Pump Systems, Farmingdale, NY, USA).

By moving the inner capillary, the volume of the reaction region was controlled, which allowed the ability to regulate the amount of reaction time after mixing. The aqueous solution of quercetin was pumped through one syringe at a flow rate of 10.0 μL/min. Hydrogen peroxide was introduced using the other syringe and was pumped at flow rates of 0.5, 1.0, and 1.5 μL/min. The most significant degradation was observed when hydrogen peroxide was pumped at 1.5 μL/min. This condition resulted in solutions that contained a quercetin concentration of 57 μM and a hydrogen peroxide concentration of 4 mM. Kinetic measurements were made by pulling the inner PEEK tubing out at 1 ft intervals. In the configuration in which the device had no extension (minimum dwell time), the total system volume was estimated to be 36 μL, based on 5 ft of inner tubing, 2 in. of outer tubing (seal union overlap), semimicro flow cell with a 10 μL capacity, and ∼1 ft of PEEK tubing (0.005″ i.d.) connecting the PDA to the ESI inlet, which made up the flow path downstream of the micromixer. At the combined flow rate of 11.5 μL/min, this allowed for measurements ranging from 3.1 to 19.4 min of reaction time.

Instrumentation. UV−vis spectra were collected using a Prominence SPD-M20A diode array detector (Shimadzu Scientific Instruments, Inc., Kyoto, Japan) set to acquire between 200 and 800 nm. Negative ion MS spectra were obtained using an ion trap−time-of-flight mass spectrometer (IT-TOF-MS, Shimadzu Scientific Instruments, Inc.) equipped with a conventional electrospray ionization (ESI) source. Analytical parameters for ionization, fragmentation, and detection were as follows: interface voltage, −3.5 kV; nebulizing gas (N_2), 1.5 L/min; drying gas (N_2), 10 L/min; curved desolvation line, 250 °C; detector voltage, 1.92 kV; ion accumulation time, 10 ms; precursor ion isolation width, 0.1 amu; collision gas (Ar), 50%; and frequency constant (q), 0.251. The estimated resolution of the instrument is 10000 at m/z 1000. A scanning rate of 100 ms was used. The estimated duty cycle at MS^3 with these settings was <0.5 s. The collision energy during collision-induced dissociation (CID) was adjusted at each tandem MS stage to determine the optimum parameters at which a maximum amount of signal information would be obtained. The IT-TOF was calibrated to <5 ppm error in mass accuracy using a solution of sodium trifluoroacetate.

dx.doi.org/10.1021/jf500619x | J. Agric. Food Chem. 2014, 62, 4322−4331

Table 1. Adduct and Degradant Ions Observed in Aqueous Solutions of Quercetin Buffered with NaOH at pH 7.4

ion identity	proposed identity	formula	m/z theor	m/z obsd	error (ppm)
Deprotonated, Sodiated, and Simple Oxidated Ions					
$[Q]$	quercetin	$C_{15}H_{10}O_7$	302.0427		
$[Q - H]^-$	quercetin monoanion	$C_{15}H_9O_7$	301.0354	301.0343	−3.7
$[2Q - H]^-$	quercetin dimer anion	$C_{30}H_{19}O_{14}$	603.0780	603.0754	−4.3
$[Q - 2H]^{2-}$	quercetin dianion	$C_{15}H_8O_7$	150.0141	150.0135	−4.0
$[Q - 2H]^{\bullet-}$	quercetin radical anion	$C_{15}H_8O_7$	300.0276	300.0263	−4.3
$[Q - H_2 - H]^-$	quercetin *o*-quinone anion	$C_{15}H_7O_7$	299.0197	299.0189	−2.7
$[Q - 2H + Na]^-$	sodiated quercetin *o*-quinone anion	$C_{15}H_8O_7Na$	323.0173	323.0154	−5.9
Hydroxylated and Peroxidated Ions					
$[Q + O - H]^-$	2,3,4-chalcan-trione monoanion	$C_{15}H_9O_8$	317.0303	317.0290	−4.1
$[Q + O - H_2 - H]^-$	*o*-quinone 2,3,4-chalcan-trione anion	$C_{15}H_7O_8$	315.0146	315.0131	−4.8
$[Q + O_2 - H]^-$	2,4-peroxyl quercetin	$C_{15}H_9O_9$	333.0252	333.0242	−3.0
$[Q + O - 2H]^{2-}$	2,3,4-chalcan-trione dianion	$C_{15}H_8O_8$	158.0115	158.0108	−4.4
$[Q + O - 2H + Na]^-$	sodiated 2,3,4-chalcan-trione anion	$C_{15}H_8O_8Na$	339.0122	339.0117	−1.5
$[Q + O_2 - 2H + Na]^-$	sodiated 2,4-peroxyl quercetin anion	$C_{15}H_8O_9Na$	355.0072	355.0058	−3.9
Degradation Products Ions					
$[Q - C_7H_5O]^-$	2,4,6-trihydroxy-2-oxo-2-phenylacetate	$C_8H_5O_6$	197.0092	197.0086	−3.0
$[Q - C_7H_7O_2]^-$	3,4-dione-2-oxo-2-phenylacetate	$C_8H_3O_5$	178.9986	178.9979	−3.9
$[Q - C_8H_5O_2]^-$	2,4,6-trihydroxybenzoate	$C_7H_5O_5$	169.0142	169.0140	−1.2
$[(Q - C_8H_5O_2)_2 + Na]^-$	sodiated 2,4,6-trihydroxybenzoate dimer	$C_{14}H_{10}O_{10}Na$	361.0177	361.0168	−2.5
$[Q - C_8H_5O_3]^-$	3,4-dihydroxybenzoate	$C_7H_5O_4$	153.0193	153.0186	−4.6
$[Q - C_8H_7O_3]^-$	3,4-dione-benzoate	$C_7H_3O_4$	151.0037	151.0031	−4.0
Small Molecule Loss Ions					
$[Q - CO - H]^-$	4-(4,6-dihydroxy-oxo-2,3-dihydro-1-benzofuran-2-yl)-2-hydroxyphenolate	$C_{14}H_9O_6$	273.0405	273.0394	−4.0
$[Q - CO - H_2 - H]^-$	2-(3,4-dioxocyclohexa-1,5-dien-1-yl)-6-hydroxy-3-oxo-2,3-dihydro-1-benzofuran-4-olate	$C_{14}H_7O_6$	271.0248	271.0239	−3.3
$[Q + O_2 - CO - H]^-$	quercetin depside anion	$C_{14}H_9O_8$	305.0303	305.0293	−3.3

Data collection and analysis were carried out using LCMS Solutions version 3.4 software. The Accurate Mass Calculator and Formula Predictor software tools were used to support determination of theoretical m/z values and elemental formulas of observed fragments. The software was configured to recommend formulaic possibilities based on the following requirements: 1−15 carbons, 0−10 oxygens, 0−15 hydrogens, 0−1 sodium, and within 25 ppm error. Isotopic ratios were also evaluated.

Computational Modeling. Three-dimensional Cartesian coordinates for structures of quercetin and related oxidated ions were submitted to Gaussian 03 for optimization using DFT/B3LYP and a 6-31G basis set.[37] The lowest energy conformation (LEC) was obtained by allowing the software to optimize the atoms in three dimensions.

RESULTS

Time-Resolved Measurements of Aqueous Quercetin Mixed with Hydrogen Peroxide. Changes in the UV and mass spectra due to increasing reaction time were evaluated by maintaining the same flow of the syringe pumps and increasing the length of the reaction chamber.

Changes in UV−Vis Spectra. The UV−vis spectral profile of quercetin in water was characterized by three distinct bands (I, II, and III) that had maxima at 384, 322, and 270 nm, respectively (Figure 3). Absorbance of band I has been associated with the cinnamoyl system of the B-ring, and the absorbance of band II has been associated with the benzoyl system of the A-ring. Band III has been connected with quinonic structures.[38,39] As H_2O_2 began to be mixed with quercetin, a decrease in the absorbance of bands I and II was observed. As the reaction time was extended, the absorbance of band I further decreased and a hypochromic shift of the maximum of band I from 384 to 360 nm was noted. A further decrease in intensity was also noted in band II as the reaction time was extended. In contrast, after the initial addition of H_2O_2, the absorbance in band III increased at the 3.1 and 6.5 min marks and then decreased at 9.9 and 16.6 min. Between 16.6 and 19.4 min, no change in band III was noted. A slight increase around 294 nm was seen at the 19.4 min mark. Two isosbestic points were noted at 285 and 364 nm.

Mass Spectral Analysis without H_2O_2. The signal for the deprotonated quercetin ion $[Q - H]^-$ (m/z 301.0343) has a significant intensity in the negative mode and can be easily observed at relatively low concentrations. This signal was the base peak observed in the spectra at room temperature. Although some quercetin-related ions were observed in the positive mode, they were not observed at significant intensity levels for informative analysis during any of the test conditions and, therefore, are not discussed in this assessment.

Evaluation of the $[Q - H]^-$ signal intensity over long periods showed that aqueous solutions of quercetin at a concentration of 65 μM and at pH 7.4 were relatively stable for >6 h at room temperature. In addition, trace signals for $[Q - 2H]^{2-}$ and $[2Q - H]^-$ (m/z 150.0135 and 603.0754) were observed at a level below 1% relative intensity. Other quercetin-related signals that could be observed at room temperature were classified into four categories: (1) simple oxidation events, (2) hydroxylated structures, (3) sodiated adducts, and (4) ions with small molecule loss (Table 1). The signals for $[Q - H_2 - H]^-$ and $[Q - 2H]^{\bullet-}$ at m/z 299.0189 and 300.0263, observed at 4 and 8% relative intensity, represent the initial oxidation events quercetin undergoes in aqueous solution. Two hydroxylated structures, $[Q + O - H]^-$ and $[Q + O - 2H]^{2-}$ at m/z

dx.doi.org/10.1021/jf500619x | J. Agric. Food Chem. 2014, 62, 4322−4331

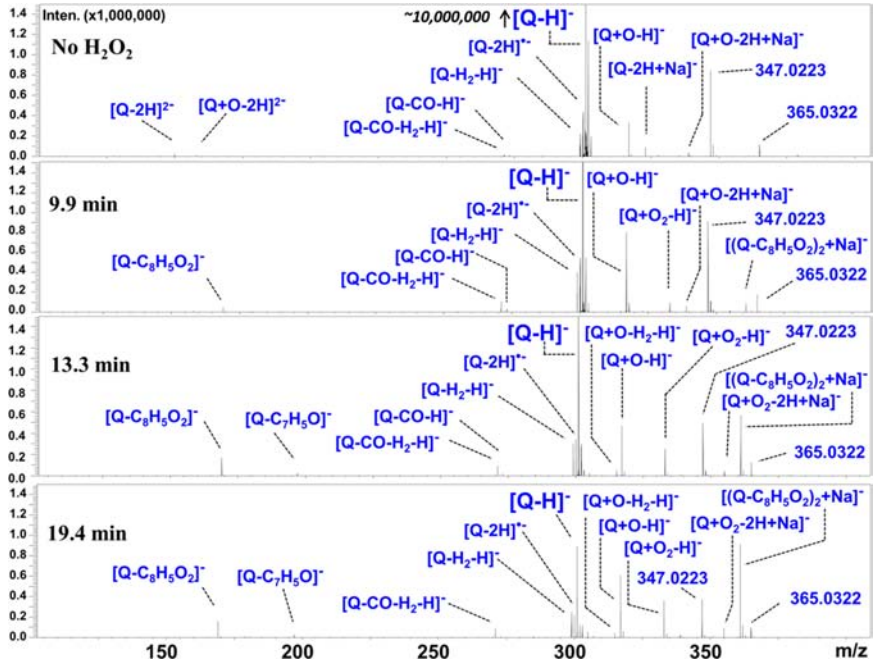

Figure 4. Comparative time-resolved spectra in the negative ionization mode after mixing 65 μM quercetin (pH 7.4) and 0.1% H_2O_2 at a ratio of 10:1.5 μL/min.

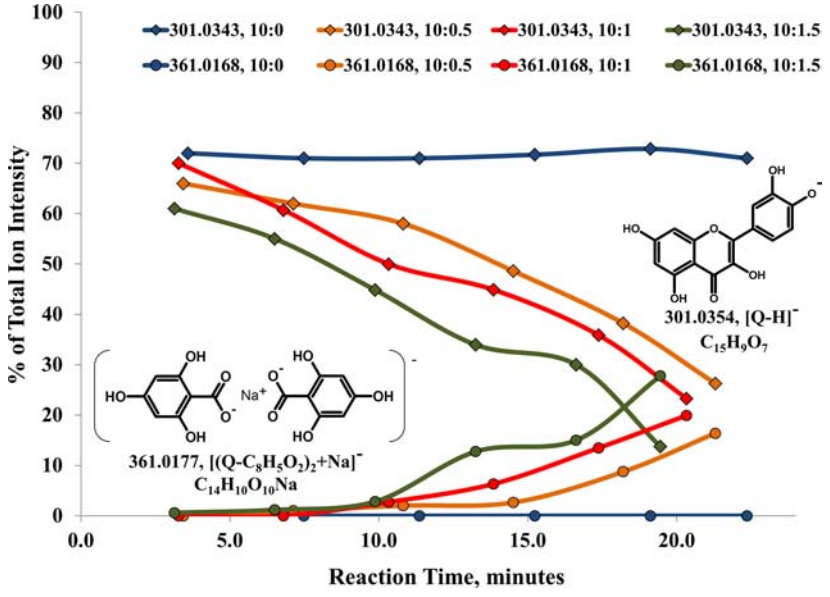

Figure 5. Plot of the H_2O_2-dependent oxidative degradation of $[Q - H]^-$ (m/z 301.0354) ion intensity (normalized against total ion intensity) over time. Formation of $[(Q - C_8H_5O_2)_2Na]^-$ (m/z 361.0177) was observed after addition of H_2O_2 and increased with increasing reaction time. The flow rate of quercetin (65 μM) was held constant at 10 μL/min while the flow rate of the 0.1% H_2O_2 solution was increased from 0.0 μL to 0.5, 1.0, and 1.5 μL/min.

317.0290 and 158.0108, were observed at 4 and ≪1% relative intensity. Two sodiated structures, $[Q - 2H + Na]^-$ (<1% relative intensity) and $[Q + O - 2H + Na]^-$ (<1%), at m/z 323.0154 and 339.0117, respectively, were observed and were believed to be formed due to influence from electrospray ionization.[40,41] An unidentified ion at m/z 347.0223 was observed at 13% relative intensity. Finally, trace amounts of signals at <1% relative intensity at m/z 273.0394 and 271.0239 were observed and were identified as $[Q - CO - H]^-$ and $[Q - CO - H_2 - H]^-$ on the basis of high mass accuracy.

Reaction with 3% Hydrogen Peroxide. Upon addition of 3% hydrogen peroxide with 65 μM quercetin (10:1; a postmixed H_2O_2 concentration of 0.3%) at the minimum dwell time allowed by the device (3.3 min), the $[Q - H]^-$ signal disappeared immediately and two signals at m/z 169.0140 and 361.0168 were observed. On the basis of mass accuracy they were determined to be ions with an elemental formula of $C_7H_5O_5$ and $C_{14}H_{10}O_{10}Na$, respectively. The latter structure was proposed to be a sodiated dimer of the former (see Discussion) and would therefore make the two ions $[Q - C_8H_5O_2]^-$ and $[(Q - C_8H_5O_2)_2 + Na]^-$, respectively. These

dx.doi.org/10.1021/jf500619x | J. Agric. Food Chem. 2014, 62, 4322−4331

two signals were seen in similar intensities and were the largest signals seen in the spectra. Numerous other quercetin-related signals could also be observed after the addition of hydrogen peroxide that were not previously observed in unmixed quercetin solutions. The concentration of hydrogen peroxide being mixed was lowered systematically until the signals for $[Q - C_8H_5O_2]^-$ and $[(Q - C_8H_5O_2)_2 + Na]^-$ were no longer observed above 1% relative intensity and the intensity of the $[Q - H]^-$ was unaffected. The postmixed concentration of hydrogen peroxide was 0.009% (~3 mM) when this was achieved. The ion signals forming from the simple oxidation events, $[Q - H_2 - H]^-$ and $[Q - 2H]^{\bullet -}$, appeared to also be unaffected at this concentration.

The presence of the hydrogen peroxide did appear to hinder the formation of some of the ions observed in the unreacted aqueous solutions, as the $[Q - 2H]^{2-}$, $[2Q - H]^-$, and $[Q - 2H + Na]^-$ ions could no longer be discernible from the baseline after mixing quercetin with even low levels of H_2O_2. The hydroxylated ion signals $[Q + O - H]^-$ and $[Q + O - 2H + Na]^-$ increased significantly (10 and 2% relative intensity), and two peroxylated ion signals, $[Q + O_2 - H]^-$ and $[Q + O_2 - 2H - Na]^-$, m/z 333.0242 and 355.0058, respectively, could be observed at trace levels below 1% relative intensity, which were previously unidentifiable before mixing. Additionally, the small molecule loss signals $[Q - CO - H]^-$ and $[Q - CO - H_2 - H]^-$ increased to 4% relative intensity.

Changes in MS Spectra Based on Increasing Reaction Time. To reduce the inherent variability of ion intensities observed over the course of many days and multiple preparations of reagents, quercetin and product ion intensities were normalized as a percent of total ion intensity. As can be seen in Figures 4 and 5, as the reaction time was increased, the intensity of the $[Q - H]^-$ signal was observed to decrease, reaching 13% of the total ion intensity at 19.4 min. In contrast, the intensity of the ions $[Q - C_8H_5O_2]^-$ and $[(Q - C_8H_5O_2)_2 + Na]^-$ grew as the reaction time was extended and reached a maximum of 7 and 28% of the total ion intensity, respectively. By 19.4 min, the signal for $[(Q - C_8H_5O_2)_2 + Na]^-$ had become the base peak observed in the spectra. At the 13.3 min mark, trace signals below 0.5% total ion intensity of $[Q - C_7H_5O]^-$ and $[Q - C_7H_7O_2]^-$, m/z 197.0086 and 178.9979, respectively, could be observed. These signals increased slightly to maxima of 0.9 and 0.6% total ion intensity by 19.4 min. At this time point, an ion at m/z 153.0186, $[Q - C_8H_5O_3]^-$, began to be observed in trace amounts below 0.5% total ion intensity.

To further investigate the origin of the signal at m/z 361.0168, believed to be $[(Q - C_8H_5O_2)_2 + Na]^-$, and to confirm it was a sodiated dimer of 2,4,6-trihydroxybenzoate (theoretical m/z 169.0142), quercetin solutions were prepared with KOH instead of NaOH and reacted with H_2O_2. The ion signal at m/z 169.0140 was observed; however, a signal near m/z 361.0177, $[(Q - C_8H_5O_2)_2 + Na]^-$, was not observed (data not shown). A small ion with ~1% relative intensity at m/z 376.9917, which would correspond to the ion $[(Q - C_8H_5O_2)_2 + K]^-$, was observed. Fragmentation of this signal returned a product ion at m/z 169.0133.

The ion $[Q + O - H]^-$ increased slightly from 3.1 to 6.5 min and reached its maximum of 11% total ion intensity at the 6.5 min mark and then steadily decreased at each time point, reaching 5% total ion intensity at 19.4 min (Figure 6). The ion $[Q + O_2 - H]^-$ also increased through 6.5 min and continued to increase at the 9.9 min mark, reaching a maximum of 6% total ion intensity, and then was observed to decrease steadily

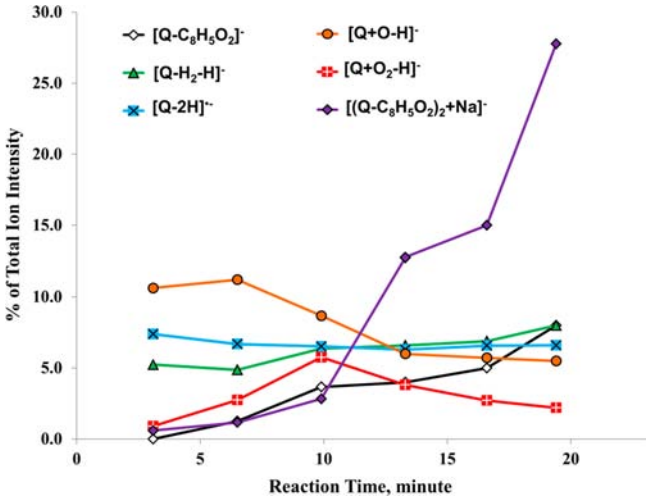

Figure 6. Plot of the H_2O_2-dependent oxidative degradation products of quercetin ion intensities (normalized against total ion intensity) over time. The flow rate of quercetin (65 μM) was held constant at 10 μL/min while the flow rate of the 0.1% H_2O_2 solution was 1.5 μL/min.

at each time point thereafter, reaching 3% at 19.4 min. At the 13.3 min mark, signals for $[Q + O - H_2 - H]^-$ and $[Q + O_2 - 2H + Na]^-$ could be distinguished above baseline at 0.5 and 1.5% total ion intensity, respectively (Figure 4). These signals remained consistent at these levels through 19.4 min. A signal at m/z 305.0293, $[Q + O_2 - CO - H]^-$, also appeared at the 13.3 min mark at 0.7% total ion intensity and remained consistent through 19.4 min.

Many ions were either unaffected or had only a slight change. The intensity for the ions representing the simple oxidation events of quercetin, $[Q - H_2 - H]^-$ and $[Q - 2H]^{\bullet -}$, increased only slightly and reached maxima of 6 and 7% total ion intensity for both ions. Ion signals at m/z 273.0394 ($[Q - CO - H]^-$) and 271.0239 ($[Q - CO - H_2 - H]^-$) also remained at a consistent level compared to the dwell time as the reaction time increased. The unidentified ion at m/z 347.0223 was consistently near 10% total ion intensity regardless of condition. Fragmentation of this ion resulted in product ions at m/z 206.9941, 299.0204, 300.0257, and 301.0314, suggesting that the parent ion was quercetin-related. On the basis of the isotopic distribution it was established that this ion was singly charged; however, no elemental formula could be determined that would agree within 20 ppm of the observed mass. Additionally, a singly charged ion at m/z 365.0322 was observed near 1.5% total ion intensity in all conditions, but its identification was also inconclusive.

DISCUSSION

Acid–Base Equilibrium and Simple Oxidation Ions. Because sample preparations were not sparged or prepared under evacuation of air, it should be assumed that aqueous quercetin would be in the presence of dissolved O_2 and ~250 nM hydroxyl ions from autoionization of water (depending on the pH). In addition to electrospray ionization effects, the presence of trace ROS may contribute to the formation of the simple oxidated quercetin ion $[Q - H_2 - H]^-$ and the radical ion $[Q - 2H]^{\bullet -}$ in fresh solutions at room temperature. The radical ion $[Q - 2H]^{\bullet -}$, which was observed to be pH-dependent in the previous evaluation of quercetin oxidation, was observed at ~2:1 higher intensities than the $[Q - H_2 -$

dx.doi.org/10.1021/jf500619x | J. Agric. Food Chem. 2014, 62, 4322–4331

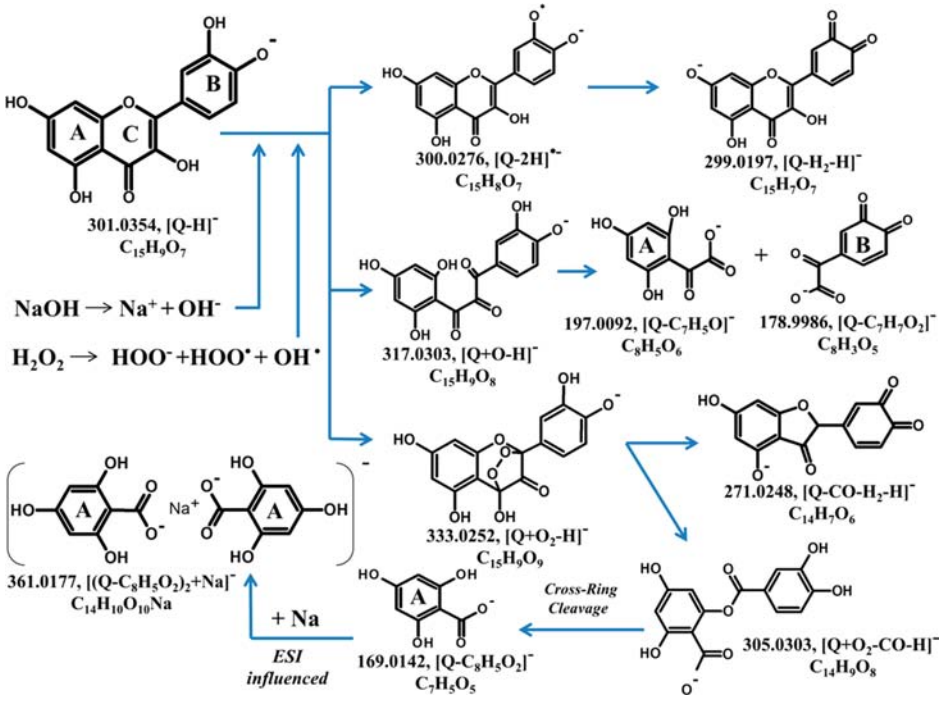

Figure 7. Proposed degradation pathways of quercetin in aqueous solutions in physiological conditions when mixed with hydrogen peroxide. Theoretical m/z values are provided.

Table 2. Estimated Mulliken Charges of the Deprotonated Quercetin Anion $[Q - H]^-$, Hydroxylated Quercetin Anion $[Q + O - H]^-$, and Peroxylated Quercetin Anion $[Q + O_2 - H]^-$ in Their Lowest Energy Configuration (LEC) Using Gaussian 03 and Optimized with DFT/B3LYP and a 6-31G Basis Set

ring	atom	Q	$[Q - H]^-$	$[Q + O - H]^{-a}$	$[Q + O - H]^{-b}$	$[Q + O_2 - H]^{-c}$	$[Q + O_2 - H]^{-C2-C4d}$	$[Q + O_2 - H]^{-C2-C3d}$
C	C2	0.27	0.25	0.21	0.25	0.15	0.22	0.30
	C3	0.22	0.19	0.34	0.24	0.37	0.36	0.30
	C4	0.24	0.22	0.23	0.24	0.21	0.23	0.29
A	C5	0.21	0.18	0.20	0.23	0.21	0.22	0.21
	C6	−0.14	−0.16	−0.16	−0.17	−0.16	−0.16	−0.17
	C7	0.27	0.25	0.26	0.26	0.27	0.25	0.26
	C8	−0.11	−0.12	−0.12	−0.12	−0.12	−0.12	−0.13
	C9	0.23	0.23	0.25	0.26	0.24	0.28	0.28
B	C1′	0.04	0.01	0.01	0.05	0.02	0.08	0.07
	C2′	−0.15	−0.16	−0.13	−0.16	−0.16	−0.12	−0.13
	C3′	0.25	0.19	0.18	0.20	0.19	0.21	0.22
	C4′	0.27	0.28	0.28	0.29	0.29	0.28	0.29
	C5′	−0.16	−0.20	−0.20	−0.19	−0.21	−0.18	−0.18
	C6′	−0.12	−0.11	−0.12	−0.09	−0.09	−0.07	−0.04
energy, kJ/mol				3093.976	3094.082	3291.182	3291.168	3291.192

[a]C-ring intact. [b]C-ring opened. [c]C-ring intact and noncyclic peroxylated. [d]C-ring intact and cyclic peroxylated.

$H]^-$ ion and demonstrates the ability of the quercetin structure to stabilize a radical at ambient temperatures. As hydrogen peroxide is introduced, the levels of ROS would significantly increase, due to the decomposition of hydrogen peroxide into hydroxyl radicals, hydroxyl ions, peroxide radicals, and hydroperoxyl radicals. The notion that ROS promote simple oxidation of quercetin is further supported by the observed increase in the intensity of $[Q - H_2 - H]^-$ and $[Q - 2H]^{\bullet -}$ after the addition of H_2O_2. These simple oxidated ions do not appear to be further affected as the reaction time increases; only a slight increase in the $[Q - H_2 - H]^-$ near 20 min of mixing was observed (Figures 4 and 6).

Hydroxylated and Peroxylated Ions. The hydroxylated adduct of quercetin, $[Q + O - H]^-$, was also observed at room temperature without the addition of hydrogen peroxide. In the previous kinetic study of thermal degradation of quercetin, the authors suggested that the formation of this ion was due to, first, hydroxylation at the C2 position to form a 2-hydroxy-3,4-flavonedione and then formation of a 2,3,4-chalcan-trione anion. This was presumably by C-ring opening of the 2-hydroxy-3,4-flavonedione at the O1−C2 bond and formation of a double-bonded oxygen at C2 (Figure 7).[11] Krishnamachari et al. suggested that this chalcan-trione structure would further stabilize into a benzofuran.[42] As H_2O_2 was mixed, the

dx.doi.org/10.1021/jf500619x | J. Agric. Food Chem. 2014, 62, 4322−4331

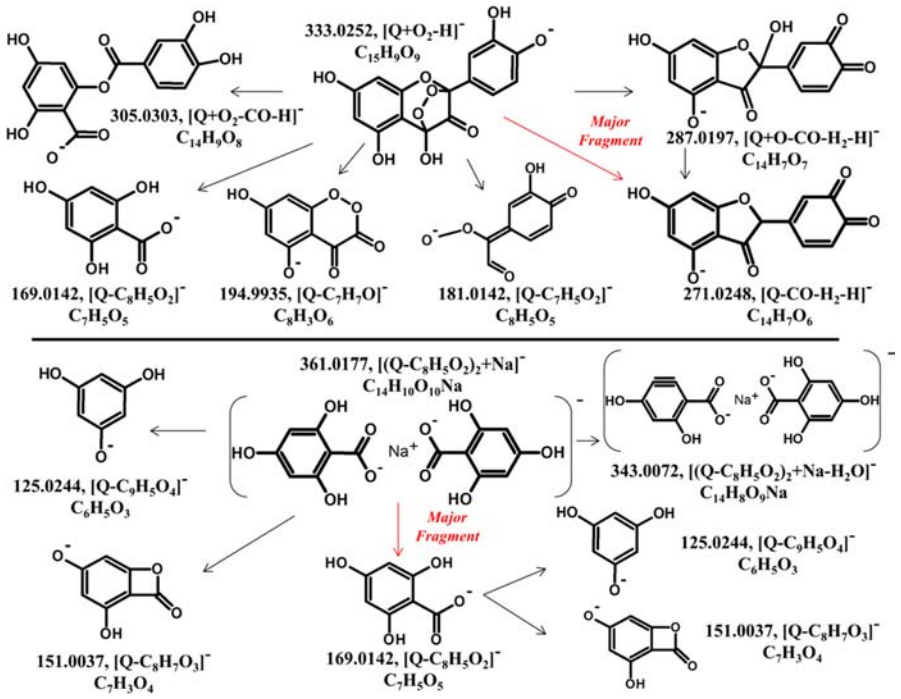

Figure 8. Proposed structures and theoretical m/z of product ions from higher order fragmentation (MS/MS and MS^3) of $[Q + O_2 - H]^-$, m/z 333.0252, and $[(Q - C_8H_5O_2)_2Na]^-$, m/z 361.0177.

concentration of hydroxyl ions and hydroxyl radicals increased, which led to increased hydroxylation of quercetin and a nearly 2-fold increase in the intensity of this ion, as compared to unreacted solutions of quercetin.

The peroxylated ion $[Q + O_2 - H]^-$ was observed only after the addition of H_2O_2. It can be assumed that the ion formation may be attributed to the reaction between quercetin and nucleophilic attack by hydrogen peroxide. Evaluation of the mulliken charges for the deprotonated quercetin $[Q - H]^-$ shows C2 as having the highest partial positive charge and represents the carbon in the C-ring that has the most carbocation characteristics and reactivity (Table 2). Additionally, many computational studies in the literature have demonstrated the charge distribution of the HOMO and LUMO located at this position.[32−36] Therefore, both hydroxylation and peroxylation would most likely occur at C2. The relationship between the increase in signal intensity for $[Q + O_2 - H]^-$ within 10 min and the decrease in the $[Q + O - H]^-$ after 6 min suggests competition between the individual ROS species for reactivity at this site on quercetin.

Decrease in the intensity of both of these ions may also suggest that these ions are only intermediates in the degradation pathway of quercetin when mixed with ROS generated by hydrogen peroxide. Decrease in intensity may be due to further oxidation of the hydroxylated and peroxylated quercetin ions, such as $[Q + O - H_2 - H]^-$ and $[Q + O_2 - 2H + Na]^-$. However, $[Q + O - H_2 - H]^-$ and $[Q + O_2 - 2H + Na]^-$ could be formed by hydroxylation or by peroxylation of simple oxidated quercetin $[Q - H_2 - H]^-$.

The structure for $[Q + O_2 - H]^-$ could exist in more than just one structure in solution. A few studies propose a cyclic peroxylated quercetin intermediate in which the peroxide reacts at the C2 position and forms a bridge across the C-ring by bonding with C4.[21,43] The fragmentation product ion of m/z 333.0242 $[Q + O_2 - H]^-$ further confirms this as a possible structure (Figure 8). The major fragment product ion of $[Q + O_2 - H]^-$ was m/z 271.0236 and represents an ion with the elemental formula $C_{14}H_7O_6$ (−4.4 ppm error). The neutral loss from fragmentation would be a loss of CH_2O and O_2. The loss of three oxygens and only one carbon suggests that the neutral loss involves the added peroxide as well as a carbonyl from either the C3 or C4 position.

Evaluation of the computationally simulated structure, in which peroxylation was only at C2 (and not bridged), suggested that bridging may also occur at C3, because C3 has a significantly higher estimated positive partial charge than C4 (Table 2). The C2 to C3 bridged peroxylated quercetin structure could also possibly lead to all of the fragmentation structures proposed in Figure 8. The calculated total energies of the noncyclic peroxylated quercetin, the 2,4-cyclic-peroxylated quercetin, and the 2,3-cyclic peroxylated quercetin were similar (within ±0.02 kJ/mol); however, the C2−C4 cyclic structure was slightly more energetically favorable than the other two (Table 2). Indeed, there may be a distribution of both the C2−C3 and C2−C4 bonded structures in solution. In a computational study of enzymatic oxygenolysis of quercetin, Fiorucci et al. concluded that the formation of cyclic peroxide would favor 1,3-cycloaddition, instead of 1,2-cycloaddition.[44]

Cleavage of the weak peroxide bond of the C2−C4 bond, followed by decarboxylation at the C3 site, would give rise to a depside structure with a m/z of 305.0303, which was observed in the late kinetic time points (Figures 4 and 7).[22,23] The computational analysis of the C2−C4 peroxylated quercetin confirms the potential reactivity and possibly decarboxylation at the C3 position on the basis of its higher partial positive charge compared to the C2 and C4 positions (Table 2). The observed ions at m/z 273.0394 and 271.0239 also suggest decarboxylation from the C-ring. The fact that the major fragment product ion seen when m/z 333.0242 was fragmented was m/z 271.0236 supports the notion that the appearance of m/z 271.0239 and 273.0394 in the initial MS scan is related to the peroxylated quercetin pathway. These ions were also observed

dx.doi.org/10.1021/jf500619x | J. Agric. Food Chem. 2014, 62, 4322−4331

in the thermal degradation study of quercetin and a study of copper-catalyzed quercetin degradation.[45]

Cross-Ring Cleavage Pathways. The structures for *m/z* 169.0140 and 361.0168 appear to be the preferred degradation products as they were observed to consistently increase as the reaction time was extended. Fragmentation of *m/z* 169.0140 resulted in *m/z* 125.0249 and 151.0044, which confirmed the precursor ion to be the A-type cross-ring cleavage product $[Q - C_8H_5O_2]^-$ (2,4,6-trihydroxybenzoate) observed in the thermal degradation study.[30] The major product ion that resulted from fragmentation of *m/z* 361.0168 was *m/z* 169.0148, and smaller intensity fragment ions included *m/z* 125.0242, 151.0045, and 343.0029. Higher order fragmentation of the product ion *m/z* 169.0148 (MS^3) provided further product ion signals at *m/z* 151.0032 and 125.0239. Refer to Figure 8 for the proposed fragment ion structures and theoretical masses. Considering the observed fragmentation data and that *m/z* 361.0168 does not form when NaOH is replaced by KOH, the ion at *m/z* 361.0168 must be due to a 2,4,6-trihydroxybenzoate dimer bridged by a sodium ion. Previously, Schug and McNair demonstrated a similar phenomenon in which they observed pseudomolecular ion formation of sodium-bridged dimers of aromatic carboxylic acids in the negative ionization mode by ESI.[40,41]

The depside generated by degradation of the 2,4-cyclic peroxylated quercetin may be the intermediate that leads to formation of the 2,4,6-trihydroxybenzoate. Additional nucleophilic attack by ROS at the C2 position of this depside could cause cleavage of the O1−C2 bond. This would make 2,4,6-trihydroxybenzoate be the charged leaving group. This preferred degradation product is different from the 2,4,6-trihydroxy-2-oxo-2-phenylacetate and 2,4,6-trihydroxy-2-hydroxy-2-phenylacetate degradation products (*m/z* 197.0092 and 199.0248) observed for the thermal degradation pathway.[30] The late kinetic time point of the hydrogen peroxide mixing study did show trace amounts of an ion at *m/z* 197.0086, along with two other A-type and B-type cross-ring cleavage product ions, *m/z* 153.0186 and 178.9979. Formation of these ions could be due to continued hydroxylation of the chalcan-trione, $[Q + O - H]^-$.

Interpretation of UV−Vis Spectral Profile. Details presented by the mass spectral data help to further explain the changes observed in the UV spectral profile. As expected, when the quercetin structure interacts with hydrogen peroxide at the C2 position and the hydroxylated and peroxylated structures are being formed, the cinnamoyl and benzoyl structures are interrupted, causing a decrease in the absorbance of bands I and II. Shift of the maxima in band I from 380 nm (Figure 3) may also be in part due to simple oxidation events and disruption of C-ring aromaticity. In addition to an effect from quinones, band III has been suggested to be influenced by the chalcone structure.[46,47] The increase in band III at the initial time points correlated with an increase in the $[Q + O - H]^-$ at the first two kinetic measurements, as well as the decrease in absorbance along with a decrease in intensity after 9.9 min. Further oxidation of the hydroxylated and peroxylated structures ($[Q + O - H_2 - H]^-$ and $[Q + O_2 - 2H + Na]^-$) may contribute to the hyperchromic shift of the maxima of band III. An HPLC-UV study by Zvezdanovic et al. identified 2,4,6-trihydroxybenzoate as a prominent quercetin degradant, which had a UV profile that consisted of a single band with a maximum at 294 nm.[47] At the last time point, the influence of the 2,4,6-trihydroxybenzoate may have begun to be seen in band III with the slight increase in absorbance at 294 nm. The trihydroxybenzoate structure would maintain the benzoyl system from the A-ring side and an absorbance near band II.[26,48]

AUTHOR INFORMATION

Corresponding Author

*(K.A.S.) Mail: 700 Planetarium Place, Box 19065, Arlington, TX 76019-0065, USA. E-mail: kschug@uta.edu. Phone: (817) 272-3541. Fax: (817) 272-3808.

Funding

We gratefully acknowledge the support of the National Science Foundation (CHE-0846310).

Notes

The authors declare no competing financial interest.

ACKNOWLEDGMENTS

We gratefully acknowledge the support of Shimadzu Scientific Instruments, Inc., for their support of instrumentation through the Shimadzu Equipment Grants for Research Program. We also appreciate the help and guidance of Prof. Purnendu K. Dasgupta with respect to device construction.

REFERENCES

(1) Day, A. J.; Williamson, G. In *Flavonoids in Health and Disease*, 2nd ed.; Rice-Evans, C. A., Packer, L., Eds.; CRC Press: Boca Raton, FL, USA, 2010; pp 391−412.

(2) Hertog, M. G. L.; Kromhout, D.; Aravanis, C.; Blackburn, H.; Buzina, R.; Fidanza, F.; Giampaoli, S.; Jansen, A.; Menotti, A.; Nedeljkovic, S.; Pekkarinen, M.; Simic, B. S.; Toshima, H.; Feskens, E. J. M.; Hollman, P. C. H.; Katan, M. B. *Arch. Intern. Med.* **1995**, *155*, 381−386.

(3) Guardia, T.; Rotelli, A. E.; Juarez, A. O.; Pelzer, L. E. *Farmaco* **2001**, *56*, 683−687.

(4) Rogerio, A. P.; Kanashiro, A.; Fontanari, C.; Silva, E. V. G.; Lucisano-Valim, Y. M.; Soares, E. G.; Faccioli, L. H. *Inflamm. Res.* **2007**, *56*, 402−408.

(5) Comalada, M.; Camuesco, D.; Sierra, S.; Ballester, I.; Xaus, J.; Galvez, J.; Zarzuelo, A. *Eur. J. Immunol.* **2005**, *35*, 584−592.

(6) Boots, A. W.; Haenen, G. R. M. M.; Bast, A. *Eur. J. Pharmacol.* **2008**, *585*, 325−337.

(7) Mitchell, A. E.; Hong, Y. J.; Koh, E.; Barrett, D. M.; Bryant, D. E.; Denison, R. F.; Kaffka, S. *J. Agric. Food Chem.* **2007**, *55*, 6154−6159.

(8) Buchner, N.; Krumbein, A.; Rohn, S.; Kroh, L. W. *Rapid Commun. Mass Spectrom.* **2006**, *20*, 3229−3235.

(9) Makris, D. P.; Rossiter, J. T. *J. Food Compos. Anal.* **2002**, *15*, 103−113.

(10) Wiberg, E.; Wiberg, N.; Holleman, A. F. *Inorganic Chemistry*; Academic Press: San Diego, CA, USA, 2001.

(11) Halliwella, B.; Clement, M. V.; Longa, L. H. *FEBS Lett.* **2000**, *486*, 10−13.

(12) Branemark, P. I.; Ekholm, R.; Albrektsson, B.; Lindstrom, J.; Lundborg, G.; Lundskog, J. *J. Bone Joint Surg. Am.* **1967**, *49*, 48−62.

(13) Sapers, G. M.; Sites, J. E. *J. Food Sci.* **2003**, *68*, 1793−1797.

(14) Duthie, S. J.; Collins, A. R.; Duthie, G. G.; Dobson, V. L. *Mutat. Res., Genet. Toxicol. Environ. Mutagen.* **1997**, *393*, 223−231.

(15) Musonda, C. A.; Chipman, J. K. *Carcinogenesis* **1998**, *19*, 1583−1589.

(16) Johnson, M. K.; Loo, G. *Mutat. Res., DNA Repair* **2000**, *459*, 211−218.

(17) Aherne, S. A.; O'Brien, N. M. *Nutr. Cancer* **1999**, *34*, 160−166.

(18) Husain, S. R.; Cillard, J.; Cillard, P. *Phytochemistry* **1987**, *26*, 2489−2491.

(19) Miura, Y. H.; Tomita, I.; Watanabe, T.; Hirayama, T.; Fukui, S. *Biol. Pharm. Bull.* **1998**, *21*, 93−96.

(20) Pignatelli, P.; Pulcinelli, F. M.; Celestini, A.; Lenti, L.; Ghiselli, A.; Gazzaniga, P. P. *Am. J. Clin. Nutr.* **2000**, *72*, 1150−1155.
(21) Zhou, A.; Kikandi, S.; Sadik, O. A. *Electrochem. Commun.* **2007**, *9*, 2246−2255.
(22) Makris, D. P.; Rossiter, J. T. *Food Chem.* **2002**, *77*, 177−185.
(23) Aliaga, C.; Lissi, E. A. *Can. J. Chem.* **2004**, *82*, 1668−1673.
(24) Jo, S.; Ka, E.; Lee, H.; Apostolidis, E.; Jang, H.; Kwon, Y. *Int. J. Appl. Res. Nat. Prod.* **2009**, *2*, 52−60.
(25) Hvattum, E.; Stenstrom, Y.; Ekeberg, D. *J. Mass Spectrom.* **2004**, *39*, 1570−1581.
(26) Zhou, A.; Sadik, O. A. *J. Agric. Food Chem.* **2008**, *56*, 12081−12091.
(27) Barnes, J. S.; Schug, K. A. *Int. J. Mass Spectrom.* **2011**, *38*, 71−80.
(28) Tedmon, L.; Barnes, J. S.; Nguyen, H. P.; Schug, K. A. *J. Am. Soc. Mass Spectrom.* **2013**, *24*, 399−409.
(29) Wilson, D. J.; Konermann, L. *Anal. Chem.* **2003**, *75*, 6408−6414.
(30) Barnes, J. S.; Foss, F. W.; Schug, K. A. *J. Am. Soc. Mass Spectrom.* **2013**, *24*, 1513−1522.
(31) Fiorucci, S.; Golebiowski, J.; Cabrol-Bass, D.; Antonczak, S. *J. Agric. Food Chem.* **2007**, *55*, 903−911.
(32) Trouillas, P.; Marsal, P.; Siri, D.; Lazzaroni, R.; Duroux, J. L. *Food Chem.* **2006**, *97*, 679−688.
(33) Markovic, Z. S.; Markovic, J. M. D.; Dolicanin, C. B. *Theor. Chem. Acc.* **2010**, *127*, 69−80.
(34) Mendoza-Wilson, A. M.; Glossman-Mitnik, D. *J. Mol. Struct.: THEOCHEM* **2005**, *716*, 67−72.
(35) Dhaouadi, Z.; Nsangou, M.; Garrab, N.; Anouar, E. H.; Marakchi, K.; Lahmar, S. *J. Mol. Struct.: THEOCHEM* **2009**, *904*, 35−42.
(36) Justino, G. C.; Vieira, A. J. S. C. *J. Mol. Model.* **2010**, *16*, 863−876.
(37) Frisch, M. J.; Trucks, G. W.; Schlegel, H. B.; Scuseria, G. E.; Robb, M. A.; Cheeseman, J. R.; Montgomery, J. A., Jr.; Vreven, T.; Kudin, K. N.; Burant, J. C.; Millam, J. M.; Iyengar, S. S.; Tomasi, J.; Barone, V.; Mennucci, B.; Cossi, M.; Scalmani, G.; Rega, N.; Petersson, G. A.; Nakatsuji, H.; Hada, M.; Ehara, M.; Toyota, K.; Fukuda, R.; Hasegawa, J.; Ishida, M.; Nakajima, T.; Honda, Y.; Kitao, O.; Nakai, H.; Klene, M.; Li, X.; Knox, J. E.; Hratchian, H. P.; Cross, J. B.; Bakken, V.; Adamo, C.; Jaramillo, J.; Gomperts, R.; Stratmann, R. E.; Yazyev, O.; Austin, A. J.; Cammi, R.; Pomelli, C.; Ochterski, J. W.; Ayala, P. Y.; Morokuma, K.; Voth, G. A.; Salvador, P.; Dannenberg, J. J.; Zakrzewski, V. G.; Dapprich, S.; Daniels, A. D.; Strain, M. C.; Farkas, O.; Malick, D. K.; Rabuck, A. D.; Raghavachari, K.; Foresman, J. B.; Ortiz, J. V.; Cui, Q.; Baboul, A. G.; Clifford, S.; Cioslowski, J.; Stefanov, B. B.; Liu, G.; Liashenko, A.; Piskorz, P.; Komaromi, I.; Martin, R. L.; Fox, D. J.; Keith, T.; M. A. Al-Laham, Peng, C. Y.; Nanayakkara, A.; Challacombe, M.; Gill, P. M. W.; Johnson, B.; Chen, W.; Wong, M. W.; Gonzalez, C.; Pople, J. A. *Gaussian 03, Revision C.02*, Gaussian, Inc.: Wallingford, CT, USA, 2004.
(38) Mabry, T. J.; Markham, K. R.; Thomas, M. B. *The Systematic Identification of Flavonoids*; Springer: London, UK, 2012.
(39) He, J. B.; Yu, C. L.; Duan, T. L.; Deng, N. *Anal. Sci.* **2009**, *25*, 373−377.
(40) Schug, K. A.; McNair, H. M. *J. Chromatogr., A* **2003**, *985*, 531−539.
(41) Schug, K. A.; McNair, H. M. *J. Sep. Sci.* **2002**, *25*, 759−766.
(42) Krishnamachari, V.; Levine, L. H.; Pare, P. W. *J. Agric. Food Chem.* **2002**, *50*, 4357−4363.
(43) Zenkevich, I. G.; Eshchenko, A. Y.; Makarova, S. V.; Vitenberg, A. G.; Dobryakov, Y. G.; Utsal, V. A. *Molecules* **2007**, *12*, 654−672.
(44) Fiorucci, S.; Golebiowski, J.; Cabrol-Bass, D.; Antonczak, S. *ChemPhysChem* **2004**, *5*, 1726−1733.
(45) Pekal, A.; Biesaga, M.; Pyrzynksa, K. *Biometals* **2011**, *24*, 41−49.
(46) Dall'Acqua, S.; Miolo, G.; Innocenti, G.; Caffieri, S. *Molecules* **2012**, *17*, 8898−8907.
(47) Zvezdanovic, J. B.; Stanojevic, J. S.; Markovic, D. Z.; Cvetkovic, D. J. *J. Serb. Chem. Soc.* **2012**, *77*, 297−312.
(48) Merken, H. M.; Beecher, G. R. *J. Agric. Food Chem.* **2000**, *48*, 577−599.

JOURNAL OF AGRICULTURAL AND FOOD CHEMISTRY

Article

pubs.acs.org/JAFC

Separation and Characterization of Phenolic Compounds from U.S. Pecans by Liquid Chromatography–Tandem Mass Spectrometry

Katherine S. Robbins,[†] Yuanyuan Ma,[†] M. Lenny Wells,[‡] Phillip Greenspan,[§] and Ronald B. Pegg*[,†]

[†]Department of Food Science & Technology, College of Agricultural and Environmental Sciences, The University of Georgia, 100 Cedar Street, Athens, Georgia 30602-2610, United States

[‡]Department of Horticulture, College of Agricultural and Environmental Sciences, The University of Georgia, 4604 Research Way, Tifton, Georgia 31793-5766, United States

[§]Department of Pharmaceutical & Biomedical Sciences, College of Pharmacy, The University of Georgia, 250 W. Green Street, Athens, Georgia 30602, United States

Supporting Information

ABSTRACT: The phenolic acids and proanthocyanidins (PACs) of pecans possess bioactive properties, which might be useful in retarding the onset of and ameliorating the status of certain chronic disease states. There is a general lack of information in the literature regarding such compounds, especially the PACs. Crude phenolic extracts pooled from eight commercially significant cultivars were selected based on their relatively high antioxidant capacities. The pooled extracts were separated via Sephadex LH-20 column chromatography into five ethanolic low-molecular-weight (LMW) fractions and one acetonic high-molecular-weight (HMW) fraction. The preparations were then characterized using RP-HPLC-ESI-MS/MS and diol-phase HPLC-ESI-MS/MS in order to determine the key constituents present in the LMW and HMW fractions, respectively. As previously observed in pecan nutmeat, ellagic acid and (+)-catechin were found to be the major phenolics in the LMW fractions. The last eluting LMW fraction did not contain phenolic acids; rather it possessed PAC monomers and dimers. The HMW fraction comprised a majority of its PACs as dimers; yet, monomers, trimers, tetramers, pentamers, and hexamers were also separated and characterized.

KEYWORDS: *pecans, proanthocyanidins (PACs), Sephadex LH-20, RP-HPLC, diol-phase-HPLC, ESI-MS/MS*

INTRODUCTION

Pecans [*Carya illinoinensis* (Wangenh.) K. Koch] and other tree nuts are receiving increased attention due to their purported health benefits[1−4] and a qualified health claim approved more than 10 years ago by the U.S. Food and Drug Administration. Most reports associate these benefits with healthful lipid profiles (*i.e.*, MUFAs, PUFAs, α-tocopherol, and γ-tocopherol), but more recently attention has turned toward the favorable phenolic profiles that tree nuts possess. Endogenous pecan phenolics can be segregated into two main classes, namely, phenolic acids (e.g., ellagic and gallic acids as well as their derivatives) and condensed tannins/proanthocyanidins (PACs) with varying degrees of polymerization (DP).[5] Characterization of these important classes, especially the PACs, is lacking in the literature.[6]

PACs, or condensed tannins, are a type of phenolic polymer. There are two main types, that is, procyanidins and prodelphinidins. Procyanidins, the most prevalent PAC found in foods, are composed of (−)-epicatechin monomers, whereas the prodelphinidins comprise (−)-epigallocatechin monomers.[7] PACs are usually not classified based on the individual compound type; rather, they are centered on the DP that exist.[8] The DP can range anywhere from 2 (i.e., dimers) to 10^+ (i.e., polymers). The antioxidant properties and antimutagenic activity of PACs can vary based upon structure and DP.[7]

Pecan PACs and their flavan-3-ol monomers have shown potential for important health-related benefits *in vivo*.[6] In a randomized controlled trial employing a crossover design with a one-week washout period between treatments, Hudthagosol et al.[6] had 16 healthy men and women (23−44 years, BMI 22.7 ± 3.4) consume a test meal composed of either whole pecans, blended pecans, or an isocaloric meal of equivalent macronutrient composition. Blood was sampled at baseline and at intervals up to 24 h postingestion. Plasma antioxidant capacities and the levels of γ-tocopherol and epigallocatechin gallate (EGCG) from the panelists' blood were determined; each increased significantly ($p < 0.05$) postprandially. While the flavan-3-ol monomers can be absorbed in the small intestine, there is evidence that all PACs with a DP of 3 and higher may not be able to be properly absorbed.[9] If this is indeed the case, larger PACs can still participate in contributing a health benefit to humans, as these compounds can be broken down into smaller secondary metabolites by colonic microflora[10] and then be absorbed.

In this study, we employed Sephadex LH-20 column chromatography to fractionate pecan phenolic acids, their derivatives, and PACs. Once separated, these fractions were characterized by the total phenolics content (TPC) assay, UV spectral analysis, and RP-HPLC-ESI-MS/MS characterization of the low-molecular-weight (LMW) fractions and diol-phase

Received: February 20, 2014
Revised: April 11, 2014
Accepted: April 15, 2014
Published: April 16, 2014

 © 2014 American Chemical Society

HPLC-ESI-MS/MS of the high-molecular-weight (HMW) fraction.

MATERIALS AND METHODS

Chemicals and Glassware. Washed sea sand, sodium carbonate, glass wool, ethanol (95%), and ACS-grade methanol, hexanes, and acetone as well as HPLC-grade water, methanol, hexanes, 2-propanol, and acetonitrile were acquired from Fisher Scientific Co., LLC (Suwanee, GA, USA). Glacial acetic acid and hydrochloric acid were purchased from VWR International, LLC (Suwanee, GA, USA). Sephadex LH-20, Folin−Ciocalteu's phenol reagent, (+)-catechin hydrate, gallic acid, ellagic acid, and protocatechuic acid were purchased from the Sigma-Aldrich Chemical Co. (St. Louis, MO, USA). Procyanidin B2 was acquired from Indofine Chemical Company, Inc. (Hillsborough, NJ, USA), and the cocoa PAC standards with both A- and B-type linkages of DP = 2−10 were obtained from Planta Analytica (Danbury, CT, USA). No differences in the composition of these PAC standards were expected compared to those endogenous to pecans.

Collection of Samples. Eighteen pecan cultivars were acquired from commercial and research pecan orchards in Georgia (11), New Mexico (2), and Texas (5) over a three-month period in the fall of 2011. All orchards had received commercial cultural management care according to the Cooperative Extension recommendations in each state. The nuts were raw and remained in-shell through transport, packaging, and storage. After arrival to the Department of Food Science & Technology, Athens, GA, the pecan samples were placed in labeled pouches (Sealed Air Corporation, Elmwood Park, NJ, USA), vacuum packed (Henkelman 600, Henkelman BV, The Netherlands) to retard oxidative degradation, and stored at −80 °C until analyzed. On the day of analysis, pecan samples were removed from the freezer, shelled, and allowed to warm to room temperature to ensure a proper mass reading. Roughly 12 g of nutmeat was placed in a −20 °C freezer and allowed to partially refreeze to facilitate grinding. Each nut sample was then combined with ∼60 g of washed sea sand and ground in a commercial coffee mill (Grind Central Coffee Grinder, Cuisinart, East Windsor, NJ, USA) to a very fine powder using an intermittent pulsing technique. In this manner, oils were not expressed from the nutmeat during the particle size reduction step.

Lipid Extraction. A Soxhlet apparatus was employed to facilitate the extraction of lipids from all pecan samples. Briefly, a known quantity of the ground matter (pecan and sand) was placed into a cellulose extraction thimble (single thickness, 43 mm *i.d.* × 123 mm *e.l.*, Whatman International Ltd., Maidstone, England) and the mass recorded. Glass wool was placed in the top of the thimble to ensure that the contents remained in place during extraction. Extraction was performed using ∼350 mL of hexanes for 20 h. Upon completion, the thimbles were removed, placed on aluminum foil, and allowed to dry overnight in a fumehood. The hexanes were removed from the lipid extract using a Büchi Rotavapor R-210 and a V-700 vacuum pump connected to a V-850 vacuum controller (Büchi Corporation, New Castle, DE, USA) at 45 °C. The lipid portion was weighed for gravimetric analysis.

Phenolic Compound Extraction. The defatted pecan nutmeat was removed from the dried thimble and placed in a beaker. As employed by Wu et al.,[11] a $(CH_3)_2CO/H_2O/CH_3COOH$ solvent mixture (70:29.5:0.5 v/v/v, 100 mL) was used to extract phenolic compounds. Extraction was carried out according to Craft et al.[12] Briefly, the contents in 250 mL Erlenmeyer flasks were heated at 50 °C for 30 min in an orbital-shaking water bath (New Brunswick Scientific, New Brunswick, NJ, USA). The extraction was performed 3×, and the supernates were pooled. Acetone was evaporated from the pooled supernate using the Rotavapor. The aqueous portion was poured into 100 × 50 mm [diameter × height] crystallizing dishes (VWR), covered with filter paper, and placed in a −80 °C freezer until frozen. The samples were then lyophilized in a FreeZone 2.5 L benchtop freeze-dryer (Labconco Corporation, Kansas City, MO, USA) to ensure all traces of moisture were removed. The dried extract was transferred to amber-colored vials, flushed with N_2, capped, and stored at 4 °C until analyzed. A total lipid and phenolic extraction was completed in triplicate for each of the 18 pecan cultivars.

Sample Selection and Extract Separation. On the basis of preliminary data (results not shown here), the eight cultivars with the best performance based on the H-ORAC$_{FL}$ assay were selected for use in this study. A 240 mg portion of each crude pecan extract was taken and pooled. The resultant extract (1.92 g) was mixed in a small volume of ∼75% (v/v) ethanol and sonicated to ensure its complete dissolution. The sample was then applied via a Pasteur pipet to the top of a chromatographic column packed with Sephadex LH-20 (bead size: 25−100 μm; Chromaflex column, 30 × 400 mm [i.d. × length], Kontes, Vineland, NJ, USA), and flow was conducted by gravity. The LMW phenolic compounds (molecular weight <600 Da) were eluted with ∼1.5 L of 95% (v/v) ethanol. Fractions (7 mL volume) were collected by a Beckman Coulter SC100 collector (Fullerton, CA, USA). The eluent was then switched to 50% (v/v) aqueous acetone, and an HMW phenolic fraction (molecular weight ≥600 Da) was eluted from the column with ∼600 mL of the second mobile phase. Total recovery of the extract from the column was 99%.

Fraction Determination. LMW phenolic fractions were analyzed using an Agilent 8453 UV−vis diode array detection (DAD) spectrophotometer (Agilent Technologies, Inc., Wilmington, DE, USA) scanning across a wavelength range of 200 to 400 nm. Spectral differences were used as a guide to group the collected fractions into five pooled lots. After combining, the ethanol was evaporated using the Rotavapor. To ensure complete removal of solvent and moisture, the pooled fractions were lyophilized with the Labconco freeze drier and then stored in amber-glass bottles at 4 °C until analyzed. Apropos the HMW fraction, acetone was also removed *in vacuo* and the aqueous residue lyophilized and stored as described above.

Total Phenolics Content Assay. The TPCs of the ethanolic fractions were determined based on a method adapted from Swain and Hillis[13] employing Folin−Ciocalteu's phenol reagent. Each fraction was diluted to 0.20 mg/mL in anhydrous CH_3OH. The assay was performed using 1 mL of methanolic extract, 7.5 mL of deionized water, 0.5 mL of Folin−Ciocalteu's phenol reagent, and 1 mL of saturated sodium carbonate. The solution was vortexed for 30 s, and the tubes sat for 1 h to allow for optimal color development. The absorbance of the resulting chromophore from this colorimetric reaction was measured at λ = 750 nm using the Agilent spectrophotometer. A standard curve was prepared using known concentrations of working solutions of (+)-catechin (1.6 to 8.0 μg/mL). TPC values are reported as g catechin equiv (CE)/g ethanolic extract.

HPLC Characterization. *Reversed-Phase HPLC Characterization (RP-HPLC-ESI-MS/MS).* The RP-HPLC method of Srivastava et al.[14] was followed to characterize the fractions of the pooled pecan cultivars. An Agilent 1200 series HPLC system consisting of a quaternary pump with degasser, autosampler, thermostated column compartment, UV−vis DAD with standard flow cell, and 3D ChemStation software (Agilent Technologies, Santa Clara, CA, USA) was employed for the chromatography. A reversed-phase Luna $C_{18}(2)$ column (4.6 × 250 mm, 5 μm particle size; Phenomenex, Torrance, CA, USA) was utilized. A gradient elution consisting of mobile phase A ($H_2O/CH_3CN/CH_3COOH$, 93:5:2, v/v/v) and mobile phase B ($H_2O/CH_3CN/CH_3COOH$, 58:40:2, v/v/v) from 0 to 100% B over a 50 min period at a flow rate of 1 mL/min was employed. A volume of 100 μL was injected for each of the crude fractions (4.0 mg/mL methanol). Detection wavelengths were λ = 255 nm (ellagic acid and ellagic acid derivatives), 280 nm (phenolic acids, (+)-catechin, (−)-epicatechin), 320 nm (phenolic acids, notably of the *trans*-cinnamic acid family), and 360 nm (flavonols). Tentative identification of separated components was made by matching UV−vis spectra and retention time (t_R) mapping with standard compounds prior to ESI-MS/MS analyses. Comparisons of chromatographed compounds were also made with those of selected published works.

RP-HPLC-ESI-MS/MS analyses of the crude extracts were performed on an Agilent 1100 HPLC system, with the same chromatography conditions as described above, coupled with a Bruker Esquire 3000^{plus} ion trap mass spectrometer (Bruker Daltonics Inc.,

Billerica, MA, USA), which was equipped with an ESI source. Instrument control and data acquisition were performed with Esquire Control 5.0 software. Raw data were analyzed using Data Analysis 4.1 (Bruker Daltonics Inc.). The dissolved crude extracts were infused into the source chamber from the HPLC via a T-junction delivering roughly one-third of the flow to the mass spectrometer. Mass spectra were acquired in the negative-ion mode with smart settings for a target mass at an m/z of 800. The voltage applied to the capillary was 4.0 kV with an end plate offset of −500 V. Nitrogen was used as the nebulizing gas at a pressure of 10 psi, a dry gas flow rate of 6 L/min, and a dry gas temperature of 280 °C. All collision-induced dissociation mass spectra were obtained at a fragmentation voltage of 1 V after isolation of the desired precursor ion. A full scan was performed over the mass range of 100 to 1000 Da at a rate of 13 000 m/z per second under standard−normal scan mode. The ion current control target was 50 000 with a maximum accumulation time of 50 ms. Each mass spectrum generated was based on an average of ten scans. The phenolic compounds were preliminarily fragmented using the auto-MS^2 mode with the following precursor ion selection parameters: two precursor ions, threshold abs of 10 000, threshold rel of 5.0%, ion excluded after two spectra, and exclusion release after 0.5 min.

Diol-Phase HPLC Characterization (Diol-Phase HPLC-ESI-MS/MS). PACs were separated based on their DP according to Kelm et al.[15] The same Agilent 1200 Series HPLC utilized for the reversed-phase analyses was employed, but with a PrincetonSPHER DIOL column (250 mm × 4.6 mm, 5 μm particle size, 60 Å; Princeton Chromatography, Inc., Cranbury, NJ, USA) equipped with a guard cartridge/holder system, a thermostated column compartment set at 30 °C, and a fluorescence detector. A gradient elution consisting of mobile phase (A) CH_3CN/CH_3COOH (98:2, v/v) and (B) $CH_3OH/H_2O/CH_3COOH$ (95:3:2, v/v/v) was utilized. The linear gradient was completed at 1.0 mL/min as follows: 0−35 min, 0−40% B; held for 5 min; 40−45 min, 40−0% B; and then an additional 5 min hold in order to equilibrate the system. A volume of 20 μL was injected for each sample; extracts were first dissolved in anhydrous CH_3OH (20 mg/mL) and then further diluted 1:9 (v/v) with mobile phase A to a final concentration of 2 mg/mL. Samples were passed through a 0.45 μm PTFE syringe filter prior to injection. Fluorescence detection was employed with excitation/emission at λ = 276/316 nm, respectively. The photomultiplier tube gain was held constant at 10 for the duration of the run time. Commercial purified standards were analyzed to determine the t_R's and area values for two monomers [(+)-catechin and (−)-epicatechin], three dimers (B2, 2a, 2b), and a set of polymers of varying DP ranging from 3 to 10. B2 is procyanidin B2, which is a B-type dimer and its structure is (−)-epicatechin-(4β→8)-(−)-epicatechin. The additional dimers, namely, 2a and 2b, are nonspecific A- and B-type dimers, respectively. Tentative identification based on the DP was made by t_R mapping of these authentic standards prior to ESI-MS/MS analysis. Quantification of samples was based on standard t_R's and area values. Further characterization of the PAC sample was accomplished by diol-phase HPLC-ESI-MS/MS. The same instrumentation and MS conditions were used as for the reversed-phase analyses described above. A full scan was performed over the mass range of 200 to 3000 Da at a rate of m/z 13 000 per second. Each mass spectrum generated was based on an average of five scans. PAC identity was determined based on t_R mapping, m/z comparison with those reported in the literature, and MS/MS fragmentations.

Statistical Analysis. All colorimetric and fluorescence assay measurements were repeated a minimum of three times. The results were expressed as mean ± standard deviation.

RESULTS AND DISCUSSION

On the basis of gravimetric analyses, the lipid content of the pecans ranged from 68 to 78 g oil/100 g nutmeat and the acetonic fraction yields ranged from 6.0 to 9.2 g fraction/100 g nutmeat. The eight best-performing defatted pecan nutmeat acetonic extracts, in terms of the H-$ORAC_{FL}$ assay, were selected to generate a composite product. The extracts selected exhibited antioxidant activities ranging from 18.0 to 25.5 mmol Trolox equivalents/100 g nutmeat. It was assumed that the antioxidant activity (comprehensive results not shown) was chiefly attributable to the phenolic constituents; hence, a pooled extract of the "top performers" likely would contain a complete phenolic profile that one could find in U.S. pecans.

Fraction Determination. Fractions eluting from the Sephadex LH-20 column with 95% (v/v) ethanol were analyzed spectrophotometrically. Pooling, based on observed similarities and differences in the spectra of the samples, yielded five fractions (Figure 1). Fraction I possesses a large band at ∼240 nm and a smaller one at ∼350 nm. As fraction I transitioned to fraction II, there appeared to be a shift to the left of the peak maximum. Fraction II can be characterized by a maximum absorbance at 208 nm and then a gradual decrease in absorbance with increasing wavelength. There is a slight increase in the absorbance at ∼260 nm. The transition from fraction II to fraction III was characterized by an increase in bands at 255 and 278 nm. Final development of fraction III was represented by a large peak at ∼210 nm and a secondary one with a maximum at 278 nm. The transition from fraction III to IV was identified by a drastic increase in absorbance at ∼250 nm. Fraction IV contained a peak maximum at ∼255 nm with minor peak maxima at 208 and 354 nm. Fraction V was highlighted by a reduction in all peaks to ∼0 with only a slight band at 210 nm. After freeze-drying, the mass of each fraction was recorded: fraction I comprised 77.4% of the total mass fractionated. The acetonic tannin fraction, referred to as VI, represented 16.5% of the mass. Fractions II, III, IV, and V each constituted less than 5% of the total mass with mass percentages of 3.6, 0.6, 1.0, and 0.7%, respectively.

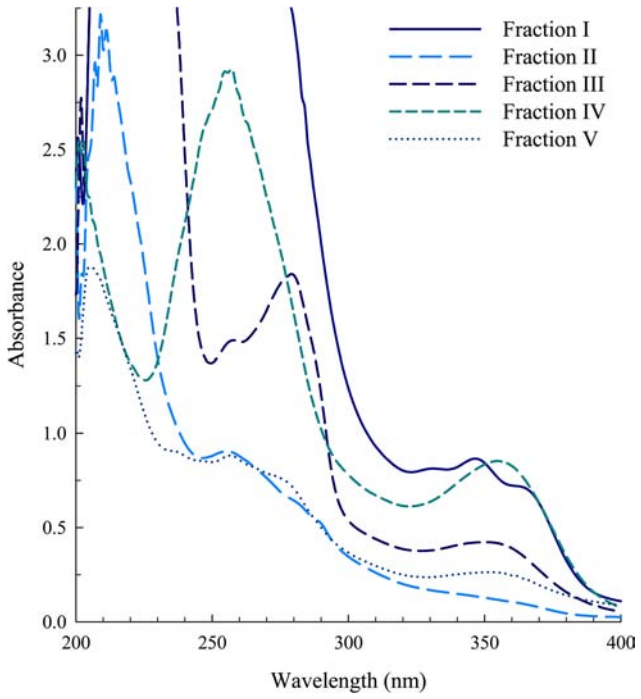

Figure 1. Spectral characteristics of five ethanolic fractions (I−V) isolated from a defatted pecan crude acetonic extract using Sephadex LH-20 column chromatography.

TPC Assay. The TPC was determined for each of the pooled fractions (Table 1). The TPC value is an indication of the quantity of phenolic compounds in a test sample, and it can potentially provide information as to the antioxidant capacity of

Table 1. Total Phenolics Content (TPC) of Five Ethanolic Fractions from a Pecan Crude Acetonic Extract Isolated by Sephadex LH-20 Column Chromatography

fraction[a]	TPC[b,c] (mg (+)-catechin equivalents/g fraction)
I	48 ± 1
II	67 ± 3
III	198 ± 4
IV	169 ± 2
V	180 ± 4

[a]Fractions I–V were eluted from the Sehpadex LH-20 column with 95% (v/v) ethanol. [b]Results are reported as mean ± standard deviation based on triplicate measurements. [c]Because of the high ellagic acid content in fractions II–IV, the TPC was also expressed as ellagic acid equivalents based on an ellagic acid standard curve. These values were 47 ± 2, 77 ± 4, 300 ± 7, 251 ± 3, and 269 ± 7 mg ellagic acid equivalents/g fraction for fractions I, II, III, IV, and V, respectively.

an extract. Fractions I and II exhibited markedly lower TPC values than fractions III–V. Fraction III gave the highest TPC value of 197 ± 4 mg CE/g fraction. Similarly, fractions IV and V exhibited marked values. This indicates that most of the phenolic compounds within the ethanolic fractions are present in fractions III–V. Because the majority of the phenolic compounds present in fractions II through IV were ellagic acid or its derivatives, the TPC was also determined in ellagic acid equivalents (EAE) (see footnote *c* of Table 1). These values ranged from 47 ± 2 mg EAE/g fraction for fraction I to 300 ± 7 mg EAE/g fraction for fraction III. Fractions IV and V had similar contents of 251 ± 3 and 269 ± 7 mg EAE/g fraction, respectively.

RP-HPLC Characterization of Pecan Phenolics. RP-HPLC was employed to profile the phenolics in the pooled ethanolic fractions. Four main groups of phenolic acids were identified across the five fractions, namely, gallic acid, protocatechuic acid, (+)-catechin, and ellagic acid. These compounds were quantified in each sample and reported as mg phenolic/g fraction (Table 2). Although fraction IV possessed only a small quantity of these four phenolic acids relative to the other fractions, it should be noted that several procyanidin dimers were identified in this fraction. Furthermore, fraction V displayed no peaks in the wavelength range of 250 to 350 nm by UV detection and did not appear to contain any phenolic acids identifiable by RP-HPLC. It was suspected that the ethanol may have eluted some of the LMW tannin compounds within the defatted pecan crude acetonic extract. This was confirmed through the use of diol-phase HPLC and by observing the spectral pattern of fraction V (Figure 1): both monomers and dimers were identifiable.

Table 2. Phenolic Acid Contents in Five Ethanolic Fractions from a Pecan Crude Acetonic Extract Isolated by Sephadex LH-20 Column Chromatography

fraction	gallic acid	protocatechuic acid	catechin[a]	ellagic acid[b]
I	nd[c]	tr[d]	nd	nd
II	tr	nd	16.5	31.7
III	nd	nd	35.5	41.3
IV	nd	nd	nd	4.97
V[e]	nd	nd	nd	nd

[a]Catechin values include free (+)-catechin, catechin hexoside, and (epi)catechin gallate. The data are expressed as mg catechin equivalents (CE)/g fraction. [b]Ellagic acid contents include free ellagic acid and all other ellagic acid derivatives. All data are reported as mg ellagic acid equivalents/g fraction. [c]nd = not detected; limit of detection (LOD) = 4.0, 0.74, 9.2, and 5.3 ng/mL for (+)-catechin (C), protocatechuic (PR) acid, gallic (G) acid, and ellagic acid (E), respectively. [d]A peak was detected, but not quantifiable. Limit of quantification (LOQ) = 12.7, 2.5, 30.6, 17.6 ng/mL for C, PR, G, and E, respectively. [e]Diol-phase HPLC-ESI-MS/MS confirmed the presence of low-molecular-weight tannin constituents in this fraction.

Fraction I contained a high amount of "filler" (i.e., nonphenolic constituents such as simple sugars) isolated from the defatted pecan crude acetonic extract. Even though it possessed the greatest mass content of the fractions, it displayed the lowest TPC. In fact, there were practically no identifiable phenolic acids present in the chromatogram of fraction I: the only two phenolic acids identified were protocatechuic acid and caffeic acid (see Table 3). Fraction II also displayed a comparatively lower TPC than that of fractions III through V. Six main phenolic acids, or their derivatives, were identified in fraction II: caffeic, gallic, protocatechuic, (+)-catechin, *p*-hydroxybenzoic, and ellagic acids (see Figure 2 and Table 3). While gallic acid was identified based on its t_R and UV spectrum, it was present below the limit of quantification. The (+)-catechin and ellagic acid (and their derivatives) contents of fraction II were determined to be 16.5 and 31.7 mg/g fraction, respectively. Both the (+)-catechin and ellagic acid derivatives were calculated as equivalents of the parent compound (NB, calculation was based on the standard curve of ellagic acid for all ellagic acid derivatives). This ellagic acid majority can be observed in the spectra of fraction II (Figure 1). There is a large peak below what could be expected for any of these phenolic acids, and then there is a slight rise around 255 nm signifying the presence of ellagic acid or a derivative. On the basis of the spectral pattern for fraction III, it was assumed that a high proportion of this fraction consisted of ellagic acid due to its peak maximum near 255 nm (Figure 1). Via RP-HPLC this was confirmed. Fraction III is composed of mainly ellagic acid and its derivatives but also includes some catechin derivatives. Table 2 shows that including the (epi)catechin gallate content, fraction III possessed 35.5 mg catechin/g extract and 41.3 mg ellagic acid/g extract. Fraction IV contained mainly procyanidin dimers along with a few ellagic acid derivatives. Originally, it was believed that this fraction contained a large quantity of catechin derivatives, based on the UV spectral pattern observed for the eluted peaks compared to that of a (+)-catechin and (−)-epicatechin commercial standard. After HPLC-ESI-MS/MS analyses, however, it was determined that these peaks were actually that of the PAC dimers (see Table 3).

No free caffeic acid was detected in any of the fractions. But a caffeic acid hexoside was identified in fractions I (F1-1), II (F2-2), III (F3-2), and IV (F4-1). The t_R's for this compound ranged from 2.69 to 4.00 min depending on the fraction analyzed. This variation in t_R may be due to slight differences in the caffeic acid hexoside structure, such as type or number of glycosidic moieties present. All four compounds exhibited a molecular ion $[M - H]^-$ at m/z 341 with a MS^2 fragment at m/z 179 corresponding to caffeic acid. Aiding in the identification of these compounds was the neutral loss of 162 amu, which is often associated by the presence of hexosides.[16] Fractions I and II both had a protocatechuic acid derivative present (F1-2 and F2-10); this identification was determined based on similarities between the UV spectrum of these peaks and that of a protocatechuic acid standard, as well as the MS^2 ion of m/z 153

Table 3. Tentative Identification of Phenolic Acids from Four Ethanolic Fractions of a Pecan Crude Acetonic Extract Isolated on a Sephadex LH-20 Column

peak	t_R[a] (min)	$[M-H]^-$	MS^2 ions (m/z)	neutral loss	tentative identification (ID)[b]
Fraction I					
F1-1	4.00	341	179	162	caffeic acid hexoside
F1-2	5.45	333	241−153	92−180	protocatechuic acid hexoside
F1-3	6.31	368	179−144−113	189−224−255	no ID
F1-4	27.69	679	619−457−323−215	60−222−356−464	no ID
F1-5	30.12	457	325−293−203−163	132−164−254−294	epigallocatechin gallate, gallocatechin gallate
Fraction II					
F2-2	2.69	341	179	162	caffeic acid hexoside
F2-3	3.82	331	169	162	gallic acid hexoside
F2-5	4.28	481	301	180	HHDP glucose
F2-6	4.89	169	153−125	16−44	gallic acid
F2-7	5.41	137	122−111−107	15−26−30	*p*-hydroxybenzoic acid
F2-8	6.16	331	169−125	162−206	gallic acid hexoside
F2-9	6.87	451	289	162	catechin hexoside
F2-10	7.31	315	153	162	protocatechuic acid hexoside
F2-11	7.91	451	289	162	catechin hexoside
F2-13	8.68	451	289	162	catechin hexoside
F2-14	9.31	451	289	162	catechin hexoside
F2-15	9.82	289	245−205−179	44−84−110	(+)-catechin
F2-17	11.95	463	301	162	ellagic acid hexoside
F2-22	16.57	433	301	132	ellagic acid pentose
F2-24	19.63	477	315−300	162−177	methyl ellagic acid hexoside
F2-25	20.64	301	217	84	ellagic acid
F2-26	21.86	491	328	163	dimethyl ellagic acid hexoside
F2-27	22.71	447	315	132	methyl ellagic acid pentose
F2-28	26.10	447	315	132	methyl ellagic acid pentose
F2-30	29.00	475	460−329−299	15−146−176	dimethyl ellagic acid pentose
F2-31	30.23	599	447−315	152−284	methyl ellagic acid galloyl pentose
F2-32	30.83	329	314	15	dimethyl ellagic acid
Fraction III					
F3-1	2.81	387	305−223−141	82−164−246	no ID
F3-2	3.35	341	179	162	caffeic acid hexoside
F3-3	3.72	481	301	180	HHDP glucose
F3-4	4.87	481	301	180	HHDP glucose
F3-5	5.64	305	261−219−179−125	44−86−126−180	(epi)gallocatechin
F3-6	6.67	577	451−425−407−289−269	126−152−170−288−308	PD2B
F3-7	9.61	289	245−205−125	44−84−164	(+)-catechin
F3-9	12.90	441	289	152	(epi)catechin gallate
F3-11	15.52	197	169	28	ethyl gallate
F3-12	15.97	433	301	132	ellagic acid pentose
F3-13	16.53	615	463−301	152−314	digalloyl ellagic acid
F3-14	20.15	441	289	152	(epi)catechin gallate
F3-15	20.65	301	217	84	ellagic acid
F3-16	22.31	441	289	152	(epi)catechin gallate
F3-17	22.70	487	469−425−407−339−301	18−62−80−148−186	valoneic acid dilactone hydrate
F3-18	24.61	477	315−300	192−177	methyl ellagic acid hexoside
F3-19	26.07	541	313−227−169	228−314−372	no ID
F3-20	26.94	585	433−301	152−284	ellagic acid galloyl pentose
F3-21	27.55	575	449−423−407−289	126−152−168−286	PD2A
F3-22	28.70	585	433−301	152−284	ellagic acid galloyl pentose
F3-23	32.34	599	447−315	152−284	methyl ellagic acid galloyl pentose
F3-24	33.44	599	447−315	152−284	methyl ellagic acid galloyl pentose
F3-25	35.13	599	447−315	152−284	methyl ellagic acid galloyl pentose
Fraction IV					
F4-1	3.72	341	179	162	caffeic acid hexoside
F4-2	3.93	577	451−425−407−289−245	126−152−170−288−332	PD2B
F4-3	4.85	481	301	180	ellagic acid HHDP glucose
F4-4	5.95	575			PD2A
F4-5	7.85	577	451−425−407−289−245	126−152−170−288−332	PD2B
F4-6	9.34	575			PD2A

dx.doi.org/10.1021/jf500909h | J. Agric. Food Chem. 2014, 62, 4332−4341

Table 3. continued

peak	t_R[a] (min)	$[M - H]^-$	MS^2 ions (m/z)	neutral loss	tentative identification (ID)[b]
Fraction IV					
F4-7	10.16	577	451−425−407−289−245	126−152−170−288−332	PD2B
F4-8	12.58	577	451−425−407−289−245	126−152−170−288−332	PD2B
F4-9	20.77	575	449−423−407−289	126−152−168−286	PD2A
F4-10	27.13	575	449−423−407−289	126−152−168−286	PD2A
F4-11	28.04	585	433−301	152−284	ellagic acid galloyl pentose
F4-12	28.89	585	433−301	152−284	ellagic acid galloyl pentose

[a]Retention time (t_R) from RP-HPLC analysis. [b]Tentative identifications were achieved using t_R mapping and fragmentation-pattern comparison to those of commercial standards as well as compounds previously reported in pecans by Boulekbache-Makhlouf et al.[16] and de la Rosa et al.[17] Abbreviations are as follows: HHDP glucose = bis(hexahydroxydiphenoyl)glucose; PD2A = proanthocyanidins A-type dimer; PD2B = proanthocyanidins B-type dimer.

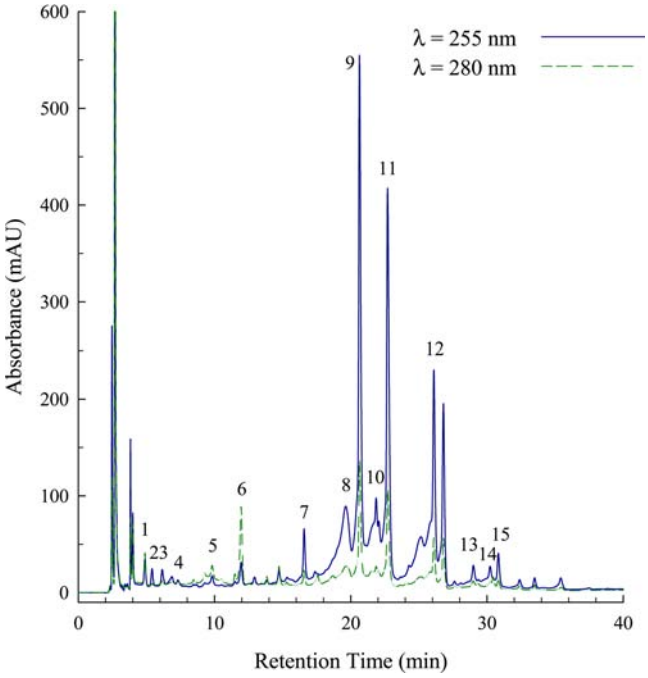

Figure 2. Reversed-phase HPLC chromatogram at λ = 255 and 280 nm of fraction II isolated from a defatted pecan crude acetonic extract on a Sephadex LH-20 column using 95% (v/v) ethanol. The phenolic acids identified were as follows: (1) gallic acid; (2) *p*-hydroxybenzoic acid; (3) a gallic acid hexoside; (4) a protocatechuic acid hexoside; (5) (+)-catechin; (6) an ellagic acid hexoside; (7) an ellagic acid pentose; (8) a methyl ellagic acid hexoside; (9) ellagic acid; (10) a dimethyl ellagic acid hexoside; (11) a methyl ellagic acid pentose; (12) a methyl ellagic pentose; (13) a dimethyl ellagic acid pentose; (14) a methyl ellagic acid galloyl pentose; and (15) dimethyl ellagic acid.

representing protocatechuic acid itself. Peak F2-10 is tentatively identified as a protocatechuic acid hexoside due to the neutral loss of 162 amu. While this loss is not observed in peak F1-2, the loss of 180 amu may be indicative of a hexoside and water group [loss of 162 + 18 amu]. The only fraction to include *p*-hydroxybenzoic acid was fraction II (F2-7), which was identified based on a comparison of its $[M - H]^-$ and UV spectral pattern to a commercial standard. Gallic acid was also identified only in fraction II and was present in two different forms: free gallic acid (F2-6) and as two gallic acid hexosides (F2-3 and F2-8). The free gallic acid eluted with a t_R of 4.90 min and had a $[M - H]^-$ of m/z 169, consistent with those observed for commercial standards. The other two peaks (F2-3 and F2-8) were identified to be gallic acid hexosides. Both hexosides were identified based on their fragment ions at m/z of 169, indicating the presence of gallic acid, as well as a neutral loss of 162 amu commonly associated with hexosides. There may be slight differences in the structure of these hexosides due to the presence of a second MS^2 fragment of m/z 125 for F2-6.

Ellagic acid and its derivatives accounted for almost one-third of the peaks present in four fractions. Fractions II, III, and IV all possessed several forms of this phenolic acid. Free ellagic acid (F2-25 and F3-15) was identified by its molecular ion $[M - H]^-$ at m/z of 301 and by matching t_R's and UV spectra with those of a commercial standard. Both ellagic acid hexoside and methyl ellagic acid hexoside were found in the analyzed samples (F2-17, F2-24, and F3-18). These could be identified at m/z 463 for $[M - H]^-$, the presence of a MS^2 fragment at m/z of 301 (or 315 in the case of a methyl ellagic acid hexoside), and a neutral loss of 162 amu indicating the cleavage of a hexose. Similar methyl ellagic acid derivatives have been previously reported in pecans by de la Rosa et al.[17] and in *Eucalyptus globulus* fruit by Boulekbache-Makhlouf et al.[16] Two ellagic acid pentoses were tentatively identified (i.e., F2-22 and F3-12) by their MS^2 fragment of m/z 301 and neutral loss of 132 amu, commonly associated with the loss of a pentoside.[16] A third group of compounds from the ellagic acid family, namely, methyl ellagic acid pentoses, were identified in fraction II, F2-27 and F2-28. These compounds displayed the same fractionation pattern as the ellagic acid pentoses with the addition of 15 amu to the m/z commonly associated with a methyl group. This "m/z increase" was also observed with the methyl ellagic acid hexosides (F2-24 and F3-18) compared against the ellagic acid hexosides reported above. These ellagic acid derivatives have been previously identified based on fragmentation patterns in other ellagic acid-rich products such as the fruit of *Eucalyptus globulus*, blackberries, and camu-camu.[16,18,19] Several other derivatives of these compounds and additional side groups were identified in the fractions isolated: dimethylellagic acid pentose (F2-30); dimethylellagic acid hexose (F2-26); methylellagic acid galloyl pentose (F2-31, F3-23, F3-24, and F3-25); digalloylellagic acid (F3-13); ellagic acid galloyl pentose (F3-20, F3-22, F4-11, and F4-12); ellagic acid HHDP glucose (F4-3); and dimethylellagic acid (F2-32). All of these compounds were identified based on key fragmentation patterns highlighted previously and comparison to literature sources.[16,19] Similar ellagic acid derivatives, namely, methyl ellagic acid, ellagic acid pentose, and ellagic acid rhamnose derivatives, were reported by de la Rosa et al.[17] in pecans from Mexico. Somewhat surprisingly, valoneic acid dilactone was identified in fraction III (F3-17) based on its key fragmentation ions of m/z 469 and 425. This compound has been previously identified in pecans and is a suspected

ellagitannin degradation product.[17] The authors were not expecting to observe this in a sample of LMW phenolic acids or a nonhydrolyzed sample. However, it should be noted that two other polymeric compounds, procyanidin A- and B-type dimers, also eluted in fraction III, signifying that it may be possible for some higher MW polymeric compounds to elute in the ethanolic fractions of a Sephadex LH-20 column.

The next prominent class of compounds found in these fractions was (+)-catechin and its derivatives. Free (+)-catechin was identified in fractions II and III with a $[M - H]^-$ at m/z 289 and a t_R of 9.61 and 9.82 min, respectively. Several catechin hexosides (F2-9, F2-11, F2-13, and F2-14) were also present in fraction II with t_R's ranging from 6.87 to 9.31 min. All of these peaks possessed a molecular ion $[M - H]^-$ at m/z 451 and were identified based on a daughter ion at m/z 289 and a neutral loss of 162 amu. In addition, several other forms of catechins were identified in the analyzed fractions. For instance, fraction I contained either epigallocatechin gallate or gallocatechin gallate at peak F1-5 with a t_R of 30.12 min and a molecular ion $[M - H]^-$ at m/z 457. Fraction III also contained (epi)gallocatechin (F3-5), (epi)catechin gallate (F3-9, F3-14, and F3-16), and ethyl gallate (F3-11).

Fraction IV contained no (+)-catechin or (−)-epicatechin monomers, but there were several peaks corresponding to procyanidin dimers (F4-2, F4-4, F4-5, F4-6, F4-7, F4-8, F4-9, and F4-10). Both procyanidin A- and B-type dimers were represented in this fraction. The A-type PAC peaks were identified by a molecular ion $[M - H]^-$ at m/z 575 and fragment ions at m/z 425, 407, and 289. No previous literature studies have identified A-type linkages present in pecan samples. However, they have been previously reported in peanut skins[20] and almonds.[21] In the peanut skin samples, Sarnoski et al.[20] also observed similar fragmentation patterns for a PAC dimer with A-type linkages. The authors found no other compounds with a similar MW and expected fragmentation patterns that would be a logical alternative to the PAC dimer. While the PD2A fragmentation patterns match well with those reported in peanut skins,[20] a more in-depth study of these compounds is warranted for a proper identification. Exact mass data and further information regarding the specific fragmentation patterns of the compound would be useful. A PAC dimer with B-type linkages, procyanidin 2B, was identified by a molecular ion $[M - H]^-$ at m/z 577 and neutral losses of 152 and 170 amu.

Currently, there is no other study in the literature that attempts to examine individual fractions of pecans separated by Sephadex LH-20 column chromatography with two mobile phases or identifies the presence of as many phenolic acid derivatives. Malik et al.[22] used Sephadex LH-20 chromatography to separate compounds within pecan extracts, but only employed a single mobile phase of 80% (v/v) methanol. The main phenolic acids identified in the present study match those previously reported in pecans[5,17,23] and also characterize others. Malik et al.[22] identified gallic acid, (+)-catechin, caffeic acid, ellagic acid, and some derivatives in their samples, but also had three additional phenolic acids that were not identified in our samples; they were catechol, *m*-coumaric acid, and chlorogenic acid. These discrepancies could be due to differences in the HPLC conditions employed as well as variations in pecan cultivar selection and growing location. Similar phenolic acids have previously been reported in other tree nut types. For example, John and Shahidi[24] identified gallic acid, protocatechuic acid, (+)-catechin, ellagic acid, and their derivatives in Brazil nut samples. Milbury et al.[25] investigated the phenolic acids in almonds and identified (+)-catechin, protocatechuic acid, and *p*-hydroxybenzoic acid, as well as other phenolic acids not identified in the pecan samples. Qualitative and quantitative comparison between our findings with those in the literature is difficult due to the chosen data reporting style. We believe that for this study it is best to present the data on a mg phenolic/g fraction basis. The current literature reports the data as mg/g pecan. Even though a gravimetric analysis was conducted and all recoveries were calculated, we believe that some phenolic material may have been lost during the spectrophotometric analysis. It is believed that accuracy would be lost if contents were extrapolated to the pecan nutmeat level.

Diol-Phase HPLC Characterization of Pecan Phenolics. The tannin fraction, isolated on Sephadex LH-20 using 50% (v/v) aqueous acetone as the mobile phase, was analyzed via diol-phase HPLC in order to tentatively identify the DP represented in the sample. Further investigation into the composition of this fraction was then accomplished by ESI-MS/MS analyses. The pooled cultivar possessed DP from monomers through hexamers (Figure 3). On the basis of a set of PAC standards,

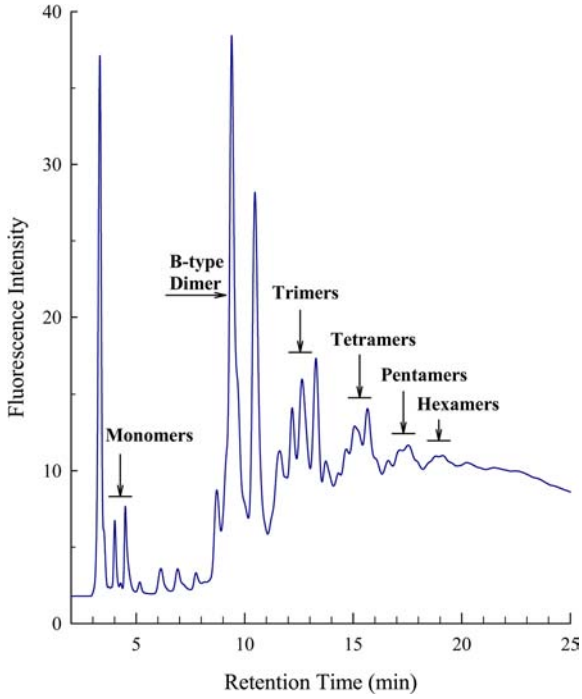

Figure 3. Diol-phase HPLC chromatograms for the tannin fraction isolated from eight pooled pecan cultivars. Fluorescence detection was employed with excitation/emission at λ = 276/316 nm, respectively.

monomers eluted from the diol-phase HPLC column roughly between 3 and 5 min; dimers, 7−11 min; trimers, 12−14 min; tetramers, 14−16 min; pentamers, 17−18 min; hexamers, 18−19 min; heptamers, 20−21 min; octamers, 21−22 min; nonamers, 22−23 min; and decamers, 23−24 min. The sample had 17.7% of its PACs represented by tetramers or larger polymers (Table 4). The greatest proportion of the tannin fraction was attributed to dimers, representing 56.6% of the tannin fraction. The next largest DP was the trimers, accounting for 25.3% of the total. The content of (+)-catechin + (−)-epicatechin monomers in the sample was only 0.289 mg/g tannin fraction. This low value was expected because the majority of the monomers should be present in the ethanolic

Table 4. Characterization and Quantification of the Tannin Fraction from a Pecan Crude Acetonic Extract Isolated by Sephadex LH-20 Column Chromatography Using 50% (v/v) Aqueous Acetone[a]

degrees of polymerization (DP)	pooled cultivars[b]
1	0.3
2	47.3
3	21.1
4−6	14.8
total	83.5

[a]Characterized by diol-phase HPLC and quantification completed using commercial standards with varying degrees of polymerization. [b]All quantities are expressed as mg compound/g tannin fraction.

fraction(s). These findings demonstrate that the tannin fractions, in particular those with higher DP, may play a role in determining the observed *in vitro* antioxidant activity of a sample.

A deeper examination of the PAC composition was completed using diol-phase HPLC-ESI-MS/MS analyses. After completing a full scan over the mass range of 200 to 3000 Da, a search of common PAC mass ions from the literature[20,26] was undertaken: nine compounds were identified in the acetonic fraction (i.e., fraction VI; see Table 5). All of the

Table 5. PAC Compounds Present in the Tannin Fraction Isolated from Eight Pooled Pecan Cultivars

t_R[a]	DP[b]	unit types[c]	linkage	$[M-H]^-$
6.5	2	2 (epi)catechin	B	577
9.7	3	3 (epi)catechin	B	865
11.0	3	2 (epi)catechin and 1 (epi)gallocatechin	B	881
13.1	4	4 (epi)catechin	B	1153
14.2	4	3 (epi)catechin and 1 (epi)gallocatechin	B	1169
16.0	5	5 (epi)catechin	B	1441
16.3	5	4 (epi)catechin and 1 (epi)gallocatechin	B	1457
18.0	6	5 (epi)catechin and 1 (epi)gallocatechin	B	1745
19.0	6	4 (epi)catechin and 2 (epi)gallocatechin	B	1761

[a]Retention time determined from diol-phase HPLC-ESI-MS analyses. [b]Degrees of polymerization. [c]Cross-checking with compounds identified in nut skins, as reported by Sarnoski et al.[20] and Monagas et al.[26]

compounds present in the sample exhibited a B-type linkage, which was to be expected based on literature reports of pecan PACs.[8] Interestingly, the tannin fraction possessed both procyanidin and prodelphinidin compounds. Two PACs, one procyanidin and one prodelphinidin, were detected for each DP with the exception of the dimer, which had a single identification, and the hexamers, which were both prodelphinidins. The single dimer is composed of two (epi)catechin units based on a t_R of 6.5 min and a molecular ion $[M-H]^-$ at m/z 577. The two trimers identified in the pecan sample had molecular ions $[M-H]^-$ at m/z 865 and 881 and eluted at a t_R of 9.7 and 11.0 min, respectively. On the basis of the $[M-H]^-$, these compounds were identified as possessing 3 (epi)catechin units and 2 (epi)catechin + 1 (epi)gallocatechin unit. The two detected trimers differed in their molecular ions by 16 amu, and this trend continued for the three larger DP of m/z at 1153−1169, 1441−1457, and 1745−1761.

Gu et al.[8] stated that PACs are present in numerous different food types including pecans. These authors reported that the monomers, dimers, trimers, 4−6mers, 7−10mers, and >10mers constituted 3.4, 8.5, 5.3, 20.5, 17.0, and 45.2%, respectively, in pecans. It should be noted that in the present study we did not find any PACs larger than hexamers. With the removal of the 7−10mers and >10 mers from the Gu et al.[8] data set, the monomers, dimers, trimers, and 4−6mers now account for 9.2, 22.5, 13.9, 54.3%, respectively. In comparison to the prevalence of tetramers through hexamers in the former study, the present one found dimers to be most abundant. Earlier methods of PAC analysis (i.e., TLC analysis, RP-HPLC, and early normal-phase HPLC methods) were discredited for failing to separate compounds with DP > 4.[27] In preparing for this research, standards were run with DP of 8, 9, and even 10 with excellent resolution and detection on the diol-phase column and the fluorescence detector. For this reason, we believe that any PACs with DP > 7 would have been visible with this methodology and no suppression of ions occurred. In a study by Kelm et al.,[15] in which the diol-phase HPLC methodology was first introduced, there was also excellent resolution up to a DP = 14. On the basis of Kelm et al.[15] and the employment of the diol-phase column, we believe that PACs with higher DP would be properly resolved if they had been present in the defatted pecan acetonic extract. This was further confirmed by the MS data. No ions corresponding to PACs with a DP higher than 6 were identified in the sample. While the authors believe that all of the PACs containing (+)-catechin and (−)-epicatechin monomers were identified and quantified, there may be some PACs that are not properly captured with the fluorescence detector. Lazarus et al.[28] points out that fluorescence detection cannot be used for the identification of PACs with gallocatechin and gallic ester components. Further HPLC investigation of these compounds using diol-phase diode-array detection is necessary. Additional information regarding specific composition, monomer position, and length of the PACs could be acquired using the thiolysis preparation technique coupled with HPLC characterization. In thiolysis, individual PAC units are separated into end units and interior units through an acid-catalyzed cleavage of the interflavan bonds.[29] After cleavage, the interior unit intermediates are reacted with toluene α-thiol, forming thiol-flavonol adducts, and the end units remain as flavanol monomers.[29,30] These thiol adducts can then be separated and identified with HPLC analysis to give a better picture of the average DP of the PACs, as well as the position and type of the monomeric units.[30] We are not aware of any literature studies that have investigated pecan PACs using a thiolysis step.

It has also been noted that when PACs are separated on Sephadex LH-20 via isocratic elution, the first compounds to elute will be those PACs with smaller MWs and the heavier ones will elute last.[31] A possible reason for a reduction in the quantity of HMW PACs in our study could be that a sufficient quantity of the aqueous acetone was not employed to elute all PACs from the column. However, based on the mass balance performed in this work, it is not possible that this could account for the extreme differences observed. A total of 1.92 g of crude extract was loaded onto the Sephadex LH-20 column, and a mass of 1.90 g comprising the various fractions was recovered after lyophilization. This signifies that 99% of the crude extract applied to the column was recovered via the chromatography and that very small quantities of higher DP, if they existed, might remain on the Sephadex LH-20 column. Unfortunately the Gu et al.[8] study is the only literature source that quantifies and characterizes PAC components of pecan nutmeat. Further

and more extensive characterization of these compounds is necessary to determine more information about the contents of pecans, in particular the HMW PACs. By utilizing exact mass HPLC/MS technologies, one might be able to further elucidate the structure of these compounds in pecans from various growing locations and cultivar types. HPLC/MS^n analysis has previously been used to gain excellent information regarding the PAC profile of peanut skins.[20]

Researchers aim to quantify and characterize phenolic compounds in natural products due to their beneficial health benefits. The PAC compounds have been shown to remain intact in the low pH environment of the stomach and arrive to the small intestine intact.[32] In this form, the PACs are unable to be absorbed in large quantities.[10] However, colon microflora is able to breakdown PAC polymers to smaller metabolites that can be absorbed and utilized.[10] The full benefit of these metabolites is not fully understood, thereby making predictions of the biological activity of higher degree polymers difficult. Hudthagosol et al.[6] demonstrated adroitly that concentrations of the main PAC monomers, (+)-catechin and (−)-epicatechin, increased in the plasma of individuals after pecan consumption; these results are encouraging. Further research on the bioaccessibility (i.e., the extent of release of nutrients/phytochemicals from the food matrix during digestion) and the bioavailability (i.e., the extent of absorption and utilization of released nutrients/phytochemicals for normal physiological functions) of phenolic constituents and PACs of pecans need to be investigated to gain better insight into the role of these compounds in disease prevention.

■ ASSOCIATED CONTENT

Supporting Information

This material is available free of charge via the Internet at http://pubs.acs.org.

■ AUTHOR INFORMATION

Corresponding Author

*Tel: 706-542-1099. Fax: 706-542-1050. E-mail: pegg@uga.edu.

Funding

The authors would like to acknowledge the Georgia Agricultural Commodity Commission for Pecans (GACCP) and the USDA-NIFA-SCRI Award No. 2011-51181-30674 for funding this research.

Notes

The authors declare no competing financial interest.

■ ACKNOWLEDGMENTS

Use of the Proteomics and Mass Spectrometry (PAMS) core facility under the direction of Dr. Dennis Phillips of UGA's Department of Chemistry is greatly appreciated; in particular, thanks are extended to Dr. Phillips for assisting Y.M. with the LC-MS/MS analyses. The authors would also like to acknowledge Dr. Agnieszka Kosińska-Cagnazzo of the Institute of Animal Reproduction and Food Research of the Polish Academy of Sciences for her assistance with setting up the diol-phase HPLC analyses.

■ REFERENCES

(1) Hu, F. B.; Stampfer, M. J. Nut consumption and risk of coronary heart disease: A review of epidemiologic evidence. *Curr. Atheroscler. Rep.* **1999**, *1*, 204−209.

(2) Kris-Etherton, P. M.; Zhao, G.; Binkoski, A. E.; Coval, S. M.; Etherton, T. D. The effects of nuts on coronary heart disease risk. *Nutr. Rev.* **2001**, *59*, 103−111.

(3) Blomhoff, R.; Carlsen, M. H.; Andersen, L. F.; Jacobs, D. R., Jr. Health benefits of nuts: potential role of antioxidants. *Br. J. Nutr.* **2006**, *96*, S52−S60.

(4) Sabaté, J.; Ros, E.; Salas-Salvadó, J. Nuts: nutrition and health outcomes. *Br. J. Nutr.* **2006**, *96*, S1−S2.

(5) Villarreal-Lozoya, J. E.; Lombardini, L.; Cisneros-Zevallos, L. Phytochemical constituents and antioxidant capacity of different pecan [*Carya illinoinensis* (Wangenh.) K. Koch] cultivars. *Food Chem.* **2007**, *102*, 1241−1249.

(6) Hudthagosol, C.; Haddad, E. H.; McCarthy, K.; Wang, P.; Oda, K.; Sabaté, J. Pecans acutely increase plasma postprandial antioxidant capacity and catechins and decrease LDL oxidation in humans. *J. Nutr.* **2011**, *141*, 56−62.

(7) Rigaud, J.; Escribano-Bailon, M. T.; Prieur, C.; Souquet, J.-M.; Cheynier, V. Normal-phase high-performance liquid chromatographic separation of procyanidins from cacao beans and grape seeds. *J. Chromatogr. A* **1993**, *654*, 255−260.

(8) Gu, L.; Kelm, M. A.; Hammerstone, J. F.; Beecher, G.; Holden, J.; Haytowitz, D.; Gebhardt, S.; Prior, R. L. Concentrations of proanthocyanidins in common foods and estimations of normal consumption. *J. Nutr.* **2004**, *134*, 613−617.

(9) Holt, R. R.; Lazarus, S. A.; Sullards, M. C.; Zhu, Q. Y.; Schramm, D. D.; Hammerstone, J. F.; Fraga, C. G.; Schmitz, H. H.; Keen, C. L. Procyanidin dimer B2 [epicatechin-(4β-8)-epicatechin] in human plasma after the consumption of a flavanol-rich cocoa. *Am. J. Clin. Nutr.* **2002**, *76*, 798−804.

(10) Déprez, S.; Brezillon, C.; Rabot, S.; Philippe, C.; Mila, I.; Lapierre, C.; Scalbert, A. Polymeric proanthocyanidins are catabolized by human colonic microflora into low-molecular-weight phenolic acids. *J. Nutr.* **2000**, *130*, 2733−2738.

(11) Wu, X.; Beecher, G. R.; Holden, J. M.; Haytowitz, D. B.; Gebhardt, S. E.; Prior, R. L. Lipophilic and hydrophilic antioxidant capacities of common foods in the United States. *J. Agric. Food Chem.* **2004**, *52*, 4026−4037.

(12) Craft, B. D.; Kosińska, A.; Amarowicz, R.; Pegg, R. B. Antioxidant properties of extracts obtained from raw, dry-roasted, and oil-roasted US peanuts of commercial importance. *Plant Foods Hum. Nutr.* **2010**, *65*, 311−318.

(13) Swain, T.; Hillis, W. E. The phenolic constituents of *Prunus domestica*. I.−The quantitative analysis of phenolic constituents. *J. Sci. Food. Agric.* **1959**, *10*, 63−68.

(14) Srivastava, A.; Greenspan, P.; Hartle, D. K.; Hargrove, J. L.; Amarowicz, R.; Pegg, R. B. Antioxidant and anti-inflammatory activities of polyphenolics from southeastern U.S. range blackberry cultivars. *J. Agric. Food Chem.* **2010**, *58*, 6102−6109.

(15) Kelm, M. A.; Johnson, J. C.; Robbins, R. J.; Hammerstone, J. F.; Schmitz, H. H. High-performance liquid chromatography separation and purification of cacao (*Theobroma cacao* L.) procyanidins according to degree of polymerization using a diol stationary phase. *J. Agric. Food Chem.* **2006**, *54*, 1571−1576.

(16) Boulekbache-Makhlouf, L.; Meudec, E.; Chibane, M.; Mazauric, J.-P.; Slimani, S.; Henry, M.; Cheynier, V.; Madani, K. Analysis by high-performance liquid chromatography diode array detection mass spectrometry of phenolic compounds in fruit of *Eucalyptus globulus* cultivated in Algeria. *J. Agric. Food Chem.* **2010**, *58*, 12615−12624.

(17) de la Rosa, L. A.; Alvarez-Parrilla, E.; Shahidi, F. Phenolic compounds and antioxidant activity of kernels and shells of Mexican pecan (*Carya illinoinensis*). *J. Agric. Food Chem.* **2011**, *59*, 152−162.

(18) Mertz, C.; Cheynier, V.; Günata, Z.; Brat, P. Analysis of phenolic compounds in two blackberry species (*Rubus glaucus* and *Rubus adenotrichus*) by high-performance liquid chromatography with diode array detection and electrospray ion trap mass spectrometry. *J. Agric. Food Chem.* **2007**, *55*, 8616−8624.

(19) Fracassetti, D.; Costa, C.; Moulay, L.; Tomás-Barberán, F. A. Ellagic acid derivatives, ellagitannins, proanthocyanidins and other phenolics, vitamin C and antioxidant capacity of two powder products

from camu-camu fruit (*Myrciaria dubia*). *Food Chem.* **2013**, *139*, 578−588.
(20) Sarnoski, P. J.; Johnson, J. V.; Reed, K. A.; Tanko, J. M.; O'Keefe, S. F. Separation and characterisation of proanthocyanidins in Virginia type peanut skins by LC−MS^n. *Food Chem.* **2012**, *131*, 927−939.
(21) Bolling, B. W.; Chen, C.-Y. O.; McKay, D. L.; Blumberg, J. B. Tree nut phytochemicals: composition, antioxidant capacity, bioactivity, impact factors. A systematic review of almonds, Brazils, cashews, hazelnuts, macadamias, pecans, pine nuts, pistachios and walnuts. *Nutr. Res. Rev.* **2011**, *24*, 244−275.
(22) Malik, N. S. A.; Perez, J. L.; Lombardini, L.; Cornacchia, R.; Cisernos-Zevallos, L.; Bradford, J. Phenolic compounds and fatty acid composition of organic and conventional grown pecan kernels. *J. Sci. Food Agric.* **2009**, *89*, 2207−2213.
(23) Senter, S. D.; Horvat, R. J.; Forbus, W. R. Relation between phenolic acid content and stability of pecans in accelerated storage. *J. Food Sci.* **1980**, *45*, 1380−1382, 1392.
(24) John, J. A.; Shahidi, F. Phenolic compounds and antioxidant activity of Brazil nut (*Bertholletia excels*). *J. Funct. Food* **2010**, *2*, 196−209.
(25) Milbury, P. E.; Chen, C.-Y.; Dolnikowski, G. G.; Blumberg, J. B. Determination of flavonoids and phenolics and their distribution in almonds. *J. Agric. Food Chem.* **2006**, *54*, 5027−5033.
(26) Monagas, M.; Garrido, I.; Lebrón-Aguilar, R.; Gómez-Cordovés, M. C.; Rybarczyk, A.; Amarowicz, R.; Bartolomé, B. Comparative flavan-3-ol profile and antioxidant capacity of roasted peanut, hazelnut, and almond skins. *J. Agric. Food Chem.* **2009**, *57*, 10590−10599.
(27) Okuda, T.; Yoshida, T.; Hatano, T. New methods of analyzing tannins. *J. Nat. Prod.* **1989**, *52*, 1−31.
(28) Lazarus, S. A.; Hammerstone, J. F.; Adamson, G. E.; Schmitz, H. H. High-performance liquid chromatography/mass spectrometry analysis of proanthocyanidins in food and beverages. *Methods Enzymol.* **2001**, *335*, 46−57.
(29) Guyot, S.; Marnet, N.; Sanoner, P.; Drilleau, J.-F. Direct thiolysis on crude apple materials for high-performance liquid chromatography characterization and quantification of polyphenols in cider apple tissues and juices. *Methods Enzymol.* **2001**, *335*, 57−70.
(30) Scioneaux, A. N.; Schmidt, M. A.; Moore, M. A.; Lindroth, R. L.; Wooley, S. C.; Hagerman, A. E. Qualitative variation in proanthocyanidin composition of *Populus* species and hybrids: Genetics is the key. *J. Chem. Ecol.* **2011**, *37*, 57−70.
(31) Lea, A. G. H.; Bridle, P.; Timberlake, C. F.; Singleton, V. L. The procyanidins of white grapes and wines. *Am. J. Enol. Vitic.* **1979**, *30*, 289−300.
(32) Rios, L. Y.; Bennett, R. N.; Lazarus, S. A.; Rémésy, C.; Scalbert, A.; Williamson, G. Cocoa procyanidins are stable during gastric transit in humans. *Am. J. Clin. Nutr.* **2002**, *76*, 1106−1110.

JOURNAL OF AGRICULTURAL AND FOOD CHEMISTRY

Article

pubs.acs.org/JAFC

Metabolic Engineering of *Escherichia coli* for Production of Butyric Acid

Mukesh Saini,[†] Zei Wen Wang,[†] Chung-Jen Chiang,*[,‡] and Yun-Peng Chao*[,†,§,∥]

[†]Department of Chemical Engineering, Feng Chia University 100 Wenhwa Road, Taichung 40724, Taiwan

[‡]Department of Medical Laboratory Science and Biotechnology, China Medical University, No. 91, Hsueh-Shih Road, Taichung 40402, Taiwan

[§]Department of Health and Nutrition Biotechnology, Asia University, Taichung 41354, Taiwan

[∥]Department of Medical Research, China Medical University Hospital, Taichung 40447, Taiwan

ABSTRACT: The butyrate production by engineered *Escherichia coli* is afflicted by both low titer and low selectivity (defined as the butyrate/acetate (B/A) ratio). To address this issue, a strategy for metabolic engineering of *E. coli* was implemented including (1) elimination of all major NADH-dependent reactions in the fermentation metabolism, (2) reconstruction of a heterologous pathway leading to butyryl-CoA, (3) recruitment of endogenous *atoDA* for conversion of butyryl-CoA to butyrate with acetate as a CoA acceptor, and (4) removal of the acetate-synthesis pathway. Grown on glucose (20 g/L) plus acetate (8 g/L), the engineered strain consumed almost all glucose and acetate and produced 10 g/L butyrate as a predominant product within 48 h. It leads to high butyrate selectivity with the B/A ratio reaching 143. The result shows that our proposed approach may open a new avenue in biotechnology for production of butyrate in *E. coli*.

KEYWORDS: *butyric acid, Escherichia coli, metabolic engineering*

INTRODUCTION

Butyric acid is a short-chain fatty acid and has a broad range of applications in industry. Its derivatives such as butyrate esters are applied for fragrant- and flavor-enhancing agents in beverages, food, and cosmetics.[1,2] A polymer prepared from butyric acid and cellulose acetate can be utilized for the manufacture of plastics and textile fibers.[3,4] Serving as therapeutic prodrugs, the derived forms of butyrate are shown to exhibit an anticancer effect.[5] In addition, the commercial value of butyric acid is greatly acknowledged for its role as a precursor of biofuels, such as *n*-butanol. The approach by catalytic conversion of butyric acid to *n*-butanol is reportedly feasible by either biotransformation with microbes or the hydrogenation reaction using chemical catalysts.[2,6] *n*-Butanol is superior to ethanol for replacing gasoline in many ways.[7] Therefore, production of *n*-butanol from renewable resources (i.e., biobutanol) has recently gained a spotlight in both the academic and industry communities. It is conceived that the commercial availability of biobutanol enables a large reduction of the greenhouse effect caused by enormous consumption of fossil fuels.

Butyric acid currently on the market is mainly produced by a chemical synthesis method with the resource coming from crude oils.[8] However, the overwhelming concern of global warming and the rising desire for natural products have driven industrial attention toward fermentative production of butyric acid. *Clostridium* species, Gram-positive and strictly anaerobic bacteria, have long been investigated for the production of butyric acid because of their higher productivity and production titers. Many fermentation strategies have been proposed to achieve high butyrate production.[9] Nevertheless, the clostridial fermentation pattern is too complicated to operate. It needs careful investigation of key factors that affect butyrate production to optimize the fermentation process.[2] A typical fermentation feature of *Clostridium* involves the acidogenesis phase followed by the solventogenesis phase.[10] In the first phase, butyrate, acetate, and hydrogen are major products. Upon entry to the stationary phase, reassimilation of produced acids at the second stage leads to production of acetone, *n*-butanol, and ethanol, known as the ABE fermentation.[11] In addition, less availability of genetic tools and physiological information also hinders the advance of the butyrate production process based on *Clostridium*.

Escherichia coli is known as a biotechnology workhorse because it can be easily cultured and genetically manipulated. Moreover, its physiological information and fermentation technique are generally available. Intensive studies have been directed toward development of *E. coli* for the production of biofuels and high-value chemicals.[12,13] To improve the production efficiency, metabolic engineering of *E. coli* for the desired trait appears to be the most commonly adopted approach. This technique enables the evolution of living cells in a short time frame.[14,15] In general, strain improvement by metabolic engineering requires a strategy that includes deletion of undesired pathways, removal of bottleneck nodes, and/or extension of metabolic pathways leading to heterologous products.[16] Based on these strategies, recent studies have illustrated functional reconstruction of the *Clostridium* pathway in *E. coli*.[17,18] This advancement is conducive to the study on

Received: January 23, 2014
Revised: April 23, 2014
Accepted: April 28, 2014
Published: April 28, 2014

ACS Publications © 2014 American Chemical Society

Table 1. Strains, Plasmids, and Primers Applied in This Study[a]

	main characteristics	source
E. coli Strain		
DH5α(pir)	*deoR endA1 gyrA96 hsdR17 supE44 thi1 recA1*	
	lacZM15 λpir	lab collection
BL21	F^- *dcm gal ompT hsdS*(r_B- m_B^-)	lab collection
BL-A1	as BL21Δ*ptsG*Δ*poxB* HK022::$\lambda P_R P_L$-*glf*	22
BuT-8L	as BL-A1Δ*ldhA*Δ*frdA* *ϕ*80*attB*:: $P\lambda P_L$-*ter* *λattB*:: $P\lambda P_L$-*crt*	
	Δ*adhE*::*ϕ*80*attB*:: $P\lambda P_L$-*pha-hbd*	this study
BuT-8LA	as BuT-8L $P\lambda P_L$-*atoDABE*	this study
BuT-8L-ato	as BuT-8LA Δ*pta*	this study
Plasmid		
pA123	*ϕ*80Int *bla*$^+$	27
pBlue-LamGn	*λattB* LE*-*gen*-RE*	23
pBlue-P80Gn	*ϕ*80*attB* LE*-*gen*-RE*	23
pCP20	λP_R-*flp* *bla*$^+$	26
pINT-ts	*λ*Int *bla*$^+$ *repA*101	27
pKD46	*λ*Red *bla*$^+$ *repA*101	26
pLam-Crt	*λattP* LE*-*kan*-R6K *ori*-RE* $P\lambda P_L$-*crt*	23
pMC-ptaKm	Δ*pta*:: FRT-*kan*-FRT	this study
pPhi-LoxKm	*ϕ*80*attP* LE*-*kan*-R6K *ori*-RE*	23
pPhi-Ter	*ϕ*80*attP* LE*-*kan*-R6K *ori*-RE* $P\lambda P_L$-*ter*	23
pPhi-PhaAHbd	*ϕ*80*attP* LE*-*kan*-R6K *ori*-RE* $P\lambda P_L$-*pha-hbd*	23
pPL-Gn	LE*-*gen*-RE*-$P\lambda P_L$	this study
pSPL-atoD	LE*-*gen*-RE*-$P\lambda P_L$-*atoD* (truncate)	this study
pTH19-CreCs	P*araBAD*-*cre* *cat*$^+$	23
Primer		
FrdA1	GAAAGTCGACGAATCCCGCCCAGG	22
FrdA2	CAAGAAAGCTTGTTGATAAGAAAGG	22
LdhA1	TCTTATGAAACTCGCCGTTTATAG	22
LdhA2	TTAAACCAGTTCGTTCGGGCAG	22
Pta1	TGTCCAAGCTTATTATGCTGATCCCTACC	22
Pta2	GTTCGACTAGTTTAGAAATGCGCGCGTC	22
AdE1	GTTCTGTCTGAAGACGACAC	22
AdE2	CCGCTCTAGAACTAGTGGATCCAGCCTGCAGAACGATATCAG	22
AdE3	GCGGCAGGAGTCTATGAACACGCAAACGTGCAGTTGCATCTG	23
AdE4	TCAGCGCACCGTTTTTCAGG	23
LPL1	TTAGAATTCATTACCTGTTCGTATAATG	this study
LPL2	AAGCTTACCCAATTCGCCCTAGGTGATAATGGTTGCATGTAATCCTAAGGAGGTTGATCCATATG	this study
LPL3	GGTGATAATGGTTGCATGTAAATGAATTCTAACACCGTGCGTGTTGACTATTTTACCTCTGGC	this study
RC13 034	CATCTCACCAGATATCATGC	this study
RC13 035	AATCGGAGCTCGAAAGTGAACTGTTTGG	this study
RC13 036	GATAACATATGAAAACAAAATTGATGACATTAC	this study
RC13 037	CGGAAGGATCCTTCTTTTACCATTGCCTG	this study

[a]Abbreviations: P*araBAD*, the *araBAD* promoter; *ori*, replication origin; $P\lambda P_R P_L$, the $\lambda P_R P_L$ promoter; $P\lambda P_L$, the λP_L promoter; *bla*, ampicillin-resistant determinant; *cat*, chloramphenicol-resistant determinant; *kan*, kanamycin-resistant determinant; *gen*, gentamicin-resistant determinant.

production of butyrate by *E. coli* with the report of the production titer in the range 1.3−4.3 g/L.[19,20] The production titer is later improved to reach 7.2 g/L by a technique combining synthetic scaffolds and fed-batch cultivation.[21]

In this study, a biosynthetic pathway leading to butyrate was reconstructed in *E. coli*. Utilizing glucose and acetate as the substrates, the engineered *E. coli* strain was able to produce >10 g/L butyrate as a predominant product. This indicates the promise of this approach for the production of butyrate in the surrogate *E. coli* strain.

MATERIALS AND METHODS

Gene Deletion and Insertion. The main strains, plasmids, and primers applied in this study are listed in Table 1. DNA manipulation was routinely conducted using strain DH5α(pir) as the intermediate strain. Derived from *E. coli* strain BL21, strain BL-A1[22] was utilized for the experiment. The *frdA* gene of strain BL-A1 was deleted essentially following the previous report.[23−25] In brief, the DNA fragment containing *frdA* inserted with the FRT-*kan*-FRT cassette was amplified by polymerase chain reaction (PCR) from strain CGSC10964 with primers FrdA1 and FrdA2. By electroporation, the PCR DNAs were introduced into the strain carrying *λ* Red-borne plasmid pKD46.[26] Under the nonpermissive condition for the plasmid, integrants with the inserted DNAs via homologous recombination were selected for resistance to kanamycin but susceptibility to ampicillin. Later removal of the integrated marker from the integrant was carried out using helper plasmid pCP20 as described previously.[26] In a similar way, the DNA bearing *ldhA* inserted with the FRT-*kan*-FRT cassette was amplified from strain CGSC9216 with primers LdhA1 and LdhA2 and utilized for elimination of *ldhA*. Furthermore, *pta* was removed by using the PCR DNA that carries *pta* integrated with FRT-*kan*-FRT from plasmid pMC-ptaKm with primers Pta1 and Pta2.

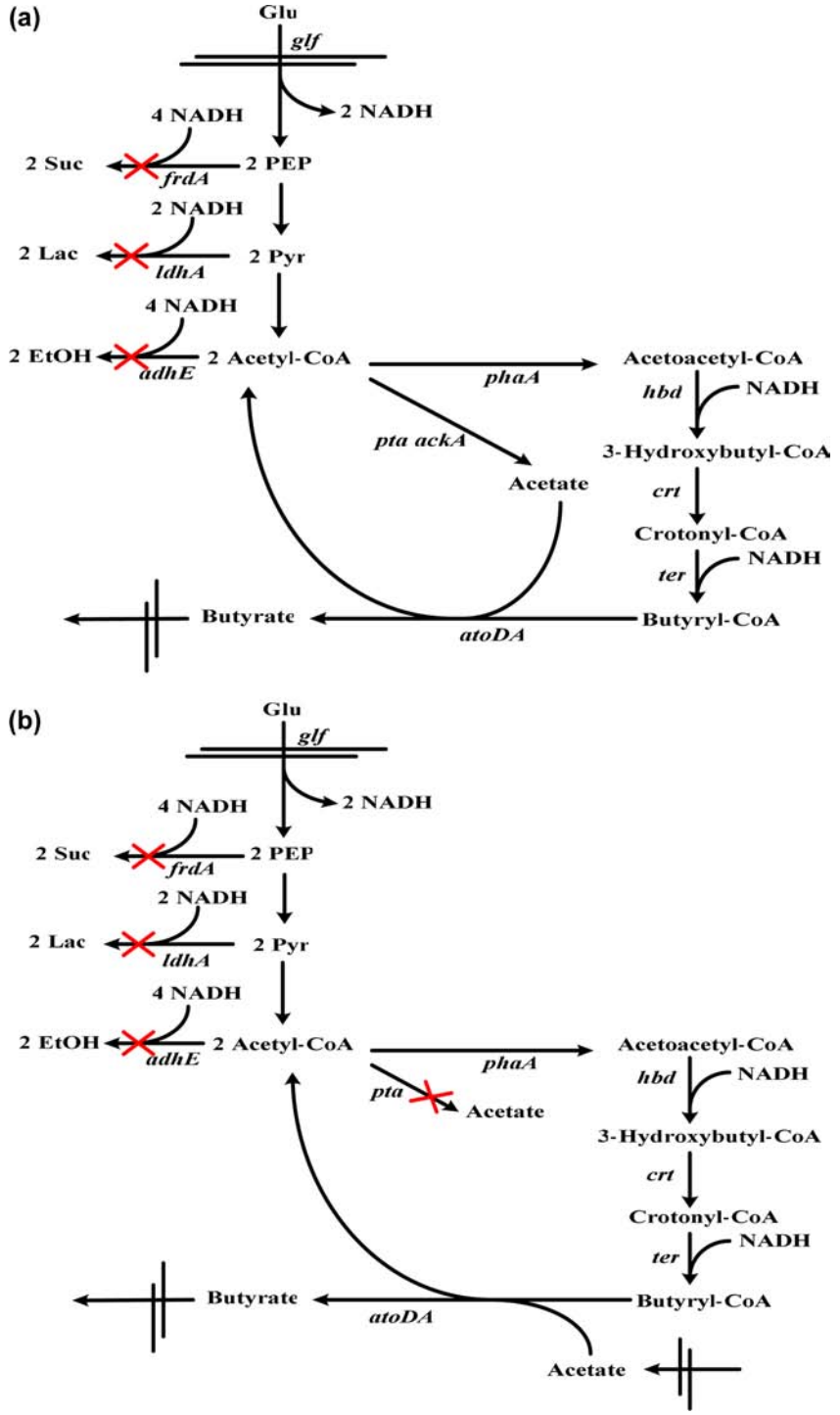

Figure 1. Metabolic pathway leading to butyrate from glucose in *E. coli*. (a) Endogenous acetate system. (b) Exogenous acetate system. The genes involved in the metabolic pathway: *ackA*, acetate kinase; *adhE*, aldehyde-alcohol dehydrogenase; *atoDA*, acetoacetyl-CoA transferase; *ldhA*, lactate dehydrogenase; *frdA*, subunit of *fumarate reductase; pta*, phosphate acetyltransferase; *phA*, *β*-ketothiolase; *hbd,* 3-hydroxybutyryl-CoA dehydrogenase; *crt*, crotonase; *ter,* trans-enoyl-CoA reductase. The deleted genes are marked by "X". Abbreviations: Glu, glucose; PEP, phosphoenolpyruvate; Pry, pyruvate; EtOH, ethanol; Lac, lactate; Suc, succinate.

Insertion of the heterologous genes into *E. coli* was conducted according to the previous report.[22] In brief, plasmid pPhi-Ter that carries the *ter* gene of *Terponema denticola* DSM14222 was transformed into the strain with helper plasmid pAH123,[27] which expresses *ϕ*80 integrase (Int). Under the nonpermissive condition for the plasmid, integrants with insertion of *ter* at *ϕ*80 *attB* were selected for resistance to kanamycin but susceptibility to ampicillin. The integrated marker of the integrant was then removed using helper plasmid pTH19-CreCs as described previously.[23] Subsequently, integration of the *crt* gene from *Clostridium acetobutylicum* DSM792 at *λ attB* was carried out in the same way. Plasmid pLam-Crt was simply transformed into the strain carrying helper plasmid pINT-ts that express phage *λ* Int.[27] Moreover, an extra *ϕ*80 *attB* site was created at *adhE* of the resulting strain. This was carried out by first amplification of the DNA comprising the *ϕ*80*attB*-LE*-*gen*-RE* cassette flanked by two homologous extensions of *adhE* from plasmid

dx.doi.org/10.1021/jf500355p | J. Agric. Food Chem. 2014, 62, 4342−4348

pBlue-P80Gn based on overlapping PCR with primers AdE1/AdE2 and AdE3/AdE4.[23] Followed by electroporation, the PCR DNA was introduced into the strain with plasmid pKD46. Integrants exhibiting the gentamicin-resistant and ampicillin-sensitive phenotype were then scored. One resulting strain was integrated with the gene cluster comprising *phaA* of *Cupriavidus necator* and *hbd* of *C. acetobutylicum* DSM792 at the created ϕ80 *attB* site by using plasmid pPhi-PhaAHbd, thus resulting in the knockout of *adhE*. Finally, removal of the inserted markers was aided with helper plasmid pTH19-CreCs.

Enhanced Expression of Endogenous Genes. Plasmid pPL-Gn was constructed by incorporation of the λP_L promoter ($P\lambda P_L$) into plasmid pBlue-LamGn. This was carried out by the first PCR with primers LPL1 and LPL2, followed by the second PCR with primers LPL1 and LPL3 using the first PCR DNA as the template. The resulting PCR DNA was digested with *Eco*RI and then self-ligated. This resulted in plasmid pPL-Gn carrying the LE*-*gen*-RE* cassette fused with $P\lambda P_L$ (LE*-*kan*-RE*-$P\lambda P_L$). Meanwhile, the DNA containing the upstream region and 5′-end structural sequence of *atoD* was amplified from *E. coli* strain BL21 by PCR with primers RC13034/RC13035. After digestion with *Eco*RV-*Sac*I, the PCR DNA and plasmid pBluescript were spliced together to obtain plasmid pBlue-atoD. The *Nde*I-*Bam*HI sites were then introduced into plasmid pBlue-atoD by PCR with primers RC13036/RC13037. Meanwhile, the DNA cassette bearing LE*-*gen*-RE*-$P\lambda P_L$ was recovered from plasmid pPL-Gn by *Nde*I-*Bam*HI and incorporated into plasmid pBlue-atoD to give plasmid pSPL-atoD. This plasmid carried the passenger DNA that contained the upstream region and the fusion of LE*-*gen*-RE*-$P\lambda P_L$ to the 5′-end structural sequence of *atoD*. By PCR with primers RC13034/RC13035, the passenger DNA was electroporated into the strain with plasmid pKD46. The resulting integrant harbored *atoDABE* driven by $P\lambda P_L$.

Bacterial Culturing. The bacterial growth was measured turbidimetrically at 550 nm (OD_{550}). *E. coli* strains were grown on Luria–Bertani (LB) medium at 37 °C overnight. The overnight culture was then inoculated into 125 mL Erlenmeyer flasks containing 50 mL of modified Terrific broth medium (12 g/L tryptone, 24 g/L yeast extract, 2.13 g/L KH_2PO_4, and 12.54 g/L K_2HPO_4) supplemented with 12 g/L glucose. The initial cell density was kept at an OD_{550} of 0.1. The oxygen-limited culture condition was performed according to our previous report.[23] Bacterial cultures were seeded into Erlenmeyer flasks (125 mL) containing 50 mL of medium and incubated at 37 °C and 100 rpm.

Analytical Methods. Glucose and organic acids (including butyric acid) were analyzed by high-performance liquid chromatography (HPLC) according to the method reported previously.[23] To determine the AtoDA activity, bacterial strains were harvested with 67 mM Tris-HCl (pH 8) by centrifugation after culturing for 24 h. Cells were disrupted using sonication and then fractioned by centrifugation. The supernatant was recovered as cell-free extract (CFX). The enzymatic reaction was then carried out by adding 10 μL of CFX into the reaction solution (90 μL), which consisted of 20 mM butyryl-coA, 0.4 mM sodium acetate, and 67 mM Tris-HCl (pH 8). The reaction proceeded for 20 min and was terminated by heating the solution at 100 °C for 10 min. The butyrate concentration in the reaction was determined by HPLC. The specific enzyme activity was defined as butyrate produced in μmol per min (U) per mg CFX.

RESULTS

Reconstruction of the Butyrate-Synthesis Pathway. The biosynthetic pathway leading to butyrate was developed by starting with *E. coli* strain BL-A1 in several steps (Figure 1). Strain BL-A1 was previously constructed by removal of *poxB*, and its native glucose uptake system was replaced by *glf* (encoding glucose facilitator) from *Zymomonas mobilis*.[22] First, *adhE*, *ldhA*, and *frdA* of strain BL-A1 were eliminated to conserve availability of NADH and to reduce production of waste byproducts. Second, heterologous genes including *phaA*, *hbd*, *crt*, and *ter* each under the control of $P\lambda P_L$ were integrated into the strain to obtain strain BuT-8L. Note that *adhE* of the strain was inactivated after insertion of the *phaA-hbd* gene cluster (see Materials and Methods). The approach resulted in the constructed pathway directing glucose flux to butyryl-CoA (Figure 1). Lastly, the expression level of endogenous *atoDA* in strain BuT-8L was enhanced by fusion of the gene cluster *atoDAEB* with $P\lambda P_L$, resulting in strain BuT-8LA. This final step was recruited to complete the butyrate-synthetic pathway by catalytic conversion of butyryl-CoA to butyrate at the expense of acetate. The functionality of AtoDA was further verified by assaying the enzyme activity. As a result, strain BuT-8LA exhibited 8-fold higher activity than control strain BuT-8L (0.56 vs 0.07 U/mg).

Production of Butyrate in Engineered *E. coli*. Production of butyrate was investigated for the engineered *E. coli* strains. Therefore, shake-flask cultures of strains BuT-8L and BuT-8LA were carried out in the presence of glucose. After 24 h of fermentation, strain BuT-8LA produced 3.4 g/L butyrate as a major product, whereas the butyrate production in control strain BuT-8L was around 1 g/L (Figure 2). The result

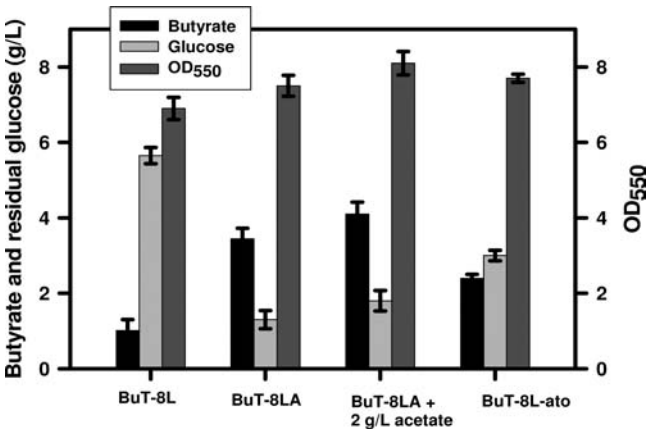

Figure 2. Production of butyrate in the engineered *E. coli* strains. The oxygen-limited fermentation was carried out with shake-flask cultures in the presence of 12 g/L glucose for 24 h. The experiments were conducted in triplicate.

indicates that the constructed pathway in *E. coli* is functional for the synthesis of butyrate. Nevertheless, AtoDA-catalyzed conversion of butyryl-CoA to butyrate requires acetate (Figure 1A). It was informative to investigate the effect of acetate on the butyrate production in strain BuT-8LA (*pta ackA* positive). First, 2 g/L acetate was supplemented in the medium, and the butyrate titer in this strain was increased to 4.1 g/L. Note that *pta and ackA* are mainly responsible for production of acetate in strain BuT-8LA. Moreover, *pta* was removed from strain BuT-8LA to obtain strain BuT-8L-ato. As a result, the *pta*-lacking strain produced less butyrate (2.5 g/L). Taken together, these results suggest that acetate plays a determining role in the synthesis of butyrate.

Effect of Acetate on Butyrate Production. Interestingly, intracellular acetate may be regenerated by coupling the Pta-AckA with AtoDA reactions (Figure 1A). However, this regeneration system in strain BuT-8LA does not seem to function sufficiently to provide acetate which meets the requirement for the butyrate production as illustrated in Figure 2 (i.e, strain BuT-8LA with acetate supplementation). This implies that the butyrate production in the strain is likely limited by the availability of acetate. Therefore, the approach by

supplementation of acetate was expected to improve the production of butyrate (Figure 1B). Strain BuT-8L-ato, deficient in *pta*, was utilized for the experiments. As shown in Figure 3, the strain consumed almost all glucose after 24 h of

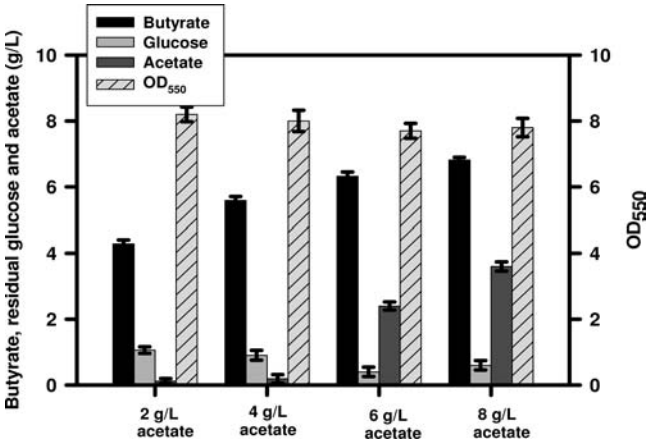

Figure 3. Effect of acetate on the butyrate production in the engineered *E. coli* strain. Strain BuT-8L-ato was grown on 12 g/L glucose supplemented with various concentrations of sodium acetate, and the oxygen-limited fermentation was carried out for 24 h. The experiments were conducted in triplicate.

fermentation, while its butyrate production increased with the increasing amount of supplemented acetate. The butyrate production reached the maximum (6.8 g/L) in the case where 8 g/L sodium acetate was augmented. The result indicates the positive contribution of acetate to the butyrate production.

Butyrate Production by Glucose Feeding. Indeed, it was found that around half of the supplemented acetate (8 g/L) still remained at the end of the fermentation, as illustrated in Figure 3. We reasoned that the strategy by supplementation of extra glucose might be useful to increase the butyrate production at the expense of remaining acetate. Therefore, strain BuT-8L-ato was initially cultured on the medium containing 12 g/L glucose plus 8 g/L sodium acetate. After 24 h, various amounts of glucose were added to the culture medium and the bacterial fermentation was continued. In general, the butyrate production in the strain increased along the time course (Figure 4). The butyrate production finally reached >10 g/L after 48 h of fermentation, when 8 and 10 g/L glucose were additionally supplemented. For the case of 10 g/L supplementation, glucose was not completely consumed by the strain. Nevertheless, there was only a trace amount of acetate (<0.07 g/L) left in the medium for both cases.

DISCUSSION

Clostridium species are native butyrate producers and carry out a butyrate-synthesis pathway typically consisting of *thl*, *hbd*, *crt*, *bcd*, *ptb*, and *buk* genes.[10] The enzymes encoded by the first four genes reduce acetyl-CoA to butyryl-CoA, while the latter two gene products convert butyryl-CoA to butyrate. In this study, the biosynthetic pathway of butyrate was reconstructed in *E. coli* by substitution of *thl* and *bcd* with *phaA* and *ter* from *C. necator* and *T. denticola* DSM14222, respectively. This heterologous pathway was previously proven functional to provide butyryl-CoA for the synthesis of *n*-butanol in *E. coli* by genomic engineering strategy.[23] Moreover, endogenous *atoDA* was employed to complete the synthetic pathway by conversion

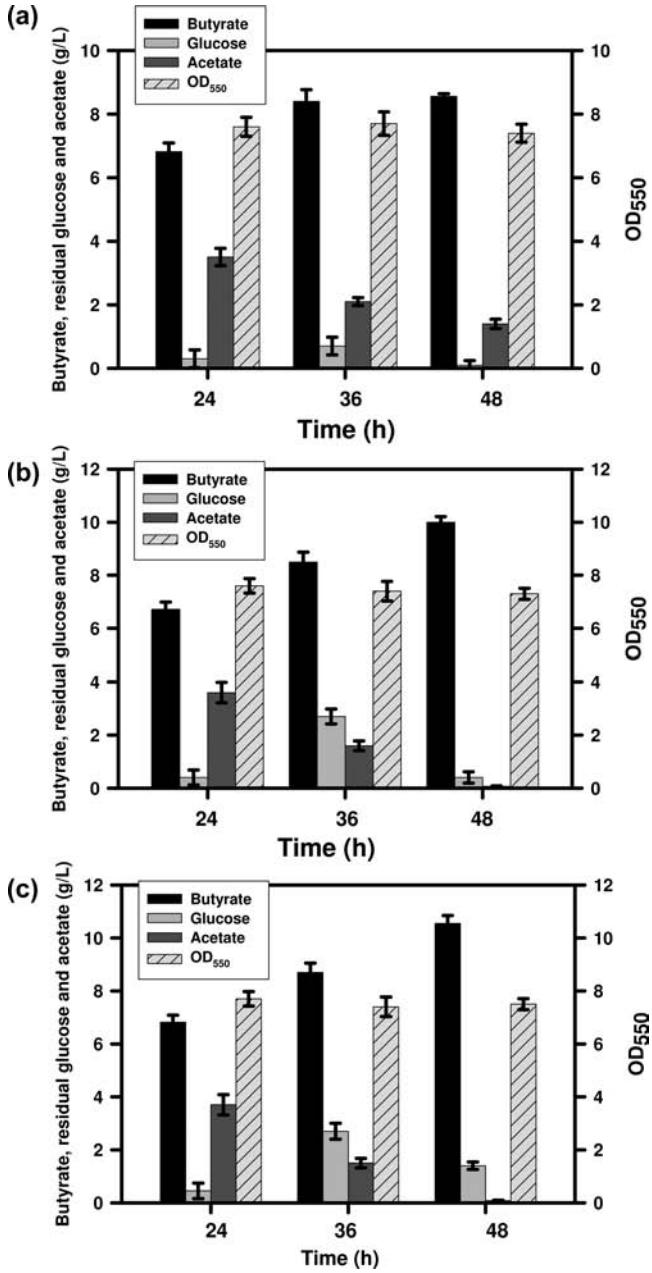

Figure 4. Time course production of butyrate in *E. coli* by glucose feeding. Under the oxygen-limited condition, strain BuT-8L-ato was cultured in the presence of 12 g/L glucose and 8 g/L sodium acetate. After 24 h, extra glucose was added into the culture broth. The experiments were conducted in triplicate. (a) Extra feeding of 6 g/L glucose; (b) extra feeding of 8 g/L glucose; (c) extra feeding of 10 g/L glucose.

of butyryl-CoA to butyrate. As known, AtoA and AtoD constitute the β and α subunits of acetoacetyl-CoA transferase, whose physiological function is responsible for activation of short-chain (C3−C6) fatty acids for their respective thioesters.[28] The *E. coli* strain cannot grow on butyrate unless it has a genotype of *fadR atoC*.[29] The *fadR* null mutation induces the *fad*-encoded β-oxidation enzymes, while the *atoC* constitutive mutation results in the expression of the *atoDAEB* operon, respectively. Therefore, *E. coli* with functional *atoDA* only is unable to assimilate butyrate, which is favorable for the butyrate production. Finally, the endogenous NADH-dependent path-

dx.doi.org/10.1021/jf500355p | J. Agric. Food Chem. 2014, 62, 4342−4348

way nodes were all removed from the central metabolism. This approach turns the heterologous pathway that reduces acetyl-CoA to butyryl-CoA into an electron sink, consequently driving carbon flux to butyrate (Figure 1). Such a strategy by balancing the redox state of cells has been proven useful for fermentative production of desired products.[30−32]

As illustrated in Figure 2, strain BuT-8LA, carrying the constructed synthetic pathway of butyrate, was able to produce butyrate. With the basal AtoDA activity (i.e., 0.07 U/mg), strain BuT-8L produced much less butyrate. AtoDA converts acetate and butyryl-CoA to butyrate and acetyl-CoA. In strain BuT-8LA, the two reactions mediated by Pta-AckA and PhaA can compete for the acetyl-CoA pool. Apparently, the reaction rate of the Pta-AckA step is not on a par with that of the PhaA step, consequently restricting the butyrate production. This view is supported by an increase in the butyrate titer for strain BuT-8LA that received extra acetate. By further removal of *pta*, the resulting strain BuT-8L-ato (*pta poxB* negative) produced 30% less butyrate than strain BuT-8LA (Figure 2). In addition, strain BuT-8L-ato deficient in *pta-ackA* and *poxB* may still synthesize acetate,[33] but perhaps limiting. Therefore, more supplemented acetate results in improvement of butyrate production for strain BuT-8L-ato (Figure 3). It should be noted that the ATP level is probably not a limiting factor in the engineered *E. coli*. As revealed from the synthetic pathway (Figure 1), the butyrate production requires NADH, and the ATP produced at the substrate-level phosphorylation is thus conserved. Acting like *atoDA*, the *ptb-buk* in the *Clostridium* pathway mediates the last synthetic step by generation of ATP per butyrate production. However, the *ptb-buk* expressed in *E. coli* exhibits a nonspecific function and generates crotonate as a byproduct.[34] Note that AtoDA may react with acetoacetyl-CoA to produce acetoacetate. Our analyses showed no detectable levels of acetoacetate and its decarboxylated product, acetone, in the culture broth.

There are a few studies centering on butyrate production in *E. coli*. One earlier approach employed the reverse β-oxidation pathway of fatty acids. Without involvement of any foreign genes, the engineered *E. coli* was shown to produce 1.3 g/L butyrate from 30 g/L glucose after 48 h of fermentation.[19] The result leads to a production yield of butyrate (g/L) on glucose (g/L), defined as $Y_{B/G}$, of 4.3%. Another study introduced the butyrate-synthesis pathway into *E. coli* using the clostridial pathway for reduction of acetoacetyl-CoA to butyryl-CoA and endogenous *tesB* (encoding thioesterase II) for consecutive conversion of butyryl-CoA to butyrate.[20] The result is encouraging, with the butyrate/acetate (B/A) weight ratio reaching 41. To improve the butyrate production based on this constructed pathway, a recent study implemented the synthetic scaffold to couple the three heterologous genes (*hbd*, *crt*, and *ter*) in a spatially organized pathway. Consequently with the fed-batch supplementation of glucose, butyrate production in the strain reached 7.2 g/L from 19 g/L glucose (i.e., $Y_{B/G}$ = 37.9%) at 84 h.[21] However, this approach is afflicted by the associated production of acetate (4 g/L) with the B/A ratio reaching 1.8. The butyrate selectivity (represented by the B/A ratio) is a key factor employed for evaluation of the clostridial fermentation performance since the lower ratio greatly increases the purification cost of butyrate.[9] Even with inactivation of the acetate synthesis, the potential butyrate producer *C. tyrobutyricum* still displayed a B/A ratio ranging between 5 and 7.[35] Most recently, a study reported the reconstruction of the whole butyrate synthetic pathway from *C. difficile* in *E. coli*. The butyrate titer was low (around 0.27 g/L) but with less acetate production.[36] Overall, the results of these previous studies are less impressive due to the low production titer and/or the low B/A ratio. In the present study, a synthetic pathway was designed to produce butyrate at the expense of acetate. This proposed approach resulted in a high butyrate titer as well as a trace amount of acetate and other known organic compounds. Consequently, 10 g/L butyrate could be obtained from 20 g/L glucose plus 8 g/L acetate within 48 h, and the B/A ratio reached 143 (Figure 4B). The butyrate production gives a $Y_{B/G}$ of 50%. In theory, one butyrate can be produced from 0.5 glucose plus one acetate according to the stoichiometry of the synthetic pathway (Figure 1). Therefore, this butyrate production on glucose and acetate accounts for 85.5% of the theoretical yield.

In conclusion, our proposed strategy for the production of butyrate in *E. coli* shows promise in terms of high production titer, productivity, and selectivity (i.e., the B/A ratio). Nevertheless, more efforts are required to improve the current approach. For instance, butyrate and acetate in the un-ionized form exhibit a similar inhibitory effect on *E. coli* metabolism.[37] Therefore, an *E. coli* strain with a high tolerance to the toxicity is expected to be useful for higher butyrate production. This work is currently being undertaken in our lab.

AUTHOR INFORMATION

Corresponding Authors

*(C.-J. Chiang) E-mail: oleosin91@yahoo.com.tw. Tel: 886-4-22053366, ext. 7227.

*(Y.-P. Chao) E-mail: ypchao@fcu.edu.tw. Tel: 886-4-24517250, ext. 3677. Fax: 886-4-24510890.

Notes

The authors declare no competing financial interest.

ACKNOWLEDGMENTS

This work is supported by Ministry of Science and Technology, Taiwan (NSC 101-2221-E-035-057-MY3 and NSC 103-2622-E-035-008-CC1).

REFERENCES

(1) Armstronga, D. W.; Yamazakib, H. Natural flavours production: a biotechnological approach. *Trends Biotechnol.* **1986**, *4*, 264−268.

(2) Dwidar, M.; Park, J. Y.; Mitchell, R. J.; Sang, B. I. The future of butyric acid in industry. *ScientificWorldJournal* **2012**, *471417*, 1−9.

(3) Cao, Y.; Li, H.; Zhang, J. Homogeneous synthesis and characterization of cellulose acetate butyrate (CAB) in 1-allyl-3-methylimidazolium chloride (AmimCl) ionic liquid. *Ind. Eng. Chem. Res.* **2011**, *50*, 7808−7814.

(4) El-Shafee, E.; Saad, G. R.; Fahmy, S. M. Miscibility, crystallization and phase structure of poly(3-hydroxybutyrate)/cellulose acetate butyrate blends. *Eur. Polym. J.* **2001**, *37*, 2091−2104.

(5) Rephaeli, A.; Zhuk, R.; Nudelman, A. Prodrugs of butyric acid from bench to bedside: synthetic design, mechanisms of action, and clinical applications. *Drug Dev. Res.* **2000**, *50*, 379−391.

(6) Kim, H. S.; Lee, S. H.; Yoon, Y. S.; Oh, S. H.; Chung, Y. M.; Kim, O. Y.; Jeon, H. J. Nanometer-sized copper-based catalyst, production method thereof, and alcohol production method using the same through direct hydrogenation of carboxylic acid. WO 11/132957, 2011.

(7) Dürre, P. Biobutanol: an attractive biofuel. *Biotechnol. J.* **2007**, *2*, 1525−1534.

(8) Cascone, R. Biobutanol-a replacement for bioethanol. *Chem. Eng. Prog.* **2008**, *104*, S4−S9.

(9) Zhang, C.; Yang, H.; Yang, F.; Ma, Y. Current progress on butyric acid production by fermentation. *Curr. Microbiol.* **2009**, *59*, 656−663.

(10) Lee, S. Y.; Park, J. H.; Jang, S. H.; Nielsen, L. K.; Kim, J.; Jung, K. S. Fermentative butanol production by *Clostridia*. *Biotechnol. Bioeng.* **2008**, *101*, 209−228.
(11) Jones, D. T.; Woods, D. R. Acetone-butanol fermentation revisited. *Microbiol Rev.* **1986**, *50*, 484−524.
(12) Clomburg, J. M.; Gonzalez, R. Biofuel production in Escherichia coli: the role of metabolic engineering and synthetic biology. *Appl. Biochem. Biotechnol.* **2010**, *86*, 419−434.
(13) Yu, C.; Cao, Y.; Zou, H.; Xian, M. Metabolic engineering of *Escherichia coli* for biotechnological production of high-value organic acids and alcohols. *Appl. Biochem. Biotechnol.* **2011**, *89*, 573−583.
(14) Bailey, J. Towards a science of metabolic engineering. *Science* **1991**, *252*, 1668−1675.
(15) Cameron, D. C.; Tong, I. T. Cellular and metabolic engineering. *Appl. Biochem. Biotechnol.* **1993**, *38*, 105−140.
(16) Stephanopoulos, G.; Vallino, J. J. Network rigidity and metabolic engineering in metabolite overproduction. *Science* **1991**, *252*, 1675−1681.
(17) Atsumi, S.; Cann, A. F.; Connor, M. R.; Shen, C. R.; Smith, K. M.; Brynildsen, M. P.; Chou, K. J.; Hanai, T.; Liao, J. C. Metabolic engineering of *Escherichia coli* for 1-butanol production. *Metab. Eng.* **2008**, *10*, 305−311.
(18) Bond-Watts, B. B.; Bellerose, R. J.; Chang, M. C. Y. Enzyme mechanism as a kinetic control element for designing synthetic biofuel pathways. *Nat. Chem. Biol.* **2011**, *7*, 222−227.
(19) Seregina, T. A.; Shakulov, R. S.; Debabov, V. G.; Mironov, A. S. Construction of a butyrate-producing *E. coli* strain without the use of heterologous genes. *Appl. Biochem. Biotechnol.* **2010**, *46*, 745−754.
(20) Lim, J. H.; Seo, S. W.; Kim, S. Y.; Jung, G. Y. Refactoring redox cofactor regeneration for high-yield biocatalysis of glucose to butyric acid in *Escherichia coli*. *Bioresour. Technol.* **2013**, *135*, 568−573.
(21) Back, J. M.; Mazumdar, S.; Lee, S. W.; Jung, M. Y.; Lim, J. H.; Seo, S. W.; Jung, G. Y.; Oh, M. K. Butyrate production in engineered *Escherichia coli* with synthetic scaffolds. *Biotechnol. Bioeng.* **2013**, *110*, 2790−2794.
(22) Chiang, C. J.; Lee, H. M.; Guo, H. J.; Wang, Z. W.; Lin, L. J.; Chao, Y. P. Systematic approach to engineer *Escherichia coli* pathways for co-utilization of the glucose-xylose mixture. *J. Agric. Food Chem.* **2013**, *61*, 7583−7590.
(23) Chiang, C. J.; Saini, M.; Lee, H. M.; Wang, Z. W.; Chen, P. T.; Chao, Y. P. Genomic engineering of *Escherichia coli* by the phage attachment site-based integration system with mutant *loxP* sites. *Proc. Biochem.* **2012**, *47*, 2246−2254.
(24) Chiang, C. J.; Chen, P. T.; Chao, Y. P. Replicon-free and markerless methods for genomic insertion of DNAs in phage attachment sites and controlled expression of chromosomal genes in *Escherichia coli*. *Biotechnol. Bioeng.* **2008**, *101*, 985−995.
(25) Chiang, C. J.; Chen, P. T.; Chen, S. Y.; Chao, Y. P. Marker-free chromosomal expression of foreign and native genes in *Escherichia coli*. In *Methods in Molecular Biology*; Williams, J. A., Ed.; Humana Press: New York, 2011; pp 113−124.
(26) Datsenko, K. A.; Wanner, B. L. One-step inactivation of chromosomal genes in *Escherichia coli* K-12 using PCR products. *Proc. Natl. Acad. Sci. U.S.A.* **2000**, *97*, 6640−6645.
(27) Haldimann, A.; Wanner, B. L. Conditional-replication, integration, excision, and retrieval plasmid-host systems for gene structure-function studies of bacteria. *J. Bacteriol.* **2001**, *183*, 6384−6393.
(28) Sramek, S. J.; Frerman, F. E. Purification and properties of *Escherichia coli* coenzyme A-transferase. *Arch. Biochem. Biophys.* **1975**, *171*, 14−26.
(29) Clark, D. P.; Cronan JR, J. E., Two-carbon compounds and fatty acids as carbon sources. In *Escherichia coli and Salmonella: Cellular and Molecular Biology*, Neidhardt, F. C.; Curtiss, R., III; Ingraham, J. L.; Lin, E. C. C.; Low, K. B.; Magasanik, B.; Reznikoff, W. S.; Riley, M.; Schaechter, M.; Umbarger, H. E., Eds.; ASM Press: Washington, DC, 1996; Vol. *1*, pp 343−357.
(30) Berríos-Rivera, S. J.; Bennett, G. N.; San, K. Y. The effect of increasing NADH availability on the redistribution of metabolic fluxes in *Escherichia coli* chemostat cultures. *Metab. Eng.* **2002**, *4*, 230−237.
(31) Jantama, K.; Zhang, X.; Moore, J. C.; Shanmugam, K. T.; Svoronos, S. A.; Ingram, L. O. Eliminating side products and increasing succinate yields in engineered strains of *Escherichia coli* C. *Biotechnol. Bioeng.* **2008**, *101*, 881−893.
(32) Shen, C. R.; Lan, E. I.; Dekishima, Y.; Baez, A.; Cho, K. M.; Liao, J. C. Driving forces enable high-titer anaerobic 1-butanol synthesis in *Escherichia coli*. *Appl. Environ. Microbial.* **2011**, *77*, 2905−2915.
(33) Phue, J. N.; Lee, S. J.; Kaufman, J. B.; Negrete, A.; Shiloach, J. Acetate accumulation through alternative metabolic pathways in *ackA* (−) *pta* (−) *poxB* (−) triple mutant in *E. coli* B (BL21). *Biotechnol. Lett.* **2010**, *32*, 1897−1903.
(34) Fischer, C. R.; Tseng, H. C.; Tai, M.; Prather, K. L.; Stephanopoulos, G. Assessment of heterologous butyrate and butanol pathway activity by measurement of intracellular pathway intermediates in recombinant *Escherichia coli*. *Appl. Microbiol. Biotechnol.* **2010**, *88*, 265−275.
(35) Liu, X.; Zhu, Y.; Yang, S. T. Construction and characterization of *ack* deleted mutant of *Clostridium tyrobutyricum* for enhanced butyric acid and hydrogen production. *Biotechnol. Prog.* **2006**, *22*, 1265−1275.
(36) Aboulnaga, E. H.; Pinkenburg, O.; Schiffels, J.; El-Refai, A.; Buckel, W.; Selmer, T. Butyrate production in *Escherichia coli*: exploitation of an oxygen tolerant bifurcating butyryl-CoA dehydrogenase/electron transferring flavoprotein complex from *Clostridium difficile*. *J. Bacteriol.* **2013**, DOI: 10.1128/JB.00321-13.
(37) Henderson, P. J. Ion transport by energy-conserving biological membranes. *Annu. Rev. Microbiol.* **1971**, *25*, 393−42.

JOURNAL OF AGRICULTURAL AND FOOD CHEMISTRY

Article

pubs.acs.org/JAFC

Influence of Amount of Starting Material for DNA Extraction on Detection of Low-Level Presence of Genetically Engineered Traits[||]

Tigst Demeke,*[,†] Anh Phan,[‡] Indira Ratnayaka,[†] Michelle Holigroski,[†] and G. Ronald Jenkins[§]

[†]Canadian Grain Commission, 1404-303 Main Street, Winnipeg, Manitoba R3C 3G8, Canada

[‡]Corporate Services, Canadian Grain Commission, 303 Main Street, Winnipeg, Mantiboa R3C 3G8, Canada

[§]Maple Woods College, 2601 NE Barry Road, Kansas City, Missouri 64156-1299, United States

ABSTRACT: Two laboratories independently examined how the amount of starting material influences DNA extraction efficiency and, ultimately, the detection of low-level presence of genetically engineered (GE) traits in commercialized grains. GE traits from one maize, two canola, and two soybean samples were used as prototypical models in the study design as well as two commonly used DNA extraction methods, a small scale (0.1 and 0.2 g samples) and a large scale (1.0 and 2.0 g samples). The DNA samples were fortified (spiked) at 0.1 and 0.01% (w/w) levels. The amount of DNA recovery varied between the two laboratories, although a sufficient amount of DNA was obtained to perform replicate PCR analysis by both laboratories. Reliable detection of all five events was achieved by both laboratories at 0.1% level using either small-scale or large-scale DNA extractions. Reliable detection of the GE events was achieved at 0.01% level for soybean and canola but not for maize. Variability was observed among the two laboratories in terms of the Ct values generated. There was no difference between small-scale and large-scale DNA extraction methods for qualitative PCR detections of all five GE events.

KEYWORDS: *genetically engineered events, PCR, A2704, HCN92, OXY235, DP305423, MIR604, canola, soybean, maize*

INTRODUCTION

As grains move through the production and distribution chain, comingling of similar types and qualities routinely occurs, making the low-level presence (formerly known as adventitious presence) of mixed varieties a reality in bulk grain handling systems. With the advances of modern agricultural biotechnology, complex challenges have been introduced into global markets when trading grains. These challenges have become self-evident between exporting countries that produce a surplus of genetically engineered (GE) agricultural products and importing countries that apply different authorization standards to the same commodities. Grain quality and product compliance measures, based on sound scientific principles and reasonable outcomes, are necessary for the purpose of facilitating marketing of GE grain products. Low-level presence of unapproved or discontinued GE materials in non-GE commercial grains, oilseeds, and foodstuffs has been a contentious regulatory issue that often affects international grain trade.[1,2] A low-level presence of differing varieties potentially occurs when (1) naturally occurring drift of GE pollen, carried by wind and insects, contaminates neighboring fields; (2) planting equipment is shared between different types of farming operations; (3) equipment such as augers, conveyors, and elevators handle both GE and non-GE crops; (4) GE crops comingle with non-GE crops in grain bins and drying equipment; (5) harvesting machinery, such as combines, are utilized to harvest both GE and non-GE crops; and (6) during the field trial stage of development, GE seeds located in test plots infiltrate nearby plots being grown to generate foundation seed.

Two examples of a low-level presence of unapproved GE events that significantly affected commercial grain trade include FP967 flax in Canada[2] and LLRice601 in the United States.[3] Many countries have developed legislation regarding tolerance and traceability requirements for GE traits. However, there is a wide variation in tolerance and traceability requirements among countries, thus affecting grain trade.[1] Some of the challenges for detection of trace levels of GE traits include sampling and sample preparation, the amount of starting material when DNA extraction is performed, the amount of DNA recovered during the extraction, and the integrity of the DNA used for PCR.

According to European Commission Regulation No. 619/2011,[4] reliable detection of GE traits can be achieved at a 0.1% level. For the detection of FP967 transgenic flax event, detection limits of 0.0035%[2] and 0.001%[5] have been reported. However, there are some controversial opinions regarding laboratories' capacity to accurately and reliably detect the low-level presence of GE materials below the 0.1% level.[6] One study in particular suggests that relatively large amounts of starting material for DNA extraction (e.g., 2.0 g) provide better reproducibility and precision in the final analytical result.[7] Many of the commercially available DNA extraction kits cannot be used for extraction of DNA from relatively large amounts of ground samples such as 2.0 g (the kits are usually limited to ≤0.2 g ground material). The traditional sodium dodecyl sulfate (SDS)- and cetylmethylammonium bromide (CTAB)-based methods can be used for extraction of DNA from relatively large amounts of samples such as 1.0−5.0 g. However, both SDS- and CTAB-based DNA extraction methods are time-consuming and tedious. In addition, toxic chemicals such as phenol and chloroform are used for the large-scale DNA extraction methods. To date, the impact of the amount of starting

Received: February 5, 2014
Revised: April 3, 2014
Accepted: April 18, 2014
Published: April 18, 2014

ACS Publications © 2014 American Chemical Society

material for DNA extraction on the reliability of detection of low concentrations of GE traits by PCR has not been systematically studied. Therefore, this study was designed to compare the effect of using small-scale (0.1 and 0.2 g of starting materials) and large-scale (1.0 and 2.0 g of starting materials) DNA extractions on the detection of the low-level presence of GE traits (0.01 and 0.1% fortified or spiked samples) using data collected from two independent laboratories. It was also aimed to determine if there was variability among different crops and GE events in terms of detection of the low-level presence of GE traits by performing statistical analysis to evaluate the results.

MATERIALS AND METHODS

Seed Sources and Sample Preparation. Seeds of Armor BX GE canola variety (event OXY235) and Innovator (event HCN92) were received from the Oilseeds Monitoring unit of the Canadian Grain Commission (CGC). Certified seeds of non-GE canola variety, Eagle, were purchased from the American Oil Chemists' Society (AOCS, Urbana, IL, USA). The OXY235 and HCN92 GE canola events were not detected in the non-GE variety. For the DP305423 soybean event, certified ground reference materials ERM-BF426C (1%) and ERM-BF426D (10%) were used for making the 0.01 and 0.1% spike samples with a non-GE soybean variety. For the A2704-12 soybean event, certified seeds of the GE soybean variety PS2295 LL (Bayer Crop Science) were used for fortification. Seeds of the non-GE soybean variety Colby, obtained from Thompsons Ltd. (Chatham, ON, Canada), were used for fortification for both soybean events. The GE events DP305423 and A2704-12 were not detected in the Colby soybean variety (data not shown). Certified heterozygous maize reference samples 0407A (non-GE variety, Syngenta) and 0607A2 (MIR604eVent, Syngenta) were purchased from AOCS and used for fortification at 0.01 and 0.1% levels.

The canola and soybean samples (with the exception of DP305423 ground certified reference material) were ground with a Retsch model ZM100 Centrifugal Grinding Mill (Fischer Scientific, Ottawa, ON, Canada) using a 1.0 mm sieve. For 0.01% GE gravimetrically fortified samples, 0.01 g of GE powder sample was mixed with 99.99 g of non-GE powder sample, whereas for 0.1% fortified GE sample, 0.1 g of GE powder sample was mixed with 99.90 g of non-GE powder sample. The fortified powder samples were placed in 500 mL autoclaved Nalgene centrifuge tubes (Thermo Fisher Scientific, Ottawa, ON, Canada) and thoroughly mixed manually to maintain homogeneity. Subsamples of the ground materials from the same source were used by USDA/GIPSA and CGC laboratories for DNA extraction and PCR.

DNA Extraction and Quantification. For extraction of DNA from 0.1 and 0.2 g samples, a Fast ID Genomic DNA Extraction Kit (Genetic ID, Fairfield, IA, USA) was used following the manufacturer's recommendations. For soybean and maize, the procedure was slightly modified at CGC as the supernatant was not sufficient for the follow-up steps. A single 0.25 in. ceramic grinding ball (Qbiogen, Carlsbad, CA, USA) was added to each 2.0 mL centrifuge tube containing the sample, plus 1400 μL of lysis buffer, and the centrifuge tubes were pulverized in a mixer mill (Qiagen TissueLyser II, Toronto, ON, Canada) at 30 Hz for 60 s before incubation.

For extraction of DNA from 1 and 2 g samples, the CTAB DNA extraction method was followed.[8] Ten milliliters of extraction buffer was used for both 1 and 2 g samples. Before PCR assay, the DNA extracted with the CTAB-based method was purified with the DNA Clean & Concentrator 25 kit (Zymo Research, Cedarlane Laboratories, Ltd., Burlington, ON, Canada; and Zymo Research Corp., Irvine, CA, USA, for CGC and USDA/GIPSA laboratories, respectively).

DNA was quantified by fluorometry with a PicoGreen Assay Kit (Molecular Probes, Eugene, OR, USA) as recommended by the manufacturer. Assays were performed in 96-well fluorescence microtiter plates (Thermo Scientific, Waltham, MA, USA), and fluorescence was measured on a SpectraMax GeminiXS (MDS Analytical Technologies, formerly known as Molecular Devices, Toronto, ON, Canada). DNA samples used for a given PCR were quantified at the same time for all methods. The Abs260/280 and Abs260/230 ratios for the genomic DNA were determined with a SpectraMax Plus 384 (MDS Analytical Technologies, Sunnyvale, CA, USA) at the CGC. At the USDA/GIPSA, DNA was quantified using a fluorometric assay with a Luminometer 20/20 instrument (Turner Biosystems Inc., Sunnyvale, CA, USA) in conjunction with the Quant-iT PicoGreen (PG) assay kit (Molecular Probes). Stock DNA samples were diluted between 1:250 and 1:500 with 0.5× TE (Tris-EDTA) buffer to a target concentration of 20−200 pg/μL. The PG reagent was prepared according to the manufacturer's protocol; the diluted stock DNA test and reference samples were mixed 1:1 with PG reagent to a final volume of 200 μL to produce 1:500 to 1:1000 final dilutions and compared with fluorometric measurements from a standard curve. A calibration curve was generated from λ phage DNA, supplied by the manufacturer (Molecular Probes) at a stock concentration of 100 ng/μL and diluted to 250, 125, 62.5, 31.3, and 0.0 pg/μL with 0.5× TE buffer. Extracted DNA test samples were diluted to a working stock concentration of 20 ng/μL.

Polymerase Chain Reaction. For qualitative real-time PCR, the 25 μL volume contained 1× TaqMan Universal Master Mix, primers, probes, and 100 ng of genomic DNA. The DNA sequences and concentration of primers and probes used are provided in Table 1. Fortified reference DNA samples (0.01 and 0.1%), non-GE DNA, and no template controls were included for each PCR experiment. Both laboratories performed PCR in triplicate using an ABI 7500 real-time PCR system. The thermal profile for all events, except the OXY235 canola event consisted of initial holds for 2 min at 50 °C and for 6 min at 95 °C, followed by 45 cycles of 15 s at 95 °C and a 1 min annealing/extension step at 60 °C. For the OXY235 canola event, the thermal profile consisted of initial holds for 2 min at 50 °C and for 10 min at 95 °C, followed by 50 cycles of 15 s at 95 °C and 1 min annealing/extension step at 60 °C.

Statistical Analysis of Data. The data set of Ct values from real-time PCR was analyzed using SAS software (version 9.2 SAS Institute Inc., Cary, NC, USA). For purposes of ignoring distinction between grain types (i.e., maize, soybean, and canola) used in the study, the potential sources of variance in observed Ct values in the combined data set were composed of (1) laboratory differences (CGC vs USDA), (2) extraction method (CTAB vs Fast ID), (3) fortification level (0.1 vs 0.01% GM), (4) starting amount of sample (0.1 and 0.2 g with Fast ID vs 1 and 2 g with CTAB-Zymo), and (5) replication (×3) of Ct measurements within each level of sample amount. As distribution-fitting based on the small number of observations (n= 6) relevant to comparisons of interest would not be robust, the Wilcoxon nonparametric test was used as it does not make assumptions about the distribution of observed Ct values.[9] The Wilcoxon option was used with PROC NPAR1WAY[10] for making relative comparison of Ct values between groups. In addition to P values for Wilcoxon one-sided and two-sided two-group comparisons, analysis outputs included chi-square probabilities for the Kruskall−Wallis test, which were used to assess statistical difference between groups, as group comparisons did not assume matched pairs for observed Ct values.

RESULTS AND DISCUSSION

DNA Yield and Quality. DNA was extracted from finely ground canola, soybean, and maize samples to determine whether adequate amounts of intact DNA could be recovered and used to detect a low-level presence of GE traits by PCR. Highly variable DNA yields were obtained and verified by both the CGC and USDA/GIPSA laboratories for the Fast ID and CTAB-based DNA extraction methods (Table 2). CGC generally recovered greater amounts of DNA that ranged from 1.6 ± 0.3 to 182.9 ± 2.2 μg, whereas USDA/GIPSA generally recovered lesser amounts of DNA that ranged from 1.1 ± 0.2 to 84.0 ± 5.8 μg. Additionally, the data revealed that in most cases the Fast ID kit provided greater quantities of recovered DNA when using larger amounts of finely ground starting material

Table 1. Primer and Probe DNA Sequences and Concentrations Used for Qualitative Real-Time PCR Assays

primer name	crop and event	sequence (5′−3′)	primer/probe concn (nM)	amplicon size (bp)	ref
MDB685-F	canola (HCN92)	GTT GCG GTT CTG TCA GTT CC	400	95	19
KVM180-R		CGA CCG GCG CTG ATA TAT GA	400		
TM 029 Taqman probe		FAM-TCC CGC GTC ATC GGC GG-TAMRA	200		
OXYRG	canola (OXY235)	GAT AGA TGG TGG TGT GAG TCT TGT	300	124	20
OXYRV		CCT AAC TTT TGG TGT GAT GAT GCT	300		
OXYRP- probe		6-FAM-TGC CAT CAG CTG ACA CGC CGT GC-TAMRA	150		
MDB510-F	canola (CruA)	GGC CAG GGT TTC CGT GAT	200	101	19
MDB 511-R		CCG TCG TTG TAG AAC CAT TGG	200		
TM 003 Taqman Probe		VIC-AGT CCT TAT GTG CTC CAC TTT CTG GTG CA 3′-TAMRA	200		
DP-305-F1	soybean (DP305423)	CGT GTT CTC TTT TTG GCT AGC	800	93	21
DP-305-R5		GTG ACC AAT GAA TAC ATA ACA CAA ACT A	500		
DP-305 probe		6-FAM-TGA CAC AAA TGA TTT TCA TAC AAA AGT CGA GA-TAMRA	220		
KVM175	soybean (A2704-12)	GCA AAA AAG CGG TTA GCT CCT	400	64	22
SMO001		ATT CAG GCT GCG CAA CTG TT	400		
TM031 TaqMan probe		6-FAM-CGG TCC TCC GAT CGC CCT TCC-TAMRA	200		
Lec for2	soybean (lectin)	CCA GCT TCG CCG CTT CCT TC	550	74	21
GMO3-126 Rev		GAA GGC AAG CCC ATC TGC AAG CC	550		
Lec TaqMan probe		6-FAM-CTT CAC CTT CTA TGC CCC TGA CAC-TAMRA	100		
MIR604 primer F	maize (MIR604)	GCG CAC GCA ATT CAA CAG	600	76	23
MIR604 primer R		GGT CAT AAC GTG ACT CCC TTA ATT CT	300		
MIR604 TaqMan probe		FAM-AGG CGG GAA ACG ACA ATC TGA TCA TG-TAMRA	200		
Zm *Adh*1 primer F	maize (Adh1)	CGT CGT TTC CCA TCT CTT CCT CC	300	135	23
Zm *Adh*1 primer R		CCA CTC CGA GAC CCT CAG TC	300		
Zm *Adh*1 TaqMan probe		VIC-AAT CAG GGC TCA TTT TCT CGC TCC TCA-TAMRA	200		

Table 2. Summary of Average DNA Yield for Fast ID and CTAB-Based DNA Extraction Methods[a]

	average DNA yield (μg)					
	DNA extraction		0.01%		0.1%	
trait	amount (g)	method	CGC	GIPSA	CGC	GIPSA
OXY235 canola	0.1	Fast ID	3.9 ± 1.1	1.3 ± 0.0	3.2 ± 0.7	1.1 ± 0.2
	0.2	Fast ID	8.2 ± 3.1	1.9 ± 0.1	9.0 ± 2.2	1.6 ± 0.1
	1.0	CTAB	81.3 ± 9.4	13.1 ± 1.4	104.5 ± 8.0	12.9 ± 1.6
	2.0	CTAB	182.9 ± 2.2	9.1 ± 2.2	164.9 ± 17.6	8.6 ± 3.4
HCN92 canola	0.1	Fast ID	3.1 ± 0.9	1.5 ± 0.1	1.6 ± 0.3	1.4 ± 0.0
	0.2	Fast ID	5.9 ± 1.8	2.3 ± 0.3	2.0 ± 0.1	1.7 ± 0.1
	1.0	CTAB	48.9 ± 1.3	8.6 ± 1.0	55.6 ± 15.4	7.2 ± 2.6
	2.0	CTAB	166.9 ± 19.7	10.8 ± 0.9	170.6 ± 6.8	10.1 ± 0.7
DP305423 soybean	0.1	Fast ID	5.2 ± 0.3	2.1 ± 0.6	6.0 ± 2.1	1.8 ± 0.2
	0.2	Fast ID	6.2 ± 0.5	3.5 ± 0.4	4.1 ± 0.4	3.4 ± 0.3
	1.0	CTAB	75.5 ± 5.9	12.6 ± 1.8	54.6 ± 29.5	13.5 ± 2.5
	2.0	CTAB	90.3 ± 10	85.5 ± 4.2	76.8 ± 16.5	74.0 ± 6.9
A2704-12 soybean	0.1	Fast ID	9.1 ± 0.2	2.0 ± 0.6	10.2 ± 1.6	1.6 ± 0.2
	0.2	Fast ID	9.3 ± 1.7	3.1 ± 1.2	7.7 ± 0.9	3.1 ± 0.3
	1.0	CTAB	49.4 ± 3.3	14.1 ± 1.5	64.9 ± 0.4	14.2 ± 0.5
	2.0	CTAB	54.9 ± 25.3	70.2 ± 23.4	73.0 ± 1.4	84.0 ± 5.8
MIR604 maize	0.1	Fast ID	3.9 ± 0.8	2.7 ± 0.4	4.6 ± 1.6	3.0 ± 0.2
	0.2	Fast ID	7.8 ± 3.3	4.2 ± 0.5	4.0 ± 2.7	4.4 ± 0.5
	1.0	CTAB	24.2 ± 1.4	18.2 ± 1.6	24.5 ± 0.7	18.6 ± 0.9
	2.0	CTAB	56.5 ± 0.4	48.1 ± 3.4	58.3 ± 3.3	50.2 ± 3.8

[a]The ± values are average of two DNA extractions. Fast ID, Fast ID DNA extraction method; CTAB, CTAB-based DNA extraction method (before Zymo purification of the DNA).

(Fast ID comparison of 0.1 vs 0.2 g). Similar observations were seen with the CTAB extraction method (comparison of 1.0 vs 2.0 g). Atypical quantities of recovered DNA were generated by CGC on the two soybean samples and the single maize sample using Fast ID kits. For CGC, consistently higher canola, soybean, and maize DNA yields were obtained for the Fast ID method

Table 3. Abs260/280 and Abs260/230 Ratios (CGC Laboratory) for Samples Fortified with GE Traits Obtained from Two DNA Extraction Methods

trait	DNA extraction method	fortification level (%)	average absorbance ratios for 260/280	260/230
OXY235 canola	Fast ID	0.01	1.77	0.55
	CTAB	0.01	1.87	2.03
	Fast ID	0.1	1.75	0.60
	CTAB	0.1	1.93	2.39
HCN92 canola	Fast ID	0.01	1.73	0.27
	CTAB	0.01	1.77	1.64
	Fast ID	0.1	1.47	0.48
	CTAB	0.1	1.92	1.83
A2704 soybean	Fast ID	0.01	1.90	1.20
	CTAB	0.01	1.90	2.20
	Fast ID	0.1	1.88	1.15
	CTAB	0.1	1.90	2.00
DP305423 soybean	Fast ID	0.01	1.84	0.40
	CTAB	0.01	1.93	2.13
	Fast ID	0.1	1.86	0.60
	CTAB	0.1	1.92	2.25
MIR604 maize	Fast ID	0.01	1.83	0.45
	CTAB	0.01	1.80	1.60
	Fast ID	0.1	1.93	0.40
	CTAB	0.1	1.83	1.50

compared with USDA/GIPSA with the exception of 0.2 g maize sample fortified at 0.1%. The likely explanation for this observation could be that the CGC extraction method included a ceramic grinding ball in the centrifuge tube containing buffer and pulverization with the Mixer Mill for soybean and maize, which created a finer particle size thereby leading to a higher extraction efficiency (see Materials and Methods). With the Fast ID DNA extraction method, the DNA yield ranged from 1.1 ± 0.2 to 10.2 ± 1.6 μg. Six hundred nanograms of DNA was sufficient to carry out the experiments in triplicate for both the transgene and the endogenous control.

As predicted, much higher yields of DNA were obtained with the large scale CTAB-based extraction method (1.0/2.0 g sample) compared with the small-scale Fast ID extraction method (0.1/0.2 g sample (Table 2)). Interestingly, there were large differences in DNA yields between CGC and USDA/GIPSA laboratories using the CTAB extraction method. The CTAB protocol used by the two laboratories had some differences that might explain these observations. The USDA/GIPSA protocol excluded the reducing agent, β-mercaptoethanol, with their CTAB method during steps that required chloroform/isoamyl alcohol extractions. For the CGC, β-mercaptoethanol (0.01 M), phenol/chloroform/isoamyl alcohol 25:24:1 (1×) and chloroform/isoamyl alcohol 24:1 (2×) were used in the extraction steps. Modification of the DNA extraction protocol may have partially contributed to the variation in total canola DNA yield, even though the soybean and maize DNA yields were not affected as much. Because DNA yield extracted from the same amount of starting material provided significant variability, the use of equivalent amounts of DNA in the PCR was critical.

Table 4. Summary of Average Threshold Cycle (Ct) Values Obtained[a]

trait	DNA extraction amount (g)	DNA extraction method	average Ct values, target gene 0.01% CGC	0.01% GIPSA	0.1% CGC	0.1% GIPSA
OXY235 canola	0.1	Fast ID	37.85 ± 0.64	38.92 ± 0.76	33.23 ± 0.90	33.37 ± 0.48
	0.2	Fast ID	37.73 ± 1.09	37.80 ± 1.54	33.22 ± 0.30	32.89 ± 0.16
	1.0	CTAB	37.21 ± 1.00	38.85 ± 0.59	32.40 ± 0.37	34.15 ± 0.11
	2.0	CTAB	36.94 ± 0.99	38.36 ± 1.70	32.82 ± 0.35	34.02 ± 0.14
HCN92 canola	0.1	Fast ID	40.20 ± 1.41	38.32 ± 1.27	33.97 ± 0.40	34.22 ± 0.49
	0.2	Fast ID	36.33 ± 1.39	38.05 ± 1.17	34.58 ± 0.36	33.90 ± 0.17
	1.0	CTAB	38.69 ± 0.67	38.94 ± 0.84	34.23 ± 0.47	35.69 ± 0.48
	2.0	CTAB	38.09 ± 0.45	38.52 ± 0.92	34.68 ± 0.36	36.12 ± 0.34
DP305423 soybean	0.1	Fast ID	38.00 ± 0.83	36.95 ± 0.87	33.31 ± 0.25	33.13 ± 0.67
	0.2	Fast ID	36.97 ± 0.90	36.08 ± 0.19	33.40 ± 0.20	32.84 ± 0.18
	1.0	CTAB	35.87 ± 0.57	37.22 ± 0.57	32.36 ± 0.15	33.95 ± 0.24
	2.0	CTAB	36.05 ± 0.40	36.95 ± 0.31	33.11 ± 0.27	33.66 ± 0.17
A2704-12 soybean	0.1	Fast ID	36.10 ± 0.39	33.95 ± 0.41	32.41 ± 0.26	30.41 ± 0.24
	0.2	Fast ID	34.15 ± 0.73	34.43 ± 0.50	31.42 ± 0.33	30.20 ± 0.07
	1.0	CTAB	35.21 ± 0.52	34.62 ± 0.51	31.04 ± 0.40	30.53 ± 0.30
	2.0	CTAB	34.90 ± 0.79	34.28 ± 0.30	31.35 ± 0.60	31.36 ± 0.21
MIR604 maize[b]	0.1	Fast ID	38.70 ± 0.95 (83%)	38.51 ± 0.20 (50%)	36.20 ± 0.72	36.14 ± 0.36
	0.2	Fast ID	38.69 ± 0.77 (67%)	39.82 ± 1.35 (67%)	35.91 ± 0.91	35.77 ± 0.23
	1.0	CTAB	37.93 ± 0.51	38.57 ± 0.67 (67%)	34.93 ± 0.19	35.79 ± 0.57
	2.0	CTAB	38.54 ± 0.65 (83%)	38.91 ± 0.69 (67%)	35.83 ± 0.42	35.43 ± 0.40

[a]The ± standard deviation values are for 6 PCR results (2 DNA extractions × 3 PCRs). Fast ID, Fast ID DNA extraction; CTAB, CTAB DNA extraction. [b]The values in parentheses indicate the percentage detected of six samples (e.g., 83% indicates that five of the six PCR samples produced detectable PCR signal and one sample did not produce detectable signal; the Ct values are the averages of detectable signals).

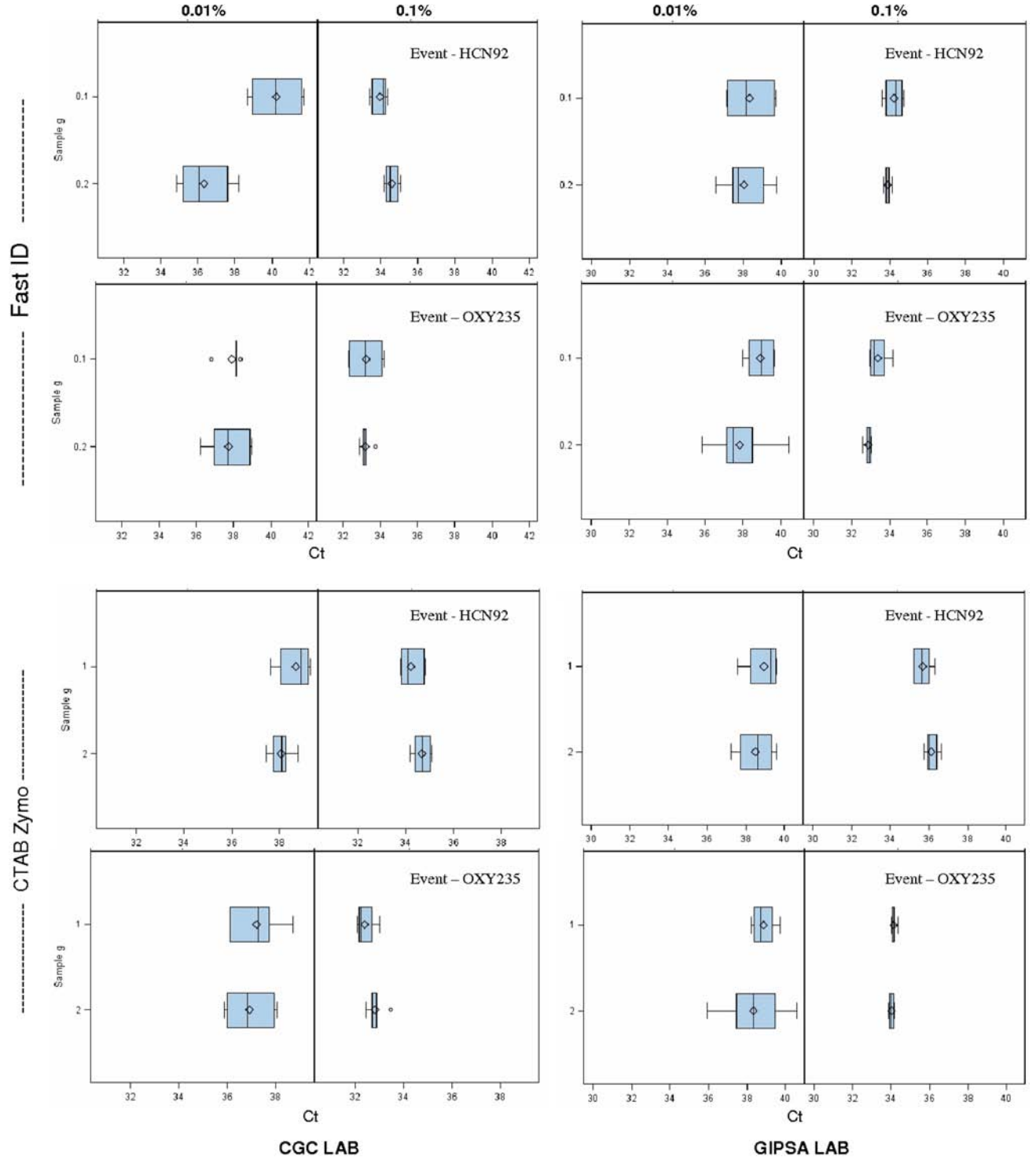

Figure 1. Distribution of Ct values from detection of two GM events in canola (HCN92 and OXY235) fortified at two levels (0.1 and 0.01% w/w), based on two DNA extraction methods (Fast ID and CTAB) conducted at two laboratories (CGC and USDA/GIPSA).

Both laboratories used a constant mass of 100 ng of DNA quantified with a PicoGreen assay for the PCR.

The Abs260/280 and Abs260/230 ratios of different DNA extractions were determined at the CGC. Most of the CTAB and Fast ID extracted DNA had relatively high Abs260/280 ratios indicative of suitable DNA quality for PCR (Table 3). The DNA extracted with the Fast ID method had low Abs260/230 values indicating the possible presence of contaminants that absorb at 230 nm. Low Abs260/230 ratios have been observed in DNA extractions using the Fast ID method on samples of canola, flax, and soybean even though this did not appear to affect PCR amplification.[11] Purification of 20 μg of CTAB DNA using a DNA Clean & Concentrator 25 kit (Zymo Research, Cedarlane Laboratories Ltd., Bulington, ON, Canada) from four canola, four soybean, and two maize samples was performed to determine the percentage of recovery at the CGC. Average DNA recoveries of 47, 74, and 80% were obtained for soybean, canola, and maize, respectively. The purification step

dx.doi.org/10.1021/jf500610w | J. Agric. Food Chem. 2014, 62, 4349−4358

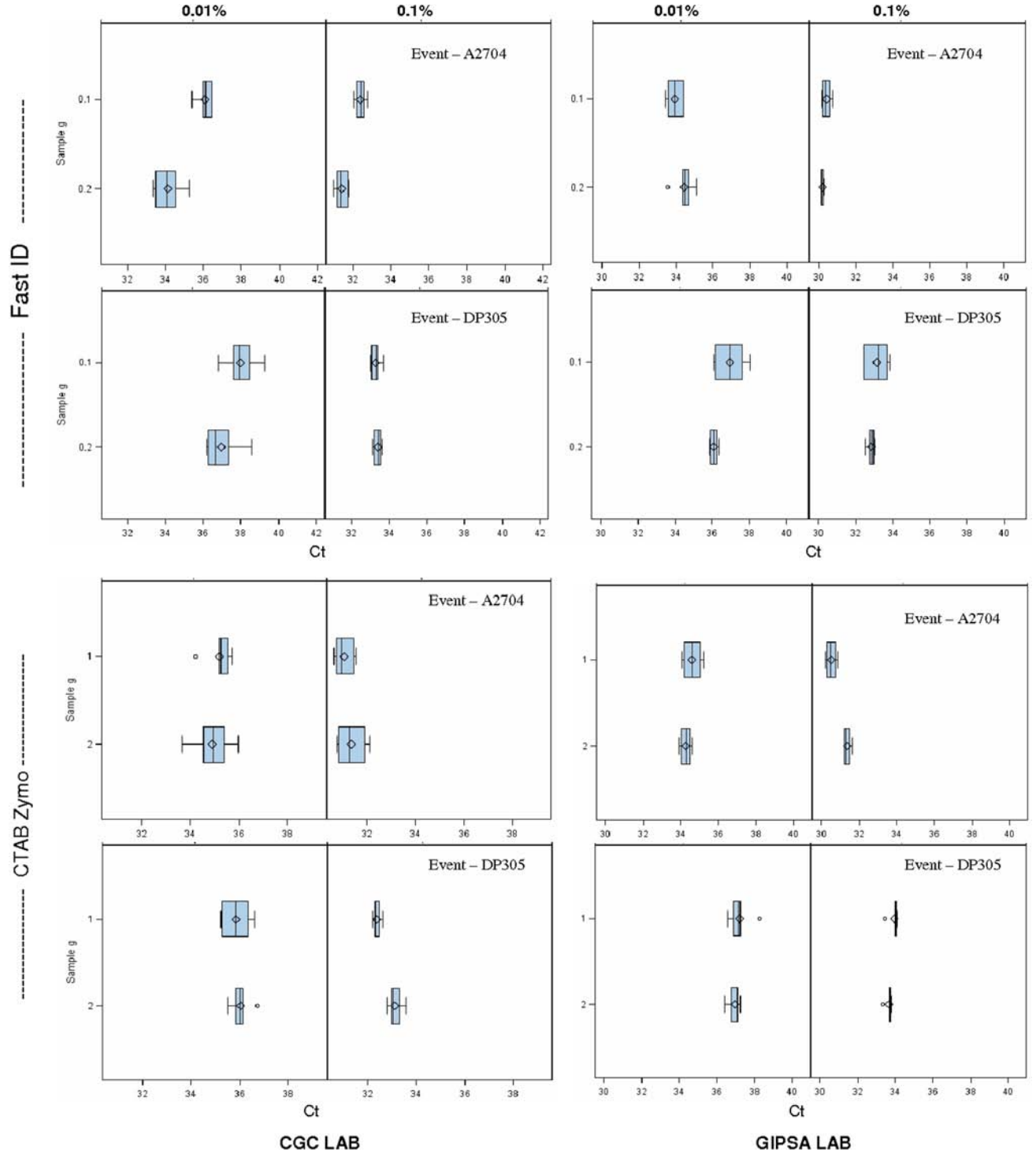

Figure 2. Distribution of Ct values from detection of two GM events in soybean (A2704 and DP305) fortified at two levels (0.1 and 0.01% w/w), based on two DNA extraction methods (Fast ID and CTAB) conducted at two laboratories (CGC and USDA/GIPSA).

used for CTAB-extracted DNA may have also contributed to the variation in DNA yield.

Small-Scale versus Large-Scale DNA Extractions for the Detection of LLP of GE Events. Comparable PCR results (in terms of Ct values) were obtained from DNA extracts using small-scale (Fast ID) and large-scale (CTAB) extraction methods. Higher Ct values were obtained for 0.01% fortified samples compared with 0.1% fortified samples as expected (Table 4). However, there was more variability among the Ct values generated by PCR for the 0.01% fortified samples (Figures 1−3). In general, detection of a low-level presence of GE events, such as 0.01% (1 in 10000), is relatively more challenging as the error rate due to DNA dilution, pipeting, etc., is amplified.[12]

For the 0.01% fortified samples and Fast ID extraction method, 0.2 g extraction samples had relatively lower Ct values (indicating a greater chance of detection) than 0.1 g extraction samples for HCN92 canola, DP305423 soybean, and A2704 soybean GE events (CGC; Table 4; Figures 1 and 2).

dx.doi.org/10.1021/jf500610w | J. Agric. Food Chem. 2014, 62, 4349−4358

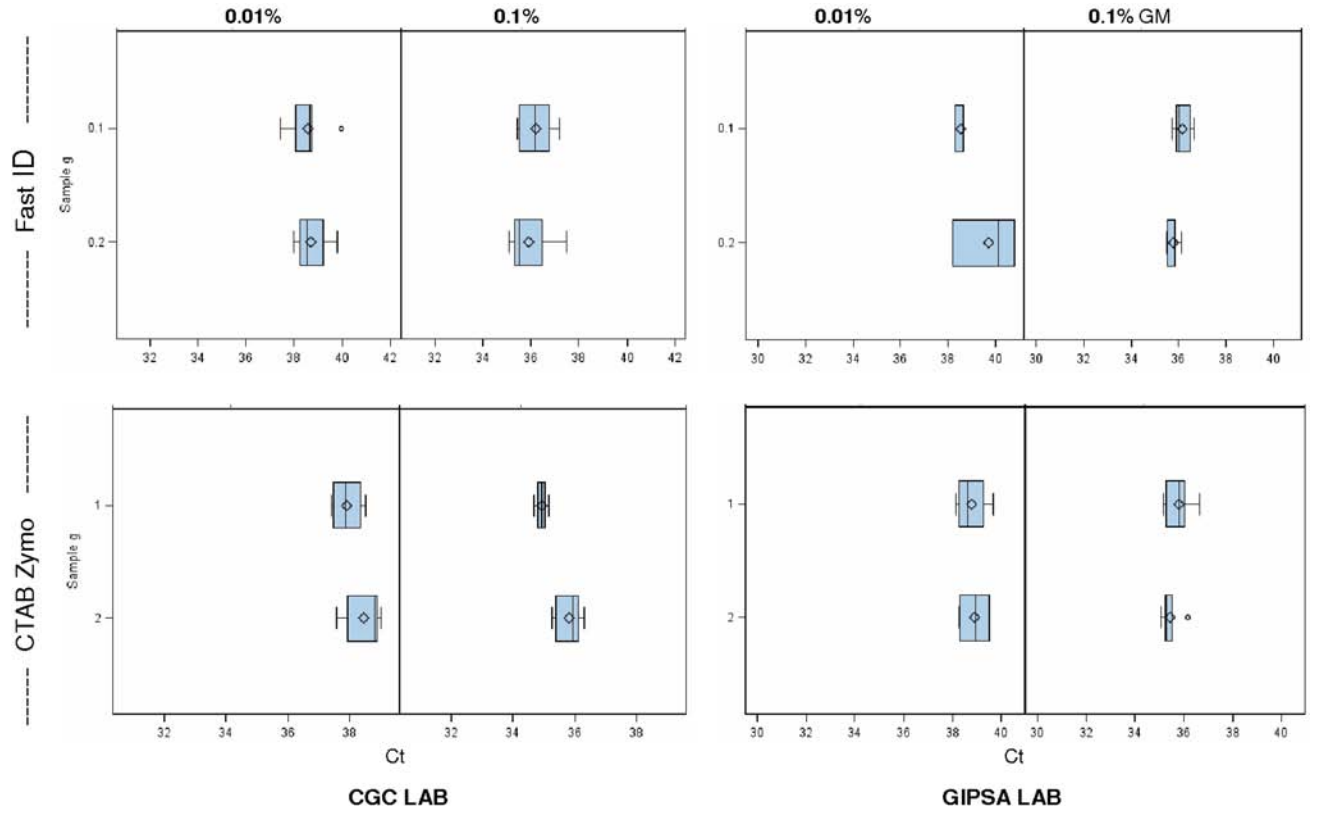

Figure 3. Distribution of Ct values from detection of GM event (MIR604) in maize fortified at two levels (0.1 and 0.01% w/w), based on two DNA extraction methods (Fast ID and CTAB) conducted at two laboratories (CGC and USDA/GIPSA).

On the basis of these data, improvement in the detection of the low-level presence of GE events may not necessarily be achieved as a result of using large-scale DNA extraction methods such as CTAB. The use of small-scale DNA extraction methods saves time and money. For the small-scale extraction method, sufficient amounts of DNA were achieved for replicate PCR and repeatable Ct values were obtained, especially for 0.1% fortified samples. Holden et al. suggested that samples prepared at the 0.1% fortification level can generate false-negative results when certain detergent-based DNA isolation methods are used.[13] The bulk of the false-negative results were attributed to the presence of inhibitors that inactivate Taq DNA polymerase in the PCR.

For the MIR604 maize event, repeatable and consistent detection by PCR was not achieved at the 0.01% fortification level regardless of the extraction method or the amount of starting material used under the conditions of this study design. In addition, significant variability was observed, including false-negative results, between the two DNA extraction methods as well as within replicates for the Ct values obtained (Table 4). The MIR604 heterozygous reference maize purchased from AOCS was reported to have a purity of 99.98%; thus, this may have also affected the fortification and in turn the detection of the MIR604 maize event at 0.01% level. Haploid genome weight for *Brassica napus* (canola), maize, and soybean has been reported to be 1.13 pg,[15] 2.3 pg,[16] and 1.12 pg,[17] respectively. On the basis of the described genome weights, 100 ng of DNA spiked at the 0.01% level will have approximately nine copies of OXY235 canola and DP305423 soybean and four copies of maize. Thus, the chance of detection of GE canola and soybean samples at low levels is higher than that of GE maize samples. This may potentially explain why we could not reliably detect 0.01% MIR604 maize samples.

In a collaborative trial validation study, 100% detection of 0.02% LLRice62 and MS8 canola (45 samples for each event were correctly identified) was reported.[14] For homogeneously prepared samples, GE trait testing laboratories can detect low concentration levels of GE events. Genetically engineered grains/seeds are not homogeneously distributed in a grain lot.[6,18] Thus, sampling is more of a challenge compared to detection of the GE traits using PCR.

Results of Statistical Analysis. With respect to statistical difference in Ct values between extraction sample amounts within Fast ID (0.1 vs 0.2 g) and CTAB (1 vs 2 g), OXY235 canola samples showed no difference for both methods, at both fortification levels and across both the CGC and USDA/GIPSA laboratories; the only exception was the 0.1% Fast ID method for the USDA/GIPSA laboratory (Table 5). For HCN92 canola, CGC results showed statistical differences for Fast ID extractions at both 0.1 and 0.01% fortifications, but no differences were seen in USDA/GIPSA results. With MIR604 maize, CGC results showed differences for CTAB extractions at the 0.1% fortification. Similar results were seen for A2704 soybean and DP305423 soybean, where one laboratory may see statistical difference but results from the other laboratory showed no difference. Although the majority of comparisons across the 0.1 and 0.01% fortification levels in both laboratories showed no statistical difference within Fast ID (0.1 and 0.2 g) and CTAB (1 and 2 g) DNA extraction methods for observed Ct values, variability for reproducibility of respective Ct values may be significant for some traits with respect to combinations of fortification level, DNA extraction method, and amount of extraction sample.

Table 5. Probability of Statistical Difference in Observed Ct Values within Fast ID (0.1 vs 0.2 g Samples) and CTAB (1 vs 2 g Samples) DNA Extraction Methods at 0.1 and 0.01% Fortification Levels Conducted at Two Laboratories (Kruskall–Wallis Test)

			CGC laboratory		GIPSA laboratory	
trait	fortification level (%)	DNA extraction method	chi-square	Pr > chi-square[a]	chi-square	Pr > chi-square[a]
OXY235 canola	0.10	Fast ID	0.0000	1.0000	4.3485	0.0370
		CTAB	3.4029	0.0651	2.3222	0.1275
	0.01	Fast ID	0.1333	0.7150	2.0769	0.1495
		CTAB	0.1026	0.7488	0.2308	0.6310
HCN92 canola	0.10	Fast ID	5.0256	0.0250	0.8333	0.3613
		CTAB	2.5641	0.1093	1.6468	0.1994
	0.01	Fast ID	7.5000	0.0062	0.0256	0.8728
		CTAB	2.0842	0.1488	0.6410	0.4233
A2704 soybean	0.10	Fast ID	8.3077	0.0039	3.1466	0.0761
		CTAB	1.8591	0.1727	5.3330	0.0209
	0.01	Fast ID	8.3077	0.0039	2.0842	0.1488
		CTAB	0.6410	0.4233	0.7500	0.3865
DP305423 soybean	0.10	Fast ID	0.6410	0.4233	0.0581	0.8095
		CTAB	8.3077	0.0039	4.3485	0.0370
	0.01	Fast ID	3.1026	0.0782	3.6923	0.0547
		CTAB	0.4103	0.5218	0.6433	0.4225
MIR604 maize	0.10	Fast ID	1.2564	0.2623	3.6923	0.0547
		CTAB	8.3368	0.0039	0.9231	0.3367
	0.01	Fast ID	0.0600	0.8065	0.4286	0.5127
		CTAB	2.7000	0.1003	0.0000	1.0000

[a]Difference within DNA extraction methods for each % GM fortification levels are deemed statistically significant where Pr > chi-square is ≤0.05 for 95% confidence.

Table 6. Probability of Statistical Difference between Fast ID and CTAB DNA Extraction Methods for Observed Ct Values from Real-Time PCR for 0.1 and 0.01% Fortification Levels with Five Traits Conducted at Two Labs (Kruskall–Wallis Test)

		CGC laboratory		GIPSA laboratory	
trait	fortification level (%)	chi-square	Pr > chi-square[a]	chi-square	Pr > chi-square[a]
OXY235 canola	0.10	6.166	0.0130	13.4584	0.0002
	0.01	3.8788	0.0489	0.2409	0.6235
HCN92 canola	0.10	0.7507	0.3863	16.5082	<0.0001
	0.01	0.1857	0.6665	1.1413	0.2854
A2704 soybean	0.10	7.5274	0.0061	8.6212	0.0033
	0.01	0.3333	0.5637	1.0067	0.3157
DP305423 soybean	0.10	10.0833	0.0015	12.0157	0.0005
	0.01	13.6533	0.0002	5.0722	0.0243
MIR604 maize	0.10	5.0744	0.0243	3.1022	0.0782
	0.01	1.2136	0.2706	0.1503	0.6982

[a]Difference within DNA extraction methods for each %GM fortification level is deemed statistically significant where Pr > chi-square is ≤0.05 for 95% confidence.

In terms of comparing DNA extraction methods (Fast ID vs CTAB) for statistical difference in Ct values across fortification levels, differences in results between laboratories were found (Table 6). Only DP305423 soybean showed statistical difference between Fast ID and CTAB for both 0.1 and 0.01% fortification levels across both CGC and USDA/GIPSA laboratories. For MIR604 maize only CGC results showed statistical differences between extraction methods at 0.1% fortification, whereas for HCN92 canola only USDA/GIPSA results showed statistical differences at the 0.1% fortification level. Both laboratories found statistical differences between extraction methods for A2704 soybean fortified at the 0.1% level. Comparisons for OXY235 canola showed statistical differences for both fortification levels in CGC results, whereas USDA/GIPSA results showed differences only for the 0.1% fortification level. For these comparisons, however, Ct results

were aggregated across sample extraction amounts, and variance in Ct values due to different amounts of starting material used within each extraction method likely contributed to the observed variance between laboratories.

Summary. In this study, the influence of starting material on the detection of low-level presence of GE traits was investigated using five GE events (two events each for canola and soybean and one event for maize). Higher DNA yields were obtained with the larger scale DNA extraction method (1.0 and 2.0 g samples) compared to the smaller scale DNA extraction method (0.1 and 0.2 g samples). There was variability in the DNA yield obtained between the CGC and USDA/GIPSA laboratories involved in this study, especially for the large-scale DNA extraction method. CTAB-extracted DNA that was further purified on a DNA Clean & Concentrator Kit had greater purity (based on Abs260/280 and Abs260/230 ratios) compared with the Fast ID extracted DNA. When the large-scale CTAB DNA extraction method (1.0 and 2.0 g samples) was compared with a small-scale Fast ID DNA extraction method (0.1 and 0.2 g samples), the data did not reveal differences in terms of detection by PCR for four of the five GE events studied at 0.1 and 0.01% fortification levels. Overall, reliable detection of the GE events was achieved at the 0.1% level. Reliable detection at the 0.01% fortification level was achieved for the four canola and soybean GE traits, but not as reliably for the MIR604 maize GE trait. The 0.01% 100 ng maize DNA has a low MIR604 copy number, which may have resulted in unreliable detection. There was more variability in Ct values generated by the duplicate DNA extractions for the 0.01% fortified samples using 0.1 g of starting material. Thus, detection of samples at this fortification level using only 0.1 g of starting material could potentially produce false-negative results in maize but not in soybean or canola. In general, a kit-based DNA extraction method (using 0.1 and 0.2 g of sample) can be used instead of the large-scale CTAB DNA extraction method for the detection of low levels of GE events in ground grain samples, which could save time and cost.

AUTHOR INFORMATION

Corresponding Author

*(T.D.) Phone: (204) 984-4582. Fax: (204) 983-0724. E-mail: tigst.demeke@grainscanada.gc.ca.

Notes

[‖]Paper No. 1076 of the Grain Research Laboratory, Canadian Grain Commission.

The authors declare no competing financial interest.

ACKNOWLEDGMENTS

Paul Wacker is acknowledged for help in carrying out the experiments at USDA/GIPSA. Stefan Wagener (Canadian Grain Commission, Grain Research Laboratory) is acknowledged for reviewing the manuscript.

ABBREVIATIONS USED

Ct, cycle threshold value; CGC, Canadian Grain Commission; CTAB, cetylmethyl-ammonium bromide; GE, genetically engineered; SDS, sodium dodecyl sulfate; USDA/GIPSA, U.S. Department of Agriculture, Grain Inspection, Packers and Stockyards Administration

REFERENCES

(1) Demeke, T.; Perry, D. J.; Scowcroft, W. R. Adventitious presence of GMOs: scientific overview for Canadian grains. *Can. J. Plant Sci.* **2006**, *86*, 1−23.

(2) Grohmann, L.; Busch, U.; Pecoraro, S.; Hess, N.; Pietsch, K.; Mankertz, J. Collaborative trail validation of a construct-specific real-time PCR method for detection of genetically modified linseed event 'CDC Triffid' FP967. *Eur. Food Res. Technol.* **2011**, *232*, 557−561.

(3) Davison, J. GM plants: science, politics and EC regulations. *Plant Sci.* **2010**, *178*, 94−98.

(4) EU Commission Regulation No. 619/2011. Laying down the methods of sampling and analysis for the official control of feed as regards presence of genetically modified material for which an authorization procedure is pending or the authorization of which has expired. *Off. J. Eur. Union* **2011** (June 24), L166/9−L1669/15.

(5) Nakamura, K.; Akiyama, H.; Yamada, C.; Satoh, R.; Nakiyama, D.; Sakata, K.; Kawakami, H.; Mano, J.; Kitta, K.; Teshima, R. Novel method to detect a construct-specific sequence of the acetolactate synthase gene in genetically-modified flax CDC Triffid (FP967). *Biol. Pharm. Bull.* **2010**, *33*, 532−534.

(6) Lipp, M.; Shillito, R.; Giroux, R.; Spiegelhalter, F.; Charlton, S.; Pinero, D.; Song, P. Polymerase chain reaction technology as analytical tool in agricultural biotechnology. *J. Agric. Food Chem.* **2005**, *88*, 136−155.

(7) Waiblinger, H.-U.; Graf, N.; Broll, H.; Grohmann, L.; Pietsch, K. Evaluation of real-time PCR results at the limit of detection. *J. Verbr. Lebensm.* **2011**, *6*, 411−417.

(8) Demeke, T.; Ratnayaka, I.; Phan, A. Effects of DNA extraction and purification methods on real-time quantitative PCR analysis of Roundup Ready soybean. *J. AOAC Int.* **2009**, *92*, 1136−1144.

(9) Juan, J. S.; Reed, A.; Chen, F.; Stewart, C. C., Jr. Statistical analysis of real-time PCR data. *BMC Bioinformatics* **2006**, *7*, 85; http://www.biomedcentral.com/1471-2105/7/85 (accessed January 24, 2014).

(10) SAS Institute. *SAS/STAT(R) 9.2 User's Guide*, 2nd ed., release 9.2; SAS Institute Inc.: Cary, NC, USA, 2013; http://support.sas.com/documentation/cdl/en/statug/63033/HTML/default/viewer.htm#statug_npar1way_sect004.htm (accessed January 24, 2014).

(11) Demeke, T.; Ratnayaka, I.; Holigroski, M.; Phan, A. Assessment of DNA extraction methods for PCR testing of discontinued or unapproved biotech events in single seeds of canola, flax and soybean. *Food Control* **2012**, *24*, 44−49.

(12) Booker, H. M.; Lamb, E. G. Quantification of low-level GM seed presence in Canadian commercial flax stocks. *AgBioForum* **2012**, *15*, 31−35.

(13) Holden, M. J.; Blasic, J. R.; Bussjaeger, L.; Kao, C.; Shokere, L. A.; Kendall, D. C.; Freese, L.; Jenkins, G. R. Evaluation of extraction methodologies for corn kernel (*Zea mays*) DNA for detection of trace amounts of biotechnology-derived DNA. *J. Agric. Food Chem.* **2003**, *51*, 2468−2474.

(14) Grohmann, L.; Brünen-Nieweler, C.; Nemeth, A.; Waiblinger, H.-U. Collaborative trial validation studies of real-time PCR-based GMO screening methods for detection of the *bar* Gene and the *ctp2-cp4epsps* construct. *J. Agric. Food Chem.* **2009**, *57*, 8913−8920.

(15) Johnston, J. S.; Pepper, A. E.; Hall, A. E.; Chen, Z. J.; Hodnett, G.; Drabek, J.; Lopez, R.; Price, H. J. Evolution of genome size in Brassicaceae. *Ann. Bot.* **2005**, *95*, 229−235.

(16) Schnable, P. S.; Ware, D.; Fulton, R. S.; Stein, J. C.; Wei, F.; Pasternak, S.; Liang, C.; Zhang, J.; Fulton, L.; Graves, T. A.; et al. The B73 maize genome: complexity, diversity, and dynamics. *Science* **2009**, *326*, 1112−1115.

(17) Arumuganthan, K.; Earle, E. D. Nuclear DNA content of some important plant species. *Plant Mol. Biol. Rep.* **1991**, *93*, 208−218.

(18) Paoletti, C.; Heissenberger, A.; Mazarra, M.; Larcher, S.; Grazioli, E.; Corbisier, P.; Hess, N.; Berben, G.; Lübeck, P. S.; De Loose, M.; Moran, G.; Henry, C.; Brera, C.; Folch, I.; Ovesna, J.; Van den Eede, G. Kernel lot distribution assessment (KeLDA): a study on the distribution of GMO in large soybean shipments. *Eur. Food Res. Technol.* **2006**, *224*, 129−139.

(19) EURL GMFF (European Union Reference Laboratory for Genetically Modified Food and Feed (2011). Event-specific method for the quantification of oilseed rape Topas 19/2using real-time PCR; http://gmo-crl.jrc.ec.europa.eu/summaries/CRLVL1204%20VP.pdf (accessed January 24, 2014).
(20) Wu, G.; Wu, Y.; Xiao, L.; Lu, C. Event-specific qualitative and quantitative PCR methods for the detection of genetically modified rapeseed Oxy-235. *Transgenic Res.* **2008**, *17*, 851−862.
(21) EURL GMFF (European Union Reference Laboratory for Genetically Modified Food and Feed (2009). Event-specific method for the quantification of soybean event DP-305423-1 using real-time PCR; http://gmo-crl.jrc.ec.europa.eu/summaries/CRLVL0707VP%20Corr2%20EURL%20web.pdf (accessed January 24, 2014).
(22) EURL GMFF (European Union Reference Laboratory for Genetically Modified Food and Feed (2009). Event-specific method for the quantification of soybean line A2704−12 using real-time PCR; http://gmo-crl.jrc.ec.europa.eu/summaries/A2704-12_soybean_validated_Method.pdf (accessed January 24, 2014).
(23) EURL GMFF (European Union Reference Laboratory for Genetically Modified Food and Feed (2009). Event-specific method for the quantification of maize line MIR604 using real-time PCR; http://gmo-crl.jrc.ec.europa.eu/summaries/MIR604_validated_Method_correctedversion1.pdf (accessed January 24, 2014).

JOURNAL OF AGRICULTURAL AND FOOD CHEMISTRY

Article

pubs.acs.org/JAFC

Effects of Soluble and Insoluble Fractions from Bilberries, Black Currants, and Raspberries on Short-Chain Fatty Acid Formation, Anthocyanin Excretion, and Cholesterol in Rats

Greta Jakobsdottir,*[,†] Ulf Nilsson,[†] Narda Blanco,[‡] Olov Sterner,[‡] and Margareta Nyman[†]

[†]Applied Nutrition and Food Chemistry, Department of Food Technology, Engineering and Nutrition, Kemicentrum, Lund University, P.O. Box 124, SE-221 00 Lund, Sweden

[‡]Centre for Analysis and Synthesis, Department of Chemistry, Kemicentrum, Lund University, P.O. Box 124, SE-221 00 Lund, Sweden

Supporting Information

ABSTRACT: Dietary fiber and flavonoids, important components in berries, are suggested to improve metabolic health. This study investigates whether soluble and insoluble fractions isolated from bilberry, black currant, and raspberry affect the formation of short-chain fatty acids (SCFAs), uptake and excretion of flavonoids, and levels of cholesterol differently. Cecal SCFA pools were higher in rats fed the soluble than the insoluble fractions (525 vs 166 μmol, $P < 0.001$), whereas higher concentrations of butyric acid were found in the distal colon and serum of rats fed the insoluble fractions (5 vs 3 μmol/g and 58 vs 29 μmol/L, respectively, $P < 0.001$). The soluble bilberry fraction gave lower amounts of liver cholesterol (56 mg) than the other berry fractions (87 ± 5 mg), formed the highest amount of SCFAs (746 vs 266 ± 21 μmol), and contributed the highest intake of anthocyanins. Cyanidin-3-glucoside monoglucuronide was detected in the urine of all groups, whereas anthocyanins were found only in groups fed soluble black currant and raspberry.

KEYWORDS: *berries, fiber, SCFAs, anthocyanins, cholesterol*

INTRODUCTION

Berries are known to be an important part of a healthy diet and a good source of many vitamins and minerals. Many other imperative compounds can be found in berries, such as dietary fiber and flavonoids.[1] Dietary fibers have been connected to many positive health effects: they help in weight loss and appetite regulation and can reduce the risk of developing diseases such as type 2 diabetes and heart disease.[2−4] The flavonoids are not essential to humans, but the health benefits of berries are often related to these components, and through their antioxidative capacity they may have a protective role against various diseases associated with oxidative stress.[1,5] More than 4000 flavonoids have been described, and anthocyanins are a common group of flavonoids. Anthocyanins are found in high amounts in bilberries and black currants, whereas raspberries contain relatively low amounts, and they are responsible for the color of fruit and berry.[6,7] Bilberries also contain high amounts of proanthocyanidins and raspberries, ellagitannins, whereas black currants contain only small amounts of these components.[8] The bioavailability of various flavonoids is an important question in this respect.

Dietary fibers are not digested in the small intestine, but reach the large intestine, where microbial fermentation takes place.[2] Some fibers are also resistant to microbial degradation. The fermentation gives rise to short-chain fatty acids (SCFAs), mainly acetic, propionic, and butyric acids. The amount of SCFAs formed is dependent upon a number of factors, for example, the kind of dietary fiber that reaches the colon, the transit time, and the microbiota composition.[9,10] Some SCFAs have been shown to have positive health effects, and butyric acid has been mostly emphasized, but propionic may also have some interesting effects.[11] Butyric acid is an energy source for the colonic epithelial cells,[12] and impaired butyric acid metabolism has been associated with colonic diseases but also connected to decreased risk of metabolic diseases.[13,14] The physicochemical properties of the dietary fiber, such as solubility, are important for the health-promoting effects and the formation of SCFAs.[15] Very few studies have been focused on dietary fiber in berries.

Some phenolic compounds, such as the flavonoids, may be absorbed in the small intestine after cleavage by intestinal esterases. The flavonoids can also be more or less tightly bound to the dietary fiber complex, which affects the bioavailability of these components.[16,17] Depending on how they are associated with the dietary fiber, the substances may be released throughout the gut, and the specific physiological activity can vary on the basis of the site of release. Like the dietary fiber per se, another fraction of the flavonoids may be resistant to colonic degradation, thereby reaching feces intact and having no biological effect.

Interest in new food components with prebiotic properties is growing. Many byproducts are formed during, for example, juice production. To get an idea of where the flavonoids in berries are located, and also which fibers are most active, we

Received: September 4, 2013
Revised: April 14, 2014
Accepted: April 27, 2014
Published: May 5, 2014

ACS Publications © 2014 American Chemical Society

dx.doi.org/10.1021/jf5007566 | J. Agric. Food Chem. 2014, 62, 4359−4368

Table 1. Composition of Test Diets (g/kg, dwb)

	soluble			insoluble		
	bilberry	black currant	raspberry	bilberry	black currant	raspberry
casein	120	120	120	120	120	120
DL-methionine	1.2	1.2	1.2	1.2	1.2	1.2
corn oil	50	50	50	50	50	50
mineral mixture[a]	48	48	48	48	48	48
vitamin mixture[b]	8	8	8	8	8	8
choline chloride	2	2	2	2	2	2
berries[c]	771	771	771	77	108	97
sucrose	0	0	0	100	100	100
wheat starch[d]	0	0	0	594	563	574
energy content (kJ/kg)	16600	16500	16400	16500	16400	16300

[a]Containing (g/kg) 0.43 $CuSO_4 \cdot 5H_2O$, 1.6 $ZnSO_4 \cdot 7H_2O$, 389 KH_2PO_4, 201.2 $NaH_2PO_4 \cdot 2H_2O$, 380 $CaCO_3$, 0.08 KI, 67 $MgSO_4$, 9 $FeSO_4 \cdot 7H_2O$, 4 $MnSO_4 \cdot H_2O$, 0.023 $CoCl \cdot 6H_2O$, 119.1 NaCl, 0.019 chromium(III)chloride, and 0.013 sodium selenate (Lantmännen AB, Sweden). [b]Containing (g/kg) 0.62 menadione, 2.5 thiamin hydrochloride, 2.5 riboflavin, 1.25 pyridoxine hydrochloride, 6.256 calcium pantothenate, 6.256 nicotinic acid, 0.25 folic acid, 12.5 inositol, 1.25 *p*-aminobenzoic acid, 0.05 biotin, 0.00375 cyanocobalamin, 0.187 retinol palmitate, 0.00613 calciferol (D3), 25 *d*-*α*-tocopheryl acetate, and 941.25 maize starch (Lantmännen AB, Sweden). [c]Corresponding to 45 g dietary fiber/kg diet (dry weight basis) in diets containing bilberry and 60 g dietary fiber/kg diet (dry weight basis) in diets containing black currant and raspberry. The berries were from Procordia AB (Eslöv, Sweden). [d]Norfoods Sweden AB, Malmö, Sweden.

Table 2. Composition and Fecal Excretion of Dietary Fiber in Rats Fed Soluble or Insoluble Fractions from Bilberry, Black Currant, or Raspberry[a]

	composition of dietary fiber						fecal excretion (%)					
	soluble			insoluble			soluble			insoluble		
	bilberry	black currant	raspberry	bilberry	black currant	raspberry	bilberry	black currant	raspberry	bilberry	black currant	raspberry
dietary fiber polysaccharides (g/100 g, dwb)	5.5c	3.4c	6.0c	18.2a	14.1b	18.5a	14bc	18bc	16bc	26a	11c	21ab
monomeric composition (%)												
rhamnose	3	5	3	1	2	1	7d	11cd	15bc	33a	18b	32a
fucose	1	2	1	<0.5	1	<0.5	16	5	13	31	15	26
arabinose	8	11	19a	5b	7	4b	10b	3c	2d	14a	5b	7b
xylose	32a	3c	7c	28ab	8c	23b	1e	8c	3d	35a	16b	27a
mannose	5b	9b	2b	3b	32a	2b	8b	3c	12b	10b	4c	18a
galactose	12	12	13	6	8	5	19a	7c	5c	19a	11b	18a
glucose	32b	25b	26b	46a	30b	51a	10c	50a	45a	23b	13bc	21b
uronic acid	7b	33a	28a	11b	12b	13b	30a	12c	5d	19ab	20ab	15bc
lignin[b] (g/100 g, dwb)	0.3a	4.4a	1.3a	39.8b	41.9b	39.5b	nd[c]	nd	nd	nd	nd	nd
total dietary fiber (g/100 g, dwb)	5.8	7.8	7.3	58	56	58						

[a]Mean values ($n = 7$) within a row with unlike letters (a–d) are significantly different ($P < 0.05$). [b]The difference between total dietary fiber (AOAC method[19]) and the sum of dietary fiber polysaccharides[18] represents lignin and other sulfuric acid resistant substances. [c]nd, not determined.

thought it would be useful to separate the raw material into soluble and insoluble fractions.

The aim of this study was to investigate whether soluble and insoluble fractions isolated from three Swedish berries, bilberry, black currant, and raspberry would affect physiological parameters associated with colonic and metabolic health. Fermentability of the dietary fiber, the formation of SCFAs in the hindgut (cecum and distal colon), and the amount of anthocyanins in blood, urine, and cecal contents were analyzed. Liver cholesterol and triglycerides and the level of SCFAs and inflammatory cytokines in portal blood of rats were also analyzed.

MATERIALS AND METHODS

Chemicals. The following chemicals were used: hexane and Triton X-100 (Sigma-Aldrich, St. Louis, MO, USA); isopropanol and 2,6-di-*tert*-butyl-4-methylphenol (BHT) (Merck, Darmstadt, Germany); Infinity Cholesterol reagent (Thermo Scientific, Middletown, VA, USA); Chemistry Calibrator (Pointe Scientific Inc., Canton, MI, USA); Hypnorm (Division of Janssen-Cilag Ltd., Janssen Phamaceutica, Beerse, Belgium); Dormicum (F. Hoffman-La Roche AG, Basel, Switzerland); Milliplex MAP rat cytokine kit (Merck Millipore, Billerica, MA, USA); serum tube (SST Advance, Plus Blood Collection Tubes, BD, Plymouth, UK); and plasma tubes containing EDTA (K2E 3.6 mg, Plus Blood Collection Tubes, BD).

Separation of Soluble and Insoluble Berry Fraction. Bilberry (*Vaccinium myrtillus*), black currant (*Ribes nigrum*), and raspberry (*Rubus ideaus*) were freeze-dried (Procordia, Eslöv, Sweden), and soluble and insoluble parts of the berries were separated before inclusion in rat diets. The following procedure resulted in three soluble and three insoluble berry fractions, and diets were formulated from the six test materials obtained. The freeze-dried berries were ground by hand in a mortar. To liberate as much soluble fiber as possible from the berries, different amounts of water, difffernt pH values, and

dx.doi.org/10.1021/jf5007566 | J. Agric. Food Chem. 2014, 62, 4359–4368

Table 3. Feed Intake, Body Weight Gain, Dietary Fiber Fermentability, and Bulking Capacity in Rats Fed a Diet Containing Soluble or Insoluble Fractions from Bilberry, Black Currant, or Raspberry[a]

	soluble			insoluble			*P*		
	bilberry	black currant	raspberry	bilberry	black currant	raspberry	berry	sol	berry × sol
feed intake (g/day)	9.3 ± 0.4	10.3 ± 0.2	10.0 ± 0.2	11.7 ± 0.2	11.9 ± 0.1	11.5 ± 0.2	NS	<0.001[b]	NS
body wt gain (g/g feed)	0.17 ± 0.04	0.21 ± 0.03	0.26 ± 0.03	0.28 ± 0.03	0.32 ± 0.02	0.28 ± 0.03	NS	0.002[b]	NS
fermentability (%)	88.6 ± 2.2a	81.9 ± 1.3ab	84.5 ± 1.8ab	73.6 ± 2.5c	89.2 ± 0.8a	79.1 ± 1.3bc	0.033	0.004	<0.001
bulking capacity (g/g fiber ingested)	1.4 ± 0.3	1.3 ± 0.0	1.0 ± 0.1	1.3 ± 0.1	0.9 ± 0.0	1.1 ± 0.0	0.033[c]	NS	NS

[a]Mean values with their SEM (n = 7). Values within a row with unlike letters (a–c) are significantly different ($P < 0.05$). [b]Values in groups fed insoluble fractions were significantly higher than in those fed soluble fractions. [c]Values in groups fed bilberries were significantly higher than in those fed raspberries.

different temperatures were tested. Another aim was to preserve the dietary fiber as intact as possible and extract all berry components. The maximal amount of fiber was referred to as the amount obtained under physiological conditions according to the dietary fiber methodology.[18,19] During the isolation and optimization process, the samples with different formulations were heated in a water bath at different pH values (1.5, 2 and 3), amounts of water (4–10 mL/g), and temperatures (70–85 °C). The test tubes were centrifuged, and the supernatant was filtered and precipitated with 95% alcohol and filtered with Celite (Fibertec System E 1023 Filtration Module) to estimate the amount of the soluble fiber fraction. The optimal parameters were found to be at pH 2 and 80 °C for all three berries, and the optimum amount of water was 5–7 L/kg freeze-dried berries. During the extraction of the dietary fiber from the berries, they were mixed with water and heated in a metal pot to 80 °C under constant stirring. The berry solution was centrifuged, and the supernatant (soluble fraction) was filtered through a sieve into plastic containers and frozen at −20 °C before subsequent evaporation in a rotary vacuum evaporator (Heidolph VV-60, Germany) and freeze-drying (Labconco Lyph-lock-18, Kansas City, MO, USA). The insoluble fraction (the pellet after centrifugation and the leftovers from the filter) was freeze-dried as well. The content of dietary fiber and anthocyanins was analyzed in the different berry fractions obtained.

Preparation of Diets. All diets contained the same amount of protein (120 g/kg casein dry weight basis, dwb) and fat (50 g/kg corn oil, dwb), and the amounts of added minerals (48 g/kg dwb) and vitamins (8 g/kg dwb) were also the same for all diets (Table 1). The energy contents of the diets were very similar (Table 1). Furthermore, the content of dietary fiber in the diets was 6 g/100 g (dwb) for the soluble and insoluble fractions of raspberries and black currants (corresponding to 771 g of the soluble berry fractions and 97–108 g of the insoluble berry fractions calculated on dwb). The dietary fiber content is shown in Table 2. For practical reasons the amount of dietary fiber in the diet containing the soluble fraction of bilberries had to be limited to 4.5 g/100 g (dwb), as it was not possible to incorporate more berries along with the chosen levels of nutrients (protein, fat, minerals, and vitamins). This also corresponded to 771 g (dwb) of the soluble bilberry fraction and 77 g (dwb) of the insoluble bilberry fraction. Because the primary goal was to compare the effects of insoluble and soluble fractions, the amount of fiber was the same in the insoluble bilberry fraction as in the soluble bilberry fraction. The amount of available carbohydrates was also more or less the same in the various diets, although from different origins. In the insoluble berry fractions the available carbohydrates were from added sucrose and wheat starch, known to be completely digested, containing no resistant starch and not giving rise to any SCFAs,[20] whereas the available carbohydrates (glucose, sucrose, and fructose) were from berries in the soluble fractions. The amount of antioxidants varied between different diets, but it would be impossible to take this into consideration, too. Despite this, the intakes of anthocyanins were quite similar for the insoluble and soluble bilberry and black currant fractions, whereas the intake was higher with the soluble raspberry fraction than with the insoluble one (see results, anthocyanins).

One diet was prepared from each soluble and insoluble dietary fiber berry fraction, resulting in six diets. The diets containing the soluble berry fractions had a slightly sour taste, especially with the soluble bilberry fraction, which the rats did not like. To retain the composition of nutrients, a sweetener was added to the diets, which resulted in good feed consumption (Table 3). The sweetener added was a mixture of Aspartame (2.0 mg/g feed, dwb) (SinoSweet Co. Ltd., Yixing, Jiangsu, China) and Acesulfam-K (0.7 mg/g feed, dwb) (Zhangjiagang Hope Chemicals Co. Ltd., Zhangjiagang, Jiangsu, China).

The content of dietary fiber (dwb) in the soluble fraction was 5.8 g/100 g in bilberry, 7.8 g/100 g in black currant, and 7.3 g/100 g in raspberry, whereas the dietary fiber content was considerably higher in the insoluble fractions: 58 g/100 g (dwb) in bilberry, 56 g/100 g in black currant, and 58 g/100 g in raspberry. The soluble fractions consisted of dietary fiber polysaccharides containing glucose (25–32%) and galactose (12–13%) (Table 2). Soluble fractions from black currant and raspberry also contained high proportions of uronic acids (28–33%) and raspberry arabinose (19%), whereas bilberry contained high amounts of xylose (32%). The insoluble fractions consisted of polysaccharides containing glucose (30–51%) and uronic acids (11–13%). Bilberry and raspberry also contained xylose (23–28%), whereas black currant contained high amounts of mannose (32%).

Experimental Design. Forty-two male Wistar rats (Taconic, Lille Skensved, Denmark), with a starting weight of 127.6 (SE 1.2) g, were randomly divided into six groups of seven animals. Each group was given one of the six diets (Table 1), and the feed intake was restricted to 12 g (dwb) per day, which is an adequate amount of feed for rats of this size,[21] but with unlimited access to water. The rats were housed individually in metabolic cages[22] in a room maintained at 22 °C, with a 12 h light–dark cycle. The animals were healthy and active throughout the experiment. The Ethics Committee for Animals Studies at Lund University approved the animal experiment (Application M 30-09).

The rats were allowed to adapt to the diets for 7 days followed by a 5 day experimental period, when feces and feed residues were collected quantitatively daily, whereas urine was collected during approximately 1–2 h every day, after the rats had been fed. The feces were stored at −20 °C, then freeze-dried and milled, before the composition of dietary fiber was analyzed. The urine samples were stored at −20 °C and analyzed for anthocyanins once the sampling was completed. To calculate the exact amount of feed ingested, the feed residues from each rat were weighed. After the experimental period, the animals were anesthetized by subcutaneous injection of a mixture (1:1:2) of Hypnorm, Dormicum, and water at a dose of 0.15 mL/100 g body weight. Blood was taken from the hepatic portal vein and placed in serum and plasma tubes containing EDTA (approximately 3 and 2 mL, respectively), which were centrifuged and stored at −40 °C until the analysis of SCFAs[23] (serum), cytokines (serum), and anthocyanins (plasma). The cecum was removed and the content transferred to a test tube and mixed, and the pH was measured with an InLab Semi-Microelectrode (Mettler Toledo, OH, USA). The cecal tissue was rinsed with water, dried, and weighed, and cecal contents were determined. The cecal content was stored at −40 °C for analysis of SCFAs and anthocyanins. The liver was removed, weighed, and stored at −20 °C, before being freeze-dried and mortared, and then analyzed

for cholesterol and triglycerides. Stool samples were collected from the distal colon and stored at −40 °C until the analysis of SCFAs.

Analytical Methods. *Dietary Fiber.* The amount of dietary fiber in the soluble and insoluble berry fractions was determined gravimetrically with the AOAC method developed at the department.[19] The composition of the isolated dietary fiber residues in raw materials was quantified by using GLC, for the neutral sugars, and a spectrophotometric method was used to analyze uronic acids.[18] The content of dietary fiber polysaccharides in feces was analyzed as for the raw materials but without the gravimetric step. Lignin was calculated as the difference between the dietary fiber content of raw materials obtained by the enzymatic gravimetric AOAC method, which include lignin in the measurements, and the sum of dietary fiber monomers analyzed by GLC. Previous studies have shown a good accordance with these two methodologies; that is, the difference should give a good measurement of lignin.[24]

SCFAs in Portal Blood. SCFAs (acetic, propionic, isobutyric, butyric, isovaleric, and valeric acid) were analyzed in serum according to the method of Zhao et al.[23] with some modifications.[25] Water (3335 mL) and 0.5 mM 2-ethylbutyric acid (internal standard) in 2 M hydrochloric acid (27 μL) were added to the serum samples (240 μL) to protonate the SCFAs. A hollow fiber, for supported liquid membrane extraction, was immersed in the serum solution for the extraction of SCFAs. After the extraction, the SCFAs were flushed from the hollow fiber and injected onto a fused-silica capillary column (DB-FFAP 125-3237; J&W Scientific, Agilent Technologies Inc., Folsom, CA, USA). GC ChemStation software (Agilent Technologies Inc., Wilmington, DE, USA) was used to analyze the data.[23]

SCFAs in Intestinal Content. The SCFAs (acetic, propionic, isobutyric, butyric, isovaleric, valeric, and caproic acids) and heptanoic acid were analyzed in the intestinal content (cecum and distal colon) using a GLC method.[26] Hydrochloric acid (0.25 M) and 2-ethylbutyric acid (internal standard) were added to the intestinal samples and homogenized with an Ultra Turrax T25 basic (IKA-Werke, Staufen, Germany) for 1 min. The homogenized samples were centrifuged (MSE Super Minor, Hugo Tillquist AB, Solna, Sweden), and the supernatant was analyzed using GLC as described above.

Multiplex Cytokine Assay. A Milliplex microbeads array system was used to analyze serum levels of six cytokines, interleukin (IL)-4, IL-12, IL-18, MCP-1, IFN-γ, and TNF-α, according to the manufacturer's instructions using Milliplex MAP rat cytokine kit assay technology, as previously described.[27]

Anthocyanins. The anthocyanins in the raw material (soluble and insoluble berry fractions) were extracted from 1 g of sample with 15 mL of methanol/water/acetic acid (85:15:0.5, v/v/v). The sample solution was sonicated for 15 min at room temperature and centrifuged (200*g*) for 15 min and the supernatant removed. This procedure was repeated using 10 mL of methanol/water/acetic acid, and the supernatants were combined and transferred into a clean flask. Methanol/water/acetic acid was used to fill to a final volume of 25 mL. One milliliter was then filtered using a 0.2 μm GH Polypro (GHP, hydrophilic polypropylene) (Pall Corp., Washington, NY, USA) membrane syringe filter (Acrodisc, Sigma-Aldrich, St. Louis, MO, USA).

Urine and plasma samples were thawed and syringe filtered with a 0.2 μm GHP membrane before analysis of anthocyanins. For the soluble berry fractions only urine samples from rats fed black currants and raspberries were analyzed for anthocyanins, because the urine from bilberries was blue, and it cannot be ruled out that the urine had been contaminated with bilberries. Cecal samples were thawed and then extracted with methanol/water (1:1, v/v) for 1 h at room temperature followed by centrifugation (15 min, 200*g*), and the supernatant was filtered using the same GPH membrane.[28]

Anthocyanins analysis was performed on an Agilent 1260 Infinity system equipped with a quaternary pump, a diode array (DAD), an autosampler, and a thermostat column compartment, coupled with an Agilent 6100 series quadrupole LC-MS operated with electrospray ionization (API-ESI-MS). A 250 × 4.6 mm i.d. Agilent Technology SB-C18 column (Santa Clara, CA, USA) was used for separation. Elution was carried out using two mobile phases, A (5% v/v formic acid in water) and B (methanol). The gradient system used has been reported by Wu et al.[28] The elution of anthocyanins was monitored at 520 nm (Agilent 6100 Infinity system equipped with a DAD detector) and then introduced into the ion-trap electrospray mass spectrometer equipped with API-ES (Agilent Technology 6120 quadrupole LC-MS). The mass spectrometer was operated in the positive ion mode, full scan, in the range m/z 100−1000 under the following conditions: capillary voltage, 3000 V; drying gas flow, 12 L/min; nebulizer pressure, 40 psig; and drying gas temperature, 300 °C. Cyanidin-3-glucoside was used to create a calibration curve for the quantification of anthocyanins.[29,30]

Liver Cholesterol. Livers were lyophilized and mortared. A 3:2 mixture of hexane and isopropanol with 0.005% (v/w) BHT (1 mL/0.1 g liver) was used to extract the liver cholesterol on an orbital shaker followed by centrifugations. The supernatant was transferred to a clean tube. The extraction was repeated four times, and the supernatants were combined and then dried under N_2 flow at room temperature. The extracted lipids were redissolved in 1 mL of isopropanol containing 1% (v/v) Triton X-100. Total liver cholesterol was determined spectrophotometrically using Infinity Cholesterol reagent and Chemistry Calibrator.

Calculations and Statistical Analysis. The design of the experiment was randomized. The berries used in the study were bilberry, black currant, and raspberry and, as the soluble and insoluble fractions of the berries were isolated, the study involved six groups of seven rats. Two-way ANOVA with Tukey's test was used to determine the effects of different berries (berry), solubility (sol), and their interactions (berry × sol) (Tables 2−8). When significant interactions (berry × sol) were found ($P < 0.05$), individual means were analyzed by one-way ANOVA using Tukey's multiple-range test ($P < 0.05$). When no interactions could be found, only P values for berries (berry) and solubility (sol) were evaluated, with Tukey's test. In Table 2 interactions were found for all components, except fucose, and therefore only results from Tukey's multiple-range test are shown in the table. All evaluations were performed with Minitab software (release 16). The results were normally distributed with the exception of some SCFAs and a few monosaccharides in fecal excretion, which became normally distributed after Box−Cox transformation of the data set. Values are presented as means and SEM in Tables 3−8, and differences with P values <0.05 are considered significant, whereas P values ≤0.1 were defined as tendency.

The level of each fatty acid (μmol/g) was multiplied by the cecal amount to obtain the cecal pool (μmol). The body weight gain was calculated in grams per gram of food consumed. The fecal excretion (Table 2) of the dietary fiber components was calculated as follows:

$$\frac{\text{g dietary fiber components in feces}_{\text{test diet}}}{\text{g dietary fiber component ingested}_{\text{test diet}}} \times 100$$

The fermentability (Table 3) of the dietary fiber was calculated as follows:

$$\left(1 - \frac{\text{g dietary fiber in feces}_{\text{test diet}}}{\text{g dietary fiber ingested}_{\text{test diet}}}\right) \times 100$$

The fecal bulking capacity (Table 3) was calculated as follows:

$$\frac{\text{fecal dry wt (g)}_{\text{test diet}}}{\text{g dietary fiber ingested}_{\text{test diet}}}$$

RESULTS

Feed Intake and Body Weight. The feed intake was lower in the groups fed the soluble fraction (mean = 9.9 ± 0.2 vs mean = 11.7 ± 0.1 g/day, dwb, $P < 0.001$) (Table 3). There was no difference between different berries. Groups fed soluble fractions also gained slightly less weight (mean = 0.21 ± 0.02 g/g feed vs mean = 0.30 ± 0.02 g/g feed for the insoluble fraction, $P = 0.002$).

Table 4. Cecal Content, Tissue Weight and pH, Cecal Pool and Proportions of SCFAs, and Ratios between Acetic and Propionic Acid and between Acetic and Propionic plus Butyric Acids in Rats Fed a Diet Containing Soluble or Insoluble Fractions of Bilberry, Black Currant, or Raspberry[a]

	soluble			insoluble			*P*		
	bilberry	black currant	raspberry	bilberry	black currant	raspberry	berry	sol	berry × sol
cecal content (g)	11.5 ± 0.9a	4.8 ± 0.4b	4.1 ± 0.4b	2.0 ± 0.1c	2.0 ± 0.1c	1.7 ± 0.1c	<0.001	<0.001	<0.0011
cecal tissue wt (g)	1.5 ± 0.0a	1.0 ± 0.0b	0.8 ± 0.0b	0.5 ± 0.0c	0.5 ± 0.0c	0.5 ± 0.0c	<0.001	<0.001	<0.001
cecal pH	7.2 ± 0.2	7.6 ± 0.1	7.4 ± 0.2	6.8 ± 0.1	6.8 ± 0.2	6.8 ± 0.1	NS	<0.001[b]	NS
Pool (μmol)									
acetic acid	660 ± 91c	280 ± 36b	390 ± 30bc	130 ± 5a	125 ± 9a	115 ± 8a	0.002	<0.001	0.007
propionic acid	53 ± 8	35 ± 3	47 ± 2	15 ± 1	15 ± 1	14 ± 1	NS	<0.001[b]	NS
butyric acid	27 ± 6	18 ± 3	30 ± 4	21 ± 2	25 ± 3	22 ± 2	NS	NS	NS
minor acids	6 ± 1a	13 ± 1b	17 ± 2b	7 ± 0a	6 ± 1a	6 ± 1a	<0.001	<0.001	<0.001
total	746 ± 104c	346 ± 41b	484 ± 33bc	173 ± 8a	171 ± 14a	157 ± 11a	0.007	<0.001	0.012
Proportion (%)									
acetic acid	90 ± 1a	84 ± 1b	83 ± 1b	78 ± 0c	76 ± 1c	76 ± 1c	<0.001	<0.001	0.004
propionic acid	7 ± 0b	11 ± 1a	10 ± 1a	9 ± 0ab	9 ± 0ab	9 ± 0ab	0.003	NS	0.001
butyric acid	3 ± 0	5 ± 0	7 ± 1	13 ± 1	15 ± 1	15 ± 1	NS	<0.001[c]	NS
Ratio									
ACE:PRO	13.2 ± 1.0a	7.9 ± 0.8b	8.2 ± 0.6b	8.5 ± 0.4b	8.7 ± 0.2b	8.2 ± 0.3b	<0.001	0.012	<0.001
ACE:(PRO+BUT)	8.9 ± 0.7a	5.2 ± 0.4b	5.1 ± 0.3bc	3.5 ± 0.1cd	3.3 ± 0.1d	3.2 ± 0.1d	<0.001	<0.001	<0.001

[a]Mean values with their SEM ($n = 7$). Mean values within a row with unlike letters (a–d) are significantly different ($P < 0.05$). [b]Values in groups fed soluble fractions were significantly higher than in those fed insoluble fractions. [c]Values in groups fed soluble fractions were significantly lower than in those fed insoluble fractions.

Table 5. Distal Colon Concentrations and Proportions of SCFAs and Ratio between Acetic and Propionic Acid and between Acetic and Propionic plus Butyric Acids in Rats Fed Soluble or Insoluble Fractions from Bilberry, Black Currant, or Raspberry[a]

	soluble			insoluble			*P*		
	bilberry	black currant	raspberry	bilberry	black currant	raspberry	berry	sol	berry × sol
Concentration (μmol/g)									
acetic acid	28 ± 3	32 ± 4	32 ± 4	32 ± 4	27 ± 1	23 ± 3	NS	NS	NS
propionic acid	3 ± 0b	4 ± 0ab	5 ± 0a	4 ± 0ab	3 ± 0b	3 ± 0b	NS	0.012	0.012
butyric acid	2 ± 0a	3 ± 0ab	4 ± 0b	5 ± 1b	5 ± 1b	4 ± 1b	NS	<0.001	0.001
minor acids	1 ± 0a	2 ± 0b	3 ± 0b	2 ± 0b	2 ± 0b	2 ± 0b	<0.001	0.004	<0.001
total	34 ± 4	41 ± 5	44 ± 4	43 ± 5	37 ± 2	32 ± 4	NS	NS	0.054
Proportion (%)									
acetic acid	85 ± 1a	82 ± 1ab	78 ± 2b	78 ± 2b	76 ± 2b	78 ± 2b	NS	0.001	0.032
propionic acid	10 ± 1b	10 ± 0b	13 ± 1a	9 ± 0b	9 ± 0b	10 ± 0b	<0.001[b]	<0.001[c]	NS
butyric acid	5 ± 0d	8 ± 1cd	10 ± 1bc	13 ± 1ab	15 ± 2a	12 ± 2abc	0.042	<0.001	0.011
Ratio									
ACE:PRO	9.0 ± 0.7	7.9 ± 0.3	6.3 ± 0.5	8.6 ± 0.5	8.6 ± 0.4	7.9 ± 0.4	0.004[d]	NS	NS
ACE:(PRO+BUT)	5.8 ± 0.5a	4.6 ± 0.3ab	3.6 ± 0.3b	3.6 ± 0.3b	3.3 ± 0.3b	3.7 ± 0.3b	0.013	<0.001	0.011

[a]Mean values with their SEM ($n = 7$, with the exception of $n = 6$ for soluble bilberry). Mean values within a row with unlike letters (a–d) are significantly different ($P < 0.05$). [b]Values in groups fed raspberries were significantly higher than in those fed bilberries or black currants. [c]Values in groups fed soluble fractions were significantly higher than in those fed insoluble fractions. [d]Values in groups fed bilberries were significantly higher than in those fed raspberries or black currants.

Cecal Content, Tissue and pH, Dietary Fiber Fermentability, and Fecal Bulking Capacity. Soluble and insoluble fractions and also the type of berry affected cecal content and tissue weights ($P < 0.001$) (Table 4), and groups fed soluble fractions generally weighed more. Rats fed soluble bilberries weighed most (11.5 and 1.5 g for the cecal content and tissue, respectively), which was higher ($P < 0.001$) than the weights in groups fed the soluble fractions of black currants and raspberries (mean = 4.5 ± 0.3 and 0.9 ± 0.0 g for the cecal content and tissue, respectively). The insoluble fractions gave considerably lower weights than the soluble fractions (mean = 1.9 ± 0.1 and 0.5 ± 0.0 g for the cecal content and tissue, respectively). Rats fed the insoluble fractions had a lower cecal pH (mean = 6.8 ± 0.1) than rats fed the soluble fractions (7.4 ± 0.1, $P < 0.001$). Dietary fibers in both the soluble and insoluble fractions were highly fermented in the hindgut of rats, but the fermentability was higher for the soluble fractions (85 ± 1 vs 81 ± 2% for the insoluble fraction, $P = 0.041$) (Table 3). The insoluble fiber fraction of black currants was more fermented (89%) than the insoluble fraction of bilberries (74%, $P < 0.001$). The fecal bulking capacity was similar for all groups, but the groups fed the two raspberry fractions had a lower fecal bulking capacity compared with the corresponding bilberry fractions (1.0 ± 0.0 vs 1.3 ± 0.1, $P = 0.042$).

SCFAs in the Hindgut. *Cecum.* The total amount of cecal SCFAs was higher in groups fed the soluble berry fractions than those fed the insoluble fractions, 525 ± 52 vs 166 ± 6 μmol for the insoluble fractions, $P < 0.001$ (Table 4). Of the soluble

dx.doi.org/10.1021/jf5007566 | J. Agric. Food Chem. 2014, 62, 4359–4368

Table 6. Serum Concentration and Proportions of SCFAs and Ratio between Acetic and Propionic Acid and between Acetic and Propionic plus Butyric Acids in Rats Fed Soluble or Insoluble Fractions from Bilberry, Black Currant, or Raspberry[a]

	soluble			insoluble			*P*		
	bilberry	black currant	raspberry	bilberry	black currant	raspberry	berry	sol	berry × sol
Concentration (μmol/L)									
acetic acid	915 ± 87a	670 ± 56b	765 ± 56ab	655 ± 24b	755 ± 48ab	605 ± 49b	NS	0.019	0.014
propionic acid	47 ± 8	45 ± 4	55 ± 3	39 ± 5	49 ± 4	44 ± 7	NS	NS	NS
butyric acid	29 ± 5ab	25 ± 2a	33 ± 4abc	48 ± 6bcd	72 ± 13d	54 ± 7cd	NS	<0.001	0.100
minor acids	15 ± 2	19 ± 1	22 ± 2	22 ± 3	27 ± 2	23 ± 3	NS	0.018	NS
total	1006 ± 93a	759 ± 58	875 ± 62	764 ± 37	903 ± 63	726 ± 64b	NS	NS	0.015
Proportion (%)									
acetic acid	92 ± 1	90 ± 1	90 ± 0	89 ± 1	86 ± 1	86 ± 1	0.004[b]	<0.001[c]	NS
propionic acid	5 ± 0	6 ± 0	6 ± 0	5 ± 0	6 ± 0	6 ± 1	0.01[d]	NS	NS
butyric acid	3 ± 17	4 ± 0	4 ± 0	6 ± 0	8 ± 19	8 ± 0	NS	<0.001[e]	NS
Ratio									
ACE:PRO	21.2 ± 2.7	15.2 ± 1.0	13.9 ± 0.8	18.1 ± 2.0	15.4 ± 0.7	15.0 ± 1.3	0.004[f]	NS	NS
ACE:(PRO+BUT)	18.3 ± 2.2	12.6 ± 0.9	11.9 ± 0.6	14.7 ± 1.5	12.7 ± 0.5	12.3 ± 1.0	0.002[f]	NS	NS

[a]Mean values with their SEM (n = 7, with the exceptions of n = 6 for soluble bilberry and n = 5 for insoluble black currant). Mean values within a row with unlike letters (a–d) are significantly different (P < 0.05). [b]Values in groups fed bilberries were significantly higher than in those fed raspberries. [c]Values in groups fed soluble fractions were significantly higher than in those fed insoluble fractions. [d]Values in groups fed raspberries were significantly higher than in those fed bilberries. [e]Values in groups fed insoluble fractions were significantly higher than in those fed soluble fractions. [f]Values in groups fed bilberries were significantly higher than in those fed black currant or raspberries.

Table 7. Total Amount (mg) of Liver Cholesterol and Triglyceride in Rats Fed Soluble or Insoluble Fractions from Bilberry, Black Currant, or Raspberry[a]

	soluble			insoluble			*P*		
	bilberry	black currant	raspberry	bilberry	black currant	raspberry	berry	sol	berry × sol
cholesterol	56 ± 3a	91 ± 9b	76 ± 4ab	91 ± 4b	85 ± 4b	89 ± 4b	0.021	0.002	0.001
triglyceride	108 ± 12a	152 ± 11ab	143 ± 11ab	175 ± 14b	129 ± 4a	146 ± 10ab	NS	NS	0.001

[a]Mean values with their SEM (n = 7). Mean values within a row with unlike letters (a,b) are significantly different (P < 0.05).

fractions, bilberries exhibited the highest cecal amount of SCFAs (746 ± 104 μmol), which was more than twice as large as for the group fed the soluble fraction of black currants (346 ± 41 μmol, P < 0.001). SCFAs formed from the insoluble berry fractions were considerably lower and rather similar between berries. Due to the higher amounts of SCFAs formed with the soluble berry fractions, the yield of the specific SCFAs was also generally higher with these fractions than with the insoluble fractions (acetic acid, propionic acid, and minor acids P < 0.001). There was a tendency toward a higher amount of butyric acid formed in rats fed soluble bilberry and raspberry fractions than in corresponding insoluble fraction, whereas the proportion of butyric acid was higher with the insoluble fraction (14 ± 0%) than with the soluble fractions (5 ± 0%, P < 0.001). Similarly, the ratio between acetic acid and propionic plus butyric acid was also lower with the insoluble fraction. The proportion of propionic acid between groups was quite similar.

Distal Colon. Higher concentrations of butyric acid and minor acids were seen with insoluble berry fractions than with soluble berry fractions in the distal colon of rats (P < 0.001 and P < 0.004, respectively), whereas the concentration of propionic acid was higher with the soluble fractions (P < 0.012) (Table 5). Of the various berries, the soluble raspberry fraction gave a higher propionic acid concentration in the rats than the soluble bilberry fraction (P < 0.05), and it was also higher than the insoluble fraction of raspberry. The proportion of propionic acid was higher with the soluble raspberry fraction than with the other berry fractions (P < 0.05).

SCFAs in Portal Blood. The concentration of acetic acid in serum was 605–915 μmol/L, that of propionic acid, 39–55 μmol/L, and that of butyric acid, 25–72 μmol/L. Smaller amounts of the minor acids were detected (15–27 μmol/L).

The soluble fraction of bilberry gave a higher concentration of acetic acid (915 μmol/L) in the rats than the insoluble fraction (655 μmol/L, P = 0.019) (Table 6). In contrast, the insoluble fractions gave higher concentrations of butyric acid (48, 54, and 72 μmol/L, respectively, for bilberry, raspberry, and black currant) than the soluble fraction (29, 33 and 25 μmol/L, respectively, P < 0.001). It is noteworthy that the soluble fraction of black currant gave the lowest concentration of butyric acid (25 ± 2 μmol/L) in the rats, whereas the insoluble fraction of black currant gave the highest concentration (72 ± 13 μmol/L, P < 0.001). No difference was seen for propionic acid.

Inflammatory Markers. No difference was seen in inflammatory cytokines (IL-12, IL-18, and MCP-1) for any of the groups (see the Supporting Information).

Liver Cholesterol and Triglyceride. The total amount of liver cholesterol was lower and triglycerides tended to be lower in rats fed the soluble berry fractions rather than the insoluble fractions (mean = 75 ± 4 mg vs 88 ± 2 mg, P = 0.002, for cholesterol and mean = 133 ± 8 vs 150 ± 7 mg, P = 0.081, for triglycerides) (Table 7). Of the different soluble berry fractions, the bilberry group had the lowest amount of cholesterol compared with the other groups (56 vs 89 ± 3 mg). Groups fed soluble bilberry and insoluble black currant also had lower amounts of triglycerides compared with the group fed insoluble bilberry (108 and 129 vs 175 mg).

Anthocyanins and Glucuronide Metabolites. The total content of anthocyanins was higher in the insoluble berry

dx.doi.org/10.1021/jf5007566 | J. Agric. Food Chem. 2014, 62, 4359–4368

Table 8. Intake (μg/5 Days, dwb) and Content (μg/g, dwb) (in Parentheses) of Anthocyanins in Soluble and Insoluble Fractions of Bilberry, Black Currant, and Raspberry and the Amount Excreted in Urine of Rats Fed Soluble Black Currant and Raspberry (μg/mL)[a]

	berry fractions						urine	
	soluble			insoluble			soluble	
	bilberry	black currant	raspberry	bilberry	black currant	raspberry	black currant	raspberry
cyanidin-3-*O*-sophoroside	–[b]	–	776 ± 15 (16)	–	–	211 ± 4 (34)		0.32 ± 0.07
delphinidin-3-galactoside	952 ± 44 (25)	–	–	977 ± 13 (196)	–	–		
delphinidin-3-*O*-glucoside	900 ± 42 (24)	303 ± 5 (6)	–	857 ± 11 (172)	475 ± 2 (65)	–	0.34 ± 0.02	
delphinidin-3-*O*-rutinoside	–	1069 ± 17 (22)	–	–	1171 ± 6 (159)	–	0.75 ± 0.05	
cyanidin-3-galactoside	980 ± 45 (26)	–	–	939 ± 12 (188)	–	–		
delphinidin-3-arabinoside	678 ± 31 (18)	–	–	705 ± 9 (141)	–	–		
cyanidin-3-*O*-glucoside	964 ± 45 (26)	179 ± 3 (4)	–	855 ± 11 (172)	183 ± 1 (25)	–	0.25 ± 0.02	
cyanidin-3-*O*-rutinoside	–	702 ± 11 (14)	258 ± 5 (5)	–	784 ± 4 (106)	71 ± 2 (11)	0.67 ± 0.05	0.15 ± 0.01
petunidin-3-galactoside	499 ± 23 (13)	–	–	372 ± 5 (75)	–	–		
cyanidin-3-arabinoside	597 ± 28 (16)	–	–	590 ± 8 (118)	–	–		
petunidin-3-glucoside	762 ± 35 (20)	–	–	598 ± 8 (120)	–	–		
peonidin-3-galactoside	238 ± 11 (6)	–	–	147 ± 2 (30)	–	–		
petunidin-3-arabinoside	288 ± 13 (8)	–	–	208 ± 3 (42)	–	–		
peonidin-3-glucoside	826 ± 38 (22)	–	–	706 ± 9 (142)	–	–		
malvidin-3-galactoside	724 ± 34 (19)	–	–	608 ± 8 (122)	–	–		
malvidin-3-glucoside	140 ± 7 (4)	–	–	56 ± 1 (11)	–	–		
malvidin-3-arabinoside	226 ± 11 (6)	–	–	147 ± 2 (30)	–	–		
total	8774 ± 407 (233)	2253 ± 36 (46)	1034 ± 20 (21)	7765 ± 100 (1559)	2613 ± 12 (355)	282 ± 6 (45)	2.01 ± 0.13	0.47 ± 0.08

[a]Mean values with their SEM (n = 7). Values in parentheses show the content of anthocyanins in the soluble and insoluble berry fractions (μg/g, dwb). [b]–, values are below the detection limit (<1.2 ng/mL).

dx.doi.org/10.1021/jf5007566 | J. Agric. Food Chem. 2014, 62, 4359−4368

fractions than in the soluble ones (1559 and 233 μg/g for the insoluble and soluble bilberry fractions, respectively; 355 and 46 μg/g for the insoluble and soluble black currant fractions, respectively; and 45 and 21 μg/g for the insoluble and soluble raspberry fractions, respectively) (Table 8). With regard to the intake of anthocyanins, it was more similar from the soluble and insoluble bilberry fractions (8774 ± 407 and 7765 ± 100 μg/5 days, respectively) and also for the soluble and insoluble black currant fractions (2253 ± 36 and 2613 ± 12 μg/5 days, respectively), whereas the intake from the soluble raspberry fraction was 4 times higher than from the insoluble fraction (1034 ± 20 vs 282 ± 6 μg/5 days, respectively). Both fractions of bilberries had the greatest number of anthocyanins (14 in both fractions), followed by black currants (4 in both fractions). Only two different anthocyanins were found in raspberries, where cyanidin-3-*O*-sophoroside was found only in raspberry, whereas delphinidin-3-*O*-rutinoside was also detected in black currants.

Anthocyanins were detected in the urine of rats fed the soluble fractions from black currant and raspberry (0.25−0.75 μg/mL for black currant and 0.15−0.32 μg/mL for raspberry) (Table 8). Rats fed soluble fractions from bilberry were contaminated with the diet; therefore, no reliable analyses on anthocyanins could be performed. No anthocyanins were detected in the urine of the rats fed the insoluble fractions. However, in the LC-MS analysis cyanidin-3-glucoside monoglucuronide (m/z 648) was detected as ($M + Na^+$) in all urine samples. No anthocyanins or glucuronide metabolites were detected in cecum or blood plasma for any of the groups.

DISCUSSION

The aim of the present study was to investigate whether soluble and insoluble fractions isolated from three Swedish berries would affect the formation and absorption of SCFAs and the uptake and utilization of flavonoids by using a rat model. Furthermore, levels of cholesterol, triglycerides, and inflammatory cytokines were analyzed. This may be important for physiological parameters associated with colonic and metabolic health and therefore of interest in the production of foods with health benefits. Interestingly, the largest differences in the physiological parameters analyzed were seen between soluble and insoluble berry fractions. The differences between different berries were also greater in the soluble fractions than in the insoluble berry fractions, which exhibited quite similar results. It is noteworthy that the soluble fractions gave lower liver cholesterol and triglycerides in the rats than the insoluble fractions, especially with the soluble bilberry fraction. This fraction also had a higher formation of SCFAs, especially of acetic acid, than the other soluble berry fractions. Furthermore, the anthocyanin intake was higher with the soluble bilberry fraction than with the other soluble fractions, which could be another reason for the lower triglycerides and cholesterol levels in the liver. Similar findings have been seen by Kim et al., who gave a soluble chokeberry extract to apo E−/− mice.[31] Thus, the plasma cholesterol and triglyceride levels decreased, which could be related to decreased antioxidant enzyme activities in the liver (glutathione peroxidase) and in plasma (paraoxonase and catalase), that is, enzymes usually linked with protection from oxidative damage. However, the gene expression connected to cholesterol metabolism, lipogenesis, and fatty acid oxidation was unaffected in that study. The cholesterol and triglyceride levels were significantly higher with the insoluble bilberry fraction than with the soluble fraction, despite a similar intake of anthocyanins, which may be due to the lower bioavailability of anthocyanins with the insoluble bilberry fraction, which unfortunately not could be evaluated. To avoid this problem in future studies, an idea would be to collect urine from the urinary bladder at the end of the experiment instead.

The amount of anthocyanins ingested was highest with bilberries, irrespective of solubility, followed by black currants and then raspberries. Although the contribution of anthocyanins from the insoluble berry fractions, at least for black currant and bilberry, was as high as from the soluble berry fractions, these could only be found in urine of rats fed soluble berry fractions from black currant and raspberry. On the other hand, cyanidin-3-glucoside monoglucuronide, detected only with LC-MS, could be seen in urine of all groups irrespective of solubility. However, this peak was not quantified. Similar results have also been found by others.[32] The presence of anthocyanins in urine of rats indicates that these components were absorbed before reaching the colon and explains why no anthocyanins could be found in the cecum of rats. The absence of anthocyanins in blood of rats may be because they are rapidly metabolized. However, the anthocyanins may have been fermented by the microbiota, leading to a different molecular structure and therefore not detectable in this study. Most anthocyanins have been reported to be absorbed to a low extent in the upper part of the gastrointestinal tract and therefore possibly degraded to phenolic acids by the colon microbiota.[33,34] This could also be a reason why none of the anthocyanins of the insoluble berry fractions could be detected in cecum, portal blood, or urine of rats. Another reason could be that anthocyanins were tightly bound to the dietary fiber and not free for extraction in the analyses or for uptake in the colon. Additionally, limited analyses of the glucuronidated form of anthocyanins and metabolites that have been methylated might also explain the low amounts detected. However, it cannot be excluded that the amounts consumed were too low, and because the levels are further diluted in the body, the compounds may have been below the detection limit of the analytical methodology used. On the other hand, the levels of anthocyanins consumed were similar to or up to 10 times higher compared with the study of Kim et al., in which apo E−/− mice got a chokeberry extract.[31] The anthocyanins were not analyzed in blood there either, only the activity of some antioxidant enzymes. The anthocyanin content in black currants and raspberries was 10 times lower than in a previous study using the same rat model.[27] A possible explanation for this is that the berries came from two different suppliers. Furthermore, the berries were treated differently in the two studies. In the previous study the whole berry was studied, whereas soluble and insoluble fractions were studied in the present study.

The somewhat lower feed intake in rats fed diets containing the soluble berry fractions than in those fed insoluble fractions may be due to the more sour taste of these diets. However, it could also be due to the soluble fractions per se absorbing more water and therefore giving greater satiety and a lower feed intake. Soluble fractions formed more SCFAs, which may affect hormones associated with appetite (e.g., adiponectin) and inflammatory factors (TNF-α and IL-6) as suggested by Galisteo et al.[14] This may explain the lower feed intake. The gut microbial metabolism is increasingly suggested to be a causative agent of obesity.[35] Furthermore, soluble and viscous dietary fibers have been shown to increase satiety in humans, and the higher the viscosity, the greater the effects, delaying the

dx.doi.org/10.1021/jf5007566 | J. Agric. Food Chem. 2014, 62, 4359−4368

gastric emptying and/or intestinal absorption of nutrients.[14,36] This may be another reason for the lower levels of cholesterol and triglycerides in the liver. A lower intake of feed containing soluble fibers than insoluble ones has been seen in rats in a previous investigation on wheat.[37]

The greater formation of SCFAs, especially acetic acid, with the soluble fractions may explain the lower liver cholesterol and triglycerides in the rats fed these fractions, as mentioned above. The lowest amounts were seen with the soluble fraction of bilberry, and this fraction exhibited the highest cecal formation and serum concentration of SCFAs. This fraction also gave the highest cecal formation of propionic acid, although not significant, which is interesting because several studies have suggested that this acid has a beneficial effect on lipid metabolism.[38] However, the proportion of propionic acid did not increase and the ratio between acetic and propionic acid did not decrease either in the cecum or in serum, factors that are considered to be important in this respect. In recent years, butyric acid has been suggested to have a positive effect on lipid metabolism,[39] but the lower amounts of lipids in the liver could not be related to this acid either. Instead, both black currants and raspberries had lower ratios of both acetic to propionic acid and acetic to propionic plus butyric acid. It may be questioned whether it is just the total amount of SCFAs formed that is important, and not the specific acids. The soluble fiber fraction in bilberries was more fermented than those in the other berries, but these types of fibers were also more prone to form SCFAs, especially acetic acid. Interestingly, the composition of the dietary fiber was different in the soluble bilberry fraction compared with the fiber in the other soluble berry fractions. Thus, bilberries contained higher amounts of polymers consisting of xylose and glucose and lesser amounts of those consisting of uronic acids, and it might be questioned if this could be why bilberries produce more acetic acid. Another important factor may be that the rats used in this study were conventional rats; that is, they were healthy, and perhaps it is more difficult to see connections between different biological parameters in such rats. The amounts of cholesterol and triglycerides in the liver of the rats were in the same range as those found in another investigation with other types of fiber (guar gum, pectin, and a mixture of the two) using a similar rat model.[40] In that study, the dietary fibers were shown to decrease the amount of liver cholesterol to the same extent and independently of the fiber type in rats, compared with a fiber-free diet. The use of conventional rats may also explain why there were no differences in inflammatory risk markers between groups.

The cecal content and cecal tissue weights were higher with the soluble berry fractions than with the insoluble ones. This is possibly due to the dietary fiber in the soluble berry fraction retaining more water than the insoluble fraction, enlarging the cecum and increasing tissue weight.[41] The cecal tissue weight has previously been shown to be more correlated to the cecal volume than the concentration of SCFAs.[27,41] However, cecal pH was lower in groups fed diets containing the insoluble fractions. This might seem strange, but the pH has been shown to be highly correlated to the cecal concentration of SCFAs.[42] Due to the considerably lower weight of cecal content in rats fed insoluble berry fractions, the cecal concentrations were considerably higher with these fractions than with the soluble ones (SCFA concentration not shown in any table). This also shows that the concentration of SCFAs is not that interesting to elucidate, at least not in this case.

The insoluble berry fractions had fewer effects, but the insoluble fraction of black currant gave the lowest amounts of triglycerides in the liver. Interestingly, this fraction also gave the highest serum concentration and distal proportion of butyric acid, where the latter may help to improve colonic health, because most colonic diseases occur in the distal part of the colon. The insoluble fraction of black currants was composed of polysaccharides containing large amounts of mannose (32%) that was more or less completely fermented. Guar gum, another type of dietary fiber, which to a great extent is composed of mannose (galactomannan), has been shown to give high amounts of both propionic and butyric acids.[25] The insoluble bilberry fraction gave higher amounts of liver triglycerides than the other insoluble berry fractions, which may be related to the higher ratio of acetic to propionic and butyric acid in the serum of rats fed this fraction. The compositions of the dietary fiber in the insoluble bilberry and raspberry fractions were quite similar, so that could not be the reason. The intake of anthocyanins was also considerably higher with bilberries. However, it may be due to other types of antioxidants present in raspberries, for example, ellagitannins, that are able to change the composition of the microbiota and also the formation of specific SCFAs.

The present study showed that the soluble berry fractions had greater impact on parameters related to dietary fiber, such as fermentation of the dietary fiber, formation and concentration of SCFAs in the blood and cecum, and lipids in the liver, than the insoluble berry fractions, indicating an influence of the colon microbiota. The type of berry was also more important for the effects of soluble berry fractions than for the insoluble ones, which had more similar effects. Only anthocyanins in the soluble berry fraction could be seen in the urine of rats.

■ ASSOCIATED CONTENT

Ⓢ Supporting Information

Additional table. This material is available free of charge via the Internet at http://pubs.acs.org.

■ AUTHOR INFORMATION

Corresponding Author

*(G.J.) Phone: 0046 46 222 47 68. Fax: 0046 46 222 45 32. E-mail: Greta.Jakobsdottir@appliednutrition.lth.se.

Funding

This study was supported by the Antidiabetic Food Centre, a VINNOVA VINN Excellence Center at Lund University.

Notes

The authors declare no competing financial interest.

■ REFERENCES

(1) Borges, G.; Degeneve, A.; Mullen, W.; et al. Identification of flavonoid and phenolic antioxidants in black currants, blueberries, raspberries, red currants, and cranberries. *J. Agric. Food Chem.* **2010**, *58*, 3901−3909.

(2) Anderson, J. W.; Baird, P.; Davis, R. H., Jr.; et al. Health benefits of dietary fiber. *Nutr Rev.* **2009**, *67*, 188−205.

(3) Lock, K.; Pomerleau, J.; Causer, L.; et al. The global burden of disease attributable to low consumption of fruit and vegetables: implications for the global strategy on diet. *Bull. WHO* **2005**, *83*, 100−108.

(4) de Mello, V. D. F.; Schwab, U.; Kolehminen, M.; et al. A diet high in fatty fish, bilberries and wholegrain products improves markers of endothelial function and inflammation in individuals with impaired glucose metabolism in a randomised controlled trial: the Sysdimet study. *Diabetologia* **2011**, *54*, 2755−2767.

(5) Landete, J. M. Updated knowledge about polyphenols: functions, bioavailability, metabolism, and health. *Crit Rev. Food Sci. Nutr.* **2012**, *52*, 936−948.
(6) Puupponen-Pimia, R.; Nohynek, L.; Meier, C.; et al. Antimicrobial properties of phenolic compounds from berries. *J. Appl. Microbiol.* **2001**, *90*, 494−507.
(7) Wang, H.; Cao, G.; Prior, R. Oxygen radical absorbing capacity of anthocyanins. *J. Agric. Food Chem.* **1997**, *45*, 304−309.
(8) Heinonen, M. Antioxidant activity and antimicorobial effects of berry phenolics − a Finnish perspective. *Mol. Nutr. Food Res.* **2007**, *51*, 684−691.
(9) Wong, J. M.; de Souza, R.; Kendall, C. W.; et al. Colonic health: fermentation and short chain fatty acids. *J. Clin. Gastroenterol.* **2006**, *40*, 235−243.
(10) Macfarlane, S.; Macfarlane, G. T. Regulation of short-chain fatty acid production. *Proc. Nutr. Soc.* **2003**, *62*, 67−72.
(11) Macfarlane, G. T.; Macfarlane, S. Bacteria, colonic fermentation, and gastrointestinal health. *J. AOAC Int.* **2012**, *95*, 50−60.
(12) Bach Knudsen, K. E.; Serena, A.; Canibe, N.; et al. New insight into butyrate metabolism. *Proc. Nutr. Soc.* **2003**, *62*, 81−86.
(13) Scheppach, W.; Bartram, H. P.; Richter, F. Role of short-chain fatty acids in the prevention of colorectal cancer. *Eur. J. Cancer* **1995**, *31A*, 1077−1080.
(14) Galisteo, M.; Duarte, J.; Zarzuelo, A. Effects of dietary fibers on disturbances clustered in the metabolic syndrome. *J. Nutr. Biochem.* **2008**, *19*, 71−84.
(15) Lunn, J.; Buttriss, J. Carbohydrates and dietary fibre. *Nutr. Bull.* **2007**, *32*, 21−64.
(16) Palafox-Carlos, H.; Ayala-Zavala, J. F.; Gonzalez-Aguilar, G. A. The role of dietary fiber in the bioaccessibility and bioavailability of fruit and vegetable antioxidants. *J. Food Sci.* **2011**, *76*, R6−R15.
(17) Wawer, I.; Wolniak, M.; Paradowska, K. Solid state NMR study of dietary fiber powders from aronia, bilberry, black currant and apple. *Solid State Nucl. Magn. Reson.* **2006**, *30*, 106−113.
(18) Theander, O.; Åman, P.; Westerlund, E.; et al. Total dietary fiber determined as neutral sugar residues, uronic acid residues, and Klason lignin (the Uppsala method): collaborative study. *J. AOAC Int.* **1995**, *78*, 1030−1044.
(19) Asp, N. G.; Johansson, C. G.; Hallmer, H.; et al. Rapid enzymatic assay of insoluble and soluble dietary fiber. *J. Agric. Food Chem.* **1983**, *31*, 476−482.
(20) Björck, I.; Nyman, E. M.; Pedersen, B.; et al. Formation of enzyme resistant starch during autoclaving of wheat starch: studies in vitro and in vivo. *J. Cereal Sci.* **1987**, *6*, 159−172.
(21) Animal Specific Training: Rats. University of Wisconsin—Milwaukee, USA; http://www4.uwm.edu/usa/acp/training/manual/manual_rats.cfm (accessed January 22, 2014).
(22) Nyman, M.; Asp, N. G. Fermentation of dietary fibre components in the rat intestinal tract. *Br. J. Nutr.* **1982**, *47*, 357−366.
(23) Zhao, G.; Liu, J. F.; Nyman, M.; et al. Determination of short-chain fatty acids in serum by hollow fiber supported liquid membrane extraction coupled with gas chromatography. *J. Chromatogr.* **2007**, *846*, 202−208.
(24) Nyman, M.; Björck, I.; Siljeström, M.; et al. Dietary fibre in cereals − composition, fermentation and effect of processing. In *Proceedings from an International Symposium in Cereal Science and Technology in Sweden*, June 13−16, 1988; Asp, N. G., Ed.; Lund University BTJ tryck: Lund, Sweden, 1989; pp 40−54.
(25) Jakobsdottir, G.; Jädert, C.; Holm, L.; et al. Propionic and butyric acids, formed in the caecum of rats fed highly fermentable dietary fibre, are reflected in portal and aortic serum. *Br. J. Nutr.* **2013**, *110*, 1565−1572.
(26) Zhao, G.; Nyman, M.; Jönsson, J. A. Rapid determination of short-chain fatty acids in colonic contents and faeces of humans and rats by acidified water-extraction and direct-injection gas chromatography. *Biomed. Chromatogr.* **2006**, *20*, 674−682.
(27) Jakobsdottir, G.; Blanco, N.; Xu, J.; et al. Formation of short-chain fatty acids, excretion of anthocyanins, and microbial diversity in rats fed blackcurrants, blackberries, and raspberries. *J. Nutr. Metab.* **2013**, DOI: 10.1155/2013/202534.
(28) Wu, X.; Gu, L.; Prior, R. L.; et al. Characterization of anthocyanins and proanthocyanidins in some cultivars of *Ribes*, *Aronia*, and *Sambucus* and their antioxidant capacity. *J. Agric. Food Chem.* **2004**, *52*, 7846−7856.
(29) Ogawa, K.; Sakakibara, H.; Iwata, R.; et al. Anthocyanin composition and antioxidant activity of the vrowberry (*Empetrum nigrum*) and other berries. *J. Agric. Food Chem.* **2008**, *56*, 4457−4462.
(30) Mullen, W.; Larcombe, S.; Arnold, K.; et al. Use of accurate mass full scan mass spectrometry for the analysis of anthocyanins in berries and berry-fed tissues. *J. Agric. Food Chem.* **2010**, *58*, 3910−3915.
(31) Kim, B.; Ku, C. S.; Pham, T. X.; et al. *Aronia melanocarpa* (chokeberry) polyphenol-rich extract improves antioxidant function and reduces total plasma cholesterol in apolipoprotein E knockout mice. *Nutr. Res. (N.Y.)* **2013**, *33*, 406−413.
(32) Felgines, C.; Talavera, S.; Texier, O.; et al. Blackberry anthocyanins are mainly recovered from urine as mthylated and glucuronidated conjugates in humans. *J. Agric. Food Chem.* **2005**, *53*, 7721−7727.
(33) Fleshhut, J.; Kratzer, F.; Rechkemmer, G.; et al. Stability and biotransformation of various dietary anthocyanins in vitro. *Eur. J. Nutr.* **2006**, *45*, 7−18.
(34) McGhie, T. K.; Walton, M. C. The bioavailability and absorption of anthocyanins: towards a better understanding. *Mol. Nutr. Food Res.* **2007**, *51*, 702−713.
(35) Bäckhed, F.; Ding, H.; Wang, T.; et al. The gut microbiota as an environmental factor that regulates fat storage. *Proc. Natl. Acad. Sci. U.S.A.* **2004**, *101*, 15718−15723.
(36) Ekström, L. M.; Björck, I. M.; Östman, E. M. On the possibility to affect the course of glycaemia, insulinaemia, and perceived hunger/satiety to bread meals in healthy volunteers. *Food Funct.* **2013**, *4*, 522−529.
(37) Haskå, L.; Andersson, R.; Nyman, M. The effect of dietary fiber from wheat processing streams on the formation of carboxylic acids and microbiota in the hindgut of rats. *J. Agric. Food Chem.* **2011**, *59*, 3406−3413.
(38) Berggren, A. M.; Nyman, E. M.; Lundquist, I.; et al. Influence of orally and rectally administered propionate on cholesterol and glucose metabolism in obese rats. *Br. J. Nutr.* **1996**, *76*, 287−294.
(39) Marcil, V.; Delvin, E.; Garofalo, C.; et al. Butyrate impairs lipid transport by inhibiting microsomal triglyceride transfer protein in Caco-2 cells. *J. Nutr.* **2003**, *133*, 2180−2183.
(40) Jakobsdottir, G.; Xu, J.; Molin, G.; et al. High-fat diet reduces the formation of butyrate, but increases succinate, inflammation, liver fat and cholesterol in rats, while dietary fibre counteracts these effects. *PLoS One* **2013**, *13*, 8−11.
(41) Nilsson, U.; Nyman, E. M. Carboxylic acids in the hindgut of rats fed higly soluble inulin and *Bifidobacterium lactis* (Bb-123), *Lactobacillus salivarius* (UCC 500) or *Lactobacillus rhamnous* (GG). *Scand. J. Food Nutr.* **2007**, *51*, 13−21.
(42) Berggren, A.; Björck, I. M. E.; Nyman, M.; et al. Short-chain fatty acid content and pH in caecum of rats given various sources of carbohydrates. *J. Sci. Food Agric.* **1993**, *63*, 397−406.

JOURNAL OF AGRICULTURAL AND FOOD CHEMISTRY

Article

pubs.acs.org/JAFC

Phenolic Composition of Vinegars over an Accelerated Aging Process Using Different Wood Species (Acacia, Cherry, Chestnut, and Oak): Effect of Wood Toasting

Ana B. Cerezo, M. Antonia Álvarez-Fernández, Ruth Hornedo-Ortega, Ana M. Troncoso, and M. Carmen García-Parrilla*

Área de Nutrición y Bromatología, Facultad de Farmacia, Universidad de Sevilla, C/P García González no. 2, Sevilla 41012, Spain

ABSTRACT: Wood shavings are widely employed in vinegar making to reduce aging time. Accordingly, this study aims to evaluate the effects of using shavings from different wood species (acacia, cherry, chestnut, and oak) and of toasting on the release of phenolic compounds into vinegar during the aging process. The study involved aging vinegars using previously toasted shavings and untoasted ones, at 0.5% and 1% (w/v), and collecting samples at 15 and 30 days. The phenolic compounds were analyzed by LC-DAD during the aging process. As a result, wood markers naringenin and kaempferol (cherry), robinetin and fustin (acacia), and isovanillin (oak) were identified for the first time in vinegars. The results also showed that toasting wood shavings decreases the concentration of most flavonoid wood markers (e.g., (+)-taxifolin, naringenin, and fustin) in vinegar, but that it is essential for the highest releases of aldehyde compounds (syringaldehyde, protocatechualdehyde, and vanillin). Remarkably, 15 days was sufficient to obtain the highest increases of most polyphenol compounds in the vinegar. Statistical analysis (linear discriminant analysis) proved that the phenolic compounds identified in vinegars are useful for discriminating vinegars regarding the wood species of the shavings used to accelerate aging.

KEYWORDS: *acacia, cherry, chestnut, oak, vinegar, polyphenol, toasting*

INTRODUCTION

Wood chips are used extensively in enology to accelerate aging.[1−4] However, there are scarce data available for vinegar making, and the majority is fairly recent.[5,6] Most studies have focused on oak chips, since this is the most commonly used species.[5,7,8] Even though other wood species, such as acacia, chestnut, cherry, mulberry, and ash, have all been crucial in producing traditional high-quality balsamic vinegars,[9] the use of chips from these woods to diversify products remains virtually unexplored in the literature concerning vinegar making.[10]

The release of polyphenol compounds from wood chips, staves, and shavings into wine and vinegar is a matter of interest in scientific literature.[5,6,11−15] The main points of interest as regards the release of polyphenol from wood chips into beverages are wood species, wood treatment in chip making, and the beverage matrix. Several recent studies have evaluated the release of polyphenol compounds from different heartwoods, such as cherry, chestnut, acacia, ash, etc., for their further use in cooperage.[16−21] Certain phenolic compounds have been established as wood markers, such as naringenin, isosakuranetin, eriodictyol, aromadendrin, and (+)-taxifolin in cherry wood;[19,21,22] (+)-dihydrorobinetin, fustin, robinetin, robtin, butin, and leucorobinetinidin in acacia wood;[10,20,21] gallic and ellagic acid and hydrolyzable tannins of both the ellagitannins and gallotannins in chestnut wood;[21,23] and oleuropein, ligstroside, olivil, verbascoside, isoverbascoside, oleoside, tyrosol, syringaresinol, and cyclolovil in ash wood.[21]

The thermic treatment of wood is a determining factor in the release of polyphenols. Indeed, aldehydes, such as protocatechualdehyde and coniferaldehyde, have not been reported in vinegars aged in untoasted oak barrels,[22] while they have been identified in vinegars aged in toasted oak barrels.[24] These studies have recorded that vanillin took 7 months longer to be released in untoasted oak barrels than in toasted ones.[22,24] Further to this, it has also been shown that toasting led to the formation of benzoic acids (protocatechuic acid, *p*-hydroxybenzoic acid, vanillic acid, and syringic acid) in cherry and chestnut heartwood, and cinnamic acids (caffeic acid and ferulic acid) in acacia and chestnut heartwood, due to lignin degradation,[19−21] while it resulted in the degradation of flavonoid markers.[19−21] To be specific, (+)-dihydrorobinetin concentration decreased 20-fold in vinegar that was aged with toasted acacia shavings.[10] What is more, the concentration of (+)-taxifolin in cherry heartwood was reduced by 97% when it was toasted.[19] Previous studies have further reported that condensed and hydrolyzable tannin concentrations diminished remarkably (70−95%) or even disappeared in toasted cherry, acacia, and chestnut heartwood when compared to seasoned heartwood, due to their heat-sensitive nature.[19−21]

WINEGAR European Project (COOP-CT-2005-017269) identified certain phenolic compounds as markers in high-quality vinegar aged in different untoasted wood barrels, such as acacia (dihydrorobinetin), cherry ((+)-taxifolin), and chestnut (high concentration of gallic acid and gallic ethyl ester). This paper aims to evaluate the effect of toasting on the release of the wood markers previously established by WINEGAR and polyphenols, in general, from acacia, cherry, chestnut, and oak shavings into vinegar. Besides this, we intend to assess the use

Received: October 18, 2013
Accepted: April 17, 2014
Published: April 17, 2014

ACS Publications © 2014 American Chemical Society

Table 1. Quantitive Evaluation of Phenolic Compounds in Vinegars Aged with Cherry and Chestnut Shavings

	concentration (mg/L)															
	cherry								chestnut							
	toasted				untoasted				toasted				untoasted			
	0.5%[a]		1%		0.5%		1%		0.5%		1%		0.5%		1%\	
compounds	15 d[b]	30 d	15 d	30 d	15 d	30 d	15 d	30 d	15 d	30 d	15 d	30 d	15 d	30 d	15 d	30 d
gallic acid	32.0 ac[c]	34.14 ac	43.6 ad	44.14 ad	38.33 be	46.9 bf	43.97 be	55.1 bf	34.1 ac	35.8 ac	54.9 ad	54.9 ad	98.2 bc	107.6 bc	157.3 bde	219.1 bdf
protocatechuic acid	ni[d]	ni	ni	ni	ni	ni	ni	ni	1.05	1.11	0.76	1.06	1.20	0.98	1.13	1.58
3-*O*-methylgallic acid	3.01	2.54	3.32	2.19	2.92	2.93	2.33	2.82	3.04	2.9	2.55	2.79	2.45	2.51	2.20	2.38
protocatechualdehyde	3.88 ac	4.02 ac	6.95 ad	6.98 ad	ni b	ni b	ni b	ni b	ni	ni	ni	ni	ni	ni	ni	ni
tyrosol	30.8	27.2	33.1	28.6	33.9	36.90	28.78	39.2	32.60	32.52	32.6	31.9	33.2	28.1	33.38	28.24
syringic acid	25.87	28.0	26.9	25.8	19.38	27.24	23.70	32.1	27.4	30.6	31.1	34.9	22.1	26.0	21.4	25.0
vanillin	ni	ni	ni	ni	ni	ni	ni	ni	0.89 a	0.71 a	0.86 a	0.89 a	0.51 b	0.55 b	0.58 b	0.46 b
gallic ethyl ester	11.3 a	10.44 a	10.3 a	9.4 a	4.9 b	5.1 b	4.8 be	3.11 bf	10.67 a	10.9 a	10.6 a	11.39 a	12.06 b	11.65 b	14.6 b	12.7 b
syringaldehyde	ni	ni	ni	ni	ni	ni	ni	ni	7.94 ac	8.04 ac	13.82 ad	14.70 ad	ni b	ni b	ni b	ni b
(+)-taxifolin	2.77 ac	2.67 ac	5.70 ad	5.2 ad	8.78 bce	9.59 bcf	17.3 bde	26.46 bdf	ni	ni	ni	ni	ni	ni	ni	ni
ellagic acid	ni	ni	ni	ni	ni	ni	ni	ni	8.04 ac	8.12 ac	10.51 ad	11.37 ad	5.63 b	4.91 b	7.77 b	5.73 b
naringenin	7.23 ac	7.4 ac	12.7 ad	12.4 ad	21.9 bc	21.7 bc	40.44 bd	40.5 bd	ni	ni	ni	ni	ni	ni	ni	ni
caftaric acid	ni	ni	ni	ni	ni	ni	ni	ni	114.5	109.9	126.63	114.8	122.0	117.11	126.18	108.4
caffeic acid	3.40	3.70	3.85	3.22	3.21	3.94	3.54	4.09	ni	ni	ni	ni	ni	ni	ni	ni
p-cuomaric acid	1.96	1.63	1.49	1.49	1.06	1.29	1.13	1.32	2.06	2.01	1.75	1.84	1.81	1.44	1.69	1.64
quercetin-3-glucoside	19.30 a	19.64 a	19.6 ae	17.2 af	15.7 be	13.77 bf	14.25 be	9.51 bf	22.7 a	19.2 a	20.9 a	18.1 a	12.27 b	13.86 b	13.9 b	14.4 b
kaempferol	10.19 ac	9.7 ac	12.79 ad	12.7 ad	6.2 bc	5.9 bc	9.7 bd	10.57 bd	ni	ni	ni	ni	ni	ni	ni	ni

[a]%, w/v. [b]Days. [c]Letters a and b in the same column indicate significant differences ($p < 0.05$) between different treatments (toasted and untoasted) within the same wood. Letters c and d in the same column indicate significant differences ($p < 0.05$) between different shaving % within the same treatment and wood. Letters e and f in the same column indicate significant differences ($p < 0.05$) between different aging time within the same treatment, shaving %, and wood. [d]Not identified.

dx.doi.org/10.1021/jf500654d | J. Agric. Food Chem. 2014, 62, 4369−4376

Table 2. Quantitive Evaluation of Phenolic Compounds in Vinegars Aged with Acacia and Oak Shavings

	concentration (mg/mL)															
	acacia								oak							
	toasted				untoasted				toasted				untoasted			
	0.5%[a]		1% (%, w/v)		0.5% (%, w/v)		1% (%, w/v)		0.5% (%, w/v)		1% (%, w/v)		0.5% (%, w/v)		1% (%, w/v)	
compounds	15 d[b]	30 d	15 d	30 d	15 d	30 d	15 d	30 d	15 d	30 d	15 d	30 d	15 d	30 d	15 d	30 d
gallic acid	29.0 ac[c]	28.8 ac	30.6 ad	32.8 ad	17.3 be	27.3 bf	20.48 be	28.16 bf	44.7 a	45.59 a	39.7 a	35.9 a	47.91 bc	47.4 bc	50.07 bd	50.2 bd
3-*O*-methylgallic acid	3.16	3.02	3.06	3.42	3.03	3.44	3.09	3.1	ni[d]	ni	ni	ni	ni	ni	ni	ni
protocatechualdehyde	30.8 ac	33.9 ac	52.1 ad	58.8 ad	18.92 b	19.45 b	19.6 b	19.6 b	ni	ni	ni	ni	ni	ni	ni	ni
tyrosol	33.8	32.65	32.9	35.6	32.9	32.6	33.66	30.95	38.5	36.5	34.72	30.3	29.4	39.4	38.2	37.12
dihydrorobinetin[e]	11.1 a	11.6 ac	20.06 ad	23.50 ad	234.6 bc	246.8 bc	388.5 bd	384.8 bd	ni	ni	ni	ni	ni	ni	ni	ni
syringic acid	23.5	26.50	25.13	29.8	22.31	25.70	21.73	23.70	25.9	29.5	29.6	32.6	23.1	26.7	22.60	26.1
vanillin	1.15 a	1.51 a	1.40 a	1.66 a	0.88 b	0.90 b	0.85 b	0.81 b	2.36 a	2.27 a	2.6 a	2.60 a	2.12 b	2.40 b	2.18 b	2.24 b
isovanillin	ni	ni	ni	ni	ni	ni	ni	ni	0.76 ac	1.11 ac	2.07 ad	2.75 ad	0.61 b	0.94 b	0.32 b	0.69 b
gallic ethyl ester	11.3	10.89	9.9	11.57	11.50	11.78	10.3	8.4	6.3 c	6.31 c	8.63 d	10.86 d	8.6 c	9.40 c	7.1 d	7.0 d
fustin	2.45 ac	2.44 ac	3.65 ade	4.08 adf	11.1 be	12.16 bf	12.18 be	29.00 bf	ni	ni	ni	ni	ni	ni	ni	ni
syringaldehyde	3.7 ac	4.28 ac	6.68 ade	7.19 adf	ni b	ni b	ni b	ni b	2.89 ac	3.03 ac	4.63 ad	4.64 ad	ni b	ni b	ni b	ni b
ellagic acid	3.42	3.55	3.6	4.2	4.3	3.7	4.06	3.7	6.13 ac	5.65 ac	8.66 ad	8.33 ad	4.8 bc	4.69 bc	6.65 bd	6.59 bd
robinetin	55.28 ace	61.74 acf	88.9 ade	102.89 adf	44.5 bc	54.3 bc	62.70 bde	73.17 bdf	ni	ni	ni	ni	ni	ni	ni	ni
caftaric acid	98.2	99.6	88.2	71.7	72.4	78.4	72.54	84.92	55.3	67.7	92.3	99.2	86.3	102.4	84.9	74.8
p-cuomaric acid	1.0	1.8	1.71	2.06	1.78	1.89	1.79	1.46	2.2	1.53	1.58	1.64	1.44	1.52	3.72	1.55
quercetin-3-glucoside	14.9	18.50	18.2	14.2	16.15	19.1	17.74	18.29	21.6	19.73	21.02	17.98	20.8	18.23	20.4	17.8

[a]%, w/v. [b]Days. [c]Letters a and b in the same column indicate significant differences ($p < 0.05$) between the different treatments (toasted and untoasted) within the same wood. Letters c and d in the same column indicate significant differences ($p < 0.05$) between the different shaving % within the same treatment and wood. Letters e and f in the same column indicate significant differences ($p < 0.05$) between the different aging time within the same treatment, shaving % and wood. [d]Not identified. [e]Previously reported (Cerezo et al., 2009).

dx.doi.org/10.1021/jf500654d | J. Agric. Food Chem. 2014, 62, 4369−4376

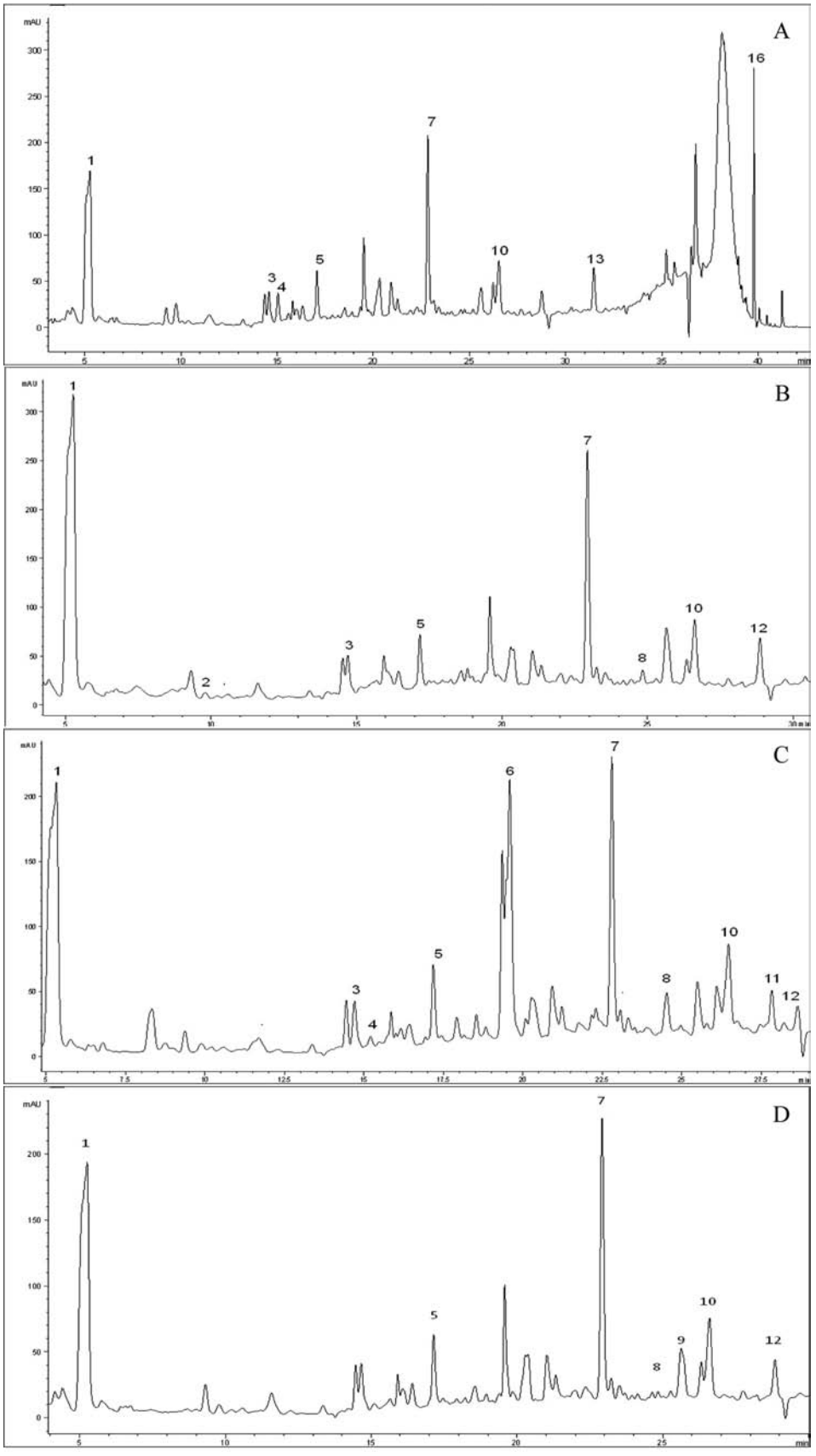

Figure 1. LC-DAD chromatograms (280 nm) of vinegars aged with 1% of cherry (A), chestnut (B), acacia (C), and oak (D) shavings along 30 days: 1, gallic acid; 2, protocatechuic acid; 3, 3-*O*-methylgallic acid; 4, protocatechualdehyde; 5, tyrosol; 6, dihydrorobinetin; 7, syringic acid; 8, vanillin; 9, isovanillin; 10, gallic ethyl ester; 11, fustin; 12, syringaldehyde; 13, (+)-taxifolin; 14, ellagic acid; 15, robinetin; 16, naringenin.

dx.doi.org/10.1021/jf500654d | *J. Agric. Food Chem.* 2014, 62, 4369−4376

of shavings as an option to shorten aging time, in order to produce differentiated high-quality products more economically.

MATERIALS AND METHODS

Woods and Vinegar. A young, monovarietal, *Cabernet Sauvignon* red wine, a 2007 vintage, produced under controlled experimental conditions by the "Rancho La Merced" research center (Jerez de la Frontera, Spain), was used to produce the vinegar samples under conditions described in a previous study.[25] The resulting vinegar had 8.97 g/100 mL of acetic acid and an alcoholic degree of 1.33° (%, v/v).

Acacia (*Robina pseudoacacia*), cherry (*Prunus avium*), chestnut (*Castanea sativa*), and oak (*Quercus sps.*) wood shavings (5−10 mm) were provided by Boteria Torner S.L. (Barcelona, Spain). Vinegar samples were aged for 15 and 30 days using previously toasted (at 180 °C for 3 h in the oven) and untoasted shavings at 0.5% and 1% (w/v). A total of 32 samples were analyzed in duplicate. Samples were filtered through a Millex-LCR 13 mm filter before injection.

LC-DAD Identification and Quantification of Phenolic Compounds. LC analyses of phenolic compounds were performed using an Agilent series 1100 system equipped with a quaternary pump (series 1100 G1311A), automatic injector (series 1100 G1313A), and degasser (series 1100 G1379A). Detection was carried out using a UV/vis diode detector (series 1100 G1315B) coupled to a Chemstation HP A.10.02 (HP/Agilent). The column was an Agilent Zorbax SB-C18, 4.6 × 250 mm and particle size 3.5 μm. The chromatographic conditions had previously been used for vinegar analysis.[5] The method uses a binary gradient, A (glacial acetic acid/water pH 2.65) and B (20% A + 80% acetonitrile), programmed for the following gradient: 0 min 0% B; 5 min 2% B; 10 min 4% B; 15 min 10% B; 30 min 20% B; 35 min 30% B; 40 min 100% B; 45 min 0% B. The sample volume injected was 50 μL. The flow rate was 1.5 mL/min, and the temperature was set at 40 °C. Quantification was performed by external calibration with respective standards, using detection at 365 nm (robinetin, quercetin-3-glucoside, and kaempferol), 320 nm (hydroxycinnamic acids and syringaldehyde), and 280 nm (the remaining compounds). Once successful spectral matching had taken place, the results were confirmed by spiking with respective standards to achieve a complete identification by means of the peak purity test. The peaks that did not fulfill these requirements were not quantified.

The standards of the identified phenolic compounds were purchased from Fluka [caffeic acid, gallic acid, *p*-coumaric acid, gallic ethyl ester, quercetin-3-glucoside, isovanillin, and tyrosol], Sigma [(+)-taxifolin, ellagic acid, syringic acid, protocatechualdehyde, kaempferol, protocatechuic acid, and syringaldehyde], Merck [vanillin], Extrasynthese [fustin and robinetin], and Chromadex [3-*o*-methylgallic acid, caftaric acid, and naringenin]. Dihydrorobinetin was isolated from vinegar.[10]

Statistical Analyses. Statistical analyses were performed using Statistica software.[26] One-way analysis of variance (ANOVA) was used to test significant differences between (i) samples aged with toasted and untoasted shavings, (ii) vinegars aged for different periods, and (iii) vinegars aged with different shaving proportions. Linear discriminant analysis (LDA) enabled functions to be constructed to classify samples according to the type of wood or wood toasting with which they were in contact. The forward stepwise method achieved the best results.

RESULTS AND DISCUSSION

A total of 21 phenolic compounds were detected in vinegars aged with cherry, acacia, chestnut, and oak wood shavings (Tables 1 and 2). Figure 1 shows the chromatograms of the vinegars aged with each wood. The concentrations of phenolic acids (gallic acid and ellagic acid) and their esters (gallic ethyl ester), phenolic aldehydes (protocatechualdehyde, vanillin, isovanillin, and syringaldehyde), and flavonoids ((+)-taxifolin, naringenin, kaempferol, quercetin-3-glucoside, robinetin, and fustin) changed depending on toasting, shaving percentage, and aging time. None of the other compounds changed under the different conditions.

Polyphenol Compounds Identified for the First Time in Vinegars. Naringenin and kaempferol were both identified for the first time in vinegars aged with cherry wood, confirming previous studies that have described them as a marker in cherry heartwood.[19,21,27] Recently, prunin and eriodictyol were established as markers of wine aged with cherry wood because they were determined after 2 months aging with cherry chips.[28] The values reported were low: concentrations ranged between 0.24 and 0.65 mg/L (eriodictyol) and between 0.31 and 0.97 mg/L (prunin). The shorter length of our experiment may account for the absence of the above-mentioned compounds in our samples. It would be worthwhile verifying whether these compounds could be a marker of the time in contact with this wood, in addition to their value as cherry species markers.

This is the first time that robinetin and fustin compounds have been determined in vinegars aged with acacia wood. They have been previously identified in acacia heartwood[20,29] and in red wine aged in acacia wood barrels,[30] but not in vinegars.

Isovanillin was detected only in vinegars aged with oak shavings. Thus, isovanillin can be proposed as a marker of vinegars in contact with oak wood. As far as we know, this is the first time isovanillin has been identified in vinegars in contact with oak wood. Hydroxycinnamic aldehydes such as coniferaldehyde and sinapaldehyde have been detected in previous studies in wood extracts using methanol/water (1:1), diethyl ether, and ethyl acetate as solvent.[19−21] They have not been not detected either in wine aged with these woods[28] or in vinegars that likely involved a matrix effect. Furthermore, in these studies, wood extracts were subsequently treated to concentrate minor compounds.[19−21] Conversely, our samples were only filtered before injection, to prevent any artifact formation during sample treatment. The absence of the sample treatment and concentration step in our experiment explains the absence of these compounds in our samples.

In summary, further to (+)-taxifolin and (+)-dihydrorobinetin, which have previously been identified in vinegars aged in cherry and acacia wood,[10,22] naringenin and kaempferol are also good markers of vinegars aged with cherry wood, and robinetin and fustin are wood markers of acacia.

Effect of Wood Toasting on Phenolic Composition. In general, toasting was crucial for decreasing the concentrations of flavonoids ((+)-taxifolin, naringenin, and fustin) and a certain phenolic acid (gallic acid). Furthermore, wood toasting is essential for the release of certain compounds, such as aldehydes, into the vinegar, which is crucial for quality and sensory purposes.[31] Indeed, vinegars that have no contact with wood maintain their polyphenolic composition with no changes.[32]

In our results, (+)-taxifolin concentration was 4−5 times higher in vinegars aged with untoasted shavings compared to vinegars aged with toasted shavings (Table 1). (+)-Taxifolin has been previously described as a marker of vinegar aged in untoasted cherry wood barrels,[22] but no studies have yet been performed to elucidate on the effect of toasting on its release into the vinegar. Sanz et al.[19] found that the (+)-taxifolin content in seasoned cherry wood was more than 35 times higher than in toasted wood. In this study, toasting showed similar effects on naringenin, where its concentration was 3 times higher in samples aged with untoasted cherry wood shavings (Table 1). Some authors have also shown toasting to

be crucial in the release of naringenin from cherry wood, its content being 9 times higher in seasoned heartwood compared to toasted heartwood.[19] A matrix effect should explain the differences in these concentration values obtained. Differences are greater if a solvent such as methanol/water (1:1), diethyl ether, or ethyl acetate[19] is used rather than wine[28] or vinegar (Table 1). In fact, red wine aged with toasted cherry chips has shown double the concentration of (+)-taxifolin[28] compared to our vinegar aged with toasted cherry chips in a similar proportion (Table 1), as a consequence of the higher solubility of this compound in an ethanol matrix. However, in similar conditions (toasting and chips content) naringenin showed similar concentrations in wine[28] and vinegar (Table 1).

The release of fustin into the vinegar was also affected by toasting; it presented a concentration 6−7 times higher in vinegars aged with untoasted acacia wood shavings (Table 2). Previous studies have reported that fustin is highly sensitive to thermic treatment; acacia heartwood toasted at medium plus conditions (185 °C for 45 min) did not show fustin content, while there was a high concentration in the seasoned one.[20] Similar thermic sensitivity has been previously described for (+)-dihydrorobinetin, which presented a concentration 20 times higher in vinegars aged with untoasted acacia shavings compared to the toasted ones.[10] In contrast, toasting had the reverse effect on robinetin content, which presented concentrations between 12 and 29% higher in vinegars aged with toasted acacia shavings (Table 2). Previous studies state that robinetin does not change significantly with toasting in acacia heartwood[20] and wine aged with acacia wood barrels,[30] appearing to be quite stable when heated.

A high concentration of gallic acid has been described as a marker of vinegars in contact with chestnut wood.[23] The present study shows that gallic acid was significantly influenced by toasting, showing concentrations more than 3 times higher in vinegars aged with untoasted shavings (Table 1). Sanz et al. agrees that gallic acid is extremely sensitive to heat treatment.[21]

On the other hand, phenolic aldehyde concentrations were higher in vinegars aged with toasted shavings, in accordance with previous data reported comparing toasted and untoasted heartwoods.[16,21] In particular, syringaldehyde was restricted to vinegars aged with toasted shavings (Tables 1 and 2). Wood species determined the release of aldehydes and their concentration in the vinegar. Specifically, protocatechualdehyde was identified in cherry and acacia; vanillin and syringaldehyde in acacia, chestnut, and oak; and isovanillin only in oak wood (Tables 1 and 2).

In addition to the aldehyde compounds, toasting significantly increased the release of ellagic acid in vinegars aged with chestnut and oak wood shavings, showing significantly higher ellagic acid concentration in those aged with chestnut wood. Previous studies also agree that toasting favors the release of this compound.[33] Kaempferol concentration was also significantly increased with toasting in vinegars aged with cherry shavings (Table 1). In contrast, Sanz et al. showed that kaempferol content was higher in seasoned cherry heartwood than in toasted heartwood.[19]

Effect of Shaving Amount and Aging Time on Phenolic Composition. It would seem likely that the higher the shaving percentage (w/v) used, the higher the content of phenolic compounds released into the vinegar. This tendency was observed for (+)-taxifolin and naringenin, whose concentrations remarkably doubled, at 1% compared to 0.5% of shavings, regardless of wood treatment (Table 1). This trend has also been described for wine aged with 3 and 6 g/L of cherry chips.[28] However, other phenolic compounds such as protocatechualdehyde, kaempferol, fustin, robinetin, and isovanillin significantly increased their concentration at 1% of shavings but not in the same proportion as the shaving amount (Tables 1 and 2). On the other hand, the concentration of other phenolic compounds, vanillin for instance, did not significantly change in accordance with shaving amount (Tables 1 and 2).

Aging time has no remarkable influence on most of the phenolic compounds released from wood (Tables 1 and 2), which is in line with previous data reported, in vinegars aged with chips.[5] Fifteen days was sufficient to obtain the highest polyphenol concentrations in the vinegar, except for gallic acid, (+)-taxifolin, syringaldehyde, robinetin, and fustin (Tables 1 and 2). Gallic acid concentration significantly increased at 30 days, when aging was performed only with untoasted chestnut (1% shaving) and cherry and acacia (0.5 and 1% shaving) wood, the highest increase being with chestnut (40%), due to the high gallic acid content present in chestnut wood species.[22] The concentration of (+)-taxifolin also increased (>50%) after 30 days of aging with untoasted cherry shavings (Table 1). Additionally, we observed that the longer the time, the higher the concentration of syringaldehyde in vinegars aged only with toasted acacia shavings (1%) (Table 2).

Remarkably, (+)-taxifolin, protocatechualdehyde and vanillin showed a higher concentration in vinegars aged with shavings (Tables 1 and 2) than in vinegars aged in barrels that were made specifically using the same untoasted wood.[22] For instance, (+)-taxifolin content was more than 7 times higher in vinegars aged with untoasted cherry shavings at 1% (v/v) for one month (Table 1) compared to vinegars aged in an untoasted cherry wood barrel for six months.[22] Additionally, vinegars aged with untoasted acacia shavings at 0.5% (v/v) for 15 days (Table 2) presented a protocatechualdehyde concentration 3 times higher than in vinegars aged in untoasted acacia wood barrels for 180 days.[22] Moreover, vanillin concentration was 4 times higher in vinegars aged with untoasted oak shavings at 0.5% (v/v) for 15 days (Table 2) compared with vinegars aged in an untoasted oak wood barrel for a year.[22] On comparing robinetin concentration in vinegars aged with toasted acacia shavings at 1% (v/v) for 15 days (Table 2) to its concentration in wines aged in toasted acacia wood barrels for 6 months,[30] its concentration was observed to be 3 times higher in the former.

These data therefore support that shaving is a useful practice to accelerate the aging process and release the highest quantity of certain polyphenol compounds, including wood markers.

Statistical Analysis. Phenolic compounds are a powerful tool for discriminating vinegars produced in different origins[34] and with different acetification processes[35] and woods.[22,24] They are chemical markers for authentication purposes.[36] Since this paper found phenolic compounds in vinegars for the first time, we analyzed their capability to be used for these purposes. In order to achieve this goal, a linear discriminant analysis (LDA) was performed on the whole set of samples, grouping the vinegars according to the species of wood shavings used for aging. By means of the forward stepwise method, 16 variables were included in the model (robinetin, kaempferol, (+)-taxifolin, naringenin, vanillin, isovanillin, syringaldehyde, gallic ethyl ester, gallic acid, ellagic acid, caffeic acid, caftaric acid, protocatechuic acid, 3-*O*-methylgallic acid, quercetin-3-glucoside, and tyrosol) and 3 factors obtained. Table 3 displays the

Table 3. Correlation of Variables with the Canonical Roots Using the Forward Stepwise LDA Analysis According to the Species of Wood Used for Vinegar Aging

variables	root 1	root 2	root 3
caffeic acid	0.392 885	0.113 208	0.107 229
tyrosol	0.095 382	−0.313 251	0.290 785
quercetin-3-glucoside	0.003 531	0.242 954	0.159 681
caftaric acid	0.085 433	−0.132 525	−0.112 586
3-*O*-methylgallic acid	0.024 167	−0.135 065	0.150 303
vanillin	−0.128 460	0.165 642	−0.089 921
robinetin	−0.054 338	−0.023 099	0.274 941
protocatechuic acid	−0.020 036	−0.206 189	−0.178 797
naringenin	0.054 986	0.015 844	0.015 007
syringaldehyde	−0.013 557	−0.030 086	−0.016 787
ellagic acid	−0.050 510	−0.034 872	−0.231 856
gallic ethyl ester	−0.019 819	−0.054 281	0.006 696
kaempferol	0.136 626	0.039 368	0.037 289
(+)-taxifolin	0.043 024	0.012 397	0.011 742
gallic acid	−0.001 211	−0.039 380	−0.057 710
isovanillin	−0.021 178	0.070 516	−0.058 782

correlation of variables with the canonical roots obtained. Figure 2 shows the scatterplot obtained plotting root 1 versus root 2. The classification functions achieved 100% correct sample classifications according to wood species. Furthermore, a statistical analysis to discriminate samples according to thermal treatment of shaving was performed. Forward stepwise LDA allowed 100% of samples to be correctly classified; the variables in the model were dihydrorobinetin, kaempferol, naringenin, isovanillin, syringaldehyde, protocatechualdehyde, gallic ethyl ester, ellagic acid, caffeic acid, syringic acid, caftaric acid, protocatechuic acid, 3-*O*-methylgallic acid, and quercetin-3-glucoside. (+)-Taxifolin has been previously used as a wood marker to classify vinegars according to the kind of wood in which they were aged.[22] This paper shows for the first time that robinetin, kaempferol, and naringenin are wood markers that are useful for authentication purposes in vinegar making.

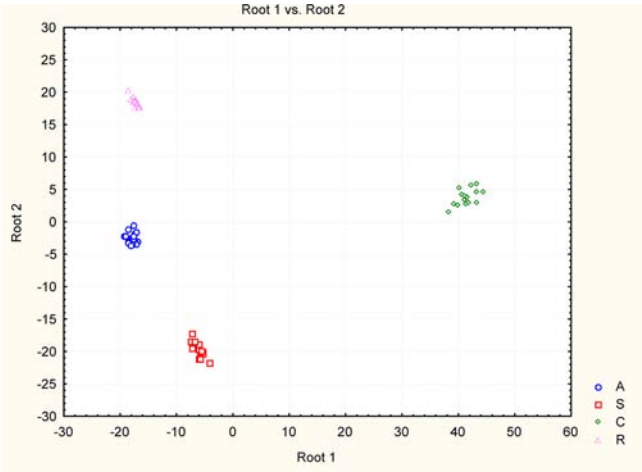

Figure 2. Plot of the first two roots issued from linear discriminant analysis (LDA): A, acacia; R, oak; S, chestnut; C, cherry.

This paper provides advanced knowledge of polyphenol composition in vinegars by describing naringenin, kaempferol, robinetin, fustin, and isovanillin in vinegars for the first time. The statistical treatment proves that certain newly detected phenolic compounds are also a useful tool for discriminating vinegars elaborated with shavings from different wood species.

Additionally, results show that toasting acacia, cherry, chestnut, and oak wood shavings mostly decreases flavonoid wood markers, such as (+)-taxifolin, naringenin, and fustin, while it is essential for the highest releases of aldehyde compounds into the vinegar. This paper provides data to develop a strategy to produce vinegars with an appropriate phenolic composition in a short time. If phenolic aldehydes are desired for their impact on the sensory properties of the product, toasting shavings is mandatory. Conversely, if the aim is to obtain a product that is rich in flavonoids, no toasting is recommended.

AUTHOR INFORMATION

Corresponding Author

*E-mail: mcparrilla@us.es. Fax: 954233765.

Funding

The authors are grateful to the European Commission (Project WINEGAR, COOP-CT-2005-017269) for financial assistance.

Notes

The authors declare no competing financial interest.

ACKNOWLEDGMENTS

The authors are grateful to Belén Puertas and Emma Cantos ("Rancho de la Merced", Jerez de la Frontera, Spain) for providing the wine.

REFERENCES

(1) Rodríguez-Bencomo, J. J.; Ortega-Heras, M.; Pérez-Magariño, S. Effect of alternative techniques to ageing on less and use of non-toasted oak chips in alcoholic fermentation on the aromatic composition of red wine. *Eur. Food Res. Technol.* **2009**, *230*, 485−496.

(2) Pérez-Magariño, S.; Ortega-Heras, M.; Cano-Mozo, E.; González-Sanjosé, M. L. The influence of oak wood chips, micro-oxygenation treatment, and grape variety on colour, and anthocyanin and phenolic composition of red wines. *J. Food Compos. Anal.* **2009**, *22*, 204−211.

(3) Del Álamo, M.; Nevares, I.; Gallego, L.; Fernández de Simón, B.; Cadahía, E. Micro-oxygenation strategy depends on origin and size of oak chips or staves during accelerated red wine aging. *Anal. Chim. Acta* **2010**, *660*, 92−101.

(4) Bautista-Ortín, A. B.; Lencina, A. G.; Cano-López, M.; Pardo-Mínguez, F.; López-Roca, J. M.; Gómez-Plaza, E. The use of oak chips during the ageing of a red wine in stainless steel tanks or used barrels: Effect of the contact time and size of the oak chips on aroma compounds. *Aust. J. Grape Wine Res.* **2008**, *14*, 63−70.

(5) Tesfaye, W.; Morales, M. L.; Benítez, B.; García-Parrilla, M. C.; Troncoso, A. M. Evolution of wine vinegar composition during accelerated aging with oak chips. *Anal. Chim. Acta* **2004**, *513*, 239−245.

(6) Durán Guerrero, E.; Castro Mejías, R.; Natera Marín, R.; Ruiz Bejarano, M. J.; Rodríguez Dodero, M. C.; García Barroso, C. Accelerated aging of a Sherry wine vinegar on an industrial scale employing microoxygenation and oak chips. *Eur. Food Res. Technol.* **2011**, *232*, 241−254.

(7) Gonalves, F. J.; Jordao, A. M. Changes in antioxidant activity and the proanthocyanidin fraction of red wine aged in contact with portuguese (Quercus Pyrenaica Willd.) and American (Quercus Alba L.) oak wood chips. *Ital. J. Food Sci.* **2009**, *21*, 51−64.

(8) Frangipane, M. T.; Santis, D. D.; Ceccarelli, A. Influence of oak woods of different geographical origins on quality of wines aged in barriques and using oak chips. *Food Chem.* **2007**, *103*, 46−54.

(9) Hillmann, H.; Mattes, J.; Brockhoff, A.; Dunkel, A.; Meyerhof, W.; Hofmann, T. Sensomics Analysis of Taste Compounds in Balsamic Vinegar and Discovery of 5-Acetoxymethyl-2-furaldehyde

as a Novel Sweet Taste Modulator. *J. Agric. Food Chem.* **2012**, *60*, 9974−9990.
(10) Cerezo, A. B.; Espartero, J. L.; Winterhalter, P.; García-Parrilla, M. C.; Troncoso, A. M. (+)-Dihydrorobinetin: a marker of vinegar ageing in acacia (Robinia pseudoacacia) Wood. *J. Agric. Food Chem.* **2009**, *57*, 9551−9554.
(11) Del Álamo, M.; Nevares, I. Wine aging in bottle from artificial systems (staves and chips) and oak woods. *Anal. Chim. Acta* **2006**, *563*, 255−263.
(12) Del Álamo, M.; Fernández, J. A.; De Castro, R. Changes in phenolic compounds and color parameters of red wine aged with oak chips and in oak barrels. *Food Sci. Technol. Int.* **2004**, *10*, 233−241.
(13) Del Álamo, M.; Nevares, I.; Cárcel, L. M.; Navas, L. Analysis for low molecular weight phenolic compounds in a red wine aged in oak chips. *Anal. Chim. Acta* **2004**, *513*, 229−237.
(14) Monedero, L.; Olalla, M.; Quesada, J. J.; López-García, H.; López, M. C. Exhaustion techniques in the selection and description of phenolic compounds in Jerez wine extracts obtained by an accelerated aging technique. *J. Agric. Food Chem.* **1998**, *46*, 1754−1764.
(15) Monedero, L.; Olalla, M.; Villalón, M.; López-García, H.; López, M. C. Standardisation of the chromatic characteristics of sobretablas wine macerates obtained by an accelerated ageing technique using heating and oak shavings. *Food Chem.* **2000**, *69*, 47−54.
(16) Alañón, M. E.; Castro-Vázquez, L.; Díaz-Maroto, M. C.; Hermosín-Gutiérrez, I.; Gordon, M. H.; Pérez-Coello, M. S. Antioxidant capacity and phenolic composition of different woods used in cooperage. *Food Chem.* **2011**, *129*, 1584−1590.
(17) De Rosso, M.; Cancian, D.; Panighel, A.; Dalla Vedova, A.; Flamini, R. Chemical compounds released from five different woods used to make barrels for aging wines and spirits: volatile compounds and polyphenols. *Wood Sci. Technol.* **2009**, *43*, 375−385.
(18) Garcia, R.; Soares, B.; Barrocas Dias, C.; Costa Freitas, A. M.; Cabrita, M. J. Phenolic and furanic compounds of Portuguese chestnut and French, American and Portuguese oak wood chips. *Eur. Food Res. Technol.* **2012**, *235*, 457−467.
(19) Sanz, M.; Cadahía, E.; Esteruelas, E.; Muñoz, A. M.; Fernández de Simón, B.; Hernández, T.; Estrella, I. Phenolic Compounds in Cherry (Prunus avium) Heartwood with a View to Their Use in Cooperage. *J. Agric. Food Chem.* **2010**, *58*, 4907−4914.
(20) Sanz, M.; Fernández de Simón, B.; Esteruelas, E.; Muñoz, A. M.; Cadahía, E.; Hernández, T.; Estrella, I.; Pinto, E. Effect of Toasting Intensity at Cooperage on Phenolic Compounds in Acacia (Robinia pseudoacacia) Heartwood. *J. Agric. Food Chem.* **2011**, *59*, 3135−3145.
(21) Sanz, M.; Fernández de Simón, B.; Cadahía, E.; Esteruelas, E.; Muñoz, A. M.; Hernández, T.; Estrella, I. Polyphenolic profile as a useful tool to identify the wood used in wine aging. *Anal. Chim. Acta* **2012**, *732*, 33−45.
(22) Cerezo, A. B.; Tesfaye, W.; Soria-Díaz, M. E.; Torija, M. J.; Mateo, E.; García-Parrilla, M. C.; Troncoso, A. M. Effect of wood on the phenolic profile and sensory properties of wine vinegars during ageing. *J. Food Compos. Anal.* **2010**, *23*, 175−184.
(23) Cerezo, A. B.; Tesfaye, W.; Torija, M. J.; Mateo, E.; García-Parrilla, M. C.; Troncoso, A. M. The phenolic composition of red wine vinegar produced in barrels made from different woods. *Food Chem.* **2008**, *109*, 606−615.
(24) Tesfaye, W.; Morales, M. L.; García-Parrilla, M. C.; Troncoso, A. M. Evolution of phenolic compounds during an experimental aging in wood of Sherry vinegar. *J. Agric. Food Chem.* **2002**, *50*, 7053−7061.
(25) Cerezo, A. B.; Cuevas, E.; Winterhalter, P.; García-Parrilla, M. C.; Troncoso, A. M. Anthocyanin composition in Cabernet sauvignon red wine vinegar obtained by submerged acetification. *Food Res. Int.* **2010**, *43*, 1577−1584.
(26) Statsoft, INC. *STATISTICA for Windows (Computer program manual)*; Staftsoft, Inc.: 2300 East 14th Street, Tulsa, OK, 2001; pp 74104−4442.
(27) Vinciguerra, V.; Luna, M.; Bistoni, A.; Zollo, F. Variation in the composition of the heartwood flavonoids of Prunus avium by on-column capillary gas chromatography. *Phytochem. Anal.* **2003**, *14*, 371−377.
(28) Fernández de Simón, B.; Sanz, M.; Cadahía, E.; Martínez, J.; Esteruelas, E.; Muñoz, A. M. Polyphenolic compounds as chemical markers of wine ageing in contact with cherry, chestnut, false acacia, ash and oak wood. *Food Chem.* **2014**, *143*, 66−76.
(29) Magel, E.; Jay-Allemand, C.; Ziegler, H. Formation of heartwood substances in the stemwood of Robinia pseudoacacia L. II. Distribution of nonstructural carbohydrates and wood extractives across the trunk. *Trees* **1994**, *8*, 165−171.
(30) Sanz, M.; Fernández de Simón, B.; Esteruelas, E.; Muñoz, A. M.; Cadahía, E.; Hernández, T.; Estrella, I.; Martinez, J. Polyphenols in red wine aged in acacia (Robinia pseudoacacia) and oak (Quercus petraea) wood barrels. *Anal. Chim. Acta* **2012**, *732*, 83−90.
(31) Giudici, P.; Gullo, M.; Solieri, L.; Falcone, P. M. Technological and Microbiological Aspects of Traditional Balsamic Vinegar and Their Influence on Quality and Sensorial Properties. *Adv. Food Nutr. Res.* **2009**, *58*, 137−182.
(32) Xu, Q.; Tao, W.; Ao, Z. Antioxidant activity of vinegar melanoidins. *Food Chem.* **2007**, *102*, 841−849.
(33) Sarni, F.; Moutounet, M.; Puech, J. L.; Rabier, P. H. Effect of heat treatment of oak wood extractable compounds. *Holzforschung* **1990**, *44*, 461−466.
(34) García-Parrilla, M. C.; González, G. A.; Heredia, F. J.; Troncoso, A. M. Differentiation of Wine Vinegars Based on Phenolic Composition. *J. Agric. Food Chem.* **1997**, *45*, 3487−3492.
(35) García-Parrilla, M. C.; Heredia, F. J.; Troncoso, A. M. The influence of the acetification process on the phenolic composition of wine vinegars. *Sci. Aliments* **1998**, *18*, 211−221.
(36) García-Parrilla, M. C.; Cerezo, A. B.; Tesfaye, W.; Troncoso, A. M. Phenolic compounds as markers for the authentication of Sherry vinegars: A foresight for high quality vinegars characterization. In *Progress in Authentication of Food and Wine*; Ebeler, S. E., Takeoka, G. R., Winterhalter, P., Eds.; American Chemical Society: Washington, DC, 2011; pp 201−213.

JOURNAL OF AGRICULTURAL AND FOOD CHEMISTRY

Article

pubs.acs.org/JAFC

Do Sun- versus Shade-Grown Kiwifruits Perform Differently upon Storage? An Overview of Fruit Maturity and Nutraceutical Properties of Whole and Fresh-Cut Produce

Marco Landi, Francesca Tardelli, Damiano Remorini, Rossano Massai, and Lucia Guidi*

Department of Agriculture, Food and Environment, University of Pisa, 56124 Pisa, Italy

ABSTRACT: Fresh-cut produce represents a good method to save about 25% of the kiwifruit not useful to meet the fresh fruit-marketing standard due to improper size and shape. For that reason, fresh-cut kiwifruit has been extensively studied. However, the comprehension of the influence of some aspects of cultivation might further increase the shelf life as well as the nutritional values of that fruit. This study explored the hypothesis that kiwifruits grown fully exposed to sunlight or partially shaded differently perform upon storage as whole fruit and as minimally processed produce. Flesh firmness (FF), total solids soluble (SSC), ascorbate (AA_T), flavonoids (TFO), and phenols (TF) contents were evaluated in sliced and whole fruit upon 3 days of storage at 4 °C after 75 days of cold chamber storage at 0 °C. The activities of two enzymes related to the softening process, polygalacturonase (PG) and pectinmethylesterase (PME), were evaluated as well. FF and SSC were constitutively higher in sun-exposed fruit, and those characteristics remained higher during the storage as whole fruit. Greater constitutive content of AA_T, TFO, and TP was found in sun-exposed whole fruit, although after cutting the reduction in their content was significantly lower in shaded fruits. PME and PG activities were higher only in whole shaded fruits, whereas no relevant differences occurred after cutting. In summary, sun-exposed fruits were more suitable for the fresh-fruit market, whereas the shaded counterpart displayed a good predisposition for use as fresh-cut produce, maintaining similar fruit maturity properties but higher nutraceutical values when sliced than fruit grown under full sun.

KEYWORDS: *Actinidia deliciosa 'Hayward', antioxidant, ascorbic acid, flavonoids, phenols, shelf life*

INTRODUCTION

Kiwifruit [*Actinidia deliciosa* (A. Chev.) C.F. Liang and A.R. Ferguson cv. 'Hayward'] is a highly nutritious fruit rich in bioactive compounds and particularly in vitamin C.[1] In fact, ascorbic acid content in kiwifruit ranges between 25 and 155 mg 100 g^{-1} of fruit fresh weight (fw).[2] Additionally, kiwifruit is a good source of a wide variety of other phytochemicals, such as polyphenols and natural antioxidant substances,[3] including β-carotene, lutein, anthocyanins, and ellagic acid.[4]

A relevant problem for the kiwifruit market is that approximately 25% of kiwifruits may not meet the fresh fruit-marketing standard due to improper size and shape. Nevertheless, these kiwifruits could be saved through processing. This is why kiwifruit importance as fresh-cut products has been targeted by several studies regarding its preservation as sliced fruit.[5,6] However, little has been reported about the physiological, microbiological, and nutritional changes that may occur in fresh-cut kiwifruit slices.[7−9] It is well-known that physical damages and wounding cause several biochemical defensive reactions where cellular decompartmentation leads to intermixing of enzymes and substrates, as well as release of acids and hydrolyzing enzymes. All of these actions limited strongly the shelf life of this kind of produce during storage,[10] kiwifruits being particularly sensitive to softening phenomena.

The amount of the bioactive compounds, as well as the maturity, is strongly influenced by different factors[11] and, among those, storage conditions have surely a great impact.[7,12] Certainly, long-term cold storage is the best method to maintain kiwifruit quality[13] considering that kiwifruit has a relatively long storage life (4−6 months at 0−4 °C). Flesh firmness (FF) is the most important parameter and the best predictor of kiwifruit ripening progress. It defines postharvest quality, considering that a 2 kg threshold is the minimum kiwifruit FF to avoid physical damage during standard postharvest handling.[14] FF is very high at harvest time (6 kg) but rapidly declines when fruit is ready to eat, between 1.3 and 1.8 kg, according to established firmness criteria.[15]

During the storage period, changes in quality characteristics are accompanied by fruit softening, a process attributable to structural changes in the cell wall. For kiwifruit, softening largely occurs as a result of the enzyme-mediated hydrolysis of cell wall, due to ethylene production.[16,17] Several enzymes are involved in this complex process, including polygalacturonase (PG; EC 3.2.1.15) and pectinmethylesterase (PME; EC 3.1.1.11). The involvement of the enzyme PG in kiwifruit softening was already confirmed;[18] PG is, indeed, the main enzyme promoting pectin solubilization as it hydrolyzes α-1,4-glycosidic bonds that hold galacturonic acid residues in de-esterified galacturonan chains produced by PME. In fact, although there is not so much clarity about that, PME activity seems to be the first involved in the softening process[19] because it is responsible for the removal of methyl groups of galacturonic acid residues from pectin,[20] leading to depolymerization.[21] After that, the rapid increase in PG activity is related to progressive increase of fruit softening.[19] PG can be classified

Received: November 8, 2013
Revised: March 21, 2014
Accepted: April 25, 2014
Published: April 25, 2014

ACS Publications © 2014 American Chemical Society

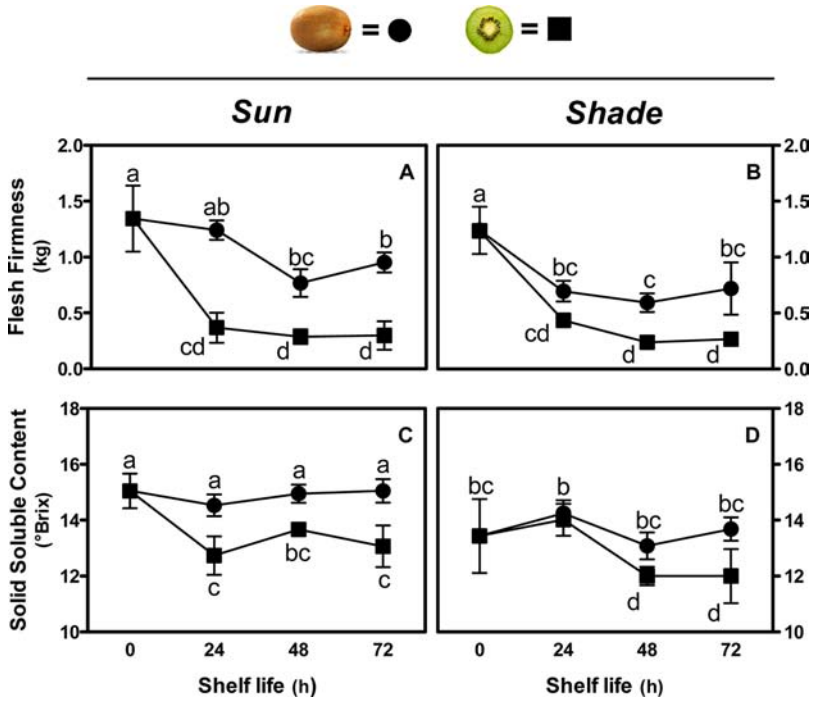

Figure 1. Flesh firmness (A, B) and solid soluble content (C, D) of full sunlight- and shade-grown Hayward kiwifruit stored for 0, 24, 48, and 72 h as fresh-cut and whole produce. Each value represents the mean of six replicates ± SD. Means were compared following two-way ANOVA test with treatment light exposure during growth and storage period as variability factors. Means flanked by the same letters are not significantly different after Fisher's least-significant difference test (LSD).

into endo-PG and exo-PG, albeit in general endo-PG is the major PG involved in kiwifruit softening.[17]

In addition to storage, canopy position, and consequently the degree of sunlight exposure of kiwifruit, represents another determinant factor to be taken into account for its influence in determining the quantity of bioactive compounds and fruit maturity characteristics. Indeed, it has been reported that fruits exposed to direct sunlight have greater sugar content when compared to fruits grown partially shaded.[22] Higher contents of AA_T, TP, and TFO were also found in full-sun-grown kiwifruits as compared to fruits collected from shade.[23] Moreover, for other fruits, a direct exposure to sunlight is responsible for making them firmer than those grown in the shade.[24]

The aim of this work was the evaluation of fruit maturity and nutritional characteristics of 75 day cold-stored kiwifruit grown under full sun or partially shaded, either as whole fruit or as minimally processed produce upon storage, to establish which was more suitable or, in other terms, less depreciable and with a reduced loss of quality for each type of market segment (as whole fruit or minimally processed produce).

■ MATERIALS AND METHODS

Fruit Material. Trials were carried out in 2009 and 2010 seasons on fruits from a commercial kiwifruit orchard located in Rigoli, Pisa, Italy (43°78′71″ N, 10°24′52″ E), where vines were treated as a free palmette. *A. deliciosa* (cultivar 'Hayward') fruits were harvested in November 2009 and 2010. Climatic parameters were continuously monitored by means of a stationary weather station from fruit set to fruit harvest; minimum and maximal temperatures averaged 20 and 28 °C, respectively, and maximum temperature reached 31−34 °C during sunny hours. Daily global radiation and mean air temperature averaged, respectively, 12.3 MJ m^{-2} and 25.7 °C. Detailed information about precipitation distribution within the growing period and relative humidity conditions are available at http://www.meteopisa.net/archivio_storico/.

To evaluate the effect of solar irradiation, fruits were harvested both from external portions of the canopy, characterized by 100% of daily intercepted solar radiation, and from partially shaded portions (−80 to −90% of incident sunlight). Immature fruits were immediately stored at 0 °C in a cold chamber, and the evaluation of quality, fruit maturity, and physiological indices was performed after 75 days of cold storage.

Slice Preparation. Forty kiwifruits, randomly chosen among 180 harvested, were removed from cold storage and kept at 25 °C for 48 h before being washed in tap water and distilled water and then dried with sterile paper. After the removal of tops and peels, each whole fruit was sliced into seven segments (~30−35 mm diameter) with a sharp knife. Slices were first held in ice-cold (4 °C) chlorine dioxide sanitizer (for 2 min), dipped in ice-cold Milli-Q water with 0.5% citric acid preservative solution (for 2 min), washed in ice-cold Milli-Q water (for 2 min), dried with paper, and randomized into clear rectangular polyethylene tetraphthalate (PET) hinged containers (750 cc, Commital Cofresco, Italy). Sliced samples[7] were put into each box. All boxes were kept at 4 °C under light, simulating the commercial conditions of sale. Whole unpeeled fruits were put in the same type of box (one fruit for each box to equalize the sample material present in fresh-cut boxes). Samples were collected from both fresh-cut and whole fruits during the storage period immediately after cutting (0 h) and at 24, 48, and 72 h. The samples were immediately frozen in liquid nitrogen and kept stored at −80 °C before the analysis.

Flesh Firmness. Measurements were carried out on a flat surface by a stand drill mounted penetrometer (8 mm probe; model 53205, TR, Forlì, Italy). FF was estimated among the mean of six readings and expressed as kilograms.

Soluble Solids Concentration. Soluble solids content (SSC) was estimated among the mean of six replicates taken from kiwi juice. A digital refractometer (model 53011, TR, Forlì, Italy) was used. Measurements were carried out at the same sites as FF and were expressed as degrees Brix.

Ascorbic Acid Content. Total ascorbic acid content (AA_T) was determined spectrophotometrically following the method described by Kampfenkel et al.[25] slightly modified by Degl'Innocenti et al.[26] Total

dx.doi.org/10.1021/jf405008c | J. Agric. Food Chem. 2014, 62, 4377−4383

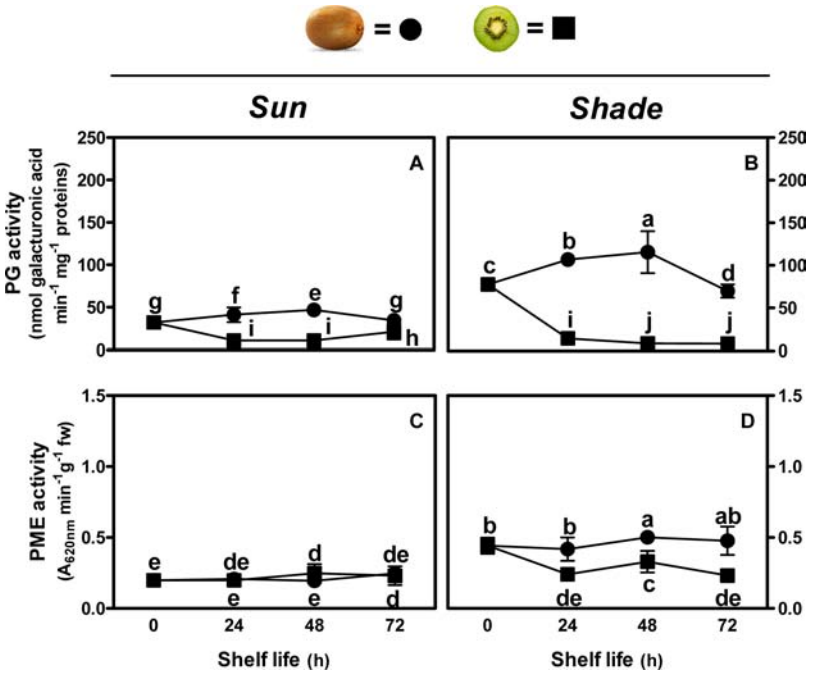

Figure 2. Polygalacturonase (PG; A, B) and pectinmethylesterase activities (PME; C, D) of full sunlight- and shade-grown Hayward kiwifruit stored for 0, 24, 48, and 72 h as fresh-cut and whole produce. Each value represents the mean of six replicates ± SD. Means were compared following two-way ANOVA test with treatment light exposure during growth and storage period as variability factors. Means flanked by the same letters are not significantly different after Fisher's least-significant difference test (LSD).

ascorbic acid was reported as milligrams of ascorbic acid per 100 g of fresh weight.

Total Polyphenols and Total Flavonoids. The extraction of TP and TFO was based on the method reported by Du et al.[27] slightly modified. Fruit tissue (ca. 3 g) was at first homogenized in 12 mL of ethanol/acetone (7:3; v/v) at 37 °C for 1 h. The extract was filtered using Whatman no. 41 paper and subsequently rinsed in 3 mL of the same extraction solution. Filtrates were collected and recovered at −20 °C and until the analysis of TP and TFO.

TP content was determined using the Folin−Ciocalteu assay, according to the method of Dewanto et al.[28] TP concentration was expressed as gallic acid equivalents (μg GAE 100 g^{-1} fw) using a calibration curve (50−600 μg mL^{-1}).

TFO concentration was determined at 506 nm. TFO content was expressed using rutin (mg RE 100 g^{-1} fw) as standard (6.25−1000 μg mL^{-1}).

Polygalacturonase and Pectinmethylesterase Activity. PG activity determination was carried out as described by Lazan et al.[29] with slight modifications. An aliquot of the extracted mixture was desalted with a Sephadex G-25 (1 cm × 10 cm) column prior to assay for polygalacturonase activity. PG activity was determined according to the original method described by Gross.[30] The assay of PG activity was based on the hydrolytic release of reducing groups from polygalacturonic acid. The absorbance was determined at 276 nm. PG activity was expressed as mole-reducing groups release per minute per milligrams of protein (nmol galacturonic acid min^{-1} mg^{-1} protein). Protein determination was performed according to the method of Lowry et al.[31]

PME extraction was carried out as described by Sanchez and Morais.[32] Frozen kiwifruit samples were homogenized in a solution of 1.5 M NaCl in an external ice bath for 6 min. The kiwifruit/NaCl solution ratio was 1:4 (w:w). The homogenate was centrifuged at 20000*g* for 30 min at 4 °C, and then the supernatant was filtered with a 6-fold cheesecloth, collected, and adjusted to pH 7.5 with a solution of 0.1 M NaOH. PME activity was spectrophotometrically determined according to the method of Zocca et al.[33] PME activity was monitored immediately after the extract addition and read at 620 nm at room temperature for 40 min. One blank was made for each sample, without bromothymol blue. Specific PME activity was defined as a decrease of A_{620} per minute per gram of fw.

Statistical Analysis. About 60 plants with different geographical orientations within the orchard (N; S; W; E) were randomly selected to collect fruits. Experiments were carried out twice with similar results, and a representative data set is reported herein. For each sample, the result is the mean of six replicates (n = 6) ± SD. Means of data were compared by two-way ANOVA considering light exposure (fully or partially shaded) and storage period (0, 24, 48, and 72 h) as treatments. Differences among treatment means were evaluated by Fisher's least-significant difference test (LSD) for P = 0.05. All statistical analyses were performed using the CoStat software package (CoHort Software, 1994; Berkeley, CA, USA).

RESULTS AND DISCUSSION

Fruit Maturity Properties and Softening-Related Enzymes. FF was constitutively similar in both sunny and shade whole kiwifruits in agreement with previous findings[18,34] (Figure 1A,B). Conversely, Tombesi et al.[34] pointed out a reduction of FF only when kiwifruits were grown almost completely shaded (<50 μmol quanta m^{-2} s^{-1}). In addition, the similar decline of FF we found in whole fruit at the end of the storage period, independent of light exposure, confirms previous results.[3,18] The process is mainly dependent on the activity of softening-related enzymes, that is, PG and PME. In addition, FF decremented strongly after cutting, in a similar way in kiwifruit collected under full sun or in shade conditions (−85 and −79%, respectively, at 72 h after cutting) when compared to the fruit before cutting. Thus, the effect of canopy position, and consequently the amount of light intercepted by fruit, does not affect the FF upon storage period.

FF is one of the most relevant parameters for consumer acceptability as well as SSC. In our experiments, SSC was constitutively greater in full sun-exposed kiwifruits than in the shaded counterpart (15.5 ± 0.62 vs 13.43 ± 0.54 °Brix, respectively; Figure 1C,D), confirming results previously

dx.doi.org/10.1021/jf405008c | J. Agric. Food Chem. 2014, 62, 4377−4383

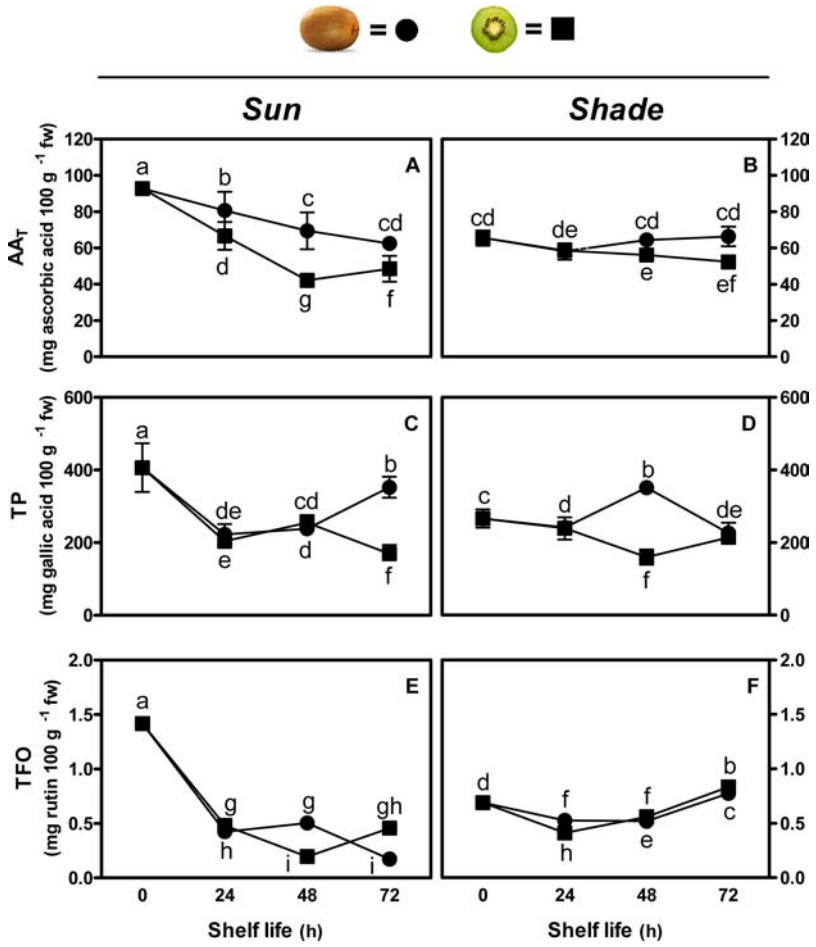

Figure 3. Total vitamin C content (AA_T; A, B), total phenols (TP; C, D), and total flavonoids (TFO; E, F) of full sunlight- and shade-grown Hayward kiwifruit stored for 0, 24, 48, and 72 h as fresh-cut and whole produce. Each value represents the mean of six replicates ± SD. Means were compared following two-way ANOVA test with treatment light exposure during growth and storage period as variability factors. Means flanked by the same letters are not significantly different after Fisher's least-significant difference test (LSD).

described.[34] In addition, SSC values were higher than 13 °Brix in both sun and shaded fruits, indicating a high acceptability level for consumers.[15] Thus, the hypothesis that the conversion of starch into soluble sugars typically characterizes ripening phenomena and leads to an increase in SSC[13,35] appeared realistic for these experiments, too. Indeed, light intensity has the potential to increase fruit photosynthesis, promoting indirectly starch synthesis and total carbohydrate content.[36] Whereas no relevant changes occurred in SSC upon storage period as whole fruit, when kiwifruits were minimally processed, the reduction in SSC values was reasonably comparable in fruit grown under full sunlight or in partially shaded condition, suggesting cutting exerts a similar effect independent of light received by fruit during the growing season (Figure 1).

Although softening is a visually evident effect, that process remained a partially unclear biochemical mechanism in which several enzyme-catalyzed mechanisms act together, inducing changes in cell wall.[37] Fruit softening is the result of a cumulative effect caused by different types of modifications that are responsible for texture changes and loss of firmness.[38] The activity of enzymes correlated with softening processes (PG and PME) was evaluated, and the results are reported in Figure 2. PG activity was statistically higher ($P < 0.05$) in fruit collected in shade canopy portions at the beginning of the experiments, and the enzymatic activity of PG upon storage time revealed a slight reduction in both types of sliced kiwifruit, independent of the degree of light exposure. On the other hand, the most remarkable result is the severe enhancement of PG activity in whole shaded fruits at 24 and 48 h, reaching at 72 h values similar to those found at the beginning of storage. The conservation as whole fruit, conversely, incremented only slightly PG activity in sun-exposed fruit (Figure 2A,B).

The PME pattern is reported in Figure 2C,D. The activity was higher in shade fruit (about +55%) before cutting. PME activity decreased upon storage period as fresh-cut produce, reaching values statistically similar to those of sun-exposed fruit stored in a similar way. Conversely, in shaded whole fruit values of PME activity remained high and even slightly increased compared with values found at time 0 upon all three storagec conditions.

Although little research has been focused on the effects of shade conditions on fruit physiology, it seems that shade determines a buildup of ethylene production, which is strictly linked to inner mesocarp firmness reduction.[38] Kiwifruit is, indeed, one of the climacteric fruits classified among the commodities with "high" ethylene production (10−100 μL C_2H_4 kg^{1-} h^{-1}) as reported by Kader.[39] In agreement with our findings, the latter author reported that processes during kiwifruit storage caused an acceleration of tissue softening when

dx.doi.org/10.1021/jf405008c | J. Agric. Food Chem. 2014, 62, 4377−4383

fruits were grown in shaded conditions. Conversely, high temperatures (i.e., during full sunlight exposure) are responsible for a general increment of heat shock protein transcription and translation,[24] metabolic processes that lead to a reduction in tissue respiration and to a decrease in ethylene production as well as in fruits' ability to respond to ethylene.[40] In accordance, we found fruit exposed to full sunlight appeared less sensitive to softening phenomena as compared to the counterpart grown under shade when stored as whole fruit. On the contrary, in fresh-cut produce no relevant differences were found in FF or in either PG or PME activity independent of the canopy position of fruit, suggesting that the activity of those enzymes is more relevant for whole fruit than for minimally processed produce.

Nutraceutical Compounds. On the one hand, the FF and the SSC, coupled with softening-related enzyme activities, draw a picture of fruit maturity of sun-exposed and shaded kiwifruits stored in different ways; on the other hand, investigation of ascorbate, phenols, and flavonoids sharpens the picture contributing to the understanding of the differences in terms of nutraceutical properties. The relevance of vitamin C content in kiwifruit is widely accepted, and it has been reported that the antioxidant capacity is mainly (but not only) attributable to that organic molecule.[18,23] In fruit grown in full sunlight we found the highest ascorbic acid content (Figure 3). Indeed, as well documented by previous studiets, fruits exposed to high light were commonly characterized by a higher vitamin C content,[7] ascorbate being directly synthesized from sugars produced at greater levels when photosynthesis highly performs.[41] However, in this work ascorbate is rapidly lost upon storage as whole fruit (−31% at 72 h) and also when fruit was stored as fresh-cut produce (−52% at 72 h). Conversely, the effect of storage was less severe in partially shaded fruit, where at the end of the storage as whole fruit AA_T was not significantly dissimilar to that found at time 0. A further confirmation of the less deleterious impact of storage period on AA_T in shaded fruit is that in minimally processed shaded kiwifruit at 72 h after cutting AA_T content (48.5 ± 7.1 mg 100 g^{-1} fw) was statistically not dissimilar from that found in full-sunlight sliced fruit (52.4 ± 2.3 mg 100 g^{-1} fw). The decrease of ascorbate is, however, commonly associated with fruit tissue degradation;[42] thus, if storage as whole fruit, and much more storage as fresh-cut produce,[43] enhances that metabolic process, the reduction of ascorbate is predictable. In addition, vitamin C content in fruit after cold storage is usually lower than the one recorded for fresh fruits,[7,13] although the degree of vitamin C degradation is strictly dependent on the length and temperature of storage.[44]

Ascorbate is usually recognized as one of the most powerful antioxidants, but the nutraceutical value of phenols and flavonoids is surely not negligible for their positive influence on human health.[45] Total phenols and flavonoids contents upon storage period are reported in Figure 3C−F. The constitutive content of those compounds (both TP and TFO) was remarkably higher in fruit grown in full sunlight when compared to the shaded counterpart (+31% for TO and +51% for TFO). These results represent clear evidence that the synthesis of phenols and flavonoids in kiwifruit is positively related to the extent of light intercepted on the canopy during the growth. However, both TP and TFO contents dramatically decreased in sun-grown fruit upon storage. Analyses of TP in shaded fruit revealed only a slight decline in the amount of those classes of metabolites in both whole and sliced fruit, whereas TFO was even increased at 72 h. In addition, despite a lower content of TP and TFO than found in shaded fruit at the beginning of storage, at 72 h inherent values of both TP and TFO were significantly greater than those found for sun fruit. A similar decline of TP was pointed out by Cocci et al.[46] after 2 days of shelf life. Other authors, conversely, found that whole and fresh-cut kiwifruits stored for 9 days had no statistically different values of phenols upon storage.[47] Thus, due to the high variability of kiwifruit material attributable to (I) orchard location, (II) agronomic practices applied in the orchard, (III) postharvest operations, and, obviously, (IV) genetic variability among plants, all of these factors might partially lead to different results.

After the necessary predication above, what we consider a useful result for scientific progress as well for direct industrial applications is the observation that shaded fruits, with an improper size and/or shape to be merchandized as whole fruit, are better suited for fresh-cut production than are fruits with similar defects grown in full sunlight. Conversely, full sun-exposed fruits, belonging to the same plants from which shaded fruits were collected, have greater amounts of ascorbate, phenols, and flavonoids, but unfortunately all of those nutraceutical compounds are rapidly lost upon storage. Thus, full sunlight grown fruits should be preferentially consumed as fresh produce to maximize their properties.

AUTHOR INFORMATION

Corresponding Author

*(L.G.) Phone: +39 050 2216613. Fax: +39 050 2216630. E-mail: lucia.guidi@unipi.it.

Notes

The authors declare no competing financial interest.

ACKNOWLEDGMENTS

We thank Azienda "Camillo Pacini e Figli" (Rigoli, Pisa, Italy) for providing kiwifruits. Moreover, we especially thank Nicola Trasacco for the helping hand in performing analyses.

ABBREVIATIONS USED

AA_T, total ascorbate; GAE, gallic acid equivalents; FF, flesh firmness; LSD, least significant difference; PG, polygalacturonase; PME, pectin methyl esterase; SSC, solid soluble content; TP, total phenols; TFO, total flavonoids; RE, rutin equivalents; SD, standard deviation

REFERENCES

(1) Nishiyama, I.; Yamashita, Y.; Yamanaka, M.; Shimohashi, A.; Fukuda, T.; Oota, T. Varietal difference in vitamin C content in the fruit of kiwifruit and other *Actinidia* species. *J. Agric. Food Chem.* **2004**, *52*, 5472−5475.

(2) Kabaluk, J. T.; Kempler, C.; Toivonen, P. M. A. *Actinidia arguta* − characteristics relevant to commercial production. *Fruit Var. J.* **1997**, *51*, 117−122.

(3) Ilina, N.; Alem, H. J.; Pagano, E.; Sozzi, G. O. Suppression of ethylene perception after exposure to cooling conditions delays the progress of softening in Hayward kiwifruit. *Postharvest Biol. Technol.* **2010**, *55*, 160−168.

(4) Nishiyama, I. Fruits of *Actinidia* genus. *Adv. Food Nutr. Res.* **2007**, *52*, 293−324.

(5) Beirão-da-Costa, S.; Steineer, A.; Correia, L.; Empis, J.; Moldão-Martins, M. Effects of maturity stage and mild heat treatments on quality of minimally processed kiwifruit. *J. Food Eng.* **2006**, *76*, 616−625.

(6) Beirão-da-Costa, S.; Steineer, A.; Correia, L.; Leitão, E.; Empis, J.; Moldão-Martins, M. Influence of moderate heat pre-treatments on physical and chemical characteristics of kiwifruit slices. *Eur. Food Res.Technol.* **2008**, *226*, 641−651.
(7) Lee, S. K.; Kader, A. A. Pre-harvest and post-harvest factors influencing vitamin C content of horticultural crops. *Postharvest Biol. Technol.* **2000**, 207−220.
(8) Toivonen, P. M. A.; Brummel, D. Biochemical bases of appearance and texture changes in fresh-cut vegetables and fruits. *Postharvest Biol. Technol.* **2008**, *48*, 1−14.
(9) Li, W.; Li, X.; Sun, Y.; Tang, Y.; Jiang, Y.; Zhang, M. Effect of packaging conditions on physiology quality and shelf-life of fresh-cut kiwifruit. *Adv. Mater. Res.* **2011**, *233*, 1985−1988.
(10) Hodges, D. M.; Toivonen, P. M. A. Quality of fresh-cut fruits and vegetables as affected by exposure to abiotic stress. *Postharvest Biol. Technol.* **2008**, *48*, 155−162.
(11) Kader, A. A. Influence of preharvest and postharvest environment on nutritional composition of fruits and vegetables. In *Horticulture and Human Health: Contributions of Fruits and Vegetables*, Proceedings of the 1st International Symposium on Horticulture and Human Health; Quebedeaux, B., Bliss, F. A., Eds.; Prentice Hall: Upper Saddle River, NJ, USA, 1988; pp 18−32.
(12) Ayala-Zavala, J. F.; Wang, S. Y.; Wang, C. Y.; Gonzales-Aguilar, A. G. Effect of storage temperatures on antioxidant capacity and aroma compounds in strawberry fruit. *LWT−Food Sci. Technol.* **2004**, *37*, 687−695.
(13) Zolfaghari, M.; Sahari, M. A.; Barzegar, M.; Samadloiy, H. Physicochemical and enzymatic properties of five kiwifruit cultivars during cold storage. *Food Bioprocess. Technol.* **2010**, *3*, 239−246.
(14) Crisosto, C. H.; Garner, D.; Saenz, K. Relationship between kiwifruit size and the rate of softening under controlled atmosphere conditions. In *Fruits Other than Apples and Pears*, Seventh International Controlled Atmosphere Research Conference; Kader, A. A., Ed.; University of California: Davis, CA, USA, 1997; Post. Hort. Series N. 17 Proceedings, 3, pp 165−169.
(15) Crisosto, C. H.; Crisosto, G. M. Understanding consumer acceptance of early harvested *Hayward* kiwifruit. *Postharvest Biol. Technol.* **2001**, *22*, 205−213.
(16) Wang, Z. Y.; MacRae, E. A.; Wright, M. A.; Bolitho, K. M.; Ross, G. S.; Atkinson, R. G. Polygalacturonase gene expression in kiwifruit: relationship to fruit softening and ethylene production. *Plant Mol. Biol.* **2000**, *42*, 317−328.
(17) Xian, L.; Changjie, X.; Schuyler, S. K.; Kungsong, C. Regulatory mechanisms of textural changes in ripening fruits. *Crit. Rev. Plant Sci.* **2010**, *29*, 222−243.
(18) Tavarini, S.; Degl'Innocenti, E.; Remorini, D.; Massai, R.; Guidi, L. Polygalacturonase and β-galactosidase activities in Hayward kiwifruit as affected by light exposure, maturity stage and storage time. *Sci. Hortic.* **2009**, *120*, 342−347.
(19) Prasanna, V.; Prabha, T. N.; Tharanathan, R. N. Fruit ripening phenomena − an overview. *Crit. Rev. Food Sci. Nutr.* **2007**, *47*, 1−19.
(20) Payasi, A.; Mishra, N. N.; Soares Chaves, A. L.; Singh, R. Biochemistry of fruit softening: an overview. *Physiol. Mol. Biol. Plants* **2009**, *15*, 103−113.
(21) De Assis, S. A.; Lima, D. C.; De Faria Oliveira, O. M. M. Activity of pectinmethylesterase, pectin content and vitamin C in acerola fruit at various stages of fruit development. *Food Chem.* **2001**, *74*, 133−137.
(22) Moretti, C. L.; Mattos, L. M.; Calbo, A. G.; Sargent, S. A. Climate changes and potential impacts on postharvest quality of fruit and vegetable crops: a review. *Food Res. Int.* **2010**, *43*, 1824−1832.
(23) Tavarini, S.; Degl'Innocenti, E.; Remorini, D.; Massai, R.; Guidi, L. Antioxidant capacity, ascorbic acid, total phenols and carotenoids changes during harvest and after storage of Hayward kiwifruit. *Food Chem.* **2008**, *107*, 282−288.
(24) Woolf, A. B.; Wexler, A.; Prusky, D.; Kobiler, E.; Lurie, S. Direct sunlight influences postharvest temperature responses and ripening of five avocado cultivars. *J. Am. Soc. Hortic. Sci.* **2000**, *125*, 370−376.
(25) Kampfenkel, K.; Van Montagu, M.; Inze, D. Extraction and determination of ascorbate and dehydroascorbate from plant tissue. *Anal. Biochem.* **1995**, *225*, 165−167.
(26) Degl'Innocenti, E.; Guidi, L.; Pardossi, A.; Tognoni, F. Biochemical study of leaf browning in minimally processed leaves of lettuce. *J. Agric. Food Chem.* **2005**, *53*, 9980−9984.
(27) Du, G.; Li, M.; Ma, F.; Liang, D. Antioxidant capacity and the relationship with polyphenol and vitamin C in *Actinidia* fruits. *Food Chem.* **2009**, *113*, 557−562.
(28) Dewanto, V.; Adom, K. K.; Liu, R. H. Thermal processing enhances the nutritional value of tomatoes by increasing total antioxidant activity. *J. Agric. Food Chem.* **2002**, *50*, 3010−3014.
(29) Lazan, H.; Selamat, M. K.; Ali, Z. M. β-Galactosidase, polygalacturonase and pectinesterase in differential softening and cell-wall modification during papaya fruit ripening. *Physiol. Plant.* **1995**, *95*, 106−112.
(30) Gross, K. A rapid and sensitive spectrophotometric metod for assaying polygalacturonase using 2-cyanoacetamide. *HortScience* **1982**, *17*, 933−934.
(31) Lowry, O. H.; Rosebrough, N. J.; Farr, N. J.; Randall, R. J. Protein measurements with the Folin phenol reagent. *J. Biol. Chem.* **1951**, *193*, 265−275.
(32) Sanchez, A. C. G.; Morais, A. M. M. B. Effects of controlled atmosphere (CA) storage on pectinmethylesterase (PME) activity and texture of 'Rocha' pears. *J. Sci. Food Agric.* **2001**, *82*, 143−145.
(33) Zocca, F.; Lomolino, G.; Curioni, A.; Spettoli, P.; Lante, A. Detection of pectinmethylesterase activity in presence of methanol during grape pomace storage. *Food Chem.* **2007**, *102*, 59−65.
(34) Tombesi, A.; Antignozzi E.; Palliotti A. Influence of light exposure on characteristic and storage life of kiwifruit. *N. Z. J. Crop Hortic. Sci.* **1993**, *21*, 85−90.
(35) Antunes, M. D. C.; Sfakiotakis, E. M. Ethylene biosynthesis and ripening behaviour of Hayward kiwifruit subjected to some controlled atmospheres. *Postharvest Biol. Technol.* **2002**, *26*, 167−179.
(36) Guan, H. P.; Janes, H. W. Light regulation of sink metabolism in tomato fruit. Growth and sugar accumulation. *Plant Physiol.* **1991**, *96*, 916−921.
(37) Giovannoni, J. J.; Della Penna, D.; Bennett, A. B.; Fisher, R. Polygalacturonase and tomato fruit ripening. *Hortic. Rev.* **1992**, *13*, 67−109.
(38) Nishizawa, T.; Taira, S.; Nakanishi, M.; Ito, M.; Togashi, M.; Motomura, Y. Acetaldehyde, ethanol and carbohydrate concentrations in developing muskmelon fruit are affected by short-term shading. *HortScience* **1998**, 992−994.
(39) Kader, A. A. Fruits in the global market. In *Quality and Its Biological Basis*; Knee, M., Ed.; Sheffield Academic Press: Sheffield, UK, 2002; pp 1−16.
(40) Lee, S. K.; Young, R. E. Temperature sensitivity of avocado firmness in relation to ethylene treatment. *J. Am. Soc. Hortic. Sci.* **1984**, *109*, 689.
(41) Harris, R. S. Effects of agricultural practises on the composition of foods. In *Nutritional Evaluation of Food Processing*, 2nd ed.; Harris, R. S., Karmas, E., Eds.; AVI: Westport, CT, USA, 1975; pp 33−57.
(42) Kalt, W. Effects of production and processing factors on major fruit and vegetable antioxidants. *J. Food Sci.* **2005**, *70*, 11−19.
(43) Plaza, L.; Crespo, I.; De Pascual-Teresa, S.; De Ancos, B.; Sánchez-Moreno, C.; Muñoz, M.; Cano, M. P. Impact of minimal processing on orange bioactive compounds during refrigerated storage. *Food Chem.* **2011**, *124*, 646−651.
(44) De Ancos, B.; Sanchez-Moreno, C.; Plaza, L.; Cano, P. Nutritional and health aspects of fresh-cut vegetables. In *Advances in Fresh-Cut Fruits and Vegetables Processing*; Martin-Belloso, O., Soliva-Fortuny, R., Eds.; CRC Press: Boca Raton, FL, USA, 2011; pp 145−165.
(45) Halliwell, B.; Rafter, J.; Jennifer, A. Health promotion by flavonoids, tocopherols, tocotrienols, and other phenols: direct or indirect effects? Antioxidant or not? *Am. J. Clin. Nutr.* **2005**, *81*, 2685−2765.

(46) Cocci, E.; Rocculi, P.; Romani, S.; Rosa, M. D. Changes in nutritional properties of minimally processed apples during storage. *Postharvest Biol. Technol.* **2006**, *39*, 265−271.
(47) Antunes, M. D. C.; Dandlen, S.; Cavaco, A. M.; Miguel, G. Effects of postharvest application of 1-MCP and post-cutting dip treatment on the quality and nutritional properties of fresh-cut kiwifruit. *J. Agric. Food Chem.* **2010**, *58*, 6173−6181.

JOURNAL OF AGRICULTURAL AND FOOD CHEMISTRY

Article

pubs.acs.org/JAFC

Stability of *trans*-Resveratrol Associated with Transport Proteins

Manuela Pantusa,[†] Rosa Bartucci,[†,‡] and Bruno Rizzuti*[,§]

[†]Department of Physics, University of Calabria, Ponte P. Bucci, Cubo 31C, 87036 Rende (CS), Italy

[‡]CNISM Unit, University of Calabria, Ponte P. Bucci, Cubo 31C, 87036 Rende (CS), Italy

[§]CNR-IPCF UOS of Cosenza, LiCryL and CEMIF.Cal, University of Calabria, Ponte P. Bucci, Cubo 33B, 87036 Rende (CS), Italy

ABSTRACT: Spectrophotometry and fluorescence combined with docking and molecular dynamics simulations are used to study the effect of the carrier proteins β-lactoglobulin and human serum albumin on the degradative *trans*-to-*cis* conversion of resveratrol. The spectroscopic measurements quantify the concentration of resveratrol isoforms after 2 h of irradiation with light at 340 nm, showing that their ratio depends linearly on temperature between 20 and 50 °C and obeys an Arrhenius law with activation energies of photoisomerization of 7.8 and 11.2 kcal/mol for β-lactoglobulin and albumin, respectively, compared to 5.1 kcal/mol in solution. Thus, both proteins protect *trans*-resveratrol from degradation, with albumin being more effective than β-lactoglobulin. The computational techniques clarify details of the binding of *trans*-resveratrol to the proteins and show that the stabilizing effect correlates with an increase of the dihedral order parameter of the ligand. These findings suggest that transport proteins are viable carriers to stabilize and deliver resveratrol *in vivo* in the biologically effective *trans* form.

KEYWORDS: *resveratrol, β-lactoglobulin, human serum albumin, absorbance, fluorescence, docking, molecular dynamics*

INTRODUCTION

Resveratrol is a phenolic compound of the stilbene family that is naturally present in some plants, such as grapes, peanuts, and mulberries, to protect against fungal infections or environmental stresses.[1,2] Resveratrol is also found in food and beverages, particularly red wine.[3,4] From a structural point of view, resveratrol consists of two aromatic rings, one single- and another double-hydroxylated joined by a methylene bridge, and can occur in two isomers, *trans*- and *cis*-resveratrol (Figure 1).

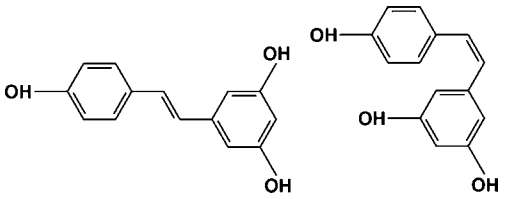

Figure 1. Chemical structures of (left) *trans*- and (right) *cis*-resveratrol.

The *trans* isomer is the natural form and converts to the *cis* isomer as a consequence of exposure to sunlight or UV radiation.[5] To the biologically active *trans* isomer are ascribed health benefits that make resveratrol particularly interesting for applications in the pharmaceutical and nutraceutical fields.[6] The beneficial health properties include antioxidant and antiatherosclerotic effects,[7] inhibition of blood platelet aggregation,[8] cardioprotective activity,[9] and chemopreventive action against cancer proliferation.[10,11]

In spite of its biological positive effects, resveratrol shows limitations such as low solubility in aqueous media, and consequently in biological fluids,[1,11] weak absorption after oral administration, and rapid metabolization *in vivo*, resulting in poor bioavailability. In addition, the conversion of the *trans* form into the less active *cis* isomer reduces resveratrol action. These limitations are overcome via loading the polyphenol into water-soluble carriers, which also offer protection from degradative processes. Among soluble carriers, proteins are optimal for the loading and cellular delivery of drugs. Resveratrol has been shown to have an affinity for various proteins, such as breast cancer resistance protein and human cyclin-dependent kinase,[12] insulin,[13] buttermilk proteins,[14,15] plasmatic lipoproteins,[16] and other transport proteins such as hemoglobin,[17] β-lactoglobulin,[18−20] and albumins.[17,21−26]

β-Lactoglobulin (βLG) and human serum albumin (HSA) are the most abundant proteins in bovine milk and in human blood plasma, respectively, and they are considered model carriers for a number of ligands. βLG (162 residues, 18.3 kDa) is a member of the lipocalin protein family, involved in the binding and transport of hydrophobic and amphiphilic molecules such as fatty acids and retinoids.[27] It is characterized by nine β-strands and a three-turn α-helix. Eight out of the nine β-strands are antiparallel and form a β-barrel sandwich with a central cavity, usually referred to as the protein calyx, which constitutes the main binding site.[28] Other external sites have been characterized or proposed for several ligands.[27] HSA (585 residues, 66 kDa) has an α-helical structure and can bind, store, and transport a wide variety of exogenous and endogenous molecules that include drugs, metals, and, with strong affinity, fatty acids.[29] Within the protein, two drug sites for binding aromatic and heterocyclic compounds[30] and 11 sites for medium- and long-chain fatty acids have been identified.[31]

In this paper we study the stability of *trans*-resveratrol bound to βLG and HSA as compared to when it is free in solution, either in aqueous buffer or in ethanol. UV light at 340 nm has

Received: December 13, 2013
Revised: April 28, 2014
Accepted: April 29, 2014
Published: April 29, 2014

ACS Publications © 2014 American Chemical Society

been used as the external perturbation to probe the photostability of *trans*-resveratrol. At this wavelength neither the two proteins nor *cis*-resveratrol absorb, and only *trans*-resveratrol is excited. Samples are investigated prior and after 2 h of continuous illumination at different temperatures, between 20 and 50 °C. The study is carried out experimentally by spectrophotometry and intrinsic resveratrol fluorescence, which allow quantifying the fraction of the two resveratrol isoforms present after irradiation and to assess the stabilizing effect of the proteins. Jointly, docking calculations and molecular dynamics (MD) simulations have been performed to gain insights into the binding modes and the dynamical behavior of resveratrol in interaction with both βLG and HSA, providing details on the mechanism of stabilization of the molecule.

MATERIALS AND METHODS

Materials and Sample Preparation. *trans*-Resveratrol (3,4′,5-trihydroxy-*trans*-stilbene), βLG (A and B variant, purity ≥90%), and HSA (fatty acid-free and globulin-free, purity approximately 99%) were from Sigma-Aldrich (St. Louis, MO, USA). The reagent-grade salts for the 10 mM phosphate buffer solution (PBS) at pH 7.4 were from Merck (Darmstadt, Germany), and ethanol was from Carlo Erba (Milan, Italy). All materials were used as purchased with no further purification. Bidistilled water was used throughout.

Solutions of *trans*-resveratrol either in PBS or in ethanol were prepared daily at a concentration of 5 μM, which is below the resveratrol solubility in water (0.023 mg/mL). A gentle stirring was used to dissolve it in PBS. Resveratrol concentration in both PBS and ethanol was determined by spectrophotometry, by using a molar extinction coefficient ε_{304} = 30 135 M^{-1} cm^{-1} and ε_{308} = 30 000 M^{-1} cm^{-1}, respectively.[5,32]

Protein−resveratrol complexes were prepared by mixing an amount of protein stock solution (at a concentration of 50 μM) and *trans*-resveratrol solution in PBS at the molar ratio of 10:1. HSA and βLG concentration were determined spectrophotometrically by using ε_{280} = 35 219 M^{-1} cm^{-1} and ε_{278} = 17 600 M^{-1} cm^{-1}, respectively.[33,34] To protect resveratrol from degradation due to radiation effects, sample handling and storage were carried out under light-protected conditions.

Absorbance and Fluorescence Measurements. Absorbance data were acquired with a JASCO 7850 spectrophotometer equipped with a TPU-436 Peltier thermostated cell holder (accuracy ±0.5 °C) and an EHC-441 temperature programmer, using 1 cm optical path quartz cuvettes. Temperature was measured directly by a YSI thermistor dipped into the cuvette.

Intrinsic *trans*-resveratrol fluorescence data were collected on an LS 50B spectrofluorometer (PerkinElmer, Beaconsfield, UK) equipped with a Peltier temperature programmer PTP-1 (accuracy ±0.5 °C) using 1 cm path length cuvettes. The excitation wavelength was 340 nm, whereas the slit widths of excitation and emission were 6 and 4 nm, respectively. Buffer background was subtracted from the raw emission spectra.

Absorbance and fluorescence measurements were carried out at temperatures of 20, 25, 37, 45, and 50 °C on either freshly prepared nonilluminated resveratrol-containing samples (t = 0 h) or samples illuminated for 2 h with light at 340 nm. Irradiation was performed within the spectrofluorometer after loading the sample into the cuvette. A 2 h time interval of irradiation was suitable for obtaining maximum conversion of the *trans*- to the *cis*-resveratrol isomer. The reproducibility of the results has been assessed by performing three independent experiments.

Docking Calculations. The binding of *trans*-resveratrol to both βLG and HSA was first predicted by molecular docking and subsequently simulated in the presence of explicit solvent. The structure of resveratrol was built by using the UCSF Chimera software.[35] The starting structures of the two proteins were modeled on the basis of their crystallographic configurations, as previously described.[36,37]

The apo form of βLG (3NPO entry[28] in the Protein Data Bank (PDB) repository) was used. Docking results were further tested with the βLG structure in complex with retinol and retinoic acid (1GX8 and 1GX9 entries,[27] respectively). For HSA, the crystallographic structures in association with palmitic acid (1E7H entry[31] of the PDB) and with both myristic acid and warfarin (1H9Z entry[38]) were considered. In particular, the latter was used to compare directly our docking results with those previously reported by Lu and co-workers.[17] Although extracted from complexes, only the coordinates of protein atoms were used in all cases.

Docking calculations to estimate the binding affinity of resveratrol and to obtain the starting structure for the protein−ligand complexes were performed by using AutoDock Vina,[39] allowing full flexibility for the ligand. Computations were repeated to ensure the reproducibility of the docking location, and the affinity energy values are calculated over multiple runs.

Molecular Dynamics Simulations. After docking, protein−resveratrol complexes were solvated in a rhombic dodecahedron with a minimum distance of 1 nm from any box edge, resulting in 6571 water molecules for βLG and 30415 for HSA. The systems were neutralized by adding 8 and 15 Na^+ counterions for βLG and HSA, respectively. Energy minimization was performed to relax the system and avoid bad atomic contacts.

Simulations were carried out by using the GROMACS 4.5 software package[40] with the AMBER ff99SB force field.[41] The GAFF force field[42] was used for resveratrol, and the TIP3P model[43] for water. Long-range electrostatic interactions were calculated through the particle-mesh Ewald (PME) method.[44]

Periodic boundary conditions were applied to avoid edge effects, and sampling was performed in the isothermal−isobaric ensemble. A Bussi−Donadio−Parrinello thermostat[45] and Berendsen barostat[46] were used, with reference values of 300 K and 10^5 Pa, respectively. Production runs were carried out for 50 ns, saving the simulation trajectories with a sampling time of 1 ps. The software package VMD[47] was used for trajectory visualization.

RESULTS AND DISCUSSION

Photostability of *trans*-Resveratrol in Solution and in the Carrier Proteins βLG and HSA. The absorbance and fluorescence spectra at 37 °C of resveratrol in PBS before illumination (black lines) and after 2 h of continuous irradiation at 340 nm (red lines) are reported in Figure 2A and B, respectively. The absorbance spectrum of nonirradiated resveratrol shows a broad maximum between 300 and 320 nm, as expected for *trans*-resveratrol in aqueous solution at

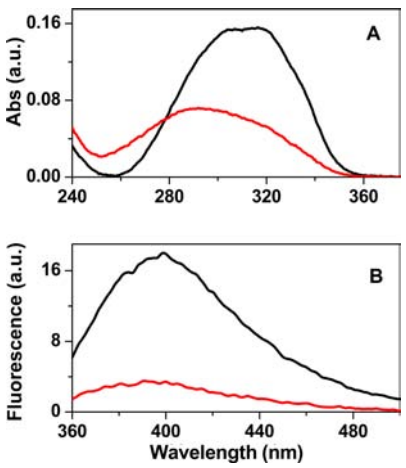

Figure 2. (A) Absorbance and (B) fluorescence spectra at 37 °C of *trans*-resveratrol in PBS before (black line) and after (red line) exposure for 2 h to radiation at 340 nm.

dx.doi.org/10.1021/jf405584a | J. Agric. Food Chem. 2014, 62, 4384−4391

neutral pH.[5,32,48] By comparing the absorbance curves of the irradiated and nonirradiated sample in Figure 2A it is evident that UV light induces in the absorbance a marked attenuation of about 55%, a shift to lower wavelength of λ_{max}, and an enhancement at 260 nm. These spectral features are typical of *cis*-resveratrol.[32,48] They indicate that resveratrol is not stable and tends to isomerize from *trans* to *cis* form when perturbed with radiation at 340 nm. The emission spectrum of the illuminated sample in Figure 2B is characterized by a pronounced quenching of the fluorescence quantum yield compared to the nonilluminated one. Similarly, this is due to the formation of the *cis* isoform upon irradiation at 340 nm, at which only *trans*-resveratrol is excited. The attenuation of fluorescence intensity cannot be attributed to resveratrol aggregation, because of the low concentration used, 5 μM. In fact, aggregation is reported to occur for resveratrol concentrations higher than 12.5 μM at pH 5.5 and 37 μM at pH 10.5.[49] Thus, the results in Figure 2 clearly indicate that *trans*-resveratrol in PBS solution, exposed for 2 h to radiation at 340 nm, partially converts to *cis*-resveratrol, resulting in a coexistence of *trans*- and *cis*-resveratrol populations in the samples.

Absorbance and fluorescence measurements have been carried out on resveratrol−PBS samples at temperatures both lower and higher than 37 °C (i.e., 20, 25, 45, and 50 °C) (curves not shown). The spectra of irradiated samples are markedly and progressively affected by the temperature increase, in a manner consistent with the progressive conversion of *trans*- to *cis*-resveratrol. In contrast, no significant spectral variations are recorded in nonilluminated samples at each temperature, indicating that the sole temperature does not affect the stability of *trans*-resveratrol, whereas it affects the ratio of the two isoforms that coexist in solution upon UV irradiation.

The stability of *trans*-resveratrol against UV irradiation has been also investigated in ethanol solution. Absorbance and fluorescence curves (not shown) indicate, also in this solvent, a temperature-dependent degradation of *trans*-resveratrol due to light irradiation.

Resveratrol binds to βLG with a binding constant[18,20] between 10^4 and 10^6 M^{-1} and to HSA with a binding constant[25] of about 10^5 M^{-1}. The number of resveratrol molecules bound per protein is 1 for HSA[25] and 1[18] or 1.1[20] for βLG. The excess of protein in solution (protein to resveratrol molar ratio is 10:1) gives a saturation in the fluorescence signal, ensuring that all *trans*-resveratrol is bound to the proteins. The absorbance and fluorescence spectra for resveratrol in βLG and the fluorescence spectra for resveratrol in HSA recorded at 37 °C before (black lines) and after 2 h (red lines) of continuous irradiation at 340 nm are shown in Figure 3A, B, and C, respectively. For the HSA−resveratrol complex the absorbance measurements are not given because of the high superposition of the spectrum of the protein with those of both *trans*- and *cis*-resveratrol.

The absorbance spectra in Figure 3A are obtained by subtracting the βLG spectrum from the spectrum of the βLG−resveratrol complex. By comparing the curves in Figure 3 (relative to resveratrol−protein complexes) with those reported in Figure 2 (relative to resveratrol−PBS samples), it emerges that the formation of *cis*-resveratrol consequent to UV illumination also occurs when the ligand is bound to the protein, although it is clearly reduced.

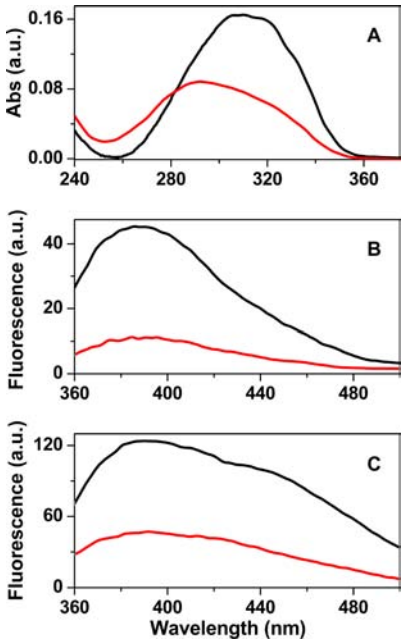

Figure 3. (A) Absorbance and (B) fluorescence spectra at 37 °C of *trans*-resveratrol bound to βLG before (black line) and after (red line) exposure for 2 h to radiation at 340 nm. (C) Fluorescence spectra of *trans*-resveratrol bound to HSA as in (B).

The absorbance and fluorescence data have been analyzed to estimate the concentration of *trans*-, C_{trans}, and *cis*-resveratrol, C_{cis}, present in solution after 2 h of exposure to light at 340 nm. The concentrations of the two resveratrol isoforms are determined from the absorbance measurements by the following formulas, which are valid when starting from a 100% *trans*-resveratrol solution of known initial concentration, $C_0 = A_0/\varepsilon_{trans}$:[5]

$$C_{trans} = \frac{1}{R-1}\left(\frac{RA}{l\varepsilon_{trans}} - C_0\right) \quad (1)$$

$$C_{cis} = \frac{1}{1-R}\left(\frac{A}{l\varepsilon_{cis}} - RC_0\right) \quad (2)$$

where $R = \varepsilon_{trans,304\ nm}/\varepsilon_{cis,304\ nm} = 30\,135/9749 \approx 3.09$ in 10 mM phosphate buffer solution[5] and $R = \varepsilon_{trans,308\ nm}/\varepsilon_{cis,308\ nm} = 30\,000/12\,500 = 2.4$ in ethanol,[32] ε_{trans} and ε_{cis} are the molar extinction coefficients of *trans*- and *cis*-resveratrol, respectively, A is the measured absorbance at 304 nm in buffer and at 308 nm in ethanol, and l is the optical path length. The fractions of the two isoforms are simply given by $f_{trans} = C_{trans}/C_0$ and $f_{cis} = C_{cis}/C_0$. From the fluorescence data, the fraction of *trans* isomers is $f_{trans} = F_t/F_0$ and the corresponding concentration is $C_{trans} = f_{trans}C_0$, where F_t is the fluorescence maximum after irradiation (t = 2 h) and F_0 the fluorescence maximum before irradiation (t = 0 h). The fraction and the concentration of *cis* isomers are given by $f_{cis} = 1 - f_{trans}$ and $C_{cis} = C_0 - C_{trans}$, respectively.

Table 1 reports the data deduced by using the equations given above. The values indicate that comparable fractions are obtained from the two techniques at each temperature. The values of f_{trans} decrease (f_{cis} increase) with a temperature increase. For resveratrol in PBS, 2 h of UV illumination promotes the formation of a marked *cis* population already at 20 °C, about 73%, which increases to 86% at 50 °C. In addition,

dx.doi.org/10.1021/jf405584a | J. Agric. Food Chem. 2014, 62, 4384−4391

Table 1. Percentage Fractions, f_{trans}, of *trans*-Resveratrol Free in PBS and in Ethanol and Bound to βLG and HSA

	PBS		ethanol		βLG		HSA
$T \pm 0.5$ (°C)	absorbance	fluorescence	absorbance	fluorescence	absorbance	fluorescence	fluorescence
20.0	27.4 ± 0.9	26.7 ± 2.1	18.7 ± 0.6	21.1 ± 0.7	38.9 ± 0.9	38.6 ± 2.3	61.2 ± 2.4
25.0	26.1 ± 0.9	27.2 ± 2.4	17.9 ± 0.6	18.8 ± 0.9	31.0 ± 0.8	32.6 ± 2.6	53.1 ± 2.1
37.0	16.9 ± 0.8	18.1 ± 1.4	11.7 ± 0.5	14.0 ± 1.0	27.9 ± 0.8	24.3 ± 1.5	37.8 ± 1.5
45.0	16.5 ± 0.8	17.2 ± 1.2	11.0 ± 0.4	13.5 ± 0.7	17.7 ± 0.6	18.1 ± 0.9	25.9 ± 1.3
50.0	13.8 ± 0.7	14.5 ± 1.0	10.2 ± 0.4	12.1 ± 0.6	15.2 ± 0.6	14.9 ± 0.7	20.4 ± 1.0

the fractions of *cis* isomer, f_{cis}, are slightly higher in ethanol, ranging from 79%−81% to 88−90% in the whole temperature range. This finding should be taken into account in the context of the possible use of ethanol in dissolving resveratrol for pharmaceutical applications.

A number of studies have dealt with the isomerization of resveratrol in solution. It has been reported that, except in buffers at high pH, *trans*-resveratrol is stable in the dark from hours to several days,[32] whereas different treatments, including exposure to sunlight,[5] direct illumination with tubular lamps that emit at all visible wavelengths,[18] and UV irradiation,[25,32,48,50] induce the formation of *cis* isomers starting from a pure *trans*-resveratrol solution. Specifically, for a UV-illuminated resveratrol solution, the formation of the *cis* isoform is influenced by physicochemical parameters such as resveratrol concentration, pH of the dispersion media, and wavelength and duration of the excitation.[25,32,48,50] In addition, it has been demonstrated that no other products are present except *trans*- and *cis*-resveratrol when UV light interacts with a resveratrol solution.[48] Within this framework, it is of interest to compare our results for resveratrol free in solution with those obtained in the above-mentioned studies. At 20 °C, upon illumination at 260 nm (i.e., a wavelength suitable to excite *cis*-resveratrol) of a 5.7 μM solution, 50.9% of *trans*-resveratrol is converted into *cis*-resveratrol after 150 min, and 59.6% is converted after 330 min.[50] By using HPLC/UV, Camont et al. report that 8 h of sunlight exposure reduces to 30% the concentration of *trans*-resveratrol starting from a pure 100 μM solution.[5] Trela and Waterhouse report that a 418 μM solution of *trans*-resveratrol in ethanol was converted to 90.6% *cis*-resveratrol after 100 min of illumination at 366 nm and to 63% after 10 h at 254 nm.[32]

The data in Table 1 relative to the two proteins clearly indicate that they decrease resveratrol isomerization induced by radiation at 340 nm. Indeed, compared to that obtained in PBS or ethanol, at any temperature the fraction of *trans*-resveratrol is increased (*cis*-resveratrol is reduced) in the presence of βLG and even more in the presence of HSA. This occurs more efficiently at low than at high temperature. For comparison, by using spectrophotometry, Liang et al. reported that complexing resveratrol with βLG provides a slight increase in photostability relative to resveratrol−buffer solution.[18] In fact, samples exposed to white light are almost stable in *trans*-configuration for up to 21 h, when absorbance at 305 nm is decreased to about 80% of the initial value in the absence of βLG and to about 90% in its presence. For the HSA−resveratrol complex, after repeated fluorescence measurements at λ_{ex} = 315 nm, the fraction of resveratrol in *trans* form is 50.5% compared to 34% for resveratrol in PBS.[25]

Arrhenius plots of the temperature dependences of C_{trans}/C_{cis} deduced from fluorescence data for resveratrol in PBS (squares), ethanol (circles), βLG (triangles), and HSA (diamonds) are given in Figure 4. In all cases, the temperature dependence is linear, conforming well to an Arrhenius law with

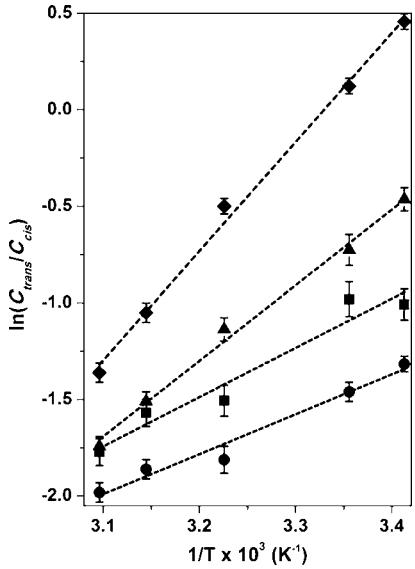

Figure 4. Temperature dependence of C_{trans}/C_{cis} ratio deduced from fluorescence data for resveratrol in PBS (squares), ethanol (circles), βLG (triangles), and HSA (diamonds). The lines are least-squares linear fits of the data according to Arrhenius law.

an activation energy of photoisomerization of 5.1 ± 0.7 and 4.1 ± 0.4 kcal/mol for resveratrol in PBS and ethanol, respectively. These values translate to 7.8 ± 0.3 and 11.2 ± 0.4 kcal/mol for resveratrol in βLG and HSA, respectively.

The activation energy of photoisomerization for *trans*-resveratrol in PBS at pH 4 was previously reported to be 3.7 ± 0.3 kcal/mol upon excitation at 260 nm for different time periods and at temperatures between 20 and 50 °C.[50] On the whole, the spectroscopic data indicate that the two proteins, although not being able to prevent the formation of the *cis* isomer, are able to protect *trans*-resveratrol from degradation, and in this respect HSA is more effective than βLG.

Docking and MD Simulations of Protein−Resveratrol Complexes. Docking of *trans*-resveratrol to βLG was carried out by using the unliganded protein form and resulted in two poses of the ligand on the protein surface, as shown in Figure 5A. Pose 1 corresponds to several slightly different binding modes with resveratrol placed at the entrance of the protein calyx and an estimated energy of −6.2 ± 0.3 kcal/mol. Pose 2 occurs in an external region on the opposite site with respect to the protein calyx, with one −OH group of resveratrol forming a hydrogen bond with the exposed carboxyl oxygen of Trp19, and a binding energy of −5.8 ± 0.2 kcal/mol.

In a single case, a binding mode of pose 1 was found with resveratrol more deeply inserted into the protein calyx. However, stable association within this site can be excluded on the basis of experimental data[19] indicating that binding of resveratrol takes place in another site because it occurs even at

dx.doi.org/10.1021/jf405584a | J. Agric. Food Chem. 2014, 62, 4384−4391

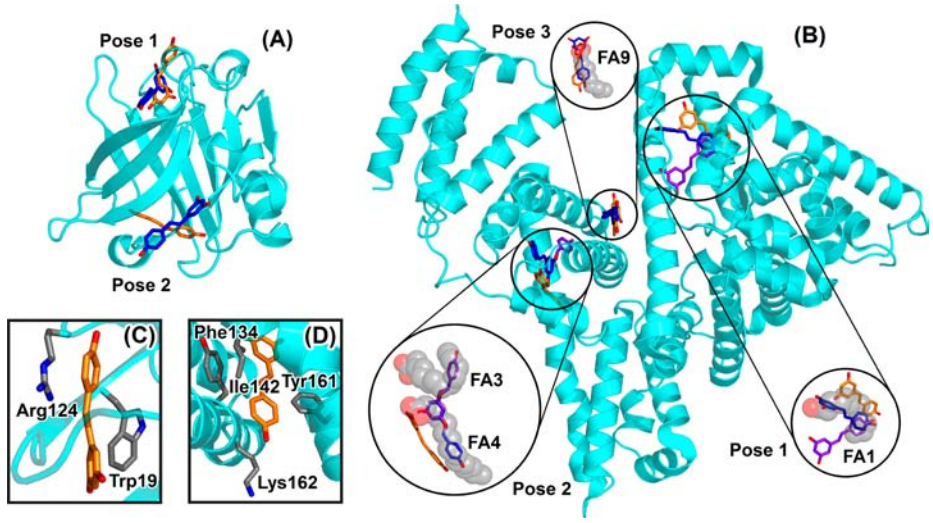

Figure 5. *trans*-Resveratrol bound to (A) βLG and (B) HSA, with the ligand in the docking poses (blue and purple) and after MD simulations (orange). For HSA, superposition with crystallographic binding sites for fatty acids (FA1, FA3, FA4, and FA9) is evidenced. Details of protein residues interacting with the ligand in (C) βLG and (D) HSA are also shown.

low pH, when the inner region of the hydrophobic cavity is inaccessible,[27] and at high temperature when the calyx is disrupted.[51] Therefore, this particular binding mode of pose 1 can be considered an artifact, possibly due to the docking scoring function not taking into account the specificity of the binding site of βLG, which is an extreme case of a large and yet completely dehydrated cavity.[52]

Additional docking calculations were carried out by using the crystallographic βLG structure containing within the protein calyx either retinol or retinoic acid, both possessing a β-ionone ring whose steric hindrance resembles that of either of the two resveratrol rings. The structure of βLG alone was extracted from the complexes with both retinol and retinoic acid and used to accommodate *trans*-resveratrol. Nevertheless, estimates for binding modes and affinity of resveratrol to these protein structures were found to be similar to the unliganded protein form.

Classical MD simulations were performed with the ligand initially placed according to the binding modes obtained by the docking procedure, to determine the main features of βLG–resveratrol interaction when all the degrees of freedom of the protein are free to move and in the presence of solvent. Figure 6 shows the simulated number of water molecules within a distance of 0.3 nm with respect to resveratrol. When the ligand is initially placed in pose 1, at the opening of the protein calyx, it is in contact on average with 40 water molecules compared with about 75 contacts when it is fully solvated in water. Thus, the curve indicates that resveratrol remains within the upper region of the funnel, without penetrating the main βLG binding site. A similar behavior was observed in five other simulation runs, with the molecule variously interacting with several protein residues, such as forming transient hydrogen bonds with either O-Met107, O-Ser116, or O^{γ}-Ser116. Migration of resveratrol deep into the binding site was never observed in simulation.

Simulations starting with the ligand in pose 2 (Figure 5A) show that resveratrol initially explores the surroundings of the docking placement while remaining in contact with the protein main chain in correspondence with the Trp19 residue. In this position, resveratrol is in contact on average with 60 water molecules (see Figure 6). Quick reduction of the number of

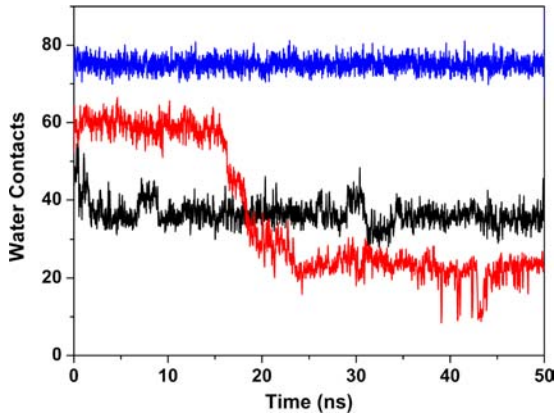

Figure 6. Number of water molecules in contact with *trans*-resveratrol (blue line) free in the solvent, (black line) at the entrance of the βLG calyx (pose 1), and (red line) close to Trp19 (pose 2), as a function of the simulation time. Data are averaged over 50 ps for clarity of presentation.

contacts, which is visible in the curve at 16–18 ns, indicates that resveratrol partially penetrates the protein surface. As shown in Figure 5C, the ligand accommodates in between the side chain of Arg124, which is exposed to the solvent, and the side chain of Trp19, which is more distant from the protein surface. In this position resveratrol is more specifically attached to the protein and protected from the solvent compared with any location at the calyx entrance. Both hydrophobic and hydrophilic contacts contribute to secure the ligand to the protein, the former playing a major role as previously suggested on the basis of experimental data.[19,20]

The docking procedure was repeated by using protein structures obtained in simulation after 20 ns. A binding energy of -7.1 ± 0.5 kcal/mol was found for resveratrol in the binding site between Trp19 and Arg124. In contrast, no appreciable variation was observed for the binding affinity of resveratrol at the entrance of the protein calyx, compared with the starting protein structure. Therefore, the overall simulation results suggest that the region close to the Trp19 residue is the most

dx.doi.org/10.1021/jf405584a | J. Agric. Food Chem. 2014, 62, 4384–4391

likely binding site for resveratrol to βLG, in agreement with fluorescence quenching[19] and other techniques.[20]

Association of *trans*-resveratrol in the protein region in between Trp19 and Arg124 residues provides a straightforward explanation of the binding mechanism and of the stabilizing effect due to βLG on the *trans*-to-*cis* transition. In fact, in this binding site the ligand molecule is restrained in its dynamics and mostly protected from the solvent. Nevertheless, the protein does not provide a complete protection from the solvent, and it does not totally inhibit the possibility of rotation around the double bond in the methylene bridge of resveratrol. Furthermore, a fraction of resveratrol molecules may bind in nonspecific or low-affinity locations on the protein surface, including the entrance of the protein calyx, thus being unrestrained in the dynamics and markedly more in contact with the solvent compared to the binding location in correspondence with Trp19 and prone to convert to the *cis* form. This hypothesis would also explain why for βLG the number of resveratrol molecules bound per protein could vary from 1 to 1.1.[18,20]

For the HSA−resveratrol complex, the docking results indicate that resveratrol can bind HSA in three different poses (see Figure 5B), corresponding to sites that can be occupied by fatty acids or other small ligands. These sites are hereafter indicated with their conventional nomenclature.[31] Pose 1 was found in correspondence with the binding site FA1 of HSA and shows the highest affinity, with an interaction energy of −8.9 ± 0.2 kcal/mol. In this site resveratrol can associate in either of two binding modes. One of the two rings of resveratrol occupies the position corresponding to a fatty acid tail, whereas the other ring is placed either instead of the lipid headgroup or pointing toward the center of the protein (see Figure 5B). Similarly, pose 2 shows an interaction energy of −8.5 ± 0.2 kcal/mol and overlaps totally or in part with the binding site FA4, with two different binding modes. In fact, one of the two resveratrol rings can alternatively be in the place of the tail of a fatty acid in the binding site FA3. Such a combination is not unusual for HSA, because the two binding sites FA3 and FA4 can accommodate ligands bulkier than fatty acids by rearranging into the single cavity DS2, or drug site 2.[30] Finally, pose 3 has a binding affinity of −7.5 ± 0.3 kcal/mol and coincides with the binding site FA9, which is a cleft in the upper region of the central protein crevice and can be occupied by capric acid, but not by other fatty acids with a longer chain.[31]

It is interesting to note that our docking results do not detect any binding mode in the cavity between subdomain IB/IIA of the protein, which was previously predicted[17] as the only binding site for resveratrol by using the AutoDock 3.5 program.[53] In contrast, the drug site DS2 was already reported as the only binding site for resveratrol in bovine serum albumin[26] by using AutoDock 4.2. Such differences in the results can probably be attributed to the improvement of the scoring function of AutoDock, as well as to the higher accuracy of the new-generation function later adopted by AutoDock Vina,[39] which was used in our calculations.

MD simulations were performed on the HSA−resveratrol complex, with the ligand placed in the different poses selected through the docking. The results show that, except when placed in pose 3 (FA9) at the central protein crevice, resveratrol partially diffuses away from the starting position due to dynamical rearrangements of the protein matrix. In particular, when initially placed in pose 1, it relocates about 0.5 nm from the starting position and ends up being surrounded by Tyr161, Ile142, Phe134, and Lys162, as shown in Figure 5D. The first two residues are close to resveratrol from the beginning of the simulation; thus they move away from their starting position. Similarly, when placed in pose 2, resveratrol moves about 0.4 nm from the starting position.

To assess the strain exerted by the protein matrix, the distribution of values of the dihedral angle involved in the *trans*-to-*cis* conversion was calculated and compared to the equilibrium value found for resveratrol free in water, θ_{eq} = 180 ± 22°. The results reported in Figure 7 show that the highest strain is found in correspondence with the binding site FA9, as indicated by both the higher difference found for the average value and the lower variance in the distribution around this value. In contrast, less strain is found in correspondence with the other two positions, indicating that resveratrol is more easily accommodated within the protein in these sites.

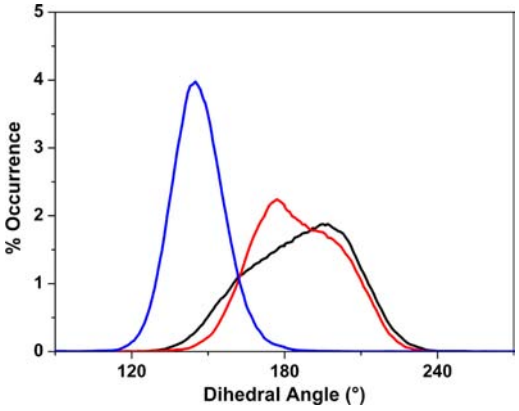

Figure 7. Distribution of dihedral angle for *trans*-resveratrol calculated in the time interval 25−50 ns in the binding sites of HSA: (black line) site FA1, (red line) site FA4, (blue line) site FA9.

Table 2 reports the dihedral order parameter S^2 and water contacts of *trans*-resveratrol in the different binding sites of HSA. Data for resveratrol free in water and associated with βLG are also reported for comparison. The parameter S^2 ranges from 0, for a dihedral angle free to sample any conformation, to 1 for a perfectly rigid system.[54] Thus, it gives a quantitative indication of the degree of inhibition for a rotation around the central methylene bridge of resveratrol.

Table 2. Dihedral Order Parameter and Solvent Contacts, Calculated in Simulation in the Time Interval 25−50 ns, for *trans*-Resveratrol Free in Water or Starting from Different Poses in Either βLG or HSA

environment	pose	binding site	order parameter	solvent contacts
water			0.86 ± 0.01	75 ± 3
βLG	2	Trp19/Arg124	0.89 ± 0.01	25 ± 6
HSA	1	FA1	0.91 ± 0.01	23 ± 7
HSA	2	FA4	0.94 ± 0.01	27 ± 6
HSA	3	FA9	0.95 ± 0.01	28 ± 8

The values found in the simulation show that the dihedral order parameter correlates with the stability of resveratrol against the *trans*-to-*cis* conversion found in our absorbance and fluorescence measurements: it is lower in the aqueous solvent, intermediate in βLG, and higher in HSA. In contrast, no clear correlation appears by comparing the contacts between *trans*-resveratrol and water in βLG and HSA. Although resveratrol

dx.doi.org/10.1021/jf405584a | J. Agric. Food Chem. 2014, 62, 4384−4391

complexed with HSA is more deeply buried and in contact with more amino acid compared to βLG, the difference of solvent contacts for the two proteins is not striking because the binding sites of HSA are hydrophobic cavities accessible to the solvent.[55]

Finally, docking of *trans*-resveratrol was performed again on HSA by using the simulation structures closer to the average configuration in the interval 25−50 ns. Only the protein structures were considered, and the search space for the docking was restricted to the region occupied by each ligand. The resulting affinity energies obtained placing the ligand in the three binding sites are, respectively, 8.9 ± 0.4, 8.1 ± 0.5, and 7.1 ± 0.3 kcal/mol. These values are consistent with the ones obtained for the three poses in the initial docking procedure. However, the energetic differences among the three binding sites in this case are more evident and in better agreement with previous experiments.[25] In fact, the stoichiometry of binding between resveratrol and HSA is not modified by the presence of 3 mol of stearic acid per mole of protein, whereas the amount of associated resveratrol is reduced when 5 mol of stearic acid is present. This suggests that the binding site FA1, which is not one of the three high-affinity binding sites for long-chain fatty acids,[56] is the one preferred by resveratrol. In contrast, the binding site FA4 has a high affinity for long-chain fatty acids;[31,56] thus it is reasonable to consider it at most a secondary binding site for resveratrol. Furthermore, the binding site FA9 cannot accommodate a long-chain fatty acid;[31] thus it cannot be a primary binding site for resveratrol, as in this case the stoichiometry of the HSA−resveratrol complex would have no or little change with varying amounts of stearic acid.

The overall results provide a possible explanation for the different degree of protection against the *trans*-to-*cis* transition of resveratrol in βLG and HSA. Limitations in the contact with the solvent, and especially restrictions in the freedom of fluctuation due to the hindrance of the protein matrix, likely stabilize the *trans*-resveratrol molecule. In this respect, the simulation data show that HSA protects resveratrol more efficiently than βLG. In particular, van der Waals interactions with a relatively high number of hydrophobic amino acid residues contribute to fasten resveratrol in HSA. Furthermore, the binding energy of *trans*-resveratrol to HSA is considerably lower than for βLG, thus providing a more stable complex. Other factors may also play an additional role, such as the fact that the binding site of HSA is more internal, so that the ligand may not easily escape back into the solvent.

In conclusion, the findings of the present work indicate that transport proteins can be conveniently used to store and deliver resveratrol in the *trans* form and suggest that other protein carriers may be further investigated with the aim of dispensing *in vivo* resveratrol or other similar ligands.

AUTHOR INFORMATION

Corresponding Author

*Phone: +39 0984 496078. Fax: +39 0984 494401. E-mail: bruno.rizzuti@cnr.it.

Funding

M.P. acknowledges financial support from EU and Regione Calabria by Regional Operative Program Calabria ESF 2007/2013, IV Axis Human Capital, Operative Objective M2, Action D5.

Notes

The authors declare no competing financial interest.

REFERENCES

(1) King, R. E.; Bomser, J. A.; Min, D. B. Bioactivity of resveratrol. *Compr. Rev. Food Sci. Food Saf.* **2006**, *5*, 65−70.

(2) Gulcin, I. Antioxidant properties of resveratrol: A structure-activity insight. *Innov. Food Sci. Emerg. Technol.* **2010**, *11*, 210−218.

(3) Langcake, P.; Pryce, R. The production of resveratrol by Vitis vinifera and other members of the vitaceae as a response to infection or injury. *J. Physiol. Plant Pathol.* **1976**, *9*, 77−86.

(4) Celotti, E.; Ferrarini, R.; Zironi, R.; Conte, L. S. Resveratrol content of some wines obtained from dried Valpolicella grapes: Recioto and Amarone. *J. Chromatogr. A* **1996**, *730*, 47−52.

(5) Camont, L.; Cottart, C. H.; Rhayem, Y.; Nivet-Antoine, V.; Djelidi, R.; Collin, F.; Beaudeux, J. L.; Bonnefont-Rousselot, D. Simple spectrophotometric assessment of the trans-/cis-resveratrol ratio in aqueous solutions. *Anal. Chim. Acta* **2009**, *634*, 121−128.

(6) Fremont, L. Minireview - Biological effects of resveratrol. *Life Sci.* **2000**, *66*, 663−673.

(7) Orallo, F. Comparative studies of the antioxidant effects of cis- and trans-resveratrol. *Curr. Med. Chem.* **2006**, *13*, 87−98.

(8) Olas, B.; Wachowicz, B. Resveratrol, a phenolic antioxidant with effects on blood platelet functions. *Platelets* **2005**, *16*, 251−260.

(9) Bradamante, S.; Barenghi, L.; Villa, A. Cardiovascular protective effects of resveratrol. *Cardiovasc. Drug Rev.* **2004**, *22*, 169−188.

(10) Jang, M. S.; Cai, E. N.; Udeani, G. O.; Slowing, K. V.; Thomas, C. F.; Beecher, C. W. W.; Fong, H. H. S.; Farnsworth, N. R.; Kinghorn, A. D.; Mehta, R. G.; Moon, R. C.; Pezzuto, J. M. Cancer chemopreventive activity of resveratrol, a natural product derived from grapes. *Science* **1997**, *275*, 218−220.

(11) Asensi, M.; Medina, I.; Ortega, A.; Carretero, J.; Bano, M. C.; Obrador, E.; Estrela, J. M. Inhibition of cancer growth by resveratrol is related to its low bioavailability. *Free Radical Biol. Med.* **2002**, *33*, 387−398.

(12) Feng, L.; Jin, J.; Zhang, L. F.; Yan, T.; Tao, W. Y. Analysis of the resveratrol-binding protein using phage-displayed random peptide library. *Acta Biochem. Biophys. Sin.* **2006**, *38*, 342−348.

(13) Chen, Y. Y.; Xiao, L.; Cui, J. H.; Chen, G. F.; Zhang, J.; Wang, P. Biological relevance of the interaction between resveratrol and insulin. *Food Biophys.* **2013**, *8*, 282−289.

(14) Ye, J. H.; Thomas, E.; Sanguansri, L.; Liang, Y. R.; Augustin, M. A. Interaction between whole buttermilk and resveratrol. *J. Agric. Food Chem.* **2013**, *61*, 7096−7101.

(15) Bourassa, P.; Bariyanga, J.; Tajmir-Riahi, H. A. Binding sites of resveratrol, genistein, and curcumin with milk α- and β-caseins. *J. Phys. Chem. B* **2013**, *117*, 1287−1295.

(16) Belguendouz, L.; Fremont, L.; Gozzelino, M. T. Interaction of transresveratrol with plasma lipoproteins. *Biochem. Pharmacol.* **1998**, *55*, 811−816.

(17) Lu, Z.; Zhang, Y. Y.; Liu, H.; Yuan, J. L.; Zheng, Z. L.; Zou, G. L. Transport of a cancer chemopreventive polyphenol, resveratrol: Interaction with serum albumin and hemoglobin. *J. Fluoresc.* **2007**, *17*, 580−587.

(18) Liang, L.; Tajmir-Riahi, H. A.; Subirade, M. Interaction of β-lactoglobulin with resveratrol and its biological implications. *Biomacromolecules* **2008**, *9*, 50−56.

(19) Liang, L.; Subirade, M. Study of the acid and thermal stability of β-lactoglobulin-ligand complexes using fluorescence quenching. *Food Chem.* **2012**, *132*, 2023−2029.

(20) Kanakis, C. D.; Tarantilis, P. A.; Polissiou, M. G.; Tajmir-Riahi, H. A. Probing the binding sites of resveratrol, genistein, and curcumin with milk β-lactoglobulin. *J. Biomol. Struct. Dyn.* **2013**, *31*, 1455−1466.

(21) Jannin, B.; Menzel, M.; Berlot, J. P.; Delmas, D.; Lancon, A.; Latruffe, N. Transport of resveratrol, a cancer chemopreventive agent, to cellular targets: Plasmatic protein binding and cell uptake. *Biochem. Pharmacol.* **2004**, *68*, 1113−1118.

(22) N'soukpoe-Kossi, C. N.; St-Louis, C.; Beauregard, M.; Subirade, M.; Carpentier, R.; Hotchandani, S.; Tajmir-Riahi, H. A. Resveratrol binding to human serum albumin. *J. Biomol. Struct. Dyn.* **2006**, *24*, 277−283.

(23) Xiao, J. B.; Chen, X. Q.; Jiang, X. Y.; Hilczer, M.; Tachiya, M. Probing the interaction of trans-resveratrol with bovine serum albumin: a fluorescence quenching study with Tachiya model. *J. Fluoresc.* **2008**, *18*, 671−678.
(24) Bourassa, P.; Kanakis, C. D.; Tarantilis, P.; Pollissiou, M. G.; Tajmir-Riahi, H. A. Resveratrol, genistein, and curcumin bind bovine serum albumin. *J. Phys. Chem. B* **2010**, *114*, 3348−3354.
(25) Pantusa, M.; Sportelli, L.; Bartucci, R. influence of stearic acids on resveratrol-HSA interaction. *Eur. Biophys. J. Biophy.* **2012**, *41*, 969−977.
(26) Liu, X. L.; Shang, Y. H.; Ren, X. D.; Li, H. Molecular modeling and spectroscopic studies on the interaction of transresveratrol with bovine serum albumin. *J. Chem.* **2013**, *2013*, 494706−1−7.
(27) Kontopidis, G.; Holt, C.; Sawyer, L. The ligand-binding site of bovine β-lactoglobulin: evidence for a function? *J. Mol. Biol.* **2002**, *318*, 1043−1055.
(28) Loch, J.; Polit, A.; Gorecki, A.; Bonarek, P.; Kurpiewska, K.; Dziedzicka-Wasylewska, M.; Lewinski, K. Two modes of fatty acid binding to bovine β-lactoglobulin − Crystallographic and spectroscopic studies. *J. Mol. Recognit.* **2011**, *24*, 341−349.
(29) Peters, T. *All about Albumin: Biochemistry, Genetics and Medical Applications*; Academic Press: San Diego, 1997.
(30) Sudlow, G.; Birkett, D. J.; Wade, D. N. Further characterization of specific drug binding sites on human serum albumin. *Mol. Pharmacol.* **1976**, *12*, 1052−1061.
(31) Bhattacharya, A. A.; Grune, T.; Curry, S. Crystallographic analysis reveals common modes of binding of medium and long-chain fatty acids to human serum albumin. *J. Mol. Biol.* **2000**, *303*, 721−732.
(32) Trela, B. C.; Waterhouse, A. L. Resveratrol: Isomeric molar absorptivities and stability. *J. Agric. Food Chem.* **1996**, *44*, 1253−1257.
(33) Pace, C. N.; Vajdos, F.; Fee, L.; Grimsley, G.; Gray, T. How to measure and predict the molar absorption-coefficient of a protein. *Protein Sci.* **1995**, *4*, 2411−2423.
(34) Dufour, E.; Roger, P.; Haertle, T. Binding of benzo(α)pyrene, ellipticine, and cis-parinaric acid to β-lactoglobulin − Influence of protein modifications. *J. Protein Chem.* **1992**, *11*, 645−652.
(35) Pettersen, E. F.; Goddard, T. D.; Huang, C. C.; Couch, G. S.; Greenblatt, D. M.; Meng, E. C.; Ferrin, T. E. UCSF chimera - A visualization system for exploratory research and analysis. *J. Comput. Chem.* **2004**, *25*, 1605−1612.
(36) Guzzi, R.; Rizzuti, B.; Bartucci, R. Dynamics and binding affinity of spin-labeled stearic acids in β-lactoglobulin: Evidences from EPR spectroscopy and molecular dynamics simulation. *J. Phys. Chem. B* **2012**, *116*, 11608−11615.
(37) Rizzuti, B.; Pantusa, M.; Guzzi, R. The role of lys525 on the head-group anchoring of fatty acids in the highest affinity binding site of albumin. *Spectrosc.-Int. J.* **2010**, *24*, 159−163.
(38) Petitpas, I.; Bhattacharya, A. A.; Twine, S.; East, M.; Curry, S. Crystal structure analysis of warfarin binding to human serum albumin − Anatomy of drug site I. *J. Biol. Chem.* **2001**, *276*, 22804−22809.
(39) Trott, O.; Olson, A. J. AutoDock Vina: Improving the speed and accuracy of docking with a new scoring function, efficient optimization, and multithreading. *J. Comput. Chem.* **2010**, *31*, 455−61.
(40) Hess, B.; Kutzner, C.; van der Spoel, D.; Lindahl, E. GROMACS 4: Algorithms for highly efficient, load-balanced, and scalable molecular simulation. *J. Chem. Theory Comput.* **2008**, *4*, 435−447.
(41) Hornak, V.; Abel, R.; Okur, A.; Strockbine, B.; Roitberg, A.; Simmerling, C. Comparison of multiple Amber force fields and development of improved protein backbone parameters. *Proteins* **2006**, *65*, 712−725.
(42) Wang, J. M.; Wolf, R. M.; Caldwell, J. W.; Kollman, P. A.; Case, D. A. Development and testing of a general Amber force field. *J. Comput. Chem.* **2004**, *25*, 1157−1174.
(43) Jorgensen, W. L.; Chandrasekhar, J.; Madura, J. D.; Impey, R. W.; Klein, M. L. Comparison of simple potential functions for simulating liquid water. *J. Chem. Phys.* **1983**, *79*, 926−935.
(44) Darden, T.; York, D.; Pedersen, L. Particle mesh Ewald: An N•log(N) method for Ewald sums in large systems. *J. Chem. Phys.* **1993**, *98*, 10089−10092.
(45) Bussi, G.; Donadio, D.; Parrinello, M. Canonical sampling through velocity rescaling. *J. Chem. Phys.* **2007**, *126*, 014101−014108.
(46) Berendsen, H. J. C.; Postma, J. P. M.; Di Nola, A.; Haak, J. R. Molecular dynamics with coupling to an external bath. *J. Chem. Phys.* **1984**, *81*, 3684−3690.
(47) Humphrey, W.; Dalke, A.; Schulten, K. VMD: Visual Molecular Dynamics. *J. Mol. Graph. Model.* **1996**, *14*, 33−38.
(48) Goldberg, D. M.; Ng, E.; Karumanchiri, A.; Yan, J.; Diamandis, E. P.; Soleas, G. J. Assay of Resveratrol glucosides and isomers in wine by direct-injection high-performance liquid-chromatography. *J. Chromatogr. A* **1995**, *708*, 89−98.
(49) Lopez-Nicolas, J. M.; Garcia-Carmona, F. Aggregation state and pK_a values of (E)-resveratrol as determined by fluorescence spectroscopy and UV-visible absorption. *J. Agric. Food Chem.* **2008**, *56*, 7600−7605.
(50) Figueiras, T. S.; Neves-Petersen, M. T.; Petersen, S. B. Activation energy of light induced isomerization of resveratrol. *J. Fluoresc.* **2011**, *21*, 1897−1906.
(51) Mousavi, S. H. A.; Bordbar, A. K.; Haertle, T. Changes in structure and in interactions of heat-treated bovine beta-lactoglobulin. *Protein Pept. Lett.* **2008**, *15*, 818−825.
(52) Qvist, J.; Davidovic, M.; Hamelberg, D.; Halle, B. A dry ligand-binding cavity in a solvated protein. *Proc. Natl. Acad. Sci. U.S.A.* **2008**, *105*, 6296−6301.
(53) Morris, G. M.; Goodsell, D. S.; Halliday, R. S.; Huey, R.; Hart, W. E.; Belew, R. K.; Olson, A. J. Automated docking using a Lamarckian genetic algorithm and an empirical binding free energy function. *J. Comput. Chem.* **1998**, *19*, 1639−1662.
(54) van der Spoel, D.; Berendsen, H. J. C. Molecular dynamics simulations of Leu-enkephalin in water and DMSO. *Biophys. J.* **1997**, *72*, 2032−2041.
(55) De Simone, F.; Guzzi, R.; Sportelli, L.; Marsh, D.; Bartucci, R. Electron spin-echo studies of spin-labelled lipid membranes and free fatty acids interacting with human serum albumin. *BBA-Biomembranes* **2007**, *1768*, 1541−1549.
(56) Simard, J. R.; Zunszain, P. A.; Ha, C. E.; Yang, J. S.; Bhagavan, N. V.; Petitpas, I.; Curry, S.; Hamilton, J. A. Locating high-affinity fatty acid-binding sites on albumin by X-ray crystallography and NMR spectroscopy. *Proc. Natl. Acad. Sci. U.S.A.* **2005**, *102*, 17958−17963.

JOURNAL OF AGRICULTURAL AND FOOD CHEMISTRY

Article

pubs.acs.org/JAFC

Mapping the Variation of the Carrot Metabolome Using ^{1}H NMR Spectroscopy and Consensus PCA

Morten Rahr Clausen,* Merete Edelenbos, and Hanne Christine Bertram

Department of Food Science, Aarhus University, Kirstinebjergvej 10, DK-5792 Aarslev, Denmark

Supporting Information

ABSTRACT: Genetic variation is the most influential factor for carrot (*Daucus carota* L.) composition. However, difference in metabolite content between carrot varieties has not been described by NMR, although primary metabolites are important for human health and sensory properties. The aim of the present study was to investigate the effect of genotype on carrot metabolite composition using a ^{1}H NMR-based metabolomics approach. After extraction using aqueous and organic solvents, 25 hydrophilic metabolites, β-carotene, sterols, triacylglycerols, and phospholipids were detected. Multiblock PCA showed that three principal components could be identified for classification of the five carrot varieties using different spectroscopic regions and the results of the two solvent extraction methods as blocks. The varieties were characterized by differences in carbohydrate, amino acid, nucleotide, fatty acid, sterol, and β-carotene contents. ^{1}H NMR spectroscopy coupled with multiblock data analysis was an efficient and useful tool to map the carrot metabolome and identify genetic differences between varieties.

KEYWORDS: *^{1}H NMR, carrots, consensus PCA, metabolite extraction*

INTRODUCTION

The appearance of carrots, their chemical composition, and quality are known to be affected by genotype and growth and storage conditions.[1,2] Recently, it was shown that genotype is the single most important factor that controls both the chemical composition (carotenes, sugars, phenolics, terpenes, falcarindiol) and sensory properties (sweetness and bitterness) of carrots.[3] Older papers, however, indicated that growing year and location also are important factors determining quality differences.[4,5]

The major aroma compounds of carrots are terpenes and sesquiterpenes.[6−8] These compounds significantly affect aroma and flavor attributes and interact with the taste attributes sweetness and bitterness.[7,9] Furthermore, phenolics and falcarinol and their derivatives have been extensively analyzed due to their implications for human health and sensory properties.[1,9−12] In fresh carrots, the sensory attribute bitterness was found to be related to the content of falcarindiol and a dicaffeic acid derivative of quinic acid.[13] Furthermore, data indicated that a high content of the carbohydrates sucrose, glucose, and fructose could mask bitterness.[6,13] Bitterness has also been attributed to the isocoumarin 6-methoxymellein, which increases after mechanical stress during handling and packaging of carrots.[1]

Although the content of secondary metabolites and carbohydrates has been extensively investigated in carrots, little is known about the variation of primary metabolites and lipids between genetically different carrots. To elucidate the effect of genotype on carrot metabolite composition, the aim of the present study was to investigate different carrot varieties by using a ^{1}H NMR-based metabolomic approach. Metabolomics is widely used as a tool to understand plant metabolism and food quality.[14,15] To understand the effects of postharvest storage and plant diseases, metabolomics has been used to investigate different root crops and their response to cold storage and microbial infections.[16−18] Furthermore, metabolomic phenotyping may lead to important information about authenticity of varieties grown under different conditions and has been used to discriminate different varieties of grass and legumes,[19] potatoes,[20] and Jerusalem artichoke tubers.[16]

MATERIALS AND METHODS

Plant Material and Sample Preparation. Five carrot varieties were selected for analyses: 'Bolero' (orange), 'Nipomo' (orange), 'Purple Haze' (purple with an orange core), 'Mello Yello' (yellow), and 'White Satin' (white). All varieties were F1-hybrids from Bejo Zaden (Warmenhuizen, The Netherlands) except for 'Bolero', which was bred by Vilmorin (La Ménitré, France). 'Bolero' was grown at the Department of Food Science, Aarhus University, Årslev, Denmark (10°27′ E, 55°18′ N) in a sandy loam soil (typical Agrudalf), whereas 'Nipomo', 'Purple Haze', 'Mello Yello', and 'White Satin' were grown at Tange Frilandsgartneri A/S, Bjerringbro, Denmark (9°34′ E, 56°20′ N) in a coarse sandy loam soil. All carrots were sown in April 2009 and hand-harvested in October 2009, when fully mature. Harvested roots were stored for 3 months at 1 °C and >95% relative humidity to keep shelf life and prevent loss of moisture. Five medium-sized roots of each variety were sampled and used for analyses. The roots had upper diameters between 31 and 41 mm and weights between 75 and 150 g. Roots were washed in tap water, and half of each root (the middle part) was sliced in approximately 0.5 cm disks, immediately frozen in liquid nitrogen and freeze-dried (48 h), vacuum-packaged in hermetically sealed aluminum foil pouches, and stored at −24 °C until analyses. Each carrot was treated as one replicate. At the time of analyses, freeze-dried material was ground using a pestle and a nitrogen-cooled mortar. Two subsamples of 50 mg of each carrot sample were weighed into 2 mL Eppendorf tubes, one tube for aqueous and one tube for organic extraction of the lyophilized carrot

Received: January 20, 2014
Revised: April 28, 2014
Accepted: April 28, 2014
Published: April 28, 2014

ACS Publications © 2014 American Chemical Society

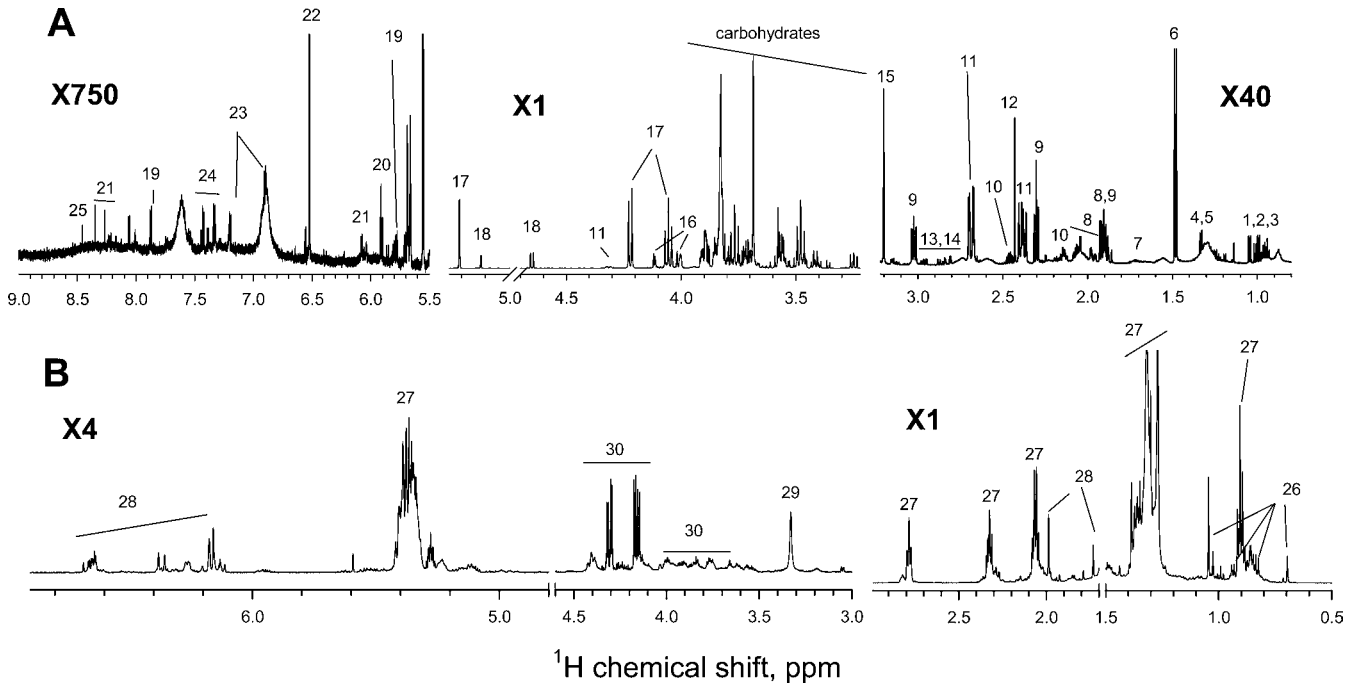

Figure 1. Representative ^{1}H NMR spectra of (A) aqueous and (B) organic extracts of 'Purple Haze' carrot. Peaks: 1, isoleucine; 2, leucine; 3, valine; 4, lactic acid; 5, threonine; 6, alanine; 7, arginine; 8, quinic acid; 9, γ-aminobutyric acid; 10, glutamine; 11, malic acid; 12, succinic acid; 13, aspartic acid; 14, asparagine; 15, choline; 16, fructose; 17, sucrose; 18, glucose; 19, uracil; 20, uridine; 21, β-adenosine; 22, fumaric acid; 23, tyrosine; 24, phenylalanine; 25, formic acid; 26, sterols; 27, fatty acid chain; 28, β-carotene; 29, phospholipids; 30, glycerol moiety triglycerides.

powder. One milliliter of unbuffered deionized water (Elga, Marlow, UK) was used for aqueous extraction. Although buffering of the solvent could have minimized variations in chemical shifts, we corrected for such variations using Icoshift. One milliliter of chloroform 99.8% D, 0.05% tetramethylsilan (TMS) (Cambridge Isotopes Laboratories Inc., Andover, MA, USA) was used for organic extraction. Samples were sonicated for 15 min at room temperature and stored at −80 °C (organic extract) or sonicated for 15 min at room temperature and then extracted overnight at 4 °C and stored at −80 °C (aqueous extract). Samples were centrifuged (10000*g*, 10 min, 4 °C) before NMR analyses. The organic supernatants were filtered through a nylon filter, and 600 μL of sample was transferred to NMR tubes. The aqueous supernatant was transferred directly to NMR tubes (500 μL) and mixed with 100 μL of D_2O containing 0.05% 3-(trimethylsilyl)propionic acid-[2,2,3,3-d_4] (TMSP) (Aldrich Chemistry, Steinheim, Germany).

NMR Spectroscopy. NMR spectra of extracts were obtained on a Bruker Avance III 600 equipped with a TXI probe (Bruker Biospin, Rheinstetten, Germany) operating at a ^{1}H frequency of 600.13 MHz and 298 K. One-dimensional (1D) proton NMR spectra of the aqueous extracts were acquired with a single 90° pulse, a relaxation delay of 5 s, and 64 scans sweeping 12.7 ppm/7288 Hz (offset 4.7 ppm) with 32K data points. The water signal was partially suppressed through irradiation with a weak presaturation pulse. NMR acquisition of the chloroform extracts was performed with a single 90° pulse, a relaxation delay of 1 s, and 64 scans sweeping 20.6 ppm/12335 Hz (offset 6.2 ppm) with 64K data points. All spectra were referenced to TMSP (aqueous extracts) or TMS (organic extracts).

Carrot metabolites were identified from pure standards, two-dimensional (2-D) NMR experiments (^{1}H−^{1}H homonuclear shift correlation (COSY) and ^{1}H−^{13}C heteronuclear single-quantum correlation spectroscopy (HSQC)), and comparison with published data.[21−25] The COSY spectra were acquired with a spectral width of 6130 Hz in both dimensions, 8K data points, and 512 increments with 32 transients per increment. The HSQC spectra were acquired with a spectral width of 8000 Hz in the F2 dimension and 25000 Hz in the F1 dimension, a data matrix with a size of 1K × 256 data points, and 64 transients per increment. All spectra were manually phased and baseline corrected.

Data Analysis. The NMR spectra of the aqueous extracts were aligned using the Icoshift procedure in Matlab version 8.1 (The Mathworks Inc., Natick, MA).[26] Alignment of NMR spectra of organic extracts was not necessary. The regions from 9.0 to 0.5 ppm were used for multivariate data analysis. Signals from residual water and nondeuterated solvents, which corresponded to the 5.0−4.7 ppm region in the aqueous extracts and the 7.24−7.14 and 1.7−1.5 ppm regions in the organic extracts, were left out. Compounds extracted from the filter at 8.02 and 4.63 ppm were also removed in the organic extracts. Prior to multivariate data analysis, NMR spectra were normalized according to the total spectrum intensity and Pareto scaled.

The multiblock method consensus PCA was performed in Matlab using the multiblock toolbox version 0.2 with full cross-validation.[27,28] With this method, the overall trend in the data was described at the super level, where the super scores (t_s) described how each sample was influenced over all blocks. The influence of each data block on this trend was described by the super block weights (w) and the weights were used to evaluate the importance of the different data blocks relative to each other. To examine the trend within blocks, block scores (t) were used to describe how each sample was influenced within each block. The influence of each variable on this trend was described by the block loadings (p).

For calculation of metabolite correlations, metabolites were integrated using an in-house developed Matlab script. Pearson correlation coefficients were calculated in Matlab using the corrcoeff function, and significant correlations are reported at $P \leq 0.01$.

RESULTS AND DISCUSSION

Figure 1 summarizes the metabolites identified in the carrot extracts; 25 hydrophilic metabolites were extracted and identified from lyophilized tissue of the carrots, and the hydrophobic metabolites identified comprised β-carotene, sterols, and peaks originating from fatty acid chains, the glycerol moiety of triacylglycrols, and the choline moiety of

dx.doi.org/10.1021/jf5014555 | J. Agric. Food Chem. 2014, 62, 4392−4398

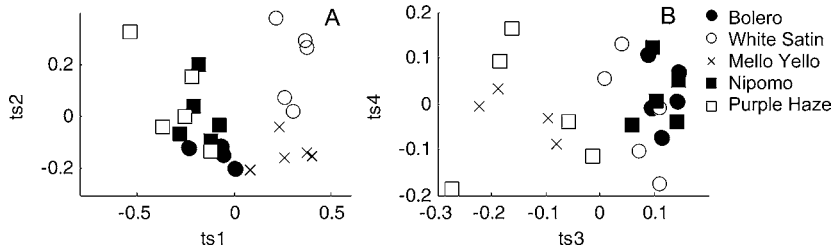

Figure 2. Consensus PCA super scores (t_s): (A) ts1 versus ts2; (B) ts3 versus ts4 of ^{1}H NMR spectra of carrot extracts divided into four blocks.

phospholipids. The detected sterol was similar to pure β-sitosterol; however, it could not be unambiguously assigned due to overlapping signals. The types of compounds in the four data blocks were as follows: block 1 covered the range 9−5.5 ppm in the aqueous extract and contained primarily aromatic amino acids, nucleotides/nucleosides, fumaric acid, and formic acid; block 2 covered the range 5.5−3.2 ppm in the aqueous extract and comprised primarily carbohydrates; block 3 covered the range 3.2−0.5 ppm in the aqueous extract and contained primarily organic acids and aliphatic amino acids; and block 4 covered the range 7.0−0.5 ppm in the organic extract and comprised sterols, fatty acids, carotene, phospholipids, and triglycerides.

In practice, extraction procedures are highly selective and will therefore not provide a complete picture of the metabolites present in a given sample.[29] In the present study the identified metabolites mainly comprised primary metabolites, whereas secondary metabolites were hardly detected; β-carotene, the primary carotenoid in orange carrots, could be detected in all orange varieties. Lutein, which is responsible for the yellow color in 'Mello Yello', and polyphenolics, which are responsible for the purple color in 'Purple Haze' were, however, not detected. Also, chlorogenic acid, which is common in carrots and reported in high concentrations in 'Purple Haze', was not identified.[13] This is in agreement with a previous study in which chlorogenic acid was detected only in trace amounts in roots using NMR,[30] whereas others found chlorogenic acid and feruloylquinic acid in leaf shoots.[31] On the other hand, we detected quinic acid, which is a precursor of chlorogenic acid, in all samples.

Multiblock methods are powerful tools to combine information from different data blocks obtained from the same objects, for example, metabolites that have similar metabolic origin or are obtained by different extraction methods.[27] In the multiblock analysis, data from the same objects are combined at a super level, and information is provided about the interrelationsships between blocks. Hence, the multiblock method may potentially reveal relationsships between metabolites extracted in different solvents or analyzed with different techniques.[27] Furthermore, multiblock analysis can be informative when minor trends in the data need to be revealed, either because they are not modeled[32] or simply because they are overlooked when loadings are inspected visually in a normal principal component analysis (PCA). The latter aspect may be corrected for by assigning data blocks the same weight in the analysis.

For this study, five carrot varieties with differences in appearance (mainly color) and chemical composition as revealed in previous studies were chosen.[6] Hydrophilic and hydrophobic metabolites were extracted using water and chloroform, and extracts were analyzed by ^{1}H NMR spectroscopy and data treated by multiblock statistical analysis. In principle, any number of blocks could be chosen to make the approach more data driven. However, that was not the purpose of the present study. The separation into blocks was mainly based on the need to integrate data from the two solvents in the same model. Furthermore, the division of the aqueous extract data into blocks was convenient because of the variation in peak intensities.

Consensus PCA was used to analyze the NMR data from the four assigned blocks. The carrot varieties could be discriminated by three principal components (PC1, PC2, and PC3) in the multiblock analysis (Figure 2), whereas no discrimination could be seen along PC4. A three-component model resulted in an acceptable cross-validated prediction error of 0.47, which did not improve significantly after inclusion of more principal components.

Along PC1, the varieties 'Mello Yello' and 'White Satin' were discriminated from the orange-colored 'Bolero', 'Nipomo', and 'Purple Haze'. A less clear discrimination was seen along PC2 between the varieties 'Bolero' and 'Mello Yello' and the rest of the varieties (Figure 2A). Along PC3, 'Nipomo' and 'Bolero' discriminated from 'Purple Haze' (Figure 2B). Overall, it was possible to separate the five genotypes by the multiblock method despite the fact that high between-root variations were observed for 'Purple Haze', 'Mello Yello', and 'White Satin' (Figure 2). The variety 'Purple Haze' is a two-colored F1-hybrid, which makes sampling of tissues of this variety challenging, for example, if the weight proportion of purple compared to orange tissues differs between roots. The other varieties were monochrome F1-hybrids with relatively even distributions of inner xylem (core) and outer phloem tissues (cortex).

The super weights (w) in Figure 3 allow us directly to extract which data blocks were most important for the discrimination

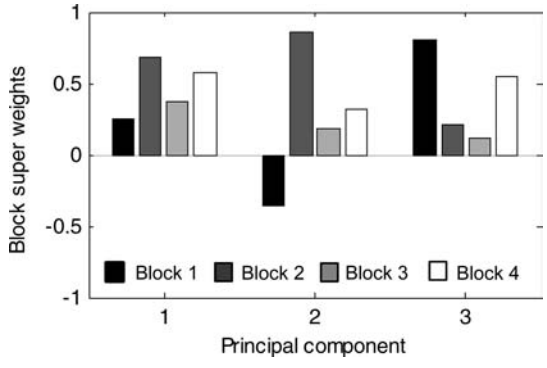

Figure 3. Consensus PCA block super weights showing the contribution of each block to the discrimination of the carrot varieties shown in Figure 2: block 1, 9−5.5 ppm in the aqueous extract; block 2, 5.5−3.2 ppm in the aqueous extract; block 3, 3.2−0.5 ppm in the aqueous extract; block 4, 7.0−0.5 ppm in the organic extract.

dx.doi.org/10.1021/jf5014555 | J. Agric. Food Chem. 2014, 62, 4392−4398

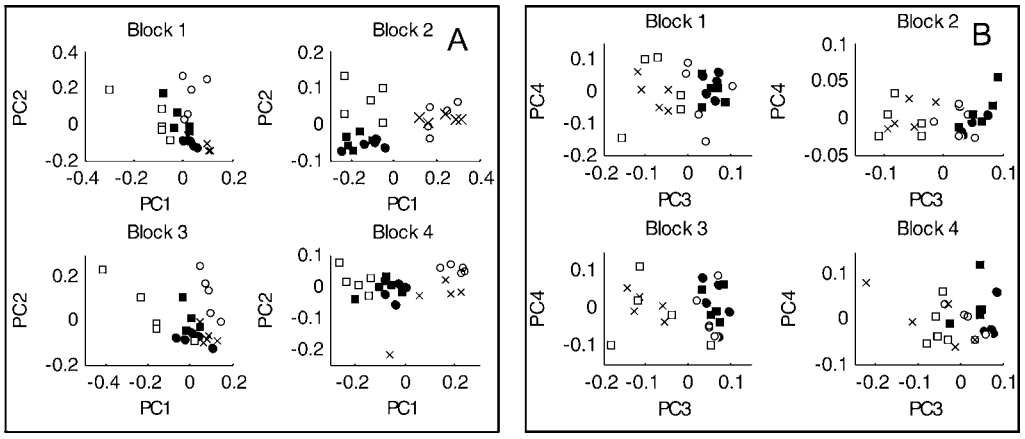

Figure 4. Block scores derived from the consensus PCA models: (A) PC1 versus PC2; (B) PC3 versus PC4; block 1, 9−5.5 ppm in the aqueous extract; block 2, 5.5−3.2 ppm in the aqueous extract; block 3, 3.2−0.5 ppm in the aqueous extract; block 4, 7.0−0.5 ppm in the organic extract. Legend is as in Figure 2.

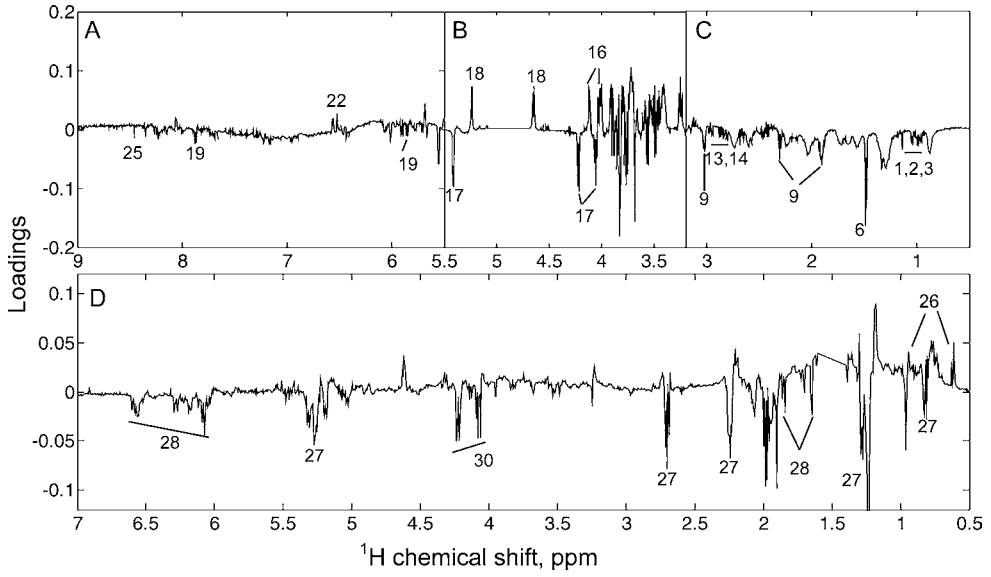

Figure 5. Block loadings for PC1 calculated on the basis of the consensus PCA for blocks 1−4. Peaks: 1, isoleucine; 2, leucine; 3, valine; 6, alanine; 9, γ-aminobutyric acid; 13, aspartic acid; 14, asparagine; 16, fructose; 17, sucrose; 18, glucose; 19, uracil; 22, fumaric acid; 25, formic acid; 26, sterols; 27, fatty acid chain; 28, β-carotene; 30, glycerol moiety triglycerides.

between varieties. Along PC1, all four blocks contributed to the discrimination of varieties; however, block 2 (carbohydrates) and block 4 (sterols, fatty acids, carotene, phospholipids, and triglycerides) had the highest super weights (Figure 3) and hence were most significant. Blocks 2 and 4 resulted in discrimination remarkably similar to that of the super level, which can be seen by comparing Figures 2A and 4A for those two blocks. The results showed that the orange varieties 'Bolero', 'Nipomo', and 'Purple Haze' discriminated from the yellow and white varieties 'Mello Yello' and 'White Satin' using information on the carbohydrate and lipid profiles. The results also indicated a connection between contents of carbohydrates and lipids in carrot roots. The block loadings in Figure 5 showed that discrimination between varieties could be attributed to differences in sucrose, fructose, glucose, and β-carotene contents. The yellow and white carrot varieties 'Mello Yello' and 'White Satin' contained no or only traces of β-carotene[6] and, furthermore, these varieties were characterized by higher contents of fructose and glucose than orange 'Bolero', 'Nipomo', and 'Purple Haze' roots, which had higher contents of sucrose and lipids, except for signals from sterols. The super weights for blocks 1 and 3 (organic acids, aromatic and aliphatic compounds) were smaller than for blocks 2 and 4 mainly due to between-root variation in 'Purple Haze' and the discrimination of this variety from the other varieties (Figures 3 and 4A). This result shows that the NMR approach using consensus PCA could reveal both major and minor metabolic phenotypes and easily assign them to the most significant data blocks.

The discrimination between orange-colored varieties and the yellow and white varieties comprised the majority of the variation in the data. This variation resulted in characteristic metabolite compositions that could be modeled. 'Mello Yello' and 'White Satin' discriminated along PC2 (Figure 2A), and after inspection of their block scores and loadings, it was clear that this was due to higher contents of fumaric acid, malic acid, β-carotene, and several lipid components in 'Mello Yello' and higher contents of two unknown peaks, phospholipids and glutamine, in 'White Satin' (Figures 4A and 6). On the other hand, no discrimination in block 2 could be observed (Figure 4A). Likewise 'Bolero' could be discriminated from 'Nipomo'

dx.doi.org/10.1021/jf5014555 | J. Agric. Food Chem. 2014, 62, 4392−4398

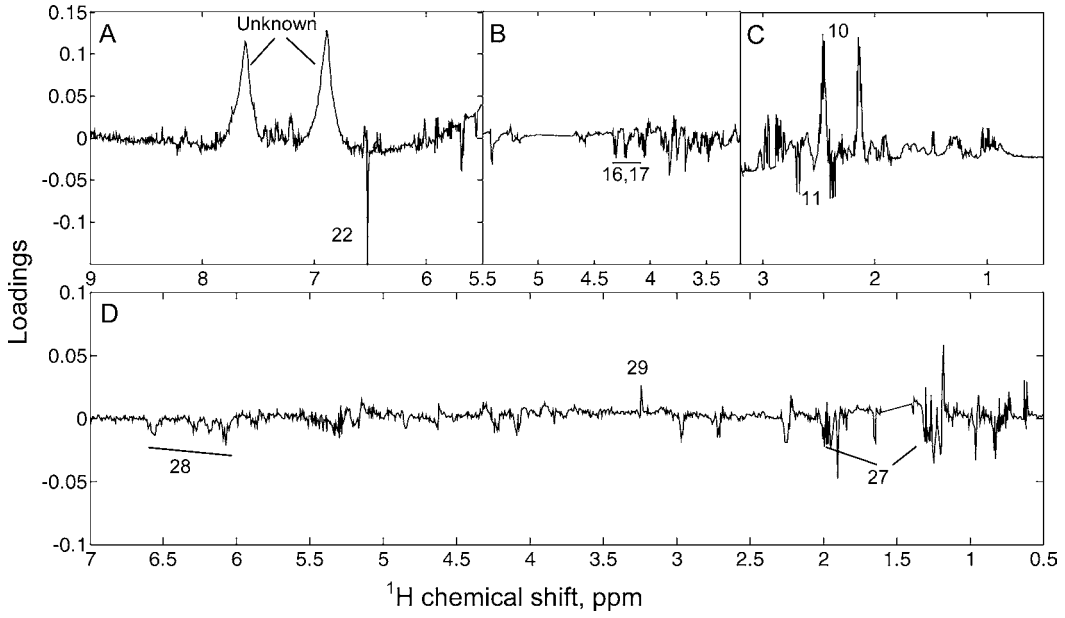

Figure 6. Block loadings for PC2 calculated on the basis of the consensus PCA for blocks 1−4. Peaks: 10, glutamine; 11, malic acid; 16, fructose; 17, sucrose; 22, fumaric acid; 27, fatty acid chain; 28, β-carotene; 29, phospholipids.

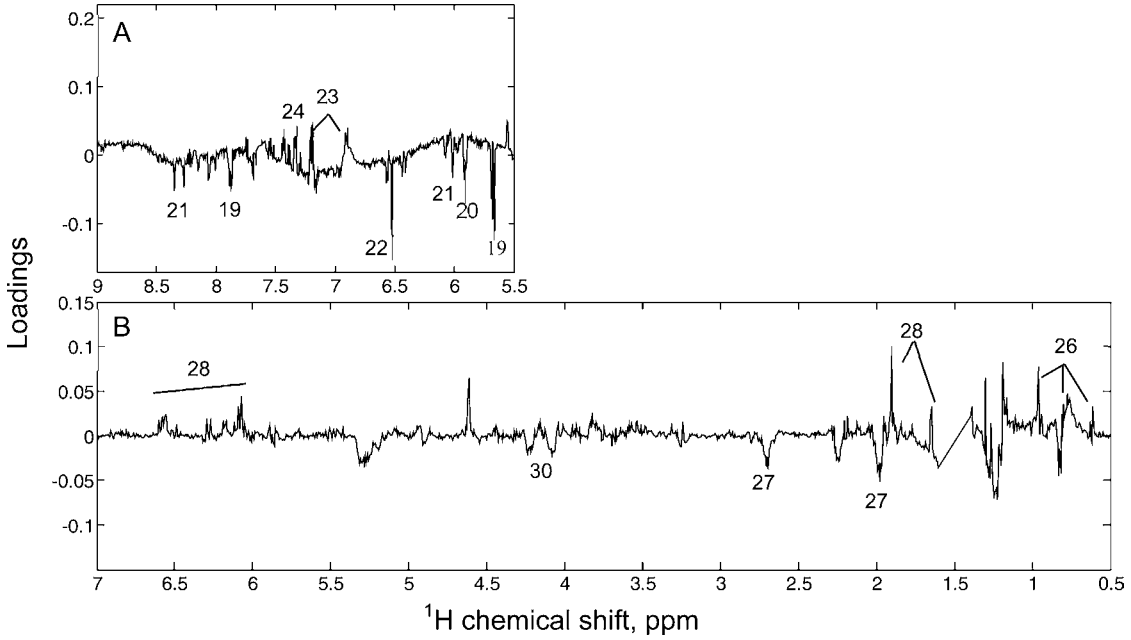

Figure 7. Block loadings for PC3 calculated on the basis of the consensus PCA. Only loadings from (A) block 1 and (B) block 4 are shown. Peaks: 19, uracil; 20, uridine; 21, β-adenosine; 22, fumaric acid; 23, tyrosine; 24, phenylalanine; 27, fatty acid chain; 28, β-carotene; 30, glycerol moiety triglycerides.

and 'Purple Haze' (blocks 1 and 3), and block 2 discriminated 'Purple Haze' from 'Bolero' and 'Nipomo'. Along PC3, Figure 2B shows a clear discrimination of 'Purple Haze' from 'Nipomo' and 'Bolero'. This separation was found in all block scores (Figure 4B). The super weights in Figure 3 clearly showed that block 1 (aromatic compounds) and block 4 (lipids) contributed most to this separation, and hence these two blocks were used for interpretation of PC3 (Figure 7). The loadings showed that 'Nipomo' and 'Bolero' were characterized by higher contents of β-carotene, sterols, fumaric acid, uridine, and β-adenosine, whereas 'Purple Haze' had higher contents of phenylalanine, tyrosine. and fatty acids, which was confirmed after integration of the corresponding peaks (data not shown).

The classifications of the carrot varieties from the carbohydrate (block 2) and lipid data (block 4) were remarkably alike (Figure 4A). This indicates that correlations between carbohydrates and lipids could exist for genetically different carrots. Hogstad et al.[2] reported a high correlation between sucrose and β-carotene in carrots grown in different years and soil types having variable supply of fertilizer. Pearson correlation analysis revealed a correlation coefficient of 0.91 between sucrose and β-carotene (Figure 8). The sucrose content was positively, and fructose and glucose contents were

dx.doi.org/10.1021/jf5014555 | J. Agric. Food Chem. 2014, 62, 4392−4398

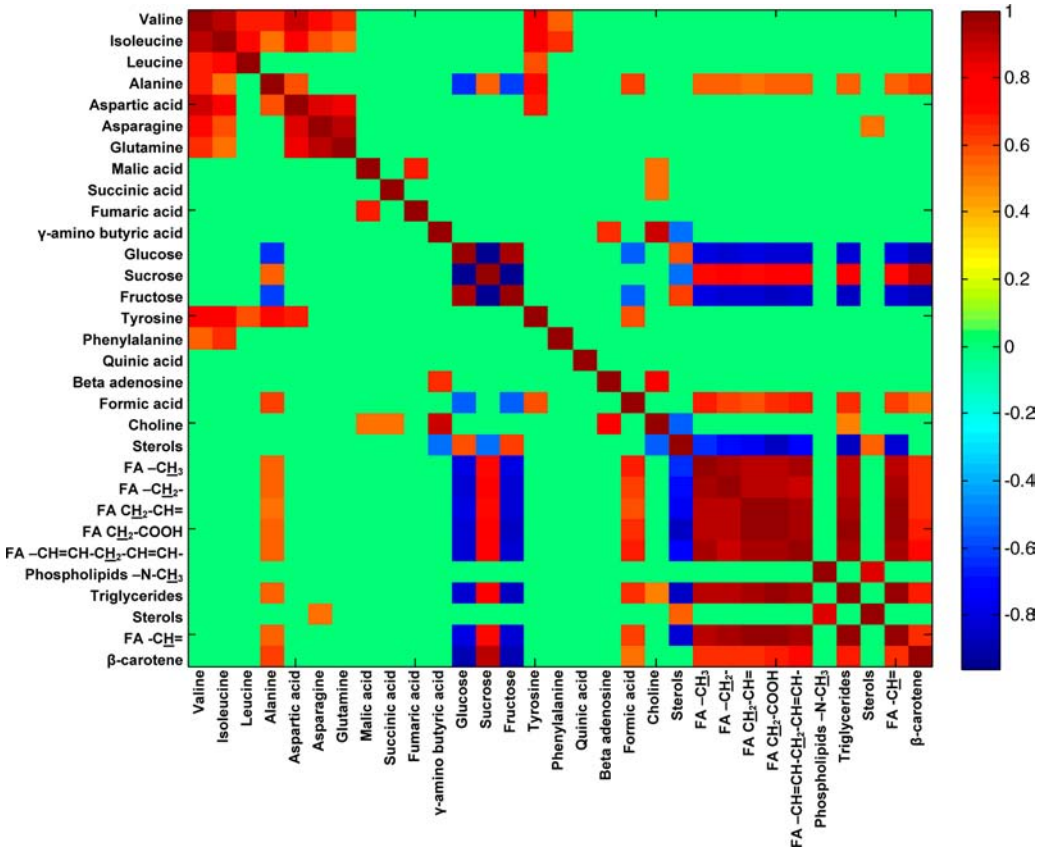

Figure 8. Pearson correlation coefficients between metabolites in carrots. Only correlations at $p \leq 0.01$ are shown. FA, fatty acid.

negatively, correlated with other metabolites in the lipid fraction (block 4), except for phospholipids and sterols, for which correlations were low and nonsignificant (Figure 8). Furthermore, the contents of most amino acids were correlated, and especially leucine/isoleucine and asparagine/glutamine were highly correlated. Many important aroma and flavor compounds are synthesized from compounds of the lipid metabolism or from degradation of lipids and amino acids.[33] Differences in these constituents may therefore be directly and/or indirectly responsible for variation in the sensory properties of carrots.

In conclusion, the present study revealed that ^{1}H NMR spectroscopy coupled with multiblock data analysis was an efficient and useful tool to map the carrot metabolome and identify compositional changes between varieties that could be determined by genetic differences, soil type, and growing strategy. The major differences were due to differences in the carbohydrate and β-carotene contents, where orange-colored varieties were characterized by relatively high contents of sucrose and β-carotene and relatively low contents of fructose and glucose. Minor differences, such as variations in the content of glutamine, fumaric acid, and malic acid, between the yellow ('Mello Yello') variety and the white ('White Satin') variety were also revealed. Consequently, because many precursors for aroma compounds were identified, the method could be used in addition to or to complement instrumental and sensory analysis of plant food products. Likewise, the methodology may find uses in studies of authenticity of plant food products and impact of terroir and growing system (e.g conventional and organic growing) as well as postharvest handling and storage on plant food quality to increase plant food quality and diversity on the market.

■ ASSOCIATED CONTENT

Supporting Information

Tables S1 and S2. This material is available free of charge via the Internet at http://pubs.acs.org.

■ AUTHOR INFORMATION

Corresponding Author

*(M.R.C.) Phone: +45 87158318. Fax +45 87154812. E-mail: MortenR.Clausen@agrsci.dk.

Funding

The research was funded by The Danish Research Council FTP through the project "Advances in Food quality and Nutrition Research through implementation of metabolomic strategies" (274-09-0169) and by the Ministry of Food, Agriculture and Fisheries through the project GOURMETROOT (Contract 3304-FVFP-08-K-04-01).

Notes

The authors declare no competing financial interest.

■ ACKNOWLEDGMENTS

We acknowedlge Nina Eggers for excellent technical assistance. We thank Christian Clement Yde for helpful discussions on the multivariate data analysis.

■ REFERENCES

(1) Seljåsen, R.; Bengtsson, G. Sensory and chemical changes in five varieties of carrot (*Daucus carota* L) in response to mechanical stress at harvest and postharvest. *J. Sci. Food Agric.* **2001**, *81*, 436−447.

(2) Hogstad, S.; Risvik, E.; Steinsholt, K. Sensory quality and chemical composition in carrots: a multivariate study. *Acta Agric. Scand.* **1997**, *47*, 253−264.
(3) Seljåsen, R.; Kristensen, H. L.; Lauridsen, C.; Wyss, G. S.; Kretzschmar, U.; Inéz, B.-A.; Kahl, J. Quality of carrots as affected by pre- and postharvest factors and processing. *J. Sci. Food Agric.* **2013**, *93*, 2611−2626.
(4) Martens, M.; Rosenfeld, H. J.; Russwurm, H., Jr. Predicting sensory quality of carrots from chemical, physical and agronomical variables: a multivariate study. *Acta Agric. Scand.* **1985**, *35*, 407−420.
(5) Rosenfeld, H.; Risvik, E. Sensory profiling of carrots from northern latitudes. *Food Res. Int.* **1997**, *30*, 593−601.
(6) Alasalvar, C.; Grigor, J.; Zhang, D.; Quantick, P. C.; Shahidi, F. Comparison of volatiles, phenolics, sugars, antioxidant vitamins, and sensory quality of different colored carrot varieties. *J. Agric. Food Chem.* **2001**, *49*, 1410−1416.
(7) Kreutzmann, S.; Thybo, A. K.; Edelenbos, M.; Christensen, L. P. The role of volatile compounds on aroma and flavour perception in coloured raw carrot genotypes. *Int. J. Food Sci. Technol.* **2008**, *43*, 1619−1627.
(8) Kjeldsen, F.; Christensen, L. P.; Edelenbos, M. Changes in volatile compounds of carrots (*Daucus carota* L.) during refrigerated and frozen storage. *J. Agric. Food Chem.* **2003**, *51*, 5400−5407.
(9) Rosenfeld, H. J.; Aaby, K.; Lea, P. Influence of temperature and plant density on sensory quality and volatile terpenoids of carrot (*Daucus carota* L.) root. *J. Sci. Food Agric.* **2002**, *82*, 1384−1390.
(10) Varming, C.; Jensen, K.; Møller, S.; Brockhoff, P. B.; Christiansen, T.; Edelenbos, M.; Bjørn, G. K.; Poll, L. Eating quality of raw carrots − correlations between flavour compounds, sensory profiling analysis and consumer liking test. *Food Qual. Prefer.* **2004**, *15*, 531−540.
(11) Young, J. F.; Duthie, S. J.; Milne, L.; Christensen, L. P.; Duthie, G. G.; Bestwick, C. S. Biphasic effect of falcarinol on Caco-2 cell proliferation, DNA damage, and apoptosis. *J. Agric. Food Chem.* **2007**, *55*, 618−623.
(12) Metzger, B. T.; Barnes, D. M.; Reed, J. D. Purple carrot (*Daucus carota* L.) polyacetylenes decrease lipopolysaccharide-induced expression of inflammatory proteins in macrophage and endothelial cells. *J. Agric. Food Chem.* **2008**, *56*, 3554−3560.
(13) Kreutzmann, S.; Christensen, L. P.; Edelenbos, M. Investigation of bitterness in carrots (*Daucus carota* L.) based on quantitative chemical and sensory analyses. *LWT−Food Sci. Technol.* **2008**, *41*, 193−205.
(14) Wishart, D. S. Metabolomics: applications to food science and nutrition research. *Trends Food Sci. Technol.* **2008**, *19*, 482−493.
(15) Hall, R. D. Plant metabolomics: from holistic hope, to hype, to hot topic. *New Phytol.* **2006**, *169*, 453−468.
(16) Clausen, M. R.; Bach, V.; Edelenbos, M.; Bertram, H. C. Metabolomics reveals drastic compositional changes during overwintering of Jerusalem artichoke (*Helianthus tuberosus*) tubers. *J. Agric. Food Chem.* **2012**, *60*, 9495−9501.
(17) Aliferis, K. A.; Jabaji, S. FT-ICR/MS and GC-EI/MS metabolomics networking unravels global potato sprout's responses to *Rhizoctonia solani* infection. *PLoS One* **2012**, DOI: 10.1371/journal.pone.0042576.
(18) Vikram, A.; Lui, L. H.; Hossain, A.; Kushalappa, A. C. Metabolic fingerprinting to discriminate diseases of stored carrots. *Ann. Appl. Biol.* **2006**, *148*, 17−26.
(19) Bertram, H. C.; Weisbjerg, M. R.; Jensen, C. S.; Pedersen, M. G.; Didion, T.; Petersen, B. O.; Duus, J. Ø.; Larsen, M. K.; Nielsen, J. H. Seasonal changes in the metabolic fingerprint of 21 grass and legume cultivars studied by nuclear magnetic resonance-based metabolomics. *J. Agric. Food Chem.* **2010**, *58*, 4336−4341.
(20) Beckmann, M.; Enot, D. P.; Overy, D. P.; Draper, J. Representation, comparison, and interpretation of metabolome fingerprint data for total composition analysis and quality trait investigation in potato cultivars. *J. Agric. Food Chem.* **2007**, *55*, 3444−3451.
(21) Fan, T.; Higashi, R.; Lane, A.; Jardetzky, O. Combined use of ^{1}H-NMR and GC-MS for metabolite monitoring and in vivo ^{1}H-NMR assignments. *Biochim. Biophys. Acta* **1986**, *882*, 154−167.
(22) Wishart, D. S.; Tzur, D.; Knox, C.; Eisner, R.; Guo, A. C.; Young, N.; Cheng, D.; Jewell, K.; Arndt, D.; Sawhney, S.; Fung, C.; Nikolai, L.; Lewis, M.; Coutouly, M. A.; Forsythe, I.; Tang, P.; Shrivastava, S.; Jeroncic, K.; Stothard, P.; Amegbey, G.; Block, D.; Hau, D.; Wagner, J.; Miniaci, J.; Clements, M.; Gebremedhin, M.; Guo, N.; Zhang, Y.; Duggan, G. E.; MacInnis, G. D.; Weljie, A. M.; Dowlatabadi, R.; Bamforth, F.; Clive, D.; Greiner, R.; Li, L.; Marrie, T.; Sykes, B. D.; Vogel, H. J.; Querengesser, L. HMDB: the Human Metabolome Database. *Nucleic Acids Res.* **2007**, *35*, D521−D526.
(23) Rivas-Ubach, A.; Sardans, J.; Pérez-Trujillo, M.; Estiarte, M.; Peñuelas, J. Strong relationship between elemental stoichiometry and metabolome in plants. *Proc. Natl. Acad. Sci. U.S.A.* **2012**, *109*, 4181−4186.
(24) Vlahov, G. Application of NMR to the study of olive oils. *Prog. Nucl. Magn. Reson. Spectrosc.* **1999**, *35*, 341−357.
(25) Ulrich, E. L.; Akutsu, H.; Doreleijers, J. F.; Harano, Y.; Ioannidis, Y. E.; Lin, J.; Livny, M.; Mading, S.; Maziuk, D.; Miller, Z.; Nakatani, E.; Schulte, C. F.; Tolmie, D. E.; Kent Wenger, R.; Yao, H.; Markley, J. L. BioMagResBank. *Nucleic Acids Res.* **2008**, *36*, D402−D408.
(26) Savorani, F.; Tomasi, G.; Engelsen, S. B. Icoshift: a versatile tool for the rapid alignment of 1D NMR spectra. *J. Magn. Reson.* **2010**, *202*, 190−202.
(27) Westerhuis, J. a.; Kourti, T.; MacGregor, J. F. Analysis of multiblock and hierarchical PCA and PLS models. *J. Chemom.* **1998**, *12*, 301−321.
(28) van den Berg, F. Multi-block Toolbox for MATLAB; http://models.life.ku.dk/MBToolbox (accessed Jan 7, 2013).
(29) Prosen, H.; Kokalj, M.; Janes, D.; Kreft, S. Comparison of isolation methods for the determination of buckwheat volatile compounds. *Food Chem.* **2010**, *121*, 298−306.
(30) Leiss, K.; Cristofori, G.; van Steenis, R.; Verpoorte, R.; Klinkhamer, P. G. L. An eco-metabolomic study of host plant resistance to Western flower thrips in cultivated, biofortified and wild carrots. *Phytochemistry* **2013**, *93*, 63−70.
(31) Grebenstein, C.; Choi, Y. H.; Rong, J.; de Jong, T. J.; Tamis, W. L. M. Metabolic fingerprinting reveals differences between shoots of wild and cultivated carrot (*Daucus carota* L.) and suggests maternal inheritance or wild trait dominance in hybrids. *Phytochemistry* **2011**, *72*, 1341−1347.
(32) Biais, B.; Allwood, J. W.; Deborde, C.; Xu, Y.; Maucourt, M.; Beauvoit, B.; Dunn, W. B.; Jacob, D.; Goodacre, R.; Rolin, D.; Moing, A. ^{1}H NMR, GC-EI-TOFMS, and data set correlation for fruit metabolomics: application to spatial metabolite analysis in melon. *Anal. Chem.* **2009**, *81*, 2884−2894.
(33) Christensen, L. P.; Edelenbos, M.; Kreutzmann, S. Fruits and vegetables in moderate climate. In *Flavours and Fragrances. Chemistry, Bioprocessing and Sustainability*; Berger, R. G., Ed.; Springer: Berlin, Germany, 2007; 648 pp.

JOURNAL OF AGRICULTURAL AND FOOD CHEMISTRY

Article

pubs.acs.org/JAFC

Terms of Use CC-BY

Effects of Genotype, Season, and Nitrogen Nutrition on Gene Expression and Protein Accumulation in Wheat Grain

G. A. Chope,*[,†] Y. Wan,[‡] S. P. Penson,[†] D. G. Bhandari,[§] S. J. Powers,[‡] P. R. Shewry,[‡] and M. J. Hawkesford[‡]

[†]Cereals and Ingredients Processing, Campden BRI, Chipping Campden, Gloucestershire, GL55 6LD, U.K.

[‡]Rothamsted Research, Harpenden, Hertfordshire, AL5 2JQ, U.K.

[§]HGCA, Stoneleigh Park, Kenilworth, Warwickshire, CV8 2TL, U.K.

Supporting Information

ABSTRACT: Six commercial U.K. cultivars of winter wheat selected to represent different abilities to partition nitrogen into grain protein were grown in replicated field trials at five different sites over three seasons. The proportion of LMW glutenin subunits decreased and the proportion of gliadins increased during grain development and in response to N application. Differences were observed between the proportions of LMW glutenin subunits and gliadins in low- and high-protein grain, these two fractions being decreased and increased, respectively. There was little effect of grain protein content on the proportions of either the HMW glutenin subunits or large glutenin polymers, which are enriched in these subunits, with the latter increasing during development in all cultivars. The proportion of total protein present in polymers in the mature grain decreased with increasing N level. Correlations were also observed between the abundances of gliadin protein transcripts and the corresponding proteins.

KEYWORDS: *wheat, grain quality, grain protein, flour functionality*

INTRODUCTION

The relationship between fertilizer inputs and harvest outputs is of vital importance for all crops, particularly in the context of increasing pressure to reduce nitrogen usage. The availability of nitrogen in the environment has an effect on the protein content and composition of wheat, which in turn affects the processing properties. The application of nitrogen fertilizer is required to achieve the 13% dry weight protein specification for breadmaking wheat in the U.K. Such applications are costly and may have a negative environmental footprint. There is therefore a need to develop new varieties that are more efficient in their uptake and utilization of nitrogen. Several studies have identified differences in the nitrogen use efficiency of modern and older cultivars, including high-quality breadmaking cultivars such as Xi19, Hereward, and Malacca.[1] Furthermore, whereas an inverse correlation is generally observed between the yield and grain protein content of bread wheat,[2] some cultivars consistently accumulate higher protein contents than would be expected based on their yields. These have been defined as exhibiting grain protein deviation[3] and may provide a basis for the future development of wheat cultivars that require less nitrogen fertilization to achieve acceptable protein contents for breadmaking. However, protein content is only one factor affecting processing quality, with protein quality (composition) also being important. It is, therefore, important to understand the relationship between N nutrition, grain protein content, grain protein composition, and processing properties.

The relationships between genetically determined differences in gluten protein composition and grain processing properties are well established.[4,5] However, wheat grain quality is also known to be highly sensitive to environmental conditions, although the basis for these effects is poorly understood.[6] Unravelling the interactions between genotype, environment, and nutrition is essential to facilitate the development of new wheat varieties having high stability to environmental fluctuations and, in particular, to maintain quality across a range of nitrogen inputs.

This paper describes multisite trials of six wheat cultivars with different levels of nitrogen over three years, to investigate the content and composition of gluten storage proteins during development and at maturity (using SDS-PAGE and size exclusion HPLC). Furthermore, transcriptome profiling of the developing caryopses at 21 days post-anthesis allowed the gliadin protein accumulated to be related to the expression levels of the corresponding genes.

MATERIALS AND METHODS

Growth and Harvesting of Wheat. Five U.K. breadmaking wheat cultivars (Cordiale, Hereward, Malacca, Marksman, and Xi19) and one feed wheat cultivar (Istabraq) were grown in randomized block with three-blocks (replicated) field trials in 2009, 2010, and 2011 at five U.K. sites: Rothamsted Research (Harpenden, Hertfordshire), RAGT (Ickleton, Cambridgeshire), KWS (Thriplow, Cambridgeshire), Syngenta (Duxford, Cambridgeshire), and Limagrain (Woolpit, Bury St Edmunds, Suffolk). Nitrogen was applied at three levels (100, 200, and 350 kg/ha in total, split in up to three applications) before anthesis. Mature grain was sampled in all years. In 2009 and 2010 at Rothamsted, main stem ears were tagged at anthesis and whole

Received: February 5, 2014
Revised: April 8, 2014
Accepted: April 15, 2014
Published: May 1, 2014

 © 2014 American Chemical Society

Table 1. Protein Composition (SDS-PAGE and SE-HPLC) and Gene Expression Data Present for All Six Cultivars (Cordiale, Hereward, Istabraq, Malacca, Marksman, and Xi19) for Combinations of Sites, Years, Time Points and N Levels[a]

analysis	year	site	N levels (kg/ha)			time points (DPA[b])				
protein composition[c]	2009	Rothamsted	100	200	350	21	28	35	42	M[d]
	2010	Rothamsted	100	200	350	21	28	35	42	M
		RAGT	100	200	350	21[e]				M
		Limagrain	100	200	350					M
		KWS	100	200	350					M
		Syngenta	100	200	350					M
	201	Rothamsted	100	200	350	21[e]				M
		RAGT	100	200	350	21[e]				M
		Limagrain	100	200	350					M
		KWS	100	200	350					M
		Syngenta	100	200	350					M
gene expression[f]	2009	Rothamsted	100	200	350	21				
	2010	Rothamsted	100	200	350	21				

[a]The sites were Rothamsted Research (Harpenden, Hertfordshire), RAGT (Ickleton, Cambridgeshire), KWS (Thriplow, Cambridgeshire), Syngenta (Duxford, Cambridgeshire), and Limagrain (Woolpit, Bury St Edmunds, Suffolk). [b]Days post-anthesis. [c]Nitrogen SDS-PAGE data: three biological replicates, two technical replicates; SE-HPLC data: one biological replicate, one technical replicate. [d]M = maturity. [e]21 DPA samples for 200 kg N/ha only. [f]Gene expression data: three biological replicates, one technical replicate.

caryopses were harvested from the middle part of the ear at 21, 28, 35, and 42 days post-anthesis (DPA). In 2010 and 2011, caryopses were harvested at 21 DPA from the RAGT site.

Total Nitrogen Determination. Total nitrogen was determined in mature grain using the Dumas combustion method,[7] using a CNS (carbon, nitrogen, sulfur) combustion analyzer (Leco Corp., St. Paul, MN, USA).

SDS-PAGE. For sodium dodecyl sulfate-polyacrylamide gel electrophoresis (SDS-PAGE), samples (35 mg) of wholemeal flour milled in a hand-operated grinder were extracted with 1 mL of 0.0625 M Tris-HCl, pH 6.8, 2% (w/v) sodium dodecyl sulfate (SDS), 1.5% (w/v) dithiothreitol, 10% (v/v) glycerol, and 0.002% (w/v) bromophenol blue. Gels (NuPAGE 12% Bis-Tris, Life Technologies, Paisley, UK) were stained with Coomassie brilliant blue and then scanned and analyzed using Total Lab TL120 version 2006F (Nonlinear Dynamics, Newcastle upon Tyne, UK) with an optical density curve calibrated using a Kodak T14 control scale (Tiffen, LLC, Rochester, NY, USA). Values for band optical density and band percent as a proportion of the total lane optical density were analyzed. Analysis was carried out for three biological replicates and two technical replicates of each gel that were run together on the same day and stained and destained together.

SE-HPLC. Size exclusion high-performance liquid chromatography (SE-HPLC) was used to determine the protein polymer size distribution of white flour samples milled using a Chopin CD 1 laboratory mill (Chopin Technologies, Villeneuve-la-Garenne Cedex, France). The analysis was performed according to the Profilblé method developed jointly by ARVALIS and l'Institut National de Recherche Agronomique.[8] Flour (160 mg) was mixed with 20 mL of 1% SDS (w/v) in 0.1 M phosphate buffer (pH 6.9), sonicated (Misonix Microson XL2000, Qsonica, LLC, Newtown, CT, USA) to solubilize the polymeric gluten proteins, and then centrifuged for 10 min at 4500*g*. An aliquot of the supernatant was sealed in a HPLC vial ready for analysis. SE-HPLC was conducted using a Jasco (Jasco Ltd, Great Dunmow, Essex, UK) system operating with a TSK gel G 4000SW column (30 cm × 7.5 mm) and a TSK gel SK guard column (7.5 cm × 7.5 mm). The flow rate was 0.7 mL/min, and detection was performed at 214 nm. Samples from the three biological replicates were pooled prior to analysis. The chromatograms were integrated using a combination of automated algorithms and manual rules developed as part of the Profilblé method. Peak ratios were calculated as reported by Millar (2003).[9]

RNA Extraction. Twenty-one DPA caryopses for RNA extraction were frozen at −80 °C until required. RNA was extracted using a method based on Chang et al. (1993).[10,11] About 1.5 g of whole caryopses was ground in a cooled mill, and RNA was extracted in CTAB buffer (2% CTAB, 2% PVP K30, 100 mM Tris-HCl, pH 8.0, 25 mM EDTA, 2.0 M NaCl, 0.5 g/L spermidine, 2% (w/v) 2-mercaptoethanol) with chloroform/isoamyl alcohol (24:1) to remove proteins. The RNA was precipitated by incubation with 10 M LiCl on ice overnight and then dissolved in SSTE buffer (1.0 M NaCl, 0.5% (w/v) SDS, 10 mM Tris HCl pH 8.0, 1 mM EDTA) to remove polysaccharides and extracted once with chloroform/isoamyl alcohol. After ethanol precipitation, total RNA was dissolved in DEPC-treated water and stored at −80 °C.

Gene Expression Profiling. Transcriptome profiling was performed using the Affymetrix GeneChip Wheat Genome Array and the standard one-cycle cDNA synthesis protocol and hybridization (as described in the GeneChip Expression Analysis Technical Manual) at the University of Bristol. Transcriptome data were analyzed using the GeneSpring version 11 (Agilent Technologies Inc., Santa Clara, CA, USA) package. The standard workflow was followed for two-factor experiments (nitrogen level, variety). Gene expression analysis was carried out for each of three biological replicates of whole caryopses harvested at 21 DPA from one site (Rothamsted Research) only, in 2009 and 2010.

Statistical Methods. Protein composition and gene expression data were determined for all six cultivars for each of different combinations of sites, years, time points, and N levels, as described in Table 1.

SDS-PAGE data were analyzed by residual maximum likelihood (REML) using GenStat (14th edition, VSN International Ltd, Hemel Hempstead, UK) to fit a linear mixed model consisting of random (design) and fixed (treatment) effects. The main effects and interactions between cultivar, N level, and time point factors formed the fixed part of the model. The effects of sites and years and further nested effects relating to blocking at the field (blocks and plots) and laboratory (gels and lanes within gels) stages were taken as design features, so that results for the combinations of cultivar, N level, and time point were effectively without issues of unequal representation across different sites and years. Data were subjected to $\log_e$ transformation to ensure a Normal distribution and homogeneity of variance. Comparisons of predicted means of statistical ($p < 0.05$, F-test) relevance from the model were made using estimated standard error of the difference values on the corresponding degrees of freedom, thus providing least significant difference (LSD) values at the 5% ($p = 0.05$) level of significance.

SE-HPLC data were transformed by using a $\log_e$-centering transformation[12] due to their compositional nature. To give an overall description and to afford a separation of the profiles of the samples in the absence of biological replication due to pooling, a multivariate method, principal coordinates analysis (PCO),[13] was applied.

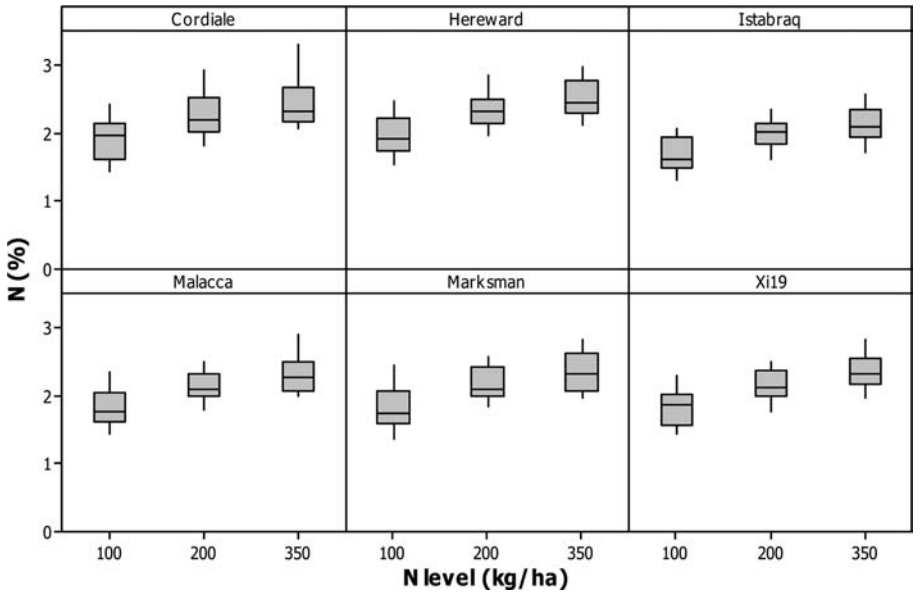

Figure 1. Box plots of the wholegrain N content (%) at maturity for each of six wheat cultivars grown at three different levels of N fertilization (100, 250, or 350 kg N/ha. Data displayed represent the distribution of means of samples collected over combinations of three years and five sites with three biological replicates (N = 594 in total, n = 11 per box plot).

Following regression analysis of the original variables on the two coordinate vectors (PCo1 and PCo2) retained, the variables were ranked, via the regression F-statistics, in order of the importance of their contribution to the principal coordinate vectors and therefore to any discrimination seen in the two dimensions. The means for the SE-HPLC data across combinations of years and sites were calculated to allow visualization of general trends over development, with standard error based on variation across years and sites.

Gene expression values were subjected to $\log_e$ transformation to ensure a Normal distribution and homogeneity of variance. The data were analyzed by REML using a model with the main effects and interaction between cultivar and N level as the treatment structure and with the field blocking (blocks and plots) nested within the two years (2009 and 2010) as the design structure.

Pearson correlations between gene expression data for the Rothamsted Research site at 21 DPA in the two years (2009 and 2010) and for all varieties and N levels, with the protein variables from either SDS-PAGE (with replication) or SE-HPLC (without replication), were calculated and tested for significance (F-tests).

RESULTS

Determination of Protein Content and Composition. The percentage N content of the wholegrain samples increased with increasing N fertilization for all varieties, from a mean of 1.83% (approximately 10.43% protein, conversion factor = 5.7) at 100 kg N/ha to 2.34% (approximately 13.34% protein) at 350 kg N/ha (Figure 1). Istabraq had the lowest protein content and Hereward the highest at all N-fertilization levels.

The content and composition of gluten proteins in the samples were determined using both SDS-PAGE and SE-HPLC.

SDS-PAGE Analysis. Quantitative gel scanning of SDS-PAGE separations of fractions extracted under reducing conditions was used to determine the proportions of bands corresponding to the major groups of gluten protein subunits: the HMW subunits of glutenin (HMW GS), LMW subunits of glutenin (LMW GS), and gliadins. Combining data from the SDS-PAGE analyses of samples from three years and five sites (with three biological and two technical replicates of each) showed broadly similar patterns for these protein groups for the six cultivars, but with some statistically significant (p < 0.05, LSD) differences (Figure 2).

The HMW GS (Figure 2A) accounted for between about 8% and 18% of the total gluten protein fraction, depending on the cultivar, stage of development, and N level (p = 0.001, F-test). Generally, the proportions of HMW GS were not strongly influenced by the N level. However, Marksman contained the highest proportion of HMW GS at all N levels and also showed a small overall increase in response to N. The LMW GS (Figure 2B and C) and gliadins (Figure 2D and E) were the major groups, accounting for between about 45% and 55% and between 30% and 40% of the total gluten protein fraction, respectively, at 21 DPA. These two fractions decreased or increased, respectively, as a proportion of the total protein during grain development.

The significance (p-values) of terms in the model fitted using REML are given in Table 2. For gliadins, the interactions between cultivar and time point and between N level and time point were significant (p < 0.001, F-test), but the interaction between cultivar and N level was not significant (p = 0.153, F-test), indicating that each cultivar responded in a similar way to increased N fertilization. During development the proportion of gliadins increased (means are presented in Figure 2D and E), with the increase being greater in Cordiale, Marksman, and Xi19 than in the other three cultivars. For all cultivars, there was a small increase between 28 and 35 DPA compared to rapid changes between 21 and 28 DPA (particularly at 200 kg N/ha) and between 35 and 42 DPA. Malacca contained the lowest proportion of gliadins throughout development and at maturity. The proportion of gliadins was lowest at the lowest N level, with little difference between the proportions at 200 and 350 kg N/ha.

The changes observed for LMW GS were the inverse of those observed for the gliadins, which is to be expected, as these two groups together accounted for over 80% of the total fraction. Thus, the interactions between cultivar and time point and between N level and time point were significant (p < 0.001, F-test), but the interaction between cultivar and N level was not

dx.doi.org/10.1021/jf500625c | J. Agric. Food Chem. 2014, 62, 4399−4407

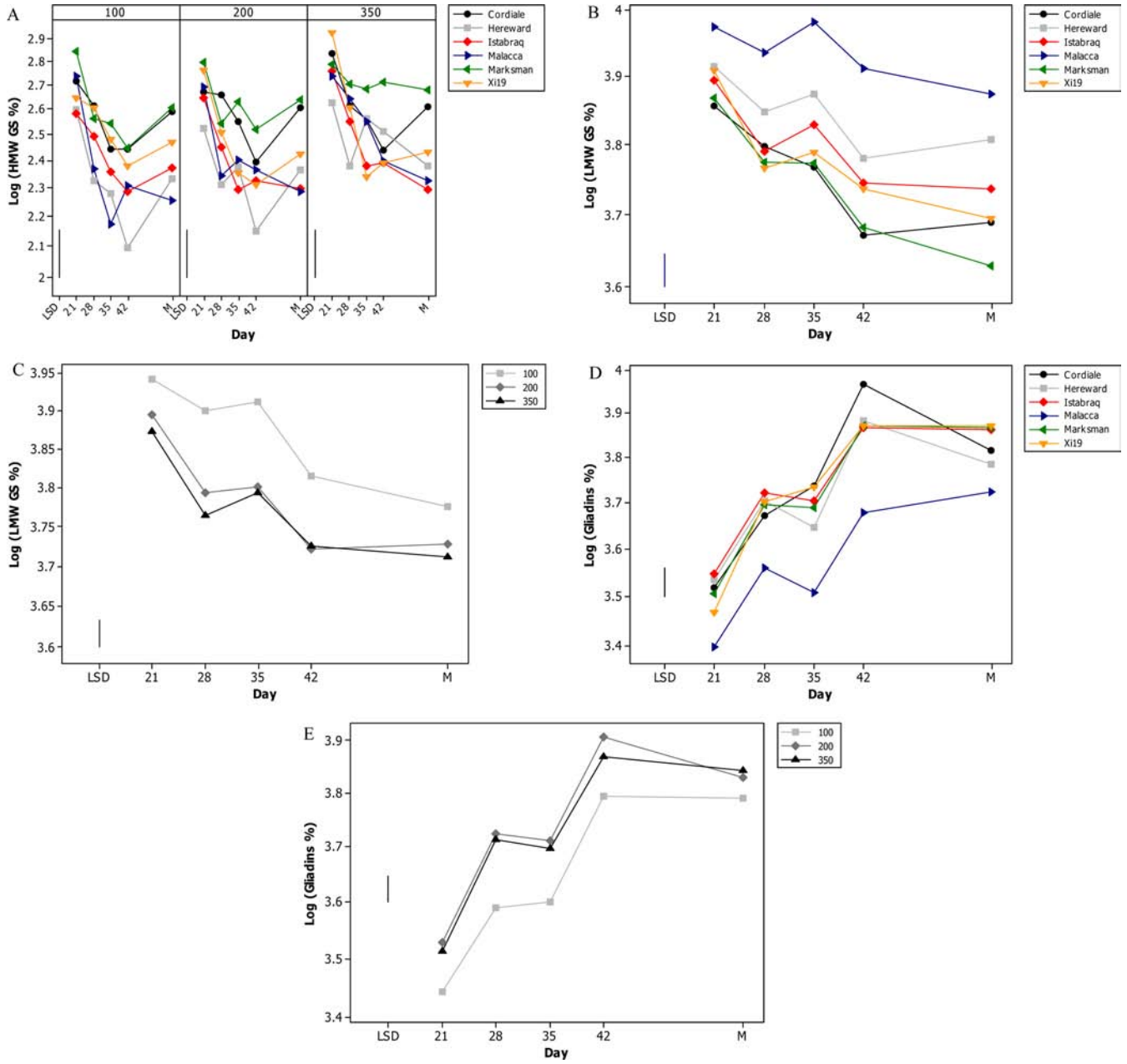

Figure 2. Log_e of the proportion of HMW glutenins (A), LMW glutenins (B, C), and gliadins (D, E) as a percentage of gluten protein in six wheat cultivars grown at three different levels of N fertilization (100, 200, or 350 kg N/ha). Data represent means of samples collected over combinations of three years and five sites with three biological replicates and two technical replicates (N = 1871 in total, n = 11 per mean). LSD (5%) bars are shown to allow comparison between means.

Table 2. Significance (F-Statistics and *p*-Values) of the Main Effects and Interactions between the Three Factors Cultivar, Time Point, and N Level for SDS-PAGE Analysis (log_e-Transformed Data)

	source					
	HMW GS		LMW GS		gliadins	
	F	*p*-value	F	*p*-value	F	*p*-value
time point	76.90	<0.001	143.50	<0.001	314.24	<0.001
cultivar	124.79	<0.001	204.75	<0.001	84.26	<0.001
N level	13.10	<0.001	91.84	<0.001	58.04	<0.001
time point·cultivar	5.41	<0.001	5.60	<0.001	5.43	<0.001
time point·N level	3.68	<0.001	4.84	<0.001	4.51	<0.001
cultivar·N level	2.94	0.001	0.90	0.532	1.46	0.153
time point·cultivar·N level	1.86	0.001	0.59	0.981	1.18	0.207

dx.doi.org/10.1021/jf500625c | J. Agric. Food Chem. 2014, 62, 4399−4407

significant (p = 0.532, F-test). A rapid decrease occurred between 21 and 28 DPA followed by little change between 28 and 35 DPA and a further rapid decrease between 35 and 42 DPA (Figure 2B). Also, Malacca contained a much higher proportion of LMW GS compared to the other cultivars. Finally, the proportion of LMW GS was highest at the lowest N level with little difference between the 200 and 350 kg N/ha levels (Figure 2C).

Consistent differences across years and sites (data not shown) were observed between Cordiale and Marksman (high proportions of HMW GS and low proportions of LMW GS) and Malacca (high LMW GS and low gliadins).

SE-HPLC Analysis. SE-HPLC was used to separate the total grain proteins (monomers and polymers) based on their size distribution, without reduction of disulfide bonds, with five peaks being recognized.[8] The first peak to elute from the column is referred to as F1 and consists of HMW polymers enriched in HMW GS, while the F2 peak comprises LMW polymers and is enriched with LMW GS. The F3 and F4 peaks are composed principally of ω-gliadins and α-, β-, and γ-gliadins, respectively, and the F5 peak comprises LMW proteins including albumins and globulins. The total area under the trace is a measure of the total protein content of the flour and is termed AT.

The SE-HPLC data were analyzed by principal coordinates analysis. The first two PCos accounted for 86.03% (63.82 and 22.21% for PCo1 and PCo2, respectively) of the variation in the distance matrix formed from the similarities between samples, so these two were retained and the data are visualized in Figure 3, with developing and mature samples highlighted in Figure 3A and N treatments highlighted in Figure 3B. The F-statistics resulting from relating the two PCos to the variables are shown in Table 3.

F1 was most important for the separation on the PCo1 axis, followed, to a lesser extent, by F2, F3, and F5, with the mature samples being clearly separated from the immature samples (Figure 3A). F4 and total gluten protein (F1+F2+F3+F4) were important for separation on the PCo2 axis, with the coordinate generally increasing with N level for each year by site by cultivar combination (Figure 3B).

Figure 4 shows changes in the proportions of polymeric gluten proteins, calculated as F1+F2 divided by F3+F4. At all N levels and for all varieties the proportion increased as the grain developed until 28 DPA, followed by a decrease between 28 and 35 DPA and a final increase between 35 DPA and maturity. Istabraq generally had the lowest proportion of polymeric gluten proteins and Hereward the highest. The proportion of polymeric proteins decreased with increasing N level at maturity.

The protein composition also differed between varieties, and these differences were consistent across sites and years (data not shown). Averaging over the site by year combinations, Istabraq had the lowest proportion of the F1 fraction (12.2–12.5% at maturity), while the highest proportion of the F2 fraction and the lowest proportion of the F5 fraction were in Malacca (F2: 25.4–25.5%; F5: 35.7–38.5% at maturity) and Hereward (F2: 25.4–25.9%; F5: 36.4–39.3% at maturity). The lowest proportion of the F3 fraction was in Cordiale (7.1–7.5% at maturity) and Xi19 (7.1–7.4% at maturity).

Gene Expression. A total of 55 probe sets on the arrays were identifiable as corresponding to gluten protein transcripts. However, because the gluten proteins showed high polymorphism both within and between cultivars, not all of the probe sets corresponded to genes present within each cultivar. For example, six probe sets corresponded to HMW GS, for genes encoding HMW GS 1Dx3, 1Dx5, 1Bx7, 1Bx14, 1By9, and 1By16, while the HMW subunits expressed in the six cultivars are 1Ax1, 1Bx14, 1By15, 1Dx5, and 1Dy10 in Marksman, 1Bx7, 1By9, 1Dx3, and 1Dy12 in Hereward, 1Ax1, 1Bx17, 1By18, 1Dx5, and 1Dy10 in Cordiale, 1Bx17, 1By18, 1Dx2, and 1Dy12 in Malacca, 1Bx14, 1By15, 1Dx5, and 1Dy10 in Xi19, and 1Bx7, 1By9, 1Dx2, and 1Dy12 in Istabraq (Supplementary Figure S1). Similarly, a high degree of sequence identity within other families of gluten proteins would be expected to have resulted in cross-hybridization with related transcripts. Therefore, Figure 5 shows the mean expression profiles of individual transcripts related to HMW GS (six elements), LMW GS (nine elements), and gliadins (40 elements).

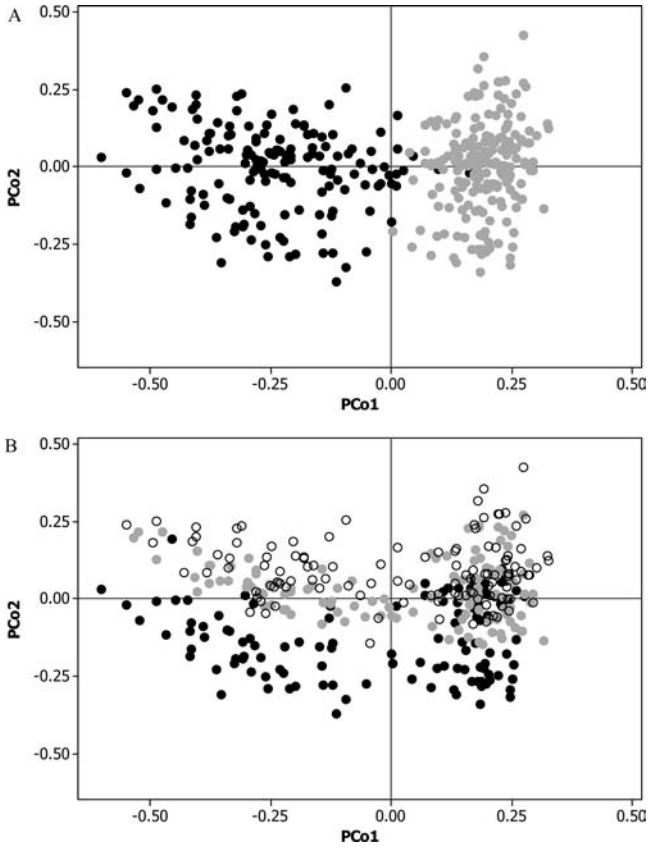

Figure 3. Coordinates for each sample determined by SE-HPLC for the first two PCos (explaining 63.82% and 22.21% of the variation in the distance matrix, respectively) showing the separation of samples according to time point (A; black = immature, gray = mature) or N level (B; black = 100 kg N/ha, gray = 200 kg N/ha, white = 350 kg N/ha).

Table 3. F Statistics from Relating the Two PCos to the ($\log_e$-Transformed) SE-HPLC Variables

variable	PCo1	PCo2
F1	3050.7	1.4
F2	1475.0	0.8
F3	1468.6	37.6
F4	9.0	979.2
F5	1065.5	80.7
gluten protein (F1+F2+F3+F4)	16.4	858.1

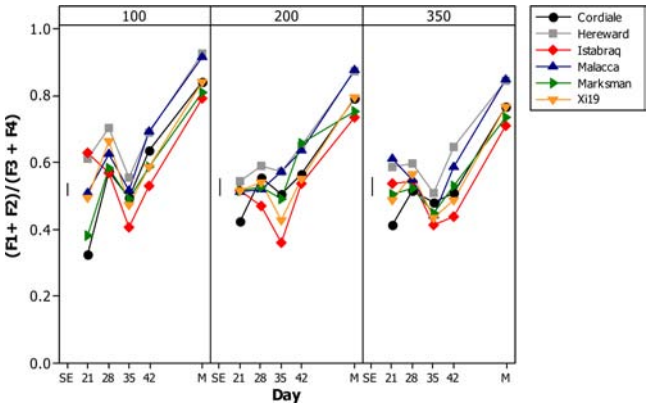

Figure 4. Ratio of polymeric (F1+F2) to monomeric (F3+F4) protein analyzed by SE-HPLC for six wheat cultivars and three levels of N fertilization (100, 200, or 350 kg N/ha). Data are means across year and site combinations. As the data are not replicated, the SEMs are based solely on the variation across years and sites (N = 354 in total, n = 11 per mean). The average SEM is shown as a vertical bar for convenience.

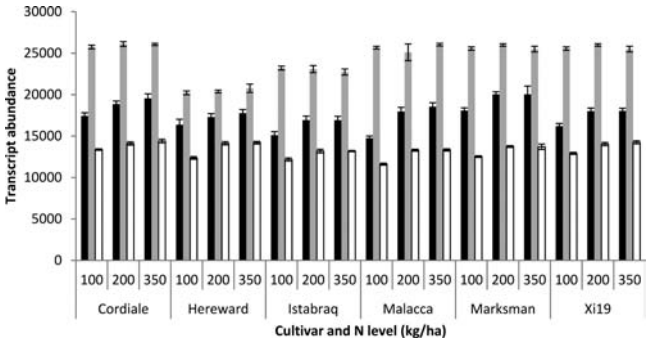

Figure 5. Gene expression values for the mean of all HMW GS (black)-, LMW GS (gray)-, and gliadin (white)-related genes for six wheat cultivars grown at one site (Rothamsted Research) only. Data are from microarray analysis and represent means of samples collected over two years with three biological replicates (N = 108 in total, n = 6 per mean). Error bars represent standard error. See Supporting Information for tables of means for statistical comparison using relevant LSD (5%) values for data on the $\log_e$-transformed scale.

The significance levels (p-values) of the main effects and the interactions between the two factors cultivar and N level are shown in Table 4 (after accounting for sources of design variation). There were independent effects of N level and cultivar (p < 0.001, F-test) for gene expression corresponding to HMW GS, which differs from the SDS-PAGE results for HMW GS, where the cultivar by N level interaction was significant. The relative levels of hybridization to the probe sets suggested that Marksman had the highest level of gene expression, but did not differ significantly (p < 0.05, LSD) from Cordiale (Supplementary Table S1). The other four cultivars appeared to have somewhat lower levels of gene expression, with Istabraq having the lowest. A trend of increasing HMW GS gene expression with increasing N was seen (Supplementary Table S1).

For LMW GS gene expression, only the main effect of cultivar was significant (p < 0.001, F-test). Cordiale, Malacca, Marksman, and Xi19 showed the highest level of LMW GS gene expression and were not significantly (p < 0.05, LSD) different from one another, while Hereward had by far the lowest level (Supplementary Table S2). There was a significant variety by N interaction (p = 0.022, F-test) for gliadin gene expression, which appeared to be lowest for Istabraq and Malacca (Supplementary Table S3). However, the validity of comparisons between cultivars can be questioned, as they may differ in the extent to which the gluten protein genes present correspond to the sequences present in the probe sets. This would result in stronger hybridization signals, indicating greater gene expression.

By contrast, comparisons of hybridization intensity within cultivars are valid, and these all showed significant increases in gene expression with increasing N. For gliadin-related gene expression, Cordiale appeared to display a more linear response with respect to increasing N than the other varieties, having the greatest hybridization intensity of all of the cultivars at 100 kg N/ha. Cordiale was also the only cultivar that showed a marked increase in gliadin gene expression between 200 and 350 kg N/ha (Supplementary Table S3).

Correlation of Gene Expression Data with Protein Composition. The proportions of gliadins measured by SDS-PAGE were significantly correlated with the corresponding data for average gliadin-related gene expression in both 2009 (r = 0.335, p = 0.013, n = 54, F-test) and 2010 (r = 0.372, p = 0.006, n = 54, F-test) (Figure 6A). In particular, the proportions of gliadin proteins and the gene expression were lowest at 100 kg N/ha, with the 200 and 350 kg N/ha samples having higher proportions of gliadin protein but more variable gliadin gene expression. Similarly, gliadin gene expression was positively correlated with the proportion of gliadin proteins measured by SE-HPLC (F4 fraction) (2009: r = 0.641, p = 0.004, n = 18, F-test; 2010: r = 0.768, p < 0.001, n = 18, F-test) (Figure 6B). No significant (p < 0.05, F-test) correlations were observed between glutenin subunit (HMW or LMW) gene expression and the proportions of the proteins determined by SDS-PAGE, but HMW subunit gene expression showed a negative correlation with the proportion of large glutenin polymers determined by SE-HPLC (Figure 6C) (2009: r = −0.387, p = 0.112, n = 18, F-test; 2010: r = −0.637, p = 0.004, n = 18, F-test), presumably because this smaller fraction, when expressed as a percentage of AT, is diluted by the increasing amounts of F4.

Table 4. Significance (F-Statistics and p-Values) of the Main Effects and Interactions between the Two Factors Cultivar and N Level for $\log_e$ Gene Expression Analysis

	source					
	HMW GS		LMW GS		gliadins	
	F	p-value	F	p-value	F	p-value
cultivar	19.88	<0.001	132.74	<0.001	27.80	<0.001
N level	45.66	<0.001	0.16	0.853	137.78	<0.001
cultivar·N level	1.48	0.163	0.93	0.507	2.24	0.022

dx.doi.org/10.1021/jf500625c | J. Agric. Food Chem. 2014, 62, 4399−4407

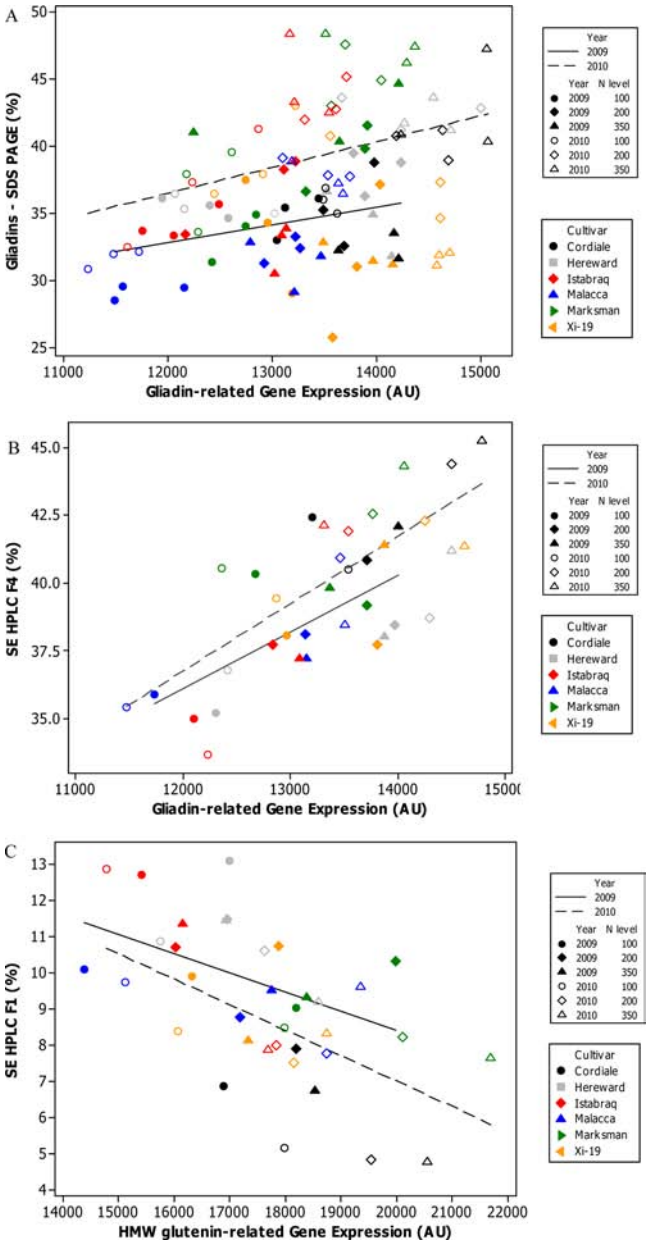

Figure 6. Correlations between gene expression values and protein contents determined by SDS-PAGE and SE-HPLC. (A) Gliadin gene expression and % gliadin proteins determined by SDS-PAGE (2009: $r = 0.335$, $p = 0.013$, $n = 54$; 2010: $r = 0.372$, $p = 0.006$, $n = 54$; for data on $\log_e$ scale). (B) Gliadin gene expression and monomeric gliadin proteins determined by SE-HPLC (F4 fraction) (2009: $r = 0.641$, $p = 0.004$, $n = 18$; 2010: $r = 0.768$, $p < 0.001$, $n = 18$; for data on $\log_e$ scale). (C) HMW subunit gene expression and large glutenin polymers (F1 fraction) measured by SE-HPLC (2009: $r = -0.387$, $p = 0.112$, $n = 18$; 2010: $r = -0.637$, $p = 0.004$, $n = 18$; for data on $\log_e$ scale). Data are for six cultivars grown at Rothamsted Research in 2009 and 2010 with three biological replicates, analyzed at 21 DPA for gene expression profiles and at maturity for protein composition.

DISCUSSION

A combination of transcriptomics and protein analysis was used to identify differences between varieties in terms of their ability to partition N into gluten proteins in response to increased N inputs. This showed a consistent and robust inverse relationship between wheat grain yield and grain %N, which is consistent with previous studies.[3,14] Although grain protein deviation (GPD) was not consistent between the two years, Marksman, Hereward, and Cordiale all tended to show positive GPD. However, both 2010 and 2011 were drier than average, particularly during the spring, which was reflected by a negative impact on N responses (on yield and/or grain N).

The relationships between genetically determined differences in gluten protein composition and grain processing properties are well established.[4,5] The most consistent effect of increased N observed in the present study was increased synthesis and accumulation of gliadins, whether determined as % gluten protein subunits by SDS-PAGE, as monomeric gluten proteins by SE-HPLC, or by gene transcript profiling. Previous studies have shown that increases in grain N result in increases in the proportions of the monomeric gliadins,[15−21] leading to increased dough extensibility. However, Pechanek et al. (1997)[22] showed that the effect of N on grain protein composition was not consistent, but varied between varieties. Our results support this conclusion, as clear statistically significant differences were observed between the six cultivars that were studied.

Less is known about the effects of nutrition on the glutenin fraction, either on the proportions of the individual subunits or on the size distribution of the glutenin polymers. Thus, both increases[23] and decreases[22] in the proportions of HMW subunits have been reported in response to N application, while Panozzo and Eagles (2000)[17] and Zhu and Khan (2001)[19] showed differential effects of N on glutenin polymers and processing properties in cultivars with different HMW subunit alleles. Our results showed that increasing grain N resulted in decreases in the % LMW GS but little effect on the % HMW GS in all cultivars, but that the absolute values and temporal patterns during development varied between the cultivars. Although these did not differ consistently between the five breadmaking cultivars and the single feed quality cultivar (Istabraq), the latter did have the lowest proportion of high molecular weight glutenin polymers (%F1 by SE-HPLC), which are known to be positively correlated with high dough strength.[24,25]

It has previously been shown that glutenin polymers increase significantly in size during the desiccation phase of seed development,[20,26,27] and the results from our study support this. Differential effects on this process could provide a mechanism for effects of the environment during the later stages of grain maturation on grain quality, but would not explain effects of the environment at earlier stages of grain development. In the present study a similar increase in gluten polymers was observed in all six wheat cultivars, with no significant difference between Hereward (which is favored by millers and bakers because it is more stable in quality between seasons), Istabraq (the feed cultivar), and the other four breadmaking wheat cultivars. Environmental effects on grain protein composition and quality that are not related to N content have also been reported by Kolster et al. (1991).[28]

In order to ensure relevance to commercial wheat production and utilization, we focused on field-grown samples of six cultivars of wheat, using material from combinations of five sites and three years (totaling 11 different environments) and three biological replicates. All cultivars showed similar trends in the relationship between N application and protein composition, but statistically significant differences were observed between the cultivars in terms of their varying trends in composition over development time. Although our data suggest that genetic differences in N utilization exist between cultivars,

dx.doi.org/10.1021/jf500625c | J. Agric. Food Chem. 2014, 62, 4399−4407

it is clear that larger scale studies are required, with more cultivar × site × year × N combinations, in order to identify and exploit genotypes that make more efficient use of applied N, in terms of efficiency of translocation to the grain and incorporation into quality-related proteins.

■ ASSOCIATED CONTENT

Supporting Information

Figure S1: SDS-PAGE analysis of reduced total gluten protein fractions from the six cultivars showing the HMW glutenin subunits expressed in the six cultivars. Table S1: Log_e-transformed raw gene expression values for the mean of all HMW GS-related genes for six wheat cultivars grown at one site (Rothamsted Research) only. Table S2: Log_e-transformed raw gene expression values for the mean of all LMW GS-related genes for six wheat cultivars grown at one site (Rothamsted Research) only. Table S3: Log_e-transformed raw gene expression values for the mean of all gliadin-related genes for six wheat cultivars grown at one site (Rothamsted Research) only. Supporting information for Figure 5: Statistical analysis of gene expression data on log_e scale. This material is available free of charge via the Internet at http://pubs.acs.org.

■ AUTHOR INFORMATION

Corresponding Author

*Tel: +44(0)1386 842000. Fax: +44(0)1386 842100. E-mail: gemma.chope@campdenbri.co.uk.

Funding

The work reported here was supported by the BBSRC Industrial Partnership Award BB/G022437 with support from the Home Grown Cereals Authority grant RD-2007-3409 "Sustainability of UK-grown wheat for breadmaking". Field trials at Rothamsted Research were supported by the Defra-funded WGIN project. Trials at KWS, Limagrain, RAGT, and Syngenta were supported by the respective breeding companies.

Notes

The authors declare no competing financial interest.

■ ABBREVIATIONS USED

cDNA, complementary DNA; DPA, days post-anthesis; GPD, grain protein deviation; HMW GS, high molecular weight glutenin subunits; LMW GS, low molecular weight glutenin subunits; LSD, least significant difference; PCO, principal coordinates analysis; REML, residual maximum likelihood; SDS, sodium dodecyl sulfate; SDS-PAGE, sodium dodecyl sulfate polyacrylamide gel electrophoresis; SE-HPLC, size exclusion high-performance liquid chromatography

■ REFERENCES

(1) Dampney, P. M. R.; Edwards, A.; Dyer, C. J. *Managing nitrogen applications to new group 1 and 2 wheat varieties*; Project Report 400; HGCA: UK, 2006.

(2) Kettlewell, P. S. Agronomy and cereal quality. In *Cereal Grain Quality*; Henry, R. J., Kettlewell, P. S., Eds.; Chapman and Hall: London, UK, 1996; pp 407−437.

(3) Monaghan, J. M.; Snape, J. W.; Chojecki, J. S.; Kettlewell, P. S. The use of grain protein deviation for identifying wheat cultivars with high grain protein concentration and yield. *Euphytica* **2001**, *122*, 309−317.

(4) Payne, P. I.; Nightingale, M. A.; Krattinger, A. F.; Holt, L. M. The relationship between HMW glutenin subunit composition and breadmaking quality of British grown wheat varieties. *J. Sci. Food Agric.* **1987**, *40*, 51−65.

(5) Shewry, P. R.; Tatham, A. S.; Barro, F.; Barcelo, P.; Lazzeri, P. Biotechnology of breadmaking: unraveling and manipulating the multi-protein gluten complex. *Biotechnology* **1995**, *13*, 1185−1190.

(6) Triboï, E.; Abad, A.; Michelena, A.; Lloveras, J.; Ollier, J.; Daniel, L. C. Environmental effects on the quality of two wheat genotypes: 1. quantitative and qualitative variation of storage proteins. *Eur. J. Agron.* **2000**, *13*, 47−64.

(7) Dumas, J. B. A. Procedes de l'analyse organique. *Ann. de Chim. Phys.* **1831**, *2*, 198−213.

(8) Morel, M. H.; Dehlon, P.; Autran, J. C.; Leygue, J. P.; Bar-L'Helgouac'h, C. Effects of temperature, sonication time and power settings on size distribution and extractability of total wheat flour proteins as determined by size-exclusion high performance liquid chromatography. *Cereal Chem.* **2000**, *77*, 685−691.

(9) Millar, S. J. *The development of near infrared (NIR) spectroscopy calibrations for the prediction of wheat and flour quality*; Project Report 310; HGCA: UK, 2003.

(10) Chang, S. J.; Puryear, J.; Cairney, J. A simple and efficient method for isolating RNA from pine trees. *Plant Mol. Biol. Rep.* **1993**, *11*, 113−116.

(11) Wan, Y.; Poole, R. L.; Huttly, A. K.; Toscano-Underwood, C.; Feeney, K.; Welham, S.; Gooding, M. J.; Mills, E. N. C.; Edwards, K. J.; Shewry, P. R.; Mitchell, R. A. C. Transcriptome analysis of grain development in hexaploid wheat. *BMC Genomics* **2008**, *9*, 121−137.

(12) Aitchison, J. *Statistical Analysis of Compositional Data*; Chapman and Hall: London, UK, 1985.

(13) Krzanowski, W. J. *Principles of Multivariate Analysis: A User's Perspective*, revised ed.; Oxford University Press: UK, 2000.

(14) Simmonds, N. W. The relation between yield and protein in cereal grain. *J. Sci. Food Agric.* **1995**, *67*, 309−315.

(15) Jia, Y. Q.; Fabre, J. L.; Aussenac, T. Effects of growing location on response of protein polymerization to increased nitrogen fertilization for the common heat cultivar Soissons: Relationship with some aspects of the breadmaking quality. *Cereal Chem.* **1996**, *73*, 526−532.

(16) Jia, Y. Q.; Masbou, V.; Aussenac, T.; Fabre, J. L.; Debaeke, P. Effects of nitrogen fertilization and maturation conditions on protein aggregates and on the breadmaking quality of Soissons, a common wheat cultivar. *Cereal Chem.* **1996**, *73*, 123−130.

(17) Panozzo, J. F.; Eagles, H. A. Cultivar and environmental effects on quality characters in wheat II protein. *Aust. J. Agric. Res.* **2000**, *51*, 629−636.

(18) Kindred, D. R.; Verhoeven, T. M. O.; Weightman, R. M.; Swanston, J. S.; Agu, R. C.; Brosnan, J. M.; Sylvester-Bradley, R. Effects of variety and fertiliser nitrogen on alcohol yield, grain yield, starch and protein content, and protein composition of winter wheat. *J. Cereal Sci.* **2008**, *48*, 46−57.

(19) Zhu, J.; Khan, K. Effects of genotype and environment on glutenin polymers and breadmaking quality. *Cereal Chem.* **2001**, *78*, 125−130.

(20) Shewry, P. R.; Underwood, C.; Wan, Y.; Lovegrove, A.; Bhandari, D.; Toole, G.; Mills, E. N. C.; Denyer, K.; Mitchell, R. A. C. Storage product synthesis and accumulation in developing grains of wheat. *J. Cereal Sci.* **2009**, *50*, 106−112.

(21) Godfrey, D.; Hawkesford, M.; Powers, S.; Millar, S.; Shewry, P. R. Nutritional effects on wheat grain composition and end use quality. *J. Agric. Food Chem.* **2010**, *58*, 3012−3021.

(22) Pechanek, U.; Karger, A.; Groger, S.; Charvat, B.; Schoggl, G.; Lelley, T. Effect of nitrogen fertilization on quantity of flour protein components, dough properties, and breadmaking quality of wheat. *Cereal Chem.* **1997**, *74*, 800−805.

(23) Weiser, H.; Seilmeier, W. The influence of nitrogen fertilisation on quantities and proportions of different protein types in wheat flour. *J. Sci. Food Agric.* **1998**, *76*, 49−55.

(24) Singh, N. K.; Donovan, G. R.; MacRitchie, F. Use of sonication and size-exclusion high-performance liquid chromatography in the

study of wheat flour proteins. II. Relative quantity of glutenin as a measure of breadmaking quality. *Cereal Chem.* **1990**, *67*, 161−170.
(25) Popineau, Y.; Cornec, M.; Lefebvre, J.; Marchylo, B. Influence of high Mr glutenin subunits on glutenin polymers and rheological properties of gluten and gluten subfractions of near-isogenic lines of wheat Sicco. *J. Cereal Sci.* **1994**, *19*, 231−241.
(26) Carceller, J. L.; Aussenac, T. SDS-insoluble glutenin polymer formation in developing grains of hexaploid wheat: the role of the ratio of high to low molecular weight glutenin subunits and drying rate during ripening. *Aust. J. Plant Physiol.* **2001**, *28*, 193−201.
(27) Daniel, C.; Triboï, E. Changes in wheat protein aggregation during grain development: effects of temperatures and water stress. *Eur. J. Agron.* **2002**, *16*, 1−12.
(28) Kolster, P.; Krechting, K. F.; Van Gelder, W. M. J. Quantitative variation of total and individual high molecular weight glutenin subunits of wheat in relation to variation in environmental conditions. *J. Sci. Food Agric.* **1991**, *57*, 405−415.

JOURNAL OF AGRICULTURAL AND FOOD CHEMISTRY

Article

pubs.acs.org/JAFC

Characterization and Quantitation of Anthocyanins and Other Phenolics in Native Andean Potatoes

M. Monica Giusti,*[,†] Maria Fernanda Polit,[†] Huseyin Ayvaz,[†] David Tay,[‡] and Ivan Manrique[‡]

[†]Department of Food Science and Technology, The Ohio State University, 110 Parker Food Science and Technology Building, 2015 Fyffe Road, Columbus, Ohio 43210, United States

[‡]International Potato Center, Avenida La Molina 1895, La Molina Apartado Postal 1558, Lima, Peru

ABSTRACT: Andean potatoes are gaining popularity not only for their appealing colors and culinary uses but also for their potential higher content of polyphenolic compounds. The objective of this study was to identify potato varieties with increased phenolic content. This was achieved through characterization and quantitation of the phenolic composition in 20 varieties of native Andean potatoes from 4 different *Solanum* species with different colors. Major quantitative and qualitative differences among evaluated samples were more dependent on the coloration of the extracted sample rather than on the species. The most predominant anthocyanidins were petunidin-3-coumaroylrutinoside-5-glucoside and pelargonidin-3-coumaroylrutinoside-5-glucoside in purple and red potato extracts, respectively, while chlorogenic acid and its isomers were the main phenolic compund (43% of the total phenolic content). Our study suggested that the appropriate selection of native potatoes could provide new sources of polyphenolics with health promoting properties and natural pigments with increased stability for food applications.

KEYWORDS: *Andean tubers, potato, anthocyanins, polyphenols, chlorogenic acid*

INTRODUCTION

Potato is the fifth most produced crop worldwide after sugar cane, maize, wheat and rice with a production of >368 million tons in 2012.[1] Potatoes are a good source of dietary energy, carbohydrates, fiber, vitamin C, vitamin B1, niacin, vitamin B6 and minerals such as potassium, phosphorus and magnesium.[2] Besides basic nutrients, potatoes also provide a good source of phenolic compounds.

Correlation between ingesting phenolic compounds and improved health has been shown in epidemiological studies.[3−6] Phenolic compounds were shown to have antioxidant activity and other characteristics that could promote health. Among phenolics, anthocyanins are of special interest not only due to their health benefits but also due to their possible utilization as natural food pigments.[7,8]

The Andes are home to a great diversity of native potato species which have been traditionally consumed and solely grown in the Andes region by locals. Native Andean potato tubers show a wide variability in tuber shape, flesh and skin color, texture and flavor. This genetic diversity also generates substantial variability in nutritional contents.[2,9] However, very little is known about the chemical nature and identity of the bioactive compounds present in native Andean potatoes.[9]

The present study was designated to evaluate and characterize polyphenolics and anthocyanin content in native Andean potato varieties. This fits into a long-term objective of enhancing nutrition through diet and delivering health-enhancing components through stable crop commodities. For this study, the objective was to monitor and compare the phenolic content and profile of 20 different native Andean potato varieties from different species, which exhibited a variety of colors. The study included the measurement of the total phenolic, monomeric and polymeric anthocyanin content as well as the qualitative characterization of the anthocyanins and nonanthocyanin phenolics fraction. The hypothesis was that among the wide variety of native Andean potatoes, there are some that could represent important sources of phenolic components and could increase consumption of phytochemicals and antioxidants in the human diet.

MATERIALS AND METHODS

Chemicals. Reagent grade trifluoroacetic acid (TFA), certified ACS grade HCl (12N), LC−MS grade 99.9% methanol, 99.9% acetonitrile and water, certified ACS grade ethyl acetate and potassium hydroxide, HPLC grade 88% formic acid, 99.9% acetone and 99.9% chloroform were purchased from Fisher Scientific (Fair Lawn, NJ). Chlorogenic acid, caffeic acid, ferulic acid, *p*-coumaric acid and protocatechuic acid standards, reagent grade gallic acid, and Folin-Ciocalteau reagent were purchased from MP Biomedical (Aurora, OH). Sinapic acid standard (98%) was purchased from Sigma-Aldrich (St. Louis, MO). Chlorogenic acid isomers were prepared as described by Nagels.[10] Anthocyanidin standards were prepared from the acid hydrolysis of strawberries and grapes as described by Wrolstad and others.[11]

Plant Materials. A total of 20 samples (Table 1) of different colors (cream, yellow, brown, pink, red and purple) and species (*S. tuberosum*, *S. stenotonum*, *S. phureja* and *S. chaucha*) were used in this study. Potatoes were harvested by the International Potato Center (CIP), lyophilized and powdered with skin before shipping. Depending on the availability of the samples, between 150 and 500 g potato tubers were washed and cut into 1 cm^3 cubes. Cubes were then mixed and a random 100 g was weighed and placed in a polyethylene bag. Samples were immediately frozen at −20 °C and kept frozen until liophilized. Following the liophilization, native Andean potato samples

Received: February 6, 2014
Revised: April 20, 2014
Accepted: April 21, 2014
Published: April 21, 2014

 © 2014 American Chemical Society

Table 1. CIP Accession Number, Species Name, Lyophilized Sample Color Description and Water Activity of Analyzed Samples

CIP accession number	species name	lyophilized sample color	aw/°T
705534	*S. stenotomum* subsp. *stenotomum*	very bright purple with white spots	0.047/22.4 °C
703640	*S. tuberosum* subsp. *andigenum*	very bright purple with white spots	0.209/20.4 °C
706726	*S. tuberosum* subsp. *andigenum*	purple with black and white spots	<0.034/22.3 °C
704733	*S. tuberosum* subsp. *andigenum*	dark purple gray	0.085/22.1 °C
703862	*S. tuberosum* subsp. *andigenum*	purple cream with dark purple spots	0.072/20.9 °C
704133	*S. stenotomum* subsp. *stenotomum*	gray purple with purple spots	0.049/21.3 °C
702556	*S. stenotomum* subsp. *stenotomum*	purple pink	0.059/20.9 °C
706630	*S. tuberosum* subsp. *andigenum*	pink purple	<0.034/21.9 °C
700234	*S. tuberosum* subsp. *andigenum*	red purple with brown and white spots	0.044/21.7 °C
705841	*S. tuberosum* subsp. *andigenum*	red purple with brown and white spots	<0.034/21.1 °C
703752	*S. tuberosum* subsp. *andigenum*	red brown with brown spots	<0.034/22.6 °C
703695	*S. tuberosum* subsp. *andigenum*	brown	<0.034/21.2 °C
705820	*S. phureja*	cream with brown spots	<0.033/20.5 °C
704537	*S. chaucha*	cream white with dark spots	<0.034/21.3 °C
705946	*S. stenotomum subsp. stenotomum*	cream purple with dark spots	0.038/23.4 °C
705500	*S. stenotomum* subsp. *goniocalyx*	cream with brown spots	0.054/22.3 °C
702464	*S. stenotomum subsp. goniocalyx*	cream with brown spots	0.053/22.9 °C
703782	*S. stenotomum* subsp. *stenotomum*	yellow with brown spots	0.069/22.5 °C
706884	*S. stenotomum* subsp. *goniocalyx*	yellow with brown spots	<0.034/21.4 °C
704481	*S. stenotomum* subsp. *goniocalyx*	bright yellow with brown spots	<0.034/22.5 °C

were shipped by the CIP to our laboratory. Samples were kept under dark and at −40 °C until analysis. Lyophilization with skin caused the presence of skin pieces irregularly distributed in the sample. In some of the samples, skin had darker colors and highly contributed to the sample pigment content. During the weighing step, samples were taken from different parts of the containers to have a final representative sample as homogeneous as possible.

Extraction of Anthocyanins and Other Phenolics from Potato Samples. Lyophilized potato powder (~3 g) was blended with 45 mL of acidified aqueous acetone (20:80 v/v acidified with 0.1% HCL and 0.2% TFA) for 5 min with a tissuemiser homogenizer (Fisher Scientific, Fair Lawn, NJ) over a water/ice bath to reduce enzymatic activity. The mixture was centrifuged for 5 min at 3400 g (Centrific centrifuge Model 225; Fisher Scientific, Fair Lawn, NJ) and the supernatant was filtered through a Whatman #1 filter by vacuum suction using a Buchner funnel. The residual cake was reextracted with 25 mL of aqueous acetone (20:80 v/v acidified with 0.1% HCL and 0.2% TFA). Filtrates were combined and transferred to a separatory funnel and gently mixed with 2 volumes of chloroform. Samples were stored at 4 °C for 4 h in the dark. The aqueous phase (top layer) was separated and centrifuged for 7 min (3400 g). The aqueous supernatant was recovered and residual acetone/chloroform was removed using a Büchii Rotavapor (New Castle, DE) at 40 °C under vacuum. The remaining aqueous potato extract was then taken to 5 mL on a volumetric flask with acidified water (0.01% HCl). Extraction was done in triplicate for each sample.

Solid Phase Purification of Phenolic Fraction. The aqueous potato extract was purified using a Sep-pak C_{18} Vac solid cartridge (6 cm^3, 1 g sorbent; Waters Corp., Milford, MA). The C_{18} cartridge was activated with 10 mL of methanol and washed with 10 mL of acidified water (0.01% HCl). Potato extract (1 mL) was passed through the cartridge, anthocyanins and other phenolics were bound to the C_{18} cartridge; sugars and other polar compounds were removed with 10 mL of acidified water (0.01% HCl). The phenolic fraction was eluted with 10 mL of acidified methanol (0.01% HCl). The procedure was performed twice for every sample. Methanol was removed in a Büchii rotary evaporator at 40 °C under vacuum and the phenolic fraction was taken to 5 mL on a volumetric flask with acidified water (0.01% HCl). Purified phenolic extract was filtered (0.45 μm Whatman polypropylene filter) for further HPLC analysis.

Saponification of Anthocyanins. Aqueous potato extracts (1 mL) were saponified in a screw-cap test tube with 10 mL of 20% aqueous KOH for 10 min at room temperature in the dark as described by Durst and Wrolstad.[12] The solution was neutralized with the addition of 4 N HCl until a red color was seen and applied to an activated Sep-pak C_{18} Vac solid cartridge. Column was rinsed with 10 mL of acidified water (0.01% HCl) and liberated acid groups were removed with 10 mL of ethyl acetate. Saponified anthocyanin fraction was eluted with acidified methanol (0.01% HCl) and rotoevaporated at 40 °C under vacuum. The saponified fraction was taken to 5 mL on a volumetric flask with acidified water and filtered (0.45 μm Whatman polypropylene filter) for further HPLC analysis.

Acid Hydrolysis of Anthocyanins. Saponified anthocyanin extracts (3 mL) were hydrolyzed with 10 mL of 4 N HCl in a screw-cap test tube. The test tube was flushed with nitrogen gas, sealed and placed in a boiling water bath for 60 min in the dark and then cooled in an ice bath.[7] The solution was applied to an activated Sep-pak C_{18} Vac solid cartridge. The column was rinsed with 10 mL of acidified water (0.01% HCl) and the hydrolyzed anthocyanidin fraction was collected with acidified methanol (0.01% HCl) and rotoevaporated at 40 °C under vacuum. The hydrolyzed anthocyanidin fraction was taken to 2 mL on a volumetric flask with acidified water and filtered (0.45 μm Whatman polypropylene filter) for immediate HPLC analysis.

Monomeric and Polymeric Anthocyanin Content. Monomeric anthocyanin content was determined using the pH differential method as described by Giusti and Wrolstad.[13] Each aqueous potato extract was appropriately diluted using pH 1.0 and pH 4.5 (0.4 M sodium acetate) buffers. Solutions were allowed to equilibrate for 15 min in the dark. Absorbance was read on 1 cm path length disposable cuvettes at 510 nm (for red potato extracts) or 520 nm (for purple potato extracts) and 700 nm using a UV−visible Spectrophotometer 2450 (Shimadzu Scientific Instruments, Inc., Columbia, MD). Monomeric anthocyanin content (MAC) (mg/L) was calculated using the equation given by Giusti and Wrolstad.[13] Analyses were performed for each extraction replication (n = 3).

Polymeric anthocyanin content was also determined using the method described by Giusti and Wrolstad.[13] Using the dilution factors previously determined, an aliquote (1.85 mL) of diluted sample in acidified water (0.01% HCl) was prepared in each of two cuvettes (1 cm path length); then 0.15 mL of water was added to one of the cuvettes and 0.15 mL of potassium metabisulfate solution to the other and allowed to equilibrate for 15 min before reading at 420, 510 nm (for red potato extracts) or 520 nm (for purple potato extracts) and 700 nm using a UV−visible spectrophotometer 2450 (Shimadzu Scientific Instruments, Inc., Columbia, MD). Polymeric anthocyanin content was calculated using the equations given by Giusti and Wrolstad.[13] Analyses were performed for each extraction replication (n = 3).

Total Phenolics Quantitation. Total phenolics were measured using the microscale protocol for Folin-Ciocalteau colorimetry as described by Waterhouse.[14] Aliquotes (20 μL) of aqueous potato extract, a gallic acid calibration standard and a water blank were placed into separate 1 cm path length (2 mL) plastic cuvettes. Then 1.58 mL

Table 2. Monomeric and Polymeric Anthocyanin and Total Phenolic Content in Potato Extracts[a]

CIP accession number	monomeric anthocyanins	% polymeric color	total phenolics mg GAE/100 g DW	% of total phenolics corresponding to monomeric anthocyanins
Section I: purple potato extracts				
705534	152.7 ± 22.3	20.0 ± 5.9	412.49 ± 40.95	37.02%
703640	145.2 ± 5.0	18.1 ± 13.5	510.20 ± 41.43	28.45%
706726	46.7 ± 3.8	20.2 ± 6.4	278.73 ± 24.00	16.77%
704733	41.1 ± 2.4	34.6 ± 2.5	379.20 ± 7.93	10.83%
703862	25.6 ± 0.9	28.8 ± 13.9	178.99 ± 11.71	14.28%
704133	16.8 ± 1.7	25.2 ± 9.9	162.19 ± 10.54	10.38%
Section II: red potato extracts				
702556	90.9 ± 8.5	12.4 ± 6.9	261.49 ± 18.63	34.76%
706630	88.7 ± 14.4	17.2 ± 4.9	337.71 ± 7.88	26.25%
700234	79.8 ± 3.5	20.5 ± 5.2	266.18 ± 7.67	29.99%
705841	75.6 ± 3.1	19.0 ± 7.6	304.17 ± 8.95	24.87%
703752	56.7 ± 3.6	24.8 ± 7.1	249.67 ± 24.24	22.72%
703695	54.6 ± 2.4	27.6 ± 8.0	241.93 ± 22.63	22.58%
705820	42.8 ± 2.4	13.9 ± 4.0	152.40 ± 14.86	28.10%
704537	38.1 ± 6.5	21.8 ± 7.0	153.36 ± 14.73	24.86%
705946	29.4 ± 2.9	34.0 ± 2.6	231.05 ± 22.00	12.71%
705500	25.9 ± 0.9	27.5 ± 10.2	199.75 ± 28.22	12.95%
702464	25.3 ± 1.0	26.2 ± 8.2	162.29 ± 9.88	15.57%
703782	8.2 ± 0.5	40.3 ± 1.1	159.15 ± 15.38	5.17%
Section III: yellow potato extracts				
706884	N/A	N/A	114.63 ± 10.75	N/A
704481	N/A	N/A	113.37 ± 6.36	N/A

[a] Section I: purple potato extracts (monomeric anthocyanin expressed as mg of cy-3-glu equivalents/100 g DW). Section II: red potato extracts (monomeric anthocyanin expressed as pg-3-glu equivalents/100 g DW). Section III: yellow potato extracts (Total phenolic content is expressed as mg of gallic acid equivalents (GAE) per 100 g of DW). Data are means ± SE (n = 3).

of water was added to each cuvette, followed by 100 μL of Folin-Ciocalteu reagent thoroughly mixed and incubated for 7 min. After incubation, 300 μL of sodium carbonate solution was added, mixed and allowed to incubate for 2 h at room temperature. Absorbance of samples, standards and blanks at 765 nm were measured on a UV−visible spectrophotometer 2450 (Shimadzu Scientific Instruments, Inc., Columbia, MD). Absorbance of the blank was subtracted from all readings and a calibration curve was created from the standards. Total phenolic content was calculated as gallic acid equivalents (GAE) based on the gallic acid calibration curve.

HPLC−MS Characterization of Samples. Samples were analyzed using a Shimadzu LCMS-2010 EV Liquid Chromatograph Mass Spectrometer (Shimadzu Scientific Instruments, Inc., Columbia, MD) equipped with LC-20AD pumps and SIL-20AC autosampler coupled with a SPDM20A photodiode array (PDA) detector and a single quadrupole electron spray ionization (ESI) mass spectrometer (MS) detector. Data was analyzed and processed using the LCMS Solutions software (Version 3, Shimadzu Scientific Instruments, Inc., Columbia, MD). Separation of anthocyanins and other phenolics in red extracts was achieved on a reverse phase Symmetry C_{18} column (3.5 um, 4.6 × 150 mm^2; Waters Corp., Milford, MA) and a Symmetry 2 micro guard column (4.6 × 22 mm^2; Waters Corp., Milford, MA). Chromatographic conditions were as follows: flow rate, 0.8 mL/min; mobile phase A, 4.5% formic acid in LCMS grade water; mobile phase B, LC−MS grade acetonitrile; gradient 0−5 min, 5% B; 5−20 min, 5−15% B; 20−30 min, 15% B; 30−40 min, 15−20% B; 40−45 min, 20−30% B; 45−48 min, 30−5% B and after each run 5 min was given to equilibrate the column to initial condition; injection volume varied according to the sample and ranged from 60 to 120 μL. Spectral data (250−700 nm) was collected during the whole run. Elution of total phenolics was monitored at wavelength 280 nm, cinnamic acids at 320 nm and anthocyanins at 510−520 nm.

Separation of anthocyanins and other phenolics in purple extracts was achieved using the following chromatographic conditions: flow rate: 0.8 mL/min; mobile phase: A, 10% formic acid in LCMS grade water; B, LC−MS grade acetonitrile; gradient: 0−5 min, 5% B; 5−16 min, 5- 13% B; 16−26 min, 13% B; 26−40 min, 13−20% B; 40−45 min, 20−30% B; 45−48 min, 30−5% B and after each run 5 min was given to equilibrate the column to initial condition; injection volume varied according to the sample and ranged from 60 to 120 μL. Spectral data (250−700 nm) was collected during the whole run. Elution of anthocyanins was monitored at wavelength 510−520 nm. Separation of anthocyanidins in hydrolyzed samples was achieved using the following chromatographic conditions: flow rate, 0.8 mL/min; mobile phase A, 4.5% formic acid in LC−MS grade water; mobile phase B, LC−MS grade acetonitrile; gradient 0−30 min, 5−35% B; 30−35 min, 35% B; 35−38 min, 35−5% B; 38−41 min, 5% B; injection volume: 120 μL. Spectral data (250−700 nm) was collected during the whole run. Elution of anthocyanins was monitored at wavelength 510−520 nm.

A 0.2 mL/min flow was diverted to the MS. Mass spectra were obtained under positive ion condition using total ion scan (SCAN) (from m/z 150 to 1300) and selective ion monitoring (SIM) modes. Eight channels including m/z 181 (caffeic acid), m/z 271 (pelargonidin), m/z 287 (cyanidin), m/z 301 (peonidin), m/z 303 (delphinidin), m/z 317 (petunidin), m/z 331 (malvidin) and m/z 355 (chlorogenic acid), were monitored in the SIM mode to detect the 6 common anthocyanin aglycone fragments and two common phenolic acids.

RESULTS AND DISCUSSION

Sample Characteristics. Detailed information about the species used in the study including water activity (aw) values of the lyophilized samples measured prior to sample extraction is shown in Table 1. All samples had aw lower than 0.086 (at ∼21 °C) except for sample 703640 which had aw of 0.209. The average moisture content in the samples was 2.07%, with sample 703640 being the only variety with moisture content higher than 4% (∼6%) (moisture data is not shown). In general the lyophilization process removed most of the moisture from the potato samples.

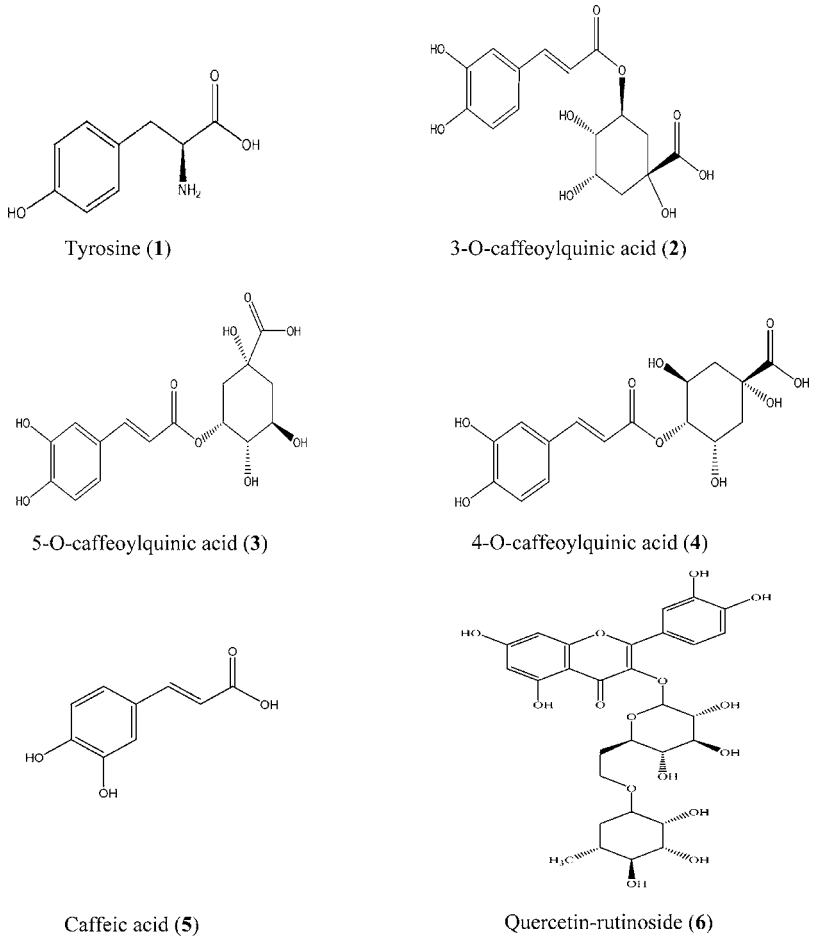

Figure 1. Chemical structures of the major phenolic compounds identified in Andean potatoes by HPLC PDA/MS. *Compound numbers refer to the peak numbers given in Figure 2.

Table 3. List of Phenolic Compounds Identified in Andean Potatoes by HPLC PDA/MS

peak no[a]	retention time (min)[a]	M^+ (m/z)	peak assignment	reference compounds
1	3.3	182	tyrosine	tentatively identified
2	7.5	355	3-*O*-caffeoylquinic acid	chlorogenic acid isomers[b]
3	12.8	355	5-*O*-caffeoylquinic acid	chlorogenic acid isomers[b]
4	14.2	355	4-*O*-caffeoylquinic acid	chlorogenic acid isomers[b]
5	15.0	181	caffeic acid	caffeic acid standard
6	26.5	611	quercetin-rutinoside derivative	tentatively identified

[a]Compound numbers and retention times refer to the numbers given in Figure 1. [b]Chlorogenic acid isomers were prepared as described by Nagels.[10]

Improvement of the Extraction. Initially, phenolic fraction of the potatoes was extracted following the procedure described by Shiroma-Kian and others.[15] However, during extraction of selected potato samples, some browning occurred and anthocyanin coloration was lost suggesting enzymatic degradation. According to Francis,[16] anthocyanins can be degraded by a number of enzymes classified as glycosidases (anthocyanases), polyphenoloxidases (PPO) and peroxidases. These enzymes are found in plant tissue and naturally occur in potatoes. Glycosidases act directly on anthocyanins hydrolyzing the pigments to sugars and anthocyanidins (aglycone).[16,17] Anthocyanidins are very unstable and degrade to colorless derivatives or condense with other phenolics to form polymeric colored compounds.[15] The action of PPO and peroxidases on anthocyanins is indirect.[11] For example, PPO oxidizes *o*-diphenols (phenolic acids, e.g., chlorogenic acid) to *o*-benzoquinone which in the presence of oxygen reacts with the anthocyanins by a nonenzymatic mechanism to form oxidized anthocyanins and degradation products.[17] In order to minimize pigment degradation, the extraction process of anthocyanins and other phenolics from potato samples was modified. The percent of acid and acetone in the aqueous acetone solution was increased and the time for the homogenization was reduced. The pH of a solution can have a marked effect on enzymatic activity. Enzymes that degrade anthocyanins have an optimum pH greater than 4.[18] The pH of 70% aqueous acetone acidified with 0.01% HCl was lower than pH 3. However, after homogenization with the potato powder, the pH of the solution was higher than pH 5. This suggested that the potato powders had high buffering capacity and were increasing the pH of the solution. In order to obtain final pH values lower than 3.5 after homogenization, the acidity of the aqueous acetone solution was increased with additional HCl and trifluoroacetic acid (TFA). A combination of 0.1% HCl and 0.2% TFA resulted on a final extract with a pH between 3−3.5 that minimized enzymatic activity and favored pigment stability.

dx.doi.org/10.1021/jf500655n | J. Agric. Food Chem. 2014, 62, 4408−4416

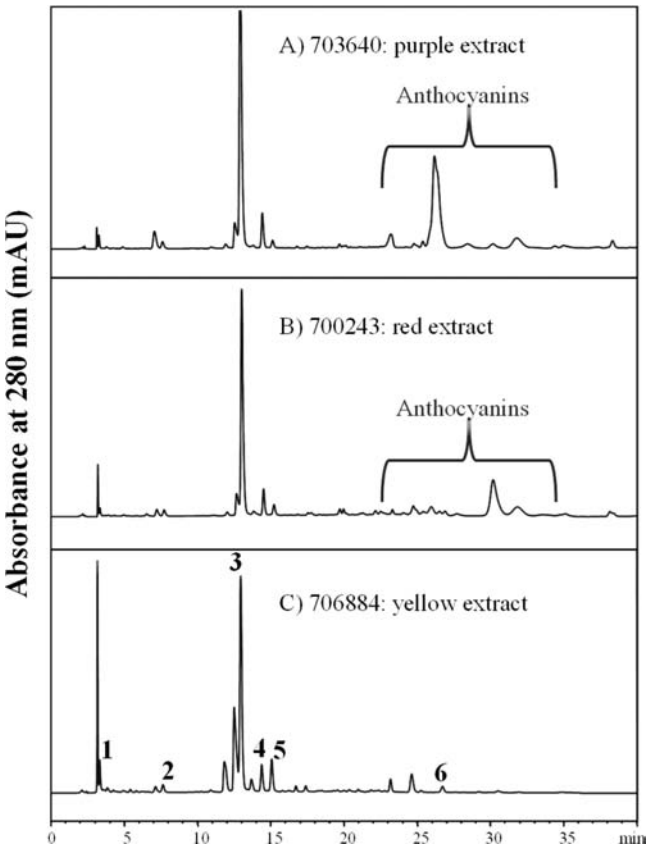

Figure 2. HPLC chromatogram at 280 nm of phenolics compounds in native Andean potatoes. *Compound 1 and 6 were tentatively identified.

Table 4. Relative Phenolic Composition of Potato Samples (% of Total Peak Area at 280 nm)[a]

CIP accession number	1[b]	2	3	4	5
705534	0.15	1.22	25.03	3.05	1.81
703640	0.77	0.95	33.76	3.88	1.12
706726	0.74	2.00	38.52	5.29	2.39
704733	0.48	0.66	39.84	3.87	5.19
703862	0.93	1.55	33.78	4.10	3.23
704133	2.73	2.43	31.73	5.90	3.33
702556	0.37	1.27	35.17	3.98	2.94
706630	0.51	3.51	38.21	8.13	1.78
700234	0.75	1.27	40.95	4.11	1.85
705841	0.80	3.63	41.83	9.75	1.70
703752	0.40	0.85	20.79	4.66	1.88
703695	1.46	0.96	30.23	4.51	1.53
705820	1.39	1.68	24.97	5.44	1.11
704537	1.13	1.24	34.93	2.92	3.67
705946	1.77	1.72	45.96	7.36	3.29
705500	1.25	4.53	45.39	8.60	3.15
702464	0.28	2.56	51.52	9.24	3.71
703782	1.46	2.21	33.34	5.16	7.85
706884	3.28	1.55	36.90	4.21	5.55
704481	1.17	1.30	31.48	6.83	8.42

[a]Compound numbers refer to the numbers given in Table 3. [b]Tentative identification.

Another important consideration was that the extracted samples were going to be concentrated after the chloroform partitioning. High concentrations of acid could hydrolyze the phenolic compounds and anthocyanins in the sample. TFA was chosen to acidify the solution since, even though it is a strong acid, it is also more volatile than HCl and could evaporate during the concentration of the sample.

To better protect the integrity of the sample and minimize enzymatic activity, higher concentrations of acetone could be used during extraction. A small trial with different concentrations of acetone in the extraction solution was performed using 70, 80, 90 and 100% of acidified acetone. The solution with 80% aqueous acidified acetone was the most efficient and was chosen as the extracting solvent for this research.

The homogenization process was also improved using a tissuemiser homogenizer and reducing the mixing time from 10 to 5 min. The previous procedure called for homogenization on a rotamixer took longer time to extract the phenolics from the samples. In addition to decreasing the time involved in the extraction, changing to a tissumizer allowed us to incorporate a water/ice bath to reduce temperature and diminish any residual enzymatic activity. Usually when chloroform partitioning is performed in a sample, two layers are formed. The top aqueous layer contains the phenolic fraction in water and the bottom layer contains the mixture of chloroform and acetone. In our extraction procedure, an additional layer was formed between the chloroform/acetone and the aqueous layers. To separate it from the phenolic (aqueous) fraction, a centrifugation step was applied.

Total Phenolic Quantitation. Phenolic content of potato samples ranged from 113.37 to 510.20 mg of gallic acid equivalents (GAE) per 100 g of DW (Table 2). From the samples evaluated, potatoes from the species *S. tuberosum* subsp. *andigenum* and *S. Stenotomum* subsp. *stenotomum* had higher levels of phenolic compounds than the other species analyzed. Since the majority of the analyzed samples belonged to the *S. tuberosum* subsp. *andigenum* and *S. Stenotomum* subsp. *stenotomum* species (13 out of 20 samples), it can not be concluded as these species will always have higher phenolic content. More research needs to be done including more samples of different species to be able to determine if indeed samples of these two species have overall higher phenolic content than samples of other species. The sample with the highest total phenolic content ($p < 0.001$) was 703640, a *S. tuberosum* subsp. *andigenum* that exhibited a dark purple coloration in the extract with 510.2 mg of GAE/100 g DW, followed by sample 705534, a *S. stenotomum* subsp. *stenotomum*, dark purple extract and 704733, a *S. tuberosum* subsp. *andigenum*, a purple extract with 412.49 and 379.2 mg of GAE/100 g DW, respectively. Samples 706884 and 704481 both belonging to the specie *S. Stenotomum* subsp. *goniocalyx* produced yellow extracts and did not contain monomeric anthocyanins. These two samples had the lowest total phenolic content with 114.63 mg and 113.37 mg of GAE per 100 g DW, respectively. Phenolic content of the potato samples evaluated seemed to be more dependent on the coloration of the samples than on the specie, with higher phenolic content being obtained from samples exhibiting more intense colors. The values found in this research were higher than those reported by Im and others[19] in 24 regular American potatoes (including Yucon gold, Russet, red and white potatoes) bought in a local store in Berkely, California finding 4.09 mg to 281 mg of total phenolics per 100 g of DW. Only one variety studied by the authors gave higher values of phenolics, which was a Peruvian purple potato with 757 mg of total phenolics per 100g of DW.

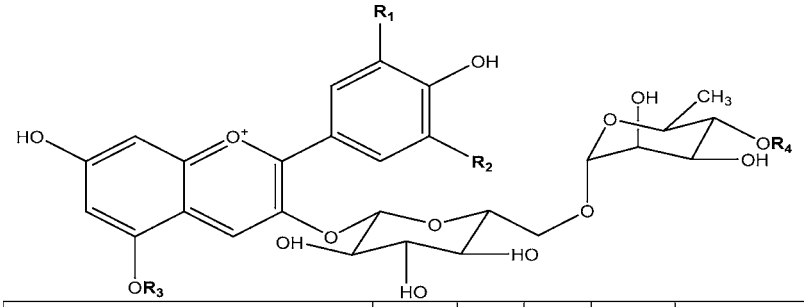

Name of Anthocyanin	Peak No	R_1	R_2	R_3	R_4
Pelargonidin-3-rutinoside-5-glucoside	7	H	H	Glucose	-
Pelargonidin-3-rutinoside	8	H	H	-	-
Pelargonidin-3-caffeoylrutinoside-5-glucoside	9	H	H	Glucose	Caffeic acid
Peonidin-3-caffeoylrutinoside-5-glucoside	10	OCH_3	H	Glucose	Caffeic acid
Cyanidin-3-coumaroylrutinoside-5-glucoside	11	OH	H	Glucose	Coumaric acid
Petunidin-3-coumaroylrutinoside-5-glucoside	11[I]	OCH_3	OH	Glucose	Coumaric acid
Pelargonidin-3-coumaroylrutinoside-5-glucoside	12	H	H	Glucose	Coumaric acid
Peonidin-3-coumaroylrutinoside-5-glucoside	13	OCH_3	H	Glucose	Coumaric acid
Pelargonidin-3-feruloylrutinoside-5-glucoside	14	H	H	Glucose	Ferulic acid
Peonidin-3-feruloylrutinoside-5-glucoside	15	OCH_3	H	Glucose	Ferulic acid
Petunidin-3-caffeoylrutinoside-5-glucoside	16	OCH_3	OH	Glucose	Caffeic acid
Petunidin-3-feruloylrutinoside-5-glucoside	17	OCH_3	OH	Glucose	Ferulic acid
Malvidin-3-coumaroylrutinoside-5-glucoside	18	OCH_3	OCH_3	Glucose	Coumaric acid

Figure 3. Chemical structures of major anthocyanins identified in red and purple potato extracts by HPLC PDA/MS. *Compound numbers refer to the peak numbers given in Figure 4.

Monomeric and Polymeric Anthocyanin Content. Based on the anthocyanin composition, colored samples have a maximum absorbance (λ_{max}) at different wavelengths. Most of the colored potato samples analyzed had their λ_{max} either at 520 nm (purple extracts) or at 510 nm (red extracts). Purple extracts with highest absorbance at 520 nm were quantitated as cy-3-glu equivalents (Table 2 Section I) while red extracts with λ_{max} at 510 nm were quantitated as pg-3-glu equivalents (Table 2 Section II).

The monomeric anthocyanin content of the different red and purple potato varieties ranged from 8.2 to 152.7 mg/100 g DW. The cultivars with the lowest monomeric anthocyanin content were 703782, a *S. stenotomum* subsp. *stenotomum* that exhibited a light purple extract and 704133, a *S. stenotomum* subsp. *Stenotomum* exhibiting a light red extract with 8.2 and 16.8 mg/100 DW, respectively. The varieties with highest pigment content were 705534, a *S. stenotomum* subsp. *stenotomum*, dark purple extract, and 703640, a *S. tuberosum* subsp. *andigenum*, dark purple extract, with more than 145 mg cy-3-glu equivalents/100 g DW. These two samples also had high content of total phenolics. Anthocyanin content of the potato samples evaluated were more related to the coloration of the samples than on the specie, since samples with more intense colors showed higher anthocyanin content. Higher monomeric anthocyanin content has been reported for other purple potato cultivars such as Urenika with average contents 507.8 and 183.6 mg/100 g FW in the skin and flesh, respectively.[20] Rodriguez-Saona and others[7] also reported higher contents of monomeric anthocyanins (>35 mg/100 g FW) in two different red potato selections. Similarly, Campos and others[9] found higher quantities of total anthocyanin content in fresh native Andean potato tubers (8 mg to 80 mg per 100 g of fresh tuber). There might be the potential to develop a red and purple potato clones through potato breeding studies with pigment content similar to those of Urenika.[7]

In the analyzed samples, the percentage of polymeric color ranged between 12.4% and 40.3% (Table 2) with an average polymeric color of 24%. The sample with the highest percentage of polymeric color was 703782 (*S. stenotomum* subsp. *stenotomum*, red extract), which was found to contain the lowest monomeric anthocyanin content as well. Polymeric color in the potato samples could be attributed to polymerization reactions during processing/lyophilization and over storage as well as some possible residual enzymatic activity during extraction.

Anthocyanin content as a percentage of the total phenolics ranged from 5.17% to 37.02% with an average of 20% of the total phenolics content (Table 2). With the exception of sample 704733, a *S. tuberosum* subsp. *andigenum* that produced a purple extract, total phenolic and anthocyanin content showed linear correlation (R^2 = 0.841, p-value = 0.0001). The reason for sample 704733 being an outlier was the high content of phenolic compounds (379.2 mg of GAE per 100 g of DW) and low content of monomeric anthocyanins (41.1 mg of cy-3-glu

dx.doi.org/10.1021/jf500655n | J. Agric. Food Chem. 2014, 62, 4408−4416

Table 5. List of Major Anthocyanins Identified in Red and Purple Potato Extracts by HPLC PDA/MS

peak no[a]	retention time (min)[a]	M^+ (m/z)	fragment ions	peak assignment[b]
7	13.4	741	271	pelargonidin-3-rutinoside-5-glucoside
8	19.5	579	271	pelargonidin-3-rutinoside
9	24.3	903	271	pelargonidin-3-caffeoylrutinoside-5-glucoside
10	25.1	933	301	peonidin-3-caffeoylrutinoside-5-glucoside
11	25.6	903	287	cyanidin-3-coumaroylrutinoside-5-glucoside
11[I]	26.3	933	317	petunidin-3-coumaroylrutinoside-5-glucoside
12	29.5	887	271	pelargonidin-3-coumaroylrutinoside-5-glucoside
13	31.1	917	301	peonidin-3-coumaroylrutinoside-5-glucoside
14	32.9	917	271	pelargonidin-3-feruloylrutinoside-5-glucoside
15	34.4	947	301	peonidin-3-feruloylrutinoside-5-glucoside
16	19.6	949	317	petunidin-3-caffeoylrutinoside-5-glucoside
17	27.3	963	317	petunidin-3-feruloylrutinoside-5-glucoside
18	31.9	948	331	malvidin-3-coumaroylrutinoside-5-glucoside

[a]Compound numbers and retention times refer to the numbers given in Figures 4 and 5. [b]All anthocyanins were identified based on the combined information on UV−vis, molecular ion, mass fragments and retention times of the anthocyanin and the anthocyanidins. Anthocyanidin identification was made using the acid hydrolysis of strawberry (for pelargonidin) and grape (for delphinidin, cyanidin, peonidin, petunidin and malvidin as references).

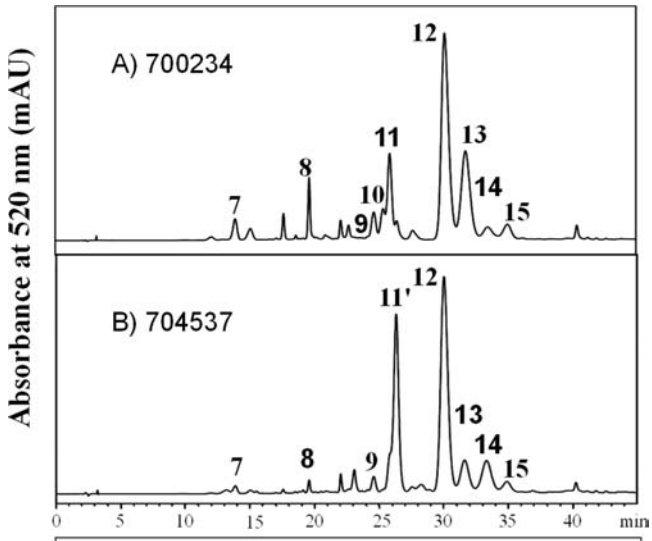

Code	7	8	9	10	11	11'	12	13	14	15
700234	2.3	4.1	3.3	3.4	10.1	ND	38.7	20.6	3.1	3.3
702464	3.4	1.2	2.5	ND	0.5	ND	69.2	1.7	14.6	1.5
702556	3.0	4.0	3.4	1.4	3.3	ND	53.5	10.7	9.5	3.8
703695	4.2	1.7	6.2	ND	2.0	ND	68.3	2.2	8.5	ND
703752	4.1	1.2	7.3	ND	2.9	ND	58.8	2.0	17.8	ND
703782	5.7	4.3	3.2	ND	4.2	ND	45.8	9.3	11.3	4.7
704537	0.9	0.7	1.7	ND	ND	28.8	43.5	7.6	8.6	2.3
705500	6.2	3.5	2.8	ND	2.0	ND	64.5	3.8	8.9	0.9
705820	11.3	15.4	4.0	ND	ND	ND	51.0	1.5	5.9	0.6
705841	5.9	6.8	3.0	1.3	7.1	ND	48.7	10.9	3.6	2.0
705946	4.4	10.6	4.4	ND	ND	ND	63.7	2.2	4.1	NQ
706630	6.3	6.8	3.2	1.5	5.9	ND	49.8	9.7	4.0	2.3

Figure 4. HPLC chromatograms at 520 nm for major anthocyanins of red potato extracts and their peak areas (% of total peak area at 520 nm). ND: not detected. Difference from 100 is due to the presence of minor peaks, each accounting for less than 2% of total area. *All anthocyanins were tentatively identified.

equivalents per 100 g of DW) it contained. This finding shows that even though the presence of anthocyanins increases the overall phenolic content, there might be potato varieties with high phenolic content that show little or no anthocyanin content.

Phenolic Characterization. Potato phenolics were characterized by monitoring the elution of compounds at 280 nm. Key structures for phenolics addressed are illustrated in Figure 1 and further detalied in Table 3. Three chromatograms representing purple, red and yellow extracts can be seen in Figure 2. Similar phenolic profiles were obtained for all potato samples besides the differences in the anthocyanin fractions (Figure 2).

The presence of chlorogenic, caffeic, *p*-coumaric, ferulic, sinapic, gallic and protocatechuic acid have been previously reported in potatoes.[7,20−22] Therefore, cocktails with these phenolic acid standards were injected in the HPLC−MS with the same separation method used for the potato samples. From the standards used, only chlorogenic and caffeic acid were identified among the phenolic acids in the samples. Chlorogenic acid isomers were prepared and injected in the HPLC−MS following the same method used for the potato samples and other standards. During the isomerization procedure, caffeic acid was also formed and eluted after the three isomers.

Phenolic identification was made based on UV, mass spectra and retention time comparisons to those of pure standards available. In addition to the anthocyanin peaks, 13 major phenolic peaks were found in the potato samples (Figure 2). From those peaks four compounds (**2**, **3**, **4** and **5**) have been clearly identified and two others (**1** and **6**) have been tentatively identified.

Relative proportions of the phenolic compounds (% of total peak area at 280 nm) identified were reported in Table 4. Proportions of the compound **6** (tentatively identified) were not included in Table 4 due to difficulty of quantitation since the compound coeluted with an anthocyanin peak. In average, **2**, **3** and **4** represented 43% of the total phenolic content. However, this value was lower than the 70% of total phenolic area reported by Rodriguez-Saona and others[7] in red potatoes and up to 90% of the total phenolic compounds in potato tubers analyzed by Malmberg and Theander.[23]

Anthocyanin Characterization. Anthocyanin profiles obtained were very similar among all samples within the same color (purple and red extracts). However, clear differences between anthocyanin profiles of purple and red samples were noticed from the HPLC chromatograms at 520 nm. Purple extracts had fewer peaks than the red extracts and in general, most predominant peaks in purple extracts eluted before the predominant peaks in red extracts. Due to their different profiles, both groups were characterized individually. To facilitate the identification of the anthocyanins, samples were saponified and hydrolyzed and analyzed through HPLC−MS. Anthocyanidin identification was made based on UV−vis and mass spectra and retention time comparisons to those of anthocyanidin standards obtained from the acid hydrolysis of

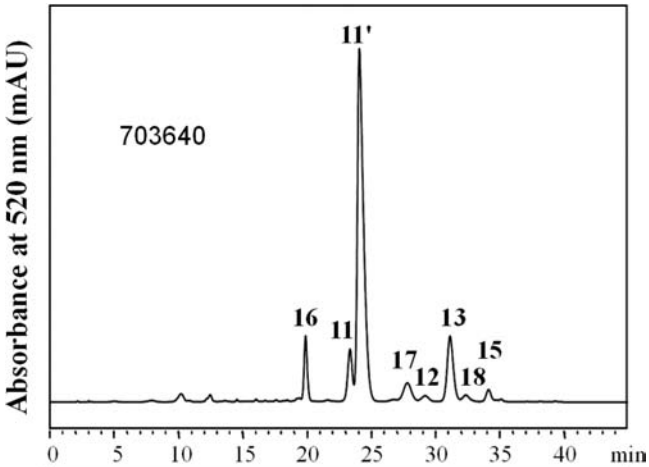

Code	16	11	11'	17	12	13	18	15
703640	6.1	7.1	63.6	4.5	1.3	11.9	1.3	1.5
703862	3.5	4.6	57.0	3.6	10.1	11.0	4.8	2.2
704133	4.0	6.3	61.6	3.0	1.2	15.9	3.0	2.0
704733	4.8	7.6	62.5	3.4	ND	15.9	2.4	1.3
705534	4.3	4.6	68.4	3.0	0.5	12.6	3.0	1.6
706726	5.3	7.4	65.7	2.8	ND	12.0	2.1	1.0

Figure 5. HPLC chromatogram at 520 nm for major anthocyanins in purple potato extract and their peak areas (% of total peal area at 520 nm). ND: not detected. Difference from 100 is due to the presence of minor peaks, each accounting for less than 2% of total area. *All anthocyanins were tentatively identified.

strawberry (pelargonidin) and grape (delphinidin, cyanidin, peonidin, petunidin and malvidin). Key structures of anthocyanins identified are illustrated in Figure 3 and further detailed in Table 5.

Red Potato Extracts. Three major anthocyanidins (cyanidin, pelargonidin and peonidin) were identified in red potato extracts. Among the saponified samples, four major peaks were identified based on UV−vis and mass spectra as cyanidin-3-rutinoside-5-glucoside, pelargonidin-3-rutinoside-5-glucoside, peonidin-3-rutinoside-5-glucoside, pelargonidin-3-rutinoside with pelargonidin-3-rutinoside-5-glucoside was being the most predominant peak in the saponified samples.

Seven of the nine anthocyanin major peaks in red potato extracts (Figure 4) were acylated with a cinnamic acid. Three different cinnamic acids were found acylating the anthocyanins in red potato extract: caffeic, *p*-coumaric and ferulic acid. Nine major anthocyanin peaks were identified based on UV−vis and mass spectra. Pelargonidin-3-*p*-coumaroyl-5-glucoside was the most predominant peak in red potato extracts after saponification which was in accordance with the findings of Rodriguez-Saona and others.[7] Five major peaks were pelargonidin derivatives: two nonacylated (compounds **7** and **8**) and three acylated (compounds **9**, **12** and **14**), while three pigments were acylated peonidin derivatives (compounds **10**, **13** and **15**) and only one major pigment was identified as acylated cyanidin derivative (compound **11**). Sample 704537, a *S. Chaucha specie*, presented slight differences in anthocyanin profile and therefore it was characterized individually. The main difference between sample 704537 and the other red potato extracts was the presence of compound $\mathbf{11^I}$ (Figure 4).

Relative proportions (% of total peak area at 520 nm) of the anthocyanin compounds previously identified were also shown in Figure 4. In average, compound **12** accounted for 54.6% of the total anthocyanin content. However, this value was lower than the range between 56.7 and 83.2% of total area reported by Rodriguez-Saona and others[7] in red potatoes.

Purple Potato Extracts. Five major anthocyanidins (cyanidin, petunidin, pelargonidin, peonidin and malvidin) were identified in purple potato extracts. From the six common anthocyanidins found in nature, only delphinidin was not present in purple potato extracts. Petunidin and peonidin were the most predominant anthocyanidins in purple potato extracts.

Four major peaks were found in the saponified samples of purple potato extracts. The peaks were identified based on UV−vis and mass spectra as the 3-rutinoside-5-glycoside derivatives of the five anthocyanidins found in the hydrolyzed samples. According to order of their elution, they were: cyanidin-3-rutinoside-5-glucoside, petunidin-3-rutinoside-5-glucoside, pelargonidin-3-rutinoside-5-glucoside and peonidin-3-rutinoside-5-glucoside, with petunidin and peonidin glycosides being the most predominant peaks in the saponified samples.

The separation and identification of the acylated anthocyanins in purple potato extracts was more challenging since some of the peaks coeluted making their identification more difficult. Accordingly, the HPLC separation method was improved by changing the aqueous solvent concentration to 10% formic acid and slightly modifying the solvent gradient. Even though fractioning of the molecules and MS data collection was better with lower acid concentrations, better separation of the compounds in the C_{18} column was achieved with higher acidity. The same three acylating groups (caffeic, p-coumaric and ferulic) identified in red potato extracts were also found in the purple potato extracts. Eight major acylated anthocyanin peaks (Figure 5) were identified in purple potato extracts: **11**, $\mathbf{11^I}$, **12**, **13**, **15**, **16**, **17**, **18**. Petunidin and peonidin acylated derivatives were the most predominant peaks in purple potato extracts.

Relative proportions (% of total peak area at 520 nm) of the anthocyanin compounds in purple potato extracts were also shown in Figure 5. In average, compound $\mathbf{11^I}$ accounted for 63.2% of the total anthocyanin content.

In conclusion, Andean potato samples from different species showed great variability in polyphenolic and anthocyanin content. Major quantitative and qualitative differences among evaluated samples seemed to be more dependent on the coloration of the sample after extraction rather than on the specie. Potato varieties with high anthocyanin content could be used as sources of natural pigments with increased stability for food applications. Due to the high consumption levels of potatoes around the world, selected native Andean potatoes could be be introduced into the market to deliver significant amounts of phenolic compounds with potential health promoting properties into the human diet.

AUTHOR INFORMATION

Corresponding Author

*Tel.: +1 614-247-8016. Fax: +1 614 292 0218. E-mail: giusti.6@osu.edu.

Notes

The authors declare no competing financial interest.

ABBREVIATIONS USED

CIP, international potato center; DW, dry weight; ESI, electron spray ionization; GAE, gallic acid equivalents; HPLC, high-pressure liquid chromatography; MS, mass spectroscopy; PDA,

photodiode array; PPO, polyphenol oxidase; SIM, selective ion monitoring; TFA, trifluoroacetic acid

REFERENCES

(1) Food and Agriculture Organization of the United Nations (FAOSTAT). http://faostat.fao.org/site/567/default.aspx#ancor (accessed January 2nd, 2014).

(2) Andre, C. M.; Ghislain, M.; Bertin, P.; Oufir, M.; Herrera, M.; Hoffmann, L.; Hausman, J. F.; Larondelle, Y.; Evers, D. Andean potato cultivars (*Solanum tuberosum* L.) as a source of antioxidant and mineral micronutrients. *J. Agric. Food Chem.* **2007**, *55*, 366−378.

(3) Boker, L. K.; Van der Schouw, Y. T.; De Kleijn, M. J.; Jacques, P. F.; Grobbee, D. E.; Peeters, P. H. Intake of dietary phytoestrogens by Dutch women. *J. Nutr.* **2002**, *132*, 1319−1328.

(4) Dragsted, L. O.; Strube, M.; Leth, T. Dietary levels of plant phenols and other nonnutritive components: could they prevent cancer? *Eur. J. Cancer Prev.* **1997**, *6*, 522−528.

(5) Hertog, M. G.; Bueno-de-Mesquita, H. B.; Fehily, A. M.; Sweetnam, P. M.; Elwood, P. C.; Kromhout, D. Fruit and vegetable consumption and cancer mortality in the Caerphilly Study. *Cancer Epidemiol., Biomarkers Prev.* **1996**, *5*, 673−677.

(6) Knekt, P.; Kumpulainen, J.; Järvinen, R.; Rissanen, H.; Heliövaara, M.; Reunanen, A.; Hakulinen, T.; Aromaa, A. Flavonoid intake and risk of chronic diseases. *Am. J. Clin. Nutr.* **2002**, *76*, 560−568.

(7) Rodriguez-Saona, L.; Giusti, M. M.; Wrolstad, R. E. Anthocyanin pigment composition of red-fleshed potatoes. *J. Food Sci.* **1998**, *63*, 458−465.

(8) Giusti, M. M.; Wrolstad, R. E. Acylated anthocyanins from edible sources and their applications in food systems. *Biochem. Eng. J.* **2003**, *14*, 217−225.

(9) Campos, D.; Noratto, G.; Chirinos, R.; Arbizu, C.; Roca, W.; Cisneros-Zevallos, L. Antioxidant capacity and secondary metabolites in four species of Andean tuber crops: native potato (*Solanum* sp.), mashua (*Tropaeolum tuberosum* Ruiz & Pavón), oca (*Oxalis tuberosa* Molina) and ulluco (*Ullucus tuberosus* Caldas). *J. Sci. Food Agric.* **2006**, *86*, 1481−1488.

(10) Nagels, L. High performance liquid chromatographic separation of naturally occurring esters of phenolic acids. *J. Chromatogr., A* **1980**, *187*, 181−187.

(11) Wrolstad, R. E.; Durst, R. W.; Lee, J. Tracking color and pigment changes in anthocyanin products. *Trends Food Sci. Technol.* **2005**, *16*, 423−428.

(12) Durst, R. W.; Wrolstad, R. E. Separation and characterization of anthocyanins by HPLC. In *Current Protocols in Food Analytical Chemistry*; Wrolstad, R. E., Ed.; John Wiley & Sons: New York, 2001; units F1.3.1−F1.3.13.

(13) Giusti, M. M.; Wrolstad, R. E. Anthocyanins. Characterization and measurement of anthocyanins by UV-visible spectroscopy. In *Current Protocos in Food Analytical Chemistry*; Wrolstad, R. E., Ed.; John Wiley & Sons: New York, 2001; unit F1.2.1−1.

(14) Waterhouse, A. L. Determination of total phenolics. In *Current Protocols in Food Analytical Chemistry*; Wrolstad, R. E., Ed.; John Wiley & Sons: New York, 2002; units I1.1.1−I1.1.8.

(15) Shiroma-Kian, C.; Tay, D.; Manrique, I.; Giusti, M. M.; Rodriguez-Saona, L. E. Improving the screening process for the selection of potato breeding lines with enhanced polyphenolics content. *J. Agric. Food Chem.* **2008**, *56*, 9835−9842.

(16) Francis, F. J. Food colorants: anthocyanins. *Crit. Rev. Food Sci. Nutr.* **1989**, *28*, 273−314.

(17) Schwartz, S. J.; von Elbe, J. H.; Giusti, M. M. Colorants. In *Fennema's Food chemistry*, 4th ed.; Fennema, O. R., Damodaran, S., Parkin, K., Eds.; CRC Press/Taylor & Francis: Boca Raton, FL, 2008.

(18) Parkin, K. L. Enzymes. In *Fennema's Food chemistry*, 4th ed.; Fennema, O. R., Damodaran, S., Parkin, K., Eds.; CRC Press/Taylor & Francis: Boca Raton, FL, 2008.

(19) Im, H. W.; Suh, B. S.; Lee, S. U.; Kozukue, N.; Ohnisi-Kameyama, M.; Levin, C. E.; Friedman, M. Analysis of phenolic compounds by high-performance liquid chromatography and liquid chromatography/mass spectrometry in potato plant flowers, leaves, stems, and tubers and in home-processed potatoes. *J. Agric. Food Chem.* **2008**, *56*, 3341−3349.

(20) Lewis, C. E.; Walker, J. R. L.; Lancaster, J. E.; Sutton, K. H. Determination of anthocyanins, flavonoids and phenolic acids in potatoes. I. Coloured cultivars of *Solanum tuberosum* L. *J. Sci. Food Agric.* **1998**, *77*, 45−47.

(21) Reddivari, L.; Hale, A. L.; Miller, J. C. J. Determination of phenolic content, composition and their contribution to antioxidant activity in specialty potato selections. *Am. J. Potato Res.* **2007**, *84*, 275−282.

(22) Reddivari, L.; Miller, J. C. J.; Hale, A. L. Genotype, location, and year influence antioxidant activity, carotenoid content, phenolic content, and composition in specialty potatoes. *J. Agric. Food Chem.* **2007**, *55*, 8073−8079.

(23) Malmberg, A. G.; Theander, O. Determination of chlorogenic acid in potato tubers. *J. Agric. Food Chem.* **1985**, *33*, 549−551.

JOURNAL OF AGRICULTURAL AND FOOD CHEMISTRY

Article

pubs.acs.org/JAFC

Self-Emulsification of Alkaline-Dissolved Clove Bud Oil by Whey Protein, Gum Arabic, Lecithin, and Their Combinations

Yangchao Luo, Yue Zhang, Kang Pan, Faith Critzer, P. Michael Davidson, and Qixin Zhong*

Department of Food Science and Technology, University of Tennessee in Knoxville, Knoxville, Tennessee 37996, United States

ABSTRACT: Low-cost emulsification technologies using food ingredients are critical to various applications. In the present study, a novel self-emulsification technique was studied to prepare clove bud oil (CBO) emulsions, without specialized equipment or organic solvents. CBO was first dissolved in hot alkaline solutions, added at 1% v/v into neutral solutions with 1% w/v emulsifier composed of whey protein concentrate (WPC), gum arabic, lecithin, or their equal mass mixtures, and adjusted to pH 7.0. The self-emulsification process did not affect UV−vis absorption spectrum, reversed-phase HPLC chromatogram, or antimicrobial activity of CBO against *Escherichia coli* O157:H7, *Listeria monocytogenes* Scott A, and *Salmonella* Enteritidis. The entrapment efficiency after extraction by petroleum ether was determined to be about 80%. Most emulsions were stable during 7 days of storage. Emulsions prepared with WPC had smaller particles, whereas emulsions prepared with emulsifier mixtures had more stable particle dimensions. The studied self-emulsification technique may find numerous applications in the preparation of low-cost food emulsions.

KEYWORDS: *self-emulsification, clove bud oil, alkaline deprotonation, neutralization, whey protein concentrate, gum arabic*

INTRODUCTION

Essential oils (EOs) are aromatic liquids derived from plants or plant parts, including leaves, flowers, buds, fruits, barks, and seeds.[1−3] EOs are well-known for their antioxidant and antimicrobial activities and have been widely used as functional ingredients in food, pharmaceutical, and cosmetic products.[1] In recent years, the application of EOs in food products has generated particular interest because of their generally recognized as safe (GRAS) regulatory status, multiple functionalities, and wide acceptance by consumers.[2,3] Clove oils are the EOs obtained by distillation of the flower buds, stems, and leaves of the clove tree (*Syzygium aromaticum*). Among clove oils, clove bud oil (CBO) is widely used and well-known for its potent antioxidant properties and antibacterial, antifungal, and antiviral activities.[4] Eugenol, 4-allyl-2-methoxyphenol, is the primary constituent (>80%) of CBO[5] and is the major contributor of the above biological functions of CBO.[4,6,7]

The poor solubility in aqueous solutions and high volatility during processing are two major obstacles of utilizing EOs as sanitizing agents or as preservatives in food matrices. Oil-in-water emulsions carefully prepared using appropriate surfactants and emulsification processes are common choices to deliver EOs in aqueous systems. Although synthetic surfactants such as polysorbates (Tweens) have demonstrated excellent emulsifying activities, their potential toxicity and regulated use in foods limit their applications in the food industry.[8,9] Therefore, there is a paradigm shift from synthetic to naturally occurring emulsifiers.

Food biopolymers, that is, proteins and polysaccharides, with appropriate surface activity are promising candidates to prepare naturally occurring and potentially GRAS emulsions for food applications.[10,11] For instance, the combination of whey protein concentrate (WPC) and gum arabic (GA) has been shown to effectively prepare chia (*Salvia hispanica*) EO microcapsules by spray-drying, and the resultant spray-dried powder can be freely reconstituted in water, greatly improving its application in aqueous systems.[12] Furthermore, nanoemulsions, with droplets smaller than approximately 200 nm in diameter, can prevent the creaming/precipitation of EO droplets and potentially enhance their antimicrobial activity.[13] Nanoemulsions are commonly prepared by high-energy methods such as high-pressure homogenization and microfluidization, but high capital and operating costs as well as scalability raise concerns about their practicality in the food industry.[14]

Therefore, the goal of the present work was to study a low-energy self-emulsifying technique to prepare EO nanoemulsions using naturally occurring emulsifiers. CBO was used as a model EO, and WPC, GA, and soy lecithin were selected as emulsifiers. The principle was based on the deprotonation of the hydroxyl group of eugenol (Scheme 1), the major component in CBO, under aqueous alkaline conditions and the self-emulsifying process during the subsequent neutralization in the presence of the natural emulsifiers. The first objective was to study the feasibility of the proposed self-emulsifying approach and characterize physicochemical properties of CBO emulsions. The second objective was to evaluate how the emulsification process affected the antimicrobial activity of CBO

Scheme 1. Chemical Structures of Native and Deprotonated Eugenol

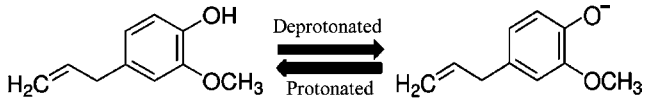

Received: February 9, 2014
Revised: April 15, 2014
Accepted: April 23, 2014
Published: April 23, 2014

ACS Publications © 2014 American Chemical Society

against the Gram-negative bacteria *Escherichia coli* O157:H7 and *Salmonella* Enteritidis and the Gram-positive bacterium *Listeria monocytogenes*.

MATERIALS AND METHODS

Materials. Organic-certified CBO with a purity of no less than 85% was purchased from Sigma-Aldrich Corp. (St. Louis, MO, USA). WPC-34, consisting of 3−4.5% fat, 34−36% protein, and 48−52% lactose, was provided by Grande Cheese Co. (Grande, WI, USA). The clear WPC dispersion was prepared by removing fat globules as described by Damodaran.[15] The 4% WPC was hydrated for 2 h in deionized water, and the pH was adjusted to 4.0. After standing for 2 h at room temperature (21 °C) and centrifugation at 5000*g* for 20 min (SORVALL RC5B Plus centrifuge, DuPont, Wilmington, DE, USA), the transparent supernatant was collected for emulsion preparation. GA was purchased from Fisher Scientific (Pittsburgh, PA, USA). Soy lecithin (Sunlipon 50) was generously provided by Perimondo, LLC (New York, NY, USA). Other chemicals and reagents were of analytical grade and purchased from Fisher Scientific and used as received.

Preparation of Emulsions. Deprotonation of CBO was accomplished by mixing 0.5 mL of CBO with 4.5 mL of 1−5 M NaOH in a glass vial and heating at 110 °C for 10 min in a glycerol bath until the mixture became transparent. The deprotonation of CBO was accelerated by heating, similarly to saponification in the edible oil industry. For emulsion preparation, 3 M NaOH was used as aqueous phase to dissolve CBO. Single or blends of emulsifiers were dissolved separately in water at an overall emulsifier concentration of 1% w/v, consisting of WPC only, GA only, lecithin only, or their equal mass mixtures (Table 1). Then 0.5 mL of alkaline-dissolved CBO was added to 4.5 mL of the emulsifier aqueous solution, preadjusted to pH 7.0 at room temperature, and mixed for 5 min on a magnetic stirring plate. Then, the pH of the mixture was adjusted to pH 7.0, using 3 or 0.3 M citric acid. The emulsion spontaneously formed during the acidification process. The emulsion formed was stirred for another 10 min and then stored at 4 °C until further analyses.

Table 1. Compositions Used To Prepare 1% w/v Emulsifier Aqueous Solutions

sample	WPC (%)	gum arabic (%)	lecithin (%)
A	1	0	0
B	0	1	0
C	0	0	1
D	0.5	0.5	0
E	0	0.5	0.5
F	0.5	0	0.5
G	0.33	0.33	0.33

Structural Changes of Clove Bud Oil after Emulsification. HPLC and UV−vis absorption spectroscopy were used to study the structure of CBO before and after self-emulsification. CBO was extracted from the emulsion prepared with WPC using ethyl acetate. The solvent was then evaporated under the fume hood, and the extracted CBO was dissolved in methanol. The unprocessed CBO was directly dissolved in methanol as a control for unprocessed CBO. The absorption spectrum of each from 200 to 600 nm was determined using a UV−vis spectrophotometer (Evolution 201, Thermo Scientific, Waltham, MA, USA). For HPLC, a reversed phase system (1200 series, Agilent Technologies, Waldbronn, Germany) was used at conditions described previously.[16] The HPLC system was composed of a quaternary pump module, a degasser, an autosampler, a temperature-controlled column chamber, and an Agilent diode array and multiple wavelength detector. Chromatograms were recorded and integrated using the 1200 LC Chromatography Data System. A ZORBAX Eclipse Plus C18 HPLC column (5 μm, 150 mm × 4.6 mm, Agilent, Palo Alto, CA, USA) equipped with a ZORBAX Eclipse Plus C-18 guard column (4.6 × 12.5 mm, 5 μm) was used in the present study. A 10 μL sample was injected, and the detector was set at a wavelength of 274 nm. The mobile phase consisting of water (solvent A) and methanol (solvent B) was applied at 0.5 mL/min as follows: a linear gradient of 20−80% B from 0 to 20 min, an isocratic step with 80% B from 20 to 25 min, and a linear gradient from 80% B to 20% B from 25 to 30 min. The column chamber was controlled at 25 °C throughout the experiments.

Entrapment Efficiency. The entrapment efficiency was determined by subtracting the free oil content from the total oil content. The free oil content in the prepared emulsion was measured according to the method of Rodea-González et al.[12] with modifications. Briefly, 0.5 mL of a freshly prepared emulsion was mixed with 2 mL of petroleum ether. The mixture was gently stirred for 10 min, and then 0.1 mL of the upper organic solvent phase was transferred to a 20 mL vial, followed by resting in a fume hood for 5 min to evaporate petroleum ether. Then, 4 mL of ethanol was added to dissolve the extracted oil, and the absorbance was measured at 280 nm, using the above spectrophotometer. A standard curve was established using CBO standard solutions in ethanol to correlate the absorbance value with the oil concentration. The entrapment efficiency was then calculated using eq 1:

$$\text{entrapment efficiency}\,(\%) = \frac{\text{total oil} - \text{free oil}}{\text{total oil}} \times 100\% \quad (1)$$

Particle Size and Stability of Emulsions. The particle size of the emulsions was measured using dynamic light scattering with a Delsa Nano analyzer (Beckman Coulter, Inc., Atlanta, GA, USA) at an angle of 165°. The hydrodynamic diameter (D_h) and polydispersity index (PDI) were measured during storage at room temperature (21 °C) for 7 days.

Surface Hydrophobicity (S_0). The S_0 of individual emulsifiers and their combinations was determined using a fluorescence probe, 8-anilinonaphthalene-1-sulfonic acid (ANS), based on the method of Luo et al.,[17] with minor modifications. Briefly, individual emulsifiers or their mixtures were dispersed in 0.01 M phosphate-buffered saline (PBS, pH 7.0) at 1 mg/mL as stock solutions, which were further diluted with PBS to various concentrations in the range of 5−100 μg/mL. The diluted samples (4 mL) were mixed with 20 μL of an ANS working solution that was previously prepared at 8 mM in 0.01 M PBS (pH 7.0). The mixtures were incubated for 2 h at room temperature (21 °C) in the dark. The fluorescence intensity was then recorded at an excitation wavelength of 355 nm and an emission wavelength of 507 nm using a spectrofluorometer (model RF-1501, Shimadzu Corp.,

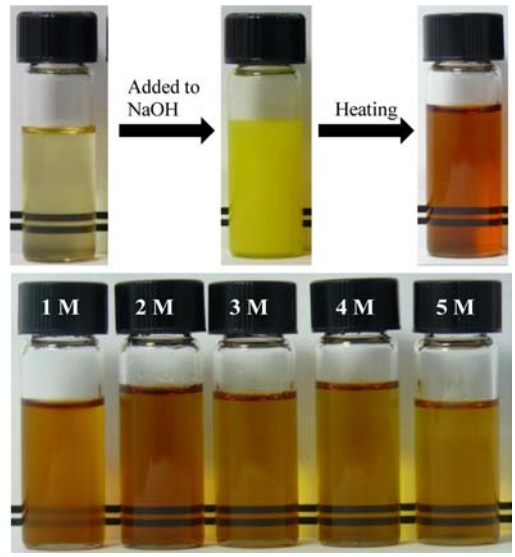

Figure 1. (a) Appearance of clove bud oil (left) after mixing at 10% v/v with 3 M NaOH (center) at 21 °C and after heating at 110 °C for 10 min (right); (b) appearance of 10% v/v clove bud oil heated at 110 °C for 10 min in 1−5 M NaOH (as labeled on vial caps).

Tokyo, Japan). The initial slope of fluorescent intensity versus sample concentration plot after linear regression with $R^2 > 0.995$ was used as an index for S_0.

Topographical Structures of Oil Droplets. The morphology of emulsion samples was studied using atomic force microscopy. The freshly prepared emulsion samples were diluted with distilled water to a final emulsifier concentration of 10 μg/mL. Ten microliters of the diluted sample was spread evenly onto freshly cleaved mica sheets mounted on a sample disk (Bruker Corp., Santa Barbara, CA, USA). A rectangular cantilever having an aluminum reflective coating on the backside and a quoted force constant of 2.80 N/m (FESPA, Bruker Corp.) and a Multimode VIII microscope (Bruker AXS, Billerica, MA, USA) were used to scan the sample. Images with a preset scan area of 10.0 × 10.0 μm were generated at a scanning speed of 1 Hz using the tapping mode.

Antimicrobial Assays. The antimicrobial activities of emulsion samples were tested against three bacterial strains in tryptic soy broth (TSB). *E. coli* O157:H7 ATCC 43895, *L. monocytogenes* Scott A, and *Salmonella* Enteritidis were obtained from the culture collection of the Department of Food Science and Technology at the University of Tennessee in Knoxville. All strains were grown in TSB and stored at −20 °C in 20% glycerol as stocks. Each strain was transferred at least twice in TSB with an interval of 24 h prior to use. Experiments were conducted at least twice for each culture, and samples were done in duplicate.

The minimum inhibitory (MIC) and minimum bactericidal (MBC) concentrations were determined using the microbroth dilution method.[18] Each culture was diluted to ca. 10^6 CFU/mL in TSB. Then, 120 μL of the diluted culture was added into wells of a 96-well microtiter plate and was mixed with 120 μL of TSB or an antimicrobial sample. Free CBO samples were prepared by dissolving 5% w/v CBO in 5% ethanol that was diluted in TSB to CBO concentrations of 250, 500, 750, 1000, 1250, 1500, 2000, or 2500 ppm. The emulsion samples were diluted in TSB directly to the same CBO concentrations. The microtiter plates were incubated at 32 °C for *L. monocytogenes* Scott A or at 37 °C for *E. coli* O157:H7 ATCC 43895 and *Salmonella* for 24 h. The absorbance at 630 nm (Abs_{630}) of each well was acquired before and after incubation using a microtiter plate reader (Titertek Multiscan MC, Labsystems, Helsinki, Finland). The MIC was defined as the lowest concentration of CBO preventing growth of the test strain, which corresponded to an Abs_{630} change of <0.05. To determine MBC, 10 μL of the mixture from negative wells (with $\Delta Abs_{630} < 0.05$) were spread-plated on tryptic soy agar (TSA) and incubated for another 24 h at temperatures referenced above. MBC was defined as the lowest concentration of CBO corresponding to no detectable colonies on TSA after incubation.

To study the growth kinetics of bacteria, 1 mL of the bacterial culture with about 10^7 CFU/mL was mixed with free CBO (predissolved in 5%) or emulsion samples and TSB to an overall volume of 10 mL, which corresponded to a population of ca. 10^6 CFU/mL. The final concentration of CBO was 750 ppm. Mixtures were incubated at 32 °C (*L. monocytogenes*) or 37 °C (*E. coli* O157:H7 and *Salmonella*). Viable bacteria were enumerated at 0, 4, 8, 24, and 48 h by spreading 0.1 mL of the mixtures on TSA plates and incubating as above for 24 h.

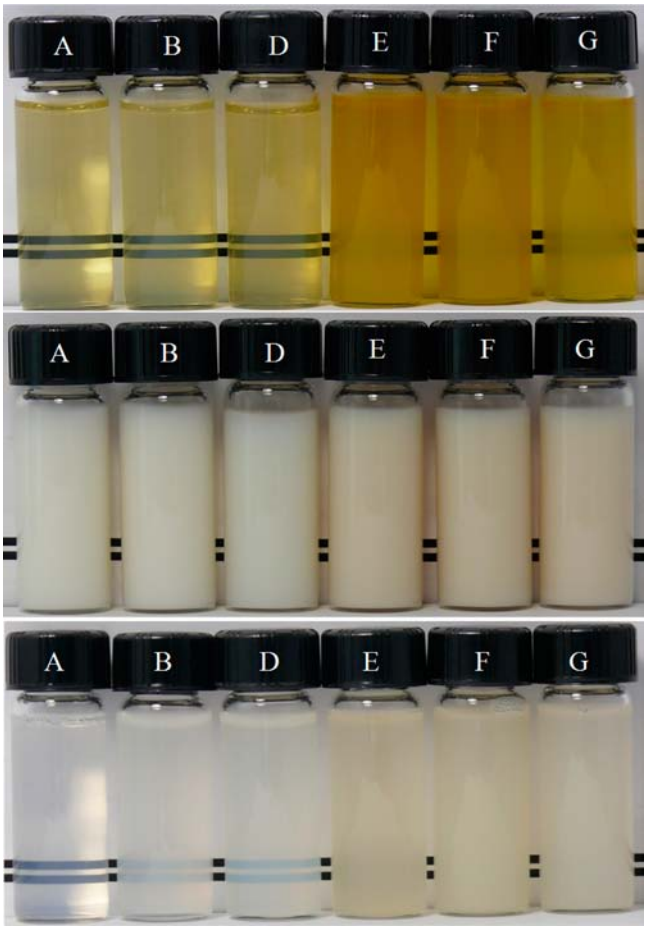

Figure 2. Appearance of samples after addition of 1% v/v alkaline-dissolved (in 3 M NaOH at 110 °C for 10 min) CBO in neutral aqueous solutions with 1% w/v emulsifier composed of (A) WPC only, (B) gum arabic only, (D) equal masses of WPC and gum arabic, (E) equal masses of gum arabic and lecithin, (F) equal masses of WPC and lecithin, and (G) equal masses of WPC, gum arabic, and lecithin (top), followed by acidification to pH 7.0 (middle), and further 5-fold dilution to 0.2% v/v oil in deionized water (bottom).

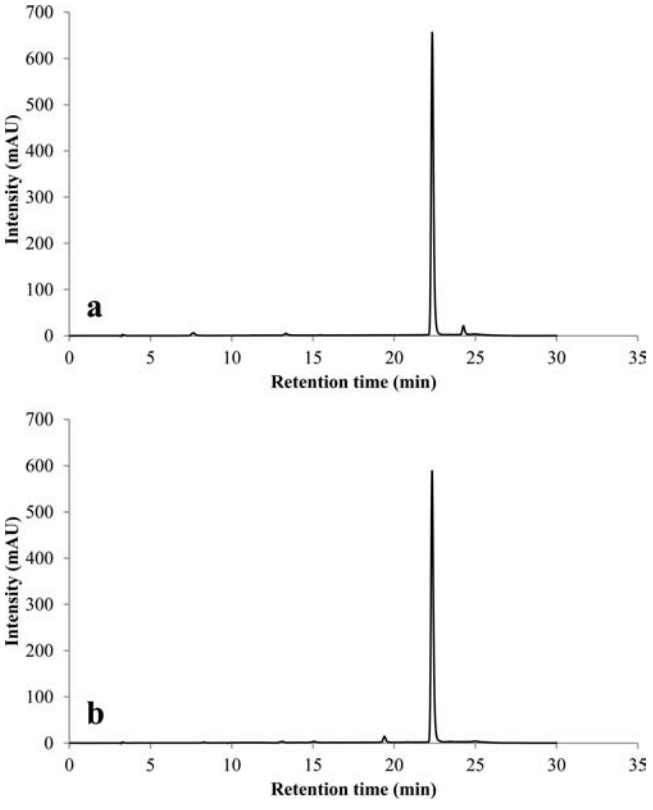

Figure 3. HPLC chromatograms of CBO before (a) and after (B) self-emulsification. The emulsion was prepared at 1% v/v CBO (predissolved in 3 M NaOH at 110 °C for 10 min) self-emulsified by 1% w/v WPC.

dx.doi.org/10.1021/jf500698k | J. Agric. Food Chem. 2014, 62, 4417−4424

Statistical Analysis. The experiments of emulsion preparation and characterization were conducted in triplicate. All results were reported as means ± standard deviations. The analysis of variance (ANOVA) and Tukey's multiple-comparison tests were performed using the SPSS 13.0 software (SPSS Inc., Chicago, IL, USA) at a significance level (P) of 0.05.

RESULTS AND DISCUSSION

Alkaline Dissolution Conditions. At room temperature, the initial aqueous mixture of CBO in 3 M NaOH was turbid (Figure 1a) but gradually became transparent if stirred for a sufficient time, ca. 10 h. Transparency was due to the deprotonation of the CBO phenolic components (primarily eugenol), making them negatively charged (Scheme 1) and therefore solubilized under alkaline conditions. At elevated temperatures, the time for the reaction was significantly shortened. Preliminary tests using 10% v/v CBO in 3 M NaOH at 60−120 °C for 10 min showed that 110 °C for 10 min was sufficient to obtain a transparent sample. The transparent solution had a darker color after heating (Figure 1a), suggesting alkaline treatment caused structural changes to CBO components. The concentration of NaOH was also varied from 1 to 5 M to evaluate its influence on the reaction. It was shown that 3 M was sufficiently high to obtain a transparent solution after heating at 110 °C for 10 min (Figure 1b). The reaction conditions of heating 10% v/v CBO in 3 M NaOH at 110 °C for 10 min were used for the remainder of the research.

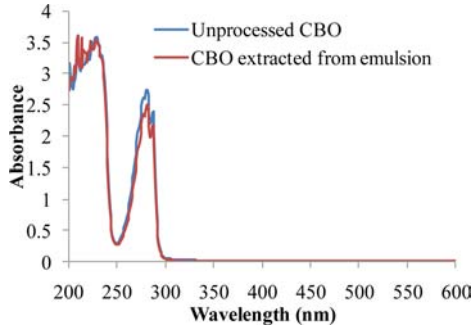

Figure 4. Comparison of UV−vis absorption spectra of CBO before and after self-emulsification. The emulsion was prepared at 1% v/v CBO (predissolved in 3 M NaOH at 110 °C for 10 min) self-emulsified by 1% w/v WPC.

Self-Emulsification of Alkaline-Dissolved CBO. The 10% v/v alkaline-dissolved CBO was mixed with a 9-fold volume of the 1% w/v emulsifier solution with compositions listed in Table 1, followed by neutralization to form emulsions containing 1% v/v CBO. When the alkaline-dissolved CBO was mixed with WPC, GA, or their blend, the mixture exhibited a lighter color than those with lecithin (Figure 2, top). This can be attributed to the color and water-insolubility of soy lecithin. When lecithin was the only emulsifier, large aggregates were observed following neutralization (data not shown), which may be due to the precipitation of lecithin by citric acid.[19] In contrast, other samples formed turbid dispersions without visible free oil or creaming, indicating successful self-emulsification (Figure 2, middle). After a 5-fold dilution to 0.2% CBO, the sample emulsified with WPC only was transparent; those with GA and WPC−GA mixture were translucent, whereas the other three samples with lecithin remained opaque, possibly due to the insoluble lecithin particles (Figure 2, bottom).

Because the self-emulsification process involved an alkaline treatment, it is essential to confirm the reversibility of the structural changes to CBO components, primarily eugenol. Therefore, HPLC was carried out to compare the retention time and peak area of eugenol in unprocessed CBO and that extracted

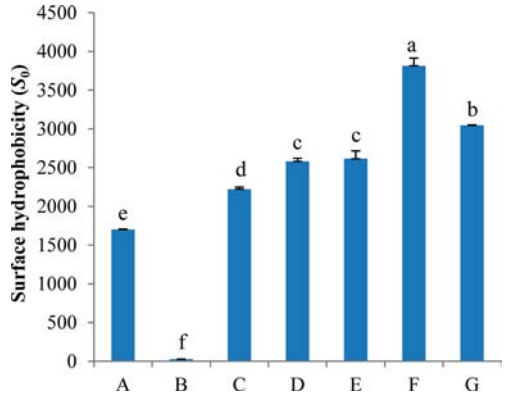

Figure 5. Surface hydrophobicity of (A) WPC only, (B) gum arabic only, (C) lecithin only, (D) equal masses of WPC and gum arabic, (E) equal masses of gum arabic and lecithin, (F) equal masses of WPC an lecithin, and (G) equal masses of WPC, gum arabic, and lecithin. Error bars are standard deviations from three replicates. Different letters above bars indicate significant differences in the mean ($P < 0.05$).

Table 2. Hydrodynamic Diameter (D_h) and Polydispersibility Index (PDI) of Clove Bud Oil Emulsions during 7 Days of Storage at 21 °C[a]

		surfactant(s)					
parameter	day	WPC	GA	WPC + GA	GA + lecithin	WPC + lecithin	WPC + GA + lecithin
D_h	0	160.2 ± 9.0a	406.4 ± 26.7b	268.6 ± 27.0a	541.1 ± 10.3b	252.3 ± 8.7a	241.0 ± 12.8a
	1	186.6 ± 32.7 a	498.0 ± 25.9a	262.1 ± 23.2a	606.7 ± 17.6ab	266.9 ± 4.9a	243.9 ± 27.1a
	3	196.6 ± 45.8 a	496.3 ± 23.1a	270.3 ± 46.1a	618.1 ± 20.7ab	264.4 ± 14.9a	251.4 ± 32.1a
	7	204.7 ± 41.9 a	550.5 ± 34.8a	283.0 ± 57.3a	688.7 ± 75.1a	273.5 ± 16.7a	257.1 ± 45.5a
PDI	0	0.298 ± 0.00a	0.209 ± 0.01c	0.292 ± 0.04a	0.325 ± 0.04a	0.312 ± 0.01a	0.289 ± 0.01a
	1	0.285 ± 0.04a	0.260 ± 0.03b	0.299 ± 0.02a	0.317 ± 0.03a	0.313 ± 0.01a	0.292 ± 0.02a
	3	0.289 ± 0.04a	0.289 ± 0.00ab	0.299 ± 0.03a	0.302 ± 0.05a	0.292 ± 0.01a	0.283 ± 0.05a
	7	0.307 ± 0.05a	0.317 ± 0.01a	0.323 ± 0.05a	0.297 ± 0.05a	0.298 ± 0.01a	0.314 ± 0.05a

[a]Emulsions with 1% v/v oil were prepared with 1% w/v of WPC, gum arabic (GA), or lecithin individually or their combinations with equal masses. Numbers are mean ± standard deviation ($n = 3$). For the same sample and parameter, numbers sharing different letters are significantly different ($P < 0.05$).

dx.doi.org/10.1021/jf500698k | J. Agric. Food Chem. 2014, 62, 4417−4424

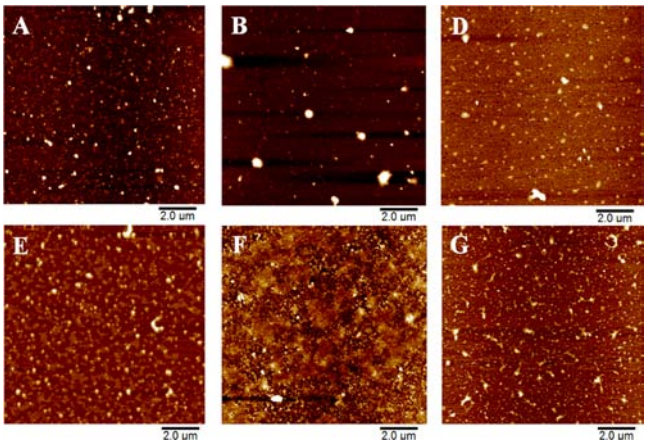

Figure 6. Topographical images of CBO emulsions prepared with (A) WPC only, (B) gum arabic only, (D) equal masses of WPC and gum arabic, (E) equal masses of gum arabic and lecithin, (F) equal masses of WPC and lecithin, and (G) equal masses of WPC, gum arabic, and lecithin.

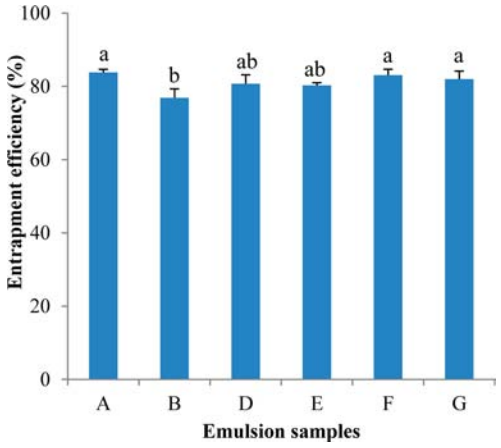

Figure 7. Entrapment efficiency of 1% v/v clove bud oil (predissolved in 3 M NaOH at 110 °C for 10 min) self-emulsified by 1% w/v emulsifier composed of (A) WPC only, (B) gum arabic only, (D) equal masses of WPC and gum arabic, (E) equal masses of gum arabic and lecithin, (F) equal masses of WPC and lecithin, and (G) equal masses of WPC, gum arabic, and lecithin. Error bars are standard deviations from three replicates. Different letters above bars indicate significant differences in the mean ($P < 0.05$).

from the emulsion. As shown in Figure 3a, the unprocessed CBO showed a sharp peak at the retention time of 22.3 min, representing eugenol.[16] The CBO extracted from the emulsion prepared with WPC (Figure 3b) had the major peak with the same retention time and peak area as the same concentration of unprocessed CBO. The same retention time revealed the same polarity of two samples, indicating that the double bond at its allyl side chain was not hydrogenated or cleaved after alkaline dissolution and neutralization. The UV−vis absorption spectra of CBO before and after emulsion preparation were also identical (Figure 4), further confirming no structural changes to CBO with the conditions studied.

Structure and Stability of Emulsions. The particle dimensions, D_h and PDI, were measured immediately after the emulsions were prepared and were monitored during the storage at ambient conditions up to 7 days (Table 2). Overall, freshly prepared emulsions exhibited D_h in the range of 160−540 nm. The sample self-emulsified with WPC alone had the smallest particles followed by the triple combination of emulsifiers and WPC−lecithin mixture, whereas that emulsified with GA alone had the largest particles. This agreed with a previous study using orange oil emulsions prepared with GA by high-pressure homogenization, which had much larger D_h than those emulsified by soy protein isolate, whey protein isolate, or sodium caseinate.[20] Compared with protein emulsifiers, the emulsification property of GA is limited by its high molecular weight and low surface hydrophobicity (Figure 5, discussed below), making it less effective in adsorbing onto the surface of oil droplets. Emulsion samples generally demonstrated good stability, showing no creaming during storage, except for the sample emulsified with GA only that demonstrated flocculated particles, which were redispersible after gentle shaking. When particle size changes were compared during storage, emulsions prepared with mixtures of emulsifiers generally showed better stability in maintaining particle size than those with individual emulsifiers. The one exception was the one emulsified with the GA−lecithin mixture, which exhibited a significant increase in particle size after 1 day of storage ($P < 0.05$). As to PDI, the emulsion prepared with GA demonstrated a significant increase in PDI ($P < 0.05$) during storage, whereas no significant changes of PDI were observed with any other emulsion. A PDI of about 0.3 indicates a relatively narrow distribution of particle sizes. Better stability of emulsions prepared with WPC−lecithin, WPC−GA, and WPC−GA−lecithin mixtures, with 8.4, 5.2, and 6.6% increases in D_h, respectively, than that of WPC

Table 3. MIC and MBC of Free and Self-Emulsified[a] Clove Bud Oil (CBO) against *E. coli* O157:H7 ATCC 43895 and *Salmonella* Enteritidis at 37 °C and against *Listeria monocytogenes* Scott A at 32 °C

	E. coli O157:H7		*Salmonella*		*L. monocytogenes*	
antimicrobial	MIC (ppm)	MBC (ppm)	MIC (ppm)	MBC (ppm)	MIC (ppm)	MBC (ppm)
free CBO[b]	750	750	750	750	1000	1250
emulsified CBO[a]						
WPC	500	500	500	750	750	1250
GA	500	500	500	750	500	1000
WPC + GA	500	500	500	750	500	1000
WPC + lecithin	500	500	500	750	750	1250
GA + lecithin	500	500	500	750	750	1000
WPC + GA + lecithin	500	500	500	750	750	1000

[a]Emulsions were prepared with 1% v/v CBO self-emulsified with 1% w/v surfactants composed of WPC, gum arabic (GA), and lecithin individually or their combinations with equal masses. [b]Predissolved in 50% ethanol, corresponding to 2.5% ethanol in the assay mixture; the 2.5% ethanol did not show inhibition against all bacteria.

dx.doi.org/10.1021/jf500698k | J. Agric. Food Chem. 2014, 62, 4417−4424

alone (27.8% increase in D_h) agreed with the reported synergistic surface activity of β-lactoglobulin (a component of WPC) and lecithin[21] and WPC and GA.[22] Overall, emulsions prepared with WPC and its mixtures with GA and/or lecithin had smaller particles than those without WPC and had no significant change in D_h during storage ($P > 0.05$, Table 2).

To better understand potential synergistic effects among natural emulsifiers, the S_0 values of the emulsifiers and their mixtures were measured (Figure 5). Both the WPC and lecithin exhibited high S_0 values, whereas GA (a mixture of polysaccharides and glycoproteins) was very hydrophilic and hence had a low S_0. Interestingly, the combination of GA with WPC or lecithin had higher S_0 values than individual emulsifiers. As discussed above, this may indicate that the complex formation between these emulsifiers may have enhanced their emulsifying and stabilizing properties.

The topography of oil particles prepared with different emulsifiers is shown in Figure 6. The treatments self-emulsified by WPC, GA, and their combination had spherical particles, verifying self-emulsification during neutralization. In contrast, emulsions prepared in the presence of lecithin had irregular structures. This is likely due to water-insoluble lecithin particles because soybean lecithin is a complex mixture composed of both water-soluble and -insoluble substances, such as phospholipids, glycerol, and triglycerides.[23]

Entrapment Efficiency. The entrapment efficiency was about 80% for all emulsifiers (Figure 7). The treatment with GA alone had significantly lower entrapment efficiency (76.8%), possibly due to its reduced ability to emulsify CBO compared to other treatments. The efficiencies of entrapping CBO using the present self-emulsification technique were comparable to, or higher than, those of many other oil-in-water emulsion systems prepared with natural emulsifiers using high-energy methods such as high-speed homogenization,[24] high-pressure homogenization,[25] and probe-type sonication.[26]

Minimum Inhibitory and Minimum Bactericidal Concentrations of Emulsions. The MICs for free CBO were 1000, 750, and 750 ppm, whereas the MBCs were 1250, 750, and 750 ppm against *L. monocytogenes* Scott A, *E. coli* O157:H7 ATCC 43895, and *Salmonella* Enteritidis, respectively (Table 3). The results are in general agreement with other studies.[2,27] The CBO emulsions had MICs and MBCs that were similar or one to two dilutions lower than free CBO, whereas no antimicrobial activity of the emulsifiers alone was observed. Therefore, emulsification did not have a negative impact on the antimicrobial activity of CBO. Because all MICs and MBCs were below the water solubility of eugenol (1350 ppm at 21 °C and likely higher at 32 or 37 °C),[16] it can be concluded that binding between the selected emulsifiers and CBO did not interfere with the antimicrobial activity of eugenol. Conversely, higher MICs or MBCs of eugenol nanoemulsions than of free eugenol were reported when Tween 80[28] or whey protein−maltodextrin conjugates[29] were used as emulsifiers. Additionally, the emulsions prepared with GA and its mixture with other emulsifiers exhibited lower MICs and/or MBCs against *L. monocytogenes* than other treatments. It has been speculated that the strong anionic properties of GA may influence surface proteins on the cell membrane of *L. monocytogenes*, which may enhance the antimicrobial activity of EOs.[30]

Growth Kinetics of Bacteria in TSB. The three transparent/translucent emulsions (WPC alone, GA alone, and WPC−GA) with 0.2% v/v CBO (Figure 2) were evaluated for the influence on the growth kinetics of the test bacteria in TSB at a final CBO level of 750 ppm. The activity was compared with free CBO predissolved in 5% ethanol. An ethanol control (0.25% v/v, equivalent to final ethanol concentration in free CBO sample) in the TSB did not show any effect on the growth of the cultures (Figure 8). Free CBO exhibited significant inhibitory effects on the growth of three bacteria. For *L. monocytogenes* (Figure 8A), the emulsion prepared with GA exhibited a significantly better reduction ($P < 0.05$) at shorter times than the

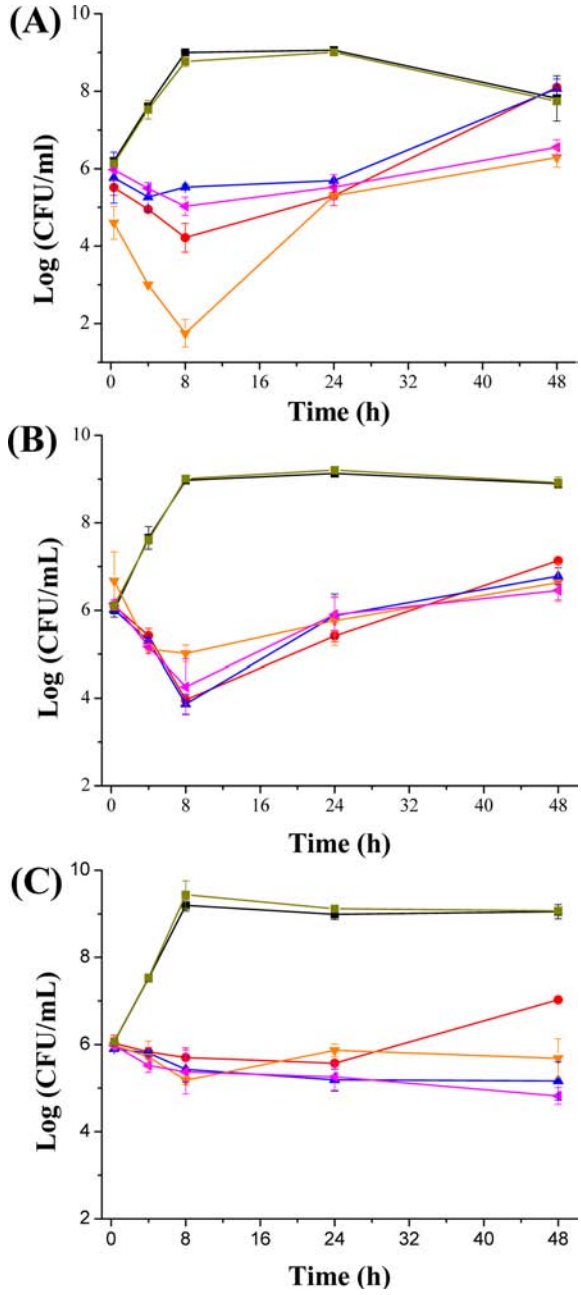

Figure 8. Growth curves of (A) *Listeria monocytogenes* Scott A at 32 °C, (B) *Escherichia coli* O157:H7 ATCC 43895 at 37 °C, and (C) *Salmonella* Enteritidis at 37 °C in TSB treated by no antimicrobials (negative control, black squares), 0.25% ethanol (positive control, as in free clove bud oil (CBO) treatment, green squares), 750 ppm free CBO (predissolved in 5% ethanol, red circles), and 750 ppm of CBO in the emulsion form prepared with WPC (blue triangles), GA (yellow triangles), and equal masses of WPC and GA (magenta triangles). Error bars are standard deviations from four replicates.

dx.doi.org/10.1021/jf500698k | J. Agric. Food Chem. 2014, 62, 4417−4424

other antimicrobial treatments, especially at 8 h, which was >2.5 log CFU/mL lower than free CBO. At 24 h, all CBO emulsions demonstrated bacteriostatic inhibition, which was 2.5−3 logs lower than the control. At the end of incubation (48 h), the antilisterial activity of WPC-emulsified sample was similar to that of free CBO and was the least effective among the three emulsions, whereas the emulsion prepared with the GA−WPC mixture exhibited significant inhibitory effects compared to the control. For *E. coli* O157:H7 (Figure 8B), all free and emulsified CBO treatments were highly inhibitory with an initial 2−2.5 log reduction in the first 8 h. After 48 h, all treatments continued to demonstrate bacteriostatic activity against the test microorganism. For *Salmonella*, no initial reduction was seen, but at the end of the incubation period, all emulsions demonstrated bacteriostatic activity, whereas the free CBO had begun to show growth (Figure 8C). Overall, at the end (48 h) of incubation, all three bacteria treated by free CBO recovered to a higher population than the three emulsion samples. Therefore, the self-emulsification technique used to prepare EO emulsions did not compromise the antimicrobial activity of CBO.

In summary, CBO emulsions were successfully prepared using a self-emulsification technique with naturally occurring food emulsifiers at ambient conditions without specialized equipment or organic solvents. The self-emulsification process (dissolving in a hot alkaline solution and neutralization) did not appear to have changed either the structure or antimicrobial activity of the major component in CBO (eugenol). WPC was effective in reducing emulsion droplet size, whereas the emulsifier mixtures were better emulsion stabilizers than single emulsifiers. Emulsions as prepared were stable during storage at room temperature and could be prepared as transparent or translucent samples upon dilution to CBO concentrations appropriate for application. Thus, the studied self-emulsification technique holds great potential in preparing EO emulsions for use as antimicrobial food preservatives or sanitizers in postharvest washing solutions for fresh produce production.

AUTHOR INFORMATION

Corresponding Author

*(Q.Z.) Mail: Department of Food Science and Technology, University of Tennessee, 2510 River Drive, Knoxville, TN 37996, USA. Phone: (865) 974-6196. Fax: (865) 974-7332. E-mail: qzhong@utk.edu.

Funding

This work was supported by the University of Tennessee and the U.S. Department of Agriculture, National Institute of Food and Agriculture, under Grant TEN02012-02247.

Notes

The authors declare no competing financial interest.

REFERENCES

(1) Dorman, H. J. D.; Deans, S. G. Antimicrobial agents from plants: antibacterial activity of plant volatile oils. *J. Appl. Microbiol.* **2000**, *88*, 308−316.

(2) Burt, S. Essential oils: their antibacterial properties and potential applications in foods − a review. *Int. J. Food Microbiol.* **2004**, *94*, 223−253.

(3) Sacchetti, G.; Maietti, S.; Muzzoli, M.; Scaglianti, M.; Manfredini, S.; Radice, M.; Bruni, R. Comparative evaluation of 11 essential oils of different origin as functional antioxidants, antiradicals and antimicrobials in foods. *Food Chem.* **2005**, *91*, 621−632.

(4) Chaieb, K.; Hajlaoui, H.; Zmantar, T.; Kahla-Nakbi, A. B.; Rouabhia, M.; Mahdouani, K.; Bakhrouf, A. The chemical composition and biological activity of clove essential oil, *Eugenia caryophyllata* (*Syzigium aromaticum* L. Myrtaceae): a short review. *Phytother. Res.* **2007**, *21*, 501−506.

(5) Srivastava, A. K.; Srivastava, S. K.; Syamsundar, K. V. Bud and leaf essential oil composition of *Syzygium aromaticum* from India and Madagascar. *Flavour Fragrance J.* **2005**, *20*, 51−53.

(6) Lee, K.-G.; Shibamoto, T. Antioxidant property of aroma extract isolated from clove buds [*Syzygium aromaticum* (L.) Merr. et Perry]. *Food Chem.* **2001**, *74*, 443−448.

(7) Ayoola, G.; Lawore, F.; Adelowotan, T.; Aibinu, I.; Adenipekun, E.; Coker, H.; Odugbemi, T. Chemical analysis and antimicrobial activity of the essential oil of *Syzigium aromaticum* (clove). *Afr. J. Microbiol. Res.* **2008**, *2*, 162−166.

(8) Csáki, K. F. Synthetic surfactant food additives can cause intestinal barrier dysfunction. *Med. Hypotheses* **2011**, *76*, 676−681.

(9) Kralova, I.; Sjöblom, J. Surfactants used in food industry: a review. *J. Disper. Sci. Technol.* **2009**, *30*, 1363−1383.

(10) Dickinson, E. Hydrocolloids as emulsifiers and emulsion stabilizers. *Food Hydrocolloids* **2009**, *23*, 1473−1482.

(11) Pan, K.; Chen, H.; Davidson, P. M.; Zhong, Q. Thymol nanoencapsulated by sodium caseinate: physical and antilisterial properties. *J. Agric. Food Chem.* **2014**, *62*, 1649−1657.

(12) Rodea-González, D. A.; Cruz-Olivares, J.; Román-Guerrero, A.; Rodríguez-Huezo, M. E.; Vernon-Carter, E. J.; Pérez-Alonso, C. Spray-dried encapsulation of chia essential oil (*Salvia hispanica* L.) in whey protein concentrate-polysaccharide matrices. *J. Food Eng.* **2012**, *111*, 102−109.

(13) Donsì, F.; Annunziata, M.; Sessa, M.; Ferrari, G. Nanoencapsulation of essential oils to enhance their antimicrobial activity in foods. *LWT−Food Sci. Technol.* **2011**, *44*, 1908−1914.

(14) McClements, D. J.; Rao, J. Food-grade nanoemulsions: formulation, fabrication, properties, performance, biological fate, and potential toxicity. *Crit. Rev. Food Sci. Nutr.* **2011**, *51*, 285−330.

(15) Damodaran, S. Straightforward process for removal of milk fat globule membranes and production of fat-free whey protein concentrate from cheese whey. *J. Agric. Food Chem.* **2011**, *59*, 10271−10276.

(16) Chen, H.; Davison, M.; Zhong, Q. Impacts of sample preparation methods on solubility and antilisterial characteristics of essential oil components in milk. *Appl. Environ. Microbiol.* **2014**, *80*, 907−916.

(17) Luo, Y.; Pan, K.; Zhong, Q. Physical, chemical and biochemical properties of casein hydrolyzed by three proteases: partial characterizations. *Food Chem.* **2014**, *155*, 146−154.

(18) Ma, Q.; Davidson, P. M.; Zhong, Q. Antimicrobial properties of lauric arginate alone or in combination with essential oils in tryptic soy broth and 2% reduced fat milk. *Int. J. Food Microbiol.* **2013**, *166*, 77−84.

(19) Pastuszewska, B.; Jabłecki, G.; Święch, E.; Buraczewska, L.; Ochtabińska, A. Nutritional value of rapeseed meal containing lecithin gums precipitated with citric acid. *Anim. Feed Sci. Technol.* **2000**, *86*, 117−123.

(20) Kim, Y. D.; Morr, C. V.; Schenz, T. W. Microencapsulation properties of gum arabic and several food proteins: liquid orange oil emulsion particles. *J. Agric. Food Chem.* **1996**, *44*, 1308−1313.

(21) Bylaite, E.; Nylander, T.; Venskutonis, R.; Jonsson, B. Emulsification of caraway essential oil in water by lecithin and β-lactoglobulin: emulsion stability and properties of the formed oil-aqueous interface. *Colloid Surf. B* **2001**, *20*, 327−340.

(22) Klein, M.; Aserin, A.; Svitov, I.; Garti, N. Enhanced stabilization of cloudy emulsions with gum arabic and whey protein isolate. *Colloid Surf. B* **2010**, *77*, 75−81.

(23) Rydhag, L.; Wilton, I. The function of phospholipids of soybean lecithin in emulsions. *J. Am. Oil Chem. Soc.* **1981**, *58*, 830−837.

(24) Carneiro, H. C. F.; Tonon, R. V.; Grosso, C. R. F.; Hubinger, M. D. Encapsulation efficiency and oxidative stability of flaxseed oil microencapsulated by spray drying using different combinations of wall materials. *J. Food Eng.* **2013**, *115*, 443−451.

(25) Hogan, S. A.; McNamee, B. F.; O'Riordan, E. D.; O'Sullivan, M. Microencapsulating properties of sodium caseinate. *J. Agric. Food Chem.* **2001**, *49*, 1934−1938.
(26) Legako, J.; Dunford, N. T. Effect of spray nozzle design on fish oil-whey protein microcapsule properties. *J. Food Sci.* **2010**, *75*, E394−E400.
(27) Ma, Q.; Davidson, P. M.; Zhong, Q. Antimicrobial properties of lauric arginate alone or in combination with essential oils in tryptic soy broth and 2% reduced fat milk. *Int. J. Food Microbiol.* **2013**, *166*, 77−84.
(28) Terjung, N.; Löffler, M.; Gibis, M.; Hinrichs, J.; Weiss, J. Influence of droplet size on the efficacy of oil-in-water emulsions loaded with phenolic antimicrobials. *Food Funct.* **2012**, *3*, 290−301.
(29) Shah, B.; Davidson, P. M.; Zhong, Q. Nanodispersed eugenol has improved antimicrobial activity against *Escherichia coli* O157:H7 and *Listeria monocytogenes* in bovine milk. *Int. J. Food Microbiol.* **2013**, *161*, 53−59.
(30) Cabanes, D.; Dehoux, P.; Dussurget, O.; Frangeul, L.; Cossart, P. Surface proteins and the pathogenic potential of *Listeria monocytogenes*. *Trends Microbiol.* **2002**, *10*, 238−245.

JOURNAL OF AGRICULTURAL AND FOOD CHEMISTRY

Article

pubs.acs.org/JAFC

Model Studies on the Oxidation of Benzoyl Methionine in a Carbohydrate Degradation System

Michael Hellwig,* Katja Löbmann, Tom Orywol, and Annegrit Voigt

Institute of Food Chemistry, Technische Universität Dresden, D-01062 Dresden, Germany

Supporting Information

ABSTRACT: The stability of benzoyl methionine was analyzed during incubation with carbohydrate compounds such as reducing sugars, dicarbonyl compounds, reductones, and Amadori rearrangement products (ARPs). The reaction products were identified and quantified by HPLC-UV and HPLC-MS. In the presence of ARPs, >40% of benzoyl methionine was oxidized to benzoyl methionine sulfoxide after 48 h at 80 °C in acetate-buffered solution (pH 6.0), whereas <10% was oxidized in the presence of mono- and disaccharides. As an important side reaction, peptide bond cleavage through α-amidation was verified. The influence of benzoyl methionine on carbohydrate degradation reactions was assessed through analysis of vicinal dicarbonyl compounds by HPLC-UV. Glyoxal, methylglyoxal, diacetyl, and 3-deoxyglucosone were quantified as the most important derivatives. The thioether group of methionine strongly influenced carbohydrate degradation pathways: Less glyoxal was formed from reducing carbohydrates, showing that benzoyl methionine can act as a radical scavenger. However, more diacetyl was formed from ARPs and reductones, indicating that also radical-dependent pathways could be influenced by benzoyl methionine. The degradation of reducing carbohydrates should thus be an important contributor to protein oxidation in food items with low fat content.

KEYWORDS: *protein oxidation, methionine, Amadori products, reductone, dicarbonyl compounds*

INTRODUCTION

The thioether group of methionine, **1**, is very prone to oxidation by reactive oxygen species (ROS), which leads to the formation of methionine sulfoxide (MetSO), **2**, and methionine sulfone, **3** (Figure 1).[1] ROS involved in methionine oxidation are hydrogen peroxide (H_2O_2), the superoxide radical anion ($^{\bullet}O_2^-$), the hydroxyl radical ($^{\bullet}OH$), and alkoxyl radicals ($^{\bullet}OR$). They result from radiation, metal-catalyzed oxidations, and oxidase-catalyzed reactions. Oxidation reactions can also occur at other amino acid side chains and at the protein backbone.[2] Protein oxidation is generally considered to have negative consequences on food quality; however, the underlying molecular mechanisms are not yet fully understood.[3] The products **2** and **3** have only rarely been analyzed in protein model systems[4] and food samples. In soy proteins, egg white powder, and whey concentrates, up to 67% of total methionine can be oxidized to the sulfoxide **2** and up to 10% to the sulfone **3**.[5−7] Methionine oxidation was proposed to result from food processing, but this has not yet been assessed systematically. Research primarily focused on oxidation reactions caused by lipid peroxidation.[8,9] The free amino acid **1** can undergo several further degradation reactions during food processing, for example, to aroma-active aldehydes.[10,11] The sulfoxide **2** can be a source of essential methionine, but the reduction to **1** was reported to be incomplete, especially in young organisms.[12]

The formation of radicals can also be observed in carbohydrate chemistry. Exposure of carbohydrates to high-temperature and extreme pH milieus leads to their degradation via different reactions such as dehydration, β-dicarbonyl cleavage, and retro-aldol reactions.[13,14] These reactions are generally referred to as caramelization, that is, sugar degradation reactions in the absence of amino compounds. The reactions are accelerated in the presence of amino compounds (amino acids, peptides, proteins) in the course of the Maillard reaction. Enolized carbohydrates can easily be oxidized to dicarbonyl compounds by molecular oxygen, which is concomitantly reduced to superoxide and hydrogen peroxide. This reaction can be accelerated by transition metal ion catalysis during monosaccharide autoxidation.[15−17] Under physiological conditions, the formation of superoxide is fastest from osones and short-chain carbohydrates and slowest from ketoses and aldoses.[18] Amadori rearrangement products (ARPs), which enolize comparatively quickly, were reported to play a key role in the formation of hydrogen peroxide and superoxide radical anions.[19−21] The possibility of superoxide generation from ARPs in glycated protein has also been discussed with respect to diabetic complications in vivo.[22]

The high susceptibility of **1** to oxidation and the importance of redox reactions in carbohydrate degradation chemistry allow the hypothesis that **1** could significantly be oxidized by intermediates of sugar degradation. It was the aim of this study to assess the stability of benzoyl methionine, **1a**, in a model of carbohydrate degradation, to identify the reaction products and to compare different carbohydrate compounds in terms of their ability to provoke methionine oxidation. Moreover, the cleavage of a peptide bond by α-amidation in a carbohydrate degradation system and the influence of the thioether group of **1** on carbohydrate degradation reactions are reported for the first time.

Received: February 13, 2014
Revised: April 23, 2014
Accepted: April 26, 2014
Published: April 26, 2014

ACS Publications © 2014 American Chemical Society

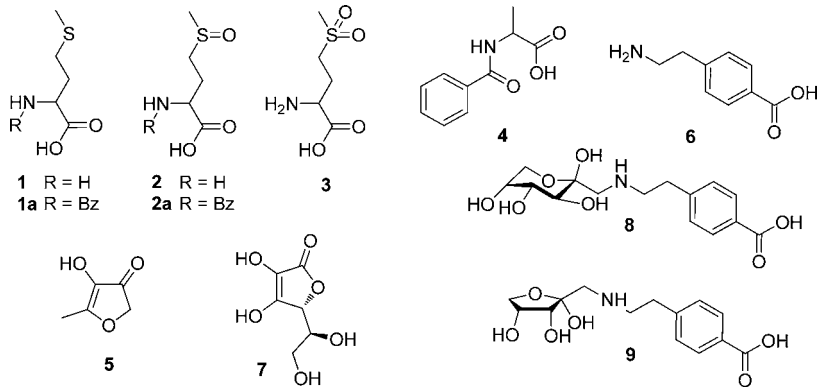

Figure 1. Chemical structures of the investigated products: **1**, methionine; **1a**, benzoyl methionine (BzMet); **2**, methionine sulfoxide (MetSO); **2a**, benzoyl methionine sulfoxide (BzMetSO); **3**, methionine sulfone; **4**, benzoyl alanine (BzAla); **5**, 4-hydroxy-5-methyl-3-furanone; **6**, 4-(2-aminoethyl)benzoic acid; **7**, ascorbic acid; **8**, 4-[2-(1-desoxyfructosyl)aminoethyl]benzoic acid; **9**, 4-[2-(1-desoxyribulosyl)aminoethyl]benzoic acid.

MATERIALS AND METHODS

Chemicals. Benzoyl succinimide (BzOSu), benzoyl methionine (BzMet, **1a**), and benzoyl alanine (BzAla, **4**) were obtained from Bachem (Bubendorf, Switzerland) and D-glucose, DL-methionine sulfoxide, and diisopropyl ethylamine (DIPEA) from Alfa Aesar (Karlsruhe, Germany). Lactose monohydrate was purchased from Roth (Karlsruhe, Germany). Fructose, lactulose, 4-hydroxy-5-methyl-3-furanone, **5**, methylglyoxal, 4-(2-aminoethyl)benzoic acid, **6**, hydrochloride (PAEBA), linolenic acid methyl ester, and ribose were obtained from Sigma-Aldrich (Steinheim, Germany). Ammonium acetate was from Grüssing (Filsum, Germany) and ascorbic acid **7** from Riedel-de-Haën (Seelze, Germany). Stearic acid methyl ester was purchased from Merck (Darmstadt, Germany). The water used for the preparation of buffers and solutions was obtained using a Purelab plus purification system (USFilter, Ransbach-Baumbach, Germany).

Synthesis of DL-Benzoylmethionine Sulfoxide, 2a. Benzoyl succinimide (1.0 g, 4.6 mmol) and 1.52 g (9.2 mmol) of DL-methionine sulfoxide, **2**, were dissolved in a mixture of 10 mL of dimethylformamide, 10 mL of dioxan, and 5 mL of water. The reaction was started by the addition of 1.56 mL (9.2 mmol) of DIPEA. The mixture was stirred for 5.5 h, evaporated to dryness in vacuo, and redissolved in 30 mL of water. The solution was extracted with ethyl acetate (4 × 20 mL). The aqueous solution was left to crystallize at 4 °C overnight. The crystals were recrystallized from water.

Analytical data: ESI-MS, positive mode, $[M + H]^+$ m/z 270.1; ^{1}H NMR (500 MHz, D_2O), δ 2.21 (m, 1H), 2.38 (m, 1H), 2.61 (s, 3H), 2.87 (m, 1H), 2.98 (m, 1H), 4.64 (m, 1H), 7.43 (m, 2H), 7.53 (m, 1H), 7.70 (m, 2H). Elemental analysis of $C_{12}H_{15}NO_4S$ (MW = 269.32) requires C, 53.52%; H, 5.61%; N, 5.20%; and S, 11.91%. Found: C, 51.95%; H, 4.71%; N, 4.98%; S, 12.11%. Content = 95.3%, based on nitrogen. Yield = 0.3 g (24.2%).

Synthesis of 4-[2-(1-Desoxyfructosyl)aminoethyl]benzoic Acid, 8. PAEBA, **6** (153.1 mg, 0.76 mmol), and 740 μL of 1 N NaOH were evaporated to dryness and redissolved in 30 mL of methanol. After the addition of 803 mg (4.5 mmol) of glucose, the mixture was heated under reflux for 4 h. The slightly brown solution was evaporated to dryness. The residue was mixed with silica gel until a fluid powder was obtained. The product was fractionated by flash chromatography on 50 g of silica gel using 350 mL of acetone/methanol (4:1, v/v), 300 mL of acetone/methanol (1:1, v/v), and 350 mL of methanol as the eluents. Fractions of 10 mL were collected manually, and product elution was monitored by spotting 1 μL of the fractions on two TLC plates and spraying either with 0.1% ninhydrin in ethanol or with 1% triphenyl tetrazolium chloride in 1 N NaOH. The product was found to elute between 510 and 690 mL. The organic solvents were removed by rotary evaporation, and the residue was lyophilized to give a slightly yellow powder, which was stored at −20 °C.

Analytical data: ESI-MS, positive mode, $[M + H]^+$ m/z 328.1; NMR data, see Table S1 in the Supporting Information. RP-HPLC content = 86.6%, calibrated with PAEBA. Yield = 185.6 mg (59.1%).

Synthesis of 4-[2-(1-Desoxyribulosyl)aminoethyl]benzoic Acid, 9. **6** (149.2 mg, 0.74 mmol) and 443.7 mg (3.0 mmol) of ribose were dissolved in 2 mL of water. The solution was slurried with 1.4 g of cellulose and lyophilized. The lyophilisate was stored at room temperature in a desiccator for 36 days in the presence of a saturated solution of calcium chloride maintaining a relative humidity of 35%.[23] The brown powder was then extracted with water (3 × 50 mL), and the combined fractions were evaporated to dryness using a rotary evaporator. The residue was dissolved in 10 mL of 0.075% acetic acid and fractionated by semipreparative HPLC using a Wellchrom high-pressure gradient system with an online degasser, a UV detector K-2501, and a fraction collector K-16 (all from Knauer, Berlin, Germany). The separation was performed at room temperature using an RP-18 column (Eurospher 100, 300 mm × 8 mm, 5 μm, Knauer) with a guard column (30 mm × 8 mm) filled with the same material. The flow rate was 1.4 mL/min, and the absorbance was read at 254 nm. Samples of 1 mL were injected manually and the eluate of the prominent peak was collected and evaporated to dryness in vacuo. Because this peak was not pure, the residue was dissolved in 75 mL of pyridinium acetate buffer, pH 3.0, and fractionated on a semi-preparative ion-exchange column in the pyridinium form (1.5 × 50 cm) as described earlier.[24] The column was eluted first with 300 mL of 0.3 M pyridinium formate buffer, pH 3.75, then with 250 mL of 0.3 M pyridinium acetate buffer, pH 4.05, and last with 500 mL of 0.4 M pyridinium acetate buffer, pH 4.35. From the collected fractions (6 mL), 1 μL was spotted on two TLC plates. Detection with ninhydrin and triphenyl tetrazolium chloride reagents revealed that the target substance eluted with 220−400 mL of the last elution buffer. The respective fractions were combined, filtered, evaporated to dryness, and finally lyophilized.

Analytical data: ESI-MS, positive mode, $[M + H]^+$ m/z 298.1; NMR data, see Table S2 in the Supporting Information. RP-HPLC content = 67.6%, calibrated with PAEBA. Yield = 28.2 mg (8.1%).

Characterization of Synthesized Products. NMR spectra were recorded on a Bruker DRX 500 instrument (Rheinstetten, Germany) at 500 MHz (^{1}H) and 125 MHz (^{13}C), respectively, using D_2O as the solvent. Chemical shifts are given in parts per million (ppm) relative to the internal HOD signal (^{1}H, 4.70 ppm), and relative to the external standard tetramethylsilane (^{13}C), respectively. Assignments of signals are based on ^{1}H−^{1}H correlation spectroscopy (COSY), distortionless enhancement by polarization transfer (DEPT) and heteronuclear single-quantum coherence (HSQC) experiments. Mass spectra were obtained on a PerSeptive Biosystems Mariner time-of-flight mass spectrometry instrument equipped with an electrospray ionization source (ESI-TOF-MS, Applied Biosystems, Stafford, TX, USA) working in the positive mode. Calibration of the mass scale was performed with a mixture of bradykinin, angiotensin I, and

neurotensin. After appropriate dilution with 1% formic acid in 50% aqueous acetonitrile, the samples were injected into the ESI source by a syringe pump. Elemental analysis was performed on a Euro EA 3000 elemental analyzer (Eurovector, Milano, Italy). Elemental analysis was used to calculate the product content of **2a**. The percentage of nitrogen in the preparation was divided by the theoretical percentage of nitrogen of the target substance and the content expressed in percent by weight. The purity and content of **8** and **9** were determined by HPLC-UV using the gradient system for benzoylated amino acids after calibration with **6**.

Incubation of Benzoylated Amino Acids with Carbohydrate Compounds. In general, benzoyl methionine (BzMet), **1a** (4 mM), was incubated with different carbohydrate compounds (sugars, dicarbonyl compounds, reductones, and ARPs, 4 mM) in 1 mL of 0.1 M sodium acetate buffer, pH 6.0, for 48 h at 80 °C in a sand bath. Stearic and linolenic acid methyl esters were dissolved in methanol before addition. The incubations were performed in screw-cap glass tubes (V = 7.5 mL). To evaluate the time course of the oxidation of **1a**, samples were prepared as above and heated for up to 6 h. For each sampling time, separate solutions were prepared, so that opening of the tubes during incubation could be avoided. In additional experiments, **1a** was substituted for 4 mM BzAla, **4**, PAEBA, **6**, or BzMetSO, **2a**. All incubations were performed in triplicate. After the incubations, the samples were cooled and stored at −20 °C until analysis. For the analysis of benzoylated amino acids, 50 μL of the incubation mixture was added to 950 μL of HPLC solvent A. The samples were centrifuged (10000 U/min, 10 min, 4 °C), transferred into HPLC vials, and measured as described below. Dicarbonyl compounds were converted to quinoxalines by incubating 500 μL of the reaction mixtures with 150 μL of 0.5 M sodium phosphate buffer, pH 7.0, and 150 μL of a solution containing 0.2% *o*-phenylenediamine and 18.5 mM DETAPAC.[25] After overnight derivatization, the samples were centrifuged (10000 U/min, 10 min, 4 °C), transferred into HPLC vials, and measured as described below.

High-Pressure Liquid Chromatography with UV Detection. HPLC-UV analyses were performed using a high-pressure gradient system from Amersham Pharmacia Biotech (Uppsala, Sweden), consisting of a pump P-900 with an online degasser (Knauer), a column oven, and a UV detector UV-900. For the analysis of benzoylated amino acids and benzamide, a stainless steel column (250 mm × 4.6 mm) filled with Eurospher-100 RP-18 material of 5 μm particle size with a guard column (5 mm × 4 mm) of the same material was used (Knauer). The mobile phases were 10 mM ammonium acetate buffer, pH 4.5 (solvent A), and methanol (solvent B). The proportion of solvent B was at 20% for 3 min, then linearly increased to 75% during 11 min, and further to 80% B during 3 min. The absorbance was read at 228 nm. The injection volume was 65 μL, and the separation was performed at room temperature and a flow rate of 0.8 mL/min. The analysis of 1,2-dicarbonyl compounds was performed as described previously.[25] For both methods, external calibration was performed. The recovery of **1a** at a concentration of 4 mM was 101% after incubation without carbohydrate compounds.

High-Pressure Liquid Chromatography with Mass Spectrometric Detection. Quinoxalines in selected incubation mixtures were analyzed with the high-pressure gradient system 1200 series (Agilent Technologies, Böblingen, Germany), consisting of a binary pump, an online degasser, a column oven, an autosampler, and a diode array detector. Samples were analyzed at room temperature on a stainless steel column (150 mm × 3 mm, 5 μm) filled with Eurospher-100 RP-18 material (Knauer, Berlin, Germany) with an integrated guard column (5 mm × 3 mm) of the same material. A solution of 0.075% acetic acid in water (solvent A) and a mixture of 80% methanol and 20% solvent A (solvent B) were used as the eluents at a flow rate of 0.3 mL/min in the gradient mode (0 min, 5% B; 30 min, 50% B; 35 min, 50% B; 39 min, 70% B; 44 min, 70% B; 46 min, 5% B; 56 min, 5% B). The injection volume was 50 μL.

The absorbance was read at 280 and 312 nm, respectively. UV spectra were recorded between 190 and 400 nm. The HPLC system was coupled to the mass spectrometer 6410 Triple Quad (Agilent Technologies), working in the positive mode with a capillary voltage of 4000 V, a source temperature of 350 °C, and a fragmentor voltage of 110 V. The mass scan (m/z 105−500) was started after 2 min. Data acquisition and evaluation were performed with the software Mass Hunter B.02.00 (Agilent).

The same device and HPLC column were used for the mass spectrometric analysis of benzoylated amino acids. As solvent A, 10 mM ammonium acetate buffer, pH 4.5 was used, whereas solvent B was methanol. Benzoylated amino acids were separated at a flow rate of 0.3 mL/min in the gradient mode (0 min, 20% B; 3 min, 20% B; 8 min, 50% B; 14 min, 65% B; 16 min, 80% B; 19 min, 20% B; 24 min, 20% B). The injection volume was 65 μL. The absorbance was read at 228 nm, and UV spectra were recorded between 190 and 400 nm. The mass scan (m/z 100−1000) was started after 2 min at a fragmentor voltage of 135 V.

RESULTS AND DDISCUSSION

Stability of Benzoyl Methionine during Sugar Degradation. The high impact of amino groups on sugar degradation reactions has long been known, but little is known about the interrelationships between other functional groups of amino acids and carbohydrate degradation. In preliminary studies on the modification of protein-bound lysine residues with 3-deoxyglucosone,[26] a certain degradation of protein-bound methionine during heating of fructosylated casein was noticed. Methionine sulfoxide formation has also been observed in glycation reactions of casein and lactose.[4] Because **1** is very susceptible to oxidation, and redox reactions are important in carbohydrate degradation chemistry, **1** should significantly be oxidized by carbohydrate degradation intermediates. To quantify the extent of oxidation reactions and to compare different carbohydrates, **1a** was utilized as a molecular probe. N-Benzoylation of methionine should suppress Maillard reactions at the amino group and enable direct analysis also of the reaction product(s) by RP-HPLC with UV detection. Hydrolysis and derivatization steps, which can favor the degradation of **2**,[12] were avoided. As carbohydrate compounds, food-relevant sugars and degradation products together with important reductones and Amadori rearrangement products (ARPs) were included in the study. Compounds **8** and **9** served as model ARPs. The need for protection of possible sites of side reactions (e.g., amino groups) led to the choice of 4-(2-aminoethyl)benzoic acid (PAEBA, **6**) as the parent amine (Figure 1). The UV-active ARPs **8** and **9** had a carboxyl group to ensure water solubility. An ethylene group was introduced between the aromatic ring and the amino group to suppress side reactions resulting from the conjugation of the amino group with the ring. NMR analysis of the ARPs **8** and **9** showed that the fructosyl residue of **8** was mainly present in the β-pyranose form, whereas the ribulosyl residue of **9** showed the α-furanose, β-furanose, and open-chain forms (data shown in Supporting Information Tables S1 and S2). Owing to the strong structural similarity of the sugar moieties of **8** and **9** to those of fructoselysine and ribuloselysine,[21,24] both products were considered suitable as ARP model compounds. The incubations were performed at equimolar concentrations (4 mM) of **1a** and carbohydrate compounds at 80 °C in sodium acetate buffer at pH 6.0. With buffer salts, traces of metals can be introduced, which are known to catalyze monosaccharide autoxidation;[15−17] however, differences between carbohydrate compounds can be assessed nevertheless. The incubation of **1a** with equimolar H_2O_2 led to the immediate and complete oxidation to **2a**. No oxidation was observed when **1a** was incubated in the absence of any carbohydrate compound. Because **2a** was stable in the presence of carbohydrate

compounds for up to 48 h, it was measured as an integral marker of the extent of oxidation. RP-HPLC allowed the separation of **1a** and **2a** (Figure 2a,b). The formation of **2a** could be followed by this method when **1a** was incubated with glucose (Figure 2c) or ribose (Figure 2d).

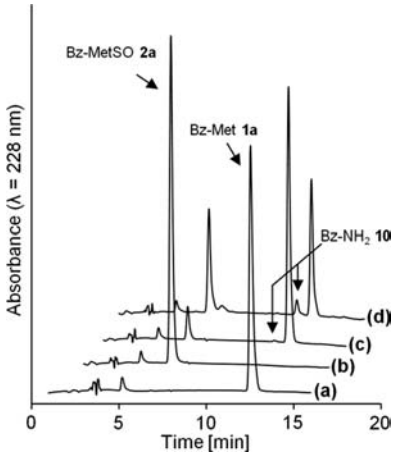

Figure 2. RP-HPLC with UV detection of (a) a standard solution of benzoyl methionine, **1a**; (b) a standard solution of benzoyl methionine sulfoxide, **2a**; (c) an incubation mixture consisting of 4 mM benzoyl methionine and 4 mM glucose after constant heating at 80 °C for 48 h; and (d) an incubation mixture consisting of 4 mM benzoyl methionine and 4 mM ribose after constant heating at 80° for 48 h.

In all incubation experiments with carbohydrate compounds, the concentration of **2a** rose in a monotone way; however, pronounced differences between compounds in their ability to induce methionine oxidation were observed both in the time course and in the extent of oxidation. Time courses for four representative carbohydrate compounds are shown in Figure 3. Aldoses and ketoses led to only very slow oxidation of **1a**. The incubation with glucose provoked no measurable oxidation in the first 4 h, and only 0.2% of **1a** had been oxidized to **2a** after 6 h (data not shown). With ribose, the oxidation of **1a** is already measurable after 1.5 h, and 8 times more **2a** is formed after 6 h (Figure 3). In contrast, dicarbonyl compounds, reductones, and ARPs showed intense initial oxidation. In the presence of **8**, 2.6% of **1a** had already been oxidized after 20 min of incubation. After the initial phase, the oxidation proceeded more slowly and linearly as indicated by the regression lines in Figure 3. This biphasic process can best be explained by a fast oxidation of the carbohydrate compounds in the first minutes by the oxygen dissolved in the solution. Assuming the production of one molecule of superoxide from one molecule of oxygen and the oxidation of one molecule of **1a** by one molecule of superoxide,[27,28] ca. 6% of **1a** can be oxidized at an oxygen solubility of 8 mg/L at 25 °C, which decreases to 2−4 mg/L at 80 °C. After the initial phase, the reaction rate is more strongly determined by the transfer of oxygen from the gas phase to the medium, which results in a linear time course. However, this effect is the same for all derivatives incubated and should not be a serious drawback.

Due to differences in the initial phase of oxidation, no reaction rates were calculated; instead, the extent of oxidation was compared through quantification of **2a** after 48 h of constant heating at 80 °C. Again, the susceptibility to oxidation of **1a** is lowest in the presence of aldoses and highest in the presence of ARPs (Table 1). Because the oxidation of **1** is a process mediated by ROS, the different carbohydrates and carbohydrate derivatives must differ in their ability to generate ROS. The differences between glucose, ribose, and methylglyoxal can be explained by their susceptibility to enolization, which precedes the oxidation of monosaccharides and

Table 1. Yields of Benzoyl Methionine Sulfoxide (BxMetSO, 2a) and Benzamide ($BzNH_2$, 10) in Incubation Mixtures of Benzoyl Methionine, 1a (4 mM), and Carbohydrate Compounds (4 mM)

	BzMetSO[a]	$BzNH_2$[a]
glucose	5.5 ± 1.9	0.4 ± 0.1
fructose	7.8 ± 0.8	0.6 ± 0.1
lactose	3.4 ± 0.3	0.2 ± 0.1
lactulose	7.3 ± 1.1	0.5 ± 0.1
ribose	9.3 ± 0.6	0.8 ± 0.1
methylglyoxal	18.1 ± 1.2	0.5 ± 0.1
glyoxal	1.5 ± 0.1	0.1 ± 0.1
HMF	1.8 ± 0.2	0.1 ± 0.1
Amadori product **8**	43.6 ± 0.8	3.3 ± 0.1
glucose and PAEBA **6**[b]	4.3 ± 0.6	0.3 ± 0.1
fructose and PAEBA **6**[b]	7.7 ± 1.1	0.7 ± 0.2
Amadori product **9**	42.4 ± 2.5	4.4 ± 0.3
reductone **5**	23.4 ± 0.2	4.2 ± 0.2
ascorbic acid **7**	25.3 ± 0.6	3.5 ± 0.3
methyl stearate	nd	nd
methyl linolenate	47.6 ± 2.6	0.1 ± 0.1

[a]Data are means ± SD given in mol % based on the initial BzMet concentration, $n = 3$. [b]Both compounds were incubated with **1a** at a concentration of 4 mM.

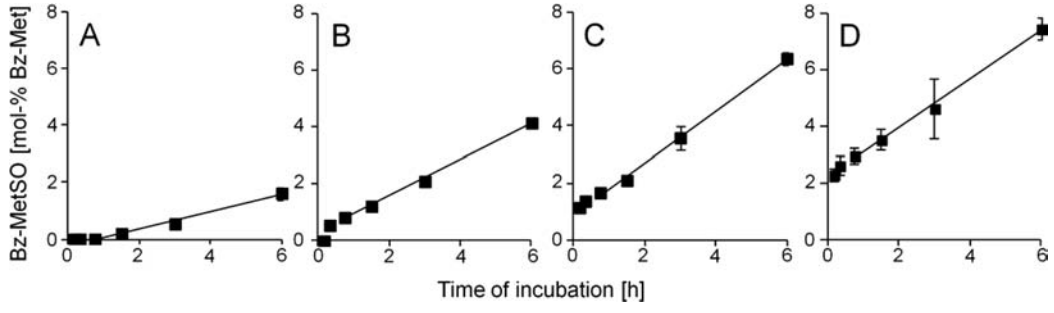

Figure 3. Time course of the formation of benzoyl methionine sulfoxide, **2a**, during incubation of benzoyl methionine **1a** in the presence of carbohydrates and their degradation products (A, ribose; B, methylglyoxal; C, 4-hydroxy-5-methyl-3-furanone; D, 4-[2-(1-desoxyfructosyl)-aminoethyl]benzoic acid, **8**). Data are mean values ± SD, $n = 3$. The regression lines were calculated by the least-squares method (45 min−6 h).

dx.doi.org/10.1021/jf500733f | J. Agric. Food Chem. 2014, 62, 4425−4433

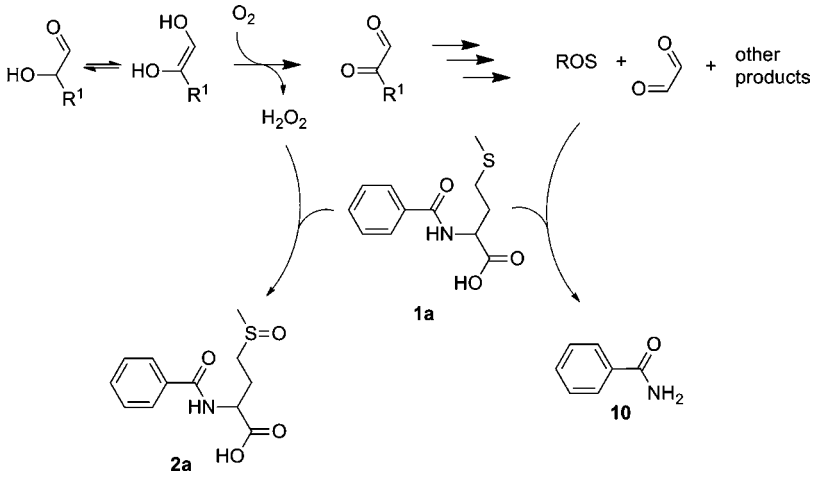

Figure 4. Proposed pathways of carbohydrate degradation, methionine oxidation, and α-amidation in heated mixtures of benzoyl methionine, **1a**, and aldoses.

correlates with the formation of superoxide radical anions.[15,21,18,27] Enolization of intact saccharides is hindered by acetal formation. Methylglyoxal cannot form ring structures and is able to enolize more easily. The low concentrations of **2a** measured after incubation of glyoxal as compared to methylglyoxal can be explained by the fact that glyoxal cannot enolize and forms stable aldehyde hydrates.

The reductones **5** and **7**, which possess an α-keto enediol structure, also invoked relatively strong oxidation. Although generally regarded as a powerful antioxidant, **7** can also act in a pro-oxidative way by generating hydrogen peroxide through autoxidation.[29] Both pro- and antioxidative properties have also been described for α-aminoketones and aminoreductones.[28,30] The antioxidative activity of aminoreductones can be at least equal to that of **7**.[30] The highest concentrations of **2a** were measured in the presence of the ARPs **8** and **9**. The 1,2-enolization of ARPs is strongly favored due to decreasing electron density at the C-1 following N-protonation under acidic conditions.[31] Moreover, aminoreductones are generated very quickly in heated solutions of carbohydrates and amino compounds as degradation products of the initially formed ARPs.[32,33] Even though aminoreductones were not measured in the present study, it can be assumed that they are responsible for the strong oxidation of **1a** in the presence of **8** and **9**. Further studies will have to show how the oxidation of the thioether group of methionine is dependent on the concentration of carbohydrate compounds and the ratio of carbohydrate compounds to methionine. Incubation of **1a** with ARPs **8** and **9** led to the same extent of oxidation as co-incubation with methyl linolenate, whereas there was no **2a** measurable on incubation with methyl stearate. The strong oxidation of methionine by intermediates of lipid peroxidation in food model systems is known from the literature.[8] A comparison of the extent of methionine oxidation in food systems caused by intermediates of lipid and carbohydrate oxidation will be part of our further studies. The fact that carbohydrate degradation products and ARPs can strongly contribute to protein oxidation should be taken into account when proteins for food applications are functionalized by glycation.[34]

Besides **2a**, a further new peak appeared during the incubation of **1a** with most of the carbohydrate compounds. This peak eluted before **1a** (Figure 2) and showed a UV spectrum similar to that of **1a**, but with a slightly hypsochromically shifted relative maximum at 225 nm. From the apparent protonated molecular ion (m/z 122.2), a relative monoisotopic molecular mass of 121.2 was calculated, leading to the assumption that the peak is caused by benzamide ($BzNH_2$, **10**). The identity of this peak as **10** was verified by comparison with a standard. In the presence of most carbohydrate compounds, **2a** and **10** are formed in a ratio of 10:1. Slightly more **10** is formed in the presence of the reductones **5** and **7**, whereas it hardly appears in incubation mixtures containing methyl linolenate. Amides such as **10** are products of the well-known α-amidation pathway, which starts by abstraction of a hydrogen radical from the α-C atom of a peptide-bound amino acid, ultimately leading to an amide (N-terminal) and a ketoacyl derivative (C-terminal).[35] Differences in the relative amounts of the reaction products **2a** and **10** could result from differences in the amounts and species of ROS produced from the different carbohydrate compounds (Figure 4).

The present study shows that oxidation reactions of carbohydrates might also strongly influence protein stability in food systems, for example, during food processing and storage. Because molecular oxygen is not able to directly oxidize **1** in solution, the role of carbohydrates in the development of the sometimes very high concentrations of **2** in food[5−7] needs to be further explored, predominantly with regard to redox, concentration, temperature, and moisture dependence.

Changes in Carbohydrate Degradation Reactions in the Presence of Benzoyl Methionine. The oxidation of carbohydrates can lead to the formation of vicinal dicarbonyl compounds.[16,17] Being the predominant products, 3-deoxyglucosone, glyoxal, methylglyoxal, and diacetyl were measured after 48 h of incubation (Figure 5). To see whether the occurrence of dicarbonyl compounds can be attributed to the thioether group of methionine, benzoyl alanine (BzAla, **4**) was incubated under the same conditions. The results are presented in Table 2. The methionine thioether group strongly alters the pattern of dicarbonyl compounds resulting from carbohydrate degradation. As a rule, mono- and disaccharides form 3−15 times more glyoxal in the presence of **4** than in the presence of **1a**. On the other hand, slightly less 3-DG is formed from fructose, lactose, and lactulose in the presence of **4** than in the presence of **1a**. As depicted in the generalized scheme in Figure 4, the enolized form of a carbohydrate compound, for example,

dx.doi.org/10.1021/jf500733f | J. Agric. Food Chem. 2014, 62, 4425−4433

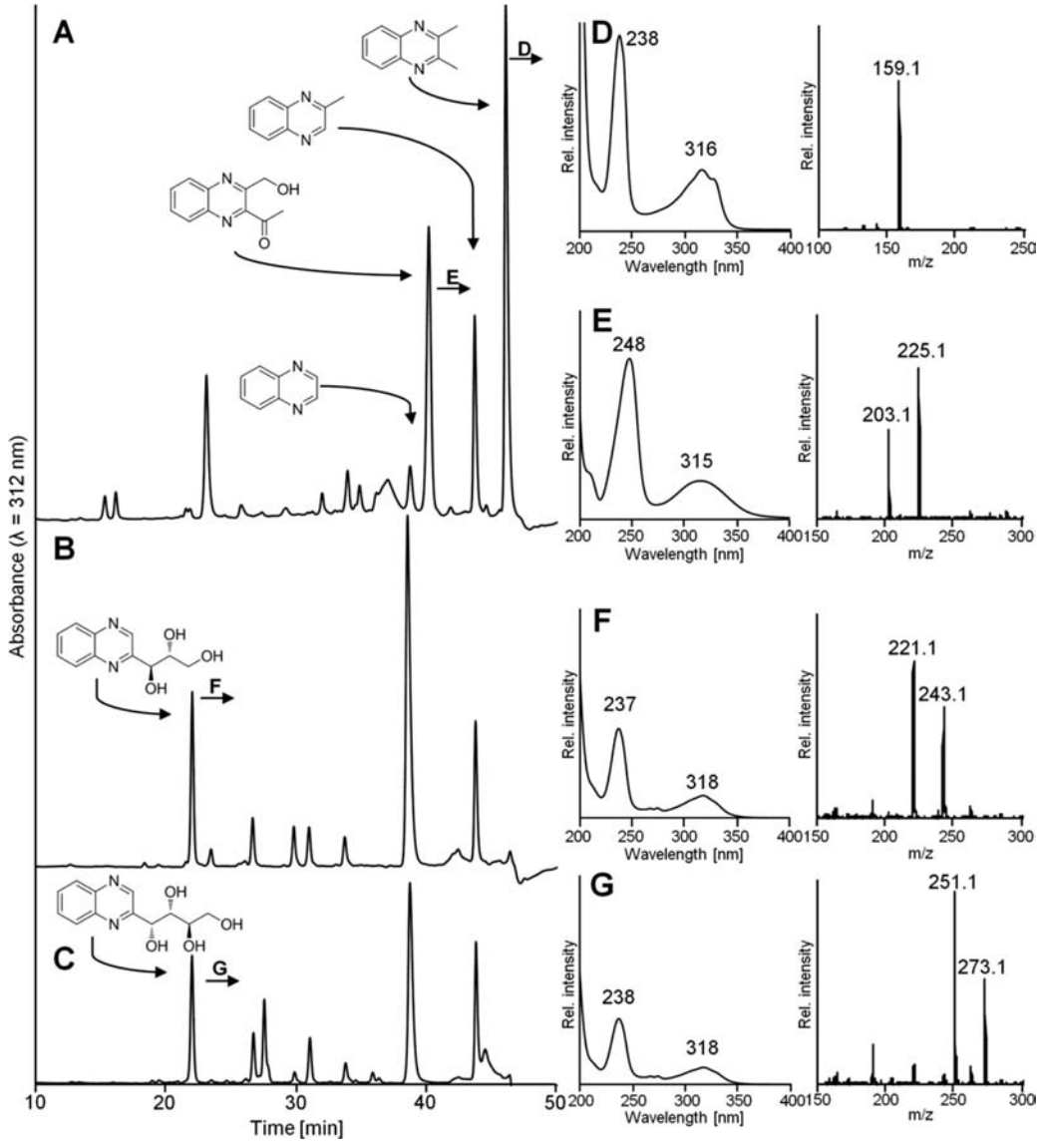

Figure 5. RP-HPLC with UV and mass spectrometric detections of incubation mixtures of benzoyl methionine (c = 4 mM), **1a**, in the presence of (A) 4-hydroxy-5-methyl-3-furanone, **5**; (B) ribose; and (C) fructose after constant heating at 80 °C for 24 h with proposed structures of quinoxalines; UV and mass spectra of quinoxalines resulting from (D) diacetyl (t_R = 46.2 min), (E) 2,3,4-trioxopentanol (t_R = 40.2 min), (F) ribosone (t_R = 22.1 min), and (G) glucosone (t_R = 22.0 min).

glucose, is oxidized to a 1,2-dicarbonyl compound, for example, glucosone, whereas molecular oxygen is reduced to hydrogen peroxide as an ROS species. Hydroperoxides have been proposed as the first intermediates in carbohydrate autoxidation.[27] In this study, the primary oxidation products 2,3,4-trioxopentanol, ribosone, and glucosone, respectively, were qualitatively identified in the reaction mixtures as the respective predominating quinoxalines resulting from the furanone **5** (Figure 5E, proposed quinoxaline structure), ribose (Figure 5F), and fructose (Figure 5G), respectively. The quinoxalines were identified on the basis of a relative UV maximum between 312 and 320 nm and their protonated molecular ions ($[M + H]^+$) or the respective sodium adducts ($[M + Na]^+$). In later stages of autoxidation, the carbohydrate chain can oxidatively be cleaved leading, for example, to the formation of glyoxal.[36−39] When **1a** is present, the reaction of ROS with the thioether group is favored. Thus, **1a** can suppress oxidative carbohydrate degradation reactions in favor of nonoxidative degradations leading, for example, to 3-deoxyglucosone or methylglyoxal.[40] In the presence of **1a**, carbohydrates behave similarly as under microaerobic conditions.[38−40]

The situation is quite diverse when ARPs and reductones are examined. In this case, glyoxal formation tends to be higher in the presence of **1a** than in the presence of **4**. Moreover, a pronounced formation of diacetyl was measured in the incubation mixtures of some carbohydrate compounds (Figure 5D). Diacetyl formation was always significantly higher when BzMet was present. Basically, diacetyl can be formed by the combination of two acetyl radicals especially at low concentrations of oxidizing agents,[41] by isomerization from 1-deoxyglucosone[42,43] and during specific glucose degradation reactions.[44] Traces of free amino groups can be formed from the ARPs **8** and **9** during the incubations. Therefore, **8** was replaced in the incubation by its parent molecules **6** and glucose as well as by **6** and fructose to assess possible interferences resulting from the early Maillard reaction. At a

dx.doi.org/10.1021/jf500733f | J. Agric. Food Chem. 2014, 62, 4425−4433

Table 2. Concentrations of Dicarbonyl Compounds in Incubation Mixtures of Benzoylated Amino Acids (4 mM) and Carbohydrate Compounds (4 mM)

amino acid	3-DG[a]	GO[a]	MGO[a]	diacetyl[a]
glucose				
BzMet	nd	2.9 ± 0.5	nd	nd
BzAla	nd	21.1 ± 1.8	3.0 ± 0.7	nd
PAEBA	1.7 ± 0.4	3.3 ± 0.5	nd	nd
fructose				
BzMet	15.2 ± 1.0	3.4 ± 0.3	12.7 ± 0.6	nd
BzAla	10.8 ± 0.7	51.8 ± 2.9	10.9 ± 0.3	nd
PAEBA	23.9 ± 1.6	5.0 ± 1.5	12.4 ± 0.7	nd
lactose				
BzMet	4.9 ± 0.4	2.0 ± 0.2	3.3 ± 0.2	nd
BzAla	1.4 ± 0.4	8.5 ± 1.3	3.6 ± 0.6	nd
lactulose				
BzMet	18.0 ± 0.2	3.6 ± 0.3	2.9 ± 0.5	nd
BzAla	14.2 ± 0.3	10.8 ± 0.6	6.0 ± 0.6	nd
ribose				
BzMet	nd	7.5 ± 1.0	3.4 ± 0.4	5.0 ± 1.5
BzAla	nd	84.4 ± 7.5	5.0 ± 0.7	nd
Amadori product **8**				
BzMet	43.1 ± 4.7	35.2 ± 8.9	11.8 ± 1.1	10.6 ± 1.7
BzAla	2.0 ± 0.3	21.5 ± 2.8	7.7 ± 0.2	7.4 ± 0.5
PAEBA	80.5 ± 2.9	20.7 ± 4.0	6.4 ± 0.3	9.1 ± 1.2
Amadori product **9**				
BzMet	nd	77.1 ± 4.6	13.1 ± 1.5	46.6 ± 0.8
BzAla	nd	72.1 ± 6.9	11.6 ± 0.8	15.1 ± 1.3
reductone **5**				
BzMet	nd	19.1 ± 1.1	5.1 ± 0.3	135.7 ± 13.6
BzAla	nd	8.8 ± 1.5	10.0 ± 1.1	76.9 ± 4.4
ascorbic acid **7**				
BzMet	nd	14.5 ± 0.7	7.8 ± 0.2	7.4 ± 0.5
BzAla	nd	21.6 ± 0.9	6.7 ± 0.5	2.7 ± 0.3

[a]Data are given in μmol/L, means ± SD, $n = 3$.

concentration of 4 mM of each compound, the incubation of glucose and **6** or of fructose and **6** with **1a** did not lead to a significant change in the oxidation to **2a** or the cleavage to **10** (Table 1). Diacetyl formation was not measurable (Table 2). The role of ARP degradation by primary amines under the incubation conditions was measured through incubation of **8** only with **6** (both at 4 mM, 48 h, 80 °C). This did not lead to the same increase in the concentration of diacetyl as on incubation of **1a** and **8** (Table 2). Thus, the thioether group of methionine must be responsible for the differences in diacetyl formation. The mechanistic basis for these changes could be a decrease in the concentration of oxygen or ROS in the mixtures after reaction with **1a**, which could favor combinations of acetyl radicals to form diacetyl.[38,41] On the other hand, the radical nature of methionine oxidation might also lead to a stabilization of intermediate reductone or acetyl radicals; however, the nature of such stabilization yet needs to be further explored.

In summary, it has been shown that **1a** can be oxidized to **2a** during incubation with reducing carbohydrates, reductones, and ARPs at moderate temperatures. The presence of **1a** leads to changes in the reaction pathways of sugar degradation in such a way that oxidation reactions are suppressed, whereas certain radical reactions, for example, the combination of acetyl radicals to form diacetyl, are favored. These findings represent novel aspects of the molecular basis of protein oxidation reactions in food systems. Even in the absence of substantial amounts of lipids, food protein oxidation should occur through the action of intermediates of carbohydrate or ARP oxidation, for example, in food items such as skimmed milk or beer, and also in solid foods such as bread (crumb) or low-fat meat products without the development of a characteristic flavor resulting from lipid peroxidation products. The determination of individual protein oxidation products needs further attention.

■ ASSOCIATED CONTENT

Supporting Information

^{13}C and ^{1}H spectroscopic data of 4-[2-(1-desoxyfructosyl)-aminoethyl]benzoic acid, **8** (Table S1), and 4-[2-(1-desoxyribulosyl)aminoethyl]benzoic acid, **9** (Table S2). This material is available free of charge via the Internet at http://pubs.acs.org.

■ AUTHOR INFORMATION

Corresponding Author

*(M.H.) Phone: +49-351-463-32122. Fax: +49-351-463-34138. E-mail: Michael.Hellwig@chemie.tu-dresden.de.

Notes

The authors declare no competing financial interest.

■ ACKNOWLEDGMENTS

We thank Prof. T. Henle, Institute of Food Chemistry, TU Dresden, for valuable discussions. We are grateful to the members of the Institute of Organic Chemistry, TU Dresden, namely, Dr. Margit Gruner and Anett Rudolph, for recording

the NMR spectra, and Anke Peritz for performing the elemental analysis.

■ ABBREVIATIONS USED

ARP, Amadori rearrangement product; Bz, benzoyl; DIPEA, diisopropylethylamine; DETAPAC, diethylenetriaminepentaacetic acid; HPLC, high-pressure liquid chromatography; NMR, nuclear magnetic resonance; PAEBA, 4-(2-aminoethyl)-benzoic acid; ROS, reactive oxygen species; t_R, retention time

■ REFERENCES

(1) Berlett, B. S.; Stadtman, E. R. Protein oxidation in aging, disease, and oxidative stress. *J. Biol. Chem.* **1997**, *272*, 20313−20316.
(2) Dean, R. T.; Fu, S.; Stocker, R.; Davies, M. J. Biochemistry and pathology of radical-mediated protein oxidation. *Biochem. J.* **1997**, *324*, 1−18.
(3) Lund, M. N.; Heinonen, M.; Baron, C. P.; Estévez, M. Protein oxidation in muscle foods: a review. *Mol. Nutr. Food Res.* **2011**, *55*, 83−95.
(4) Meltretter, J.; Seeber, S.; Humeny, A.; Becker, C. M.; Pischetsrieder, M. Site-specific formation of Maillard, oxidation, and condensation products from whey proteins during reaction with lactose. *J. Agric. Food Chem.* **2007**, *55*, 6096−6103.
(5) Hayashi, R.; Suzuki, F. Determination of methionine sulfoxide in protein and food by hydrolysis with *p*-toluenesulfonic acid. *Anal. Biochem.* **1985**, *149*, 521−528.
(6) Todd, J. M.; Marable, N. L.; Kehrberg, N. L. Methionine sulfoxide determination after alkaline hydrolysis of amino acid mixtures, model protein systems, soy products and infant formulas. *J. Food Sci.* **1984**, *49*, 1547−1551.
(7) Baxter, J. H.; Lai, C.-S.; Phillips, R. R.; Dowlati, L.; Chio, J. J.; Luebbers, S. T.; Dimler, S. R.; Johns, P. W. Direct determination of methionine sulfoxide in milkproteins by enzyme hydrolysis/high-performance liquid chromatography. *J. Chromatogr., A* **2007**, *1157*, 10−16.
(8) Tannenbaum, S. R.; Barth, H.; Le Roux, J. P. Loss of methionine in casein during storage with autoxidizing methyl linoleate. *J. Agric. Food Chem.* **1969**, *17*, 1353−1354.
(9) Ametani, A.; Shimizu, M.; Kaminogawa, S.; Yamauchi, K.; Takahashi, S. Methionine oxidation and proline cis-trans isomerization in α_{S1}-casein on emulsification with oxidized lipid. *Agric. Biol. Chem.* **1987**, *51*, 477−481.
(10) Yaylayan, V. A.; Keyhani, A. Carbohydrate and amino acid degradation pathways in L-methionine/D-[^{13}C]glucose model systems. *J. Agric. Food Chem.* **2001**, *49*, 800−803.
(11) Pfeiffer, Y. V.; Kroh, L. W. Investigation of reactive α-dicarbonyl compounds generated from the Maillard reactions of L-methionine with reducing sugars via their stable quinoxaline derivatives. *J. Agric. Food Chem.* **2010**, *58*, 8293−8299.
(12) Cuq, J.-L.; Besancon, P.; Chartier, L.; Cheftel, C. Oxidation of methionine residues of food proteins and nutritional availability of protein-bound methionine sulfoxide. *Food Chem.* **1978**, *3*, 85−102.
(13) Kroh, L. W. Caramelisation in food and beverages. *Food Chem.* **1994**, *51*, 373−379.
(14) Weenen, H. Reactive intermediates and carbohydrate fragmentation in Maillard chemistry. *Food Chem.* **1998**, *62*, 393−401.
(15) Wolff, S. P.; Crabbe, M. J. C.; Thornalley, P. J. The autoxidation of glyceraldehydes and other simple monosaccharides. *Experientia* **1984**, *40*, 244−246.
(16) Wolff, S. P.; Dean, R. T. Glucose autoxidation and protein modification − the potential role of autoxidative glycosylation in diabetes. *Biochem. J.* **1987**, *245*, 243−250.
(17) Thornalley, P. J.; Langborg, A.; Minhas, H. S. Formation of glyoxal, methylglyoxal and 3-deoxyglucosone in the glycation of proteins by glucose. *Biochem. J.* **1999**, *344*, 109−116.
(18) Ortwerth, B. J.; James, H.; Simpson, G.; Linetsky, M. The generation of superoxide anions in glycation reactions with sugars, osones, and 3-deoxyosones. *Biochem. Biophys. Res. Commun.* **1998**, *245*, 161−165.
(19) Azevedo, M.; Falcão, J.; Raposo, J.; Manso, C. Superoxide radical generation by Amadori compounds. *Free Radical Res. Commun.* **1988**, *4*, 331−335.
(20) Elgawish, A.; Glomb, M.; Friedlander, M.; Monnier, V. M. Involvement of hydrogen peroxide in collagen cross-linking by high glucose in vitro and in vivo. *J. Biol. Chem.* **1996**, *271*, 12964−12971.
(21) Mossine, V. V.; Linetsky, M.; Glinsky, G. V.; Ortwerth, B. J.; Feather, M. S. Superoxide free radical generation by Amadori compounds: the role of acyclic forms and metal ions. *Chem. Res. Toxicol.* **1999**, *12*, 230−236.
(22) Gillery, P.; Monboisse, J. C.; Maquart, F. X.; Borel, J. P. Glycation of proteins as a source of superoxide. *Diabetes Metab.* **1988**, *14*, 25−30.
(23) Rockland, L. B. Saturated salt solutions for static control of relative humidity between 5 and 40 °C. *Anal. Chem.* **1960**, *32*, 1375−1376.
(24) Hellwig, M.; Henle, T. Formyline, a new glycation compound from the reaction of lysine and 3-deoxypentosone. *Eur. Food Res. Technol.* **2010**, *230*, 903−914.
(25) Hellwig, M.; Degen, J.; Henle, T. 3-Deoxygalactosone, a "new" 1,2-dicarbonyl compound in milk products. *J. Agric. Food Chem.* **2010**, *58*, 10752−10760.
(26) Hellwig, M.; Henle, T. Release of pyrraline in absorbable peptides during simulated gastrointestinal digestion of casein glycated by 3-deoxyglucosone. *Eur. Food Res. Technol.* **2013**, *237*, 47−55.
(27) Dubourg, J.; Naffa, P. Oxydation des hexoses reducteurs par l'oxygène en milieu alcalin. *Bull. Soc. Chim. Fr.* **1959**, *9*, 1353−1362.
(28) Bechara, E. J. H.; Dutra, F.; Cardoso, V. E. S.; Sartori, A.; Olympio, K. P. K.; Penatti, C. A. A.; Adhikari, A.; Assunção, N. A. The dual face of endogenous α-aminoketones: pro-oxidizing metabolic weapons. *Comp. Biochem. Physiol. C* **2007**, *146*, 88−110.
(29) Liao, M.-L.; Seib, P. A. Chemistry of L-ascorbic acid related to foods. *Food Chem.* **1988**, *30*, 289−312.
(30) Pischetsrieder, M.; Rinaldi, F.; Gross, U.; Severin, T. Assessment of the antioxidative and prooxidative activities of two aminoreductones formed during the Maillard reaction: effects on the oxidation of β-carotene, N^{α}-acetylhistidine, and *cis*-alkenes. *J. Agric. Food Chem.* **1998**, *46*, 2945−2950.
(31) Yaylayan, V. A.; Huyghues-Despointes, A. Chemistry of Amadori rearrangement products: analysis, synthesis, kinetics, reactions, and spectroscopic properties. *Crit. Rev. Food Sci. Nutr.* **1994**, *34*, 321−369.
(32) Hodge, J. E.; Rist, C. E. The Amadori rearrangement under new conditions and its significance for non-enzymatic browning reactions. *J. Am. Chem. Soc.* **1953**, *75*, 316−322.
(33) Pischetsrieder, M.; Schoetter, C.; Severin, T. Formation of an aminoreductone during the Maillard reaction of lactose with N^{α}-acetyllysine or proteins. *J. Agric. Food Chem.* **1998**, *46*, 928−931.
(34) Oliver, C. M.; Melton, L. D.; Stanley, R. A. Creating proteins with novel functionality via the Maillard reaction: a review. *Crit. Rev. Food Sci. Nutr.* **2006**, *46*, 337−350.
(35) Garrison, W. M.; Bennett, W.; Jayko, M. E. Radiation-induced oxidation of protein in aqueous solution. *Radiat. Res.* **1962**, *16*, 483−502.
(36) Hofmann, T.; Bors, W.; Stettmaier, K. Studies on radical intermediates in the early stage of the nonenzymatic browning reaction of carbohydrates and amino acids. *J. Agric. Food Chem.* **1999**, *47*, 379−390.
(37) Glomb, M. A.; Tschirnich, R. Detection of α-dicarbonyl compounds in Maillard reaction systems and in vivo. *J. Agric. Food Chem.* **2001**, *49*, 5543−5550.
(38) Smuda, M.; Glomb, M. A. Novel insights into the Maillard catalyzed degradation of maltose. *J. Agric. Food Chem.* **2011**, *59*, 13254−13264.
(39) Gobert, J.; Glomb, M. A. Degradation of glucose: reinvestigation of reactive α-dicarbonyl compounds. *J. Agric. Food Chem.* **2009**, *57*, 8591−8597.

(40) Voigt, M.; Smuda, M.; Pfahler, C.; Glomb, M. A. Oxygen-dependent fragmentation reactions during the degradation 1-deoxy-D-erythro-hexo-2,3-diulose. *J. Agric. Food Chem.* **2010**, *58*, 5685−5691.
(41) Nukaya, H.; Inaoka, Y.; Ishida, H.; Tsuji, K.; Suwa, Y.; Wakabayashi, K.; Kosuge, T. Modification of the amino group of guanosine by methylglyoxal and other α-ketoaldehydes in the presence of hydrogen peroxide. *Chem. Pharm. Bull.* **1993**, *41*, 649−653.
(42) Weenen, H. Reactive intermediates and carbohydrate fragmentation in Maillard chemistry. *Food Chem.* **1998**, *62*, 393−401.
(43) Hollnagel, A.; Kroh, L. W. Formation of α-dicarbonyl fragments from mono- and disaccharides under caramelization and Maillard reaction conditions. *Z. Lebensm. Unters. Forsch.* **1998**, *207*, 50−54.
(44) Yaylayan, V. A.; Keyhani, A. Origin of 2,3-pentanedione and 2,3-butanedione in D-glucose/L-alanine Maillard model systems. *J. Agric. Food Chem.* **1999**, *47*, 3280−3284.

JOURNAL OF AGRICULTURAL AND FOOD CHEMISTRY

Article

pubs.acs.org/JAFC

Chitin Microfibers Reinforce Soy Protein Gels Cross-Linked by Transglutaminase

Yang Yuan,[†] Ying-En Sun,[†] Zhi-Li Wan,[†] Xiao-Quan Yang,*[,†,‡] Jun-Feng Wu,[†] Shou-Wei Yin,[†] Jin-Mei Wang,[†] and Jian Guo[†]

[†]Research and Development Center of Food Proteins, College of Light Industry and Food, South China University of Technology, Guangzhou 510640, PR China

[‡]State Key Laboratory of Pulp and Paper Engineering, South China University of Technology, Guangzhou 510640, PR China

ABSTRACT: To improve the gel strength, we attempt to introduce the microcomposite concept into the food gel system. A stable positively charged chitin microfibers (CMFs) suspension was fabricated by a facile microfluidizer approach without changing its chemical structure. The obtained CMFs bearing width of about 0.5−5 μm and length of more than 500 μm were then developed in a transglutaminase cross-linked β-conglycinin (7S) gel. The morphological and rheological characterizations of the 7S-CMF composited gels were done as a function of the protein and CMFs concentrations. Results showed that the presence of the CMFs network improved the gel strength significantly. This effect was CMFs content dependent and was related to the formation of a sponge-like porous microstructure. We inferred that the CMFs provided an initial framework for gel formation and added structural rigidity to the protein gel. The role of protein was to participate in network development as an electrostatic coating and gelation component.

KEYWORDS: *β-conglycinin, chitin, microfiber, reinforce, composite, gel*

INTRODUCTION

Foods should be understood as soft materials.[1] It is no surprise that food technologists are getting or will be getting inspiration from other scientific fields such as material science. Novel functional properties are expected to be created by high performance composite materials in polymer-based food systems. Recently, the application of the nano- or micro-structured composite concept has been observed in biopolymer-based films, hydrogels, and scaffolds.[2−6] As novel functional renewable materials, natural cellulose and chitin nano- or microfibers have received increasing interest because of their abundance, biocompatibility, and specific properties.[7] In addition to their high mechanical strength, they have several useful advantages such as high aspect ratio and facile chemical modification, showing a potential application in the material and food industry.[4]

According to previous research, the top-down method is applicable to the production of nano- or microfibers, involving physical, enzymatic, chemical, and mechanical ways.[8] Compared to other approaches, microfluidization, as a novel mechanical method, has attracted a great deal of interest in recent years because it is convenient. Lee et al.[9] reported that cellulose nanofibers can be prepared by the application of a microfluidizer at 138 MPa. Liu et al.[10] also found that the joint treatment of wet-grinding and high-pressure homogenization can effectively disassemble chitosan particles into nanofibers.

Chitin (poly-β-(1,4)-*N*-acetyl-D-glucosamine) is the second most abundant natural polysaccharide next to cellulose. As the waste products of the seafood industry, crab and shrimp shells are the main commercial sources of chitin, implying that there is a great profit if chitin can be used as a food ingredient. Chitin has shown a great deal of functional and nutritional benefits such as the reduction of plasma cholesterol and intestinal lipid absorption.[11] However, chitin is insoluble in all common solvents due to its rigid crystalline structure, which is a major problem in developing its uses. Even though it can be dissolved in some specific solvents such as saturated calcium solvent,[12] using them by this means in food industry can be challenging. Recently, for promotion of the use of chitin, fibrillar chitin provides another interesting pathway because a lot of novel functional properties have been reported after the formation of chitin and chitosan nano- or microfibers.[4,10,13−15] Araki et al.[4] reported that the presence of chitin nanowhiskers significantly enhanced the gel strength of the cross-linked chitosan hydrogel. Zhou et al.[14] found that the chitosan nanofibers played a role like a cross-linker and a reinforcing agent in the polyacrylamide hydrogel, resulting a significant increase in compression strength and storage modulus. Most recently, reports on using chitin nanofibers suspensions as metal sorbents have been first published.[15] However, as far as we know, fibrillar chitin as food compositions have seldom been investigated until now. The applications of nano- or microfibers in the above-mentioned investigations provide a novel route, and we attempt to introduce this nano- or microcomposite concept into a food system for reinforcing the food gel.

Soy proteins (SP) are the most important representative of legume proteins and have been widely used to formulate foods to improve their nutritional and functional qualities. Microbial transglutaminase (MTGase), because of its low-cost mass production and is "Generally Recognized As Safe", has been largely utilized as a food processing tool in the past few years.[16]

Received: February 21, 2014
Revised: April 26, 2014
Accepted: April 26, 2014
Published: April 27, 2014

ACS Publications © 2014 American Chemical Society

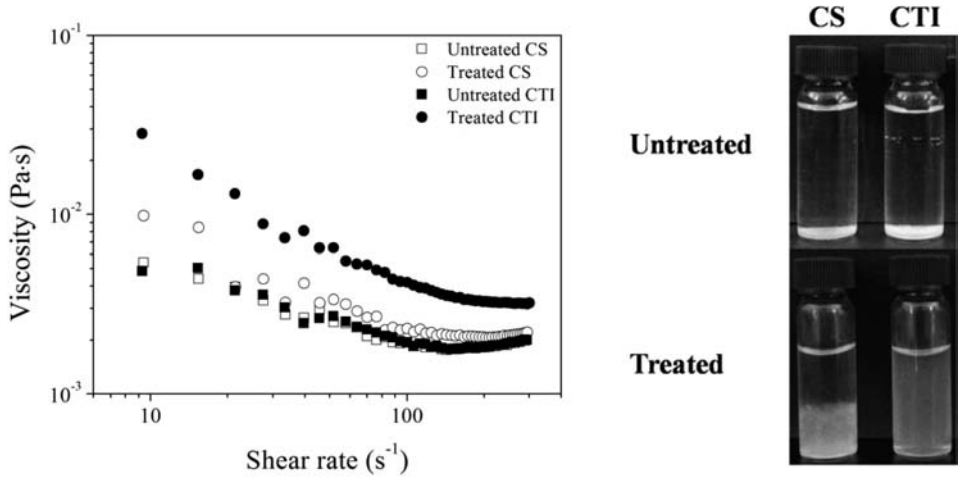

Figure 1. Observation and viscosity of the raw suspension and treated suspension of chitosan (CS) and chitin (CTI), respectively (0.1 wt % dry sample weight).

There have been several reports on the gelation of SP induced by MTGase.[17,18] Tang et al.[18] found that MTGase cross-linked glycinin-rich SP gel showed significantly higher gel strength than β-conglycinin-rich SP gel. In recent years, MTGase induced SP-polysaccharide composite gels, which showed notably improved gel strength, are attracting increased attention. Guo et al.[19] introduced a novel method regarding MTGase induced SP-based hydrogel by complexing SP with dextran sulfate. Most recently, Zhang et al.[20] investigated the combined cross-linking of MTGase and Maillard cross-linking, indicating that denser and finer networks of combined-treated gels were formed compared to those of the SP gels.

β-Conglycinin (7S), one of the main fractions of SP, is a glycoprotein, showing a great potential in delivery of hydrophilic nutrients. However, 7S gels show poor gel strength, which could limit its uses. In this study, we prepared a chitin microfibers (CMFs) network in an aqueous system by a facile mechanical top-down approach and investigated the morphology and structure of the obtained CMFs network. Subsequently, use of CMFs for reinforcement of MTGase cross-linked 7S gels was investigated to reveal its potentially attractive application in food. Small and large deformation rheological analyses were used to investigate gelation kinetics and mechanical properties. The microstructures of the gels were characterized by using scanning electron microscopy.

MATERIALS AND METHODS

Materials. Defatted soybean flakes were purchased from Shandong Xinjiahua Industrial and Commercial Co. Ltd., China. The β-conglycinin-rich SP was prepared according to Nagano's procedure.[21] Protein content of 7S lyophilized powder was 89.7 ± 0.4% determined by the Dumas method (N × 5.71) in a Rapid N Cube (Elementar France, Villeurbanne, France). The chitosan (molecular weight about 300 kDa; degree of deacetylation of 95%; moisture 8.0%; ash content 0.7%) and chitin (degree of deacetylation ≤50%; moisture 9.0%; ash content 0.9%) used for experiment were purchased from Shandong Aokang Industrial and Commercial Co. Ltd., China. MTGase was purchased from Ajinomoto Co., Japan. The activity of the enzyme product was 100 U/g as determined according to the method proposed by Folk et al.[22] All chemicals used were of analytical or better grade.

Preparation of Chitin and Chitosan Fiber Suspensions. A certain amounts of raw chitin and/or chitosan powders were suspended into distilled water to obtain a slurry with 0.1%, 0.25%, and 0.5% (w/w) dry sample weight. After 10 min of stirring, the slurries were homogenized using an Ultraturrax (T25, IKA, Staufen, Germany) at 10 000 rpm for 5 min. The obtained predispersed slurries were then passed through a homogenizer (Microfluidizers M-110 EH Processor Co., Lampertheim, Germany) under a constant pressure of 150 MPa and at a flow rate of 100 mL/min for 10 passes. The obtained chitin and chitosan fiber suspensions were stored at 4 °C prior to further analysis.

Preparation of 7S-CMF Composite Gels. The gel solutions were prepared by dissolving the 7S powders into the chitin fiber suspensions directly. A certain amount of 7S powders was dissolved into a certain amount of chitin fiber suspensions (0.1%, 0.25%, and 0.5%, w/w) under continuous stirring (200 rpm) for 3 h. The pHs of mixtures were adjusted to 7.0, and then the mixtures were stored overnight at 4 °C to allow a complete hydration. For the gelation step, a MTGase concentration of 30 unit/g of 7S was used in each reaction according to the pretest. In all mixtures, 7S reached a final concentration of 4%, 6%, and 8% (w/v), respectively. After vacuum degassing, the mixtures were incubated in a water bath (45 °C, 4 h) for gel formation.

ζ-Potential. The ζ-potentials of the samples were determined according to previous publications by using a Nanosizer ZS instrument (Malvern Instruments Ltd., Worcestershire, UK).[10,23] The electrophoretic mobility was determined by Laser Doppler Velocimetry, and the maximum working voltage on the electrode was ±160 V. The Henry equation was then applied for calculating the ζ-potential. All measurements were conducted in triplicate.

Fourier Transform Infrared Measurements (FTIR). FTIR measurements were performed on flakes of sample powder mixed with KBr. The sample quantity (about 5 mg) in KBr (200 mg) was chosen in order to optimize the flake transmittance and to obtain a well detectable absorption in the spectral region of 4000−400 cm^{-1}. All spectra were recorded at 25 °C, with a resolution of 4 cm^{-1}, using a Vector-33 interferometer (Bruker Optics, Ettlingen, Germany) working under a vacuum to avoid intense spectral components.

Low Amplitude Dynamic Oscillatory Measurements. Steady shear viscosities and dynamic rheological measurements were conducted by a HAAKE RheoStress 600 rheometer (Thermo electron GmbH, Karlsruhe, Germany) equipped with a parallel plates geometry (plate sensor PP35 Ti, 35 mm diameter, 1 mm gap) and a circulating system for temperature control. In the steady shear experiment, the apparent viscosity was measured across a range of shear rates (0.01−300 s^{-1}) at 25 °C. As for dynamic rheological analyses, time-sweep analysis was used to monitor the gelation kinetics of gel samples, which were induced by MTGase. The sample solutions were placed on the plate immediately after the addition of MTGase. Subsequently, the test at a frequency of 1 Hz and a strain of 0.5% (within linear

dx.doi.org/10.1021/jf500922n | J. Agric. Food Chem. 2014, 62, 4434−4442

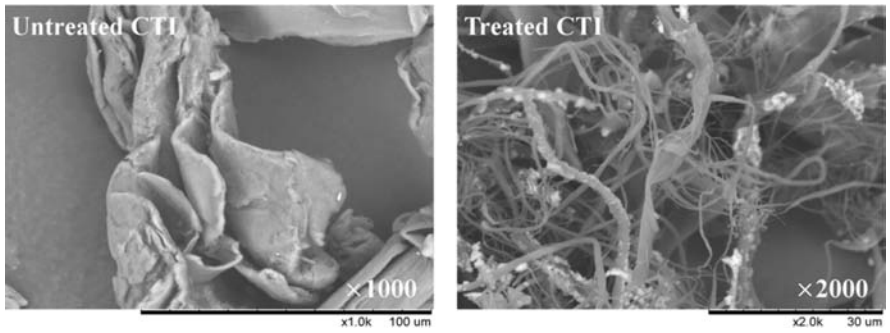

Figure 2. SEM micrographs of the raw chitin sample and high-pressure homogenized treated sample.

viscoelastic region) was started when the temperature was stable at 45 °C.

Uniaxial Compression. The gel samples (cubes with an edge length of 10 mm) were compressed between lubricated plates fitted to a TA.TX2 texture analyzer (Stable 194 Micro System, Surrey, U.K.) with a cylinder measuring probe (P/20a) which had a diameter of 20.0 mm. The breakdown pattern of the gels was observed by compressing the gels at a constant speed of 0.2 mm/s to 20% of their initial height at room temperature. Stress and strain were calculated according to the following equations: stress = $(F/A_i) \times ((L_i - \Delta L)/L_i)$; strain = $|\ln(L_i/(L_i - \Delta L))|$, where F(N) is the force measured during compression; A_i (m^2) is the initial cross sectional area of the specimen; L_i (m) is the initial specimen height; ΔL (m) is the deformation. At least two gel samples were tested per treatment, and each treatment was replicated two times.

Scanning Electron Microscopy (SEM) Observations. According to a previous publication,[18] chitin microfibers and gel samples were immersed in liquid nitrogen for 5 min to minimize the impact of ice crystals and then freeze-dried. Lyophilized samples were cut carefully and stuck onto an SEM aluminum plate through the double-sided conductive carbon tabs. Samples were coated with gold in a E-1010 ion sputter (Hitachi High-Technologies Corporation, Tokyo, Japan) before the test. The SEM images were recorded at 25 °C using a TM-3000 tabletop low vacuum scanning electron microscope (Hitachi High-Technologies Corporation, Tokyo, Japan) at an accelerating voltage of 15 kV.

Statistical Analysis. All the data were subjected to one-way analysis of variance, and correlations between the results were carried out using Statistical Analysis System Software (SAS version 9.0, SAS Institute, Cary, NC); significant differences were determined by Duncan's multiple range test and accepted at $P < 0.05$.[24]

RESULTS AND DISCUSSION

Characterization of Chitin Microfibers. Figure 1 shows the observations and viscosities of the raw suspensions and treated suspensions of chitosan and chitin, respectively. As shown in photograph, raw chitosan and chitin particles, without any treatment, both settled quickly in water (less than 2 min). After being processed by high-pressure homogenization, chitosan and chitin suspensions displayed totally different stabilities in water. Large and millimeter-scale fibers were obtained in treated chitosan suspension coupled with the settlement of these fibrils after 5 min. Treated chitin, however, was macroscopically well suspended in water and did not precipitate during 2 months of storage at 4 °C. The viscosities of these samples also can be seen in Figure 1. As a control, samples showed very low shear viscosities before high-pressure homogenization treatment. No significant increase in viscosity can be found in treated chitosan suspension. In contrast, chitin fiber suspension showed a significant increase in viscosity, suggesting that the internal structure of chitin spread out after the treatment and the increased steric hindrance effect resulted

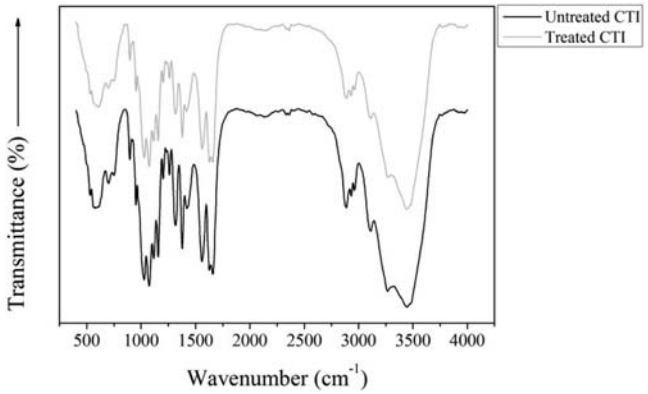

Figure 3. FTIR spectra of the raw chitin sample and its microfibers after mechanical treatment.

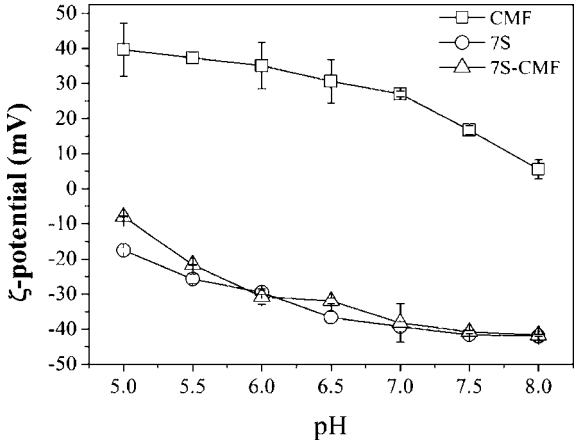

Figure 4. Effects of pH on ζ-potential of chitin microfibers (CMFs) suspension (1 mg/mL), β-conglycinin (7S) suspension (5 mg/mL), and 7S-CMFs mixture (5 mg/mL, 7S/CMFs ratio = 5/1).

in a higher viscostiy.[25] Chitin fiber suspension showed a decrease in viscosity for higher shear rates, meaning that the samples were shear thinning. It could indicate that the shear reduced the connections between chitin fibers and made the suspension flow more easily.[25,26]

Figure 2 shows the SEM micrographs of raw chitin powder and high-pressure treated chitin sample. Large and irregular-shaped particles which were millimeter sized were observed in Figure 2A. After treatment, the irregular-shaped chitin particles disassembled into chitin fibers. These fibers intertwined with each other, and the diameter of these fibers were distributed over a range from approximately 0.5 to 5 μm (Figure 2B),

dx.doi.org/10.1021/jf500922n | J. Agric. Food Chem. 2014, 62, 4434−4442

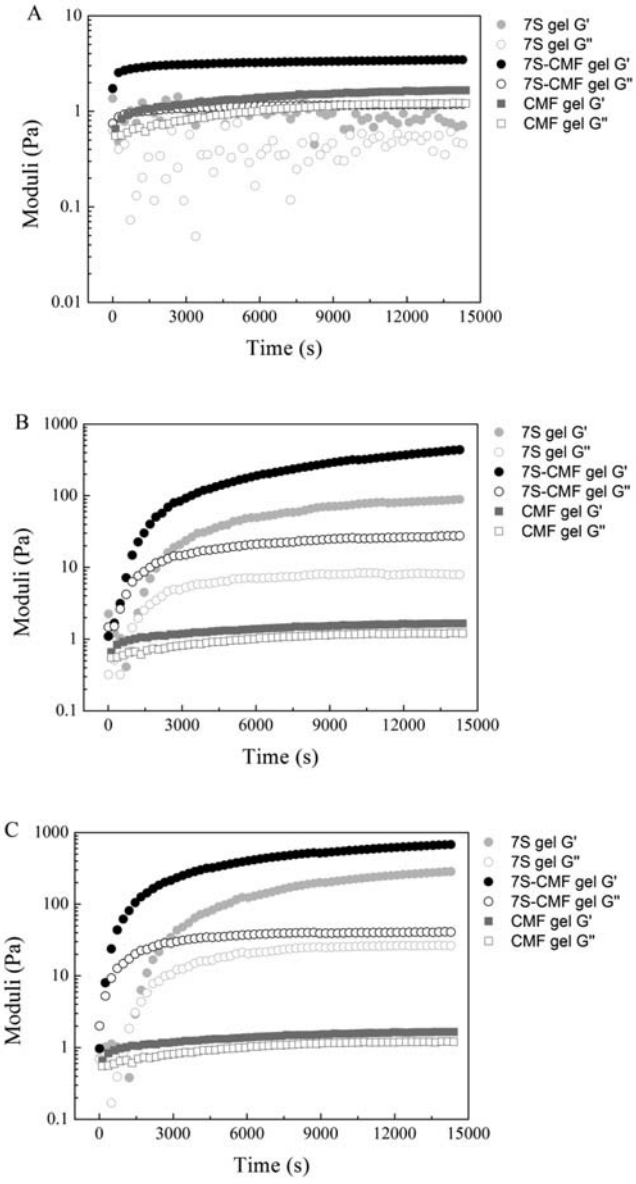

Figure 5. Time sweep rheological profiles of 7S-CMF composite gels as a function of 7S concentrations (A: 4%, B: 6%, and C: 8%).

meaning that chitin microfibers (CMFs) were obtained. Many research studies have clarified several advantages regarding high-pressure homogenization for obtaining chitin nano- or microfibers such as high mechanical strength, high aspect ratio, and adsorption of protein and metal ions.[15] Most recently, Tzoumaki et al.[27] successfully fabricated an oil-in-water Pickering emulsion which was stabilized by chitin nanocrystal. Overall, high-pressure homogenization successfully disassembled the chitin particles into stable water suspensible chitin microfibers, which could be used in food as a thickening and reinforced filler.

The chemical composition of chitin was obviously unchanged during the high-pressure homogenization treatments, which can be seen in Figure 3. The chemical composition analysis of chitin was based on the identification of bands related to the functional groups present in chitin: the OH stretching band at 3480 cm^{-1}, NH stretching band at 3270 cm^{-1}, amide band I at 1660 and 1620 cm^{-1}, and amide II band at 1560 cm^{-1}. Both the position and relative intensity of characteristic bands of the CMFs are similar to those of the raw chitin particle, indicating the original chemical and molecular structures of chitin were retained in the case of mechanical treatment. Liu et al.[10,14] also reported that the chemical compositions of both chitosan and chitin were unchanged during the mechanical treatments at neutral pH.

Stability of 7S-CMF Mixture. Electrostatic forces have been shown to have a significant effect on colloid stability in many studies regarding protein and polysaccharide interaction.[28] There appears to be no investigation on the ζ-potential of chitin colloid suspension, which is probably because measurements of ζ-potential of insoluble chitin particles are unreliable. However, the ζ-potentials were successfully measured after the chitosan and chitin particles were disassembled into micro- or nanofibers.[10,29] The ζ-potential–pH patterns of CMFs are shown in Figure 4, which show that CMFs were positively charged microfibers at all tested pHs (from pH 5.0 to 8.0). The pK_a of amino groups was reported as 6.2–7.0.[30] At a pH below the pK_a, chitin microfibers carry a positive charge due to the protonation of amino groups, and the charged groups provide electrostatic repulsion between fibers.[29] With pH elevation, the ζ-potentials of CMFs decreased from 39.6 ± 5.5 mV at pH 5.0 to 5.5 ± 1.9 mV at pH 8.0. It is noteworthy that CMFs showed high ζ-potentials above 27 mV during a long pH region from 5.0 to 7.0 and then decreased to 5.5 mV rapidly. This phenomenon was due to the deprotonation of the amino groups. Concomitantly, the suspended CMFs were stable at a long pH region and then settled down in 5 min at high pH (pH 8.0), suggesting that CMFs were also electrically stabilized and aggregates were obtained at high pH due to the decrease electrostatic repulsion.

The ζ-potential–pH patterns of 7S are shown in Figure 4 as well. It is well-known that 7S particles carry a negative charge at pH above their pI (pH 4.3). Electrostatic interaction between 7S and CMFs should occur at all tested pH values because they carry a complementary charge. The strength of the electrostatic interaction (SEI) between oppositely charged polyelectrolytes can be estimated by calculating the absolute value of the product of the measured ζ-potential of both polymers at each pH.[28] The SEI–pH curves indicated that the interactions between 7S and CMFs should be strongest at pH 6.5 and coacervates should be obtained (data not shown). However, the 7S-CMFs mixture was stable, and no coacervates were found at all tested pHs. The ζ-potential curve of 7S-CMFs mixture suggested that the charge of the mixture was protein charge dominant because it showed similar values as the 7S ζ-potential curve.

Moreover, the thermal stability of CMFs was also investigated by macroscopic observation. Macroscopic observation suggested that CMFs suspension was stable at 45 °C and became unstable at the temperature above 70 °C. This phenomenon can be ascribed to the increasing attractive interaction between the chitin fiber when increasing the system temperature.[25] As a result, cold-set MTGase cross-linked gelation method was used to form the 7S-CMF composite gel because it can effectively avoid the impact of heat treatment on the stability of the microfibers

7S-CMF Composite Gel. In this study, we attempted to investigate the effect of CMFs on gelation rate and extent of soy 7S globulin. Therefore, dynamic viscoelastic properties of the 7S-CMF composite gels were investigated by small deformation rheological measurements. Storage modulus (G') and loss modulus (G'') values represent the elastic and viscous

dx.doi.org/10.1021/jf500922n | J. Agric. Food Chem. 2014, 62, 4434–4442

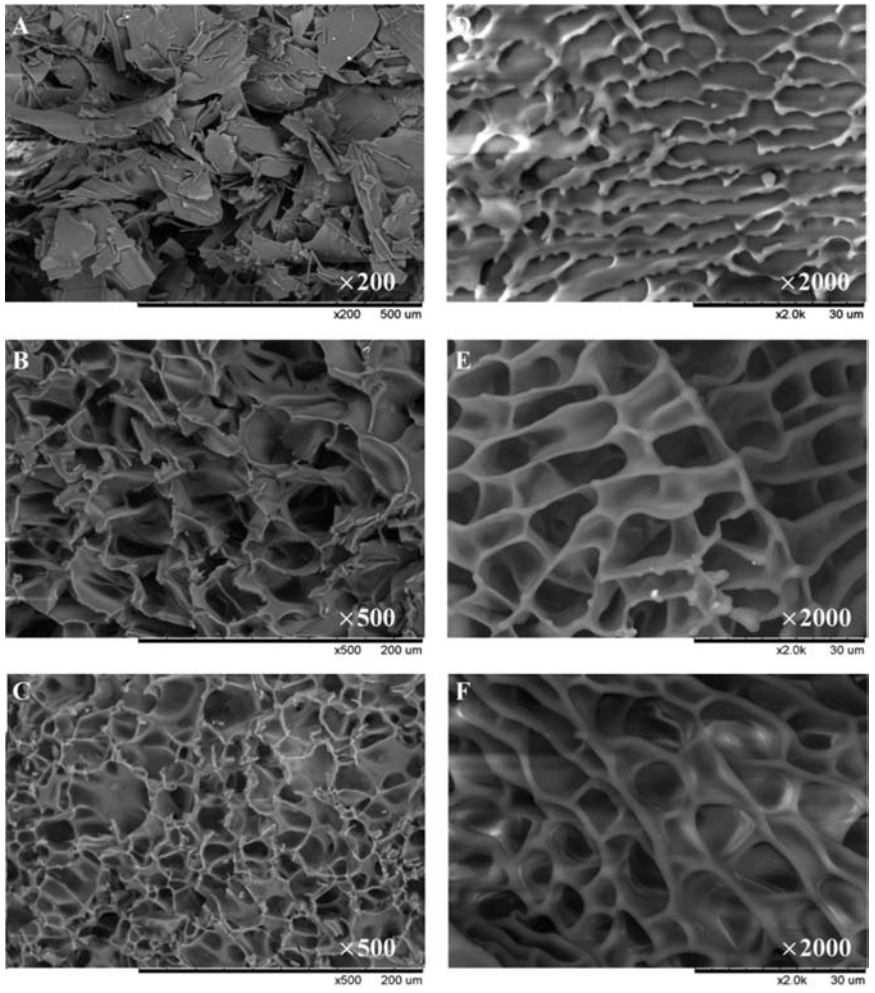

Figure 6. SEM images of 7S-CMF composite gels as a function of 7S concentrations (A and D: 4%; B and E: 6%; C and F: 8%; A, B, and C: 7S gels; D, E, and F: CMFs composited 7S gels).

components in the network.[31] As shown in Figure 5, 7S dispersion showed different rheological profiles at different protein contents. Irregular scatter diagrams were obtained at 7S concentration of 4%, suggesting that the 7S dispersion was still in the liquid state, and no gelation networks were obtained at such a low concentration. As long as the protein content (6% and 8%, w/v) exceeded the critical gelation concentration, G' and G'' of 7S dispersion developed similarly, and the G' values were significantly greater in magnitude than the G'' values. As for 7S-CMF composite gels, significant enhancements of gel strength were observed in Figure 5. As shown in Figure 5A, compared to the 7S gel, the 7S-CMF composite gel displayed a more organized pattern even though it was still liquid state in appearance. This phenomenon may be related to the presence of CMFs network that provided an initial framework and the G' values were stable around 1 Pa (CMFs gel in Figure 5). However, the lack of protein reacting sites resulted in a low elastic and viscous modulus. Significant increases of viscoelastic modulus were found at a higher protein concentration, representing an evident increase in G' values of the 7S-CMF composite gel of about 10 times compared with those of the 7S gel at both protein content of 6% and 8%. Meanwhile, the gelation time (t_{gel}), which is generally accepted as the time when the value of G' becomes greater than that of G'' and is greater than 10 Pa,[32] was significantly ($p < 0.05$) shortened in the presence of CMFs. In detail, the values of t_{gel} at protein content of 6% and 8% decreased from 2000 and 1900 s (7S gel) to 800 and 300 s (7S-CMF composite gel), respectively.

The changes in rheological and mechanical properties of gels are highly related to the changes in microstructure. One way to look at the inside of a gel is with SEM. Typically, SEM showed better resolution than confocal laser scanning microscopy (CLSM), but the sample used in SEM requires rather a severe and time-consuming sample preparation including freeze-drying.[33] The porous and cellular microstructures observed with SEM are probably induced by ice crystal formation during the freezing step in sample preparation.[34] As presented in Figure 6, the results of SEM showed that microstructural modifications occur in 7S-CMF composite gels, in particular, changes in porosity, including an increase in the amount and a decrease in size. In detail, 7S gels showed disordered and lamellar structures at 4%, while showed typical interconnected macroporous morphologies with pore sizes ranging from 10 to 40 μm at 6% and 8%, indicating that the more protein the gel had the more compact and homogeneous the microstructure was. Sponge-like pore structures were formed as seen in 7S-CMF composite gels (Figure 6D−F). The size of the pores is around 3−9 μm. Beginning with the thin and shallow networks at low protein content, thicker and smoother networks and deeper pores were observed with an increase in protein content. Such changes in microstructure could affect gel rheological properties and explain the increase in gel viscoelastic modulus.

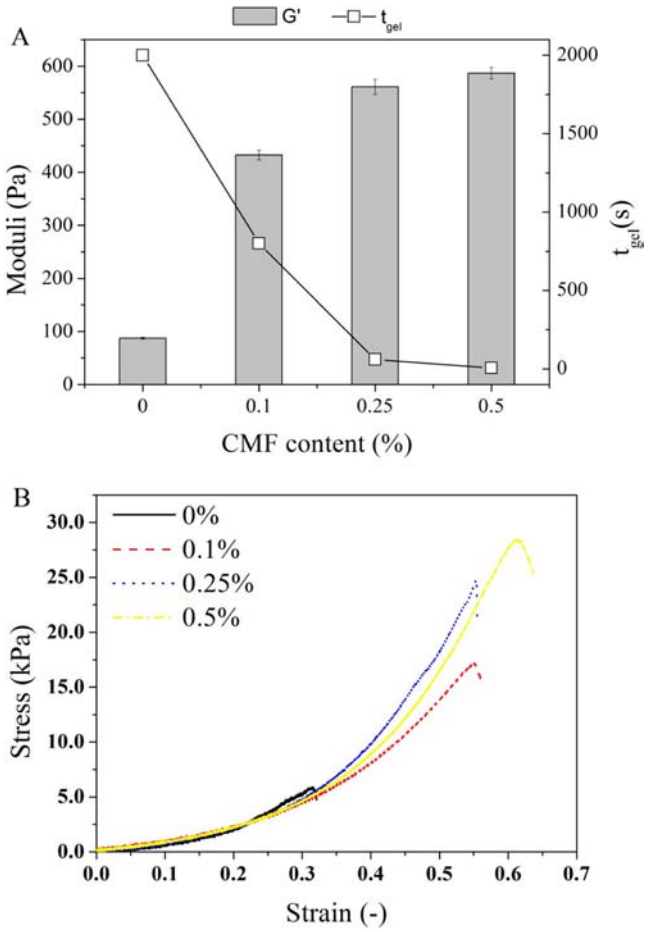

Figure 7. (A) G', t_{gel}, and (B) stress−strain curves of 7S-CMF composite gels as a function of CMFs concentrations at a 7S concentration of 6%.

Aouada et al.[5] also found a three-dimensional, well-oriented porous microstructure when they added cellulose nanofibers into a hydrogel, showing a similar decreases in pore size and increases in gel strength.

Figure 7A showed that the elastic modulus increased while the t_{gel} decreased significantly ($p < 0.05$) with increased concentrations of CMFs, suggesting that the formation of gel was significantly influenced by the CMFs content. Previous papers have clarified the effect of polysaccharide concentration on the formation of protein−polysaccharide mixed gel. Guo et al.[19] showed that the gelation of soy protein was accelerated by adding dextran sulfate, and the strengths of the formed gels were dextran sulfate amount dependent. Le et al.[35] found the β-lactoglobulin and xanthan gum ratio strongly affected gelation kinetics and was a main factor controlling the gelation process and the gel structure. Uniaxial compression measurements were performed to investigate the fracture properties (Figure 7B). 7S gel fractured at relatively low strain and stress values which coincided with previous investigations,[36] suggesting a weak and brittle gel was formed. 7S-CMF composite gel showed different stress−strain curves. As expected, increasing CMFs concentration caused an increase in both fracture stress and fracture strain. The value of the fracture stress increased from 5.8 to 17.0 kPa, 24.7 and 28.4 kPa, while the fracture strain increased from 0.315 to 0.551, 0.553, and 0.614 with CMFs content elevation. These agreed with the small deformation rheological investigations that showed a similar trend of G' values for 7S-CMF composite gels.

To further confirm the data of small and large deformation tests, SEM images of 7S-CMF composite gels were recorded as a function of CMFs contents. As shown in Figure 8, a significantly different microstructure can be found between the 7S-CMF composite gels and control sample, and then smaller and regular pores were obtained when the CMFs concentration increased. The overall data suggested that the great enhancement in gel strength may be related to the modification of gel microstructure, and this modification was ratio dependent.

General Discussion. In this work, a stable chitin microfibers suspension was obtained by passing chitin particles through a high-pressure homogenization equipment. The

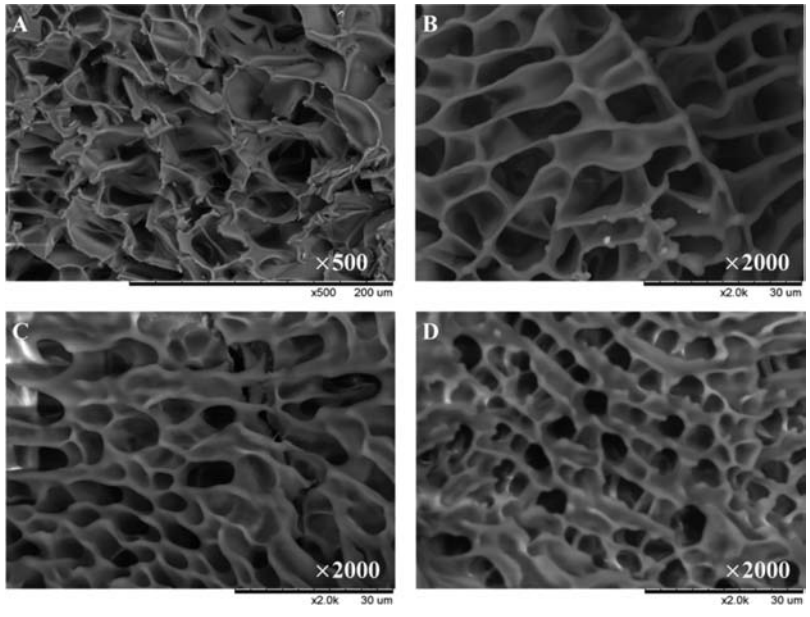

Figure 8. SEM images of 7S-CMF composite gels as a function of CMFs concentrations at 7S concentration of 6% (A: 0%, B: 0.1%, C: 0.25%, and D: 0.5%).

dx.doi.org/10.1021/jf500922n | J. Agric. Food Chem. 2014, 62, 4434−4442

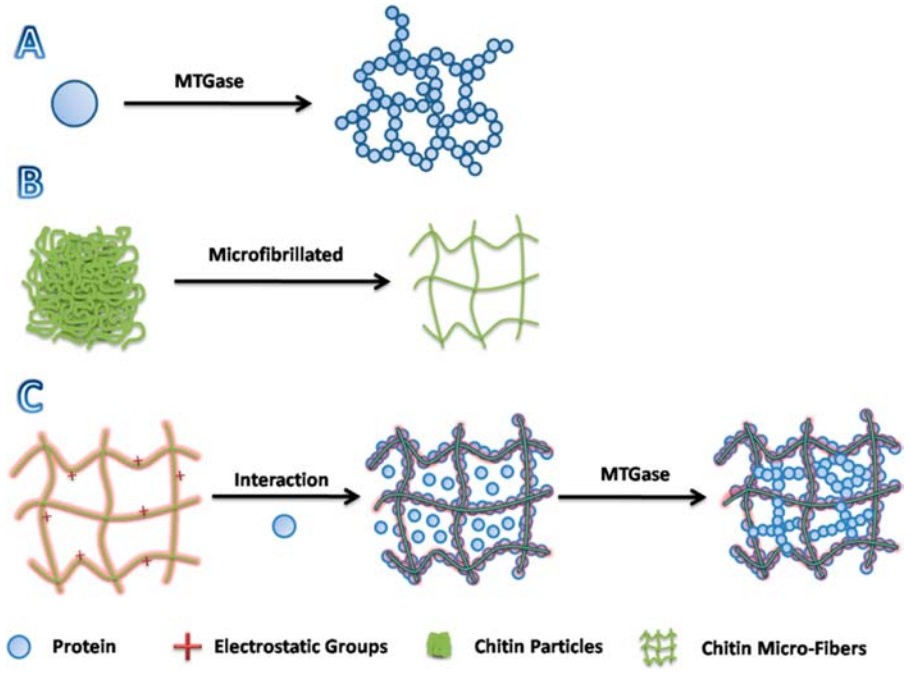

Figure 9. Schematic illustration of the formation of 7S-CMF composite gel (A: the formation of MTGase induced 7S gel; B: the formation of CMFs; C: the formation of 7S-CMF composite gel).

obtained novel fiber material was used in 7S gel as a thickening and reinforced filler because the advantages such as high viscosity, high aspect ratio, and facile electrostatic modification (Figures 1, 2, and 4). Compared to MTGase induced 7S gel, the addition of CMFs enhanced the gel strength and modified the gel structure. To clarify a reasonable understanding of this improvement, a schematic illustration of the formation of 7S-CMF composite gel is proposed and shown in Figure 9.

β-Conglycinin is one of the main fractions of SP. MTGase induced 7S gelation has been fully investigated in past 20 years, concluding that transglutaminase catalyzed an acyl-transfer reaction between the γ-carbonyl group of a glutamine residue and the ε-amino group of a lysine residue. The resultant covalent connections between the protein molecules formed the three-dimensional networks of the gel.[16] If protein underwent a heat treatment, more groups were exposed from the hydrophobic core of the molecules, and this treatment favored the MTGase cross-linking reaction.[19] In this paper, heating cannot be used, and this type of MTGase cross-linked unheated 7S gel showed typical interconnected macroporous protein backbone and relatively weak gel strength which were proven by means of SEM and rheology technique (Figure 9A). As shown in Figures 1 and 2, high-pressure homogenization disassembled the chitin particles into stable water suspensible chitin microfibers (Figure 9B). Most interestingly, the result of ζ-potentials showed that the obtained CMFs still carried a positive charge at neutral pHs. The reason for this phenomenon is probably because the release, from within the chitin particles, of some unacetylated amino groups increased the protonation on the microfiber surfaces.[37] Liu et al.[10] reported a similar result using chitosan and chitin suspension. The adsorption of metal ions by these materials have been reported due to the microfibrous structure and electrostatic attraction.[15] Most interestingly, some researchers suggested that the presence of nano- or microfiber significantly increased the mechanical and swelling properties of biomaterial hydrogel.[38,39] From this viewpoint, a hypothesis is proposed in Figure 9C.

When a 7S-CMF mixture was obtained at neutral pH, the presence of a CMFs network provided an initial framework, and then the protein coated on the CMFs network via electrostatic attractive force because protein carried a complementary charge in this case. However, the presence of excessive protein in the aqueous phase might exist around the CMFs framework and produce a net negative charge of the whole system (Figure 4). After MTGase induced covalent cross-linking, the 7S-CMF composite gel system was achieved. The CMFs played a key role as a gel backbone, while the role of the 7S protein was to participate in network development as a coating and gelation component. Thanks to the presence of CMFs, a more organized and rigid microstructure was remodeled, resulting a shorter gelation time and stronger gel strength. This reinforced behavior indicated that CMFs in this work had a similar reinforcing effect with other nano- or microfillers such as nanoparticles and nanocrystals, which can indicate that the uniformly dispensed nano- or microfillers can transfer the load from the polymer chain to themselves and stop the growing of microcracks.[38−40] Moreover, Zhou et al.[39] suggested that the mechanical properties of composite hydrogels depend not only on the reinforced properties of fillers, but also on interactions between the filler and the matrix, resembling the electrostatic coating of SP on rthe CMFs network in this paper.

In conclusion, a stable chitin microfibers suspension was successfully fabricated by passing chitin particles through a microfluidizer. As shown in the morphology analysis, high-pressure treatment disassemble the chitin particles into chitin microfibers. As a result, the enlarged steric structure and released amino groups improved the colloidal stability by a steric stabilizing and electrostatic repulsion effect. The most interesting finding in this paper was that the presence of the CMFs network improved the gel strength of the MTGase

cross-linked 7S gel significantly. The amount of CMFs was found to be a factor that affected the gel properties as well. The more CMFs the gel contained, the faster and the tougher the gel formed. The fracture stress and fracture strain also increased as a function of CMFs content. We inferred that the presence of CMFs provided an initial framework for gel formation and added structural rigidity to the 7S gel. The role of protein was to participate in network development as an electrostatic coating and gelation component. These findings will provide a new path for application of chitin in food.

AUTHOR INFORMATION

Corresponding Author

*Tel: (+86 20) 87114262. Fax: (+86 20) 87114263. E-mail: fexqyang@163.com; fexqyang@scut.edu.cn.

Funding

This work is part of the research projects of Chinese National Natural Science Fund (Serial Number: 31371744 and 31130042, sponsored by the NSFC) and National High Technology Research and Development Program of China (863 Program: 2013AA102208-3).

Notes

The authors declare no competing financial interest.

REFERENCES

(1) Mezzenga, R.; Schurtenberger, P.; Burbidge, A.; Michel, M. Understanding foods as soft materials. *Nat. Mater.* **2005**, *4*, 729−740.

(2) Shams, M. I.; Nogi, M.; Berglund, L. A.; Yano, H. The transparent crab: preparation and nanostructural implications for bioinspired optically transparent nanocomposites. *Soft Matter* **2012**, *8*, 1369−1373.

(3) Fernandes, S. C. M.; Oliveira, L.; Freire, C. S. R.; Silvestre, A. J. D.; Neto, C. P.; Gandini, A.; Desbriéres, J. Novel transparent nanocomposite films based on chitosan and bacterial cellulose. *Green Chem.* **2009**, *11*, 2023−2029.

(4) Araki, J.; Yamanaka, Y.; Ohkawa, K. Chitin-chitosan nanocomposite gels: reinforcement of chitosan hydrogels with rod-like chitin nanowhiskers. *Polym. J.* **2012**, *44*, 713−717.

(5) Aouada, F. A.; de Moura, M. R.; Orts, W. J.; Mattoso, L. H. Preparation and characterization of novel micro- and nanocomposite hydrogels containing cellulosic fibrils. *J. Agric. Food Chem.* **2011**, *59*, 9433−9442.

(6) Yano, H.; Sugiyama, J.; Nakagaito, A. N.; Nogi, M.; Matsuura, T.; Hikita, M.; Handa, K. Optically transparent composites reinforced with networks of bacterial nanofibers. *Adv. Mater.* **2005**, *17*, 153−155.

(7) Pääkkö, M.; Ankerfors, M.; Kosonen, H.; Nykänen, A.; Ahola, S.; Österberg, M.; Ruokolainen, J.; Laine, J.; Larsson, P. T.; Ikkala, O.; Lindstrom, T. Enzymatic hydrolysis combined with mechanical shearing and high-pressure homogenization for nanoscale cellulose fibrils and strong gels. *Biomacromolecules* **2007**, *8*, 1934−1941.

(8) Zeng, J. B.; He, Y. S.; Li, S. L.; Wang, Y. Z. Chitin whiskers: an overview. *Biomacromolecules* **2012**, *13*, 1−11.

(9) Lee, S. Y.; Chun, S. J.; Kang, I. A.; Park, J. Y. Preparation of cellulose nanofibrils by high-pressure homogenizer and cellulose-based composite films. *J. Ind. Eng. Chem.* **2009**, *15*, 50−55.

(10) Liu, D. G.; Chang, P. R.; Chen, M. D.; Wu, Q. L. Chitosan colloidal suspension composed of mechanically disassembled nanofibers. *J. Colloid Interface Sci.* **2011**, *354*, 637−643.

(11) Koide, S. S. Chitin-chitosan: properties, benefits and risks. *Nutr. Res. (N.Y.)* **1998**, *18*, 1091−1101.

(12) Nagahama, H.; Nwe, N.; Jayakumar, R.; Koiwa, S.; Furuike, T.; Tamura, H. Novel biodegradable chitin membranes for tissue engineering applications. *Carbohyd. Polym.* **2008**, *73*, 295−302.

(13) Liu, D. G.; Wu, Q. L.; Chang, P. R.; Gao, G. Z. Self-assembled liquid crystal film from mechanically defibrillated chitosan nanofibers. *Carbohyd. Polym.* **2011**, *84*, 686−689.

(14) Zhou, C. J.; Wu, Q. L. A novel polyacrylamide nanocomposite hydrogel reinforced with natural chitosan nanofibers. *Colloid. Surface. B* **2011**, *84*, 155−162.

(15) Liu, D. G.; Zhu, Y.; Li, Z. H.; Tian, D. L.; Chen, L.; Chen, P. Chitin nanofibrils for rapid and efficient removal of metal ions from water system. *Carbohyd. Polym.* **2013**, *98*, 483−489.

(16) Motoki, M.; Seguro, K. Transglutaminase and its use for food processing. *Trends Food Sci. Technol.* **1998**, *9*, 204−210.

(17) Tang, C. H.; Li, L.; Wang, J. L.; Yang, X. Q. Formation and rheological properties of 'cold-set' tofu induced by microbial transglutaminase. *LWT–Food Sci. Technol.* **2007**, *40*, 579−586.

(18) Tang, C. H.; Wu, H.; Chen, Z.; Yang, X. Q. Formation and properties of glycinin-rich and β-conglycinin-rich soy protein isolate gels induced by microbial transglutaminase. *Food Res. Int.* **2006**, *39*, 87−97.

(19) Guo, J.; Zhang, Y.; Yang, X. Q. A novel enzyme cross-linked gelation method for preparing food globular protein-based transparent hydrogel. *Food Hydrocolloids* **2012**, *26*, 277−285.

(20) Zhang, J. B.; Wu, N. N.; Yang, X. Q.; He, X. T.; Guo, J.; Zhu, J. H. Improvement of microbial transglutaminase-induced gelation of β-conglycinin by conjugation with dextran. *Int. J. Food Sci. Technol.* **2014**, *49*, 976−982.

(21) Nagano, T.; Hirotsuka, M.; Mori, H.; Kohyama, K.; Nishinari, K. Dynamic viscoelastic study on the gelation of 7S globulin from soybeans. *J. Agric. Food Chem.* **1992**, *40*, 941−944.

(22) Folk, J. E.; Cole, P. W. Structural requirements of specific substrates for guinea pig liver transglutaminase. *J. Biol. Chem.* **1965**, *240*, 2951−2960.

(23) Yuan, Y.; Wan, Z. L.; Yang, X. Q.; Yin, S. W. Associative interactions between chitosan and soy protein fractions: Effects of pH, mixing ratio, heat treatment and ionic strength. *Food Res. Int.* **2014**, *55*, 207−214.

(24) Duncan, D. B. Multiple Range and Multiple F Tests. *Biometrics* **1955**, *11*, 1−42.

(25) Tzoumaki, M. V.; Moschakis, T.; Biliaderis, C. G. Metastability of nematic gels made of aqueous chitin nanocrystal dispersions. *Biomacromolecules* **2009**, *11*, 175−181.

(26) Kuijk, A.; Koppert, R.; Versluis, P.; van Dalen, G.; Remijn, C.; Hazekamp, J.; Nijsse, J.; Veikov, K. P. Dispersions of attractive semiflexible fiberlike colloidal particles from bacterial cellulose microfibrils. *Langmuir* **2013**, *29*, 14356−14360.

(27) Tzoumaki, M. V.; Moschakis, T.; Kiosseoglou, V.; Biliaderis, C. G. Oil-in-water emulsions stabilized by chitin nanocrystal particles. *Food Hydrocolloids* **2011**, *25*, 1521−1529.

(28) Espinosa-Andrews, H.; Enríquez-Ramírez, K. E.; García-Márquez, E.; Ramírez-Santiago, C.; Lobato-Calleros, C.; Vernon-Carter, J. Interrelationship between the zeta potential and viscoelastic properties in coacervates complexes. *Carbohyd. Polym.* **2013**, *95*, 161−166.

(29) Li, J.; Revol, J.; Naranjo, E.; Marchessault, R. Effect of electrostatic interaction on phase separation behaviour of chitin crystallite suspensions. *Int. J. Biol. Macromol.* **1996**, *18*, 177−187.

(30) Hejazi, R.; Amiji, M. Chitosan-based gastrointestinal delivery systems. *J. Controlled Release* **2003**, *89*, 151−165.

(31) Leksrisompong, P. N.; Foegeding, E. A. How micro-phase separation alters the heating rate effects on globular protein gelation. *J. Food Sci.* **2011**, *76*, 318−327.

(32) Abbasi, S.; Dickinson, E. Influence of sugars on high-pressure induced gelation of skim milk dispersions. *Food Hydrocolloids* **2001**, *15*, 315−319.

(33) Van den Berg, L.; Rosenberg, Y.; Van Boekel, M. A.; Rosenberg, M.; Van de Velde, F. Microstructural features of composite whey protein/polysaccharide gels characterized at different length scales. *Food Hydrocolloids* **2009**, *23*, 1288−1298.

(34) Van Kleef, F. S. M. Thermally induced protein gelation: gelation and rheological characterization of highly concentrated ovalbumin and soybean protein gels. *Biopolym.* **1986**, *25*, 31−59.

(35) Le, X. T.; Turgeon, S. L. Rheological and structural study of electrostatic cross-linked xanthan gum hydrogels induced by β-lactoglobulin. *Soft Matter* **2013**, *9*, 3063−3073.
(36) Renkema, J. M. S.; Knabben, J. H. M.; Van Vliet, T. Gel formation by β-conglycinin and glycinin and their mixtures. *Food Hydrocolloids* **2001**, *15*, 407−414.
(37) Marchessault, R. H.; Morehead, F. F.; Walter, N. M. Liquid crystal systems from fibrillar polysaccharides. *Nature* **1959**, *184*, 632−633.
(38) Shin, M. K.; Spinks, G. M.; Shin, S. R.; Kim, S. I.; Kim, S. J. Nanocomposite hydrogel with high toughness for bioactuators. *Adv. Mater.* **2009**, *21*, 1712−1715.
(39) Zhou, C. J.; Wu, Q. L.; Yue, Y. Y.; Zhang, Q. G. Application of rod-shaped cellulose nanocrystals in polyacrylamide hydrogels. *J. Colloid Interface Sci.* **2011**, *353*, 116−123.
(40) Wu, Y. T.; Zhou, Z.; Fan, Q. Q.; Chen, L.; Zhu, M. F. Facile in-situ fabrication of novel organic nanoparticle hydrogels with excellent mechanical properties. *J. Mater. Chem.* **2009**, *19*, 7340−7346.

JOURNAL OF AGRICULTURAL AND FOOD CHEMISTRY

Article

pubs.acs.org/JAFC

Variation in Amylose Fine Structure of Starches from Different Botanical Sources

Kai Wang,[†,‡] Jovin Hasjim,[†,‡] Alex Chi Wu,[†,‡] Robert J. Henry,[‡] and Robert G. Gilbert*[,†,‡]

[†]Tongji School of Pharmacy, Huazhong University of Science and Technology, Wuhan, Hubei 430030, People's Republic of China

[‡]Queensland Alliance for Agriculture and Food Innovation, Centre for Nutrition and Food Sciences, The University of Queensland, , Brisbane, Queensland 4072, Australia

Supporting Information

ABSTRACT: The molecular structures of amylose and amylopectin have an impact on functional properties of starch-containing food. This is the first study comparing amylose size distributions from various plant sources. Chain-length distributions (CLDs) of amylose and amylopectin branches ("fine structure") are characterized using size-exclusion chromatography [sometimes termed gel permeation chromatography (GPC)] and parametrized by both biosynthesis-based and empirical fits, to understand the starch biosynthesis mechanism and identify associations with starch digestibility. All starches show bimodal amylose weight CLDs, varying with plant sources, with potato tuber and sweet potato root starch having relatively longer branches than the others. The digestograms of all starches fit first-order kinetics. Unlike what has been seen in cooked grains/flours, amylose and amylopectin fine structures have no association with the digestibility of freshly gelatinized starch. This suggests that the observed effect in cooked grains/flours arises from a secondary interaction between amylose fine structure and higher order structural features.

KEYWORDS: *starch, amylose, size-exclusion chromatography, chain-length distribution, biosynthesis, digestibility*

INTRODUCTION

Starch is the main carbohydrate reserve in plants, is a major source of energy in human diet and animal feed, and has wide applications in industry. It is a polysaccharide, wherein the D-glucose monomer units are linearly extended by α-(1 → 4) glycosidic linkages and the branches are connected by α-(1 → 6) glycosidic linkages as branching points. Starch consists of two main molecules: amylose, mostly linear with a molecular weight of 10^5−10^6 and a few long branches, and amylopectin, the main component of normal starches, which is hyper-branched with a much higher molecular weight (10^7−10^8) and a vast number of short-chain branches. Both components have broad distributions of size and molecular weight. A common means of characterizing structure is the chain-length distribution (CLD), the weight or number distribution of individual chains following enzymatic debranching. We use the term "fine structure" to describe this.

Starch is synthesized in plants in various organs, including seeds, roots, tubers, and fruits, and in a wide range of species. Its structure of starch varies with plant source, contributed by the differences in the coordinated action of a series of enzymes involved in starch biosynthesis, including starch synthases (SS), starch branching enzymes (SBE), and starch debranching enzymes (DBE).[1] The molecular structure of amylopectin and the amylose content of many starches have been widely reported. However, amylose fine structure from different botanical sources is essentially unexplored.

The molecular structure of starch has significant impacts on its nutritional properties for humans, especially digestibility.[2] Rapidly digested starch leads to a high postprandial glycemic response and is believed to be related to some chronic diseases, including insulin resistance, diabetes, and obesity. Slowing down the digestion rate of starch, on the other hand, is beneficial in preventing diet-related metabolic diseases.[3,4] Similar to other dietary fibers, resistant starch (RS), the component of a starch that is not digested in the small intestine, is associated with the reduced risk of acquiring colorectal cancer.[5]

Some relationships between starch structure and digestibility have been reported; e.g., starches with short amylopectin branches are more susceptible to enzyme digestion.[6] It has also been reported that so-called "high-amylose" starches tend to have more RS compared to normal and waxy starches.[7,8] It is noted in this context that "high-amylose" starches are in fact starches containing a significant number of long chains, which could either belong to true amylose or be long amylopectin chains. Relationships between amylose fine structure and digestibility are still lacking because of limited data on amylose, with only a few studies on the impacts of amylose molecular fine structure on starch digestibility.[9−11]

This paper is the first study comparing amylose fine structures from different plant species and botanical origins and discussing their impacts on starch digestion properties. The CLDs of amylose and amylopectin branches are characterized using size-exclusion chromatography (SEC) after enzymatic debranching. The amylopectin CLDs were fitted with a mathematical model based on starch biosynthetic processes to reduce the CLDs to a few parameters from which the entire CLD was reproduced using the model and which are based on

Received: March 9, 2014
Revised: April 21, 2014
Accepted: April 23, 2014
Published: April 23, 2014

ACS Publications © 2014 American Chemical Society

the underlying biosynthetic processes;[12,13] having just a few parameters rather than a whole curve greatly facilitates a statistically meaningful comparison between different starch samples. The *in vitro* enzymatic digestion of freshly cooked starch samples is investigated, and correlations between amylose fine structure and starch digestibility are investigated.

MATERIALS AND METHODS

Materials. Four varieties of sorghum grains (RTx2737, B296, ICSV400, and BTx3054) grown in Narrabri (New South Wales, Australia) were provided by Dr. Alan Cruickshank from the Department of Agriculture, Fisheries and Forestry Queensland, Warwick, Queensland, Australia. One sorghum variety (S10) grown in Liverpool (New South Wales, Australia) was supplied by Professor Ian D. Godwin, the University of Queensland, Brisbane, Queensland, Australia. Barley grains from two commercial cultivars (Shepherd and Mackay) and two breeding lines (ND18076 and ND19119-5), developed by Dr. Jerome D. Franckowiak, were grown at Hermitage Research Facility, Warwick, Queensland, Australia, and provided by Dr. Glen Fox from the University of Queensland, who also supplied commercially available barley grain (Schooner) from an alternate location (Toowoomba, Queensland, Australia). Rice grains from four breeding lines (YRI08-04-10, YRJ08-03-13, YRA08-03-10, and YRD08-05-05) were supplied by Yanco Agricultural Institute, Department of Primary Industries, Yanco, New South Wales, Australia. In addition, Nipponbare rice grain, maize grain, wheat grain, field pea, and cow pea samples were supplied by Dr. Matthew K. Morell, Commonwealth Scientific and Industrial Research Organisation (CSIRO), Canberra, Australia. Potato tuber and sweet potato root samples were purchased from a grocery store in Brisbane, Queensland, Australia.

Protease from *Streptomyces griseus* (type XIV), pancreatin from porcine pancreas, and LiBr (ReagentPlus) were purchased from Sigma-Aldrich Pty. Ltd. (Castle Hill, New South Wales, Australia). Isoamylase (from *Pseudomonas* sp.), amyloglucosidase (from *Aspergillus niger*), and D-glucose (GOPOD Format) kit were purchased from Megazyme International, Ltd. (Bray Co., Wicklow, Ireland). A series of pullulan standards with peak molecular weights ranging from 342 to 2.35×10^6 were purchased from Polymer Standards Service (PSS) GmbH (Mainz, Germany). Dimethyl sulfoxide [DMSO, guaranteed reagent (GR) grade for analysis] was purchased from Merck Co., Inc. (Kilsyth, Victoria, Australia). All other chemicals were reagent-grade and used as received.

Extraction, Dissolution, and Debranching of Starch Molecules for Structural Analysis. All starch samples were extracted and dissolved in DMSO solution with 0.5% (w/w) LiBr (DMSO/LiBr), following a method described elsewhere,[14,15] with minor modifications. Legume seeds were used as harvested; cereal grains were manually dehulled; while potato tubers and sweet potato roots were manually peeled, cut into smaller cubes, and then freeze-dried. Each sample was then ground into fine flour using a cryo-mill (Freezer/Mill 6850 SPEX, Metuchen, NJ) in a liquid nitrogen bath. Milling was for 5 min at 10 s^{-1}. Each milled flour was treated with protease and sodium bisulfite solution, followed by centrifugation to remove protein. The treated flour was dissolved in DMSO/LiBr solution and precipitated using ethanol (each treatment followed by centrifugation) to remove insoluble and soluble non-starch components, respectively. The precipitate (extracted starch) was debranched using isoamylase, following the method by Hasjim et al.,[16] neutralized to pH ~7 using 0.1 M NaOH, heated in a water bath at 80 °C for 2 h, freeze-dried, and then dissolved in DMSO/LiBr solution for subsequent analysis by SEC.

SEC. The SEC weight distribution of debranched starch was analyzed in duplicate using an Agilent 1100 series SEC system (Agilent Technologies, Waldbronn, Germany) equipped with a refractive index detector (RID, ShimadzuRID-10A, Shimadzu Corp., Kyoto, Japan), as described elsewhere.[25,26] The background theory for the following treatment has been given in detail by Castro et al.[27] A series of SEC columns (GRAM precolumn and GRAM 100 and GRAM 1000 columns, PSS) placed in an oven at 80 °C were used to separate the debranched starch molecules. DMSO/LiBr solution was used as the mobile phase with a flow rate of 0.6 mL/min. Pullulan standards were used for calibration to convert from the SEC elution volume to the hydrodynamic volume V_h or the corresponding radius R_h using the Mark–Houwink equation. The Mark–Houwink parameters K and α of pullulan in DMSO/LiBr solution at 80 °C are 2.424×10^{-4} dL g^{-1} and 0.68, respectively.[25] This relation was also used to calculate the degree of polymerization (DP) of debranched starch molecules from R_h. The Mark–Houwink parameters K and α for linear starch in DMSO/LiBr at 80 °C are 0.0150 mL g^{-1} and 0.743, respectively.[28] For linear polymers (such as debranched starch), the number distribution, $N(X)$, can be obtained from the corresponding weight distribution obtained from the RID using the relation[26,27] $w(\log X) = X^2N(X)$.

Fitting Amylopectin Number CLDs with a Biosynthesis Model. The number CLD of amylopectin as a function of DP can be used to understand the enzymatic biosynthetic processes of amylopectin molecules in the plants. Each number CLD of amylopectin branches was fitted with a model of amylopectin biosynthesis,[12,13] using a publicly available code.[29] The model considers the activities of the three core starch biosynthetic enzymes: soluble starch synthases that elongates glucan chains of amylopectin [termed SS, a role for amylose taken by granule-bound starch synthase (GBSS)], SBE (which introduces branches), and DBE (which trims excess branches). By fitting the number CLD of amylopectin with this model, a series of parameters can be obtained characterizing the enzymatic processes of the amylopectin biosynthesis. The activity ratios of SBE/SS and DBE/SS are denoted β and γ, respectively. From the mathematical development, each value of γ is associated with a value of β, so that γ is eliminated from the fitting.[12] In addition, SBE can only form branches with lengths longer than a certain minimum DP, X_{min}, and the length of moiety retained after branching must be more than a certain minimum DP, X_0. X_{min} and X_0 are also used as parameters to describe the enzymatic processes. It has been shown[30] that the CLD of amylopectin branches with DP $\lesssim$ 70 obtained using SEC is contributed by two enzyme sets, denoted enzyme sets i and ii, and the relative contribution of each is termed $h_{(ii,i)}$. In actuality, more enzyme sets are involved, but the band broadening in SEC is such that the components of the chains confined to a single lamella arising from two enzyme sets[30] cannot be distinguished. Thus, the parameters characterizing the single-lamellar SEC CLDs are in fact averages over those for the two underlying enzyme sets.

Isolation of Starch Granules by Wet Milling. Starch granules were isolated from cryo-milled flours by wet milling, following the slightly modified method by Syahariza et al.[15] Each flour sample (2 g) was steeped in 6 mL of sodium bisulfite solution (0.45% sodium metabisulfite, w/v) overnight and then milled using a homogenizer (T-25 ULTRA-TURRAX, IKA, Wilmington, NC) for 3 min. The homogenized slurry was filtered through a 53 μm screen. The flour particles that remained on the screen were homogenized and filtered, and this process was repeated 3 times or more, until no flour particles were visible on the screen. All filtrate fractions were combined and mixed with NaCl solution (0.1 M) and toluene at a ratio of 9:1 to remove proteins and lipids. The mixture was stirred for 1 h and then allowed to stand until the starch granules settled at the bottom. The toluene layer and most of the NaCl solution layer were siphoned off, and the NaCl solution/toluene steps were repeated several times until the toluene layer seemed clear, indicating no proteins or lipids. The isolated starch granules were washed repeatedly with water and ethanol, followed by air-drying at room temperature for 1 day.

***In Vitro* Starch Digestibility.** Isolated starch granules (50 mg, dry weight basis) were suspended in 2 mL of distilled water and gelatinized in a boiling water bath for 30 min with stirring and occasional vortex mixing. Each freshly gelatinized starch sample was dissolved with 7.5 mL of sodium acetate buffer (0.2 M, pH 6.0, containing 0.49 mM $MgCl_2$, 200 mM $CaCl_2$, and 0.02% NaN_3) and equilibrated at 37 °C for 15 min. An enzyme solution (0.5 mL) containing 25 μg of pancreatin and 12.5 μL of amyloglucosidase in sodium acetate buffer solution was added to the starch suspension, and the mixture incubated in a water bath at 37 °C with stirring at 200

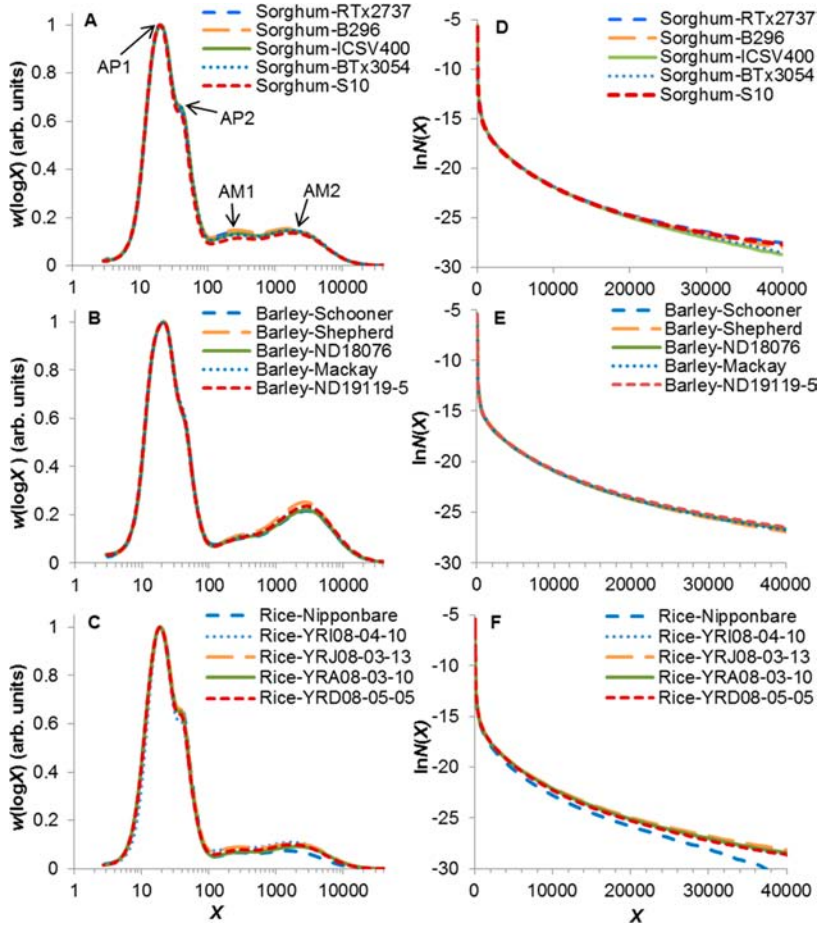

Figure 1. SEC weight and number CLDs of debranched starches extracted from (A and D) sorghum, (B and E) barley, and (C and F) rice varieties, respectively. All distributions were normalized to yield the same height of the first peak to avoid the effect of different sample concentrations.

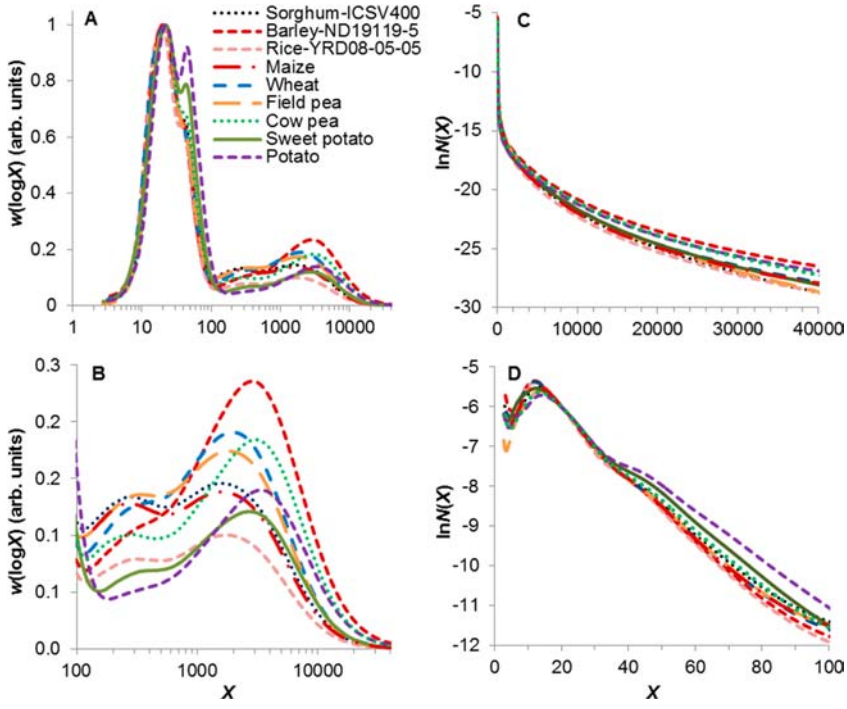

Figure 2. SEC weight CLDs of (A) debranched starch and (B) amylose and number CLDs of (C) starch and (D) amylopectin extracted from different species. All distributions were normalized to yield the same height of the first peak to avoid the effect of different sample concentrations.

dx.doi.org/10.1021/jf5011676 | J. Agric. Food Chem. 2014, 62, 4443−4453

rpm. Starch digesta (0.1 mL) were collected at 0, 10, 20, 40, 60, 90, 120, 180, 240, and 300 min, and the digestion was stopped by adding 0.9 mL of absolute ethanol. The digestibility of freshly gelatinized starch (g/100 g of dry starch) was determined from the amount of glucose released in the supernatant, tested using the Megazyme D-glucose kit, with a conversion factor of 0.9 (the ratio of the molecular weight of the anhydroglucose monomer unit in starch to that of glucose). The digestogram, for C = concentration of digested starch at time t, was fitted to first-order kinetics[31]

$$\ln(dC/dt) = \ln(C_\infty k) - kt \quad (1)$$

where k is the digestion rate coefficient and C_∞ is the concentration at long times.

Statistical Analysis. Each analysis was carried out in duplicate. Mean value and standard deviation were analyzed by Minitab 16 (Minitab, Inc., State College, PA) using analysis of variance (ANOVA) with the general linear model and Tukey's pairwise comparisons. Significant differences of the mean values were determined at $p < 0.05$. Box plots were also performed using Minitab 16 to compare the structural differences among barley, sorghum, and rice starches. Pearson's and Spearman's rank correlations were conducted using SPSS version 21 software (SPSS, Inc., Chicago, IL).

RESULTS AND DISCUSSION

CLDs. The amylose fine structural features of particular interest in the present paper are the SEC weight distribution and number distribution (termed SEC weight CLD and number CLD) of glucan chains from debranched starch as a function of the DP, X, denoted $w(\log X)$ and $N(X)$ (see Figures 1 and 2). There are a number of experimental points in this regard. Amylose branches readily retrograde (reassociate into a double helical structure) in water because of the long linear structure[17] and become less soluble, resulting in overestimation of their molecular size. Aqueous solutions with some additional treatments, including alkaline pH, high temperature, microwave, and autoclave, have been used to improve the solubility of amylose in water.[18−21] However, degradation of starch molecules may happen under these harsh conditions. Dissolution in DMSO with lithium salts has been shown to dissolve starch molecules completely without significant degradation and retrogradation.[15,22] Finally, the amylose CLD here is obtained using SEC. While fluorophore-assisted carbohydrate electrophoresis (FACE) gives very accurate CLDs for amylopectin chains,[23] this method is inapplicable to the longer chains in amylose, a problem that does not exist with SEC. However, SEC suffers from inaccuracies arising from band broadening and from calibration to relate the DP to elution volume.[24] The latter problem cannot be overcome using light-scattering detection for smaller chains, because of signal/noise limitations. These two problems are fortunately not significant for the semi-quantitative objectives of the present paper.

The CLDs of debranched starches from several sorghum, barley, and rice varieties are presented in Figure 1, and those from other botanical sources are presented in Figure 2. All starch samples show typical SEC weight and number CLDs of debranched starch. The components with $X < 100$ are amylopectin chains, while those with $X \geq 100$ are amylose chains. The SEC weight CLDs of debranched starches from all samples show four peaks or shoulders (panels A−C of Figure 1 and Figure 2A). The first peak (denoted by AP1) is the global maximum, which comprises the shorter amylopectin branches with lengths up to DP of 30, normally confined to one amorphous/crystalline lamella. The second peak or shoulder (denoted by AP2) represents the longer amylopectin branches with DPs ranging from 30 to 100, which span more than one crystalline lamella. There are also two peaks for amylose CLDs, the shorter and longer amylose branches, AM1 (X = 100−700) and AM2 (X = 700−40 000). This implies that these arise from potentially discrete enzymatic starch biosynthetic processes,[9] whose nature is unknown. For instance, one possibility is that the branches belonging to AM1 and AM2 originate from different isoforms of GBSS, the main enzyme synthesizing amylose; however, further investigations are needed to verify such speculation and to unveil the nature of the underlying mechanism.

Both SEC weight (panels A−C of Figure 1) and number (panels of Figure 1D-F) CLDs of debranched starches from cereal grains of different varieties within the same plant species generally show small differences. To compare this fine structure between starches, a set of empirical parameters was defined and obtained from the SEC weight CLDs.[9,10] These are the DP at the maximum of each peak, donated by X_{AP1}, X_{AP2}, X_{AM1}, and X_{AM2}, and the height of the each maximum relative to that of AP1, $h_{AP2/AP1}$, $h_{AM1/AP1}$, and $h_{AM2/AP1}$. The DP at the maximum of each peak reflects the relative size of chains in each group of branches, while the height ratio of each peak maximum to AP1 represents the relative amount of chains in each group of branches. As noted, because of band broadening, the two peaks/shoulders from the shorter and longer amylopectin branches and the two peaks/shoulders from the shorter and longer amylose branches are overlapping. The amylose content was calculated by the ratio of the area under the curve (AUC) of amylose branches to that of the overall SEC weight CLD of debranched starch.[32]

Structural parameters of starches from sorghum, barley, and rice varieties are compared in Figure 3. There are small differences in the parameters among the starches from different varieties within the same species (see Table S1 of the Supporting Information); however, some significant differences are observed among the starches from sorghum, barley, and rice grains (Figure 3). The X_{AM1} and $h_{AM1/AP1}$ values of barley starches cannot be obtained because the AM1 peak in the SEC weight CLDs of debranched barley starches is too small and broad; therefore, structural parameters of barley starches are not included in the comparison. Rice starches have higher X_{AM1} than sorghum starches, but the opposite trend is observed for $h_{AM1/AP1}$ values. The X_{AM2} values of barley starches are significantly higher than those of sorghum and rice starches. Barley starches have the largest amylose contents and $h_{AM2/AP1}$ values among the starches from the three cereal grains, whereas rice starches have the lowest. The X_{AP1} values show a similar trend to amylose content and $h_{AM2/AP1}$ values, suggesting that there are probably interrelationships between amylopectin and amylose CLDs. Rice starches also have significantly smaller X_{AP2} than barley and sorghum starches. On the other hand, the $h_{AP2/AP1}$ values are not significantly different among the starches from the three cereal grains.

The same analysis was performed for a series of starches extracted from a range of plant species and organs, including maize grain, wheat grain, cow pea, field pea, potato tuber, and sweet potato root. Because all samples are normal starches, the effects of varieties within the same species are less significant and, hence, only one variety of each sorghum, barley, and rice (ICSV400, ND19119-5, and YRD08-05-05, respectively), with structural parameters near the average among all varieties within each cereal grain, was chosen as the representative for comparison to the starches from other botanical sources. The weight and number CLDs of these starch samples are presented

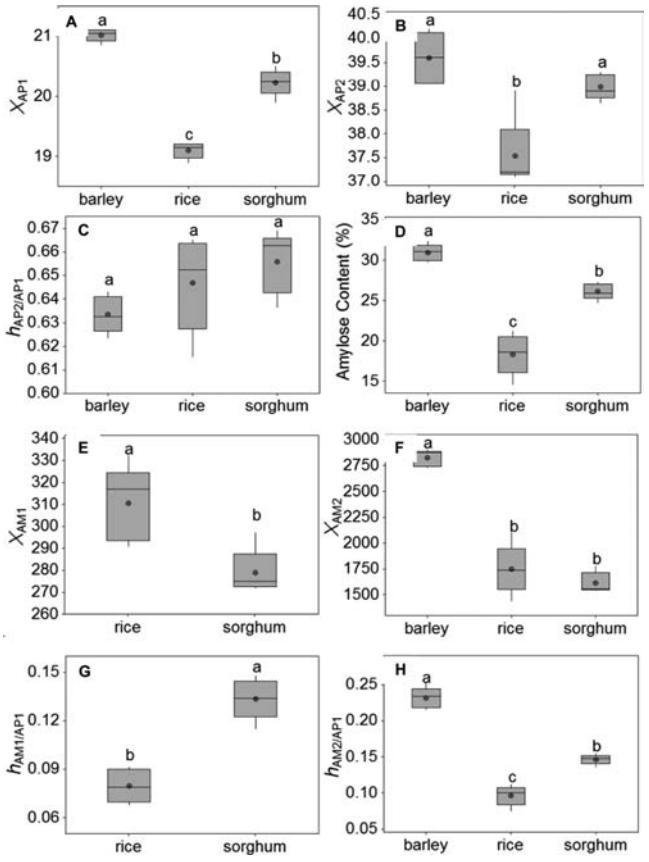

Figure 3. Comparison of the structural parameters from SEC weight CLDs among the starches extracted from sorghum, barley, and rice: (A) X_{AP1}, (B) X_{AP2}, (C) $h_{AP2/AP1}$, (D) amylose content, (E) X_{AM1}, (F) X_{AM2}, (G) $h_{AM1/AP1}$, and (H) $h_{AM2/AP1}$. Panels A, B, and C, amylopectin chains; panels E, F, G, and H, amylose chains. Samples with different letters above the boxes are significantly different at $p < 0.05$.

in Figure 2. The structural parameters are given in Table 1. Although some differences can be observed among the CLDs of starches from different botanical sources presented as number distributions $N(X)$ (Figure 2C), more details in the differences are apparent in the weight CLDs $w(\log X)$ (panels A and B of Figure 2). Differences in amylopectin CLDs among samples can also be seen from the number CLDs of amylopectin branches (Figure 2D). Presenting the same data in different ways can emphasize the different features of the CLD. The weight CLD shows the variations in the structure of amylose branches better than the number CLD.

The amylose contents vary substantially among the starch samples from different botanical sources (Table 1). This is a well-known observation and will only be briefly discussed here; all results are consistent with the literature. Legume seed starches contain the highest amylose,[33] whereas potato tuber and sweet potato root starches have the lowest.[34] The amylose contents of the starches in cereal grains are widely distributed, from barley starch having similar amylose content to legume seed starches to rice starch similar to potato tuber and sweet potato root starches. The amylose content of potato starch was reported to vary from 23 to 31%,[33−35] and that of wheat starch in the literature ranges from 19.3 to 32.7%.[34,36,37] Different values of the amylose content in rice and maize starches have also been reported, e.g., by Fitzgerald et al.[38] In addition the differences in the genetic background of the plant sources,

Table 1. Structural Parameters Obtained from SEC Weight CLDs of Debranched Starches from Different Botanical Origins[a]

		DP of peak maximum in SEC weight molecular size distribution of debranched starch				height of peak maximum in SEC weight molecular size distribution of debranched starch as a ratio to AP1 peak height		
plant species	amylose content (%)	X_{AP1}	X_{AP2}	X_{AM1}	X_{AM2}	$h_{AP2/AP1}$	$h_{AM1/AP1}$	$h_{AM2/AP1}$
barley (ND19119-5)	31.3 ± 0.8 a	20.9 ± 0.1 cd	39.6 ± 0.0 b	–	2875 ± 64 b	0.633 ± 0.008 e	–	0.236 ± 0.008 a
sorghum (ICSV400)	25.9 ± 0.3 cd	20.5 ± 0.3 de	39.2 ± 0.0 bc	275 ± 5 d	1560 ± 28 c	0.663 ± 0.012 cd	0.134 ± 0.001 a	0.146 ± 0.001 c
rice (YRD08-05-05)	18.6 ± 0.6 e	18.9 ± 0.0 f	37.2 ± 0.3 c	317 ± 4 bc	1740 ± 113 c	0.640 ± 0.001 de	0.079 ± 0.001 bc	0.101 ± 0.006 e
maize	25.2 ± 0.4 d	20.2 ± 0.1 e	38.8 ± 1.1 bc	270 ± 9 d	1550 ± 170 c	0.654 ± 0.010 de	0.128 ± 0.006 a	0.139 ± 0.001 cd
wheat	28.1 ± 0.0 bc	21.4 ± 0.4 bc	39.8 ± 0.0 b	354 ± 17 b	1965 ± 163 c	0.635 ± 0.001 e	0.129 ± 0.008 a	0.191 ± 0.001 b
cow pea	27.8 ± 0.9 bc	21.6 ± 0.0 ab	40.1 ± 0.6 b	291 ± 13 cd	3010 ± 156 ab	0.689 ± 0.001 c	0.101 ± 0.007 b	0.185 ± 0.012 b
field pea	29.5 ± 0.8 ab	21.2 ± 0.1 bc	39.1 ± 0.6 bc	335 ± 2 b	1785 ± 21 c	0.644 ± 0.009 de	0.136 ± 0.006 a	0.174 ± 0.006 b
potato	18.2 ± 0.3 e	22.2 ± 0.1 a	44.9 ± 0.0 a	–	3365 ± 106 a	0.921 ± 0.004 a	–	0.140 ± 0.003 cd
sweet potato	17.9 ± 0.5 e	22.1 ± 0.0 a	43.3 ± 0.2 a	433 ± 6 a	2665 ± 134 b	0.790 ± 0.004 b	0.069 ± 0.004 c	0.121 ± 0.001 de

[a]Mean ± standard deviation is calculated from duplicate measurements. "–" means the parameters cannot be identified, because the peak is too small and/or broad to determine the local maximum, which appears as a shoulder of the adjacent larger peak. Values with different letters in the same column are significantly different at $p < 0.05$.

dx.doi.org/10.1021/jf5011676 | J. Agric. Food Chem. 2014, 62, 4443−4453

multiple methods were used to test the amylose content in the literature and different methods measure different properties of starch that are then converted to the amylose content.[38,39]

The fine structures of amylose molecules and their relationships with amylopectin fine structure and starch properties are largely unexplored. The AM1 peaks of potato tuber and barley grain starches, as mentioned above, appear only as the shoulders of the AM2 peaks; therefore, the X_{AM1} and $h_{AM1/AP1}$ values of potato tuber and barley grain starches cannot be determined. With this exception, sweet potato root starch shows the highest X_{AM1} value but the lowest $h_{AM1/AP1}$ value among all starches. The X_{AM1} values of the other starches are quite similar, ranging from 270 to 354. Sorghum grain, maize grain, wheat grain, and field pea starches show similar $h_{AM1/AP1}$ values (around 0.13), while those for sweet potato root, rice grain, and cow pea starches are significantly lower. The X_{AM2} of potato tuber starch is the highest, followed by cow pea, barley grain, and sweet potato root starches in decreasing order, all of which are above 2600; on the other hand, those of wheat grain, field pea, rice grain, sorghum grain, and maize grain starches are markedly lower (between 1550 and 1965). The $h_{AM2/AP1}$ values of the AM2 peaks differ significantly among all samples, ranging from 0.101 to 0.236 and without clear distinctions among cereal grain, legume seed, tuber, and root starches. These results imply that the amylose molecules of potato tuber and sweet potato root starches have relatively longer branches than most cereal grain and legume seed starches, although their amylose contents are smaller.

In general, potato tuber and sweet potato root starches have the highest values of X_{AP1}, and cereal grains starches have the lowest values; although the differences are statistically significant ($p < 0.05$), the difference is only three monomer units between the largest and smallest X_{AP1}. On the other hand, both X_{AP2} and $h_{AP2/AP1}$ of potato tuber and sweet potato root starches are significantly and substantially higher than the other starches (from three to eight monomer units larger for X_{AP2} and 115−145% higher for $h_{AP2/AP1}$), with less significant differences among cereal grain and legume seed starches. That is, the amylopectin chains of potato tuber and sweet potato root starches are relatively longer than those of cereal grain (barley, sorghum, rice, maize, and wheat) and legume seed (cow pea and field pea). This might be related to the crystalline structure of starch. The crystalline structure of native starch granules can be grouped into three polymorphisms: A-, B-, and C-type polymorphs. The A-type polymorphic starch has a crystalline structure with monoclinic unit cells, whereas the B-type polymorphic starch has a crystalline structure with hexagonal unit cells and a water channel in the middle of each unit cell. The B-type starches, for instance, potato tuber starch, have longer average amylopectin chains and greater proportions of longer amylopectin chains than the A-type starches (barley, sorghum, rice, maize, and wheat).[40,41] This is probably because the larger proportion of long amylopectin branches requires more space, which is satisfied by the water channel in the unit cells of the B-type crystalline structure aligning into a stable crystalline structure. Because the C-type polymorph is a mixture of A- and B-type polymorphs, the average chain lengths of amylopectin chains of the C-type starches (cow pea, field pea, and sweet potato root starches) are in between those of A- and B-type polymorphic starches.[42−44]

Treating Amylopectin CLD with the Biosynthesis Model. Fitting the number CLDs of amylopectin (Figure 2D) with the amylopectin biosynthesis model[12,13] provides information on the activities of the core starch synthesizing enzymes and gives key insights into starch biosynthesis, the mechanism of which is still largely unclear. It also provides predictions for studies on enzymatic requirements for producing starch with targeted structure. Furthermore, the fitted parameters thus obtained, along with the structural parameters in Table 1, can be used to obtain the interrelationship between amylose and amylopectin fine structures. The fitted number CLD quantitatively reproduces the significant features of the experimental SEC number CLD of amylopectin branches (see Figure S1 of the Supporting Information). The $X_{0(i)}$ and $X_{0(ii)}$ values were set to 4 and 1, respectively, for all starch samples, as reported by Wu and Gilbert.[12] The $X_{min(i)}$ and $X_{min(ii)}$ values are similar among all starch samples (10−12 and 7−8, respectively), and in some cases, the fitting was not dramatically changed by altering X_{min} slightly. Hence, $X_{min(i)}$ and $X_{min(ii)}$ were excluded for the comparison among different starch samples. As discussed, SEC band broadening hides subtler features in the amylopectin CLD. There are extensive literature discussions on fine-structure features (e.g., by Jane et al.[40] and Cuevas et al.[45]).

Significant differences are observed in the fitted enzymatic activities among the three cereal grain (sorghum, barley, and rice) starches (Figure 4), suggesting that there are systematical differences in the enzymatic processes of starch biosynthesis in different plant species. Slight differences are also present in the fitting parameters among different varieties within the same species, reflecting the effects of genetic variations and/or environmental conditions in starch biosynthesis (see Table S2

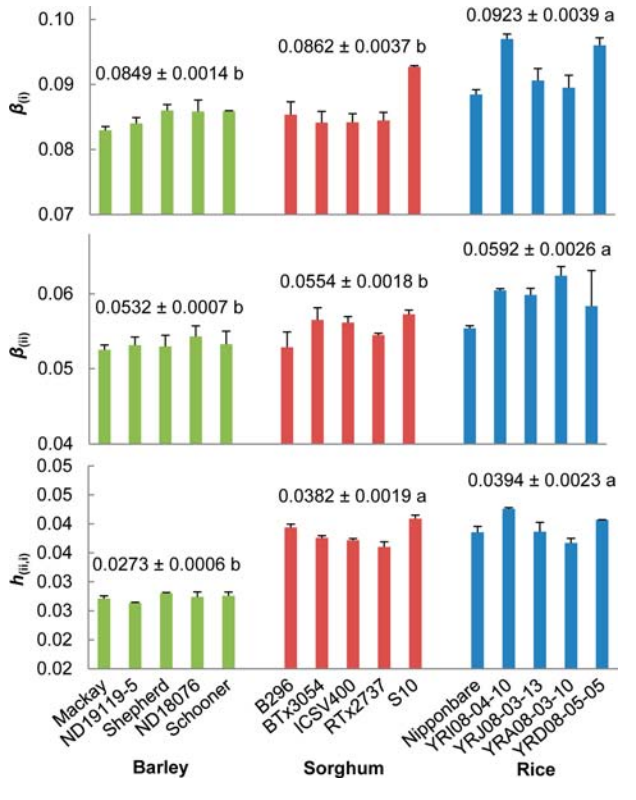

Figure 4. Parameters obtained from fitting the number CLD of barley (green), sorghum (red), and rice (blue) starches to the mathematical model: $\beta_{(i)}$, $\beta_{(ii)}$, and $h_{(ii,i)}$. Mean ± standard deviation is calculated from the five varieties of each plant species. Values with different letters are significantly different at $p < 0.05$.

dx.doi.org/10.1021/jf5011676 | J. Agric. Food Chem. 2014, 62, 4443−4453

Table 2. Parameters Obtained from Fitting the Number CLDs of Starches from Different Botanical Origins to the Mathematical Model[a]

plant species	botanical organ	fitting parameters		
		$\beta_{(i)}$	$\beta_{(ii)}$	$h_{(ii,i)}$
barley (ND19119-5)	cereal grain	0.0840 ± 0.0009 bc	0.0531 ± 0.0011 ab	0.0263 ± 0.0001 h
sorghum (ICSV400)	cereal grain	0.0842 ± 0.0010 bc	0.0562 ± 0.0008 a	0.0372 ± 0.0003 d
rice (YRD08-05-05)	cereal grain	0.0960 ± 0.0012 a	0.0584 ± 0.0048 a	0.0407 ± 0.0001 c
maize	cereal grain	0.0863 ± 0.0002 b	0.0570 ± 0.0009 a	0.0347 ± 0.0003 ef
wheat	cereal grain	0.0837 ± 0.0004 bc	0.0534 ± 0.0002 ab	0.0284 ± 0.0007 g
cow pea	legume seed	0.0797 ± 0.0002 d	0.0529 ± 0.0008 ab	0.0405 ± 0.0001 c
field pea	legume seed	0.0825 ± 0.0002 cd	0.0544 ± 0.0012 ab	0.0332 ± 0.0007 f
potato	tuber	0.0735 ± 0.0002 e	0.0477 ± 0.0002 b	0.0700 ± 0.0004 a
sweet potato	root	0.0754 ± 0.0010 e	0.0523 ± 0.0021 ab	0.0462 ± 0.0001 b

[a]Mean ± standard deviation is calculated from duplicate measurements. Values with different letters in the same column are significantly different at $p < 0.05$.

Table 3. Correlation Coefficients among Starch Fine Structures and Digestion Rate Coefficient

		amylose content	X_{AP1}	X_{AP2}	X_{AM1}	X_{AM2}	$h_{AP2/AP1}$	$h_{AM1/AP1}$	$h_{AM2/AP1}$	$\beta_{(i)}$	$\beta_{(ii)}$	$h_{(ii,i)}$
Pearson's correlation	amylose content	1										
	X_{AP1}	0.444[a]	1									
	X_{AP2}	−0.022	0.842[b]	1								
	X_{AM1}	−0.324	0.437	0.559[a]	1							
	X_{AM2}	0.280	0.708[b]	0.638[b]	0.541[a]	1						
	$h_{AP2/AP1}$	−0.443[a]	0.506[a]	0.832[b]	0.572[a]	0.427	1					
	$h_{AM1/AP1}$	0.904[b]	0.333	0.041	−0.490	−0.367	−0.314	1				
	$h_{AM2/AP1}$	0.915[b]	0.617[b]	0.225	−0.066	0.598[b]	−0.221	0.750[b]	1			
	$\beta_{(i)}$	−0.179	−0.886[b]	−0.885[b]	−0.311	−0.547[a]	−0.697[b]	−0.299	−0.326	1		
	$\beta_{(ii))}$	−0.362	−0.858[b]	−0.822[b]	−0.181	−0.612[b]	−0.547[a]	−0.412	−0.552[b]	0.811[b]	1	
	$h_{(ii,i)}$	−0.662[b]	0.101	0.513[a]	0.229	0.090	0.855[b]	−0.544[a]	−0.559[b]	−0.314	−0.187	1
	k	−0.043	0.081	0.208	−0.006	−0.052	0.017	−0.032	−0.029	−0.170	−0.129	−0.072
Spearman's rank correlation	amylose content	1										
	X_{AP1}	0.455[a]	1									
	X_{AP2}	0.367	0.888[b]	1								
	X_{AM1}	−0.192	0.090	0.128	1							
	X_{AM2}	0.376	0.636[b]	0.623[b]	0.650[b]	1						
	$h_{AP2/AP1}$	−0.497[a]	0.168	0.177	−0.342	−0.155	1					
	$h_{AM1/AP1}$	0.842[b]	0.393	0.185	−0.487	−0.324	−0.080	1				
	$h_{AM2/AP1}$	0.964[b]	0.632[b]	0.566[b]	−0.154	0.502[a]	−0.359	0.770[b]	1			
	$\beta_{(i)}$	−0.310	−0.889[b]	−0.826[b]	−0.104	−0.417	−0.411	−0.380	−0.492[a]	1		
	$\beta_{(ii)}$	−0.422	−0.824[b]	−0.776[b]	−0.041	−0.522[a]	−0.284	−0.312	−0.606[b]	0.788[b]	1	
	$h_{(ii,i)}$	−0.767[b]	−0.173	−0.145	0.132	−0.203	0.531[a]	−0.486	−0.703[b]	0.077	0.121	1
	k	−0.043	0.088	0.152	−0.091	−0.120	0.013	−0.108	−0.007	−0.071	−0.078	−0.203

[a]Correlation is significant at the 0.05 level. [b]Correlation is significant at the 0.01 level.

of the Supporting Information). These show that fitting the SEC number CLDs to this model not only allows for a quantitative comparison of the differences in the enzymatic processes in amylopectin biosynthesis among different species but also shows the small variations among different varieties within the same species.

Similar to the previous section, one variety of each of the sorghum, barley, and rice grain starches (ICSV400, ND19119-5, and YRD08-05-05, respectively) is compared to those from other botanical sources (maize grain, wheat grain, cow pea, field pea, potato tuber, and sweet potato root). The fitting parameters are summarized in Table 2. The $\beta_{(i)}$ values of cereal grain starches are significantly higher than those of the potato tuber and sweet potato root starches, and those of legume seed starches lie in between the other two groups. That is, the activity of SBE in relative to that of SS during amylopectin biosynthesis is higher (or equivalently there is a greater relative branching rate) in cereal grains than in potato tuber or sweet potato root, producing a greater fraction of single-lamella amylopectin branches and/or shorter length of amylopectin chains in cereal grains. This is consistent with the trends of X_{AP1}, X_{AP2}, and $h_{AP2/AP1}$ values (Table 1). The $\beta_{(ii)}$ values compared to the $\beta_{(i)}$ values show no clear trends among the different starch samples, whereas the $h_{(ii,i)}$ values show the opposite trend to the $\beta_{(i)}$ values. The effects of the enzyme set i on the number CLD are more significant than those of enzyme set ii, indicating that the differences in the proportion of longer amylopectin branches among all starch samples, as observed from the SEC weight CLDs (Figure 2A), are mainly due to the differences in the reaction rates of enzyme set i.

Understanding Starch Biosynthesis through Parametrization. The coefficients from Pearson's and Spearman's

dx.doi.org/10.1021/jf5011676 | J. Agric. Food Chem. 2014, 62, 4443−4453

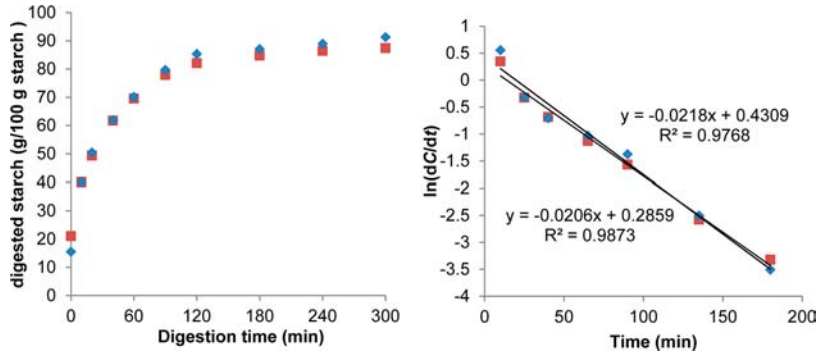

Figure 5. Digestogram of freshly cooked barley starch (shepherd) in duplicates, and the fitting of these digestograms to first-order kinetics.

rank correlation tests among the starch structural and fitting parameters are summarized in Table 3. Pearson's correlation test detects linear relations, while Spearman's rank correlation test is also able to reveal non-linear relations.

In general, the amylose content has little or no significant correlation with DPs at local peak maxima and $h_{AP2/AP1}$ of amylopectin, suggesting that the increased biosynthesis of amylose has only minor effects on amylopectin fine structure. The amylose content is positively and significantly correlated with $h_{AM1/AP1}$ and $h_{AM2/AP1}$, simply because these contribute to the amylose content. In addition, the amylose content, $h_{AM1/AP1}$, and $h_{AM2/AP1}$ are strongly and negatively correlated with $h_{(ii,i)}$, implying a competitive relationship between the biosynthesis of longer amylopectin chains and those of amylose. This is consistent with a proposed mechanism where amylopectin chains are elongated by GBSS, then cleaved from amylopectin molecules, and become amylose molecules when a sufficient size is reached.[46]

The X_{AP1}, X_{AP2}, X_{AM2}, $h_{AM2/AP1}$, $\beta_{(i)}$, and $\beta_{(ii)}$ are significantly and positively correlated and are correlated with X_{AM1} and $h_{AP2/AP1}$. It has been hypothesized that shorter amylopectin chains are elongated by SSI and SSII, longer amylopectin branches are elongated by SSIII, and amylose is elongated by GBSS. SBE isoforms introduce new branches on starch molecules, while DBE isoforms trim excess branches during amylopectin biosynthesis. The correlations might indicate that some of these enzymes (or enzyme isoforms) share the same pool of substrates and/or are in complex formation with one another (for example, SSIIa, SSIII, SBEIIa, and SBEIIb have been found in the same complex[47]).

It is noteworthy that $\beta_{(i)}$ and $\beta_{(ii)}$ are negatively correlated with X_{AM2}, meaning that the decreased SBE activity and/or increased SS activity leads to an increase in the length of longer amylose chains. SS is believed to be responsible for synthesizing amylopectin and not associated with amylose synthesis. SBE, on the other hand, acts on both amylose and amylopectin. Thus, it is more likely that the length of longer amylose chains is negatively associated with SBE activity. Because amylose is synthesized in starch granules by GBSS,[46] this relationship between the length of longer amylose chains and SBE activity provides evidence for the presence of SBE within starch granules, although SBE is found mainly as a soluble form in plastid stroma.[48] In contrast to what is seen for X_{AM2}, X_{AM1} has no significant correlation with either $\beta_{(i)}$ or $\beta_{(ii)}$, indicating that SBE does not participate in the synthesis of short amylose chains. The explanation of this phenomenon might be because GBSS and SBE activities become low in the late stage of starch synthesis.[49] In this point of starch biosynthesis, GBSS probably tends to synthesize short amylose chains, while SBE activity within starch granules becomes too low to act on these short amylose chains. As a result, the length of short amylose chains is not affected by SBE activity. However, the amylose synthesis process during starch development is still unclear, requiring further study.

In addition, the relationships among X_{AP1}, X_{AP2}, X_{AM1}, and X_{AM2} suggest that the elongation of each group of branches is not strictly by one type of enzyme; one such example is the contribution of enzyme set i to longer amylopectin chains, although enzyme set i mainly contributes to short amylopectin chains (see Figure S1 of the Supporting Information). Hence, if enzyme set i favors elongation to branching ($\beta < 1$), it will increase both X_{AP1} and X_{AP2}. This is the first study that has shown the chain-length dependency between amylopectin and amylose chains. Further studies are needed to understand the mechanism behind this observation.

***In Vitro* Digestibility and Its Correlations with Starch Structure.** In human diet, starch-containing foods are normally consumed after cooking, where starch granules have been gelatinized. During gelatinization, starch granules swell and the amylose molecules leach out into the supernatant and form a network surrounding the swollen granules, which inhibits further swelling of starch granules. At the same time, the semi-crystalline ordered structure of starch is disrupted, leading to an amorphous structure.[41] The swelling of starch granules and the melting of the crystalline structure after gelatinization increase the accessibility of starch molecules for enzymatic digestion, leading to a higher digestion rate. The granular architecture of native starch granules, on the other hand, provides a physical barrier to the diffusion of the enzymes and results in a lower digestion rate.[50,51] In addition, the starch molecules in a double helical crystalline structure, such as native starch granules and retrograded starch, are more restricted and bind less readily with amylolytic enzymes.[52]

To simulate the digestion process of starch in foods, starch samples were enzymatically digested using an *in vitro* method, after being thoroughly cooked in sufficient water. The typical digestogram of freshly gelatinized starches is present in Figure 5, showing duplicates of a barley starch as an example of repeatability. All digestograms are well-fitted by first-order kinetics (exemplified for barley starch in Figure 5), and the digestion rate coefficients k are listed in Table S3 of the Supporting Information. Pearson's and Spearman's rank correlation analyses were performed to obtain the linear and non-linear relationships, respectively, between the starch digestion rate and starch structural parameters, and the correlation coefficients are summarized in Table 3.

dx.doi.org/10.1021/jf5011676 | J. Agric. Food Chem. 2014, 62, 4443−4453

Both Pearson's and Spearman's rank correlation tests show that there are no significant correlations between the digestion rate of freshly gelatinized starch and starch structural parameters, suggesting that the digestion rate of freshly gelatinized starch is not affected by the amylose content and amylopectin and amylose fine structures. These results contrast those for cooked rice grains and sorghum flours, showing that the digestion rate was positively correlated with X_{AM2} but negatively correlated with $h_{AM2/AP1}$ and $h_{AP2/AP1}$.[9−11] The plant cell wall, protein, and lipids in grains and flours can greatly influence starch digestibility, such as creating a physical barrier and/or molecular interaction that prevents starch granules from swelling and starch molecules from leaching out during gelatinization or cooking. The presence of a plant cell wall and protein in grains and flours can also restrict water penetration and heat diffusion, increasing the resistance of starch granules to gelatinization and retaining some of the native granular structure after cooking.[53] Most of these non-starch components have been removed during isolation of starch granules, and thus, the starch granules have more freedom to swell and to be completely gelatinized during cooking. The digestion profiles of freshly gelatinized starch from the current study are also different from those of native starch granules[41,54] and retrograded starch,[6,8] showing that, in general, a higher proportion of long amylopectin branches and/or higher amylose content decreases starch digestibility. This is due to the presence of the crystalline structure in native starch granules and retrograded starch, which is enhanced or stabilized by long amylopectin chains and amylose, restricting the ability of the starch molecules to bind with amylolytic enzymes. Freshly gelatinized starch has lost almost all of the crystalline structure, and thus, the effects of long amylopectin chains and amylose are less apparent. This implies that the observed correlation between amylose fine structure in rice and sorghum flour/cooked grain can be ascribed to a secondary interaction between this fine structure and higher order structural features, as discussed above.

In conclusion, this study examines, for the first time, the fine molecular structure of amylose extracted from different plant sources. Two amylose peaks are observed on the SEC weight CLDs of all starch samples. In comparison to the SEC number CLD, the SEC weight CLD is better in exhibiting the structural features of amylose molecules. The amylose CLD differs dramatically with plant source, showing biosynthetic enzyme activities among different plant sources. Fitting the amylopectin number CLDs to a biosynthesis model gives new insight into the enzymatic processes involved in amylopectin biosynthesis. The fitted parameters obtained vary to different extents depending upon the plant sources. Enzyme set i plays a more dominant role than enzyme set ii in controlling amylopectin CLD. Correlations among starch structural and amylopectin fitting parameters suggest that amylopectin is probably the primer of amylose biosynthesis, and multiple enzymes might share the same substrate pool or work in the same complexes. *In vitro* digestion results show that the digestion rate of thoroughly cooked starch-containing food is not attributed to the fine molecular structure of amylose and amylopectin; instead, a secondary interaction between starch fine structure and higher order structural features might be a key factor.

■ ASSOCIATED CONTENT

Supporting Information

Fitting a representative number CLD of amylopectin branches (Figure S1), structural parameters obtained from SEC weight CLDs of debranched barley, sorghum, and rice starches (Table S1), parameters obtained from fitting the number CLDs of barley, sorghum, and rice starches to the mathematical model (Table S2), and digestion rate coefficient (k) of starch samples (Table S3). This material is available free of charge via the Internet at http://pubs.acs.org.

■ AUTHOR INFORMATION

Corresponding Author

*Telephone: +61-7-3365-4809. Fax: +61-7-3365-1188. E-mail: b.gilbert@uq.edu.au.

Funding

Partial support by Australian Research Council Discovery Grant DP130102461 is appreciated. Alex Chi Wu gratefully acknowledges the supported of an Australian Postgraduate Award and a CSIRO Food Future Flagship Postgraduate (top-up) Scholarship, while Kai Wang is supported by a Ph.D. scholarship provided by the China Scholarship Council and the University of Queensland.

Notes

The authors declare no competing financial interest.

■ ACKNOWLEDGMENTS

The authors gratefully acknowledge Alan Cruickshank, Glen Fox, Ian D. Godwin, Matthew K. Morell, and Yanco Agricultural Institute for providing the samples and Peter Gous, Enpeng Li, and Frederick J. Warren for useful discussions.

■ ABBREVIATIONS USED

ANOVA, analysis of variance; AUC, area under the curve; CLD, chain-length distribution; DBE, starch debranching enzymes; DMSO, dimethyl sulfoxide; DP, degree of polymerization; FACE, fluorophore-assisted carbohydrate electrophoresis; GBSS, granule-bound starch synthases; GPC, gel permeation chromatography; SBE, starch branching enzymes; SEC, size-exclusion chromatography; SS, starch synthases

■ REFERENCES

(1) Ball, S. G.; Morell, M. K. From bacterial glycogen to starch: Understanding the biogenesis of the plant starch granule. *Annu. Rev. Plant Biol.* **2003**, *54*, 207−233.

(2) Wang, K.; Henry, R. J.; Gilbert, R. G. Causal relations between starch biosynthesis, structure and properties. *Springer Sci. Rev.* **2014**, DOI: 0.1007/s40362-014-0016-0.

(3) Higgins, J. A.; Brown, I. L. Resistant starch: a promising dietary agent for the prevention/treatment of inflammatory bowel disease and bowel cancer. *Curr. Opin. Gastroenterol.* **2013**, *29*, 190−194.

(4) Johnston, K. L.; Thomas, E. L.; Bell, J. D.; Frost, G. S.; Robertson, M. D. Resistant starch improves insulin sensitivity in metabolic syndrome. *Diabetic Med.* **2010**, *27*, 391−397.

(5) Winter, J.; Nyskohus, L.; Young, G. P.; Hu, Y.; Conlon, M. A.; Bird, A. R.; Topping, D. L.; Le Leu, R. K. Inhibition by resistant starch of red meat-induced promutagenic adducts in mouse colon. *Cancer Prev. Res.* **2011**, *4*, 1920−1928.

(6) Benmoussa, M.; Moldenhauer, K. A. K.; Hamaker, B. R. Rice amylopectin fine structure variability affects starch digestion properties. *J. Agric. Food Chem.* **2007**, *55*, 1475−1479.

(7) Hu, P. S.; Zhao, H. J.; Duan, Z. Y.; Zhang, L. L.; Wu, D. X. Starch digestibility and the estimated glycemic score of different types of rice differing in amylose contents. *J. Cereal Sci.* **2004**, *40*, 231−237.
(8) Witt, T.; Gidley, M. J.; Gilbert, R. G. Starch digestion mechanistic information from the time evolution of molecular size distributions. *J. Agric. Food Chem.* **2010**, *58*, 8444−8452.
(9) Syahariza, Z. A.; Sar, S.; Tizzotti, M.; Hasjim, J.; Gilbert, R. G. The importance of amylose and amylopectin fine structures for starch digestibility in cooked rice grains. *Food Chem.* **2013**, *136*, 742−749.
(10) Syahariza, Z. A.; Sar, S.; Warren, F. J.; Zou, W.; Hasjim, J.; Tizzotti, M. J.; Gilbert, R. G. Corrigendum to "The importance of amylose and amylopectin fine structures for starch digestibility in cooked rice grains", [Food Chem. 136 (2013) 742−749]. *Food Chem.* **2014**, *145*, 617−618.
(11) Li, E.; Hasjim, J.; Gilding, E. K.; Godwin, I. D.; Gilbert, R. G. Plant pullulanase debranching enzyme plays a crucial role in starch biosynthesis in sorghum endosperm. *J. Agric. Food Chem.* **2014**.
(12) Wu, A. C.; Gilbert, R. G. Molecular weight distributions of starch branches reveal genetic constraints on biosynthesis. *Biomacromolecules* **2010**, *11*, 3539−3547.
(13) Wu, A. C.; Morell, M. K.; Gilbert, R. G. A parameterized model of amylopectin synthesis provides key insights into the synthesis of granular starch. *PLoS One* **2013**, *8*, No. e65768.
(14) Tran, T. T. B.; Shelat, K. J.; Tang, D.; Li, E.; Gilbert, R. G.; Hasjim, J. Milling of rice grains: The degradation on three structural levels of starch can be independently controlled during grinding. *J. Agric. Food Chem.* **2011**, *59*, 3964−3973.
(15) Syahariza, Z. A.; Li, E.; Hasjim, J. Extraction and dissolution of starch from cereal grains for accurate structural analysis. *Carbohydr. Polym.* **2010**, *82*, 14−20.
(16) Hasjim, J.; Cesbron-Lavau, G.; Gidley, M. J.; Gilbert, R. G. In vivo and in vitro starch digestion: Are current in vitro techniques adequate? *Biomacromolecules* **2010**, *11*, 3600−3608.
(17) Gidley, M. J. Molecular mechanisms underlying amylose aggregation and gelation. *Macromolecules* **1989**, *22*, 351−358.
(18) Jackson, D. S.; Chotoowen, C.; Waniska, R. D.; Rooney, L. W. Characterization of starch cooked in alkali by aqueous high-performance size-exclusion chromatography. *Cereal Chem.* **1988**, *65*, 493−496.
(19) Hanselmann, R.; Ehrat, M.; Widmer, H. M. Sedimentation field-flow fractionation combined with multi-angle laser-light scattering applied for characterization of starch polymers. *Starch* **1995**, *47*, 345−349.
(20) Kim, H.-S.; Huber, K. C.; Higley, J. S. Alkaline dissolution of starch facilitated by microwave heating for analysis by size-exclusion chromatography. *J. Agric. Food Chem.* **2006**, *54*, 9664−9669.
(21) You, S.; Lim, S.-T. Molecular characterization of corn starch using an aqueous HPSEC-MALLS-RI system under various dissolution and analytical conditions. *Cereal Chem.* **2000**, *77*, 303−308.
(22) Schmitz, S.; Dona, A. C.; Castignolles, P.; Gilbert, R. G.; Gaborieau, M. Quantification of the extent of starch dissolution in dimethylsulfoxide by ^{1}H NMR spectroscopy. *Macromol. Biosci.* **2009**, *9*, 506−514.
(23) O'Shea, M. G.; Samuel, M. S.; Konik, C. M.; Morell, M. K. Fluorophore-assisted carbohydrate electrophoresis (FACE) of oligosaccharides—Efficiency of labelling and high-resolution separation. *Carbohydr. Res.* **1998**, *307*, 1−12.
(24) Gilbert, R. G. Size-separation characterization of starch and glycogen for biosynthesis−structure−property relationships. *Anal. Bioanal. Chem.* **2011**, *399*, 1425−1438.
(25) Cave, R. A.; Seabrook, S. A.; Gidley, M. J.; Gilbert, R. G. Characterization of starch by size-exclusion chromatography: The limitations imposed by shear scission. *Biomacromolecules* **2009**, *10*, 2245−2253.
(26) Vilaplana, F.; Gilbert, R. G. Characterization of branched polysaccharides using multiple-detection size separation techniques. *J. Sep. Sci.* **2010**, *33*, 3537−3554.
(27) Castro, J. V.; Ward, R. M.; Gilbert, R. G.; Fitzgerald, M. A. Measurement of the molecular weight distribution of debranched starch. *Biomacromolecules* **2005**, *6*, 2260−2270.
(28) Liu, W.-C.; Halley, P. J.; Gilbert, R. G. Mechanism of degradation of starch, a highly branched polymer, during extrusion. *Macromolecules* **2010**, *43*, 2855−2864.
(29) Wu, A. C.; Gilbert, R. G. *Program "APCLDFIT"*; The University of Queensland: Brisbane, Queensland, Australia, 2013.
(30) Witt, T.; Doutch, J.; Gilbert, E. P.; Gilbert, R. G. The relations between molecular, crystalline and lamellar structures of amylopectin. *Biomacromolecules* **2012**, *13*, 4273−4282.
(31) Butterworth, P. J.; Warren, F. J.; Grassby, T.; Patel, H.; Ellis, P. R. Analysis of starch amylolysis using plots for first-order kinetics. *Carbohydr. Polym.* **2012**, *87*, 2189−2197.
(32) Vilaplana, F.; Hasjim, J.; Gilbert, R. G. Amylose content in starches: Towards optimal definition and validating experimental methods. *Carbohydr. Polym.* **2012**, *88*, 103−111.
(33) Fredriksson, H.; Silverio, J.; Andersson, R.; Eliasson, A. C.; Aman, P. The influence of amylose and amylopectin characteristics on gelatinization and retrogradation properties of different starches. *Carbohydr. Polym.* **1998**, *35*, 119−134.
(34) Bello-Perez, L. A.; Roger, P.; Colonna, P.; Paredes-Lopez, O. Laser light scattering of high amylose and high amylopectin materials, stability in water after microwave dispersion. *Carbohydr. Polym.* **1998**, *37*, 383−394.
(35) Wiesenborn, D. P.; Orr, P. H.; Casper, H. H.; Tacke, B. K. Potato starch paste behavior as related to some physical/chemical properties. *J. Food Sci.* **1994**, *59*, 644−648.
(36) Ao, Z.; Jane, J.-l. Characterization and modeling of the A- and B-granule starches of wheat, triticale, and barley. *Carbohydr. Polym.* **2007**, *67*, 46−55.
(37) Soulaka, A. B.; Morrison, W. R. The amylose and lipid contents, dimensions, and gelatinisation characteristics of some wheat starches and their A- and B-granule fractions. *J. Sci. Food Agric.* **1985**, *36*, 709−718.
(38) Fitzgerald, M. A.; Bergman, C. J.; Resurreccion, A. P.; Muller, J.; Jimenez, R.; Reinke, R. F.; Martin, M.; Blanco, P.; Molina, F.; Chen, M.-H.; Kuri, V.; Romero, M. V.; Habibi, F.; Umemoto, T.; Jongdee, S.; Graterol, E.; Reddy, K. R.; Bassinello, P. Z.; Sivakami, R.; Rani, N. S.; Das, S.; Wang, Y. J.; Indrasari, S. D.; Ramli, A.; Ahmad, R.; Dipti, S. S.; Xie, L.; Lang, N. T.; Singh, P.; Toro, D. C.; Tavasoli, F.; Mestres, C. Addressing the dilemmas of measuring amylose in rice. *Cereal Chem.* **2009**, *86*, 492−498.
(39) Vilaplana, F.; Gilbert, R. G. Analytical methodology for multidimensional size/branch-length distributions for branched glucose polymers using off-line 2-dimensional size-exclusion chromatography and enzymatic treatment. *J. Chromatogr., A* **2011**, *1218*, 4434−4444.
(40) Jane, J. L.; Chen, Y. Y.; Lee, L. F.; McPherson, A. E.; Wong, K. S.; Radosavljevic, M.; Kasemsuwan, T. Effects of amylopectin branch chain length and amylose content on the gelatinization and pasting properties of starch. *Cereal Chem.* **1999**, *76*, 629−637.
(41) Srichuwong, S.; Sunarti, T. C.; Mishima, T.; Isono, N.; Hisamatsu, M. Starches from different botanical sources II: Contribution of starch structure to swelling and pasting properties. *Carbohydr. Polym.* **2005**, *62*, 25−34.
(42) McPherson, A. E.; Jane, J. Comparison of waxy potato with other root and tuber starches. *Carbohydr. Polym.* **1999**, *40*, 57−70.
(43) Ratnayake, W. S.; Hoover, R.; Shahidi, F.; Perera, C.; Jane, J. Composition, molecular structure, and physicochemical properties of starches from four field pea (*Pisum sativum* L.) cultivars. *Food Chem.* **2001**, *74*, 189−202.
(44) Huang, J.; Schols, H. A.; van Soest, J. J. G.; Jin, Z.; Sulmann, E.; Voragen, A. G. J. Physicochemical properties and amylopectin chain profiles of cowpea, chickpea and yellow pea starches. *Food Chem.* **2007**, *101*, 1338−1345.
(45) Cuevas, R. P.; Daygon, D.; Morell, M.; Gilbert, R. G.; Fitzgerald, M. A. Using chain-length distributions to diagnose genetic

perturbations in starch biosynthesis. *Carbohydr. Polym.* **2010**, *81*, 120−127.
(46) Ball, S. G.; van de Wal, M. H. B. J.; Visser, R. G. F. Progress in understanding the biosynthesis of amylose. *Trends Plant Sci.* **1998**, *3*, 462−467.
(47) Hennen-Bierwagen, T. A.; Lin, Q.; Grimaud, F.; Planchot, V.; Keeling, P. L.; James, M. G.; Myers, A. M. Proteins from multiple metabolic pathways associate with starch biosynthetic enzymes in high molecular weight complexes: A model for regulation of carbon allocation in maize amyloplasts. *Plant Physiol.* **2009**, *149*, 1541−1559.
(48) MuForster, C.; Huang, R. M.; Powers, J. R.; Harriman, R. W.; Knight, M.; Singletary, G. W.; Keeling, P. L.; Wasserman, B. P. Physical association of starch biosynthetic enzymes with starch granules of maize endosperm—Granule-associated forms of starch synthase I and starch branching enzyme II. *Plant Physiol.* **1996**, *111*, 821−829.
(49) Hwang, J. W.; Kim, S. K.; Lee, J. S.; Kim, I. S. Gene expression of the biosynthetic enzymes and biosynthesis of starch during rice grain development. *J. Plant Biol.* **2005**, *48*, 448−455.
(50) Blazek, J.; Gilbert, E. Effect of enzymatic hydrolysis on native starch granule structure. *Biomacromolecules* **2010**, *11*, 3275−3289.
(51) Zhang, B.; Dhital, S.; Gidley, M. J. Synergistic and antagonistic effects of α-amylase and amyloglucosidase on starch digestion. *Biomacromolecules* **2013**, *14*, 1945−1954.
(52) Jane, J. L.; Robyt, J. F. Structure studies of amylose-V complexes and retro-graded amylose by action of α-amylases, and a new method for preparing amylodextrins. *Carbohydr. Res.* **1984**, *132*, 105−118.
(53) Hasjim, J.; Li, E. P.; Dhital, S. Milling of rice grains: Effects of starch/flour structures on gelatinization and pasting properties. *Carbohydr. Polym.* **2013**, *92*, 682−690.
(54) Chavez-Murillo, C. E.; Mendez-Montealvo, G.; Wang, Y. J.; Bello-Perez, L. A. Starch of diverse Mexican rice cultivars: Physicochemical, structural, and nutritional features. *Starch* **2012**, *64*, 745−756.

JOURNAL OF AGRICULTURAL AND FOOD CHEMISTRY

Article

pubs.acs.org/JAFC

Metabolomic Analysis of Antimicrobial Mechanisms of ε-Poly-L-lysine on *Saccharomyces cerevisiae*

Tao Bo,[†,‡] Miao Liu,[†,‡] Cheng Zhong,[†,‡] Qian Zhang,[†,‡] Qin-Zhi Su,[†,‡] Zhi-Lei Tan,[†,‡] Pei-Pei Han,[†,‡] and Shi-Ru Jia*[,†,‡]

[†]Key Laboratory of Industrial Fermentation Microbiology, Ministry of Education, and [‡]College of Biotechnology, Tianjin University of Science and Technology, Tianjin 300457, People's Republic of China

Supporting Information

ABSTRACT: ε-Poly-L-lysine (ε-PL), a naturally occurring amino acid homopolymer, has been widely used as a food preservative. However, its antimicrobial mechanism has not been fully understood. This study investigated the antimicrobial mode of action of ε-PL on a yeast, *Saccharomyces cerevisiae*. When treated with ε-PL at the concentration of 500 μg/mL, cell mortality was close to 100% and the phospholipid bilayer curvature, pores, and micelles on the surface of *S. cerevisiae* were clearly observed by scanning electron microscopy (SEM). At the level of 200 μg/mL, ε-PL significantly inhibited the cell growth of *S. cerevisiae*. When treated with 50 μg/mL ε-PL, the yeast cell was able to grow but the cell cycle was prolonged. A significant increase in cell membrane permeability was induced by ε-PL at higher concentrations. Metabolomics analysis revealed that the ε-PL stress led to the inhibition of primary metabolic pathways through the suppression of the tricarboxylic acid cycle and glycolysis. It is therefore proposed that the microbiostatic effect of ε-PL at lower levels on *S. cerevisiae* is achieved by inducing intracellular metabolic imbalance via disruption of cell membrane functions. Moreover, the results suggested that the antimicrobial mechanism of ε-PL on *S. cerevisiae* can in fact change from microbiostatic to microbicidal when the concentration of ε-PL increased, and the mechanisms of these two modes of action were completely different.

KEYWORDS: *ε-poly-L-lysine, Saccharomyces cerevisiae, antimicrobial mechanism, microbicidal, microbiostatic, metabolomics*

INTRODUCTION

ε-PL is a linear L-lysine homopolymer biosynthesized by actinomyces, and it has a unique structure linking ε-amino and α-carboxylic acid functional groups. It is a polycationic peptide, containing 25−35 amino acid residues. ε-PL was first discovered as a secreted product from a strain of *Streptomyces albulus* no. 346, now designated *S. albulus* NBRC 14147.[1]

Currently, ε-PL has been widely applied to food preservation because of its strong antimicrobial activity,[2] safety, and high thermostability. The antimicrobial activity of ε-PL was not affected after heat treatment at 120 °C for 20 min.[3] ε-PL has been approved by agencies of the United States, Japan, and Korea as a preservative in food.[4,5] In addition to food applications, ε-PL has a good potential application in the medical field due to some of its unique capabilities, such as selectively removing endotoxins to reduce cell toxicity, improving cell adhesion, inhibiting pancreatic lipase activity, and inhibiting the production of oral bacterial toxin.[4]

ε-PL exhibits antimicrobial activities against a wide spectrum of microorganisms including Gram-positive and Gram-negative bacteria, yeasts, and molds.[2] Research has shown that the α-amino groups of ε-PL are very important for its antimicrobial activity. However, the antimicrobial activity of ε-PL is greatly affected by pH, ionic strength, and the presence of anionic compounds. Muto[6] found that ε-PL induced the leakage of cytoplasmic malate dehydrogenase (MDH) from *Escherichia coli* cells, and such leakage had a good correlation with the decrease in cell survival rate. The microbicidal activities of ε-PL was dependent on microbial cell size, rather than the microbial species. Yamanaka and Hamano[4] reported that the antimicrobial activity of ε-PL was caused by a physical action on the cytoplasmic membrane, and the antimicrobial mechanism of ε-PL was electrostatic interaction with the microbial cell surface, followed by disorganization of the membrane and abnormal distribution of the cytoplasm, ultimately leading to physiological damage of the microbial cells. Up to now, the detailed antimicrobial mechanism of ε-PL remains unclear.

Metabolomics aims to systematically analyze the entire small molecule metabolite composition and dynamic response in microorganisms.[7] Metabolomics analysis also assess the last step in the series of changes under an external stress[8] or a pathological insult,[9] and the composition of metabolites directly reveals the phenotypic changes in a living system. We can understand the impact of ε-PL on microbial metabolism through the study of variation of intracellular metabolites, and it is important for further understanding of the antimicrobial mechanism of ε-PL.

Saccharomyces cerevisiae has also proven to be a good model eukaryote to study the inhibition effects of and the cellular responses to antimicrobial preservatives. After more than a decade of postgenomic research in our laboratory, *S. cerevisiae* has turned out to be a powerful model microbial system to study the effects and targets of many antimicrobial drugs. In this study, a common yeast strain of *S. cerevisiae*, AS2399, was treated with ε-PL at different concentrations, and the

Received: February 1, 2014
Revised: April 13, 2014
Accepted: April 15, 2014
Published: April 15, 2014

ACS Publications © 2014 American Chemical Society

antimicrobial activity and mechanisms of ε-PL were analyzed. *S. cerevisiae* cells in the ε-PL-treated groups and the control group were compared by scanning electron microscopy (SEM). The membrane permeability was investigated by propidium iodide (PI) assay. A GC-MS-based metabolomics approach and a multivariate analysis were then utilized to compare the global metabolite profiles of *S. cerevisiae* in response to ε-PL at different levels. It was surprisingly found that the antimicrobial mechanism of ε-PL on *S. cerevisiae* seemed to be more complicated than in previous studies; it actually changed depending on the concentration of ε-PL. At lower concentrations, ε-PL mainly exhibited a microbiostatic effect; at higher concentrations it clearly showed a microbicidal effect.

MATERIALS AND METHODS

Microorganism, Media, and Incubation Conditions. *S. cerevisiae* AS2399 was precultured in YPD liquid medium (2% glucose, 1% yeast extract, 2% peptone, w/v, pH 6.0) with a rotary speed of 180 rpm at 28 °C for 12 h. Then, the precultured yeast cells were transferred to a fresh YPD liquid medium, and the initial cell density was adjusted to 0.3−0.4 measured by a 722S visible spectrophotometer (Shanghai Precision Scientific Instrument Co. Ltd., Shanghai, China) at 600 nm. The cells were cultivated at 28 °C on a rotary shaker at 180 rpm in 500 mL cotton-plugged flasks containing 100 mL of YPD liquid medium either with or without ε-PL. The ε-PL used in this study was a powder provided by Silver Elephant Bioengineering Corp. (Zhejiang, China), and it had 25−35 residues with an isoelectric point of 9.0. The ε-PL solution was prepared with deionized water. For the ε-PL-treated cells, ε-PL was added to the liquid medium before cultivation at final concentrations of 50, 200, and 500 μg/mL, respectively. The experiments were conducted in triplicates.

Dose−Response Assay and Cell Fatality Rate and Viability Determination. The dose−response curve of the yeast cells was determined by measuring cellular OD_{600}. The cell fatality rate was determined using a methylene blue staining method.[10] The plate count method was used to determine yeast cell viability.

Scanning Electron Microscopy. SEM was used to observe *S. cerevisiae* cells according to a modified method of Shimada et al.[11] In brief, after ε-PL treatment, *S. cerevisiae* cells were harvested by centrifugation at 3000*g* for 3 min and washed with 0.1 M phosphate buffer. Then, cells were resuspended in 1 mL of 2.5% (v/v) glutaraldehyde (pH 7.1) at 4 °C for 2 h. After centrifugation, the cells were washed with 0.1 M phosphate buffer and then dehydrated in a progressive ethanol solution and were finally dried. Cells were then sputter-coated with gold (Hitachi E-1010) and observed with a Hitachi SU1510 microscope.

Determination of Membrane-Disrupting Activity of ε-PL (PI Assay). The membrane-disrupting activity of ε-PL was determined by measuring the fluorescence enhancement of PI (Sigma Corp., USA) in ε-PL-treated cells according to a modified method of Veerman et al.[12] It was based on the principle that the PI enters only membrane-compromised cells, after which the fluorescence of this probe is enhanced by 20−30-fold due to its binding to nucleic acids. Cells were harvested by centrifugation at 3000*g* for 3 min and washed twice with phosphate buffer saline (PBS). Cells were then resuspended in PBS, and the final cell density was adjusted to OD_{600} 0.3−0.5. One hundred microliters of the cell suspension was mixed with 100 μL of PI (initial concentration was 12 μg/mL) and was then incubated at room temperature for 5 min. The fluorescence intensity was measured at excitation and emission wavelengths of 535 and 617 nm, respectively, by a SYNERGY4 multifunctional enzyme mark instrument (Bioteck). Each experiment was conducted in triplicate.

$$\text{membrane-disrupting activity} = \frac{\text{fluorescence intensity}}{OD_{600}} \quad (1)$$

Extraction of Intracellular Metabolites. Cell samples were collected at 4, 8, and 12 h either with or without ε-PL. Yeast cells were quenched and extracted as described previously[13] with some modifications. Four biological replicates were performed for each sample. First, cell suspensions were immediately quenched at −40 °C for 5 min with 40% (v/v) methanol in water. The quenching solution was prechilled at −40 °C and used at a ratio of 4:1 (v/v) of quenching solution to cell suspension. Then cells were harvested by centrifugation at 5000*g* for 5 min and washed with PBS twice to remove the residual culture medium, followed by washing with ultrapure water to remove the salts from PBS. Then, cells were ground into fine powder in liquid nitrogen. Ground cells (50 mg) were first suspended in 1 mL of extraction buffer containing methanol/water (1:1, v/v, −40 °C) and then mixed thoroughly. The mixture was frozen in liquid nitrogen for 1 min and then was thawed, and this freeze−thaw process was repeated four times. After centrifugation at 5000*g* for 3 min, the supernatant was collected; 0.5 mL of extraction buffer was added into the precipitate for further extraction. After mixing and centrifugation at 10000*g* for 5 min, the additional supernatant extract was combined with the previously collected supernatant extract. To correct minor variations that occurred during analysis, 20 μL of internal standard solution (succinic-d_4 acid, 1.4 mg/mL, Sigma) was added to 100 μL aliquots before lyophilization.

Derivatization. Before GC-MS analysis, a two-stage chemical derivatization was carried out as described previously.[13] First, methoximation was performed by dissolving the dried metabolite samples in 50 μL of methoxamine hydrochloride (20 mg/mL in pyridine, Sigma), and the solution was incubated at 40 °C for 80 min. Then, 80 μL of *N*-methyl-*N*-(trimethylsilyl)trifluoroacetamide (MSTFA, Sigma) was added to the samples, which were subsequently incubated at 40 °C for 80 min for trimethylsilylation.

GC-MS Analysis. GC-MS analysis was performed by a GC-MS system (Agilent Technologies, Palo Alto, CA, USA) equipped with an HP-5 capillary column (60 m × 320 μm i.d., 0.25 μm film thickness; Agilent J&W Scientific, Folsom, CA, USA). Samples (1 μL) were injected with a split ratio of 1:10. Helium was used as the carrier gas at a constant flow of 1 mL/min. The injection, ion source, and ion source surface temperatures were set to 280, 250, and 280 °C, respectively. The GC oven temperature was set to 70 °C for 2 min, then raised to 290 °C at a rate of 5 °C/min, and maintained at 290 °C for 3 min. The electron impact ionization (70 eV) was set at a full scan mode (m/z 50−800). MSD Oroductivity ChemStation software (version E.02 01.1177, Agilent Technologies) was used to acquire mass spectrometric data. Compound identification was performed by comparing the mass spectra with a commercially available standard library, the National Institute of Standards and Technology mass spectral library 2008. The compounds were also identified by comparing their mass spectra and retention times with those of commercially available reference compounds.

Data Analysis. All of the areas of acquired peaks were normalized against the internal standard for further data processing. The generated normalized peak areas (variables) were imported into SIMCA package (ver. 11.5) (Umetrics, Umea, Sweden) for multivariate statistical analysis. Principal component analysis (PCA) and partial least-squares (PLS) analysis were applied to the data after mean-centering and orthogonal signal correction preprocessing. An unsupervised PCA was initially performed to obtain an overview of the GC-MS data from the control and different groups of ε-PL-treated *S. cerevisiae* cells, and the differences between the samples were detected in the PCA scores plots. Moreover, another unsupervised hierarchical cluster analysis (HCA) was performed using HCE 3.5 software. To identify the metabolites that were associated with ε-PL stress, a supervised PLS was subsequently carried out. On the basis of the loadings plots and variable importance in the projection (VIP) value threshold (VIP > 1) from the PLS models, variables that were responsible for distinguishing between the ε-PL-treated and control (without ε-PL) groups were selected. *T* tests were performed on specific metabolites and their ratios to assess the statistical significance of the metabolic changes.

Statistical Analysis. Data were analyzed using SPSS20.0 statistical software packages (http://www-01.ibm.com/software/analytics/spss/). Differences with a P value of <0.05 were considered statistically significant.

RESULTS

Dose−Response Curve, Fatality Rate, and Viability of *S. cerevisiae* in the Presence of ε-PL. As shown in Figure 1A, the addition of ε-PL inhibited cell growth, and the inhibition became increasingly significant as the concentration of ε-PL increased. The stationary phase of *S. cerevisiae* was delayed in the ε-PL-treated group at 50 μg/mL compared with the control group without ε-PL. The cell death rate of *S. cerevisiae* was increased slightly (Figure1B) by 50 μg/mL ε-PL, but most of the cells could still manage to survive. When the concentration of ε-PL was increased to 200 μg/mL, the cell growth was significantly inhibited, and cell mortality was increased by 30−40% (Figure1B). When the ε-PL concentration was increased to 500 μg/mL, the cell mortality rate climbed to nearly 100%. As shown in Figure 1C, *S. cerevisiae* cell viability decreased over time, especially in treatment groups with ε-PL at concentrations of 200 and 500 μg/mL.

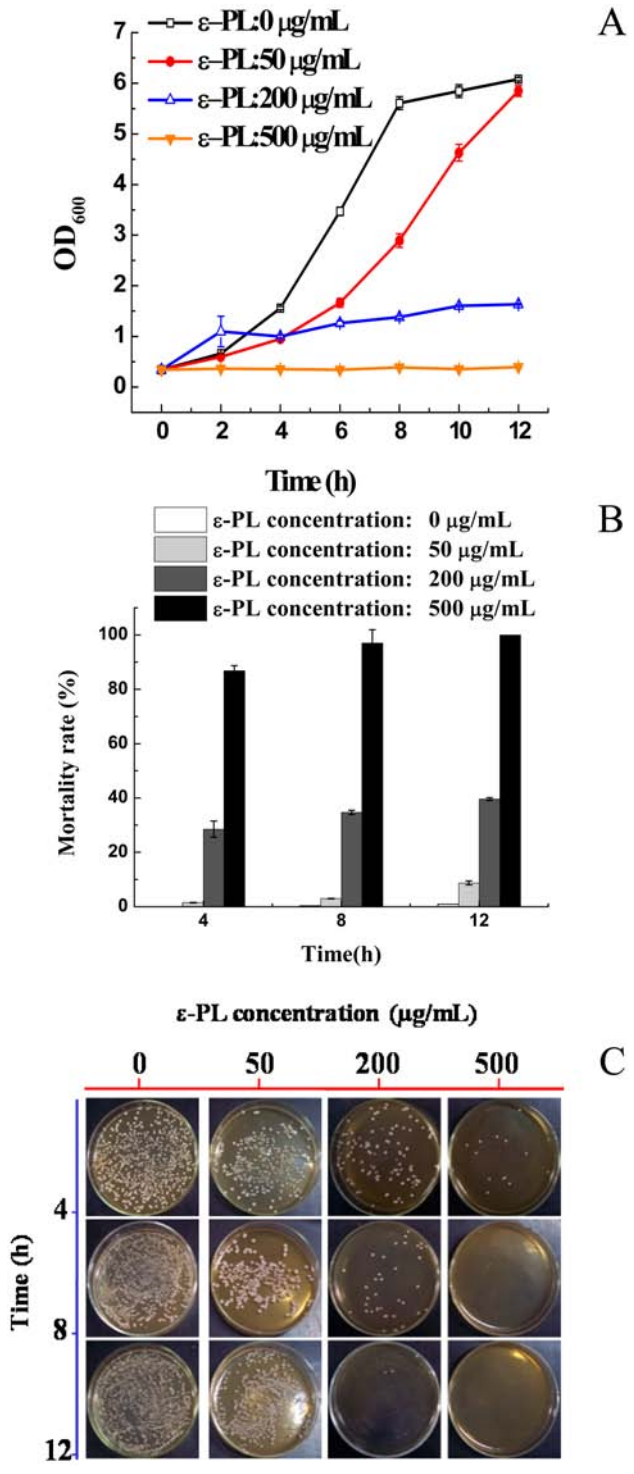

Figure 1. Effects of different concentrations of ε-PL on *S. cerevisiae*: (A) dose−response of ε-PL against *S. cerevisiae*; (B) microbicidal activities of the different concentrations of ε-PL at time points of 4, 8, and 12 h (each value is the mean of three replicates ± SD); (C) vitality of *S. cerevisiae* treated with different concentrations of ε-PL at different sampling times.

Morphological Changes in Yeast Cells Induced by ε-PL. The effect of ε-PL on *S. cerevisiae* morphology changes was investigated with SEM. In the control group a normal surface of *S. cerevisiae* was observed, and there was no apparent cellular debris (Figure 2A) on the cell surface. Compared with the control group, the size of *S. cerevisiae* cells did not change significantly for ε-PL-treated groups (Figure2B−E), but cell deformation and morphological changes became obvious as the concentration of ε-PL increased to 200 μg/mL and above. Rough and sunken surfaces were observed in some cells treated with 200 μg/mL ε-PL (Figure 2C). When the cells were treated with 500 μg/mL ε-PL, the surface of the cells was clearly rougher, and multiple pores and micelles on the surfaces could

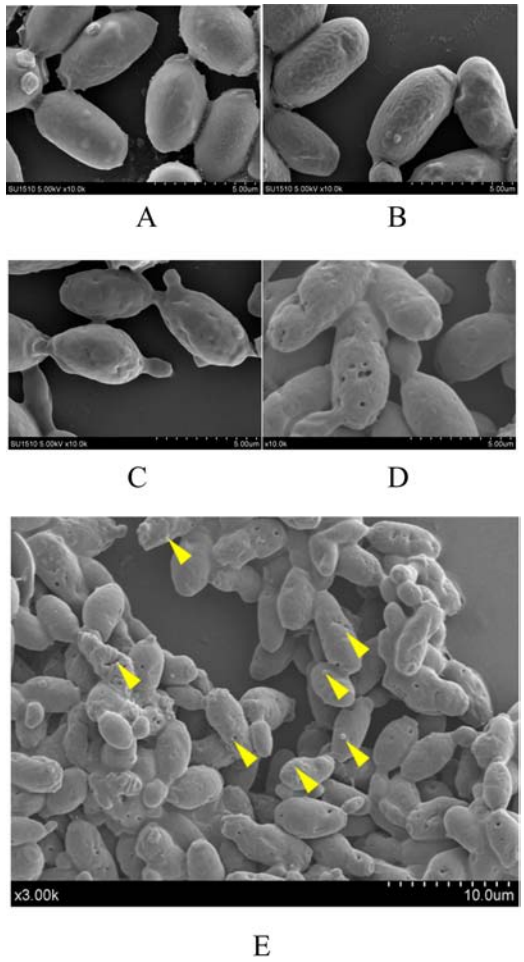

Figure 2. Scanning electron microscopy (SEM) images of *S. cerevisiae* cells without ε-PL treatment (A) treated and with ε-PL treatment at 50 μg/mL (B), 200 μg/mL (C), and 500 μg/mL (D, E) for 8 h.

dx.doi.org/10.1021/jf500505n | J. Agric. Food Chem. 2014, 62, 4454−4465

be easily seen. In addition, certain membrane disruption was observed in some cells, indicating that disruption of the bilayer curvature (Figure 2D,E) by ε-PL at higher concentrations had occurred. The pore on the cell membrane was about 0.3 μm in diameter. However, the morphology of the cells treated with 50 μg/mL ε-PL did not change significantly (Figure 2B).

Membrane-Permeabilizing Activity of ε-PL. The membrane-permeabilizing activity of ε-PL was investigated by using the PI assay. A significant increase in fluorescence intensity was observed in the ε-PL-treated groups at concentrations of 200 and 500 μg/mL for 4 h (Figure 3). In

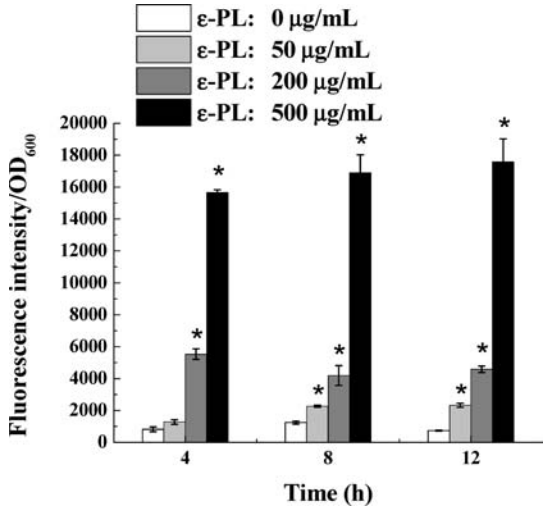

Figure 3. Membrane-permeabilizing effects of ε-PL as determined in the PI assay. Each value is the mean of three replicates ± SD. The asterisk (*) indicates significant difference from equivalent control point (t test, $P < 0.05$).

ε-PL-treated groups the fluorescence intensity increased significantly as the treatment time extended. A dramatic increase in fluorescence intensity was observed in the 500 μg/mL ε-PL treatment group.

Effect of ε-PL Treatment on Intracellular Metabolite Profiles of *S. cerevisiae*. Typical GC-MS total ion chromatograms (TIC) of the *S. cerevisiae* cells treated with various concentrations of ε-PL are shown in Figure S1 in the Supporting Information. Many fewer metabolites were found in the 500 μg/mL ε-PL treatment group than in the control and low ε-PL treatment groups. As illustrated in Figure 1, *S. cerevisiae* cells did not grow, and the cell mortality was close to 100%, probably due to the termination of metabolism of the cells by 500 μg/mL ε-PL. Therefore, the GC-MS data from the sample of 500 μg/mL ε-PL treatment group were not included in the multivariate statistical analysis.

A total of 72 metabolites were analyzed. PCA was used to investigate the metabolic differences between ε-PL-treated cells and control cells. PCA, an unsupervised clustering method, identifies and ranks major sources of variance within data sets and allows clustering of biological samples into both expected and unexpected groups on the basis of similarities and differences in the measured parameters.[14] Figure 4 shows the PCA scores plot of samples taken at different sampling time points, and the PC1/PC2 scores plot was performed to represent the sample distribution in the new multivariate space. Distinct clustering was observed among different groups at the 4 and 8 h time points (Figure 4A,B). There was no clear

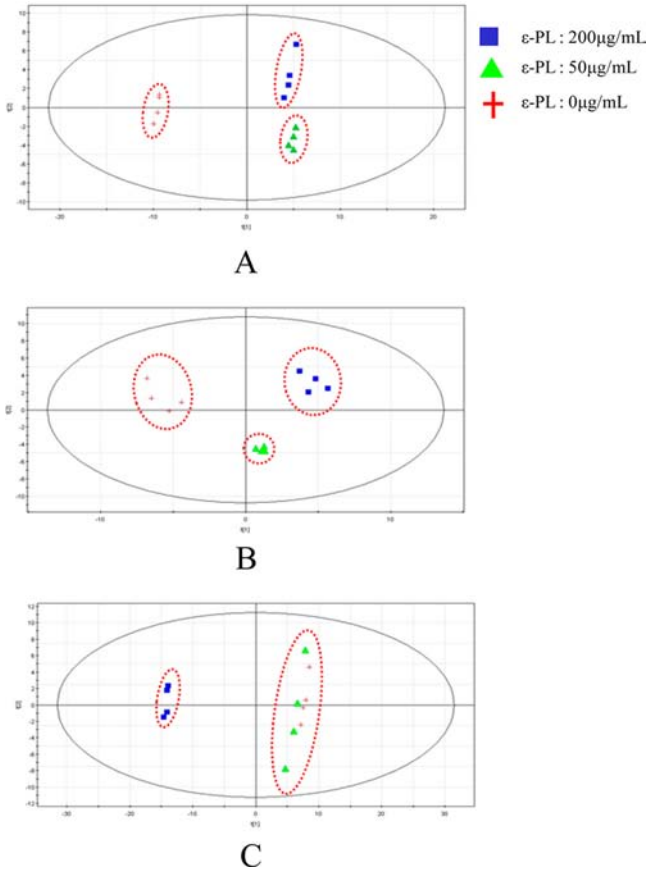

Figure 4. PCA scores plot for control group without ε-PL and ε-PL treated group. (A) sampling time at 4 h (PC1, 76.6% of total variance; PC2, 16.4% of total variance); (B) sampling time at 8 h (PC1, 50.1% of total variance; PC2, 30.8% of total variance); (C) sampling time at 12 h (PC1, 83.7% of total variance; PC2, 10.6% of total variance). In the scores plot, the confidence interval is defined by Hotelling's T2 ellipse (95% confidence interval), and observations outside the confidence ellipse are considered outliers.

difference between the 50 μg/mL treatment and the control group at the 12 h time point. The 200 μg/mL treatment group had a significantly different clustering compared with the other groups at the 12 h time point (Figure 4C). Meanwhile, multivariate data analysis was also performed by HCA. The HCA plot of the 72 differential metabolites reflected a clustering pattern that was similar to the result of the PCA (Figure 5). The ε-PL-treated groups were different from the control group at 4 and 8 h, and the ε-PL-treated group at 200 μg/mL was different from the other two groups at 12 h. The results of HCA also validated the predictive accuracy of the PCA models.

To further verify the differences and identify the metabolites that were mainly responsible for discrimination between the ε-PL-treated cells and the control cells, PLS analysis, a supervised clustering method, was performed. The clustering results were consistent with the PCA and HCA models, suggesting that the cell exposure to ε-PL might have led to systematic changes in cell metabolism pathways (Figure 6A,C,E).

Changes in Intracellular Metabolites in ε-PL-Treated Cells. The major metabolic perturbations that caused these discriminations were identified from the PLS loading plot (Figure 6B,D,F). In the PLS model, the VIP coefficient reflects the contribution of each metabolite. A higher VIP value means

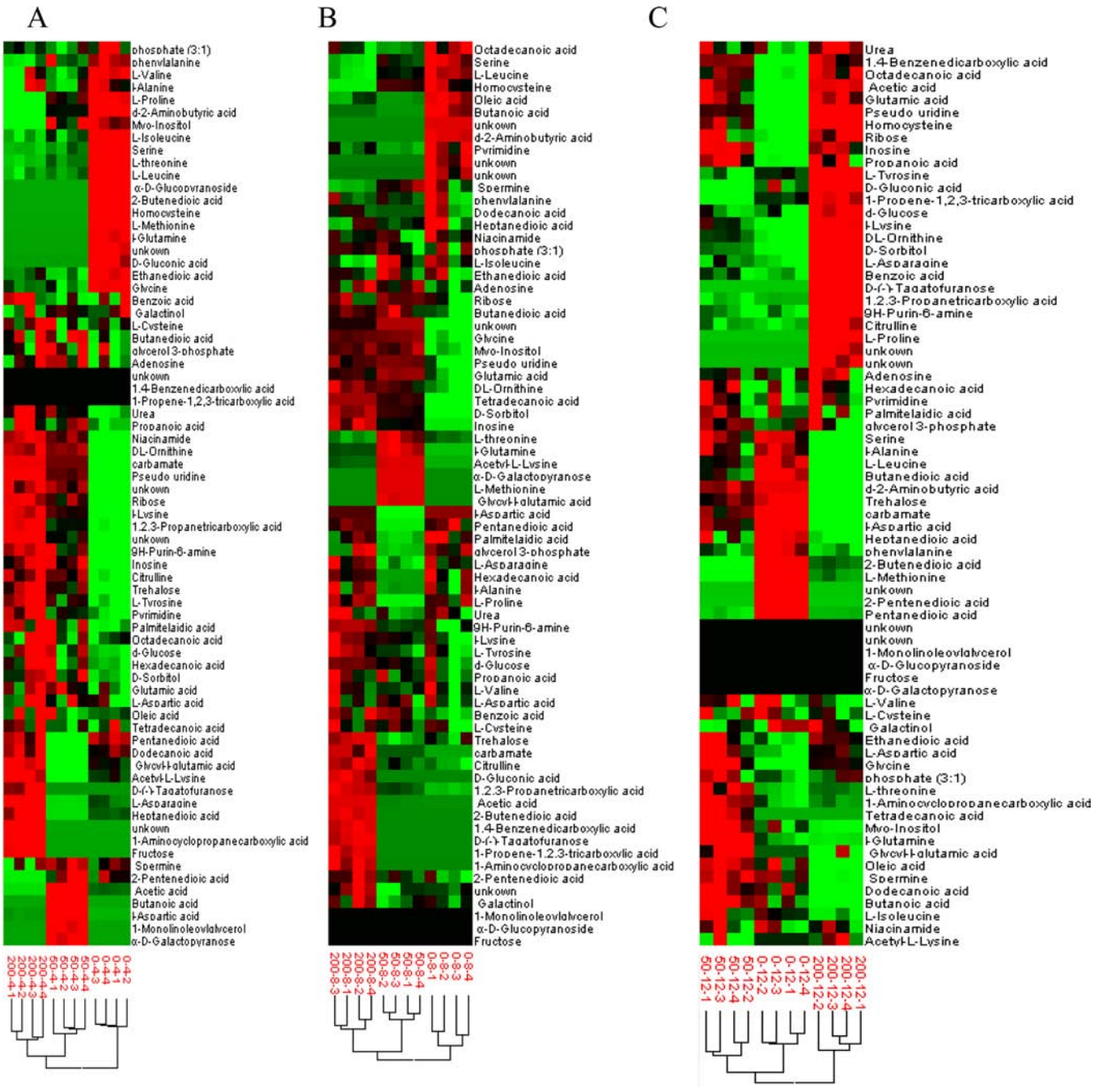

Figure 5. Hierarchical cluster analysis of the 72 identified differential metabolites: (A) sampling time at 4 h; (B) sampling time at 8 h; (C) sampling time at 12 h.

a higher contribution of the metabolite to the differentiation. A metabolite with a VIP value >1 suggests a major contribution to discriminating groups within PLS models.[15] Ornithine, phosphate, lysine, ethanedioic acid, aspartic acid, citrulline, acetic acid, citrate, glutamic acid, serine, and trehalose were found to be the most influential metabolites that were responsible for the differentiation between ε-PL-treated cells and control cells by PLS (Figure 7).

To evaluate the significant differences of metabolites in the ε-PL-treated cells compared with the control cells, a total of 30 identified typical metabolites were analyzed by *t* test (Figure8 and Table 1). These metabolites are divided into different categories based on the type of compounds and their position in the metabolic pathway, such as central carbon metabolism, urea cycle, amino acid, membrane structure, carbohydrate, and alcohols.

As illustrated in Figure 8 and Table 1, glucose is involved in glycolysis. It, as the origin of glycolysis, was found to accumulate in the ε-PL-treated groups. When compared with the control group, glucose concentration increased to 1.54- and 1.6-fold at 4 and 12 h in the 200 μg/mL ε-PL-treated group. Citrate and butanedioic acid are related to the TCA cycle. The levels of citrate compared with control increased dramatically to 3.12- and 2.75-fold at 4 and 8 h in the 50 μg/mL ε-PL-treated group and to 5.92-, 8.19-, and 4.54-fold at 4, 8, and 12 h in the 200 μg/mL ε-PL-treated group. On the contrary, when compared with the control group, the levels of butanedioic

dx.doi.org/10.1021/jf500505n | J. Agric. Food Chem. 2014, 62, 4454−4465

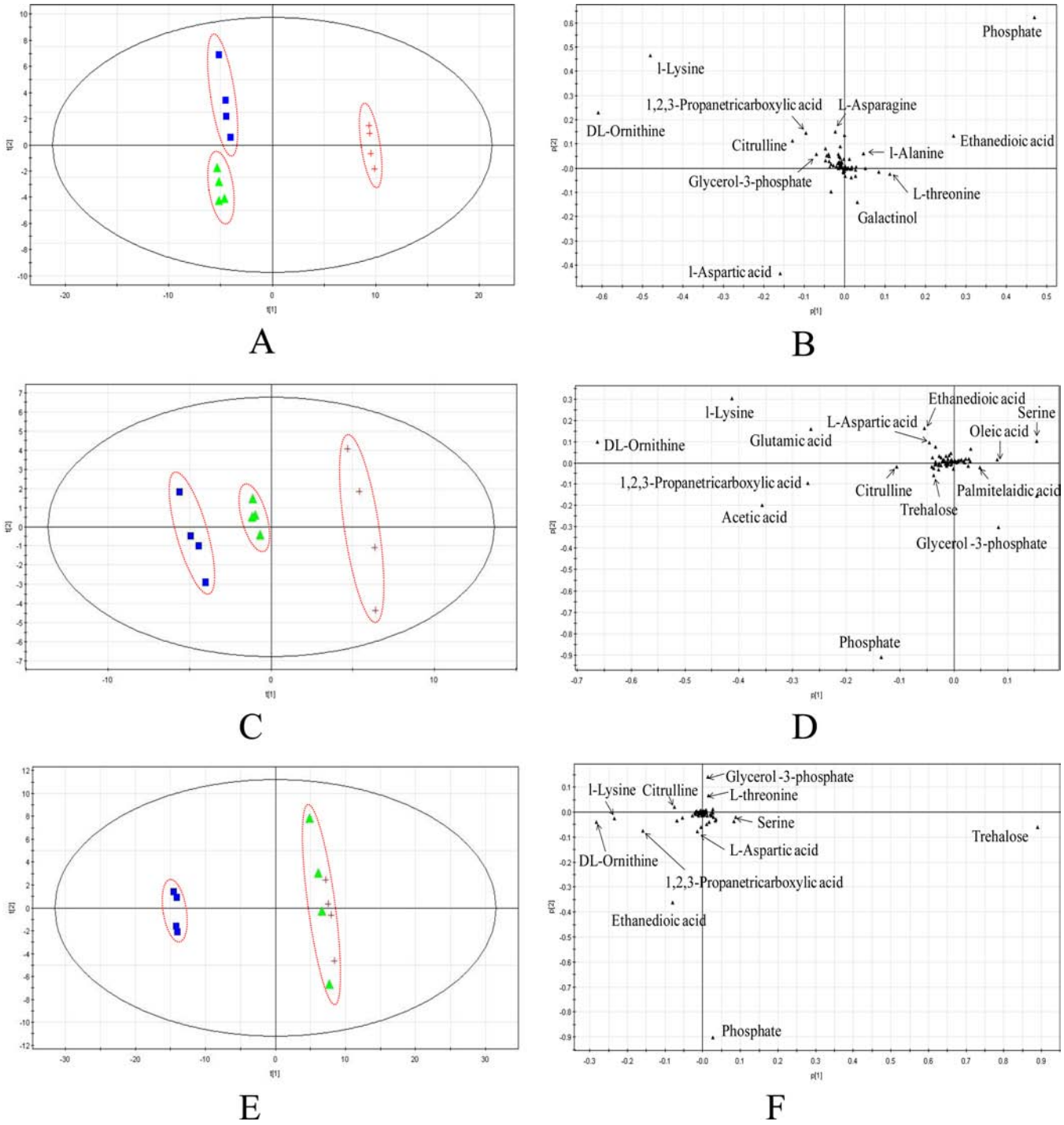

Figure 6. Scores plot and loading plot generated by PLS: (A, B) sampling time at 4 h (R^2X_{cum} = 0.929, Q^2_{cum} = 0.999); (C, D) sampling time at 8 h (R^2X_{cum} = 0.646, Q^2_{cum} = 0.984); (E, F) sampling time at 12 h (R^2X_{cum} = 0.942, Q^2_{cum} = 1.000). In the scores plot, the confidence interval is defined by Hotelling's T2 ellipse (95% confidence interval), and observations outside the confidence ellipse are considered outliers. Square represents the 200 μg/mL ε-PL-treated groups; Triangle represents the 50 μg/mL ε-PL-treated groups; Cross represents the control groups.

acid markedly decreased to 0.52- and 0.25-fold at 12 h in the 50 and 200 μg/mL ε-PL-treated groups, respectively.

Ornithine, citrulline, and urea are all involved in the urea cycle. The levels of these compounds were all elevated in ε-PL-treated groups. In the 50 μg/mL ε-PL-treated group, the levels of ornithine at 4, 8, and 12 h compared with control were 3.27-, 1.85-, and 1.53-fold, respectively. In the 200 μg/mL ε-PL-treated group, the levels of ornithine at 4, 8, and 12 h compared with control were 3.54-, 2.19-, and 2.48-fold, respectively. The levels of citrulline compared with control were significantly elevated to 3.11-, 1.93-, and 2.6-fold at 4, 8, and 12 h in the 200 μg/mL ε-PL-treated group, respectively.

A total of 13 amino acids were detected, and the most notable one was glutamic acid. Glutamic acid was accumulated in ε-PL-treated groups. When compared with the control group, it notably rose to 1.13-, 1.62-, and 1.51-fold at 4, 8, and 12 h in the 200 μg/mL ε-PL-treated groups, respectively.

dx.doi.org/10.1021/jf500505n | J. Agric. Food Chem. 2014, 62, 4454−4465

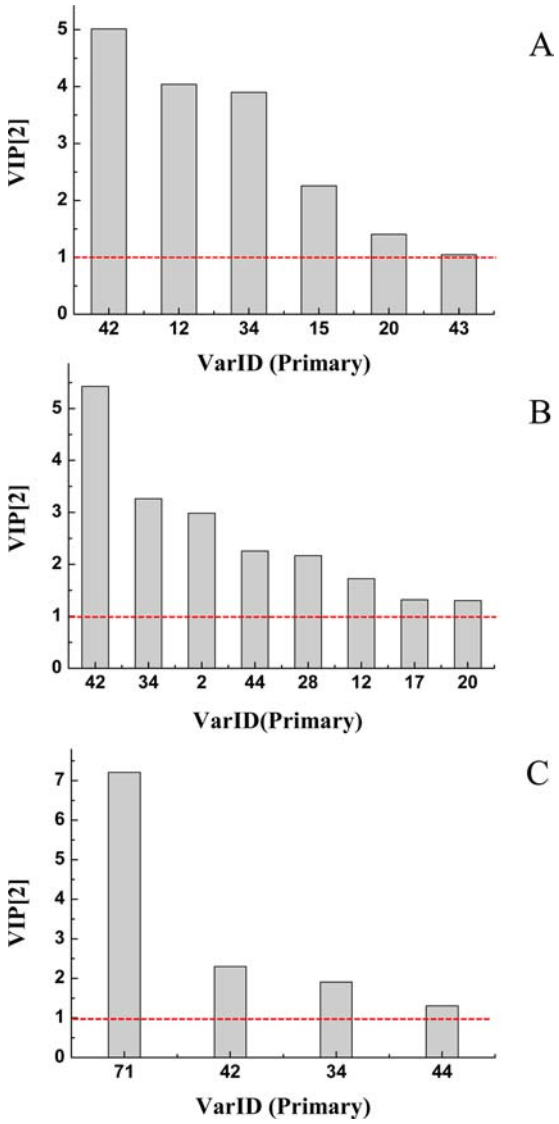

Figure 7. VIP plot generated by PLS: (A) sampling time at 4 h; (B) sampling time at 8 h; (C) sampling time at 12 h. *X*-axis represents each metabolite. 42, ornithine; 12, phosphate; 34, lysine; 15, ethanedioic acid; 20, aspartic acid; 43, citrulline; 2, acetic acid; 44, citrate; 28, glutamic acid; 17, serine; 71, trehalose.

There are two alcohols detected in *S. cerevisiae* cells. The levels of sorbitol compared with control in 50 and 200 μg/mL ε-PL-treated groups were increased to 1.86- and 4.92-fold at 12 h, respectively. The levels of inositol in 50 and 200 μg/mL ε-PL-treated groups compared with control were 2.06- and 2.01-fold at 8 h, respectively.

The detected trehalose in 50 and 200 μg/mL ε-PL-treated groups compared with control was notably decreased to 0.68- and 0.03-fold at 12 h, respectively.

DISCUSSION

The growth of cells was greatly inhibited by ε-PL. ε-PL at lower concentrations could lead to a delay in cell growth cycle of *S. cerevisiae* (Figure 1A). The cell mortality rate increased gradually, and cell viability decreased as the ε-PL concentration and treatment time increased. *S. cerevisiae* cells were killed when the ε-PL concentration reached a certain level (500 μg/mL), suggesting a fungicidal effect of ε-PL. These results indicated that the antimicrobial mode of action of ε-PL against *S. cerevisiae* was concentration-dependent. The membrane-permeabilizing activity of ε-PL was consistent with the PI assay. In the PI assay, the fluorescence intensity significantly increased as the ε-PL concentration increased (Figure 3).

Pore Formation on the Surface of *S. cerevisiae* Cells by ε-PL. The morphology of the yeast cells treated with ε-PL was also examined by SEM. Compared with the 500 μg/mL ε-PL-treated group, similar morphological alterations have been reported with *E. coli* treated with HAHp2-3-I, and micelles and pores on the surface of *E. coli* were clearly observed under SEM.[16] Currently, the antimicrobial peptides are divided into membrane disruption and nonmembrane disruption mechanism classes, depending on whether the reorientation of peptide leads to perturbation of the integrity of the cell membrane or peptide translocation into the cytoplasm.[16] The SEM observation results suggested that ε-PL at the 500 μg/mL concentration had a microbicidal activity via the membrane-damaging model. In the membrane disruption mechanism, "barrel-stave", "carpet", or "toroidal-pore" mechanisms are well studied.[16] In the barrel-stave model, peptide helices form a bundle in the membrane with a central lumen, much like a barrel composed of helical peptides as the staves. This type of transmembrane pore does not make the phospholipid bilayer curvature and is induced by hydrophobic peptides. In the toroidal-pore model, peptide can induce the phospholipid bilayer curvature, but without micelles appearing on the membrane surfaces. In the case of the carpet model, antimicrobial peptides with net charges will be attached to the membrane surface by electrostatic attraction and then accumulate on the bilayer surface like a carpet. Finally, the bilayer is disrupted in a detergent-effect manner, and phospholipid bilayer curvature, pores, and micelles are usually observed on the membrane surface.[16−18] In this study, the phospholipid bilayer curvature, pores, and micelles on the surface of *S. cerevisiae* after incubation in the medium containing 500 μg/mL ε-PL were clearly observed (Figure 2D,E). Moreover, in a previous study, Shima et al.[2] thought that ε-PL attached to the membrane surface due to electrostatic effects, which was consistent with the binding mode of antimicrobial peptides on the membrane surface in the carpet model. Thus, we presume that the microbicidal mechanism of ε-PL is more likely the carpet model. Interestingly, the *S. cerevisiae* cells could well be inhibited by low concentrations of ε-PL (<200 μg/mL), and the permeability of the cell membrane was increased, although pores or micelles on the surface of *S. cerevisiae* after incubation with low concentrations of ε-PL were not observed, and the cell shape did not change. These results also suggest that the basic mechanisms for fungicidal effect of ε-PL at higher concentrations are different from those of fungistatic effect at lower concentrations. In addition, the high concentration of antimicrobial peptides is necessary in the carpet model,[18] which also supports our speculation on the microbicidal mechanism of ε-PL.

After initial membrane binding, researchers found that peptides must locally concentrate to exert their microbiostatic activity, until they reach a concentration that enables their microbicidal action. Such a feature is commonly described as the threshold concentration concept. At this concentration, peptides begin to rearrange and alter cell membrane permeability.[17] This type of threshold concentration has been shown for some pore-forming peptides, such as Bac8c.[19] This

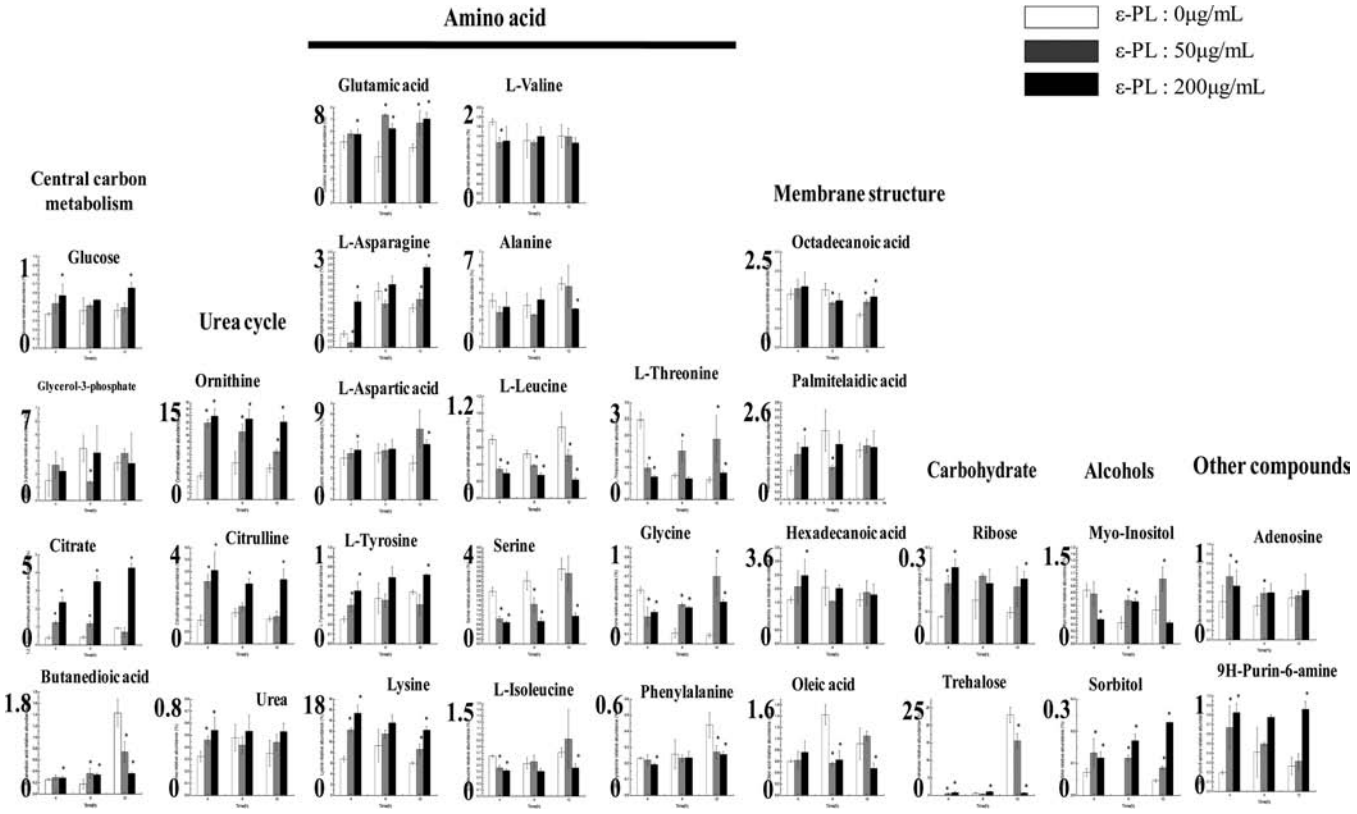

Figure 8. Variations of intracellular metabolites under the influence of ε-PL at 4, 8, and 12 h. Each value is the mean of four replicates ± SD. The asterisk (∗) indicates significant difference from equivalent control point (*t* test, $P < 0.05$).

study provides one of the best illustrations for the threshold concentration theory.

ε-PL Imposes Restrictions on Primary Metabolic Pathways. On the other hand, the microbiostatic mechanism of ε-PL has not been fully understood so far. When the concentration of ε-PL is not high enough to kill *S. cerevisiae* cells, such as at 50 and 200 μg/mL levels, it remains unclear how ε-PL inhibited the growth of the yeast. The aim of a metabolomics approach is to characterize or quantify as many as possible metabolites present in a biological sample in an unbiased manner.[20] Metabolomics analysis also assesses the last step in the series of changes that occur following an external stimulus[8] or a pathological insult,[9] and the composition of metabolites directly reveals the phenotypic changes that occur in a living system. Therefore, metabolomics studies are critical to reveal the antimicrobial mechanism of ε-PL on *S. cerevisiae*.

A perturbation in these intracellular metabolites caused by ε-PL could be detected by a GC-MS-based metabolomics approach. In this study, GC-MS combined with multivariate statistical analysis was used to investigate metabolic changes that occurred in *S. cerevisiae* as a result of exposure to different concentrations of ε-PL. The results demonstrated that there were clearly many differences at the level of intracellular metabolites among different treatment groups. Moreover, there was a clear distinction between the control and ε-PL-treated groups based on PCA, HCA, and PLS analysis. Compared with the control group, ε-PL treatment induced many metabolic changes, especially in the metabolism of carbohydrates, alcohols, lipids, and amino acids.

To investigate potential linkages between these metabolic changes and ε-PL treatment, the measured metabolite variations were mapped onto the metabolic pathways (Figure 9). As shown in Figure 9, these changes were not randomly distributed; instead, they occurred coordinately in distinct localized regions of the network. In ε-PL-treated groups, ε-PL promoted the intracellular accumulation of glucose, which indicated that glycolysis was inhibited by ε-PL. This might account for the growth inhibition of *S. cerevisiae* that was observed in the presence of ε-PL at a lower level. Furthermore, ε-PL caused decreases in the contents of serine, phenylalanine, leucine, isoleucine, and valine (Table 1). Moreover, the levels of glycine and threonine also decreased in the early stage of ε-PL treatment (Table 1). These metabolites could be converted from 3-P-glycerate and pyruvate (Figure 9), which are both metabolic intermediates of the Embden−Meyerhof−Parnas (EMP) pathway. As seen from another perspective, to some extent, the levels of metabolic intermediates of the EMP pathway decreased under ε-PL treatment. Such results also indicated the inhibition of EMP pathway by ε-PL. In the TCA cycle, the level of citric acid was increased by ε-PL (Figure 9 and Table 1). Citric acid was then transformed into α-ketoglutarate (α-KG), but α-KG might not be further involved in TCA. As shown in Figure 9, the levels of TCA cycle intermediate glutamic acid (Glu) and urea cycle intermediates ornithine, citrulline, and urea increased, whereas the level of succinate decreased upon exposure to ε-PL. The results indicated that α-KG was mainly transmuted into glutamic acid (Glu), leading to the inhibition of the TCA cycle by ε-PL. In previous studies, *S. cerevisiae* EMP pathway and TCA cycle were also inhibited by alcohol, acetic acid, and other external stimulants.[21−23]

It is our hypothesis that the central carbon metabolism of *S. cerevisiae* can be inhibited by low concentrations of ε-PL. Here are the possible explanations. First, because of ε-PL tiled on the

dx.doi.org/10.1021/jf500505n | J. Agric. Food Chem. 2014, 62, 4454−4465

Table 1. Metabolic Profiles of *S. cerevisiae* Cells Treated with ε-PL

		metabolite abundance[a] (relative to value of control groups)					
		4 h		8 h		12 h	
class	compound	50 μg/mL	200 μg/mL	50 μg/mL	200 μg/mL	50 μg/mL	200 μg/mL
central carbon metabolism	glucose	1.30	**1.54**	1.14	1.29	1.07	**1.60**
	glycerol-3-phosphate	1.78	1.47	**0.36**	0.91	1.26	0.99
	citrate	**3.12**	**5.92**	**2.75**	**8.19**	0.76	**4.54**
	butanedioic acid	1.15	**1.13**	**2.07**	**1.94**	**0.52**	**0.25**
urea cycle	ornithine	**3.27**	**3.54**	**1.85**	**2.19**	**1.53**	**2.48**
	citrulline	**2.63**	**3.11**	1.20	**1.93**	1.10	**2.60**
	urea	**1.42**	**1.67**	0.87	1.11	1.25	1.51
amino acids	glutamic acid	1.13	**1.13**	**1.91**	**1.62**	**1.44**	**1.51**
	L-asparagine	**0.35**	**3.37**	**0.77**	1.12	**1.21**	**2.03**
	L-aspartic acid	1.11	**1.19**	1.05	1.09	1.94	**1.52**
	L-tyrosine	**1.57**	**2.16**	0.96	1.46	0.76	**1.33**
	lysine	**1.79**	**2.25**	1.23	1.45	**1.43**	**2.03**
	L-valine	**0.74**	0.77	0.96	1.06	0.99	0.90
	alanine	0.75	0.87	0.77	1.14	0.96	**0.61**
	L-leucine	**0.49**	**0.42**	**0.74**	**0.52**	**0.60**	**0.26**
	serine	**0.47**	**0.41**	**0.63**	**0.36**	0.94	**0.37**
	L-isoleucine	**0.71**	**0.64**	1.05	0.76	1.31	**0.65**
	L-threonine	**0.40**	**0.29**	**2.03**	0.87	**3.09**	**1.37**
	glycine	**0.50**	**0.59**	**3.69**	**3.39**	**7.88**	**4.89**
	phenylalanine	0.95	**0.83**	0.90	0.92	**0.61**	**0.58**
membrane structure	octadecanoic acid	1.11	1.15	**0.77**	0.81	**1.40**	**1.56**
	palmitelaidic acid	1.56	**1.81**	**0.47**	0.80	1.09	1.06
	hexadecanoic acid	1.30	**1.56**	0.75	0.99	1.17	1.12
	oleic acid	1.03	1.26	**0.40**	**0.44**	1.15	**0.52**
carbohydrate	ribose	**2.21**	**2.81**	1.55	1.38	1.82	**2.08**
	trehalose	**0.48*†**	**0.80*†**	0.65	**1.86**	**0.68**	**0.03**
alcohols	*myo*-inositol	0.93	**0.45**	**2.06**	**2.01**	**1.92**	0.62
	sorbitol	**1.84**	**1.62**	**0.12*†**	**0.17*†**	**1.86**	**4.92**
other compounds	adenosine	**1.66**	**1.41**	**1.37**	1.39	1.05	1.18
	9*H*-purin-6-amine	**3.39**	**4.18**	1.21	1.90	1.18	**3.24**

[a]Metabolite abundance in bold indicates significant difference from equivalent control point (*t* test, $P < 0.05$). An asterisk (*) indicates abundance of metabolite is relative to internal standard succinic-d_4 acid; a dagger (†) indicates the metabolite corresponding to the control group was undetermined.

cell membrane, ε-PL can inhibit the membrane functions through changes in membrane fluidity and permeability. However, the cell membrane plays an important role in cell life activities, particularly in the transportation of amino acids, sugars, and ions into the *S. cerevisiae* cell through the cell membrane.[24] Thus, ε-PL can indirectly inhibit the central carbon metabolism due to the disruption of membrane functions. In addition, the plasma membrane ATPase (Pma1p) is the major protein in the plasma membrane.[24] Normally, H^+-ATPase functions to ensure the homeostasis of ions in the cytoplasm, and hence its malfunction would affect the permeability barrier of the yeast membrane; it is believed to play an important role in *S. cerevisiae* cells in response to stresses.[25,26] Inositol can increase ATPase activity to counteract the impact of ethanol on *S. cerevisiae* cell membrane permeability.[25−27] In the present study, inositol was also detected, and it was found to accumulate in the cells with prolonged action time in the ε-PL-treated groups (Figure 8). It may be a stress response in *S. cerevisiae* in the presence of ε-PL. Because ATPase activity affects the permeability of cell membrane and energy supply and there is a close relationship between inositol and ATPase activity,[28] the rise in the inositol level in *S. cerevisiae* in response to ε-PL would strongly support our hypothesis.

Second, ε-PL may induce apoptosis in yeast cells by stimulating a burst of reactive oxygen species (ROS), and thus the central carbon metabolism was indirectly inhibited. Currently, many studies have shown that the mechanism of antimicrobial peptides is very complicated, which involves their effects on multiple targets.[17,18] For instance, there are many research papers on antimicrobial peptides inducing cell apoptosis through activation of ROS, such as PAF26, coprisin, and melittin.[29−31] In our study, the levels of sorbitol and inositol in the *S. cerevisiae* cells increased by ε-PL treatment (Table 1). Sorbitol and inositol as compatible solutes are common polyhydric alcohols, which may also protect the

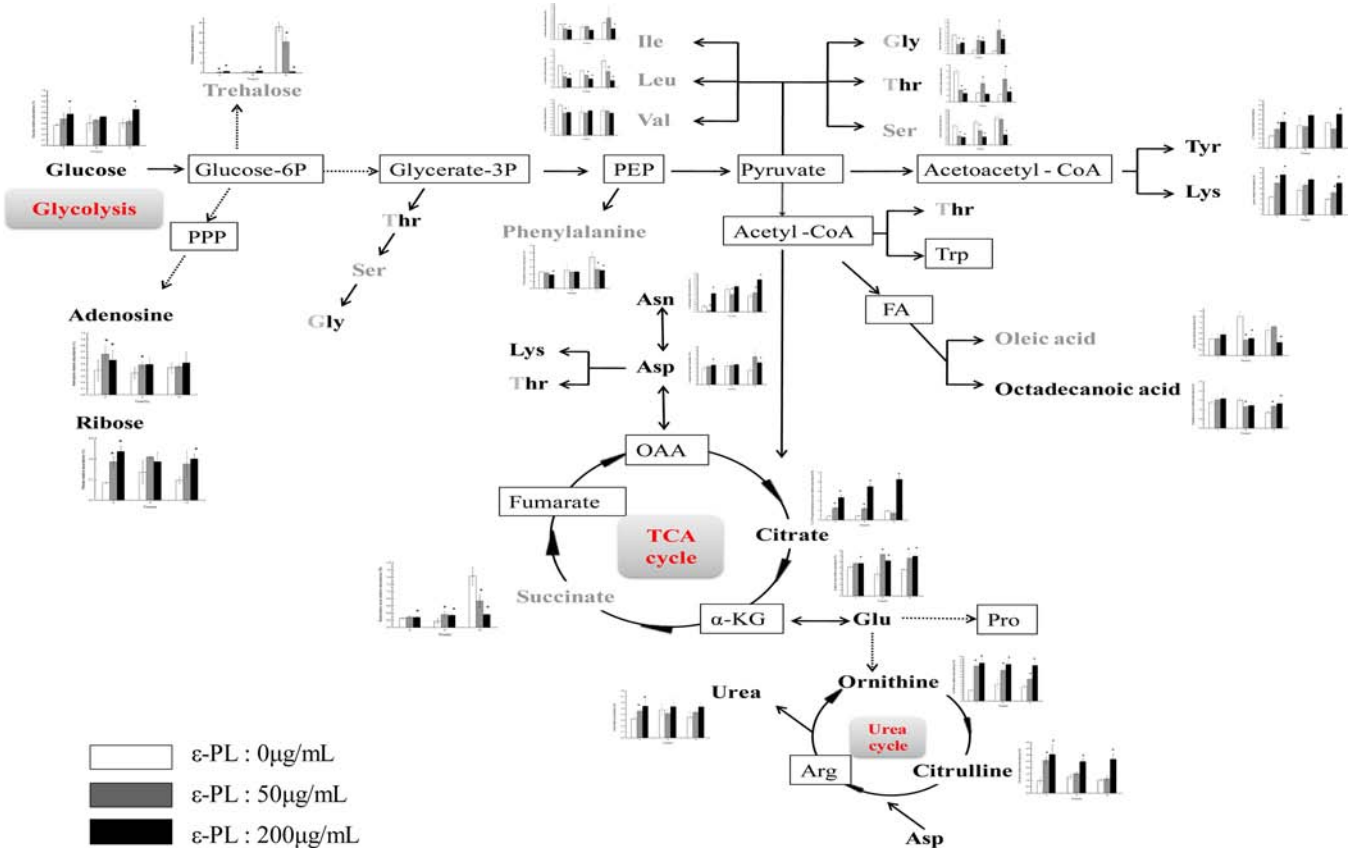

Figure 9. Schematic showing changes of metabolite abundance mapped onto the metabolic network at sampling times of 4, 8, and 12 h. Solid arrows in the network indicate a single step connecting two metabolites; dashed arrows represent multiple steps. Metabolites shown in bold black indicate a significant increase in value, bold gray indicates a significant decrease; a gray first letter only of the metabolite indicates that it is first decreased and then increased under ε-PL stress. Metabolites undetected are boxed. PPP, pentose phosphate pathway; PEP, phosphoenolpyruvate; OAA, oxaloacetate; α-KG, α-ketoglutarate; FA, fatty acid; Ile, isoleucine; Leu, leucine; Val, valine; Arg, arginine; Asn, asparagine; Asp, aspartic acid; Glu, glutamic acid; Gly, glycine; Lys, lysine; Pro, proline; Ser, serine; Thr, threonine; Trp, tryptophan; Tyr, tyrosine.

intracellular enzyme activity and cell membrane integrity through their ROS scavenging activities.[14,32] These results support our proposed ROS burst hypothesis in the *S. cerevisiae* cells.

Finally, the abnormal distribution of the cytoplasm induced by ε-PL through electrostatic interaction with the microbial cell surface may also be one of the factors responsible for the intracellular metabolic disturbances.

Variations of Protective Metabolites. Trehalose is a nonreducing disaccharide and is also commonly considered to be a protective substance of yeast cells responding to multiple external stresses.[33,34] However, trehalose is not always accumulated under external stress in the cells of *S. cerevisiae*; for example, trehalose is not accumulated in response to H_2O_2.[35,36] In the current study, trehalose was detected at 12 h in cells. However, compared with the control group, the level of trehalose did not increase in response to ε-PL treatment. This might be due to the fact that trehalose is converted from glucose-6-phosphate, an intermediate metabolite of EMP pathway.[33,36] However, the EMP pathway was inhibited by ε-PL from the beginning; therefore, the level of trehalose did not increase in the ε-PL-treated groups. The result also suggests that trehalose was unrelated to the stress induced by ε-PL.

Glutamic acid is usually considered to be a protective metabolite in cells, and it plays an important role in various stress responses; its role is largely accomplished by enhancing the stability of the cell membrane.[13,37−39] In the ε-PL-treated groups, the level of glutamic acid increased as a response tobetter protect the cells (Table 1). These results once again confirmed our hypothesis that ε-PL indirectly inhibited central carbon metabolism through disrupting the membrane functions.

Proposed Antimicrobial Mechanism of ε-PL. On the basis of our research results, we found that fungistatic and fungicidal mechanisms of ε-PL on *S. cerevisiae* cells were completely different. Thus, we are proposing two possible antimicrobial mechanisms of ε-PL as shown in Figure 10. First, ε-PL binds to anionic components of the cell membrane through electrostatic interaction. When ε-PL reached a threshold concentration, ε-PL quickly acted on the cell membrane of *S. cerevisiae* following a mode of action of the carpet model, causing micelle formation and phospholipid bilayer bending and perforation on the cell membrane, eventually leading to cell death. This is the fungicidal effect. On the other hand, when ε-PL concentration is below the threshold level, ε-PL can cause changes in the fluidity, structure, and permeability of the cell membrane. Membrane function is then disrupted due to these changes. Disruption of membrane function will lead to the inhibition of intracellular central carbon metabolism. At the same time, ε-PL may induce cell apoptosis by stimulating intracellular ROS generation. These combined actions caused by ε-PL will lead to its inhibiting the growth of *S. cerevisiae* cells, but not necessarily killing the cells.

dx.doi.org/10.1021/jf500505n | J. Agric. Food Chem. 2014, 62, 4454−4465

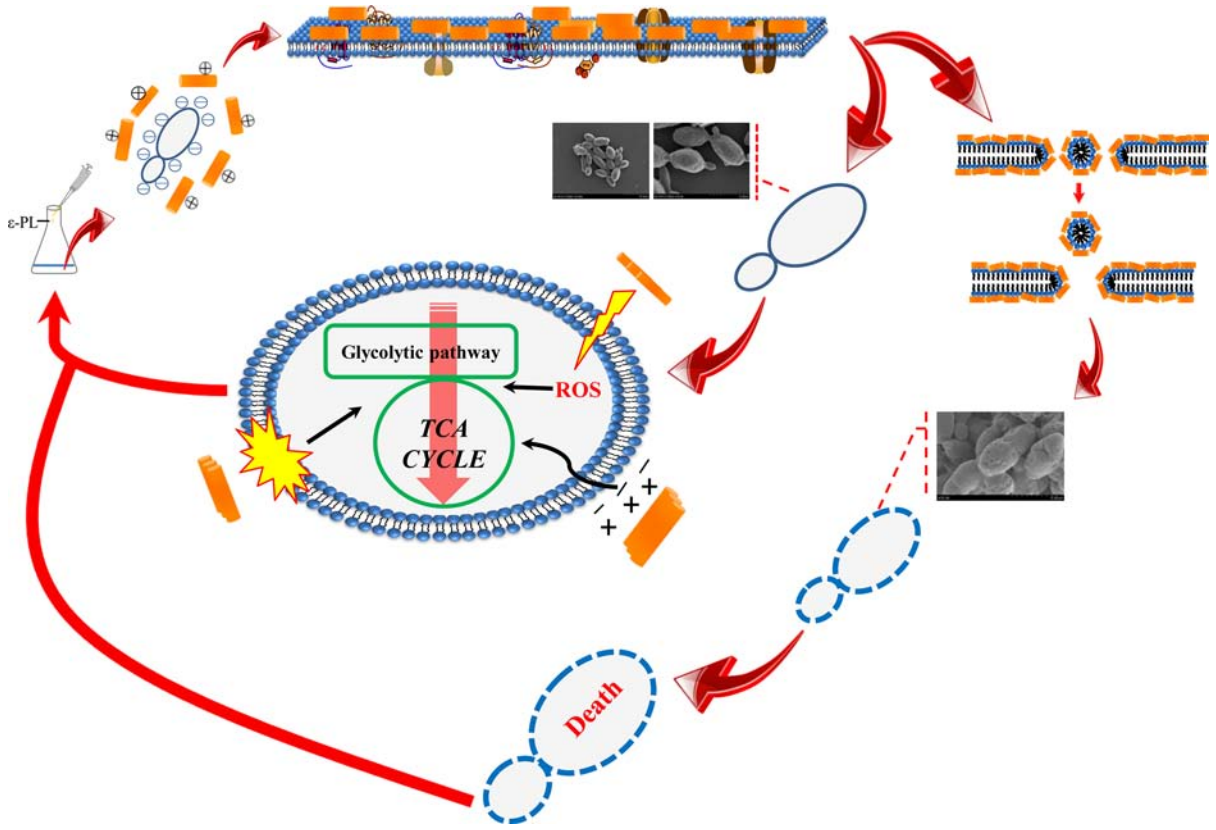

Figure 10. Possible mode of action of the ε-PL on *S. cerevisiae*.

Such mode of action is called fungistatic or a microbiostatic effect.

It is also noteworthy that most known antimicrobial peptides, or bacteriocins, generally consist of a variety of amino acids. In contrast, ε-PL is a homopolymer of a single amino acid, lysine. It also occurs in nature. In the current study, we found the action mode of ε-PL was similar to that of some other antimicrobial peptides.

In summary, this study provides a good example of antimicrobial mechanism investigation at the metabolite level with high-throughput methods. It also provides new insight into ways of understanding the modes of action of known or new antimicrobials. These results suggest that the metabolomics approach is a powerful tool to study antimicrobial mechanisms and can provide a new perspective at the molecular level on how microorganisms respond to biological preservatives including antimicrobial peptides.

■ ASSOCIATED CONTENT

Supporting Information

Figure S1. This material is available free of charge via the Internet at http://pubs.acs.org.

■ AUTHOR INFORMATION

Corresponding Author

*(S.-R.J.) Mail: Key Laboratory of Industrial Fermentation Microbiology, Ministry of Education, College of Biotechnology, Tianjin University of Science and Technology, No. 29 13th Avenue, Tianjin Economic-Technological Development Area, Tianjin 300457, People's Republic of China. Fax: 86-22-60602298. Phone: 86-22-60601598. E-mail: jiashiru@tust.edu.cn.

Funding

We are grateful for financial support from the National Natural Science Foundation of China (Project 21276197).

Notes

The authors declare no competing financial interest.

■ ACKNOWLEDGMENTS

We thank Dr. Ming-Zhu Ding for her support and contributions to the study.

■ ABBREVIATIONS USED

ε-PL, ε-poly-L-lysine; γ-PGA, γ-polyglutamic acid; *S. cerevisiae*, *Saccharomyces cerevisiae*; *S. albulus*, *Streptomyces albulus*; EMP, Embden−Meyerhof−Parnas; TCA, tricarboxylic acid cycle; PPP, pentose phosphate pathway; MDH, malate dehydrogenase; PEP, phosphoenolpyruvate; OAA, oxaloacetate; α-KG, α-ketoglutarate; FA, fatty acid; Ile, isoleucine; Leu, leucine; Val, valine; Arg, arginine; Asn, asparagine; Asp, aspartic acid; Glu, glutamic acid; Gly, glycine; Lys, lysine; Pro, proline; Ser, serine; Thr, threonine; Trp, tryptophan and; Tyr, tyrosine; ATPase, adenosinetriphosphatase; ROS, reactive oxygen species; UFAs, unsaturated fatty acids; MUFAs, mono-UFAs; PI, propidium iodide; SEM, scanning electron microscopy; GC-MS, gas chromatography−mass spectrometry; TIC, total ion chromatograms; PBS, phosphate buffer saline; MSTFA, *N*-methyl-*N*-(trimethylsilyl)trifluoroacetamide; PCA, principal component analysis; PLS, partial least-squares; HCA, hierarchical cluster analysis; VIP, variable importance in the projection; SD, standard deviation

REFERENCES

(1) Shima, S.; Sakai, H. Polylysine produced by *Streptomyces*. *Agric. Biol. Chem.* **1977**, *41*, 1907−1909.

(2) Shima, S.; Matsuoka, H.; Iwamoto, T.; Sakai, H. Antimicrobial action of ε-poly-L-lysine. *J. Antibiot.* **1984**, *37*, 1449−1455.

(3) Hiraki, J. ε-poly-L-lysine, its antimicrobial activity and utilization. *Jpn. Food Addit. Assoc. News* **1999**, 223−233.

(4) Yamanaka, K.; Hamano, Y. Biotechnological production of poly-ε-L-lysine for food and medical applications. In *Amino-acid Homopolymers Occurring in Nature*; Springer-Verlag: Berlin, Germany, 2010; pp 61−75.

(5) Purac Biochem b.v. ε-Polylysine GRAS notice (USFDA), 2010.

(6) Muto, M. Chemical technology for preservation of food products; food preservative, ε-poly-L-lysine. *Boukin Boubai* **2009**, *37*, 765−772.

(7) Fiehn, O. Metabolomics − the link between genotypes and phenotypes. *Plant Mol. Biol.* **2002**, *48* (1−2), 155−171.

(8) Van Ravenzwaay, B.; Cunha, G.; Leibold, E.; Looser, R.; Mellert, W.; Prokoudine, A.; Walk, T.; Wiemer, J. The use of metabolomics for the discovery of new biomarkers of effect. *Toxicol. Lett.* **2007**, *172* (1), 21−28.

(9) Saghatelian, A.; Cravatt, B. F. Global strategies to integrate the proteome and metabolome. *Curr. Opin. Chem. Biol.* **2005**, *9* (1), 62−68.

(10) Painting, K.; Kirsop, B. A quick method for estimating the percentage of viable cells in a yeast population, using methylene blue staining. *World J. Microbiol. Biotechnol.* **1990**, *6* (3), 346−347.

(11) Shimada, S.; Andou, M.; Naito, N.; Yamada, N.; Osumi, M.; Hayashi, R. Effects of hydrostatic pressure on the ultrastructure and leakage of internal substances in the yeast *Saccharomyces cerevisiae*. *Appl. Microbiol. Biotechnol.* **1993**, *40* (1), 123−131.

(12) Veerman, E. C.; Valentijn-Benz, M.; Van't Hof, W.; Nazmi, K.; van Marle, J.; Nieuw Amerongen, A. V. Phytosphingosine kills *Candida albicans* by disrupting its cell membrane. *Biol. Chem.* **2010**, *391* (1), 65−71.

(13) Ding, M. Z.; Zhou, X.; Yuan, Y. J. Metabolome profiling reveals adaptive evolution of *Saccharomyces cerevisiae* during repeated vacuum fermentations. *Metabolomics* **2010**, *6* (1), 42−55.

(14) Han, P. P.; Yuan, Y. J. Metabolic profiling as a tool for understanding defense response of *Taxus cuspidata* cells to shear stress. *Biotechnol. Prog.* **2009**, *25* (5), 1244−1253.

(15) Szeto, S. S.; Reinke, S. N.; Sykes, B. D.; Lemire, B. D. Mutations in the *Saccharomyces cerevisiae* succinate dehydrogenase result in distinct metabolic phenotypes revealed through ^{1}H NMR-based metabolic footprinting. *J. Proteome Res.* **2010**, *9* (12), 6729−6739.

(16) Song, R.; Wei, R. B.; Luo, H. Y.; Wang, D. F. Isolation and characterization of an antibacterial peptide fraction from the pepsin hydrolysate of half-fin anchovy (*Setipinna taty*). *Molecules* **2012**, *17* (3), 2980−2991.

(17) Teixeira, V.; Feio, M. J.; Bastos, M. Role of lipids in the interaction of antimicrobial peptides with membranes. *Prog. Lipid Res.* **2012**, *51* (2), 149−177.

(18) Brogden, K. A. Antimicrobial peptides: pore formers or metabolic inhibitors in bacteria? *Nat. Rev. Microbiol.* **2005**, *3* (3), 238−250.

(19) Spindler, E.; Hale, J.; Giddings, T.; Hancock, R.; Gill, R. Deciphering the mode of action of the synthetic antimicrobial peptide Bac8c. *Antimicrob. Agents Chemother.* **2011**, *55* (4), 1706−1716.

(20) Want, E. J.; Nordström, A.; Morita, H.; Siuzdak, G. From exogenous to endogenous: the inevitable imprint of mass spectrometry in metabolomics. *J. Proteome Res.* **2007**, *6* (2), 459−468.

(21) Kubota, S.; Takeo, I.; Kume, K.; Kanai, M.; Shitamukai, A.; Mizunuma, M.; Miyakawa, T.; Shimoi, H.; Iefuji, H.; Hirata, D. Effect of ethanol on cell growth of budding yeast: genes that are important for cell growth in the presence of ethanol. *Biosci., Biotechnol., Biochem.* **2004**, *68* (4), 968−972.

(22) Li, H.; Ma, M. L.; Luo, S.; Zhang, R. M.; Han, P.; Hu, W. Metabolic responses to ethanol in *Saccharomyces cerevisiae* using a gas chromatography tandem mass spectrometry-based metabolomics approach. *Int. J. Biochem. Cell Biol.* **2012**, *44* (7), 1087−1096.

(23) Ding, M. Z.; Wang, X.; Yang, Y.; Yuan, Y. J. Metabolomic study of interactive effects of phenol, furfural, and acetic acid on *Saccharomyces cerevisiae*. *Omics: J. Integr. Biol.* **2011**, *15* (10), 647−653.

(24) Van der Rest, M.; Kamminga, A. H.; Nakano, A.; Anraku, Y.; Poolman, B.; Konings, W. N. The plasma membrane of *Saccharomyces cerevisiae*: structure, function, and biogenesis. *Microbiol. Rev.* **1995**, *59* (2), 304−322.

(25) Furukawa, K.; Obata, H.; Kitano, H.; Mizoguchi, H.; Hara, S. Effect of cellular inositol content on ethanol tolerance of *Saccharomyces cerevisiae* in sake brewing. *J. Biosci. Bioeng.* **2004**, *98* (2), 107−113.

(26) Ding, J.; Huang, X.; Zhang, L.; Zhao, N.; Yang, D.; Zhang, K. Tolerance and stress response to ethanol in the yeast *Saccharomyces cerevisiae*. *Appl. Microbiol. Biotechnol.* **2009**, *85* (2), 253−263.

(27) Fernandes, A. R.; Sá-Correia, I. Transcription patterns of PMA1 and PMA2 genes and activity of plasma membrane H^{+}-ATPase in *Saccharomyces cerevisiae* during diauxic growth and stationary phase. *Yeast* **2003**, *20* (3), 207−219.

(28) Gancedo, C.; Serrano, R. Energy-yielding metabolism. *Yeasts* **1989**, *3*, 205−259.

(29) Carmona, L.; Gandía, M.; López-García, B.; Marcos, J. F. Sensitivity of *Saccharomyces cerevisiae* to the cell-penetrating antifungal peptide PAF26 correlates with endogenous nitric oxide (NO) production. *Biochem. Biophys. Res. Commun.* **2012**, *417* (1), 56−61.

(30) Lee, J.; Hwang, J. S.; Hwang, I. S.; Cho, J.; Lee, E.; Kim, Y.; Lee, D. G. Coprisin-induced antifungal effects in *Candida albicans* correlate with apoptotic mechanisms. *Free Radical Biol. Med.* **2012**, *52* (11), 2302−2311.

(31) Park, C.; Lee, D. G. Melittin induces apoptotic features in *Candida albicans*. *Biochem. Biophys. Res. Commun.* **2010**, *394* (1), 170−172.

(32) Chen, Z.; Cuin, T. A.; Zhou, M.; Twomey, A.; Naidu, B. P.; Shabala, S. Compatible solute accumulation and stress-mitigating effects in barley genotypes contrasting in their salt tolerance. *J. Exp. Bot.* **2007**, *58* (15−16), 4245−4255.

(33) Singer, M. A.; Lindquist, S. Thermotolerance in *Saccharomyces cerevisiae*: the Yin and Yang of trehalose. *Trends Biotechnol.* **1998**, *16* (11), 460−468.

(34) Hounsa, C. G.; Brandt, E. V.; Thevelein, J.; Hohmann, S.; Prior, B. A. Role of trehalose in survival of *Saccharomyces cerevisiae* under osmotic stress. *Microbiology* **1998**, *144* (3), 671−680.

(35) Parrou, J. L.; Teste, M. A.; François, J. Effects of various types of stress on the metabolism of reserve carbohydrates in *Saccharomyces cerevisiae*: genetic evidence for a stress-induced recycling of glycogen and trehalose. *Microbiology* **1997**, *143* (6), 1891−1900.

(36) Godon, C.; Lagniel, G.; Lee, J.; Buhler, J. M.; Kieffer, S.; Perrot, M.; Boucherie, H.; Toledano, M. B.; Labarre, J. The H_2O_2 stimulon in *Saccharomyces cerevisiae*. *J. Biol. Chem.* **1998**, *273* (35), 22480−22489.

(37) Natera, V.; Sobrevals, L.; Fabra, A.; Castro, S. Glutamate is involved in acid stress response in *Bradyrhizobium* sp. SEMIA 6144 (*Arachis hypogaea* L.) microsymbiont. *Curr. Microbiol.* **2006**, *53* (6), 479−482.

(38) Yap, S.; Lim, S. Response of *Rhizobium* sp. UMKL 20 to sodium chloride stress. *Arch. Microbiol.* **1983**, *135* (3), 224−228.

(39) Takagi, H.; Iwamoto, F.; Nakamori, S. Isolation of freeze-tolerant laboratory strains of *Saccharomyces cerevisiae* from proline-analogue-resistant mutants. *Appl. Microbiol. Biotechnol.* **1997**, *47* (4), 405−411.

JOURNAL OF AGRICULTURAL AND FOOD CHEMISTRY

Article

pubs.acs.org/JAFC

Feasibility of Surface-Enhanced Raman Spectroscopy for Rapid Detection of Aflatoxins in Maize

Kyung-Min Lee,*[,†] Timothy J. Herrman,[†] Yordanos Bisrat,[‡] and Seth C. Murray[§]

[†]Office of the Texas State Chemist, Texas A&M AgriLife Research, Texas A&M University System, College Station, Texas 77841, United States

[‡]Materials Characterization Facility, Texas A&M University, College Station, Texas 77843, United States

[§]Department of Soil and Crop Sciences, Texas A&M University, College Station, Texas 77843, United States

Supporting Information

ABSTRACT: Rapid and sensitive surface-enhanced Raman spectroscopy (SERS) for aflatoxin detection was employed for development of the models to classify and quantify aflatoxin levels in maize at concentrations of 0 to 1,206 μg/kg. Highly effective SERS substrate (Ag nanosphere) was prepared and mixed with a sample extract for SERS measurement. Strong Raman bands associated with aflatoxins and changes in maize kernels induced by aflatoxin contamination were observed in different SERS spectroscopic regions. The *k*-nearest neighbors (KNN) classification model yielded high classification accuracy and lower prediction error with no misclassification of contaminated samples as aflatoxin negative. The multiple linear regression (MLR) models showed a higher predictive accuracy with stronger correlation coefficients (r = 0.939−0.967) and a higher sensitivity with lower limits of detection (13−36 μg/kg) and quantitation (44−121 μg/kg) over other quantification models. Paired sample *t* test exhibited no statistically significant difference between the reference values and the predicted values of SERS in most chemometric models. The proposed SERS method would be a more effective and efficient analytical tool with a higher accuracy and lower constraints for aflatoxin analysis in maize compared to other existing spectroscopic methods and conventional Raman spectroscopy.

KEYWORDS: *aflatoxin, surface-enhanced Raman spectroscopy (SERS), nanostructure, chemometrics, food safety*

INTRODUCTION

Aflatoxins as secondary metabolites produced by the *Aspergillus* strains have been causing a major problem for agriculture in many countries. Aflatoxins in contaminated food and feed products are carcinogens as recognized by the International Agency for Research on Cancer (IARC) as well as other health hazards for animals and humans, leading to substantial economic losses to relevant industries.[1] Like fumonisins and other mycotoxins, maximum levels for aflatoxins in grains and oilseeds destined for animal and human consumptions have been set by the Food and Drug Administration (FDA) and European Commission (EC).[2]

The aflatoxin detection methods currently available in laboratory and nonlaboratory sites such as high performance liquid chromatography (HPLC) and enzyme-linked immunosorbent assay (ELISA) are highly selective, very accurate, and precise with good detection limits.[3] However, these methods are not practical and convenient for a real-time response due to long analysis time, low cost-effectiveness, analysis complexity, and requirement of trained personnel. Therefore, numerous studies have been continuously conducted to develop rapid, simple, and inexpensive methods with high sensitivity and specificity for early detection and identification of aflatoxins. A method employing portable equipment and nonhazardous solvents for aflatoxin analysis would be more suitable for application at the sites where the samples are collected.[4]

Spectroscopic methods are very promising and excellent tools for screening of aflatoxin contaminated samples because they are inherently rapid, specific, and possibly partially or completely computerized. Among spectroscopic methods, Raman spectroscopy is valuable due to its great possibilities and advantages in detecting mycotoxins in grains and oilseeds.[5−7] Compared to other spectroscopic methods used for mycotoxin analysis such as near-infrared spectroscopy (NIR) and Fourier-transform infrared spectroscopy (FTIR), Raman spectroscopy can provide well-resolved bands of mycotoxin molecules and allow acquisition of spectra in aqueous environments. However, conventional Raman spectroscopy has a small cross-section of Raman scattering compared to that of Rayleigh scattering, resulting in lack of sensitivity and thus requiring a longer collection time for improvement of spectral quality. Surface-enhanced Raman spectroscopy (SERS) has been considered as one of the most promising techniques to greatly improve the sensitivity of conventional Raman spectroscopy.

SERS is an advanced technique that uses nanostructural surface phenomena to enhance a weak inelastic-scattering Raman effect of molecules adsorbed on and/or at the vicinity of metal particles like silver, gold, and copper.[4,8,9] SERS can measure samples with great sensitivity and rapidity to provide comprehensive information, even on orientation of single

Received: February 18, 2014
Revised: April 28, 2014
Accepted: April 28, 2014
Published: April 28, 2014

ACS Publications © 2014 American Chemical Society

molecules adsorbed on nanometallic particles. However, detection ability and accuracy of target molecule are greatly influenced by a morphological variation of nanostructures and adsorption variation of the molecule where it is located.

The acceptability of SERS is largely determined by the methods to prepare SERS substrates.[10−17] A typical SERS enhancement factor reported in previous studies is about order of 10^7 and up to 10^{14} at extremely high enhancement levels enough for single molecule detection and identification. For SERS measurement, nanoparticles should agglomerate or aggregate prior to sample introduction. Previous studies showed that metallic nanoparticles are initially precipitated and their growth takes place with the progress of the reaction.[11,13,17] The size and stability of nanoparticles can be further optimized by altering the environments around the particles such as pH of reaction solutions, concentrations of reducing and stabilizing agents, and ratio of nanoparticle/molecule.[11]

Due to its high sensitivity, specificity, and rapidity, SERS has been broadly applied in biochemistry, molecular biology, environmental science, and food science for detection and discrimination of a wide variety of target agents.[4] Unfortunately, SERS methods are not readily available as a screening method for routine use and on-site analysis for aflatoxin detection due to use of costly metal substrates and technical difficulties in producing stable SERS substrate and obtaining reproducible results.[16,18] Wu et al.[18] obtained high quality SERS spectra of aflatoxins with a low detection limit and excellent differentiation ability with comparison of actual SERS spectra and theoretical Raman spectra.

The objective of this research is to employ a rapid and sensitive SERS method for detection of the level of aflatoxins in maize by extracting ground maize samples using a simple and fast one-step extraction procedure to explore the possibility of the method implementation for on-site analysis. The proposed SERS method could serve as a powerful tool for a high-throughput analysis with a great accuracy and convenience for aflatoxin detection at many sample collection points requiring rapid routine analysis.

MATERIALS AND METHODS

Materials. The standards of aflatoxin B_1, B_2, G_1, and G_2 were purchased from Sigma-Aldrich (St. Louis, MO). The Aflatest immunoaffinity column used for HPLC analysis was obtained from VICAM (Watertown, MA). All chemicals, reagents, and organic solvents were of analytical grade and used without any further purification.

Sample Preparation and Extraction. Maize samples naturally contaminated with aflatoxins were obtained from Office of the Texas State Chemist regulatory samples collected by Texas Feed and Fertilizer Control Service according to the State's plan of work. A total of 132 samples with aflatoxin concentration range of 0−1,126 μg/kg were selected for HPLC analysis and SERS measurements. A ZM 200 ultra centrifugal mill (Retsch, Haan, Germany) with a 0.075 mm diameter screen was used to grind each sample of approximately 4.5 kg. The ground samples contained in a polyethylene bottle were stored in a refrigerator of 4 °C prior to use and between sample measurements. The samples with higher moisture content were dried to below 15% at 40 °C for 12 h to ensure inhibition of fungal growth in the samples. The samples were equilibrated to a room temperature at least 1 h prior to analysis.

Twenty grams of ground sample was placed in a plastic bottle to which 100 mL of methanol/water (70:30, v/v) extraction solvent was added for sample extraction by vigorously shaking for 5 min. The resultant mixture was filtered through the filter paper (Whatman #1). The sample extract was directly used for SERS measurement.

Preparation of SERS Substrate. Ag nanosphere (NS) for SERS measurements was prepared with slight modifications to the previous methods.[10,19,20] In brief, 0.5 g of $AgNO_3$, 10 mL of deionized water, 0.8 g of sodium oleate, 1 mL of oleic acid, and 5 mL of ethanol were added to a 20 mL glass vial in order under agitation. The glass vial was air-tightly sealed and placed in the oven at 150 °C for 24 h. Afterward the system was cooled down to room temperature. The products inside the vial were washed with ethanol three times and dried to form Ag nanocrystals (NC) at the bottom. The collected 4 mg of AgNC was added to 1 mL of cyclohexane. This solution was added to a solution of 28 mg of sodium dodecyl sulfate (SDS) in 1 mL of deionized water. The system containing AgNC was subjected to ultrasonic treatment for emulsification for about 1 h and subsequently heated at 70 °C with stirring until the cyclohexane was removed to manufacture AgNSs.

HPLC Analysis of Aflatoxins. Fifty grams of ground maize sample was shaken for 1 h at 200 rpm for sample extraction using a solvent of methanol:water (70:30, v/v). The resultant mixture was filtered through the folded filter paper (Whatman #1). Ten milliliters of the filtered extract was mixed with 20 mL of deionized water and 1 g of sodium chloride and filtered to obtain the clean sample extract for loading onto an Aflatest immunoaffinity column (Vicam, Watertown, MA). The eluate from the column though washing with water and methanol was diluted with 1 mL of HPLC water and injected into a Waters 2695 HPLC system (Waters, Milford, MA). The HPLC system was equipped with a Spherisorb 4.6 × 150 mm, C18 column connected with Waters Spherisorb guard column 4.6 × 10 mm. The mobile phase consisted of a mixture of water:acetonitrile:methanol (3:1:1), flowing at a rate of 1.0 mL/min. Empower software (Milford, MA) was used to obtain and analyze chromatographic data. The mixture of standard aflatoxins B_1, B_2, G_1, and G_2 was prepared to build a standard calibration curve for quantification of aflatoxins in ground maize samples.

SERS Measurement. The mixture of AgNSs and the extract at the ratio of 1:1 (v/v) in volume was prepared. A 300 μL volume of the mixture was placed on 96 wells for SERS measurements in quadruplicate using spectroscopy with a RamanStation 400F (PerkinElmer, Beaconsfield, Buckinghamshire, U.K.). The Raman system was interfaced with the Spectrum (v. 6.3) software for data acquisition and analysis and consisted of a 256 × 1024 pixel CCD detector and a near-infrared laser source of 785 nm wavelength, with 175 mW output power focused on the sample. The software-controlled motorized sample stage was operated at <2 micro step resolution in an *x*-*y*-*z* direction for optimal spectral acquisition. The spectrum collected with exposure time of 2 and 5 scans at the sample location was recorded at the spectral resolution of 4 cm^{-1} in the Raman shift range of 200 to 2,000 cm^{-1}. The spectra from 7 different spots on the sample were averaged to obtain a representative spectrum of each sample.

Scanning electron microscopy (SEM) images of the samples were also made with a JSM 7500F microscope (JEOL Ltd., Tokyo, Japan) to characterize the size and morphology of AgNS and its mixture with the extracts.

Spectral Data Preprocessing. The SERS spectrum was corrected for background at the time of its acquisition. The spectrum was further baseline-corrected and normalized to minimize the influence of instrumental and environmental changes in the laboratory on the Raman signal. The background-corrected SERS spectrum was also preprocessed by a 9-point Savitzky−Golay filtering function to obtain first and second derivatives of spectra, which eliminates baseline and linear slope effects. The deconvolution preprocessing method was applied to the normalized spectra to improve a band resolution by diminishing interference between unresolved bands.

Development and Validation of Chemometric Models. For application of statistical analyses, the preprocessed spectral data were converted to an ASCII file. Prior to the development of classification models, the samples were divided into 5 subgroups according to the level of aflatoxins in maize samples: below 20 μg/kg (regarded as negative), 20−200 μg/kg, 300−450 μg/kg, 550−700 μg/kg, and above

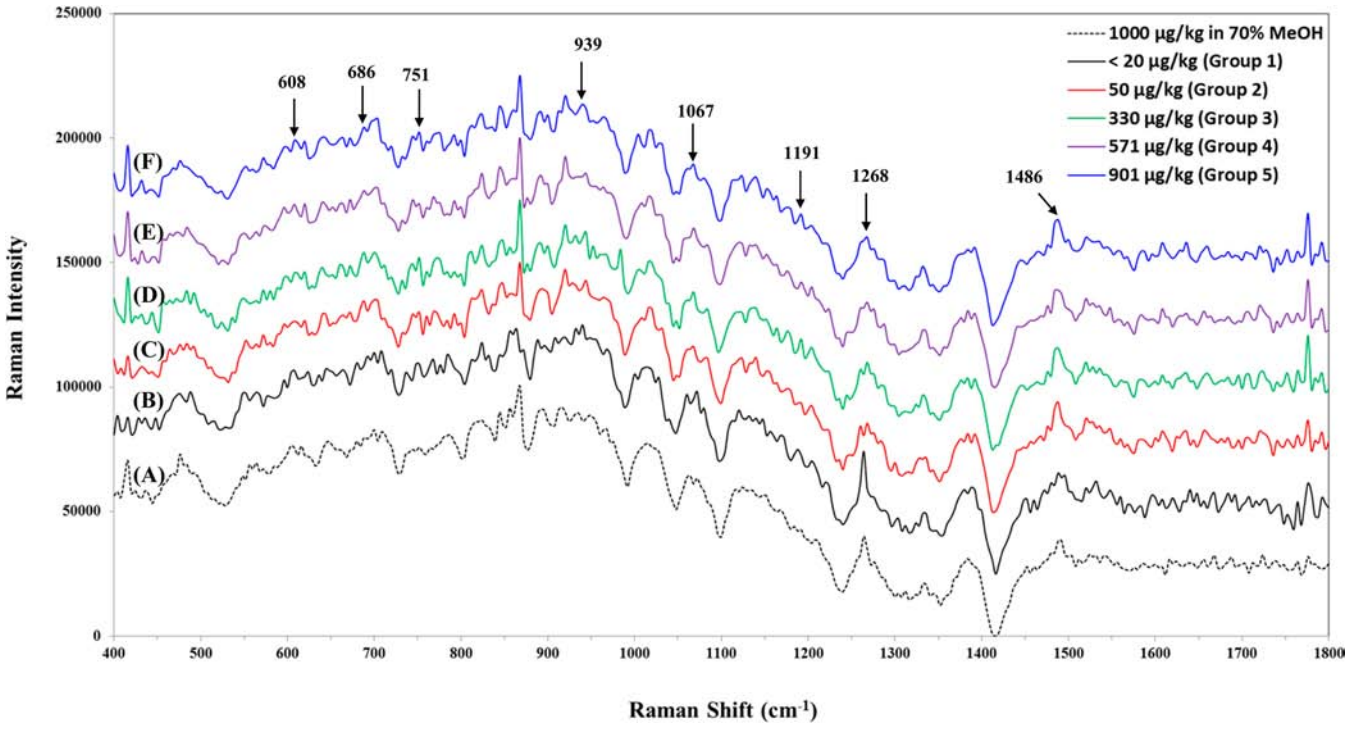

Figure 1. SERS spectra of 1,000 μg/kg pure aflatoxin in extract solvent (70% MeOH) (A) and aflatoxin contaminated sample at concentrations of (B) below 20 μg/kg (group 1), (C) 50 μg/kg (group 2), (D) 330 μg/kg (group 3), (E) 571 μg/kg (group 4), and (F) 901 μg/kg (group 5).

850 μg/kg. Principal component analysis (PCA), partial least-squares (PLS), and cluster analysis were employed to see if the samples could be well grouped into the predefined subgroups. A total of 115 spectral data were partitioned into a training data set (n = 85) for developing a calibration model and validation data set (n = 35) for testing the model. The chemometric calibration models for classification of samples by aflatoxin level were developed using two chemometric methods as proposed in previous research:[21−23] k-nearest neighbor (KNN) and linear discriminant analysis (LDA). The models were evaluated by comparing their classification accuracy and false negative error to select the model most suitable for the classification of aflatoxin contaminated maize samples.

The calibration models for aflatoxin quantification in maize were developed for the preprocessed spectral data by applying multiple linear regression (MLR), principal components regression (PCR), and partial least-squares regression (PLSR) algorithms. Prior to the chemometric application, a whole spectroscopic data set (n = 132) was randomly split into a 75% training data set and 25% validation data set. In the development of calibration models, SERS spectra were correlated with total aflatoxin concentrations (a sum of aflatoxins B_1, B_2, G_1, and G_2) in maize determined by HPLC reference methods using the chemometric methods. PCR and PLSR calibration models were cross-validated by leave-one-out validation method and evaluated based on coefficient of determination (r^2) and the predicted residual sum of squares (PRESS). The calibration models from MLR analysis using a stepwise regression option included the selected wavelengths as input variables in the equation based on partial r^2 values, partial F values, and PRESS. All chemometric models were externally validated by applying the models to predict total aflatoxin concentrations of the validation sample set and assessed by comparing the root-mean-square error of calibration (RMSEC), the root mean standard error of prediction (RMSEP), and correlation coefficient of determination (r^2). The limit of detection (LOD) and the limit of quantitation (LOQ) to assess the sensitivity of the models were determined using LOD = $3s/r$ and LOQ = $10s/r$, respectively, where s is the standard deviation of the predicted aflatoxin concentration and r is the slope of the corresponding regression equation.

Statistical Analysis. All data analyses and the development and validation of chemometric models were performed using SAS software. Statistical comparison between the SERS predicted and HPLC reference values were carried out using paired sample t test, Pearson's correlation coefficients, and the ratio of the standard deviation of the reference data to the standard error of cross-validation (RPD).[24]

RESULTS AND DISCUSSION

Spectral Data Analysis. Figure 1 shows normalized SERS spectra of ground maize sample extracts representing each aflatoxin contamination group. Common spectral features were observed among samples, but simultaneously, a distinctive change of Raman band intensities was also noticed among the sample extracts, particularly between below and above 20 μg/kg samples. Qualitative spectral differences in the normalized and derivative spectra were observed in the Raman shift ranges of 400−530 cm^{-1}, 800−980 cm^{-1}, 1100−1250 cm^{-1}, and 1500−1800 cm^{-1}. The major bands in these Raman shift regions may be associated with fungal cellular metabolites and modified cell membrane and inhibited protein and starch synthesis due to the effects of fungal and aflatoxin infection of kernels.[25]

The observed Raman bands in the SERS spectra were well assigned to the main vibrational modes associated with aflatoxin molecules according to the previously reported results.[18,26] However, shifts of some aflatoxin bands, in particular, in the aflatoxin-related Raman spectral regions, were easily observed compared to corresponding bands of conventional Raman spectroscopy. The shifts of Raman bands can be attributed to the effect of charge transfer between adsorbed aflatoxin molecules and silver metal in combination with the resonance excitation of surface plasmon.[11,27] The methyl moiety present in the extraction solution seems to add the complexity of Raman bands shift as well.[9] Nevertheless, some assignments for the major bands of interest can be tentatively determined (Table 1). The bands at 1557 and 1596 cm^{-1} corresponded to the stretching mode between carbons. The ν(C═C) mode was observed at 1486 cm^{-1}. The C−O bond at 939 cm^{-1} was

dx.doi.org/10.1021/jf500854u | J. Agric. Food Chem. 2014, 62, 4466−4474

Table 1. Tentative SERS Spectral Assignments for Aflatoxin Molecules

Raman shift (cm^{-1})	band assignments[a]
608	ring deformation
686	C−H in-plane bending
751	C−H out-of-plane bending
812	ring deformation
835	ring deformation
939	ring breath, ν(C−O)
1029	$\nu(CH_2-CH_2)$
1067	ν(C−C−C) ring deformation
1139	ν(C−O−C)(H_2) (cyclopentene ring)
1191	γ(C−H) (ring)
1268	β(C−H) ring deformation; νC−O−C; $\nu C-O-C(H_3)$
1310	$A(C-H_2)$(ring)(C−H)
1343	δCH_3
1445	$\beta(C-H)(CH_3)$, β(C−H)(ring)
1486	ν(C═C), ring deformation
1557	ν(C−C) and ring deformation
1596	ν(C−C) and ν(C−C−C)
1635	νC(H)═C(H); rings and special ring stretching
1695	ν(C═O) (cyclopentene ring) and νC═C

[a]SERS band assignments are made according to Wu et al.[23] and Móricz et al.[31]

significantly different between contaminated and noncontaminated samples in the spectra. Also, the C−H in-plane and out-of-plane bending modes found at 686 and 751 cm^{-1} appeared to be largely influenced by aflatoxin contamination. The vibration mode at 608 cm^{-1} is assigned to the ring deformation mode. However, Raman band intensity does not increase in proportion to aflatoxin concentration. This nonlinear relationship might be due to the variation in adsorption of aflatoxin molecules onto the SERS active sites and differences in sample matrices, silver nanoparticle concentration, and agglomerate morphology.[14]

Such irreproducibility of SERS signal can arise from several different conditions. If a SERS substrate contains uneven distribution of hot spots, only some portions of active sites may contribute to the SERS signal.[18] Different surface orientation and placement of target molecules on agglomerates of metal nanoparticles can also induce a slight change of SERS signal.[13,28] One obstacle in common applications of SERS is due to its inherent instability caused by metal nanoparticle aggregation with aging.[15] Our study revealed that the stability of metal nanoparticles can be significantly subject to the environments around the nanoparticles, such as a pH of the reacting solutions and nanoparticle/target molecule ratio as reported in previous studies.[11,28] The fungi producing aflatoxins obtain necessary nutrients from contaminated grains, diminishing protein, carbohydrates, and other micronutrients in the grains.[29] If the molecules other than target molecules, for example, in the sample extract for the present study, bind SERS active sites, SERS signal may respond to the concentration of the target molecules in a nonproportional way.[17] In the present study, the spectra obtained from Ag nanosphere (NS) displayed a good repeatability because hot spots are basically evenly distributed around the AgNSs and can yield a reproducible enhanced signal. Figure 2 shows representative SEM images of the AgNSs and their mixture with maize extract for the morphological analysis. In Figure 2, dispersed AgNC with various diameters were observed and they form blocks into

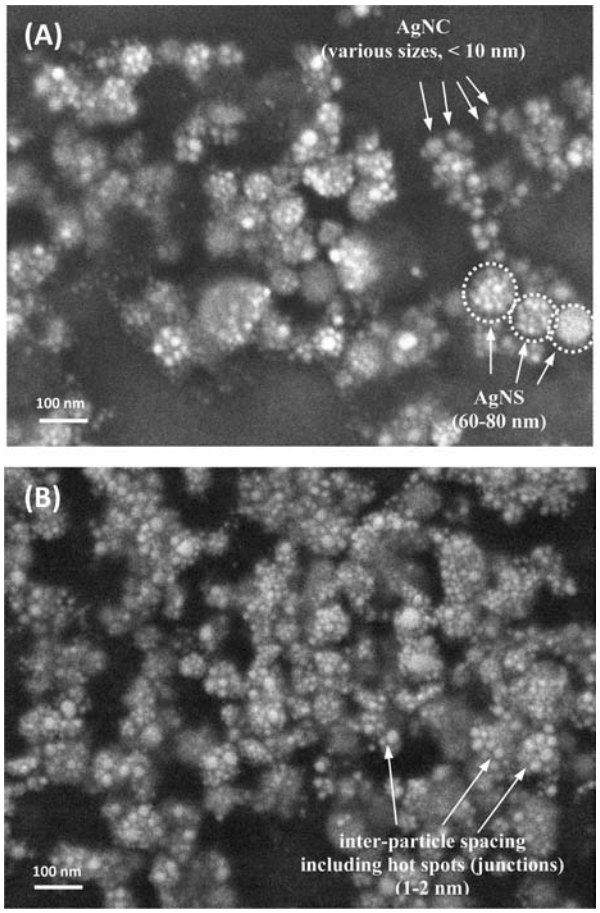

Figure 2. Scanning electron microscope (SEM) images of the mixtures of AgNSs and sample extracts at aflatoxin concentrations of (A) 50 μg/kg and (B) 901 μg/kg.

AgNSs with the diameters of 60−80 nm at an interparticle spacing of 1−2 nm. The AgNSs with the packed AgNC contain periodic hot spots or junctions which provide surface areas to adsorb aflatoxin or bioactive molecules. The previous studies reported that nanoparticles with a diameter of <10 nm produce a weak and irreproducible Raman signal due to a smaller size and the surface characteristics of nanoparticle clusters.[9,10] Meanwhile, the AgNS with a large diameter containing smaller AgNC within a microemulsion of oil droplets can produce a strong electromagnetic coupling effect for significant signal enhancement.[6,19] Further research needs to be conducted to determine the effect of structure modification of AgNSs on the spectroscopic characteristics after the sample extract introduction.

Our study shows that conventional Raman spectra obtained from the same samples were much weaker than SERS spectra and shifted in different SERS spectral regions. This indicates that aflatoxin and other extracted molecules adsorbed on the surface of nanoparticles are excited in different vibrational modes in SERS along with surface plasmon phenomenona.[9,28] In our previous studies,[30,31] a conventional Raman spectroscopy required a larger sample area and longer scanning time to obtain better spectral surface and subsurface features of ground maize samples, particularly at lower concentrations. The difference in intensity of a conventional Raman spectrum largely depended on the changes in physical, chemical, and structural properties of aflatoxin contaminated samples rather

dx.doi.org/10.1021/jf500854u | J. Agric. Food Chem. 2014, 62, 4466−4474

Table 2. Correct Classification Rates for Aflatoxin Contamination Groups Using the *k*-Nearest Neighbor Method Applied to Different Preprocessed Spectral Data

	predicted group						
	training data		validation data				
aflatoxin groups	actual	prediction[a]	actual	normal	1st deriv	2nd deriv	deconvolution
1 (<20 μg/kg)	25	25	10	10	9	7	9
2 (20−200 μg/kg)	14	14	7	5	4	5	6
3 (300−450 μg/kg)	16	16	7	4	5	6	6
4 (550−700 μg/kg)	14	14	6	5	4	4	6
5 (>850 μg/kg)	11	11	5	5	4	3	5
total (% correct)	80	80 (100.0)	35	29 (82.9)	26 (74.3)	25 (71.4)	32 (91.4)

[a]All maize samples were 100% correctly classified to their groups in the training data set regardless of the spectral preprocessing method.

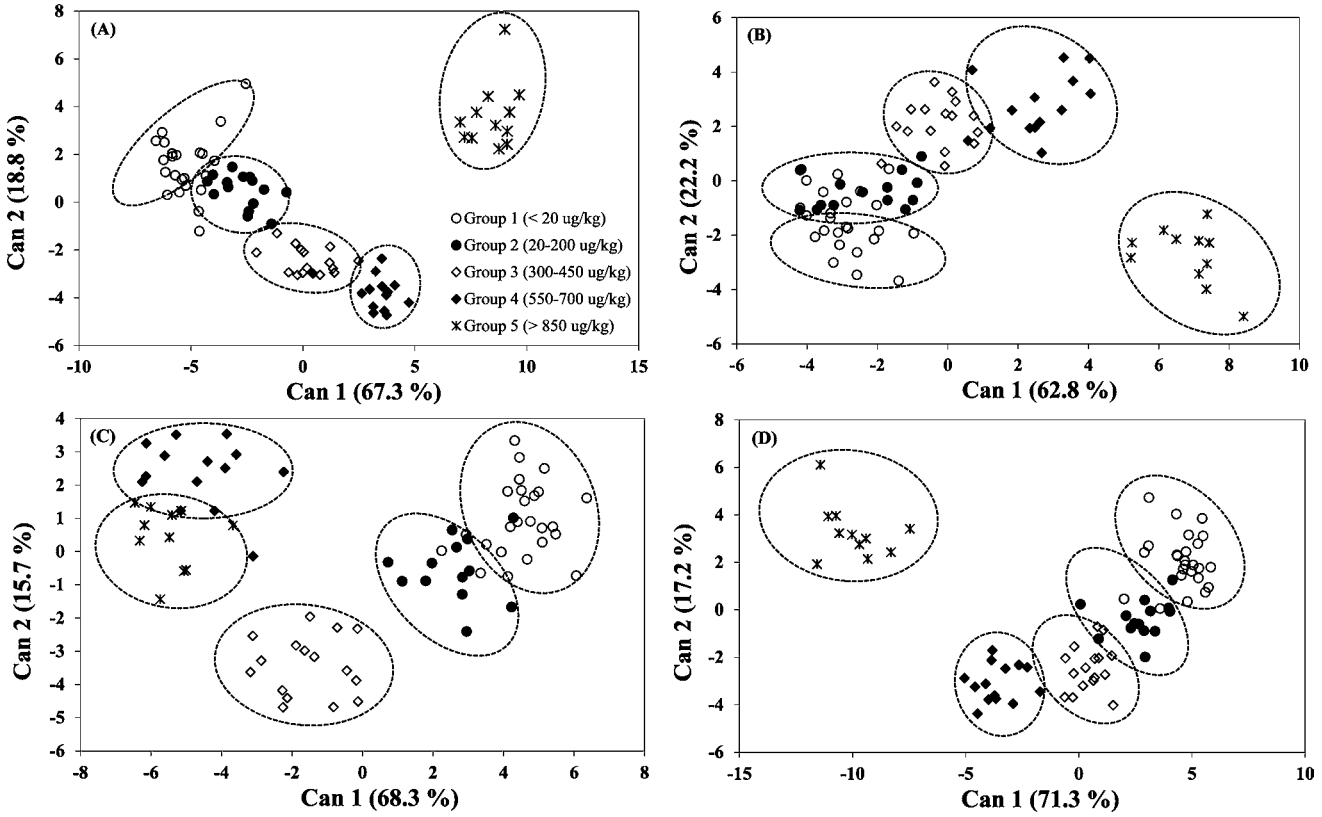

Figure 3. A scatter plot of the first two canonical discriminant scores obtained from LDA developed with four preprocessed spectra for classification of 5 different aflatoxin contamination groups: (A) normalized, (B) first derivative, (C) second derivative, and (D) deconvolution spectra.

than aflatoxin concentration.[6] Therefore, the Raman SERS method is considered as a more effective and highly efficient analytical tool for direct aflatoxin detection compared to conventional Raman spectroscopy.

Classification of Aflatoxin Contaminated Maize Samples. The classification models for aflatoxin contaminated and noncontaminated maize sample groups were developed by applying the *k*-nearest neighbors (KNN) algorithm for the four preprocessed SERS spectra in the Raman shift region of 400−1800 cm^{-1}. The KNN method was selected as a chemometric modeling technique for classification of aflatoxin contaminated maize samples because it showed outperformance over other chemometric methods such as linear discriminant analysis, partial least-squares, and principal component analysis in our previous studies.[30,31] In the present study, the KNN models exhibited stable classification accuracies from the number of neighbors greater than 5. Table 2 shows the classification accuracies of the KNN models for all preprocessed spectral data tested. As observed in Table 2, the performance of the classification models was largely determined by the mathematical pretreatment of the spectra. The correct classification rate of all calibration models was 100% for a training data set regardless of the spectral preprocessing method while rather lower classification accuracies (71.4−91.4%) were achieved when the calibration models were applied to validation data. The KNN models offering higher classification accuracy in classifying aflatoxin contaminated samples, as determined by the number of errors in an external validation data set, were obtained using normalized and deconvolution spectral data (Table 2). These two models displayed excellent classification results for maize samples with <20 μg/kg and >850 μg/kg. However, the model using the deconvolution spectra yielded higher classification accuracies for maize samples of groups 2, 3, and 4 than the model developed with normalized spectra,

dx.doi.org/10.1021/jf500854u | J. Agric. Food Chem. 2014, 62, 4466−4474

which may be attributed to the enhanced-resolution of the unresolved bands by the deconvolution pretreatment of the spectra. In these two models, no samples with greater than 20 μg/kg were misclassified as aflatoxin negative. This was in accordance with the finding in our previous study[31] with conventional Raman spectroscopy, indicating Raman spectroscopy is a promising technique to offer a rapid screening of large number of samples for aflatoxin contamination. The higher error rates were found in the models developed with first and second derivative spectra. These two KNN models displayed rather higher misclassification rate for the samples from all aflatoxin groups. This may be attributed to the excessive amplification of the noise and other extraneous peaks in the derivative spectra, resulting in a significant difference in the relative intensity of aflatoxin peaks with the original spectra despite improvement of spectroscopic resolution. However, even these models misclassified only one or two samples belong to group 2 into noncontaminated samples (group 1) considered as aflatoxin negative.

As opposed to what would be expected, the correct classification rates of the KNN models developed with the preprocessed spectra obtained from highly sensitive SERS technique were not greater and in fact were even slightly lower than those of the same chemometric models in our previous study[31] with conventional Raman spectroscopy. This can be in part explained by binding of bioactive molecules in the extracts to SERS active sites to lower SERS signal for aflatoxin molecules.[17] However, as mentioned above, the SERS method requires much smaller area and shorter scanning time than conventional Raman spectroscopy to yield equivalent results. Therefore, the calibration models can be further improved and become more robust by adding more training samples.

Because maize samples were not adequately clustered to the predefined aflatoxin group on the principal component score plot, the canonical discriminant scores derived from linear discriminant analysis of the preprocessed spectra were used to build a scatter plot (Figure 3). The canonical variable is the combination of original variables that can allow us to distinguish among the groups.[23] Figure 3 shows the actual distance between aflatoxin groups in a reduced, two-dimensional space. Maize samples within the same group are grouped closely together on the plot while the samples with very different concentrations are remotely grouped. On the whole, the grouping of the samples on the scatter plot is in agreement with the results of correct classification rates for the KNN models developed with the preprocessed spectral data (Table 2). Regions of overlap among aflatoxin groups and the degree of the overlap appear to be associated with the misclassification rate of the relevant groups. As expected, each aflatoxin group was better separated by two canonical functions for normalized and deconvolution spectra than those for first and second derivative spectra. The first two canonical variables were significant ($P < 0.001$) in all KNN models, implying its substantial contribution to discriminating aflatoxin contamination groups. The first canonical function in all models accounts for the highest percentages (62.8−71.3%) of the total variation of the groups (Figure 3). Consequently, the first and second canonical functions can explain a total of from 84.0 to 88.5% variations in the spectral data.

The PCA and PLS results also provide some additional information on the particular spectral subranges and bands corresponding to the level of aflatoxins in maize sample extracts (data not shown). Some spectral regions and wavelengths with higher loading values in PCA and with higher absolute regression coefficient value in PLS are associated with an increased level of aflatoxins and changes in maize kernels induced by aflatoxins.[25] Cluster analysis performed using all the preprocessed spectra allowed classification of aflatoxin contamination samples, which was basically configured by the aflatoxin group. However, the classification results obtained from the best clustering algorithm employed (hierarchical Ward's minimum variance method) were not as good as those from the canonical functions.

Quantification of Aflatoxins in Maize Samples. The relationships between actual aflatoxin concentrations and SERS values predicted by the models for four preprocessed spectra are shown in Table 3 and Figure 4. The chemometric methods including multiple linear regression (MLR), principal components regression (PCR), and partial least-squares regression (PLSR) algorithms, employed for development of aflatoxin quantification models, extract meaningful information from SERS spectra to correlate the spectra with aflatoxins and modified physicochemical features of maize kernels caused by aflatoxin contamination, which allows us to detect a subtle difference between aflatoxin contaminated samples for aflatoxin quantification.[6,32,33] The MLR models showed better regression quality, higher predictive accuracy, and lower error rate than other chemometric methods while the PCR models yielded far less satisfactory results compared to the MLR and PLSR models.

Table 3. Statistical Results of PLSR Models Developed with Four SERS Preprocessed Spectra for Predicting Aflatoxin Concentrations in Ground Maize Sample Extract[a]

	normalization	1st deriv	2nd deriv	deconvolution
no. of factors	5	3	4	4
RMSEC (μg/kg)[b]	65.1	77.0	47.9	55.6
RMSEP (μg/kg)[c]	107.2	139.6	150.6	142.0
LOD (μg/kg)[d]	14	25	64	34
LOQ (μg/kg)[e]	46	85	213	115
slope				
training	0.951	0.932	0.974	0.965
validation	0.741	0.703	0.709	0.625
r^{2}[f]				
training	0.951	0.932	0.974	0.965
validation	0.915	0.823	0.820	0.866
paired differences[g]				
mean	11.3	29.7	63.2	30.3
std deviation	108.5	138.8	139.1	141.2
std error	20.1	25.8	25.8	26.2
r[h]	0.956	0.907	0.906	0.931
t	0.559	1.151	2.447	1.154
sig (2-tailed)	0.580	0.259	0.021	0.258
RPD[i]	2.893	2.340	2.057	2.305

[a]Savitzky−Golay and deconvolution filtering functions were applied to normalized data to yield derivative and deconvolution spectra. [b]RMSEC: root-mean-square error of calibration. [c]RMSEP: root-mean-square error of prediction. [d]LOD: limit of detection. [e]LOQ: limit of quantitation. [f]r^2: correlation coefficient of determination. [g]Statistical comparison between reference HPLC values and predicted values of SERS. [h]r: Pearson correlation coefficient. [i]RPD: ratio of the standard deviation of the reference values to the standard error of cross-validation values.

dx.doi.org/10.1021/jf500854u | J. Agric. Food Chem. 2014, 62, 4466−4474

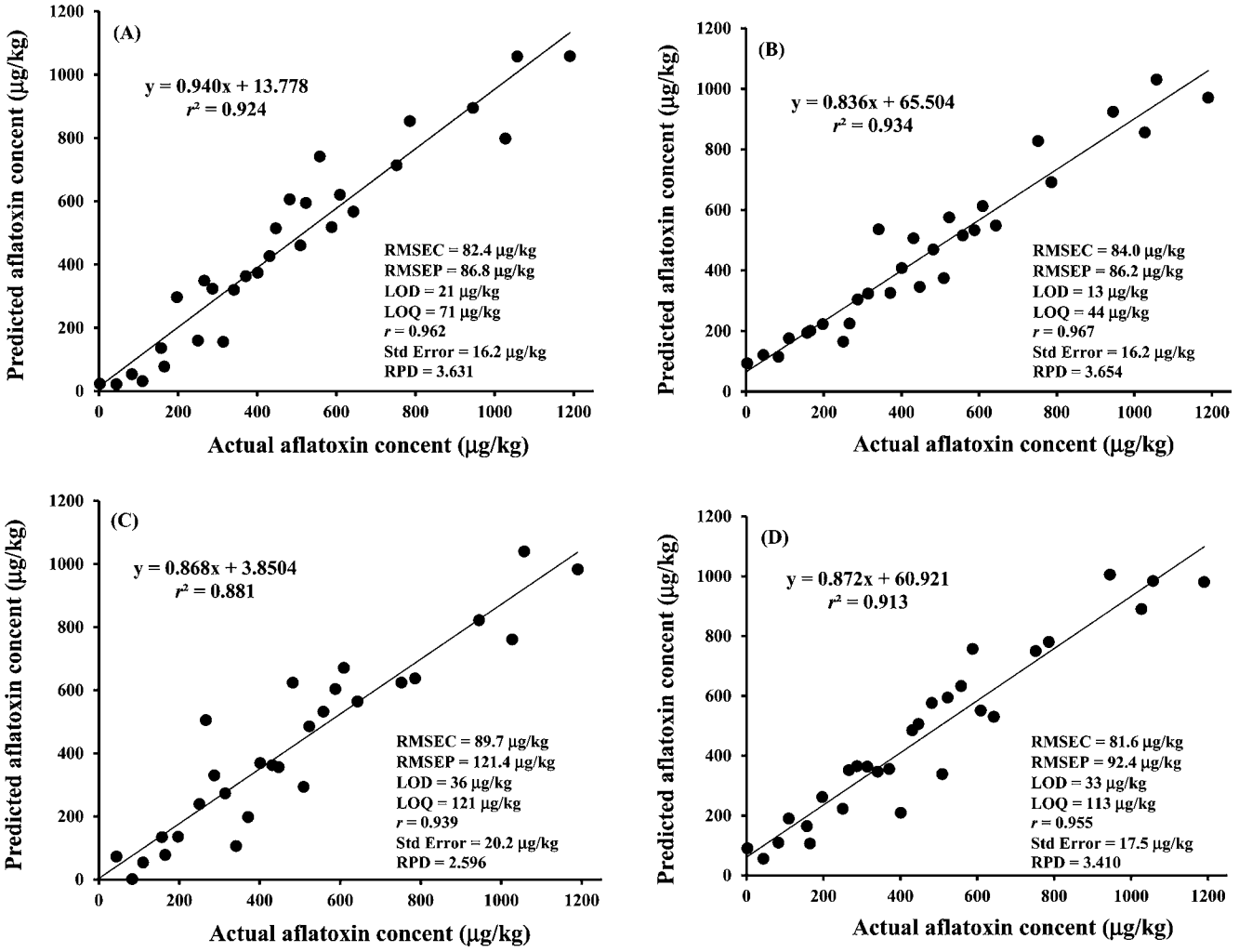

Figure 4. A linear regression plot of reference HPLC versus SERS predicted aflatoxin concentrations of the validation data set in the MLR models developed with four preprocessed spectra: (A) normalization; (B) first derivative; (C) second derivative; and (D) deconvolution.

In the MLR models, selection of optimal wavelengths was carried out using STEPWISE regression procedure and the selected wavelengths were further examined to eliminate collinearity and overfitting problems using variance inflation factor (VIF) and tolerance options. The final combination of the wavelengths was then determined by comparing with the results of the SQUARE (R^2 selection) method. All MLR models developed with the preprocessed spectra could account for more than 90% of variation in both training and validation data set, except for second derivative spectra in the validation data set (Figure 4). As would be expected, the calibration models of normalized, first derivative, and deconvolution spectra displayed better statistical performance than the model for second derivative spectra. Coefficients of determination (r^2) and predictive error rate (RMSEP) of the former three calibration models applied to the validation data set were in the range of 0.913−0.934 and 86.2−92.4 μg/kg, respectively. Meanwhile, the model for second derivative data yielded lower r^2 (0.881) and higher predictive error rate (RMSEP = 150.6 μg/kg). The slope of the linear regressions for the training data set was in the range of 0.908 to 0.923 while the calibration models applied to the validation data set produced a slightly lower slope (0.836−0.940) (Figure 4). These observations indicate a good quality of the regressions and high predictive capability of selected MLR models suitable for screening of aflatoxin contaminated samples. It appears that the MLR models include several prominent wavelengths relevant to starch molecules extracted with 70% methanol as well as aflatoxin molecules in the extract. These results enable us to carefully infer that current MLR models developed from SERS spectra may reasonably predict low and high aflatoxin concentration in extracted maize sample with the selected solvent if the models are further improved by optimized instrumental and measurement experimental conditions. However, as observed in our previous studies[30,31] with conventional Raman spectroscopy, the SERS technique was also not very accurate in predicting very low aflatoxin concentrations, particularly below the FDA action level (20 μg/kg) for aflatoxins. But the reason for inaccurate prediction of very low aflatoxin concentration with SERS might be different with conventional Raman spectroscopy. The low predictive accuracy of the SERS results may be in part explained by adsorption variation of aflatoxin molecules on or in the vicinity of the SERS active site.[8,10,14] On the other hand, conventional Raman spectroscopy could not accurately predict aflatoxin concentration due to its insufficient sensitivity and inherently weak signal to detect aflatoxin molecules as well as inhomogeneous fungal contamination and aflatoxin distribution in ground maize samples.[34,35] Therefore, it would be expected that the SERS requires less effort and attention than

conventional Raman spectroscopy in optimizing sample preparation procedure and measurement conditions to obtain reproducible and representative spectra and to improve the repeatability of the spectra.

The detailed statistical results of the PLSR models are presented in Table 3. The PLSR calibration models yielded comparable results to the MLR calibration models for the training data set, resulting in high r^2 values (0.932−0.974), lower error rate (RMSEC: 47.9−77.0 μg/kg), and a linear regression slope in the range of close to 1 (Table 3). However, the predictive accuracy of the PLSR calibration models predicting the validation samples was not as good. The PLSR calibration models applied to the validation data set produced lower r^2 values and linear regression slopes, accounting for the variation of the preprocessed spectra in the range of 82.0−91.5%. Besides, the predictive error rate (RMSEP) and quality of linear regression were not sufficiently good to use the models for predicting aflatoxin concentrations. The PCR models revealed a poor predictive performance for the training and validation samples irrespective of the preprocessing method (data not shown). The PCR calibration models applied to the validation data set yielded much lower coefficients of determinations and higher prediction errors than the MLR and PLSR models.

Paired sample t test for the validation data set showed no statistically significant difference ($p > 0.01$) between the reference HPLC values and the predicted values of SERS in all aflatoxin quantification models, except for the MLR model for second derivative spectra, but the statistical results were very subject to the chemometric and/or preprocessed methods (Table 3 and Figure 4). The MLR models showed higher p values and stronger correlation coefficients (r = 0.906−0.967) with the HPLC reference values than the PLSR and PCR models, indicating that the MLR models produced more comparable results to the HPLC method at aflatoxin levels tested. The limit of detection (LOD) and the limit of quantitation (LOQ) of the MLR models are in the ranges of 13−36 μg/kg and 44−121 μg/kg, respectively, indicating that the models are more sensitive for quantification of aflatoxins in maize. Standard errors of paired differences between the reference and predicted values were also lowest in the MLR models. According to the criterion of RPD (ratio of the standard deviation of the reference data to the standard error of cross-validation) values described in previous literature,[24,36] the MLR models may be effective for screening of aflatoxin contaminated samples. Despite the chemometric models developed by conventional Raman spectroscopy showing a slightly higher predictive accuracy than those of SERS at aflatoxin concentrations tested in this study,[31] the effectiveness and efficiency of the SERS would be better if more considerations were given to sensitivity, analysis speed, reproducibility of spectra, and potential improvement of SERS substrate.

In conclusion, the research results prove that SERS can be an alternative rapid and highly sensitive analytical method for classification and quantification of aflatoxins in contaminated maize samples over standard wet chemical methods. Compared to other spectroscopic techniques and conventional Raman spectroscopy, this technique seems to be able to provide more comprehensive information on the structural and electronic properties of aflatoxin molecules. However, the problem of spectral variation induced by instability of nanoparticles and differences in sampling and sample batches should be minimized or resolved prior to application of SERS for aflatoxin analysis. Besides, inexpensive nanomaterials and nanostructures that can give better Raman signal and stronger enhancement factor need to be found. It may also be useful to develop the SERS method combining automated spectral processing and statistical analysis algorithms for the on-site testing to facilitate real-time monitoring at critical locations in grain supply chains. Certainly, SERS is a promising and potentially powerful tool for detecting aflatoxins in maize and other grains which can greatly help improve the safety and quality of food and feed products.

■ ASSOCIATED CONTENT

Supporting Information

Tables S1 (correct classification rates of the PCR models), S2 (correct classification rates of the PLSR models), S3 (RSD of spectral intensity measurements), and S4 (statistical results of PCR models) and Figures S1 (PCA loading values), S2 (principal component score plots), and S3 (absolute regression coefficients of PLS models for four preprocessed spectra). This material is available free of charge via the Internet at http://pubs.acs.org.

■ AUTHOR INFORMATION

Corresponding Author

*Tel: 979-845-1121. Fax:979-845-1389. E-mail: kml@otsc.tamu.edu.

Funding

The authors acknowledge that this research was supported by the Andersons Endowment administered through the Ohio Agricultural Research and Development Center of The Ohio State University and the National Corn Growers Association (Aflatoxin Mitigation Center of Excellence Research Program).

Notes

The authors declare no competing financial interest.

■ ABBREVIATIONS USED

AgNC, Ag nanocrystal; AgNS, Ag nanosphere; CCD, charged coupled device; EM, electromagnetic; FTIR, Fourier transform infrared spectroscopy; HPLC, high-performance liquid chromatography; KNN, k-nearest neighbors; LDA, linear discriminant analysis; MLR, multiple linear regression; NIR, near-infrared reflectance; PCA, principal component analysis; PCR, principal components regression; PLS, partial least-squares; PLSDA, partial least-squares discriminant analysis; PLSR, partial least-squares regression; PRESS, predicted residual sum of squares; r, Pearson correlation coefficient; r^2, correlation coefficient of determination; RMSEC, root-mean-square error of calibration; RMSEP, root mean standard error of prediction; RPD, ratio of the standard deviation of the reference data to the standard error of cross-validation; SERS, surface-enhanced Raman spectroscopy

■ REFERENCES

(1) Kensler, T. W.; Roebuck, B. D.; Wogan, G. N.; Groopman, J. D. Aflatoxin: a 50-year odyssey of mechanistic and translational toxicology. *Toxicol. Sci.* **2011**, *120*, S28−S48.

(2) EC, European Commission. Commission Regulation (EC) No. 165/2010 of 26 February 2010 Amending Regulation (EC) No 1881/2006 setting maximum levels for certain contaminants in foodstuffs as regards Aflatoxins. *Off. J. Eur. Commun.* **2010**, *L50*, 11−12.

(3) Zheng, Z.; Richard, J. L.; Binder, J. A review of rapid methods for the analysis of mycotoxins. *Mycopathologia* **2006**, *161*, 261−273.

(4) Craig, A. P.; Franca, A. S.; Irudayaraj, J. Surface-enhanced Raman spectroscopy applied to food safety. *Annu. Rev. Food Sci. Technol.* **2013**, *4*, 369−380.
(5) Golightly, R. S.; Doering, W. E.; Natan, M. J. Surface-enhanced Raman spectroscopy and homeland security: a perfect match? *ACS Nano* **2009**, *3*, 2859−2869.
(6) Liu, Y.; Delwiche, S. R.; Dong, Y. Feasibility of FT-Raman spectroscopy for rapid screening for DON toxin in ground wheat and barley. *Food Addit. Contam.* **2009**, *26*, 1396−1401.
(7) Sohn, M.; Himmelsbach, D. S.; Barton, F. E., II. A comparative study of Fourier transform Raman and NIR spectroscopic methods for assessment of protein and apparent amylose in rice. *Cereal Chem.* **2004**, *81*, 429−433.
(8) He, L.; Deen, B.; Rodda, T.; Ronningen, I.; Blasius, T.; Haynes, C.; Diez-Gonzalez, F.; Labuza, T. P. Rapid detection of ricin in milk using immunomagnetic separation combined with surface-enhanced Raman spectroscopy. *J. Food Sci.* **2011**, *76*, N49−N53.
(9) Lee, P. C.; Meisel, D. Adsorption and surface-enhanced Raman of dyes on silver and gold sols. *J. Phys. Chem.* **1982**, *86*, 3391−3395.
(10) Wang, Y.; Lee, K.; Irudayaraj, J. Silver nanosphere SERS probes for sensitive identification of pathogens. *J. Phys. Chem. C* **2010**, *114*, 16122−16128.
(11) Plieth, W.; Dietz, H.; Anders, A.; Sandmann, G.; Meixner, A.; Weber, M.; Kneppe, H. Electrochemical preparation of silver and gold nanoparticles: Characterization by confocal and surface enhanced Raman microscopy. *Surf. Sci.* **2005**, *597*, 119−126.
(12) Sandmann, G.; Dietz, H.; Plieth, W. Preparation of silver nanoparticles on ITO surfaces by a double-pulse method. *J. Electroanal. Chem.* **2000**, *491*, 78−86.
(13) Sondi, I.; Goia, D. V.; Matijević, E. Preparation of highly concentrated stable dispersions of uniform silver nanoparticles. *J. Colloid Interface Sci.* **2003**, *260*, 75−81.
(14) Chen, L. M.; Liu, Y. N. Ag-nanoparticle-modified single Ag nanowire for detection of melamine by surface-enhanced Raman spectroscopy. *J. Raman Spectrosc.* **2012**, *43*, 986−991.
(15) Tang, H.; Fang, D.; Li, Q.; Cao, P.; Geng, J.; Sui, T.; Wang, X.; Iqbal, J.; Du, Y. Determination of tricyclazole content in paddy rice by surface enhanced Raman spectroscopy. *J. Food Sci.* **2012**, *77*, T105−T109.
(16) Esumi, K.; Tano, T.; Torigoe, K.; Meguro, K. Preparation and characterization of bimetallic Pd-Cu colloids by thermal decomposition of their acetate compounds in organic solvents. *Chem. Mater.* **1990**, *2*, 564−567.
(17) Yuan, W.; Ho, H. P.; Lee, R. K. Y.; Kong, S. K. Surface-enhanced Raman scattering biosensor for DNA detection on nanoparticle island substrates. *Appl. Opt.* **2009**, *48*, 4329−4337.
(18) Wu, X.; Gao, S.; Wang, J. S.; Wang, H.; Huang, Y. W.; Zhao, Y. The surface-enhanced Raman spectra of aflatoxins: spectral analysis, density functional theory calculation, detection and differentiation. *Analyst* **2012**, *137*, 4226−4234.
(19) Wang, X.; Zhuang, J.; Peng, Q.; Li, Y. A general strategy for nanocrystal synthesis. *Nature* **2005**, *437*, 121−124.
(20) Bai, F.; Wang, D.; Huo, Z.; Chen, W.; Liu, L.; Liang, X.; Chen, C.; Wang, X.; Ping, Q.; Li, Y. A versatile bottom-up assembly approach to colloidal spheres from nanocrystals. *Angew. Chem., Int. Ed.* **2007**, *46*, 6650−6653.
(21) Delwiche, S. R.; Hareland, G. A. Detection of scab-damaged red spring wheat kernels by near-infrared reflectance. *Cereal Chem.* **2004**, *5*, 643−649.
(22) Dowell, F. E.; Pearson, T. C.; Maghirang, E. B.; Xie, F.; Wicklow, D. T. Reflectance and transmittance spectroscopy applied to detecting fumonisin in single corn kernels infected with Fusarium verticillioides. *Cereal Chem.* **2002**, *79*, 222−226.
(23) Johnson, D. E. (1998). Discriminant analysis. In *Applied Multivariate Methods for Data Analyst*; Johnson, D. E., Eds.; Duxbury Press: Pacific Grove, CA, 1998; pp 217−285.
(24) Williams, P. C. Implementation of near-infrared technology. In *Near-Infrared Technology in the Agricultural and Food Industries*; Williams, P. C., Norris, K., Eds.; American Association of Cereal Chemists: St. Paul, MN, 2001; pp 145−169.
(25) McLean, M. Aflatoxin Bl-induced ultrastructural alterations in mature *Zea mays* embryos. *Mycopathologia* **1994**, *128*, 181−192.
(26) Móricz, Á.M.; Horváth, E.; Ott, P. G.; Tyihák, E. 2008. Raman spectroscopic evaluation of the influence of *Pseudomonas* bacteria on aflatoxin B1 in the BioArena complex bioautographic system. *J. Raman Spectrosc.* **2008**, *39*, 1332−1337.
(27) Xu, K.; Abell, J.; Zhao, Y.; Qian, J.; Brenneman, K.; Meshik, X.; Dutta, M.; Stroscio, M. Surface-enhanced Raman spectroscopy as a tool for characterizing nanostructures containing molecular components. *AIP Conf. Proc.* **2012**, *1506*, 57−61.
(28) Mecker, L. C.; Tyner, K. M.; Kauffman, J. F.; Arzhantsev, S.; Mans, D. J.; Gryniewicz-Ruzicka, C. M. Selective melamine detection in multiple sample matrices with a portable Raman instrument using surface enhanced Raman spectroscopy-active gold nanoparticles. *Anal. Chim. Acta* **2012**, *733*, 48−55.
(29) DiCostanzo, A.; Johnston, L. F.; Murphy, M. Effects of molds on nutrient content of feeds reviewed. *Feedstuffs* **1995**, *16*, 17−54.
(30) Lee, K. M.; Herrman, T. J.; Nansen, C.; Yun, U. Application of Raman spectroscopy for qualitative and quantitative detection of fumonisins in ground maize samples. *Int. J. Regul. Sci.* **2013**, *1*, 1−14.
(31) Lee, K. M.; Herrman, T. J.; Yun, U. Application of Raman spectroscopy for qualitative and quantitative analysis of aflatoxins in ground maize samples. *J. Cereal Sci.* **2014**, *59*, 70−78.
(32) Abramović, B.; Jajić, I.; Abramović, B.; Cosić, J.; Jurić, V. Detection of deoxynivalenol in wheat by Fourier transform infrared spectroscopy. *Acta Chim. Slov.* **2007**, *54*, 859−867.
(33) Cramer, R. D. Partial least squares (PLS): Its strengths and limitations. *Perspect. Drug Discovery Des.* **1993**, *1*, 269−278.
(34) Gowen, A. A.; O'Donnella, C. P.; Cullenb, P. J.; Downeyc, G.; Frias, J. M. Hyperspectral imaging - an emerging process analytical tool for food quality and safety control. *Trends Food Sci. Technol.* **2007**, *18*, 590−598.
(35) Kos, G.; Lohninger, H.; Mizaikoff, B.; Krska, R. Optimisation of a sample preparation procedure for the screening of fungal infection and assessment of deoxynivalenol content in maize using mid-infrared attenuated total reflection spectroscopy. *Food Addit. Contam.* **2007**, *24*, 721−729.
(36) Armstrong, P. R.; Lingenfelser, J. E.; McKinney, L. The effect of moisture content on determining corn hardness from grinding time, grinding energy, and near-infrared spectroscopy. *Appl. Eng. Agric.* **2007**, *23*, 793−799.

JOURNAL OF AGRICULTURAL AND FOOD CHEMISTRY

Article

pubs.acs.org/JAFC

Compositional Equivalency of RNAi-Mediated Virus-Resistant Transgenic Soybean and Its Nontransgenic Counterpart

Xiuchun Zhang,[†,∥] Pingjuan Zhao,[†,∥] Kunxin Wu,[†] Yuliang Zhang,[†] Ming Peng,*[,†,‡] and Zhixin Liu*[,†]

[†]Institute of Tropical Bioscience and Biotechnology, Chinese Academy of Tropical Agricultural Sciences/Key Laboratory of Biology and Genetic Resources of Tropical Crops, Ministry of Agriculture, Haikou, China

[‡]Environmental Safety Supervision and Inspection Centre for Genetically Modified Plants and Microorganisms Used in Plants, Ministry of Agriculture, Haikou, China

ABSTRACT: RNA silencing or RNA interference (RNAi), which is triggered by double-stranded RNA (dsRNA), is an evolutionarily conserved process that is active in a wide variety of eukaryotic organisms. Engineering plants with hairpin construct in which the viral gene is arranged in inverted repeats (IR) renders plants resistant to plant virus infection. However, there is no report on whether biologically important changes occurred by the insertion of IR, which confer transgenic plants virus resistance. In the present study, the compositions of virus-resistant transgenic soybean seeds developed by insertion of three short IRs, each containing the specific, highly conserved sequences derived from one virus, were compared with those of nontransgenic counterparts by applying the principle of substantial equivalence to determine whether significant undesirable biological changes occurred by IR insertion. The results revealed that the nutrient components as well as antinutrient contents of these virus-resistant soybean lines are substantially equivalent to those of the nontransgenic counterparts, and the majority of the measured amounts of nutritional components and antinutrient contents are well within the range of values reported for other commercial soybean lines. The results imply that no biologically important changes occurred by the insertion of IRs in the RNAi-mediated virus-resistant transgenic soybeans. The results can serve as baseline information for developing RNAi-mediated transgenic soybean cultivars or other crops with broader spectrum virus resistance.

KEYWORDS: *inverted repeats, virus-resistant transgenic soybean, composition, substantial equivalence*

INTRODUCTION

Research during the past decade has firmly established that land plants use an RNA-targeting defense mechanism termed RNA silencing (or RNA interference, RNAi) to combat virus infections. The trigger of RNA silencing is a double-stranded RNA (dsRNA), which is processed into small interfering RNAs (siRNAs), which direct Argonaute protein silencing corresponding genes or genetic elements in a sequence-specific manner.[1,2] On the basis of RNAi machinery, engineering plants with hairpin construct in which the transgenes are arranged in inverted repeats (IR) offers a promising alternative for controlling most major virus disease problems in crops.[3]

Considering the history of traditional breeding on safety, the likelihood that safety concern might arise due to unintended compositional changes resulting from transgenes is negligible. However, compositional studies continue to be required, and regulatory requirements for composition studies are becoming increasingly complex in some regions.[4] Soybean (*Glycine max* L. Merrill) is an important staple source of vegetable protein in food and animal feed as well as for industry because the abundance and nutritional quality of seed proteins in soybean exceed those in other grain crops. To our best knowledge, there is no report on whether biologically important changes occurred by the insertion of IR that conferred transgenic plants virus resistance. The present study was designed to evaluate the composition of the RNAi-mediated virus-resistant transgenic soybeans engineered with hairpin construct and their nontransgenic counterpart through a series of chemical analyses to determine whether significant undesirable biologically changes occurred by the IR insertion in transgenic soybeans, using the concept of "substantial equivalence", which was developed by the Organisation for Economic Co-operation and Development (OECD) in 1993 and was elaborated further by FAO/WHO.[5,6] The concept suggests that if no meaningful difference from the conventional counterpart is found, then the transgenic crop is as safe and nutritious as its traditional counterpart, which is generally accepted as safe on the basis of human food use history. Substantial equivalent analysis has been studied for different events of transgenic crops, such as corn,[7,8] soybean,[9−15] rice,[16] and papaya.[17]

MATERIALS AND METHODS

Soybean Used for Analysis. The transgenic soybeans and respective nontransgenic counterparts were cultivated in cultivation pots, which were 30 cm in diameter and 23 cm in height, in the greenhouse of the Chinese Academy of Tropical Agriculture in Hainan, China. Each cultivar (one transgenic soybean line or its nontransgenic line) was composed of 10 cultivation pots of soybeans. The arrangement of soybean cultivation pots was randomly assigned. The transgenic soybean lines were T4 generation of self-crossing progenies from T0 generation of soybean transformants, which were developed through the *Agrobacterium*-mediated transformation with transgene construct dsABS.[18] The construct contains three hairpins, which derived from the highly conserved regions of replicase genes of

Received: February 18, 2014
Revised: April 9, 2014
Accepted: April 22, 2014
Published: April 23, 2014

ACS Publications © 2014 American Chemical Society

Table 1. Proximate Composition[a] of Virus-Resistant Transgenic Soybean and Nontransgenic Counterpart Seeds (Mean ± SD; $n = 3$)

component	Throne	729-3	729-4	729-5	lit. range[b]
moisture	7.06 ± 0.08	7.11 ± 0.05	7.08 ± 0.06	7.05 ± 0.03	7−11
ash	4.73 ± 0.06	4.69 ± 0.09	4.66 ± 0.04	4.72 ± 0.07	4.61−5.37
crude fat	13.81 ± 0.11	13.62 ± 0.19	13.87 ± 0.13	13.66 ± 0.17	13.2−22.5
crude protein	37.28 ± 0.15	37.43 ± 0.12	37.37 ± 0.09	37.33 ± 0.18	36.9−46.4
carbohydrate	37.12 ± 0.16	37.15 ± 0.11	37.02 ± 0.14	37.24 ± 0.19	22.0−46.1

[a]Grams per 100 g of dry weight (moisture based on fresh weight). [b]From ref 29.

Table 2. Amino Acid Composition[a] of Virus-Resistant Transgenic Soybean and Nontransgenic Counterpart Seeds (Mean ± SD; $n = 3$)

component	Throne	729-3	729-4	729-5	lit. range[b]
alanine	1.70 ± 0.03	1.78 ± 0.04	1.72 ± 0.03	1.74 ± 0.03	1.21−1.72
arginine	2.55 ± 0.04	2.57 ± 0.03	2.64 ± 0.02	2.59 ± 0.02	1.91−3.13
asparagine	4.25 ± 0.10	4.35 ± 0.09	4.38 ± 0.11	4.39 ± 0.10	3.02−4.66
cysteine	0.58 ± 0.01	0.57 ± 0.02	0.59 ± 0.02	0.58 ± 0.02	0.34−0.72
glutamic acid	6.99 ± 0.13	7.13 ± 0.15	7.10 ± 0.14	6.97 ± 0.12	4.78−7.40
glycine	1.66 ± 0.02	1.65 ± 0.01	1.69 ± 0.03	1.71 ± 0.02	1.19−1.74
histidine	0.85 ± 0.01	0.82 ± 0.02	0.81 ± 0.03	0.84 ± 0.02	0.75−1.08
isoleucine	1.77 ± 0.02	1.79 ± 0.03	1.82 ± 0.02	1.80 ± 0.03	1.21−1.90
leucine	2.88 ± 0.05	2.97 ± 0.03	2.93 ± 0.02	2.85 ± 0.06	2.15−3.15
lysine	2.45 ± 0.03	2.49 ± 0.03	2.54 ± 0.02	2.48 ± 0.02	1.73−2.66
methionine	0.56 ± 0.02	0.57 ± 0.03	0.55 ± 0.03	0.56 ± 0.01	0.37−0.61
phenylalanine	1.88 ± 0.01	1.91 ± 0.02	1.90 ± 0.02	1.86 ± 0.03	1.36−2.05
proline	1.94 ± 0.01	2.02 ± 0.02	1.99 ± 0.01	1.96 ± 0.03	1.31−2.12
serine	1.81 ± 0.02	1.82 ± 0.03	1.81 ± 0.02	1.85 ± 0.02	0.98−2.28
threonine	1.59 ± 0.01	1.63 ± 0.02	1.60 ± 0.01	1.58 ± 0.02	1.01−1.51
tryptophan	0.54 ± 0.02	0.56 ± 0.01	0.56 ± 0.02	0.55 ± 0.02	0.28−0.47
tyrosine	1.18 ± 0.01	1.16 ± 0.03	1.15 ± 0.03	1.20 ± 0.01	0.87−1.43
valine	1.78 ± 0.02	1.71 ± 0.01	1.73 ± 0.02	1.75 ± 0.02	1.24−2.05

[a]Grams per 100 g of dry weight. [b]From ref 29.

Alfalfa mosaic virus (AMV, a member of the family Bromoviridae), *Bean pod mottle virus* (BPMV, a member of the family Secoviridae), and *Soybean mosaic virus* (SMV, a member of the family Potyviridae), respectively, and the *bar* gene isolated from *Streptomyces hygroscopicus* as a selectable marker.

Compositional Analyses. *Proximate.* Moisture content was determined gravimetrically by drying the samples in a vacuum oven at approximately 100 °C.[19] For ash determination, the samples were placed in an electric furnace at 550 °C and ignited in air. The residual ash was quantified gravimetrically.[20] The Kjeldahl method was employed to determine total nitrogen and protein of the sample. The percent nitrogen was calculated and converted to equivalent protein using a factor of 6.25.[21] The crude fat content of the soybean seed samples was determined using the Soxhlet extraction method.[22] The carbohydrates content was calculated by difference using the fresh weight-derived data according to the following equation:

$$\%\ \text{carbohydrates} = 100 - (\%\ \text{protein} + \%\ \text{fat} + \%\ \text{ash} + \%\ \text{moisture})$$

Amino Acid Profile. Protein hydrolysis was performed before ninhydrin derivatization to analyze total amino acid composition, with the exception of cysteine, methionine, and tryptophan. The samples were hydrolyzed with 1 mL of 6 M hydrochloric acid at 110 °C for 22 h under a nitrogen atmosphere. The hydrolysate was dried under reduced pressure, dissolved in 0.02 M HCl, and subjected to analysis using a UV detector and a Hitachi L-8800 automatic amino acid analyzer (Hitachi High-Technologies, Tokyo, Japan). The cystine and cysteine in the samples were oxidized to cysteic acid, and methionine was oxidized to methionine sulfone through dithiodipropionic acid treatment for 16 h at approximately 0 °C. Tryptophan is hydrolyzed from proteins by heating at approximately 110 °C in 4.2 M sodium hydroxide for 20 h. After acid hydrolysis, the sample was separated on an anion exchange column and detected with a ninhydin reaction as described in the literature.[23]

Fatty Acid Profile. Up to 20 g of ground powder of transgenic or nontransgenic soybean seeds was analyzed through gas chromatography according to the procedures from the literature.[24]

Antinutrients. Lectins were determined by measuring the agglutinating properties of soybean sample extract on rabbit red blood cells according to modified procedures from the literature.[25,26] Trypsin inhibitor activity was determined by using a modified method described previously in the literature.[27]

Isoflavones Profile. The profiles of isoflavones of soybean seeds were determined through liquid chromatography according to procedures from the literature.[28]

Statistical Analysis. After harvest, the seeds of 10 cultivation pots of each cultivar were put together. Half of each cultivar's harvested dried seeds, which were selected randomly, were milled into powder using a high-speed tissue masher for nutrient compositional analysis. All statistical data analyses were performed employing the SPSS 19.0 software package. All analytical determinations were conducted in triplicate, and results are expressed as the mean ± standard deviation. Differences between samples were tested using one-way analysis of variance (ANOVA). $P \leq 0.05$ was considered to be statistically significant.

RESULTS AND DISCUSSION

Proximate Compositions. Table 1 shows the proximate analyses, including moisture, ash content, crude protein, crude fat, and carbohydrates, of the three virus-resistant transgenic

Table 3. Fatty Acid Composition[a] of Virus-Resistant Transgenic Soybean and Nontransgenic Counterpart Seeds (Mean ± SD; n = 3)

fatty acid	Throne	729-3	729-4	729-5	lit. range[b]
14:0 myristic	0.079 ± 0.003	0.080 ± 0.003	0.079 ± 0.003	0.079 ± 0.003	0.071−0.238
16:0 palmitic	10.8 ± 0.13	10.6 ± 0.13	10.7 ± 0.15	10.6 ± 0.13	9.55−15.77
16:1 palmitoleic	0.082 ± 0.002	0.084 ± 0.003	0.083 ± 0.003	0.082 ± 0.003	0.086−0.194
17:0 heptadecanoic	0.116 ± 0.003	0.119 ± 0.002	0.119 ± 0.002	0.118 ± 0.001	0.085−0.146
17:1 heptadecenoic	0.065 ± 0.002	0.062 ± 0.002	0.065 ± 0.003	0.064 ± 0.002	0.073−0.087
18:0 stearic	4.2 ± 0.22	4.2 ± 0.22	4.2 ± 0.22	4.1 ± 0.22	2.70−5.88
18:1 oleic	20.2 ± 1.32	19.9 ± 1.38	19.8 ± 1.32	20.1 ± 1.32	14.3−32.2
18:2 linoleic	55.1 ± 2.43	55.8 ± 2.49	55.6 ± 2.43	55.1 ± 2.53	42.3−58.8
18:3 linolenic	8.4 ± 0.35	8.6 ± 0.35	8.5 ± 0.37	8.5 ± 0.35	3.00−12.52
20:0 arachidic	0.33 ± 0.01	0.33 ± 0.02	0.33 ± 0.02	0.32 ± 0.02	0.16−0.48
20:1 eicosenoic	0.17 ± 0.01	0.17 ± 0.01	0.17 ± 0.01	0.17 ± 0.01	0.14−0.35
22:0 behenic	0.35 ± 0.02	0.34 ± 0.02	0.35 ± 0.02	0.35 ± 0.02	0.163−0.482
24:0 lignoceric	0.12 ± 0.01	0.11 ± 0.01	0.12 ± 0.01	0.12 ± 0.02	

[a]Percent total fatty acid. [b]From ref 29.

Table 4. Trypsin Inhibitor and Lectin Composition of Virus-Resistant Transgenic Soybean and Nontransgenic Counterpart Seeds (Mean ± SD; n = 3)

component	Throne	729-3	729-4	729-5	lit. range[c]
lectin (HU/mg)[a]	6.06 ± 0.08	6.05 ± 0.10	6.10 ± 0.11	6.09 ± 0.15	0.09−8.46
trypsin inhibitor (TIU/mg)[b]	33.15 ± 0.12	32.98 ± 0.16	34.01 ± 0.14	33.57 ± 0.15	18−108

[a]Fresh weight basis. HU, hemagglutinating units. HU/mg denotes lectin units per milligram of fresh weight of soybean seeds. [b]TIU, trypsin inhibitor units. [c]From ref 29.

Table 5. Contents[a] of Isoflavones in Virus-Resistant Transgenic Soybean and Nontransgenic Counterpart Seeds (Mean ± SD; n = 3)

isoflavone	Throne	729-3	729-4	729-5	lit. range[b]
daidzin	81.6 ± 0.6	82.2 ± 0.5	81.8 ± 0.5	82.1 ± 0.7	35.8−360
glycitin	13.3 ± 0.4	12.9 ± 0.6	13.4 ± 0.6	13.2 ± 0.5	10.5−46.7
genistin	100 ± 1.2	102 ± 1.1	99 ± 1.3	98 ± 1.0	74.8−442.3
daidzein	8.9 ± 0.2	8.8 ± 0.1	9.1 ± 0.3	8.9 ± 0.2	2.2−47.7
glycitein	4.0 ± 0.1	4.1 ± 0.0	4.1 ± 0.1	3.9 ± 0.2	1.1−6.2
genistein	8.8 ± 0.2	8.9 ± 0.1	8.8 ± 0.0	8.9 ± 0.1	1.5−18.3

[a]Micrograms per gram dry weight. [b]From ref 30.

soybean lines and their nontransgenic counterpart seeds. In terms of these compositions, with a confidence level of 95%, no statistically significant differences were observed not only between the transgenic soybean seeds and the control but also among the different transgenic soybean lines. Individual values were within the tolerance interval determined for commercial varieties and within published literature ranges.[29] These results implied that no biologically important changes occurred for the proximate compositions of the transgenic soybean lines 729-3, 729-4, and 729-5 compared with their nontransgenic counterpart.

Amino Acid Contents. Table 2 presents the content of 18 amino acids of transgenic virus-resistant soybean and nontransgenic seeds. The content of individual amino acids in soybean seeds was expressed as percentage with respect to the total protein. The contents of the majority of the measured amino acids fell within the ranges of the ILSI database,[29] except threonine and tryptophan; the contents of these were higher than the maximum values. However, no significant differences in the levels of any of the 18 amino acids measured were found between the virus-resistant soybean seeds and their nontransgenic counterparts. These results demonstrated that the amino acid contents of the transgenic soybean cultivars were substantially equivalent to those of nontransgenic counterparts.

Fatty Acids. Individual fatty acids of soybean samples were estimated by GC-MS analysis. All fatty acids were expressed as percentage with respect to the total fatty acids (Table 3). Among them, consistent with previous results,[14−20] palmitic acid (C16:0), oleic acid (C18:1), and linoleic acid (C18:3) were the most abundant fatty acids of transgenic virus-resistant soybeans and their nontransgenic counterpart. The percentage values of the majority of the measured fatty acids fell within the ranges of the ILSI database,[29] except palmitoleic and heptadecenoic; the contents of these two fatty acids were lower than the minimum values. However, with a confidence level of 95% no statistical differences were found in fatty acid composition. The contents of the fatty acids in harvested seeds of the virus-resistant soybeans 729-3, 729-4, and 729-5 were comparable to those observed in the seeds of conventional control.

Antinutrients. The results for two important antinutritional factors (lectin and trypsin inhibitors) are presented in Table 4. Both of them were generally low and did not exceed the range reported previously,[29] which might not affect the nutritional potential of soybean seeds. The contents of lectin and trypsin

inhibitor in the harvested seeds of virus-resistant transgenic soybeans were comparable with those observed in the harvested seeds of the nontransgenic control with a confidence level of 95%. These results exhibited that the antinutrient composition of the transgenic lines was substantially equivalent to that of the nontransgenic counterpart.

Isoflavones Profile. The contents of isoflavones including daidzin, glycitin, genistin, daidzein, glycitein, and genistein in the harvested seeds of virus-resistant transgenic soybeans were comparable to those observed in the harvested seeds of the conventional control (Table 5). The level of these isoflavones fell within the ranges of other commercially available soybeans reported in previous literature.[30] No significant statistical difference was observed in any of the isoflavones levels between the transgenic and nontransgenic soybean seeds.

In conclusion, the results of compositional analyses show no meaningful differences had been found in the transgenic soybean lines with glyphosate tolerance and virus resistance from the conventional counterpart with a confidence level of 95%. On the basis of the principle of substantial equivalence,[5,6] the transgenic soybean lines with glyphosate tolerance and virus resistance are substantially equivalent to those nontransgenic counterparts. The results reported herein, together with previous findings that the composition of transgenic glyphosate-tolerant soybeans with the *bar* gene is equivalent with that of conventional soybeans,[9−15] support the conclusion that no significant undesirable biological changes occurred by the insertion of IR conferring transgenic soybean with robust resistance to mixed infection of AMV, BPMV, and SMV.

RNA silencing or RNA interference (RNAi), a form of gene suppression that occurs at transcriptional and post-transcriptional levels, is an evolutionarily conserved process that is active in a wide variety of eukaryotic organisms.[1,2] One of the advantages of RNAi-mediated virus resistance is the relatively small size of the transgene required for silencing, enabling more than one short IR containing different viruses' conserved sequences to be stacked to a single construct and enabling a broader spectrum of resistance to be developed with a single transgene.[3] RNAi has been an important tool to render plants resistant to plant virus infection,[31] although there are three main factors that can determine the practical usefulness of antiviral strategies: efficiency, durability, and safety.[32] The results showed that the transgenic soybeans with IR insertion are substantially equivalent to nontransgenic counterparts. The concept of "substantial equivalence" suggests that the RNAi-mediated virus-resistant transgenic soybeans are as safe and nutritious as their traditional counterpart. The results can serve as baseline information for developing RNAi-mediated transgenic soybean cultivars or other crops with broader spectrum virus resistance.

AUTHOR INFORMATION

Corresponding Authors

*(M.P.) Phone: +86-898-66890770. Fax: +86-898-66890978. E-mail: mmpeng_2000@yahoo.com.

*(Z.L.) Phone: +86-898-66890770. Fax: +86-898-66890978. E-mail: liuzhixin@itbb.org.cn.

Author Contributions

∥X.Z. and P.Z. contributed equally to this work.

Funding

This work was financially supported by the Natural Science Foundation of China (31201264) and the Major Science and Technology Program of Hainan Province (ZDZX2013010-3 and ZDZX2013023-1).

Notes

The authors declare no competing financial interest.

ACKNOWLEDGMENTS

We greatly appreciate the generosity of Feng Qu at The Ohio State University for providing the experimental material for this study.

REFERENCES

(1) Ding, S. RNA-based antiviral immunity. *Nat. Rev. Immunol.* **2010**, *10* (9), 632−644.

(2) Qu, F. Plant viruses versus RNAi: simple pathogens reveal complex insights on plant antimicrobial defense. *Wiley Interdiscip. Rev. RNA* **2010**, *1*, 22−23.

(3) Mansoor, S.; Amin, I.; Hussain, M.; Zafar, Y.; Briddon, R. W. Engineering novel traits in plants through RNA interference. *Trends Plant Sci.* **2006**, *11* (11), 559−565.

(4) EFSA Panel on Genetically Modified Organisms (GMO). Statistical considerations for the safety evaluation of GMOs. *EFSA J.* **2010**, *8* (1), 1250.

(5) OECD (Organisation for Economic Cooperation and Development). *Concepts and Principles*; Paris, France, 1993.

(6) FAO/WHO. *Evaluation of Allergenicity of Genetically Modified Foods*; report of a joint FAO/WHO expert consultation on allergenicity of foods derived from biotechnology; Rome, Italy, 2001.

(7) Tang, M.; He, X.; Luo, Y.; Ma, L.; Tang, X.; Huang, K. Nutritional assessment of transgenic lysine-rich maize compared with conventional quality protein maize. *J. Sci. Food Agric.* **2013**, *93* (5), 1049−1054.

(8) George, C.; Ridley, W. P.; Obert, J. C.; Nemeth, M. A.; Breeze, M. L.; Astwood, J. D. Composition of grain and forage from corn rootworm-protected corn event MON 863 is equivalent to that of conventional corn (*Zea mays* L.). *J. Agric. Food Chem.* **2004**, *52* (13), 4149−4158.

(9) Qin, F.; Kang, L.; Guo, L.; Lin, J.; Song, J.; Zhao, Y. Composition of transgenic soybean seeds with higher γ-linolenic acid content is equivalent to that of conventional control. *J. Agric. Food Chem.* **2012**, *60* (9), 2200−2204.

(10) Berman, K. H.; Harrigan, G. G.; Riordan, S. G.; Nemeth, M. A.; Hanson, C.; Smith, M.; Sorbet, R.; Zhu, E.; Ridley, W. P. Compositions of forage and seed from second-generation glyphosate-tolerant soybean MON 89788 and insect-protected soybean MON 87701 from Brazil are equivalent to those of conventional soybean (*Glycine max*). *J. Agric. Food Chem.* **2010**, *58* (10), 6270−6276.

(11) Lepping, M. D.; Herman, R. A.; Potts, B. L. Compositional equivalence of DAS-444Ø6-6 (AAD-12 + 2mEPSPS + PAT) herbicide-tolerant soybean and nontransgenic soybean. *J. Agric. Food Chem.* **2013**, *61* (46), 11180−11190.

(12) Berman, K. H.; Harrigan, G. G.; Nemeth, M. A.; Oliveira, W. S.; Berger, G. U.; Tagliaferro, F. S. Compositional equivalence of insect-protected glyphosate-tolerant soybean MON 87701 × MON 89788 to conventional soybean extends across different world regions and multiple growing seasons. *J. Agric. Food Chem.* **2011**, *59* (21), 11643−11651.

(13) Herman, R. A.; Phillips, A. M.; Lepping, M. D.; Sabbatini, J. Compositional safety of DAS-68416-4 (AAD-12) herbicide-tolerant soybean. *J. Nutr. Food Sci.* **2011**, DOI: 10.4172/2155-9600.1000103.

(14) Taylor, N. B.; Fuchs, R. L.; MacDonald, J.; Shariff, A. R.; Padgette, S. R. Compositional analysis of glyphosate-tolerant soybeans treated with glyphosate. *J. Agric. Food Chem.* **1999**, *47* (10), 4469−4473.

(15) Harrigan, G. G.; Ridley, W. P.; Riordan, S. G.; Nemeth, M. A.; Sorbet, R.; Trujillo, W. A.; Breeze, M. L.; Schneider, R. W. Chemical composition of glyphosate-tolerant soybean 40-3-2 grown in Europe

remains equivalent with that of conventional soybean (*Glycine max* L.). *J. Agric. Food Chem.* **2007**, *55* (15), 6160−6168.
(16) Gayen, D.; Sarkar, S. N.; Datta, S. K.; Datta, K. Comparative analysis of nutritional compositions of transgenic high iron rice with its non-transgenic counterpart. *Food Chem.* **2013**, *138* (2−3), 835−840.
(17) Roberts, M.; Minott, D. A.; Pinnock, S.; Tennant, P. F.; Jackson, J. C. Physicochemical and biochemical characterization of transgenic papaya modified for protection against papaya ringspot virus. *J. Sci. Food Agric.* **2014**, *94*, 1034−1038.
(18) Zhang, X.; Sato, S.; Ye, X.; Dorrance, A. E.; Morris, T. J.; Clemente, T. E.; Qu, F. Robust RNAi-Based resistance to mixed Infection of three viruses in soybean plants expressing separate short hairpins from a single transgene. *Phytopathology* **2011**, *101* (11), 1264−1269.
(19) GB 5009.3-2010. Determination of moisture in foods. Standardization Administration of the People's Republic of China, Beijing, China, 2010.
(20) GB 5009.4-2010. Determination of ash in foods. Standardization Administration of the People's Republic of China, Beijing, China, 2010.
(21) GB 5009.5-2010. Determination of protein in foods. Standardization Administration of the People's Republic of China, Beijing, China, 2010.
(22) GB 5009.6-2003. Determination of fat in foods. Standardization Administration of the People's Republic of China, Beijing, China, 2003.
(23) GB/T 5009.124-2003. Determination of amino acids in foods. Standardization Administration of the People's Republic of China, Beijing, China, 2003.
(24) GB/T 17377-2008. Animal and vegetable fats and oils − analysis by gas chromatography of methyl esters of fatty acids. Standardization Administration of the People's Republic of China, Beijing, China, 2008.
(25) Klurfeld, D. M.; Kritchevski, D. Isolation and quantitation of lectins from vegetable oils. *Lipids* **1987**, *22*, 667−668.
(26) Martin, S.; Jost, W.; Hans-Curt, F. Application of fluorescently labelled lectins for the visualization and biochemical characterization of polysaccharides in biofilms of *Pseudomonas aeruginosa*. *J. Microbiol. Methods* **2002**, *50*, 237−248.
(27) Hamerstrand, G. E.; Black, L. T.; Glover, J. D. Trypsin inhibitors in soy products: Modification of the standard analytical procedure. *Cereal Chem.* **1981**, *58*, 42−45.
(28) GB/T 23788-2009. Determination of soybean isoflavone in health-care food − High-performance liquid chromatography. Standardization Administration of the People's Republic of China, Beijing, China, 2009.
(29) ILSI International Life Sciences Institute (ILSI) Crop Composition Database, version 4.0; http://www.cropcomposition.org (search criteria: soybean seed, all locations, all years) (accessed Feb 10, 2014).
(30) Kim, J. K.; Kim, E. H.; Park, I.; Yu, B. R.; Lim, J. D.; Lee, Y. S.; Lee, J. H.; Kim, S. H.; Chung, I. M. Isoflavones profiling of soybean [*Glycine max* (L.) Merrill] germplasms and their correlations with metabolic pathways. *Food Chem.* **2014**, *153*, 258−264.
(31) Collinge, D. B.; Jørgensen, H. J.; Lund, O. S.; Lyngkjaer, M. F. Engineering pathogen resistance in crop plants: current trends and future prospects. *Annu. Rev. Phytopathol.* **2010**, *48*, 269−291.
(32) Simón-Mateo, C.; García, J. A. Antiviral strategies in plants based on RNA silencing. *Biochim. Biophys. Acta* **2011**, *1809* (11−12), 722−731.

JOURNAL OF AGRICULTURAL AND FOOD CHEMISTRY

Review

pubs.acs.org/JAFC

Glucosinolates, Myrosinase Hydrolysis Products, and Flavonols Found in Rocket (*Eruca sativa* and *Diplotaxis tenuifolia*)

Luke Bell* and Carol Wagstaff

Department of Food and Nutritional Sciences and the Centre for Food Security, University of Reading, Whiteknights, Reading, Berkshire RG6 6AH, United Kingdom

ABSTRACT: Rocket species have been shown to have very high concentrations of glucosinolates and flavonols, which have numerous positive health benefits with regular consumption. This review highlights how breeders and processors of rocket species can utilize genomic and phytochemical research to improve varieties and enhance the nutritive benefits to consumers. Plant breeders are increasingly looking to new technologies such as HPLC, UPLC, LC-MS, and GC-MS to screen populations for their phytochemical content to inform plant selections. This paper collates the research that has been conducted to date in rocket and summarizes all glucosinolate and flavonol compounds identified in the species. The paper emphasizes the importance of the broad screening of populations for phytochemicals and myrosinase degradation products, as well as unique traits that may be found in underutilized gene bank resources. This review also stresses that collaboration with industrial partners is becoming essential for long-term plant breeding goals through research.

KEYWORDS: *Brassicaceae, isothiocyanates, plant breeding, indoles, nitriles*

INTRODUCTION

In recent years, several species of minor leafy crops have risen to prominence as potentially important commercial and edible species. One example is rocket, which has quickly gained popularity in the Western diet. Originally found as an obscure crop in Mediterranean and Middle Eastern countries, rocket has become popular largely due to the pungent aromas and tastes associated with it. Glucosinolates (GSLs)/isothiocyanates (ITCs) and flavonols derived from many species[1−4] have been shown to impart significant protection against cancer and heart disease.[4−11] In Western countries, diets are generally lacking in fruits and vegetables. Despite government initiatives (such as the "5-a-day" campaign in the United Kingdom and the United States), these diseases are increasingly leading to premature deaths.[12] Plant breeders aim to maximize levels of such beneficial compounds, but with little genomic information about rocket species presently available, this is a formidable task. This review will give an overview of research in rocket, an outbreeding crop, and how breeders and processors can utilize it to enhance beneficial compounds.

ROCKET SPECIES

Rocket (also known as arugula, rucola, and roquette) is a leafy vegetable crop that has gained substantial popularity across the world, particularly over the past 15 years.[13−16] Two main species are predominantly farmed as salad crops; these are *Eruca sativa* ("salad" or "cultivated" rocket; sometimes referred to as *Eruca vesicaria* subsp. *sativa*) and *Diplotaxis tenuifolia* ("wild" rocket). Both species share a peppery taste and aroma that is very distinctive.[17] They have been reported to contain high levels of vitamin C, GSLs, flavonols, and phenolics.[18−25] These are all known to have both antioxidant and anticancer properties and are also implicated in lowering the risk of cardiovascular and cognitive diseases. For excellent information on these beneficial effects and their underlying causes, see Drewnowski and Gomez-Carneros,[26] Keum et al.,[27] D'Antuono et al.,[28] Egea-Gilbert et al.,[29] Degl'Innoocenti et al.,[30] Bjorkman et al.,[31] and Jeffery et al.[32]

TAXONOMY AND DOMESTICATION

A distinction should be made that both *Eruca* and *Diplotaxis* species have overlapping characteristics and that one can be easily mistaken for the other by the untrained eye and/or before a certain level of maturity has been reached.[28] It is also arguable that *D. tenuifolia* is the least "wild" of the two species even though the common name is "wild rocket". It is featured and favored in commercial products and breeding programs and is likely to be more domesticated than *Eruca* species as a result. *Diplotaxis* varieties are generally uniform phenotypically, with *Eruca* varieties being more diverse in this respect.[23] No direct genomic evidence has been presented in the literature to suggest one species is any more or less genetically variable than the other. Variability in GSL data seems to support the hypothesis that *Diplotaxis* species are more "wild",[33] although it is not conclusive, as only a relatively small number of cultivars have been tested. This is a point that needs clarification through research and extensive breeding, as neither species can be considered fully domesticated.[29] For example, germination rates are variable, reproductive organs are typically small, seedpods shatter and disperse freely (rather than staying on the plant), and physical defenses such as leaf hairs are still present in many commercial varieties.[34]

Received: October 6, 2013
Revised: April 28, 2014
Accepted: April 29, 2014
Published: April 29, 2014

ACS Publications © 2014 American Chemical Society

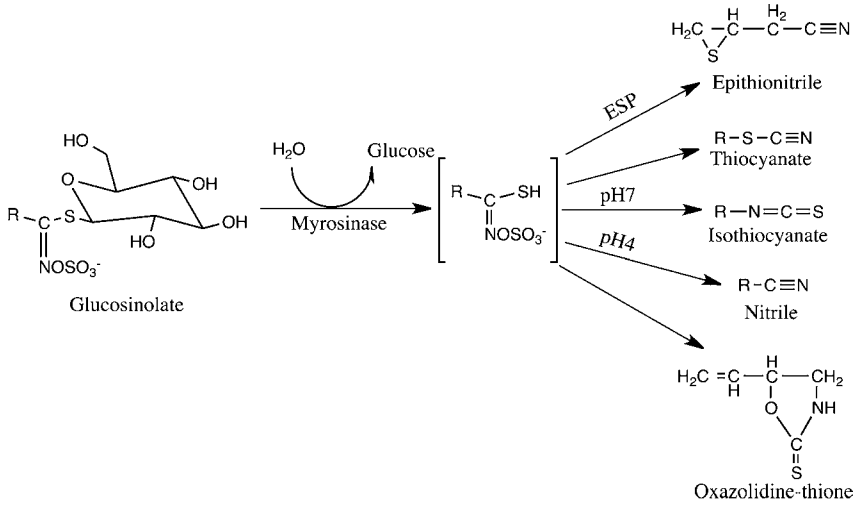

Figure 1. Glucosinolate–myrosinase reaction and some of the subsequent compounds produced under different conditions, such as pH and the influence of epithiospecifier proteins (ESP). Adapted from Zhang[9] and Hall et al.[185]

PHYTOCHEMICALS IN *ERUCA SATIVA* AND *DIPLOTAXIS TENUIFOLIA*: TYPES AND STRUCTURES

Glucosinolates. GSLs are β-thioglucoside *N*-hydrosulfates that are responsible for the sharp and bitter-tasting flavors found in cruciferous vegetables.[35,36] In combination with the enzyme myrosinase (thioglucoside glucohydrolase, EC 3.2.1.147), GSLs are hydrolyzed to create isothiocyanates, nitriles, thiocyanates, epithionitriles, indoles, oxazolidine-2-thiones, cyanopithioalkanes, ascorbigens, goitrogens, and epithioalkanes[37−49] (see Figure 1). Many of these hydrolysis products have antibacterial, antifungal, and insect-repellant effects.[50−55] GSLs and ITCs are being increasingly used as "biofumigants" to suppress soilborne pathogens, nematodes, and weeds. Some of the volatile products have the opposite effect of attracting species that can tolerate high GSL concentrations, such as types of ovipositing insects.[56,57]

The conditions under which hydrolysis of GSLs occurs will affect the respective proportions of the chemicals produced; pH, iron ions, thiol ions, temperature, and hydration play a particularly prominent role in this process in vivo.[58] The separation of GSLs in specialist "S-cells" from myrosinase in myrosin cells means that the two components come into contact only upon tissue disruption, for example, when damaged via chewing or digestion.[59−69] It is the biological activity of the ITC hydrolysis products in humans that is of most interest in rocket.[50] GSLs can be hydrolyzed within the intestinal tract by gut microflora that are known to have specific myrosinase activity,[70−73] but the efficacy of their action is not yet well determined.

GSL concentrations can vary and change over time depending on environmental conditions and stress.[7] Other factors affecting GSL profiles include plant age, organ type, developmental stage, ambient air temperature, level of water stress, photoperiod, agronomic practice, degree of wounding, and geographical origin of the variety/species.[74−81] These can often affect the profiles of *all* phytonutrients contained within tissue, not just GSLs,[82] and they are all factors that plant breeders aim to mitigate through development of genetically advanced and uniform breeding lines.

GSLs and the ITC derivatives have been an integral part of the human diet for millennia because of their presence in the family Brassicaceae.[64−66,83−89] GSLs are evolutionarily recent secondary metabolic products, having arisen 10−15 million years ago,[90,91] acting to prevent pathogen attack and dissuade herbivory. They are known in only a few angiosperm families of the order Brassicales, which includes the Brassicaceae,[92−100] and of which *Eruca* and *Diplotaxis* are members.

A study by Pasini et al.[33] of 37 rocket accessions (*Diplotaxis* and *Eruca*) showed that GSL profiles were all very similar, regardless of the species. In total, 12 GSL compounds were found across all accessions; Table 1 illustrates all known GSL compounds identified to date in rocket. These include 4-mercaptobutyl GSL (glucosativin),[21] 4-methylthiobutyl GSL (glucoerucin),[101] and 4-methylsulfinylbutyl GSL (glucoraphanin),[28] which constitute the three most abundant GSLs in rocket.

Flavonols. Flavonols are diphenylpropanes (C_6–C_3–C_6)[102] and are another important group of chemicals found within rocket species. Flavonols in rocket are found with sugar conjugates and typically occur in relatively large quantities.[103] The aglycones found (such as quercetin and kaempferol) are glycosylated and acylated, which in turn affects their biological properties.[18] A study by Martínez-Sánchez et al.[18] identified over 50 different flavonol compounds across four different species. Watercress, mizuna, and two species of rocket were all found to accumulate very different compounds within their leaves and in varying quantities. Wild rocket showed high levels of quercetin-3,3′,4-triglucosyl (43.5 mg 100 g^{-1} fw), and salad rocket had mostly kaempferol-3,4′-diglucosyl (97.8 mg 100 g^{-1} fw). The group also showed a correlation between quercetin derivatives and high antioxidant activity, despite the significant variations seen between species.

Studies conducted on rocket tissues have identified significant concentrations of polyglycosylated flavonols. The core aglycones of these are kaempferol, quercetin, and isorhamnetin;[102] Table 2 provides an up-to-date list of all flavonol compounds identified in rocket. Martínez-Sanchez et al.[18] showed that *Eruca* species accumulate kaempferol derivatives, whereas *D. tenuifolia* accumulates predominantly quercetin instead, meaning that the two chemicals could be used as identification markers between the two species.[104] Isorhamnetin aglycones are common to both species but typically in much lower concentrations.[33] The specific aglycones also impart various degrees of antioxidant activity. For example, quercetin derivatives have a higher activity than kaempferol and isorhamnetin. The differences in structure

dx.doi.org/10.1021/jf501096x | J. Agric. Food Chem. 2014, 62, 4481−4492

(the arrangement of hydroxyl groups and glycosylation) affect antioxidant activity by allowing the molecules to act as hydrogen/electron donors, single-oxygen scavengers, or reducing agents.[105]

PHYTOCHEMICALS AND THE RELATIONSHIP WITH QUALITY: TASTE AND AROMA

It is thought that the presence of glucosativin, glucoerucin, and their hydrolysis products within rocket leaves is what gives

Table 1. Intact Glucosinolates Identified within Leaves of Rocket, *Eruca* and *Diplotaxis* Species, by LC-MS (Negative Ion Mode)

R-group	Common name	R-group structure [x]	Mass parent ion	MS² spectrum ions (signature ions in bold)	Reference
2-(benzoyloxy) ethyl	-	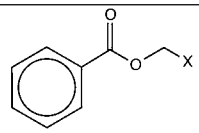	466	386	33
3-hydroxy-5-(methylsulfinyl) pentyl	-	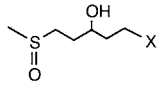	482	403	
4-(β-D-glucopyranosyldisulfanyl) butyl	Diglucothiobeinin	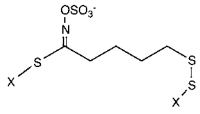	600	521	33,186
5-(methylsulfinyl) pentyl	Glucoalyssin	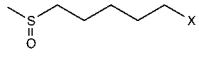	450	371	
N-butyl	Dihydrogluconapin	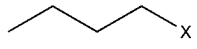	374	294	
4-phenylbutyl	Glucoamoracin	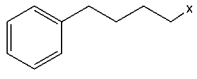	450	371	28
7-(methylsulfinyl) heptyl	Glucoibarin	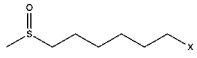	494	414	
Ethyl	Glucolepiidin	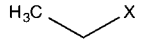	346	266	
2-phenylethyl	Gluconasturtiin	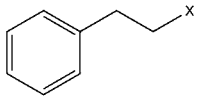	422	343	
1-methylethyl	Glucoputranjivin	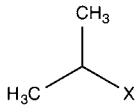	360	280	28
4-(methylsulfinyl)-3-butenyl	Glucoraphenin	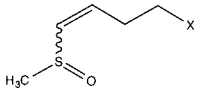	434	354	
Dimeric 4-mercaptobutyl	DMB		811	731, 569, **405**	21,33,186
4-mercaptobutyl	Glucosativin	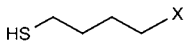	406	**259**, 209, 194, 138 97, 96	
4-hydroxy-3-indolymethyl	4-Hydroxyglucobrassicin	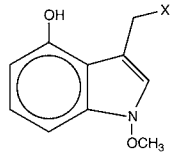	463	383, **285**, 275, 267, **259**, 240	33,178
4-(methylthio) butyl	Glucoerucin	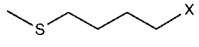	420	340, 291, 275, **259**, 242, 227, 195, 178, 163	
4-hydroxybenzyl	Glucosinalbin	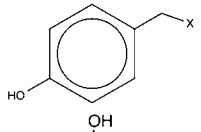	424	344, 291, 275, 261, **259**, 246, 231, 228, 182	33,178
(R,S)-2-hydroxy-3-butenyl	Progoitrin/epiprogoitrin	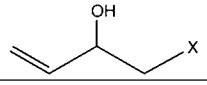	388	332, 308, 301, 275, 259, 210, 195, 136	

dx.doi.org/10.1021/jf501096x | J. Agric. Food Chem. 2014, 62, 4481−4492

Table 1. continued

R-group	Common name	R-group structure [x]	Mass parent ion	MS² spectrum ions (signature ions in bold)	Reference
3-indolymethyl	Glucobrassicin	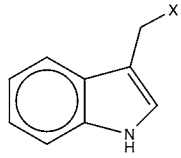	447	275, **259**, 251, 205	33,178,187
1-methylpropyl	Glucocochlearin	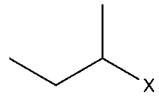	374	294	85,186
2-methylbutyl	Glucojiaputin	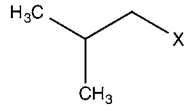	388	308	
5-(methylsulfonyl) pentyl	Glucoerysihienin	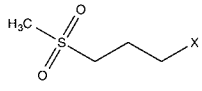	466	386	28,33
3-(methylthio) propyl	Glucoiberverin	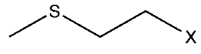	406	326, 275, **259**, 228, 145	85,178
3-butenyl	Gluconapin	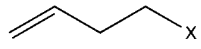	372	292, 275, **259**, 227, 195, 194, 176	28,178
Benzyl	Glucotrapaeolin	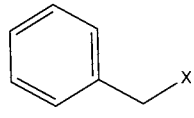	408	328, 275, **259**, 241, 230, 212, 195, 166	
1-methoxyindol-3-ylmethyl	Neoglucobrassicin	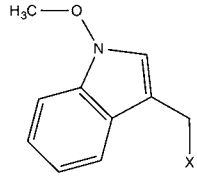	477	447, **466**, 284, **259**	28,178
2-propenyl	Sinigrin	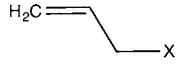	358	278, 275, **259**, 227, 195, 180, 162	
4-(methylsulfinyl) butyl	Glucoraphanin	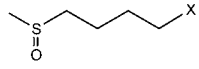	436	**372**, 291, **259**, 97, 96	21,33,178,187
4-methoxy-3-indolymethyl	4-Methoxyglucobrassicin	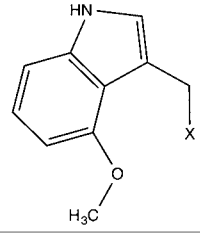	477	291, 275, **259**, 235, 227, 195	178, 188

[x]Standard GSL molecule according to IUPAC nomenclature.

them a characteristic flavor.[44] Many of the health beneficial GSLs and ITCs are thought to be responsible for strong tastes that some consumers find repellant.[106] It seems that to many people, these compounds contribute very little to a pleasurable eating experience and are actively avoided.[83] Conversely, however, some people prefer these strong tastes and aromas and will actively seek to consume rocket when it is available. Growers in Italy often prefer the subsequent cuts because of the more intense tastes and aromas that are produced,[107] and some will even "sacrifice" the first cut in favor of the subsequent leaf growth. This highlights a divide between consumers that may be indicative of underlying genotype(s) for taste perception and preference.

The breeding process in rocket varieties to date has effectively made the species "milder" in taste when compared to plants that grow naturally in the wild. Whether this has been intentional or as a result of selecting for other unrelated traits (such as leaf morphology) is debatable. Some recent commercial varieties have been bred for a "hotter" taste, such as 'Wildfire', by Tozer Seeds (Surrey, UK).

A study by Pasini et al.[17] demonstrated how breeding for sensory traits could be achieved by highlighting which glucosinolates contribute to specific taste and aroma elements in rocket. It was found that progoitrin/epiprogoitrin is responsible for bitter taste attributes, despite being only a minor component of the overall GSL profile of rocket (4.3−11.4% of total

dx.doi.org/10.1021/jf501096x | J. Agric. Food Chem. 2014, 62, 4481−4492

Table 2. Flavonol Compounds Identified in Leaves of *Eruca* and *Diplotaxis* Species by LC-MS (Negative Ion Mode)

flavonol compound[a]	*Eruca*[b]	*Diplotaxis*[b]	mass parent ion	MS^2 spectrum ions (signature ion in bold)	refs
I 3,4′-diGlc	X	X	639	**477**	18, 33
I 3-Glc	X		477		
K 3-(2-Sinp-Glc)-4′-Glc	X		817		
K 3,4′-diGlc	X	X	609		
K 3-Glc	X		447	**285**	
Q 3-Glc	X		463	301	
K 3-diGlc-7-Glc	X		771	609	33
K 3-Sinp-triGlc-7-Glc	X		1139	977, 771, 609, 429	
Q 3,4′-diGlc-3′-(6-Caf-Glc)		X	949	787, **625**, 463, 301	
M	X		317	151	189
Q	X		301	151	
R	X		609	300	
Q 3-(2-Caf-Glc)-3′-(6-Sinp-Glc)-4′-Glc		X	1155	993, 831, 787, 669, **625**, 463, 301	18, 25
Q 3-(2-Mcaf-Glc)-3′-(6-Sinp-Glc)-4′-Glc		X	1185	1023, 817, 669, 655	
Q 3-(2-Fer-Glc)-3′-(6-Fer-Glc)-4′-Glc		X	1139	977, 639, 463	18, 25, 33
Q 3-(2-Fer-Glc)-3′-(6-Sinp-Glc)-4′-Glc		X	1169	1007, 831, 669, 639, 463, 301	
Q 3-(2-Sinp-Glc)-3′-(6-Sinp-Glc)-4′-Glc		X	1199	1037, 831, 669, 463, 301	18, 25, 33
Q 3,3′,4-triGlc		X	787	625, 463, 301	
Q 3,4′-diGlc-3′-(6-Fer-Glc)		X	963	801, 639, 463, 301	
Q 3,4′-diGlc-3′-(6-Mcaf-Glc)		X	979	817, 655, 463, 301	
Q 3,4′-diGlc-3′-(6-*p*.Coum-Glc)		X	933	771, 609, 463, 301	
Q 3,4′-diGlc-3′-(6-Sinap-Glc)		X	993	831, 669, 463, 301	

[a]Abbreviations: Caf, caffeyol; Mcaf, methoxycaffeyol; *p*.Coum, *p*-coumaroyl; Fer, feruloyl; Sinp, sinapoyl; Glc, glucoside; Q, quercetin; K, kaempferol; I, isorhamnetin; M, myricetin; R, rutin. [b]Compound positively identified in species.

GSL concentration). The perceived pungency of leaves was positively related to the overall GSL content of accessions, and the levels of glucoraphanin negatively contributed to the typical "rocket" flavor. The study also highlighted an important difference between rocket and other *Brassica* sensory studies[108] in that bitterness was perceived as a favorable characteristic according to panelists. The flavonol compound kaempferol-3-(2-sinapoylglucoside)-4′-glucoside also significantly and positively contributed to flavor attributes in *Eruca* accessions. This would indicate that GSL compounds are not totally responsible for flavor in rocket. The study itself stopped short of saying how or if the information obtained would be used in breeding programs, but with study into rocket flavor components, milder (and/or stronger) varieties could be bred more efficiently once the responsible compounds are properly identified.[26]

HEALTH-PROMOTING PROPERTIES OF GLUCOSINOLATE–MYROSINASE PRODUCTS AND FLAVONOLS OF ROCKET

Isothiocyanates. ITC hydrolysis products have been identified in rocket,[45] such as 4-(methylthio)butyl ITC (erucin),[109,110] which is known to show antiproliferative activity in human lung carcinoma A549 cells, hepatoma (HepG2) cells, colon cancer cells, prostate cancer cell lines (PC3, BPH-1, and LnCap), and leukemia cells.[111] Erucin is a structurally reduced analogue of sulforaphane (which is predominantly found in broccoli) and has shown promising anticancer properties in vitro (e.g., antiproliferation of human erytroleukemic K562 cells).[112] Research into the chemopreventative and antigenotoxic nature of ITCs has shown promising results[113] (see Figure 2). Other studies involving chemically induced genotoxicity have shown very strong antigenotoxic effects of *E. sativa* extracts,[13] which is in agreement with other Brassicaceae studies.[114,115] Identifying specific cultivars of rocket with elevated levels of erucin and glucoraphanin would be an important first step in developing superior varieties from a human nutrition standpoint.

The results of GSL/ITC research prompted an investment in broccoli breeding in the past decade. A similar concerted effort could be made for rocket, which contains similar compounds that are potentially just as efficacious in humans.[116] Erucin, for example, has been shown to have a very similar, and even superior, biological activity to that of sulforaphane.[117] One paper has specifically demonstrated that the concentration of rocket ingested in an average daily diet is significant enough to impart a cancer preventative effect.[13] The metabolism of ITCs in humans via the mercapturic acid pathway has been investigated. ITCs are conjugated with glutathione and degraded by N-acetylation, initiating an increase of phase II detoxification enzymes; see Figure 3 for the detailed pathway breakdown of erucin.[113]

Nitriles. Along with ITCs, nitriles are the most abundant bioactive compounds produced by GSL hydrolysis.[116] The hydrolysis of glucoraphanin, for example, yields predominantly sulforaphane and sulforaphane nitrile. The ratio in which the two are formed depends greatly upon the environmental conditions and the plant cultivar that is used.[117] A low-pH medium tends toward the formation of nitriles, whereas high pH forms ITCs.[118,119] The presence of thiol and iron ions favors nitriles, and high temperature and hydration produce more ITCs.[120,121] This can have substantial consequences for any potential health benefits that might be imparted by the consumption of rocket.[119] The nitrile form is approximately 3 orders of magnitude less efficacious than the ITC in inducing quinone

dx.doi.org/10.1021/jf501096x | J. Agric. Food Chem. 2014, 62, 4481−4492

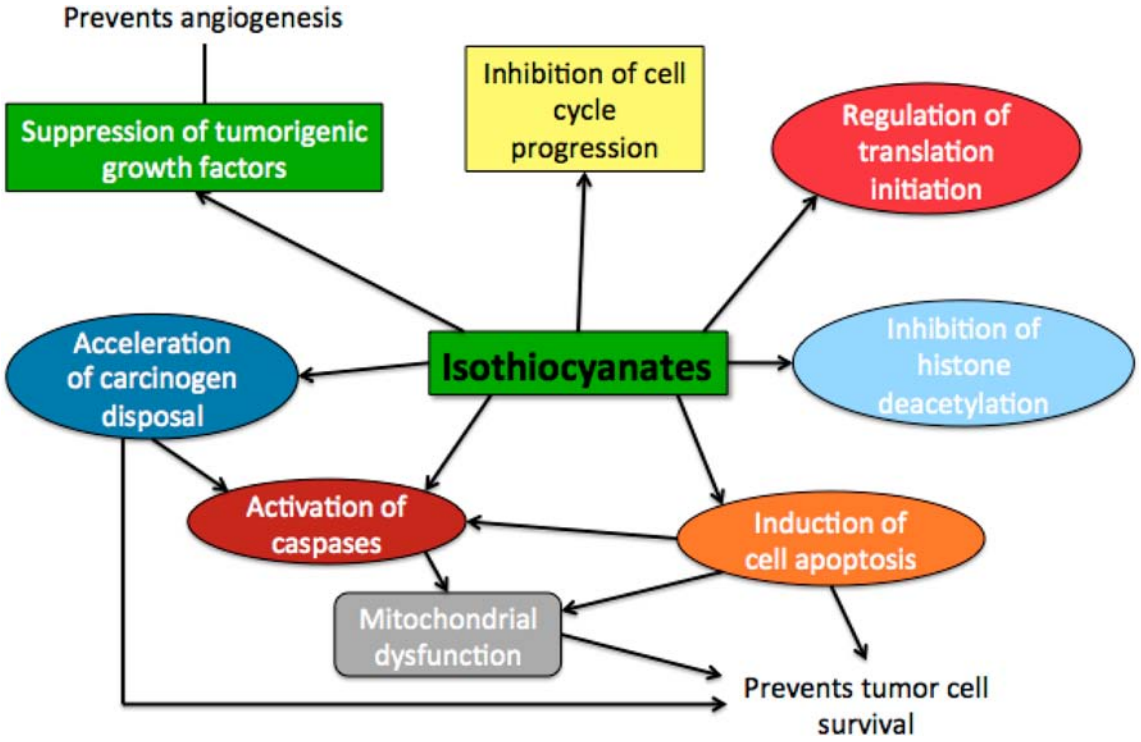

Figure 2. Pathways of documented ITC action in tumorigenic cells. See Wu et al.[113] for a detailed review of the roles ITCs play in cancer prevention.

reductase (phase II enzyme) and thus imparts a reduced enzymatic and anticarcinogenic response. Nitriles also compete with ITCs in this induction and reduce potential positive effects further.[38] As the ratio of these compounds may depend on plant variety, care must be taken in rocket breeding when plants are selected for GSL content, as this may not be reflective of the bioactives produced in subsequent hydrolysis reactions.[122] Other underlying genetic factors may influence which degradation pathway is taken.[123,124]

Indoles. Indoles are the predominant autolysis product of indole glucosinolates such as glucobrassicin, as their ITC counterparts are unstable.[85] Glucobrassicin has been detected as a minor GSL in rocket species,[33] and the predominant indole species produced is indole-3-carbinol. This compound is known to be cancer-preventative,[125,126] particularly in reproductive organs in vitro and in vivo. A condensation product of indole-3-carbinol, 3,3′-diindolymethane, is also responsible for beneficial physiological effects. Both compounds have been shown to reduce cell proliferation in breast, prostate, cervical, and colon cancer cell lines. They also show distinct differences from ITCs such as sulforaphane[127] and inhibition of tumor development in the stomach, breast, uterus, tongue, and liver of rodents.[128−135] Experiments in rodents have shown an increase in drug-metabolizing enzymes in the stomach, liver, and small intestines of individuals consuming both ITCs and indoles. This is suggestive of enhanced detoxification phase II enzymes (such as quinone reductase, glutathione reductase, and glutathione transferase)[134] and a mechanism by which these phytochemicals impart chemopreventative effects.[135,136]

Typically indoles inhibit cell proliferation through cytostatic mechanisms, whereas ITCs induce cytotoxicity within cell lines (at >12.5 μM concentrations), which ultimately leads to increased apoptosis.[137,138] This indicates that both types of compound could act and be effective at different stages of cancer development.[11] Indoles have been shown to induce programmed cell death in prostate, breast, and osteocarcinoma cell lines[139] and G_1 cell cycle arrest in breast and prostate cancer cell lines.[140,142,143] It is these cytostatic effects on cell proliferation that have been suggested as the mechanism responsible for the lack of apoptosis effects in indoles.[141]

Using information on GSL content in rocket, the ITC and indole effects can be potentially maximized in new varieties and be of greater benefit to human health when considered in tandem, rather than separately.[127]

Oxazolidine-2-thiones and Goitrogens. The hydrolysis of β-hydroxy-alkyl GSL compounds (e.g., progoitrin; a minor GSL in rocket) can produce oxazolidine-2-thiones such as goitrin (5-vinyloxazolidine-2-thione).[142−148] It is these compounds that are largely attributed to the thyroid condition of goiter in mammals,[149] but the action of microflora in the gut is thought to mediate the problems associated with high oxazolidine-2-thione intake.[150−153] That being said, oxazolidine-2-thiones interfere with thyroxine synthesis[154] and are therefore likely to have an adverse biological effect regardless of gut microflora action or bodily iodine status.[3] A study by Nishie and Daxenbilcher[155] showed that these compounds are not teratogenic or embryotoxic, however.

These molecules contribute significantly to the bitter taste of rocket that some people perceive quite strongly.[154] The detection of these compounds may be mediated in a similar genetic fashion as PROP (propylthiouracil), for example.[155,156] By using phytochemical data in rocket breeding programs these oxazolidine-2-thione components could be reduced, potentially improving consumer acceptance (depending on the target consumer) and avoiding any possible adverse health effects associated with overconsumption.

Ascorbigens. Ascorbigens are formed via the reaction of indole-3-carbinol and 3,3′-diindolymethane with ascorbic acid in the stomach during myrosinase-catalyzed degradation of indolyl-3-methyl glucosinolates.[157,158] In this manner it is

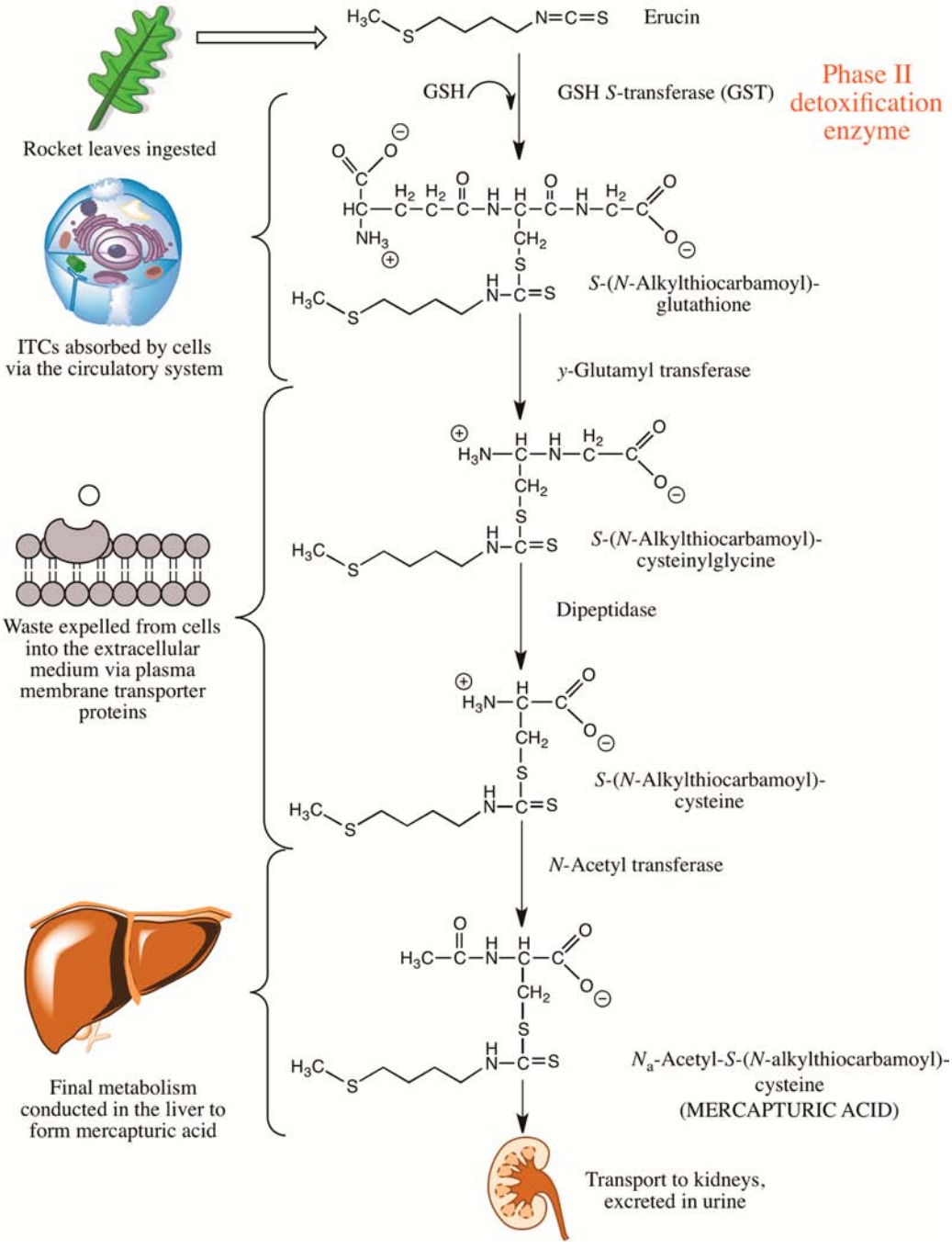

Figure 3. Mercapturic acid pathway of ITC metabolism in the human body. After ingestion of rocket leaves, glucoerucin is hydrolyzed by myrosinase to form erucin. This is released and absorbed in the ileum, where it is transported in the blood to cells around the body. ITCs initiate phase II detoxification enzymes in this pathway and are known to aid in cancer prevention. Adapted from Wu et al.[113]

thought that ascorbigens have a role in cancer modulation[159] via quinone reductase induction.[114] As has been highlighted previously, this has important implications for breeding for plant varieties with enhanced chemopreventative effects.

Epithioalkanes. Epithioalkanes are formed as part of the myrosinase reaction with GSLs at low pH with epithiospecifier protein and ferrous ions. These GSLs typically have a side chain with a double bond, such as sinigrin.[160−163] It is uncertain whether these compounds produce any significant bioactive effect in humans, but the ratio in which they are produced alongside ITCs, nitriles, and indoles may affect on these compounds' efficacy as anticarcinogens.

Flavonols. The antioxidant and anti-inflammatory function of flavonols in the human diet are well-known and include protecting the colonic epithelium from free radical damage.[164−167] They can induce the up-regulation of enzymes (such as cytochrome P450), which may lead to a decreased risk of cancer, cardiovascular disease, immune dysfunction, atherosclerosis, and chronic inflammation.[168,169]

FACTORS AFFECTING PHYTOCHEMICAL CONTENT

Breeding and Cultivation. Rocket has been consistently shown to be a good dietary source for flavonols, GSLs, and antioxidants. However, there can be large differences between

dx.doi.org/10.1021/jf501096x | J. Agric. Food Chem. 2014, 62, 4481−4492

plants of the same germplasm accession due to a combination of genetic and environmental variability. This is probably due to the outbreeding nature of the species[104] and a lack of overall uniformity in varieties. Commercial varieties cannot be considered truly domesticated because of this tendency for outcrossing, and the susceptibility of plants to inbreeding depression (a loss of genetic variability due to repeated self-pollination or crossing with a closely related individual). Development of advanced open-pollinating breeding lines (lines that are allowed to cross-pollinate freely in a population of selected individuals), or even F_1 hybrids (superior varieties produced by crossing distinctly different, elite inbred lines), could potentially minimize such variation.

Throughout the food chain there are many aspects that can have an adverse effect on GSL levels within leaves (Figure 4). These include cultivar choice, cultivation practice, climatic conditions, photoperiod, sulfur and nitrogen availability, harvest date, time spent in storage, temperature of wash water, levels of physical damage to leaves, packaging atmosphere, and food preparation methods.[30−32,170−173]

Harvesting. Rocket species have the ability to regrow their leaves repeatedly after cutting, which allows for several harvests to take place under optimal conditions.[107] In parts of southern Italy, it is not unheard of for up to seven harvests to occur from a single planting. This has obvious cost-saving benefits for growers, but multiple harvests also induce stress responses in rocket that may be detrimental to the flavor and aesthetics of the crop. Stress drives up the production of secondary metabolites such as GSLs and anthocyanins, which will produce very strong, bitter tastes. There are other detrimental effects of multiple harvests; leaves become progressively smaller and more "skeletal" in appearance with each cutting, for example. High anthocyanin levels also affect the color of leaves, turning them an undesirable pink, purple, or red. Color has been found to be one of the most important characteristics consumers look for in rocket,[174] and so the loss of fresh appearance can ultimately lead to rejection of crops by supermarkets and processors.

Industrial and Culinary Processing. There are five main influences that have been identified as affecting GSL levels during processing.[94] These are the action of myrosinase hydrolysis, myrosinase inactivation, the lysis and leaching of GSLs into wash water, thermal degradation of GSLs, and the loss of ascorbic acid, iron, and other enzyme cofactors. Myrosinase inactivation and thermal degradation of GSLs is probably less of an issue in rocket species, as the leaves are not typically cooked. The leaves are not ordinarily frozen, and so freeze−thaw hydrolysis is not likely to be a major factor either. Other factors almost certainly play a significant role in GSL and phytochemical loss in rocket. Verkerk et al.[94] highlighted four key areas that affect GSL levels before reaching the end consumer: (1) variety/cultivar used; (2) storage and packaging (postharvest, post-processing, and in shops/supermarkets); (3) industrial processing; and (4) consumer preparation methods.

If each of these areas can be mitigated through breeding superior varieties, consumers will receive an end product that is of higher nutritive quality and thus provides increased health benefits.

Postharvest Storage. Studies on both *Diplotaxis* and *Eruca* species have been conducted to determine the effects of postharvest storage conditions on chlorophyll content and respiration rates.[15] Both species of rocket have been found to have high respiration rates,[107] leading to rapidly impaired visual quality, such as stem browning, tissue yellowing, and general decay.[175] Provided initial GSL loss can be mitigated through breeding, ITC formation has been shown to increase over nitrile formation during the storage period.[176]

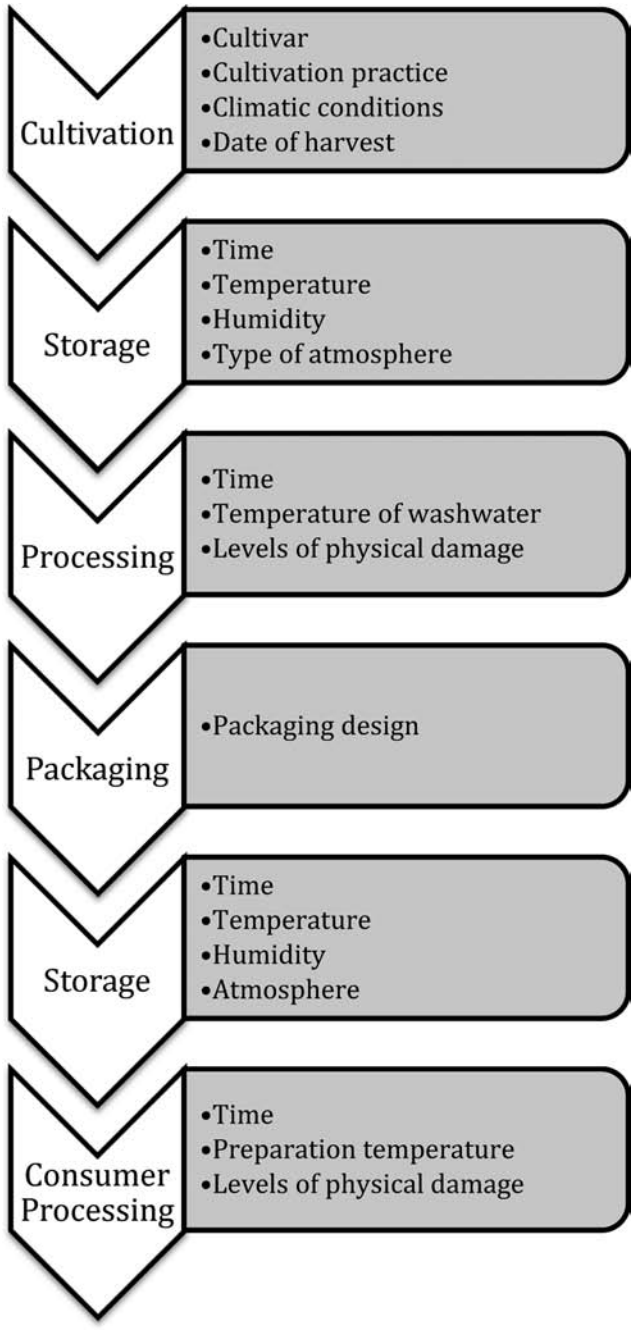

Figure 4. Factors and conditions within the commercial supply chain that affect GSL and flavonol levels within rocket leaves.

Time, temperature, humidity, and atmospheric conditions are all optimized for specific crops within the logistics chain, but these factors are often designed to prevent only visual degradation and not phytochemical breakdown.[100] Getting producers, packagers, and transporters to change their current practices to better preserve the health-promoting compounds in rocket would be a difficult task. Treatments and storage conditions are often integrated parts of protocols and procedures, and changing these would require significant testing on a commercial scale.

NEW SELECTION TOOLS FOR BREEDERS

Phytochemical Selection. It should not be forgotten that some GSLs and their breakdown products are thought to be toxic, and even carcinogenic, at high concentrations.[128] Breeders and researchers should be mindful that more of a certain compound does not necessarily mean "better".[177] Humans seem to be able to tolerate GSLs much better than pigs, rats, and rabbits, for example, but overconsumption of these compounds may have serious health consequences[64] as high-dose−effect relationships are as yet unknown in humans.[94] Few papers in GSL research (regardless of species) have acknowledged the potential for plant breeders to utilize HPLC/UPLC/LC-MS/GC-MS methods within breeding programs to "monitor" and select plants for their phytochemical content in this manner. These techniques would provide valuable information on breeding lines relatively rapidly, especially for GSL and flavonol breeding.[178] It is not common practice to select rocket plants on the basis of their phytochemical profile at present, but as interest in these compounds increases, it will be necessary for breeders to modify their selection criteria and information sources to remain competitive in the salad vegetable market.[94] This has been achieved with 'Beneforte' broccoli (Seminis Vegetable Seeds; subsidiary of Monsanto Co., St. Louis, MO, USA; www.beneforte.com) for example. It has also been indicated in hybrid varieties of *Brassica* that ITC/nitrile ratios can be selected for.[179]

Genetic Resources and Marker-Assisted Breeding. European initiatives (such as the EU GENRES project "Leafy vegetables germplasm, stimulating use"; http://documents.plant.wur.nl/cgn/pgr/leafyveg/) have included rocket species within their remit, indicating the rising prominence of the species and the desire for more work to be conducted on them. The germplasm accessions stored in gene banks are a valuable genetic resource for breeders to take advantage of.[180] The accessions contained within these collections are highly variable and have unique visual and sensory characteristics that could be introgressed into breeding lines relatively easily.[181]

Genetic information about rocket within the published literature is very scarce. Some molecular marker techniques such as random amplification of polymorphic DNA (RAPD), inter-simple sequence repeats (ISSR), and amplified fragment length polymorphisms (AFLP) have been used to analyze morphological characteristics of *E. vesicaria*.[29] ISSR and AFLP are relatively robust for screening variable populations and discriminating between cultivars,[180] but RAPD is notoriously unreliable and suffers from a lack of reproducibility and resolution. Perhaps one of the most underutilized marker types is sequence related amplified polymorphism (SRAP). The forward and reverse primers are designed to target arbitrary GC- and AT-rich sequences of the genome, respectively, and are therefore more likely to anneal to active genomic regions.[182] This could be of use in understudied crops such as rocket, as it provides a simple, repeatable, and reliable way of screening large populations.

These techniques are now for the most part, however, obsolete in advanced molecular plant breeding, as next-generation sequencing (NGS) and single-nucleotide polymorphism (SNP)/quantitative trait loci (QTL) analyses are far more specific, reliable, and cost-effective. SNPs are the most abundant marker type within genomes, and their high density is ideal for studying specific regions in detail.[183] NGS techniques are now relatively affordable, even for relatively small companies. They are widely available in academic institutions, but many companies are bypassing these in favor of dedicated private commercial services[184] or are developing their own in-house facilities. The inability of some research institutions to provide adequate customer service, cost-effectiveness, data storage, and results on time is jeopardizing how much knowledge is in the public domain. Increasingly, both large and small breeding companies are collaborating privately and advancing techniques far beyond those found in academic institutions. Future work by institutes in advanced genomics, sequencing, and genotyping is likely to be obsolete in some cases because private research is already finding new innovations, for example, for data storage and bioinformatics. Because private companies have no obligation to share their knowledge, many of these advances may be unobserved by the mainstream scientific community. Institutes and universities need to do more to attract business from industry to keep up with the pace of private advances in this area.

Transcriptome sequences are now (generally) adequate for breeders to use and make huge advances in only a few years. Linkage mapping and QTL analyses can be conducted on desktop computers, making integration into breeding companies relatively straightforward from an IT point of view, even if the actual sequencing and genotyping are outsourced. Again, this may typically be to private companies providing a dedicated service. The availability of software licenses and advanced training courses from private companies also means plant breeders do not necessarily need the expertise found in universities and research institutes to attain their goals.

SUMMARY

Of all the research papers concerning rocket species and their phytochemistry, none have directly addressed how information could be used within a working breeding population. Often it is explained or postulated purely as theory rather than actual practice or given only a cursory mention. Only very rarely is a plant breeding program reflective of theory, due to the large number of environmental factors affecting plant growth, development, and reproduction. The progressive selection of rocket plants through conventional/molecular breeding would be a valuable tool for the research community and provide an excellent incentive for breeding companies to fund research. The actual monitoring and quantification of GSL/flavonol levels through successive generations (i.e., not just one as has been the case with most studies) would not only validate the heritability of such traits in rocket but also provide a "roadmap" for how other minor crops might be developed for commercial use.

Attention must be paid to the phytochemical content of varieties within breeding populations of rocket. By focusing solely on morphological traits, important phytochemical genotypes may be inadvertently lost from populations; this could be said of all Brassicaceae species, not just rocket. The balance of glucosinolate−myrosinase degradation products does seem to have a genetic component to it and so could be selected for also. Utilizing genetic resources, the falling costs of sequencing and bioinformatics can soon produce nutritively superior varieties of rocket. Plant breeding typically takes longer than the average research project allows for, even with the use of advanced genomic selection methods. This is a situation that could be remedied by long-term industrial collaboration and sponsorship by plant-breeding firms.

AUTHOR INFORMATION

Corresponding Author

*(L.B.) Phone: +44(0) 7909447654. E-mail: luke.bell@pgr.reading.ac.uk.

Funding

L.B. is supported by a BBSRC Case Award (Reference BB/J012629/1) in partnership with Elsoms Seeds Ltd. (Spalding, UK) and Bakkavor Group Ltd. (Spalding, UK).

Notes

The authors declare no competing financial interest.

REFERENCES

(1) Chaudhary, A.; Rampal, G.; Sharma, U.; Thind, T. S.; Singh, B.; Vig, A. P.; Arora, S. *Med. Chem. Drug Discovery* **2012**, *2*, 30−37.
(2) Gross, H. B.; Dalebout, T.; Grubb, C. D.; Abel, S. *Plant Sci.* **2000**, *159*, 265−272.
(3) Jongen, W. M. F. *Proc. Nutr. Soc.* **1996**, *55*, 433−446.
(4) Vinson, J. A.; Dabbagh, Y. A.; Serry, M. M.; Jang, J. H. *J. Agric. Food Chem.* **1995**, *43*, 2800−2802.
(5) Clarke, J. D.; Dashwood, R. H.; Ho, E. *Cancer Lett.* **2008**, *269*, 291−304.
(6) Hayes, J. D.; Kelleher, M. O.; Eggleston, I. M. *Eur. J. Nutr.* **2008**, *47*, 73−88.
(7) Herr, I.; Buechler, M. W. *Cancer Treat. Rev.* **2010**, *36*, 377−383.
(8) Melchini, A.; Traka, M. H. *Toxins (Basel)* **2010**, *2*, 593−612.
(9) Zhang, Y. S. *Mutat. Res. Mol. Mech. Mutagen.* **2004**, *555*, 173−190.
(10) Yang, Y. M.; Conaway, C. C.; Chiao, J. W.; Wang, C. X.; Amin, S.; Whysner, J.; Dai, W.; Reinhardt, J.; Chung, F. L. *Cancer Res.* **2002**, *62*, 2−7.
(11) Pappa, G.; Lichtenberg, M.; Iori, R.; Barillari, J.; Bartsch, H.; Gerhauser, C. *Mutat. Res. Mol. Mech. Mutagen.* **2006**, *599*, 76−87.
(12) Casagrande, S. S.; Wang, Y.; Anderson, C.; Gary, T. L. *Am. J. Prev. Med.* **2007**, *32*, 257−263.
(13) Lamy, E.; Schroder, J.; Paulus, S.; Brenk, P.; Stahl, T.; Mersch-Sundermann, V. *Food Chem. Toxicol.* **2008**, *46*, 2415−2421.
(14) D'Antuono, L. F.; Elementi, S.; Neri, R. *J. Sci. Food Agric.* **2009**, *89*, 713−722.
(15) Koukounaras, A.; Siomos, A. S.; Sfakiotakis, E. *Postharvest Biol. Technol.* **2007**, *46*, 167−173.
(16) Hall, M. K. D.; Jobling, J. J.; Rogers, G. S. *Veg. Crop. Res. Bull.* **2012**, *76*, 21−41.
(17) Pasini, F.; Verardo, V.; Cerretani, L.; Caboni, M. F.; D'Antuono, L. F. *J. Sci. Food Agric.* **2011**, *91*, 2858−2864.
(18) Martinez-Sanchez, A.; Gil-Izquierdo, A.; Gil, M. I.; Ferreres, F. *J. Agric. Food Chem.* **2008**, *56*, 2330−2340.
(19) Kim, S. J.; Ishii, G. *J. Sci. Food Agric.* **2007**, *87*, 966−973.
(20) Bennett, R. N.; Carvalho, R.; Mellon, F. A.; Eagles, J.; Rosa, E. A. S. *J. Agric. Food Chem.* **2007**, *55*, 67−74.
(21) Bennett, R. N.; Mellon, F. A.; Botting, N. P.; Eagles, J.; Rosa, E. A. S.; Williamson, G. *Phytochemistry* **2002**, *61*, 25−30.
(22) Cataldi, T. R. I.; Rubino, A.; Lelario, F.; Bufo, S. A. *Rapid Commun. Mass Spectrom.* **2007**, *21*, 2374−2388.
(23) Bennett, R. N.; Rosa, E. A. S.; Mellon, F. A.; Kroon, P. A. *J. Agric. Food Chem.* **2006**, *54*, 4005−4015.
(24) Chun Arasu, M. V.; Lim, Y.-P.; Kim, S.-J.; J.-H. *Hortic. Environ. Biotechnol.* **2013**, *54*, 206−213.
(25) Martinez-Sanchez, A.; Llorach, R.; Gil, M. I.; Ferreres, F. *J. Agric. Food Chem.* **2007**, *55*, 1356−1363.
(26) Drewnowski, A.; Gomez-Carneros, C. *Am. J. Clin. Nutr.* **2000**, *72*, 1424−1435.
(27) Keum, Y. S.; Jeong, W. S.; Kong, A. N. T. *Mutat. Res. Mol. Mech. Mutagen.* **2004**, *555*, 191−202.
(28) D'Antuono, L. F.; Elementi, S.; Neri, R. *Phytochemistry* **2008**, *69*, 187−199.
(29) Egea-Gilabert, C.; Fernandez, J. A.; Migliaro, D.; Martinez-Sanchez, J. J.; Vicente, M. J. *Sci. Hortic. (Amsterdam)* **2009**, *121*, 260−266.
(30) Degl'Innoocenti, E.; Pardossi, A.; Tattini, M.; Guidi, L. *J. Food Biochem.* **2008**, *32*, 642−653.
(31) Bjorkman, M.; Klingen, I.; Birch, A. N. E.; Bones, A. M.; Bruce, T. J. A.; Johansen, T. J.; Meadow, R.; Molmann, J.; Seljasen, R.; Smart, L. E.; Stewart, D. *Phytochemistry* **2011**, *72*, 538−556.
(32) Jeffery, E. H.; Brown, A. F.; Kurilich, A. C.; Keck, A. S.; Matusheski, N.; Klein, B. P.; Juvik, J. A. *J. Food Compos. Anal.* **2003**, *16*, 323−330.
(33) Pasini, F.; Verardo, V.; Caboni, M. F.; D'Antuono, L. F. *Food Chem.* **2012**, *133*, 1025−1033.
(34) Gepts, P. What is a crop?: the Domestication Syndrome; http://www.plantsciences.ucdavis.edu/gepts/pb143/LEC16/Pb143l16.htm.
(35) Rungapamestry, V.; Duncan, A. J.; Fuller, Z.; Ratcliffe, B. *Proc. Nutr. Soc.* **2007**, *66*, 69−81.
(36) Velasco, P.; Cartea, M. E.; Gonzalez, C.; Vilar, M.; Ordas, A. *J. Agric. Food Chem.* **2007**, *55*, 955−962.
(37) Hecht, S. S. *J. Nutr.* **1999**, *129*, 768S−774S.
(38) Matusheski, N. V.; Jeffery, E. H. *J. Agric. Food Chem.* **2001**, *49*, 5743−5749.
(39) Rangkadilok, N.; Nicolas, M. E.; Bennett, R. N.; Premier, R. R.; Eagling, D. R.; Taylor, P. W. J. *Sci. Hortic. (Amsterdam)* **2002**, *96*, 27−41.
(40) Yuan, G. F.; Sun, B.; Yuan, J.; Wang, Q. M. *J. Zhejiang Univ. B* **2009**, *10*, 580−588.
(41) Jia, C. G.; Xu, C. J.; Wei, J.; Yuan, J.; Yuan, G. F.; Wang, B. L.; Wang, Q. M. *Food Chem.* **2009**, *114*, 28−37.
(42) McNaughton, S. A.; Marks, G. C. *Br. J. Nutr.* **2003**, *90*, 687−697.
(43) Zhang, Y. S.; Talalay, P.; Cho, C. G.; Posner, G. H. *Proc. Natl. Acad. Sci. U.S.A.* **1992**, *89*, 2399−2403.
(44) Bones, A. M.; Rossiter, J. T. *Phytochemistry* **2006**, *67*, 1053−1067.
(45) Jirovetz, L.; Smith, D.; Buchbauer, G. *J. Agric. Food Chem.* **2002**, *50*, 4643−4646.
(46) Grubb, C. D.; Abel, S. *Trends Plant Sci.* **2006**, *11*, 89−100.
(47) Yan, X. F.; Chen, S. X. *Planta* **2007**, *226*, 1343−1352.
(48) Baik, H. Y.; Juvik, J.; Jeffery, E. H.; Wallig, M. A.; Kushad, M.; Klein, B. P. *J. Food Sci.* **2003**, *68*, 1043−1050.
(49) Taiz, L.; Zeiger, E. *Plant physiology*, 4th ed.; Sinauer: Sunderland, MA, USA, 2006; p xxvi, 764 pp.
(50) Halkier, B. A.; Gershenzon, J. *Annu. Rev. Plant Biol.* **2006**, *57*, 303−333.
(51) Mithen, R.; Campos, H. *Entomol. Exp. Appl.* **1996**, *80*, 202−205.
(52) Newman, R. M.; Hanscom, Z.; Kerfoot, W. C. *Oecologia* **1992**, *92*, 1−7.
(53) Ostrofsky, M. L.; Zettler, E. R. *J. Ecol.* **1986**, *74*, 279−287.
(54) Jeffries, M. *Freshwater Biol.* **1990**, *23*, 265−269.
(55) Newman, R. M.; Kerfoot, W. C.; Hanscom, Z. *J. Chem. Ecol.* **1990**, *16*, 245−259.
(56) Brown, P. D.; Morra, M. J. *J. Agric. Food Chem.* **1995**, *43*, 3070−3074.
(57) Vaughn, S. F.; Isbell, T. A.; Weisleder, D.; Berhow, M. A. *J. Chem. Ecol.* **2005**, *31*, 167−177.
(58) Foo, H. L.; Gronning, L. M.; Goodenough, L.; Bones, A. M.; Danielsen, B. E.; Whiting, D. A.; Rossiter, J. T. *FEBS Lett.* **2000**, *468*, 243−246.
(59) Song, L.; Thornalley, P. J. *Food Chem. Toxicol.* **2007**, *45*, 216−224.
(60) Verkerk, R.; Dekker, M.; Jongen, W. M. F. *J. Sci. Food Agric.* **2001**, *81*, 953−958.
(61) Andreasson, E.; Jorgensen, L. B.; Hoglund, A. S.; Rask, L.; Meijer, J. *Plant Physiol.* **2001**, *127*, 1750−1763.
(62) Husebye, H.; Chadchawan, S.; Winge, P.; Thangstad, O. P.; Bones, A. M. *Plant Physiol.* **2002**, *128*, 1180−1188.
(63) Kliebenstein, D. J.; Kroymann, J.; Mitchell-Olds, T. *Curr. Opin. Plant Biol.* **2005**, *8*, 264−271.

(64) Tripathi, M. K.; Mishra, A. S. *Anim. Feed Sci. Technol.* **2007**, *132*, 1−27.
(65) Talalay, P.; Fahey, J. W. *J. Nutr.* **2001**, *131*, 3027S−3033S.
(66) Chen, S.; Andreasson, E. *Plant Physiol. Biochem.* **2001**, *39*, 743−758.
(67) Hoglund, A. S.; Lenman, M.; Falk, A.; Rask, L. *Plant Physiol.* **1991**, *95*, 213−221.
(68) Getahun, S. M.; Chung, F. L. *Cancer Epidemiol. Biomarkers Prev.* **1999**, *8*, 447−451.
(69) Fenwick, G. R.; Heaney, R. K. *Food Chem.* **1983**, *11*, 249−271.
(70) Rabot, S.; Nugonbaudon, L.; Raibaud, P.; Szylit, O. *Br. J. Nutr.* **1993**, *70*, 323−331.
(71) Shapiro, T. A.; Fahey, J. W.; Wade, K. L.; Stephenson, K. K.; Talalay, P. *Cancer Epidemiol. Biomarkers Prev.* **1998**, *7*, 1091−1100.
(72) Fahey, J. W.; Zhang, Y. S.; Talalay, P. *Proc. Natl. Acad. Sci. U.S.A.* **1997**, *94*, 10367−10372.
(73) Heaney, R. K.; Fenwick, G. R. *J. Sci. Food Agric.* **1980**, *31*, 593−599.
(74) Kushad, M. M.; Brown, A. F.; Kurilich, A. C.; Juvik, J. A.; Klein, B. P.; Wallig, M. A.; Jeffery, E. H. *J. Agric. Food Chem.* **1999**, *47*, 1541−1548.
(75) Rosa, E.; Heaney, R. *Anim. Feed Sci. Technol.* **1996**, *57*, 111−127.
(76) Rangkadilok, N.; Nicolas, M. E.; Bennett, R. N.; Premier, R. R.; Eagling, D. R.; Taylor, P. W. J. *Sci. Hortic. (Amsterdam)* **2002**, *96*, 11−26.
(77) Agerbirk, N.; Olsen, C. E.; Nielsen, J. K. *Phytochemistry* **2001**, *58*, 91−100.
(78) Coogan, R. C.; Wills, R. B. H.; Nguyen, V. Q. *Food Chem.* **2001**, *72*, 1−3.
(79) Ahuja, I.; de Vos, R. C. H.; Bones, A. M.; Hall, R. D. *Trends Plant Sci.* **2010**, *15*, 664−674.
(80) Hasegawa, T.; Yamada, K.; Kosemura, S.; Yamamura, S.; Hasegawa, K. *Phytochemistry* **2000**, *54*, 275−279.
(81) Bartlet, E.; Kiddle, G.; Williams, I.; Wallsgrove, R. *Entomol. Exp. Appl.* **1999**, *91*, 163−167.
(82) Jin, J.; Koroleva, O. A.; Gibson, T.; Swanston, J.; Magan, J.; Zhang, Y.; Rowland, I. R.; Wagstaff, C. *J. Agric. Food Chem.* **2009**, *57*, 5227−5234.
(83) Holst, B.; Williamson, G. *Nat. Prod. Rep.* **2004**, *21*, 425−447.
(84) Stoewsand, G. S. *Food Chem. Toxicol.* **1995**, *33*, 537−543.
(85) Fahey, J. W.; Zalcmann, A. T.; Talalay, P. *Phytochemistry* **2001**, *56*, 5−51.
(86) Cartea, M. E.; Francisco, M.; Soengas, P.; Velasco, P. *Molecules* **2011**, *16*, 251−280.
(87) Zhang, Y. S.; Talalay, P. *Cancer Res.* **1994**, *54*, S1976−S1981.
(88) Rose, P.; Won, Y. K.; Ong, C. N.; Whiteman, M. *Nitric Oxide−Biol. Chem.* **2005**, *12*, 237−243.
(89) Conaway, C. C.; Yang, Y. M.; Chung, F. L. *Curr. Drug Metab.* **2002**, *3*, 233−255.
(90) Windsor, A. J.; Reichelt, M.; Figuth, A.; Svatos, A.; Kroymann, J.; Kliebenstein, D. J.; Gershenzon, J.; Mitchell-Olds, T. *Phytochemistry* **2005**, *66*, 1321−1333.
(91) Wheat, C. W.; Vogel, H.; Wittstock, U.; Braby, M. F.; Underwood, D.; Mitchell-Olds, T. *Proc. Natl. Acad. Sci. U. S. A.* **2007**, *104*, 20427−20431.
(92) Rodman, J. E.; Karol, K. G.; Price, R. A.; Sytsma, K. J. *Syst. Bot.* **1996**, *21*, 289−307.
(93) Wittstock, U.; Halkier, B. A. *Trends Plant Sci.* **2002**, *7*, 263−270.
(94) Verkerk, R.; Schreiner, M.; Krumbein, A.; Ciska, E.; Holst, B.; Rowland, I.; De Schrijver, R.; Hansen, M.; Gerhauser, C.; Mithen, R.; Dekker, M. *Mol. Nutr. Food Res.* **2009**, *53*, S219−S265.
(95) Rosa, E. A. S. *Phytochemistry* **1997**, *44*, 1415−1419.
(96) Clarke, D. B. *Anal. Methods* **2010**, *2*, 310−325.
(97) Mithen, R. F.; Dekker, M.; Verkerk, R.; Rabot, S.; Johnson, I. T. *J. Sci. Food Agric.* **2000**, *80*, 967−984.
(98) Charron, C. S.; Saxton, A. M.; Sams, C. E. *J. Sci. Food Agric.* **2005**, *85*, 671−681.
(99) Schreiner, M. *Eur. J. Nutr.* **2005**, *44*, 85−94.
(100) Schouten, R. E.; Zhang, X. B.; Verkerk, R.; Verschoor, J. A.; Otma, E. C.; Tijskens, L. M. M.; van Kooten, O. *Postharvest Biol. Technol.* **2009**, *53*, 1−10.
(101) Graser, G.; Schneider, B.; Oldham, N. J.; Gershenzon, J. *Arch. Biochem. Biophys.* **2000**, *378*, 411−419.
(102) Arabbi, P. R.; Genovese, M. I.; Lajolo, F. M. *J. Agric. Food Chem.* **2004**, *52*, 1124−1131.
(103) Podsedek, A. *LWT−Food Sci. Technol.* **2007**, *40*, 1−11.
(104) Cartea, M. E.; Velasco, P.; Obregon, S.; Padilla, G.; de Haro, A. *Phytochemistry* **2008**, *69*, 403−410.
(105) Salah, N.; Miller, N. J.; Paganga, G.; Tijburg, L.; Bolwell, G. P.; Riceevans, C. *Arch. Biochem. Biophys.* **1995**, *322*, 339−346.
(106) Hansen, M.; Laustsen, A. M.; Olsen, C. E.; Poll, L.; Sorensen, H. *J. Food Qual.* **1997**, *20*, 441−459.
(107) Martinez-Sanchez, A.; Allende, A.; Cortes-Galera, Y.; Gil, M. I. *Postharvest Biol. Technol.* **2008**, *47*, 382−388.
(108) Schonhof, I.; Krumbein, A.; Bruckner, B. *Nahrung−Food* **2004**, *48*, 25−33.
(109) Iori, R.; Bernardi, R.; Gueyrard, D.; Rollin, P.; Polmieri, S. *Bioorg. Med. Chem. Lett.* **1999**, *9*, 1047−1048.
(110) Cerny, M. S.; Taube, E.; Battaglia, R. *J. Agric. Food Chem.* **1996**, *44*, 3835−3839.
(111) Melchini, A.; Costa, C.; Traka, M.; Miceli, N.; Mithen, R.; De Pasquale, R.; Trovato, A. *Food Chem. Toxicol.* **2009**, *47*, 1430−1436.
(112) Leoni, O.; Iori, R.; Palmieri, S.; Esposito, E.; Menegatti, E.; Cortesi, R.; Nastruzzi, C. *Bioorg. Med. Chem.* **1997**, *5*, 1799−1806.
(113) Wu, X.; Zhou, Q. H.; Xu, K. *Acta Pharmacol. Sin.* **2009**, *30*, 501−512.
(114) Zhu, C. Y.; Loft, S. *Food Chem. Toxicol.* **2003**, *41*, 455−462.
(115) Kassie, F.; Rabot, S.; Uhl, M.; Huber, W.; Qin, H. M.; Helma, C.; Schulte-Hermann, R.; Knasmuller, S. *Carcinogenesis* **2002**, *23*, 1155−1161.
(116) Alqasoumi, S.; Ai-Sohaibani, M.; Ai-Howiriny, T.; Al-Yahya, M.; Rafatullah, S. *World J. Gastroenterol.* **2009**, *15*, 1958−1965.
(117) Hanlon, N.; Coldham, N.; Sauer, M. J.; Ioannides, C. *Chem.−Biol. Interact.* **2009**, *177*, 115−120.
(118) Cole, R. A. *Phytochemistry* **1976**, *15*, 759−762.
(119) Matusheski, N. V.; Wallig, M. A.; Juvik, J. A.; Klein, B. P.; Kushad, M. M.; Jeffery, E. H. *J. Agric. Food Chem.* **2001**, *49*, 1867−1872.
(120) Uda, Y.; Kurata, T.; Arakawa, N. *Agric. Biol. Chem.* **1986**, *50*, 2735−2740.
(121) Macleod, A. J.; Rossiter, J. T. *Phytochemistry* **1986**, *25*, 1047−1051.
(122) Tookey, H. L.; Wolff, I. A. *Can. J. Biochem.* **1970**, *48*, 1024.
(123) Uda, Y.; Kurata, T.; Arakawa, N. *Agric. Biol. Chem.* **1986**, *50*, 2741−2746.
(124) Gil, V.; Macleod, A. J. *Phytochemistry* **1980**, *19*, 227−231.
(125) Cashman, J. R.; Xiong, Y.; Lin, J.; Verhagen, H.; van Poppel, G.; van Bladeren, P. J.; Larsen-Su, S.; Williams, D. E. *Biochem. Pharmacol.* **1999**, *58*, 1047−1055.
(126) Graham, S. *Cancer Res.* **1983**, *43*, 2409−2413.
(127) Bonnesen, C.; Eggleston, I. M.; Hayes, J. D. *Cancer Res.* **2001**, *61*, 6120−6130.
(128) Kim, D. J.; Han, B. S.; Ahn, B.; Hasegawa, R.; Shirai, T.; Ito, N.; Tsuda, H. *Carcinogenesis* **1997**, *18*, 377−381.
(129) Wattenberg, L. W.; Loub, W. D. *Cancer Res.* **1978**, *38*, 1410−1413.
(130) Bresnick, E.; Birt, D. F.; Wolterman, K.; Wheeler, M.; Markin, R. S. *Carcinogenesis* **1990**, *11*, 1159−1163.
(131) Bradlow, H. L.; Michnovicz, J. J.; Telang, N. T.; Osborne, M. P. *Carcinogenesis* **1991**, *12*, 1571−1574.
(132) Kojima, T.; Tanaka, T.; Mori, H. *Cancer Res.* **1994**, *54*, 1446−1449.
(133) Tanaka, T.; Kojima, T.; Morishita, Y.; Mori, H. *Jpn. J. Cancer Res.* **1992**, *83*, 835−842.
(134) Tanaka, T.; Mori, Y.; Morishita, Y.; Hara, A.; Ohno, T.; Kojima, T.; Mori, H. *Carcinogenesis* **1990**, *11*, 1403−1406.

(135) Kim, D. J.; Lee, K. K.; Han, B. S.; Ahn, B.; Bae, J. H.; Jang, J. J. *Jpn. J. Cancer Res.* **1994**, *85*, 578−583.
(136) Staack, R.; Kingston, S.; Wallig, M. A.; Jeffery, E. H. *Toxicol. Appl. Pharmacol.* **1998**, *149*, 17−23.
(137) Verhoeven, D. T. H.; Verhagen, H.; Goldbohm, R. A.; vandenBrandt, P. A.; vanPoppel, G. *Chem.−Biol. Interact.* **1997**, *103*, 79−129.
(138) Wattenberg, L. W. *Cancer Res.* **1985**, *45*, 1−8.
(139) Kuang, Y. F.; Chen, Y. H. *Food Chem. Toxicol.* **2004**, *42*, 1711−1718.
(140) Gamet-Payrastre, L.; Lumeau, S.; Gasc, N.; Cassar, G.; Rollin, P.; Tulliez, J. *Anticancer Drugs* **1998**, *9*, 141−148.
(141) Ge, X. K.; Fares, F. A.; Yannai, S. *Anticancer Res.* **1999**, *19*, 3199−3203.
(142) Cover, C. M.; Hsieh, S. J.; Tran, S. H.; Hallden, G.; Kim, G. S.; Bjeldanes, L. F.; Firestone, G. L. *J. Biol. Chem.* **1998**, *273*, 3838−3847.
(143) Sarkar, F. H.; Li, Y. W. *J. Nutr.* **2004**, *134*, 3493S−3498S.
(144) Lijang, S.; Iori, R.; Thornalley, P. J. *J. Sci. Food Agric.* **2006**, *86*, 1271−1280.
(145) Zhao, D. Y.; Tang, J.; Ding, X. L. *LWT−Food Sci. Technol.* **2007**, *40*, 439−447.
(146) Wink, M. *Biochemistry of Plant Secondary Metabolites*; Wiley-Blackwell: Chichester, UK, 2010; Vol. 40.
(147) Greer, M. A. *Arch. Biochem. Biophys.* **1962**, *99*, 369−371.
(148) Grubb, C. D.; Gross, H. B.; Chen, D. L.; Abel, S. *Plant Sci.* **2002**, *162*, 143−152.
(149) Ghawi, S. K.; Methven, L.; Niranjan, K. *Food Chem.* **2013**, *138*, 1734−1741.
(150) Higdon, J. V.; Delage, B.; Williams, D. E.; Dashwood, R. H. *Pharmacol. Res.* **2007**, *55*, 224−236.
(151) Mcdanell, R.; Mclean, A. E. M.; Hanley, A. B.; Heaney, R. K.; Fenwick, G. R. *Food Chem. Toxicol.* **1988**, *26*, 59−70.
(152) Lanzani, A.; Piana, G.; Piva, G.; Cardillo, M.; Rastelli, A.; Jacini, G. *J. Am. Oil Chem. Soc.* **1974**, *51*, 517−518.
(153) Mawson, R.; Heaney, R. K.; Zdunczyk, Z.; Kozlowska, H. *Food/Nahrung* **1993**, *37*, 336−344.
(154) Dewick, P. M. *Medicinal Natural Products: A Biosynthetic Approach*, 3rd ed.; Wiley: Hoboken, NJ, USA, 2009; 539 pp.
(155) Nishie, K.; Daxenbichler, M. E. *Food Cosmet. Toxicol.* **1980**, *18*, 159−172.
(156) Fenwick, G. R.; Griffiths, N. M. *Z. Lebensm. Unters. -Forsch.* **1981**, *172*, 90−92.
(157) Fenwick, G. R.; Griffiths, N. M.; Heaney, R. K. *J. Sci. Food Agric.* **1983**, *34*, 73−80.
(158) Lewis, J.; Fenwick, G. R. *Food Chem.* **1987**, *25*, 259−268.
(159) Buskov, S.; Hansen, L. B.; Olsen, C. E.; Sørensen, J. C.; Sørensen, H.; Sørensen, S. *J. Agric. Food Chem.* **2000**, *48*, 2693−2701.
(160) Hrncirik, K.; Valusek, J.; Velisek, J. *Eur. Food Res. Technol.* **2001**, *212*, 576−581.
(161) Preobrazhenskaya, M. N.; Bukhman, V. M.; Korolev, A. M.; Efimov, S. A. *Pharmacol. Ther.* **1993**, *60*, 301−313.
(162) Smith, T. K.; Lund, E. K.; Clarke, R. G.; Bennett, R. N.; Johnson, I. T. *J. Agric. Food Chem.* **2005**, *53*, 3895−3901.
(163) Lambrix, V.; Reichelt, M.; Mitchell-Olds, T.; Kliebenstein, D. J.; Gershenzon, J. *Plant Cell* **2001**, *13*, 2793−2807.
(164) Hollman, P. C. H.; Katan, M. B. *Biomed. Pharmacother.* **1997**, *51*, 305−310.
(165) Hollman, P. C. H.; Katan, M. B. *Food Chem. Toxicol.* **1999**, *37*, 937−942.
(166) Harborne, J. B.; Williams, C. A. *Phytochemistry* **2000**, *55*, 481−504.
(167) Olsson, L. C.; Veit, M.; Weissenbock, G.; Bornman, J. F. *Phytochemistry* **1998**, *49*, 1021−1028.
(168) Manach, C.; Scalbert, A.; Morand, C.; Remesy, C.; Jimenez, L. *Am. J. Clin. Nutr.* **2004**, *79*, 727−747.
(169) Kroon, P. A.; Clifford, M. N.; Crozier, A.; Day, A. J.; Donovan, J. L.; Manach, C.; Williamson, G. *Am. J. Clin. Nutr.* **2004**, *80*, 15−21.
(170) Engelen-Eigles, G.; Holden, G.; Cohen, J. D.; Gardner, G. *J. Agric. Food Chem.* **2006**, *54*, 328−334.
(171) Palaniswamy, U.; McAvoy, R.; Bible, B. *HortScience* **1997**, *32*, 222−223.
(172) Aires, A.; Rosa, E.; Carvalho, R. *J. Sci. Food Agric.* **2006**, *86*, 1512−1516.
(173) Palaniswamy, U.; McAvoy, R.; Bible, B.; Singha, S.; Hill, D. *Phytochem. Health* **1995**, *15*, 280−283.
(174) Koukounaras, A.; Siomos, A. S.; Sfakiotakis, E. *J. Food Qual.* **2010**, *33*, 768−779.
(175) Koukounaras, A.; Siomos, A. S.; Sfakiotakis, E. *Postharvest Biol. Technol.* **2006**, *41*, 109−111.
(176) Howard, L. A.; Jeffery, E. H.; Wallig, M. A.; Klein, B. P. *J. Food Sci.* **1997**, *62*, 1098.
(177) Kassie, F.; Parzefall, W.; Musk, S.; Johnson, I.; Lamprecht, G.; Sontag, G.; Knasmuller, S. *Chem.−Biol. Interact.* **1996**, *102*, 1−16.
(178) Rochfort, S. J.; Trenerry, V. C.; Imsic, M.; Panozzo, J.; Jones, R. *Phytochemistry* **2008**, *69*, 1671−1679.
(179) Faulkner, K.; Mithen, R.; Williamson, G. *Carcinogenesis* **1998**, *19*, 605−609.
(180) Xu, Y. *Molecular Plant Breeding*; CABI: Wallingford, UK, 2010.
(181) Bozokalfa, M. K.; Yagmur, B.; Ilbi, H.; Esiyok, D.; Kavak, S. *Crop Breed. Appl. Biotechnol.* **2009**, *9*, 372−381.
(182) Li, G.; Quiros, C. F. *Theor. Appl. Genet.* **2001**, *103*, 455−461.
(183) Baird, N. A.; Etter, P. D.; Atwood, T. S.; Currey, M. C.; Shiver, A. L.; Lewis, Z. A.; Selker, E. U.; Cresko, W. A.; Johnson, E. A. *PLoS One* **2008**, *3*.
(184) Glenn, T. C. *Mol. Ecol. Resour.* **2011**, *11*, 759−769.
(185) Hall, C.; McCallum, D.; Prescott, A.; Mithen, R. *Theor. Appl. Genet.* **2001**, *102*, 369−374.
(186) Lelario, F.; Bianco, G.; Bufo, S. A.; Cataldi, T. R. I. *Phytochemistry* **2012**, *73*, 74−83.
(187) Botting, C. H.; Davidson, N. E.; Griffiths, D. W.; Bennett, R. N.; Botting, N. P. *J. Agric. Food Chem.* **2002**, *50*, 983−988.
(188) Kim, S. J.; Ishii, G. *Soil Sci. Plant Nutr.* **2006**, *52*, 394−400.
(189) Villatoro-Pulido, M.; Priego-Capote, F.; Alvarez-Snachez, B.; Saha, S.; Philo, M.; Obregon-Cano, S.; De Haro-Bailon, A.; Font, R.; Del Rio-Celestino, M. *J. Sci. Food Agric.* **2013**.

JOURNAL OF AGRICULTURAL AND FOOD CHEMISTRY

Letter

pubs.acs.org/JAFC

Oxygen and Hydrogen Isotope Composition of Silage Water

ABSTRACT: Silage is an important dietary water source that influences the oxygen and hydrogen isotopic composition of domestic herbivores and their products. Silage sampled fresh from the silo had ^{18}O- and ^{2}H-depleted tissue water when compared with fresh pasture grass sampled around midday during the silage-making seasons. During exposure in the feed bunk, silage water became increasingly enriched in ^{18}O and ^{2}H. When $\delta^{18}O$ was plotted against $\delta^{2}H$, the slope of the regression was less during daytime than during night-time. Exposure to ^{18}O- and ^{2}H-enriched or -depleted water vapor inside sealed glass containers led to strong changes in the isotope composition of silage water. The results resembled predictions from the Craig–Gordon isotope model of evaporation. The atmospheric conditions during exposure (relative humidity, exposure time, and isotopic composition of the air vapor) in the feed bunk thus strongly affect the isotopic composition of silage water ingested by domestic herbivores.

KEYWORDS: *feedwater, labeling, evaporation, turnover, pool kinetic, water isotopes*

INTRODUCTION

Dietary water or feed moisture is an important source of water for herbivorous animals.[1] The oxygen (^{18}O) and hydrogen (^{2}H) isotope composition of ingested water is reflected in animal body water,[2] in fecal water,[3] and in tissues such as bones and teeth,[4] hair,[5,6] and milk.[7] The isotopic composition of dietary water is affected by that of precipitation (meteoric water), which is influenced by geographic features,[8] and also by local environmental conditions and vegetation characteristics.[9,10] Latitudinal, altitudinal, and seasonal variation in the isotope composition of meteoric water depends on temperature for rain and snow formation.[11] The isotopic composition of water in plant roots, tubers, and stems closely reflects that of the water taken up by roots,[12] but leaf water is isotopically enriched in comparison with source water due to isotope fractionation effects during evaporation.[13] Similarly, free surface water, such as water in puddles on pastures and dew on the leaves,[14] is subject to evaporative enrichment. Enrichment is influenced by relative humidity (RH) and the isotopic composition of water vapor.[10,13,15,16] Local humidity can also have an important effect on the oxygen isotope composition of biogenic phosphate.[17,18] Because of the above relationships there is much interest in food science, ecology, anthropology, and forensic science in using the hydrogen and oxygen stable-isotope composition of animal tissues and animal products as a tracer for the geographic origin of foodstuffs[19] as well as for the detection of adulteration of foodstuffs,[20,21] the geographic movements of animals (e.g., in birds),[8] the behavioral/nutritional ecology of herbivores,[3] and the production ecology of livestock systems.[22]

Silage is an important feedstuff in cattle production, and silage moisture can contribute a significant fraction of the total water intake of cattle.[23] Therefore, the isotopic composition of silage water affects that of body water and tissues, including milk and meat.[2] To our best knowledge, the isotopic composition of silage water has not been studied to date. Accordingly, there is no empirical knowledge on the relationship between the ^{18}O and ^{2}H of silage water and that of other water sources, such as fresh grass and drinking water, which have been studied comparatively well.[24,25] Also, there is no empirical knowledge about the main environmental controls of silage-water isotope composition. Thus, for instance, we do not know to what extent observed geographic, seasonal, and production ecology-related patterns in the ^{18}O and ^{2}H composition of milk or beef and lamb meat[7,20] are related to isotope effects emanating from silage-water consumption.

We hypothesize that silage-water isotope composition is strongly affected by RH and the isotopic composition of atmospheric humidity, as plant tissue becomes disconnected from the (liquid) soil water source when the stand is cut, and subsequent water exchange is dominated by vapor fluxes. RH may vary by 50% during a day,[26] whereas the isotopic composition in air humidity typically varies by 40‰ for hydrogen and 6‰ for oxygen during a year,[11] suggesting that RH and isotopic composition could well be a main control of silage-water isotope composition.

This study presents results derived from data collected on grassland farms in southern Germany and also the results from an experiment conducted under controlled conditions. The work addresses the following specific questions: What is the water isotope composition of silage when taken fresh from the silo? Does its isotope composition differ from that of leaf water sampled in the period of silage production? How does silage-water isotope composition change when silage is exposed to atmospheric conditions in the feed bunk? And, how does silage-water isotope composition respond to altered vapor isotope composition in controlled experiments? The observed changes of silage-water isotope composition were compared with predictions from the Craig–Gordon model. This model has been used extensively to explain the water isotope relationships during evaporation of open water bodies[27] and leaves,[28] and it provides a mechanistic treatment of evaporative fractionation, RH, and vapor isotope composition on water isotope composition at the evaporating surfaces.

THEORY

Assuming that silage water is a well-mixed reservoir, the change in water-mass per surface area (W, mol m^{-2}) over an increment of time dt is given by the rates of input (I, mol m^{-2} s^{-1}) by rain

Received: December 31, 2013
Revised: April 28, 2014
Accepted: May 5, 2014
Published: May 5, 2014

ACS Publications © 2014 American Chemical Society

or dew formation, and by the rate of evaporation (E, mol m^{-2} s^{-1}):

$$dW/dt = I - E \quad (1)$$

For the conditions in our feed bunk underneath a roof we can neglect I. The evaporation flux E is proportional to the vapor concentration difference between the water−air interface (evaporating surface) and the turbulent atmospheric region and, thus, to RH:[29]

$$E = C_s(1 - h)/\rho \quad (2)$$

where C_s denotes the saturation concentration of vapor (which depends on temperature), h is RH in equations, and ρ is a resistance coefficient.

The isotope composition of the evaporation flux is given by the Craig−Gordon model,[16] which accounts for the equilibrium isotope fractionation between liquid and vapor, the kinetic fractionation resulting from the diffusion across the air boundary layer, and the back flux of atmospheric moisture:[11]

$$R_E = (\alpha^* R_s - hR_a)/((1 - h)\rho_i/\rho) \quad (3)$$

R denotes the ratio of the abundances of the heavy and light isotopes (^{2}H/^{1}H or ^{18}O/^{16}O), and α^* is the temperature-dependent fractionation factor (α^*_O = 1.0095, α^*_H = 1.0804 at T = 24 °C).[30] The subscripts indicate the evaporated water (E), silage-water in our case (s), atmospheric vapor (a), and the heavy isotope (i).

Equation 3 can be translated into δ notation, the conventional notation for the natural abundance of stable isotopes.[29] Thus, δ^{18}O (or δ^2H) is given as δ^{18}O (or δ^2H) = $R_{sample}/R_{standard}$ − 1, where standard refers to the international SMOW standard. Then

$$\delta_E \approx (\delta_s - h\delta_a - \varepsilon^* - \Delta\varepsilon)/(1 - h) \quad (4)$$

where ε^* and $\Delta\varepsilon$ represent the equilibrium enrichment calculated from α^* and the kinetic enrichment in the diffusive layer under fully turbulent air (calculated from α_k; α_{kO} = 1.0189 and α_{kH} = 1.017)[31,32] that are associated with the phase change and diffusion. The change in δ_s is then given by[33]

$$d(WR_s)/dt = -ER_E \quad (5)$$

This means that for silage, the volume and isotopic ratio in the remaining water are controlled only by the evaporation rate E and the isotopic composition of the evaporation flux R_E, both of which depend on RH (eqs 2 and 3). The remaining fraction of the initial amount of water, W_0, is defined as $f = W/W_0$. Equation 5 can be rearranged to describe the change in isotopic composition of the remaining silage water, $d\delta_s$, with f:[34,35]

$$d\delta_s/d\ln f = \delta_E - \delta_s \quad (6)$$

As f approaches zero, δ_s approaches a steady state isotopic composition, δ_{steady},[33] under local atmospheric conditions due to the return from the atmosphere. The change of δ_s, $d\delta_s$, thus approaches zero, which, by integrating with respect to f, yields[35]

$$(\delta_s - \delta_{steady})/(\delta_{s0} - \delta_{steady}) = f^m \quad (7)$$

where δ_{s0} is the initial isotopic composition of silage water (at f = 1), δ_s is the isotopic composition of silage water at any instant in f < 1, and $m = (h - \varepsilon_k - \varepsilon^*)/(1 - h + \varepsilon_k)$ as defined by Welhan and Fritz,[34] Gonfiantini,[29] and Gibson et al.[35]

In the case of evaporation in completely dry air (h = 0), the so-called Rayleigh fractionation results and eq 7 reduces to[11]

$$(\delta_s + 1)/(\delta_{s0} + 1) = f^{\alpha^* - 1} \quad (8)$$

With vapor-saturated air (RH 100%), isotopic exchange between vapor and silage water would occur without evaporative water loss. Then, δ_s would approach the equilibrium with the air vapor if the air vapor reservoir is infinite.

With high humidity, when the water potential of the air is less negative than the (osmotic and matrix) water potential of the silage,[36,37] condensation may occur. In this case, the isotopic value of silage water (δ_s') is a mixture of condensed air vapor (δ_{cond}) and initial silage water (δ_s) until δ_s becomes equilibrated with air vapor and also reaches δ_{cond}. Thus

$$\delta_s = \frac{(M_s + M_{cond}) \times \delta_s' - M_{cond} \times \delta_{cond}}{M_s} \quad (9)$$

where M_s and M_{cond} represent the mass of initial silage water and the mass of condensed water. The equilibrium fractionation controls the isotopic composition of water condensed in saturated air[14] and thus δ_{cond}.

When silage becomes exposed to an infinite vapor source that is not in equilibrium with the water pool in the silage, this silage-water pool will gradually exchange and turn over until an equilibrium is reached. We used the reaction progress method to describe the turnover of O and H in silage water. An advantage of the reaction progress approach is that it provides half-life estimates for multiple pool systems.[38] In addition, results from experiments with isotopically different vapors (labeling experiments) can be combined. The reaction progress $1 - F$ depends on the fraction F of the water pool that has already been turned over. It is given by[38,39]

$$\frac{\delta_s - \delta_{eq}}{\delta_{s0} - \delta_{eq}} = 1 - F \quad (10)$$

where δ_{eq} is the isotopic composition of water that is in equilibrium with air vapor and F = 0 and F = 1 represent the beginning of the exchange reaction and its final steady state (equilibrium). The exchange of a single pool follows

$$1 - F = e^{-\lambda t} \quad (11)$$

where λ is the first-order rate constant. Equations 10 and 11 are particularly useful when expressed as

$$\ln(1 - F) = -\lambda t \quad (12)$$

which follows a straight line in the case of a single pool system, and a graph composed of several straight line segments in systems with several pools.

MATERIALS AND METHODS

Silage. Silage was obtained from the Grünschwaige Experimental Station, Germany: 48°23′ N, 11°50′ E (for details regarding the site, see Schnyder et al.[40]). All grassland was used for beef cattle husbandry with Limousin suckler cows. During the grazing season (approximately from the end of April to the end of October) all cattle were kept on permanent pastures. Meadows and surplus pasture growth were used for silage and hay production. Silage cuts were mainly taken in June and August (yielding 40 and 35% of total on-farm silage production). Silage production generally followed the practices described by Wilkinson.[41] Grass was mowed at around 10:00 a.m., followed by spreading and tedding. In the afternoon of the same day it was raked into rows, and on the following day the wilted grass (approximately 45% dry matter content) was collected using a forage harvester, cut to a length of 4−8 cm, transferred to a drive-in silo without addition of

other fermentable substrates, and consolidated. The silo was sealed not later than 5:00 p.m., and it remained closed until opening for feeding. Silage was the main feed source during the period of sward dormancy when the cattle were housed.

Fresh pasture grass was sampled at approximately biweekly intervals during the growing seasons (from April to October) of 2006 to 2012. All grass samples were collected around noon, immediately put into extraction vials, and sealed in the field.

Silage samples were taken randomly from silos on the experimental farm in March/April of 2011, 2012, and 2013. In addition, 28 samples of silage were obtained from silos of regional farms within a radius of about 20 km around the experimental farm. The samples comprised silage from 2012 and 2013, from different months (May−October), from the first to the fourth cut, and from grass−clover mixtures and seminatural grasslands to capture the range that can be expected.

Experiment A: Isotopic Composition of Silage Water in the Feed Bunk. This experiment assessed the variation of the isotopic composition of silage water after distribution in a feed bunk during a day. During the period of sward dormancy when cattle were housed, the daily requirement of silage was distributed on the cleaned feed bunk in the open-front stall once every morning. Silage was sampled on three consecutive days (April 25, 26, and 27, 2012) immediately after distribution in the feed bunk and at 0.5, 1, 2, 4, and 24 h thereafter. On a given day, the last sample (of the 24 h period) was collected on the next day just before the leftovers were removed and new silage was provided. A handful of silage was sampled from the upper layer of silage in the feed bunk where the cattle tended to consume. Each sample was conserved in a self-sealing bag and kept at −4 °C until water extraction started.

Weather data, including RH and air temperature, which exhibited clear diurnal cycles (Figure 1), were obtained from a meteorological station in Freising (distance = 7 km; http://www.lfl.bayern.de/agm/daten.php?statnr=8).

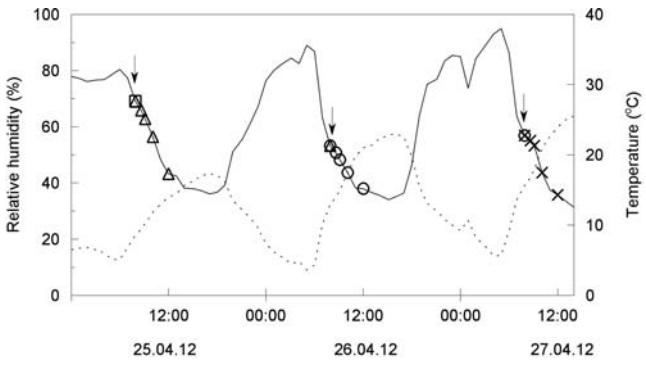

Figure 1. Weather conditions (RH, solid line; air temperature, dashed line) for four consecutive days during the feed bunk experiment. The arrows indicate the removal of leftovers from the previous day and the distribution of fresh silage in the feed bunk when 0-h and 24-h samples were taken. Markers show sampling after 0, 0.5, 1, 2, 4, and 24 h since distribution in the morning (8:00 a.m.) on April 24 (□), 25 (△), 26 (○), and 27 (×) of 2012, respectively.

Additionally, air vapor was sampled by cryogenic distillation in April (from 2006 to 2011) to assess its variation in $\delta^{18}O$ and $\delta^{2}H$ during this time of the year. Rain was sampled and measured every month from 2006 to 2011 for construction of the local meteoric water line (LMWL).

Experiment B: Vapor Labeling of Silage Water. The second experiment analyzed how the isotopic composition of air vapor influences the isotopic composition of silage water. Silage, which had been produced the year before, was collected from the silo of the experimental farm using a silage corer on March 31, 2011, and then kept in a self-seal bag at 4 °C until placement in a closed container (an exsiccator vessel with drying agent removed). To allow quick sampling from the container during the experiment, about 2 g of silage was allocated to each of six or eight aluminum trays per container as individual samples (see below). The container was then closed for about 12 h to effect a homogenization of moisture content and isotopic composition in all of the samples.

The silage samples were placed on the perforated shelf of the (exsiccator) container. Under the shelf, 40 mL of labeling water was placed in a plate of 10 cm diameter. To promote air mixing, a fan was installed in the headspace of the container. The labeling water and silage samples were quickly placed in the container and the lid was closed. Thus, the initial conditions in the container were the same as in the room with temperature, RH, $\delta^{18}O$, and $\delta^{2}H$ around 24 °C, 40%, −18‰, and −130‰, respectively.

The experiment was divided into two groups, with different sampling intervals. Each group had two containers with differing isotope composition of the labeling water. The labeling water was either enriched (in ^{18}O and ^{2}H) or depleted (heavy or light water) relative to silage water. In the first group with short time intervals between openings, six samples were exposed to the labeling atmosphere and two were removed randomly after 1, 2, and 4 h from each container. In the second group with long intervals between openings, each container contained eight samples and two samples were collected after 8, 24, 48, and 96 h. In each case, one of the duplicate samples was used to measure the isotopic composition of water and the other was used to measure relative moisture content (g/g, water mass in fresh mass of silage). The labeling water in each container was sampled at the beginning and end of the labeling experiment.

In a preliminary experiment, air-tightness of the containers was verified by filling the containers with N_2 and measuring CO_2 and humidity changes using a LiCor LI-6262 infrared gas analyzer. The evolution of humidity inside containers was examined after placing a dish of water in the container. Humidity increased rapidly from an initial 48 to 100% with a half-life of 1.8 min (r^2 = 0.96 with n = 233). The measurements were not repeated during the experiments with silage, because it would have required additional fittings, hoses, pumps, and instruments, increasing the probability of leaks and failure.

Extraction and Measurement of Silage Water. Silage water was extracted by cryogenic vacuum distillation. For the regional samples and for experiment A, $\delta^{2}H$ and $\delta^{18}O$ were measured using a L2120-*i* Analyzer (Picarro, Santa Clara, CA, USA). Mean analytical uncertainties quantified as SD of about four replicate measurements for each sample were ±0.1‰ for $\delta^{18}O$ and ±0.5‰ for $\delta^{2}H$. To examine whether the measurements using the L2120 are biased by organic volatiles in the water extracts, we compared the measurements of the L2120 with measurements of an IsoPrime isotope ratio mass spectrometer that was interfaced to a multiflow equilibration unit (both GVI, Manchester, UK). This comparison was made for a large number of samples (n = 177 for O and n = 58 for H) of differing origins. We found no indication that water samples extracted from plants or soil were subject to a larger error than pure water (rain, tap water, groundwater, air humidity). The mean bias (difference) between both instruments for 55 plant samples (O, 1.1‰; H, 1.6‰) and 51 soil samples (O, 0.0‰; H, −2.4‰) did not differ from the mean bias of 70 pure water samples (O, 0.4‰; H, −1.4‰). Also, the scatter between both measurement methods as quantified by the root mean squared error did not differ between plant samples (O, 1.4‰; H, 5.8‰), soil samples (O, 0.2‰; H, 2.5‰), and pure water samples (O, 0.6‰; H, 3.5‰).

For experiment B, which was more sensitive to such bias by organic volatiles, ^{2}H and ^{18}O values were determined by IRMS with a Thermo Finnigan DELTA^{plus} XL with TC/EA converter (Finnigan MAT, Bremen, Germany). Analytical uncertainties were ±0.5‰ for $\delta^{18}O$ and ±2‰ for $\delta^{2}H$ in this case.

All three measurement systems were calibrated using secondary isotope standards (i.e., V-SMOW, SLAP, and GISP) and checked at regular intervals using previously calibrated (again against secondary isotope standards) laboratory water standards for possible instrument drift. These laboratory standards were produced from local deionized tap water by evaporation/condensation, so that their isotope range spanned the range of samples.

dx.doi.org/10.1021/jf405703g | J. Agric. Food Chem. 2014, 62, 4493−4501

RESULTS

Comparison of Fresh Grass and Silage. The water isotope composition of fresh grass sampled in June and August, the two main periods of silage making, differed slightly (about 1.2‰ in ^{18}O), reflecting the differences in weather conditions between the two periods. In contrast, for silage there was a pronounced depletion by about 14‰ in ^{18}O and 60‰ in ^{2}H relative to fresh grass (Table 1). In the feed bunk, the silage became less depleted but, on average, the effect was small (about 1‰ in ^{18}O).

Table 1. Oxygen and Hydrogen Isotopic Composition ($\delta^{18}O$ and $\delta^{2}H$) of Water in Silage of Regional Farms and on the Experimental Farm and in Fresh Grass[a]

		$\delta^{18}O$ (‰)		$\delta^{2}H$ (‰)	
	n	mean	SD	mean	SD
regional farms					
silage from silo	28	−12.9	5.4	−109.1	51.5
experimental farm					
silage from silo	24	−9.1	2.8	−80.0	23.0
silage from feed bunk	36	−8.1	1.7	−71.5	12.4
fresh grass in June	23	2.8	3.7	−22.7	16.2
fresh grass in August	32	4.0	1.9	−11.6	10.0

[a]Silage was directly taken from either the silo or the feed bunk. Fresh grass was collected at around noon in the months when grass was cut for silage production (June and August).

The silage from the regional farms, on average, was even more depleted than the silage of the experimental farm. The standard deviation was large, and the range included the silage of the experimental farm. A pattern caused by the year or month of production or by the cut or the type of silage was not evident.

Experiment A: Feed Bunk Experiment. The isotope composition of silage water changed in a similar way on the three consecutive days. After distribution in the feed bunk, it became increasingly enriched in ^{18}O and ^{2}H (Figure 2). At 1 day after distribution, $\delta^{18}O$ and $\delta^{2}H$ of silage water had increased by 4‰ and 30‰, but was still depleted relative to the fresh grass (Table 1).

The silage water extracted from samples taken fresh from the silo in April lay at the right side of the LMWL. On average, air vapor in April had a $\delta^{18}O$ of −18 ‰ (SD 2‰) and a $\delta^{2}H$ of −132‰ (SD 16‰), respectively, whereas the water estimated from air vapor and equilibrium fractionation was very close to the LMWL and exhibited almost identical $\delta^{18}O$ but higher $\delta^{2}H$ than the water of silage taken fresh from the silo. The silage-water samples from the feed bunk were divided into two groups according to the RH of the air (Figure 3). During the morning hours (8:00 a.m. to 12:00 p.m.) the RH was relatively low and decreasing (from about 60 to 40%; Figure 1), thereby accelerating evaporation. Samples taken in this time fitted an evaporation line with a slope of 5.95 (standard error of the slope, 0.45, $r^2 = 0.76$; Figure 3a). During the night-time the RH increased to about 80% and remained at this level for several hours (Figure 1). The slope of the $\delta^{2}H$ versus $\delta^{18}O$ regression for samples taken at daily intervals, between 8:00 a.m. of 1 day and 8:00 a.m. of the next day, was significantly steeper (7.61 with a standard error of 0.55, $r^2 = 0.96$; Figure 3b).

Experiment B: Vapor Labeling Experiment. The moisture content of the silage decreased in the sealed glass containers with short opening intervals of 1, 2, and 4 h ($y = -0.03x^{0.5} + 0.47$, $r^2 = 0.46$), probably due to exchange of vapor-saturated air with vapor-depleted air when the container was opened frequently (Figure 4). In contrast, when the container was opened infrequently, silage moisture content increased with time due to condensation ($y = 0.41x^{0.06}$, $r^2 = 0.45$).

The water from silage sampled before exposure to the labeling water did not fall on the LMWL (Figures 5 and 6), as had been observed in experiment A (Figure 3). With the exception of the samples taken after 1 h, the successive samples showed a gradual exchange of the initial silage water with vapor derived from the labeling water (Figure 5). Thus, silage water became gradually enriched when exposed to heavy labeling water and depleted when exposed to light labeling water.

The gradual exchange of silage water with labeling water via vapor fluxes was especially evident when plotted as a function of labeling duration (Figure 6). A different isotopic trend of silage water was apparent, however, in the container with short intervals between openings compared with the container with long intervals between openings (compare panels a and b of Figure 6 and panels c and d of Figure 6). During the first hour,

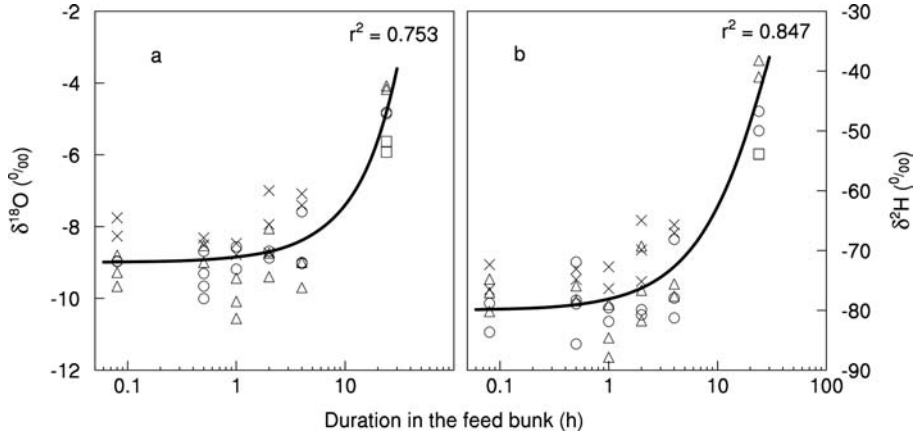

Figure 2. Changes in oxygen (a) and hydrogen (b) isotopic composition of silage water following distribution in the feed bunk at 8:00 a.m. Samples were taken immediately after distribution of silage in the feed bunk (~5 min after distribution, $n = 7$) on April 24 (□), 25 (△), 26 (○), and 27 (×) and at 0.5 h ($n = 8$), 1 h ($n = 7$), 2 h ($n = 8$), 4 h ($n = 7$), and 24 h ($n = 6$) after distribution. *x*-axes are log scaled. Lines denote second-order polynomial regressions.

dx.doi.org/10.1021/jf405703g | J. Agric. Food Chem. 2014, 62, 4493−4501

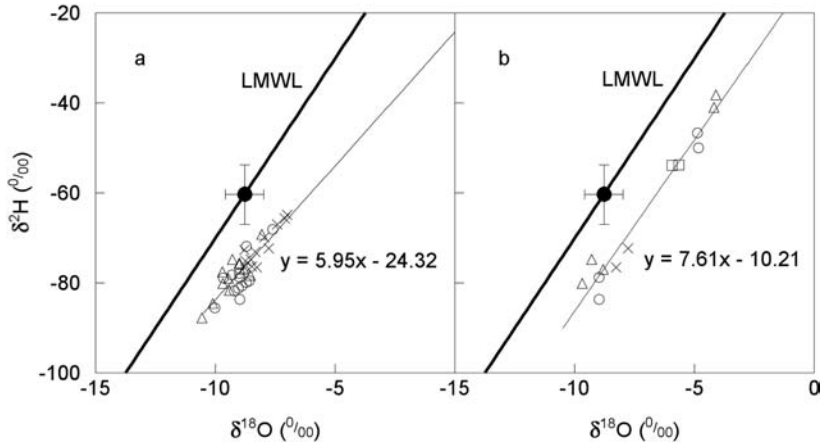

Figure 3. Relationship between $\delta^{18}O$ and $\delta^{2}H$ (evaporation line) of silage water. (a) Samples were taken immediately after distribution in the feed bunk at about 8:00 a.m. and 0.5, 1, 2, and 4 h later (n = 37). (b) Samples were taken immediately after distribution and 24 h later (n = 13). Explanation of symbols is given in Figure 2. The isotopic composition of water at 22 °C that would be in equilibrium with the measured air vapor is shown as a solid circle (●) with standard errors. The bold line represents the local meteoric water line (LMWL) derived from monthly rainwater samples between 2006 and 2011 (n = 73, r^2 = 0.99). The thin lines are regression lines for the silage water.

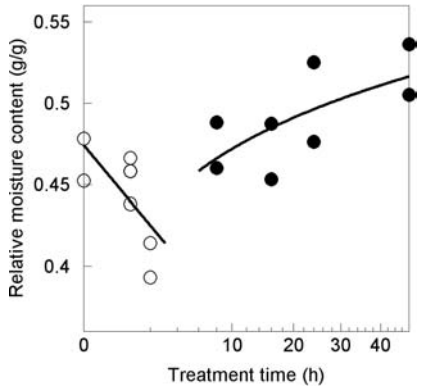

Figure 4. Moisture content of the silage as a function of time since the start of labeling: (○) data from short intervals between openings of the sealed glass containers; (●) data from long intervals between openings of the glass containers. The time axis is square-root scaled.

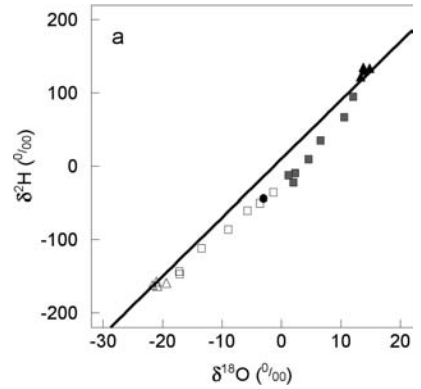

Figure 5. $\delta^{2}H$ versus $\delta^{18}O$ plot of the silage water extracted from silage exposed to heavy water and light water for 1−96 h. The black circle (●) denotes the initial silage water, triangles indicate the heavy (▲) and the light (△) labeling water. Gray and white squares represent the water in silage exposed to heavy and light labeling water, respectively. The line is the local meteoric water line (LMWL).

the silage water became enriched in ^{18}O by on average 3‰ and in ^{2}H by on average 17‰ (Figure 6a,c). However, the initial enrichment was less (only about one-third) when the labeling water was isotopically depleted (Figure 6a,c). With longer exposure time, the silage water approached the corresponding labeling water (Figure 6a,c). In the second group, where the first sample from the sealed containers was taken after 8 h, the silage water exponentially approached the corresponding labeling water (Figure 6b,c) and almost attained the value of labeling water after 48 h in the case of light labeling water. Conversely, a notable change still occurred with the heavy labeling water due to the larger isotopic spacing between silage water and heavy labeling water.

For the containers with long opening intervals and long exposure times, it was assumed that the disturbance due to the opening was very small and, hence, did not affect the estimation of reaction progress (Figure 7). The effect of condensation, however, had to be considered, as this was evident from the increasing moisture content (Figure 4). After exclusion of this effect (eq 9), the transformed data fell on one straight line during the first 48 h (Figure 7). The slope of the regression line was −0.035 (standard error 0.002, r^2 = 0.957), which corresponds to a half-life of approximately 20 h. The measurements after 96 h of exposure time fell clearly outside the range that could be expected from the prediction interval of the regression. Following the reaction progress approach, the intercept of the regression for the slow pool indicated that approximately 10% of the total silage water had a half-life longer than 20 h.

Model Simulations. Under zero humidity, the δ values follow a Rayleigh line when plotted against the remaining fraction of silage water (Figure 8). With RH increasing up to 50%, the convexity of the line decreased as compared to the Rayleigh line until a straight line was reached at RH = 50%, with a positive slope in the case of labeling water being heavier than the silage water and a negative slope in the opposite case (Figure 8a,b). With RH > 50%, the silage water approached a constant value during drying. This constant value was lower and was reached earlier at higher RH. At 100% humidity the water in the silage approached the isotopic composition of the labeling water.

The influence of RH on the pattern of slopes for the relationship between $\delta^{2}H$ versus $\delta^{18}O$ (evaporation line) depended on the relation of the initial composition of silage

dx.doi.org/10.1021/jf405703g | J. Agric. Food Chem. 2014, 62, 4493−4501

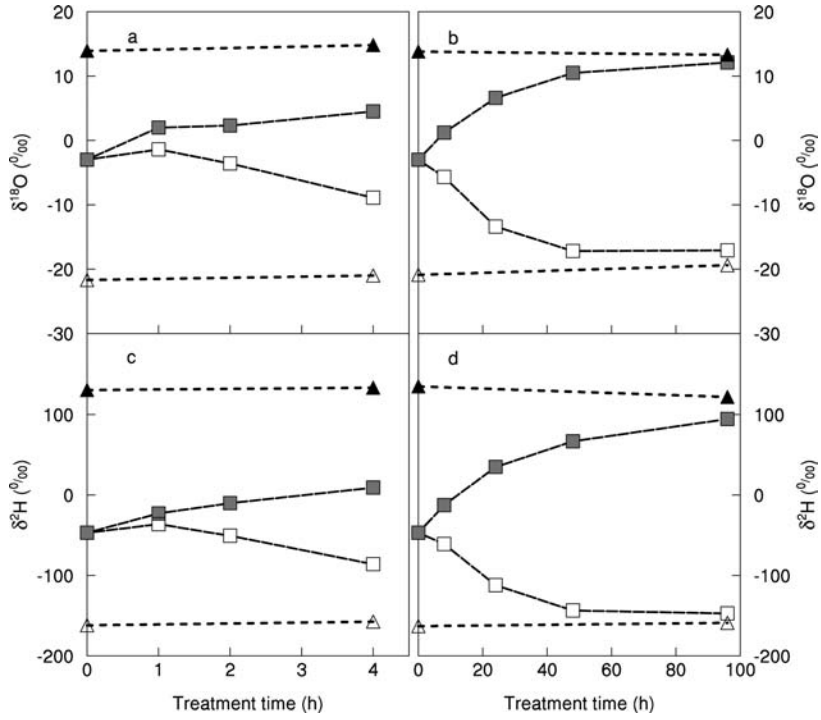

Figure 6. Time course of oxygen and hydrogen isotopic composition ($\delta^{18}O$ and $\delta^{2}H$) of silage water (squares) and labeling water (triangles) for up to 4 h (a, c) and for up to 96 h (b, d). Solid and open symbols indicate heavy and light labeling water, respectively; variation of $\delta^{18}O$ and $\delta^{2}H$ of silage water for up to 4 h and labeling water are represented by dashed lines connecting the data points, whereas the silage water for up to 96 h is represented by solid lines with exponential functions.

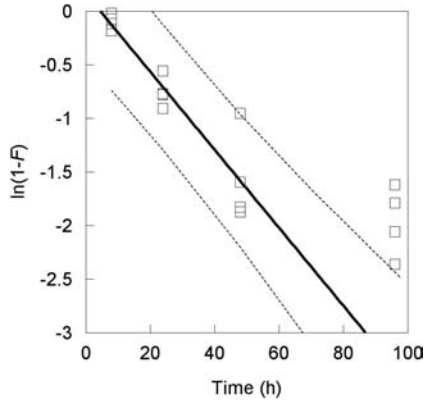

Figure 7. Reaction progress variable ($\ln(1 - F)$) calculated from data obtained from the container with long opening intervals and long labeling time after exclusion of the effect of condensation. Dashed lines represent the 95% prediction intervals of the regression (solid line, $y = 0.2 - 0.02x$; $r^2 = 0.785$; the intercept is not significant) as calculated from the measurements after 8, 24, and 48 h of labeling.

water and the isotopic composition of the vapor (Figure 8c,d). When the water in equilibrium with air vapor was isotopically heavier than the silage water, the slopes increased with RH (Figure 8c). In contrast, the $\delta^{2}H$ versus $\delta^{18}O$ line of remaining water rotated clockwise as RH increased if the silage became exposed to vapor, resulting in equilibrium water that was more depleted than the silage water (Figure 8d). For the isotopic composition chosen for Figure 8c, the line became almost vertical at about 60% RH, indicating that under this condition only $\delta^{2}H$ would change while $\delta^{18}O$ would remain constant.

DISCUSSION

This work presents the first analysis of silage-water isotope composition. It demonstrates a large contrast to the isotopic composition of fresh grass and a dominant role of RH and atmospheric water-vapor isotope composition on the isotopic composition of silage water. The changes in the isotope composition of silage water behaved similarly with the expectations from the simulation with the Craig–Gordon evaporative model, a classical mechanistic framework which has been applied extensively in empirical studies of the water isotope composition of open bodies of water and leaf water.[11]

Silage water, extracted from silage removed fresh from the silo, was strongly depleted in ^{18}O and ^{2}H relative to water extracted from fresh grass that was collected at about the same time of day as grass mowing for silage production took place, even though the moisture content of fresh grass (approximately 80%) was much higher than that of silage (about 50%). Thus, silage water must have become depleted in ^{18}O and ^{2}H at one or more stages of the production process between mowing and storage. Such processes may have involved vapor exchange with soil and atmosphere and condensation–evaporation cycles involving dew rise (vapor flux from the soil) and dew fall (atmosphere) during diurnal periods between mowing and carting of silage to the silo. Both atmospheric vapor and soil water are depleted in ^{18}O and ^{2}H relative to leaf water collected at noon.[42] Also, leaf water follows strong diurnal cycles,[42] with predawn values of $\delta^{18}O$ approximately 10‰ depleted relative to leaf water collected at noon (Inga Schleip, Ulrike Gamnitzer, Hans Schnyder, unpublished data). Certainly, additional empirical studies of diurnal vapor exchange fluxes, and related condensation–evaporation phenomena on silage water $\delta\ ^{18}O$ and $\delta\ ^{2}H$ between mowing and closing of the silo are needed.

dx.doi.org/10.1021/jf405703g | J. Agric. Food Chem. 2014, 62, 4493–4501

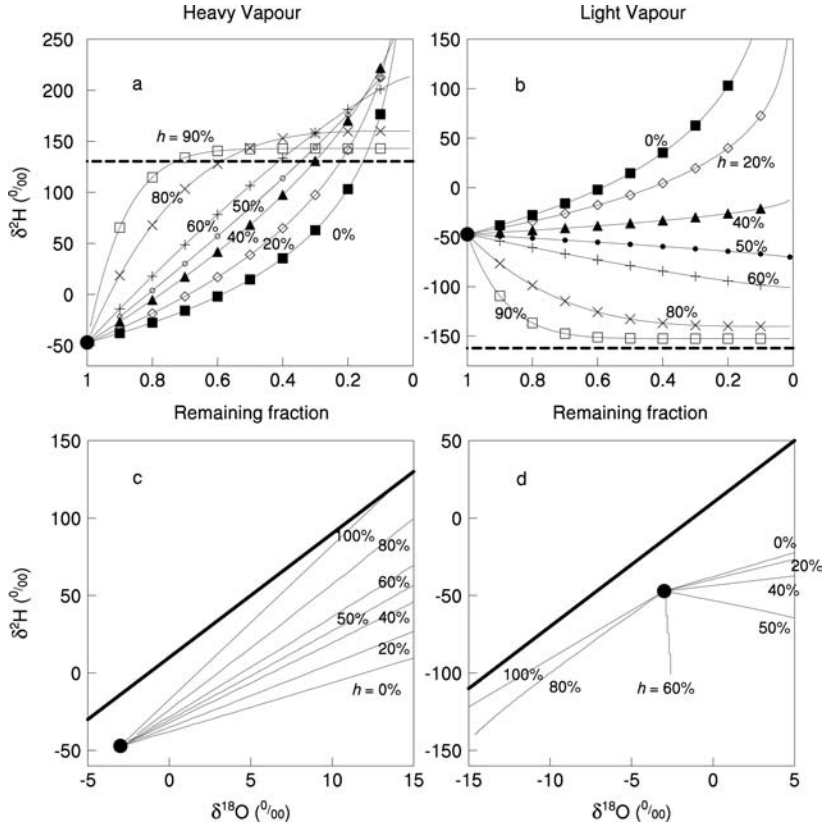

Figure 8. Effect of relative humidity (h) and isotopic composition of air vapor on the change of the hydrogen isotopic composition of silage water (δ^2H_s) (a, b) and on the slope of the δ^2H–$\delta^{18}O$ relationship (c, d) during drying. The air vapor was assumed to be in equilibrium with either heavy water (heavy vapor, $\delta^{18}O_a$ = 4.2‰, δ^2H_a = 42.9‰; a, c) or light water (light vapor, $\delta^{18}O_a$ = −31.1‰, δ^2H_a = −226.9‰; b, d) of experiment B. All calculations assume T = 24 °C, initial $\delta^{18}O_s$ = −3.0‰, initial δ^2H_s = −47.1‰, and kinetic fractionation α_{kO} = 1.0189 and α_{kH} = 1.017 (see refs 31 and 32). Dashed lines in panels a and b represent the labeling water, which was also the equilibrated state for silage water at h = 100%. Solid lines in panels c and d represent the local meteoric water line. The solid circle represents the same initial silage water in all panels.

After removal from the silo, the isotopic composition changed depending on the moisture conditions of the surrounding air, including its isotopic composition and the duration of exposure. In a vapor-labeling experiment, initial drying led to a transient enrichment but, with continuing exposure to the high humidity environment, exchange reactions became predominant (Figure 6). The Craig–Gordon model accounts for the effects of RH and isotopic composition of the vapor (Figure 8), and it was able to explain the results of all experiments. For instance, the silage in the feed bunk followed a steeper trend during the night, when RH was high, than during the daytime when humidity was low, in agreement with the prediction of the Craig–Gordon model (Figure 8). Also, in experiment B, the data points at 1 h cannot be explained as a pure exchange with vapor, but considering drying, they conformed to expectations from the Craig–Gordon model (Figure 8).

Depending on the amount and the isotopic composition of the air vapor and the degree of drying of the silage after removal from the silo, a large variation of silage water is possible. This variation may span >200‰ for δ^2H, as suggested by the simulations with the Craig–Gordon model (Figure 8). Under more realistic scenarios, where the atmospheric vapor did not differ strongly from the equilibrium vapor of silage water and drying on the feed bunk was limited, the observed variation of silage-water isotope composition in the feed bunk was much smaller (approximately 40‰ for δ^2H; Figure 2).

Vapor labeling and pool modeling indicated that the bulk of silage water comprised a pool that could be exchanged rapidly with the surrounding vapor. With a half-life of 20 h, 75% of the water inside this pool was exchanged within about 1.7 days. The fast change of the isotopic composition after exposure of the silage to an environment with altered vapor isotope composition is not unexpected given that the tissue/cell structures of the leaf are weakened or disrupted due to the mechanical and chemical modifications of the production process.[36] The vapor-labeling study also suggested that a minor fraction of the silage water (corresponding to approximately 10% of total silage water or 5% of the initial amount of tissue water in the cut grass if it is assumed that moisture decreases from an initial 80 to 40% during silage production) was included in a less rapidly exchanging water pool. We do not know the actual physical identity of this pool. Numerically it is similar in size to the water content of air-dry grass (hay),[43] which is probably associated with the bound-water fraction of cell walls.

The increase in silage moisture in the sealed containers is likely to have been due to condensation induced by the more negative osmotic and matrix potential of the silage water, relative to that of the deionized labeling water of zero potential[36,37] but not to dew formation, which was excluded in the isothermal containers. Dew could possibly provide air humidity much more rapidly to the leaves. This may explain the much shorter (apparent) half-life (1–3 h) of leaf water in intact leaves under pronounced dew formation.[44] Dew formation is

dx.doi.org/10.1021/jf405703g | J. Agric. Food Chem. 2014, 62, 4493–4501

likely to occur during the wilting phase of silage production, especially at night-time, but may also occur in open feed lots.

In each case, the silage water was found to be considerably more depleted in ^{18}O and ^{2}H than the water in fresh leaves (Table 1; Figure 2). The use of water isotopes as an indicator of the geographical origin, which has been well demonstrated in wildlife,[45] may be useful in domestic animals only if the type of feed is known (i.e., fresh grass vs silage). In domestic animals, water isotopes are better suited to indicate the type of feeding: A small seasonal variation can be expected when silage is fed throughout the year, whereas water isotopes in feed will show pronounced variation with season in the case of summer-grazed animals. In turn, the isotopic composition of the body water of an animal also changes when the diet is switched, for example, as occurs between the grazing period and the stall-feeding period in late autumn. Thus, barn-fed and pasture-fed lambs from the United Kingdom differed more than pasture-fed lambs from the United Kingdom and from Sicily in $\delta^{2}H$,[46] and the isotope composition of milk water changed significantly between winter and summer.[47] Large seasonal changes in $\delta^{18}O$ and $\delta^{2}H$ related to a diet switch were also found in cow hair[48] and beef.[20] A change in feed moisture content may also influence body-water isotope composition via a changed requirement and intake of drinking water.[49] However, both factors, the changed isotopic composition and an altered drinking water requirement, would probably change the isotopic composition of body water in the same direction as silage water, as drinking water is isotopically depleted relative to leaf water. Also, silage-water isotope composition plotted close to the LMWL. Drinking water should also plot on this line if it is derived from local meteoric water. In accordance with this, we also expect that the lower water requirements of animals during winter than during summer, due to lower temperature,[50,51] would not modify the picture.

In summary, our study demonstrated that silage water differs markedly from leaf water, and it can change during the feeding process. Thus, body water in domestic animals will differ depending on whether the feed is silage or fresh grass. This feeding pattern will overlay the geographic pattern. Given that this is the first study on silage water, more information would be useful about the influence of the production process on isotope composition of silage water.

Luanzi Sun
Karl Auerswald*
Rudi Schäufele
Hans Schnyder

Lehrstuhl für Grünlandlehre, Technische Universität München, Alte Akademie 12, Freising-Weihenstephan 85350, Germany

AUTHOR INFORMATION

Corresponding Author

*(K.A.) Phone: +49 (0) 81 617 13965. Fax: +49 (0) 81 617 13243. E-mail: auerswald@wzw.tum.de.

Funding

We acknowledge the China Scholarship Council (CSC) for supporting L.S.

Notes

The authors declare no competing financial interest.

ACKNOWLEDGMENTS

We acknowledge Jiří Šantrůček, Budweis CZ, for measuring some of the silage water samples and Alan Hopkins, Exeter, UK, for linguistic help.

REFERENCES

(1) Hyder, D. N.; Bement, R. E.; Norris, J. J. Sampling requirements of the water-intake method of estimating forage intake by grazing cattle. *J. Range Manage.* **1968**, *21*, 392−397.

(2) Kohn, M. J. Predicting animal $\delta^{18}O$: accounting for diet and physiological adaptation. *Geochim. Cosmochim. Acta* **1996**, *60*, 4811−4829.

(3) Nippert, J. B.; Culbertson, T. S. F.; Orozco, G. L.; Ocheltree, T. W.; Helliker, B. R. Identifying the water sources consumed by bison: implications for large mammalian grazers worldwide. *Ecosphere* **2013**, *4*, 1−13.

(4) Daux, V.; Lécuyer, C.; Héran, M.-A.; Amiot, R.; Simon, L.; Fourel, F.; Martineau, F.; Lynnerup, N.; Reychler, H.; Escarguel, G. Oxygen isotope fractionation between human phosphate and water revisited. *J. Hum. Evol.* **2008**, *55*, 1138−1147.

(5) Podlesak, D. W.; Torregrossa, A.-M.; Ehleringer, J. R.; Dearing, M. D.; Passey, B. H.; Cerling, T. E. Turnover of oxygen and hydrogen isotopes in the body water, CO_2, hair, and enamel of a small mammal. *Geochim. Cosmochim. Acta* **2007**, *72*, 19−35.

(6) Ehleringer, J. R.; Bowen, G. J.; Chesson, L. A.; West, A. G.; Podlesak, D. W.; Cerling, T. E. Hydrogen and oxygen isotope ratios in human hair are related to geography. *Proc. Natl. Acad. Sci. U.S.A.* **2008**, *105*, 2788−2793.

(7) Camin, F.; Perini, M.; Colombari, G.; Bontempo, L.; Giuseppe, V. Influence of dietary composition on the carbon, nitrogen, oxygen and hydrogen stable isotope ratios of milk. *Rapid Commun. Mass Spectrom.* **2008**, *22*, 1690−1696.

(8) Bowen, G. J.; Wassenaar, L. I.; Hobson, K. A. Global application of stable hydrogen and oxygen isotopes to wildlife forensics. *Oecologia* **2005**, *143*, 337−348.

(9) Barbour, M. M.; Farquhar, G. D. Do pathways of water movement and leaf anatomical dimensions allow development of gradients in $H_2{}^{18}O$ between veins and the sites of evaporation within leaves? *Plant Cell Environ.* **2003**, *27*, 107−121.

(10) Barbour, M. M. Stable oxygen isotope composition of plant tissue: a review. *Funct. Plant Biol.* **2007**, *34*, 83−94.

(11) Gat, J. R. Oxygen and hydrogen isotopes in the hydrologic cycle. *Annu. Rev. Earth Planet. Sci.* **1996**, *24*, 225−262.

(12) Dawson, T. E.; Ehleringer, J. R. Streamside trees that do not use stream water: evidence from hydrogen isotope ratios. *Nature* **1991**, *350*, 335−337.

(13) Dongmann, G.; Nurnberg, H. W.; Wagner, K. On the enrichment of $H_2{}^{18}O$ in the leaves of transpiring plants. *Radiat. Environ. Biophys.* **1974**, *11*, 41−52.

(14) Wen, X. F.; Lee, X.; Sun, X. M.; Wang, J. L.; Hu, Z. M.; Li, S. G.; Yu, G. R. Dew water isotopic ratios and their relationships to ecosystem water pools and fluxes in a cropland and a grassland in China. *Oecologia* **2012**, *168*, 549−561.

(15) Craig, H.; Gordon, L. I.; Horibe, Y. Isotopic exchange effects in the evaporation of water. *J. Geophys. Res.* **1963**, *68*, 5079−5087.

(16) Craig, H.; Gordon, L. Deuterium and oxygen-18 variations in the ocean and marine atmosphere. *Proceedings of Conference on Stable Isotope and Paleotemperatures*; Laboratory of Geology and Nuclear Science: Pisa, Italy, 1965; pp 9−130.

(17) Ayliffe, L. K.; Chivas, A. R. Oxygen isotope composition of the bone phosphate of Australian kangaroos: potential as a palaeoenvironmental recorder. *Geochim. Cosmochim. Acta* **1990**, *54*, 2603−2609.

(18) Luz, B.; Cormie, A. B.; Schwarcz, H. P. Oxygen isotope variations in phosphate of deer bones. *Geochim. Cosmochim. Acta* **1990**, *54*, 1723−1728.

(19) Renou, J.-P.; Bielicki, G.; Deponge, C.; Gachon, P.; Micol, D.; Ritz, P. Characterization of animal products according to geographic

origin and feeding diet using nuclear magnetic resonance and isotope ratio mass spectrometry. Part II: Beef meat. *Food Chem.* **2004**, *86*, 251−256.
(20) Boner, M.; Förstel, H. Stable isotope variation as a tool to trace the authenticity of beef. *Anal. Bioanal. Chem.* **2004**, *378*, 301−310.
(21) Chesson, L. A.; Podlesak, D. W.; Thompson, A. H.; Cerling, T. E.; Ehleringer, J. R. Variation of hydrogen, carbon, nitrogen, and oxygen stable isotope ratios in an American diet: fast food meals. *J. Agric. Food Chem.* **2008**, *56*, 4048−4091.
(22) Sharp, Z. D.; Cerling, T. E. Fossil isotope records of seasonal climate and ecology: straight from the horse's mouth. *Geology* **1998**, *26*, 219−222.
(23) Harb, M. Y.; Reynolds, V. S.; Campling, R. C. Eating behavior, social dominance and voluntary intake of silage in group-fed milking cattle. *Grass Forage Sci.* **1985**, *40*, 113−118.
(24) Allison, G. B.; Gat, J. R.; Leaney, F. W. J. The relationship between deuterium and oxygen-18 delta values in leaf water. *Chem. Geol.* **1985**, *58*, 145−156.
(25) Gammons, C. H.; Poulson, S. R.; Pellicori, D. A.; Reed, P. J.; Roesler, A. J.; Petrescu, E. M. The hydrogen and oxygen isotopic composition of precipitation, evaporated mine water, and river water in Montana, USA. *J. Hydrol.* **2006**, *328*, 319−330.
(26) Ephrath, J. E.; Goudriaan, J.; Marani, A. Modelling diurnal patterns of air temperature, radiation wind speed and relative humidity by equations from daily characteristics. *Agric. Syst.* **1996**, *51*, 377−393.
(27) Horita, J.; Rozanski, K.; Cohen, S. Isotope effects in the evaporation of water: a status report of the Craig-Gordon model. *Isot. Environ. Health Stud.* **2008**, *44*, 23−49.
(28) Roden, J. S.; Ehleringer, J. R. Observation of hydrogen and oxygen isotopes in leaf water confirm the Craig-Gordon model under wide-ranging environmental conditions. *Plant Physiol.* **1999**, *120*, 1165−1174.
(29) Gonfiantini, R. The δ-notation and the mass-spectrometric measurement techniques. In *Stable Isotope Hydrology: Deuterium and Oxygen-18 in the Water Cycle*; Gat, J. R., Gonfiantini, R., Eds.; International Atomic Energy Agency: Vienna, Austria, 1981; pp 35−84.
(30) Majzoub, M. Fractionnement en oxygen-18 et en deuterium entre l'eau et sa vapeur. *J. Chem. Phys.* **1971**, *68*, 1423−1436.
(31) Kays, W. M.; Crawford, M. E. *Convective Heat and Mass Transfer*; McGraw-Hill: New York, 1980.
(32) Merlivat, L. Molecular diffusivities of $H_2{}^{18}O$ in gases. *J. Chem. Phys.* **1978**, *69*, 2864−2871.
(33) Helliker, B.; Griffith, H. Toward a plant-based proxy for the isotope ratios of atmospheric water vapor. *Glob. Change Biol.* **2007**, *13*, 723−733.
(34) Welhan, J. A.; Fritz, P. Evaporation pan isotopic behavior as an index of isotopic evaporation conditions. *Geochim. Cosmochim. Acta* **1977**, *41*, 682−686.
(35) Gibson, J. J.; Prowse, T. D.; Edwards, T. W. D. Development and validation of an isotopic method for estimating lake evaporation. *Hydrol. Processes* **1996**, *10*, 1369−1382.
(36) Greenhill, W. L. Plant juices in relation to silage fermentation. III. Effect of water activity of juice. *J. Br. Grassland Soc.* **1964**, *19*, 336−339.
(37) Scanlon, B. R.; Andraski, B. J.; Bilskie, J. Miscellaneous methods for measuring matric or water potential. In *Methods of Soil Analysis, Part 4, Physical Methods*, no. 5; Dane, J. H., Topp, G. C., Eds.; Soil Science Society of America, Inc.: Madison, WI, USA, 2002; pp 643−670.
(38) Cerling, T. E.; Ayliffe, L. K.; Dearing, M. D.; Ehleringer, J. R.; Passey, B. H.; Podlesak, D. W.; Torregrossa, A.-M.; West, A. G. Determining biological tissue turnover using stable isotopes: the reaction progress variable. *Oecologia* **2007**, *151*, 175−189.
(39) Criss, R. E. *Principles of Stable Isotope Distribution*; Oxford University Press: Oxford, UK, 1999.
(40) Schnyder, H.; Schwertl, M.; Auerswald, K.; Schäufele, R. Hair of grazing cattle provides an intergrated measure of the effects of site conditions and interannual weather variability on $\delta^{13}C$ of temperate humid grassland. *Glob. Change Biol.* **2006**, *12*, 1315−1329.
(41) Wilkinson, J. M. *Silage*; Chalcombe Publications: Lincoln, UK, 2005, 254 pp.
(42) Cernusak, L. A.; Pate, J. S.; Farquhar, G. D. Diurnal variation in the stable isotope composition of water and dry matter in fruiting *Lupinus angustifolius* under field conditions. *Plant Cell Environ.* **2002**, *25*, 893−907.
(43) Jarrige, R. *Ruminant Nutrition: Recommended Allowances and Feed Tables*; John Libbey: London, UK, 1989.
(44) Kim, K.; Lee, X. Transition of stable isotope ratios of leaf water under simulated dew formation. *Plant Cell Environ.* **2011**, *34*, 1790−1801.
(45) Hobson, K. A. Tracing origins and migration of wildlife using stable isotopes: a review. *Oecologia* **1998**, *120*, 314−326.
(46) Camin, F.; Bontempo, L.; Heinrich, K.; Horacek, M.; Kelly, S. D.; Schilicht, C.; Thomas, F.; Monahan, F. J.; Hoogewerff, J.; Rossmann, A. Multi-element (H,C,N,S) stable isotope characteristics of lamb meat from different European regions. *Anal. Bioanal. Chem.* **2007**, *389*, 309−320.
(47) Kornexl, B. E.; Werner, T.; Roßmann, A.; Schmidt, H.-L. Measurement of stable isotope abundances in milk and milk ingredients − a possible tool for origin assignment and quality control. *Z. Lebensm. Unters. Forsch. A* **1997**, *205*, 19−24.
(48) Auerswald, K.; Rossmann, A.; Schäufele, R.; Schwertl, M.; Monahan, F. J.; Schnyder, H. Does natural weathering change the stable isotope composition (^2H, ^{13}C, ^{15}N, ^{18}O and ^{34}S) of cattle hair? *Rapid Commun. Mass Spectrom.* **2011**, *25*, 3741−3748.
(49) Cardot, V.; Le Roux, Y.; Jurjanz, S. Drinking behaviour of lactating dairy cows and prediction of their water intake. *J. Dairy Sci.* **2008**, *91*, 2257−2264.
(50) Winchester, C. F.; Morris, M. J. Water intake rates of cattle. *J. Anim. Sci.* **1956**, *15*, 722−740.
(51) Sun, L. Z.; Auerswald, K.; Wenzel, R.; Schnyder, H. Drinking water intake of grazing steers − the role of environmental factors controlling canopy wetness. *J. Anim. Sci.* **2013**, *91*, 1−10.

JOURNAL OF AGRICULTURAL AND FOOD CHEMISTRY

Article

pubs.acs.org/JAFC

Selenium-Enriched Probiotics Improve Antioxidant Status, Immune Function, and Selenoprotein Gene Expression of Piglets Raised under High Ambient Temperature

Fang Gan,[†] Xingxiang Chen,[†] Shengfa F. Liao,[‡] Chenhui Lv,[†] Fei Ren,[†] Gengping Ye,[†] Cuiling Pan,[†] Da Huang,[†] Jun Shi,[†] Xiuli Shi,[†] Hong Zhou,[†] and Kehe Huang*[,†]

[†]Institute of Nutritional and Metabolic Disorders in Domestic Animals and Fowls, Nanjing Agricultural University, Nanjing, Jiangsu 210095, China

[‡]Department of Animal and Dairy Sciences, Mississippi State University, Mississippi State, Mississippi 39762-9815, United States

Supporting Information

ABSTRACT: This research was conducted to evaluate the effects of selenium-enriched probiotics (SP) on growth performance, antioxidant status, immune function, and selenoprotein gene expression of piglets under natural high ambient temperature in summer. Forty-eight crossbred weanling piglets randomly allocated to four groups were fed for 42 days ad libitum a basal diet without (Con, 0.16 mg Se/kg) and with supplementation of probiotics (P, 0.16 mg Se/kg), sodium selenite (SS, 0.46 mg Se/kg), and SP (0.46 mg Se/kg). From each group, three piglets were randomly selected for blood collection on days 0, 14, 28, and 42 and tissue collection on day 42. The SP improved growth performance of piglets. Both SS and SP increased blood glutathione peroxidase activity and tissue thioredoxin reductase 1 mRNA expression, with SP being higher than SS. All P, SS, and SP supplementation increased the superoxide dismutase activity (40.1, 53.0, and 64.5%), glutathione content (84.6, 104, and 165%), TCR-induced T lymphocyte proliferation (20.8, 26.4, and 50.0%), and IL-2 concentration (24.9, 27.2, and 46.2%) and decreased malondialdehyde content (25.1, 26.3, and 49.3%), respectively. The greatest effects of SP supplementation suggest that SP may serve as a better feed additive than P or SS for piglets under high-temperature environments.

KEYWORDS: *selenium-enriched probiotics, antioxidant status, immune function, high-temperature environment, piglet*

INTRODUCTION

High ambient temperature, which can cause heat stress to pigs, especially during the summer in southern China, is a major detrimental factor that negatively affects pig health and production performance.[1] The global warming climate change as recently claimed may exacerbate this situation. A major health problem caused by heat stress in pigs is the reduction in their antioxidant capacity and immunity,[2] which could result in enormous economic losses to the swine industry.[3]

It is known that the activities of glutathione peroxidase (GPX) and superoxide dismutase (SOD) and the content of glutathione (GSH) represent the competence of animal antioxidant status because these proteins participate in the clearing of superoxide anion free radicals in cells to protect cells from being injured.[4] The malondialdehyde (MDA) content manifests the level of lipid peroxidation and indirectly represents the level of cell or tissue damage.[4] T lymphocyte proliferation and interleukin 2 (IL-2) secretion play important roles in animal immune function.[5] IL-2, a cytokine secreted by activated T lymphocytes, is an essential factor for the growth, proliferation, and differentiation of regulatory T cells.[6]

As an essential trace element nutrient for mammalian animals, selenium (Se) plays a key role in redox regulation, antioxidant defense, and immune function through GPX enzymes that catalyze the removal of the excess potentially damaging radicals produced during stress situation.[7,8] The biological effects of Se are mainly exerted through its incorporation into selenocysteine (a special amino acid) and further into selenoproteins,[9] of which some function as antioxidant enzymes with selenocysteine in the catalytic centers.[10] Selenoproteins such as glutathione peroxidase 1 (GPx1), GPx4, and thioredoxin reductase 1 (TR1) are thought to play important roles in animal antioxidant status and immune responses via the altered physiological Se status.[11] Dietary Se supplementation has been reported to increase the GPX and SOD activities, decrease MDA levels,[12] improve immunocompetence[13] of broilers under heat stress, and enhance GPx1 and TR1 selenoprotein gene expression in livers of young pigs.[14] A better effect of organic Se than inorganic Se has been reported in improving animal growth performance, as well as antioxidant and immune functions.[15−17] However, little research has been conducted to explore the effects of Se on the antioxidant status, immune function, and selenoprotein gene expression of young piglets under high ambient temperature.

Probiotics (P) are nonpathogenic microorganisms that can resist host small intestinal digestion and reach the colon alive, where they perform beneficial effects for the health of the host animals.[18] Previous studies of probiotic lactobacillus bacteria and yeasts have demonstrated that either *Lactobacillus acidophilus* or *Saccharomyces cerevisiae* has strong effects on animal

Received: March 31, 2013
Revised: May 1, 2014
Accepted: May 2, 2014
Published: May 9, 2014

ACS Publications © 2014 American Chemical Society

antioxidant status and immunity and can inhibit lipid peroxidation in pigs under normal conditions.[19,20] Likewise, a previous study in poultry also indicated that probiotics can reduce the adverse effects of heat stress.[21] However, similar studies have scarcely been conducted in pigs under high ambient temperature.

To combine the beneficial effects of both Se and probiotics, we have newly developed a feed additive product called Se-enriched probiotics (SP) in our laboratory (Chinese patent no. ZL 2005 1 0040990.2).[21] The probiotic *L. acidophilus* and *S. cerevisiae* strains we used are very efficient in transforming inorganic Se to organic Se.[22,23] Previous studies have demonstrated that dietary SP supplementation has beneficial effects on inhibiting heat shock protein (hsp) mRNA expression in piglets[24] and improving blood lipid profile in mice.[25]

The objective of this study was to investigate the potential effects of SP on the growth performance, antioxidant status, immune function, and selenoprotein gene expression of piglets raised under a high-temperature environment.

MATERIALS AND METHODS

Chemicals. The antioxidant assay kits were purchased from Nanjing Jiancheng Bioengineering Institute (Nanjing, China). Both the WST-8 Cell Counting Kit-8 and the total protein assay kit were purchased from Biyuntian Institute (Nanjing, China). Lymphocyte Separation Medium was purchased from Tianjin Hematology Institute, Chinese Academy of Medical Sciences (Tianjin, China). The interleukin-2 (IL-2) assay kit was obtained from YuanYe Biotechnology Co., Ltd. (Shanghai, China). The inorganic sodium selenite (SS) used in this study was purchased from Sigma (Shanghai, China). The stock solution of sodium selenite as a Se standard [GBW(E) 080215] and the certified Se reference material, pork liver (GBW 08551), were provided by the National Research Center for Standard Materials (Beijing, China) and the Institute of Food Examination of the Ministry of Commerce (Beijing, China), respectively. Reagents used for real-time PCR were purchased from TaKaRa (Dalian, China). All reagents for the Se assay were of analytical grade.

P, SS, and SP Products. Both P and SP products used were obtained from our own laboratory in Nanjing Agricultural University (Jiangsu, China) and contain two probiotic strains, *L. acidophilus* and *S. cerevisiae*. The colony-forming units (CFU) of *L. acidophilus* and *S. cerevisiae* strains in both products were approximately 10^{11} and 10^{9} CFU/mL, respectively. The total Se content in SS stock solution was 100 mg/L. The total Se content in SP was 10.0 mg/L, with >90% being organic Se and >75% being selenomethionine (Se-Met).[23]

Experimental Design and Animal Trial. According to a completely randomized experimental design, 48 crossbred [(Landrace × Yorkshire) × Duroc] weanling barrows (4 weeks old, body weight = 7.9 ± 0.5 kg) were randomly divided into four groups of 12 in each. Piglets in each group were further allotted into three feeding pens (as three replicates) with four piglets in each pen or replicate. All piglets received a basal diet that contained 0.16 mg Se/kg for 2 weeks prior to the feeding trial. The ingredient composition of the basal diet has been previously reported.[24]

Piglets of the four treatment groups were fed the basal diet without or with supplementation of P, SS, or SP product. The SP product provided 0.3 mg total Se/kg diet, and so did the SS product. The final calculated total Se concentration in either the SS- or the SP-supplemented diet was 0.46 mg/kg. The P product provided *L. acidophilus* and *S. cerevisiae* to the diet at doses equivalent to that provided by the SP product with the total cell counts of *L. acidophilus* and *S. cerevisiae* being 3×10^{11} and 3×10^{9} CFU/kg, respectively.

The animal feeding trial lasted for a total of 6 weeks (42 days, from June 19 to July 30, 2011) and was conducted at Bangcheng Swine Farm located in Xinghua (32°93′ N latitude and 119°82′ E longitude), Jiangsu, China. During the first 33 days, the daytime temperature in the pig shed (with natural ventilation) ranged from 25 to 38 °C, and during the last 9 days, the daytime temperature ranged from 31 to 40 °C.

All of the diets for the piglets were replenished daily, and fresh water was accessible at all times throughout the trial. Each pig was weighed at the beginning and the end of the feeding trial. Feed intake was recorded daily. Average daily gain (ADG), average daily feed intake (ADFI), and feed/gain (F/G) ratio were calculated for each group and each pig.

All experimental protocols were approved by the Committee for the Care and Use of Experimental Animals of Nanjing Agriculture University, and the Animal Ethical Number granted was SYXK (Su) 2011-0036.

Sample Collection and Preparation. From each of four treatment groups three piglets were randomly selected for blood sample collection at 2:00 to 4:00 p.m. on days 0, 14, 28, and 42 from the precaval vein. From each piglet approximately 5 mL of blood was collected in a syringe primed with EDTA, and another 5 mL of blood was collected in a syringe without EDTA. Both blood samples with and without EDTA were gently ejected into 10 mL Eppendorf tubes, respectively.

Approximately 2 mL of EDTA-primed blood samples was directly stored at −20 °C until analysis of GPX activity. To prepare erythrocyte lysates, 1 mL EDTA-primed whole blood samples were centrifuged at 700*g* for 10 min, and the resulting red blood cells were washed three times with physiological saline, resuspended in 4 mL of ice-cold distilled water, shaken vigorously to force hemolysis, and then centrifuged at 700*g* for 10 min. The resulting supernatant was the erythrocyte lysate sample required and stored at −20 °C until analysis of GSH content.

To obtain serum samples, 5 mL of whole blood sample (without EDTA) was kept in a slanting position at 37 °C for 2 h and then at 4 °C overnight, followed by centrifugation at 700*g* for 15 min. The resulting supernatant was the serum sample required and stored at −20 °C until analysis of SOD activity, MDA content, and IL-2 concentration.

At the end of the experiment (on day 42), three piglets from each of the four treatment groups were randomly selected and euthanized. Half of the spleen from each pig was harvested and stored at 37 °C until isolation of primary porcine splenocytes for analysis T lymphocyte proliferation. One-fourth of each liver, kidney, and spleen tissue was rapidly excised and rinsed with ice-cold isotonic saline, then snap-frozen in liquid nitrogen, and stored at −70 °C until analysis of GPx1, GPx4, and TR1 mRNA expression.

Analysis of GPX and SOD Activities and GSH and MDA Contents. The GPX activity in whole blood, the GSH content in erythrocyte, the SOD activity, and MDA contents in serum were respectively determined using the commercial kits in accordance with the manufacturers' instructions. GPX activity, SOD activity, and GSH and MDA contents were expressed as U/L, U/mL, μmol/g protein, and nmol/mL, respectively.

TCR-Induced T Lymphocyte Proliferation Assay. The lymphocytes of peripheral blood and spleen were collected by using a commercial Lymphocyte Separation Medium (Tianjin Hematology Institute). The T lymphocyte proliferation induced by T-cell receptor (TCR) was analyzed using a WST-8 Cell Counting Kit-8 (Beyotime) according to the manufacturer's instructions as previously described by Zhang and Sun.[26] Briefly, 5.0×10^{5} cells suspended in RPMI-1640 medium (100 μL) containing 10% fatal bovine serum were seeded in 96-well plates and treated in the absence (control) or presence of 2 μg/mL stimulatory anti-pig-CD3 mAb (clone PPT3; Abcam). After incubation for 44 h, CCK-8 solution (10 μL) was added to each well, and the cells were incubated at 37 °C for 4 h with 5% CO_2. At the end, the cells in each well were measured by Vis spectrophotometer at 450 nm.

Determination of IL-2 Concentrations in Serum. The IL-2 concentrations in the serum samples were measured by using a commercial porcine IL-2 enzyme-linked immunosorbent assay (ELISA) kit in accordance with the manufacturer's protocol (YuanYe

Biotechnology Co., Ltd.). The concentration units were expressed as pg/mL.

Determination of Selenoprotein mRNA Expression. Real-time quantitative PCR method was employed for selenoprotein mRNA detection. The PCR primers (Table 1) for two selenoprotein genes (GPx4 and TR1) and one reference gene (β-actin) were designed using Primer Premier Software (PREMIER Biosoft International, Palo Alto, CA, USA) on the basis of the known porcine sequences reported in the NCBI database (http://www.ncbi.nlm.nih.gov).

Table 1. Primers Used for Real-Time Quantitative PCR

gene	accession no.[a]	primer sequence (5′−3′)	product (bp)
β-actin	DQ845171.1	forward: CTGCGGCATCCACGAAACT reverse: AGGGCCGTGATCTCCTTCTG	147
GPx4	NM_214407.1	forward: GATTCTGGCCTTCCCTTGC reverse: TCCCCTTGGGCTGGACTTT	183
TR1	NM_214 154	forward: CCCTGGTGACAAAGAGTA reverse: GTCCTGGTCAAATCCTCT	184

[a]For retrieving the corresponding cDNA or gene sequences from the GenBank database (http://www.ncbi.nlm.nih.gov).

Total RNA was isolated from the frozen tissue samples using the RNAiso Plus (TaKaRa) reagent according to the manufacturer's protocol. The isolated RNA pellets were resuspended in 30 μL of diethyl pyrocarbonate-treated water, quantified by measurement of the absorbance ratio at 260/280 nm, and then stored at −70 °C prior to cDNA synthesis. First-strand cDNA was synthesized from 1 μg of total RNA using Oligo dT primers and M-MLV reverse transcriptase (TaKaRa) according to the manufacturer' instructions. Real-time PCR was performed on an ABI PRISM 7300 detection system (Applied Biosystems, USA). Reactions were performed in a 25 μL reaction mixture containing 12.5 μL of 2× SYBR Green I PCR Master Mix (TaKaRa), 10 μL of cDNA, 1 μL of each primer (10 μM), and 0.5 μL of PCR-grade water. The PCR procedure consisted of a 95 °C step for 30 s followed by 40 cycles consisting of 95 °C for 5 s and 60 °C for 31 s. A dissociation curve was run for each plate to confirm the production of a single product. A nontemplate reaction served as the negative control.

The relative levels of selenoprotein mRNA were determined using the Δ cycle threshold (ΔCt) method with β-actin serving as a reference gene. For each of the target selenoprotein genes, the ΔΔCt values of all the samples were calculated by subtracting the average ΔCt of the Con group from the average ΔCt of the P, SS, or SP group. The ΔΔCt values were converted to fold differences by raising 2 to the power of $-\Delta\Delta Ct$ (i.e., $2^{-\Delta\Delta Ct}$).

Statistical Analysis. Data were analyzed by the one-way ANOVA model followed by Duncan's multiple-range tests to separate the means using the SPSS computer program for Windows (version 17.0). Data for each treatment group are presented as means ± SE, and the statistical significance was set at $P < 0.05$.

RESULTS

Animal Growth Performance. The initial body weight (BW) and final BW, ADG, ADFI, and F/G in different groups of pigs are shown in Table 2. As expected, there was no difference in initial BW among the four treatment groups. Among the Con, P, and SS treatment groups, there were no differences in all of the growth performance parameters including ADFI, ADG, final BW, and F/G. Although there was no difference in ADFI when the SP group was compared with the other three groups, the SP group had higher ($P < 0.05$) final BW and ADG and lower ($P < 0.05$) F/G.

GPX Activity of Whole Blood. The GPX activities of whole blood from the four treatment groups are shown in Table 3. As expected, on day 0 there was no difference in GPX activities among the four treatment groups. On days 14, 28, and 42, the GPX activities in the P group were not higher than that in the Con group, but significant increases ($P < 0.05$) were observed in the SS and SP groups when compared to the P or Con group. Furthermore, the SP group was even higher ($P < 0.05$) than the SS group in GPX activities by approximately 23.8, 21.3, and 17.8% on days 14, 28, and 42, respectively.

Table 3. GPX Activity of Whole Blood of Piglets[a]

	GPX activity (U/L)			
group	day 0	day 14	day 28	day 42
Con	117 ± 3.22a	112 ± 2.36a	109 ± 5.43a	111 ± 4.72a
P	114 ± 4.47a	117 ± 3.89a	121 ± 3.22a	121 ± 2.68a
SS	115 ± 4.09a	147 ± 3.09b	155 ± 4.73b	163 ± 5.58b
SP	116 ± 4.97a	182 ± 2.68c	188 ± 4.64c	192 ± 3.57c

[a]The GPX activities in whole blood (U/L) of piglets fed the normal basal diet (Con group), the basal diet supplemented with probiotics (P group), the basal diet supplemented with sodium selenite (SS group), and the basal diet supplemented with selenium-enriched probiotics (SP group). Data presented are means ± SE ($n = 3$). Within a column means followed by different letters are significantly different ($P < 0.05$).

GSH Content of Erythrocytes. The erythrocyte GSH contents in the four treatment groups are shown in Table 4. As expected, on day 0 there was no difference in GSH contents among the four groups. Although there were no differences

Table 2. Growth Performance of Piglets[a]

	group			
	Con	P	SS	SP
initial BW (kg)	7.46 ± 0.29a	8.04 ± 0.15a	7.96 ± 0.23a	8.00 ± 0.22a
final BW (kg)	20.96 ± 0.79a	21.83 ± 0.61a	21.79 ± 0.65a	24.25 ± 0.83b
ADG (g/day)	321 ± 25a	328 ± 12a	329 ± 10a	387 ± 17b
ADFI (g/day)	770 ± 51a	786 ± 36a	794 ± 38a	807 ± 41a
F/G	2.40 ± 0.03a	2.39 ± 0.08a	2.41 ± 0.11a	2.09 ± 0.12b

[a]Growth performance of piglets fed the normal basal diet (Con group), the basal diet supplemented with probiotics (P group), the basal diet supplemented with sodium selenite (SS group), and the basal diet supplemented with selenium-enriched probiotics (SP group). Data presented are means ± SE ($n = 3$). Within a column means followed by different letters are significantly different ($P < 0.05$).

Table 4. GSH Content of Erythrocytes of Piglets[a]

	GSH content (μmol/g protein)			
group	day 0	day 14	day 28	day 42
Con	17.4 ± 1.93a	18.5 ± 1.95a	20.2 ± 1.85a	21.2 ± 1.97a
P	16.0 ± 2.30a	31.3 ± 2.05b	39.1 ± 2.30b	40.5 ± 2.55b
SS	18.4 ± 1.90a	33.5 ± 1.59b	43.6 ± 2.75b	45.4 ± 1.92b
SP	17.3 ± 2.06a	44.9 ± 1.97c	56.6 ± 2.10c	57.9 ± 2.14c

[a]The GSH contents in erythrocytes (μmol/g protein) of piglets fed the normal basal diet (Con group), the basal diet supplemented with probiotics (P group), the basal diet supplemented with sodium selenite (SS group), and the basal diet supplemented with selenium-enriched probiotics (SP group). Data presented are means ± SE (n = 3). Within a column means followed by different letters are significantly different (P < 0.05).

between the SS and P groups, either the SS or P group was higher (P < 0.05) than the Con group on days 14, 28, and 42. Furthermore, the SP group was even higher (P < 0.05) than the SS or the P group in erythrocyte GSH contents by approximately 38.5, 36.7, and 34.7% on days 14, 28, and 42, respectively.

SOD Activity of Serum. The SOD activities of serum from the four treatment groups are shown in Table 5. As expected, on day 0, there were no differences in SOD activities among the four treatment groups. Although there were no differences between the SS and P groups and between the SP and SS groups, either the P or SS group was higher (P < 0.05) than the Con group in SOD activities on days 14, 28, and 42. Furthermore, the SP group was even higher (P < 0.05) than the P group by approximately 18.3, 19.7, and 14.5% on days 14, 28, and 42, respectively.

MDA Content of Serum. The MDA contents of serum from four treatment groups are shown in Table 6. As expected, on day 0, there was no difference in MDA contents among the four groups. Although there were no differences between the SS and P groups, either the SS or P group was lower (P < 0.05) than the Con group on days 14, 28, and 42. Furthermore, the SP group was even lower (P < 0.05) than the SS or P group by approximately 34.3, 32.4, and 29.0% on days 14, 28, and 42, respectively.

TCR-Induced T Lmphocyte Proliferation. The TCR-induced T lymphocyte proliferation in the peripheral blood lymphocytes and the splenocytes collected from the four treatment groups on day 42 postfeeding are shown in Figure 1. When compared to the Con group, significant promotions (P < 0.05) were observed in the TCR-induced T lymphocyte proliferations in both tissues in the P, SS, and SP groups. Although there was no difference in promoting T lymphocyte proliferation between the P and SS groups in both tissues, a

Table 6. MDA Content in Serum of Piglets[a]

	MDA content (nmol/mL)			
group	day 0	day 14	day 28	day 42
Con	2.59 ± 0.17a	4.12 ± 0.21a	4.14 ± 0.13a	4.24 ± 0.10a
P	2.69 ± 0.10a	3.02 ± 0.22b	3.11 ± 0.18b	3.23 ± 0.17b
SS	2.54 ± 0.13a	2.97 ± 0.17b	3.06 ± 0.15b	3.18 ± 0.18b
SP	2.64 ± 0.09a	1.97 ± 0.19c	2.09 ± 0.24c	2.28 ± 0.13c

[a]The MDA contents in serum (nmol/mL) of piglets fed with the normal basal diet (Con group), the basal diet supplemented with probiotics (P group), the basal diet supplemented with sodium selenite (SS group), and the basal diet supplemented with selenium-enriched probiotics (SP group). Data presented are means ± SE (n = 3). Within a column means followed by different letters are significantly different (P < 0.05).

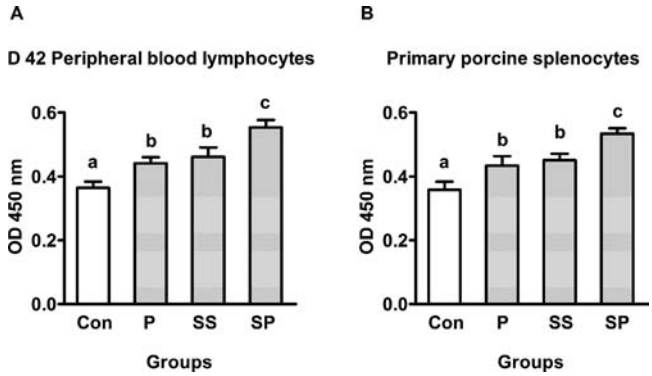

Figure 1. TCR-induced T lymphocyte proliferation in the peripheral blood lymphocytes (A) and splenocytes (B) of piglets fed the normal basal diet (Con group), the basal diet supplemented with probiotics (P group), the basal diet supplemented with sodium selenite (SS group), and the basal diet supplemented with selenium-enriched probiotics (SP group). Data presented are means ± SE (n = 3). Within a panel bars labeled with different letters differ (P < 0.05).

significant promotion (P < 0.05) was observed in the SP group when compared to the P or SS group in either tissue. In the peripheral blood lymphocytes (Figure 1A), the magnitudes of promotion were 25.0 and 19.6% for the P and SS groups, respectively. In the splenocytes (Figure 1B), the magnitudes of promotion were 23.3 and 17.8% for the P and SS groups, respectively.

IL-2 Concentration in Serum. The IL-2 concentrations in serum from four treatment groups are shown in Table 7. As expected, on day 0, there were no differences in IL-2 concentrations among the four groups. Although there were no differences between the SS and P groups, either the SS or P group was higher (P < 0.05) than the Con group on days 14–42. Furthermore, the SP group was even higher (P < 0.05) than

Table 5. SOD Activity in Serum of Piglets[a]

	SOD activity (U/mL)			
group	day 0	day 14	day 28	day 42
Con	106 ± 4.61a	96.3 ± 4.44a	105 ± 2.54a	102 ± 4.24a
P	108 ± 5.03a	131 ± 6.27b	142 ± 5.71b	152 ± 5.89b
SS	107 ± 3.66a	143 ± 3.96bc	155 ± 5.63bc	166 ± 3.38bc
SP	106 ± 3.52a	155 ± 3.56c	170 ± 3.22c	174 ± 3.26c

[a]The SOD activities in serum (U/mL) of piglets fed with the normal basal diet (Con group), the basal diet supplemented with probiotics (P group), the basal diet supplemented with sodium selenite (SS group), and the basal diet supplemented with selenium-enriched probiotics (SP group). Data presented are means ± SE (n = 3). Within a column means followed by different letters are significantly different (P < 0.05).

dx.doi.org/10.1021/jf501065d | J. Agric. Food Chem. 2014, 62, 4502–4508

Table 7. IL-2 Concentration in Serum of Piglets[a]

	IL-2 concentration (pg/mL)			
group	day 0	day 14	day 28	day 42
Con	102 ± 4.28a	99.3 ± 3.23a	100 ± 2.85a	101 ± 3.33a
P	103 ± 3.54a	122 ± 2.47b	126 ± 3.61b	127 ± 2.47b
SS	97.2 ± 2.93a	124 ± 3.73b	128 ± 3.17b	130 ± 3.06b
SP	100 ± 3.52a	139 ± 3.54c	147 ± 3.07c	153 ± 3.73c

[a]The IL-2 concentrations in serum (pg/mL) of piglets fed with the normal basal diet (Con group), the basal diet supplemented with probiotics (P group), the basal diet supplemented with sodium selenite (SS group), and the basal diet supplemented with selenium-enriched probiotics (SP group). Data presented are means ± SE (n = 3). Within a column means followed by different letters are significantly different (P < 0.05).

the SS or P group in serum IL-2 concentrations by approximately 13.0, 15.7, and 19.5% on days 14, 28, and 42, respectively.

GPx4 mRNA Expression. The expression levels of GPx4 mRNA in liver, kidney, and spleen tissues from four treatment groups on day 42 postfeeding are shown in Figure S1 (see the Supporting Information). Although some numerical increases in the GPx4 mRNA expression levels can be seen for the SS and SP groups in all three tissues, there were no statistically significant increases found in these tissues.

TR1 mRNA Expression. The expression levels of TR1 mRNA in liver, kidney, and spleen tissues collected from four different treatment groups on day 42 postfeeding are shown in Figure 2. There were no differences in terms of TR1 mRNA expression levels between the P and Con groups in any of the three tissues. However, significant increases (P < 0.05) of TR1 mRNA expression were observed for the SS and SP groups in all three tissues. When compared to the SS group, the SP group showed further increases (P < 0.05) in TR1 mRNA expression by 51.4, 23.5, and 27.5% in liver, kidney, and spleen tissues, respectively.

DISCUSSION

Earlier studies demonstrated that high-temperature environments could decrease egg production and compromise the immune function of poultry, pigs, and dairy calves,[3,27,28] and supplementation of vitamin E, vitamin C, amino acids, or Se can reduce the negative effects such as immune and physiological responses of high temperature on poultry and sheep.[13,29,30] It has been reported that probiotics can also relieve the adverse effects in poultry such as decreased growth performance and immune response under heat stress.[21] Another SP product, also developed in our laboratory, was reported to have additive beneficial effect of P and Se in terms of hens' egg-laying performance.[22] However, there is very limited knowledge concerning the effects of SP on piglets exposed to high-temperature environments.

Previous studies found no difference in ADG, ADFI, and F/G between control pigs and the pigs fed extra probiotics or inorganic Se at 0.3 mg/kg diet, whereas decreased F/G was observed with the pigs fed organic Se at 0.3 mg/kg diet.[31,32] Consistent with those data obtained from normal temperature conditions, the P or SS supplementation did not affect final BW, ADG, ADFI, and F/G in the current study under high-temperature condition; however, SP supplementation improved final BW and ADG and decreased F/G of these piglets. This discrepancy is not easily explained. One may hypothesize that the improved growth performance resulting from SP supplementation is due to the organic Se in the SP product because organic Se could affect thyroid hormone (TH) secretion, which directly or indirectly leads to a decreased F/G. Although TH was not determined in this study, it was reported that thyroxine (T4) and tri-iodothyronine (T3) could be responsible for anabolic metabolism of nutrients in lambs, with T3 being the most active form, and the Se-dependent enzyme, type I deiodinase, is needed when T4 is deiodinated to the active T3.[33] Supplemental Se caused a decrease in T4 and an increase in T3, and organic Se may be superior to inorganic Se in facilitating the T4 to T3 conversion through the action of selenoenzyme,[15] because sodium selenite had no effects on T3, T4, and T4/T3 ratio.[34]

The present study of piglets raised under high ambient temperature showed that dietary P supplementation increased GSH content and SOD activity and decreased MDA content, which is consistent with previous results on pigs raised under normal temperature conditions.[35,36] Besides these GSH, SOD, and MDA parameters, dietary SS and SP supplementation additionally increased GPX activity. Although the mechanism of probiotics on increasing GSH content and SOD activity is still unclear, the reduced MDA content may be associated with the increased GSH content and SOD activity and is further evidence of the role of probiotics (*L. acidophilus*) in improving the function of swine antioxidant defense system.[35] The effects of SS on GPX and SOD activities and GSH and MDA contents

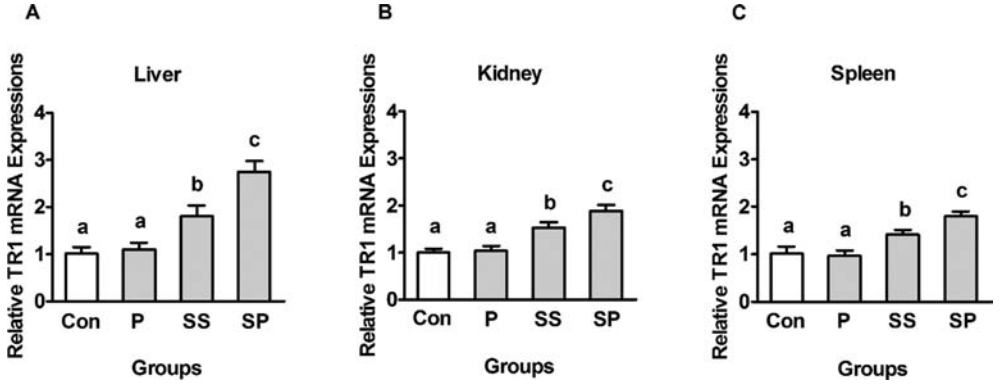

Figure 2. TR1 mRNA expression in the liver (A), kidney (B), and spleen (C) from the piglets fed with the normal basal diet (Con group), the basal diet supplemented with probiotics (P group), the basal diet supplemented with sodium selenite (SS group), and the basal diet supplemented with selenium-enriched probiotics (SP group). Data presented are means ± SE (n = 3). Within a panel bars labeled with different letters differ (P < 0.05).

in pigs raised under high-temperature conditions have not been reported until this study. It is known that the GPX activity in which Se plays a crucial role is strongly associated with animal antioxidant status,[10] as previous studies indicated that Se can elevate the antioxidant status of pigs under normal temperature conditions.[36]

That the SP supplementation further increased GPX and SOD activities and GSH content and reduced MDA content in this study strongly suggests that the SP used has more robust beneficial effects in terms of improving animal antioxidant status than P or SS alone. Our previous study also demonstrated that SP could improve murine blood lipid profile of mice and that the beneficial effects of SP are more robust than that of P or SS used alone.[25]

The effects of Se on promoting T lymphocyte proliferation and increasing IL-2 concentration in pigs raised under a high-temperature condition have not been reported either until this study. The data obtained from this study showed that dietary supplementation of P, SS, or SP promoted TCR-induced T lymphocyte proliferation in both blood and spleen and increased serum IL-2 concentrations, which are consistent with some previous studies under normal temperature conditions.[9,37] Although the mechanism is not very clear, these positive effects were thought to be due to the effects of Se on increasing Ca^{2+} flux[38] and involving cellular free thiols.[39] Furthermore, this study also showed that the effects of SP supplementation in increasing lymphocyte number and IL-2 secretion were more dramatic than that of P or SS supplementation alone, suggesting that SP is more effective in boosting pig immune function than P or SS used alone. The reason may be because there was a synergistic effect of Se and P in T lymphocyte proliferation and IL-2 secretion. It was reported that a probiotics of *L. acidophilus* increased lymphocyte number and IL-2 secretion in pigs raised under normal temperature conditions.[40,41]

The results of this study showed that TR1, but not GPx4, mRNA expressions were up-regulated by dietary supplementations of SS or SP for piglets. The mechanism of Se regulation on the expression of selenoprotein mRNA is not very clear. However, it is known that this is due to neither the transcriptional regulation nor the mRNA processing and exports from the nucleus.[42] On the other hand, it has been suggested that the explanation of Se affecting mRNA expression is that selenoprotein transcripts are affected via nonsense-mediated mRNA decay mechanism.[43]

This study found that SP supplementation has a more dramatic effect in up-regulation of TR1 mRNA expressions than SS supplementation, which may be due to the better bioavailability of the organic Se in the SP product than that of the inorganic Se in the SS product.[43] That the GPx4 mRNA expression was not affected by dietary SS or SP supplementation, as found in this study, is also consistent with previous research results.[14] But why the GPx4 mRNA expression is not sensitive to dietary Se supplementation is unknown.

In summary, the present study indicated that dietary supplementation of SP improved animal growth performance, antioxidant status, immune function, and some selenoprotein mRNA expression in piglets raised under high ambient temperature, suggesting that this SP product is a feasible dietary supplementation for piglets during hot seasons. The more robust beneficial effects of the SP product than the P or SS product used alone may be explained by two possible reasons: (i) there is an additivity or a synergistic effect between probiotics and Se in these beneficial effects, and (ii) the more robust antioxidant effects of the SP product may be due to the organic Se it contained relative to the inorganic Se contained in the SS.

■ ASSOCIATED CONTENT

Ⓢ Supporting Information

Figure S1. This material is available free of charge via the Internet at http://pubs.acs.org.

■ AUTHOR INFORMATION

Corresponding Author

*(K.H.) College of Veterinary Medicine, Nanjing Agricultural University, Nanjing 210095, Jiangsu Province, China. Phone: +86-25-84395507. Fax: +86-25-84398669. E-mail: khhuang@njau.edu.cn.

Funding

This work was supported by the National Natural Science Foundation of China (30871892 and 31272627), the Research Fund for Doctoral Program of Higher Education in China (20110097110014 and 20120097130002), the Special Fund for Agro-scientific Research in the Public Interest of China (201003011), the Priority Academic Program Development of Jiangsu Higher Education Institutions (Jiangsu, China), and the research fund from the Mississippi Agricultural and Forestry Experiment Station (027000901200; approved for publication as Journal Article 12355; Mississippi State University, USA).

Notes

The authors declare no competing financial interest.

■ REFERENCES

(1) Lucas, E.; Randall, J.; Meneses, J. Potential for evaporative cooling during heat stress periods in pig production in Portugal (Alentejo). *J. Agric. Eng. Res.* **2000**, *76*, 363−371.

(2) Ju, X. H.; Yong, Y. H.; Xu, H. J.; An, L. L.; Xu, Y. M. Impacts of heat stress on baseline immune measures and a subset of T cells in Bama miniature pigs. *Livest. Sci.* **2011**, *135*, 289−292.

(3) Yu, J.; Yin, P.; Liu, F.; Cheng, G.; Guo, K.; Lu, A.; Zhu, X.; Luan, W.; Xu, J. Effect of heat stress on the porcine small intestine: a morphological and gene expression study. *Comp. Biochem. Physiol. A: Mol. Integr. Physiol.* **2010**, *156*, 119−128.

(4) Su, Li.; Wang, M.; Yin, S. T.; Wang, H. L.; Chen, Liang.; Sun, L. G.; Ruan, D. Y. The interaction of selenium and mercury in the accumulations and oxidative stress of rat tissues. *Ecotox. Environ. Saf.* **2008**, *70*, 483−489.

(5) Grimble, R. F. Modification of inflammatory aspects of immune function by nutrients. *Nutr. Res. (N.Y.)* **1998**, *18*, 1297−1317.

(6) Kim, H. P.; Imbert, J.; Leonard, W. J. Both integrated and differential regulation of components of the IL-2/IL-2 receptor system. *Cytokine Growth Factor Rev.* **2006**, *17*, 349−366.

(7) Danesi, F.; Malaguti, M.; Nunzio, M. D.; Maranesi, M.; Biagi, P. L.; Bordoni, A. Counteraction of adriamycin-induced oxidative damage in rat heart by selenium dietary supplementation. *J. Agric. Food Chem.* **2006**, *54*, 1203−1208.

(8) Maggini, S.; Wintergerst, E. S.; Beveridge, S.; Hornig, D. H. Selected vitamins and trace elements support immune function by strengthening epithelial barriers and cellular and humoral immune responses. *Br. J. Nutr.* **2007**, *98*, 29−35.

(9) Hoffmann, F. K. W.; Hashimoto, A. C.; Shafer, L. A.; Dow, S.; Berry, M. J.; Hoffmann, P. R. Dietary selenium modulates activation and differentiation of CD4+ T cells in mice through a mechanism involving cellular free thiols. *J. Nutr.* **2010**, *140*, 1155−1161.

(10) Rotruck, J. T.; Pope, A. L.; Ganther, H. E.; Swanson, A. B.; Hafeman, D. G.; Hoekstra, W. G. Selenium: biochemical role as a component of glutathione peroxidase. *Science* **1973**, *179*, 588−590.

(11) Banerjee, S.; Yang, S.; Foster, C. B. A luciferase reporter assay to investigate the differential selenium-dependent stability of selenoprotein mRNAs. *J. Nutr. Biochem.* **2011**, *23*, 1294−1301.
(12) Ghazi, H. S.; Habibiyan, M.; Moeini, M. M.; Abdolmohammadi, A. R. Effects of dietary selenium, vitamin E, and their combination on growth, serum metabolites, and antioxidant defense system in skeletal muscle of broilers under heat stress. *Biol. Trace Elem. Res.* **2012**, *148*, 322−330.
(13) Niu, Z.; Liu, F.; Yan, Q.; Li, L. Effects of different levels of selenium on growth performance and immunocompetence of broilers under heat stress. *Arch. Anim. Nutr.* **2009**, *63*, 56−65.
(14) Zhou, J. C.; Zhao, H.; Li, J. G.; Xia, X. J.; Wang, K. N.; Zhang, Y. J.; Liu, Y.; Zhao, Y.; Lei, X. G. Selenoprotein gene expression in thyroid and pituitary of young pigs is not affected by dietary selenium deficiency or excess. *J. Nutr.* **2009**, *139*, 1061−1066.
(15) Zhan, X. A.; Qie, Y. Z.; Wang, M.; Li, X.; Zhao, R. Q. Selenomethionine: an effective selenium source for sow to improve Se distribution, antioxidant status, and growth performance of pig offspring. *Biol. Trace Elem. Res.* **2011**, *142*, 481−491.
(16) Jiang, Z. Y.; Lin, Y. C.; Zhou, G. L.; Luo, L. H.; Jiang, S. Q.; Chen, F. Effects of dietary selenomethionine supplementation on growth performance, meat quality and antioxidant property in yellow broilers. *J. Agric. Food Chem.* **2009**, *57*, 9769−9772.
(17) Montgomery, J. B.; Wichtel, J. J.; Wichtel, M. G.; McNiven, M. A.; McClure, J. T.; Markham, F.; Horohov, D. W. Effects of selenium source on measures of selenium status and immune function in horses. *Can. J. Vet. Res.* **2012**, *76*, 281−291.
(18) Musa, H. H.; Wu, S. L.; Zhu, C. H.; Seri, H. I.; Zhu, G. Q. The potential benefits of probiotics in animal production and health. *J. Anim. Vet. Adv.* **2009**, *8*, 313−321.
(19) Zhang, W.; Azevedo, M. S. P.; Wen, K.; Gonzalez, A.; Saif, L. J.; Li, G. H.; Yousefc, A. E.; Yuan, L. J. Probiotic *Lactobacillus acidophilus* enhances the immunogenicity of an oral rotavirus vaccine in gnotobiotic pigs. *Vaccine* **2008**, *26*, 3655−3661.
(20) Lessard, M.; Dupuis, M.; Gagnon, N.; Nadeau, É.; Matte, J. J.; Goulet, J.; Fairbrother, J. M. Administration of *Pediococcus acidilactici* or *Saccharomyces cerevisiae boulardii* modulates development of porcine mucosal immunity and reduces intestinal bacterial translocation after *Escherichia coli* challenge. *J. Anim. Sci.* **2009**, *87*, 922−934.
(21) Zulkifli, I.; Abdullah, N.; Mohd, N.; Ho, Y. Growth performance and immune response of two commercial broiler strains fed diets containing Lactobacillus cultures and oxytetracycline under heat stress conditions. *Br. Poult. Sci.* **2000**, *41*, 593−597.
(22) Pan, C.; Zhao, Y.; Liao, S. F.; Chen, F.; Qin, S.; Wu, X.; Zhou, H.; Huang, K. Effect of selenium-enriched probiotics on laying performance, egg quality, egg selenium content, and egg glutathione peroxidase activity. *J. Agric. Food Chem.* **2011**, *59*, 11424−11431.
(23) Gao, J.; Huang, K.; Qin, S. Determination of selenomethionine in selenium-enriched yeast by gas chromatography-mass spectrometry [in Chinese]. *Se Pu* **2006**, *24*, 235−238.
(24) Gan, F.; Ren, F.; Chen, X.; Lv, C.; Pan, C.; Ye, G.; Shi, J.; Shi, X.; Zhou, H.; Shituleni, S. A.; Huang, K. Effects of selenium-enriched probiotics on heat shock protein mRNA levels in piglet under heat stress conditions. *J. Agric. Food Chem.* **2013**, *61*, 2385−2391.
(25) Ibrahim, H. A. M.; Zhu, Y. X.; Wu, C.; Lu, C. H.; Ezekwe, M. O.; Liao, S. F.; Haung, K. H. Selenium-enriched probiotics improves murine male fertility compromised by high fat diet. *Biol. Trace Elem. Res.* **2012**, *147*, 251−260.
(26) Zhang, H. Y.; Sun, H. Up-regulation of Foxp3 inhibits cell proliferation, migration and invasion in epithelial ovarian cancer. *Cancer Lett.* **2010**, *287*, 91−97.
(27) Yoshida, N.; Fujita, M.; Nakahara, M.; Kuwahara, T.; Kawakami, S. I.; Bungo, T. Effect of high environmental temperature on egg production, serum lipoproteins and follicle steroid hormones in laying hens. *J. Poult. Sci.* **2011**, *48*, 207−211.
(28) Tao, S.; Monteiro, A. P.; Thompson, I. M.; Hayen, M. J.; Dahl, G. E. Effect of late-gestation maternal heat stress on growth and immune function of dairy calves. *J. Dairy. Sci.* **2012**, *95*, 7128−7136.
(29) Niu, Z. Y.; Liu, F. Z.; Yan, Q. L.; Li, W. C. Effects of different levels of vitamin E on growth performance and immune responses of broilers under heat stress. *Poult. Sci.* **2009**, *88*, 2101−2107.
(30) Alhidary, I.; Shini, S.; Al, J. R.; Gaughan, J. Effect of various doses of injected selenium on performance and physiological responses of sheep to heat load. *J. Anim. Sci.* **2012**, *90*, 2988−2994.
(31) Lähteinen, T.; Lindholm, A.; Rinttilä, T.; Junnikkala, S.; Kant, R.; Pietilä, T. E.; Levonen, K.; Ossowski, I.; Solano, A. G.; Jakava, V. M. Effect of *Lactobacillus brevis* ATCC 8287 as a feeding supplement on the performance and immune function of piglets. *Vet. Immunol. Immunopathol.* **2014**, *158*, 14−25.
(32) Speight, S. M.; Estienne, M. J.; Harper, A. F.; Barb, C. R.; Pringle, T. D. Effects of organic selenium supplementation on growth performance, carcass measurements, tissue selenium concentrations, characteristics of reproductive organs, and testis gene expression profiles in boars. *J. Anim. Sci.* **2012**, *90*, 533−542.
(33) Chadio, S. E.; Kotsampasi, B. M.; Menegatos, J. G.; Zervas, G. P.; Kalogiannis, D. G. Effect of selenium supplementation on thyroid hormone levels and selenoenzyme activities in growing lambs. *Biol. Trace Elem. Res.* **2006**, *109*, 145−154.
(34) Kumar, N.; Garg, A. K.; Mudgal, V.; Dass, R. S.; Chaturvedi, V. K.; Varshney, V. P. Effect of different levels of selenium supplementation on growth rate, nutrient utilization, blood metabolic profile, and immune response in lambs. *Biol. Trace. Elem. Res.* **2008**, *126*, 44−56.
(35) Wang, A.; Yi, X.; Yu, H.; Dong, B.; Qiao, S. Free radical scavenging activity of *Lactobacillus fermentum in vitro* and its antioxidative effect on growing-finishing pigs. *J. Appl. Microbiol.* **2009**, *107*, 1140−1148.
(36) Wang, J.; Ji, H.; Wang, S.; Zhang, D.; Liu, H.; Shan, D.; Wang, Y. *Lactobacillus plantarum* ZLP001: *in vitro* assessment of antioxidant capacity and effect on growth performance and antioxidant status in weaning piglets. *J. Anim. Sci.* **2012**, *25*, 1153−1158.
(37) Ren, F.; Chen, X.; Hesketh, J.; Gan, F.; Huang, K. Selenium promotes T-Cell response to TCR-stimulation and ConA, but not PHA in primary porcine splenocytes. *PLoS One* **2012**, *7*, DOI: 10.1371/journal.pone.0035375.
(38) Huang, Z.; Rose, A. H.; Hoffmann, P. R. The role of selenium in inflammation and immunity: from molecular mechanisms to therapeutic opportunities. *Antioxid. Redox Signal.* **2012**, *16*, 705−743.
(39) Mahan, D. C. Effect of organic and inorganic selenium sources and levels on sow colostrum and milk selenium content. *J. Anim. Sci.* **2000**, *78*, 100−105.
(40) Babinska, I.; Rotkiewicz, T.; Otrocka, D. I. The effect of *Lactobacillus acidophilus* and *Bifidobacterium* spp. administration on the morphology of the gastrointestinal tract, liver and pancreas in piglets. *Pol. J. Vet. Sci.* **2005**, *8*, 29−35.
(41) Tortuero, F.; Rioperez, J.; Fernandez, E.; Rodriguez, M. L. Response of piglets to oral administration of lactic acid bacteria. *J. Food Prot.* **1995**, *58*, 1369−1374.
(42) Christensen, M. J.; Burgener, K. W. Dietary selenium stabilizes glutathione peroxidase mRNA in rat liver. *J. Nutr.* **1992**, *122*, 1620.
(43) Maquat, L. E. Evidence that selenium deficiency results in the cytoplasmic decay of GPx1 mRNA dependent on pre-mRNA splicing proteins bound to the mRNA exon-exon junction. *Biofactors.* **2001**, *14*, 37−42.

JOURNAL OF AGRICULTURAL AND FOOD CHEMISTRY

Article

pubs.acs.org/JAFC

Antioxidative, Hemocompatible, Fluorescent Carbon Nanodots from an "End-of-Pipe" Agricultural Waste: Exploring Its New Horizon in the Food-Packaging Domain

Manashi Das Purkayastha,[†] Ajay Kumar Manhar,[‡] Vijay Kumar Das,[#] Anjan Borah,[†] Manabendra Mandal,[‡] Ashim Jyoti Thakur,[#] and Charu Lata Mahanta*[,†]

[†]Department of Food Engineering and Technology, School of Engineering, [‡]Department of Molecular Biology and Biotechnology, School of Science, and [#]Department of Chemical Sciences, School of Science, Tezpur University, Assam, India 784028

Supporting Information

ABSTRACT: The attention of researchers is burgeoning toward oilseed press-cake valorization for its high protein content. Protein removal from oil-cakes generates large quantities of fibrous residue (oil-and-protein spent meal) as a byproduct, which currently has very limited practical utility. In the wake of increasing awareness in waste recycling, a simple environmentally benign hydrothermal carbonization process to convert this "end-of-pipe" waste (spent meal) into antioxidative, hemocompatible, fluorescent carbonaceous nanoparticles (FCDs) has been described. In the present investigation, an interesting application of FCDs in fabricating low-cost rapeseed protein-based fluorescent film, with improved antioxidant potential (17.5−19.3-fold) and thermal stability has been demonstrated. The nanocomposite film could also be used as forgery-proof packaging due to its photoluminescence property. For assessing the feasibility of antioxidative FCDs in real food systems, a comparative investigation was further undertaken to examine the effect of such nanocarbon-loaded composite film on the oxidative shelf life of rapeseed oil. Oil samples packed in nanocomposite film sachets showed significant delay in oxidative rancidity compared to those packed in pristine protein-film sachet (free fatty acids, peroxide value, and thiobarbituric acid-reactive substances reduced up to 1.4-, 2-, and 1.2-fold, respectively). The work presents a new concept of biobased fluorescent packaging and avenues for harnessing this potent waste.

KEYWORDS: *rapeseed press-cake, carbon nanodots, hydrothermal carbonization, nanocomposite film, rapeseed protein*

INTRODUCTION

Currently, fluorescent nanoparticles (NPs) (also known as quantum dots (QDs) due to their typical sizes below 10 nm), a young smart member of the nanomaterial family, is gaining attention, especially in the fields of optoelectronics, bioimaging, biomedicines, etc. Unfortunately, application of NPs in foods[1−5] and their packaging materials is still in its infancy. The reason behind this seems to be the raised toxicity concern and environmental hazard of the fluorescent semiconductor QDs, which are based on metallic elements and heavy metals (elements from the periodic groups II−IV, III−V, and IV−VI). Alternatively, fluorescent carbon NPs (called fluorescent carbon dots or FCDs or C-dots or simply CNPs) can become an exciting option, because they are greener for the environment and show aqueous dispersibility, numerous possible applications in nanobiotechnology, and far less toxicicty to living organisms. Recently, Sk et al.[6] reported the presence of FCDs in regular carbohydrate-based food items such as bread, jaggery, sugar caramel, cornflakes, and biscuits and also showed their biocompatibility. This novel discovery alleviated the misapprehension that all fluorescent NPs are toxic and revealed that humans have been consuming fluorescent nanomaterials in the form of food caramels for centuries, and thus they can be considered safe.

Recently, procurement of novel C-dots from greener sources such as egg,[7] orange juice,[8] banana juice,[9] soy milk,[10] glucose, sucrose, starch,[11] citric acid,[12] chitosan,[13] etc., has been the center of attraction. Although they are the current state of the art, most of these methods suffer to some degree from certain drawbacks such as the requirement of sophisticated and expensive equipment such as a laser beam, microwave, or high-power autoclave; neat chemicals as precursors for synthesis; or even multisteps of operation along with surface passivation to improve the water solubility and photoluminescent properties of C-dots. Moreover, use of such food/feed or other edible stuffs as raw materials for FCD preparation is expensive for bulk use, and in the long run would create undue strains on the food resource system and food security scheme. This is a major drawback to the commercial synthesis of NPs from these edible resources, which is unlikely to be extended in the near future. This motivated us to search for a simple economical technique for the production of FCDs from industrial or agricultural byproducts. This is a challenging but worthy concept as the use of waste materials is one of the most attractive options to reduce the raw material cost and also seems benign from an ecological point of view. In this context, very few papers are available. Lu et al.[14] reported such an endeavor from pomelo peel, and the resulting CNP was used for the detection of mercury ions in water. Wang et al.[15]

Received: January 9, 2014
Revised: April 28, 2014
Accepted: May 1, 2014
Published: May 1, 2014

 © 2014 American Chemical Society

prepared C-dots from egg-shell membrane and used it for designing a fluorescent probe for glutathione detection. In a closely related work, FCDs were prepared from used coffee grounds,[16] and their practicality in cell imaging and detection of angiotensin I and insulin was assessed. Most reported C-dots have been prepared for bioimaging, which limits their application in other fields. As such, it has become urgent to develop effective routes to create functional C-dots as well as expand their applications.[10] Explicitly, the role of FCDs in the food packaging domain is unexplored to date.

Industrially, mechanical pressing of the oilseeds produces the oil (main product) and the press-cake (byproduct). Due to the high quantity of protein, the oil-cake or meal is being used mainly as animal feed. Recently, owing to the high nutritive value of the meal protein, techniques are now being devised to harness it. After the extraction of meal protein, the residual fibrous waste material (protein spent meal) is discarded and is not extensively used in industries. At present there are very few possibilities for the utilization of this waste; usually the residue is disposed of as landfill and, hence, is as an "end-of-pipe" waste. In this work, the synthesis of green fluorescent quantum-sized carbonaceous NPs from "oil-and-protein spent" rapeseed meal by a facile hydrothermal process has been reported for the first time. These NPs are referred to as "carbogenic" because of their high oxygen content along with carbon.[12]

Undeniably, the most active area of food nanoscience research and development is "packaging". This is likely connected to the fact that the public has been shown in some studies to be more willing to embrace nanotechnology in "out-of-food" applications than those in which NPs are directly added to food.[17] Therefore, the practicality of the synthesized FCDs for making green-fluorescent edible biopackaging material was investigated in this study, thereby expanding the potential application of C-dots. Synthetic plastic packaging is beginning to be replaced by biodegradable ones because of environmental concerns. Films made of carbohydrates and protein are long and have empirically been used to make food grade biodegradable packaging materials. A recent approach to this technology involves the use of vegetable protein from different types of oil-cakes such as cottonseed,[18] pumpkin seed,[19] soybean,[20] and rapeseed/canola.[21] In this milieu, edible films using rapeseed protein were developed in the current investigation, because this biopolymer can be obtained as a value-added product from the underutilized meal. As such, the study was extended to evaluate the effect of such a nanoadditive on the physicochemical properties of rapeseed protein film.

Mostly, consumers have to rely on holograms and other displays on the packets to segregate authentic products from their duplicate inferior counterparts. Often, fluorescent dyes are incorporated into the packaging to help customers easily detect authentic products (e.g., erythrosine); however, many of these dyes have been shown to be cytotoxic to a variety of mammalian cell types.[22] The unique "green" photoluminescence property of the here-in synthesized carbogenic NPs, along with high antioxidative potential and hemocompatibility, offer a solution to this problem. It is envisioned that FCD-incorporated edible films would not only be useful for quality control to ensure that consumers are able to purchase authenticated products, but would also improve the oxidative stability of the produce/commodity. To justify this possibility, further study was conducted to see the effect of FCD−protein composite film on the oxidative shelf life of an oil sample. For simplicity, the preparative protocol along with the summarization of the complete investigation is depicted pictorially in Supplementary Figure S1 in the Supporting Information.

MATERIALS AND METHODS

Chemicals. All solvents and reagents were obtained from E. Merck (India), of either high-performance liquid chromatography (HPLC) grade or analytical reagent grade, and were used without further purification.

Materials and Sample Preparation. Cold-pressed rapeseed oil and press-cake were obtained from Assam Khadi and Village Industries Board, Guwahati, India. Press-cake was detoxified prior to protein extraction according to the reported procedure[23] and then stored at −20 °C until use.

Protein Extraction from Detoxified Meal. Aqueous suspension of detoxified meal was prepared with water (30:1 v/w), followed by the addition of 0.1 M NaCl and 0.4% sodium sulfite. The pH of the suspension was adjusted to 11 ± 0.1 with 1 N NaOH solution; the suspension was mixed (200 rpm) for 1 h at 25 °C in the orbital shaker (Sartorius Stedin Biotech, CERTOMAT IS), followed by centrifugation (Sigma 3-18K centrifuge) at 7000 rpm for 20 min at 4 °C. The solid residue (oil-and-protein spent meal) was vacuum-dried (lab companion model OV-12, Jeiotech Co., Korea) for 48 h at 40 °C, ground to pass through a sieve having 250 μm pores, and then stored at −20 °C for further use. On the other hand, the protein-rich supernatant was filtered through Whatman filter no. 41, and then ammonium sulfate was added up to 85% saturation. The mixture was kept in an ice bath for 3 h with gentle stirring and then centrifuged at 10000 rpm for 20 min at 4 °C. The obtained protein precipitate was redispersed in Milli-Q water (Millipore Water Purification System, Model-Elix, USA), neutralized to pH 7, dialyzed against water at 4 °C, and finally freeze-dried, which was subsequently used for making the composite film.

Synthesis of C−Dots from Oil-and-Protein Spent Meal. FCDs were synthesized by hydrothermal carbonization (HTC) of spent meal using the reported protocols[8,24] with slight modification. In a typical procedure, oil-and-protein spent meal (10 g) was dispersed in 1 N NaOH solution (solvent) at a solvent/meal ratio of 463:1 (v/w). The suspension was refluxed in an oil bath under magnetic stirring at 180 °C for 3 h (details of the optimal production of FCDs using response surface methodology are given in supplementary section 1 in the Supporting Information). After the reaction is over, the resultant black solution was allowed to cool and then centrifuged at 3000 rpm for 10 min to separate the unreacted residue. The brownish supernatant was washed with dichloromethane to remove the unreacted organic moieties. Subsequently, the aqueous phase was mixed with acetone (water/acetone ratio =1:3 v/v), and the acetonic extract was finally reduced to dryness under vacuum. The residue was dispersed in Milli-Q water, dialyzed against water (using 1 kDa membrane, Himedia, India), and finally dried under vacuum at 40 °C to obtain FCDs (≈0.942 g).

Characterization of C−Dots. High-resolution transmission electron microscopy (HRTEM; JEOL, JEMCXII) images along with the selected-area electron diffraction (SAED) pattern were obtained at an accelerating voltage of 200 kV, and the sample was prepared by drop casting 2 μL of NP solution (0.25 mg/mL) on a 300 mesh carbon-coated copper grid and subsequent air-drying before analysis.

X-ray diffraction (XRD) measurement was carried out in thin film mode of powdered sample using a Rigaku Miniflex model (Japan), operated at 30 kV voltage and a current of 15 mA with Cu Kα radiation source (λ = 1.54 Å) at a scan rate of 5° (2θ) min^{-1} over the range of 10−70°.

Thermogravimetric analysis (TGA) curves were collected on a TG 50 model (Shimadzu, Japan). The samples were combusted under nitrogen flow (10 mL/min, to avoid thermo-oxidative reactions) at temperatures ranging from 25 to 600 °C, at a rate of 3 °C/min.

Fourier transform infrared (FTIR) spectra were obtained on a FTIR Nicolet Magna 5PC spectrometer (Impact-410, Madison, WI, USA), coupled to a PC with Omnic analysis software and having a deuterated triglycine sulfate (DTGS) detector and Nernst filament as the IR light

source. The sample was ground with KBr powder to form well-defined pellets for IR measurement, with 32 scans from 4000 to 400 cm^{-1} at a resolution of 4 cm^{-1}.

Micrographs of the sample were obtained using a JSM-6390LV scanning electron microscope (SEM; JEOL, Japan) at an accelerating voltage of 15 kV. Prior to SEM observation, samples were mounted on stubs with double-sided adhesive tape, followed by coating the samples with a thin layer of gold. For determining the elemental composition and purity, sample was prepared on a carbon-coated copper grid and kept under vacuum desiccation for 3 h before they were loaded onto a specimen holder. Elemental analysis on single particles was carried out using electron dispersive an X-ray spectroscopy (EDX, JSM-6390LV) attachment equipped with SEM.

^{1}H and ^{13}C nuclear magnetic resonance (NMR) spectra were detected at 400 MHz by a JEOL NMR system (Japan), using the inbuilt DELTA (δ) software (version G4.3.6, Japan) provided by the manufacturer.

The ultraviolet−visible (UV−vis) absorption spectrum of aqueous NP solution (0.1 mg/mL) was recorded on a UV−vis spectrophotometer (CECIL 7400, 7000 series, Aquarius).

The photoluminescence (PL) spectrum of aqueous NP solution (0.1 mg/mL) was measured on a photoluminescent spectrophotometer (model LS 55, PerkinElmer, Singapore PTE Ltd., Singapore). Illumination of the aqueous NP dispersion for detecting its fluorescence property was done inside a UV cabinet (BD-198 model, Test Master, Kolkata, India).

Quantum yield (QY) of C-dots was measured in reference to quinine sulfate in 0.1 M H_2SO_4 (QY = 58% at 354 nm excitation).[6,25] The formula used for QY is

$$(QY)_{Sm} = (QY)_{St} \times [(PL\ area/OD)_{Sm}/(PL\ area/OD)_{St}] \times \eta_{Sm}^2/\eta_{St}^2 \quad (1)$$

where Sm indicates the sample, St indicates the standard, η is the refractive index of the solvent, and PL area and OD are the fluorescence area and absorbance value, respectively. For aqueous solutions $\eta_{sm}/\eta_{st} = 1$ was chosen.[6]

Antioxidant activity was measured by using the modified 2,2-diphenyl-1-picrylhydrazyl (DPPH) radical method.[26] Briefly, 3 mL of sample solution was mixed with 1 mL of 1 mM methanolic solution of DPPH. The mixture was then vortexed and incubated in the dark at ambient temperature for 30 min. The absorbance was measured at 517 nm in a UV−vis spectrophotometer. In the case of FCDs or ascorbic acid (as standard), the amount was varied from 10 to 180 μg/mL of reaction mixture,[27] whereas for film samples, 25 mg of each film was dissolved in 3 mL of Milli-Q water.[26] The DPPH scavenging percentage was calculated using the formula

$$\text{scavenging activity}(\%) = \{(A_D - A_S) \times 100\}/A_D \quad (2)$$

where A_D and A_S are the absorbance of the DPPH solution and the standard/sample, respectively.

The hemolytic activity assay was performed according to the reported procedure.[23] Briefly, fresh goat blood from a slaughterhouse was collected in a centrifuge tube containing anticoagulant, trisodium citrate (3.2%), and was centrifuged at 3000 rpm for 10 min. The supernatant was discarded, and only the red blood corpuscles (RBCs or erythrocytes) were collected. RBCs were further washed three times with phosphate buffer solution (PBS, pH 7.4). A 10% (v/v) suspension of erythrocytes in PBS was prepared, and 1.9 mL of this erythrocyte solution was placed in a 2 mL centrifuge tube; 0.1 mL of FCDs in PBS was added to it. The tubes were then incubated for 1 h at 37 °C. For comparison, Triton X-100 (0.2%) and PBS were taken as positive and negative controls, respectively. After incubation, the tubes were subjected to centrifugation at 3000 rpm for 10 min, and finally the absorbance of the supernatant was taken at 570 nm in the UV−visible spectrophotometer.

Cell labeling with FCDs was done according to the procedure of Chandra et al.[28] The erythrocytes enriched fraction was centrifuged twice (3000 rpm, 15 min) at 4 °C to remove the residual plasma and buffy coat. RBCs were washed three times with PBS (pH 7.4) and resuspended in the same buffer to make a packed cell volume of ≈10% (w/v) as stock. Then, cell labeling was carried out by mixing different aliquots of the above RBC stock suspension with different volumes of FCDs (30.4, 45.5, 60.8, and 75.8 μL) from its stock solution (660 mg/mL) for making the final concentrations of FCDs as 20, 30, 40, and 50 mg/mL by addition of PBS in each set of experiments. Afterward, the erythrocytes were incubated for 4 h at room temperature, centrifuged (3000 rpm, 15 min) at 4 °C, and then washed three timeswith PBS. Finally, 20 μL of the cell suspension was taken and used to prepare a smear on glass slides, which were viewed under a fluorescent microscope (LEICA DM 3000, power = ebq 50 qc, USA) attached to a LEICA DFC 450C camera.

Preparation of Rapeseed Protein−FCD Composite Film and Its Application for Oil Packaging. Rapeseed protein film solution was prepared by using the methodology reported by Cho and Rhee.[20] Freeze-dried rapeseed protein powder (8 g) and glycerol (4 g) were dissolved in 100 mL of Milli-Q water. The suspension was heated on a hot-plate magnetic stirrer for 10 min at 80 °C until a homogeneous clear solution was obtained. FCDs (20 or 30 mg) were added to the mixture, and blending was further continued for 15 min at 80 °C. The mixture (40 mL each) was cast onto glass Petri plates and then dried in an oven at 35 °C for 48 h. Films were conditioned in an environmental chamber (plant growth chamber HB 303DH, K&K Scientific Supplier, India) set at 25 °C with 50% relative humidity (RH) for 48 h. The composite films with 20 and 30 mg of FCDs/100 mL of film-forming solution were accordingly coded F1 and F2, respectively. Film without FCDs served as control and was designated F0.

Films were drawn into small rectangular sachets/pouches (5 cm × 3.5 cm), each of which was filled with 4 mL of cold-pressed rapeseed oil, and then sealed after the headspace had been flushed with nitrogen gas. Oil-containing sachets were stored for 28 days in the environmental chamber (25 °C, 50% RH), and the oil samples were analyzed after every 7 days. Oil samples packed in F0, F1, and F2 were accordingly labeled S0 (control), S1, and S2, respectively.

Characterization of the Composite Films. Film thickness was measured at five random positions with a micrometer (Mitutoyo Corp., Japan). The mean thickness was used to calculate the mechanical and barrier properties of films.

For moisture content determination, film samples were weighed into aluminum pans and dried at 105 °C in an oven for 24 h (until the equilibrium weight). The weight loss of the sample was determined, from which the moisture content was calculated.

Water vapor permeability (WVP) was determined gravimetrically following the standard method of the American Society for Testing and Materials (ASTM).[26] Conditioned film samples were sealed to glass cups (4.7 cm diameter) containing water. The film-covered cups were placed in the environmental chamber (25 °C, 75% RH). Cups were weighed periodically using an analytical balance (Denver Instrument, Bohemia, NY, USA), until steady state was reached (±0.0001 g). Once the steady state was reached, the water vapor transmission rate (WVTR, ng/m^2 s) of the film (eq 3) was determined from the slope obtained from the regression analysis of moisture weight gain (Δw) transferred through the film area (A) during a definite time (Δt). WVTR was then used to calculate WVP using eq 4.

$$WVTR = \Delta w/A(\Delta t) \quad (3)$$

$$WVP = WVTR(x/\Delta p) \quad (4)$$

x is the average thickness of the film, and Δp is the partial water vapor pressure between the two sides of the film.

Oxygen permeability of the films was determined by using the wet chemical procedure of Ayranci and Tunc.[29]

Tensile strength (TS, in MPa) and *Elongation at break* (EB, %) of the film was measured according to ASTM D-882-91.[30] For evaluating *puncture strength* (PS, given as force in Newton (N)), film was punctured with a 2 mm probe in a Texture Analyzer (TA HD Plus, Stable Micro Systems, UK).

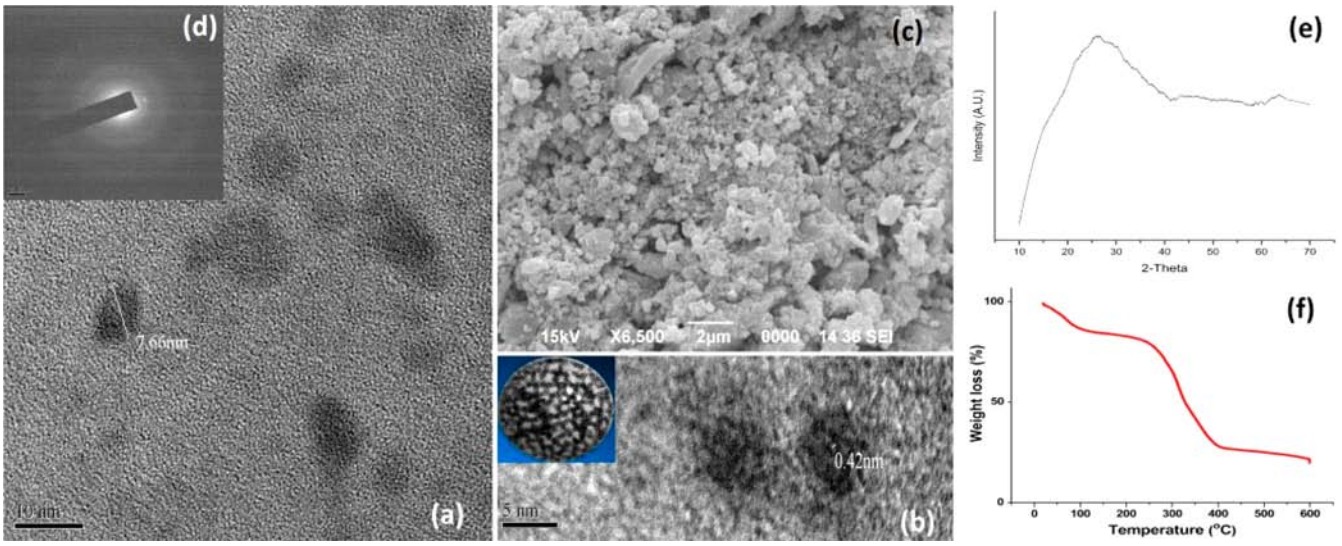

Figure 1. (a) TEM image of FCDs thus formed; (b) corresponding HRTEM image of two nanoparticles (inset, pictorial representation of the morphology of one nanoparticle); (c) SEM image of the clusters of nanoparticles obtained after drying; (d) SAED image; (e) XRD pattern; (f) TGA curve of FCDs.

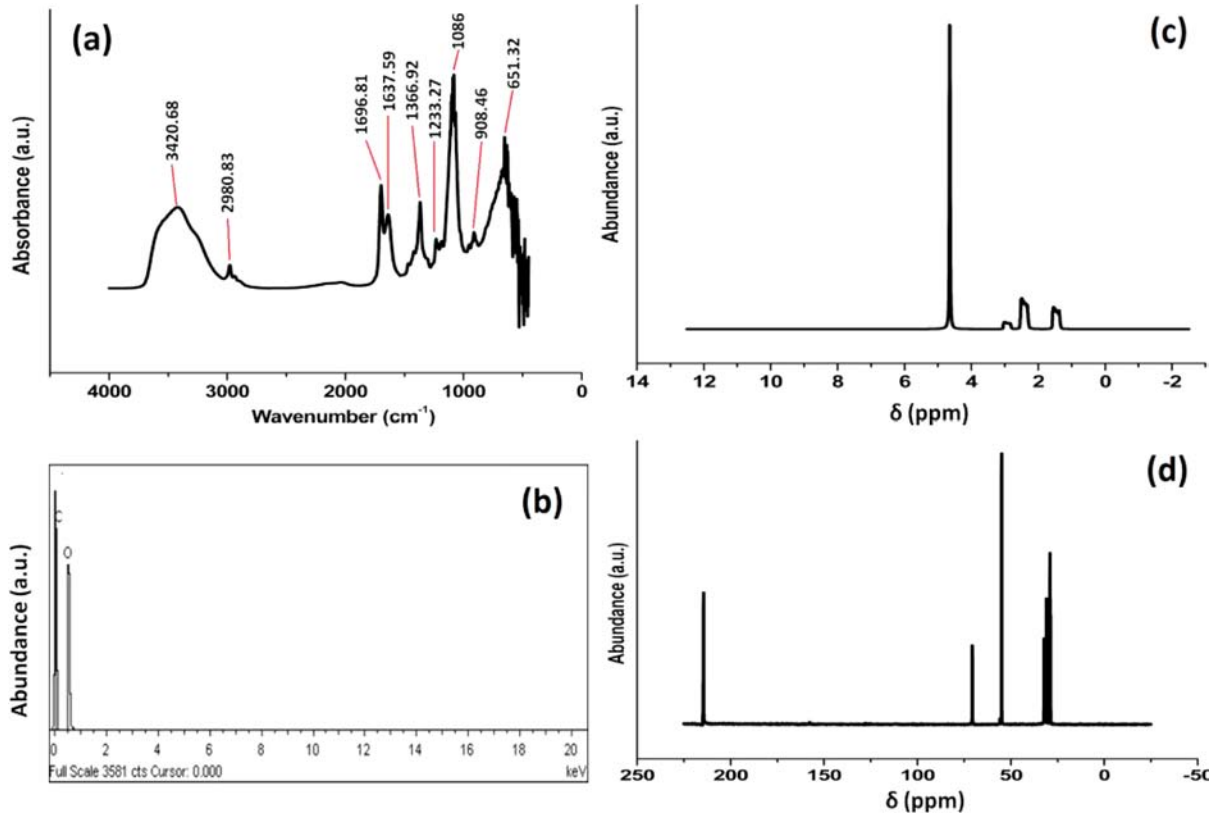

Figure 2. (a) FTIR spectrum, (b) EDX data, (c) ^{1}H NMR, and (d) ^{13}C NMR of FCDs.

Color intensity of the film was measured using a Hunter Lab Colorimeter (Ultrascan, VIS-Hunter Associates Lab., USA), fitted with a large area port (2.5 cm diameter aperture). The instrument (including 65°/0° geometry, D25 optical sensor, 10° observer, specular light) was calibrated using white and black reference tiles provided by the manufacturer.

For determining *opacity*, film absorbance was measured at 600 nm using a UV−vis spectrophotometer.[26] The sample was cut into a rectangle piece and directly placed in a spectrophotometer test cell, using an empty test cell as the reference. The opacity index of the film was calculated by using the equation

$$\text{opacity} = \text{Abs}_{600}/x \quad (5)$$

where Abs_{600} is the absorbance at 600 nm and x is the average film thickness (mm).

Analytical Tests for Oil Sample. *Free fatty acid* (FFA) and *peroxide value* (PV) were determined according to the method of Chaijan et al.[31] and expressed as grams per 100 g of lipid and milliequivalents (mequiv) of free iodine per kilogram of lipid, respectively.

Conjugated diene (CD) was estimated from the absorbance value at 233 nm using cyclohexane as the solvent blank.[32]

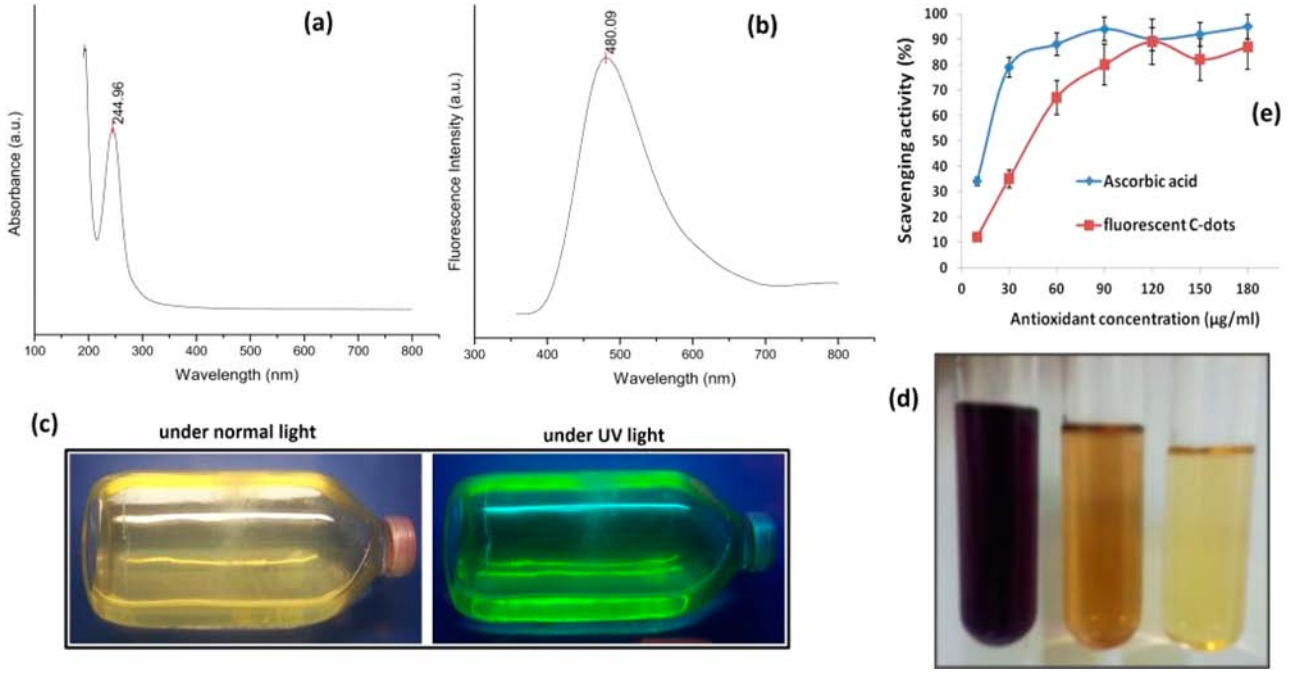

Figure 3. (a) UV−vis spectrum; (b) PL spectrum of aqueous dispersion of FCDs (0.1 mg/mL); (c) photographs of aqueous FCD dispersion (0.25 mg/mL) observed under white light and the same under UV light; (d) gradual bleaching of DPPH solution by FCDs; (e) DPPH scavenging activity of FCDs in comparison to that of ascorbic acid.

For *thiobarbituric acid-reactive substances (TBARS) assay*,[31,33,34] oil sample (0.5 g) was mixed with 2.5 mL of a solution containing 0.375% thiobarbituric acid, 15% trichloroacetic acid, and 0.25 N HCl. The mixture was heated in a boiling water bath (95−100 °C) for 10 min to develop a pink color, cooled with running tap water, and then centrifuged (3600*g*) at 25 °C for 20 min. The absorbance value of the supernatant at 532 nm was expressed as the result (A_{532}).

Statistical Analysis. All analyses were performed in triplicate, and the mean value was calculated. Analysis of variance (ANOVA) and separation of means were carried out by Tukey test, using SPSS software (version 16.0, SPSS Inc., Chicago, IL, USA) and considered significantly different at $p < 0.05$.

RESULTS AND DISCUSSION

Characterization of FCDs. The formation of C-dots was confirmed by TEM measurement (Figure 1a). HRTEM images clearly revealed that the NPs are spherical in shape; their diameters mainly lay in the range of 4.71−10.77 nm with maximum population at 7.66 nm. It can be seen that there are holes or crevices on the surface of C-dots, giving them an appearance of a puffer-like hollow ball (Figure 1b). The average diameter of these surface holes was calculated to be 0.42 nm (approximately). SEM image (Figure 1c) indicates that dried FCD powder is an aggregate of small carbon grains hundreds of nanometers in size. The entities appear to be nonhomogeneous in size and shape. This asymmetry is probably due to the effect of drying, because of which the NPs formed clusters of various sizes and shapes.[24]

The absence of any discernible lattice fringes in the HRTEM image suggests an amorphous nature of the as-prepared NPs. Concomitantly, the SAED pattern of the C-dots showed diffused rings (Figure 1d), revealing an amorphous carbon phase,[7] which agrees well with the HRTEM analysis. Furthermore, the XRD pattern (Figure 1e) presented a broad hump-like peak near 25.8°, which is attributed to amorphous carbon.[11]

The thermal behavior of FCDs was investigated by TGA. The thermogram (Figure 1f) exhibited a two-step degradation pattern with the initial degradation (<100 °C) ascribed to the loss of moisture and volatile products, whereas the final degradation (286.24−358.21 °C) was associated with the decomposition of oxygen-containing groups.[35]

The FTIR spectrum was acquired to gain further structural insights and the surface state of the synthesized FCDs. In this spectrum (Figure 2a), the stretching frequencies observed at 651, 908, 1086, 1233, 1367, 1638, 1697, 2981, and 3421 cm^{-1} indicate the presence of olefinic C−H (out-of-plane), epoxy ring, C−O or C−O—C, carboxylate group, C−N, C═O, C−H, and hydroxyl (−OH) stretch, respectively.[9] The different oxygenous functional groups as evident from FTIR prove that the surface of the FCD is partially oxidized. The origin of these functional groups can be ascribed to the degradation of the carbohydrates, crude fibers, and residual protein present in the spent meal through hydrothermal treatment.[10,14] Additionally, the presence of these hydrophilic functional groups imparts excellent water solubility to the C-dots without further chemical modification, which in turn promotes the environmental friendliness of the product.[9]

EDX data (Figure 2b) further confirm the fact that the as-prepared NPs mainly consist of carbon (47.81 wt %) and oxygen (52.18 wt %).

NMR spectra highlighted the presence of two different kinds of chemical environments or regions, which are discussed as follows. In the ^{1}H NMR spectrum (Figure 2c), the regions found are δ 1−3 (for sp^3 C−H protons) and δ 3−6 (for protons attached with hydroxyl, ether, and carbonyl groups).[9] Also, in the ^{13}C NMR spectrum (Figure 2d), similar regions were found; namely, δ 20−100 (for sp^3 carbons and for carbons attached with a hydroxyl group or ether linkage) and δ 214−215 (for keto, −C═O carbon atoms).[9] Specifically, the peaks within δ 28−33 depict the presence of methyl groups in the

dx.doi.org/10.1021/jf500138f | J. Agric. Food Chem. 2014, 62, 4509−4520

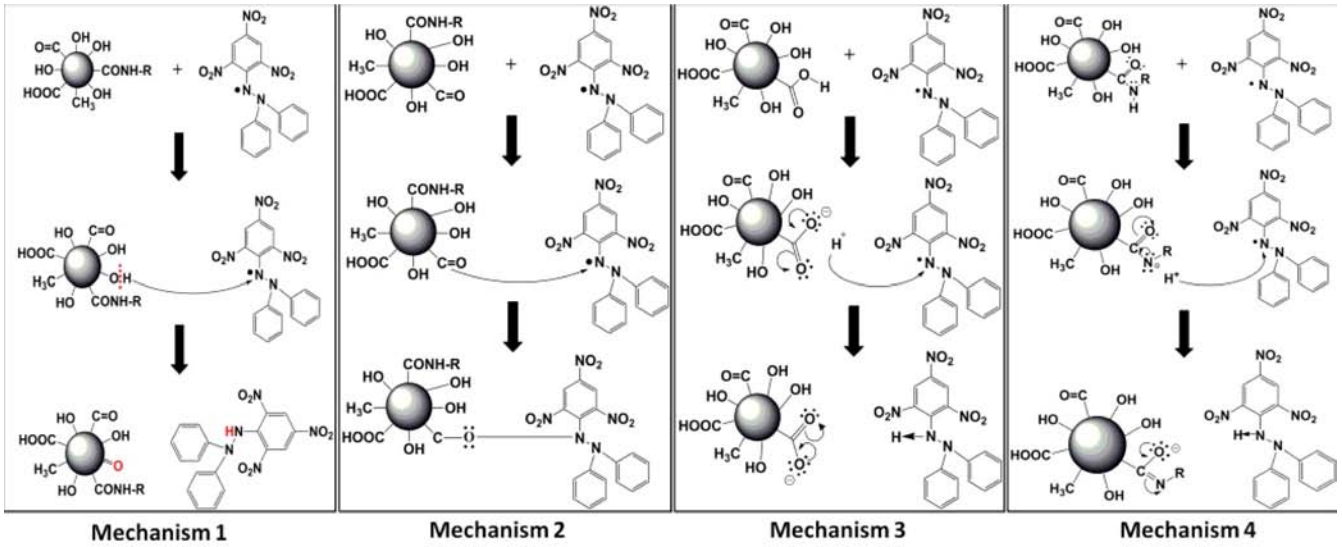

Figure 4. Plausible mechanism for the DPPH scavenging activity of FCDs.

surface functional moieties, and the singlet peak at δ 70.67 indicates the occurrence of carbohydrate units in FCDs.[6]

To explore the optical properties of FCDs, UV−vis absorption (Figure 3a) and PL studies were carried out. FCDs showed maximum UV absorption peak at 244.96 nm, which is likely to have originated from the formation of multiple polyaromatic groups where $\pi-\pi^*$ transitions of the aromatic C−C bond occur.[8] Most C-dots are excited in the UV region (330−420 nm) and yield photoluminescence in the wavelength range of 400−600 nm depending on the size of the C-dots.[16] Figure 3b shows the PL emission peak of FCDs centered at 480.09 nm, with excitation at 350 nm. This is consistent with the literature. From the fundamental as well as application viewpoint, fluorescence is one of the most fascinating behaviors of C-dots. The aqueous solution of FCDs is bright yellow and transparent in normal light but changes to an intense green color under UV light (Figure 3c), signifying the NPs to be fluorescent. It is worth noting that the origin of fluorescence from the obtained dispersion could be attributed only to the presence of C-dots because the preparatory ingredients (spent rapeseed meal, water, and NaOH) are known to be nonfluorescent materials (i.e., nonemissive under UV light), further confirming the formation of luminescent NPs. QY measured using quinine sulfate as a reference was found to be 9.2%, which is comparable with those of the reported luminescent C-dots. The fundamental mechanism of fluorescence of C-dots is still an open question; however, it is thought that the presence of quantum size and different surface trap sites could be the main factors. It is believed that radiative recombination between electrons and holes (excitons) take place at the particle surface, under the illumination of excitation light, and thus fluorescence emission occurs.[36]

With the aim of detecting the radical scavenging activity of FCDs, the DPPH assay was performed. As known, a freshly prepared DPPH solution exhibits a deep purple color with an absorption maximum at 517 nm. This purple color generally fades/disappears as soon as an antioxidant is added into the medium, resulting in a decrease in absorbance at 517 nm. Interestingly, it was found that unlike other antioxidants, FCDs first turned the purple color of fresh DPPH solution into a reddish-brown color and then gradually into a colorless (bleached) product (Figure 3d). Compared to ascorbic acid, the reaction of DPPH with FCDs proceeded at a slower rate. Nevertheless, the decrease in absorbance is detectable within minutes of reaction. This observation corroborates the DPPH radical scavenging activity of carbonaceous fullerenes (C_{60}).[37] As shown in Figure 3e, the scavenging activity of ascorbic acid and FCDs increased in a dose-dependent manner up to 94% at the dose level of 90 μg/mL and to 89% at the dose level of 120 μg/mL, respectively. The EC_{50} value was determined from the plotted graph of scavenging activity versus the concentration of sample/standard, which is defined as the amount of antioxidant necessary to decrease the initial DPPH radical concentration by 50%. EC_{50} values of ascorbic acid and FCDs were found to be 35.83 $\pm$ 4.17 and 56.16 $\pm$ 2.97 μg/mL, respectively ($p < 0.05$), confirming that the scavenging potential of FCDs was lower than that of ascorbic acid. Nonetheless, this noble facet of FCDs raises the prospects of its incorporation into oxidation-prone food models. Indeed, the nanochemistry involved in radical scavenging property of C-dots needs further investigation; however, from the knowledge gained so far, it could be explained that the quenching behavior of FCDs may be attributed to its quantum size with increased surface-to-volume ratio, providing more available reaction sites, and also to the presence of different functional moieties on the surface (−OH, C═O, −CONR, −COOH, etc.), which tends to interact with and reduce DPPH species. It has been reported that among the water-soluble fullerenes, nanomaterials of C_{60} $(C(COOH)_2)_2$, $C_{60}(OH)_{22}$, and metallofullerenes possess high antioxidative function and can wipe out different types of reactive oxygen species (ROS) depending on surface modification.[36] Amino acid-functionalized multiwalled carbon nanotubes were found to be more potent antioxidants than butylated hydroxyanisole and reduced glutathione.[38] A schematic illustrating the probable mechanism(s) is proposed in Figure 4. Data from the literature suggest that similar to fullerenes, ROS or free radicals may be "grafted" or adsorbed at the surface of C-dots by radical addition to the carbon framework, which is due to their high electron affinity.[37,39] Thus, the mechanism of scavenging reaction is not straightforward in the case of NPs, and a generalized inference can be drawn that the organic

dx.doi.org/10.1021/jf500138f | J. Agric. Food Chem. 2014, 62, 4509−4520

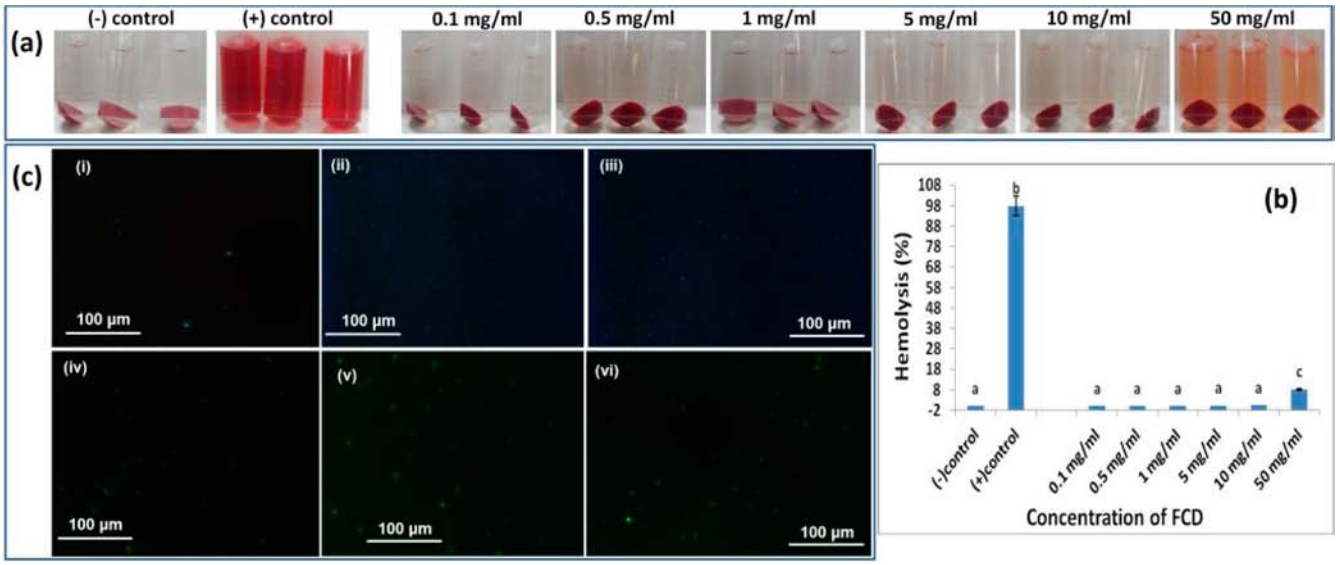

Figure 5. (a) Photographs of RBCs treated with FCDs at different concentrations. The released hemoglobin from the damaged cells in the supernatant can be seen in the photographs. (b) Hemolysis percentages of FCDs at different concentrations; (c) RBCs treated with various concentrations of FCDs observed under fluorescence microscope by excitation at 405 nm (i−(iii) and 488 nm (iv−vi).

functionalities of NPs can quench DPPH radicals (perhaps by providing hydrogen atom or by electron donation, conceivably via a free radical attack on the DPPH molecule, or by grafting/linking of radicals to C-dot's surface) and convert them to a colorless/bleached product (i.e., 2,2-diphenyl-1-picrylhydrazine, or a substituted analogous hydrazine).

Hemocompatibility. A hemolysis test was used to determine the toxicity of FCDs on mammalian RBCs. Because there are concerns about the health implication of NPs, it is important to understand how FCDs interact specifically with RBCs, as it would eventually come in direct/indirect contact with blood as soon they are exposed to the host's body. Hemolytic activity of NPs is usually determined by measuring the absorption peak of hemoglobin at 570 nm, which is released to the solution from hemolyzed cells.[40] Photographs showing precipitated RBCs at the end of the hemolysis experiment are given in Figure 5a. The red color of the released hemoglobin from damaged cells is clearly observable for positive control and 50 mg/mL concentration of FCDs. For the rest of the samples (negative control and 0.1−10 mg/mL of FCDs), the supernatants are almost colorless, confirming the intactness of the RBC membrane in these cases. This result is in conformity with that of Figure 5b. According to ASTM E2524-08 standard (standard test method for analysis of hemolytic products of NPs), hemolysis >5% indicates that the test material causes damage to RBCs; this criterion was exceeded at the FCD concentration of 50 mg/mL. Hence, FCDs were found to exhibit hemolytic activity only at higher concentration (≥50 mg/mL), which is much lower than that reported for their other counterparts (fullerenes, carbon nanotubes, etc.) and several similar NPs.[41] This benevolent feature may be due to the presence of congenial surface functional groups, making FCDs tolerable at low concentration. Yildirim et al.[40] also found that surface functionalization of nanostructures can render them completely nonhemotoxic.

To get a closer insight into the FCD-induced biological effect on RBC, the uptake of FCDs by the RBCs was examined by fluorescence microscope (Figure 5c). With increasing dosages (20, 30, and 40 mg/mL), no marked changes in the morphological shape of RBCs was detected; however, higher concentration (50 mg/mL) caused dramatic hemolysis, showing ruptured cell membranes and patches of released cell content (Supporting Information Supplementary Figure S9). It is possible that mechanical pressure exerted by excess permeation and accumulation of FCDs inside the cells caused lysis, especially at higher dosage. Thus, FCDs were found to be biocompatible in a dose-dependent manner, with no detectable hemotoxic effect up to 40 mg/mL. The C-dots were likely internalized into the RBCs through endocytosis,[16] and even after entering into the cells, the C-dots retained their fluorescence property and turned bright green under UV excitation (488 nm). In addition, when the laser excitation was changed to 405 nm, a fluorescent blue color was observed. A similar observation was obtained by Sahu et al.[8] in the case of orange juice-derived CNP. All of these preludes demonstrate that the FCDs obtained from spent rapeseed meal can serve as a potential substitute for organic dyes or semiconductor QDs in bioimaging applications.

Characterization of Rapeseed Protein Film, with (F1 and F2) or without (F0) Added FCDs. Having established the biocompatibility, we introduced the FCDs into a biopolymer matrix (rapeseed protein) in a pursuit to make fluorescent biopackaging material. One of the most important and difficult tasks in the incorporation of active compounds and new materials in a matrix is understanding if they will be miscible with the matrix and if they will not influence the processability and their structure.[42] In this study, the preliminary experiments allowed the determination of FCD concentrations that when added to the protein-based matrix do not affect significantly their appearance and processability (Supporting Information Supplementary section 3). Accordingly, composite films having 20 or 30 mg FCDs/100 mL of film-forming solution were prepared for further analyses.

On the basis of visual inspection, all of the examined films (F0, F1, and F2) showed similar homogeneity, transparency, and flexibility, with the exception of color. The color of the film changed from slightly yellow to dark brown-yellow when FCDs were added (Figure 6a−c). Generally, CNPs are blackish-

dx.doi.org/10.1021/jf500138f | J. Agric. Food Chem. 2014, 62, 4509−4520

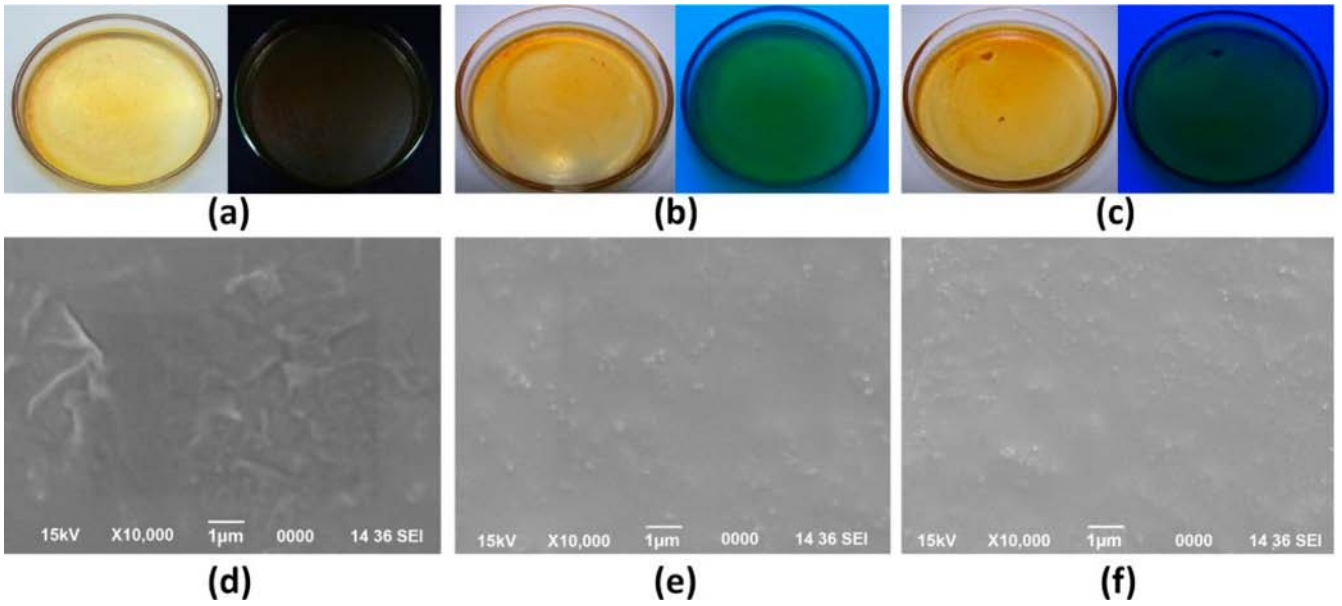

Figure 6. Photograph showing the pristine protein film and the nanocomposite films under normal light (on left) and UV light (on right) (F0 (a), F1 (b), F2 (c)) and their corresponding SEM images (F0 (d), F1 (e), F2 (f)).

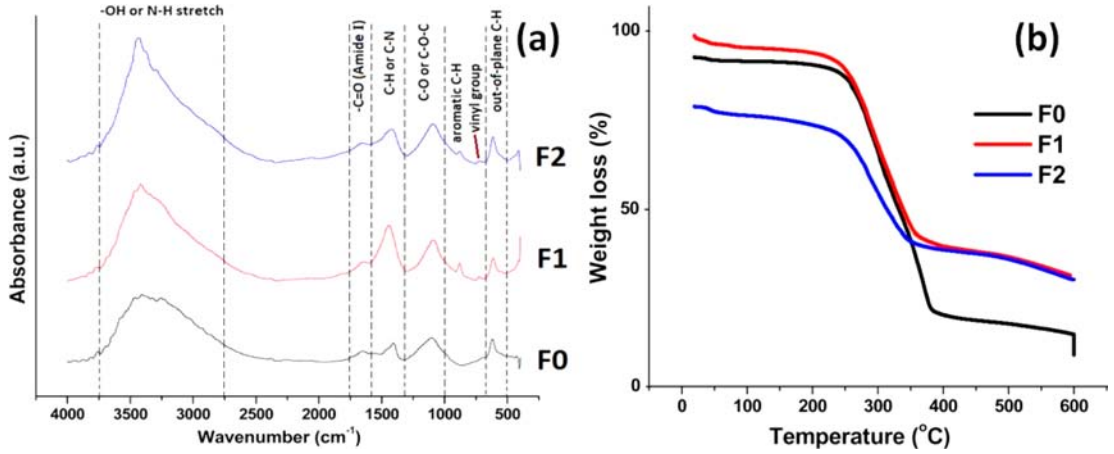

Figure 7. (a) FTIR spectra and (b) TGA curves of F0, F1, and F2.

brown, which might be the cause for dark coloration. As anticipated, F0 did not show any green glow under UV light, whereas under the same condition, F1 and F2 appeared as intense green-light-emitting films. From this it is clear that a homogeneous dispersion of the nanocomponent in the film matrix is obtained, without the presence of any visible green-colored fluorescent patches or clusters. Thus, we were successful in fabricating fluorescent glowing edible films based on the luminescent C-dots, which is envisioned to be used in forgery-proof packaging. It is expected that such packaging would benefit consumers, industry stakeholders, and food regulators. At this point, one of the objectives in this work was accomplished, and the comparative study of the physicochemical properties of these films was undertaken.

SEM was used to characterize the topography and morphology of the films (Figure 6d–f). The microstructure of F0 presented rough ridge-like protrusions on the surface, typical of protein films, as has been also reported for films prepared with soy protein,[43] rapeseed protein,[21] and pumpkin seed protein.[19] Surprisingly, F1 and F2 did not show any such ridge structures; rather, a good distribution of the additive (FCDs) in the matrix was found. FCDs appeared to be embedded on the polymeric matrix and exhibited a heterogeneous size distribution most likely due to some agglomeration. Such problems of agglomeration of nanomaterials in composite films have often been reported.[44] Agglomeration usually occurs when a relatively high loading of the nanomaterial is added to the matrix, as is the case here. Apparently, such tiny clustering did not affect the green fluorescence of the films.

The effect of the addition of FCDs into protein film was initially evaluated by FTIR. When different compounds are mixed, physical bonds and chemical interactions are reflected by changes in characteristic spectral peaks.[42] FTIR spectra of F0, F1, and F2 are shown in Figure 7a. The main broad peaks are maintained, the spectra of the films with FCDs being similar to that of the control. Special mention should be made of the peaks between 3500 and 3000 cm^{-1}, corresponding to the hydroxyl groups or hydrogen bonds or to the N–H group, that are weaker in F0 when compared to F1 or F2. This stretch appeared to be more recognizable with increasing FCD concentration. This indicates higher amounts of O–H or N–

dx.doi.org/10.1021/jf500138f | J. Agric. Food Chem. 2014, 62, 4509–4520

H groups in F1 and F2 than in F0. Derived from this fact, it is feasible to believe that FCDs, with hydrophilic surface moieties, may form hydrogen bonding between themselves or with amino groups of protein, especially when the protein is partially unfolded (denatured) during heating of a film-forming solution. This might be one of the possible reasons that F1 and F2 had more compact, uniform, and homogeneous surface morphologies compared to F0, as viewed under SEM (Figure 6d–f), mainly due to high compatibility of FCDs in the protein matrix. Addition of FCDs led to the emergence of a few new peaks in the region of 717–727 cm^{-1} (ascribable to out-of-plane C–H bending in aromatic substitution) and 878–881 cm^{-1} (correlating to the presence of vinyl groups). Moreover, in F1 and F2, the intensity of C–H or C–N stretching at 1400–1450 cm^{-1} increased and seemed to be more distinguishable than that in F0. All of these facets signify the possibility of new interactions and cross-links between FCDs and polymeric matrix.

The thermal stability of the composite films was tested by TGA. The thermograms in Figure 7b show that all of the film samples follow a similar degradation pattern, indicating uniform dispersion and high interactions of FCDs with the film (polymer) matrix.[45] Surprisingly, in all three samples, no significant mass loss was noted up to ∼260 °C, beyond which decomposition of glycerol and protein occurred.[18] The char yield is the nonvolatile carbonaceous material generated on pyrolysis, which is indicated by the residual weight after the decomposition step. It is worth mentioning that the increase of the residual yield (the char) with the increase of FCD concentration was detected, which points to the thermo-insulating nature of the C-dots as a nanofiller for the polymer matrix, a property similar to that of carbon nanotubes.[46] After degradation, the net weight loss of F0 was found to be ∼80.58%, whereas those of F1 and F2 were ∼59.73 and ∼45.65%, respectively. Thus, with the increase in FCD content, significant ($p < 0.05$) reduction in weight loss was observed, thereby proving FCDs as potent thermo-insulators for proteinaceous films, a desirous property for high-temperature processing.

Adding FCDs to the film matrix had little or no influence on film thickness ($p > 0.05$) (Table 1). This might be due to their small size. Although the same amount of film-forming solution was used, the slightly higher thickness of F0 may be due to its ridges-like rough outgrowths on its surface, as seen under SEM. The presence of FCDs led to an increase of water affinity of edible films, showing that moisture content increases in F1 and F2 significantly ($p < 0.05$) as compared to F0 (Table 1). This may be due to the hydrophilic behavior of the –OH groups in FCDs, which probably influenced WVP, increasing the adsorption of water molecules[42] in FCD-incorporated films when compared with F0. As a consequence, the water vapor barrier property of F1 and F2 is less than that of F0 (Table 1). The opposite behavior was observed for O_2 permeability, leading to a significant decrease ($p < 0.05$) of the values for FCD-containing films when these were compared with F0. Usually it is perceived that higher WVP would render higher O_2 permeability;[42] however, in this case, the radical scavenging functional groups of FCDs probably created additional sites in the film favoring the removal of oxygen, thereby minimizing the influence of adsorbed moisture in the film's transport properties. Thus, the oxygen barrier property is improved due to the presence of FCDs.

Table 1. Physicochemical Properties of Pristine Protein (F0) and Nanocomposite Films (F1 and F2)[a]

property	F0	F1	F2
thickness (μm)	54.1 ± 0.2a	48.8 ± 0.15a	49.7 ± 0.09a
moisture content (% dry basis)	28.26 ± 1.64a	35.84 ± 1.09b	36.91 ± 1.38c
WVP (ng m/m^2 s Pa)	1.43 ± 0.62a	2.47 ± 1.56b	2.85 ± 1.42b
oxygen permeability (ng day^{-1} Pa^{-1} m^{-1})	8.6 ± 0.3a	4.7 ± 0.2b	2.9 ± 0.2c
tensile strength, TS (MPa)	3.55 ± 0.51a	2.10 ± 1.78b	2.12 ± 1.15b
puncture strength, PS (N)	1.18 ± 0.03a	0.87 ± 0.01b	0.53 ± 0.09c
elongation at break, EB (%)	9.64 ± 0.02a	17.78 ± 0.69b	16.09 ± 1.03b
Hunter *L*	81.00 ± 0.13a	78.17 ± 0.16b	77.24 ± 0.09b
Hunter *a*	0.34 ± 0.01a	1.24 ± 0.03b	1.58 ± 0.05c
Hunter *b*	11.98 ± 0.12a	10.92 ± 0.07b	8.60 ± 0.04c
opacity	2.39 ± 0.17a	2.45 ± 0.13b	2.56 ± 0.02b
DPPH scavenging activity (%)	3.72 ± 1.61a	64.91 ± 2.83b	71.73 ± 4.01c

[a]Results are the mean ± standard deviation of three replicates. Values followed by same letter within a row are not significantly different ($p > 0.05$).

TS, PS, and EB of a material are used to study their resistance to tensile stress, to determine the breaking force, and to express the percentage of increase in length that occurs before the sample breaks (i.e., film's ability to stretch), respectively. The presence of FCDs in F1 and F2 influences their mechanical properties, decreasing the values of TS and PS ($p < 0.05$); on the other hand, an increase of EB values was observed. The reason behind the decreases in TS and PS by the addition of FCDs was the hydrophilic nature of C-dots, which favors the interaction with water molecules,[42] as explained by the higher moisture content of the films. Due to its small size, FCDs fit easily into the polymer chains. Due to the hydrophilic groups of FCDs (especially –OH), it is likely to be strongly bonded by hydrogen bridges with glycerol and protein molecules especially at amine, amide, carboxyl, and hydroxyl sites.[47] As a result, protein–protein interaction decreases and polymer segmental mobility increases (flexibility or EB enhances).

Good optical properties of film are extremely important in food packaging for ensuring that consumers can clearly see the food product. The darkness of the FCD-loaded films was significantly higher ($p < 0.05$), as evidenced by the lower Hunter *L* values compared to the control. Meanwhile, in comparison with F0, increase in FCD concentration increased Hunter *a* (indicator of the tendency toward redness) and decreased Hunter *b* (indicator of the reduction of yellowness) values. F0 was more transparent (lower opacity value) than F1 and F2 (Table 1). The opacity of the film samples significantly increased ($p < 0.05$) with increasing FCD concentration. This observation could be explained by the fact that a higher amount of added FCDs hinders light passage through the film. This result accords with several published studies in which addition of antioxidants, polyphenols, plant extracts, or other additives to film matrices has been found to affect the optical properties severely.

As the level of FCDs increased in the film formulation, so did the expected antioxidant character of the composite film (Table 1). In relation to F0, the DPPH scavenging activity increased by 17.5- and 19.3-fold in F1 and F2, respectively. F0 also showed

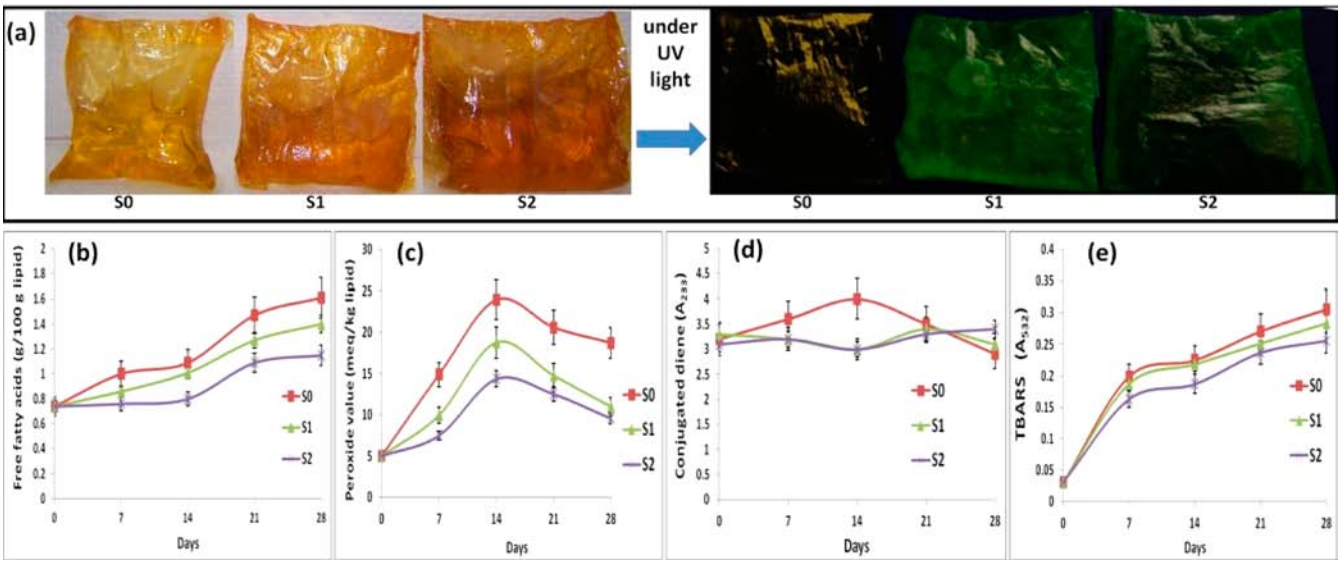

Figure 8. (a) Oil sample packed in F0, F1, and F2, as viewed under normal white light and UV light; changes in (b) free fatty acids (FFA), (c) peroxide value (PV), (d) conjugated dienes (CD), and (e) TBARS values of S0, S1, and S2 during storage.

some scavenging activity on DPPH. This is related to the fact that free radicals can react with the residual free amino ($-NH_2$) groups to form stable macromolecular radicals, and the $-NH_2$ groups can form ammonium (NH_3^+) groups by absorbing a hydrogen ion from the solution.[26] It should be noted that although a high amount of FCDs was incorporated into the film, the FCDs in the protein film showed much lower antioxidant capacity than in the free form (aqueous dispersion) at much lower concentration (Figure 3e). This could be due to interaction between FCDs and the film matrix formed via hydrogen bonds and other cross-links, thereby reducing the availability of free structural factors such as hydroxyl, keto, and carboxylic groups,[48] which imparts a scavenging feature to FCDs.

Oxidative Stability Analyses of Rapeseed Oil Packed in Nanocomposite Films. On the basis of the above results, it was presumed that the use of FCD-incorporated composite packaging could be helpful in improving the oxidative shelf life of lipid food items during storage. As such, rapeseed oil, packed in small pouches made of either nanocomposite films (F1 and F2) or pristine protein film (F0), was monitored over time to assess the antioxidative effect of these films on a real food system. The samples packaged in nanocomposite film (S1 and S2) can easily be segregated from the control (S0) under UV light, on the basis of the inherent green luminescence of C-dots (Figure 8a). To consider the complexity of the lipid oxidation process, both the primary and secondary oxidation products have been assessed.

Within the first 14 days of storage, FFA content increased perpetually in both S0 and S1 ($p < 0.05$); however, S2 showed negligible changes as compared to day 0 ($p > 0.05$) (Figure 8b). Subsequently, a gradual increase was found up to 21 days, and the highest FFA value was obtained on day 28. Possibly, lipid hydrolysis, catalyzed by lipases, occurred to a greater extent at the end of the storage period. On day 28, the respective FFA values of S1 and S2 were ~1.2- and ~1.4-fold less than that of S0. A small amount of FFA is usually noticeable in cold-pressed oil due to the release of enzymes from crushed seeds along with the oil. Alternatively, the accumulation of FFA could be attributable to the lipases from micro-organisms, which was probably enhanced with extended storage.[31]

Unsaturated fatty acids react with molecular oxygen, usually via a free radical mechanism, to form hydroperoxides, the primary oxidation products.[49] A marked increase in PV was observed in all of the tested samples for up to 14 days ($p < 0.05$) (Figure 8c). Thereafter, a decrease in PV was noticeable with extended storage ($p < 0.05$), which was presumed to be due to degradation of hydroperoxides, yielding a wide variety of secondary decomposition products including aldehydes. On day 28, the PV of S0 was almost 2 times higher than those of S1 and S2, which indicates the higher deterioration rate of S0 compared to the other samples.

During oxidation of PUFAs containing methylene-substituted dienes and polyenes, there is a shift in the position of the double bond due to isomerization and conjugate bond formation (conjugated dienes).[32] This is accompanied by increased UV absorption at 233 nm. It is an indicator of autoxidation and is reported to increase with uptake of oxygen and formation of peroxides, during the early stages of oxidation. Chaijan et al.[31] reported that almost immediately after peroxides are formed, the nonconjugated double bonds (C═C−C—C═C) that are present in natural unsaturated lipids are converted to conjugated double bonds (C═C−C═C). Thus, conjugated dienes are the primary oxidation products formed. A_{233} of S0 increased slightly up to 14 days of storage, after which its value showed a decreasing trend (Figure 8d). S1 and S2 exhibited similar profiles up to 21 days. From day 21 onward, A_{233} of S1 decreased and that of S2 continued to increase, until the end of the storage period ($p < 0.05$). This decrease probably occurred because of their decomposition into secondary oxidation products.

Secondary lipid oxidation was studied by the TBARS value. Traditionally, the absorbance at 532 nm of the pink pigment formed in the reaction is measured. In all of the samples, the TBARS value increased sharply throughout the storage ($p < 0.05$) (Figure 8e). The marked increase in TBARS during 14−28 days of storage was coincidental with the decrease in PV (Figure 8c). This was probably due to the destruction of hydroperoxides into relatively polar secondary products,

dx.doi.org/10.1021/jf500138f | J. Agric. Food Chem. 2014, 62, 4509−4520

especially aldehydes in the later stages of lipid oxidation. It was most likely that a higher rate of lipid oxidation might be taking place at the end of the storage period (days 14−28). Additionally, the loss in natural antioxidants (such as tocopherol, polyphenols, etc.) of rapeseed oil during extended storage might contribute to the increased lipid oxidation.

On the basis of the available data, it can be interpreted that the antioxidative FCDs in F1 and F2 retarded the lipid oxidation rate in S1 and S2 by quenching the free radicals. The formation of free radicals, which precedes lipid hydroperoxides, is the initial step in lipid oxidation.[34] Abstraction of hydrogen atoms from allylic carbon atoms in unsaturated lipids generates a lipid radical, which in turn has the potential to initiate the chain reactions of the autoxidation cycle.[49] The cycle is terminated either through a recombination of two radicals or by a reaction of the radical with antioxidant, leading to the formation of more stable radicals. The chain-breaking antioxidant, therefore, interrupts the oxidation chain reaction to enhance stability. Thus, FCD-incorporated packaging materials showed a profound impact on the oxidative shelf life of lipid product. Further studies need to be undertaken to improve the antioxidative and antimicrobial properties of these composite films.

From this work it is concluded that high-value CNP can be easily synthesized from spent rapeseed meal by a simple green hydrothermal route. The obtained NP was found to be multifunctional, such as water solubility, high reductive potential, photoluminescence, and biocompatibility. This is due to the rich functionalities attached to the nanocarbons. The literature enumerates biopolymer-based films as good vehicles for the incorporation of active compounds; however, inclusion of fluorescent carbon nanostructures has rarely been evaluated. The present investigation shows the incorporation of FCDs into rapeseed protein film matrix, which adds new features to the film, for instance, photoluminescence, enhancement in antioxidant potential, and thermal stability. Moreover, oil samples packed in sachets made of FCD−protein composite film are able to resist oxidation better than those stored in pristine protein-based sachets. The work opens up new possibilities for agricultural residues as a valuable precursor of useful nanomaterials and can subsequently give rise to a new concept of biobased edible fluorescent food packaging, suggesting new scalable and simple approaches to improve environmental sustainability in industrial processes. Further studies should be undertaken to analyze the release behavior of FCDs from the film into different food model systems, their effect on organoleptic properties and the gastrointestinal tract, and toxicological assessment using in vitro and in vivo models.

■ ASSOCIATED CONTENT

Supporting Information

Optimal production of FCDs using response surface methodology (RSM), mechanism of C-dot formation from rapeseed spent meal, EDX spectrum of "oil-and-protein" spent meal, hemolytic activity of FCDs using 50 mg/mL concentration, standardization of the preparation of protein−FCD composite film, and biodegradation study of nanocomposite film. This material is available free of charge via the Internet at http://pubs.acs.org.

■ AUTHOR INFORMATION

Corresponding Author

*(C.L.M.) Phone: +91 3712 267008 (5702). Fax: +91 3712 267005. E-mail: charu@tezu.ernet.in.

Funding

M.D.P. is grateful to DST-INSPIRE (India) and A.K.M. and V.K.D. are thankful to UGC-RGNF for meritorious fellowships.

Notes

The authors declare no competing financial interest.

■ ACKNOWLEDGMENTS

We are thankful to the Research staff of the Department of Physics, Tezpur University, for valuable suggestions and PL study. We gratefully acknowledge Joston P. Nongkynrih and SAIF, NEHU, Shillong, for TEM imaging.

■ REFERENCES

(1) Chen, Y.-C.; Yu, S.-H.; Tsai, G.-J.; Tang, D.-W.; Mi, F.-L.; Peng, Y.-P. Novel technology for the preparation of self-assembled catechin/gelatin nanoparticles and their characterization. *J. Agric. Food Chem.* **2010**, *58* (11), 6728−6734.

(2) Gangwar, R. K.; Tomar, G. B.; Dhumale, V. A.; Zinjarde, S.; Sharma, R. B.; Datar, S. Curcumin conjugated silica nanoparticles for improving bioavailability and its anticancer applications. *J. Agric. Food Chem.* **2013**, *61* (40), 9632−9637.

(3) Luo, Y.; Teng, Z.; Wang, T. T. Y.; Wang, Q. Cellular uptake and transport of zein nanoparticles: effects of sodium caseinate. *J. Agric. Food Chem.* **2013**, *61* (31), 7621−7629.

(4) Teng, Z.; Luo, Y.; Wang, Q. Nanoparticles synthesized from soy protein: preparation, characterization, and application for nutraceutical encapsulation. *J. Agric. Food Chem.* **2012**, *60* (10), 2712−2720.

(5) Teng, Z.; Luo, Y.; Wang, T.; Zhang, B.; Wang, Q. Development and application of nanoparticles synthesized with folic acid conjugated soy protein. *J. Agric. Food Chem.* **2013**, *61* (10), 2556−2564.

(6) Sk, M. P.; Jaiswal, A.; Paul, A.; Ghosh, S. S.; Chattopadhyay, A. Presence of amorphous carbon nanoparticles in food caramels. *Sci. Rep.* **2012**, DOI: 10.1038/srep00383.

(7) Wang, J.; Wang, C.-F.; Chen, S. Amphiphilic egg-derived carbon dots: rapid plasma fabrication, pyrolysis process, and multicolor printing patterns. *Angew. Chem., Int. Ed.* **2012**, *51*, 9297−9301.

(8) Sahu, S.; Behera, B.; Maiti, T. K.; Mohapatra, S. Simple one-step synthesis of highly luminescent carbon dots from orange juice: application as excellent bio-imaging agents. *Chem. Commun.* **2012**, *48*, 8835−8837.

(9) De, B.; Karak, N. A green and facile approach for the synthesis of water soluble fluorescent carbon dots from banana juice. *RSC Adv.* **2013**, *3*, 8286−8290.

(10) Zhu, C.; Zhai, J.; Dong, S. Bifunctional fluorescent carbon nanodots: green synthesis via soy milk and application as metal-free electrocatalysts for oxygen reduction. *Chem. Commun.* **2012**, *48*, 9367−9369.

(11) He, X.; Li, H.; Liu, Y.; Huang, H.; Kang, Z.; Lee, S.-T. Water soluble carbon nanoparticles: hydrothermal synthesis and excellent photoluminescence properties. *Colloids Surf., B* **2011**, *87*, 326−332.

(12) Bourlinos, A. B.; Stassinopoulos, A.; Anglos, D.; Zboril, R.; Karakassides, M.; Giannelis, E. P. Surface functionalized carbogenic quantum dots. *Small* **2008**, *4* (4), 455−458.

(13) Chowdhury, D.; Gogoi, N.; Majumdar, G. Fluorescent carbon dots obtained from chitosan gel. *RSC Adv.* **2012**, *2*, 12156−12159.

(14) Lu, W.; Qin, X.; Liu, S.; Chang, G.; Zhang, Y.; Luo, Y.; Asiri, A. M.; Al-Youbi, A. O.; Sun, X. Economical, green synthesis of fluorescent carbon nanoparticles and their use as probes for sensitive and selective detection of mercury(II) ions. *Anal. Chem.* **2012**, *84*, 5351−5357.

(15) Wang, Q.; Liu, X.; Zhang, L.; Lv, Y. Microwave-assisted synthesis of carbon nanodots through an eggshell membrane and their fluorescent application. *Analyst* **2012**, *137*, 5392−5397.

(16) Hsu, P.-C.; Shih, Z.-Y.; Lee, C.-H.; Chang, H.-T. Synthesis and analytical applications of photoluminescent carbon nanodots. *Green Chem.* **2012**, *14*, 917−920.
(17) Duncan, T. V. Applications of nanotechnology in food packaging and food safety: barrier materials, antimicrobials and sensors. *J. Colloid Interface Sci.* **2011**, *363*, 1−24.
(18) Yue, H.-B.; Cui, Y.-D.; Shuttleworth, P. S.; Clark, J. H. Preparation and characterization of bioplastics made from cottonseed protein. *Green Chem.* **2012**, *14*, 2009−2016.
(19) Popović, S.; Peričin, D.; Vaštag, Ž.; Popović, L.; Lazić, V. Evaluation of edible film-forming ability of pumpkin oil cake: effect of pH and temperature. *Food Hydrocolloids* **2011**, *25*, 470−476.
(20) Cho, S. Y.; Rhee, C. Mechanical properties and water vapour permeability of edible films made from fractionated soy proteins with ultrafiltration. *Lebensm. Wiss. Technol.* **2004**, *37*, 833−839.
(21) Jang, S.-A.; Lim, G.-O.; Song, K. B. Preparation and mechanical properties of edible rapeseed protein films. *J. Food Sci.* **2011**, *76* (2), C218−C223.
(22) Alford, R.; Simpson, H. M.; Duberman, J.; Hill, G. C.; Ogawa, M.; Regino, C.; Kobayashi, H.; Choyke, P. L. Toxicity of organic fluorophores used in molecular imaging: literature review. *Mol. Imaging* **2009**, *8* (6), 341−354.
(23) Das Purkayastha, M.; Das, S.; Manhar, A. K.; Deka, D.; Mandal, M.; Mahanta, C. L. Removing anti-nutrients from rapeseed press-cake and their benevolent role in waste cooking oil-derived biodiesel: conjoining the valorization of two disparate industrial wastes. *J. Agric. Food Chem.* **2013**, *61*, 10746−10756.
(24) Ray, S. C.; Saha, A.; Jana, N. R.; Sarkar, R. Fluorescent carbon nanoparticles: synthesis, characterization, and bioimaging application. *J. Phys. Chem. C* **2009**, *113* (43), 18546−18551.
(25) Bhunia, S. K.; Saha, A.; Maity, A. R.; Ray, S. C.; Jana, N. R. Carbon nanoparticle-based fluorescent bioimaging probes. *Sci. Rep.* **2013**, DOI: 10.1038/srep01473.
(26) Siripatrawan, U.; Harte, B. R. Physical properties and antioxidant activity of an active film from chitosan incorporated with green tea extract. *Food Hydrocolloids* **2010**, *24*, 770−775.
(27) Ju, K.-Y.; Lee, Y.; Lee, S.; Park, S. B.; Lee, J.-K. Bioinspired polymerization of dopamine to generate melanin-like nanoparticles having an excellent free-radical-scavenging property. *Biomacromolecules* **2011**, *12*, 625−632.
(28) Chandra, S.; Das, P.; Bag, S.; Laha, D.; Pramanik, P. Synthesis, functionalization and bioimaging applications of highly fluorescent carbon nanoparticles. *Nanoscale* **2011**, *3*, 1533−1540.
(29) Ayranci, E.; Tunc, S. A method for the measurement of the oxygen permeability and the development of edible films to reduce the rate of oxidative reactions in fresh foods. *Food Chem.* **2003**, *80*, 423−431.
(30) Hernández-Muñoz, P.; López-Rubio, A.; Lagarón, J. M.; Gavara, R. Formaldehyde cross-linking of gliadin films: effects on mechanical and water barrier properties. *Biomacromolecules* **2004**, *5*, 415−421.
(31) Chaijan, M.; Benjakul, S.; Visessanguan, W.; Faustman, C. Changes of lipids in sardine (*Sardinella gibbosa*) muscle during iced storage. *Food Chem.* **2006**, *99*, 83−91.
(32) Weber, J.; Bochi, V. C.; Ribeiro, C. P.; Victório, A. M.; Emanuelli, T. Effect of different cooking methods on the oxidation, proximate and fatty acid composition of silver catfish (*Rhamdia quelen*) fillets. *Food Chem.* **2008**, *106*, 140−146.
(33) Sun, Q.; Faustman, C.; Senecal, A.; Wilkinson, A. L.; Furr, H. Aldehyde reactivity with 2-thiobarbituric acid and TBARS in freeze-dried beef during accelerated storage. *Meat Sci.* **2001**, *57*, 55−60.
(34) Stapelfeldt, H.; Nielsen, B. R.; Skibsted, L. H. Effect of heat treatment, water activity and storage temperature on the oxidative stability of whole milk powder. *Int. Dairy J.* **1997**, *7*, 331−339.
(35) Wang, G.; Yang, J.; Park, J.; Gou, X.; Wang, B.; Liu, H.; Yao, J. Facile synthesis and characterization of graphene nanosheets. *J. Phys. Chem. C* **2008**, *112*, 8192−8195.
(36) Yan, L.; Zhao, F.; Li, S.; Hu, Z.; Zhao, Y. Low-toxic and safe nanomaterials by surface-chemical design, carbon nanotubes, fullerenes, metallofullerenes, and graphenes. *Nanoscale* **2011**, *3*, 362−382.
(37) Bhoi, V. I.; Kumar, S.; Murthy, C. N. The self-assembly and aqueous solubilization of [60]fullerene with disaccharides. *Carbohydr. Res.* **2012**, *359*, 120−127.
(38) Amiri, A.; Memarpoor-Yazdi, M.; Shanbedi, M.; Eshghi, H. Influence of different amino acid groups on the free radical scavenging capability of multi-walled carbon nanotubes. *J. Biomed. Mater. Res.−A* **2013**, *101A*, 2219−2228.
(39) Fenoglio, I.; Tomatis, M.; Lison, D.; Muller, J.; Fonseca, A.; Nagy, J. B.; Fubini, B. Reactivity of carbon nanotubes: free radical generation or scavenging activity? *Free Radical Biol. Med.* **2006**, *40*, 1227−1233.
(40) Yildirim, A.; Ozgur, E.; Bayindir, M. Impact of mesoporous silica nanoparticle surface functionality on hemolytic activity, thrombogenicity and non-specific protein adsorption. *J. Mater. Chem. B* **2013**, *1*, 1909−1920.
(41) Sayes, C. M.; Fortner, J. D.; Guo, W.; Lyon, D.; Boyd, A. M.; Ausman, K. D.; Tao, Y. J.; Sitharaman, B.; Wilson, L. J.; Hughes, J. B.; West, J. L.; Colvin, V. L. The differential cytotoxicity of water-soluble fullerenes. *Nano Lett.* **2004**, *4* (10), 1881−1887.
(42) Cerqueira, M. A.; Costa, M. J.; Fuciños, C.; Pastrana, L. M.; Vicente, A. A. Development of active and nanotechnology-based smart edible packaging systems: physical-chemical characterization. *Food Bioprocess. Technol.* **2013**, DOI: 10.1007/s11947-013-1117-5.
(43) Denavi, G.; Tapia-Blácido, D. R.; Añón, M. C.; Sobral, P. J. A.; Mauri, A. N.; Menegalli, F. C. Effects of drying conditions on some physical properties of soy protein films. *J. Food Eng.* **2009**, *90*, 341−349.
(44) Busolo, M. A.; Lagaron, J. M. Oxygen scavenging polyolefin nanocomposite films containing an iron modified kaolinite of interest in active food packaging applications. *Innovative Food Sci. Emerging Technol.* **2012**, *16*, 211−217.
(45) Deka, H.; Karak, N.; Kalita, R. D.; Buragohain, A. K. Biocompatible hyperbranched polyurethane/multi-walled carbon nanotube composites as shape memory materials. *Carbon* **2010**, *48*, 2013−2022.
(46) Dutta, S.; Karak, N.; Saikia, J. P.; Konwar, B. K. Biocompatible epoxy modified bio-based polyurethane nanocomposites: mechanical property, cytotoxicity and biodegradation. *Bioresour. Technol.* **2009**, *100*, 6391−6397.
(47) Guerrero, P.; de la Caba, K. Thermal and mechanical properties of soy protein films processed at different pH by compression. *J. Food Eng.* **2010**, *100*, 261−269.
(48) Giménez, B.; Gómez-Estaca, J.; Alemán, A.; Gómez-Guillén, M. C.; Montero, M. P. Improvement of the antioxidant properties of squid skin gelatin films by the addition of hydrolysates from squid gelatin. *Food Hydrocolloids* **2009**, *23*, 1322−1327.
(49) Choe, E.; Min, D. B. Mechanisms and factors for edible oil oxidation. *Compr. Rev. Food Sci. Food Saf.* **2006**, *5*, 169−186.

JOURNAL OF AGRICULTURAL AND FOOD CHEMISTRY

Article

pubs.acs.org/JAFC

Synthesis of Rotenone-*O*-monosaccharide Derivatives and Their Phloem Mobility

Pei-Wen Qin,[†,‡,§] Jie Wang,[†,‡,§] Hao Wang,[†,‡] Ying-Jie Wen,[†,‡] Meng-Ling Lu,[†,‡] Yu-Feng Li,[†,‡] Yue-Shuo Xu,[†,‡] and Han-Hong Xu*[,†,‡]

[†]State Key Laboratory for Conservation and Utilization of Subtropical Agro-Bioresources, and [‡]Key Laboratory of Natural Pesticide and Chemical Biology, Ministry of Education, South China Agricultural University, Guangzhou, Guangdong 510642, People's Republic of China

ABSTRACT: Six monosaccharide derivatives of rotenone were designed and synthesized to assess whether rotenone could become phloem mobile by the addition of a monosaccharide group. Phloem mobility experiments showed that only D-glucose conjugates exhibit phloem transport properties in castor bean (*Ricinus communis* L.) seedlings. Two D-glucose conjugates, 2-*O*-*β*-D-glucopyranosyldemethylrotenone and 6′-*O*-*β*-D-glucopyranosyldalpanol, had significantly obtained systemicity compared with that of rotenone, and 6′-*O*-*β*-D-glucopyranosyldalpanol was more mobile than 2-*O*-*β*-D-glucopyranosyldemethylrotenone. Coupling with a monosaccharide core is a reasonable method for conferring phloem mobility on insecticides, but phloem mobility is also affected by the parent molecule and the position of the monosaccharide.

KEYWORDS: *rotenone, monosaccharide, glycosylation reaction, phloem-mobility*

INTRODUCTION

Phloem-mobile insecticides are both economical and efficient,[1−3] but there are only a few phloem systemic insecticides obtained because the development of new pesticides with that systemicity is often expensive and complicated. Two strategies have been adopted for conferring phloem mobility to nonsystemic insecticides. One strategy consists of introducing a carboxyl group to a nonsystemic pesticide. For example, after conjugating oxamyl with glucuronic acid, the oxamyl derivative exhibits an improved phloem mobility higher than that of the parent compound in transgenic tobacco.[4] The other strategy is using the endogenous plant transporters to confer phloem mobility on nonphloem-mobile insecticides or to confer a phloem mobility different from that of the parent compound.[5−7]

In plants, sugar-transport proteins play a key role not only in long-distance transportation but also in cell-to-cell distribution of sugars throughout the plant.[8] Recently, researchers found that a plant hexose-transporter bound in plasmalemma was involved in the transportation of the 2-deoxyglucose-NBD conjugate in *E. coli*.[9] Moreover, we have reported the synthesis of a novel fipronil-glucose conjugate (GTF) and demonstrated that linking glucose can change fipronil into a phloem systemicity type, which was mediated by monosaccharide transporters.[2,10] In addition, 10 kinds of fipronil-monosaccharide derivatives were synthesized in our previous work (Figure 1).[11] Most of these derivatives have been verified as having phloem systemicity. These studies revealed that conjugating glucose or another monosaccharide can confer phloem mobility on a nonphloem-mobile insecticide.

It remains to investigate whether any nonmobile insecticide can be converted into a phloem-mobile one by the coupling of a glucose group or other monosaccharide in the same manner as that done to fipronil. Therefore, this study focuses on rotenone, a natural product of the isoflavone family and a botanical insecticide obtained from the root extracts of some leguminous plants such as *Derris* and *Lonchocarpus*.[12−15] Rotenone was linked with five kinds of monosaccharides (glucose, galactose, mannose, xylose, and arabinose) to obtain

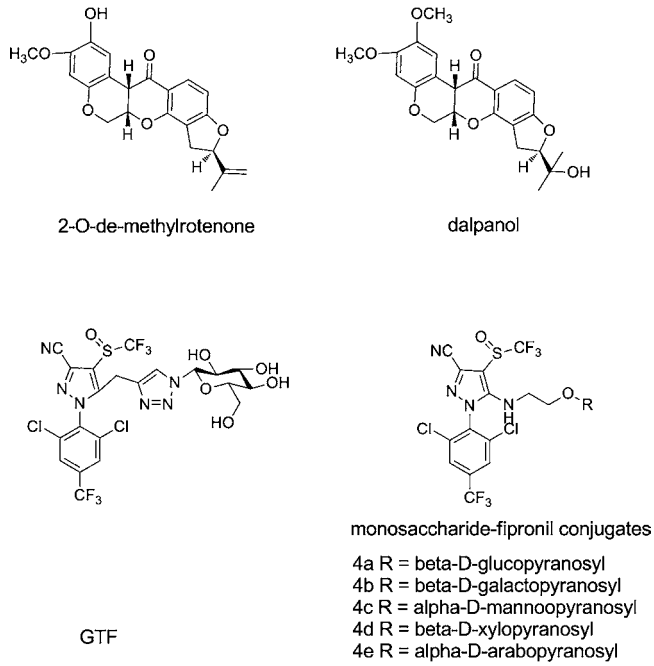

Figure 1. Chemical structure of 2-*O*-demethylrotenone, dalpanol, GTF, and monosaccharide-fipronil conjugates.

Received: January 12, 2014
Revised: April 28, 2014
Accepted: April 29, 2014
Published: April 29, 2014

ACS Publications © 2014 American Chemical Society

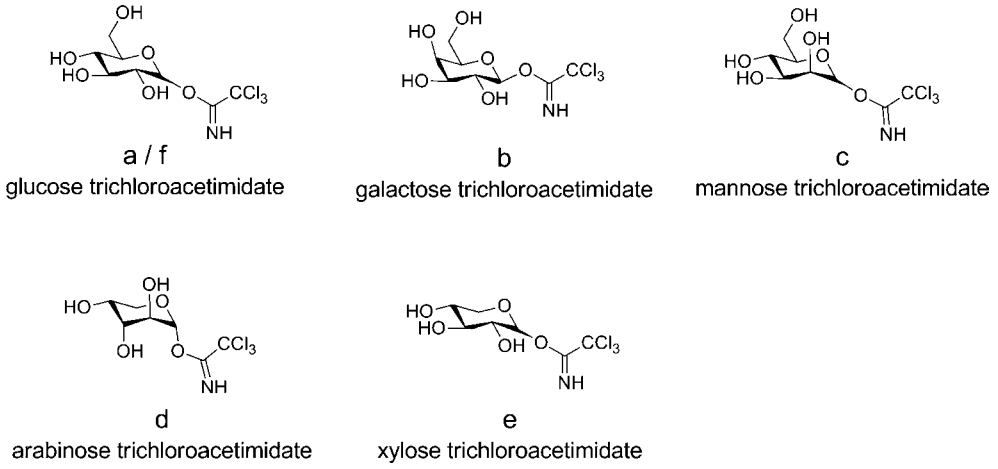

Figure 2. Structures of monosaccharide trichloroacetimidate donors.

Scheme 1[a]

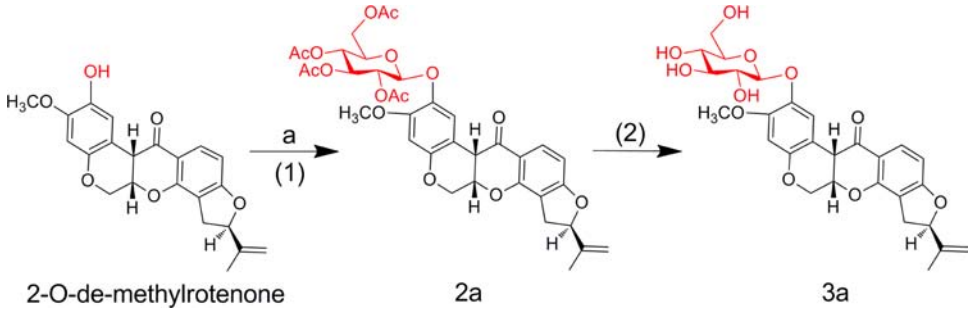

[a]Reagents and conditions: (1) $BF_3{\cdot}OEt_2$, CH_2Cl_2, and 4 Å molecular sieves, −30 °C and (2) CH_3OH and CH_3COCl, and 25 °C.

Scheme 2[a]

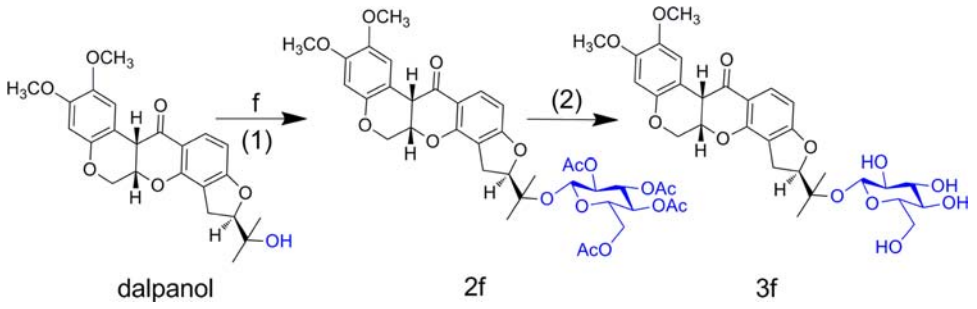

[a]Reagents and conditions: (1) TMSOTf, CH_2Cl_2, and 4 Å molecular sieves, −30 °C and (2) CH_3OH and CH_3COCl, and 25 °C.

six rotenone-glucosides linked with an *O*-glycosidic bond, including a natural product, dalpanol-*O*-glucoside.[16] Their phloem mobilities were tested in a *Ricinus* system.

MATERIALS AND METHODS

General Methods. TLC was taken on a silica gel plate (GF_{254}, Qingdao, China). Silica gel (200−300 mesh) was used for flash column chromatography. The ^1H and ^{13}C NMR spectra were provided by a Bruker AVANCE III 600 (Brunker Corporation, Switzerland) spectrometer with tetramethylsilane (TMS) as the internal standard, and chemical shifts were recorded. The mass spectrographic analysis was recorded on a Waters ZQ4000 (Waters, MA, USA) with electron-spray ionization.

Materials. The seeds of castor bean No. 9, provided by the Agricultural Science Academy of Zibo (Zibo, China), and the cultivation of seedlings were followed by a previous method.[17] Then, six day-old seedlings (the hypocotyl was about 20 mm length) were selected for further experiments.

General procedure for the Preparation of Compounds (2a−2f). Trichloroacetimidate donors[18] (Figure 2), 2-de-*O*-methylrotenone[19,20] and dalpanol[21] (Figure 1) were synthesized as previously described.

The trichloroacetimidate donor (1.2 mmol), activated 4 Å molecular sieve, and 2-de-*O*-methylrotenone (1 mmol), or dalpanol (1 mmol) were added in anhydrous CH_2Cl_2 (10 mL) under nitrogen atmosphere. The mixtures were carried out at 25 °C for 0.5 h, then cooled to −30 °C. Next, boron trifluoride etherate ($BF_3{\cdot}OEt_2$, 0.05 mL) was injected into the solution containing 2-de-*O*-methylrotenone to produce compounds **2a**−**2e** (Scheme 1). Trimethylsilyl trifluoromethanesulfonate (TMSOTf, 0.05 mL) was injected to the solution containing dalpanol to produce compound **2f** (Scheme 2). The mixtures were kept in this condition for 4 h and stirred another 1 h at 25 °C. After filtering the suspension, the filtrate was collected and

dx.doi.org/10.1021/jf500197k | J. Agric. Food Chem. 2014, 62, 4521−4527

dried in vacuo, followed by chromatography (chloroform−methanol, 99:1) to produce compounds **2a−2f** as solids.

*2-O-(2,3,4,6-Tetra-O-acetyl)-β-D-glucopyranosyldemethylrotenone (**2a**).* White solid; yield 88%. ^{1}H NMR ($CDCl_3$) δ: 7.81(d, J = 8.4 Hz, 1H), 7.07 (s, 1H), 6.52 (d, J = 8.4 Hz, 1H), 6.43 (s, 1H), 5.26−5.20 (m, 3H), 5.16 (m, 1H), 5.07 (brs, 1H), 4.93−4.92 (m, 2H), 4.76 (dd, J = 6.0, 2.4 Hz, 1H), 4.60 (dd, J = 12.0, 3.6 Hz, 1H), 4.30 (dd, J = 12.0, 4.8 Hz, 1H), 4.19−4.14 (m, 2H), 3.80(d, J = 4.2 Hz, 1H), 3.74 (s, 3H), 3.70(ddd, J = 10.2, 4.8, 2.4 Hz, 1H), 3.31 (dd, J = 15.6, 9.6 Hz, 1H), 2.95 (dd, J = 15.6, 8.4 Hz, 1H), 2.14, 2.04, 2.03, and 2.01 (s, both 3H, Ac), 1.76 (s, 3H). ^{13}C NMR ($CDCl_3$) δ: 188.50, 171.09, 170.46, 169.62, 169.57, 167.51, 157.94, 151.17, 150.25, 143.19, 141.11, 130.04, 118.89, 113.49, 113.19, 112.80, 105.74, 105.18, 101.57, 101.44, 88.03, 72.91, 72.17, 72.13, 71.27, 68.39, 66.54, 61.95, 56.18, 44.57, 31.47, 20.98, 20.83, 20.80 (2C), 17.31. EI-MS, m/z: 711.7 $[M + 1]^+$, 733.7 $[M + Na]^+$.

*2-O-(2,3,4,6-Tetra-O-acetyl)-β-D-galactopyranosyldemethylrotenone (**2b**).* White solid; yield 85%. ^{1}H NMR ($CDCl_3$) δ: 7.81 (d, J = 8.4 Hz, 1H), 7.05 (s,1H), 6.50 (d, J = 8.4 Hz, 1H), 6.42 (s, 1H), 5.41 (dd, J = 10.2, 7.8 Hz 1H), 5.39 (d, J = 3.0 Hz, 1H), 5.23 (t, J = 8.4 Hz, 1H), 5.06 (s, 1H), 5.03 (dd, J = 10.2, 3.0 Hz, 1H), 4.92 (m, 2H), 4.71 (d, J = 8.4 Hz 1H), 4.59 (dd, J = 12.0, 3.0 Hz, 1H), 4.22 (dd, J = 10.8, 7.2 Hz, 1H), 4.16 (d, J = 12.0 Hz, 1H), 4.11 (dd, J = 10.8, 6 Hz, 1H), 3.88 (t, J = 6.6 Hz, 1H), 3.79 (d, J = 4.2 Hz, 1H), 3.74 (s, 3H), 3.29 (dd, J = 15.6, 9.6 Hz, 1H), 2.94 (dd, J = 15.6, 7.8 Hz, 1H), 2.16, 2.07, 2.04, and 1.98 (both s, 3H, Ac), 1.75 (s, 3H). ^{13}C NMR ($CDCl_3$) δ: 188.46, 170.62, 170.50, 170.30, 169.65, 167.46, 157.89, 151.23, 150.24, 143.18, 141.07, 130.05, 119.26, 113.45, 113.13, 112.74, 105.70, 105.13, 101.98, 101.49, 87.97, 72.13, 70.96 (2C), 68.85, 67.03, 66.50, 61.18, 56.12, 44.55, 31.43, 20.87, 20.85 (2C), 20.76, 17.27. EI-MS, m/z: 711.7 $[M + 1]^+$, 733.7 $[M + Na]^+$.

*2-O-(2,3,4,6-Tetra-O-acetyl))-α-D-mannopyranosyldemethylrotenone (**2c**).* White solid; yield 85%. ^{1}H NMR ($CDCl_3$) δ: 7.81 (d, J = 8.4 Hz, 1H), 6.94 (s,1H), 6.49 (d, J = 8.4 Hz, 1H), 6.43 (s, 1H), 5.51−5.45 (m, 2H), 5.32 (t, J = 9.6 Hz, 1H), 5.24 (s, 1H), 5.23 (t, J = 9.0 Hz, 1H), 5.05 (s, 1H), 4.92−4.89 (m, 2H), 4.60 (dd, J = 12.0, 3.0 Hz, 1H), 4.31 (ddd, J = 10.2, 4.8, 2.4 Hz, 1H), 4.24 (dd, J = 12.0, 4.8 Hz, 1H), 4.17 (d, J = 12.0 Hz, 1H), 4.06 (dd, J = 12.0, 2.4 Hz, 1H), 3.77 (d, J = 3.6 Hz, 1H), 3.75 (s, 3H), 3.29 (dd, J = 15.6, 9.6 Hz, 1H), 2.93 (dd, J = 15.6, 7.8 Hz, 1H), 2.16, 2.09, 2.05, and 1.99 (both s, 3H, Ac), 1.75 (s, 3H). ^{13}C NMR ($CDCl_3$) δ: 188.60, 170.95, 170.10, 170.01, 169.97, 167.54, 157.92, 151.78, 150.55, 143.16, 139.32, 130.21, 120.04, 113.36, 113.08, 112.71, 105.76, 105.15, 101.64, 98.67, 87.97, 72.04, 69.55(2C), 69.17, 66.51, 66.15, 62.45, 55.92, 44.49, 31.40, 21.08, 20.89 (2C), 20.83, 17.28. EI-MS, m/z: 733.7 $[M + Na]^+$.

*2-O-(2,3,4,-Tri-O-acetyl)-β-D-xylopyranosyldemethylrotenone (**2d**).* White solid; yield 82%. ^{1}H NMR ($CDCl_3$) δ: 7.78 (d, J = 8.4 Hz, 1H), 6.95 (s, 1H), 6.48 (d, J = 8.4 Hz, 1H), 6.41 (s, 1H), 5.22 (t, J = 9.0 Hz, 1H), 5.16 (t, J = 7.8 Hz, 1H), 5.10 (dd, J = 8.4, 6.6 Hz, 1H), 5.04 (s, 1H), 4.96 (td, J = 7.8, 4.8 Hz, 1H), 4.92−4.88 (m, 3H), 4.57 (dd, J = 12.0, 3.0 Hz, 1H), 4.18 (dd, J = 12.0, 6.4 Hz, 1H), 4.16 (d, J = 12.6 Hz, 1H), 3.78 (d, J = 3.6 Hz, 1H), 3.72 (s, 3H), 3.39 (dd, J = 12.0, 7.8 Hz, 1H), 3.28 (dd, J = 15.6, 9.6 Hz, 1H), 2.93 (dd, J = 15.6, 7.8 Hz, 1H), 2.05−2.02 (m, 9H), 1.74 (s, 3H). ^{13}C NMR ($CDCl_3$) δ: 188.68, 170.22, 170.05, 169.60, 167.52, 157.96, 151.31, 150.07, 143.15, 140.55, 130.10, 118.69, 113.43, 113.14, 112.76, 105.74, 105.11, 101.58, 100.78, 88.00, 72.15, 70.96, 70.33, 68.79, 66.47, 62.06, 56.10, 44.51, 31.42, 20.94, 20.91, 20.86 17.28. EI-MS, m/z: 639.8 $[M + 1]^+$, 661.8 $[M + Na]^+$.

*2-O-(2,3,4,-Tri-O-acetyl)-α-D-arabopyranosyldemethylrotenone (**2e**).* White solid; yield 81%. ^{1}H NMR ($CDCl_3$) δ: 7.79 (d, J = 8.4 Hz, 1H), 7.00 (s, 1H), 6.48 (d, J = 8.4 Hz, 1H), 6.43 (s, 1H), 5.35 (dd, J = 8.4, 6 Hz, 1H), 5.25 (m, 1H), 5.22 (t, J = 9 Hz, 1H), 5.09 (dd, J = 8.4, 3.6 Hz, 1H), 5.05 (s, 1H), 4.91 (m, 1H), 4.90 (m, 1H), 4.82 (d, J = 6.6 Hz, 1H), 4.60 (dd, J = 12, 3.0 Hz, 1H), 4.17 (d, J = 12 Hz, 1H), 4.08 (dd, J = 12.6, 3.6 Hz, 1H), 3.78 (d, J = 3.6 Hz, 1H), 3.74 (s, 3H), 3.60 (dd, J = 12.6, 1.8 Hz, 1H), 3.28 (dd, J = 15.6, 10.2 Hz, 1H), 2.92 (dd, J = 15.6, 7.8 Hz, 1H), 2.13, 2.07, and 2.04 (both s, 3H, Ac), 1.75 (s, 3H). ^{13}C NMR ($CDCl_3$) δ: 188.60, 170.61, 170.40, 169.67, 167.47, 157.88, 151.61, 150.44, 143.17, 140.09, 130.18, 120.75, 113.39, 113.03, 112.69, 105.72, 105.06, 101.57, 101.07, 87.94, 72.05, 69.89, 69.27, 67.42, 66.55, 62.80, 55.99, 44.53, 31.40, 21.08, 20.94, 20.87, 17.27. EI-MS, m/z: 639.8 $[M + 1]^+$, 661.7 $[M + Na]^+$.

*6′-O-(2,3,4,6-Tetra-O-acetyl)-β-D-glucopyranosyldalpanol (**2f**).* White solid; yield 87%. ^{1}H NMR ($CDCl_3$) δ: 7.77 (d, J = 8.4 Hz, 1H), 6.72 (s, 1H), 6.42 (s, 1H), 6.41 (d, J = 9.0 Hz, 1H), 5.16 (t, J = 9.6 Hz, 1H), 4.98 (t, J = 9.6 Hz, 1H), 4.92−4.88 (m, 2H), 4.76 (d, J = 7.8 Hz, 1H), 4.66 (t, J = 9.0 Hz, 1H), 4.58 (dd, J = 12.0, 2.4 Hz, 1H), 4.17 (dd, J = 12.0, 10.0 Hz, 1H), 4.15 (d, J = 12.0 Hz, 1H), 4.09 (dd, J = 12.0, 2.4 Hz, 1H), 3.81 (d, J = 3.6 Hz, 1H), 3.77 (s, 3H), 3.72 (s, 3H), 3.67 (ddd, J = 9.6, 6.0, 2.4 Hz, 1H), 3.07 (d, J = 9.0 Hz, 2H), 2.00, 1.99, 1.95, and 1.80 (both s, 3H, Ac), 1.28 (s, 3H), 1.27(s, 3H). ^{13}C NMR ($CDCl_3$) δ: 189.20, 170.75, 170.44, 169.67, 169.22, 167.42, 158.08, 149.69, 147.63, 144.03, 129.97, 113.61, 113.54, 110.55, 104.95, 104.82, 101.14, 95.83, 90.62, 78.62, 73.08, 72.38, 71.83, 71.55, 68.97, 66.46, 62.53, 56.53, 56.05, 44.80, 27.52, 24.09, 21.43, 20.83, 20.79(2C) 20.56. EI-MS, m/z: 743.7 $[M + 1]^+$, 765.7 $[M + Na]^+$.

General Procedure for the Preparation of Title Compounds (3a−3f). The solid (**2a−2f**, 1 mmol) in a mixture of acetyl chloride (0.1 mL) in anhydrous methanol (10 mL) was left to stand for 4 h at 25 °C, then concentrated to dryness at 25 °C (Schemes 1 and 2). The solid was chromatographed on a silica gel column (chloroform−methanol, 15:1), and after removing solvents and washing with cooled methanol, the desired products **3a−3f** were obtained.

*2-O-β-D-Glucopyranosyldemethylrotenone (**3a**).* White solid; yield 37%. ^{1}H NMR (DMSO) δ: 7.71 (d, J = 8.4 Hz, 1H), 6.82 (s, 1H), 6.57 (d, J = 8.4 Hz, 1H), 6.51 (s, 1H), 5.33 (t, J = 9.0 Hz, 1H), 5.15−5.14 (m, 1H), 5.12 (d, J = 5.4 Hz, 1H), 5.05−5.02 (m, 2H), 4.94 (d, J = 5.4 Hz, 1H), 4.92 (s, 1H), 4.51 (dd, J = 12.0, 3.0 Hz, 1H), 4.51 (d, J = 7.8 Hz, 1H, G_1H), 4.41 (t, J = 5.4 Hz, 1H), 4.24 (d, J = 12.0 Hz, 1H), 3.92 (d, J = 3.6 Hz, 1H), 3.70 (s, 3H), 3.66−3.62 (m, 1H), 3.53 (m, 1H), 3.27 (dd, J = 15.6, 9.6 Hz, 1H), 3.23−3.13 (m, 3H), 3.08−3.05 (m, 1H), 2.88 (dd, J = 15.6, 7.8 Hz, 1H), 1.71 (s, 3H). ^{13}C NMR (DMSO) δ: 188.60, 166.51, 157.58, 149.78, 148.51, 143.12, 140.71, 129.25, 115.01, 113.18, 112.78, 112.36, 105.49, 104.34, 101.59, 101.54, 87.18, 76.93, 76.85, 73.15, 71.69, 69.31, 65.76, 60.32, 55.78, 43.54, 30.52, 16.91. EI-MS, m/z: 565.8 $[M + Na]^+$.

*2-O-β-D-Galactopyranosyldemethylrotenone (**3b**).* White solid; yield 33%. ^{1}H NMR (DMSO) δ: 7.71 (d, J = 8.4 Hz, 1H), 6.82 (s, 1H), 6.57 (d, J = 8.4 Hz, 1H), 6.51 (s, 1H), 5.33 (t, J = 9.0 Hz, 1H), 5.15−5.13 (m, 1H), 5.04 (s, 1H), 4.96−4.93 (m, 1H), 4.93−4.91 (m, 1H), 4.78−4.76 (m, 1H), 4.55−4.49 (m, 2H), 4.47 (d, J = 7.8 Hz, 1H, G_1H), 4.45 (d, J = 4.2 Hz, 1H), 4.24 (d, J = 12.0 Hz, 1H), 3.92 (d, J = 3.6 Hz, 1H), 3.70 (brs, 4H), 3.56−3.52 (m, 1H), 3.49−3.45 (m, 1H), 3.37−3.30 (m, 3H), 3.28 (dd, J = 15.6, 10.2 Hz, 1H), 2.88 (dd, J = 15.6, 7.8 Hz, 1H), 1.71 (s, 3H). ^{13}C NMR (DMSO) δ: 188.54, 166.48, 157.55, 150.10, 148.66, 143.11, 140.50, 129.21, 115.95, 113.14, 112.75, 112.31, 105.51, 104.29, 101.59, 87.15, 75.02, 73.35, 71.68, 70.40, 67.55, 65.73, 59.59, 55.78, 43.51, 40.05, 30.51, 16.89. EI-MS, m/z: 565.8 $[M + Na]^+$.

*2-O-α-D-Mannopyranosyldemethylrotenone (**3c**).* White solid; yield 30%. ^{1}H NMR (MeOD) δ: 7.78 (d, J = 8.4 Hz, 1H), 6.92 (d, J = 1.0 Hz, 1H), 6.51 (s, 1H), 6.50 (d, J = 8.4 Hz, 1H), 5.31 (t, J = 9.0 Hz, 1H), 5.18 (d, J = 1.8 Hz, 1H, G_1H), 5.06 (s, 1H), 5.02−5.00 (m, 1H), 4.93−4.91 (m, 1H), 4.58 (dd, J = 12.0, 3.0 Hz, 1H), 4.23 (d, J = 12.0 Hz, 1H), 4.01 (dd, J = 3.0, 1.8 Hz, 1H), 3.85−3.83 (m, 2H), 3.77 (s, 3H), 3.75−3.68 (m, 4H), 3.31 (dd, J = 15.6, 9.6 Hz, 1H), 2.95 (dd, J = 15.6, 7.8 Hz, 1H), 1.75 (s, 3H). ^{13}C NMR δ: 191.40, 169.11, 159.66, 153.06, 151.58, 145.17, 141.33, 130.96, 120.12, 114.53, 114.48, 112.79, 107.11, 105.78, 102.83, 102.71, 89.38, 75.43, 73.72, 72.54, 72.16, 68.28, 67.58, 62.60, 56.52, 45.71, 32.22, 17.23. EI-MS, m/z: 543.8 $[M + 1]$+, 565.8 $[M + Na]$+.

*2-O-β-D-Xylopyranosyldemethylrotenone (**3d**).* Brown solid; yield 23%. ^{1}H NMR (MeOD) δ: 7.79 (d, J = 8.6 Hz, 1H), 6.91 (s, 1H), 6.51 (s, 1H), 6.50 (d, J = 8.4 Hz, 1 H), 5.30 (d, J = 9.0 Hz, 1H), 5.05 (s, 1H), 5.00 (t, J = 3.0 Hz, 1H), 4.92−4.91 (m, 1H), 4.58(dd, J = 12.0, 3.0 Hz, 1H), 4.57 (d, J = 7.2 Hz, 1H, G_1H), 4.22 (d, J = 12.0 Hz, 1H), 3.87 (dd, J = 11.4, 5.4 Hz, 1H), 3.84 (d, J = 3.6 Hz, 1H), 3.78 (s, 3H), 3.55−3.50 (m, 1H), 3.41−3.38 (m, 1H), 3.37−3.33 (m, 1H), 3.31(dd, J = 15.6, 9.6 Hz, 1H), 3.19 (dd, J = 11.4, 10.2 Hz, 1H), 2.95 (dd, J =

dx.doi.org/10.1021/jf500197k | J. Agric. Food Chem. 2014, 62, 4521−4527

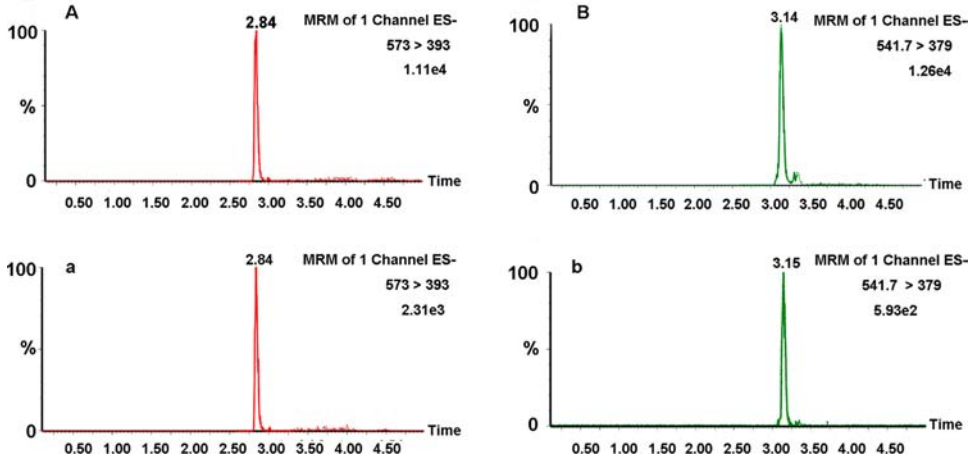

Figure 3. MRM chromatograms of conjugates glucopyranosyldemethylrotenone (**3a**) and glucopyranosyldalpanol (**3f**). (A) Standard solution of conjugates **3f** (RT, 2.84 min) and (B) standard solution of conjugates **3a** (RT, 3.14 min); (a) conjugates **3f** in phloem sap (RT, 2.84 min) and (b) conjugates **3a** in phloem sap (RT, 3.14 min) whose cotyledons were incubated in a buffered solution for 6 h including 100 μM conjugates **3a** and **3f**, respectively.

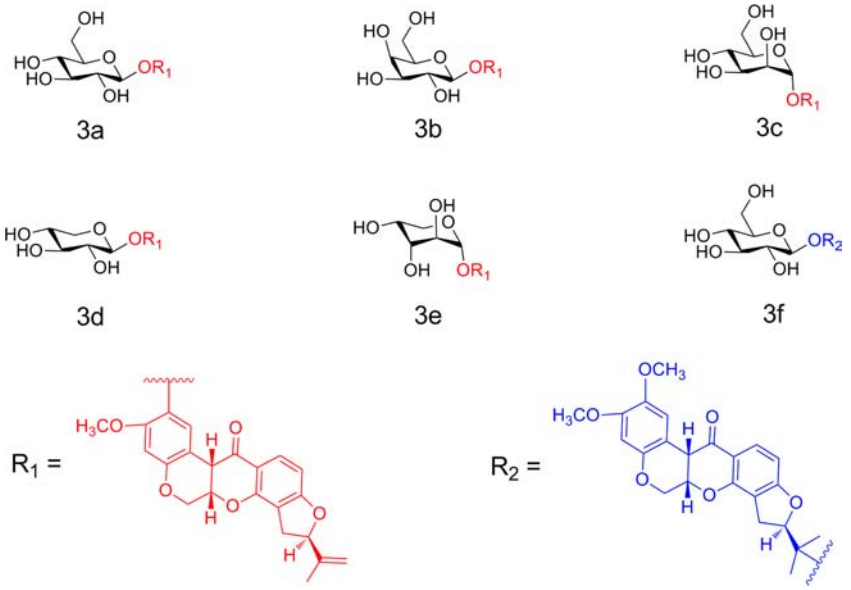

Figure 4. Structures of designed rotenone-*O*-monosaccharide conjugates: (**3a**) 2-*O*-*β*-D-glucopyranosyldemethylrotenone; (**3b**) 2-*O*-*β*-D-galactopyranosyldemethylrotenone; (**3c**) 2-*O*-*β*-D-mannopyranosyldemethylrotenone; (**3d**) 2-*O*-*β*-D-xylopyranosyldemethylrotenone; (**3e**) 2-*O*-*β*-D-arabopyranosyldemethylrotenone; and (**3f**) 6′-*O*-*β*-D-glucopyranosyldalpanol.

15.6, 7.8 Hz, 1H), 1.75 (s, 3H). ^{13}C NMR δ: 191.34, 169.08, 159.68, 152.18, 151.26, 145.15, 142.03, 130.92, 118.51, 114.59, 114.49, 112.79, 107.15, 105.76, 104.50, 102.76, 89.38, 77.56, 74.74, 73.77, 71.17, 67.59, 66.98, 56.71, 45.75, 32.21, 17.24. EI-MS, *m*/*z*: 535.8 [M + Na]$^+$.

*2-O-α-D-Arabopyranosyldemethylrotenone (**3e**).* White solid; yield 28%. ^{1}H NMR (MeOD) δ: 7.77 (d, J = 8.4 Hz, 1H), 6.91 (s, 1H), 6.51 (s, 1H), 6.50 (d, J = 8.4 Hz, 1H), 5.29 (t, J = 9.0 Hz, 1H), 5.05 (s, 1H), 5.01−4.98 (m, 1H), 4.91 (br s, 1H), 4.66 (d, J = 6.0 Hz, 1H, G$_1$H), 4.58 (dd, J = 12.6, 3.0 Hz, 1H), 4.22 (d, J = 12.6 Hz, 1H), 3.88−3.83 (m, 3H), 3.80−3.77 (m, 4H), 3.62 (dd, J = 8.4, 3.0 Hz, 1H), 3.55 (dd, J = 12.0, 1.8 Hz, 1H), 3.30 (dd, J = 15.6, 9.6 Hz, 1H), 2.94 (dd, J = 15.6, 7.8 Hz, 1H), 1.75 (s, 3H). ^{13}C NMR (DMSO) δ: 188.55, 166.51, 157.58, 150.65, 149.18, 143.09, 139.68, 129.19, 117.91, 113.16, 112.79, 112.32, 105.56, 104.33, 101.92, 101.59, 87.17, 71.97, 71.59, 70.38, 66.54, 65.79, 64.06, 55.78, 43.43, 30.54, 16.90. EI-MS, *m*/*z*: 535.8 [M + Na]$^+$.

*6′-O-β-D-Glucopyranosyldalpanol (**3f**).* White solid; yield 35%.^{1}H NMR (CDCl$_3$) δ: 7.72 (d, J = 8.4 Hz, 1H), 6.72 (s, 1H), 6.40 (s, 1H), 6.39 (d, J = 8.4 Hz, 1H), 4.94 (s, 1H), 4.74 (t, J = 9.0 Hz, 1H), 4.60−4.55 (m, 1H), 4.53 (d, J = 7.2 Hz, 1H, G$_1$H), 4.12 (d, J = 11.4 Hz, 1H), 3.83−3.76 (m, 3H), 3.76 (s, 3H), 3.73 (s, 3H), 3.58−3.48 (m, 2H), 3.31 (t, J = 7.8 Hz, 1H), 3.28 (s, 1H), 3.11 (dd, J = 15.6, 9.6 Hz, 1H), 3.00 (dd, J = 15.6, 8.4 Hz, 1H), 1.22 (s, 3H), 1.21 (s, 3H). ^{13}C NMR (CDCl$_3$) δ: 189.29, 167.16, 158.02, 149.73, 147.61, 144.09, 130.07, 113.61, 113.35, 110.63, 104.99, 104.86, 101.16, 97.38, 90.31, 79.10, 76.53, 75.66, 73.56, 72.44, 69.69, 66.42, 61.75, 56.56, 56.05, 44.73, 28.01, 22.59, 21.77.EI-MS, *m*/*z*: 597.8 [M + Na]$^+$.

Assessment of Membrane Potential. The membrane potential of protoplast was estimated by the previously reported method.[2] Duncan's multiple range test was employed to determine statistical differences between the control and treatments at a 5% probability level.

Collection and Analysis of Phloem Sap. The phloem sap collection method was as previously reported with some modifications.[2,5] The buffered solution contained 100 μM monosaccharide-rotenone conjugates or rotenone (1% Tween-80 V/V).

The phloem sap was analyzed by the previously described method with some modifications.[2] A C$_8$ reversed-phase column (Agilent, 5 μm,

dx.doi.org/10.1021/jf500197k | J. Agric. Food Chem. 2014, 62, 4521−4527

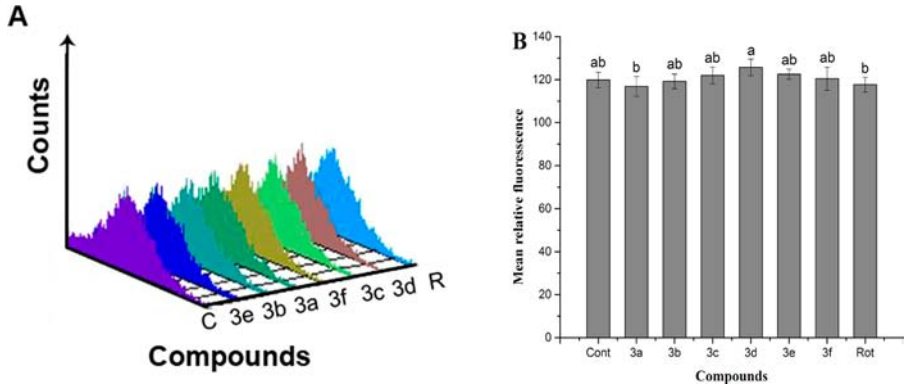

Figure 5. Membrane potential of protoplasts treated with conjugates **3a**−**3f** at 6 h. (A) Fluorescent intensity histogram. (B) Mean relative fluorescence. Protoplasts in buffer (pH 5.8) with conjugates **3a**−**3f** and rotenone (100 μM) were suspended for 6 h. Cont = control, without any treatment; Rot = rotenone. The letters on tops the columns show that there were not significant differences between treatment and the control by Duncan's multiple range test ($P > 0.05$). Mean ± SE; $n = 3$.

Table 1. Analysis of Phloem Sap

compds	incubation medium (μM)	phloem sap[a] (μM)	compds	incubation medium (μM)	phloem sap[b] (μM)
3a	100	4.90 ± 0.58	**4a**	100	23.0 ± 1.9
3b	100	ND	**4b**	100	ND
3c	100	ND	**4c**	100	7.6 ± 1.6
3d	100	ND	**4d**	100	21.8 ± 1.9
3e	100	ND	**4e**	100	15.3 ± 2.2
3f	100	14.71 ± 0.77			
rotenone	100	ND			

[a]The collection of phloem sap started from 2 h to the end of 6 h (mean ± SE; $n = 3$). ND represents not detected. [b]Data are from Yuan et al.,[11] and the phloem sap collection of monosaccharide-fipronil conjugates lasted for 2 h.

250 mm × 4.6 mm i.d.) was used at 25 °C for separation. The eluting solvent was composed of CH_3CN and H_2O (40/60, v/v). The method of standard curve was employed to determine the concentrations of 2-*O*-β-D-glucopyranosyldemethylrotenone (**3a**) and 6′-*O*-β-D-glucopyranosyldalpanol (**3f**). The linear equations of **3a** and **3f** were $y = 24.153x + 4.3533$ ($r = 0.9997$) and $y = 19.078x + 2.1597$ ($r = 0.9996$), respectively.

The conjugates **3a** of **3f** in phloem sap were identified by a previously reported method with some modifications.[10] The eluting solvent was composed of CH_3CN and H_2O (5/95, v/v, at 0.5 min; 80/20, v/v, at 3 min; and 5/95, v/v, at 4.5 min). The optimized parameters were as follows: capillary voltage, 300 kV; cone voltage, 35 V; desolvation temperatures, 350 °C; and source temperatures, 105 °C. At last, the molecule ion peaks of compounds **3a** and **3f** were determined as 541.7 and 573 (Figure 3), and those of the fragment ion peak were 379 and 393, respectively.

RESULTS AND DISCUSSION

Synthesis and Characterization. The trichloroacetimidate method[22] was adopted to couple monosaccharide with rotenone producing the conjugates **2a**−**2f** in yields of over 80%. A widely used catalyst, $BF_3{\cdot}OEt_2$, was used to prepare compounds **2a**−**2e**, but it was not efficient enough to obtain conjugate **2f** because the hydroxyl group of dalpanol is less active than that of 2-de-*O*-methylrotenone. Therefore, a more effective catalyst, TMSOTf, was introduced to the condensation of dalpanol with glucose, resulting in a yield of 87%. A classic reaction system of acetyl deprotection, NaOMe/MeOH, was attempted in the preparation of compounds **3a**−**3f**; however, it was unsuccessful because rotenone is unstable under strong alkaline conditions. Therefore, an unusual system, AcCl/MeOH, was used to prepare the desired products, with a yield of 23−37%. Finally, a series of rotenone-*O*-monosaccharide derivatives with *O*-glycosidic linkage (**3a**−**3f**, Figure 4) was obtained.

The structures of conjugates **2a**−**2f** and **3a**−**3f** were confirmed by mass spectrometry, ^1H and ^{13}C NMR. The characteristic signal of the acetyl groups could be observed in the ^1H and ^{13}C NMR spectra of compounds **2a**−**2f**. The ^1H NMR spectrum of conjugate **2a** showed signals of the acetyl groups at 2.14, 2.04, 2.03, and 2.01 ppm, and the ^{13}C NMR spectrum showed them at 171.09, 170.46, 169.62, 169.57, 20.98, 20.83, and 20.80 ppm. Compared with compounds **2a**−**2f**, there were no peaks corresponding to acetyl groups in the ^1H NMR and ^{13}C NMR spectra in compounds **3a**−**3f**. This demonstrates that the acetyl groups were totally removed in the desired products. The characteristic signal of G_1H was also confirmed in ^1H NMR spectra. For example, in compound **3a**, the signal of G_1H was observed at 4.51 ppm with $J = 7.8$ Hz, indicating that the glucosidic linkage is in the β configuration.

Phloem Mobility. Phloem mobility of conjugates **3a**−**3f** was measured using the castor bean system. The previously reported method[2] was used to measure the membrane potential of the protoplast after treatment with conjugates **3a**−**3f**. Each treatment was repeated three times, each repetetition was taken twice, and then the data were analyzed by the Duncan's multiple range test (Figure 5). Figure 5B indicates that there is no significant difference in relative fluorescence within the treatment period compared to that of the control. Consequently, they can be used to test their phloem mobility using the *Ricinus* system.

The detection results in Table 1 showed that only **3a** (4.90 ± 0.58 μM at 6h) and **3f** (14.71 ± 0.77 μM at 6 h) exhibited phloem mobility, whereas the other conjugates were not found

dx.doi.org/10.1021/jf500197k | J. Agric. Food Chem. 2014, 62, 4521−4527

Table 2. Physicochemical Properties of Tested Compounds[a]

properties	3a	3b	3c	3d	3e	3f	rotenone	dalpanol
molecular mass	542.53	542.53	542.53	512.51	512.51	574.57	394.42	412.43
log $K_{o/w}$	1.67	1.67	1.67	2.64	2.64	1.19	4.24	3.35
pK_a	12.7 ± 07 (acid)	12.7 ± 0.7 (acid)	12.7 ± 0.7 (acid)	12.9 ± 0.7 (acid)	12.9 ± 0.7 (acid)	12.9 ± 0.7 (acid)	no	14.3 ± 0.3 (acid)
PSA(A^2)	153.37	153.37	153.37	133.14	133.14	162.60	63.22	83.45
HBD	4	4	4	3	3	4	0	1
HBA	11	11	11	10	10	12	6	7

[a]The physicochemical properties of tested compounds were predicted by ACD Laboratories Perceptaprogram, version 14.0. log $K_{o/w}$ and pK_a values were classic values.

in the phloem sap. The mobility of **3f** was about three times that of **3a**, proving that the position of glucose coupling with rotenone significantly affected the phloem mobility of conjugates. Both **3a** and **3f** are D-glucose-rotenone conjugates, indicating that D-glucose is better as a substrate for conferring phloem mobility on rotenone than the other monosaccharides. However, in our previous work,[11] almost any kind of monosaccharide-fipronil conjugate exhibited phloem mobility. The wide discrepancy of phloem mobility between monosaccharide-fipronil and monosaccharide-rotenone suggests that the parent compound is involved in phloem mobility. Furthermore, fipronil is transported in the sunflower xylem,[23] while there are no reports of rotenone xylem mobility in any plant. Therefore, the results above demonstrate that phloem mobility can be acquired by a molecule by coupling it with a monosaccharide but that the extent of phloem mobility is affected by the parent molecule. Whether the influence of the parent molecule could be weakened by conjugating another monosaccharide needs further research.

"Rule of Five" was widely employed to predict whether the endogenous compounds or xenobiotics can cross membranes.[24−26] Given the physicochemical properties of tested compounds **3a−3f**, rotenone, and dalpanol in Table 2, the tested compounds are predicted to exhibit a very poor diffusion through the membranes. The Kleier model is widely utilized to predict the phloem mobility of a xenobiotic based on its physicochemical properties (pK_a and log $K_{o/w}$).[10,27] Most of the tested xenobiotics fit well, except for several xenobiotics whose transport is carrier-mediated.[5,27] Taking the physicochemical properties (pK_a and log $K_{o/w}$) of tested compounds into consideration (Table 2), compounds **3a−3f**, rotenone and dalpanol were predicted to be nonphloem mobile in terms of the Kleier Model (Figure 6). However, both **3a** and **3f** were demonstrated to be phloem mobile using the *Ricinus* system and therefore violate both this model (Figure 6) and "Rule of Five" (Table 2). The phloem mobility of some small xenobiotics were proved to involve active carrier processes, which can recognize and load these compounds into phloem sieve tubes.[28,29] Therefore, it is likely that an active carrier-mediated mechanism is also involved in glucose-rotenone conjugate uptake as well as in the systemicity of glucose-fipronil conjugates.[10] The carrier-mediated mechanisms of these large xenobiotics deserved further research.

In summary, six conjugates containing both rotenone or dalpanol and monosaccharide moieties were obtained. The tests of phloem systemicity demonstrate that conjugates with different monosaccharides have different phloem mobility and that only D-glucose-type conjugates exhibit phloem systemicity. By contrast, conjugating hexoses, pentoses, and deoxysugars to fipronil can confer phloem transport (Table 1).[11] The data suggest that this mobility is affected by the parent compound.

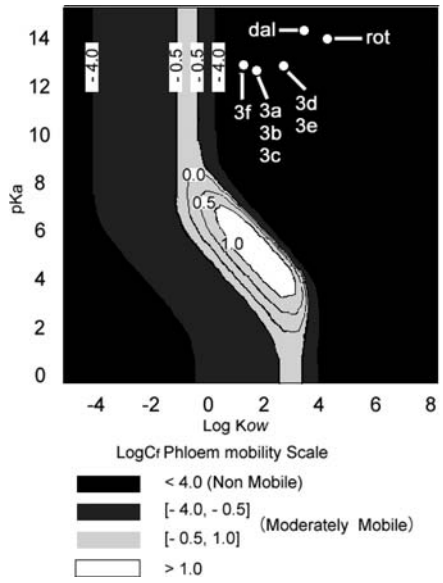

Figure 6. Prediction of phloem mobility of the tested compounds (**3a−3f**, rotenone and dalpanol) using the Kleier model.[30] Log $K_{o/w}$ and pK_a in Table 2. rot = rotenone; dal = dalpanol.

The current article offers examples of successful conversions of nonphloem-transport natural pesticide molecules into phloem-transport ones and presents useful data for developing novel insecticides with phloem mobility.

AUTHOR INFORMATION

Corresponding Author

*Tel: +86-20-85285127. E-mail: hhxu@scau.edu.cn.

Author Contributions

§P.-W.Q. and J.W. contributed equally to this work.

Funding

Financial support was from the National Natural Science Foundation of China (grant 31171886) and the Specialized Research Fund for the Doctoral Program of Education of China (grants 20114404110020 and 20134404130003).

Notes

The authors declare no competing financial interest.

ABBREVIATIONS USED

NBD, 7-nitrobenz-2-oxa-1,3-diazole; GTF, *N*-[3-cyano-1-[2,6-dichloro-4-(trifluoromethyl)phenyl]-4-[(trifluoromethyl) sulfinyl]-1*H*-pyrazol-5-yl]-1-(β-D-gluco-pyranosyl)-1*H*-1,2,3-triazole-4-methanamine; TMSOTf, trimethylsilyl trifluoromethanesulfonate; MRM, multiple reaction monitoring

REFERENCES

(1) Nauen, R.; Reckmann, U.; Thomzik, J.; Thielert, W. Biological profile of spirotetramat (Movento®)—a new two-way systemic (ambimobile) insecticide against sucking pest species. *Bayer Crop Sci. J.* **2008**, *2*, 245−278.

(2) Yang, W.; Wu, H. X.; Xu, H. H.; Hu, A. L.; Lu, M. L. Synthesis of glucose−fipronil conjugate and its phloem mobility. *J. Agric. Food Chem.* **2011**, *59*, 12534−12542.

(3) Smith, K.; Evans, D. A.; El-Hiti, G. A. Role of modern chemistry in sustainable arable crop protection. *Philos. Trans. R. Soc., B* **2008**, *1491*, 623−637.

(4) Hsu, F. C.; Sun, K.; Kleier, D. A.; Fielding, M. J. Phloem mobility of xenobiotics VI. A phloem-mobile pro-nematicide based on oxamyl exhibiting root-specific activation in transgenic tobacco. *Pestic. Sci.* **1995**, *44*, 9−19.

(5) Deletage-Grandon, C.; Chollet, J. F.; Faucher, M.; Rocher, F.; Komor, E.; Bonnemain, J. L. Carrier-mediated uptake and phloem systemy of a 350-Dalton chlorinated xenobiotic with an α-amino acid function. *Plant Physiol.* **2001**, *125*, 1620−1632.

(6) Chollet, J. F.; Deletage, C.; Faucher, M.; Miginiac, L.; Bonnemain, J. L. Synthesis and structure-activity relationships of some pesticides with an α-amino acid function. *Biochim. Biophys. Acta* **1997**, *1336*, 331−341.

(7) Jiang, D. X.; Lu, X. L.; Hu, S.; Zhang, X. B.; Xu, H. H. A new derivative of fipronil: Effect of adding a glycinyl group to the 5-amine of pyrazole on phloem mobility and insecticidal activity. *Pestic. Biochem. Physiol.* **2009**, *95*, 126−130.

(8) Williams, L. E.; Lemoine, R.; Sauer, N. Sugar transporters in higher plants − a diversity of roles and complex regulation. *Trends Plant Sci.* **2000**, *5*, 283−290.

(9) Yoshioka, K.; Takahashi, H.; Homma, T.; Saito, M.; Oh, K. B.; Nemoto, Y.; Matsuoka, H. A novel fluorescent derivative of glucose applicable to the assessment of glucose uptake activity of *Escherichia coli*. *Biochim. Biophys. Acta* **1996**, *1289*, 5−9.

(10) Wu, H. X.; Yang, W.; Zhang, Z. X.; Huang, T.; Yao, G. K.; Xu, H. H. Uptake and phloem transport of glucose-fipronil conjugate in *Ricinus communis* involve a carrier-mediated mechanism. *J. Agric. Food Chem.* **2012**, *60*, 6088−6094.

(11) Yuan, J. G.; Wu, H. X.; Lu, M. L.; Song, G. P.; Xu, H. H. Synthesis of a series of monosaccharide-fipronil conjugates and their phloem mobility. *J. Agric. Food Chem.* **2013**, *61*, 4236−4241.

(12) Isman, M. B. Botanical insecticides, deterrents, and repellents in modern agriculture and an incresasingly regulated world. *Annu. Rev. Entomol.* **2006**, *51*, 45−66.

(13) Dimetry, N. Z. Prospects of botanical pesticides for the future in integrated pest management programme (IPM) with special reference to neem uses in Egypt. *Arch Phytopathol. Plant Prot.* **2012**, *10*, 1138−1161.

(14) Sariaslani, F. S.; Rosazza, J. P. Microbial transformations of natural antitumor agents: products of rotenone and dihydrorotenone transformation by *Cunninghamella blakesleeana*. *Appl. Environ. Microbiol.* **1983**, *2*, 616−621.

(15) CaboniLi, P.; Sherer, T. B.; Zhang, N.; Taylor, G.; Na, H. M.; Greenamyer, J. T.; Casida, J. E. Rotenone, deguelin, their metabolites, and the rat model of Parkinson's disease. *Chem. Res. Toxicol.* **2004**, *17*, 1540−1548.

(16) Li, L.; Wang, H. K.; Chang, J.-J.; Mcphail, A. T.; Mcphnl, D. R.; Estes, J. R.; Lee, K.-H. Antitumor agents, 138. Rotenoids and isoflavones as cytotoxic constituents from *Amorpha fruticosa*. *J. Nat. Prod.* **1993**, *5*, 690−698.

(17) Kallarackal, J.; Orlich, G.; Schobert, C.; Komor, E. Sucrose transport into the phloem of *Ricinus communis* L. seedlings as measured by the analysis of sieve-tube sap. *Planta* **1989**, *3*, 327−335.

(18) Tian, Q.; Zhang, S.; Yu, Q.; He, M.; Yang, J. Amberlyst 15 as a mild and effective activator for the glycosylation with disarmed glycosyl trichloroacetimidate donors. *Tetrahedron* **2007**, *10*, 2142−2147.

(19) Carson, D.; Crombie, L.; Kilbee, G. W.; Moffatt, F.; Whiting, D. A. Regioselective ether cleavages of rotenoids: spiro-ether formation and stereoselective isotopic labelling of (E)- or (Z)-prenyl methyl groups in (6aS, 12aS)-rot-2′-enonic acid. J. *Chem. Soc. Perkin Trans.* **1982**, *1*, 779−788.

(20) Unai, T.; Cheng, H. M.; Yamamoto, I.; Casida, J. E. Chemical and biological O-demethylation of rotenone derivatives. *Agric. Biol. Chem.* **1972**, *8*, 1937−1944.

(21) Crombie, L.; Kilbee, G. W.; Moffatt, F.; Proudfoot, G.; Whiting, D. A. Identification and isotopic labelling of the diastereotopic methyl groups of the prenyl-derived 2-hydroxyisopropyl residues of natural products: the rotenoid dalpanol. *J. Chem. Soc., Perkin Trans.* **1991**, *1*, 3143−3148.

(22) Ješelnik, M.; Plavec, J.; Polanc, S.; Kočevar, M. Novobiocin-related compounds: synthesis of 3-benzoylamino-2-oxo- 2H-1-benzopyran-7-yl D-glycopyranosides by the trichloroacetimidate methodology. *Carbohydr. Res.* **2000**, *4*, 591−597.

(23) Aajoud, A.; Raveton, M.; Aouadi, H.; Tissut, M.; Ravanel, P. Uptake and xylem transport of fipronil in sunflower. *J. Agric. Food Chem.* **2006**, *54*, 5055−5060.

(24) Bhal, S. K.; Kassam, K.; Peirson, L. G.; Pearl, G. M. The rule of five revisited: Applying log *D* in place of log *p* in drug-likeness filters. *Mol. Pharmaceutics* **2007**, *4*, 556−560.

(25) Palm, K.; Stenberg, P.; Luthman, K.; Artursson, P. Polar molecular surface properties predict the intestinal absorption of drugs in humans. *Pharm. Res.* **1997**, *5*, 568−571.

(26) Lei, Z. W.; Wang, J.; Mao, G. L.; Wen, Y. J.; Xu, H. H. Phloem mobility and translocation of fluorescent conjugate containing glucose and NBD in castor bean (*Ricinus communis*). *J. Photochem. Photobiol., B* **2014**, 10−16.

(27) Rocher, F.; Chollet, J. F.; Legros, S.; Jousse, C.; Lemoine, R.; Faucher, M.; Bush, D. R.; Bonnemain, J. L. Salicylic acid transport in *Ricinus communis* involves a pH-dependent carrier system in addition to diffusion. *Plant Physiol.* **2009**, *4*, 2081−2091.

(28) Besson, J.; Delrot, S.; El Ibaoui, H.; Bonnemain, J. L. Uptake and release of a phloem-mobile (glyphosate) and of a non-phloem-mobile (iprodione) xenobiotic by broad bean leaf tissues. *Physiol. Veg.* **1986**, *24*, 431−432.

(29) Hart, J. J.; DiTomaso, J. M.; Linscott, D. L.; Kochian, L. V. Transport interactions between paraquat and polyamines in roots of intact maize seedlings. *Plant Physiol.* **1992**, *4*, 1400−1405.

(30) Kleier, D. A.; Hsu, F. C. Phloem mobility of xenobiotics. VII. The design of phloem systemic pesticides. *Weed Sci.* **1996**, *44*, 749−756.

JOURNAL OF AGRICULTURAL AND FOOD CHEMISTRY

Article

pubs.acs.org/JAFC

Characterization of the Key Aroma Compounds in Shiraz Wine by Quantitation, Aroma Reconstitution, and Omission Studies

Christine M. Mayr,[†] Jason P. Geue,[§] Helen E. Holt, Wes P. Pearson, David W. Jeffery,[‡] and I. Leigh Francis*

The Australian Wine Research Institute, P.O. Box 197, Glen Osmond (Adelaide), South Australia 5064, Australia

ABSTRACT: The key aroma compounds of premium Australian Shiraz wines from the warm Barossa Valley and cooler Margaret River regions were characterized. GC−Olfactometry was conducted to determine the most important volatile compounds, which were then quantitated. The wine from the Barossa Valley had higher concentrations of ethyl propanoate, dimethyl sulfide (DMS), and oak-derived compounds, whereas the Margaret River wine contained above threshold concentrations of the 'cheesy' compounds 2- and 3-methylbutanoic acid, as well as rotundone, the 'pepper'-smelling compound. The aromas were reconstituted by combining 44 aroma compounds, and sensory descriptive analysis was used to investigate the importance of the omission of several compounds, including DMS, rotundone, fatty acids, and β-damascenone, and the influence of nonvolatiles was also assessed. The study showed that the aroma of the Shiraz wines could be reconstituted in both cases, with the changes in the nonvolatile fraction having a large influence.

KEYWORDS: *Shiraz, wine, omission tests, aroma reconstitution, sensory descriptive analysis, nonvolatiles*

INTRODUCTION

Shiraz is one of the most important grape varieties in Australia and accounts for about 40% of all red wines made each year. This variety is also important to wines from several regions in France and is of growing significance worldwide. The flavor of Shiraz, also known as Syrah, is commonly described as 'spicy', 'dark fruit'- and 'berry'-like, with different styles produced depending on the region of origin and winemaking and viticultural decisions. Despite the importance of Shiraz to the world wine industry, little is known about the volatile compounds that are the key contributors to its aroma.

Of the >800 volatiles in wine,[1] only a relatively small number of specific key aroma active compounds have been identified by sensory analysis.[2,3] Guth was among the first who comprehensively determined the important flavor compounds in wine, studying the white wine varieties Scheurebe and Gewürztraminer and reconstituting their aroma.[4] The success of gas chromatography−olfactometry (GC-O), often using aroma extract dilution analysis (AEDA), coupled with careful quantitative analysis of the aroma active compounds and knowledge of aroma threshold values, has allowed significant advances in understanding of the often subtle differences in aroma between wine types. Performing a reconstitution study is an important step in modern flavor research, to confirm the identification and quantitation experiments and, therefore, to verify that all important compounds have been detected.[5] Subsequently, the key aroma compounds of another white wine (from Maccabeo) have been investigated in detail, alongside reconstitution experiments,[6] and the same group also conducted thorough studies on a Grenache rosé[7] as well as on red wine from Rioja.[8] Recently the key flavor and taste compounds of the red wine variety Dornfelder were decoded and a full reconstitution was successfully conducted.[9] For each of these studies reporting detailed and comprehensive examination of the key aroma compounds, a common finding has been that a relatively small number of yeast metabolism-derived fatty acid ethyl esters, acetate esters, fatty acids, alcohols, and the grape-derived norisoprenoid β-damascenone are of notable importance to wine aroma. For some individual wine types, the sulfur-containing compounds 3-mercaptohexanol, 3-mercaptohexyl acetate, and dimethyl sulfide, the monoterpenes *cis*-rose oxide and linalool, oak volatiles such as *cis*-oak lactone and vanillin, and the nitrogen-containing isobutylmethoxypyrazine can also have a strong influence on aroma.

Despite its importance for the wine industry, information on the aroma compounds of wines made from Shiraz grapes is very limited.[10] It is known that Shiraz wines do not contain an appreciable concentration of methoxypyrazines,[11] a characteristic that sets this variety apart from some other highly valued grape varieties such as Cabernet Sauvignon, Merlot, and Cabernet Franc, and some Shiraz wines can have sensorially important levels of rotundone, which gives a distinctive 'spicy'/'peppercorn' flavor.[12] To our knowledge no comprehensive characterization of Shiraz wine flavor has been conducted. The objective of this study was to determine the key aroma compounds of two ultrapremium (highly priced, high reputation for quality) Australian Shiraz wines, representative of two different styles: one from a relatively cooler climate in Western Australia and the other from a warmer grape-growing region in South Australia. Reconstitution studies were performed, and the reconstitutions were compared to the real wines by means of sensory descriptive analysis. In the sensory study the relative influence of the aroma compounds dimethyl sulfide, β-damascenone, linalool, and rotundone, as well as the

Received: January 3, 2014
Revised: April 16, 2014
Accepted: April 20, 2014
Published: April 20, 2014

ACS Publications © 2014 American Chemical Society

dx.doi.org/10.1021/jf405731v | J. Agric. Food Chem. 2014, 62, 4528−4536

role of oak-derived compounds, fatty acids, and nonvolatiles, was investigated via omission experiments.

MATERIALS AND METHODS

Wine. Two ultrapremium commercial 2006 vintage Shiraz wines from Margaret River, Western Australia (AUD$40), and Barossa Valley, South Australia (AUD$80), were selected in 2010 following an informal blind tasting with expert technical staff of the AWRI with extensive wine assessment experience, where a range of potential wines of long-standing reputation were considered, and selected on the basis of having characteristic sensory properties expected of wines of their respective regions. The basic composition of the wines was as follows: Barossa Valley Shiraz, pH 3.50, titratable acidity (TA, as tartaric acid) 6.8 g/L, alcohol 14.6% v/v, glucose + fructose (G + F) 0.7 g/L, volatile acidity (VA, as acetic acid) 0.68 g/L, free SO_2 14 mg/L, total SO_2 64 mg/L; Margaret River Shiraz, pH 3.50, TA 6.3 g/L, alcohol 14.2% v/v, G + F 0.6 g/L, VA 0.51 g/L, free SO_2 22 mg/L, total SO_2 91 mg/L.

Chemicals. All chemicals were of analytical reagent grade unless otherwise stated, and water was obtained from a Milli-Q purification system (Millipore, North Ryde, NSW, Australia). Ethyl propanoate, ethyl 2-methylpropanoate, ethyl butanoate, ethyl 2-methylbutanoate, ethyl 3-methylbutanoate, 2-methylpropyl acetate, 2-methylbutyl acetate, 3-methylbutyl acetate, 2-methyl-1-butanol, 3-methyl-1-butanol, ethyl hexanoate, hexyl acetate, ethyl lactate, 1-hexanol, propanoic acid, ethyl decanoate, ethyl dodecanoate, butanoic acid, 2-methylbutanoic acid, 3-methylbutanoic acid, 2-phenylethanol, decanoic acid, linalool, acetic acid, guaiacol, 4-ethylphenol, 5-methylfurfural, furfural, carbon disulfide, α-terpineol, β-damascenone, *cis*- and *trans*-oak lactone, vanillin, eugenol, sotolon, methionol, and methional were supplied by Sigma-Aldrich (Castle Hill, NSW, Australia). Ethyl acetate, 1-butanol, β-ionone, and 2-phenylethyl acetate were supplied by Merck (Kilsyth, Victoria, Australia). 2-Methyl-1-propanol was supplied by Riedel-de Haën (Seelze, Germany). Ethyl octanoate, hexanoic acid, and octanoic acid were supplied by Hopkin and Williams (London, UK). 4-Ethylguaiacol and dimethyl sulfide were supplied by Apin Chemicals (Abingdon, UK). Due to the difficulties of working with gaseous hydrogen sulfide and methanethiol, a suitable alternative employed the sodium salts of these analytes (sodium hydrosulfide hydrate, purity > 71%, and sodium thiomethoxide, purity > 96.4%, both supplied by Sigma-Aldrich), which were dissolved in cooled water and used immediately.

Basic Wine Composition. The basic chemical composition of all wines was determined by AWRI Commercial Services using methods as detailed in Iland et al.[13] TA, VA, pH, G + F, and alcohol were measured using FTIR WineScan (FOSS, Hillerød, Denmark).

Gas Chromatography−Olfactometry. GC-O was performed using an Agilent 6890 GC, equipped with a Gerstel MPS2 multipurpose sampler and coupled to an Agilent 5973N mass selective detector. The GC was also fitted with a Gerstel olfactory detection port (ODP series 1), and the flow was split between MS and ODP in a 1:1 ratio. The instrument was controlled with Agilent G1701DA ChemStation software with Maestro software integrated version 1.3.3.51/3.3. For GC analysis and GC-O DB-Wax and DB-5MS columns (both Agilent, dimensions of 60 m × 0.25 mm, 0.25 μm film) were used. The mass spectrometer quadrupole temperature was set at 150 °C, and the source was set at 230 °C. Positive ion electron impact spectra at 70 eV were recorded in the range of m/z 35−350. The carrier gas was helium (ultra high purity, BOC, Adelaide, Australia), and constant pressure mode set to 31.1 psi (nominal initial flow 2.1 mL/min) was used. For liquid injection, the samples (2 μL) were applied by splitless injection technique; the oven was held at 40 °C for 2 min and heated at 6 °C/min to 240 °C.

GC-O−Dynamic Headspace (Purge-Trap) Technique. Dynamic headspace analysis was used to analyze flavor compounds by means of GC-O as well as for identification by GC-MS. A 10 mL aliquot of wine was used in a 20 mL amber glass headspace vial, and the sample was equilibrated at 30 °C for 1 min. The volatiles were purged with helium for 20 min at 30 °C at a flow rate of 60 mL/min and 500 rpm agitation. A Tenax-TA trap was used, and its temperature was held at 30 °C during purging. After the sample purging was completed, the trap was dry-purged for 10 min at 50 mL/min to remove condensed water on the trap. The sample was then desorbed from the trap at 280 °C for 5 min to the splitless injection port using a Gerstel MPS2 multipurpose sampler of the gas chromatograph. Columns and temperature program were as described for the liquid injections.

Isolation of Volatiles for Liquid Injection. The volatiles were extracted from wine samples (500 mL) by liquid−liquid extraction with 3 × 250 mL of diethyl ether using a separation funnel and shaking vigorously for 10 min at room temperature. The combined organic phases were washed with brine and dried over anhydrous sodium sulfate. After filtration and concentration on a Vigreux column to approximately 200 mL, the volatiles were isolated by means of the solvent-assisted flavor evaporation technique (SAFE).[14] The SAFE extract was concentrated to about 1 mL at 40 °C using a Vigreaux column.

Identification of Volatiles and Aroma Extract Dilution Analysis. GC-O was conducted on the headspace samples as well as on the liquid extracts, and the odor active regions were evaluated by 15 (Margaret River wine) or 17 (Barossa Valley wine) panelists using both DB-Wax and DB-5MS columns. The wine headspace sample was then diluted stepwise (1:10) with 14% v/v aqueous ethanol/saturated potassium hydrogen tartrate, and each dilution was investigated by GC-O by three panelists using the DB-Wax column only. Identification was performed by comparing a compound's mass spectra, linear retention indices (LRI) using the n-alkane C_{5-30} series, and the odor quality with those of reference compounds.

Quantitation of Volatiles. The fermentation-derived volatile ethyl esters (ethyl acetate, ethyl lactate, ethyl hexanoate, ethyl octanoate, ethyl decanoate, ethyl 3-methylbutanoate, ethyl 2-methylbutanoate, ethyl butanoate, ethyl 2-methylpropanoate, ethyl propanoate), acetates (2-methylbutyl acetate, 3-methylbutyl acetate, 2-methylpropyl acetate, 2-phenylethyl acetate, hexyl acetate), acids (butanoic acid, hexanoic acid, octanoic acid, decanoic acid, 2-methylpropanoic acid, 2-methylbutanoic acid, 3-methylbutanoic acid), and alcohols (2-methyl-1-propanol, 1-butanol, 2-methy-1-lbutanol, 3-methyl-1-butanol, 1-hexanol) were quantitated as described previously.[15] The analysis of the monoterpenes linalool and α-terpineol was as described,[16] and the sesquiterpene rotundone was quantitated as described by Siebert et al.[17] The norisoprenoids β-damascenone and β-ionone were analyzed according to the method of Ugliano et al.[18] The low-molecular-weight sulfur compounds hydrogen sulfide, dimethyl sulfide, and methanethiol were determined as described by Siebert et al.[19] Quantitation of the volatiles acetic acid, 4-ethylguaiacol, guaiacol, 4-ethylphenol, 5-methylfurfural, furfural, *cis*- and *trans*-oak lactone, eugenol, and vanillin was according to the method of Pollnitz et al.[20] conducted by AWRI Commercial Services.

Sotolon, methionol, and methional were quantitated by means of stable isotope dilution assays as follows. After the addition of the respective labeled standard (synthesized in-house as described elsewhere, Mayr et al. in preparation) to wine samples (300 mL), the samples were equilibrated for 30 min and then extracted with diethyl ether (3 × 150 mL). The combined organic phases were washed with brine and finally dried over anhydrous sodium sulfate. After filtration and concentration on a Vigreaux column to 200 mL, the volatiles were isolated by SAFE. The SAFE extract was concentrated to about 1 mL at 40 °C using a Vigreaux column and analyzed by two-dimensional GC-MS using the following conditions. GC/GC-MS was performed using a gas chromatograph type Agilent 7890A, equipped with a Gerstel MPS2 XL multipurpose sampler and coupled to an Agilent 5975C mass selective detector (MSD). The instrument was controlled with Agilent G1701EA ChemStation software in conjunction with Gerstel Maestro software (version 1.4.8.14). For quantitation, a DB-5MS column and a DB-Wax column (both Agilent, dimensions of 30 m × 0.25 mm, 0.25 μm film) were used. Heart-cutting was performed by means of a Deans switch microfluidic plate with a flame ionization detector. The SAFE extracts were injected (2 μL) by splitless injection technique; the oven temperature was held at 40 °C for 2 min and heated at 6 °C/min to 240 °C. The carrier gas was helium (ultrahigh purity, BOC, Adelaide,

dx.doi.org/10.1021/jf405731v | J. Agric. Food Chem. 2014, 62, 4528−4536

Australia), in constant pressure mode with the 1D column head pressure at 46.5 psi and the 2D column at 34.95 psi. The Agilent GC split/splitless inlet was fitted with a resilanized borosilicate glass SPME inlet liner (Supelco) and was held at 250 °C. The MS transfer line was held at 250 °C. The cryotrap (Gerstel cryotrap system CTS2) was cooled to 0 °C with liquid N_2 and held at 0 °C as the 0.6 min heart-cut from the 1D column was transferred to the retention gap of the 2D column and while the oven was cooled to 130 °C, and then the cryotrap temperature was increased to 300 °C at 20 °C/s and held at 300 °C for 1 min.

Aroma Reconstitution. For sensory experiments the quantitated aroma compounds of the two wines were spiked into a winelike matrix according to their respective occurring concentrations. The model system of ethanol/water at the ethanol concentrations of the respective wines (14.2 and 14.6% v/v) was saturated with potassium hydrogen tartrate and adjusted to pH 3.50 using aqueous tartaric acid (40% w/v). To imitate more closely the nonvolatile matrix acids, fructose, glucose, glycerol, succinic acid, malic acid, lactic acid, sodium chloride, potassium hydrogen phosphate, and potassium thiosulfate were added, in the concentrations measured in the wines, as shown in Table 1. Organic acids were quantitated as published recently.[21]

Table 1. Major Organic Acid, Sugar, and Salt Concentrations in the Two Wine Samples

	concentration (g/L)	
compound	Barossa Valley Shiraz	Margaret River Shiraz
glycerol	12.4	8.8
glucose	nd[a]	0.18
fructose	0.59	0.25
lactic acid	1.6	1.9
succinic acid	3.9	5.2
NaCl	0.1	0.1
K_2HPO_4	1.0	1.0
$K_2S_2O_3$	0.02	0.02

[a]Not detected.

Sensory Descriptive Analysis. Eleven panelists were recruited (nine females, two males, ages 32−61 years), all of whom were part of the AWRI trained descriptive analysis panel. All panelists attended four training sessions to generate and refine appropriate aroma descriptors, their definitions, and reference standards, for rating in the formal sessions. The assessors rated 12 aroma attributes (shown in Table 2). The intensity of each aroma attribute was rated using an unstructured 15 cm line scale, with indented anchor points of "low" to "high" placed at 10 and 90%, respectively.

Samples were presented to panelists in 30 mL aliquots in three-digit-coded, covered, International Organization for Standardization black wine glasses at 22−24 °C, in isolated booths under daylight lighting, with randomized presentation order within each tray of samples across judges, except in the practice sessions, when there was a constant presentation order. In practice booth sessions the panelists assessed nine samples in duplicate, which were presented as six trays of three wines per tray. For both practice and formal testing sessions, assessors were forced to take a 60 s rest between samples. There was a 10 min rest between trays, during which assessors were requested to leave the booths. For the formal sensory sessions assessors were presented with six trays of three wines per tray each day for three days of assessment by aroma only. Eighteen samples were assessed each day in a complete randomized block design, presented to assessors three times on separate days. FIZZ software (version 2.46, Biosystemes, France) were used for the collection of all data.

Data Analysis. Sensory descriptive data for each attribute were analyzed using an analysis of variance (ANOVA) (JMP 7.0, SAS Institute, 2007) testing for the effects of sample, judge, replicate, and their interactions treating judge as a random effect, using sample by judge as the error term for the sample effect in a mixed model. Principal component analyses (PCAs) were conducted on the mean values averaged over panelists and replicates, using the correlation matrix. PCA was conducted using The Unscrambler software (CAMO Inc., Oslo, Norway).

Table 2. Aroma Descriptors and Definitions Used in the Sensory Analysis

attribute	description (reference standard composition[a])
overall fruit	overall intensity of fruit aroma of the wine
red fruit	aroma of red fruit (3 fresh raspberries, Sara Lee)
dark fruit	aroma of dark fruit (1 fresh blueberry, 2 fresh blackberries, Sara Lee)
oaky	aroma of oak (1 tsp French oak wood shavings)
smoky/ bacon	aroma of smoke, bacon (5 drops, Liquid Smoke hickory flavor)
chocolate	aroma of dark chocolate (1/3 of a square 70% cocoa chocolate, Lindt & Sprüngli)
pepper	aroma of black pepper, peppercorns (1/5 tsp freshly ground black pepper)
cooked vegetable	aroma of cooked/tinned vegetables, vegetable water (1/2 tsp water from canned green beans)
plastic	aroma of plastic, glue (4 μg/L 2,6-dichlorophenol)
green	aroma of green wood, pine, grass (freshly cut pine wood, 4 cm × 1 cm, 10 × 1 cm piece cut grass, no wine)
spices	aroma of sweet spices (equal parts aniseed, cinnamon, cloves, mixed spice; total 1/5 tsp)
nail polish remover	aroma of solvent, nail polish remover (150 μg/L ethyl acetate)
geranium	aroma of geranium (3 × 3 cm piece geranium leaf)

[a]All standards made up in 30 mL of neutral dry red wine unless otherwise stated. tsp, teaspoon.

RESULTS AND DISCUSSION

Identification and Quantitative Analysis. Aroma compounds in the concentrated liquid extracts as well as the headspace of both wines were analyzed by GC-O. Table 3 shows data from the dynamic headspace analysis. Odor active regions that could be detected in diluted samples were further identified by their mass spectra, retention time, and odor quality in comparison to reference compounds. Approximately 100 odorants could be detected, but those for which <20% of assessors reported an aroma are not listed in Table 3. Comparison of the identification by the assessors of odor active compounds in the two different wines, as indicated by GC-O, showed only slight differences and almost all identified compounds could be detected in both wines, with exception of hexyl acetate, methionol, 2,3-butanediol, 5-methylfurfural, α-terpineol, 2-phenylethyl acetate, and ethyl 4-methylpentanoate. To gain insight into the aroma differences of the two Shiraz wines, 48 of the most important compounds, from the GC-O data of the two GC column types and also evaluation of the liquid extract GC-O data (data not shown), were quantitated and the odor activity values (OAVs) were calculated by dividing actual concentrations with the published odor detection threshold concentration. Table 4 shows the concentration levels, odor thresholds in wine or model wine, and the resulting OAVs of both wines.

Of the 48 quantitated compounds, in the Barossa Valley Shiraz 28 compounds were found with an OAV >1, whereas in the Shiraz from Margaret River 27 compounds reached concentrations higher than their odor threshold. As expected, the highest concentrations in both wines were found for acetic acid (680 mg/L for BV and 510 mg/L for MR), followed by ethyl lactate (366 mg/L for BV and 247 mg/L for MR) and ethyl acetate (164 mg/L for BV and 103 mg/L for MR). The

dx.doi.org/10.1021/jf405731v | J. Agric. Food Chem. 2014, 62, 4528−4536

Table 3. Main Odorants for the Two Wines from the GC-O Dynamic Headspace Study Using the DB-Wax Column, with Percentage of Assessors Perceiving an Aroma in an Undiluted Sample and Aroma Extract Dilution Analysis (AEDA) Values

			Margaret River Shiraz		Barossa Valley Shiraz	
linear retention index (DB-Wax)	odor description	identity	percentage response (n = 17)	AEDA value[a]	percentage response (n = 15)	AEDA value[a]
880	fruity	ethyl acetate[b]	35	1	0	–
959	red berry, fruity	ethyl 2-methylpropanoate[b]	76	100	67	1000
967	butter, caramel	2,3-butanedione[b]	65	1	60	1000
1034	fruity, pineapple	ethyl butanoate[b]	88	1000	100	1000
1050	candy, apple,	ethyl 2-methylbutanoate[b]	71	1000	67	1000
1052	caramel, sweet	2,3-pentanedione[e]	59	1	47	1
1066	red berry, violet	ethyl 3-methylbutanoate[b]	82	1000	67	1000
1121	candy, banana	2/3-methylbutylacetate[b]	76	10	87	100
1134	raspberry candy	ethyl pentanoate[c]	82	100	67	100
1162	compost	ethyl 2-butenoate[e]	53	1	40	1
1187	blueberry, fruity, floral	methyl hexanoate[c]	47	1000	80	100
1191	peach, sweet, woody	ethyl 4-methylpentanoate[c]	41	1	0	-
1208	earthy, solvent	2/3-methyl-1-butanol[b]	59	1000	87	1000
1233	pineapple, candy	ethyl hexanoate[b]	88	1000	80	1000
1272	red berry	hexyl acetate[e]	47	1	0	-
1285	solvent, lemon	furfuryl ethyl ether[c]	100	1000	100	1000
1299	spicy, candy, earthy	ethyl *cis*-3-hexenoate[c]	24	1	40	1
1313	fruity, berry	4-methylpentanol[b]	29	1	47	1
1320	savory, coconut	2-heptanol[c]	35	1	27	1
1339	solvent	ethyl lactate[b]	18	1	0	-
1355	floral, green, spice	hexanol[b]	0	1	40	1
1356	floral, rose	*cis*-rose oxide[b]	24	1	0	-
1383	grass, solvent	*cis*-hex-3-en-1-ol[b]	82	1	47	1
1390	rose, leather	3-octanol[c]	41	1	33	1
1403	mushroom, grass	*trans*-hex-2-en-1-ol[b]	47	1	27	1
1425	fruity, candy	ethyl 2-hydroxy-3-methylbutanoate[c]	94	100	87	10
1439	melon, wood	ethyl octanoate[b]	65	1	93	10
1449	vinegar	acetic acid[b]	29	1	60	1
1458	cooked meat, mushroom	3-methylbutylhexanoate[c]	24	1	33	1
1463	earthy, wood	furfural[d]	29	10	87	1000
1469	flower, earth, almond	ni[f]	53	1	20	1
1499	solvent, wood, green	furfuryl butyrate[c]	65	1	60	1
1507	smoky, leather	acetylfuran[c]	35	1	27	1
1530	capsicum, herbaceous	ni	88	1	73	1
1542	berry, sweet	2,3-butanediol[b]	35	1	0	-
1544	floral, lemon	linalool[b]	59	10	40	1
1563	baked apple, floral	ethyl 3-methylthiopropanoate[c]	35	1	0	-
1573	berry candy, woody	5-methylfurfural[b]	24	100	0	-
1630	sweaty, cheese	butanoic acid[b]	59	100	0	1000
1638	smoky, cheese	ethyl decanoate[b]	35	1	40	1
1673	sweaty, cheese	2/3-methylbutanoic acid[b]	88	10	87	10
1697	spicy	α-terpineol[b]	0	-	20	1
1713	savory, potato	methionol[b]	88	1	0	-
1732	fruity, sweet	ni	29	1	80	1
1752	floral, solvent	TDN[b]	41	1	33	1
1757	herbal, fruit	ni	12	1	27	1
1822	jammy, plum, floral	2-phenylethyl acetate[b]	35	1	0	-
1827	rose, candy, citrus	β-damascenone[b]	53	1000	13	1000
1842	leafy, wood, varnish	hexanoic acid[b]	29	1	73	1
1866	smoky, medicinal	guaiacol[b]	94	1000	87	1000
1900	coconut, raspberry	*cis*-oak lactone[b]	47	100	33	100
1913	floral, rose	2-phenylethanol[b]	76	1000	40	1000
1950	coconut, green, wood	*trans*-oak lactone[b]	82	10	93	100
2011	burnt toffee, caramel	furaneol[b]	24	10	60	1
2051	cloves, jam, musty	diethyl malate[c]	35	1	47	1

dx.doi.org/10.1021/jf405731v | J. Agric. Food Chem. 2014, 62, 4528−4536

Table 3. continued

linear retention index (DB-Wax)	odor description	identity	Margaret River Shiraz		Barossa Valley Shiraz	
			percentage response (n = 17)	AEDA value[a]	percentage response (n = 15)	AEDA value[a]
2062	butter, almond	octanoic acid[b]	18	10	47	1
2143	fruity, floral, spicy	ethyl cinnamate[b]	29	1	40	10
2181	spicy	eugenol[b]	35	1	27	10
2182	spice, floral	ni	29	1	40	1
2285	earthy, caramel	decanoic acid[b]	24	1	33	1

[a]Aroma extract dilution analysis values: − indicates aroma not perceived at 1:1 dilution; 1, 10, 100, and 1000 indicate aroma perceived in undiluted sample and 1:10; 1:100, and 1:1000 dilutions, respectively (n = 3 assessors). [b]Identification based on retention time and mass spectrometric data compared to that of reference standards. [c]Identification based on retention time and mass spectrometric data reported in the literature. [d]Identification based only on mass spectrometric data. [e]Identification based on retention time and odor description; no clear mass spectrum recorded. [f]Not identified.

fermentation alcohols 2- and 3-methylbutanol, 2-methylpropanol, and 2-phenylethanol were found in concentrations in the milligrams per liter range, and in the Shiraz from Margaret River those compounds were at a higher concentration. As the odor thresholds of those compounds are between 14 and 65 mg/L, the high concentration in which they occur does not necessarily reflect their importance for the overall flavor. Taking the odor threshold into account, the highest OAV in the Shiraz from the Barossa Valley was determined for the fruity-smelling ethyl octanoate, which was 76 times the threshold concentration, followed by β-damascenone (OAV 44), which has an apple-like aroma. The fruity esters 3-methylbutyl acetate (OAV 17), ethyl hexanoate (OAV 26), and ethyl 3-methylbutanoate (OAV 18) also had high OAVs and are therefore important contributors to the overall flavor. Phenolic compounds, such as the primarily oak-derived compounds guaiacol (OAV 1.5), vanillin (OAV 1.5), and eugenol (OAV 6.8), were also found in concentrations above their threshold.

The compounds with the highest OAVs in the Shiraz from Margaret River were similar to those of the Barossa Valley Shiraz. Ethyl octanoate (OAV 88) had the highest odor activity value, followed by the other esters including ethyl hexanoate (OAV 28), ethyl propanoate (OAV 24), ethyl 3-methylbutanoate (OAV 33), and β-damascenone (OAV 24). The BV Shiraz was much higher in the concentration of ethyl propanoate. Considering other acetate esters and ethyl esters, which are important for fruity characters,[22,23] there were no significant concentration differences between the two Shiraz wines. Unlike the BV Shiraz, in the wine from Margaret River the 'cheesy', 'sweaty'-like isomers 2- and 3-methylbutanoic acid were found with high OAVs around 28. The Barossa Valley wine was higher in oak-derived compounds such as *cis*-oak lactone and eugenol and notably higher in dimethyl sulfide. The sesquiterpene rotundone, which was reported to be responsible for the 'pepper' flavor in Shiraz,[12] was detected in an above threshold concentration only in the cooler climate Shiraz.

Reconstitution Test. To confirm that the compounds were indeed key aroma compounds in Shiraz wine, they were recombined and compared with the corresponding real wine. For each wine different reconstitutions were prepared in a wine-like matrix, always adding 44 of the quantitated compounds in the amount in which they appear in Table 4, excluding those compounds occurring in concentrations far below their odor threshold (notably furfural, α-terpineol, and hexyl acetate).

The reconstitutions were first evaluated in informal blind tastings by eight expert panelists, with initial assessment of the samples presented in black glasses in silence followed by open discussion of the characteristics of the samples. The aroma of the reconstituted samples containing 44 aroma compounds in a wine-like matrix (containing ethanol, water, and tartaric acid and also organic acids, salts, and glycerol as described above) was considered in good agreement with the real wine. The overall aroma of the Barossa Valley Shiraz reconstitution was judged more wine-like by these experts than the Margaret River reconstitution. As shown below, the descriptive analyses confirmed this observation as most sensory attributes were better modeled in the BV samples.

Omission Tests. The relative sensory importance of the aroma compounds rotundone, dimethyl sulfide, β-damascenone, linalool, fatty acids, and oak-derived compounds, as well as nonvolatile compounds, was investigated by omission experiments. These compounds were selected on the basis of the differences in concentration between the two wines, as well as from bench tastings, which were used to assess different aroma compounds. Table 5 shows the different combinations of the reconstituted wines and the codes used.

From the ANOVA of the sensory descriptive study results there were significant differences ($P<0.05$) across the samples for all attributes with the exceptions of 'plastic' and 'pepper'. For the 'pepper' attribute, considering this is caused by a compound for which approximately 20% of the population are anosmic,[12] the ANOVA was rerun treating judge as a fixed effect; with this approach the pepper aroma was then rated significantly different across the samples.

The results of the descriptive study for the 16 reconstitution samples, excluding the real wines, are shown in Figure 1 in the form of a PCA plot to show the differences between the two wine types. The real wines were not included in the PCA as they were generally rated higher in several attributes, notably 'dark fruit', which dominated the PCA, making the differences among the reconstituted samples less clear. The sensory profiles of the two wines had been studied in an earlier sensory descriptive analysis.[24]

The Barossa Valley wine reconstitution samples were rated higher than the Margaret River samples in the fruity attributes 'overall fruit' and 'dark fruit', and the mean ratings for 'oaky' and 'chocolate' were also higher in this wine. For the samples mimicking the Margaret River wine the attributes 'green' and 'geranium' were more important. In both sample sets the reconstitutions without nonvolatiles (BV-NV, MR-NV) were clearly separated from their counterparts with nonvolatiles and showed a higher 'chocolate' and 'dark fruit' aroma, with lower 'green' and 'pepper' ratings. The higher rating for 'dark fruit' in the Barossa Valley wine in comparison to the wine from the Margaret River could be caused by higher concentrations of

Table 4. Odor Threshold, Concentration, and Odor Activity Values (OAVs) of Key Compounds for the Barossa Valley and Margaret River Shiraz Wines

		Barossa Valley Shiraz		Margaret River Shiraz	
compound	odor threshold[a] (μg/L)	concentration[b] (μg/L)	OAV[c]	concentration (μg/L)	OAV
acetic acid	200000[4]	680000	3.4	510000	2.6
ethyl lactate	155000[27]	366500	2.4	247250	1.6
ethyl acetate	12300[6]	164400	13.4	103100	8.4
3-methyl-1-butanol	30000[4]	161250	5.4	208400	6.9
2-methyl-1-butanol	65000[4]	40150	<1	76000	1.2
2-methyl-1-propanol	40000[3]	26750	<1	56200	1.4
2-phenylethanol	14000[3]	26350	1.9	56450	4.0
1-butanol	150000[27]	2625	<1	1939	<1
1-hexanol	8000[4]	2030	<1	2008	<1
methionol	1000[3]	2018	2.0	3061	3.1
hexanoic acid	420[3]	1840	4.4	1900	4.5
ocatanoic acid	500[3]	1480	3.0	1680	3.4
2-methylpropanoic acid	2300[3]	929	<1	1634	<1
ethyl propanoate	2100[23]	723	<1	318	<1
3-methylbutyl acetate	30[4]	508	17.0	465	15.5
3-methylbutanoic acid	33[3]	438	13.0	946	28.3
butanoic acid	173[3]	433	2.5	174	1.0
ethyl octanoate	5[3]	378	76.0	439	87.8
ethyl hexanoate	14[3]	369	26.0	391	27.9
2-methylbutanoic acid	33[3]	335	10.0	907	27.5
cis-oak lactone	24[28]	313	13.0	243	10.0
ethyl butanoate	20[4]	305	15.0	234	11.7
vanillin	200[4]	301	1.5	149	<1
furfural	14100[3]	278	<1	149	<1
decanoic acid	1000[3]	224	<1	350	<1
ethyl 2-methylpropanoate	15[3]	207	14.0	353	23.5
dimethyl sulfide	10[4]	130	13.0	37	3.7
ethyl decanoate	200[3]	127	<1	115	<1
trans-oak lactone	172[28]	116	<1	85	<1
2-methylbutyl acetate	160[27]	67	<1	85	<1
ethyl 3-methylbutanoate	3[4]	54	18.0	100	33.3
4-ethylphenol	13[29]	45	3.5	11	<1
eugenol	6[3]	41	6.8	28	4.7
ethyl 2-methylbutanoate	1[4]	36	36.0	76	76.0
2-phenylethyl acetate	250[4]	35	<1	53	<1
guaiacol	23[30]	35	1.5	28	1.2
linalool	15[4]	15	1.0	13	<1
4-methylguaiacol	65[31]	11	<1	8	<1
sotolon	0.49[29]	9	1.8	3	<1
α-terpineol	250[3]	8	<1	8	<1
hexyl acetate	670[18]	5	<1	5	<1
methanethiol	1.8[32]	2.5	1.4	1.7	<1
β-damascenone	0.05[4]	2.2	44.0	1.2	24.0
hydrogen sulfide	1.13[33]	0.6	<1	1.8	1.6
cis-rose oxide	0.2[4]	0.1	<1	0.1	<1
rotundone	0.008[12]	0.001	<1	0.038	4.0

[a]Odor threshold; reference given. In aqueous ethanol except for refs 24 29, in water, and ref 28 30, in wine. [b]Calculated as the mean value of two different workups. [c]Concentration/threshold concentration.

esters and also DMS, as the removal of DMS (BV-DMS) shifted the rating toward 'green', with lower fruit ratings. That the wine from the Barossa valley was rated more 'oaky' was also reflected in higher concentrations for *cis*-oak lactone and eugenol. There were only relatively small effects of omitting several of the compounds tested, and these will be discussed below.

Comparing the Reconstitution and the Real Wines. To assess in more detail the effects of the omissions, data from the two wines are presented separately for the most important attributes for each wine based on the PCA and the attributes that showed significant differences (Figures 2 and 3). Of all the aroma attributes, the highest rating for the real wine sample of the Barossa Valley was given for the attribute 'overall fruit' (Figure 2), which was significantly higher than the reconstituted samples. The omission of 'oaky' compounds decreased the rating significantly, as well as the omission of dimethyl sulfide. Dimethyl sulfide had a concentration of 130

dx.doi.org/10.1021/jf405731v | J. Agric. Food Chem. 2014, 62, 4528−4536

Table 5. Samples Presented to Assessors during Formal Sensory Assessment Sessions for the Reconstitution Study

sample code[a]	sample description
BV wine, MR wine	real wine
BV, MR	complete reconstitution, including nonvolatiles[b]
BV-NV, MR-NV	reconstitution without nonvolatiles[c]
BV-D, MR-D	reconstitution without β-damascenone
BV-DMS, MR-DMS	reconstitution without dimethyl sulfide
BV-FA, MR-FA	reconstitution without octanoic acid, decanoic acid, hexanoic acid
BV-L, MR-L	reconstitution without linalool
BV-O, MR-O	reconstitution in without guaiacol, *cis*-oak lactone, vanillin, eugenol, 4-methylguaiacol
BV-R, MR-R	reconstitution without rotundone

[a]BV, Barossa Valley Shiraz; MR, Margaret River Shiraz. [b]Ethanol, water, tartaric acid, glycerol, fructose, glucose, succinic acid, malic acid, lactic acid, NaCl, K_2HPO_4, $K_2S_2O_3$ concentrations shown in Table 1; aroma compounds as shown in Tables 4 and 5. [c]Matrix consisting only of ethanol, water, and tartaric acid.

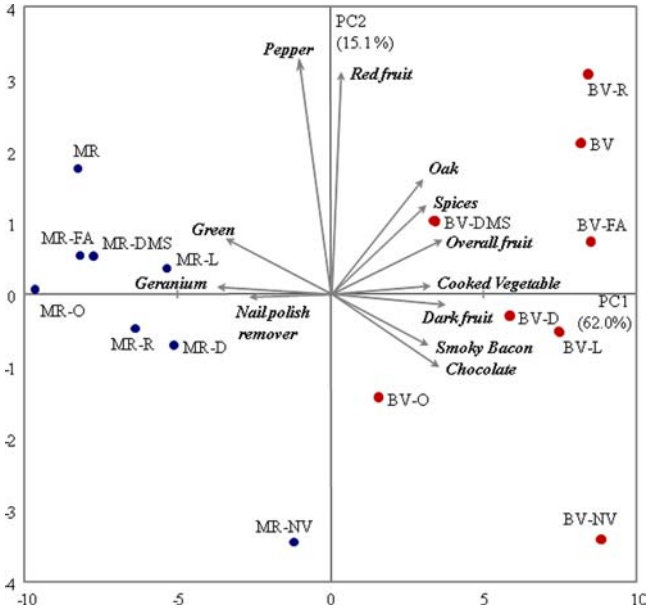

Figure 1. PCA scores and loadings biplot of all samples in the Shiraz reconstitution and omission study. Abbreviations for reconstitution treatments are as listed in Table 5.

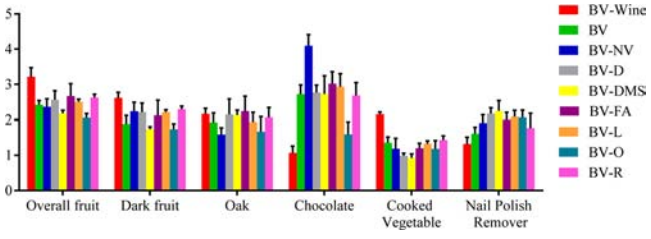

Figure 2. Mean ratings of important aroma attributes in Barossa Valley Shiraz reconstitution samples. Abbreviations for reconstitution treatments are as listed in Table 5. Error bars are one standard error.

μg/L in this wine and was well above the odor threshold. Its aroma can be described as 'cabbage-like', 'corn', and 'asparagus', depending on the matrix as well as the concentration. Our study shows that dimethyl sulfide also contributes to or enhances the fruit flavor, which is in agreement with findings of

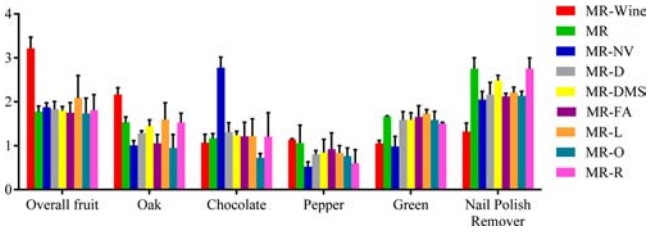

Figure 3. Mean ratings of important aroma attributes in Margaret River Shiraz reconstitution samples. Abbreviations for reconstitution treatments are as listed in Table 5. Error bars are one standard error.

others.[22,25] Although the concentration of β-damascenone is 44 times above the odor threshold and we would therefore expect that it has an influence on the fruity flavor, it does not seem to contribute substantially to the 'overall fruit' flavor as the omission of this compound led to only a marginal increase. In contrast, Pineau et al.[26] found an indirect effect of β-damascenone on fruit flavor, and Escudero et al.[22] showed that β-damascenone and β-ionone also enhance the fruitiness of wines.

Besides 'overall fruit', the attribute 'dark fruit' was an important descriptor for the BV reconstitutions and the real wine. In particular, the mean rating of the reconstitution without the nonvolatiles (BV-NV) is very similar to the real wine sample, whereas the full reconstitution (BV) has a lower intensity in 'dark fruit'. Surprisingly, the subtraction of DMS (BV-DMS) does not change the rating, whereas the reconstitution without β-damascenone (BV-D) increased the rating for the 'dark fruit' character. The omission of either linalool or rotundone led to a higher rating in this attribute, likely caused by a masking effect of these compounds on the dark fruit character.

The rating of 'oaky' is in good agreement within all samples, without any significant differences. Only the sample without nonvolatiles (BV-NV) and, as expected, the omission of oaky compounds (BV-O) were rated lower in 'oaky'. Interestingly, as discussed above, the rating for the 'chocolate' character showed significant differences and especially the sample with the omission of the nonvolatiles (BV-NV) had a very high rating in this attribute. The real wine was rated significantly lower in 'chocolate', and also the omission of 'oaky' compounds resulted in a rating similar to that of the real wine.

In contrast to this, the real wine sample (BV-wine) was rated significantly higher in the 'cooked vegetable' attribute, and the omission of either dimethyl sulfide or β-damascenone decreased the intensity for this attribute in comparison to all other reconstitutions. That dimethyl sulfide contributes to the 'cooked vegetable' character was not surprising. 'Nail polish remover' was an attribute used to describe the aroma of ethyl acetate, which is generally an undesirable character of wine. As Figure 2 shows, all reconstituted samples showed a much higher rating for this attribute than the original wine sample. The attribute 'geranium' was rated a low intensity in all samples, and the differences between the reconstitutions and the original wine sample were not significant.

The mean ratings for important sensory attributes for the reconstitutions of the wine from Margaret River are shown in Figure 3. Similarly to the wine from the Barossa Valley, 'overall fruit' was an important flavor attribute and rated highly in the real wine. The reconstituted samples were all scored significantly lower for this attribute, with only a marginal increase of the rating for the omission of linalool. Whereas the

dx.doi.org/10.1021/jf405731v | J. Agric. Food Chem. 2014, 62, 4528−4536

'oaky' character was very well modeled in the BV samples, for the MR sample set there were significant differences. The real wine was rated higher than all other samples, and the omission of nonvolatiles (MR-NV) and 'oaky' compounds (MR-O) resulted in the lowest rating. The sample without fatty acids (MR-FA) also showed a lower rating for the 'oaky' attribute. The 'chocolate' attribute for the reconstitution was in good agreement with the score for the real wine with only the omission of nonvolatiles (MR-NV) showing a significant increase for this rating. The same effect was seen for the Barossa Valley Shiraz samples; the nonvolatiles seem to have an important influence on the aroma perception of the compounds responsible for the 'chocolate' character.

The attribute 'pepper' in the wine from Margaret River was rated higher than in the BV Shiraz, which is reflected in the concentrations of the pepper-smelling compound rotundone. In the MR Shiraz rotundone was found at 38 ng/L, a concentration well above the odor threshold,[24] whereas the concentration in the BV Shiraz was only 1 ng/L. For this attribute, the rating of the full reconstitution (MR) is in good agreement with the real wine (MR-Wine). As for other attributes the fraction of nonvolatiles has a significant influence on the rating for 'pepper', which was in this case decreased. Also, the omission of rotundone led to a lower mean rating for the 'pepper' attribute. Considering the 'green' aroma descriptor, the omission of nonvolatiles (MR-NV) resulted in a rating very similar to that of the real wine; all other samples showed a higher rating.

As seen for the reconstitution of the BV samples, the attribute 'nail polish remover' was rated much higher in all samples. In this case, especially the full reconstitution (MR) and the samples MR-DMS and MR-R had increased ratings in this attribute. The perception of this flavor compound seems to be increased in reconstituted samples, presumably due to the lack of masking aroma compounds such as DMS. It is also possible that the equilibration between acetic acid and ethanol is different in the model wine from that in the real wine matrix or that different SO_2 levels contribute to the intensity of the attribute 'nail polish remover'.

This study has found that by mixing 44 aroma compounds in concentrations measured in Shiraz, the aroma of two different Australian Shiraz wines could be reconstituted. A relatively small number of critical compounds were found, providing optimism that predictive models can be developed to relate wine composition to flavor attribute intensities. Different omission experiments were analyzed by sensory descriptive analysis, and the greatest differences related to the omission of nonvolatiles. Compounds such as β-damascenone, linalool, and fatty acids had only small effects on aroma, highlighting the complexity of the behavior of mixtures of odorants even when present well above detection threshold. The omission of the mixture of organic acids, sugars, minerals, and glycerol increased the rating for the 'chocolate' character in both sample sets significantly and decreased the 'pepper' and 'green' attributes of the wine from the cooler region. Further research is needed to investigate which component of the nonvolatile fraction is the main cause of this effect, which may be of great importance in understanding and controlling undesirable 'green' flavors in wines.

AUTHOR INFORMATION

Corresponding Author

*(I.L.F.) Phone: +61 883136600. Fax: +61 883136601. E-mail: leigh.francis@awri.com.au.

Present Addresses

†(C.M.M.) Cara Technology Limited, Leatherhead Enterprise Centre, Randalls Road, Leatherhead, Surrey KT22 7RY, United Kingdom.

§(J.P.G.) CPR Pharma Services Pty Ltd., 28 Dalgleish Street, Thebarton South Australia, Australia, 5031.

‡(D.W.J.) School of Agriculture, Food and Wine, Waite Research Institute, The University of Adelaide, Waite Campus, PMB 1, Glen Osmond, South Australia 5064, Australia.

Funding

The Australian Wine Research Institute (AWRI), a member of the Wine Innovation Cluster at the Waite Precinct in Adelaide, is supported by Australian grapegrowers and winemakers through their investment body, the Grape and Wine Research and Development Corporation (GWRDC), with matching funds from the Australian government.

Notes

The authors declare no competing financial interest.

ACKNOWLEDGMENTS

We thank the sensory panelists and colleagues from the AWRI for participating in the sensory and GC-O studies.

REFERENCES

(1) Maarse, H.; Visscher, C. A.; Willemsens, L. C.; Boelens, M. H. *Volatile Compounds in Food: Qualitative and Quantitative Data, Suppl. 4*; TNO-CIVO Food Analysis Institute: The Netherlands, 1992.

(2) Guth, H. Identification of character impact odorants of different white wine varieties. *J. Agric. Food Chem.* **1997**, *45*, 3022−3026.

(3) Ferreira, V.; Lopez, R.; Cacho, J. F. Quantitative determination of the odorants of young red wines from different grape varieties. *J. Sci. Food. Agric.* **2000**, *1667*, 1659−1667.

(4) Guth, H. Quantitation and sensory studies of character impact odorants of different white wine varieties. *J. Agric. Food Chem.* **1997**, *45*, 3027−3032.

(5) Schieberle, P. New developments in methods for analysis of volatile flavor compounds and their precursors. In *Characterization of Food: Emerging Methods*; Gaonkar, A. G., Ed.; CABI: Wallingford, UK, 1995; pp 403−431.

(6) Escudero, A.; Gogorza, B.; Melús, M. A.; Ortín, N.; Cacho, J.; Ferreira, V. Characterization of the aroma of a wine from Maccabeo. key role played by compounds with low odor activity values. *J. Agric. Food Chem.* **2004**, *52*, 3516−3524.

(7) Ferreira, V.; Ortín, N.; Escudero, A.; López, R.; Cacho, J. Chemical characterization of the aroma of Grenache rosé wines: aroma extract dilution analysis, quantitative determination, and sensory reconstitution studies. *J. Agric. Food Chem.* **2002**, *50*, 4048−4054.

(8) Aznar, M.; López, R.; Cacho, J. F.; Ferreira, V. Identification and quantification of impact odorants of aged red wines from Rioja. GC-olfactometry, quantitative GC-MS, and odor evaluation of HPLC fractions. *J. Agric. Food Chem.* **2001**, *49*, 2924−2929.

(9) Frank, S.; Wollmann, N.; Schieberle, P.; Hofmann, T. Reconstitution of the flavor signature of Dornfelder red wine on the basis of the natural concentrations of its key aroma and taste compounds. *J. Agric. Food Chem.* **2011**, *59*, 8866−8874.

(10) Parker, M.; Pollnitz, A. P.; Cozzolino, D.; Francis, I. L.; Herderich, M. J. Identification and quantification of a marker compound for "pepper" aroma and flavor in Shiraz grape berries by combination of chemometrics and gas chromatography-mass spectrometry. *J. Agric. Food Chem.* **2007**, *55*, 5948−5955.

(11) Koch, A.; Doyle, C. L.; Matthews, M. A.; Williams, L. E.; Ebeler, S. E. 2-Methoxy-3-isobutylpyrazine in grape berries and its dependence on genotype. *Phytochemistry* **2010**, *71*, 2190−2198.
(12) Wood, C.; Siebert, T. E.; Parker, M.; Capone, D. L.; Elsey, G. M.; Pollnitz, A. P.; Eggers, M.; Meier, M.; Voessing, T.; Widder, S.; Krammer, G.; Sefton, M. A.; Herderich, M. J. From wine to pepper: rotundone, an obscure sesquiterpene, is a potent spicy aroma compound. *J. Agric. Food Chem.* **2008**, *56*, 3738−3744.
(13) Iland, P.; Bruer, N.; Edwards, G.; Weeks, S.; Wilkes, E. *Chemical Analysis of Grapes and Wine: Techniques and Concepts*; Patrick Iland Wine Promotions: Campbelltown, SA, Australia, 2004; pp 32−58.
(14) Engel, W.; Bahr, W.; Schieberle, P. Solvent assisted flavor evaporation − a new and versatile technique for the careful and direct isolation of aroma compounds from complex food matrices. *Eur. Food Res. Technol.* **1999**, *209*, 237−241.
(15) Siebert, T. E.; Smyth, H. E.; Capone, D. L.; Neuwöhner, C.; Pardon, K. H.; Skouroumounis, G. K.; Herderich, M. J.; Sefton, M. A.; Pollnitz, A. P. Stable isotope dilution analysis of wine fermentation products by HS-SPME-GC-MS. *Anal. Bioanal. Chem.* **2005**, *381*, 937−947.
(16) Pedersen, D. S.; Capone, D. L.; Skouroumounis, G. K.; Pollnitz, A. P.; Sefton, M. A. Quantitative analysis of geraniol, nerol, linalool, and α-terpineol in wine. *Anal. Bioanal. Chem.* **2003**, *375*, 517−522.
(17) Siebert, T. E.; Wood, C.; Elsey, G. M.; Pollnitz, A. P. Determination of rotundone, the pepper aroma impact compound, in grapes and wine. *J. Agric. Food Chem.* **2008**, *56*, 3745−3748.
(18) Ugliano, M.; Siebert, T.; Mercurio, M.; Capone, D.; Henschke, P. A. Volatile and color composition of young and model-aged Shiraz wines as affected by diammonium phosphate supplementation before alcoholic fermentation. *J. Agric. Food Chem.* **2008**, *56*, 9175−9182.
(19) Siebert, T. E.; Solomon, M. R.; Pollnitz, A. P.; Jeffery, D. W. Selective determination of volatile sulfur compounds in wine by gas chromatography with sulfur chemiluminescence detection. *J. Agric. Food Chem.* **2010**, *58*, 9454−9462.
(20) Pollnitz, A. P.; Pardon, K. H.; Sykes, M.; Sefton, M. A. The effects of sample preparation and gas chromatograph injection techniques on the accuracy of measuring guaiacol, 4-methylguaiacol and other volatile oak compounds in oak extracts by stable isotope dilution analyses. *J. Agric. Food Chem.* **2004**, *52*, 3244−3252.
(21) Marangon, M.; Lucchetta, M.; Waters, E. J. Protein stabilisation of white wines using zirconium dioxide enclosed in a metallic cage. *Aust. J. Grape Wine Res.* **2011**, *17*, 28−35.
(22) Escudero, A.; Campo, E.; Fariña, L.; Cacho, J.; Ferreira, V. Analytical characterization of the aroma of five premium red wines. insights into the role of odor families and the concept of fruitiness of wines. *J. Agric. Food Chem.* **2007**, *55*, 4501−4510.
(23) Pineau, B.; Barbe, J.-C.; Van Leeuwen, C.; Dubourdieu, D. Examples of perceptive interactions involved in specific "red-" and "black-berry" aromas in red wines. *J. Agric. Food Chem.* **2009**, *57*, 3702−3708.
(24) Herderich, M. J.; Siebert, T. E.; Parker, M.; Capone, D. L.; Jeffery, D. W.; Osidacz, P.; Francis, I. L. Spice up your life: analysis of key aroma compounds in Shiraz. In *Flavor Chemistry of Wine and Other Alcoholic Beverages*; Qian, M., Shellhammer, T. H., Eds.; American Chemical Society: Washington, DC, USA, 2012; pp 3−13.
(25) Segurel, M. A.; Razungles, A. J.; Riou, C.; Salles, M.; Baumes, R. L. Contribution of dimethyl sulfide to the aroma of Syrah and Grenache noir wines and estimation of its potential in grapes of these varieties. *J. Agric. Food Chem.* **2004**, *52*, 7084−7093.
(26) Pineau, B.; Barbe, J.-C.; van Leeuwen, C.; Dubourdieu, D. Which impact for β-damascenone on red wines aroma? *J. Agric. Food Chem.* **2007**, 4103−4108.
(27) Etievant, P. X. Wine. In *Volatile Compounds in Foods and Beverages*; Maarse, H., Ed.; Dekker: New York, 1991; pp 483−546.
(28) Brown, R. C.; Sefton, M. A.; Taylor, D. K.; Elsey, G. M. An odour detection threshold determination of all four possible stereoisomers of oak lactone in a white and a red wine. *Aust. J. Grape Wine Res.* **2006**, *12*, 115−118.
(29) Czerny, M.; Christlbauer, M.; Christlbauer, M.; Fischer, A.; Granvogl, M.; Hammer, M.; Hartl, C.; Hernandez, N. M.; Schieberle, P. Re-investigation on odour thresholds of key food aroma compounds and development of an aroma language based on odour qualities of defined aqueous odorant solutions. *Eur. Food Res. Technol.* **2008**, *228*, 265−273.
(30) Parker, M.; Osidacz, P.; Baldock, G.; Hayasaka, Y.; Black, C.; Pardon, K. H.; Jeffery, D. W.; Geue, J. P.; Herderich, M. J.; Francis, I. L. Contribution of several volatile phenols and their glycoconjugates to smoke-related sensory properties of red wine. *J. Agric. Food Chem.* **2012**, *60*, 2629−2637.
(31) Boidron, J. N.; Chatonnet, P.; Pons, M. Influence du bois sur certaines substances odorantes des vins. *Vigne Vin* **1988**, *22*, 275−293.
(32) Solomon, M. R.; Geue, J.; Osidacz, P.; Siebert, T. E. Aroma detection threshold study of methanethiol in white and red wine. *AWRI Tech. Rev.* **2010**, *186*, 8−10.
(33) Siebert, T.; Bramley, B. R.; Solomon, M. Hydrogen sulfide: aroma detection threshold study in white and red wine. *AWRI Tech. Rev.* **2009**, *183*, 14−16.

JOURNAL OF AGRICULTURAL AND FOOD CHEMISTRY

Article

pubs.acs.org/JAFC

Aroma Active Volatiles in Four Southern Highbush Blueberry Cultivars Determined by Gas Chromatography−Olfactometry (GC-O) and Gas Chromatography−Mass Spectrometry (GC-MS)

Xiaofen Du and Russell Rouseff*

Citrus Research and Education Center, University of Florida, 700 Experiment Station Road, Lake Alfred, Florida 33850, United States

ABSTRACT: Aroma active volatiles in four southern highbush blueberry cultivars ('Prima Dona', 'Jewel', 'Snow Chaser', and 'Kestrel') were determined using solid phase microextraction (SPME) in combination with gas chromatography−olfactometry (GC-O) and identified via GC-PFPD and GC-MS using retention indices of reference compounds and mass spectral data. The aromas of total, unseparated SPME extracts evaluated using GC-O were rated 8.2−9.0/10 for the four cultivars in terms of similarity to the original blueberry homogenates. In terms of GC-O aroma similarity, those aroma active volatile groups characterized as green, fruity, and floral were most intense. Of the 43 volatiles found to have aroma activity, 38 were identified and 13 had not been previously reported in blueberries. Although linalool and (*E*)-2-hexenal were common major aroma impact volatiles, dominant aroma-active volatiles were different for each cultivar. Principal component analysis confirmed that each cultivar possessed a unique aroma active profile as each cultivar was clustered into a separate score plot quadrant.

KEYWORDS: *southern highbush blueberry, blueberry aroma, GC-O, SPME*

INTRODUCTION

Next to strawberries, blueberries are the second most important berry crop in the United States.[1] The cultivated blueberry market has more than tripled since the 1970s. It has increased at a rate of 10−20% annually since 2000. The U.S. 2012 crop was worth $781.8 million.[2] The rapid increase in blueberry consumption is mainly driven by its reported nutraceutical functions, health benefits, and unique flavor.[3]

Blueberry is a plant native to North America. It is in the genus *Vaccinium*, section Cyanococcus. In this section, there are three main commercialized blueberries: highbush (*Vaccinium corymbosum*), lowbush (*Vaccinium angustifolium*), and rabbiteye (*Vaccinium ashei*). Highbush blueberry is the major planted cultivar, which accounts for approximately 95% of the total commercial production in the United States. Highbush blueberry can be further divided into northern highbush and southern highbush blueberry. Northern highbush is a high-chill blueberry, which has been optimized for high-chill zones. High-chill zones are those climates that experience a minimum of 800 h below 7.2 °C. Southern highbush is a hybrid between the northern highbush and various low-chill Cyanococcus species.[4] The northern highbush blueberry is the predominant cultivar grown in the major blueberry production areas in the northern United States: Maryland, Michigan, New Jersey, North Carolina, and Washington. The southern highbush blueberry is primarily grown in California and Florida.

Florida's southern highbush blueberries ripen earlier than blueberries in other growing areas and are the major producers of U.S. blueberries from the middle of April to late May. The early-market fruit commands a high price, and this has led to the expansion of Florida's blueberry acreage.[5] To be competitive in the blueberry market the fruit should be early ripening and of good quality. Flavor and aroma are two of the most important fruit quality characteristics and ultimately determine consumer acceptability and purchase decision. However, to the best of our knowledge, there is no study that evaluates the aroma volatiles of Florida southern highbush blueberry.

The study of blueberry flavor has been quite limited. A few of the major volatiles have been identified in various blueberry types. In highbush blueberries, the major volatile compounds were reported as ethyl acetate, (*E*)-2-hexenal, (*E*)-2-hexenol, hexanal, (*Z*)-3-hexenol, linalool, and geraniol.[6−8] Other compounds such as citronellol, α-terpineol, 2-phenylethanol, and vanillin have also been suggested to contribute to the typical aroma of highbush blueberries.[9] Few studies have examined the aroma composition in lowbush blueberries. Acetaldehyde, methyl acetate, ethyl acetate, methyl 2-methylbutanoate, methyl 3-methylbutanoate, ethyl 2-methylbutanoate, ethyl 3-methylbutanoate, methyl butanoate, and linalool were reported as the major aroma compounds.[10−12] A greater number of esters have been reported in lowbush compared to highbush blueberries. Studies on rabbiteye blueberry aroma are also very limited. The major volatiles identified in rabbiteye blueberry are ethyl acetate, *p*-cymene, hexanol, (*Z*)-2-hexenol, heptanol, cinerolone, β-ionone, terpene-4-ol, 2-undecanone, α-terpineol, carveol, nerol, and eugenol.[13−15] A combination of (*E*)-2-hexenal, (*E*)-2-hexenol, (*Z*)-3-hexenol, and linalool has been reported as being responsible for the characteristic blueberry flavor.[14]

Because the identification of blueberry aroma active volatiles is limited and conflicting, especially because there seem to be no studies on the aroma composition of southern highbush blueberry, the object of this study was to investigate the aroma active compounds in two common and two new Florida

Received: January 21, 2014
Revised: April 17, 2014
Accepted: April 23, 2014
Published: April 23, 2014

ACS Publications © 2014 American Chemical Society

southern highbush blueberry cultivars using a combination of SPME, GC-O, and GC-MS. A secondary goal was to evaluate the aroma active volatiles of these cultivars using GC-O to determine how similar or different the aroma profiles of these four cultivars were.

MATERIALS AND METHODS

Chemicals. Pure standards of ethyl propionate, methyl 2-methylbutanoate, methyl 3-methylbutanoate, ethyl 2-methylbutanoate, ethyl 3-methylbutanoate, (*Z*)-3-hexenyl acetate, (*E*)-2-hexenyl acetate, linalool, citronellol, nerol, geranylacetone, hexanal, (*Z*)-3-hexenal, (*E*)-2-hexenal, (*E*,*E*)-2,4-hexadienal, (*E*,*Z*)-2,6-nonedienal, (*E*,*E*)-2,4-nonedienal, (*Z*)-3-hexenol, 2-heptanol, 2-heptanone, 1-octen-3-one, 2-methylbutanoic acid, hexanoic acid, methional, Furaneol, *p*-cresol, and eugenol were purchased from Aldrich Chemical Co. Inc. (Milwaukee, WI, USA). Geranyl acetate, 1,8-cineole, α-terpineol, octanal, and decanal were supplied from Sunpure (Lakeland, FL, USA). Geraniol, pentanal, and dimethyl disulfide were purchased from Acros Organics (Fair Lawn, NJ, USA). 2-Nonanone was from Eastman Chemical Co. (Kingsport, TN, USA), whereas β-damascenone was from Givaudan Roure Corp. (Whippany, NJ, USA). Sodium fluoride (ACS grade) were obtained from Acros Organics. Sodium chloride and methanol were purchased from Fisher Scientific (Fair Lawn, NJ, USA).

Blueberry Samples. Highbush blueberry plants 'Jewel' and 'Prima Dona' were grown at a local blueberry farm in Haines City, FL, USA, whereas 'Snow Chaser' and 'Kestrel' were grown at a blueberry breeding center at the University of Florida, Gainesville, FL, USA. Blueberry samples were hand-harvested on April 27 (for 'Jewel' and 'Prima Dona') and May 10 (for 'Snow Chaser' and 'Kestrel') of 2011. All blueberries were grown in mounded pine bark and received similar fertilization. To obtain equal levels of fruit maturity, the berries were harvested in the more northern location (Gainesville) 2 weeks later than the berries grown in Haines City.

Blueberry samples were washed with distilled water and gently dried with tissue paper. Two hundred grams of distilled water and 200 g of berries were homogenized along with sodium chloride and sodium fluoride (final concentrations 20 and 1%, respectively) in a glass blender (Waring Products Div., Dynamics Corp. of America, New Hartford, CT, USA). Samples were blended in a high-speed pulse mode for 20 s. The puree was used for analysis.

SPME Blueberry Volatiles. SPME has been successfully coupled with GC-O to identify aroma active volatiles in foods for approximately 15 years now.[16] In this study 10 g of blueberry puree was added into a 40 mL vial and a 4 mm stir bar, which was flushed with nitrogen before sealing with a septum screw top. It was found that gentle stirring of the sample reduced equilibrium times and improved analytical precision. Samples were equilibrated at 40 °C in a water bath for 20 min. After equilibration, a 2 cm fiber coated with divinylbenzene/carboxen/polydimethylsiloxane (DVB/CAR/PDMS, Supelco, Bellefonte, PA, USA) was exposed to the headspace of the vial for 40 min at the same temperature. The three-phase fiber was chosen as it consistently produced the most representative collection of headspace volatiles compared to other fiber types. Forty minutes was chosen as an extraction time as it produced the largest amounts of volatiles and at the same time produced the most consistent results. The fiber was then introduced into the GC injection port for a 3 min desorption.

Direct GC-O. A 1 m deactivated silica column (0.32 mm i.d.) was installed on an Agilent 6890N gas chromatograph system (Palo Alto, CA, USA) directly from the injector to a high volume sniffing port (Datu, Geneva, NY, USA). The flow rate of the helium carrier gas was 20 mL/min. The injection port temperature was 220 °C, and the oven temperature was 150 °C (isothermal). The configuration allows for the evaluation of global odor of the extracts without chromatographic separation, and the entire analysis was completed in <30 s. Two trained panelists smelled the odor of the unseparated SPME extract at the GC sniffing port. Then, panelists opened a 40 mL vial to smell the original blended blueberry puree. Panelists rated the similarity between the unseparated SPME extract and the original puree odors using an 11-point scale ranging from 0 (far from the sample) to 10 (identical to the original sample). Each panelist had been screened from a larger pool of potential panelists using a set of 15 common fruit aroma active volatiles. Accepted panelists demonstrated that they could detect all separated volatiles in the training set and could reproduce the intensity of each volatile. Training time was approximately 3 weeks.

Time−Intensity GC-O Procedure. GC-O analysis was conducted using an Agilent 6890N gas chromatograph system equipped with a flame ionization detector (FID) with the previously described olfactometer. Samples were separated using a DB-Wax column (30 m × 0.32 mm i.d. cross-linked poly(ethylene glycol), 0.50 μm film thickness, J&W Scientific, Folsom, CA, USA). The column effluent was split 1:2 (by volume) into the FID and a heated sniffing port block, where the flow was mixed with humidified air. The column flow rate was 2.0 mL/min (helium) with injection in the splitless mode. Injector and detector temperatures were 220 and 250 °C. The initial oven temperature was 35 °C and held for 1 min before increasing to 190 °C at 4 °C/min and then to 240 °C at a rate of 8 °C/min, and holding at 240 °C for 5 min before cooling back to 35 °C.

Olfactometry analyses were performed by two trained panelists. Assessors rated aroma intensity continuously throughout the chromatographic run using a linear potentiometer from which output was recorded and quantified using Chromperfect software (Justice Innovations, Palo Alto, CA, USA). Retention times and verbal descriptors were recorded to permit aroma descriptors to be coupled with computerized aroma time−intensity plots. Triplicate analyses were performed for each sample by each panelist. Volatiles were not considered to be aroma active unless detected during at least half of the total sniffing trials. The intensity was the average from all panelists when an aroma was registered. Compound identification was based on matching retention times and aroma character with authentic pure standards, retention indices (RIs) that were determined using a series of standard linear alkanes C_5−C_{25}, GC-MS, or GC-PFPD (pulsed flame photometric detector).

GC-MS Identification Aroma Active Compounds. GC-MS analyses were performed using a PerkinElmer Clarus 500 gas chromatograph and a quadropole mass spectrometer (PerkinElmer, Waltham, MA, USA). Compound separation was achieved with a DB-WAX column (60 m × 0.25 mm i.d. cross-linked poly(ethylene glycol), 0.50 μm film thickness, J&W Scientific, Agilent Technique, Foster City, CA, USA). Column flow rate (helium) was 1.5 mL/min. Initial oven temperature was 35 °C. After holding for 1 min, the oven temperature was increased to 190 °C at 4 °C/min and then to 240 °C at 8 °C/min. The oven was maintained at 240 °C for 5 min before returning to 35 °C. Injection, MS transfer line, and ion source temperatures were 230, 240, and 180 °C, respectively. Fragmentation data from m/z 25 to 300 were collected in the scan mode. Compound identifications were made by comparing mass spectral data from the Wiley 275.L (G1035) database and confirmed by authentic pure standards and reported linear retention index (LRI; Kovats) values found in the literature.

GC-PFPD Identification of Sulfur Compounds. Sulfur volatile analyses were achieved using an Agilent 7890A gas chromatograph system equipped with a sulfur-specific detector: a PFPD (model 5380, OI Analytical Co., College Station, TX, USA). Volatiles were separated using a Stable-WAX column (30 m × 0.32 mm i.d. cross-linked poly(ethylene glycol), 0.50 μm film thickness, Restek, Bellefonte, PA, USA). Column flow was 1.5 mL/min (helium). Initial oven temperature was 35 °C. After holding for 1 min, the oven temperature was increased to 65 °C at a rate of 3 °C/min, then increased to 170 °C at a rate of 6 °C/min, and finally to 240 °C at a rate of 10 °C/min with a 5 min hold. The GC injection temperature was 200 °C, and the detector temperature was 250 °C. Sulfur gate time was 6−24.9 ms, and pulse frequency was approximately 3 pulses/s. Sulfur peaks from the PFPD detector were integrated using Chromperfect software version 5.0 (Justin Innovations, Inc., CA). Compound identification was based on matching LRI values from authentic sulfur standards and LRIs reported in the literature with those observed in the samples.

Multivariate Statistics. The aroma active volatile data set used average intensity ratings from the olfactory panel. Principal component

analysis (PCA) was carried out using Unscrambler version 10 from Camo (Woodbridge, NJ, USA). All 43 aroma active volatile values were used in the calculations. Graphical score and loading plots were superimposed into a single figure using the Unscrambler biplot graphing feature.

RESULTS AND DISCUSSION

Global Blueberry Aroma Using SPME. Although blueberry volatile composition has been studied by several groups, there is some disagreement, some of which can be attributed to volatile extraction and identification techniques employed. Traditional techniques such as distillation, liquid−liquid extraction, and headspace sampling are frequently used for volatile isolation in berry fruit.[17] However, most of these techniques are labor-intensive and can produce artifacts. All aroma extraction techniques produce extracts favoring some chemical classes and minimizing others or (in the case of solvent extraction) extract volatiles that have very little volatility at room temperatures but are 100% volatilized in the GC injector. Thus, GC-O results need to be interpreted with care. Static headspace solid phase microextraction (SPME) is an alternative volatile extraction technique that employs a fused silica fiber coated with an appropriate sorbent stationary phase which collects and concentrates only volatiles. The main advantages of SPME are speed, simplicity of operation, and lack of a solvent peak to obscure highly volatile components from the sample. SPME has been widely used to extract volatiles in a wide range of food samples.[18] However, not all SPME fibers produce the same results. The three-phase fiber was used in this study as we have found it to produce the most representative extracts.

When static headspace volatile collection is employed, berry samples can be present as whole fruit, sliced fruit, or blended puree. Blending is more commonly employed for berries because blending can increase volatile release from the berry matrix. However, the reaction of native enzyme activity can distort the original aroma by converting nonvolatiles into aroma active volatiles. In this study, 20% sodium chloride and 1% sodium fluoride (w/w) were added as part of the blending mixture to prevent or reduce this effect. Sodium chloride was used to inhibit lipoxygenase activity, whereas sodium fluoride was used to inhibit polyphenol oxidase activity and microbial growth during equilibrium and volatile extraction. Preliminary experiments indicated that when these salts were not employed, blueberry purees had more than 200 times the total "green volatiles" (hexanal, (*Z*)-2-hexenal, (*E*)-2-hexenal, hexanol, (*Z*)-3-hexenol, and (*E*)-2-hexenol). The rate of formation for each "green compound" appeared to be cultivar and time dependent. Informal sensory evaluations of these samples (blended with or without salts) indicated that berry purees with no added salt had much stronger "green" flavor than those with the added salt. Therefore, salts were added to the berries during blending to prevent the distortion of the native aroma profile.

After blending, blueberry puree volatiles were extracted in the static headspace mode using a 2 cm, triphase SPME fiber (DVB/CAR/PDMS). This fiber was chosen because it had been found to extract the most representative strawberry volatiles.[19] To confirm the representativeness of the SPME extracts, the global aromas of the extracts were evaluated using the unseparated GC-O method and compared to the original blended samples. The global aroma of the extracts and aroma description of the original blended samples including 'Jewel', 'Prima Dona', 'Snow Chaser', and 'Kestrel' are presented in Table 1. Overall, the aroma of the homogenized blueberry samples could be described as "fresh green", "grassy", "fruity", "floral", "blueberry-like", and "tea-like". However, the top aroma impression for each blueberry cultivar was different. 'Jewel' gave the strongest aroma notes of "grassy" and "fresh green", whereas 'Snow Chaser' had the highest level of "floral" note. 'Prima Dona' had the top aroma notes of "fresh green" and "fruity". 'Kestrel' had a similar top aroma of "fresh green" and "fruity"; however, its intensity was much higher than that of 'Prima Dona'. Overall, the global aroma of SPME extracts was quite similar to that of the original blueberry homogenates (Table 1). Compared to the reference purees, the global aroma of SPME extracts had average rates of 8.5, 9.0, 8.2, and 8.9 for 'Jewel', 'Prima Dona', 'Snow Chaser', and 'Kestrel', respectively (Table 1). The results suggested that collected SPME volatiles generated an odor that was representative of the original sample.

Table 1. Global Aroma of SPME Headspace Extracts of Four Florida Southern Highbush Blueberries Scores Compared to Aroma of Original Blended Samples

cultivar	aroma of original blended sample	global aroma of SPME extract	score
Jewel	grassy, fresh green, fruity, blueberry-like	grassy, green, fruity, blueberry-like, red tea-like	8.5
Prima Dona	fresh green, fruity, blueberry-like, green tea-like	fresh green, blueberry-like, fruity, red tea-like	9.0
Snow Chaser	floral, fruity, fresh green, blueberry-like	rosy, fresh green, floral, fruity	8.2
Kestrel	fresh green, fruity, floral, green tea-like, blueberry-like	fresh green, fruity, blueberry-like, floral, red tea-like	8.9

GC-O Analysis. Shown in Figure 1 are the average aromagrams from 'Prima Dona' and 'Kestrel' southern highbush blueberry cultivars. The 'Kestrel' aromagram is inverted for comparison purposes. Both qualitative (missing aroma volatiles) and quantitative (aroma intensity) differences are apparent. One of the more obvious features is the high number

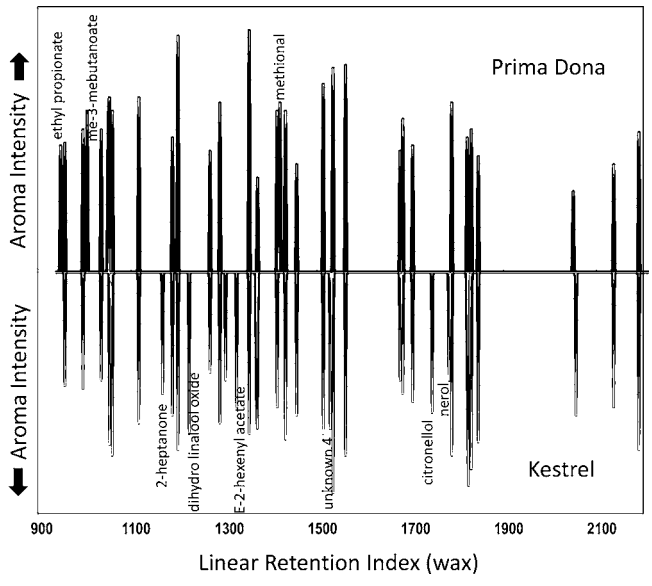

Figure 1. Aromagrams of average aroma intensities from 'Prima Dona' (upper) and 'Kestrel' (lower and inverted).

dx.doi.org/10.1021/jf500315t | J. Agric. Food Chem. 2014, 62, 4537−4543

Table 2. Identified GC-O Aroma-Active Compounds in 'Jewel', 'Prima Dona', 'Snow Chaser', and 'Kestrel' Blueberries

LRI	identity	aroma descriptors	Jewel	Prima Dona	Snow Chaser	Kestrel	identification basis[a]
949	ethyl propionate[b]	sweet, fruity, apple	5.5	4.7			RI, Std, AD
959	pentanal	malty, almond, sulfuric	5.6	4.8	4.6	4.2	RI, Std, AD, MS
997	methyl 2-methylbutanoate	green, fruity, pear		5.3	4	4.3	RI, Std, AD, MS
1005	methyl 3-methylbutanoate	fruity, apple, pineapple	6	6	5.3		RI, Std, AD, MS
1036	ethyl 2-methylbutanoate	fruity, apple	5.8	5.3		4	RI, Std, AD, MS
1050	ethyl 3-methylbutanoate	fruity, apple, sweet	6.5	5.5			RI, Std, AD, MS
1054	dimethyl disulfide	sulfuric, rotten egg	8.3	6.4	5.8	6.4	RI, Std, AD, PFPD
1061	hexanal	fresh, green, fruity	6.3	6	5.5	6.8	RI, Std, AD, MS
1117	(*Z*)-3-hexenal	green, leafy	7	6.5	5	5.6	RI, Std, AD, MS
1168	2-heptanone	fruity, spicy, cheesy	4			4.5	RI, Std, AD, MS
1188	1,8-cineole	minty, woody, herbaceous	3.7	5	6	5.3	RI, Std, AD, MS
1202	(*E*)-2-hexenal	grassy, pungent	8.3	8.8	8	6.6	RI, Std, AD, MS
1224	dihydrolinalool oxide	moldy, fatty, fruity	5.8		6.3	6	RI, MS
1270	octanal	citrus, fatty	4	4.5		3.7	RI, Std, AD, MS
1291	1-octen-3-one[a]	mushroom	6.3	6.3	5.2	5.6	RI, Std, AD
1302	(*Z*)-3-hexenyl acetate	green, fruity, woody	4.5		5	4	RI, Std, AD, MS
1326	(*E*)-2-hexenyl acetate	green, leafy, apple			4.7	5	RI, Std, AD, MS
1353	unknown 1	sulfurous, grassy	8.5	9	6.8	6	
1370	(*Z*)-3-hexenol	green, grassy				4.8	RI, Std, AD, MS
1373	2-nonanone	fruity, earthy, herb	4.3	3.5	4	5.7	RI, Std, AD, MS
1413	(*E*,*E*)-2,4-hexadienal	leaf, fatty, green	6	6	5	5	RI, Std, AD, MS
1419	unknown 2	floral, perfume	5.6	6.3			
1432	methional	cooked potato	6	6	5.8	6.2	RI, Std, AD, PFPD
1456	unknown 3	fresh, fruity, rosy	5.7	4	5.3	5.3	
1513	2-heptanol[b]	woody, musty, moldy	6.7	7	5.3	6	RI, Std, AD
1528	unknown 4	fresh green, fruity, fatty	4.8	-	4.5	5.8	
1534	linalool	green, rosy, floral	8	7.6	8	8.2	RI, Std, AD, MS
1561	(*E*,*Z*)-2,6-nonadienal	fresh, green, cucumber	6.8	7.7	6.3	6.8	RI, Std, AD, MS
1651	2-methylbutanoic acid[b]	cheesy, sour	5		3.5		RI, Std, AD
1677	α-terpineol	woody, piney, citrus	4	4.5	4	4	RI, Std, AD, MS
1684	(*E*,*E*)-2,4-nonedienal	fatty, green, cucumber	6.3	5.7	6	4.5	RI, Std, AD, MS
1706	geranyl acetate	woody, floral, rosy	5	4.7	5	4.8	RI, Std, AD, MS
1747	citronellol	floral, rosy, sweet				5.2	RI, Std, AD, MS
1783	nerol	floral, citrus, sweet				4	RI, Std, AD, MS
1790	β-damascenone[b]	floral, fruity, tea	7.2	6.3	5.8	6.8	RI, Std, AD
1824	hexanoic acid	cheesy, sour	4	5	6	4.5	RI, Std, AD, MS
1825	geraniol	sweet, fruity, berry			6	7.8	RI, Std, AD, MS
1832	geranylacetone	floral, rosy, sweet	5.9	5.3	6.2	7.3	RI, Std, AD, MS
1846	decanal	fruity, citrus, orange	5.6	4.3	4	6.3	RI, Std, AD, MS
2049	Furaneol[b]	sweet, candy, camarel	4.8	3			RI, Std, AD
2057	*p*-cresol[b]	fecal, sulfurous			3.5	5.3	RI, Std, AD
2138	eugenol	sweet, clove, tobacco	4	4	6.5	5	RI, Std, AD, MS
2191	unknown 5	smoky, earthy, moldy	6.7	5.2	6.6	6.6	

[a]RI, retention index; Std, standard; AD, aroma description. [b]Tentatively identified.

(28) of shared aroma active volatiles. It is also worth noting that the aroma strengths of these aroma active volatiles are quite different. For example, the most intense odorant in the 'Kestrel' cultivar was linalool, whereas the most intense odorant for 'Prima Dona' was an unknown described as having a sulfurous, grassy aroma and eluted at a wax LRI of 1353. There were, however, nine volatiles that were found in only one cultivar and not the other. The relatively new 'Kestrel' cultivar contained six aroma active volatiles that were not observed in the more established 'Prima Dona' cultivar. This is not to say that the six aroma active volatiles labeled in Figure 1 were not present in 'Prima Dona'; it means only if they were present, their concentrations were below their respective thresholds. Conversely, the 'Prima Dona' cultivar contained three aroma active volatiles not observed in the 'Kestrel' cultivar. These peaks are labeled as well.

Aroma Volatiles in Southern Highbush Blueberry. A summary of aroma active volatile from all four southern highbush blueberry cultivars is shown in Table 2. A total of 43 aroma active volatiles are observed in the GC-O experiments. Thirty-eight of these aroma active compounds were identified using the techniques listed in the last column in the table. Five aroma active volatiles remain unidentified/unknown. There were nine aldehydes, eight esters, seven terpenes, five ketones, two alcohols, two acids, two sulfurs, and three miscellaneous compounds.

Aldehydes are the most abundant chemical group with aroma activity found in southern highbush blueberry. Hexanal, (*Z*)-3-hexenal, (*E*)-2-hexenal, (*E*,*Z*)-2,6-nonadienal, and (*E*,*E*)-2,4-

nonedienal contributed "fresh green", "grassy", and "fruity" aroma notes, whereas pentanal, octanal, (*E*,*E*)-2,4-hexadienal, and decanal contributed "fatty" and "citrus" aroma notes (Table 2). Unsaturated aldehydes such as (*Z*)-3-hexenal, (*E*,*E*)-2,4-hexadienal, (*E*,*Z*)-2,6-nonadienal, and (*E*,*E*)-2,4-nonedienal have not been previously reported in blueberries. These unsaturated aldehydes are generally considered as the oxidized products of unsaturated fatty acids and should be considered as natural in vivo products of blueberry maturation as the added salt should have inhibited enzyme activity during and after sample blending. Aldehydes as a group make a major contribution to blueberry aroma, in agreement with previous results.[14]

Esters are the next most abundant group, including ethyl propanoate, methyl 2-methylbutanoate, methyl 3-methylbutanoate, ethyl 2-methylbutanoate, ethyl 3-methylbutanoate, (*Z*)-3-hexyl acetate, (*E*)-2-hexyl acetate, and geranyl acetate contributing "green", "sweet", "fruity", "apple", "banana", "pear", and "floral" aroma notes (Table 2). Ethyl propanoate, methyl 2-methylbutanoate, (*E*)-2-hexyl acetate, and geranyl acetate have not been previously reported in blueberry. Ethyl 2-methylbutanoate has been identified in northern highbush and lowbush blueberry,[6,10] whereas methyl 3-methylbutanoate, ethyl 3-methylbutanoate, and (*Z*)-3-hexyl acetate have been reported in lowbush blueberries.[10] Generally, esters are the major aroma components of fruits such as strawberry,[20] apple, and banana.[21] However, few esters have been identified in highbush blueberry. Esters are not considered as important as aldehydes to the aroma in northern highbush blueberries. They have been identified as important volatiles in some lowbush blueberries.[10] In terms of ester composition, the southern highbush blueberry is more similar to lowbush blueberry than to the northern highbush blueberry.

Terpenes such as linalool, citronellol, nerol, and geraniol contributed "sweet", "floral", "fruity", "citrus", and "berry-like" aroma notes. 1,8-Cineole, dihydrolinalool oxide, and α-terpineol contributed "woody", "herbaceous", and "piney" aroma notes (Table 2). Except for dihydrolinalool oxide, all of the other six terpenes had been previously reported in various blueberry types.[6,7,10,14] Linalool was a major aroma active volatile in all four southern highbush blueberry cultivars examined. This is consistent with literature data.[14] Geraniol was a major aroma volatile only in 'Snow Chaser' and 'Kestrel'.

Only two alcohols, including (*Z*)-3-hexenol and 2-heptanol, were aroma active (Table 2). We confirmed earlier reports that 2-heptanol contributed a "musty", "moldy" aroma to southern highbush blueberries. (*Z*)-3-Hexenol had been reported as one of the major "green compounds" in blueberries. However, in this study, it was observed in only a single cultivar ('Kestrel)' and only at midlevel intensity.

Only three ketones were found to have aroma activity. They included 2-heptanone, 1-octen-3-one, and 2-nonanone. They contributed "fruity" "mushroom", "earthy", and "cheese-like" aroma. These carbonyl compounds have not been previously reported as contributing to blueberry aroma. Acids such as hexanoic acid and 2-methylbuanoic acid contributed "cheesy" and "sour" sensory attributes and have been previously reported in blueberry.[7]

Sulfur compounds were identified using a special sulfur-specific detector, a PFPD. Using this highly sensitive and selective detector, several sulfur volatiles were tentatively identified using retention index matching. Identified volatiles included hydrogen sulfide, methanethiol, dimethyl sulfide, dimethyl disulfide, and methional. However, only dimethyl disulfide and methional were found to possess aroma actively in parallel GC-O studies. They were described as possessing "sulfurous rotten egg" and "cooked potato" aromas, respectively (Table 2). Methional had not been previously reported in blueberries, but dimethyl sulfide had been reported in some wild blueberries.[22]

Furaneol was tentatively identified in two southern highbush blueberries ('Jewel' and 'Prima Dona', Table 2). Furaneol has "sweet", "candy", and "caramel" aroma notes, with a very low organoleptic threshold, 10 μg/kg in water.[23] Furaneol has been reported in fruits such as strawberry,[23] pineapple,[24] and blackberry.[25] However, it has not been previously identified in blueberry. Two phenolic compounds, including *p*-cresol and eugenol, contributed "fecal" and "clove" aroma attributes to southern highbush blueberries. Both of these two compounds have been previously reported in blueberries.[7]

Comparison of Chemical Groups and Total Intensities. Not surprisingly, the four southern highbush blueberry cultivars share many common aroma volatiles. Of the 43 aroma active volatiles, 33 were common to at least three of the four cultivars. There were a total of 37 aroma volatiles in 'Kestrel', 36 in 'Jewel', 33 in 'Snow Chaser', and 32 in 'Prima Dona'. Aldehydes (9) were the most abundant volatile group, closely followed by esters (8) and terpenes (7). There was more variation within the terpene group than in any other chemical group. Only three aroma active terpenes were observed in 'Prima Dona', but seven terpenes were observed in 'Kestrel'.

Not only did the number of aroma active compounds vary among the four cultivars, but the aroma intensities also varied. 'Jewel' and 'Kestrel' had the highest total aroma intensities from all aroma active volatiles (both identified and unknown) of 209 and 204, respectively. In contrast, the total aroma intensities due to 'Prima Dona' and 'Snow Chaser' were only 180 and 179, respectively. The major contributors to total aroma intensity were aldehydes, esters, and terpenes. The aldehyde and terpene intensity values observed in this study were in agreement with literature reports that aldehydes and terpenes are considered the major volatiles contributing to blueberry aroma.[14]

Aroma Profiles of 'Jewel', 'Prima Dona', 'Snow Chaser', and 'Kestrel'. No single aroma active volatile was that much more intense than all the others. Only linalool and (*E*)-2-hexenal had aroma intensity >7.5 in all four cultivars. It has been previously reported that an aroma recombination of (*E*)-2-hexenal, (*E*)-2-hexenol, (*Z*)-3-hexenol, and linalool conveys the characteristic blueberry flavor.[14] In the current study (*E*)-2-hexenol was not detected and (*Z*)-3-hexenol was observed only as a midlevel aroma active volatile in a single cultivar ('Kestrel').

Shown in Figure 2 is a summary of the total aroma intensities of all 43 aroma active volatiles grouped into eight groups based on aroma similarities. It can be seen that green, fruity, and floral aroma characters are the major contributors to blueberry aroma. Sulfury and moldy/musty are midlevel aroma attributes with the remaining three aroma categories contributing to background blueberry aroma. Therefore, blueberry aroma is more complex than a single aldehyde and a few 6- and 10-carbon alcohols.

The relative aroma strengths of these eight aroma categories varied somewhat between the four cultivars. 'Jewel' and 'Kestrel' possessed similar aroma strengths in the five strongest aroma categories. However, 'Jewel' contained relatively greater intensities in the low-level aroma categories of sweet and

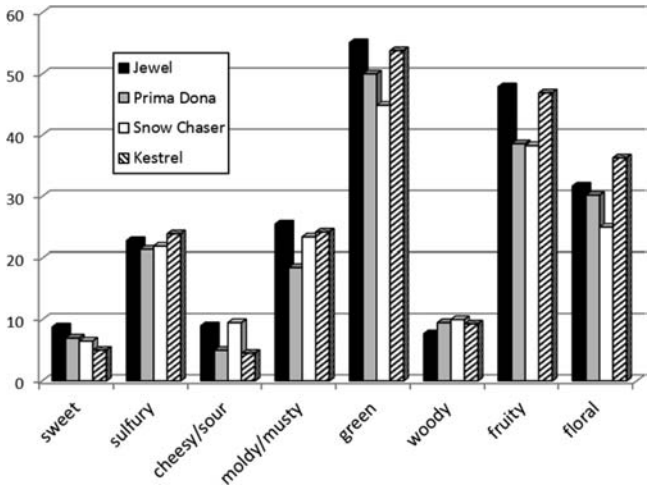

Figure 2. Comparison of GC-O aroma group profiles of four southern highbush blueberry cultivars grown in Florida.

cheese/sour than 'Kestral'. In a similar fashion, the aroma profile of 'Prima Dona' was similar to that of 'Snow Chaser", but 'Prima Dona' exhibited higher total levels in the major green and floral aroma categories.

Principal Component Analysis. To determine if there were appreciable differences in the aroma profiles of the four cultivars used in this study, the aroma volatile data were analyzed using PCA. Shown in Figure 3 are the score and

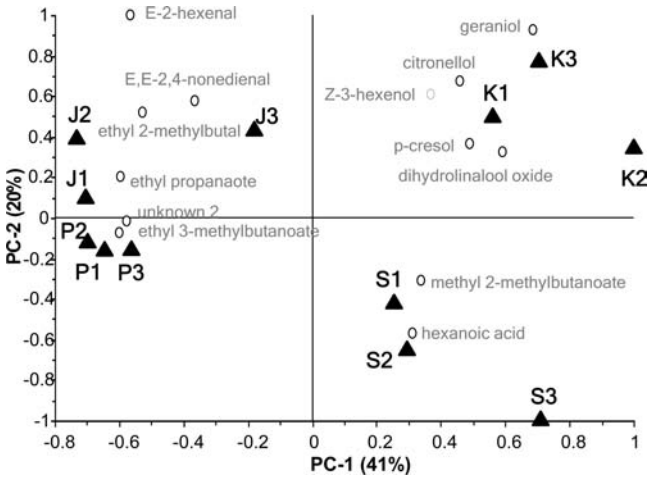

Figure 3. PCA biplot of eigenvalue score values (open triangles) and major loading values (solid circles). P, 'Prima Dona'; J, 'Jewel'; K, 'Kestrel'; S, 'Snow Chaser'.

loading plots of triplicate results for the four blueberry cultivars examined in this study. The first two principal components described 61% of the total variance. Furthermore, each of the four cultivars was clustered in the score plot with no overlap. This indicated that each of the four cultivars possessed a unique aroma profile. PC-1 cleanly separated 'Kestrel' and 'Snow Chaser' on the right-hand (+) side from the more commercially common 'Jewel' and 'Prima Dona' cultivars. The PC-1 axis was defined primarily by geraniol and dihydrolinalool oxide load values on the positive side and ethyl-3-methylbutanoate and unknown 2 loading values on the negative side. PC-2 completely separated 'Kestrel' from 'Snow Chaser' and 'Jewel' from 'Prima Dona'. However, as shown in Figure 3, the degree of separation in the latter case was not as profound. PC-2 was defined primarily but not exclusively by the loading values of citronellol, (*Z*)-3-hexenol, and *p*-cresol on the positive side and by hexanoic acid and methyl-2-methylbutanoate on the negative side. It should be kept in mind that the eigenvector values shown in the score plots were the results of many other variables with smaller loading values. Nevertheless, the complete separation of all four cultivars indicated that each possessed a unique aroma profile and that the close proximity (but not overlapping) of the 'Jewel' and 'Prima Dona' clusters indicated that their overall aroma profiles were similar but still distinct.

AUTHOR INFORMATION

Corresponding Author

*Phone: (863) 956-1151. E-mail: rrouseff@ufl.edu.

Funding

This project was funded in part by a USDA Specialty Crops Research Initiative titled "Increasing Consumption of Fresh Fruits & Vegetables by Enhancing Their Quality and Safety" as a joint research project with the University of California, Davis, and the University of Florida.

Notes

The authors declare no competing financial interest.

ACKNOWLEDGMENTS

We thank Kendra Blaker and James Olmstead (Department of Horticulture Science, University of Florida) for supplying blueberry samples.

REFERENCES

(1) Krewer, G.; NeSmith, D. S. The Georgia blueberry industry: its history, present state, and potential for development in the next decade. *Acta Hortic.* **2002**, *574*, 101−106.

(2) USDA National Agricultural Statistics Service, Blueberry statistics. March 2013, 395; http://www.nass.usda.gov/Statistics_by_Subject.

(3) Diegidio, V.; Sinelli, N.; Casiraghi, E.; Spinardi, A.; Mignani, I. Evaluation of quality and nutraceutical content in blueberries (*Vaccinium corymbosum*) by near and mid infrared spectroscopy. *Postharvest Biol. Technol.* **2008**, *50*, 31−36.

(4) Lyrene, P. M. Breeding southern highbush and rabbiteye blueberries. *Acta Hortic.* **2006**, *715*, 29−37.

(5) Williamson, J. G.; Lyrene, P. M. Blueberry varieties for Florida. *Univ. Fla. IFAS Extension* **2004**, *No. HS967*, 1−9.

(6) Parliment, T. H.; Kolor, M. G. Identification of the major volatile components of blueberry. *J. Food Sci.* **1975**, *40*, 762−763.

(7) Hirvi, T.; Honkanen, E. The aroma of blueberries. *J. Sci. Food Agric.* **1983**, *34*, 992−996.

(8) Hirvi, T.; Honkanen, E. The aroma of some hybrids between high-bush blueberry (*Vaccinium corymbosum*, L.) and bog blueberry (*Vaccinium uliginosum*, L.). *Z. Lebensm. Unters. Forsch.* **1983**, *176*, 346−349.

(9) Hanoglu, A.; Pucarelli, F. Determination of key aroma-active compounds by GCO-aroma extract dilution analysis (AEDA) in cranberry and blueberry fruits. *Chem. Flavors* **2007**, 269−275.

(10) von Sydow, E.; Anjou, K. The aroma of bilberries (*Vaccinium myrtillus* L.). I. Identification of volatile compounds. *Food Sci. Technol. (London)* **1969**, *2*, 78−81.

(11) Von Sydow, E.; Andersson, J.; Anjou, K.; Karlsson, G. The aroma of bilberries (*Vaccinium myrtillus* L.). II. Evaluation of the press juice by sensory methods and by gas chromatography and mass spectrometry. *Food Sci. Technol. (London)* **1970**, *3*, 11−17.

(12) Hall, I. V.; Forsyth, F. R.; Lightfoot, H. J. Volatiles from developing fruit of *Vaccinium angustifolium*. *Can. Inst. Food Sci. Technol. J.* **1970**, *3*, 1−3.
(13) Horvat, R. J.; Senter, S. D.; Dekazos, E. D. GLC-MS analysis of volatile constituents in rabbiteye blueberries. *J. Food Sci.* **1983**, *48*, 278−279.
(14) Horvat, R. J.; Senter, S. D. Comparison of the volatile constituents from rabbiteye blueberries (*Vaccinium ashei*) during ripening. *J. Food Sci.* **1985**, *50*, 429−431.
(15) Horvat, R. J.; Schlotzhauer, W. S.; Chortyk, O. T.; Nottingham, S. F.; Payne, J. A. Comparison of volatile compounds from rabbiteye blueberry (*Vaccinium ashei*) and deerberry (*V. stamineum*) during maturation. *J. Essent. Oil Res.* **1996**, *8*, 645−648.
(16) Bazemore, R.; Goodner, K.; Rouseff, R. Volatiles from unpasteurized and excessively heated orange juice analyzed with solid phase microextraction and GC-olfactometry. *J. Food Sci.* **1999**, *64*, 800−803.
(17) Du, X. F.; Qian, M. Flavor chemistry of small fruits: blackberry, raspberry, and blueberry. In *Flavor and Health Benefits of Small Fruits*; ACS Symposium Series 1035; Qian, M. C., Rimando, A. M., Eds.; American Chemical Society: Washington, DC, USA, 2010; pp 27−43.
(18) Ferreira, I. M. P. L. V. O.; Pinho, O. Headspace solid-phase microextraction (HE-SPME) in combination with GC/MS or GC/FID for quantification of volatile compounds in food matrices. *Trends Chromatogr.* **2006**, *2*, 31−42.
(19) Jouquand, C.; Chandler, C.; Goodner, K.; Plotto, A. Optimization of strawberry volatile sampling by direct gas chromatography olfactometry. *Proc. Fla. State Hortic. Soc.* **2008**, *121*, 260−264.
(20) Latrasse, A. Fruits III. In *Volatile Composition in Foods and Beverages*; Maarse, H., Ed.; Dekker: New York, 1991; pp 329−387.
(21) Berger, R. G. Fruits I. In *Volatile Compounds in Foods and Beverages*; Maarse, H., Ed.; Dekker: New York, 1991; pp 283−304.
(22) Baloga, D. W.; Vorsa, N.; Lawter, L. Dynamic headspace gas chromatography-mass spectrometry analysis of volatile flavor compounds from wild diploid blueberry species. In *Fruit Flavors*; ACS Symposium Series 596; Rouseff, R. L., Leahy, M. M., Eds.; American Chemical Society: Washington, DC, USA, 1995; pp 235−247.
(23) Larsen, M.; Poll, L. Odor thresholds of some important aroma compounds in strawberries. *Z. Lebensm. Unters. Forsch.* **1992**, *195*, 120−1123.
(24) Pickenhagen, W.; Velluz, A.; Passerat, J. P.; Ohloff, G. Estimation of 2,5-dimethyl-4-hydroxy-3(2*H*)-furanone (Furaneol) in cultivated and wild strawberries, pineapples, and mangoes. *J. Sci. Food Agric.* **1981**, *32*, 1132−1134.
(25) Du, X. F.; Qian, M. Quantification of 2,5-dimethyl-4-hydroxy-3(2*H*)-furanone using solid-phase extraction and direct microvial insert thermal desorption gas chromatography-mass spectrometry. *J. Chromatogr., A* **2008**, *1208*, 197−201.

JOURNAL OF AGRICULTURAL AND FOOD CHEMISTRY

Article

pubs.acs.org/JAFC

Characterization of the Major Aroma-Active Compounds in Mango (*Mangifera indica* L.) Cultivars Haden, White Alfonso, Praya Sowoy, Royal Special, and Malindi by Application of a Comparative Aroma Extract Dilution Analysis

John P. Munafo, Jr.,[†] John Didzbalis,[†] Raymond J. Schnell,[†] Peter Schieberle,[‡] and Martin Steinhaus*[,‡]

[†]Mars Global Chocolate Science and Technology, Mars, Incorporated, 800 High Street Hackettstown, New Jersey 07840, United States

[‡]Deutsche Forschungsanstalt für Lebensmittelchemie (German Research Center for Food Chemistry), Lise-Meitner-Strasse 34, 85354 Freising, Germany

ABSTRACT: The aroma-active compounds present in tree-ripened fruits of the five mango (*Mangifera indica* L.) cultivars Haden, White Alfonso, Praya Sowoy, Royal Special, and Malindi were isolated by solvent extraction followed by solvent-assisted flavor evaporation (SAFE) and analyzed by gas chromatography−olfactometery (GC-O). Application of a comparative aroma extract dilution analysis (cAEDA) afforded 54 aroma-active compounds in the flavor dilution (FD) factor range from 4 to ≥2048, 16 of which are reported for the first time in mango. The results of the identification experiments in combination with the FD factors revealed 4-hydroxy-2,5-dimethyl-3(2*H*)-furanone as an important aroma compound in all cultivars analyzed. Twenty-seven aroma-active compounds were present in at least one mango cultivar at an FD factor ≥128. Clear differences in the FD factors of these odorants between each of the mango cultivars suggested that they contributed to the unique sensory profiles of the individual cultivars.

KEYWORDS: *mango, Mangifera indica, aroma extract dilution analysis, 4-hydroxy-2,5-dimethyl-3(2H)-furanone*

INTRODUCTION

Mangoes are the fruits of *Mangifera indica* L., a tropical tree native to South Asia and a member of the sumac family (Anacardiaceae). Mango cultivation is said to have started more than 4000 years ago in the region of eastern India. Today, mango trees are grown throughout the tropical and selected subtropical parts of the world, and mangoes are among the most important fruit crops of the tropics with the major producers being India, China, Thailand, and Pakistan.[1−3]

Mango fruits grow at the end of a long, string-like stem. They are drupes, consisting of a leathery exocarp, a fleshy, juicy mesocarp representing the edible part, and a stony endocarp encasing a single large, flat, oblong seed. The pulp normally sticks to the pit, as fibers extend from the endocarp into the flesh. Size, shape, skin color, skin smoothness, and flesh color strongly depend upon the cultivar. Today, several hundred different mango cultivars are known, over 350 of which are propagated in commercial nurseries. In general, mangoes are between 6 and 25 cm long and weigh up to 2 kg. Typically, the shape is slightly kidney-like and somewhat flattened, with a beak at the apex, but sometimes also nearly round, oval, or ovoid-oblong. The immature fruit has a green skin that gradually turns yellow, orange, red, or purple as the fruit matures. Combinations of several colors in one fruit also occur. The skin surface may be velvety or smooth and waxy. The flesh color ranges from whitish yellow to orange. Mangoes are usually picked before they are fully ripe to prevent them from falling and being damaged. After the fruits have ripened, they can be stored under refrigeration for up to 3 weeks. Mangoes are mainly consumed as fresh fruits. A minor percentage is processed to preserves, juice, dried fruit, or chutney. The mango flesh consists of ∼80% water and up to 20% sugar. It is a rich source of dietary fiber, vitamin C, and β-carotene.[1,2]

A major factor contributing to the popularity of mango is its flavor. In Western countries, mangoes are generally considered high in quality if they combine a low fiber content with a strong sweet taste, a balanced acidity, and an aroma profile high in fruity and low in terpeny notes. Similar to phenotypical traits such as fruit size, shape, and color, the flavor properties of mangoes are strongly influenced by the cultivar.[3]

Numerous studies have been conducted on mango volatiles of different cultivars,[3,4] which has led to the identification of several hundred compounds to date.[4] It has been demonstrated that besides the cultivar,[3,5−26] the maturity,[3,18,22,23] and the geographic origin[26] have an influence on the volatile profile of fresh mangoes.

Despite the large number of investigations on mango volatiles, studies aimed at evaluating the contribution of individual volatile compounds to mango aroma are surprisingly scarce.[15−17,20,25] Application of an aroma extract dilution analysis (AEDA)[27,28] to headspace extracts obtained from mangoes of different cultivars grown in Brazil, (Carlota, Haden, Espada, Coração de Boi, Rubi, and Tommy Atkins) revealed the fruity-smelling ethyl butanoate as an important aroma-active compound in all samples investigated, whereas the

Received: February 19, 2014
Revised: April 22, 2014
Accepted: April 28, 2014
Published: April 28, 2014

ACS Publications © 2014 American Chemical Society

dx.doi.org/10.1021/jf5008743 | J. Agric. Food Chem. 2014, 62, 4544−4551

importance of ethyl 2- and 3-methylbutanoates, δ-3-carene, and α-pinene clearly depended on the cultivar.[15] On the basis of odor activity values (OAVs; ratio of concentration to odor threshold), hexanal, (*E*)-2-hexenal, (*Z*)-3-hexenal, (*E*)-2-decenal, γ-terpinene, and (*E*)-β-ocimene were suggested as key aroma compounds in Thai Khieo Sawoei mangoes[16] and β-damascenone, terpinolene, ethyl hexanoate, (*E*,*Z*)-2,6-nonadienal, 4-methoxy-2,5-dimethyl-3(2*H*)-furanone (MDMF), (*R*)-linalool, and ethyl butanoate were proposed as characteristic aroma components in yellow Thai Keaw mango fruits.[17] A detailed study including the analysis of 20 mango cultivars followed by OAV calculation resulted in the identification of ethyl 2-methylpropanoate, ethyl butanoate, (*E*,*Z*)-2,6-nonadienal, (*E*)-2-nonenal, methyl benzoate, (*E*)-β-ionone, decanal, and MDMF as potentially most important mango aroma compounds.[20] A more recent study on odor-active compounds in Corazón mangoes showed high OAVs for β-damascenone, ethyl butanoate, (*E*,*Z*)-2,6-nonadienal, ethyl 2-methylpropanoate, (*E*)-2-nonenal, (*E*)-β-ionone, and terpinolene.[25]

A major deficiency in the body of previously published work on aroma-active compounds in mango is the application of simultaneous distillation−extraction (SDE) for the isolation of the volatile fraction.[16,17,20,25] The elevated temperatures acting on the fruit material during the SDE procedure are known to lead to compound degradation and artifact formation.[29] The use of mild volatile compound isolation techniques, such as solvent-assisted flavor evaporation (SAFE),[30] therefore, is an important factor in the identification of the authentic aroma-active compounds present in the fruits.

The aim of the present study was to apply a comparative AEDA (cAEDA) on the volatiles obtained by SAFE distillation from fresh, tree-ripened mangoes of different cultivars. To our knowledge, there are no reports on the aroma-active compounds in fresh mango fruit that employ the SAFE isolation technique to date. To gain insight into the compounds contributing to the specific sensory profiles of different mango cultivars, five cultivars exhibiting clear organoleptic differences were chosen for this investigation, namely, Haden, White Alfonso, Praya Sowoy, Royal Special, and Malindi.

The cultivar Haden was initially introduced in Florida in 1910 and inspired the creation of the large-scale mango industry in southern Florida. Haden is a seedling of the Indian cultivar Mulgoba and probably resulted from Mulgoba × Turpentine. Haden is the seed parent of numerous other U.S. cultivars.[31] Haden mango fruits are ∼10 × 8 cm in size and weigh up to 500 g. The skin is thick and tough, yellow in color, with crimson blush and numerous whitish-yellow glands. The fruit shape is egg-like with a depressed beak. The flesh is yellowish-orange, firm, and juicy, with a moderate fiber content and a pleasant aroma.[2]

Alfonso, also known as Appus, Badami, Gundu, Haphus, Kagdi, Khader, and Khader Pasand, is a small and traditional Indian cultivar dating back to the early 16th century. It is considered one of the finest dessert mangoes. The cultivar White Alfonso, also referred to as Safeda Afoos, originated in India, too, as a descendant of Alfonso and was collected in 1908 close to Mumbai. White Alfonso mangoes are large, with a weight up to 2 kg. They are yellow with a red blush skin, which is thick and tough. The orange colored flesh is sweet, firm, and juicy with minimal fiber.

Praya Sowoy is a typical Southeast Asian mango cultivar originating in Thailand. Fruits are big, weighing up to 1 kg, and have an oblong shape. The skin is yellow and thin, and the flesh is firm with little fiber.

Royal Special is a lesser known Indian mango cultivar that is mainly used for mango products such as pickles, dried mangoes, and canned juice.[32] The skin is thick and tough, and the flesh is juicy and fibrous.

The cultivar Malindi is a chance seedling of unknown parentage from the Kenyan coastline. It is also known as apple mango due to the round fruit shape resembling an apple. Malindi mangoes grow to approximately 1 kg. The skin is smooth and thin and the flesh yellow, juicy, and low in fiber.

MATERIALS AND METHODS

Mango Fruits. All samples were provided by the USDA ARS Station in Miami, FL, USA. Fruits were harvested by hand when fully ripe. State of ripeness was estimated by experienced ARS personnel through sensory evaluation of color, firmness, taste, and aroma. Fruits were shipped overnight by air freight to the Mars Global Chocolate Science and Technology Laboratory (Hackettstown, NJ, USA). Sensory analyses and preparation of aroma isolates were performed on the day of arrival.

Reference Aroma Compounds. The following reference aroma compounds were purchased from the commercial vendors given in parentheses: **1**−**2**, **4**−**8**, **10**−**16**, **19**−**24**, **26**−**36**, **38**−**45**, **47**, **49**−**54** (Sigma-Aldrich, St. Louis, MO, USA); **37** (Penta Manufacturing Company, Livingston, NJ, USA). Compounds **3**,[33] **9**,[34] **17**,[35] **18**,[36] **46**,[37] and **48**[37] were synthesized as described in the literature.

Miscellaneous Chemicals and Reagents. Diethyl ether and pentane were freshly distilled before use. Mercurated agarose gel was prepared from Affi-Gel 10 (Bio-Rad, Munich, Germany) using a procedure provided by Bio-Rad.

Sensory Analyses. Fresh mango samples (15 g) were cut into cubes (2 cm) and placed into 20 mL borosilicate glass scintillation vials (Thermo Fisher Scientific, Fair Lawn, NJ, USA). Each sample was orthonasally evaluated by free choice profiling and in a quantitative descriptive analysis (QDA) by 12 trained sensory panelists. The descriptors used in the QDA were defined on the basis of the odor of a reference compound dissolved in water at a concentration of 100 times above the respective threshold value or using a standard reference material. Reference odorants used in the sensory experiments were ethyl butanoate (fruity), 4-hydroxy-2,5-dimethyl-3(2*H*)-furanone (HDMF) (caramel, sweet), butanoic acid (sweaty), linalool (floral, citrus), (*Z*)-3-hexenal (green), myrcene (terpeny), γ-octalactone (coconut), and 4-mercapto-4-methyl-2-pentanone (tropical). The standard sensory reference materials used in the study were fresh pineapple cubes (2 cm) (pineapple) and fresh raspberries (raspberry). Panelists rated the descriptor for each of the samples on a seven-point scale in 0.5 increments from 0 to 3, with 0 = not detectable, 1 = weak, 2 = moderate, and 3 = strong.

Preparation of the Aroma Isolates. Fresh ripe mangoes (3 fruits) were peeled, seeds were removed, and the flesh was cut into sections (4 cm). The sections were immediately frozen in liquid nitrogen and ground into a fine powder with a laboratory mill. A portion of the powder (25 g) was sequentially extracted with freshly distilled diethyl ether (1 × 100 mL, 1 × 50 mL) on an autoshaker at ambient temperature for 10 min. After centrifugation (5000 rpm; 5 min), the supernatants were combined and the residue was discarded. The organic layer was isolated in a separatory funnel, and the aqueous layer was discarded. The ether extract was then subjected to high-vacuum distillation using SAFE.[30] The distillation apparatus was thermostated at 40 °C and kept under high vacuum (10^{-3} Pa). The sample was dropped into the evaporation flask of the device over 40 min. After an additional 30 min, the vacuum was broken, and the distillate was thawed at room temperature and dried over anhydrous sodium sulfate. The sample was then concentrated to approximately 2 mL using a Vigreux column (50 × 1 cm) and finally to 200 μL under a gentle stream of nitrogen. The aroma profile of the isolate was then

evaluated to ensure that it closely matched the profile of the fresh ripe mango flesh.

Gas Chromatography–Olfactometry (GC-O). A 6890 series GC system (Agilent Technologies, Santa Clara, CA, USA) was equipped with a DB-5 or an HP-FFAP capillary (each 30 m × 0.32 mm, 0.25 μm film thickness) (Agilent). The samples (1 μL) were injected cold-on-column at 35 °C using helium as the carrier gas. The flow rate was set to 1.0 mL/min. After 1 min at 35 °C, the oven temperature was increased at 60 °C/min to 60 °C, then increased at 6 °C/min to 230 °C, and held for 10 min. The effluent was split 1:1 by volume at the end of the capillary by a Y-type splitter into two 50 cm sections of uncoated deactivated fused silica capillaries. One section was directed to the flame ionization detector (FID) held at 250 °C and the other part to a heated sniffing port held at 180 °C. The sniffing port was mounted on the front FID detector base and consisted of a custom-machined aluminum cylindrical cone (80 mm × 25 mm i.d.) housing the capillary. During GC-O analysis, the odor of the effluent from the sniffing port was evaluated by a panelist. As an odor was detected, the retention time and the odor quality were recorded. Linear retention indices (RI) were calculated from these retention times and the retention times of adjacent *n*-alkanes by linear interpolation.

Comparative Aroma Extract Dilution Analysis. Aroma isolates were diluted to obtain serial dilutions of 1:2, 1:4, 1:8, ..., 1:2048. Dilutions 1:4, 1:8, 1:32, 1:128, 1:512, and 1:2048 were additionally analyzed by GC-O using the FFAP column and the conditions described above. For best comparison, corresponding dilutions of each cultivar were analyzed consecutively. For each cultivar, each aroma-active region was assigned an FD factor corresponding to the dilution factor of the highest diluted sample in which the odor was detectable.[27,28]

Fractionation of the Mango Aroma Isolates. Samples prepared as described above were concentrated to 1 mL with the use of a Vigreux column and applied to a silica gel solid phase extraction (SPE) cartridge (Phenomenex, Torrance, CA, USA) that was conditioned sequentially with pentane (5 mL), diethyl ether (5 mL), and a second portion of pentane (5 mL). Elution was performed with pentane (5 mL; fraction A) followed by pentane/diethyl ether (98:2, v/v; 5 mL; fraction B), pentane/diethyl ether (95:5, v/v; 5 mL; fraction C), pentane/diethyl ether (9:1, v/v; 5 mL; fraction D), pentane/diethyl ether (1:1, v/v; 5 mL; fraction E), and finally diethyl ether (5 mL; fraction F). Each fraction was then concentrated, first to 2 mL using a Vigreux column and finally to 200 μL under a gentle stream of nitrogen prior to analysis.

The volatile thiol fraction (fraction T) of each mango cultivar was isolated from a SAFE distillate obtained from 25 g of fruit pulp by affinity chromatography.[38] The SAFE distillate was concentrated (Vigreux column; 5 mL) and applied onto mercurated agarose gel (1 g) in a glass column (0.5 cm i.d.). After the column had been rinsed with dichloromethane (50 mL), the thiols were eluted with dithiothreitol (10 mmol/L) in dichloromethane (50 mL). The excess of dithiothreitol was removed by SAFE distillation, and the distillate was concentrated to 200 μL using a Vigreux column (60 cm) and a microdistillation device.[39]

The odorants detected during AEDA were localized in fractions A–F and T by GC-O, and mass spectra were recorded by gas chromatography-mass spectrometry (GC-MS) or two-dimensional heart-cut gas chromatography–olfactometry/mass spectrometry (GC-O/GC-O/MS).

Gas Chromatography–Mass Spectrometry. An Agilent 6890 series GC system equipped with an HP-FFAP column (30 m × 0.25 mm, 0.25 μm film thickness) (Agilent) was coupled via a heated (250 °C) transfer line to an Agilent 5973 mass spectrometer detector. Helium at 1 mL/min constant flow was used as the carrier gas. One minute after on-column injection at 35 °C, the oven temperature was increased at 60 °C/min to 60 °C and then at 6 °C/min to 230 °C. The final temperature was held for 10 min. The mass spectrometer was operated in electron impact (EI) ionization mode at 70 eV and a scan range of *m*/*z* 50–550.

Two-Dimensional Heart-Cut Gas Chromatography-Olfactometry/Mass Spectrometry. A gas chromatograph Mega 2 (Fisons Instruments, Mainz, Germany), equipped with a cold-on-column injector, a column DB-FFAP (30 m × 0.32 mm, 0.25 μm film thickness) (Agilent Technologies, Waldbronn, Germany), a moving column stream switching system (MCSS), and an FID plus a sniffing port as monitor detectors, was coupled via a heated (250 °C) deactivated fused silica capillary serving as transfer line to a CP 3800 gas chromatograph (Varian, Darmstadt, Germany) equipped with a cold trap and a column DB-5 (30 m × 0.25 mm, 0.25 μm film thickness) (Agilent). The column end was connected via a Y-shaped glass splitter and deactivated fused silica capillaries to a sniffing port and a Saturn 2000 mass spectrometer (Varian) operated in the EI mode. The sniffing ports each consisted of a cylindrical aluminum device with a beveled top and a central drill hole for the capillary and were mounted on a heated detector base of the GC. The tailor-made trap consisted of a piece of steel tubing housing the capillary and, when active, was cooled (−100 °C) by means of liquid nitrogen. The length and diameter of the splitting capillaries in the second oven were adjusted to ensure simultaneous detection of eluted compounds at the sniffing port and in the MS, which was confirmed by the analysis of test odorants.

For the structural assignment of compounds **3** and **9**, in a first run, the mango fractions containing the target compounds were separated on the first column while the MCSS conveyed the eluate to the monitor detectors. The retention times of the target compounds were determined by sniffing the eluate at the sniffing port. In a second run, during the elution of the target compounds, the eluate of the first column was transferred to the precooled trap where the heart-cut was condensed. After trap cooling had been turned off, the second oven was started. The eluate was monitored by sniffing, and when the target compound was detected at the sniffing port, the mass spectrum was recorded.

RESULTS AND DISCUSSION

Sensory Characteristics of the Mango Cultivars. Freshly cut pieces of the flesh of tree-ripened fruits of each of the five mango cultivars were evaluated by trained panelists, first using free-choice profiling (Table 1) and subsequently a QDA (Figure 1). Results showed distinct differences between the cultivars. The aroma of Haden mangoes was characterized as typical sweet mango-like with strong fruity, tropical, coconut-like notes. White Alfonso also showed a characteristic sweet mango-type aroma, but was less fruity than Haden, instead showing a pronounced terpeny note that distinguished it from all other varieties investigated. The sensory profile of Praya Sowoy was clearly dominated by a strong green, grassy odor note, whereas the scores of the other aroma notes were rather low in this cultivar. The overall aroma of Royal Special mangoes included the characteristic sweet mango-like note, a pronounced fruity note, pineapple-like and floral notes, and, in

Table 1. Sensory Characterization of the Five Mango Cultivars by Orthonasal Free-Choice Profiling (12 Experienced Panelists)

cultivar	aroma description
Haden	sweet mango aroma with fruity, tropical, coconut, and pineapple notes
White Alfonso	sweet mango aroma with terpeny, green, and coconut notes
Praya Sowoy	mildest sweet mango aroma with green and mild fruity notes
Royal Special	sweet mango aroma with some terpeny, fruity, and raspberry notes
Malindi	sweet mango aroma with some mild terpeny, green, pineapple, and tropical notes

dx.doi.org/10.1021/jf5008743 | J. Agric. Food Chem. 2014, 62, 4544–4551

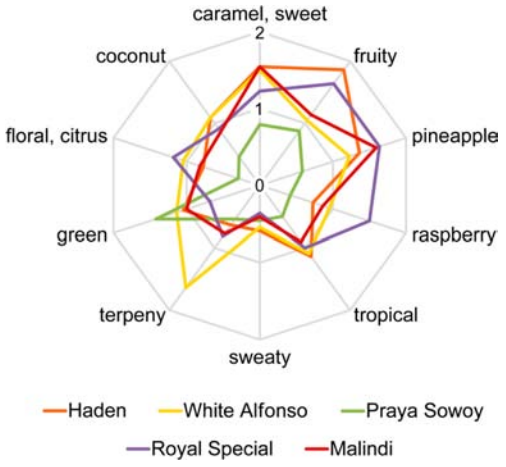

Figure 1. Aroma profiles of fresh fruit flesh obtained from five mango cultivars. Panelists rated the intensity of each attribute on a scale from 0 to 3 in 0.5 increments, with 0 = not detectable, 1 = weak, 2 = moderate, and 3 = strong.

particular, an intense and unique raspberry note. The aroma of Malindi was characterized as having a very balanced sweet mango aroma profile with pineapple-like, fruity, green, tropical, and mild terpeny notes, but lacking any special note.

Screening the Mango Volatiles for Aroma-Active Compounds. Tree-ripened mango fruits of each cultivar were peeled, the seeds were removed, and the flesh was cut into small sections. To stop enzymatic reactions, the sections were immediately frozen in liquid nitrogen and ground into a fine powder, which was subsequently extracted with diethyl ether. Nonvolatile compounds were removed from the extracts by SAFE,[30] and the distillates were concentrated. Elevated temperatures were avoided throughout the entire workup to avoid artifact formation and compound degradation. In particular, the extraction was performed at ambient temperature, and SAFE was carried out at 40 °C. As a result, the smell of the aroma isolates still clearly represented the typical aroma characteristics of the fresh flesh of the corresponding mango cultivars. Aroma isolates were submitted to a cAEDA,[27,28] which resulted in 54 aroma-active compounds in the FD factor range from 4 to ≥2048 (Table 2).

To assign the structures of the odorous compounds, their RIs, odor characteristics, and mass spectra were compared to data obtained from authentic reference substances. To separate aroma-active compounds from coeluted components and to aid in their identification by GC-MS, each of the aroma isolates was fractionated over silica gel to afford six fractions (A−F). Further aroma isolates of each cultivar were submitted to affinity chromatography[38] on mercurated agarose gel to selectively enrich thiols (fraction T). All fractions were subsequently analyzed by GC-O to localize the odorants and then by GC-MS to obtain their mass spectra. This procedure allowed for the structural assignment of 42 of the 54 aroma-active compounds (Table 2). When mass spectra could not be obtained using this procedure, due to either insufficient selectivity or sensitivity of the approach, fractions were further concentrated and analyzed by two-dimensional GC-O with heart-cutting and MS detection. This GC-O/GC-O/MS approach led to the structural identification of two further compounds, namely, compounds **3** and **9**. For nine compounds (**16**, **18**, **20**, **24**, **28**, **46**, **48**, **52**, and **53**) sufficiently pure mass spectra for identification could not be obtained, but unequivocal structural assignments were achieved on the basis of the comparison of RIs and odor characteristics as determined by GC-O on two capillaries of different polarities (FFAP, DB-5) with data of reference compounds analyzed in parallel. No reference compound was available for (*E*,*Z*,*Z*)-1,3,5,8-undecatetraene (**25**); thus, its structure was tentatively assigned by comparing RIs, odor characteristics, and mass spectra with published data.[40−42]

The results of the identification experiments in combination with the FD factors revealed the 27 compounds depicted in Figure 2 as the most potent aroma-active compounds in the five mango cultivars, all of which exhibited an FD factor of ≥128 in at least one of the samples analyzed. Among them, sweet, caramel-like-smelling HDMF (**47**) exhibited the highest FD factor (≥2048) in all five mango cultivars. HDMF, therefore, might be a major contributor to the characteristic sweet mango aroma note common to all cultivars investigated. HDMF has been reported in mangoes before[43] but has never been recognized as a major aroma-active compound yet. This might be associated with the volatile isolation techniques applied in previous GC-O studies. Hot steam distillation procedures such as SDE not only imply the problem of artifact formation and compound deterioration but also give rise to low recovery of rather polar odorants such as HDMF.[30] For the same reason, most probably, 4-hydroxy-3-methoxybenzaldehyde (vanillin, **54**), had never been identified in mangoes before.

High FD factors were further determined for some fruity-smelling esters including ethyl butanoate (**5**), ethyl 3-methylbutanoate (**7**), ethyl 2-methylpropanoate (**1**), and ethyl 2-methylbutanoate (**6**). These compounds most probably accounted for the general fruity note in the mango aroma profiles. All of these have already been reported as potent aroma-active compounds in mango,[15,20,25] and particularly the importance of ethyl butanoate for the aroma of Haden has been suggested before.[15] Similarly, lactones such as γ-octalactone (**43**) and δ-octalactone (**45**) have already been held responsible for the coconut-like odor note in mangoes.[20,25]

The particular pineapple-like aroma note clearly detected in Haden, White Alfonso, Royal Special, and Malindi corresponded quite well to high FD factors of the pineapple-like-smelling odorants (*E*,*Z*)-1,3,5-undecatriene (**21**) and/or (*E*,*Z*,*Z*)-1,3,5,8-undecatetraene (**25**) in these cultivars. A peculiar raspberry note perceived in the sensory profile of Royal Special might be explained by high FD factors of violet-like-smelling aroma compounds β-ionone (**44**, FD 512) and dihydro-β-ionone (**40**, FD 128). Whereas β-ionone is known to be an important contributor to the aroma of raspberries[44] and has already been reported as an aroma-active compound in mangoes,[20,25] dihydro-β-ionone is reported here for the first time in *M. indica*.

Although β-ionone was also detected as a potent odorant in White Alfonso (FD 512), no such strong raspberry note was present in the sensory profile of this cultivar, probably due to a dominating terpeny odor note. This note might most likely be caused by the terpeny-smelling compounds (*Z*)-β-ocimene (**14**) and (*E*)-β-ocimene (**15**), which were present in high amounts (FD 512 and 128) in White Alfonso, but rather low (FD ≤32 and ≤4) in the other four cultivars. (*E*)-β-Ocimene had already been shown to contribute to the aroma of Thai Khieo Sawoei mangoes.[16] The tropical aroma note detected in the mango samples might be associated with the tropical, passionfruit-like-smelling 4-mercapto-4-methyl-2-pentanone

dx.doi.org/10.1021/jf5008743 | J. Agric. Food Chem. 2014, 62, 4544−4551

Table 2. Aroma-Active Compounds (FD ≥4) in the SAFE Distillates Obtained from Mangoes of Five Different Cultivars: Haden (H), White Alfonso (WA), Praya Sowoy (PS), Royal Special (RS), and Malindi (M)

			RI[d]		FD factor[e]						
no.[a]	odorant[b]	odor quality[c]	FFAP	DB-5	H	WA	PS	RS	M	fraction[f]	ref[g]
1	ethyl 2-methylpropanoate	fruity	950	750	512		32		4	C	7
2	2,3-butanedione	buttery	985	<600	4	8	32	8	4	D	9
3	(*E*)-2-butene-1-thiol	sulfurous	1008	717	32					A, T	
4	(*R*)-α-pinene	pine-like	1010	930		8		8	8	A	6
5	ethyl butanoate	fruity	1015	802	≥2048	128	128	32		C	7
6	ethyl 2-methylbutanoate	fruity	1020	851	512	4				C	10
7	ethyl 3-methylbutanoate	fruity	1055	850	≥2048	4		4	4	C	7
8	hexanal	green	1085	802	8					B	7
9	3-methyl-2-butene-1-thiol	sulfurous	1090	820	128		8			A, T	
10	(*E*)-3-hexenal	green	1130	800	8	4	512	8	8	B	16
11	(*Z*)-3-hexenal	green	1140	790	8	8	128			B	8
12	myrcene	terpeny	1155	990	32	128		4	128	A	5
13	ethyl hexanoate	fruity	1200	1002	8	32			4	C	7
14	(*Z*)-β-ocimene	terpeny	1250	1043	32	512	8		4	A	5
15	(*E*)-β-ocimene	terpeny	1270	1050	4	128				A	5
16	1-octen-3-one[h]	mushroom	1295	975		8	4			D	14
17	2-acetyl-1-pyrroline	cooked rice	1350	920	512	32	128	8	512	D	
18	(*Z*)-1,5-octadien-3-one[h]	geranium	1360	988	4			32		D	
19	dimethyl trisulfide	cabbage	1385	968	8					A	12
20	4-mercapto-4-methyl-2-pentanone[h]	tropical	1388	942	32	8	32	4	4	A	
21	(*E*,*Z*)-1,3,5-undecatriene	pineapple	1400	1170	512	512		8	8	A	
22	ethyl octanoate	fruity	1419	1195	32	8				C	7
23	acetic acid	vinegar	1420	600	32	8	8		4	F	5
24	2-isopropyl 3-methoxypyrazine[h]	earthy	1430	1091	4	4				D	
25	(*E*,*Z*,*Z*)-1,3,5,8-undecatetraene[i]	pineapple	1435	1172		128	8	512	512	A	42
26	3-(methylthio)propanal	cooked potato	1450	902	512	32	8	4	8	B	
27	(*Z*)-3-hexenyl butanoate	fruity	1460	1010	4		8			C	7
28	2,3-diethyl-5-methylpyrazine[h]	earthy	1495	1158	8	4		128	4	D	
29	decanal	soapy	1480	1160	4					B	10
30	(*E*)-2-nonenal	fatty	1530	1161	8	32	128	4	4	B	7
31	linalool	floral, citrus	1550	1101	4	8	8	4	4	E	5
32	MDMF	caramel	1578	1040	32	8	8	128	4	F	5
33	(*E*,*Z*)-2,6-nonadienal	cucumber	1580	1150	4	4	128	8	4	B	7
34	butanoic acid	sweaty, rancid	1610	820	32	32	128	8	4	F	11
35	phenylacetaldehyde	floral, honey	1640	1045	4	4				B	7
36	2- and 3-methylbutanoic acid[j]	sweaty, rancid	1660	885	32	8	128		4	F	11
37	3-methyl-2,4-nonanedione	hay	1715	1246	8	4	128		32	D	
38	2-phenylethyl acetate	floral	1785	1256	4	4				D	7
39	(*E*)-β-damascenone	cooked apple	1810	1385	4	4	8			E	7
40	dihydro-β-ionone	violet	1825	1433				128		E	
41	2-methoxyphenol	smoky	1860	1187		4	8			E	13
42	2-phenylethanol	floral, rose	1901	1117	128	8	32	4		E	5
43	γ-octalactone	coconut	1910	1260	512	512	128	512	512	E	5
44	β-ionone	violet	1930	1492		512		512	32	E	5
45	δ-octalactone	coconut	1963	1289	512	128		32	128	E	5
46	*trans*-4,5-epoxy-(*E*)-2-decenal[h]	metallic	2005	1380	4	8		8		B	
47	HDMF	caramel	2015	1080	≥2048	≥2048	≥2048	≥2048	≥2048	F	43
48	*trans*-4,5-epoxy-(*E*)-2-undecenal[h]	metallic	2095	1485		8		8		B	
49	4-methylphenol	barnyard	2070	1078	8	4	4	4	4	E	14
50	γ-decalactone	peach	2140	1470		4	4	4		E	5
51	δ-decalactone	coconut	2190	1495	4	4	4	4		E	7
52	sotolon[h]	maple	2195	1135	32	8	8	4		F	
53	2-aminoacetophenone[h]	floral	2200	1305	4	4		8		E	
54	4-hydroxy-3-methoxybenzaldehyde	vanilla	2600	1411	4	4	8	4	4	F	

[a]Odorants numbered according to retention time on the FFAP column. [b]Identified by comparing retention indices on FFAP and DB-5 columns and mass spectra, as well as aroma quality and intensity, with data obtained from authentic reference standards analyzed in parallel. [c]Odor quality as perceived during GC-O. [d]Linear retention index. [e]Flavor dilution factor. [f]Fraction(s) in which odorant was detected by GC-O after fractionation. [g]Reference providing the first report of the compound as a mango volatile. [h]Mass spectra could not be obtained in the mango isolates. Identification

dx.doi.org/10.1021/jf5008743 | J. Agric. Food Chem. 2014, 62, 4544−4551

Table 2. continued

was based on remaining criteria as indicated above. [i]Reference compound was not available. The structure was tentatively assigned by comparing retention indices, mass spectra, and odor characteristics with literature data.[40−42] [j]Odorants not separated on either GC column.

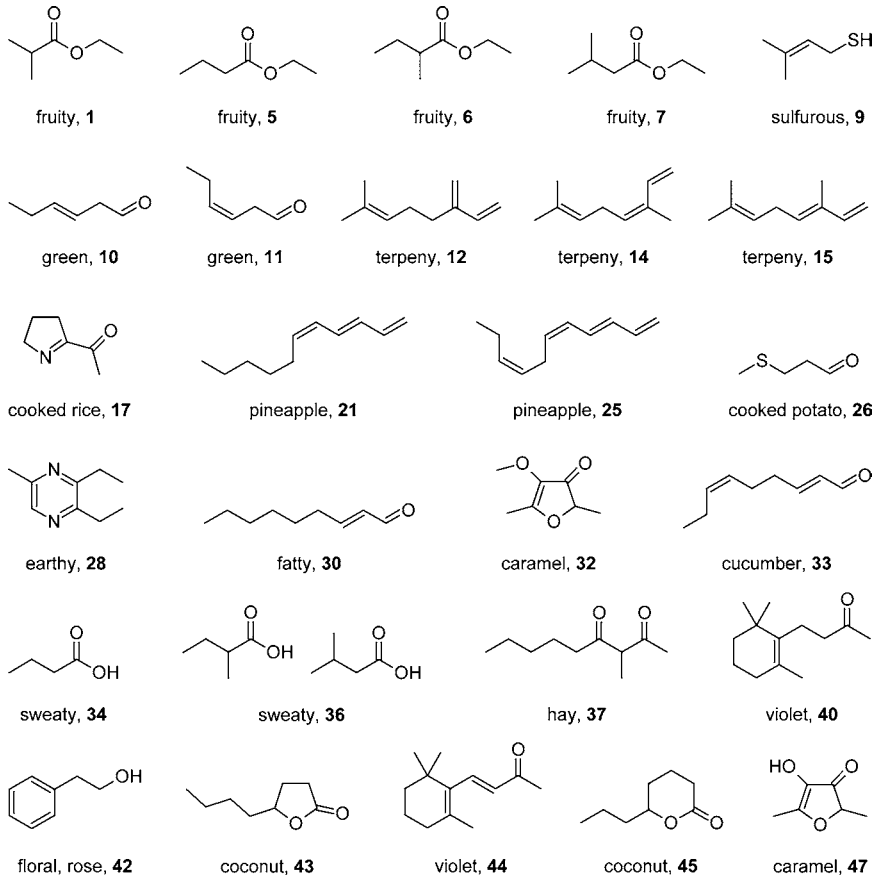

Figure 2. Aroma-active compounds with an FD factor ≥128 in at least one of the five mango cultivars analyzed.

(**20**). In Haden, however, sulfurous, skunk-like-smelling compounds (*E*)-2-butene-1-thiol (**3**) and 3-methyl-2-butene-1-thiol (**9**), previously unknown in mango, might further contribute to this specific odor character.

In good agreement with the dominating green, grassy odor note associated with Praya Sowoy mangoes, considerably high FD factors were determined for the green, grassy-smelling (*E*)-3-hexenal (**10**, FD 512) and (*Z*)-3-hexenal (**11**, FD 128). Cucumber-like-smelling (*E*,*Z*)-2,6-nonadienal (**33**, FD 128), fatty-smelling (*E*)-2-nonenal (**30**, FD 128), and hay-like-smelling 3-methyl-2,4-nonanedione (**37**, FD 128) might further contribute to the unique odor properties of Praya Sowoy. On the other hand, the sweaty, rancid-smelling butanoic acid (**34**) and 2-/3-methylbutanoic acid (**36**), although also present in rather high amounts (FD 128) compared to the other four varieties (FD ≤32), obviously did not have a vital influence on the overall aroma profile of Praya Sowoy.

In summary, the application of the cAEDA on the five mango cultivars resulted in 54 odor-active compounds, among which, to the best of our knowledge, 16 substances (**3**, **9**, **17**, **18**, **20**, **21**, **26**, **37**, **40**, **46**, **48**, **52**−**54**) are reported here for the first time as mango constituents. The FD factors provided useful ideas on the compounds responsible for the typical olfactory profile of mangoes in general and the compounds accounting for the aroma characteristics of individual cultivars. Nevertheless, the role of some odorants detected with high FD factors during cAEDA, such as the cooked rice-like-smelling 2-acetyl-1-pyrroline (**17**, FD ≤512), cooked potato-like-smelling 3-(methylthio)propanal (**26**, FD 512 in Haden), earthy-smelling 2,3-diethyl-5-methylpyrazine (**28**, FD 128 in Royal Special), and hay-like-smelling 3-methyl-2,4-nonanedione (**37**, FD 128 in Praya Sowoy), all of which had not been reported in mangoes before, is yet unclear. To fill this gap and to unequivocally confirm the hypotheses discussed before, further studies are required. Investigations on the role of individual odorants in the aroma of the five different mango cultivars, including exact quantitation of odor-active compounds by stable isotope dilution assays, aroma reconstitution experiments, and omission tests,[28] are currently under way.

AUTHOR INFORMATION

Corresponding Author

*(M.S.) Phone: +49 8161 71 2991. Fax: +49 8161 71 2970. E-mail: martin.steinhaus@lrz.tum.de.

Notes

The authors declare no competing financial interest.

ABBREVIATIONS USED

AEDA, aroma extract dilution analysis; ARS, Agricultural Research Service; cAEDA, comparative aroma extract dilution analysis; FD factor, flavor dilution factor; FFAP, free fatty acid phase; FID, flame ionization detector; GC-O, gas chromatog-

raphy−olfactometry; GC-O/GC-O/MS, two-dimensional heart-cut gas chromatography−olfactometry/mass spectrometry; MCSS, moving column stream switching system; OAV, odor activity value; QDA, quantitative descriptive analysis; RI, retention index; SAFE, solvent-assisted flavor evaporation; SDE, simultaneous distillation−extraction; SPE, solid phase extraction; USDA, United States Department of Agriculture

Nomenclature

2-acetyl-1-pyrroline, 1-(3,4-dihydro-2*H*-pyrrol-5-yl)ethanone; (*E*)-*β*-damascenone, (2*E*)-1-(2,6,6-trimethylcyclohexa-1,3-dien-1-yl)but-2-en-1-one; *γ*-decalactone, 5-hexyldihydrofuran-2(3*H*)-one; *δ*-decalactone, 6-pentyltetrahydro-2*H*-pyran-2-one; dihydro-*β*-ionone, 4-(2,6,6-trimethylcyclohex-1-en-1-yl)butan-2-one; *trans*-4,5-epoxy-(*E*)-2-decenal, (2*E*)-3-[(2*R*,3*R*)/(2*S*,3*S*)-3-butyloxiran-2-yl]prop-2-enal; *trans*-4,5-epoxy-(*E*)-2-undecenal, (2*E*)-3-[(2*R*,3*R*)/(2*S*,3*S*)-3-pentyloxiran-2-yl]prop-2-enal; HDMF, 4-hydroxy-2,5-dimethyl-3(2*H*)-furanone; *β*-ionone, (3*E*)-4-(2,6,6-trimethylcyclohex-1-en-1-yl)but-3-en-2-one; linalool, 3,7-dimethylocta-1,6-dien-3-ol; MDMF, 4-methoxy-2,5-dimethyl-3(2*H*)-furanone; myrcene, 7-methyl-3-methylideneocta-1,6-diene; (*E*)-*β*-ocimene, (3*E*)-3,7-dimethylocta-1,3,6-triene; (*Z*)-*β*-ocimene, (3*Z*)-3,7-dimethylocta-1,3,6-triene; *γ*-octalactone, 5-butyldihydrofuran-2(3*H*)-one; *δ*-octalactone, 6-propyltetrahydro-2*H*-pyran-2-one; (*R*)-*α*-pinene, (1*R*,5*R*)-2,6,6-trimethylbicyclo[3.1.1]hept-2-ene; sotolon, 3-hydroxy-4,5-dimethyl-2(5*H*)-furanone

REFERENCES

(1) Mukherjee, S. K.; Litz, R. E. Introduction: Botany and importance. In *The Mango. Botany, Production and Uses*, 2nd ed.; Litz, R. E., Ed.; CAB International: Wallingford, UK, 2009; pp 1−18.

(2) Common Fund for Commodities, Amsterdam, The Netherlands; International Tropical Fruits Network (TFNet), Serdang, Selangor, Malaysia. G-Fruit, Tropical Fruit Global Information System; http://www.itfnet.org/gfruit (Feb 2014).

(3) Chauhan, O. P.; Raju, P. S.; Bawa, A. S. Mango flavor. In *Handbook of Fruit and Vegetable Flavors*; Hui, Y. H., Ed.; Wiley: Hoboken, NJ, USA, 2010; pp 319−343.

(4) *VCF Volatile Compounds in Food: Database*, version 14.1; Nijssen, L. M., Ingen-Visscher, C. A. v., Donders, J. J. H., Eds.; TNO Triskelion: Zeist, The Netherlands, 1963−2013; http://www.vcf-online.nl (Feb 2014).

(5) Hunter, G. L. K.; Bucek, W. A.; Radford, T. Volatile components of canned Alphonso mango. *J. Food Sci.* **1974**, *39*, 900−903.

(6) MacLeod, A. J.; Gonzalez de Troconis, N. Volatile flavour components of mango fruit. *Phytochemistry* **1982**, *21*, 2523−2526.

(7) Engel, K. H.; Tressl, R. Studies on the volatile components of two mango varieties. *J. Agric. Food Chem.* **1983**, *31*, 796−801.

(8) Yamaguchi, K.; Nishimura, O.; Toda, H.; Mihara, S.; Shibamoto, T. Chemical studies on tropical fruits. In *Instrumental Analysis of Foods: Recent Progress*; Charalambous, G., Inglett, G., Eds.; Academic Press: Orlando, FL, USA, 1983; pp 93−117.

(9) Ackerman, L. G. J.; Torline, P. A. Volatile components in the headspace of 8 mango cultivars. *Lebensm. Wiss. Technol.* **1984**, *17*, 339−341.

(10) Idstein, H.; Schreier, P. Volatile constituents of Alphonso mango (*Mangifera indica*). *Phytochemistry* **1985**, *24*, 2313−2316.

(11) Idstein, H.; Bauer, C.; Schreier, P. Volatile acids in tropical fruits: cherimoya (*Annona cherimolia*, Mill.), guava (*Psidium guajava*, L.), mango (*Mangifera indica*, L., var. Alphonso), papaya (*Carica papaya*, L.) (in German). *Z. Lebensm. Unters. Forsch.* **1985**, *180*, 394−397.

(12) Yukawa, C.; Imayoshi, Y.; Miyazaki, T.; Iwabuchi, H. Volatile components of two mango varieties (in Japanese). *Foods Food Ingred. J. Jpn.* **1994**, *162*, 93−97.

(13) Ollé, D.; Baumes, R. L.; Bayonove, C. L.; Lozano, Y. F.; Sznaper, C.; Brillouet, J.-M. Comparison of free and glycosidically linked volatile components from polyembryonic and monoembryonic mango (*Mangifera indica* L.) cultivars. *J. Agric. Food Chem.* **1998**, *46*, 1094−1100.

(14) Ansari, S. H.; Ali, M.; Velasco-Negueruela, A.; Pérez-Alonso, M. J. Volatile constituents of the fruits of three mango cultivars, *Mangifera indica* L. *J. Essent. Oil Res.* **1999**, *11*, 65−68.

(15) Lopes, D. C.; Fraga, S. R.; Rezende, C. M. Aroma impact substances in commercial brazilian mangoes by HRGC-O-AEDA-MS (in Portuguese). *Quim. Nova* **1999**, *22*, 31−36.

(16) Tamura, H.; Boonbumrung, S.; Yoshizawa, T.; Varanyanond, W. The volatile constituents in the peel and pulp of a green Thai mango, Khieo Sawoei cultivar (*Mangifera indica* L.). *Food Sci. Technol. Res.* **2001**, *7*, 72−77.

(17) Boonbumrung, S.; Tamura, H.; Mookdasanit, J.; Nakamoto, H.; Ishihara, M.; Yoshizawa, T.; Varanyanond, W. Characteristic aroma components of the volatile oil of yellow keaw mango fruits determined by limited odor unit method. *Food Sci. Technol. Res.* **2001**, *7*, 200−206.

(18) Lalel, H. J. D.; Singh, Z.; Tan, S. C. Aroma volatiles production during fruit ripening of 'Kensington Pride' mango. *Postharvest Biol. Technol.* **2003**, *27*, 323−336.

(19) Pino, J. A.; Mesa, J.; Munoz, Y.; Marti, M. P.; Marbot, R. Volatile components from mango (*Mangifera indica* L.) cultivars. *J. Agric. Food Chem.* **2005**, *53*, 2213−2223.

(20) Pino, J. A.; Mesa, J. Contribution of volatile compounds to mango (*Mangifera indica* L.) aroma. *Flavour Fragrance J.* **2006**, *21*, 207−213.

(21) Quijano, C. E.; Salamanca, G.; Pino, J. A. Aroma volatile constituents of Colombian varieties of mango (*Mangifera indica* L.). *Flavour Fragrance J.* **2007**, *22*, 401−406.

(22) Lebrun, M.; Plotto, A.; Goodner, K.; Ducamp, M.-N.; Baldwin, E. Discrimination of mango fruit maturity by volatiles using the electronic nose and gas chromatography. *Postharvest Biol. Technol.* **2008**, *48*, 122−131.

(23) Pandit, S. S.; Kulkarni, R. S.; Chidley, H. G.; Giri, A. P.; Pujari, K. H.; Köllner, T. G.; Degenhardt, J.; Gershenzon, J.; Gupta, V. S. Changes in volatile composition during fruit development and ripening of 'Alphonso' mango. *J. Sci. Food Agric.* **2009**, *89*, 2071−2081.

(24) Pandit, S. S.; Chidley, H. G.; Kulkarni, R. S.; Pujari, K. H.; Giri, A. P.; Gupta, V. S. Cultivar relationships in mango based on fruit volatile profiles. *Food Chem.* **2009**, *114*, 363−372.

(25) Pino, J. A. Odour-active compounds in mango (*Mangifera indica* L. cv. Corazón). *Int. J. Food Sci. Technol.* **2012**, *47*, 1944−1950.

(26) Kulkarni, R. S.; Chidley, H. G.; Pujari, K. H.; Giri, A. P.; Gupta, V. S. Geographic variation in the flavour volatiles of Alphonso mango. *Food Chem.* **2012**, *130*, 58−66.

(27) Schieberle, P.; Grosch, W. Evaluation of the flavor of wheat and rye bread crusts by aroma extract dilution analysis. *Z. Lebensm. Unters. Forsch.* **1987**, *185*, 111−113.

(28) Schieberle, P. Recent developments in methods for analysis of flavor compounds and their precursors. In *Characterization of Food: Emerging Methods*; Gaonkar, A., Ed.; Elsevier: Amsterdam, The Netherlands, 1995; pp 403−431 (review).

(29) Derail, C.; Hofmann, T.; Schieberle, P. Differences in key odorants of handmade juice of yellow-flesh peaches (*Prunus persica* L.) induced by the workup procedure. *J. Agric. Food Chem.* **1999**, *47*, 4742−4745.

(30) Engel, W.; Bahr, W.; Schieberle, P. Solvent assisted flavour evaporation − a new and versatile technique for the careful and direct isolation of aroma compounds from complex food matrices. *Eur. Food Res. Technol.* **1999**, *209*, 237−241.

(31) Schnell, R.; Brown, J. S.; Olano, C.; Meerow, A.; Campbell, R.; Kuhn, D. Mango genetic diversity analysis and pedigree inferences for Florida cultivars using microsatellite markers. *HortScience* **2006**, *41*, 993−993.

(32) Morton, J. F. *Fruits of Warm Climates*; Echo Point Books and Media: Brattleboro, VT, USA, 1987.

(33) Tamura, H.; Fujita, A.; Steinhaus, M.; Takahisa, E.; Watanabe, H.; Schieberle, P. Identification of novel aroma-active thiols in pan-roasted white sesame seeds. *J. Agric. Food Chem.* **2010**, *58*, 7368−7375.
(34) Holscher, W.; Vitzthum, O. G.; Steinhart, H. Prenyl alcohol source for odorants in roasted coffee. *J. Agric. Food Chem.* **1992**, *40*, 655−658.
(35) Buttery, R. G.; Ling, L. C.; Juliano, B. O.; Turnbaugh, J. G. Cooked rice aroma and 2-acetyl-1-pyrroline. *J. Agric. Food Chem.* **1983**, *31*, 823−826.
(36) Ullrich, F.; Grosch, W. Identification of the most intense odor compounds formed during autoxidation of methyl linolenate at room temperature. *J. Am. Oil Chem. Soc.* **1988**, *65*, 1313−1317.
(37) Steinhaus, M.; Sinuco, D.; Polster, J.; Osorio, C.; Schieberle, P. Characterization of the aroma-active compounds in pink guava (*Psidium guajava*, L.) by application of the aroma extract dilution analysis. *J. Agric. Food Chem.* **2008**, *56*, 4120−4127.
(38) Full, G.; Schreier, P. Covalent chromatography. A valuable method for the aroma analysis of thiols at trace levels (in German). *Lebensmittelchemie* **1994**, *48*, 1−4.
(39) Bemelmans, J. M. H. Review of isolation and concentration techniques. In *Progress in Flavour Research*; Land, G. G., Nursten, H. E., Eds.; Applied Science Publishers: London, UK, 1979; pp 79−98.
(40) Marner, F. J.; Boland, W.; Jaenicke, L. Synthesis of isomeric 1,3,5,8-undecatetraenes. *Liebigs Ann. Chem.* **1982**, 579−584.
(41) Berger, R. G.; Drawert, F.; Kollmannsberger, H.; Nitz, S.; Schraufstetter, B. Novel volatiles in pineapple fruit and their sensory properties. *J. Agric. Food Chem.* **1985**, *33*, 232−235.
(42) Berger, R. G.; Drawert, F.; Kollmannsberger, H.; Nitz, S. Natural occurrence of undecaenes in some fruits and vegetables. *J. Food Sci.* **1985**, *50*, 1655−1656, 1667.
(43) Pickenhagen, W.; Velluz, A.; Passerat, J. P.; Ohloff, G. Estimation of 2,5-dimethyl-4-hydroxy-3(2*H*)-furanone (Furaneol®) in cultivated and wild strawberries, pineapples and mangoes. *J. Sci. Food Agric.* **1981**, *32*, 1132−1134.
(44) Klesk, K.; Qian, M.; Martin, R. R. Aroma extract dilution analysis of cv. Meeker (*Rubus idaeus* L.) red raspberries from Oregon and Washington. *J. Agric. Food Chem.* **2004**, *52*, 5155−5161.

JOURNAL OF AGRICULTURAL AND FOOD CHEMISTRY

Article

pubs.acs.org/JAFC

Development and Application of 3-Chloro-1,2-propandiol Electrochemical Sensor Based on a Polyaminothiophenol Modified Molecularly Imprinted Film

Xiulan Sun,*[,†] Lijuan Zhang,[†] Hongxia Zhang,[§] He Qian,[†] Yinzhi Zhang,[†] Lili Tang,[†] and Zaijun Li[‡]

[†]State Key Laboratory of Food Science and Technology, School of Food Science of Jiangnan University, Synergetic Innovation Center of Food Safety and Nutrition, Wuxi, Jiangsu 214122, China

[‡]School of Chemical and Material Engineering of Jiangnan University, Wuxi, Jiangsu 214122, China

[§]School of Foreign Studies, Shaanxi University of Technology, Han'zhong, Shaanxi 723000, China

Supporting Information

ABSTRACT: In this work, a novel electrochemical sensor for 3-chloro-1,2-propandiol (3-MCPD) detection based on a gold nanoparticle-modified glassy carbon electrode (AuNP/GCE) coated with a molecular imprinted polymer (MIP) film was constructed. *p*-Aminothiophenol (*p*-ATP) and 3-MCPD were self-assembled on a AuNP/GCE surface, and then a MIP film was formed by electropolymerization. The 3-MCPD template combined with *p*-ATP during self-assembly and electropolymerization, and the cavities matching 3-MCPD remained after the removal of the template. The MIP sensor was characterized by cyclic voltammetry (CV), differential pulse voltammetry (DPV) and scanning electron microscopy (SEM). Many factors that affected the performance of the MIP membrane were discussed and optimized. Under optimal conditions, the DPV current was linear with the log of the 3-MCPD concentration in the range from 1.0×10^{-17} to 1.0×10^{-13} mol L^{-1} ($R^2 = 0.9939$), and the detection limit was 3.8×10^{-18} mol L^{-1} ($S/N = 3$). The average recovery rate of 3-MCPD from spiked soy sauce samples ranged from 95.0% to 106.4% (RSD < 3.49%). Practically, the sensor showed high sensitivity, good selectivity, excellent reproducibility, and stability during the quantitative determination of 3-MCPD.

KEYWORDS: *molecularly imprinted polymer, electropolymerization, polyaminothiophenol, gold nanoparticles, 3-MCPD*

INTRODUCTION

3-Chloro-1,2-propandiol (3-MCPD) belongs to the chloropropanol chemicals that are formed by the reaction between hydrochloric acid and residual vegetable fat in the process of producing acid hydrolyzed vegetable protein (HVP).[1] Chloropropanols do not exist in the natural brew sauce produced by microbial fermentation. In recent years, HVP as a common savory ingredient is widely added to soy sauce and various composite seasonings. Therefore, 3-MCPD has been detected in a wide range of blended soy sauces.[2] However, there have been many studies on the toxicity of 3-MCPD such as neurotoxicity,[3] nephrotoxicity,[4] genotoxicity,[5] immunotoxicity,[6] and reproductive toxicity. Recently, 3-MCPD was classified by the IARC as group 2B and is thus "probably carcinogenic to humans".[7] The European Union (EU) established a limit level of 20 μg kg^{-1} for 3-MCPD in HVP and soy sauce.[8]

It is thus necessary to establish a simple and rapid analytical method for the trace detection of 3-MCPD. Several conventional techniques such as capillary electrophoresis with electrochemical detection,[9] gas chromatography combined with mass spectrometry (GC-MS),[10−12] and GC with electron capture detection (GC-ECD)[13] have been developed to detect 3-MCPD. Nevertheless, these methods are usually expensive and require highly trained technical personnel and complex sample pretreatment. In contrast, molecularly imprinted polymer (MIP) based electrochemical sensors have advantages such as rapid response, time savings, low cost, and high sensitivity and selectivity.

MIP sensors are currently widely used for the recognition and detection of template molecules.[14−17] In electrochemical sensors, MIPs can either accumulate the template molecules on the surface of the electrode, which makes the sensor more sensitive, or separate the template molecules from other analytes to improve the selectivity of the sensor. These advantages of MIPs make them ideal recognition elements for sensors. For the preparation of MIP sensors, electropolymerization can be used to directly synthesize MIP films in situ on the surface of the electrode.[18] The constructed imprinted films are stable and their thickness is easily controlled. And the quantity of effective recognition cavities on the surface of the sensor determines the sensitivity of MIP sensors. It is well-known that more binding cavities form with increasing MIP film thickness, but thick MIP films can make communication inefficient between the imprinted cavities and the transducer and result in slow analyte diffusion to the binding cavities.[19] Au nanoparticles (AuNPs) have been used to obtain higher surface area electrodes and thus increase the amount of effective imprinted sites.[18] This occurs by electrodeposition of AuNPs onto the electrode surface, which presents important advantages such as a large number of reactive sites, catalytic properties, large surface area, and high conductivity.[16,20] Self-

Received: December 8, 2013
Revised: March 27, 2014
Accepted: April 28, 2014
Published: April 28, 2014

ACS Publications © 2014 American Chemical Society

dx.doi.org/10.1021/jf4055159 | J. Agric. Food Chem. 2014, 62, 4552−4557

assembled monolayer (SAM) based chemically modified electrodes can also improve the performance of the solid electrodes. SAMs can be produced by strong chemisorption between organic molecules and a substrate. Moreover, SAMs have excellent stability, can be integrated with biomolecular electronic devices, and are widely used in sensors.[21−23]

In this study, self-assembly and electropolymerization were combined to prepare a MIP sensor for the determination of 3-MCPD. AuNPs were first electrodeposited onto a glassy carbon electrode (GCE) surface to obtain a higher surface area electrode to increase the number of effective binding cavities. Subsequently, *p*-aminothiophenol (*p*-ATP) was self-assembled onto the AuNP/GCE surface by the formation of Au−S bonds between gold and the thiol groups (-SH) of the *p*-ATP molecules. The 3-MCPD template was then further assembled onto the monolayer of *p*-ATP through hydrogen bonding between the amino groups of *p*-ATP and the hydroxyls of 3-MCPD. Finally, a MIP film was formed on the surface of the AuNP/GCE with *p*-ATP and 3-MCPD assembly by electropolymerization in an ethanol solution with *p*-ATP, 3-MCPD template, and tetrabutylammonium perchlorate (TBAP). A novel MIP sensor was thus obtained after removing the 3-MCPD template. The electrochemical behavior of the imprinted sensor was characterized by cyclic voltammetry (CV) and differential pulse voltammetry (DPV). The electrochemical experimental results indicate that the MIP sensor has high sensitivity and excellent selectivity toward 3-MCPD. And the MIP sensor was successfully used to detect trace amounts of 3-MCPD in real soy sauce, and it showed good reproducibility, stability, and recovery. This study provides a promising approach for preparing sensors and makes the fabricated sensor an ideal candidate for 3-MCPD detection.

MATERIALS AND METHODS

Reagents and Chemicals. 3-MCPD (97%), 1,3-dichloro-2-propanol (1,3-DCP, 97%), 2,3-dichloro-1-propanol (2,3-DCP, 97%), glycerol (99%), and 1,2-propanediol (99%) were purchased from J&K Chemical. Tetrabutylammonium perchlorate (TBAP, 99%) and *p*-ATP (97%) were obtained from Sigma (Aldrich, Spain). Tetrachloroaurate-(III) acid ($HAuCl_4$), potassium ferricyanide, and potassium ferrocyanide ($K_3[Fe(CN)_6]$ and $K_4[Fe(CN)_6]$, 99.5%) were provided by Sinopharm Chemical Reagent Co., Ltd. (Shanghai, China). All other reagents were chromatography analytical grade and prepared with ultrapure water. Ultrapure water was used throughout this work. Stock solutions of 100 mM analytes were prepared and kept in brown bottles at 4 °C. Soy sauce was purchased from a local supermarket.

Instruments. CV and DPV experiments were carried out with a CHI-760C electrochemical workstation (CH Inc., Shanghai, China). The conventional three-electrode system was employed with a modified glass carbon electrode (GCE, Φ2 mm) as working electrode, a platinum wire as auxiliary electrode, and a saturated calomel electrode (SCE) as reference one. The morphology of the modified GCE surface was observed using a scanning electron microscope (SEM) (Hitachi S-4800, Japan). All experiments were performed at ambient temperature.

Fabrication of a AuNP Modified GCE. Before electrode modification, a bare GCE was immersed in a fresh piranha solution of H_2SO_4/30% H_2O_2 (3:1, v/v) for 15 min and then rished with redistilled water. The GCE was polished to a mirror-finish with a slurry of alumina (0.30 and 0.05 μm), washed with ultrapure water, and then ultrasonicated in ethanol and ultrapure water for 2 min. The polished GCE was then dipped in 2.43 mmol L^{-1} aqueous $HAuCl_4$ solution with 0.1 mol L^{-1} H_2SO_4 and treated at −0.2 V constant potential for 200 s. After being rinsed several times with ultrapure water and absolute ethanol, the modified GCE was immersed in H_2SO_4/30% H_2O_2 (3:1, v/v) solution for 5 min, washed with ultrapure water, and then dried under nitrogen flow at room temperature.

***p*-ATP and 3-MCPD Self-Assembly on the AuNP/GCE.** The *p*-ATP-modified electrode was prepared according to the reported methods.[19,24,25] The prepared AuNP/GCE was immersed in an ethanol solution containing 5 mM *p*-ATP for 24 h at room temperature, removed, and then washed with ethanol and redistilled water to remove physically absorbed *p*-ATP. Then, the *p*-ATP-modified AuNP/GCE was immersed in an ethanol solution with 1 mmol L^{-1} 3-MCPD for 4 h. The electrode was removed, rinsed with ethanol and redistilled water to remove physically absorbed 3-MCPD, and then dried under nitrogen gas at ambient temperature.

Fabrication of Imprinted PATP−AuNP/GCE. The *p*-ATP−3-MCPD modified AuNP/GCE was immersed in an ethanol solution containing 0.1 mmol L^{-1} *p*-ATP, 0.05 mmol L^{-1} 3-MCPD, and 50 mmol L^{-1} TBAP. After the polymer solution was deoxygenated under nitrogen flow for 15 min, electropolymerization was carried out by 10 CV scannings between −0.3 V and +1.2 V (scan rate 50 mV s^{-1}). Then, the imprinted PATP−AuNP/GCE was immersed in methanol/water (2:1) solution containing 4 mol L^{-1} HNO_3 for 25 min to remove the 3-MCPD template. For comparison, a nonimprinted PATP−AuNP/GCE was fabricated and treated in the same way without adding the 3-MCPD template.

Electrochemical Measurements. CV and DPV measurements were carried out to evaluate the current response of the modified electrodes immersed in a solution of 2.5 mmol L^{-1} $[Fe(CN)_6]^{3-/4-}$ with 0.1 mol L^{-1} KCl as the supporting electrolyte over an applied potential range from −0.2 to +0.6 V. All measurements were carried out at ambient temperature. Cyclic voltammograms (CVs) of the MIP film were performed by scanning the potential between −0.3 and +1.2 V at a scan rate of 50 mV s^{-1}.

Detection of 3-MCPD in Real Soy Sauce Samples. Soy sauce samples provided by a local market were used to evaluate the developed MIP sensor. All samples were determined to be free of 3-MCPD by GC-ECD detection before performing spiking and recovery studies. Soy sauce samples (1.0 mL) were spiked with a 3-MCPD standard solution at concentration levels of 10^{-16}, 10^{-15} and 10^{-14} mol L^{-1}. After mixing with a vortex mixer, the samples were centrifuged at 4000 rpm for 10 min at room temperature. The supernatants were ultrasonicated with ethyl acetate (3 mL) three times for 15 min each. After keeping steady for 10 min, the resulting extractants were collected, dried under nitrogen flow at room temperature, and then dissolved in 1 mL of ethanol solution. The mixture was then centrifuged at 4000 rpm for 10 min, and the clear solution was analyzed using the MIP sensor.

RESULTS AND DISCUSSION

Fabrication of the AuNP Modified GCE. During electrodeposition of AuNPs onto the GCE surface, efficient coverage of AuNPs was obtained by controlling the deposition time. The deposition time was optimized by testing the DPV signals of the AuNP/GCE in 2.5 mmol L^{-1} $[Fe(CN)_6]^{3-/4-}$

Scheme 1. Scheme of the Imprinted PATP−AuNP/GCE

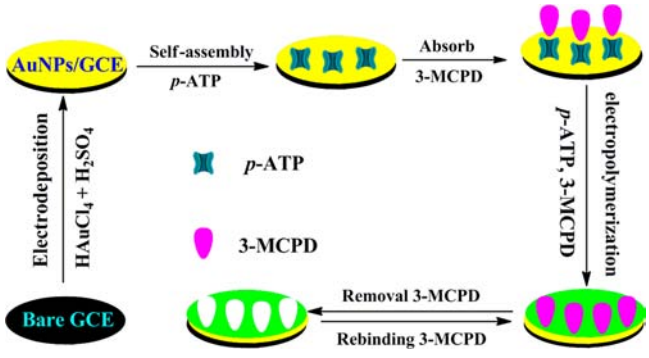

dx.doi.org/10.1021/jf4055159 | J. Agric. Food Chem. 2014, 62, 4552−4557

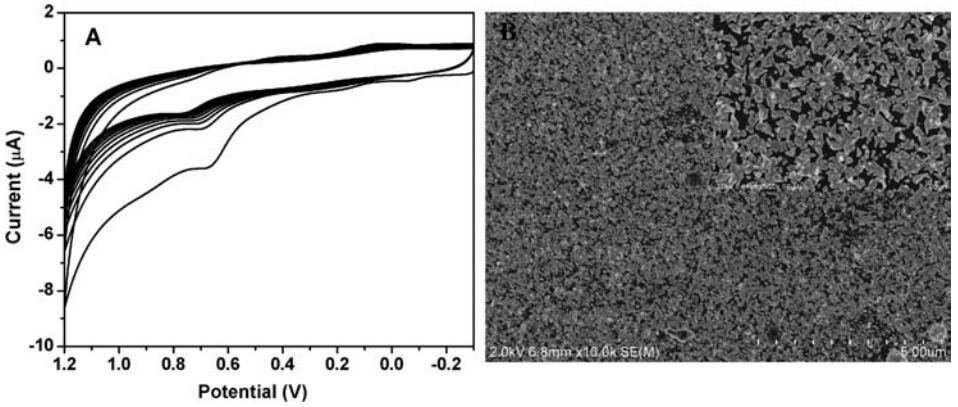

Figure 1. (A) Cyclic voltammograms and (B) SEM images of the imprinted PATP film formed on the AuNP/GCE surface in ethanol solution containing 0.1 mmol L^{-1} *p*-ATP, 0.05 mmol L^{-1} 3-MCPD, and 50 mmol L^{-1} TBAP. Potential range, −0.3 to 1.2 V; scan rate, 50 mV s^{-1}; scan cycles, 10.

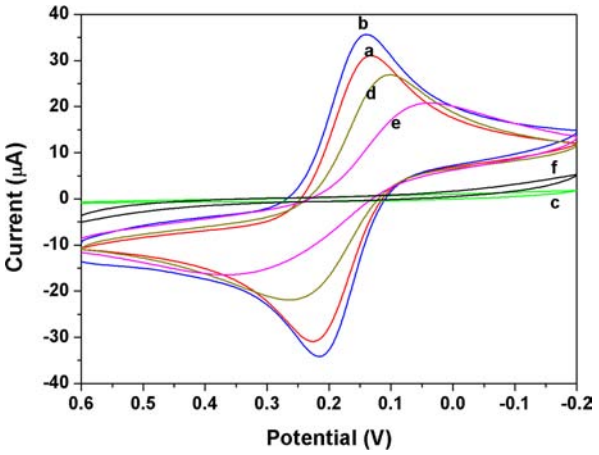

Figure 2. Cyclic voltammograms of 2.5 mmol L^{-1} $[Fe(CN)_6]^{3-/4-}$ with 0.1 mol L^{-1} KCl at (a) bare GCE, (b) AuNP modified GCE, MIP sensor before (c) and after (d) template removal, (e) MIP sensor after template rebinding, (f) NIP sensor after template removal. Scan rate 100 mV s^{-1}.

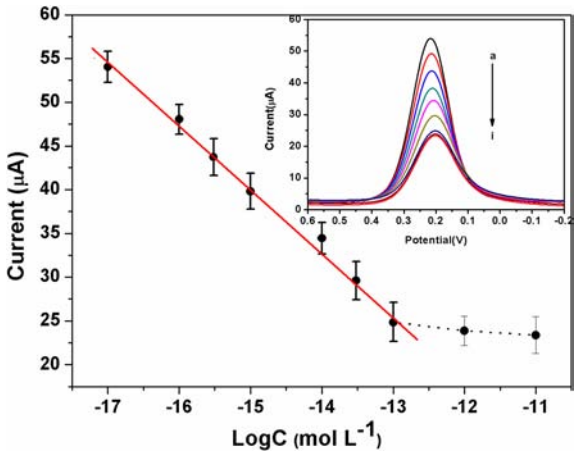

Figure 4. DPV of the PATP−AuNP/GCE incubated using different concentrations of 3-MCPD: (a−i) 10^{-17}, 10^{-16}, 10^{-15}, 10^{-14}, 10^{-13}, 10^{-12}, or 10^{-11} mol L^{-1} 3-MCPD in an aqueous solution for 6 min.

with 0.1 mol L^{-1} KCl. As shown in Figure s1A, Supporting Information, the DPV response of $[Fe(CN)_6]^{3-/4-}$ reached the maximum at 1400 s and then decreased. Although the number of AuNPs on the electrode surface increased with the longer deposition time, the further accumulation of AuNPs would decrease the surface area of the AuNPs, which would reduce the current response of the modified electrode. The obtained SEM images showed that the AuNPs had a uniform dispertion on the electrode surface (Figure s1B, Supporting Information). Since the current response of $[Fe(CN)_6]^{3-/4-}$ slightly increased

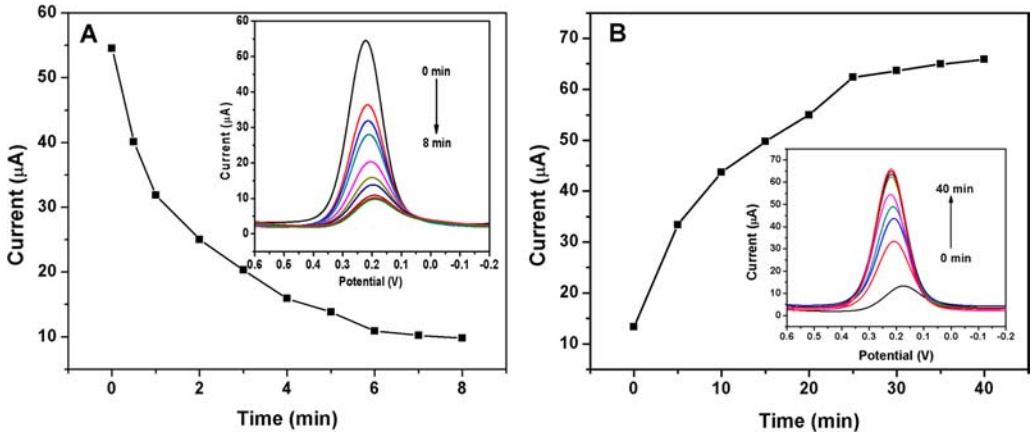

Figure 3. DPV corresponding to the PATP−AuNP/GCE immersed in (A) 2×10^{-15} mol L^{-1} 3-MCPD over different times (time from 0 to 8 min) and (B) a methanol/water (2:1) solution containing 4 mol L^{-1} HNO_3 over different times (time from 0 to 40 min).

dx.doi.org/10.1021/jf4055159 | J. Agric. Food Chem. 2014, 62, 4552−4557

Table 1. Comparison with Other Reported Methods for 3-MCPD Detection

extraction method[a]	analytical method	sample type	LOD ($\mu g\ kg^{-1}$)	ref
SPME	GC/MS	soy sauces	4.62	8
SPE	GC/MS	hydrolysate	1.0	10
PLE	GC/MS	bakery foods	1.7	12
MIP	chemosensing	soya sauces	*b*	28
liquid phase extraction	electrochemical sensor	soy sauce	4.2×10^{-10}	this work

[a]SPME, solid-phase microextraction; SPE, solid phase extraction; PLE, pressurized liquid extraction. [b]The LOD was not mentioned in the article.

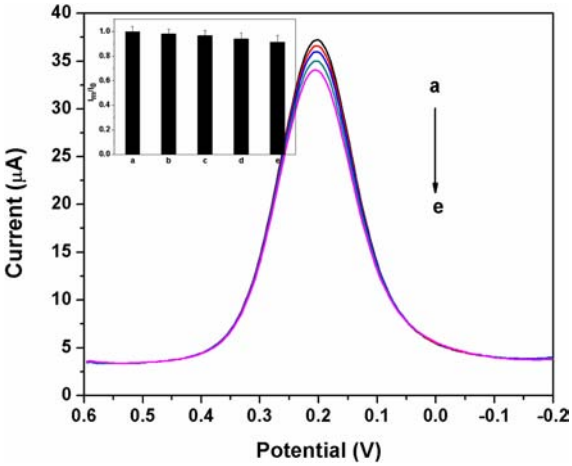

Figure 5. DPV of the PATP−AuNP/GCE immersed in (a) 2×10^{-15} mol L^{-1} 3-MCPD, (b−e) 2×10^{-15} mol L^{-1} 3-MCPD in the presence of 2×10^{-14} mol L^{-1} 2,3-DCP, 1,3-DCP, 1,2-propanediol, and glycerol. Preconcentration time was 6 min before measurement. The inset shows the anodic peak current ratio (I_m/I_o) of the MIP sensor as 2×10^{-15} mol L^{-1} 3-MCPD and 2×10^{-15} mol L^{-1} 3-MCPD in the presence of 2×10^{-14} mol L^{-1} glycerol, 1,2-propanediol, 1,3-DCP and 2,3-DCP.

Table 2. Average Recovery and Relative Standard Deviation of 3-MCPD in Soy Sauce (n = 3)

spiked ($\times 10^{-15}$ mol L^{-1})	found ($\times 10^{-15}$ mol L^{-1})	recovery (%)	RSD (%)
0.1	0.095	95	3.15
1	0.98	98	2.87
10	10.64	106.4	3.49

from 200 to 1400 s, a deposition time of 200 s was selected to fabricate the AuNP modified GCE.

Fabrication of Imprinted PATP−AuNP/GCE. Scheme 1 shows the preparation procedure used to produce the imprinted PATP−AuNP/GCE. The preparation procedure can be summarized in four steps: *p*-ATP self-assembly on the AuNP/GCE surface; hydrogen bonding adsorption of 3-MCPD template onto the *p*-ATP−AuNP/GCE surface; electropolymerization of PATP on the AuNP/GCE surface with *p*-ATP and 3-MCPD assembly; removal of 3-MCPD template from the MIP film. Before electropolymerization, the AuNP/GCE was immersed in a *p*-ATP solution for 24 h. A SAM of *p*-ATP molecules was formed on the surface of AuNP/GCE by Au−S bonds between the gold particles and the thiol groups (-SH) of the *p*-ATP molecules. Then, the *p*-ATP monolayer was chemisorbed onto the AuNP/GCE surface, and this exposed an array of amino groups to the solution. Subsequently, the *p*-ATP−AuNP/GCE was immersed in the 3-MCPD solution for 4 h. The 3-MCPD template assembled on the *p*-ATP−AuNP/GCE surface through hydrogen bonding between the amino groups ($-NH_2$) of *p*-ATP and the hydroxyls of 3-MCPD. The self-assembly of 3-MCPD increased the number of the binding sites in the MIP film and enhanced the sensitivity of the sensor. Furthermore, the SAM formed by *p*-ATP and 3-MCPD served as an initial polymerizable monolayer to drive selective electropolymerization on the AuNP/GCE surface.[26]

The imprinted PATP membrane was electrodeposited onto the surface of AuNP/GCE followed by *p*-ATP and 3-MCPD assembly in an ethanol solution with 0.1 mmol L^{-1} *p*-ATP, 0.05 mmol L^{-1} 3-MCPD, and 50 mmol L^{-1} TBAP by ten CV scannings over the potential range of −0.3 and +1.2 V with a scan rate of 50 mV s^{-1}. Figure 1A showed the representative CV response of the electropolymerization process that was used to form a PATP membrane on the surface of AuNP/GCE. During electropolymerization, radical anions were produced at a certain scan potential, and they initiated the polymerization of *p*-ATP. The CV behavior of *p*-ATP showed that it undergoes an entirely irreversible oxidation process. The oxidation peak of *p*-ATP was clearly observed at a 0.658 V potential on the first scanning. The peak current gradually reduced with increasing the scan cycles, and it eventually reached a steady state after 10 scan cycles. The oxidation peak potential of *p*-ATP slightly shifted to more anodic potential from 0.658 to 0.747 V. The results showed that a polymeric PATP membrane was formed on the AuNP/GCE surface. The decrease in the current response seemed to be related to the continuous formation of the PATP film, which suppressed the oxidation reaction of *p*-ATP. The morphology of the PATP−AuNP/GCE surface was observed using SEM, as shown in Figure 1B. The roughness of the PATP−AuNP/GCE surface increased obviously compared with the surface of the AuNP/GCE, indicating that the polymer membrane was successfully deposited onto the surface of the electrode. To evaluate the hydrophilic property of the MIP film, a contact angle experiment was provided. The contact angle θ was 98.5°, which indicated that the MIP film was hydrophobic (Figure s2, Supporting Information).

The cyclic voltammograms of the film formed with and without 3-MCPD were similar, which indicated that 3-MCPD did not have any effect on the electroactivity on the AuNP/GCE in the polymerization potential window range. Therefore, the structure of 3-MCPD was not electrochemically changed during the polymerization process.

Characterization of the Electrochemical Behavior of the MIP Sensor. The CV responses of the bare and modified electrodes were recorded in 2.5 mmol L^{-1} $[Fe(CN)_6]^{3-/4-}$ with 0.1 mol L^{-1} KCl to confirm whether 3-MCPD was embedded in the MIP membrane, where the redox current of $[Fe(CN)_6]^{3-/4-}$ was used to evaluate the procedure. Figure 2 showed the relationship between the surface modification conditions of the GCE and the peak current. The bare electrode showed a couple of redox peaks with a peak potential separation (ΔE_p) of 93 mV and an I_p ratio of about 1:1 in curve a. After covering with AuNPs, a decrease in the ΔE_p (75 mV) and an increase in the I_p were obtained, as shown in curve b. This could be attributed to an increase in electrocatalytic effect and the effective surface area of the AuNPs, which could greatly increase the electron transfer rate of $[Fe(CN)_6]^{3-/4-}$. Curve c

dx.doi.org/10.1021/jf4055159 | J. Agric. Food Chem. 2014, 62, 4552−4557

shows the current response of the MIP sensor before the removal of 3-MCPD. By comparison with the current response of the AuNP/GCE, almost no redox peak was observed, which indicated that the MIP film had been formed on the AuNP/GCE surface. After removing 3-MCPD (curve d), a decrease in ΔE_p (129 mV) and an obvious increase in I_p were observed. A possible reason was that the cavities after 3-MCPD removal enhanced the diffusion of $[Fe(CN)_6]^{3-/4-}$ through the MIP film and promoted the redox reaction of $[Fe(CN)_6]^{3-/4-}$ on the sensor. The emergence of curve e can be ascribed to the limited access of $[Fe(CN)_6]^{3-/4-}$ to the imprinted membrane after recombining 3-MCPD. This can be explained by the interaction between 3-MCPD and the imprinted membrane, which determines the electron transfer properties of $[Fe(CN)_6]^{3-/4-}$ on the surface of the electrode. In contrast, for the NIP sensor after template removal (curve f), almost no electrochemical response was obtained because the PATP membrane covered the GCE surface polymerized in the absence of 3-MCPD, which caused that no cavities with binding sites to be available. The eluted nonpolymerized *p*-ATP in the NIP film lead to a minor change in redox current, which was negligible after template removal. This indicates that the NIP sensor is nonselective and fails to recognize 3-MCPD.[27]

Optimization of the Incubation and Elution Time. The incubation time is an important factor that influences the adsorption of the targets on the sensor. To determine the optimum incubation time for the detection of 3-MCPD, the imprinted PATP−AuNP/GCE was incubated over different times in 2×10^{-15} mol L^{-1} 3-MCPD. As shown in Figure 3A, the current decreased significantly with an increase in incubation time and reached a stable response after 6 min, which indicated that an adsorption equilibrium was obtained. Therefore, the optimum incubation time for 3-MCPD determination was 6 min.

After electropolymerization, the PATP membrane modified GCE was immersed in a methanol/water (2:1) solution containing 4 mol L^{-1} HNO_3, which was used to remove the template. As shown in Figure 3B, the current gradually increased and reached a maximum at about 25 min, and it remained stable over 15 min, which means that the template was completely removed at about 25 min in this elution solution. As a result, an adsorption time of 6 min and an elution time of 25 min were selected in the following sections.

Electrochemical Detection of 3-MCPD. To detect 3-MCPD, the proposed PATP−AuNP/GCE was immersed in different concentrations of 3-MCPD solution from 1×10^{-17} to 1×10^{-11} mol L^{-1}, and a significant decrease in peak current was observed as shown in the inset of Figure 4. This indicated that when 3-MCPD was recombined, a compact film appeared on the electrode surface, which prevented $[Fe(CN)_6]^{3-/4-}$ from accessing the electrode surface. The formed PATP film resulted in a lower electrochemical response for the $[Fe(CN)_6]^{3-/4-}$ probe.

For quantitative analysis, the proposed PATP−AuNP/GCE was incubated at different concentrations of 3-MCPD for 6 min. DPVs of the sensor were recorded in a 2.5 mmol L^{-1} $[Fe(CN)_6]^{3-/4-}$ solution containing 0.1 mol L^{-1} KCl. After a 6 min preconcentration, because the binding sites in the membrane were occupied by 3-MCPD template, the redox peak current decreased with an increase in 3-MCPD concentration. As shown in Figure 4, the decrease in DPV signals is directly related to the increase of 3-MCPD concentration. A linear behavior between the DPV current and the log of the 3-MCPD concentration was obtained from 1×10^{-17} to 1×10^{-13} mol L^{-1} (R^2 = 0.9939). The lowest detectable concentration was 3.8×10^{-18} mol L^{-1}, which was more sensitive than most available 3-MCPD detection methods (Table 1).

The Adsorption Characteristics of the MIP Sensor. The adsorption curves of the MIP and NIP sensor for 3-MCPD were plotted in Figure s3, Supporting Information. With the increase of concentration of 3-MCPD, the adsorption capacity of the MIP sensor gradually increased and reached the stability. It showed that the MIP sensor had an excellent adsorption for 3-MCPD and the NIP sensor had almost no adsorption.

The selectivity of the MIP sensor, based on the specific interaction between the template and the binding cavities, is an important factor to be considered. The selectivity of the MIP sensor toward 3-MCPD was evaluated by determining its DPV signals in the presence of analogues including glycerol, 1,2-propanediol, 1,3-DCP, and 2,3-DCP. It was calculated using the peak current ratio (I_m/I_o) where I_m and I_o are the anodic peak current of $[Fe(CN)_6]^{3-/4-}$ at about 0.2 V potential with and without structural analogues. A 10-fold excess of glycerol, 1,2-propanediol, 1,3-DCP, and 2,3-DCP in the presence of 3-MCPD hardly changed the peak current of $[Fe(CN)_6]^{3-/4-}$, as shown in Figure 5. The I_m/I_o only varied slightly between 0.91 and 0.98 (inset of Figure 5). The results indicated that the proposed sensor had a higher recognition selectivity for 3-MCPD than for analogues. This may be explained by the fact that the delicate binding cavities of the 3-MCPD template in the MIP film are able to recognize the template molecules through their shape, size, and functional group distribution, which can be used to detect 3-MCPD from a complex matrix without separation.

The Reproducibility and Stability of the MIP Sensor. To evaluate the reproducibility and repeatability of the MIP sensor, experiments were carried out in 10^{-15} mol L^{-1} 3-MCPD solution. The MIP sensor was regenerated with a peak current RSD of 3.12% using four different GCE electrodes. The excellent reproducibility was obtained with a relative standard deviation of 2.93% after 20 washes and measurements. Therefore, the MIP sensor has good reversibility. Moreover, the good stability of the sensor is a key factor for the 3-MCPD detection. To evaluate its stability, the MIP sensor was stored at room temperature for 10 days, and the peak current did not significantly change. After a month, it decreased to 92%. All measurements indicate that the MIP sensor possesses excellent stability.

Application to Real Soy Sauce Samples. The proposed method was used to determine the amount of 3-MCPD in soy sauce samples. The soy sauce samples were directly spiked with 10^{-16}, 10^{-15}, and 10^{-14} mol L^{-1} 3-MCPD, respectively. The result showed that the average recovery of 3-MCPD from the soy sauce samples was excellent and ranged from 95.0% to 106.4% with less RSD (<3.49%) in Table 2. Therefore, the established method can be used to detect the trace content of 3-MCPD in soy sauce without sample pretreatment.

■ ASSOCIATED CONTENT

Ⓢ Supporting Information

DPV and SEM image of the AuNP modified GCE, Result of the contact angle experiment of the MIP film, and MIP and NIP sensor responses to the incubation concentration of 3-MCPD. This material is available free of charge via the Internet at http://pubs.acs.org.

AUTHOR INFORMATION

Corresponding Author

*Tel: +86 510-85329015. Fax: +86 510-85328726. E-mail: sxlzzz@jiangnan.edu.cn.

Funding

This work was supported by the "'973'" National Basic Research Program of China (No. 2012CB720804), the National Research Program (Nos. 201003008-08 and 201203069-1), the Program for New Century Excellent Talent, Qing Lan Project in Jiangnan University, and the Priority Academic Program Development of Jiangsu Higher Education Institutions.

Notes

The authors declare no competing financial interest.

REFERENCES

(1) Crews, C.; Hasnip, S.; Chapman, S.; Hough, P.; Potter, N.; Todd, J.; Brereton, P.; Matthews, W. Survey of chloropropanols in soy sauces and related products purchased in the UK in 2000 and 2002. *Food Addit. Contam.* **2003**, *20*, 916−922.

(2) Nyman, P. J.; Diachenko, G. W.; Perfetti, G. A. Survey of chloropropanols in soy sauces and related products. *Food Addit. Contam.* **2003**, *20*, 909−915.

(3) Cavanagh, J. B.; Nolan, C. C. The neurotoxicity of α-chlorohydrin in rats and mice: II. Lesion topography and factors in selective vulnerability in acute energy deprivation syndromes. *Neuropathol. Appl. Neurobiol.* **1993**, *19*, 471−479.

(4) Velisek, J.; Davidek, J.; Kubelka, V.; Janicek, G.; Svobodova, Z.; Simicova, Z. New chlorine-containing organic compounds in protein hydrolysates. *J. Agric. Food Chem.* **1980**, *28*, 1142−1144.

(5) El Ramy, R.; Ould Elhkim, M.; Lezmi, S.; Poul, J. M. Evaluation of the genotoxic potential of 3-monochloropropane-1,2-diol (3-MCPD) and its metabolites, glycidol and β-chlorolactic acid, using the single cell gel/comet assay. *Food Chem. Toxicol.* **2007**, *45*, 41−48.

(6) Lee, J. K.; Byun, J. A.; Park, S. H.; Kim, H. S.; Park, J. H.; Eom, J. H.; Oh, H. Y. Evaluation of the potential immunotoxicity of 3-monochloro-1,2-propanediol in Balb/c mice: I. Effect on antibody forming cell, mitogen-stimulated lymphocyte proliferation, splenic subset, and natural killer cell activity. *Toxicology* **2004**, *204*, 1−11.

(7) Grosse, Y.; Baan, R.; Secretan-Lauby, B.; El Ghissassi, F.; Bouvard, V.; Benbrahim-Tallaa, L.; Guha, N.; Islami, F.; Galichet, L.; Straif, K. Carcinogenicity of chemicals in industrial and consumer products, food contaminants and flavourings, and water chlorination byproducts. *Lancet Oncol.* **2011**, *12*, 328−329.

(8) Lee, M.-R.; Chiu, T.-C.; Dou, J. Determination of 1,3-dichloro-2-propanol and 3-chloro-1,2-propandiol in soy sauce by headspace derivatization solid-phase microextraction combined with gas chromatography−mass spectrometry. *Anal. Chim. Acta* **2007**, *591*, 167−172.

(9) Xing, X.; Cao, Y. Determination of 3-chloro-1,2-propanediol in soy sauces by capillary electrophoresis with electrochemical detection. *Food Control* **2007**, *18*, 167−172.

(10) Meierhans, D. C.; Bruehlmann, S.; Meili, J.; Taeschler, C. Sensitive method for the determination of 3-chloropropane-1,2-diol and 2-chloropropane-1,3-diol by capillary gas chromatography with mass spectrometric detection. *J. Chromatogr. A* **1998**, *802*, 325−333.

(11) Abu-El-Haj, S.; Bogusz, M. J.; Ibrahim, Z.; Hassan, H.; Al Tufail, M. Rapid and simple determination of chloropropanols (3-MCPD and 1,3-DCP) in food products using isotope dilution GC−MS. *Food Control* **2007**, *18*, 81−90.

(12) Racamonde, I.; González, P.; Lorenzo, R. A.; Carro, A. M. Determination of chloropropanols in foods by one-step extraction and derivatization using pressurized liquid extraction and gas chromatography−mass spectrometry. *J. Chromatogr. A* **2011**, *1218*, 6878−6883.

(13) Pesselman, R. L.; Feit, M. J. Determination of residual epichlorohydrin and 3-chloropropanediol in water by gas chromatography with electron-capture detection. *J. Chromatogr. A* **1988**, *439*, 448−452.

(14) Kan, X.; Xing, Z.; Zhu, A.; Zhao, Z.; Xu, G.; Li, C.; Zhou, H. Molecularly imprinted polymers based electrochemical sensor for bovine hemoglobin recognition. *Sens. Actuators, B* **2012**, *168*, 395−401.

(15) Liu, Y.; Song, Q.-J.; Wang, L. Development and characterization of an amperometric sensor for triclosan detection based on electropolymerized molecularly imprinted polymer. *Microchem. J.* **2009**, *91*, 222−226.

(16) Xie, C.; Li, H.; Li, S.; Wu, J.; Zhang, Z. Surface Molecular Self-Assembly for Organophosphate Pesticide Imprinting in Electropolymerized Poly(p-aminothiophenol) Membranes on a Gold Nanoparticle Modified Glassy Carbon Electrode. *Anal. Chem.* **2010**, *82*, 241−249.

(17) Pan, M.-F.; Fang, G.-Z.; Liu, B.; Qian, K.; Wang, S. Novel amperometric sensor using metolcarb-imprinted film as the recognition element on a gold electrode and its application. *Anal. Chim. Acta* **2011**, *690*, 175−181.

(18) Liu, J.-q.; Wulff, G. Molecularly Imprinted Polymers with Strong Carboxypeptidase A-Like Activity: Combination of an Amidinium Function with a Zinc-Ion Binding Site in Transition-State Imprinted Cavities. *Angew. Chem., Int. Ed.* **2004**, *43*, 1287−1290.

(19) Riskin, M.; Tel-Vered, R.; Bourenko, T.; Granot, E.; Willner, I. Imprinting of Molecular Recognition Sites through Electropolymerization of Functionalized Au Nanoparticles: Development of an Electrochemical TNT Sensor Based on π-Donor−Acceptor Interactions. *J. Am. Chem. Soc.* **2008**, *130*, 9726−9733.

(20) Qian, J.; Wang, C.; Pan, X.; Liu, S. A high-throughput homogeneous immunoassay based on Förster resonance energy transfer between quantum dots and gold nanoparticles. *Anal. Chim. Acta* **2013**, *763*, 43−49.

(21) Xu, S.; Han, X. A novel method to construct a third-generation biosensor: self-assembling gold nanoparticles on thiol-functionalized poly(styrene-co-acrylic acid) nanospheres. *Biosens. Bioelectron.* **2004**, *19*, 1117−1120.

(22) Retna Raj, C.; Ohsaka, T. Voltammetric detection of uric acid in the presence of ascorbic acid at a gold electrode modified with a self-assembled monolayer of heteroaromatic thiol. *J. Electroanal. Chem.* **2003**, *540*, 69−77.

(23) Li, Y.; Li, J.; Xia, X.-H.; Liu, S.-Q. Direct electrochemistry of cytochrome c immobilized on a novel macroporous gold film coated with a self-assembled 11-mercaptoundecanoic acid monolayer. *Talanta* **2010**, *82*, 1164−1169.

(24) Rubinstein, I.; Rishpon, J.; Sabatani, E.; Redondo, A.; Gottesfeld, S. Morphology control in electrochemically grown conducting polymer films. 1. Precoating the metal substrate with an organic monolayer. *J. Am. Chem. Soc.* **1990**, *112*, 6135−6136.

(25) Huang, Z.; Chen, F.; Bennett, P. A.; Tao, N. Single Molecule Junctions Formed via Au−Thiol Contact: Stability and Breakdown Mechanism. *J. Am. Chem. Soc.* **2007**, *129*, 13225−13231.

(26) Yuan, L.; Zhang, J.; Zhou, P.; Chen, J.; Wang, R.; Wen, T.; Li, Y.; Zhou, X.; Jiang, H. Electrochemical sensor based on molecularly imprinted membranes at platinum nanoparticles-modified electrode for determination of 17β-estradiol. *Biosens. Bioelectron.* **2011**, *29*, 29−33.

(27) Wang, Z.; Li, H.; Chen, J.; Xue, Z.; Wu, B.; Lu, X. Acetylsalicylic acid electrochemical sensor based on PATP−AuNPs modified molecularly imprinted polymer film. *Talanta* **2011**, *85*, 1672−1679.

(28) Leung, M. K. P.; Chiu, B. K. W.; Lam, M. H. W. Molecular sensing of 3-chloro-1,2-propanediol by molecular imprinting. *Anal. Chim. Acta* **2003**, *491*, 15−25.

JOURNAL OF AGRICULTURAL AND FOOD CHEMISTRY

Article

pubs.acs.org/JAFC

Comparison of Extraction Protocols To Determine Differences in Wine-Extractable Tannin and Anthocyanin in *Vitis vinifera* L. cv. Shiraz and Cabernet Sauvignon Grapes

Keren A. Bindon,* Stella Kassara, Wieslawa U. Cynkar, Ella M. C. Robinson, Neil Scrimgeour, and Paul A. Smith

The Australian Wine Research Institute, P.O. Box 197, Glen Osmond, SA 5064, Australia

Supporting Information

ABSTRACT: Cabernet Sauvignon and Shiraz grapes were sourced from different regions within Australia, and microvinified with a skin contact period of 6 days. Grape samples were extracted using two protocols: a 15% v/v ethanol, 10 g/L tartaric acid extract of gently crushed berries (wine-like, WL) and a 50% v/v ethanol, pH 2 extract of grape berry homogenate. It was found that in WL extracts, grape tannin and anthocyanin concentrations were strongly related to wine tannin, anthocyanin and color density achieved during the skin contact period. No relationship was observed for grape tannin concentration analyzed in homogenate extracts and wine tannin, but a strong, positive relationship was found for anthocyanin concentration. When the data obtained from homogenate extraction was treated separately by grape variety, a stronger relationship between grape and wine tannin concentration was observed. Tannin compositional analysis in wines indicated that higher tannin concentrations were due to the extraction of tannin of higher molecular mass during fermentation, most likely from grape skins.

KEYWORDS: *anthocyanin, tannin, color, grape, wine, extractability, (−)-epigallocatechin, (−)-epicatechin-3-O-gallate, prodelphinidin, molecular mass, methyl cellulose, phloroglucinolysis*

INTRODUCTION

In the production of red wines, it is crucial to optimize the extraction of grape-derived phenolic compounds, primarily anthocyanin and condensed tannin (proanthocyanidin) in order to ensure the development of stable wine color and desirable textural properties. Tannins extracted during wine-making potentially originate from grape skins, seeds and pulp[1] while in most commercially-produced grape varieties, anthocyanins occur only in the grape skins. The extraction of phenolics from these respective grape components during fermentation differs significantly, with anthocyanin and skin tannin being extracted early,[2,3] and seed tannin being extracted later. While a significant amount of tannin is present in grape pulp, this appears to remain nonextractable during fermentation, potentially due to a strong association with pulp cell wall constituents.[1] Interactions between tannin and cell wall constituents may also occur in grape skins (and potentially seeds), which limits tannin extraction into the wine.[1] Apart from exerting a limiting effect on tannin extractability, cell wall constituents from grape and yeast cells which become suspended during fermentation can bind, and remove tannin and anthocyanin as these settle to form wine lees.[1,4,5]

There are only a limited number of published studies which have directly explored the relationship between grape phenolic concentration and wine composition. Studies which have attempted to draw correlations between an exhaustive extract of homogenized grape samples (50% v/v ethanol) and the corresponding wines[6,7] have shown positive relationships for grape anthocyanin analysis and wine color indices. However, for tannin analysis in 50% v/v ethanol extracts of whole-grape homogenates, the relationship between grape and wine tannin has been found to be weak[7] or absent.[6] Some studies have explored the relationship between only grape skin tannin concentration and wine tannin concentration.[8−12] These have shown a strong relationship, in which higher grape skin tannin concentrations were correlated with higher wine tannin concentrations. Interestingly, a cocorrelation between higher grape skin tannin concentration, grape anthocyanin concentration and wine color density was a common observation by these authors.[8−12]

Color, as well as anthocyanin and tannin concentrations in wine, have been shown to be positively associated with market value grade, and they are therefore useful as objective markers for wine quality.[13,14] Higher wine tannin, anthocyanin and polymeric pigment concentrations have been shown to be strongly correlated with wine color density and overall quality score as defined by a sensory panel.[10] Yet, despite this clear indication that the strategic management of wine tannin and anthocyanin is important, a rapid analytical method to predict wine phenolic profile from grapes has not yet been developed.

Various factors may have hindered progress in this area. Foremost, rapid, high-throughput analysis methods which are specific for tannin have only recently been developed.[15−18] Another important consideration is that most analytical methods aim to achieve as close to an exhaustive extraction as possible, and this is evident in techniques applied for grape tannin and anthocyanin.[15,16] Wine, on the other hand,

Received: January 16, 2014
Revised: April 27, 2014
Accepted: April 29, 2014
Published: April 29, 2014

ACS Publications © 2014 American Chemical Society

represents a partial extraction from the grape solids. As a result, using an exhaustive extraction method might not capture information regarding the intrinsic variability in the kinetics of tannin and anthocyanin extraction during fermentation, as well as potential back-binding events to cell wall constituents. In light of this, a desirable, commercially relevant outcome for wine industry producers would be a procedure for the prediction of anthocyanin and tannin concentrations achievable during fermentation, specifically, the stage during which skin tannin extraction approaches a plateau and is proportionally higher than tannin extraction from seeds.[2,3,19] In addition, considering that certain winemaking techniques may increase extraction of tannin from the grape solids,[20] a measure of total grape tannin (i.e., exhaustive extraction) is also of relevance for decision-making in the winery. Both measures could inform producers how best to approach processing, e.g. guiding pressing decisions or for benchmarking winemaking procedures. Conceptually, the idea of an "extractability" assay is not new, and methods have been proposed by other authors to represent phenolics extractable under aqueous conditions, in comparison with a harsh, high-solvent extraction.[21−23] However, this has yet to be demonstrated as relevant across a sufficiently wide range of grape and wine phenolic compositions. There exists a significant knowledge gap in understanding the grape to wine relationship: in terms of both tannin and anthocyanin extractability, their retention in wine and the development of wine color.

The current study aimed to validate an extraction protocol which mimics the conditions of fermentation, and apply it to grape samples representing a wide a wide range of phenolic composition. To do this, a large sample set from two commercial grape varieties at different ripeness grades were sourced across a number of grape-growing regions within South Australia. Grape batches were subjected to extraction in dilute 15% v/v alcohol (wine-like extract, WL), as well as to a more exhaustive extraction protocol using homogenized grapes and 50% v/v ethanol, and were microvinified. Tannin and anthocyanin concentrations in grape extracts and wines were compared, and they provide a proof of concept that grape compositional parameters can be measured to predict wine phenolic outcomes. This indicates the scope for the development of a commercially-relevant analytical approach.

MATERIALS AND METHODS

Grape Sampling and Processing. A total of 39 batches of fruit (approximately 8 kg) were sourced from two grape varieties in the 2012−2013 growing season: 20 samples of Cabernet Sauvignon grapes and 19 samples of Shiraz grapes. Grape regions and vineyards were selected by a commercial wine producer (Accolade Wines, Reynella, SA, Australia). Grapes were harvested at commercial ripeness from five growing regions within South Australia: Riverland, McLaren Vale, Clare, Padthaway, and Langhorne Creek. The temperature and rainfall data for these regions for the 2012−2013 growing season are shown as S1 in the Supporting Information. Following harvesting, batches of fresh fruit were stored sealed, and they were then immediately transported to Adelaide, South Australia. On arrival, fruit batches were stored at 4 °C for no more than 6 days. In order to facilitate sample processing and small-scale winemaking, no more than 10 batches of grapes were processed within a week. Fruit batches were therefore processed at five time points over a period of 2 months, for which the dates of sample preparation are shown in Table 1. Grape batches were completely destemmed by hand, and thereafter, subsamples were taken for analysis and winemaking. For analysis of average berry weight, juice pH, titratable acidity (TA) and total soluble solids (as °Brix), a 200-berry sample was collected and weighed. This was then transferred to a plastic bag equipped with a resealable zipper and gently crushed by hand. Expressed juice was collected through a 0.5 mm sieve, and then centrifuged at 1730*g* for 5 min. Juice °Brix was determined using a digital refractometer. TA and pH were determined using a pH meter and combination electrode. The TA was determined by titrating with 0.33 M sodium hydroxide solution to a pH end-point of 8.2, and expressed in g/L of tartaric acid equivalents. From each destemmed grape berry sample, triplicate 50 g (±0.5 g) and 200 g batches were sampled and the weight recorded, and these were then transferred to plastic bags equipped with a resealable zipper or in screw-cap polypropylene containers, respectively. The triplicate 50 and 200 g samples were stored at 4 °C and processed fresh within 3 h, as described below. For certain grape samples, further triplicate batches of 50 and 200 g were collected as described above, but they were immediately frozen at −20 °C. These grape batches were stored for either 24 h, 1 month or 3 months in order to determine the effect of freezing on anthocyanin and tannin concentration measured by different analytical methodologies. Finally, triplicate 1 kg samples were collected from each destemmed grape batch and transferred to sealed plastic bags. Care was taken to minimize grape crushing, and samples were stored at 4 °C overnight, before being processed for microvinification, as described below.

Extraction of Whole Berry Samples under Wine-like Conditions. To simulate the extraction of tannin and anthocyanin from gently crushed grapes under wine-like conditions, a WL extraction protocol in model wine solution was developed. The extraction solvent was prepared containing 400 mL/L absolute ethanol and 10 g/L tartaric acid, pH 3.4. Frozen 50 g berry samples were brought to room temperature by placing them sealed, within a 25 °C water bath for 1 h. Defrosted or fresh triplicate 50 g berry samples, retained in a plastic bag equipped with a resealable zipper, were gently crushed by hand. Crushed grape berries and juice were transferred to a 70 mL polypropylene jar, and 15 mL of extraction solvent was added, to each sample. This addition was based on an approximate juice yield of 0.5 mL per g of fruit, in order to extract in 15% v/v ethanol. Samples were sealed under screw cap and extracted on a platform shaker at 25 °C in the dark for 40 h. After extraction, samples were pressed by hand through a 0.5 mm sieve and the volume of recovered extract recorded. For the sample set studied, the percentage standard deviation of the average recovered extraction volume was 7%. The grape skin and seed residue were recovered and re-extracted in 30 mL of 50% v/v aqueous ethanol pH 2 (with HCl) for a further 18 h. The 50% ethanol extract was recovered as described above, but the volume was not recorded. The WL and 50% ethanol extracts were centrifuged at 1730*g* for 5 min, and thereafter aliquots were removed for the analysis of tannin and anthocyanin as described below.

Optimization of Extraction Volume and Time for Model Wine Extracts. Before the main experiment was commenced, the effect of extraction volume and the length of the extraction on tannin concentration per unit berry fresh mass were investigated for a single Cabernet Sauvignon grape sample obtained from a vineyard located at the Waite Campus, University of Adelaide. Grape samples were prepared as outlined above, but the extraction volume per 50 g sample was adjusted between 35 and 75 mL, maintaining the ethanol concentration at 15% v/v. Extractions were performed in triplicate, and tannin and anthocyanin concentrations were monitored at five time points over a 64 h period and then analyzed as outlined below (Supporting Information S2).

Extraction of Grape Berry Homogenates. Homogenate extractions were performed according to a published protocol.[5,15,16] The selection of a 200 g grape sample for homogenization was required for the type of homogenizer used, which was a Retsch Grindomix GM200 (Retsch GmbH & Co., Germany). Frozen 200 g berry samples were defrosted by placing them at 4 °C for 18 h. Both fresh and defrosted triplicate 200 g samples were homogenized cold (<10 °C) and analyzed on the day of homogenization. Berry samples were homogenized in at 8000 rpm for 20 s. A 1 g portion of homogenate was weighed into a pretared centrifuge tube and the mass recorded. The homogenate was then extracted in 10 mL of 50% v/v, aqueous ethanol, pH 2. Tubes were capped and extractions carried out

on a suspension mixer for 1 h at room temperature. The tube was then centrifuged at 1730*g* for 10 min, and the supernatant analyzed as described below.

Microvinification. The triplicate 1 kg grape batches were retained in the plastic bag equipped with a resealable zipper which had been used for storage at 4 °C overnight, and crushed by hand, ensuring that no leakage of juice occurred. All grape juice and solids (skin, seeds) were transferred to sterile 1.5 L glass French Press coffee plungers (Bodum, Triengen, Switzerland) using a glass funnel. A standard addition of 50 mg potassium metabisulfite (PMS) (Enartis Pacific Pty Ltd., Nuriootpa, South Australia) was made per 1 kg ferment. The ferments were adjusted to a pH of 3.5 by the addition of tartaric acid (Australian Tartaric Products Pty Ltd., Red Cliffs, Victoria, Australia). *Saccharomyces cerevisiae* PDM yeast (Maurivin, Sydney, Australia) and diammonium phosphate (DAP) were added at a rate of 300 mg/kg must. Each ferment, including the glass French Press and plunger, was weighed. Fermentation was initiated at a constant temperature of 25 °C, and the progress of fermentation was monitored daily by the reduction in ferment weight. On a daily basis the plunger was gently lifted to mix the wine, and thereafter the fermentation cap was resubmerged leaving approximately 1 cm of wine above the plunger surface. After 6 days of fermentation the plunger was lowered to press off the wine from the grape solids. Wine was carefully transferred to a 500 mL bottle equipped with an oxygen trap and kept at 25 °C for a further 24 h. For the first sample series undergoing fermentation, 5 out of 6 grape batches had completed fermentation within the 7-day period, with residual glucose and fructose levels below 0.5 g/L (Table 2). In order to prevent oxidation or film yeast growth, and well as to retain consistency in processing between the various fermentation experiments, all ferments were stopped at 7 days. This was also an important consideration to prevent the introduction of skin contact time as an additional variable in the study. To stop fermentation, an 80 mg addition of total SO_2 as PMS (as a 10% w/v solution in water) was added to each ferment, stirred, and allowed to equilibrate for 2 h. Wine was decanted into sterile 100 and 200 mL glass bottles, sealed under screw-cap with no ullage, and stored for 4 weeks at 4 °C. Thereafter, wine was sampled for analysis of pH and TA as described above. Residual sugar in each wine was determined as glucose and fructose equivalents using an automated analyzer (Daytona) with the enzymatic method of Randox (Randox Laboratories, Crumlin, United Kingdom). Volatile acidity was measured using a multispectral wine analyzer (Microdom, Taverny, France) and was between 0.2 and 0.7 g/L across the wine sample range. Wine tannin, anthocyanin and color were analyzed as described below. A further 10 mL aliquot of each wine was frozen at −80 °C for later analysis of tannin composition. The decision to freeze wine samples for analysis was based on the previous observation that tannin concentration in both WL grape extracts and wines are stable within 18 months (Supporting Information S3).

Analysis of Anthocyanin, Tannin and Wine Color Properties. Tannin, anthocyanin and color properties in triplicate grape extracts and wines were analyzed using a standard high-throughput method.[16] Each analysis was performed in duplicate. Briefly, tannin concentration was analyzed following precipitation by methyl cellulose (MCP) in 1.1 mL 96-well plate. A 25 μL sample of grape extract or wine was combined with 300 μL of 0.04% (w/v) methyl cellulose (Sigma-Aldrich, St. Louis, MO, USA) solution, mixed on an automated plate shaker and left to stand for 3 min. A sample control was included where water was added in place of the methyl cellulose solution. A 200 μL aliquot of saturated ammonium sulfate (Sigma-Aldrich, St. Louis, MO, USA) was added, followed by 475 μL water. Where tannin concentration was below detection limit, the sample was increased up to 100 μL and the volume of water adjusted accordingly to give a final volume of 1 mL. Samples were mixed on an automated plate shaker and left to stand for 10 min. Centrifugation was performed for 5 min at maximum speed on a Hettich Universal 32 R centrifuge equipped with a Hettich 1645 rotor for 96-well plates (Adelab Scientific). A 300 μL aliquot of supernatant from the methyl-cellulose treated and control samples were transferred into a 370 μL 96-well UV plate and the 280 nm absorbance measured using a SpectraMax M2Microplate Reader (Molecular Devices, Australia). Quantification was performed by analyzing the difference in 280 nm absorbance between control and MCP-treated samples, using (−)-epicatechin (Sigma-Aldrich, St. Louis, MO, USA) as the quantitative standard. To ensure standardization of the tannin analysis across the staggered time points at which grape and wine sampling and extraction took place, a purified commercial seed extract (Tarac Technologies, Nuriootpa, Australia) was included for each 96-well plate assayed.

For the measurement of grape and wine color, the procedure was as follows. For total anthocyanin, a 20 μL of wine or a 50 μL aliquot of grape extract was added to 1 M HCL to a final volume of 1 mL, and mixed. Samples were left to stand in the dark for 1 h. The 1 h period was modified from the original method stipulating 3 h,[16] as we had demonstrated that maximal ionization of anthocyanins was achievable within this period (data not shown). For wine analyses only, a further 100 μL of wine was added to 900 μL of buffer solution containing 0.5% (w/v) tartaric acid and 12% (v/v) ethanol (pH 3.4), mixed and analyzed immediately. Buffer solution was also prepared containing 0.1% (v/v) acetaldehyde or 0.375% (w/v) sodium metabisulfite, and 900 μL of the respective solutions were combined with 100 μL wine, mixed, left to stand in the dark for 1 h, and then analyzed. For spectral analysis of color measures, a 300 μL aliquot was transferred to a 370 μL 96-well UV plate and the 420 and 520 nm absorbances measured using a SpectraMax M2Microplate Reader (Molecular Devices, Australia), corrected using an appropriate sample blank and a water constant correct function to approximate a 1 cm path length. Estimates of wine anthocyanin, modified wine color density and nonbleachable (bisulfite-resistant) pigment were determined from spectral data according to the calculations outlined in the published method.[16] The estimate of grape anthocyanin was also according to the published method[16] but without correction for bisulfite.

Following the analysis of tannin concentration in wines, a subsample of 8 high-concentration and 8 low-concentration wines (a single replicate of a triplicate ferment batch) were identified for subsequent tannin compositional analysis, of which equal proportions were from the Shiraz and Cabernet Sauvignon grape varieties. The 10 mL frozen (−80 °C) aliquots of each of the 16 wines identified were rapidly defrosted in a water bath at room temperature, and centrifuged at 1730*g* for 5 min. Duplicate analyses of wine aliquots were performed. Total tannin (approximately 1 mg based on MCP analysis) was isolated using solid-phase extraction with the modifications outlined in Kassara et al. (2011).[14] Purified tannin was reconstituted in 100 μL methanol and analyzed by high-throughput phloroglucinolysis[24] and high-performance liquid chromatography (HPLC), as described previously.[25,26] For HPLC, an Agilent model 1100 (Agilent Technologies Australia Pty Ltd., Melbourne, Australia) was used, equipped with Chemstation software. For phloroglucinolysis, (−)-epicatechin (Sigma-Aldrich, St. Louis, MO, USA) was the quantitative standard.

Statistical Analysis. Significant differences between samples and treatments were determined by one-way analysis of variance (ANOVA) or Student's *t*-test. For analysis of unbalanced sample numbers, the weighted mean was used. For these analyses the JMP 5.0.1 (SAS, Cary, NC, USA) and Graph Pad Prism 6.02 (GraphPad Software, Inc., La Jolla, CA, USA) software packages were used. For linear regression and multiple linear regression analysis, Unscrambler X 10.2.0 (CAMO Software, Oslo, Norway) or Microsoft Excel 2007 was used.

RESULTS AND DISCUSSION

Effect of Extraction Volume and Time on Tannin and Anthocyanin Concentration in Model Wine Extracts. The effect of extraction volume and the length of the extraction on tannin and anthocyanin concentration in WL extracts were investigated for a single Cabernet Sauvignon grape sample. The extraction volume was between 35 and 75 mL, maintaining the ethanol concentration at 15% v/v, sampled five times during 64 h (Supporting Information S2). For all extraction volumes

Table 1. General Grape Composition, Anthocyanin and Tannin Concentration Determined for Shiraz and Cabernet Sauvignon Samples Obtained from Different Growing Regions within South Australia during 2013[b]

Grape Variety	Region	Date processed	pH	Titratable acidity (g/L)	Total soluble solids (° Brix)	Berry F. Wt (g)	Wine-like extraction method[a]		Homogenate extraction method	
							Tannin (mg/g)	Anthocyanin (mg/g)	Tannin (mg/g)	Anthocyanin (mg/g)
Shiraz	Riverland	18th January	3.86	3.9	23.9	0.74	1.28 ± 0.08	0.52 ± 0.03	3.03 ± 0.33	1.38 ± 0.03
			3.83	5.2	24.0	1.30	1.34 ± 0.02	0.39 ± 0.01	1.60 ± 0.14	1.01 ± 0.01
			3.78	3.6	25.1	1.14	1.38 ± 0.08	0.48 ± 0.02	2.52 ± 0.03	1.24 ± 0.06
			3.62	5.0	22.9	1.04	0.88 ± 0.02	0.32 ± 0.01	2.25 ± 0.06	0.88 ± 0.06
			3.89	4.1	24.2	1.18	1.16 ± 0.06	0.35 ± 0.02	2.17 ± 0.13	0.95 ± 0.01
			3.68	4.4	22.8	1.17	1.42 ± 0.06	0.42 ± 0.02	2.70 ± 0.30	1.09 ± 0.01
	McLaren Vale	25th February	3.64	5.5	32.0	0.83	2.53 ± 0.10	0.87 ± 0.01	6.54 ± 0.17	2.15 ± 0.02
			3.64	5.5	31.7	0.80	2.46 ± 0.08	0.82 ± 0.03	6.61 ± 0.01	1.95 ± 0.06
			3.43	5.7	30.0	0.84	2.40 ± 0.07	0.92 ± 0.01	5.99 ± 0.10	2.10 ± 0.04
			3.48	5.4	30.9	0.82	2.60 ± 0.09	1.03 ± 0.05	6.04 ± 0.18	2.24 ± 0.02
			3.52	5.6	31.1	0.79	2.65 ± 0.12	0.99 ± 0.02	6.73 ± 0.14	2.26 ± 0.03
			3.52	5.3	31.0	0.78	2.75 ± 0.04	1.05 ± 0.02	6.42 ± 0.23	2.24 ± 0.08
Cabernet Sauvignon	Riverland	4th March	3.91	4.2	23.9	0.93	1.14 ± 0.04	0.48 ± 0.01	3.14 ± 0.11	1.18 ± 0.04
			3.89	3.9	26.1	1.12	1.80 ± 0.04	0.63 ± 0.01	4.02 ± 0.23	1.32 ± 0.04
			3.55	4.4	23.4	1.27	1.35 ± 0.05	0.45 ± 0.01	3.76 ± 0.43	1.09 ± 0.05
			3.83	3.8	24.2	0.82	1.59 ± 0.06	0.61 ± 0.01	3.58 ± 0.02	1.44 ± 0.02
			3.89	4.4	23.7	0.83	1.07 ± 0.07	0.32 ± 0.00	4.75 ± 0.25	0.84 ± 0.00
			3.69	4.3	24.4	0.89	1.50 ± 0.04	0.44 ± 0.03	4.83 ± 0.13	0.96 ± 0.01
			3.81	4.4	24.5	0.95	1.11 ± 0.04	0.36 ± 0.01	4.82 ± 0.09	0.90 ± 0.03
			3.79	4.0	23.4	0.89	1.29 ± 0.07	0.39 ± 0.00	5.58 ± 0.05	0.95 ± 0.02
			3.78	4.0	24.6	0.91	1.11 ± 0.02	0.36 ± 0.01	5.26 ± 0.31	1.03 ± 0.02
			3.82	4.0	24.8	0.84	1.13 ± 0.02	0.41 ± 0.01	4.83 ± 0.22	1.10 ± 0.01
	McLaren Vale		3.74	4.1	25.6	0.83	1.86 ± 0.05	0.67 ± 0.02	6.63 ± 0.03	1.88 ± 0.06
			3.72	4.0	25.6	0.88	1.89 ± 0.06	0.67 ± 0.01	6.77 ± 0.14	1.71 ± 0.03
Shiraz	Langhorne Creek		3.58	4.6	22.8	1.42	1.94 ± 0.14	0.67 ± 0.02	4.55 ± 0.02	1.65 ± 0.05
			3.52	5.0	22.2	1.37	1.98 ± 0.03	0.63 ± 0.01	3.87 ± 0.20	1.68 ± 0.05
Cabernet Sauvignon	Riverland	12th March	3.82	5.0	23.3	0.69	0.83 ± 0.06	0.42 ± 0.02	3.73 ± 0.08	0.89 ± 0.03
			3.81	4.1	24.8	0.71	1.14 ± 0.03	0.46 ± 0.01	4.88 ± 0.21	0.91 ± 0.01
			3.63	3.5	24.6	0.83	1.39 ± 0.03	0.48 ± 0.02	5.50 ± 0.11	1.01 ± 0.04
			3.83	3.0	26.1	1.13	2.50 ± 0.15	0.93 ± 0.02	8.69 ± 0.53	2.06 ± 0.04
	Clare		3.94	2.7	25.8	1.03	2.27 ± 0.09	0.96 ± 0.01	8.55 ± 0.40	2.09 ± 0.09
			3.74	3.3	25.0	0.94	1.77 ± 0.08	0.84 ± 0.01	7.66 ± 0.21	1.71 ± 0.04
	McLaren Vale	18th March	3.82	3.7	24.8	0.89	1.95 ± 0.02	0.75 ± 0.03	6.34 ± 0.12	1.94 ± 0.02
			3.75	3.6	24.4	0.98	1.88 ± 0.10	0.73 ± 0.01	6.06 ± 0.17	1.91 ± 0.01
			3.92	3.2	24.5	0.81	2.06 ± 0.06	0.80 ± 0.02	5.82 ± 0.26	1.95 ± 0.05
			3.77	4.3	24.3	0.88	1.93 ± 0.02	0.78 ± 0.02	5.66 ± 0.28	1.76 ± 0.02
Shiraz	Langhorne Creek		3.92	3.2	26.1	1.18	2.90 ± 0.18	0.85 ± 0.02	5.76 ± 0.12	2.05 ± 0.06
Cabernet Sauvignon	Padthaway		3.60	5.0	25.6	0.90	1.80 ± 0.14	0.69 ± 0.02	5.94 ± 0.23	1.65 ± 0.05
			3.71	4.0	25.9	0.84	1.95 ± 0.03	0.82 ± 0.01	6.22 ± 0.31	1.99 ± 0.03
All samples										
	Mean		3.74	4.28	25.49	0.95	1.74	0.64	5.12	1.52
	Maximum		3.94	5.70	32.00	1.42	2.90	1.05	8.69	2.26
	Minimum		3.43	2.70	22.20	0.69	0.83	0.32	1.60	0.84
Mean by variety										
	Shiraz		3.68	4.70	26.43	1.00	1.83	0.66	4.47	1.57
	Cabernet Sauvignon		3.78	3.92	24.62	0.92	1.66	0.61	5.65	1.45
	ANOVA P =		<0.05	<0.01	ns	<0.01	ns	ns	<0.01	ns
Mean by region										
	Riverland		3.78	4.22^{a}	24.14^{b}	0.96^{b}	1.26^{b}	0.44^{c}	3.84^{d}	1.06^{b}
	McLaren Vale		3.66	4.66^{a}	27.99^{a}	0.84^{c}	2.25^{a}	0.84^{ab}	6.3^{b}	2.01^{a}
	Langhorne Creek		3.67	4.27^{a}	23.7^{b}	1.33^{a}	2.27^{a}	0.72^{b}	4.73^{cd}	1.79^{a}
	Clare		3.84	3.00^{b}	25.63^{ab}	1.03^{bc}	2.18^{a}	0.91^{a}	8.3^{a}	1.96^{a}
	Padthaway		3.66	4.50^{a}	25.75^{ab}	0.87^{bc}	1.88^{a}	0.76^{ab}	6.08^{bc}	1.82^{a}
	ANOVA P =		ns	<0.05	<0.001	<0.001	<0.0001	<0.0001	<0.0001	<0.0001

[a]Wine-like tannin extract corrected for differences in extraction volume recovery. [b]ANOVA, $n = 39$, different superscripted letters after the mean within a column indicate significant differences by a post-hoc Student's t-test, ns = not significant.

tested, tannin concentration increased up to the 40 h time point. At the 40 h time point the standard error of the triplicate extractions was low, and differences in tannin quantity between extracts of different volumes were negligible. Before and after the 40 h time point, higher extraction volumes (65 or 75 mL) were found to have lower tannin concentrations when normalized for differences in total solvent volume. However, it was also observed that at the 45 and 64 h assay time points, there was a large increase in the standard error for the tannin assay triplicates. Thus, the estimated tannin quantity at these time points was found to be more variable for the different extraction volumes tested, either increasing, decreasing or reaching a plateau. Since this may have reflected instability or oxidation of the extract at the 45 and 64 h time points, a 40 h

dx.doi.org/10.1021/jf5002777 | J. Agric. Food Chem. 2014, 62, 4558−4570

extraction period was selected as optimal to maximize tannin extraction but prevent extract instability. For the extract volumes tested, the 40 mL volume extract was more stable across sampling time points, and standard error was low across all time points evaluated. Therefore, a 40 mL extraction volume (15 mL addition of solvent, as outlined above) was selected to optimize for tannin extraction. It should be noted, however, that this gave a slightly lower estimated anthocyanin concentration than the higher extraction volumes evaluated (Supporting Information S2). The estimated anthocyanin quantity was found to be directly related to extract volume, and it decreased as solvent volume decreased. Losses of anthocyanin at lower solvent volumes may have been due to a greater adsorption of anthocyanin to grape constituents, or potentially oxidation, but this was not investigated further. Anthocyanin in all extract volumes tested was found to decline after a 40 h extraction time, which confirmed that this was an optimal extraction period to ensure extract stability.

Compositional Variation in Grape and Wine Samples. Since the objective of the research was to source grapes with a diverse range of phenolic compositions on which extraction protocols could be validated, it was considered that regional and maturity differences might introduce significant variability. Differences in phenolics by grape variety were a further important consideration, and two principal commercial grape varieties were selected for the study.

To better define the regions within South Australia from which grapes were sourced, seasonal minimum and maximum temperatures, and rainfall data for the 2012−2013 growing season are shown as S1 of the Supporting Information. It was evident that the regions selected for the study had differences in the maximum and minimum temperatures during the growing season. In particular, McLaren Vale was characterized by higher minimum temperatures during the ripening period, which was noted anecdotally to be associated with a compression of the ripening period, which may account for the higher average °Brix levels for the region, and higher residual sugar levels in wines due to only a partial completion of fermentation in the 7-day period (Tables 1 and 2).

The Padthaway region had lower minimum temperatures than the other regions studied throughout grape development, but this was not associated with measurable differences in juice composition. Similarly, differences in maximum temperature during the grape development period were not associated with regional differences in juice composition. Only the Riverland and Langhorne Creek regions differed in maximum daily temperature from the other regions sampled, being higher and lower, respectively. All the regions sampled received intermittent rain events during the grape development period, but only Clare, Riverland and Padthaway had high rainfall during the ripening phase. Riverland had the lowest total seasonal rainfall of the regions, and Clare the highest. Albeit from a low sample number, Clare grape samples were characterized by lower juice titratable acidity, but they had no difference in pH. Small differences in general grape and wine composition were found by grape variety, with Shiraz having slightly lower juice pH, higher berry weight, and higher juice titratable acidity than Cabernet Sauvignon (Table 1), but no significant difference was found in juice °Brix. Due to acid adjustment prior to winemaking, titratable acidity was not significantly different between varieties, but it was found that after vinification, Shiraz wines had a slightly higher average pH than Cabernet Sauvignon wines.

For the range of grape and wine samples analyzed, the variation in measured tannin and anthocyanin concentration was greater than the variation in juice compositional properties (pH, titratable acidity, °Brix) or berry weight (Tables 1 and 2). For tannin determined in WL extracts, the difference between the maximum and minimum concentrations across all samples varied by a factor of 3.5. For homogenate extracts and wines, this factor was 5.5. For anthocyanin concentration determined in WL extracts, homogenate extracts and wines, maximum and minimum values differed by a factor of 3 across the whole range of samples (Tables 1 and 2). As might be expected, the concentration of tannin and anthocyanin determined using the homogenate extraction procedure was higher than the corresponding analysis using WL extracts.

There were no significant differences observed in the averages by grape variety for tannin and anthocyanin concentrations determined using WL extraction. However, for homogenate extracts, the average tannin concentration for Cabernet Sauvignon grapes was higher than that in Shiraz, but no difference was found by variety in terms of anthocyanin concentration. Grape tannin and anthocyanin concentrations determined using both the WL and homogenate extraction protocols showed regional variation, and grape samples with the lowest concentrations were from the Riverland compared with all other regions (Table 1).

In comparing the anthocyanin and tannin concentrations of the corresponding wines, regional differences were consistent with what was observed in the grape extracts: the lowest concentrations for both parameters were found in Riverland wines, and the highest in McLaren Vale wines (Table 2). A consideration in interpreting this result is that the McLaren Vale sample was composed of grapes of a higher average °Brix, and the corresponding wines contained higher residual sugar, a natural result of stopping the fermentation 24 h after the 6-day skin contact period. The possibility that higher grape maturity could be related to higher concentrations of phenolics in WL extracts and wines cannot be excluded, and this will be discussed later. It would not be expected that the presence of higher sugar concentrations in WL extracts, or higher residual sugar in the ferments, might have influenced either tannin or anthocyanin concentration by altering the sample matrix, and this is supported by our observations that wine tannin concentration does not change significantly after press (unpublished data, see Supporting Information S4).

Since collecting data regarding the management practices of each vineyard from which the grapes were sourced was not practicable, it is not possible to suggest any causative effect for the observed regional differences. The Riverland is a highly irrigated region, with greater water application and therefore potentially a higher vineyard vigor, which could have reduced grape anthocyanin, and possibly tannin.[27,28] However, it is noteworthy that the average berry weight for Riverland fruit was not significantly greater than the berry weights from the other regions, and it would be expected that this would increase in response to irrigation.[29,30] As noted previously, the main climatic variable which distinguished the Riverland region from the others was higher maximum daily temperatures during the developmental period (Supporting Information S1). Higher temperatures during berry development are well-known to be associated with lowered grape anthocyanin concentration[31] but an effect on tannin is less clear, and might be expected to result in higher grape tannin concentration.[32] The regional effect is

Table 2. General Composition, Anthocyanin, Tannin and Color Properties Determined for Shiraz and Cabernet Sauvignon Wines Made Using a Standard Microvinification Protocol under Controlled Conditions[a]

Grape Variety	Region	Ferment start date	pH	Titratable acidity (g/L)	Residual sugar (g/L)	Tannin (mg/L)	Anthocyanin (mg/L)	Wine Colour Density (A.U.)	Non-bleachable pigments (A.U.)
Shiraz	Riverland	19th January	3.82 ± 0.00	6.9 ± 0.12	0.1 ± 0.00	850 ± 94	741 ± 7	14.9 ± 0.44	1.82 ± 0.05
			3.69 ± 0.02	7.6 ± 0.13	0.1 ± 0.00	552 ± 46	517 ± 8	8.9 ± 0.34	1.05 ± 0.06
			3.57 ± 0.00	6.6 ± 0.06	0.2 ± 0.03	856 ± 27	638 ± 5	11.8 ± 0.04	1.43 ± 0.03
			3.47 ± 0.01	7.2 ± 0.03	0.5 ± 0.15	446 ± 33	436 ± 7	7.9 ± 0.13	0.93 ± 0.01
			3.61 ± 0.01	7.3 ± 0.09	0.3 ± 0.06	697 ± 34	496 ± 5	8.8 ± 0.14	1.15 ± 0.01
			3.64 ± 0.01	5.6 ± 0.09	66.1 ± 6.46	777 ± 36	499 ± 15	9.7 ± 0.39	1.25 ± 0.02
	McLaren Vale	26th February	3.46 ± 0.05	9.0 ± 0.15	98.1 ± 1.78	2185 ± 142	1105 ± 7	28.6 ± 0.58	3.25 ± 0.12
			3.47 ± 0.01	8.9 ± 0.07	67.8 ± 4.22	2100 ± 112	1016 ± 27	25.2 ± 1.15	3.19 ± 0.10
			3.48 ± 0.01	8.6 ± 0.06	54.7 ± 5.13	1985 ± 104	1138 ± 6	27.8 ± 0.51	3.09 ± 0.07
			3.50 ± 0.02	8.6 ± 0.09	57.3 ± 2.83	2248 ± 81	1241 ± 9	28.9 ± 0.22	3.25 ± 0.03
			3.57 ± 0.00	8.8 ± 0.09	90.5 ± 1.07	2318 ± 108	1217 ± 11	29.9 ± 0.37	3.47 ± 0.03
			3.55 ± 0.01	8.6 ± 0.07	124.2 ± 1.67	2396 ± 80	1186 ± 14	29.1 ± 0.31	3.46 ± 0.07
Cabernet Sauvignon	Riverland	5th March	3.66 ± 0.00	7.2 ± 0.09	0.1 ± 0.00	439 ± 36	514 ± 4	9.8 ± 0.09	1.22 ± 0.02
			3.67 ± 0.01	7.2 ± 0.06	21.4 ± 2.42	1525 ± 61	798 ± 15	17.2 ± 0.39	2.35 ± 0.06
			3.45 ± 0.01	6.3 ± 0.07	81.8 ± 0.60	829 ± 113	438 ± 4	9.4 ± 0.23	1.19 ± 0.04
			3.68 ± 0.01	6.7 ± 0.09	0.1 ± 0.00	973 ± 15	725 ± 3	14.7 ± 0.18	1.85 ± 0.03
			3.49 ± 0.00	7.5 ± 0.00	0.1 ± 0.00	621 ± 24	488 ± 8	10.1 ± 0.25	1.76 ± 0.07
			3.33 ± 0.02	8.5 ± 0.19	1.5 ± 0.98	873 ± 45	571 ± 17	11.1 ± 0.05	1.71 ± 0.09
			3.38 ± 0.01	8.4 ± 0.03	0.5 ± 0.12	719 ± 28	531 ± 6	10.4 ± 0.21	1.70 ± 0.01
			3.34 ± 0.01	7.5 ± 0.23	0.1 ± 0.00	845 ± 120	561 ± 6	11.7 ± 0.84	1.92 ± 0.15
			3.44 ± 0.01	7.7 ± 0.09	0.3 ± 0.12	690 ± 6	550 ± 6	10.6 ± 0.07	1.88 ± 0.03
			3.52 ± 0.01	7.4 ± 0.06	11.0 ± 0.52	799 ± 11	579 ± 10	10.4 ± 0.39	1.93 ± 0.07
	McLaren Vale		3.40 ± 0.02	7.9 ± 0.27	1.4 ± 0.28	1429 ± 42	961 ± 3	18.7 ± 0.48	2.24 ± 0.03
			3.37 ± 0.02	7.7 ± 0.20	1.6 ± 0.70	1429 ± 71	894 ± 19	17.7 ± 0.21	2.23 ± 0.05
Shiraz	Langhorne Creek		3.36 ± 0.01	7.3 ± 0.03	3.2 ± 1.04	1056 ± 35	814 ± 16	16.1 ± 0.29	1.62 ± 0.02
			3.43 ± 0.01	7.2 ± 0.12	13.2 ± 2.92	1345 ± 71	822 ± 2	16.4 ± 0.37	1.67 ± 0.06
Cabernet Sauvignon	Riverland	13th March	3.45 ± 0.01	8.9 ± 0.03	0.1 ± 0.00	440 ± 48	556 ± 6	9.9 ± 0.25	1.38 ± 0.03
			3.44 ± 0.01	8.0 ± 0.15	27.6 ± 5.70	794 ± 56	577 ± 12	10.4 ± 0.14	1.77 ± 0.03
			3.40 ± 0.00	7.3 ± 0.10	38.3 ± 2.45	878 ± 63	738 ± 176	14.3 ± 4.45	1.98 ± 0.34
	Clare		3.32 ± 0.01	7.9 ± 0.06	35.9 ± 0.90	1602 ± 72	1000 ± 21	21.6 ± 0.64	2.56 ± 0.04
			3.25 ± 0.00	7.9 ± 0.05	36.1 ± 2.85	1641 ± 85	1140 ± 15	23.7 ± 0.55	2.47 ± 0.02
			3.32 ± 0.00	7.4 ± 0.07	35.1 ± 6.13	1311 ± 94	939 ± 15	19.1 ± 0.40	2.06 ± 0.03
	McLaren Vale	19th March	3.41 ± 0.00	7.6 ± 0.12	9.8 ± 4.46	1530 ± 111	941 ± 24	18.3 ± 0.85	2.26 ± 0.07
			3.38 ± 0.01	7.6 ± 0.07	9.8 ± 4.14	1256 ± 134	859 ± 7	17.2 ± 0.09	2.14 ± 0.04
			3.39 ± 0.01	7.7 ± 0.22	5.6 ± 2.99	1379 ± 69	976 ± 15	19.5 ± 0.36	2.28 ± 0.02
			3.39 ± 0.00	7.8 ± 0.06	16.2 ± 4.32	1297 ± 85	890 ± 30	17.3 ± 0.55	2.25 ± 0.13
Shiraz	Langhorne Creek		3.37 ± 0.01	8.0 ± 0.12	36.5 ± 5.47	1967 ± 30	912 ± 24	19.8 ± 0.31	2.30 ± 0.08
Cabernet Sauvignon	Padthaway		3.31 ± 0.01	7.3 ± 0.00	5.7 ± 1.52	1059 ± 65	776 ± 13	15.3 ± 0.34	1.60 ± 0.06
			3.35 ± 0.01	6.9 ± 0.06	36.2 ± 2.41	1439 ± 22	880 ± 19	18.4 ± 0.31	1.96 ± 0.01
All samples									
Mean			3.46	7.65	25.35	1220	786	16.4	2.0
Maximum			3.82	9.00	124.17	2396	1241	29.9	3.5
Minimum			3.25	5.63	0.10	439	436	7.9	0.9
Mean by variety									
Shiraz			3.54	7.62	38.01	1332	810	17.7	2.1
Cabernet Sauvignon			3.40	7.72	13.42	1108	760	15.2	2.0
ANOVA P =			<0.0001	ns	<0.05	ns	ns	ns	ns
Mean by region									
Riverland			3.53^{a}	7.35	13.16	769^{c}	576^{c}	11.17^{c}	1.59^{c}
McLaren Vale			3.45^{ab}	8.23	44.75	1796^{a}	1035^{a}	23.20^{a}	2.76^{a}
Langhorne Creek			3.39^{bc}	7.51	17.61	1456^{ab}	849^{b}	17.44^{b}	1.86^{bc}
Clare			3.30^{c}	7.71	35.67	1518^{ab}	1026^{ab}	21.46^{ab}	2.36^{ab}
Padthaway			3.33^{bc}	7.10	20.95	1249^{b}	828^{b}	16.83^{b}	1.78^{bc}
ANOVA P =			<0.01	ns	ns	<0.0001	<0.0001	<0.0001	<0.0001

[a]ANOVA, $n = 39$, different superscripted letters after the mean within a column indicate significant differences by a post-hoc Student's t-test, ns = not significant.

nonetheless evident, and it most likely reflects the interaction of climate, cultural practices, and possibly grape maturity.

Correlation of Grape and Wine Compositional Parameters. The primary aim of this study was to observe whether a relationship could be found between a grape-based measure of tannin or anthocyanin and the corresponding analysis in wine. Since most anthocyanin not only remains in the monomeric form in wine but also forms colored derivatives,[33] analyzing only wine anthocyanin concentration might not capture the range of colored products which were

dx.doi.org/10.1021/jf5002777 | J. Agric. Food Chem. 2014, 62, 4558−4570

Table 3. Relationships between Grape and Wine Compositional Parameters Determined for Shiraz and Cabernet Sauvignon Grapes and Wines by Linear Regression Analysis

		R^2 value range				
Grape or Wine Analytical Parameter	code[a]	0.79–0.7	0.84–0.8	0.89–0.85	0.94–0.9	≥0.95
Wine-like tannin (uncorrected)[b]	**A**	G, I	D	C, F	E, H	B
Wine-like tannin (corrected)[c]	**B**	G	F	C, D, E	H	A
Homogenate anthocyanin	**C**		H	A, B, E	D, F	
Wine-like anthocyanin (corrected)[c]	**D**	G	A, H	B, E	C.F	
Wine Color Density[d]	**E**	I		B, C, D, G	A, H	F
Wine anthocyanin[d]	**F**		B, G	A, H	C, D	E
Wine nonbleachable pigment[d]	**G**	A, B, D, I	F	E, H		
Wine tannin[e]	**H**	I	C, D	F, G	A, B, E	
Grape Total Soluble Solids[f]	**I**	A, E, G, H				

[a]Letter code for each grape or wine: analytical parameter where letters in columns which follow show associated linear regression coefficient R^2 values in increasing order of significance. [b]Analysis of tannin in wine-like extracts assuming a constant juice yield per unit berry fresh mass. [c]Analysis of tannin or anthocyanin in wine-like extracts corrected for differences in final extraction volume. [d]Wine color compositional measures determined as absorbance units. [e]Wine tannin concentration determined by methyl cellulose precipitation. [f]Grape must total soluble solids preferment determined as °Brix.

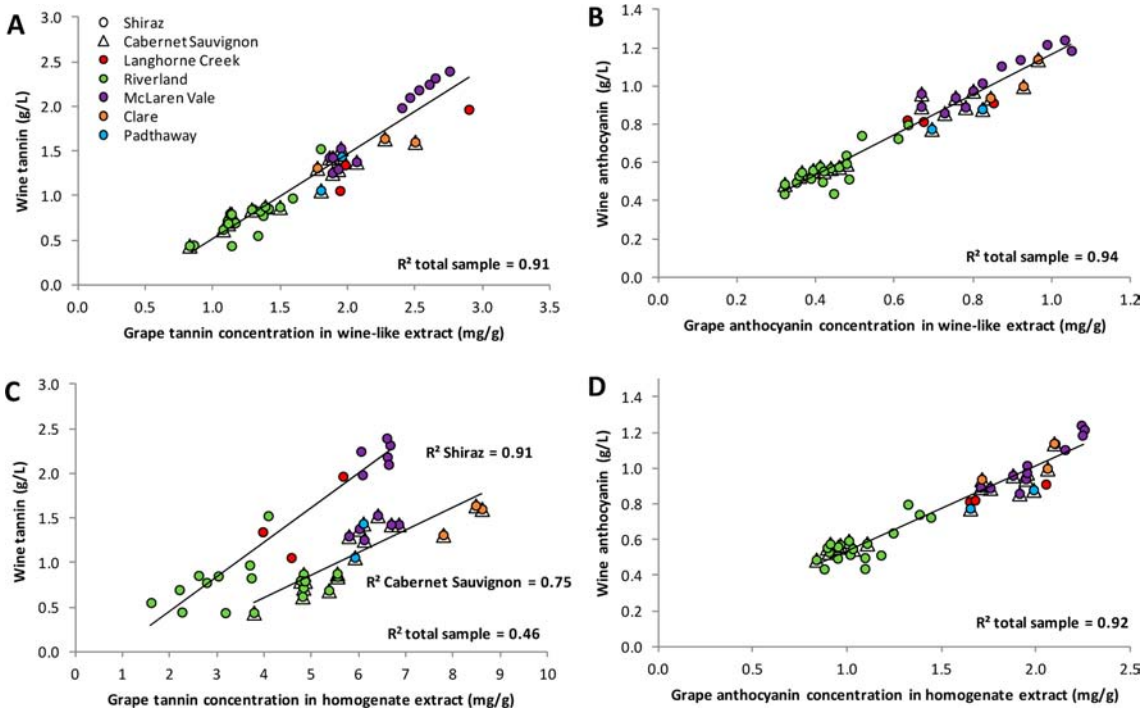

Figure 1. Linear regression analysis showing distribution of data by grape variety and region of (A) wine-like grape tannin and wine tannin; (B) wine-like grape anthocyanin and wine anthocyanin; (C) homogenate grape tannin and wine tannin; (D) homogenate grape anthocyanin and wine anthocyanin.

formed during fermentation. Therefore, the relationships of grape-based measures of tannin and anthocyanin to a range of wine parameters were investigated: tannin, monomeric anthocyanin, modified wine color density[16] and nonbleachable pigments.[16] The wine color properties of the sample series are shown in Table 2. A summary table of key significant relationships between measured grape and wine parameters obtained following linear regression analysis is presented as *R*-squared (R^2) values (Table 3), and for reference, the full correlation table is provided as S5 of the Supporting Information.

In the development of the WL extraction protocol, an important consideration was that some variability in juice yield might exist between grape samples, which could influence the dilution of tannin extracted, as well as the alcohol concentration of the extraction medium, since the addition of ethanol was kept constant. Therefore, tannin concentration (as mg/g berry fresh weight) was expressed as a volume-corrected measure, as well as an uncorrected measure which assumed a constant juice yield per gram of grapes. Strong relationships were found using linear regression analysis for corrected and uncorrected tannin concentration determined across the whole range of grape samples ($R^2 \geq 0.95$) (Table 3), and both these analytical measures were strongly related to wine tannin concentration ($R^2 > 0.9$). The calculated root-mean-square error (RMSE) of prediction of wine tannin concentration from the WL assays was 0.18 g/L for the volume-corrected corrected assay, and 0.15 g/L for the uncorrected assay. This is of relevance, since in

dx.doi.org/10.1021/jf5002777 | J. Agric. Food Chem. 2014, 62, 4558–4570

a commercial application of the WL extraction protocol, the estimate of juice volume or recovered extract volume would be tedious and time-consuming, and possibly hinder its uptake. The current results indicate that this volume correction step may not be necessary in order to compare compositional differences between grape samples. The relationship between grape tannin concentration determined using the WL tannin protocol and wine tannin concentration is shown graphically (Figure 1A), and it demonstrates the distribution of samples by grape variety, maturity and regional origin, as discussed previously.

Re-extraction of the WL extract residues with 50% v/v ethanol increased the estimate of total grape tannin concentration by 52% (±13%) but reduced the strength of the relationship with wine tannin slightly to give an R^2 value of 0.86 (Supporting Information S5). With sample homogenization and extraction in 50% v/v ethanol, the grape tannin concentration was on average 204% (±92%) higher than that determined in the WL extracts. Interestingly, a poor relationship was observed between grape tannin concentration determined from homogenate extracts and wine tannin concentration (R^2 = 0.46 for total sample) (Figure 1C, Supporting Information S5). A "tannin extractability" estimate was calculated as follows: [WL tannin ×100] ÷ [homogenate tannin]. This measure expresses the extractable grape tannin concentration as a proportion of total grape tannin, and we considered that this might correlate with wine tannin concentration. However, no relationship was found with the "tannin extractability" estimate and wine tannin concentration (data not shown, see Supporting Information S5).

From the scatter-plot shown in Figure 1C, a separation of tannin data by grape variety could be observed, which indicates that there may be different responses for grape tannin concentration determined in homogenate extracts for the Shiraz and Cabernet Sauvignon varieties. Indeed, separation of the samples by variety brought an improvement in the R^2 values for grape tannin determined in homogenate extracts and wine tannin following linear regression, and this was better modeled for Shiraz (R^2 > 0.9) than for Cabernet Sauvignon (R^2 = 0.75). It is likely that at high ethanol concentration (50% v/v) and with homogenization, a significantly increased seed tannin was extracted than can be expected with WL extraction. Since seed tannin is not readily extracted during the early stages of fermentation[2,19] (Supporting Information S6), it is unlikely that seed tannin was significantly extracted in the wines, and this will be discussed in more detail at a later stage. The WL extraction protocol is therefore more accurate in predicting the concentration of grape tannin that is extractable during primary fermentation, in this case during a set 6-day skin contact period.

Differences in the concentration and proportional distribution of tannin within the grape berry (skin versus seed) may account for somewhat higher concentrations of homogenate-extract grape tannin in the Cabernet Sauvignon samples, possibly reflecting a higher seed tannin concentration. The relatively strong relationship found for homogenate-extracted tannin concentration and wine tannin concentration for the respective grape varieties treated as distinct sample sets shows that this extraction protocol may still have relevance for the prediction of wine-extractable tannin, but only when the calibration is determined for a given variety.

For grape anthocyanin, the homogenate extraction, corrected WL (Table 3) and uncorrected WL protocols (Supporting Information S5) were strongly correlated to one another. Both grape-based measures were strongly related to wine anthocyanin concentration ($R^2 \geq 0.9$) and wine color density (R^2 > 0.85) (Table 3, Figure 1B, D). A weaker relationship was found for the grape-based measures of anthocyanin and nonbleachable wine pigments, with WL and homogenate extracts giving R^2 = 0.7 (Table 3) and 0.65, respectively.

Rather, a stronger relationship was found for wine tannin concentration and nonbleachable pigments (R^2 > 0.85). Nonbleachable pigment and wine tannin concentration also strongly contributed to wine color density, as evidenced by similarly high R^2 values. Since wine color was analyzed in young wines, a significant proportion of anthocyanin was still in the monomeric form (Table 2), and it had not yet undergone the reactions associated with aging which significantly increase nonbleachable pigments.[34] Hence, the greatest contribution of nonbleachable pigments in young wines was potentially from anthocyanin-tannin condensation products (polymeric pigments) formed during fermentation[35] as opposed to smaller, anthocyanin-derived pigments. Since both anthocyanin and tannin are required for the formation of stable wine color, their analysis in WL extracts may be a good predictor of wine color density, as well as nonbleachable pigments. Multiple linear regression analysis revealed an improvement of the R^2 of prediction for both wine color density and nonbleachable pigments to 0.87 when both WL tannin and anthocyanin concentration measures were used (data not shown).

A further important consideration was how basic grape compositional differences in terms of either ripeness or berry weight were related to measured color and tannin in grapes or wine. It was found that the degree of grape sugar ripeness (as juice °Brix) was related (R^2 > 0.7) (Table 3) to uncorrected WL tannin concentration, wine tannin concentration, wine color density and nonbleachable pigments. Interestingly, juice °Brix had a weaker relationship with concentrations of corrected WL tannin, grape anthocyanin and wine anthocyanin (Supporting Information S5). No relationship was found for juice °Brix and the recovered volume of WL extracts, so the strong relationship to uncorrected WL tannin concentration is not accounted for simply by changes in juice volume. A further important observation was that no correlation was found between berry weight and any measure of grape or wine tannin and color (data not shown). This is of particular relevance for grapes of the Shiraz variety,[36] since shrivel in the later stages of ripening may increase the relative concentration of tannin and sugar per unit fresh mass.

As discussed previously, both the corrected and uncorrected measures of grape WL tannin concentration were strongly related to wine tannin concentration, but the R^2 value was slightly higher for the uncorrected measure (0.94 compared to 0.91). Therefore, the correlation between wine tannin and °Brix may simply indicate that increases in grape ripeness may have been associated with increased extractability of tannin.

Since all ferments were pressed off skins before the completion of alcoholic fermentation, and wines made from higher °Brix grapes had high residual sugar levels, ethanol concentration was unlikely to have influenced tannin extraction. The relationship between grape ripeness (°Brix) and tannin concentration in grapes is unclear, and reports in the literature are variable, showing that tannin can increase, remain constant or decrease during ripening.[26,37−43] While our results do not demonstrate a causative effect, the current data indicate that changes in grape composition associated with ripening may

Table 4. Tannin Compositional Properties Determined by Phloroglucinol Analysis for Selected High-Tannin and Low-Tannin Shiraz and Cabernet Sauvignon Wine Samples Obtained from a Variety of Regions within South Australia[k]

Grape Variety	Region	Tannin concentration range[a]	MCP tannin[c] (g/L)	Subunit tannin[d] (g/L)	MC[e] (%)	MM[f] (g/mol)	mDP[g]	Prodelphinidin[h] (mole %)	Prodelphinidin[i] (% of EXT)	Galloylation[j] (mole %)
Shiraz	McLaren Vale	HIGH	2.18	0.88	40.48	4609	15.3	37.4	43.2	3.4
			2.25	0.79	35.28	4335	14.4	37.5	43.1	3.5
			2.40	0.88	36.91	4905	16.3	39.4	43.9	3.4
	Langhorne Creek		1.97	0.69	34.98	5004	16.6	34.1	42.5	3.7
	Riverland	LOW	0.85	0.22	25.49	3129	10.4	33.9	43.5	3.7
			0.45	0.26	58.27	2872	9.5	31.2	43.0	4.0
			0.70	0.32	45.86	3465	11.5	36.1	41.4	3.5
			0.44	0.13	29.83	1721	5.7	26.5	39.2	3.6
Cabernet Sauvignon	McLaren Vale	HIGH	1.43	0.71	49.99	5015	16.7	44.3	44.7	1.8
	Clare		1.60	0.96	59.81	4809	16.0	44.9	45.3	1.7
			1.64	0.89	54.11	4959	16.5	45.8	43.4	1.7
	Padthaway		1.44	0.83	57.85	4884	16.3	42.1	41.7	1.9
	Riverland	LOW	0.62	0.36	58.47	3123	10.4	42.1	43.5	2.3
			0.72	0.43	59.39	3763	12.5	40.1	42.3	2.3
			0.69	0.38	55.20	3454	11.5	38.9	40.4	2.4
			0.44	0.32	72.72	2857	9.5	37.5	39.1	2.2
	Mean Shiraz HIGH		2.20^{a}	0.81^{a}	36.91^{b}	4713^{a}	15.6^{a}	37.1^{b}	43.19	3.5^{a}
	Mean Shiraz LOW		0.61^{c}	0.23^{c}	39.86^{b}	2797^{b}	9.3^{b}	31.9^{c}	41.78	3.7^{a}
	Mean Cabernet Sauvignon HIGH		1.53^{b}	0.85^{a}	55.44^{a}	4917^{a}	16.4^{a}	44.3^{a}	43.79	1.8^{c}
	Mean Cabernet Sauvignon LOW		0.62^{c}	0.37^{b}	61.44^{a}	3299^{b}	11.0^{b}	39.7^{b}	41.33	2.3^{b}
	ANOVA[b]		<0.0001	<0.0001	<0.01	<0.0001	<0.0001	<0.001	ns	<0.0001

[a]Analysis of a subsample of wines designated HIGH or LOW in tannin concentration based on methyl cellulose precipitation analysis. [b]Significant differences are indicated by different superscripted letters alongside the mean and were determined by one-way ANOVA, followed by a post-hoc unpaired Student's *t*-test, ns = not significant. [c]Tannin concentration determined by methyl cellulose precipitation as epicatechin equivalents. [d]Tannin concentration as the sum of flavan-3-ol subunits by phloroglucinolysis expressed as epicatechin equivalents. [e]Mass conversion is the recovery of tannin as its component subunits by phloroglucinolysis, as a proportion of the total tannin concentration by methyl cellulose precipitation. [f]Molecular mass as determined by phloroglucinolysis. [g]Mean degree of polymerization in epicatechin units. [h]Molar proportion of extension (−)-epigallocatechin subunits. [i]Molar proportion of (−)-epigallocatechin subunits of extension (EXT) subunits only. [j]Molar proportion of terminal and extension (−)-epicatechin-3-*O*-gallate subunits. [k]ANOVA, $n = 16$, different letters after the mean within a column indicate significant differences determined by a post-hoc Student's *t*-test.

influence the extraction of grape tannin into wine during fermentation, and this warrants ongoing investigation.

Compositional Differences between High- and Low-Tannin Wines. A subset of wine samples were analyzed for subunit compositional analysis following solid-phase extraction[14] and phloroglucinolysis[24] to determine whether differences in wine tannin concentration observed using the MCP tannin assay could be (1) confirmed using an alternative method of quantification and (2) associated with changes in tannin subunit composition or molecular mass. A subset of wine samples from both grape varieties studied were selected, having high- or low-tannin concentration based on the MCP assay. The Shiraz wines had higher tannin concentration, as measured by MCP, than Cabernet Sauvignon wines (Table 4). However, when tannin concentration was determined by phloroglucinolysis for these samples, high-tannin Shiraz and Cabernet Sauvignon wines showed similar concentrations based on subunit yield. On the other hand, for the low-tannin samples, the Cabernet Sauvignon wines had a somewhat higher subunit yield by phloroglucinolysis than Shiraz wines. Nevertheless, it was evident that differences in high and low wine tannin concentrations determined using the MCP tannin assay were confirmed by the phloroglucinolysis assay.

The differences in the phloroglucinolysis yield point to varietal differences in the extent to which the tannin could be cleaved to its component subunits by acid-catalyzed depolymerization (tannin mass conversion). It is well-known that wine tannin mass conversion can vary by grape variety, ripeness[1,26,38,44−47] and decreases during winemaking,[1,45] following oxidation[48] or during wine aging.[47] This consequently affects wine tannin concentration as determined by subunit yield. It was evident that tannin mass conversion was similar by variety for both low- and high-tannin wines (Table 4), and was higher in Cabernet Sauvignon wines than in Shiraz wines. Varietal differences in tannin mass conversion may not necessarily be incurred during winemaking, and they can be found in tannin extracts from grape.[1,26,45,46] The differences in phloroglucinolysis yield between high- and low-tannin wines may therefore be a varietal effect. Varietal differences in tannin composition were also observed for the degree of tannin galloylation ((−)-epicatechin-*O*-gallate), which was significantly higher for Shiraz wines. Since seed tannins contain proportionally higher levels of epicatechin gallate than skin tannin,[40,44] this could be considered to reflect a greater extraction of seed tannin in Shiraz wines. However, this is unlikely to be the case, since our work to date with Shiraz grapes has shown minimal extraction of seed tannin during a similar skin contact period to that used in the current study (Supporting Information S6). Furthermore, the degree of galloylation in skin tannin can be up to 10% in Shiraz grapes,[1,44,47] but it is generally low in ripe Cabernet Sauvignon grapes[26,43,49] (also see Supporting Information S7).

Tannin molecular mass, which gives similar information to the mean degree of polymerization (mDP) increased as wine tannin concentration increased, and this was associated with a minor increase in the proportion of prodelphinidin ((−)-epigallocatechin) of total tannin subunits. However, when prodelphinidin was expressed as a proportion of extension

dx.doi.org/10.1021/jf5002777 | J. Agric. Food Chem. 2014, 62, 4558−4570

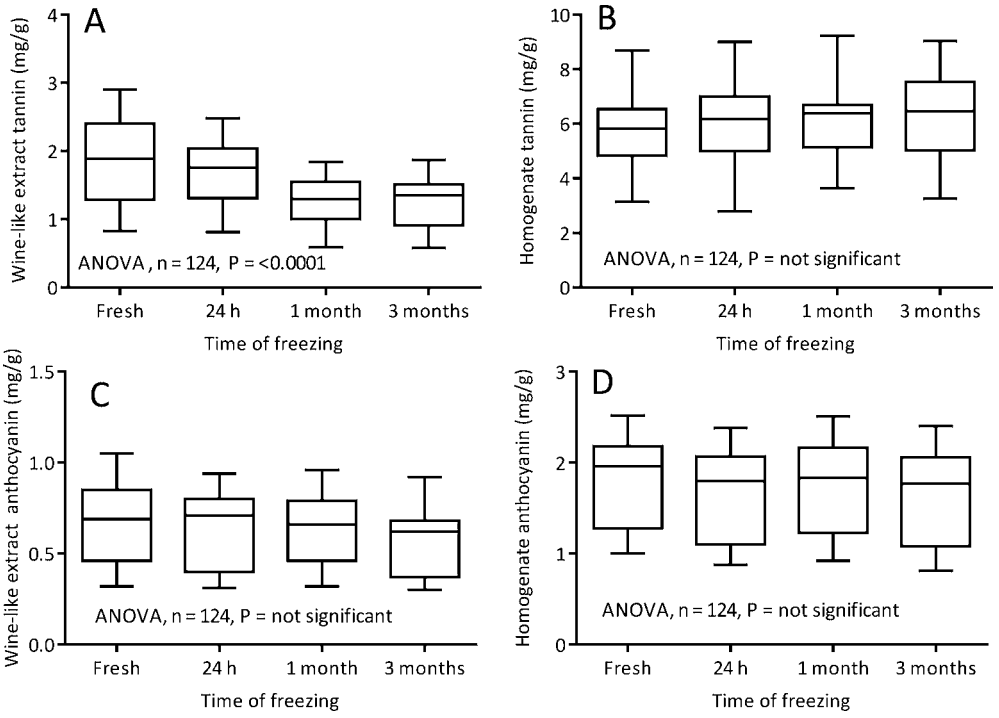

Figure 2. Effect of a 3 month freezing period at −20 °C on grape composition determined by one-way ANOVA (n = 124) showing the distribution of samples as box and whisker plots (mean, maximum, minimum): (A) tannin concentration determined following wine-like extraction; (B) tannin concentration determined following homogenate extraction; (C) anthocyanin concentration determined following wine-like extraction; (D) anthocyanin concentration determined following homogenate extraction.

units only, this was unchanged by either grape variety or tannin concentration. The proportion of prodelphinidin as a proportion of extension units can range considerably in skin tannins, and it is quite variable by season and grape variety[1,26,42−45,49] (Supporting Information S7). For the current wine sample set, therefore, the high values for prodelphinidin as a proportion of tannin extension units, together with a low percent galloylation are strong evidence that the wine tannin extracted during the 6-day skin contact period was primarily derived from the grape skins. This is expected based on published work[2] as well as our unpublished data (Supporting Information S6), which indicate that skin tannin extraction predominates within the early skin contact period.

Effect of Freezing on the Analysis of Grape Tannin and Anthocyanin. The effect of storing grape samples at low temperature is an important consideration when samples are collected at a faster rate than analytical capacity and throughput allow, such as in a commercial or research context. Previous studies have shown that grape samples can be frozen at −20 °C for up to 3 months without measuring a loss in anthocyanin, when this was determined following a homogenate extraction protocol.[50] At the outset of the current study, the effect of freezing grapes on tannin concentration was unknown.

The analysis of tannin and anthocyanin in homogenate and WL extracts was performed on a subset of grape samples that had been frozen at −20 °C for 24 h, 1 month and 3 months (Figure 2). Due to the previous observations that anthocyanin concentration declines after 3 months of freezing,[50] the storage period was not extended further. It was found that freezing grape samples for 24 h brought about a small reduction in grape tannin concentration measured using the WL extraction protocol, and this decreased further by 1 month and 3 months (Figure 2A). In observing the distribution of measured WL tannin concentration at 24 h of freezing, the most significant decreases (14% loss) in tannin concentration were found for the grape samples with the highest tannin, while samples with lower tannin were unchanged. After 1 month and 3 months of freezing, losses in measured tannin concentration measured in WL extracts were consistent for both high- and low-tannin grape samples, between 34% and 37%.

Unlike the WL extraction protocol, frozen grape samples analyzed using the homogenate extraction procedure showed no significant loss in measured grape tannin concentration (Figure 2B). This indicates that the effect on tannin concentration in WL extracts was not likely to be due to tannin degradation, but rather due to changes in tannin extractability brought about by freezing. This is also supported by the observation that tannin concentration is stable in frozen extracts (and wines) at −20 °C (Supporting Information S2). Speculatively, freezing of grapes may increase the adsorption of tannin by grape cell walls,[1] since breakdown of subcellular compartments during freezing and defrosting may occur. In contrast to the effect on WL tannin, no impact of freezing was found for WL anthocyanin extracts (Figure 2C). Similar to a previously published study,[50] freezing up to 3 months caused no reduction in measured anthocyanin concentration in homogenate extracts. This indicates that following limited time periods of frozen storage, the homogenization extraction protocol can be used for grape tannin and anthocyanin analysis, but the WL extraction protocol is acceptable only for anthocyanin analysis.

Implications of the Results for Commercial Wine-making Practice. The reported results have shown that for fresh grape samples, the application of a WL extraction provides a good indication of tannin and anthocyanin concentrations extractable during fermentation (in this study during a 6-day

dx.doi.org/10.1021/jf5002777 | J. Agric. Food Chem. 2014, 62, 4558−4570

skin contact period). It was found that there was no benefit in correcting tannin or anthocyanin concentration in WL extracts for variation in juice (extract) volume. This means that extractions and analyses could be implemented in situations which demand high sample throughput, such as commercial or research laboratories. A limitation of the WL extraction protocol for tannin analysis, however, was that grape samples could not be frozen. It is therefore recommended that where delays in sample analysis occur, whole grape bunches are sealed and stored short-term at 4 °C before being destemmed. Alternatively, if WL extractions can be immediately conducted on fresh grapes, the extract appears to be stable at −20 °C, enabling the tannin analysis to be performed later (Supporting Information S3).

The use of a homogenate extraction protocol was also found to be of value for predicting wine anthocyanin concentration, and when the calibration is adjusted for a particular cultivar, it could be used to predict wine tannin concentration. The benefit found for the use of the homogenate extraction protocol was that samples could be frozen before analysis. A further advantage of homogenate extraction is that this method has been used to develop calibrations for rapid analytical methods such as near-infrared spectroscopy[51] and UV−visible spectroscopy.[52]

The WL and homogenate extraction techniques were shown to be of value in the prediction of tannin and anthocyanin concentrations extractable during the fermentation period. However, it is important to note that in commercial winemaking practice, different winemaking approaches can increase tannin concentration[20] beyond that extracted during fermentation. Some studies have shown that skin tannin concentration tends to reach a maximum during primary ferment,[2,3] but others have shown that it can increase continuously during both fermentation[49,53] and extended maceration.[39] On the other hand, seed tannin is poorly extracted during primary fermentation, but a late, rapid increase in extraction is observed after approximately 6 days, suggested to be facilitated by hydration of the seeds rather than an increase in wine ethanol concentration.[19,54] Hence, seed tannin extraction could potentially increase until maceration is stopped, but it has been observed that a maximum in total wine tannin concentration is generally reached by 20 days of maceration.[39,55]

Given this variability in the kinetics of tannin extraction, a key question is whether the magnitude of the effect of a winemaking technique on final wine tannin concentration is in fact dependent upon grape tannin composition and extractability. In collating data from a limited number of studies which have explored the effect of extended maceration on wine tannin extraction,[20,39,49,55−57] it was found that a strong positive relationship exists between tannin extracted during fermentation and the maximum tannin extracted following extended maceration (Supporting Information S8).

Based on this, it appears viable that in a commercial context, decision-making regarding the optimal winemaking approach for particular grape batches could be enhanced by knowledge of the tannin and anthocyanin extractable during fermentation. For example, for high-tannin grapes, adequate extraction of phenolics may be obtained during a short skin contact period, whereas for low-tannin grapes extending maceration time or applying thermovinification[20] may be required. The benchmarking of grape samples for their predicted wine tannin, anthocyanin, and color could facilitate comparisons by season, region, vineyard, grape variety or management practices, and it would be of great advantage in commercial winemaking.

■ ASSOCIATED CONTENT

Supporting Information

S1: Climatic data for the regions studied in the 2012−2013 growing season. S2: Extraction of anthocyanin and tannin from a crushed, whole-berry grape sample under wine-like conditions over 64 h. S3: Tannin concentration determined in fresh and frozen samples of small-scale wines and 15% ethanol extracts. S4: Evolution of wine tannin during small scale fermentation. S5: Correlation table showing linear regression coefficients for grape and wine analytical parameters. S6: Extraction of skin tannin during the fermentation of two red grape varieties. S7: Distribution of galloylation and prodelphinidin in purified skin tannin isolates. S8: Review of wine tannin concentration data taken at the end of primary ferment and the maximum tannin concentration reached following extended maceration (>20 days). This material is available free of charge via the Internet at http://pubs.acs.org.

■ AUTHOR INFORMATION

Corresponding Author

*Tel: +61-8-83136190; Fax: +61-8-83136601; E-mail: keren.bindon@awri.com.au.

Funding

The Australian Wine Research Institute, a member of the Wine Innovation Cluster in Adelaide, is supported by Australian grape-growers and winemakers through their investment body, the Grape and Wine Research and Development Corporation, with matching funds from the Australian Government.

Notes

The authors declare no competing financial interest.

■ ACKNOWLEDGMENTS

The authors would like to thank Accolade Wines, Reynella, South Australia for the donation of grape samples. Chris Bevin, formerly of Accolade Wines, coordinated the logistics of vineyard selection, harvesting and transport of grape samples. Bob Dambergs is recognized for conceptualizing and developing the small-scale “French Press” winemaking method. Michael Coode is acknowledged for small-scale winemaking, and Ruchita Shah, for technical support in both the laboratory and winery. Ross Kolouch, Michael McBryde and Jennifer Baldock assisted in the preparation and handling of grape and wine samples. Eric Wilkes and Peter Godden of the AWRI are thanked for proof-reading the manuscript.

■ REFERENCES

(1) Bindon, K. A.; Smith, P. A.; Holt, H.; Kennedy, J. A. Interaction between Grape-Derived Proanthocyanidins and Cell Wall Material. 2. Implications for Vinification. *J. Agric. Food Chem.* **2010**, *58*, 10736−10746.

(2) Cerpa-Calderon, F. K.; Kennedy, J. A. Berry Integrity and Extraction of Skin and Seed Proanthocyanidins during Red Wine Fermentation. *J. Agric. Food Chem.* **2008**, *56*, 9006−9014.

(3) Peyrot des Gachons, C.; Kennedy, J. A. Direct Method for Determining Seed and Skin Proanthocyanidin Extraction into Red Wine. *J. Agric. Food Chem.* **2003**, *51*, 5877−5881.

(4) Guerrero, R.; Smith, P.; Bindon, K. Application of insoluble fibers in the fining of wine phenolics. *J. Agric. Food Chem.* **2013**, *61*, 4424−4432.

(5) Holt, H.; Cozzolino, D.; McCarthy, J.; Abrahamse, C.; Holt, S.; Solomon, M.; Smith, P.; Chambers, P. J.; Curtin, C. Influence of yeast strain on Shiraz wine quality indicators. *Int. J. Food Microbiol.* **2013**, *165*, 302−311.
(6) Fragoso, S.; Guasch, J.; Acena, L.; Mestres, M.; Busto, O. Prediction of red wine colour and phenolic parameters from the analysis of its grape extract. *Int. J. Food Sci. Technol.* **2011**, *46*, 2569−2575.
(7) du Toit, W. J.; Visagie, M. Correlations between South African Red Grape and Wine Colour and Phenolic Composition: Comparing the Glories, Iland and Bovine Serum Albumin Tannin Precipitation Methods. *S. Afr. J. Enol. Vitic.* **2012**, *33*, 33−41.
(8) Ristic, R.; Downey, M.; Iland, P. G.; Bindon, K.; Francis, I. L.; Herderich, M.; Robinson, S. P. Exclusion of sunlight from Shiraz grapes alters wine colour, tannin and sensory properties. *Austr. J. Grape Wine Res.* **2007**, *13*, 53−65.
(9) Cortell, J. M.; Sivertsen, H. K.; Kennedy, J. A.; Heymann, H. Influence of Vine Vigor on Pinot noir Fruit Composition, Wine Chemical Analysis, and Wine Sensory Attributes. *Am. J. Enol. Vitic.* **2008**, *59*, 1−10.
(10) Ristic, R.; Bindon, K.; Francis, L. I.; Herderich, M. J.; Iland, P. G. Flavonoids and C-13-norisoprenoids in Vitis vinifera L. cv. Shiraz: relationships between grape and wine composition, wine colour and wine sensory properties. *Austr. J. Grape Wine Res.* **2010**, *16*, 369−388.
(11) Cortell, J. M.; Halbleib, M.; Gallagher, A. V.; Righetti, T. L.; Kennedy, J. A. Influence of vine vigor on grape (Vitis vinifera L. cv. Pinot noir) and wine proanthocyanidins. *J. Agric. Food Chem.* **2005**, *53*, 5798−5808.
(12) Cortell, J. M.; Halbleib, M.; Gallagher, A. V.; Righetti, T. L.; Kennedy, J. A. Influence of Vine Vigor on Grape (*Vitis vinifera* L. Cv. Pinot Noir) Anthocyanins. 2. Anthocyanins and Pigmented Polymers in Wine. *J. Agric. Food Chem.* **2007**, *55*, 6585−6595.
(13) Mercurio, M. D.; Dambergs, R. G.; Cozzolino, D.; Herderich, M. J.; Smith, P. A. Relationship between Red Wine Grades and Phenolics. 1. Tannin and Total Phenolics Concentrations. *J. Agric. Food Chem.* **2010**, *58*, 12313−12319.
(14) Kassara, S.; Kennedy, J. A. Relationship between Red Wine Grade and Phenolics. 2. Tannin Composition and Size. *J. Agric. Food Chem.* **2011**, *59*, 8409−8412.
(15) Sarneckis, C.; Dambergs, R. G.; Jones, P.; Mercurio, M.; Herderich, M. J.; Smith, P. Quantification of condensed tannins by precipitation with methyl cellulose: development and validation of an optimized tool for grape and wine analysis. *Austr. J. Grape Wine Res.* **2006**, *12*, 39−49.
(16) Mercurio, M. D.; Dambergs, R. G.; Herderich, M. J.; Smith, P. A. High Throughput Analysis of Red Wine and Grape Phenolics-Adaptation and Validation of Methyl Cellulose Precipitable Tannin Assay and Modified Somers Color Assay to a Rapid 96 Well Plate Format. *J. Agric. Food Chem.* **2007**, *55*, 4651−4657.
(17) Heredia, T. M.; Adams, D. O.; Fields, K. C.; Held, P. G.; Harbertson, J. F. Evaluation of a comprehensive red wine phenolics assay using a microplate reader. *Am. J. Enol. Vitic.* **2006**, *57*, 497−502.
(18) Cozzolino, D.; Cynkar, W. U.; Dambergs, R. G.; Mercurio, M. D.; Smith, P. A. Measurement of Condensed Tannins and Dry Matter in Red Grape Homogenates Using Near Infrared Spectroscopy and Partial Least Squares. *J. Agric. Food Chem.* **2008**, *56*, 7631−7636.
(19) Hernandez-Jimenez, A.; Kennedy, J. A.; Bautista-Ortin, A. B.; Gomez-Plaza, E. Effect of Ethanol on Grape Seed Proanthocyanidin Extraction. *Am. J. Enol. Vitic.* **2012**, *63*, 57−61.
(20) Sacchi, K. L.; Bisson, L. F.; Adams, D. O. A review of the effect of winemaking techniques on phenolic extraction in red wines. *Am. J. Enol. Vitic.* **2005**, *56*, 197−206.
(21) Bautista-Ortin, A. B.; Busse-Valverde, N.; Rodriguez-Rodriguez, P.; Jimenez-Pascual, E.; Gil-Munoz, R.; Gomez-Plaza, E. Qualitative composition and extractability of grape skin tannins during the ripening period. Role of the extraction solvent. *J. Int. Sci. Vigne Vin.* **2013**, *47*, 137−143.
(22) Ortega-Regules, A.; Romero-Cascales, I.; Ros-Garcia, J. M.; Lopez-Roca, J. M.; Gomez-Plaza, E. A first approach towards the relationship between grape skin cell-wall composition and anthocyanin extractability. *Anal. Chim. Acta* **2006**, *563*, 26−32.
(23) Joutei, K. A.; Glories, Y. Étude en conditions modèles de l'extractibilité des composés phénoliques des pellicules et des pépins de raisins rouges. *J. Int. Sci. Vigne Vin.* **1994**, *28*, 303−317.
(24) Kennedy, J. A.; Jones, G. P. Analysis of Proanthocyanidin Cleavage Products Following Acid-Catalysis in the Presence of Excess Phloroglucinol. *J. Agric. Food Chem.* **2001**, *49*, 1740−1746.
(25) Bindon, K. A.; Smith, P. A.; Kennedy, J. A. Interaction between Grape-Derived Proanthocyanidins and Cell Wall Material. 1. Effect on Proanthocyanidin Composition and Molecular Mass. *J. Agric. Food Chem.* **2010**, *58*, 2520−2528.
(26) Bindon, K. A.; Kennedy, J. A. Ripening-Induced Changes in Grape Skin Proanthocyanidins Modify Their Interaction with Cell Walls. *J. Agric. Food Chem.* **2011**, *59*, 2696−2707.
(27) Roby, G.; Harbertson, J. F.; Adams, D. A.; Matthews, M. A. Berry size and vine water deficits as factors in winegrape composition: Anthocyanins and tannins. *Austr. J. Grape Wine Res.* **2004**, *10*, 100−107.
(28) Ojeda, H.; Andary, C.; Kraeva, E.; Carbonneau, A.; Deloire, A. Influence of pre- and postveraison water deficit on synthesis and concentration of skin phenolic compounds during berry growth of Vitis vinifera cv. Shiraz. *Am. J. Enol. Vitic.* **2002**, *53*, 261−267.
(29) Ojeda, H.; Deloire, A.; Carbonneau, A. Influence of water deficits on grape berry growth. *Vitis* **2001**, *40*, 141−146.
(30) Roby, G.; Matthews, M. A. Relative porportions of seed, skin and flesh, in ripe berries from Cabernet Sauvignon grapevines grown in a vineyard either well irrigated or under water deficit. *Austr. J. Grape Wine Res.* **2004**, *10*, 74−82.
(31) Mori, K.; Goto-Yamamoto, N.; Kitayama, M.; Hashizume, K. Loss of anthocyanins in red-wine grape under high temperature. *J. Exp. Bot.* **2007**, *58*, 1935−1945.
(32) Cohen, S. D.; Tarara, J. M.; Kennedy, J. A. Assessing the impact of temperature on grape phenolic metabolism. *Anal. Chim. Acta* **2008**, *621*, 57−67.
(33) Cheynier, V.; Duenas-Paton, M.; Salas, E.; Maury, C.; Souquet, J. M.; Sarni-Manchado, P.; Fulcrand, H. Structure and properties of wine pigments and tannins. *Am. J. Enol. Vitic.* **2006**, *57*, 298−305.
(34) Hayasaka, Y.; Birse, M.; Eglinton, J.; Herderich, M. The effect of Saccharomyces cerevisiae and Saccharomyces bayanus yeast on colour properties and pigment profiles of a Cabernet Sauvignon red wine. *Austr. J. Grape Wine Res.* **2007**, *13*, 176−185.
(35) Eglinton, J.; Griesser, M.; Henschke, P.; Kwiatkowski, M.; Parker, M.; Herderich, M. Yeast-mediated formation of pigmented polymers in red wine. In *Red Wine Color: Revealing the Mysteries*; Waterhouse, A. L., Kennedy, J. A., Eds.; ACS Symposium Series 886; American Chemical Society: Washington, DC, 2004; pp 7−21.
(36) Sadras, V. O.; McCarthy, M. G. Quantifying the dynamics of sugar concentration in berries of Vitis vinifera cv. Shiraz: a novel approach based on allometric analysis. *Austr. J. Grape Wine Res.* **2007**, *13*, 66−71.
(37) Downey, M. O.; Harvey, J. S.; Robinson, S. P. Analysis of tannins in seeds and skins of Shiraz grapes throughout berry development. *Austr. J. Grape Wine Res.* **2003**, *9*, 15−27.
(38) Bindon, K.; Varela, C.; Kennedy, J.; Holt, H.; Herderich, M. Relationships between harvest time and wine composition in *Vitis vinifera* L. cv. Cabernet Sauvignon 1. Grape and wine chemistry. *Food Chem.* **2013**, *138*, 1696−1705.
(39) Gil, M.; Kontoudakis, N.; Gonzalez, E.; Esteruelas, M.; Fort, F.; Miguel Canals, J.; Zamora, F. Influence of Grape Maturity and Maceration Length on Color, Polyphenolic Composition, and Polysaccharide Content of Cabernet Sauvignon and Tempranillo Wines. *J. Agric. Food Chem.* **2012**, *60*, 7988−8001.
(40) Kennedy, J. A.; Matthews, M. A.; Waterhouse, A. L. Changes in grape seed polyphenols during fruit ripening. *Phytochemistry* **2000**, *55*, 77−85.
(41) Kennedy, J. A.; Matthews, M. A.; Waterhouse, A. L. Effect of Maturity and Vine Water Status on Grape Skin and Wine Flavonoids. *Am. J. Enol. Vitic.* **2002**, *53*, 268−274.

(42) Hanlin, R.; Downey, M. Condensed Tannin Accumulation and Composition in Skin of Shiraz and Cabernet Sauvignon Grapes during Berry Development. *Am. J. Enol. Vitic.* **2009**, *60*, 11.
(43) Bordiga, M.; Travaglia, F.; Locatelli, M.; Coisson, J. D.; Arlorio, M. Characterisation of polymeric skin and seed proanthocyanidins during ripening in six Vitis vinifera L. cv. *Food Chem.* **2011**, *127*, 180−187.
(44) Kennedy, J. A.; Hayasaka, Y.; Vidal, S.; Waters, E. J.; Jones, G. P. Composition of Grape Skin Proanthocyanidins at Different Stages of Berry Development. *J. Agric. Food Chem.* **2001**, *49*, 5348−5355.
(45) Hanlin, R. L.; Kelm, M. A.; Wilkinson, K. L.; Downey, M. O. Detailed Characterization of Proanthocyanidins in Skin, Seeds, and Wine of Shiraz and Cabernet Sauvignon Wine Grapes (Vitis vinifera). *J. Agric. Food Chem.* **2011**, *59*, 13265−13276.
(46) Bindon, K. A.; Smith, P. A. Comparison of the affinity and selectivity of insoluble fibres and commercial proteins for wine proanthocyanidins. *Food Chem.* **2013**, *136*, 917−28.
(47) McRae, J. M.; Falconer, R. J.; Kennedy, J. A. Thermodynamics of Grape and Wine Tannin Interaction with Polyproline: Implications for Red Wine Astringency. *J. Agric. Food Chem.* **2010**, *58*, 12510−12518.
(48) Poncet-Legrand, C.; Cabane, B.; Bautista-Ortin, A. B.; Carrillo, S.; Fulcrand, H.; Perez, J.; Vernhet, A. Tannin Oxidation: Infra- versus Intermolecular Reactions. *Biomacromolecules* **2010**, *11*, 2376−2386.
(49) Busse-Valverde, N.; Bautista-Ortin, A. B.; Gomez-Plaza, E.; Fernandez-Fernandez, J. I.; Gil-Munoz, R. Influence of skin maceration time on the proanthocyanidin content of red wines. *Eur. Food Res. Technol.* **2012**, *235*, 1117−1123.
(50) Cynkar, W.; Cozzolino, D.; Dambergs, R.; Janik, L.; Gishen, M. The Effects of Homogenisation Method and Freezing on the Determination of Quality Paramenters in Red Grape Berries of *Vitis Vinifera*. *Austr. J. Grape Wine Res.* **2004**, *10*, 236−242.
(51) Cozzolino, D.; Cynkar, W. U.; Dambergs, R. G.; Mercurio, M. D.; Smith, P. A. Measurement of condensed tannins and dry matter in red grape homogenates using near infrared spectroscopy and partial least squares. *J. Agric. Food Chem.* **2008**, *56*, 7631−7636.
(52) Dambergs, R. G.; Mercurio, M. D.; Kassara, S.; Cozzolino, D.; Smith, P. A. Rapid Measurement of Methyl Cellulose Precipitable Tannins Using Ultraviolet Spectroscopy with Chemometrics: Application to Red Wine and Inter-Laboratory Calibration Transfer. *Appl. Spectrosc.* **2012**, *66*, 656−664.
(53) Aron, P. M.; Kennedy, J. A. Compositional Investigation of Phenolic Polymers Isolated from Vitis vinifera L. Cv. Pinot Noir during Fermentation. *J. Agric. Food Chem.* **2007**, *55*, 5670−5680.
(54) Busse-Valverde, N.; Gomez-Plaza, E.; Lopez-Roca, J. M.; Gil-Munoz, R.; Fernandez-Fernandez, J. I.; Bautista-Ortin, A. B. Effect of Different Enological Practices on Skin and Seed Proanthocyanidins in Three Varietal Wines. *J. Agric. Food Chem.* **2010**, *58*, 11333−11339.
(55) Casassa, L. F.; Larsen, R. C.; Beaver, C. W.; Mireles, M. S.; Keller, M.; Riley, W. R.; Smithyman, R.; Harbertson, J. F. Impact of Extended Maceration and Regulated Deficit Irrigation (RDI) in Cabernet Sauvignon Wines: Characterization of Proanthocyanidin Distribution, Anthocyanin Extraction, and Chromatic Properties. *J. Agric. Food Chem.* **2013**, *61*, 6446−6457.
(56) Joscelyne, V. L. Consequences of extended maceration for red wine colour and phenolics. Ph.D. Thesis, School of Agriculture, Food and Wine, The University of Adelaide, 2009.
(57) Dambergs, R.; Sparrow, A.; Carew, A.; Scrimgeour, N.; Wilkes, E.; Godden, P.; Herderich, M.; Johnson, D. Quality in a cool climate—maceration techniques in Pinot Noir production. *Wine Vitic. J.* **2012**, *27*, 18−26.

JOURNAL OF AGRICULTURAL AND FOOD CHEMISTRY

Article

pubs.acs.org/JAFC

Assessment of the Degree of Interference of Polyphenolic Compounds on Glucose Oxidation/Peroxidase Assay

Adeline Ik Chian Wong[†] and Dejian Huang*[,†,‡]

[†]Food Science and Technology Program, Department of Chemistry, National University of Singapore, 3 Science Drive 3, Singapore 117543, Singapore

[‡]National University of Singapore (Suzhou) Research Institute, 377 Lin Quan Street, Suzhou Industrial Park, Jiangsu 215123, China

ABSTRACT: The glucose oxidase/peroxidase assay (GOP) is a coupled enzymatic assay commonly used in measuring glucose concentrations in biological sciences and food chemistry, particularly for quantification of α-glucosidase activity. However, we found that the GOP assay is prone to interference, especially from reducing substances such as polyphenolic compounds, which are commonly found in botanical materials. To establish the scope and limitation of the assay in measuring α-glucosidase inhibition activity, we systematically investigated the structural features of the polyphenolic compounds that can lead to false positives. Utilizing sodium dodecyl sulfate (SDS) as surrogate for the meriquinone intermediate formed during the reaction, we measured the reactivity of this redox active intermediate toward common flavonoids. Our results show that flavonoids with *o*-dihydroxy groups in the B-ring cause strong interference and that compounds with little DPPH scavenging activity do not have interference. Our results highlight the need for checking the suitability of the GOP assay first before it is applied in measuring α-glucosidase inhibition activity. In addition, when the literature data on α-glucosidase inhibition activity of botanical extracts or polyphenolic compounds using GOP assay are interpreted, potential false positives due to interference on the assay will need to be taken into consideration.

KEYWORDS: *α-glucosidase, glucose oxidase/peroxidase assay, o-dianisidine, flavonoids*

INTRODUCTION

Due to the increasing global population of type II diabetes patients, research on finding ways to mitigate this dreadful disease have intensified in recent years.[1] One way to control hyperglycemia is through starch hydrolase inhibitors from edible plants, which contain structurally diverse α-glucosidase inhibitors including sugar mimics[2] and polyphenolic compounds.[3,4] To uncover novel α-glucosidase inhibitors from plants, particularly edible plants, the *p*-nitrophenyl glucopyranose (*p*NPG) assay and coupled glucose oxidase/peroxidase (GOP) bienzyme assay are widely applied as convenient guides to fractionation and purification of inhibitors. Whereas the *p*NPG assay uses a synthetic probe that may not be truly reflective of natural substrates of the enzymes, the GOP assay was developed initially to quantitate the amount of D-glucose in human fluids.[5] Principally, this assay uses glucose oxidase to oxidize β-D-glucose by molecular oxygen to D-glucono-δ-lactone and hydrogen peroxide. In the presence of peroxidase (e.g., horseradish peroxidase), hydrogen peroxide reacts with colorless chromogenic molecules to form colorful dyes that can be quantified conveniently by colorimeters. Many chromogenic compounds have been used as substrates for horseradish peroxidase.[6] Among them, *o*-dianisidine has been more widely applied than others. In acidic conditions, the oxidized *o*-dianisidine becomes rose-pink with absorbance maximum at 540 nm (Figure 1).[7] Due to its convenience, the GOP assay has been applied in many other systems including measurement of α-glucosidase activity and screening for its inhibitors.

Although the GOP assay is highly substrate specific and relatively convenient to use, it is highly susceptible to various interferences.[8,9] The GOP assay utilizes two oxidases and involves complicated redox reaction mechanisms; as such, any compounds that can inhibit the two enzymes or react with the reactive intermediates of reaction will cause interferences.[10] Indeed, there are scattered reports on the interference issue of the GOP assay. Using 4-aminoantipyrine and 3-hydroxybenzoic acid as chromogenic substrates in the GOP assay, Shaukat and co-workers recently found that green tea polyphenolic compounds cause interferences and lead to false-negative results in blood serum glucose concentrations, and the interference was suggested to be due to the radical scavenging activity of the polyphenolic compounds.[11] In another study, polyphenols were also found to interfere because of their reducing activity.[12] Despite the number of studies addressing the issue of interferences, the GOP assay continues to be applied in the quantification of α-glucosidase inhibitory activity of natural products due to its convenience and selectivity of glucose.[13] Because natural products often contain polyphenolic compounds, it is important to systematically address the scope and limitations of the GOP assay in quantifying botanical samples on α-glucosidase inhibitory activity. Therefore, we investigated the interference of common polyphenolic compounds found in the plant kingdom on the degree of interference on GOP assays by adding sodium dodecyl sulfate (SDS) to stabilize meriquinone intermediates formed during the oxidation of *o*-dianisidine by peroxidase. Our results reported herein will help researchers in using the GOP assay in plant extracts to assess the suitability of

Received: January 28, 2014
Revised: March 29, 2014
Accepted: April 27, 2014
Published: April 28, 2014

ACS Publications © 2014 American Chemical Society

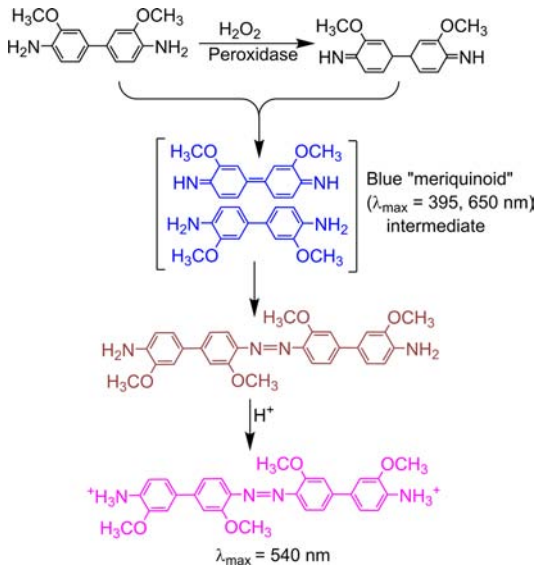

Figure 1. Reaction scheme of *o*-dianisidine oxidation. Hydrogen peroxide reacts with colorless reduced *o*-dianisidine in the presence of peroxidase to form the dianisidine quinonediimine intermediate. Application of SDS suspends the meriquinoid complex intermediate (λ_{max}= 395; 650 nm). Irreversible coupling reaction with two quinonediimines forms the brown bisazobiphenyl product. Bisazobiphenyl product reacts with H_2SO_4 to form a more stable pink product (λ_{max}= 540 nm).

the assays and provide a guide for avoiding unnecessary false results.

MATERIALS AND METHODS

Reagents and Instruments. Chemical reagents were obtained from commercial sources. These compounds include caffeic acid, ferulic acid, rutin, apigenin, chrysin, coumaric acid, gallic acid, hesperedin, hesperetin, kaempferol, luteolin, morin, naringin, quercetin, hydrogen peroxide solution, *o*-dianisidine dihydrochloride, glucose oxidase, and peroxidase from horseradish, sodium dodecyl sulfate, (-)-Epigallocatechin gallate, (-)-Epigallocatechin, (-)-Epicatechin, Quinic acid (Sigma-Aldrich, Singapore); 3,5-dihydroxyflavone, 3,7-dihydroxyflavone, 3′,3,4-trihydroxyflavone, 5,3′,4′-trihydroxyflavone, 5,7,3′,4′,5′-pentahydroxyflavone, 7,3′,4′-trihydroxyflavone, 7,8-dihydroxyflavone, fisetin, galangin, gossypetin, and myricetin (Indofine Chem. Co., Hillsborough, NJ, USA); tannic acid (Merck, Germany); and ascorbic acid, chlorogenic acid (Spectrum Chemical Co., Singapore). A microplate reader (Bio-Tek Instruments Inc., Winooski, VT, USA) was used to measure the spectrophotometric readings.

Generation of the Meriquinone Intermediate and Its Reactivity with Polyphenolic Compounds. *o*-Dianisidine (0.1 mM), SDS (1.0 mM), H_2O_2 (0.1 mM), and peroxidase (0.25 units) in citrate buffer (pH 4) were reacted for 1 min to generate the meriquinone intermediate, which was quantified by UV absorbance at 395 nm. Polyphenolic compounds with various concentrations were reacted with meriquinone. The decrease of the UV absorbance over time was monitored for selected compounds including vitamin C, coumaric acid, caffeic acid, gallic acid, and EGCG. For the rest of the samples, end point readings were carried out at 650 nm. The final concentrations of the polyphenolic compounds were kept at 100 μM. The absorbance readings were taken after 5 min of reaction. The degree of interference was quantified through the equation

$$\%\ \text{interference} = 100(A_{blk} - A_s)/A_{blk}$$

where A_s is the absorbance of the reaction mixture of the sample with meriquinone at 650 nm and A_{blk} is the absorbance of blank (water). All measurements were performed in triplicates, and the results were expressed as mean ± standard deviation.

RESULTS AND DISCUSSION

During the quantification of α-glucosidase activity and measurment of the activity of inhibitors, maltose or sucrose was hydrolyzed into glucose (and fructose in the case of sucrose). The α-glucosidase activity was measured by the generated glucose by the GOP assay. The commonly used chromophore in GOP assay is *o*-dianisidine, which is oxidized by peroxidase to give brown azo dye via a blue charge transfer complex, meriquinone (Figure 1). The polyphenolic compounds may interfere with the assay by reacting with meriquinone, which will lead to false negatives of the glucose or false positives in α-glucosidase inhibitory activity. To assess the severity of interference by different polyphenolic compounds by reducing meriquinone intermediate, we applied SDS at pH 4 according to literature studies to stabilize the positively charged meriquinone intermediates through electrostatic interaction with the negatively charged surfactant.[14,15]

Ascorbic Acid. When ascorbic acid was added to the meriquinone solution at concentrations of 25 and 50 μM (1:4 and 1:2 ratios with reference to H_2O_2), there was an initial marked decrease in absorbance but also a regain of the blue color from 10 to 250 s (Figure 2A). Apparently, the ascorbic acid is consumed

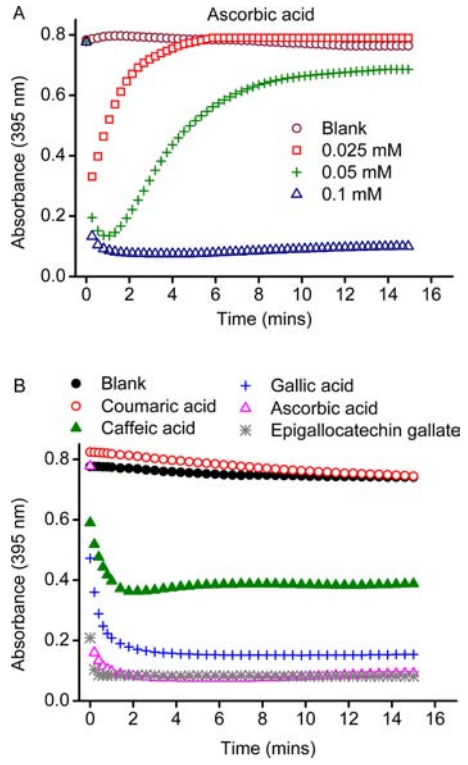

Figure 2. (A) Reduction kinetics of the meriquinone structure monitored at 395 nm for 15 min at various stoichiometries of H_2O_2 concentration to ascorbic acid (ratios of 4:1, 2:1, and 1:1). (B) Reduction kinetics (monitored at 395 nm for 15 min) of the meriquinone structure of coumaric acid, caffeic acid, gallic acid, ascorbic acid, and EGCG at a stoichiometric ratio of 1:1 H_2O_2/sample concentration.

quickly by oxidation with meriquinone, leading to the fading of blue color. The increase in absorbance is due to the regeneration of meriquinone intermediates formed by enzymatically catalyzed oxidation of *o*-dianisidine as there was a surplus of H_2O_2. When ascorbic acid was added at a ratio of 1:1 with H_2O_2 (100 μM), there was a dramatic reduction in the meriquinone solution to a colorless solution without any regain of color. This finding

dx.doi.org/10.1021/jf500431z | J. Agric. Food Chem. 2014, 62, 4571−4576

suggests that vitamin C reacts only with meriquinone but does not inhibit peroxidase.

We further monitored the reduction kinetics of the meriquinone intermediate reaction with coumaric acid, caffeic acid, gallic acid, and epigallocatechin gallate with concentration equal to that of H_2O_2 (Figure 2B). Coumaric acid with only one hydroxy group (OH) did not show much reactivity, whereas caffeic acid can lead to 50% interference at steady state throughout the remaining time. A further addition of an OH group in gallic acid was shown to reduce 75% of the absorbance values, from 0.8 to 0.2. The dependence on the number of OH groups in the phenolic acid is consistent with the increasing reducing activity from mono- to tri-OH moieties. These preliminary results prompted us to systematically evaluate the interference of common polyphenolic compounds.

Reduction of Meriquinone Intermediate by Polyphenolic Compounds. To delineate the structure−activity relationship, we measured 31 commonly found polyphenolic compounds, and the results are shown in Figures 3 and 4 arranged by their structural groups. We will discuss each class of compounds, respectively.

Flavones. As shown in Figure 3A, chrysin and apigenin have no interference ($p < 0.05$) indicating that the A ring OH groups at the 5- and 7-positions do not enable reduction of meriquinone. In contrast, apigenin isomer, 7(or 5),3′,4′-trihydroxyflavone, exhibits significant activity. This plus the fact that luteolin has a similar activity suggests that the catecholic unit is sufficient for the reduction of meriquinone. In agreement with this, 7,8-dihydroxyflavone also has a comparable activity, although it has only two OH groups. In this series, pentahydroxyflavone possesses the strongest activity because it has three *o*-OH groups at the B ring.

Flavanones. The common flavanones naringin, hesperetin, and its glycoside counterpart hesperedin all showed intermediate interference activity as shown in Figure 3B. The reason was that the B rings of the tested flavones do not contain catecholic units. Apparently, methoxylation of the catechol unit will lead to a reduced activity. In addition, there was no difference between hesperidin and hesperetin, suggesting that the OH group in the C-7 position of the A ring does not contribute to the activity of reducing meriquinones. These flavanones do possess some antioxidant activity, although the activity is much weaker compared with those of many other flavonoids.[16,17] Similar to the case of rutin, the glycosylation of hesperedin did not influence the interference percentage ($p > 0.05$).

Phenolic Acids. Coumaric acid shows a partial interference even though it has only one OH group; this is very different from that of isoflavones, which have multiple OH groups but have only very weak interferences (Figure 3C). In addition, ferulic acid and caffeic acid show stronger interferences that are comparable to that of chlorogenic acid. Gallic acid also exhibits strong interference. Therefore, it is reasonable to conclude that hydrolyzable tannins, which are the major group of polyphenolic compounds in the plant kingdom, will also have strong interference because gallates are the main moiety in hydrolyzable tannins. Indeed, tannic acid shows a strong interference. Similarly, caffeic acid has two OH groups arranged in the ortho position and was shown to have a percent interference of 88.91 ± 2.35, which was comparatively high. The percent interference of caffeic acid was not significantly different ($p > 0.05$) from those of gallic acid (due to the additional OH group) and ferulic acid (due to the CH_3O group). In the case of ferulic acid, one methoxy substitution at the ortho position relative to the hydroxyl group slightly decreased the interference (84.89 ± 2.8), but the decrease was not significant ($p > 0.05$). Ortho substitution with an electron donor of a methoxy group stabilizes the aryloxyl radical and thus its antioxidative action. However, the impact of a methoxy group is far from being equivalent to the addition of a hydroxy group. The removal of either the methoxy or hydroxy group from the phenolic ring resulted in a sharp decrease in the percent interference as seen by the coumaric acid structure. Monophenols are known to be less efficient in antioxidant activity.[19]

Flavan-3-ols. Similar to previous results, we found that all flavan-3-ols (catechins) exhibit strong interferences (Figure 3D). At the tested concentration, there was no difference among the catechins. The catecholic units in the B ring and/or the *o*-trihydroxy groups in the B ring and galloyl units are certainly potent in reducing meriquinones.[20]

Flavonols. With 11 compounds, this group is the largest category, and all of them exhibit a certain degree of interference (Figure 3E). The degree of interference is roughly correlated to the number of OH groups except rutin, which has four OH groups, but the interference activity is much weaker than that of its aglycone quercetin. Therefore, the 3-OH group contributes significantly to the activity. In this series, the *o*-OH group at the B ring increases the activity as is apparent by comparing the values of kaempferol and quercetin. 3,5-Dihydroxyflavone, 3,7-dihydroxyflavone, and galangin showed intermediate interference. These three compounds have a similar feature in that they lack any hydroxy group in the B ring of its structure but differ in the OH group present in the A and C rings. The hydroxy position of 3,7-dihydroxyflavone showed a significantly stronger interference compared to 3,5-dihydroxyflavone. Galangin, which has OH groups on the 3-, 5-, and 7-positions, did not significantly increase interference compared to 3,7-dihydroxyflavone. The addition of a hydroxyl group (monohydroxyl substitution) in the B ring as seen in kaempferol increased the percent interference significantly ($p < 0.05$). It has been proposed that the single 4′-hydroxy group in the B ring has the potential to conjugate with the 3-hydroxy group through conjugation of the C ring. The phenoxyl radical formed could abstract an electron from the radical cation to generate a dication and the phenolate.[18] The addition of another hydroxyl group in the 5′-position of the B ring as seen in myricetin did not significantly ($p > 0.05$) alter the interference as compared to quercetin. This is on par with other studies, which have shown that the presence of a third hydroxy group in the B ring at the C-5 position did not enhance the effectiveness of myricetin compared to quercetin.[19] The stabilizing effect of the extra radical is provided by only one of the two hydroxyls ortho to the hydrogen-donating hydroxyl group.[20] Studies have also suggested that a hydrogen atom is most likely donated from the 3-OH, which leads to a more stable radical tautomer.[21,22]

In a broad stroke, there seems to be an overall structure−activity relationship between the compound and its ability to reduce the meriquinone radical. Within the "high interference" category, the compounds generally possess a larger number of hydroxy groups (OH). The radical scavenging property of flavonoids has been attributed to the number of OH groups that are present in the ring structure.[23,24] In addition, the configuration of the H-donating hydroxy groups is also one of the main structural features, which influences the antioxidant capacity of phenolics.[25] Furthermore, compounds in the "high interference" group possess many OH groups that are in the ortho position. The ortho arrangement of OH groups causes the development of an intramolecular hydrogen bond (IHB), which is able to stabilize the radical, leading to a lower O−H bond dissociation enthalpy (BDE). The BDE governs the ability of a particular flavonoid to

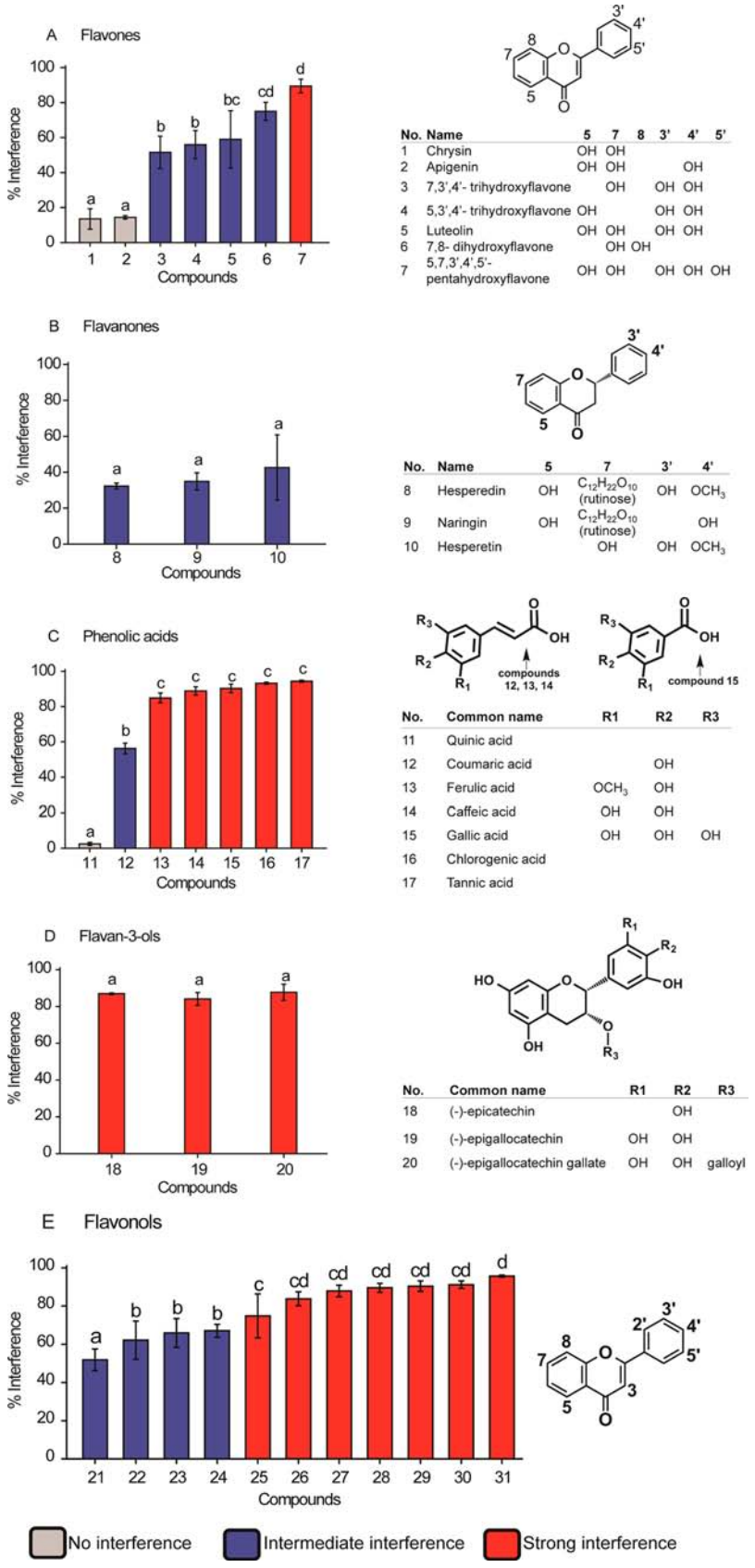

No.	Name	5	7	8	3'	4'	5'
1	Chrysin	OH	OH				
2	Apigenin	OH	OH			OH	
3	7,3',4'- trihydroxyflavone		OH		OH	OH	
4	5,3',4'- trihydroxyflavone	OH			OH	OH	
5	Luteolin	OH	OH		OH	OH	
6	7,8- dihydroxyflavone		OH	OH			
7	5,7,3',4',5'- pentahydroxyflavone	OH	OH		OH	OH	OH

No.	Name	5	7	3'	4'
8	Hesperedin	OH	$C_{12}H_{22}O_{10}$ (rutinose)	OH	OCH_3
9	Naringin	OH	$C_{12}H_{22}O_{10}$ (rutinose)		OH
10	Hesperetin		OH	OH	OCH_3

compounds 12, 13, 14

compound 15

No.	Common name	R1	R2	R3
11	Quinic acid			
12	Coumaric acid		OH	
13	Ferulic acid	OCH_3	OH	
14	Caffeic acid	OH	OH	
15	Gallic acid	OH	OH	OH
16	Chlorogenic acid			
17	Tannic acid			

No.	Common name	R1	R2	R3
18	(-)-epicatechin		OH	
19	(-)-epigallocatechin	OH	OH	
20	(-)-epigallocatechin gallate	OH	OH	galloyl

Figure 3. Interference of various compounds (represented in numerics) and subdivided according to their respective classes: (A) flavones; (B) flavanones; (C) phenolic acids; (D) flavan-3-ols; (E) flavanols. Compound identities for Figure 3E are: **21**, 3,5-dihydroxyflavone; **22**, rutin; **23**, 3,7-dihydroxyflavone; **24**, galangin; **25**, kaemferol; **26**, 3'3,4-trihydroxyflavone; **27**, morin; **28**, gossypetin; **29**, fisetin; **30**, myricetin; **31**, quercetin.

dx.doi.org/10.1021/jf500431z | J. Agric. Food Chem. 2014, 62, 4571−4576

donate hydrogen atoms, and the lower the BDE value, the higher the ability of a flavonoid to donate hydrogen.[26]

Correlation of Degree of Interference and Antioxidant Activity Measured by DPPH Radical Scavenging Activity. Because meriquinone is an oxidant, its reaction with polyphenolic compounds has some similarity to the reaction used in measuring the antioxidant activity with the DPPH assay. If there is a good correlation of interference and the DPPH assay, one might be able to apply the DPPH assay to conveniently distinguish the likelihood of interference of any given plant extract. Therefore, we attempted to correlate the degree of the interference and the IC_{50} of the polyphenolic compounds for DPPH assay, and the results are shown in Figure 4. In general,

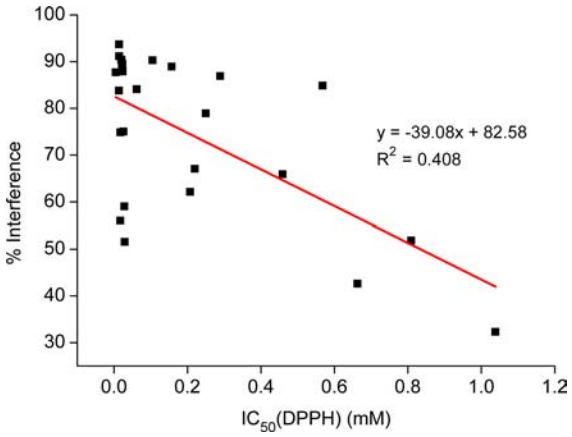

Figure 4. Correlation between percent interference of compounds and the IC_{50} of DPPH (mM).

those compounds with a high interference also had a high antioxidant activity (i.e., low IC_{50} of DPPH assay), but there was no linear correlation. Therefore, DPPH may be qualitatively applied to judge the potential interference of the GOP assay. Measuring the turbidity decrease during enzymatic starch hydrolysis is an accurate way to test enzyme activity, and it is not subject to interference due to reducing activity of the phenolic compounds. We applied this method to evaluate the inhibitory activity of α-glucosidase and found that these compounds have no measurable activity. These results highlighted the limitation of the GOP assay in natural products.

In conclusion, we have illustrated that the majority of polyphenolic compounds found in the plant kingdom have a significant interference in the GOP assay. Because the reaction with the free radical intermediate is likely to be a reduction reaction, it is reasonable to assume that radical scavengers will have a false-positive interaction. This effectively makes the GOP assay not useful in measuring the α-glucosidase inhibition activity of botanical extracts. It is essential to test the interference first before the GOP assay is applied for quantification of α-glucosidase activity. Recently, our group developed a high-throughput method for screening α-glucosidase and α-amylase inhibition activity of natural products using turbidity changes.[27] In this assay, natural starch was applied as the substrate and acarbose was used as a reference standard. Because turbidity is a physical parameter of the starch solution, one would expect that it would be more resistant to the interference of chemical reactions.

AUTHOR INFORMATION

Corresponding Author

*(D.H.) E-mail: chmhdj@nus.edu.sg.

Funding

The authors would like to acknowledge the financial support from the National University of Singapore (Suzhou) Research Institute under the grant number NUSRI2011-007 and The Industrialization-Academic-Research Platform grant of Jiangsu Province, China.

Notes

The authors declare no competing financial interest.

REFERENCES

(1) Bailey, C. J.; Aschner, P.; Del Prato, S.; LaSalle, J.; Ji, L. N.; Matthaei, S. Individualized glycaemic targets and pharmacotherapy in type 2 diabetes. *Diabetes Vasc. Disease Res.* **2013**, *10*, 397−409.

(2) Wardrop, D. J.; Waidyarachchi, S. L. Synthesis and biological activity of naturally occurring α-glucosidase inhibitors. *Nat. Prod. Rep.* **2010**, *27*, 1431−1468.

(3) Xiao, J.; Kai, G.; Yamamoto, K.; Chen, X. Advance in dietary polyphenols as α-glucosidases inhibitors: a review on structure-activity relationship aspect. *Crit. Rev. Food Sci. Nutr.* **2013**, *53*, 818−836.

(4) Williamson, G. Possible effects of dietary polyphenols on sugar absorption and digestion. *Mol. Nutr. Food Res.* **2013**, *57*, 48−57.

(5) Huggett, A. G.; Nixon, D. A. Use of glucose oxidase, peroxidase, and *o*-dianisidine in determination of blood and urinary glucose. *Lancet* **1957**, *2*, 386−370.

(6) Conyers, S. M.; Kidwell, D. A. Chromogenic substrates for horseradish peroxidase. *Anal. Biochem.* **1991**, *192*, 207−211.

(7) Cooper, G. R. Methods for determining the amount of glucose in blood. *Crit. Rev. Clin. Lab. Sci.* **1973**, *4*, 101−145.

(8) Kaufmann-Raab, I.; Jonen, H. G.; Jahnchen, E.; Kahl, G. F.; Groth, U. Interference by acetaminophen in the glucose oxidase-peroxidase method for blood glucose determination. *Clin. Chem.* **1976**, *22*, 1729−1731.

(9) Nakashima, E.; Nakamura, J.; Hamada, Y.; Koh, N.; Sakakibara, F.; Hotta, N. Interference by gliclazide in the glucose oxidase/peroxidase method for glucose assay. *Diabetes Res. Clin. Prac.* **1995**, *30*, 149−152.

(10) Fales, F. W. Glucose (enzymatic). In *Standard Methods of Clinical Chemistry*; Seligson, D., Ed.; Academic Press: New York, 1963; pp 101−112.

(11) Shaukat, S.; Waqar, M. A. Green tea phenols interference in the glucose oxidase/peroxidase test. *J. Food Biochem.* **2011**, *35*, 1170−1185.

(12) Xu, H.; Leng, X.; Wang, M.; Zhang, G. Glucose measurement in the presence of tea polyphenols. *Food Anal. Methods* **2011**, *5*, 1027−1032.

(13) Fatmawati, S.; Shimizua, K.; Kondo, R. Ganoderol B: a potent α-glucosidase inhibitor isolated from the fruiting body of *Ganoderma lucidum*. *Phytomedicine* **2011**, *18*, 1053−1055.

(14) Claiborne, A.; Fridovich, I. Chemical and enzymatic intermediates in the peroxidation of *o*-dianisidine by horseradish peroxidase. 1. Spectral properties of the products of dianisidine oxidation. *Biochemistry* **1979**, *18*, 2324−2329.

(15) Kireyko, A. V.; Veselova, I. A.; Shekhovtsova, T. N. Mechanisms of peroxidase oxidation of *o*-dianisidine, 3,3′,5,5′-tetramethylbenzidine, and *o*-Phenylenediamine in the presence of sodium dodecyl sulfate. *Russ. J. Bioorg. Chem.* **2006**, *32*, 71−77.

(16) Miyake, Y.; Yamamoto, K.; Tsujihara, N.; Osawa, T. Protective effects of lemon flavonoids on oxidative stress in diabetic rats. *Lipids* **1998**, *33*, 689−695.

(17) Jeon, S. M.; Bok, S. H.; Jang, M. K.; Kim, Y. H.; Nam, K. T.; Jeong, T. S. Comparison of antioxidant effects of naringin and probucol in cholesterol-fed rabbits. *Clin. Chim. Acta* **2002**, *317*, 181−190.

(18) Soobrattee, M. A.; Neergheen, V. S.; Luximon-Ramma, A.; Aruoma, O. I.; Bahorun, T. Phenolics as potential antioxidant therapeutic agents: mechanism and actions. *Mutat. Res.* **2005**, *579*, 200−213.

(19) Pannala, A. S.; Chan, T. S.; O'Brien, P. J.; Rice-Evans, C. A. Flavonoid B-ring chemistry and antioxidant activity: fast reaction kinetics. *Biochem. Biophys. Res. Commun.* **2001**, *282*, 1161−1168.

(20) Seyoum, A.; Asres, K.; El-Fiky, F. K. Structure-radical scavenging activity relationships of flavonoids. *Phytochemistry* **2006**, *67*, 2058−2070.
(21) Amic, D.; Davidovic-Amic, D.; Beslo, D.; Trinajstic, N. Structure-radical scavenging activity relationships of flavonoids. *Croatian Chem. Acta* **2003**, *76*, 55−61.
(22) Van Acker, S. A. B. E.; De Groot, M. J.; Van De Berg, D. J.; Tromp, M. N. J. L.; Den Kelder, G. D. O.; Van Der Vijgh, W. J. F.; Bast, A. A quantum chemical explanation of the antioxidant activity of flavonoid. *J. Chem. Res. Toxicol.* **1996**, *9*, 1305−1312.
(23) Rice-Evans, C. A.; Miller, N. J.; Bolwell, P. G.; Bramley, P. M.; Pridham, J. B. The relative antioxidant activities of plant-derived polyphenolic flavonoids. *Free Radical Res.* **1995**, *22*, 375−383.
(24) Rasulev, B. F.; Abdullaev, N. D.; Syrov, V. N.; Leszczynski, J. A quantitative structure-activity relationship (QSAR) study of the antioxidant activity of flavonoids. *QSAR Comb. Sci.* **2005**, *24*, 1056−1065.
(25) Cao, G.; Sofic, E.; Prior, R. L. Antioxidant and prooxidant behavior of flavonoids: structure-activity relationships. *Free Radical Biol. Med.* **1997**, *22*, 749−760.
(26) Thavasi, V.; Leong, L. P.; Bettens, R. P. Investigation of the influence of hydroxyl groups on the radical scavenging ability of polyphenols. *J. Phys. Chem. A* **2006**, *110*, 4918−4923.
(27) Liu, T.; Song, L.; Wang, H.; Huang, D. A high-throughput assay for quantification of starch hydrolase inhibition based on turbidity measurement. *J. Agric. Food Chem.* **2011**, *59*, 9756−9762.

JOURNAL OF AGRICULTURAL AND FOOD CHEMISTRY

Article

pubs.acs.org/JAFC

Distribution of Branches in Whole Starches from Maize Mutants Deficient in Starch Synthase III

Fan Zhu,[†] Eric Bertoft,[‡] and Koushik Seetharaman*[,‡]

[†]School of Chemical Sciences, University of Auckland, Private Bag 92019, Auckland, New Zealand

[‡]Department of Food Science and Nutrition, University of Minnesota, 1334 Eckles Avenue, St. Paul, Minnesota 55108, United States

ABSTRACT: An earlier study explored the possibility of analyzing the distribution of branches directly in native, whole starch without isolating the amylopectin component. The aim of this study was to explore if this approach can be extended to include starch mutants. Whole starches from *du1* maize mutants deficient in starch synthase III (SSIII) with amylose content of ∼30−40% were characterized and compared with the wild type of the common genetic background W64A. Clusters were produced from whole starch by hydrolysis with α-amylase of *Bacillus amyloliquefaciens*. Their compositions of building blocks and chains were analyzed further by complete α-amylolysis and by debranching, respectively, whereafter the products were subjected to gel permeation and anion exchange chromatography. The size and structure of the clusters were compared with those of their isolated amylopectin component. Whereas the whole starch of the wild type sample had a branched structure similar to that of its amylopectin component, the results showed that the *du1* mutation resulted in more singly branched building blocks in the whole starch compared to the isolated amylopectin. This suggested that amylose and/or intermediate materials in whole *du1* starches likely contributed to the composition of branches. This study explored an alternative procedure to characterize the composition of branches in the whole starch without fractionating the components.

KEYWORDS: *whole starch, starch synthase III, structure, cluster, building block*

INTRODUCTION

Starch is a complex mixture of diverse biopolymers of glucose ranging from linear to branched molecules.[1] However, separation of these components in mutant starches can be a challenge. One of the most commonly employed methods for normal starches is based on butanol precipitation as originally developed by Schoch.[2] By this method the starch components are fractionated into a butanol-precipitated fraction, referred to as amylose, and a butanol-non-precipitated fraction, commonly known as amylopectin. Variations in the butanol precipitation based methods have been developed over the years. For example, Klucinec and Thompson used a mixture of isoamyl alcohol and butanol to obtain a precipitate consisting of amylose and intermediate material, whereas the supernatant consisted of amylopectin.[3] The amylose was then separated from the intermediate material by precipitation in butanol. When research is conducted on different mutant samples, however, the definitions and the isolation of the different starch components become more confounding.

Analysis of starch samples from mutant plants with detailed genetics presents an opportunity to understand biosynthesis−structure relationships. However, the analysis of the branched structure of the starch components down to the cluster and building block levels[4] requires a relatively large amount of sample. Whereas starches from plants most often are available in comparatively large amounts, starches from organisms such as algae or leaves[5,6] are available only in small quantities and do not in practice permit a separation into amylopectin and other components. This seriously hinders further exploration of the structure of starch from interesting mutants or pursuing other research questions. A possible alternative could be to analyze whole starch samples ("whole" denotes the native starch isolated from flour as opposed to the fractionated starch components) without separating the amylose and amylopectin. In a previous study with normal and waxy maize,[7] we explored the opportunity to understand starch structure without separating the amylose and amylopectin fractions from whole starch. We showed that the branching pattern in whole normal maize starch was comparable to that of waxy maize starch. One of the critiques of that research, however, was that the comparison of the whole normal starch was not with the amylopectin component from the same normal starch. In this study we therefore isolated the amylopectin component and compared it with the same whole maize starch of the genetic background W64A. We further used *du1* mutants of maize with the same genetic background that are deficient in starch synthase III (SSIII)[8,9] as a test material to study if analyses of the branching pattern in mutant whole starches are useful for the understanding of the effect of the mutation. The mutations were detailed by Lin et al.,[10] and the molecular structure of the starches was reported previously by Zhu et al.[11] Further studies on the cluster and building block structure of amylopectin from the same samples were also presented.[12] It was shown that the *du1* mutation altered the structure of starch and its amylopectin component and that it also increased the apparent amylose content. This study compares the cluster and building block structure of whole *du1* maize starches with the data for clusters and building blocks in amylopectin presented previously.[12]

Received: February 10, 2014
Revised: March 31, 2014
Accepted: March 31, 2014
Published: March 31, 2014

ACS Publications © 2014 American Chemical Society

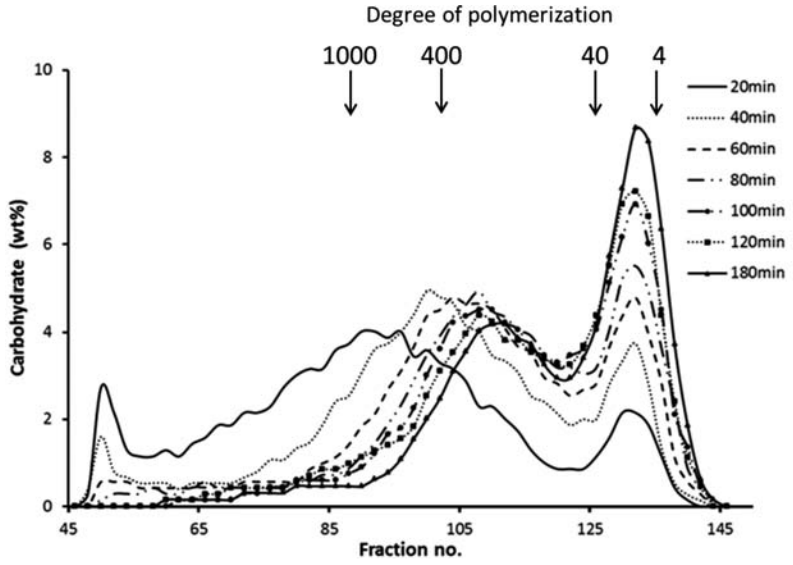

Figure 1. Time course of α-amylolysis of whole starch from W64A by GPC on Sepharose CL 6B. wt %, weight-based percentage.

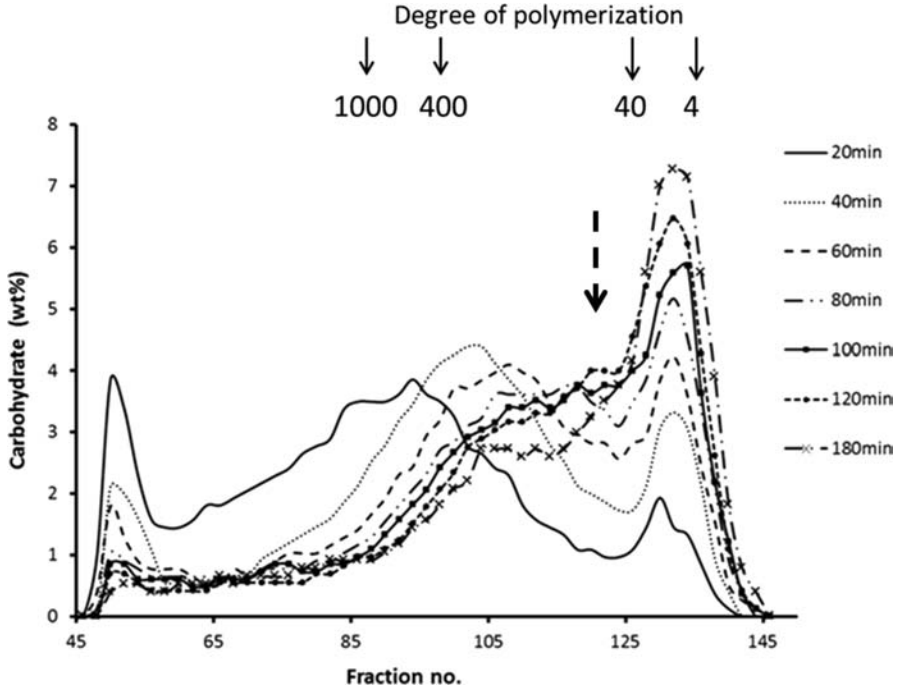

Figure 2. Time course of α-amylolysis of whole starch from *du1-M3* by GPC on Sepharose CL 6B. wt %, weight-based percentage. Dashed arrow indicates the boundary region between linear and branched fractions.

MATERIALS AND METHODS

Starches and Enzymes. The maize samples including one wild type (W64A) and two single *dull1* mutants (*du1-Ref* and *du1-M3*) were the same specimens used in a previous study.[10] They were of the W64A inbred genetic background. Both *dull1* mutations caused complete loss of SSIII enzyme activity, but *du1-Ref* expressed the protein at low level, whereas *du1-M3* produced no protein.[10] The molecular structure of the starches and the cluster and building block structure of amylopectins were reported previously.[11,12]

α-Amylase of *Bacillus amyloliquefaciens* (EC 3.2.1.1), β-amylase of barley (EC 3.2.1.2, specific activity = 705 U/mg), isoamylase of *Pseudomonas amyloderamosa* (EC 3.2.1.68, specific activity = 210 U/mg), and pullulanase of *Klebsiella pneumoniae* (EC 3.2.1.41, specific activity = 699 U/mg) were from Megazyme (Wicklow, Ireland). The activity of the α-amylase (413 U/mL at pH 6.5, 25 °C) was determined on the basis of a previous description.[13] The given activities of other enzymes were according to the supplier.

Time Course Analysis of α-Amylolysis for Cluster Production from Whole Starch. Whole starch (20 mg) was dissolved in 400 μL of 90% dimethyl sulfoxide (DMSO) by gentle heating and then constant stirring for 3 days at room temperature (~22 °C) to ensure the complete dissolution of starch before hot double-distilled water (1.4 mL) was added. After cooling, α-amylase (200 μL, 0.9 U/mL) in NaOAc buffer (0.01 M, pH 6.5) was added to start the reaction in a water bath (25 °C) with magnetic stirring. The concentrations for substrate and α-amylase in the reaction system were 10 mg/mL and 0.09 U/mL. Samples (200 μL) were taken from 20 to 150 min. If not analyzed immediately, NaOH solution (4 μL, 5.0 M) was added and mixed to destroy the α-amylase, and then the sample was stored at −18 °C. Before analysis, the sample was diluted in water (200 μL), conditioned by NaOH solution (40 μL, 5.0 M), and analyzed by GPC

on Sepharose CL 6B as described below under Chromatographic Techniques.

Production and Characterization of α-Dextrins and β-Limit Dextrins of Clusters from Whole Starch. Whole starch (160 mg) was dissolved in 3.2 mL of 90% DMSO by gentle heating and then constant stirring for 3 days at room temperature (~22 °C) to ensure the complete dissolution of starch. Hot double-distilled water (11.2 mL) was added and, after cooling, α-amylase (1.6 mL, 0.9 U/mL) in NaOAc buffer (0.01 M, pH 6.5) was added to start the reaction in a water bath (25 °C) with magnetic stirring. The reaction was continued for 90 min before being stopped by the addition of NaOH (320 μL, 5.0 M) and standing at room temperature for 2 h to destroy the α-amylase. Pure methanol (80 mL) was added to precipitate the α-dextrins of clusters. The sample was left at 4 °C for 3 h before the precipitate was recovered by centrifugation (4000*g*, 20 min) at room temperature. The precipitate was washed twice with pure methanol (10 mL) and allowed to stand in a fume hood to remove the methanol through evaporation.

The external chain segments of α-dextrins of clusters were removed by β-amylase to obtain the β-limit dextrins of clusters as previously described.[7] Briefly, α-dextrins were dissolved in hot water to a carbohydrate concentration of 10 mg/mL and mixed with NaOAc buffer (0.01 M, pH 6.0) and β-amylase (1 μL/10 mg of dextrins). The β-amylolysis reaction was conducted at room temperature overnight, then boiled for 5 min, condensed by rotary evaporation at 50 °C, and purified through two coupled PD-10 columns (GE Healthcare Life Sciences, Piscataway, NJ, USA) to remove maltose and buffer salt. The β-amylolysis was repeated, and the resulting hydrolysate solution was run twice through the PD-10 columns to completely remove maltose and buffer salt from the β-LDs. The solution of β-LDs of clusters was condensed to a smaller volume for a suitable concentration for further analysis and stored in a freezer (−30 °C) before use.

Debranching. Solutions of β-LDs and building blocks with a carbohydrate amount of 1 mg were diluted in hot water to make up a volume (225 μL). After cooling, NaOAc buffer (25 μL, 0.01 M, pH 5.5), pullulanase (1 μL), and isoamylase (1 μL) were added. The reaction was at room temperature for 20 h with stirring to completely break the α-(1,6)-linkages before analysis by high-performance anion exchange chromatography (HPAEC). The reaction was terminated by boiling for 10 min.

Chromatographic Techniques. The molecular weight distributions of the clusters and building blocks were analyzed by gel permeation chromatography (GPC) of Sepharose CL 6B (Pharmacia, Uppsala, Sweden) and of Superdex 30 (Pharmacia), respectively, as described previously.[12] The column was calibrated as described previously.[14] The building block mixtures and also the debranched samples were analyzed by HPAEC as described previously.[12]

Statistical Analysis. Tests were conducted in triplicate and analyzed using SPSS version 19.0 software (IBM Corp., Armonk, NY, USA). Differences between means of data were compared by least significant difference at a significance level of $p < 0.05$.

RESULTS

Time Course Analysis of α-Amylolysis of Whole Starch. Hydrolysis kinetics of whole starches treated with α-amylase of *B. amyloliquefaciens* by using GPC is presented in Figure 1 (W64A) and Figure 2 (*du1-M3*). The hydrolysis profile for *du1-Ref* was similar to that of *du1-M3*. The fractions prior to 125 are primarily branched dextrins, whereas those after that are mostly linear dextrins.[15] These latter dextrins were likely the product of both amylose and the external and intercluster segments of amylopectin or intermediate materials. Figure 3 shows the kinetics of starch degradation over time. The hydrolysis was rapid in the initial stage and then became slower. The average DP of the branched dextrins leveled off around DP 150. On the basis of these observations, 90 min of α-amylolysis was chosen for large-scale cluster production for all whole maize starches.

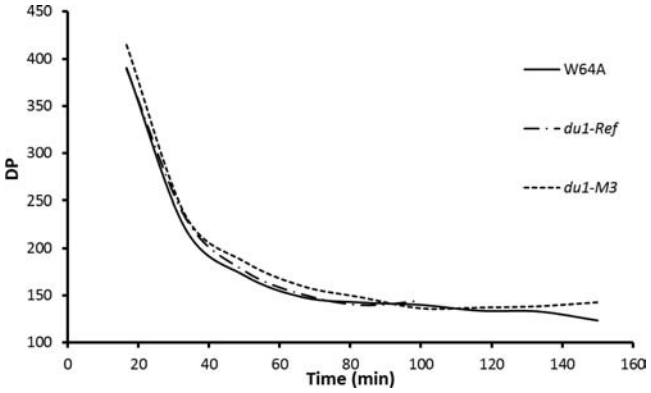

Figure 3. Development of average DP (degree of polymerization) of branched dextrins as a function of time during α-amylolysis.

Characterization of Clusters. Isolated clusters from whole starch were subjected to β-amylolysis to remove external chains that remained after α-amylolysis. The molecular weight distribution of the resulting β-limit dextrins (β-LDs) is shown in Figure 4. The average DP of clusters from W64A (64.6) was

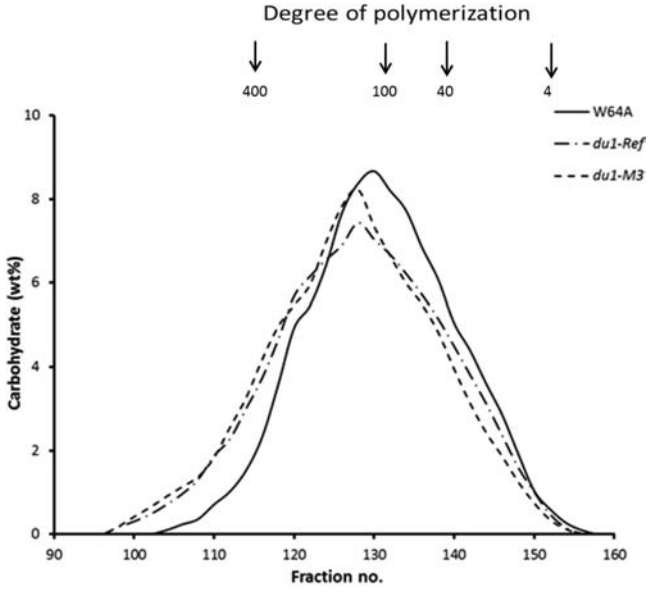

Figure 4. Molecular weight distribution obtained by GPC on Sepharose CL 6B of β-limit dextrins of clusters. wt %, weight-based percentage.

smaller than that of *du1-Ref* (78.3) and *du1-M3* (86.9) (Table 1). The same trend was also found for the peak DP (120 for W64A and 140 for *du1* mutants). *du1* mutant samples had a higher average number of chains per cluster (NC 13.2−15.2) than W64A (NC 10.9). Average chain length (CL 5.7−5.9), internal chain length (ICL 3.0−3.3), and total internal chain length (TICL 9.9−10.3) were similar for all genotypes.

Unit chains of clusters can be categorized into a- (carrying no other chains) and b-chains (carrying other chains).[16] These chains are different from "A" and "B" chains typically designated in amylopectin molecules.[17] The a-chains are completely external chains and have DP 2 and 3 in the β-LDs,[18] whereas the b-chains represent the internal unit chain profiles of the clusters and are presented in Figure 5. The b-chains can be further divided into different categories according

dx.doi.org/10.1021/jf500697g | J. Agric. Food Chem. 2014, 62, 4577−4583

Table 1. Characterization of β-Limit Dextrins of Clusters from Whole Maize Starches[a]

genotype	DP	peak-DP	NC	peak-NC	CL	ICL	TICL
W64A	64.6c	120b	10.9c	20.2b	5.9a	3.3a	10.3a
du1-Ref	78.3b	140a	13.2b	23.7a	5.9a	3.2ab	10.1ab
du1-M3	86.9a	140a	15.2a	24.4a	5.7a	3.0b	9.9b

[a]DP, average degree of polymerization (DP) estimated by GPC; NC, number of chains estimated as DP/CL; CL, average chain length estimated by HPAEC; ICL, internal chain length = (CL − ECL) × NC/(NC − 1) − 1, in which ECL is 2 for β-limit dextrin; TICL, total internal chain length = CL of b-chains in β-LD − 1.5. Different lower case letters within a column indicate significant differences ($p < 0.05$).

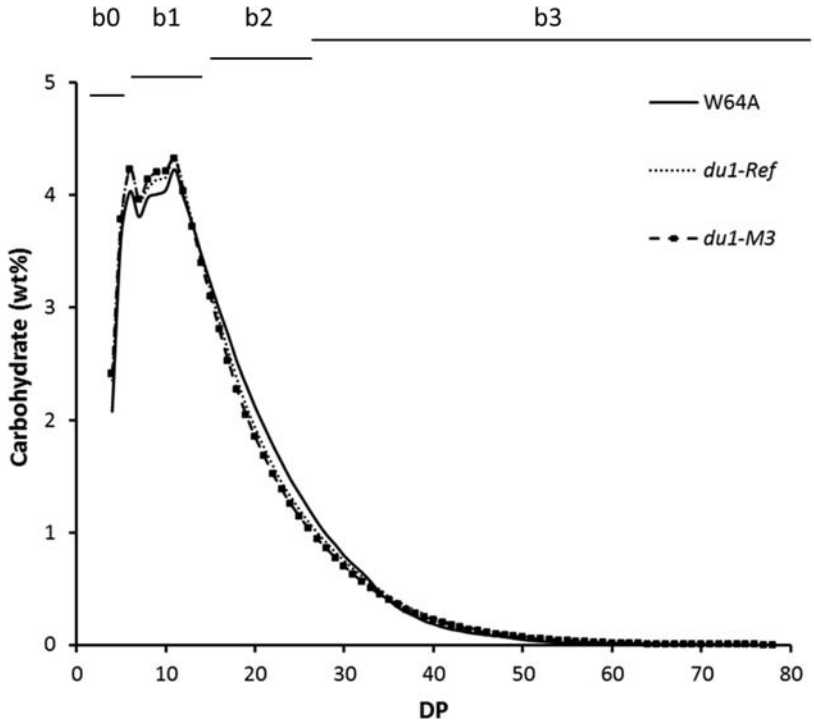

Figure 5. Fractionation by HPAEC of unit chains of debranched β-limit dextrins of clusters from whole starches. b0 = 4−6, b1 = 7−18, b2 = 19−27, b3 ≥ 28. wt %, weight-based percentage.

to their length and on the basis of their possible function as a part of the cluster structure (Table 2).[16] The amounts of a-chains in the clusters of whole starch of all different genotypes were similar (59.6−60.3%), and this was also the case for b1- and b3-chains. However, *du1* mutant samples had somewhat lower amounts of b2-chains (3.3−3.6%) and higher amount of b0-chains (11.8−12.2%) than W64A (b2 = 4% and b0 = 11.4%).

Table 2. Relative Molar Composition (Percent) of Chain Categories in β-Limit Dextrins of Clusters from Whole Maize Starches in Comparison with That from the Amylopectin[a]

genotype	a	b0	b1	b2	b3
W64A	60.3a	11.4b	22.8a	4.0a	1.4a
du1-Ref	59.6a	12.2a	23.0a	3.6b	1.5a
du1-M3	61.0a	11.8ab	22.3b	3.3b	1.3a
$W64A_{AP}$	51.4	10.2	19.6	3.5	1.4
$du1\text{-}Ref_{AP}$	51.7	9.0	19.2	4.5	2.1
$du1\text{-}M3_{AP}$	52.5	9.5	19.4	4.4	2.3

[a]For the whole starch of W64A, *du1-Ref*, and *du1-M3*, the DP range of *a* = 2−3, b0 = 4−6, b1 = 7−18, b2 = 19−27, and b3 ≥28 for β-LDs; for the amylopectin ($W64A_{AP}$, $du1\text{-}Ref_{AP}$, and $du1\text{-}M3_{AP}$), the composition was from the φ,β-LDs as detailed previously, the DP range of a = 2, b0 = 4−6, b1 = 7−18, b2 = 19−27, b3 ≥28 for φ,β-LDs.[12] Different lower case letters within a column of whole starches (W64A, *du1-Ref*, and *du1-M3*) indicate significant differences ($p < 0.05$).

Characterization of Building Blocks in Clusters. To further understand the organization of chains in clusters, the clusters were subjected to extensive hydrolysis to release the small and tightly branched building blocks. As expected, the building block profile exhibited two distinguishable peaks with the one around fraction 123 (DP ∼ 8) representing singly branched building blocks and the one around fraction 136 (DP ∼ 2) representing linear dextrins (Figure 6). The branched building blocks can generally be categorized into five groups (groups 2−6), of which groups 2−4 have a corresponding number of chains and groups 5 and 6 are more heterogeneous with ≥5 chains per block.[19,20] The molecular structure of building blocks is presented in Table 3. The branched building blocks had an average DP of 11.0−11.2 and the NC ranged from 2.8 to 3.0 for all genotypes. The chain length parameters of the building blocks were also very similar.

From the structures of clusters and their building blocks, the interconnection and composition of branched building blocks in clusters were calculated (Table 4). The interblock chain length (IB-CL) was similar for all of the genotypes (6.5−6.6). The number of blocks per cluster ranged from 5.5 (*du1-M3*) to

dx.doi.org/10.1021/jf500697g | J. Agric. Food Chem. 2014, 62, 4577−4583

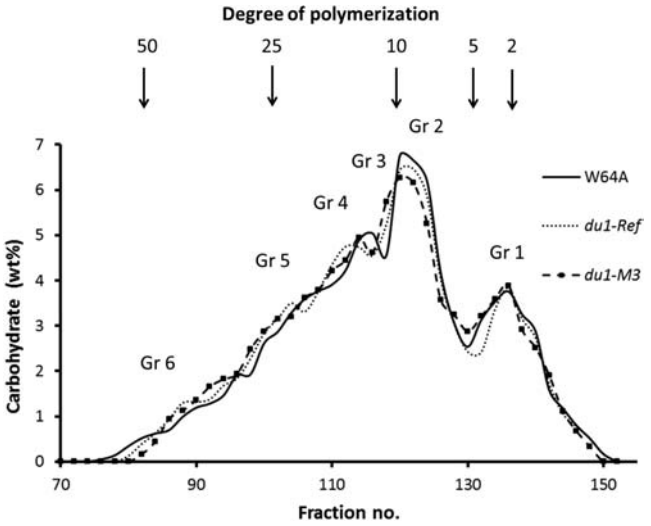

Figure 6. Fractionation of building blocks in β-limit dextrins of clusters of whole maize starches on Superdex 30. Groups (Gr) of building blocks are shown. wt %, weight-based percentage.

4.2 (W64A). All genotypes had a density of blocks per cluster around 6.4−6.5. Clusters in the *du1* mutant samples had somewhat less of group 2 blocks (57.6−58.0%) compared with W64A (60.4%), but more of groups 3−6 blocks.

DISCUSSION

In a previous study, we highlighted that the cluster and building block attributes were similar between whole normal and waxy maize starches.[7] Results from this study, in which the amylopectin was isolated from normal starch (W64A) and compared with the same starch, confirmed that the cluster and building block data from whole normal starch are reflective of the structure of the corresponding amylopectin (Figure 7). This study also takes this approach further with mutant starch that affects the structure of the amylopectin component. Results in this study will be compared with the fine structure of amylopectin from these same samples reported in a previous publication.[12]

The pattern of α-amylolysis of samples in this study agreed with the previous result for normal maize starch with an apparent amylose content of 23%.[7] However, there remained large dextrins (fractions 45−70) toward the end of hydrolysis (Figures 1 and 2) that are typically not observed with pure amylopectin samples[7,15] and even from these samples[12] as compared in Figure 8. This may therefore be attributed to the amylose and/or the intermediate components of starch. Hayashi et al.[21] reported that amylose could reassociate and precipitate when whole starch in DMSO solution is diluted in water and cooled. In this aggregated physical form it would become resistant to α-amylolysis. Nevertheless, these remnants were hydrolyzed by subsequent dissolution and β-amylolysis as shown by their absence in the purified cluster fractions (Figure 4). Another noticeable difference was the larger amount of dextrins produced by the α-amylase at the boundary between the branched and linear dextrins[15] (fractions 120−125) with whole starches compared to amylopectin, especially for the *du1-M3* sample toward later stages of α-amylolysis (Figure 2). This may be attributed to extensive hydrolysis of both amylose and intermediate fractions[22] to DP ~40. The large production of this material from the *du1* samples may be attributed to the higher amounts of amylose (36.5 and 40.5% for mutants vs 29.6% for normal maize) with altered molecular structure as a result of SSIII deficiency as shown previously.[11]

The external chain segments that remain in the clusters after the action of α-amylase can largely be removed either with β-amylase or sequentially with phosphorylase *a* and then β-amylase.[23] The external chain lengths (ECL) of a- and b-chains in β-LDs are slightly different from that of φ,β-LDs: In β-LDs a-chains have DP 2 or 3 and the ECL of the b-chains is 1 or 2, whereas in φ,β-LDs all a-chains have DP 2 and the ECL of all b-chains is 1.[23] The internal structure of the LDs is, however, identical in β-LDs and φ,β-LDs. In this study, β-LDs of the clusters were produced as opposed to φ,β-LDs in our previous study on the purified amylopectin,[12] as this saves 2 days of analysis time. A comparison of the clusters from the two protocols is presented in Figures 7 and 9. The differences in the profiles in the region of the short chains (<DP 15) are due to minor differences in ECL of the LDs rather than differences in the internal chain distributions. The profiles of the b-chains at DP >15 (where the small differences in ECL of β-LDs and φ,β-LDs diminish) of clusters from whole normal maize were very

Table 4. Composition of Building Blocks in β-Limit Dextrins of Clusters of Whole Maize Starches[a]

				distribution of block categories (%)			
genotype	IB-CL	DBbl	NBbl	Gr 2	Gr 3	Gr 4	Gr 5 and Gr 6
W64A	6.6a	6.5a	4.2b	60.4a	21.3b	8.8b	9.5b
du1-Ref	6.5a	6.5a	5.1a	58.0b	22.3a	9.1a	10.6a
du1-M3	6.5a	6.4a	5.5a	57.6b	22.7a	9.1a	10.5a

[a]IB-CL, interblock chain length per cluster = mol $\%_{linear} \times DP_{linear}$/mol $\%_{branched}$ + 4; DBbl, density of building blocks per cluster = NBbl/$DP_{cltr} \times 100$, in which DP_{cltr} is the average DP of φ,β-LDs of clusters; NBbl, number of building blocks per cluster = wt $\%_{Bbl}/100 \times DP_{cluter}/DP_{Bbl}$, in which wt $\%_{Bbl}$ is the weight percent of branched building blocks. Categorization of groups 2−6 of building blocks is based on their number of chains per block. Different lower case letters within a column indicate significant differences ($p < 0.05$).

Table 3. Characterization of Building Blocks in β-Limit Dextrins of Clusters from Whole Maize Starches[a]

	linear		branched						
genotype	mol %	DP	wt %	mol %	DP	CL	ICL	TICL	NC
W64A	56.4a	2.0a	80.8b	43.6b	11.0a	3.8ab	1.7b	4.3ab	3.0a
du1-Ref	56.1a	2.0a	81.2ab	43.9b	11.2a	3.7b	1.6b	4.2b	3.0a
du1-M3	55.1b	2.1a	81.5b	44.9a	11.1a	4.0a	2.1a	4.5a	2.8a

[a]Linear dextrins have DP 1, 2, and 3, and branched building blocks have DP ≥ 5. DP, average DP estimated by GPC; CL, average chain length estimated by HPAEC; ICL, internal chain length = (CL − ECL) × NC/(NC − 1) − 1, in which external chain length (ECL) is estimated as 2; TICL, total internal chain length; NC, number of chains = DP/CL. Different lower case letters within a column indicate significant differences ($p < 0.05$).

dx.doi.org/10.1021/jf500697g | J. Agric. Food Chem. 2014, 62, 4577−4583

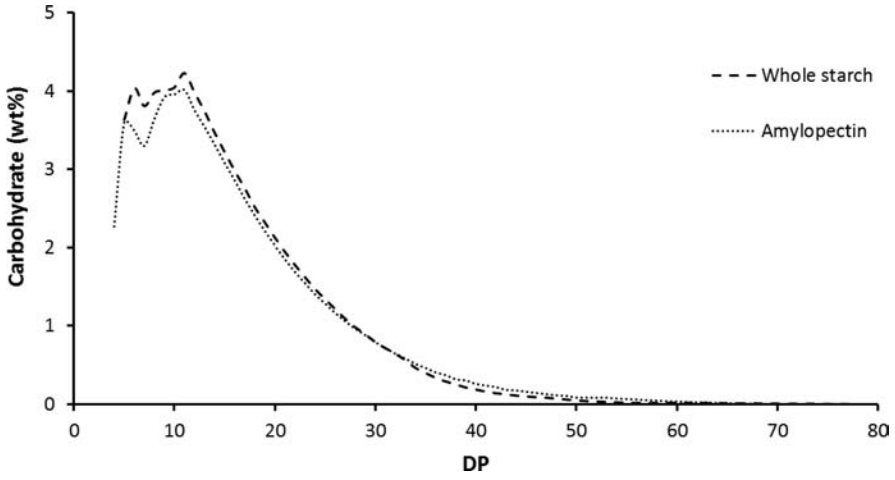

Figure 7. Unit chain length distribution comparison of clusters from whole starch (β-limit dextrins) and its amylopectin (φ,β-limit dextrins) of W64A. Data for amylopectin are from a previous paper.[12] wt %, weight-based percentage.

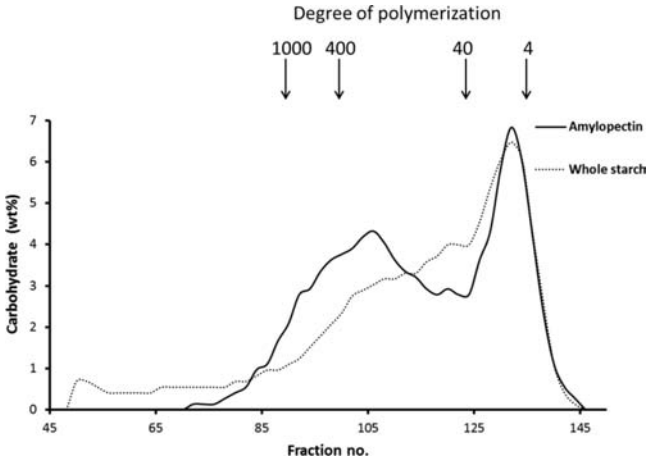

Figure 8. Comparison of α-dextrins of whole starch and its amylopectin from *du1-M3* during α-amylolysis at 120 min. Data for amylopectin are from a previous paper.[12] wt %, weight-based percentage.

similar to those of the clusters from amylopectin isolated from the same starch (Figure 7).

The amounts of a-chains in the clusters of whole starch of different genotypes were, however, significantly higher than the amount of a-chains in clusters of amylopectin (Table 2). This can be attributed to the fact that chains with DP 3 in the β-LDs are mixtures of a- and b-chains[24] and therefore overestimate the number of a-chains in the β-LDs, whereas in the φ,β-LDs, all a-chains have DP 2. In general, the *du1* mutation resulted in an elevated amount of shorter b-chains around DP 5−15 and a decreased amount of intermediate-length b-chains around DP 15−30 (Figure 9). This did not agree with the previous results on the cluster structure of amylopectin of the same samples (Table 2).

The effect of *du1* mutation on the cluster size and NC (Table 1) was consistent with the previous result on the φ,β-LDs of clusters from amylopectin,[12] although minor differences in the exact values for the *du1* mutant starches were noted. The pattern of the influence of *du1* mutation on the CL, ICL, and TICL of whole starch clusters was partially inconsistent with the results of amylopectin.[12] Apparently, this might be attributed to clusters from branched components in either

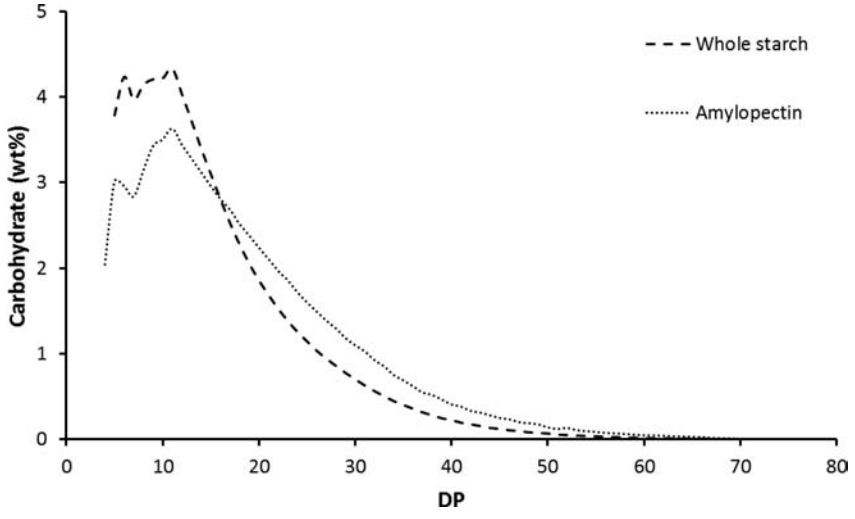

Figure 9. Unit chain length distribution comparison of clusters from whole starch (WS) (β-limit dextrins) and its amylopectin (φ,β-limit dextrins) of *du1-M3*. Data for amylopectin are from a previous paper.[12] wt %, weight-based percentage.

intermediate materials or branched amylose molecules, which likely had relatively higher amounts of shorter chains.

When the building blocks from whole starch (Table 3) were compared to those from amylopectin,[12] their structures were similar, but there were compositional differences in the small building blocks. Group 2 building blocks was more abundant in whole starch compared to clusters from purified amylopectin, and group 3 building blocks were correspondingly lower.

The difference in the composition and structure of clusters and building blocks from whole starch and isolated amylopectin, although small, do reflect the influence of amylose and intermediate components. The deficiency in SSIII probably resulted in altered levels of other enzymes related to biosynthesis of amylose, as suggested by Fujita et al. and Szydlowski et al.[25,26] This likely influenced the branching pattern of several starch components, which ultimately gave rise to different structural characteristics of the clusters when whole starch was analyzed as test material.

In conclusion, the cluster and building block structures of whole starches deficient in starch synthase III were compared with those of isolated amylopectin from a previous study. Structural and compositional similarities were observed but with some minor differences. The structural differences included a higher proportion of singly branched building blocks (group 2) in clusters of whole starch with a corresponding reduction of group 3 building blocks compared to isolated amylopectin. This difference was likely due to changes in the structural features in the amylose and/or intermediate components as affected by the deficiency in SSIII. On the basis of these results, it is apparent that the use of whole starches to explore branching patterns cannot replace the analysis of purified amylopectins, especially in mutant samples. However, it could be used as a complement and will provide useful information in the analysis of samples obtained in only small quantities like from leaf starches, from which purified amylopectin cannot be obtained in large enough quantities.

AUTHOR INFORMATION

Corresponding Author

*(K.S.) E-mail: kseethar@umn.edu.

Funding

The financial support of the Natural Sciences and Engineering Research Council of Canada (NSERC) is gratefully acknowledged.

Notes

The authors declare no competing financial interest.

ACKNOWLEDGMENTS

Maize starch samples were kindly provided by Professor Alan M. Myers at the Department of Biochemistry, Biophysics, and Molecular Biology, Iowa State University, Ames, IA, USA.

REFERENCES

(1) Buléon, A.; Colonna, P.; Planchot, V.; Ball, S. Starch granules: structure and biosynthesis. *Int. J. Biol. Macromol.* **1998**, *23*, 85−112.

(2) Schoch, T. J. Fractionation of starch by selective precipitation with butanol. *J. Am. Chem. Soc.* **1942**, *64*, 2957−2961.

(3) Klucinec, J. D.; Thompson, D. B. Fractionation of high-amylose maize starches by differential alcohol precipitation and chromatography of the fractions. *Cereal Chem.* **1998**, *75*, 887−896.

(4) Pérez, S.; Bertoft, E. The molecular structures of starch components and their contribution to the architecture of starch granules: A comprehensive review. *Starch/Staerke* **2010**, *62*, 389−420.

(5) Ball, S.; Colleoni, C.; Cenci, U.; Raj, J. N.; Tirtiaux, C. The evolution of glycogen and starch metabolism in eukaryotes gives molecular clues to understand the establishment of plastid endosymbiosis. *J. Exp. Bot.* **2011**, *62*, 1775−1801.

(6) Smith, A. M. Starch in the *Arabidopsis* plant. *Starch/Staerke* **2012**, *64*, 421−434.

(7) Zhu, F.; Bertoft, E.; Seetharaman, K. Characterization of internal structure of maize starch without amylose and amylopectin separation. *Carbohydr. Polym.* **2013**, *97*, 475−481.

(8) Gao, M.; Wanat, J.; Stinard, P. S.; James, M. G.; Myers, A. M. Characterization of dull1, a maize gene coding for a novel starch synthase. *Plant Cell* **1998**, *10*, 399−412.

(9) Keeling, P. L.; Myers, A. M. Biochemistry and genetics of starch synthesis. *Annu. Rev. Food Sci. Technol.* **2010**, *1*, 271−303.

(10) Lin, Q.; Huang, B.; Zhang, M.; Zhang, X.; Rivenbark, J.; Lappe, R. L.; James, M. G.; Myers, A. M.; Hennen-Bierwagen, T. A. Functional interactions between starch synthase III and isoamylase-type starch-debranching enzyme in maize endosperm. *Plant Physiol.* **2012**, *158*, 679−692.

(11) Zhu, F.; Bertoft, E.; Källman, A.; Myers, A. M.; Seetharaman, K. Molecular structure of starches from maize mutants deficient in starch synthase III. *J. Agric. Food Chem.* **2013**, *61*, 9899−9907.

(12) Zhu, F.; Bertoft, E.; Seetharaman, K. Composition of clusters and building blocks in amylopectins from maize mutants deficient in starch synthase III. *J. Agric. Food Chem.* **2013**, *61*, 12345−12355.

(13) Bertoft, E.; Manelius, R.; Qin, Z. Studies on the structure of pea starches. Part 1: initial stages in α-amylolysis of granular smooth pea starch. *Starch/Staerke* **1993**, *45*, 215−220.

(14) Bertoft, E.; Spoof, L. Fractional precipitation of amylopectin alpha-dextrins using methanol. *Carbohydr. Res.* **1989**, *189*, 169−180.

(15) Bertoft, E. Composition of clusters and their arrangement in potato amylopectin. *Carbohydr. Polym.* **2007**, *68*, 433−446.

(16) Bertoft, E.; Koch, K.; Åman, P. Building block organisation of clusters in amylopectin from different structural types. *Int. J. Biol. Macromol.* **2012**, *50*, 1212−1223.

(17) Peat, S.; Whelan, W. J.; Thomas, G. J. Evidence of multiple branching in waxy maize starch. *J. Chem. Soc., Chem. Commun.* **1952**, 4546−4548.

(18) Summer, R.; French, D. Action of β-amylase on branched oligosaccharides. *J. Biol. Chem.* **1956**, *222*, 469−477.

(19) Bertoft, E. Composition of building blocks in clusters from potato amylopectin. *Carbohydr. Polym.* **2007**, *70*, 123−136.

(20) Bertoft, E.; Koch, K.; Åman, P. Structure of building blocks in amylopectins. *Carbohydr. Res.* **2012**, *361*, 105−113.

(21) Hayashi, A.; Kotani, Y.; Cho, C. H. The rate of amylose precipitation from a dilute solution. *Agric. Biol. Chem.* **1984**, *48*, 949−954.

(22) Poutanen, K.; Lauro, M.; Suortti, T.; Autio, K. Partial hydrolysis of gelatinized barley and waxy barley starches by alpha-amylase. *Food Hydrocolloids* **1996**, *10*, 269−275.

(23) Bertoft, E. Partial characterisation of amylopectin alpha-dextrins. *Carbohydr. Res.* **1989**, *189*, 181−193.

(24) Bertoft, E. On the nature of categories of chains in amylopectin and their connection to the super helix model. *Carbohydr. Polym.* **2004**, *57*, 211−224.

(25) Fujita, N.; Yoshida, M.; Kondo, T.; Saito, K.; Utsumi, Y.; Tokunaga, T.; Nishi, A.; Satoh, H.; Park, J. H.; Jane, J. L.; Miyao, A.; Hirochika, H.; Nakamura, Y. Characterization of SSIIIa-deficient mutants of rice: the function of SSIIIa and pleiotropic effects by SSIIIa deficiency in the rice endosperm. *Plant Physiol.* **2007**, *144*, 2009−2023.

(26) Szydlowski, N.; Ragel, P.; Hennen-Bierwagen, T. A.; Planchot, V.; Myers, A. M.; Mérida, A.; d'Hulst, C.; Wattebled, F. Integrated functions among multiple starch synthases determine both amylopectin chain length and branch linkage location in *Arabidopsis* leaf starch. *J. Exp. Bot.* **2011**, *62*, 4547−4559.

JOURNAL OF AGRICULTURAL AND FOOD CHEMISTRY

Article

pubs.acs.org/JAFC

Concentration- and Time-Dependent Effects of Isothiocyanates Produced from Brassicaceae Shoot Tissues on the Pea Root Rot Pathogen *Aphanomyces euteiches*

Shakhawat Hossain,*[,†] Göran Bergkvist,[†] Kerstin Berglund,[‡] Robert Glinwood,[†] Patrick Kabouw,[§] Anna Mårtensson,[‡] and Paula Persson[†]

[†]Department of Crop Production Ecology, Swedish University of Agricultural Sciences, P.O. Box 7043, SE-750 07 Uppsala, Sweden

[‡]Department of Soil and Environment, Swedish University of Agricultural Sciences, P.O. Box 7014, SE-750 07 Uppsala, Sweden

[§]Department of Terrestrial Ecology, Netherlands Institute of Ecology (NIOO-KNAW), Boterhoeksestraat 48, 6666 GA Heteren, The Netherlands

ABSTRACT: Isothiocyanates (ITCs) hydrolyzed from glucosinolates (GSLs) in Brassicaceae tissue are toxic to soil organisms. In this study, the effect of aliphatic and aromatic ITCs from hydrated dry Brassicaceae shoot tissues on the mycelium and oospores of the pea root rot pathogen *Aphanomyces euteiches* was investigated. The profile and concentrations of GSLs in two test Brassicaceae species, *Sinapis alba* and *Brassica juncea*, and the ITCs from the dominant hydrolyzed parent GSLs were monitored. The concentrations of dominant ITCs and pathogen exposure time were evaluated in in vitro experiments. The greatest effect on the pathogen was observed from aliphatic ITCs hydrolyzed from *B. juncea* tissue, and the effect depended on the ITC concentration and exposure time. ITCs were more effectively hydrolyzed from *B. juncea* GSLs than from *S. alba* GSLs; i.e., the ITC/GSL ratio was higher in *B. juncea* than in *S. alba* tissue, giving a different release pattern. The release of phenylethyl isothiocyanate, which was common to both species, followed a pattern similar to that of the dominant ITC in each crop species. This suggests that traits other than GSL content, e.g., plant cell structure, may affect the release of ITCs and should therefore influence the choice of species used for biofumigation purposes.

KEYWORDS: *Brassicaceae, glucosinolate, isothiocyanate, Aphanomyces euteiches, pea root rot*

INTRODUCTION

Pea root rot caused by the pathogen *Aphanomyces euteiches* Drechs is a serious problem in pea production worldwide.[1−3] The pathogen can persist in the soil for long periods without a host plant due to the thick protective cell walls of the *Aphanomyces* oospores. When oospores are stimulated to germinate by pea root exudates,[4] a short mycelium strand and a sporangium are produced. The sporangium releases zoospores that attack the pea roots.[5] Pea root rot is difficult to control as there are no available pea cultivars with an acceptable level of resistance.[6] Furthermore, synthetic fungicides may have a negative environmental impact, and certain agents have been prohibited, for example, within the European Union.[7] The commonly recommended way to control *A. euteiches* is therefore to leave intervals (6−8 years) between pea crops in the rotation.[8]

Many plants of the family Brassicaceae (brassica) can suppress soil-borne organisms when grown as cover crops or when added as plant residues to infested soil.[9−11] In field studies, *Sinapis alba* (white mustard) reduced the development of *Aphanomyces* pea root rot when used as green manure. This reduction was enhanced when white mustard was used for a second consecutive year.[12] Studies under greenhouse conditions showed that incorporating cabbage tissue after growth in contaminated soil gave close to a 10-fold reduction in pea root rot disease severity.[13] Suppressive effects of brassica tissues are associated with the glucosinolate class of chemicals (GSLs) present in the tissues.[10] The biofumigation concept in agricultural systems was introduced by Australian scientists in the 1990s and includes practices to relieve the pressure of soil pests and pathogens by the use of brassica crops.[14] The concept is based on the toxic volatile compounds produced from hydrolyzed GSLs.[10,13,15,16] When brassica crop tissues are damaged, GSLs are hydrolyzed by myrosinase to form volatile isothiocyanates (ITCs), thiocyanates, water-soluble nitriles, and epithionitriles.[10,17] The composition and quantity of the produced substances depend on the parent GSL. The type and concentration of GSLs vary between brassica species, cultivars, and vegetative parts and are also influenced by the plant development stage.[16,18,19] The GSLs are classified as aliphatic, aromatic, or indolyl on the basis of their chemical structure.[10,20] Isothiocyanates suppress a wide range of organisms, including the soil-borne pathogen *A. euteiches*.[21] A study has demonstrated that volatile compounds from decomposing cabbage tissues inhibit hyphal growth of *A. euteiches* and that the pathogen is unable to grow further when placed in fresh air after exposure, although the active substance was not specified.[9] The suppressive effects depend on the composition and concentration of ITCs.[22] The chemical structure of ITCs influences their mode of action, meaning that different ITCs may show varying levels of toxicity at the

Received: December 5, 2013
Revised: May 6, 2014
Accepted: May 7, 2014
Published: May 13, 2014

 © 2014 American Chemical Society

same concentration.[23−25] An aliphatic structural group attached to the nitrogen in the basic ITC structure generally confers greater toxicity than an aromatic structure.[26] Generally, the toxicity of ITCs decreases as the size of the organic group increases.[27,28] Aliphatic ITCs bind directly with protein molecules inside cells and inhibit their activity, whereas aromatic ITCs first interact with the cell membrane, changing its electrophilic properties, before entering the cell[23] and reducing cell activity.[29]

Many different brassica-derived materials have been used to study aspects of biofumigation, such as fresh plant tissues, rape seed meal, freeze-dried plant tissues, and oil extracts, but pure ITCs have also been used.[18,30−32] Shoot tissue comprises the greater part of the brassica plant material when it is used for biofumigation in practice. Here, we evaluate a simple, reproducible system for studying shoot tissue effects on a plant pathogen in vitro using low-temperature drying of the plant material.[13,33]

Our overall aim was to discover how brassica plant tissues can be used for biofumigation to reduce the occurrence of root rot on peas caused by *A. euteiches*. Our specific objectives were to compare crop species with different GSL compositions to generate knowledge on the choice of brassica crop for biofumigation in the control of pea root rot. We tested the hypotheses that (1) ITCs from hydrolyzed aliphatic GSLs in *Brassica juncea* shoot tissue are more effective than ITCs from aromatic GSLs in *S. alba* shoot tissue at reducing the ability of *A. euteiches* oospores to cause pea root rot, (2) the lethal effect of aliphatic ITCs from shoot tissues on the growth of *A. euteiches* depends on the concentration of ITCs and time of pathogen exposure, and (3) the release patterns of ITCs from *B. juncea* and *S. alba* are different and influence the suppressive effects on *A. euteiches*.

MATERIALS AND METHODS

Plant Materials. Air-dried shoot tissues of two GSL-containing plant species, *B. juncea* (cv. Pacific Gold) and *S. alba* (cv. Architect), a non-GSL plant species, *Secale cereale* (cv. Amilo), and a water control were compared for their effect on the oospores and mycelium of *A. euteiches*. The effect of volatile compounds produced from hydrated shoot tissues was studied in in vitro experiments. The most effective plant species was chosen for dose and exposure-time experiments, compared with the effect of chemical solutions of the dominant ITCs from the two brassica species. The composition of GSLs in *B. juncea* and *S. alba* dry shoot tissues and of ITCs produced from hydrated tissues were analyzed.

Shoot Tissue Production. Three cover crops, *S. alba*, *B. juncea*, and *Se. cereale*, were grown in garden soil (Hasselfors Garden AB, Sweden) in the greenhouse. A complete nutrient solution (Cederroth International AB, Sweden) was applied at regular intervals together with additional $(NH_4)_2SO_4$ to enhance GSL production. Shoot tissues were harvested at soil level when *B. juncea* and *S. alba* reached the flowering stage. The tissues were dried at 35 °C for 72 h and then ground separately four times at 6000 rpm to a fine powder. The ground shoot tissues were stored in airtight containers and kept in a dark and dry place until use.

***A. euteiches* Inoculum.** *A. euteiches* strain 5035:2A was used in all experiments (obtained from F. Heyman, Department of Forest Mycology and Plant Pathology, Swedish University of Agricultural Sciences, Uppsala, Sweden). The strain was maintained on corn meal agar (CMA) (Oxoid Ltd., United Kingdom) at 6 °C and was used for soil inoculation.[34,35] For the production of oospore inoculum, the *A. euteiches* strain was cultured in oat meal broth for 4 weeks. It was homogenized, the oospore concentration was calculated, and then it was mixed with talcum powder (VWR International AB, Sweden) and dried. The dry inoculum material was sieved through a 1 mm mesh net and stored at 4 °C until use.

Field Soil. Soil was collected from an agricultural field in Giresta, Enköping, Sweden, and tested for the absence of *A. euteiches*. The soil consisted of 46% clay, 48% silt, 2% sand, and 4% organic matter. The organic matter content was estimated by loss on ignition. The soil contained 1.5 mg of N/mL, and the pH (H_2O) was 7.7. The soil was sieved through a 0.6 cm mesh and stored at 4 °C with the soil moisture content maintained at 21% during storage. For some experiments the soil was sterilized by autoclaving twice at 121 °C for 30 min.

Oospore Volatile Exposure and Bioassay. A 1 g mass of dry shoot tissue of *B. juncea*, *S. alba*, and *Se. cereale* was transferred separately to 220 mL plastic cups (8.9 cm diameter). A 4 g mass of talcum powder containing about 2.8×10^4 oospores was spread homogeneously on a filter paper placed in a 9 cm diameter sieve (1 mm mesh) and placed on top of the cup. At the start of the experiment 5 mL of sterilized deionized water was added to the tissue, and another plastic cup was immediately placed upside down on top of the sieve as a lid. The container was sealed with several layers of Parafilm (Sigma-Aldrich Sweden AB) and placed in the dark at 24 °C for 10 days. Sterilized deionized water was used as the control, and three replicates per treatment were performed.

After 10 days of incubation, the oospore−talcum powder mixture was removed from the container, and 0.8 g of the 4 g of treated powder was mixed with 80 mL of sterilized and nonsterilized soil. Four subsamples, 20 mL each, of the two infested soils were transferred to 85 mL pots. One pea seed (cv. Clare) was sown on top of the infested soils in each pot and was covered with an additional 5 mL of noninfested soil. The pots were placed in a greenhouse with a light/dark period of 14 h/10 h at a temperature of 24/19 ± 2 °C and relative humidity (RH) of 85 ± 5%. The soil moisture was adjusted daily to field levels to obtain optimal infection conditions. All pea seedling roots were evaluated for root rot disease severity 3 weeks after sowing. Each pea seedling was assigned a DSI (disease severity index) value on the basis of the mean disease symptoms of the individual pea seedlings in the four tubes representing each experimental unit. The scale for DSI ranges from 0% to 100%, but each individual plant can only be assigned one of five scores for disease severity: 0%, healthy plant; 25%, root slightly discolored; 50%, root extensively discolored but not shrunken; 75%, root extensively discolored and shrunken; 100%, root partly or completely rotted or plant dead.[36]

In Vitro Exposure of the Mycelium to Volatiles: Effect of Dose. Dry shoot tissue, 60, 100, and 140 mg, of *B. juncea*, *S. alba*, and *Se. cereale* was transferred separately to 220 mL plastic cups and mixed with 5 mL of sterilized, deionized water. A water control was included, and all treatments had three replicates. The doses were determined after a pilot study with *B. juncea* shoot tissues in which a 140 mg dose completely inhibited pathogen growth. A plug (7 mm diameter) from actively growing *A. euteiches* culture was placed in the center of a 9 cm CMA dish and placed as a lid on the top of the cup immediately after water was added to the dry plant tissues. The cup and dish were sealed with Parafilm and incubated in a growth cabinet at 24 °C for 4 days. The colony diameter of *A. euteiches* was measured on the lid daily using a measuring scale. After 4 days, the culture dish lids were removed from the cups, placed in the same growth cabinet at 24 °C, and observed for further growth of *A. euteiches*.

In Vitro Exposure of the Mycelium to Volatiles: Effect of Exposure Time. Hydrated *B. juncea* shoot tissue (140 mg) was used to produce volatile compounds which were exposed to an actively growing *A. euteiches* plug (7 mm diameter) put on fresh CMA dishes as in the dose experiment described above. Three exposure times were used, 40, 80, and 120 min, with three replicates of each. After exposure, the dishes were incubated at 24 °C, and the colony diameter of *A. euteiches* was measured daily using a measuring scale on the lid. After 4 days, the culture dish lids were removed from the cups, placed in the same growth cabinet at 24 °C, and observed for further growth of *A. euteiches*.

Exposure with ITC Chemical Standards. An in vitro experiment was performed using authentic chemical standards (CSs) of volatile

Table 1. Major Isothiocyanates Detected from 140 mg of Hydrated Dried Plant Tissues of *S. alba* and *B. juncea* and Their Chemical Standard Mixtures (1 mL Each) (S.alba-CS and B.juncea-CS)[a]

treatment	allyl (μg/min)	SE[b]	benzyl (μg/min)	SE	phenylethyl (μg/min)	SE
S. alba at 0−10 min	0.0003	0.00002	0.0245	0.00299	0.0026	0.00009
S.alba-CS[c] at 0−10 min	0.0013	0.00013	0.2051	0.05291	0.0123	0.00483
B. juncea at 60−70 min	0.3650	0.00710	nd[e]		0.0003	0.00005
B.juncea-CS[d] at 60−70 min	0.4310	0.01100	ni[f]		nd	

[a]Samples were taken 0−10 and 60−70 min after addition of water according to the highest peaks with 140 mg of dried plant tissues of *S. alba* and *B. juncea*, respectively. [b]Standard error. [c]Mixture of chemicals standard for predominant ITCs from *S. alba* denoted as "S.alba-CS". [d]Mixture of chemicals standard for predominant ITCs from *B. juncea* denoted as "B.juncea-CS". [e]Not detected. [f]Not included in mixture.

compounds produced from *B. juncea* and *S. alba* tissues, identified as described below. Standard solution mixtures were designed to give concentrations of volatile compounds that closely resembled those recorded from hydrated dry shoot tissue by collecting volatile compounds from plant tissue and CSs under the same conditions and quantifying the major components by gas chromatography (Table 1). The *B. juncea* chemical standard mixture (B.juncea-CS) contained allyl isothiocyanate (40 μg/μL, >98% purity, Sigma-Aldrich Sweden AB) and phenylethyl isothiocyanate (2 μg/μL, 99% purity, Sigma-Aldrich Sweden AB). The *S. alba* chemical standard mixture (S.alba-CS) contained benzyl isothiocyanate (30 μg/μL, 98% purity, Sigma-Aldrich Sweden AB), phenylethyl isothiocyanate (5 μg/μL) and allyl isothiocyanate (0.2 μg/μL). All chemical standard mixtures were dissolved in hexane.

A 1 μL volume of each B.juncea-CS and S.alba-CS standard mixture was placed in the center of a filter paper in a sealed plastic cup containing an actively growing *A. euteiches* mycelium (7 mm plug) placed on a fresh CMA dish and incubated in the dark at 22 °C. Hyphal growth was measured daily for 4 days using a measuring scale. The growth was compared with the growth of an *A. euteiches* volatile-exposed culture where the volatiles originated from 140 mg of hydrated dried tissues of *B. juncea* and *S. alba* using water and hexane as control treatments. For details of ITC analyses, see below.

Glucosinolate Analysis. Glucosinolates were extracted from ground shoot tissue.[37] In brief, GLSs were extracted from 100 mg of dry shoot tissue by 70% MeOH which was heated to 90 °C to deactivate myrosinase and therefore avoid degradation of the GSLs. The extracts were transferred to a DEAE-Sephadex 25 column (Sigma, St. Louis, MO) before desulfating. Desulfoglucosinolates were separated and identified using HPLC with an acetonitrile/Milli-Q water gradient. GSL detection was performed with a photodiode array detector with 229 nm wavelength. The correction factors at 229 nm to calculate the concentrations of GSLs were followed.[38,39] The peaks of desulfoglucosinolates were identified by comparison with standards on the basis of retention times and ultraviolet spectra. Different concentrations of sinigrin (2-propenyl) (Acros Organics, Fair Lawn, NJ) were used as an external standard and extracted following the same procedure as that for the shoot tissue. The levels of GSLs were calculated on the basis of the dry weight of the tissues.

Isothiocyanate Analysis. Ground shoot tissue (140 mg) was placed in a glass dish and moistened with 5 mL of Milli-Q water. The suspension was immediately placed under a bell-shaped glass vessel (380 mL) with two openings and sealed with bulldog clips at 24 ± 2 °C in the dark. Volatile compounds were collected by pulling air from the outlet of the jar through a glass liner containing Tenax TA (50 mg, 60/80 mesh, Supelco, Bellefont, PA).

A positive pressure push−pull system was used, with charcoal-filtered air pushed through an inlet into the vessel at 500 mL/min and pulled out through the adsorbent at 350 mL/min. The greater push rate prevented entry of contaminating volatiles. All glassware and Teflon tubes (connecting air flow tubes) were washed with detergent, distilled water, and acetone and baked in an oven at 175 °C for at least 16 h prior to the entrainment. Charcoal filters and glass liners with Tenax TA were baked at 175 and 220 °C, respectively, under N_2 flow for 16 h. Volatiles were collected for periods of 10 min at 0−10, 30−40, 60−70, and 120−130 min after addition of water to the tissue. The rest of the time the outlet of the glass vessel was open, preventing the buildup of released volatiles.

Concentrations of ITCs arising from the dosing of CS solutions as described above were determined by analyzing 1 μL of either B.juncea-CS or S.alba-CS mixture put on a filter paper placed inside a sealed plastic cup (220 mL). A glass liner (with Tenax TA) was inserted through a hole in the plastic cup, and air was pulled from the cup at a flow rate of 350 mL/min. The aim was to sample at the peak concentration of the major ITCs, which was after 60−70 min of incubation for B.juncea-CS and 0−10 min of incubation for S.alba-CS as indicated by previous analysis of volatiles from *B. juncea* and *S. alba* plant tissues. Volatiles were collected for 10 min and analyzed by gas chromatography as described below.

For quantification, collected volatiles were analyzed by gas chromatography (GC) on an Agilent 6890N with a flame ionization detector equipped with an HP-1 column (100% dimethylpolysiloxane, 50 m, 0.32 mm i.d., 0.52 μm film thickness, J&W Scientific, Folsom, CA) and fitted with an Optic 3 thermal desorption system (Atas GL International, Veldhoven, The Netherlands). An internal standard, 50 ng of decane, was injected onto the glass liner containing the sample prior to desorption. The liner containing the Tenax with absorbed volatiles was placed directly into the injector, and volatiles were thermally desorbed starting at 30 °C for 0.5 min and rising at 16 °C/s to 250 °C. The GC temperature program was 30 °C for 3 min, 5 °C/min to 150 °C for 0.1 min, and then 10 °C/min to 250 °C for 15 min using hydrogen as the carrier. The amount of each compound was calculated relative to the internal standard.

For tentative compound identification, volatile samples from the treatments, *B. juncea* hydrated plant tissue, B.juncea-CS mixture, *S. alba* hydrated plant tissue, and S.alba-CS mixture, were collected as described above and analyzed by coupled GC−mass spectrometry using an Agilent 7890N gas chromatograph coupled to an Agilent 5975C mass-selective detector (electron impact 70 eV) fitted with an Optic 3 thermal desorption system (Atas GL International). The thermal desorption and GC oven temperature programs were as described above. The carrier gas was helium with a flow rate of 1.3 mL/min. Volatile compounds were identified by comparison against a commercially available library (National Institute of Standards and Technology, NIST 08, Gaithersburg, MD) and by comparison of mass spectra and retention indices with commercially available authentic standards where available (Sigma-Aldrich Sweden AB). Where standards were unavailable, in some cases the retention index (Kovats Index, KI) of the substance could be matched with a previously published KI for the compound on the type of GC column used in the current study (HP-1) (Figure 5).

ITC/GSL Ratios. ITC/GSL ratios were calculated for selected GSLs. 2-Propenyl glucosinolate was the dominant GSL in *B. juncea* shoot tissues, and *p*-hydroxybenzyl glucosinolate was dominant in *S. alba* shoot tissues. 2-Phenylethyl was detected in both plant tissues as a common GSL. The detected GSLs were recorded as micromoles per gram of dry tissue in the GC analysis (Table 2) and converted to micrograms for the selected GSLs using their molecular weights. Estimated amounts of ITCs produced from their parent GSLs in hydrated plant tissues during the initial 130 min were calculated (Figure 5). Total amounts of each ITC (μg) produced in the initial 130 min of hydrolysis from 1 g of hydrated dry tissue was divided by

Table 2. Different Glucosinolates and Concentrations (μmol/g) in Dry Shoot Tissue of *B. juncea* (cv. Pacific Gold) and *S. alba* (cv. Architect)

compd	*B. juncea*	SE	*S. alba*	SE
	Aliphatic			
2-(*S*)-2-hydroxybutenyl	nd[a]	nd	0.515	0.023
5-(methylsulfinyl)pentyl	nd	nd	0.008	0.005
4-pentenyl	0.011	0.006	nd	nd
n-butyl	0.032	0.011	nd	nd
3-(methylthio)propyl	nd	nd	0.013	0.004
3-butenyl	0.012	0.007	0.062	0.005
2-hydroxy-3-butenyl	nd	nd	0.018	0.001
2-propenyl	3.909	0.497	nd	nd
unknown	0.019	0.007	nd	nd
	Aromatic			
2-phenylethyl	0.119	0.016	0.068	0.005
benzyl	nd	nd	0.483	0.054
p-hydroxybenzyl	nd	nd	7.935	0.981
	Indolyl			
(4-hydroxy-3-indolyl)methyl	0.006	0.004	nd	nd
(4-methoxy-3-indolyl)methyl	0.001	0.001	0.008	0.001
3-indolylmethyl	0.040	0.007	0.016	0.002
(1-methoxy-3-indolyl)methyl	0.008	0.002	0.009	0.002
total	4.156		9.136	

[a]Not detected.

the amount of each GSL (μg) in 1 g of dry tissue and multiplied by 100 to determine the ITC/GSL ratios.

Statistical Analysis. The mean DSI and radial growth of hyphae were transformed to their natural logarithms. The experiments were generally analyzed in accordance with their completely randomized design. However, the soil treatment (sterilized vs nonsterilized) in the test of disease development on peas after oospore exposure to ITC volatile compounds was treated as a subplot factor and the cover crops were treated as the main plot factor in a split plot design. The effect of the cover crop, dose of cover crops, and time of exposure to the volatile and cover crop/chemical were treated as fixed factors in all experiments, and each replicate was treated as a random factor. Analyses of variances were made using the procedure linear model, and least-squares means were compared using Tukey's test with a $P \leq 0.05$ significance limit in R version 2.15.1 (The R Foundation, 2012).

RESULTS

Effects of Volatile Compounds on Oospores. Volatile compounds from hydrated *B. juncea* dry tissue strongly reduced the inoculum potential of *A. euteiches* oospores, shown by a significant reduction in pea root rot symptoms compared to that of control shoot tissues from the other species ($P < 0.001$, SE ± 0.120; Figure 1). The other cover crops or soil sterilization before the experiment started had no significant effect on disease development.

Effect of Volatile Compounds on Hyphal Growth: Effect of Dose. *B. juncea* shoot tissue suppressed the hyphal growth of *A. euteiches* more efficiently than tissue from the other species ($P < 0.001$) (Figure 2). The hyphal growth of *A. euteiches* was more affected by shoot tissue dose with *B. juncea* than with *S. alba* (dose × cover crop interaction, $P < 0.001$). The highest dose of *B. juncea* shoot tissue completely inhibited growth, and no further growth was registered when these cultures were placed in fresh air. The volatile compounds produced from the lower doses of *B. juncea* and the highest dose of *S. alba* also reduced the hyphal growth of *A. euteiches*

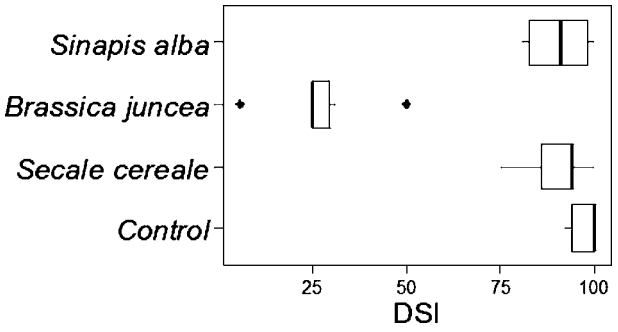

Figure 1. Pea root rot symptoms registered in a bioassay depending on pretreatment of *Aphanomyces* oospores with volatile compounds from hydrated dry plant tissues. Pea seedlings were rated for pea root rot 3 weeks after pea seed sowing. The scale for disease severity index (DSI) is 0−100%: 0%, healthy plant; 25%, root slightly discolored; 50%, root extensively discolored but not shrunken; 75%, root extensively discolored and shrunken; 100%, root partly or completely rotted or plant dead.[36] The value of DSI is back-transformed from the natural logarithm. Control = water.

significantly compared with the water control. No effect was found in the *Se. cereale* tissue treatment.

Effect of Volatile Compounds on Hyphal Growth: Effect of Exposure Time. The hyphal growth of *A. euteiches* was affected by the time of exposure to volatile compounds produced from hydrolyzed *B. juncea* shoot tissue ($P = 0.002$). The volatile compounds from the 140 mg dose of hydrated *B. juncea* shoot tissue completely inhibited the growth of *A. euteiches* after exposure for 120 min (Figure 3). No further growth was observed during the following days when the cultures were placed in fresh air.

Effects of Chemical Standard Mixtures. Volatile compounds arising from the chemical standard mixtures suppressed the growth of *A. euteiches* in vitro ($P < 0.001$). Volatile compounds from hydrated *B. juncea* dried shoot tissue and both chemical standard mixtures, B.juncea-CS and S.alba-CS, completely inhibited the growth of *A. euteiches* (Figure 4). There was no further growth in the following days when the cultures were placed in fresh air. Volatile compounds from hydrated *S. alba* tissue also caused some reduction of hyphal growth compared to the water control. No inhibition of pathogen growth was observed when exposed to the solvent hexane.

Glucosinolates in *B. juncea* and *S. alba* Shoot Tissues. Both species contained aliphatic, aromatic, and indolyl GSLs. Total extracted GSL concentrations in *S. alba* were higher than the concentration of GSLs in *B. juncea*. *S. alba* contained one more GSL compound than *B. juncea*. The aliphatic 2-propenyl glucosinolate dominated in *B. juncea*, and the aromatic *p*-hydroxybenzyl glucosinolate dominated in the *S. alba* tissue (Table 2).

Isothiocyanates from *B. juncea* and *S. alba*. *S. alba* shoot tissue produced more volatile compounds and a greater total amount of ITCs than *B. juncea*. *S. alba* and *B. juncea* were dominated by aromatic benzyl isothiocyanate hydrolyzed from *p*-hydroxybenzyl and benzyl glucosinolates and aliphatic allyl isothiocyanate from 2-propenyl glucosinolate, respectively. Both plant species produced the aromatic phenylethyl isothiocyanate (Table 3).

Pattern of ITC Release from *B. juncea* and *S. alba* Hydrated Tissues. ITCs were released faster from the GSLs in *S. alba* than from the GSLs in *B. juncea* tissue at the

dx.doi.org/10.1021/jf501776c | J. Agric. Food Chem. 2014, 62, 4584−4591

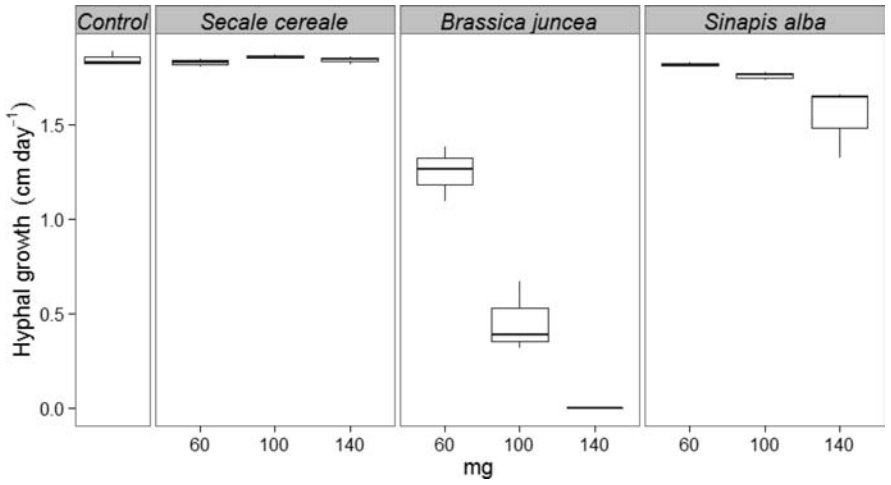

Figure 2. Effects of volatile compounds from 60, 100, and 140 mg of hydrated *B. juncea*, *S. alba*, and *S. cereale* dry shoot tissues on the hyphal growth (cm/day) of *A. euteiches* at 24 °C in vitro. Control = water.

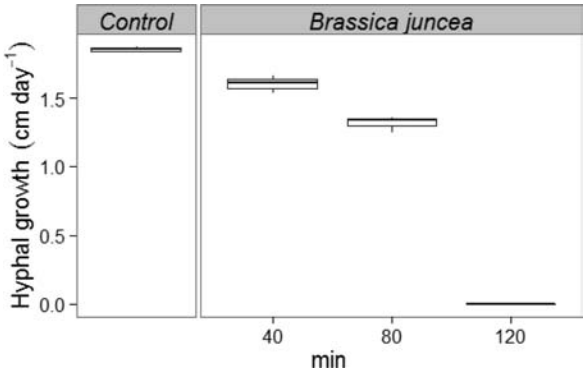

Figure 3. Effects of volatile compounds from 140 mg of hydrated *B. juncea* dry shoot tissues exposed for 40, 80, and 120 min on the hyphal growth (cm/day) of *A. euteiches* at 24 °C in vitro. Control = water.

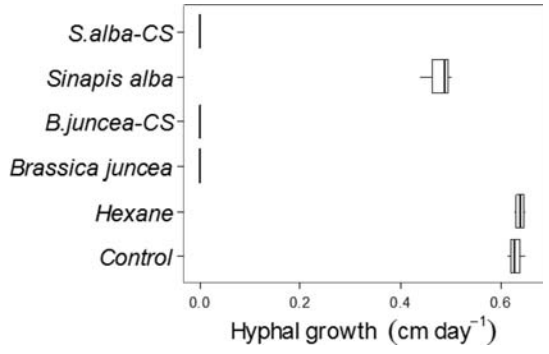

Figure 4. Effects of volatile compounds from 140 mg of hydrated *B. juncea* and *S. alba* dry shoot tissues and the chemical standard mixtures B.juncea-CS and S.alba-CS on the hyphal growth (cm/day) of *A. euteiches* at 22 °C in vitro. Control = water.

Table 3. Volatile Compounds (μg/min) in the First 2 h after Addition of Water in 1 g of Dry Shoot Tissue of *B. juncea* (cv. Pacific Gold) and *S. alba* (cv. Architect)

compd	*B. juncea*	SE	*S. alba*	SE
	Aliphatic ITC			
3-butenyl[b]	0.0024	0.0003	0.0352	0.0104
4-methylpentyl[b]	nd[e]		0.005	0.0014
allyl[a]	0.2077	0.0211	0.0016	0.0007
n-heptyl[a]	nd		0.0005	0.0001
n-hexyl[a]	nd		0.0024	0.0009
n-pentyl[a]	nd		0.0008	0.0002
sec-butyl[c]	0.0022	0.0004	0.0007	0.0003
	Aromatic ITC			
benzyl[a]	nd		0.1851	0.0404
phenylethyl[a]	0.0112	0.0021	0.0289	0.0046
	Others			
(*Z*)-3-hexen-1-ol[a]	nd		0.0017	0.0002
(*Z*)-3-hexenal[a]	0.0019	0.0006	0.0024	0.0007
3,5-octadien-2-one[d]	0.0014	0.0003	0.0023	0.0005
allyl thiocyanate[b]	0.0211	0.0022	nd	
benzaldehyde[a]	0.0024	0.0004	0.0058	0.0011
benzyl isocyanate[a]	nd		0.0014	0.0003
2-phenylpropane[d]	0.0088	0.0047	0.0054	0.0032
diallyl disulfide[a]	nd		0.0003	0.0001
dimethyl disulfide[a]	nd		0.0005	0.0003
total	0.2591		0.28	

[a]Mass spectrum and retention index (Kovats Index, KI) match with National Institute of Standards and Technology standard library (NIST 08) and with an authentic standard. [b]Mass spectrum match in NIST 08 and KI concurs with published KI.[40] [c]No satisfactory match in NIST 08, but mass spectrum matches published spectrum.[41] [d]Match in NIST 08. [e]Not determined.

beginning of hydrolysis (Figure 5). The GSLs of *B. juncea* produced ITCs over a longer time with increasing rate compared to ITCs from *S. alba* tissue. The estimated ITC/GSL ratio of the dominant aliphatic 2-propenyl producing allyl isothiocyanate in *B. juncea* was 1.82. The ITC/GSL ratio for the dominant aromatic *p*-hydroxybenzyl and benzyl producing benzyl isothiocyanate in *S. alba* was 0.56. The ratio of the aromatic 2-phenylethyl glucosinolate producing phenylethyl isothiocyanate, which was common to both species, was 11.51 for *B. juncea* and 15.51 for *S. alba*.

The release patterns of phenylethyl isothiocyanate were different for the two species, even though the originating 2-phenylethyl glucosinolate was the same in both species. Instead, it followed the same pattern as the dominant allyl isothiocyanate in *B. juncea* and benzyl isothiocyanate in *S. alba* (Figure 5).

dx.doi.org/10.1021/jf501776c | J. Agric. Food Chem. 2014, 62, 4584−4591

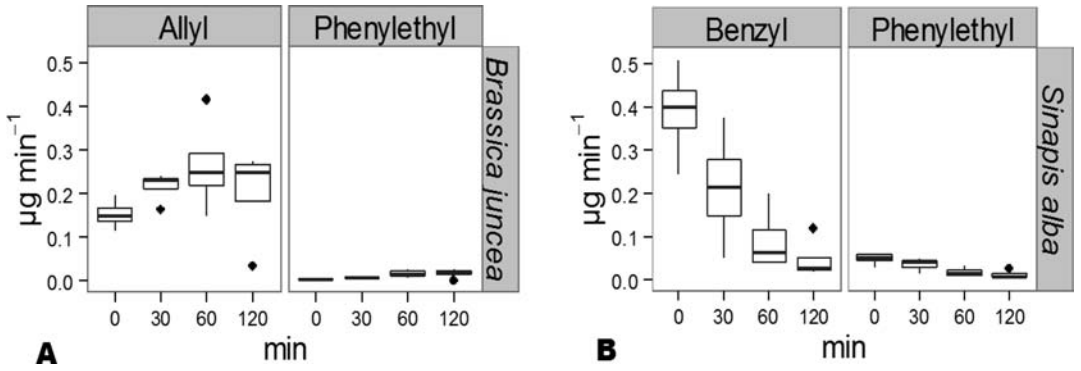

Figure 5. Release pattern and concentration of allyl, benzyl, and phenylethyl isothiocyanates at different time (min) points after addition of water to 1 g of dry shoot tissue of (A) *B. juncea* (cv. Pacific Gold) and (B) *S. alba* (cv. Architect).

DISCUSSION

This study shows that volatile compounds produced by brassica shoot tissue have a strong inhibitory effect on *A. euteiches*. However, the results also highlight the importance of understanding the mechanisms behind the suppression when designing systems where plants containing GSLs are used to control soil-borne pathogens. We show that the brassica species, dose of ITC, and time of exposure interact in determining the effect of the volatile compounds on the *A. euteiches* mycelium or oospores.

We used shoot tissues from two brassica species with different GSL profiles. Although we used cultivars different from those in earlier investigations, produced the plant tissue under greenhouse conditions, partly with artificial light, and dried the material to standardized dosages, the variety and concentration of GSLs in *B. juncea* and *S. alba* shoot tissues were similar to those found in earlier studies.[10,15,42−45] This indicates that the GSL composition remains consistent in the plant species despite differences in cultivar, growing conditions, and low-temperature drying of the plant material. As a consequence of the composition of GSLs, we found that the volatile compounds produced from *B. juncea* and *S. alba* were dominated by allyl and benzyl isothiocyanates, respectively, which is in line with earlier studies.[10] The thick-walled, long-lived oospores of *A. euteiches* are structures very different from the thin-walled *A. euteiches* hyphae. Nevertheless, suppression by direct exposure to volatile compounds was shown for both these reproductive structures. For both mycelium and oospore exposures, volatiles hydrolyzed from *B. juncea* tissue were more effective than volatiles from *S. alba* tissue. Previous investigations comparing the effects of aliphatic and aromatic ITCs tested the survival of weevil larvae.[30] The conclusion was that the aliphatic allyl isothiocyanate is likely to have greater biological activity than the aromatic ITCs, which is in line with the biological responses observed in the current study.

The in vitro data from the current study show that the amount of *B. juncea* tissue used was lethal to *A. euteiches*, whereas the equivalent amount of *S. alba* tissue did not completely prevent pathogen growth. This indicates that the highest dose of *S. alba* dry shoot tissue did not produce a high enough concentration of volatile compounds to prevent pathogen growth. However, in the experiment with chemical standards, the volatile compounds released from the *S. alba* chemical mixture completely prevented hyphal growth. The analysis of collected volatile compounds showed that the *S. alba* chemical mixture produced 10 times more ITCs than *S. alba* hydrated dry shoot tissue. It can be assumed that the concentration of ITCs contributes to their suppressive effects.

Our ITC analysis revealed differences in the pattern of ITC release between *B. juncea* and *S. alba* hydrated dry tissues. The calculated ITC/GSL ratios indicate that 2-propenyl glucosinolate is more efficient than *p*-hydroxybenzyl and benzyl glucosinolates at producing ITCs. The chemical structure and size of GSLs mainly regulate their efficiency of conversion into ITCs.[25,48] Our chemical analysis also shows the hydrated dry shoot tissue of *S. alba* released volatile compounds more rapidly, with the highest concentration recorded within a much shorter time than for *B. juncea*. The dominant ITC released by *B. juncea* tissue, allyl isothiocyanate, has a lower molecular weight and lower boiling point than benzyl isothiocyanate, the dominant compound released by *S. alba*. However, despite the expected higher volatility of allyl isothiocyanate, its concentration in the headspace of hydrolyzed powder of the respective plants was comparable to that of benzyl isothiocyanate. Although it is likely that the volatility of these ITCs does influence their toxicity, our results suggest that other factors inherent to the dry powders themselves are also important.

The hydrolysis process for the dominant aliphatic GSL in *B. juncea* shoot tissue seemed to follow a longer time course than that for the dominant aromatic GSL in *S. alba*. Furthermore, we observed that the release pattern of phenylethyl isothiocyanate differed between plant species, following the same pattern as the dominant ITC for each species. The ITC/GSL ratio (indicating the efficiency of production) of the species' common aromatic phenylethyl isothiocyanate from the parent 2-phenylethyl glucosinolate was lower in *B. juncea* tissue than in *S. alba*. This suggests that other traits inherent to the dry powders, such as plant cell structure or water-absorbing capacity, influence GSL hydrolysis and ITC release. These factors probably interact with the characteristics of the chemicals themselves, such as volatility, to determine the eventual ITRC release.[48] These factors, however, require further investigation.

Toxic effects from incorporated *B. juncea* plant tissue in *A. euteiches* contaminated soil have been shown to reduce the development of pea root rot, but an effect of ITCs has not always been established.[12,46] In a closed system, volatile ITCs can easily interact directly with the exposed pathogen. We show that the degree of detrimental effects from ITCs was enhanced as the time of pathogen exposure increased. For *A. euteiches* growing on CMA agar medium, the lethal dose of ITCs from *B. juncea* was reached after 2 h of exposure, showing the importance of keeping the concentration of effective ITCs

dx.doi.org/10.1021/jf501776c | J. Agric. Food Chem. 2014, 62, 4584−4591

high for this period. For an optimal effect in a biofumigation process, this suggests the use of a cover after incorporation of plant biomass to minimize evaporation of volatiles. This measure was also suggested in earlier studies.[47]

The current study shows that brassica plant tissue, its dominant ITCs, their concentration and release pattern, and exposure time are important factors for the suppression of *A. euteiches*. The results highlight the importance of choosing plant species with the most effective production ratio but also high biomass production to reach optimal concentration levels when GSL-containing plants are used for biofumigation. The results support the use of a cover to minimize dispersal of ITCs, which should allow the ITCs to interact directly with the pathogen for a longer period. However, the findings from this study need further verification under field conditions.

AUTHOR INFORMATION

Corresponding Author

*Phone: +46-1867-2349. Fax: +46-1867-2890. E-mail: Shakhawat.Hossain@slu.se.

Funding

This project was funded by the research program SLU EkoForsk at the Swedish University of Agricultural Sciences.

Notes

The authors declare no competing financial interest.

ACKNOWLEDGMENTS

We thank Erika Qvarfordt for technical assistance.

REFERENCES

(1) Papavizas, G. C.; Ayres, W. A. *Aphanomyces euteiches. Aphanomyces Species and Their Root Diseases in Pea and Sugarbeet: A Review*; Technical Bulletin 1485; U.S. Department of Agriculture: Washington, DC, 1974; pp 8−9.

(2) Persson, L.; Bodker, L.; Larson-Wikstrom, M. Prevalence and pathogenicity of foot and root rot pathogens of pea in southern Scandinavia. *Plant Dis.* **1997**, *81*, 171−174.

(3) Gaulin, E.; Jacquet, C.; Bottin, A.; Dumas, B. Root rot disease of legumes caused by *Aphanomyces euteiches*. *Mol. Plant Pathol.* **2007**, *8*, 539−548.

(4) Shang, H.; Grau, C. R.; Peters, R. D. Oospore germination of *Aphanomyces euteiches* in root exudates and on the rhizoplanes of crop plants. *Plant Dis.* **2000**, *84*, 994−998.

(5) Hardham, A. R.; Hyde, G. J. Asexual sporulation in the oomycetes. *Adv. Bot. Res.* **1997**, *24*, 353−398.

(6) McGee, J. R.; Coyne, C.; Pilet-Nayel, M.-L.; Moussart, A.; Tivoli, B.; Baranger, A.; Hamon, C.; Vandemark, G.; McPhee, K. Registration of pea germplasm lines partially resistant to Aphanomyces root rot for breeding fresh or freezer pea and dry pea types. *J. Plant Regist.* **2012**, *6*, 203−207.

(7) European Parliament, Council of the European Union. *Regulation (EC) No 1107/2009 of the European Parliament and of the Council of 21 October 2009, Concerning the Placing of Plant Protection Products on the Market and Repealing Council Directives 79/117/EEC and 91/414/EEC*; Brussels, Belgium, 2009.

(8) Hossain, S.; Bergkvist, G.; Berglund, K.; Mårtensson, A.; Persson, P. Aphanomyces pea root rot disease and control with special reference to impact of Brassicaceae cover crops. *Acta Agric. Scand., B* **2012**, *62*, 477−487.

(9) Lewis, J. A.; Papavizas, G. C. Evolution of volatile sulfur-containing compounds from decomposition of crucifers in soil. *Soil Biol. Biochem.* **1970**, *2*, 239−246.

(10) Brown, P. D.; Morra, M. J. Control of soil-borne plant pests using glucosinolate-containing plants. *Adv. Agron.* **1997**, *61*, 167−231.

(11) Kirkegaard, J. A.; Matthiessen, J. N. Developing and refining the biofumigation concept. *Agroindustria* **2005**, *3*, 5−11.

(12) Muehlchen, A. M.; Rand, R. E.; Parke, J. L. Evaluation of green manures for controlling Aphanomyces root rot of peas. *Plant Dis.* **1990**, *74*, 651−654.

(13) Lewis, J. A.; Papavizas, G. C. Effect of sulfur-containing volatile compounds and vapors from cabbage decomposition on *Aphanomyces euteiches*. *Phytopathology* **1971**, *61*, 208−214.

(14) Angus, J. F.; Gardner, P. A.; Kirkegaard, J. A.; Desmarchelier, J. M. Biofumigation: isothiocyanates released from *Brassica* roots inhibit growth of the take-all fungus. *Plant Soil* **1994**, *162*, 107−112.

(15) Fahey, J. W.; Zalcmann, A. T.; Talalay, P. The chemical diversity and distribution of glucosinolates and isothiocyanates among plants. *Phytochemistry* **2001**, *56*, 5−51.

(16) van Dam, N. M.; Tytgat, T. O. G.; Kirkegaard, J. A. Root and shoot glucosinolates: a comparison of their diversity, function and interactions in natural and managed ecosystems. *Phytochem. Rev.* **2009**, *8*, 171−186.

(17) Kiddle, G.; Bennett, R. N.; Botting, N. P.; Davidson, N. E.; Robertson, A. A. B.; Wallsgrove, R. M. High-performance liquid chromatographic separation of natural and synthetic desulphoglucosinolates and their chemical validation by UV, NMR and chemical ionisation-MS methods. *Phytochem. Anal.* **2001**, *12*, 226−242.

(18) Smolinska, U.; Morra, M. J.; Knudsen, G. R.; Brown, P. D. Toxicity of glucosinolate degradation products from *Brassica napus* seed meal towards *Aphanomyces euteiches* f. sp *pisi*. *Phytopathology* **1997**, *87*, 77−82.

(19) Malik, S. M.; Riley, B. M.; Norsworthy, K. J.; Bridges, W., Jr. Glucosinolate profile variation of growth stages of wild radish (*Raphanus raphanistrum*). *J. Agric. Food Chem.* **2010**, *58*, 3309−3315.

(20) Wittstock, U.; Halkier, B. A. Glucosinolate research in the *Arabidopsis era*. *Trends Plant Sci.* **2002**, *7*, 263−270.

(21) Brown, P. D.; Morra, M. J. Glucosinolate-containing plant tissues as bioherbicides. *J. Agric. Food Chem.* **1995**, *43*, 3070−3074.

(22) Sang, J. P.; Minchinton, P.; Johnstone, P.; Truscott, R. J. W. Glucosinolate profiles in the seed, root and leaf tissue of cabbage, mustard, rapeseed, radish and swede. *Can. J. Plant Sci.* **1984**, *64*, 77−93.

(23) Kawakishi, S.; Kaneko, T. Interaction of oxidized glutathione with allyl isothiocyanate. *Phytochemistry* **1985**, *24*, 715−718.

(24) Kirkegaard, J. A.; Sarwar, M.; Matthiessen, J. N. Assessing the biofumigation potential of crucifers. *Acta Hortic.* **1998**, *459*, 105−111.

(25) Smith, B. J.; Kirkegaard, J. A. *In vitro* inhibition of soil microorganisms by 2-phenylethyl isothiocyanate. *Plant Pathol.* **2002**, *51*, 585−593.

(26) Smolinska, U.; Morra, M. J.; Knudsen, G. R.; James, R. L. Isothiocyanates produced by *Brassica* species as inhibitors of *Fusarium oxysporum*. *Plant Dis.* **2003**, *87*, 407−412.

(27) Falk, K. L.; Vogel, C.; Textor, S.; Bartram, S.; Hick, A. Glucosinolate biosynthesis: demonstration and characterization of the condensing enzyme of the chain elongation cycle in *Eruca sativa*. *Phytochemistry* **2004**, *65*, 1073−84.

(28) Yuesheng, Z. The molecular basis that unifies the metabolism, cellular uptake and chemopreventive activities of dietary isothiocyanates. *Carcinogenesis* **2012**, *33*, 2−9.

(29) Abreu, A. C.; Borges, A.; Simoes, L. C.; Saavedra, M. J.; Simoes, M. Antibacterial activity of phenyl isothiocyanate on *Escherichia coli* and *Staphylococcus aureus*. *Med. Chem.* **2013**, *9*, 756−761.

(30) Matthiessen, J. N.; Shackleton, M. A. Biofumigation: environmental impacts on the biological activity of diverse pure and plant-derived isothiocyanates. *Pest Manage. Sci.* **2005**, *61*, 1043−1051.

(31) Gimsing, A. L.; Kirkegaard, J. A. Glucosinolate and isothiocyanate concentration in soil following incorporation of *Brassica* biofumigants. *Soil Biol. Biochem.* **2006**, *38*, 2255−2264.

(32) Rongai, D.; Cerato, C.; Lazzeri, L. A natural fungicide for the control of *Erysiphe betae* and *Erysiphe cichoracearum*. *Eur. J. Plant Pathol.* **2009**, *124*, 613−619.

(33) Bång, U. *Rhizoctonia solani* soil infestation in Sweden and biofumigation studies *in vitro*. *Abstracts of Papers and Posters*, 17th

Triennial Conference of the European Association of Potato Researchers, Brasov, Romania, July 6−10, 2008; European Association of Potato Researchers: Leuven, Belgium, 2008; pp 144−146.
(34) Schneider, C. L. Use of oospore inoculum of *Aphanomyces cochloides* to initiate blackroot disease in sugar beet seedlings. *J. Am. Soc. Sugar Beet* **1978**, *20*, 55−62.
(35) Persson, L.; Larsson-Wikström, M.; Gerhardson, B. Assessment of soil suppressiveness to Aphanomyces root rot of pea. *Plant Dis.* **1999**, *83*, 1108−1112.
(36) Parke, J. L.; Rand, R. E.; Joy, A. E.; King, E. B. Biological control of Pythium damping-off and Aphanomyces root rot of peas by application of *Pseudomonas cepacia* or *P. fluorescens* to seed. *Plant Dis.* **1991**, *75*, 987−992.
(37) Kabouw, P.; Biere, A.; van der Putten, W. H.; van Dam, N. M. Intra-specific differences in root and shoot glucosinolate profiles among white cabbage (*Brassica oleracea* var. *capitata*) cultivars. *J. Agric. Food Chem.* **2010**, *58*, 411−417.
(38) Buchner, R. Approach to determination of HPLC response factors for glucosinolates. In *Glucosinolates in Rapeseeds: Analytical Aspects*; Wathelet, J.-P., Ed.; Martinus Nijho Publishers: Boston, 1987; pp 50−58.
(39) Brown, P. D.; Tokuhisa, J. G.; Reichelt, M.; Gershenzon, J. Variation of glucosinolate accumulation among different organs and developmental stages of *Arabidopsis thaliana*. *Phytochemistry* **2003**, *62*, 471−481.
(40) Valette, L.; Fernandez, X.; Poulain, S.; Lizzani-Cuvelier, L.; Loiseau, A. M. Chemical composition of the volatile extracts from *Brassica oleracea* L. var. *botrytis* 'Romanesco' cauliflower seeds. *Flavour Fragrance J.* **2006**, *21*, 107−110.
(41) Kjaer, A.; Ohashi, M.; Wilson, J. M.; Djerassi, C. Mass spectra of isothiocyanates. *Acta Chem. Scand.* **1963**, *17*, 2143−2154.
(42) Bodnaryk, R. P. Developmental profile of sinalbin (*p*-hydroxybenzyl glucosinolate) in mustard seedlings, *Sinapis alba* L., and its relationship to insect resistance. *J. Chem. Ecol.* **1991**, *17*, 1543−1556.
(43) Morra, M. J.; Kirkegaard, J. A. Isothiocyanate release from soil incorporated *Brassica* tissues. *Soil Biol. Biochem.* **2002**, *34*, 163−1690.
(44) Kirkegaard, J. A.; Sarwar, M. Biofumigation potential of brassicas. I. Variation in glucosinolate profiles of diverse field-grown brassicas. *Plant Soil* **1998**, *201*, 71−89.
(45) Rosa, E. A. S.; Heaney, R. K.; Fenwick, G. R.; Portas, C. A. M. Glucosinolates in crop plants. *Horic. Rev.* **1997**, *19*, 99−215.
(46) Papavizas, G. C. Suppression of Aphanomyces root rot of peas by cruciferous soil amendments. *Phytopathology* **1966**, *56*, 1071−1075.
(47) Njoroge, S. M. C.; Riley, M. B.; Keinath, A. P. Effect of incorporation of *Brassica* spp. residues on population densities of soilborne microorganisms and on damping-off and Fusarium wilt of watermelon. *Plant Dis.* **2008**, *92*, 287−294.
(48) Sarwar, M.; Kirkegaard, J. A.; Wong, P. T. W.; Desmarchelier, J. M. Biofumigation potential of brassicas: in vitro toxicity of isothiocyanates to soil-borne fungal pathogens. *Plant Soil* **1998**, *201*, 103−112.

JOURNAL OF AGRICULTURAL AND FOOD CHEMISTRY

Article

pubs.acs.org/JAFC

Polyphenols in Strawberry (*Fragaria* × *ananassa*) Leaves Induced by Plant Activators

Anna Kårlund,[†] Juha-Pekka Salminen,[‡] Piia Koskinen,[‡] Jeffrey R. Ahern,[‡] Maarit Karonen,[‡] Kari Tiilikkala,[§] and Reijo O. Karjalainen*[,†]

[†]Department of Biology, University of Eastern Finland, P.O. Box 1627, FI-70211 Kuopio, Finland

[‡]Department of Chemistry, University of Turku, FI-20014 Turku, Finland

[§]Plant Production Research, MTT AgriFood Research Finland, FI-31600 Jokioinen, Finland

Supporting Information

ABSTRACT: Strawberry leaves contain high amounts of diverse phenolic compounds potentially possessing defensive activities against microbial pathogens and beneficial properties for human health. In this work, young strawberry plants were treated with two plant activators, *S*-methylbenzo-1,2,3-thaidiazole-7-carbothiate (BTH) and birch wood distillate. Phenolic compounds from activator-treated and control leaves were subjected to quantitative analyses by HPLC-DAD, HPLC-ESI-MS, and microQTOF ESI-MS. Thirty-two different phenolic compounds were detected and characterized, and 21 different ellagitannins constituted the largest group of compounds in the strawberry leaves (37.88−45.82 mg/g dry weight, 47.0−54.3% of total phenolics). Treatment with BTH resulted in higher levels of individual ellagitannins, whereas treatment with birch wood distillate strongly increased the levels of chlorogenic acid in strawberry leaves compared with the control. The results suggest that different plant activators may be useful tools for the activation of different branches in the phenylpropanoid biosynthesis in strawberry.

KEYWORDS: *polyphenols, strawberry (Fragaria × ananassa), leaves, BTH, activators*

INTRODUCTION

During the evolutionary history of terrestrial plants, plant surfaces have been continuously exposed to abiotic and biotic stresses caused by environmental factors such as ultraviolet-B (UV-B) radiation, ozone, and numerous plant pathogens and insects. In agriculture, pesticides are extensively used to control diseases, insects, and weeds to protect and improve yields and might be considered a necessity of modern farming.[1−3] Despite the benefits of pesticides to crop yields, these chemicals can additionally cause some health hazards to pesticide-manufacturing workers and farmers, and also consumers and workers in the food industry are exposed daily to plant pesticides and pesticide residues via plants or food of plant origin.[1−3] In the future, changing climatic variables, such as altered wind patterns and rising temperatures, may further increase pest outbreaks and the need for pesticide application and directly or indirectly alter the behavior of pesticides, for example, fungicides, in agricultural lands and plant surfaces.[4−6] Altogether, application of pesticides can also cause some external, delayed costs from damage to the environment, human health, and other production sectors.[3,5] Apart from better awareness and safety practices, there is likely a growing need and demand for inexpensive and effective but at the same time more natural pesticides. Phenolic compounds, a large class of plant secondary metabolites, are an important component of plants' natural defense against pathogens. Elicitor molecules are exogenous or endogenous compounds that can activate defense compounds, secondary metabolites, or their synthesis in an organism. Elicitors that induce pathways enhancing the accumulation of phenolic compounds can be utilized to protect plants from infections.[7]

Polyphenolic compounds have been, and still are, important mediators in the adaptation and survival responses of plants in acute and chronic challenges. Polyphenols, such as ellagitannins, appear to play an important role in plant defense against insect pests[8] and plant pathogens.[9] Also, plants growing naturally in high latitudes,[10] high temperature, and high light conditions[11] or under low nitrogen and phosphorus availability[12,13] may contain relatively high concentrations of phenolic compounds. UV-B radiation[14] and ozone-induced stress[15,16] are capable of causing variable changes in polyphenol profiles. Polyphenols also act in plants regulating cell growth, differentiation, pollen fertility, and nodulation and thus may contribute some vital features of plant fitness.[17,18] The concentration of polyphenols in plants varies widely during plant development and in different plant organs.[19] The concentration of antimicrobial polyphenols can be increased by exposing plants to mild microbial infection or infection mimicking treatment, that is, by application of elicitor-active compounds capable of activation of defensive pathways. For example, *S*-methylbenzo-1,2,3-thaidiazole-7-carbothiate (BTH) is successfully used in numerous plants to activate plant defense systems, increasing concentrations of different polyphenols.[20]

Recently it has been found that leaves of berry plants are rich in bioactive polyphenols. High concentrations of polyphenols have been measured from black currant (*Ribes nigrum*),[21] raspberry (*Rubus ideaus*),[22] bilberry (*Vaccinium myrtillus*),[10]

Received: December 16, 2013
Revised: April 16, 2014
Accepted: April 16, 2014
Published: April 16, 2014

ACS Publications © 2014 American Chemical Society

saskatoon (*Amelanchier alnifolia*),[23] and strawberry (*Fragaria* × *ananassa*)[24] leaves. Strawberries are extensively grown horticultural crop plants possessing a wide range of bioactive compounds. In strawberry, antioxidant capacity in leaves has been found higher than in berries,[19] and the extract made from wild strawberry leaves has demonstrated a direct, endothelium-dependent vasodilator activity.[25] Potentially beneficial health effects of strawberry polyphenols against, for example, cancer,[26] cardiovascular diseases,[27] inflammation-related diseases,[28] and Alzheimer's disease,[29] have been reported. These observations suggest that strawberry leaves may be a promising bioresource for diverse health-related applications; this could increase the level of utilization and the value of the plant material. Although polyphenols from strawberry fruits have been extensively analyzed from different cultivars during the past few years, little is known about the individual phenolic compounds occurring in strawberry leaves.[30,31] We previously analyzed some of the phenolic compounds in greenhouse-grown strawberry leaves.[32] We also detected improved resistance of strawberry leaves to powdery mildew (*Sphaerotheca macularis* Wall. ex. Fr) after BTH exposure.[32]

Byproducts of a slow thermal conversion process, also known as pyrolysis of wood material, have been used in Asian countries for centuries as growth stimulants, fertilizers, fungicides, herbivore repellents, and herbicides, and today they are marketed globally as biological control agents.[33,34] Birch wood distillate is a byproduct of birch wood processing formed during pyrolysis,[33] and its tar-free fraction contains mainly acetic acid, methanol, hydroxypropanone, furfural, and acetone.[34] Fractions of birch wood distillate may act as plant-based biological control agents that can possibly be used as a commercial plant-protecting agent of low environmental risk.[34,35]

In the present study, extensive analysis using powerful liquid chromatography coupled to diode array detection and electrospray ionization mass spectrometry (HPLC-DAD, HPLC-ESI-MS, and microQTOF ESI-MS) was conducted to further identify and characterize the induced polyphenols from BTH- and birch wood distillate-treated strawberry leaves to clarify the potential of strawberry leaves as a source of health-beneficial compounds and BTH and birch wood distillate as plant-protecting agents.

MATERIALS AND METHODS

Plant Material. Strawberries (cv. Polka) were grown at the MTT AgriFood Research Finland (Jokioinen, Finland) greenhouses in 7 cm pots in a peat−sand mixture (3:1) and fertilized weekly with Superflex-9 fertilizer (19% N, 5% P, 20% K). The following growth conditions were used: relative humidity, 50−70% (night−day); daylight, 16 h; and temperature, 19−22 °C (night−day). Plants were grown until they had at least four fully developed leaves before the treatments were begun.

Two hundred strawberry plants were randomly divided into three groups of 40−80 plants. One group was sprayed with 0.5 g/L active BTH (Bion 50 WG, Syngenta, ca. 5 mL per plant) according to our previous work.[32] One group was sprayed with 10% birch wood distillate (ca. 5 mL per plant) containing, for example, acids, ether-solubles, ether-insolubles ("wood syrup"), and polycyclic aromatic hydrocarbons.[34] Further composition of the distillate is described in Fagernäs et al.[34] The control group was sprayed with water until runoff (ca. 5 mL per plant). Samples for chemical analysis were collected from control plants immediately after treatment (day 0) and from control and BTH- and birch wood distillate-treated plants 7 days after treatment (day 7).[32] All samples were collected at the same time of day (at 12−2 p.m.) under uniform light conditions. For each treatment/sampling date combination, we randomly selected 10 plants and destructively harvested leaves for chemical analyses. From these 10 plants, leaves from 2−3 plants were pooled, creating four unique sample replicates per treatment/sampling date combination. Samples were immediately frozen with liquid nitrogen and stored at −80 °C until they were freeze-dried.

Sample Preparation, Extraction, and Fractionation. Freeze-dried samples were homogenized into a fine powder using a ball grinder (Retsch MM200, Haan, Germany) and stored in a −20 °C freezer until the chemical analyses were conducted. Our analytic workflow was as follows: (1) initial sample screening; (2) preparative scale extraction, fractionation, and MRM method development; (3) quantitative analysis of phenolic compounds by UPLC-DAD-MS/MS; and (4) qualitative analysis of phenolics by HPLC-ESI-QTOF-MS.

Initial Sample Screening. For initial screening and subsequent quantitative analysis, analytical scale extractions were used: samples of 10 mg were extracted with 2 × 1400 μL of acetone/water (80:20, v/v). The extracts were concentrated into water phase with a vacuum concentrator (Eppendorf concentrator 5301, Hamburg, Germany), freeze-dried (Christ Alpha 2-4, Osterode, Germany), redissolved into 1 mL of water, and filtered through 0.20 μm PTFE filters (VWR International, Darmstadt, Germany). We first conducted preliminary analyses to identify the major phenolic compounds present in all samples using UPLC-MS/MS (see experimental methods below).

Preparative Scale Extraction, Fractionation, and MRM Method Development. For preparative scale extractions, 8 g of ground leaf material was extracted with 5 × 200 mL acetone/water (80:20, v/v). Acetone was evaporated from the pooled extracts by rotary evaporation and the water phase freeze-dried. Two grams of the freeze-dried extract was dissolved into 30 mL of water and fractionated with Sephadex LH-20 (Pharmacia, Uppsala, Sweden) gel chromatography as described by Salminen and Karonen.[36] The Sephadex fractions containing the polyphenols were further fractionated by semipreparative HPLC using a Waters Delta 600 (Waters, Milford, MA, USA) system equipped with Fraction Collector III. The column used was Phenomenex Gemini C18 (10 μm, 150 × 21.2 mm, Phenomenex, Torrance, CA, USA) with 0.1% formic acid and acetonitrile as eluents. These purified compounds were used by direct infusion with a Waters XEVO triple-quadrupole mass spectrometer to develop compound-specific multiple reaction monitoring (MRM) methods and quantitative calibration curves for the specific measurement of each major metabolite in our samples (Table 1).[37] Isomeric compound pairs with the same molecular masses were quantified using the same calibration curve for both of the compounds.

Quantitative Analysis of Phenolic Compounds by UPLC-DAD-MS/MS. For quantitative analyses, phenolic extracts from each sample (after 30× dilution with water) were analyzed using ultraperformance liquid chromatography with an electrospray triple-quadrupole mass spectrometry detector (UPLC-MS/MS) and compound-specific MRM methods. The Waters Acquity Xevo UPLC-MS/MS (Waters, Milford, MA, USA) system utilized a Waters Acquity UPLC BEH Phenyl column (1.7 μm, 2.1 × 100 mm, Waters, Dublin, Ireland) column with acetonitrile (A) and 0.1% formic acid (B) as eluents. The gradient was as follows: 0−0.5 min, 0.1% A (isocratic); 0.5−5 min, 0.1−30% A in B (linear gradient); 5−5.1 min, 30−90% A in B (linear gradient); 5.1−7.1 min, 90% A (isocratic); 7.1−7.2 min, 90−0.1% A in B (linear gradient); 7.2−8.5 min, 0.1% A (isocratic). The flow rate was 0.500 mL/min. Five microliters of the sample extract was injected into the UPLC column. Phenolic concentrations were calculated as milligrams per gram dry weight.

Qualitative Analysis of Phenolics by HPLC-ESI-QTOF-MS. All fractions and extracts were analyzed by the HPLC-DAD-ESI-QTOF-MS system consisting of an Agilent 1200 series HPLC equipped with a diode array detector (Agilent Technologies, Waldbronn, Germany) and micrOTOF-Q ESI-mass spectrometer (Bruker Daltonics, Bremen, Germany). Chromatographic separations were performed using a Waters Acquity UPLC BEH C18 column (1.7 μm, 50 mm × 2.1 mm, Waters, Dublin, Ireland). The binary mobile phase consisted of acetonitrile (A) and 0.1% formic acid (B). The elution profile was as follows: 0−0.1 min, 0% A (isocratic); 0.1−5 min, 0−30% A in B

Table 1. Phenolic Compounds Quantified from Strawberry Leaves, Their Molecular Formulas, High-Resolution Mass Spectral Data, Composition, Retention Times in the UPLC-MS/MS Analysis, and Multiple Reaction Monitoring (MRM) Methods Used for Their Selective Quantification[a]

no.	code	compd identity	mol formula	calcd	measd	error (ppm)	composition	retention time in UPLC-MS/MS analysis (min)	quantitative MRM method: *m/z* of the mother ion → *m/z* of the daughter ion	cone voltage (V)	collision energy (eV)
1	G1	1-*O*-galloylglucose	$C_{13}H_{16}O_{10}$	332.0743	332.072	6.9	GLUC + G	1.25 (*1.47*, *2.00*, *2.44*)	331.03 → 168.92	34	22
2	G2	monogalloyl quinic acid	$C_{14}H_{16}O_{10}$	344.0743	344.0729	4.1	GLUC + Q	1.73	343.03 → 191.00	38	20
3	G3	trigalloyl glucose	$C_{27}H_{24}O_{18}$	636.0963	636.0980	−2.7	GLUC + 3G	3.35	634.97 → 464.97	32	24
4	E1	2,3-(*S*)-HHDP-glucose	$C_{20}H_{18}O_{14}$	482.0697	482.0669	5.8	GLUC + HHDP	1.02, 1.10	481.03 → 301.00	26	26
5	E2	pedunculagin	$C_{34}H_{24}O_{22}$	784.0759	784.0760	−0.1	GLUC + 2HHDP	2.49, 2.82	782.97 → 301.04	56	44
6	E3a	galloyl-HHDP-glucose **a**	$C_{27}H_{22}O_{18}$	634.0806	634.0802	−0.1	GLUC + G + HHDP	2.52	632.97 → 300.92	46	32
7	E3b	galloyl-HHDP-glucose **b**	$C_{27}H_{22}O_{18}$	634.0806	634.0802	0.6	GLUC + G + HHDP	2.71	632.97 → 300.92	46	32
8	E3c	galloyl-HHDP-glucose **c**	$C_{27}H_{22}O_{18}$	634.0806	634.0809	0.6	GLUC + G + HHDP	3.08	632.97 → 300.92	46	32
9	E4	tellimagrandin I	$C_{34}H_{26}O_{22}$	786.0916	786.0916	0.0	GLUC + 2G + HHDP	3.08, 3.31	784.97 → 300.97	55	40
10	E5	dimeric ellagitannin 1416 Da	$C_{61}H_{44}O_{40}$	1416.1409	1416.141	−0.1	2GLUC + G + 3HHDP	3.18	707.16 → 300.97	32	40
11	E6a	dimeric ellagitannin 1718 Da **a**	$C_{75}H_{50}O_{48}$	1718.1472	1718.1596	−7.2	2GLUC + G + 4HHDP	3.26	858.10 → 300.96	36	42
12	E6b	dimeric ellagitannin 1718 Da **b**	$C_{75}H_{50}O_{48}$	1718.1472	1718.1494	−1.3	2GLUC + G + 4HHDP	3.65	858.10 → 300.96	36	42
13	E6c	dimeric ellagitannin 1718 Da **c**	$C_{75}H_{50}O_{48}$	1718.1472	1718.1545	−4.2	2GLUC + G + 4HHDP	3.74	858.10 → 300.96	36	42
14	E7a	dimeric ellagitannin 2020 Da **a**	$C_{89}H_{56}O_{56}$	2020.1534	2020.1615	−4.0	2GLUC + 2G + 4HHDP + GA − H_2O	3.77	1009.16 → 300.99	40	54
15	E7b	dimeric ellagitannin 2020 Da **b**	$C_{89}H_{56}O_{56}$	2020.1534	2020.1583	−2.4	2GLUC + 2G + 4HHDP + GA − H_2O	4.16	1009.16 → 300.99	40	54
16	E7c	dimeric ellagitannin 2020 Da **c**	$C_{89}H_{56}O_{56}$	2020.1534	2020.1556	−1.1	2GLUC + 2G + 4HHDP + GA − H_2O	4.44	1009.16 → 300.99	40	54
17	E7d	dimeric ellagitannin 2020 Da **d**	$C_{89}H_{56}O_{56}$	2020.1534	2020.1523	0.5	2GLUC + 2G + 4HHDP + GA − H_2O	4.63	1009.16 → 300.99	40	54
18	E8**a**	dimeric ellagitannin 2038 Da **a**	$C_{89}H_{58}O_{57}$	2038.1640	2038.1623	0.8	2GLUC + 2G + 4HHDP + GA	3.84 (*3.90*)	996.16 → 300.96	42	55
19	E8**b**	dimeric ellagitannin 2038 Da **b**	$C_{89}H_{58}O_{57}$	2038.1640	2038.1676	−1.8	2GLUC + 2G + 4HHDP + GA	3.90	996.16 → 300.96	42	55
20	E9a	dimeric ellagitannin 1870 Da	$C_{82}H_{54}O_{52}$	1870.1581	1870.1616	−1.9	2GLUC + 2G + 4HHDP	3.95	934.10 → 300.99	38	46
21	E9b	agrimoniin	$C_{82}H_{54}O_{52}$	1870.1581	1870.1538	2.3	2GLUC + 2G + 4HHDP	4.15	934.10 → 300.99	38	46
22	E10	trimeric ellagitannin 2502 Da	$C_{109}H_{74}O_{70}$	2502.2231	2502.2216	0.6	3GLUC + 3G + 5HHDP	4.01	1250.40 → 301.00	45	65
23	E11	trimeric ellagitannin 2804 Da	$C_{123}H_{80}O_{78}$	2804.2293	2804.2282	0.4		4.31	933.90 → 300.99	32	44
24	F1	catechin	$C_{15}H_{14}O_6$	290.0790	290.0797	−2.4		2.86	289.03 → 245.07	32	16
25	F2	quercetin diglycoside 610 Da	$C_{26}H_{26}O_{17}$	610.1170	610.1164	1.0		3.75	609.03 → 301.00	45	30

dx.doi.org/10.1021/jf405589f | J. Agric. Food Chem. 2014, 62, 4592−4600

Table 1. continued

no.	code	compd identity	mol formula	calcd	measd	error (ppm)	composition	retention time in UPLC-MS/MS analysis (min)	quantitative MRM method: m/z of the mother ion → m/z of the daughter ion	cone voltage (V)	collision energy (eV)
26	F3	kaempferol diglycoside 594 Da	$C_{26}H_{26}O_{16}$	594.1221	594.1195	4.4		4.06	593.03 → 284.99	34	25
27	F4	quercetin glycoside 478 Da	$C_{21}H_{18}O_{13}$	478.0747	478.0733	2.9		4.08	477.03 → 301.01	32	22
28	F5	flavonoid glycoside 446 Da	$C_{23}H_{26}O_{9}$	446.1577	446.1544	7.4		4.99	445.10 → 144.98	40	28
29	P1	trimeric proanthocyanidin	$C_{45}H_{38}O_{18}$	866.2058	866.2061	−0.3		2.18	865.07 → 289.05	40	36
30	P2a	dimeric proanthocyanidin **a**	$C_{30}H_{26}O_{12}$	578.1424	578.1439	−2.6		2.89	577.09 → 425.10	30	16
31	P3b	dimeric proanthocyanidin b	$C_{30}H_{26}O_{12}$	578.1424	578.1430	−1.0		3.44	577.09 → 425.10	30	16
32	CH	chlorogenic acid a[6]	$C_{16}H_{18}O_{9}$	354.0951	354.0928	6.5		2.90 (3.28)	353.03 → 191.00	24	18

[a]Isomeric compounds with the same molecular mass that were quantified with the same calibration curves are denoted in their identifying code (e.g. E6a, E6b). Compounds with multiple reported retention times are known epimers (e.g., tellimagrandin I) or other isomers that were detected in samples but below the limits of quantification (in parentheses, e.g., 1-*O*-galloylglucose). Ellagitannin and galloyl derivative characterization based on Moilanen, Sinkkonen, and Salminen, 2013. GA, gallic acid; G, galloyl; Q, quinic acid; GLUC, glucose; HHDP, hexahydroxydiphenoyl.

(linear gradient); 5−6 min, 30−70% A in B (linear gradient); 6−8 min, 70% A in B (isocratic). The flow rate was 0.45 mL/min, and the injection volume was 5 μL. Chromatograms were recorded at 280 nm. The HPLC system was controlled by Hystar software (version 3.2., Bruker BioSpin, Rheinstetten, Germany). The mass spectrometer was controlled by Compass micrOTOF control software (Bruker Daltonics) and operated in negative ion mode. The capillary voltage was maintained at +4000 V with the end plate offset at −500 V. The pressure for the nebulizer gas (N_2) was set at 1.6 bar, and the drying gas (N_2) flow rate was 12.0 L/min and temperature, 200 °C. The full scan mass ranged from m/z 100 to 3000. Calibration with 5 mM sodium formate injected via a six-port valve was used at the end of the LC-MS experiment to provide high-accuracy mass measurements. The data were handled by Compass DataAnalysis software (version 4.0, Bruker Daltonics).

Data Handling. The phenolic chemical data set contained both quantitative variation (in the total concentrations of phenolics in a sample) and qualitative variation (relative amounts of different chemical in comparison to the total concentration). To distinguish between these two effects, for each sample we divided the concentration of each individual compound by the total concentration of phenolics in the sample (the sum of all compounds combined). These values were used in further analysis as measures of qualitative variation in the phenolic profile of each sample. In addition to this, we included the total concentration of phenolics as a measure of quantitative variation between samples.

Statistical Analysis. Our data set contained a large number of response variables (concentrations of individual chemicals), with strong positive and negative correlations between individual traits. This correlated data structure precluded the use of multiple univariate analysis of variance (ANOVA) analyses. Similarly, because the number of response variables (P = 33) exceeded our sample size (N = 16), we did not have the statistical power to utilize standard statistical methods such as MANOVA. Thus, we opted to utilize principal component analysis (PCA) to explain observed variation between samples in phenolic profiles. PCA uses orthogonal transformation to generate linearly uncorrelated principal components.[38] We used the PRINCOMP procedure in SAS to perform a PCA with all of our treatment levels together. We selected the optimum number of principal component axes using a scree plot,[38] which resulted in two axes (Supporting Information Table S1).

To test whether groups of samples separated in the PCA were significantly different, from one another we used the GLM procedure in SAS to perform ANOVA. We used our treatment levels as predictor variables and the two PC axes as response variables. We used the LSMEANS statement to test for differences between treatments, correcting for multiple comparisons using the Tukey adjustment.

RESULTS AND DISCUSSION

Identification and Characterization of Strawberry Leaf Phenolics. The phenolic compounds from strawberry leaves were characterized and tentatively identified according to their characteristic UV spectra, molecular masses, and MS fragmentation patterns. In total, 32 phenolic compounds were quantified using sensitive and compound-specific MRM methods that were separately developed for each compound (Figure 1; Table 1). Isomeric compounds with the same molecular mass were treated as unique compounds, but separate analyses pooling these compounds resulted in qualitatively similar results (results not shown). Strawberry leaves contained a diverse suite of polyphenols, including gallic acid derivatives (6), ellagitannins (21), flavonoids (5), proanthocyanidins (3), and chlorogenic acids (2).

The total amounts and percentages of different groups of phenolic compounds in different treatment groups are presented in Table 2. Twenty-one different ellagitannins constituted the largest group of the compounds in the leaves,

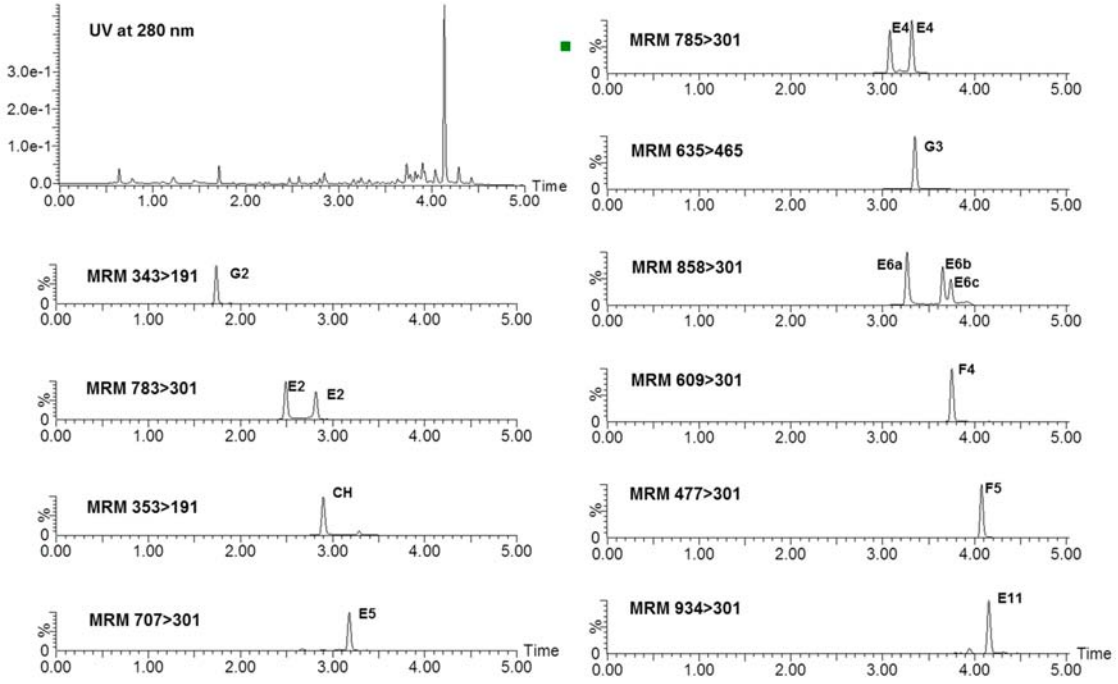

Figure 1. Representative UV and compound-specific MRM chromatograms. The use of MRM allowed the highly sensitive and selective quantification of a number of phenolic compounds simultaneously. Pictures are selected MRM chomtograms, with individual measured compounds identified.

representing 47.0−54.3% of the total phenolic compounds in differently treated strawberry leaves. Ellagitannins occur in high levels also in strawberry fruits (9.7−22.9 mg/100 g).[30] Sanguiin H-6, lambertianin C, galloyl bis-hexahydroxydiphenic acid (HHDP) glucose,[30] agrimoniin, and five other ellagitannins[31] were recently detected in fruits of different strawberry cultivars. In this work, agrimoniin (Table 2, code E9b) was the most abundant compound in the strawberry leaves, supporting the previous findings[32] and agrimoniin was also recently found to be the main ellagitannin in both wild and cultivated strawberry fruits.[31,39]

In the present study, flavonoids were found to be the second largest group of polyphenols in strawberry leaves, and their percentage of the total phenolic compounds in different treatment groups was 36.4−41.4%. However, Oszmiański et al.[22] found quercetin derivatives as the most abundant group of phenolic compounds in the strawberry leaves.

Proanthocyanidins are the most abundant phenolic compounds in strawberry fruits; the concentrations vary among cultivars between 53.9 and 163.2 mg/100 g.[30] Proanthocyanidins have also been detected in strawberry leaves[32] and in the leaves of white strawberry.[24] In the present study, proanthocyanidins represented the third largest group of phenolic compounds in strawberry leaves (4.7−8.0% of total, Table 2). Galloyl derivatives and chlorogenic acids were the other phenolic compounds identified from the strawberry leaf samples, and their percentages of total phenolic compounds altered between 0.9 and 3.1%.

When compared to the recent information about polyphenols analyzed from the leaves of other berries, strawberry appears to be a rich source of different ellagitannins. For example, leaves of bilberry contain mainly quercetin-3-*O*-glucuronide, *trans*-chlorogenic acid, *cis*-chlorogenic acid, cinchonain, and some other minor phenolics, whereas the main compound in the lingonberry leaves seems to be quercetin-3-*O*-glucuronide, and these leaves contain also many other quercetin drivatives and other flavonols.[40] The saskatoon leaves consisted mainly of quercetin- and kaempferol-derived glycosides (41% of the phenols), hydroxycinnamic acids (36%), and minor amounts of catechins and neolignans.[23]

In general, we observed strong positive correlations between the concentrations of gallic acid derivatives and ellagitannins (Supporting Information Table S2). This was expected, because these compounds are formed along the same hydrolyzable tannin biosynthetic pathway that uses the metabolic flux of one branch of the shikimate pathway.[36] In contrast, all of the hydrolyzable tannins showed negative correlations with the concentrations of flavonoids, proanthocyanidins, and chlorogenic acids. This finding is in agreement with flavonoids, proanthocyanidins, and chlorogenic acids needing the metabolic flux of the shikimate pathway that is not directed toward hydrolyzable tannins. Similarly, we found strong positive correlations between the relative concentrations of flavonoids, proanthocyanidins, and chlorogenic acids as they all need the shikimate pathway for their biosynthesis. However, flavonoids and proanthocyanidins were more strongly correlated with each other than with chlorogenic acids, because they utilize also the acetate/malonate pathway that is not needed for the biosynthesis of chlorogenic acids. Among the correlations between individual compounds there were three exceptions that did not fit well with the general pattern: HHDP-glucose (E1), ellagitannin 2038 Da (E13), and flavonoid glycoside 594 Da (F3). Of these, only the pattern observed with HHDP-glucose and other HTs is explained by HHDP-glucose being the catabolic product of ellagitannins.[41] To explain the patterns observed with E13 and F3 would need further investigation of the specific structures.

The PCA and subsequent ANOVA were able to detect significant differences in the polyphenolic profiles of different treatments (Figure 2). The first two PCA axes were able to

Table 2. Concentrations of Phenolic Compounds Measured in Strawberry Leaves in Different Treatments[a]

			concentrations (mg/g dw)			
no.	code	compound	control day 0	control day 7	BTH day 7	birch day 7
1	G1	1-*O*-galloylglucose	0.84 ± 0.01 (1.0)	0.38 ± 0.03 (0.5)	0.78 ± 0.03 (0.9)	0.35 ± 0.02 (0.4)
2	G2	monogalloyl quinic acid	1.38 ± 0.08 (1.7)	1.25 ± 0.04 (1.5)	1.50 ± 0.04 (1.8)	1.14 ± 0.03 (1.4)
3	G3	trigalloyl glucose	0.31 ± 0.02 (0.4)	0.19 ± 0.01 (0.2)	0.31 ± 0.02 (0.4)	0.21 ± 0.01 (0.3)
4	E1	2,3-(*S*)-HHDP-glucose	1.14 ± 0.07 (1.4)	1.43 ± 0.01 (1.8)	1.41 ± 0.03 (1.7)	1.33 ± 0.03 (1.7)
5	E2	pedunculagin	2.83 ± 0.14 (3.5)	2.72 ± 0.04 (3.4)	2.87 ± 0.08 (3.4)	2.85 ± 0.06 (3.5)
6	E3a	galloyl-HHDP-glucose a	0.07 ± 0.01 (0.1)	0.05 ± 0.01 (0.1)	0.06 ± 0.01 (0.1)	0.05 ± 0.01 (0.1)
7	E3b	galloyl-HHDP-glucose b	0.10 ± 0.01 (0.1)	0.08 ± 0.01 (0.1)	0.10 ± 0.01 (0.1)	0.06 ± 0.01 (0.1)
8	E3c	galloyl-HHDP-glucose c	0.26 ± 0.02 (0.3)	0.18 ± 0.01 (0.2)	0.33 ± 0.02 (0.4)	0.13 ± 0.01 (0.2)
9	E4	tellimagrandin I	0.20 ± 0.01 (0.2)	0.16 ± 0.01 (0.2)	0.17 ± 0.02 (0.2)	0.17 ± 0.01 (0.2)
10	E5	dimeric ellagitannin 1416 Da	0.89 ± 0.04 (1.1)	0.93 ± 0.04 (1.2)	0.95 ± 0.08 (1.1)	0.90 ± 0.05 (1.1)
11	E6a	dimeric ellagitannin 1718 Da	1.24 ± 0.08 (1.5)	1.14 ± 0.02 (1.4)	1.47 ± 0.06 (1.7)	1.06 ± 0.03 (1.3)
12	E6b	dimeric ellagitannin 1718 Da	0.84 ± 0.02 (1.0)	0.57 ± 0.04 (0.7)	0.70 ± 0.05 (0.8)	0.59 ± 0.04 (0.7)
13	E6c	dimeric ellagitannin 1718 Da	0.71 ± 0.02 (0.9)	0.45 ± 0.03 (0.6)	0.50 ± 0.02 (0.6)	0.46 ± 0.03 (0.6)
14	E7a	dimeric ellagitannin 2020 Da a	0.15 ± 0.02 (0.2)	0.13 ± 0.01 (0.2)	0.10 ± 0.03 (0.1)	0.13 ± 0.02 (0.2)
15	E7b	dimeric ellagitannin 2020 Da b	0.8 ± 0.05 (1.0)	0.72 ± 0.04 (0.9)	0.84 ± 0.03 (1.0)	0.75 ± 0.05 (0.9)
16	E7c	dimeric ellagitannin 2020 Da c	1.00 ± 0.07 (1.2)	0.80 ± 0.06 (1.0)	1.12 ± 0.08 (1.3)	0.88 ± 0.05 (1.1)
17	E7d	dimeric ellagitannin 2020 Da d	0.21 ± 0.01 (0.3)	0.19 ± 0.01 (0.2)	0.21 ± 0.01 (0.2)	0.20 ± 0.01 (0.2)
18	E8a	dimeric ellagitannin 2038 Da a	1.39 ± 0.14 (1.7)	1.49 ± 0.04 (1.8)	1.64 ± 0.13 (1.9)	1.53 ± 0.14 (1.9)
19	E8b	dimeric ellagitannin 2038 Da b	0.21 ± 0.03 (0.3)	0.29 ± 0.03 (0.4)	0.25 ± 0.03 (0.3)	0.25 ± 0.05 (0.3)
20	E9a	dimeric ellagitannin 1870 Da	1.94 ± 0.06 (2.4)	1.17 ± 0.11 (1.4)	2.46 ± 0.13 (2.9)	0.92 ± 0.06 (1.1)
21	E9b	agrimoniin	27.85 ± 0.2 (34.3)	23.33 ± 0.58 (28.9)	28.02 ± 0.50 (32.8)	23.61 ± 0.87 (29.3)
22	E10	trimeric ellagitannin 2502 Da a	1.65 ± 0.08 (2.0)	1.64 ± 0.07 (2.0)	2.03 ± 0.02 (2.4)	1.66 ± 0.06 (2.1)
23	E11	trimeric ellagitannin 2804 Da	0.63 ± 0.06 (0.8)	0.41 ± 0.02 (0.5)	0.59 ± 0.08 (0.7)	0.44 ± 0.05 (0.5)
24	F1	catechin	6.89 ± 0.28 (8.5)	9.68 ± 0.27 (12.0)	8.35 ± 0.23 (9.8)	8.92 ± 0.40 (11.1)
25	F2	quercetin diglycoside 610 Da	10.51 ± 0.28 (12.9)	12.36 ± 0.17 (15.2)	11.09 ± 0.29 (12.9)	11.88 ± 1.00 (14.7)
26	F3	kaempferol diglycoside 594 Da	8.56 ± 0.23 (10.6)	5.25 ± 0.27 (6.5)	7.60 ± 0.35 (8.9)	5.54 ± 0.49 (6.9)
27	F4	quercetin glycoside 478 Da	3.79 ± 0.18 (4.7)	5.86 ± 0.17 (7.3)	3.86 ± 0.12 (4.5)	5.99 ± 0.21 (7.4)
28	F5	flavonoid glycoside 446 Da	0.22 ± 0.04 (0.3)	0.30 ± 0.06 (0.4)	0.25 ± 0.03 (0.3)	0.36 ± 0.07 (0.4)
29	P1	trimeric proanthocyanidin	0.28 ± 0.07 (0.3)	0.50 ± 0.09 (0.6)	0.30 ± 0.07 (0.4)	0.44 ± 0.07 (0.5)
30	P2a	dimeric proanthocyanidin a	3.23 ± 0.13 (4.0)	5.51 ± 0.47 (6.8)	3.87 ± 0.24 (4.5)	5.11 ± 0.19 (6.3)
31	P2b	dimeric proanthocyanidin b	0.29 ± 0.03 (0.4)	0.49 ± 0.05 (0.6)	0.36 ± 0.02 (0.4)	0.36 ± 0.04 (0.4)
32	CH	chlorogenic acid	0.74 ± 0.02 (0.9)	1.07 ± 0.03 (1.3)	1.26 ± 0.08 (1.5)	2.26 ± 0.04 (2.8)
33	TOTAL	total phenolics	81.15 ± 0.64	80.7 ± 0.32	85.36 ± 1.75	80.57 ± 2.40

[a]Values are presented as the mean ± standard deviation with percent concentration in parentheses. Sample size for each treatment was 4. BTH, BTH-treated leaves; Birch, birch wood distillate-treated leaves.

summarize 77% of the variance in the data set (Supporting Information Table S1). These principal components were able to separate samples into unique clusters corresponding to different treatments (Figure 2A). ANOVA and Tukey's pairwise comparisons revealed these clusters formed significantly different groups. The first principal component (PC1) separated samples into three clusters, corresponding to different treatments. All treatments were differentiated in PC1 except for control day 7 and birch wood distillate-treated day 7 (Figure 2A, *x*-axis). The second principal component (PC2) further differentiated groups on the basis of their combined phenolic profiles. Here, control day 7 and birch wood distillate-treated day 7 were differentiated (Figure 2A, *y*-axis). The individual traits with the highest and lowest loading values contributed most to these differences (Figure 2B; Supporting Information Table S1).

Impact of BTH Treatment on Strawberry Leaf Phenolics. The total amount of phenolic compounds in untreated control leaves was not much altered in 7 days, but in the BTH-treated leaves the concentration of total phenolic compounds was increased 7 days after the BTH exposure (Table 2). Interestingly, in a previous work[32] using strawberry cultivar 'Jonsok', the concentration of phenolics in BTH-treated plants was found to be reduced to the same level as in control plants within 7 days even if the concentration was higher in treated than in untreated plants after 2 days of exposure. This is in line with the recent data demonstrating that majority of the phenolic compounds accumulated in plants in a genotype-dependent manner[42] because a different cultivar (cv. 'Polka') was used in the present study.

The total amount of ellagitannins in BTH-treated strawberry leaves was found to increase within the 7 days after BTH exposure, but the total content of galloyl derivatives was not much altered in BTH-treated plants over the test period. In control plants, the total contents of both ellagitannins and galloyl derivatives were somewhat decreased during the 7 day experiment. Instead, the total amount of proanthocyanidins was increased in all leaf samples within the 7 day test period, but the increase was more pronounced in control samples than in BTH-exposed samples.

In our previous work[32] we found that the most significant early accumulation of strawberry leaf phenolic compounds after BTH application occurred in the ellagitannin group but that the increased total ellagitannin content of BTH-treated plants did not persist over 7 days. However, the total amounts of tannin groups do not indicate any specific biological activities in a

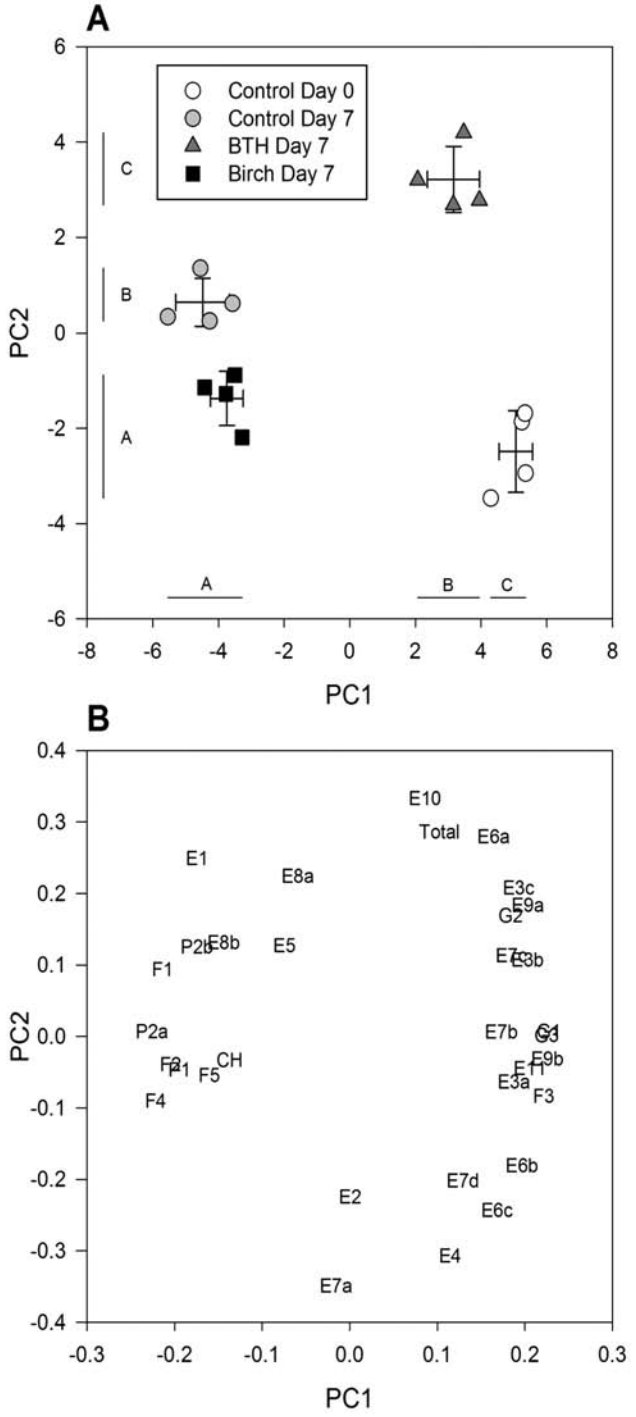

Figure 2. Results of principal component analysis. Panel A shows the sample scores on PC1 and PC2 from PCA. Bars and letters on each PC axis show the results of ANOVA analyses, groups with different letters were significantly different at α = 0.05. BTH, BTH-treated strawberry leaves; Birch, birch wood distillate-treated strawberry leaves. Panel B shows the loading values of response values (phenolic compound concentrations and total phenolics) on the same PCA axes.

plant sample because the activity of an individual tannin compound is affected by its chemical structure and the contents of different active and nonactive compound forms may vary.[41] It is known that the contents of individual phenolics in tree leaves can change during leaf development and in a season-dependent manner, even though the total amount of phenolic compounds is not necessarily altered.[41]

Salicylic acid (SA), a 2-hydroxyl derivative of benzoic acid, is an important player not only in plant innate immunity but also in systemic-acquired resistance (SAR), and both SA and its analogue BTH as well as incompatible microbial interaction are known to induce rapid oxidative burst (OB) in plants.[43,44] OB is a plant defense mechanism causing rapid and extensive production of reactive oxygen species, mainly superoxide radical ($^{\bullet}O_2^-$), hydrogen peroxide (H_2O_2), and hydroxyl radical ($^{\bullet}OH$), which destroy invading pathogens and act as signal molecules in further stress-related reactions in plant cells; however, they can also damage plant tissues and organelles.[45,46] Proanthocyanidins, ellagitannins, and galloyl-glucose esters are strong radical scavengers.[43] For example, in sugar cane (*Saccharum* spp.), exposure to H_2O_2 has been shown to cause up-regulation of phenylpropanoid pathways and, hence, increase the production of phenolic metabolites in the plants 24 h after the H_2O_2 treatment.[46] Ellagitannins generally play protective roles in plants against microbial pathogens and insects pests.[8,9] It was recently found that a penta-esterified ellagitannin, identified as 1-*O*-galloyl-2,3;4,6-bis-hexahydroxydiphenoyl-β-D-glucopyranose, is strongly accumulated in strawberry leaves as a result of infection by nonvirulent *Colletotrichum fragariae*;[47] this ellagitannin may have properties of common plant defense molecule and capability of activating defense cascades perhaps via the transcription factor WRKY1 following elicitor treatment or pathogen infection.[48] In addition, (+)-catechin previously isolated from strawberry leaves was shown to contribute the induced resistance against fungal diseases.[49] Proanthocyanidins are oligomers and polymers of flavan-3-ol units, such as (+)-catechin, and flavan-3-ols are products of the flavonoid biosynthesis pathway.[50] Like total proanthocyanidins, total flavonoid compounds in the control and BTH-treated plants were increased 7 days after the exposure, but the flavonoid level in the BTH-exposed samples stayed lower than in the control plants. In a previous study,[32] the amount of catechin was not altered upon BTH application. Stress factors, such as competition, herbivory, and diseases, can cause changes in allocation patterns in plants and plant leaves, and these changes are often dependent on both plant genotype and resource availability.[51]

Effect of Birch Wood Distillate on Leaf Phenolics. To examine if plant-derived natural elicitors are capable of activation of the phenolic defense compound production in strawberry, leaves were treated with birch wood distillate. Interestingly, our data clearly indicate that birch wood distillate exposure increased the concentrations of chlorogenic acids in strawberry leaves. Chlorogenic acids were increased in control plants as well, but the increase in distillate-treated plants was much more pronounced (Table 2). The other phenolic compounds exhibited no changes in response to birch wood distillate treatment.

In plants, chlorogenic acid has been demonstrated to play an important role in plant resistance to fungal diseases.[52] The strong antibacterial activity of chlorogenic acid appears to be based on its ability to modulate outer and plasma membrane permeability, resulting in the loss of the important barrier function.[53] In peach (*Prunus persica*), another member of the Rosaceae family, neochlorogenic acid, an isomer of chlorogenic acid, has been found to inhibit brown rot (*Monilinia laxa*) infections, and also chlorogenic acid has a reducing effect on melanin production and, hence, on the growth of the fungus.[54]

Collectively, our data demonstrate that strawberry leaves possess a substantial amount of ellagitannins and that the accumulation of specific ellagitannins in young strawberry leaves can be further increased by elicitor treatments such as BTH application. Our data also suggest that plant-derived activators such as birch wood distillate can activate different branches in the strawberry phenylpropanoid biosynthetic pathway from synthetic ones (such as BTH); treatments of young plants in greenhouses with different types of plant activators may, hence, hold great potential for enhancing specific compounds in plants for the production of valuable biomaterial for industrial applications, for example, cosmetics, dietary supplements, pharmaceuticals, and animal feed. Consequently, young greenhouse-grown strawberry plants provide a homogeneous and inexpensive material for the production of specific ellagitannins. BTH treatments have also been found to improve resistance in grape plants to gray mold and in strawberry to powdery mildew.[32,55] In addition, some studies support the idea of using pyrolysis byproducts as environmentally and economically sustainable plant-protecting agents.[33] Hence, more extensive study on the application and mechanisms of action of BTH and wood-derived biological activators in protecting plants from fungal diseases could also be worthwhile.

■ ASSOCIATED CONTENT

Supporting Information

Tables S1 and S2. This material is available free of charge via the Internet at http://pubs.acs.org.

■ AUTHOR INFORMATION

Corresponding Author

*(R.O.K.) E-mail: reijo.karjalainen@uef.fi.

Funding

This study was financially supported by the Academy of Finland (Grant 258992 to J.P.S. and Grant 251388 to M.K.). We thank the Maiju and Yrjö Rikala Horticultural Foundation and the Northern Savo ELY-center for financial support. Chemical analyses on the ultraperformance liquid chromatography−mass spectrometry system were made possible by a Strategic Research Grant of University of Turku (Ecological Interactions) to J.P.S.

Notes

The authors declare no competing financial interest.

■ REFERENCES

(1) Laakso, J.; Lavinto, M.; Rasikari, H.; Karlström, U.; Siivinen, K.; Lukkarinen, T.; Ovaskainen, M.-L.; Sinkko, H.; Tapanainen, H.; Virtanen, S. Dietary exposure to plant protection products − a cumulative risk assessment (in Finnish). In *Evira Research Reports 3/2010*; Finnish Food Safety Authority Evira: Helsinki, Finland, 2010; 3, 110 pp.

(2) Khan, D. A.; Hashmi, I.; Mahjabeen, W.; Naqvi, T. A. Monitoring health implications of pesticide exposure in factory workers in Pakistan. *Environ. Monit. Assess.* **2010**, *168*, 231−240.

(3) Wilson, C.; Tisdell, C. Why farmers continue to use pesticides despite environmental, health and sustainability costs. *Ecol. Econ.* **2001**, *39*, 449−462.

(4) Olesen, J. E.; Bindi, M. Consequences of climate change for European agricultural productivity, land use and policy. *Eur. J. Agron.* **2002**, *16*, 239−262.

(5) Koleva, N. G.; Schneider, U. A.; McCarl, B. A. Pesticide externalities from the US agricultural sector − the impact of internalization, reduced pesticide application rates, and climate change. *Proc. Environ. Sci.* **2011**, *6*, 153−161.

(6) Steffens, K.; Larsbo, M.; Moeys, J.; Jarvis, N.; Lewan, E. Predicting pesticide leaching under climate change: Importance of model structure and parameter uncertainty. *Agric. Ecosyst. Environ.* **2013**, *172*, 24−34.

(7) Krishna, V. V.; Kumar, K. G.; Pradeepa, K.; Kumar, S. R. S.; Kumar, R. S. Biochemical markers assisted screening of *Fusarium* wilt resistant *Musa paradisiacal* (L.) cv. Puttabale micropropagated clones. *Indian J. Exp. Biol.* **2013**, *51*, 531−542.

(8) Ruuhola, T.; Salminen, P.; Salminen, J.-P.; Ossipov, V. Ellagitannins: defences of *Betula nana* against *Epirrita autumnata* folivory? *Agric. For. Entomol.* **2013**, *15*, 187−196.

(9) Daglia, M. Polyphenols as antimicrobial agents. *Curr. Opin. Biotechnol.* **2012**, *23*, 174−181.

(10) Martz, F.; Jaakola, L.; Julkunen-Tiitto, R.; Stark, S. Phenolic composition and antioxidant capacity of bilberry (*Vaccinium myrtillus*) leaves in Northern Europe following foliar development and along environmental gradients. *J. Chem. Ecol.* **2010**, *36*, 1017−1028.

(11) Wang, S. Y.; Chen, C.-T.; Wang, C. Y. The influence of light and maturity on fruit quality and flavonoid content of red raspberries. *Food Chem.* **2009**, *112*, 676−684.

(12) Anttonen, M.; Hoppula, K.; Nestby, R.; Verheul, M.; Karjalainen, R. Influence of fertilization, mulch color, early forcing, fruit order, planting date, shading, growing environment, and genotype on the contents of selected phenolics in strawberry (*Fragaria* × *ananassa* Duch.) fruits. *J. Agric. Food Chem.* **2006**, *54*, 2614−2620.

(13) Lillo, C.; Lea, U.; Ruoff, P. Nutrient depletion as a key factor for manipulating gene expression and product formation in different branches of the flavonoid pathway. *Plant Cell Environ.* **2008**, *31*, 587−601.

(14) Jansen, M. A. K.; Hectors, K.; O'Brien, N. M.; Guisez, Y.; Potters, G. Plant stress and human health: do human consumers benefit from UV-B acclimated crops? *Plant Sci.* **2008**, *175*, 449−458.

(15) Kangasjärvi, J.; Talvinen, J.; Utriainen, M.; Karjalainen, R. Plant defense systems induced by ozone: review. *Plant Cell Environ.* **1994**, *17*, 783−794.

(16) Agati, G.; Azzarello, E.; Pollastri, S.; Tattini, M. Flavonoids as antioxidants in plants: location and functional significance. *Plant Sci.* **2012**, *196*, 67−76.

(17) Boudet, A.-M. Evolution and current status of research in phenolic compounds. *Phytochemistry* **2007**, *68*, 2722−2735.

(18) Pourcel, L.; Routaboul, J.-M.; Cheynier, V.; Lepiniec, L.; Debeaujon, I. Flavonoid oxidation in plants: from biochemical properties to physiological functions. *Trends Plant Sci.* **2007**, *12*, 29−36.

(19) Wang, Y.; Lin, H. H. Antioxidant activity in fruits and leaves of blackberry, raspberry, and strawberry varies with cultivar and developmental stage. *J. Agric. Food Chem.* **2000**, *48*, 140−146.

(20) Walters, D. R.; Fountaine, J. M. Practical application of induced resistance to plant diseases: an appraisal of effectiveness under field conditions. *J. Agric. Sci.* **2009**, *147*, 523−535.

(21) Tabart, J.; Franck, T.; Kevers, C.; Pincemail, J.; Serteyn, D.; Defraigne, J.-O.; Dommes, J. Antioxidant and anti-inflammatory activities of *Ribes nigrum* extracts. *Food Chem.* **2006**, *131*, 1116−1122.

(22) Oszmiański, J.; Wojdyło, A.; Gorzelany, J.; Kapusta, I. Identification and characterization of low molecular weight polyphenols in berry leaf extracts by HPLC-DAD and LC-ESI/MS. *J. Agric. Food Chem.* **2011**, *59*, 12830−12835.

(23) Lavola, A.; Karjalainen, R.; Julkunen-Tiitto, R. Bioactive polyphenols in leaves, stems and berries of Saskatoon (*Amelancier alnifolia* Nutt) cultivars. *J. Agric. Food Chem.* **2012**, *60*, 1020−1027.

(24) Simirgiotis, M. J.; Schmeda-Hirschmann, G. Determination of phenolic composition and antioxidant activity in fruits, rhizomes and leaves of the white strawberry (*Fragaria chiloensis* spp. *chiloensis* form *chiloensis*) using HPLC-DAD-ESI-MS and free radical quenching techniques. *J. Food Compos. Anal.* **2010**, *23*, 545−553.

(25) Mudnic, I.; Modun, D.; Brizic, I.; Vukovic, J.; Generalic, I.; Katalinic, V.; Bilusic, T.; Ljubenkov, I.; Boban, M. Cardiovascular

effects in vitro of aqueous extract of wild strawberry (*Fragaria vesca*, L.) leaves. *Phytomedicine* **2009**, *16*, 462−469.
(26) Zhang, Y.; Seeram, N. P.; Lee, R.; Feng, L.; Heber, D. Isolation and identification of strawberry phenolics with antioxidant and human cancer cell antiproliferative properties. *J. Agric. Food Chem.* **2008**, *56*, 670−675.
(27) Edirisinghe, I.; Burton-Freeman, B.; Varelis, P.; Kappagoda, T. Strawberry extract caused endothelium-dependent relaxation through the activation of PI3 kinase/Akt. *J. Agric. Food Chem.* **2008**, *56*, 9383−9390.
(28) Edirisinghe, I.; Banaszewski, K.; Cappozzo, J.; Sandhya, K.; Ellis, C. L.; Tadapaneni, R.; Kappagoda, C. T.; Burton-Freeman, B. M. Strawberry anthocyanin and its association with postprandial inflammation and insulin. *Br. J. Nutr.* **2011**, *106*, 913−922.
(29) Maher, P.; Akaishi, T.; Abe, K. Flavonoid fisetin promotes ERK-dependent long-term potentiation and enhances memory. *Proc. Natl. Acad. Sci. U.S.A.* **2006**, *103*, 16568−16573.
(30) Buendía, B.; Gil, M. I.; Tudela, J. A.; Gady, A. L.; Medina, J. J.; Soria, C.; López, J. M.; Tomás-Barberán, F. A. HPLC-MS analysis of proanthocyanidin oligomers and other phenolics in 15 strawberry cultivars. *J. Agric. Food Chem.* **2010**, *58*, 3916−3926.
(31) Aaby, K.; Mazur, S.; Nes, A.; Skrede, G. Phenolic compounds in strawberry (*Fragaria* × *ananassa* Duch.) fruits: composition in 27 cultivars and changes during ripening. *Food Chem.* **2012**, *132*, 86−97.
(32) Hukkanen, A. T.; Kokko, H. I.; Buchala, A. J.; McDougall, G. J.; Stewart, D.; Kärenlampi, S. O.; Karjalainen, R. O. Benzothiadiazole induces the accumulation of phenolics and improves resistance to powdery mildew in strawberries. *J. Agric. Food Chem.* **2007**, *5*, 1862−1870.
(33) Tiilikkala, K.; Fagernäs, L.; Tiilikkala, J. History of use of wood pyrolysis liquids as biocide and plant protecting product. *Open Agric. J.* **2010**, *4*, 111−118.
(34) Fagernäs, L.; Kuoppala, E.; Tiilikkala, K.; Oasmaa, A. Chemical composition of birch wood slow pyrolysis products. *Energy Fuels* **2012**, *26*, 1275−1283.
(35) Hagner, M.; Penttinen, O.-P.; Pasanen, T.; Tiilikkala, K.; Setälä, H. Acute toxicity of birch tar oil on aquatic organisms. *Agric. Food Sci.* **2010**, *19*, 24−33.
(36) Salminen, J.-P.; Karonen, M. Chemical ecology of tannins and other phenolics: we need a change in approach. *Funct. Ecol.* **2011**, *25*, 325−338.
(37) Moilanen, J.; Sinkkonen, J.; Salminen, J.-P. Characterization of bioactive plant ellagitannins by chromatographic, spectroscopic and mass spectrometric methods. *Chemoecology* **2013**, *23*, 165−179.
(38) Legendre, P.; Legendre, L. In *Numerical Ecology, 20*; Elsevier: Amsterdam, The Netherlands, 1998; 853 pp.
(39) Vrhovsek, U.; Guella, G.; Gasperotti, M.; Pojer, E.; Zancato, M.; Mattivi, F. Clarifying the identity of the main ellagitannin in the fruit of the strawberry, *Fragaria vesca* and *Fragaria ananassa* Duch. *J. Agric. Food Chem.* **2012**, *60*, 2507−2516.
(40) Hokkanen, J.; Mattila, S.; Jaakola, L.; Pirttilä, A. M.; Tolonen, A. Identification of phenolic compounds from lingonberry (*Vaccinium vitis-idaea* L.), bilberry (*Vaccinium myrtillus* L.) and hybrid bilberry (*Vaccinium* × *intermedium* Ruthe L.) leaves. *J. Agric. Food Chem.* **2009**, *57*, 9437−9447.
(41) Salminen, J.-P.; Ossipov, V.; Haukioja, E.; Pihlaja, K. Seasonal variation on the content of hydrolysable tannins in leaves of *Betula pubescens*. *Phytochemistry* **2001**, *57*, 15−22.
(42) Muñoz, C.; Sánchez-Sevilla, J. F.; Botella, M. A.; Hoffmann, T.; Schwab, W.; Valpuesta, V. Polyphenol composition in the ripe fruits of *Fragaria* species and transcriptional analyses of key genes in the pathway. *J. Agric. Food Chem.* **2011**, *59*, 12598−12604.
(43) Vogt, T. Phenylpropanoid biosynthesis. *Mol. Plant* **2010**, *3*, 2−20.
(44) Faoro, F.; Maffi, D.; Cantu, D.; Iriti, M. Chemical-induced resistance against powdery mildew in barley: the effects of chitosan and benzothiadiazole. *BioControl.* **2008**, *53*, 387−401.
(45) Wojtaszek, P. Oxidative burst: an early plant response to pathogen infection. *Biochem. J.* **1997**, *322*, 681−692.
(46) Arencibia, A. D.; Bernal, A.; Zayas, C.; Carmona, E.; Cordero, C.; González, G.; García, R.; Santana, I. Hydrogen peroxide induced phenylpropanoids pathway eliciting a defensive response in plants micropropagated in Temporary Immersion Bioreactors (TIBs). *Plant Sci.* **2012**, *195*, 71−79.
(47) Mamaní, A.; Filippone, M. P.; Grellet, C.; Welin, B.; Castagnaro, A. P.; Ricci, J. C. Pathogen-induced accumulation of an ellagitannin elicits plant defense response. *Mol. Plant−Microbe Interact.* **2012**, *25*, 1430−1439.
(48) Encinas-Villarejo, S.; Maldonado, A. M.; Amil-Ruiz, F.; de los Santos, B.; Romero, F.; Pliego-Alfaro, F.; Muñoz-Blanco, J.; Caballero, J. L. Evidence for a positive regulatory role of strawberry (*Fragaria* × *ananassa*) Fa WRKY1 and *Arabidopsis* At WRKY75 proteins in resistance. *J. Exp. Bot.* **2009**, *60*, 3043−3065.
(49) Yamamoto, M.; Nakatsuka, S.; Otani, H.; Kohmoto, K.; Nishimura, S. (+)-Catechin acts as an infection-inhibiting factor in strawberry leaf. *Phytopathology* **2000**, *90*, 595−600.
(50) Xie, D.-Y.; Dixon, R. A. Proanthocyanidin biosynthesis − still more questions than answers? *Phytochemistry* **2005**, *66*, 2127−2144.
(51) Donaldson, J. R.; Kruger, E. L.; Lindroth, R. L. Competition- and resource-mediated tradeoffs between growth and defensive chemistry in trembling aspen (*Populus tremuloides*). *New Phytol.* **2006**, *169*, 561−570.
(52) Maher, E. A.; Bate, N. J.; Ni, W.; Elkind, Y.; Dixon, R. A.; Lamb, C. J. Increased disease susceptibility of transgenic tobacco plants with suppressed levels of preformed phenylpropanoid products. *Proc. Natl. Acad. Sci. U.S.A.* **1994**, *91*, 7802−7806.
(53) Lou, Z.; Wang, H.; Zhu, S.; Ma, C.; Wang, Z. Antibacterial activity and mechanism of action of chlorogenic acid. *J. Food Sci.* **2011**, *76*, 398−403.
(54) Villarino, M.; Sandín-España, P.; Melgarejo, P.; De Cal, A. High chlorogenic and neochlorogenic acid levels in immature peaches reduce *Monilinia laxa* infection by interfering with fungal melanin biosynthesis. *J. Agric. Food Chem.* **2011**, *59*, 3205−3213.
(55) Iriti, M.; Rossoni, M.; Borgo, M.; Faoro, F. Benzothiadiazole enhances resveratrol and anthocyanin biosynthesis in grapevine, meanwhile improving resistance to *Botrytis cinerea*. *J. Agric. Food Chem.* **2004**, *52*, 4406−4413.

JOURNAL OF AGRICULTURAL AND FOOD CHEMISTRY

Article

pubs.acs.org/JAFC

Chemical Compositions by Using LC-MS/MS and GC-MS and Biological Activities of *Sedum sediforme* (Jacq.) Pau

Abdulselam Ertaş,*[,†] Mehmet Boğa,[‡] Mustafa Abdullah Yılmaz,[§] Yeter Yeşil,[⊥] Nesrin Haşimi,[∥] Meryem Şeyda Kaya,[▽] Hamdi Temel,[§,#] and Ufuk Kolak[○]

[†]Department of Pharmacognosy, Faculty of Pharmacy, Dicle University, 21280 Diyarbakır, Turkey

[‡]Department of Pharmaceutical Technology, Faculty of Pharmacy, Dicle University, 21280 Diyarbakır, Turkey

[§]Dicle University Science and Technology Research and Application Center (DÜBTAM), Dicle University, 21280 Diyarbakır, Turkey

[⊥]Department of Pharmaceutical Botany, Faculty of Pharmacy, Istanbul University, Istanbul 34116, Turkey

[∥]Department of Nutrition and Dietetics, School of Health, Batman University, 72060 Batman, Turkey

[▽]Department of Pharmacology, Faculty of Pharmacy, Dicle University, 21280 Diyarbakır, Turkey

[#]Department of Pharmaceutical Chemistry, Faculty of Pharmacy, Dicle University, 21280 Diyarbakır, Turkey

[○]Department of General and Analytical Chemistry, Faculty of Pharmacy, Istanbul University, Istanbul 34116, Turkey

Supporting Information

ABSTRACT: In this research, the chemical composition and biological activities of various extracts obtained from whole parts of *Sedum sediforme* (Jacq.) Pau were compared. The amounts of total phenolic and flavonoid components in crude extracts were determined by expression as pyrocatechol and quercetin equivalents, respectively. All of the extracts (petroleum ether, acetone, methanol, and water) obtained from *S. sediforme* showed strong antioxidant activity in four tested methods. Particularly, the IC_{50} values of the methanol extract, which was the richest in terms of total phenolic and flavonoid contents, were found to be lower than those of α-tocopherol and BHT in β-carotene bleaching (9.78 ± 0.06 μg/mL), DPPH free radical scavenging (9.07 ± 0.07 μg/mL), and ABTS cation radical scavenging (5.87 ± 0.03 μg/mL) methods. Furthermore, the methanol extract of *S. sediforme* showed higher inhibition activity than galanthamine against acetyl- and butyryl-cholinesterase enzymes. Also, acetone and methanol extracts exhibited moderate antimicrobial activity against *Candida albicans*. The main constituents of fatty acid and essential oil were identified as palmitic acid (C16:0) (28.8%) and α-selinene (20.4%), respectively, by GC-MS. In the methanol extract of *S. sediforme*, quercetin, rutin, naringenin, and protocatechuic, *p*-coumaric, caffeic, and chlorogenic acids were detected and quantified by LC-MS/MS. Results of the current study showed that the methanol extract of *S. sediforme* may also be used as a food supplement.

KEYWORDS: *Sedum sediforme, phenolic content, essential oil, fatty acid, antioxidant, anticholinesterase, antimicrobial, quercetin, LC-MS/MS, GC-MS*

INTRODUCTION

Belonging to the Crassulaceae family, the genus *Sedum* L. comprises approximately 348 species in the world and 33 species in Turkey. Additionally, it is named Kayakoruğu and Damkoruğu in Anatolia.[1,2] *Sedum* species have been known as both vegetables and folk medicines. They are used for the treatment of many diseases such as wounds, hemorrhoids, constipation, and foot fungi and as a laxative and diuretic.[3−5] Being a Mediterranean element, *Sedum sediforme* (Jacq.) Pau is named Altın otu (goldherb) due to its yellow flowers and is used as a food[4−6] and ornamental globally.[7]

Previous phytochemical studies indicated that *Sedum* species contained different natural compounds such as new isoflavone derivatives sedacins A and B,[8] arbutin and hydroquinone,[9] phenolic acids and flavonoids,[10] flavonol glycosides and sarmenosides V−VII,[11] and alkaloids.[12] In addition, several studies exhibited that *Sedum* species had strong antioxidant potential.[5,8,10,13,14]

Several papers can be found on *S. sediforme* in the literature. In the study of Sakar et al., it is reported that two new compounds, the structures of which were elucidated by spectroscopic means as (2*R*,3*R*)-7,4′-dihydroxy-5,3′,5′-trimethoxyflavan 3-*O*-gallate and 1-β-D-glucopyranosyloxy-3-methoxy-5-hydroxybenzene, were isolated from *S. sediforme* flowers.[15] They were accompanied by limocitrin 3-glucoside, 1-β-D-glucopyranosyloxy-3,5-dihydroxybenzene, kaempferol 3-rhamnoside, quercetin 3-rhamnoside, (−)-epicatechin 3-gallate, (−)-epigallocatechin 3-gallate, myricetin 3-rhamnoside, and gallic acid.[15]

In a former study, an HPLC method was established to determine quercetin, which is a common hydrolysate of the flavonoid glycosides in *Sedum sarmentosum*, *Sedum lineare*, and *Sedum erythrostictum*.[16] Besides, Romojaro et al. reported that *S. sediforme* had a high phenol content and hydrophilic total antioxidant activity.[5] These aforementioned studies triggered us

Received: January 5, 2014
Revised: April 11, 2014
Accepted: April 28, 2014
Published: April 28, 2014

ACS Publications © 2014 American Chemical Society

Table 1. Analytical Parameters of UHPLC-ESI-MS/MS Method

analyte	RT[a]	equation	R^2[b]	RSD%[c]	linearity range (mg/L)	LOD/LOQ[d] (μg/L)	recovery (%)	U[e] (%)
quercetin	5.369	$f(x) = 1829.35x + 32208.90$	0.999 75	1.33	0.025−1.000	0.63/1.93	97.1	7.6
protocatechuic acid	1.380	$f(x) = 783.913x + 9758.52$	0.999 70	2.19	0.025−1.000	0.74/2.25	102.3	10.1
chrysin	10.086	$f(x) = 520.665x + 866.55$	0.999 68	3.59	0.025−1.000	0.60/1.85	98.4	5.9
rutin	4.373	$f(x) = 788.005x - 9096.62$	0.999 27	0.95	0.025−1.000	0.53/1.59	99.0	7.1
hesperetin	6.445	$f(x) = 570.363x + 2835.74$	0.999 72	2.16	0.025−1.000	0.68/2.10	101.2	6.5
naringenin	6.112	$f(x) = 1298.14x - 6598.05$	0.999 82	1.50	0.025−1.000	0.80/2.45	96.5	3.5
rosmarinic acid	4.609	$f(x) = 168.107x - 428.04$	0.999 59	2.60	0.025−1.000	0.93/2.86	91.2	4.9
vanillin	4.207	$f(x) = 52.7804x + 1089.93$	0.999 82	2.75	0.025−1.000	0.85/2.61	100.8	5.1
p-coumaric acid	4.407	$f(x) = 69.0997x + 264.38$	0.999 97	1.24	0.025−1.000	0.76/2.34	99.3	4.6
caffeic acid	2.580	$f(x) = 2783.56x + 45880.00$	0.999 50	1.10	0.025−1.000	0.66/2.01	95.9	5.9
chlorogenic acid	1.661	$f(x) = 1448.01x + 2695.90$	0.999 86	0.62	0.025−1.000	0.72/2.22	97.8	9.5

[a]Retention time. [b]Coefficient of determination. [c]Relative standard deviation. [d]Limit of deteection/limit of quantification. [e]Percent relative uncertainty at 95% confidence level ($k = 2$).

to focus on *S. sediforme*, which is an edible species. The high phenolic content of *S. sediforme* and the quercetin content of *Sedum* species show that chemical and biological activities of these species are worth studying deeply. It is a known fact that phenolic compounds, especially quercetin, show high antioxidant and anticholinesterase activities.[17−19] Thus, we aimed to investigate the relationship between the chemical composition and biological activities of *S. sediforme*.

To the best of our knowledge, there are no studies on the essential oil, fatty acid, and phenolic profiles and antioxidant (β-carotene−linoleic acid test system, DPPH free radical scavenging activity, and cupric reducing antioxidant capacity (CUPRAC)), anticholinesterase and antimicrobial activities of *S. sediforme* in the literature. At the beginning, the fatty acid and essential oil compositions of *S. sediforme* were determined by using GC-MS in the current study. In the next step, related antioxidant, anticholinesterase, and antimicrobial activities and total phenolic and flavonoid contents were analyzed. Moreover, the phenolic and flavonoid contents of *S. sediforme* methanol extract was also determined using UHPLC-ESI-MS/MS for quantitative and qualitative purposes.

MATERIALS AND METHODS

Chemicals and Instruments. The phenolic content and fatty acid composition of *S. sediforme* were determined by using LC-ESI-MS/MS (Shimadzu, Kyoto, Japan) and GC-MS (Thermo Scientific Polaris Q) instruments, respectively. A Shimadzu UV spectrophotometer and a BioTek Power Wave XS microplate reader (USA) were used for the activity assays. 2,2′-Azinobis(3-ethylbenzothiazoline-6-sulfonic acid) diammonium salt (ABTS) (purity = 97.5%) and butylated hydroxytoluene (BHT) (≥99%) were purchased from Merck (Darmstadt, Germany); quercetin (95%), protocatechuic acid (97%), chrysin (97%), rutin (94%), hesperetin (95%), naringenin (95%), rosmarinic acid (96%), vanillin (99%), *p*-coumaric acid (98%), caffeic acid (98%), chlorogenic acid (95%), formic acid (≤100%), 2,2-diphenyl-1-picrylhydrazyl (DPPH) (≥95%), β-carotene (≥93%), linoleic acid (≥99%), Tween 40, pyrocathecol (≥99%), 5,5-dithiobis-(2-nitrobenzoic acid) (DTNB) (≥98%), copper(II) chloride dihydrate ($CuCl_2 \cdot 2H_2O$) (≥99%), neocuproine (2,9-dimethyl-1,10-phenanthroline) (≥98%), ethylenediaminetetraacetic acid (EDTA) (≥98%), acetylcholinesterase (AChE) (type VI-S, EC 3.1.1.7, 425.84 U/mg), and butyrylcholinesterase (BChE) (EC 3.1.1.8, 11.4 U/mg) were obtained from Sigma (Germany); α-tocopherol (≥95.5%) and acetylthiocholine iodide (≥98%) were from Aldrich (Germany); galanthamine hydrobromide (≥94%) was from Sigma-Aldrich (Germany); Folin−Ciocalteu phenol reagent was from Applichem (Germany); butyrylthiocholine iodide (≥99%) was from Fluka (Germany).

Plant Material. *S. sediforme* (Jacq.) Pau was collected by Dr. A. Ertaş from western Turkey (Istanbul) in May 2012 and characterized by Dr. Y. Yeşil (Department of Pharmaceutical Botany, Faculty of Pharmacy, Istanbul University). Voucher specimens have been strored in the Herbarium of Istanbul University, Faculty of Pharmacy (ISTE: 9805).

Identification and Quantitation of Phenolic Compounds. *Instruments and Chromatographic Conditions.* LC-ESI-MS/MS analysis of the methanol extract was performed by using a Shimadzu UHPLC instrument coupled to a tandem MS instrument. The liquid chromatograph was equipped with LC-30AD binary pumps, a DGU-20A3R degasser, a CTO-10ASvp column oven, and an SIL-30AC autosampler.

For the chromatographic separation, a C18 reversed-phase Inertsil ODS-4 (100 mm × 2.1 mm i.d., 2 μm) analytical column was used. The column temperature was fixed at 40 °C. The elution gradient consisted of mobile phases (A) water (5 mM ammonium acetate and 0.1% formic acid) and (B) acetonitrile (0.1% formic acid). The following gradient was used: at $t = 0.00$ min, 20% B; at $t = 3.00$ min, 20% B; at $t = 3.01$ min, 50% B; at $t = 8.99$ min, 50% B; at $t = 9.01$ min, 90% B; at $t = 11.99$ min, 90% B; at $t = 12.00$ min, 20% B; at $t = 14.99$ min, 20% B. The solvent flow rate was maintained at 0.5 mL/min, and the injection volume was settled as 10 μL.

MS Instrumentation. MS detection was performed using a Shimadzu LCMS 8040 model triple-quadrupole mass spectrometer equipped with an ESI source operating in negative ion mode. LC-ESI-MS/MS data were collected and processed by LabSolutions software (Shimadzu). The multiple reaction monitoring (MRM) mode was used to quantify the analytes: the assay of phenolic compounds was performed following two or three transitions per compound, the first one for quantitative purposes and the second and/or third one for confirmation.

Optimization of LC-ESI-MS/MS Method. Subsequent to several combinations of trials, a gradient acetonitrile (0.1% formic acid, 5 mM ammonium acetate) and water (0.1% formic acid) system was concluded to be the best mobile phase solution. For rich ionization and the separation of the molecules, the mentioned mobile phase proved to be the best of all. ESI source was chosen instead of atmospheric pressure chemical ionization (APCI) and atmospheric pressure photoionization (APPI) sources as the phenolic compounds were small and relatively polar molecules. Tandem mass spectrometry was chosen to be used for the current study because this system is commonly used for its fragmented ion stability.[17] The working conditions were determined as interface temperature, 350 °C; DL temperature, 250 °C; heat block temperature, 400 °C; nebulizing gas flow (nitrogen), 3 L/min; and drying gas flow (nitrogen), 15 L/min.

Method Validation Parameters. In the current study, 11 phenolic compounds (quercetin, protocatechuic acid, chrysin, rutin, hesperetin, naringenin, rosmarinic acid, vanillin, *p*-coumaric acid, caffeic acid, and chlorogenic acid) were quantified in *S. sediforme*. In the chromatographic analysis of phenolic compounds, gradient separation was

applied. Linear regression equations of the phenolic compound standards are represented in Table 1. The linearity of the LC-MS/MS conditions for phenolic compounds was affirmed in the range from 0.025 to 1 mg/L by the high coefficient of determination ($R^2 > 0.999$) obtained. The limit of detection (LOD) and limit of quantitation (LOQ) of the method reported in this study were dependent on the calibration curve established from six measurements. The LOD and LOQ of the method were determined by using the equations 3S/N and 10S/N, respectively (S/N refers to the signal to noise ratio) (Table 1). For different compounds, LOD ranged from 0.53 to 0.93 μg/L and LOQ ranged from 1.59 to 2.86 μg/L (Table 1). Furthermore, the recovery of the phenolic compound standards ranged from 91.2 to 102.3%.

Estimation of Uncertainty. *Identification of Uncertainty Sources.* The sources of the uncertainty for the applied method were evaluated and calculated using EURACHEM Guide, 2004.[17,20,21]

The following parameters were used for the calculations of uncertainties: (1) calibration curve (cal); (2) purity of reference standards (pur); (3) stock solutions (Css); (4) weighing of samples (m_{sample}); (5) repeatabilitity (rep); (6) recovery (rec).

Standard combined uncertainty is a function of the individual uncertainties of each parameter and calculated by using eq 1:

$$u(C) = \sqrt{u^2(\text{cal}) + u^2(\text{pur}) + u^2(\text{Css}) + u^2(\text{w}) + u^2(\text{rep}) + u^2(\text{rec})} \quad (1)$$

Main uncertainty sources are defined as purity of standards and calibration curve. Standard combined uncertainties are multiplied by 2 for the calculation of expanded uncertainties by accepting a 95% confidence level. Calculated uncertainties are shown in Table 1.

Preparation of Plant Extracts for LC-ESI-MS/MS. For sample preparation, initially, the whole parts of the dried and powdered plants (10 g) were extracted by MeOH (3 × 50 mL) in 24 h at room temperature (extraction yield, 8.3%). The extract was subsequently filtered and evaporated under reduced pressure. Then, dry filtrate was diluted until 250 mg/L and passed through the 0.2 μm microfiber filter for LC-ESI-MS/MS.

Esterification of Total Fatty Acids and GC-MS Conditions. Esterification of petroleum ether extract (100 mg) of *S. sediforme* was performed according to the report of Kılıc et al.[22] In this study, Thermo Scientific Polaris Q GC-MS was used. GC-MS study conditions and comparison of identification and quantification of the compounds were done in exactly same manner according to Kılıc et al.[22]

Preparation of Plant Extracts for Biological Activities and GC-MS. In this analysis, primarily, whole plant material was dried and powdered, and 100 g of plant material was sequentially macerated with petroleum ether (3 × 250 mL), acetone (3 × 250 mL), methanol (3 × 250 mL), and water (3 × 250 mL) for 24 h at room temperature. Subsequent to filtration, the solvents were evaporated to handle the crude extracts.

Preparation of Essential Oil and GC-MS Conditions. Essential oil was obtained using a Clevenger apparatus from the whole parts of plant (100 g), which was crumbled into small pieces and soaked in distilled water (500 mL) for 3 h. The obtained essential oil was dried over anhydrous Na_2SO_4 and stored at 4 °C for a sufficient period of time. The essential oil was diluted using CH_2Cl_2 (1:3 v/v) prior to gas chromatography–flame ionization detector (GC-FID) and GC-MS analysis. GC-FID analysis was performed using a Thermo Electron Trace GC-FID detector, and GC-MS analysis was performed using the same GC and Thermo Electron DSQ MS.

The following GC conditions were applied for both GC-MS and GC-FID analyses. The GC oven temperature was kept at 60 °C for 10 min and programmed to 280 °C at a rate of 4 °C/min and then kept constant at 280 °C for 10 min. A nonpolar Phenomenex DB5 fused silica column (30 m × 0.32 mm, 0.25 μm film thickness) was used with helium at 1 mL/min (20 psi) as a carrier gas. The split ratio was adjusted to 1:50, the injection volume was 0.1 μL, and EI/MS was recorded at 70 eV ionization energy. The mass range was m/z 35–500 amu. Alkanes (C8–C24) were used as reference points in the calculation of Kovats indices (KI) by the same conditions.[23,24]

Identification of the compounds was based on comparing their retention times and mass spectra with those obtained from authentic samples and/or the NIST and Wiley spectra as well as data from the published literature. GC-FID and GC-MS analyses were replicated three times (mean RSD% < 0.1).

Determination of Total Phenolic and Flavonoid Contents. Total phenolic and flavonoid amounts in the crude extracts expressed as pyrocatechol and quercetin equivalents, respectively, were calculated according to the following equations:[25,26]

$$\text{absorbance} = 0.0126\ \text{pyrocatechol}\ (\mu\text{g}) + 0.0314\ (R^2 = 0.9936)$$

$$\text{absorbance} = 0.1495\ \text{quercetin}\ (\mu\text{g}) - 0.0958\ (R^2 = 0.9994)$$

Antioxidant Activity of the Extracts. To determine the antioxidant activity, the following tests were applied: β-carotene–linoleic acid test system, DPPH free radical and ABTS cation radical scavenging activity, and cupric reducing antioxidant capacity (CUPRAC) methods.[27−30]

Anticholinesterase Activity of the Extracts. A spectrophotometric method developed by Ellman et al. was used to indicate the acetyl- and butyryl-cholinesterase inhibitory activities.[31]

Determination of Antimicrobial Activity and Minimum Inhibitory Concentration (MIC). Five different microorganisms including Gram-positive bacteria (*Streptococcus pyogenes* ATCC19615 and *Staphylococcus aureus* ATCC 25923), Gram-negative bacteria (*Pseudomonas aeruginosa* ATCC 27853, *Escherichia coli* ATCC 25922), and yeast (*Candida albicans* ATCC10231), which were purchased from Refik Saydam Sanitation Center (Turkey), were used for detecting the antimicrobial activity of the samples. The disc diffusion method was employed for this purpose.[32] The minimum inhibitory concentration was determined by the broth macrodilution method according to NCCLS.[33] Ampicillin and fluconazole were used as positive controls for bacteria and yeast, respectively.

Statistical Analysis. The results of the antioxidant and anticholinesterase activity assays were represented as means ± SD. The results were evaluated using an unpaired t test and ANOVA variance analysis with the NCSS statistical computer package. The differences were considered statistically significant at $p < 0.05$.

RESULTS AND DISCUSSION

Quantitative Analysis of Phenolic and Flavonoid Compounds by UHPLC-ESI (QqQ)/MS/MS. Having the same general structure with an aromatic hydroxyl nucleus, almost 8000 phenolic compounds exist in nature.[17] Phenolic compounds that exist in plants constitute one of the most important groups acting as free radical terminators and primary antioxidants. Plant polyphenols are multifunctional in that they act as reducing agents, hydrogen atom donors, and singlet oxygen scavengers. Besides being the most diverse and prevalent natural compounds, flavonoids are the most important phenolics. Being members of the polyphenol family, flavonoids have more than 4000 species that exist in the roots, flowers, and leaves of plants.[17]

A literature survey reveals several studies on the use of liquid chromatography electrospray ionization tandem mass spectrometry to perform quantitative analyses.[17,34] Therefore, for quantitative purpose, the analyses of 11 phenolic and flavonoid compounds in the methanol extract of *S. sediforme* were done by an accurate method on a mass spectrometer equipped with a triple-quadrupole analyzer. Due to the fact that negative ionization mode was more sensitive and selective for phenolics and flavonoids, it was preferred in the current study.

The specific fragmentation reactions were selected to monitor the aforesaid phenolic and flavonoid compounds by

MRM. Eleven compounds, which were five flavonoids, five phenolic acids, and one phenolic aldehyde, were monitored by the transition from the specific deprotonated molecular ions to the corresponding fragment ions. Molecular ions, fragments observed in MS/MS, related collision energies for these fragments, and the quantified result for *S. sediforme* are presented in Table 2.

Table 2. Identification and Quantification of Phenolic Compounds of Methanol Extract of *S. sediforme* by UHPLC-ESI-MS/MS

compound	parent ion (m/z)[a]	MS^2(CE)[b]	quantification[c] (μg analyte/g extract)
quercetin	**300.90**	**151.0 (22), 121.0 (26), 107.0 (29)**	**1813.51 ± 137.82**
protocatechuic acid	152.90	108.9 (15), 90.9 (25)	71.23 ± 7.22
chrysin	252.90	62.9 (33),143.0 (28) ,107.0 (26)	ND[d]
rutin	609.00	300.1 (39), 271.0 (53)	138.62 ± 8.17
hesperetin	300.90	164.0 (24), 136.0 (30), 108.0 (37)	ND
naringenin	270.90	151.0 (18), 119.0 (25), 107.0 (26)	39.67 ± 1.38
rosmarinic acid	358.90	132.9 (41), 161.0 (17)	ND
vanillin	150.90	136.0 (17), 92.0 (21), 107.8 (26)	ND
p-coumaric acid	162.90	119.1 (15), 92.9 (28)	94.08 ± 4.33
caffeic acid	178.90	134.9 (14), 134.0 (25)	151.25 ± 8.93
chlorogenic acid	353.00	191.1 (15), 84.8 (45)	23.30 ± 2.18

[a]Molecular ions of the standard compounds (mass to charge ratio). [b]MRM fragments for the related molecular ions (CE refers to related collision energies of the fragment ions). [c]Values in μg/g (w/w) of plant methanol extract. [d]Not detected.

Quercetin, rutin, and naringenin were detected and quantified of five flavonoids; however, chrysin, hesperetin, and vanillin were not found. Furthermore, four phenolic acids (protocatechuic acid, *p*-coumaric acid, caffeic acid, and chlorogenic acid) were characterized in *S. sediforme* (Table 2; Figure 1; Figure S1 in the Supporting Information). Quercetin was found to be the most abundant flavonoid compound (1813.51 ± 137.82 μg/g extract) in the methanol extract of *S. sediforme* (Table 2; Figure 1). Besides, caffeic acid (151.25 ± 8.93 μg/g extract) was found to be the most plentiful phenolic acid in *S. sediforme* (Table 2; Figure 1).

In the literature, there are few studies on phenolic and flavonoid compounds of *Sedum* species by HPLC and LC-MS techniques.[16,35] Xu et al. reported a HPLC methodology that was established to determine quercetin, which is a common hydrolysate of the flavonoid glycosides in *S. sarmentosum*, *S. lineare*, and *S. erythrostictum*.[16]

Fatty Acid and Essential Oil Composition by GC-MS. GC-MS analysis was used to determine the fatty acid composition of the petroleum ether extract. As represented in Table 3, 10 components were identified, constituting 100.0% of the petroleum ether extract of *S. sediforme*, and the major

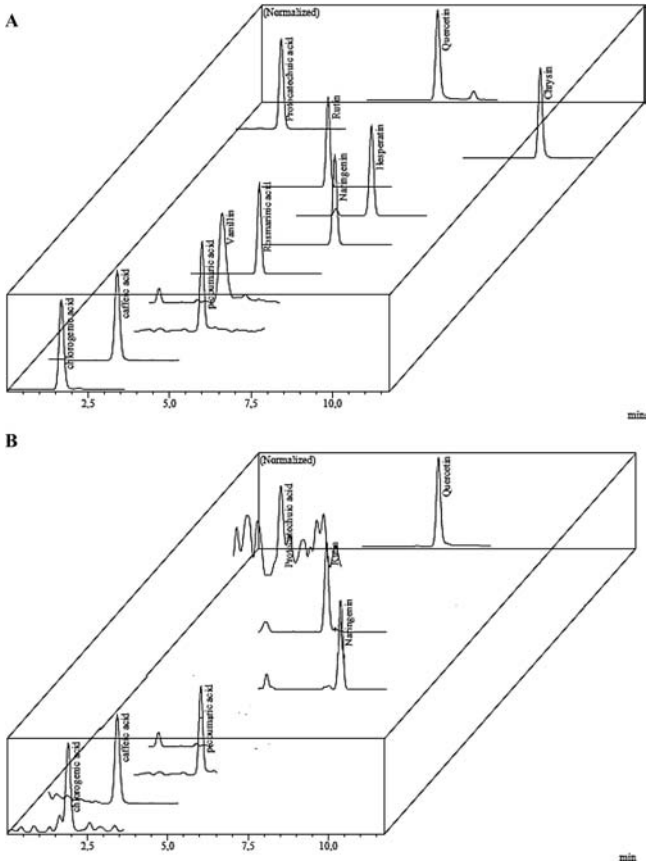

Figure 1. UHPLC-ESI-MS/MS chromatograms of (A) 250 μg/mL standard mix and (B) *S. sediforme* methanol extract.

Table 3. GC-MS Analysis of *S. sediforme* Petroleum Ether Extract

t_R[a] (min)	constituent[b]	composition[c] (%)
9.69	octanedioic acid	1.2 ± 0.05
14.39	10-undecenoic acid	1.2 ± 0.06
18.60	myristic acid	2.5 ± 0.04
25.27	**palmitic acid**	**28.8 ± 0.30**
30.64	linoleic acid	9.7 ± 0.18
30.77	oleic acid	12.6 ± 0.12
30.86	linolenic acid	12.9 ± 0.15
31.54	stearic acid	24.6 ± 0.29
37.38	arachidic acid	3.3 ± 0.06
43.82	behenic acid	3.2 ± 0.10
	total	100.0

[a]Retention time (in minutes). [b]Nonpolar Phenomenex DB-5 fused silica colum. [c]Percentage of relative weight.

constituents were characterized as palmitic acid (C16:0) (28.8%), stearic acid (C18:0) (24.6%), and linolenic acid (C18:3 omega-3) (12.9%). This is the first report on the fatty acid composition of *S. sediforme*. The amount of saturated fatty acids was found to be greater than the amount of unsaturated fatty acid in the present study. There have been no reports regarding direct fatty acid analysis of *Sedum* species by GC-MS, except the lipophilic extract obtained from *Sedum hispanicum*.[36] However, in this study, 0.89% of the fatty acid content was identified in the lipophilic extract of *S. hispanicum*. In that sense,

dx.doi.org/10.1021/jf500067q | J. Agric. Food Chem. 2014, 62, 4601−4609

it could be said that the current study is the first report on the fatty acid composition of *Sedum* species.

The essential oil composition was examined by GC-MS analysis. Twenty-four components were determined, constituting 91.6% of the essential oil composition of *S. sediforme*. The main components of the essential oil of *S. sediforme* were identified as α-selinene (20.4%), 2,5-di-*tert*-octyl-*p*-benzoquinone (13.1%), valencene (6.3%), and carvone oxide (4.3%) (Table 4). There have been few papers regarding GC-MS analysis of essential oil composition of *Sedum* species.[37,38] Yaylı et al. reported that 38 and 35 components were identified in the essential oils of *S. pallidum* var. *bithynicum* and *S. spurium*, respectively. Besides, in their study, the main components of these species were found to be caryophyllene oxide for *S. pallidum* var. *bithynicum* and hexahydrofarnesyl acetone for *S. spurium* in the ratios of 12.8 and 15.7%, respectively.[38]

Table 4. Chemical Composition of the Essential Oil from *S. sediforme*

RI[a]	constituent[b]	composition[c] (%)
865	isononane	2.1 ± 0.02
954	camphene	1.2 ± 0.03
1193	mrytenal	1.0 ± 0.01
1197	mrytenol	1.1 ± 0.03
1249	1,3-di-*tert*-butylbenzene	3.5 ± 0.04
1276	carvone oxide	4.3 ± 0.04
1299	carvacrol	1.3 ± 0.01
1376	α-copaene	1.8 ± 0.02
1409	longifolene	3.2 ± 0.03
1442	aromadendrene	3.5 ± 0.03
1481	α-curcemene	1.3 ± 0.01
1484	valencene	6.3 ± 0.02
1498	**α-selinene**	**20.4 ± 0.09**
1677	cadalene	2.1 ± 0.03
1712	curcumen-15-al	1.5 ± 0.03
1746	2-methylheptadecane	4.0 ± 0.02
1890	2-methyl-1-hexadecanol	2.3 ± 0.02
2109	heneicosane	4.2 ± 0.04
2156	1-nonadecanol	2.1 ± 0.03
2259	2,5-di-*tert*-octyl-*p*-benzoquinone	13.1 ± 0.07
2366	arachidic acid	2.6 ± 0.05
2407	tetracosane	4.2 ± 0.03
2896	choleic acid	2.1 ± 0.04
2900	nonacosane	2.4 ± 0.01
	total	91.6

[a]Retention indices (DB-5 column). [b]Nonpolar Phenomenex DB-5 fused silica column. [c]Percentage of relative weight.

Antioxidant Activity and Total Phenolic and Flavonoid Content. The antioxidant activity studies of the petroleum ether (SSP), acetone (SSA), methanol (SSM), and water (SSW) extracts prepared from the whole plant of *S. sediforme* were carried out by β-carotene bleaching, DPPH free radical scavenging, ABTS cation radical decolorisation, and CUPRAC assays. The SSM extract showed the highest extraction yield, but no significant differences in the extraction yields of other extracts were observed.

In the crude extracts, total phenolic and flavonoid amounts were determined and expressed as pyrocatechol and quercetin equivalents, respectively (y = 0.0126 pyrocatechol (μg) + 0.0314, R^2 = 0.9936 and y = 0.1495 quercetin (μg) − 0.0958, R^2 = 0.9994). The phenolic and flavonoid amounts of the SSM extract were identified to be the richest. The amounts of total phenolic and flavonoid from SSM were 335.71 ± 4.81 and 26.66 ± 0.75 μg/mg extract, respectively. The amount of phenolic components was seen to be higher than that of flavonoid components. The results are shown in Table 5. In the literature, total phenolic and flavonoid contents in the examined *Sedum acre* extracts were expressed in terms of gallic acid and rutin equivalents, respectively.[14] Moreover, Stankovic et al. reported that the total phenolic and flavonoid amounts in the examined acetone extract of *S. acre* were 181.75 and 173.42 mg/g, respectively.[14] Additionally, in the study of Romojaro et al. *S. sediforme* showed high levels of total phenolic content, 191.53 mg/100 g fresh weight (gallic acid equivalent).[5] In this regard, the richness of *Sedum* species in terms of phenolic and flavonoid compounds, which are known for their important pharmacological properties, increases the importance of these species.

As indicated in Table 6, the SSP and SSA extracts showed moderate lipid peroxidation activity (IC_{50} = 51.34 ± 0.92 and

Table 6. Antioxidant Activity of the Extracts and Standards[a]

	IC_{50} (μg/mL)		
sample	lipid peroxidation	DPPH free radical	ABTS cation radical
SSP	51.34 ± 0.92a	174.55 ± 0.91a	75.03 ± 0.45a
SSA	54.61 ± 0.31b	17.20 ± 0.33b	8.76 ± 0.52b
SSM	9.78 ± 0.06c	9.07 ± 0.07c	5.87 ± 0.03c
SSW	153.05 ± 1.71d	104.45 ± 1.28d	9.01 ± 0.29b
α-TOC	15.54 ± 0.21e	18.76 ± 0.31e	9.88 ± 0.08d
BHT	10.35 ± 0.03f	48.86 ± 0.09f	10.67 ± 0.11e

[a]Values are means ± SD, n = 3; values with different letters in the same column are significantly different (p < 0.05).

Table 5. Total Phenolic and Flavonoid Contents, Extraction Yield, and Anticholinesterase Activity of Extracts and Galanthamine at 200 μg/mL[a]

sample	inhibition % against AChE	inhibition % against BChE	phenolic content (μg PEs[b]/mg extract)	flavonoid content (μg QEs[c]/mg extract)	extraction yield % (w/w)
SSP	NA[d]	11.53 ± 0.20a	137.30 ± 0.85a	10.91 ± 0.14a	3.02
SSA	28.31 ± 1.12a	65.69 ± 2.91b	254.37 ± 2.30b	21.23 ± 0.71b	3.11
SSM	**85.09 ± 0.21b**	**89.57 ± 0.86c**	**335.71 ± 4.81c**	**26.66 ± 0.75c**	**7.20**
SSW	40.61 ± 0.60c	12.32 ± 1.01a	184.92 ± 5.91d	15.93 ± 0.81d	2.31
galanthamine[e]	79.91 ± 0.42d	81.21 ± 0.59d			

[a]Values expressed are means ± SD of three parallel measurements, and values were calculated according to negative control. Values with different letters in the same column are significantly different (p < 0.05). [b]Pyrocatechol equivalents (y = 0.0126x + 0.0314, R^2 = 0.9936). [c]Quercetin equivalents (y = 0.1495x − 0.0958, R^2 = 0.9994). [d]Not active. [e]Standard drug.

dx.doi.org/10.1021/jf500067q | J. Agric. Food Chem. 2014, 62, 4601−4609

54.61 ± 0.31 μg/mL, respectively) and the SSW extract showed weak lipid peroxidation activity (153.05 ± 1.71 μg/mL) in the β-carotene bleaching method. However, the SSM extract showed very strong lipid peroxidation activity (9.78 ± 0.06 μg/mL) in the β-carotene bleaching method. Furthermore, the SSM extract exhibited higher activity than α-tocopherol (15.54 ± 0.21 μg/mL) and BHT (10.35 ± 0.03 μg/mL), which were used as standards in the β-carotene bleaching method. As seen in Table 6, the SSP and SSW extracts showed weak and moderate activity (174.55 ± 0.91 and 104.45 ± 1.28 μg/mL) in DPPH free radical scavenging activity, respectively. On the other hand, the SSA and SSM extracts exhibited very strong DPPH free radical scavenging activity. Besides, the SSA (17.20 ± 0.33 μg/mL) and SSM (9.07 ± 0.07 μg/mL) extracts showed higher activity than α-tocopherol (18.76 ± 0.31 μg/mL) and BHT (48.86 ± 0.09 μg/mL). In previous studies, Mavi et al. reported that *S. sempervivoides* showed very strong activity (88.9 and 86.0% inhibition, respectively) in the DPPH free radical scavenging assay and lipid peroxidation−thiobarbituric acid method at 200 μg/mL concentration.[13] In addition, Stankovic et al. reported that the acetone extract of *S. acre* exhibited very strong activity in the DPPH free radical scavenging assay.[14] The largest capacity to neutralize DPPH radicals was found for the acetone extract, which neutralized 50% of free radicals at the concentration of 29.57 μg/mL.[14] Morover, in the study of Thuong et al., the MeOH-, EtOAc-, and BuOH-soluble fractions exhibited significant scavenging activities against free radicals (DPPH and superoxide) as well as remarkable inhibitory effects on lipid peroxidation.[10]

As shown in Table 6, the SSP extract indicated moderate activity (75.03 ± 0.45 μg/mL) in the ABTS cation radical scavenging assay. However, the SSA, SSM, and SSW extracts exhibited very strong effects in the ABTS cation radical scavenging assay. In addition to that, the SSA (8.76 ± 0.52 μg/mL), SSM (5.87 ± 0.03 μg/mL), and SSW (9.01 ± 0.29 μg/mL) extracts showed higher activity than α-tocopherol (9.88 ± 0.08 μg/mL) and BHT (10.67 ± 0.11 μg/mL). According to Romojaro et al., *S. sediforme* showed very strong effects in hydrophilic and lipophilic total antioxidant activities, with 588.87 ± 35.52 mg of Trolox equivalent 100 g^{-1} FW.[5] Morover, *S. sediforme* showed good activity (81.60% inhibition) in peroxyl radical (H_2O_2) scavenging potential assay.[5] The SSM extract and α-tocopherol indicated 1.73 and 1.62 absorbance in CUPRAC at 100 μg/mL, respectively (Figure 2). According to our literature survey this is the first study about the cupric reducing antioxidant capacity of *Sedum* species. Therefore, this study is important in this field.

When we look at the antioxidant results of the four tested extracts, we can see the parallelism between antioxidant activities and total phenolic content. In particular, looking at the quantitative phenolic analysis of the methanol extract by LC-MS/MS, it can be deduced that this high activity may be related to the quercetin content. Quercetin is known to have various pharmacological effects.[17−19] Particularly, flavonoids are present in plant sources as flavonoid glycosides. Therefore, this high activity also might be said to arise from quercetin gycosides. If we were to express this in a different way, this high activity can be attributed to the synergic effect between quercetin, quercetin glycosides, and other phenolic compounds.[39] In further studies, our group plans to purify, structurally determine, and quantify the secondary metabolites, especially flavonoid glycosides of *Sedum* species. Furthermore, we also aim to study in vivo pharmacological effects of the purified compounds.

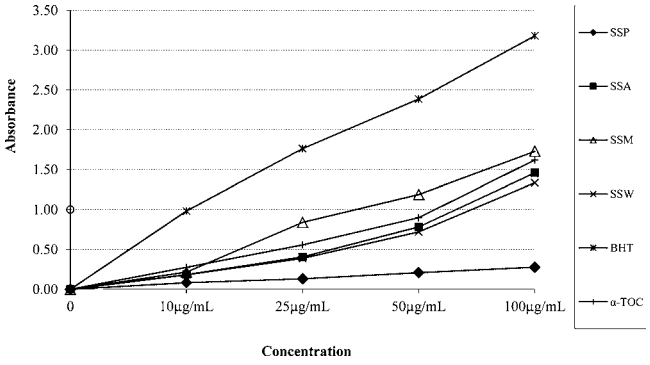

Figure 2. Cupric reducing antioxidant capacity of *S. sediforme*, α-tocopherol, and BHT.

Anticholinesterase Activity. As demonstrated in Table 5, the SSA extract exhibited good inhibitory activity (65.69% inhibition) against butyrylcholinesterase enzyme. The SSW extract showed moderate inhibitory activity (40.61% inhibition) against acetylcholinesterase enzyme, at 200 μg/mL. On the other hand, the SSM extract showed 85.09 and 89.57% inhibition activities, which are higher than galanthamine inhibitory activity against acetyl- and butyryl-cholinesterase enzymes at 200 μg/mL, respectively.

The anticholinesterase activity of the SSM extract shows parallelism to its high total phenolic and flavonoid contents. This high activity of the SSM extract might be related not only to its high total phenolic and flavonoid contents but also to its quercetin content directly or to the synergic effect of quercetin with other phenolic compounds.[39] When previous studies are examined, it can be seen that quercetin has strong antioxidant properties as well as an anticholinesterase effect.[17−19] Additionally, Min et al. reported that quercetin had shown potential inhibitory activity against AChE.[18] Furthermore, Choi et al. reported that quercetin might improve cognitive ability against TMT-induced neuronal deficit and also had an inhibitory action against AChE.[19] To our knowledge, there are no reports about the anticholinesterase activity of *Sedum* species. Because our results were higher than those for galanthamine and there has been no such study about *Sedum* species, the anticholinesterase activity results of *S. sediforme* will be important data in this field.

Antimicrobial Activity. The antimicrobial activities of *S. sediforme* extracts against different microorganisms were measured by using the disc diffusion method, and the results were assessed according to inhibition zone diameter. Results are presented in Table 7. No antimicrobial activity of the water extract against the five tested microorganisms was detected (data not shown). However, the petroleum ether, acetone, and methanol extracts were active on tested microorganisms, and the sensitivity of active extracts was found not to differ significantly among tested microorganisms. Whereas the petroleum ether extract exhibited weak antimicrobial activity (inhibition zone < 12) against all tested microorganisms, the acetone and methanol extracts showed moderate antimicrobial activity against *C. albicans* (inhibition zone < 20−12) and weak antimicrobial activity against Gram-positive and -negative bacteria. The highest activities were exhibited by acetone and methanol extracts against *C. albicans*, with 18 ± 0 and 15 ± 0.1 mm inhibition zone diameters, respectively.

dx.doi.org/10.1021/jf500067q | J. Agric. Food Chem. 2014, 62, 4601−4609

Table 7. Zones of Growth Inhibition (mm) and MIC Values Showing the Antimicrobial Activity of *S. sediforme* Extracts Compared to Positive Controls

	petroleum ether extract		acetone extract		methanol extract		positive controls	
	DD[a]	MIC	DD[a]	MIC	DD[a]	MIC	DD[b]	MIC
Gram-positive								
S. aureus	10 ± 0.4	18 ± 0.2	7 ± 0.2	8 ± 0.2	9 ± 0.3	5 ± 0.6	35 ± 0.2	1.95 ± 0.3
S. pyogenes	9 ± 0.4	19 ± 0.7	9 ± 0.1	7 ± 0.1	9 ± 0.3	8 ± 0.5	19 ± 0.2	7.815 ± 0.1
Gram-negative								
E. coli	9 ± 0.3	18 ± 0.5	7 ± 0.1	17 ± 0.3	10 ± 0.1	9 ± 0.4	20 ± 0.1	7.815 ± 0.4
P. aeruginosa	7 ± 0.2	8 ± 0.5	10 ± 0	5 ± 0.5	10 ± 0.2	6 ± 0.2	NA[c]	NA
yeast								
C. albicans	8 ± 0.3	8 ± 0.4	18 ± 0	1 ± 0.2	15 ± 0.1	1 ± 0.3	30 ± 0.3	3.125 ± 0.2

[a]Inhibition zone in diameter (mm) around the disks (6 mm) impregnated with 30 mg/mL of plant extracts. [b]Inhibition zone in diameter (mm) of positive controls that are ampicillin for bacteria and fluconazole for yeast. Minimum inhibitory concentration (MIC) values are given as mg/mL for plant extracts and as μg/mL for antibiotics. [c]Not active.

For a more reliable assessment of antimicrobial activity, a broth dilution assay was carried out. The sensitivity of the test microorganisms against active extracts was evaluated, and results are shown as MIC (Table 7). Values ranged from 8 to 19 mg/mL for the petroleum ether extract, from 1 to 17 mg/mL for the acetone extracts, and from 1 to 9 mg/mL for the methanol extracts. The MIC results indicate that the methanol extract was found to be the most active extract. The lowest MIC value was recorded by the acetone and methanol extracts against *C. albicans* (1 mg/mL). This is the first study dealing with the antimicrobial activity of *S. sediforme*. On the other hand, in a previous paper, the methanol, acetone, and ethyl acetate extracts of *S. acre* revealed high antibacterial activity against Gram-positive bacteria and low to moderate antifungal activity.[14] Besides, the essential oils of *S. pallidum* Bieb. var. *bithynicum* and *S. spurium* showed low antimicrobial activity against Gram-negative and -positive bacteria and yeast-like fungi,[38] and *S. sormentosum* Bunge showed weak inhibitory activity against *B. subtilis* and *S. aureus*.[40]

The present study concluded that the methanol extract of *S. sediforme* showed very strong antioxidant and anticholinesterase activities. These properties of the methanol extract of *S. sediforme* were parallel to the total phenolic content. On the basis of our results, quercetin was found to be the most abundant phenolic compound in *S. sediforme*. Many studies in the literature showed that quercetin and its glycosides had potent biological properties, in particular antioxidant and anticholinesterase activities. Thus, these high activities of *S. sediforme* may be related to either high total phenolic or quercetin contents.[17−19,41] From a broader perspective, these high activities of *S. sediforme* might be related not only to its high total phenolic and flavonoid contents but also directly to its quercetin content or to the synergic effect of quercetin with other phenolic compounds.[39]

Furthermore, protocatechuic, *p*-coumaric, and chlorogenic acids were found for the first time in *Sedum* species. Although the total phenolic content was found as very rich in *S. sediforme*, phenolic constituents were detected in low amounts. Therefore, these results could be the effect of some other phenolic constituents such as flavonoid glycosides that we have not studied yet.

In conclusion, it is found that *S. sediforme* had very high antioxidant and anticholinesterase activities. Therefore, the results of the current study showed that the methanol extract of *S. sediforme* can also be used as a food source because of its high quercetin amount, total phenolic content, strong antioxidant, and anticholinesterase properties.

All in all, the rich total phenolic content and high antioxidant and anticholinesterase capacities of the methanol extract of *S. sediforme* indicated that more future studies should be done in this field.

■ ASSOCIATED CONTENT

Supporting Information

Figures S1−S5. Equations S1−S7. Antioxidant and anticholinesterase activities methods. Tables S1−S14. This material is available free of charge via the Internet at http://pubs.acs.org.

■ AUTHOR INFORMATION

Corresponding Author

*(A.E.) Phone: +90 412 2488030/7512. E-mail: abdulselamertas@hotmail.com or abdulselam.ertas@dicle.edu.tr.

Funding

We acknowledge the Dicle University for financial support (Research University Grant DUBAP: 13-ASMYO-61). We thank Dicle University Science and Technology Research and Application Center (DÜBTAM) for the partial support of this study.

Notes

The authors declare no competing financial interest.

■ ABBREVIATIONS USED

LC-MS/MS, liquid chromatography−tandem mass spectrometry; GC-MS, gas chromatography−mass spectrometry; GC-FID, gas chromatography−flame ionization detector; UHPLC-ESI-MS/MS, ultrahigh-performance liquid chromatography−electrospray ionization−tandem mass spectrometry; ABTS, 2,2′-azinobis(3-ethylbenzothiazoline-6-sulfonic acid) diammonium salt; BHT, butylated hydroxytoluene; DPPH, 2,2-diphenyl-1-picrylhydrazyl; DTNB, 5,5′-dithiobis(2-nitrobenzoic acid); $CuCl_2 \cdot 2H_2O$, copper(II) chloride dihydrate; neocuproine, 2,9-dimethyl-1,10-phenanthroline; EDTA, ethylenediaminetetraacetic acid; APCI, atmospheric pressure chemical ionization; APPI, atmospheric pressure photoionization; LOD, limit of detection; LOQ, limit of quantitation; CUPRAC, cupric reducing antioxidant capacity; BChE, butyrylcholinesterase enzyme; AChE, acetylcholinesterase enzyme; MIC, minimum inhibitory concentration; NCCLS, National Committee for Clinical Laboratory Standards; SD, standard deviation; MRM,

multiple reaction monitoring; SSP, petroleum ether extract of *S. sediforme*; SSA, acetone extract of *S. sediforme*; SSM, methanol extract of *S. sediforme*; SSW, water extract of *S. sediforme*

REFERENCES

(1) Alpınar, K. *Sedum* L. In *Türkiye Bitkileri Listesi/Damarlı Bitkiler*; Güner, A., Aslan, S., Ekim, T., Vural, M., Babaç, M. T., Eds.; Nezahat Gökyiğit Botanik Bahçesi ve Flora Araştırmaları Derneği Yayını: Istanbul, Turkey, 2012; pp 384−386.

(2) Chamberlain, D. F. *Sedum* L. In *Flora of Turkey and the East Aegean Islands*; Davis, P. H., Ed.; Edinburgh University Press: Edinburgh, Scotland, 1972; 4, pp 224−244.

(3) Baser, K. H. C. *The Medicinal Plants of Korea*; Kyo-Hak Publishing: Seoul, Korea, 1999; pp 198−203.

(4) Baytop, T. *Türkçe Bitki Adları Sözlüğü*; Türk Tarih Kurumu Basımevi: Ankara, Turkey, 1994; p 163.

(5) Romojaro, A.; Botella, M. A.; Obon, C.; Pretel, M. T. Nutritional and antioxidant properties of wild edible plants and their use as potential ingredients in the modern diet. *Int. J. Food Sci. Nutr.* **2013**, *64* (8), 944−952.

(6) Elmadfa, I. In *Local Mediterranean Food Plants and Nutraceuticals*; Heinrich, M., Müller, W. E., Galli, C., Eds.; Karger Medical and Scientific Publishers: Basel, Switzerland, 2006; 59, p 49.

(7) Andry, H.; Yamamoto, T.; Inoue, M. Effectiveness of hydrated lime and artificial zeolite amendments and *Sedum* (*Sedum sediforme*) plant cover in controlling soil erosion from an acid soil. *Aust. Soil Res.* **2007**, *45* (4), 266−279.

(8) Li, W. L.; Luo, Q. Y.; Wu, L. Q. Two new prenylated isoflavones from *Sedum aizoon* L. *Fitoterapia* **2011**, *82* (3), 405−407.

(9) Stanislaw, G.; Wanda, D. M.; Joanna, K. Occurrence of arbutin and hydroquinone in the genus *Sedum* L. *Farm. Pol.* **1984**, *40*, 211−213.

(10) Thoung, P. T.; Kang, J. H.; Na, M.; Jin, W.; Youn, U. J.; Seeong, Y. H.; Song, K. S.; Min, B. K.; Bae, K. Anti-oxidant constituents from *Sedum takesimense*. *Phytochemistry* **2007**, *68* (19), 2432−2438.

(11) Morikawa, T.; Ninomiya, K.; Zhang, Y.; Yamada, T.; Nakamura, S.; Matsuda, H.; Muraoka, O.; Hayakawa, T.; Yoshikawa, M. Flavonol glycosides with lipid accumulation inhibitory activity from *Sedum sarmentosum*. *Phytochem. Lett.* **2012**, *5* (1), 53−58.

(12) Gill, S.; Raszeja, W.; Szynkiewicz, G. Occurrence of nicotine in some species of the genus *Sedum*. *Farm. Polym.* **1979**, *35*, 151−153.

(13) Mavi, A.; Terzi, Z.; Ozgen, U.; Yıldırım, A.; Coskun, M. Antioxidant properties of some medicinal plants: *Prangos ferulacea* (Apiaceae), *Sedum sempervivoides* (Crassulaceae), *Malva neglecta* (Malvaceae), *Cruciata taurica* (Rubiaceae), *Rosa pimpinellifolia* (Rosaceae), *Galium verum* subsp. *verum* (Rubiaceae), *Urtica dioica* (Urticaceae). *Biol. Pharm. Bull.* **2004**, *27* (5), 702−705.

(14) Stanković, M.; Radojević, I.; Ćurčić, M.; Vasić, S.; Topuzović, M.; Čomić, L.; Marković, S. Evaluation of biological activities of goldmoss stonecrop (*Sedum acre* L.). *Turk. J. Biol.* **2012**, *36* (5), 580−588.

(15) Sakar, M. K.; Petereit, F.; Nahrstedt, A. Two phloroglucinol glucosides, flavan gallates and flavonol glycosides from *Sedum sediforme* flowers. *Phytochemistry* **1993**, *33* (1), 171−174.

(16) Xu, R.; Chen, Y. J.; Wan D. R.; Wang, J. HPLC determination of quercetin in three plant drugs from genus *Sedum*. In *Proceedings of 2009 International Conference of Natural Product and Traditional Medicine*, Xian, China; Liu, J., Vittori, S., Yang, C., Eds.; Scientific & Technical Development Inc: Flushing, NY, 2009; 1 and 2, pp 643−646.

(17) Gulcin, I.; Bursal, E.; Sehitoglu, H. M.; Goren, A. C. Polyphenol contents and antioxidant activity of lyophilized aqueous extract of propolis from Erzurum, Turkey. *Food Chem. Toxicol.* **2010**, *48* (8−9), 2227−2238.

(18) Min, B. S.; Cuong, T. D.; Lee, J. S.; Shin, B. S.; Woo, M. H.; Hung, T. M. Cholinesterase inhibitors from *Cleistocalyx operculatus* buds. *Arch. Pharm. Res.* **2010**, *33* (10), 1665−1670.

(19) Choi, G. N.; Kim, J. H.; Kwak, J. H.; Jeong, C. H.; Jeong, J. H.; Jeong, H. R.; Lee, U.; Heo, H. J. Effect of quercetin on learning and memory performance in ICR mice under neurotoxic trimethyltin exposure. *Food Chem.* **2012**, *132* (2), 1019−1024.

(20) Binici, B.; Bilsel, M.; Karakas, M.; Koyuncu, I.; Goren, A. C. An efficient GC-IDMS method for determination of PBDEs and PBB in plastic materials. *Talanta* **2013**, *116*, 417−426.

(21) EURACHEM CITAC Guide CG4. *Quantifiying Uncertainty in Analytical Measurement*, 3rd ed.; Ellison, S. L. R., Williams, A.,, Eds.; 2004; available from www.eurachem.org.

(22) Kılıc, T.; Dirmenci, T.; Goren, A. C. Chemotaxonomic evaluation of species of Turkish *Salvia*: fatty acid composition of seed oils. II. *Rec. Nat. Prod.* **2007**, *1* (1), 17−23.

(23) Altun, M.; Goren, A. C. Essential oil composition of *Satureja cuneifolia* by simultaneous distillation-extraction and thermal desorption GC-MS techniques. *J. Essent. Oil Bearing Plants* **2007**, *10* (2), 139−144.

(24) Polatoglu, K.; Demirci, B.; Demirci, F.; Goren, N.; Baser, K. H. C. The essential oil composition of *Tanacetum densum* (Labill.) Heywood ssp. *eginense* Heywood from Turkey. *Rec. Nat. Prod.* **2012**, *6* (4), 402−406.

(25) Slinkard, K.; Singleton, V. L. Total phenol analyses: automation and comparison with manual methods. *Am. J. Enol. Vitic.* **1977**, *28* (49), 49−55.

(26) Moreno, M. I. N.; Isla, M. I.; Sampietro, A. R.; Vattuone, M. A. Comparison of the free radical-scavenging activity of propolis from several regions of Argentina. *J. Ethnopharmacol.* **2000**, *71* (1−2), 109−114.

(27) Miller, H. E. A simplified method for the evaluation of antioxidants. *J. Am. Oil Chem. Soc.* **1971**, *48*, 91−98.

(28) Blois, M. S. Antioxidant determinations by the use of a stable free radical. *Nature* **1958**, *181*, 1199−1200.

(29) Re, R.; Pellegrini, N.; Proteggente, A.; Pannala, A.; Yang, M.; Rice-Evans, C. Antioxidant activity applying an improved ABTS radical cation decolorization assay. *Free Radical Biol. Med.* **1999**, *26* (9−10), 1231−1237.

(30) Apak, R.; Guclu, K.; Ozyurek, M.; Karademir, S. E. Novel total antioxidant capacity index for dietary polyphenols and vitamins C and E, using their cupric ion reducing capability in the presence of neocuproine: CUPRAC method. *J. Agric. Food Chem.* **2004**, *52* (26), 7970−7981.

(31) Ellman, G. L.; Courtney, K. D.; Andres, V.; Featherstone, R. M. A new and rapid colorimetric determination of acetylcholinesterase activity. *Biochem. Pharmacol.* **1961**, *7*, 88−95.

(32) NCCLS (National Committee for Clinical Laboratory Standards). *Performance Standards for Antimicrobial Disk Susceptibility Test*, 6th ed.; Wayne, PA, USA, 1997; M2-A6.

(33) NCCLS (National Committee for Clinical Laboratory Standards). *Methods for Dilution Antimicrobial Susceptibility Tests for Bacteria That Grow Aerobically*, 8th ed.; Wayne, PA, USA, 2009; M08-A8.

(34) Onder, F. C.; Ay, M.; Sarker, S. D. Comparative study of antioxidant properties and total phenolic content of the extracts of *Humulus lupulus* L. and quantification of bioactive components by LC-MS/MS and GC-MS. *J. Agric. Food Chem.* **2013**, *61* (44), 10498−10506.

(35) Sturm, S.; Mulinacci, N.; Vincieri, E. E.; Stuppner, H. Analysis of flavonols of *Sedum telephium* L. leaves by capillary electrophoresis and HPLC-mass spectrometry. *Chromatographia* **1999**, *50* (7/8), 433−438.

(36) Orhan, I.; Deliorman-Orhan, D.; Ozcelik, B. Antiviral activity and cytotoxicity of the lipophilic extracts of various edible plants and their fatty acids. *Food Chem.* **2009**, *115* (2), 701−705.

(37) Mesicek, N.; Perpar, M. Essential oils from the orpine *Sedum maximum*. *Farm. Vestn.* **1973**, *24*, 123−124.

(38) Yaylı, N.; Yasar, A.; Yılmaz Iskender, N.; Yaylı, N.; Cansu, T. B.; Coskuncelebi, K.; Karaoglu, S. Chemical constituents and antimicrobial activities of the essential oils from *Sedum allidum* var. *bithynicum* and *S. spurium* grown in Turkey. *Pharm. Biol.* **2010**, *48* (2), 191−194.

(39) Ginsburg, H.; Deharo, E. A call for using natural compounds in the development of new antimalarial treatments-an introduction. *Malaria J.* **2011**, *10* (Suppl.1), S1.
(40) Kim, S. J.; Cho, A. R.; Han, J. Antioxidant and antimicrobial activities of leafy green vegetable extracts and their applications to meat product preservation. *Food Control* **2013**, *29* (1), 112−120.
(41) Rice-Evans, C. A.; Miller, N. J.; Paganga, G. Structure antioxidant activity relationships of flavonoids and phenolic acids. *Free Radical Biol. Med.* **1996**, *20* (3), 933−956.

JOURNAL OF AGRICULTURAL AND FOOD CHEMISTRY

Article

pubs.acs.org/JAFC

In Vitro Inhibitory Effect on Digestive Enzymes and Antioxidant Potential of Commonly Consumed Fruits

Anna Podsędek,* Iwona Majewska, Małgorzata Redzynia, Dorota Sosnowska, and Maria Koziołkiewicz

Institute of Technical Biochemistry, Department of Biotechnology and Food Sciences, Lodz University of Technology, Stefanowskiego 4/10, 90-924 Łódź, Poland

ABSTRACT: Dietary inhibitors of fats and carbohydrates degrading enzymes can reduce obesity and type 2 diabetes. In this study, we screened crude extracts from 30 commonly consumed fruits to test their in vitro inhibitory effect against key enzymes relevant for obesity (pancreatic lipase) and type 2 diabetes (α-glucosidase and α-amylase), total phenolic content (Folin–Ciocalteu method), and antioxidant capacity (ABTS and FRAP). The IC_{50} values of the fruits tested varied from 39.91 to >400 mg/mL, from 1.04 to >80 mg/mL, and from 0.72 to 135.07 mg/mL against α-glucosidase, α-amylase, and pancreatic lipase, respectively. Antioxidant capacity ranged from 0.66 to 124.66 μmol of TE/g of fruit and strongly correlated with phenolic content, while the enzyme inhibition was poorly correlated with total phenolic and antioxidant capacity. Among fruits tested, blue honeysuckle and red gooseberry exhibited the highest inhibitory activity with respect to the carbohydrate degrading enzymes, while lingonberry had the strongest anti-lipase activity.

KEYWORDS: *fruits, enzyme inhibition, pancreatic lipase, α-glucosidase, α-amylase, antioxidant capacity, phenolic compounds*

INTRODUCTION

Overweight and obesity are the fifth leading risk of global deaths. In addition, 44% of the diabetes burden, 23% of the ischemic heart disease burden, and between 7% and 41% of certain cancer burdens are attributable to overweight and obesity (http://www.who.int). According to the World Health Organization (WHO) overweight and obesity as well as their related diseases can be reduced by limiting energy intake from total fats and sugars, engaging in regular physical activity, and increasing consumption of fruits, vegetables, legumes, whole grains, and nuts. Dietary intervention seems to be a reasonable option for treatment of obesity and type 2 diabetes.

Inhibition of dietary fat and sugar absorption from the intestine seems to be an effective way to prevent obesity and type 2 diabetes. In the continuing search for novel effective antiobesity and antidiabetes agents, medicinal plants or inedible parts of plants have been screened for potential lipase, α-amylase, or α-glucosidase inhibitory activities.[1−5] Pancreatic lipase (EC 3.1.1.3; triacylglycerol acyl hydrolase) produced by the pancreatic acinar cells hydrolyzes triglycerides mainly into 2-monoacylglycerols and free fatty acids, and it is responsible for the hydrolysis of 50−70% of total dietary fats in the intestinal lumen.[1,6] The plant derived pancreatic lipase inhibitors are classified into the following classes of chemical compounds: saponins, terpenes, and phenolics.[1] However, it is increasingly recognized that among different classes of phytochemicals phenolic compounds are the most active lipase inhibitors. Consistently with this statement, several in vitro studies have shown that white, green, oolong, and black tea polyphenols[7−9] as well as green coffee and cocoa polyphenols[10,11] inhibit pancreatic lipase.

Phenolic compounds affect also digestive enzymes involved in the hydrolysis of dietary carbohydrates. The inhibition of α-amylase and α-glucosidase by polyphenolic-rich plant extracts or isolated phenolic compounds may offer a natural dietary approach to preventing type 2 diabetes. Pancreatic α-amylase [EC 3.2.1.1; α-1,4-glucan-4-glucanohydrolase] is an endoglucosidase that is delivered into the intestinal lumen as a constituent of pancreatic juices and catalyzes the hydrolysis of starch to maltose and maltotriose.[12] α-Glucosidase [EC 3.2.1.20] is a membrane-bound enzyme located in the epithelium of the small intestine, and it catalyzes the cleavage of glycosidic bonds and releases of glucose from disaccharides and oligosaccharides.[13] The inhibitory activity of plant origin phenolic compounds against carbohydrate degrading enzymes is being increasingly documented. For example, cocoa,[11] colored grains[14] and almond seed skin[15] as well as herbal polyphenolic-rich fractions[16] have shown inhibitory effects on α-amylase and/or α-glucosidase activities in vitro. It is reasonable to hypothesize that a phenolic-rich diet may reduce absorption of fats and sugars via an inhibition of the enzymes degrading these substrates. For this reason the interest in studying the inhibition of digestive enzymes by these phytochemicals has recently increased.

It is well-known that fruits are very important components of the human diet as well as the sources of dietary phenolics. There is some evidence that polyphenols from fruits and fruit products can also inhibit digestive enzymes. McDoughall et al.[17] reviewed that berry anthocyanins, ellagitannins, and proanthocyanidins inhibit α-glucosidase, α-amylase, and pancreatic lipase, respectively. Additionally, strawberry, raspberry, blueberry, rowanberry, blackcurrant, and red grape extracts showed inhibitory effects on carbohydrate degrading enzymes.[18−23] Some information is also available about anti-lipase potential of fruit extracts, because such inhibitory activity

Received: February 17, 2014
Revised: May 1, 2014
Accepted: May 2, 2014
Published: May 2, 2014

ACS Publications © 2014 American Chemical Society

dx.doi.org/10.1021/jf5008264 | J. Agric. Food Chem. 2014, 62, 4610−4617

was demonstrated for blueberry,[24] lingonberry, Arctic bramble, cloudberry, strawberry, raspberry,[25] and Cornelian cherries.[4]

Therefore, it is reasonable to hypothesize that consumption of fruits may decrease α-glucosidase, α-amylase, and/or pancreatic lipase activities and may be an important support in the management of postprandial hyperglycemia and obesity. The objective of this study was to screen the different fruits commonly consumed in Poland as well as all over the world for their pancreatic lipase, α-glucosidase, and α-amylase inhibitory activities and determine the correlation of the inhibitory effect to antioxidant capacity and phenolic content.

MATERIALS AND METHODS

Materials. The list of fruits used in this study is given in Table 1. Gallic acid, intestinal acetone powder from rat source of α-glucosidase (EC 3.2.1.20), α-amylase (from porcine pancreas type VI-B, lipase (EC 3.1.1.3) from porcine pancreas type II, *p*-nitrophenyl-α-D-glucopyranoside (pNPG), *p*-nitrophenyl acetate, 4-methylumbelliferyl oleate, *p*-nitrophenyl-α-D-glucopiranoside, 2,2′-azinobis(3-ethyl-benzthiazoline-6-sulfonic acid) (ABTS), 2,4,6-tris-2-pyridyl-*s*-triazine (TPTZ), potassium persulfate, trolox, TRIS-base, dimethyl sulfoxide (DMSO), and acetonitrile were obtained from Sigma-Aldrich. Acetone and sodium carbonate were purchased from Chempur (Piekary Śląskie, Poland). Folin−Ciocalteu reagent, potato starch, hydrochloric acid, sodium chloride, calcium chloride, and ferric chloride of analytical grade were purchased from POCH (Gliwice, Poland). Ultrapurity water was prepared in the laboratory using a Simplicity Water Purification System (Millipore, Marlborough, MA, USA).

Table 1. Popular Name, Scientific Name, Origin, and Purchased Place of Fruits Tested

fruit sample	scientific name	origin	place of purchase
apple cv. Golden Delicious	*Malus domestica*	Poland	local farmers
banana	*Musa*	not known	local supermarket
bilberry	*Vaccinium myrtillus*	Poland	local market
black currant	*Ribes nigrum*	Poland	local market
blackberry	*Rubus fruticosus*	Poland	local farmers
blueberry cv. Toro	*Vaccinium corymbosum*	Poland	Research Institute of Horticulture
blue honeysuckle cv. Wojtek	*Lonicera caerulea* var..*kamtschatica*	Poland	Research Institute of Horticulture
cranberry	*Vaccinium oxycoccus*	Poland	local market
chokeberry	*Aronia melanocarpa*	Poland	local market
gooseberry green	*Ribes uva-crispa*	Poland	local market
gooseberry red	*Ribes uva-crispa*	Poland	local market
grape pink	*Vitis vinifera*	Chile	local supermarket
grapefruit red	*Citrus paradis*	not known	local supermarket
kiwi	*Actinidia chinensis*	Chile	local supermarket
lingonberry	*Vaccinium vitis-idaea*	Poland	local market
mandarine	*Citrus reticulata*	not known	local supermarket
orange	*Citrus sinensis*	not known	local supermarket
peach	*Prunus persica*	not known	local supermarket
pear cv. Lukasówka	*Pyrus communis*	Poland	local supermarket
pear cv. Nashi	*Pyrus communis*	Chile	local supermarket
pineapple	*Ananas sativus*	Costa Rica	local supermarket
plum cv. Renkloda	*Prunus domestica*	Poland	local market
plum cv. Węgierka Zwykła	*Prunus domestica*	Poland	local market
pomegranate	*Punica granatum*	Tunisia	local supermarket
pomelo	*Citrus maxima*	not known	local supermarket
raspberry cv. Polka	*Rubus idaeus*	Poland	local farmers
red currant	*Ribes rubrum*	Poland	local market
sour cherry	*Prunus cerasus*	Poland	local farmers
strawberry cv. Onebor	*Fragaria x ananassa*	Poland	local farmers
sweet cherry cv. Regina	*Prunus avium*	Poland	local farmers

Preparation of Fruit Extracts. Extraction from the edible, mixed part of fruits (20 g) was done with 70% acetone (200 mL) at room temperature for 60 min with constant stirring. After centrifuging at 4000 rpm for 10 min, and filtration through Munktell filter AB, the supernatants were concentrated at 40 °C (vacuum rotary evaporator RII, Büchi, Switzerland) to remove the acetone and the aqueous phase was diluted to 25 mL with water. For further analytical and biological activity assays, a gradient of concentrations was prepared via serial dilution of the fruit extracts in pure water. Finally, 1 mL of extract corresponded to 0.8 mg of fruit.

Pancreatic Lipase Inhibition in Vitro Assay. The inhibition of lipase activity was determined by measuring the release of 4-methylumbelliferone from 4-methylumbelliferyl oleate or *p*-nitrophenol from *p*-nitrophenyl acetate by using a fluorimetric or spectrophotometric method, respectively. The amount of the inhibitor (expressed as mg of fruit per 1 mL of reaction mixture under assay conditions) required to inhibit 50% of the enzyme activity is defined as the IC_{50} value. The IC_{50} of the fruits tested was obtained from the line of the plot of the fruit concentration in 1 mL of reaction mixture versus the % inhibition. All samples were assayed in triplicate.

Fluorimetric assay using 4-methylumbeliferyl oleate as substrate (4-MUO) was carried out according to previous papers[26,27] with some modification. Lipase from porcine pancreas type II was dissolved in buffer consisting of 20 mM Tris-base, 150 mM NaCl, and 1.3 mM $CaCl_2$ (pH 7.4) at 1 mg/mL, and then the supernatant was used after centrifugation at 13 000 rpm for 5 min. The 0.1 mM substrate solution was prepared by dissolving 1.1 mg of 4-MUO in 0.5 mL of DMSO and diluting 50-fold with the above Tris buffer. For the pancreatic lipase assay, in a 96-well plate 25 μL of the varying concentrations of the fruit extracts were combined with 25 μL of enzyme solution, mixed, and incubated at 37 °C for 5 min. Then, 50 μL of 0.1 mM 4-MUO solution was added, mixed, and incubated at 37 °C for 20 min. The amount of 4-methylumbelliferone released by lipase was measured with a microplate reader (Synergy2, BioTek Instruments Inc.) at an excitation wavelength of 360 nm and at an emission wavelength of 460 nm. The sample blank and the control blank (without substrate) were performed in the same way. The inhibition (%) was calculated by using the following formula:

$$\text{inhibition (\%)} = \frac{(F_{\text{control}} - F_{\text{control blank}}) - (F_{\text{sample}} - F_{\text{sample blank}})}{(F_{\text{control}} - F_{\text{control blank}})} \times 100$$

where F_{control} and $F_{\text{control blank}}$ are a fluorescence value of the solvent control with and without 4-MUO, respectively; F_{sample} and $F_{\text{sample blank}}$ are a fluorescence value of the extract with and without 4-MUO, respectively.

The procedure of Umezawa et al.[28] for lipase activity determination using *p*-nitrophenyl acetate as substrate was modified. The 50 mM stock solution of *p*-nitrophenyl acetate in DMSO was prepared. Pure water was added to reach a final concentration of 10 mM. Lipase from porcine pancreas type II was dissolved in water at 10 mg/mL, and then centrifuged at 13 000 rpm for 5 min. The composition of the reaction mixture was as follows: 0.2 mL of fruit extract, 0.2 mL of lipase solution, 1.4 mL of 0.1 M Tris buffer (pH 7.4), and 0.2 mL of 10 mM *p*-nitrophenyl acetate solution. The absorbance at 400 nm was read immediately against water after incubation at 37 °C for 10 min. In the control sample, the extract was replaced with 0.2 mL of water. A blank

dx.doi.org/10.1021/jf5008264 | J. Agric. Food Chem. 2014, 62, 4610−4617

Table 2. Pancreatic Lipase, α-Amylase, and α-Glucosidase Inhibitory Activities of Fruits[a]

fruit	enzyme inhibition IC_{50} (mg of fresh fruit/mL)			
	pancreatic lipase[b]	pancreatic lipase[c]	α-amylase	α-glucosidase
apple	14.01 ± 0.53 f	>80	>200	385.70 ± 23.12 lm
banana	32.54 ± 1.30 j	>80	>200	399.10 ± 8.14 lm
bilberry	0.82 ± 0.12 a	25.12 ± 0.09 k	29.57 ± 0.80 f	75.76 ± 4.83 bcd
black currant	1.73 ± 0.14 a	7.53 ± 0.04 b	3.88 ± 0.05 b	85.79 ± 1.10 cde
blackberry	6.23 ± 0.58 bcd	23.13 ± 0.38 j	18.47 ± 1.02 de	219.73 ± 17.68 h
blueberry	1.33 ± 0.09 a	14.53 ± 0.17 d	46.40 ± 1.08 h	68.18 ± 1.91 bc
blue honeysuckle	8.03 ± 0.44 de	15.53 ± 0.08 e	50.20 ± 1.29 i	39.91 ± 2.54 a
cranberry	1.04 ± 0.10 a	9.03 ± 0.07 c	7.99 ± 0.26 c	204.15 ± 9.83 gh
chokeberry	1.24 ± 0.05 a	>80	1.18 ± 0.09 a	204.55 ± 19.14 gh
grape pink	0.93 ± 0.07 a	21.13 ± 0.10 i	18.92 ± 0.56 e	98.93 ± 2.13 e
green gooseberry	2.01 ± 0.13 a	19.52 ± 0.20 h	1.92 ± 0.09 a	63.36 ± 0.63 b
kiwi	9.53 ± 0.36 e	16.12 ± 0.09 ef	>200	319.98 ± 2.26 k
lingonberry	0.72 ± 0.03 a	4.07 ± 0.07 a	32.71 ± 0.86 g	102.68 ± 8.98 e
mandarine	29.53 ± 1.83 i	61.56 ± 0.64 p	>200	>400
orange	15.06 ± 0.26 f	26.52 ± 0.47 l	>200	>400
peach	41.52 ± 1.69 k	>80	>200	264.44 ± 3.66 j
pear Lukasówka	58.10 ± 1.69 l	>80	>200	>400
pear Nashi	135.07 ± 3.40 m	>80	>200	369.11 ± 7.10 l
pineapple	20.05 ± 0.73 g	37.21 ± 0.27 n	>200	>400
plum Renkloda	20.03 ± 0.37 g	76.53 ± 1.11 s	>200	>400
plum Węgierka Zwykła	9.81 ± 0.44 e	60.06 ± 0.23 o	>200	167.88 ± 8.22 f
pomegranate	4.24 ± 0.31 b	18.53 ± 0.12 g	32.15 ± 2.17 g	191.88 ± 0.23 g
pomelo	23.24 ± 4.10 h	34.13 ± 1.26 m	>200	>400
raspberry	0.91 ± 0.06 a	22.54 ± 0.58 j	17.25 ± 1.01 d	241.04 ± 17.70 i
red currant	0.78 ± 0.04 a	9.54 ± 0.08 c	1.14 ± 0.02 a	159.76 ± 5.33 f
red gooseberry	1.42 ± 0.03 a	20.06 ± 0.60 h	1.04 ± 0.04 a	99.76 ± 6.49 e
red grapefruit	7.83 ± 0.31 de	21.16 ± 0.58 i	>200	>400
sour cherry	6.42 ± 0.26 cd	16.54 ± 0.36 f	>200	258.18 ± 21.20 ij
strawberry	5.72 ± 0.05 bc	73.04 ± 0.60 r	18.18 ± 0.29 de	156.36 ± 5.99 f
sweet cherry	14.22 ± 0.07 f	>80	>200	91.51 ± 3.56 de

[a]Values are means ± standard deviations. Mean values with different letters within the same column are statistically different ($p < 0.05$). [b]4-Methylumbelliferyl oleate based assay. [c]*p*-Nitrophenyl acetate based assay.

sample without the *p*-nitrophenyl acetate was measured for each extract. The results were expressed as inhibition (%) of lipase activity according to the following formula:

$$\text{inhibition (\%)} = \frac{A_{\text{control}} - (A_{\text{sample}} - A_{\text{sample blank}})}{A_{\text{control}}} \times 100$$

Alpha-Glucosidase Inhibition Assay. The inhibition of α-glucosidase activity was determined by measuring the amount of glucose hydrolyzed from *p*-nitrophenyl-α-D-glucopyranoside. An α-glucosidase enzyme solution was prepared by dissolving 0.5 g of intestinal acetone powder from rat in 10 mL of saline (0.9% w/v) and sonicated 12 times at regular intervals (30 s sonications and 30 s off) in an ice bath. After centrifugation at 3000 rpm for 30 min at 4 °C, the resulting supernatant was diluted two times with 0.1 M potassium phosphate buffer (pH 6.9) and was used as the enzyme solution. For the α-glucosidase assay, in a 96-well plate 50 μL of the fruit extract was combined with 50 μL of a fresh prepared enzyme solution and incubated for 10 min. The enzyme reaction was initiated by adding 50 μL of 5 mM *p*-nitrophenyl-α-D-glucopyranoside solution in the above buffer (pH 6.9). The mixtures were incubated at 37 °C for 20 min. Finally, 100 μL of 0.1 M sodium carbonate solution was added and the absorbance (A_A) was read at 405 nm (Synergy2, BioTek Instruments Inc.). Blank and α-glucosidase controls were also included. α-Glucosidase control (A_C) consisted of buffer, substrate, and enzyme. Blank (A_B) consisted of the fruit extract, substrate, and enzyme added after stopping of the reaction with 0.1 M sodium carbonate solution. Blank to control (A_D) consisted of the buffer, substrate, and enzyme added after stopping of the reaction with 0.1 M sodium carbonate solution. All samples were assayed in triplicate.

The rate of α-glucosidase inhibition activity was calculated as a percentage of the control by the following equation:

$$\text{inhibition (\%)} = 100 \times \left[1 - \frac{(A_A - A_B)}{(A_C - A_D)}\right]$$

where A_C, A_A, A_B, and A_D were the absorbance of control, sample, blank sample, and blank control, respectively. The inhibitory activity was expressed as the IC_{50} value.

Alpha-Amylase Inhibition Assay. The α-amylase inhibitory effect of the fruit extracts was assayed according to the procedure described previously by Xiao et al.,[29] with slight modifications. Briefly, 40 μL of 0.2% (w/v) potato starch solution, 20 μL of the fruit extract, or 0.1 M phosphate buffer containing 6 mM $CaCl_2$ (pH 6.9) (control) was mixed with 20 μL of α-amylase from porcine pancreas type VI-B dissolved in the above buffer in a 96-well plate to start the enzyme reaction. After incubation at 37 °C for 10 min, the reaction was stopped by the addition 80 μL of 0.4 M HCl. After that, 100 μL of 5 mM I_2 in 5 mM KI was added, and the absorbance was read at 600 nm (Synergy2, BioTek Instruments Inc.). All samples were assayed in triplicate. The α-amylase inhibitory activity was calculated as follows:

$$\text{inhibition (\%)} = 100 \times \left[1 - \frac{(A_B - A_A)}{(A_D - A_C)}\right]$$

where A_A and A_B were the absorbance of incubated mixture containing fruit extract and starch with or without amylase, respectively. A_C and

A_D were the absorbance of incubated mixture containing starch and amylase or only starch. The inhibitory activity was expressed as the IC_{50} value.

Determination of Antioxidant Capacity. The fruit extracts were assessed for antioxidant capacity by the following two methods: 2,2′-azinobis(3-ethylbenzthiazoline-6-sulfonic acid) radical scavenging activity (ABTS method) and ferric reducing antioxidant power (FRAP method). In both methods, trolox (6-hydroxy-2,5,7,8-tetramethychroman-2-carboxylic acid) was used as a standard and the antioxidant capacity was expressed as μmol of trolox equivalents (TE) per 1 g fresh weight of fruit. All samples were assayed in triplicate.

ABTS Method. $ABTS^{\bullet+}$ radical cation scavenging activity was determined according to the procedure described by Re et al.[30] 2,2′-Azinobis(3-ethylbenzthiazoline-6-sulfonic acid) radical cation ($ABTS^{\bullet+}$) was produced by the reacting of 7 mM ABTS water solution with 2.45 mM potassium persulfate (final concentration) followed by an incubation of the mixture in the dark for 12−16 h at room temperature. Stock solution of $ABTS^{\bullet+}$ was diluted with methanol until an absorbance of 0.76 ± 0.02 at 734 nm was reached. Then, 20 μL of fruit extract or water (control) was mixed with 1 mL of diluted $ABTS^{\bullet+}$ solution, and after 6 min at 30 °C absorbance of this mixture was measured at 734 nm.

FRAP Method. The FRAP assay developed by Benzie and Strain[31] was performed with some modification. Briefly, 2.7 mL of FRAP reagent, prepared freshly and warmed to 30 °C, was mixed with water (0.27 mL) and the fruit extract (0.09 mL). The FRAP reagent was prepared by mixing 2.5 mL of a 10 mM solution of 2,4,6-tris-2-pyridyl-*s*-triazine (TPTZ) in 40 mM HCl with 2.5 mL of 20 mM $FeCl_3$ and diluting with 25 mL of 0.3 mM acetate buffer (pH 3.6). Absorbance at 593 nm was recorded after 10 min incubation of the solution at 30 °C.

Total Phenolic Content. The content of the total phenolics was evaluated by using the Folin−Ciocalteu method. Each fruit extract (0.1−1.0 mL) was mixed with 25 mL of distilled water followed by 0.5 mL of Folin−Ciocalteu reagent and 5 mL of 20% (w/w) Na_2CO_3. The volume of reaction mixture was adjusted to 50 mL with distilled water. The absorbance was then measured at 760 nm after incubation at room temperature for 20 min. Total phenolic content was expressed as mg of gallic acid equivalent (GAE) per 100 g of fresh weight of fruit. All samples were assayed in triplicate.

Phenolic Profile. Phenolic profiles were determined using a high-performance liquid chromatography system (Waters, Milford, MA) that consisted of a gradient pump (1525), photodiode array detector (2998), autoinjector (2707) and Breeze 2 system controller equipped with a 250 × 4.6 mm i.d., 5 μm Symmetry C18 column (Waters). The mobile phase was a binary gradient with A, water/formic acid (90:10, v/v), and B, water/acetonitrile/formic acid (40:50:10, v/v/v), with a flow rate of 1 mL/min.[32] The binary gradient was as follows: 12% B (0 min), 12−30% B (0−26 min), 30−100% B (26−40 min); 100% B (40−43 min), 12% B (43−48 min), and 12% B (48−50 min). Phenolics were qualified into one of the four subclasses and quantified on the base of maximum of UV−vis absorption and spectra recorded from 200 to 600 nm. The hydroxybenzoic acid derivatives and flavanols were quantified at 280 nm and expressed as gallic acid equivalents, hydroxycinnamic acids at 320 nm as chlorogenic acid equivalents, flavonols at 360 nm as rutin equivalents, and anthocyanins at 520 nm as cyanidin 3-glucoside equivalents. The results were expressed as mg/100 g fresh weight of fruit. All samples were assayed in triplicate.

Statistical Analysis. The results are given as the means ± standard deviations. Data were analyzed by means of a one-way ANOVA using Statistica Ver. 6.0 (USA), and Duncan's post hoc test was used to assess the differences between the means with significance level $p < 0.05$. Pearson's correlation coefficients were determined using Microsoft Excel XP.

RESULTS AND DISCUSSION

Pancreatic Lipase Inhibitory Activity. Pancreatic lipase is the most important enzyme responsible for digestion of dietary fat, so its inhibition can lead to beneficial effects on overweight and obesity. In the present work the anti-lipase activity of fruits was investigated using *p*-nitrophenyl acetate (spectrophotometric method) and 4-methylumbelliferyl oleate (fluorimetric method) as substrates. Significant differences ($p < 0.05$) were found among the analyzed fruits in the inhibitory activities toward pancreatic lipase type II (Table 2). The IC_{50} values varied from 0.72 to 135.07 mg of fruit/mL in the fluorimetric method and from 4.07 to more than 80 mg of fruit/mL in the spectrophotometric method. Among the 30 fruits examined, only lingonberry and red currant strongly inhibited pancreatic lipase activity in both methods. They showed IC_{50} values less than 0.8 mg/mL in the fluorimetric assay, and less than 10 mg/mL in the spectrophotometric assay. In addition, bilberry, pink grape, raspberry, cranberry, chokeberry, blueberry, red gooseberry, and black currant showed a relatively high inhibitory effect with their IC_{50} values less than 2 mg/mL in the fluorimetric assay. Black currant and cranberry showed also high inhibitory activity with IC_{50} less than 10 mg/mL in the assay of *p*-nitrophenol release. On the other hand, seven fruits used at 80 mg/mL concentration (the maximum dose of fruit extract in the assay condition) inhibited in this assay pancreatic lipase activity less than 50%.

Few reports have been published about pancreatic lipase inhibitory activity of crude fruit extracts in vitro. Slanc et al.[33] reported that 20 mg/mL of blueberry and apple fruits provided 70% inhibitory activity, while raspberry and banana extracts provided between 40 and 70% inhibitory activity against pancreatic lipase, measured with *p*-nitrophenyl palmitate. Methanolic extract of the Carols muscadine inhibited pancreatic lipase activity with IC_{50} 34.41 mg/mL.[34] Roh and Jung[4] demonstrated a relatively high anti-lipase activity (34.8%) for Cornelian cherries at a concentration of 0.1 mg/mL when *p*-nitrophenyl butyrate was used as a substrate. On the other hand, seven raspberry cultivars examined by Zhang et al.[23] did not show anti-lipase activity measured by fluorimetric assay. Other in vitro studies also demonstrated that lipase activity was effectively inhibited by phenolic-rich extracts of raspberry, strawberry, cloudberry, and Arctic bramble, while black currant and rowanberry extracts had no effect in *p*-nitrophenyl laurate-based assay.[25] These opposite effects can result from the use of different analytical methods (different type and concentration of synthetic substrate, concentration of lipase) and type of extraction solvent. For this reason, there is a need to standardize the method, and further studies with the use of dietary lipids as substrates should be carried out to compare and/or confirm anti-lipase activity of fruit extracts evaluated using artificial substrates.

α-Glucosidase and α-Amylase Inhibitory Activity. In human, dietary carbohydrates are hydrolyzed by pancreatic α-amylase and intestinal α-glucosidase enzymes responsible for the breakdown of oligosaccharides and disaccharides into monosaccharides suitable for absorption.[3] The inhibition of these enzymes is specifically useful for the treatment of non-insulin-dependent diabetes because it will slow down the release of glucose in the blood. In the present work the anti-glucosidase or anti-amylase activity of fruits was investigated using *p*-nitrophenyl-α-D-glucopyranoside or potato starch as substrates, respectively. Significant differences ($p < 0.05$) were found among the analyzed fruits in the inhibitory activities toward α-glucosidase and α-amylase (Table 2). The inhibition of α-glucosidase was in a wide range with the IC_{50} values from 39.91 to more than 400 mg fruit/mL. Blue honeysuckle showed

Table 3. Antioxidant Capacity and Total Phenolic Content of Fruits[a]

fruit	antioxidant capacity (μmol of TE/g fruit)		total phenolics (mg of GAE/100 g)
	ABTS	FRAP	
apple	8.77 ± 0.86 de	4.98 ± 0.43 def	126.80 ± 4.99 g
banana	1.83 ± 0.11 ab	1.15 ± 0.06 ab	30.61 ± 1.27 ab
bilberry	54.17 ± 4.50 m	41.70 ± 2.88 m	487.45 ± 9.27 m
black currant	35.75 ± 2.60 l	29.93 ± 1.33 l	473.64 ± 12.44 m
blackberry	28.91 ± 1.14 k	23.36 ± 1.29 k	288.82 ± 20.65 j
blueberry	27.09 ± 2.05 jk	16.86 ± 0.80 j	337.05 ± 20.92 k
blue honeysuckle	51.54 ± 4.02 m	49.52 ± 4.69 n	540.04 ± 27.73 n
cranberry	20.43 ± 1.14 h	12.74 ± 0.37 i	239.01 ± 23.35 i
chokeberry	124.66 ± 8.27 n	94.24 ± 6.87 o	1423.74 ± 87.83 o
grape pink	10.38 ± 0.55 e	6.10 ± 0.30 ef	117.71 ± 5.40 g
green gooseberry	18.56 ± 1.21 gh	12.28 ± 0.45 hi	245.99 ± 21.13 i
kiwi	1.97 ± 0.10 ab	1.46 ± 0.08 abc	46.40 ± 2.75 abcd
lingonberry	34.82 ± 3.85 l	22.28 ± 2.57 k	410.73 ± 14.53 l
mandarine	3.54 ± 0.28 abc	1.66 ± 0.11 abc	64.93 ± 1.56 cde
orange	4.80 ± 0.11 bc	3.50 ± 0.06 abcde	86.27 ± 2.75 ef
peach	1.59 ± 0.17 ab	0.79 ± 0.06 a	24.83 ± 1.42 a
pear Lukasówka	1.46 ± 0.06 ab	0.81 ± 0.06 a	23.76 ± 1.39 a
pear Nashi	1.65 ± 0.14 ab	0.76 ± 0.07 a	27.20 ± 1.37 a
pineapple	4.02 ± 0.18 abc	4.01 ± 0.20 bcde	62.14 ± 2.64 bcde
plum Renkloda	0.84 ± 0.09 a	0.66 ± 0.06 a	22.78 ± 1.35 a
plum Węgierka Zwykła	2.03 ± 0.20 ab	1.49 ± 0.08 abc	36.55 ± 2.49 abc
pomegranate	14.02 ± 0.88 f	7.62 ± 0.32 fg	183.32 ± 10.05 h
pomelo	3.25 ± 0.07 abc	2.22 ± 0.19 abcd	60.18 ± 2.20 bcde
raspberry	20.36 ± 0.50 h	16.81 ± 0.20 j	183.98 ± 10.42 h
red currant	23.45 ± 1.44 i	16.68 ± 1.25 j	261.95 ± 31.89 ij
red gooseberry	24.39 ± 1.78 ij	16.99 ± 0.53 j	319.63 ± 12.94 k
red grapefruit	3.69 ± 0.13 abc	3.08 ± 0.09 abcd	105.49 ± 4.03 fg
sour cherry	10.70 ± 0.28 e	9.12 ± 0.53 g	120.80 ± 11.37 g
strawberry	16.56 ± 0.84 fg	9.95 ± 0.78 gh	192.95 ± 19.67 h
sweet cherry	6.00 ± 0.33 cd	4.34 ± 0.11 cde	77.53 ± 4.87 def

[a]Values are means ± standard deviations. Mean values with different letters within the same column are statistically different ($p < 0.05$).

the strongest α-glucosidase inhibitory activity with an IC_{50} value of 39.91 mg/mL, and the order of the most potent α-glucosidase inhibitors was as follows: blue honeysuckle > green gooseberry >blueberry > bilberry > black currant > sweet cherry > pink grape > red gooseberry.

Although the fruits tested appeared to have anti-α-glucosidase activities, our experiments have shown that they are weak inhibitors of pancreatic α-amylase. Among 30 fruits tested, half of them at concentration 200 mg/mL inhibited α-amylase activity below 50%. The findings showed that red and green gooseberries, chokeberry, and red currant were the most effective inhibitors of this enzyme with IC_{50} values less than 2 mg/mL.

α-Amylase and/or α-glucosidase inhibitory activities of raspberry, strawberry, lingonberry, black currant, pomegranate, and blueberry extracts have been confirmed by other authors,[18,22] although the inhibitory effect ranks are different from those obtained in our experiments. Similarly to our results, Da Silva Pinto et al.[35] reported red and black currants and red and green gooseberries as the good inhibitors of α-glucosidase and α-amylase, while red currant was the strongest inhibitor of both enzymes. In the present study red currant has indicated very high α-amylase inhibitory activity, but a moderate inhibitory effect against α-glucosidase. Zhang and co-workers[23] observed strong α-glucosidase inhibitory effect for the phenol-rich extracts from raspberries, while none of the seven extracts showed detectable inhibitory effect against pancreatic α-amylase. Contrarily, in our study raspberry crude extract inhibited activity of both enzymes at the moderate level. This observation is consistent with the report of McDougall et al.[18] that the raspberry extract inhibited activity of pancreatic α-amylase. In addition, α-glucosidase inhibitory activity was also demonstrated for Carols muscadine[34] and apple,[36] while α-amylase inhibitory effect was demonstrated for rowanberry, cloudberry, and Arctic bramble.[22]

Antioxidant Capacity. The contribution of fruits to health improvement has been partly attributed to their antioxidant capacity. Antioxidant properties of fruits tested were estimated as scavenging potential toward $ABTS^{\bullet+}$ radical cation and the potential to reduce ferric to ferrous ion (FRAP), and were expressed as trolox (soluble analogue of vitamin E) equivalents (TE): Table 3. Significant differences ($p < 0.05$) were found among the analyzed fruits in the antioxidant capacity. The trolox equivalents (TE) values varied from 0.84 to 124.66 μmol/g of fresh fruit and from 0.66 to 94.24 μmol/g in ABTS and FRAP methods, respectively. Chokeberry had the highest antioxidant capacity, while plum Renkloda showed the lowest TE values, regardless of assay method. Antioxidant capacities of the fruits have been studied in vitro by many authors,[37−39] and our results are consistent with published data.

Total Phenolic Content and Phenolic Profile. The health benefits of fruits are mainly attributed to their vitamins, carotenoids, and phenolic compounds. Phenolic compounds range from simple, low molecular weight, single aromatic

dx.doi.org/10.1021/jf5008264 | J. Agric. Food Chem. 2014, 62, 4610−4617

Table 4. Pearson's Correlation Coefficients (r) between Total Phenolic Content, Antioxidant Capacities, and Digestive Enzymes Inhibitory Activities of Thirty Fruits

	total phenolics	α-amylase	α-glucosidase	pancreatic lipase[a]	pancreatic lipase[b]	ABTS	FRAP
total phenolics	1						
α-amylase	−0.2482	1					
α-glucosidase	−0.3322	−0.1331	1				
pancreatic lipase[a]	−0.3469	0.5322	0.5312	1			
pancreatic lipase[b]	−0.5302	−0.0253	0.0788	0.6254	1		
ABTS	0.9920	−0.2054	−0.3372	−0.3434	−0.4726	1	
FRAP	0.9792	−0.1600	−0.3405	−0.3290	−0.4384	0.9917	1

[a]4-Methylumbelliferyl oleate based assay. [b]-*p*-Nitrophenyl acetate based assay.

Table 5. Phenolic Profiles Determined by HPLC[a]

	phenolics (mg/100 g)			
fruit	HBA and flavanols[b]	HCA[c]	flavonols[d]	anthocyanins[e]
blue honeysuckle	58.62 ± 2.43	55.04 ± 0.81	26.33 ± 3.08	335.37 ± 4.35
lingonberry	106.67 ± 3.55	26.16 ± 1.72	5.94 ± 0.83	25.82 ± 0.75
red gooseberry	77.38 ± 0.23	12.48 ± 2.47	3.12 ± 0.48	4.15 ± 0.37

[a]Values are means ± standard deviations. [b]Determined at 280 nm as gallic acid equivalents. HBA: hydroxbenzoic acids. [c]Determined at 320 nm as chlorogenic acid equivalents. HCA: hydroxycinnamic acids. [d]Determined at 360 nm as rutin equivalents. [e]Determined at 520 nm as cyanidin 3-glucoside equivalents.

ringed compounds to large and complex flavonoids and tannins, with a wide range of biological activities. In this study, the total extractable phenolic contents of 30 different fruits were determined by colorimetric method with Folin−Ciocalteu reagent, and expressed as gallic acid equivalents (GAE). Although the Folin−Ciocalteu reagent is nonspecific to phenolic compounds, and can react with a wide range of thiol derivatives, some vitamins, especially vitamin C, and aromatic amino acids, it is still the most widely used reagent to determine total phenolic content.[40] Moreover, the responses of phenolic compounds to this assay were affected by both the position and degree of hydroxylation in the phenolic molecule. In the present study significant differences ($p < 0.05$) were found among the analyzed fruits in the total phenolic content. The phenolic contents for the fruits studied ranged from 22.78 to 1423.74 mg of GAE/100 g fresh weight (Table 3). Among the fruits, chokeberry contained the highest amount of phenolics followed by blue honeysuckle, bilberry, black currant, and lingonberry, whereas the lowest levels (less than 30 mg of GAE/100 g) were found in plum Renkloda, pears Lukasówka and Nashi, and peach. In general, the present findings are consistent with literature data,[39,41−43] wherein phenolic content in fruits may be affected by a large number of factors such as climatic conditions, agrotechnical processes, cultivars, harvest time, and storage conditions.

Evaluation of Parameters across Tests. In the present study a highly positive correlation between phenolic content and antioxidant capacities measured by ABTS and FRAP assays was reported with a Pearson's correlation coefficient of $r \geq 0.97$ when used for 30 fruit extracts (Table 4). Others researchers also noticed good correlation between total phenolic content and antioxidant potential of fruits as well as a strong correlation between ABTS and FRAP assays.[38,44−46] Some authors postulated that the Folin−Ciocalteu (FC) assay should not be viewed as a measure of total phenolic content, but rather a measure of overall antioxidant capacity.[46] Therefore, it could be expected to find excellent linear correlations between the total phenolic content obtained by the FC method and the antioxidant activity determined by FRAP and ABTS assays. We also observed a high positive correlation between antioxidant capacities measured by ABTS and FRAP assays with a Pearson's correlation coefficient of $r \geq 0.992$.

In contrast to the high correlation between phenolic content and antioxidant capacity, a weaker correlation was observed between phenolic content and inhibition of pancreatic lipase, α-glucosidase, or α-amylase ($r < -0.530$), as well as between antioxidant capacity and the inhibitory effect ($r < -0.473$); Table 4. Our results are consistent with the data for blueberry anthocyanin extract for which α-amylase inhibitory activity correlated poorly with both total phenolic content and FRAP.[24] Lack of correlation between α-glucosidase inhibitory activity and antioxidant activity and total phenolic content has been reported for the phenol-rich extracts from seven raspberry cultivars.[23] In contrast, Wang and co-workers[20] noted a positive correlation (averaging $r = 0.89$) between α-glucosidase inhibitory activity and scavenging activity for peroxyl and hydroxyl radicals as well as for hydrogen peroxide and singlet oxygen in blueberry peel tissue. Flores et al.[24] also observed high correlation between α-glucosidase inhibition by blueberry anthocyanin extract and both its total phenolic content and FRAP.

Results of the present and previous studies suggest that the type of phenolics is more important for the inhibitory effects against digestive enzyme than total phenolic amounts. Moreover, phenolic compounds present in the crude extracts may show synergistic and/or antagonist effects which can influence results of measurements in the assay system. Remarkable differences not only in content but also in composition of phenolic compounds for fruits affect their biological activity. Moreover, a large diversity in the structure between the different subclasses of phenolic compounds as well as within the group influences their stability, solubility, and bonding ability with the digestive enzymes. For example, significant differences in anti-lipase activity were dependent upon the procyanidin degree of polymerization.[47] Previous study also demonstrated that anthocyanidin has much stronger anti-lipase and anti-glucosidase activities than the glycoside form.[48] Among nine phenolic acids tested by Zhang et al.[23] only

ellagic acid inhibited α-glucosidase activity, and according to You et al.[34] ellagic acid was a stronger inhibitor of this enzyme than catechin and quercetin. Therefore, phenolic composition may have a significant importance for inhibition of digestive enzymes by fruits.

For the above-mentioned reason, the three extracts with the highest inhibitory activity against enzymes tested were analyzed for the phenolic profile by HPLC (Table 5). The most abundant phenolic compounds found in the blue honeysuckle extract (the highest α-glucosidase inhibitory activity) were anthocyanins. The inhibitory effectiveness of anthocynins against α-glucosidase has also been reported for other colored fruits such as black currant, strawberry, raspberry, and blueberry fruit extracts.[18,20] This may suggest that anthocyanins are important constituents regarding anti-glucosidase activity. Although chokeberries are known as the most rich source of anthocyanins among fruits[49] in the present study they showed higher IC_{50} value compared to blue honeysuckle. This difference in the IC_{50} values may result from different anthocyanin profile for these two fruits. The major anthocyanin in chokeberry is cyanidin 3-galactoside (66.7% of total anthocyanins),[42,49] while cyanidin 3-glucoside dominates in the blue honeysuckle fruit (71−89% of total anthocyanins).[50] According to Bräunlich et al.[51] cyanidin-3-galactoside possessed 1.8-fold lower α-glucosidase inhibitory activity than cyanidin-3-glucoside. So, inhibitory activity of anthocyanins is strongly influenced by the sugar units linked to the anthocyanidin.

Phenolics with maximum at 280 nm, i.e., flavanols and/or hydroxybenzoic acids, are the main phenolic compounds in red gooseberries which exhibited the highest α-amylase inhibitory activity (Tables 2 and 5). According to literature data[52] proanthocyanidins are important phenolics in gooseberry fruit. α-Amylase inhibitory activity of strawberry and red raspberry was associated with tannins, especially ellagitannins.[35,53] However, a high level of ellagitannins in yellow raspberries did not increase amylase inhibition.[22] Probably the presence of anthocyanins potentiated the enzyme inhibition by ellagitannins. The authors also suggested that high α-amylase inhibitory activity of rowanberry is related to proanthocyanidins.

The high pancreatic lipase inhibitory activity of lingonberries may be caused by proanthocyanidins.[25] In the present study the flavanols were the main phenolic compounds in these berries (Table 5). Sugiyama et al.[54] suggested that the oligomeric procyanidins present in apple polyphenol extract inhibited triglyceride absorption by inhibiting pancreatic lipase activity in mice and humans.

AUTHOR INFORMATION

Corresponding Author

*Tel: 48 426313435. Fax: 48 42 6366618. E-mail: anna.podsedek@p.lodz.pl.

Funding

The work was funded by the National Science Centre allocated on the basis of Decision No. DEC-2011/01/B/NZ9/02046 and grant No. N N312 340740.

Notes

The authors declare no competing financial interest.

REFERENCES

(1) Birari, R. B.; Bhutani, K. K. Pancreatic lipase inhibitors from natural sources: unexplored potential. *Drug Discovery Today* **2007**, *12*, 879−889.

(2) Kumar, S.; Narwal, S.; Kumar, V.; Prakash, O. α-Glucosidase inhibitors from plants: A natural approach to treat diabetes. *Pharmacogn. Rev.* **2011**, *5*, 19−29.

(3) De Sales, P. M.; Souza, P. M.; Simeoni, L. A.; Silveira, D. α-Amylase inhibitors: a review of raw material and isolated compounds from plant source. *J. Pharm. Pharm. Sci.* **2012**, *15*, 141−183.

(4) Roh, C.; Jung, U. Screening of crude plant extracts with anti-obesity activity. *Int. J. Mol. Sci.* **2012**, *13*, 1710−1719.

(5) Yun, J. W. Possible anti-obesity therapeutics from nature—a review. *Phytochemistry* **2010**, *71*, 1625−1641.

(6) Mukherjee, M. Human digestive and metabolic lipases—a brief review. *J. Mol. Catal. B: Enzym.* **2003**, *22*, 369−376.

(7) Gondoin, A.; Grussu, D.; Stewart, D.; McDougall, G. J. White and green tea polyphenols inhibit pancreatic lipase in vitro. *Food Res. Int.* **2010**, *43*, 1537−1544.

(8) He, Q.; Lv, Y.; Yao, K. Effects of tea polyphenols on the activities of α-amylase, pepsin, trypsin and lipase. *Food Chem.* **2007**, *101*, 1178−1182.

(9) Uchiyama, S.; Taniguchi, Y.; Saka, A.; Yoshida, A.; Yajima, H. Prevention of diet-induced obesity by dietary black tea polyphenols extract in vitro and in vivo. *Nutrition* **2011**, *27*, 287−292.

(10) Almoosawi, S.; McDougall, G. J.; Fyfe, L.; Al-Dujaili, E. A. S. Investigating the inhibitory activity of green coffee and cacao bean extracts on pancreatic lipase. *Nutr. Bull.* **2010**, *35*, 207−212.

(11) Gu, Y.; Hurst, W. J.; Stuart, D. A.; Lambert, J. D. Inhibition of key digestive enzymes by cocoa extracts and procyanidins. *J. Agric. Food Chem.* **2011**, *59*, 5305−5311.

(12) Damager, I.; Numao, S.; Chen, H.; Brayer, G. D.; Withers, S. G. Synthesis and characterisation of novel chromogenic substrates for human pancreatic α-amylase. *Carbohydr. Res.* **2004**, *339*, 1727−1737.

(13) Li, Y.; Wen, S.; Kota, B. P.; Peng, G.; Li, G. Q.; Yamahara, J.; Roufogalis, B. D. Punicagranatum flower extract, a potent alpha-glucosidase inhibitor, improves postprandial hyperglycemia in Zucker diabetic fatty rats. *J. Ethnopharmacol.* **2005**, *99*, 239−244.

(14) Yao, Y.; Sang, W.; Zhou, M.; Ren, G. Antioxidant and alpha-glucosidase inhibitory activity of colored grains in China. *J. Agric. Food Chem.* **2010**, *58*, 770−774.

(15) Tsujita, T.; Shintani, T.; Sato, H. α-Amylase inhibitory activity from nut seed skin polyphenols. 1. Purification and characterization of almond seed skin polyphenols. *J. Agric. Food Chem.* **2013**, *61*, 4570−4576.

(16) Wongsa, P.; Chaiwarit, J.; Zamaludien, A. In vitro screening of phenolic compounds, potential inhibition against α-amylase and α-glucosidase of culinary herbs in Thailand. *Food Chem.* **2012**, *131*, 964−971.

(17) McDougall, G. J.; Kulkarni, N. N.; Stewart, D. Current developments on the inhibitory effects of berry polyphenols on digestive enzymes. *BioFactors* **2008**, *34*, 73−80.

(18) McDougall, G. J.; Shpiro, F.; Dobson, P.; Smith, P.; Blake, A.; Stewart, D. Different polyphenolic components of soft fruits Inhibit α-amylase and α-glucosidase. *J. Agric. Food Chem.* **2005**, *53*, 2760−2766.

(19) Johnson, M. H.; Lucius, A.; Meyer, T.; de Mejia, E. G. Cultivar evaluation and effect of fermentation on antioxidant capacity and in vitro inhibition of α-amylase and α-glucosidase by highbush blueberry (Vaccinium corombosum). *J. Agric. Food Chem.* **2011**, *59*, 8923−8930.

(20) Wang, S. Y.; Camp, M. J.; Ehlenfeldt, M. K. Antioxidant capacity and α-glucosidase inhibitory activity in peel and flesh of blueberry (Vaccinium spp.) cultivars. *Food Chem.* **2012**, *132*, 1759−1768.

(21) Cheplick, S.; Kwon, Y.-I.; Bhowmik, P.; Shetty, K. Phenolic-linked variation in strawberry cultivars for potential dietary management of hyperglycemia and related complications of hypertension. *Bioresour. Technol.* **2010**, *101*, 404−413.

(22) Grussu, D.; Stewart, D.; McDougall, G. J. Berry polyphenols inhibit α-amylase in vitro: identifying active components in rowanberry and raspberry. *J. Agric. Food Chem.* **2011**, *59*, 2324−2331.

(23) Zhang, L.; Li, J.; Hogan, S.; Chung, H.; Welbaum, G. E.; Zhou, K. Inhibitory effect of raspberries on starch digestive enzyme and their antioxidant properties and phenolic composition. *Food Chem.* **2010**, *119*, 592−599.

(24) Flores, F. P.; Singh, R. K.; Kerr, W. L.; Pegg, R. B.; Kong, F. Antioxidant and enzyme inhibitory activities of blueberry anthocyanins prepared using different solvents. *J. Agric. Food Chem.* **2013**, *61*, 4441−4447.
(25) McDougall, G. J.; Kulkarni, N. N.; Stewart, D. Berry polyphenols inhibit pancreatic lipase activity in vitro. *Food Chem.* **2009**, *115*, 193−199.
(26) Cha, K. H.; Song, D.-G.; Kim, S. M.; Pan, C.-H. Inhibition of gastrointestinal lipolysis by green tea, coffee, and gomchui (Ligularia fischeri) tea polyphenols during simulated digestion. *J. Agric. Food Chem.* **2012**, *60*, 7152−7157.
(27) Ivanov, S. A.; Nomura, K.; Malfanov, I. L.; Sklyar, I. V.; Ptitsyn, L. R. Isolation of a novel catechin from Bergenia rhizomes that has pronounced lipase-inhibiting and antioxidative properties. *Fitoterapia* **2011**, *82*, 212−218.
(28) Umezawa, H.; Aoyagi, T.; Hazato, T.; Uotani, K.; Kojima, F.; Hamada, M.; Takeuchi, T. Esterastin, an inhibitor of esterase, produced by actinomycetes. *J. Antibiot. (Tokyo)* **1978**, *31*, 639−641.
(29) Xiao, Z.; Storms, R.; Tsang, A. A quantitative starch-iodine method for measuring alpha-amylase and glucoamylase activities. *Anal. Biochem.* **2006**, *351*, 146−148.
(30) Re, R.; Pellegrini, N.; Proteggente, A.; Pannala, A.; Yang, M.; Rice-Evans, C. Antioxidant activity applying an improved ABTS radical cation decolorization assay. *Free Radical Biol. Med.* **1999**, *26*, 1231−1237.
(31) Benzie, I. F. F.; Strain, J. J. The ferric reducing ability of plasma (FRAP) as a measure of "antioxidant power": the FRAP assay. *Anal. Biochem.* **1996**, *239*, 70−76.
(32) Dyrby, M.; Westergaard, N.; Stapelfeldt, H. Light and heat sensitivity of red cabbage extract in soft drink model systems. *Food Chem.* **2001**, *72*, 431−437.
(33) Slanc, P.; Doljak, B.; Kreft, S.; Lunder, M.; Janeš, D.; Štrukelj, B. Screening of selected food and medicinal plant extracts for pancreatic lipase inhibition. *Phytother. Res.* **2009**, *23*, 874−877.
(34) You, Q.; Chen, F.; Wang, X.; Jiang, Y.; Lin, S. Anti-diabetic activities of phenolic compounds in muscadine against alpha-glucosidase and pancreatic lipase. *LWT—Food Sci. Technol.* **2012**, *46*, 164−168.
(35) Da Silva Pinto, M.; Kwon, Y.-I.; Apostolidis, E.; Lajolo, F. M.; Genovese, M. I.; Shetty, K. Evaluation of red currants (Ribes rubrum L.), black currants (Ribes nigrum L.), red and green gooseberries (Ribes uva-crispa) for potential management of type 2 diabetes and hypertension using in vitro models. *J. Food Biochem.* **2010**, *34*, 639−660.
(36) Barbosa, A. C. L.; Pinto, M.; da, S.; Sarkar, D.; Ankolekar, C.; Greene, D.; Shetty, K. Varietal influences on antihyperglycemia properties of freshly harvested apples using in vitro assay models. *J. Med. Food* **2010**, *13*, 1313−1323.
(37) Nilsson, J.; Pillai, D.; Onning, G.; Persson, C.; Nilsson, A.; Akesson, B. Comparison of the 2,2′-azinobis-3-ethylbenzotiazo-line-6-sulfonic acid (ABTS) and ferric reducing anti-oxidant power (FRAP) methods to asses the total antioxidant capacity in extracts of fruit and vegetables. *Mol. Nutr. Food Res.* **2005**, *49*, 239−246.
(38) Floegel, A.; Kim, D.-O.; Chung, S.-J.; Koo, S. I.; Chun, O. K. Comparison of ABTS/DPPH assays to measure antioxidant capacity in popular antioxidant-rich US foods. *J. Food Compos. Anal.* **2011**, *24*, 1043−1048.
(39) Wu, X.; Gu, L.; Prior, R. L.; McKay, S. Characterization of anthocyanins and proanthocyanidins in some cultivars of Ribes, Aronia, and Sambucus and their antioxidant capacity. *J. Agric. Food Chem.* **2004**, *52*, 7846−7856.
(40) Everette, J. D.; Bryant, Q. M.; Green, A. M.; Abbey, Y. A.; Wangila, G. W.; Walker, R. B. Thorough study of reactivity of various compound classes toward the Folin−Ciocalteu reagent. *J. Agric. Food Chem.* **2010**, *58*, 8139−8144.
(41) Sun, J.; Chu, Y.-F.; Wu, X.; Liu, R. H. Antioxidant and antiproliferative activities of common fruits. *J. Agric. Food Chem.* **2002**, *50*, 7449−7454.
(42) Wu, X.; Beecher, G. R.; Holden, J. M.; Haytowitz, D. B.; Gebhardt, S. E.; Prior, R. L. Lipophilic and hydrophilic antioxidant capacities of common foods in the United States. *J. Agric. Food Chem.* **2004**, *52*, 4026−4037.
(43) Kähkönen, M. P.; Hopia, A. I.; Heinonen, M. Berry phenolics and their antioxidant activity. *J. Agric. Food Chem.* **2001**, *49*, 4076−4082.
(44) Hwang, S. J.; Yoon, W. B.; Lee, O.-H.; Cha, S. J.; Kim, J. D. Radical-scavenging-linked antioxidant activities of extracts from black chokeberry and blueberry cultivated in Korea. *Food Chem.* **2014**, *146*, 71−77.
(45) Gorinstein, S.; Haruenkit, R.; Poovarodom, S.; Vearasilp, S.; Ruamsuke, P.; Namiesnik, J.; Leontowicz, M.; Leontowicz, H.; Suhaj, M.; Sheng, G. P. Some analytical assays for the determination of bioactivity of exotic fruits. *Phytochem. Anal.* **2010**, *21*, 355−362.
(46) Dudonné, S.; Vitrac, X.; Coutiére, P.; Woillez, M.; Mérillon, J.-M. Comparative study of antioxidant properties and total phenolic content of 30 plant extracts of industrial interest using DPPH, ABTS, FRAP, SOD, and ORAC assays. *J. Agric. Food Chem.* **2009**, *57*, 1768−1774.
(47) Gonçalves, R.; Mateus, N.; de Freitas, V. Study of the interaction of pancreatic lipase with procyanidins by optical and enzymatic methods. *J. Agric. Food Chem.* **2010**, *58*, 11901−11906.
(48) You, Q.; Chen, F.; Wang, X.; Luo, P. G.; Jiang, Y. Inhibitory effects of muscadine anthocyanins on α-glucosidase and pancreatic lipase activities. *J. Agric. Food Chem.* **2011**, *59*, 9506−9511.
(49) Wu, X.; Beecher, G. R.; Holden, J. M.; Haytowitz, D. B.; Gebhardt, S. E.; Prior, R. L. Concentrations of anthocyanins in common foods in the United States and estimation of normal consumption. *J. Agric. Food Chem.* **2006**, *54*, 4069−4075.
(50) Wojdyło, A.; Jáuregui, P. N. N.; Carbonell-Barrachina, Á. A.; Oszmiański, J.; Golis, T. Variability of phytochemical properties and content of bioactive compounds in Lonicera caerulea L. var. kamtschatica berries. *J. Agric. Food Chem.* **2013**, *61*, 12072−12084.
(51) Braunlich, M.; Slimestad, R.; Wangensteen, H.; Brede, C.; Malterud, K. E.; Barsett, H. Extracts, anthocyanins and procyanidins from Aronia melanocarpa as radical scavengers and enzyme inhibitors. *Nutrients* **2013**, *5*, 663−678.
(52) Hellström, J. K.; Törrönen, A. R.; Mattila, P. H. Proanthocyanidins in common food products of plant origin. *J. Agric. Food Chem.* **2009**, *57*, 7899−7906.
(53) McDougall, G. J.; Stewart, D. The inhibitory effects of berry polyphenols on digestive enzymes. *BioFactors* **2005**, *23*, 189−195.
(54) Sugiyama, H.; Akazome, Y.; Shoji, T.; Yamaguchi, A.; Yasue, M.; Kanda, T.; Ohtake, Y. Oligomeric procyanidins in apple polyphenol are main active components for inhibition of pancreatic lipase and triglyceride absorption. *J. Agric. Food Chem.* **2007**, *55*, 4604−4609.

JOURNAL OF AGRICULTURAL AND FOOD CHEMISTRY

Article

pubs.acs.org/JAFC

Phenolic Acids Identified in Sorghum Distillery Residue Demonstrated Antioxidative and Anti-Cold-Stress Properties in Cultured Tilapia, *Oreochromis mossambicus*

Shin-Mei Lee,[†] Jing-Jen Lin,[‡] Chih-Yuan Liao,[‡] Hui-Ling Cheng,[‡] and Bonnie Sun Pan*[,‡]

[†]Department of Food Science, National Quemoy University, Kinmen 892, Taiwan

[‡]Department of Food Science, National Taiwan Ocean University, Keelung 202, Taiwan

ABSTRACT: This study aimed to identify the bioactive compounds and evaluate the anti-cold-stress function of the sorghum distillery residue (SDR) using tilapia as an alternative animal model. The highest contents of water-soluble bioactive compounds in SDR were polyphenols, followed by tannins, anthocyanins, and flavonoids. SDR was extracted with double-distilled water, 95% ethanol, and ethyl acetate, separately. The ethanol extract (SDR−E) yielded the highest polyphenol content [15.03 mg/g of SDR dry weight (dw)], of which the EC_{50} value of *R*,*R*-diphenyl-*β*-picrylhydrazyl (DPPH) radical scavenging efficiency was 0.56 ± 0.04 mg/mL. The SDR−E suppressed the oxidation of low-density lipoproteins (LDLs) more efficiently than that of other extracts. Tilapia fed a diet containing 3.6% SDR−E decreased accumulative mortality during cold stress, of 46.2%. The accumulative morality of the control was 92.9%. The phenolic acids identified in SDR included gallic acid (0.36 ± 0.08 mg/g of SDR dw), 3,4-dihydroxybenzoic acid (0.16 ± 0.12 mg/g of SDR dw), and 4-hydroxybenzoic acid (0.49 ± 0.23 mg/g of SDR dw). Diets supplemented with 0.5% 4-hydroxybenzoic acid fed to tilapia showed a lower mortality rate than that fed 1.0% 4-hydroxybenzoic acid, comparable to that of the tilapia fed 20% SDR. The latter showed lower mortality than that of the control. These results suggested that 4-hydroxybenzoic acid is one of the major anti-cold-stress compounds in SDR.

KEYWORDS: *sorghum distillery residue, phenolic acids, 4-hydroxybenzoic acid, tilapia, anti-cold stress*

INTRODUCTION

Sorghum distillery residue (SDR), a byproduct of sorghum liquor production, has not been used to add value to it. Sorghum contains high levels of flavonoids, anthocyanins, and phenolic acids.[1,2] The antioxidant activity significantly correlates to the total phenolic content of sorghum.[3] The antioxidative properties of polyphenols allow them to suppress low-density lipoprotein (LDL) oxidation and scavenge free radicals.[4,5] Polyphenols demonstrate antioxidative activities better than vitamin C and vitamin E[4]. Grey mullet (*Mugil cephalus*) fed SDR improved blood fluidity and cold adaptation during winter.[6] A grey mullet fed diet containing 20% SDR resulted in significantly increased total antioxidant capacity of blood plasma and prolonged the lag phase of *ex vivo* tilapia LDL oxidation compared to those fed the control diet.[5] SDR extracts were found to have free-radical-scavenging and tyrosinase-inhibiting effects.[5,7] Both *in vitro* and *ex vivo* LDL oxidation of tilapia were inhibited by the hot-water extract of freshwater clam in a similar dose-dependent pattern. Therefore, the *in vitro* study could serve as a quick screening test to predict the *in vivo* protective effect on LDL oxidation.[8,9]

This research targeted the identity of the natural-occurring antioxidants present in SDR. Different solvents were used to extract polyphenols from SDR to obtain the highest yield and to identify the bioactive compounds extracted. *R*,*R*-Diphenyl-*β*-picrylhydrazyl (DPPH) free-radical-scavenging activity and prolongation of the lag phase of LDL oxidation may be used as bioindicators to evaluate the antioxidative properties of the SDR. Tilapia was used as an alternative animal model to assess the anti-cold-stress activity of SDR when the fish were exposed to cold stress.

MATERIALS AND METHODS

SDR. SDR collected from the Kinmen Distillery was dried at 145 °C at 5 rpm with a double drum dryer (Sung-Hsing Enterprise, Taiwan). The moisture content of SDR reached less than 10%. The dried SDR was ground at room temperature (Yuan Tai Chi dump-style mill, Yu Chi Machinery, Taiwan) and sieved to 60 mesh.

SDR Extracts. SDR was added with 10 times double-distilled (dd) H_2O (w/v) (SDR−W), 95% ethanol (SDR−E), and ethyl acetate (SDR−EA), separately. The SDR extracts were then heated at the boiling point of the solvent for 2 h. The extract was filtered with Advantec 5C filter paper. The residue was extracted repeatedly. Each extract was collected and combined. The solvents were removed under vacuum, while the concentrate was freeze-dried (Kingmech Co., Ltd., Taiwan) and stored at −20 °C for later use.

Chemical. DPPH, gallic acid, 3,4-dihydroxybenzoic acid, 4-hydroxybenzoic acid (4-HB), caffeic acid, cyanidin, quercetin, and epigallocatechin-3-gallate (EGCG) were purchased from Sigma Chemical Co. (St. Louis, MO). All solvents/chemicals used were of analytical grade and obtained from Merck, Taiwan, Ltd. [Taipei, Taiwan, Republic of China (ROC)].

DPPH Free-Radical-Scavenging Properties. The method by Shimada et al.[10] was applied. SDR−W and SDR−EA were dissolved in 200 μL of ddH_2O and dimethyl sulfoxide (DMSO), respectively, and the volume was adjusted to 1000 μL by adding methanol. SDR−E was dissolved in 1000 μL of methanol. A total of 50 μL of each sample or

Received: February 22, 2014
Revised: April 23, 2014
Accepted: May 2, 2014
Published: May 2, 2014

ACS Publications © 2014 American Chemical Society

Trolox as the positive control was taken to a 96-well microplate. The volume was adjusted to 150 μL by adding methanol. A total of 50 μL of 100 mM methanolic solution of DPPH was added to these wells and shaken vigorously. The wells were placed at room temperature for 30 min in the dark prior to being detected at 517 nm using an enzyme-linked immunosorbent assay (ELISA) reader (Spectramax 190, Maxline Microplate Reader System Devices, Sunnyvale, CA). Samples of lower absorbance at 517 nm ($A_{517\ nm}$) indicate higher DPPH scavenging activity.

Total Phenolic Content. A volume of 500 μL of SDR methanolic extract (1 mg/mL) was added to 1 mL of 1:10 (v/v) diluted Folin–Ciocalteu phenol reagent to react at 25 °C for 5 min. Na_2CO_3 was added to the mixture solution to adjust the pH to 9.70–9.85 and allowed to stand for 2 h at 25 °C. Absorbance at 675 nm was measured. The results were expressed as milligrams of gallic acid equivalent per gram of SDR dry weight (dw).[11]

Total Anthocyanin Content. A total of 5.0 g of SDR was added to 50 mL of 0.1% HCl methanol, shaken for 1 h in the dark, and then filtered (Whatman No. 4 filter paper). Residues were extracted repeatedly until the red color disappeared. The solvent extracts were combined, of which 20 mL was taken, and its pH was adjusted to 1.0 and 4.5 with HCl and NaOH, respectively. The sample was analyzed at 520 nm. Cyanidin was used to calibrate the standard curve.[12]

The non-anthocyanin compounds did not absorb at 520 nm, as shown in Figure 2.

Total Flavonoids. A sample of 5.0 g was added to 100 mL of methanol, shaken for 1 h, and then filtered. Residues were extracted twice. The two aliquots were mixed, of which 1 mL was added to 1 mL of 2% methanolic $AlCl_3{\cdot}6H_2O$. The conjugation of Al^{3+} and flavonoids stabilized the color appearance and produced the bathochromic shift for identification. Absorbance was measured at 430 nm, 10 min later. The results were expressed as milligrams of quercetin equivalent per gram of SDR dw.[13]

Tannins. A total of 0.2 g of SDR was added to 10 mL of 1% HCl methanol and shaken for 24 h at room temperature. The mixture was centrifuged at 2200*g* for 10 min. A total of 100 μL of crude extract was added to 5 mL of vanillin reagent (Sigma, St. Louis, MO). The color of the mixture developed after 20 min. The absorbance was read at 500 nm. A standard curve of epigallocatechin-3-gallate (EGCG) in milligrams per milliliter (Sigma) was prepared for quantification. Concentrations were calculated as EGCG (milligrams of equivalent per gram of dw) from the standard curve.[13,14]

Quantification of Phenolic Acids. A sample of 5.0 g was added to 400 mL of 50% aqueous acetone,[15] ultrasonicated (Ultrasonic Cleaner, model D200H, 40 kHz, power at 200 W, heater at 250 W, Delta Co., Taipei, Taiwan) for extraction at 45 °C for 1 h, and then filtered (Whatman No. 4 filter paper). Residues were extracted twice. The extracts were mixed and evaporated at 60 °C using a rotary evaporator. The concentrate was added to 200 mL of butanol and ultasonicated for 2 min, and then the butanol fraction was allowed to separate from the aqueous fraction. Butanol was removed from the butanol extract under vacuum and then dissolved in methanol to 100 mL. High-performance liquid chromatography (HPLC) analysis was carried out after filtering the sample through a 0.45 μm nylon filter. A total of 10 μL of the filtrate was injected into a Luna C18 column (25 cm × 4.6 mm, 5 μm particles, Phenomenex, Torrance, CA), eluted with mobile phase A (2:98, v/v, acetic acid/water) and mobile phase B (8:92, v/v, butanol/methanol) using a gradient program: 0–10 min (95:5, v/v, A/B), 10–17.5 min (85:15, v/v, A/B), 17.6–30.5 min (85:15, v/v, A/B), and 30.6–40 min (50:50, v/v, A/B). The flow rate was 1.0 mL/min. The UV absorbance was monitored at 254 nm (Thermo UV 6000 LP, Finnigan Spectra System, Riviera Beach, FL).[16]

Isolation and Cu^{2+}-Induced Oxidation of LDL. LDL was obtained by ultracentrifugation of human blood plasma from a density range of $1.019 < d < 1.063$ adjusted with NaBr.[17] LDL was dialyzed for 24 h against 5 mM phosphate-buffered saline (PBS) containing 125 mM NaCl (pH 7.4) at 4 °C. The concentration of the dialyzed LDL was determined enzymatically using a commercial kit (Randox Laboratories, San Francisco, CA) and adjusted to 0.15 mg of cholesterol/mL. A total of 100 μL of LDL was added to SDR extract in each well, of which the volume was adjusted to 240 μL with PBS. Then, 10 μL of 125 μM $CuSO_4$ solution was added to make a final volume of 250 μL in each well. The time course of LDL oxidation was monitored, as indicated by the increased absorbance at 232 nm in the 96-well quartz microliter plate (Spectramax 190, Maxline Microplate Reader System Devices, Sunnyvale, CA) at 25 °C for 12 h. The LDL oxidation lag phase was calculated.[5,8]

Cold-Stress Trials. *SDR Feeding Trial.* Tilapia (*Oreochromis mossambicus*) were transferred from a fish farm to the laboratory and acclimated for 2 weeks. Each fish was hand-collected from aquaria with a net onto a plastic tray. The eye of the fish was covered with a piece of cheesecloth and weighed. Seven fish of similar sizes were kept in each of four glass aquaria (92 × 56 × 61 cm) with constant-aerated fresh water of 24 °C. Commercial eel powder (Tai Roum Co., Taichung, Taiwan, ROC) was used as the control diet, which contained 44% protein, 25% carbohydrates, 6% lipid, and 12.0% ash. Dextrin was added in the control diet to balance the 3.6% SDR–E–poly(ethylene glycol) (PEG) diet (Table 1). Both diets were isocaloric and of equal protein content. After acclimation, tilapia were divided into two groups in duplicated aquaria with six fish per aquarium. For 3 months, the two groups of tilapia were fed with the control diet or test diet at 1% body weight per day. The latter contained 3.6% SDR–E–PEG (on a dw basis), which was the SDR–E treated with PEG to counteract the inhibitory effect of the tannins in SDR.[14] The control diet and 4-HB diet did not contain tannin; thus, PEG was not added to them. All groups of fish were exposed to a temperature drop from 24.5 to 13 °C within 10 h, then maintained for 5 days at 13 °C, followed by readjustment of the water temperature to 24 °C, and held for 2 days.

Table 1. Formulation of Tilapia Feed in the SDR–E Feeding Trial

component	control	SDR–E–PEG
formulation (g)		
SDR–E		3.6
PEG[a]		0.1
eel powder	100.0	96.3
dextrin	3.7	
composition		
protein (%)	42.3	42.3
gross energy (kcal/g)	3.8	3.8

[a]PEG = poly(ethylene glycol).

4-HB Feeding Trial. Tilapia were separated into three groups, with each of them consisting of 16 fish/glass aquarium, and fed a diet at 1% body weight per day. The 20% SDR–PEG diet was used as a positive control, in which casein was added for adjusting the diet to isocaloric and of equal protein content with the test diets (Table 2). SDR itself contained 27% crude protein. The test diet contained 0.5% authentic 4-HB or 1.0% 4-HB, separately.

Table 2. Formulation of Tilapia Feed in the 4-HB Feeding Trial

component	20% SDR–PEG	0.5% 4-HB	1.0% 4-HB
formulation (g)			
SDR	20.0		
4-HB[a]		0.5	1.0
PEG[b]	0.1		
eel powder	73.0	99.5	99.5
casein	7.0		0.5
composition			
protein (%)	44.0	44.0	44.0
gross energy (kcal/g)	3.8	3.8	3.8

[a]4-HB = 4-hydroxybenzoic acid. [b]PEG = poly(ethylene glycol).

Statistical Analysis. All values are presented as the mean ± standard deviation (SD). Analysis of variance (ANOVA) was used for comparison of multiple samples. A least significant difference (LSD) test was applied for significant analysis at the 95% level. Sigma 9.0 for Windows was used for statistical analysis of data.

RESULTS AND DISCUSSION

Bioactive Compounds of SDR. The antioxidant compounds in SDR were identified, as shown in Table 3.

Table 3. Bioactive Compounds of SDR in Comparison to Sorghum[a]

compound	sorghum (mg of equivalent/g of dw)	SDR (mg of equivalent/g of dw)
polyphenols as gallic acid	6.51 ± 1.55 b	3.13 ± 0.62 a
anthocyanins as cyanidin	0.07 ± 0.05 a	0.05 ± 0.03 a
flavonoids as quercetin	0.04 ± 0.02 a	0.06 ± 0.01 b
tannins as EGCG	1.60 ± 0.13 b	1.25 ± 0.38 a

[a]All data are shown as the mean ± SD (n = 3).

Polyphenols contributed the highest content, followed by tannins in sorghum and SDR. Anthocyanins and flavonoids were much lower in content, each of which contributed only 20% of the polyphenols. In comparison to the bioactive compounds of sorghum, the SDR was significantly ($p < 0.05$) lower in polyphenols and tannins than sorghum. No significant ($p > 0.05$) difference in anthocyanin content was found between sorghum and SDR.

Yield of Total Polyphenols Varied with Extraction Solvents. Polyphenols were extracted from SDR with water, ethanol, or ethyl acetate, separately, as shown in Table 4. The water extract showed the highest yield, followed by the ethanol extract and then the ethyl acetate extract. However, the ethanol extract contained the highest amount of polyphenols. A recent study on SDR also showed that the water extract had a higher yield than the ethanol extract (SDR−E).[7] Their phenolic content in SDR−E was 19.20 ± 3.22 mg of gallic acid equivalent (GAE)/g of extract, while ours was 15.03 mg of GAE/g of extract (Table 4). Both results were in a similar range.

Table 4. Yield and Polyphenol Content Extracted from Sdr Water, 95% Ethanol, Or Ethyl Acetate Extracted from Sdr

extract[a]	yield[b] (% dw)	SDR extract (mg of GAE/g)[c]	SDR dw (mg of GAE/g)[c]
SDR−W	30.8	4.74	1.46
SDR−E	18.6	15.03	2.80
SDR−EA	9.8	10.07	0.99

[a]SDR, sorghum distillery residue; W, double-distilled water; E, ethanol; and EA, ethyl acetate. [b]Yield (%) = (dry weight of SDR extract/SDR dry weight) × 100. [c]The polyphenol content was expressed as gallic acid equivalent (GAE).

Inhibition of LDL Oxidation and DPPH Scavenging Activity. Cu^{2+}-induced oxidation of human LDL was used for evaluation of the LDL protective effect. The *in vitro* model showed that all of the extracts of SDR prolonged the lag phase of LDL oxidation, being 2−13 times the control, 69.9 ± 11.0 min (Table 5), and reduced the oxidation rate at the propagation stage in a dose-dependent manner (Figure 1). At the same concentration (0.04 mg/mL) of the SDR extract, SDR−E had the longest lag time for human *in vitro* LDL oxidation (903.6 ± 21.2 min), followed by SDR−EA (894.5 ± 24.2 min). Both were significantly ($p < 0.05$) higher than that of Trolox, the positive control (624.9 ± 25.3 min), as shown in Table 5. The lag time of LDL oxidation increased with the total polyphenols of SDR−E (15.03 mg of GAE/g of SDR dw) in comparison to that of SDR−W (4.74 mg of GAE/g of SDR dw), as shown in Table 4, and its lag time was only 135.3 ± 56.7 min, as shown in Table 5.

Table 5. *In Vitro* Effects of the SDR Extract on the Lag Time of Human LDL Oxidation and DPPH Scavenging Activity

treatment[a]	lag time (min)[b]	DPPH scavenging, EC_{50} (mg/mL)
control	69.9 ± 11.0 a	
SDR−W	135.3 ± 56.7 b	1.22 ± 0.06 c
SDR−E	903.6 ± 21.2 d	0.56 ± 0.04 b
SDR−EA	894.5 ± 24.2 d	2.67 ± 0.06 d
Trolox	624.9 ± 25.3 c	0.03 ± 0.00 a

[a]SDR, sorghum distillery residue; W, double-distilled water; E, ethanol; and EA, ethyl acetate. [b]A comparison was made at an equal concentration of 0.04 mg/mL extract. Values in the same column with different letters are significantly different ($p < 0.05$), as analyzed with Duncan's test.

Trolox is able to protect the endogenous antioxidants of LDL from oxidation and prolong the oxidation lag phase[18] and, thus, was used as positive control in this study. SDR−W contained mainly water-soluble substances and resulted in a lag phase 2 times the control, while SDR−E extended the lag phase 12.9-fold that of the control and 1.45-fold that of Trolox.

The antioxidative effect of SDR−E on LDL oxidation was significantly stronger than that of SDR−W, indicative of the fact that the 95% ethanol extract contained more active compounds or the polarity was lower than the water-soluble compounds in SDR. SDR−E was similar in polarity and efficiency to SDR−EA to protect the LDL from oxidation. The SDR−E and SDR−EA extracts are comparatively nonpolar and can readily enter into the core of the LDL to protect the LDL endogenous antioxidants, such as α-tocopherol.[8] From the oxidation lag time, SDR−E and SDR−EA both showed higher antioxidative activity on LDL than that of Trolox.

SDR−E showed the lowest EC_{50} or the higher DPPH free-radical-scavenging activity than SDR−W and SDR−EA (Table 5). SDR−E demonstrated the highest efficacy in both prolonging the oxidation lag time and the DPPH free-radical-scavenging ability. A high content of polyphenol in SDR−E (Table 4) seemed to contribute to the antioxidative activity in prolonging the LDL oxidation lag time and free-radical-scavenging effect. However, no significant correlation was found between the lag time of LDL oxidation and free-radical-scavenging activity (Table 5), indicative of the fact that the antioxidative activity of sorghum involved in retarding the initiation of LDL oxidation[3] came from mechanisms other than scavenging free radicals.

Phenolic Acids of SDR. The phenolic acids of SDR were identified using reversed-phase high-pressure liquid chromatography equipped with a photodiode array detector (RP-HPLC−PDA), as shown in Figure 2A. The chromatogram of the 4-HB standard is shown in Figure 2B, and the chromatogram of the mixture of authentic phenolic acids, including gallic acid, 3,4-dihydroxybenzoic acid, and caffeic acid, is shown in Figure 2C.

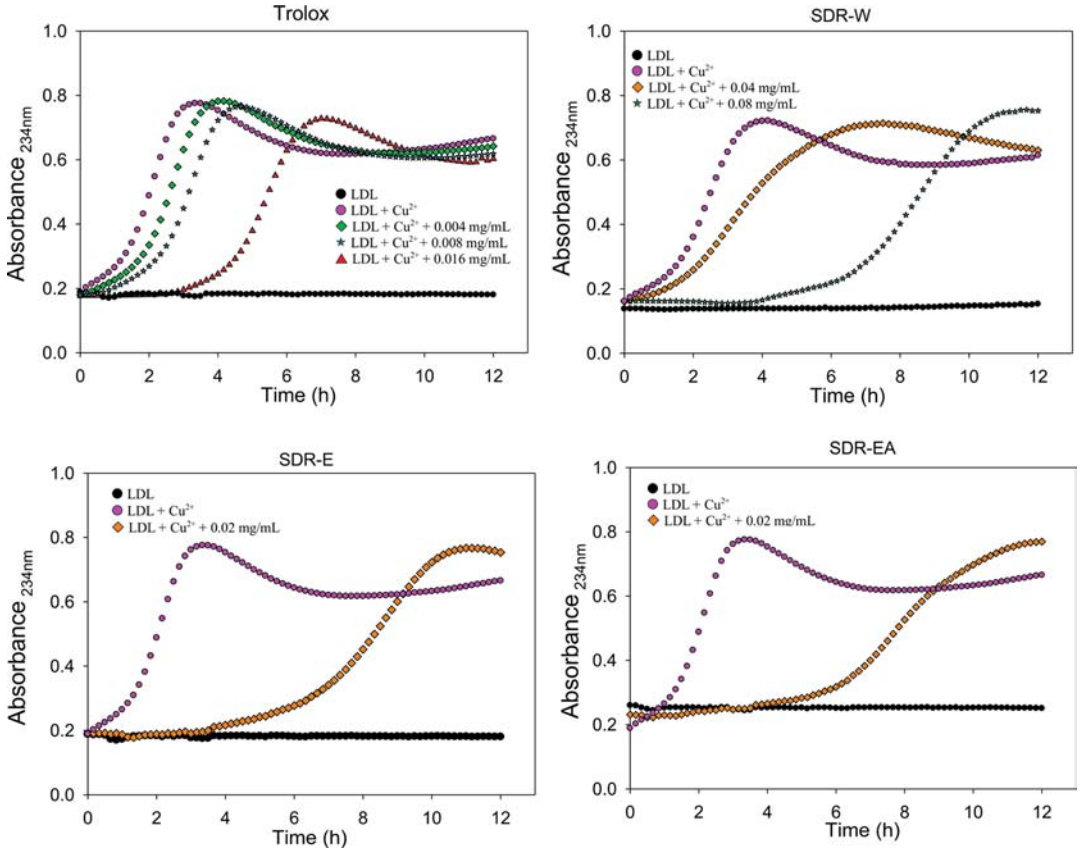

Figure 1. *In vitro* oxidation of human LDL treated with SDR extracts in comparison to Trolox.

The compound in each peak was identified by comparing the retention time and absorption spectrum to those of the authentic standards. Gallic acid (5.308 min), 3,4-dihydroxybenzoic acid (11.172 min), and 4-HB (17.71 min) were verified as present in SDR. An unknown compound was observed at 20.78 min, to be identified. SDR showed a pronounced increase in 4-HB after fermentation of the cooked sorghum. The highest content of phenolic acid in SDR was 4-HB (0.49 ± 0.23 mg/g of dw), followed by gallic acid (0.36 ± 0.08 mg/g of dw) and 3,4-dihydroxybenzoic acid (0.16 ± 0.12 mg/g of dw), as shown in Table 6.

Sorghum of white, lemon yellow, red, and brown varieties contains phenolic acids, which are located in the pericarp, testa, aleurone layer, and endosperm. A total of 10 phenolic acids, including 4-HB and gallic acid, were identified from sorghum.[19] These two phenolic acids were both found in SDR but not in cooked sorghum before fermentation (Table 6). The phenolic acids in sorghum are present mostly in the bound form.[20] Bilberry (European blueberry) fermented with *Lentinus edodes* having β-glycosidase activity also increased in phenolic content, including gallic acid, 4-HB, chlorogenic acid, and *p*-coumaric acid.[21]

The anti-inflammatory activity of sorghum bran correlated with their phenolic content and antioxidant activity.[22] 4-HB showed antimicrobial[23] and antifungal activity[24] and inhibited pre-adipocyte growth.[25] Fermentation of sorghum is a way to produce phenolic acids for enhancing its bioactivities.

Tilapia Fed SDR−E−PEG Reduced Mortality after Cold Stress. Because a fish diet containing 20% SDR−PEG fed to grey mullet (*Mugil cephalus*) prolonged the lag phase of LDL oxidation,[5] tilapia were tested by feeding the diet equivalent to the 20% SDR−PEG diet. The yield of SDR−E in the SDR was 18.6% (Table 4). The test diet fed to tilapia was adjusted to contain 3.6% SDR−E−PEG in comparison to feeding with the control diet made of commercial eel powder. Both diet groups were fed for 3 months at 24.5 °C. During the cold-stress trial, the water temperature was monitored to 13 °C, held for 5 days, and then recovered to 24 °C for 2 days. The accumulative mortality of tilapia is shown in Figure 3. When the water temperature stayed at 13 °C for 5 days, the accumulative mortality of the SDR−E−PEG group was 38.4%, which was much lower than that of the control group (64.3%). As the temperature returned to 24 °C for 2 days, the accumulative morality of the SDR−E−PEG group increased to 46.2%, significantly different ($p < 0.05$) from the control group (92.9%), indicating that SDR−E fed to tilapia improved the adaptability of the fish to temperature fluctuation.

4-HB as an Anti-Cold-Stress Component of SDR. To reduce the consumption of ethanol during preparation of the bioactive feed for practical application, SDR−PEG was used for feeding trials at a level of 0.5 or 1% (w/w) 4-HB of feed. The bioactive compound of SDR responsible for the anti-cold-stress effect in fish was assessed. The highest content of phenolic acids in SDR was 4-HB; therefore, it was speculated to be the major contributor of the anti-cold-stress activity. Tilapia were fed diets containing 20% SDR−PEG,[14] 0.5% 4-HB, or 1.0% 4-HB for 37 days at 25 °C, and then the water temperature was dropped to 13 °C, maintained for 13 days, and followed by recovering to 25 °C. The accumulative mortality is shown in Figure 4. Tilapia fed with 0.5 and 1.0% 4-HB started to die after days 6 and 7, while the accumulated mortality increased to 25 and 37.5%, respectively. Tilapia fed with 20% SDR−PEG

dx.doi.org/10.1021/jf500876k | J. Agric. Food Chem. 2014, 62, 4618−4624

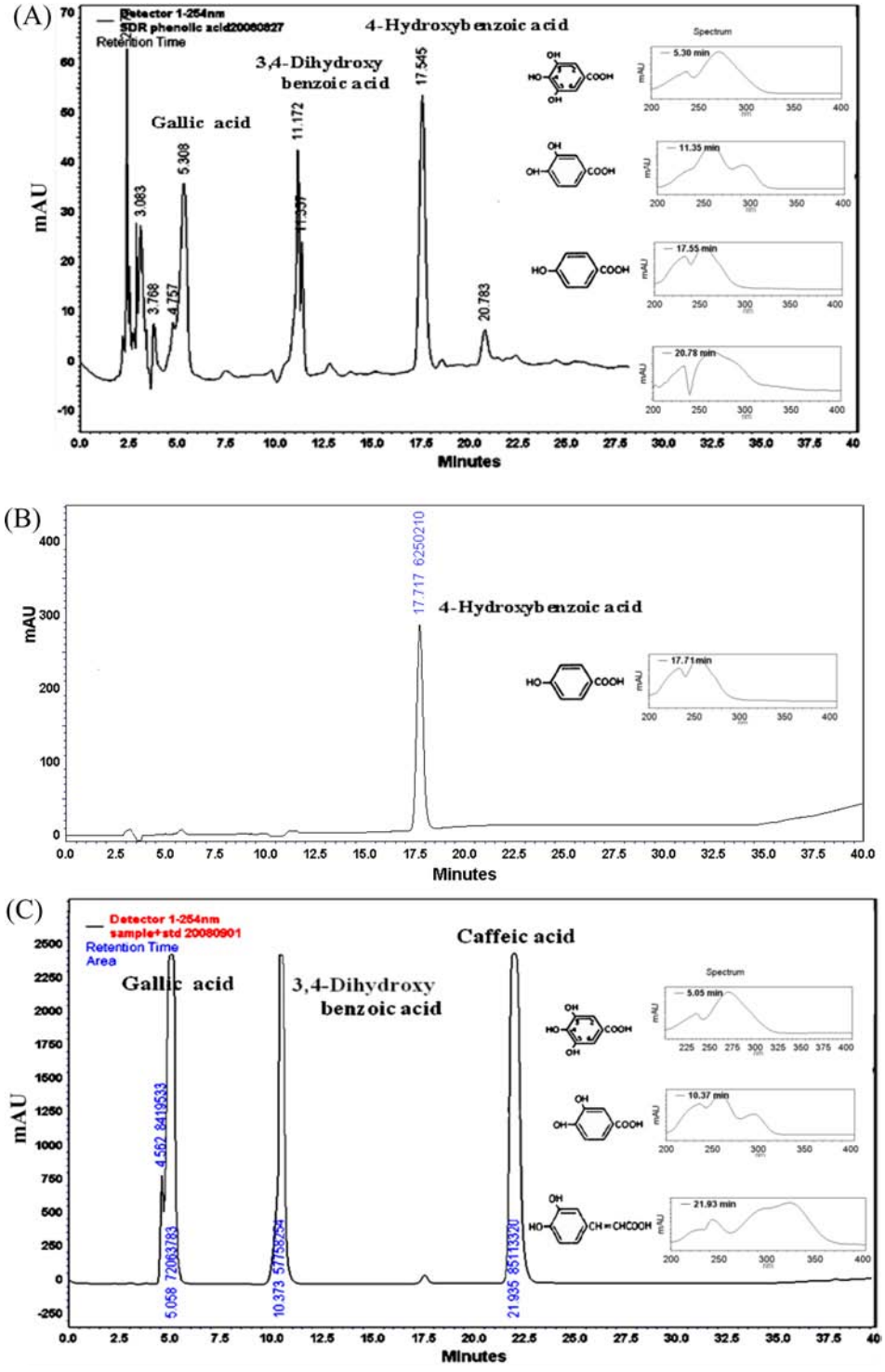

Figure 2. RP-HPLC−PDA chromatogram of phenolic acids of (A) SDR and (B and C) authentic standards.

Table 6. Phenolic Acid Content of Cooked Sorghum Seed and SDR (mg/g of dw)[a]

compound	cooked sorghum seed	SDR
gallic acid		0.36 ± 0.08
3,4-dihydroxybenzoic acid	0.05 ± 0.04	0.16 ± 0.12
4-HB		0.49 ± 0.23

[a]The data are shown as the mean ± SD (n = 3).

started to die after day 10, and the final accumulative mortality was 18.75%, indicated that SDR was stronger in anti-cold-stress capacity than that of 0.5 or 1.0% 4-HB.

The diet containing 0.5% 4-HB was less effective to fish with regard to anti-cold-stress capacity than the diet containing 20% SDR−PEG (Figure 4). While the bioactive content of SDR−PEG was comparable to that of SDR−E−PEG, which showed lower accumulative mortality than those fed the control diet (Figure 3), we summarized that SDR, SDR−E, and 0.5% 4-HB could all improve fish survivability during cold stress. However,

dx.doi.org/10.1021/jf500876k | J. Agric. Food Chem. 2014, 62, 4618−4624

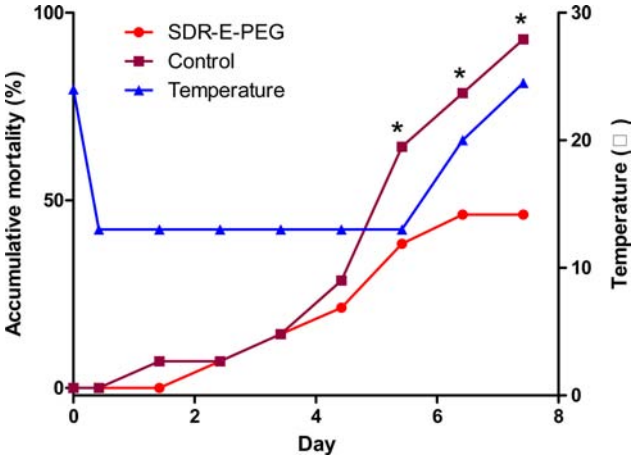

Figure 3. Mortality of tilapia fed for 3 months between September and November with diet containing 95% SDR–E–PEG, followed by exposure of tilapia to cold stress at 13 °C for 5 days and then recovered to 24.5 °C. (*) Values significantly different ($p < 0.05$) between the control and test groups.

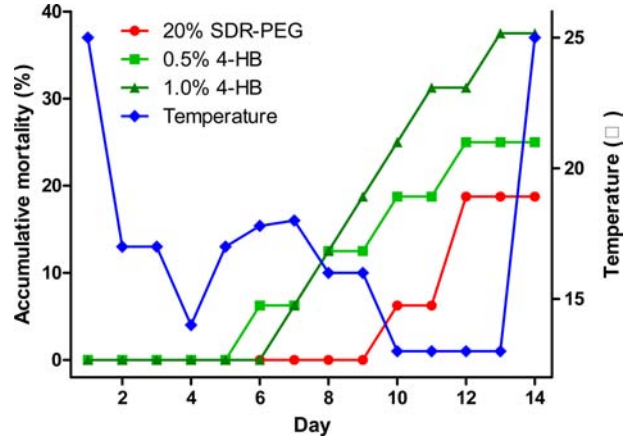

Figure 4. Accumulative mortality of the tilapia fed diet containing 20% SDR–PEG, 0.5% 4-HB, and 1.0% 4-HB for 37 days, followed by exposure to cold stress.

there could be other effective components present in SDR to better enhance the anti-cold-stress effect than 0.5% 4-HB alone. This is our ongoing study to identify these other anti-cold-stress compounds and possibly the mechanism of this effect.

Consumption of cranberry juice increased the concentration of 2-hydroxybenzoic acid (salicylic acid) in plasma[26] and urine of human volunteers.[27] The phytochemical constituents of the cranberry extract showed antiproliferative and synergistic effects against human tumor cell lines.[28] The phenolic acids demostrated anti-inflammatary[29] and antioxidant[30] activities and enhanced gut health.[31]

This study is the first investigation to elucidate the potential applicability of SDR–E to be used as a feed additive to enhance the cold adaptability of cultured tropical fish. It is indicated that the mortality occurred mainly when the temperature was recovered from cold stress, while 4-HB in SDR enhanced the cold adaptability of fish. It seemed that there are bioactive compounds other than 4-HB present in SDR that amplified the efficacy of 4-HB, which deserve further investigation.

AUTHOR INFORMATION

Corresponding Author

*E-mail: bonnie@ntou.edu.tw.

Funding

This study is funded with Project 100-EC-17-A-17-S1-177 by the Ministry of Economic Affairs of Taiwan, ROC.

Notes

The authors declare no competing financial interest.

REFERENCES

(1) Dykes, L.; Rooney, L. W.; Waniska, R. D.; Rooney, W. L. Phenolic compounds and antioxidant activity of sorghum grains of varying genotypes. *J. Agric. Food Chem.* **2005**, *53*, 6813–6818.

(2) Dykes, L.; Seitz, L. M.; Rooney, W. L.; Rooney, L. W. Flavonoid composition of red sorghum genotypes. *Food Chem.* **2009**, *116*, 313–317.

(3) Awika, J. M.; Rooney, L. W.; Wu, X.; Prior, R. L.; Cisneros-Zevallos, L. Screening methods to measure antioxidant activity of sorghum (*Sorghum bicolor*) and sorghum products. *J. Agric. Food Chem.* **2003**, *51*, 6657–6662.

(4) Sánchez-Moreno, C.; Jiménez-Escrig, A.; Saura-Calixto, F. Study of low-density lipoprotein oxidizability indexes to measure the antioxidant activity of dietary polyphenols. *Nutr. Res. (N. Y., NY, U. S.)* **2000**, *20*, 941–953.

(5) Lee, S. M.; Cheng, H. L.; Pan, B. S. LDL oxidation, antioxidant capacity and growth of cultured grey mullet (*Mugil cephalus*) fed dietary sorghum distillery residue pretreated with polyethylene glycol. *J. Agric. Food Chem.* **2009**, *57*, 7877–7882.

(6) Lee, S. M.; Pan, B. S. Effect of dietary sorghum distillery residue on hematological characteristics of cultured grey mullet (*Mugil cephalus*); an animal model for pre-screening antioxidant and blood thinning activities. *J. Food Biochem.* **2003**, *27*, 1–18.

(7) Wang, C. Y.; Ng, C. C.; Lin, H. T.; Shyu, Y. T. Free radical-scavenging and tyrosinase-inhibiting activities of extracts from sorghum distillery residue. *J. Biosci. Bioeng.* **2011**, *111*, 554–556.

(8) Chen, T. Y.; Pan, B. S. *Ex vivo* inhibitory effect on tilapia LDL oxidation and hypolipidemia properties of *Glycine tomentella* root extract. *Comp. Biochem. Physiol., Part A: Mol. Integr. Physiol.* **2007**, *148*, 189–195.

(9) Chen, T. Y.; Shiao, M. S.; Pan, B. S. Inhibition of 12- and 15-lipoxygenase activities and protection of human and tilapia low density lipoprotein oxidation by I-Tiao-Gung (*Glycine tomentella*). *Lipids* **2005**, *40*, 1171–1177.

(10) Shimada, K.; Fujikawa, K.; Yahara, K.; Nakamura, T. Antioxidative properties of xanthan on the antioxidation of soybean oil in cyclodextrin emulsion. *J. Agric. Food Chem.* **1992**, *40*, 945–948.

(11) Singleton, V. L.; Rossi, J. A., Jr. Colorimetry of total phenolics with phosphomolybdic–phosphotungstic acid reagents. *Am. J. Enol. Vitic.* **1965**, *16*, 144–153.

(12) Fuleki, T.; Francis, F. J. Quantitative methods for anthocyanins. *J. Food Sci.* **1968**, *33*, 78–83.

(13) Price, M.; Socoyoc, S. V.; Butler, L. G. A critical evaluation of the vanillin reaction as an assay for tannin in sorghum grain. *J. Agric. Food Chem.* **1978**, *26*, 1214–1218.

(14) Lee, S. M.; Pan, B. S. Inhibitory effect of tannin in dietary sorghum distillery residue and preliminary treatment with PEG on *in vitro* digestibility of grey mullet (*Mugil cephalus*). *J. Food Biochem.* **2003**, *27*, 485–500.

(15) Christel, Q. D.; Bernard, G.; Jacques, V.; Thierry, D.; Claude, B.; Michel, L.; Micheline, C.; Jean, C. C.; Francois, B.; Francis, T. Phenolic compounds and antioxidant activities of buckwheat (*Fagopyrum esculentum* Moench) hulls and flour. *J. Ethnopharmacol.* **2000**, *72*, 35–42.

(16) Hahn, D. H.; Faubion, J. M.; Rooney, L. W. Sorghum phenolic acids, their high performance liquid chromatography separation and their relation to fungal resistance. *Cereal Chem.* **1983**, *60*, 255–259.

(17) Kleinveld, H. A.; Hak-Lemmers, H. L. M.; Stalenhoef, A. F. H.; Demacker, P. N. M. Improved measurement of low-density-lipoprotein susceptibility to copper-induced oxidation: Application of a short procedure for isolating low density lipoprotein. *Clin. Chem.* **1992**, *38*, 2066−2072.
(18) Bergmann, A. R.; Ramos, P.; Esterbauer, H.; Winklhofer-Roob, B. M. *RRR-α*-Tocopherol can be substituted for by Trolox in determination of kinetic parameters of LDL oxidizability by copper. *J. Lipid Res.* **1997**, *38*, 2580−2588.
(19) Dykes, L.; Rooney, L. W. Sorghum and millet phenols and antioxidants. *J. Cereal Sci.* **2006**, *44*, 236−251.
(20) Hahn, D. H.; Faubion, J. M.; Rooney, L. W. Sorghum phenolic acids, their high performance liquid chromatography separation and their relation to fungal resistance. *Cereal Chem.* **1983**, *60*, 255−259.
(21) Zheng, Z.; Shetty, K. Solid-state bioconversion of phenolics from cranberry pomace and role of *Lentinus edodes β*-glucosidase. *J. Agric. Food Chem.* **2000**, *48*, 895−900.
(22) Burdette, A.; Garner, P. L.; Mayer, E. P.; Hargrove, J. L.; Hartle, D. K.; Greenspan, P. Anti-inflammatory activity of select sorghum (*Sorghum bicolor*) brans. *J. Med. Food.* **2010**, *13*, 879−887.
(23) Cho, J. Y.; Moon, J. H.; Seong, K. Y.; Park, K. H. Antimicrobial activity of 4-hydroxybenzoic acid and *trans*-4-hydroxycinnamic acid isolated and identified from rice hull. *Biosci., Biotechnol., Biochem.* **1998**, *62*, 2273−2276.
(24) Chong, K. P.; Rossall, S.; Atong, M. *In vitro* antimicrobial activity and fungitoxicity of syringic acid, caffeic acid and 4-hydroxybenzoic acid against *Ganoderma boninense*. *J. Agric. Sci.* **2009**, *1*, 15−20.
(25) Hsu, C. L.; Huang, S. L.; Yen, G. C. Inhibitory effect of phenolic acids on the proliferation of 3T3-L1 preadipocytes in relation to their antioxidant activity. *J. Agric. Food Chem.* **2006**, *54*, 4191−4197.
(26) Zhang, K.; Zuo, Y. GC−MS determination of flavonoids and phenolic and benzoic acids in human plasma after consumption of cranberry juice. *J. Agric. Food Chem.* **2004**, *52*, 222−227.
(27) Duthie, G. G.; Kyle, J. A.; Jenkinson, A. M.; Duthie, S. J.; Baxter, G. J.; Paterson, J. R. Increased salicylate concentrations in urine of human volunteers after consumption of cranberry juice. *J. Agric. Food Chem.* **2005**, *53*, 2897−2900.
(28) Seeram, N. P.; Adams, L. S.; Hardy, M. L.; Heber, D. Total cranberry extract versus its phytochemical constituents: Antiproliferative and synergistic effects against human tumor cell lines. *J. Agric. Food Chem.* **2004**, *52*, 2512−2517.
(29) Anson, N. M.; Aura, A. M.; Selinheimo, E.; Mattila, I.; Poutanen, K.; Van Den Berg, R.; Havenaar, R.; Bast, A.; Haenen, G. R. M. M. Bioprocessing of wheat bran in whole wheat bread increases the bioavailability of phenolic acids in men and exerts anti-inflammatory effects *ex vivo*. *J. Nutr.* **2011**, *141*, 137−143.
(30) Gruz, J.; Ayaz, F. A.; Torun, H.; Strnad, M. Phenolic acid content and radical scavenging activity of extracts from medlar (*Mespilus germanica* L.) fruit at different stages of ripening. *Food Chem.* **2011**, *124*, 271−277.
(31) Russell, W.; Duthie, G. Plant secondary metabolites and gut health: The case for phenolic acids. *Proc. Nutr. Soc.* **2011**, *70*, 389−396.

JOURNAL OF AGRICULTURAL AND FOOD CHEMISTRY

Article

pubs.acs.org/JAFC

Asiatic Acid Ameliorates Hepatic Lipid Accumulation and Insulin Resistance in Mice Consuming a High-Fat Diet

Sheng-Lei Yan,[†,∥] Hui-Ting Yang,[#,∥] Yi-Ju Lee,[§] Chun-Che Lin,[○] Ming-Hui Chang,[○] and Mei-Chin Yin*[,#,⊥]

[†]Division of Gastroenterology, Department of Internal Medicine, Chang Bing Show-Chwan Memorial Hospital, Changhua County, Taiwan

[#]Department of Nutrition, China Medical University, Taichung City, Taiwan

[§]Department of Pathology, Chung Shan Medical University Hospital, Taichung City, Taiwan

[○]Division of Gastroenterology and Hepatology, Department of Internal Medicine, Chung Shan Medical University Hospital, Taichung City, Taiwan

[⊥]Department of Health and Nutrition Biotechnology, Asia University, Taichung City, Taiwan

ABSTRACT: Effects of asiatic acid (AA) at 10 or 20 mg/kg/day upon hepatic steatosis in mice consuming a high-fat diet (HFD) were examined. AA intake decreased body weight, water intake, feed intake, epididymal fat, and plasma and hepatic triglyceride levels in HFD-treated mice ($P < 0.05$). HFD enhanced 2.85-fold acetyl coenzyme A carboxylase (ACC1), 3.34-fold fatty acid synthase (FAS), 3.71-fold stearoyl CoA desaturase (SCD)-1, 3.62-fold 3-hydroxy-3-methylglutaryl coenzyme A reductase, 2.91-fold sterol regulatory element-binding protein (SREBP)-1c, and 2.75-fold SREBP-2 expression in liver ($P < 0.05$). Compared with HFD groups, AA intake at two doses reduced 18.9−45.7% ACC1, 25.1−49.8% FAS, 24.7−57.1% SCD-1, and 21.8−53.3% SREBP-1c protein expression ($P < 0.05$). Histological results indicated AA intake at two doses reduced hepatic lipid accumulation and inflammatory infiltrate. HFD increased hepatic production of reactive oxygen species, interleukin (IL)-1β, IL-6, and tumor necrosis factor-α, as well as decreased hepatic glutathione content and glutathione peroxidase and catalase activities ($P < 0.05$). AA intake at two doses reversed these alterations ($P < 0.05$). AA intake suppressed 32.4−58.8% nuclear factor kappa (NF-κ)B p65 and 24.2−56.7% p-p38 expression ($P < 0.05$) and at high dose down-regulated 29.1% NF-κB p50 and 40.7% p-JNK expression in livers from HFD-treated mice. AA intake at two doses lowered plasma insulin secretion and HOMR-IR ($P < 0.05$). These results suggest that AA is a potent hepatic protective agent against HFD-induced hepatic injury.

KEYWORDS: *asiatic acid, high-fat diet, hepatic steatosis, insulin resistance*

INTRODUCTION

Hepatic steatosis, hyperlipidemia, and obesity due to lipid accumulation are risk factors associated with the prevalence of cardiovascular diseases and metabolic disorders,[1,2] in which both oxidative and inflammatory reactions are involved.[3] Enhanced lipogenesis is a major contributor to lipid accumulation in the liver and other organs. Thus, any agent with antilipogenic, antioxidative, and anti-inflammatory effects may improve lipid metabolism disorders and alleviate hepatic steatosis and related injury.

Asiatic acid (AA, Figure 1) is a pentacyclic triterpene naturally occurring in many vegetables and fruits such as basil (*Ocimum basilicum*), brown mustard (*Brassica juncea*), and centella (*Centella asiatica* L.).[4,5] It has been reported that this triterpene could provide antioxidative and anti-inflammatory protection for mouse liver against D-galactosamine or lipopolysaccharide-induced acute liver injury.[6,7] Wei et al.[8] observed that AA intragastrical administration protected liver against ethanol-induced hepatotoxicity through attenuating oxidative stress. Pakdeechote et al.[9] indicated that 3 weeks of AA intake at 10 or 20 mg/kg/day improved high-carbohydrate and high-fat diet induced metabolic abnormalities including glucose intolerance, hypertension, and circulating oxidative and inflammatory stress in rats. However, it remains unknown whether AA could suppress high-fat diet caused hepatic lipogenesis or oxidative and inflammatory injury.

Acetyl coenzyme A carboxylase (ACC), fatty acid synthase (FAS), stearoyl CoA desaturase (SCD)-1, and 3-hydroxy-3-methylglutaryl coenzyme A (HMG-CoA) reductase are lipogenic enzymes and involved in the biosynthesis of triglyceride and cholesterol in the liver and adipose tissue.[10,11]

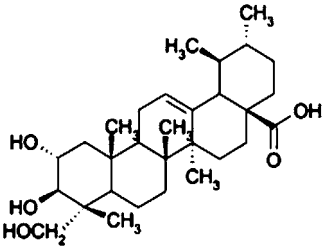

Figure 1. Structure of AA.

Received: March 8, 2014
Revised: April 24, 2014
Accepted: April 29, 2014
Published: April 29, 2014

ACS Publications © 2014 American Chemical Society

Table 1. Body Weight, Water Intake, Feed Intake, Liver Weight, and Epididymal Fat in Mice Treated with Normal Diet (ND), High-Fat Diet (HFD), or HFD with AA-Low or AA-High for 7 Weeks[a]

	ND	HFD	HFD + AA-low	HFD + AA-high
body wt (g/mouse)	24.6 ± 1.1a	36.4 ± 1.7d	32.8 ± 0.9c	28.5 ± 1.2b
water intake (mL/mouse/day)	2.0 ± 0.4a	5.8 ± 0.6c	4.7 ± 0.3b	4.5 ± 0.5b
feed intake (g/mouse/day)	1.5 ± 0.3a	5.3 ± 0.8d	4.5 ± 0.4c	3.8 ± 0.5b
liver wt (g/mouse)	1.28 ± 0.13a	2.16 ± 0.23c	2.01 ± 0.14c	1.74 ± 0.18b
epididymal fat (g/mouse)	0.24 ± 0.05a	1.41 ± 0.15d	1.12 ± 0.10c	0.72 ± 0.09b

[a]Values are means ± SD, $n = 10$. Means in a row without a common letter differ, $P < 0.05$.

Sterol regulatory element-binding protein (SREBP)-1c and SREBP-2 are important transcription factors responsible for the expression of genes encoded for fatty acid and cholesterol biosynthesis, respectively.[12,13] In addition, hormones such as insulin, leptin, and adiponectin also affect lipid metabolism. Abnormal levels of these hormones in circulation due to a high-fat diet enhance lipogenesis.[14] So far, less information is available regarding the influence of AA upon these lipogenic enzymes, SREPBs, and hormones. It is reported that a high-fat diet promoted hepatic oxidative and inflammatory stress by activating nuclear factor kappa (NF-κ)B and mitogen-activated protein kinase (MAPK) pathways.[15,16] Our previous study found that a high-fat diet decreased hepatic glutathione (GSH) content, lowered catalase and glutathione peroxidase (GPx) activities, and increased cytokine release.[17] If AA could alleviate high-fat diet caused oxidative and inflammatory injury, it may protect the liver against the development of steatohepatitis.

The major purpose of this study was to investigate the effects of AA at 10 or 20 mg/kg/day on lipid deposit and protein expression of lipogenic enzymes and SREBPs in livers from high-fat diet treated mice. The influence of this triterpene upon hepatic oxidative and inflammatory stress, as well as the variation of insulin, leptin, adiponectin, and ghrelin in circulation, was also evaluated.

MATERIALS AND METHODS

Materials. Asiatic acid (AA, 98%) was purchased from Sigma-Aldrich Co. (St. Louis, MO, USA). High-fat diet (HFD) containing 60% of calories as fat was purchased from Research Diets Co. (New Brunswick, NJ, USA), in which saturated fat and monounsaturated fat were 55 and 35% of total fat, respectively.

Animals and Diets. Male 3-week-old C57BL/6 mice were obtained from the National Laboratory Animal Center (National Science Council, Taipei City, Taiwan). Use of the mice was reviewed and approved by the China Medical University animal care committee. After 1 week of acclimation, mice were used for experiments.

Experimental Design. Mice were divided into four groups: normal group (normal diet); HFD group (high-fat diet); AA-low group (high-fat diet plus AA at 10 mg/kg/day); AA-high group (high-fat diet plus AA at 20 mg/kg/day). AA, suspended in 1.2% methyl cellulose (MC), was administered daily by oral gavage. After 7 weeks, mice were killed with carbon dioxide. Blood, liver, and epididymal fat from each mouse were collected and weighed. Protein concentration of tissue homogenate was determined by a commercial assay kit (Pierce Biotechnology Inc., Rockford, IL, USA) with bovine serum albumin as standard. Our preliminary study found that there was no significant difference in all measurements between mice consuming the normal diet and normal diet plus AA-high or between mice consuming the high-fat diet and the high-fat diet plus vehicle (1.2% MC). Thus, two groups, normal diet plus AA-high and high-fat diet plus vehicle were omitted in the present study.

Blood Analysis. Triglyceride (TG) and total cholesterol (TC) levels in plasma were assayed by kits purchased from Wako Pure Chemical Co. (Osaka, Japan). Plasma activity of alanine aminotransferase (ALT) and aspartate aminotransferase (AST) was determined by commercial kits (Randox Laboratories Ltd., Crumlin, UK). Plasma levels of glucose (mmol/L) and insulin (nmol/L) were measured by using a glucose HK kit (Sigma Chemical Co., St. Louis, MO, USA) and mouse ultrasensitive ELISA kit (DRG Instruments GmbH, Marburg, Germany), respectively. Insulin resistance, expressed as homeostasis model assessment-insulin resistance (HOMA-IR), was calculated via the formula [glucose (mmol/L) × insulin (mU/L)]/22.5. Plasma leptin and adiponectin levels were measured using a Mouse Leptin Quantikine ELISA kit (R&D Systems, Minneapolis, MN, USA) and a Rat/mouse Adiponectin ELISA kit (Phoenix Europe GmbH, Karlsruhe, Germany), respectively. Plasma immunoreactive ghrelin concentration was measured using a radioimmunoassay kit (Phoenix Pharmaceuticals, Belmont, CA, USA).

Hepatic TG and TC. Liver homogenate, 1 mL, was mixed with 2.5 mL of chloroform/methanol (2:1, v/v). The chloroform layer was collected and concentrated. After mixing with 10% Triton X-100 in isopropanol, the sample was assayed by using Wako Triglyceride E-Test and Total Cholesterol E-Test kits (Wako Pure Chemical).

Fecal Lipid Analysis. Feces, at 0.5 g, were mixed with 3.5 mL of deionized water. After sitting at 4 °C overnight, feces were homogenized by vortexing. The fecal lipid was extracted with methanol/chloroform (2:1, v/v) using a method described in Tsujita et al.[18] The lipophilic layer was collected and dried under a nitrogen stream.

Measurement of Oxidative and Inflammatory Factors in Liver. Liver tissue was homogenized with cold phosphate-buffered saline containing 0.05% Tween 20 and 1 mM EDTA. After centrifuging, the supernatants were used for measurements. Sample was mixed with 25 mM 2′,7′-dichlorofluorescein diacetate. After 30 min of incubation at room temperature, reactive oxygen species (ROS) level was determined by monitoring fluorescence change at an excitation wavelength of 488 nm and an emission wavelength of 515 nm. GSH content was measured by using a commercial kit (OxisResearch, Portland, OR, USA). The activities of GPX and catalase were assayed by GPX and catalase kits (Calbiochem, EMD Biosciences, Inc., San Diego, CA, USA). Levels of interleukin (IL)-1β, IL-6, and tumor necrosis factor (TNF)-α were determined using ELISA kits (R&D Systems).

Western Blot Analysis. Liver tissue was homogenized in buffer containing 0.5% Triton X-100 and protease-inhibitor cocktail (1:1000, Sigma-Aldrich Chemical Co.). This homogenate was further mixed with buffer (60 mM Tris-HCl, 2% SDS, and 2% β-mercaptoethanol, pH 7.2) and boiled for 5 min. Sample at 40 μg protein was applied to 10% SDS−polyacrylamide gel electrophoresis and transferred to a nitrocellulose membrane (Millipore, Bedford, MA, USA) for 1 h. After blocking with a solution containing 5% nonfat milk for 1 h to prevent nonspecific binding of antibody, membrane was incubated with mouse anti-ACC1, anti-FAS, anti-SCD-1 (1:1000), anti-HMG-CoA reductase, anti-SREBP-1c, anti-SREBP-2 (1:2000), and anti-NF-κB and anti-MAPK (1:1000) monoclonal antibodies (Boehringer-Mannheim, Indianapolis, IN, USA) at 4 °C overnight and followed by reaction with horseradish peroxidase-conjugated antibody for 3.5 h at room temperature. The detected bands were quantified by an image analyzer (ATTO, Tokyo, Japan), and glyceraldehyde-3-phosphate dehydrogenase (GAPDH) was used as a loading control. The blot was quantified by densitometric analysis. Results were normalized to GAPDH and given as arbitrary units (AU).

Table 2. Plasma Levels of ALT, AST, TG, and TC, Hepatic Levels of TG and TC, and Fecal Lipid Level in Mice Treated with Normal Diet (ND), High-Fat Diet (HFD), or HFD with AA-Low or AA-High for 7 Weeks[a]

	ND	HFD	HFD + AA-low	HFD + AA-high
plasma				
ALT (U/L)	33 ± 3a	118 ± 10d	91 ± 5c	60 ± 6b
AST (U/L)	36 ± 4a	104 ± 8d	82 ± 7c	51 ± 4b
TG (g/L)	2.24 ± 0.08a	5.76 ± 0.21d	5.01 ± 0.13c	3.98 ± 0.10b
TC (g/L)	1.28 ± 0.05a	3.90 ± 0.11c	3.56 ± 0.06c	2.94 ± 0.07b
hepatic				
TG (mg/g wet wt)	25.9 ± 1.2a	64.5 ± 2.5d	51.1 ± 1.6c	38.2 ± 0.9b
TC (mg/g wet wt)	2.8 ± 0.2a	7.6 ± 0.4c	7.1 ± 0.3c	6.4 ± 0.2b
fecal				
lipid (mg/g feces)	8.3 ± 0.5a	13.6 ± 0.4b	14.0 ± 0.6b	15.7 ± 0.5c

[a]Values are means ± SD, $n = 10$. Means in a row without a common letter differ, $P < 0.05$.

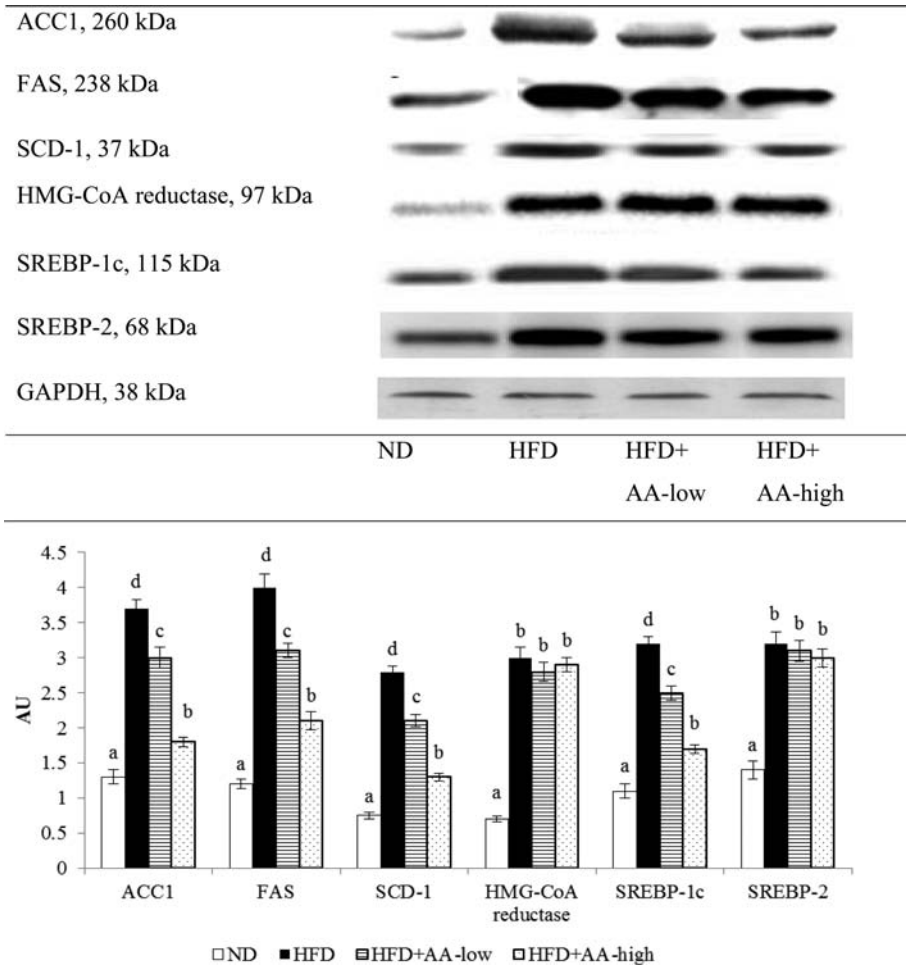

Figure 2. Hepatic protein expression of ACC1, FAS, SCD-1, HMG-CoA reductase, SREBP-1c, and SREBP-2 in mice treated with normal diet (ND), high-fat diet (HFD), or HFD with AA-low or AA-high for 7 weeks. Values are means ± SD, $n = 10$. Means among bars without a common letter differ, $P < 0.05$.

Histological Analysis. Partial liver tissue from each mouse was fixed in 10% phosphate-buffered formalin and embedded in paraffin. Paraffin section at 5 μm thickness was cut and stained with Oil Red O (ORO) stain and hematoxylin-eosin (H&E) stain, and followed by examination under a light microscope for histological analysis.

Statistical Analysis. The effect of each treatment was analyzed from 10 mice ($n = 10$) in each group. All data were expressed as the mean ± standard deviation (SD). Statistical analysis was done using one-way analysis of variance, and post-hoc comparisons were carried out using Dunnet's t test. Statistical significance was considered at $P < 0.05$.

RESULTS

Effects of AA on Body Weight. HFD increased mouse body weight, water intake, feed intake, liver weight, and epididymal fat (Table 1, $P < 0.05$). Compared with HFD groups, AA intake at low and high doses decreased body weight, water intake, feed intake, and epididymal fat in HFD-treated mice ($P < 0.05$). AA intake only at high dose lowered liver weight of mice treated with HFD ($P < 0.05$).

dx.doi.org/10.1021/jf501165z | J. Agric. Food Chem. 2014, 62, 4625−4631

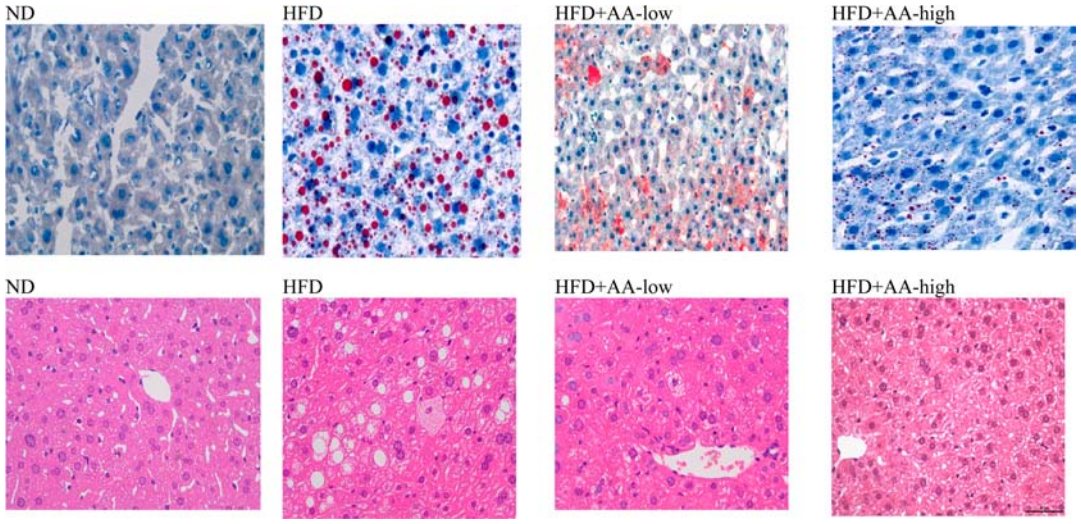

Figure 3. Effects of AA upon hepatic lipid accumulation (upper row), determined by ORO statin; hepatic inflammation (lower row), determined by H&E stain in mice treated with normal diet (ND), high-fat diet (HFD), or HFD with AA-low or AA-high for 7 weeks. Magnification: 200×.

Table 3. Plasma Level of Glucose, Insulin, HOMA-IR, Leptin, Adiponectin, and Ghrelin in Mice Treated with Normal Diet (ND), High Fat Diet (HFD), or HFD with AA-Low or AA-High for 7 Weeks[a]

	ND	HFD	HFD + AA-low	HFD + AA-high
glucose (mmol/L)	7.2 ± 0.3a	7.8 ± 0.5a	7.6 ± 0.2a	7.5 ± 0.4a
insulin (nmol/L)	14.2 ± 0.6a	25.8 ± 1.8d	22.5 ± 1.1c	17.8 ± 0.9b
HOMA-IR	4.3 ± 0.8a	33.4 ± 2.1d	26.1 ± 1.7c	15.0 ± 1.0b
leptin (ng/mL)	1.21 ± 0.20a	2.19 ± 0.17b	2.10 ± 0.11b	1.98 ± 0.08b
adiponectin (μg/mL)	8.3 ± 0.5b	4.7 ± 0.2a	4.8 ± 0.4a	5.1 ± 4a
ghrelin (fmol/mL)	152 ± 13b	96 ± 7a	101 ± 6a	105 ± 9a

[a]Values are means ± SD, n = 10. Means in a row without a common letter differ, $P < 0.05$.

Table 4. Hepatic Levels of ROS and GSH, Activities of Catalase and GPX, and Levels of IL-1β, IL-6, and TNF-α in Mice Treated with Normal Diet (ND), High-Fat Diet (HFD), or HFD with AA-Low or AA-High for 7 Weeks[a]

	ND	HFD	HFD + AA-low	HFD + AA-high
ROS (RFU/mg protein)	0.26 ± 0.04a	1.30 ± 0.12d	1.02 ± 0.10c	0.66 ± 0.08b
GSH (nmol/mg protein)	12.4 ± 0.6d	7.3 ± 0.4a	8.4 ± 0.5b	10.1 ± 0.7c
GPX (U/mg protein)	18.6 ± 0.5d	12.5 ± 0.3a	14.1 ± 0.4b	15.5 ± 0.5c
catalase (U/mg protein)	17.1 ± 0.7d	11.3 ± 0.4a	12.5 ± 0.6b	14.3 ± 0.6c
IL-1β (pg/mg protein)	19 ± 3a	108 ± 10d	87 ± 8c	60 ± 5b
IL-6 (pg/mg protein)	15 ± 2a	94 ± 7d	77 ± 5c	52 ± 4b
TNF-α (pg/mg protein)	18 ± 4a	103 ± 11d	85 ± 9c	56 ± 5b

[a]Values are means ± SD, n = 10. Means in a row without a common letter differ, $P < 0.05$.

Effects of AA on Lipid Levels. HFD raised plasma ALT, AST, TG, and TC levels; hepatic TG and TC levels; and fecal lipid content (Table 2, $P < 0.05$). Compared with HFD groups, AA intake at two doses decreased plasma ALT, 22.9−48.5%; AST, 21.2−50.1%; and TG levels, 12.4−30.4%; and lowered hepatic TG level, 20.8−41.3% ($P < 0.05$). Plasma TC level and hepatic TC level were reduced by AA intake at high dose ($P < 0.05$). AA intake only at high dose increased fecal lipid content ($P < 0.05$).

Effects of AA on Hepatic Lipogenesis. As shown in Figure 2, HFD enhanced 2.85-fold ACC1, 3.34-fold FAS, 3.71-fold SCD-1, 3.62-fold HMG-CoA reductase, 2.91-fold SREBP-1c, and 2.75-fold SREBP-2 expression in liver ($P < 0.05$). Compared with HFD groups, AA intake at two doses reduced ACC1, 18.9−45.7%; FAS, 25.1−49.8%; SCD-1, 24.7−57.1%; and SREBP-1c, 21.8−53.3%, protein expression ($P < 0.05$). AA intake did not affect hepatic protein expression of HMG-CoA reductase and SREBP-2 ($P > 0.05$). As shown in Figure 3, HFD led to a great amount of fat deposition in liver, determined by ORO stain (upper row), and caused obvious foci of inflammatory cell infiltration in liver, determined by H&E stain (lower row). AA intake at two doses decreased hepatic lipid droplets and inflammatory infiltration. HFD increased plasma levels of insulin, leptin, and HOMA-IR and decreased adiponectin and ghrelin levels (Table 3, $P < 0.05$). AA intake at two doses lowered plasma insulin secretion and HOMR-IR ($P < 0.05$) but did not affect plasma glucose, leptin, ghrelin, or adiponectin levels ($P > 0.05$).

Effects of AA on Hepatic Oxidative and Inflammatory Stress. HFD increased hepatic production of ROS, IL-1β, IL-6, and TNF-α as well as decreased hepatic GSH content and GPX and catalase activities (Table 4, $P < 0.05$). Compared with HFD

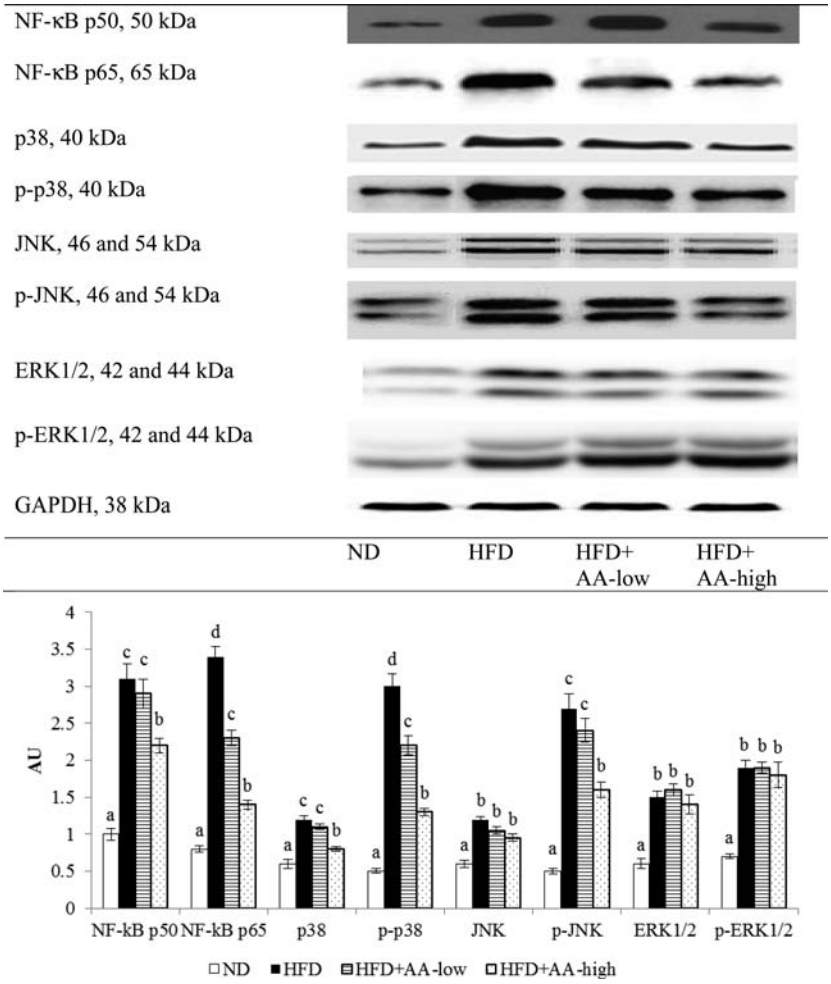

Figure 4. Hepatic protein expression of NF-κB and MAPK in mice treated with normal diet (ND), high-fat diet (HFD), or HFD with AA-low or AA-high for 7 weeks. Values are means ± SD, $n = 10$. Means among bars without a common letter differ, $P < 0.05$.

groups, AA intake at two doses lowered hepatic ROS, 21.5−49.2%; IL-1β, 19.4−44.3%; IL-6, 18.1−44.7%; and TNF-α, 17.5−45.6%, levels but retained 15.1−38.4% GSH content and maintained 12.8−24.1% GPX and 10.6−26.5% catalase activities ($P < 0.05$). As shown in Figure 4, HFD up-regulated hepatic NF-κB and MAPK expression ($P < 0.05$). AA intake dose-dependently suppressed NF-κB p65, 32.4−58.8%, and p-p38, 24.2−56.7%, expression ($P < 0.05$) and at high dose down-regulated NF-κB p50, 29.1%, and p-JNK, 40.7%, expression. AA intake did not affect ERK1/2 and p-ERK1/2 expression ($P > 0.05$).

DISCUSSION

The high-fat diet we used enhanced hepatic protein expression of lipogenic enzymes and factors including ACC1, FAS, SCD-1, HMG-CoA reductase, SREBP-1c, and SREBP-2, which clearly explained the observed lipid accumulation in liver, circulation, and epididymal white adipose tissue. We further found that the intake of AA markedly attenuated high-fat diet caused hyperlipidemia, hepatic steatosis, and epididymal fat deposit. Our Western blot data revealed that AA intake effectively suppressed hepatic expression of ACC1, FAS, SCD-1, and SREBP-1c. Our histological data indicated that AA intake reduced fat deposits in hepatocytes. Furthermore, AA intake alleviated high-fat diet induced insulin resistance and hepatic oxidative and inflammatory stress. These findings supported that AA could protect liver via antilipogenic, antioxidative, and anti-inflammatory activities to improve high-fat diet caused injury.

ACC1 mediates the initial step of fatty acid synthesis via converting acetyl-CoA to malonyl-CoA.[11] FAS is responsible for the last step in fatty acid biosynthesis and plays a determinant role for hepatic fatty acid generation in de novo lipogenesis.[10] SCD-1 catalyzes the rate-limiting step in the cellular biosynthesis of monounsaturated fatty acids, primarily oleate and palmitoleate, which could be incorporated into and stored as triglyceride in liver.[19] SREBP-1c is the major upstream transcription factor involved in hepatic triglyceride biosynthesis and modulates the expression of downstream targets including FAS, ACC1, and SCD-1.[20−22] Thus, the suppression on the expression of these enzymes and SREBP-1c could inhibit hepatic lipogenesis and lower fat accumulation in liver. Our present study found that AA treatments effectively down-regulated hepatic expression of ACC1, FAS, SCD-1, and SREBP-1c, which subsequently decreased triglyceride biosynthesis and deposit in liver, adipose tissue, and circulation and finally attenuated hepatic steatosis and lowered body weight. These findings indicated that AA was an effective agent against triglyceride biosynthesis. Obviously, the antilipogenic activities of AA could be mainly ascribed to its suppression upon hepatic SREBP-1c, an upstream lipogenic factor, and the less available SREBP-1c subsequently declined the expression of downstream

factors, ACC1, FAS, and SCD-1 in the liver. On the other hand, HMG-CoA reductase, regulated by SREBP-2, is responsible for cholesterol biosynthesis.[23] Our present study found AA intake did not affect hepatic SREBP-2 and HMG-CoA reductase expression. SREBP-1c is produced from a single gene, *SREBF-1*, located on chromosome 17p11.2, but SREBP-2 is generated from another gene, *SREBF-2*, located on chromosome 22q13.[24] It is speculated that AA had less affinity to chromosome 22q13 and/or less interference with gene *SREBF-2*, which caused failure in regulating SREBP-2 in HFD-treated mice liver. However, it is interesting to find that AA at high dose lowered hepatic and circulating cholesterol levels. It is likely that AA at high dose mildly mediated other factor(s) involved in cholesterol biosynthesis. These results implied that AA was a weak inhibitor against cholesterol biosynthesis. In addition, our data revealed AA intake at high dose increased fecal lipid content. Thus, the lipid-lowering effect of this triterpene was slightly due to an increase in lipid excretion.

Other studies[25,26] and our present study found that a high-fat diet altered circulating levels of several hormones. Our data indicated that AA intake substantially alleviated hyperinsulinemia. It is highly possible that this triterpene suppressed hepatic lipogenesis and reduced lipid accumulation in liver and adipose tissue, which in turn restored insulin sensitivity and lowered the requirement for insulin. The reduction of HOMA-IR in AA-treated mice we observed also agreed with this agent improving high-fat diet induced insulin resistance. In addition, a high-fat diet stimulates the release of inflammatory cytokines such as IL-1β and TNF-α, which blocks adipocyte insulin action and contributes to the development of obesity-related insulin resistance.[27,28] Thus, the improved insulin resistance in AA-treated mice could partially result from the diminished hepatic release of these inflammatory cytokines. AA treatments did not affect high-fat diet induced hyper-leptinemia, hypo-adiponectinemia, and hypo-ghrelinemia in our present study. Obviously, AA was not able to mediate these hormones.

It is reported that excessive energy from a high-fat diet promoted oxidative enzyme activities, disturbed tricarboxylic acid cycle electron transport chain, and impaired mitochondrial respiratory capability in liver and other organs such as the heart, which led to the overproduction of ROS and enhanced oxidative stress and consequently activated MAPK and NF-κB pathways.[29,30] The activation of these two pathways further augmented hepatic oxidative and inflammatory stress and contributed to the progression of liver disorders including steatohepatitis.[30,31] The results of our present study agreed with those previous studies because our molecular analyses data revealed that a high-fat diet enhanced hepatic expression of NF-κB p50, NF-κB p65, p38, JNK, and ERK1/2, which in turn evoked the generation of ROS and inflammatory cytokines including IL-6 and TNF-α. Furthermore, we found that AA intake limited phosphorylation of NF-κB p50, NF-κB p65, p38, and JNK in liver, which subsequently decreased the activation of NF-κB and MAPK. Because both NF-κB and MAPK pathways have been suppressed, the lower formation of ROS and inflammatory cytokines in livers from AA-treated mice could be explained. Our histological results indicated that AA intake ameliorated lobular inflammation and diffuse ballooning degeneration in hepatocytes. The restored antioxidative defenses such as GPX and catalase activities and lowered plasma ALT and AST levels in AA-treated mice also indicated that hepatic oxidative and inflammatory stress had been mitigated. These findings showed that dietary AA could be absorbed and exerted its hepatic protection through regulating hepatic NF-κB and MAPK pathways.

AA is a triterpene naturally occurring in many plant foods and herbs. Ramachandran and Saravanan[32] reported that AA intake at 10 or 20 mg/kg body weight altered hepatic enzyme activities of carbohydrate metabolism in diabetic rats. In our present study, AA intake also at 10 or 20 mg/kg body weight markedly protected THE liver against high-fat diet induced injury in mice. On the basis of its natural property and support from other studies and our data, the application of this compound seems safe. The doses used in our present study were approximately equal to 0.7 or 1.4 g/day for a 70 kg man. Our previous study found that gynura (*Gynura bicolor* DC), brown mustard (*Brassica juncea*), and daylily (*Hemerocallis fulva* L.) contained AA in the range of 55−102 mg/g dry weight.[4] Thus, the consumption of these vegetables, rich in AA, might also benefit the prevention of diet-induced lipid disorders. On the other hand, we noted that AA intake lowered mouse feed intake. It seems that this agent, a tasteless compound, was able to affect appetite and contributed to decreased body weight.

In conclusion, high-fat diet caused hyperlipidemia, hepatic steatosis, and insulin resistance. The intake of asiatic acid markedly lowered lipid accumulation in the circulation, liver, and adipose tissue via suppressing the protein expression of ACC1, FAS, SCD-1, and SREBP-1c. This triterpene also improved insulin resistance and attenuated hepatic oxidative and inflammatory injury. These results suggest that asiatic acid is a potent hepatic protective agent against high-fat diet induced steatohepatitis.

AUTHOR INFORMATION

Corresponding Author

*(M.-C.Y.) Mail: Department of Nutrition, China Medical University, 91 Hsueh-shih Road, Taichung City, Taiwan. Phone: 886-4-22053366, ext. 7510. Fax: 886-4-22062891. E-mail: mcyin@mail.cmu.edu.tw.

Author Contributions

‖S.-L.Y. and H-T.Y. contributed equally to this study.

Notes

The authors declare no competing financial interest.

REFERENCES

(1) Daskalopoulou, S. S.; Mikhailidis, D. P.; Elisaf, M. Prevention and treatment of the metabolic syndrome. *Angiology* **2004**, *55*, 589−612.

(2) Sullivan, S. Implications of diet on nonalcoholic fatty liver disease. *Curr. Opin. Gastroenterol.* **2010**, *26*, 160−164.

(3) Samaha, F. F.; Foster, G. D.; Makris, A. P. Low-carbohydrate diets, obesity, and metabolic risk factors for cardiovascular disease. *Curr. Atheroscler. Rep.* **2007**, *9*, 441−447.

(4) Yin, M. C.; Lin, M. C.; Mong, M. C.; Lin, C. Y. Bioavailability, distribution, and antioxidative effects of selected triterpenes in mice. *J. Agric. Food Chem.* **2012**, *60*, 7697−7701.

(5) Hashim, P.; Sidek, H.; Helan, M. H.; Sabery, A.; Palanisamy, U. D.; Ilham, M. *Triterpene composition and bioactivities of* Centella asiatica. *Molecules* **2011**, *16*, 1310−1322.

(6) Gao, J.; Tang, X.; Dou, H.; Fan, Y.; Zhao, X.; Xu, Q. Hepatoprotective activity of *Terminalia catappa* L. leaves and its two triterpenoids. *J. Pharm. Pharmacol.* **2004**, *56*, 1449−1455.

(7) Ma, K.; Zhang, Y.; Zhu, D.; Lou, Y. Protective effects of asiatic acid against D-galactosamine/lipopolysaccharide-induced hepatotoxicity in hepatocytes and kupffer cells co-cultured system via redox-regulated leukotriene C4 synthase expression pathway. *Eur. J. Pharmacol.* **2009**, *603*, 98−107.

(8) Wei, J.; Huang, Q.; Huang, R.; Chen, Y.; Lv, S.; Wei, L.; Liang, C.; Liang, S.; Zhuo, L.; Lin, X. Asiatic acid from *Potentilla chinensis* attenuate ethanol-induced hepatic injury via suppression of oxidative stress and Kupffer cell activation. *Biol. Pharm. Bull.* **2013**, *36*, 1980−1989.
(9) Pakdeechote, P.; Bunbupha, S.; Kukongviriyapan, U.; Prachaney, P.; Khrisanapant, W.; Kukongviriyapan, V. Asiatic acid alleviates hemodynamic and metabolic alterations via restoring eNOS/iNOS expression, oxidative stress, and inflammation in diet-induced metabolic syndrome rats. *Nutrients* **2014**, *6*, 355−370.
(10) Jensen-Urstad, A. P.; Semenkovich, C. F. Fatty acid synthase and liver triglyceride metabolism: housekeeper or messenger? *Biochim. Biophys. Acta* **2012**, *1821*, 747−753.
(11) Mao, J.; DeMayo, F. J.; Li, H.; Abu-Elheiga, L.; Gu, Z.; Shaikenov, T. E.; Kordari, P.; Chirala, S. S.; Heird, W. C.; Wakil, S. J. Liver-specific deletion of acetyl-CoA carboxylase 1 reduces hepatic triglyceride accumulation without affecting glucose homeostasis. *Proc. Natl. Acad. Sci. U.S.A.* **2006**, *103*, 8552−8557.
(12) Ji, C.; Chan, C.; Kaplowitz, N. Predominant role of sterol response element binding proteins (SREBP) lipogenic pathways in hepatic steatosis in the murine intragastric ethanol feeding model. *J. Hepatol.* **2006**, *45*, 717−724.
(13) Jump, D. B.; Botolin, D.; Wang, Y.; Xu, J.; Christian, B.; Demeure, O. Fatty acid regulation of hepatic gene transcription. *J. Nutr.* **2005**, *135*, 2503−2506.
(14) Mong, M. C.; Chao, C. Y.; Yin, M. C. Histidine and carnosine alleviated hepatic steatosis in mice consumed high saturated fat diet. *Eur. J. Pharmacol.* **2011**, *653*, 82−88.
(15) Shih, P. H.; Hwang, S. L.; Yeh, C. T.; Yen, G. C. Synergistic effect of cyanidin and PPAR agonist against nonalcoholic steatohepatitis-mediated oxidative stress-induced cytotoxicity through MAPK and Nrf2 transduction pathways. *J. Agric. Food Chem.* **2012**, *60*, 2924−2933.
(16) Leclercq, I. A.; Farrell, G. C.; Sempoux, C.; dela Peña, A.; Horsmans, Y. Curcumin inhibits NF-κB activation and reduces the severity of experimental steatohepatitis in mice. *J. Hepatol.* **2004**, *41*, 926−934.
(17) Lin, C. C.; Yin, M. C. Effects of cysteine-containing compounds on biosynthesis of triglyceride and cholesterol and anti-oxidative protection in liver from mice consuming a high fat diet. *Br. J. Nutr.* **2008**, *99*, 37−43.
(18) Tsujita, T.; Takaichi, H.; Takaku, T.; Aoyama, S.; Hiraki, J. Antiobesity action of ε-polylysine, a potent inhibitor of pancreatic lipase. *J. Lipid Res.* **2006**, *47*, 1852−1858.
(19) Paton, C. M.; Ntambi, J. M. Biochemical and physiological function of stearoyl-CoA desaturase. *Am. J. Physiol. Endocrinol. Metab.* **2009**, *297*, E28−E37.
(20) Bettzieche, A.; Brandsch, C.; Hirche, F.; Eder, K.; Stangl, G. I. L-Cysteine down-regulates SREBP-1c-regulated lipogenic enzymes expression via glutathione in HepG2 cells. *Ann. Nutr. Metab.* **2008**, *52*, 196−203.
(21) Sekiya, M.; Yahagi, N.; Matsuzaka, T.; Najima, Y.; Nakakuki, M.; Nagai, R.; Ishibashi, S.; Osuga, J.; Yamada, N.; Shimano, H. Polyunsaturated fatty acids ameliorate hepatic steatosis in obese mice by SREBP-1 suppression. *Hepatology* **2003**, *38*, 1529−1539.
(22) Bellenger, J.; Bellenger, S.; Clément, L.; Mandard, S.; Diot, C.; Poisson, J. P.; Narce, M. A new hypotensive polyunsaturated fatty acids dietary combination regulates oleic acid accumulation by suppression of stearoly CoA desaturase 1 gene expression in the SHR model of genetic hypertension. *FASEB J.* **2004**, *18*, 773−775.
(23) Eberlé, D.; Hegarty, B.; Bossard, P.; Ferré, P.; Foufelle, F. SREBP transcription factors: master regulators of lipid homeostasis. *Biochimie* **2004**, *86*, 839−848.
(24) Eberlé, D.; Hegarty, B.; Bossard, P.; Ferré, P.; Foufelle, F. SREBP transcription factors: master regulators of lipid homeostasis. *Biochimie* **2004**, *86*, 839−848.
(25) Handjieva-Darlenska, T.; Boyadjieva, N. The effect of high-fat diet on plasma ghrelin and leptin levels in rats. *J. Physiol. Biochem.* **2009**, *65*, 157−164.
(26) Parra, P.; Palou, A.; Serra, F. Moderate doses of conjugated linoleic acid reduce fat gain, maintain insulin sensitivity without impairing inflammatory adipose tissue status in mice fed a high-fat diet. *Nutr. Metab. (London)* **2010**, *20*, 7−5.
(27) Shoelson, S. E.; Lee, J.; Goldfine, A. B. Inflammation and insulin resistance. *J. Clin. Invest.* **2006**, *116*, 1793−1801.
(28) Cersosimo, E.; DeFronzo, R. A. Insulin resistance and endothelial dysfunction: the road map to cardiovascular diseases. *Diabetes Metab. Res. Rev.* **2006**, *22*, 423−436.
(29) Peairs, A. T.; Rankin, J. W. Inflammatory response to a high-fat, low-carbohydrate weight loss diet: effect of antioxidants. *Obesity (Silver Spring)* **2008**, *16*, 1573−1578.
(30) Sinha-Hikim, I.; Sinha-Hikim, A. P.; Shen, R.; Kim, H. J.; French, S. W.; Vaziri, N. D.; Crum, A. C.; Rajavashisth, T. B.; Norris, K. C. A novel cystine based antioxidant attenuates oxidative stress and hepatic steatosis in diet-induced obese mice. *Exp. Mol. Pathol.* **2011**, *91*, 419−428.
(31) Yogalakshmi, B.; Bhuvaneswari, S.; Sreeja, S.; Anuradha, C. V. Grape seed proanthocyanidins and metformin act by different mechanisms to promote insulin signaling in rats fed high calorie diet. *J. Cell Commun. Signal.* **2014**, *8*, 13−22.
(32) Ramachandran, V.; Saravanan, R. Efficacy of asiatic acid, a pentacyclic triterpene on attenuating the key enzymes activities of carbohydrate metabolism in streptozotocin-induced diabetic rats. *Phytomedicine* **2013**, *20*, 230−236.

JOURNAL OF AGRICULTURAL AND FOOD CHEMISTRY

Article

pubs.acs.org/JAFC

Cysteine-Conjugated Metabolites of Ginger Components, Shogaols, Induce Apoptosis through Oxidative Stress-Mediated p53 Pathway in Human Colon Cancer Cells

Junsheng Fu,[†] Huadong Chen,[†,§] Dominique N. Soroka,[†,§] Renaud F. Warin,[†] and Shengmin Sang*[,†,‡]

[†]Center for Excellence in Post-Harvest Technologies, North Carolina Agricultural and Technical State University, North Carolina Research Campus, 500 Laureate Way, Kannapolis, North Carolina 28081, United States

[‡]Lineberger Comprehensive Cancer Center, The University of North Carolina at Chapel Hill, 450 West Drive, CB# 7295, Chapel Hill, North Carolina 27599, United States

ABSTRACT: Shogaols, the major constituents of thermally processed ginger, have been proven to be highly effective anticancer agents. Our group has identified cysteine-conjugated shogaols (M2, M2′, and M2″) as the major metabolites of [6]-, [8]-, and [10]-shogaol in human and found that M2 is a carrier of its parent molecule [6]-shogaol in cancer cells and in mice, while being less toxic to normal colon fibroblast cells. The objectives of this study are to determine whether M2′ and M2″ behave in a similar manner to M2, in both metabolism and efficacy as anticancer agents, and to further explore the biological pro-apoptotic mechanisms of the cysteine-conjugated shogaols against human colon cancer cells HCT-116 and HT-29. Our results show that [8]- and [10]-shogaol have similar metabolic profiles to [6]-shogaol and exhibit similar toxicity toward human colon cancer cells. M2′ and M2″ both show low toxicity against normal colon cells but retain potency against colon cancer cells, suggesting that they have similar activity to M2. We further demonstrate that the cysteine-conjugated shogaols can cause cancer cell death through the activation of the mitochondrial apoptotic pathway. Our results show that oxidative stress activates a p53 pathway that ultimately leads to p53 up-regulated modulator of apoptosis (PUMA) induction and down-regulation of B-cell lymphoma 2 (Bcl-2), followed by cytochrome *c* release, perturbation of inhibitory interactions of X-linked inhibitor of apoptosis protein (XIAP) with caspases, and finally caspase 9 and 3 activation and cleavage. A brief screen of the markers attenuated by the proapoptotic activity of M2 revealed similar results for [8]- and [10]-shogaol and their respective cysteine-conjugated metabolites M2′ and M2″. This study highlights the cysteine-conjugated metabolites of shogaols as novel dietary colon cancer preventive agents.

KEYWORDS: *ginger, cysteine-conjugated metabolites, shogaols, colon cancer, apoptosis*

INTRODUCTION

Ginger, the rhizome of *Zingiber officinale*, has been cultivated as both a ubiquitous spice and a traditional medicinal food for thousands of years.[1] Its many curative properties include treatment of nausea and dyspepsia, ameliorating symptoms of arthritis via anti-inflammation, and therapeutic activity against asthma, respiratory disorders, and rheumatic ailments.[2−5] Most recently, pharmacologically active components of ginger have been implicated in chemoprevention via numerous mechanisms. Gingerols and shogaols have been identified as the most active ingredients in ginger. Shogaols, the products of ginger thermal processing, consistently show greater anticarcinogenic activity than gingerols, with [6]-shogaol (6S) being the most abundant one followed by [10]- and [8]-shogaol (10S and 8S) (Figure 1A).[6−10] In particular, 6S has repeatedly shown strong chemopreventive activity against colorectal cancer, the third most common cancer diagnosed in the United States.[11−15]

Therapeutics with high anticancer potency often come under scrutiny for their accompanying toxicity against noncancerous cells in the viable organism. Consequently, there is escalating interest in employing dietary components and their metabolic constituents as less noxious treatments toward chemoprevention.[16−18] Our group has recently established that the reactive ginger component 6S is extensively metabolized in mice and in cancer cells[19,20] and that redox transformation and a phase II mercapturic acid pathway (MAP) are its major metabolic routes.[19,20] As previously reported, an initial reaction between the α,β-unsaturated ketone functional group of 6S and the cysteine sulfhydryl component of GSH takes place in the MAP, giving rise to the corresponding conjugates. The conjugates then undergo series of enzymatic modifications on the GSH moiety, forming cysteinylglycine, cysteine, and finally *N*-acetylcysteine conjugates. Additional studies show that both 8S and 10S are also metabolized in humans through the MAP and the cysteine-conjugated metabolites, M2′ and M2″, respectively (Figure 1B), were identified as their major metabolites in human urine.[21] Phase II metabolism products such as thiol conjugates are more water-soluble and often less toxic and pungent than their parent compounds, making them preferable for chemoprevention trials.[22] Our group recently investigated the bioactivity of the cysteine-conjugated metabolite of [6]-shogaol (M2) and its putative mode of action as a hydrophilic carrier of the parent molecule to its site of efficacy. We established that cysteine-conjugation reduced the toxicity of 6S against normal human colon and lung fibroblast cells while

Received: March 18, 2014
Revised: May 2, 2014
Accepted: May 2, 2014
Published: May 2, 2014

ACS Publications © 2014 American Chemical Society

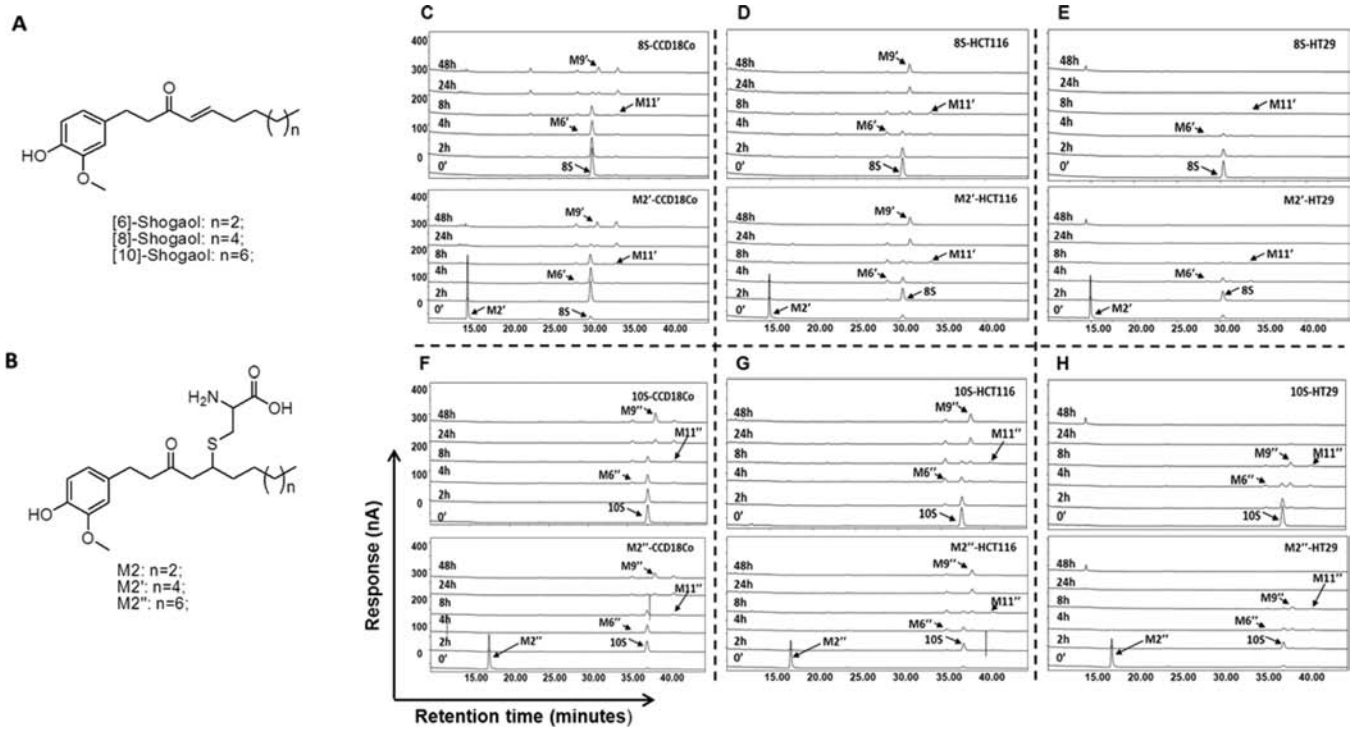

Figure 1. M2′ and M2″ serve as a carrier to their parent compounds [8]- and [10]-shogaol (8S and 10S), respectively. Chemical structures of shogaols (A) and their cysteine-conjugated metabolites (B); HPLC-ECD chromatograms representing the metabolic profiles of 8S, M2′, 10S, and M2″ in human colon normal cells, CCD-18Co (C, F), and human colon cancer cells, HCT-116 (D, G) and HT-29 (E, H).

still retaining efficacy against human colon and lung cancer cells.[13] Through a series of chemical stability and biological assays, we demonstrated the function of M2 as a carrier of 6S to its active site, wherein the parent compound is rendered less toxic but regains potency and similar bioactivity upon deconjugation.[23] It is still unknown whether M2′ and M2″ behave in a similar manner to M2, in both efficacy as anticancer agents and metabolically. As an expansion of our proposed chemical mechanism for cysteine conjugates as carriers of their parent molecule shogaols, we investigated whether M2′ and M2″ are the respective carriers of 8S and 10S in cancer cells and can induce apoptosis through a mechanism similar to M2.

Although we have established the functionality and importance of M2, its mechanism of action against colon cancer cells has not been completely elucidated. There have been studies implicating 6S as a pro-apoptotic agent, via reactive oxygen species (ROS) production and subsequent growth arrest and DNA damage (GADD)-inducible transcription factor 153 (GADD153) expression in COLO 205 cells,[15] an inducer of G_2/M arrest and aberrant mitotic cell death associated with tubulin aggregation in HCT-116 colon carcinoma cells,[14] and an inhibitor of colon cancer cell proliferation through activation of peroxisomal proliferator activated receptor γ (PPARγ).[12] Given the significance of M2 as a potential therapeutic with selective toxicity toward cancerous cells, the impetus of this study is also to determine the mechanistic role M2 plays in promoting apoptosis in human colon cancer cells HCT-116 and HT-29. In particular, examining the impact of M2 in colon cancer cells containing wild-type *p53* (HCT-116) and mutant *p53* (HT-29) will be emphasized. The progressive loss or inactivation of *p53* is well associated with the corresponding advancement of cancer to more aggressive stages, and is one of the most prevalent genetic defects in human malignancies that often correlates to chemotherapeutic resistance.[24−26] Thus, determining whether the bioactivity of M2, M2′, or M2″ is dependent upon *p53* status is of critical concern in terms of cancer prevention, since usable compounds must be able to exert their activity through the early mutations stages of cancer.

MATERIALS AND METHODS

Cell Culture. HCT-116 and HT-29 human colon cancer cells, CCD-18Co human fibroblast cells derived from colon, and Eagle's minimum essential media (EMEM) were obtained from American Type Tissue Culture (Manassas, VA). McCoy's 5A medium was purchased from Thermo Fisher Scientific (Waltham, MA). Supplements of fetal bovine serum (FBS) and penicillin/streptomycin were purchased from Gemini Bio-Products (West Sacramento, CA).

Reagents. 6S, 8S, and 10S were purified from ginger extract in our laboratory.[10] M2 was synthesized in our laboratory, as previously reported.[13] HPLC-grade solvents and other reagents were obtained from VWR International (South Plainfield, NJ). LC/MS grade solvents and other reagents were obtained from Thermo Fisher Scientific (Rockford, IL). Glutathione was obtained from Sigma-Aldrich (St. Louis, MN). Crystal violet, glutaraldehyde, MTT [3-(4,5-dimethylthiaxol-2-yl)-2,5-diphenyltetrazolium bromide], and propidium iodide were procured from Thermo Fisher Scientific (Waltham, MA). Primary antibodies against β-actin, B-cell lymphoma 2 (Bcl-2), caspase 9, caspase 3, cytochrome *c*, PUMA (p53 up-regulated modulator of apoptosis), p53, XIAP (X-linked inhibitor of apoptosis protein), as well as secondary antibodies conjugated to HRP (horseradish peroxidase) against mouse and rabbit were purchased from Cell Signaling Technology (Beverly, MA).

HPLC-ECD Analysis. A high-performance liquid chromatrography/ESA electrochemical detector (HPLC-ECD) (ESA, Chelmsford, MA) consisting of an ESA model 584 HPLC pump, an ESA model 542 autosampler, an ESA organizer, and an ESA electrochemical detector (ECD) coupled with two ESA model 6210 four sensor cells was used. A Gemini C18 column (150 mm × 4.6 mm, 5 μm; Phenomenex, Torrance, CA) was used for chromatographic analysis at

dx.doi.org/10.1021/jf501351r | J. Agric. Food Chem. 2014, 62, 4632−4642

Table 1. δ_H (600 MHz) and δ_C (150 MHz) NMR Spectra Data of M2′ and M2″[a]

	M2′		M2″	
	δ_H, multi (J)	δ_C	δ_H, multi (J)	δ_C
1	2.81, m	31.6	2.81, m	31.8
2	2.81, m	48.1	2.81, m	48.1
3		210.4		210.4
4	2.88, m	53.8	2.89, m	53.8
	2.81, m		2.81, m	
5	3.11, m	40.9	3.11, m	40.9
6	1.56, m	34.9	1.56, m	34.9
7	1.42, m	27.4	1.42, m	
8	1.31, m	31.8	1.31, m	31.8
9	1.31, m	29.2[b]	1.31, m	29.3[b]
10	1.31, m	28.9[b]	1.31, m	29.3[b]
11	1.31, m	28.9[b]	1.31, m	29.2[b]
12	1.31, m	26.4[b]	1.31, m	29.1[b]
13	0.92, t (6.9)	22.3	1.31, m	28.9[b]
14		13.0	1.31, m	26.4[b]
15			1.31, m	22.3
16			0.92, t (6.9)	13.0
1′		132.4		132.4
2′	6.80, d (2.0)	111.7	6.80, d (2.0)	111.8
3′		147.8		147.7
4′		144.4		144.4
5′	6.71, d (7.98)	115.0	6.71, d (7.98)	115.0
6′	6.65, dd (7.98, 2.0)	120.4	6.65, dd (7.98, 2.0)	120.5
1″	(a) 3.21, m	32.0	(a) 3.21, m	32.1
	(b) 2.81, m		(b) 2.81, m	
2″	3.66, m	54.9	3.66, m	54.9
3″		171.1		171.2
*O*Me	3.85, s	55.1	3.85, s	55.0

[a]CD_3OD; δ in ppm and J in Hz. [b]Assignments interchangeable.

a flow rate of 1.0 mL/min. The mobile phases consisted of solvent A (30 mM sodium phosphate buffer containing 1.75% ACN and 0.125% THF, pH 3.35) and solvent B (15 mM sodium phosphate buffer containing 58.5% ACN and 12.5% THF, pH 3.45). The gradient elution had the following profile: 20% B from 0 to 3 min; 20−55% B from 3 to 11 min; 55−60% B from 11 to 12 min; 60−65% B from 12 to 13 min; 65−100% B from 13 to 40 min; 100% B from 40 to 45 min; then 20% B from 45.1 to 50 min. The cells were then cleaned at a potential of 1000 mV for 1 min. The injection volume of the sample was 10 μL. The eluent was monitored by the Coulochem electrode array system (CEAS) with potential settings at 200, 250, 300, 350, 400, 450, and 500 mV. Data for Figure 1 were from the channel set at 350 mV of the CEAS.

LC/MS Analysis. LC/MS analysis was carried out with a Thermo-Finnigan Spectra System, which consisted of an Accela high-speed MS pump, an Accela refrigerated autosampler, and an LTQ Velos ion trap mass detector (Thermo Electron, San Jose, CA) incorporated with heated electrospray ionization (H-ESI) interfaces. A Gemini C_{18} column (50 mm × 2.0 mm i.d., 3 μm; Phenomenex, Torrance, CA) was used for separation at a flow rate of 0.2 mL/min. The column was eluted from 100% solvent A (5% aqueous methanol with 0.2% acetic acid) for 3 min, followed by linear increases in B (95% aqueous methanol with 0.2% acetic acid) to 40% from 3 to 15 min, to 91% from 15 to 49 min, and to 100% from 49 to 50 min, and then with 100% B from 50 to 55 min. The column was then re-equilibrated with 100% A for 5 min. The LC eluent was introduced into the H-ESI interface. The positive ion polarity mode was set for the H-ESI source with the voltage on the H-ESI interface maintained at approximately 4.5 kV. Nitrogen gas was used as the sheath gas and auxiliary gas. Optimized source parameters, including ESI capillary temperature (300 °C), capillary voltage (50 V), ion spray voltage (3.6 kV), sheath gas flow rate (30 units), auxiliary gas flow rate (5 units), and tube lens (120 V), were tuned using authentic 6S. The collision-induced dissociation (CID) was conducted with an isolation width of 2 Da and normalized collision energy of 35 for MS^2 and MS^3. Default automated gain control target ion values were used for $MS-MS^3$ analyses. The mass range was measured from 50 to 1000 m/z. Data acquisition was performed with Xcalibur 2.0 version (Thermo Electron, San Jose, CA).

Chemical Synthesis of M2′ and M2″. The experimental procedure to synthesize M2′ and M2″ was similar to that of M2.[13] In brief, a catalytic amount of $NaHCO_3$ (1.3 mg, 0.015 mmol) was added to a mixture of 8S (91.2 mg, 0.3 mmol) and cysteine (54 mg, 0.45 mmol) in methanol/water (6 mL, 1:1, v/v). The mixture was stirred at room temperature for 24 h, and adjusted to pH 6 with a diluted acetic acid solution (0.1 M). The mixture was then purified by preparative HPLC to give M2′ as a white solid (70 mg, yield 55%). Shogaol 10S (100 mg, 0.3 mmol) instead of 8S was used in the above reaction to give M2″ (73 mg, yield 54%).

Purification of M2′ or M2″ Using Preparative HPLC. Waters preparative HPLC systems with 2545 binary gradient module, Waters 2767 sample manager, Waters 2487 autopurification flow cell, Waters fraction collector III, dual injector module, and 2489 UV/Visible detector were used to separate M2′ or M2″ from the reaction mixture. A Phenomenex Gemini-NX C_{18} column (250 mm × 30.0 mm i.d., 5 μm) was used with a flow rate of 20.0 mL/min. The wavelength of the UV detector was set at 280 nm. The injection volume was 1.0 mL for each run. The mobile phase consisted of solvent A (H_2O + 0.1% formic acid) and solvent B (MeOH + 0.1% formic acid). The reaction mixture of M2′ was injected to the preparative column and eluted with a gradient solvent system (75% to 87% B from 0 to 12 min; to 75% B from 12 to 12.5 min; then 75% B from 12.5 to 15 min). A total of six runs resulted in 70 mg of M2′ (t_R 9.45 min). Similarly, reaction mixture of M2″ was injected to the preparative column and eluted with a gradient solvent system (85% to 100% B from 0 to 15 min; then

dx.doi.org/10.1021/jf501351r | J. Agric. Food Chem. 2014, 62, 4632−4642

100% B from 15 to 16 min; to 85% B from 16 to 16.5 min; then 85% B from 16.5 to 20 min). A total of seven runs resulted in 73 mg of M2″ (t_R 8.13 min).

Nuclear Magnetic Resonance (NMR). ^{1}H (600 MHz), and ^{13}C (150 MHz) NMR spectra of M2′ and M2″ in CD_3OD were acquired on a Bruker AVANCE 600 MHz NMR spectrometer (Bruker, Inc., Silberstreifen, Rheinstetten, Germany). The ^{1}H and ^{13}C NMR data of M2′ and M2″ are listed in Table 1.

Metabolism of 8S, 10S, M2′, and M2″ in Human Colon Cancer Cells. Cells (1.0×10^6) were plated in six-well culture plates and were allowed to attach for 24 h at 37 °C in 5% CO_2 incubator. Shogaol 8S or 10S in DMSO or the corresponding cysteine-conjugated metabolites M2′ and M2″ were diluted in McCoy's 5A medium (containing 10% fetal bovine serum, 1% penicillin/streptomycin, and 1% glutamine) to reach a final concentration of 10 μM and were incubated with different colon cancer cell lines (HCT-116 or HT-29). At different time points (0, 2, 4, 8, 24, and 48 h), 190 μL samples of supernatant were taken and transferred to vials containing 10 μL of 2% acetic acid to stabilize these compounds and their respective metabolites. An equal volume of acetonitrile was added to the samples before centrifugation. The supernatant was harvested, and the samples were then analyzed by HPLC-ECD.

Evaluation of Toxicity in Human Colon Cancer and Normal Colon Cells. Cell viability was determined by an MTT colorimetric assay as described previously.[27] Briefly, human colon fibroblast cells, CCD-18Co, or human colon cancer cells, HCT-116 or HT-29, were plated in 96-well microtiter plates with 3000 cells/well and allowed to attach for 24 h at 37 °C and 5% CO_2. The test compounds (in DMSO) were added to cell culture medium to desired final concentrations (final DMSO concentrations for control and treatments were 0.1%). After the cells were cultured for 24 h, the medium was aspirated, and cells were treated with 200 μL of fresh medium containing 2.41 mmol/L MTT. After incubation for 3 h at 37 °C, the medium containing MTT was aspirated, 100 μL of DMSO was added to solubilize the formazan precipitate, and the plates were shaken gently for an hour at room temperature. Absorbance values were derived from the plate reading at 550 nm on a Biotek (Winooski, VT) microtiter plate reader. The reading reflected the number of viable cells and was expressed as a percentage of viable cells in the control. CCD-18Co cells were grown in EMEM. Both HCT-116 and HT-29 cells were cultured in McCoy's 5A medium. All of the above media were supplemented with 10% fetal bovine serum, 1% penicillin/streptomycin, and 1% glutamine, and the cells were kept in a 37 °C incubator with 95% humidity and 5% CO_2.

Apoptosis Analysis. Apoptosis was determined by FACS analysis of propidium iodide (PI)-stained cells. In brief, cells were trypsinized, washed with cold phosphate-buffered saline (PBS), fixed in ice-cold 70% ethanol for 1 h, and then resuspended in 2 mL of PBS supplemented with 10 μL of RNase (100 mg/mL) and incubated at 37 °C for 30 min. After incubation, DNA was stained with 1 mg/mL PI in PBS. Cell staining was analyzed using a Cell Lab QuantaTM SC flow cytometer (Beckman Coulter, Danvers, MA), and data were processed using FCS Express software (DeNovo Software, Los Angeles, CA). The percentage of apoptotic cells in each sample was determined based on the sub-G_0 peaks detected in monoparametric histograms.

Measurement of Reactive Oxygen Species. This assay employed the cell-permeable fluorogenic probe 2′,7′-dichlorodihydrofluorescein diacetate [DCFH-DA] (Sigma-Aldrich, St. Louis, MO) to measure the relative changes in O_2^- and H_2O_2 levels in HCT-116 or HT-29 cells after treatment with 5, 10, and 20 μM 6S or M2 (or DMSO) over 0, 2, 4, 8, and 24 h. In brief, DCFH-DA is diffused into cells and is deacetylated by cellular esterases to nonfluorescent 2′,7′-dichlorodihydrofluorescein (DCFH), which is rapidly oxidized to highly fluorescent 2′,7′-dichlorofluorescein (DCF) by intracellular hydrogen peroxide or other low molecular weight peroxides.[13,28] Measured fluorescence intensity is thus proportional to the amount of such peroxides in the cell at a given time. Human colon cancer cells HCT-116 or HT-29 were seeded in 96-well black-sided, clear-bottomed culture plates, with 5000 cells/well and were allowed to adhere for 24 h in a 37 °C incubator with 5% CO_2. Media was aspirated, and 5, 10, or 20 μM M2, 6S, or DMSO diluted in media was added to designated wells, which were run in triplicate. After desired incubation times of 0, 2, 4, 8, or 24 h, media and test compounds were aspirated. Cells were washed three times with 200 μL of PBS before addition of 100 μL of 1 mM DCFH-DA. The fluorogenic probe permeated cell membranes and was processed to DCF for 1 h at 37 °C. After incubation, plates were immediately placed in a Biotek microplate reader to measure fluorescence at wavelengths of 485 (excitation) and 528 (emission). Raw values were normalized to DMSO control for each time point and are presented as fold induction versus 0 h time point (n = 3).

Western Blot Analysis. Cell lysates were prepared in ice-cold RIPA lysis buffer [25 mM Tris-HCl (pH 7.6), 150 mM NaCl, 1% NP-40, 1% sodium deoxycholate, 0.1% SDS, Thermo Fisher Scientific] supplemented with a protease inhibitor cocktail (AEBSF, aprotinin, bestatin, E-64, leupeptin, and pepstatin A in DMSO with EDTA, Thermo Fisher Scientific). Protein content was measured by a Pierce BCA Assay Kit (Thermo Fisher Scientific). Protein contents of cell lysates (30 μg of protein/lane) were resolved by SDS-PAGE. Proteins were then electro-transferred onto PVDF membranes, and blots were blocked for 1 h at room temperature in 1 × TBS with 1% casein (Bio-Rad Laboratories, Berkeley, CA). Blots were then incubated overnight at 4 °C with the desired primary antibody diluted in TBS with 0.5% Tween-20. Blots were then washed with TBS-Tween 20 and probed for 1 h with the appropriate secondary antibody (1:1000). Protein bands were visualized with chemiluminescence using West Femto maximum detection substrate (Thermo Fisher Scientific). To confirm equal protein loading in each lane, immunoblots were stripped and reprobed for β-actin. Protein fold-induction was calculated by normalizing the intensity of the band of interest to β-actin first and then to DMSO control lanes.

Colony Formation Assay. Human colon cancer cells HCT-116 or HT-29 (1000 cells per well) were seeded in 6-well culture plates for 24 h and then incubated with M2 (0, 1, 5, 10, 20, or 40 μM) in DMSO in a 37 °C incubator with 5% CO_2. After 2 weeks, colonies were washed with phosphate-buffered saline (PBS), then stained with a mixture of 6.0% glutaradehyde and 0.5% crystal violet for 30 min at room temperature, rinsed in water, air-dried, and then photographed.

Statistical Analysis. Student's t-test or two-way analysis of variance (ANOVA) with the Bonferroni post-test were used to determine the statistical significance of data, which was performed on GraphPad Prism version 5.00 for Windows (GraphPad Software, San Diego, CA).

RESULTS

Synthesis and Structure Elucidation of M2′ and M2″. A similar experimental procedure was used for the syntheses of M2′ and M2″ as the previous protocol used for M2.[13] M2′ showed the molecular formula $C_{22}H_{35}NO_5S$ on the basis of positive ESI-MS at m/z 426 $[M + H]^+$ and its ^{1}H and ^{13}C NMR data. The molecular weight of M2′ was 121 mass units more than that of 8S (MW 304), indicating that M2′ was the cysteine-conjugated 8S, which is an expected result from the reaction between 8S and L-cysteine. This was also supported by the observation of the absence of a double bond in the ^{1}H and ^{13}C NMR spectra of M2′. Therefore, M2′ was confirmed to be 5-cysteinyl-8S. In the same way, M2″ was identified as 5-cysteinyl-10S, based on its positive ESI-MS at m/z 454 $[M + H]^+$ and its ^{1}H and ^{13}C NMR data (Table 1).

M2′ and M2″ Give Similar Metabolic Profiles as Their Parent Compounds 8S and 10S. Recent work in our group has focused on the biotransformation of the cysteine-conjugated metabolite of 6S, M2. The metabolic profiles of M2 in cancer cells HCT-116 and H-1299 resembled those of 6S, indicating that its biotransformation route was initiated by deconjugation.[23] Evidence supporting the identification of M2′ and M2″ as carriers of their respective shogaols is presented in

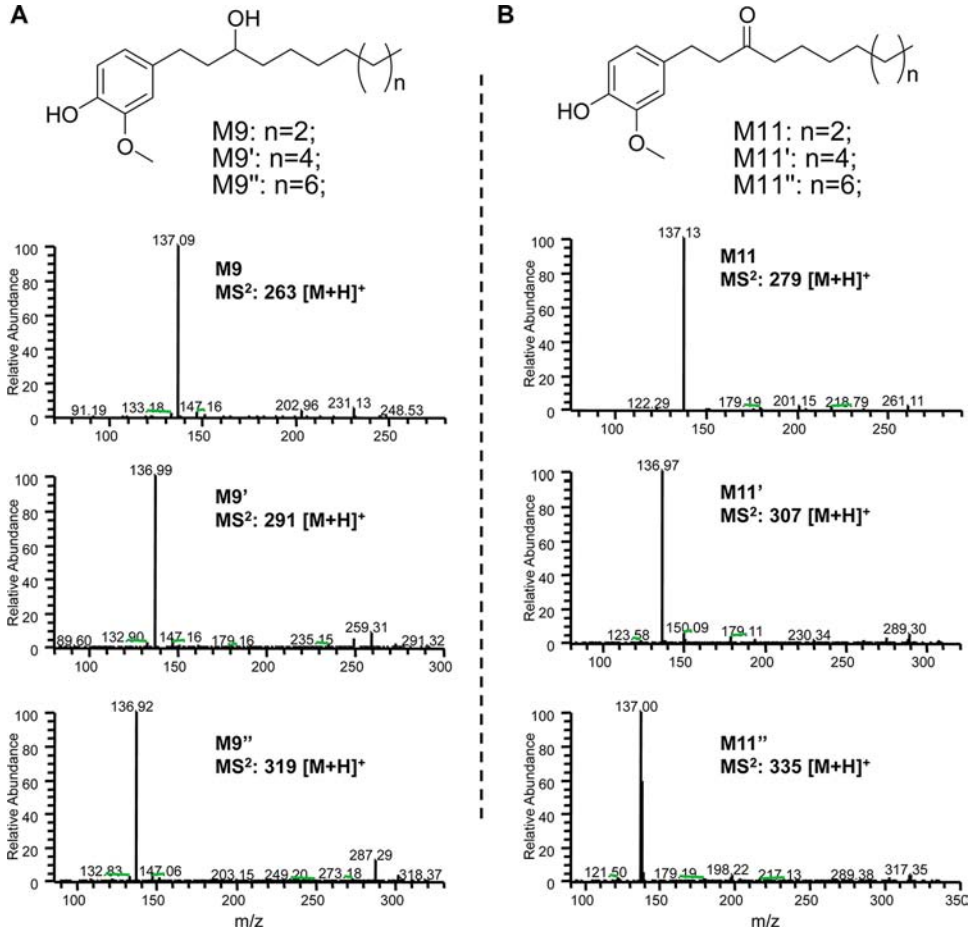

Figure 2. Chemical structures and MS/MS spectra of M9, M9′, and M9″ (A) and M11, M11′, and M11″ (B).

Figure 1, in which the metabolic profiles of 8S and 10S in human colon fibroblast cells CCD18Co (Figure 1C,F) or human colon cancer cells HCT-116 (Figure 1D,G) and HT-29 (Figure 1E,H) are compared with the profiles of M2′ and M2″ in the same respective cell lines. Upon removal of the cysteine residue, which occurs after less than 2 h of treatment, M2′ and M2″ are metabolized in an almost identical fashion as their parent shogaols. We have reported that M9 and M11 are the major metabolites of 6S in cancer cells; M11 is the double bond reduced metabolite of 6S, and M9 is the ketone group reduced metabolite of M11.[19] In the present study, reduced products were also identified as the major metabolites of 8S and 10S in human colon fibroblast cells and cancer cells, M9′ and M11′ for 8S and M9″ and M11″ for 10S. Their structures were confirmed by comparing their MS/MS spectra with those of M9 and M11 (Figure 2).

M2′ and M2″ Exert Similar Bioactivities as Their Parent Compounds 8S and 10S. We have reported that M2 has low toxicity in normal human fibroblast colon and lung cells while still remaining toxic against colon cancer and lung cancer cells.[13] As the structure of the cysteine-conjugated metabolites of 8S and 10S only differ from 6S by their respective increases in side chain length, we hypothesized that M2′ and M2″ should have similar activities compared with their parent molecules as M2 has compared with 6S.

Our results from measurement of cell viability by MTT assay show that 8S and 10S and their respective cysteine-conjugated metabolites M2′ and M2″ have low toxicity in normal colon cells CCD-18Co (Figure 3A), with IC_{50} values of 104.66 and 135.53 μM for 8S and 10S, respectively, and IC_{50} values greater than 200 μM for M2′ and M2″. All compounds were highly potent against human colon cancer cells HCT-116 (Figure 3B) and HT-29 (Figure 3C), with slightly different efficacy profiles between the two types of cells. M2′ and M2″ show higher activity against HCT-116 than their parent molecules, with IC_{50} values of 15.21 and 13.28 μM, respectively, versus values of 22.8 and 25.09 μM for 8S and 10S, respectively. Similar results were observed in the *p53* mutant HT-29 cell line, albeit slightly more resistant to treatment from all compounds. The IC_{50} values for 8S and 10S, 27.88 and 23.92 μM, were about 10−16% lower than those for M2′ and M2″, at 31.15 and 28.75 μM, respectively.

M2 Induces Apoptosis in Human Colon Cancer Cells HCT-116 and HT-29. In order to compare the biological similarities of M2, M2′, and M2″, we first needed to acquire a more accurate view of the mechanisms of action of M2. To study the impact of M2 on induction of apoptosis in both HCT-116 and HT-29 colon cancer cells, the percent of apoptotic cells were quantified after 24 h treatment of increasing doses of M2 (Figure 3D). A dose-dependent effect of M2 was observed with HCT-116 cells being notably more sensitive to M2 treatment than HT-29 cells. Treatment with 40 μM M2 gave the greatest induction of apoptosis in HCT-116 and HT-29 cells, with 26.34% or 14.38% apoptotic cells, respectively. The 10 and 20 μM treatments also yielded twice as many apoptotic HCT-116 cells compared with HT-29 cells (Figure 3D).

dx.doi.org/10.1021/jf501351r | J. Agric. Food Chem. 2014, 62, 4632−4642

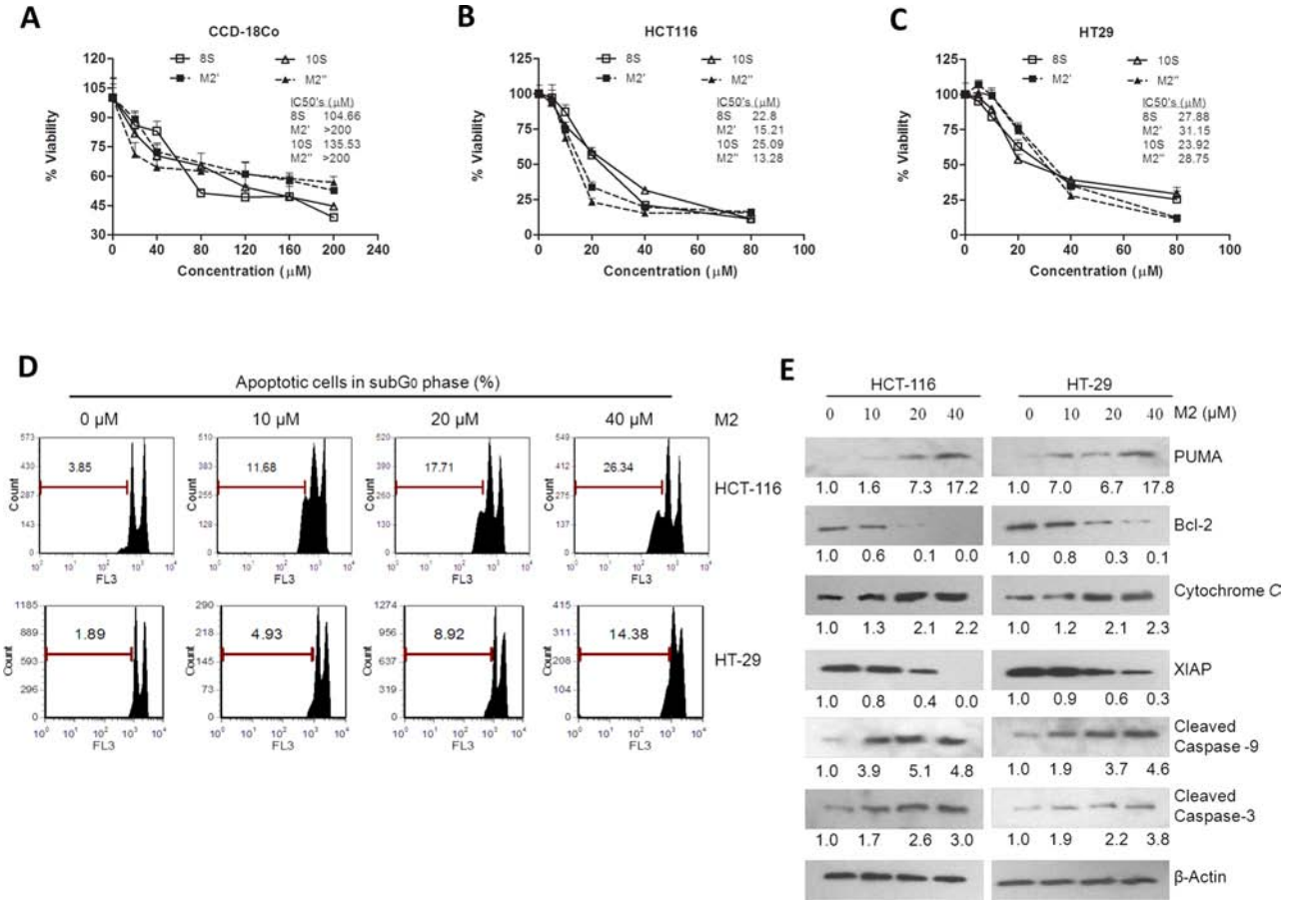

Figure 3. M2′ and M2″ remain bioactive to human colon cancer cells but less toxic to human normal colon cells than 8S and 10S and M2 induces apoptosis on HCT-116 and HT-29 human colon cancer cells. Growth inhibitory effects of 8S, M2′, 10S, and M2″ against human normal colon cells CCD-18Co (A) and human colon cancer cells HCT-116 (B) and HT-29 (C) treated with 8S, M2′, 10S, or M2″ for 24 h at different doses (n = 6) (measured by MTT assay). (D) Effect of M2 on apoptosis in human colon cancer cells HCT-116 and HT-29 treated with M2 (0, 10, 20, and 40 μM) for 24 h measured by PI staining; data represent mean ± SD. (E) Western blot analysis of HCT-116 and HT-29 cell extracts treated with DMSO, 10, 20, and 40 μM of M2 for 24 h. Fold induction for each marker compared with DMSO is indicated under the corresponding line.

Induction of apoptosis was further confirmed by Western blot analysis of markers of the intrinsic mitochondrial apoptosis pathway (Figure 3E). Increasing doses of M2 led to PUMA induction (up to ∼17-fold increase in both cell lines when treated with 40 μM M2) and progressive reduction of Bcl-2 levels (undetectable in HCT-116 and ∼0.1-fold in HT-29 cells when treated with 40 μM M2). We detected a progressive increase in cytochrome c release with increasing doses of M2 (up to ∼2.2-fold increase in both cell lines when treated with 40 μM M2). We also observed a clear, progressive reduction in XIAP expression with increasing doses of M2 (undetectable in HCT-116 and ∼0.3-fold in HT-29 cells when treated with 40 μM M2). Finally, increasing concentration of the cleaved forms of caspase 9 (up to ∼4.6-fold increase in both cell lines when treated with 40 μM M2) and caspase 3 (∼3−4-fold increase in both cell lines when treated with 40 μM M2) were detected with increasing doses of M2. Overall, these results show that markers of the mitochondrial pathway (PUMA, Bcl-2) of apoptosis were activated upon exposure to M2 and ultimately led to the release of the corresponding apoptosis markers (cytochrome c, cleaved caspases 3 and 9).

8S, 10S, M2′, and M2″ Activate Apoptosis. Our results on M2′ and M2″ are consistent with our previous observation that M2 has low toxicity in normal colon cells while still retaining strikingly similar potency to 6S in cancer cell growth inhibition.[13] Thus, we could tentatively propose that M2′ and M2″ have similar biological roles as the function we previously proposed for M2, as low toxicity carriers of parent molecular 8S and 10S to active sites, where function is restored upon removal of the cysteine group.[23] To verify this hypothesis, we studied the apoptotic markers modulated by M2 (described Figure 3E) in HCT-116 and HT-29 cells treated with 8S, M2′, 10S, or M2″ for 24 h. We chose a dose of 20 μM since it is close to the IC_{50} values of all compounds.

Screening of the markers modulated by the pro-apoptotic activity of M2 gave similar results for 8S and 10S and their respective cysteine-conjugated metabolites M2′ and M2″(Figure 4A). In other words, PUMA and cleaved caspase-3 were up-regulated, with concomitant down-regulation of Bcl-2. The changes in marker expression was observed in both cell lines in a nearly identical amplitude between the parent compound and its corresponding metabolite.

Shogaols and Their Cysteine-Conjugated Metabolites Affect Wild-Type and Mutant *p53* Expression in Human Colon Cancer Cells HCT-116 and HT-29. Since we established that the cysteine-conjugated shogaols could activate apoptosis through the same pathway, we wanted to further study their mechanisms of action using 6S and its metabolite M2 as a model. We established that PUMA, a transcriptional target of p53, accumulated almost identically in *p53* wild-type

dx.doi.org/10.1021/jf501351r | J. Agric. Food Chem. 2014, 62, 4632−4642

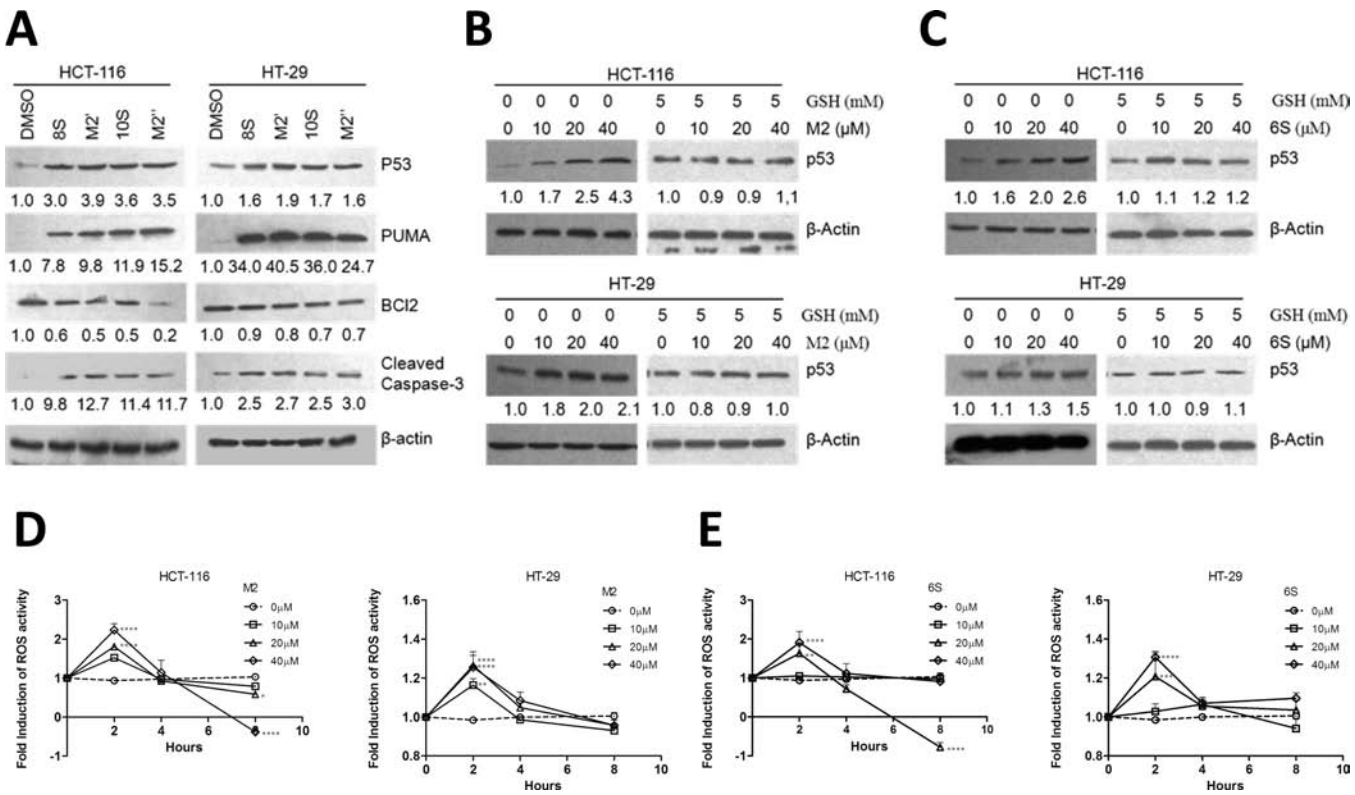

Figure 4. Cysteine conjugated shogaols induce apoptosis via oxidative stress-mediated p53 pathway. Western blot analysis of HCT-116 or HT-29 cell extracts treated with DMSO or 20 μM of 8S, M2′, 10S, or M2″ for 24 h on apoptosis-related protein (A) or with 0, 10, 20, and 40 μM of M2 or 6S on p53 expression with or without the presence of GSH (5 mM) (B and C). Protein levels were relatively quantitated by densitometric analysis using β-actin as a loading control. Fold induction for each marker compared with DMSO is indicated under the corresponding line. (D, E) Induction of ROS by M2 or 6S. HCT-116 and HT-29 cells were treated with indicated concentrations of 6S or M2 for different time periods, and the intracellular ROS levels were determined as described under Materials and Methods. (*$p < 0.05$, **$p < 0.01$, ***$p < 0.001$, and ****$p < 0.0001$).

HCT-116 and *p53* mutant HT-29 cell lines, with both showing greater than 17-fold induction of PUMA after 24 h treatment with 40 μM M2 (Figure 3E). To study the impact of M2 on p53 regulation in human colon cancer cells and its dependency on p53 integrity, *p53* wild-type HCT-116 or *p53* mutant HT-29 cells were cultured with M2 or 6S for 24 h at concentrations of 10, 20, or 40 μM. The p53 response in colon cancer cells to 6S treatment (10, 20, or 40 μM for 24 h) was observed in HCT-116 and HT-29. After M2 or 6S treatment, a dose-dependent up-regulation of p53 is noted in both wild-type and mutant cancer cell lines (Figure 4B,C), indicating that M2 or 6S regulation of p53 does not require a wild-type gene, although induction of p53 expression by M2 or 6S is dramatic in HCT-116 cells and slightly less striking (but still significant) in HT-29 cells (Figure 4B,C). Consistent with our premise, we then studied p53 expression in HCT-116 and HT-29 cells after exposure to 20 μM of 8S, M2′, 10S, or M2″. We observed an increase in p53 accumulation for all compounds (Figure 4A). The cysteine-conjugated metabolites were able to increase p53 accumulation in a similar manner to their parent compound.

6S and Its Cysteine-Conjugated Metabolite M2 Affect Reactive Oxygen Species Generation in Human Colon Cancer Cells HCT-116 and HT-29. Our observations up to this point indicated that M2 induces apoptosis in colon cancer cells through modulation of p53 expression and subsequent activation of the mitochondrial apoptotic pathway through PUMA and Bcl-2. However, the mechanism triggering the p53 accumulation was still unclear. Because overabundance of reactive oxygen species has been implicated as a genotoxic stressor and trigger for p53 activation,[29−33] we observed the production of ROS by M2 (compared with parent compound 6S for reference) in HCT-116 and HT-29 cells. As shown in Figure 4D,E, the trends of ROS induction by both M2 and 6S are strikingly similar, with the greatest peak at 2 h after treatment and a steady decline thereafter, which is consistent with the changes of glutathione levels in cancer cells that we reported previously.[23] In this case, treatment of HCT-116 cells with 40 μM M2 produced the greatest ROS activity after 2 h, with greater than 2-fold induction (with statistical significance, $p < 0.0001$). The scales of induction of ROS by M2 or 6S are parallel to the p53 induction response in the two respective cell lines. That is, in HCT-116 cells, ROS activity is induced 2-fold or greater by M2 or 6S treatment, while in HT-29 cells, ROS activity is induced less than 1.5-fold.

To demonstrate that ROS induction was indeed the trigger to p53 accumulation, we treated HCT-116 and HT-29 cells for 24 h with M2 or 6S (10, 20, or 40 μM) and supplemented with 5 mM GSH in order to suppress ROS accumulation in the cells. As shown on Figure 4B,C, addition of GSH suppressed p53 induction in both cell lines for all concentrations of M2 or 6S, establishing that p53 does not accumulate if there is no ROS generation.

M2 Inhibits Colony Formation in Human Colon Cancer Cells HCT-116 and HT-29. While we established that the cysteine conjugate of 6S can activate apoptosis, it is possible that other mechanisms leading to cancer cell death are triggered, especially in light of the specific activation of the multiacting p53. Since p53 is one of the major regulators of the

dx.doi.org/10.1021/jf501351r | J. Agric. Food Chem. 2014, 62, 4632−4642

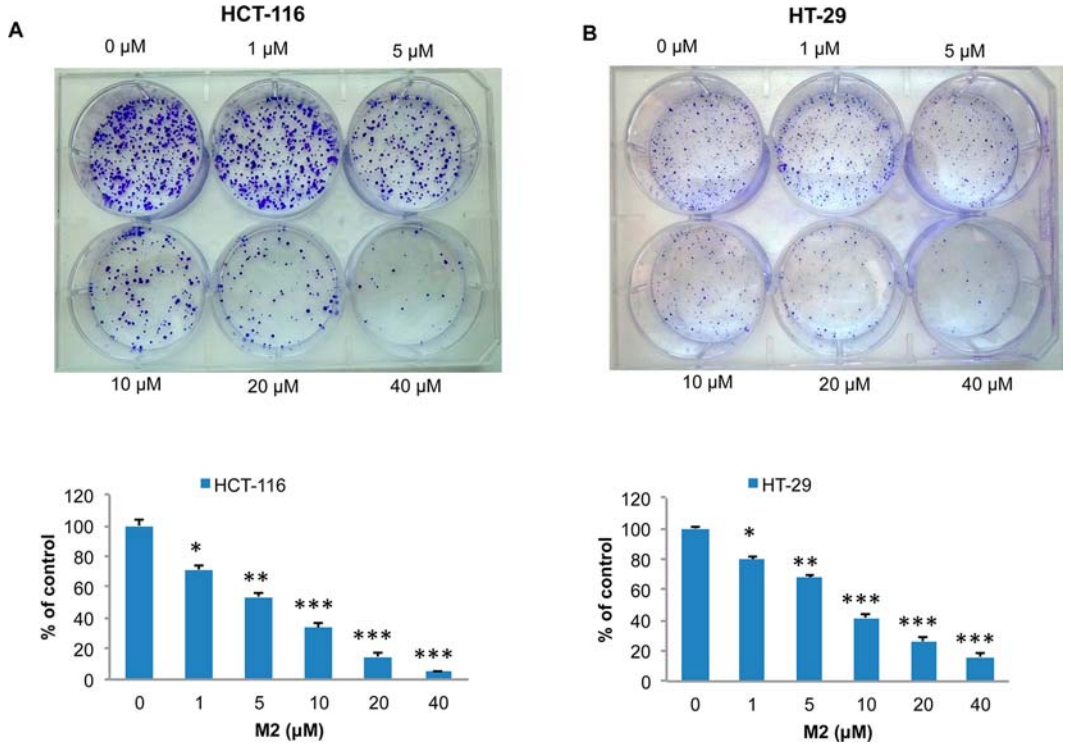

Figure 5. Dose dependent inhibition of human colon cancer cell colony formation by M2 in HCT-116 (A) and HT-29 (B) cells. HCT-116 (A) and HT-29 (B) cells were treated with M2 (0, 1, 5, 10, 20, and 40 μM) and incubated in 6-well plates for 2 weeks, and the cells were then stained with crystal violet and counted for colony formation. Each column represents a mean ± SD (n = 3; *p < 0.05; **p < 0.01; ***p < 0.001).

cell cycle, we further investigated the potential of our cysteine conjugated metabolites to inhibit cancer cell proliferation, using a colony assay and M2 as a model. Human colon cancer cells HCT-116 (Figure 5A) and HT-29 (Figure 5B) were treated with M2 with doses ranging from 0 to 40 μM for 2 weeks. Inhibition of colony formation was observed in a dose-dependent manner in both cell lines, with 50% inhibition between 5 and 10 μM treatments. Following a trend underlined previously, HCT-116 cells are slightly more sensitive to M2 than HT-29 cells.

DISCUSSION

There is currently considerable interest in developing cancer therapeutics and preventive agents from dietary sources, with extensive research over the past few decades focusing on plant derivatives.[34−38] Ginger has been comprehensively studied in recent years for its chemopreventive properties, particularly against colorectal cancer.[39−42] Our group and others have identified active constituents of ginger, with our most recent focus on shogaols, especially 6S.[12,13,19,20,23,39,43,44] The metabolism and biotransformation of 6S was investigated thoroughly, providing further insight into its means of exerting bioactivity.[19] Upon testing the efficacy of the major metabolites of 6S, we found that 5-cysteinyl-conjugated 6S (M2) exerted strong antiproliferative activity against human colon cancer cells, while having significantly lessened toxicity in normal human colon cells.[13] Further, M2 was shown to act as a carrier of parent molecule 6S.[23] The discovery of M2 was via correlation of 6S metabolism as a highly electrophilic xenobiotic through the detoxifying mercapturic acid pathway (MAP). We also found that increased chain length of shogaols does not cause a departure from the MAP. M2′ and M2″ were identified as the major metabolites of 8S and 10S, respectively, from humans upon consumption of ginger tea.[21] The current study shows that M2′ and M2″ are the carriers of 8S and 10S, respectively, and have similar antiproliferative activity against human colon cancer cells and less toxicity in normal human colon cells to their respective parent compounds. Our results clearly indicate that this portion of phase II metabolism transforms electrophiles to less reactive and more water-soluble intermediates, thus aiding in their mobility and decreasing their toxicity en route.[45]

It has already been established through many studies that 6S induces apoptosis in cancer cells via several pathways,[12−15] and thus our focus was to identify the pathway that encompasses the mode of activity of M2. We demonstrated that M2 treatment could induce ROS generation, which in turn up-regulated p53 expression and induced apoptosis through the mitochondrial pathway. This proposed mechanism is summarized in Figure 6. Since tumor suppressor gene *p53* is one of the most frequent mutations in cancers, leading to resistance to pharmacological interventions and more aggressive progression,[46−49] we were interested in testing the efficacy of M2 in wild-type *p53* HCT-116 human colon cancer cells as well as mutant *p53* HT-29 human colon cancer cells. In what could be a fortunate outcome for the putative roles of ginger constituents and metabolites toward chemoprevention, M2 induced apoptosis in both cell lines. It is notable that although the p53 pro-apoptotic pathway was exploited for at least some of M2's bioactivity and that we observed a general trend of superior bioactivity in HCT-116 cells, the metabolite's efficacy was ultimately not compromised by *p53* mutation. This is particularly attractive in terms of cancer chemoprevention, since it suggests that the cysteine-conjugated metabolite of 6S would still be able to activate a p53 apoptotic response even in cancer cells containing mutations of the *p53* gene.

dx.doi.org/10.1021/jf501351r | J. Agric. Food Chem. 2014, 62, 4632−4642

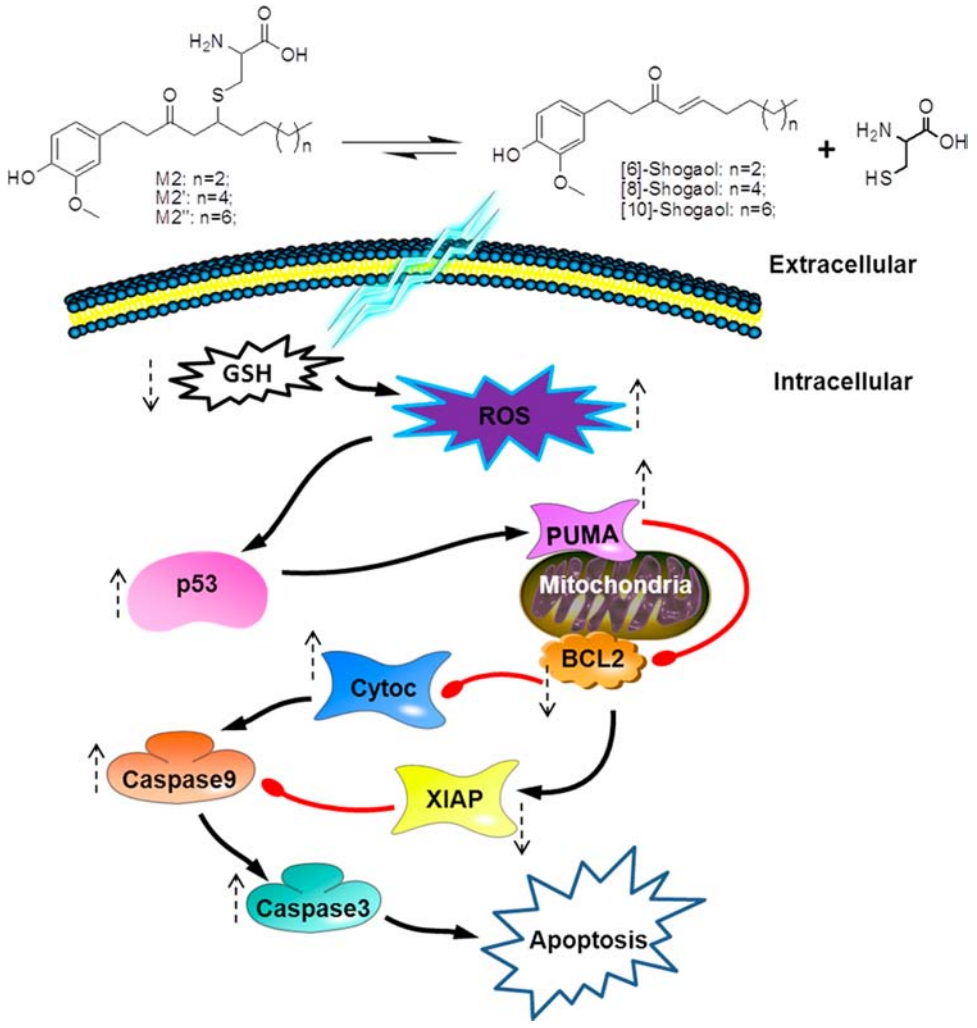

Figure 6. Schematic representation of the mechanisms of action of shogaols and their cysteine-conjugated metabolites in regulating apoptosis by p53 induction, activation of PUMA via p53 translocation to the mitochrondrial surface, Bcl-2 down-regulation, cytochrome *c* release, XIAP inhibition, and finally caspases 9 and 3 activation and cleavage.

A commonly proposed p53-induced apoptosis mechanism involves direct interaction with Bcl-2 family members and down-regulation of antiapoptotic genes, such as Bcl-2, which was also noted in the current study.[47,50−52] Both HCT-116 and HT-29 human colon cancer cells experienced a dramatic down-regulation of Bcl-2 after M2 treatment. Interestingly, PUMA, a transcriptional target of p53,[53] was also up-regulated in both colon cancer cell lines after treatment with M2. Upon a transcriptionally induced signal from p53, PUMA assists in promoting apoptosis by disrupting the association restraints Bcl-xL exerts on p53, thus liberating the molecule to exert pro-apoptotic activity, but binding to Bcl-xL in the process.[54] This evidence supports the strong role of M2 as a chemopreventive agent against colon cancer cells that induces p53 expression and downstream regulation.

Treatment of colon cancer cells HCT-116 and HT-29 with M2 in this study lead to apoptosis, through early production of reactive oxygen species. Overabundance of ROS combined with a cancer cell's reduced detoxification ability can often lead to oxidative stress sufficient to induce programmed cell death.[55] Apoptosis induced by p53 is at least partially dependent upon accumulation of ROS,[56] and we demonstrated this to be also true in our model. Therefore, we can conclude that M2 causes p53 induction of apoptosis via ROS production in both HCT-116 and HT-29 human colon cancer cells. Since we demonstrated that the other metabolites M2′ and M2″ activate similar markers of apoptosis (Figure 4A) and contain the same chemical reactivity as M2, it is reasonable to conclude that these metabolites would behave in a similar way and could also activate cancer cell apoptosis through ROS induction and the subsequent p53 accumulation. In addition, we also demonstrated that M2 does not exclusively induce cancer cell death through apoptosis and can also influence other major mechanisms such as cell proliferation (Figure 5); it follows that other cysteine conjugated metabolites originating from the same MAP have that potential as well. These compounds are worthy of further investigation, and further studies could examine commonly consumed ginger mixtures containing these compounds for more direct translation of these data to *in vivo* dietary models.

Ginger components are highly lauded for their vast and varied chemopreventive properties. Because shogaols have been proven as highly effective anticancer agents, the continued study of their mechanisms of activity can allow us to discover novel anticancer targets. Further, investigation of the metabolic products of shogaols can provide new therapeutic routes that are less toxic, while retaining high efficacy. This study has shown that cysteine-conjugated shogaols are novel compounds

with a putative role as natural pharmaceuticals with low-toxicity, high-potency, and at least partial indifference to *p53* integrity in colon cancer cells.

AUTHOR INFORMATION

Corresponding Author

*Tel: 704-250-5710. Fax: 704-250-5709. E-mail: ssang@ncat.edu.

Author Contributions

§H.C. and D.N.S. contributed equally to this work.

Notes

The authors declare no competing financial interest.

ACKNOWLEDGMENTS

This work was supported by NIH Grants CA138277 and CA138277S1 to S. Sang.

ABBREVIATIONS

6S, [6]-shogaol; 8S, [8]-shogaol; 10S, [10]-shogaol; GSH, glutathione; HPLC, high-performance liquid chromatography; LC/MS, liquid chromatrography/mass spectrometry; M2, 5-cysteinyl-6S; M2′, 5-cysteinyl-8S; M2″, 5-cysteinyl-10S; p53, tumor protein 53; ROS, reactive oxygen species

REFERENCES

(1) Park, E. J.; Pezzuto, J. M. Botanicals in cancer chemoprevention. *Cancer Metastasis Rev.* **2002**, *21*, 231−255.

(2) Kubra, I. R.; Rao, L. J. An impression on current developments in the technology, chemistry, and biological activities of ginger (*Zingiber officinale* Roscoe). *Crit. Rev. Food Sci. Nutr* **2011**, *52*, 651−688.

(3) Ali, B. H.; Blunden, G.; Tanira, M. O.; Nemmar, A. Some phytochemical, pharmacological and toxicological properties of ginger (*Zingiber officinale* Roscoe): A review of recent research. *Food Chem. Toxicol.* **2008**, *46*, 409−420.

(4) Altman, R. D.; Marcussen, K. C. Effects of a ginger extract on knee pain in patients with osteoarthritis. *Arthritis Rheum.* **2001**, *44*, 2531−2538.

(5) Lantz, R. C.; Chen, G. J.; Sarihan, M.; Solyom, A. M.; Jolad, S. D.; Timmermann, B. N. The effect of extracts from ginger rhizome on inflammatory mediator production. *Phytomedicine* **2007**, *14*, 123−128.

(6) Kim, J. S.; Lee, S. I.; Park, H. W.; Yang, J. H.; Shin, T. Y.; Kim, Y. C.; Baek, N. I.; Kim, S. H.; Choi, S. U.; Kwon, B. M.; Leem, K. H.; Jung, M. Y.; Kim, D. K. Cytotoxic components from the dried rhizomes of *Zingiber officinale* Roscoe. *Arch Pharm. Res.* **2008**, *31*, 415−418.

(7) Bak, M. J.; Ok, S.; Jun, M.; Jeong, W. S. 6-Shogaol-rich extract from ginger up-regulates the antioxidant defense systems in cells and mice. *Molecules* **2012**, *17*, 8037−8055.

(8) Dugasani, S.; Pichika, M. R.; Nadarajah, V. D.; Balijepalli, M. K.; Tandra, S.; Korlakunta, J. N. Comparative antioxidant and anti-inflammatory effects of [6]-gingerol, [8]-gingerol, [10]-gingerol and [6]-shogaol. *J. Ethnopharmacol.* **2010**, *127*, 515−520.

(9) Wu, H.; Hsieh, M. C.; Lo, C. Y.; Liu, C. B.; Sang, S.; Ho, C. T.; Pan, M. H. 6-Shogaol is more effective than 6-gingerol and curcumin in inhibiting 12-O-tetradecanoylphorbol 13-acetate-induced tumor promotion in mice. *Mol. Nutr. Food Res.* **2010**, *54*, 1296−1306.

(10) Sang, S.; Hong, J.; Wu, H.; Liu, J.; Yang, C. S.; Pan, M. H.; Badmaev, V.; Ho, C. T. Increased growth inhibitory effects on human cancer cells and anti-inflammatory potency of shogaols from Zingiber officinale relative to gingerols. *J. Agric. Food Chem.* **2009**, *57*, 10645−10650.

(11) Siegel, R.; Ward, E.; Brawley, O.; Jemal, A. Cancer statistics, 2011: The impact of eliminating socioeconomic and racial disparities on premature cancer deaths. *Ca—Cancer J. Clin.* **2011**, *61*, 212−36.

(12) Tan, B. S.; Kang, O.; Mai, C. W.; Tiong, K. H.; Khoo, A. S.; Pichika, M. R.; Bradshaw, T. D.; Leong, C. O. 6-Shogaol inhibits breast and colon cancer cell proliferation through activation of peroxisomal proliferator activated receptor gamma (PPARgamma). *Cancer Lett.* **2013**, *336*, 127−39.

(13) Zhu, Y.; Warin, R. F.; Soroka, D. N.; Chen, H.; Sang, S. Metabolites of ginger component [6]-shogaol remain bioactive in cancer cells and have low toxicity in normal cells: chemical synthesis and biological evaluation. *PloS One* **2013**, *8*, No. e54677.

(14) Gan, F. F.; Nagle, A. A.; Ang, X.; Ho, O. H.; Tan, S. H.; Yang, H.; Chui, W. K.; Chew, E. H. Shogaols at proapoptotic concentrations induce G(2)/M arrest and aberrant mitotic cell death associated with tubulin aggregation. *Apoptosis* **2011**, *16*, 856−867.

(15) Pan, M. H.; Hsieh, M. C.; Kuo, J. M.; Lai, C. S.; Wu, H.; Sang, S.; Ho, C. T. 6-Shogaol induces apoptosis in human colorectal carcinoma cells via ROS production, caspase activation, and GADD 153 expression. *Mol. Nutr. Food Res.* **2008**, *52*, 527−537.

(16) Bansal, P.; Khoobchandani, M.; Kumar, V.; Srivastava, M. M., Cruciferous Vegetables: Novel Cancer Killer and Guardians of Our Health. In *Chemistry of Phytopotentials: Health, Energy and Environmental Perspectives*, Khemani, L. D., Srivastava, M. M., Srivastava, S., Eds.; Springer: Berlin Heidelberg, 2012; pp 3−7.

(17) Tan, X.-L.; Spivack, S. D. Dietary chemoprevention strategies for induction of phase II xenobiotic-metabolizing enzymes in lung carcinogenesis: A review. *Lung Cancer* **2009**, *65*, 129−137.

(18) Zhang, Y. Allyl isothiocyanate as a cancer chemopreventive phytochemical. *Mol. Nutr. Food Res.* **2010**, *54*, 127−135.

(19) Chen, H.; Lv, L.; Soroka, D.; Warin, R. F.; Parks, T. A.; Hu, Y.; Zhu, Y.; Chen, X.; Sang, S. Metabolism of [6]-shogaol in mice and in cancer cells. *Drug Metab. Dispos.* **2012**, *40*, 742−753.

(20) Chen, H.; Sang, S. Identification of phase II metabolites of thiol-conjugated [6]-shogaol in mouse urine using high-performance liquid chromatography tandem mass spectrometry. *J. Chromatogr. B: Anal. Technol. Biomed. Life Sci.* **2012**, *907*, 126−139.

(21) Chen, H.; Soroka, D. N.; Hu, Y.; Chen, X.; Sang, S. Characterization of thiol-conjugated metabolites of ginger components shogaols in mouse and human urine and modulation of the glutathione levels in cancer cells by [6]-shogaol. *Molecular Nutr. Food Res.* **2013**, *57*, 447−458.

(22) Conaway, C. C.; Krzeminski, J.; Amin, S.; Chung, F. L. Decomposition rates of isothiocyanate conjugates determine their activity as inhibitors of cytochrome p450 enzymes. *Chem. Res. Toxicol.* **2001**, *14*, 1170−1176.

(23) Chen, H.; Soroka, D. N.; Zhu, Y.; Hu, Y.; Chen, X.; Sang, S. Cysteine-conjugated metabolite of ginger component [6]-shogaol serves as a carrier of [6]-shogaol in cancer cells and in mice. *Chem. Res. Toxicol.* **2013**, *26*, 976−985.

(24) Soussi, T.; Lozano, G. p53 mutation heterogeneity in cancer. *Biochem. Biophys. Res. Commun.* **2005**, *331*, 834−842.

(25) Toledo, F.; Wahl, G. M. Regulating the p53 pathway: in vitro hypotheses, in vivo veritas. *Nat. Rev. Cancer* **2006**, *6*, 909−923.

(26) Seemann, S.; Maurici, D.; Olivier, M.; Caron de Fromentel, C.; Hainaut, P. The tumor suppressor gene TP53: Implications for cancer management and therapy. *Crit. Rev. Clin. Lab. Sci.* **2004**, *41*, 551−583.

(27) Mosmann, T. Rapid colorimetric assay for cellular growth and survival: Application to proliferation and cytotoxicity assays. *J. Immunol Methods* **1983**, *65*, 55−63.

(28) Brandt, R.; Keston, A. S. Synthesis of diacetyldichlorofluorescin: A stable reagent for fluorometric analysis. *Anal. Biochem.* **1965**, *11*, 6−9.

(29) Qin, H.; Yu, T.; Qing, T.; Liu, Y.; Zhao, Y.; Cai, J.; Li, J.; Song, Z.; Qu, X.; Zhou, P.; Wu, J.; Ding, M.; Deng, H. Regulation of apoptosis and differentiation by p53 in human embryonic stem cells. *J. Biol. Chem.* **2007**, *282*, 5842−5852.

(30) Speidel, D.; Helmbold, H.; Deppert, W. Dissection of transcriptional and non-transcriptional p53 activities in the response to genotoxic stress. *Oncogene* **2006**, *25*, 940−953.

(31) Tao, Y.; Li, W.; Liang, W.; Van Breemen, R. B. Identification and quantification of gingerols and related compounds in ginger dietary supplements using high-performance liquid chromatography-

tandem mass spectrometry. *J. Agric. Food Chem.* **2009**, *57*, 10014−10021.
(32) Waster, P. K.; Ollinger, K. M. Redox-dependent translocation of p53 to mitochondria or nucleus in human melanocytes after UVA- and UVB-induced apoptosis. *J. Invest. Dermatol.* **2009**, *129*, 1769−1781.
(33) Zhao, Y.; Chaiswing, L.; Velez, J. M.; Batinic-Haberle, I.; Colburn, N. H.; Oberley, T. D.; St Clair, D. K. p53 translocation to mitochondria precedes its nuclear translocation and targets mitochondrial oxidative defense protein-manganese superoxide dismutase. *Cancer Res.* **2005**, *65*, 3745−3750.
(34) Cerella, C.; Radogna, F.; Dicato, M.; Diederich, M. Natural compounds as regulators of the cancer cell metabolism. *Int. J. Cell Biol.* **2013**, *2013*, No. 639401.
(35) Cohen, S.; Flescher, E. Methyl jasmonate: A plant stress hormone as an anti-cancer drug. *Phytochemistry* **2009**, *70*, 1600−1609.
(36) Elkady, A. I.; Abuzinadah, O. A.; Baeshen, N. A.; Rahmy, T. R. Differential control of growth, apoptotic activity, and gene expression in human breast cancer cells by extracts derived from medicinal herbs Zingiber officinale. *J, Biomed. Biotechnol.* **2012**, *2012*, No. 614356.
(37) Karna, P.; Chagani, S.; Gundala, S. R.; Rida, P. C.; Asif, G.; Sharma, V.; Gupta, M. V.; Aneja, R. Benefits of whole ginger extract in prostate cancer. *Br. J. Nutr.* **2012**, *107*, 473−484.
(38) Orlikova, B.; Diederich, M. Power from the garden: Plant compounds as inhibitors of the hallmarks of cancer. *Curr. Med. Chem.* **2012**, *19*, 2061−2087.
(39) Stoner, G. D. Ginger: Is it Ready for Prime Time? *Cancer Prev. Res.* **2013**, *6*, 257−262.
(40) Citronberg, J.; Bostick, R.; Ahearn, T.; Turgeon, D. K.; Ruffin, M. T.; Djuric, Z.; Sen, A.; Brenner, D. E.; Zick, S. M. Effects of Ginger Supplementation on Cell-Cycle Biomarkers in the Normal-Appearing Colonic Mucosa of Patients at Increased Risk for Colorectal Cancer: Results from a Pilot, Randomized, and Controlled Trial. *Cancer Prev. Res.* **2013**, *6*, 271−281.
(41) Yogosawa, S.; Yamada, Y.; Yasuda, S.; Sun, Q.; Takizawa, K.; Sakai, T. Dehydrozingerone, a structural analogue of curcumin, induces cell-cycle arrest at the G2/M phase and accumulates intracellular ROS in HT-29 human colon cancer cells. *J. Nat. Prod.* **2012**, *75*, 2088−2093.
(42) Ramos, S. Cancer chemoprevention and chemotherapy: Dietary polyphenols and signalling pathways. *Mol. Nutr Food Res.* **2008**, *52*, 507−526.
(43) Park, G.; Kim, H. G.; Ju, M. S.; Ha, S. K.; Park, Y.; Kim, S. Y.; Oh, M. S. 6-Shogaol, an active compound of ginger, protects dopaminergic neurons in Parkinson's disease models via anti-neuroinflammation. *Acta Pharmacol. Sin.* **2013**, *34*, 1131−1139.
(44) Chen, H.; Soroka, D.; Zhu, Y.; Sang, S. Metabolism of ginger component [6]-shogaol in liver microsomes from mouse, rat, dog, monkey, and human. *Molecular Nutr. Food Res.* **2013**, *57*, 865−876.
(45) Xu, C.; Li, C.-T.; Kong, A.-N. Induction of phase I, II and III drug metabolism/transport by xenobiotics. *Arch. Pharmacal Res.* **2005**, *28*, 249−268.
(46) Wang, B.; Xiao, Z.; Ko, H. L.; Ren, E. C. The p53 response element and transcriptional repression. *Cell Cycle (Georgetown, Tex.)* **2010**, *9*, 870−879.
(47) Vousden, K. H.; Prives, C. Blinded by the Light: The Growing Complexity of p53. *Cell* **2009**, *137*, 413−431.
(48) Lane, D.; Levine, A. p53 Research: The past thirty years and the next thirty years. *Cold Spring Harbor Perspect. Biol.* **2010**, *2*, No. a000893.
(49) Garritano, S.; Inga, A.; Gemignani, F.; Landi, S. More targets, more pathways and more clues for mutant p53. *Oncogenesis* **2013**, *2*, No. e54.
(50) Laptenko, O.; Prives, C. Transcriptional regulation by p53: One protein, many possibilities. *Cell Death Differ.* **2006**, *13*, 951−961.
(51) Vazquez, A.; Bond, E. E.; Levine, A. J.; Bond, G. L. The genetics of the p53 pathway, apoptosis and cancer therapy. . *Nat. Rev. Drug Discovery* **2008**, *7*, 979−987.
(52) Youle, R. J.; Strasser, A. The BCL-2 protein family: Opposing activities that mediate cell death. . *Nat. Rev. Mol. Cell Biol.* **2008**, *9*, 47−59.
(53) Nakano, K.; Vousden, K. H. PUMA, a Novel Proapoptotic Gene, Is Induced by p53. *Mol. Cell* **2001**, *7*, 683−694.
(54) Speidel, D. Transcription-independent p53 apoptosis: An alternative route to death. *Trends Cell Biol.* **2010**, *20*, 14−24.
(55) Ozben, T. Oxidative stress and apoptosis: Impact on cancer therapy. *J. Pharm. Sci.* **2007**, *96*, 2181−2196.
(56) Oren, M. Decision making by p53: Life, death and cancer. *Cell Death Differ.* **2003**, *10*, 431−442.

JOURNAL OF AGRICULTURAL AND FOOD CHEMISTRY

Article

pubs.acs.org/JAFC

Enhanced Ethanol Production from Pomelo Peel Waste by Integrated Hydrothermal Treatment, Multienzyme Formulation, and Fed-Batch Operation

Renliang Huang,[‡,∥] Ming Cao,[†,∥] Hong Guo,[†] Wei Qi,[†,#] Rongxin Su,*[,†,#] and Zhimin He[†]

[†]State Key Laboratory of Chemical Engineering, Tianjin Key Laboratory of Membrane Science and Desalination Technology, School of Chemical Engineering and Technology, Tianjin University, Tianjin 300072, People's Republic of China

[‡]School of Environmental Science and Engineering, Tianjin University, Tianjin 300072, People's Republic of China

[#]Collaborative Innovation Center of Chemical Science and Engineering (Tianjin),Tianjin 300072, People's Republic of China

ABSTRACT: Pomelo peel is an abundant pectin-rich biomass waste in China and has the potential to serve as a source of fuels and chemicals. This study reports a promising way to deal with pomelo peel waste and to utilize it as raw material for ethanol production via simultaneous saccharification and fermentation (SSF). An integrated strategy, incorporating hydrothermal treatment, multienzyme formulation, and fed-batch operation, was further developed to enhance the ethanol production. The results show that hydrothermal treatment (120 °C, 15 min) could significantly reduce the use of cellulase (from 7 to 3.8 FPU g^{-1}) and pectinase (from 20 to 10 U g^{-1}). A multienzyme complex, which consists of cellulase, pectinase, β-glucosidase, and xylanase, was also proven to be effective to improve the hydrolysis of pretreated pomelo peel, leading to higher concentrations of fermentative sugars (36 vs 14 g L^{-1}) and galacturonic acid (23 vs 9 g L^{-1}) than those with the use of a single enzyme. Furthermore, to increase the final ethanol concentration, fed-batch operation by adding fresh substrate was employed in the SSF process. A final solid loading of 25% (w/v), which is achieved by adding 15% fresh substrate to the SSF system at an initial solid loading of 10%, produced 36 g L^{-1} ethanol product in good yield (73.5%). The ethanol concentration is about 1.73-fold that at the maximum solid loading of 14% for batch operation, whereas both of them have a closed ethanol yield. The results indicate that the use of the fed-batch mode could alleviate the decrease in ethanol yield at high solid loading, which is caused by significant mass transfer limitation and increased inhibition of toxic compounds in the SSF process. The integrated strategy demonstrated in this work could open a new avenue for dealing with pectin-rich biomass wastes and utilization of the wastes to produce ethanol.

KEYWORDS: *pomelo peel, ethanol, cellulase, pectinase, enzymatic hydrolysis, SSF*

INTRODUCTION

Citrus production and consumption worldwide have grown strongly over the past few decades. According to the statistical data from the Food and Agriculture Organization of the United Nations (FAOSTAT), the world production of citrus fruits in 2010 was over 100 million tons.[1] With the heavy consumption of these fruits (e.g., juice/sugar production), a large amount of citrus waste is generated, which accounts for about 50% of the fruit weight. The wastes include fruit peel, membrane residues, and other byproducts.[2] Traditionally, the wastes are disposed of through a burning process or used as raw material for active substance extraction and animal feed manufacturing.[3−6] However, these means are not satisfactory as the market demand may be limited or secondary contamination and low-value products result. Up to now, the majority of citrus wastes are still deposited or disposed of simply as mentioned before, leading to serious environmental pollution and great wastage of resources. Therefore, it is highly desirable to develop green and economical ways to deal with citrus wastes, as well as to utilize the wastes to produce staple or value-added products.

Citrus wastes mainly consist of soluble mono- and disaccharides (e.g., glucose, fructose, sucrose), insoluble polysaccharides (e.g., cellulose, hemicellulose, pectin), and lignin.[7] This chemical composition renders the wastes to be a potential candidate for the production of biofuels and other sugar-based chemicals.[2,8] Ethanol, being one of the most promising biofuels, has received great attention with the increasing fuel demand and environmental concerns globally. In recent years, much effort has been invested to develop second-generation ethanol fuel from nonfood crops. Most of this research focuses on the use of recalcitrant lignocellulosic biomass, such as corn cobs,[9,10] corn stover,[11−13] wood chips,[14,15] switchgrass,[16] and rice straw,[17] due to their large-scale availability and low raw material cost. In these cases, the high content of lignin and the recalcitrant structure of these feedstocks greatly hinder enzymatic hydrolysis and fermentation. Generally, harsh pretreatment and high enzyme loading are required in ethanol production. In comparison with recalcitrant lignocellulosic biomass, citrus wastes, such as citrus peel, contain less lignin and more pectin, which enable a facile hydrolysis of the wastes into fermentable sugars by the use of several hydrolytic enzymes in combination.[18,19] With the large sugar content generated from highly degradable polysaccharides and the elimination of harsh pretreatment, citrus wastes could prove to be an attractive source of bioethanol.[20] This

Received: November 18, 2013
Revised: May 2, 2014
Accepted: May 2, 2014
Published: May 6, 2014

ACS Publications © 2014 American Chemical Society

Table 1. Chemical Compositions (Percent of Dry Matter) of Different Citrus Wastes

citrus waste	cellulose	hemicellulose	pectin	lignin	soluble sugars	ash
orange peel[47]	37.08	11.04	23.02	7.52	9.57	2.56
orange waste[23]	22.0	11.1	25.0	2.19	22.9	3.73
Kinnow mandarin peel[27]	10.72	3.88	22.88	1.91	29.66	3.52
mandarin peel[28]	20.8	17.2	14.2	8.9	21.6	3.0
grapefruit waste[47]	26.57	5.59	8.53	11.56	8.02	8.09
pomelo peel (this work)	16.50	6.86	35.42	3.16	12.62	4.14

study aims to provide a practical approach to utilize citrus wastes as biomass source for ethanol production.

In previous studies, citrus wastes from orange (*Citrus sinensis*),[21−25] Kinnow mandarins (*Citrus reticulata*),[26−28] and grapefruit (*Citrus paradisi*)[29] have been successfully used to produce ethanol via enzymatic hydrolysis and fermentation. As we know, the technological package (e.g., pretreatment, enzymatic hydrolysis, fermentation) utilized in ethanol production is generally specific to the feedstocks, due to the significant structural differences among various biomass materials. The technology, together with the properties of the feedstock (e.g., degradability, availability, locality, price), determine the economic feasibility of ethanol production. Pomelo (*Citrus maxima*), a characteristic fruit of China, has a large annual production of >2 million tons (pomelo and grapefruit production are estimated at 3.6 million tons in 2011 from FAOSTAT, with China being the largest producer). Pomelo has more peel and segment membrane than most other citrus fruits, generating a significant quantity of pomelo waste in China. However, to date, no report has discussed the utilization of these wastes for ethanol production.

Pomelo peel has a higher pectin content than other citrus wastes (see Table 1). Although pectin can be easily hydrolyzed, the high pectin content could still limit the hydrolysis of cellulose and hemicellulose because it acts as a physical barrier to restrict the access of enzymes to the substrate.[30] Furthermore, pectin can increase the viscosity of substrate slurry and limit mass transfer during hydrolysis and fermentation. The lower sugar content (~36%, including cellulose, hemicellulose, and soluble sugars) in pomelo peel as compared to other citrus wastes could also result in a lower final ethanol concentration. Therefore, to focus on using pomelo peel as the feedstock for ethanol production, it is essential to develop efficient and economic approaches to improve the hydrolysis efficiency and increase the final ethanol concentration.

Herein, we report a green and economical way to deal with pomelo peel waste and utilize it for ethanol production via a simultaneous saccharification and fermentation (SSF) process. An integrated strategy, incorporating hydrothermal treatment, multienzyme formulation, and fed-batch operation, was proposed to enhance ethanol production. Specifically, to reduce the enzyme dosage in the process, we introduced a simple hydrothermal treatment at a high temperature (120 °C) before performing SSF. Multienzyme formulation and fed-batch operation were further employed to improve the hydrolysis efficiency and increase the final ethanol concentration. In addition, the effects of the initial D-limonene concentration, pH value, and dry yeast concentration on ethanol production were also investigated.

MATERIALS AND METHODS

Chemicals, Enzymes, and Yeast. Glucose (>99.5%), cellobiose (>99%), sucrose (>99.5%), fructose (>99%), xylose (>99%), galactose (>99%), arabinose (>99%), rhamnose (>99%), and galacturonic acid (>97%) were purchased from Sigma. D-Limonene (>97%) was obtained from Aladdin Industrial Corp. (Shanghai, China). Cellulase (GC220, 123 FPU mL^{-1}) was purchased from Genencor International (Palo Alto, CA, USA) in 2009. Pectinase (Multifect pectinase, 597 U mL^{-1}) was graciously provided by Genencor International in 2009. Commercial ethanol instant active dry yeast powder (*Saccharomyces cerevisiae*, yeast cells concentration ~ 20 billion cells/g, water content ~ 6%) was purchased from Angel Yeast Co., Ltd. (Wuhan, China). All of the other chemicals, such as ethanol, sulfuric acid, hydrochloric acid, and oxalate ammonium, were of analytical grade and were obtained from commercial sources.

Sample Preparation. Mature yellow pomelos (*C. maxima*) were collected from a local fruit market in Tianjin, China. Pomelo peels were manually separated and washed with deionized water to remove any extraneous matter. Then the peels were cut into small pieces (~1 cm) and dried in a hot-air oven at 70 °C to a constant weight. The dried pomelo peels were ground to a fine powder (500−600 μm) using an electric mill and stored in an enclosed container for subsequent use.

Hydrothermal Treatment. To facilitate the operation of pretreatment and subsequent enzymatic hydrolysis or SSF, as well as to enhance the break of biomass structure, sodium acetate buffer (50 mM, pH 4.8) was chosen as acidic medium to pretreat pomelo peels. In a typical experiment, 10 g of dried pomelo peels was placed in a screw-capped laboratory bottle (Pyrex bottles) and mixed with sodium acetate buffer (50 mM, pH 4.8) solution at a final concentration of 10% (w/v). The solid/liquid slurry was then put into a stainless steel autoclave at 120 °C for 15 min. After cooling, the treated pomelo peels were directly used for subsequent enzymatic hydrolysis or SSF processing. To prepare the sample for compositional analysis, the solid residue after hydrothermal treatment was separated by filtering, washed with deionized water, and dried in a hot-air oven at 70 °C to a constant weight.

Enzymatic Hydrolysis by Multienzyme Complex. The pomelo peels were first treated under different solid loadings, 5, 7, 10, and 14% (w/v), according to the procedure mentioned above. After hydrothermal treatment, two commercial enzymes, GC220 and Multifect pectinase, were added into the resulting pomelo peel samples over loading ranges of 0−4.6 FPU g^{-1} dry matter (DM) and 0−25 U g^{-1} DM, respectively. Digestive reactions were carried out in an air-bath shaker at 150 rpm and 50 °C for the appropriate time. Five hundred microliter aliquots were taken out at different time points for high-performance liquid chromatography (HPLC) analysis. To investigate the effect of hydrothermal treatment on sugar release, raw pomelo peels without pretreatment were used as a control sample for enzymatic hydrolysis.

Ethanol Production via SSF Process. All of the SSF experiments with a loading volume of 30 mL were carried out in 100 mL glass bottles. The pomelo peels was mixed with sodium acetate buffer (50 mM, pH 4.8) containing 1 g L^{-1} $(NH_4)_2HPO_4$, 1 g L^{-1} $MgSO_4 \cdot 7H_2O$, and 2.0 g L^{-1} yeast extract at the desired initial DM concentrations (5−14%, w/v, based on the dry weight of raw pomelo peels). After hydrothermal treatment, GC220 (3.8 FPU g^{-1} DM) and Multifect pectinase (15 U g^{-1} DM) were added into the treated pomelo peel samples and then incubated at 50 °C for 10 h with continuous shaking

at 150 rpm. After prehydrolysis, the temperature was reduced to 30 °C, and the pH of the medium was controlled at 5.0. The initial pH of the prehydrolyzed medium was between 4.0 and 4.3, and sodium hydroxide was added to the mixture to adjust the pH. The SSF experiments were started by adding 2−6 g L^{-1} dry yeast at 30 °C and 150 rpm. The time of yeast addition was referred to as time zero. The experiments were run for another 48 h. Five hundred microliter aliquots were taken out at different time points for HPLC analysis (e.g., ethanol, sugars, galacturonic acid). After SSF processing, the residue solid was washed, filtered, dried, and weighed. Ethanol volumetric productivity (grams per liter per hour, g L^{-1} h^{-1}) was calculated as the ratio of the final ethanol concentration (g L^{-1}) to the fermentation time (h).

The fed-batch SSF experiments were started with an initial 10% solid loading. Another 10 or 15% dry matter was added during the SSF process, giving a final solid loading of 20 or 25%. The final solid loading of 20% is achieved by adding 0.6 g (3%, w/v), 0.6 g (3%), 0.6 g (3%), and 0.2 g (1%) of fresh pretreated pomelo peel at 8, 18, 24, and 30 h, respectively. The final solid loading of 25% is achieved by adding 0.6 g (3%, w/v), 0.6 g (3%), 0.6 g (3%), 0.5 g (2.5%) 0.5 g (2.5%), and 0.2 g (1%) fresh pretreated pomelo peel at 8, 18, 24, 30 , 36, and 42 h, respectively. The fermentation conditions, enzyme loadings, and nutrient concentrations were the same as in the batch experiments.

Analytical Methods. The ethanol-soluble fraction was extracted by using repeated extractions of pomelo peels at 10% solid-to-liquid ratio using 80% ethanol at 80 °C. All of the filtrate was collected and centrifuged at 13000 rpm for 10 min and then analyzed for sugars by using HPLC. The contents of cellulose, hemicellulose, lignin, and ash in pomelo peels were determined in accordance with the standardized methods of the National Renewable Energy Laboratory (NREL, Golden, CO, USA).[31] Pectin content was determined by sequential extraction of water (60 °C, 2 h, two times), 0.5% oxalate ammonium (60 °C, 2 h, two times), and 0.05 M HCl (80 °C, 1 h).[32] The extracts were recovered by filtration and precipitated by ethanol with 4 times volume, respectively. The resulting pectin were then dried and weighed. D-Limonene content in pomelo peels was estimated using the Scott oil method.[33]

Sugars, such as glucose, xylose, galactose, and arabinose, were quantified by a HPLC system (Agilent, USA) using a refractive index detector and Aminex HPX-87P column (Bio-Rad, Hercules, CA, USA) at 85 °C with ultrapure water as the mobile phase at a flow rate of 0.8 mL min^{-1}. Peaks were detected and quantified on the basis of the area and retention time of the sugar standards (e.g., sucrose, glucose, fructose, arabinose, galactose, xylose, and rhamnose). Ethanol and galacturonic acid were determined by HPLC equipped with a refractive index detector on an Aminex HPX-87H column (Bio-Rad) at 65 °C. The mobile phase was 0.005 mol L^{-1} sulfuric acid, and the flow rate was 0.6 mL min^{-1}. All of the samples were centrifuged and filtered through 0.45 μm membranes.

The activities of GC220 and Multifect pectinase were determined on the basis of the different substrates because both of them contain many different enzymes. Cellulase and β-glucosidase activities of enzymes were determined using filter paper and cellobiose as substrate, respectively, according to the methods suggested by Ghose.[34] Xylanase and pectinase activities (U mL^{-1}, 1 U = 1 μmol min^{-1} of substrate converted) of enzymes were assayed using birchwood xylan and polygalacturonic acid as substrate, respectively, as previously described.[35,36] The protein content in enzyme solution was measured using Bradford's method with bovine serum albumin as the standard.[37] Each datum was represented as the mean of three replicate analyses. Especially, cellulase activity (FPU mL^{-1}) and β-glucosidase activity (CBU mL^{-1}) were given by[34]

$$\text{cellulase activity} = \frac{0.37}{[\text{enzyme}]\ \text{releasing 2.0 mg of glucose}}\ \text{FPU mL}^{-1} \quad (1)$$

$$\beta\text{-glucosidase activity} = \frac{0.0926}{[\text{enzyme}]\ \text{releasing 1.0 mg of glucose}}\ \text{CBU mL}^{-1} \quad (2)$$

where [enzyme] represents the proportion of original enzyme solution present in the directly tested enzyme dilution.

RESULTS AND DISCUSSION

Chemical Composition of Pomelo Peel. We have determined the chemical composition of raw pomelo peel and its compositional changes after hydrothermal treatment. As shown in Figure 1, raw pomelo peel consists of cellulose

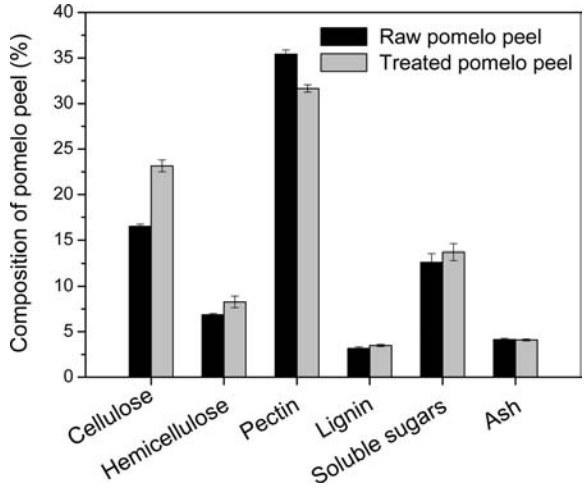

Figure 1. Compositional change of pomelo peel after hydrothermal treatment. Treatment conditions: solid loading 10% (w/v), 50 mM sodium acetate buffer (pH 4.8), 120 °C, 15 min.

(16.5%, based on dry matter), hemicellulose (6.86%), pectin (35.42%), lignin (3.16%), soluble sugars (12.62%), and ash (4.14%). Especially, the soluble sugars in ethanol extract are mainly composed of glucose (5.6% of dry matter) and fructose (6.9%). After treatment, the overall weight loss of solid components is 29.88%. Compositional analysis shows that the pectin content decreased to 31.65%, indicating the partial hydrolysis of pectin during the treatment. On the basis of the change in soluble sugars contents (12.62 vs 13.71%, Figure 1) and overall weight loss of solid components, we found that 23.8% of soluble sugars were released from solid fractions to liquid phase. In addition, cellulose and hemicellulose, generally, are difficult to be degraded during the treatment process (120 °C, 15 min). Their content in residual solid increased to 23.14 and 8.27% after treatment, respectively, remaining 98.2 and 84.4% of their initial weight in raw materials. In general, no significant change in chemical composition of pomelo peel was found during the hydrothermal treatment.

Enzymatic Hydrolysis of Pomelo Peel via Multi-enzyme Complex. In this study, two commercial enzymes, namely, GC220 and Multifect pectinase, were used to hydrolyze the pomelo peel waste. Protein concentrations and specific activities of the enzymes are presented in Table 2. GC220 has a high cellulase activity of 123 FPU mL^{-1}, and Multifect pectinase has a high pectinase activity of 597.4 U mL^{-1}. Both of them have β-glucosidase and xylanase activities, which are sufficient to degrade cellobiose and xylan, making the addition of β-glucosidase and xylanase for this hydrolysis process unnecessary. When the cellulase and pectinase loadings

Table 2. Protein Concentrations and Specific Activities of Enzymes

enzyme	protein concn (mg mL^{-1})	cellulase (FPU mL^{-1})	β-glucosidase (CBU mL^{-1})	xylanase (U mL^{-1})	pectinase (U mL^{-1})
GC220	64.9	123	74.5	908.6	0.1
Multifect pectinase	23.8	0.1	232.1	207.1	597.4

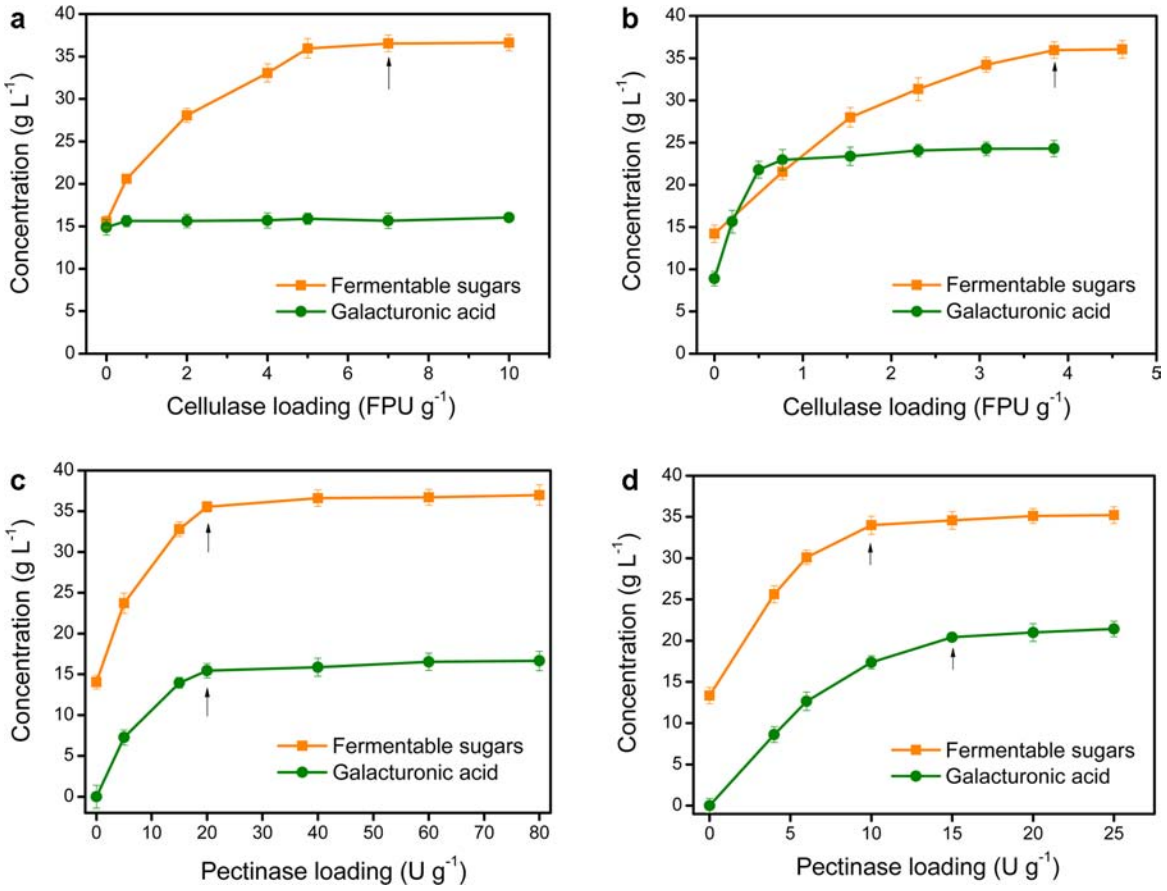

Figure 2. (a, b) Effect of cellulase loading on the release of fermentable sugars and galacturonic acid from raw pomelo peel (a) and treated pomelo peel (b) at 10% (w/v) solid concentration. Other default conditions unless otherwise noted: pectinase 20 U g^{-1}, pH 4.8, 50 °C, 150 rpm, 24 h. (c, d) Effect of pectinase loading on the release of fermentable sugars and galacturonic acid from raw pomelo peel (c) and treated pomelo peel (d) at 10% (w/v) solid concentration. Other default conditions unless otherwise noted: cellulase 3.8 FPU g^{-1}, pH 4.8, 50 °C, 150 rpm, 24 h.

were 3.8 FPU g^{-1} and 15 U g^{-1}, respectively, the hydrolysate after 24 h of reaction at 5% solid loading contained glucose (13.7 g L^{-1}), fructose (5.9 g L^{-1}), galactose (2.6 g L^{-1}), rhamnose (1.0 g L^{-1}), xylose (1.0 g L^{-1}), arabinose (1.3 g L^{-1}), and galacturonic acid (10.8 g L^{-1}). To calculate the sugars content for ethanol production, we defined the sum of glucose, fructose, galactose, and rhamnose as fermentable sugars, which can be transformed into ethanol by *S. cerevisiae*.

Figure 2 shows the effect of cellulase and pectinase loading on the release of fermentable sugars and galacturonic acid from pomelo peel at a 10% solid concentration. When the pectinase loading was 20 U g^{-1}, the concentrations of fermentable sugars increased with increasing cellulase loading for both untreated and treated pomelo peel (Figure 2a,b). The sugars concentration was measured at about 15 g L^{-1} only by using pectinase alone (zero points in Figure 2a,b). The increased fermentable sugars after cellulase addition are mainly attributed to the release of glucose from cellulose chains on the basis of the HPLC results (data not shown). In the case of treated pomelo peel, 3.8 FPU g^{-1} cellulase loading can produce a high sugar concentration (~36 g L^{-1}), and this loading is lower than that for raw pomelo peel (~7 FPU g^{-1}) to produce the same sugar concentration. In addition, the treated pomelo peel has a higher galacturonic acid concentration than raw pomelo peel (23 vs 15 g L^{-1}) at a low cellulase loading (e.g., 1 FPU g^{-1}). Generally, galacturonic acid is localized in pectic fractions of citrus peels.[38] Higher galacturonic acid concentration suggests that hydrothermal treatment together with cellulose degradation may allow pectinase to become more accessible to pectin and thus improve its hydrolysis.

The changes in the concentration of fermentative sugars and galacturonic acid with increasing pectinase loading are shown in Figure 2c,d, and the cellulase loading was kept at 3.8 FPU g^{-1}. When cellulase was used alone, the sugars concentration was about 14 g L^{-1} (zero points in Figure 2c,d), which mainly resulted from cellulose and hemicellulose. As the pectinase loading was increased to 20 U g^{-1}, the sugar concentration for raw pomelo peel increased to about 35 g L^{-1} (Figure 2c). It is noted that the same concentration can be reached using a lower enzyme loading of 10 U g^{-1} for pretreated pomelo peel sample (Figure 2d). The higher sugar concentration after pectinase addition is attributed to the release of glucose and galactose in pectin-branched chains, as well as the enhanced hydrolysis of cellulose and hemicellulose. On the other hand, the

concentration of galacturonic acid was directly correlated with pectinase loading. For raw and pretreated pomelo peel, the saturated pectinase dosages were 20 and 15 U g^{-1} respectively. These results indicate that the application of hydrothermal treatment could significantly reduce the use of cellulase (from 7 to 3.8 FPU g^{-1}) and pectinase (from 20 to 10 U g^{-1}). This treatment process, combined with a multienzyme complex, could further improve the hydrolysis of pectin and cellulose, leading to high concentrations of fermentative sugars (from 14 to 36 g L^{-1}) and galacturonic acid (from 9 to 23 g L^{-1}).

Enzymatic Hydrolysis of Pomelo Peel at High Solid Loadings. High concentrations of fermentable sugars are often required to obtain high ethanol concentrations. A promising approach to increase sugar concentrations involves the operation of enzymatic hydrolysis at high solid loadings. For pomelo peel, when the solid loading exceeded 14%, almost all of the buffer solution was absorbed. The high viscosity will prevent efficient mixing and mass transfer, resulting in more power consumption, poor solid and enzyme distribution, and localized product buildup. In this work, we investigated the enzymatic hydrolysis of pretreated pomelo peel over the solid loading range of 5−14%. As shown in Figure 3, the final

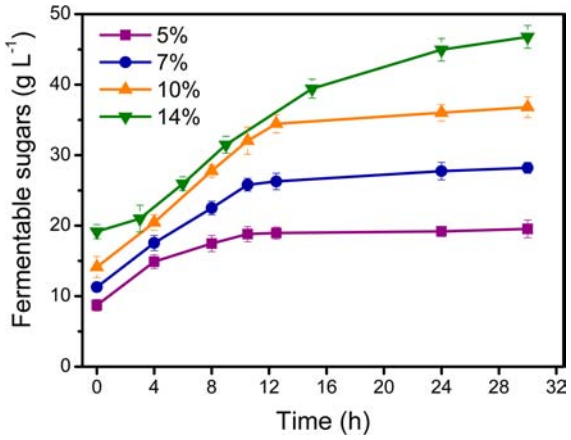

Figure 3. Time course of the release of fermentable sugars from pretreated pomelo peel at different solid loadings. Conditions: cellulase 3.8 FPU g^{-1}, pectinase 15 U g^{-1}, pH 4.8, 50 °C, 150 rpm.

concentrations of fermentable sugar obtained after 24 h of hydrolysis could reach 19, 28, 36, and 44 g L^{-1} at solid loadings of 5, 7, 10, and 14%, respectively. The hydrolysis rates were notably higher within the first 12 h of hydrolysis than at the later stage. The enzymatic hydrolysis could be nearly finished within 12 h when the solid loading was <10%. However, efficiency was reduced when the solid loading was at 14%, and >30 h was necessary for the entire hydrolysis reaction. The results suggest that high solid loading (e.g., 14%) could cause significant mass transfer limitation, leading to decreased hydrolysis efficiency. Therefore, in this case, a solid loading of 10% is appropriate for enzymatic hydrolysis of pomelo peel.

Ethanol Production from Pomelo Peel via a SSF Process. SSF is a promising process for ethanol production from lignocellulosic biomass due to its reduced catabolite repression, simplicity of operation, low capital investment, and improved process economics. In this study, we therefore employed SSF to produce ethanol using pectin-rich pomelo peel as substrate. Prior to the SSF process, a prehydrolysis operation was performed at 50 °C for 10 h with 3.8 FPU g^{-1} cellulase and 15 U g^{-1} pectinase loadings; the temperature was then reduced to 30 °C, and the yeast was added to initiate SSF process.

Previous studies had demonstrated that D-limonene in citrus wastes was toxic to yeast cells and thus reduced the alcoholic fermentation ability.[22] Therefore, citrus wastes are often required to remove D-limonene below inhibitory levels for yeasts prior to SSF. For example, steam explosion can be used to remove >90% of the D-limonene in citrus waste because it is highly volatile.[22] In this work, the hydrothermally treated pomelo peel contains 0.045% (v/w, of dry matter) D-limonene, which could lead to a maximum concentration of 0.0045% during the SSF process at a 10% solid loading. To determine the inhibition threshold amount of D-limonene to *S. cerevisiae*, we investigated the effect of initial concentration of D-limonene on ethanol production. The commercial D-limonene (97%) was added to pomelo peel at the beginning of SSF to achieve different D-limonene concentrations, ranging from 0.01 to 0.15% (v/v). As shown in Figure 4a, ethanol concentrations in fermentations decreased for initial D-limonene concentrations >0.06% (v/v). Because the D-limonene concentration in pomelo peel slurry (0.0045%) is much lower the critical value (0.06%), additional removal of D-limonene is not required in further study.

To obtain high alcoholic fermentation ability, two key operating parameters, the initial pH value and the yeast concentration, were optimized in this study. As shown in Figure 4b, the initial pH had a significant effect on both ethanol and galacturonic acid concentrations. Alcoholic fermentation at an initial pH of 4.5 produced the least ethanol. In this case, the final pH at the end of fermentation was 4.2. The result indicated that pH 4.2−4.5 greatly repressed yeast vitality and thus reduced the ethanol production. When the initial pH increased to 5.0 or 5.5, the final pH values in fermentation broth were 4.71 and 5.05, respectively. In both cases, we could obtain high ethanol concentrations within the pH range of 4.7−5.5. However, further increase of initial pH to ≥6.0 could reduce the ethanol yield. Meanwhile, we found that the galacturonic acid concentrations decreased as the pH increased, because pectinase is more effective at a lower pH (e.g., pH 4.5). Therefore, the initial pH of 5.0 is ideal for both *S. cerevisiae* and pectinase and was used in the following study.

A series of SSF experiments were further carried out using different dry yeast inoculations to determine the most appropriate yeast concentration. As shown in Figure 4c, when the yeast concentration was 2 g L^{-1}, 9.83 g L^{-1} ethanol was produced after 36 h of SSF process using 3.8 FPU g^{-1} cellulase and 15 U g^{-1} pectinase loadings. Final ethanol levels increased with increasing yeast concentration up to 5 g L^{-1}. When using 5 g L^{-1} yeast, we obtained 17.3 g L^{-1} ethanol product after 36 h of SSF. Nevertheless, as the yeast amount reached 6 g L^{-1}, the production rate and concentration of ethanol decreased. This finding can be explained by increased sugar consumption for cell growth under an oxygen circumstance and a large amount of seed.

During the SSF process, glucose, fructose, and galactose can be fermented to ethanol by *S. cerevisiae* cells (no sucrose was detected in the samples). The glucose consumption rate is higher than that of fructose and galactose.[26] The maximum concentration of fermentable sugars was 38.4 g L^{-1} at a 10% solid loading. A theoretical ethanol concentration of 19.6 g L^{-1} could be obtained if all fermentable sugars were fermented to ethanol. Using the optimized parameters as described before,

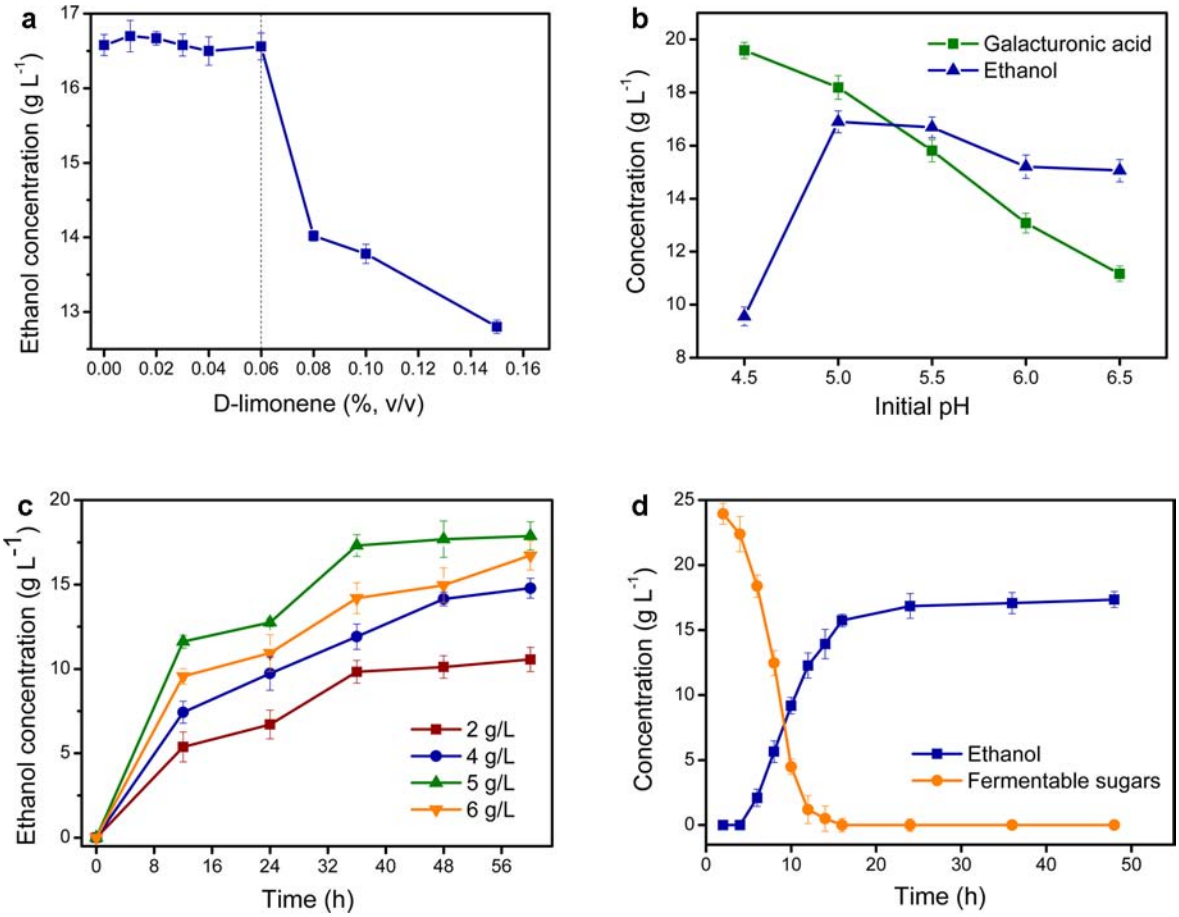

Figure 4. (a–c) Effects of initial D-limonene concentrations (a), pH values (b), and yeast concentrations (c) on ethanol production in the SSF process. (d) Time course of ethanol production and sugars consumption in the SSF process. Default conditions unless otherwise noted: (1) prehydrolysis conditions: cellulase 3.8 FPU g^{-1}, pectinase 15 U g^{-1}, pH 4.8, 50 °C, 150 rpm, 10 h; (2) SSF conditions: solid loading 10%, yeast 5 g L^{-1}, pH 5.0, 30 °C, 150 rpm, 48 h.

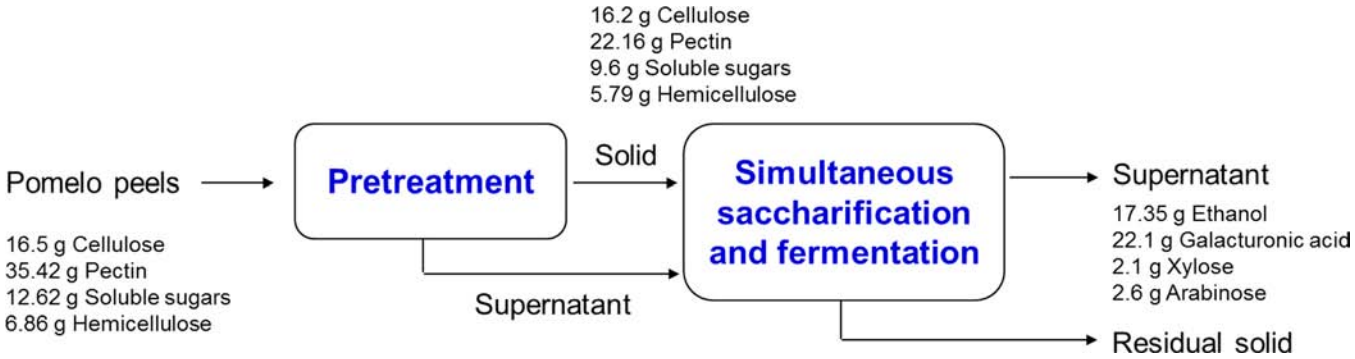

Figure 5. Mass flow for key components of pomelo peels during the hydrothermal pretreatment and SSF process. Pretreatment conditions: solid loading 10% (w/v), 50 mM sodium acetate buffer (pH 4.8), 120 °C, 15 min. SSF conditions: (1) prehydrolysis: 10% solid loading, cellulase 3.8 FPU g^{-1}, pectinase 15 U g^{-1}, pH 4.8, 50 °C, 150 rpm, 10 h; (2) SSF: yeast 5 g L^{-1}, pH 5.0, 30 °C, 150 rpm, 48 h.

17.35 g L^{-1} ethanol was obtained after 48 h of SSF (Figure 4d), accounting for 88.4% of the theoretical yield. Within the first 16 h, >90% of the total ethanol could be produced (the volumetric ethanol productivity is 0.98 g L^{-1} h^{-1}), which suggests that yeast cells may have utilized most of the sugars at this stage and then switched into stationary mode due to nutrient exhaustion and changes in environmental conditions in the medium. Figure 5 shows the mass flow for key components of pomelo peels during the hydrothermal pretreatment and SSF process. As shown in Figure 5, the main products are ethanol (17.35 g, equivalent to 34.02 fermentable sugars) and galacturonic acid (22.1 g), indicating that approximately 80.5% of the original components (cellulose, pectin, and soluble sugars) was transferred to product.

Ethanol Production via SSF with Batch and Fed-Batch Operation. For ethanol production, an important objective is to increase the final ethanol concentration, thus reducing the costs of downstream processing. Generally, operating SSF at high solid loadings is a promising way to increase ethanol concentrations. In this work, we investigated the ethanol

dx.doi.org/10.1021/jf405172a | J. Agric. Food Chem. 2014, 62, 4643–4651

production with batch operation at different solid loadings. As described before, the maximum solid loading for batch operation is 14% due to the high viscosity of pomelo peel slurry. The ethanol concentrations and yields at the solid loadings of 5−14% are shown in Figure 6. When the initial solid

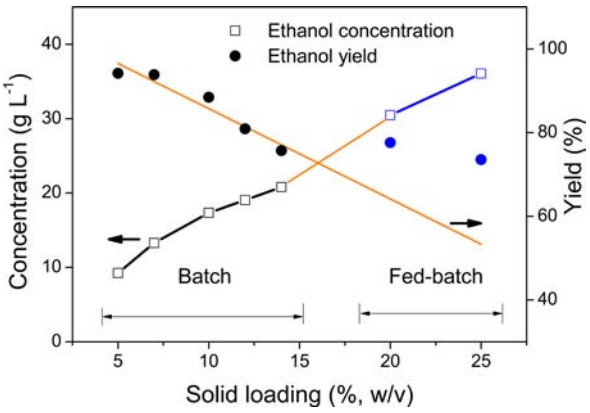

Figure 6. Final ethanol concentrations and yields in the batch (5−14% solid loading) and fed-batch SSF process. Final solid loadings of 20 and 25% were achieved by adding another 10 and 15% to the SSF system with an initial solid loading of 10%, as described under Materials and Methods. Other default conditions unless otherwise noted: (1) prehydrolysis: cellulase 3.8 FPU g^{-1}, pectinase 15 U g^{-1}, pH 4.8, 50 °C, 150 rpm, 10 h; (2) SSF: yeast 5 g L^{-1}, pH 5.0, 30 °C, 150 rpm, 48 h.

concentration is 5% (w/v), the ethanol concentration reached 9.24 g L^{-1}, being 94.2% of the theoretical concentration. At the highest solid loading (14%), we can obtain 20.8 g L^{-1} ethanol product. However, the ethanol yield decreased significantly from 94.2 to 75.7% with increasing solid loadings. The yields would further decrease if the solid loading was increased under batch operation. The worsened performance of yeast and enzymes should be mainly attributed to the lowered mass transfer efficiency (high viscosity). Additionally, the accumulation of yeast inhibitors, such as ethanol,[39,40] and D-limonene (Figure 4a),[22] at high solid loading could also limit the ethanol production.

To further increase the final ethanol concentration while avoiding an increase in viscosity, fed-batch operation by adding fresh substrate was used in the SSF process. As shown in Figure 6, on the basis of the initial solid concentration of 10%, an additional 10% of fresh substrate was added during the first 30 h. The final ethanol concentrations after 48 h increased to 30.45 g L^{-1}, which is nearly 2 times higher than that at 10% solid loading (17.35 g L^{-1}, Figure 6). The concentration could further increase to 36.06 g L^{-1} (the volumetric ethanol productivity is 0.75 g L^{-1} h^{-1}) at a 25% final solid loading via fed-batch operation. In these cases, the yields can reached 77.6 and 73.5%, respectively, which is close to that at 14% solid loading and much higher than the predicted value (at 25% solid loading) under batch operation. Our results demonstrated that use of the fed-batch mode could alleviate the technical problem, as mentioned before, which is caused by high loading of pomelo peel in the SSF process.

Previous studies had employed separate hydrolysis and fermentation (SHF) to produce ethanol from citrus wastes (e.g., orange peel[41,42]) hydrolysate. Although SHF could achieve high ethanol concentration, it has low volumetric ethanol productivity (e.g., 37−40 g L^{-1}, 0.50−0.55 g L^{-1} h^{-1};[41] 35−38 g L^{-1}, 0.42−0.8 g L^{-1} h^{-1}[42]). In this study, SSF with batch operation could obtain higher volumetric ethanol productivity (0.98 g L^{-1} h^{-1}) compared with the SHF process. However, batch SSF produces only 17.35 g L^{-1} ethanol due to the low sugar content in pomelo peel. Other citrus wastes and the mixed fruit wastes have higher sugar content and lower pectin content (Table 1); therefore, simple batch SSF could be used for ethanol production, achieving high ethanol concentration and high ethanol productivity (e.g., Kinnow waste and banana peel, 26.84 g L^{-1}, 0.56 g L^{-1} h^{-1};[43] citrus peel, 38.68 g L^{-1}, 1.61 g L^{-1} h^{-1};[22] Kinnow mandarin peel, 33.87 g L^{-1}, 2.82 g L^{-1} h^{-1};[27] Kinnow waste, 42 g L^{-1}, 3.5 g L^{-1} h^{-1}[26]). For pomelo peel, however, it is difficult to obtain high ethanol concentration in the batch SSF process, as mentioned before, due to the high viscosity at high solid loading. Here, we proposed fed-batch SSF strategy, combined with hydrothermal treatment and multienzyme formulation, to enhance the ethanol production, obtaining 36 g L^{-1} ethanol product as close to that from other citrus peels. Additionally, the fed-batch SSF had an ethanol productivity of 0.75 g L^{-1} h^{-1} within 48 h, which is higher than that in batch-SSF with 14 wt % solid loading (0.43 g L^{-1} h^{-1}, within 48 h).

In this study, *S. cerevisiae*, a robust yeast strain, was used to produce ethanol from pomelo peel. It presents many advantages, including high ethanol tolerance and favorable performance at relatively low pH and oxygen levels. However, *S. cerevisiae* has no ability to naturally ferment galacturonic acid and pentose sugars.[44] Citrus wastes, such as pomelo peel in this work, contain significantly large amounts of galacturonic acid. If galacturonic acid can be converted to ethanol, it would further increase the final ethanol concentration and thus increase the feasibility of these feedstocks for large-scale ethanol production. Whereas engineering *S. cerevisiae* to utilize galacturonic acid is a solution, it is still currently a challenge to develop efficiently engineered *S. cerevisiae* for ethanol production from galacturonic acid.[45] However, successful attempts have been made to ferment galacturonic acid to ethanol using recombinant bacteria, such as *Escherichia coli* KO11.[19,46] Therefore, these strains can be employed to utilize the galacturonic acid in the residual fermentation broth after SSF process.

In summary, we have developed an integrated strategy, incorporating hydrothermal treatment, multienzyme formulation, and fed-batch operation, to enhance ethanol production from pomelo peel. Hydrothermal treatment helped in partial hydrolysis of pectin and helped in reducing the use of cellulase and pectinase. Multienzyme complex was also proven to be effective in improving the hydrolysis of pretreated pomelo peel to fermentative sugars and galacturonic acid. Moreover, to overcome the drawback of low ethanol concentration, we employed fed-batch SFF to produce ethanol from pomelo peel, achieving 36 g L^{-1} ethanol product in good yield (73.5%) and ethanol productivity (0.75 g L^{-1} h^{-1}). The strategy demonstrated in our work, combined with subsequent galacturonic acid conversion, could open a new avenue for utilization of the abundant pectin-rich biomass available to produce ethanol.

AUTHOR INFORMATION

Corresponding Author

*(R.S.) E-mail: surx@tju.edu.cn. Phone: +86 22 27407799. Fax: +86 22 27407599.

Author Contributions

‖R.H. and M.C. contributed equally to this work.

Funding

We acknowledge the financial supports received from the National Natural Science Foundation of China (No. 21276192), the Ministry of Science and Technology of China (Nos. 2012BAD29B05 and 2013AA102204), Open Funding Project of the State Key Laboratory of Chemical Engineering (No. SKL-ChE-11B01), and the Ministry of Education (Nos. NCET-11-0372, 20110032130004, and B06006).

Notes

The authors declare no competing financial interest.

REFERENCES

(1) Food and Agriculture Organization of the United Nations. Medium-term prospects for agricultural commodities, http://www.fao.org/docrep/006/y5143e/y5143e12.htm.

(2) Siles Lopez, J. A.; Li, Q.; Thompson, I. P. Biorefinery of waste orange peel. *Crit. Rev. Biotechnol.* **2010**, *30*, 63−69.

(3) Lapuerta, M.; Hernandez, J. J.; Pazo, A.; Lopez, J. Gasification and co-gasification of biomass wastes: effect of the biomass origin and the gasifier operating conditions. *Fuel Process. Technol.* **2008**, *89*, 828−837.

(4) Tsai, H.-L.; Chang, S. K. C.; Chang, S.-J. Antioxidant content and free radical scavenging ability of fresh red pummelo *Citrus grandis* (L.) Osbeck juice and freeze-dried products. *J. Agric. Food Chem.* **2007**, *55*, 2867−2872.

(5) Khan, M. K.; Abert-Vian, M.; Fabiano-Tixier, A.-S.; Dangles, O.; Chemat, F. Ultrasound-assisted extraction of polyphenols (flavanone glycosides) from orange (*Citrus sinensis* L.) peel. *Food Chem.* **2010**, *119*, 851−858.

(6) Geerkens, C. H.; Schweiggert, R. M.; Steingass, H.; Boguhn, J.; Rodehutscord, M.; Carle, R. Influence of apple and citrus pectins, processed mango peels, a phenolic mango peel extract, and gallic acid as potential feed supplements on in vitro total gas production and rumen methanogenesis. *J. Agric. Food Chem.* **2013**, *61*, 5727−5737.

(7) Ting, S. V.; Deszyck, E. J. The carbohydrates in the peel of oranges and grapefruita. *J. Food Sci.* **1961**, *26*, 146−152.

(8) Pourbafrani, M.; McKechnie, J.; MacLean, H. L.; Saville, B. A. Life cycle greenhouse gas impacts of ethanol, biomethane and limonene production from citrus waste. *Environ. Res. Lett.* **2013**, *8*, DOI: 10.1088/1748-9326/8/1/015007.

(9) Zhang, M.; Wang, F.; Su, R.; Qi, W.; He, Z. Ethanol production from high dry matter corncob using fed-batch simultaneous saccharification and fermentation after combined pretreatment. *Bioresour. Technol.* **2010**, *101*, 4959−4964.

(10) Huang, R.; Su, R.; Qi, W.; He, Z. Understanding the key factors for enzymatic conversion of pretreated lignocellulose by partial least square analysis. *Biotechnol. Prog.* **2010**, *26*, 384−392.

(11) Zhang, M. J.; Su, R. X.; Li, Q.; Qi, W.; He, Z. M. Enzymatic saccharification of pretreated corn stover in a fed-batch membrane bioreactor. *BioEnergy Res.* **2010**, *4*, 134−140.

(12) Garlock, R. J.; Chundawat, S. P. S.; Balan, V.; Dale, B. E. Optimizing harvest of corn stover fractions based on overall sugar yields following ammonia fiber expansion pretreatment and enzymatic hydrolysis. *Biotechnol. Biofuels* **2009**, *2*, 29.

(13) Roche, C. M.; Dibble, C. J.; Stickel, J. J. Laboratory-scale method for enzymatic saccharification of lignocellulosic biomass at high-solids loadings. *Biotechnol. Biofuels* **2009**, *2*, 28.

(14) Yanase, H.; Miyawaki, H.; Sakurai, M.; Kawakami, A.; Matsumoto, M.; Haga, K.; Kojima, M.; Okamoto, K. Ethanol production from wood hydrolysate using genetically engineered *Zymomonas mobilis*. *Appl. Microbiol. Biotechnol.* **2012**, *94*, 1667−1678.

(15) Monavari, S.; Galbe, M.; Zacchi, G. The influence of solid/liquid separation techniques on the sugar yield in two-step dilute acid hydrolysis of softwood followed by enzymatic hydrolysis. *Biotechnol. Biofuels* **2009**, *2*, 6.

(16) Bals, B.; Rogers, C.; Jin, M.; Balan, V.; Dale, B. Evaluation of ammonia fibre expansion (AFEX) pretreatment for enzymatic hydrolysis of switchgrass harvested in different seasons and locations. *Biotechnol. Biofuels* **2010**, *3*, 1.

(17) Singh, A.; Bishnoi, N. R. Optimization of enzymatic hydrolysis of pretreated rice straw and ethanol production. *Appl. Microbiol. Biotechnol.* **2012**, *93*, 1785−1793.

(18) Mohnen, D. Pectin structure and biosynthesis. *Curr. Opin. Plant Biol.* **2008**, *11*, 266−277.

(19) Doran, J. B.; Cripe, J.; Sutton, M.; Foster, B. Fermentations of pectin-rich biomass with recombinant bacteria to produce fuel ethanol. *Appl. Biochem. Biotechnol.* **2000**, *84*−*6*, 141−152.

(20) Edwards, M. C.; Doran-Peterson, J. Pectin-rich biomass as feedstock for fuel ethanol production. *Appl. Microbiol. Biotechnol.* **2012**, *95*, 565−575.

(21) Grohmann, K.; Cameron, R. G.; Buslig, B. S. Fermentation of sugars in orange peel hydrolysates to ethanol by recombinant *Escherichia coli* KO11. *Appl. Biochem. Biotechnol.* **1995**, *51*−*2*, 423−435.

(22) Wilkins, M. R.; Widmer, W. W.; Grohmann, K. Simultaneous saccharification and fermentation of citrus peel waste by *Saccharomyces cerevisiae* to produce ethanol. *Process Biochem.* **2007**, *42*, 1614−1619.

(23) Pourbafrani, M.; Forgacs, G.; Horvath, I. S.; Niklasson, C.; Taherzadeh, M. J. Production of biofuels, limonene and pectin from citrus wastes. *Bioresour. Technol.* **2010**, *101*, 4246−4250.

(24) Widmer, W.; Zhou, W.; Grohmann, K. Pretreatment effects on orange processing waste for making ethanol by simultaneous saccharification and fermentation. *Bioresour. Technol.* **2010**, *101*, 5242−5249.

(25) Oberoi, H. S.; Vadlani, P. V.; Madl, R. L.; Saida, L.; Abeykoon, J. P. Ethanol production from orange peels: two-stage hydrolysis and fermentation studies using optimized parameters through experimental design. *J. Agric. Food Chem.* **2010**, *58*, 3422−3429.

(26) Oberoi, H. S.; Vadlani, P. V.; Nanjundaswamy, A.; Bansal, S.; Singh, S.; Kaur, S.; Babbar, N. Enhanced ethanol production from Kinnow mandarin (*Citrus reticulata*) waste via a statistically optimized simultaneous saccharification and fermentation process. *Bioresour. Technol.* **2011**, *102*, 1593−1601.

(27) Sandhu, S. K.; Oberoi, H. S.; Dhaliwal, S. S.; Babbar, N.; Kaur, U.; Nanda, D.; Kumar, D. Ethanol production from Kinnow mandarin (*Citrus reticulata*) peels via simultaneous saccharification and fermentation using crude enzyme produced by *Aspergillus oryzae* and the thermotolerant *Pichia kudriavzevii* strain. *Ann. Microbiol.* **2012**, *62*, 655−666.

(28) Boluda-Aguilar, M.; Garcia-Vidal, L.; Gonzalez-Castaneda, F. D.; Lopez-Gomez, A. Mandarin peel wastes pretreatment with steam explosion for bioethanol production. *Bioresour. Technol.* **2010**, *101*, 3506−3513.

(29) Wilkins, M. R.; Widmer, W. W.; Grohmann, K.; Cameron, R. G. Hydrolysis of grapefruit peel waste with cellulase and pectinase enzymes. *Bioresour. Technol.* **2007**, *98*, 1596−1601.

(30) Carpita, N. C.; Gibeaut, D. M. Structural models of primary cell walls in flowering plants: consistency of molecular structure with the physical properties of the walls during growth. *Plant J.* **1993**, *3*, 1−30.

(31) Sluiter, A.; Hames, B.; Ruiz, R.; Scarlata, C.; Sluiter, J.; Templeton, D.; Crocker, D. *Determination of Structural Carbohydrates and Lignin in Biomass*; Laboratory Analytical Procedure, NREL/TP-510-42618; National Renewable Energy Laboratory: Golden, CO, USA, 2008 (revised July 2011).

(32) Happi Emaga, T.; Robert, C.; Ronkart, S. N.; Wathelet, B.; Paquot, M. Dietary fibre components and pectin chemical features of peels during ripening in banana and plantain varieties. *Bioresour. Technol.* **2008**, *99*, 4346−4354.

(33) Scott, W. C.; Veldhuis, M. Rapid estimation of recoverable oil in citrus juices by bromate titration. *J. Assoc. Off. Anal. Chem.* **1966**, *49*, 628−633.

(34) Ghose, T. K. Measurement of cellulase activities. *Pure Appl. Chem.* **1987**, *59*, 257−268.

(35) Berlin, A.; Gilkes, N.; Kilburn, D.; Bura, R.; Markov, A.; Skomarovsky, A.; Okunev, O.; Gusakov, A.; Maximenko, V.; Gregg, D.; Sinitsyn, A.; Saddler, J. Evaluation of novel fungal cellulase

preparations for ability to hydrolyze softwood substrates − evidence for the role of accessory enzymes. *Enzyme Microb.Technol.* **2005**, *37*, 175−184.
(36) Semenova, M. V.; Grishutin, S. G.; Gusakov, A. V.; Okunev, O. N.; Sinitsyn, A. P. Isolation and properties of pectinases from the fungus *Aspergillus japonicus*. *Biochemistry (Moscow)* **2003**, *68*, 559−569.
(37) Bradford, M. M. A rapid and sensitive method for the quantitation of microgram quantities of protein utilizing the principle of protein-dye binding. *Anal. Biochem.* **1976**, *72*, 248−254.
(38) Grohmann, K.; Cameron, R. G.; Buslig, B. S. Fractionation and pretreatment of orange peel by dilute acid hydrolysis. *Bioresour. Technol.* **1995**, *54*, 129−141.
(39) Bezerra, R. F.; Dias, A. Enzymatic kinetic of cellulose hydrolysis: inhibition by ethanol and cellobiose. *Appl. Microbiol. Biotechnol.* **2005**, *126*, 49−59.
(40) Hoppe, G.; Hansford, G. Ethanol inhibition of continuous anaerobic yeast growth. *Biotechnol. Lett.* **1982**, *4*, 39−44.
(41) Wilkins, M.; Suryawati, L.; Maness, N.; Chrz, D. Ethanol production by *Saccharomyces cerevisiae* and *Kluyveromyces marxianus* in the presence of orange-peel oil. *World J. Microbiol. Biotechnol.* **2007**, *23*, 1161−1168.
(42) Grohmann, K.; Cameron, R.; Buslig, B. Fermentation of orange peel hydrolysates by ethanologenic *Escherichia coli*. In *Seventeenth Symposium on Biotechnology for Fuels and Chemicals*; Wyman, C., Davison, B., Eds.; Humana Press: Totowa, NJ, USA, 1996; Vol. 57/58, pp 383−388.
(43) Sharma, N.; Kalra, K. L.; Oberoi, H.; Bansal, S. Optimization of fermentation parameters for production of ethanol from Kinnow waste and banana peels by simultaneous saccharification and fermentation. *Indian J. Microbiol.* **2007**, *47*, 310−316.
(44) Huang, R.; Su, R.; Qi, W.; He, Z. Bioconversion of lignocellulose into bioethanol: process intensification and mechanism research. *BioEnergy Res.* **2011**, *4*, 225−245.
(45) van Maris, A. J. A.; Abbott, D. A.; Bellissimi, E.; van den Brink, J.; Kuyper, M.; Luttik, M. A. H.; Wisselink, H. W.; Scheffers, W. A.; van Dijken, J. P.; Pronk, J. T. Alcoholic fermentation of carbon sources in biomass hydrolysates by *Saccharomyces cerevisiae*: current status. *Antonie Van Leeuwenhoek* **2006**, *90*, 391−418.
(46) Richard, P.; Hilditch, S. D-Galacturonic acid catabolism in microorganisms and its biotechnological relevance. *Appl. Microbiol. Biotechnol.* **2009**, *82*, 597−604.
(47) Marin, F. R.; Soler-Rivas, C.; Benavente-Garcia, O.; Castillo, J.; Perez-Alvarez, J. A. By-products from different citrus processes as a source of customized functional fibres. *Food Chem.* **2007**, *100*, 736−741.

JOURNAL OF AGRICULTURAL AND FOOD CHEMISTRY

Article

pubs.acs.org/JAFC

Synthesis and Evaluation of Novel Acyl Derivatives from Jatropha Oil as Potential Lubricant Basestocks

Arukali Sammaiah, Korlipara V. Padmaja, and Rachapudi B. N. Prasad*

Centre for Lipid Research, CSIR−Indian Institute of Chemical Technology, Hyderabad 500007, Andhra Pradesh, India

ABSTRACT: A novel class of jatropha oil-based acylated derivatives from hydroxy alkyl esters of jatropha fatty acids (C_1, C_3, C_4, and C_8) and various anhydrides (C_2, C_3, C_4, and C_6) were synthesized and their physicochemical and lubricant properties reported. Jatropha fatty acid alkyl esters were dihydroxylated using the in situ performic acid method and further acylated with different anhydrides to produce acylated derivatives. Acylated derivatives of dihydroxy jatropha fatty acid alkyl esters were charaterized by NMR, FTIR, GC, and GC-MS analysis and were evaluated for their viscosity, viscosity index, pour and flash points, and oxidation stability. Most of the derivatives are either in ISO VG 22 or 32 viscosity grade with good viscosity index. It was observed that increase in acyl chain length and branching in the end-chain ester improved the pour point of the diacyl derivatives. All of the hexanoylated esters exhibited better oxidation stability compared to other acylated products, and their pour points are comparable to those of synthetic esters such as TMP trioleates. In general, isoalcohol esters with longer acyl chains showed promise as potential candidates for hydraulic fluids and metal-working fluids in ISO VG 22 and 32 viscosity range.

KEYWORDS: *jatropha oil, hydroxy fatty acid alkyl esters, acylated derivatives, viscosity index, pour point, oxidation stability*

INTRODUCTION

With increasing oil prices, global warming, and other environmental problems, the field of lubricants derived from nonpetrochemical feedstock has recently attracted a great deal of interest. Vegetable oils are considered to be one of the cheapest and most abundant biological sources available.[1] The use of vegetable oils as platform chemicals for biolubricant synthesis has numerous advantages, including inherent biodegradability and limited toxicity. In this context, increasing efforts have been focused on the use of vegetable oils as platform chemicals for the development of lubricant basestocks. On the other hand, vegetable oils exhibit poor oxidative stability[2,3] due to the presence of unsaturation. These active sites are highly susceptible to radical attack, and subsequently the molecules undergo oxidative degradation and form polar oxy compounds, which results in insoluble deposits and increase in oil acidity and viscosity. The functionalization at unsaturation with hydroxyl moieties through reactions involving the C−C double bonds is the most used methodology for the preparation of plant oil-derived lubricant basestocks.[4−14] Most of the work reported on acylated derivatives is based on edible oils such as soy and corn or nonedible oils such as milkweed, which are high-viscous fluids. Biolubricant basestocks have more demand for lower viscosity grades such as ISO VG 32 and 64. Therefore, with a view to develop lower viscosity grade base fluids, we have chosen a nonedible oil, namely, jatropha oil, as feedstock. *Jatropha curcus* (Linnaeus), a tropical, oilseed-bearing tree belonging to the Euphorbiaceae family, has attracted considerable attention as a potential source for biodiesel production. Jatropha oil is looked upon as one of the most appropriate renewable alternative sources not only for biodiesel but also for biolubricants.[15−17] In this study, we report the synthesis of different acylated derivatives of dihydroxy fatty acid alkyl esters (C_1−C_8; Scheme 1) from jatropha oil utilizing various acid anhydrides for acylation to study the effect of branching on the lubricant properties of the products.

MATERIALS AND METHODS

Materials. Jatropha oil (JO, iodine value = 92 mg I_2/g) was purchased from M/s Sanjeevani Herbal Heath Society (Hyderabad, India). Sodium hydroxide, hydrochloric acid (HCl), sulfuric acid, *p*-toluenesulfonic acid (*p*-TSA), propan-2-ol, butan-1-ol, 2-methylpropan-1-ol, 2-ethylhexan-1-ol, dimethylaminopyridine (DMAP), xylene, aqueous hydrogen peroxide (30%), formic acid (85%), acetic acid, acetic anhydride, sodium bicarbonate, and sodium sulfate were purchased from s.d.Fine-Chem Ltd. (Mumbai, India). Propionic, butyric, and hexanoic anhydrides were procured from Sigma-Aldrich (St. Louis, MO, USA). Hexane, methanol, and ethyl acetate were purchased from Industrial Solvents and Chemicals Pvt. Ltd. (Mumbai, India).

Methods. *Instrumental Analysis.* ^{1}H NMR spectra were obtained using a Bruker AR X 400 spectrometer (500, 300 MHz), and TMS was used as an internal standard. ^{13}C NMR spectra were recorded in $CDCl_3$ on a Varian spectrometer (75 MHz). IR spectra were recorded in chloroform on a PerkinElmer (Norwalk, CT, USA) model Spectrum BX FTIR spectrometer neat as thin film. The spectrum was recorded in absorbance mode.

The fatty acid composition was analyzed by using gas chromatograph 6890N series of Agilent making using an HP-1 column (30 m × 0.25 mm × 0.5 μm). The injector and flame ionization detector were at 300 °C. The oven temperature was programmed at 150 °C for 2 min and then increased to 300 °C at 10 °C/min. The carrier gas used was nitrogen at a flow rate of 1.5 mL/min. The GC-MS analysis was performed using an Agilent 6890 gas chromatograph with an HP-1 MS capillary column (30 m × 0.25 mm × 0.5 μm) connected to an Agilent 5973 mass spectrophotometer at 70 eV (*m*/*z* 50−600; source at 230 °C, and quadruple at 150 °C) in the EI mode. The oven temperature

Received: December 4, 2013
Revised: May 2, 2014
Accepted: May 5, 2014
Published: May 5, 2014

ACS Publications © 2014 American Chemical Society

Scheme 1. Synthesis of Acylated Derivatives of Dihydroxy Jatropha Fatty Acid Alkyl Esters

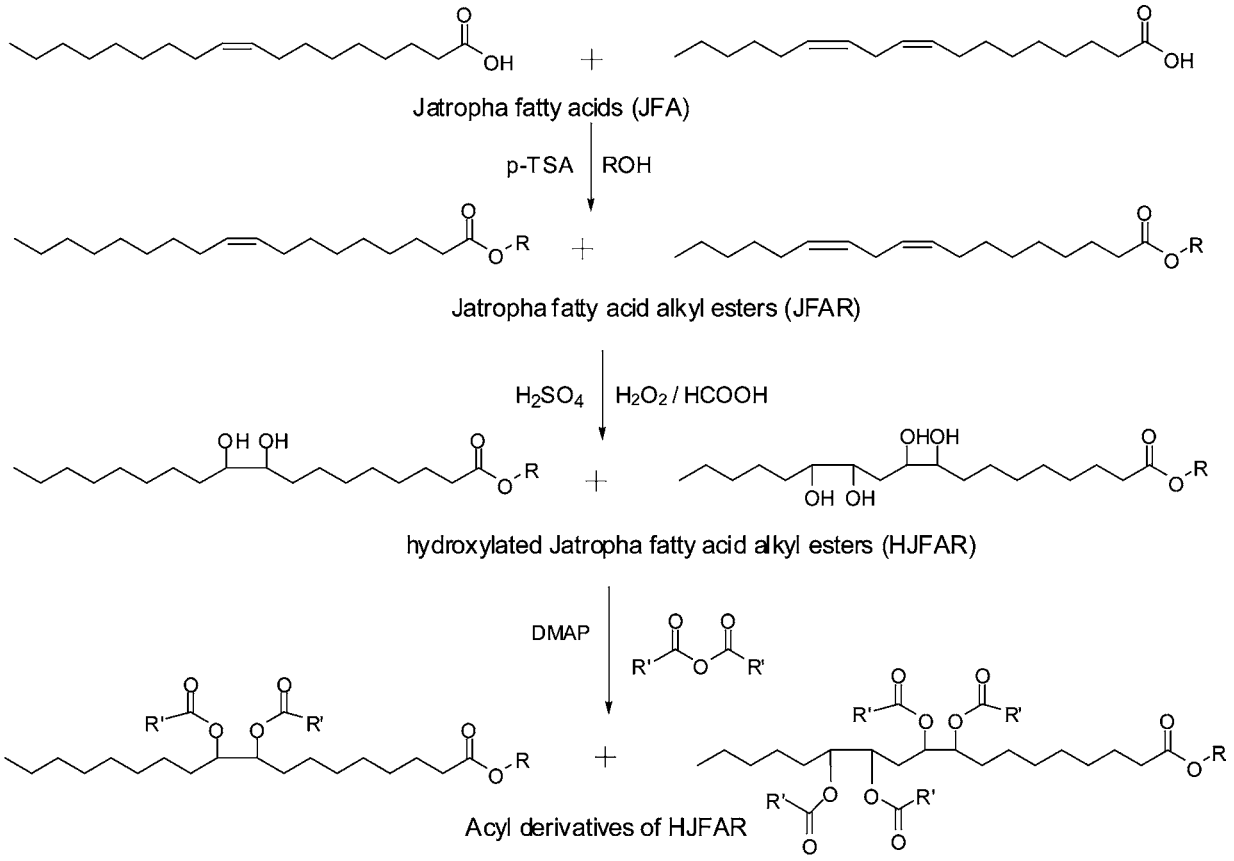

was programmed at 150 °C for 2 min, raised at 10 °C/min to 300 °C, and held for 20 min at 300 °C. The carrier gas used was helium at a flow rate of 1.0 mL/min.

The hydroxyl values of hydroxy and acylated jatropha fatty acid alkyl esters were determined as per the AOCS Cd 13-60 standard method. The iodine and acid values of products were determined as per the AOCS Cd 1-25 and Cd 3d-63 standard methods. Quantitative analysis was always carried out in three replicants.

Hydrolysis of Jatropha Oil. Jatropha oil (107.20 g, 0.12 mol) and sodium hydroxide (19.2 g, 0.48 mol) dissolved in 215 mL of distilled water were stirred mechanically for 6 h. The substrate and reagent were taken in 1:4 mol/mol ratio, and substrate to water was taken in 1:2 vol/vol ratio. The course of the reaction was monitored by TLC using the solvent system hexane/ethylacetae (90:10 v/v) until the complete disappearance of triglyceride. After completion of the reaction, the reaction mixture was acidified with concentrated HCl. The product was extracted in ethyl acetate and washed with water to remove excess HCl, and the solvent was evaporated to obtain 101.2 g of product.

Preparation of Jatropha Fatty Acid Alkyl Esters. Jatropha fatty acids (JFAs; 100 g, 0.37 mol), alcohol (0.74 mol), *p*-TSA (1 g based on 1% weight of JFA), and 150 mL of xylene were stirred at reflux under nitrogen atmosphere until a theoretical amount of water was collected. The crude product was distilled at 60−150 °C and 5 mmHg to remove excess alcohol and xylene. The resultant product was dissolved in hexane, washed with $NaHCO_3$ solution, filtered over Na_2SO_4, concentrated in vacuo, and dried under vacuum to afford alkyl esters of jatropha fatty acids. Short-chain alcohols were esterified without using xylene, H_2SO_4 for methyl esters and *p*-TSA for 2-propyl esters. The product was passed over basic alumina using hexane to recover the product having an acid value of <0.1.

Hydroxylation of Jatropha Fatty Acid Alkyl Esters. Jatropha fatty acid alkyl esters (110 g, 0.388 mol), formic acid (0.582 mol), and concentrated sulfuric acid (2% weight of formic acid and hydrogen peroxide) were taken into a three-necked round-bottom flask, and the temperature of the medium was maintained at 15 °C. Hydrogen peroxide solution, 30% concentration (1.164 mol), was added slowly to the contents under mechanical stirring at 15 °C for 1 h. After addition, the contents were stirred at 85 °C for 15 h. The final product was extracted with ethyl acetate and washed with water until it was acid free. The reaction was monitored hourly by oxirane value, hydroxyl value, and IR and gas chromatography studies. The formation of hydroxyl product was confirmed by IR, ^{1}H NMR, ^{13}C NMR, and GC and GC-MS studies after silylation of the hydroxyl product.

Hydroxy Jatropha Fatty Acid Methyl Esters. ^{1}H NMR ($CDCl_3$) δ 0.89 (t, $-CH_2-C\underline{H}_3$), 1.24−1.4 (m, $-C\underline{H}_2-CH_3$), 1.55−1.65 (m, $C\underline{H}_2-CH_2-CO-$), 2.27 (t, $-C\underline{H}_2-C{=}O$), 3.2−3.4 (m, $-C\underline{H}-OH$), 3.65 (s, $O-CH_3$); ^{13}C NMR ($CDCl_3$) δ 14 ($\underline{C}H_3-CH_2-$), 22−32.2 ($-CH_2-$), 34.3 ($-\underline{C}H_2-C{=}O$), 51.5 ($\underline{C}H_3O-C{=}O$), 74.2 ($-\underline{C}H-OH$), 174.5 ($-COO-$); IR (neat, cm^{-1}) 3445 (−OH), 2925 (C−H), 1743 (C=O), 1168 (C−C (=O)−O).

Hydroxy Jatropha Fatty Acid 2-Propyl Esters. ^{1}H NMR ($CDCl_3$) δ 0.88 (t, $-CH_2-C\underline{H}_3$), 1.21 (d, $-CH-(C\underline{H}_3)_2$), 1.24−1.4 (m, $-C\underline{H}_2-CH_3$), 1.56−1.65 (m, $C\underline{H}_2-CH_2-CO-$), 2.22 (t, $-CH_2-C{=}O$), 3.2−3.4 (m, $-C\underline{H}-OH$), 4.9−5.0 (m, $-C\underline{H}-O-C{=}O$); ^{13}C NMR ($CDCl_3$) δ 14 ($\underline{C}H_3-CH_2-$), 21.7 ($(\underline{C}H_3)_2-CH-$), 22.6−32.2 ($-CH_2-$), 34.5 ($-\underline{C}H_2-C{=}O$), 67.3 ($-\underline{C}HO-C{=}O$), 74.4 ($-\underline{C}H-OH$), 174.3 ($-COO-$); IR (neat, cm^{-1}) 3448 (−OH), 2925 (C−H), 1736 (C=O), 1112 (C−C(=O)−O).

dx.doi.org/10.1021/jf501388d | J. Agric. Food Chem. 2014, 62, 4652−4660

Hydroxy Jatropha Fatty Acid 1-Butyl Esters. ^{1}H NMR ($CDCl_3$) δ 0.88 (t, $-CH_2-CH_3$), 0.94 (t, $-CH_2-CH_3$), 1.24−1.4 (m, $-CH_2-CH_3$), 1.56−1.65 (m, CH_2-CH_2-CO-), 2.25 (t, $-CH_2-C=O$), 3.3−3.4 (m, $-CH-OH$), 4.03 (d, $-CH_2O-C=O$); ^{13}C NMR ($CDCl_3$) δ 13.6 (CH_3-CH_2-), 14 (CH_3-CH_2-), 19.1−31.8 ($-CH_2-$), 34.3 ($-CH_2-C=O$), 64.1 ($-CH_2O-C=O$), 74.5 ($-CH-OH$), 174 ($-COO-$); IR (neat, cm^{-1}) 3446 (−OH), 2925 (C−H), 1743 (C=O), 1172 (C−C(=O)−O).

Hydroxy Jatropha Fatty Acid 2-Methyl-1-propyl Esters. ^{1}H NMR ($CDCl_3$) δ 0.88 (t, $-CH_2-CH_3$), 0.93 (d, $-CH-(CH_3)_2$), 1.24−1.4 (m, $-CH_2-CH_3$), 1.56−1.65 (m, CH_2-CH_2-CO-), 1.93 (m, $-CH-(CH_3)_2$), 2.3 (t, $-CH_2-C=O$), 3.3−3.4 (m, $-CH-OH$), 3.85 (d, $-CH_2-O-C=O$); ^{13}C NMR ($CDCl_3$) δ 14 (CH_3-CH_2-), 19 (($CH_3)_2-CH-$), 22.6−32.2 ($-CH_2-$), 34.5 ($-CH_2-C=O$), 70.3 ($-CH-O-C=O$), 74.5 ($-CH-OH$), 173.5 ($-COO-$); IR (neat, cm^{-1}) 3445 (−OH), 2925 (C−H), 1742 (C=O), 1172 (C−C(=O)−O).

Hydroxy Jatropha Fatty Acid 2-Ethyl-1-hexyl Esters. ^{1}H NMR ($CDCl_3$) δ 0.88 (t, $-CH_2-CH_3$), 0.90 (t, $-CH_2-CH_3$), 1.24−1.4 (m, $-CH_2-CH_3$), 1.5−1.65 (m, CH_2-CH_2-CO-), 2.25 (t, $-CH_2-C=O$), 3.2−3.3 (m, $-CH-OH$), 3.95 (d, $-CH_2-O-C=O$); ^{13}C NMR ($CDCl_3$) δ 10.8 (CH_3-CH_2-), 14 (CH_3-CH_2-), 22.1−32.4 ($-CH_2-$), 38.5 ($-CH_2-C=O$), 66.5 ($-CHO-C=O$), 74.5 ($-CH-OH$), 174 ($-COO-$); IR (neat, cm^{-1}) 3446 (−OH), 2925 (C−H), 1741 (C=O), 1171 (C−C(=O)−O).

Acylation of Hydroxy Jatropha Fatty Acid Alkyl Esters. Hydroxylated jatropha fatty acid alkyl esters (100.1 g, 0.32 mol), alkanoic anhydride (0.8 mol), DMAP (0.1 g, 0.1% DMAP based on weight of hydroxylated jatropha fatty acid alkyl esters), and xylene (150 mL) were taken in a three-necked round-bottom flask and stirred at 140−150 °C for 6−8 h. The reaction was monitored by TLC using as solvent system hexane/ethyl acetae (90:10 v/v) and IR. The crude product was distilled at 140 °C and 5 mmHg to remove excess alkanoic anhydride and xylene. The residue was extracted with ethyl acetate and washed with water, filtered over Na_2SO_4, and concentrated in vacuo to obtain diacyl jatropha fatty acid alkyl esters. The product was further purified to remove traces of alkanoic acid by passage through a basic alumina column to obtain diacyl jatropha fatty acid alkyl esters with an acid value of <0.1. The product was confirmed by IR, ^{1}H NMR, ^{13}C NMR, and GC and GC-MS studies.

Acetylated Esters of Jatropha Fatty Acid Methyl Esters (AOJFAME). ^{1}H NMR ($CDCl_3$) δ 0.88 (t, $-CH_2-CH_3$), 1.24−1.4 (m, $-CH_2-CH_3$), 1.55−1.65 (m, CH_2-CH_2-CO-), 2.07 (s, $-CH_3-C=O$), 2.27 (t, $-CH_2-C=O$), 3.65 (s, $O-CH_3$), 4.9−4.96 (m, $-CH-O-C=O$); ^{13}C NMR ($CDCl_3$) δ 14 (CH_3-CH_2-), 20.5 ($CH_3-C=O$), 22.5−31.7 ($-CH_2-$), 33.5−35 ($-CH_2-C=O$), 51.5 ($CH_3O-C=O$), 73.5−75 ($-CH-O-C=O$), 170.3(CH_3-COO-), 174.1 ($-COO-CH_3$); IR (neat, cm^{-1}) 2928 (C−H), 1742 (C=O), 1172 (C−C (=O)−O).

Propionylated Esters of Jatropha Fatty Acid Methyl Esters (POJFAME). ^{1}H NMR ($CDCl_3$) δ 0.88 (t, $-CH_2-CH_3$), 1.16 (t, $-CO-CH_2-CH_3$), 1.24−1.35 (m, $-CH_2-CH_3$), 1.44−1.65 (m, CH_2-CH_2-CO-), 2.25 (t, $-CH_2-C=O$), 3.66 (s, $O-CH_3$), 4.93−4.98 (m, $-CH-O-C=O$); ^{13}C NMR ($CDCl_3$) δ 9.3 (CH_3-CH_2-), 14 (CH_3-CH_2-), 22.3−32.6 ($-CH_2-$), 33.8−35.2 ($-CH_2-C=O$), 51.4 ($CH_3O-C=O$), 73.3−74.8 ($-CH-O-C=O$), 173.9 (CH_2-COO-), 174.2 ($-COO-CH_3$); IR (neat, cm^{-1}) 2928 (C−H), 1740.5 (C=O), 1180 (C−C (=O)−O).

Butanoylated Esters of Jatropha Fatty Acid Methyl Esters (BOJFAME). ^{1}H NMR ($CDCl_3$) δ 0.88 (t, $-CH_2-CH_3$), 0.96 (t, $-CO-(CH_2)_2-CH_3$), 1.24−1.35 (m, $-CH_2-CH_3$), 1.44−1.65 (m, CH_2-CH_2-CO-), 2.26 (t, $-CH_2-C=O$), 3.64 (s, $O-CH_3$), 4.92−4.96 (m, $-CH-O-C=O$); ^{13}C NMR ($CDCl_3$) δ 13.6 (CH_3-CH_2-), 14 (CH_3-CH_2-), 18.5−32.1 ($-CH_2-$), 33.9−36.2 ($-CH_2-C=O$), 51.4 ($CH_3O-C=O$), 73.4−75.1 ($-CH-O-C=O$), 173.5 (CH_2-COO-), 174.1 ($-COO-CH_3$); IR (neat, cm^{-1}) 2928 (C−H), 1735 (C=O), 1176 (C−C (=O)−O).

Hexanoylated Esters of Jatropha Fatty Acid Methyl Esters (HOJFAME). ^{1}H NMR ($CDCl_3$) δ 0.88 (t, $-CH_2-CH_3$), 0.90 (t, $-CO-(CH_2)_4-CH_3$), 1.2−1.36 (m, $-CH_2-CH_3$), 1.42−1.64 (m, CH_2-CH_2-CO-), 2.28 (t, $-CH_2-C=O$), 3.64 (s, $O-CH_3$), 4.91−4.96 (m, $-CH-O-C=O$); ^{13}C NMR ($CDCl_3$) δ 13.8 (CH_3-CH_2-), 14 (CH_3-CH_2-), 22.2−32.2 ($-CH_2-$), 34.6−35.6 ($-CH_2-C=O$), 51.5 ($CH_3O-C=O$), 73.3−74.6 ($-CH-O-C=O$), 173.2 (CH_2-COO-), 174.1 ($-COO-CH_3$); IR (neat, cm^{-1}) 2928 (C−H), 1740 (C=O), 1171 (C−C (=O)−O).

Acetylated Esters of Jatropha Fatty Acid 2-Propyl Esters (AOJFAiPE). ^{1}H NMR ($CDCl_3$) δ 0.88 (t, $-CH_2-CH_3$), 1.21 (d, $-CH-(CH_3)_2$), 1.24−1.4 (m, $-CH_2-CH_3$), 1.56−1.65 (m, CH_2-CH_2-CO-), 2.04 (s, $-CH_3-C=O$), 2.2 (t, $-CH_2-C=O$), 4.92−4.98 (m, $-CH-O-C=O$); ^{13}C NMR ($CDCl_3$) δ 14 (CH_3-CH_2-), 21.7 (($CH_3)_2$ −CH−), 22.6−32.2 ($-CH_2-$), 34.5 ($-CH_2-C=O$), 34.5−35.2 ($-CH_2-C=O$), 67.15 (($H_3C)_2-CHO-C=O$), 73.5−75.2 ($-CH-O-C=O$), 170.3 (CH_3-COO-), 173.3 ($-COO-$); IR (neat, cm^{-1}) 2928 (C−H), 1730 (C=O), 1108 (C−C (=O)−O).

Propionylated Esters of Jatropha Fatty Acid 2-Propyl Esters (POJFAiPE). ^{1}H NMR ($CDCl_3$) δ 0.88 (t, $-CH_2-CH_3$), 1.16 (t, $-CO-CH_2-CH_3$), 1.21 (d, $-CH-(CH_3)_2$), 1.24−1.4 (m, $-CH_2-CH_3$), 1.56−1.65 (m, CH_2-CH_2-CO-), 2.25 (t, $-CH_2-C=O$), 4.93−4.98 (m, $-CH-O-C=O$); ^{13}C NMR ($CDCl_3$) δ 9.25 (CH_3-CH_2-), 14 (CH_3-CH_2-), 21.7 (($CH_3)_2$ −CH−), 22.6−32.2 ($-CH_2-$), 34.25−35.4 ($-CH_2-C=O$), 67.2 ($-CHO-C=O$), 73.5−75.2 ($-CH-O-C=O$), 173.3 ($-COO-$), 173.8 (CH_2-COO-); IR (neat, cm^{-1}) 2928 (C−H), 1734 (C=O), 1183 (C−C (=O)−O).

Butanoylated Esters of Jatropha Fatty Acid 2-Propyl Esters (BOJFAiPE). ^{1}H NMR ($CDCl_3$) δ 0.88 (t, $-CH_2-CH_3$), 0.96 (t, $-CO-(CH_2)_2-CH_3$), 1.21 (d, $-CH-(CH_3)_2$), 1.24−1.4 (m, $-CH_2-CH_3$), 1.56−1.65 (m, CH_2-CH_2-CO-), 2.2−2.36 (t, $-CH_2-C=O$), 4.93−4.99 (m, $-CH-O-C=O$); ^{13}C NMR ($CDCl_3$) δ 13.6 (CH_3-CH_2-), 14 (CH_3-CH_2-), 21.7 (($CH_3)_2$ −CH−), 18.6−32.02 ($-CH_2-$), 34.35−36.2 ($-CH_2-C=O$), 67.2 ($-CHO-C=O$), 73.3−74.8 ($-CH-O-C=O$), 172.5 (CH_2-COO-), 173.5 ($-COO-$); IR (neat, cm^{-1}) 2929 (C−H), 1729 (C=O), 1180 (C−C (=O)−O).

Hexanoylated Esters of Jatropha Fatty Acid 2-Propyl Esters (HOJFAiPE). ^{1}H NMR ($CDCl_3$) δ 0.88 (t, $-CH_2-CH_3$), 0.90 (t, $-CO-(CH_2)_4-CH_3$), 1.21 (d, $-CH-(CH_3)_2$), 1.24−1.4 (m, $-CH_2-CH_3$), 1.56−1.65 (m, CH_2-CH_2-CO-), 2.22 (t, $-CH_2-C=O$), 2.27 (t, $-CH_2-C=O$), 4.90−4.99 (m, $-CH-O-C=O$); ^{13}C NMR ($CDCl_3$) δ 13.8 (CH_3-CH_2-), 14 (CH_3-CH_2-), 21.7 (($CH_3)_2$ −CH−), 22.2−32.2 ($-CH_2-$), 33.90−35.5 ($-CH_2-C=O$), 67.15 ($-CHO-C=O$), 73.3−74.8 ($-CH-O-C=O$), 173.2 ($-COO-$); IR (neat, cm^{-1}) 2929 (C−H), 1734 (C=O), 1174 (C−C (=O)−O).

Acetylated Esters of Jatropha Fatty Acid 2-Methyl-1-Propyl Esters (AOJFAiBE). ^{1}H NMR ($CDCl_3$) δ 0.88 (t, $-CH_2-CH_3$), 0.93 (d, $-CH-(CH_3)_2$), 1.24−1.5 (m, $-CH_2-CH_3$), 1.56−1.65 (m, CH_2-CH_2-CO-), 1.93 (m, $-CH-(CH_3)_2$), 2.05 (s, $-CH_3-C=O$), 2.25 (t, $-CH_2-C=O$), 3.82 (d, $-CH_2O-C=O$), 4.92−4.96 (m, $-CH-O-C=O$); ^{13}C NMR ($CDCl_3$) δ 14 (CH_3-CH_2-), 19 (($CH_3)_2$ −CH−), 20.5 ($CH_3-C=O$), 22.5−31.7 ($-CH_2-$), 34.1−35.2 ($-CH_2-C=O$), 70.5 ($-CHO-C=O$), 73.7−75.2 ($-CH-O-C=O$), 170.3 (CH_3-COO-), 173.8 ($-COO-$); IR (neat, cm^{-1}) 2928 (C−H), 1740 (C=O), 1174 (C−C (=O)−O).

Propionylated Esters of Jatropha Fatty Acid 2-Methyl-1-propyl Esters (POJFAiBE). ^{1}H NMR ($CDCl_3$) δ 0.88 (t, $-CH_2-CH_3$), 0.93 (d, $-CH-(CH_3)_2$), 1.16 (t, $-CO-CH_2-CH_3$), 1.24−1.5 (m, $-CH_2-CH_3$), 1.56−1.65 (m, CH_2-CH_2-CO-), 1.93 (m, $-CH-(CH_3)_2$), 2.24−2.38 (m, $-CH_2-C=O$), 3.82 (d, $-CH_2O-C=O$), 4.92−4.98 (m, $-CH-O-C=O$); ^{13}C NMR ($CDCl_3$) δ 9.3 ($-CH_3$), 14 (CH_3-CH_2-), 19 (($CH_3)_2$ −CH−), 22.2−32.2 ($-CH_2-$), 34.3−35.5 ($-CH_2-C=O$), 70.5 ($-CHO-C=O$), 73.5−75.2 ($-CH-O-C=O$), 173.8 ($-COO-$), 173.95 (CH_2-COO-); IR (neat, cm^{-1}) 2929 (C−H), 1739 (C=O), 1182 (C−C (=O)−O).

Butanoylated Esters of Jatropha Fatty Acid 2-Methyl-1-propyl Esters (BOJFAiBE). ^{1}H NMR ($CDCl_3$) δ 0.88 (t, $-CH_2-CH_3$), 0.93 (d, $-CH-(CH_3)_2$), 0.96 (t, $-CO-(CH_2)_2-CH_3$), 1.24−1.5 (m, $-CH_2-CH_3$), 1.56−1.65 (m, CH_2-CH_2-CO-), 1.93 (m,

dx.doi.org/10.1021/jf501388d | J. Agric. Food Chem. 2014, 62, 4652−4660

−C<u>H</u>−$(CH_3)_2$), 2.24−2.27 (m, −C<u>H</u>$_2$−C=O), 3.82 (d, −C<u>H</u>$_2$O−C=O), 4.92−4.98 (m, −C<u>H</u>−O−C=O); ^{13}C NMR ($CDCl_3$) δ 13.6 (<u>C</u>H$_3$−CH$_2$−), 14 (<u>C</u>H$_3$−CH$_2$−), 19 ((<u>C</u>H$_3$)$_2$ −CH−), 22.4−32.2 (−CH$_2$−), 34.3−36.2 (−<u>C</u>H$_2$−C=O), 70.5 (−<u>C</u>HO−C=O), 73.3−75.2 (−<u>C</u>H−O−C=O), 173.15 (CH$_2$−<u>C</u>OO−), 173.8 (−<u>C</u>OO−); IR (neat, cm^{-1}) 2929 (C−H), 1736 (C=O), 1178 (C−C (=O)−O).

Hexanoylated Esters of Jatropha Fatty Acid 2-Methyl-1-propyl Esters (HOJFAiBE). ^{1}H NMR ($CDCl_3$) δ 0.88 (t, −CH$_2$−C<u>H</u>$_3$), 0.90 (t, −CO−(CH$_2$)$_4$−C<u>H</u>$_3$), 0.93 (d, −CH−(C<u>H</u>$_3$)$_2$), 1.24−1.5 (m, −C<u>H</u>$_2$−CH$_3$), 1.56−1.65 (m, C<u>H</u>$_2$−CH$_2$−CO−), 1.93 (m, −C<u>H</u>−(CH$_3$)$_2$), 2.24−2.32 (m, −C<u>H</u>$_2$−C=O), 3.82 (d, −C<u>H</u>$_2$O−C=O), 4.92−4.98 (m, −C<u>H</u>−O−C=O); ^{13}C NMR ($CDCl_3$) δ 13.8 (<u>C</u>H$_3$−CH$_2$−), 14 (<u>C</u>H$_3$−CH$_2$−), 19 ((<u>C</u>H$_3$)$_2$ −CH−), 22.15−32.2 (−CH$_2$−), 34.3−35.7 (−<u>C</u>H$_2$−C=O), 70.5 (−<u>C</u>HO−C=O), 73.3−75.2 (−<u>C</u>H−O−C=O), 173.35 (CH$_2$−<u>C</u>OO−), 173.8 (−<u>C</u>OO−); IR (neat, cm^{-1}) 2929 (C−H), 1738 (C=O), 1171 (C−C (=O)−O).

Acetylated Esters of Jatropha Fatty Acid 1-Butyl Esters (AOJFAnBE). ^{1}H NMR ($CDCl_3$) δ 0.88 (t, −CH$_2$−C<u>H</u>$_3$), 0.94 (t, −CH$_2$−C<u>H</u>$_3$), 1.22−1.5 (m, −C<u>H</u>$_2$−CH$_3$), 1.54−1.63 (m, C<u>H</u>$_2$−CH$_2$−CO−)m 2.05 (s, −C<u>H</u>$_3$−C=O), 2.25 (t, −C<u>H</u>$_2$−C=O), 4.05 (t, −C<u>H</u>$_2$−O−C=O), 4.92−4.98 (m, −C<u>H</u>−O−C=O); ^{13}C NMR ($CDCl_3$) δ 13.6 (<u>C</u>H$_3$−CH$_2$−), 13.85 (<u>C</u>H$_3$−CH$_2$−), 20.5 (<u>C</u>H$_3$−C=O), 18.9−32.4 (−CH$_2$−), 34.1−35.25 (−<u>C</u>H$_2$−C=O), 63.8 (−<u>C</u>H$_2$O−C=O), 73.4−75.1 (−<u>C</u>H−O−C=O), 170.2 (CH$_3$−<u>C</u>OO−), 173.5 (−<u>C</u>OO−); IR (neat, cm^{-1}) 2928 (C−H), 1740 (C=O), 1177 (C−C (=O)−O).

Propionylated Esters of Jatropha Fatty Acid 1-Butyl Esters (POJFAnBE). ^{1}H NMR ($CDCl_3$) δ 0.88 (t, −CH$_2$−C<u>H</u>$_3$), 0.94 (t, −CH$_2$−C<u>H</u>$_3$), 1.16 (t, −CO−CH$_2$−C<u>H</u>$_3$), 1.22−1.50 (m, −C<u>H</u>$_2$−CH$_3$), 1.54−1.64 (m, C<u>H</u>$_2$−CH$_2$−CO−), 2.22−2.38 (m, −C<u>H</u>$_2$−C=O), 4.05 (t, −C<u>H</u>$_2$−O−C=O), 4.92−5.0 (m, −C<u>H</u>−O−C=O); ^{13}C NMR ($CDCl_3$) δ 9.1 (CH−<u>C</u>H$_3$), 13.6 (<u>C</u>H$_3$−CH$_2$−), 13.95 (<u>C</u>H$_3$−CH$_2$−), 19.2−32.7 (−CH$_2$−), 34.2−35.7 (−<u>C</u>H$_2$−C=O), 63.8 (−<u>C</u>H$_2$O−C=O), 73.3−74.8 (−<u>C</u>H−O−C=O), 173.7 (−COO−); IR (neat, cm^{-1}) 2929 (C−H), 1739 (C=O), 1182 (C−C (=O)−O).

Butanoylated Esters of Jatropha Fatty Acid 1-Butyl Esters (BOJFAnBE). ^{1}H NMR ($CDCl_3$) δ 0.88 (t, −CH$_2$−C<u>H</u>$_3$), 0.94 (t, −CH$_2$−C<u>H</u>$_3$), 0.96 (t, −CO−(CH$_2$)$_2$−C<u>H</u>$_3$), 1.21−1.46 (m, −C<u>H</u>$_2$−CH$_3$), 1.55−1.67 (m, C<u>H</u>$_2$−CH$_2$−CO−), 2.21−2.28 (m, −C<u>H</u>$_2$−C=O), 4.05 (t, −C<u>H</u>$_2$−O−C=O), 4.92−4.98 (m, −C<u>H</u>−O−C=O); ^{13}C NMR ($CDCl_3$) δ 13.6 (<u>C</u>H$_3$−CH$_2$−), 13.95 (<u>C</u>H$_3$−CH$_2$−), 18.85−32.7 (−CH$_2$−), 35.2−36.8 (−<u>C</u>H$_2$−C=O), 63.8 (−<u>C</u>H$_2$O−C=O), 73.3−74.5 (−<u>C</u>H−O−C=O), 172.9 (CH$_2$−<u>C</u>OO−), 173.6 (−<u>C</u>OO−); IR (neat, cm^{-1}) 2930 (C−H), 1727 (C=O), 1178 (C−C (=O)−O).

Hexanoylated Esters of Jatropha Fatty Acid 1-Butyl Esters (HOJFAnBE). ^{1}H NMR ($CDCl_3$) δ 0.88 (t, −CH$_2$−C<u>H</u>$_3$), 0.95 (t, −CH$_2$−C<u>H</u>$_3$), 1.2−1.43 (m, −C<u>H</u>$_2$−CH$_3$), 1.56−1.65 (m, C<u>H</u>$_2$−CH$_2$−CO−), 2.21−2.33 (m, −C<u>H</u>$_2$−C=O), 4.05 (t, −C<u>H</u>$_2$−O−C=O), 4.92−4.99 (m, −C<u>H</u>−O−C=O); ^{13}C NMR ($CDCl_3$) δ 13.6 (<u>C</u>H$_3$−CH$_2$−), 13.95 (<u>C</u>H$_3$−CH$_2$−), 18.8−32.4 (−CH$_2$−), 34.3−35.7 (−<u>C</u>H$_2$; IR (neat, cm^{-1}) 2930 (C−H), 1734 (C=O), 1173 (C−C (=O)−O).

Acetylated Esters of Jatropha Fatty Acid 2-Ethyl-1-Hexyl Esters (AOJFAEHE). ^{1}H NMR ($CDCl_3$) δ 0.88 (t, −CH$_2$−C<u>H</u>$_3$), 0.90 (t, −CH$_2$−C<u>H</u>$_3$), 1.22−1.50 (m, −C<u>H</u>$_2$−CH$_3$), 1.54−1.64 (m, C<u>H</u>$_2$−CH$_2$−CO−), 2.05 (s, −C<u>H</u>$_3$−C=O), 2.25 (t, −C<u>H</u>$_2$−C=O), 3.95 (d, −C<u>H</u>$_2$−O−C=O), 4.91−4.97 (m, −C<u>H</u>−O−C=O); ^{13}C NMR ($CDCl_3$) δ 10.9 (<u>C</u>H$_3$−CH$_2$−), 14 (<u>C</u>H$_3$−CH$_2$−), 20.5 (<u>C</u>H$_3$−C=O), 22.7−32.1 (−CH$_2$−), 34.3−38.7 (−<u>C</u>H$_2$−C=O), 66.5 (−<u>C</u>HO−C=O), 73.7−75.2 (−<u>C</u>H−O−C=O), 170.5 (CH$_3$−<u>C</u>OO−), 173.8 (−<u>C</u>OO−); IR (neat, cm^{-1}) 2929 (C−H), 1732 (C=O), 1180 (C−C (=O)−O).

Propionylated Esters of Jatropha Fatty Acid 2-Ethyl-1-hexyl Esters (POJFAEHE). ^{1}H NMR ($CDCl_3$) δ 0.88 (t, −CH$_2$−C<u>H</u>$_3$), 1.14 (t, −CO−CH$_2$−C<u>H</u>$_3$), 1.22−1.48 (m, −C<u>H</u>$_2$−CH$_3$), 1.50−1.62 (m, C<u>H</u>$_2$−CH$_2$−CO−), 2.22−2.34 (m, −C<u>H</u>$_2$−C=O), 3.95 (d, −C<u>H</u>$_2$−O−C=O), 4.91−4.98 (m, −C<u>H</u>−O−C=O); ^{13}C NMR ($CDCl_3$) δ 9.05 (<u>C</u>H$_3$−), 10.9 (<u>C</u>H$_3$−CH$_2$−), 14 (<u>C</u>H$_3$−CH$_2$−), 22.1−32.2 (−CH$_2$−), 34.2−38.8 (−<u>C</u>H$_2$−C=O), 66.5 (−<u>C</u>HO−C=O), 73.3−75.1 (−<u>C</u>H−O−C=O), 173.8 (−COO−); IR (neat, cm^{-1}) 2929 (C−H), 1736 (C=O), 1182 (C−C (=O)−O).

Butanoylated Esters of Jatropha Fatty Acid 2-Ethyl-1-hexyl Esters (BOJFAEHE). ^{1}H NMR ($CDCl_3$) δ 0.89 (t, −CH$_2$−C<u>H</u>$_3$), 0.96 (t, −CO-(CH$_2$)$_2$−C<u>H</u>$_3$), 1.2−1.38 (m, −C<u>H</u>$_2$−CH$_3$), 1.40−1.68 (m, C<u>H</u>$_2$−CH$_2$−CO−), 2.23−2.34 (m, −C<u>H</u>$_2$−C=O), 3.95 (d, −C<u>H</u>$_2$−O−C=O), 4.93−4.98 (m, −C<u>H</u>−O−C=O); ^{13}C NMR ($CDCl_3$) δ 10.9 (<u>C</u>H$_3$−CH−), 13.5 (<u>C</u>H$_3$−CH$_2$−), 14 (<u>C</u>H$_3$−CH$_2$−), 18.4−32.4 (−CH$_2$−), 34.2−38.9 (−<u>C</u>H$_2$−C=O), 66.5 (−<u>C</u>HO−C=O), 73.0−74.7 (−<u>C</u>H−O−C=O), 173.0 (CH$_2$−<u>C</u>OO−), 173.8 (−<u>C</u>OO−); IR (neat, cm^{-1}) 2929 (C−H), 1734 (C=O), 1178 (C−C (=O)−O).

Hexanoylated Esters of Jatropha Fatty Acid 2-Ethyl-1-hexyl Esters (HOJFAEHE). ^{1}H NMR ($CDCl_3$) δ 0.90 (t, −CH$_2$−C<u>H</u>$_3$), 1.24−1.38 (m, −C<u>H</u>$_2$−CH$_3$), 1.43−1.65 (m, C<u>H</u>$_2$−CH$_2$−CO−), 2.24−2.35 (m, −C<u>H</u>$_2$−C=O), 3.95 (d, −C<u>H</u>$_2$−O−C=O), 4.92−4.98 (m, −C<u>H</u>−O−C=O); ^{13}C NMR ($CDCl_3$) δ 10.8 (<u>C</u>H$_3$−CH$_2$−), 14 (<u>C</u>H$_3$−CH$_2$−), 22.7−32.02 (−CH$_2$−), 34.2−38.4 (−<u>C</u>H$_2$−C=O), 66.6 (−<u>C</u>HO−C=O), 73.35−74.8 (−<u>C</u>H−O−C=O), 173.2 (CH$_3$−<u>C</u>OO−), 173.8 (−<u>C</u>OO−); IR (neat, cm^{-1}) 2930 (C−H), 1729 (C=O), 1174 (C−C (=O)−O).

Density. The density of the hydroxy products was measured following ASTM method D-4052. The measurements were carried out at 25 °C by using an Anton Paar DMA 4500 M density meter, and distilled water was used to verify the exact volume. The measurements were conducted three times for each sample, and the results were averaged.

Kinematic Viscosity. The kinematic viscosities were determined on a Cannon Constant Temperature Viscosity Bath (Cannon Instrument Co., State College, PA, USA) at 40 and 100 °C using a Cannon Fenske viscometer tubes per ASTM method D-445. The viscosity index (VI) was calculated from the kinematic viscosity data at 40 and 100 °C using ASTM method D-2270. Triplicate measurements were made, and the average values were reported.

Pour Point. The pour points of acylated products were measured per ASTM method D-97 with an accuracy of ±3 °C using on Automatic Pour Point Tester manufactured by Dott. Gianni Scavini & Co., Italy. Pour points were measured in 3 °C increments, and all the runs were carried out in duplicate.

Flash Point. Flash point of the products was measured per ASTM D-93 method using a Koehler Inc. apparatus. Duplicate measurements were made, and the average values were reported.

Rotating Pressurized Vessel Oxidation Test (RPVOT). Oxidation stability of acylated products was determined with RPVOT tests per ASTM test method D-2272. The experiments were carried out in the presence of copper catalyst at 150 °C and 5.0 mL of reagent grade water, and the vessel was sealed and charged with oxygen to 90 psi pressure.

RESULTS AND DISCUSSION

Jatropha oil containing oleic (45.7%) and linoleic (33%) acids as major fatty acids was converted into its corresponding fatty acids by a saponification route. Jatropha fatty acids (acid value, 193 mg KOH/g) were esterified with different alcohols, namely, methanol, propan-2-ol, butan-1-ol, 2-methylpropan-1-ol, and 2-ethylhexan-1-ol using H_2SO_4 for methyl esters and *p*-TSA for the other esters. The fatty acid esters were hydroxylated by using Prilezhaev dihydroxylation using in situ generated performic acid from hydrogen peroxide and formic acid. Synthesis of dihydroxy jatropha fatty acid alkyl esters was done in a single step, without isolating the intermediate epoxide, and they were analyzed for their physicochemical characteristics and chromatographic (GC, GC-MS) and spectral data. The low iodine value (1.2−1.8 g I_2/100 g) and higher hydroxyl values (195−220 mg KOH/g) of the esters indicated almost complete hydroxylation of fatty acid esters. Hydroxy alkyl esters were characterized using GC after silylation with *N*,*O*-bis(trimethylsilyl)trifluoroacetamide. The formation of the hydroxyl group was observed in the FTIR

dx.doi.org/10.1021/jf501388d | J. Agric. Food Chem. 2014, 62, 4652−4660

absorption at 3445−3463 cm^{-1} wavenumbers. The double-bond carbon was no longer detected at 3004 cm^{-1} in the products. ^{1}H NMR spectra of products exhibited the following peaks: 3.2−3.4 (−C<u>H</u>−OH), 2.25 ($-CH_2-C{=}O$), 1.60−1.2($-CH_2-$), and 0.85−0.93 ppm (CH_3). ^{13}C NMR confirmed the presence of the following groups: carbonyl at around 173−174.5 ppm, C_9 and C_{10} hydroxyl carbons at 74.2 and 75.5 ppm, $-CH_2-$ carbon over the range from 21.5 to 34.5 ppm, and terminal methyl carbon at 11−14 ppm.

The density and kinematic viscosities of the oil's hydroxylated esters from which the VI values were calculated are summarized in Table 1. Density and viscosity values were low for esters with branched alcohols and high for esters with straight-chain alcohols.

Table 1. Physicochemical Properties of Hydroxy Jatropha Fatty Acid Alkyl Esters

	hydroxy JFA esters				
	methyl	*n*-butyl	isopropyl	isobutyl	2-ethylhexyl
hydroxyl values (mg KOH/g)	220.13	224.46	220.46	222.52	195.37
iodine value	1.3	1.8	1.2	1.5	1.5
density 25 °C	0.9638	0.9367	0.9380	0.9374	0.9244
kinematic viscosity (cSt)					
40 °C	167.88	84.62	51.22	58.85	67.34
100 °C	15.02	9.86	6.94	7.66	8.81
viscosity index	87	95	89	92	103

In the second step, hydroxy alkyl esters were acylated with acetic, propionic, butyric, and hexanoic anhydrides. Reaction progress was monitored using FTIR for checking the disappearance of the O−H stretching band in the region of 3700−3100 cm^{-1} and by determination of the hydroxyl number. The prominent alkyl and carbonyl frequencies around 2940−2850 and 1740 cm^{-1}, respectively, indicated the substituent moieties' contributions to the spectra. The completion of reaction was confirmed by hydroxyl value (<2) of the products and also by their respective ^{1}H NMR and ^{13}C NMR spectra. New peaks at 4.91−4.98 ppm (protons at the point of substitution −CH−O−CO−R in the FA chain) appeared in all acylated products.

The FTIR spectra of the acylated products (Figure 1) did not exhibit hydroxy bands at 3447 cm^{-1} and a corresponding increase in the ester carbonyl at ∼1739 cm^{-1}, confirming more ester structures in the products. The FTIR spectra (Figure 1) of all these products have some common peaks at 2928 and 2856 cm^{-1} (methylene asymmetric stretching), 1465 cm^{-1} (CH_2 bending vibration), 1372 cm^{-1} (CH_3 symmetrical bending vibration), and 722 cm^{-1} (CH_2 rocking vibrations) and additional peaks at 1234, 1174, and 1106 cm^{-1} due to stretching vibrations of the C−O group in esters. Formation of the acylated products was also confirmed by the increase in peak intensity ratio 1465:1372 cm^{-1}. Also, the intensities of peaks such as 1739 (ester carbonyl) and 1174 cm^{-1} (C−O stretching of esters) relative to that of the 2928 cm^{-1} peak have increased in acylated products compared to starting materials (Figure 1). This is due to the increase in ester functionalities in the products. This trend was observed in spectra of all acylated

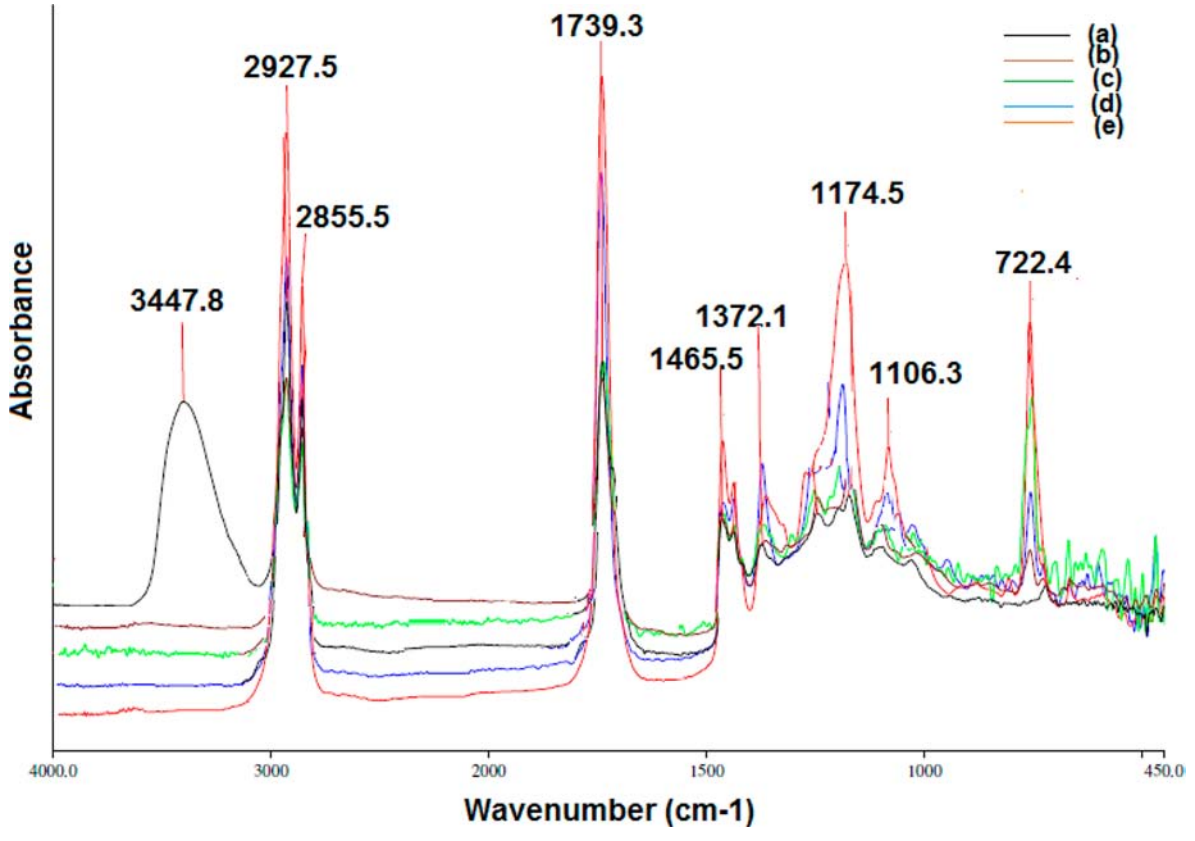

Figure 1. IR spectra of (a) hydroxy jatropha fatty acid methyl esters, (b) acetylated jatropha fatty acid methyl esters, (c) propionylated jatropha fatty acid methyl esters, (d) butanoylated jatropha fatty acid methyl esters, and (e) hexanoylated jatropha fatty acid methyl esters.

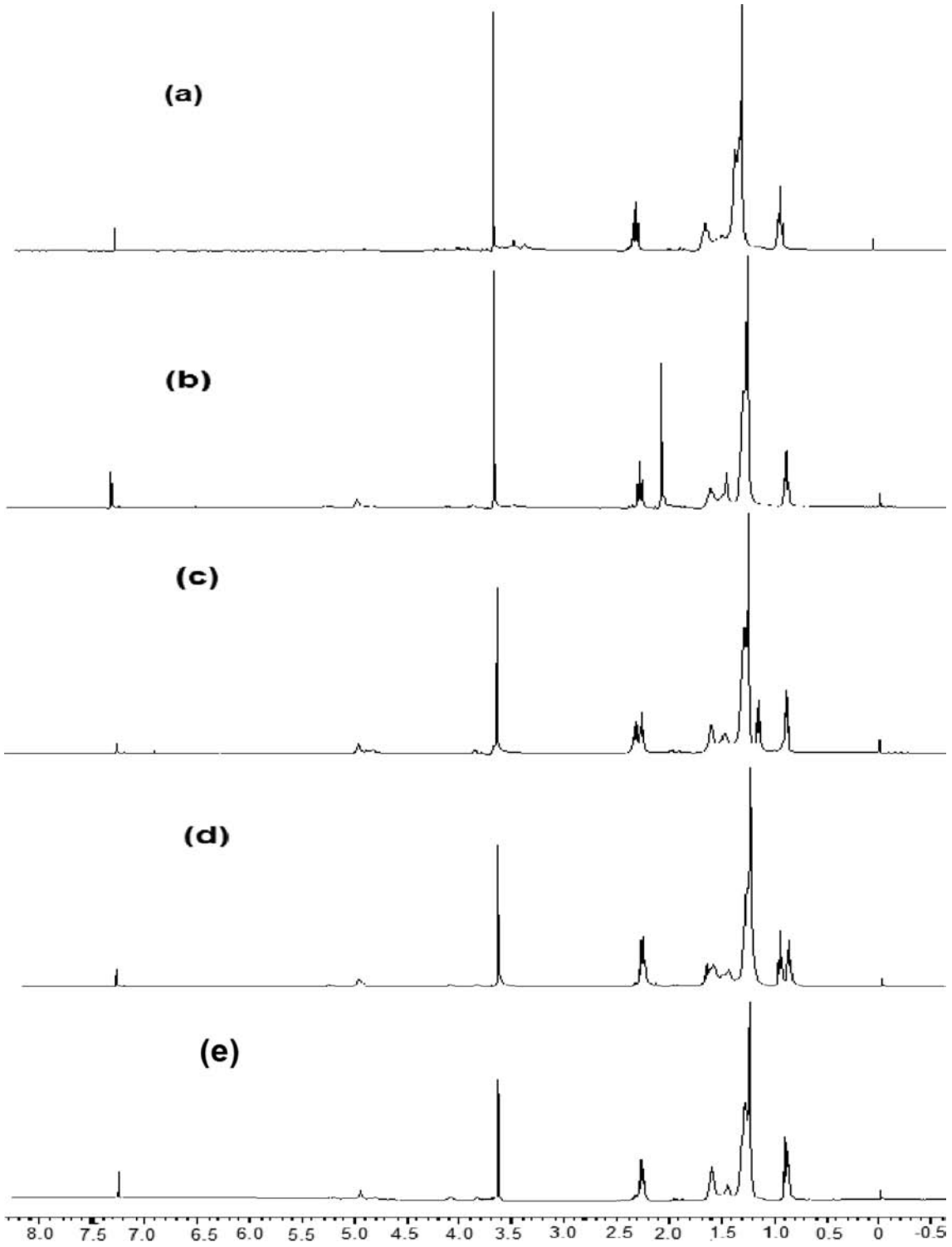

Figure 2. ^{1}H NMR spectra of (a) hydroxy jatropha fatty acid methyl esters, (b) acetylated jatropha fatty acid methyl esters, (c) propionylated jatropha fatty acid methyl esters, (d) butanoylated jatropha fatty acid methyl esters, and (e) hexanoylated jatropha fatty acid methyl esters.

products, confirming the formation of the acyl group in all of the products.

In the ^{1}H NMR spectra (Figure 2) the presence of additional peaks in acetylated products at 2.07 ppm is due to methyl protons of the $-COCH_3$ group and corresponding methyl carbons at 21.2 ppm, and carbonyl carbons at 170.3 ppm in ^{13}C NMR (Figure 3) confirm the formation of the acetoxy groups. Additional peaks also appeared at 2.23−2.36 ppm due to the $-CH_2$ protons α to the carbonyl group. The formation of propionylated products is confirmed by an increase in the area of the peak at 2.25−2.36 ppm due to CH_2 protons α to the carboxy group of the acyl side chain, the appearance of a new peak at 1.14−1.18 ppm due to methyl protons on the end of the acyl side chain, and the corresponding methyl carbon peak at 9.3 ppm in the ^{13}C NMR spectrum. The butanoylated products are confirmed by an increase in area of the peak at

dx.doi.org/10.1021/jf501388d | J. Agric. Food Chem. 2014, 62, 4652−4660

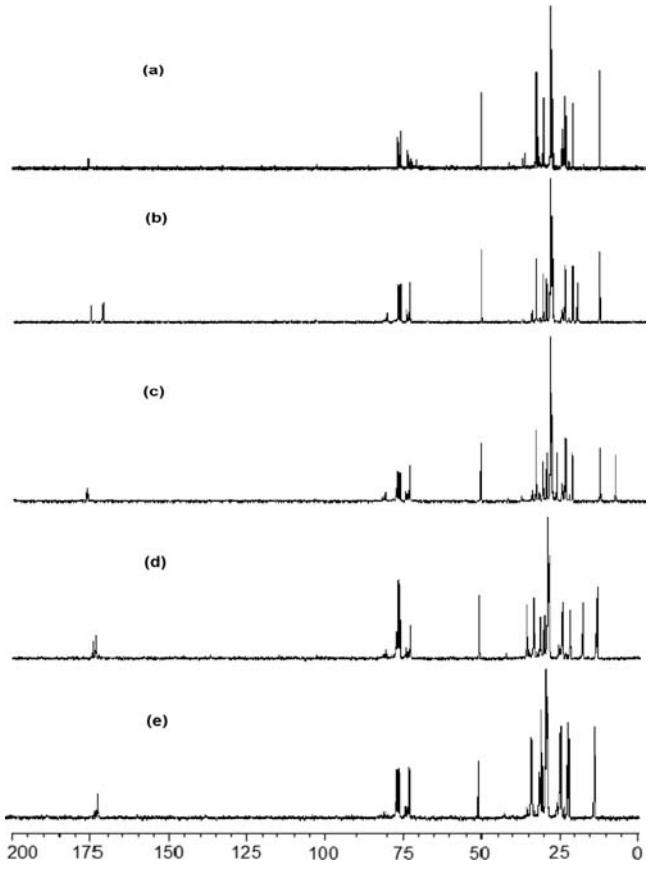

Figure 3. ^{13}C NMR spectra of (a) hydroxyl jatropha fatty acid methyl esters, (b) acetylated jatropha fatty acid methyl esters, (c) propionylated jatropha fatty acid methyl esters, (d) butanoylated jatropha fatty acid methyl esters, and (e) hexanoylated jatropha fatty acid methyl esters.

2.37−2.21 ppm due to CH_2 protons α to the carboxy group of the acyl side chain, the appearance of a new peak at 0.93−0.98 ppm due to CH_3 protons of the acyl side chain, and a new peak at 18.2 ppm in the ^{13}C NMR spectrum due to the CH_2 carbon α to the end carbon of the acyl side chain. The hexanyolated products are confirmed by an increase in the area of peaks at 2.25−2.32 ppm due to CH_2 protons α to carboxy group of acyl side chain and 0.93−0.98 ppm due to CH_3 protons of acyl side chain in their ^1H NMR spectra. In the ^{13}C NMR spectra, the appearance of a new peak at 34.4 ppm due to the CH_2 carbon α to the carboxy group of the acyl side chain confirms their formation. The peaks at 3.2−3.4 ppm in hydroxy products due to hydroxy protons in the −CHOH group are not present in acylated derivatives. Both the NMR and the infrared spectra of these acyl derivatives indicated the absence of residual hydroxyl groups in the acylated derivatives. The GC-MS spectra also indicated the absence of hydroxylated products indicating complete acylation of hydroxyl groups. Acylated derivatives were evaluated for their lubricant properties such as viscosity, viscosity index, pour and flash points, and oxidation stability by RPVOT test. The results are summarized in Table 2.

Kinematic Viscosity. Acylation of dihydroxylated products resulted in a reduction of kinematic viscosity at both 40 and 100 °C. The kinematic viscosity of acylated derivatives was found to be in the ranges of 19.45−30.06 cSt at 40 °C and 4.24−5.92 cSt at 100 °C as shown in Table 2. These ranges are lower than that of the original oil because of the difference in molecular size. Most of the acylated derivatives are found to be in the range of either ISO VG 22 or 32 viscosity grade and of hydraulic base fluids. Among the alkyl acylated derivatives 2-ethylhexyl esters with the longest chain length exhibited the highest observed viscosity relative to the other products. Viscosity attenuation was observed with an increase in chain length of the acyl chain up to C_4. This is due to the effect of branching in the chain, which tends to introduce sphericity in the molecule, causing attenuation in the viscosity.[14] Increase in viscosity in hexanoylated esters is in accord with the expectation that materials with longer chain lengths generally exhibit higher viscosities because of their extended sweep in the medium. Similar observations of the effect of branching on viscosity had been reported in branched polysaccharides,[18] branched synthetic polymers[19,20] and oligomerized estolides of oleic acid.[21] The viscosity index of hydroxylated jatropha fatty acid alkyl esters varied from 87 to 103. The VI value is increased (104−150) in the acylated derivatives. The VI of acylated products increased with increasing chain length of the acyl group. Even though the VI increased with the molecular weight of the acyl group, it decreased with branching. A similar trend was reported by Yao et al.[22] for ricinoleic acid-based acylated products. The VI values of the reported acylated derivatives are comparable to those of synthetic oils and superior to those of mineral oils.[23,24]

Table 2. Lubricant Properties of Acylated Derivatives of Jatropha Fatty Acid Alkyl Esters

	viscosity (cSt)					
sample	40 °C	100 °C	viscosity index	pour point (°C)	flash point (°C)	RPVOT (min)
JO	35.4	7.9	205	−6	186	5
AOJFAME	22.72	4.42	104	9	202	5
POJFAME	20.15	4.30	121	6	208	5
BOJFAME	19.45	4.24	125	6	210	5
HOJFAME	23.55	4.86	132	3	220	15
AOJFAiPE	22.86	4.46	106	0	210	10
POJFAiPE	20.83	4.41	123	0	210	10
BOJFAiPE	20.24	4.38	128	0	216	10
HOJFAiPE	24.02	4.97	136	−3	222	15
AOJFAiBE	25.74	4.92	116	0	216	10
POJFAiBE	23.78	4.87	129	0	220	10
BOJFAiBE	23.26	4.84	134	−3	226	10
HOJFAiBE	26.36	5.32	140	−3	230	15
AOJFAnBE	26.76	5.14	123	6	218	10
POJFAnBE	24.69	5.08	138	3	228	10
BOJFAnBE	24.20	5.06	142	3	230	10
HOJFAnBE	28.58	5.78	150	0	234	15
AOJFAEHE	28.72	5.36	122	−9	236	10
POJFAEHE	26.84	5.26	131	−12	244	10
BOJFAEHE	26.02	5.22	136	−12	248	10
HOJFAEHE	30.06	5.92	146	−15	254	15

Pour Point. Pour point measurement provides a good estimate of low-temperature fluidity of the lubricants. The pour points of acylated products were found to be in the range from 9 to −15 °C (Table 2). Acylated products esterified with straight-chain alcohols (methyl and *n*-butyl) exhibited higher pour points (from 9 to 0 °C). The basestocks with higher pour points are suitable for high-temperature and radiation resistance applications.[25] The pour point improved in the case of esters with isoalcohols such as 2-propyl, 2-methyl-1-propyl, and 2-

dx.doi.org/10.1021/jf501388d | J. Agric. Food Chem. 2014, 62, 4652−4660

ethyl-1-hexyl (from 0 to −15 °C) due to the presence of branching. The basestocks with low pour points are useful for machine tool and hydraulic systems applications.[25] All acylated products of 2-ethylhexyl esters exhibited low pour points. A similar trend was also reported by Erhan et al.[26] In general, isoalcohol esters with longer acyl chain lengths exhibited lower pour points.

Flash Point. Flash point measurement provides a good estimate of volatility and fire resistance of the lubricants. The flash point of acylated products was found to be in the range of 202−254 °C, which is observed to be much higher than that of the JO (Table 2). The flash points increased with increasing chain length of the end-chain ester group and the acyl group. All of the acylated products with flash point ≥165 °C lie well within the range of hydraulic oils.[27] High flash point ensures greater safety in the handling and storage of the fuel, which is a desirable requirement for lubricants.

Oxidation Stability. Oxidation stability is another important property that determines the lubricant's stability. The oxidation stability of acylated derivatives and JO obtained using the RPVOT method was found to be in the range of 5−15 min (Table 2). Acetylated, propionylated, and butanoylated methyl esters exhibited lower oxidation stability values (5 min) similar to that of JO, and hexanoylated derivatives exhibited higher values (15 min). No significant change was observed with increasing chain length of the end-chain ester group from C_3 to C_8. The oxidative stability of hexanoylated esters was found to be similar to that of synthetic esters such as TMP trioleate.[24]

In conclusion, we have synthesized a series of novel acyl derivatives from jatropha oil in two simple steps. In the first step we prepared different hydroxylated jatropha fatty acid alkyl esters by in situ generated performic acid method followed by their acylation with anhydrides of different chain lengths to prepare their acyl derivatives. Preliminary investigations on these products have shown that these are promising candidates for low-viscosity grade applications either as such or after formulations.

AUTHOR INFORMATION

Corresponding Author

*(R.B.N.P.) E-mail: rbnprasad@iict.res.in. Phone: +91 040 27193179. Fax: +91 040 27193370.

Funding

A.S. thanks the University Grants Commission (UGC), New Delhi, India, for financial support through a Senior Research Fellowship (SRF).

Notes

The authors declare no competing financial interest.

REFERENCES

(1) Biermann, U.; Friedt, W.; Lang, S.; Lühs, W.; Machmüller, G.; Metzger, J. O.; Rüsch gen Klaas, M.; Schäfer, H. J.; Schneider, M. P. New syntheses with oils and fats as renewable raw materials for the chemical industry. *Angew. Chem. Int. Ed.* **2000**, *39*, 2206−2224.

(2) Gapinski, R. E.; Joseph, I. E.; Layzell, B. D. A vegetable oil based tractor lubricant. *SAE Tech. Pap.* **1994**, *No. 941758*, 1−9.

(3) Becker, R.; Knorr, A. An evaluation of antioxidants for vegetable oils at elevated temperatures. *Lubr. Sci.* **1996**, *8* (2), 95−117.

(4) Harry-O'kuru, R. E.; Holser, R. A.; Abbott, T. P.; Weisleder, D. Synthesis and characterization of polyhydroxy triglycerides from milkweed oil. *Ind. Crops Prod.* **2002**, *15*, 51−58.

(5) Harry-O'kuru, R. E.; Carriere, C. J. Synthesis, rheological characterization and constitutive modeling of polyhydroxy triglycerides derived from milkweed oil. *J. Agric. Food Chem.* **2002**, *50*, 3214−3221.

(6) Harry-O'kuru, R. E.; Mohamed, A.; Xu, J.; Sharma, B. K. Synthesis and characterization of corn oil polyhydroxy fatty acids designed as additive agent for many applications. *J. Am. Oil Chem. Soc.* **2011**, *88*, 1211−1221.

(7) Dahlke, B.; Hellbardt, S.; Paetow, M.; Zech, W. H. Polyhydroxy fatty acids and their derivatives from plant oils. *J. Am. Oil Chem. Soc.* **1995**, *72*, 349−353.

(8) Adhvaryu, A.; Liu, Z.; Erhan, S. Z. Synthesis of novel alkoxylated triacylglycerols and their lubricant base oil properties. *Ind. Crops Prod.* **2005**, *21*, 113−119.

(9) Teeter, H. M.; Gast, L. E.; Bell, E. W.; Cowan, J. C. Synthetic lubricants from hydroxy stearic acids. *Ind. Eng. Chem.* **1953**, *45*, 1777−1779.

(10) Hwang, H.; Erhan, S. Z. Modification of epoxidized soybean oil for lubricant formulations with improved oxidative stability and low pour point. *J. Am. Oil Chem. Soc.* **2001**, *78*, 1179−1184.

(11) Sharma, B. K.; Adhvaryu, A.; Liu, Z.; Erhan, S. Z. Chemical modification of vegetable oils for lubricant applications. *J. Am. Oil Chem. Soc.* **2006**, *83*, 129−136.

(12) Sharma, B. K.; Liu, Z.; Adhvaryu, A.; Erhan, S. Z. One-pot synthesis of chemically modified vegetable oils. *J. Agric. Food Chem.* **2008**, *56*, 3049−3056.

(13) Hwang, H.; Adhvaryu, A.; Erhan, S. Z. Preparation and properties of lubricant basestocks from epoxidized soybean oil and 2-ethylhexanol. *J. Am. Oil Chem. Soc.* **2003**, *80*, 811−815.

(14) Harry-O'kuru, R. E.; Biresaw, G.; Cermak, S. C.; Gordon, S. H.; Vermillion, K. Investigation of some characteristics of polyhydroxy milkweed triglycerides and their acylated derivatives in relation to lubricity. *J. Agric. Food Chem.* **2011**, *59*, 4725−4735.

(15) Daniel, L.; Ardiyanti, A. R.; Schuur, B.; Manurung, R.; Broekhuis, A. A.; Heeres, H. J. Synthesis and properties of highly branched *Jatropha curcas* L. oil derivatives. *Eur. J. Lipid Sci. Technol.* **2011**, *113*, 18−30.

(16) Hafizah, N. A.; Salimon, J. Synthesis and characterization of ester trimethylolpropane based *jatropha curcas* oil as biolubricant base stocks. *J. Sci. Technol.* **2010**, *2*, 47−58.

(17) Ghazi, T. I. M.; Resul, M. F. M. G.; Syam, A. M.; Idris, A. Synthesis of biodegradable lubricant from jatropha oil with high content of free fatty acids. *Environmental Division Annual Meeting*; American Institute of Chemical Engineers: New York, 2008; pp 524−530.

(18) Whistler, R. L.; BeMiller, J. N. Factors influencing gum costs and application. In *Industrial Gums, Polysaccharides and Their Derivatives*; Whistler, R. L., Ed.; Academic Press: New York, 1959; pp 1−13.

(19) Jonsson, U. J. Lubrication of rolling element bearings with HFC-polyester mixtures. *Wear* **1999**, *232*, 185−191.

(20) Wood-Adams, P. The effect of long chain branches on the shear flow behavior of polyethylene. *J. Rheol.* **2001**, *45*, 203−210.

(21) Harry-O'kuru, R. E.; Isbell, T. A.; Weisleder, D. Synthesis of estolide esters from *cis*-9-octadecenoic acid estolides. *J. Am. Oil Chem. Soc.* **2001**, *78*, 219−222.

(22) Yao, L.; Hammond, E. G.; Wang, T.; Bhuyan, S.; Sundararajan, S. Synthesis and physical properties of potential biolubricants based on ricinoleic acid. *J. Am. Oil Chem. Soc.* **2010**, *87*, 937−945.

(23) Rudnick, L. R. Polyalphaolefins. In *Synthetics, Mineral Oils and Bio-Based Lubricants*; Rudnick, L. R., Ed.; CRC Press, Taylor & Francis Group: Boca Raton, FL, USA, 2006; pp 1−33.

(24) Mckeon, T. A.; Sharma, B. K.; Lin, J. T.; Erhan, S. Z.; Alander, J.; Gunstone, F. D. Non food uses of oils and fats. In *The Lipid Hand Book*; Gunstone, F. D., Harwood, J. L., Dijkstra, A. L., Eds.; CRC Press: New York, 2007; pp 615−620.

(25) Booser, E. R. Lubrication and lubricants. In *Kirk−Othmer Encyclopedia of Chemical Technology*, 4th ed.; Grant, M. H., Ed.;Wiley-Interscience: Chichester, UK, 1992; Vol. 15, pp 463−517.

(26) Erhan, S. Z.; Sharma, B. K.; Liu, Z.; Adhvaryu, A. Lubricant base stock potential of chemically modified vegetable oils. *J. Agric. Food Chem.* **2008**, *56*, 8919−8925.
(27) Tālis, P.; Karabeško, P.; Mieriņa, I.; Seržane, R.; Strēle, M.; Tupureina, V.; Jure, M. Composition of hydraulic fluids based on rapeseed oil and its derivatives. *Eng. Rural Dev. Jelgava* **2009**, 171−175.

JOURNAL OF AGRICULTURAL AND FOOD CHEMISTRY

Article

pubs.acs.org/JAFC

Combined Deacetylation and PFI Refining Pretreatment of Corn Cob for the Improvement of a Two-Stage Enzymatic Hydrolysis

Yuedong Zhang,[†,‡] Xindong Mu,[†] Haisong Wang,[†] Bin Li,*[,†] and Hui Peng*[,†]

[†]CAS Key Laboratory of Bio-based Materials, Qingdao Institute of Bioenergy and Bioprocess Technology, Chinese Academy of Sciences (CAS), Qingdao, Shandong 266101, People's Republic of China

[‡]University of Chinese Academy of Sciences, Beijing 100049, People's Republic of China

Supporting Information

ABSTRACT: A combined deacetylation and PFI refining pretreatment was applied to corn cob for the improvement of a two-stage enzymatic hydrolysis. In stage 1, the pretreated corn cob was first hydrolyzed by xylanase to produce xylo-oligosaccharides (XOS). In stage 2, the solid residue isolated from stage 1 was further hydrolyzed by cellulase and β-glucosidase. NaOH, Na_2CO_3, and $Ca(OH)_2$ were tested to remove acetyl groups in the process of deacetylation, and it was found that $Ca(OH)_2$ could be the most suitable alkali for deacetylation in this work. After deacetylation using 0.8 mmol of $Ca(OH)_2$/g of substrate and PFI refining, 50.5% xylan in the raw material could be hydrolyzed into XOS. The corresponding xylan yield of stage 1, the glucan yield of stage 2, and the total sugar yield (all sugars released in the hydrolyzate) after the two-stage enzymatic hydrolysis were 0.306, 0.305, and 0.661 g/g of corn cob, respectively.

KEYWORDS: *corn cob, deacetylation, PFI refining, enzymatic hydrolysis, pretreatment, xylo-oligosaccharides (XOS)*

INTRODUCTION

Xylo-oligosaccharides (XOS) are widely used as food and feed additives, which are considered soluble dietary fibers that have prebiotic activity, favoring the improvement of bowel and immune functions and having antimicrobial and other health benefits.[1] Currently, XOS are usually produced from the separated xylan or pretreated xylan-rich biomass through acidic or enzymatic hydrolysis.[2−7] Corn cob is an inexpensive and widely available resource of hemicellulose, which is usually chosen to produce XOS.[2−4,6] In comparison to the chemical technologies (e.g., acid hydrolysis), the enzymatic hydrolysis is a better route for the food industries, because no toxic and undesired byproducts, such as furfural, are generated during the enzymatic process.[1] However, the enzymatic substrates are mostly prepared by severe processes, which would not be friendly to the environment. Furthermore, the cellulose in the xylan-deprived corn cob residue should be used in a more economical and environmentally benign method.

For enzymatic hydrolysis of biomass, pretreatment is an important technology to alter the structure of cellulosic biomass to make cellulose/hemicellulose more accessible to enzymes.[8] Nowadays, most commercially promising pretreatment processes [e.g., dilute acid/alkali pretreatment,[9,10] steam explosion,[11] sulfite pretreatment to overcome recalcitrance of lignocellulose (SPORL) method,[12] etc.] are mainly aimed to remove the lignin or hemicellulose through severe chemical reactions or mechanical treatment with respect to the properties of feedstock and the goal of end use. For corn cob, which has a high hemicellulose (32−39%) and low lignin content (9−14%),[3,4,6] the acetyl groups on hemicellulose would be the main recalcitrance barrier, because the steric hindrance of acetyl groups could lower the activity of xylanase.[13] Thus, the selective removal of acetyl groups from the backbone of xylan in feedstock by deacetylation can significantly improve the xylan digestibility and cellulose enzymatic hydrolysis.[14] Acetyl xylan esterase,[15,16] hydroxylamine solutions,[17] and dilute alkali[13] can be used for deacetylation, and the conditions of deacetylation are usually milder compared to the traditional pretreatments, because acetyl groups are more reactive than the other enzymatic hydrolysis hinders (e.g., lignin).[18] Furthermore, deacetylation could reduce the acetic acid generated during pretreatment and enzymatic hydrolysis, which could restrain the growth of microbes in the ethanol fermentation.[19,20]

On the other hand, many mechanical refining technologies that have been widely applied in the pulp industry were used to increase enzymatic hydrolysis of various pretreated biomass. The applied technologies included disk-mill,[12,21,22] PFI mill,[22−24] food processor blender,[22] extruder,[22,25,26] Szego mill,[23] etc. It was reported that all of the refining technologies could improve the biomass digestibility by 10−20%.[22] Among them, the PFI mill was a commonly used laboratory mechanical refiner, which could provide accurate control and induce homogeneous refining effects on the substrate.[27] As a lab equipment, the PFI mill could refine a small quantity of biomass and be easily handled. Also, the PFI mill was usually used to simulate a disc refiner, which could be used at a large scale, although the refining of the PFI mill differed from disc and conical refiners (PFI mill imposed a greater proportion of compressive to shear forces). It has been know that the PFI mill is a high-energy and low-intensity refiner and normally uses 10 times the energy typically consumed in industrial refiners.[27]

Received: January 14, 2014
Revised: April 3, 2014
Accepted: May 1, 2014
Published: May 1, 2014

 © 2014 American Chemical Society dx.doi.org/10.1021/jf500189a | J. Agric. Food Chem. 2014, 62, 4661−4667

Table 1. Component of Corn Cob before and after Deacetylation

sample		chemical composition (wt %)					
	alkali charge (mmol/g of od substrate)	C_{glucan} (R_{glucan})	C_{xylan} (R_{xylan})	C_{arabin} (R_{arabin})	C_{acetyl} ($R_{deacetylation}$)	C_{lignin} ($R_{delignification}$)	R_{solid} (%)
NaOH[a]	0.8	44.72 (92.9)	40.98 (84.50)	3.62 (90.81)	0.08 (97.89)	5.06 (63.68)	72.50
	0.6	42.02 (99.44)	39.95 (93.84)	3.15 (90.02)	0.30 (90.99)	8.36 (31.64)	82.59
	0.4	40.06 (100.43)	38.45 (95.68)	3.29 (99.60)	0.62 (80.27)	8.29 (28.19)	87.49
	0.2	39.23 (101.72)	37.49 (96.49)	3.11 (97.38)	1.80 (40.77)	8.90 (20.23)	90.49
Na_2CO_3[a]	0.8	39.32 (98.23)	37.81 (93.76)	3.08 (92.92)	0.79 (74.95)	8.66 (25.24)	87.19
	0.6	37.5 (99.71)	36.96 (97.55)	2.79 (89.59)	1.02 (65.58)	8.00 (26.50)	92.80
	0.4	39.33 (101.19)	37.57 (95.94)	3.09 (96.00)	1.76 (42.53)	8.47 (24.70)	89.79
	0.2	38.77 (100.75)	37.1 (95.69)	2.97 (93.20)	2.33 (23.16)	8.76 (21.34)	90.69
$Ca(OH)_2$	0.8	39.6 (96.76)	37.06 (89.89)	3.36 (99.15)	0.13 (95.97)	7.97 (32.70)	85.28
	0.6	39.44 (97.91)	37.05 (91.30)	2.75 (82.44)	0.57 (82.04)	8.62 (26.02)	86.64
	0.4	39.27 (98.25)	37.26 (92.54)	3.17 (95.78)	0.86 (72.69)	8.63 (25.37)	87.32
	0.2	38.51 (98.60)	36.51 (92.79)	3.11 (96.16)	1.90 (38.26)	8.83 (21.88)	89.36
raw material		34.90	35.16	2.89	2.75	10.10	

[a]Measured as Na_2O.

Therefore, in this work, to improve the XOS yield and efficiently use cellulose from corn cob, a combined deacetylation and PFI refining pretreatment process was established and a two-stage enzymatic hydrolysis for the pretreated corn cob were carried out. The two-stage enzymatic hydrolysis was also used to evaluate the effectiveness of the combined pretreatment method. In the first stage of enzymatic hydrolysis (stage 1), just xylanase was added to release XOS, while in the second stage of hydrolysis (stage 2), both cellulase and β-glucosidase were used to digest the solid residue obtained from stage 1, aiming for the full utilization of the corn cob.

MATERIALS AND METHODS

Materials. The corn cob was harvested in 2012, in Shandong province (China), further milled by an agriculture use hammer mill, and screened to obtain the fraction with a particle size between the meshes of 20 and 80 (i.e., 0.18−0.85 mm). The screened corn cob was stored in sealed plastic bags at room temperature to be ready for the component analysis and pretreatment. The solid content of the prepared corn cob was 93.9%.

Xylanase was generously provided by Habio Enzyme (Mianyang, Sichuan province, China), and its activity was 38 international units (IU)/mL. Celluclast 1.5 L (cellulase) and Novozyme 188 (β-glucosidase) were bought from Sigma-Aldrich (St. Louis, MO). The activities of cellulase and β-glucosidase were 121 filter paper units (FPU)/mL and 741 IU/mL, respectively. All of the enzyme activities were measured using the methods reported by Ghose.[28] Other chemicals were of analytical quality and were bought from Sinopharm Chemical Reagent Co., Ltd. All of the enzymes and chemicals were used as received.

Deacetylation Treatment. The deacetylation treatment of corn cob was carried out following the previous procedure,[14] with slight modifications. Briefly, 10 g of screened dry corn cob was put into a 250 mL bottle with 120 mL of alkali solution of different alkali charge. The alkali charge ranged from 0.2 to 0.8 mmol/g of oven-dried (od) substrate. Then, the bottle was placed in an incubator shaker with 160 rpm at 70 °C for 3 h. After deacetylation, the corn cob was filtered and washed with tap water 4 times through a 300-mesh nylon cloth until neutrality. For each time, the ratio of washing water/deacetylated corn cob was 3:1 (w/w). Finally, the solid samples were collected and weighed for further analysis and tests. As a control, the corn cob was treated in water at 70 °C for 3 h. In deacetylation treatment, two weak bases Na_2CO_3 and $Ca(OH)_2$ and one strong base NaOH were used. The alkali charges of NaOH and Na_2CO_3 were measured as Na_2O (mmol/g of od substrate), and the alkali charges of $Ca(OH)_2$ (mmol/g of od substrate) were considered to be the same as that of Na_2O in this work, because although the solubility of $Ca(OH)_2$ is low (about 1.4×10^{-3} mmol/L in 70 °C), the ionization degree is high ($k_1 = 3.72 \times 10^{-3}$, and $k_2 = 3.98 \times 10^{-2}$). For example, 0.6 mmol of NaOH or Na_2CO_3 (as Na_2O)/g of substrate and 0.6 mmol of $Ca(OH)_2$/g of substrate could be considered to have the same alkali charge.

Mechanical Refining. To further increase enzymatic digestibility, the deacetylated and washed corn cob was modified by a PFI beating machine (mode PL11-00, Xianyang TEST Equipment Co., Ltd., Xianyang, China). The beating conditions were as follows: beating revolution was 4000 according to the studies by Chen et al.[14] and Jones et al.[23]; beating consistency was 10 wt %; revolution speed was 1400 rpm; and beating gap was 0.24 mm.

Enzymatic Hydrolysis. The corn cob was hydrolyzed in two stages. In stage 1, the corn cob was first hydrolyzed by xylanase. A total of 20 mL of a mixture of substrate (with 2% solid loading), sodium citrate buffer (0.1 M, pH 4.8), and xylanase was added in a 50 mL bottle for the National Renewable Energy Laboratory (NREL) procedure.[29] The xylanase dose was 66 IU/g of od biomass. The xylanase hydrolysis was carried out at 50 °C with the agitation at 120 rpm for 24 h. Upon completion, the hydrolyzate was separated by filtration, and the solid residue was washed and further hydrolyzed by cellulase and β-glucosidase in stage 2. All hydrolyzed residues were added together with sodium citrate buffer (0.1 M, pH 4.8), cellulase, and β-glucosidase to a 50 mL bottle. Then, the slurry was diluted to 20 mL. The cellulase and β-glucosidase doses were 18 FPU/g and 9 IU/g of od biomass, respectively, on the basis of the corn cob added in stage 1. The other conditions were the same as stage 1. After 48 h of hydrolysis, the hydrolyzate was collected by filtration to be ready for sugar analysis.

Analytical Methods. Glucan, xylan, acetyl, and lignin contents of biomass were determined using the NREL procedure.[30] The oligosaccharide and monosaccharide in the hydrolyzate were examined by high-performance liquid chromatography (HPLC, model 1200, Agilent, Santa Clara, CA) on a carbohydrate analysis column (Waters SunFire, 4.6 × 250 mm, 5 μm) with 50 mg/L ethylenediaminetetraacetic acid (EDTA) calcium salts as the mobile phase. A 10 μL sample of the hydrolyzate was injected into the column, and XOS were detected by a refractive index detector. Glucose, xylose, arabinose (Sigma, St. Louis, MO), xylobiose, xylotriose, and xylotetraose (Suntory Co., Ltd., Kyoto, Japan), with retention times of 9.7, 10.8, 12.2, 8.9, 7.7, and 7.0 min, respectively, were used as standards.

The crystallinities of corn cobs were measured using a Bruker D8 ADVANCE X-ray diffractometer (Bruker Co., Germany). The specimen was prepared by placing approximately 0.1 g of the freeze-dried and milled biomass sample on a glass sample holder and then placing a drop of acetone on the sample to fix it on the holder. The specimen was scanned at 2°/min from $2\theta = 10-26°$ with a step size of 0.05°.

dx.doi.org/10.1021/jf500189a | J. Agric. Food Chem. 2014, 62, 4661−4667

RESULTS AND DISCUSSION

Effect of the Pretreatment on Structural Features of Corn Cob. Table 1 shows the compositions of native and deacetylated corn cobs, as well as the recovery or removal rate of the corresponding component. In most cases, the deacetylation process could not efficiently remove the lignin, which was a main barrier of enzymatic hydrolysis, except using NaOH at an alkali charge of 0.8 mmol/g of substrate. A total of 63% delignification was achieved when using 0.8 mmol of NaOH/g of substrate, while the lignin removal at other conditions was just 20−32%. This was probably due to the fact that the acetyl groups were easier to remove compared to lignin. A lower dosage of NaOH (e.g., 0.6 mmol/g of substrate) could only sufficiently remove acetyl groups, while a higher dosage of NaOH (e.g., 0.8 mmol/g of substrate) could also provide enough alkali to remove much more lignin during deacetylation. Under these relatively mild alkaline conditions, the recovery rates of glucan and xylan after deacetylation were all higher than 92 and 84%, respectively (Table 1), because there was only a small amount of carbohydrates degraded in deacetylation (particularly for glucan). The glucan and xylan compositions of the samples were all improved by the removal of ash, lignin, soluble sugars, and other water-soluble extractives. Also, as shown in Table 2, after deacetylation, there was a slight increase (1−2%) of the crystallinity index of corn cob. This was because of the removal of amorphous components (i.e., acetyl groups and lignin) in deacetylated corn cob.[24] However, the decrease of cellulose crystallinity after deacetylation was due to the increase of the cellulose content in the deacetylated corn cob (Table 1). After PFI refining, both the crystallinity index and cellulose crystallinity of deacetylated corn cob were decreased (Table 2). This was mainly due to the destruction of the crystalline region in cellulose caused by the compression and shear forces during PFI refining.[18]

Table 2. Crystallinity Index of Corn Cob before and after Deacetylation and PFI Refining

	raw corn cob	deacetylated corn cob[a]	deacetylated and PFI refined corn cob[a]
crystallinity index (CrI) (%)	35.7	37.1	34.3
cellulose crystallinity (CCr) (%)	102.3	94.5	87.3

[a]Deacetylation condition: $Ca(OH)_2$ of 0.4 mmol/g of substrate alkali charge.

Unlike the delignification and crystallinity, the deacetylation increased significantly with the increase of alkali charge. For example, when the alkali charge was increased from 0.2 to 0.8 mmol/g of substrate using Na_2CO_3, the degree of deacetylation was increased from 23 to 74%. For the two weak alkali [Na_2CO_3 and $Ca(OH)_2$], the effect of $Ca(OH)_2$ on deacetylation was closer to that of NaOH compared to Na_2CO_3, because of the higher pH derived from $Ca(OH)_2$ at the same alkali charge. For instance, 96% deacetylation could be achieved after $Ca(OH)_2$ treatment with the alkali charge of 0.8 mmol/g of substrate at 70 °C for 3 h, suggesting that the mild process could efficiently remove the acetyl groups in corn cob.

Two-Stage Enzymatic Hydrolysis of Deacetylated Corn Cob. Low solids (2%) enzymatic hydrolysis was performed to test the digestibility of deacetylated corn cob in the near-ideal conditions, in which the mass transfer limitations between enzymes and substrate as well as the inhibition from products could be negligible. Figures 1 and 2 show the effect of the alkali charge on the percentage of enzymatic hydrolysis and the sugar yields of the two-stage hydrolysis of corn cobs, which were deacetylated by NaOH, Na_2CO_3, and $Ca(OH)_2$, respectively. Both the percentage of enzymatic hydrolysis and the sugar yields were increased with the increase of the alkali charge. When the corn cobs were deacetylated by NaOH, Na_2CO_3, and $Ca(OH)_2$ at the alkali charge of 0.8 mmol/g of substrate, the hydrolysis percentages of xylan in stage 1 were 93, 71, and 85%, respectively. The hydrolysis percentages of glucan in stage 2 were 86, 58, and 74%, respectively. For the case of $Ca(OH)_2$, although the enzymatic hydrolysis percentage of xylan was lower than that for NaOH, the sugar yield (0.293 g/g of corn cob at 0.8 mmol/g of substrate) was similar to the sugar yield using NaOH (0.300 g/g of corn cob at 0.8 mmol/g of substrate) because of the high recovery of xylan after the

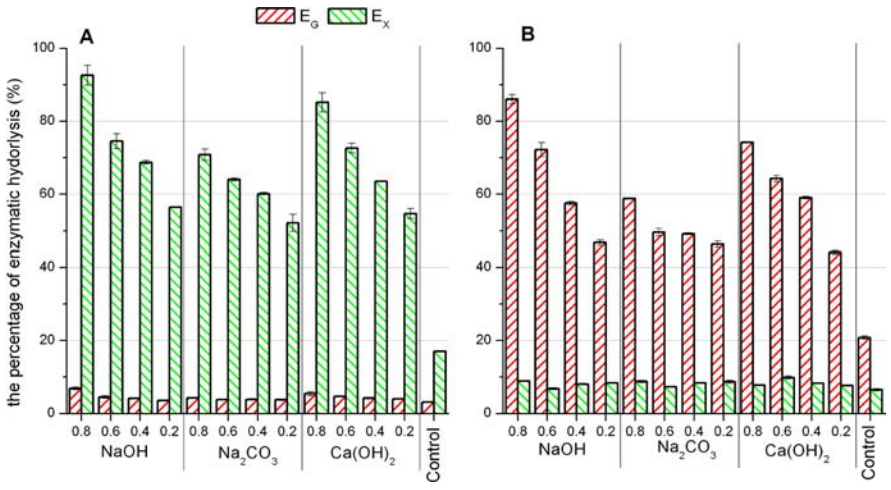

Figure 1. Percentages of enzymatic hydrolysis (E_G and E_X) of the two-stage hydrolysis of corn cob deacetylated by different bases and alkali charges. (A) Percentages of enzymatic hydrolysis of stage 1 (xylanase hydrolysis). (B) Percentages of enzymatic hydrolysis of stage 2 (cellulase and β-glucosidase hydrolysis). Values of 0.8−0.2, samples deacetylated with the alkali charge of 0.8−0.2 mmol/g of substrate (NaOH and Na_2CO_3 were calculated as Na_2O); control, water-treated sample.

dx.doi.org/10.1021/jf500189a | J. Agric. Food Chem. 2014, 62, 4661−4667

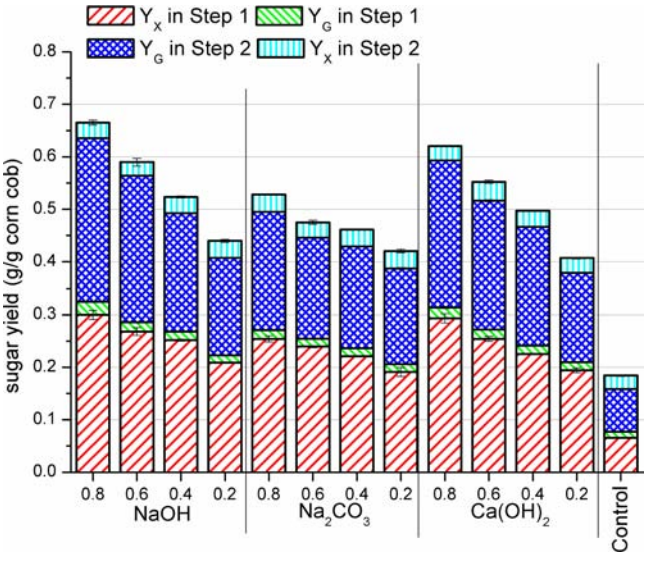

Figure 2. Sugar yields (Y_G and Y_X) of the two-stage hydrolysis of corn cob deacetylated by different bases and alkali charges. Values of 0.8–0.2, samples deacetylated with the alkali charge of 0.8–0.2 mmol/g of substrate (NaOH and Na_2CO_3 were calculated as Na_2O); control, water-treated sample.

deacetylation process using $Ca(OH)_2$. In comparison to other cellulosic material (such as corn stover[14] and aspen wood[31]), the corn cob could be highly digested in enzymatic hydrolysis after mild deacetylation treatment without any severe pretreatment (such as acid-assisted steam explosion[11] and acidified sodium chloride delignification[12,21]) because of the low lignin and high hemicellulose contents. In the two-stage hydrolysis, most xylan was separated in stage 1 by xylanase, leaving most of the glucan in the hydrolyzed solid residue because of the selectivity of xylanase. All of the proportions of sugars in the hydrolyzates after stage 1 were similar to the proportion deacetylated by $Ca(OH)_2$ with the alkali charge of 0.8 mmol/g of substrate (Table 3). XOS accounted for about 50% soluble

Table 3. Sugar Content of the Hydrolyzate after Xylanase Hydrolysis[a]

saccharide	glucose	xylose	X2[b]	X3[b]	X4–X7[b]	arabinose
content (wt %)[c]	6.25	33.93	41.88	10.12	2.47	5.33
conversion (%)[d]	5.3	27.7	36.5	9.0	2.2	

[a]From the PFI refined corn cob [deacetylated by $Ca(OH)_2$ with the alkali charge of 0.8 mmol/g of substrate]. [b]X2, xylobiose; X3, xylotriose; and X4–X7, xylotetraose, xylopentaose, xylohexaose, and xyloheptaose. [c]On the basis of the total sugar weight in the hydrolyzate. [d]On the basis of xylan or glucan in the raw corn cob.

sugar in the hydrolyzate. The comparatively low percentage of XOS could be caused by the long hydrolysis time, which could obtain a higher xylan yield because XOS could be further hydrolyzed into xylose by β-xylosidase in crude xylanase. The enzymatic digestions of the solid residues (stage 2) obtained from xylanase hydrolysis had a trend similar to stage 1. Because most of the digestible xylan was removed in stage 1 by xylanase, the percent of xylose in the hydrolyzate of stage 2 was much lower than the hydrolyzate directly obtained from the traditional one-stage enzymatic hydrolysis without the xylan-removing process. As presented in Table 4, the final sugar

Table 4. Comparison of the Sugar Yields Obtained from Different Enzymatic Hydrolysis Processes[a]

two-stage hydrolysis							
stage 1 (24 h)		stage 2 (48 h)		total yield[b]		one-stage hydrolysis (48 h)[c]	
Y_{G1}	Y_{X1}	Y_{G2}	Y_{X2}	Y_G	Y_X	Y_G	Y_X
0.021	0.293	0.278	0.028	0.299	0.321	0.336	0.340

[a]Hydrolysis substrate: PFI refined corn cob [deacetylated by $Ca(OH)_2$ at the alkali charge of 0.8 mmol/g of substrate]. [b]The total yield of two-stage hydrolysis (Y_G or Y_X) was calculated as follows: $Y_G = Y_{G1} + Y_{G2}$; $Y_X = Y_{X1} + Y_{X2}$. [c]Enzyme doses: cellulase, 18 FPU/g of od biomass; β-glucosidase, 9 IU/g of od biomass; and xylanase, 66 IU/g of od biomass.

yields obtained from the two-stage enzymatic hydrolysis were somewhat lower compared to the traditional one-stage hydrolysis. This was likely because used cellulase and β-glucosidase contained some xylanases, which had the ability to hydrolyze xyloligomers into xylose, thus removing the inhibition from xyloligomers during hydrolysis. This was in agreement with the fact that there were no xyloligomers detected in the hydrolyzate after one-stage hydrolysis. On the other hand, in the one-stage hydrolysis, three enzymes (cellulase, β-glucosidase, and xylanase) were added together, and the addition of xylanase may reduce the ineffective adsorption of cellulase to xylan and lignin, thus leading to the relative increase of cellulase activity.[18,32−34] Therefore, a higher final sugar yield could be achieved by the one-stage enzymatic hydrolysis. However, in stage 1 of the two-stage enzymatic hydrolysis, used xylanase had a lower ability to hydrolyze xyloligomers to xylose. Thus, many xyloligomers could be obtained after the hydrolysis of stage 1. Furthermore, in stage 2, the glucan yield was lower compared to the one-stage hydrolysis. This was possibly due to the relatively increased proportion of lignin in the xylan-deprived corn cob residue. The increased proportion of lignin might increase the ineffective adsorption of cellulase to lignin, thus lowering the glucan yield. However, although the sugar yields from the two-stage hydrolysis were lower than the one-stage hydrolysis, using xylanase and cellulase to "tailor" the deacetylated corn cob in two separated processes could make the component of the product more simplified, which is good for the further microbial or chemical utilizations. In addition, the optimization of enzymatic hydrolysis and the study of the inhibition of the XOS product in high solid loading (≥15%) hydrolysis will be conducted in the future.

Impact of Refining on the Enzymatic Hydrolysis. As shown in Figures 3 and 4, the enzymatic hydrolysis percentages of xylan (E_X) in stage 1, the enzymatic hydrolysis percentages of glucan (E_G) in stage 2, and the total sugar yields (Y_S) were all increased after PFI refining. The increased extents of sugar yields ranged from 0.023 to 0.212 g/g of corn cob (Figure 4), which were comparable to the previous reports.[18] However, the increased extents of hydrolysis percentages and sugar yields for the samples treated at hash conditions were lower than that for the samples treated with mild conditions. For example, as shown in Figure 4A, 9.7% improvement of the enzymatic hydrolysis percentage of xylan could be obtained for the samples treated with 0.2 g of $Ca(OH)_2$/g of substrate, while only 3.6% improvement could be achieved for the samples treated with 0.8 g of $Ca(OH)_2$/g of substrate. Also, for the

dx.doi.org/10.1021/jf500189a | J. Agric. Food Chem. 2014, 62, 4661−4667

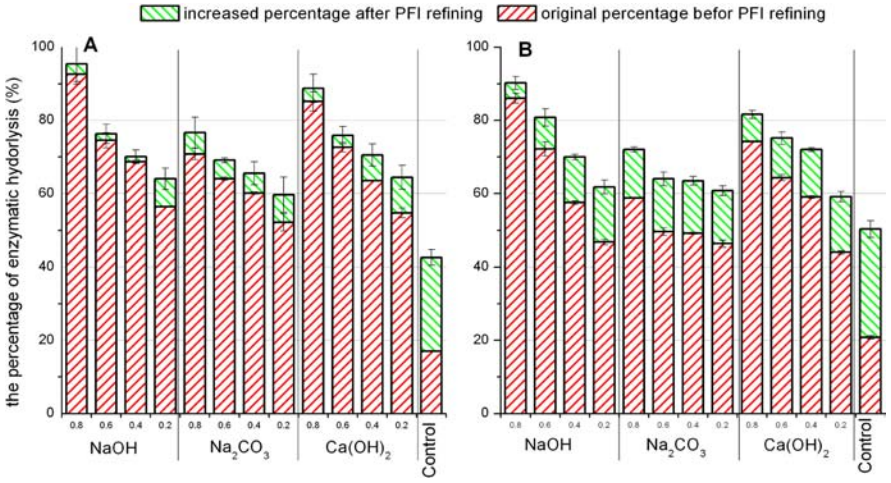

Figure 3. Effect of PFI refining on the rates of enzymatic hydrolysis (E_G and E_X) of the two-stage hydrolysis of deacetylated corn cob. (A) E_X of stage 1 (xylanase hydrolysis). (B) E_G of stage 2 (cellulase and β-glucosidase hydrolysis) Values of 0.8−0.2, samples deacetylated with the alkali charge of 0.8−0.2 mmol/g of substrate (NaOH and Na_2CO_3 were calculated as Na_2O); control, water-treated sample.

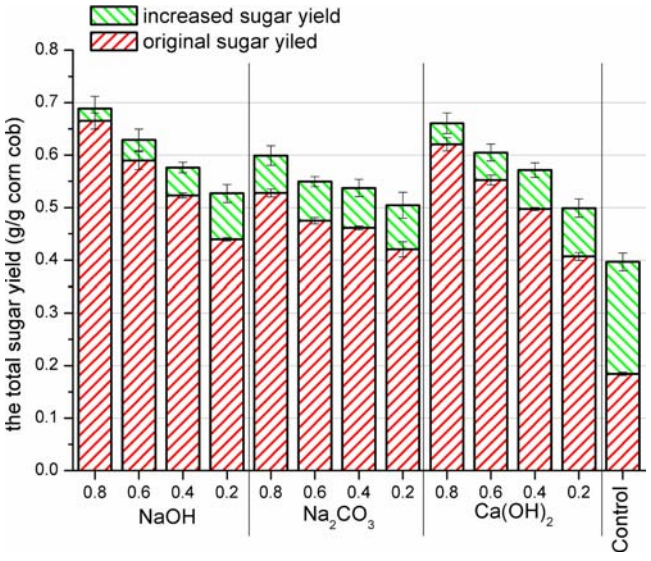

Figure 4. Effect of PFI refining on the total sugar yields (all of the sugars in hydrolyzate) obtained from the two-stage hydrolysis of deacetylated corn cob. Values of 0.8−0.2, samples deacetylated with the alkali charge of 0.8−0.2 mmol/g of substrate (NaOH and Na_2CO_3 were calculated as Na_2O); control, water-treated sample.

control sample, the total sugar yield was 0.212 g/g of corn cob, while after PFI refining, the total sugar yield could be 2.7 times higher than that of the unrefined sample (Figure 4). This was because the size reduction that resulted from the PFI refining increased the reactive surface area for enzymes, thus leading to an increase of xylan and glucan yields.[18] On the other hand, the decrease of crystallinity of cellulose (Table 2) caused by the compression and shear force of the PFI mill could also make cellulose more digestible.[13] In addition, as presented in Figure 4, a total sugar yield of 0.661 g/g of corn cob could be obtained from the samples treated by 0.8 mmol of $Ca(OH)_2$/g of substrate, which was comparable to the yield (0.688 g/g of corn cob) obtained from the sample treated by NaOH with the same alkali charge. This was due to the fact that higher sugar recovery could be achieved in the deacetylation process by the use of $Ca(OH)_2$. Therefore, it can be concluded that $Ca(OH)_2$ is the more appropriate alkali for deacetylation and the suitable alkali charge is 0.8 mmol/g of substrate based on the results obtained in this study. Other benefits using $Ca(OH)_2$ are that (1) $Ca(OH)_2$ is an inexpensive and milder base compared to NaOH and (2) $Ca(OH)_2$ can be easily recovered. Although some calcium ions may precipitate as calcium salts, precipitated calcium could be removed by sufficient washing (e.g., using vacuum washing equipment at large-scale production) after deacetylation. Another possible solution to avoid the precipitation of calcium is to add a small amount of chelating agent (e.g., EDTA) before deacetylation, so that the released calcium ions could be chelated and then removed during washing.

Mass Balance Analysis. The overall process and mass balance for the combined deacetylation [on the basis of $Ca(OH)_2$] and PFI refining pretreatment of corn cob plus the two-stage enzymatic hydrolysis are presented in Figure 5. For theoretical calculation, the sugar loss in PFI refining was neglected. As demonstrated in Figure 5, after $Ca(OH)_2$ deacetylation (with the alkali charge of 0.8 mmol/g of substrate) and PFI refining, 79.8% xylan was hydrolyzed in

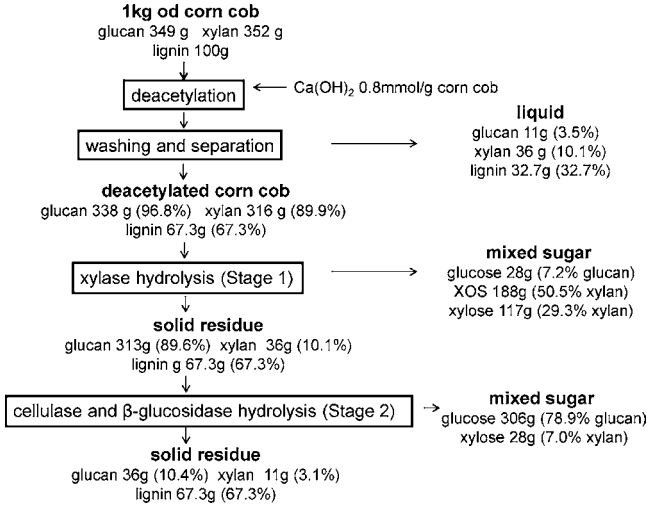

Figure 5. Mass balance of the overall process (deacetylation + PFI refining + two-stage hydrolysis).

dx.doi.org/10.1021/jf500189a | J. Agric. Food Chem. 2014, 62, 4661−4667

stage 1 of enzymatic hydrolysis and 50.5% hemicellulose was converted to XOS. The cellulose in the solid residue separated from stage 1 could be highly digested by cellulase and β-glucosidase in stage 2. In total, 86.8% xylan and 86.1% glucan in the raw corn cob were hydrolyzed in the two-stage enzymatic hydrolysis, indicating that the combined $Ca(OH)_2$ deacetylation and PFI refining pretreatment process was a relatively effective method to improve the enzymatic digestion of corn cob. In addition, in comparison to the traditional one-stage enzymatic hydrolysis, the two-stage hydrolysis can make the resulting sugar products simpler and easier to be used in the downstream processes.

■ ASSOCIATED CONTENT

Ⓢ Supporting Information

X-ray diffraction (XRD) pattern of raw corn cob (Figure S1) and detailed calculations. This material is available free of charge via the Internet at http://pubs.acs.org.

■ AUTHOR INFORMATION

Corresponding Authors

*Telephone/Fax: +86-532-80662725. E-mail: libin@qibebt.ac.cn.

*E-mail: penghui@qibebt.ac.cn.

Funding

This research was funded by the Natural Science Foundation of China (21206184, 31370582, and 21306216), the Shandong Provincial Natural Science Foundation for Distinguished Young Scholar (China) (JQ201305), and the National High Technology Research and Development Program ("863" Program) of China (2012AA022301).

Notes

The authors declare no competing financial interest.

■ ABBREVIATIONS USED

XOS, xylo-oligosaccharides; SPORL, sulfite pretreatment to overcome recalcitrance of lignocellulose; NREL, National Renewable Energy Laboratory; HPLC, high-performance liquid chromatography; R_{solid}, recovery rate of solid after deacetylation; R_{glucan}, recovery rate of glucan; R_{xylan}, recovery rate of xylan; R_{arabin}, recovery rate of arabinan; $D_{delignification}$, delignification percentage after deacetylation; $D_{deacetylation}$, deacetylation percentage after deacetylation; E_X, enzymatic hydrolysis percentage of xylan; E_G, enzymatic hydrolysis percentage of glucan; Y_X, xylan yield; Y_G, glucan yield; Y_S, total sugar yield

■ REFERENCES

(1) Carvalho, A. F. A.; de Oliva Neto, P.; da Silva, D. F.; Pastore, G. M. Xylo-oligosaccharides from lignocellulosic materials: Chemical structure, health benefits and production by chemical and enzymatic hydrolysis. *Food Res. Int.* **2013**, *51*, 75−85.

(2) Chapla, D.; Pandit, P.; Shah, A. Production of xylooligosaccharides from corncob xylan by fungal xylanase and their utilization by probiotics. *Bioresour. Technol.* **2012**, *115*, 215−221.

(3) Aachary, A. A.; Prapulla, S. G. Value addition to corncob: Production and characterization of xylooligosaccharides from alkali pretreated lignin−saccharide complex using *Aspergillus oryzae* MTCC 5154. *Bioresour. Technol.* **2009**, *100*, 991−995.

(4) Yang, R.; Xu, S.; Wang, Z.; Yang, W. Aqueous extraction of corncob xylan and production of xylooligosaccharides. *LWT—Food Sci. Technol.* **2005**, *38*, 677−682.

(5) Akpinar, O.; Erdogan, K.; Bostanci, S. Enzymatic production of xylooligosaccharide from selected agricultural wastes. *Food Bioprod. Process.* **2009**, *87*, 145−151.

(6) Samanta, A. K.; Senani, S.; Kolte, A. P.; Sridhar, M.; Sampath, K. T.; Jayapal, N.; Devi, A. Production and in vitro evaluation of xylooligosaccharides generated from corn cobs. *Food Bioprod. Process.* **2012**, *90*, 466−474.

(7) Brienzo, M.; Carvalho, W.; Milagres, A. M. F. Xylooligosaccharides production from alkali-pretreated sugarcane bagasse using xylanases from *Thermoascus aurantiacus*. *Appl. Biochem. Biotechnol.* **2010**, *162*, 1195−1205.

(8) Mou, H. Y.; Orblin, E.; Kruus, K.; Fardim, P. Topochemical pretreatment of wood biomass to enhance enzymatic hydrolysis of polysaccharides to sugars. *Bioresour. Technol.* **2013**, *142*, 540−545.

(9) Li, B.; Liu, H.; Xu, H.; Pang, B.; Mou, H. Y.; Wang, H.; Mu, X. Characterization of the detailed relationships of the key variables in the process of the alkaline sulfite pretreatment of corn stover by multivariate analysis. *BioResources* **2014**, *9*, 2757−2771.

(10) Mou, H. Y.; Heikkilä, E.; Fardim, P. Topochemistry of alkaline, alkaline-peroxide and hydrotropic pretreatments of common reed to enhance enzymatic hydrolysis efficiency. *Bioresour. Technol.* **2013**, *150*, 36−41.

(11) Alvira, P.; Tomas-Pejo, E.; Ballesteros, M.; Negro, M. J. Pretreatment technologies for an efficient bioethanol production process based on enzymatic hydrolysis: A review. *Bioresour. Technol.* **2010**, *101*, 4851−4861.

(12) Zhu, J. Y.; Pan, X. J.; Wang, G. S.; Gleisner, R. Sulfite pretreatment (SPORL) for robust enzymatic saccharification of spruce and red pine. *Bioresour. Technol.* **2009**, *100*, 2411−2418.

(13) Chang, V. S.; Holtzapple, M. T. Fundamental factors affecting biomass enzymatic reactivity. *Appl. Biochem. Biotechnol.* **2000**, *84*−*6*, 5−37.

(14) Chen, X. W.; Tao, L.; Shekiro, J.; Mohaghaghi, A.; Decker, S.; Wang, W.; Smith, H.; Park, S.; Himmel, M. E.; Tucker, M. Improved ethanol yield and reduced minimum ethanol selling price (MESP) by modifying low severity dilute acid pretreatment with deacetylation and mechanical refining: 1) Experimental. *Biotechnol. Biofuels* **2012**, *5*, 60.

(15) Agger, J.; Vikso-Nielsen, A.; Meyer, A. S. Enzymatic xylose release from pretreated corn bran arabinoxylan: Differential effects of deacetylation and deferuloylation on insoluble and soluble substrate fractions. *J. Agric. Food Chem.* **2010**, *58*, 6141−6148.

(16) Selig, M. J.; Adney, W. S.; Himmel, M. E.; Decker, S. R. The impact of cell wall acetylation on corn stover hydrolysis by cellulolytic and xylanolytic enzymes. *Cellulose* **2009**, *16*, 711−722.

(17) Grohmann, K.; Mitchell, D. J.; Himmel, M. E.; Dale, B. E.; Schroeder, H. A. The role of ester groups in resistance of plant cell wall polysaccharides to enzymatic hydrolysis. *Appl. Biochem. Biotechnol.* **1989**, *20*−*21*, 45−61.

(18) Leu, S. Y.; Zhu, J. Y. Substrate-related factors affecting enzymatic saccharification of lignocelluloses: Our recent understanding. *BioEnergy Res.* **2013**, *6*, 405−415.

(19) Larsson, S.; Palmqvist, E.; Hahn-Hägerdal, B.; Tengborg, C.; Stenberg, K.; Zacchi, G.; Nilvebrant, N.-O. The generation of fermentation inhibitors during dilute acid hydrolysis of softwood. *Enzyme Microb. Technol.* **1999**, *24*, 151−159.

(20) Nigam, J. N. Development of xylose-fermenting yeast *Pichia stipitis* for ethanol production through adaptation on hardwood hemicellulose acid prehydrolysate. *J. Appl. Microbiol.* **2001**, *90*, 208−215.

(21) Zhu, W.; Zhu, J. Y.; Gleisner, R.; Pan, X. J. On energy consumption for size-reduction and yields from subsequent enzymatic saccharification of pretreated lodgepole pine. *Bioresour. Technol.* **2010**, *101*, 2782−2792.

(22) Chen, X.; Kuhn, E.; Wang, W.; Park, S.; Flanegan, K.; Trass, O.; Tenlep, L.; Tao, L.; Tucker, M. Comparison of different mechanical refining technologies on the enzymatic digestibility of low severity acid pretreated corn stover. *Bioresour. Technol.* **2013**, *147*, 401−408.

(23) Jones, B. W.; Venditti, R.; Park, S.; Jameel, H.; Koo, B. Enhancement in enzymatic hydrolysis by mechanical refining for pretreated hardwood lignocellulosics. *Bioresour. Technol.* **2013**, *147*, 353−60.

(24) Mou, H. Y.; Li, B.; Fardim, P. Pretreatment of corn stover with modified hydrotropic method to enhance enzymatic hydrolysis. *Energy Fuels* **2014**, DOI: 10.1021/ef5001634.
(25) Liu, C.; van der Heide, E.; Wang, H.; Li, B.; Yu, G.; Mu, X. Alkaline twin-screw extrusion pretreatment for fermentable sugar production. *Biotechnol. Biofuels* **2013**, *6*, 97.
(26) Zhang, Y.; Hou, T.; Li, B.; Liu, C.; Mu, X.; Wang, H. Acetone−butanol−ethanol production from corn stover pretreated by alkaline twin-screw extrusion pretreatment. *Bioprocess Biosyst. Eng.* **2013**, 1−9.
(27) Kerekes, R. J. Characterizing refining action in PFI mills. *Tappi J.* **2005**, *4* (3), 9−14.
(28) Ghose, T. K. Measurement of cellulase activities. *Pure Appl. Chem.* **1987**, *59*, 257−268.
(29) Selig, M.; Weiss, N.; Ji, Y. *Enzymatic Saccharification of Lignocellulosic Biomass*; National Renewable Energy Laboratory (NREL): Golden, CO, 2008; NREL/TP-510-42629.
(30) Sluiter, A.; Hames, B.; Ruiz, R.; Scarlata, C.; Sluiter, J.; Templeton, D.; Crocker, D. *Determination of Structure Carbohydrates and Lignin in Biomass*; National Renewable Energy Laboratory (NREL): Golden, CO, 2008; NREL/TP-510-42618.
(31) Kong, F. R.; Engler, C. R.; Soltes, E. J. Effects of cell-wall acetate, xylan backbone, and lignin on enzymatic-hydrolysis of aspen wood. *Appl. Biochem. Biotechnol.* **1992**, *34*−*5*, 23−35.
(32) Qing, Q.; Wyman, C. E. Supplementation with xylanase and β-xylosidase to reduce xylo-oligomer and xylan inhibition of enzymatic hydrolysis of cellulose and pretreated corn stover. *Biotechnol. Biofuels* **2011**, *4*, 18.
(33) Segal, L.; C. J; Martin, A. E.; Conrad, C. M. An empirical method for estimating the degree of crystallinity of native cellulose using the X-ray diffractometer. *Text. Res. J.* **1959**, *29*, 786−794.
(34) Xu, F.; Shi, Y. C.; Wang, D. X-ray scattering studies of lignocellulosic biomass: A review. *Carbohydr. Polym.* **2013**, *94*, 904−917.

JOURNAL OF AGRICULTURAL AND FOOD CHEMISTRY

Article

pubs.acs.org/JAFC

Effects of Monomers and Homopolymer Contents on the Dry and Wet Tensile Properties of Starch Films Grafted with Various Methacrylates

Zhen Shi,[†,‡] Narendra Reddy,[‡] Li Shen,[§] Xiuliang Hou,[†] and Yiqi Yang*[,†,‡,§,∥,⊥]

[†]Key Laboratory of Eco-textiles, Ministry of Education, College of Textiles and Garments, Jiangnan University, Lihu Road #1800, Wuxi 214122, People's Republic of China

[‡]Department of Textiles, Merchandising, and Fashion Design, 234 HECO Building, East Campus, University of Nebraska—Lincoln, Lincoln, Nebraska 68583-0802, United States

[§]College of Chemistry, Chemical Engineering, and Biotechnology, Donghua University, No. 1882 West Yan'an Road, Shanghai 200051, People's Republic of China

[∥]Department of Biological Systems Engineering and [⊥]Nebraska Center for Materials and Nanoscience 234 HECO Building, East Campus, University of Nebraska—Lincoln, Lincoln, Nebraska 68583-0802, United States

ABSTRACT: Starch grafted with four different methacrylates was compression molded to form thermoplastic films with good strength and water stability. Starch is an inexpensive and biodegradable polymer but is nonthermoplastic and needs to be chemically modified to make starch suitable for various applications. In this research, starch was grafted with four methacrylates (methyl, ethyl, butyl, and hexyl), and the effect of the length of the alkyl ester group on grafting parameters, thermoplasticity, and properties of thermoplastic films developed have been studied. Influence of grafting conditions on % grafting efficiency, % homopolymers, and % monomer conversion were studied, and the grafted starch was characterized using thermogravimetric analysis (TGA), differential scanning calorimetry (DSC), and nuclear magnetic resonance (^{1}H NMR). At similar grafting ratios, butyl methacrylate (BMA) provided better strength and elongation to the starch films than the other three methacrylates. Grafting of methacrylates appears to be an economical approach to develop thermoplastic products from starch.

KEYWORDS: *starch, thermoplastics, methacrylates, grafting*

INTRODUCTION

Starch is one of the most widely used biopolymers for food and nonfood applications. Large availability, low cost, and easy biodegradability are some of the major features that make starch attractive for various applications. Starch is found in several sources, including cereal grains, vegetables, and fruits, but the basic structure and properties of starch are the same. Nonfood applications of starch include paper, pharmaceutical, biofuel, textile, and packaging, in addition to many others. Although ethanol production, paper, and other applications use starch in its native form, many types of physical and/or chemical modifications are done to make starch suitable for processing and to develop products. Modifications are also necessary to improve the properties, such as increasing its tensile strength and hydrophobicity, and to obtain starch-based products with desired features.[1] Modified or unmodified starches are made into products mainly by the wet or dry approach. Wet processing of starch includes dissolving or dispersing starch and casting the solution, mainly to form films. Dry processing of starch includes extrusion, injection, and compression molding to form foams, sheets, films, and other products.

Although dry processing of starch is preferred over wet processing, native starch is nonthermoplastic, and it is necessary to modify starch to produce thermoplastic products.[2] Thermoplastic starch, commonly referred to as TPS, is made by mixing starch with water and plasticizers under heat and can be extruded or processed into products.[3,4] TPS could be used to manufacture films for food packing, extrudates for secondary packing, and micro and nanofibers for textile and medical applications. Similarly, TPS could be used as a resin, and natural fibers could be used as reinforcement to obtain completely degradable composites. However, thermoplastic starch has several limitations. For instance, TPS is mostly water-soluble and provides products with poor strength.[3,5] Blending of synthetic polymers, inorganic materials, and additives such as lignin and nanoclay have been used to improve the properties of products developed from thermoplastic starch.[6] Cross-linking is another approach that has been commonly used to improve the properties of starch products.[7] It was previously shown that solution cast starch films, after being cross-linked with citric acid, had much higher tensile strength and water stability.[7]

Chemical modifications, such as acetylation, hydroxypropylation, and grafting, have also been used to modify starch and develop thermoplastic products.[8,9] Starch acetates have been produced on a commercial scale and used in pharmaceutical, food, and other industries. Although acetylation makes starch thermoplastic and provides products with good tensile

Received: March 20, 2014
Revised: April 29, 2014
Accepted: May 1, 2014
Published: May 12, 2014

ACS Publications © 2014 American Chemical Society

dx.doi.org/10.1021/jf5013709 | J. Agric. Food Chem. 2014, 62, 4668−4676

properties and water stability, acetylation is expensive and not affordable to develop commodity products such as films. Recently, acylation of starch using enzymes has been done to avoid the harsh conditions necessary during other chemical modifications.[1] Grafting of polymers is another approach that has been commonly used to develop products from starch. Both natural and synthetic polymers have been grafted onto starch to impart desired properties to starch.[9] A multitude of synthetic monomers such as acrylamide, polyurethane, polystyrene, acrylonitrile, and vinyl monomers have been grafted onto starch, and the thermal behavior of the grafted materials have been compared to the unmodified starch.[9−11]

Among the various types of monomers grafted onto starch, acrylic monomers such as methyl, ethyl, and butyl acrylates, and the corresponding methacrylates, are preferred due to their lower cost and ability to provide good performance properties.[12] Grafting of acrylic monomers onto starch and other biopolymers has been extensively studied, and the influence of catalysts, initiators, and monomers on the grafting parameters and properties of the products obtained has also been investigated. For example, methyl methacrylate (MMA) was grafted onto sago starch in aqueous media using different initiators of ceric ammonium nitrate and potassium persulfate under nitrogen atmosphere.[12] On the basis of FTIR studies, it was suggested that MMA was successfully grafted onto starch and that the grafted starch was suitable for developing thermoplastic products.[12] In another study, cassava starch was grafted with poly(methyl methacrylate) using benzoyl peroxide as initiator.[13] Starch with 37.2% grafting ratio, 95.5% yield, and 54.3% homopolymer was obtained after the reaction. Ethyl acrylate and acrylamide were grafted onto starch by copolymerization using potassium permanganate-citric acid as initiator, and the reaction conditions were optimized. Grafting of the copolymers onto starch was proven using FTIR.[9] In another study, corn starch was first alkenylsuccinylated to different degrees of substitutions and was later graft-copolymerized with acrylic acid.[14] Alkenylsuccinylation resulted in higher grafting efficiency and stronger films.

The influence of the alkyl chain length on the grafting efficiency was studied using three vinyl monomers [methyl methacrylate (MMA), ethyl methacrylate (EMA), and butyl methacrylate (BMA)] using ceric ammonium nitrate as the initiator. Optimum grafting conditions were developed, and it was found that the reactivity of the methacrylates increased with increasing alkyl group length.[15] It was also suggested that the monomers were grafted onto the amorphous and crystalline regions. Crystallinity and thermal stability of the grafted starch were found to decrease after grafting. Starch was graft copolymerized with methacrylonitrile and MMA, EMA, BMA, and HMA. Among the four methacrylates studied, HMA was found to have considerably lower % grafting, which was inferred to result from the lesser accessibility of HMA to the active sites of the carbohydrate.[16]

Efforts have also been made to develop thermoplastics from grafted starch.[17] Starch grafted with methyl acrylates and methacrylates has been injection molded into ribbons, and the properties of the extruded ribbons have been investigated.[18,19] Films with tensile values ranging from 8 to 17 MN/mm^2 and with elongations from 2% to 150% were obtained, depending on the level of grafting and the aging time.[18] In other research, starch-*g*-PMA with PMA contents between 59% and 67% provided films with tensile strengths ranging from 9 to 24 MN/m^2 and elongations of 30−265%.[19] Bagley et al. grafted methyl acrylate, methyl methacrylate, and a mixture of methyl and butyl acrylate and extruded them into ribbons.[20] Plastics obtained from starch-*g*-methyl methacrylate were described as being brittle, but those grafted with methyl acrylate and butyl acrylate were flexible and leathery.[20] As seen from the literature discussed above, limited study has been done on developing thermoplastics products from grafted starch, and only a few monomers have been studied. The influence of different acrylic monomers, their structures, and chain lengths, and the amount of homopolymers on the tensile properties of compression-molded films is not known. More importantly, the resistance of the films to water and high humidity and the suitability of the starch films for various applications have not been investigated. In this research, a series of vinyl monomers with increasing alkyl chain lengths were grafted onto starch. Grafting conditions were optimized, and the grafted starch was characterized for thermal behavior and structural changes. Grafted starch was compression molded into thermoplastic films, and the influences of % homopolymers on the dry and wet tensile properties were studied. The ability of the different monomers to improve the strength and water stability were also investigated.

MATERIALS AND METHODS

Materials. Corn starch (regular) was purchased from the National Starch Company and used as received. Four vinyl monomers (MMA, EMA, BMA, and HMA) were selected for grafting onto starch based on our previous studies on grafting vinyl monomers onto chicken feathers and camelina meal.[21,22] Monomers, potassium persulfate used as initiator, sodium bisulfite used as reductant, and other chemicals required for the study were reagent grade.

Methods. *Grafting.* Starch was first dispersed in water, and the required ratios of monomers were added into a four-necked flask along with the initiator and reductant. Oxygen in the flask was removed by displacing it with nitrogen, and the entire reaction was performed under nitrogen atmosphere. Grafting conditions such as monomer concentration to starch (30−140%), reaction time (0.5 to 4 h), and reaction temperature were varied to obtain the optimum grafting conditions. After the required grafting time, the reaction was stopped by adding 2% paradioxybenzene. Grafted starch was thoroughly washed in water to remove unreacted monomers and inorganic salts and later dried and collected. Grafting parameters, such as grafting efficiency, molar grafting ratio (mol/g), monomer conversion (%), and % homopolymers were calculated using equations reported in our previous researches.[21]

Thermal Analysis. Grafted starch was analyzed to determine the thermal behavior using differential scanning calorimeter (DSC) and thermogravimetric analysis (TGA). DSC studies were done on a Mettler Toledo calorimeter (Model D822e; Mettler Toledo, Columbus, OH) under nitrogen atmosphere with temperatures ranging from 25 °C to 250 °C. Three scans were done for each sample, and the average data were used to draw the melting curves. TGA studies were done on a Sigma T300 analyzer with 10 mg of sample, and three samples were analyzed under nitrogen for each condition. An average of the three samples were used to plot the thermal degradation curves.

Fourier Transform Infrared (FTIR). Grafted and ungrafted starch samples were analyzed on a Fourier Transform Infrared Spectrophotometer (Thermo Scientific Model: iS10; Thermo Scientific, Waltham, MA) on an attenuated total reflectance mode using a diamond cell. Samples were scanned 32 times from 500 to 4000 cm^{-1} at a resolution of 8 cm^{-1}. Three spectras were collected for each sample, and the average values were used for comparison.

^{1}H NMR. Nuclear magnetic resonance studies were conducted to confirm grafting of the monomers onto starch. For the NMR analysis, samples were dissolved in acetone (1 wt %) and scanned on a Avance 600 MHz Digital NMR spectrometer (Bruker Co. Ltd. Switzerland). A

dx.doi.org/10.1021/jf5013709 | J. Agric. Food Chem. 2014, 62, 4668−4676

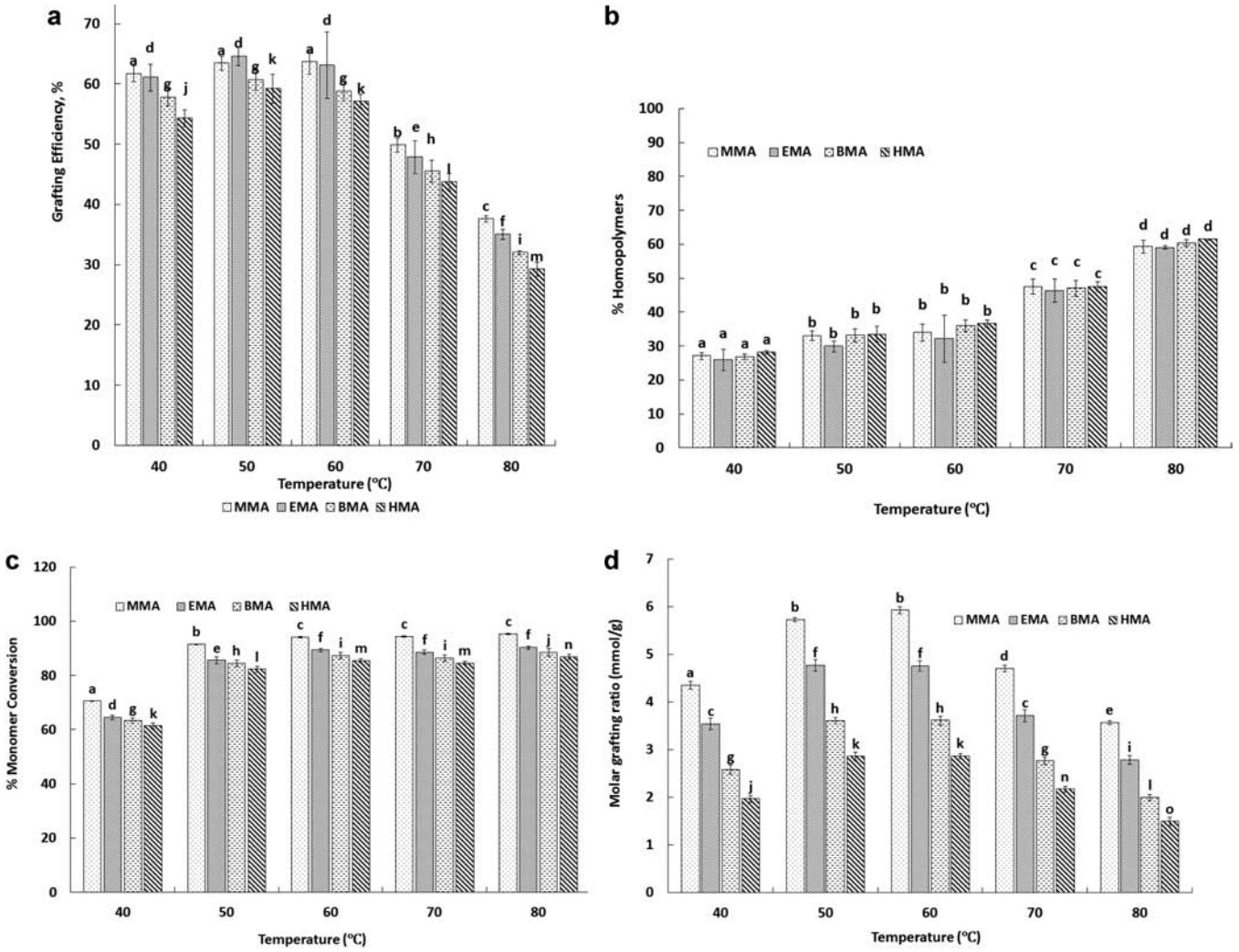

Figure 1. Influence of grafting temperature on % grafting efficiency (a), % homopolymers (b), % monomer conversion (c), and molar grafting ratio (d). Grafting was performed using 100% of monomers based on weight of starch for 180 min at various temperatures. For each monomer, data points with the different letters indicate statistically significant difference.

basic proton pulse sequence (zg30) was used with a relaxation delay of 1 s and acquisition time of 3 s and operated at 600 MHz. Spectra were phase corrected interactively using TOPSPIN. Baseline correction was carried out manually using the appropriate factors.

Influence of Homopolymers. Homopolymers formed by the reaction between the monomers will affect the thermal behavior and properties of the thermoplastic films developed. To understand the influence of homopolymers, starch was treated (Soxhlet extracted for 24 h) using acetone to remove the homopolymers. The amount of homopolymers in the grafted starch was determined based on the weight differences before and after extraction. A known amount of homopolymers (25−75%) was first dissolved in acetone, and the grafted samples were later added into the solution. Acetone was evaporated, and the samples containing homopolymers were dried and later powdered in a Wiley mill (20 mesh) before being compression molded into films.

Developing Thermoplastics. Grafted starch with and without a known amount of homopolymers was compression molded to form films. Samples (about 10−12 g) were placed between two aluminum foils and compression molded on a carver press at different temperatures for 5 min at a pressure of 20 000−40 000 PSI. The different compression conditions were because of the varying thermoplasticities of the grafted samples. After compression, the press was cooled by running cold water, and samples were collected for further analysis.

Dry and Wet Tensile Properties. Compression-molded films were first conditioned at 21 °C and 65% relative humidity for at least 48 h before being tested. To determine the stability under wet conditions, samples were conditioned at 90% humidity for 24 h in a Caron environmental chamber and then immediately tested. Tensile tests to determine the strength, elongation, and modulus were done on an MTS tensile tester (Model Qtest 10, MTS Corporation, Duluth, MN) according to ASTM standard D 882. The gauge length was 5 cm, and the crosshead speed was 10 mm/min. At least 20 samples from three different films were tested, and the average and standard deviations of the strength, elongation, and modulus were reported.

STATISTICS

Data obtained was analyzed using SAS by the Tukey's pairwise comparison method. The significance level was set at 95% with α = 0.05, and a P value of less than 5% were considered insignificant.

RESULTS AND DISCUSSION

Effect of Grafting Conditions on Grafting Parameters.

Effect of Grafting Temperature. Figure 1a,d shows the influence of temperature on grafting parameters. Increasing the temperature decreased the % grafting efficiency for all four monomers studied, as seen from Figure 1a. There was no

dx.doi.org/10.1021/jf5013709 | J. Agric. Food Chem. 2014, 62, 4668−4676

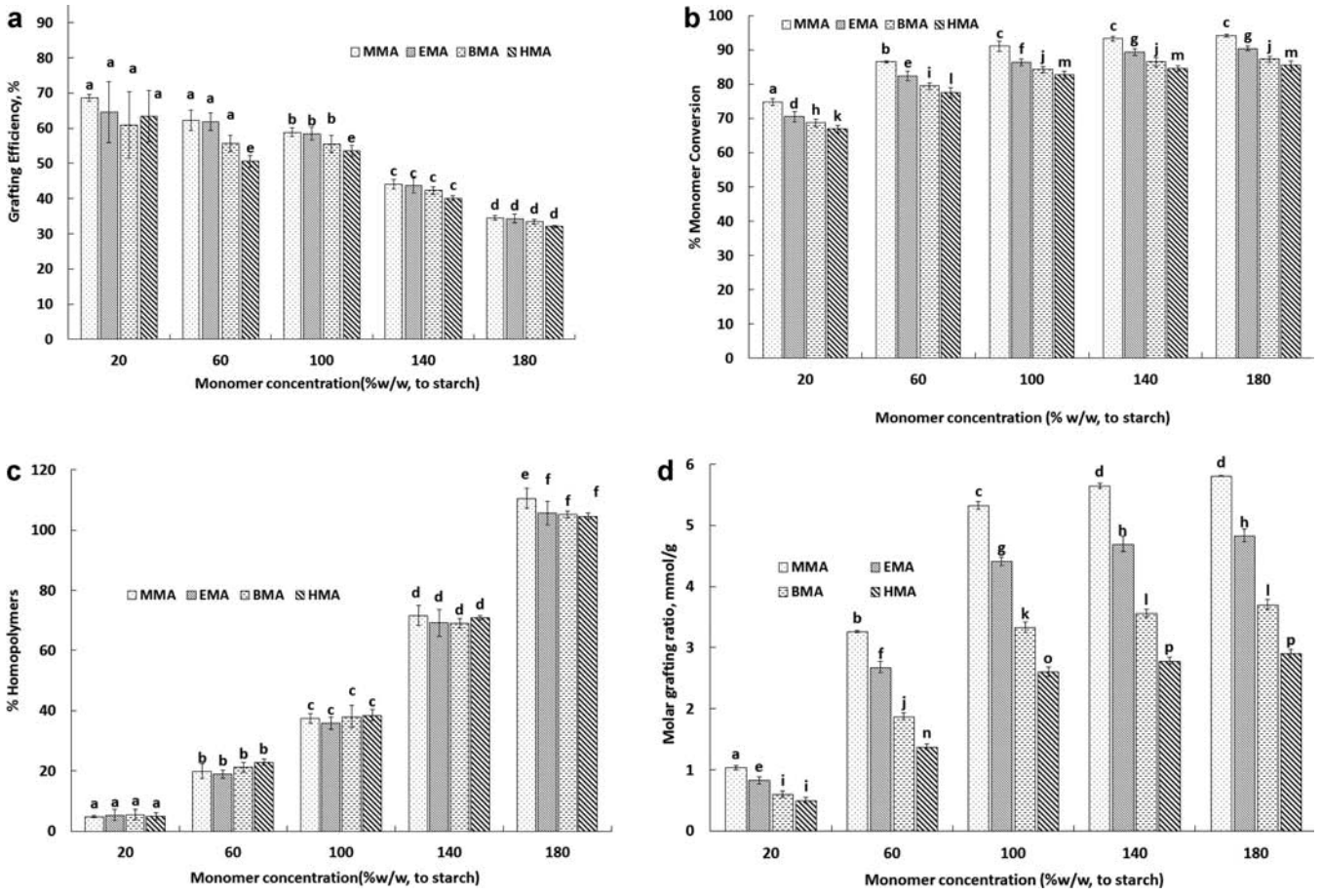

Figure 2. Influence of monomer concentration during grafting on % grafting efficiency (a), % homopolymers (b), % monomer conversion (c), and molar grafting ratio (d). Grafting was performed at 60 °C for 60 min using different concentrations of monomers. For each monomer, data points with the different letters indicate statistically significant difference.

significant change in the grafting efficiency when the temperature was between 40 °C and 60 °C, but the grafting efficiency decreased at 70 °C and 80 °C. Increasing the length of alkyl chain from 2 to 6 (MMA to HMA) decreased the % grafting efficiency at all temperatures studied. Previous studies on the grafting of starch with methacrylates have also shown that increasing temperature increased the grafting efficiency up to a certain temperature, and the % grafting efficiency (GE%) decreased at high temperature.[15] Therefore, a decrease in % GE at high temperatures was attributed to the increase in termination rate of the starch grafted polymeric chain or due to chain transfer to monomer molecules.[15] A decrease in the % GE leads to an increase in % homopolymers when the grafting temperature was 70 °C and 80 °C as seen from Figure 1b. At high temperatures, the monomers move faster and more readily react with each other and form the homopolymers. The % monomer conversion was considerably lower when the temperature was 40 °C, but increased to above 70% for all the monomers when the temperature was 80 °C or higher. Increasing the length of the alkyl chain decreased the % monomer conversion at all temperatures studied, as seen from Figure 1c due to the steric hindrance as the length of the carbon chain increases.[16] This is more evident when the molar grafting ratio is considered for the different monomers. Increasing the temperature increased the molar grafting ratio for all the monomers, as seen from Figure 1d. More interestingly, the grafting ratios decreased as the length of the alkyl chain increased, although the grafting conditions were similar. At a temperature of 60 °C, MMA had a grafting ratio of 5.9 mmol/g, compared to 2.9 mmol/g for HMA. MMA, being a much smaller molecule than HMA, was more easily accessible to starch and was easily grafted and provided higher % grafting. A temperature of 60 °C was found to provide the most optimum grafting for all four monomers studied.

Effect of Monomer Concentration. Increasing monomer concentration continually decreased the % grafting efficiency and increased the % homopolymers, as seen from Figure 2a,b. The % homopolymers were less than 5% for all the monomers when the monomer concentration was 20%. Increasing the monomer concentration leads to a substantial increase in % homopolymers up to about 105−110% when the monomer concentration is 180%. When the monomer concentration was increased above 20%, a higher number of monomer molecules are available for reaction, and therefore, higher numbers of monomers were grafted onto starch. When the monomer concentration increased above an optimum level, the monomers collide with each other and form homopolymers because the growing poly(methacrylate) chain has greater compatibility with the monomer molecules.[15,16] At low monomer concentrations (20%), the % monomer conversion is significantly lower (Figure 2c) because there are fewer molecules in solution that can react and form grafted chains or homopolymers. The molar grafting ratio increased with increasing monomer concentration for all the monomers, as

dx.doi.org/10.1021/jf5013709 | J. Agric. Food Chem. 2014, 62, 4668−4676

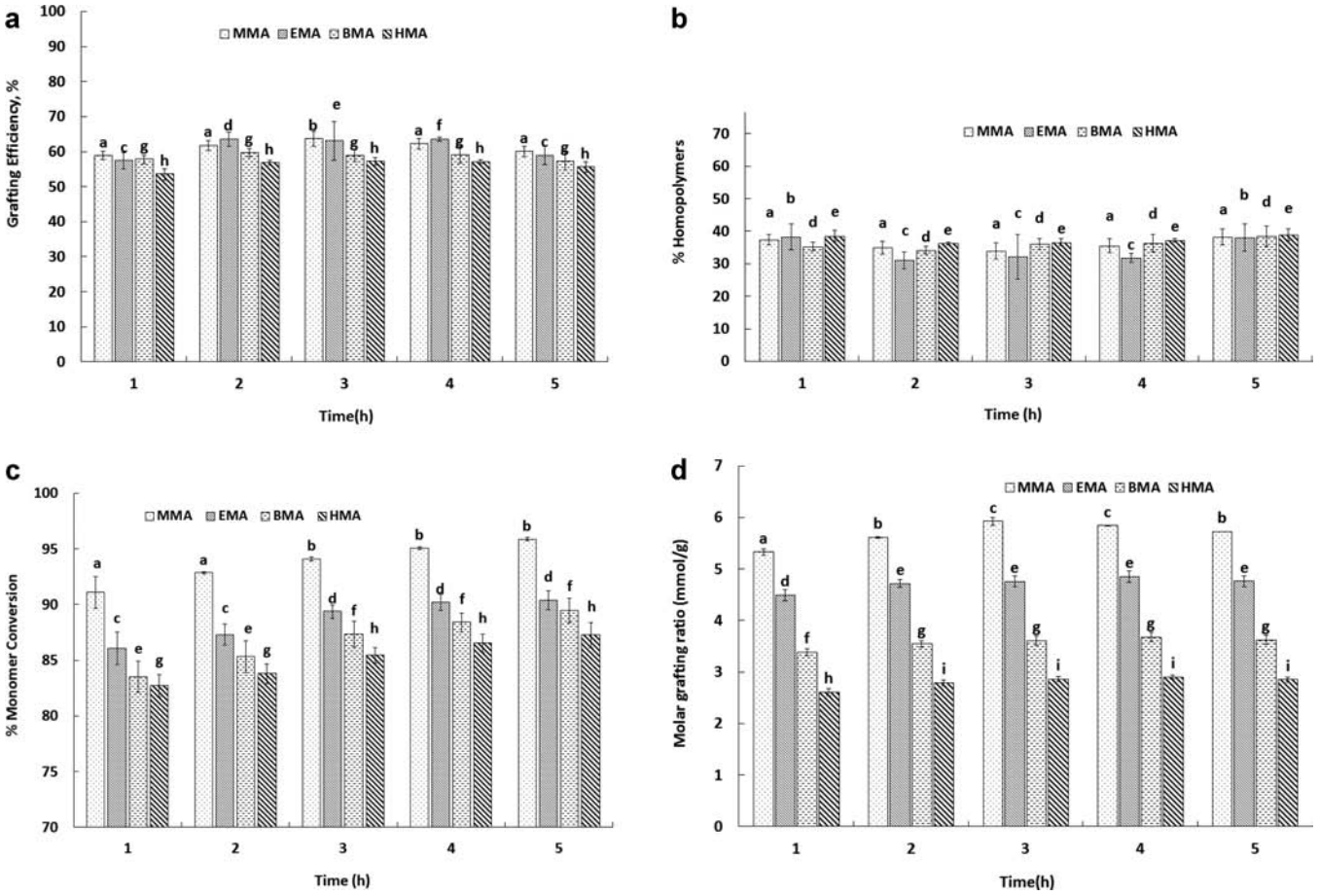

Figure 3. Influence of reaction time on % grafting efficiency (a), % homopolymers (b), % monomer conversion (c), and molar grafting ratio (d). Grafting was performed at 60 °C with 1:1 ratio of monomer to starch. For each monomer, data points with the different letters indicate statistically significant difference.

seen from Figure 2d. However, the grafting ratio decreased substantially with increasing length of the alkyl chain due to steric hindrance of the longer chain monomers and subsequent difficulty in being grafted onto starch.

Effect of Grafting Time. Grafting time did not show a major effect on % grafting efficiency, as seen from Figure 3a. Similarly, the % homopolymers (Figure 3b) also did not show any significant change with increasing reaction time. However, monomer conversion marginally increased with increasing reaction time, as seen from Figure 3c. Previous studies had shown that increasing reaction time from 30 to 60 min significantly increased % GE for MMA, EMA, and BMA. In our reaction, we added the monomers gradually for almost 30 min, and we therefore did not study a reaction time lower than 1 h. Most of the monomers have either been grafted or converted into homopolymers within 1 h, and we therefore do not observe any major change in grafting parameters with increasing reaction time. As observed before, higher alkyl chain length decreased the grafting ratio, and reaction time did not affect the grafting ratio, as seen from Figure 3d.

Characterizing the Grafted Starch. *Fourier Transform Infrared Spectroscopy.* The characteristic carbonyl group in the methacrylates that appears as C═O stretching at about 1730 cm^{-1} is seen in Figure 4 for all four spectra for the grafted starch. The intensity of this peak is highest for HMA, similar for EMA and MMA, and considerably lower for BMA. Presence of the additional peak in the grafted samples that belongs to the

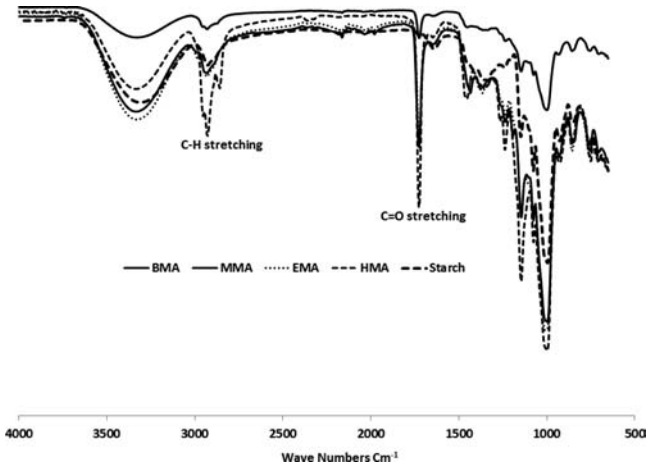

Figure 4. FTIR spectrum of the unmodified and grafted starch depicting the characteristic peaks belonging to the carbonyl group in the monomers. The spectrum was recorded after extracting the homopolymers from the grafted samples.

methacrylates confirms grafting of the monomers onto starch.[9,13] Broad peaks seen between 3500 and 3100 cm^{-1} are due to the hydroxyl groups in starch and the sharp peaks at about 2900 cm^{-1} are due to the C−H stretching from the grafted polymers, also suggesting successful grafting.[12,13]

dx.doi.org/10.1021/jf5013709 | J. Agric. Food Chem. 2014, 62, 4668−4676

Thermal Behavior. Thermal degradations of the grafted starch samples were similar as seen from Figures 5 and 6. A

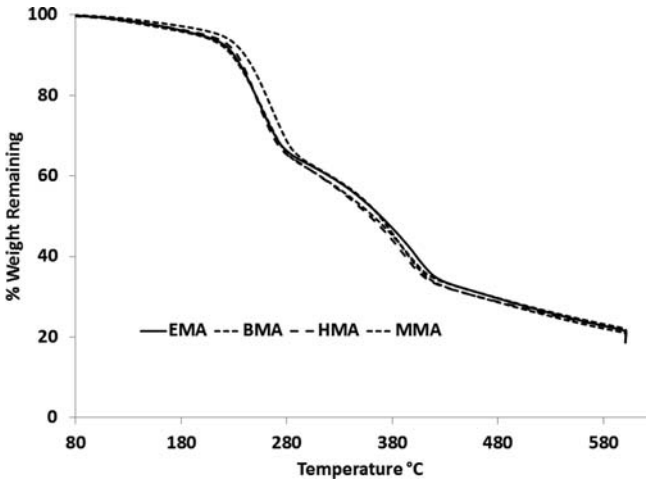

Figure 5. Thermal degradation (% weight loss) of the grafted starch samples when heated to 580 °C.

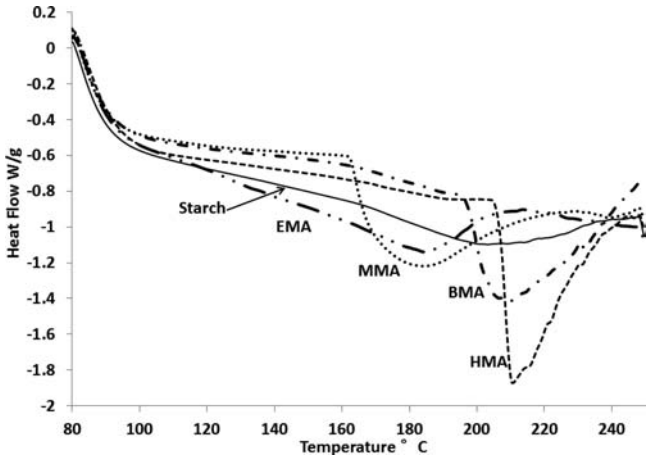

Figure 6. DSC thermograms illustrating that the starches grafted with higher lengths of alkyl chains had better melting when heated to 250 °C.

sharp decrease in the curve is seen around 220 °C, suggesting the start of degradation. MMA showed a slightly lower weight loss than the other samples up to about 300 °C, whereas HMA and EMA showed lower weight loss between 300 °C and 400 °C. An overall weight loss of about 80% was obtained after heating to 600 °C. DSC thermograms clearly show that starch grafted with longer lengths of alkyl esters (BMA and HMA) melted at higher temperatures and had sharper peaks compared to the starch grafted with MMA and EMA. Among the four monomers studied, EMA-grafted starch had a relatively lower melting enthalpy of about 12.6 J/g compared to 50−53 J/g for the other three monomers. As seen from Figure 6, HMA had a sharp and large melting peak at about 210 °C, whereas MMA and EMA produced broad melting peaks ranging from 160 °C to 200 °C. BMA and HMA are more thermally stable than MMA and EMA and therefore melt at higher temperatures. The sharp melting peaks for HMA and BMA suggest that these two polymers may provide better thermoplastic products but need higher processing temperatures. Although the melting peaks for the grafted starch were between 160 °C and 200 °C, the grafted starch could be compression molded into films at 165 °C under pressure, thereby preventing excessive thermal damage to starch at high temperatures.

^{1}H NMR. Grafting of the poly(acrylates) onto starch was evident from the NMR spectra in Figure 7a−d below. As shown in Figure 7a, the H NMR resonances at 3.2−3.8 (protons 2,3,4,5,6), 4.3 (proton 7) and 5.0−5.3 (proton 1) were the characteristic signals from starch. The resonances at 3 and 2.5 ppm were from water and DMSO, respectively. Figure 7b−e illustrated that the H NMR spectrum for the MMA-, EMA-, BMA-, and HMA-grafted starch, respectively. It could be seen that polyacrylates and starch moieties were present in the spectrum. After grafting with acrylates, resonances at 0.9−2.0 ppm appeared, which were the signals of CH_3, CH_2, and CH groups in the polyacrylate. The resonance of 4.3 ppm (proton 7) decreased or disappeared in the spectra, which clearly confirmed the grafting of polyacrylates onto the hydroxyl group of starch. The signal of $COOCH_3$ group of polyacrylate overlapped with protons 2−6 of the starch, which made the resonance at 3.2−3.8 ppm more complicated.

Tensile Properties of Compression Molded Starch Films. Table 1 provides a comparison of the tensile strength of the starch films grafted with the four different monomers and containing different levels of homopolymers. On the basis of the tensile strength in Table 1, it can be observed that increasing the length of alkyl chains from 2 to 4 increased the strength of the films when there was no homopolymer but HMA grafted starch films had considerably lower strength than BMA-grafted films. BMA had strength of 1 MPa compared to 0.2 and 0.3 MPa for MMA and EMA, respectively, whereas HMA-grafted films have a strength of 0.5 MPa. Addition of homopolymers continually increased the strength for all the monomers. With 50% homopolymers, the strength of the MMA- and EMA-grafted films were nearly 10 times higher, 3 times higher for BMA films, and twice higher for HMA films. Films made from the 100% homopolymers showed that increasing the length of the alkyl chain considerably decreased the tensile strength. For instance, MMA-homopolymer films had a strength of 12.8 MPa, compared to 3 MPa for HMA-homopolymer films. MMA- and EMA-grafted films showed considerably lower elongation than BMA and HMA films, especially with the addition of homopolymers. With 50% homopolymers, BMA films had the highest strength, although HMA-grafted films showed higher elongation than the films containing the other monomers.

Although MMA and EMA provided films with good dry tensile properties, the films containing up to 75% homopolymers were unstable in water, became too weak, and could not be tested even after conditioning at 90% humidity for 24 h at 21 °C. BMA- and HMA-grafted films showed good stability to moisture, especially in the presence of homopolymers, as seen from Table 1. In fact, the wet strength of the films grafted with HMA and containing 50% and 75% homopolymers is similar to or higher than the dry strength of the films. Tensile properties of the grafted starch films will depend on the extent of grafting, amount of homopolymers, and the inherent properties of the monomers and homopolymers. BMA provides better thermoplasticity, melts the starch and therefore provides the films with good tensile strength. In addition, increasing the alkyl chain length decreased the hydrophilicity, and therefore, BMA- and HMA-grafted films had better water stability than MMA and EMA films.

dx.doi.org/10.1021/jf5013709 | J. Agric. Food Chem. 2014, 62, 4668−4676

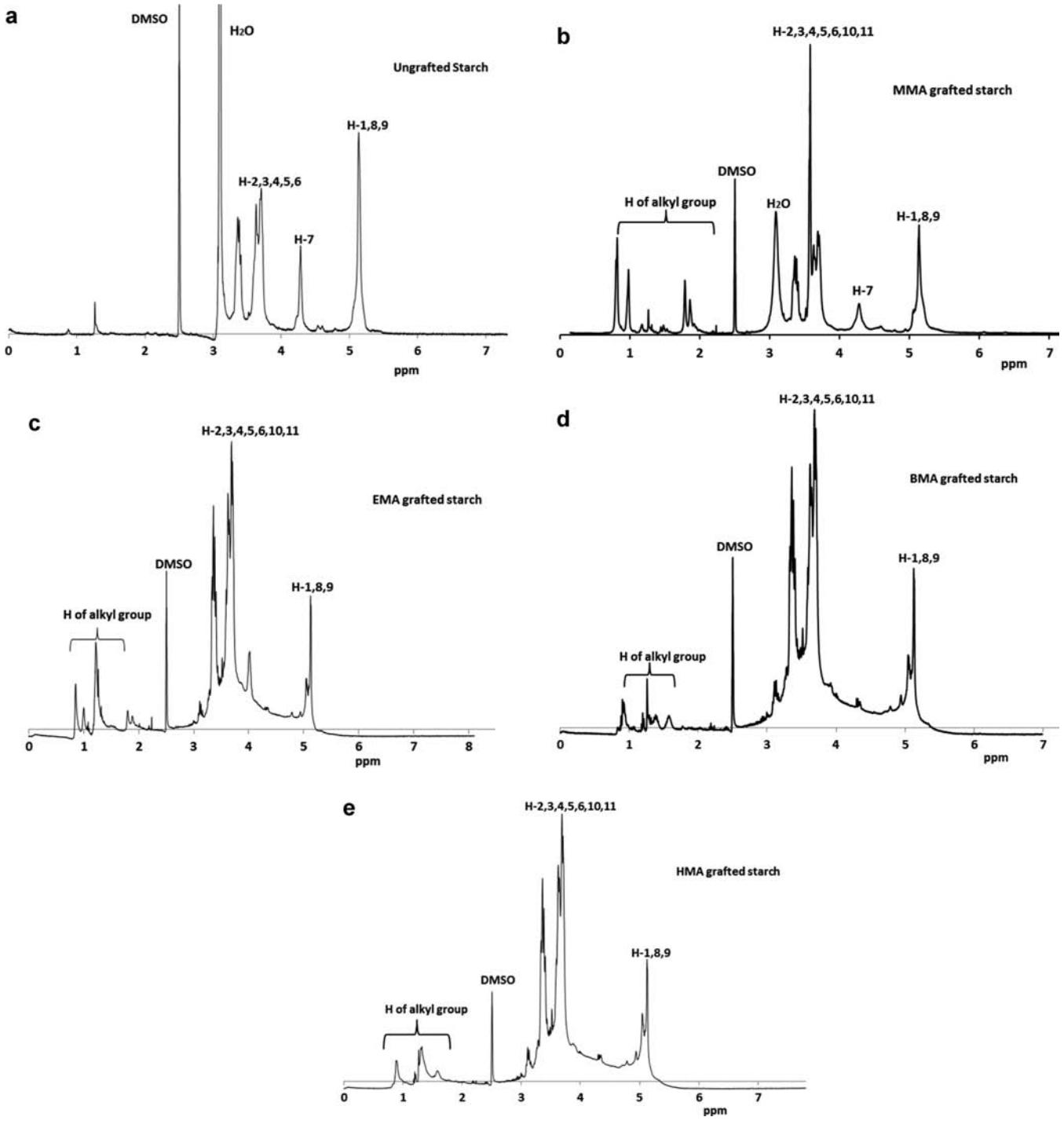

Figure 7. [1]H NMR spectra of the ungrafted starch (a), MMA-grafted starch (b), EMA-grafted starch (c), BMA-grafted starch (d), and HMA-grafted starch (e) with the position of the various hydrogen atoms.

Elongation of the films also showed that increasing the alkyl chain length and amount of monomers increases elongation. Without any homopolymers, MMA had an elongation of 2.8%, compared to 3.2% for HMA. Starch films grafted with HMA were considerably softer and therefore had lower strength but higher elongation (than BMA containing films). Increasing the length of alkyl chains increases the flexibility of the side chains, and therefore, the elongation of the films with BMA and HMA was higher than those of MMA- and EMA-containing homopolymers. Addition of homopolymers did not show an increase in the elongation of MMA- or EMA-grafted films, but the elongation of the BMA- and HMA-grafted films increased up to 10 times. BMA-grafted films without homopolymers had an elongation of 3.1%, compared to 8.5% when 50% homopolymers were added. HMA-grafted films without any homopolymers had an elongation of 3.2%, compared to 10.4% when the homopolymer content was 50%. Increase in elongation for the BMA and HMA films should be due to the high elongation of the BMA (71%) and HMA (111%) homopolymers. Wet elongation of the BMA- and HMA-grafted films also showed a similar trend with elongations of 8.6 and

dx.doi.org/10.1021/jf5013709 | J. Agric. Food Chem. 2014, 62, 4668−4676

Table 1. Dry and Wet Tensile Strength of Starch Films Grafted (2.7 mmol/(g) with Four Different Monomers and Containing Different Ratios of Homopolymers[a]

	breaking stress, MPa							
	MMA		EMA		BMA		HMA	
% homo polymers	dry	wet	dry	wet	dry	wet	dry	wet
0	0.23 ± 0.04^{a}	0	0.36 ± 0.09^{a}	0	1.0 ± 0.1^{b}	0.4 ± 0.03^{E}	0.5 ± 0.1^{a}	0.4 ± 0.09^{E}
25	0.45 ± 0.01^{a}	0	2.4 ± 0.7^{c}	0	2.5 ± 0.4^{c}	1.9 ± 0.6^{D}	0.8 ± 0.1^{b}	1.4 ± 0.5^{D}
50	2.9 ± 0.6^{d}	0	3.0 ± 0.4^{d}	0	3.4 ± 0.2^{e}	1.6 ± 0.7^{D}	1.0 ± 0.1^{b}	1.6 ± 0.7^{D}
75	4.1 ± 0.5^{f}	0	3.9 ± 0.5^{f}	0	4.3 ± 0.4^{f}	2.1 ± 0.6^{C}	1.5 ± 0.4^{b}	2.1 ± 0.6^{C}
100	12.8 ± 1.0^{h}	5.0 ± 1.2^{H}	8.5 ± 0.9^{g}	5.5 ± 0.7	5.8 ± 0.6^{c}	2.5 ± 0.6^{C}	3.0 ± 0.8^{e}	2.5 ± 0.6^{C}

[a]Films were compression molded at 165 °C for 5 min. For each monomer, data points with the different letters indicate statistically significant difference.

16.4% for the BMA and HMA films containing 50% homopolymers.

On the basis of the strength and elongation of starch films grafted with various monomers, BMA was found to be more suitable to obtain films with good strength and elongation. A digital picture of a film made by compression molding starch grafted with BMA is shown in Figure 8. The film is transparent,

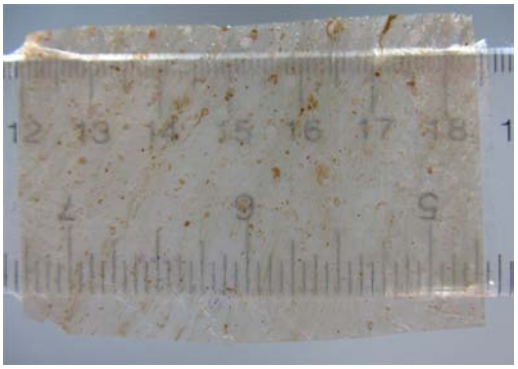

Figure 8. A digital picture of a film made by compression molding starch grafted with BMA.

indicating that the grafted starch could be melted and made into thermoplastic products. Further studies were done to develop films from BMA with different grafting ratios and study the dry and wet tensile properties, since films grafted with MMA and EMA were weak and could not be tested after conditioning at 90% humidity for 24 h.

Increasing the % grafting from 2.1 to 4.2 mmol/g (30% to 60% grafting) substantially increased the strength and elongation of the BMA grafted starch films from 1 to 3.2 MPa. There was also a considerable increase in the wet strength of the films (from 0.4 to 1.8 MPa) because of the increase in the amount of the hydrophobic polymer with increasing % grafting. When the grafting was 50%, the wet strength of the films was about 30% of the dry strength. Elongation of the films also increased from 3% to 12% when the grafting ratio was increased from 2.1 to 4.2 mmol/g. The corresponding increase in the wet elongation was from 6.7% to 25%. Strength and elongation of the films increased with increasing % grafting, since the grafted starch became more thermoplastic and formed better films. In addition, the grafted polymer had better strength and elongation than starch, and increasing the % of the grafted polymer therefore increased the tensile properties. Stability of the films under high humidities and in water is important for various applications, especially for food packaging. BMA-grafted films showed good dry and wet tensile properties even when the grafting was 30%. Therefore, BMA grafted starch films could be useful for food and other applications.

Starch grafted with BMA provided thermoplastic films with good strength and water stability. At similar grafting ratios, although increasing the length of the alkyl esters provided higher thermoplasticity and increased water stability, HMA homopolymers were considerably softer and decreased the strength of the starch films. Increasing the chain length also decreased the grafting ratio due to stearic hindrance from the monomers with longer side chains. Homopolymers considerably affected the tensile properties and water stability. Increasing the % of homopolymers generally increased the tensile strength and elongation. Films grafted with EMA were considerably brittle with elongation of 1−3%, whereas films grafted with BMA and HMA had elongations between 5% and 35%, depending on the amount of homopolymers. Overall, BMA was found to be more suitable for developing thermoplastic starch products with good tensile properties and water stability.

AUTHOR INFORMATION

Corresponding Author

*Fax: 402-472-0640; e-mail: yyang2@unl.edu.

Notes

The authors declare no competing financial interest.

ACKNOWLEDGMENTS

The authors thank the Program for Changjiang Scholars and Innovative Research Team in University (No. IRT1135) at Jiangnan University, Scientific Support Program of Jiangsu Province (BE2011404), the Graduate student innovation plan of Jiangsu Province (CX10B_222Z), the Doctor Candidate Foundation of Jiangnan University (JUDCF10004), agricultural research division, and the USDA-HATCH act and Multistate project S1054(NEB 37-037) at the University of Nebraska—Lincoln for their financial support. The China scholarship council is also acknowledged for providing the living expenses for the visiting scholar (Z.S.).

REFERENCES

(1) Alissandratos, A.; Halling, P. J. Enzymatic acylation of starch. *Biores. Technol.* **2012**, *115*, 41−47.

(2) Jimenez, A.; Jose Fabra, M.; Talens, P.; Chiralt, A. Edible and biodegradable starch films: A Review. *Food Bioproc. Technol.* **2012**, *5* (6), 2058−2076.

(3) Cyras, V. P.; Manfredi, L. B.; Ton-That, M.-T.; Vazquez, A. Physical and mechanical properties of thermoplastic starch/montmorillonite nanocomposite films. *Carbohyd. Polymr.* **2008**, *73* (1), 55−63.
(4) Arvanitoyannis, I. S.; Vlachos, A. Maize Authentication: Quality Control Methods and Multivariate Analysis (Chemometrics). *Crit. Rev. Food Sci. Nutr.* **2009**, *49* (6), 501−537.
(5) He, G. J.; Liu, Q.; Thompson, M. R. Characterization of structure and properties of thermoplastic potato starch film surface cross-linked by UV irradiation. *Starch-Starke* **2013**, *65* (3−4), 304−311.
(6) Soares, F. C.; Yamashita, F.; Mueller, C. M. O.; Pires, A. T. N. Thermoplastic starch/poly(lactic acid) sheets coated with cross-linked chitosan. *Polym. Test.* **2013**, *32* (1), 94−98.
(7) Reddy, N.; Yang, Y. Citric acid cross-linking of starch films. *Food Chem.* **2010**, *118* (3), 702−711.
(8) Singh, A. V.; Nath, L. K.; Guha, M. Synthesis and characterization of highly acetylated sago starch. *Starch-Starke* **2011**, *63* (9), 523−527.
(9) Zhang, B.; Zhou, Y. Synthesis and characterization of graft copolymers of ethyl acrylate/acrylamide mixtures onto starch. *Polym. Comp.* **2008**, *29* (5), 506−510.
(10) Jyothi, A. N. Starch graft copolymers: Novel applications in industry. *Comp. Interface* **2010**, *17* (2−3), 165−174.
(11) Kaewtatip, K.; Tanrattanakul, V.; Szecsenyi, K. M.; Pavlicevic, J.; Budinski-Simendic, J. Thermal properties and morphology of cassava starch grafted with different content of polystyrene. *J. Thermal Anal. Calorim.* **2010**, *102* (3), 1035−1041.
(12) Fakhru'l-Razi, A.; Qudsieh, I. Y. M.; Yunus, W.; Ahmad, M. B.; Rahman, M. Z. A. Graft copolymerization of methyl methacrylate onto sago starch using ceric ammonium nitrate and potassium persulfate as redox initiator systems. *J. Appl. Polym. Sci.* **2001**, *82* (6), 1375−1381.
(13) Pimpan, V.; Thothong, P. Synthesis of cassava starch-*g*-poly(methyl methacrylate) copolymers with benzoyl peroxide as an initiator. *J. Appl. Polym. Sci.* **2006**, *101* (6), 4083−4089.
(14) Zhu, Z.; Zhang, L.; Li, M.; Zhou, Y. Effects of starch alkenylsuccinylation on the grafting efficiency, paste viscosity, and film properties of alkenylsuccinylated starch-*g*-poly(acrylic acid). *Starch-Starke* **2012**, *64* (9), 704−712.
(15) Athawale, V. D.; Rathi, S. C. Effect of chain length of the alkyl group of alkyl methacrylates on graft polymerization onto starch using ceric ammonium nitrate as initiator. *Eur. Polym. J.* **1997**, *33* (7), 1067−1071.
(16) Vazquez, B.; Goni, I.; Gurruchaga, M.; Valero, M.; Guzman, G. M. Synthesis and characterization of graft-copolymers of methacrylonitrile methacrylate mixtures onto amylomaize by the ceric ion method. *J. Polym. Sci., Part A: Polym. Chem.* **1992**, *30* (8), 1541−1548.
(17) Willet (Willett, J. L. Starch in Polymer Compositions. In *Starch: Chemistry and Technology*, 3rd ed.; BeMiller, J., Whistler, R., Eds.; Academic Press: New York, 2009; pp 715−737.
(18) Trimnell, D.; Swanson, C. L.; Shogren, R. L.; Fanta, G. F. Extrusion processing of granular starch-*g*-poly(methylacrylate)-effect of extrusion conditions on morphology and properties. *J. Appl. Polym. Sci.* **1993**, *48* (9), 1665−1675.
(19) Dennenberg, R. J.; Bothast, R. J.; Abbott, T. P. A new biodegradable plastic made from starch graft poly(methyl acrylate) copolymers. *J. Appl. Polym. Sci.* **1978**, *22*, 459−465.
(20) Bagley, E. B.; Fants, G. F.; Burr, R. C.; Doane, W. M.; Russell, C. R. Graft copolymers of polysaccharides with thermopalastic polymers, a new type of filled plastic. *Polym. Engg. Sci.* **1977**, *17* (5), 311−315.
(21) Jin, E.; Reddy, N.; Zhu, Z.; Yang, Y. Graft polymerization of native chicken feathers for thermoplastic applications. *J. Agric. Food Chem.* **2011**, *59* (5), 1729−1738.
(22) Reddy, N.; Jin, E.; Chen, L.; Jiang, X.; Yang, Y. Extraction, characterization of components, and potential thermoplastic applications of camelina meal grafted with vinyl monomers. *J. Agric. Food Chem.* **2012**, *60* (19), 4872−4879.

JOURNAL OF AGRICULTURAL AND FOOD CHEMISTRY

Article

pubs.acs.org/JAFC

Fabrication of Epigallocatechin-3-gallate Nanocarrier Based on Glycosylated Casein: Stability and Interaction Mechanism

Jin Xue, Chen Tan, Xiaoming Zhang, Biao Feng, and Shuqin Xia*

State Key Laboratory of Food Science and Technology, School of Food Science and Technology, Jiangnan University, Lihu Road 1800, Wuxi, Jiangsu 214122, China

Supporting Information

ABSTRACT: Polyphenols normally have strong binding affinity with proteins, which may lead to protein precipitation. Glycosylation of protein via Maillard reaction in mild condition may inhibit the precipitation. This study prepared nanocomplexes of epigallocatechin-3-gallate (EGCG) and protein, and their stability against environmental stress was investigated. Subsequently, these findings were correlated with the interactions between EGCG and casein. Results showed that glycosylated casein displayed strong encapsulating and retaining capacity to EGCG, and no obvious aggregation or fusion appeared in the concentration range of 0.25−5.00 mg/mL during storage. The in vitro release demonstrated that casein, especially glycosylated casein, could effectively protect EGCG from degradation in alkaline pH and displayed a slow and sustained release in intestinal fluid, which may be attributed to the inhibiting effects of casein binding on the motion freedom of EGCG. Fluorescence quenching spectra demonstrated that the steric hindrance induced by dextran could inhibit the interaction between casein and EGCG. These findings demonstrated that glycosylated casein could be used as a promising and effective nanocarrier for EGCG.

KEYWORDS: *epigallocatechin-3-gallate, casein, glycosylation, Maillard reaction, stability, nanocarrier, fluorescence quenching*

INTRODUCTION

Tea polyphenols are being consumed by over two-thirds of the world's population and have shown versatile beneficial bioactivities.[1,2] The typical polyphenols in green tea include epigallocatechin-3-gallate (EGCG), epigallocatechin (EGC), epicatechin (EC), and epicatechin-3-gallate (ECG). Among these ingredients, EGCG is the most abundant and effective one.[3] However, EGCG is sensitive to pH, temperature, and oxygen, which limits its commercial applications in the food industry.[4] The lack of stability presents a significant challenge to design a vehicle that can protect EGCG from oxidation and degradation and thereby expand its industrial application.[1,3]

Encapsulation has been recognized as an effective approach to enhance the stability of EGCG against pro-oxidant elements.[5] So far, several delivery carriers have been applied to encapsulate EGCG, including liposomes,[6] polysaccharides,[7] proteins, and denatured protein.[8] Among these carriers, protein molecules can cross-link to each other, forming colloidal particles to encapsulate tea polyphenols effectively. EGCG binds to a wide variety of proteins, especially to those having random coil conformations (e.g., casein with 30−35% random coil) with a high content of proline.[9] The phenolic groups and associated aromatic rings in protein structure enable EGCG to build bridges between protein molecules.[10] Milk proteins have been mainly reported as possible carriers for bioactive compounds. It was proposed that EGCG may associate with heated β-lactoglobulin through hydrophobic interactions and hydrogen bonds, leading to the formation of visible microfibrilar structures.[8] Recently, casein has become rapidly recognized due to its unique unfolded structure under native conditions from the family of unstructured proteins. Fluorescence quenching,[11] single-molecule force microscopy,[10] dynamic laser light scattering,[12] small-angle X-ray scattering,[12] and some other biophysical techniques have demonstrated that EGCG has a strong binding affinity with α-casein and β-casein. Thus, casein seemed to be a promising carrier for EGCG.

Nevertheless, casein is sensitive to the variations of the ionic strength and pH in the aqueous phase. In protein-based cases, it is difficult to control the size and colloidal stability of the protein−polyphenol nanoparticles with a high loading capacity of polyphenols.[13] The precipitation of polyphenols at high loading capacity with proteins can be partly inhibited by polysaccharides through the formation of ternary protein−polyphenol−carbohydrate complexes and/or blocking of the interactions between polyphenols and proteins.[14] However, the combination of hydrophilic polysaccharide and protein creates mostly noncovalent interactions, which are sensitive to environment conditions. Accordingly, the aggregation or phase separation might take place arising from the binding at high EGCG loading capacity. Additionally, delivery systems with average sizes smaller than 100 nm and high loading capacity have scarcely been reported, and an effective system for the delivery of EGCG in clear aqueous system is still being probed. The Maillard reaction via conjugation with polysaccharide is one of the most effective methods that can obviously improve protein properties, such as emulsifying ability, solubility, stability, and antioxidation.[15] In addition, it is noted that the high hydration capacity and the presence of uncharged polysaccharide exert contrasting effects on these functional properties of casein, probably

Received: July 25, 2013
Revised: February 6, 2014
Accepted: March 26, 2014
Published: March 26, 2014

ACS Publications © 2014 American Chemical Society

dx.doi.org/10.1021/jf405157x | J. Agric. Food Chem. 2014, 62, 4677−4684

depending on the anchorage of the hydrophobic residues of protein molecule and the orientation of the polysaccharide moiety to the aqueous layer.[13,16] Glycosylated proteins have been devoted to the encapsulated application of anthocyanin[17] and drug molecules[18] and have provided a good reference for an intestinal-targeted delivery system of vulnerable functional ingredients. Many research studies have been carried out on the interaction between proline-rich salivary glycoprotein[19] and polyphenols, but fewer papers concern the interaction between polyphenols and glycosylated proteins obtained via Maillard reaction.

In this work, EGCG nanocarrier was developed on the basis of glycosylated casein (casein−dextran conjugate) via Maillard reaction aiming to improving the stability of EGCG in the food industry, especially in clear beverages. The encapsulating properties of native and glycosylated casein were compared by using dynamic light scattering (DLS) and transmission electron microscopy (TEM). The entrapment efficiency and in vitro release behavior of EGCG were determined by high-performance liquid chromatography (HPLC). To gain insights into the influence of glycosylation, the interactions between EGCG and protein (native and glycosylated casein) were investigated by means of fluorescence spectroscopy. Some important pieces of information such as the binding constants and binding site values were compared.

MATERIALS AND METHODS

Materials. EGCG (98% purity) was purchased from Shanghai Qiangsheng Biochemical Ltd. (Shanghai, China). Casein (molecular mass 25−30 kDa, 99% purity) and dextran (molecular mass 20 kDa) were purchased from Sino-pharm Chemical Reagent Co., Ltd. (Shanghai, China). Methanol and acetonitrile were of HPLC grade (Sino-pharm Chemical Reagent Co., Ltd.). *o*-Phthaldialdehyde (OPA) of chemical grade was obtained from Sino-pharm Chemical Reagent Co., Ltd. Sodium chloride, hydrochloric acid, sodium hydroxide, monopotassium phosphate, and cholate were purchased from Sino-pharm Chemical Reagent Co., Ltd. Pepsin (activity 3000−3500 U mg^{-1}) and pancreatin consisting of protease (activity 285 U mg^{-1}), amylase (activity 288 U mg^{-1}), and lipase (activity 56 U mg^{-1}) were purchased from Sangong Biotech Co., Ltd. (Shanghai, China). Other reagents used were of analytical grade. All aqueous solutions were prepared using deionized water.

Synthesis of Casein−Dextran Conjugates. Casein−dextran (20 kDa) conjugates were synthesized via Maillard reaction as reported by Nakamura et. al with minor modification.[20] Research showed that dextran of 20 kDa supported a higher grafted degree than monosaccharide with a small molecule weight and more moderate viscosity than macromolecular polysaccharide.[21] Specifically, casein and dextran at the fixed mass ratio of 1:7 (corresponding to a molar ratio 1:6) were dissolved together in phosphate buffer solution (0.2 mol/L) at room temperature, and the pH of the mixture was adjusted to 7.0. After continuous stirring for 12 h, the solution was freeze-dried for 2 days at −50 °C. The lyophilized powder was heated at 60 °C for 20 h under 79% relative humidity in a desiccator containing saturated KBr solution. Samples were stored at −20 °C in the dark. The related mixtures were then dispersed in distilled water to a concentration of 0.5 mg/mL. To obtain the pure glycosylated casein, the sample was conducted with a 50 mL Microsep Advance Centrifugal Device (molecular weight cutoff of 100 K; Pall Corp., Port Washington, NY, USA) at 7000 rpm for 30 min until 15 mL of the initial volume remained followed by the addition of deionized water to the original volume. These procedures were repeated three times, and then the retentates were freeze-dried and stored at 4 °C.

OPA Assay. The grafting degree of casein−dextran conjugate was analyzed through an OPA assay, which was expressed as the changes in free amino group contents per gram of casein after Maillard reaction as previously reported.[22] Four milliliters of free OPA reagent was added in 200 μL of casein−dextran conjugate solutio,n and the mixture was incubated at 35 °C for 2 min. Then, the absorbance of the mixture was measured at 340 nm immediately using a spectrophotometer (UV-1600, Mapada Instruments Co., Ltd., China). The OPA reagent was used as the blank. The L-lysine curve was measured as a standard.

Molecular Weight Determination of Glycosylated Casein. The weight-average molecular weight ($\bar{M}_w$) and number-average molecular weight ($\bar{M}_n$) of glycosylated casein after modification were analyzed by aqueous high-performance size exclusion chromatography (HPSEC)[23,24] with a multiangle laser light scattering (MALLS) setup (Wyatt Technology Corp., Santa Barbara, CA, USA). The refractive index increment (dn/dc) of glycosylated casein and its molecular fraction determined experimentally was used. $\bar{M}_w$, $\bar{M}_n$, and radius of gyration (R_g) were calculated by Astra 1.4 software (MALLS). Glycosylated casein and its molecular fraction were analyzed with a SEC protein column (5 μm, 300 Å, 7.8 × 300 nm). The mobile phase was determined using 0.1 mol/L NaCl containing 0.04% NaN_3 with a flow rate of 0.4 mL/min, and the injection volume was determined at 200 μL. Each sample was analyzed at least three times.

Preparation of EGCG Nanocomplexes Composed of Casein and Glycosylated Casein. Casein−EGCG and glycosylated casein−EGCG nanocomplexes were prepared according to a previous paper with a slight modification.[25] Briefly, casein and glycosylated casein were dissolved in the 0.2 mol/L phosphate buffer at pH 7.0 and stirred overnight at room temperature. The weight concentration of casein was adjusted to 1.0 mg/mL. EGCG solution was prepared using acetate buffer (0.2 mol/L, pH 4.5). EGCG solution was mixed with the two kinds of proteins (1:19, v/v) respectively at room temperature to obtain different weight concentrations according to EGCG/protein molar ratios (0:1, 1:1, 2:1, 6:1, 10:1, 16:1, 32:1, 64:1, 128:1, 256:1). Samples were stored at 4 °C under N_2 atmosphere in a dark environment.

Size Measurement. The *z*-average diameter and size distribution of casein−EGCG and glycosylated casein−EGCG complexes were carried out at 25 ± 0.1 °C using a Nano-ZS90 particle size analyzer (Malvern Instruments Ltd., Malvern, UK) with a He/Ne laser (λ = 633 nm), scattering angle 90°. Aliquots of 1 mL of sample were diluted to 10 mL with the same buffer solution to avoid multiple scattering phenomena due to interparticle interaction.[26] Immediately, the diluted sample was transferred into the polystyrene curet for size determination, and then the *z*-average diameter (D_z) and particle size distribution (polydispersity index, PDI) were recorded by DLS.

Entrapment Efficiency. Aliquots of protein−EGCG complex solution (2 mL) were transferred into an Amicon Ultra-3K centrifugal filter device (Pall Corp.). After centrifugation at 4000 rpm for 30 min, free EGCG penetrated through the Ultracel membrane into the centrifuge tube, which was determined by HPLC. The elution was carried out on a C_{18} column (5 μm, 39 × 150 mm, Atlantis, Waters, Milford, MA, USA), the mobile phase was methanol/water (99.9:0.1, v/v), the injection volume was 5 μL, and the wavelength was set at 280 nm. EGCG standard curve was $Y = 10^7X - 15669$ (R^2 = 0.9985) in the concentration range of 0.01−0.1 mg/mL and $Y = 10^7X - 90217$ (R^2 = 0.9984) in the concentration range of 0.1−1.0 mg/mL, where X is the concentration and Y is the peak area. The entrapment efficiency was determined using the following equation:

$$\text{entrapment efficiency (\%)} = \frac{\text{amount of entrapped EGCG}}{\text{total amount of EGCG}} \times 100$$

Storage Stability. During the 10 days of storage at 4 °C under N_2 atmosphere in a dark environment, an aliquot of samples was used for size and retention rate measurements. The retention rate and change of *z*-average diameter (ΔD_Z) were determined respectively using the following equations:

$$\text{retention rate (\%)} = \frac{\text{amount of entrapped EGCG after storage}}{\text{amount of entrapped EGCG initially prepared}} \times 100$$

$$\Delta D_z\ (\%) = \frac{D_z \text{ after incubation at predetermined time} - D_z \text{ initially prepared}}{D_z \text{ initially prepared}} \times 100$$

After 15 days storage, the samples of EGCG−casein (mole ratio 64:1), direct mixture of EGCG/casein/dextran (64:1:6), and EGCG−glycosylated casein (64:1) were taken out to observe the state of suspension.

In Vitro Release. The simulated gastric fluid (SGF) or intestinal fluids (SIF) were prepared according to a previous study.[27] SGF consisted of sodium chloride (2 g/L), hydrochloric acid 37% (0.008 L/L), and pepsin (3.2 g/L). The pH was adjusted to 1.3 using hydrochloric acid. SIF consisted of sodium hydroxide (1.81 g/L), potassium dihydrogen phosphate (8.09 g/L), pancreatin (4.76 g/L), and bile salts (5.16 g/L). The pH was adjusted to 7.5 using sodium hydroxide. The release profile of EGCG from protein was assessed using a dialysis method (cutoff molecular weight of 8000 Da). A solution of 10.0 mL of EGCG−casein and EGCG−glycosylated casein nanocomplexes with EGCG/protein molar ratio 10:1 was transferred into a dialysis bag and dialyzed against 40 mL of SGF or SIF. Then the release medium was incubated at 37 °C in a multipoint stirrer (SKY-110WX, Shanghai, China) equipped with a water bath. At a predetermined sampling time, 200 μL of release medium was drawn out and replenished with 200 μL of fresh buffer. All of the samples were protected from light. The amount of released EGCG was measured by HPLC as described above. The cumulative release rate was determined by using the calculation[28]

$$\text{cumulative release percentage}_t\ (\%) = \frac{\sum_{i=1}^{i=t-1} c_i V_i + c_t V_t}{\text{total EGCG (mg)}} \times 100$$

#tab;where c_i and c_t are the concentrations of EGCG in the release medium at times i and t, respectively. V_i is the withdrawn volume from release medium at time i. V_t is the release medium volume at time t.

Transmission Electron Microscopy. TEM micrographs were conducted on a Hitachi-7650 at an accelerating voltage of 200 kV. The samples were prepared with a casein concentration of 1.0 mg/mL, and the EGCG/casein molar ratios were 0:1 and 4:1, respectively. An aqueous suspension of the samples was deposited upon a carbon-coated copper grid, followed by air-drying for 1 min. Then, the sample was instantly stained with 1 wt % ammonium molybdate.[29]

Fluorescence Quenching of Protein by EGCG. To investigate the interaction between EGCG and casein, a fluorescence quenching method was used with a fluorescence spectrometer (Hitachi F-7000, Japan). The fluorescence spectra of casein, glycosylated casein, and their EGCG complexes at different EGCG/casein molar ratios (0:1, 0.5:1, 1:1, 2:1, 6:1, 10:1, 16:1, 32:1) were scanned, respectively. All measurements were performed at 15 °C. Emission spectra were recorded from 285 to 500 nm with an excitation wavelength of 280 nm and from 290 to 500 nm with an excitation wavelength of 295 nm, employing excitation slit widths of 2.5 nm and emission slit widths of 5.0 nm.

Statistical Analysis. In this study all samples were prepared and analyzed in triplicate. The data are presented as means ± standard deviation of three determinations. Statistical significance ($p < 0.05$) was determined with the analysis of variance (one-way ANOVA) using SPSS 16.0 (SPSS Inc., Chicago, IL, USA).

RESULTS AND DISCUSSION

Synthesis of Casein−Dextran Conjugate. The Maillard reaction is a chemical reaction that involves linking polysaccharide and peptides or proteins by reducing end carbonyl groups and amino groups.[30] Herein, casein and dextran were used to prepare Maillard reaction products (MRPs), which were confirmed by the grafting degree (GD) assessed via OPA assay. It was found that the GD was about 22.97 ± 2.01% in the casein−dextran conjugate at the mass ratio of 1:7 (molar ratio of 1:6). Rival and his co-workers have demonstrated with a fluorometric method that casein consisted of four principal proteins, α_{s1}-casein, α_{s2}-casein, β-casein, and κ-casein, in the weight ratio of 3:0.8:3:1, corresponding with lysine residue numbers of 14, 24, 11, and 9, respectively.[31] According to the calibration and calculations of the molecular weight of casein and free lysine, the milligrams of lysine to milligrams of casein factor is $F = \sum((R_L W_L)/(W_C R_P)) = 0.08484$, where R_L is residues of lysine in each casein, $W_C = 5$, and W_L is the molecular weight of lysine.[32] This implied that the average number of free lysine residues of casein was up to 13.[33] After Maillard reaction, 3.2 ± 0.05 free amino groups were consumed. The decrease in average number of free lysine residues directly proved that these dextran molecules were grafted to casein molecules.[24]

The weight-average ($\bar{M}_w$) and number-average weights ($\bar{M}_n$) of casein and glycosylated casein had been determined by HPSEC, which demonstrated that the molecular weight of casein via Maillard reaction had changed and also gave information about the effects of modification indirectly. This presented that the weight-average molecular weights of casein and glycosylated casein were $(2.8045 \pm 0.2758) \times 10^4$ and $(2.5665 \pm 0.3855) \times 10^5$ g/mol, respectively. The number-average molecule weights were $(2.5794 \pm 0.3740) \times 10^4$ and $(2.1388 \pm 0.3212) \times 10^5$ g/mol, respectively, and the refractive index increment was $dn/dc = 1.20 \pm 0.17$. The obvious change of molecular weight further demonstrated that glycosylated casein became a bigger and more complicated micelle in solution than native casein.

Influence of Casein Glycosylation on Their Aggregation and Binding Capability with EGCG. The effects of different mixing molar ratios on EGCG−casein and EGCG−glycosylated casein were studied at pH 7.0 by DLS and HPLC (Table 1). It was found that casein and glycosylated casein displayed strongest encapsulating ability on EGCG at the ratios of 10:1 and 128:1, respectively, corresponding to EE values of 85.63 ± 0.88 and 89.36 ± 4.28%. The higher encapsulation efficiency and concentration of glycosylated casein indicated that glycosylation can improve the binding capacity of casein to EGCG. On the other hand, when the molar ratio of EGCG−casein was up to 32:1, the particle size greatly increased and cloud could be observed. When the molar ratio was further increased to the threshold of 64:1, aggregation took place and phase separation happened 4 h later. This may be due to a direct

Table 1. Entrapment Efficiency (EE) of EGCG−Casein and EGCG−Glycosylated Casein Complexes at Different Mixing Molar Ratios[a]

	EE (%)	
molar ratio (EGCG:protein)	EGCG−casein	EGCG−glycosylated casein
0:1	ND[b]	ND
1:1	38.41 ± 2.31a	48.32 ± 2.71a
2:1	47.66 ± 2.82b	50.38 ± 5.24a
6:1	58.82 ± 2.06c	58.88 ± 7.13b
10:1	85.63 ± 0.88d	70.41 ± 1.93c
16:1	73.78 ± 2.11e	78.91 ± 0.98d
32:1	72.84 ± 0.31e	87.19 ± 2.19e
64:1	ND	89.36 ± 4.28e
128:1	ND	75.99 ± 4.20d
256:1	ND	66.30 ± 1.88f

[a]Results are expressed as mean value ± standard deviation ($n = 3$). Values in a column followed by different letters are significantly different ($p < 0.05$). Casein concentration was fixed at 1.0 mg/mL (pH 7.0). [b]ND, not detected.

dx.doi.org/10.1021/jf405157x | J. Agric. Food Chem. 2014, 62, 4677−4684

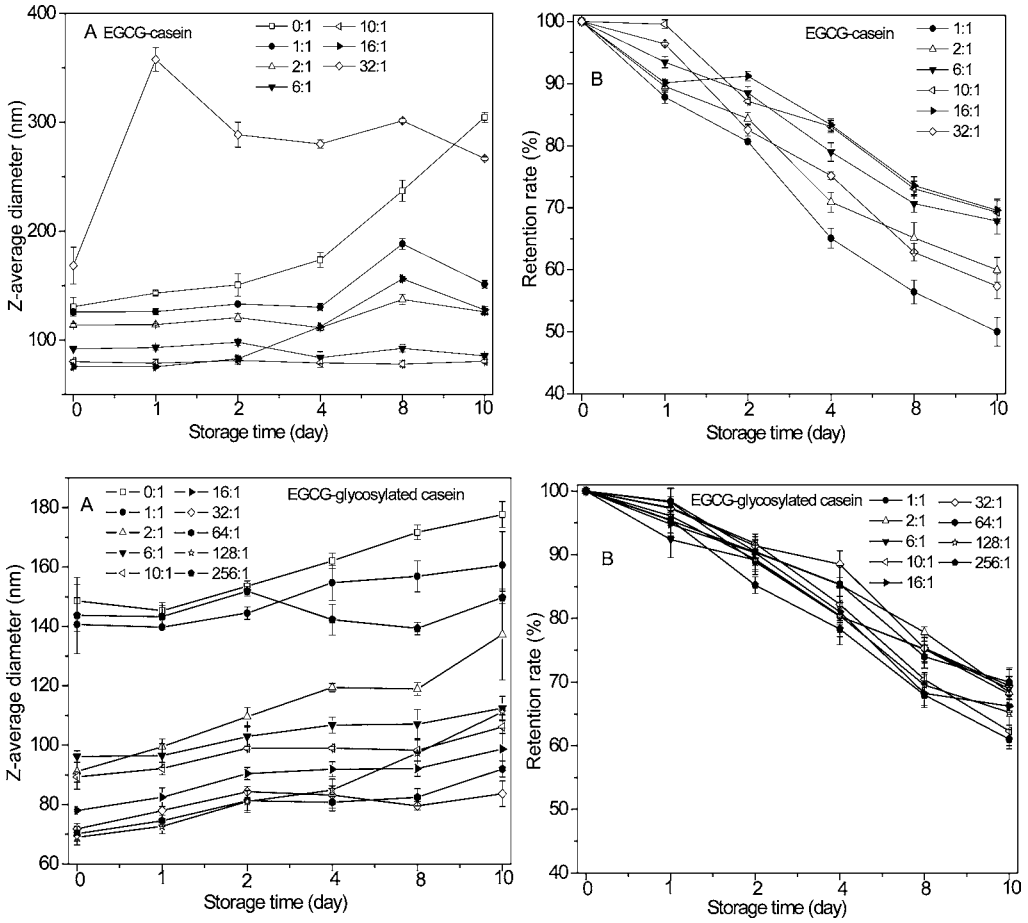

Figure 1. Change of *z*-average diameter (A) and retention rate (B) of EGCG−casein and EGCG−glycosylated casein nanocomplexes with different EGCG/casein molar ratios during storage at 4 °C in the dark.

bridging of unstructured casein by EGCG-coated proteins at higher EGCG−protein ratios.[34] When the molar ratio increased to 256:1, the system of EGCG−glycosylated casein nanocomplex was still transparent and colloidally stable. This is related to the dextran grafted on the surface of casein, which shields the casein surface from EGCG bridging by forming a steric hindrance effect.[14]

To further evaluate the stability of EGCG−casein and EGCG−glycosylated casein nanocomplexes, *z*-average diameter and retention rate during storage were compared, respectively. From Figure 1, it was observed that both *z*-average diameter and retention rate of EGCG−glycosylated casein nanocomplex became more stable than those of EGCG−casein nanocomplex. When the EGCG−casein molar ratio increased to 32:1, the retention rate of EGCG−casein nanocomplex decreased to <60%, whereas that of the EGCG−glycosylated casein nanocomplex decreased to 70%. This result indicated that casein protected EGCG from degradation. Previous study also demonstrated that the glycosylated casein played a positive role in inhibiting oxidation due to their shell structure.[35,36] As shown in Figure 2, the cloud appeared when EGCG−casein and EGCG−casein/dextran mixtures were initially prepared, whereas the EGCG−glycosylated casein nanocomplex remained clear as the same EGCG−casein molar ratio of 64:1. After 15 days of storage, the aggregation and phase separation were apparent for the EGCG−casein and EGCG−casein/dextran mixtures, whereas the EGCG−glycosylated casein nanocomplex was transparent as initially prepared.

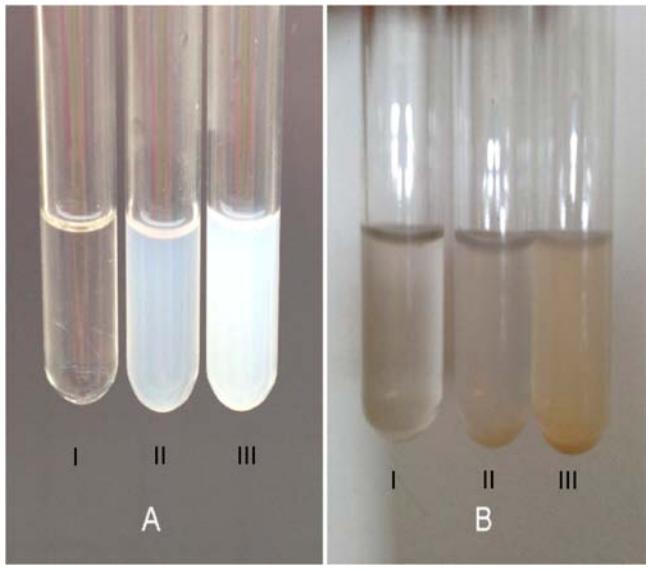

Figure 2. Photographs of the EGCG−casein complex initially prepared (A) and after 15 days of storage at 4 °C in the dark (B). (I) EGCG−glycosylated casein; (II) EGCG−casein/dextran mixture; (III) EGCG−casein nanocomplex. The samples were prepared at pH 7.0, casein concentration = 1.0 mg/mL, molar ratio of EGCG/casein 64:1.

The stabilizing role of casein to EGCG was highly concentration dependent upon the EGCG−casein molar ratio.

dx.doi.org/10.1021/jf405157x | J. Agric. Food Chem. 2014, 62, 4677−4684

Polyphenols are multidentate ligands that are able to bind simultaneously, via different phenolic groups. Upon addition of EGCG, casein binding to EGCG on more than one binding site causes intermolecular cross-linking, particle contraction, and then diameter decreasing.[22] Moreover, a higher EGCG−casein molar ratio may lead to aggregation and precipitation. Herein, the glycosylation effectively suppressed the aggregation and precipitation behavior of casein in the presence of EGCG. Thus, the steric hindrance through covalent attachment of dextran played an important role in colloidal stability. Pascal and his co-workers[37] also confirmed that the location of glycosyl moieties in salivary glycoprotein, which were strongly hydrophilic with regard to the interaction site and created steric hindrance. This property limited the extent of protein affinity to EGCG, and thereby a much higher EGCG concentration was used to cause protein aggregation. Moreover, glycosyl moieties must remain exposed to the aqueous phase at the outer surface of aggregation, and this could limit the size of the aggregates.

In Vitro Release. Due to the chemical degradation at the intestinal pH and microbial metabolism in the gastrointestinal tract, EGCG always exhibited low bioavailability.[38] One of the approaches to improve bioavailability is to encapsulate the EGCG in a carrier matrix[39] or bind it to form insoluble complexes.[40] In the present study, the effects of casein and glycosylated casein binding on the EGCG release in both SGF andSIF were investigated. Figure 3A shows that the free EGCG underwent a burst release within 0.5 h in SGF and the release rate reached 45% after 4 h of incubation. After binding with casein and glycosylated casein, the release of EGCG was inhibited, with release rates of 38 and 32% after 4 h, respectively. Obviously, the decreased release was attributed to their interaction with casein through hydrogen binding. Furthermore, this effect was more pronounced in the case of glycosylated casein. It can be elucidated in terms of earlier conclusion that casein was less susceptible to gastric enzyme degradation after glycosylation.[31]

When incubating in SIF, free EGCG exhibited a rapid release process within 1 h (Figure 3B). Note that the EGCG bound with casein or glycosylated casein exhibited a relatively slow and sustained release, and the release rates were around 65 and 58% after 5 h, respectively. Besides the inhibition of molecular mobility of EGCG, another probable reason was that the glycosylation brought steric hindrance and covered the binding sites of enzyme on protein, thus leading to a low degree of hydrolysis.[41] These results confirmed that the sustained release of EGCG from the nanocomplexes may lead to the minimization of its chemical degradation in the gut conditions. Thus, the capacity of the casein nanocomplexes (especially glycosylated casein) to stabilize EGCG suggested that much more EGCG can be delivered to the human digestive system.[22]

Morphology of EGCG−Casein Nanocomplexes at Different Molar Ratios. TEM image shows that the shapes of EGCG−casein and −glycosylated casein nanocomplexes are both spherical (Figure 4). Most of the casein and EGCG−casein nanocomplexes had a diameter of <200 nm, and the diameters decreased with the addition of EGCG. The decrease of diameter was probably due to the fact that the interactions between EGCG and casein led to the conformation transition of proline-rich casein so that the linear molecules were compact,[42] which was in agreement with the DLS data. In addition, the particle size of the EGCG−glycosylated casein nanocomplex was much smaller than that of the EGCG−casein nanocomplex, which also indicated that the glycosylation of casein had an influence on

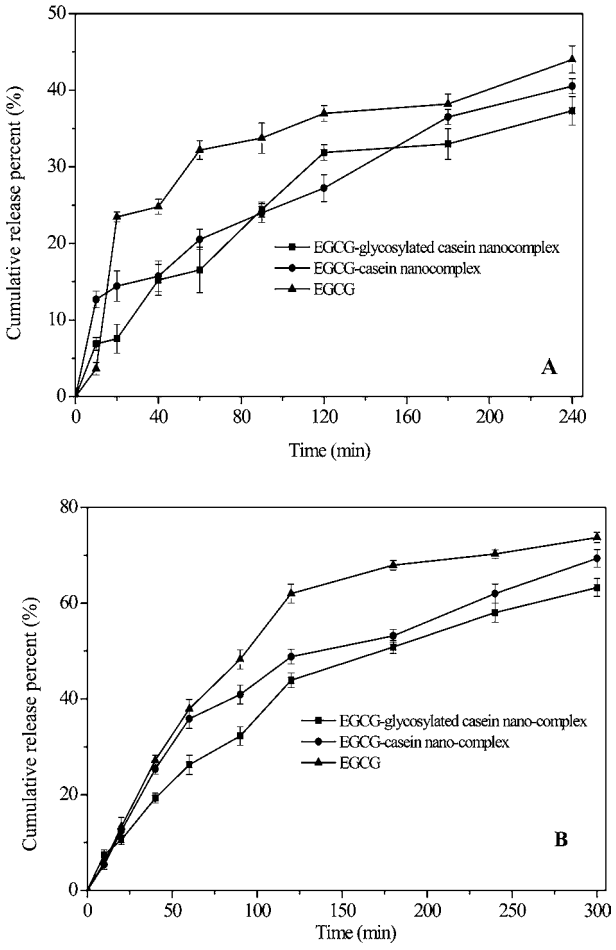

Figure 3. In vitro release of EGCG from EGCG−casein nanocomplexes in SGF (A) and SIF (B) over 4 h of incubation. The protein concentration was 1.0 mg/mL, and EGCG/casein molar ratio was 10:1.

the interaction between EGCG and casein, leading the system to be more colloidally stable.

Fluorescence Quenching of Casein by EGCG. The intrinsic fluorescence contributed by tyrosine (Tyr) and tryptophan (Trp) is an effective tool for investigating the interaction and binding of polyphenol and protein in an attempt to characterize the nature of tea polyphenol complexion. Herein, we mainly compared the binding affinities of EGCG to casein, as well as glycosylated casein. As is well-known, tryptophan has intrinsic fluorescence residues when exciting at 280 nm and tyrosine has intrinsic fluorescence residues when exciting at 295 nm in casein protein.[8] As shown in Figure 5, the fluorescence quenching of casein and glycosylated casein was induced by EGCG, which also suggested that when other molecules interacted with casein, Trp and Tyr fluorescence may change depending on the impact of such interaction on the casein conformation.[11] With increasing concentration of EGCG, the fluorescence intensity of two kinds of proteins decreased gradually upon excitement at both 280 and 295 nm, whereas the fluorescence quantum yield of Tyr at 295 nm was much smaller than that of Trp at 280 nm, which was probably because Trp residues were located on casein surfaces.

Quencher molecules produce two kinds of quenching effects, static and dynamic quenching. Static quenching frequently results in encountering pair formation between quencher and fluorophore molecules, whereas dynamic quenching requires

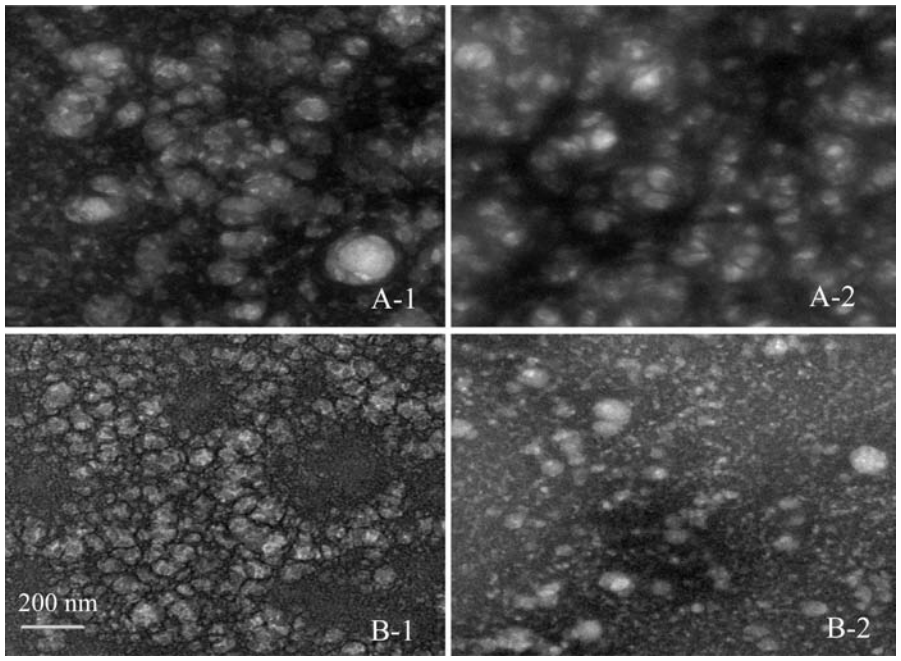

Figure 4. TEM images of EGCG−casein complexes: EGCG−casein nanocomplex (A); EGCG−glycosylated casein nanocomplex (B); EGCG/protein molar ratio 0:1 (1); EGCG/protein molar ratio 4:1 (2). The casein concentration was 1.0 mg/mL.

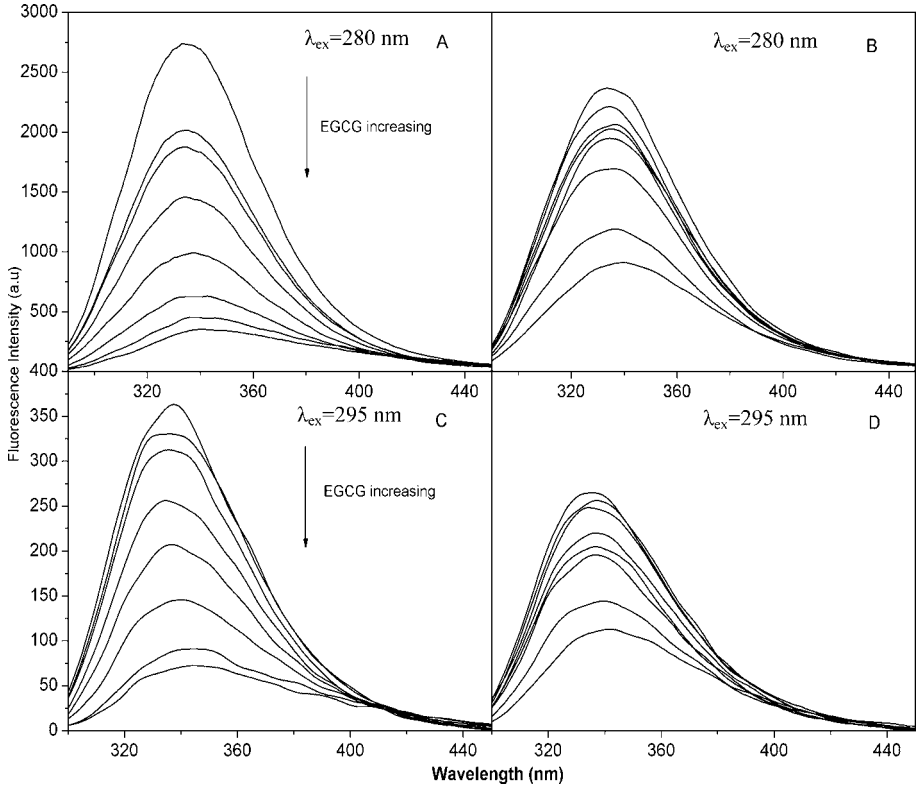

Figure 5. Quenching effect of EGCG on casein (A, C) and glycosylated casein (B, D) fluorescence intensity. The EGCG/casein molar ratios were 0:1, 0.5:1, 1:1, 2:1, 6:1, 10:1, 16:1, and 32:1 (from the top down). Casein concentration was 0.2 mg/mL.

bimolecular collisions.[43] Fluorescence quenching can be often described by the Stern−Volumer equation[8]

$$\frac{F_0}{F} = 1 + K_{sv}[Q]$$

where F_0 and F are the fluorescence intensities before and after the addition of quencher, respectively. K_{sv} is the Stern−Volumer quenching constant, and [Q] is the concentration of the quencher. The value of K_{sv} is compared with 2×10^{10} L mol^{-1} s^{-1} to determine whether the quenching type is dynamic or static quenching through the above equation. We therefore calculated that no matter Tyr or Trp, casein or casein−dextran conjugate, the K_{sv} was always $>2 \times 10^{10}$ L mol^{-1} s^{-1}, which meant it was

dx.doi.org/10.1021/jf405157x | J. Agric. Food Chem. 2014, 62, 4677−4684

Table 2. Binding Constants and Binding Sites between Different EGGC−Casein Protein Complexes at Excitation Wavelengths of 280 and 295 nm

	λ_{ex} = 280 nm			λ_{ex} = 295 nm		
casein	K_a ($\times 10^3$ L mol^{-1})	n	R^2	K_a ($\times 10^3$ L mol^{-1})	n	R^2
native	4.653	0.7679	0.9077	9.339	0.9880	0.9790
glycosylated	3.632	0.6712	0.9458	5.935	0.8685	0.9562

static quenching that decided the binding affinity between EGCG and casein.

Results from fluorescence measurements can be used to estimate the binding constant of polyphenol−protein complex from followed equation:

$$\mathrm{Lg}[(F_0 - F)/F] = \mathrm{Lg}\, K_a + n\, \mathrm{Lg}\,[\mathrm{Q}]$$

According to this equation, the binding constants and binding sites between EGCG and casein (including native and glycosylated casein) are shown in Table 2. The binding constants gave information about the molecular environment in the vicinity of the chromophore molecule, suggesting a strong affinity of EGCG with casein, which might be attributed to the presence of more OH groups in EGCG than in other catechins.[44] At 280 and 295 nm excitation wavelengths, the binding constants and binding sites of EGCG−casein were larger than those of EGCG−glycosylated casein, which suggested that EGCG had a lower affinity with glycosylated casein due to the presence of dextran grafted. With dextran grafting via Maillard reaction, little shift of emission maximum wavelength of tryptophan and tyrosine was observed in the glycosylated casein, suggesting that there was little change about the interior hydrophobic environment of protein. However, the fluorescence intensity of glycosylated casein was weakened compared with that of the native casein. Thus, it was considered that the grafting of dextran on the surface of the casein molecule presented a shielding effect on the fluorescence of casein. The tightening of casein protein structure through intramolecular interactions, such as hydrogen bonds, seemed to bury Trp and Tyr in a more hydrophobic environment, which was related to unfolding of casein structure and displayed the gradually decreasing z-average diameters in DLS measurement.

■ ASSOCIATED CONTENT

Supporting Information

Additional experimental details. This material is available free of charge via the Internet at http://pubs.acs.org.

■ AUTHOR INFORMATION

Corresponding Author

*(S.X.) E-mail: sqxia2006@hotmail.com. Phone: 86-510-85884496. Fax: 86-510-85884496.

Funding

This research was financially supported by projects of the National 125 Program of China (2011BAD23B04), the National Natural Science Foundation for Young Scholars of China (31000815), SKLF-TS200904, and PAPD.

Notes

The authors declare no competing financial interest.

■ REFERENCES

(1) Yang, C. S.; Pan, E. The effects of green tea polyphenols on drug metabolism. *Expert Opin. Drug Met.* **2012**, *8*, 677−689.

(2) Wang, X.; Ho, C.-T.; Huang, Q. Investigation of adsorption behavior of (−)-epigallocatechin gallate on bovine serum albumin surface using quartz crystal microbalance with dissipation monitoring. *J. Agric. Food Chem.* **2007**, *55*, 4987−4992.

(3) Wang, Y.; Li, M.; Xu, X.; Song, M.; Tao, H.; Bai, Y. Green tea epigallocatechin-3-gallate (EGCG) promotes neural progenitor cell proliferation and sonic hedgehog pathway activation during adult hippocampal neurogenesis. *Mol. Nutr. Food Res.* **2012**, *56*, 1292−1303.

(4) Su, Y. L.; Leung, L. K.; Huang, Y.; Chen, Z.-Y. Stability of tea theaflavins and catechins. *Food Chem.* **2003**, *83*, 189−195.

(5) Quintanilla-Carvajal, M. X.; Camacho-Díaz, B. H.; Meraz-Torres, L. S.; Chanona-Pérez, J. J.; Alamilla-Beltrán, L.; Jimenéz-Aparicio, A.; Gutiérrez-López, G. F. Nanoencapsulation: a new trend in food engineering processing. *Food Eng. Rev.* **2009**, *2*, 39−50.

(6) Kajiya, K.; Kumazawa, S.; Nakayama, T. Effects of external factors on the interaction of tea catechins with lipid bilayers. *Biosci., Biotechnol., Biochem.* **2002**, *66*, 2330−2335.

(7) Li, T.; Hu, W.; Li, J.; Zhang, X.; Zhu, J.; Li, X. Coating effects of tea polyphenol and rosemary extract combined with chitosan on the storage quality of large yellow croaker (*Pseudosciaena crocea*). *Food Control* **2012**, *25*, 101−106.

(8) Shpigelman, A.; Israeli, G.; Livney, Y. D. Thermally-induced protein-polyphenol co-assemblies: β-lactoglobulin-based nanocomplexes as protective nanovehicles for EGCG. *Food Hydrocolloids* **2010**, *24*, 735−743.

(9) Siebert, K. J. Effects of protein-polyphenol interactions on beverage haze, stabilization, and analysis. *J. Agric. Food Chem.* **1999**, *47*, 353−362.

(10) Jöbstl, E.; Howse, J. R.; Fairclough, J. P. A.; Williamson, M. P. Noncovalent cross-linking of casein by epigallocatechin gallate characterized by single molecule force microscopy. *J. Agric. Food Chem.* **2006**, *54*, 4077−4081.

(11) Hasni, I.; Bourassa, P.; Hamdani, S.; Samson, G.; Carpentier, R.; Tajmir-Riahi, H.-A. Interaction of milk α- and β-caseins with tea polyphenols. *Food Chem.* **2011**, *126*, 630−639.

(12) Jöbstl, E.; O'Connell, J.; Fairclough, J. P. A.; Williamson, M. Molecular model for astringency produced by polyphenol/protein interactions. *Biomacromolecules* **2004**, *5*, 942−949.

(13) Akinshina, A.; Ettelaie, R.; Dickinson, E.; Smyth, G. Interactions between adsorbed layers of $\alpha S1$-casein with covalently bound side chains: a self-consistent field study. *Biomacromolecules* **2008**, *9*, 3188−3200.

(14) Yan, Y.; Hu, J.; Yao, P. Effects of casein, ovalbumin, and dextran on the astringency of tea polyphenols determined by quartz crystal microbalance with dissipation. *Langmuir* **2009**, *25*, 397−402.

(15) Dong, S.; Wei, B.; Chen, B.; McClements, D. J.; Decker, E. A. Chemical and antioxidant properties of casein peptide and its glucose Maillard reaction products in fish oil-in-water emulsions. *J. Agric. Food Chem.* **2011**, *59*, 13311−13317.

(16) Aminlari, M.; Ramezani, R.; Jadidi, F. Effect of Maillard-based conjugation with dextran on the functional properties of lysozyme and casein. *J. Sci. Food Agric.* **2005**, *85*, 2617−2624.

(17) Wang, Z.; Li, Y.; Chen, L.; xiulan, X.; Yuan, Q. A study of controlled uptake and release of anthocyanins by oxidized starch microgels. *J. Agric. Food Chem.* **2013**, *61*, 5880−5887.

(18) García-López, J. J.; Hernández-Mateo, F.; Isac-García, J.; Kim, J. M.; Roy, R.; Santoyo-González, F.; Vargas-Berenguel, A. Synthesis of per-glycosylated β-cyclodextrins having enhanced lectin binding affinity. *J. Org. Chem.* **1999**, *64*, 522−531.

(19) Canon, F.; Ballivian, R.; Chirot, F.; Antoine, R.; Sarni-Manchado, P.; Lemoine, J. R. M.; Dugourd, P. Folding of a salivary intrinsically

disordered protein upon binding to tannins. *J. Am. Chem. Soc.* **2011**, *133*, 7847−7852.
(20) Nakamura, S.; Kato, A.; Kobayashi, K. New antimicrobial characteristics of lysozyme-dextran conjugate. *J. Agric. Food Chem.* **1991**, *39*, 647−650.
(21) Dickinson, E. Emulsion stabilization by polysaccharides and protein-polysaccharide complexes. In *Food Science and Technology*; Dekker: New York, 1995; p 501.
(22) Zhou, H.; Sun, X.; Zhang, L.; Zhang, P.; Li, J.; Liu, Y.-N. Fabrication of biopolymeric complex coacervation core micelles for efficient tea polyphenol delivery via a green process. *Langmuir* **2012**, *28*, 14553−14561.
(23) Pereyra, R.; Schmidt, K. A.; Wicker, L. Interaction and stabilization of acidified casein dispersions with low and high methoxyl pectins. *J. Agric. Food Chem.* **1997**, *45*, 3448−3451.
(24) Renard, D.; Lavenant-Gourgeon, L.; Ralet, M.-C.; Sanchez, C. *Acacia senegal* gum: continuum of molecular species differing by their protein to sugar ratio, molecular weight, and charges. *Biomacromolecules* **2006**, *7*, 2637−2649.
(25) Li, B.; Du, W.; Jin, J.; Du, Q. Preservation of (−)-epigallocatechin-3-gallate antioxidant properties loaded in heat treated β-lactoglobulin nanoparticles. *J. Agric. Food Chem.* **2012**, *60*, 3477−3484.
(26) Tan, C.; Xue, J.; Eric, K.; Feng, B.; Zhang, X.; Xia, S. Dual effects of chitosan decoration on the liposomal membrane physicochemical properties as affected by chitosan concentration and molecular conformation. *J. Agric. Food Chem.* **2013**, *61*, 6901−6910.
(27) Zhao, L.; Xiong, H.; Peng, H.; Wang, Q.; Han, D.; Bai, C.; Liu, Y.; Shi, S.; Deng, B. PEG-coated lyophilized proliposomes: preparation, characterizations and in vitro release evaluation of vitamin E. *Eur. Food Res. Technol.* **2011**, *232*, 647−654.
(28) Ding, B.; Xia, S.; Hayat, K.; Zhang, X. Preparation and pH stability of ferrous glycinate liposomes. *J. Agric. Food Chem.* **2009**, *57*, 2938−2944.
(29) Yue, L.; Zhang, X.-M. Structural characterization and photocatalytic behaviors of doped CeO_2 nanoparticles. *J. Alloy. Compd.* **2009**, *475*, 702−705.
(30) ter Haar, R.; Schols, H. A.; Gruppen, H. Effect of saccharide structure and size on the degree of substitution and product dispersity of α-lactalbumin glycated via the Maillard reaction. *J. Agric. Food Chem.* **2011**, *59*, 9378−9385.
(31) Rival, S. G.; Fornaroli, S.; Boeriu, C. G.; Wichers, H. J. Caseins and casein hydrolysates. 1. Lipoxygenase inhibitory properties. *J. Agric. Food Chem.* **2001**, *49*, 287−294.
(32) Ferrer, E.; Alegría, A.; Farré, R.; Abellán, P.; Romero, F.; Clemente, G. Evolution of available lysine and furosine contents in milk-based infant formulas throughout the shelf-life storage period. *J. Sci. Food Agric.* **2003**, *83*, 465−472.
(33) Eigel, W.; Butler, J.; Ernstrom, C.; Farrell, H., Jr.; Harwalkar, V.; Jenness, R.; Whitney, R. M. Nomenclature of proteins of cow's milk: fifth revision. *J. Dairy Sci.* **1984**, *67*, 1599−1631.
(34) Pascal, C.; Poncet-Legrand, C.; Imberty, A.; Gautier, C.; Sarni-Manchado, P.; Cheynier, V.; Vernhet, A. Interactions between a non glycosylated human proline-rich protein and flavan-3-ols are affected by protein concentration and polyphenol/protein ratio. *J. Agric. Food Chem.* **2007**, *55*, 4895−4901.
(35) Wu, S.; Sun, K.; Wang, X.; Wang, D.; Wan, X.; Zhang, J. Protonation of epigallocatechin-3-gallate (EGCG) results in massive aggregation and reduced oral bioavailability of EGCG-dispersed selenium nanoparticles. *J. Agric. Food Chem.* **2013**, *61*, 7268−7275.
(36) Zhong, Y.; Shahidi, F. Lipophilized epigallocatechin gallate (EGCG) derivatives as novel antioxidants. *J. Agric. Food Chem.* **2011**, *59*, 6526−6533.
(37) Pascal, C.; Poncet-Legrand, C. l.; Cabane, B.; Vernhet, A. Aggregation of a proline-rich protein induced by epigallocatechin gallate and condensed tannins: effect of protein glycosylation. *J. Agric. Food Chem.* **2008**, *56*, 6724−6732.
(38) van't Slot, G.; Humpf, H.-U. Degradation and metabolism of catechin, epigallocatechin-3-gallate (EGCG), and related compounds by the intestinal microbiota in the pig cecum model. *J. Agric. Food Chem.* **2009**, *57*, 8041−8048.
(39) Patel, A.; Heussen, P.; Hazekamp, J.; Velikov, K. P. Stabilisation and controlled release of silibinin from pH responsive shellac colloidal particles. *Soft Matter* **2011**, *7*, 8549−8555.
(40) Patel, A. R.; Seijen-ten-Hoorn, J.; Velikov, K. P. Colloidal complexes from associated water soluble cellulose derivative (methylcellulose) and green tea polyphenol (epigallocatechin gallate). *J. Colloid Interface Sci.* **2011**, *364*, 317−323.
(41) Acosta, E. Bioavailability of nanoparticles in nutrient and nutraceutical delivery. *Curr. Opin. Colloid Interface Sci.* **2009**, *14*, 3−15.
(42) Bourassa, P.; Bariyanga, J.; Tajmir-Riahi, H. Binding sites of resveratrol, genistein, and curcumin with milk α-and β-caseins. *J. Phys. Chem. B* **2013**, *117*, 1287−1295.
(43) Lakos, Z.; Szarka, Á.; Koszorús, L.; Somogyi, B. Quenching-resolved emission anisotropy: a steady state fluorescence method to study protein dynamics. *J. Photochem. Photobiol. B* **1995**, *27*, 55−60.
(44) Kanakis, C. D.; Hasni, I.; Bourassa, P.; Tarantilis, P. A.; Polissiou, M. G.; Tajmir-Riahi, H.-A. Milk β-lactoglobulin complexes with tea polyphenols. *Food Chem.* **2011**, *127*, 1046−1055.

JOURNAL OF AGRICULTURAL AND FOOD CHEMISTRY

Article

pubs.acs.org/JAFC

Improvement of *Alcaligenes faecalis* Nitrilase by Gene Site Saturation Mutagenesis and Its Application in Stereospecific Biosynthesis of (*R*)-(−)-Mandelic Acid

Zhi-Qiang Liu,[†] Xin-Hong Zhang,[†] Ya-Ping Xue,[†] Ming Xu,[‡] and Yu-Guo Zheng*[,†]

[†]Institute of Bioengineering, Zhejiang University of Technology, Hangzhou, Zhejiang 310014, People's Republic of China

[‡]Zhejiang Laiyi Biotechnology Co., Ltd, Shengzhou, Zhejiang 312400, People's Republic of China

Supporting Information

ABSTRACT: Nitrilases have recently received considerable attention as the biocatalysts for stereospecific production of carboxylic acids. To improve the activity, the nitrilase from *Alcaligenes faecalis* was selected for further modification by the gene site saturation mutagenesis method (GSSM), based on homology modeling and previous reports about mutations. After mutagenesis, the positive mutants were selected using a convenient two-step high-throughput screening method based on product formation and pH indicator combined with the HPLC method. After three rounds of GSSM, Mut3 (Gln196Ser/Ala284Ile) with the highest activity and ability of tolerance to the substrate was selected. As compared to the wild-type *A. faecalis* nitrilase, Mut3 showed 154% higher specific activity. Mut3 could retain 91.6% of its residual activity after incubation at pH 6.5 for 6 h. In a fed-batch reaction with 800 mM mandelonitrile as the substrate, the cumulative production of (*R*)-(−)-mandelic acid after 7.5 h of conversion reached 693 mM with an enantiomeric excess of 99%, and the space-time productivity of Mut3 was 21.50-fold higher than that of wild-type nitrilase. The K_m, V_{max}, and k_{cat} of wild-type and Mut3 for mandelonitrile were 20.64 mM, 33.74 μmol mg^{-1} min^{-1}, 24.45 s^{-1}, and 9.24 mM, 47.68 μmol mg^{-1} min^{-1}, and 34.55 s^{-1}, respectively. A homology modeling and molecular docking study showed that the diameter of the catalytic tunnel of Mut3 became longer and that the tunnel volume was smaller. These structural changes are proposed to improve the hydrolytic activity and pH stability of Mut3. Mut3 has the potential for industrial applications in the upscale production of (*R*)-(−)-mandelic acid.

KEYWORDS: *nitrilase, molecular modification, gene site saturation mutagenesis, mandelonitrile, (R)-(−)-mandelic acid*

INTRODUCTION

Nitrilases (EC 3.5.5.1) are important industrial enzymes used to convert nitriles directly into corresponding carboxylic acids and ammonia in a single step with mild conditions.[1,2] Occurrences, catalytic mechanisms, applicabilities, and molecular modifications of nitrilases have been widely reported.[3−5] By far, all known nitrilases can be classified as aromatic nitrilases, aliphatic nitrilases, and arylacetonitrilases according to substrate specificity.[6] Nitrilases are found in many plants and microorganisms, and their applications have been widely explored.[6] Recently, screening new nitrilases, exploring their applications, and the molecular modification of nitrilases are becoming hot issues because of the important application of nitrilases.[4,5,7−10]

It was reported that one of the important industrial applications of nitrilases is the conversion of (*R*,*S*)-mandelonitrile to (*R*)-(−)-mandelic acid.[11] This reaction exhibits excellent enantioselectivity, low-cost starting material, and most especially the possibility of performing a dynamic kinetic resolution of racemic substrate which provides theoretically 100% yield of the product.[11,12] (*R*)-(−)-mandelic acid has been used as an important intermediate for the production of pharmaceuticals such as semisynthetic penicillins, cephalosporins, antitumor agents, antiobesity agents, and chiral resolving agent for the resolution of racemic alcohols and amines.[12,13] (*R*)-(−)-mandelic acid can be produced by two routes including chemical and biosynthetic methods.[14] Biocatalytic synthesis of (*R*)-(−)-mandelic acid has been widespread because of its industrial development and application prospects.[11,12,15,16] The production of (*R*)-(−)-mandelic acid by nitrilases has the most potential for the industrial application.[11,15,17] There are several reported strains with abilities for the bioproduction of (*R*)-(−)-mandelic acid, including *Alcaligenes* sp. ECU0401,[18] *Pseudomonas putida* MTCC 5110[7,19] *A. faecalis* ZJUTB10,[5,11] *A. faecalis* ATCC 8750,[20] *P. fluorescens* EBC191,[8] *A. faecalis* JM3,[21] *Bradyrhizobium japonicum* USDA110,[22] and *Burkholderia cenocepacia* J2315.[23] However, the reported nitrilases still cannot meet the requirement for the industrial production of (*R*)-(−)-mandelic acid because of their poor activity and lower stability under low pH. To resolve this problem, nitrilases from different origins have been modified by various approaches.[3,5,24]

The gene site saturation mutagenesis method (GSSM) is widely used in the modification of proteins based on the PCR method, which has made a series of high-profile achievements on nitrilases.[25] Yeom et al. had mentioned that a positively charged amino acid at position 129 in nitrilase from *Rhodococcus rhodochrous* ATCC 33278 was an essential residue for the activity with meta-substituted benzonitriles by the

Received: December 24, 2013
Revised: March 29, 2014
Accepted: April 27, 2014
Published: April 28, 2014

ACS Publications © 2014 American Chemical Society

GSSM.[26] Wu et al. obtained a mutant nitrilase with increased activity, specificity, and stability by modification at sites Thr210 and Leu201 located in α6, and Phe168 at the junction of the β10 helix and α6.[27,28] Nolan et al. found that the active sites for cyanide hydratase and nitrilase activity in the protein were the same by the GSSM.[29] The cyanide dihydratase completely lost its activity by the replacement of Cys163 to Ser, and the replacement of Tyr53 to Phe caused an increase of the K_m value of the enzyme for cyanide when the conserved amino acid residues in the cyanide dihydratase from *P. stutzeri* AK61 were altered by GSSM.[30]

In this study, the recombinant nitrilase from *A. faecalis* was selected to improve activity by using GSSM. On the basis of the secondary and three-dimensional structures, interactions between the substrate and nitrilase, and previous reports,[5,31,32] three sites in the α-helix (Leu175, Ala197, and Val305) and one site in the β-sheet (Ala284) located after Cys163 were selected for further mutagenesis. The site Gln196 was also selected using the software HotSpot Wizard to identify the point that plays an important role in enzyme catalysis and substrate specificity. After mutagenesis, the mutants were screened by a two-step screening method based on bromocresol purple as the pH indicator combined with liquid chromatography, and the best mutant Mut3 with serendipitously improved activity and pH stability was obtained. The characteristics of purified wild-type and Mut3 were studied and compared. The homology modeling and molecular docking were further studied to elucidate the interactions between substrate and nitrilase. Finally, the potential application in the kinetic resolution of racemic mandelonitrile to prepare *R*-(−)-mandelic acid was evaluated as well.

MATERIALS AND METHODS

Strains, Plasmids, and Medium. *E. coli* BL21 (DE3) (F-ompT gal dcm lon, hsdSB (rB- mB-) λ (DE3 (lacI lacUV5-T7 gene 1 ind1 sam7 nin5))) (Invitrogen, Karlsruhe, Germany) was used for heterologous expression. *E. coli* and recombinant *E. coli* strains were grown in Luria−Bertani (LB) medium (tryptone 10 g/L, yeast extract 5 g/L, and NaCl 10 g/L). The pET28b-NIT plasmid and recombinant nitrilase from *A. faecalis* was constructed and stored in our laboratory.[5] *Dpn* I and PrimeSTAR HS DNA polymerase were provided by the TaKaRa company (Dalian, China). (*R,S*)-mandelonitrile, (*R*)-(−)-mandelic acid, and (*S*)-(−)-mandelic acid were purchased from Sigma (St. Louis, MO). All other reagents and chemicals were commercially available and of analytic grade.

Table 1. Primers for the Gene Site Saturation Mutagenesis

positions of mutant	primers
Leu175	L175 (F): 5′-CTCTGTACTCCGAANNNGCGCACGCTCTGTC-3′
	L175 (R): 5′-GACAGAGCGTGCGCNNNTTCGGAGTACAGAG-3′
Ala197	A197 (F): 5′-CTGTACTCCGAACAGNNNCACGCTCTGTC-3′
	A197 (R): 5′-CAGAGCGTGNNNCTGTTCGGAGTACAGAGA-3′
Val305	V305 (F): 5′-GTCTAAATACGCCNNNTACTCCCAGCACGAAG-3′
	V305 (R): 5′-CTTCGTGCTGGGAGTANNNGGCGTATTTAGAC-3′
Ala284	A284 (F): 5′-GAAGCCACTCGTCTGNNNCTGGATCTGGGTC-3′
	A284 (R): 5′-GACCCAGATCCAGNNNCAGACGAGTGGCTTC-3′
Gln196	Q196 (F): 5′-CATGGAAGAGATCNNNTTCGCTAAGGCTATC-3′
	Q196 (R): 5′-GATAGCCTTAGCGAANNNGATCTCTTCCATG-3′

Gene Site Saturation Mutagenesis. Random mutations were introduced to the nitrilase gene by GSSM at positions of Leu175, Ala197, Val305, Ala284, and Gln196 using PrimeSTAR HS DNA polymerase (Takara) and pET28b-NIT plasmid as a template. The five pairs of primers carrying mutations are listed in Table 1. The plasmids with positive mutations from the previous round of mutations were used as a template for the next step of mutation. The PCR reaction mixture consisted of 200 μM for each dNTP, 0.2 μM primers, 10 μL of 5× PrimeSTAR Buffer (Mg^{2+} plus), and 1.25 U PrimeSTAR HS DNA polymerase (Takara) in 50 μL. The reaction was carried out at 94 °C for 5 min, followed by 30 cycles of 98 °C for 10 s, 55 °C for 15 s for amplifying the nitrilase gene, 72 °C for 8 min, and then 72 °C for 10 min in a PCR thermocycler (Biometra, Göttingen, Germany). PCR products were subjected to 0.9% agarose electrophoresis and then purified by a PCR purification kit (Simgen, Hangzhou, China). After purification, the DNA fragment was digested with *Dpn* I at 37 °C for 3 h to remove the template plasmid containing the methylation sites. The plasmid pET28b-NIT_{mut} was then transformed into *E. coli* BL21 (DE3) by the heat-shock method.[33]

Screening Method. A two-step screening method which was constructed to screen the mutants was described below: Each single colony was picked from the plate with 50 mg/mL kanamycin (Kan) to 96-well plates with LB broth and incubated overnight with vigorous shaking (500 rpm) at 37 °C. One part of the culture was transferred to the new 96-well plates with 50 mg/mL Kan, 0.1 mM isopropyl-β-D-thiogalactoside (IPTG), 100 mM (*R,S*)-mandelonitrile, and LB medium, and then thermomixed for 8−10 h at 30 °C. (*R,S*)-Mandelonitrile would be catalyzed to (*R*)-(−)-mandelic acid by nitrilase expressed by IPTG induction. The final concentration of 0.01% (w/v) bromocresol purple solution was added for high-throughput and rapid screening. The pH of the medium in the 96-well plate was kept at 7.0, and the screening method was based on the formation of yellow caused by mandelic acid as a result of hydrolysis by positive mutants. When the pH became lower and lower with the hydrolysis process of the (*R,S*)-mandelonitrile to produce mandelic acid, the medium with purple background would change the color to yellow. Finally, the positive mutants were selected by the formation of yellow. At the same time, the mutants which made the color of bromocresol purple solution change from purple to yellow were picked from the corresponding plates and grown at 37 °C in 50 mL of LB media containing 50 μL of 50 mg/mL Kan for further tests. The nitrilase was induced by the addition of 0.1 mM IPTG when optical density (OD) at 600 nm of the culture broth reached between 0.6 and 0.8. The cells were then incubated at 28 °C for 12 h and harvested by centrifugation at 9000 rpm for 10 min. The reaction was carried out with free cells in 1 mL of pure water at 40 °C, 500 rpm for 10 min. After reaction, the reaction mixture was centrifuged at 12000 rpm for 5 min, and then the amount of (*R*)-(−)-mandelic acid in the supernatant was subsequently determined by high-performance liquid chromatography (HPLC) mentioned below to further confirm the positive mutants with improved nitrilase activity.

Nitrilase Purification and Sodium Dodecyl Dulfate−Polyacrylamide Gel Electrophoresis (SDS−PAGE). After being induced by 0.1 mM IPTG, the cells harboring recombinant nitrilases were collected by centrifugation and then were resuspended in 30 mL of pure water and lysed by sonication with a Vibra-Cell VC 505 ultrasonic processor (Sonics and Materials Inc., Newtown, CT) at 400 W for 15 min. The resulting slurry was centrifuged at 12000 rpm for 20 min, and the supernatant was loaded to a nickel-NTA superflow column, which has been equilibrated with buffer (20 mM NaH_2PO_4 and 300 mM NaCl; and pH 8.0). Unbound proteins were washed out from the column with buffer (20 mM NaH_2PO_4, 300 mM NaCl, 50 mM imidazole, and pH 8.0). The active enzyme was eluted with buffer by a linear gradient from 50 to 500 mM imidazole at a flow rate of 1 mL/min. The purified enzymes were analyzed using 12% SDS−PAGE.

Enzyme Assays and Protein Assay. The standard activity assay was carried out using (*R*,*S*)-mandelonitrile (100 mM) as substrate and 0.2 mg/mL of purified enzyme mixed in potassium phosphate buffer (100 mM and pH 8.0). The reaction mixture (total volume 10 mL) was incubated at 45 °C for 10 min and stopped by HCl solution (final 2 M). Then, 200 μL of the mixture was centrifuged at 12000 rpm for 20 min, and the supernatant was subjected to HPLC analysis as described below for assaying the nitrilase activity. The amount of (*R*)-(−)-mandelic acid was determined by a LC-20AD prominence liquid chromatography instrument (Shimadzu, Kyoto, Japan) using a C18 column (5 μm × 250 nm × 4.6 nm, Elite Analytical Instruments Co., Ltd., Dalian, China) and equipped with a SPD-2A prominence UV/vis detector. Each sample (20 μL) was eluted at 30 °C with 0.01 M $(NH_4)H_2PO_4/CH_3OH$ = 13:7 (v/v, 1 mL/min) as the mobile phase, and absorbance at 228 nm was measured. The retention time for (*R*)-(−)-mandelic acid was 3.2 min. The optical purity of (*R*)-(−)-mandelic acid was determined by an analysis of the enantiomers on a CHIRALEL-OD-H column (250 × 4.6 mm) (Daicel Chemical Industries, Shinzaike, Japan) at a flow rate of 0.8 mL/min with a mobile phase containing hexane, 2-propanol, and trifluoroacetic acid (90:10:0.1, v/v) at a wavelength of 228 nm.

One unit of nitrilase activity was defined as the amount of enzyme that produces 1 μmol of (*R*)-(−)-mandelic acid per minute under the conditions described above. Protein quantitative analysis was conducted using the Bradford method[34] with bovine serum albumin as a standard.

Optimum pH and pH Stability. To investigate the optimal pH and the effect of pH on the activity of nitrilase, four buffers including citrate buffer (pH 3.0−6.0), phosphate buffer (pH 6.0−8.5), Tris-HCl buffer (pH 7.0−8.5), and glycine-NaOH buffer (pH 8.5−10.0) with a concentration of 100 mM were used, and the reactions were performed at 45 °C using 100 mM (*R*,*S*)-mandelonitrile as substrate. To investigate pH stability, the enzyme was dissolved in buffers of pHs ranging from 6.5 to 8.5 and incubated at 0 °C from 0.5 to 6 h, and then the relative activities were performed with standard assay conditions. Activity without treatment obtained at pH 8.0 was used as a blank and regarded as 100%.

Optimum Temperature and Thermal Stability. The optimal temperature of the enzyme was determined by assaying enzyme activities at temperatures ranging from 25 to 65 °C. Thermal stability was investigated by incubating enzymes at temperatures ranging from 30 to 60 °C. The enzyme was incubated in a heat-block at the specified temperature for a certain time. The relative activities were examined at 45 °C for 10 min.

Circular Dichroism (CD) Measurements. CD spectra were recorded on a JASCO J-815 Spectropolarimeter (JASCO Inc., Easton, MD) with Spectra Manager 228 software. The temperature was controlled from 10 to 60 °C using a Fisher Isotemp Model 3016S water bath (Fisher Scientific, Waltham, MA). A lyophilized powder (purity >95%, w/w) was prepared. A stock solution of 0.02 mg/mL nitrilase was generated in ddH_2O. The spectra were recorded from 190 to 250 nm.

Homology Modeling and Molecular Docking. The three-dimensional homology model of nitrilase was constructed using Build Homology Models (MODELER) in Discovery studio (DS) 2.1 (Accelrys Software, San Diego) and the crystal structure of a hypothetical protein PH0642 (PDB accession code 1J31) was used as the template. The catalytic tunnel size was analyzed using software HotSpot Wizard to identify the residues essential for protein function, enzyme activity, and substrate specificity. Autodock 4.0 was used to study the interaction between substrate and nitrilase, and to predict the spatial structure and catalytic mechanism of the nitrilase.

Time Course of (*R*,*S*)-Mandelonitrile Hydrolysis. The reaction mixture (10 mL) contained 0.1 g of wet cells of wild-type or evolved nitrilase suspended in 100 mM potassium phosphate buffer (pH 8.0) containing 100 mM (*R*,*S*)-mandelonitrile. These reactions were carried out at 40 °C in a reciprocal shaker at 150 rpm. Samples were removed at predetermined times, and the yield was determined by HPLC.

Fed-Batch Production of (*R*)-(−)-Mandelic Acid Using Mut3 as the Catalyst. The fed-batch reaction was performed at 40 °C and 150 rpm in 200 mL reaction volume. The reaction mixture contained 100 mM potassium phosphate buffer (pH 8.0), 100 mM (*R*,*S*)-mandelonitrile, and 5% wet cells of Mut3. (*R*,*S*)-mandelonitrile (100 mM) was fed in the subsequent 7 batches (total 800 mM) once an hour. The reaction mixture (100 μL) was periodically withdrawn and analyzed by HPLC.

Isolation and Identification of (*R*)-(−)-Mandelic Acid. The isolation procedure of (*R*)-(−)-mandelic acid was performed according to the following procedure: 2% (w/v) activated carbon was added into the fed-batch reaction mixture (200 mL) to remove the cells. After filtration, the filtrate adjusted to pH 9.0−10.0 with 2 M NaOH was extracted with an equal volume of ethyl acetate twice to obtain the aqueous phase, which was acidified to pH 1.0−2.0 with 2 M HCl. The aqueous phase suffered from vacuum filtration (SHB-III, Zhengzhou trade Co., LTD, China) to remove the proteins in the solvent, and then the filtrate was extracted with isopyknic ethyl acetate three times. After the organic extract was dried by anhydrous sodium sulfate, the solvent was removed through vacuum distillation (Adyantag ML, Heidolph, Germany) in a rotary evaporator, and the crystal of (*R*)-mandelic acid was subsequently obtained.

The ^{13}C and ^{1}H nuclear magnetic resonance (NMR) spectra of (*R*)-(−)-mandelic acid were obtained on a NMR spectrometer (AVANCE 500 MHz, Bruker, Fallanden, Switzerland) with DMSO as the solvent, using 500 and 125 MHz for carbon and proton determinations, respectively. The FTIR spectrum for (*R*)-(−)-mandelic acid was recorded on a Fourier transform infrared spectrometer (Nicolet 6700; Thermo, Waltham, MA) with a Contimμm FTIR Micro system in the region of 4000−400 cm^{-1} using KBr pellets. The LC-MS spectrum for (*R*)-mandelic acid was recorded on a high performance liquid chromatography−time-of-flight mass spectrometer (Agilent Technologies 1200 Series, 6210 Time-of-Flight MS spectrometer) (Agilent Technologies, Waldbronn, Germany), and the experimental parameters were used as follows: ionization mode, ESI scan; gas temperature, 300 °C; fragmentor, 80 V; drying gas, 3.5 L/min; skimmer, 65 V; nebulizer, 20 psig; OCTIRFV pp, 250 V; and Vcap, 3000 V.

Statistical Analysis. If not specifically noted, all experiments in this study were performed in triplicate. Analysis of variance (ANOVA) was carried out using the SAS program, version 8.1 (SAS Institute Inc., Cary, NC). Least significant differences (LSD) were computed at $P < 0.05$.

RESULTS

Construction and Screening of Mutant Libraries. The PCR products of GSSM were purified and digested by *Dpn* I to remove the template plasmid containing the methylation sites and to create the recombination library of pET28b-NIT_{mut}. Single colonies of positive mutants were picked from LB agar plates containing Kan resistance to 96-well plates with 200 μL of LB broth supplemented with 50 mg/mL of Kan and incubated overnight with vigorous shaking (500 rpm) at 37 °C. Ten microliters of the culture was transferred to the new 96-

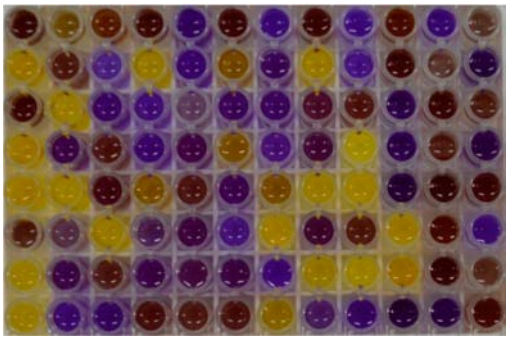

Figure 1. Mutant library screening for the high activity of nitrilases in a 96-well plate.

dx.doi.org/10.1021/jf405683f | J. Agric. Food Chem. 2014, 62, 4685−4694

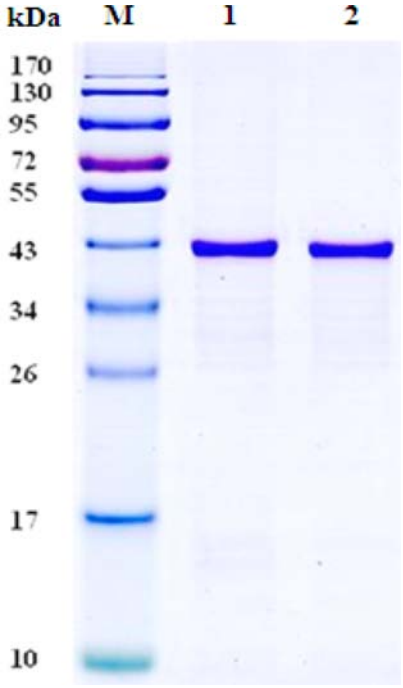

Figure 2. SDS−PAGE analysis of purified nitrilases. Gels with 30% polyacrylamide were subjected to protein analysis, and the protein bands were stained with Coomassie blue R250. Lanes 1 and 2 stand for Mut3 and the wild-type nitrilase, respectively.

well plates with 50 mg/mL Kan and 500 μL of LB medium, and then was incubated at 37 °C until the OD at 600 nm of the culture broth reached between 0.6 and 0.8 for retesting the activity and pH stability. In addition, plates containing both 100 mM (*R*,*S*)-mandelonitrile and 0.1 mM IPTG were incubated for 10 h at 28 °C. The final concentration of 0.01% (w/v) bromocresol purple solution was added for screening. The wells containing positive colonies with improved properties could become yellow and the negative mutants remain in the purple background (Figure 1 and Figure S1 in the Supporting Information). Over 6300 colonies in total were screened, and 55 clones could make the wells turn yellow. Among these clones, 10 better ones were retested using HPLC, and the clone with the greatest improvement in activity was selected (Table S1 in the Supporting Information). At the same time, selected variants were sequenced, and their amino acid substitutions are listed in Table S1 (Supporting Information). After three rounds of GSSM followed by screening, a best mutant Mut3 (Gln196Ser/Ala284Ile), with 200% relative activity than the wild-type, was selected as the targeted evolved nitrilase for further studies.

Expression and Purification of Nitrilases. The wild-type and evolved nitrilases were subjected to Nickel-NTA affinity chromatography. As shown in SDS−PAGE (Figure 2), there is only one pure band with a molecular weight of around 43 kDa observed for both of the purified wild-type and evolved nitrilases, which is consistent with the predicted molecular weight.

Influences of pH Values on the Activites of Nitrilases. It is well-known that the pH values affect the ionic environment of the enzyme, thus acting on its interaction between substrate and enzyme activity. To investigate the effect of pH on nitrilase activity, the reaction was performed in buffers including citrate buffer (pH 3.0−6.0), phosphate buffer (pH 6.0−8.5), Tris-HCl buffer (pH 7.0−8.5), and glycine-NaOH buffer (pH 8.5−10.0) with a concentration of 100 mM at 45 °C. As shown in Figure 3A, both wild-type nitrilase and Mut3 showed almost the same trends of activities under different pH conditions. The maximum specific activity of the evolved and wild-type nitrilases was observed at pH 8.0. Compared to wild-type nitrilase, the activity of Mut3 has increased significantly ranging from pH 3.0 to 10.0. Moreover, at pH 8.0, the specific activity of Mut3 (42.77 U/mg) was improved 154% compared to that of wild-type nitrilase (27.79 U/mg).

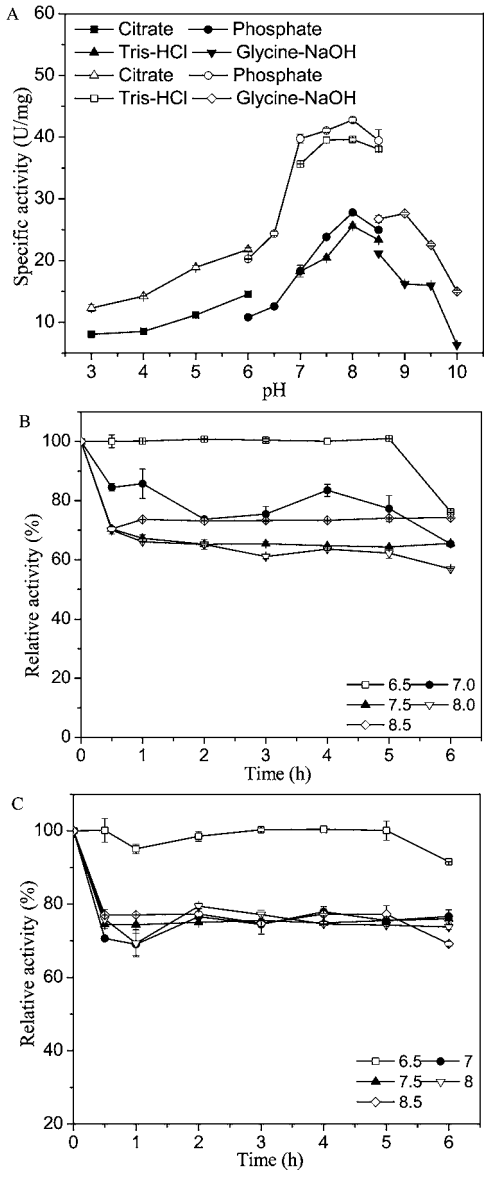

Figure 3. Influence of pH on the activity of nitrilases and stability. (A) Reactions were performed at 45 °C with different buffers. Hollow and solid represent the mutant Mut3 and the wild-type nitrilase, respectively. (B) pH stability was investigated by dissolving the wild-type nitrilase in phosphate buffers of pHs ranging from 6.5 to 8.5 and incubated at 0 °C from 0.5 to 6 h. (C) pH stability was investigated by dissolving Mut3 in phosphate buffers of pHs ranging from 6.5 to 8.5 and incubated at 0 °C from 0.5 to 6 h.

The pH stability study (Figure 3B and C) showed that Mut3 was more stable at pH 6.5 with about 90% residual activity after 6 h than the wild-type nitrilase with only 76% residual activity.

dx.doi.org/10.1021/jf405683f | J. Agric. Food Chem. 2014, 62, 4685−4694

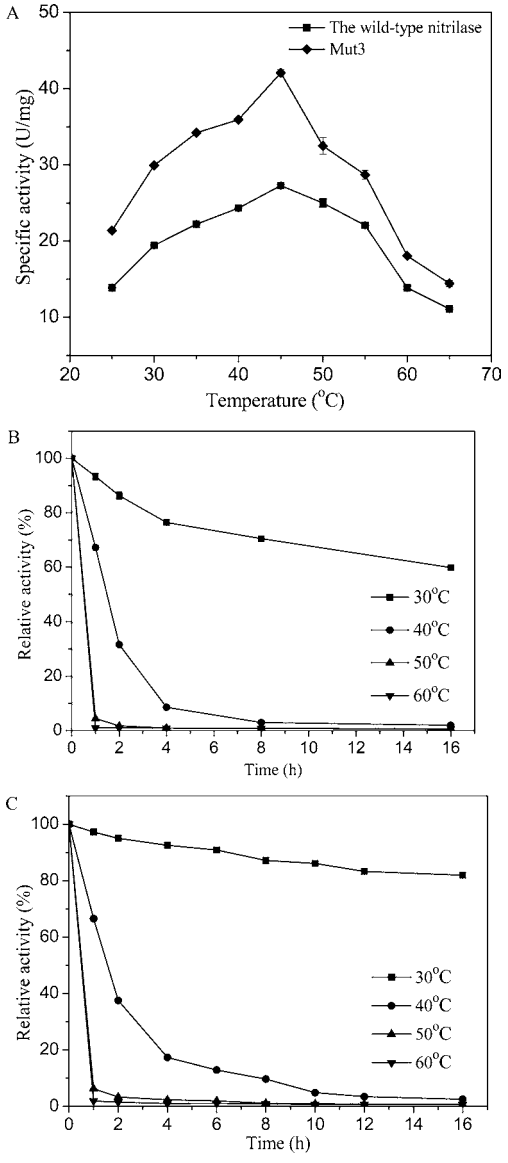

Figure 4. Effect of temperature on the activity of nitrilases and stability. (A) Reactions were performed in 100 mM at pH 8.0 phosphate buffer at various temperatures ranging from 25 to 65 °C. (B) Thermal stability was investigated by incubating the wild-type nitrilase at temperatures ranging from 30 to 60 °C. (C) Thermal stability was investigated by incubating Mut3 at temperatures ranging from 30 to 60 °C.

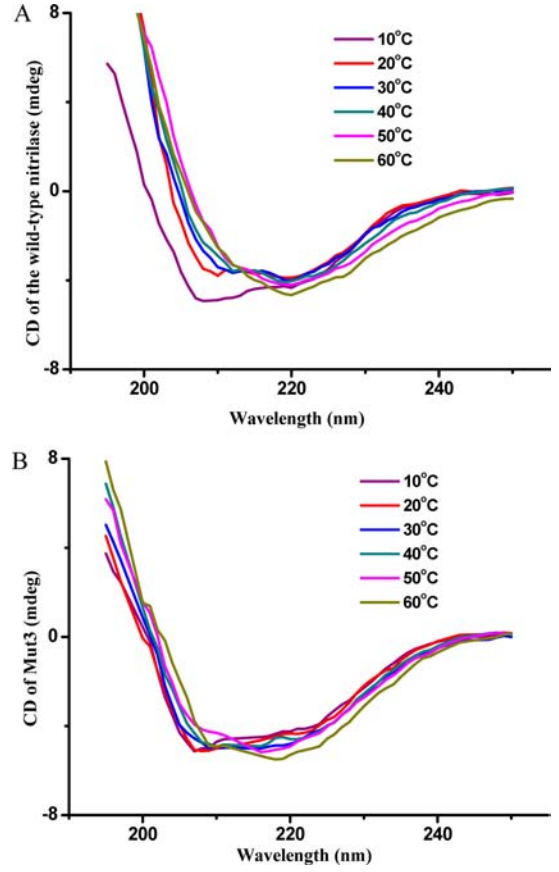

Figure 5. spectroscopic structural analyses of nitrilases. CD wavelength scans of the wild-type nitrilase (A) and Mut3 (B) at pH 7.5.

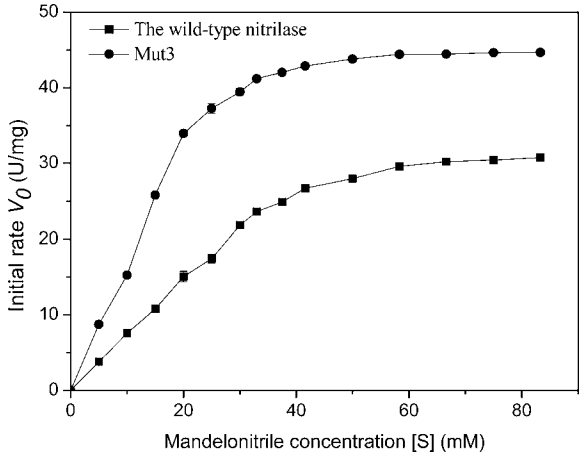

Figure 6. Reaction rate at different mandelonitrile concentrations. Reactions were performed at 45 °C, 150 rpm, with 100 mM potassium phosphate buffer (pH 8.0).

Effects of Temperatures on the Activities. The effects of temperatures on nitrilase activities of the wild-type and Mut3 were investigated. Enzyme (0.2 mg/mL) was dissolved in 100 mM phosphate buffer (pH 8.0) and incubated for 5 min at a temperature ranging from 25 to 65 °C before reaction. The reaction was started by adding 100 mM (*R*,*S*)-mandelonitrile under the corresponding temperature at 150 rpm for 10 min in a reciprocal shaker. As shown in Figure 4A, the optimum temperatures were 45 °C for both the wild-type and Mut3. The activities of nitrilases decreased significantly when the temperature was above 45 °C, and the specific activity of Mut3 was about 154% higher as compared to the wild-type nitrilase under the optimal temperature and pH.

The study of thermostability showed that the activity of wild-type nitrilase maintained about 60% incubation after 16 h, while the residual activity of Mut3 was 75% at 30 °C. After incubation for 1 h at 50 and 60 °C, the relative activity of wild-type nitrilase was sharply reduced to 4.40% and 1.03%, and Mut3 was 6.30% and 1.92%, respectively. Mut3 was unstable at higher temperature as revealed by a half-life of 54 h at 30 °C, 1.9 h at 40 °C, and 0.4 h at 50 °C, which was better than that of the wild-type nitrilase with half-lives of 21 h at 30 °C, 1.8 h at 40 °C, and 0.2 h at 50 °C (Figure 4B and C). The results corresponded to the circular dichroism data, indicating the

dx.doi.org/10.1021/jf405683f | J. Agric. Food Chem. 2014, 62, 4685−4694

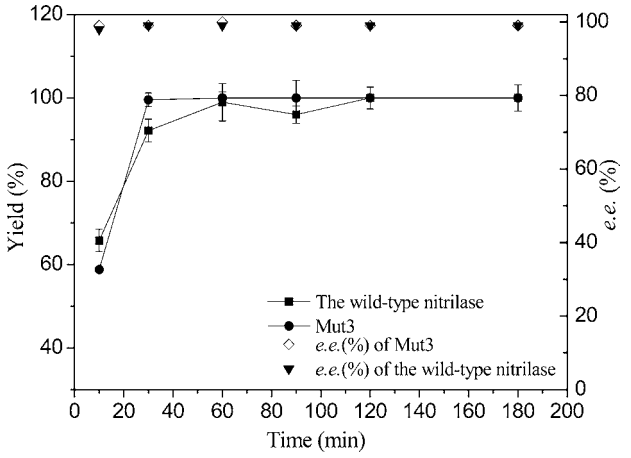

Figure 7. Time course analysis of (*R*,*S*)-mandelonitrile biotransformation by wild-type nitrilase and Mut3 under optimal conditions with a pH of 8.0, a temperature of 40 °C, and a concentration of (*R*,*S*)-mandelonitrile of 100 mM.

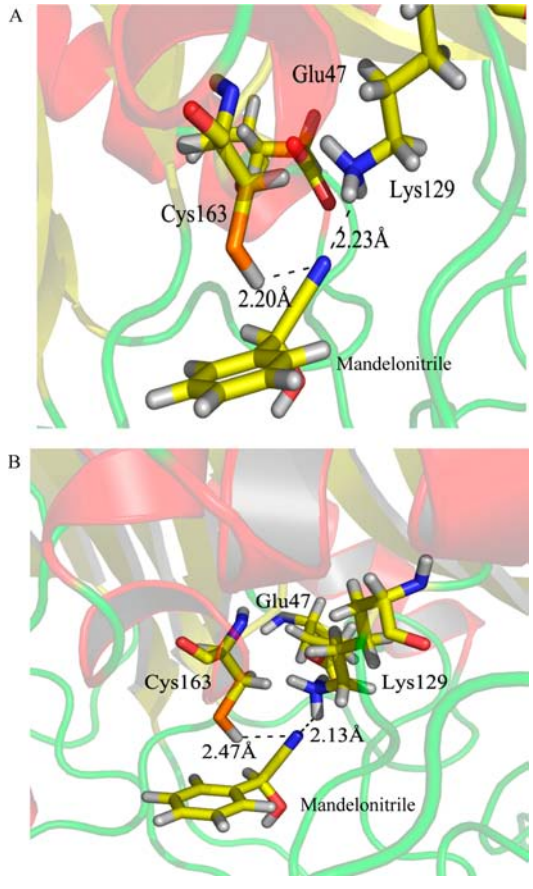

Figure 8. Homology modeling and docking analysis of nitrilases with mandelonitrile docking into the active site of the wild-type nitrilase (A) and Mut3 (B).

nitrilases were sensitive to heat (Figure 5 and Table S2, Supporting Information).

Kinetic Analysis of Wild-Type and Evolved Nitrilase. To determine the kinetics of reaction catalyzed by nitrilases, the initial rate V_0 was investigated at different concentrations (0–100 mM) of (*R*,*S*)-mandelonitrile (Figure 6). The experimental data were fitted to the Michaelis–Menten equation ($V_0 = (V_{max}[S])/(K_m + [S])$), and the values of K_m and V_{max} were

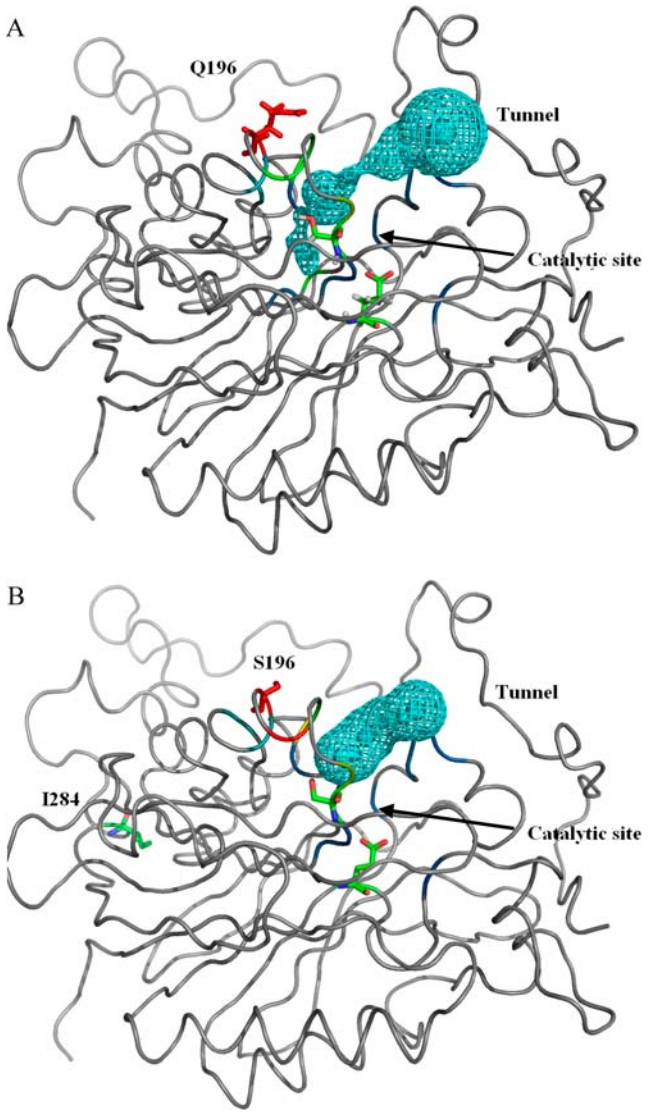

Figure 9. Tunnel analyses of wild-type nitrilase (A) and Mut3 (B).

calculated according to the Lineweaver–Burk plots. The values of K_m, V_{max}, and k_{cat} were calculated to be 20.64 mM, 33.74 μmol mg^{-1} min^{-1}, and 24.45 s^{-1} for wild-type nitrilase, while they were 9.24 mM, 47.68 μmol mg^{-1} min^{-1}, and 34.55 s^{-1} for Mut3, respectively.

Time Course of (*R*,*S*)-Mandelonitrile Hydrolysis. Wet cells of wild-type or Mut3 (0.1 g) was suspended in the 10 mL reaction mixture containing 100 mM potassium phosphate buffer (pH 8.0) and 100 mM (*R*,*S*)-mandelonitrile. The reactions were carried out at 40 °C in a reciprocal shaker at 150 rpm. Samples were removed at predetermined times, and the yield was determined by HPLC analysis. As shown in Figure 7, the yield of Mut3 could reach 100% in 0.5 h which was higher than that of the wild-type, and the enantiomeric excess (e.e.) of (*R*)-(−)-mandelic acid was >99%.

Fed-Batch Production of (*R*)-(−)-Mandelic Acid. To obtain efficient production of (*R*)-(−)-mandelic acid and reduce the potential inhibition on enzyme at high substrate concentration, a fed-batch reaction was performed using Mut3 as catalyst. (*R*,*S*)-Mandelonitrile (100 mM) was fed to the subsequent 7 batches (total concentration of substrate: 800 mM) once an hour. The accumulative concentration of (*R*)-

dx.doi.org/10.1021/jf405683f | J. Agric. Food Chem. 2014, 62, 4685–4694

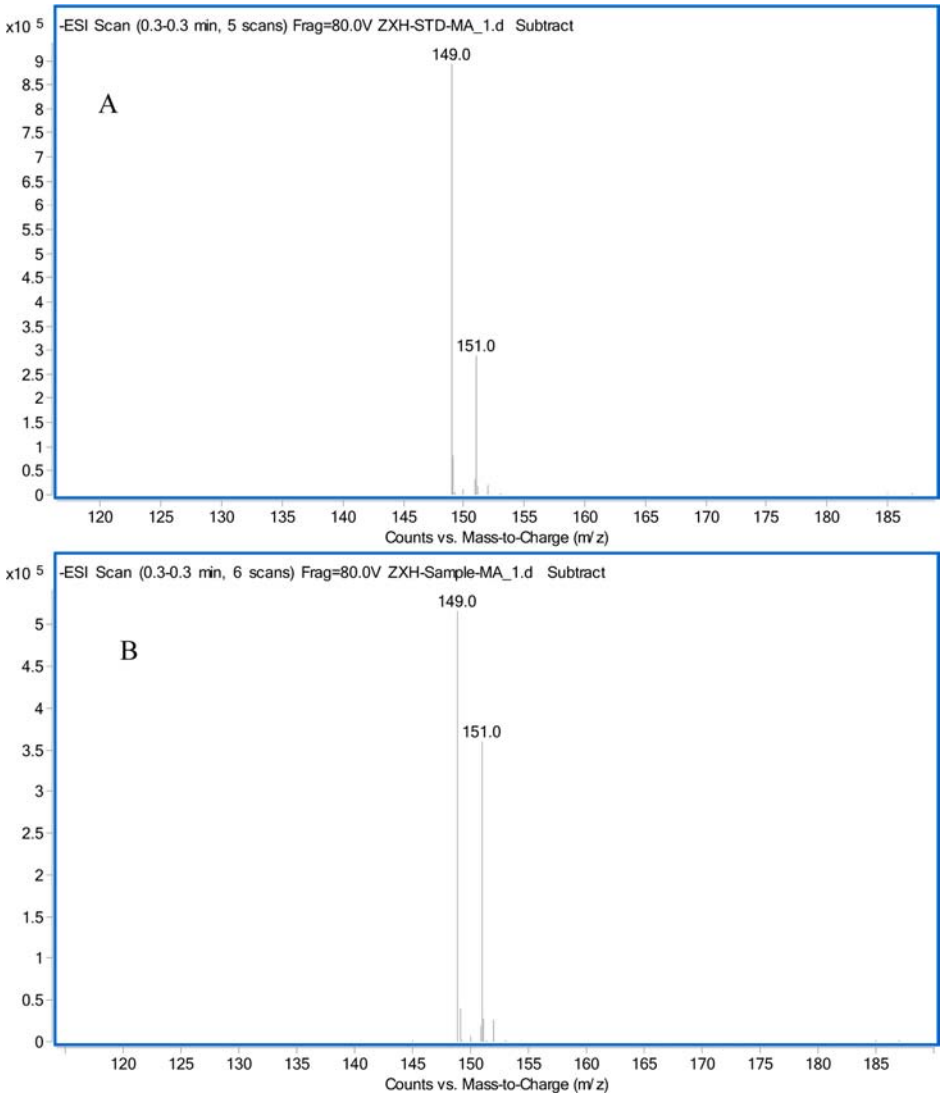

Figure 10. Identification of (*R*)-(−)-mandelic acid. LC-MS spectrum of (*R*)-(−)-mandelic acid, standard (*R*)-(−)-mandelic acid (A), and separated (*R*)-(−)-mandelic acid (B).

(−)-mandelic acid reached 585 mM after 5.5 h of biotransformation (Figure S2, Supporting Information). Compared to the previous report,[35] 693 mM of (*R*)-(−)-mandelic acid concentration at 7.5 h in this work displayed the highest productivity in terms of the nitrilase catalyzing asymmetric hydrolysis of (*R,S*)-mandelonitrile, and the optical purity of the (*R*)-(−)-mandelic acid was maintained above 99% during the reaction process. In addition, considering the cost of industrial application, Mut3 with excellent tolerance against high product concentration is more favorable for applications because the separation cost of product will be reduced substantially. Taking the volumetric productivity and product concentration tolerance into account, the mutant Mut3 was potential for industrial application.

Isolation and Identification of (*R*)-Mandelic Acid. After isolation and purification of (*R*)-(−)-mandelic acid according to the method described in Materials and Methods, (*R*)-(−)-mandelic acid with 99% purity was obtained (Figure S3, Supporting Information). The LC-MS spectrum of the separated (*R*)-(−)-mandelic acid was presented in Figure 10A and B, LC-MS showed that the molecular ion peak of (*R*)-(−)-mandelic acid was *m/z* 151.0, which was in accordance with the mass of (*R*)-(−)-mandelic acid. The FTIR spectrum of the separated (*R*)-(−)-mandelic acid is presented in Figure 11A and B; the two sharp peaks presented at 3448 and 1724 cm^{-1} could be assigned to the O−H and C═O stretching vibrations, respectively. The two peak absorption bands at 1495 and 1455 cm^{-1} were due to the C═C stretching vibration on the phenyl group. When ^{13}C NMR was performed, the isolated product gave one signal at 174 ppm, which referred to the C positions of the carboxyl group. The absorption bands between 126 and 140 ppm were due to the C positions on the phenyl group (Figure S4, A and B, Supporting Information). Figure S5, A and B (Supporting Information) shows four different kinds of H atoms, which corresponded to the structure of (*R*)-(−)-mandelic acid, one peak at chemical shift δ = 12.6356 ppm representing one H atom at the carboxyl group. The split peaks at chemical shifts between δ = 7.2797 ppm and δ = 7.4522 ppm represented the H positions on the phenyl group, and the peak at chemical shift δ = 2.50 ppm referred to the H position of the hydroxyl group. Accordingly, it was concluded that the isolated product was (*R*)-(−)-mandelic acid.

dx.doi.org/10.1021/jf405683f | J. Agric. Food Chem. 2014, 62, 4685−4694

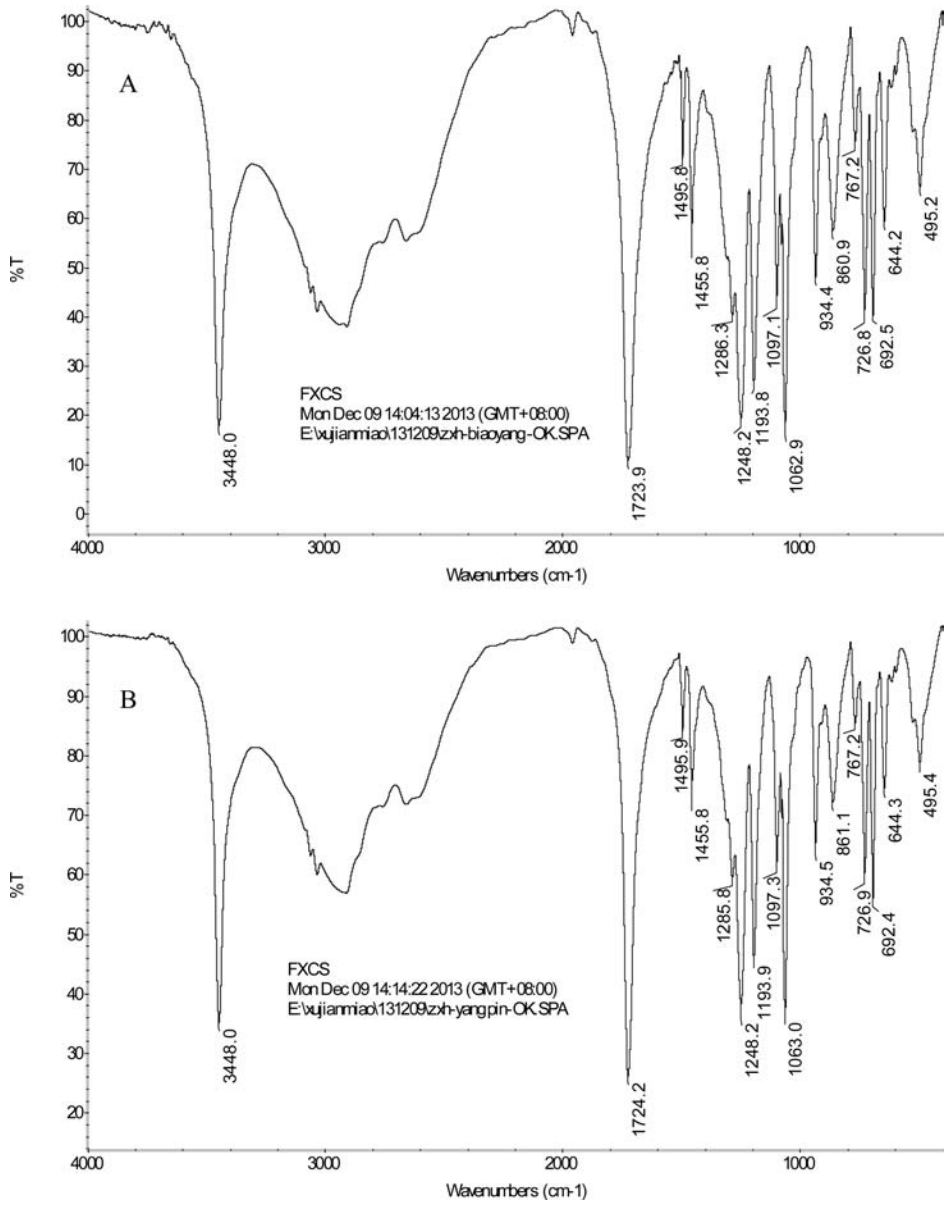

Figure 11. Identification of (*R*)-(−)-mandelic acid. Infrared spectroscopy of (*R*)-(−)-mandelic acid, standard (*R*)-(−)-mandelic acid (A), and separated (*R*)-mandelic acid (B).

Table 2. Comparison of Wild-Type Nitrilase and Mut3 with Reported Nitrilases

substrate (mM)	bacteria	resting cells (g)	reaction time (h)	the volume of reaction (mL)	yield (%)	reference
100	*E. coli* JM109/pNLE	0.01	2	1	100	15
100	*E. coli* M15/BCJ2315	0.1	1	10	99.1	37
100	the wild-type nitrilase	0.1	1	10	100	this work
100	Mut3	0.1	0.5	10	100	this work

DISCUSSION

Nitrilases have recently drawn considerable attention due to their ability to transform nitriles to carboxylic acids with chemo-, region-, and enantioselectivity.[36,37] Nitrilases, as important industrial enzymes, have more significant improvements than traditional chemical catalysts,[38] which have mediated the industrial conversion of aliphatic, arylaliphatic, aromatic, and heterocyclic nitriles.[6,37] One of the important industrial applications of nitrilases is the conversion of (*R*,*S*)-mandelonitrile to (*R*)-(−)-mandelic acid with high enantioselectivity, low cost, and almost 100% yield.[5,11,12] The goal of this study is to improve the nitrilase from *A. faecalis* to meet the requirement of an upscale production of (*R*)-(−)-mandelic acid.

On the basis of the secondary structure, relationships between substrate and the nitrilase, and previous reports,[5,31,32] five sites (Leu175, Ala197, Val305, Ala284, and Gln196) were selected to carry out mutations for improving activity of nitrilase. After screening by a two step screening method, the best mutant Mut3 was selected. Mut3 displayed dramatic improvement in activity, pH stability, and tolerance to the

substrate. In a fed-batch reaction with 800 mM (*R*,*S*)-mandelonitrile as the substrate, the cumulative concentration of (*R*)-(−)-mandelic acid in the reaction mixture after 5.5 h of biotransformation reached 585 mM with an e.e. of 99%, which was higher than that in a previous report with 520 mM after 18 h. At the same time, the space-time productivity of Mut3 (10.64 mmol L^{-1} h^{-1} g^{-1}) was 7.40-fold higher than that in a previous report (1.44 mmol L^{-1} h^{-1} g^{-1}).[35]

CD results confirmed that these nitrilases are sensitive to heat and that the thermostability of Mut3 was better than that of wild-type nitrilase. The nitrilase activites of both wild-type and Mut3 shared almost the same trends under different pH conditions. The specific activity of Mut3 (42.77 U/mg) was 154% higher than that of wild-type nitrilase (27.79 U/mg) at pH 8.0. The analysis of the time course of (*R*,*S*)-mandelonitrile hydrolysis indicated that the yield of Mut3 could reach 100% in 0.5 h, which was shorter than that of wild-type nitrilase with 1 h. Especially, the time-space productivity of (*R*)-(−)-mandelic acid by Mut3 was superior to those in previous reports (Table 2).[35,39]

Homology modeling and molecular docking analysis can predict spatial structure and the catalytic mechanism of nitrilase (Figure 8). Modeling and mutation studies showed that conserved catalytic residues Cys163, Glu47, and Lys129 are the catalytic triad of the nitrilase. Cys163 attacks cyano as affinity reagents with hydrogen bonds, Lys129 has a stabilizing effect on the triplet complex with hydrogen bonds, and Glu47 plays a leading role in catalysis.[5] The tunnel analysis indicated that the diameter of the catalytic tunnel and tunnel volume for Mut3 were 1.70 and 16.0 $Å^3$ compared with 0.43 and 23.0 $Å^3$ for the wild-type (Figure 9). The larger catalytic tunnel and smaller tunnel volume can improve the nitrilase to hold and selectively catalyze the substrate.[30,32]

In summary, we genetically engineered the nitrilase originated from *A. faecalis* nitrilase by GSSM for the production of (*R*)-(−)-mandelic acid. A mutant, Mut3 with high activity, enantioselectivity, and stability in high concentrations of substrate or product, had been obtained. The thermostability of Mut3 was better than that of wild-type nitrilase. After mutation, Mut3 achieved the highest space-time productivity (10.64 mmol L^{-1} h^{-1} g^{-1}). The results in this work indicated that Mut3 was a promising biocatalyst for the production of (*R*)-(−)-mandelic acid in industrial applications. This study paved a foundation for the large-scale biotransformation of (*R*,*S*)-mandelonitrile to (*R*)-(−)-mandelic acid. Further studies will focus on the upscale production of (*R*)-(−)-mandelic acid using Mut3 as the biocatalyst and are underway in our laboratory.

■ ASSOCIATED CONTENT

Supporting Information

Relative activities of wild-type and evolved nitrilases, comparison of θ208, θ222, and θ216 at different temperatures of nitirilases, color images of bromocresol purple responding to increasing mandelic acid concentration, time-course profile for the preparation of (*R*)-(−)-mandelic acid which was fed in the subsequent 7 feeds (total 800 mM), crystal of (*R*)-(−)-mandelic acid, and ^1H and ^{13}C NMR of (*R*)-(−)-mandelic acid. This material is available free of charge via the Internet at http://pubs.acs.org.

■ AUTHOR INFORMATION

Corresponding Author

*Tel: +86-571-88320630. Fax: +86-571-88320630. E-mail: zhengyg@zjut.edu.cn.

Funding

This work was financially supported by the National High Technology Research and Development Program of China (863 Program) (No. 2011AA02A210), Natural Science Foundation of Zhejiang Province (No. R3110155, Z4090612 and Y4110409), and Qianjiang Talent Project of Zhejiang Province.

Notes

The authors declare no competing financial interest.

■ REFERENCES

(1) Kirk, O.; Borchert, T. V.; Fuglsang, C. C. Industrial enzyme applications. *Curr. Opin. Biotechnol.* **2002**, *13* (4), 345−351.

(2) Straathof, A. J.; Panke, S.; Schmid, A. The production of fine chemicals by biotransformations. *Curr. Opin. Biotechnol.* **2002**, *13* (6), 548−556.

(3) Gong, J. S.; Lu, Z. M.; Li, H.; Shi, J. S.; Zhou, Z. M.; Xu, Z. H. Nitrilases in nitrile biocatalysis: recent progress and forthcoming research. *Microb. Cell Fact.* **2012**, *11* (1), 142.

(4) Liu, Z. Q.; Baker, P. J.; C, F.; Xue, Y. P.; Zheng, Y. G.; Shen, Y. C. Screening and improving the recombinant nitrilases and application in biotransformation of iminodiacetonitrile to iminodiacetic acid. *PLoS One* **2013**, *8* (6), e67197.

(5) Liu, Z. Q.; Dong, L. Z.; Cheng, F.; Xue, Y. P.; Wang, Y. S.; Ding, J. N.; Zheng, Y. G.; Shen, Y. C. Gene cloning, expression, and characterization of a nitrilase from *Alcaligenes faecalis* ZJUTB10. *J. Agric. Food. Chem.* **2011**, *59* (21), 11560−11570.

(6) O'Reilly, C.; Turner, P. D. The nitrilase family of CN hydrolysing enzymes - a comparative study. *J. Appl. Microbiol.* **2003**, *95* (6), 1161−1174.

(7) Kaul, P.; Banerjee, A.; Mayilraj, S.; Banerjee, U. C. Screening for enantioselective nitrilases: kinetic resolution of racemic mandelonitrile to (*R*)-(−)-mandelic acid by new bacterial isolates. *Tetrahedron: Asymmetry* **2004**, *15* (2), 207−211.

(8) Rustler, S.; Muller, A.; Windeisen, V.; Chmura, A.; Fernandes, B. C. M.; Kiziak, C.; Stolz, A. Conversion of mandelonitrile and phenylglycinenitrile by recombinant *E. coli* cells synthesizing a nitrilase from *Pseudomonas fluorescens* EBC191. *Enzyme Microb. Technol.* **2007**, *40* (4), 598−606.

(9) Zhang, H. J.; Q, W.; Zhou, Q. W.; Zhou, G. C. Biotransformation of the neonicotinoid insecticide thiacloprid by the *Bacterium Variovorax* boronicumulans strain J1 and mediation of the major metabolic pathway by nitrile hydratase. *J. Agric. Food. Chem.* **2012**, *60* (1), 153−159.

(10) Mullaney, J. A.; Kelly, W. J.; Mcghie, T. K. Lactic acid bacteria convert glucosinolates to nitriles efficiently yet differently from enterobacteriaceae. *J. Agric. Food. Chem.* **2013**, *61* (12), 3039−3046.

(11) Xue, Y. P.; Liu, Z. Q.; Xu, M.; Wang, Y. J.; Zheng, Y. G.; Shen, Y. C. Enhanced biotransformation of (*R*,*S*)-mandelonitrile to (*R*)-(−)-mandelic acid with in situ production removal by addition of resin. *Biochem. Eng. J.* **2010**, *53* (1), 143−149.

(12) Xiao, M. T.; Huang, Y. Y.; Ye, J.; Guo, Y. H. Study on the kinetic characteristics of the asymmetric production of *R*-(−)-mandelic acid with immobilized *Saccharomyces cerevisiae* FD11b. *Biochem. Eng. J.* **2008**, *39* (2), 311−318.

(13) Tang, K.; Yi, J.; Huang, K.; Zhang, G. Biphasic recognition chiral extraction: A novel method for separation of mandelic acid enantiomers. *Chirality* **2009**, *21* (3), 390−395.

(14) Xue, Y. P.; Xu, S. Z.; Liu, Z. Q.; Zheng, Y. G.; Shen, Y. C. Enantioselective biocatalytic hydrolysis of (R,S)-mandelonitrile for production of (R)-(-)-mandelic acid by a newly isolated mutant strain. *J. Ind. Microbiol. Biotechnol.* **2011**, *38* (2), 337−345.

(15) Schmid, A.; Dordick, J. S.; Hauer, B.; Kiener, A.; Wubbolts, M.; Witholt, B. Industrial biocatalysis today and tomorrow. *Nature* **2001**, *409* (6817), 258−268.
(16) Takahashi, E.; Nakamichi, K.; Furui, M.; Mori, T. *R*-(−)-Mandelic acid production from racemic mandelic acids by *Pseudomonas polycolor* with asymmetric degrading activity. *J. Ferment. Bioeng.* **1995**, *79* (5), 439−442.
(17) Williams, D. J.; Critchley, C.; Pun, S.; Chaliha, M. Key role of Fe^{2+} in epithiospecifier protein activity. *J. Agric. Food. Chem.* **2010**, *85* (15), 8512−8521.
(18) He, Y. C.; Xu, J. H.; Xu, Y.; Ouyang, L. M.; Pan, J. Biocatalytic synthesis of R-(-)-mandelic acid from racemic mandelonitrile by a newly isolated nitrilase-producer *Alcaligenes* sp. ECU0401. *Chinese Chem. Lett.* **2007**, *18* (6), 677−680.
(19) Naik, S. C.; Kaul, P.; Barse, B.; Banerjee, A.; Banerjee, U. C. Studies on the production of enantioselective nitrilase in a stirred tank bioreactor by *Pseudomonas putida* MTCC 5110. *Bioresour. Technol.* **2008**, *99* (1), 26−31.
(20) Yamamoto, K.; Oishi, K.; Fujimatsu, I.; Komatsu, K. Production of *R*-(−)-mandelic acid from mandelonitrile by *Alcaligenes faecalis* ATCC 8750. *Appl. Environ. Microbiol.* **1991**, *57* (10), 3028−3032.
(21) Nagasawa, T.; Mauger, J.; Yamada, H. A novel nitrilase, arylacetonitrilase, of *Alcaligenes faecalis* JM3 - purification and characterization. *Eur. J. Biochem.* **1990**, *194* (3), 765−772.
(22) Zhu, D. M.; Mukherjee, C.; Biehl, E. R.; Hua, L. Discovery of a mandelonitrile hydrolase from *Bradyrhizobium japonicum* USDA110 by rational genome mining. *Biochem. J.* **2007**, *129* (4), 645−650.
(23) Wang, H. L.; Sun, H. H.; Wei, D. Z. Discovery and characterization of a highly effcient enantioselective mandelonitrile hydrolase from *Burkholderia cenocepacia* J2315 by phylogeny-based enzymatic substrate specificity prediction. *BMC Biotechnol.* **2013**, *13*, 14.
(24) Liu, Z. Q.; Sun, Z. H.; Leng, Y. Directed evolution and characterization of a novel D-pantonohydrolase from *Fusarium moniliforme*. *J. Agric. Food. Chem.* **2006**, *54* (16), 5823−5830.
(25) Zoller, M. J.; Smith, M. Oligonucleotide-directed mutagenesis using M13-derived vectors: an efficient and general procedure for the production of point mutations in any fragment of DNA. *Nucleic Acids Res.* **1982**, *10* (20), 6487−6500.
(26) Yeom, S. J.; Lee, J. K.; Oh, D. K. A positively charged amino acid at position 129 in nitrilase from *Rhodococcus rhodochrous* ATCC 33278 is an essential residue for the activity with meta-substituted benzonitriles. *FEBS Lett.* **2010**, *584* (1), 106−110.
(27) Wu, S. J.; Fogiel, A. J.; Petrillo, K. L.; Hann, E. C.; Mersinger, L. J.; DiCosimo, R.; O'Keefe, D. P.; Ben-Bassat, A.; Payne, M. S. Protein engineering of *Acidovorax facilis* 72W nitrilase for bioprocess development. *Biotechnol. Bioeng.* **2007**, *97* (4), 689−693.
(28) Wu, S. J.; Fogiel, A. J.; Petrillo, K. L.; Jackson, R. E.; Parker, K. N.; DiCosimo, R.; Ben-Bassat, A.; O'Keefe, D. P.; Payne, M. S. Protein engineering of nitrilase for chemoenzymatic production of glycolic acid. *Biotechnol. Bioeng.* **2008**, *99* (3), 717−720.
(29) Nolan, L. M.; Harnedy, P. A.; Turner, P.; Hearne, A. B.; O'Reilly, C. The cyanide hydratase enzyme of *Fusarium lateritium* also has nitrilase activity. *FEMS Microbiol. Lett.* **2003**, *221* (2), 161−165.
(30) Watanabe, A.; Yano, K.; Ikebukuro, K.; Karube, I. Investigation of the potential active site of a cyanide dihydratase using site-directed mutagenesis. *Biochim. Biophys. Acta* **1998**, *1382* (1), 1−4.
(31) Schreiner, U.; Hecher, B.; Obrowsky, S.; Waich, K.; Klempier, N.; Steinkellner, G.; Gruber, K.; Rozzell, J. D.; Glieder, A.; Winkler, M. Directed evolution of *Alcaligenes faecalis* nitrilase. *Enzyme Microb. Technol.* **2010**, *47* (4), 140−146.
(32) Williamson, D. S.; Dent, K. C.; Weber, B. W.; Varsani, A.; Frederick, J.; Thuku, R. N.; Cameron, R. A.; van Heerden, J. H.; Cowan, D. A.; Sewell, B. T. Structural and biochemical characterization of a nitrilase from the thermophilic bacterium, *Geobacillus pallidus* RAPc8. *Appl. Microbiol. Biotechnol.* **2010**, *88* (1), 143−153.
(33) Chung, C. T.; Niemela, S. L.; Miller, R. H. One-step preparation of competent *Escherichia coli*: transformation and storage of bacterial cells in the same solution. *Proc. Natl. Acad. Sci. U.S.A.* **1989**, *86* (7), 2172−2175.
(34) Bradford, M. M. A rapid and sensitive method for the quantitation of microgram quantities of protein utilizing the principle of protein-dye binding. *Anal. Biochem.* **1976**, *72* (1−2), 248−254.
(35) Zhang, Z. J.; Xu, J. H.; He, Y. C.; Ouyang, L. M.; Liu, Y. Y.; Imanaka, T. Efficient production of (*R*)-(−)-mandelic acid with highly substrate/product tolerant and enantioselective nitrilase of recombinant *Alcaligenes sp. Process Biochem.* **2010**, *45* (6), 887−891.
(36) Wang, M. X. Enantioselective biotransformations of nitriles in organic synthesis. *Top. Catal.* **2005**, *35* (1−2), 117−130.
(37) Thuku, R. N.; Brady, D.; Benedik, M. J.; Sewell, B. T. Microbial nitrilases: versatile, spiral forming, industrial enzymes. *J. Appl. Microbiol.* **2009**, *106* (3), 703−727.
(38) Martinkova, L.; Kren, V. Biotransformations with nitrilases. *Curr. Opin. Chem. Biol.* **2010**, *14* (2), 130−137.
(39) Ni, K. F.; Wang, H. L.; Zhao, L.; Zhang, M. J.; Zhang, S. Y.; Ren, Y. H.; Wei, D. Z. Efficient production of (*R*)-(−)-mandelic acid in biphasic system by immobilized recombinant *E.coli*. *J. Biotechnol.* **2013**, *167* (4), 433−440.

JOURNAL OF AGRICULTURAL AND FOOD CHEMISTRY

Article

pubs.acs.org/JAFC

Drying and Denaturation Characteristics of α-Lactalbumin, β-Lactoglobulin, and Bovine Serum Albumin in a Convective Drying Process

M. Amdadul Haque,[†,‡] Peter Aldred,[§] Jie Chen,[#] Colin Barrow,[⊥] and Benu Adhikari*[,†]

[†]School of Applied Sciences, RMIT University, Melbourne City Campus, Melbourne, VIC 3001, Australia

[‡]Department of Agro-processing, BSMRAU, Gazipur 1706, Bangladesh

[§]School of Health Sciences, University of Ballarat, Mount Helen, VIC 3353, Australia

[#]State Key Laboratory for Food Science and Technology, Jiangnan University, Wuxi, China

[⊥]School of Life and Environmental Sciences, Deakin University, Geelong, VIC 3217, Australia

ABSTRACT: Drying and denaturation kinetics of aqueous droplets of α-lactalbumin (α-lac), β-lactoglobulin (β-lg), and bovine serum albumin (BSA) were measured in a convective drying environment. Single droplets having an initial droplet diameter of 2 ± 0.1 mm and containing 10% (w/v) protein concentration were dried using conditioned air (65 and 80 °C, 2−3% RH, 0.5 m/s velocity) for 600 s. The denaturation of these proteins was measured by using reversed-phase HPLC. At the end of 600 s of drying 13.3 and 19.4% α-lac was found to be lost due to denaturation at 65 and 80 °C, respectively. Up to 31.0% of β-lg was found to be denatured, whereas BSA was not found to be significantly ($p > 0.05$) denatured in these drying conditions. The formation and strength of skin and the associated morphological features were found to be linked with the degree of denaturation of these proteins. The secondary structure of these proteins was significantly ($p < 0.05$) affected and altered by the drying stresses. The β-sheet and random coil contents were increased in α-lac by 6.5 and 4.0%, respectively, whereas the α-helix and β-turn contents decreased by 5.5 and 5.0%, respectively. The β-sheet and random coil contents in β-lg were increased by 7.5 and 2.0%, respectively, whereas the α-helix and β-turn contents decreased by 3.5 and 6.0%, respectively. In the case of BSA the β-sheet, α-helix, and random coil contents were found to increase, whereas the β-turn content decreased.

KEYWORDS: *bovine serum albumin, α-lactalbumin and β-lactoglobulin denaturation, drying, single droplet, β-sheet, β-turn, α-helix, morphology*

INTRODUCTION

Whey is a heterogeneous mix of proteins. Among these proteins, α-lactalbumin (α-lac, 20%), β-lactoglobulin (β-lg, 65%), and bovine serum albumin (BSA, 8%) are the major constituents and comprise >90% of total whey protein. There are numerous studies in the literature reporting the denaturation of whey protein during thermal processing including drying.[1−3] However, these studies do not provide the drying and denaturation kinetics of individual whey protein fractions. A limited number of works are reported in the literature that provide the extent of denaturation of individual whey proteins (when they are treated separately), especially during isothermal heat treatment and high-pressure treatment processes.[4−6] There is little, if any, published work in the literature quantifying and analyzing the denaturation kinetics of individual whey protein components at the droplet level during convective drying. The quantification and understanding of drying and denaturation kinetics of individual whey protein components can help minimize the denaturation of individual whey proteins during powder formation and also help in designing better spray-dryers.

The spray-drying process involves atomization of a solution into droplets in a drying chamber and subsequent removal of the solvent through evaporation and finally formation of powder product. The formation of particles from a solution in the convective drying process such as spray-drying involves both equilibrium thermodynamic and kinetic processes. The vapor pressure and temperature gradients within a drying droplet and the drying medium are the key driving forces for the mass transfer from, and heat transfer to, the droplet. In an actual drying process, unique and complex evolution of particle shape and morphology takes place, which affects the mass and heat transport process. On the other hand, the magnitude of the vapor pressure and temperature gradients and the resultant heat and mass transfer fluxes also greatly affect the development of morphology in drying droplets.

In the spray-drying process, the operating parameters (or even the design of dryer to less extent) have to be judiciously selected to control the particle morphology. This is because the characteristics of the product such as particle density, particle size distribution, and residual final moisture content are greatly affected by the morphology of dried particles.[7] During spray-drying, the particle morphology is greatly affected by the drying conditions as well as by the nature and concentration of feed and the mode of atomization used. For example, the skin-forming and crust-forming materials develop quite different

Received: January 5, 2014
Revised: May 1, 2014
Accepted: May 1, 2014
Published: May 2, 2014

ACS Publications © 2014 American Chemical Society

dx.doi.org/10.1021/jf405603c | J. Agric. Food Chem. 2014, 62, 4695−4706

morphological features.[8] Hence, the monitoring and analysis of the evolution of morphology during the particle formation process can provide very important information. However, it is not yet technologically feasible to capture the evolution of morphology during the particle formation process in situ during spray-drying. To date, the morphological features of spray-dried powders are acquired and analyzed using final powder particles.[9] However, these morphological features cannot be used to explain the evolution of morphology during the particle formation process. Thus, the relationships among the drying kinetics, morphology, physicochemical characteristics, and denaturation of protein are poorly understood. Single-droplet drying experiments are commonly carried out to capture the evolution of morphological features in drying droplets in convective drying processes.[10] Despite some limitations such as much larger droplet size and much longer drying time, single droplet drying experiments provide very important information regarding the development of morphological features during the convective drying process which is a much simplified and idealized model of spray-drying.[11−14]

Reversed-phase high-performance liquid chromatography (RP-HPLC) is an effective tool to separate denatured and native proteins. The chemical resin in the stationary phase of this column (i.e., presence of C8, C18) successfully retards migration of the denatured protein.[3,15] The strong affinity of these chemicals toward the hydrophobic portion of denatured proteins helps to separate the denatured and native proteins.

The functionality of protein predominantly depends on its specific molecular composition and structure. The polypeptide chains acquire a folded form to perform their biological functions. However, the stress generated during processing such as spray-drying can alter the structure of protein. Fourier transform infrared (FTIR) spectroscopy has been commonly used to identify and explain the structural characteristics of proteins. It is used to quantify the change in the secondary structure of proteins.[16] The polypeptide and protein repeat units give raise to nine characteristic IR absorption bands, namely, amides A and B and amides I−VII. The amide I region ranging between 1600 and 1700 cm^{-1} is commonly chosen to measure qualitative and quantitative changes in secondary structure of proteins because of its very high signal-to-noise ratio.[17,18] Furthermore, the absorption at this band is able to give considerable variation in IR signal even at small alterations in the molecular configuration of analytes.[19]

Although the IR spectra obtained are intrinsic and complex, mathematical tools such as derivatization and Fourier self-deconvolution (FSD) analyses are available to determine the unique structural features such as α-helix, β-sheets, β-turns, and random coils of a protein.[20,21] The derivatization and FSD can be applied to quantify alteration in structural features of proteins due to processing stresses.[16,17]

In this context, the key aim of this study was to measure the denaturation and drying kinetics of major whey proteins (α-lac, β-lg, and BSA) in convective air-drying environments. FTIR spectroscopy was used to quantify and explain the alteration in the secondary structure of these proteins caused by drying-induced stresses. The evolution of droplet morphology was captured and analyzed using single-droplet drying experiments.

EXPERIMENTAL PROCEDURES

Materials. The protein samples (α-lac, β-lg, and BSA) with high purity (≥95% pure) were purchased from Sigma-Aldrich (New South Wales, Australia). The HPLC solvents acetonitrile and trifluoroacetic acid (TFA) were purchased from Sigma-Aldrich and Fisher Scientific (Victoria, Australia), respectively. Deuterium oxide (D_2O) was purchased from Sigma-Aldrich. All proteins and chemicals were used as received without further purification.

Methods. *Single-Droplet Drying (SDD).* Details of the SDD instrument and its working procedure are provided elsewhere.[22,23] Aqueous droplets of 5 ± 0.1 μL initial volume (2 ± 0.1 mm initial droplet diameter) containing 10% (w/v) protein were suspended on the tip of a glass filament with a 0.2 ± 0.01 mm diameter. This droplet-suspending filament was supported by a droplet suspension system made up of a bored Teflon cylinder. The droplets were then subjected to conditioned drying air. The drying air was cleaned and heated by passing through a series of columns containing dried molecular sieve and dried silica gel. The temperature of the drying air was controlled by a proportional-integral-derivative (PID) controller. The droplets were dried at two different air temperatures (65 and 80 °C) at a constant velocity of 0.5 m/s. The relative humidity of the drying air was measured by using an EL-USB relative humidity data logger (Lascar Electronics, UK) and was found to be 2.5 ± 0.5% at these two drying temperatures. The wet bulb temperatures corresponding to air temperatures of 65 and 80 °C were 26 and 30 °C, respectively. The droplets were dried for 600 s, and the denaturation was measured at every 60 s interval. The temperature and mass loss histories were recorded in a computer. Images of the droplets during drying were captured at every 50 s interval using a digital camera (EOS 60D, Canon, NSW, Australia) at 40−50× magnification.

Determination of Denaturation of Proteins. The convectively dried droplets were diluted to 100 μg/mL with deionized water. Then, the pH of the diluted protein solutions was lowered to 4.6 by adding 0.1 M HCl to assist in separating the native and denatured proteins.[23,24] After the pH of protein solutions was adjusted, they were kept for 30 min and centrifuged at 11500g for 10 min. The supernatant was collected and injected onto the RP-HPLC column to separate the denatured and undenatured proteins. A control sample without drying was treated in the same way including pH treatment and centrifugation. The supernatant of the control sample was also subjected to RP-HPLC separation in the same way as dried protein. Residual native protein content was calculated using the ratio between the area under the peak of the treated protein and the area under the peak of untreated (control) protein (100%), as suggested by Parris and Baginski.[3]

The experiments were carried out in triplicate, and the average values are reported in the ensuing sections. The statistical analyses were carried out by using data analysis tools, Microsoft Office Excel 2010. The significance difference between two mean values was determined using one-way analysis of variance at 95% confidence level ($p < 0.05$). The inbuilt program in Microsoft Excel was used for this purpose.

Acquiring the IR Spectra. The IR spectra were acquired using a PerkinElmer Frontier FT-IR instrument operated by CPU32 M software. The SDD samples subjected to single-droplet drying and control samples were diluted to 5 mg/mL concentration using deuterium oxide (D_2O) containing 100 mM sodium chloride (NaCl).[18] The samples used in these tests were collected after 500 s of drying at both drying (air) temperatures. This time of sample collection (500 s) was chosen on the basis of the fact that both WPI (as a whole) and its major component β-lg were found to reach their maximum levels of denaturation at this time at both drying temperatures.[25] The samples were scanned within 650−4000 cm^{-1} using triglycine sulfate (TGS) detector. A total of four scans at 4 cm^{-1} resolution were accumulated at 0.2 cm/s scanning speed.

Analysis of IR Spectra. The blank spectrum (D_2O + NaCl) was subtracted from the spectrum of each sample. The baseline-subtracted protein spectra were analyzed by using PerkinElmer's proprietary software (version 10.03.06) and OPUS 6.5.92 (Bruker Biosciences Pty Ltd., Victoria, Australia). A 9-point second-derivative analysis using the PerkinElmer software was used to locate the peak position in the spectra. The OPUS software was used for quantitative analysis of secondary structure of protein by Fourier self-deconvolution. The original spectra (of amide region I, 1600−1700 cm^{-1}) without any

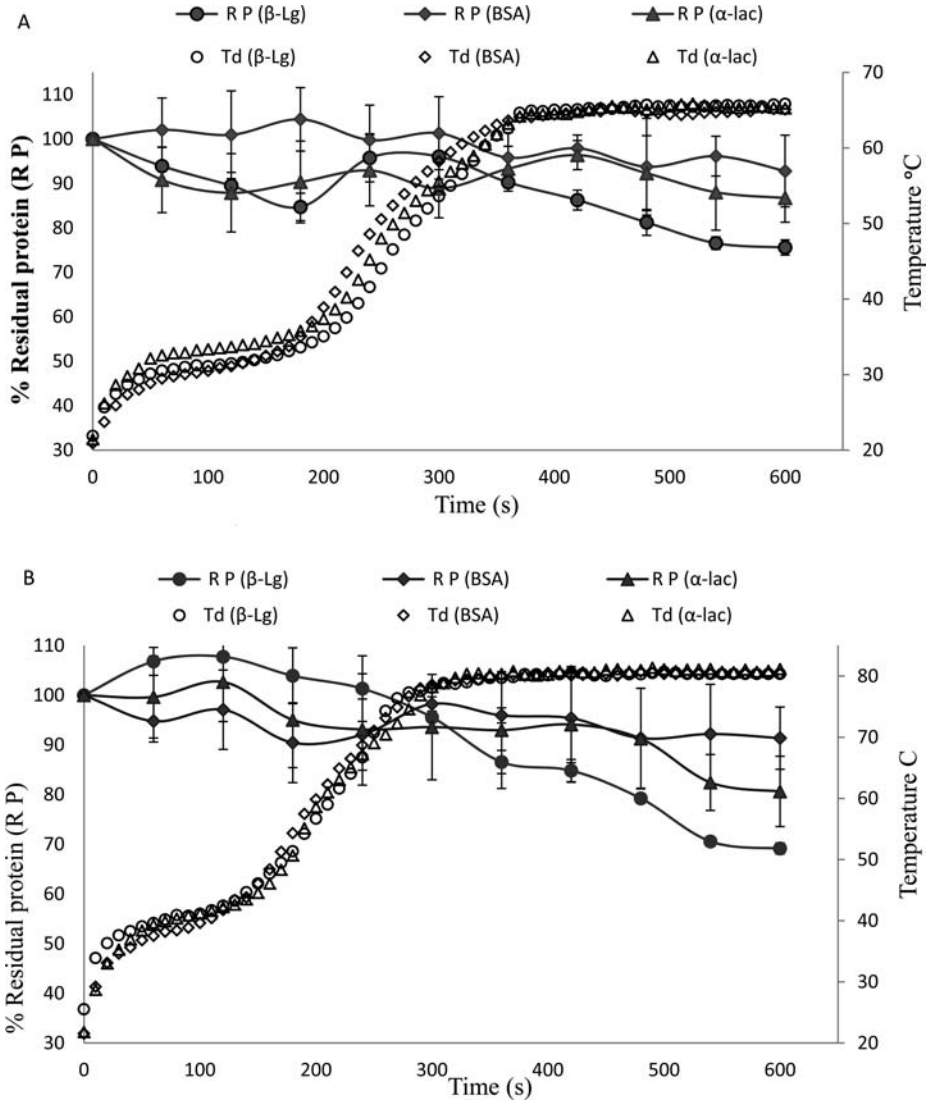

Figure 1. Denaturation of BSA, α-lac, and β-lg with drop temperature increment during drying at (A) 65 and (B) 80 °C air temperatures. The error bars show the standard deviation (SD) of experimental values.

smoothing were deconvoluted by gamma factor 2. The FSD curves were fitted with Gaussian shape and were analyzed by local least-squares (LLS) algorithm. Percentage of secondary structures (α-helix, β-sheets, β-turns, and random coils) was estimated using eq 1[16,26]

$$\text{secondary structure (\%)} = A_{\text{ind}}/A_{\text{total}} \times 100 \quad (1)$$

where A_{ind} = sum of area of individual secondary structure in amide I band and A_{total} = sum of area of total secondary structure in amide I band.

The position or location of bands for each secondary structure (β-sheets, α-helix, and β-turns) of tested proteins in D_2O were determined as suggested in the literature.[19,27,28] The bands from 1620 to 1640 cm^{-1} and from 1674 to 1680 cm^{-1} were assigned to β-sheets. The bands from 1641 to 1647 cm^{-1} were assigned to random coil. The bands within 1648−1660 cm^{-1} were assigned to α-helix. Similarly, the bands appearing at and in the vicinity of 1663, 1671, 1683, 1688, and 1694 cm^{-1} were assigned to β-turns.

RESULTS AND DISCUSSION

Denaturation of BSA, β-Lg, and α-Lac during Convective Drying. The denaturation kinetics of BSA, β-lg, and α-lac due to convective drying at droplet level were measured by RP-HPLC. As presented in Figure 1, a different extent of denaturation was observed in these whey protein fractions. Among these three proteins, BSA showed the highest stability as determined by the highest level of residual protein. β-Lg showed the least stability, that is, the lowest level of residual protein during drying. The stability of α-lac against denaturation remained between those of BSA and β-lg at both 65 and 80 °C (Figure 1). There was no significant ($p > 0.05$) loss of BSA and α-lac when dried at 65 and 80 °C for up to 480 s. At the end of 600 s, 13.26 and 19.37% of α-lac was found to be denatured at 65 and 80 °C, respectively. When the solution of β-lg was dried at these two drying temperatures, 24.40 and 30.85% of this protein was found to be denatured at 65 and 80 °C drying temperatures, respectively, when dried for 600 s. The difference in molecular configuration of these protein fractions might have played an important role for these differences in the observed denaturation. Specifically, the difference in the number of cysteine (amino acid) molecules and sulfur bridges in the structure of these proteins can be attributed to the variation in the denaturation. β-Lg starts to show significant ($p < 0.05$) loss due to denaturation (Figure 1B) when it reaches a state of irreversible denaturation (for example, 240 s at 80 °C). Before this state of irreversible denaturation is reached,

dx.doi.org/10.1021/jf405603c | J. Agric. Food Chem. 2014, 62, 4695−4706

Table 1. Model Constants To Predict the Evaporation Rate from Droplets during Drying of α-Lac, β-Lg, and BSA

		model constants				
drying temp (°C)	protein	*A*	*B*	*C*	*D*	R^2
65	α-lac	$6.65e^{-6}$	0.00507	0.9740		0.98 ± 0.02
	β-lg	$7.5e^{-6}$	0.0055	0.9940		
	BSA	$8.6e^{-6}$	0.0058	0.9770		
80	α-lac	$1.3e^{-8}$	$1.75e^{-5}$	0.0074	0.9968	0.97 ± 0.03
	β-lg	$1.6e^{-8}$	$2.00e^{-5}$	0.0078	0.9728	
	BSA	$1.6e^{08}$	$2.00e^{-5}$	0.0078	0.9728	

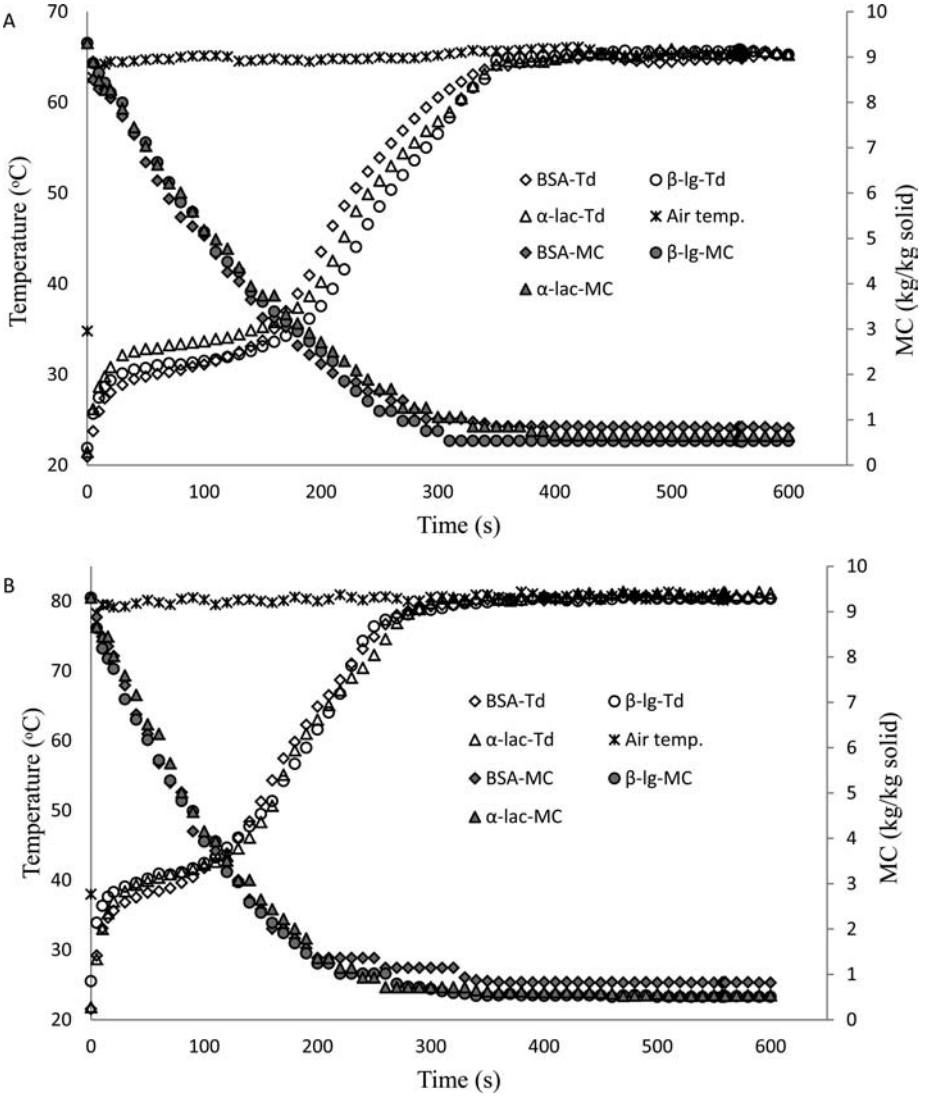

Figure 2. Moisture content and temperature profiles of BSA, α-lac, and β-lg during drying at (A) 65 and (B) 80 °C drying temperature. MC, moisture content; Td, drop temperature.

reversible denaturation occurs, and it involves excitation (due to the affinity of reaction of the thiol group of free cysteine with the adjacent sulfur bonds) of free cysteine molecules present in the β-lg and BSA structures. Due to prolonged drying stress, the peptides of β-lg are exposed to such an extent that they start to aggregate. On the other hand, the presence of 17 sulfur bridges helps to keep BSA relatively stable. Due to the absence of any free cysteine in α-lac structure, this protein is comparatively less excited or perturbed when it is subjected to dehydration stresses and it is less affected by thiol−disulfide interaction.[29] A more detailed explanation of the factors causing different extents of denaturation of these whey protein constituents during convective drying is presented elsewhere.[25]

Drying Kinetics and Its Relationship with Protein Denaturation. It is shown in Figure 1 that all of the denaturation−time curves exhibit some degree of fluctuation or perturbation from the very beginning of the drying process. When the droplet temperature was about 40 ± 5 °C, the denaturation--time curves started to fluctuate due to the impact of drying on the surface hydrophobicity. β-lg started to be lost

dx.doi.org/10.1021/jf405603c | J. Agric. Food Chem. 2014, 62, 4695−4706

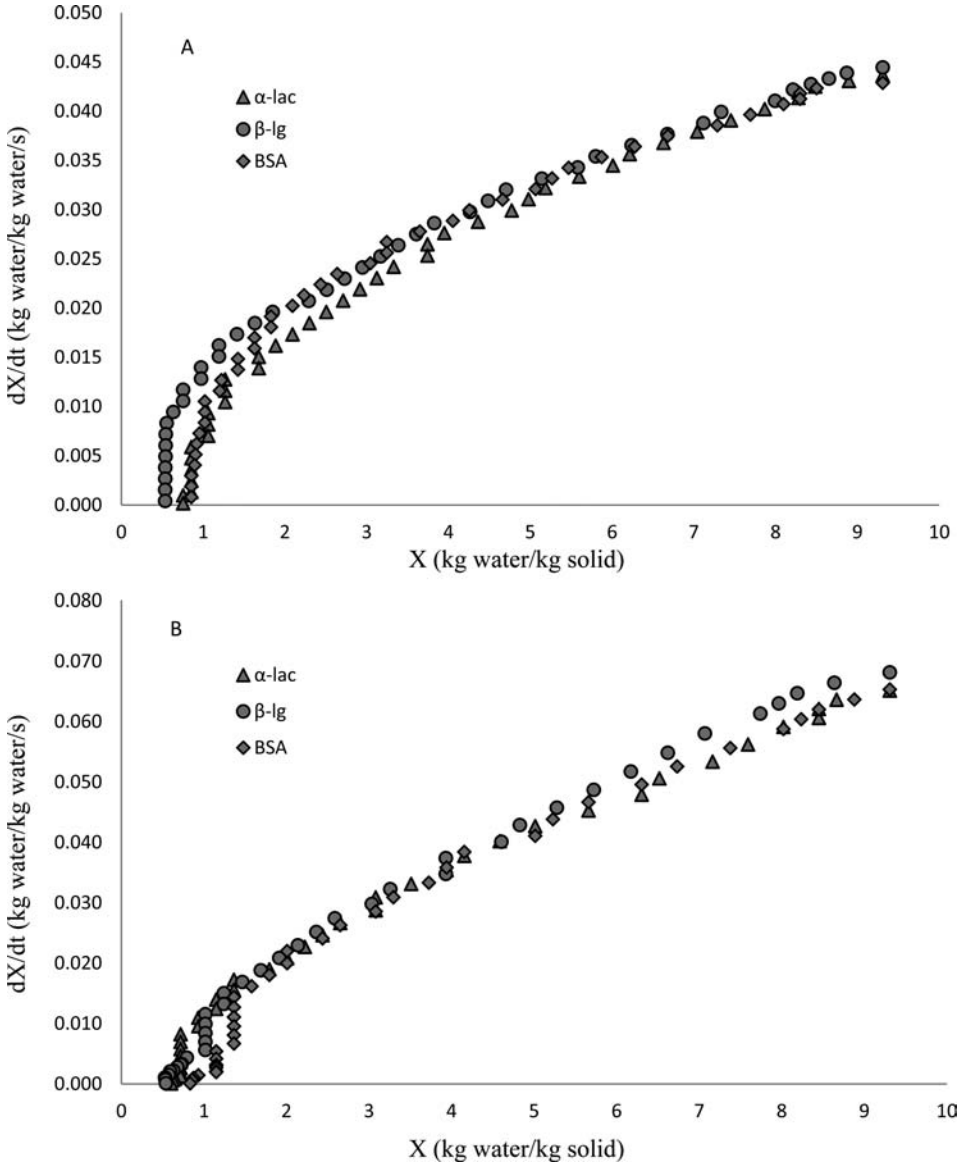

Figure 3. Evaporation rate profiles as a function of water content during drying of α-lac, β-lg, and BSA droplets at (A) 65 and (B) 80 °C air temperature.

due to irreversible denaturation and subsequent coagulation when the droplet temperature reached 55 ± 5 °C (Figure 1A). This irreversible denaturation started becoming prominent at 290 and 240 s of drying at 65 and 80 °C, respectively. We had previously reported the relationship between denaturation and droplet temperature in the case of WPI.[25] A similar trend in the relationship between denaturation and drying temperature was observed in this study only in the case of β-lg. The trends in the relationship between drying temperature and denaturation in the case of BSA and α-lac are quite different. In our earlier study,[25] WPI was dried and the individual fractions of WPI (α-lac, β-lg, and BSA) were dried as a part of whole. In the current study, intact and native individual proteins (α-lac, β-lg, and BSA) were dried individually as starting materials and the denaturation kinetics of one is not affected by the presence of the others.

To better understand the effect of drying rate on the protein denaturation, we determined the drying rate (dX_t/dt) from the experimental moisture loss versus time data. Polynomial models were fitted with the experimental moisture ratio (MR), and the drying rate was determined as shown by eqs 3 and 5 below.

For 65 °C drying temperature:

$$\mathrm{MR} = \frac{X_t - X_\infty}{X_0 - X_\infty} = At^2 - Bt + C \tag{2}$$

$$\frac{dX_t}{dt} = (X_0 - X_\infty)(2At - B) \tag{3}$$

For 80 °C drying temperature:

$$\mathrm{MR} = \frac{X_t - X_\infty}{X_0 - X_\infty} = -At^3 + Bt^2 - Ct + D \tag{4}$$

$$\frac{dX_t}{dt} = (X_0 - X_\infty)(-3At^2 + 2Bt - C) \tag{5}$$

X_t = moisture content of the droplet being dried at a given time (kg/kg solid), X_∞ = final moisture content of the dried droplet at the end of drying (kg/kg solid), and X_0 = initial moisture

dx.doi.org/10.1021/jf405603c | J. Agric. Food Chem. 2014, 62, 4695−4706

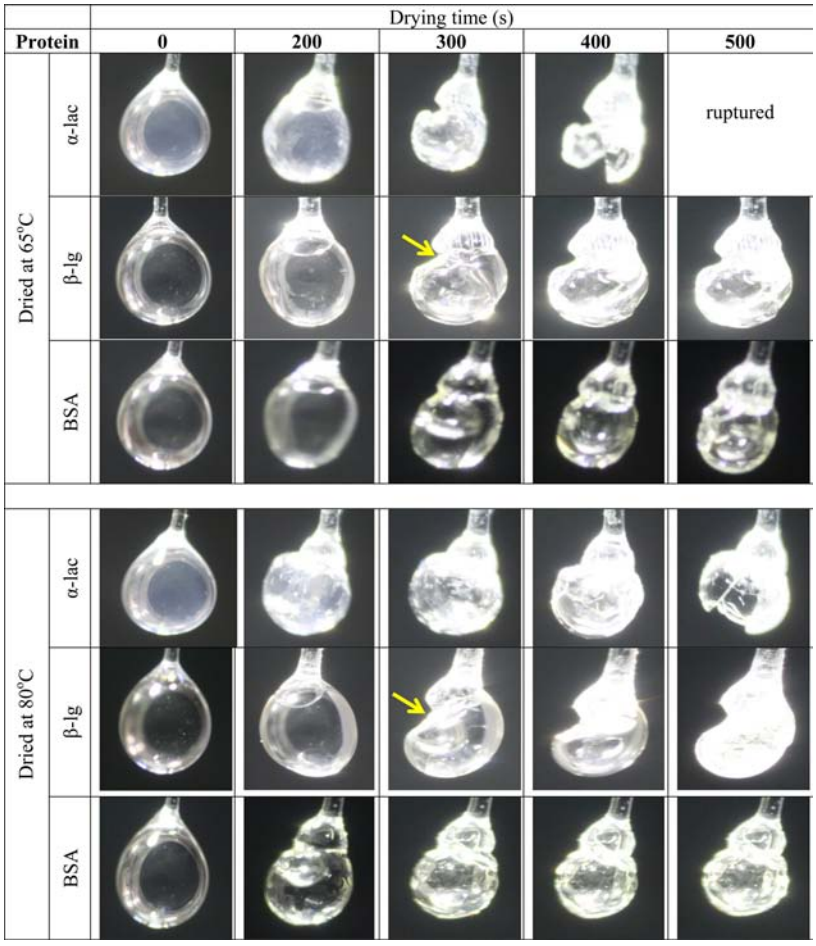

Figure 4. Development of morphological features in α-lac, β-lg, and BSA during single droplet drying at 65 and 80 °C. The arrows show partial loss of spherical shape.

content of the droplet being dried (kg/kg solid). Similarly, t = drying time (s), and A, B, C and D are the model constants. After fitting the moisture ratio curves with acceptable R^2 values, the drying rates (dX_t/dt) for all of the protein samples were calculated as shown by eqs 3 and 5. The estimated model constants along with the R^2 values are listed in Table 1.

The drying kinetics (moisture content and temperature histories) of BSA, β-lg, and α-lac are presented in Figures 2 and 3. It can be seen from Figures 2A and 3A that the BSA and β-lg tended to show higher rate of moisture loss (0.0218 and 0.0213 kg water/kg dry solid/s, respectively) than α-lac (0.0200 kg water/kg dry solid/s), and their droplet temperature remained close to the wet bulb temperature up to around 200 s. It also appears that an increase in BSA concentration offers greater resistance to moisture removal. The difference in the drying kinetics between these two proteins is observed after 200 s, and the drying rate of BSA became lower than that of β-lg (Figure 3A). After about 390 s of drying at 65 °C, the moisture content of both proteins did not decrease further and the droplet temperatures also reached very close to the drying air temperature. After the transition period of 200 s, the trends in the droplet temperature histories of these two proteins also changed remarkably. The temperature of the BSA droplet increased more rapidly than that of β-lg. In the case of α-lac the drop temperature started to increase more quickly than those of BSA and β-lg. The α-lac also showed similar reversible−irreversible transition at 200 s while drying at 65 °C. After this point, the droplet temperature of α-lac increased very rapidly and reached close to the drying air temperature. The rate of increase in droplet temperature in α-lac was faster than that of β-lg but slower than that of BSA.

These transitions in the temperature history curves (Figure 2A) of these proteins stem from the increased "drop side resistance" to the outward diffusion of moisture content.[8] The increased resistance to outward moisture diffusion gives rise to the "profile reversal", which means that the droplet temperature of the usually slower drying droplet is higher. Before the profile reversal, the drop temperature of β-lg droplet is slightly higher than that of BSA. After the profile reversal, the temperature of the BSA droplet is higher than that of the β-lg droplet. This phenomenon is more prominent in the cases of α-lac and BSA. The morphological changes of these protein droplets during convective drying, to some extent, might also be responsible for these interesting features observed in the drying profiles.

The morphological features of droplets of BSA, β-lg, and α-lac while drying at 65 and 80 °C are presented in Figure 4. It can be seen from this figure that the original spherical shape of the droplet remained more or less intact up to 200 s in all of the protein droplets. It has to be pointed out here that so long as the moisture content of the droplet is high and the droplet temperature is not too close to the drying air temperature (Figures 2 and 3), the morphology of the droplet remains more or less spherical (Figure 4). The morphology of these protein droplets showed different trends after 200 s. The BSA was

dx.doi.org/10.1021/jf405603c | J. Agric. Food Chem. 2014, 62, 4695−4706

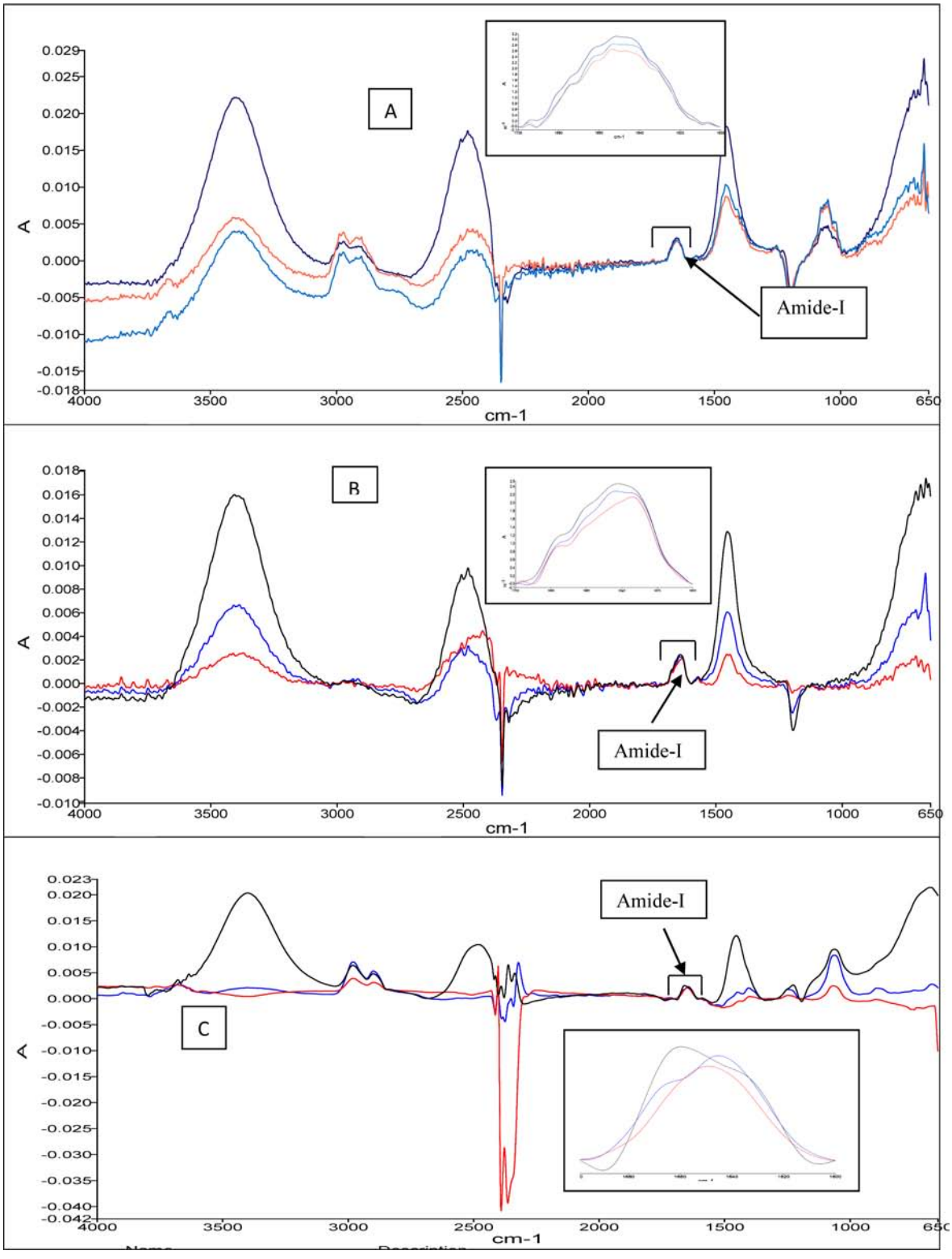

Figure 5. Absorbance spectra from FTIR of original and dried (A) α-lac, (B) β-lg, and (C) BSA (black, blue, and red lines indicate native and 65 and 80 °C treated spectra, respectively). Amide I regions are zoomed in the insets.

capable of retaining more moisture in its matrix and exhibited a sharper increase in droplet temperature. It is commonly accepted that a droplet with a lower drying rate (retains more moisture content) shows faster increase in droplet temperature due to a lesser degree of evaporative cooling. One of the interesting features associated with the morphology and drying kinetics was that the protein (BSA) containing more water in droplet for longer time was found to retain its spherical shape longer. In addition, the entrapped water inside the drying droplet of this protein caused a buildup of vapor pressure, which developed wrinkles and troughs or uneven surface morphology.[30] The interplay between the force generated by

dx.doi.org/10.1021/jf405603c | J. Agric. Food Chem. 2014, 62, 4695−4706

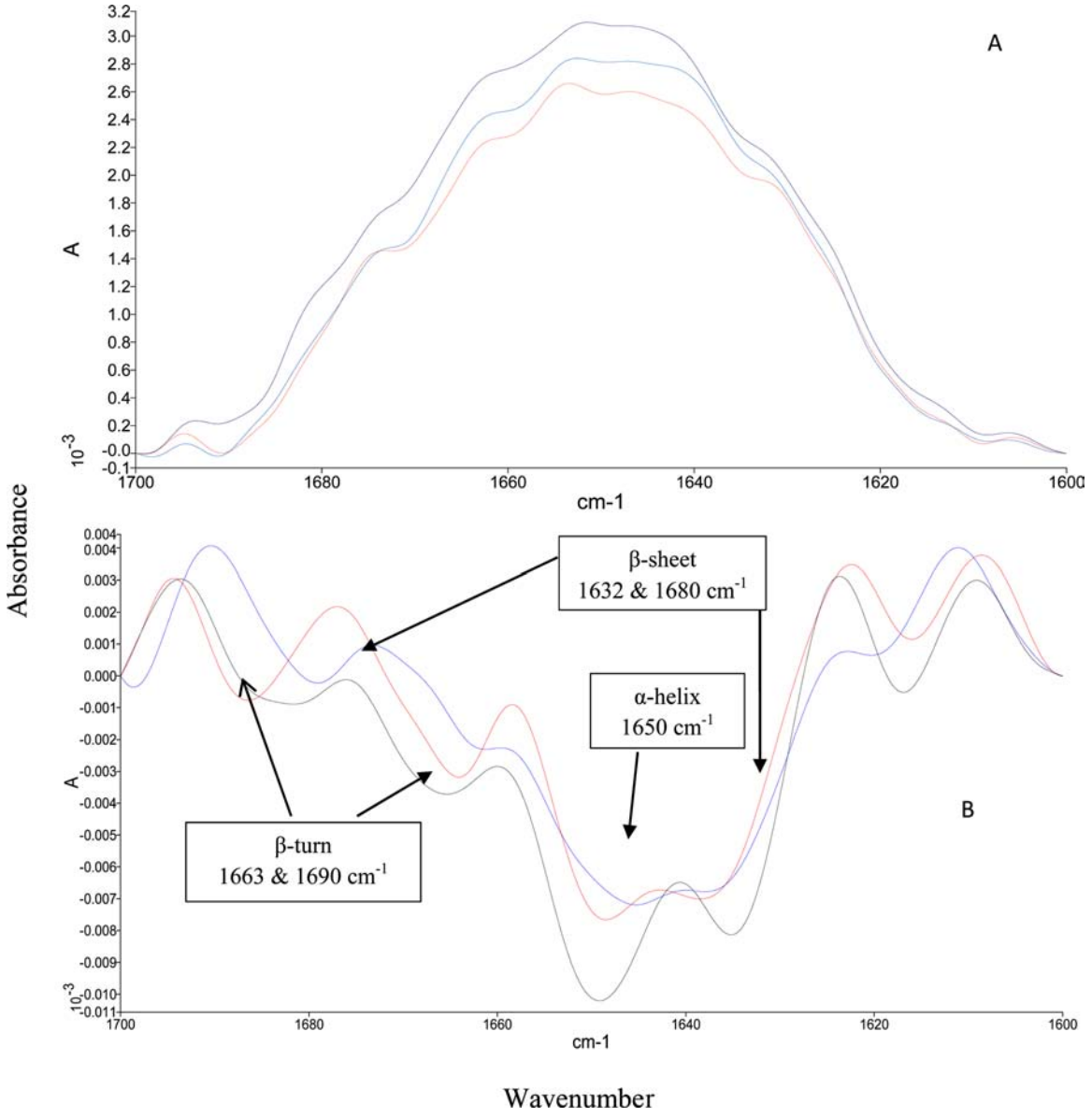

Figure 6. (A) Absorbance and (B) second-derivative spectra of amide I region of the native and single droplet dried α-lac (black, blue, and red lines indicate native and 65 and 80 °C treated spectra, respectively).

this vapor built up within the droplet, and the thermoplastic nature of the protein skin is the one of the main causes giving rise to the wrinkled morphology in BSA. A similar trend regarding the relationship between the surface morphology and drying kinetics was observed in these proteins at 80 °C as well. The only difference was that the development of morphological features occurred much mor rapidly while drying at 80 °C. After 360 s of drying at 80 °C, the moisture loss of all three proteins was almost ceased.

Denaturation of BSA, α-Lac, and β-Lg and Droplet Morphology. The evolution of morphology in BSA, α-lac, and β-lg droplets when dried at 65 and 80 °C is presented in Figure 4. As can be seen from this figure, these three proteins produced three different types of morphological features. The surface of the BSA droplet showed the ability to resist the stress exerted by the drying process and, hence, maintained spherical feature and resisted surface folding and wrinkling to a greater extent at both temperatures until the end of drying. β-Lg was least capable of resisting the deformation of droplet/particle surface during drying at both temperatures. β-Lg partially lost its spherical shape after 300 and 200 s when dried at 65 and 80 °C, respectively, and resulted in a buckled particle. α-Lac maintained its spherical shape during the early stage of drying. However, it started becoming increasingly fragile, and the particle surface was ruptured when the drying progressed.

The whey protein BSA acquired a rigid structure immediately after the start of drying (Figure 4), which might be responsible for much slower moisture evaporation in this protein. The rigidity of the BSA droplet surface during drying might be explained by its large molecular mass. BSA has a higher molecular mass (66.27 kDa) than those of α-lac (14.18 kDa) and β-lg monomer (18.28 kDa). Besides, the high number of sulfur bridges present in the BSA structure might provide greater resistance against outward moisture diffusion and maintain a moist interior. The preservation of its spherical shape by α-lac in the early stage of drying can also be attributed to its skin-forming behavior. The subsequent rupture of the α-lac particle suggests that this protein forms a thinner skin. The

dx.doi.org/10.1021/jf405603c | J. Agric. Food Chem. 2014, 62, 4695−4706

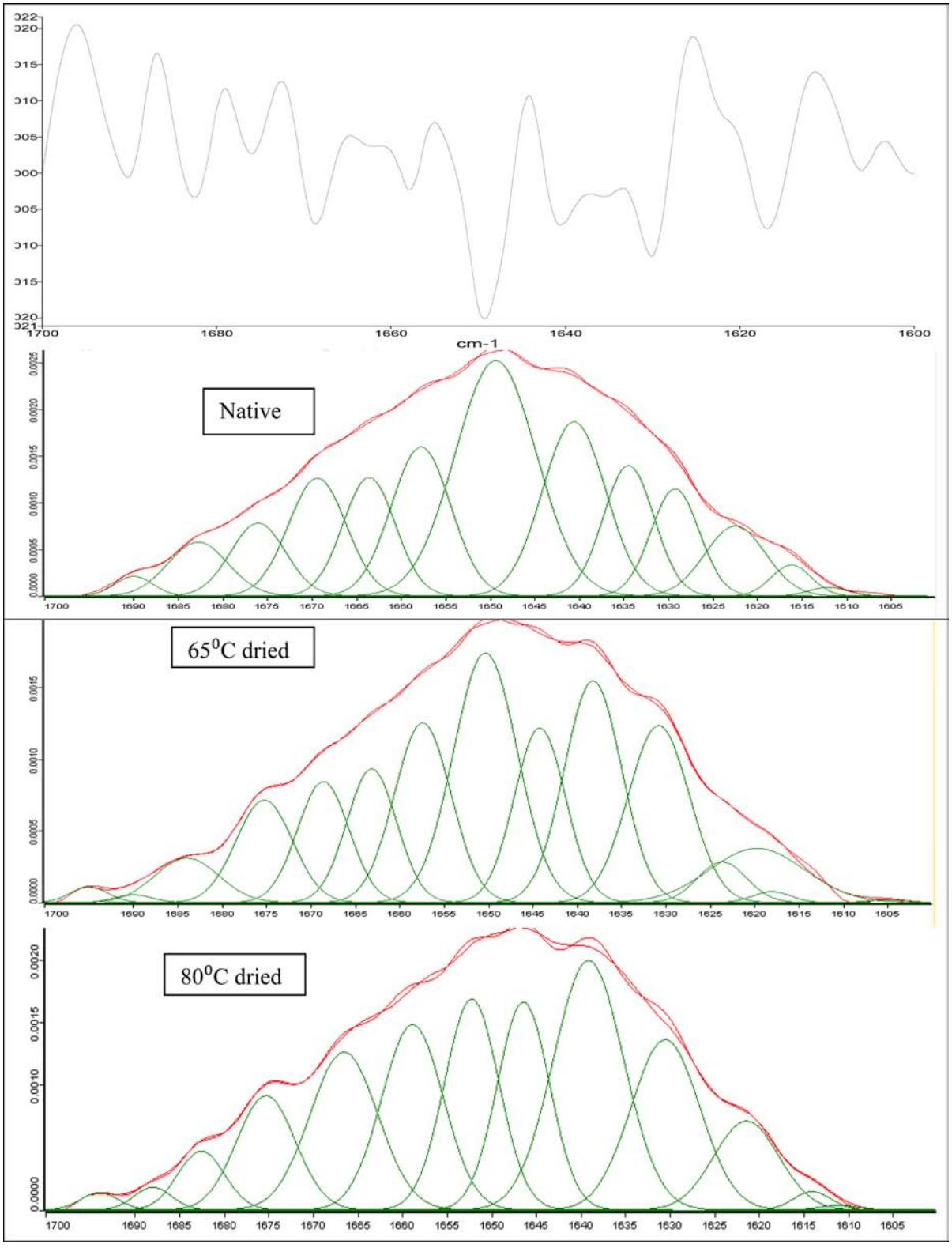

Figure 7. Fitted spectra of native and dried α-lac (a sample of second-derivative spectra of native α-lac is at the top).

irreversible denaturation of proteins and their agglomerates is capable of forming a thick skin at the outer surface of droplets being dried.[9] It can be observed from Figure 1 that α-lac denatured only marginally at 500 s when the skin was ruptured due to drying (a 65 °C). This lack of denaturation and, hence, the lack of formation of a rigid wall (or skin) produced α-lac particles with a hollow crust. The dried particles with a hollow crust are known to collapse or shrivel quite easily.[9] This is why the particles of α-lac ruptured quite easily at both drying temperatures. On the other hand, β-lg experienced significant ($p < 0.05$) denaturation at both drying temperatures and the denaturation and aggregation occurred as early as 250 s of drying. Because the denatured proteins conveniently form a rigid skin, the formation of skin in this protein also started after

dx.doi.org/10.1021/jf405603c | J. Agric. Food Chem. 2014, 62, 4695−4706

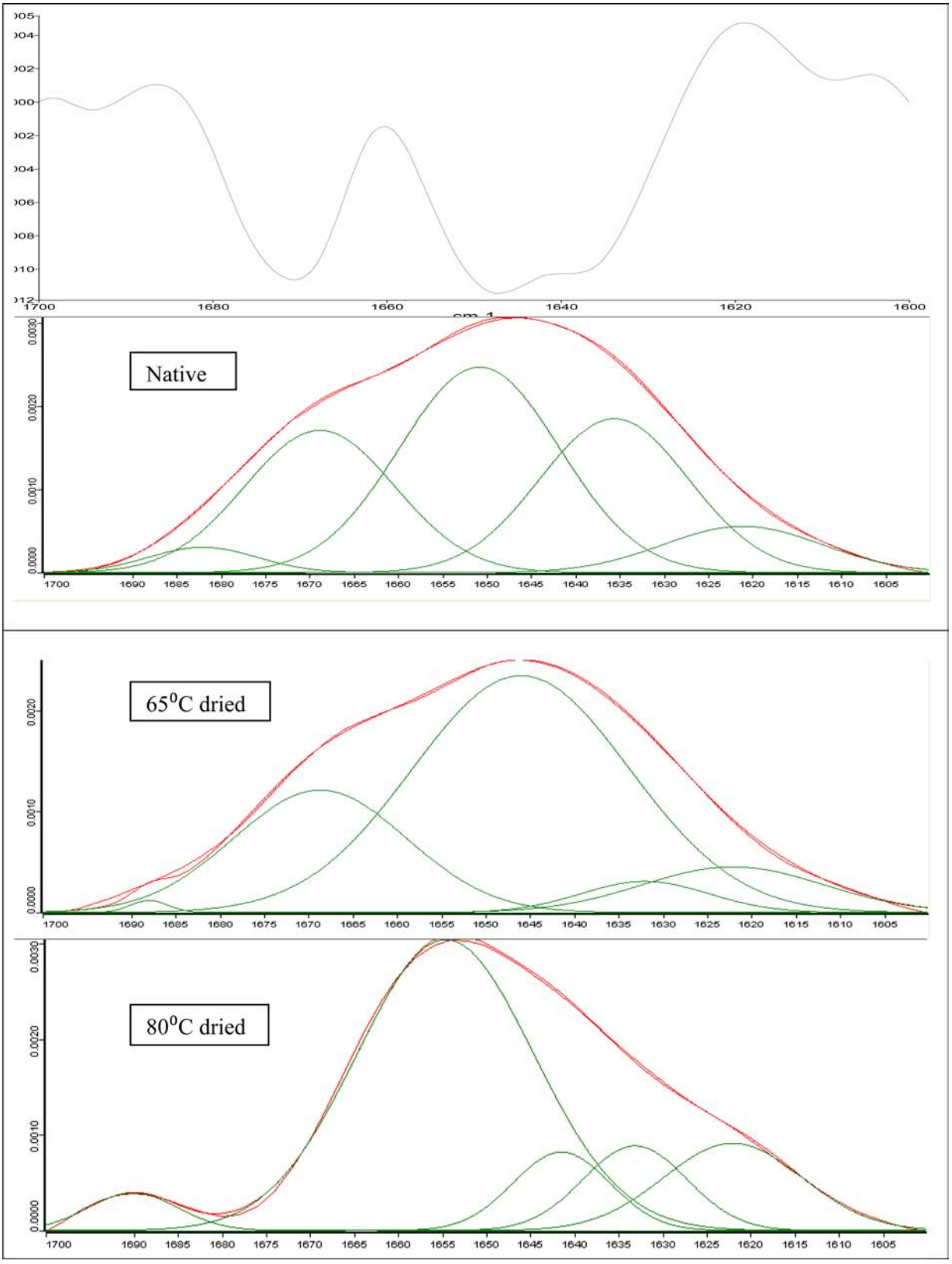

Figure 8. Fitted spectra of native and dried BSA (a sample of second-derivative spectra of native BSA is at the top).

200 s. This explains why the partial wrinkling appeared on the surface of this protein after 200 s. The better stability of α-lac droplet/particle (lack of rupture) at 80 °C compared to 65 °C (Figure 4, 500 s) can be attributed to the significantly ($p <$ 0.05) higher extent of denaturation of α-lac at 80 °C than at 65 °C.

Alteration in Secondary Structure of BSA, α-Lac, and β-Lg. Figure 5 shows the IR spectra of native and dried BSA, α-lac, and β-lg. The second derivatives of the IR spectra were

dx.doi.org/10.1021/jf405603c | J. Agric. Food Chem. 2014, 62, 4695−4706

used to identify the individual structural features of these proteins. For example, the derivative spectra (Figure 6B) derived from intrinsic absorbance spectra (Figure 6A) are able to clearly assign some specific bands in both native and dried proteins. The derivative spectra are also able to quantify the magnitude and direction of change occurring in a specific band due to drying-related stresses. For example, when α-lac was dried at 65 °C for 500 s (Figure 6B), the proportion of its β-sheet increased (around 1680 cm^{-1}), and this increase was compensated by the decrease in α-helix (around 1650 cm^{-1}) and β-turn (around 1663 and 1690 cm^{-1}). After assigning the bands using nine-point second-derivative analysis, the FTIR spectra were deconvoluted and fitted with OPUS software to quantify the individual peaks (Figures 7 and 8). The derivative spectrum of each untreated (or not dried) protein was overlaid on top of the corresponding dried protein. The assignment of each band to the secondary structural features after deconvolution is provided in Table 2. The peaks between

Table 2. Peak Assignments for Secondary Structure of Protein in D_2O of Deconvoluted Spectra in Amide I Region

component	wavenumber (cm^{-1})
β-sheet (low frequency)	1620−1640
random coil	1641−1647
α-helix	1648−1660
β-turns (low frequency)	1661−1673
β-sheet (high frequency)	1674−1680
β-turns (high frequency)	1681−1699

1600 and 1619 cm^{-1} are known to be generated from aromatic side chains and are not considered during the quantification of secondary structure.[16,31] The changes in the secondary structural features due to drying are provided in Table 3.

Table 3. Percentage Breakdown of Different Fractions of Secondary Structures in Native and Dried Whey Proteins

		secondary structures (%)			
protein	treatment	α-helix	β-sheet	β-turns	random coil
α-lac	native	35.00	39.50	20.00	5.50
	65 °C (dried)	32.50	41.50	18.50	7.50
	80 °C (dried)	29.50	46.00	15.00	9.50
B-lg	native	25.00	47.00	17.00	11.00
	65 °C (dried)	22.00	54.50	12.00	11.50
	80 °C (dried)	21.50	54.50	11.00	13.00
BSA	native	53.50	20.50	26.00	0.00
	65 °C (dried)	59.00	17.00	24.00	0.00
	80 °C (dried)	62.00	22.50	12.50	3.00

Thirteen bands were required to produce best fitting to α-lac and β-lg's IR spectra (Figure 7). On the other hand, BSA produced only five major bands in both native and dried states in the amides I region (Figure 8). Although the band numbers are similar in both native and dried proteins, they showed differences in magnitude and the location of the bands. Through the band fitting and quantification, it was found that the secondary structures of α-lac and β-lg are dominated by β structure, whereas the secondary structure of BSA is dominated by helix structure (Table 3). The observed composition of secondary structural features of BSA, α-lac, and β-lg is in agreement with earlier studies.[17,27,32] It has been reported that α-lac contains 41.0% β structure and 33.0% helix structure and that β-lg contains 50.0% β structure and 10.0% helix structure.[27] Similarly, BSA contains 24.0% β-sheet and 57.0% helix in its structure.[17,32] Our observations suggest that the secondary structural properties of BSA, α-lac, and β-lg were affected by the convective drying quite differently. The drying process increased the β-sheet and random coil contents in β-lg by 7.5 and 2.0%, respectively. At the same time, the α-helix and β-turn contents decreased by 3.5 and 6.0%, respectively. In the case of α-lac, the drying stress decreased the α-helix content by 5.5% and the β-turn content by 5.0%. These decreased secondary structural contents were compensated by increases in β-sheet by 6.5% and random coil by 4.0%. The β-sheet, helix, and coil contents of BSA were found to increase (up to 2.0, 8.5, and 3.0%, respectively), whereas the β-turn content decreased (up to 13.5%).

In conclusion, the kinetics of major whey proteins revealed that at the end of 600 s of convective drying 13.3 and 19.4% α-lac was found to denature at 65 and 80 °C, respectively, whereas up to 31.0% of β-lg was denatured. No significant ($p > 0.05$) amount of BSA was found to be lost by denaturation under these drying conditions. The secondary structural properties of all the studied proteins were found to be significantly ($p < 0.05$) affected and altered by the drying stresses. In the case of α-lac and β-lg, the β-sheet and random coil contents were found to increase, which were compensated by the decrease in α-helix and β-turn. On the other hand, β-sheet, helix, and coil contents were found to increase in the case of BSA, whereas the β-turn content decreased. A highly wrinkled skin was formed on the surface of BSA, whereas a hollow fragile skin was formed on the surface of α-lac. The whey protein β-lg droplet lost its spherical shape initially but developed a firm outer surface skin afterward. The correlations among denaturation kinetics, drying kinetics, and particle morphology during drying at droplet level reported in this study will be important in producing structurally intact and functionally superior milk protein powders through spray-drying. The fundamental information on the denaturation kinetics of bovine serum albumin, α-lactalbumin, and β-lactoglobulin presented in this study will broaden the application of these proteins as nutritional and functional ingredients, especially in food and pharmaceutical applications.

AUTHOR INFORMATION

Corresponding Author

*E-mail: benu.adhikari@rmit.edu.au; Phone: +61 3 9925 9940; Fax: +61 3 992 53747.

Funding

M.A.H. thanks the Australian government for providing him with an Endeavour Postgraduate Scholarship.

Notes

The authors declare no competing financial interest.

ACKNOWLEDGMENTS

We thank Bruce Armstrong, Technical officer, Federation University Australia, for technical help during experiments.

REFERENCES

(1) Oldfield, D. J.; Taylor, M. W.; Singh, H. Effect of preheating and other process parameters on whey proteins reactions during skim milk powder manufacture. *Int. Dairy J.* **2005**, *15*, 501−511.

(2) Anandharamakrishnan, C.; Riellya, C. D.; Stapleya, A. G. F. Effects of process variables on the denaturation of whey proteins during spray drying. *Drying Technol.* **2007**, *25*, 799−807.
(3) Parris, N.; Baginski, M. A. A rapid method for the determination of whey protein denaturation. *J. Dairy Sci.* **1991**, *74*, 58−64.
(4) Wehbi, Z.; Perez, M.; Sanchez, L.; Pocovi, C.; Barbana, C.; Calvo, M. Effect of heat treatment on denaturation of bovine α-lactalbumin: determination of kinetic and thermodynamic parameters. *J. Agric. Food Chem.* **2005**, *53*, 9730−9736.
(5) Takeda, K.; Wada, A.; Yamamoto, K.; Moriyama, Y.; Aoki, K. Conformational changes of bovine serum albumin by heat treatment. *J. Protein Chem.* **1989**, *8*, 653−659.
(6) Hosseini-nia, T.; Ismail, A. A.; Kubow, S. Pressure-induced conformational changes of β-lactoglobulin by variable-pressure Fourier transform infrared spectroscopy. *J. Agric. Food Chem.* **1999**, *47*, 4537−4542.
(7) Lin, J.; Gentry, J. W. Spray drying drop morphology: experimental study. *Aerosol Sci. Technol.* **2003**, *37*, 15−32.
(8) Adhikari, B.; Howes, T.; Bhandari, B. R.; Troung, V. Effect of addition of maltodextrin on drying kinetics and stickiness of sugar and acid-rich foods during convicting drying: experiments and modelling. *J. Food Eng.* **2004**, *62*, 53−68.
(9) Walton, D. E. The morphology of spray dried particles a qualitative view. *Drying Technol.* **2000**, *18*, 1943−86.
(10) Ranz, W. E.; Marshall, W. R. Evaporation from drops. *Chem. Eng. Process.* **1952**, *48*, 141−146.
(11) Sano, Y.; Keey, R. B. The drying of a spherical particle containing colloidal material into a hollow sphere. *Chem. Eng. Sci.* **1982**, *37*, 881−889.
(12) Lin, S. X. Q.; Chen, X. D. Improving the glass-filament method for accurate measurement of drying kinetics of liquid droplets. *Chem. Eng. Res. Design* **2002**, *80*, 401−410.
(13) Mezhericher, M.; Levy, A.; Borde, I. Theoretical models of single droplet drying kinetics: a review. *Drying Technol.* **2010**, *28*, 278−293.
(14) Lin, S. X. Q.; Chen, X. D. A model for drying of an aqueous lactose droplet using the reaction engineering approach. *Drying Technol.* **2006**, *24*, 1329−1334.
(15) Ferreira, I. M. P. L. V. O.; Caçote, H. Detection and quantification of bovine, ovine and caprine milk percentages in protected denomination of origin cheeses by reversed-phase high-performance liquid chromatography of β-lactoglobulins. *J. Chromatogr., A* **2003**, *1015*, 111−118.
(16) Ngarize, S.; Herman, H.; Adams, A.; Howell, N. Comparison of changes in the secondary structure of unheated, heated, and high-pressure-treated β-lactoglobulin and ovalbumin proteins using fourier transform raman spectroscopy and self-deconvolution. *J. Agric. Food Chem.* **2004**, *52*, 6470−6477.
(17) Fu, F.; Deoliveira, D. B.; Trumble, W. R.; Sarkar, H. K.; Singh, B. R. Secondary structure estimation of proteins using the amide III region of Fourier transform infrared spectroscopy: application to analyze calcium binding-induced structural changes in calsequestrin. *Appl. Spectrosc.* **1994**, *48*, 1432−1441.
(18) van de Weert, M.; Haris, P. I.; Hennink, W. E.; Crommelin, D. J. A. Fourier transform infrared spectrometric analysis of protein conformation: effect of sampling method and stress factors. *Anal. Biochem.* **2001**, *297*, 160−169.
(19) Kong, J.; Yu, S. Fourier transform infrared spectroscopic analysis of protein secondary structures. *Acta Biochem. Biophys. Sin.* **2007**, *39*, 549−559.
(20) Huson, M. G.; Strounina, E. V.; Kealley, C. S.; Rout, M. K.; Church, J. S.; Appelqvist, I. A. M.; Gidley, M. J.; Gilbert, E. P. Effects of thermal denaturation on the solid-state structure and molecular mobility of glycinin. *Biomacromolecules* **2011**, *12*, 2092−2102.
(21) Yang, W.; Griffiths, P. R.; Byler, D. M.; Susi, H. Protein conformation by infrared spectroscopy: resolution enhancement by Fourier self-deconvolution. *Appl. Spectrosc.* **1985**, *39*, 282−287.
(22) Adhikari, B.; Howes, T.; Bhandari, B. R. Use of solute fixed coordinate system and method of lines for prediction of drying kinetics and surface stickiness of single droplet during convective drying. *Chem. Eng. Process.* **2007**, *46*, 405−419.
(23) Haque, M. A.; Putranto, A.; Aldred, P.; Chen, J.; Adhikari, B. Drying and denaturation kinetics of whey protein isolate (WPI) during convective air drying process. *Drying Technol.* **2013**, *31*, 1532−1544.
(24) Anandharamakrishnan, C.; Rielly, C. D.; Stapley, A. G. F. Loss of solubility of α-lactalbumin and β-lactoglobulin during the spray drying of whey proteins. *LWT−Food Sci. Technol.* **2008**, *41*, 270−277.
(25) Haque, M. A.; Aldred, P.; Chen, J.; Barrow, C. J.; Adhikari, B. Comparative study of denaturation of whey protein isolate (WPI) in convective air drying and isothermal heat treatment processes. *Food Chem.* **2013**, *141*, 702−711.
(26) Yazdanpanah, N.; Langrish, T. A. G. Comparative study of deteriorative changes in the ageing of milk powder. *J. Food Eng.* **2013**, *114*, 14−21.
(27) Byler, D. M.; Susi, H. Examination of the secondary structure of proteins by deconvolved FTIR spectra. *Biopolymers* **1986**, *25*, 469−487.
(28) Boye, J. I.; Alli, I.; Ismail, A. A.; Gibbs, B. F.; Konish, Y. Factors affecting molecular characteristics of whey protein gelation. *Int. Dairy J.* **1995**, *5*, 337−353.
(29) Ng-Kwai-Hang, K. F. *Milk Proteins Heterogeneity, Fractionation, and Isolation*; McGill Univ. Mont. QC; Elsevier: Canada, 2011; pp 751−764.
(30) Adhikari, B.; Howes, T.; Bhandari, B. R.; Troung, V. Surface stickiness of drops of carbohydrate and organic acid solutions during convective drying: experiments and modeling. *Drying Technol.* **2003**, *21*, 839−873.
(31) Susi, H.; Byler, D. M. Fourier deconvolution of the amide I Raman band of proteins as related to conformation. *Appl. Spectrosc.* **1988**, *42*, 819−826.
(32) Grdadolnik, J. Saturation effects in FTIR spectroscopy: intensity of amide I and amide II bands in protein spectra. *Acta Chim. Slov.* **2003**, *50*, 777−788.

JOURNAL OF AGRICULTURAL AND FOOD CHEMISTRY

Article

pubs.acs.org/JAFC

Effects of Storage Temperature, Storage Duration, and Subsequent Ripening on the Physicochemical Characteristics, Volatile Compounds, and Phytochemicals of Western Red Nectarine (*Prunus persica* L. Batsch)

Christophe Aubert,* Philippe Bony, Guillaume Chalot, Pierre Landry, and Sebastien Lurol

Centre Technique Interprofessionnel des Fruits et Légumes, route de Mollégès, 13210 Saint-Rémy-de-Provence, France

ABSTRACT: Western Red nectarines, harvested at commercial maturity, were stored for up to 20 days at 1, 4, or 8 °C and then transferred to 25 °C for 0 or 4 days. The main physicochemical attributes, phytochemicals, and volatile compounds were then determined. During storage and ripening, firmness, titratable acidity, organic acids, and C_6 volatile compounds decreased, whereas ethylene production, lactones, and C_{13} norisoprenoids greatly increased. Soluble solids content, sugars, and polyphenols remained quite constant during both stages. During storage, vitamin C decreased and carotenoids did not significantly change, whereas both greatly increased during ripening. Increased time of low-temperature storage has been found to decrease lactones and C_{13} norisoprenoids in nectarine and, consequently, to limit its aroma during maturation. Finally, Western Red nectarine was found hardly chilling injury sensitive, and trends for sugars, polyphenols and lactones observed in this study were contrary to those generally reported in the literature for chilling-injured fruit.

KEYWORDS: *Prunus persica, nectarine, volatile compounds, carotenoids, polyphenolic compounds, vitamin C, shelf life, cold storage*

INTRODUCTION

Nowadays, there is a wide consensus that a greater consumption of fruits and vegetables contributes to improved health and well-being by reducing the risk of diseases such as cardiovascular diseases and some forms of cancer.[1,2] The health benefits of fruits and vegetables have been attributed to their specific chemical composition, particularly phytochemicals such as vitamin C, carotenoids, and polyphenolics, which act as antioxidants by scavenging harmful free radicals, which are implicated in most degenerative diseases.[3] On the basis of this evidence, in 2003 the Joint FAO/WHO (Food and Agriculture Organization of the United Nations/World Health Organization) report on diet, nutrition, and the prevention of chronic diseases recommended the intake of a minimum of 400 g of fruits and vegetables per day, ideally 800 g, for the prevention of chronic diseases such as cancer, diabetes, heart diseases, and obesity.

In peaches and nectarines, the major phenolic compounds are catechin, epicatechin, and caffeoylquinic acids, whereas predominant carotenoids are α- and β-carotene, zeaxanthin, and lutein. Chlorogenic acid (5-caffeoylquinic acid) and neochlorogenic acid (3-caffeoylquinic acid) have been found to be chemopreventive against breast cancer, whereas β-carotene has been suggested to have preventive benefits against lung and colorectal cancer.[4−6] Peaches and nectarines are also sources of vitamin C and vitamin A precursors. Because humans are unable to synthesize their own vitamin C, unlike most animals, this compound is considered the most important vitamin in fruits and vegetables for human nutrition, and >90% of the vitamin C in human diets is supplied by fruits and vegetables.[7] Among carotenoids, β-carotene (primarily), α-carotene, and β-cryptoxanthin are vitamin A precursors. Vitamin A is essential for normal growth, reproduction, and resistance to infection. It also plays a role in vision, and a severe deficiency can lead to irreversible blindness.[8]

Although peaches and nectarines are an important source of fibers, vitamins, and other phytochemical compounds with beneficial effects on health, these fruits are mainly appreciated by consumers for their sweetness, juiciness, and characteristic flavor. Aroma is one of the essential factors contributing to peach quality, and peach volatiles have been thoroughly investigated. More than 100 compounds have been identified, and among them, some lactones (mainly γ- and δ-decalactone, γ-dodecalactone, γ-octalactone, and γ-jasmolactone), some C_{13} norisoprenoids (β-damascenone, β-ionone, and 8,9-dehydrothea-spirone), and some C_6 aldehydes ((*Z*)-3-hexenal and (*E*)-2-hexenal) have been reported to be important compounds in peach aroma.[9,10]

Because they soften quickly at room temperature, peaches and nectarines have a short shelf life, and low-temperature storage is the most common current method for delaying ripening after harvest and extending their commercial life. However, several physiological disorders, collectively known as chilling injury (CI), can develop under low temperature during storage and affect fruit quality. These disorders, particularly lack of juiciness and flesh browning, mainly develop during fruit ripening after cold storage and are of commercial importance because the problem is not noticed until the fruit reaches consumers.[11]

Levels of phytochemicals in fruits and vegetables are known to be influenced by numerous pre- and postharvest factors such

Received: January 7, 2014
Revised: April 11, 2014
Accepted: April 14, 2014
Published: April 14, 2014

ACS Publications © 2014 American Chemical Society

dx.doi.org/10.1021/jf4057555 | J. Agric. Food Chem. 2014, 62, 4707−4724

as genetic background, maturity, environmental factors, and culture practices, as well as by storage conditions.[7,12,13] Variability of volatiles in peaches and nectarines has likewise been reported to depend on cultivar, maturity, and storage conditions.[14−23] Even though changes in volatiles during low-temperature storage have been the subject of some studies, those on carotenoids, polyphenols, or vitamin C in nectarines are relatively scarce.[24−28]

Despite their importance for the overall quality of nectarine, to our best knowledge, to date no study carried out on the evolution of both volatiles and phytochemicals during storage has been reported in the literature. The aim of this work was to evaluate the effects of different storage conditions (3 temperatures × 5 durations) followed or not by 4 days of ripening at 25 °C on several nectarine quality attributes, such as sugars, organic acids, volatile compounds, carotenoids, polyphenolics, and vitamin C. Firmness, ethylene production, soluble solids content, and titratable acidity have also been determined.

MATERIALS AND METHODS

Chemicals. Chloroform (99.9%), ethyl acetate (99.8%), ethanol (99.8%), 2-octanol (98%), formic acid (96%), KH_2PO_4 (99.5%), H_3PO_4 (33.5−36.5%), tris(2-carboxyethyl)phosphine (TCEP; 98%), $(NH_4)_2SO_4$ (≥99%), and *n*-alkane standards (C_8−C_{40}) were obtained from Sigma-Aldrich (Saint-Quentin-Fallavier, France). Acetonitrile (99.99%), hexane (99.99%), acetone (99.98%), dichloromethane (99.9%), and methanol (99.99%) were all of HPLC gradient grade (Fisher Chemical, Leicestershire, UK). Reference compounds were obtained from Sigma-Aldrich (sucrose, glucose, fructose, citric acid, malic acid, quinic acid, ascorbic acid, (*Z*)-3-hexenyl acetate, (*Z*)-3-hexenal, hexanal, (*E*)-2-hexenal, (*E*)-2-hexenol, benzaldehyde, linalool, 2,4-hexadienal, 6-pentyl-α-pyrone, γ-octalactone, γ-decalactone, γ-jasmolactone, β-carotene, 3-caffeoylquinic acid, 4-caffeoylquinic acid, 5-caffeoylquinic acid, (+)-catechin, procyanidin dimer B2, quercetin-3-*O*-galactoside, quercetin-3-*O*-glucoside, and quercetin-3-*O*-rutinoside), Interchim (Montluçon, France) (hotrienol, γ-hexalactone, γ-heptalactone, δ-octalactone, and δ-decalactone), and Extrasynthese (Lyon, France) (β-cryptoxanthin, cyanidin-3-glucoside, and procyanidin dimer B1). Deionized water (0.050 $\mu S \cdot cm^{-1}$) used in all experiments was obtained from a Purelab Flex system (ELGA Labwater, Antony, France).

Samples. Yellow-fleshed nectarines (*Prunus persica* L. Batsch cv. Western Red) were hand-harvested at commercial ripeness stage on August 24, 2012, from the experimental orchard of the Ctifl of Balandran (Gard, France). Commercial ripeness represented fruit harvested with firmness of about 50 N to withstand handling, transport, and storage conditions. Immediately after harvest, fruits (~350 kg) were transported to the laboratory and healthy fruits were then selected on the basis of skin color, uniformity, and size and randomly placed in trays of 30 fruit. Three batches of ~100 kg (~600 fruit) were then made. Two of them were stored at temperatures outside the "killing temperature zone",[11] respectively at 1 and 8 °C, and the third was stored at 4 °C to induce development of CI symptoms. The fruit were stored at these temperatures for up to 3 weeks (3, 6, 10, 13, and 20 days). After storage, samples were then transferred to 25 °C and analyses were carried out after 0 (SL0) or 4 days (SL4). All measurements were performed on 30 fruits (3 replications of 10 fruits) at harvest and for each combination of factors (5 storage durations × 3 cold storage durations × 2 shelf life durations).

Ethylene Production (EP). Whole nectarines were weighed and placed in 10 L jars (3 jars per treatment containing 10 fruits each) hermetically sealed for 60 min before measurements using a gas chromatograph equipped with a flame ionization detector (FID-GC). Five hundred microliter gas samples were collected from the outlet port of each jar and directly injected into a Varian 3800 gas chromatograph fitted with a CP-PoraPLOT Q-HT column (0.53 mm × 10 m × 20 μm) (Varian). Oven, injector, and FID temperatures were 30, 50, and 250 °C, respectively.

Evaluation of Fruit and Physicochemical Analyses. Flesh firmness was determined on two opposite sides of each fruit after the removal of a 1 mm thick slice of skin using a fruit texture analyzer (FTA GS-15, Güss Ltd.) fitted with an 8 mm diameter plunger tip. The results were expressed in newtons (N). Fruits were then cut into two halves through the suture plane, and flesh browning was immediately evaluated on the mesocarp and the area around the pit. The score of CI was then calculated according to the method of Zhang et al.[19] Fruits were then freed from the stone, cut in small cubes (~1 cm^3), immediately frozen in liquid nitrogen and reduced to powder using a mortar grinder (Pulverisette 2, Fritsch) with liquid nitrogen. The frozen powders were then stored at −80 °C until analysis. About 15 g of frozen tissue (−80 °C) was thawed for ~30 min at room temperature, homogenized in a blender (Waring, USA), and then centrifuged (8500*g*, 5 min, 4 °C). Soluble solids content (SSC) was determined from the supernatant with an Atago PR-32 digital refractometer. The results were expressed in °Brix. Titratable acidity (TA) was determined by diluting 5 mL of supernatant with 30 mL of deionized water and titrating to pH 8.1 with 0.1 N NaOH using a Titroline 7000 automatic titrator with autosampler (SI Analytics). Results were given as grams of malic acid per 100 g of fresh weight (FW).

Determination of Sugars and Organic Acids. The levels of individual sugars (glucose, fructose, sucrose, and sorbitol) and organic acids (malic, citric, and quinic acid) were simultaneously determined by HPLC. One gram of frozen powder added to 20 mL of deionized water was homogenized for 60 s using an Ultra-Turrax (T25, Ika). After centrifugation (14000*g*, 10 min, 4 °C), the supernatant was filtered (RC 0.2 μm Phenex; Phenomenex, Le Pecq, France) and directly injected into HPLC. A Waters Acquity UPLC H-Class liquid chromatograph was used with a photodiode array detector (PDA) and a refractive index (RI) detector connected in series. The PDA was set at 210 nm. The RI temperature was set at 34 °C. Ten microliters of each sample was injected using a sample manager on a 300 mm × 7.8 mm i.d. ion-exclusion Rezex ROA-Organic H+ column equipped with a Carbo-H guard column (Phenomenex). The column oven temperature was set at 27 °C. The flow of mobile phase (0.005 N H_2SO_4) was 0.4 mL/min. Identifications were performed by comparing retention times (t_R) with those of standards and by spiking samples with pure compounds. Quantifications were carried out using calibration curves based on different injected amounts of standards.

Determination of Vitamin C. One gram of frozen powder added to 10 mL of metaphosphoric acid (MPA, 6%) was homogenized for 60 s at 20000 rpm with an Ultra-Turrax (T25, Ika). After centrifugation (10000*g*, 5 min, 4 °C), the supernatant was filtered (RC 0.2 μm Phenex; Phenomenex). Ascorbic acid (AA) was determined by direct injection in HPLC (see conditions below) of 500 μL of extract added to 500 μL of MPA (6%). Total vitamin C was determined by HPLC after 3 h of reduction under agitation at room temperature of 500 μL of extract added to 500 μL of TCEP (10 mM) in MPA (6%).[29] Dehydroascorbic acid (DHA) was then calculated by subtracting AA determined in the absence of reducing agent from total vitamin C content. A Varian ProStar 230 liquid chromatograph was used with a photodiode area detector (Varian PDA detector 330). The PDA was set at 245 nm. Ten microliters of each sample was injected using a Varian 410 autosampler on a 250 mm × 4.6 mm i.d. (5 μm) Supelcosil C18 column (Sigma-Aldrich). The column oven temperature was set at 25 °C. The flow of mobile phase (0.2 M KH_2PO_4; pH adjusted to 3.0 with H_3PO_4) was 1 mL/min. Identifications were performed by comparing retention times (t_R) with those of standards and by spiking samples with pure compounds. Quantifications were carried out using calibration curves based on different injected amounts of standards.

Determination of Carotenoids. Two grams of frozen powder and 40 mL of a mixture of hexane/acetone/ethanol (40:20:40 v/v/v) were homogenized for 30 s at 20000 rpm using an Ultra-Turrax (T25, Ika). After the addition of 6 mL of deionized water, agitation, and centrifugation (10000*g*, 5 min, 4 °C), 10 mL of hexanic extract was concentrated to dryness under vacuum directly into a 2 mL HPLC autosampler vial using an evaporator−concentrator (Rocket, Genevac Ltd.). After the addition of 1 mL of CH_2Cl_2/MeOH (50:50 v/v) and solubilization, the carotenoid extract was directly injected into UPLC.

Separation and characterization of carotenoid compounds were carried out using a Waters Acquity UPLC equipped with a photodiode array detector (detection at 475 nm) and a Phenomenex Kinetex C18 column (100 mm × 2.1 mm i.d., 1.7 μm) protected by a precolumn filter (Phenomenex). The column oven temperature was set at 15 °C. A binary solvent system was used at a 0.5 mL/min flow rate with solvent A (acetonitrile/water; 96:4 v/v) and solvent B (ethyl acetate). The elution gradient was as follows: 0−2.5 min, isocratic 0% B; 2.5−11 min, linear 0−51% B; 11−16 min, isocratic 51% B. The volume of injection was 2 μL. Identifications were performed by comparing retention times (t_R) with those of standards and by spiking samples with pure compounds. Quantifications were carried out using calibration curves based on different injected amounts of standards.

Determination of Polyphenols. Four grams of frozen powder and 20 mL of a mixture of MeOH/H_2O/formic acid (60:38:2 v/v/v) were homogenized for 60 s at 20000 rpm with an Ultra-Turrax (T25, Ika) and centrifuged (10000*g*, 5 min, 4 °C). Ten milliliters of supernatant was concentrated to dryness under vacuum directly into a 2 mL HPLC autosampler vial using an evaporator−concentrator (Rocket, Genevac Ltd.). After the addition of 1 mL of mixture of MeOH/formic acid (95:5 v/v) and solubilization, the polyphenolic extract was directly injected into UPLC and UPLC-MS as described below. Separation and characterization of phenolic compounds were carried out using a Waters Acquity UPLC equipped with a photodiode array detector (detection at 280, 330, and 520 nm) and a Waters Acquity HSS T3 column (100 mm × 2.1 mm i.d., 1.8 μm) protected by a precolumn filter (Waters), in a 45 °C heated oven. A binary solvent system was used at a 0.4 mL/min flow rate with solvent A (water/formic acid; 98.5:1.5 v/v) and solvent B (methanol). The elution gradient was as follows: 0−6 min, linear 1−21% B; 6−14.5 min, linear 21−70% B; 14.5−19 min, isocratic 95%; 19−24 min, isocratic 1% B. The volume of injection was 1 μL. The hydroxycinnamic acids and flavanols were detected at 280 nm, flavonols at 330 nm, and anthocyanins at 530 nm. Compound identification was achieved by comparing the retention times (t_R) and their UV−vis spectra from 200 to 600 nm with those of standards and by spiking samples with pure compounds whenever possible. The identification of the phenolic compounds was also achieved through the coupling of a Waters Acquity UPLC with an ion trap mass spectrometer Bruker Daltonics HCT ultra equipped with an electrospray ionization source. Chromatographic conditions were the same as above. A capillary voltage of 2 kV was used in the negative and positive ion modes for polyphenol and anthocyanin characterization, respectively. Nitrogen was used as drying and nebulizing gas with a flow rate of 9 L/min. The desolvation temperature was set at 365 °C and the nebulization pressure at 40 psi. The ion trap was operated in the Ultrascan mode from m/z 150 to 1200. The volume of injection was 1 μL. Quantification was achieved according to the concentrations of a corresponding external standard. For the compounds lacking reference compounds, related compounds were used as standards for the quantification. Therefore, *p*-coumaroylquinic acid and caffeoylquinic acid derivative were quantified in equivalents of 5-caffeoylquinic acid. Levels of phenolic compounds were expressed as milligrams per 100 g of FW.

Isolation of Volatiles. Samples were analyzed according to the liquid−liquid microextraction (LLME) method previously described[30] with some modifications. Briefly ∼20 g of frozen powder, 20 mL of $(NH_4)_2SO_4$ saturated solution, and 20 μL of 2-octanol (411.6 μg/mL) (internal standard) were homogenized at 20000 rpm with an Ultra-Turrax (T25, Ika) and centrifuged (13000*g*, 5 min, 4 °C). The supernatant was then transferred into a 50 mL screw-capped conical centrifuge tube (34 × 98 mm glass borosilicate) containing a magnetic stir bar (15 × 6 mm). Two hundred microliters of $CHCl_3$ was added, and the mixture was extracted for 60 min under magnetic stirring at room temperature. After removal of the magnetic stir bar, the tube was sonicated for 1 min in a Branson Ultrasonic Cleaner 5510 and centrifuged (1000*g*, 5 min, 4 °C). Chloroform extract was then recovered with a 50 μL syringe, transferred to a 100 μL vial, and immediately injected into GC-MS and GC-FID. Separation of volatile compounds was carried out using a Varian 3800 gas chromatograph equipped with an Rtx-Wax (Restek) capillary column (30 m × 0.25 mm i.d., 0.25 μm film thickness). The flow of hydrogen 5.7 carrier gas was 1 mL/min. The oven temperature was kept at 40 °C for 3 min, then programmed to 250 °C at 5 °C/min, and kept at 250 °C for 15 min. Injections (1 μL) were performed at 220 °C in splitless mode (1.5 min) using a CombiPAL autosampler equipped with a Peltier cooling rack at 4 °C (CTC Analytics). The FID was kept at 250 °C. The levels of the volatile compounds were expressed as 2-octanol equivalent (assuming all of the response factors were 1). The concentrations are to be considered as relative data because recovery after extraction and calibration factors related to the standard were not determined. Identification of volatiles was achieved using GC-MS. A PerkinElmer Clarus 680 gas chromatograph was used with the same capillary column as above. Injections (1 μL) were performed at 220 °C in splitless mode (1.5 min) using a 108-vial integrated liquid autosampler (PerkinElmer). The oven temperature program was as above. A PerkinElmer Clarus SQ8C mass spectrometer was used. Mass spectra were acquired over the 30−350 amu range at 1 scan/s, with an ionizing electron energy of 70 eV and ion source at 220 °C. The transfer line temperature was set at 250 °C, and the flow of helium 6.0 carrier gas was 1 mL/min. Compounds were first identified using NIST/EPA/NIH MS Search 2.0 and our own mass spectra libraries. Identities of most of them were then confirmed by comparison of their linear retention indices and EI mass spectra with those of reference compounds.

Statistical Analysis. Analyses of variance and principal component analysis (PCA) were performed using Statbox 7.2.2 (FBC Software).

RESULTS AND DISCUSSION

The effects of different cold storage conditions and subsequent shelf life on the physicochemical attributes and the levels of the main phytochemicals and volatile compounds of a yellow-fleshed nectarine were investigated in this study. The fruits, harvested at commercial ripeness stage, were stored for up to 3 weeks in cold chambers at 1, 4, or 8 °C and then subjected to a postharvest ripening at 25 °C and 80−90% relative humidity in a ripening chamber for 0 (SL0) or 4 days (SL4). Fruit evaluation, firmness, SSC, TA, EP, and the levels of the main sugars (sucrose, glucose, fructose, and sorbitol) and organic acids (malic, citric, and quinic acid) have been determined. A total of 25 volatile compounds including 4 C_6-compounds, 9 lactones, 6 C_{13} norisoprenoids, 3 terpenols, 2 carbonyl compounds, and 1 ester were extracted using LLME and analyzed by GC-FID and GC-MS. Among phytochemicals, both forms of vitamin C (ascorbic and dehydroascorbic acid), 2 carotenoids (β-carotene and β-cryptoxanthin), and 12 polyphenolic compounds, including 5 hydroxycinnamic acids, 1 anthocyanin, 3 flavan-3-ols, and 3 flavonols, have been determined by HPLC, UPLC, and UPLC-MS.

A PCA was performed to graphically summarize the distribution of the 50 variables (11 physicochemical attributes, 39 volatiles and phytochemicals) within the different samples of nectarines (31 samples) (Figure 1). As shown in Figure 1A, 57% of the total variance was explained by the first two axes. The first axis (PC1), with 41% of the variance explained, mainly discriminates SL0 from SL4 samples, whereas the second axis (PC2), with 16% of the variance explained, mainly discriminates samples according to the duration of storage. The distribution of the variables is shown in Figure 1B, and most of them are well correlated on the first two axes (60% of the variables showed a squared factor loading >0.50). As shown, SL4 samples positively located on PC1 are particularly characterized by high levels of lactones and C_{13} norisoprenoids. With an average squared factor loading of ∼0.92, the nine lactones were highly positively correlated on PC1, particularly 7-decen-5-olide (L8; 0.943), γ-octalactone (L3; 0.937), γ-heptalactone (L2; 0.935), hexalactone (L1; 0.934), δ-octalactone (L4; 0.928), and γ-decalactone

dx.doi.org/10.1021/jf4057555 | J. Agric. Food Chem. 2014, 62, 4707−4724

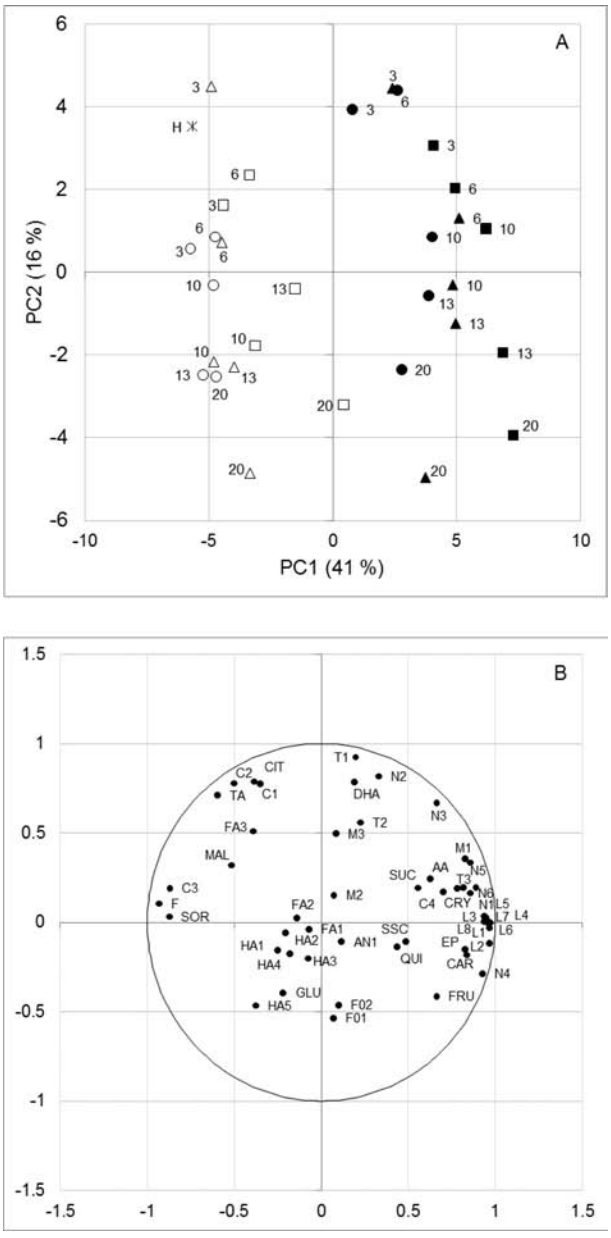

Figure 1. Results from PCA: (A) projection of the samples at harvest (H) and during storage at 1 °C (○, ●), 4 °C (△, ▲), or 8 °C (□, ■) (numbers represent days of cold storage, after 0 days at 25 °C (open symbols) or 4 days at 25 °C (solid symbols); (B) factor loadings of variables (EP, ethylene production; F, firmness; SSC, soluble solids; TA, titratable acidity; for other codes see Tables 1−4).

(L5; 0.902). Most of the C_{13} norisoprenoids were also highly correlated on PC1, in particular, 3-hydroxy-β-ionone (N4, 0.859), dehydrovomifoliol (N6; 0.791), 8,9-dehydrotheaspirone (N1, 0.733), and 3-hydroxy-5,6-epoxy-β-ionone (N5; 0.686). Among other variables, (*Z*)-3-hexenyl acetate (M1; 0.733), β-carotene (CAR; 0.701), EP (0.682), 3,7-dimethyl-1,5-octadien-3,7-diol (T3; 0.665), and β-cryptoxanthin (CRY; 0.608) were also well positively correlated on PC1. SL0 samples, negatively located on the first axis, are mainly defined by high levels of firmness (F; 0.868), sorbitol (SOR, 0.764), and (*E*)-2-hexenal (C3, 0.756). Samples at harvest and those stored for 3 or 6 days, positively located on PC2, are mainly discriminated from those stored for 20 days by higher levels of linalool (T1; 0.856), 3-hydroxy-7,8-dihydro-β-ionone (N2; 0.669), citric acid (CIT; 0.622), dehydroascorbic acid (DHA; 0.616), (*Z*)-3-hexenal (C2; 0.606), hexanal (C1; 0.602), and TA (0.506).

Fruit Evaluation, Firmness, Ethylene Production, Soluble Solids Content, Titratable Acidity, Sugars, and Organic Acids. Up to 13 days of storage, whatever the temperature, no flesh browning was detected in our samples at both SL0 and SL4. For longer storage, a slight internal browning appeared in a limited number of fruits after ripening. After 20 days of storage and 4 days at 25 °C, the CI scores for the samples stored at 1, 4, or 8 °C were between 4 and 6% and were found very low in comparison to those generally reported in the literature for CI-sensitive peaches.[19,20,27,28] In a previous work, Red Diamond nectarine and May Diamond nectarine, respectively the seed parent and the pollen parent of Western Red nectarine (U.S. Plant Patent 8,196), have been found to not develop any symptoms of CI after 5 weeks of storage at 0 or 5 °C.[31] The effects of storage and/or postharvest ripening on the main physicochemical attributes and the levels of predominant sugars and organic acids of Western Red nectarines are given in Table 1 and Figure 2. As shown, the variations of firmness and EP are the most important changes observed in response to the different treatments. Globally, the effects are characterized by opposite changes in these two parameters. With increasing storage time and temperature, flesh firmness decreased while EP increased at the same time. For up to 2 weeks, firmness was generally maintained at 1 and 4 °C, whereas it decreased drastically after 10 days of storage at 8 °C. These results indicate that as the fruit softened there was a typical ethylene climacteric rise, which is in agreement with previous works.[19,20] The rate of softening of nectarines during cold storage was found to be very similar for lower temperatures (Figure 2). For storage at 1 and 4 °C, the average decrease of firmness was about ∼0.3 N per day over the 3 weeks, whereas it was 6 times higher (∼1.8 N per day) during storage at 8 °C. After 13 and 20 days of storage at this temperature, the loss of firmness was respectively about 45 and 70%, and, according to Crisosto,[32] the corresponding nectarines are to be considered respectively as "ready to buy" (26.6 N) and "ready to eat" (13.5 N). The firmness of fruit after cold storage followed by 4 days at 25 °C ranged from 2.7 to 11.9 N and, as expected, overall firmness decreased with days at 25 °C. The rate of softening of nectarines during postharvest ripening at 25 °C was found to be very similar for fruits cold-stored at 1 or 4 °C. The results also indicated that the longer the samples are prestored at 1 or 4 °C, the greater the decrease of firmness during the phase of ripening at 25 °C (up to ∼11 N per day for 20 days of storage).

As presented in Figure 2, EP increased as the fruit softened, particularly during storage at 8 °C or postharvest ripening at 25 °C. No significant difference was observed for EP in the nectarines maintained at 1 or 4 °C for up to 3 weeks of storage, whereas it markedly increased in fruits stored at 8 °C even after only 3 days of storage. For 13 and 20 days of storage, the levels of EP were 50−65-fold higher in fruits stored at 8 °C than in fruits stored at lower temperatures. After 4 days at 25 °C, levels of EP significantly increased whatever the temperature of prestorage. Levels of EP were significantly higher in fruits prestored at 8 °C than in those maintained at 1 or 4 °C, but in comparison the increases were markedly more important for prestored fruits at these latter temperatures.

SSC ranged from 11.5 to 13.4 °Brix with a mean of 12.3 °Brix, which is greater than the minimum (8 °Brix) established by the European Union to market peaches and nectarines (R-CE no. 1861/2004), although most previous findings

dx.doi.org/10.1021/jf4057555 | J. Agric. Food Chem. 2014, 62, 4707−4724

Table 1. Levels of Sugars and Organic Acids in Nectarine Samples at Harvest and after 3, 6, 10, 13, or 20 Days of Cold Storage followed by 0 (SL0) or 4 (SL4) Days at 25 °C

				SL0					SL4					
code	compound	at harvest	temp (°C)	3 days	6 days	10 days	13 days	20 days	3 days	6 days	10 days	13 days	20 days	signif
				Sugars (g/100 g)										
SUC	sucrose	5.27 ± 0.10	1	5.07	5.32	5.42	5.15	5.36	5.39	5.43	5.43	5.61	5.35 A[a]	ns
			4	5.29 ab[b]	5.63 a	5.22 ab	5.45 ab	5.08 ab	5.38 ab	5.77 a	5.70 a	5.44 ab	4.86 bB	**
			8	5.43	5.31	5.40	5.47	5.43	5.72	5.45	5.80	5.36	5.50 A	ns
			signif	ns	ns	ns	ns	ns	ns	ns	ns	ns	*	
GLU	glucose	1.49 ± 0.04	1	1.52	1.47	1.50 B	1.58	1.52	1.60	1.48	1.44	1.50	1.45 C	ns
			4	1.50 b	1.52 b	1.56 bA	1.61 b	1.78 a	1.51 b	1.48 a	1.50 b	1.47 b	1.89 aA	***
			8	1.60	1.48	1.55 A	1.56	1.53	1.56	1.50	1.55	1.47	1.59 B	ns
			signif	ns	ns	*	ns	ns	ns	ns	ns	ns	**	
FRU	fructose	1.53 ± 0.05	1	1.64	1.57	1.59	1.72	1.66	1.85	1.71	1.68	1.80	1.72 C	ns
			4	1.59 c	1.60 c	1.69 c	1.73 c	1.96 c	1.72 c	1.69 c	1.77 c	1.79 c	2.22 aA	***
			8	1.70 bc	1.57 c	1.69 bc	1.71 bc	1.75 bc	1.79 abc	1.74 bc	1.85 ab	1.80 abc	1.95 aB	**
			signif	ns	ns	*	ns	ns	ns	ns	ns	ns	**	
SOR	sorbitol	1.32 ± 0.01	1	1.17 a	1.29 a	1.17 a	1.20 a	1.14 a	0.75 b	0.75 b	0.67 b	0.70 b	0.71 bB	***
			4	1.30 a	1.42 a	1.15 a	1.28 a	1.28 a	0.74 b	0.81 b	0.73 b	0.64 b	0.92 bA	***
			8	1.28 a	1.10 bc	1.18 ab	1.27 a	1.02 c	0.77 d	0.67 de	0.69 de	0.57 e	0.56 eA	***
			signif	ns	ns	ns	ns	ns	ns	ns	ns	ns	**	
	total sugars	9.61 ± 0.04	1	9.40	9.66	9.68	9.65	9.68	9.59	9.37	9.22	9.61	9.23 B	ns
			4	9.68	10.18	9.61	10.06	10.11	9.36	9.74	9.70	9.34	9.88 A	ns
			8	10.02	9.47	9.81	10.00	9.73	9.84	9.35	9.89	9.20	9.59 A	ns
			signif	ns	ns	ns	ns	ns	ns	ns	ns	ns	**	
				Organic Acids (g/100 g)										
CIT	citric acid	0.41 ± 0.00	1	0.40 b	0.41 b	0.41 b	0.41 b	0.37 bc	0.48 aA	0.44 ab	0.39 bc	0.36 bcA	0.33 c	***
			4	0.41 a	0.37 ab	0.37 ab	0.37 ab	0.32 bc	0.43 aAB	0.40 ab	0.36 ab	0.32 bcB	0.27 c	***
			8	0.40 ab	0.41 a	0.37 ab	0.37 abc	0.34 bc	0.40 abB	0.42 a	0.36 abc	0.33 bcAB	0.30 c	***
			signif	ns	ns	ns	ns	ns	ns	ns	ns	ns	**	
MAL	malic acid	0.46 ± 0.01	1	0.39	0.42	0.41	0.36	0.37	0.37	0.37	0.35	0.35 B	0.39 A	ns
			4	0.45	0.46	0.39	0.41	0.37	0.38	0.40	0.39	0.40 A	0.39 A	ns
			8	0.44 a	0.42 ab	0.42 ab	0.44 a	0.36 bcd	0.40 abc	0.37 bcd	0.37 bcd	0.34 cdB	0.32 dB	***
			signif	ns	ns	ns	ns	ns	ns	ns	ns	ns	ns	
QUI	quinic acid	0.20 ± 0.01	1	0.21	0.22	0.22	0.21	0.22	0.22	0.22	0.22	0.21	0.21	ns
			4	0.21	0.23	0.22	0.22	0.21	0.22	0.23	0.22	0.22	0.23	ns
			8	0.21 a	0.21 a	0.22 a	0.22 a	0.22 a	0.23 a	0.21 a	0.23 a	0.22 a	0.23 a	ns
			signif	ns	ns	ns	ns	ns	ns	ns	ns	ns	ns	

dx.doi.org/10.1021/jf4057555 | J. Agric. Food Chem. 2014, 62, 4707−4724

Table 1. continued

code	compound	at harvest	temp (°C)	SL0				SL4				signif
				3 days	6 days	10 days	13 days	20 days	3 days	6 days	10 days	13 days	20 days	
							Organic Acids (g/100 g)							
	total organic acids	1.07 ± 0.01	1	1.00 abc	1.05 ab	1.04 abc	0.98 abc	0.95 abc	1.07 aA	1.02 abc	0.96 abc	0.92 c	0.93 bcA	**
			4	1.07 a	1.06 a	0.97 bcd	1.00 abc	0.90 d	1.03 abB	1.03 ab	0.96 bcd	0.93 cd	0.90 dA	***
			8	1.06 a	1.05 a	1.01 ab	1.02 ab	0.91 cd	1.02 adB	1.00 ab	0.96 bc	0.89 de	0.85 eB	***
			signif	ns	ns	ns	ns	ns	*	ns	ns	ns	*	

[a]Means within the same days of cold storage + days at 25 °C followed by different capital letters are significantly different (SNK test, $p < 0.05$). [b]Means within the same temperature of cold storage followed by different small letters are significantly different (SNK test, $p < 0.05$).

considered that a mean value of SSC over 10 °Brix is the minimum value for consumer acceptance.[33] No significant change was observed for SSC during storage and/or postharvest ripening at 25 °C, and the levels in samples were found to be overall similar to those observed at harvest (Figure 2). These results are consistent with those observed by Robertson et al.[17] and Cano-Salazar et al.[21−23] Sucrose was found as the major soluble sugar, ranging from 49 to 59% of the total sugar content, followed by reducing sugars, fructose (16−22%) and glucose (15−19%), and sorbitol (6−14%). As shown in Table 1, the level of total sugar contents was not affected by storage and shelf life. Some significant differences have been observed for the levels of sucrose and reducing sugars during storage and/or shelf life, but on average their levels have been found to be very similar to those observed at harvest (Table 1). In contrast, although the levels of sorbitol did not change significantly during storage, a significant decrease of about 30−50% was observed during shelf life at 25 °C. Sorbitol, a polyalcohol sugar, has been previously reported to play an important role in the texture and flavor of peach and nectarine fruits and also in terms of nutrition for special dietary purposes, such as diet control and dental health.[34] Because the levels of CI were very low in our samples, our results differ from those recently reported by Wang et al.,[28] who observed, after 28 days of storage at 5 °C, significant changes in the levels of sucrose and reducing sugars in peaches exhibiting severe internal browning symptoms. As previously mentioned,[28] our results support that probably close relationships between soluble carbohydrate metabolism and CI exist in peaches exposed to cold stresses.

The levels of TA ranged from 0.51 to 0.76 g malic acid/100 g. These levels have been found to be lower than the maximum limit (0.9%) generally admitted between peaches with low and high levels of acidity.[33] The average level of TA found in ripened Western Red nectarine (SL4) was about 0.64 g malic acid/100 g and was consistent with most of those previously reported in the literature for other yellow-flesh nectarines.[21−23,33−35] The main organic acids detected in Western Red nectarines were citric and malic acid, which each represent about 40% of the total organic acids, and quinic acid. The results were consistent with those previously reported,[34] but shikimic acid was not detected in our sample. As shown in Figure 2 and Table 1, TA, total organic acids, and malic and citric acid significantly decreased during storage and shelf life at 25 °C, whereas levels of quinic acid were not affected by postharvest treatments and were found similar to those observed at harvest. As previously observed for Californian and Chilean yellow flesh peaches,[33] approximately 30% of the harvest titratable acidity (HTA) in mature fruit has been lost during ripening. These results also agree with those previously reported by Robertson et al.[16] and Cano-Salazar et al.[21−23]

Phytochemical Compounds. Total vitamin C content ranged from 2.9 to 6.5 mg/100 g and ascorbic acid (AA) was predominant (81−90%). The average level of vitamin C in ripened samples (SL4) was about 5.6 mg/100 g. Similar levels have been previously found in different cultivars of yellow-fleshed nectarines from California.[35] As indicated in Table 2, regardless of the temperature, the levels of AA, and consequently those of vitamin C, decreased significantly with days of storage, but losses were significantly more important at 1 or 4 °C. For 20 days of storage, the levels of vitamin C observed in nectarines stored at 8 °C were about 18% lower than those observed at harvest, but the levels were, respectively, 46 and 40% lower for samples prestored at 1 or 4 °C. These results are consistent with those previously reported by Dalla Valle et al.,[24] who observed a

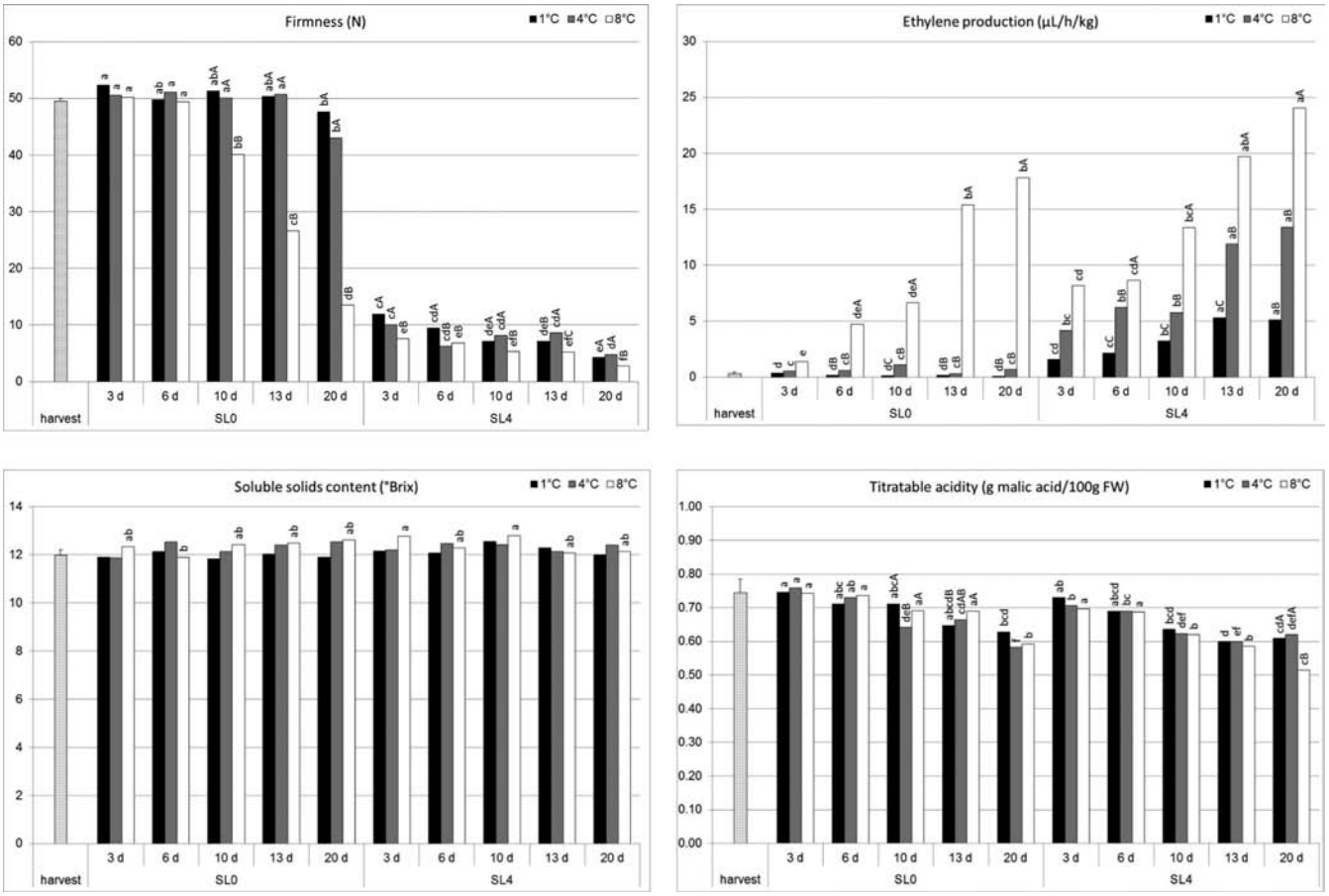

Figure 2. Physicochemical attributes in nectarine samples at harvest and after 3, 6, 10, 13, or 20 days of cold storage followed by 0 (SL0) or 4 (SL4) days at 25 °C. Similar vertical bars followed by different small letters are significantly different (SNK test, $p < 0.05$). Vertical bars within the same days of storage + days at 25 °C followed by different capital letters are significantly different (SNK test, $p < 0.05$).

significant decrease in the levels of vitamin C in three different peach cultivars stored for up to a week at 4 °C after harvest. Recently, significant lower levels of AA in peaches stored at 0 °C have been also reported in comparison to the levels observed in fruits stored at 5 °C.[27] These results also confirm that although low-temperature storage is the most important tool to extend shelf life and maintain fruit quality, freshly harvested fruits contain more vitamin C than those held in cold storage.[7] Our results also indicated that levels of AA increased significantly during postharvest ripening. After 4 days at 25 °C, vitamin C levels in the nectarines were on average 22% higher than those observed in the corresponding samples before ripening. After 20 days of storage, these values were 80 and 60% higher for samples prestored at 1 or 4 °C, respectively. Peaches and nectarines are climacteric fruit and therefore may ripen either on- or off-tree. Although it is generally admitted that maturity is one of the major factors determining the compositional quality of fruit, and consequently influences the content of AA in fruit, its accumulation during ripening depends on the type of fruit. Our results are in agreement with Lee and Kader,[7] who previously reported that AA content decreased with ripening in apple and mango, but increased in papaya, apricot, and peach. They also reported that fruit accumulated AA during ripening on or off the plant, even if the increase was much greater in the fruit left on the plant. Our results also confirm that, sometimes, fruits stored at room temperature after cold storage may improve their nutritional attributes such as vitamin C content. Similar results have been observed in kiwifruit maintained for a week at 25 °C after a cold storage during 2−6 months at 0 °C.[36] Toor and Savage[37] also observed a slight accumulation of AA in tomatoes stored at 7, 15, or 25 °C for up to 10 days.

As indicated in Table 2, total carotenoid content ranged from 126 to 197 μg/100 g; β-carotene was predominant and accounted for 95−97% of the total carotenoid content in our samples. These levels are consistent with those previously observed in different cultivars of yellow-fleshed nectarines from California.[35] No significant change was observed for carotenoid content during cold storage, but in contrast they increased significantly during the postharvest ripening at 25 °C, with a more pronounced effect for samples prestored at 4 or 8 °C. On average, the levels of carotenoids in samples after 4 days at 25 °C were 13, 21, and 32% higher than those observed at harvest in the nectarines prestored at 1, 4, and 8 °C, respectively. The changes in carotenoid levels during cold storage have not been studied much, but similar results have been observed in two cultivars of yellow nectarines,[25] in carrots,[38] or in mangoes.[39] With regard to evolution of carotenoids during shelf life, increases of β-carotene and β-cryptoxanthin in peaches held in air at 20 °C for 8 days after harvest were already observed by Caprioli et al.[26] Similar results have also been described previously for kiwifruit stored for 2 months at 0 °C and maintained for 7 days at 25 °C.[36]

As shown in Table 3, total polyphenol content ranged from 8.6 to 10.4 mg/100 g. Hydroxycinnamic acids, accounting for

dx.doi.org/10.1021/jf4057555 | J. Agric. Food Chem. 2014, 62, 4707−4724

Table 2. Levels of Vitamin C and Carotenoids in Nectarine Samples at Harvest and after 3, 6, 10, 13, or 20 Days of Cold Storage followed by 0 (SL0) or 4 (SL4) Days at 25 °C

				SL0					SL4					
code	compound	at harvest	temp (°C)	3 days	6 days	10 days	13 days	20 days	3 days	6 days	10 days	13 days	20 days	signif
				Vitamin C (mg/100 g)										
AA	ascorbic acid	4.50 ± 0.53	1	4.52 a[a]	4.43 a	3.80 ab	3.30 b	2.37 cB[b]	4.21 a	4.08 ab	4.40 a	4.73 a	4.64 aB	***
			4	4.56 ab	4.68 ab	3.67 bc	3.34 cd	2.75 dB	4.54 ab	4.61 ab	5.03 a	5.02 a	4.65 abB	***
			8	4.78 abc	4.24 bcd	4.14 cd	3.93 cd	3.70 dA	5.07 ab	4.67 abc	5.18 a	5.29 a	5.53 aA	***
			signif	ns	ns	ns	ns	*	ns	ns	ns	ns	**	
DHA	dehydroascorbic acid	0.85 ± 0.03	1	0.82 ab	0.60 bc	0.72 abc	0.66 bc	0.51 cB	0.97 a	0.86 ab	0.81 ab	0.72 abc	0.49 c	***
			4	0.86 ab	0.67 abcd	0.72 abcd	0.63 bcd	0.46 dB	0.92 a	0.79 abc	0.74 abc	0.71 abcd	0.54 cd	***
			8	0.84 ab	0.88 ab	0.80 ab	0.74 ab	0.69 abA	0.90 ab	1.06 a	1.09 a	0.61 b	0.76 ab	*
			signif	ns	ns	ns	ns	*	ns	ns	ns	ns	ns	
	total vitamin C	5.34 ± 0.51	1	5.34 a	5.02 a	4.51 ab	3.96 b	2.87 cB	5.17 a	4.95 a	5.21 a	5.45 a	5.14 aB	***
			4	5.42 ab	5.35 ab	4.38 bc	3.97 cd	3.21 dB	5.45 ab	5.40 ab	5.77 a	5.73 a	5.19 abB	***
			8	5.62 abc	5.11 bcd	4.94 cd	4.67 d	4.39 dA	5.97 ab	5.73 abc	6.27 a	5.89 ab	6.28 aA	***
			signif	ns	ns	ns	ns	*	ns	ns	ns	ns	**	
				Carotenoids (mg/100 g)										
CRY	*β*-cryptoxanthin	5.3 ± 0.3	1	5.0 bc	4.8 bc	5.2 bc	5.3 bc	4.5 c	6.9 a	7.5 a	7.6 a	7.7 a	6.3 abB	***
			4	5.1 d	5.4 d	4.5 d	4.1 d	4.7 d	6.5 c	7.2 bc	8.2 ab	8.8 a	7.1 bcB	***
			8	4.5 c	5.0 c	5.0 c	4.1 c	4.6 c	7.0 b	6.7 b	8.0 ab	7.4 ab	8.5 aA	***
			signif	ns	ns	ns	ns	ns	ns	ns	ns	ns	*	
CAR	*β*-carotene	130.7 ± 7.4	1	130.6 b	130.7 b	131.9 b	129.5 b	121.8 b	141.1 ab	137.6 abC	137.4 ab	161.3 a	158.0 a	**
			4	132.3 bc	134.4 bc	123.9 c	151.9 abc	138.4 abc	141.6 abc	151.8 abcB	155.3 abc	172.0 a	166.8 ab	**
			8	126.7 d	123.7 d	124.8 d	148.3 cd	149.2 cd	157.4 c	162.4 bcA	167.0 abc	189.5 a	184.7 ab	***
			signif	ns	ns	ns	ns	ns	ns	**	ns	ns	ns	
	total carotenoids	136.0 ± 7.1	1	135.7 b	135.5 b	137.1 b	134.8 b	126.3 b	148.0 ab	145.1 abC	144.9 ab	169.0 a	164.3 a	***
			4	137.5 c	139.8 bc	128.4 c	156.0 abc	143.1 bc	148.1 abc	159.0 abcB	163.6 abc	180.8 a	173.8 ab	**
			8	131.2 d	128.6 d	129.8 d	152.4 cd	153.8 cd	164.4 c	169.1 bcA	175.0 abc	197.0 a	193.2 ab	***
			signif	ns	ns	ns	ns	ns	ns	**	ns	ns	ns	

[a]Means within the same temperature of cold storage followed by different small letters are significantly different (SNK test, $p < 0.05$). [b]Means within the same days of cold storage + days at 25 °C followed by different capital letters are significantly different (SNK test, $p < 0.05$).

dx.doi.org/10.1021/jf405755s | J. Agric. Food Chem. 2014, 62, 4707−4724

Table 3. Levels of Polyphenolic Compounds in Nectarine Samples at Harvest and after 3, 6, 10, 13, or 20 Days of Cold Storage followed by 0 (SL0) or 4 (SL4) Days at 25 °C

				SL0					SL4					
code	compound	at harvest	temp (°C)	3 days	6 days	10 days	13 days	20 days	3 days	6 days	10 days	13 days	20 days	signif
				Hydroxycinnamic Acids (mg/100 g)										
HA1	3-caffeoylquinic acid	2.93 ± 0.17	1	3.11	3.05	3.03	3.13	2.98	3.02	2.86	3.03 B[b]	2.95	2.88 B	ns
			4	3.05 abc[a]	3.06 abc	3.20 a	2.97 abcd	2.77 d	2.95 abcd	2.88 bcd	2.94 abcdB	2.79 cd	3.14 abA	***
			8	3.02	3.01	3.03	2.95	2.91	2.86	2.93	3.14 A	3.09	3.14 A	ns
			signif	ns	ns	ns	ns	ns	ns	ns	*	ns	**	
HA2	*p*-coumaroylquinic acid	0.07 ± 0.01	1	0.07	0.06 B	0.07	0.07	0.07	0.07	0.07	0.07	0.07	0.06	ns
			4	0.07 ab	0.06 abB	0.07 a	0.07 ab	0.06 ab	0.06 ab	0.06 b	0.07 ab	0.06 ab	0.06 ab	*
			8	0.07	0.07 A	0.07	0.06	0.07	0.06	0.07	0.07	0.07	0.07	ns
			signif	ns	*	ns	ns	ns	ns	ns	ns	ns	ns	
HA3	5-caffeoylquinic acid	3.98 ± 0.13	1	4.30	4.31	4.39	4.02 B	4.79	4.09	3.93	4.38 A	4.02	3.94	ns
			4	3.96	4.83	4.47	4.33 A	4.14	4.28	4.61	3.84 B	3.90	4.53	ns
			8	4.22	3.97	4.32	3.95 B	4.26	4.49	4.04	4.39 A	4.36	4.31	ns
			signif	ns	ns	ns	**	ns	ns	ns	*	ns	ns	
HA4	4-caffeoylquinic acid	0.04 ± 0.01	1	0.04 ab	0.04 b	0.04 ab	0.04 a	0.03 b	0.04 abA	0.04 ab	0.04 b	0.04 ab	0.04 b	*
			4	0.04 ab	0.03 ab	0.04 a	0.04 ab	0.03 ab	0.04 abA	0.03 b	0.04 ab	0.03 ab	0.04 ab	*
			8	0.04 a	0.04 a	0.04 a	0.03 a	0.04 a	0.03 aB	0.03 a	0.04 a	0.04 a	0.04 a	*
			signif	ns	ns	ns	ns	ns	*	ns	ns	ns	ns	
HA5	caffeoylquinic acid derivative	0.09 ± 0.01	1	0.10	0.09	0.10	0.10 A	0.10	0.09	0.09	0.09	0.08	0.09	ns
			4	0.09 cd	0.10 abc	0.11 ab	0.10 bcA	0.12 a	0.09 cd	0.10 abc	0.09 bcd	0.08 d	0.10 bc	***
			8	0.09 ab	0.09 ab	0.10 a	0.08 bB	0.10 a	0.10 a	0.09 ab	0.09 ab	0.09 ab	0.09 ab	*
			signif	ns	ns	ns	**	ns	ns	ns	ns	ns	ns	
	total hydroxycinnamic acids	7.10 ± 0.29	1	7.62	7.55	7.62	7.35	7.98	7.31	6.98	7.60 A	7.16	7.00 B	ns
			4	7.20 a	8.10 a	7.89 a	7.51 a	7.12 a	7.42 a	7.68 a	6.98 aB	6.87 a	7.87 aA	*
			8	7.44	7.17	7.56	7.08	7.37	7.56	7.15	7.72 A	7.65	7.65 AB	ns
			signif	ns	ns	ns	ns	ns	ns	ns	*	ns	*	
				Anthocyanins (mg/100 g)										
AN1	cyanidin-3-glucoside	1.13 ± 0.05	1	1.07 ab	0.73 b	0.98 ab	0.93 ab	1.12 ab	1.25 ab	1.03 ab	1.16 ab	0.73 b	1.44 a	*
			4	1.20 abc	1.16 abc	0.92 bc	0.79 c	1.29 ab	1.09 abc	1.15 abc	0.83 bc	0.82 bc	1.52 a	***
			8	1.12	0.90	0.87	0.89	1.14	1.13	1.00	0.86	1.24	1.21	ns
			signif	ns	ns	ns	ns	ns	ns	ns	ns	ns	ns	
				Flavanols (mg/100 g)										
FA1	procyanidin dimer B1	0.22 ± 0.01	1	0.25	0.27	0.25	0.21	0.29	0.20 B	0.22	0.24	0.21	0.23	ns
			4	0.20	0.28	0.25	0.23	0.23	0.27 AB	0.25	0.21	0.21	0.25	ns
			8	0.23 ab	0.21 b	0.24 ab	0.22 b	0.23 ab	0.31 aA	0.21 b	0.28 ab	0.26 ab	0.21 b	*
			signif	ns	ns	ns	ns	ns	*	ns	ns	ns	ns	

dx.doi.org/10.1021/jf4057555 | J. Agric. Food Chem. 2014, 62, 4707−4724

Table 3. continued

code	compound	at harvest	temp (°C)	SL0 3 days	SL0 6 days	SL0 10 days	SL0 13 days	SL0 20 days	SL4 3 days	SL4 6 days	SL4 10 days	SL4 13 days	SL4 20 days	signif
						Flavanols (mg/100 g)								
FA2	(+)-catechin	0.22 ± 0.01	1	0.24	0.28	0.25	0.22	0.28	0.21	0.23	0.23	0.21	0.23	ns
			4	0.21	0.26	0.25	0.23	0.23	0.26	0.24	0.22	0.21	0.24	ns
			8	0.23 ab	0.23 ab	0.24 ab	0.23 ab	0.24 ab	0.30 a	0.22 ab	0.26 ab	0.25 ab	0.20 b	*
			signif	ns	ns	ns	ns	ns	ns	ns	ns	ns	ns	
FA3	procyanidin dimer B2	0.023 ± 0.001	1	0.026	0.027 B	0.024	0.021	0.023	0.020 B	0.022	0.019	0.017	0.018 AB	ns
			4	0.021 bc	0.037 aA	0.021 bc	0.020 bc	0.017 c	0.027 bA	0.023 bc	0.019 bc	0.019 bc	0.020 bcA	***
			8	0.024 b	0.021 bcB	0.020 bc	0.018 bc	0.017 bc	0.029 aA	0.020 bc	0.023 b	0.021 bc	0.015 cB	***
			Sign.	ns	*	ns	ns	ns	*	ns	ns	ns	*	
	total flavanols	0.457 ± 0.019	1	0.515	0.566	0.519	0.450	0.589	0.430	0.475	0.488	0.440	0.471	ns
			4	0.428	0.571	0.519	0.473	0.472	0.560	0.518	0.449	0.446	0.504	ns
			8	0.485 ab	0.457 b	0.502 ab	0.470 b	0.478 ab	0.638 a	0.451 b	0.561 ab	0.526 ab	0.427 b	*
			signif	ns	ns	ns	ns	ns	ns	ns	ns	ns	ns	
						Flavonols (mg/100 g)								
FO1	quercetin-3-*O*-galactoside	0.17 ± 0.03	1	0.20	0.20	0.19	0.21 A	0.20	0.19	0.17	0.19	0.17	0.19	ns
			4	0.17	0.19	0.20	0.21 A	0.20	0.17	0.22	0.20	0.17	0.22	ns
			8	0.18 a	0.16 a	0.22 a	0.14 aA	0.22 a	0.20 a	0.22 a	0.16 a	0.21 a	0.20 a	*
			signif	ns	ns	ns	*	ns	ns	ns	ns	ns	ns	
FO2	quercetin-3-*O*-glucoside + quercetin-3-*O*-rutinoside	0.25 ± 0.04	1	0.26	0.24	0.22 B	0.28	0.23	0.25	0.22	0.23	0.23	0.25	ns
			4	0.22	0.25	0.24 A	0.27	0.26	0.23	0.28	0.27	0.25	0.29	ns
			8	0.23	0.22	0.26 A	0.20	0.27	0.26	0.28	0.22	0.26	0.25	ns
			Sign.	ns	ns	*	ns	ns	ns	ns	ns	ns	ns	
	total flavonols	0.42 ± 0.07	1	0.46	0.44	0.40	0.49	0.43	0.44	0.39	0.42	0.40	0.44	ns
			4	0.39	0.45	0.44	0.48	0.47	0.40	0.50	0.47	0.42	0.51	ns
			8	0.41	0.38	0.48	0.34	0.49	0.46	0.50	0.37	0.47	0.45	ns
			signif	ns	ns	ns	ns	ns	ns	ns	ns	ns	ns	
	total polyphenols	9.11 ± 0.27	1	9.67	9.28	9.51	9.22	10.11	9.43	8.88	9.66 A	8.72	9.36	ns
			4	9.22 ab	10.27 ab	9.77 ab	9.25 ab	9.35 ab	9.47 ab	9.85 ab	8.72 abB	8.55 b	10.41 a	*
			8	9.45	8.90	9.40	8.78	9.48	9.78	9.10	9.52 A	9.88	9.74	ns
			signif	ns	ns	ns	ns	ns	ns	ns	**	ns	ns	

[a]Means within the same temperature of cold storage followed by different small letters are significantly different (SNK test, $p < 0.05$). [b]Means within the same days of cold storage + days at 25 °C followed by different capital letters are significantly different (SNK test, $p < 0.05$).

dx.doi.org/10.1021/jf4057555 | J. Agric. Food Chem. 2014, 62, 4707−4724

75−82% of the total polyphenol content, were found to be predominant, followed by anthocyanins (8−16%), flavanols (4−7%), and flavonols (4−5%). Among hydroxycinnamic acids, 5- and 3-caffeoylquinic acids, and cyanidin-3-glucoside (anthocyanin) accounted, respectively, for 42−47, 29−34, and 8−15% of the total polyphenol content. In all samples, the amount of chlorogenic acid was larger than that of neochlorogenic acid. These results are consistent with those previously reported by Tomás-Barberán et al.[40] and confirm that this compound is the main hydroxycinnamate of peaches. Cryptochlorogenic (4-caffeoylquinic) acid was also detected in our samples. Catechin was found as the main monomeric flavanol as previously mentioned. Procyanidins B1 and B2 have also been detected in our samples, but not epicatechin, gallocatechin, and epigallocatechin. Among flavonols, quercetin 3-glucoside, 3-galactoside, and 3-rutinoside have been quantified in our samples but no kaempferol derivatives have been detected. As previously mentioned,[40] cyanidin 3-glucoside was found as the main anthocyanin pigment, but anthocyanin 3-rutinoside was not found in our extracts. As shown in Table 3, although some individual polyphenol results were statistically different between samples, the changes observed during storage and/or postharvest ripening were relatively weak and the levels in samples were found to be overall similar to those observed at harvest. These results are consistent with those previously reported by Asami et al.[41] in peaches stored during 2 weeks at 4 °C, but differ from those reported by Tsantili et al.,[27] who reported significant changes in total phenolic and flavonoid concentrations in peaches stored at 5 °C for 2 or 4 weeks. Because this latter work supports a possible role of polyphenols in cell wall metabolism in chilling-injured peaches, it is not surprising, given the CI scores observed in our samples, that no significant change was found for these compounds.

Volatile Compounds. As indicated in Table 4, the effects of storage and/or postharvest ripening on Western Red volatiles are mainly characterized by opposite changes in two major groups of volatiles, the first group consisting of C_6 compounds and the second of lactones and C_{13} norisoprenoids. Except for 20 days of storage at 8 °C, C_6 compounds, aldehydes, and alcohols, products of enzymatic breakdown of unsaturated fatty acids, are the main compounds isolated in unripened nectarines (SL0), from 44% in samples stored for 13 days at 8 °C to 86% in nectarines at harvest (Figure 3). During storage and/or postharvest ripening, the relative proportions of these so-called green components, in particular those of (*Z*)-3-hexenal and (*E*)-2-hexenal (Table 4), decreased drastically by up to ∼8% in samples stored for 20 days at 8 °C with 4 days of ripening at 25 °C. These results agree with those previously reported in peaches by Zhang et al.[19] With decreasing concentrations of C_6 compounds during storage and/or ripening, lactones and C_{13} norisoprenoids increase during the same time and become the major volatiles in "ready to eat" nectarines. Whereas the levels of lactones and C_{13} norisoprenoids in the samples stored at 1 or 4 °C have been found to be very similar to those observed at harvest, they significantly increased during storage at 8 °C and after ripening, with a much more marked effect during this latter stage (Table 4). After 4 days of ripening at 25 °C, the relative proportions of lactones and C_{13} norisoprenoids were, respectively, 76 and 13% in samples prestored for 20 days at 8 °C (Figure 3). Among lactones, γ-hexalactone, γ- and δ-octalactone, γ- and δ-hexalactone, γ-jasmolactone, 6-pentyl-α-pyrone, and (*Z*)-7-decen-5-olide, previously reported to be major contributors to peach aroma,[9,10] are the ones that mainly increased during postharvest ripening, reaching their highest amounts in samples stored for 13 or 20 days at 8 °C followed by 4 days at 25 °C. These results are consistent with those previously reported by Raffo et al.[18] and confirm that increasing times of low-temperature storage (2−3 weeks, 1−4 °C) significantly reduce the fruit's ability to perform lactone accumulation and, consequently, to develop its aroma after being exposed to ripening temperature. These results also indicated that storage at a moderate temperature (8 °C) does not decrease the fruit's ability to ripen normally when they are removed from storage and exposed to a ripening temperature. Previous works reported significantly lower levels of volatiles, especially lactones, in chilling-injured peaches during the shelf life period after transfer from low temperature.[19,20] Our results indicate that in lack of CI, or at least in the case of very low levels of development, the levels of lactones do not drastically decrease during shelf life. As recently proposed by Xi et al.,[20] these results support that loss of fruity aromas in peaches and nectarines during cold storage is a symptom of CI. In agreement with the results previously reported by Engel et al.,[14] γ-hexalactone was already present at high levels in fruits at harvest and increased steadily during maturation, whereas γ- and δ-decalactone, present at very low levels in unripened fruit, mainly increased during the last stages of ripening (SL4).

A similar trend was observed for C_{13} norisoprenoids, and particularly for 8,9-dehydrotheaspirone, 3-hydroxy-β-ionone, 3-hydroxy-5,6-epoxy-β-ionone, and dehydrovomifoliol. These compounds, generally considered to be derived from carotenoids by oxidative degradations, are important aroma constituents, and most of those reported in this study have been previously identified in numerous natural products.[42] Oxygenated carotenoids, neoxanthin (an allenic xanthophyll), violaxanthin (an epoxy xanthophyll), and lutein (a nonepoxy xanthophyll) have been previously identified in nectarines,[43] and partial characterization of carotenoid cleavage enzymes in nectarine[44] has been shown. The occurrence of free and glycosidically bound C_{13} norisoprenoid compounds has been previously described in peaches and nectarines.[9,14,16,45−47] Several authors have pointed out the importance of these compounds for the aroma of peaches and nectarines. 8,9-Dehydrotheaspirone has been previously reported as a major constituent in white-fleshed nectarines. The importance of this spirocyclic C_{13} ether, and those of β-ionone and β-damascenone for the specific flavor of these cultivars, has been clearly demonstrated by Takeoka et al.[48] and Knapp et al.[49] Except in the research done by Raffo et al.[18] on peach, to our best knowledge no data about the impact of low-temperature storage and/or postharvest ripening on the levels of C_{13} norisoprenoids in nectarines have been reported. As shown in Table 4, no significant change was observed for C_{13} norisoprenoids content during cold storage, but in contrast they increased significantly during the postharvest ripening at 25 °C, with a more pronounced effect for samples prestored at 4 or 8 °C.

Regardless of temperature, the levels of linalool significantly decreased with increasing duration of storage, whereas they increased when fruit were transferred to 25 °C. After 13 days of storage at 1 or 4 °C, the concentrations of linalool were under the limits of detection, and only very low levels of this compound were detected after ripening at 25 °C. These results were in agreement with those previously reported in peaches.[17,18] Lastly, with the exception of the increase of (*Z*)-3-hexenyl acetate when fruits were transferred to 25 °C, the changes of other compounds during storage and/or ripening

Table 4. Levels[a] of Volatile Compounds in Nectarine Samples at Harvest and after 3, 6, 10, 13, or 20 Days of Cold Storage followed by 0 (SL0) or 4 (SL4) Days at 25 °C

						SL0					SL4					
code	compound	LRI[b]	ID[c]	at harvest	temp (°C)	3 days	6 days	10 days	13 days	20 days	3 days	6 days	10 days	13 days	20 days	signif
						C_6 Compounds										
C1	hexanal	1072	A	1081.6 ± 101.3	1	636.5 a[d]	340.0 bc	226.3 cdB[e]	306.7 bcA	225.4 cd	619.9 a	692.0 aA	425.2 b	237.9 cdA	109.0 dB	***
					4	807.9 a	541.8 b	377.8 cdA	344.6 cdeA	270.7 de	464.7 bc	287.3 deB	310.9 de	125.9 fB	211.7 efA	***
					8	521.4 a	546.5 a	273.6 cB	210.4 cB	163.5 c	629.8 a	471.8 adB	322.5 bc	236.6 cA	83.8 cB	***
					signif	ns	ns	*	*	ns	ns	*	ns	**	***	
C2	(*Z*)-3-hexenal	1140	A	1759 ± 11.6	1	950.3 a	1031.0 a	466.0 c	159.9 d	15.3 d	677.6 b	516.2 cA	103.5 d	53.7 dA	15.6 dA	***
					4	779.6 b	971.1 a	396.6 cd	108.7 e	13.1 e	532.3 c	212.6 deC	109.1 e	20.0 eB	5.7 eB	***
					8	697.8 b	991.0 a	453.9 bc	141.8 cd	18.0 d	593.1 b	369.9 bcdB	150.4 cd	63.5 dA	7.1 dB	***
					signif	ns	ns	ns	ns	ns	ns	*	ns	*	**	
C3	(*E*)-2-hexenal	1225	A	1381.1 ± 195.7	1	1222.0 abA	1236.7 ab	1192.2 abA	1472.2 aA	1188.3 abA	686.1 cd	852.2 bcA	774.7 cd	433.0 deA	283.9 eA	***
					4	1365.2 aA	924.9 b	946.0 bB	1135.2 bB	1096.6 bA	566.1 c	418.3 cdB	595.6 c	221.2 dc	328.7 cdA	***
					8	833.3 aB	716.9 ab	474.7 abcdC	543.4 abcdC	570.0 abcdB	613.3 abc	368.1 bcdB	402.6 bcd	306.3 cdB	210.6 dB	***
					signif	*	ns	**	**	*	ns	***	ns	**	*	
C4	(*E*)-2-hexenol	1405	A	0.6 ± 0.1	1	1.0 cB	2.0 bB	1.0 cB	1.2 cB	1.2 cB	2.2 bB	2.1 bB	3.4 aB	2.1 bB	2.0 bB	***
					4	1.4 cdB	1.8 cB	1.4 cdB	1.1 dB	1.1 dB	2.7 bB	2.5 bB	3.9 aB	2.5 bB	2.3 bB	***
					8	8.1 dA	13.6 cA	6.1 dA	5.8 dA	6.2 dA	25.9 abA	31.8 aA	28.7 abA	23.8 bA	17.6 cA	***
					signif	**	***	**	***	*	***	**	**	***	***	
	total C_6 compounds			4222.3 ± 305.2	1	2809.8 a	2609.8 a	1885.5 bA	1940.0 bA	1430.2 bc	1985.8 b	2062.6 bA	1306.7 c	726.8 dA	410.6 dB	***
					4	2954.2 a	2439.5 b	1721.8 cA	1589.7 cB	1381.4 cd	1565.9 c	920.7 deB	1019.6 de	369.6 fB	548.4 efA	***
					8	2060.6 a	2268.0 a	1208.3 bcB	901.4 cC	757.6 c	1862.0 ab	1241.5 bcB	904.3 c	630.3 cA	319.2 cC	***
					signif	ns	ns	*	***	ns	ns	**	ns	**	**	
						Lactones										
L1	γ-hexalactone	1706	A	312.9 ± 34.6	1	259.5 d	391.2 d	399.0 dAB	335.5 d	394.7 dB	752.3 cB	839.1 bcB	1101.2 aB	909.3 bB	848.1 bcB	***
					4	293.1 e	410.0 cd	346.6 deB	430.1 cd	471.5 cB	919.4 bAB	1132.7 aA	1093.9 aB	898.6 bB	871.4 bB	***
					8	369.5 e	450.5 e	463.6 eA	464.6 e	696.6 dA	1092.2 cA	1161.0 cA	1383.9 bA	1486.9 bA	1791.2 aA	***
					signif	ns	ns	*	ns	*	*	**	**	***	***	
L2	γ-heptalactone	1810	A	10.8 ± 1.6	1	10.7 e	16.9 de	16.2 deB	15.7 de	20.4 d	30.4 c	35.5 cB	49.4 a	42.7 dB	47.2 ab	***
					4	10.2 e	19.3 d	18.5 dB	22.3 d	22.6 d	36.7 c	47.6 abA	53.3 a	49.6 abA	43.9 b	***
					8	15.5 d	21.5 cd	24.0 bcA	27.1 bc	32.0 b	44.2 a	46.5 aA	51.2 a	51.7 aA	48.2 a	***
					signif	ns	ns	*	ns	ns	ns	*	ns	**	ns	
L3	γ-octalactone	1918	A	7.3 ± 2.1	1	6.6 e	11.6 e	8.6 eB	8.7 eb	11.5 eB	68.4 dB	94.6 cB	133.1 a	111.0 bB	98.6 c	***
					4	6.4 d	9.0 d	8.0 dB	10.9 dB	16.5 dB	89.8 cAB	129.2 abA	134.6 a	119.1 bB	86.3 c	***
					8	9.6 d	14.1 d	19.7 dA	31.7 dA	52.2 cA	114.4 bA	132.5 abA	133.9 ab	143.9 aA	122.5 ab	***
					signif	ns	ns	***	*	**	*	*	ns	**	*	
L4	δ-octalactone	1966	A	4.2 ± 1.1	1	5.1 d	9.7 d	8.4 dC	6.3 dB	5.6 dB	42.4 cB	66.4 bB	103.4 a	92.1 aC	99.8 aB	***
					4	8.0 b	12.0 d	10.3 dB	10.1 dAB	7.5 dB	62.7 cB	106.3 aA	108.4 a	110.2 aB	89.0 bB	***
					8	9.2 c	14.8 c	12.6 cA	18.4 cA	30.9 cA	84.9 bA	97.9 bA	119.9 a	137.1 aA	138.2 aA	***
					signif	ns	ns	**	*	**	*	*	ns	***	*	

dx.doi.org/10.1021/jf405755s | J. Agric. Food Chem. 2014, 62, 4707−4724

Table 4. continued

code	compound	LRI[b]	ID[c]	at harvest	temp (°C)	SL0 3 days	SL0 6 days	SL0 10 days	SL0 13 days	SL0 20 days	SL4 3 days	SL4 6 days	SL4 10 days	SL4 13 days	SL4 20 days	signif
								Lactones								
L5	γ-decalactone	2142	A	6.9 ± 2.2	1	4.0 d	7.3 d	4.3 dB	4.4 dB	4.3 dB	104.8 cB	194.3 b	270.7 a	260.7 a	223.3 b	***
					4	6.1 e	3.8 e	6.1 eB	7.2 eB	9.2 eB	148.1 dB	256.1 b	264.0 b	308.7 a	213.5 c	***
					8	5.7 c	14.3 c	23.4 cA	52.2 cA	75.9 cA	204.0 bA	244.4 ab	229.6 b	293.6 a	208.3 b	***
					signif	ns	ns	***	***	***	*	ns	ns	ns	ns	
L6	6-pentyl-α-pyrone + γ-jasmolactone	2180	A	21.5 ± 5.4	1	10.8 e	11.2 eB	6.2 eC	6.0 eB	4.9 eB	163.6 dC	303.4 c	465.0 aA	418.7 ab	374.5 b	***
					4	10.2 e	7.6 eB	12.1 eB	13.6 eB	14.6 eB	213.4 dB	309.0 c	461.9 abA	488.5 a	421.8 b	***
					8	13.6 e	22.5 eA	32.4 eA	83.3 eA	143.3 dA	266.7 cA	388.4 ab	320.5 bcB	425.2 a	337.5 b	***
					signif	ns	*	***	**	***	**	ns	*	ns	ns	
L7	δ-decalactone	2195	A	16.3 ± 3.1	1	2.6 cB	7.3 cB	3.8 cC	3.3 cB	5.7 cB	155.1 bB	295.3 a	336.3 a	336.6 a	300.6 aA	***
					4	6.1 eB	10.2 eB	20.7 eB	24.8 eB	17.5 eB	216.9 dAB	338.1 b	320.7 bc	386.0 a	303.9 cA	***
					8	16.9 dA	58.9 cdA	51.2 cdA	114.4 cA	82.9 cdA	281.6 abA	297.4 a	277.8 ab	347.7 a	216.6 bA	***
					signif	*	**	***	***	***	*	ns	ns	ns	*	
L8	7-decen-5-olide	2261	B (47)	6.1 ± 1.2	1	1.4 d	3.2 dB	2.3 dC	1.7 dB	2.5 dB	65.5 cB	111.2 b	160.2 aB	147.3 aB	115.5 bB	***
					4	1.5 c	2.5 cB	4.3 cB	6.0 cB	6.0 cB	96.8 bAB	150.3 a	154.9 aB	147.7 aB	113.3 bB	***
					8	3.2 e	11.9 eA	11.8 eA	36.8 eA	74.1 dA	132.9 cA	188.3 b	221.9 bA	304.0 aA	323.2 aA	***
					signif	ns	**	***	**	***	*	ns	*	***	***	
	total lactones			385.9 ± 45.7	1	300.5 e	458.4 e	448.9 eB	381.6 eB	449.7 eB	1382.5 dC	1940.0 cB	2619.3 a	2318.4 bB	2107.5 bcB	***
					4	341.6 d	474.3 d	426.6 dB	525.0 dB	565.5 dB	1783.7 cB	2469.2 aA	2591.9 a	2508.5 aB	2143.0 bB	***
					8	443.2 e	608.6 e	638.7 eA	828.6 eA	1187.9 dA	2220.8 cA	2556.4 bA	2738.7 b	3190.2 aA	3185.7 aA	***
					signif	ns	ns	**	*	**	*	*	ns	**	**	
								C_{13} Norisoprenoids								
N1	8,9-dehydrothea-spirone	2045	B (49)	41.7 ± 12.3	1	33.3 d	49.9 bcd	40.6 cd	29.6 d	56.4 bcd	100.1 b	139.8 a	89.9 bc	73.9 bcdA	78.8 bcd	***
					4	25.0 e	40.8 de	40.7 de	55.7 cde	52.0 cde	122.0 b	190.7 a	119.8 b	74.6 cdA	93.1 bc	***
					8	29.6 c	58.9 abc	46.3 bc	87.1 ab	91.4 ab	114.6 a	117.9 a	115.4 a	92.3 abA	110.2 a	***
					signif	ns	ns	ns	ns	ns	ns	ns	ns	*	ns	
N2	3-hydroxy-7,8-dihy-dro-β-ionone	2560	B (46)	16.2 ± 4.5	1	13.4 cdB	18.0 bc	11.6 cd	7.1 dB	12.4 cd	28.8 a	25.1 ab	19.8 bc	16.5 c	12.3 cdB	***
					4	43.2 aA	13.5 cd	13.5 cd	12.2 dA	10.8 d	32.7 b	21.1 c	17.1 cd	15.1 cd	16.0 cdA	***
					8	24.7 abB	18.8 abc	14.8 bc	14.2 bcA	15.4 bc	30.8 a	24.5 ab	19.6 abc	17.9 abc	10.0 cB	***
					signif	**	ns	ns	**	ns	ns	ns	ns	ns	*	
N3	3-hydroxy-7,8-dihy-dro-β-ionol	2668	B (46)	3.3 ± 2.0	1	3.1 dB	4.3 cdB	1.1 dB	0.4 d	0.3 d	26.9 a	26.6 a	8.4 bc	10.2 b	5.7 cdA	***
					4	3.1 cB	1.3 cC	0.8 cB	nd[f]	nd	31.2 a	20.0 b	10.0 c	7.6 c	4.9 cA	***
					8	4.8 bA	7.5 bA	2.2 bA	1.6 b	1.4 b	22.2 a	19.8 a	7.2 b	6.1 b	2.3 bB	***
					signif	*	**	**	***	***	ns	ns	ns	ns	*	

dx.doi.org/10.1021/jf405755s | J. Agric. Food Chem. 2014, 62, 4707−4724

Table 4. continued

code	compound	LRI[b]	ID[c]	at harvest	temp (°C)	SL0 3 days	SL0 6 days	SL0 10 days	SL0 13 days	SL0 20 days	SL4 3 days	SL4 6 days	SL4 10 days	SL4 13 days	SL4 20 days	signif
									C_{13} Norisoprenoids							
N4	3-hydroxy-β-ionone	2684	B (*46*)	2.3 ± 0.6	1	1.5 d	3.0 d	2.6 dB	2.1 dB	3.8 dB	16.5 cB	24.4 bB	41.1 a	40.1 aB	35.2 aB	***
					4	0.9 d	2.2 d	2.4 dB	4.1 dB	38.1 bA	26.5 cAB	38.7 bA	44.5 b	45.2 bB	69.3 aA	***
					8	1.8 d	3.3 d	4.4 dA	10.8 dA	33.6 cA	32.7 cA	38.5 cA	51.1 b	63.4 aA	65.6 aA	***
					signif	ns	ns	**	**	*	*	*	ns	**	*	
N5	3-hydroxy-5,6-epoxy-β-ionone	2724	B (*46*)	35.9 ± 17.5	1	16.1 c	21.4 cB	11.2 cC	6.8 cC	7.5 cB	61.0 b	82.5 a	72.4 ab	68.1 b	68.3 bB	***
					4	22.7 b	19.8 bB	15.9 bB	18.7 bB	9.8 bB	75.7 a	74.1 a	72.8 a	74.0 a	90.8 aA	***
					8	24.1 b	35.9 bA	23.2 bA	33.2 bA	34.8 bA	73.4 a	71.3 a	65.7 a	67.4 a	57.5 aC	***
					signif	ns	*	***	**	****	ns	ns	ns	ns	***	
N6	dehydrovomifoliol	2992	B (*46*)	30.6 ± 14.2	1	34.3 dB	48.8 dB	46.8 dC	73.3 dA	36.4 d	296.2 b	356.8 a	342.8 a	292.3 b	233.3 cB	***
					4	44.7 dAB	53.0 dB	53.0 dB	50.2 dB	61.6 d	340.0 a	373.5 a	354.1 a	272.1 b	227.6 cB	***
					8	51.1 cA	68.7 Ca	77.0 cA	71.4 cA	76.8 c	371.2 a	360.2 a	371.0 a	337.0 a	284.0 bA	***
					signif	*	*	***	*	ns	ns	ns	ns	ns	**	
	total C_{13} norisoprenoids			130.0 ± 49.3	1	101.7 d	145.5 d	113.9 dB	119.4 d	116.8 dC	529.4 b	655.2 a	574.4 b	501.1 b	433.7 cB	***
					4	139.6 d	130.7 d	126.4 dB	140.9 d	172.4 dB	628.1 b	718.1 a	618.2 b	488.6 c	501.6 cAB	***
					8	136.0 b	193.1 b	167.9 bA	218.4 b	253.4 bA	644.9 a	632.2 a	629.9 a	584.2 a	529.6 aA	***
					signif	ns	ns	*	ns	***	ns	ns	ns	ns	*	
									Terpenols							
T1	linalool	1530	A	50.2 ± 4.8	1	24.7 c	9.8 dB	5.1 d	nd	nd	79.9 a	61.4 b	9.2 d	6.8 d	1.7 d	***
					4	28.7 bc	5.9 cB	nd	nd	nd	83.1 a	40.3 b	7.6 c	2.5 c	1.5 c	***
					8	22.5 c	15.6 cdA	1.7 e	1.1 e	0.3 e	63.3 a	44.4 b	11.0 de	6.7 de	0.6 e	***
					signif	ns	*	***			ns	ns	ns	ns	ns	
T2	hotrienol	1612	A	2.7 ± 0.4	1	1.7 aB	6.9 a	6.0 a	2.7 a	3.1 a	7.8 aB	7.7 a	4.3 a	3.0 a	3.5 a	*
					4	15.1 aA	6.4 b	2.4 b	2.3 b	3.4 b	9.3 bA	9.5 b	4.2 b	2.3 b	3.0 b	***
					8	4.0 bcdeB	5.4 abc	1.7 e	2.3 de	8.0 a	6.5 abcC	6.7 ab	5.8 abc	5.1 abcd	3.3 cde	***
					signif	*	ns	ns	ns	ns	**	ns	ns	ns	ns	
T3	3,7-dimethyl-1,5-octadien- 3,7-diol	1953	A	55.0 ± 9.2	1	36.1 d	59.6 cA	62.2 cB	33.8 dC	63.0 c	72.8 cB	95.9 ab	109.8 a	79.0 bc	71.3 c	***
					4	50.0 c	59.8 bcA	47.6 cC	49.2 cB	51.6 c	101.7 aA	99.3 a	84.5 ab	69.4 bc	74.2 abc	***
					8	38.9 b	86.8 aA	72.3 aA	69.9 aA	96.5 a	78.5 aB	83.6 a	93.7 a	90.3 a	96.8 a	***
					signif	ns	*	**	**	ns	*	ns	ns	ns	ns	
	total terpenols			107.9 ± 4.8	1	62.6 cd	76.3 cd	73.4 cdA	36.5 dC	66.1 cdB	160.5 aB	165.0 a	123.3 b	88.9 c	76.4 cd	***
					4	93.8 c	72.1 c	50.0 cB	51.6 cB	55.1 cB	194.1 aA	149.1 b	96.3 c	74.1 c	78.7 c	***
					8	65.4 d	107.8 bcd	75.7 cdA	73.3 cdA	104.9 bcdA	148.3 aB	134.6 ab	110.5 bc	102.1 bcd	100.7 bcd	***
					signif	ns	ns	*	**	*	*	ns	ns	ns	ns	

dx.doi.org/10.1021/jf405555 | J. Agric. Food Chem. 2014, 62, 4707−4724

Table 4. continued

code	compound	LRI[b]	ID[c]	at harvest	temp (°C)	SL0 3 days	SL0 6 days	SL0 10 days	SL0 13 days	SL0 20 days	SL4 3 days	SL4 6 days	SL4 10 days	SL4 13 days	SL4 20 days	signif
									Miscellaneous							
M1	(Z)-3-hexenyl acetate	1321	A	4.0 ± 0.4	1	2.9 c	4.8 cA	4.7 cA	4.0 c	2.5 cB	16.2 bC	27.1 a	28.0 aB	25.8 aB	18.2 bB	***
					4	5.3 d	4.7 dA	3.5 dB	3.3 d	2.4 dB	20.6 bB	31.3 a	29.4 aB	27.2 aB	15.8 cB	***
					8	4.3 d	7.9 dA	3.7 dB	4.5 d	3.6 dA	26.3 cA	27.2 c	39.6 aA	40.9 aA	33.2 bA	***
					signif	ns	*	*	ns	**	**	ns	*	**	*	
M2	2,4-hexadienal	1403	A	2.8 ± 0.2	1	1.9 b	3.6 ab	4.7 ab	5.5 aA	1.9 b	2.5 b	4.9 ab	6.0 aA	3.4 ab	2.5 bB	***
					4	3.4 ab	3.4 ab	2.5 ab	4.2 abA	1.9 b	2.8 ab	2.8 ab	3.9 abAB	2.4 ab	4.3 aA	*
					8	2.3 abc	2.2 abc	2.2 abc	1.3 cB	1.2 c	2.3 abc	1.6 bc	2.9 abB	3.3 a	2.6 abcB	**
					signif	ns	ns	ns	*	ns	ns	ns	*	ns	**	
M3	benzaldehyde	1524	A	61.9 ± 1.8	1	71.2 bc	35.9 de	26.6 eC	52.8 cd	55.0 cd	85.4 abA	73.2 bc	101.0 a	58.9 cdA	43.7 de	***
					4	86.8 a	54.1 c	46.1 cdA	61.7 c	48.7 cd	56.1 cB	57.0 c	74.6 b	36.4 dB	44.6 cd	***
					8	77.8 a	41.3 b	35.8 bB	57.1 ab	48.5 ab	67.5 abAB	52.5 ab	76.4 a	60.3 abA	39.0 b	**
					signif	ns	ns	**	ns	ns	*	ns	ns	*	ns	
	total miscellaneous			68.6 ± 1.5	1	76.1 cd	44.3 ef	36.0 fB	62.3 de	59.4 de	104.1 bA	105.2 b	135.0 a	88.2 bcA	64.4 de	***
					4	95.6 b	62.2 de	52.0 eA	69.1 de	53.0 e	79.5 cdB	91.2 bc	107.8 a	66.0 deB	64.6 de	***
					8	84.4 bcd	51.4 de	41.7 eAB	62.9 cde	53.3 de	96.1 abcAB	81.3 bcd	119.0 a	104.5 abA	74.8 bcde	***
					signif	ns	ns	*	ns	ns	*	*	ns	*	ns	
	total volatiles			4914.6 ± 284.3	1	3350.6 c	3334.3 c	2557.6 de	2539.7 de	2122.2 e	4162.4 b	4928.0 a	4758.7 a	3723.3 bcB	3092.6 cdB	***
					4	3624.8 b	3178.8 b	2376.8 c	2376.3 c	2227.3 c	4251.3 a	4348.3 a	4433.8 a	3506.8 bB	3336.3 bB	***
					8	2789.6 bc	3228.9 b	2132.3 c	2084.6 c	2357.1 c	4972.1 a	4646.2 a	4502.4 a	4611.3 aA	4210.0 aA	***
					signif	ns	ns	ns	ns	ns	ns	ns	ns	**	**	

[a]Values expressed in μg/kg equivalent of 2-octanol. [b]Linear retention index calculated using a series of *n*-hydrocarbons. [c]A, identities confirmed by comparing mass spectra and retention time with those of authentic standards; B, identities tentatively assigned by comparing mass spectra with those obtained from the literature numbered and italicized within parentheses. [d]Means within the same temperature of cold storage followed by different small letters are significantly different (SNK test, $p < 0.05$). [e]Means within the same days of cold storage + days at 25 °C followed by different capital letters are significantly different (SNK test, $p < 0.05$). [f]Not detected.

dx.doi.org/10.1021/jf405755s | J. Agric. Food Chem. 2014, 62, 4707−4724

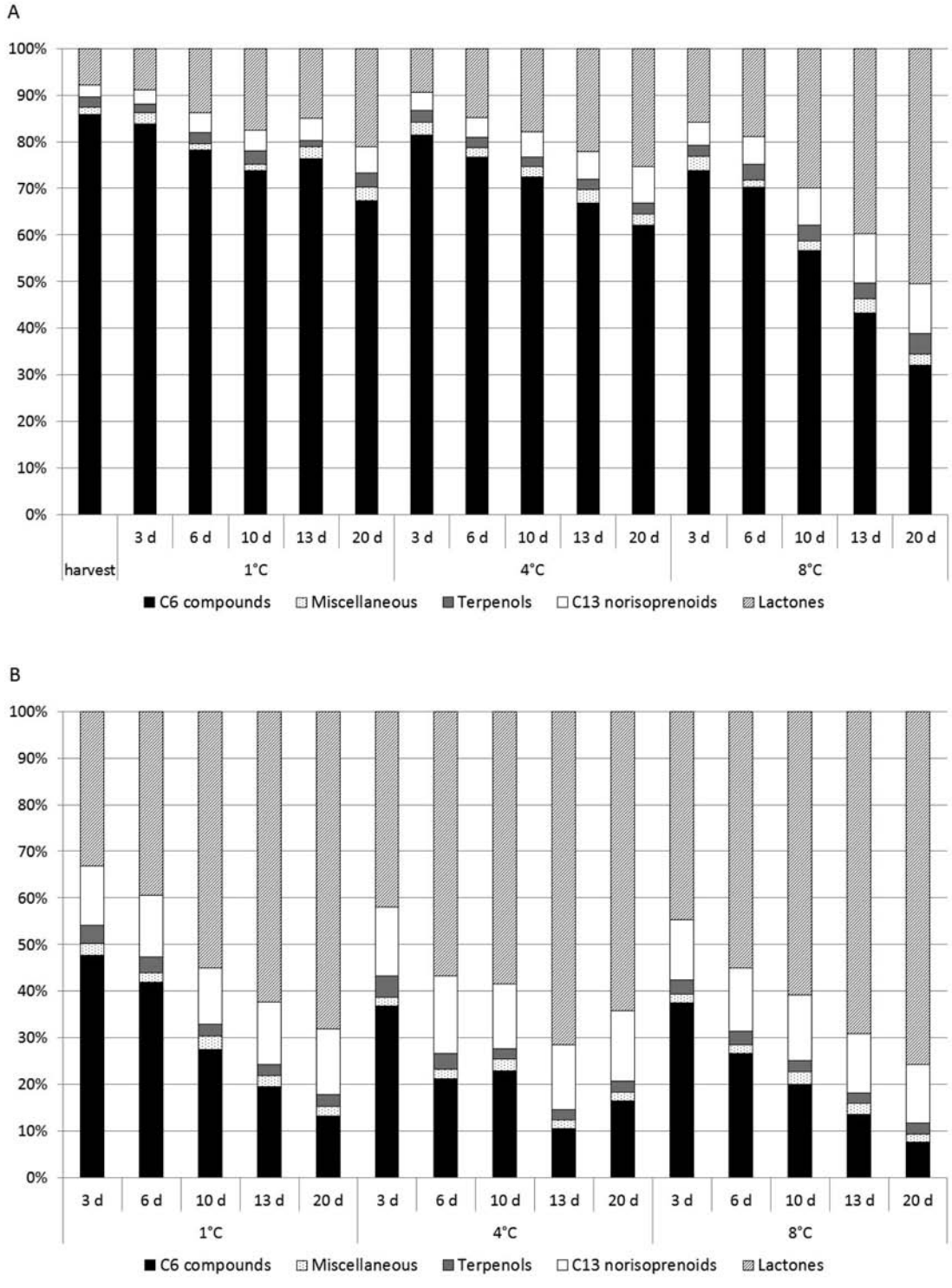

Figure 3. Relative proportions (percent) of the main classes of volatile compounds in nectarine samples at harvest and after 3, 6, 10, 13, or 20 days of cold storage followed by 0 (A) or 4 (B) days at 25 °C.

have been found to be erratic, and no univocal trends have been observed.

In this study, great numbers of data have been obtained under different storage conditions of Western Red nectarine and/or subsequent ripening. The results showed that the most significant changes, those being significant decreases of firmness, TA, organic acids, and C_6 volatile compounds and a significant increase of EP, lactones, and C_{13} norisoprenoids, took place during storage and postharvest maturation, whereas SSC, sugars, and polyphenolic compounds remained quite constant during the same time. This study also clearly indicates that in the case of a very low level of CI development, the trends observed for the levels of sucrose, reducing sugars, polyphenols, and lactones are different from those generally observed in chilling-injured nectarines. As previously mentioned by other studies, the present results tend to confirm that there are close relationships between soluble carbohydrate metabolism and CI in peach fruit exposed to cold stresses.

dx.doi.org/10.1021/jf4057555 | J. Agric. Food Chem. 2014, 62, 4707−4724

They also support a possible role of phenolics in cell wall metabolism in chilling-injured peaches. Lastly, they confirm that the decrease of lactones and the loss of fruity aromas generally observed during shelf life after removal from cold storage are symptoms of CI in peach fruit.

AUTHOR INFORMATION

Corresponding Author

*(C.A.) Phone: +33 490 920 582. Fax: +33 490 924 887. E-mail: aubert@ctifl.fr.

Notes

The authors declare no competing financial interest.

ACKNOWLEDGMENTS

We thank Claire Dufour and Michele Loonis for LC-MS identifications and Nelly Ottens for assistance with English.

REFERENCES

(1) Riboli, E.; Norat, T. Epidemiologic evidence of the protective effect of fruit and vegetables on cancer risk. *Am. J. Clin. Nutr.* **2003**, *78*, 559S−569S.

(2) Hung, H. C.; Joshipura, K. J.; Jiang, R.; Hu, F. B.; Hunter, D.; Smith-Warner, S. A.; Colditz, G. A.; Rosner, B.; Spiegelman, D.; Willett, W. C. Fruit and vegetable intake and risk of major chronic disease. *J. Natl. Cancer. Inst.* **2004**, *96*, 1577−1584.

(3) Rice-Evans, C. A.; Miller, N. J.; Paganga, G. Structure-antioxidant activity relationships of flavonoids and phenolic acids. *Free Radical Biol.* **1996**, *20*, 933−956.

(4) Potter, J. D.; Slattery, M. L.; Bostick, R. M.; Gapstur, S. M. Colon cancer: a review of the epidemiology. *Epidemiol. Rev.* **1993**, *15*, 499−545.

(5) Fraser, P. D.; Bramley, P. M. The biosynthesis and nutritional uses of carotenoids. *Prog. Lipid Res.* **2004**, *43*, 228−265.

(6) Noratto, G.; Porter, W.; Byrne, D.; Cisneros-Zevallos, L. Identifying peach and plum polyphenols with chemopreventive potential against estrogen-independent breast cancer cells. *J. Agric. Food Chem.* **2009**, *57*, 5219−5226.

(7) Lee, S. K.; Kader, A. A. Preharvest and postharvest factors influencing vitamin C content of horticultural crops. *Postharvest Biol. Technol.* **2000**, *20*, 207−220.

(8) Tee, E.-S. Carotenoids and retinoids in human nutrition. *Crit. Rev. Food Sci. Nutr.* **1992**, *31*, 103−163.

(9) Eduardo, I.; Chietera, G.; Bassi, D.; Rossini, L.; Vecchietti, A. Identification of key odor volatile compounds in the essential oil of nine peach accessions. *J. Sci. Food Agric.* **2010**, *90*, 1146−1154.

(10) Sánchez, G.; Besada, C.; Badenes, M. L.; Monforte, A. J.; Granell, A. A non-targeted approach unravels the volatile network in peach fruit. *PLoS One* **2012**, *7*, e38992.

(11) Lurie, S.; Crisosto, C. H. Chilling injury in peach and nectarine. *Postharvest Biol. Technol.* **2005**, *37*, 195−208.

(12) Manach, C.; Scalbert, A.; Morand, C.; Rémésy, C.; Jiménez, L. Polyphenols: food sources and bioavailability. *Am. J. Clin. Nutr.* **2004**, *79*, 727−747.

(13) Poiroux-Gonord, F.; Bidel, L. P. R.; Fanciullino, A.-L.; Gautier, H.; Lauri-Lopez, F.; Urban, L. Health benefits of vitamins and secondary metabolites of fruit and vegetables and prospects to increase their concentrations by agronomic approaches. *J. Agric. Food Chem.* **2010**, *58*, 12065−12082.

(14) Engel, K. H.; Ramming, D. W.; Flath, R. A.; Teranashi, R. Investigation of volatile constituents in nectarines. 2. Changes in aroma composition during nectarine maturation. *J. Agric. Food Chem.* **1988**, *36*, 1003−1006.

(15) Visai, C.; Vanoli, M. Volatile compound production during growth and ripening of peaches and nectarines. *Sci. Hortic.* **1997**, *70*, 15−24.

(16) Aubert, C.; Günata, Z.; Ambid, C.; Baumes, R. Changes in physicochemical characteristics and volatile constituents of yellow- and white-fleshed nectarines during maturation and artificial ripening. *J. Agric. Food Chem.* **2003**, *51*, 3083−3091.

(17) Robertson, J. A.; Meredith, F. I.; Horvat, R. J.; Senter, S. D. Effect of cold storage and maturity on the physical and chemical characteristics and volatile constituents of peaches (cv. Cresthaven). *J. Agric. Food Chem.* **1990**, *38*, 620−624.

(18) Raffo, A.; Nardo, N.; Tabilio, M. R.; Paoletti, F. Effects of cold storage on aroma compounds of white- and yellow-fleshed peaches. *Eur. Food Res. Technol.* **2008**, *226*, 1503−1512.

(19) Zhang, B.; Xi, W. P.; Wei, W. W.; Shen, J. Y.; Ferguson, I.; Chen, K. S. Changes in aroma-related volatiles and gene expression during low temperature storage and subsequent shelf-life of peach fruit. *Postharvest Biol. Technol.* **2011**, *60*, 7−16.

(20) Xi, W. P.; Zhang, B.; Liang, L.; Shen, J. Y.; Wei, W. W.; Xu, C. J.; Allan, A. C.; Ferguson, I. B.; Chen, K. S. Postharvest temperature influences volatile lactone production via regulation of acyl-CoA oxidases in peach fruit. *Plant Cell Environ.* **2012**, *35*, 534−545.

(21) Cano-Salazar, J.; Echeverría, G.; Crisosto, C. H.; López, L. Cold-storage potential of four yellow-fleshed peach cultivars defined by their volatile compounds emissions, standard quality parameters, and consumer acceptance. *J. Agric. Food Chem.* **2012**, *60*, 1266−1282.

(22) Cano-Salazar, J.; López, M. L.; Echeverría, G. Relationships between the instrumental and sensory characteristics of four peach and nectarine cultivars stored under air and CA atmospheres. *Postharvest Biol. Technol.* **2013**, *75*, 58−67.

(23) Cano-Salazar, J.; López, M. L.; Crisosto, C. H.; Echeverría, G. Volatile compound emissions and sensory attributes of 'Big Top' nectarine and 'Early Rich' peach fruit in response to a pre-storage treatment before cold storage and subsequent shelf-life. *Postharvest Biol. Technol.* **2013**, *76*, 152−162.

(24) Dalla Valle, A. Z.; Mignani, I.; Spinardi, A.; Galvano, F.; Ciappellano, S. The antioxidant profile of three different peaches cultivars (*Prunus persica*) and their short-term effect on antioxidant status in human. *Eur. Food Res. Technol.* **2007**, *225*, 167−172.

(25) Di Vaio, C.; Graziani, G.; Marra, L.; Cascone, A.; Ritieni, A. Antioxidant capacities, carotenoids and polyphenols evaluation of fresh and refrigerated peach and nectarine cultivars from Italy. *Eur. Food Res. Technol.* **2008**, *227*, 1225−1231.

(26) Caprioli, I.; Lafuente, M. T.; Rodrigo, M. J.; Mencarelli, F. Influence of postharvest treatments on quality, carotenoids, and abscisic acid content of stored 'Spring Belle' peach (*Prunus persica*) fruit. *J. Agric. Food Chem.* **2009**, *57*, 7056−7063.

(27) Tsantili, E.; Shin, Y.; Nock, J. F.; Watkins, C. B. Antioxidant concentrations during chilling injury development in peaches. *Postharvest Biol. Technol.* **2010**, *57*, 27−34.

(28) Wang, K.; Shao, X.; Gong, Y.; Zhu, Y.; Wang, H.; Zhang, X.; Yu, D.; Yu, F.; Qiu, Z.; Lu, H. The metabolism of soluble carbohydrates related to chilling injury in peach fruit exposed to cold stress. *Postharvest Biol. Technol.* **2013**, *86*, 53−61.

(29) Wechtersbach, L.; Cigić, B. Reduction of dehydroascorbic acid at low pH. *J. Biochem. Biophys. Methods* **2007**, *70*, 767−772.

(30) Aubert, C.; Baumann, S.; Arguel, H. Optimization of the analysis of flavor volatile compounds by liquid−liquid microextraction (LLME). Application to the aroma analysis of melons, peaches, grapes, strawberries, and tomatoes. *J. Agric. Food Chem.* **2005**, *53*, 8881−8895.

(31) Crisosto, C. H.; Mitchell, F. G.; Ju, Z. Susceptibility to chilling injury of peach, nectarine, and plum cultivars grown in California. *HortScience* **1999**, *34*, 1116−1118.

(32) Crisosto, C. H. How do we increase peach consumption? In *Proceedings of the 5th International Peach Symposium*, Acta Horticulturae 592; Johnson, R. S., Crisosto, C. H., Eds.; ISHS: Davis, CA, USA, 2002; pp 601−605.

(33) Crisosto, C. H.; Crisosto, G. M. Relationship between ripe soluble solids concentration (RSSC) and consumer acceptance of high and low acid melting flesh peach and nectarine (*Prunus persica* (L.) Batsch) cultivars. *Postharvest Biol. Technol.* **2005**, *38*, 239−246.

(34) Reig, G.; Iglesias, I.; Gatius, F.; Alegre, S. Antioxidant capacity, quality, anthocyanins and nutrients content of several peach cultivars

[*Prunus persica* (L.) Batsch] grown in Spain. *J. Agric. Food Chem.* **2009**, *61*, 6344−6357.
(35) Gil, M.; Tomàs-Barberàn, F. A.; Hess-Pierce, B.; Kader, A. A. Antioxidant capacities, phenolic compounds, carotenoids, and vitamin C contents of nectarine, peach, and plum cultivars from California. *J. Agric. Food Chem.* **2002**, *50*, 4976−4982.
(36) Tavarini, S.; Degl'Innocenti, E.; Remorini, D.; Massai, R.; Guidi, L. Antioxidant capacity, ascorbic acid, total phenols and carotenoids changes during harvest and after storage of Hayward kiwifruit. *Food Chem.* **2008**, *107*, 282−288.
(37) Toor, R. K.; Savage, G. P. Changes in major antioxidant components of tomatoes during post-harvest storage. *Food Chem.* **2006**, *99*, 724−727.
(38) Kopas-Lane, L. M.; Warthesen, J. J. Carotenoid photostability in raw spinach and carrots during cold storage. *J. Food Sci.* **1995**, *60*, 773−776.
(39) Thomas, P.; Joshi, M. R. Reduction of chilling injury in ripe Alphonso mango fruit in cold storage by temperature conditioning. *Int. J. Food Sci. Technol.* **1988**, *23*, 447−455.
(40) Tomás-Barberán, F. A.; Gil, M. I.; Cremin, P.; Waterhouse, A. L.; Hess-Pierce, B.; Kader, A. A. HPLC-DAD-ESIMS analysis of phenolic compounds in nectarines, peaches, and plums. *J. Agric. Food Chem.* **2001**, *49*, 4748−4760.
(41) Asami, D. K.; Hong, Y.-J.; Barrett, D. M.; Mitchell, A. E. Processing-induced changes in total phenolics and procyanidins in clingstone peaches. *J. Sci. Food Agric.* **2003**, *83*, 56−63.
(42) Winterhalter, P.; Rouseff, R. Carotenoid-derived aroma compounds: an introduction. In *Carotenoid-Derived Aroma Compounds*; ACS Symposium 802; Winterhalter, P., Rouseff, R., Eds.; American Chemical Society: Washington, DC, USA, 2001; pp 1−18.
(43) Müller, H. Determination of the carotenoid content in selected vegetables and fruit by HPLC and photodiode array detection. *Z. Lebensm. Unters. Forsch. A* **1997**, *204*, 88−94.
(44) Baldermann, S.; Naim, M.; Fleischmann, P. Enzymatic carotenoid degradation and aroma formation in nectarines (*Prunus persica*). *Food Res. Int.* **2005**, *38*, 833−836.
(45) Krammer, G.; Winterhalter, P.; Schwab, M.; Schreier, P. Glycosidally bound aroma compounds in the fruits of *Prunus* species apricot (*P. armenica* L.), peach (*P. persica* L.), yellow plum (P. *domestica* L. *srp Syriaca*). *J. Agric. Food Chem.* **1991**, *39*, 778−781.
(46) Aubert, C.; Ambid, C.; Baumes, R.; Günata, Z. Investigation of bound aroma constituents of yellow-fleshed nectarines (*Prunus persica* l. cv. Springbright). Changes in bound aroma profile during maturation. *J. Agric. Food Chem.* **2003**, *51*, 6280−6286.
(47) Aubert, C.; Milhet, C. Distribution of the volatile compounds in the different parts of a white-fleshed peach (*Prunus persica* L. Batsch). *Food Chem.* **2007**, *102*, 375−384.
(48) Takeoka, G. R.; Flath, R. A.; Buttery, R. G.; Winterhalter, P.; Güntert, M.; Ramming, D. W.; Teranishi, R. Free and bound flavor constituents of white-fleshed nectarines. In *Flavor Precursors − Thermal and Enzymatic Conversions*; ACS Symposium Series 490; Teranishi, R., Takeoka, G. R., Güntert, M., Eds.; American Chemical Society: Washington, DC, USA, 1992; pp 116−138.
(49) Knapp, H.; Weigand, C.; Gloser, J.; Winterhalter, P. 2-Hydroxy-2,6,10,10-tetramethyl-1-oxaspiro[4.5]dec-6-en-8-one: precursor of 8,9-dehydrotheaspirone in white-fleshed nectarines. *J. Agric. Food Chem.* **1997**, *45*, 1309−1313.

JOURNAL OF AGRICULTURAL AND FOOD CHEMISTRY

Article

pubs.acs.org/JAFC

Toward an Understanding of Mechanisms Involved in Non-Polyphenol Oxidase (Non-PPO) Darkening in Yellow Alkaline Noodles (YAN)

Robert E. Asenstorfer,*[,†] Marie J. Appelbee,[‡,§] Christine A. Kusznir,[†] and Daryl J. Mares[†]

[†]School of Agriculture, Food and Wine, The University of Adelaide, Waite Campus, PMB 1, Glen Osmond, SA 5064, Australia

[‡]South Australian Research and Development Institute, Grain Quality Research Laboratory, Waite Research Precinct, Glen Osmond, SA 5064, Australia

ABSTRACT: Asian noodles prepared from bread wheat flour darken over time due to a combination of polyphenol oxidase (PPO) activity and non-PPO effects. Although the enzymatic mechanism associated with the PPO reaction is well established, the non-PPO component consists of both physical (e.g., changes in surface properties) and chemical reactions. Variations in pH and solvents were used to gain a quantitative estimate of the contribution of physical and chemical components to non-PPO darkening in yellow alkaline noodles (YAN). In a set of five common high-PPO Australian wheat cultivars it was estimated that on average non-PPO darkening accounted for 69% of total darkening, with approximately two-thirds of this due to physical darkening and one-third had a chemical origin. Data from the chemical portion of non-PPO darkening is consistent with the presence of a PPO-like enzyme that oxidizes tyrosine, has a pH maximum of 8.1, and is inhibited by 50% methanol or ethanol but in the noodle is insensitive to PPO inhibitors such as tropolone. Therefore, with low-PPO and PPO-free wheat varieties becoming available, it may be possible to further reduce darkening in YAN by breeding for wheat varieties with low or zero levels of this PPO-like enzyme.

KEYWORDS: *yellow alkaline noodle (YAN), polyphenol oxidase (PPO), non-PPO darkening*

INTRODUCTION

Yellow alkaline noodles (YAN) are made from bread wheat (*Triticum aestivum* L.) flour treated with alkaline salts. A bright yellow color free from dark specks is highly desirable. YAN are usually sold as a fresh product, although they can be parboiled and refrigerated to extend storage time. Fresh YAN darken over time, which decreases their marketability. Polyphenol oxidase (PPO), which is inhibited by tropolone and salicylhydroxamic acid, causes about one-third to half of the darkening.[1] It is, however, possible to reduce PPO darkening by the selection of wheat varieties with low or zero PPO activity.[2,3] The remaining darkening is non-PPO darkening and results from both physical and chemical factors.[1] The physical component of non-PPO darkening involves changes in the noodle matrix, which alter the reflectance properties of the noodle surface, whereas the chemical component of non-PPO darkening is thought to arise from oxidation of tyrosine to yield black pigments.[4]

In previous studies, non-PPO darkening as measured by a change in the CIE-*Lab L** value was described using two time periods, 0−4 and 4−24 h.[1,4] Non-PPO darkening during the first time period was correlated with protein content[1] and was related to physical changes in the noodle.[1] Non-PPO darkening in the second time period (4−24 h) was independent of total protein content and was thought to be predominantly due to chemical oxidation rather than physical changes in the noodle. Oxidation of tyrosine groups within the glutenin and gliadin proteins with subsequent polymerization provides a possible mechanism for darkening during the 4−24 h time period.[1] Possible evidence for this was the addition of *n*-propanol extracts (containing predominantly gliadin and traces of unpolymerized glutenin), tyrosine, or the peptide GQQGYYPTS (an analogue of the consensus motifs GYYPTS(L/G)QQ) to YAN increased darkening during the 4−24 h time period.[1] Because a lack of specific inhibitors for non-PPO darkening,[5] it has been difficult to determine the contribution of the chemical component to total non-PPO darkening in YAN. The aim of this paper is to gain an estimate of the proportion of physical and chemical components of non-PPO darkening and to examine the origin of the chemical portion of non-PPO darkening.

MATERIALS AND METHODS

Materials. A hard white bread wheat with high-PPO activity (*Triticum aestivum* L. cv. Tasman) and a durum wheat with a near-zero PPO activity (*Triticum durum* Desf. cv. Kamilaroi) were selected. Grains of both cultivars were produced in field trials at the Waite Campus of the University of Adelaide.[1,4] Four hard white high-PPO bread wheat cultivars (Lark, Sunvale, Janz, and Yitpi) and a hard white low-PPO bread wheat (Axe) produced in field trials at the Waite Campus of the University of Adelaide were also examined for chemical and physical components of non-PPO darkening. PPO activities for the cultivars as determined according to the method of Bernier and Howes[2,6,7] were measured as an increase in absorbance of a tyrosine solution at 415 nm after 3 h: Tasman, 0.27 ± 0.05; Kamilaroi, 0.02 ± 0.01; Lark, 0.15 ± 0.02; Sunvale, 0.20 ± 0.01; Janz, 0.15 ± 0.09; Yitpi, 0.15 ± 0.02; Axe, 0.06 ± 0.01. Absorbance for Kamilaroi was not significantly different from control (solution with no grains), and indeed there was no visible change in color of the incubation solution or the grain coat.

Received: January 13, 2014
Revised: April 4, 2014
Accepted: May 1, 2014
Published: May 1, 2014

ACS Publications © 2014 American Chemical Society

Flour Milling and Noodle Sheet Preparation. Grain was conditioned overnight to 15% moisture and milled on a Bühler experimental mill (Bühler AG, Uzwil, Switzerland). The break and reduction flour streams were combined. The pollard stream was resieved on a shaker, and the recovered flour was added to the combined streams from the mill. Different batches of grain gave slightly different color responses, and therefore the same batch was used for each experiment and, when possible, for the different experiments. Flour (10 g) and 3.6 mL of 2% sodium carbonate solution, with or without the PPO inhibitor tropolone (0.01 mol L^{-1}), were mixed into a dough in a cylindrical mixing bowl using a drill press with a modified mixing paddle. The dough was mixed for 105 s with intermittent pauses to clean dough adhering to the paddle. The dough was rolled into a ball and made into a noodle sheet using a domestic pasta maker (Atlas 150, Marcato S.P.A., Campodarego, Italy). The noodle sheet was then placed in a resealable plastic bag to prevent drying and to make noodle handling easier. Processing and storage were at room temperature (22 °C).

Darkening Rates. CIE-*Lab* color measurements of raw noodles were made using a Dataflash 100 (Datacolor International, Lawrenceville, NJ, USA) reflectance spectrophotometer. Each data point represents the average of two noodle sheets, each of which was measured twice. The rates of darkening for the two time periods were determined from the L^* value of the noodle sheets measured at 2, 5, 10, 15, 20, 30, 40, 50, 60, 90, 120, 150, 180, 210, 240, and 1440 min. Mixed-order rate equations ($\Delta L^* = kt^n + c$, where ΔL^* is the change in darkening between time 2 min and time t of darkening, k is the rate, t is time in h, and n and c are constants) were fitted to the noodle darkening and standard errors estimated using WinCurveFit.[8]

pH Analysis. Noodles from near-zero-PPO Kamilaroi flour were made in a series of buffers: 2% HCl, 0.2 mol L^{-1} sodium citrate (pH 4.0, 5.0, 6.0); 0.2 mol L^{-1} Tris (pH 7.0, 8.0, 9.0, 10.0); 0.2 mol L^{-1} $NaCO_3$; 1% NaOH; 1.5% NaOH; 2% NaOH. The L^* values were measured at 0, 2, 4, and 24 h. Noodles (1 g) were extracted in 2 mL of water and centrifuged, and the pH was measured. A curve[9]

$$\Delta L^* = \frac{a + b10^{(\mathrm{pH}-\mathrm{p}K_{a1})} + c10^{(2\mathrm{pH}-\mathrm{p}K_{a1}-\mathrm{p}K_{a1})}}{1 + 10^{(\mathrm{pH}-\mathrm{p}K_{a1})} + 10^{(\mathrm{pH}-\mathrm{p}K_{a1}-\mathrm{p}K_{a2})}}$$

where a represents the ΔL^* plateau at low pH, b is the theoretical maximum ΔL^* value, and c represents the plateau at high pH, was fitted to the change in darkening (ΔL^*) using WinCurveFit,[8] which allowed estimation of pK_a (acid dissociation constant) values and maximum and minimum ΔL^* values.

Incorporation of Solvents into Noodle Preparation. The 2% sodium carbonate solution used to prepare the noodles was made up with different nonaqueous solvents. These were glycerol (Merck Pty Ltd., Kilsyth, VIC, Australia), ethylene glycol (Ajax Chemicals Pty Ltd., Sydney, Australia), methanol (Chem-Supply, Gilman, SA, Australia), ethanol (Chem-Supply), *n*-propanol (Scharlab S.L., Sentimenat, Spain), and dimethyl sulfoxide (Merck Pty Ltd.). The rates of darkening were measured using the method described above.

Mid-infrared (Mid-IR) Spectroscopy. Mid-IR frequencies used to examine changes in the protein quaternary structure were the amide I band (1580−1720 cm^{-1}; 80% C−O stretch, 10% C−N bend, and 10% N−H bend) and amide II band (1480−1580 cm^{-1}; 60% N−H bend and 40% C−N stretch).[10,11] The spectrum of noodle sheets was obtained using a PerkinElmer (Waltham, MA, USA) Spectrum One FT-IR spectrometer equipped with a Pike Technologies (Madison, WI, USA) diffuse reflectance autosampler. The data were transferred to GRAMS/AI[12] software, and the areas of the amide bands were determined manually.

***n*-Propanol Extract Fractionation.** Initial separation was based on the Osborne method.[13] Flour (200 g) was extracted with water (1.5 L) for 30 min at 60 °C and then centrifuged at 1500*g* for 10 min to give an albumin fraction. A globulin fraction was obtained by extracting the precipitate with a 0.2 mol L^{-1} NaCl solution (750 mL) for 30 min at 60 °C and then centrifuged at 1500*g* for 10 min. To the precipitate was added 30% ethanol (750 mL), and the mixture was extracted for 30 min at 60 ° and , then centrifuged at 1500*g* for 10 min to give gliadin fraction (A). The 50% propanol fraction (gliadin fraction B) was obtained by adding *n*-propanol (750 mL) to the precipitate and extracting for 30 min at 60 °C. This extract was centrifuged at 1500*g* for 10 min and the supernatant retained (if dried by rotary evaporation this yielded ≈10−12 g). In preference to drying, different amounts of water or propanol were added, and the precipitates and supernatants were analyzed for noodle darkening activity. A fraction with the highest activity was obtained by diluting the supernatant to 9% propanol and allowed to stand for 72 h. The supernatant was decanted, and both supernatant and precipitate were dried by rotary evaporation (yields: precipitate, ≈1.5 g; supernatant, ≈9 g). The precipitate was washed with 200 mL of chloroform to give two fractions, chloroform soluble (≈0.7 g) and chloroform insoluble (≈0.7 g), which were dried by rotary evaporation. The chloroform-insoluble material was subsequently redissolved in warm 20% propanol (50 mL) and fractioned using a C18 column (90 mm × 20 mm dia., Bodesil-C18 40 μm, Varian, Palo Alto, CA, USA), collecting the elution with 100 mL of 20% propanol fraction (≈0.3 g) and then eluting with 50% propanol (100 mL) to obtain a 50% propanol fraction (≈0.4 g). Both fractions were dried by rotary evaporation.

PPO Analysis. PPO analyses of protein extracts were based on the 96-well method of Bernier and Howes.[6] A tyrosine solution (100 mL) was made with 0.01 mol L^{-1} tyrosine in 0.1 mol L^{-1} Tris base buffer (pH 9) with ≈40 μL of Tween 20 added. Protein extract (2 mg) was dissolved in 300 μL of tyrosine solution per microplate well and incubated for 3 h at 37 °C. Portions (100 μL) from each well were transferred into a new microplate, and the optical density was read by a microplate reader.

Polyacrylamide Gel Electrophoresis (PAGE). SDS-PAGE separation was achieved byusing the method of Singh et al.[14] with minor modifications.[15] Acid-PAGE was performed according to the method of Clements.[16] Gliadins were extracted from *T. aestivum* cv. Chinese Spring, Gabo, Cheyenne, and Tasman as reference standards.

RESULTS AND DISCUSSION

Effect of pH on YAN Non-PPO Darkening. It was necessary to establish the amount of physical and chemical components of non-PPO darkening. A higher proportion of chemical than physical darkening occurred during the 4−24 h time period.[4] The pH data (Figure 1) indicated that there are

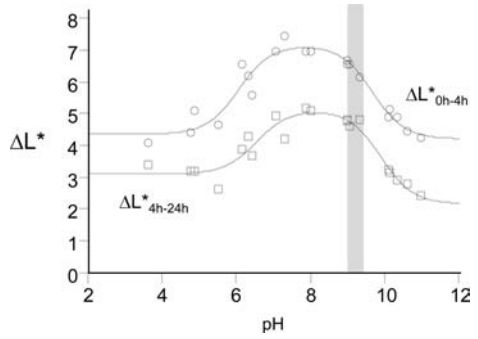

Figure 1. Effect of pH on darkening during the 4−24 h time period in noodles made from near-zero-PPO Kamilaroi durum flour (gray area indicates the approximate pH of YAN).

both pH-dependent and pH-independent components to non-PPO darkening during the 4−24 h time period. The maximum darkening of noodles made from Kamilaroi flour occurs at pH 8.1, which is slightly lower than the pH of normal YAN (pH ≈9−9.2) but similar to the pH of maximum PPO activity in noodles (pH ≈8.2).[4] Plateaus associated with minima of non-PPO darkening were observed at pH values <5 and >11. These plateaus represent the pH-independent component of non-PPO darkening associated with physical darkening, whereas the pH-dependent portion is associated with chemical darkening. In YAN, the chemical portion of non-PPO darkening was estimated

Table 1. Maximum and Minimum (Plateaus pH <5 and >11) Darkening (ΔL^*) Values and pK_a Values for Non-PPO Darkening in Noodles Made with Near-Zero-PPO Kamlaroi Durum with a Range of pH Values for Three Time Periods (0−4, 4−24, and 0−24 h)

		ΔL^*_{min}		pK_a values	
time period	ΔL^*_{max} (pH)	pH <5	pH >11	pK_{a1}	pK_{a2}
0−4 h	7.07 (7.86)	4.35 ± 0.21	4.20 ± 0.30	6.07 ± 0.18	9.67 ± 0.21
4−24 h	5.02 (8.14)	3.10 ± 0.17	2.16 ± 0.36	6.54 ± 0.22	9.91 ± 0.22
0−24 h	12.09 (7.99)	7.49 ± 0.28	6.34 ± 0.48	6.27 ± 0.13	9.81 ± 0.16

by calculating the difference between maximum and minimum darkening, whereas the physical portion of non-PPO darkening was estimated by the difference between the minimum and zero darkening. Both of these were expressed as a percentage of maximum darkening. Without knowing the actual baseline darkening at alkaline noodle pH (9−9.2), two preliminary estimates for the chemical portion of non-PPO darkening were calculated by comparing maximum darkening at pH 8.1 with each of the plateaus. On the basis of the low-pH plateau, 38% of non-PPO darkening, or on the basis of the high-pH plateau, 57% of non-PPO darkening, was due to chemical processes during the 4−24 h time period. A similar analysis of the 0−4 and 0−24 h time periods suggested chemical darkening was responsible for approximately 38% (low-pH plateau) to 41% (high-pH plateau) and 38% (low-pH plateau) to 47% (high-pH plateau) of total non-PPO darkening, respectively (Table 1).

pK_a (acid dissociation constant) values were used to measure the midpoints between maximum and minimum darkening in YAN relative to pH (Figure 1; Table 1). The maximum for non-PPO darkening at pH 8.1 was flanked by a pK_a measured for chemical darkening on the low-pH side of the peak (pK_{a1} = 6.54 ± 0.22) and one on the high-pH side of the peak (pK_{a2} = 9.91 ± 0.22), which are similar to the pK_a values reported for PPO darkening in YAN made from Tasman flour (pK_{a1} = 7.0; pK_{a2} = 9.8).[4] This suggests the chemical component of non-PPO darkening may be due to an enzyme.

Effect of Solvents on YAN Non-PPO Darkening. In preliminary investigations, it was noted that different solvents have an effect on YAN darkening. The solvents investigated can be divided into two groups according to their effects on darkening in noodles made from Kamilaroi flour during the 4−24 h time period (Figure 2). Methanol, ethanol, and propanol show a linear inhibition of darkening with higher concentration until a critical concentration of solute was reached. This coincided with a concentration at which there is inadequate water to make a noodle. Dimethyl sulfoxide (DMSO) and ethylene glycol both showed a lower rate of inhibition until a critical concentration, when the inhibition of darkening increased rapidly (Figure 2). Glycerol at 10% showed a slight enhancement of darkening, and at lower concentrations a curve similar to DMSO and ethylene glycol could be fitted.

In YAN made with near-zero-PPO Kamilaroi flour, the maximum inhibition of darkening by methanol or ethanol (50% solution) indicated that 61−64% of darkening during the 4−24 h time period (Figure 2A) and 33−39% of total darkening for the 0−24 h time period were due to non-PPO chemical reaction (Table 2). Whereas the estimate for the chemical portion of non-PPO darkening achieved by methanol/ethanol addition for the 4−24 h time period was slightly higher than the estimate derived from the pH data for the same period (38−57%), the estimates obtained for the 0−24 h time period by 50% methanol/ethanol addition and by pH (38−47%) method were in reasonable agreement. For the 4−24 h time period, the level of

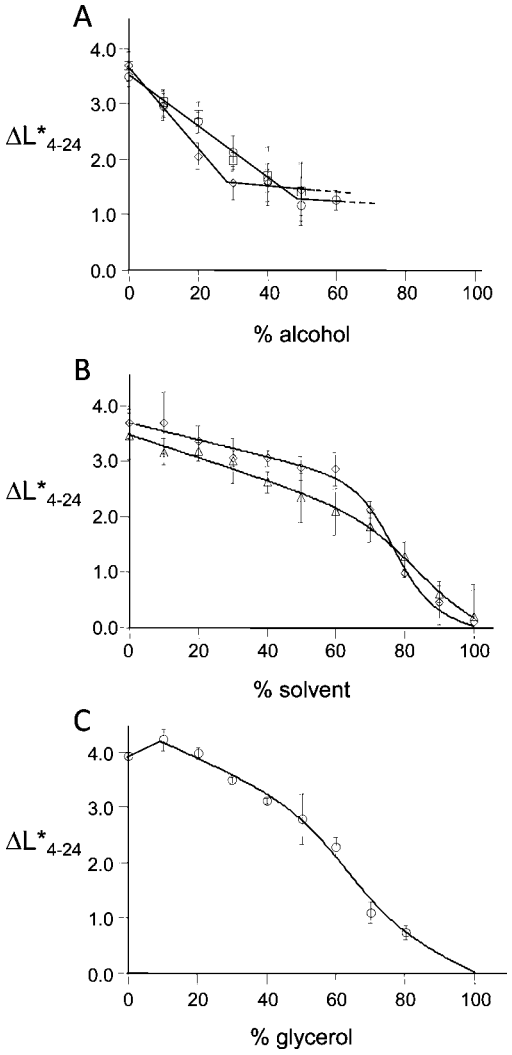

Figure 2. Effects of different solvents on YAN darkening in noodles made from near-zero-PPO Kamilaroi durum flour during the 4−24 h time period: (A) methanol (circles), ethanol (squares), propanol (diamonds); (B) ethylene glycol (diamonds) and dimethyl sulfoxide (triangles); (C) glycerol; panels B and C are fitted with modified logistic curves (bars represent standard error of the mean).

non-PPO darkening inhibited by 50% methanol or ethanol was similar to the high range for the pH data, indicating the plateau at high pH was a more appropriate baseline for physical non-PPO darkening than the low-pH plateau. Contrary to previous suggestions,[1] a considerable amount of physical darkening occurred during the 4−24 h time period.

Addition of nonaqueous solvents can displace water from the surface of the protein and cause changes in protein structure, which should be detected by IR spectroscopy.[17−19] Whereas the amide II band is strongly influenced by hydration,[19,20] no

Table 2. Comparison of Various Components of Total Darkening (ΔL^*_{0-24}) in YAN Made from a Near-Zero-PPO Durum Variety (Kamilaroi), Five High-PPO Bread Wheat Varieties (Tasman, Lark, Sunvale, Janz, and Yitpi), and a Low-PPO Bread Wheat Variety (Axe)

	Kamilaroi (near-zero PPO)		av *T. aestivum* var. (high PPO)		Axe (low PPO)	
darkening	ΔL^*_{0-24}	%	ΔL^*_{0-24}	%	ΔL^*_{0-24}	%
total	10.68 ± 0.08	100	12.6 ± 0.32	100	7.78 ± 0.38	100
PPO	0.04 ± 0.15	0	3.93 ± 0.71	31	0.27 ± 0.58	3
non-PPO total	10.64 ± 0.07	100	8.67 ± 0.39	69	7.51 ± 0.20	97
physical	6.82 ± 0.19	64	5.93 ± 0.31	47	5.71 ± 0.51	73
chemical	3.82 ± 0.26	36	2.74 ± 0.70	22	1.80 ± 0.31	23

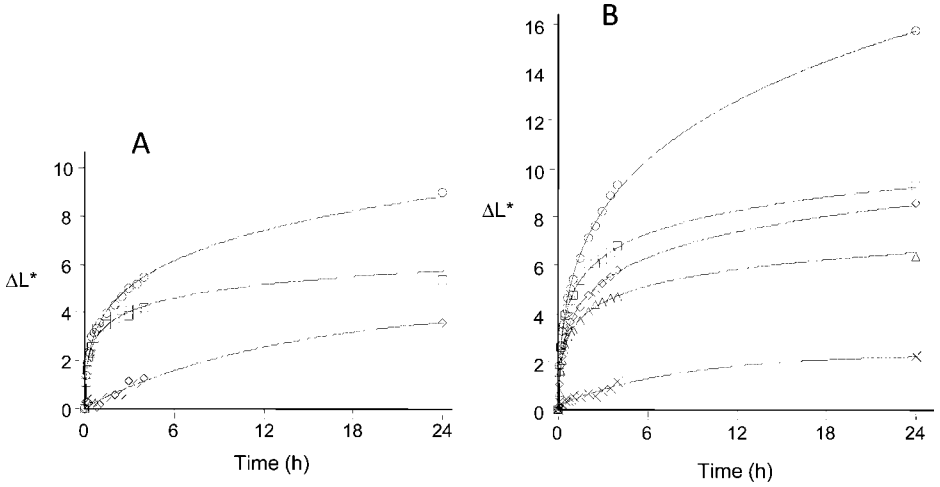

Figure 3. (A) Darkening in noodles made from zero-PPO Kamilaroi flour with 50% methanol (squares), and control (circles) with mixed-order rate equations fitted and their difference (diamonds) fitted with a first-order rate equation. (B) Darkening in noodles made from high-PPO Tasman flour with 0.1 mol L^{-1} tropolone (squares), 50% methanol (diamonds), 0.1 mol L^{-1} tropolone and 50% methanol (triangles), and control (circles) with mixed-order rate equations fitted. The difference between YAN made from Tasman flour with 0.1 mol L^{-1} tropolone and YAN made from Tasman flour with 0.1 mol L^{-1} tropolone and 50% methanol (cross) fitted a first-order rate equation.

Table 3. Rate (k_1) and Order of the Rate Equations Fitted to the Difference in the Darkening (ΔL^*) of the Control (0%) and Different Amounts of Alcoholic Solvent Added in YAN Noodles Made from Near-Zero-PPO Kamilaroi Flour

	methanol		ethanol		propanol	
alcohol	order	k_1 (h^{-1})	order	k_1 (h^{-1})	order	k_1 (h^{-1})
10%	1st	0.13 ± 0.06	1st	0.05 ± 0.04	0th	
20%	1st	0.12 ± 0.06	1st	0.11 ± 0.01	1st	0.03 ± 0.03
30%	1st	0.08 ± 0.03	1st	0.05 ± 0.02	1st	0.02 ± 0.03
40%	1st	0.11 ± 0.02	1st	0.08 ± 0.01	1st	0.05 ± 0.03
50%	1st	0.07 ± 0.02	1st	0.11 ± 0.02	mixed	
60%	mixed					

differences were observed in the band areas of either the amide I or the amide II bands between 50% methanol or 50% ethanol and the control (data not shown), suggesting conformational changes in gluten structure were not involved in non-PPO darkening but rather a chemical reaction was involved. Noodles made with very high concentrations of DMSO, ethylene glycol, and glycerol showed little or no darkening, which clearly indicated that there is a requirement for water for both the physical and chemical components of non-PPO darkening to proceed.

By calculating the difference in darkening between the control noodle (0% alcohol) and the noodle made with an inhibitor (or organic solvent), it is possible to estimate the rate of inhibition of darkening. For example, Figure 3A shows that the control noodle exhibits darkening at a faster rate and amount than the noodle made with 50% methanol. The difference between these curves indicates the effects of 50% methanol only. This curve fits a first-order rate equation ($\Delta L^* = a \exp(-kt)$, where k is the rate, t is time in hours, and a is a constant), and from this it is possible to estimate the rate of darkening (0.07 ± 0.02 h^{-1}). These difference rate data suggest that although there is sufficient water to make a noodle, methanol or ethanol inhibit first-order or pseudo-first-order reactions at all concentrations (Table 3). The rates of darkening for methanol and ethanol are similar. Additional darkening attributed to PPO, which was estimated by difference in the darkening of Tasman noodles made with and without 0.01 mol L^{-1} tropolone (a PPO inhibitor; Figure 3B), indicated that PPO darkening also follows a first- or pseudo-first-order reaction, and the rate is similar to that for inhibition by methanol and ethanol (0.11 ± 0.01 h^{-1}). A first-order or pseudo-first-order reaction is often indicative of an enzyme-catalyzed reaction.

dx.doi.org/10.1021/jf500206e | J. Agric. Food Chem. 2014, 62, 4725−4730

Ethanol and methanol have the potential to alter enzyme conformation, leading to inhibition. Whereas the chemical portion of non-PPO darkening is inhibited by ethanol and methanol, PPO activity is only partially inhibited by both methanol and ethanol in noodles made from Tasman flour (Figure 3B). It is known that wheat PPO is resistant to inactivation by quite high levels of methanol and ethanol.[21] By using a combination of 50% methanol and tropolone it is possible to estimate the contribution of the different processes to YAN darkening. For example, YAN made from Tasman flour with 0.01 mol L^{-1} tropolone compared (ΔL^* = 9.26) with the control (ΔL^* = 15.7) gave an estimate that 41% of darkening was due to PPO. Any darkening in YAN not inhibited by 50% methanol and 0.01 mol L^{-1} tropolone gives an estimate of the physical portion of non-PPO darkening (ΔL^* = 6.36), which is about 41% in Tasman. The remaining darkening (18%) is due to the chemical portion of non-PPO darkening (Figure 3B).

In this way, YAN made from five common high-PPO wheat varieties (including Tasman) and a low-PPO variety (Axe) were measured and compared with the near-zero-PPO Kamilaroi to give an estimate of the contribution of the PPO and the physical and chemical portions of non-PPO darkening in YAN (Table 2). There was no significant difference in noodle darkening in the presence or absence of the PPO inhibitor, tropolone. The relative contribution of the chemical portion of non-PPO darkening to total non-PPO darkening was similar in the high-PPO wheat varieties and Kamilaroi but not in the low-PPO wheat variety, Axe (Table 2).

Other Possible Methods for Estimating the Chemical Portion of YAN Non-PPO Darkening. Asenstorfer et al.[5] published the effects of a variety of enzyme inhibitors on noodle darkening, and although no specific non-PPO inhibitor was identified, the enzyme inhibitor phenylhydrazine (0.01 mol L^{-1}) decreased darkening in Kamilaroi by an amount similar to the chemical portion of non-PPO darkening (ΔL_{0-24} = 4.16) and in Tasman by an amount similar to the combined contributions of PPO darkening and the chemical portion of non-PPO darkening (ΔL_{0-24} = 8.84). Phenylhydrazine is a PPO inhibitor;[22] however, it appears to be inhibiting an enzyme in addition to PPO. This was further evidence that the chemical portion of non-PPO darkening is catalyzed by an enzyme, possibly an enzyme with PPO-like activity but which is insensitive to the PPO inhibitor, tropolone. Phenylhydrazine (or a less toxic alternative) may provide another method of estimating the contribution of the enzymatic (PPO and non-PPO) to YAN darkening.

Extraction of YAN Darkening Components. Initial results suggested that gliadins and glutenins were involved in the chemical portion of non-PPO darkening.[1] When the gliadin-rich extracts from *Triticum durum* cv. Kamilaroi were dried and added back to YAN, there was an increase in non-PPO darkening. The fraction with the highest YAN darkening activity was derived from a 50% propanol extract of Tasman flour. This 50% propanol extract was subsequently further fractionated by C18 chromatography with 20% propanol and 50% propanol. The fraction obtained from the 20% propanol was active with a ΔL^*_{0-24} value of 3.10 ± 0.46, whereas the fraction obtained from the 50% propanol was inactive with a ΔL^*_{0-24} value of −0.82 ± 0.52 (Table 4). These two propanol fractions were also analyzed for tyrosine darkening using the PPO assay. The 20% propanol fraction oxidized some tyrosine, whereas the 50% propanol fraction showed no darkening. Subsequent work confirmed the relationship between tyrosine darkening, as measured by the PPO assay, and the amount of noodle darkening (Figure 4) and therefore indicated that the active fractions contained enzyme(s) rather than substrate.

Table 4. Comparison of Fractions Obtained from *T. aestivum* cv. Tasman Flour on the Darkening (ΔL^*_{0-24}) of Yellow Alkaline Noodles (YAN) Made with Near-Zero-PPO Kamilaroi Flour (Adjusted to 0.1 g/10 g equiv) and the Oxidation of Tyrosine As Measured at 415 nm

fraction	ΔL^*_{0-24}	ΔOD ($mg^{-1}\ h^{-1} \times 10^{-3}$)
supernatant	0.14 ± 0.08	nd[a]
precipitate	0.36 ± 0.06	nd
$CHCl_3$ soluble	−1.10 ± 0.02	nd
$CHCl_3$ insoluble	0.90 ± 0.12	nd
50% propanol	−0.82 ± 0.52	−0.1 ± 0.8
20% propanol	3.10 ± 0.46	14.0 ± 2.5

[a]Not determined.

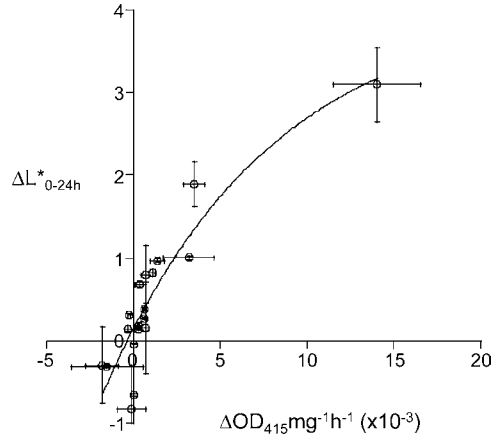

Figure 4. Darkening of YAN (ΔL^*_{0-24}) made from zero-PPO Kamilaroi flour with a range of propanol extracts from Tasman flour added (adjusted to 0.1 g/10 g equiv) compared with the oxidation of tyrosine (ΔOD_{415}) by the same extracts (bars represent standard error of the mean).

Analysis by SDS-PAGE and acid-PAGE showed that the 20% propanol fraction contained a higher proportion of α/β-gliadins than the 50% propanol fraction (data not shown). Mass spectrometry of the 20% propanol fraction revealed that the main constituents of this fraction were proteins with mass 30000−35000 (m/z), which was consistent with the presence of gliadins[23] (data not shown). Typically wheat PPO enzymes are associated with the water-soluble (albumin/globulin) fraction[24] and not the gliadin fraction. The active fractions appeared to contain an enzyme inhibited both by tropolone and by methanol (Table 5). In agreement with previous studies,[21] PPO in YAN made from Tasman flour was only slightly inhibited by methanol (Figure 3B). However, partial purification of the unknown enzyme involved in non-PPO darkening may have increased its sensitivity to tropolone inhibition. It is therefore possible that this enzyme is a type of PPO. Anderson et al.[25] reported a tropolone-insensitive PPO in immature wheat kernels. However, if this enzyme is indeed a PPO, it belongs to a different class of PPO enzymes than previously described in wheat bran.[25,26]

Data presented here are consistent with the suggestion that the chemical component of non-PPO darkening involves the presence of a PPO-like enzyme with a hydrophobicity similar to that of gliadin which is able to oxidize tyrosine, has a pH maximum of 8.1, and is sensitive to 50% methanol, ethanol, and

Table 5. Difference in Darkening ΔL^* as a Result of Crude Enzyme Extract from Tasman Wheat Added to YAN Made from near-Zero-PPO Kamilaroi at a Concentration of 0.1 g/10 g[a]

	ΔL^*
extract (0.1 g/10 g)	0.60 ± 0.37
tropolone + extract	0.04 ± 0.35
methanol control	−2.41 ± 0.52
methanol + extract	−2.54 ± 0.43
expected methanol + extract	−1.81

[a]Tropolone (PPO inhibitor) and 50% methanol were added to noodles containing the extract and compared with control noodles made with and without 50% methanol.

phenylhydrazine but is insensitive to tropolone in situ. With low-PPO and PPO-free wheat varieties becoming available, it may be possible to further reduce darkening in YAN by breeding for wheat varieties with low or zero levels of this PPO-like enzyme.

AUTHOR INFORMATION

Corresponding Author

*(R.E.A.) Phone: +61 8 83137480. Fax: +61 8 83137109. E-mail: robert.asenstorfer@adelaide.edu.au.

Present Address

[§](M.J.A.) LongReach Plant Breeders, Unit 1/18 Waddikee Road, Lonsdale, SA 5160, Australia.

Funding

We thank The University of Adelaide (Adelaide, SA, Australia) and the Grains Research and Development Corporation (Barton, ACT, Australia) for research funding and support.

Notes

The authors declare no competing financial interest.

ACKNOWLEDGMENTS

We gratefully acknowledge the use of a Bühler mill from the Australian Grain Technologies' Wheat Grain Laboratory (Urrbrae, SA, Australia).

REFERENCES

(1) Asenstorfer, R. E.; Appelbee, M. J.; Mares, D. J. Impact of protein on darkening in yellow alkaline noodles. *J. Agric. Food Chem.* **2010**, *58*, 4500−4507.

(2) Mares, D. J.; Mrva, K. Genetic variation for quality traits in synthetic wheat germplasm. *Aust. J. Agric. Res.* **2008**, *59*, 406−412.

(3) Mares, D. J.; Panozzo, J. F. Impact of selection for low grain polyphenol oxidase activity on darkening in Asian noodles. In *Proceedings of the Ninth Assembly Wheat Breeding Society of Australia*; Williamson, P., Banks, P., Haak, I., Thompson, J., Campbell, A., Eds.; Wheat Breeding Society of Australia: Toowoomba, QLD, Australia, 1999; pp32−34.

(4) Asenstorfer, R. E.; Appelbee, M. J.; Mares, D. J. Physical-chemical analysis of non-polyphenol oxidase (non-PPO) darkening in yellow alkaline noodles. *J. Agric. Food Chem.* **2009**, *57*, 5556−5562.

(5) Asenstorfer, R. E.; Kumaratilake, A.; Mares, D. J. An inhibitor study of the non-polyphenoloxidase darkening of yellow alkaline noodles. In *Cereals 2006, Proceedings of the 56th Australian Cereal Chemistry Conference and Indian Ocean Rim Symposium*; Blanchard, C. L., Solah, V. A., Crosbie, G. B., Eds.; Charles Sturt University: Wagga Wagga, NSW, Australia, 2007; pp 64−69.

(6) Bernier, A.-M.; Howes, N. K. Quantification of variation in tyrosinase activity among durum and common wheats. *J. Cereal Sci.* **1994**, *19*, 157−159.

(7) Mares, D. J.; Campbell, A. W. Mapping components of flour and noodle colour in Australian wheat. *Aust. J. Agric. Res.* **2001**, *52*, 1297−1309.

(8) *WinCurveFit*, version 1.1.8; Kevin Raner Software: Mt. Waverley, VIC, Australia, 2002.

(9) Rossotti, F. J. C.; Rossotti, H. *The Determination of Stability Constants and Other Equilibrium Constants in Solution*; McGraw-Hill: New York, 1961.

(10) Li, W.; Dobraszczyk, B. J.; Dias, A.; Gil, A. M. Polymer conformational structure of wheat proteins and gluten subfractions revealed by ATR-FTIR. *Cereal Chem.* **2006**, *83*, 407−410.

(11) Robertson, G. H.; Gregorski, K. S.; Cao, T. K. Changes in secondary protein structures during mixing development of high absorption (90%) flour and water mixtures. *Cereal Chem.* **2006**, *83*, 136−142.

(12) *GRAMS/AI*, version 9.00 R2; Thermo Fisher Scientific: Waltham, MA, USA, 2009.

(13) Osborne, T. B. *The Proteins of the Wheat Kernel*; Publication 84; Carnegie Institution of Washington: Washington, DC, USA, 1907.

(14) Singh, N. K.; Shepherd, K. W.; Cornish, G. B. A simplified SDS-PAGE procedure for separating LMW subunits of glutenin. *J. Cereal Sci.* **1991**, *14*, 203−208.

(15) Appelbee, M. J.; Mekuria, G. T.; Nagasandra, V.; Bonneau, J. P.; Eagles, H. A.; Eastwood, R. F.; Mather, D. E. Novel allelic variants encoded at the *Glu-D3* locus in bread wheat. *J. Cereal Sci.* **2009**, *49* (2), 254−261.

(16) Clements, R. L. A continuous acetic acid system for polyacrylamide gel electrophoresis of gliadins and other prolamines. *Electrophoresis* **1988**, *9*, 90−93.

(17) Pézolet, M.; Bonenfanta, S.; Dousseaua, F.; Popineau, Y. Conformation of wheat gluten proteins. Comparison between functional and solution states as determined by infrared spectroscopy. *FEBS Lett.* **1992**, *299*, 247−250.

(18) Belton, P. S.; Gil, A. M.; Grant, A.; Alberti, E.; Tatham, A. S. Proton and carbon NMR measurements of the effects of hydration on the wheat protein omega-gliadin. *Spectrochim. Acta Mol. Biomol. Spectrosc.* **1998**, *54*, 955−966.

(19) Wellner, N.; Belton, P. S.; Tatham, A. S. Fourier transform IR spectroscopic study of hydration induced structure changes in the solid state of omega gliadins. *Biochem. J.* **1996**, *319*, 741−747.

(20) Almutawah, A.; Barker, S. A.; Belton, P. S. Hydration of gluten: a dielectric, calorimetric, and Fourier transform infrared study. *Biomacromolecules* **2007**, *8*, 1601−1606.

(21) Okot-Kotber, M.; Liavoga, A.; Yong, K.-J.; Bagorogoza, K. Activation of polyphenol oxidase in extracts of bran from several wheat (*Triticum aestivum*) cultivars using organic solvents, detergents, and chaotropes. *J. Agric. Food Chem.* **2002**, *50*, 2410−2417.

(22) Lerner, H. R.; Harel, E.; Lehman, E.; Mayer, A. M. Phenylhydrazine, a specific irreversible inhibitor of catechol oxidase. *Phytochemistry* **1971**, *10*, 2637−2640.

(23) Hayasaka, Y. The Australian Wine Research Institute, Glen Osmond, SA 5064, Australia, 2011.

(24) Strelec, I.; Ugarčić-Hardi, Ž.; Balkić, J.; Šimunić, N. Enzymatic activity in wheat seeds of different protein content. *Agric. Conspec. Sci.* **2007**, *72* (3), 239−243.

(25) Anderson, J. V.; Fuerst, E. P.; Hurkman, W. J.; Vensel, W. H.; Morris, C. F. Biochemical and genetic characterization of wheat (*Triticum* spp.) kernel polyphenol oxidases. *J. Cereal Sci.* **2006**, *44*, 353−367.

(26) Yamasaki, Y.; Konno, H.; Kazuhiko, N. Polyphenol oxidase from wheat bran is a serpin. *Acta Biochim. Polym.* **2008**, *55*, 325−328.

JOURNAL OF AGRICULTURAL AND FOOD CHEMISTRY

Article

pubs.acs.org/JAFC

Red Wine and Oenological Extracts Display Antimicrobial Effects in an Oral Bacteria Biofilm Model

Irene Muñoz-González,[†] Thomas Thurnheer,[‡] Begoña Bartolomé,[†] and M. Victoria Moreno-Arribas*[,†]

[†]Instituto de Investigación en Ciencias de la Alimentación (CIAL), CSIC-UAM, C/Nicolás Cabrera, 9 Campus de Cantoblanco, 28049 Madrid, Spain

[‡]Center of Dental Medicine, Institute of Oral Biology, Section of Oral Microbiology and Immunology, University of Zürich, Plattenstrasse 11, CH-8032 Zürich, Switzerland

ABSTRACT: The antimicrobial effects of red wine and its inherent components on oral microbiota were studied by using a 5-species biofilm model of the supragingival plaque that includes *Actinomyces oris*, *Fusobacterium nucleatum*, *Streptococcus oralis*, *Streptococcus mutans* and *Veillonella dispar*. Microbiological analysis (CFU counting and confocal laser scanning microscopy) of the biofilms after the application of red wine, dealcoholized red wine, and red wine extract solutions spiked or not with grape seed and inactive dry yeast extracts showed that the solutions spiked with seed extract were effective against *F. nucleatum*, *S. oralis* and *A. oris*. Also, red wine and dealcoholized wine had an antimicrobial effect against *F. nucleatum* and *S. oralis*. Additional experiments showed almost complete and early degradation of flavan-3-ol precursors [(+)-catechin and procyanidin B2] when incubating biofilms with the red wine extract. To our knowledge, this is the first study of antimicrobial properties of wine in an oral biofilm model.

KEYWORDS: *wine, polyphenols, oral bacteria biofilm, antimicrobials*

INTRODUCTION

The oral cavity is an enormously complex habitat with several hundred commensal microbial species colonizing it, and furthermore, it is unique in the human body in possessing nonshedding surfaces, the teeth, allowing microorganisms to adhere to the surface of teeth for long periods of time, embedded in a self-produced matrix of extracellular polymeric substances,[1] and thus leading to extensive biofilm formation, dental plaque,[2] which is more resistant than planktonic cells to mechanical stress or antibiotic treatment.[3] The microorganisms of dental plaque live with one another in a commensal or mutualistic symbiotic relationship, allowing a mixture of aerobic and anaerobic bacteria to live in the same environment. Some of these oral bacteria, such as streptococci or lactobacilli, are able to produce high levels of organic acids following fermentation of dietary sugars. Acids released from dental plaque lead to demineralization of the tooth surface and consequently to dental caries, periodontal disease or tooth loss,[4] which are the most prevalent oral diseases in humans, affecting up to 60−90% of the world population.[5]

Even using mechanical removal, dental biofilms cannot be eliminated completely. Antimicrobial agents are complementarily used to control dental plaque.[6−8] Until now, several substances have been tested for the control of oral biofilms, including essential oils, amine fluoride, triclosan, etc., but one of the most widely used and effective antibiofilm agents is chlorhexidine.[9] However, chlorhexidine has been associated with some secondary effects, namely the reduction of human taste perception and the pigmentation of oral tissues, which limits its application. Therefore, the search for new antimicrobials has arisen, and natural products are preferable due to the lack of secondary effects and, therefore, the potential for long-term usage in the oral cavity.

The inherent matrix of the biofilm, such as extracellular polymeric substances that reduce penetration of antimicrobial agents and the presence of persistent cells surviving at low metabolic rates, contributes to the widely described phenomenon of reduced sensitivity to antimicrobial agents.[10] Because of this, biofilm models including bacteria and fungi from different species, have proven both useful and reliable in predicting *in vivo* efficacy of antimicrobials. In this sense, most experimental models for short-term studies involve a solid surface for the adhesion of bacteria.[11]

Although there is substantial literature reporting the antimicrobial properties of phenolic compounds or polyphenols against bacteria isolates,[12−14] information about their effect on oral pathogens is still scarce.[15] Studies carried out with tea and cranberry polyphenols have shown an inhibitory effect on biofilm formation by oral pathogens such as *Streptococcus mutans*, *Streptococcus oralis*, *Streptococcus sobrinus* and *Porphyromonas gingivalis*.[16] Grapes and wines are good dietary sources of polyphenolic compounds, including hydroxybenzoic and hydroxycinnamic acids, phenolic alcohols, flavan-3-ol monomers, oligomeric and polymeric procyanidins, flavonols, stilbenes and anthocyanins (only present in red varieties).[17] Recently, it has been found that wine and grape phenolic extracts, as well as pomace phenolic extracts, were able to inhibit the growth of different *Streptococcus* spp. strains associated with dental caries.[18,19]

On the other hand, interactions between wine phenolics and oral microbiota can also include a possible bacterial catabolism

Received: January 15, 2014
Revised: April 28, 2014
Accepted: April 29, 2014
Published: April 29, 2014

ACS Publications © 2014 American Chemical Society

of wine phenolics into less complex phenolic metabolite structures, as seems to happen with flavonol glycosides.[15] With regard to anthocyanins, their degradation in human saliva at 37 °C has been described, being structure-dependent, largely mediated by oral microbiota, and partially suppressed after oral rinsing with antibacterial chlorhexidine.[8]

With the final aim of seeking natural products that could be used in oral hygiene and to ascertain interactions between wine components and oral microbiota, in this study the antimicrobial effects of red wine and dealcoholized red wine were investigated using a biofilm model of the supragingival plaque that integrates five bacteria species commonly associated with oral disease. A wine phenolic extract (Provinols), especially rich in anthocyanins, was also tested using the same model, and in both the absence and presence of other enological extracts from grape seeds (Vitaflavan) and yeast (inactive dry yeast, IDY). Additional experiments were carried out to determine any possible phenolic metabolism during the formation of the bacterial biofilm.

MATERIALS AND METHODS

Red Wines. The red wine used in this study was a young red wine (var. Pinot Noir, vintage 2010), kindly provided by Bodegas Miguel Torres S.A. (Catalonia, Spain). The wine was elaborated following the winery's own winemaking procedures and was selected because of its relatively high phenolic content: total polyphenols = 1758 mg of gallic acid equiv/L, total anthocyanins = 447 mg of malvidin-3-glucoside/L, and total catechins = 1612 mg of (+)-catechin/L. The main individual phenolic compounds found in this wine included anthocyanins, flavan-3-ols, flavonols, alcohols, stilbenes and hydroxycinnamic acids[20] (Table 1).

For the preparation of dealcoholized red wine, ethanol was removed using a rotary evaporator and then distilled water was added until the original volume was reached.

Oenological Extracts. A wine extract, Provinols, was kindly supplied by Safic-Alcan Especialidades S.A.U. (Barcelona, Spain). A grape seed extract, Vitaflavan, was kindly provided by Piriou (Les Dérivés Resiniques & Terpéniques S.A., France). The total phenolic content of the extracts was 474 mg of gallic acid equiv/g for Provinols and 629 mg of gallic acid equiv/g for Vitaflavan. The main phenolic compounds identified in both extracts are reported in Table 1. Also, two inactive dry yeast (IDY) commercial preparations (*Saccharomyces cerevisiae*), IDY 1 and IDY 2, rich in mannoproteins, amino acids and peptides, respectively, were kindly provided by Lallemand S.A. (Blagnac, France) and Agrovin S.A. (Alcázar de San Juan, Ciudad Real, Spain).

The wine extract was dissolved in distilled water containing 2.5% DMSO (v/v), at a concentration of 1.6 g/L. The wine extract solution was fortified in grape seed polyphenols by adding 2.5 g of grape seed extract to 100 mL of the wine solution. Also, the wine extract solution was enriched in wine matrix components (mainly polysaccharides and nitrogen compounds) by adding the IDY preparations to the wine extract solution at a final concentration of 0.4 g/L.

Bacterial Strains and Culture (Growth) Conditions. *Actinomyces oris* OMZ 745, *Fusobacterium nucleatum* OMZ 598, *Streptococcus oralis* OMZ 607, *Streptococcus mutans* UA159 (OMZ 918) and *Veillonella dispar* ATCC 17748^T (OMZ 493) were obtained from the culture collection of the Institute of Oral Biology, University of Zürich. Prior to the experiment, precultures were prepared by transferring the strains on Columbia Blood Agar plates and incubating them for 96 h at 37 °C under anaerobic conditions. After this time, the strains were transferred from the Columbia Blood Agar plates to broth cultures (1 × 9 mL of modified fluid universal medium (mFUM) + 0.3% glucose) (OMZ 493 + 1% sodium lactate) and incubated overnight at 37 °C. After incubation, 200 μL of bacteria from each working culture was individually inoculated in 5 mL of fresh mFUM and incubated at 37 °C anaerobically (7 h maximum). In order to obtain an inoculum

Table 1. Main Phenolic Compounds in Wine and Extracts

	wine (mg/L)[20]	wine extract (mg/g)[34]	grape seed extract (mg/g)[35]
	Benzoic Acids		
Gallic acid	27.30 ± 0.20	1.06 ± 0.05	9.11 ± 0.01
Protocatechuic acid	3.88 ± 0.01	*n.a*[a]	*n.a*[a]
3-*O*-Methylgallic acid	1.06 ± 0.06	*n.a*[a]	*n.a*[a]
4-Hydroxybenzoic acid	0.57 ± 0.01	*n.a*[a]	*n.a*[a]
Vanillic acid	1.85 ± 0.03	*n.a*[a]	*n.a*[a]
Syringic acid	2.30 ± 0.13	*n.a*[a]	*n.a*[a]
Benzoic acid	1.14 ± 0.06	*n.a*[a]	*n.a*[a]
Salicylic acid	0.21 ± 0.01	*n.a*[a]	*n.a*[a]
	Phenols		
Phloroglucinol	0.33 ± 0.03	*n.a*[a].	*n.a*[a]
Tyrosol	31.40 ± 1.40	18.90 ± 1.30	*n.a*[a]
Dihidroxyphenyl propan-2-ol	0.30 ± 0.04	*n.a*[a]	*n.a*[a]
	Cinnamic Acids		
Caffeic acid	6.97 ± 0.26	*n.a*[a].	*n.a*[a]
p-Coumaric acid	1.39 ± 0.02	*n.a*[a].	*n.a*[a]
Ferulic acid	0.22 ± 0.02	*n.a*[a].	*n.a*[a]
Coutaric acid	8.64 ± 0.01	2.00 ± 0.12	*n.a*[a]
Caftaric acid	4.98 ± 0.33	0.19 ± 0.07	*n.a*[a]
	Stilbenes		
Resveratrol	7.12 ± 0.29	0.43 ± 0.02	*n.a*[a]
Resveratrol-3-*O*-glucoside	*n.a*[a]	9.17 ± 0.17	*n.a*[a]
	Flavan-3-ols and Others		
(+)-Catechin	51.60 ± 1.70	9.90 ± 0.32	74.60 ± 0.09
(−)-Epicatechin	34.90 ± 2.90	6.87 ± 0.15	67.70 ± 0.75
(−)-Epicatechin-3-*O*-gallate	*n.a*[a]	0.23 ± 0.02	26.20 ± 0.41
Procyanidin B1	79.10 ± 0.90	11.10 ± 0.10	61.00 ± 1.42
Procyanidin B2	44.70 ± 0.60	4.69 ± 0.10	45.10 ± 0.95
B2-3-*O*-gallate	*n.a*[a]	0.03 ± 0.01	1.80 ± 0.06
B2-3′-*O*-gallate	*n.a*[a]	0.03 ± 0.00	1.61 ± 0.01
Procyanidin B3	16.00 ± 1.00	1.23 ± 0.02	20.40 ± 0.33
Procyanidin B4	12.90 ± 0.30	0.83 ± 0.02	15.00 ± 0.13
Procyanidin B5	2.67 ± 0.01	*n.a*[a]	*n.a*[a]
Procyanidin B7	5.75 ± 0.15	*n.a*[a].	*n.a*[a]
Procyanidin C1	14.00 ± 0.40	1.07 ± 0.04	7.07 ± 0.08
Other trimers	7.96 ± 1.05	1.24 ± 0.09	6.81 ± 0.06 (t2)
	Flavonols		
Quercetin	1.92 ± 0.01	22.40 ± 0.60	*n.a*[a]
Myricetin	0.70 ± 0.03	2.55 ± 0.07	*n.a*[a]
Kaempherol	*n.d*[b]	0.04 ± 0.01	*n.a*[a]
Quercetin-3-*O*-glucoside	*n.a*[a]	0.14 ± 0.02	*n.a*[a]
Quercetin-3-*O*-galactoside	*n.a*[a]	0.11 ± 0.01	*n.a*[a]
	Anthocyanins		
Delphinidin-3-*O*-glucoside	2.58 ± 0.11	0.57 ± 0.012	*n.a*[a]
Cyanidin-3-*O*-glucoside	0.76 ± 0.04	0.27 ± 0.01	*n.a*[a]
Petunidin-3-*O*-glucoside	4.06 ± 0.13	1.47 ± 0.03	*n.a*[a]
Peonidin-3-*O*-glucoside	18.90 ± 2.00	1.78 ± 0.01	*n.a*[a]
Malvidin-3-*O*-glucoside	36.70 ± 3.40	9.01 ± 0.50	*n.a*[a]

[a]Not analyzed. [b]Not detected.

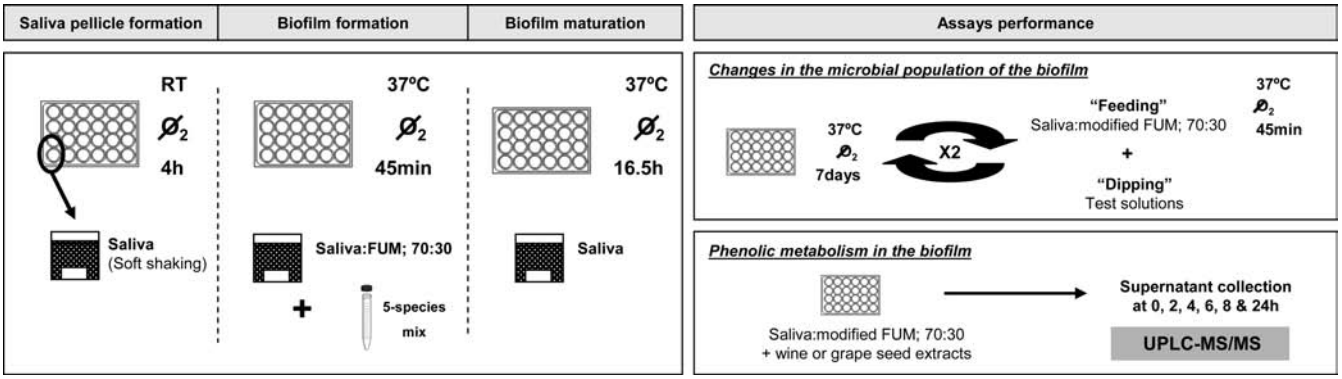

Figure 1. Biofilm formation/maturation and assays diagram.

containing cultures in the exponential growth phase of approximately 10^7 CFU/mL, a microbial suspension with equal volumes and densities of each strain was prepared.

Saliva Processing. Saliva was collected from five volunteers and processed according to the protocol of Guggenheim et al.[21] Briefly, whole unstimulated saliva was collected for 1 h each morning, over several days, at least 1.5 h after eating, drinking, or teeth cleaning. Saliva samples were collected in sterile 50 mL polypropylene tubes, chilled in an ice bath or frozen at −20 °C. After 500 mL of saliva had been collected, it was pooled and centrifuged (30 min, 4 °C, 27,000*g*); the supernatant was pasteurized (60 °C, 30 min) and recentrifuged in sterile tubes. The resulting supernatant was stored in sterile 50 mL polypropylene tubes at −80 °C. The efficiency of the process was assessed by plating the processed saliva samples onto CBA agar; after 72 h at 37 °C, no CFUs were observed on the incubated plates. A sterile 1:1 dilution in H_2O + 25% physiological NaCl was used for the biofilm formation and throughout the experimentation.

In Vitro Biofilm Experiments. Figure 1 shows a sequence chart regarding the biofilm formation prior to assays for determining changes in the microbial population of the biofilm and for assessing phenolic metabolism in the biofilm.

Biofilm Formation. Biofilms were grown using the slightly modified protocol described by Guggenheim et al.[21] and Thurnheer et al.[22] In brief, the 5-species biofilms were grown in 24-well polystyrene cell-culture plates on hydroxyapatite (HA) discs of 9 mm Ø (Clarkson Chromatography Products, South Williamsport, USA) previously preconditioned in 800 μL of whole unstimulated pooled saliva (as described in the previous section) during 4 h at room temperature, with shaking (95 rpm) in order to promote pellicle formation. To initiate the biofilm formation, the discs were covered for 45 min with 1.6 mL of a mixture comprising 30% saliva, 70% mFUM and 200 μL of the bacterial inoculum described above. mFUM corresponds to a well-established tryptone yeast-based broth medium designated as FUM[23] and modified by supplementing 67 mM Sørensen's buffer (final pH 7.2). The carbohydrate concentration in mFUM was 0.3% (w/v) and consisted of glucose for the first 16 h and from then on of a 1:1 (w/w) mixture of glucose and sucrose.

After this first incubation, discs were subjected to three consecutive 1 min dip-washes in 2 mL 0.9% NaCl to remove growth medium and free-floating cells but not microorganisms adhering firmly to the HA discs. Then, they were incubated anaerobically for 16.5 h at 37 °C in preconditioned and processed saliva to form the biofilm (Figure 1).

Assay for Determining Changes in the Microbial Population of the Biofilm. Once the biofilm was formed, discs were maintained in a 24-well plate with preconditioned and processed saliva in anaerobic conditions for 7 days. Twice a day, and with 7 h of difference in between, discs were "fed" by immersing them into a preconditioned fresh growth medium (30% saliva, 70% mFUM (v/v) containing 0.15% glucose and 0.15% sucrose) for 45 min, at 37 °C, under anaerobic conditions, After each "feeding", discs were dipped in the different test solutions (1 mL) for 2 min and while being gently shaken by hand. After this time, the discs were dipped once in the preconditioned-processed saliva in order to clean any remains of the test solutions. Immediately after, discs were returned to the "old" 24-well plate with preconditioned and processed saliva and incubated anaerobically until the next "feeding" (Figure 1). After 7 days, biofilms were either stained for confocal laser scanning microscopy (see below) or harvested, at room temperature, in 1 mL of 0.9% NaCl by scratching with a special odontological instrument. Cell viability was tested using a Live/Dead BacLight Viability Kit (Molecular Probes Inc.) The total CFU, streptococci and all taxa were assessed by anaerobic culture (37 °C) using selective (Mitis Salivarious for *Streptococcus oralis* and *Streptococcus mutans*; Fastidious Anaerobe Agar for *Fusobacterium nucleatum*) and nonselective media (Columbia Blood Agar for *Actinomyces oris*, *Veillonella dispar* and total CFU) and colonies were counted.

Distilled water was used as the negative antimicrobial control, and 0.2% chlorhexidine-gluconate solution (Sigma-Aldrich, Steinheim, Germany) in water was the positive antimicrobial control. In order to discard a possible antimicrobial effect of the alcohol, a 12%-ethanol-in-water solution was also tested. For both, test solutions and controls, experiments were carried out in triplicate.

Assay for Assessing Phenolic Metabolism in the Biofilm. After initiating biofilm formation as described above, the 70:30 saliva:mFUM media was enriched with the wine extract (1.6 g/L) in the absence of the presence of grape seed extract (10 g/L) and added into the wells containing the discs (Figure 1). Then, plates were incubated at 37 °C under anaerobic conditions and aliquots of enriched media were taken at 0, 2, 4, 6, 8, and 24 h.

Analysis of Wine Compounds and Bacterial/Microbial Metabolites. Phenolic compounds were analyzed using an UPLC-ESI-MS/MS following a previously reported method.[20] The liquid chromatographic system was a Waters Acquity UPLC (Milford, MA) equipped with a binary pump, an autosampler thermostated at 10 °C, and a heated column compartment (40 °C). The column employed was a BEH-C18, 2.1 × 100 mm and 1.7 μm particle size from Waters (Milford, MA). The mobile phases were 2% acetic acid in water (A) and 2% acetic acid in acetonitrile (B). The gradient program was as follows: 0 min, 0.1% B; 1.5 min, 0.1% B; 11.17 min, 16.3% B; 11.5 min, 18.4% B; 14 min, 18.4% B; 14.1 min, 99.9% B; 15.5 min, 99.9% B; 15.6 min, 0.1% B. Equilibrium time was 2.4 min resulting in a total runtime of 18 min. The flow rate was set constant at 0.5 mL/min and injection volume was 2 μL.

The LC effluent was pumped to an Acquity TQD tandem quadrupole mass spectrometer equipped with a Z-spray electrospray ionization (ESI) source operated in negative polarity mode. The ESI parameters were set as follows: capillary voltage, 3 kV; source temperature, 130 °C; desolvation temperature, 400 °C; desolvation gas (N_2) flow rate, 750 L/h; cone gas (N_2) flow rate, 60 L/h. The ESI was operated in negative ionization mode. For quantification purposes, data were collected in the multiple reaction monitoring (MRM) mode, tracking the transition of parent and product ions specific to each compound. The MS/MS parameters (cone voltage, collision energy and MRM transition) of the 60 phenolic compounds targeted in the present study (mandelic acids, benzoic acids, phenols, hippuric acids, phenylacetic acids, phenylpropionic acids, cinnamic acids, 4-hydrox-

dx.doi.org/10.1021/jf501768p | J. Agric. Food Chem. 2014, 62, 4731−4737

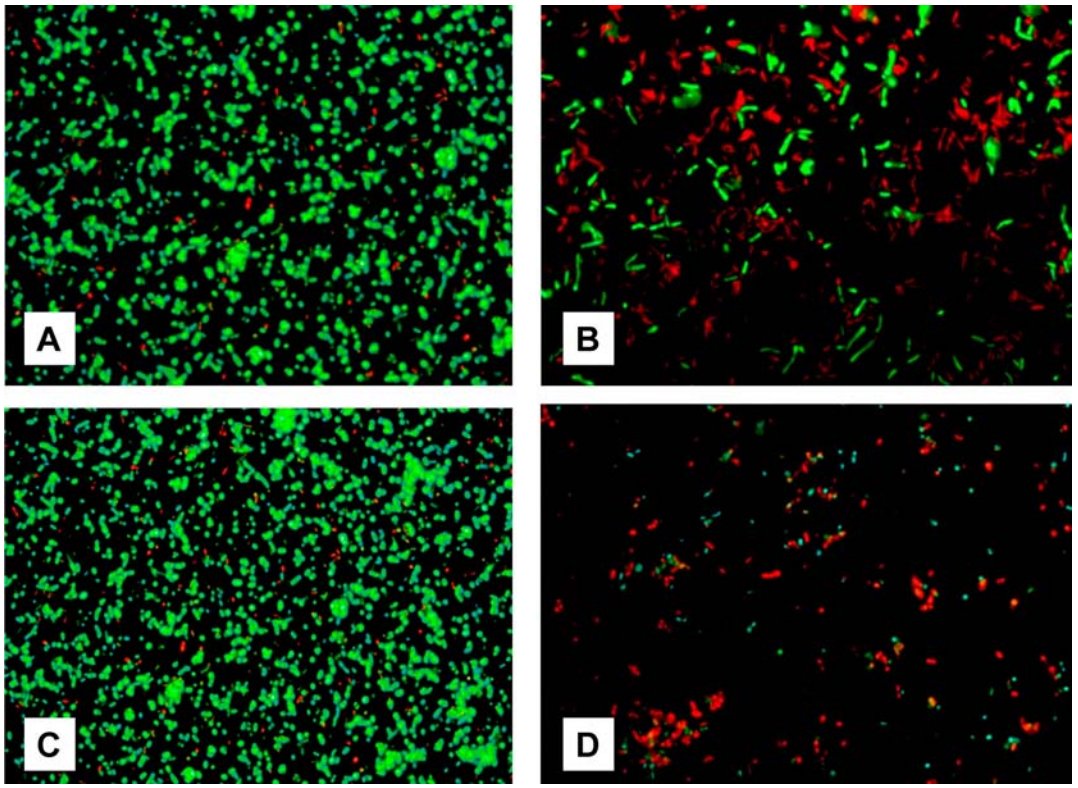

Figure 2. Confocal scanned segment of biofilm stained with LIVE/DEAD kit after exposure to (A) negative control (water), (B) red wine, (C) wine extract (Provinols, 1.6 g/L), and (D) grape seed extract (Vitaflavan, 2.5 g/L) in wine extract solution (1.6 g/L).

Table 2. Bacterial Populations (Log_{10}CFU) of *S. mutans*, *S. oralis*, *A.oris*, *F. nucleatum*, and *V. dispar* in the Biofilm, after Treatments with Water, Ethanol 12% in Water, Wine, Dealcoholized Wine and 0.2% Clorhexidine-gluconate

	S. mutans	*S. oralis*	*F. nucleatum*	*A. oris*	*V. dispar*
Water	8.09 ± 0.09	8.42 ± 0.17	5.90 ± 0.89	8.40 ± 0.32	7.36 ± 0.37
Ethanol 12% in water	8.01 ± 0.16	8.20 ± 0.37	<1.30 ± 0.00[a]	8.75 ± 0.64	7.92 ± 0.12
Wine	7.89 ± 0.07	5.77 ± 0.63[a]	<1.30 ± 0.00[a]	8.37 ± 0.20	6.94 ± 0.38
Dealcoholized wine	7.68 ± 0.22	4.79 ± 0.80[a]	<1.30 ± 0.00[a]	8.24 ± 0.07	7.12 ± 0.88
Clorhexidine-gluconate 0.2%	<1.30 ± 0.00[a]	<1.30 ± 0.00[a]	<1.30 ± 0.00[a]	<1.30 ± 0.00[a]	<1.30 ± 0.00[a]

[a]Significant differences (Dunnett's test) in the population in comparison to the negative control (water).

yvaleric acids and valerolactones) were previously reported.[24] Data acquisition and processing was realized with MassLynx 4.1 software.

Staining of Biofilms and Confocal Laser Scanning Microscopy (CLSM). For CLSM, treated as well as untreated, biofilms were stained using the LIVE/DEAD BacLight bacterial viability assay (Invitrogen, Zug, Switzerland) according to the instructions of the manufacturer. After 20 min staining, excess dye was gently aspirated from the discs without touching the biofilms. They were embedded upside-down in 20 μL of Mowiol[25] and stored at room temperature in the dark for at least 6 h prior to microscopic examination.

Stained biofilms were examined by CLSM at randomly selected positions using a Leica TCS SP5 (Leica Microsystems, Heidelberg GmbH, Germany) with a ×20/0.8 numerical aperture (NA) and a ×63/1.4 NA oil immersion objective lens in conjunction with 488 nm laser excitation and 530 nm emission filters for Syto 9 (live stain) and 561 nm laser excitation, and 640 nm emission filters for propidium iodide (dead stain). Image acquisition was done in 8-line average mode, and the data were processed using Imaris 7.2.2 (Bitplane AG, Zurich, Switzerland).

Statistical Analysis. Means and standard deviations were calculated using Microsoft Excel 2007. Statistical analyses were performed through Statistica©. To compare the antimicrobial effects of the different treatments with the control (water), the Dunnett test was applied. Graphs were performed with Microsoft Excel 2007.

RESULTS AND DISCUSSION

Antimicrobial Properties of Red Wine on the Biofilm. The effects of a red wine and the same wine without ethanol on a biofilm model composed of five representative species commonly encountered in supragingival plaque, including Gram-positive (*A. oris, S. mutans, S. oralis*) as well as Gram-negative (*F. nucleatum, V. dispar*) bacteria,[21] were investigated. Among these bacteria were the so-called early colonizers, *A. oris*, *S. oralis* and *V. dispar*, and late colonizers, *S. mutans* and *F. nucleatum*, the latter also designated as a bridging organism due to its capability to coaggregate with a wide range of early and late colonizers.[26] In comparison to the control biofilm (Figure 2A), when biofilms were dipped into red wine (Figure 2B) and dealcoholized red wine, some decrease in cell viability of the whole biofilm was visually estimated. However, no visually changes were observed when applying the wine extract solution (Figure 2C). CFU values for the five bacteria comprising the biofilm indicated an important reduction in *F. nucleatum* and *S. oralis* population when applying red wine and dealcoholized red wine to the biofilm, in comparison to the negative control (distilled water) (Table 2). The Dunnett test confirmed

Table 3. Bacterial Populations ($Log_{10}CFU$) of *S. mutans*, *S. oralis*, *A.oris*, *F. nucleatum*, and *V. dispar* in the Biofilm, after Treatments with Provinols, Provinols + Vitaflavan, Provinols + IDY 1 and Provinols + IDY 2

	S. mutans	*S. oralis*	*F. nucleatum*	*A. oris*	*V. dispar*
Water + 2.5% DMSO	8.02 ± 0.05	8.47 ± 0.09	6.77 ± 0.07	8.55 ± 0.07	7.74 ± 0.04
Provinols	8.11 ± 0.08	8.59 ± 0.11	6.54 ± 0.57	8.34 ± 0.39	7.68 ± 0.39
Provinols + Vitaflavan	7.77 ± 0.18	6.49 ± 0.07[a]	<1.30 ± 0.00[a]	<3.30 ± 0.00[a]	7.95 ± 0.09
Provinol + IDY 1	8.18 ± 0.03	8.60 ± 0.01	7.13 ± 0.13	8.89 ± 0.02	8.15 ± 0.15
Provinols + IDY 2	8.13 ± 0.07	8.44 ± 0.07	7.14 ± 0.04	8.68 ± 0.03	8.11 ± 0.11

[a]Significant differences (Dunnetts test) in the population in comparison to the negative control (water + 2.5% DMSO).

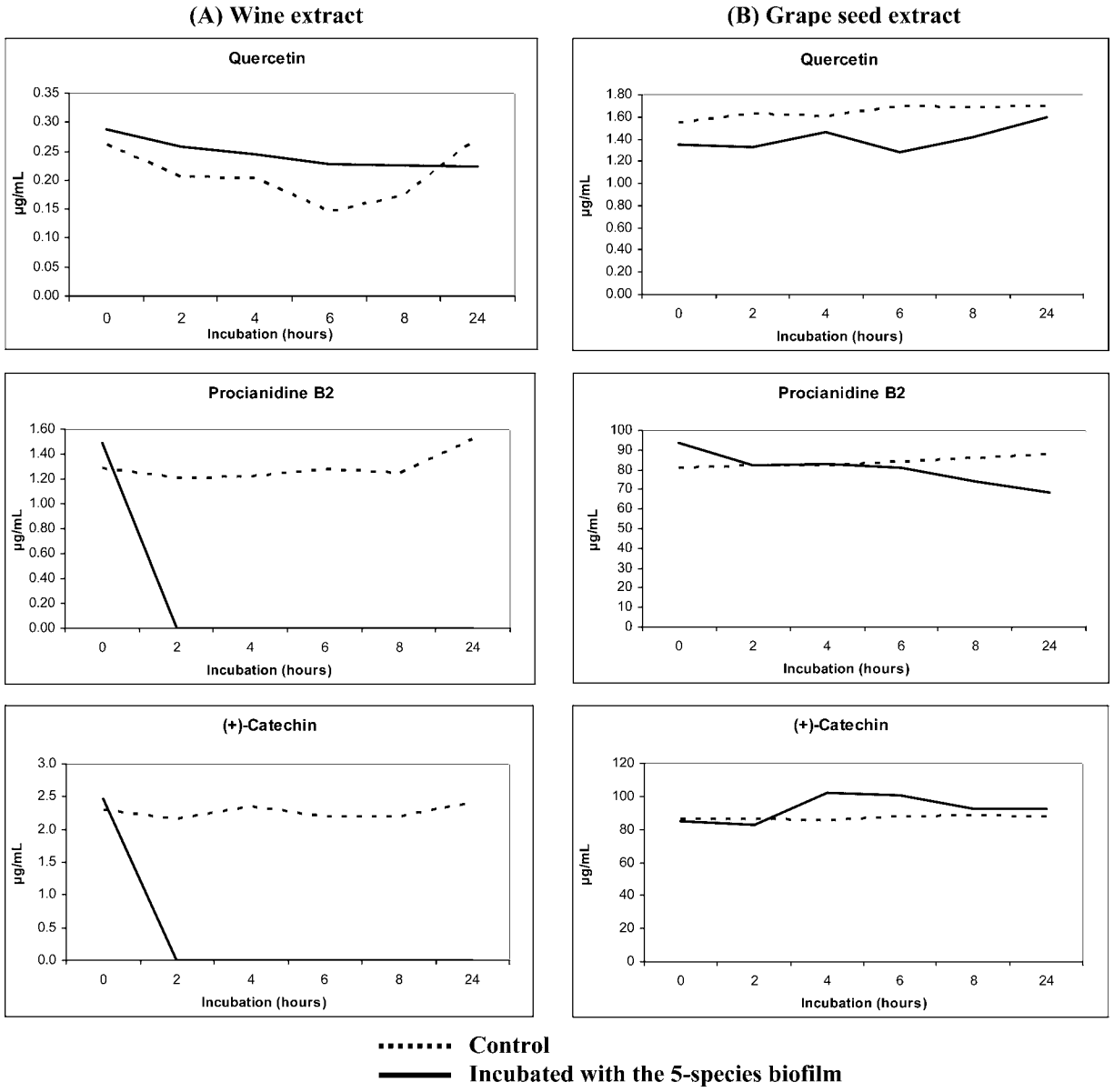

Figure 3. Metabolism of precursors (+)-catechin, quercetin and procyanidin B2 after 0, 2, 4, 6, 8, and 24 h of incubation in FUM media enriched with (A) wine extract (Provinols) and (B) grape seed extract (Vitaflavan, 1%) in wine extract solution.

significant differences in the population of these two strains after the treatment with wine and dealcoholized wine. Generally, wines contain between 10 and 12% of ethanol, which have antimicrobial properties. To understand the action mechanism of red wines in more depth, the effects of ethanol of the bacteria biofilm were investigated. The treatment with 12% ethanol resulted in a significant decrease in the population of *F. nucleatum* (Table 2). However, since treatments of the biofilm with both wine and dealcoholized wine inhibited *F. nucleatum* growth, it was likely that other wine components—apart from ethanol—had antimicrobial properties against this bacteria species. As expected, all the strains were eradicated after the treatment with the positive control (0.2% chlorexidine-gluconate solution) (Table 2).

In an intervention study with 75 volunteers, Signoretto et al.[27] analyzed the microbial population of supragingival and

dx.doi.org/10.1021/jf501768p | J. Agric. Food Chem. 2014, 62, 4731−4737

subgingival plaque using PCR-DGGE and found that *F. nucleatum* was less frequent in wine drinkers compared with water drinkers. Other authors, such as Daglia et al.,[28] have also shown antimicrobial properties of dealcoholized wine against oral streptococci. Both studies were consistent with our results in that wine selectively inhibited the growth of *F. nucleatum* and *S. oralis* in the presence of other species, such as *S. mutans*, *A. oris* and *V. dispar* in an oral biofilm model.

Given the antimicrobial effects of wine observed in the first experiment, the next step was to study the influence of some wine-specific components, such as polyphenols, including flavan-3-ols, peptides or yeast polysaccharides. For that purpose, a red wine extract solution spiked with different extracts rich in those specific components of wine (grape seed extract rich in flavan-3-ols, and two inactive dry yeasts rich in peptides and mannoproteins, respectively) was used. Table 3 reports the CFU values of the five bacteria species of the tested biofilm after treatments with wine extract and wine extract solution spiked with different extracts (grape seed extract, IDY1 and IDY2). Dunnett's test showed significant differences in *F. nucleatum, S. oralis and A. oris* with the application of the wine extract spiked with the grape seed extract rich in flavan-3-ols.[17] However, wine extract solutions spiked with IDY1 and IDY2 did not show any effect in the populations of the five-strain biofilm. Notably, a great decrease in the viability of the cell was visually appreciated in the biofilm recovered from the discs that were dipped in the grape seed extract solution (Figure 2D). Cueva et al.[29] reported significant inhibition in the growth of some oral streptococci, such as *Streptococcus mutans* and *Streptococcus sobrinus*, when incubating planktonic cultures with flavan-3-ols precursors, (+)-catechin and (−)-epicatechin, in which grape seed extract is particularly rich. Moreover, they showed that extracts from grape seed, especially Vitaflavan and its oligomeric fraction, exerted higher antimicrobial activity against various oral pathogens than the rest of the extracts tested (red wine extract and grape pomace extract). Similarly, Rotava et al.[30] and Baydar et al.[31] reported antimicrobial effects of grape seed extracts against pathogenic bacteria such as *S. aureus* and *E. coli*. It has been suggested that the high concentration of flavonoids and their derivatives in grape seeds could be responsible for the antimicrobial activity of grape seed extracts.[32] These observations raise the question of how the hydroxyl groups (structure) of flavonoids affect oral bacterial biofilm.

The search for new antimicrobial agents to control the formation of dental plaque requires appropriate screening models that include orally relevant organisms. The mode used in this study is not only useful for investigating ecological shifts in plaque composition in response to plaque composition but also for testing the efficacy of antimicrobial agents under conditions of repeated short-term exposure.[11] Other oral biofilm models that use flow chamber systems or in-mouth dispositives have also been used. Among these, flow chamber systems allowing biofilm formation/maturation under hydrodynamic conditions, and careful control and easy changes of the environment, are very useful for analysis of structural biofilm formation. In-mouth dispositives allow *in vivo* formation of the biofilm including the endogenous microbiota of the volunteer. Although these models are the most realistic in miming oral biofilms, the high interindividual variability in the composition of the biofilms may provoke high deviations in the results.

Changes in Wine Phenolic Metabolism. Because wine and its polyphenols diminished bacteria population in the oral biofilm, a new assay was performed in order to gain a deeper understanding about microbial metabolism of polyphenols in the tested extracts.

First, the wine extract solution was added to the growth media and the progress of the phenolic metabolism by the five-species biofilm was studied by monitoring changes in the main phenolic compounds present in the wine extract (Table 1): flavan-3-ols monomers ((+)-catechin, (−)-epicatechin and (−)-epicatechin-3-*O*-gallate), dimeric procyanidins (B1, B2, B3, B4, B5, B7, B2-3-*O*-gallate and B2-3-*O*-gallate), trimeric procyanidins (C1 and other trimers) and flavonols (quercetin, myricetin, kaempherol, quercetin-3-*O*-glucoside and quercetin-3-*O*-galactoside). As a brief example, Figure 3A shows the differences in the degradation by the five-strain biofilm of three of the analyzed precursors, (+)-catechin, procyanidin B2 and quercetin, when growing in media enriched with the wine extract solution (1.6 g/L). The UPLC-MS analysis of these three compounds showed high degradation rates, almost completely during the first 2 h of incubation, in the flavan-3-ol precursors, (+)-catechin and procyanidin B2, probably because of their low concentration in the media, which permitted the bacteria of the biofilm to ues them as a carbon source. However, no degradation of the precursor quercetin was observed during the incubation period.

To gain further knowledge about the metabolism of grape polyphenols, specifically in flavan-3-ols metabolism, the growing media was enriched by adding, to the red wine extract solution, a concentration of 10 g/L of grape seed extract, which is especially rich in flavan-3-ol precursors (Figure 3B). Despite the greater concentration of flavan-3-ol precursors, no degradation of the flavan-3-ol precursors was observed. Nor was degradation of precursor quercetin observed during the incubation period.

The emergence of antibiotic resistance by some oral bacteria biofilm species presents a worldwide problem, and thus, novel strategies are required. The use of natural antimicrobials may contribute to controlling the disordered growth of oral microbiota; thus, overcoming problems caused by species resistant to conventional antimicrobials.[33] To our knowledge, this is the first report on the antimicrobial properties of wine in an oral biofilm model. Our results show that red wine, at moderate concentration, inhibits the growth of some pathogenic species in an oral biofilm model. These findings contribute to existing knowledge about the beneficial effects of red wines (one of the most important products of agriculture and food industries) on human health. Moreover, the promising results concerning grape seed extract, which showed the highest antimicrobial activity, open promising ways toward a natural ingredient in the formulation of oral care products specifically indicated for the prevention of caries, due to its antimicrobial properties.

AUTHOR INFORMATION

Corresponding Author

*E-mail: victoria.moreno@csic.es. Tel: 34 91 0017900. Fax: 34 910017905.

Funding

This work was funded by the MINECO (Spanish National Projects AGL2012-04172-C02-01), CONSOLIDER INGENIO 2010 (FUN-C-FOOD, CSD2007-063, Spain), and the Comunidad de Madrid (ALIBIRD P2009/AGR-1469) Project. I.M.-G. would like to thank the FPI Program for its research contract.

Notes

The authors declare no competing financial interest.

■ ACKNOWLEDGMENTS

We would like to thank Ruth Graf and Andy Meier for their support with the maintenance of the bacteria as well as the cultivation of the biofilms.

■ REFERENCES

(1) Abee, T.; Kovacs, A. T.; Kuipers, O. P.; van der Veen, S. Biofilm formation and dispersal in Gram-positive bacteria. *Curr. Opin. Biotechnol.* **2011**, *22*, 172−179.

(2) Marsh, P. D. Are dental diseases examples of ecological catastrophes? *Microbiology-Sgm* **2003**, *149*, 279−294.

(3) Roberts, A. M. Peter Oral biofilms: a reservoir of transferable, bacterial, antimicrobial resistance. *Expert Rev. Anti. Infec. Ther.* **2010**, *8*, 1441−50.

(4) Hardie, J. Oral Microbiology—Current Concepts in the Microbiology of Dental-Caries and Periodontal-Disease. *Br. Dent. J.* **1992**, *172*, 271−278.

(5) Da Silva, B. R.; Abreu de Freitas, V. A.; Carneiro, V. A.; Sousa Arruda, F. V.; Lorenzon, E. N.; Walter de Aguiar, A. S.; Cilli, E. M.; Cavada, B. S.; Teixeira, E. H. Antimicrobial activity of the synthetic peptide Lys-a1 against oral streptococci. *Peptides* **2013**, *42*, 78−83.

(6) Furiga, A.; Lonvaud-Funel, A.; Dorignac, G.; Badet, C. In vitro anti-bacterial and anti-adherence effects of natural polyphenolic compounds on oral bacteria. *J. Appl. Microbiol.* **2008**, *105*, 1470−1476.

(7) Marsh, P. D. Controlling the oral biofilm with antimicrobials. *J. Dent.* **2010**, *38*, S11−S15.

(8) Kamonpatana, K.; Giusti, M. M.; Chitchumroonchokchai, C.; MorenoCruz, M.; Riedl, K. M.; Kumar, P.; Failla, M. L. Susceptibility of anthocyanins to ex vivo degradation in human saliva. *Food Chem.* **2012**, *135*, 738−747.

(9) Corbin, A.; Pitts, B.; Parker, A.; Stewart, P. S. Antimicrobial Penetration and Efficacy in an In Vitro Oral Biofilm Model. *Antimicrob. Agents Chemother.* **2011**, *55*, 3338−3344.

(10) Hoyle, B. D.; Costerton, J. W. Bacterial resistance to antibiotics: the role of biofilms. *Prog. Drug Res.* **1991**, *37*, 91−105.

(11) Guggenheim, B.; Guggenheim, M.; Gmur, R.; Giertsen, E.; Thurnheer, T. Application of the Zurich biofilm model to problems of cariology. *Caries Res.* **2004**, *38*, 212−222.

(12) Jayaprakasha, G.; Selvi, T.; Sakariah, K. Antibacterial and antioxidant activities of grape (Vitis vinifera) seed extracts. *Food Res. Int.* **2003**, *36*, 117−122.

(13) Ozkan, G.; Sagdic, O.; Baydar, N.; Kurumahmutoglu, Z. Antibacterial activities and total phenolic contents of grape pomace extracts. *J. Sci. Food Agric.* **2004**, *84*, 1807−1811.

(14) Cueva, C.; Moreno-Arribas, M. V.; Martin-Alvarez, P. J.; Bills, G.; Francisca Vicente, M.; Basilio, A.; Lopez Rivas, C.; Requena, T.; Rodriguez, J. M.; Bartolome, B. Antimicrobial activity of phenolic acids against commensal, probiotic and pathogenic bacteria. *Res. Microbiol.* **2010**, *161*, 372−382.

(15) Requena, T.; Monagas, M.; Pozo-Bayon, M. A.; Martin-Alvarez, P. J.; Bartolome, B.; del Campo, R.; Avila, M.; Martinez-Cuesta, M. C.; Pelaez, C.; Moreno-Arribas, M. V. Perspectives of the potential implications of wine polyphenols on human oral and gut microbiota. *Trends Food Sci. Technol.* **2010**, *21*, 332−344.

(16) Bodet, C.; Grenier, D.; Chandad, F.; Ofek, I.; Steinberg, D.; Weiss, E. I. Potential oral health benefits of cranberry. *Crit. Rev. Food Sci. Nutr.* **2008**, *48*, 672−680.

(17) Monagas, M.; Gomez-Cordoves, C.; Bartolome, B.; Laureano, O.; Ricardo-Da-Silva, J. Monomeric, oligomeric, and polymeric flavan-3-ol composition of wines and grapes from Vitis vinifera L. cv. Graciano, Tempranillo, and Cabernet Sauvignon. *J. Agric. Food Chem.* **2003**, *51*, 6475−6481.

(18) Thimothe, J.; Bonsi, I. A.; Padilla-Zakour, O. I.; Koo, H. Chemical characterization of red wine grape (Vitis vinifera and Vitis interspecific hybrids) and pomace phenolic extracts and their biological activity against Streptococcus mutans. *J. Agric. Food Chem.* **2007**, *55*, 10200−10207.

(19) Furiga, A.; Lonvaud-Funel, A.; Badet, C. In vitro study of antioxidant capacity and antibacterial activity on oral anaerobes of a grape seed extract. *Food Chem.* **2009**, *113*, 1037−1040.

(20) Munoz-Gonzalez, I.; Jimenez-Giron, A.; Martin-Alvarez, P. J.; Bartolome, B.; Moreno-Arribas, M. V. Profiling of Microbial-Derived Phenolic Metabolites in Human Feces after Moderate Red Wine Intake. *J. Agric. Food Chem.* **2013**, *61*, 9470−9479.

(21) Guggenheim, B.; Giertsen, E.; Schupbach, P.; Shapiro, S. Validation of an in vitro biofilm model of supragingival plaque. *J. Dent. Res.* **2001**, *80*, 363−370.

(22) Thurnheer, T.; van der Ploeg, J.; Giertsen, E.; Guggenheim, B. Effects of Streptococcus mutans gtfC deficiency on mixed oral biofilms in vitro. *Caries Res.* **2006**, *40*, 163−171.

(23) Gmur, R.; Guggenheim, B. Antigenic Heterogeneity of Bacteroides-Intermedius as Recognized by Monoclonal-Antibodies. *Infect. Immun.* **1983**, *42*, 459−470.

(24) Jimenez-Giron, A.; Isabel Queipo-Ortuno, M.; Boto-Ordonez, M.; Munoz-Gonzalez, I.; Sanchez-Patan, F.; Monagas, M.; Martin-Alvarez, P. J.; Murri, M.; Tinahones, F. J.; Andres-Lacueva, C.; Bartolome, B.; Moreno-Arribas, M. V. Comparative Study of Microbial-Derived Phenolic Metabolites in Human Feces after Intake of Gin, Red Wine, and Dealcoholized Red Wine. *J. Agric. Food Chem.* **2013**, *61*, 3909−3915.

(25) Thurnheer, T.; Gmur, R.; Shapiro, S.; Guggenheim, B. Mass transport of macromolecules within an in vitro model of supragingival plaque. *Appl. Environ. Microbiol.* **2003**, *69*, 1702−1709.

(26) Kolenbrander, P. E.; Palmer, R. J., Jr.; Rickard, A. H.; Jakubovics, N. S.; Chalmers, N. I.; Diaz, P. I. Bacterial interactions and successions during plaque development. *Periodontol. 2000* **2006**, *42*, 47−79.

(27) Signoretto, C.; Bianchi, F.; Burlacchini, G.; Sivieri, F.; Spratt, D.; Canepari, P. Drinking Habits Are Associated with Changes in the Dental Plaque Microbial Community. *J. Clin. Microbiol.* **2010**, *48*, 347−356.

(28) Daglia, M.; Papetti, A.; Grisoli, P.; Aceti, C.; Dacarro, C.; Gazzani, G. Antibacterial activity of red and white wine against oral streptococci. *J. Agric. Food Chem.* **2007**, *55*, 5038−5042.

(29) Cueva, C.; Mingo, S.; Munoz-Gonzalez, I.; Bustos, I.; Requena, T.; del Campo, R.; Martin-Alvarez, P. J.; Bartolome, B.; Moreno-Arribas, M. V. Antibacterial activity of wine phenolic compounds and oenological extracts against potential respiratory pathogens. *Lett. Appl. Microbiol.* **2012**, *54*, 557−563.

(30) Rotava, R.; Zanella, I.; da Silva, L. P.; Manfron, M. P.; Ceron, C. S.; Alves, S. H.; Karkow, A. K.; Aquino Santos, J. P. Antibacterial, antioxidant and tanning activity of grape by-product. *Ciencia Rural* **2009**, *39*, 941−944.

(31) Baydar, N. G.; Sagdic, O.; Ozkan, G.; Cetin, S. Determination of antibacterial effects and total phenolic contents of grape (Vitis vinifera L.) seed extracts. *Int. J. Food Sci. Technol.* **2006**, *41*, 799−804.

(32) Anastasiadi, M.; Chorianopoulos, N. G.; Nychas, G. E.; Haroutounian, S. A. Antilisterial Activities of Polyphenol-Rich Extracts of Grapes and Vinification Byproducts. *J. Agric. Food Chem.* **2009**, *57*, 457−463.

(33) Nascimento, G.; Locatelli, J.; Freitas, P.; Silva, G. Antibacterial activity of plant extracts and phytochemicals on antibiotic-resistant bacteria. *Brazilian J. Microbiol.* **2000**, *31*, 247−256.

(34) Sánchez-Patán, F.; Cueva, C.; Monagas, M.; Walton, G. E.; Gibson, G. R.; Quintanilla-López, J. E.; Lebron-Aguilar, R.; Martin-Alvarez, P. J.; Moreno-Arribas, M. V.; Bartolome, B. In Vitro Fermentation of a Red Wine Extract by Human Gut Microbiota: Changes in Microbial Groups and Formation of Phenolic Metabolites. *J. Agric. Food Chem.* **2012**, *60*, 2136−2147.

(35) Sánchez-Patán, F.; Cueva, C.; Monagas, M.; Walton, G. E.; Gibson, G. R.; Martin-Alvarez, P. J.; Moreno-Arribas, M. V.; Bartolome, B. Gut microbial catabolism of grape seed flavan-3-ols by human faecal microbiota. Targetted analysis of precursor compounds, intermediate metabolites and end-products. *Food Chem.* **2012**, *131*, 337−347.

JOURNAL OF AGRICULTURAL AND FOOD CHEMISTRY

Article

pubs.acs.org/JAFC

Effects of Nitrogen on the Distribution and Chemical Speciation of Iron and Zinc in Pearling Fractions of Wheat Grain

Yan-Fang Xue,[†,‡] Tristan Eagling,[‡] Jibin He,[‡] Chun-Qin Zou,[†] Steve P. McGrath,[‡] Peter R. Shewry,[‡,§] and Fang-Jie Zhao*[,∥]

[†]Key Laboratory of Plant-Soil Interactions, Ministry of Education, Center for Resources, Environment and Food Security, China Agricultural University, Beijing 100193, China

[‡]Rothamsted Research, Harpenden, Hertfordshire AL5 2JQ, United Kingdom

[§]School of Agriculture, Policy and Development, University of Reading, P.O. Box 237, Reading RG6 6AR, United Kingdom

[∥]State Key Laboratory of Crop Genetics and Germplasm Enhancement, College of Resources and Environmental Sciences, Nanjing Agricultural University, Nanjing 210095, China

Supporting Information

ABSTRACT: Increasing nitrogen supply can increase Fe and Zn concentrations in wheat grain, but the underlying mechanisms remain unclear. Size-exclusion chromatography coupled with inductively coupled plasma mass spectrometry was used to determine Fe and Zn speciation in the soluble extracts of grain pearling fractions of two wheat cultivars grown at two N rates (100 and 350 kg of N ha^{-1}). Increasing N supply increased the concentrations of total Fe and Zn and the portions of Fe and Zn unextractable with a Tris−HCl buffer and decreased the concentrations of Tris−HCl-extractable (soluble) Fe and Zn. Within the soluble fraction, Fe and Zn bound to low molecular weight compounds, likely to be Fe−nicotianamine and Fe−deoxymugineic acid or Zn−nicotianamine, were decreased by 5−12% and 4−37%, respectively, by the high N treatment, whereas Fe and Zn bound to soluble high molecular weight or soluble phytate fractions were less affected. The positive effect of N on grain Fe and Zn concentrations was attributed to an increased sink in the grain, probably in the form of water-insoluble proteins.

KEYWORDS: *wheat, iron, zinc, speciation, distribution*

INTRODUCTION

Iron and zinc deficiencies are widespread nutritional disorders, affecting over two billion people in the world.[1,2] Insufficient dietary intakes of Fe and Zn and limited dietary diversity are thought to be responsible for human micronutrient deficiencies, especially in developing countries, where high proportions of cereal grains with inherently low concentrations of Fe and Zn, such as wheat and rice, are consumed as staple foods.[1,3] The bioavailability of Fe and Zn in cereal grains is also relatively low due to the presence of antinutritional compounds such as phytic acid and phenolic compounds.[1] Additionally, milling of wheat grain into white flour further results in reduced concentrations of Fe and Zn, because they are enriched in the outer parts of the grains, consisting mainly of the aleurone layer, embryo, pericarp, and testa.[4−6] Therefore, increasing Fe and Zn concentrations and/or their bioavailability in white flour is desirable for tackling the problem of micronutrient malnutrition.

Recent studies have shown that nitrogen supply is an important factor affecting the concentrations of Fe and Zn in wheat grain. For example, under both field and glasshouse conditions, increasing N supply generally enhances Fe and Zn concentrations in wheat grain.[5,7−9] It has been reported that N increases Zn uptake by roots, Zn translocation from roots to shoots and Zn remobilization from leaves to grain in wheat,[4,10] but the mechanisms are not well understood.

Nicotianamine (NA), a nonprotein amino acid, is an important nitrogenous compound involved in Fe and Zn transport via the phloem and subsequent loading into seeds.[11−15] Increasing NA concentration in the rice seed by overexpression of the rice NA synthase genes (*OsNAS*) was found to enhance not only Fe and Zn concentrations in the seed but also their bioavailability.[16−18] The increased Fe and Zn concentrations in the endosperm of the transgenic rice seed were mainly present as complexes with NA and deoxymugineic acid (DMA).[12,16] DMA is synthesized from NA and is involved not only in the acquisition of Fe from the rhizosphere but also in the phloem transport of Fe.[19,20] There is evidence that DMA is the major Fe chelate in rice phloem sap.[21] Therefore, it is possible that the beneficial effect of N results from an increased synthesis of NA and/or DMA facilitating the transport of Fe and Zn to the grain via the phloem. Another possible explanation is that increased N supply may create a larger sink in the grain for Fe and Zn, as there is evidence of positive correlations between protein and Fe and Zn concentrations among diverse wheat cultivars.[22−24]

The bioavailability of a given element is determined by both its total concentration and its distribution among various chemical species;[25] both the concentration and speciation may vary among different tissues or milling fractions of cereal grains. The effects of N on the total concentrations of Fe and Zn in

Received: January 16, 2014
Revised: May 5, 2014
Accepted: May 7, 2014
Published: May 7, 2014

 © 2014 American Chemical Society

different milling fractions of wheat grain have been studied, with the results showing generally positive effects in different grain fractions such as in the embryo, endosperm, and bran.[5,8,26] However, little is known about the effect of the N supply on the chemical speciation of Fe and Zn in different wheat grain fractions. This information could provide an important clue to understanding the effect of N on Fe and Zn distribution in the grain. Recently, size-exclusion chromatography coupled with inductively coupled plasma mass spectrometry (SEC−ICP-MS) has been used to identify the soluble forms of Fe complexed with soluble phytate and Zn bound to peptides in barley embryos,[27] Fe and Zn bound to NA and DMA in rice endosperm,[12,16] and Fe and Zn bound to NA/DMA, soluble phytate, and high molecular weight compounds in wheat flour.[28] If increasing N supply increases the transport of NA- or DMA-chelated forms of Fe and Zn to the grain, one may expect increased levels of these complexes in wheat grain.

The objective of the present study was therefore to investigate how the N supply affects the chemical speciation of Fe and Zn in the soluble extracts of whole wheat grain and fractions prepared by sequential pearling of the grain.

MATERIALS AND METHODS

Field Experiment. Two wheat cultivars (*Triticum aestivum* cv. Hereward and Paragon) were grown in the Wheat Genetic Improvement Network (WGIN) trial at Rothamsted, United Kingdom, in October 2008. Hereward is a winter wheat, and Paragon is a spring wheat, both being hard wheat with good bread-making properties.[29] The information about the experimental site, climate, and crop husbandry for the experiment has been previously described.[30] The soil was a clay loam with a pH of 8.1, a total Zn concentration of 88.8 mg kg^{-1}, and a DTPA-extractable Zn concentration of 1.6 mg kg^{-1}. Each cultivar was sown in three replicate plots (each 3 × 10 m) with two N application rates (100 and 350 kg of N ha^{-1}, recorded as N100 and N350, respectively). A completely randomized block design was used for the experiment. Nitrogen fertilizer, as ammonium nitrate, was applied in split top dressings in March (nominal growth stage (GS) 24), April (GS 31), and May (GS 32) 2009.[31] In addition, 145 kg of P_2O_5 ha^{-1} and 120 kg of K_2O ha^{-1} as potassium dihydrogen phosphate were applied in March 2009. All plots received 111 kg of sulfate ha^{-1} as kieserite in March 2009.

Pearling of Wheat Grain. The grain was harvested at crop maturity and air-dried to 12% moisture content before pearling. Wholemeal was produced using a ball mill (Glen Creston, Stanmore, England). Pearling was carried out as described by Tosi et al.[32] using a Streckel and Schrader (Hamburg, Germany) pearling mill. This gave fractions 1−6 corresponding to 7%, 6%, 7%, 10%, 10%, and 10% of the grain weight. Previous studies have shown that these fractions are enriched in the pericarp tissue (bran), the aleurone layer, the subaleurone layer, and three progressively more central areas of the starchy endosperm, respectively.[32] The grain remaining after pearling, representing the core endosperm and accounting for about 50% of the total grain weight, was ground in a ball mill and called fraction 7. Between 95% and 97% of the initial mass was recovered in the seven fractions after pearling.

Chemical Analysis. Whole grain (WG) and grain pearling fractions (oven-dried at 50 °C for 10 h) were digested with HNO_3/$HClO_4$ (87/13, v/v) in a heating block.[33] Total Fe, Zn, and P concentrations in digested solutions were determined by inductively coupled plasma optical emission spectrometry (ICP-OES; PerkinElmer Optima 7500 DV, Waltham, MA). Two blanks and a certified reference material (NIST1567a, wheat flour) were included in each batch of digestion to ensure analytical quality. Repeated analysis (n = 7) of NIST 1567a gave mean values (±SD) of 14.1 ± 1.7 mg of Fe kg^{-1}, 11.7 ± 0.5 mg of Zn kg^{-1}, and 1.33 ± 0.03 g of P kg^{-1}, which are in good agreement with the certified values of 14.1 ± 0.5 mg of Fe kg^{-1}, 11.6 ± 0.4 mg of Zn kg^{-1}, and 1.34 ± 0.06 g of P kg^{-1}, respectively. The nitrogen concentration in the samples was determined with the American Society for Testing and Materials (ASTM) standard protocol E1019 using a LECO combustion analysis system based on the Dumas method.[31] Phytate P in the samples was determined according to the method of Haug and Lantzsch.[34]

Wholemeal and three selected grain pearling fractions (fractions 3, 5, and 7, corresponding to the subaleurone layer, central endosperm, and core endosperm, respectively) of both cultivars with two N treatments were extracted according to Eagling et al.[28] Approximately 70 mg (subaleurone layer), 100 mg (whole grain flour), and 140 mg (endosperm) of the selected fractions were extracted with 7 mL of 50 mM Tris−HCl buffer (pH 7.5) in sterile vials. The extracts were incubated at 37 °C for 18 h with shaking at 120 rpm. At the end of the incubation period, the extracts were centrifuged (21000g, 13 °C, 10 min) and the supernatant was filtered through a 0.2 μm filter (Minisart). Total Fe and Zn concentrations in the soluble extracts were determined using ICP-MS (Agilent 7500ce, Agilent Technologies, Palo Alto, CA). Fe and Zn speciation in the soluble extracts was analyzed using SEC−ICP-MS. A Superdex 75 10/300 GL size-exclusion column (glass, 10 × 300 mm, 13 μm cross-linked agarose/dextran, Amersham Biosciences, United States) was used to obtain an optimum separation range between 0.7 and 70 kDa. Tris−HCl buffer (50 mM, pH 7.5) was used as the mobile phase with a flow rate of 0.47 mL min^{-1} at a controlled temperature of 18 °C. The volume of the sample injected was 100 μL. SEC−ICP-MS analyses were performed on a high-performance liquid chromatograph (Agilent 1100 series, Agilent Technologies, Waltham, MA) coupled to an ICP mass spectrometer with the following conditions: rf power, 1.5 kW; carrier gas flow rate, 0.85 L min^{-1}; nebulizer pump speed, 0.2 L min^{-1}; collision/reaction gas, H_2 (3 mL min^{-1}) and He (2 mL min^{-1}). A mixture of He and H_2 was used as the collision/reaction gas to minimize polyatomic interferences on the isotope signals.

Molecular size calibration was performed using a UV detector (Agilent Technologies, Palo Alto, CA) at 214 nm and the standards apoprotein (6.6 kDa), cytochrome c (12.4 kDa), vitamin B12 (1.35 kDa), triglycine (0.19 kDa), and glycine (0.075 kDa) (all from Sigma-Aldrich). A log-linear regression curve was constructed from molecular size versus retention time. A 100 μL volume of 20 mM EDTA/50 mM Tris−HCl buffer (pH 7.5) was injected between flour samples to remove residual metals adsorbed to the column. The column was rinsed twice after bran samples due to the higher levels of Fe and Zn. To remove any residual metals retained by the column, it was cleaned rigorously between batches with 100 μL of pepsin (1 mg mL^{-1}), phytase (2 mg mL^{-1}), NaCl (0.5 M), and acetic acid (10%) (all from Sigma-Aldrich) at a flow rate of 0.2 mL min^{-1} at 36 °C. EDTA (10 mM)/Tris−HCl (50 mM) buffer (pH 7.5) was injected through the column for 1 h each day.

As Tris−HCl provided a pH buffer only, Tris−HCl-extractable Fe and Zn can be considered to represent the water-soluble fraction. Insoluble Fe and Zn concentrations were estimated by the difference between the total and soluble concentrations. The concentrations of Fe and Zn bound to the individual peaks in the Tris--HCl-extractable fractions were estimated by multiplying the relative peak areas by the soluble concentrations of these elements in the extracts.

Statistical Analysis. The significance of the effects of N application rates, cultivars, and pearling fractions and their interactions on Fe and Zn concentrations was evaluated by analysis of variance (ANOVA). Significant differences between treatment means were determined using Tukey's honest significant difference (HSD) test at the 5% level (P < 0.05) using GenStat, 14th ed. (VSN International, Hemel Hempstead, U.K.).

RESULTS

Grain Yields. Increasing the N dose from 100 to 350 kg ha^{-1} increased the grain yield by 33% and 27% in the cultivars Hereward and Paragon, respectively (P < 0.001; Supplementary Figure 1, Supporting Information). There was no significant

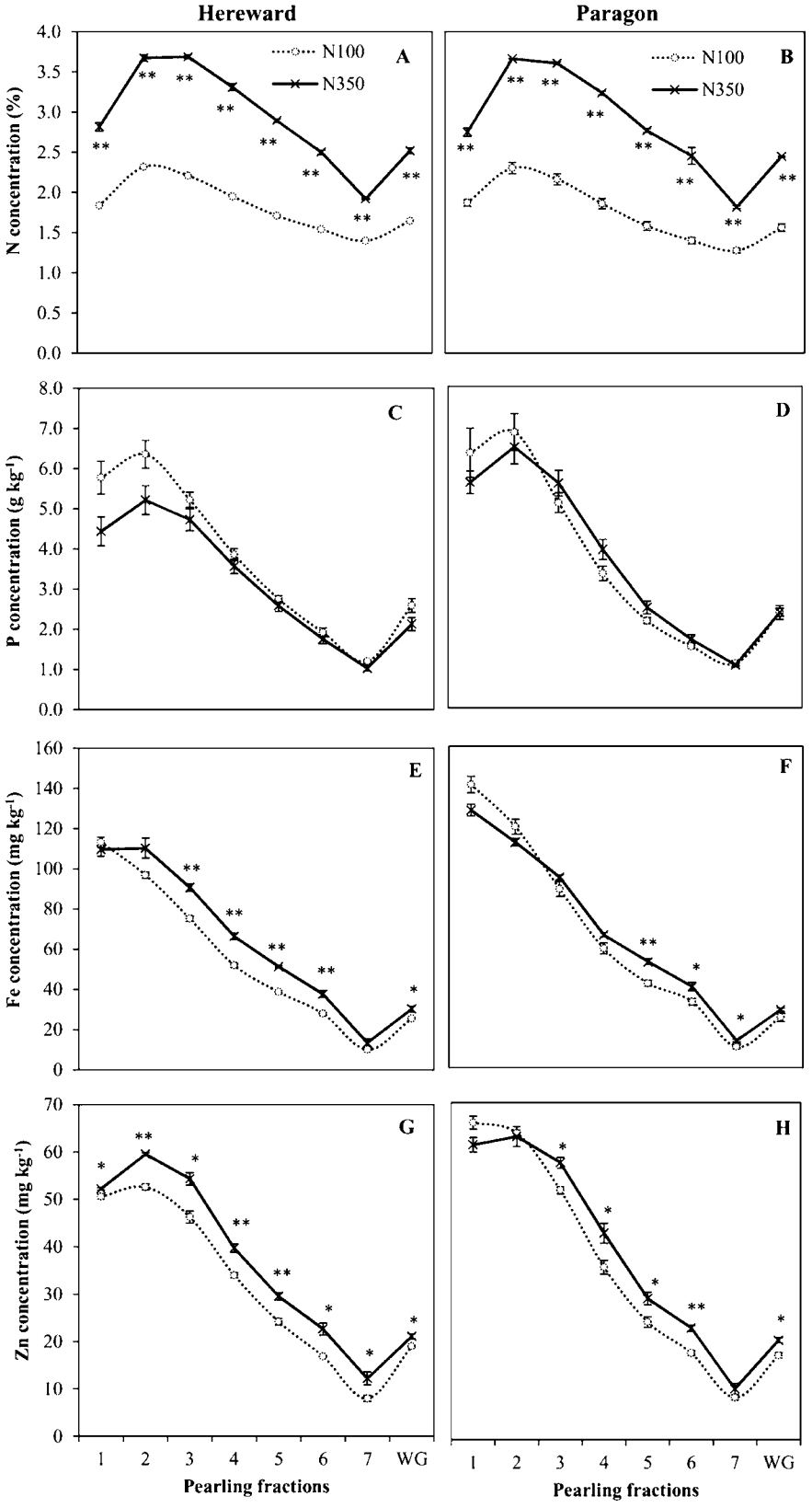

Figure 1. Effects of N treatments (low N, 100 kg of N ha^{-1}; high N, 350 kg of N ha^{-1}) on the N, P, Fe, and Zn concentrations in the pearling fractions and whole grain of the wheat cultivars Hereward and Paragon. Data are means ± SE of three independent replications. One and two asterisks indicate significant differences between the two N treatments for the same pearling fraction at $P < 0.05$ and $P < 0.01$, respectively. Key: fraction 1, bran; fraction 2, aleurone layer; fraction 3, subaleurone layer; fractions 4–6, three progressively more central areas of the starchy endosperm; fraction 7, core endosperm; WG, whole grain.

dx.doi.org/10.1021/jf500273x | J. Agric. Food Chem. 2014, 62, 4738–4746

difference between the two cultivars in grain yield at either level of N treatment.

Distributions of Fe and Zn in Different Pearling Fractions. Figure 1 shows the effects of the N supply on the total concentrations of N, P, Fe, and Zn in WG and pearling fractions of the two wheat cultivars. Two-way ANOVA revealed significant effects of the N supply on the N, P, Fe, and Zn concentrations and significant effects of the cultivar on the N and Zn concentrations of WG (Supplementary Table 1, Supporting Information). The interactions between N supply and cultivar were also significant for the P and phytate P concentrations of WG. Three-way ANOVA showed significant effects of the interactions of N supply, cultivar, and pearling fraction on the Fe and Zn concentrations with the exception of the nonsignificant effect of the interaction between N and cultivar on the Zn concentration (Supplementary Table 1). The high N treatment (350 kg of N ha^{-1}) significantly increased the N concentrations in all pearling fractions and WG of both cultivars, the effect being more pronounced in the outer layers (pearling fractions 2 and 3) than in the core endosperm (Figure 1A,B). There was no significant difference in the P concentration of WG or pearling fractions between the two N treatments (Figure 1C,D). The high N treatment significantly decreased the phytate P concentration in the core endosperm (fraction 7) in Hereward, but had no significant effects in Paragon (Figure 2). The high N treatment significantly increased the total Zn concentration in WG of both cultivars and the total Fe concentration in Hereward (Figure 1E–H). There were also significant and positive effects of the N supply on the Fe and Zn concentrations in most of the pearling fractions of Hereward (Figure 1E–G). In Paragon N decreased the Fe and Zn concentrations in the bran and/or aleurone layer but increased their concentrations in the inner fractions (Figure 1F,H). In general, the effect of N was larger and more consistent in Hereward than in Paragon.

There was a progressive decrease in the concentrations of N, P, Fe, and Zn from the outer to the inner part of the grain (Figure 1). For example, the highest concentrations of N, P, Fe, and Zn in the outermost bran or aleurone layer (fraction 1 or 2) were 0.7-, 4.3-, 10.4-, and 5.6-fold higher than those in the inner core endosperm (fraction 7) in the low N treatment, while the corresponding values were 0.9-, 4.1-, 7.2-, and 3.9-fold higher in the high N treatment, respectively, in Hereward. Similar results were also found in Paragon.

Supplementary Table 2 (Supporting Information) presents the effects of the two N treatments on the distributions of Fe and Zn in different pearling fractions. In Hereward, the outermost three layers (bran, aleurone layer, and subaleurone layer) constituted about 20% of the grain mass, but accounted for 54% and 47%, respectively, of the total Fe and Zn contents in the low N treatment. In the high N treatment, these outer layers accounted for slightly less of the grain Fe (48%) and Zn (41%) than in the low N treatment. By contrast, the remaining core endosperm, constituting about 50% of the grain mass, contained only 14–16% and 19–24%, respectively, of the total Fe and Zn contents (Supplementary Tables 2 and 3, Supporting Information). Similar results were also found in Paragon.

Fe and Zn Speciation in Grain Pearling Fractions. Figures 3 and 4 show SEC–ICP-MS analysis of the Fe and Zn species in the Tris–HCl extracts of wholemeal (Figures 3A,B and 4A,B) and pearling fractions 3 (Figures 3C,D and 4C,D), 5 (Figures 3E,F and 4E,F), and 7 (Figures 3G,H and 4G,H). Due to the long run time for each sample, the samples of the two cultivars were analyzed in two separate batches. For this reason, the absolute peak heights or peak areas were not comparable between the two cultivars.

For Fe speciation, the extracts of all samples contained a low molecular weight (LMW; 1.5 ± 0.1 kDa) complex which eluted at ~36 min. Our previous study[28] showed that this LMW peak probably contains a mixture of Fe–DMA and Fe–NA. Similarly, the LMW peak has been shown to contain a mixture of Fe–DMA and Fe–NA in rice extracts.[12,16] The wheat extracts also contained one or two high molecular weight (HMW) forms of Fe at retention times of ~16 and 18 min (corresponding to >70 ± 0.4 and 20 ± 0.4 kDa, respectively). The identities of these HMW peaks are unknown, but could be soluble proteins.[28] Additionally, the extracts from some fractions, such as the subaleurone layer and the central endosperm of Hereward and the subaleurone layer of Paragon, showed the presence of a medium molecular weight (MMW) complex at a retention time of ~29 min (corresponding to 5.0 ± 0.1 kDa) (Figure 3C–E). The study by Eagling et al.[28] showed that this peak coeluted with P, suggesting that it is a soluble iron phytate. Persson et al.[27] identified a similar MMW peak in the extracts of barley embryo as a soluble iron phytate oligomer.

For Zn speciation, the extracts of all samples contained an HMW complex (>70 kDa) at a retention time of ~16 min and an LMW complex at a retention time of ~35 min (1.9 ± 0.2 kDa) (Figure 4); the latter has been identified as a mixture of Zn–NA and Zn–DMA complexes in rice endosperm.[12] A

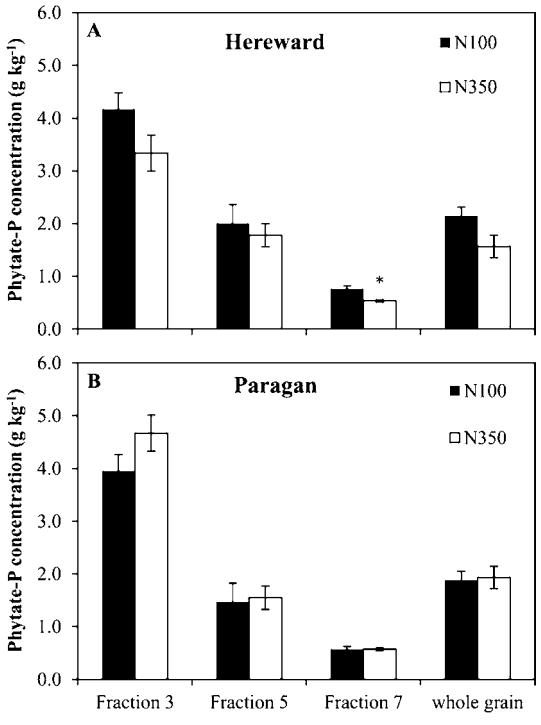

Figure 2. Effects of N treatments (low N, 100 kg of N ha^{-1}; high N, 350 kg of N ha^{-1}) on the phytate P concentrations in the selected pearling fractions and wholemeal flour of the wheat cultivars Hereward and Paragon. Data are means ± SE of three independent replications. An asterisk indicates a significant difference between the two N treatments for the same pearling fraction at $P < 0.05$. Key: fraction 3, subaleurone layer; fraction 5, central endosperm; fraction 7, core endosperm.

dx.doi.org/10.1021/jf500273x | J. Agric. Food Chem. 2014, 62, 4738–4746

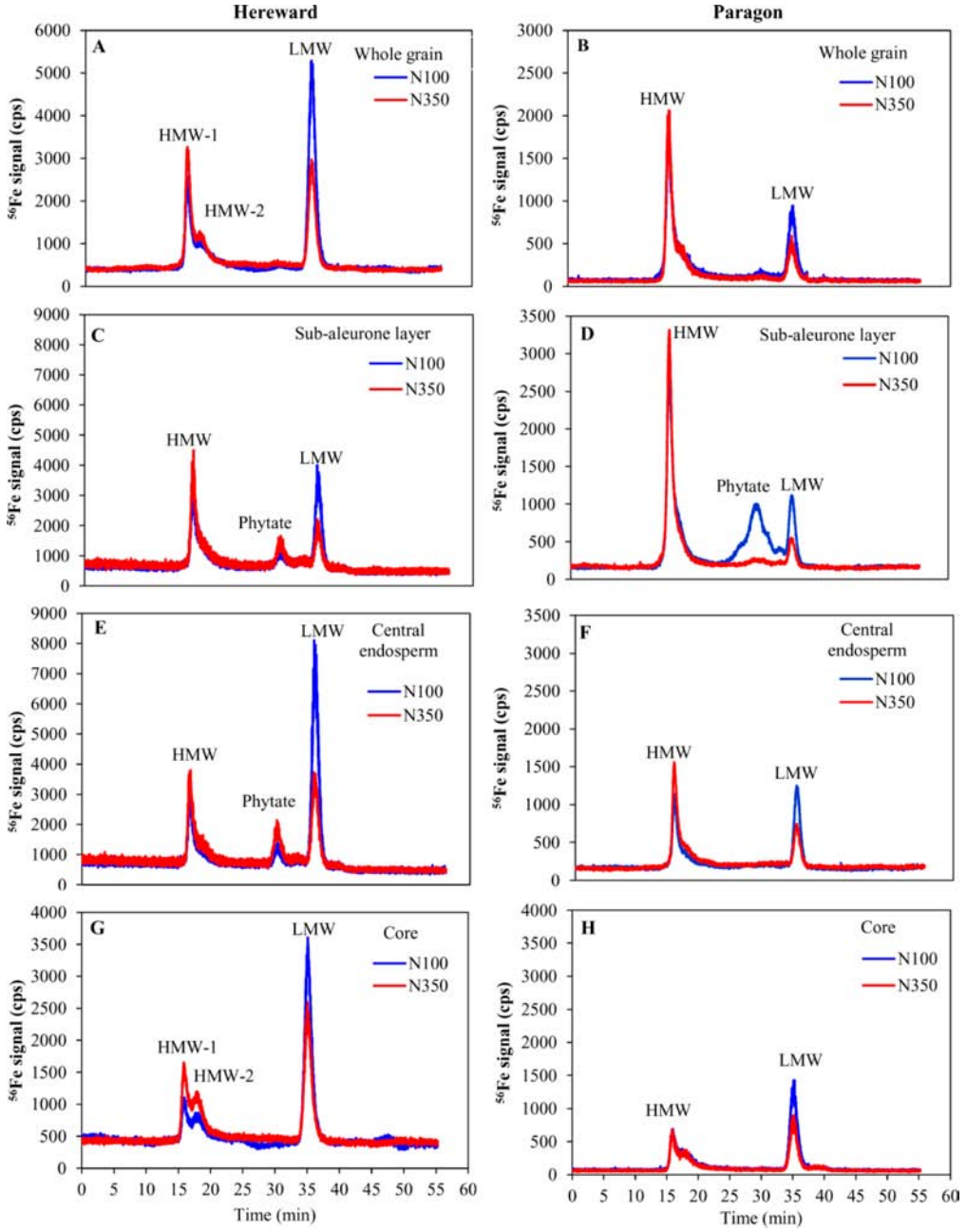

Figure 3. Chromatograms of Fe speciation in the 50 mM Tris−HCl buffer (pH 7.5) extracts of wheat fractions (wholemeal flour, subaleurone layer, central endosperm, and core endosperm) as determined by SEC−ICP-MS.

comparison with the Zn−NA and Zn−DMA standards suggests that the LMW peak in wheat extract is more likely to be only Zn−NA.[28]

The nitrogen supply had a distinct effect on Fe species in the soluble extracts. The high N treatment significantly enhanced the peak area of HMW Fe, but decreased that of LMW Fe in both cultivars, as well as that of the soluble iron phytate (MMW) in the subaluerone layer of Paragon (Figure 3). Generally, the effect of N on Zn species was similar to that for Fe species, although less pronounced (Figure 4).

Tables 1 and 2 present the concentrations and percentage distributions of Fe and Zn species, respectively, in the selected samples of both cultivars. The nitrogen supply had opposite effects on the soluble (extracted in 50 mM Tris−HCl buffer, pH 7.5) and insoluble fractions of Fe and Zn. In the wholemeal and all pearling fractions except the core endosperm of Hereward, the concentrations of soluble Fe were significantly lower in the high N than in the low N treatment. Similar but less pronounced results were also found for the soluble Zn concentration. By contrast, the insoluble fractions of Fe and Zn were significantly increased by the high N treatment. In the wholemeal of Hereward, soluble Fe represented 33.5% and 21.6% of the total Fe concentrations in the low and high N treatments, respectively, with the remainder being the insoluble fractions. For Zn, the soluble fraction accounted for 46.2% and 35.3%, respectively, in the low and high N treatments. There was a general trend of increasing percentage of soluble Fe and Zn from the subaleurone/central endosperm layer to the inner core endosperm. For Paragon, the effects of N on insoluble and soluble Fe and Zn concentrations were similar to those

dx.doi.org/10.1021/jf500273x | J. Agric. Food Chem. 2014, 62, 4738−4746

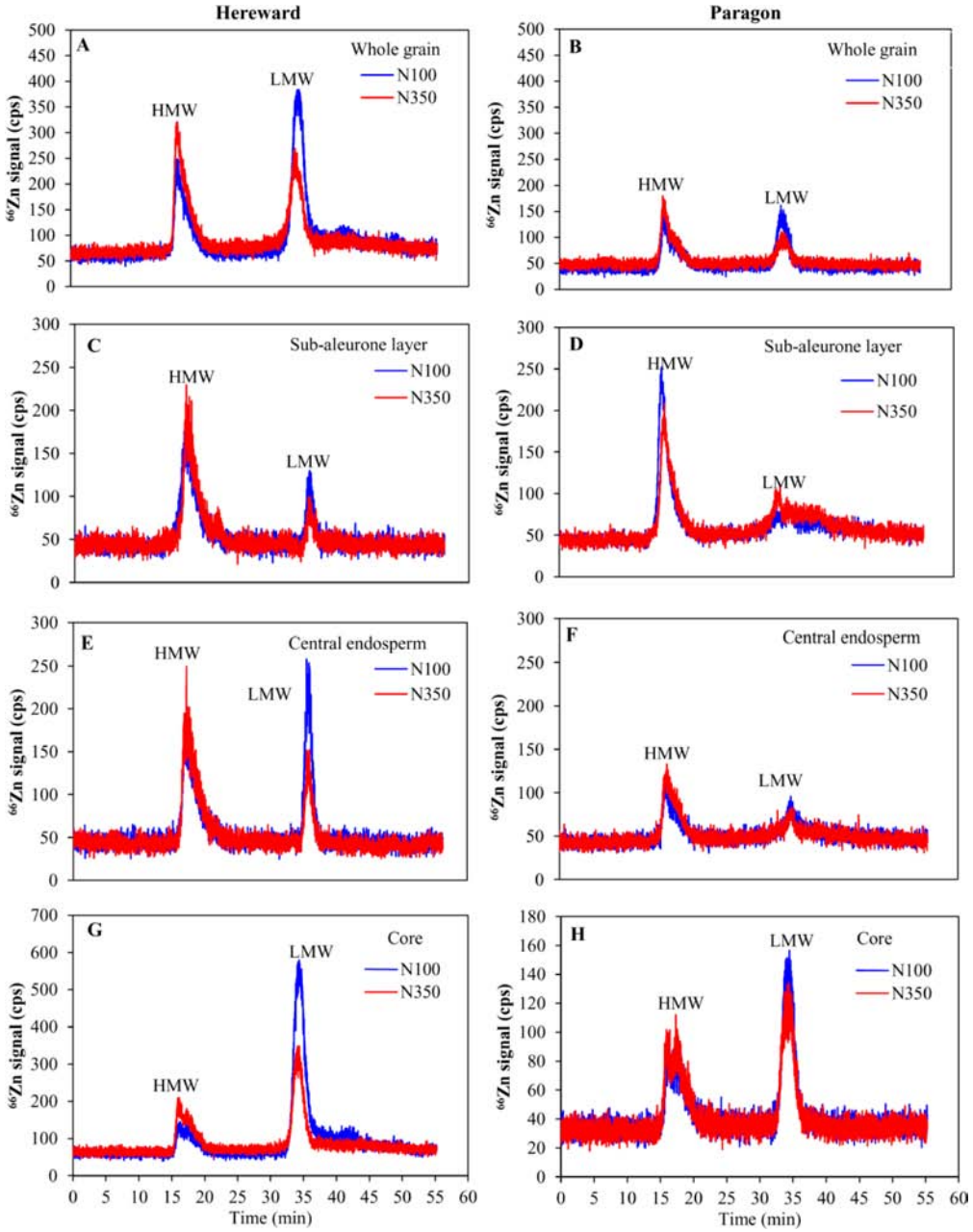

Figure 4. Chromatograms of Zn speciation in the 50 mM Tris−HCl buffer (pH 7.5) extracts of wheat fractions (wholemeal flour, subaleurone layer, central endosperm, and core endosperm) as determined by SEC−ICP-MS.

observed in Hereward with the exception of the wholemeal, where the soluble Zn concentration was significantly increased by the high N treatment. In general, the effects of N were more significant and consistent in Hereward than in Paragon.

Among the soluble species, the concentrations of LMW Fe (likely Fe−NA and Fe−DMA complexes) and LMW Zn (likely Zn−NA) were lower in the high N than in the low N treatment, the differences being significant in most of the pearling fractions and the wholemeals of both cultivars (Tables 1 and 2). Among all pearling fractions of the two cultivars, soluble LMW Fe accounted for 1.5−24.8% of the total Fe concentration; this percentage was the highest in the core endosperm and was significantly decreased by the high N treatment in most pearling fractions. Soluble LMW Zn accounted for 4.8−58.4% of the total Zn concentration, which was also significantly decreased by the high N treatment in most pearling fractions. The effects of N on other soluble species of Fe or Zn (i.e., those associated with HMW and soluble phytate) were not significant.

DISCUSSION

The present study has shown that increasing the N application rate from 100 to 350 kg ha^{-1} generally increased the concentrations of Fe and Zn in wheat grain, although there were some subtle differences between the two wheat cultivars and between the different pearling fractions (Figure 1). The positive effect of N is generally consistent with other studies,[5,8] although the extent of increase was relatively small in the present study possibly due to a dilution effect of increased yield and limited availability of Zn and Fe in the soil with a high pH. Similar to previous studies,[26,35] both Fe and Zn concentrations were found to decrease from the outer layer of the grain to the

dx.doi.org/10.1021/jf500273x | J. Agric. Food Chem. 2014, 62, 4738−4746

Table 1. Insoluble Fe Concentration, Soluble Fe Concentration, Soluble Fe Chemical Speciation Concentrations, and Fe Species Content (%) in Different Wheat Grain Pearling Fractions of the Two Cultivars As Affected by N Treatments[a]

					soluble Fe chemical speciation concn (mg kg^{-1})				Fe species content (%)				
cultivar	fraction	N level (kg ha^{-1})	insoluble Fe concn (mg kg^{-1})	soluble Fe concn (mg kg^{-1})	HMW-1	HMW-2	iron phytate	LMW	insoluble Fe	HMW-1	HMW-2	iron phytate	LMW
Hereward	whole grain	100	16.9 e	8.5 bc	2.0 bc	1.0 a	–	5.5 a	66.5 c	7.8 ab	4.0 a	–	21.7 a
		350	24.3 d	6.7 c	2.9 b	0.9 a	–	2.9 b	78.4 b	9.1 a	3.1 a	–	9.4 c
	subaleurone layer	100	60.2 b	13.7 a	6.7 a	–	1.2 ab	5.8 a	81.5 ab	9.1 a	–	1.6 a	7.9 cd
		350	81.7 a	10.8 b	7.1 a	–	1.4 a	2.3 bc	88.3 a	7.6 ab	–	1.5 a	2.5 e
	central endosperm	100	29.6 d	8.4 bc	2.2 bc	–	0.6 b	5.6 a	77.9 b	5.9 ab	–	1.5 a	14.7 b
		350	45.2 c	6.3 c	2.9 b	–	1.1 ab	2.3 bc	87.7 a	5.7 ab	–	2.2 a	4.4 de
	core endosperm	100	6.8 f	3.3 d	0.4 c	0.4 a	–	2.5 bc	67.1 c	4.2 b	3.8 a	–	24.8 a
		350	11.5 ef	3.5 d	0.9 bc	0.7 a	–	1.8 c	76.8 b	5.8 ab	4.9 a	–	12.5 bc
Paragon	whole grain	100	19.6 de	6.7 c	4.8 b	–	–	1.9 bc	74.0 de	18.6 a	–	–	7.4 bc
		350	23.6 d	5.0 dc	4.1 b	–	–	0.9 c	82.4 abcd	14.3 ab	–	–	3.3 dc
	subaleurone layer	100	64.0 b	27.4 a	15.0 a	–	8.7	3.7 a	70.0 e	16.4 a	–	9.5	4.0 dc
		350	80.0 a	14.6 b	13.2 a	–	–	1.4 c	84.6 abc	13.9 abc	–	–	1.5 d
	central endosperm	100	36.9 c	6.5 c	3.2 bc	–	–	3.3 ab	85.0 ab	7.4 bcd	–	–	7.6 bc
		350	48.6 c	5.1 dc	3.8 b	–	–	1.2 c	90.6 a	7.1 bcd	–	–	2.3 d
	core endosperm	100	8.3 e	2.9 d	0.7 d	0.4 a	–	1.8 c	74.4 cde	6.3 dc	3.6 a	–	15.6 a
		350	10.8 e	2.8 d	0.9 dc	0.5 a	–	1.4 c	79.3 bcde	6.3 d	4.1 a	–	10.3 b

[a]A dash means not detected. Means in a column followed by different letters are significantly different among different pearling fractions and N treatments ($P < 0.05$).

Table 2. Insoluble Zn Concentration, Soluble Zn Concentration, Soluble Zn Chemical Speciation Concentrations, and Zn Species Content (%) in Different Wheat Grain Pearling Fractions of the Two Cultivars As Affected by N Treatments[a]

					soluble Zn chemical speciation concn (mg kg^{-1})		Zn species content (%)		
cultivar	fraction	N level (kg ha^{-1})	insoluble Zn concn (mg kg^{-1})	soluble Zn concn (mg kg^{-1})	HMW Zn	LMW Zn	insoluble Zn	HMW Zn	LMW Zn
Hereward	whole grain	100	10.2 de	8.8 b	3.3 bcd	5.5 a	53.8 ab	17.4 ab	28.8 b
		350	14.0 de	7.6 bc	4.3 bc	3.3 dc	64.7 a	20.0 ab	15.3 bcd
	subaleurone layer	100	30.8 b	14.2 a	10.3 a	3.8 bc	68.5 a	23.0 a	8.5 dc
		350	40.6 a	12.9 a	10.4 a	2.6 de	75.8 a	19.4 ab	4.8 d
	central endosperm	100	16.1 d	7.6 bc	4.2 bc	3.5 bcd	67.9 a	17.6 ab	14.5 bcd
		350	22.3 c	7.1 bcd	5.4 b	1.7 e	75.9 a	18.2 ab	5.9 d
	core	100	2.4 f	5.1 dc	0.7 d	4.3 b	31.6 b	10.0 b	58.4 a
		350	8.2 ef	4.9 d	2.1 dc	2.8 d	62.5 a	15.8 ab	21.7 bc
Paragon	whole grain	100	7.2 b	10.9 d	6.5 bcd	4.4 ab	39.7 bc	35.9 bc	24.4 abc
		350	5.4 b	15.6 c	8.8 bc	6.8 a	25.5 dc	42.4 bc	32.1 ab
	subaleurone layer	100	6.8 b	45.5 a	39.1 a	6.3 ab	12.9 d	75.0 a	12.1 c
		350	19.1 a	39.5 b	33.4 a	6.1 ab	32.6 bc	56.9 ab	10.4 c
	central endosperm	100	14.9 a	9.8 d	6.5 bcd	3.2 ab	60.5 a	26.5 c	13.0 bc
		350	19.0 a	11.6 d	9.9 b	1.7 b	62.1 a	32.5 c	5.5 c
	core	100	3.8 b	5.5 e	1.9 d	3.6 ab	41.2 bc	19.8 c	39.0 a
		350	5.5 b	5.9 e	3.2 dc	2.7 ab	47.8 ab	27.8 c	24.4 abc

[a]Means in a column followed by different letters are significantly different among different pearling fractions and N treatments ($P < 0.05$).

central endosperm, a pattern that reflects the localization of the phytate granules in the aleurone layer and their role in sequestering Fe and Zn.[36] It should be noted that, due to the presence of a crease in the wheat grain, the pearling method used may not completely remove the bran and the aleurone layer from the central endosperm fraction, thus explaining the presence of some soluble phytate P in this fraction (Figure 3E). However, the positive effect of the N supply on the Fe and Zn concentrations was not related to phytate, because its concentration was unaffected or even slightly decreased by

dx.doi.org/10.1021/jf500273x | J. Agric. Food Chem. 2014, 62, 4738−4746

the high N treatment (Figure 2). Small concentrations of soluble iron phytate complexes were found in some of the pearling fractions, but they were not significantly affected by N treatments.

It has been shown that Fe and Zn are likely to be complexed with NA and/or DMA during their transport in the phloem, an important process for the translocation of these minerals from leaves to grains.[13,15,19,20] A high N supply may enhance NA and/or DMA biosynthesis and therefore its availability for the phloem transport of Fe and Zn.[4,10,37] However, contrary to this hypothesis, we found that the concentrations of LMW Fe (likely Fe−NA/Fe−DMA) and LMW Zn (likely Zn−NA) in the different pearling fractions and in the whole grain were significantly decreased by the high N treatment (Figures 3 and 4, Tables 1 and 2). Mainly due to this negative effect, N also significantly decreased the concentrations and percentages of soluble Fe and Zn. These results suggest that enhanced NA and/or DMA availability is not the reason for the positive effect of N on Fe and Zn accumulation in wheat grain. Alternatively, it is possible that elevated NA and/or DMA are responsible for the Fe and Zn transport into the grain but that Fe and Zn are then sequestered in other forms.

Interestingly, insoluble forms of Fe and Zn were significantly increased by the high N treatment, especially in Hereward (Tables 1 and 2). This effect was much larger than the negative effect of N on the soluble Fe and Zn, resulting in an overall increase in the total concentrations (Figure 1). This N effect may be explained by an increased content of protein (Figure 1A,B), which may bind Fe and Zn in the grain. A recent study using high-resolution secondary ion mass spectrometry (NanoSIMS) showed that Fe in the wheat endosperm is associated with the protein matrix surrounding the starch granules and the protein bodies.[38] The identities of the proteins that bind Fe and Zn in the endosperm are not known, but the lack of Fe signals inside the protein bodies in the NanoSIMS images suggests that they are not storage proteins. Ferritins are Fe storage proteins, but they are soluble[39] and represent only a small proportion of the total Fe in cereals such as wheat.[40,41] Other compounds such as tannins and certain types of insoluble fiber may also interact with Fe and Zn,[42] but may not explain the effect of N. Taken together, the results of the present study suggest that a high N supply provides a larger protein sink for the storage of Fe and Zn in the wheat grain. This larger sink may also sequester Fe and Zn at the expense of the soluble forms, including Fe and Zn complexes with NA/DMA, resulting in lower concentrations of the soluble Fe and Zn.

The effect of N in influencing the distribution of Fe and Zn between the soluble species and the insoluble fraction on their bioavailability to humans remains to be investigated. Previous studies have shown that the Fe−NA and Zn−NA complexes in rice are bioavailable using an in vitro digestion/Caco-2 cell culture model and mouse feeding experiments.[12,16,18] Therefore, decreased NA−Fe and NA−Zn may have negative effects on Fe and Zn bioavailability. However, Fe and Zn bound to insoluble proteins may become bioavailable during gastrointestinal digestion processes. Additionally, the positive effect of N was not associated with an increased phytate level, which may be favorable to Fe and Zn bioavailability.

■ ASSOCIATED CONTENT

Supporting Information

Grain yield of two wheat cultivars as affected by N treatments (Supplementary Figure 1), two-way and three-way ANOVA) of the effects of the N supply, cultivars, and pearling fractions on the concentrations of N, P, Fe, and Zn in the whole grain and pearling fractions of wheat (Supplementary Table 1), effects of N treatments on the distributions of Fe and Zn in different pearling fractions of the two wheat cultivars (Supplementary Table 2), and relative weight percentage of each grain tissue after pearling (Supplementary Table 3). This material is available free of charge via the Internet at http://pubs.acs.org.

■ AUTHOR INFORMATION

Corresponding Author

*E-mail: Fangjie.Zhao@njau.edu.cn. Phone: +86 (0)25 84396509. Fax: +86 (0)25 84399551.

Funding

This research was funded by HarvestPlus Project 8055, "Optimizing the quality, species and availability of Fe in modern bread wheat cultivars in order to prevent global Fe deficiencies". Y.-F.X. acknowledges funding by the China Scholarship Council. Grain samples were from field trials at Rothamsted Research supported by the Defra-funded Wheat Genetic Improvement Network (WGIN) project. Rothamsted Research receives strategic funding from the Biotechnological and Biological Sciences Research Council (BBSRC).

Notes

The authors declare no competing financial interest.

■ ACKNOWLEDGMENTS

We thank Adrian Crosland for assistance in sample analysis and Rodger White for statistical advice.

■ REFERENCES

(1) Welch, R. M.; Graham, R. D. Breeding for micronutrients in staple food crops from a human nutrition perspective. *J. Exp. Bot.* **2004**, *55*, 353−364.

(2) White, P. J.; Broadley, M. R. Biofortification of crops with seven mineral elements often lacking in human diets—iron, zinc, copper, calcium, magnesium, selenium and iodine. *New Phytol.* **2009**, *182*, 49−84.

(3) Cakmak, I. Enrichment of cereal grains with zinc: agronomic or genetic biofortification? *Plant Soil* **2008**, *302*, 1−17.

(4) Cakmak, I.; Pfeiffer, W. H.; McClafferty, B. Biofortification of durum wheat with zinc and iron. *Cereal Chem.* **2010**, *87*, 10−20.

(5) Kutman, U. B.; Yildiz, B.; Cakmak, I. Improved nitrogen status enhances zinc and iron concentrations both in the whole grain and the endosperm fraction of wheat. *J. Cereal Sci.* **2011**, *53*, 118−125.

(6) Zhang, Y. Q.; Shi, R. L.; Rezaul, K. M.; Zhang, F. S.; Zou, C. Q. Iron and zinc concentrations in grain and flour of winter wheat as affected by foliar application. *J. Agric. Food Chem.* **2010**, *58*, 12268−12274.

(7) Gooding, M. J.; Fan, M. S.; McGrath, S. P.; Shewry, P. R.; Zhao, F. J. Contrasting effects of dwarfing alleles and nitrogen availability on mineral concentrations in wheat grain. *Plant Soil* **2012**, *360*, 93−107.

(8) Shi, R. L.; Zhang, Y. Q.; Chen, X. P.; Sun, Q. P.; Zhang, F. S.; Römheld, V.; Zou, C. Q. Influence of long-term nitrogen fertilization on micronutrient density in grain of winter wheat (*Triticum aestivum* L.). *J. Cereal Sci.* **2010**, *51*, 165−170.

(9) Xue, Y. F.; Yue, S. C.; Zhang, Y. Q.; Cui, Z. L.; Chen, X. P.; Yang, F. C.; Cakmak, I.; McGrath, S. P.; Zhang, F. S.; Zou, C. Q. Grain and shoot zinc accumulation in winter wheat affected by nitrogen management. *Plant Soil* **2012**, *361*, 153−163.

(10) Erenoglu, E. B.; Kutman, U. B.; Ceylan, Y.; Yildiz, B.; Cakmak, I. Improved nitrogen nutrition enhances root uptake, root-to-shoot translocation and remobilization of zinc (^{65}Zn) in wheat. *New Phytol.* **2011**, *189*, 438−448.

(11) Borg, S.; Brinch-Pedersen, H.; Tauris, B.; Holm, P. B. Iron transport, deposition and bioavailability in the wheat and barley grain. *Plant Soil* **2009**, *325*, 15−24.
(12) Lee, S.; Persson, D. P.; Hansen, T. H.; Husted, S.; Schjoerring, J. K.; Kim, Y. S.; Jeon, U. S.; Kim, Y. K.; Kakei, Y.; Masuda, H.; Nishizawa, N. K.; An, G. Bio-available zinc in rice seeds is increased by activation tagging of nicotianamine synthase. *Plant Biotechnol. J.* **2011**, *9*, 865−873.
(13) Curie, C.; Cassin, G.; Couch, D.; Divol, F.; Higuchi, K.; Le Jean, M.; Misson, J.; Schikora, A.; Czernic, P.; Mari, S. Metal movement within the plant: contribution of nicotianamine and yellow stripe 1-like transporters. *Ann. Bot.* **2009**, *103*, 1−11.
(14) Tauris, B.; Borg, S.; Gregersen, P. L.; Holm, P. B. A roadmap for zinc trafficking in the developing barley grain based on laser capture microdissection and gene expression profiling. *J. Exp. Bot.* **2009**, *60*, 1333−1347.
(15) Trampczynska, A.; Kuepper, H.; Meyer-Klaucke, W.; Schmidt, H.; Clemens, S. Nicotianamine forms complexes with Zn(II) in vivo. *Metallomics* **2010**, *2*, 57−66.
(16) Lee, S.; Jeon, U. S.; Lee, S. J.; Kim, Y. K.; Persson, D. P.; Husted, S.; Schjorring, J. K.; Kakei, Y.; Masuda, H.; Nishizawa, N. K.; An, G. Iron fortification of rice seeds through activation of the nicotianamine synthase gene. *Proc. Natl. Acad. Sci. U.S.A.* **2009**, *106*, 22014−22019.
(17) Johnson, A. A. T.; Kyriacou, B.; Callahan, D. L.; Carruthers, L.; Stangoulis, J.; Lombi, E.; Tester, M. Constitutive overexpression of the *OsNAS* gene family reveals single-gene strategies for effective iron- and zinc-biofortification of rice endosperm. *PLoS One* **2011**, *6*.
(18) Zheng, L. Q.; Cheng, Z. Q.; Ai, C. X.; Jiang, X. H.; Bei, X. S.; Zheng, Y.; Glahn, R. P.; Welch, R. M.; Miller, D. D.; Lei, X. G.; Shou, H. X. Nicotianamine, a novel enhancer of rice iron bioavailability to humans. *PLoS One* **2010**, *5*.
(19) Bashir, K.; Ishimaru, Y.; Nishizawa, N. K. Iron uptake and loading into rice grains. *Rice* **2010**, *3*, 122−130.
(20) Inoue, H.; Kobayashi, T.; Nozoye, T.; Takahashi, M.; Kakei, Y.; Suzuki, K.; Nakazono, M.; Nakanishi, H.; Mori, S.; Nishizawa, N. K. Rice OsYSL15 is an iron-regulated iron(III)-deoxymugineic acid transporter expressed in the roots and is essential for iron uptake in early growth of the seedlings. *J. Biol. Chem.* **2009**, *284*, 3470−3479.
(21) Nishiyama, R.; Kato, M.; Nagata, S.; Yanagisawa, S.; Yoneyama, T. Identification of Zn-nicotianamine and Fe-2′-deoxymugineic acid in the phloem sap from rice plants (*Oryza sativa* L.). *Plant Cell Physiol.* **2012**, *53*, 381−390.
(22) Morgounov, A.; Gomez-Becerra, H. F.; Abugalieva, A.; Dzhunusova, M.; Yessimbekova, M.; Muminjanov, H.; Zelenskiy, Y.; Ozturk, L.; Cakmak, I. Iron and zinc grain density in common wheat grown in Central Asia. *Euphytica* **2007**, *155*, 193−203.
(23) Peleg, Z.; Saranga, Y.; Yazici, A.; Fahima, T.; Ozturk, L.; Cakmak, I. Grain zinc, iron and protein concentrations and zinc-efficiency in wild emmer wheat under contrasting irrigation regimes. *Plant Soil* **2008**, *306*, 57−67.
(24) Zhao, F. J.; Su, Y. H.; Dunham, S. J.; Rakszegi, M.; Bedo, Z.; McGrath, S. P.; Shewry, P. R. Variation in mineral micronutrient concentrations in grain of wheat lines of diverse origin. *J. Cereal Sci.* **2009**, *49*, 290−295.
(25) Theil, E. C. Iron, ferritin, and nutrition. *Annu. Rev. Nutr.* **2004**, *24*, 327−343.
(26) Cakmak, I.; Kalayci, M.; Kaya, Y.; Torun, A. A.; Aydin, N.; Wang, Y.; Arisoy, Z.; Erdem, H.; Yazici, A.; Gokmen, O.; Ozturk, L.; Horst, W. J. Biofortification and localization of zinc in wheat grain. *J. Agric. Food Chem.* **2010**, *58*, 9092−9102.
(27) Persson, D. P.; Hansen, T. H.; Laursen, K. H.; Schjoerring, J. K.; Husted, S. Simultaneous iron, zinc, sulfur and phosphorus speciation analysis of barley grain tissues using SEC-ICP-MS and IP-ICP-MS. *Metallomics* **2009**, *1*, 418−426.
(28) Eagling, T.; Neal, A. L.; McGrath, S. P.; Fairweather-Tait, S.; Shewry, P. R.; Zhao, F. J. Distribution and speciation of iron and zinc in grain of two wheat genotypes. *J. Agric. Food Chem.* **2014**, *62*, 708−716.
(29) National Association of British and Irish Millers Wheat Guide. www.nabim.org.uk (accessed on May 2, 2014).
(30) Barraclough, P. B.; Howarth, J. R.; Jones, J.; Lopez-Bellido, R.; Parmar, S.; Shepherd, C. E.; Hawkesford, M. J. Nitrogen efficiency of wheat: genotypic and environmental variation and prospects for improvement. *Eur. J. Agron.* **2010**, *33*, 1−11.
(31) He, J.; Penson, S.; Powers, S. J.; Hawes, C.; Shewry, P. R.; Tosi, P. Spatial patterns of gluten protein and polymer distribution in wheat grain. *J. Agric. Food Chem.* **2013**, *61*, 6207−6215.
(32) Tosi, P.; Gritsch, C. S.; He, J.; Shewry, P. R. Distribution of gluten proteins in bread wheat (*Triticum aestivum*) grain. *Ann. Bot.* **2011**, *108*, 23−35.
(33) Zhao, F. J.; McGrath, S. P.; Crosland, A. R. Comparison of three wet digestion methods for the determination of plant sulphur by inductively coupled plasma atomic emission spectroscopy (ICP-AES). *Commun. Soil Sci. Plant Anal.* **1994**, *25*, 407−418.
(34) Haug, W.; Lantzsch, H. J. Sensitive method for the rapid determination of phytate in cereals and cereal products. *J. Sci. Food Agric.* **1983**, *34*, 1423−1426.
(35) Liu, Z. H.; Wang, H. Y.; Wang, X. E.; Zhang, G. P.; Chen, P. D.; Liu, D. J. Phytase activity, phytate, iron, and zinc contents in wheat pearling fractions and their variation across production locations. *J. Cereal Sci.* **2007**, *45*, 319−326.
(36) Brinch-Pedersen, H.; Borg, S.; Tauris, B.; Holm, P. B. Molecular genetic approaches to increasing mineral availability and vitamin content of cereals. *J. Cereal Sci.* **2007**, *46*, 308−326.
(37) Aciksoz, S. B.; Ozturk, L.; Gokmen, O. O.; Roemheld, V.; Cakmak, I. Effect of nitrogen on root release of phytosiderophores and root uptake of Fe(III)-phytosiderophore in Fe-deficient wheat plants. *Physiol. Plant.* **2011**, *142*, 287−296.
(38) Moore, K. L.; Zhao, F. J.; Gritsch, C. S.; Tosi, P.; Hawkesford, M. J.; McGrath, S. P.; Shewry, P. R.; Grovenor, C. R. M. Localisation of iron in wheat grain using high resolution secondary ion mass spectrometry. *J. Cereal Sci.* **2012**, *55*, 183−187.
(39) Theil, E. C. Ferritin: structure, gene regulation, and cellular function in animals, plants, and microorganisms. *Annu. Rev. Biochem.* **1987**, *56*, 289−315.
(40) Lukac, R. J.; Aluru, M. R.; Reddy, M. B. Quantification of ferritin from staple food crops. *J. Agric. Food Chem.* **2009**, *57*, 2155−2161.
(41) May, L.; Morris, E. R.; Ellis, R. Chemical identity of iron in wheat by Moessbauer spectroscopy. *J. Agric. Food Chem.* **1980**, *28*, 1004−1006.
(42) Lestienne, I.; Caporiccio, B.; Bresancon, P.; Rochette, I.; Trechet, S. Relative contribution of phytates, fibers, and tannins to low iron and zinc in vitro solubility in pearl millet (*Pennisetum glaucum*) flour and grain fractions. *J. Agric. Food Chem.* **2005**, *53*, 8342−8348.

JOURNAL OF AGRICULTURAL AND FOOD CHEMISTRY

Article

pubs.acs.org/JAFC

Lettucenin Sesquiterpenes Contribute Significantly to the Browning of Lettuce

Franziska Mai and Marcus A. Glomb*

Institute of Chemistry, Food Chemistry, Martin-Luther-University Halle-Wittenberg, Kurt-Mothes-Straße 2, 06120 Halle, Germany

ABSTRACT: Wound-induced changes in the composition of secondary plant compounds cause the browning of processed lettuce. Cut tissues near the lettuce butt end clearly exhibit increased formation of yellow−brown pigments. This browning reaction is typically been attributed to the oxidation of polyphenols by the enzyme polyphenol oxidase (PPO). However, in our previous study on Iceberg lettuce, we showed that, besides the enzymatic polyphenol browning, other reactions must be involved in the formation of colored structures. With the present study for the first time, we isolated yellow sesquiterpenes by multilayer countercurrent chromatography (MLCCC), followed by preparative high-performance liquid chromatography (HPLC). Further analyses by nuclear magnetic resonance (NMR) and mass spectrometry (MS) techniques identified lettucenin A and three novel derivatives. We call these compounds lettucenins A1, B, and B1. Color-dilution analyses revealed these lettucenins as key chromophores in the browning of Iceberg lettuce. A time formation curve showed the accumulation of lettucenins A and B within 40 h after cutting. Thereafter, these structures were degraded to unknown colored compounds. Lettucenin A was verified in five varieties of *Lactuca*. In contrast to that, lettucenin A was present only at trace levels in five varieties of *Cichorium*. Therefore, lettucenin A might be used as a chemosystematic marker of the genus *Lactuca*.

KEYWORDS: *Iceberg lettuce, Lactuca sativa, multilayer countercurrent chromatography (MLCCC), enzymatic browning, lettucenin, color-dilution analyses*

INTRODUCTION

Besides tomato, potato, and carrot, lettuce (*Lactuca sativa* L.) is one of the most popular vegetables in the world.[1] Favorite species are Butterhead, Romaine, and most importantly, Iceberg lettuce. In 2010, the consumption per private household in Germany amounted to 2.8 kg.[1]

Browning is one of the main causes of quality loss during the postharvest storage of lettuce and minimally processed lettuce.[2] In general, lettuce tends toward very rapid browning specifically on the lettuce butt end after harvesting.[3] Yellowish brown pigments are usually formed on bruises and cut surfaces. The huge economic loss encouraged researchers to conduct studies to understand lettuce-browning mechanisms. Numerous studies have focused on the typical enzymatic browning triggered by polyphenol oxidase (PPO). Furthermore, extensive investigations were carried out to describe beneficial effects of specific physical or chemical treatments on the prevention of discoloration.[3,4] However, for lettuce and also other kinds of fruits or vegetables, no precise relationship was found between browning potential, PPO activity, and total or individual phenol accumulation or degradation.[5−7] Besides the chemistry of black tea fermentation, specific products of enzymatic browning have hardly been scientifically researched.

In our recent study, the relationship between discoloration of Iceberg lettuce and enzymatic browning was thoroughly investigated.[8] This was based on literature that described enzymatic browning as the reaction between phenolic substances and enzymes.[4,9,10] Unexpectedly, the total concentration of polyphenols and the activity of PPO were not directly related to the browning processes. Model incubation experiments of plant extract solutions supported the argument that, in addition to the typical enzymatic browning induced by PPOs, further mechanisms must be considered to explain total browning of lettuce.[8]

Post-infectious defense induces the formation of antimicrobial substances in plants. The German plant pathologist K. O. Müller established the term "phytoalexin" in 1940.[11] The induction of the secondary metabolites is often caused by biotic (microorganisms) and abiotic agents, such as heavy metals (e.g., cupric chloride), but also physical injuries (such as cutting or brushing).[13]

Lettucenin A was first reported to be a sesquiterpenoid phytoalexin of lettuce by Takasugi et al. and found to be produced by lettuce and dandelion leaves in response to stress induced by pathogenic fungus or cupric chlorid.[12,13] Another fungitoxin was isolated and identified as costunolid from lettuce infected with *Pseudomonas cichorii*.[12] In addition, lettucenin A showed strong bioactivity against different pathogenic fungi *in vivo*.[14]

Monde et al. and Ahmad et al. described non-colored phytoalexins from *Cichorium intybus* and *Taraxacum wallichii*.[15,16] Bennet et al. hypothesized further phytoalexins of the sesquiterpenoid group to be involved in defense reactions in Iceberg lettuce but were not able to show any specific structures.[14] Up until now, lettucenin A is the only colored structure that might be responsible for the discoloration of lettuce.

With the present work, we were able to isolate colored sesquiterpenes from lettuce and correlate the intensive tissue

Received: January 24, 2014
Revised: April 27, 2014
Accepted: May 2, 2014
Published: May 12, 2014

ACS Publications © 2014 American Chemical Society

browning to the formation of phytoalexins. The formation of lettucenin A and three novel derivatives was induced solely by mechanical injury. With color-dilution analyses, we established the significance of lettucenins in the browning of lettuce. Finally, lettucenin A was quantitated in different varieties of Cichorieae.

MATERIALS AND METHODS

Chemicals. Chemicals of the highest quality available were obtained from Roth (Karlsruhe, Germany), unless otherwise indicated. High-performance liquid chromatography (HPLC)-grade methanol was purchased from Sigma-Aldrich (Taufenkirchen, Germany). Deuterated $CDCl_3$ was obtained from Chemotrade (Leipzig, Germany). For all experiments, ultrapure water was used.

Plant Materials. Commercial varities of lettuce (*L. sativa* L., Romaine, Butterhead, Iceberg, Lollo Rosso, and Lollo Bionda; *C. intybus* L., Radicchio, Sugar Loaf, and Chicory; and *Cichorium endivia* L., Endive and Frisee) were obtained from local markets in Germany. The lettuce heads were prepared for further processing by removing and discarding wrapper leaves and brown spots. For some experiments, the fresh lettuce head was separated into four tissue types: green leaves, yellow leaves, leaf panicles, and butt end. Each lot was cut into squares (1 × 1 cm) using a sharp ceramic knife and mixed thoroughly. For browning, the processed plant materials were packed into Petri dishes and kept at room temperature for 24 and 48 h, respectively. The brown material was stored in freeze bags, freeze-dried, and stored at −20 °C until used.

Extraction of Plant Material. For isolation of colored structures, 100 g of the freeze-dried mix of the entire head of Iceberg was extracted with acetone/water (7:3, v/v, 1.5 L) at 5 °C for 24 h under an argon atmosphere. The filtrates were concentrated under reduced pressure (<30 °C) until complete evaporation of acetone. The residual aqueous solution was successively extracted with diethyl ether (2 × 200 mL) and ethyl acetate (2 × 200 mL). The diethyl ether and ethyl acetate extracts were evaporated to dryness, and the residues (1500 mg of diethyl ether extract and 600 mg of ethyl acetate extract) were used for multilayer countercurrent chromatography (MLCCC).

For comparative studies on browning, 1 g of freeze-dried material of 24 and 40 h aged sliced tissue types of Iceberg lettuce was extracted with 10 mL of acetone/water (7:3, v/v) at 5 °C under an argon atmosphere. After 24 h, the samples were centrifuged at 4500 rpm for 10 min. A 1 mL aliquot of the clarified supernatant was dried under argon stream. The residue was extracted 2 times with 2 mL of diethyl ether. The combined diethyl ether phases were dried under an argon stream.

Analytical HPLC−Diode Array Detection (DAD)−Mass Spectrometry (MS). A Jasco system (Jasco, Gross-Umstadt, Germany) with a quaternary gradient unit PU 2080, a degasser DG 2080-54, an autosampler AS 2055, a column oven (Jasco Jetstream II), and a multiwavelength detector MD 2015 was used. Alternatively, the detector was coupled to an API 4000 triple quadruple mass spectrometer (Applied Biosystems, Foster City, CA). Chromatographic separations were performed on stainless-steel columns (Vydac CRT, 218TP54, 250 × 4.0 mm, RP-18, 5 μm, Hesperia, CA) using a flow rate of 1.0 mL/min. The mobile phase consisted of water (solvent A) and MeOH/water (7:3, v/v, solvent B). To both solvents (A and B), 0.8 mL/L of formic acid was added. Samples were analyzed using a gradient system: samples were injected at 50% B and held for 10 min. The gradient was changed linear to 100% B in 60 min and held at 100% B for 10 min. The column temperature was always 25 °C. The effluent was monitored at 280 and 420 nm.

MS ionization was achieved using the turbospray ionization source operated in positive-ion mode. Turbospray settings were as follows: curtain gas (N_2) at 40 psi, ion source gas 1 at 50 psi, ion source gas 2 at 60 psi, source temperature at 500 °C, and ion spray voltage at 4500 V. The total ion current (TIC) chromatogram with a scan range between m/z 100 and 700 and mass spectral data on precursor ions were detected. Declustering potential, entrance potential, collision energy, and cell exit potential were optimized for each analyte. For evaluation, we used Analyst software and Borwin−PDA software.

Quantitation of Lettucenins A and B. For quantitation, the samples were analyzed with HPLC using DAD, as described above. The phytoalexins eluted with a retention time of 22.8 min (lettucenin B) and 27.0 min (lettucenin A). Standard solutions were prepared in methanol. The amounts of lettucenins A and A1 were calculated on the basis of the published molar extinction coefficient of lettucenin A.[12] For quantitation of lettucenins B and B1, the authentic isolated standards were used.

MLCCC. The MLCCC system (Ito, multilayer separator−extractor model, P.C., Inc., Potomac, MD) was equipped with a constant flow pump (Waters 6000 A, Waters Corporation, Milford, MA), a Kontron spectrophotometer (Kontron 432, Kontron-Instruments, Rossdorf, Germany) operating at 420 nm, and a sample injection valve with a 10 mL sample loop. Eluted liquids were collected in fractions of 8 mL with a fraction collector (LKB Ultrorac 7000, LKB-Producter AB, Stockholm-Bromma, Sweden). Chromatograms were recorded on a plotter (Servogor 200, GMC, Nürnberg, Germany). The multilayer coil was prepared from a 1.6 mm inner diameter polytetrafluoroethylene (PTFE) tubing. The total capacity was 290 mL. MLCCC was run at a revolution speed of 790 rpm and a flow rate of 2 mL/min in head-to-tail modus.

Samples of 500 mg of dried extract were dissolved in a 1:1 mixture of light and heavy phase (10 mL) and injected into the system. Diethyl ether extracts were separated using *n*-hexane/ethyl acetate/methanol/water (3:5:3:5, v/v/v/v, solvent system A), and ethyl acetate extracts were isolated using *n*-hexane/ethyl acetate/methanol/water (4:5:4:5, v/v/v/v, solvent system B). The purified materials (fractions 35−40) were evaporated to dryness, and the residues (5−15 mg) were used for preparative HPLC−ultraviolet (UV).

Preparative HPLC−UV. A Besta HD 2-200 pump (Besta, Wilhelmsfeld, Germany) was used at a flow rate of 15 mL/min. Elution of materials was monitored by an UV detector set at 420 nm (Jasco UV-2075, Gross-Umstadt, Germany). Up to 20 mg of the above material from MLCCC was injected. Chromatographic separations were performed on a stainless-steel column (Vydac CRT, 218TP1022, 250 × 23 mm inner diameter, RP-18, 10 μm, Hesperia, CA). The mobile phases used were solvents A and B, identical to the analytical HPLC−DAD system. An isocratic method was chosen according to the characteristics of the target structures. From the individual chromatographic fractions, solvents were removed under reduced pressure. After the addition of diethyl ether, combined solutions of lettucenins were dried under argon stream.

Accurate Mass Determination [High-Resolution Mass Spectrometry (HRMS)]. The high-resolution positive- and negative-ion electrospray ionization (ESI) mass spectra were obtained from a Bruker Apex III Fourier transform ion cyclotron resonance (FT-ICR) mass spectrometer (Bruker Daltonics, Billerica, MA) equipped with an infinity cell, a 7.0 T superconducting magnet (Bruker, Karlsruhe, Germany), a radio frequency (RF)-only hexapole ion guide, and an external electrospray ion source (APOLLO, Agilent, off-axis spray). Nitrogen was used as the drying gas at 150 °C. The samples were dissolved in methanol, and the solutions were introduced continuously via a syringe pump at a flow rate of 120 μL/h. The data were acquired with 256 000 data points and zero-filled to 1 024 000 by averaging 32 scans.

Nuclear Magnetic Resonance (NMR) Spectroscopy. NMR experiments were performed on a Bruker Avance III 800 NMR spectrometer (Bruker, Rheinstetten, Germany) operating at 800 MHz for ^1H and 200 MHz for ^{13}C, respectively. Samples were dissolved in $CDCl_3$, and all spectra were run at 27 °C. Chemical shifts are given relative to external Me_4Si and were referenced to internal $CDCl_3$ (^1H, δ = 7.260 ppm; ^{13}C, δ = 77.160 ppm).

Color-Dilution Analysis. An aliquot (50 μL) of diethyl ether extract was analyzed by HPLC−DAD for determination of the color-dilution factor (CD factor). Fractions (1 mL) with material exhibiting absorption maxima at 420 nm were then stepwise 1:1 diluted with solvent B. The test was carried out in daylight against a white background. Each dilution was visually judged until the color

difference between the diluted fraction and two blanks of solvent B could just be visually detected using a triangle test. This dilution was defined as the CD factor. The CD factors evaluated by five different panelists in two independent sessions were averaged. For assignment of the total color-dilution factor (CD_{total} factor), 50 μL of diethyl ether extract was diluted to 1 mL and treated as described above.[19]

RESULTS AND DISCUSSION

Browning of Lettuce Tissues. For the following studies, conventional Iceberg lettuce was sliced and browned at room temperature. After 24 h, the sliced and bruised areas of the plant material showed significant discoloration. To explain the discoloration, 24 h aged sliced Iceberg lettuce was compared to fresh sliced Iceberg lettuce. For this purpose, freeze-dried plant material was extracted as described above. The final diethyl ether extracts were screened for colored structures by analytical HPLC–DAD (Figure 1). A direct comparison of chromatograms A and B at 420 nm shows that, in browned lettuce, different visible absorbing compounds were detected. Because of the absorption maxima between 400 and 440 nm, these structures are indeed responsible for the discoloration (Figure 2). In the context of enzymatic browning, yellow structures with similar UV/vis spectra were previously presented in the literature but structural analysis was not performed.[17] For structure elucidation, the brown soluble compounds were isolated from the diethyl ether and ethyl acetate extracts of Iceberg lettuce.

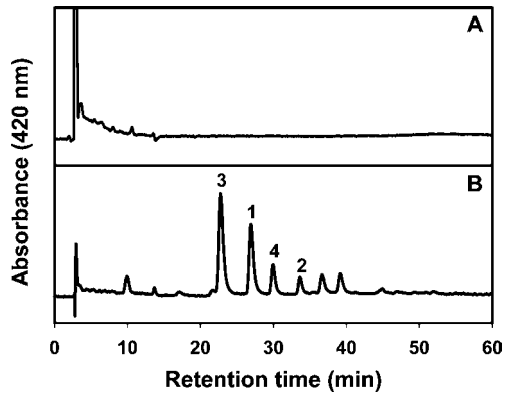

Figure 1. HPLC–DAD chromatogram of (A) acetone/water extract from fresh sliced Iceberg lettuce at λ = 420 nm and (B) acetone/water extract from 24 h aged sliced Iceberg lettuce at λ = 420 nm. Retention times are given in parentheses: (**1**) lettucenin A (27.0 min), (**2**) lettucenin A1 (33.7 min), (**3**) lettucenin B (22.8 min), and (**4**) lettucenin B1 (30.0 min).

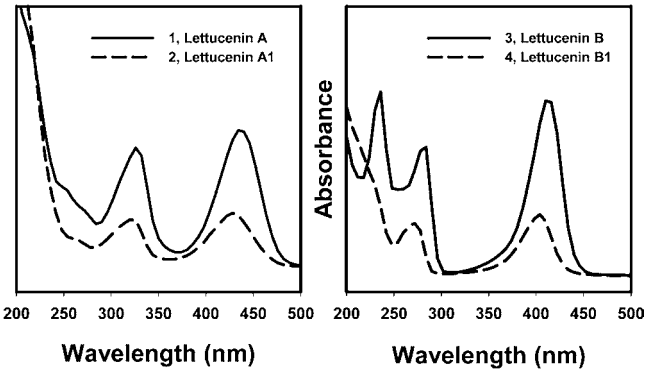

Figure 2. UV/vis spectra of (**1**) lettucenin A, (**2**) lettucenin A1, (**3**) lettucenin B, and (**4**) lettucenin B1.

Isolation and Elucidation of Colored Compounds. The first step of purification was separation by MLCCC using solvent system A for ethyl acetate extracts and solvent system B for *n*-butanol extracts. Afterward, fractions containing the yellowish brown material were separated by preparative HPLC to isolate pure substances. The final structural evidence was achieved by ^{1}H and ^{13}C NMR measurements, as well as heteronuclear single-quantum coherence (HSQC), heteronuclear multiple-bond correlation (HMBC), and homonuclear correlation spectroscopy (H,H COSY) techniques.

Four structures were verified (Figure 1): lettucenin A (**1**) and three derivatives A1 (**2**), B (**3**), and B1 (**4**). Thus far, only compound **1** has been isolated from Iceberg lettuce. NMR data of compound **1** were in line with the study by Takasugi et al. Lettucenin A is a phytoalexin that was identified in Iceberg lettuce for the first time in 1985,[12] but no other structures have yet been published.

Compounds **1**–**4** were isolated as unstable yellowish crystalline substances with concentrations ranging between 0.1 and 6.0 μg/g of fresh weight (FW) as determined by HPLC–DAD. HPLC/ESI–MS delivered for compound **1** a pseudo-molecular ion of m/z 241.2 $[M + H]^+$. This finding was confirmed by HRMS (found, m/z 241.08608 $[M + H]^+$; calculated, m/z 241.08592 $[M + H]^+$, for $C_{15}H_{13}O_3$). In comparison, HRMS gave a pseudo-molecular ion of m/z 243.2 $[M + H]^+$ for compound **3** (found, m/z 243.10157 $[M + H]^+$; calculated, m/z 243.10157 $[M + H]^+$ for $C_{15}H_{15}O_3$). HPLC/ESI(+)–tandem mass spectrometry (MS^2) experiments verified a dominant CO loss of 28 mass units for both compounds $[M + H - 28]^+$ (Table 1). The degree of unsaturation (DU) was calculated from the molecular formulas. The DUs of compounds **1** and **3** were 10 and 9, respectively. The absence of a double bond in compound **3** was also reflected in the UV/vis spectrum. The absorption maximum shifted from 440 nm for compound **1** to 416 nm for compound **3** (Figure 2). ^{1}H NMR experiments of compounds **1** and **3** confirmed the difference of a double bond between C-4 and C-15. For compound **3**, at position C-4, an additional proton was detected and, at position C-15, a methyl group was identified, which coupled with the proton at C-4 to give a doublet (1.35 ppm, d; Table 2). This was different from lettucenin A, which clearly showed a methylene signal for H-15 (5.92 ppm, m; 6.67 ppm, m). The remaining signals of compound **3** corresponded to the pattern of lettucenin A.

With regard to all results, compound **3** boasts the same basic ring structure as lettucenin A with the difference of saturation between C-4 and C-15 (Figure 3) and was unequivocally assigned to 2,7,8,9-tetrahydro-6,9-dimethyl-2-oxo-azuleno[4,5-*b*]furan-3-carboxaldehyde. We have named compound **3** lettucenin B because of the structural similarity to lettucenin A.

HPLC/ESI–MS delivered for compounds **2** and **4** pseudo-molecular ions of m/z 271.1 and 273.1 $[M + H]^+$, respectively. These findings were confirmed by HRMS (found for compound **2**, m/z 271.09649 $[M + H]^+$; calculated, m/z 271.09649 $[M + H]^+$, for $C_{16}H_{15}O_4$; found for compound **4**, m/z 273.11214 $[M + H]^+$; calculated, m/z 273.11214 $[M + H]^+$, for $C_{16}H_{17}O_4$; Table 1). In parallel to compounds **1** and **3**, compounds **2** and **4** also showed a difference of m/z 2 to indicate an absent double bond. HPLC/ESI(+)–MS^2 experiments verified parallel losses of 14 and 32 mass units for both

dx.doi.org/10.1021/jf500413h | J. Agric. Food Chem. 2014, 62, 4747–4753

Table 1. UV Spectral Data and Mass Spectrometric Data of Lettucenins

compound number	compound	HPLC–DAD, λ_{max} (nm)	HRMS $[M + H]^+$ (m/z)	HPLC/ESI(+)–MS^2 (m/z)
1	lettucenin A	440, 326	241.08608	241.2, 213.6
2	lettucenin A1	428, 326	271.09649	271.2, 257.2, 239.1
3	lettucenin B	416, 284, 236	243.10157	243.2, 215.1
4	lettucenin B1	404, 272	273.11214	273.2, 259.1, 241.2

Table 2. ^{1}H NMR Spectroscopic Data[a] of Lettucenin A (1), Lettucenin B (3), and Lettucenin B1 (4)

C	1	3	4
1			
2	3.25 (m, 2H)	3.21 (m, 1H)	3.17 (m, 1H)
		3.08 (m, 1H)	3.03 (m, 1H)
3	2.99 (m, 2H)	1.93 (m, 1H)	2.24 (m, 1H)
		2.28 (m, 1H)	1.90 (m, 1H)
4		3.93 (m, 1H)	3.91 (m, 1H)
5			
6			
7			
8	8.91 (d, 1H, ^3J = 11.3 Hz)	8.86 (d, 1H, ^3J = 11.3 Hz)	8.73 (d, 1H, ^3J = 11.7 Hz)
9	7.94 (d, 1H, ^3J = 11.3 Hz)	7.67 (d, 1H, ^3J = 11.3 Hz)	7.55 (d, 1H, ^3J = 11.7 Hz)
10			
11			
12			
13	9.91 (s, 1H)	10.40 (s, 1H)	
14	2.60 (s, 3H)	2.52 (s, 3H)	2.48 (s, 3H)
15	5.92 (m, 1H)	1.35 (d, 3H, ^3J = 7.2 Hz)	1.32 (d, 3H, ^3J = 7.1 Hz)
	6.67 (m, 1H)		
16			3.93 (s, 3H)

[a]All spectra were recorded at 800 MHz in $CDCl_3$ in ppm. δ, chemical shift; J, coupling constant. Hydrogen/carbon assignments were verified by HMBC, HSQC, H,H COSY, and attached proton test (APT) measurements.

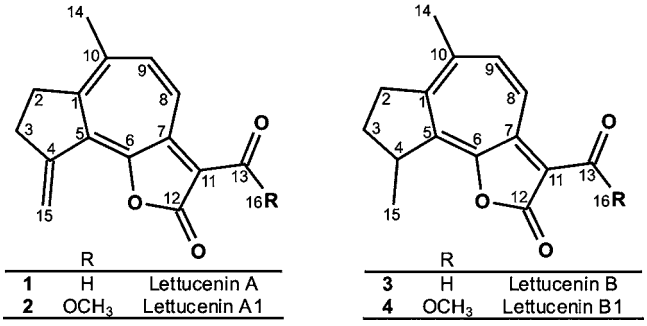

Figure 3. Isolated chromophores from processed Iceberg lettuce.

compounds **2** and **4** (Table 1). $[M + H - 32]^+$ is a characteristic fragment of methyl esters.[18]

Indeed, a methoxy group was verified for compound **4** by ^{1}H and ^{13}C NMR experiments downfield at 3.93 and 51.7 ppm, respectively, in addition to the ^{1}H and ^{13}C NMR signal pattern of lettucenin B (Tables 2 and 3). A simultaneous high-field shift of C-13 from 186.0 to 165.0 ppm and HMBC correlations between C-16 and C-13 as well as C-11 unequivocally established the proposed methyl ester and was assigned to 2,7,8,9-tetrahydro-6,9-dimethyl-2-oxo-azuleno[4,5-*b*]furan-3-carboxylic acid methyl ester. Therefore, we call compound **4** lettucenin B1.

Because of the low quantities of compound **2** found in processed lettuce, it was not possible to isolate enough material for NMR studies. Nevertheless, in comparison of the UV/vis spectra of compound **1** to compound **3** and compound **2** to compound **4**, the absorption maxima shift from 440 to 416 nm and from 428 to 404 nm, respectively; i.e., there was the same difference of 24 nm in both pairs (Figure 2). In parallel to compound **1**, this indicated an extra double bond for compound **2**. In comparison of compound **1** to compound **2** and compound **3** to compound **4**, each with an identical UV/vis pattern, compounds **2** and **4** showed a hypsochromic shift of 12 nm. These parallels together with the HRMS, MS^2, and UV/

Table 3. ^{13}C NMR Spectroscopic Data[a] of Lettucenin A (1), Lettucenin B (3), and Lettucenin B1 (4)

C	1	3	4
1	148.1	145.9	154.5
2	34.4	35.5	35.1
3	30.9	31.0	31.0
4	157.9	41.3	41.1
5	134.5	153.3	144.2
6	152.6	156.5	152.3
7	150.5	149.5	152.2
8	128.3	129.1	128.3
9	144.8	143.9	142.6
10	143.6	143.6	141.8
10	100.0	100.5	92.4
12	170.2	169.5	166.4
13	186.3	186.0	165.0
14	24.3	26.0	25.8
15	120.0	19.6	19.5
16			51.7

[a]All spectra were recorded at 200 MHz in $CDCl_3$. δ, chemical shift. Hydrogen/carbon assignments were verified by HMBC, HSQC, H,H COSY, and APT measurements.

dx.doi.org/10.1021/jf500413h | J. Agric. Food Chem. 2014, 62, 4747–4753

vis data strongly proposed compound **2** as the methyl ester of lettucenin A, as shown in Figure 3.

Influence of Lettucenins to Discoloration. To determine the contribution of lettucenins to the overall color of browned Iceberg lettuce, color-dilution analysis was performed (Figure 4).[19,20] CD factors were analyzed in the diethyl ether

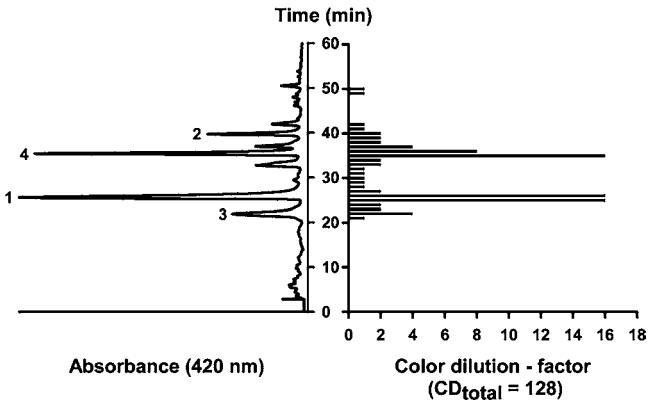

Figure 4. HPLC–DAD chromatogram (λ = 420 nm; left side) and color-dilution chromatogram (right side) of the diethyl ether extract of 24 h aged sliced Iceberg lettuce.

extract by a panel of five people. At 420 nm, chromophores were detected, which accounted for more than 50% of the total color of the diethyl ether extract. The structurally identified compounds **1**–**4** contributed 40% to the overall color (with the lead compound lettucenin A even at 25%). This means that the difference of 10% was related to the remaining unknown signals. In addition, in the total water/acetone extract, compounds **1**–**4** explained 25% of the overall color. This means that lettucenins are important coloring agents in the browning of Iceberg lettuce.

Formation of Lettucenin A in Different Lettuce. To understand the formation of lettucenin A in the plant more accurately, three varieties of lettuce were divided into four parts (green and yellow leaves, leaf panicle, and butt end) and browned at room temperature. After a browning period of 24 or 40 h, samples were collected and freeze-dried. From the samples, the lettucenins were extracted and lettucenin A as a specific marker was quantitated (Figure 5). As shown in the graphic, different concentrations of compound **1** occurred in the different parts of the Iceberg lettuce. A similar distribution was found in the varieties Butterhead and Lollo Bionda. After 24 h, the highest concentrations of compound **1** and all other lettucenin derivatives were analyzed, always in the lettuce butt end. This confirmed the visual impression of strong browning in the lettuce butt end.[8]

Because compound **1** is a reactive intermediate, there was no accumulation in the plant. This was proven by comparison to the lettuce butt end browning after 40 h. Only 5% of the concentration found in the 24 h sample could be quantitated. Figure 6 shows the time-course formation of compounds **1** and **3**, where concentrations of compound **1** reached a maximum after 24 h. After that, compound **1** degraded almost to the initial level at 40 h. This also confirmed the difference between the butt end samples in Figure 5. In contrast to compound **1**, compound **3** reached a maximum 16 h later at significantly lower concentrations. This strongly suggested compound **1** as the precursor structure in the formation of compound **3**.

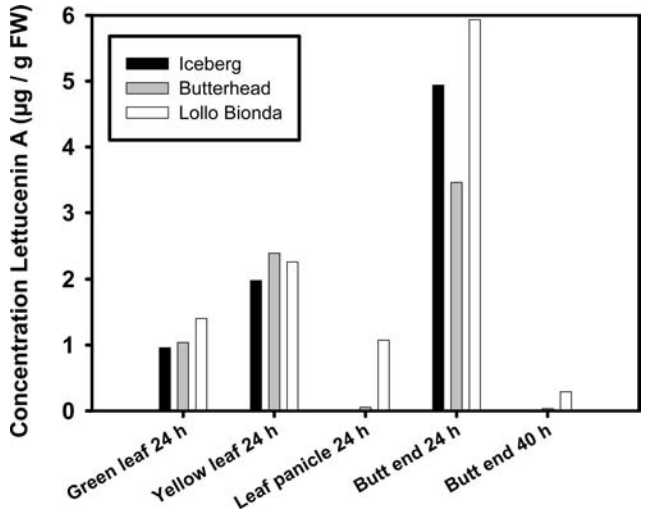

Figure 5. Lettucenin A accumulation in different parts of three varieties of lettuce after 24 and 40 h of cutting.

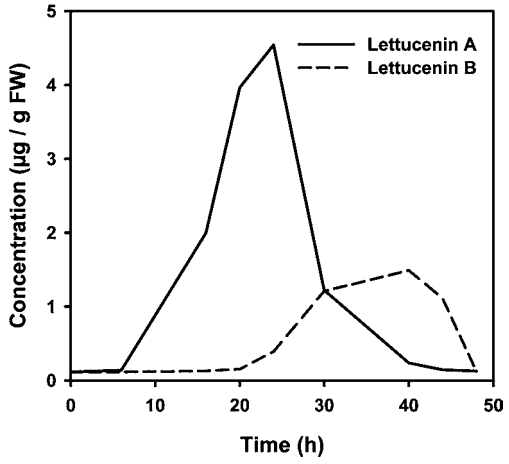

Figure 6. Time-course formation of lettucenin A and lettucenin B in sliced Iceberg lettuce.

The temperature is a crucial factor in the formation of lettucenins. At elevated temperature, the maximum concentration of compound **1** was reached much earlier (data not shown). According to studies by Tahara et al., Takasugi et al., and Sessa et al., the pathogenic bacterium *P. cichorii* or cupric chlorid and cupric sulfate also increase the concentration of lettucenin A with a maximum of 3 μg/g of FW.[12,13,21] Other microorganisms (*Pseudomonas syringae* pv. *phaseolicola* and *Botrytis cinerea*) generated yields reaching up to 9 μg/g of FW. Lettucenin A was found within cotyledons with the red spot syndrome (6.2 μg/g of FW) and is therefore related to a microbial infestation.[22] Observations by Bestwick et al. suggest that there is a correlation of irreversible membrane damage and induction of phytoalexin accumulation.[23] Thereby, threshold levels of membrane dysfunction lead to the induction of endogenous mechanisms that cause the lettucenin biosynthesis.[23] In the present paper, samples were mechanically injured, by cutting them with a ceramic knife. Thus, a deliberate infection with microorganisms or heavy metals has to be excluded.

Importance of Lettucenin A in Different Varieties of Lettuce. In previous studies, lettucenin A was one of the most important phytoalexins in the group of composites.[14,15] It was

dx.doi.org/10.1021/jf500413h | J. Agric. Food Chem. 2014, 62, 4747–4753

identified in some European and Asian species: *Taraxacum officinale*, *Taraxacum hondoense*, *L. sativa*, *Lactuca dentate*, *Lactuca scariola*, *Sonchus oleraceus*, *Sonchus asper*, and *Ixeris repens*.[12,13,24] As depicted in Figure 7, 10 types of Cichorieae, a

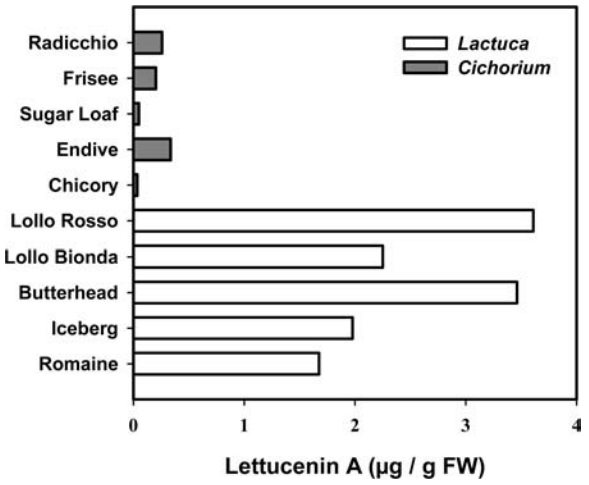

Figure 7. Lettucenin A accumulation in 24 h aged sliced stem material of 10 varieties of Cichorieae (5 varieties of *Lactuca* and 5 varieties of *Cichorium*).

tribe of flowering plants in the daisy family Asteraceae, were examined for lettucenin A, all of which are popular commercial lettuce, with 5 species belonging to the genus *Chichorium* and 5 species belonging to the genus *Lactuca*. In the genus *Cichorium*, compound **1** was detected with a maximum of 0.34 μg/g of FW, whereas in the genus *Lactuca*, concentrations ranged from 1.68 to 3.61 μg/g of FW. The levels of compound **1** in varieties of *Lactuca* were at least 5 times higher than those in varieties of *Cichorium*. Thus, there is a significant difference between these two genera. Thus far, lettucenin A was not found in uninfected samples of *L. sativa* L. (Iceberg) and, therefore, was not considered as a chemosystematic marker.[25] However, the present data strongly suggest that lettucenin A can indeed be used as an identity marker within the genus *Lactuca*.

In conclusion, we succeeded to extend the range of sesquiterpene yellow chromophores in Iceberg lettuce. In contrast to published data on microbial and heavy metal stress, lettucenin formation was induced solely by mechanical distortion. The main compound was confirmed to be the phytoalexin lettucenin A. In addition, we identified unequivocally two novel colored derivatives of lettucenin A. A third structure related to lettucenins was assigned on the basis of mass spectrometric data. Color-dilution analyses revealed the major importance of lettucenins as key chromophores in browned Iceberg lettuce. Thus, sesquiterpene-based discoloration has to be added as a new aspect to the concept of enzymatic browning in vegetables previously only attributed to polyphenolic chemistry.

AUTHOR INFORMATION

Corresponding Author

*Fax: ++49-345-5527341. E-mail: marcus.glomb@chemie.uni-halle.de.

Notes

The authors declare no competing financial interest.

ACKNOWLEDGMENTS

The authors thank M. Kovermann and S. Gröger from the Institute of Physics, Biophysics Research Group, Martin-Luther-University Halle-Wittenberg (Germany), for recording NMR spectra. The authors are also grateful to J. Schmidt from the Leibniz Institute of Plant Biochemistry, Halle (Germany), for performing accurate mass analysis.

REFERENCES

(1) Agrarmarkt Informations-GmbH. *AMI-Marktbilanz Gemüse 2010*; Agrarmarkt Informations-GmbH: Bonn, Germany, 2011.

(2) Mateos, M.; Ke, D.; Cantwell, M.; Kader, A. A. Phenolic metabolism and ethanolic fermentation of intact and cut lettuce exposed to CO_2-enriched atmospheres. *Postharvest Biol. Technol.* **1993**, *3*, 225−233.

(3) Castaner, M.; Gil, M. I.; Ruiz, M. V.; Artes, F. Browning susceptibility of minimally processed Baby and Romaine lettuces. *Eur. Food Res. Technol.* **1999**, *209*, 52−56.

(4) Ke, D.; Saltveit, M. E. Wound-induced ethylene production, phenolic metabolism and susceptibility to russet spotting in Iceberg lettuce. *Physiol. Plant.* **1989**, *76*, 412−418.

(5) Tavarini, S.; Degl'Innocenti, E.; Pardossi, A.; Guidi, L. Biochemical aspects in two minimally processed lettuces upon storage. *Int. J. Food Sci. Technol.* **2007**, *42*, 214−219.

(6) Amiot, M. J.; Tacchini, M.; Aubert, S.; Nicolas, J. Phenolic composition and browning susceptibility of various apple cultivars at maturity. *J. Food Sci.* **1992**, *57*, 958−962.

(7) Cantos, E.; Espin, J. C.; Tomas-Barberan, F. A. Effect of wounding on phenolic enzymes in six minimally processed lettuce cultivars upon storage. *J. Agric. Food Chem.* **2001**, *49*, 322−330.

(8) Mai, F.; Glomb, M. A. Isolation of phenolic compounds from Iceberg lettuce and impact on enzymatic browning. *J. Agric. Food Chem.* **2013**, *61*, 2868−2874.

(9) Toivonen, P. M. A.; Brummell, D. A. Biochemical bases of appearance and texture changes in fresh-cut fruit and vegetables. *Postharvest Biol. Technol.* **2008**, *48*, 1−14.

(10) Tomas-Barberan, F.; Espin, J. C. Phenolic compounds and related enzymes as determinants of quality in fruits and vegetables. *J. Sci. Food Agric.* **2001**, *81*, 853−876.

(11) Müller, K. O.; Börger, H. Experimentelle untersuchungen über die *Phytophthora*-resistenz der kartoffel. *Arb. Biol. Reichsanst. Land-Forstwirtsch.* **1940**, *23*, 189−231.

(12) Takasugi, M.; Okinaka, S.; Katsui, N.; Masamune, T.; Shirata, A.; Ohuchi, M. Isolation and structure of lettucenin-A, a novel guaianolide phytoalexin from *Lactuca sativa* var. *capitata* (Compositae). *J. Chem. Soc., Chem. Commun.* **1985**, *10*, 621−622.

(13) Tahara, S.; Hanawa, F.; Harada, Y.; Mizutani, A. Fungitoxin inducibly produced by dandelion leaves treated with cupric chlorid. *J. Agric. Biol. Chem.* **1988**, *52*, 2947−2948.

(14) Bennett, M. H.; Gallagher, M. D. S.; Bestwick, C. S.; Rossiter, J. T.; Mansfield, J. W. The phytoalexin response of lettuce to challenge by *Botrytis cinerea*, *Bremia lactucae* and *Pseudomonas syringae* pv. *phaseolicola*. *Physiol. Mol. Plant Pathol.* **1994**, *44*, 321−333.

(15) Monde, K.; Oya, T.; Shirata, A.; Takasugi, M. Studies on stress metabolites. 10. A guaianolide phytoalexin, cichoralexin, from *Cichorium intybus*. *Phytochem.* **1990**, *29*, 3449−3451.

(16) Ahmad, V. U.; Yasmeen, S.; Ali, Z. Taraxacin, a new guaianolide from *Taraxacum walichii*. *J. Nat. Prod.* **2000**, *63*, 1010−1011.

(17) Tomás-Barberán, F. A.; Gil, M. I.; Castaner, M.; Artes, F.; Saltveit, M. E. Effect of selected browning inhibitors on phenolic metabolism in stem tissue of harvested lettuce. *J. Agric. Food Chem.* **1997**, *45*, 583−589.

(18) Zeeh, B.; Meier, H.; Hesse, M. *Spektroskopische Methoden in der Organischen Chemie*; Thieme: Stuttgart, Germany, 2011.

(19) Heinrich, T.; Willenberger, I.; Glomb, M. Chemistry formation during rooibos fermentation. *J. Agric. Food Chem.* **2012**, *60*, 5221−5228.

(20) Frank, O.; Jezussek, M.; Hofmann, T. Characterisation of novel 1*H*,4*H*-quinolizinium-7-olate chromophores by application of colour dilution analysis and high-speed countercurrent chromatography on thermally browned pentose/L-alanine solutions. *Eur. Food Res. Technol.* **2001**, *213*, 1−7.
(21) Sessa, R. A.; Bennett, M. H.; Lewis, M. J.; Mansfield, J. W.; Beale, M. H. Metabolite profiling of sesquiterpene lactones from *Lactuca* species—Major latex components are novel oxalate and sulphate conjugates of lactucin and its derivatives. *J. Biol. Chem.* **2000**, *275*, 26877−26884.
(22) Bestwick, L.; Bennett, M. H.; Mansfiel, W. Accumulation of the phytoalexin lettucenin A and changes in 3-hydroxy-3-methylglutaryl coenzyme A reductase activity in lettuce seedlings with the red spot disorder. *Phytochemistry* **1995**, *39*, 775−777.
(23) Bestwick, C. S.; Bennett, M. H.; Mansfield, J. W. Hrp mutant of *Pseudomonas syringae* pv. *phaseolicola* induces cell-wall alterations but not membrane damage leading to the hypersensitive reaction in lettuce. *Plant Physiol.* **1995**, *108*, 503−516.
(24) Hanawa, F.; Kanauchi, M.; Tahara, S.; Mizutani, J. Lettucenin A as a phytoalexin of dandelion and its elicitation in dandelion cell cultures. *J. Fac. Agric., Hokkaido Univ.* **1995**, *66* (2), 151−162.
(25) Zidorn, C. Sesquiterpene lactones and their precursors as chemosystematic markers in the tribe Cichorieae of the Asteraceae. *Phytochemistry* **2008**, *69*, 2270−2296.

JOURNAL OF AGRICULTURAL AND FOOD CHEMISTRY

Article

pubs.acs.org/JAFC

5-Hydroxymethyl-2-furfural and Derivatives Formed during Acid Hydrolysis of Conjugated and Bound Phenolics in Plant Foods and the Effects on Phenolic Content and Antioxidant Capacity

Peter X. Chen,[†,‡] Yao Tang,[†,§] Bing Zhang,[†,∥] Ronghua Liu,[†] Massimo F. Marcone,[‡] Xihong Li,[§] and Rong Tsao*[,†]

[†]Guelph Food Research Centre, Agriculture and Agri-Food Canada, 93 Stone Road West, Guelph, Ontario, Canada N1G 5C9

[‡]Department of Food Science, Ontario Agricultural College, University of Guelph, 50 Stone Road East, Guelph, Ontario, Canada, N1G 2W1

[§]Key Laboratory of Food Nutrition & Safety, Tianjin University of Science & Technology, Ministry of Education, Tianjin 300457, China

[∥]State Key Laboratory of Food Science and Technology, Nanchang University, Nanchang 330047, Jiangxi, China

ABSTRACT: A common protocol for the extraction of phenolic aglycons or bound phenolics in plants generally involves hydrothermal hydrolysis in an aqueous methanol or ethanol solution containing 2−4 N HCl. However, as shown in the present study, this process also forms 5-(hydroxymethyl)furan-2-carbaldehyde (HMF) and its derivative products 5-(methoxymethyl)-furan-2-carbaldehyde (MMF) and 5-(ethoxymethyl)furan-2-carbaldehyde (EMF), as identified by HPLC-DAD−ESI-MS/MS and NMR. These compounds are commonly misidentified as phenolics due to similar UV absorption at 280 nm. In this study, production of HMF, MMF, and EMF was shown to be dependent on the solvent condition and duration and temperature of hydrolysis. Fruits and vegetables produced HMF more readily than grains. HMF and its derivatives were subjected to various spectrophotometric antioxidant assays [2-diphenyl-1-picryhydrazyl radical scavenging activity (DPPH), ferric-reducing antioxidant power (FRAP), and oxygen radical absorbing capacity (ORAC)] and displayed antioxidant activity mainly in the ORAC assay. Results of this study help avoid overestimation of phenolic content and antioxidant activities of plant foods.

KEYWORDS: *hydroxymethylfurfural, methoxymethylfurfural, ethoxymethylfurfural, furans, HPLC-DAD, LC−MS, NMR, dehydration, fructose, plant extraction*

INTRODUCTION

Plants produce a wide variety of secondary metabolites known as phenolic compounds or polyphenols that possess various biological functions in plants, including phytoalexins, attractants for pollinators, plant pigmentation, antioxidants, and protection against UV light.[1,2] Extraction of phenolic compounds depends on the specific forms in which they are present in plants. Extractable phenolics can be in free or in conjugated forms; the latter are generally soluble glycosides of phenolic acids and flavonoids.[3] Many phenolic compounds are insoluble, being bound to cell wall polymers through ester and glycosidic links, and are therefore not extractable using organic solvents alone.[3] Hydrolysis under alkaline, acidic, or enzymatic conditions is often performed to release these bound phenolics.[2] Typical acid hydrolysis conditions for cleaving glycosidic bonds of conjugated phenolic acids or flavonoids to obtain their respective aglycons involve heating at high temperature (>80 °C) for 1−3 h in an aqueous methanol or ethanol solution containing 2−4 N HCl.[4,5]

Chemical hydrolysis under acid and alkaline conditions has been a major tool commonly used when studying conjugated and bound phenolics in many food crops. The HPLC-DAD phenolic profiles of plant-derived acid hydrolysates consistently showed at least one or two major peaks, dependent on solvent used, eluting at comparable retention times as certain benzoic acids when monitored at 280 nm.[6] In fact, acid hydrolysis performed by other investigators of dry bean (*Phaseolus vulgaris* L.),[6,7] quinoa (*Chenopodium quinoa* Willd.),[8] red clover (*Trifolium pretense* L.),[9] wheat bran,[10] and cranberry juice[11] all showed the presence of peaks bearing LC−UV characteristics similar to those of simple phenolic acids. Our efforts in identifying the structures of these peaks have led to the conclusion that these peaks are not those of phenolics. Such misidentification of phenolics in the literature can lead to significant overestimation of total phenolic content and could affect the outcome of chemical antioxidant assays.[3,6,12]

Under similar hydrothermal acidic conditions, sugar molecules (e.g., fructose, glucose, sucrose) undergo dehydration reactions to form 5-hydroxymethyl-2-furfural (HMF, **1**; Figure 1).[12,13] This furanic compound can also be formed during a Maillard reaction;[14] therefore, it is found in many processed foods, particularly sugar- or starch-rich foods.[15,16] Like other furan derivatives, HMF has been found to induce a significant number of chromosome aberrations and a lowering of mitotic activity.[17] HMF and its derivatives have found their use as intermediates for the production of plastics, polymers,

Received: February 6, 2014
Revised: April 29, 2014
Accepted: May 5, 2014
Published: May 5, 2014

ACS Publications © 2014 American Chemical Society

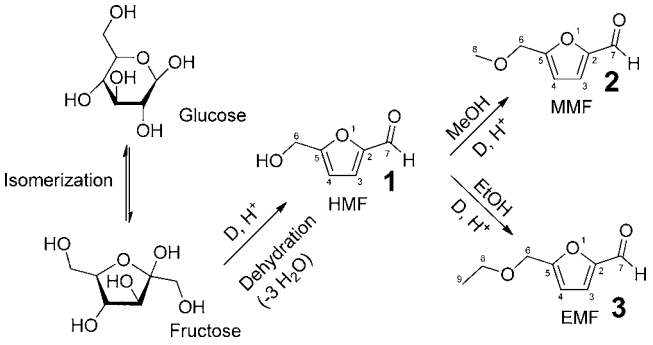

Figure 1. Formation of HMF, MMF, and EMF during thermal acid hydrolysis of conjugated polyphenols in food samples.

pharmaceuticals, and transportation fuel. The ability to produce HMF from carbohydrate-rich biomass is of great interest.[18] Reaction conditions can dictate the formation of methyl or ethyl ethers of HMF such as 5-methoxymethylfuran-2-carbaldehyde (MMF, **2**) or 5-ethoxymethylfuran-2-carbaldehyde (EMF, **3**).[19,20] MMF and EMF can be converted to a wide range of mono- and dialkoxymethyl ethers for biofuels[20] and has been used for the synthesis of novel biomass-based vinyl polymers.[21−23]

In our current study, we have identified major compounds in the acid hydrolysates of cranberry bean (*Phaseolus vulgaris* L.), quinoa (*Chenopodium quinoa* Willd), lentil (*Lens culinaris* L.), and buckwheat (*Fagopyrum esculentum* Moench) seed extracts to be HMF and its methyl and ethyl ethers. A previous report on the acid hydrolysis of flax seed led to the accurate identification of HMF; however, its derivatives remained unknown.[24] In this study, we have obtained evidence for the formation of HMF and its derivatives MMF and EMF, in model systems and in actual food samples, using HPLC-DAD−ESI-MS/MS and NMR. Overestimation of total phenolic content and antioxidant capacity in these food extracts due to HMF and its derivatives was investigated using in vitro chemical methods. Our results will help others to accurately assess the phenolic composition of food, especially those in bound or conjugated forms, and the antioxidant and other biological activities of acid hydrolysis products.

METHODS AND METHODS

Chemicals and Reagents. HPLC-grade acetonitrile was obtained from EMD Chemicals (Gibbstown, NJ), anhydrous ethyl alcohol (ethanol) from Commercial Alcohols (Brampton, Canada), and methanol from Caledon Laboratories (Georgetown, Canada). MMF standard was obtained from Enamine LLC (Monmouth Jct, NJ). Hydrochloric acid (HCl) and sodium carbonate were supplied by Fischer Scientific (Nepean, Canada). Formic acid, 2-diphenyl-1-picryhydrazyl radical (DPPH), fluorescein, Folin−Ciocalteu reagent, L-ascorbic acid, 2,4,6-tri(2-pyridyl)-*s*-triazine, 2,2′-azobis(2-amidinopropane) dihydrochloride, 6-hydroxy-2,5,7,8-tetramethlchroman-2-carboxylic acid (Trolox), anhydrous methylene chloride, deuterated chloroform ($CDCl_3$), gallic acid, catechin, furfural, HMF, EMF, fructose, glucose, sucrose, and inulin standards were obtained from Sigma-Aldrich Chemical Co. (St. Louis, MO). Distilled and deionized water was obtained in house from a Thermo Scientific Barnstead Nanopure ultrapure water purification system (Ottawa, Canada).

Food Materials. Whole cranberry bean seeds ("Hooter") were kindly provided by Dr. Peter Pauls, Department of Plant Agriculture, University of Guelph. Quinoa, lentil, and buckwheat seeds were purchased from local stores. Fruit and vegetables including apple, cucumber, and carrot were also purchased from local stores. The grain samples were ground directly using a commercial grinder (Stanley Black & Decker Inc., New Britain, CT). The fruit samples were lyophilized using a Bulk Tray Dryer (Labconco, Kansas City, MO) prior to grinding. The powdered samples were kept at −20 °C until analyzed.

Extraction and Acid Hydrolysis. Briefly, powdered plant materials (0.25 g) were accurately weighed and mixed with 10 mL of 2 N HCl in either 70% methanol or 70% ethanol (v/v). The mixture was vortexed for 10 s using a minishaker (IKA Works, Wilmington, NC), sonicated for 15 min (VWR, Mississauga, Canada), and then shaken by rotatory mixing at room temperature for 2 h (Scientific Industries, Bohemia, NY). Hydrolysis was carried out at 85 °C for 1 h using a hot water bath (IKA, Wilmington, NC), and the extract was syringe filtered using 0.45 μm PVDF filters (Sigma-Aldrich Co., St. Louis, MO) prior to HPLC analysis. The effect of hydrolysis duration and temperature on HMF and MMF formation was further studied by adjusting reaction time (30, 60, 120 min) and temperature (65, 75, 85, 95 °C) in a model system using quinoa seeds. All extractions were carried out in triplicates.

Identification and Quantitation with HPLC. HPLC analysis was carried out using an Agilent 1100 series HPLC system (equipped with a model G1329A auto sampler, a model G1322A degasser, a model G1311A quaternary solvent delivery system, and a model G1315B diode-array detector) and using Agilent ChemStation software. The analytical column used was a Phenomenex Luna phenyl-hexyl 5 U (250 × 4.6 mm). The binary mobile phase consisted of 5% formic acid in water (v/v) (solvent A) and 95% methanol:5% acetonitrile (v/v) (solvent B). The gradient solvent system used was as follows: 0−40 min, 80% B; 40−42 min, 80%−100% B; 42−44 min, 100% B; 44−44.5 min, 100%−0% B. Peaks were monitored at 280 nm. Flow rate was kept at 1.0 mL/min for a run time of 50 min.

HMF, MMF, and EMF were first identified by comparing the retention time and UV absorption spectrum of individual peaks with those of the standards. Quantitation was performed with external standards using HPLC analysis data and establishing a standard curve by plotting peak areas against the concentrations (0.78−200 mg/L) of the standards.

Liquid Chromatography−Mass Spectrometry Analysis. Quinoa seed sample from previously described extraction and acid hydrolysis was injected into a Dionex UHPLC UltiMate 3000 liquid chromatograph interfaced to an amaZon SL ion trap mass spectrometer (Bruker Daltonics, Billerica, MA). A C18 column (Agilent Poroshell 120 2.7 μm particle size, 150 mm × 4.6 mm) was used for chromatographic separation. The initial mobile phase conditions were 0.1% formic acid in water (v/v; mobile phase A) and 0.1% formic acid in acetonitrile (v/v; mobile phase B). The gradient went to 98% solvent B, with the flow rate maintained at 0.4 mL/min, in 30 min. The mass spectrometer electrospray capillary voltage was maintained at 4.5 kV and the drying temperature at 220 °C with a flow rate of 10 L/min. The nebulizer pressure was 40 psi. Nitrogen was used as both nebulizing and drying gas and helium was used as collision gas at 60 psi. The mass-to-charge ratio was scanned across the range m/z 50−1200 in enhanced resolution positive ion auto MS/MS mode. The smart parameter setting (SPS) was used to automatically optimize the trap drive level for precursor ions. The instrument was externally calibrated with the ESI TuneMix (Agilent). UV monitoring was at 280 nm for HMF derivatives.

NMR Preparation and Analysis. HMF, MMF, and EMF formed during extraction under thermal acidic conditions of quinoa seeds were prepared using 2 N HCl in deionized water, methanol, and ethanol, respectively, in separate experiments as described above. Samples were neutralized using sodium bicarbonate prior to liquid−liquid extraction with methylene chloride. The organic layer was subsequently dried over magnesium sulfate and filtered with anhydrous methylene chloride rinses. The resulting extract was dried using rotary evaporation in vacuo. Prior to acquisition of NMR spectra, each dried sample was mixed with $CDCl_3$. ^{1}H NMR spectra were recorded on a Bruker Avance 400 MHz spectrometer equipped with a Cryoplatform Prodigy cryoprobe. Chemical shift (δ) values for ^{1}H NMR spectra are reported in parts per million (ppm) from

dx.doi.org/10.1021/jf500518r | J. Agric. Food Chem. 2014, 62, 4754−4761

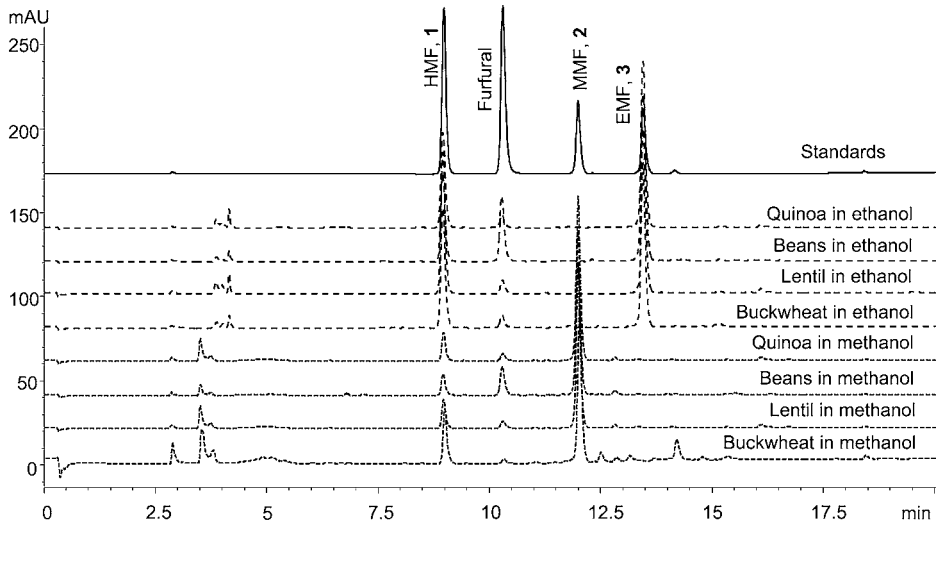

Figure 2. Representative HPLC-DAD chromatograms of a standard mixture of 5-hydroxymethyl-2-furan-2-carbaldehyde (HMF), furfural, 5-methoxymethylfuran-2-carbaldehyde (MMF), and 5-ethoxymethylfuran-2-carbaldehyde (EMF) and profiles of selected grains (cranberry beans, quinoa, lentil and buckwheat seed) extracts following acid hydrolysis in methanol and ethanol solution.

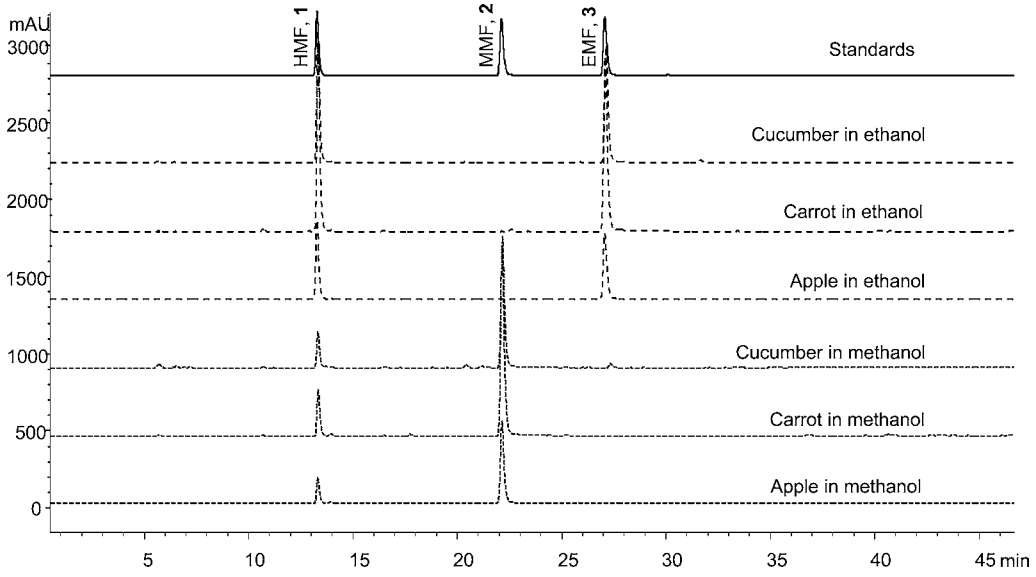

Figure 3. Representative HPLC-DAD chromatograms of a standard mixture of 5-hydroxymethyl-2-furan-2-carbaldehyde (HMF), 5-methoxymethylfuran-2-carbaldehyde (MMF), and 5-ethoxymethylfuran-2-carbaldehyde (EMF) and profiles of selected fruits and vegetable (cucumber, carrot, and apple) extracts following acid hydrolysis in ethanol and ethanol solution.

tetramethylsilane with the solvent resonance as the internal standard ($CDCl_3$, 7.24 ppm).

Total Phenolic and Flavonoid Contents. Total phenolic (TPC) and total flavonoid (TFC) content of authenticated HMF, MMF, and EMF standards was determined using a model EL 340 UV/vis microplate reader (Biotek, Inc., Winooski, VT). A modified Folin–Ciocalteu assay was employed to determine the TPC value measured at 765 nm against reagent blank.[25] TPC was expressed as milligrams of gallic acid equivalents per gram of standard (mg GAE/g) determined using the standard calibration curve of gallic acid with a linear range of 0.0156–0.5 mg/mL (r = 0.999).

Total flavonoid content (TFC) was determined using a modified 96-well microplate method.[26] Absorbance was measured at 510 nm and TFC value was expressed as milligrams of catechin equivalents per gram of standard (mg CAE/g) using a calibration curve of (+)-catechin with linear range of 0.0156–0.5 mg/mL (r = 0.999).

Antioxidant Assays. Radical DPPH scavenging activity and ferric-reducing antioxidant power (FRAP) of authenticated HMF, MMF, and EMF standards were determined using a UV/vis microplate reader (Biotek, Inc., Winooski, VT).[26,27] The DPPH value was expressed as micromoles of Trolox per gram of standard (μmol TE/g) calculated on the basis of the Trolox standard calibration curve. Absorbance was measured at 517 nm against reagent blank. The FRAP value was expressed as micromoles of ascorbic acid equivalent (AAE) per gram of standard (μmol AAE/g). DPPH and FRAP values were determined using respective Trolox and L-ascorbic acid standard curves with a linear range of 62.5–1000 μM (r = 1.0).

Oxygen radical absorbing capacity (ORAC) of authenticated HMF, MMF, and EMF standards was measured using a fluorescence method. The excitation wavelength was set to 485 nm and emission wavelength was 520 nm.[27] A PLX 800 fluorescence spectrophotometer equipped with an automatic thermostatic holder (Bio-Tek, Inc., Winooski, VT) was used. The ORAC value was expressed as micromoles of Trolox

dx.doi.org/10.1021/jf500518r | J. Agric. Food Chem. 2014, 62, 4754–4761

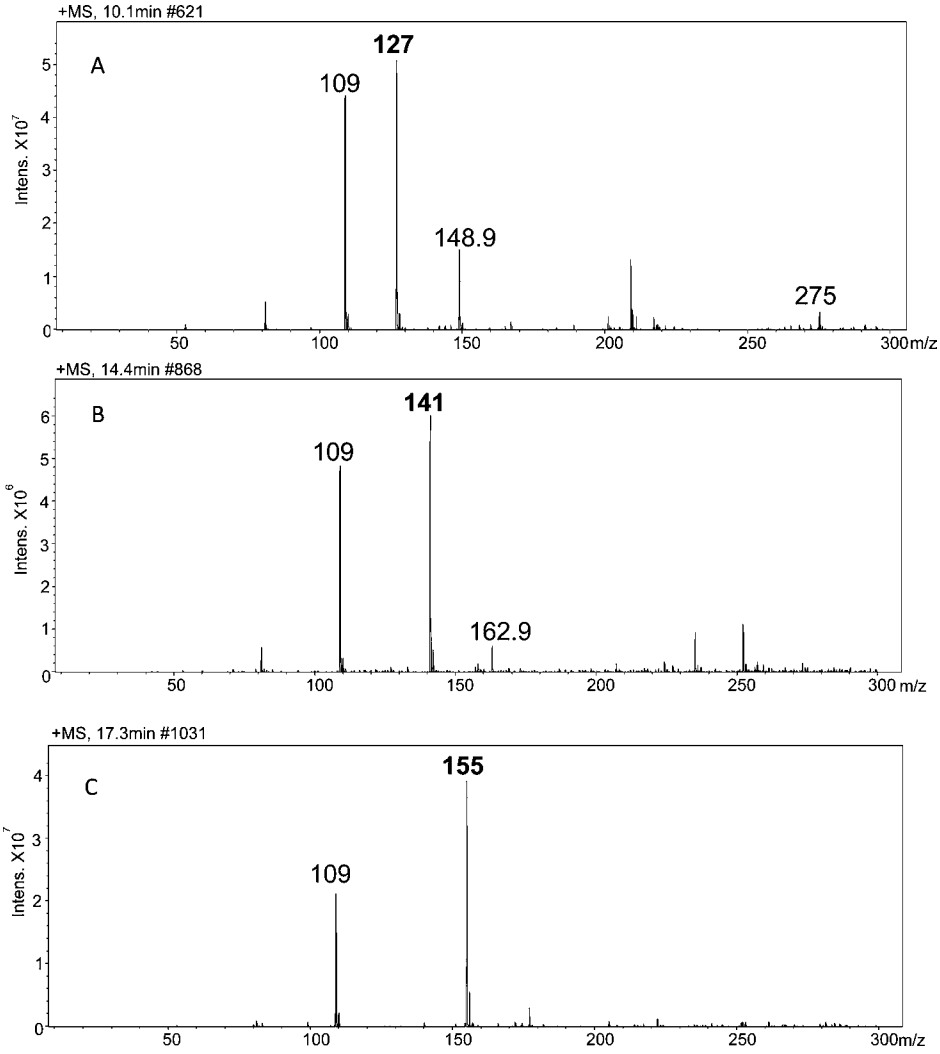

Figure 4. LC−ESI-MS spectra of (A) HMF, (B) MMF, and (C) EMF from hydrolysis of quinoa seeds scanned from m/z 50−1200 in enhanced resolution positive ion auto-MS/MS mode.

per gram of standard (μmol TE/g) calculated on the basis of the Trolox standard calibration curve with linear range of 6.25−100 μM (r = 0.973).

Statistical Analysis. Significant differences among grain samples and standards for each of the parameters were assessed with a one-way analysis of variance (ANOVA test) using SPSS Version 18.0 statistical package for Windows (IBM, Chicago, IL). Statistical differences among the means were evaluated using the LSD test at the $p \leq 0.05$ level to evaluate the significance of the analysis.

RESULTS AND DISCUSSION

Detection and Identification of HMF and HMF Derivatives. Acid hydrolysis of plant materials contains major peaks that are early eluting and detected at 280 nm. These compounds tend to be mistaken for phenolic acids bearing similar retention times.[6] Our results show that these peaks are in fact furans and not phenolic compounds and that this distinction should be made clear in order to prevent the overestimation or interference when quantitating phenolics or assaying for chemical antioxidant activity.

Figure 2 shows a representative chromatogram overlay of the acid hydrolysis products of cranberry bean, quinoa, lentil, and buckwheat seeds along with a standard reference mixture consisting of HMF and its derivatives measured at 280 nm. In fruit and vegetable samples (carrot, cucumber and apple), HMF and its derivatives were also identified and were produced at significantly higher levels compared to grain samples (Figure 3). The high concentration of HMF, MMF, and EMF in fruit and vegetable samples is due to the high presence of carbohydrate sugars acting as substrate.[18] Plant materials and acidic solvent solution were refluxed at 85 °C for 1−3 h (final HCl concentration 2 N). These conditions are commonly used for hydrolysis of various plant materials in the extraction of aglycons or bound phenolics from various plant materials.[28,29] Sequential and direct 2 N HCl hydrolysis of dry beans also undoubtedly yielded HMF and its derivative product in a previous report by Ross et al., although this finding remained unreported.[6] The authors noted that these compounds (denoted X and Y) coeluted with gallic acid and protocatechuic acid, respectively; however, the UV spectra did not agree. HMF has also previously been reported in flaxseed extracts following 40−140 min acid hydrolysis (final HCl concentration of 1 N) at 95 °C.[24] However, the structure and identity of derivative products remained unknown. In our current study, extraction and hydrolysis of cranberry bean, quinoa, lentil, and buckwheat seeds in a solution of 70% methanol (v/v) in 2 N HCl produced three major peaks, corresponding to HMF, furfural, and MMF upon HPLC separation and detection at 280 nm.

dx.doi.org/10.1021/jf500518r | J. Agric. Food Chem. 2014, 62, 4754−4761

Similarly, the presence of 70% ethanol (v/v) in 2 N HCl produced three major peaks in all samples tested detected at 280 nm.

It is likely that the formation of HMF in our study was the result of a dehydration reaction converting sugars to HMF (Figure 1).[18] This is all the more likely as cranberry bean seeds previously soaked in water, therefore leaching them of their sugar content, only contained trace amounts of HMF upon acid hydrolysis. This was verified by subjecting fructose, glucose, sucrose, and inulin standards to acid hydrolysis conditions and detecting the formation of HMF (data not shown). Additionally, the conversion of HMF to its respective derivatives MMF and EMF in the presence of methanol and ethanol has previously been established.[13,19,30] The identity of HMF, MMF, and EMF in all samples studied was verified by comparing retention times and UV spectra against authenticated standards (Figure 2).

ESI-MS analysis of quinoa seeds hydrolyzed under acidic conditions showed that the peak corresponding to HMF (**1**) (t_R = 9 min) (Figure 2) had an abundance of molecular ions with m/z 127 $[M + H]^+$ and 148.9 $[M + Na]^+$ and MS/MS fragment m/z 109 (Figure 4), matching it with authenticated HMF standard. The fragment ion m/z 109 is likely formed after loss of a water molecule (H_2O). The secondary product formed in the presence of methanol (t_R 12 min) (Figure 2) showed a molecular ion of m/z 141 $[M + H]^+$ and 162.9 $[M + Na]^+$ and a fragment ion of m/z 109 and was identified as MMF (**2**). In the presence of ethanol, EMF (**3**) (t_R 13.5 min) (Figure 2) was identified and showed molecular mass of m/z 155 $[M + H]^+$ and 177 $[M + Na]^+$, exactly one CH_2 (m/z 14) unit more than MMF. The same fragment ion of m/z 109 was observed (Figure 4). This common fragment ion is from the furan ($C_6H_5O_2^-$) backbone structure, further confirming that these three peaks are furan derivatives. In the case of MMF, fragmentation resulted in a loss of m/z 32 (CH_3−OH), while EMF lost m/z 46 (CH_3−CH_2−OH). MMF and EMF were produced from pure HMF under the same thermal acidic conditions in aqueous methanol and ethanol, respectively, as opposed to actual food samples, such as quinoa. All MS data for the HMF, MMF, and EMF formed during thermal acidic reaction matched those of the standards, further supporting the identification of the HMF derivatives.

HMF and its derivatives MMF and EMF were prepared from quinoa seeds under optimal conditions so as to maximize the yield and purity of each individual compound for ^{1}H NMR analysis for further structural confirmation (Table 1). NMR spectra show the presence of a furanic ring in all samples denoted by the presence of protons at C3 and C4. Other common protons include a pair of protons on C6 and a single proton on C7. NMR data of HMF also was previously reported, and results are comparable.[31] However, samples were dissolved in D_2O. In the present study we used $CDCl_3$, which allowed for the weak signal of the hydroxyl proton attached to C6 of HMF to be intensified. Distinguishing structural features of MMF and EMF are observed by the presence of methyl protons on C8 in the case of MMF, and methylene protons (C8) and methyl protons (C9) are present in EMF (Table 1, Figure 1).

Table 1. Proton NMR Data of HMF, MMF, and EMF Produced during Acid Hydrolysis of Aqueous Methanol or Ethanol Mixture of Quinoa Seed Flower

	^{1}H NMR data, δ (ppm)		
proton	HMF, **1**	MMF, **2**	EMF, **3**
C3−H	7.22 (d, 1, H)	7.18 (d, 1, H)	7.20 (d, 1, H)
C4−H	6.52 (d, 1, H)	6.49 (d, 1, H)	6.51 (d, 1, H)
C6−H	4.71 (s, 2, H)	4.44 (s, 2, H)	4.51 (s, 2, H)
C6−OH	2.62 (s, 1, H)		
C7−H	9.58 (d, 1, H)	9.54 (s, 1, H)	9.59 (s, 1, H)
C8−H		3.40 (s, 3, H)	3.57 (q, 2, H)
C9−H			1.22 (t, 3, H)

Previous reports have thoroughly demonstrated the production of EMF from the etherification of HMF with ethanol.[19,30] This one-pot reaction is catalyzed under heat and addition of organic acids, producing EMF, which is a good candidate as a biofuel alternative due to its high energy potential.[22] MMF is not as useful and popular as EMF as a biofuel alternative; however, its precursor methanol is widely used in the extraction of polyphenols from plant matter.[6,7,12,17,19,32,33] Extraction of phenolic compounds in the presence of alcohol, acid, and heat may catalyze the formation of HMF and its furanic derivatives that are otherwise unidentified and may impact identification of coeluting phenolic compounds. Identification of HMF, MMF, and EMF as described above led us to the hypothesis that, during the acid hydrolysis of conjugated plant polyphenols, a methyl or ethyl ether was formed through further acid catalyzed condensation between the methanol or ethanol molecule and the HMF molecule (Figure 1).

HMF, MMF, and EMF Formation As Affected by Temperature, Duration, and Solvent Conditions. Table 2 shows the amount of HMF and derivatives produced in a one-pot reaction involving quinoa, buckwheat, lentils, and beans at 85 °C for 2 h in the presence of either acidified aqueous methanol or ethanol. The results suggest that MMF is produced more readily than EMF. Buckwheat in the presence of methanol yielded significantly less HMF and MMF compared to the other samples tested ($p < 0.05$). This may be due to buckwheat's relatively low sugar content.[34,35] While other catalysts are commonly used, such as Al^{3+} and Z-SBA-15, HCl provides higher EMF yield (93%) in one-pot reaction in hydrothermal conditions.[18,30]

The effects of temperature and duration of reaction on the formation of HMF and MMF were further studied using quinoa seeds (Table 3). At temperature extremes (65 and 95 °C), HMF formation is not favored. Increasing the reaction time slightly increased HMF yield at 65 °C but reduced the yield at 95 °C. Increasing the temperature to 75 and 85 °C produces the highest concentration of HMF in quinoa seeds and is optimal when reaction duration is between 0.5 and 1 h. A further increase in time or temperature of hydrolysis resulted in decreased HMF content mirrored by the increased MMF content. Optimal MMF production was observed at 95 °C for 30 min. However, increased reaction duration may compensate for lowered reaction temperature. Low water content typically favors HMF production, as the formation of 1 mol of HMF from 1 mol of fructose or glucose releases 3 mol of water; therefore, the presence of too much water may inhibit the reaction producing HMF.[36] HMF formation generally starts at an average water activity of 0.40, independent of temperature.[32] In our study, water content was kept consistent among all the samples, as the reaction took place in sealed glass vials and in a closed system, preventing loss of water due to evaporation at high temperatures.

Table 2. Concentrations of HMF, MMF, and EMF in the Hydrolysate of Grain Samples Subjected to 2 N HCl Hydrolysis at 85 °C for 2 h in 70% Methanol or Ethanol[a]

	methanol		ethanol	
samples	HMF, **1** (μg/mL)	MMF, **2** (μg/mL)	HMF, **1** (μg/mL)	EMF, **3** (μg/mL)
Quinoa	0.88 ± 0.16 a	9.86 ± 0.79 E	5.54 ± 0.38 d	5.31 ± 0.41 C
Buckwheat	0.36 ± 0.01 a	2.06 ± 0.05 A	4.57 ± 0.00 c	3.09 ± 0.34 B
Lentil	0.49 ± 0.02 a	8.22 ± 0.55 D	4.66 ± 0.75 c	3.74 ± 0.54 B
Cranberry beans	0.61 ± 0.00 a	9.77 ± 0.04 E	3.72 ± 0.11 b	5.34 ± 0.01 C

[a] $n = 3$. Results are reported as mean ± SD. Values followed by the same letter for the same compound are not significantly different ($p < 0.05$).

Table 3. Concentrations of HMF and MMF in the Hydrolysates of Quinoa Seeds and the Influence of Temperature and Duration on the One-Pot Reaction in the Presence of 70% Methanol and 2 N HCl[a]

	HMF, **1** (μg/mL)			MMF, **2** (μg/mL)		
temp (°C)	0.5 h	1 h	2 h	0.5 h	1 h	2 h
65	3.52 ± 0.21 c	4.05 ± 0.22 d	4.35 ± 0.08 de	1.82 ± 0.29 A	3.57 ± 0.48 B	9.28 ± 0.19 C
75	5.20 ± 0.46 f	5.20 ± 0.02 f	4.11 ± 0.28 d	4.43 ± 0.32 B	11.10 ± 0.82 D	16.34 ± 2.34 EF
85	4.82 ± 0.61 ef	3.28 ± 0.30 c	1.26 ± 0.05 a	14.90 ± 0.52 E	16.91 ± 0.94 F	15.82 ± 0.83 EF
95	2.08 ± 0.10 b	1.70 ± 0.26 ab	1.65 ± 0.03 ab	20.86 ± 0.83 G	17.07 ± 0.82 F	15.02 ± 0.51 E

[a] $n = 3$. Results are reported as mean ± SD. Values followed by the same letter for the same compound (HMF and MMF treated separately) are not significantly different ($p < 0.05$).

Effect of HMF, MMF, and EMF on in Vitro Chemical Assays. Colorimetric assays such as TPC and TFC are commonly used to quantitate general classes of phenolic compounds;[1,10] however, these assays are not necessarily highly specific to the phenolic or flavonoid groups and are often interfered by other coexisting chemical classes. Because acid hydrolysis is a common practice in studying phenolics, and HMF and its ether derivatives can be formed under the hydrolysis conditions, the effect of these compounds on the TPC and TFC content must be studied to avoid overestimation. Similarly, HMF derivatives may also affect the total antioxidant capacity in chemical-based assays (Table 4). When HMF, MMF, and EMF standards were examined in both TPC and TFC assays, no interfering effect was found below 200 μg/mL. However, the effect was compound- and concentration-dependent. For example, MMF showed a TPC value of 2.9 mg GAE/g at 625 μg/mL. HMF and EMF only began to show TPC values at 2500 and 1250 μg/mL, respectively. In terms of the antioxidant assays, while HMF and its derivatives MMF and EMF did not show any antioxidant activity in DPPH and FRAP assays at concentrations below 200 μg/mL, they did significantly affect the ORAC assay even at the lowest concentration tested (1.563 μg/mL), and the effect was also dose-dependent. At elevated concentrations, however, HMF, MMF, and EMF began to show FRAP values as well. At 625 μg/mL, MMF and EMF showed 7.71 and 10.32 μmol AAE/g, respectively, while HMF did not show any interference with the FRAP assay until 1250 μg/mL. The effect of these compounds on FRAP values was also dose-dependent. This should be considered in future studies, as concentrations of HMF, MMF, and EMF can reach >2500 μg/mL during common acid hydrolysis assisted extraction procedures for many food samples (data not shown). ORAC is one of the most frequently used antioxidant assay methods. At its lowest concentration tested (1.563 μg/mL), HMF displayed antioxidant activity comparable to that previously reported in the insoluble-bound phenolic extract in quinoa seeds extracted in 3 M HCl at 80 °C for 2 h.[37] This would suggest that the presence of HMF in the acid hydrolysate could be contributing to the majority if not all of the reported antioxidant activity misappropriated to insoluble-bound phenolics. Chemical antioxidant assays function on the basis of two major mechanisms, hydrogen atom transfer (HAT) and single electron transfer (SET).[1] ORAC exploits the HAT reaction mechanism, while FRAP relies totally on an SET-based reaction mechanism, and DPPH color loss occurs through either HAT or SET reaction. DPPH acts both as the radical probe and oxidant and is limited by its steric accessibility favoring smaller molecules. The structure of HMF contains a hydroxyl group that has hydrogen atom donating potential and some electron-dense groups such as double bonds, an aldehyde group, and an oxygenated furan ring.[38] DPPH activity in HMF was previously reported, and the activity was time- and dose-dependent.[38,39]

Table 4. ORAC, TPC, and FRAP values of HMF, MMF, and EMF Authenticated Standards[a]

μg/mL	HMF	MMF	EMF
	ORAC (μmol TE/g)		
1.563	5.21 ± 0.18	3.28 ± 0.70	3.81 ± 1.28
3.125	5.32 ± 0.44	6.65 ± 0.96	4.62 ± 2.21
6.25	7.45 ± 1.46	6.89 ± 0.25	5.08 ± 0.70
12.5	7.98 ± 0.46	7.22 ± 1.62	5.30 ± 0.77
25	13.91 ± 1.45	10.81 ± 1.40	5.68 ± 0.53
50	19.17 ± 0.32	16.87 ± 1.46	8.66 ± 1.50
100	31.59 ± 0.23	30.17 ± 1.13	15.33 ± 2.32
200	38.33 ± 0.51	50.54 ± 1.25	31.55 ± 1.58
	TPC (mg GAE/g)		
625	0	2.90 ± 0.12	0
1250	0	8.01 ± 0.18	4.91 ± 0.13
2500	3.97 ± 0.08	17.11 ± 1.26	10.02 ± 0.56
5000	9.04 ± 0.23	36.02 ± 0.94	19.89 ± 0.98
	FRAP (μmol AAE/g)		
625	0.00	7.71 ± 0.20	10.32 ± 0.78
1250	0.00	21.15 ± 0.26	20.22 ± 0.47
2500	5.29 ± 0.35	57.43 ± 0.72	46.85 ± 1.95
5000	10.14 ± 0.44	100.37 ± 0.81	109.71 ± 2.94

[a] $n = 3$. Results are reported as mean ± SD.

dx.doi.org/10.1021/jf500518r | J. Agric. Food Chem. 2014, 62, 4754−4761

The present study revealed that HMF can be produced from hydrothermal acid hydrolysis of plant materials during extraction of phenolic aglycons or bound phenolics. When the extraction was in aqueous methanol or ethanol, two of the most frequently used solvent systems for phenolic extraction, the hydrolysis conditions favored the production of MMF or EMF, respectively. HMF and its two ether derivatives were confirmed by HPLC-DAD−ESI-MS/MS and NMR. Under the same conditions, methanol was more reactive than ethanol with HMF, forming higher concentrations of MMF than EMF in different foods. Formation of HMF and its derivative products are dependent on temperature and reaction duration. Indisputable identification of HMF and its ether derivatives in the hydrolysate of plant foods helps avoid misidentification as phenolics; this is particularly important when using acid hydrolysis to study aglycons and bound phenolics. Misidentification can lead to overestimation when using HPLC in quantitating phenolic compounds as HMF and its derivatives also show absorption at 280 nm, at which wavelength many phenolics are detected. HMF, MMF, and EMF also displayed a dose-dependent response to ORAC at low concentrations ($\geq$1.563 μg/mL) and to TPC and FRAP at high concentrations ($\geq$625 μg/mL). Caution must therefore be taken when using in vitro chemical assays to assess antioxidant activity and phenolic content of plant materials after acid hydrolysis.

AUTHOR INFORMATION

Corresponding Author

*E-mail: rong.cao@agr.gc.ca. Tel: +1-226-217-8108. Fax: +1-226-217-8183.

Funding

This project is supported by the A-Base research (RBPI 1004) of Agriculture & Agri-Food Canada.

Notes

The authors declare no competing financial interest.

ACKNOWLEDGMENTS

We thank Dr. Dyanne Brewer and Dr. Armen Charchoglyan, Advanced Analysis Center, University of Guelph, for providing mass spectra reports and Emily Carlson from the University of Guelph for assisting us with NMR analysis.

ABBREVIATIONS USED

HMF, 5-(hydroxymethyl)furan-2-carbaldehyde; MMF, 5-(methoxymethyl)furan-2-carbaldehyde; EMF, 5-(ethoxymethyl)furan-2-carbaldehyde.

REFERENCES

(1) Naczk, M.; Shahidi, F. Phenolics in cereals, fruits and vegetables: Occurrence, extraction and analysis. *J. Pharm. Biomed. Anal.* **2006**, *41*, 1523−1542.

(2) Tsao, R. Chemistry and biochemistry of dietary polyphenols. *Nutrients* **2010**, *2*, 1231−1246.

(3) Khoddami, A.; Wilkes, M.; Roberts, T. Techniques for analysis of plant phenolic compounds. *Molecules* **2013**, *18*, 2328−2375.

(4) Naczk, M.; Shahidi, F. Extraction and analysis of phenolics in food. *J. Chromatogr. A* **2004**, *1054*, 95−111.

(5) Nyman, N. A.; Kumpulainen, J. T. Determination of anthocyanidins in berries and red wine by high-performance liquid chromatography. *J. Agric. Food Chem.* **2001**, *49*, 4183−4187.

(6) Ross, K. A.; Beta, T.; Arntfield, S. D. A comparative study on the phenolic acids identified and quantified in dry beans using HPLC as affected by different extraction and hydrolysis methods. *Food Chem.* **2009**, *113*, 336−344.

(7) Lin, L.-Z.; Harnly, J. M.; Pastor-Corrales, M. S.; Luthria, D. L. The polyphenolic profiles of common bean (*Phaseolus vulgaris* L.). *Food Chem.* **2008**, *107*, 399−410.

(8) Repo-Carrasco-Valencia, R.; Hellström, J. K.; Pihlava, J.-M.; Mattila, P. H. Flavonoids and other phenolic compounds in Andean indigenous grains: Quinoa (*Chenopodium quinoa*), kañiwa (*Chenopodium pallidicaule*) and kiwicha (*Amaranthus caudatus*). *Food Chem.* **2010**, *120*, 128−133.

(9) Tsao, R.; Papadopoulos, Y.; Yang, R.; Young, J. C.; McRae, K. Isoflavone profiles of red clovers and their distribution in different parts harvested at different growing stages. *J. Agric. Food Chem.* **2006**, *54*, 5797−5805.

(10) Kim, K.-H.; Tsao, R.; Yang, R.; Cui, S. W. Phenolic acid profiles and antioxidant activities of wheat bran extracts and the effect of hydrolysis conditions. *Food Chem.* **2006**, *95*, 466−473.

(11) Chen, H.; Zuo, Y.; Deng, Y. Separation and determination of flavonoids and other phenolic compounds in cranberry juice by high-performance liquid chromatography. *J. Chromatogr. A* **2001**, *913*, 387−395.

(12) Murkovic, M.; Pichler, N. Analysis of 5-hydroxymethylfurfual in coffee, dried fruits and urine. *Mol. Nutr. Food Res.* **2006**, *50*, 842−846.

(13) Chheda, J. N.; Dumesic, J. A. An overview of dehydration, aldol-condensation and hydrogenation processes for production of liquid alkanes from biomass-derived carbohydrates. *Catal. Today* **2007**, *123*, 59−70.

(14) Surh, Y.-J.; Tannenbaum, S. R. Activation of the Maillard reaction product 5-(hydroxymethyl)furfural to strong mutagens via allylic sulfonation and chlorination. *Chem. Res. Toxicol.* **1994**, *7*, 313−318.

(15) Capuano, E.; Fogliano, V. Acrylamide and 5-(hydroxymethyl)-furfural (HMF): A review on metabolism, toxicity, occurrence in food and mitigation strategies. *Food Sci. Technol.-LWT* **2011**, *44*, 793−810.

(16) Bordajandi, L. R.; Gómara, B.; González, M. J., Analysis of dioxins and furans (PCDDs and PCDFs) in food. In *Analysis of Endocrine Disrupting Compounds in Food*; Wiley-Blackwell: Chichester, U.K., 2010; pp 49−73.

(17) Nässberger, L. Influence of 5-hydroxymethylfurfural (5-HMF) on the overall metabolism of human blood cells. *Hum. Exp. Toxicol.* **1990**, *9*, 211−214.

(18) Li, Y.; Liu, H.; Song, C.; Gu, X.; Li, H.; Zhu, W.; Yin, S.; Han, C. The dehydration of fructose to 5-hydroxymethylfurfural efficiently catalyzed by acidic ion-exchange resin in ionic liquid. *Bioresour. Technol.* **2013**, *133*, 347−353.

(19) Balakrishnan, M.; Sacia, E. R.; Bell, A. T. Etherification and reductive etherification of 5-(hydroxymethyl)furfural: 5-(Alkoxymethyl)furfurals and 2,5-bis(alkoxymethyl)furans as potential bio-diesel candidates. *Green Chem.* **2012**, *14*, 1626−1634.

(20) Huber, G. W.; Iborra, S.; Corma, A. Synthesis of transportation fuels from biomass: Chemistry, catalysts, and engineering. *Chem. Rev.* **2006**, *106*, 4044−4098.

(21) Yoshida, N.; Kasuya, N.; Haga, N.; Fukuda, K. Brand-new biomass-based vinyl polymers from 5-hydroxymethylfurfural. *Polym. J.* **2008**, *40*, 1164−1169.

(22) Mascal, M.; Nikitin, E. B. Direct, high-yield conversion of cellulose into biofuel. *Angew. Chem., Int. Ed.* **2008**, *47*, 7924−7926.

(23) Ras, E.-J.; Maisuls, S.; Haesakkers, P.; Gruter, G.-J.; Rothenberg, G. Selective hydrogenation of 5-ethoxymethylfurfural over alumina-supported heterogeneous catalysts. *Adv. Synth. Catal.* **2009**, *351*, 3175−3185.

(24) Li, X.; Yuan; Xu, S. P.; Wang, J. H.; Liu, X. Separation and determination of secoisolariciresinol diglucoside oligomers and their hydrolysates in the flaxseed extract by high-performance liquid chromatography. *J. Chromatogr. A* **2008**, *1185*, 223−232.

(25) Li, H.; Deng, Z.; Wu, T.; Liu, R.; Loewen, S.; Tsao, R. Microwave-assisted extraction of phenolics with maximal antioxidant activities in tomatoes. *Food Chem.* **2012**, *130*, 928−936.

(26) Herald, T. J.; Gadgil, P.; Tilley, M. High-throughput micro plate assays for screening flavonoid content and DPPH-scavenging activity in sorghum bran and flour. *J. Sci. Food Agric.* **2012**, *92*, 2326−2331.
(27) Li, H.; Deng, Z.; Zhu, H.; Hu, C.; Liu, R.; Young, J. C.; Tsao, R. Highly pigmented vegetables: Anthocyanin compositions and their role in antioxidant activities. *Food Res. Int.* **2012**, *46*, 250−259.
(28) Mattila, P.; Kumpulainen, J. Determination of free and total phenolic acids in plant-derived foods by HPLC with diode-array detection. *J. Agric. Food Chem.* **2002**, *50*, 3660−3667.
(29) Soong, Y.-Y.; Barlow, P. J. Quantification of gallic acid and ellagic acid from longan (*Dimocarpus longan* Lour.) seed and mango (*Mangifera indica* L.) kernel and their effects on antioxidant activity. *Food Chem.* **2006**, *97*, 524−530.
(30) Lanzafame, P.; Temi, D. M.; Perathoner, S.; Centi, G.; Macario, A.; Aloise, A.; Giordano, G. Etherification of 5-hydroxymethyl-2-furfural (HMF) with ethanol to biodiesel components using mesoporous solid acidic catalysts. *Catal. Today* **2011**, *175*, 435−441.
(31) Serra-Cayuela, A.; Castellari, M.; Bosch-Fusté, J.; Riu-Aumatell, M.; Buxaderas, S.; López-Tamames, E. Identification of 5-hydroxymethyl-2-furfural (5-HMF) in Cava sparkling wines by LC-DAD−MS/MS and NMR spectrometry. *Food Chem.* **2013**, *141*, 3373−3380.
(32) Ameur, L. A.; Tyrstram, G.; Birlouez-Aragon, I. Accumulation of 5-hydroxymethyl-2-furfural in cookies during the backing process: Validation of an extraction method. *Food Chem.* **2006**, *98*, 790−796.
(33) Gao, L.; Mazza, G. Rapid method for complete chemical characterization of simple and acylated anthocyanins by high-performance liquid chromatography and capillary gas−liquid chromatography. *J. Agric. Food Chem.* **1994**, *42*, 118−125.
(34) Tahir, I.; Farooq, S. Grain composition in some buckwheat cultivars (*Fagopyrum* spp.) with particular reference to protein fractions. *Plant Food Hum Nutr* **1985**, *35*, 153−158.
(35) Vidal-Valverde, C.; Frias, J.; Sierra, I.; Blazquez, I.; Lambein, F.; Kuo, Y.-H. New functional legume foods by germination: Effect on the nutritive value of beans, lentils and peas. *Eur. Food Res. Technol.* **2002**, *215*, 472−477.
(36) Kroh, L. W. Caramelisation in food and beverages. *Food Chem.* **1994**, *4*, 373−379.
(37) Laus, M. N.; Gagliardi, A.; Soccio, M.; Flagella, Z.; Pastore, D. Antioxidant activity of free and bound compounds in quinoa (*Chenopodium quinoa* Willd.) seeds in comparison with durum wheat and emmer. *J. Food Sci.* **2012**, *77*, C1150−C1155.
(38) Li, Y. X.; Li, Y.; Qian, Z. J.; Kim, M. M.; Kim, S. K. In vitro antioxidant activity of 5-HMF isolated from marine red alga *Laurencia undulata* in free-radical-mediated oxidative systems. *J. Microbiol.* **2009**, *19*, 1319−1327.
(39) Zhao, L.; Chen, J.; Su, J.; Li, L.; Hu, S.; Li, B.; Zhang, X.; Xu, Z.; Chen, T. In vitro antioxidant and antiproliferative activities of 5-hydroxymethylfurfural. *J. Agric. Food Chem.* **2013**, *61*, 10604−10611.

JOURNAL OF AGRICULTURAL AND FOOD CHEMISTRY

Article

pubs.acs.org/JAFC

Factors Limiting the Enzymatic Hydrolysis of Wheat Gluten

L. Giesler,* D. Linke, and R. G. Berger

Institut für Lebensmittelchemie, Leibniz Universität Hannover, Callinstraße 5, Hannover 30167, Germany

ABSTRACT: The enzymatic hydrolysis of wheat gluten for the production of seasonings using mixtures of endo- and exopeptidases results in yields typically below 40%. Possible limiting parameters, such as an increasing product inhibition, autopeptidolysis of the enzymes, and lack of cleavage sites, were studied using novel peptidases from *Flammulina velutipes* or the commercial Flavourzyme preparation. Seven intermittent electrodialysis steps (10 g/L gluten and 10 kaU/mL) for the in situ removal of amino acids minimized the product inhibition. During 16 h, hydrolysis progressed nearly linearly. Compared to the batch control, a 3-fold yield of amino acids released was obtained indicating that an integrated product removal alleviates the problem of product inhibition. Autopeptidolysis, as shown using sodium dodecyl sulfate polyacrylamide gel electrophoresis and enzyme activity assays, was suppressed with increasing concentrations of competing gluten substrate. Peptidases of *F. velutipes* showed product inhibition only, whereas a combined effect of product inhibition and lack of cleavage sites was observed for Flavourzyme.

KEYWORDS: *wheat gluten, hydrolysis, electrodialysis, autopeptidolysis, cleavage site, Flavourzyme, Flammulina velutipes*

INTRODUCTION

Enzymatic protein hydrolysis is widely used in the food industry for applications such as the production of seasonings from soy or wheat proteins or the improvement of the functional properties of dairy products and confectionary.[1] So far, total hydrolysis of the protein as obtained by the former hydrochloric acid catalyzed process was not achieved, even if complex enzyme preparations were used.[2] Previous studies suggested limitations, such as product inhibition, autopeptidolysis, and the decline of sufficient cleavage sites in the substrate in the course of the process.[3−5] An advanced cleavage of peptide bonds might result in the formation of bitter tasting peptides. Thus, the technical aim is often not just to improve the degree of hydrolysis but preferably to bring the reaction to completion.

To date, research focused on product inhibition as the limiting factor.[6] As shown previously, Flavourzyme and *Flammulina velutipes* peptidases were both inhibited by the hydrophobic L-amino acids L-isoleucine, L-leucine, L-valine, and L-phenylalanine. L-Serine inhibited only *F. velutipes* peptidases, while L-histidine and L-glutamine inhibited only Flavourzyme peptidases.[4] The same study[4] confirmed that electrodialysis (ED) equipped with four ultrafiltration membranes (UF, cutoff 4 kDa) was suitable to minimize the product inhibition. After applying the ED twice for 1 h during the 20 h of hydrolysis, a large increase of the degree of hydrolysis (DH) of up to 145% for *F. velutipes* peptidases and of 70% for Flavourzyme compared to the control batch was observed.[4] To fully explore the potential of ED, the membrane surface was increased,[7] and the ED step repeatedly was implemented during the hydrolysis.

The phenomenon of autopeptidolysis was described for individual enzymes, such as subtilisin-like serine peptidases,[8] retroviral aspartyl proteases,[9] or neutral peptidases.[10] A pure peptidase is generally not susceptible to autopeptidolysis under native conditions. After an irreversible inactivation by high temperature or chemical denaturants, the native structure becomes impaired, and autopeptidolysis by residual active peptidase may occur.[10,11] Thus, the application of mixtures of endo- and exopeptidases bears the risk of peptidases degrading each other. In this study, the robustness and reaction behavior of Flavourzyme, a commercial preparation from *Aspergillus oryzae*, was compared to a mixture of peptidases from the edible basidiomycete *F. velutipes*, previously proven for the hydrolysis of wheat gluten.[4] Autopeptidolysis and the availability of cleavage sites in the substrate were studied.

MATERIALS AND METHODS

Materials. All chemicals and solvents were of analytical or HPLC grade and obtained from Carl Roth (Karlsruhe, Germany), Merck (Darmstadt, Germany), Sigma−Aldrich (Taufkirchen, Germany), and VWR International GmbH (Darmstadt, Germany), respectively.

Cultivation of *F. velutipes*. Cultivations were carried out as described previously.[4]

Peptidase Activity. The peptidolytic activity was determined with the azocasein assay as a photometric end-point method following ref. 4.

Two more specific peptidase assays were performed in 96-well microtiter plates: first, 50 mM Tris buffer pH 7 and 10 μL of *Z*-Ala-Ala-Pro-Phe-*p*-nitroanilide (2 mM AAPF), or second, 25 mM sodium acetate buffer pH 5 and *Z*-Gly-Pro-*p*-nitroanilide (2 mM) from Sigma−Aldrich (Taufkirchen, Germany) with each substrate in dimethyl sulfoxide and 20 μL of enzyme preparation in a total volume of 150 μL. The molar extinction coefficient of *p*-nitroaniline was determined at $\varepsilon^* = 4567\ \mu L/\mu M$ at 405 nm in a BioTek Synergy 2 microtiter plate reader (Bad Friedrichshall, Germany). The absorption was measured at 37 °C and 405 nm over 90 min. One unit of peptidolytic activity was calculated as the amount of enzyme required to produce 1 μM *p*-nitroaniline per minute.

Preparation of Wheat Gluten Hydrolysate. Various hydrolysis experiments were carried out with dry sterilized (130−135 °C, 8 h) wheat gluten (5−100 g/L) at 180 rpm, 45 °C, and pH 6.0 in 25 mM

Received: February 20, 2014
Revised: April 22, 2014
Accepted: April 30, 2014
Published: April 30, 2014

ACS Publications © 2014 American Chemical Society

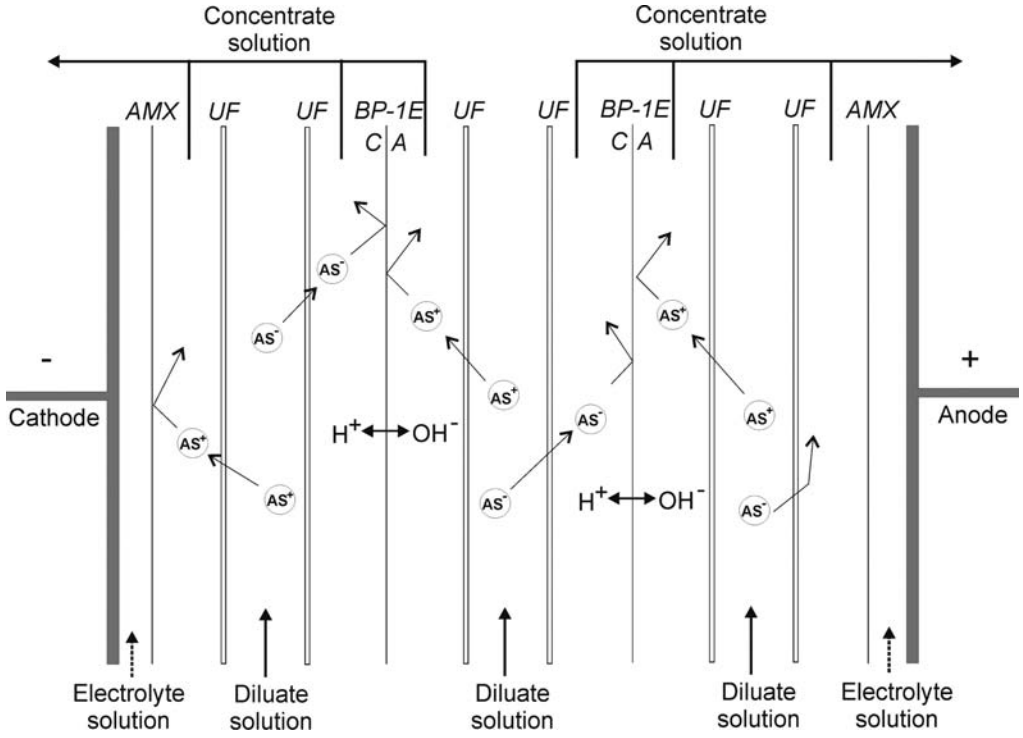

Figure 1. Configuration of the ED stack for the separation of amino acids (AS), anionic membrane (AMX), bipolar membrane (BP-1E) to block ion migration and delivery of the counterion, and six ultrafiltration membranes (UF).

sodium acetate buffer with two different peptidase mixtures, *F. velutipes* or Flavourzyme from Novozymes (Copenhagen, Denmark), using standardized peptidase activities per milliliter of hydrolysate. For each hydrolysate, the concentration of L-amino acids (mM), soluble protein (mg/L), and the DH were investigated over time as described in ref 4.

Electrodialysis. ED equipped with six ultrafiltration membranes (UF, cutoff 4 kDa, UH004P from Microdyn-Nadir, Wiesbaden, Germany) was used to increase the transfer rate of L-amino acids from the diluate into the concentrate solution. The stack configuration with UF membranes is shown in Figure 1.[4] To check the transfer increase, the recovery of the model solution consisting of L-glutamic acid, L-asparagine, L-serine, and L-leucine (50 mM in 25 mM sodium acetate buffer, pH 6) was calculated. ED experiments were carried out using the laboratory-scale EDL02 (Hescon GmbH, Engstingen, Germany), equipped with a DSE electrode at pH 6, 12 V with a current density of 14.0 mA/cm^2 and 0.25% Na_2SO_4 as electrolyte solution, to separate the L-amino acids from the wheat gluten hydrolysates during the hydrolysis following. The recovery of the L-amino acids was calculated as reported previously.[4] Two alternating hydrolysis samples (sample 1 (S1) and sample 2 (S2)) were used, and the ED was integrated alternating 4-fold or 7-fold into the 20 or 26 h hydrolysis process. For every experiment, a batch control was carried along.

Autopeptidolysis and Thermal Stability. The peptidase mixtures of *F. velutipes* or Flavourzyme were incubated in 25 mM sodium acetate buffer pH 6 at different temperatures (4, 20, and 45 °C) over 20 h with or without addition of gluten (10 or 100 g/L) as substrate. After the incubation at defined temperatures or substrate concentrations, residual peptidase activity was assayed with the azocasein and the AAPF assay as described above. Gycerol, $(NH_4)_2SO_4$, $MgC1_2$, $CaC1_2$, ethylenediaminetetraacetic acid (EDTA), and phenylmethylsulfonyl fluoride (PMSF) were tested as protectants against thermal inactivation of the peptidases. The inactivation (%) was calculated using the change in activity compared to the initial activity. Sodium dodecyl sulfate polyacrylamide gel electrophoresis (SDS-PAGE) was used to follow autopeptidolytic process of the enzymes.

Sodium Dodecyl Sulfate Polyacrylamide Gel Electrophoresis. SDS-PAGE analyses were performed using 12% (*w*/*v*) polyacrylamide separation gels after Laemmli.[12] Samples were prepared by mixing 10 μL of enzyme solution and 10 μL of loading buffer (0.1 M Tris/HCl (pH 6.8), 0.2 M DTT, 4% SDS, 20% glycerol, 0.2% bromophenol blue) and boiling for 10 min. After electrophoresis at 18 mA per gel, the gels were stained with Instant Blue (Gentaur GmbH, Aachen, Germany). Marker proteins from 10 to 250 kDa (BioRad, Munich, Germany) were used for molecular mass determination.

Cleavage Sites. To determine whether enough cleavage sites for the peptidases were present in the wheat gluten, the following hydrolysis experiments were performed. Prehydrolysis for 3 h was performed at 180 rpm, 45 °C, and pH 6 in 25 mM sodium acetate buffer with two different peptidase mixtures from either *F. velutipes* or Flavourzyme. Thereafter, the hydrolysate was centrifuged (10 min, 5000 rpm, 4 °C). Fresh peptidases and buffer were added to the gluten that was already partly hydrolyzed (C1). To the already used peptidases and buffer solution, fresh wheat gluten was added (C2). Both mixtures were then further incubated for 17 h. For every experiment, a batch control was carried out. Hydrolyzed samples were analyzed for peptidolytic activity, the concentration of L-amino acids (mM) and the soluble peptides (mg/mL).

Statistical Analysis. The ED, autopeptidolysis, and cleavage site studies were subjected to statistical analysis (error probability $p < 0.05$) using the one-way ANOVA of the Origin 6.1 software (OriginLab Corporation, Northampton, MA, USA). All data presented are averages of duplicate measurements. Numerous experiments were conducted, and single parameters, such as enzyme activity, were changed to distinguish critical from insignificant factors; for the bulk of these measurements, the standard deviation of repetitions was typically below 5%.

RESULTS AND DISCUSSION

Electrodialysis Using Six Ultrafiltration Membranes. In order to reduce inhibition by the recently identified amino acids (L-isoleucine, L-leucine, L-valine, L-phenylalanine, L-histidine, and L-glutamine) for *F. velutipes* and Flavourzyme peptidases, the transfer rate of the ED unit was increased by using six UF

dx.doi.org/10.1021/jf500901a | J. Agric. Food Chem. 2014, 62, 4762−4768

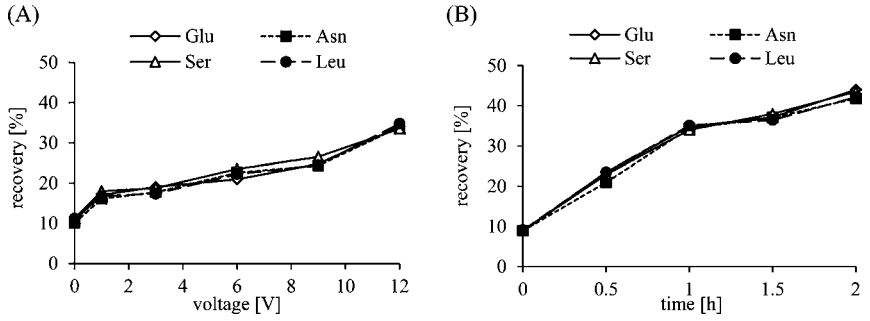

Figure 2. Effect of different voltages on the transport from diluate into concentrate using UF membranes (A) at different voltages per hour or (B) over 2 h at 12 V, expressed as recovery of the L-amino acids: L-asparagine, L-glutamic acid, L-serine, and L-leucine (50 mM model solution, pH 6).

membranes (previously four).[4] The three diluate circuits and six concentrate circuits of the ED stack led to an enhanced recovery (Figure 1). As previously described,[4] all of the L-amino acids measured were transported at similar rates, and the recovery increased with higher voltages (Figure 2A). After 1 h of ED at 12 V with six UF membranes, the best transfer rates were achieved: L-asparagine, 34 ± 1%; L-glutamic acid, 34 ± 2%; L-serine, 34 ± 3%; and L-leucine, 35 ± 2% per hour. Without an electric potential applied, the transfer rates varied between 8% and 9%. With increased time of ED, the recovery increased as well, as did the conductivity of the concentrate. After 2 h of ED at 12 V, transfer rates of 42−44% were reached (Figure 2B), and a higher conductivity in the concentrate solution (16.2 mS/cm) compared to the diluate (13.5 mS/cm) was observed. With converging conductivity in both circuits, the transport of ions through the membranes slowed down (Figure 2B). With the commonly used stack configurations, that is, AMX/CMX (anionic/cationic membrane) or four UF membranes, lower transfer rates of 8−10% and 22−30%, respectively, were obtained.[4] Similar results were reported by Poulin et al.[7] who found a 4-fold increase of the peptide transfer when stacking four UF membranes instead of one.

L-Amino acids possessing inhibitory properties were effectively removed from the hydrolysates obtained using either Flavourzyme or/ *F. velutipes* peptidases: L-isoleucine (34%/33%), L-leucine (33%/33%), L-valine (34%/32%), L-phenylalanine (34%/31%), L-glutamine (33%/33%), L-histidine (34%/35%), and L-serine (32%/34%). Furthermore, soluble peptides less than 4 kDa were transported, with transfer rates ranging from 10% to 12% per hour.

A further improvement of the efficiency of hydrolysis was achieved by combining the increased area of the UF membranes with a more frequent application of the ED step. During 20 h of hydrolysis (10 g/L gluten and 1 kaU/mL peptidase mixture) and a 4-fold ED, each for 1 h, an increased release of L-amino acids of 94% for Flavourzyme and of 153% for *F. velutipes* was recorded (Table 1). These results indicated an improvement compared to previous studies with 2-fold ED and four UF membranes (Flavourzyme: 70%; *F. velutipes*: 145%[4]). The best yields of hydrolysis (batch: DH 35%; ED: DH 76%) were achieved with a low substrate concentration (5 g/L gluten) and a high peptidase activity of 75 kaU/mL *F. velutipes* peptidases. With a 7-fold integrated ED (10 g/L gluten and 10 kaU/mL), a nearly linear progression for the first 16 h of the hydrolysis process (Figure 3A) and a 3-fold concentration of amino acids released was obtained (Table 1). Thus, the manifold integration of ED proved to be suitable for overcoming product inhibition.

Table 1. Efficiency of Electrodialysis (ED) Compared to the Batch Process[a]

peptidase	activity (kaU/mL hydrolysate)	wheat gluten (g/L)	no. of ED cycles (each 1 h)	amino acids released (mM)	
				batch	ED
Fx	1	10	4	14.1	27.5
Fx	10	10	4	20.7	40.7
Fve	1	10	4	14.8	37.5
Fve	10	10	4	19.5	39.2
Fve	10	10	7	**19.5**	**56.4**
Fve	75	5	4	14.1	30.8

[a]Hydrolysis of wheat gluten for 20 h plus electrodialysis (1 h prehydrolysis) at pH 6 and 45 °C using Flavourzyme (Fx) or *F. velutipes* (Fve) peptidases, respectively.

Transfer rates decreased during the seven steps of the ED from initially 32−35% to 26−27%. This is explained by clogging of the membrane pores over time, as there was no washing step after each step. Poulin et al.[13] reported a weak fouling, if one UF membrane was used in the ED stack, which was removed by rinsing the membrane with distilled water. Although fouling is of minor importance due to the absence of pressure in a ED stack with UF membranes, various interactions between the clogging membranes and the peptides may take place that influence the migration.[14]

Peptidase activity decreased in the batch as well as in the ED process over time. After 26 h, around 9% of the introduced peptidase activity remained in the ED experiment and about 18% in the batch (Figure 3B). Cui et al.[15] also observed a decrease of Alcalase activity during the hydrolysis of wheat gluten in an enzyme membrane reactor. There are two possible explanations: First, some peptidases remained adsorbed at the membranes, which would explain the difference between the ED and batch experiments. Second, peptidases were lost due to a high autopeptidolytic activity. Hence, two washing steps were integrated after every ED step. The first washing step, refreshing the buffer solution in the diluate and rinsing for 10 min, recovered 3−4% of initial *F. velutipes* and 8−9% of initial Flavourzyme peptidase activity. Afterward, the buffer solution was refreshed for a second time, and the poles were switched for a further 10 min. One percent of the initial *F. velutipes* peptidase activity and up to four percent of Flavourzyme activity were recovered. The recovery rate showed no differences with or without the use of wheat gluten as the substrate.

dx.doi.org/10.1021/jf500901a | J. Agric. Food Chem. 2014, 62, 4762−4768

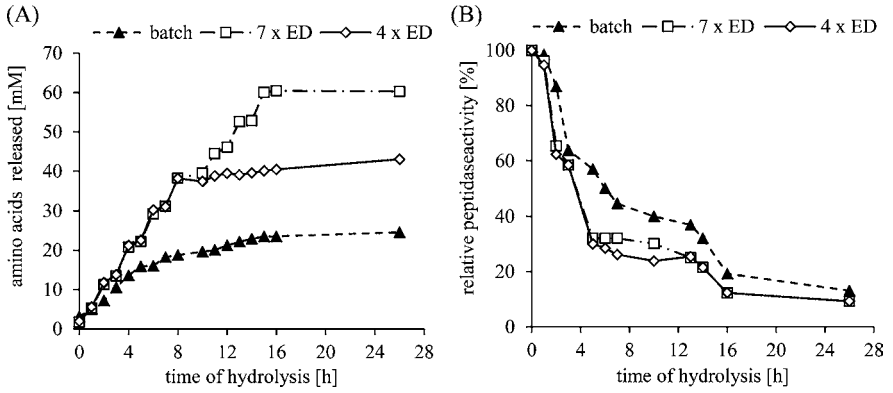

Figure 3. Hydrolysis of wheat gluten combined with ED (UF configuration) using *F. velutipes* peptidases (10 kaU/mL hydrolysate each) for 26 h, 10 g/L gluten at pH 6, 45 °C, 1 h prehydrolysis, 4-fold or 7-fold ED for 1 h at 12 V, 35 °C. (A) Released amino acid concentration; (B) change of the relative peptidase activity (%) quantified using the azocasein assay.

Table 2. Peptidase Inactivation (%) at Different Incubation Temperatures (4, 20, 45 °C), with Different Additives and Wheat Gluten Concentrations (0, 10, 100 g/L) after 20 h Incubation at 45 °C and pH 6 by Using Different Initial Peptidase Activities (A: High Activity; B: Low Activity) of Flavourzyme and *F. velutipes*, Quantified with Azocasein and AAPF Assay

	peptidase inactivation (%) (azocasein assay)			
	Flavourzyme		*F. velutipes*	
	A [250 kaU/mL]	B [10 kaU/mL]	A [80 kaU/mL]	B [10 kaU/mL]
Temperature				
4 °C	65.4 ± 1.2	4.7 ± 0.5	60.7 ± 1.2	7.0 ± 0.4
20 °C	65.9 ± 1.6	6.4 ± 0.9	69.8 ± 1.1	10.4 ± 1.7
45 °C	72.7 ± 2.6	34.3 ± 1.1	96.1 ± 2.9	86.2 ± 3.1
Substrate				
0 g/L		32.1 ± 1.0		85.2 ± 0.2
10 g/L		28.3 ± 0.5		79.3 ± 0.2
100 g/L		30.3 ± 1.9		62.0 ± 0.1
	peptidase inactivation (%) (AAPF assay)			
	Flavourzyme		*F. velutipes*	
	A [15 U/L]	B [1 U/L]	A [15 U/L]	B [1 U/L]
Temperature				
4 °C	2.6 ± 0.3	3.8 ± 0.7	0.0 ± 0.1	0.0 ± 0.2
20 °C	28.9 ± 1.4	17.4 ± 1.4	16.4 ± 1.3	5.8 ± 1.5
45 °C	50.5 ± 2.9	27.5 ± 1.9	97.1 ± 2.8	65.0 ± 2.9
Substrate				
0 g/L		28.1 ± 0.2		66.2 ± 1.3
10 g/L		25.5 ± 3.0		48.4 ± 0.4
100 g/L		17.2 ± 0.2		43.1 ± 6.7
Additives				
control		27.5 ± 1.9		61.3 ± 0.5
glycerol (1.9 M)		58.8 ± 2.5		69.9 ± 1.0
$(NH_4)_2SO_4$ (0.5 M)		41.6 ± 6.9		63.3 ± 3.4
$MgC1_2$ (9 mM)		18.4 ± 1.8		58.2 ± 1.1
EDTA (100 μM)		98.9 ± 0.5		99.5 ± 0.2
PMSF (100 μM)		89.1 ± 0.3		96.6 ± 0.1
$CaC1_2$ (36 mM)		5.8 ± 0.2		35.5 ± 1.2

Autopeptidolytic Activity of Peptidase Mixtures. An extensive hydrolysis, preferably using mixtures of endo- and exopeptidases, is desired to reduce the bitterness of the hydrolysate as well as to obtain a high DH.[2] Besides the degradation of the substrate, peptidases may hydrolyze each other. An intermolecular mechanism by which peptidases digest other peptidases has been suggested.[8] The autopeptidolysis of *F. velutipes* and Flavourzyme peptidases was monitored by measuring the residual activity after different incubation studies at various temperatures without substrate and at different substrate concentrations (Table 2). With increasing incubation temperature, the recovered peptidase activity decreased. Incubation at 45 °C, corresponding to the temperature optimum of the applied peptidases, showed a decrease of the peptidase activity (initially 10 kaU/mL) of 86.2% for *F. velutipes* and 34.3% for Flavourzyme. Bajorath et al.[16] observed a constant slow decrease in proteinase K (initial concentration 0.01 mg/mL) activity at room temperature. With higher initial

dx.doi.org/10.1021/jf500901a | J. Agric. Food Chem. 2014, 62, 4762−4768

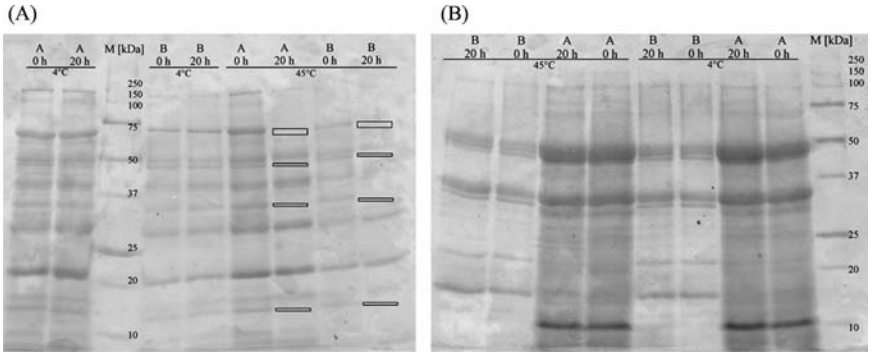

Figure 4. SDS-PAGE (12%) to study autopeptidolysis without substrate at 4 and 45 °C with two different initial peptidase activities (A: high activity; B: low activity) for (A) *Flammulina velutipes* and (B) Flavourzyme; changes in the band pattern after 20 h were marked with a box. M [kDa] Precision Plus Protein-Standard unstained (BioRad, Germany).

peptidase activity, the residual activity for *F. velutipes* and Flavourzyme peptidases decreased (Table 2). The absence of gluten in these incubations implied that the peptidase breakdown was an autopeptidolytic event. These data were confirmed with a second peptidase activity test using AAPF, in addition to the azocasein assay, as the substrate. Similar results were obtained by Abraham and Breuil.[8] The incubation with different substrate concentrations (10 and 100 g/L wheat gluten) resulted in the competitive minimization of autolysis (Table 2). Thus, autolysis became negligible in the presence of excess substrate.

To achieve a more detailed picture of the products of autopeptidolysis, the enzyme solutions without substrate were analyzed by SDS-PAGE. At the lower incubation temperature (4 °C), no changes of the electrophoretic patterns were detected, neither for *F. velutipes*, nor for Flavourzyme peptidases (Figure 4A, B). After 20 h at 45 °C, four bands (73, 48, 32, and 15 kDa, Figure 4A, black boxes) of the mixture from *F. velutipes* disappeared in the SDS-PAGE gel. The bands at 20, 27, 37, and 50 kDa did not change after 20 h. Gelatin zymography visualized active peptidases in the supernatant of *F. velutipes* at 15, 27, 32, 37, 75, and 150 kDa.[17] Flavourzyme showed no modifications of the pattern on the SDS-PAGE gel (Figure 4B) and in the gelatin zymography after 20 h of incubation at 45 °C. Thus, it is supposed that hypothetical degradation products were smaller than 10 kDa.

At 45 °C and an initial peptidase activity of 10 kaU/mL, *F. velutipes* and Flavourzyme released 80 and 110 μM L-amino acids, respectively. With increased initial peptidase activity, the release of L-amino acids increased as well: *F. velutipes* [80 kaU/mL] and Flavourzyme [250 kaU/mL] gave 0.76 and 0.84 mM L-amino acids, respectively).

To minimize autopeptidolysis, the peptidase mixtures (1 U/L) were incubated with various presumed protectants:[8] glycerol (1.9 M), $(NH_4)_2SO_4$ (0.5 M), $MgCl_2$ (9 mM), and $CaCl_2$ in different concentrations. Glycerol (1.9 M), $(NH_4)_2SO_4$ (0.5 M), and $MgCl_2$ (9 mM) did not protect the peptidases from *F. velutipes* or Flavourzyme, as proven by AAPF peptidase activity assay (Table 2). Additionally, the effects of the specific serine peptidase inhibitor PMSF and the metallopeptidase inhibitor EDTA on the degradation of *F. velutipes* or Flavourzyme peptidases were studied. The peptidase mixtures were completely inhibited by PMSF (100 μM) and EDTA (100 μM). No protection against autopeptidolysis was detected. A similar study reported that the addition of a protease inhibitor did not lead to an increased stability, as the autopeptidolysis is usually not sufficiently suppressed.[18] Only $CaCl_2$ significantly extended the peptidase activity of both enzyme mixtures. Increasing $CaCl_2$ concentrations (0.9, 3.9, 9.0, 18.0, 27.0 mM) minimized the loss of initial activity (1 U/L). A 25% lower inactivation for *F. velutipes* peptidases and 22% for Flavourzyme compared to the control without supplementation was determined at 27 mM $CaCl_2$. A further increase of $CaCl_2$ up to 36 mM had no better effect (Table 2). When the peptidases of *F. velutipes* were incubated with 9 mM $CaCl_2$, the protein band at 32 kDa in the SDS gel (Figure 4A) was not degraded as in the control without $CaCl_2$ (data not shown). Calcium ions are required by some peptidases for folding of the peptide chain and hence activity (for example, thermolysin and proteinase K). Abraham and Breuil[8] showed an improvement of the half-life time of the purified subtilisin-like serine protease secreted by *Ophiostoma piceae* (7.7 min at 40 °C) by adding 27 mM $CaCl_2$ up to 2 h at 40 °C.

To prevent peptidases against autopeptidolysis, two strategies are available: the identification and removal of the primary cleavage sites and restricting their accessibility. It has been suggested that especially the loop with the peptidolysis site could be stabilized by Ca^{2+}-binding against unfolding.[8] Braxton and Wells[19] identified two sites of autopeptidolysis of subtilisin BPN′. They also evaluated stabilization by site-directed mutagenesis in regions of autolytic susceptibility. The data indicated that the peptidase mixtures of *F. velutipes* and Flavourzyme contained subtilisin-like peptidases that were stabilized by Ca^{2+} ions.

It was examined how $CaCl_2$ (9 mM) affected the hydrolysis of wheat gluten (10 g/L) with *F. velutipes* or Flavourzyme peptidases (10 kaU/mL). The loss of peptidase activity was minimized in the presence of $CaCl_2$ (without gluten) by 6% for *F. velutipes* and by 4% for Flavourzyme. During the incubation of wheat gluten in the presence of $CaCl_2$, the autopeptidolysis was lowered by around 4% for *F. velutipes* and 2% for Flavourzyme peptidases. However, the DH was not significantly increased (*F. velutipes*: 12.6 ± 1.0%; Flavourzyme: 14.7 ± 0.4%) compared to the control without supplementation (*F. velutipes*: 11.3 ± 0.1%; Flavourzyme: 14.9 ± 0.9%). Neither autopeptidolysis nor product inhibition were significantly affected by the presence of Ca^{2+} ions. It was concluded that the lack of cleavage sites in wheat gluten was another factor likely to limit hydrolysis.

Cleavage Sites. Since no single purified peptidase was used for the hydrolysis of wheat gluten, the incubations were evaluated by adding either substrate or peptidases after 3 h of

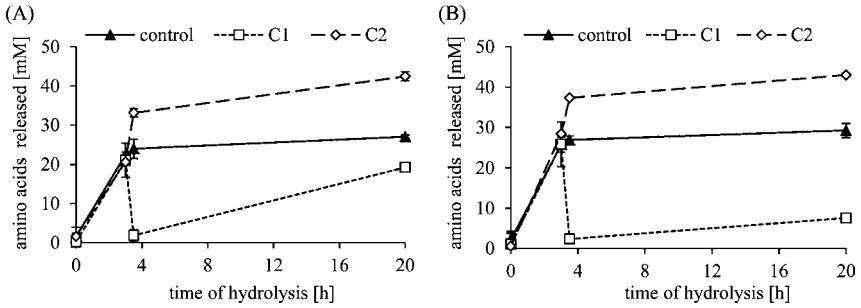

Figure 5. Cleavage sites study: Release of L-amino acids [mM] using peptidases of (A) *F. velutipes* and (B) Flavourzyme (28 kaU/mL hydrolysate each) for 20 h, 10 g/L gluten at pH 6, 45 °C. After 3 h of prehydrolysis, (C1) addition of fresh peptidases and buffer to the prehydrolyzed gluten and (C2) addition of fresh wheat gluten to the already used peptidases and buffer solution compared to the control.

preincubation. The initial rate of hydrolysis was affected in a positive way by the additional supplementation of substrate (C2, Figure 5A, B). Product inhibition increased because of a higher release of L-amino acid compared to the control. This observation was also described by Ravallec-Plé et al.[20] for the hydrolysis of cod (*Gadus morhua*) muscle with alcalase. They assumed that the substrate cleavage sites were limiting, as the DH did not increase upon another addition of enzyme. Different observations were made in the present study for the two enzyme preparations after the second addition: In the case of peptidases from *F. velutipes*, the addition of fresh enzyme and buffer after 3 h of prehydrolysis led to a further increase of the rate of hydrolysis. A similar release of L-amino acids after 20 h of hydrolysis between the sample C1 (additional enzyme) and the control was observed (Figure 5A). This is an indication that there were still enough cleavage sites in the substrate for the action of the peptidases from *F. velutipes*. Flavourzyme showed the opposite effect. Despite the elimination of inhibitory L-amino acids and the supply of fresh enzyme, the DH of the control was not reached within another 17 h of hydrolysis (C1, Figure 5B). Similar experiments with a higher activity of Flavourzyme (280 kaU/mL) confirmed the results. After 9 h of hydrolysis, no further increase of the DH was determined for C1 (data not shown). With a higher initial enzyme activity, it is expected that the lack of cleavage sites appears even earlier. An increased substrate concentration will delay the effect. Overall, the lack of suitable cleavage sites in wheat gluten limited the efficiency of the peptidases in Flavourzyme. A possible explanation could be a lack of prolyl-specific peptidases in the enzyme mixture. L-Glutamine and L-proline (13−23%) together account for half or more of the peptide-bound amino acids in wheat gluten.[21] Due to the unique structure of L-proline, peptide bonds involving L-proline are often less susceptible to the action of peptidases. Using *Z*-Gly-Pro-*p*-nitroanilide as a substrate for prolyl-specific peptidases,[22] no activity was detected in Flavourzyme, whereas the culture supernatant of *F. velutipes* possessed an activity of 1.8 ± 0.3 U/L. The supernatant of *F. velutipes* contained numerous gelatin-cleaving peptidases that were not purified yet,[17] a glutaminase (85 kDa with 13 kDa subunits indicating a hexameric protein)[23] and a serine protease (34.5 kDa) with caspase- and legumain-like activities.[24] Flavourzyme is a commercial enzyme preparation of *A. oryzae* with endo- and exopeptidolytic activity. So far, the sequence analysis of peptidases of *A. oryzae* demonstrated about 18 peptidases, while the genome of *A. oryzae* was supposed to code for 134 putative peptidases.[25] Depending on the cultivation conditions, different peptidases were expressed. Liang et al.[26] described extracellular peptidases of *A. oryzae*, for example, oryzin, aspergillus-pepsin O, chain A of deuterolysin, leucine aminopeptidase, glutaminase, metallopeptidase, alanyl dipeptidyl peptidase, and Xaa-Pro aminopeptidase from the culture of a soybean koji. There are no data on which of these peptidases is present in Flavourzyme.

The peptidase mixtures used in the past were unable to hydrolyze wheat gluten completely. To compose an ideal peptidase mixture for the total hydrolysis, the peptidases of Flavourzyme or *F. velutipes*[17] will have to be purified individually and biochemically characterized for substrate specificity. The presence of a prolyl-specific peptidases[22] and a glutaminase[27] and a balanced ratio of exo- to endopeptidases appears essential to produce taste-active amino acids and peptides.[2]

Compared to *F. velutipes* peptidases (Table 1), the experiments showed that Flavourzyme peptidases suffered from a combination of a lack of cleavage sites, pronounced product inhibition, and the lack of prolyl-specific activity. Peptidases of *F. velutipes* were adversely affected by product inhibition only.

The integration of electrodialysis equipped with UF membranes was shown to be an effective means to overcome product inhibition. The autopeptidolytic activity of the peptidase mixtures is a minor issue, because it is easily suppressed by increased dosages of substrate.

AUTHOR INFORMATION

Corresponding Author

*Phone: +49(0)511 762 4585; fax: +49(0)511 762 4547; e-mail: lucienne.giesler@lci.uni-hannover.de.

Notes

The authors declare no competing financial interest.

ACKNOWLEDGMENTS

Cooperation of the Nestlé Product Technology Centre, Singen/Hohentwiel, Germany, is gratefully acknowledged.

ABBREVIATIONS USED

Fve, *Flammulina velutipes*; Fx, Flavourzyme; ED, electrodialysis; MM, mineral salt medium; DH, degree of hydrolysis; SDS-PAGE, sodium dodecyl sulfate polyacrylamide gel electrophoresis

REFERENCES

(1) Clemente, A. Enzymatic protein hydrolysates in human nutrition. *Trends Food Sci. Technol.* **2000**, *11*, 254−262.

(2) Kong, X.; Zhou, H.; Qian, H. Enzymatic hydrolysis of wheat gluten by proteases and properties of the resulting hydrolysates. *Food Chem.* **2007**, *102*, 759−763.
(3) Souissi, N.; Bougatef, A.; Triki-Ellouz, Y.; Nasri, M. Biochemical and functional properties of Sardinella (Sardinella aurita) by-product hydrolysates. *Food Technol. Biotechnol.* **2007**, *45*, 187.
(4) Giesler, L.; Linke, D.; Rabe, S.; Appel, D.; Berger, R. G. Hydrolysis of wheat gluten by combining peptidases of *Flammulina velutipes* and electrodialysis. *J. Agric. Food Chem.* **2013**, *61*, 8641−8649.
(5) Nchienzia, H.; Morawicki, R.; Gadang, V. Enzymatic hydrolysis of poultry meal with endo- and exopeptidases. *Poult. Sci.* **2010**, *89*, 2273−2280.
(6) Apar, D. K.; Ozbek, B. Corn gluten hydrolysis by alcalase: Kinetics of hydrolysis. *Chem. Eng. Commun.* **2010**, *197*, 963−973.
(7) Poulin, J.-F.; Amiot, J.; Bazinet, L. Improved peptide fractionation by electrodialysis with ultrafiltration membrane: Influence of ultrafiltration membrane stacking and electrical field strength. *J. Membr. Sci.* **2007**, *299*, 83−90.
(8) Abraham, L. D.; Breuil, C. Factors affecting autolysis of a subtilisin-like serine proteinase secreted by *Ophiostoma piceae* and identification of the cleavage site. *Biochim. Biophys. Acta, Gen. Subj.* **1995**, *1245*, 76−84.
(9) Rose, J. R.; Salto, R.; Craik, C. S. Regulation of autoproteolysis of the HIV-1 and HIV-2 proteases with engineered amino acid substitutions. *J. Biol. Chem.* **1993**, *268*, 11939−11945.
(10) Dürrschmidt, P.; Mansfeld, J.; Ulbrich-Hofmann, R. Refolding of the non-specific neutral protease from *Bacillus stearothermophilus* proceeds via an autoproteolytically sensitive intermediate. *Biophys. Chem.* **2010**, *147*, 66−73.
(11) Tatsumi, H.; Ikegaya, K.; Murakami, S.; Kawabe, H.; Nakano, E.; Motai, H. Elucidation of the thermal stability of the neutral proteinase II from *Aspergillus oryzae*. *Biochim. Biophys. Acta, Protein Struct. Mol. Enzymol.* **1994**, *1208*, 179−185.
(12) Laemmli, U. K. Cleavage of structural proteins during the assembly of the head of bacteriophage T4. *Nature* **1970**, *227*, 680−685.
(13) Poulin, J.-F.; Amiot, J.; Bazinet, L. Simultaneous separation of acid and basic bioactive peptides by electrodialysis with ultrafiltration membrane. *J. Biotechnol.* **2006**, *123*, 314−328.
(14) Doyen, A.; Beaulieu, L.; Saucier, L.; Pouliot, Y.; Bazinet, L. Impact of ultrafiltration membrane material on peptide separation from a snow crab byproduct hydrolysate by electrodialysis with ultrafiltration membranes. *J. Agric. Food Chem.* **2011**, *59*, 1784−1792.
(15) Cui, J.; Kong, X.; Hua, Y.; Zhou, H.; Liu, Q. Continuous hydrolysis of modified wheat gluten in an enzymatic membrane reactor. *J. Sci. Food Agric.* **2011**, *91*, 2799−2805.
(16) Bajorath, J.; Saenger, W.; Pal, G. P. Autolysis and inhibition of proteinase K, a subtilisin-related serine proteinase isolated from the fungus *Tritirachium album Limber*. *Biochim. Biophys. Acta, Protein Struct. Mol. Enzymol.* **1988**, *954*, 176−182.
(17) Grimrath, A.; Berends, P.; Rabe, S.; Berger, R.; Linke, D. Koji fermentation based on extracellular peptidases of *Flammulina velutipes*. *Eur. Food Res. Technol.* **2011**, *232*, 415−424.
(18) Fujimura, S.; Oshikawa, K.; Terada, S.; Kimoto, E. Primary structure and autoproteolysis of brevilysin H6 from the venom of *Gloydius halys brevicaudus*. *J. Biochem.* **2000**, *128*, 167−173.
(19) Braxton, S.; Wells, J. A. Incorporation of a stabilizing Ca^{2+}-binding loop into subtilisin BPN′. *Biochemistry* **1992**, *31*, 7796−7801.
(20) Ravallec-Plé, R.; Gilmartin, L.; Van Wormhoudt, A.; Le Gal, Y. Influence of the hydrolysis process on the biological activities of protein hydrolysates from cod *(Gadus morhua)* muscle. *J. Sci. Food Agric.* **2000**, *80*, 2176−2180.
(21) Woychik, J.; Boundy, J. A.; Dimler, R. Wheat gluten proteins, amino acid composition of proteins in wheat gluten. *J. Agric. Food Chem.* **1961**, *9*, 307−310.
(22) Edens, L.; Dekker, P.; Van Der Hoeven, R.; Deen, F.; de Roos, A.; Floris, R. Extracellular prolyl endoprotease from *Aspergillus niger* and its use in the debittering of protein hydrolysates. *J. Agric. Food Chem.* **2005**, *53*, 7950−7957.
(23) Eisele, N.; Linke, D.; Bitzer, K.; Na'amnieh, S.; Nimtz, M.; Berger, R. G. The first characterized asparaginase from a basidiomycete, *Flammulina velutipes*. *Bioresour. Technol.* **2011**, *102*, 3316−3321.
(24) Iketani, A.; Nakamura, M.; Suzuki, Y.; Awai, K.; Shioi, Y. A novel serine protease with caspase-and legumain-like activities from edible basidiomycete *Flammulina velutipes*. *Fungal Biol.* **2013**, *117*, 173−181.
(25) Kobayashi, T.; Abe, K.; Asai, K.; Gomi, K.; Juvvadi, P. R.; Kato, M.; Kitamoto, K.; Takeuchi, M.; Machida, M. Genomics of *Aspergillus oryzae*. *Biosci., Biotechnol., Biochem.* **2007**, 0702090305.
(26) Liang, Y.; Pan, L.; Lin, Y. Analysis of extracellular proteins of *Aspergillus oryzae* grown on soy sauce koji. *Biosci., Biotechnol., Biochem.* **2009**, 0812271225.
(27) Aaslyng, M. D.; Poll, L.; Nielsen, P. M.; Flyge, H. Sensory, chemical and sensometric studies of hydrolyzed vegetable protein produced by various processes. *Eur. Food Res. Technol.* **1999**, *209*, 227−236.

JOURNAL OF AGRICULTURAL AND FOOD CHEMISTRY

Article

pubs.acs.org/JAFC

Purification, Characterization, cDNA Cloning and *In Vitro* Expression of a Serine Proteinase from the Intestinal Tract of Sea Cucumber (*Stichopus japonicus*) with Collagen Degradation Activity

Long-Jie Yan,[†] Chun-Lan Zhan,[†] Qiu-Feng Cai, Ling Weng, Cui-Hong Du, Guang-Ming Liu, Wen-Jin Su, and Min-Jie Cao*

College of Biological Engineering, Jimei University, Jimei, Xiamen 361021, China

Fujian Provincial Key Laboratory of Food Microbiology and Enzyme Engineering, Xiamen, Fujian Province 361021, China

ABSTRACT: Sea cucumber (*Stichopus japonicus*) autolysis during transportation and processing is a major problem and the specific proteinases responsible for autolysis have not yet been identified. In the present study, a 34 kDa serine proteinase (SP) was isolated to high purity from sea cucumber intestinal tract by a series of column chromatographies. Peptide mass fingerprinting revealed that six peptide fragments were identical to a proprotein convertase subtilisin/kexin type 9 preproprotein from sea cucumber *A. japonicus*. The enzyme hydrolyzed gelatin effectively at pH 6.0−9.0 and 35−40 °C, and the enzyme activity was strongly inhibited by SP inhibitors. Sea cucumber collagen was hydrolyzed significantly by purified SP at 37 °C and more gradually at 4 °C, suggesting that SP may be involved in autolysis. In addition, the SP gene that codes for 377 amino acid residues was cloned into an *E. coli* expression vector and expressed *in vitro*. A polyclonal antibody against rSP was prepared and found to react specifically against both rSP and endogenous SP, which may prove useful for future studies on the physiological functions of SP.

KEYWORDS: *sea cucumber intestinal tract, serine proteinase, purification, molecular cloning, in vitro expression, autolysis*

INTRODUCTION

Sea cucumber (*Stichopus japonicus*) is traditionally regarded as a seafood delicacy and is widely consumed in China, Japan, Korea, and other Asian countries.[1] In China, the total output of sea cucumber production is increasing annually to meet consumer demand.[2] However, sea cucumbers are easily subject to autolysis, which is a major problem in transportation and processing.[3]

Autolysis, or self-digestion, is a common phenomenon that occurs in various aquatic products[4−6] and some species of fish.[7] After the death of these animals, biochemical reactions responsible for anabolism cease while endogenous proteinases involved in catabolism retain their function. Major digestive organs secrete proteinases such as trypsin, chymotrysin, and cathepsin. Among these proteolytic enzymes, serine proteinase (SP) have significant activity in the hydrolysis of collagen[8−10] and myofibrillar proteins.[11,12]

In the edible portions of sea cucumbers, the highly insoluble collagen fibers account for about 70% of total protein.[13] As a result, collagen hydrolysis is likely the main factor in sea cucumber autolysis. Recently, we identified a gelatinolytic metalloproteinase (GMP) from the body wall of sea cucumber active in collagen degradation.[14] Considering the significant autolysis rate of harvested sea cucumbers, we propose that yet unidentified proteinases in the sea cucumber intestinal tract may also play an important role during collagen degradation. Although several reports regarding enzymes from the intestinal tract of sea cucumber have been published, including a highly alkaline proteinase,[15] a novel β-1,3-glucanase,[16] and a cathepsin L-like proteinase,[17] little information exists on how they may act on collagen.

In this paper, we report the identification of a unique SP from the intestinal tract of sea cucumber and investigated its enzymatic characteristics while focusing in on its activity on collagen. The gene encoding this SP was cloned, overexpressed in *Escherichia coli*, and the recombinant SP (rSP) was purified to homogeneity. A specific polyclonal antibody against rSP was produced, which reacted positively with SP purified from sea cucumber. Our present study provides valuable information for further analysis of the relationship between SPs and sea cucumber autolysis.

MATERIALS AND METHODS

Intestinal Tract Removal. Sea cucumbers with body weight of 150−200 g were purchased alive from January to March from an aquaculture base in Quangang, Fujian Province, China. Following purchase, the sea cucumbers were placed in cold seawater and transported to the laboratory within 4 h. The digestive tracts were immediately removed, rinsed carefully with cold distilled water and either used for experiments or stored at −80 °C.

Chemicals. DEAE-Sephacel, Sephacryl S-200 HR, Mini-Q, HisTrap HP, and Protein A Sepharose were purchased from GE Healthcare (Waukesha, WI, U.S.A.). Protein markers and bovine serum albumin were purchased from Bio-Rad (Richmond, CA, U.S.A.). The t-Butyloxy-carbonyl-Phe-Ser-Arg-4-methyl-coumaryl-7-amide (Boc-Phe-Ser-Arg-MCA) and other synthetic fluorogenic peptide substrates (MCA-substrates) were purchased from Peptide Institute (Osaka, Japan). Benzamidine, 1,10-phenanthroline monohydrate,

Received: February 21, 2014
Revised: April 25, 2014
Accepted: April 28, 2014
Published: April 28, 2014

ACS Publications © 2014 American Chemical Society

EDTA, EGTA were purchased from Sigma (St. Louis, MO, U.S.A.). Bovine gelatin, L-3-carboxytrans-2, 3-epoxypropionyl-L-leucine-4-guanidinobutylamide (E-64), and Triton X-100 were products of Amresco (Solon, OH, U.S.A.). Pepstatin A was purchased from Roche (Mannheim, Germany). The 4-(2-aminoethyl)-benzenesulfonyl fluoride hydrochloride (Pefabloc SC) was a product of Merck (Darmstadt, Germany).

Purification of SP. All procedures were performed at 4 °C. Briefly, the digestive tracts of sea cucumbers (200 g) were homogenized in 4-fold (v/w) of 20 mM Tris-HCl (pH 8.0) with 0.02% NaN_3 (buffer A) and centrifuged at 10000 g for 20 min. The supernatant was then collected as the crude enzyme fraction and subsequently applied to an ion-exchange column DEAE-Sephacel (2.5 × 10 cm) previously equilibrated with buffer A. After washing the column with buffer A until the absorbance at 280 nm reached baseline, bound proteins were eluted with a 0 to 0.5 M linear NaCl gradient in buffer A. Active fractions were pooled and concentrated by ultrafiltration using a YM-10 membrane (Millipore) and loaded on a gel filtration column of Sephacryl S-200 (2.5 × 98 cm) equilibrated with buffer A containing 0.15 M NaCl. Active fractions were collected, dialyzed against buffer A, and applied to a Mini-Q high performance ion exchange column (1 mL). A linear gradient elution using 0−0.5 M NaCl was performed at a flow rate of 0.5 mL/min. Active fractions were collected as purified proteinase and were used for enzymatic characterization.

Protein Concentration Analysis. Protein concentrations were estimated by measuring the absorbance at 280 nm using a Lambda 35 spectrophotometer (PerkinElmer, U.S.A.). The concentration of proteins after each purification step except the Mini-Q was determined by the method of Lowry[18] using bovine serum albumin as the standard.

Assay of Enzyme Activity. SP activity was measured as described by Guo et al.,[11] using Boc-Phe-Ser-Arg-MCA as a substrate. The reaction was initiated by adding 50 μL of enzyme solution to the reaction mixture containing 900 μL of 20 mM Tris-HCl (pH 8.0) and 50 μL of 10 μM substrate and incubated at 37 °C for 10 min. The reaction was stopped by adding 1.5 mL stopping agent (methyl alcohol/*n*-butyl alcohol/distilled water = 35:30:35, v/v/v), and enzyme activity was detected by measuring the fluorescence intensity of the liberated 7-amino-4-methylcoumarin (AMC) at an excitation wavelength of 380 nm and emission wavelength of 450 nm in a fluorescence spectrophotometer (FP-6200, Jasco, Japan). One unit of enzyme is defined as the amount of enzyme required to liberate 1 nmol of AMC per min.

SDS-PAGE and Gelatin Zymography. SDS-PAGE was performed based on the protocol of Laemmli.[19] Samples were separated using 12% polyacrylamide gels and stained with silver. Gelatin zymography was performed according to the method described by Herron et al.[20] Samples were mixed 3:1 with 4 × SDS sample buffer (200 mM Tris-HCl, pH 6.8 containing 8% SDS, 0.4% brommophenol blue and 40% glycerol) and were electrophoresed in 12% polyacrylamide gels containing 0.1% bovine gelatin at 4 °C. After electrophoresis, the gels were washed with 2.5% (v/v) Triton X-100 for 30 min by gently shaking to remove SDS, followed by a deionized water rinse. After incubation at 37 °C for 12 h in 20 mM Tris-HCl (pH 8.0), the gel was stained with Coomassie Brilliant Blue (CBB) R-250. The area of enzyme activity appeared as a clear band on the CBB-stained dark blue background, and the clarity of the band correlates positively to enzyme activity.

MALDI-TOF/TOF-MS/MS Analysis. Purified SP was separated on a 12% SDS-PAGE gel and stained with silver and the target protein band was selected for mass spectrometry analysis.[21] The target protein band was excised and destained using 30 mM $K_3Fe(CN)_6$ and 100 mM $Na_2S_2O_3$, followed by addition of 100 mM NH_4HCO_3 and incubated at room temperature for 15 min. The band was digested with trypsin at 37 °C overnight. Peptides were extracted with 100 μL of extraction solution containing 50% acetonitrile and 0.1% trifluoroacetic acid for 15 min. Obtained peptide solution was desalted using Ziptip C-18 columns (Pierce), lyophilized, and analyzed by 4800 plus MALDI-TOF analyzer (Applied Biosystems, Foster City, U.S.A.) in the School of Life Science, Sun Yat-Sen University, China.

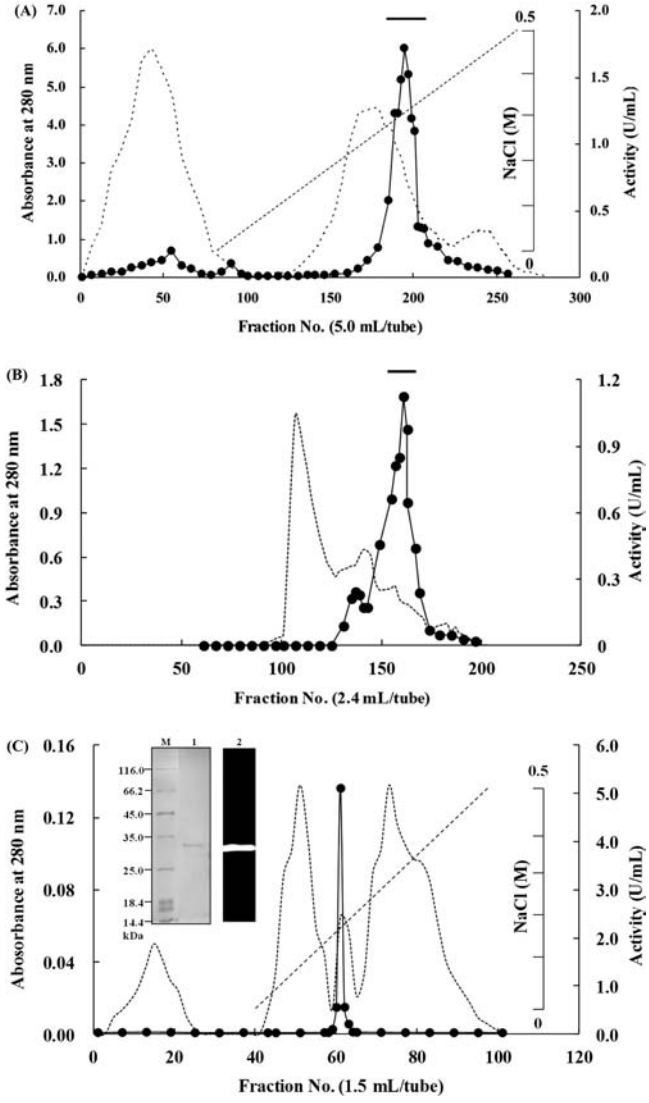

Figure 1. Column chromatography purification of the SP from the intestinal tract of sea cucumber. (A) DEAE-Sephacel chromatography. (B) Sephacryl S-200 chromatography. (C) Mini-Q chromatography. Absorbance at 280 nm (---); Enzymatic activity to Boc-Phe-Ser-Arg-MCA (-●-). SDS-PAGE and gelatin zymography of purified proteinase are shown in the inset of part C. Lane M, protein marker; lane 1, purified SP on silver stained 12% SDS-PAGE gel; lane 2, purified SP on gelatin zymography.

The resulting data were searched against the NCBI database using Matrix Science's Mascot 2.2 search engine.

Effect of Proteinase Inhibitors. To investigate the effects of different proteinase inhibitors on the proteinase, gels resulting from gelatin zymography gel electrophoresis were washed and rinsed as described above and subsequently allowed to incubate in buffer A with inhibitors at 37 °C for 12 h, followed by CBB staining. Control tests were performed in the absence of proteinase inhibitor. The effect of proteinase inhibitors on the proteinase was also analyzed using Boc-Phe-Ser-Arg-MCA as substrate. Briefly, purified SP was preincubated with corresponding inhibitors at different final concentrations for 30 min at 4 °C in 20 mM Tris-HCl buffer (pH 8.0), and the remaining enzymatic activity was determined as described above.

Preparation of Sea Cucumber Collagen. All procedures were performed at 4 °C as described.[14] Briefly, sea cucumber body wall (80 g wet weight) was minced and orderly washed by distilled water, 0.1 M Tris-HCl (pH 8.0) containing 5 mM EDTA, distilled water and 0.1 M NaOH with continuous stirring to remove noncollagenous material and pigment. The insoluble component was digested with

dx.doi.org/10.1021/jf500923y | J. Agric. Food Chem. 2014, 62, 4769−4777

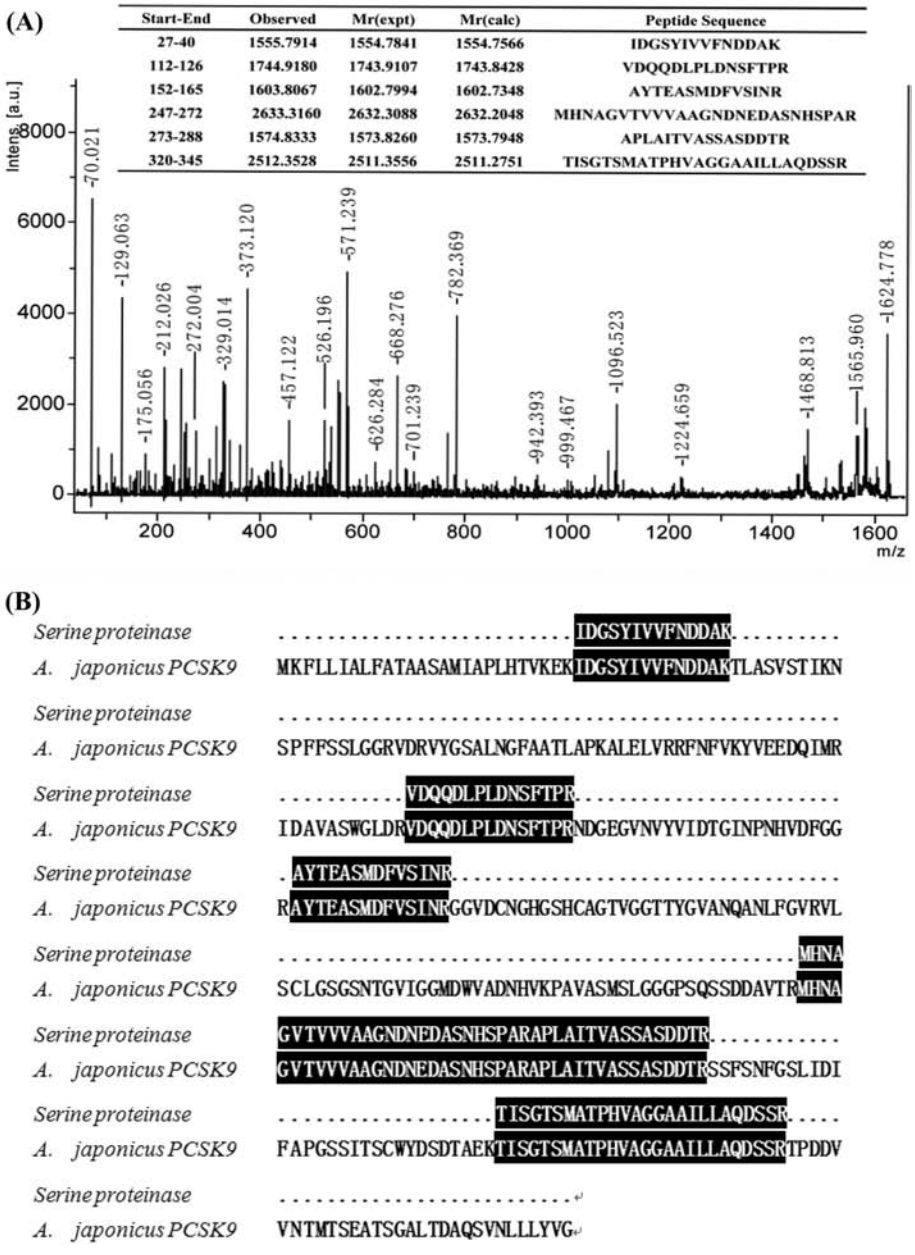

Figure 2. Peptide mass fingerprinting of purified SP. (A) Ions identified using mass spectrometry (MS). The sequences of six peptide fragments are shown in the above table. (B) Protein sequence alignment of SP with the sequence of proprotein convertase subtilisin/kexin type 9 preproprotein (gi:86277304) from *A. japonicus*. Identical amino acid residues are shown with black background.

porcine pepsin in 0.5 M acetic acid overnight, followed by centrifugation at 12000 g for 30 min. Collagen in the supernatant was salted out by adding NaCl to a final concentration of 0.8 M. After centrifugation, the collagen was collected and dissolved in 0.5 M acetic acid, and extensively dialyzed against 0.02 M sodium phosphate buffer (pH 8.0). The purified collagen was lyophilized and stored at −80 °C until analysis.

Degradation of Sea Cucumber Collagen. The purified enzyme was allowed to react with sea cucumber collagen in buffer A at 37 °C for different time intervals. After incubation, samples were applied to 7.5% gel for electrophoresis followed by CBB staining.

RNA Preparation and cDNA Synthesis. Total RNA was isolated from the intestinal tract of sea cucumber using the Trizol method.[11] First strand cDNA was synthesized with TIANScript RT Kit according to the manufacturer's instructions.

Reverse Transcription Polymerase Chain Reaction (RT-PCR). Degenerate primers (PF1 5′-TTGACCAACAAGACTTACCTC-3′ and PR1 5′-GTCATCACTAGCAGAGGAAGC-3′) to amplify partial sequences of the SP gene were designed according to the MALDI-TOF mass spectra results. Using these primers and the synthesized cDNA, a 500 bp fragment of the SP gene was amplified by PCR in a Gene Amp 9700 (Applied Biosystems, U.S.A.) thermal cycler. The PCR program was as follows: 5 min at 94 °C followed by 30 cycles of 30 s at 94 °C, 45 s at 55 °C, 60 s at 72 °C, and a final extension of 10 min at 72 °C. The PCR product was purified by agarose gel electrophoresis and cloned into pMD-18T vector (TakaRa) followed by DNA sequence analysis. DNA sequencing was performed at Invitrogen Biotechnological Co. Ltd. (Guangzhou, China) using the ABI Prism 3730 (CA, U.S.A.) DNA sequencer.

5′- and 3′- Rapid Amplification of cDNA Ends (5′- and 3′- RACE). The full-length sequence was obtained by 5′-RACE and 3′-RACE with several gene-specific primers (PF 5′-TGCTCCTC-TGGCTATCACTG-3′ and PR 5′-CACAGTGAGAACCATGTC-CAT-3′). RACE and RACE-PCR were performed with the SMART RACE cDNA Amplification Kit and Advantage 2 PCR Kit (Clontech, U.S.A.). Touchdown PCR was used to improve the

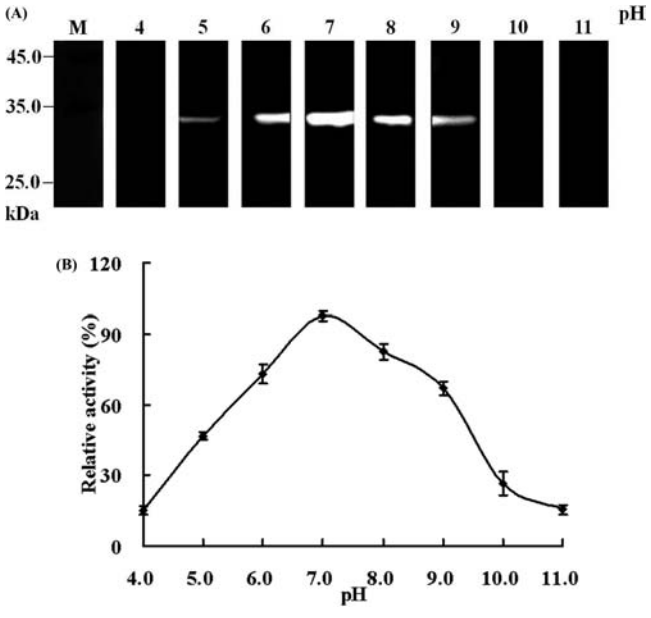

Figure 3. Optimal pH of SP. (A) Gelatin zymography analysis of pH on SP. Gelatin-incorporated gels were allowed to incubate at 37 °C for 12 h in different buffers at pH 4.0−10.0. (B) Effect of pH on purified SP using Boc-Phe-Ser-Arg-MCA as substrate.

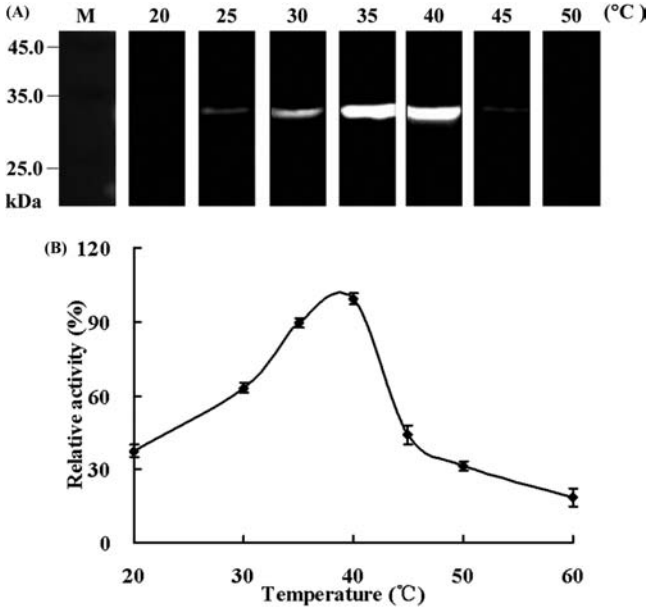

Figure 4. Optimal temperature of SP. (A) Gelatin zymography analysis of temperature on SP. Gelatin-incorporated gels were allowed to incubate in buffer A for 12 h at different temperatures from 20 to 50 °C. (B) Effect of temperature on purified SP using Boc-Phe-Ser-Arg-MCA as substrate.

specificity of SMARTer RACE amplification. The PCR products, 5′-RACE (550 bp) and 3′-RACE (500 bp) were purified, cloned and sequenced. The RT-PCR fragments as well as the 3′-RACE and 5′-RACE fragments were combined using the DNAman program to generate the full-length SP cDNA.

Construction of Recombinant Plasmids. The SP fragment without signal peptide was amplified by primers P5F 5′-CATATGATTGCACCTCTCCAC −3′ (containing the *Nde*I site) and P3R 5′- GAATTCACCAACATACAAGAGCAG −3′ (containing the *Eco*RI site). The plasmids containing PCR products and the pET-28a plasmid were digested with restriction enzymes *Nde*I and *Eco*RI.

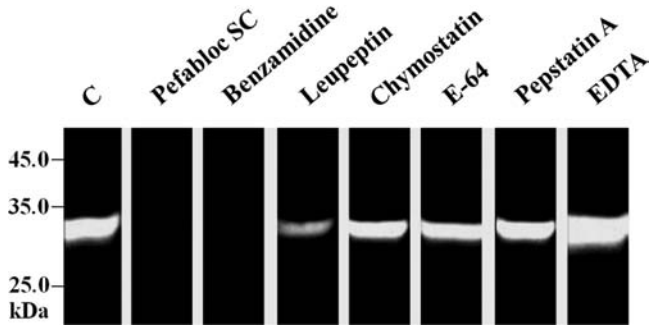

Figure 5. Effect of proteinase inhibitors on the purified SP. Gelatin zymography was conducted to investigate the inhibitory effect of proteinase inhibitors on the purified SP at 37 °C for 12 h in buffer A, followed by CBB staining. Lane C, control (without inhibitor); Lane 1, Pefabloc SC (2 mM); Lane 2, benzamidine (5 mM); Lane 3, Leupeptin (5 mM); Lane 4, Chymostatin (5 mM); Lane 5, E-64 (0.01 mM); Lane 6, Pepstatin A (0.015 mM); and Lane 7, EDTA (10 mM).

PCR products were ligated into the digested pET-28a (+) plasmid to generate pET-28a-*SP* recombinant plasmids.

Expression and Purification of the Recombinant SP. pET-28a-*SP* was transformed into *E. coli* BL21 (DE3) to make the expression strain BL-pET-*SP*. Overnight culture of the transformants (2 mL) was transferred into 200 mL kanamycin-containing Luria−Bertani broth for large scale culture while shaking at 37 °C. When the optical density at 600 nm reached 0.6, isopropyl β-D-1-thiogalactopyranoside (IPTG) was added to the final concentration of 1 mM for induction of recombinant proteinase expression. After culturing at 37 °C for 4 h, bacteria were collected by centrifugation at 9000 g for 5 min and resuspended in 1/10 cold buffer (50 mM Tris-HCl, 150 mM NaCl, pH 8.0). The bacteria were lysed by sonication and centrifuged at 12000 g for 20 min to remove the supernatant. The inclusion bodies were solubilized in a denaturing solution (20 mM Tris-HCl, pH 8.0 containing 150 mM NaCl and 4 M urea) and the His-tagged recombinant proteinase was purified using a Ni-NTA agarose affinity column and eluted with denaturing solution containing 100 mM imidazole. Following elution, the purified rSP was dialyzed against a renaturation buffer (20 mM Tris-HCl, 150 mM NaCl, pH 8.0) and its enzyme activity and purity were analyzed.

Preparation of Antiserum Against rSP. Purified rSP was used as antigen to produce polyclonal antibodies. Approximately 100 μg highly purified rSP was mixed with 1 mL complete Freund's adjuvant. The thoroughly mixed samples were subcutaneously injected into a rabbit. The same amount of antigen (100 μg) was mixed with incomplete Freund's adjuvant and injected subcutaneously into the rabbit on a biweekly basis and repeated four times. Blood sample was collected after the last booster. Anti-rSP polyclonal antibodies were purified by passing the sera through a Protein A Sepharose column.

RESULTS

Purification of SP. Following a series of column chromotogaphy purifications, a SP was purified to homogeneity. As shown in Figure 1**A**, SP was eluted from DEAE-Sephacel with a linear gradient of 0−0.5 M NaCl. Active fractions from the first column were further purified by Sephacryl S-200 gel filtration (Figure 1**B**). After Mini-Q ion exchange column purification, the enzymatically active peak migrated as a single band with a molecular mass of 34 kDa on SDS-PAGE (Figure 1**C**). Gelatin zymography analysis showed a corresponding gelatinolytic active band, suggesting that the proteinase was purified to homogeneity. The purification steps were summarized in Table 1. Approximately 0.1 mg of highly purified SP was obtained from 200 g of sea cucumber intestinal tract, the specific activity was 85.0 U/mg with a 331.7-fold increase and 1.6% recovery.

Table 1. Summary of the Purification of SP from the Intestinal Tract of Sea Cucumber

purification steps	total protein (mg)	total activity (U)	specific activity (U/mg)	yield (%)	purification (fold)
crude enzyme	2024.8	518.8	0.3	100.0	1.0
DEAE-Sephacel	302.4	125.9	0.4	24.3	1.6
Sephacryl S-200	9.9	23.7	2.4	4.6	9.3
Mini-Q	0.1	8.5	85.0	1.6	331.7

MALDI-TOF/TOF-MS/MS. To determine the amino acid sequence of the purified protein, the protein band was excised from SDS-PAGE and in-gel digested with trypsin. The resulting peptide mixture was analyzed by MALDI-TOF/TOF-MS/MS. Peptide mass fingerprinting (PMF) shown in Figure 2A revealed peptide fragments in the 800−5000 Da m/z range, and peaks with signal-to-noise ratios (SNR) > 50 were compared with the NCBI. It is interesting to note that the amino acid sequence of six peptide fragments containing a total of 111 amino acid residues were 100% identical to a proprotein convertase subtilisin/kexin type 9 preproprotein (gi:86277304) from *Apostichopus japonicus*, which is also a SP (Figure 2B).

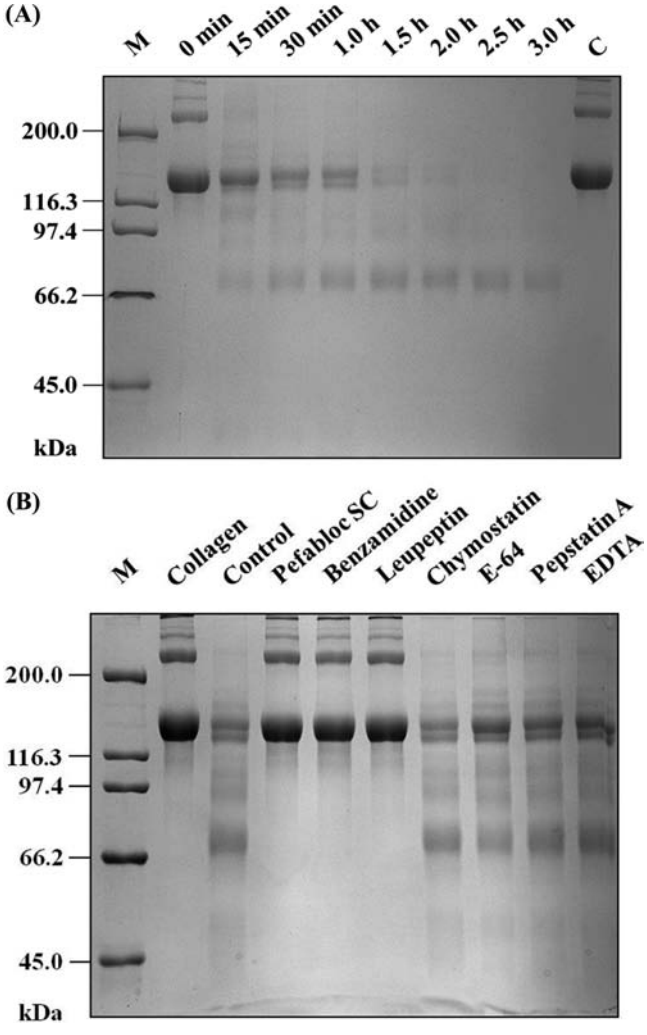

Figure 6. Degradation of sea cucumber collagen by SP. (A) SP (≈20 ng) and sea cucumber collagen (≈40 μg) were incubated in buffer A at 37 °C for different intervals. (B) Proteolysis patterns of collagen incubated with or without SP in the presence of various proteinase inhibitors at 37 °C in buffer A for 15 min. Lane M, protein marker; Lane 1, sea cucumber collagen; Lane 2, control (without inhibitor); Lane 3, Pefabloc SC (2 mM); Lane 4, benzamidine (5 mM); Lane 5, leupeptin (5 mM); Lane 6, chymostatin (5 mM); Lane 7, E-64 (0.01 mM); Lane 8, pepstatin A (0.015 mM); and Lane 9, EDTA (10 mM).

Effects of pH and Temperature. We sought to determine the maximum gelatinolytic activity of the purified SP. At 37 °C, a clear proteolytic band can be observed between pH 4.0−11.0. As shown in Figure 3A, the clearest band can be seen at pH 7.0 and the proteolytic band is negligible below pH 5.0 or above pH 9.0. Using Boc-Phe-Ser-Arg-MCA as the substrate, the maximum activity of SP was also detected at pH 7.0 (Figure 3B). The temperature-dependence of SP activity was determined using gelatin zymography (Figure 4A) and fluorogenic substrate hydrolyzing activity (Figure 4B). The results from both methods demonstrated that SP is maximally active at 40 °C.

Effect of Proteinase Inhibitors on the Purified SP. By gelatin zymography (Figure 5) and fluorogenic substrate hydrolyzing activity assays as readouts, the purified SP was almost completely suppressed by Pefabloc SC and benzamidine, which are known as specific SP inhibitors (Table 2). As an inhibitor both to serine and cysteine proteinases, leupeptin could not completely suppress the activity of purified SP. On the other hand, inhibitors to the other three types of proteinases (cysteine proteinase, aspartic proteinase, and metalloproteinase) did not show any inhibitory effect toward SP. These results strongly suggest that the purify enzyme is a SP.

Table 2. Effect of Proteinase Inhibitors on the SP Activity

inhibitor	concn. (mM)	relative activity (%)
control	0	100
Pefabloc SC	0.2	12.5 + 0.1
	2	7.4 + 0.4
benzamidine	0.5	15.9 + 0.3
	5	9.1 + 0.5
leupeptin	0.01	55.2 + 0.8
	0.1	43.5 + 1.2
chymostatin	0.01	85.7 + 0.6
	0.1	86.9 + 1.4
E-64	0.015	90.4 + 2.0
	0.1	91.2 + 1.2
pepstatinA	0.015	86.3 + 3.6
	0.1	84.7 + 2.8
EDTA	1	103.6 + 2.8
	10	127.6 + 2.3

Collagen Hydrolysis by SP. To confirm the involvement of SP in sea cucumber autolysis, its activity in the hydrolysis of collagen was investigated. As shown in Figure 6A, in the presence of SP, the β- and γ-chains of sea cucumber collagen were hydrolyzed after incubation at 37 °C for 15 min, and the original collagen bands (α, β and γ) completely disappeared after 3 h incubation. However, in the presence of SP inhibitors, collagen hydrolysis was completely suppressed when incubated with SP (Figure 6B). Leupeptin also significantly suppressed collagen hydrolysis although it only partially inhibited the activity of SP in gelatin zymography. Aspartic proteinase, cysteine proteinase and metalloproteinase inhibitors, on the other hand, did not show any inhibitory effects on collagen

dx.doi.org/10.1021/jf500923y | J. Agric. Food Chem. 2014, 62, 4769−4777

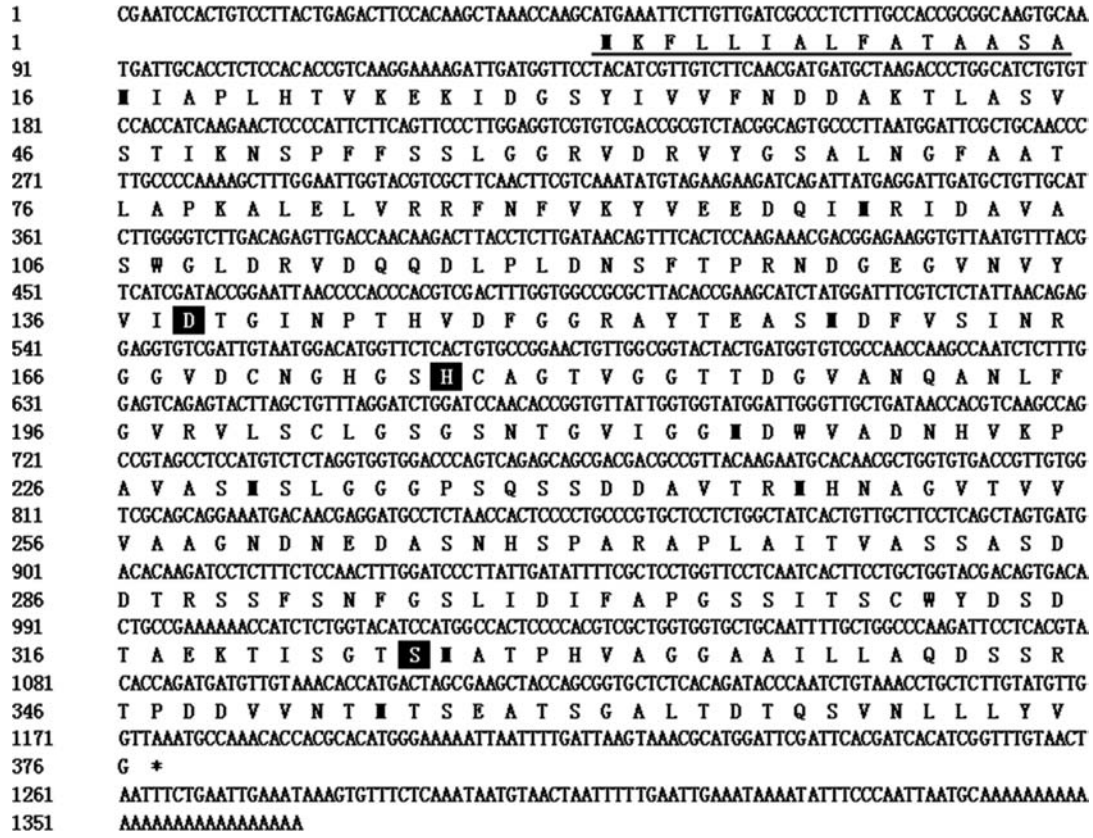

Figure 7. Nucleic acid and deduced amino acid sequences of SP. Base pair numbers and amino acid residue numbers are indicated to the left of each row. The signal peptide sequence is underlined. The Asp[138], His[176] and Ser[325] that form the catalytic triad of SP are shown with a black background.

hydrolysis. Proteolysis of collagen by SP at 4 °C was slower than that at 37 °C, but a similar proteolysis pattern was also be observed (data not shown).

cDNA Cloning of SP. The complete sequence of SP was cloned from *S. japonicus* and has been deposited in GenBank under the accession number KF888630. The full-length sequence of SP (1367 bp) contains an open reading frame (ORF) of 1131 bp encoding a putative protein of 377 amino acid residues with a 15 amino acids signal peptide located at the N-terminus (Figure 7). The molecular mass of mature SP is predicted to be 37.51 kDa and the p*I*, 4.44. BLASTp analysis showed that SP shares 99% identity to proprotein convertase subtilisin/kexin type 9 preproprotein (serine proteinnase-like) from sea cucumber (*A. japonicus*), 53% to an extracellular serine proteinase-like from sea urchin (*Strongylocentrotus purpuratus*) (Figure 8).

Expression and Purification of rSP. The recombinant BL-pET28a-*SP* was induced with IPTG for 4 h. The molecular mass of rSP is about 42 kDa when the 6 × His-tag (4.5 kDa) is taken into account, a mass that is similar to the theoretical value. Though the recombinant protein was mainly found in inclusion bodies, the His-tagged protein was easily purified using affinity chromatography to high purity. Subsequently, anti-rSP polyclonal antibody was successfully prepared using purified rSP as the antigen.

Western Blot Analysis. Western blot analysis showed that the anti-rSP polyclonal antibody specifically reacts both to rSP, native SP and even crude extract from the intestinal tract of sea cucumber (Figure 9), suggesting its high specificity.

DISCUSSION

Sea cucumbers are exceptionally sensitive to autolysis upon changing environmental factors such as increased temperature, change of salinity, and UV exposure. Hydrolysis of the collagen causes the disintegration of sea cucumber microstructures and the reduction of texture. As the body wall of sea cucumbers is mainly composed of collagen,[13] we propose that sea cucumber autolysis is mainly due to collagen hydrolysis. Though previous studies on sea cucumber proteinases have been reported,[14,22] information on the possible roles they play on autolysis is not available. Consequently, discovering and characterizing endogenous collagenolytic proteinases in sea cucumber may be beneficial to the elucidation of the mechanism behind sea cucumber autolysis.

Recently, we identified a GMP from the body wall of the sea cucumber *S. japonicus* and found that GMP maintains collagen proteolytic activity even at 4 °C. Considering the rapid rate of autolysis in harvested sea cucumbers, we proposed that the intestinal tract, which contains various proteinases, may be involved in autolysis. To find out what types of endogenous collagenolytic proteinases are responsible for collagen proteolysis, various proteinase inhibitors were added to crude extract from sea cucumber intestinal tract. The results showed that SP inhibitors and metalloproteinase inhibitors effectively suppressed collagen proteolysis, while other inhibitors exhibited no inhibitory effects (data not shown). It is clear then that serine proteinase and metalloproteinase are the major proteinases responsible for collagen proteolysis, which agrees well to a previously published report using casein-zymography.[23] In the present study, we purified the SP from the intestinal tract of sea cucumbers and characterized its enzymatic

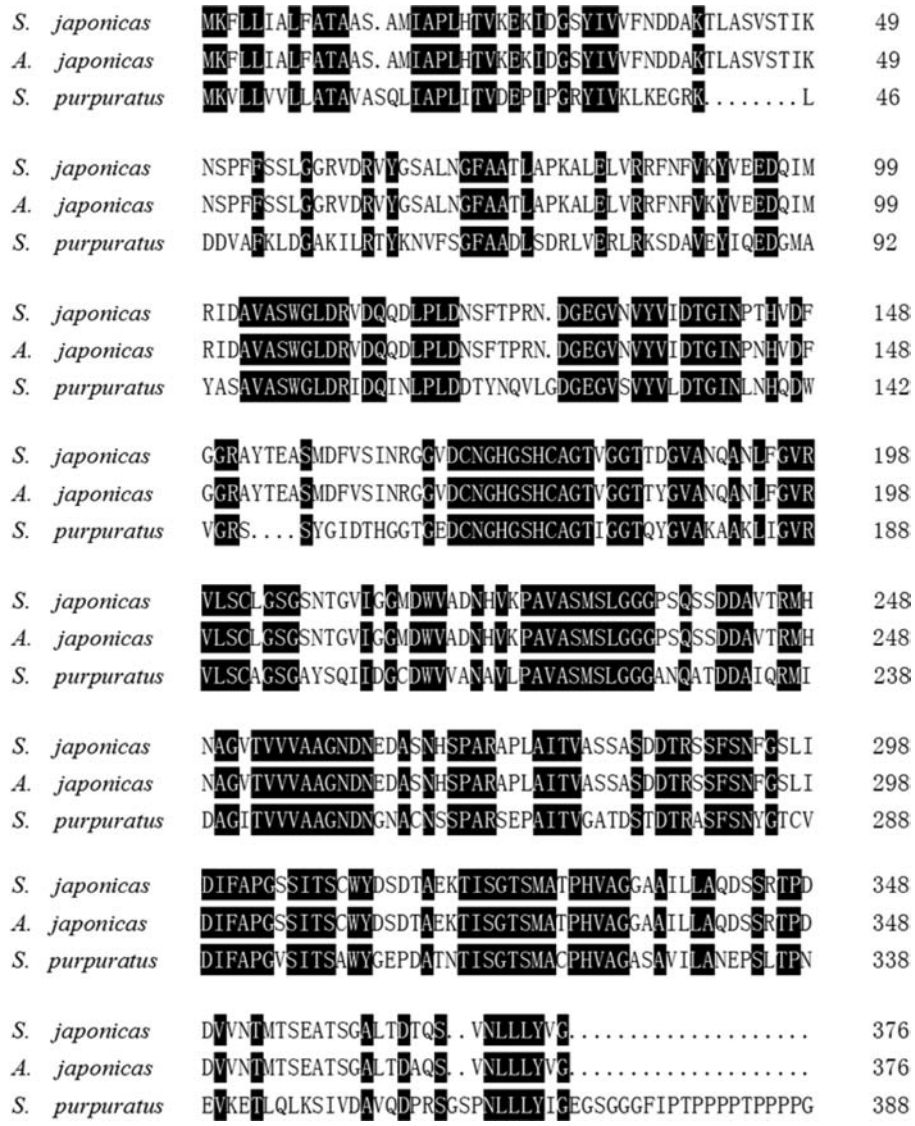

Figure 8. Alignment of primary structures of SP. The sequence of sea cucumber SP was compared with that of proprotein convertase subtilisin/kexin type 9 preproprotein (ABC87995, *A. japonicus*) and extracellular serine proteinase-like (XP_791416, *Strongylocentrotus purpuratus*). Identical amino acid residues are shown with black background.

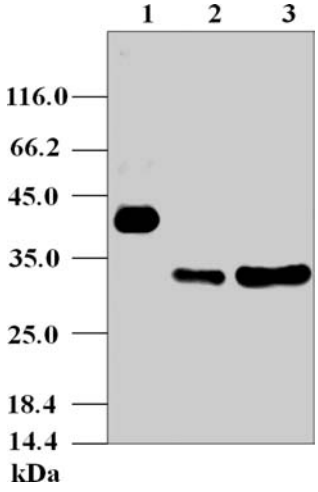

Figure 9. Western blotting analysis using anti-rSP polyclonal antibody. Lane 1, purified rSP; Lane 2, crude extract from the intestinal tract of sea cucumber; Lane 3, purified native SP.

properties. Based on an enzyme activity assay using Boc-Phe-Ser-Arg-MCA as the substrate, a SP with a molecular mass of approximately 34 kDa was purified through a series of column chromatographies. The molecular mass of the purified proteinase was close to that of a SP from sea urchin (*Strongylocentrotus purpuratus*, 35 kDa).[24]

According to the MALDI-TOF/TOF-MS/MS spectrum analysis, six peptide fragments consisting of 111 amino acid residues were identical to the sequence of a proprotein convertase subtilisin/kexin type 9 preproprotein (PCSK 9) (gi: 86277304) from *A. japonicus* (Figure 3A). PSCK9 belongs to the family of mammalian secretory kexin-like subtilases[25] and shares high homology with the C family of serine proteases.[26] Recently, Sun et al.[27] reported that PCSK9 is one of the top 10 down-regulated genes during sea cucumber regeneration.

The optimum pH for SP activity was 7.0 (Figure 4A) and the highest enzymatic activity was found at 35 °C (Figure 5A) using both gelatin zymography and fluorogenic substrates. The optimum pH of SP is similar to SPs from filefish (*Novoden modestrus*)[28] and fresh water prawn (*Macrobrachium rosenbergii*).[8]

dx.doi.org/10.1021/jf500923y | J. Agric. Food Chem. 2014, 62, 4769−4777

Meanwhile, the optimum temperature of purified SP is similar to another SP from the hepatopancreas of the northern shrimp.[10]

The enzymatic activity of the purified SP was strongly inhibited by SP inhibitors such as Pefabloc SC and benzamidine, while no significant inhibitory effects were observed using aspartic proteinase, cysteine proteinase and metalloproteinase inhibitors. Different from specific SP inhibitors such as Pefabloc SC and benzamidine, leupeptin is a reversible, competitive inhibitor both to serine and cysteine proteinases. Leupeptin could not completely suppress the purified SP during the 12 h incubation of gelatin-zymography (Figure 5). However, in collagen hydrolysis, as the reaction was performed only for 30 min, thus, no obvious degradation by SP could be observed on SDS-PAGE in the presence of leupeptin (Figure 6B). These indicate that the purified proteinase is different from trypsin-type collagenolytic SPs. Previous study showed that serine collagenase can be inhibited by metalloproteinase inhibitor EDTA as well as by SP inhibitors such as TLCK, DFP and soybean trypsin inhibitor.[7,9,28]

To ascertain the biological function of SP in sea cucumber autolysis, sea cucumber collagen hydrolysis patterns was examined using purified SP. With longer reaction times, significant degradation of the original band (α, β, and γ) of collagen was found when SP was incubated with sea cucumber collagen both at 37 °C (Figure 6A) and 4 °C (data not shown). Collagen proteolysis is completely suppressed by SP inhibitors (Figure 6B). Because SP from sea cucumber intestinal tract showed highly collagenolytic activity, we infer that endogenous SP is responsible for the degradation of collagenous fibrils in sea cucumber autolysis.

To further understand the underlying mechanism of sea cucumber autolysis, we successfully cloned the full-length cDNA (Figure 7) of SP. It contained a signal peptide, a prodomain, a catalytic domain and a carboxyl-terminal. Comparing the primary sequence of SP with other SPs, the purified SP shared relatively high identities to proprotein convertase subtilisin/kexin type 9 preproprotein and an extracellular serine proteinase from sea urchin (Figure 8), suggesting their close relationship. Like other SPs,[11] the catalytic domain consists Asp^{138}, His^{176} and Ser^{325}, which is the active site responsible for the enzymatic activity of SP. There are 4 cysteine residues at positions 170, 177, 202, and 310 that may form two intramolecular disulfide bonds in the tertiary structure. The difference in molecular mass between the native SP (34 kDa) and the calculated molecular weight from the nucleotide sequence (37.51 kDa) may be attributed to a cleavage site at ASA_{15}-MI, which may be where the signal peptide is cleaved from the protein. The theoretical p*I* of the mature protein is 4.44, which is consistent with the observation that we were able to purify SP in Tris-HCl pH 8.0 using DEAE-Sephacel weak anion exchange chromatography and Mini-Q strong anion exchange chromatography.

Thereafter, we used the *E. coli* expression vector pET28a to produce rSP. Although rSP revealed very low biological activity after following purification using denaturation buffer followed by renaturation, we were able to prepare a polyclonal antibody using rSP as the antigen and Western blot analysis (Figure 9) showed that both native SP and rSP reacted specifically with the rabbit anti-rSP polyclonal antibody. Based on its specificity, the antibody prepared in the present work can be applied to investigate the existence of SP in different tissues of sea cucumber by immunohistochemical study. It is also possible to prepare an immunoaffinity column for purification of native SP more effectively.

AUTHOR INFORMATION

Corresponding Author

*Tel.: +86-592-6180378. Fax: +86-592-6180470. Email: mjcao@jmu.edu.cn.

Author Contributions

†L.J.Y. and C.L.Z. contributed equally to this manuscript.

Notes

The authors declare no competing financial interest.

ACKNOWLEDGMENTS

This work was sponsored by the National Natural Scientific Foundation of China (Nos. 31271838), the Key Project of the Ministry of Science and Technology of China (2012BAD38B09), Public Science and Technology Research Funds Projects of Ocean (201305015-3), and the Science and Technology Bureau of Xiamen (3502Z20133020).

REFERENCES

(1) Yu, L.; Ge, L.; Xue, C.; Chang, Y.; Zhang, C.; Xu, X.; Wang, Y. Structural study of fucoidan from sea cucumber *Acaudina molpadioides*: A fucoidan containing novel tetrafucose repeating unit. *Food Chem.* **2014**, *142*, 197−200.

(2) *China Fisheries Yearbook*; China Agricultural Press: Beijing, China, 2013 (in Chinese).

(3) Wu, H. T.; Li, D. M.; Zhu, B. W.; Sun, J. J.; Zheng, J.; Wang, F. J.; Konno, K.; Jiang, X. Proteolysis of noncollagenous proteins in sea cucumber, *Stichopus japonicus*, body wall: Characterization and the effects of cysteine protease inhibitors. *Food Chem.* **2013**, *141*, 1287−1294.

(4) Eakpetch, P.; Benjakul, S.; Visessanguan, W.; Kijroongrojana, K. Autolysis of Pacific white shrimp (*Litopenaeus vannamei*) meat: Characterization and the effects of protein additives. *J. Food Sci.* **2008**, *73*, 95−103.

(5) Wang, J. H.; Ma, W. C.; Su, J. C.; Chen, C. S.; Jiang, S. T. Comparison of the properties of m-calpain from tilapia and grass shrimp muscles. *J. Agric. Food Chem.* **1993**, *41*, 1379−1384.

(6) Kimio, N.; Yukio, K.; Teruyoshi, M.; Daizo, Y. Classification of proteases in antarctic krill (*Euphausia superba*). *Agric. Biol. Chem.* **1983**, *47*, 2577−2583.

(7) Siringan, P.; Raksakulthai, N.; Yongsawatdigul, J. Autolytic activity and biochemical characteristics of endogenous proteinases in Indian anchovy (*Stolephorus indicus*). *Food Chem.* **2006**, *98*, 678−684.

(8) Sriket, C.; Benjakul, S.; Visessanguan, W.; Kishimura, H. Collagenolytic serine protease in fresh water prawn (*Macrobrachium rosenbergii*): Characteristics and its impact on muscle during iced storage. *Food Chem.* **2011**, *124*, 29−35.

(9) Hayet, B. K.; Rym, N.; Ali, B.; Sofiane, G.; Moncef, N. Low molecular weight serine protease from the viscera of sardinelle (*Sardinella aurita*) with collagenolytic activity: Purification and characterisation. *Food Chem.* **2011**, *124*, 788−794.

(10) Aoki, H.; Ahsan, M. N.; Matsuo, K.; Hagiwara, T.; Watabe, S. Purification and characterization of collagenolytic proteases from the hepatopancreas of northern shrimp (*Pandalus eous*). *J. Agric. Food Chem.* **2002**, *51*, 777−783.

(11) Guo, C.; Cao, M. J.; Liu, G. M.; Lin, X. S.; Hara, K.; Su, W. J. Purification, characterization, and cDNA cloning of a myofibril-bound serine proteinase from the skeletal muscle of crucian carp (*Carassius auratus*). *J. Agric. Food Chem.* **2007**, *55*, 1510−1516.

(12) Cao, M. J.; Jiang, X. J.; Zhong, H. C.; Zhang, Z. J.; Su, W. J. Degradation of myofibrillar proteins by a myofibril-bound serine proteinase in the skeletal muscle of crucian carp (*Carasius auratus*). *Food Chem.* **2006**, *94*, 7−13.

(13) Saito, M.; Kunisaki, N.; Urano, N.; Kimura, S. Collagen as the major edible component of sea cucumber (*Stichopus japonicus*). *J. Food Sci.* **2002**, *67*, 1319−1322.
(14) Wu, H. L.; Hu, Y. Q.; Shen, J. D.; Cai, Q. F.; Liu, G. M.; Su, W. J.; Cao, M. J. Identification of a novel gelatinolytic metalloproteinase (GMP) in the body wall of sea cucumber (*Stichopus japonicus*) and its involvement in collagen degradation. *Process Biochem.* **2013**, *48*, 871−877.
(15) Fu, X. Y.; Xue, C. H.; Miao, B. C.; Li, Z. J.; Yang, W. G.; Wang, D. F. Study of a highly alkaline protease extracted from digestive tract of sea cucumber (*Stichopus japonicus*). *Food Res. Int.* **2005**, *38*, 323−329.
(16) Zhu, B. W.; Zhao, J. G.; Yang, J. F.; Mikiro, T.; Zhang, Z. S.; Zhou, D. Y. Purification and partial characterization of a novel β-1,3-glucanase from the gut of sea cucumber *Stichopus japonicus*. *Process Biochem.* **2008**, *43*, 1102−1106.
(17) Zhou, D. Y.; Chang, X. N.; Bao, S. S.; Song, L.; Zhu, B. W.; Dong, X. P.; Zong, Y.; Li, D. M.; Zhang, M. M.; Liu, Y. X.; Murata, Y. Purification and partial characterisation of a cathepsin L-like proteinase from sea cucumber (*Stichopus japonicus*) and its tissue distribution in body wall. *Food Chem.* **2014**, *158*, 192−199.
(18) Lowry, O. H.; Rosebrough, N.; Farr, A.; Randall, R. Protein measurement with the Folin phenol reagent. *J. Biol. Chem.* **1951**, *193*, 265−275.
(19) Laemmli, U. Cleavage of structural proteins during the assembly of the head. *Nature* **1970**, *227*, 680−685.
(20) Herron, G. S.; Banda, M. J.; Clark, E. J.; Gavrilovc, J.; Werb, Z. Secretion of metalloproteinases by stimulated capillary endothelial cells. *J. Biol. Chem.* **1986**, *261*, 2814−2818.
(21) Mortz, E.; Krogh, T. N.; Vorum, H.; Görg, A. Improved silver staining protocols for high sensitivity protein identification using matrix-assisted laser desorption/ionization-time of flight analysis. *Proteomics* **2001**, *1*, 1359−1363.
(22) Zhu, B. W.; Yu, J. W.; Zhang, Z.; Zhou, D. Y.; Yang, J. F.; Li, D. M.; Murata, Y. Purification and partial characterization of an acid phosphatase from the body wall of sea cucumber *Stichopus japonicus*. *Process Biochem.* **2009**, *44*, 875−879.
(23) Fu, X. Y.; Xue, C. H.; Miao, B. C.; Li, Z. J.; Gao, X.; Hirata, T. Distribution and seasonal activity variation of proteases in digestive tract of sea cucumber *Stichopus japonicus*. *Fish. Sci.* **2006**, *72*, 1130−1132.
(24) Haley, S. A.; Wessel, G. W. The cortical granule serine protease CGSP1 of the sea urchin, *Strongylocentrotus purpuratus,* is autocatalytic and contains a low-density lipoprotein receptor-like domain. *Dev. Biol.* **1999**, *211*, 1−10.
(25) Seidah, N. G.; Benjannet, S.; Wickham, L.; Marcinkiewicz, J.; Jasmin, S. B.; Stifani, S.; Basak, A.; Prat, A.; Chrétien, M. The secretory proprotein convertase neural apoptosis-regulated convertase 1 (NARC-1): Liver regeneration and neuronal differentiation. *Proc. Natl. Acad. Sci. U.S.A.* **2003**, *100*, 928−933.
(26) Timms, K. M.; Wagner, S.; Samuels, M. E.; Forbey, K.; Goldfine, H.; Jammulapati, S.; Skolnick, M. H.; Hopkins, P. N.; Hunt, S. C.; Shattuck, D. M. A mutation in PCSK9 causing autosomal-dominant hypercholesterolemia in a Utah pedigree. *Hum. Genet.* **2004**, *114*, 349−353.
(27) Sun, L.; Chen, M.; Yang, H.; Wang, T.; Liu, B.; Shu, C.; Gardiner, D. M. Large scale gene expression profiling during intestine and body wall regeneration in the sea cucumber (*Apostichopus japonicus*). *Comp. Biochem. Physiol. D* **2011**, *6*, 195−205.
(28) Kim, S.; Park, P.; Kim, J.; Shahidi, F. Purification and characterization of a collagenolytic protease from the filefish, *Novoden modestrus*. *J. Biochem. Mol. Biol.* **2002**, *35*, 165−171.

JOURNAL OF AGRICULTURAL AND FOOD CHEMISTRY

Article

pubs.acs.org/JAFC

Blue Light Irradiation Affects Anthocyanin Content and Enzyme Activities Involved in Postharvest Strawberry Fruit

Feng Xu,[†] Shifeng Cao,[‡] Liyu Shi,[§] Wei Chen,[§] Xinguo Su,[#] and Zhenfeng Yang*,[§]

[†]School of Marine Sciences, Ningbo University, Ningbo 315211, People's Republic of China

[‡]Nanjing Research Institute for Agricultural Mechanization, Ministry of Agriculture, Nanjing 210014, People's Republic of China

[§]College of Biological and Environmental Sciences, Key Laboratory of Fruits and Vegetables Postharvest and Processing Technology Research of Zhejiang Province, Zhejiang Wanli University, Ningbo 315100, People's Republic of China

[#]Guangdong Food and Drug Vocational College, Guangzhou 510520, People's Republic of China

ABSTRACT: Blue light irradiation was applied to postharvest strawberry fruit to explore its influence on anthocyanin content and anthocyanin biosynthetic enzyme activities. Strawberry fruit was irradiated with blue light at 40 μmol m^{-2} s^{-1} for 12 days at 5 °C. The results indicated that blue light treatment improved total anthocyanin content in strawberry fruit during storage. Meanwhile, the treatment increased the activities of glucose-6-phosphate, shikimate dehydrogenase, tyrosine ammonia-lyase, phenylalanine ammonia-lyase, cinnamate-4-hydroxylase, 4-coumarate/coenzyme A ligase, dihydroflavonol-4-reductase, chalcone synthase, flavanone-3-β-hydroxylase, anthocyanin synthase, and UDP-glycose flavonoid-3-*O*-glycosyltranferase, which suggested that the enhancement of anthocyanin concentration by blue light might result from the activation of its related enzymes. Blue light might be proposed as a supplemental light source in the storage of strawberry fruit to improve its anthocyanin content.

KEYWORDS: *strawberry fruit, blue light, anthocyanin, postharvest*

INTRODUCTION

Anthocyanins are red, orange, purple, or blue water-soluble pigments occurring in fruits and vegetables, which play important biological roles in protecting plants against various biotic and abiotic stresses and in furnishing flowers and fruits with distinct colors to attract insects and animals for pollination and seed dispersal.[1] In addition to colorant properties, interest in anthocyanins has intensified due to their reported role in reducing the risk of coronary heart disease, cancer, and stroke.[2] Therefore, consumption of fruit rich in anthocyanins may be beneficial to human health.[3] It is vital to understand the regulation of anthocyanin biosynthesis thoroughly to develop anthocyanin-rich foods, thereby meeting the increasing demand for health-promoting compounds in our diet. To date, the biosynthesis pathway of anthocyanins and flavonoids has been almost completely elucidated as shown in Figure 1, and most of the structural genes encoding the enzymes responsible for each step have been isolated from different sources.[4,5]

Light is one of the most important environmental factors for plants, as a source of energy and in many other respects including anthocyanin synthesis.[6] Various types of lights might have distinct effects.[7−9] Among the different light wavelengths, blue light is one of the most effective in enhancing anthocyanin biosynthesis.[10,11] For example, anthocyanin production in apples had a strong dependence on both intensity and quality of light. Blue-violet and UV light were most effective, and far red was least effective, or even inhibitory.[7] Illumination with blue (both 455 and 470 nm) light-emitting diodes (LEDs) light resulted in higher anthocyanins content in red lettuce.[12] It is also reported that anthocyanin accumulation showed higher induction levels under blue light (465 nm) relative to green and red light during fruit development in strawberries.[14]

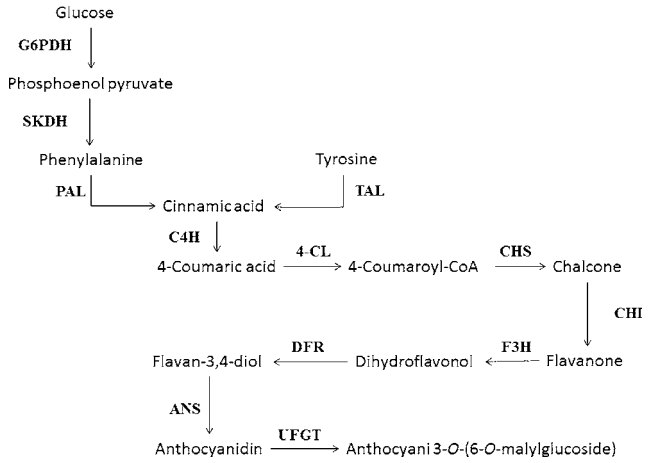

Figure 1. Simplified pathway for anthocyanin and flavonoid biosynthesis. G6PDH, glucose-6-phosphate; SKDH, shikimate dehydrogenase; PAL, phenylalanine ammonia-lyase; TAL, tyrosine ammonia-lyase; C4H, cinnamate-4-hydroxylase; 4CL, 4-coumarate:-CoA ligase; CHS, chalcone synthase; CHI, chalcone isomerase; F3H, flavanone 3-hydroxylase; DFR, dihydroflavonol 4-reductase; ANS, anthocyanidin synthase; UFGT, UDP-glucose:flavonoid glucosyltransferase.

Strawberry is one of the most commonly consumed berries and a good source of anthocyanins, which have shown potent antioxidant properties against chemically generated radicals.[13]

Received: March 5, 2014
Revised: April 29, 2014
Accepted: April 30, 2014
Published: April 30, 2014

ACS Publications © 2014 American Chemical Society

Previous literature showed that anthocyanin composition and anthocyanin contents in strawberries can be enhanced by ultraviolet radiation, altered gas composition, benzothiadiazole-7-carbothioic acid *S*-methylester (BTH), or application of signaling molecules.[14−18] Anthocyanin accumulation in response to different visible light wavelengths (e.g., blue, red, and green) has been investigated in strawberries during fruit development.[14] However, no information is available on the effect of blue light on anthocyanin content in postharvest strawberry fruit. In this paper, blue LED light was applied to the postharvest strawberry fruit, and the effects on anthocyanin content and related enzymes of anthocyanin synthesis were explored.

MATERIALS AND METHODS

Plant Materials. Strawberry (*Fragaria ananassa* Duch. cv. Fengguang) fruits were harvested by hand at stage of three-fourths colored based on the first appearance of red color on the fruit surface. Fruit were harvested and removed from a farm at Ningbo, Zhejiang province, and transported within 2 h to the laboratory. Fruits were selected for uniform size and color and then divided into two groups randomly.

LED Blue Light Irradiation. The first group of strawberries was irradiated with blue (470 nm) light at an intensity of 40 μmol m^{-2} s^{-1} for 12 days at 5 °C (80−90% relative humidity); this dose was chosen in our present study on the basis of our preliminary research (data not shown). GreenPower LED Research Module Blue (Koninklijke Philips Electronics N.V., The Netherlands) was used in blue light irradiation, and the flux intensity of the LEDs at the level of samples was measured with a digital visible light meter (model 9.4 Blue Light, Solartech Inc., USA). The second group of fruit was stored at 5 °C in the dark (80−90% relative humidity) and considered as the control. There were three replicates of 5 kg of fruit each per treatment, and the experiment was conducted twice. Samples were taken initially and at 2 day intervals during storage, immediately frozen in liquid nitrogen, and kept at −80 °C until required.

Total Anthocyanin Content Determination. The pH differential method[19] was applied to measure the total anthocyanin concentration of strawberry fruit. One gram samples from each replicate were homogenized with 5 mL of precooled acidified water (3% formic acid), and after centrifugation at 10000*g* for 15 min (4 °C), then another 5 mL of precooled acidified water was used to extract the residue again. The supernatant was combined to make the final volume of 25 mL for analysis. Results were expressed as milligrams of cyanidin-3-glucoside (Cy-3-Glu) equivalents per gram of fresh weight.

Enzyme Assays. G6PDH and SKDH were extracted with 0.1 M potassium phosphate buffer (pH 7.4) containing 2 mM cysteine, 2 mM EDTA, and 0.5 mM dithiothreitol (DTT). PAL and TAL were extracted with 0.2 mM sodium borate buffer (pH 8.7), containing 20 mM β-mercaptoethanol. Fruit flesh (5 g) was ground with 200 mM Tris-HCl buffer (pH 7.5) containing 25% (v/v) glycerol and 0.1 M DTT for C4H, 4-CL, F3H, and DFR. The CHS extraction was carried out by grinding the tissue with 300 μL of 50 mM KH_2PO_4 (pH 8.0) containing 20 mM ascorbic acid. The mixture was ultrasonicated in ice for 2 min. For UFGT, the samples were suspended in the buffer solution, including 100 mM Tris-HCl (pH 7.5), 10 mM sodium ascorbate, 5 mM dithiothreitol, 0.1% β-mercaptoethanol (v/v), and 10 μM *p*-aminophenylmethanesulfonyl fluoride (*p*-APMSF). The extracts were homogenized at 4 °C and centrifuged (12000*g*, 15 min). The supernatants were used for enzyme assays.

G6PDH activity was determined in reaction mixtures containing 5.88 μM NADP, 53.7 μM gluose-6-phosphate, and 88.5 mM $MgCl_2$, which followed the method of Debham and Emes with slight modification.[20] One unit of enzyme activity was equivalent to the oxidation of 1 μmol of NADPH per minute. SKDH activity was performed at 25 °C in the presence of 4 mM shikimic acid and 2.0 mM NADP in 0.1 mM Tris-HCl buffer at pH 9.0 as previously described.[21]

PAL and TAL assays were conducted according to the methods of Zucker and Kozukue et al.,[22,23] respectively. One unit of PAL activity was expressed as the amount of enzyme causing an increase in A_{290} of 0.001 unit h^{-1}. One unit of TAL was defined as the amount of enzyme causing an increase in A_{333} of 0.01 unit h^{-1}.

According to the method of Lamb et al.,[24] C4H activity was assayed in 50 mM phosphate buffer containing 2 mM 2-mercaptoethanol, 0.5 mM NADPH, and 2 mM *trans*-cinnamic acid, in a final volume of 2 mL of reaction buffer. The mixture was incubated for 1 h at 37 °C. The reaction was terminated by adding 6 M HCl, and 1 unit of C4H activity was expressed as the amount of enzyme causing an increase in A_{290} of 0.001 unit h^{-1}.

4-CL activity was determined spectrophotometrically in the presence of 50 μL of crude enzyme, 0.2 mM *p*-coumarate, 7.5 mM $MgCl_2$, 0.8 mM ATP, and 38 mM CoA in 100 mM Tris-HCl buffer (pH 7.5), as described previously.[25] One unit of 4-CL was defined as the amount of enzyme causing a decrease in A_{333} of 0.01 unit h^{-1}.

CHS activity was determined according to the method of Edwards and Kessman.[26] F3H and DFR activities were measured using the method of Liu et al.,[27] which determined the contents of F3H substrate (naringenin) and DFR substrate (dihydroquertin) with high-performance liquid chromatography (HPLC) analysis. UFGT activity was measured according to the method of Lister et al. with slight modification.[28] The reaction mixture consisted of enzyme solution (100 μL), 50 mM bicine buffer (100 μL, pH 8.5), substrate (quercetin 15 μL of 2 mg/mL), and UDP-galactose (10 μL of 15 mg/mL). Reaction tubes were incubated at 30 °C for 30 min, and the reaction was terminated by adding 75 μL of 20% (v/v) trichloroacetic acid in methanol.

The determination of ANS activity was based on that described previously.[29] The reaction mixture (500 μL) consisting of 20 mM K-Pi (pH 7.0), 200 mM NaCl, 10 mM maltose, 5 mM DTT, 40 mM sodium ascorbate, 1 mM 2-oxoglutaric acid, 0.4 mM $FeSO_4$, 1 M leucocyanidin, and ANS protein in 2 mg of crude cell extract was incubated at 30 °C for 30 min. The reaction was terminated by the addition of 5 μL of 36% (v/v) HCl, and the cyanidin formed was extracted by 500 μL of isoamyl alcohol for HPLC analysis. Cyanidin analysis was carried out by using a Waters 2695 HPLC equipped with a 2998 photodiode array detector (Waters Corp., Milford, MA, USA) according to the method of Saito et al.[29]

Protein content in the enzyme extracts was estimated using the Bradford method,[30] using bovine serum albumin as a standard.

Statistical Analysis. All statistical analyses were processed using SPSS (SPSS Inc., Chicago, IL, USA). Data were analyzed by one-way analysis of variance (ANOVA). The means were separated by Duncan's multiple-range test, and differences at $P < 0.05$ were considered to be significant.

RESULTS

Effect of Blue Light Treatment on Total Anthocyanin Content in Strawberry Fruit. The total anthocyanin content was quantitatively determined in strawberry fruit over 12 days of storage (Figure 2). The concentration of total anthocyanin in the control group increased sharply during the first 4 days of storage, but did not consistently afterward. In contrast, the content in the blue light-treated strawberry fruit increased during the whole storage. As compared to the control fruit, the values of total anthocyanin concentration were significantly ($p < 0.05$) higher after 2 days of storage.

Effect of Blue Light Treatment on G6PDH and SKDH Activities in Strawberry Fruit. G6PDH activity in both the control and blue light treatment increased during the first 8 days of storage and then declined (Figure 3A). SKDH activity increased in both blue light treatment and control samples as the storage progressed (Figure 3B). Blue light treatment enhanced the activities of both enzymes significantly ($P < 0.05$) after 2 days of storage.

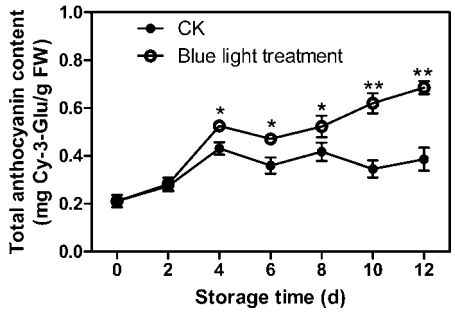

Figure 2. Effect of blue light treatment on total anthocyanin content in strawberry fruit during storage at 5 °C. Values are means ± SE. Vertical bars represent standard errors of the means. Asterisks indicate significant differences between blue light-treated and control samples (Duncan's multiple-range test; *, $P < 0.05$; **, $P < 0.01$; and ***, $P < 0.001$).

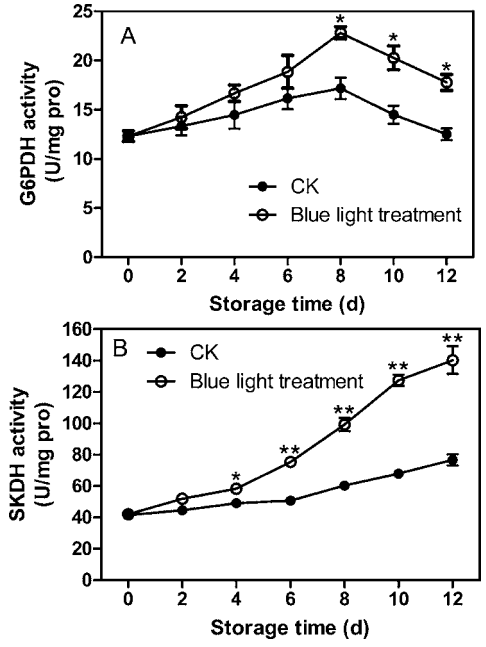

Figure 3. Effect of blue light treatment on G6PDH and SKDH activities in strawberry fruit during storage at 5 °C. Values are means ± SE. Vertical bars represent standard errors of the means. Asterisks indicate significant differences between blue light-treated and control samples (Duncan's multiple-range test; *, $P < 0.05$; **, $P < 0.01$; and ***, $P < 0.001$).

Effect of Blue Light Treatment on TAL, PAL, C4H, and 4-CL Activities in Strawberry Fruit. TAL and PAL activities in both control and blue light treatment increased during the initial 6 days of storage; thereafter they declined gradually (Figure 4A,B). In comparison with the control berries, significantly ($P < 0.05$) higher activities of TAL and PAL were observed in blue light-treated fruit after 4 and 2 days of storage, respectively.

C4H activity in the control strawberry fruit increased gradually in the first 6 days and then decreased over the next 6 days. On the other hand, the activity in blue light-treated samples increased rapidly, reached a maximum level at 8 days, and then declined afterward (Figure 4C). When compared to the control fruit, blue light treatment maintained significantly ($P < 0.05$) higher C4H activity after 6 days of storage.

4-CL activity increased in all strawberry fruits regardless of treatment at the first 2 days of storage and declined thereafter. The activity in the blue light-treated fruit was significantly ($P < 0.05$) higher than that in the control during the whole storage (Figure 4D).

Effect of Blue Light Treatment on CHS and F3H Activities in Strawberry Fruit. CHS and F3H activities in control strawberry fruit began to increase after 4 days of storage. However, a significant enhancement of these two enzymes was found in the blue light-treated fruit, and the treatment maintained higher activities of CHS and F3H after 2 days of storage (Figure 5).

Effect of Blue Light Treatment on DFR, ANS, and UFGT Activities in Strawberry Fruit. DFR activity in both control and blue light-treated fruits increased first and declined after 4 and 6 days of storage, respectively (Figure 6A). No significant changes of ANS and UFGT activities in control fruit were observed throughout the storage time. However, the activities of ANS and UFGT in blue light-treated fruit increased during the first 10 and 8 days of storage, respectively, and decreased afterward (Figure 6B,C). There was a positive effect of blue light treatment on all three enzymes whereby the treatment maintained significantly ($P < 0.05$) higher enzyme activities after 2 days of storage as compared to the control fruit.

DISCUSSION

Anthocyanins represent a group of natural flavonoid compounds in plants and are responsible for the coloration of strawberry fruit. Environmental conditions are known to induce anthocyanin accumulation across the major groups of higher plants, of these light being the best studied. It was reported that blue LED light regulated the metabolic pathways causing both increased concentrations of bioprotective compounds and plant growth of red leaf lettuce.[31] Similar to the previous study at different development stages of strawberries,[14] in our present work, we also found blue light treatment could enhance anthocyanin content in postharvest strawberries after 2 days of storage (Figure 2), which suggested that blue light could be a potential method to enhance anthocyanin accumulation and maintain a high-quality product of postharvest strawberry fruit.

Anthocyanins are secondary metabolites, primarily synthesized via the pentose phosphate pathway and shikimate, phenylpropanoid, and flavonoid pathways. These pathways consist of a number of enzymatic steps, each catalyzed by a sequential reaction for anthocyanin synthesis (Figure 1). Therefore, in this study, we examined the possible role of key regulatory enzymes in anthocyanin metabolism in response to blue light treatment. G6PDH and SKDH are the crucial enzymes in the pentose phosphate and shikimate pathways, which are both involved in anthocyanin biosynthesis. CO_2 stress enhanced phenolic accumulation in the root of *Panax ginseng* via induction of G6PDH activity. In addition, BTH treatment increased the activities of G6PDH and SKDH in postharvest strawberry fruit,[14] which was responsible for the enhancement of anthocyanin biosynthesis. Similarly, in our present study, the increased anthocyanin content in blue light-treated strawberry fruit was probably associated with the induction of these two enzymes as well.

The phenylpropanoid pathway plays an important role in anthocyanin synthesis. The result of the coordinated action of many related enzymes in the phenylpropanoid pathway might be attributed to the accumulation of anthocyanin in

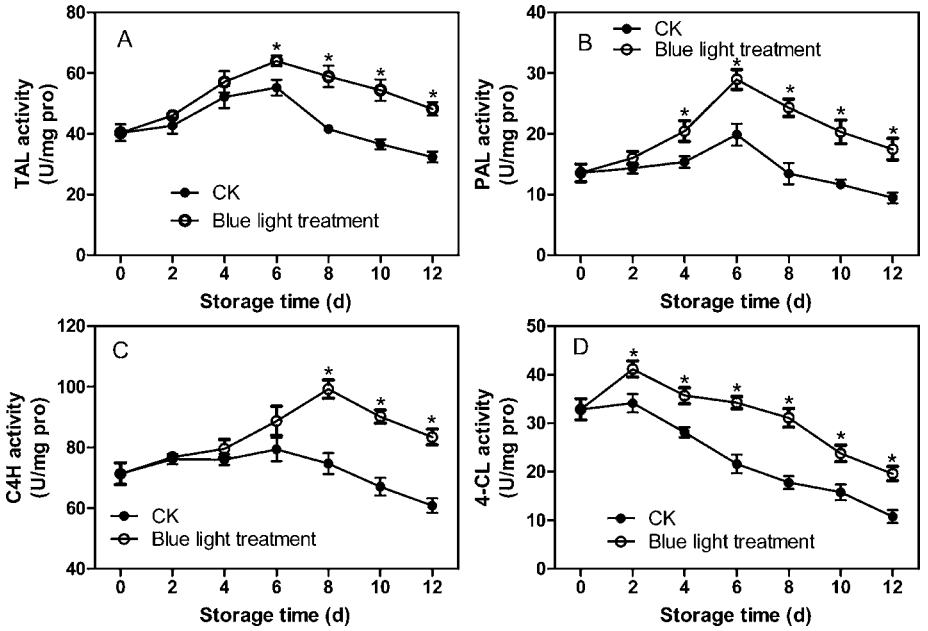

Figure 4. Effect of blue light treatment on TAL, PAL, C4H, and 4-CL activities in strawberry fruit during storage at 5 °C. Values are means ± SE. Vertical bars represent standard errors of the means. Asterisks indicate significant differences between blue light-treated and control samples (Duncan's multiple-range test; *, $P < 0.05$; **, $P < 0.01$; and ***, $P < 0.001$).

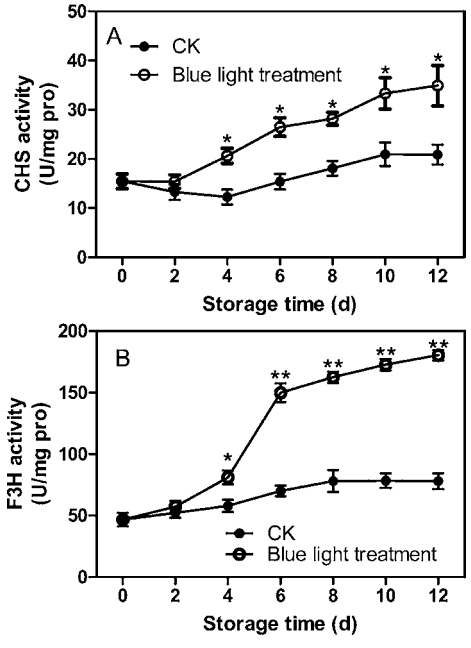

Figure 5. Effect of blue light treatment on CHS and F3H activities in strawberry fruit during storage at 5 °C. Values are means ± SE. Vertical bars represent standard errors of the means. Asterisks indicate significant differences between blue light-treated and control samples (Duncan's multiple-range test; *, $P < 0.05$; **, $P < 0.01$; and ***, $P < 0.001$).

strawberries after blue light treatment. Therefore, the four pivotal enzymes involved in this pathway, PAL, TAL, C4H, and 4-CL, were investigated. It has been shown that treatment with gibberellic acid increased PAL and TAL activities, which was correlated with the anthocyanin accumulation in ripening strawberries.[32] BTH induced anthocyanin content in postharvest strawberry fruit by enhancing activities of the four enzymes of phenylpropanoid metabolism.[14] Thus, in our present study, the higher PAL and TAL activities as well as the increased activities of C4H and 4-CL observed in blue light-treated strawberries indicated that an enhancement in anthocyanin production by blue light was accompanied by induction of the four key enzymes in the phenylpropanoid pathway of strawberry fruit.

Anthocyanin accumulation is also thought to be the result of interaction of the multiple key enzymes in the flavonoid pathway.[33] An increase of enzyme activities or gene expression involved in this pathway along with an increase in anthocyanin accumulation in response to light exposure has been reported. For example, Ju et al. have shown in 'Fuji' apples that light-reflecting mulches increased anthocyanin concentration and UFGT activity.[34] Ubi et al. demonstrated that increase in the expression levels of all five biosynthetic genes, *CHS*, *F3H*, *DFR*, *ANS*, and *UFGT*, in fruit skin of five apple cultivars coincided with increases of anthocyanin concentration.[35] When the fruit was bagged about 1 month prior to commercial harvest to prevent anthocyanin biosynthesis, the expression of *CHS*, *ANS*, and *UFGT* was substantially depressed in fruit skin, whereas that of all five genes was enhanced by UV-B treatment with the accumulation of anthocyanins.[35] Our results agreed with these authors because we found that blue light enhanced the activities of CHS, F3H, DFR, ANS, and UFGT in postharvest strawberries during storage, resulting in anthocyanin biosynthesis.[11] Previous study has revealed that blue light induced anthocyanin accumulation in strawberries during fruit development by regulating the expression of anthocyanin biosynthetic genes. Together with this study, our results suggested that blue light regulated multiple key enzymes in the anthocyanin pathway, thereby enhancing anthocyanin biosynthesis in strawberries during both fruit development and postharvest storage; however, the possible differences in regulatory mechanisms of anthocyanin accumulation by blue light applied before or after harvest need further study.

In conclusion, blue light was effective for stimulating anthocyanin accumulation in postharvest strawberry fruit. The

dx.doi.org/10.1021/jf501120u | J. Agric. Food Chem. 2014, 62, 4778−4783

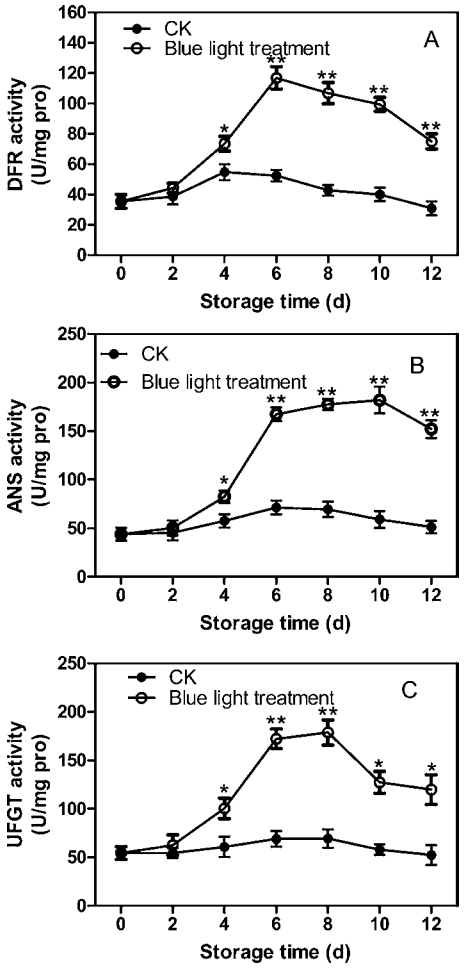

Figure 6. Effect of blue light treatment on DFR, ANS, and UFGT activities in strawberry fruit during storage at 5 °C. Values are means ± SE. Vertical bars represent standard errors of the means. Asterisks indicate significant differences between blue light-treated and control samples (Duncan's multiple-range test; *, $P < 0.05$; **, $P < 0.01$; and ***, $P < 0.001$).

enhancement in anthocyanin content by blue light might result from the activation of key enzymes in the pentose phosphate, shikimate, phenylpropanoid, and flavonoid pathways. Blue light could be considered as a supplemental light source in postharvest strawberry fruit to improve levels of health-promoting compounds, especially anthocyanin accumulation.

AUTHOR INFORMATION

Corresponding Author

*(Z.Y.) Phone:+86-574-88222229. Fax: +86-574-88222991. E-mail: yangzf@zwu.edu.cn.

Funding

This study was supported by the National Science Foundation of China (31101356), the Natural Science Foundation of Ningbo City (2013A610155, 2013A610159), the Induction of Talent Project (ZX2012000031), and the K. C. Wong Magna Fund at Ningbo University.

Notes

The authors declare no competing financial interest.

REFERENCES

(1) Harborne, J. B.; Williams, C. A. Advances in flavonoid research since 1992. *Phytochemistry* **2000**, *55*, 481−504.
(2) Chaovanalikit, A.; Wrolstad, R. Anthocyanin and polyphenolic composition of fresh and processed cherries. *J. Food Sci.* **2004**, *69*, 419−421.
(3) Surh, Y. J. Cancer chemoprevention with dietary phytochemicals. *Nat. Rev. Cancer* **2003**, *3*, 768−780.
(4) Winkel-Shirley, B. Flavonoid biosynthesis. A colorful model for genetics, biochemistry, cell biology, and biotechnology. *Plant Physiol.* **2001**, *126*, 485−493.
(5) Schijlen, E. G.; Ric de Vos, C.; van Tunen, A. J.; Bovy, A. G. Modification of flavonoid biosynthesis in crop plants. *Phytochemistry* **2004**, *65*, 2631−2648.
(6) Nascimento, L.; Leal-Costa, M. V.; Coutinho, M. A.; Moreira Ndos, S.; Lage, C. L.; Barbi, N. d. S.; Costa, S. S.; Tavares, E. S. Increased antioxidant activity and changes in phenolic profile of *Kalanchoe pinnata* (Lamarck) persoon (Crassulaceae) specimens grown under supplemental blue light. *Photochem. Photobiol.* **2013**, *89*, 391−399.
(7) Saure, M. C. External control of anthocyanin formation in apple. *Sci. Hortic.* **1990**, *42*, 181−218.
(8) Feng, S. Q.; Wang, Y. L.; Yang, S.; Xu, Y. T.; Chen, X. S. Anthocyanin biosynthesis in pears is regulated by a R2R3-MYB transcription factor PyMYB10. *Planta* **2010**, *232*, 245−255.
(9) Kataoka, I.; Beppu, K. UV irradiance increases development of red skin color and anthocyanins in 'Hakuho' peach. *HortScience* **2004**, *39*, 1234−1237.
(10) Chen, D. Q.; Li, Z. Y.; Pan, R. C.; Wang, X. J. Anthocyanin accumulation mediated by blue light and cytokinin in *Arabidopsis* seedlings. *J. Integr. Plant Biol.* **2006**, *48*, 420−425.
(11) Kadomura-Ishikawa, Y.; Miyawaki, K.; Noji, S.; Takahashi, A. Phototropin 2 is involved in blue light-induced anthocyanin accumulation in *Fragaria* × *ananassa* fruits. *J. Plant Res.* **2013**, *126*, 847−857.
(12) Samuolienė, G.; Sirtautas, R.; Brazaitytė, A.; Duchovskis, P. LED lighting and seasonality effects antioxidant properties of baby leaf lettuce. *Food Chem.* **2012**, *134*, 1494−1499.
(13) Wang, S. Y.; Zheng, W. Effect of plant growth temperature on antioxidant capacity in strawberry. *J. Agric. Food Chem.* **2001**, *49*, 4977−4982.
(14) Cao, S.; Hu, Z.; Zheng, Y.; Lu, B. Effect of BTH on anthocyanin content and activities of related enzymes in strawberry after harvest. *J. Agric. Food Chem.* **2010**, *58*, 5801−5805.
(15) Gil, M. I.; Holcroft, D. M.; Kader, A. A. Changes in strawberry anthocyanins and other polyphenols in response to carbon dioxide treatments. *J. Agric. Food Chem.* **1997**, *45*, 1662−1667.
(16) Ayala-Zavala, J. F.; Wang, S. Y.; Wang, C. Y.; González-Aguilar, G. A. Methyl jasmonate in conjunction with ethanol treatment increases antioxidant capacity, volatile compounds and postharvest life of strawberry fruit. *Eur. Food Res. Technol.* **2005**, *221*, 731−738.
(17) Zheng, Y. H.; Wang, S. Y.; Wang, C. Y.; Zheng, W. Changes in strawberry phenolics, anthocyanins, and antioxidant capacity in response to high oxygen treatments. *LWT−Food Sci. Technol.* **2007**, *40*, 49−57.
(18) Erkan, M.; Wang, S. Y.; Wang, C. Y. Effect of UV treatment on antioxidant capacity, antioxidant enzyme activity and decay in strawberry fruit. *Postharvest Biol. Technol.* **2008**, *48*, 163−171.
(19) Cheng, G. W.; Breen, P. J. Activity of phenylalanine ammonia-lyase (PAL) and concentrations of anthocyanins and phenolics in developing strawberry fruit. *J. Am. Soc. Hortic. Sci.* **1991**, *116*, 865−869.
(20) Debnam, P. M.; Emes, M. J. Subcellular distribution of enzymes of the oxidative pentose phosphate pathway in root and leaf tissues. *J. Exp. Bot.* **1999**, *50*, 1653−1661.
(21) Díaz, J.; Merino, F. Shikimate dehydrogenase from pepper (*Capsicum annuum*) seedlings. Purification and properties. *Physiol. Plant.* **1997**, *100*, 147−152.

(22) Zucker, M. Sequential induction of phenylalanine ammonia-lyase and a lyase-inactivating system in potato tuber disks. *Plant Physiol.* **1968**, *43*, 365−374.
(23) Kozukue, N.; Kozukue, E.; Kishiguchi, M. Changes in the contents of phenolic substances, phenylalanine ammonia-lyase (PAL) and tyrosine ammonia-lyase (TAL) accompanying chilling-injury of eggplant fruit. *Sci. Hortic.* **1979**, *11*, 51−59.
(24) Lamb, C.; Rubery, P. A spectrophotometric assay for trans-cinnamic acid 4-hydroxylase activity. *Anal. Biochem.* **1975**, *68*, 554−561.
(25) Knobloch, K. H.; Hahlbrock, K. 4-Coumarate:CoA ligase from cell suspension cultures of *Petroselinum hortense* Hoffm: partial purification, substrate specificity, and further properties. *Arch. Biochem. Biophys.* **1977**, *184*, 237−248.
(26) Edwards, R.; Kessmann, H. *Molecular Plant Pathology: A Practical Approach*; IRL Press: Oxford, UK, 1992; pp 45−62.
(27) Liu, M. L.; Liu, Y. B.; Cao, B. Determination of *Reaumuria soongorica* leaf F3H and DFR activities under drought stress by using RP-HPLC-MS (in Chinese). *Chin. J. Ecol.* **2012**, *31*, 2158−2162.
(28) Lister, C. E.; Lancaster, J. E.; Walker, J. R. Developmental changes in enzymes biosynthesis in the skins of red and green apple cultivars. *J. Sci. Food Agric.* **1996**, *71*, 313−320.
(29) Saito, K.; Kobayashi, M.; Gong, Z.; Tanaka, Y.; Yamazaki, M. Direct evidence for anthocyanidin synthase as a 2-oxoglutarate-dependent oxygenase: molecular cloning and functional expression of cDNA from a red forma of *Perilla frutescens*. *Plant J.* **1999**, *17*, 181−189.
(30) Bradford, M. M. A rapid and sensitive method for the quantitation of microgram quantities of protein utilizing the principle of protein-dye binding. *Anal. Biochem.* **1976**, *72*, 248−254.
(31) Stutte, G. W.; Edney, S.; Skerritt, T. Photoregulation of bioprotectant content of red leaf lettuce with light-emitting diodes. *HortScience* **2009**, *44*, 79−82.
(32) Montero, T.; Mollá, E.; Martín-Cabrejas, M. A.; López-Andréu, F. J. Effects of gibberellic acid (GA_3) on strawberry PAL (phenylalanine ammonia-lyase) and TAL (tyrosine ammonia-lyase) enzyme activities. *J. Sci. Food Agric.* **1998**, *77*, 230−234.
(33) Ju, Z. G. Fruit bagging, a useful method for studying anthocyanin synthesis and gene expression in apples. *Sci. Hortic.* **1998**, *77*, 155−164.
(34) Ju, Z. Q.; Duan, Y. S.; Ju, Z. G. Effects of covering the orchard floor with reflecting films on pigment accumulation and fruit coloration in 'Fuji' apples. *Sci. Hortic.* **1999**, *82*, 47−56.
(35) Ubi, B. E.; Honda, C.; Bessho, H.; Kondo, S.; Wada, M.; Kobayashi, S.; Moriguchi, T. Expression analysis of anthocyanin biosynthetic genes in apple skin: effect of UV-B and temperature. *Plant Sci.* **2006**, *170*, 571−578.

JOURNAL OF AGRICULTURAL AND FOOD CHEMISTRY

Article

pubs.acs.org/JAFC

Sesquiterpenes Inhibiting the Microglial Activation from *Laurus nobilis*

Hongqiang Chen,[†,‡] Chunfeng Xie,[†,‡] Hao Wang,[†,‡] Da-Qing Jin,[‡,§] Shen Li,[†,‡] Meicheng Wang,[†] Quanhui Ren,[†] Jing Xu,*[,†] Yasushi Ohizumi,[∥] and Yuanqiang Guo*[,†]

[†]College of Pharmacy and Tianjin Key Laboratory of Molecular Drug Research and [§]School of Medicine, Nankai University, Tianjin 300071, People's Republic of China

[∥]Graduate School of Pharmaceutical Sciences, Tohoku University, Sendai 980-8578, Japan

Supporting Information

ABSTRACT: The inhibitory reagents to inhibit the activation of microglial cells may be potentially useful for the treatment of neurodegenerative diseases. The leaves of the plant *Laurus nobilis* belonging to the family Lauraceae, namely, bay leaves, have been used as a popular spice, and their extract showed moderate inhibition on microglial activation. A further phytochemical investigation of the leaves led to the isolation of two new (**1**, **2**) and eight known (**3**−**10**) sesquiterpenes. Their structures were elucidated on the basis of extensive 1D and 2D NMR (HMQC, HMBC, ^{1}H−^{1}H COSY, and NOESY) spectroscopic data analyses and Chem3D modeling. The following biological studies disclosed that these isolated compounds showed inhibitory activities on LPS-induced microglial activation. The results of our phytochemical investigation, including two new sesquiterpenes (**1** and **2**) and the first report of two compounds (**3** and **4**) from this species, further revealed the chemical composition of bay leaves as a popular spice, and the biological studies implied that bay leaves, containing bioactive substances with the inhibition of microglial activation, were potentially beneficial to human health.

KEYWORDS: *Laurus nobilis, bay leaf, sesquiterpenes, microglial activation, neurodegenerative diseases*

INTRODUCTION

As human longevity increases, chronic neurodegenerative disorders are having an increasing impact on public health. Among these neurodegenerative disorders, Alzheimer's disease (AD) and Parkinson's disease (PD) are the most common representatives, which have an about 2% incidence of the population over 65 years of age.[1] Though the mechanism of neurodegenerative diseases remains unclear, accumulating evidence strongly supports that the pathway leading to neurodegenerative diseases, such as PD and AD, involves the activation of microglial cells.[2] Microglial cells, the resident immune cells of the central nervous system (CNS), play a major role in host defense and tissue repair in CNS. The activated microglial cells release neurotoxic and inflammatory mediators, such as nitric oxide (NO), reactive oxygen species (ROS), and proinflammatory cytokines, and overproduction of these inflammatory mediators in the CNS can cause various severe neurodegenerative diseases.[3] The activation of microglial cells in the CNS is an early sign that often precedes neuronal death.[3,4] Therefore, the inhibition of microglial activation can halt the following neuronal damage in the CNS, and the inhibitory reagents to inhibit the microglial activation may be potentially effective for the treatment of neurodegenerative diseases.[5]

Laurus nobilis, belonging to the family Lauraceae, is an evergreen tree widely distributed in the Mediterranean area and Europe.[6] The leaves of *L. nobilis*, namely, bay leaves, have been used as not only one of the most popular culinary spices in all western countries but also a folk medicine for asthma, digestive disorders, cardiac diseases, diarrhea, and rheumatic pains.[7,8] Previous phytochemical investigations on *L. nobilis* revealed the main presence of sesquiterpenes, megastigmane and phenolic components, and flavonoids,[7−14] which showed NO inhibitory effects,[7,9] cytotoxic activities,[8,11−13] and inhibitory effects on alcohol absorption.[15] In the course of our survey on biologically active substances in medicinal plants, considerable attention has been given to the occurrence of compounds with inhibitory effects of the microglial activation, since these substances are expected to be potentially useful for the treatment of neurodegenerative diseases. As a continuation of our work on the search for bioactive substances from traditional folk medicines or medicinal food,[16−18] we investigated the chemical constituents of the ethyl acetate soluble part of the methanol extract from the leaves of *L. nobilis*, which showed moderate inhibitory effects on LPS-induced microglial activation. This investigation led to the isolation and identification of two new sesquiterpenes, named laurupenes A and B (**1** and **2**), and eight known analogues (**3**−**10**) (Figure 1). Their structures were elucidated on the basis of spectroscopic data analyses (IR, ESI-MS, HR-ESI-MS, and 1D and 2D NMR). This paper herein describes their isolation, structure elucidation, and inhibitory activities on lipopolysaccharide (LPS)-induced microglial activation.

Received: March 31, 2014
Revised: May 5, 2014
Accepted: May 6, 2014
Published: May 6, 2014

ACS Publications © 2014 American Chemical Society

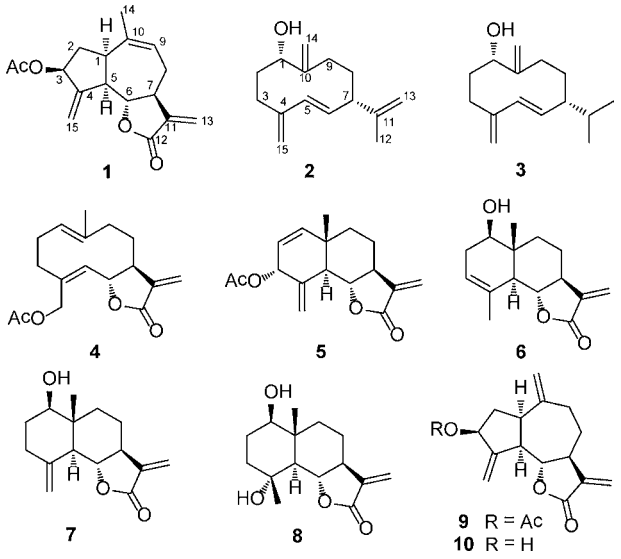

Figure 1. Structures of compounds **1**−**10** from *L. nobilis*.

MATERIALS AND METHODS

General. The optical rotations were measured in CH_2Cl_2 using a Rudolph Autopol IV automatic polarimeter. The IR spectra were taken on a Bruker Tensor 27 FT-IR spectrometer with KBr disks. The ESI-MS spectra were obtained on an LCQ-Advantage mass spectrometer (Finnigan Co. Ltd., U.S.A.). HR-ESI-MS spectra were recorded by an Agilent 6520 Q-TOF LC/MS (Agilent, U.S.A.). 1D and 2D NMR spectra were recorded on a Bruker AV 400 instrument (400 MHz for ^{1}H and 100 MHz for ^{13}C) with TMS as an internal standard. HPLC separations were performed on a CXTH system, equipped with a UV3000 detector at 210 nm (Beijing Chuangxintongheng Instruments Co. Ltd., China), and a YMC-pack ODS-AM (20 × 250 mm) column (YMC Co. Ltd., Japan). Silica gel was used for column chromatography (200−300 mesh, Qingdao Marine Chemical Group Co. Ltd., China). Chemical reagents for isolation were of analytical grade and purchased from Tianjin Chemical Reagent Company, China. Biological reagents were from Sigma Company. The murine microglial BV-2 cell line was from Shanghai Institutes for Biological Sciences, Chinese Academy of Sciences (China).

Plant Material. The leaves of *L. nobilis* were purchased in July 2011 from Bozhou Materia Medica Market, Anhui province, China. A voucher specimen (No. 20110919) was identified by Dr. Yuanqiang Guo (College of Pharmacy, Nankai University, China) and deposited at the laboratory of the Research Department of Natural Medicine, College of Pharmacy, Nankai University, China.

Extraction and Isolation. The air-dried leaves of *L. nobilis* (6.0 kg) were powdered and extracted were with MeOH (3 × 48 L) under reflux. The organic solvent was evaporated to obtain a crude extract (375 g). The extract was suspended in H_2O (0.7 L) and partitioned with EtOAc (3 × 0.7 L). The EtOAc soluble part (260 g) was subjected to a silica gel column chromatography, using a gradient of acetone in petroleum ether (1%−30%), to give ten fractions (F_1−F_{10}) based on TLC analyses. F_2 was fractionated by middle pressure liquid chromatography (MPLC) over octadecylsilyl (ODS) eluting with a step gradient from 70% to 90% MeOH in H_2O to give four subfractions (F_{2-1}−F_{2-4}). F_{2-2} was further purified by preparative HPLC (YMC-pack ODS-AM, 20 × 250 mm, 75% MeOH in H_2O) to afford compound **1** (t_R = 22 min, 11.4 mg). Compound **2** (t_R = 26 min, 4.0 mg) was obtained from the subfraction F_{2-3} using the same HPLC system (82% MeOH in H_2O), and compound **3** (t_R = 28 min, 8.1 mg) was obtained from F_{2-4} (85% MeOH in H_2O). F_3, F_4, F_5, F_6, and F_8 were also subjected to the same MPLC over ODS, eluting with a step gradient from 60% to 90% MeOH in H_2O, to give subfractions F_{3-1}−F_{3-4}, F_{4-1}−F_{4-6}, F_{5-1}−F_{5-5}, F_{6-1}−F_{6-9}, and F_{8-1}−F_{8-8}, respectively. The further purification of subfraction F_{4-2} (73% MeOH in H_2O) with the same HPLC system led to afford compound **4** (t_R = 24 min, 23.9 mg). Compounds **5** (t_R = 21 min, 18.9 mg) and **9**

Table 1. ^{1}H and ^{13}C NMR Data of Compounds 1 and 2 (δ ppm in $CDCl_3$ and J in Hz)[a]

	1		2	
position	^{13}C	^{1}H	^{13}C	^{1}H
1	43.7	α 2.63 m	76.2	β 3.78 dd (11.8, 3.3)
2	37.5	α 2.72 m	36.2	α 2.08 m
		β 1.53 m		β 2.01 m
3	73.8	α 5.52 m	30.1	α 2.44 ddd (17.6, 12.8, 4.8)
				β 2.21 m
4	147.8		146.4	
5	51.0	α 2.71 m	129.6	6.08 d (15.8)
6	83.3	β 4.08 dd (10.7, 9.4)	136.6	5.54 dd (15.8, 10.3)
7	45.6	α 2.69 m	52.4	β 2.68 m
8	29.1	α 2.57 m	37.1	α 1.82 m
		β 2.65 m		β 2.11 m
9	121.4	5.58 d (7.6)	34.5	α 2.66 m
				β 1.71 m
10	137.0		153.1	
11	139.8		147.4	
12	169.8		21.3	1.72 s
13	119.6	6.22 d (3.3)	109.4	4.73 s
		5.49 d (3.3)		4.71 s
14	28.0	1.82 s	110.9	5.30 s
				5.04 s
15	117.2	5.48 s	113.5	4.96 s
		5.38 s		4.87 s
OAC	171.0			
	21.3	2.06 s		

[a]The assignments of NMR data are based on ^{1}H, ^{13}C, DEPT, ^{1}H−^{1}H COSY, HMQC, and HMBC NMR experiments.

dx.doi.org/10.1021/jf501515v | J. Agric. Food Chem. 2014, 62, 4784−4788

(t_R = 23 min, 35.6 mg) were obtained from subfraction F_{3-2} using the above HPLC system (73% MeOH in H_2O). With the same protocols, compounds **6** (t_R = 24 min, 32.2 mg) and **10** (t_R = 20 min, 13.2 mg) were isolated from subraction F_{5-1} (65% MeOH in H_2O), and compound **7** (t_R = 21 min, 64.2 mg) was obtained from F_{6-1} (62% MeOH in H_2O). The further purification of F_{8-1} with the above HPLC system (60% MeOH in H_2O) resulted in the isolation of compound **8** (t_R = 15 min, 41.6 mg).

Laurupene A (1). Colorless oil; $[\alpha]_D^{12}$ = +27.3 (*c* 0.55, CH_2Cl_2); IR (KBr) ν_{max} cm^{-1} 2967, 2930, 1768, 1736, 1666, 1372, 1240, 1137, 1015; ^1H NMR (400 MHz, $CDCl_3$) and ^{13}C NMR (100 MHz, $CDCl_3$) data, see Table 1; ESI-MS *m*/*z* 289 $[M + H]^+$; HR-ESI-MS *m*/*z* 289.1437 $[M + H]^+$, calcd for $C_{17}H_{21}O_4$, 289.1440.

Laurupene B (2). Colorless oil; $[\alpha]_D^{12}$ = −17.7 (*c* 0.26, CH_2Cl_2); IR (KBr) ν_{max} cm^{-1} 2968, 2929, 1658, 1372, 1276, 1261, 764; ^1H NMR (400 MHz, $CDCl_3$) and ^{13}C NMR (100 MHz, $CDCl_3$) data, see Table 1; ESI-MS *m*/*z* 219 $[M + H]^+$; HR-ESI-MS *m*/*z* 219.1742 $[M + H]^+$, calcd for $C_{15}H_{23}O$, 219.1749.

Bioassay for Inhibitory Activities on LPS-Induced Microglial Activation. The activated microglial cells release neurotoxic and inflammatory mediators, such as nitricoxide (NO). The amount of released NO production indicate the level of microglial activation or inhibition degree. Murine microglial BV-2 cells were selected for the experiments. The cells were cultured at 37 °C in DMEM supplemented with 10% (v/v) inactivated fetal bovine serum and 100 U/mL penicillin/streptomycin under a water-saturated atmosphere of 95% air and 5% CO_2. The cells were seeded in 96-well culture plates (5×10^4 cells/well) and allowed to adhere for 24 h at 37 °C. The cells were incubated for 20 h with or without 0.2 μg/mL of LPS (Sigma Chemical Co., St. Louis, MO, U.S.A.) in the absence or presence of the test compounds. 2-Methyl-2-thiopseudourea, sulfate (SMT), was used as a positive control. As a parameter of NO synthesis, the nitrite concentration was measured by the Griess reaction using the supernatant of the BV-2 cells. Briefly, 50 μL of the cell culture supernatant was reacted with 50 μL of Griess reagent [1:1 mixture of 0.1% *N*-(1-naphthyl)ethylenediamine in H_2O and 1% sulfanilamide in 5% phosphoric acid] in a 96-well plate, and the absorbance was read with a microplate reader (Thermo Fisher Scientific Inc., U.S.A.) at 550 nm. The experiment was performed three times, and the IC_{50} values for the inhibition of NO production were determined on the basis of linear or nonlinear regression analysis of the concentration−response data curves.

RESULTS AND DISCUSSION

Compound **1** was isolated as a colorless oil. Its HR-ESI-MS provided the molecular formula $C_{17}H_{20}O_4$, through the presence of a peak at *m*/*z* 289.1437 $[M + H]^+$ (calcd for $C_{17}H_{21}O_4$ 289.1440). The molecular formula indicated eight unsaturation degrees for **1**. The IR spectrum evidenced the presence of an α,β-saturated γ-lactone moiety (1736 cm^{-1}). The ^1H NMR spectrum of **1** exhibited two methyl singlets at δ_H 1.82 (3H, s, H_3-14) and 2.06 (3H, s, $COCH_3$), five olefinic protons at δ_H 5.58 (1H, d, *J* = 7.6 Hz, H-9), 6.22 and 5.49 (each 1H, d, *J* = 3.3 Hz, H_2-13), and 5.48 and 5.38 (each 1H, s, H_2-15), and two oxygenated methine protons at δ_H 5.52 (1H, m, H-3) and 4.08 (1H, dd, *J* = 10.7, 9.4 Hz, H-6) (Table 1). The ^{13}C NMR spectrum of **1** showed 17 carbon resonances. From the ^1H and ^{13}C NMR spectra, one acetoxy group was obvious. Apart from the two carbons (δ_C 171.0, 21.3) for the acetoxy group, there were 15 residual resonances in the ^{13}C NMR spectrum, which were classified into one methyl [δ_C 28.0 (C-14)], four methylenes [δ_C 37.5 (C-2), 29.1 (C-8), 119.6 (C-13), and 117.2 (C-15)], six methines [δ_C 43.7 (C-1), 73.8 (C-3), 51.0 (C-5), 83.3 (C-6), 45.6 (C-7), and 121.4 (C-9)], and four quaternary carbons [δ_C 147.8 (C-4), 137.0 (C-10), 139.8 (C-11), and 169.8 (C-12)] based on the DEPT and HMQC spectra. According to the unsaturation degrees, the aforementioned spectroscopic features, and the sesquiterpenes isolated from the genus *Laurus*,[8−12] compound **1** might be a sesquiterpene with three rings and an acetoxy group. In order to confirm the above assumption and elucidate the structure, the following HMBC and $^1H-^1H$ COSY experiments were performed. In the HMBC spectrum, the long-range correlations of H-1 to C-2, C-3, C-4, C-5, C-6, C-9, C-10, and C-14, and H-5 to C-1, C-2, C-3, C-4, C-6, C-7, C-10, and C-15, revealed the fusion of a five-membered ring and a seven-membered ring, which bonded with the α,β-saturated γ-lactone ring via the C-6 and C-7 unit. By the HMBC correlations of H_2-15 to C-3, C-4, and C-5, and H_2-13 to C-7, C-11, and C-12, the two terminal double bonds were accordingly assigned to C-4 and C-15, and C-11 and C-13, respectively. The oxygenated carbon at δ_C 73.8 and the residual olefinic carbons at δ_C 121.4 and 137.0 were ascribable to C-3, C-9, and C-10, respectively, by the interpretation of the HMBC spectrum. Consequently, the substituted acetoxy group was attached at C-3 by the HMBC correlation of H-3 to the carbonyl carbon at δ_C 171.0. By further analyzing the HMQC, HMBC, and $^1H-^1H$ COSY spectra (Figure 2), all the proton and carbon signals were assigned unambiguously. Thus, the planar structure of a guaianolide-type sesquiterpene for compound **1** was established.

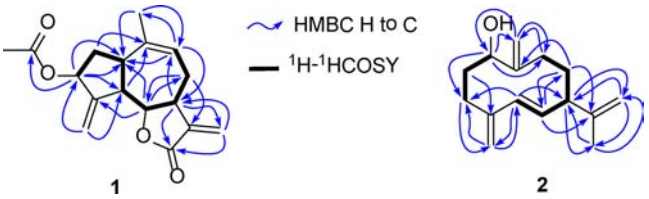

Figure 2. Selected HMBC and $^1H-^1H$ COSY correlations of compounds **1** and **2**.

The relative configuration of **1** was elucidated as follows. For the reported natural guaianolide sesquiterpene, the five-membered lactone ring, the seven-membered ring, and the other five-membered ring are *trans*- and *cis*-fused with each other, respectively, H-1, H-5, and H-7 are in α-positions on the same side, and H-6 is in β-position on the opposite side.[19] The NOESY correlations observed for H-5/H-7, H-5/H-1, H-1/H-3, H-6/H-2β, H-6/H-8β, and H-9/H_3-14 (Figure 3) and the

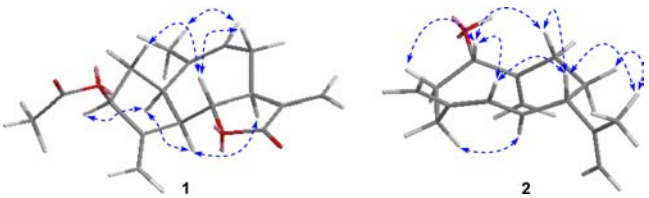

Figure 3. Key NOESY correlations of compounds **1** and **2**.

further Chem3D modeling suggested a conformation for compound **1** as depicted in Figure 3, where the C-3 acetoxy group was in a β-position. The structure of compound **1** was therefore characterized and named laurupene A.

Compound **2** possessed a molecular formula $C_{15}H_{22}O$ as determined by the HR-ESI-MS (*m*/*z* 219.1742 $[M + H]^+$, calcd for $C_{15}H_{23}O$, 219.1749), which implied five unsaturation degrees. The ^1H NMR spectrum of **2** exhibited one methyl group at δ_H 1.72 (3H, s, H_3-12), eight olefinic protons at δ_H

dx.doi.org/10.1021/jf501515v | J. Agric. Food Chem. 2014, 62, 4784−4788

6.08 (1H, d, J = 15.8 Hz, H-5), 5.54 (1H, dd, J = 15.8, 10.3 Hz, H-6), 4.73 and 4.71 (each 1H, s, H_2-13), 5.30 and 5.04 (each 1H, s, H_2-14), and 4.96 and 4.87 (each 1H, s, H_2-15), and one oxygenated methine proton at δ_H 3.78 (1H, dd, J = 11.8, 3.3 Hz, H-1) (Table 2). The ^{13}C NMR spectrum of **2** showed 15

Table 2. IC_{50} Values of Compounds 1 and 3−10 Inhibiting the Microglial Activation Indicated by the Amount of NO Production[a]

compd	IC_{50} (μM)	compd	IC_{50} (μM)
1	>100	**7**	22.0 ± 1.1
3	>100	**8**	30.5 ± 0.8
4	23.3 ± 3.2	**9**	14.0 ± 0.5
5	39.9 ± 6.0	**10**	35.4 ± 4.1
6	25.3 ± 1.9	SMT[b]	8.1 ± 1.2

[a]Data are presented as mean ± SD based on three experiments. Compound **2** was not assayed for the inhibitory effects because of inadequate amount. [b]SMT (2-methyl-2-thiopseudourea, sulfate) was used as a positive control.

carbon signals, comprising one methyl (C-12), seven methylenes (C-2, C-3, C-8, C-9, C-13, C-14, and C-15), four methines (C-1, C-5, C-6, and C-7), and three quaternary carbons (C-4, C-10, and C-11) based on the DEPT and HMQC spectra. According to the molecular, unsaturation degrees, and the above spectroscopic features, compound **2** might be a germacrane-type sesquiterpene.[8−13] In order to confirm the germacrane-type skeleton and achieve the assignments of proton and carbon signals, a following HMBC experiment was performed. By the interpretation of HMQC and HMBC spectroscopic data, the ten-membered ring and the isopropenyl moiety attached at C-7 were deduced and defined. The additional two terminal double bonds were accordingly assigned to C-4 and C-15, and C-10 and C-14, respectively, by the HMBC correlations of H_2-15 to C-3, C-4, and C-5, and H_2-14 to C-1, C-9, and C-10. Based on the above deductions, the germacrane skeleton consisting of one ten-membered ring and an isopropenyl moiety was inferred, where the methylene groups of two terminal double bonds between C-4 and C-15, and C-10 and C-14, replaced the characteristic C-14 and C-15 methyl groups of the common germacrane skeleton. Consequently, the oxygenated carbon at δ_C 76.2 and the olefinic carbons at δ_C 129.6 and 136.6 were assigned to C-1, C-5, and C-6, respectively, by the long-range correlations of H-1 to C-9, C-10, C-14, C-2, and C-3, H-5 to C-3, C-4, C-6, C-7, and C-15, and H-6 to C-4, C-5, C-7, C-8, and C-11. The further analyses of 2D NMR spectra led to the assignments of all the protons and carbons. Thus, the planar structure of a germacrane-type sesquiterpene for **2** was established.

The relative configuration of **2** was deduced as follows. The coupling constant between H-5 and H-6 ($J_{5,6}$ = 15.8 Hz) revealed an *E*-configuration for the C-5−C-6 double bond. The NOESY correlations observed for H-5/H-1, H-5/H-7, H-7/H-9β, H-9β/H-1, H-7/H_3-12, H-8β/H_3-12, and H-6/H-3α (Figure 3) and the Chem3D modeling suggested a conformation for **2** as depicted in Figure 3, where the H-7 and H-1 were both in β-positions. The structure of compound **2** was therefore characterized, which has been named laurupene B.

Based on the spectroscopic analyses and the comparison with the literature, the known compounds were identified as *ent*-germacra-4(15),5,10(14)-trien-1α-ol (**3**),[20] 15-acetoxycostunolide (**4**),[21] 3α-acetoxyeudesma-1,4(15),11(13)-trien-12,6α-olide (**5**),[21] santamarine (**6**),[8] reynosin (**7**),[8] 1β-hydroxy arbusculin A (**8**),[22] zaluzanin D (**9**),[23] and zaluzanin C (**10**).[23]

Studies on the inhibition of microglial activation have demonstrated that reagents with inhibitory activities of microglial activation can halt the neuronal damage in the CNS and may be potentially useful for the treatment of neurodegenerative diseases.[5] In order to search for and obtain the bioactive substances inhibiting the microglial activation as candidates for the treatment of neurodegenerative diseases, these sesquiterpenes isolated from *L. nobilis* were evaluated for their inhibitory effects on LPS-induced microglial activation using murine microglial BV-2 cells (Figure 4). The level of

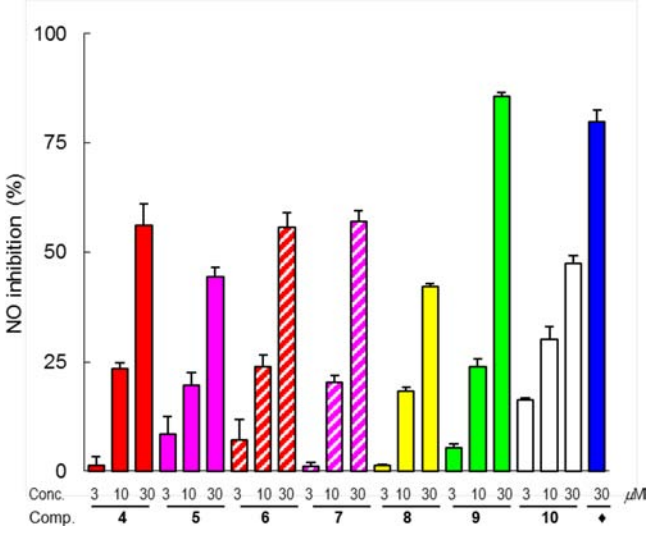

Figure 4. Inhibitory effects of compounds **4−10** on LPS-induced microglial activation. The inhibition levels of microglial activation were indicated by the amount of released NO production in BV-2 cells. BV-2 cells were treated with LPS alone or together with each compound at the concentrations indicated. After 20 h incubation, the supernatants were tested by Griess assay and the NO inhibitory rates were calculated. The experiment was performed three times, and the data are expressed as mean ± SD values. The inhibitory rate on NO production was calculated as follows: inhibitory rate (%) = (1 − (LPS/sample − untreated)/(LPS − untreated)) × 100. ◆ indicates positive control, SMT.

microglial activation or inhibition degree was indicated by the amount of released NO production.[24] 2-Methyl-2-thiopseudourea sulfate (SMT) was used as a positive control (IC_{50} 8.1 μM). All the evaluated sesquiterpenes exhibited inhibitory effects on LPS-induced microglial activation, and the inhibitory effects indicated by the amount of NO production are shown in Table 3. Compounds **4−10** inhibited LPS-induced microglial activation dose-dependently with IC_{50} values of 23.3, 39.9, 25.3, 22.0, 30.5, 14.0, and 35.4 μM, respectively. Compounds **1** and **3** showed weak activities (IC_{50} values >100 μM). Compound **2** was not assayed for the inhibitory effects because of inadequate amount. MTT assay indicated that all the assayed compounds had no significant cytotoxicity to the BV-2 cells at their effective concentration for the inhibition of microglial activation (data not shown).

In summary, two new and eight known sesquiterpenes were successfully isolated from the leaves of *L. nobilis*. Their structures were elucidated by 1D and 2D NMR spectra and Chem3D modeling. Biological studies disclosed that all of the evaluated isolates exhibited inhibitory effects on LPS-induced

microglial activation and compound **9** exerted the most inhibition against microglial activation indicated by the amount of NO production, which was comparable to the positive control (SMT). The results of our chemical investigation, including two new sesuqiterpenes (**1** and **2**) and the first report of two compounds (**3** and **4**) from this species, further revealed the chemical composition of *L. nobilis*, and the biological screening of these isolates exhibited that the leaves of *L. nobilis*, used as a popular spice, may be beneficial to human health, while the current biological data suggest that these sesquiterpenes from *L. nobilis*, especially compounds **4**, **6**, **7**, and **9** with strong inhibitory activities of microglial activation, may probably be considered as candidate agents for neurodegenerative diseases. Further biological studies on these compounds are still underway by our group.

■ ASSOCIATED CONTENT

Supporting Information

The 1D and 2D NMR and HR-ESI-MS spectra of compounds **1** and **2**. This material is available free of charge via the Internet at http://pubs.acs.org.

■ AUTHOR INFORMATION

Corresponding Authors

*Tel/fax: +86-22-23502595. E-mail: xujing611@nankai.edu.cn.
*Tel/fax: +86-22-23502595. E-mail: victgyq@nankai.edu.cn.

Author Contributions

‡These authors contributed equally to this work.

Notes

The authors declare no competing financial interest.

■ REFERENCES

(1) Fratiglioni, L.; Qiu, C. Prevention of common neurodegenerative disorders in the elderly. *Exp. Gerontol.* **2009**, *44*, 46−50.

(2) Perry, V. H.; Nicoll, J. A.; Holmes, C. Microglia in neurodegenerative disease. *Nat. Rev. Neurol.* **2010**, *6*, 193−201.

(3) González-Scarano, F.; Baltuch, G. Microglia as mediators of inflammatory and degenerative diseases. *Annu. Rev. Neurosci.* **1999**, *22*, 219−240.

(4) Block, M. L.; Zecca, L.; Hong, J. S. Microglia-mediated neurotoxicity: uncovering the molecular mechanisms. *Nat. Rev. Neurosci.* **2007**, *8*, 57−69.

(5) Dheen, S. T.; Kaur, C.; Ling, E. A. Microglial activation and its implications in the brain diseases. *Curr. Med. Chem.* **2007**, *14*, 1189−1197.

(6) Garg, S. N.; Siddiqui, M. S.; Agarwal, S. K. New fatty acid esters and hydroxy ketones from fruits of *Laurus nobilis*. *J. Nat. Prod.* **1992**, *55*, 1315−1319.

(7) De Marino, S.; Borbone, N.; Zollo, F.; Ianaro, A.; Di Meglio, P.; Iorizzi, M. Megastigmane and phenolic components from *Laurus nobilis* L. leaves and their inhibitory effects on nitric oxide production. *J. Agric. Food Chem.* **2004**, *52*, 7525−7531.

(8) Fang, F.; Sang, S.; Chen, K. Y.; Gosslau, A.; Ho, C. T.; Rosen, R. T. Isolation and identification of cytotoxic compounds from bay leaf (*Laurus nobilis*). *Food Chem.* **2005**, *93*, 497−501.

(9) De Marino, S.; Borbone, N.; Zollo, F.; Ianaro, A.; Di Meglio, P.; Iorizzi, M. New sesquiterpene lactones from *Laurus nobilis* leaves as inhibitors of nitric oxide production. *Planta Med.* **2005**, *71*, 706−710.

(10) Appendino, G.; Tagliapietra, S.; Nano, G. M.; Cisero, M. A sesquiterpene alcohol from the fruits of *Laurus nobilis*. *Phytochemistry* **1992**, *31*, 2537−2538.

(11) Barla, A.; Topçu, G.; Öksüz, S.; Tümen, G.; Kingston, D. G. I. Identification of cytotoxic sesquiterpenes from *Laurus nobilis* L. *Food Chem.* **2007**, *104*, 1478−1484.

(12) Dall'Acqua, S.; Viola, G.; Giorgetti, M.; Loi, M. C.; Innocenti, G. Two new sesquiterpene lactones from the leaves of *Laurus nobilis*. *Chem. Pharm. Bull.* **2006**, *54*, 1187−1189.

(13) Julianti, E.; Jang, K. H.; Lee, S.; Lee, D.; Mar, W.; Oh, K. B.; Shin, J. Sesquiterpenes from the leaves of *Laurus nobilis* L. *Phytochemistry* **2012**, *80*, 70−76.

(14) Fiorini, C.; David, B.; Fouraste, I.; Vercauteren, J. Acylated kaempferol glycosides from *Laurus nobilis* leaves. *Phytochemistry* **1998**, *47*, 821−824.

(15) Yoshikawa, M.; Shimoda, H.; Uemura, T.; Morikawa, T.; Kawahara, Y.; Matsuda, H. Alcohol absorption inhibitors from bay leaf (*Laurus nobilis*): structure-requirements of sesquiterpenes for the activity. *Bioorg. Med. Chem.* **2000**, *8*, 2071−2077.

(16) Xu, J.; Jin, D. Q.; Liu, C.; Xie, C.; Guo, Y.; Fang, L. Isolation, characterization, and NO inhibitory activities of sesquiterpenes from *Blumea balsamifera*. *J. Agric. Food Chem.* **2012**, *60*, 8051−8058.

(17) Wang, S.; Jin, D. Q.; Xie, C.; Wang, H.; Wang, M.; Xu, J.; Guo, Y. Isolation, characterization, and neuroprotective activities of sesquiterpenes from *Petasites japonicus*. *Food Chem.* **2013**, *141*, 2075−82.

(18) Guo, P.; Li, Y.; Xu, J.; Liu, C.; Ma, Y.; Guo, Y. Bioactive *neo*-clerodane diterpenoids from the whole plants of *Ajuga ciliata* Bunge. *J. Nat. Prod.* **2011**, *74*, 1575−1583.

(19) Ando, M.; Ibayashi, K.; Minami, N.; Nakamura, T.; Isogai, K.; Yoshimura, H. Studies on the synthesis of sesquiterpene lactones, 16. The syntheses of 11β,13-dihydrokauniolide, estafiatin, isodehydrocostuslactone, 2-oxodesoxyligustrin, arborescin, 1,10-epiarborescin, 11β,13-dihydroludartin, 8-deoxy-11β,13-dihydrorupicolin B, 8-deoxyrupicolin B, 3,4-epiludartin, ludartin, kauniolide, dehydroleucodin, and leucodin. *J. Nat. Prod.* **1994**, *57*, 433−445.

(20) Lee, S. O.; Choi, S. Z.; Chio, S. U.; Kim, G. H.; Kim, Y. C.; Lee, K. R. Cytotoxic terpene hydroperoxides from the aerial parts of *Aster spathulifolius*. *Arch. Pharm. Res.* **2006**, *29*, 845−848.

(21) Zdero, C.; Bohlmann, F. Sesquiterpene lactones from *Dicoma species*. *Phytochemistry* **1990**, *29*, 183−187.

(22) Choi, J. Y.; Choi, E. H.; Jung, H. W.; Oh, J. S.; Lee, W. H.; Lee, J. G.; Son, J. K.; Kim, Y.; Lee, S. H. Melanogenesis inhibitory compounds from *Saussureae radix*. *Arch. Pharm. Res.* **2008**, *31*, 294−299.

(23) Krishna Kumari, G. N.; Masilamani, S.; Ganesh, M. R.; Aravind, S. Microbial transformation of zaluzanin D. *Phytochemistry* **2003**, *62*, 1101−1104.

(24) Schmidt, H. H. H. W.; Kelm, M. Determination of nitrite and nitrate by the Griess reaction. In *Methods in Nitric Oxide Research*; Feelisch, M., Stamler, J. S., Eds.; John Wiley and Sons: West Sussex, U.K., 1996; pp 491−497.

JOURNAL OF AGRICULTURAL AND FOOD CHEMISTRY

Article

pubs.acs.org/JAFC

A Comprehensive Study To Explore Differences in Mycotoxin Patterns from Agro-ecological Regions through Maize, Peanut, and Cassava Products: A Case Study, Cameroon

Emmanuel Njumbe Ediage,*[,†] Kerstin Hell,[‡] and Sarah De Saeger[†]

[†]Laboratory of Food Analysis, Faculty of Pharmaceutical Sciences, Ghent University, Harelbekestraat 72, 9000 Gent, Belgium

[‡]International Institute of Tropical Agriculture, 08 B.P. 0932, Cotonou, Benin

ABSTRACT: A total of 420 samples were collected from agrarian households. Whereas 51% (215/420) of the samples were contaminated with one or more toxins, the contamination rates for maize, peanut, and cassava products were 74, 62, and 24%, respectively. The fumonisins (20−5412 μg/kg), aflatoxin B_1 (6−645 μg/kg), roquefortine C (1−181 μg/kg), and deoxynivalenol (27−3842 μg/kg) were the most prevalent contaminants in maize. For peanut samples, aflatoxin B_1 (6−125 μg/kg) and ochratoxin A (0.3−12 μg/kg) were the main contaminants, whereas aflatoxin B_1 (6−194 μg/kg) and penicillic acid (25−184 μg/kg) were detected in the cassava products. Exposures calculated through maize intake for fumonisin B_1 and aflatoxin B_1 were several-fold higher (2−5 for fumonisin B_1 and 10^4−10^5 for aflatoxin B_1) than the health-based guidance values of 2 μg/kg bw/day and 0.15 ng/kg bw/day, respectively. The study design constitutes a good model that can be implemented in other sub-Saharan African countries.

KEYWORDS: *aflatoxin, fumonisin, ochratoxin A, mass spectrometry, feremented cassava, Africa*

INTRODUCTION

Mycotoxins are a heterogeneous group of toxic secondary metabolites produced by toxigenic fungi that contaminate a wide range of cereals, nuts, and their derived processed products with over 400 having been characterized. The aflatoxins (for example, B_1, B_2, G_1, and G_2), ochratoxin A (OTA), fumonisins (for example, B_1, B_2, and B_3), zearalenone (ZEA), and trichothecenes (deoxynivalenol, T2 toxin, HT2 toxin, and nivalenol) are considered to be significant.[1] This is due to their relatively acute and chronic effects observed in experimental animal studies and their frequent occurrence in food and feed worldwide.[2]

Formation of mycotoxins begins at preharvest plants and continues through postharvest in stored and processed products. Their occurrence in agricultural products and also in processed products significantly affects economies of developing countries and poses a serious risk for animal and human health. Preharvest and postharvest management strategies have therefore been recommended not only to reduce mycotoxin levels but also to control mycotoxin-related risks. Monitoring or surveillance of mycotoxin levels in crops and derived products is an important management tactic that is implemented along the food chain from farm to consumer.

Since the year 2000, mycotoxin monitoring programs have been carried out in several West African countries such as Benin Republic and Togo.[3,4] No surveys were done in Cameroon until 1994, when the fungal diversity in different maize species was characterized for the first time.[5−7] The presence of leaf, stem, and ear diseases in maize production areas in Cameroon was also reported.[8,6] The first data on multimycotoxin occurrence in dietary staples was reported in 2001.[6] Trace levels of aflatoxin B_1 (AFB_1) were detected in a few samples, whereas quantifiable levels of deoxynivalenol (DON; <100−1300 μg/kg), fumonisin B_1 (FB_1; 300−26000 μg/kg), and ZEA (50−110 μg/kg) were reported in maize.[6] Since 2007 there have been increasing numbers of reports on the occurrence of mycotoxins in dietary staples and their derived products from Cameroon.[9−12] Despite this upsurge in contamination data, the principal agricultural products (other than maize) such as cassava and peanuts have not yet been comprehensively investigated.

Cassava (*Manihot esculenta*) and cassava products constitute one of the main dietary staples consumed throughout West Africa, especially in Cameroon.[13] It accounts for 13% of the total energy intake of the Cameroonian population.[14] Despite its high consumption, very little is known about its mycotoxin profile. Recently, a large number of fungi (*Aspergillus* spp.) were isolated from stored cassava products, which raised serious concerns on the potential of this commodity as a natural substrate liable to mycotoxin contamination.[9] With respect to agricultural practices, cassava is often cultivated in a mixed-cropping system, which is a common practice among subsistence farmers in Cameroon. It is well documented that such practices increase the potential of mycological cross contamination.[9,15]

Cameroon is known as the bread basket of West and Central Africa with tens of thousands of tons of unprocessed agricultural food crops being exported daily to adjoining African and European countries. Traders often infiltrate the villages to purchase their desired products at low bargained prices. During trading, good-quality products are purchased for

Received: January 9, 2014
Revised: May 4, 2014
Accepted: May 5, 2014
Published: May 5, 2014

ACS Publications © 2014 American Chemical Society

dx.doi.org/10.1021/jf501710u | J. Agric. Food Chem. 2014, 62, 4789−4797

export while the poor-quality products are rejected and left behind for household consumption by the local farmers. The poor-quality products could consist of insect-infected and/or fungi-infested grains with possibly very high mycotoxin contamination. For the export products, usually minimal or no quality control is carried out at the points of entry of the importing African countries.

Although the European Union through the European Food Safety Authority (EFSA) and other advisory and legislative bodies have established maximum levels for certain mycotoxins in some foodstuffs,[16,17] these legislations are nonbinding in countries outside the European Union. On the African continent, by the year 2003, only 15 of the 54 African countries were known to have specific mycotoxin regulations,[18] mostly for controlling aflatoxin contamination. Meanwhile, for the majority of African countries, no specific mycotoxin regulations exist, including Cameroon. The absence of elaborate surveys and reports on economic consequences (losses) resulting from rejection of poor-quality products at the international market has hindered the establishment of mycotoxin legislations in most African countries.

All surveys on mycotoxin contamination carried out in Cameroon over the past decade so far have been based on random sampling of food commodities from street vendors.[10−12] Only one study[5] assessed the occurrence of mycotoxins (aflatoxins, DON, and ZEA) in 72 maize samples from farmers in three villages. An additional drawback was that this was not a household survey. Household surveys reflect direct exposure of individuals at the household level, but surveys of street vendors do not. In remote villages, the raw food used to prepare a family meal is usually cultivated at the household level in small plots, and for this, exposure is envisaged to be constant throughout the year with the exception of some perishable seasonal crops. The bottleneck with household surveys in developing countries is the difficulty in gaining access for sampling to these the remote villages, which are often the most affected with the mycotoxin problem, due to very poor nonexisting infrastructure. Studies were therefore limited to urban and/or semiurban areas.

This study was aimed to go beyond the boundaries of previous studies by providing a comprehensive insight into the differences in mycotoxin patterns from three agro-ecological regions in Cameroon using maize, peanut, and cassava products as model food staples. Sampling in very remote areas with a potentially higher risk of the mycotoxin problem tends to give more added value to the proposed study. Furthermore, this is so far the only report on the occurrence of mycotoxins in cassava and its products from Cameroon.

MATERIALS AND METHODS

Sampling. Cameroon has five agro-ecological zones, from which three were selected for this study: the western highland (WH), the humid forest with monomodal rainfall (HFM), and the humid forest with bimodal rainfall (HFB). The climatic conditions of the three regions sampled have been described by IRA-NCRE.[19] Figure 1 shows the map of Cameroon with the five agro-ecological zones.

The WH is characterized by an annual rainfall from 1300 to >3000 mm/year depending on the topography of the land with atmospheric temperature varying from <15 to 27 °C. In the HFM, the annual rainfall is about 10000 mm/year in Debuncha, which is the fourth wettest locality in the world, with an atmospheric temperature varying from 20 to 28 °C. Rainfall in the HFB ranges between 2000 and 4000 mm/year, and mean atmospheric temperature is 23 °C. The climate of this zone comprises four seasons (unlike the two other zones, which have just two seasons), a long dry season from December to May, a short wet season from May to June, a short dry season from July to October, and a long and heavy wet season from October to November.[19]

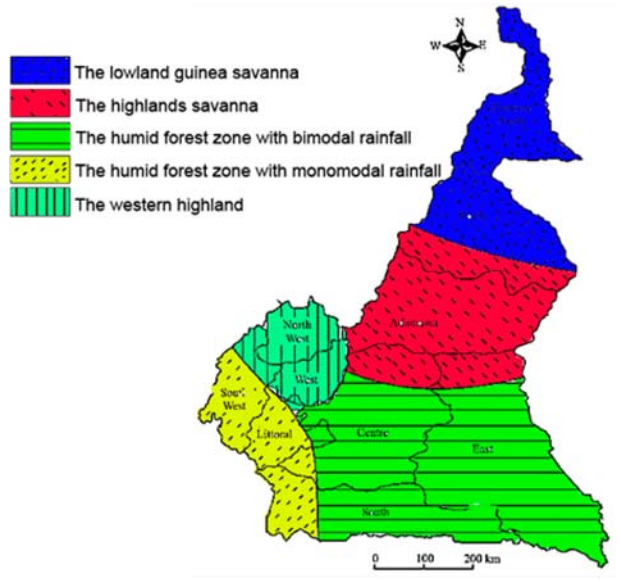

Figure 1. Map of Cameroon, showing the different agro-ecological regions.

The selection of these three zones was based on their agricultural contributions to the national food supply, which have always been greater than those of the two other nonselected regions. From these agro-ecological zones, a total of 10 villages were selected with 3 villages from each of the zones with the exception of the HFB zone, from which four villages were selected. A total of 165 maize grain (*Zea mays*), 90 peanut (*Arachis hypogaea*), and 165 cassava (*Manihot esculenta*; flakes (fermented cassava) and/or chips (nonfermented cassava)) samples intended for human consumption were collected from randomly selected households during two separate sampling sessions; July−August 2009 (rainy season) and December 2010−January 2011 (dry season). Sampling was performed by experienced and well-trained field facilitators. The villages included Malende, Kossala, and Ikiliwindi for the HFM; Bambui, Mbengwi, and Dschang for the WH; and Ndokayoka, Nkolbikong, Ngonai, and Nkolo for the HFB.

Sampling of maize and peanuts was carried out on the basis of the official guidelines described in Commission Regulation EC 401/2006[20] with some modifications. Briefly, the whole content of a traditional bag of stored maize and peanuts was considered as a lot. An aggregate sample size of 0.5 kg was composed of five incremental samples. Each incremental portion was about 100 g, and one incremental portion was taken for every 25 kg of product. In cases when the weight of the traditional bag exceeded 25 kg, the bag was subdivided into portions of 25 kg, and each section was sampled. Subsamples were taken at different depths or positions and then mixed together in a plastic container, and the 0.5 kg final sample was taken. During the first sampling session, peanuts were not collected due to time constraints. Maize and peanut samples were carefully labeled and sealed in paper bags. All samples were stored at −18 °C prior to their transportation to the Laboratory of Food Analysis, Ghent University, Belgium, by air shipment. Table 1 shows the distribution of collected samples across the three agro-ecological regions during the two sampling periods. Prior to analysis, 250 g of maize and peanut samples (unshelled) were milled to a sieve size of 0.5−1 mm using an IKA M20 universal mill (Sigma-Aldrich, Bornem, Belgium), from which a representative portion (250 g) was taken for analysis.

Materials and Reagents. Ammonium acetate was supplied by Grauwmeer (Leuven, Belgium). Acetic acid was purchased from Merck (Darmstadt, Germany). Dichloromethane, *N*,*N*-dimethylforma-

Table 1. Distribution of Samples Collected from Individual Households across the Different Agro-ecological Zones

	no. of samples						
	sampling period 1: July–August 2009			sampling period 2: December 2010–January 2011			
product	HFM[a]	HFB[a]	WH[a]	HFM	HFB	WH	total no. of samples collected
maize	26	23	26	30	30	30	165
peanut	–[a]	–	–	30	30	30	90
cassava flakes	20	15	18	20	22	21	115
cassava chips	6	8	8	10	8	9	50
subtotal	52	46	52	90	90	90	420

[a]HFM, humid forest with monomodal rainfall; HFB, humid forest with bimodal rainfall; WH, western highland; –, no samples were collected.

mide, and ethyl acetate were supplied by Acros Organics (Geel, Belgium). Methanol and *n*-hexane, both of HPLC grade, as well as Whatman glass microfiber filters (GFA, 125 mm) were purchased from VWR International (Zaventem, Belgium). Ultrafree centrifugal filter devices (0.22 μm) from Millipore (Billerica, MA, USA) were used. Bakerbond aminopropyl (NH_2) solid phase extraction (SPE) cartridges were obtained from Grace Discovery Sciences (Lokeren, Belgium). Water was purified on a Milli-Q Plus apparatus (Millipore, Brussels, Belgium).

Analytical standards, namely, 3-acetyldeoxynivalenol (3-AcDON), 15-acetyldeoxynivalenol (15-AcDON), alternariol (AOH), alternariol methyl ether (AME), altenuene (ALT), aflatoxin B_1 (AFB_1), aflatoxin B_2 (AFB_2), aflatoxin G_1 (AFG_1), aflatoxin G_2 (AFG_2), beauvericin (BEA), deoxynivalenol (DON), deepoxy-deoxynivalenol (DOM), fumonisin B_1 (FB_1), fumonisin B_2 (FB_2), fusarenone-X (FUS-X), nivalenol (NIV), HT2 toxin (HT2), neosolaniol (NEO), ochratoxin A (OTA), sterigmatocystin (STE), zearalenone (ZEA), and zearalanone (ZAN) were purchased from Sigma-Aldrich (Bornem, Belgium). Diacetoxyscirpenol (DAS) and T2 toxin (T2) were purchased from Biopure (Tulln, Austria). Fumonisin B_3 (FB_3) was obtained from Promec Unit (Tygerberg, South Africa). Penicillic acid (PA) was purchased from Fermentek (Jerusalem, Israel), whereas roquefortine C (ROQC) was obtained from Enzo Life Science (Lorrach, Germany). FB_2 and FB_3 standards (1 mg) were prepared in 1 mL of acetonitrile/water (50:50, v/v). Stock solutions of 3-AcDON, 15-AcDON, ALT, AFB_1, AFB_2, AFG_1, AFG_2, BEA, DON, DOM, FB_1, FUS-X, HT2, OTA, PA, ROQC, STE, T2, ZAN, and ZEA were prepared in methanol at a concentration of 1 mg/mL. AOH and AME stock solutions (1 mg/mL) were prepared in methanol/dimethylformamide (60:40, v/v). NIV, NEO, DOM, and DAS were obtained as solutions (100 μg/mL) in acetonitrile. All stock solutions were stored at −18 °C except FB_2 and FB_3, which were stored at 4 °C. New stock solutions were prepared every 6 months. From the individual stock standard solutions, a standard mixture was prepared at the following concentrations: AME, 20 ng/μL; AOH, FUS-X, HT2, NIV, and NEO, 10 ng/μL; ALT, 5 ng/μL; 15-AcDON, 2.5 ng/μL; AFB_2, 3-AcDON, DON, and ZEA, 2 ng/μL; T2, 1 ng/μL; DAS and STE, 0.5 ng/μL; FB_1, FB_2, and FB_3, 0.5 ng/μL; ROQC, AFB_1, AFB_2, AFG_1, and AFG_2, 0.2 ng/μL; BEA, 0.1 ng/μL; PA and OTA, 0.05 ng/μL. The standard mixtures were stored at −18 °C and renewed every 3 months.

Sample Preparation. The protocol used for sample preparation has been described.[21] One gram of homogenized sample was spiked with internal standards ZAN and DOM at 20 and 300 μg/kg, respectively. The fortified sample was kept in the dark for 15 min. DOM was used as internal standard (IS) for DON, 3-AcDON, and 15-AcDON, whereas ZAN was used for the other toxins. Both internal standards were used to correct for small volume changes during sample preparation.

All samples were extracted with 15 mL of extraction solvent methanol/ethyl acetate/water (70:20:10, v/v/v) for 30 min using an end-over-end shaker and centrifuged for 15 min at 3170*g*. The supernatant was transferred into a new extraction tube and evaporated at 40 °C. The residue was reconstituted in 5 mL of methanol/water (85:15, v/v) to which 10 mL of dichloromethane/hexane (30:70, v/v) solution was added. The mixture was shaken for 10 min and centrifuged at 3200*g* for 10 min. The dichloromethane/hexane phase was discarded, whereas the methanol/water phase was kept for further cleanup. The defatted extract (5 mL) was split into two parts of 2.5 mL each, for sample enrichment (cleanup). One part (of the split extract) was cleaned by passing it through a glass fiber filter, whereas the second part was cleaned up using amino propyl (NH_2) cartridges. After the equilibration step with 6 mL of methanol/water (85:15, v/v), the sample extract was loaded onto the SPE cartridge and the eluate collected in a test tube. Both parts (the NH_2 SPE and the glass fiber) of the cleaned extracts were recombined and evaporated at 40 °C. The residue was redissolved in 300 μL of mobile phase consisting of methanol/water/acetic acid (57.2:41.8:1, v/v/v) and 5 mM ammonium acetate. Ultrafree MC centrifugal devices were used to further filter the resulting solution prior to injection into the LC-MS/MS system; this was performed for 15 min at 10000*g*.

LC-MS/MS Method. Both the chromatographic and mass spectrometric conditions and settings were described previously.[21] Briefly, a Symmetry RP-C18 column of 150 mm × 2.1 mm, 5 μm, and a 10 mm × 2.1 mm Sentry guard column of the same material (Waters, Zellik, Belgium) were used for the chromatographic separation. The mobile phase constituted two solvent mixtures both containing 5 mM ammonium acetate. Solvent A was composed of water/methanol/acetic acid (94:5:1, v/v/v), whereas methanol/water/acetic acid (97:2:1, v/v/v) was used as solvent B. The solvent flow rate of 0.3 mL/min was adopted for a total gradient run time of 28 min. A 20 μL injection volume was applied.

Detection and quantitation were performed with a Waters Acquity UPLC apparatus coupled to a Micromass Quattro Micro triple-quadrupole mass spectrometer (Waters, Milford, MA, USA). The mass spectrometry analyses were carried out using selected reaction monitoring (SRM) channels in positive electrospray ionization (ESI +) mode. The following were the instrumental settings: source and desolvation temperatures, 130 and 350 °C, respectively; capillary voltage, 3.2 kV; cone nitrogen and desolvation gas flows, 200 and 800 L/h, respectively.

Commission Decision 2002/657/EC[22] and Commission Regulation 401/2006/EC[20] were used as guidelines for the validation of the analytical method. The performance characteristics of the method were in good agreement with both guidelines as earlier described.[21] Table 2 shows the limit of detection (LOD) and limit of quantitation (LOQ) of the target analytes.

Food Frequency Questionnaire (FFQ). A FFQ was administered by trained interviewers. The FFQ was developed on the basis of the consumption habits regarding the target food matrices. In addition to the target food matrices, other food items such as rice, yams, and plantain were also included to cover as many traditional foods as possible. Consumption frequency was measured by a range starting from less than once a month to three times a day. Portion sizes were chosen for each food item according to usual measures: cups for rice and peanuts, slices for yams, and weights for cereal grains and cassava products (pictures depicting the different portion sizes were presented during the interview). The FFQ was applied to 30 randomly selected households living in each village. A total of 300 households (520 individuals) from the 10 villages investigated were collected. The 300 households were evenly distributed throughout the two sampling seasons. Each participating household was expected to provide at least one of the three dietary staples. The body weight of a child and that of an adult (from the same household) were recorded together with the food intake and were used for risk assessment using the deterministic approach.

Table 2. Limit of Detection (LOD) and Limit of Quantitation (LOQ) of the Target Analytes

	LOD (μg/kg)			LOQ (μg/kg)		
analyte	maize	cassava	peanut	maize	cassava	peanut
NIV	35	31	25	106	93	76
DON	9	15	12	27	46	37
PA	8	8	8	25	25	24
NEO	5	8	21	16	15	64
FUS-X	14	5	23	43	15	70
ΣAcDON	10	10	9	30	30	27
AFG_2	1	2	0.3	4	6	1
AFG_1	2	1	1	5	2	3
AFB_2	0.5	1	1	2	3	4
ALT	1	1	1	3	2	2
AFB_1	2	0.3	2	6	0.8	6
DAS	1	0.4	0.1	2	1	0.4
ALT	3	3	2	10	8	5
HT-2	13	9	11	39	28	34
FB_1	6	6	5	20	20	15
T2	0.4	0.1	0.3	1	0.4	1
FB_3	15	15	15	45	45	45
OTA	0.1	0.3	0.1	0.3	0.8	0.3
FB_2	15	15	15	45	45	45
AME	2	1	1	6	4	4
BEA	5	3	0.2	15	10	1
STE	2	3	1	5	9	2
ROQC	0.3	0.1	0.2	1	0.3	1
ZEA	9	6	10	27	20	30

Statistical Analysis. The SPSS software version 20.0 (SPSS Inc., Chicago, IL, USA) program was used for statistical analysis. For exposure assessment, the mean of the entire sample population was used for the calculations with samples <LOD given a value of LOD/2. A nonparametric Mann–Whitney test for two independent samples and a Kruskal–Wallis test for k independent samples were used to evaluate possible differences in the mean (mean rank) mycotoxin levels across the different agro-ecological zones and sampling sessions, after evaluation of the homogeneity of variances with Levene's test. In addition, a contingency test was used to evaluate the possible differences between the incidences of each mycotoxin within the different sample categories. The mean values were calculated for the different sample categories, taking into consideration the negative samples. A p value of 0.05 was used to determine the statistical significance.

RESULTS AND DISCUSSION

General Mycotoxin Contamination Pattern. Of all food samples, 51% (215/420) were found to be contaminated with at least one of the 25 mycotoxins. The contamination rates for each sample matrix were as follows: 74, 62, and 24% for maize, peanut, and cassava products, respectively (Table 3).

Occurrence of Mycotoxins in Maize Samples. DON and its acetylated derivatives (sum of 3-AcDON and 15-AcDON (∑AcDON)), ZEA, ROQC, BEA, aflatoxins (AFB_1 and AFB_2), and fumonisins (FB_1, FB_2, and FB_3)) were detected in the maize samples. The fumonisins (sum of FB_1, FB_2, and FB_3) had the highest occurrence rate (74%, 122/165) in maize samples (Table 3) with the concentration FB_1 in all positive samples being greater than those of FB_2 and FB_3. The highest concentrations of FB_1, FB_2, and FB_3 detected were 5412, 2890, and 2180 μg/kg, respectively (Table 4), which were higher than the levels recently reported (2313 μg/kg) from the same country.[12]

Table 3. Occurrence of Mycotoxins in Different Sample Matrices[a]

sample matrix/mycotoxin[b]	no. of positive samples[c]	% positive samples
maize		
$FB_1 + FB_2 + FB_3$	122/165	74
AFB_1	37/165	22
ROQC	32/165	19
AFB_2	30/165	18
ZEA	23/165	14
DON	20/165	12
∑AcDON	17/165	10
BEA	16/165	10
peanut		
AFB_1	26/90	29
OTA	12/90	13
cassava		
AFB_1	42/165	25
PA	10/165	6

[a]Data summarized from the two sampling periods. [b]DON, deoxynivalenol; PA, penicillic acid; 3-AcDON, 3-acetyldeoxynivalenol; 15-AcDON acetyldeoxynivalenol; AFB_2, aflatoxin B_2; AFB_1, aflatoxin B_1; FB_1, fumonisin B_1; FB_3, fumonisin B_3; OTA, ochratoxin A; FB_2, fumonisin B_2; BEA, beauvericin; ROQC, roquefortine C; ZEA, zearalenone; ΣAcDON, sum of 3-AcDON and 15-AcDON. [c]Ratio of positive samples to the total number of samples analyzed for that particular matrix.

For every DON positive sample, co-occurrence of 3-AcDON and/or 15-AcDON was also detected except in five samples for which the levels of ∑AcDON were below the method LOQ (16 μg/kg). The presence of DON (20/165; 27–3842 μg/kg) and its metabolites (∑AcDON (17/165)) in maize has often been associated with samples originating from temperate regions such as northern Europe and North America.[23] However, reports emerging from tropical countries, especially from sub-Saharan Africa, continue to reveal the occurrence of DON in maize and maize products.[24] Furthermore, the detection of DON in the urine of toddlers (1.5–5 years) from Cameroon[13] also affirms its presence in food commodities originating from sub-Saharan Africa. The maximum level for DON in unprocessed maize was set by Commission Regulation 1881/2006[16] at 1750 μg/kg. Despite its relatively low occurrence rate (12%), eight samples were contaminated above the maximum level set by the European Commission.[20]

AFB_1 and AFB_2 were detected in maize samples at rates of 22 and 18%, respectively, and mean levels and the range detected for AFB_1 and AFB_2 are presented in Table 4. Between the different years of sampling, there were no statistically significant differences in the mean concentrations; 111 and 127 μg/kg for AFB_1 and 23 and 18 μg/kg for AFB_2 in sampling periods 1 and 2, respectively. A total of 35% (13/37) and 24% (9/37) of the aflatoxin positive samples obtained in sampling periods 1 and 2, respectively, exceeded the maximum level of 10 μg/kg of total aflatoxins in maize as specified in Commission Regulation 1881/2006.[16]

Members of the *Penicillium* spp. are well-known colonizers of maize silages, leading to the production of ROQC. Recently, ROQC production in maize fields prior to harvesting was demonstrated, contradicting the belief that *Penicillium* toxin formation occurs exclusively during storage.[25] This might possibly explain the occurrence of ROQC in maize samples originating from Cameroon. Its presence in 19% (32/165; 1–

Table 4. Mycotoxin Pattern in Cameroon from Three Agro-ecological Regions through Maize, Peanut, and Cassava Products

	mean concentration (CI, 95%) range (μg/kg) of mycotoxins detected in the different staples[a]							
	sampling period 1: 2009				sampling period 2: 2010−2011			
sample matrix/ mycotoxin[b]	HFM	HFB	WH	mean	HFM	HFB	WH	mean
maize								
DON	207 (27−2141)	60 (212−918)	275(27−2741)	181	612(27−2411)	161(27−1084)	452 (218−3842)	408
FB_1	1418 (75−3716)	468 (20−1418)	2102 (112−5412)	1329	2601 (20−4030)	665 (314−2841)	2949 (20−3212)	2072
FB_2	1157 (112−2268)	370 (50−843)	965 (75−2882)	831	2555 (10−2890)	663 (50−915)	1742 (112−1846)	1653
FB_3	398 (50−1442)	156 (75−482)	357 (65−412)	303	993 (112−2180)	604 (132−864)	376 (50−698)	657
AFB_1	22 (6−184)	59 (6−345)	26 (6−195)	35	100 (6−645)	96 (6−216)	47 (6−210)	81
AFB_2	7 (2−108)	8 (2−215)	6 (2−85)	7	23 (2−225)	14 (2−120)	29 (2−75)	22
ZEA	61 (75−279)	58 (27−228)	65 (85−262)	61	113 (35−334)	111 (27−242)	86 (55−286)	103
∑AcDON	44 (65−231)	36 (30−187)	47 (54−170)	42	71 (30−115)	62 (30−176)	46 (30−186)	60
ROQC	20 (1−94)	15 (1−137)	25 (1−145)	20	48 (1−84)	44 (1−118)	55 (1−181)	49
BEA	39 (15−412)	33 (15−384)	35 (15−264)	35	69 (15−312)	66 (15−284)	51 (15−385)	62
peanut								
OTA	ns	ns	ns	ns	5 (0.3−12)	3 (0.3−10)	4 (0.3−4)	4
AFB_1	ns	ns	ns	ns	26 (6−125)	22 (6−77)	22 (6−110)	23
cassava								
AFB_1	12 (6−194)	2 (6−95)	5 (6−193)	6	10 (6−125)	1 (6−32)	10 (6−141)	7
PA	7 (25−184)	3 (25−96)	3 (25−72)	4	4 (25−76)	2 (25−46)	4 (25−44)	4

[a]Samples < LOD were given the LOD/2 value. CI, confidence interval; HFM, humid forest region with monomodal rainfall; HFB, humid forest region with bimodal rainfall; WH, western highland; ns, no samples. [b]DON, deoxynivalenol; PA, penicillic acid; 3-AcDON, 3-acetyldeoxynivalenol; 15-AcDON, 15-acetyldeoxynivalenol; AFB_2, aflatoxin B_2; AFB_1, aflatoxin B_1; FB_1, fumonisin B_1.

181 μg/kg) (Tables 3 and 4) of the maize samples should not be underestimated.

BEA was detected in 16/165 (10%) of the maize samples at levels of 15−412 μg/kg. BEA, a cyclic hexadepsipeptide, is produced by various *Fusarium* spp. such as *Fusarium avenaceum*, *Fusarium lateritium*, *Fusarium scirpi*, and *Fusarium oxysporum* and structurally relates to the enniatins.[26−28] Three percent of maize samples originating from southern Nigeria were found to be contaminated with the enniatins.[29] In this study, the majority of the BEA positive samples were detected in the HFM. Considering the close geographical location of both southern Nigeria and the HFM of Cameroon (latitude 0−10° N) the presence of BEA in maize samples from Cameroon further strengthens earlier reports that BEA and enniatins are natural contaminants in maize samples originating from sub-Saharan Africa. Recently, a 93% occurrence rate of these mycotoxins was found in maize beer from Cameroon.[12] With very little or no information on its potential toxic effects in humans and no legislation with regard to its maximum level, the potential health risk associated with its exposure cannot be estimated.

The occurrence of ZEA in agricultural commodities has not been rigorously investigated in sub-Saharan Africa. It was first reported in South African maize and subsequently recovered in maize and other commodities elsewhere on the continent.[30] The maize samples analyzed in this study showed a 14% (23/165) occurrence rate for ZEA, with none of the samples exceeding the maximum level of 350 μg/kg for unprocessed maize products.[20] The detected concentration range was 27−334 μg/kg (Table 4). Compared to other reports on the occurrence of ZEA in maize samples from sub-Saharan Africa, the levels detected in this study were lower than levels previously reported[29] in maize samples from Nigeria (up to 779 μg/kg). ZEA was also reported in maize samples from Cameroon with a mean of 68 μg/kg and a maximum concentration of 309 μg/kg.[12]

Occurrence of Mycotoxins in Peanut Samples. AFB_1 and OTA were the main contaminants in peanut samples. The occurrence rate and levels of AFB_1 (26/90, 6−125 μg/kg) were considerably higher than those of OTA (12/90, 0.3−12 μg/kg) (Tables 3 and 4). From this study, the concentrations of aflatoxins detected in peanut samples can be said to be comparatively low when compared with data from other sub-Saharan African countries. Similar results have been reported in Kenya, where 96% of raw podded peanuts had levels <4 μg/kg and only 4% had levels >10 μg/kg.[31] Meanwhile, in Botswana, concentrations of 12−329 mg/kg in raw peanuts were reported.[32]

The European Commission has fixed stringent maximum levels for total aflatoxins and AFB_1 in peanuts intended for direct human consumption at 2 and 4 μg/kg, respectively, which has led to a serious impact (export products have plummeted) on the economy of several African countries.[33] The Codex Alimentarius Commission also adopted the limit for total aflatoxins at 15 μg/kg in peanuts;[34] nevertheless, the WHO prescribed the maximum level of 5 μg/kg for AFB_1 in various foodstuffs.[35] The levels of AFB_1 in 13 of the 26 AFB_1-positive samples exceeded the maximum level as specified in Commission Regulation No. 1881/2006[16] with 8 samples exceeding 100 μg/kg.

Occurrence of Mycotoxins in Cassava Products. Fermented cassava (flakes) had a higher contamination rate (32%) than cassava chips (nonfermented products) (15%). For cassava flakes, AFB_1 and PA were detected at concentrations that ranged between 6 and 194 μg/kg and between 25 and 184 μg/kg, respectively (Table 4), whereas for the nonfermented cassava products, AFB_1 was the sole contaminant with levels of 6−95 μg/kg. PA was not detected in any of the nonfermented products, suggesting that cassava flakes constitute a suitable substrate for growth of *Penicillium* spp. and hence mycotoxin production. Significant levels of other acidic mycotoxins such as tenuazonic acid, cyclopiazonic acid, and patulin have also been

reported[36] in dried cassava products originating from Ghana. The levels of PA reported herein (25−184 μg/kg) were lower than levels (60−230 μg/kg) previously reported[36] from Ghana.

The occurrence of aflatoxins in cassava products is still a topic of debate. Studies conducted in Tanzania,[37] Nigeria,[38] and Benin[39,40] reported no aflatoxins in market cassava products. In contrast, a recent survey conducted in Tanzania and the Republic of Congo showed the occurrence of AFB_1 in market cassava samples.[41] Furthermore, studies with dried cassava products (Kokonte) from markets in Ghana[36] showed the presence of STE, a precursor of AFB_1. This necessitates further research be carried out in other African countries on cassava products to fully comprehend the aflatoxin problem in cassava products. Cassava fermentation is thought to lower the microbial load and hence mycotoxin contamination. However, if appropriate storage systems are not implemented, this might lead to fungal growth and possibly mycotoxin contamination.[42]

Given that only 3/65 nonfermented cassava samples had AFB_1 above 10 μg/kg, it can be said that consumption of nonfermented cassava products might not pose a serious risk to the populations concerned, compared with maize and peanut. However, continuous monitoring and surveys are needed to mitigate any future disease outbreaks and adverse health effects. At this moment, there are no existing regulations on mycotoxins in cassava products.

Differences in the Mycotoxin Pattern across the Different Agro-ecological Zones and Sampling Years. The mean (geometric mean) and concentration range of each of the detected toxins for a given sample matrix and agro-ecological zone are given in Table 4. To understand the distribution of mycotoxins across the different agro-ecological zones, a pairwise comparison of the mean mycotoxin concentration from a given agro-ecological zone and sample matrix was compared with the levels detected across the other two agro-ecological zones. Differences between the two different sampling years were also evaluated.

Maize Samples. Irrespective of the year of sampling, the mean FB_1 levels in samples from the HFM and WH regions were significantly higher (p = 0.01 for HFM and 0.032 for WH) than the mean levels detected in samples from the HFB (Table 4). The same trend was also observed when the sum of the fumonisins was considered. Although differences in climatic conditions across the different agro-ecological regions can explain the observed distribution of fumonisins, other determinants such as differences in preferred storage conditions across the different regions cannot be ruled out. The HFB is a transition zone from rain forest to savanna, which is characterized by four seasons, unlike the two other agro-ecological regions. Taking into consideration the prevailing weather conditions and agricultural practices in the HFB region, one would anticipate a high rate of mycotoxin occurrence as this region is characterized by two periods of seasonal rainfall during which harvesting is carried out under intense rainy conditions. Furthermore, data extracted from prevalidated questionnaires revealed that 84% of the households harvested the matured cobs while still fresh, with the remaining 16% of the cobs left in the farms to dry before being harvested. A combination of the prevailing weather conditions (four seasons), agricultural practices such as harvesting under intense rainy conditions, and allowing the cobs to dry in the field could have favored potential mold growth, but it was not the case in this study. Samples from this region showed lower levels of FB_1 contamination than samples from the two other regions.

With regard to the different years of sampling, significant differences were observed in the mean fumonisin levels (sum of FB_1 + FB_2 + FB_3) between the first and second years of sampling (p = 0.02), with significantly higher levels in the second year than in the first year of sampling. This can be explained by the long and heavy seasonal rains, which occurred from February to September 2010, whereas in 2009 the duration of seasonal rains was considered to be moderate for that time of the year.[43] Similarly, the mean levels of DON and ∑AcDON were significantly higher (p = 0.001 for DON and 0.01 for ∑AcDON) in the second year than in samples obtained during the first year of sampling. Just like the fumonisins, heavy rains, insufficient drying conditions to reach the safe water content levels, and poor storage conditions could be the contributing factors that accounted for these differences in contamination between the two sampling periods. Because *Fusarium* spp. are primarily field mycotoxin producers, mycotoxin production could have occurred in the field.

With regard to aflatoxin contamination in maize samples, the mean concentration of aflatoxins in samples from the HFB was significantly higher (p > 0.05) than those detected in samples collected from the two other regions (Table 4). This trend was not observed for samples obtained during the second sampling year.

No significant differences were observed in the mean levels of ROQC, ZEA, and BEA between the different sampling years (p > 0.05). With respect to the agro-ecological zones, a trend was observed; the mean levels of ROQC in samples from the WH region were significantly higher than those obtained from HFM and HFB. For ZEA and BEA, no significant differences were found across the different agro-ecological zones (Table 4).

Mycotoxins in Peanut and Cassava Products. The mean AFB_1 levels detected in peanut samples from the HFM were significantly higher than those detected in samples from the HFB (p = 0.012), but no significant differences (p > 0.05) were observed when levels of the toxins detected in peanut samples from the WH and the HFM were compared (Table 4). Likewise, no significant differences were observed in the mean OTA levels in peanut (p > 0.05) across the different agro-ecological zones.

Given that cassava is a root crop, the levels of mycotoxins in cassava are less known to be associated with seasonal and climatic conditions. Hence, contamination could occur only during and/or after processing.

Significant differences in the mean AFB_1 levels were observed across the different agro-ecological zones. Fermented cassava products (flakes) are mostly consumed in the WH and HFM regions, whereas cassava chips are predominantly eaten in the HFB. Irrespective of the sampling year, the mean AFB_1 levels in the fermented cassava products from the WH and HFM regions were significantly higher (p = 0.021 and 0.015, respectively) than those detected in nonfermented samples. This observation suggests that fermentation increases the microbial load, which might have led to AFB_1 production. Similar observations highlighted the fact that the distribution of aflatoxin in positive samples depended on parameters such as pH, moisture content, storage duration, type of chips (fermented cassava), size of chips, level of contamination by aflatoxin-producing fungi, processing practices, and storage facilities.[9] No significant differences (p > 0.05) were found in the mean AFB_1 levels in cassava samples (both cassava chips

and flakes) originating from both the WH and tHFM regions. As previously mentioned, PA was not detected in the nonfermented cassava products.

Consumer Risk Assessment. Exposure to mycotoxins of the different subpopulations was estimated by considering the consumption data obtained from the FFQ and the mean concentrations of mycotoxin (including samples with concentrations <LOD) for the different agro-ecological zones (deterministic approach). Data were computed for infants as well as for adults. The calculated exposure was compared with health-based guidance values (tolerable daily intake (TDI))[44−49] and also expressed as percentage of the analyte-specific TDI exceeded (%TDI calculated as ((calculated exposure/TDI) × 100)). %TDI < 100 implies the TDI for the specific mycotoxin was not exceeded.

Because AFB_1 is a genotoxic carcinogen, there is no set TDI. However, a provisional range of 0.11−0.19 ng/kg bw/day was proposed[49] for the African and Asian populations that might also be predisposed to hepatitis B virus (HBV). For the purpose of this study and for comparing the risk of the different populations, a mean value of 0.15 ng/kg bw/day was used.

Portion sizes of 0.03 and 0.2 kg per day were considered average for an infant and adult, respectively (average intake from the FFQ). Median weights of 60 and 15.2 kg were also assumed to be representative for an adult and infant (<2 years), respectively.

The calculated average exposure for all of the mycotoxins for households in the HFM and WH were in general higher than the average exposure for households in the HFB except for the aflatoxins (Tables 5 and 6). For the aflatoxins, exposure was in the order HFB > WH > HFM and HFM > HFB > WH for years 1 and 2, respectively, for both adults and infants. With regard to maize intake, the calculated exposure for FB_1 calculated for both adults and infants in both the HFM and WH regions exceeded the TDI (Tables 5 and 6). In general, exposure was higher in adults than in infants despite the higher body weight of the adults. Likewise, the TDI for AFB_1 was exceeded in the range of 10^4−10^5% TDI (Tables 5 and 6) irrespective of the agro-ecological region and growth category (infant or adult). The TDIs for ZEA, OTA, DON, and ΣAcDON were not exceeded (<100% TDI) for both the infant and adult populations for the different sampling seasons and agro-ecological regions.

With respect to peanut consumption, exposure to AFB_1 calculated for both the infant and adult populations was in the range of 2.8×10^3−5.7×10^4% TDI. On the other hand, exposure calculated for OTA was not exceeded (<100% TDI) for both the infant and adult populations (Tables 5 and 6). With respect to cassava consumption, data from Tables 5 and 6 reveal that the TDI for AFB_1 was exceeded (1.3×10^3−1.3×10^4% TDI) by both the infant and the adult populations in all three agro-ecological regions and during the different sampling seasons. The potential consequences that might arise following chronic exposure to these mycotoxins should not be underestimated.

A putative mycotoxin contamination pattern from three agro-ecological regions in Cameroon using maize, peanut, and cassava products as food models was established. Whereas significant differences in the mean mycotoxin levels were observed across the different agro-ecological zones, exposure was significantly higher in the HFM and WH regions and lowest in the HFB (but not for the aflatoxins), irrespective of the sampling period. Furthermore, the mean concentration of

Table 5. Risk Associated with Adults Following Consumption of Dietary Staples

		calculated exposure[a] (%TDI[b])						
		sampling period 1			sampling period 2			
matrix/mycotoxin		HFM	HFB	WH	HFM	HFB	WH	health-based guidance values; TDI[c]
maize								
	DON + ∑AcDON	0.7 (69)	0.2 (20)	0.9 (92)	2 (204)	1.81 (54)	1.5 (151)	1 μg/kg bw/day[d]
	FB_1	4.7 (236)	1.6 (78)	7 (350)	9 (434)	1.45 (112)	9.8 (491)	2 μg/kg bw/day[e]
	AFB_1	$0.07(5 \times 10^4)$	$0.2\ (1.3 \times 10^3)$	$0.1\ (6 \times 10^4)$	$0.3\ (2.2 \times 10^5)$	$0.34\ (2.1 \times 10^5)$	$0.2\ (1.0 \times 10^5)$	0.15 ng/kg bw/day[f]
	ZEA	0.2 (81)	0.2 (77)	0.2 (87)	0.4 (151)	0.58 (148)	0.3 (115)	0.25 μg/kg bw/day[g]
peanut								
	OTA	NA[i]	NA	NA	0.02 (98)	0.01 (59)	0.013 (78)	0.017 μg/kg bw/day[h]
	AFB_1	NA	NA	NA	0.1 (5.7×10^5)	0.19 (4.8×10^5)	0.07 (48×10^5)	0.15 ng/kg bw/day[f]
cassava								
	AFB_1	$0.04\ (2.6 \times 10^4)$	$0.01\ (4 \times 10^3)$	$0.02\ (1.1 \times 10^4)$	$0.03\ (2.2 \times 10^4)$	$0.002\ (2.2 \times 10^3)$	$0.04\ (2.2 \times 10^4)$	0.15 ng/kg bw/day[f]

[a]Calculated exposure expressed as μg/kg bw/day. [b]%TDI calculated as (calculated exposure/TDI) × 100. %TDI < 100 implies the TDI for the specific mycotoxin was not exceeded. HFM, humid forest with monomodal rainfall; HFB, humid forest with bimodal rainfall; WH, western highland. [c]Tolerable daily intake (TDI). [d]Based on scientific opinion released by SCF, 2002. [e]Levels based on scientific opinion released by SCF, 2000. [f]Based on Kuiper Goodman et al.[49] [g]Based on scientific opinion released by EFSA, 2011. [h]Based on toxicity levels based on scientific opinion released by EFSA, 2006. [i]NA, not applicable.

dx.doi.org/10.1021/jf501710u | J. Agric. Food Chem. 2014, 62, 4789−4797

Table 6. Risk Associated with Infants Following Consumption of Dietary Staples

	calculated exposure[a] (%TDI[b])						
	sampling period 1			sampling period 2			
matrix/mycotoxin	HFM	HFB	WH	HFM	HFB	WH	health-based guidance values; TDI[c]
maize							
DON + ∑AcDON	0.4 (237)	0.1 (46)	0.5 (309)	1.2 (120)	0.3 (32)	4.81 (89)	1 μg/kg bw/day[d]
FB_1	2.8 (145)	0.9 (54)	4 (215)	5.1 (257)	1.3 (66)	5.24 (291)	2 μg/kg bw/day[e]
AFB_1	0.04 (24)	0.1 (71)	0.05 (20)	0.2 (1.3×10^5)	0.20 (1.2×10^5)	0.17 (6.1×10^4)	0.15 ng/kg bw/day[f]
ZEA	0.1 (133)	0.1 (151)	0.13 (149)	0.2 (89)	0.2 (87)	0.53 (67)	0.25 μg/kg bw/day[g]
peanut							
OTA	NA[i]	NA	NA	0.01 (592)	0.006 (35)	0.008 (47)	0.017 μg/kg bw/day[h]
AFB_1	NA	NA	NA	0.05 (3.4×10^4)	0.043 (2.8×10^4)	0.043 (2.8×10^4)	0.15 ng/kg bw/day[f]
cassava							
AFB_1	0.02 (23)	0.002 (10)	0.01 (21)	0.02 (1.3×10^4)	0.002 (1.3×10^3)	0.02 (1.3×10^4)	0.15 ng/kg bw/day[f]

[a]Calculated exposure expressed as μg/kg bw/day. [b]%TDI, calculated as (calculated exposure/TDI) × 100. %TDI < 100 implies the TDI for the specific mycotoxin was not exceeded. HFM, humid forest with monomodal rainfall; HFB, humid forest with bimodal rainfall; WH, western highland. [c]Tolerable daily intake (TDI). [d]Based on scientific opinion released by SCF, 2002. [e]Levels based on scientific opinion released by SCF, 2000. [f]Based on Kuiper Goodman et al.[49] [g]Based on scientific opinion released by EFSA, 2011. [h]Based on toxicity levels based on scientific opinion released by EFSA, 2006. [i]NA, not applicable.

the mycotoxins detected in maize samples obtained from the second year (2010−2011) of sampling was significantly higher than those of the first year (2009) of sampling, which suggests a possible influence of preharvest (e.g., climatic changes) and/or postharvest (e.g., storage practices) practices on mycotoxin contamination from year to year. To summarise, a total of 51% of the samples were contaminated with one or more mycotoxins. The rates of contamination were 74, 62, and 24% for maize, peanut, and cassava products, respectively. Hence, mycotoxin contamination constitutes a major problem in agricultural staples from Cameroon. The relative abundance of the mycotoxins was as follows: FB1 > FB2 > FB3 > AFB1 > AFB2 > ROQC > ZEA > OTA > DON > ∑AcDON > BEA > PA.

Data from the deterministic risk assessment showed that the calculated exposure for infants as well as adults exceeded the TDI through maize, peanut, and cassava consumption. On the basis of the calculated exposure, the TDI was exceeded for FB_1 and AFB_1 following maize consumption. Likewise, exposure to AFB_1 through cassava consumption was also exceeded. Particular attention should be paid to AFB_1, especially in populations with a very high prevalence of HBV (10%). Vulnerable groups and/or individuals (such as elderly or immune-compromised people and pregnant women) living in these study zones should be alerted to the potential danger arising from the consumption of mycotoxin-contaminated foodstuffs. There is a need to carry out periodic surveys and awareness campaigns in the high-risk regions (HFM and WH) to educate subsistence farmers as well as other agricultural stakeholders on the merits of good agricultural practices in relation to reducing mycotoxin exposure.

AUTHOR INFORMATION

Corresponding Author

*(E.N.E.) Phone: +32 9 264 81 33. Fax: +32 9 264 81 99. E-mail: emmanuel.njumbeediage@ugent.be.

Notes

The authors declare no competing financial interest.

REFERENCES

(1) CAST. Mycotoxins − risk in plants, animal and human systems. Task Force Report, Ames, IA, USA. 2003; No. 139, pp 1−191.

(2) Hussein, H. S.; Brasel, J. M. Toxicity, metabolism, and impact of mycotoxins on humans and animals. *Toxicology* **2001**, *167*, 101−134.

(3) Hell, K.; Cardwell, K. F.; Setamou, M.; Schulthess, F. Influence of insect infestation on aflatoxin contamination of stored maize in four agro-ecological regions in Benin. *Afr. Entomol.* **2000b**, *8*, 169−177.

(4) Egal, S.; Hounsa, A.; Gong, Y. Y.; Turner, P. C.; Wild, C. P.; Hall, A. J.; Hell, K.; Cardwell, K. F. Dietary exposure to aflatoxin from maize and groundnut in young children from Benin and Togo, West Africa. *Int. J. Food Microbiol.* **2005**, *104*, 215−224.

(5) Ngoko, Z. Mycotoxin contamination of maize in relation with fungal infection, cultural practices and agro-ecology in Cameroon. Ph.D. Thesis, University of Orange Free State, South Africa, 1999.

(6) Ngoko, Z.; Cardwell, K. F.; Marasas, W. F. O.; Wingfield, M. J.; Ndemah, R.; Schulthess, F. Biological and physical constraints on maize production in the humid forest and western highlands of Cameroon. *Eur. J. Plant Pathol.* **2001**, *108*, 893−902.

(7) Tagne, A.; Kongsdal, O.; Ngoko, Z.; The, C.; Mathur, S. B. *Fusarium pallidoroseum* in maize samples of three agro-ecological zones of Cameroun. *J. Stored Prod. Res.* **2003**, *39*, 367−374.

(8) Cardwell, K. F.; Schulthess, F.; Ndemah, R.; Ngoko, Z. A systems approach to assess crop health and maize yield losses due to pests and diseases in Cameroon. *Agric. Ecosyst. Environ.* **1997**, *65*, 33−47.

(9) Essono, G.; Ayodele, M.; Akoa, A.; Foko, J.; Olembo, S.; Gockowski, J. *Aspergillus* species on cassava chips in storage in rural areas of southern Cameroon: their relationship with storage duration, moisture content and processing methods. *Afr. J. Microbiol. Res.* **2007**, *1*, 1−8.

(10) Ngoko, Z.; Daoudo, H.; Imele, P. T.; Kamga, S.; Mendi, M.; Mwangi, R.; Bandyopadhyay, R.; Marasas, W. F. O. Fungi and mycotoxins associated with food commodities in Cameroon. *J. Appl. Biosci.* **2008**, *6*, 164−168.

(11) Njobeh, P. B.; Dutton, M. F.; Koch, S. K.; Chuturgoo, n A. A.; Stoev, S. D.; Mosonik, J. S. Simultaneous occurrence of mycotoxins in human food commodities from Cameroon. *Mycotoxin Res.* **2010**, *26*, 47−57.

(12) Abia, W. A.; Warth, B.; Sulyok, M.; Krska, R.; Tchana, A. N.; Njobeh, P. B.; Dutton, M. F.; Moundipa, P. F. Determination of multi-mycotoxin occurrence in cereals, nuts and their products in Cameroon by liquid chromatography tandem mass spectrometry (LC-MS/MS). *Food Control* **2013**, *31*, 438−453.

(13) Njumbe Ediage, E.; Diana Di Mavungu, J.; Song, S.; Sioen, I.; De Saeger, S. Multimycotoxin analysis in urines to assess infant exposure; a case study in Cameroon. *Environ. Int.* **2013**, *57*−*58*, 50−59.
(14) Westby, A. Chapter 14. Cassava utilisation, storage and processing. In *Cassava: Biology, Production and Utilsation*; Hillocks, R. J., Thresh, J. M., Bellotti, A. C., Eds.; CAB International: Wallingford, UK, 2001; pp 281−300; ISBN 0851995241.
(15) Njobeh, P. B.; Dutton, M. F.; Koch, S. H.; Chuturgoon, A.; Stoev, S.; Seifert, K. Contamination with storage fungi of human food from Cameroon. *Int. J. Food Microbiol.* **2009**, *135*, 193−198.
(16) Commission Regulation No. 1881/2006 of 19 December 2006 setting maximum levels for certain contaminants in foodstuffs. *Off. J. Eur. Union* **2006**, *L364*, 5.
(17) Commission Regulation (EC) No. 1126/2007 of 28 September 2007 amending Regulation (EC) No. 1881/2006 setting maximum levels for certain contaminants in foodstuffs as regards *Fusarium* toxins in maize and maize products. *Off. J. Eur. Union* **2007**, *L255*, 14.
(18) FAO. *Worldwide Regulations for Mycotoxins in Food and Feed*; FAO Food and Nutrition Paper 81; Rome, Italy, 2004.
(19) NCRE (National Cereal Research Extension). *Annual Report*; The National Cereal Research and Extension Project. IITA-IRA-USAID, 1992; 193 pp.
(20) European Commission (EC). Commission Regulation No. 401/2006 of 23 February 2006 laying down the methods of sampling and analysis for the official control of the levels of mycotoxins in foodstuffs. *Off. J. Eur. Union* **2006**, *L70*, 12−34.
(21) Njumbe Ediage, E.; Diana Di Mavungu, J.; Monbaliu, S.; Van Peteghem, C.; De Saeger, S. A validated multianalyte LC−MS/MS method for quantification of 25 mycotoxins in cassava flour, peanut cake and maize samples. *J. Agric. Food Chem.* **2011**, *59*, 5173−5180.
(22) European Commission (EC). Commission Decision 2002/657 of 12 August 2002 implementing Council Directive 96/23/EC concerning the performance of analytical methods and the interpretation of results. *Off. J. Eur. Union* **2002**, *L221*, 8−36.
(23) Perkowski, J.; Plattner, R. D.; Goliński, P.; Vesonder, R. F.; Chelkowski, J. Natural occurrence of deoxynivalenol, 3-acetyl-deoxynivalenol, 15-acetyl-deoxynivalenol, nivalenol, 4,7-dideoxynivalenol, and zearalenone in Polish wheat. *Mycotoxin Res.* **1990**, *6*, 7−12.
(24) Shephard, G. S.; van der Westhuizen, L.; Katerere, D. R.; Herbst, M.; Pineiro, M. Preliminary exposure assessment of deoxynivalenol and patulin in South Africa. *Mycotoxin Res.* **2010**, *26*, 181−185.
(25) Mansfield, M. A.; Jones, A. D.; Kulda, G. A. Contamination of fresh and ensiled maize by multiple Penicillium mycotoxins. *Postharvest Pathol. Mycotoxicol.* **2008**, *98*, 330−336.
(26) Bottalico, A.; Perrone, G. Toxigenic Fusarium species and mycotoxins associated with head blight in small-grain cereals in Europe. *Eur. J. Plant Pathol.* **2002**, *108*, 611−624.
(27) Logrieco, A.; Mule, G.; Moretti, A.; Bottalico, A. Toxigenic *Fusarium* species and mycotoxins associated with maize ear rot in Europe. *Eur. J. Plant Pathol.* **2002**, *108*, 597−609.
(28) Nicholson, P.; Chandler, E.; Draeger, R. C.; Gosman, N. E.; Simpson, D. R.; Thomsett, M.; Wilson, A. H. Molecular tools to study epidemiology and toxicology of *Fusarium* head blight of cereals. *Eur. J. Plant Pathol.* **2003**, *109*, 691−703.
(29) Adejumo, T. O.; Hettwer, U.; Karlovsky, P. Occurrence of *Fusarium* species and trichothecenes in Nigerian maize. *Int. J. Food Microbiol.* **2007**, *116*, 350−357.
(30) Placinta, C. M.; D'Mello, J. P. F.; Macdonald, A. C. M. A review of worldwide contamination of cereal grains and animal feed with *Fusarium* mycotoxins. *Anim. Feed Sci. Technol.* **1999**, *78*, 21−37.
(31) Mutegi, C. K.; Wagacha, M.; Kimani, J.; Otieno, G.; Wanyama, R.; Hell, K.; Christiee, M. E. Incidence of aflatoxin in peanuts (*Arachis hypogaea Linnaeus*) from markets in Western, Nyanza and Nairobi Provinces of Kenya and related market traits. *J. Stored Prod. Res.* **2013**, *52*, 118−127.
(32) Barro, N.; Quattara, C. A.; Nikiema, P. A.; Quattara, A. S.; Traore, A. S. Microbial quality assessment of some street food widely consumed in Ouagadougou, Burkina Faso. *Sante* **2002**, *12*, 369−374.
(33) Otsuki, T.; Wilson, J. S.; Sewadeh, M. What price precaution? European harmonization of aflatoxin regulations and African groundnut exports. *Eur. Rev. Agric. Econ.* **2001**, *28*, 263−283.
(34) Codex Alimantarius Commission. Proposed draft code of practice for the prevention (reduction) of mycotoxin contamination in cereals, including annexes on ochratoxin A, zearalenone, fumonisins, and trichothecenes, CX/FAC 02/21, Joint FAO/WHO Food Standards Programme, Rotterdam, the Netherlands, 2002.
(35) Papp, E.; H-Otta, G.; Zaray, G.; Mincsovics, E. Liquid chromatographic determination of aflatoxins. *Microchem J.* **2002**, *73*, 39−46.
(36) Wareing, P. W.; Westby, A.; Gibbs, J. A.; Allotey, L. T.; Halm, M. Consumer preferences and fungal and mycotoxin contamination of cassava products from Ghana. *Int. J. Food Sci. Technol.* **2001**, *36*, 1−10.
(37) Muzanila, Y. C.; Brennan, J. G.; King, R. D. Residual cyanogens, chemical composition and aflatoxins in cassava flour from Tanzanian villages. *Food Chem.* **2000**, *70*, 45−49.
(38) Jimoh, K. O.; Kolapo, A. L. Mycoflora and aflatoxin production in market samples of some selected Nigerian foodstuffs. *Res. J. Microbiol.* **2008**, *3*, 169−174.
(39) Gnonlonfin, G. J. B.; Hell, K.; Fandohan, P.; Siame, A. B. Mycoflora and natural occurrence of aflatoxins and fumonisin B1 in cassava and yam chips from Benin, West Africa. *Int. J. Food Microbiol.* **2008**, *122*, 140−147.
(40) Gnonlonfin, G. J. B.; Adovi, Y.; Katerere, D. R.; Shephard, G. S.; Sanni, A.; Brimer, L. Mycoflora and absence of aflatoxin contamination of commercialized cassava chips in Benin, West Africa. *Food Control* **2012**, *23*, 333−337.
(41) Manjula, K.; Hell, K.; Fandohan, P.; Abass, A.; Bandyopadhyay, R. Aflatoxin and fumonisin contamination of cassava products and maize grain from markets in Tanzania and Republic of the Congo. *Toxin Rev.* **2009**, *28*, 63−69.
(42) Kaaya, A. N.; Eboku, D. Mould and aflatoxin contamination of dried cassava chips in Eastern Uganda: association with traditional processing and storage practices. *J. Biol. Sci.* **2010**, *10*, 718−729.
(43) FAO. Interpolated Estimated Dekadal Rainfall − By Region/Province Cameroon. NOAA/FEWSNet (2013), http://www.fao.org/giews/english/ierf/list_cross.asp?code=45 (accessed Jan 2014).
(44) Scientific Committee on Food. Opinion on *Fusarium* Toxins − Part 3: Fumonisin B1 (expressed on 17 October 2000). 2000, http://europa.eu.int/comm/food/fs/sc/scf/out73_en.pdf (accessed Jan 2014).
(45) EFSA Panel on Contaminants in the Food Chain (CONTAM). Scientific opinion on the risks for public health related to the presence of zearalenone in food. *EFSA J.* **2011**, *2197*, 124.
(46) European Food Safety Authority (EFSA). Opinion of the scientific panel on the contaminants in the food chain on a request from the commission related to ochratoxin A in food. *EFSA J.* **2006**, *365*, 56.
(47) European Commission (EC). Opinion of the Scientific Committee on Food on *Fusarium* toxins. Part 6: Group evaluation of T-2 toxin, HT-2 toxin, nivalenol and deoxynivalenol, 2002, http://ec.europa.eu/food/fs/sc/scf/out123_en.pdf (accessed Jan 2014).
(48) IARC. Ochratoxin A. In *IARC Monographs on the Evaluation of Carcinogenic Risks to Humans*; IARC Press: Lyon, France, 1993; Vol. 56, pp 489−521.
(49) Kuiper-Goodman, T. Mycotoxins: risk assessment and legislation. *Toxicol. Lett.* **1995**, *82*−*83*, 853−859.

JOURNAL OF AGRICULTURAL AND FOOD CHEMISTRY

Article

pubs.acs.org/JAFC

Effects of Antioxidants of Bamboo Leaves and Flavonoids on 2-Amino-1-methyl-6-phenylimidazo[4,5-*b*]pyridine (PhIP) Formation in Chemical Model Systems

Yan Zhang, Zhou Luo, Zeping Shao, Chundi Yu, and Shuo Wang*

Key Laboratory of Food Nutrition and Safety, Ministry of Education of China, Tianjin University of Science and Technology, Tianjin 300457, China

ABSTRACT: The inhibitory effects of antioxidants of bamboo leaves (AOB) and flavonoids against 2-amino-1-methyl-6-phenylimidazo[4,5-*b*]pyridine (PhIP) formation were investigated in creatinine and phenylalanine model systems. AOB and the tested flavonoids (orientin, homoorientin, vitexin, isovitex, apigenin, luteolin, isorhamnetin, fisetin, and hesperetin) had significant dose-dependent inhibition effects on PhIP formation with different IC_{50} values. The superoxide anion ($O_2^{\bullet-}$) scavenging activities of these nine flavonoids were evaluated using the pyrogallol autoxidation system. The EC_{50} values of compounds that showed antioxidant activity were found to correlate well (R^2 = 0.8003) with the corresponding IC_{50} values representing their inhibition of PhIP formation. It was assumed that the inhibitory effects of flavonoids on PhIP formation were probably achieved by scavenging free radicals generated in the reaction system. These findings provide valuable information for the development of effective strategies to minimize heterocyclic amine content in thermally processed food.

KEYWORDS: *heterocyclic amines, 2-amino-1-methyl-6-phenylimidazo[4,5-b]pyridine (PhIP), antioxidants of bamboo leaves (AOB), flavonoid, free radical scavenging, chemical model systems*

INTRODUCTION

About 30 years ago, Japanese scientist Sugimura discovered a new group of highly mutagenic compounds by means of an Ames test, which were classified as heterocyclic amines (HAs).[1] HAs are generally formed in a wide variety of heated proteinaceous foods and are known to be carcinogenic and mutagenic in rodents and are considered to be potential human carcinogens. Epidemiological studies have provided evidence that the risks of colorectal adenoma and lung cancer were increased by the intake of well-done or grilled meats containing HAs mutagens.[2,3] There are two main categories of HAs, polar and nonpolar HAs. The latter category has been shown to be responsible for most of the HA-associated mutagenic activity detected in food. Among these, 2-amino-1-methyl-6-phenylimidazo[4,5-*b*]pyridine (PhIP), which is generally found in the highest abundance from normal cooking procedures, induces mammary and colon carcinomas in rats in a clear dose-dependent manner.[4,5]

In 1987, Shioya[6] discovered that PhIP was produced by heating a mixture of creatinine, phenylalanine, and glucose. It was suggested that the Maillard reaction between phenylalanine and glucose was responsible for producing the intermediates that condense with creatinine to form PhIP. In the following years, using ^{13}C-labeled phenylalanine and creatine, it was demonstrated that phenylalanine and creatine were precursors of PhIP formation under conditions of dry heating.[7] Although the complete reaction mechanism is still not fully established, phenylacetaldehyde is believed to play a key role by undergoing an aldol condensation with creatinine.[8]

In view of their potent mutagenic activity as well as the fact that they can even be formed during ordinary household cooking, a great deal of attention has been focused on developing strategies which can effectively lower the content of HAs in foods, to reduce overall human exposure.[9] Ever since the early 1980s, scientists have been researching methods such as microwave cooking marinated foods and antioxidant compounds to reduce the level of HAs generated in daily diets. Felton[10] discovered that the mutagenicity of beef cooked by microwave heating was reduced by 95% compared with beef prepared by normal cooking methods, suggesting that the amount of HAs generated by microwave cooking was reduced. Salmon[11] demonstrated that pretreating chicken with marinade reduced the amount of HAs formed. Kato[12] discovered that in a creatinine/glycine/glucose model system with butylated hydroxyanisole, propyl gallate, and other spiked antioxidants, the formation of HAs was reduced. Cheng also found that both naringenin and epigallocatechin gallate can inhibit the formation of PhIP in chemical model system, which was presumably achieved by scavenging or trapping of phenylacetaldehyde via polyphenol−phenylacetaldehyde adduct formation. This study presented a key mechanism of polyphenol to inhibit PhIP formation.[8,13]

Antioxidants of bamboo leaves (AOB) is a complex mixture of natural antioxidants that was listed in the Chinese Standard GB-2760 as a legal and safe food additive in 2004. AOB was reported to possess strong antioxidant activity and inhibition toward transition metal ions and free radical induced deterioration of macromolecules in vitro.[14] Our prior study discovered that AOB could effectively inhibit HA formation in fried pork, including PhIP formation.[15] In this study, the effects of AOB in combination with flavonoids on the formation of

Received: January 28, 2014
Revised: April 23, 2014
Accepted: May 7, 2014
Published: May 7, 2014

ACS Publications © 2014 American Chemical Society

PhIP were explored using a PhIP-forming chemical model system. The relationship between the inhibition effect of flavonoids on PhIP formation and superoxide anion ($O_2^{\bullet-}$) scavenging ability was also investigated in an effort to determine the inhibitory mechanism of flavonoids toward PhIP formation.

MATERIALS AND METHODS

Chemicals and Apparatus. Phenylalanine, diethylene glycol, creatinine, luminol, and pyrogallol were obtained from Sigma-Aldrich Co. (St. Louis, MO, USA). PhIP was from Toronto Research Chemicals (Toronto, Canada). Antioxidants of bamboo leaves were from Shengshi Biology (Huzhou, China). Orientin, homoorientin, vitexin, and isovitex were purchased from Bestbiotech (Tianjin, China). Apigenin, luteolin, isorhamnetin, and fisetin were purchased from J&K Chemical (Beijing, China).

Si-SCX-2 cartridges (200 mg, 3 mL) were purchased from Silicycle Inc. (Quebec, Canada). Hypersep C18 cartridges (200 mg, 3 mL) were obtained from Thermo Electron Corp. (Bellefonte, KY, USA).

LC-MS/MS was performed on an Agilent 1200 series HPLC system coupled to an Agilent 6410 triple-quadrupole mass spectrometer equipped with electrospray ionization (ESI) (Waldbronn, Germany). Chemiluminescence analysis was carried out on a Thermo Fluoroskan Ascent FL. The vortex was purchased from IKA (Baden, Germany). The block heater (Stuart SBH200D) was purchased from a dealer of Stuart, Beijing XinKaiLong Bio Co. Ltd. (Beijing, China).

Effects of AOB and Flavonoids on PhIP Formation in Chemical Model System. The PhIP-producing model system consisted of 2.08 mg of creatinine and 3.2 mg of phenylalanine, weighed and mixed in 2 mL of diethylene glycol in Hach Cod digestion vials by vortexing. The vials were inserted into a block heater set at 120 °C and heated for 2 h. After heating, the vials were cooled in water.[16,17]

The effects of AOB and flavonoids on PhIP formation were investigated using the PhIP-producing model system. The amounts of added AOB and flavonoids (orientin, homoorientin, vitexin, isovitex, apigenin, luteolin, isorhamnetin, fisetin, and hesperetin) were 0.25, 0.5, 1, 1.5, 2, 2.5, and 5 mg/mL. Samples without any AOB or flavonoids were used as the controls. All experiments were performed in triplicate.

Extraction of PhIP from the Model System. The procedure was carried out according to that of Zhang et al. with minor modifications. Solid phase extraction (SPE) was used to extract the PhIP from the solution where the chemical reaction was conducted in the presence of precursors. The Si-SCX-2 cartridge was prewashed with 5 mL of MeOH followed by 5 mL of H_2O/0.1 M HCl (1:1, v/v). The cartridge was then dried under vacuum and washed with 3 mL of 0.01 M HCl followed by 3 mL of 0.1 M HCl/MeOH (9:1, v/v). PhIP was eluted with 10 mL of 1.5 M NH_4AC/MeOH (9:1, v/v) and further purified by C18 cartridge. C18 cartridge was preconditioned with 5 mL of MeOH followed by 5 mL of H_2O, and then the PhIP eluent from the Si-SCX-2 cartridge was loaded onto the C18 cartridge. After washing with 10 mL of ultrapure water, the PhIP was eluted with 2 mL of MeOH/NH_3H_2O (25%) (9:1, v/v). The eluent was then evaporated to dryness under nitrogen and redissolved in 1 mL of MeOH. After filtering through a 0.22 μm organic filter, 1 μL of the purified extract was analyzed by LC-MS/MS.[18]

Quantitation of PhIP by LC-MS/MS. A C18 column (2.1 × 150 mm, 3.5 μm; Agilent) was selected for the chromatographic separation and quantitation of PhIP. To achieve stable and better separation, the column temperature was 25 °C, with a binary mobile phase at a flow rate of 0.2 mL/min. Mobile phases A and B consisted of acetonitrile and 10 mM ammonium formate/formic acid (pH 3.5), respectively. The gradient program was as follows: 0 min, 10% A; 10 min, 60% A; 14 min, 10% A. The post-time re-equilibration was 9 min. Positive ion mode and multiple reaction monitoring mode were used for MS/MS detection. The electrospray ionization parameters were optimized as nebulizer pressure of 40 psi and capillary voltage of 4000 V. Nitrogen was used as the nebulizer, drying, and collision gas. The drying gas flow rate was 10 L/min, and the drying temperature was 350 °C. For each transition, the dwell time was 80 ms.

Free Radical Scavenging Activity Determination. A pyrogallol autoxidation system, in which superoxide anion ($O_2^{\bullet-}$) was generated by pyrogallol autoxidation and used to oxidize luminol to produce a proportional strong chemiluminescence signal, was employed to determine the free radical scavenging activities of AOB and flavonoids according to the method of Li et al.[19,20] with some modifications. The scavenging effect of flavonoids on ($O_2^{\bullet-}$) could be obtained by observing the decease of emission light intensity. The reaction mixture contained 50 μL of pyrogallol (1×10^{-3} M) in 10 mmol/L HCl, 140 μL of carbonate buffer (50 mM, pH 10.2), and 20 μL of luminol (1×10^{-3} M) in 50 mmol/L NaOH.

The sample solution was first placed in a Costar 96-well plate, then the carbonate buffer and luminol were added, and the contents were mixed. Then, pyrogallol was added and chemiluminescence analysis was started immediately. The emission light intensity was recorded every 5 s, and the total integral of the light intensity over 60 s was determined. The control reaction was performed in the same manner as the mixture without the sample solution, and the background was measured without pyrogallol addition.

Statistical Analysis. Data were reported as the mean ± SD for triplicate determinations. One-way ANOVA and Duncan's test were employed to identify differences in means. Statistical analyses were performed using IBM SPSS for Windows (version rel. 19.0, 2010, SPSS Inc., Chicago, IL, USA). Statistical significance was declared at $P < 0.05$.

RESULTS AND DISCUSSION

Effects of AOB on PhIP Formation in Chemical Model System. HAs can be formed when creatine, a specific amino acid, and a monosaccharide are allowed to react at elevated temperatures (usually >100 °C). In this study, the effects of AOB and flavonoids on PhIP formation were evaluated in a chemical model system. AOB comprise a complex mixture that is extracted from specific bamboo leaves from southern China. AOB is of interest as an emerging food additive because of its effects in reducing the level of toxic compounds that accompany food processing. In 2008, Zhang reported that AOB had a significant inhibition effect (percent inhibition ≥ 70%) on acrylamide formation in a low-moisture asparagine−glucose model system.[21] Previously we reported that AOB was better at inhibiting HA formation than some synthesized antioxidants in the fried pork model.[15] However, the food matrix included components such as lipids, proteins, and other unknown substances, which may interfere with HA formation. Thus, in this study, the effects of AOB on PhIP formation were evaluated in a chemical model system. As expected, AOB could effectively inhibit the generation of PhIP in the chemical model system in a similar fashion as exposure to the fried pork. There was a positive correlation between the level of AOB and the reduction in PhIP formation; that is, the more AOB was added, the less PhIP was generated. The PhIP contents were reduced by 13.49, 36.13, 41.82, 45.81, and 52.42% in the system compared with the control as the AOB levels increased (Figure 1). The percent inhibition exceeded 50% when 2.5 mg/mL of AOB was spiked in the chemical model system.

Effects of Reactive Components from AOB on PhIP Formation in a Chemical Model System. AOB, which exhibited good dose-dependent inhibition of PhIP formation in a chemical model system, mainly consists of flavone glycosides, phenolic acids, and lactones. To identify the active components of AOB that inhibited PhIP formation, four flavone glycosides from AOB, orientin, homoorientin, vitexin, and isovitex, were further evaluated. The amount of each flavone glycoside added

dx.doi.org/10.1021/jf500483y | J. Agric. Food Chem. 2014, 62, 4798−4802

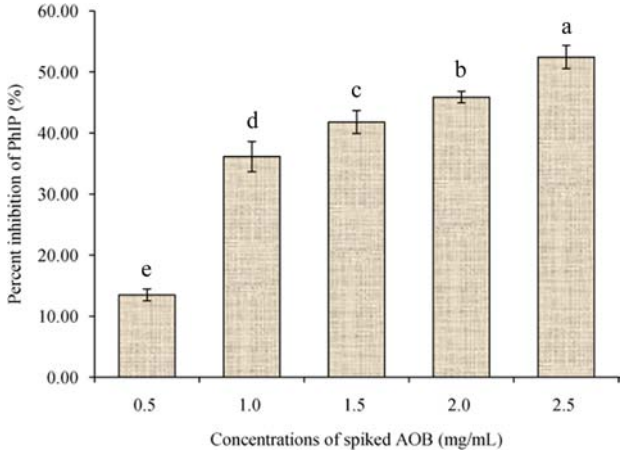

Figure 1. Inhibition effects of AOB on PhIP formation in a chemical model system. Percent inhibition results were statistically analyzed by one-way ANOVA and Duncan's test. Values with different letters are significantly different ($P < 0.05$).

was the same as their levels in the AOB. The results showed that each flavone glycoside obviously inhibited PhIP generation, and the percent inhibition increased with increases in the spiked flavonoids in a similar fashion as with AOB. As shown in Table 1, the dose−effect relationship between the spiked level

Table 1. Inhibition of PhIP Formation by Flavonoids Reported as IC_{50} Values

flavonoid	regression eq	R^2	IC_{50} (mg/mL)
orientine	$Y = e^{(4.514-0.195/x)}$	0.960	0.162
homoorientine	$Y = e^{(4.52-0.194/x)}$	0.971	0.160
vitexin	$Y = e^{(4.52-0.392/x)}$	0.978	0.301
isovitexin	$Y = e^{(4.515-0.364/x)}$	0.993	0.322
fisetin	$Y = e^{(4.729-4.481/x)}$	0.989	2.743
isorhamnetin	$Y = e^{(4.101-0.633/x)}$	0.956	1.675
apigenin	$Y = e^{(4.679-1.136/x)}$	0.981	0.382
luteolin	$Y = e^{(4.574-0.356/x)}$	0.886	0.269
hesperetin	$Y = e^{(4.326-3.519/x)}$	0.959	4.251

of flavonoids and the inhibition of PhIP formation was obtained with a high correlation coefficient. The IC_{50}, the half-maximal inhibitory concentration, was used as the index to evaluate the inhibition effect of flavonoids against PhIP formation. The larger the IC_{50} value, the smaller the inhibition effect. The IC_{50} values of the four flavone glycosides were between 0.16 and 0.322 mg/mL, suggesting slight differences in their inhibition activities on PhIP formation. Orientin and homoorientin were better inhibitors of PhIP generation than vitexin and isovitex. There was no difference in inhibiting PhIP formation between orientin and homoorientin or between vitexin and isovitex at the tested concentrations.

The IC_{50} values of the four flavone glycosides were all smaller than that of AOB, which contains 40% (m/m) flavones. When the spiked AOB was 2.5 times the amount of the added flavone glycosides, the inhibition by AOB was less effective than that of the flavone glycosides alone. This indicated that flavone glycosides may be the dominant components in AOB inhibiting the formation of PhIP.

Effects of Other Flavonoids on PhIP Formation in the Chemical Model System. Because four flavone glycosides (orientin, homoorientin, vitexin, and isovitex) all had dose-dependent effects on PhIP formation, five other flavonoids (apigenin, luteolin, isorhamnetin, fisetin, and hesperetin) were chosen to further explore the relationship between flavonoids and inhibition effects on PhIP formation. The results indicated that apigenin, luteolin, isorhamnetin, fisetin, and hesperetin all inhibited PhIP formation (data not shown). The inhibition activity increased gradually with increases in the amount of flavonoids. Luteolin was the strongest, with 87.06% inhibition at 2.5 mg/mL concentration. Apigenin showed an almost equivalent inhibition effect as that for luteolin, with 85.06% inhibition of PhIP formation. Isorhamnetin also effectively inhibited PhIP formation. Hesperetin and fisetin were weaker inhibitors at the same spiked levels, but when spiked at 5 mg/mL, their potency increased.

The IC_{50} values were obtained from fits to the data using S-curves, which provided the best correlation coefficients. The regression equations and parameters are shown in Table 1. The inhibition of PhIP formation was also found to be strongly dose-dependent upon the concentration of flavonoid added in all cases. Luteolin exhibited the strongest inhibition of PhIP formation followed by apigenin; their IC_{50} values were both <1.0 mg/mL. In summary, the order for the inhibition of PhIP formation was luteolin > apigenin > isorhamnetin > fisetin > hesperetin.

Relationship between Radical Scavenging Activity and Effects of Flavonoids on PhIP Inhibition. Chemiluminescence has been widely used as a sensitive assay for monitoring free radical scavenging by flavonoids. It is commonly accepted that flavonoids may exert their strong antioxidant activity by scavenging free radicals. To explore the connection between free radical scavenging ability and inhibition of PhIP formation, the superoxide anion ($O_2^{\bullet-}$) scavenging ability of flavonoids was investigated. The half-maximal effective concentration (EC_{50}), which is defined as the concentration required for inhibition of 50% of the chemiluminescence intensity, is normally used to express radical scavenging activities. The greater the EC_{50} value, the weaker the radical scavenging activities. Because the emission light intensity reached a maximum after 5 s and was stable, the light intensity at 5 s was selected to calculate the EC_{50} values. The results (Table 2) showed that the nine tested flavonoids

Table 2. Free Radical Scavenging Activities of Nine Flavonoids As Determined by Chemiluminescence Analysis

flavonoid	linear fitting eq	R^2	EC_{50} (μg/mL)
luteolin	$Y = -0.0008x + 0.2834$	0.959	116.9
hesperetin	$Y = -0.0002x + 0.3036$	0.999	566.7
fisetin	$Y = -0.0009x + 0.4497$	0.984	288.3
apigenin	$Y = -0.0006x + 0.2694$	0.882	131.9
isorhamnetin	$Y = -0.0006x + 0.2985$	0.962	180.4
orientin	$Y = -0.0006x + 0.3025$	0.809	187.1
homoorientin	$Y = -0.0006x + 0.2986$	0.869	180.6
vitexin	$Y = -0.0006x + 0.3104$	0.903	200.2
isovitexin	$Y = -0.0007x + 0.3342$	0.945	205.6

had different EC_{50} values, indicating their different radical scavenging activities. The order of the flavonoid EC_{50} values from large to small was luteolin, apigenin, isorhamnetin, orientin, homoorientin, vitexin, isovitexin, fisetin, and hesperetin.

To investigate the relationship between radical scavenging activity and the effects of flavonoids on PhIP formation, the

dx.doi.org/10.1021/jf500483y | J. Agric. Food Chem. 2014, 62, 4798−4802

IC_{50} and EC_{50} values were analyzed by regression analysis. A significant correlation (R^2 = 0.8003) was observed as shown in Figure 2. This indicated that the capacity of flavonoids to

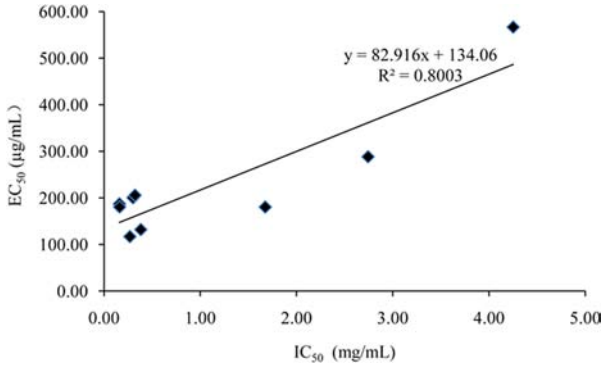

Figure 2. Linear fit of the relationship between IC_{50} (mg/mL) and EC_{50} (μg/mL) in the PhIP model system.

inhibit PhIP formation was highly correlated with their superoxide anion ($O_2^{\bullet-}$) scavenging ability, and the flavonoid-driven inhibition of PhIP formation was likely a result of free radical scavenging during the reaction. This was consistent with the postulated pathway for PhIP formation in which phenylalanine is first converted into phenylacetaldehyde, which then reacts with creatinine to produce the corresponding aldol adduct, which then forms PhIP; there may be free radicals generated during the skeleton degradation.[16] Each flavonoid has a distinct chemical structure, which results in unique antioxidant and free radical scavenging activities and, ultimately, different potencies of inhibition of PhIP formation. It was reported that the degree of hydroxylation and location of the hydroxy groups were the critical factors for determining the antioxidant capacities of flavonoids. The IC_{50} values are likely similar between the specific pairs of isomerides, orientin and homoorientin and vitexin and isovitex, because the chemical structures of the pairs differ only in the position of a hydroxyl group on the sugar moiety.

In conclusion, this study demonstrated that AOB may inhibit PhIP formation in a chemical model system. The results were consistent with previous results that AOB could effectively inhibit PhIP formation better than synthetic antioxidants in fried pork. Four flavone glycosides (orientin, homoorientin, vitexin, and isovitex) from AOB and five flavonoids (apigenin, luteolin, isorhamnetin, fisetin, and hesperetin) all showed dose-dependent inhibition of PhIP formation. The flavonoids varied in their inhibition and superoxide anion ($O_2^{\bullet-}$) scavenging abilities. The IC_{50} and EC_{50} values of the flavonoids correlated, indicating that flavonoids may inhibit PhIP formation via their free radical scavenging abilities. Our explanation is not consistent with the previously proposed mechanism whereby polyphenols were suggested to trap or scavenge phenylacetaldehyde, via adduct formation, to inhibit PhIP formation.[8,13] Indeed, free radical scavenging and phenylacetaldehyde scavenging can occur simultaneously, which may have a synergistic effect on inhibiting the formation of PhIP.

AUTHOR INFORMATION

Corresponding Author

*(S.W.) Phone: +86 22 60601456. Fax: +86 22 60601332. E-mail: s.wang@tust.edu.cn.

Funding

This work was supported by the Ministry of Science and Technology of the People's Republic of China (Project 2011AA100806), the Special Fund for Agro-scientific Research in the Public Interest (Project 201203069), and the program for Changjiang Scholars and Innovative Research Team in University (IRT1166).

Notes

The authors declare no competing financial interest.

REFERENCES

(1) Sugimura, T.; Nagao, M.; Kawachi, T.; Honda, M.; Yahag, T.; Seino, Y.; Sato, S.; Matsukura, N.; Matsushima, T.; Shirai, A.; Sawamura, M.; Matsumoto, H. Mutagens-carcinogens in food, with special reference to highly mutagenic pyrolytic products in broiled foods. *Origins Hum. Cancer* **1977**, *4*, 1561−1577.

(2) Sinha, R.; Rothman, N. Role of well-done, grilled red meat, heterocyclic amines (HCAs) in the etiology of human cancer. *Cancer Lett.* **1999**, *143*, 189−194.

(3) Layton, D. W.; Bogen, K. T.; Knize, M. G.; Hatch, F. T.; Johnson, V. M.; Felton, J. S. Cancer risk of heterocyclic amines in cooked foods: an analysis and implications for research. *Carcinogenesis.* **1995**, *16*, 39−52.

(4) Ni, W.; McNaughton, L.; LeMaster, D. M.; Sinha, R.; Turesky, R. J. Quantitation of 13 heterocyclic aromatic amines in cooked beef, pork, and chicken by liquid chromatography-electrospray ionization/tandem masss spectrometry. *J. Agric. Food Chem.* **2008**, *56*, 68−78.

(5) Zamora, R.; Alcón, E.; Hidalgo, J. F. Effect of amino acids on the formation of 2-amino-1-methyl-6-phenylimidazo[4,5-*b*]pyridine (PhIP) in creatinine/phenylalanine and creatinine/phenylalanine/4-oxo-2-nonenal reaction mixture. *Food Chem.* **2013**, *141*, 4240−4245.

(6) Shioya, M.; Wakabayashi, K.; Sato, S.; Nagao, M.; Sugimura, T. Formation of a mutagen, 2-amino-1-methyl-6-phenylimidazo[4,5-*b*]pyridine (PhIP) in cooked beef, by heating a mixture containing creatinine, phenylalanine and glucose. *Mutat. Res.* **1987**, *191*, 133−138.

(7) Felton, J. S.; Knize, M. G. Mutagen formation in muscle meats and model heating systems. In *Mutagens in Food: Detection and Prevention*; Hayatsu, H., Ed.; CRC Press: Boca Raton, FL, USA, 1991; pp 57−66.

(8) Cheng, K. W.; Wong, C. C.; Cho, C. K.; Chu, I. K.; Sze, K. H.; Lo, C.; Chen, F.; Wang, M. Trapping of phenylacetaldehyde as a key mechanism responsible for naringerin's inhibitory activity in mutagenic 2-amino-1-methyl-6-phenylimidazo[4,5-*b*]pyridine formation. *Chem. Res. Toxicol.* **2008**, *21*, 2026−2034.

(9) Skog, K. I.; Johansson, M. A. E.; Jägerstad, M. I. Carcinogenic heterocyclic amines in model systems and cooked foods: a review on formation, occurrence and intake. *Food Chem. Toxicol.* **1998**, *36*, 879−896.

(10) Felton, J. S.; Fultz, E.; Dolbeare, F. A.; Knize, M. G. Effect of microwave pretreatment on heterocyclic aromatic amine mutagens/carcinogens in fried beef patties. *Food Chem. Toxicol.* **1994**, *32*, 897−903.

(11) Salmon, C. P.; Knize, M. G.; Felton, J. S. Effects of marination on the of heterocyclic amine carcinogen formation in grilled chicken. *Food Chem. Toxicol.* **1997**, *35*, 433−441.

(12) Kato, T.; Harashima, T.; Moriya, N.; Kikugawa, K.; Hiramoto, K. Formation of the mutagenoic/carcinogenic imidazoquinoxaline-type heterocyclic amine through the unstable free radical Maillard intermediates and its inhibition by phenolic antioxidants. *Carcinogenesis* **1996**, *11*, 2469−2476.

(13) Cheng, K. W.; Wong, C. C.; Chao, J.; Lo, C.; Chen, F.; Chu, I. K.; Che, C. M.; Ho, C.-T.; Wang, M. Inhibition of mutagenic PhIP formation by epigallocatechin gallate via scavenging of phenylacetaldehyde. *Mol. Nutr. Food Res.* **2009**, *53*, 716−725.

(14) Hu, C.; Zhang, Y.; Kitts, D. D. Evaluation of antioxidant and prooxidant activities of bamboo *Phyllostachys nigra* var. henonis leaf extract in vitro. *J. Agric. Food Chem.* **2008**, *48*, 3170−3176.

(15) Zhang, Y.; Yu, C. D.; Mei, J. B.; Wang, S. Formation and mitigation of heterocyclic aromatic amines in fried pork. *Food Addit. Contam.* **2013**, *30*, 1501−1507.
(16) Zochling, S.; Murkovic, M. Formation of the heterocyclic aromatic amine PhIP: identification of precursors and intermediates. *Food Chem.* **2002**, *79*, 125−134.
(17) Wong, D.; Cheng, K. W.; Wang, M. F. Inhibition of heterocyclic amine formation by water-soluble vitamins in Maillard reaction model systems and beef patties. *Food Chem.* **2012**, *133*, 760−766.
(18) Zhang, Y.; Lin, C. P.; Fang, G. Z.; Mei, J. B.; Wang, X.; Wang, S. Tandem solid phase extraction coupled to LC-ESI-MS/MS for the accurate simultaneous determination of five heterocyclic aromatic amines in processed meat products. *Eur. Food Res. Technol.* **2012**, *234*, 197−205.
(19) Li, H. P.; Zhang, M. M.; Ma, G. J. Radical scavenging activity of flavonoids from *Trollius chinensis* Bunge. *Nutrition* **2011**, *27*, 1061−1065.
(20) Marklund, S.; Marklund, G. Involvement of the superoxide anion radical in the autoxidation of pyrogallol and a convenient assay for superoxide dismutase. *Eur. J. Biochem.* **1974**, *47*, 469−474.
(21) Zhang, Y.; Zhang, Y. Effect of natural antioxidants on kinetic behavior of acrylamide formation and elimination in low-moisture asparagine-glucose model system. *J. Food Eng.* **2008**, *85*, 105−115.

JOURNAL OF AGRICULTURAL AND FOOD CHEMISTRY

Article

pubs.acs.org/JAFC

In Vitro Adsorption of Aluminum by an Edible Biopolymer Poly(γ-glutamic acid)

Yesudoss Christu Rajan,[†] Baskaran Stephen Inbaraj,[†] and Bing Huei Chen*[,†,‡]

[†]Department of Food Science and [‡]Graduate Institute of Medicine, Fu Jen University, Taipei 242, Taiwan

ABSTRACT: Accumulation of aluminum in human has been reported to be associated with dementia, Parkinson's disease, and Alzheimer's disease. The objectives of this study were to evaluate an edible biopolymer poly(γ-glutamic acid) (γ-PGA) for aluminum removal efficiency under in vitro conditions as affected by pH, contact time, aluminum concentration, temperature, ionic strength, and essential metals in both aqueous aluminum solution and simulated gastrointestinal fluid (GIF). A low aluminum adsorption occurred at pH 1.5−2.5, followed by a maximum adsorption at pH 3.0−4.0 and precipitating thereafter as aluminum hydroxide at pH > 4. Adsorption was extremely fast with 81−96% of total adsorption being attained within 1 min, reaching equilibrium in 5−10 min. Kinetic data at low (10 mg/L) and high (50 mg/L) concentrations were well described by pseudo-first-order and pseudo-second-order models, respectively. Equilibrium adsorption isotherms at different temperatures were precisely fitted by both Langmuir and Redlich−Peterson models with the maximum adsorption capacities at 25, 37, and 50 °C being 35.85, 38.68, and 44.23 mg/g, respectively. Thermodynamic calculations suggested endothermic and spontaneous nature of aluminum adsorption by γ-PGA with increased randomness at the solid/solution interface. Variation in ionic strengths did not alter the adsorption capacity, however, the incorporation of essential metals significantly reduced the aluminum adsorption by following the order copper > iron > zinc > calcium > potassium. Compared to aqueous solution, the aluminum adsorption from simulated GIF was high at all studied pH (1−4) with Langmuir monolayer adsorption capacity being 49.43 mg/g at 37 °C and pH 4. The outcome of this study suggests that γ-PGA could be used as a safe detoxifying agent for aluminum.

KEYWORDS: *poly(γ-glutamic acid), aluminum, detoxification, gastrointestinal pH, kinetics, isotherms, essential metals*

INTRODUCTION

Aluminum is one of the most common and abundant metallic elements in the Earth's crust.[1] Until a decade ago aluminum was regarded as an inert and insoluble mineral that does not pose any threat to human health. Consequently, aluminum containing agents have been used in many applications including food, drinking water, and medicine.[2−4] Moreover, acid rain in recent years has transformed the insoluble aluminum-containing minerals into a more soluble form resulting in accumulation of aluminum in food through drinking water sources.[3,4] Though aluminum compounds are currently used in industrial and pharmaceutical sectors as cosmetics, food additives, and household products, the major route of exposure of aluminum to human is through food.[3,4] Unprocessed foods typically contribute less than 5 mg of Al/kg, however, the use of aluminum-based foils, bowls, vessels, trays, and pans in the presence of acids and salts may elevate the level of aluminum in food.[3] For a 60 kg adult, the mean dietary exposure from food and water was estimated to range from 1.6 to 13 mg of Al/day, which corresponded to 0.2−2.3 mg/kg body weight per week.[3] Nevertheless, the tolerable weekly aluminum intake recommended by EFSA is only 1 mg of aluminum/kg body weight/week.[3] Moreover, several studies have implicated that aluminum accumulation can cause neurotoxicity leading to increased risk of neurological and bone disorders such as Alzheimer's disease, Parkinson's disease, dementia, and osteomalacia.[3−6] Thus, it is important to explore new therapeutic methods to minimize aluminum accumulation in human body.

Theoretically, aluminum mainly exists as a soluble species $Al[(H_2O)_6]^{3+}$ at pH ≤ 4, but at pH > 4, it can be precipitated as $Al(OH)_3$ through transient formation of $Al(OH)^{2+}$ and $Al(OH)_2^+$.[3,7] Accordingly, at physiological pH (5.5−7.4), aluminum should precipitate, preventing its absorption through the gastrointestinal tract. However, several in vivo studies have demonstrated increased accumulation of aluminum during simultaneous administration of aluminum hydroxide and fruit juices or organic acids (citric, ascorbic, and glutamic acids).[7−10] This is because various dietary ligands in conjugation with gastric juice solubilize the aluminum cations, resulting in the equilibrium formation of a soluble complex of aluminum for enhanced absorption and bioavailability.[8,9] Chelation therapy is one of the most common methods used for treatment of patients with metal poisoning. Several chelators such as desferrioxamine and feralex have been found beneficial for reduction of tissue accumulation of aluminum in human.[11,12] Nevertheless, these chelators may cause potential side effects including kidney overload, mineral deficiency, and cardiac arrest.[13] Therefore, it is essential to develop potential and safe detoxifying agents for treatment of aluminum poisoning.

In this study, an edible and biodegradable biopolymer poly(γ-glutamic acid) (γ-PGA) was evaluated as a safe detoxifying agent for aluminum in a batch mode under in vitro conditions. The γ-PGA consists of repetitive glutamic acid

Received: March 12, 2014
Revised: May 2, 2014
Accepted: May 5, 2014
Published: May 5, 2014

ACS Publications © 2014 American Chemical Society

dx.doi.org/10.1021/jf5011484 | J. Agric. Food Chem. 2014, 62, 4803−4811

units connected by γ-amide linkages facilitating α-carboxyl groups for conjugation to different compounds (−[−NH−CH(COOH)−$(CH_2)_2$−CO−]$_n$−).[14,15] It is commercially synthesized in different ionic forms (H, Ca, Na, Mg, and NH_4) and varying molecular masses (up to 2 million daltons) using *Bacillus* species by either the de novo method in solid state fermentation or the salvage bioconversion pathway in submerged fermentation.[15,16] Owing to its biocompatible nature, γ-PGA finds application to a wide variety of fields such as food, medicine, hygiene, agriculture, cosmetics, and the environment.[15,16] More specifically, γ-PGA has been used a drug carrier in various biomedical applications.[14−16] Our previous studies on γ-PGA as a metal-adsorbing agent have mainly focused on adsorption of divalent cations like lead (Pb^{2+}), cadmium (Cd^{2+}), and mercury (Hg^{2+}).[14,17] However, its application in adsorbing a trivalent cation like aluminum (Al^{3+}) has not been explored for possible treatment of aluminum intoxication in human. The present work aims to perform an in vitro study to evaluate the adsorbing ability of aluminum by γ-PGA as affected by different parameters like pH, contact time, aluminum concentration, temperature, ionic strength, and essential metals in both aqueous aluminum solution and simulated gastrointestinal fluid (GIF).

MATERIALS AND METHODS

Materials. Aluminum sulfate used for preparation of stock and working solutions was obtained from Sigma-Aldrich (St. Louis, MO). To study the effect of essential metals on aluminum adsorption by γ-PGA, metal salts such as anhydrous copper(II) sulfate and zinc(II) sulfate heptahydrate were procured from Sigma-Aldrich, while potassium chloride, calcium(II) chloride, and iron(II) sulfate heptahydrate were from Nacalai Tesque, Inc. (Kyoto, Japan), JT Baker (Phillipsburg, NJ), and Ajax Finechem (Sydney, Australia), respectively. Chemicals such as sodium acetate, thiourea, and 1,8-dihydroxy-2-(4-sulfophenylazo)naphthalene-3,6-disulfonic acid trisodium salt (SPADNS) used for analysis of aluminum were purchased from Sigma-Aldrich. Sodium chloride and pepsin (a 700 FIP U/g digestive enzyme) used for simulating GIF were obtained from JT Baker and Merck (Taipei, Taiwan). For preparation of different aluminum concentrations and making necessary dilution during analysis, the deionized water collected from a Milli-Q purification system from Millipore Co. (Bedford, MA) was used. The pH of aluminum solution and simulated GIF was adjusted using chemicals such as nitric acid, sodium hydroxide, and sodium bicarbonate obtained from Lab-Scan Analytical Sciences (Bangkok, Thailand), Nacalai Tesque, and Sigma-Aldrich, respectively.

Poly(γ-glutamic acid) As an Adsorbent. The acid form of γ-PGA produced from *Bacillus subtilis* var. Natto was supplied by Vedan Enterprise Corp. (Taichung, Taiwan), and a detailed procedure for synthesis of γ-PGA and its physicochemical characteristics were reported elsewhere.[15] Briefly, the γ-PGA was synthesized by a salvage bioconversion pathway through submerged fermentation generating γ-PGA mostly during the stationary phase of cell growth, and its physicochemical characteristics as provided by the manufacturer are as follows: physical appearance, white and granulate free flow powder; MW, 990 kDa; purity, 95%; particle size, 1−150 μm; clarity (OD_{400}), 0.18; moisture content, 5%; bulk density, 0.32 mg/mL; decolorizing ability (methylene blue dye), 135 mg/g; total heavy metal (as Pb), 15 mg/L; *Escherichia coli* and *Salmonella*, not detectable/1 g; pH_{zpc} value, 4.09; elemental analysis (found/calculated, %): 44.86/46.51 C; 5.91/5.43 H; 10.49/10.85 N; 0/0 S.

Batch-Mode Adsorption Experiments and Aluminum Analysis. Aluminum adsorption experiments by γ-PGA were carried out in a batch-mode by preparing initially 1000 mg/L stock solution using 6.3408 g of aluminum sulfate (Formula weight: 342.15 g) and eventually diluting with deionized water to obtain working solutions with specific concentration. Then, 50 mL of aluminum solution was taken in 125 mL Erlenmeyer flasks and the solution pH was adjusted to a desired value using a Suntex 701 pH meter (Suntex Instruments Co., Ltd., Taipei, Taiwan) connected with a Horiba 9611-10D glass electrode (Horiba Instruments Inc., CA). To the aluminum solution, a known weight of γ-PGA was added, followed by shaking in a Firstek B601D reciprocating water bath shaker (Firstek Scientific Co., Tau-Yen, Taiwan) for predetermined time intervals with speed at 150 rpm and temperature at 37 °C, and filtration through a 0.2 μm membrane filter, and the filtrate was analyzed for aluminum concentration. After several trial experiments were performed, a γ-PGA dose of 0.6 g/L was chosen based on the concentration range (5−100 mg/L) used in the equilibrium study. Blank experiments without addition of γ-PGA were also performed to nullify the possible adsorption of aluminum on experimental flask and membrane filter.

For determination of aluminum in solution, a colorimetric method reported by Rizk et al.[18] was modified and used. To 5 mL of aluminum solution, 2 mL of acetate buffer (pH 5.5), 1 mL of 0.1% (w/v) thiourea, and 2 mL of 0.002 M SPADNS reagent were added sequentially for development of purple color. Next, the intensity of color, which is directly proportional to aluminum concentration in solution, was measured using a Beckman DU 640 spectrophotometer (Beckman Instruments Inc., CA) at a wavelength of 580 nm. Prior to adsorption experiments, a calibration curve for a range of aluminum concentration (0.25−5.0 mg/L) was developed and a linear regression equation ($y = 0.2887x + 0.0377$, $r^2 = 0.995$) obtained was used for quantitative determination of aluminum (Figure 1).

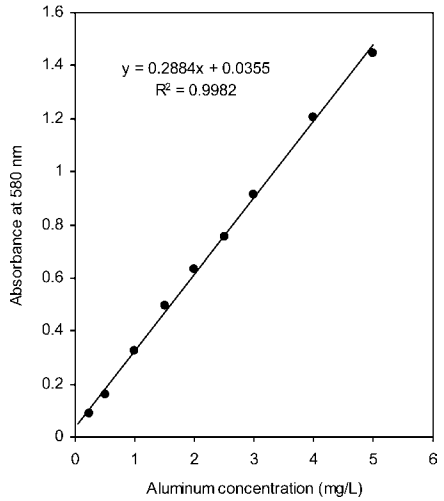

Figure 1. Standard calibration curve for aluminum obtained for a concentration range of 0.25−5.0 mg/L at 580 nm.

Scanning Electron Microscopy. Scanning electron microscopic (SEM) images of pure γ-PGA and aluminum-adsorbed γ-PGA were recorded by adding a few milligrams of each sample in dichloromethane and casting 1 μL of dispersed sample on a silicon wafer. After drying overnight, the samples were coated with platinum using Auto Fine Coater (JEO, JFC-1600, Japan) at 10 mA for 90 s and placed on the sample mount for capturing images using a JEOL JSM-6700F SEM instrument (Japan) at 10 kV. In addition, the energy dispersive X-ray spectroscopy (EDX) was done for aluminum-adsorbed γ-PGA by using an EDX machine from Oxford Instruments (X-max, Oxfordshire, U.K.) connected to the SEM instrument.

Aluminum Adsorption at Different pH. Fifty milliliters of aluminum solutions were adjusted to different pH values at 1, 1.5, 2, 2.5, 3, 3.5, 4, 5, 6, and 7 and shaken with 0.6 g/L of γ-PGA for 2 h at 37 °C. After equilibrium, the aluminum-loaded γ-PGA was filtered for analyzing free aluminum in solution. As precipitation of aluminum as aluminum hydroxide occurred at pH > 4, the pH of aluminum solution was adjusted to pH 4 in all the other adsorption experiments.

Aluminum Adsorption Kinetics. Adsorption kinetics was conducted at two different aluminum concentrations (10 and 50

mg/L) by adjusting 50 mL of aluminum solutions to pH 4 and shaking with 0.6 g/L γ-PGA at 37 °C for different intervals of time (1, 2, 5, 10, 20, 30, 60, 90, and 120 min). After each predetermined time interval, a portion of the aliquot was collected, filtered, and analyzed for aluminum remaining in solution.

Aluminum Adsorption Isotherms and Determination of Thermodynamic Parameters. For developing adsorption isotherms, the equilibrium data were obtained at 9 different aluminum concentrations (5, 10, 20, 30, 40, 50, 60, 80, and 100 mg/L) by adjusting each to pH 4 first, followed by adding 0.6 g/L γ-PGA and shaking for 2 h in a 37 °C water bath. At equilibrium, the unadsorbed aluminum in solution was analyzed for determination of adsorption capacity at each concentration. To determine the thermodynamic parameters such as enthalpy change ($\Delta H°$), entropy change ($\Delta S°$), and free energy change ($\Delta G°$), the adsorption isotherms were also constructed at two different temperatures (25 and 50 °C) and the equilibrium constants obtained were fitted into the classical Van't Hoff equation and Gibbs free energy equation.[17]

Aluminum Adsorption at Different Ionic Strengths. Aluminum removal as affected by the ionic strength encountered in biological matrix was studied based on a method reported by Inbaraj and Chen.[13] Briefly, aluminum solution at 50 mg/L was spiked into four different concentrations (0.001, 0.01, 0.1, and 1 M) of sodium acetate solution and adjusted to pH 4.0. Then, 0.6 g/L γ-PGA was added to each mixture, shaken for 2 h at 37 °C, and filtered and residual aluminum in solution was determined.

Aluminum Adsorption As Affected by Essential Metals. The effect of several biologically essential metals (potassium, calcium, zinc, iron, and copper) on aluminum adsorption by γ-PGA was studied by taking a 1:1 mixture of aluminum and an essential metal as a bisolute system at four different concentrations (5, 25, 50, and 100 mg/L) and adjusting the pH of each to 4.0. To the binary mixture, 0.6 g/L of γ-PGA was added and shaken for 2 h in a 37 °C water bath.

Aluminum Adsorption from Simulated Gastrointestinal Fluid. Initially, gastrointestinal fluid was simulated by adopting a method prescribed by US Pharmacopeia for drug dissolution studies and eventually modified as reported by Inbaraj and Chen.[13] The simulation of GIF involved mixing sodium chloride, hydrochloric acid, and pepsin for a final concentration of 0.03 M, 0.085 M, and 0.32% (w/v), respectively. For assessing the adsorption efficiency of γ-PGA toward aluminum at different gastrointestinal pH, the aluminum solution at 50 mg/L was spiked into GIF, followed by adjusting to different pH values 1, 2, 3, 3.5, and 4, adding 0.6 g/L γ-PGA to each, shaking for 2 h at 37 °C, and analyzing the filtrate for residual aluminum in GIF. Adsorption isotherm was also developed by preparing 9 different aluminum concentrations (5, 10, 20, 30, 40, 50, 60, 80, and 100 mg/L) in GIF, adjusting to pH 4.0, shaking with 0.6 g/L γ-PGA for 2 h, and determining the remaining free aluminum in GIF after adsorption to γ-PGA.

Aluminum Release at Different pH. To elucidate the nature of aluminum adsorption on γ-PGA, aluminum release from aluminum-adsorbed γ-PGA was studied by initially conducting an adsorption experiment with a mixture of 50 mg/L aluminum solution (50 mL) and 0.6 g/L γ-PGA shaking for 2 h at 37 °C. After equilibrium, the aluminum-adsorbed γ-PGA was carefully separated and the supernatant was measured for aluminum concentration. The aluminum-adsorbed γ-PGA was then washed several times with deionized water to remove any unadsorbed aluminum and shaken with 50 mL of deionized water adjusted to different pH values (1, 2, 3, 4, and 5) for 1 h for determining the level of aluminum release.

Data Analyses and Modeling. All the adsorption experiments were carried out in duplicate, and the mean values showed a maximum deviation of only ±5%. Aluminum adsorption capacity at different time intervals (q_t, mg/g) was determined based on the mass balance equation, $q_t = (C_i - C_t)/(V/W)$, where C_i and C_t are aluminum concentration at time 0 and time t, respectively, V (L) is the volume of aluminum solution, and W (g) is the weight of γ-PGA. Similarly, by replacing C_t with C_e and q_t with q_e, aluminum adsorption at equilibrium can be calculated using the equation $q_e = (C_i - C_e)/(V/W)$, where C_e and q_e are concentration and adsorption capacity at equilibrium, respectively.[13,14] Both kinetic and isotherm data were fitted with several theoretical models by using a GNUPLOT program (Copyright Thomas Williams and Colin Kelley, version 4.0 for windows) involving a nonlinear regression method based on the Marquardt–Levenberg algorithm.[13,14] The extent of deviation of theoretical models from experimental data was estimated by obtaining coefficient of determination (r^2) directly from Microsoft Excel and chi-square statistic (χ^2) by substituting the experimental (q_{ex}, mg/g) and predicted (q_{pr}, mg/g) adsorption capacities in the equation $\chi^2 = \sum((q_{ex} - q_{pr})^2/q_{pr})$.[14,17]

RESULTS AND DISCUSSION

Scanning Electron Microscopy for Pure γ-PGA and Aluminum-Adsorbed γ-PGA. Scanning electron microscopic images were recorded for pure γ-PGA and aluminum-adsorbed γ-PGA to visualize the surface changes (Figures 2A and 2B). In addition, the energy dispersive X-ray spectroscopy (EDX) was done for aluminum-adsorbed γ-PGA to confirm aluminum adsorption and its elemental weight percentage on the γ-PGA surface (Figure 2C). The surface of pure γ-PGA seems to be smooth and soft, while aluminum-adsorbed γ-PGA appears rough and agglomerated probably because of conformational change from helix into random coil during aluminum

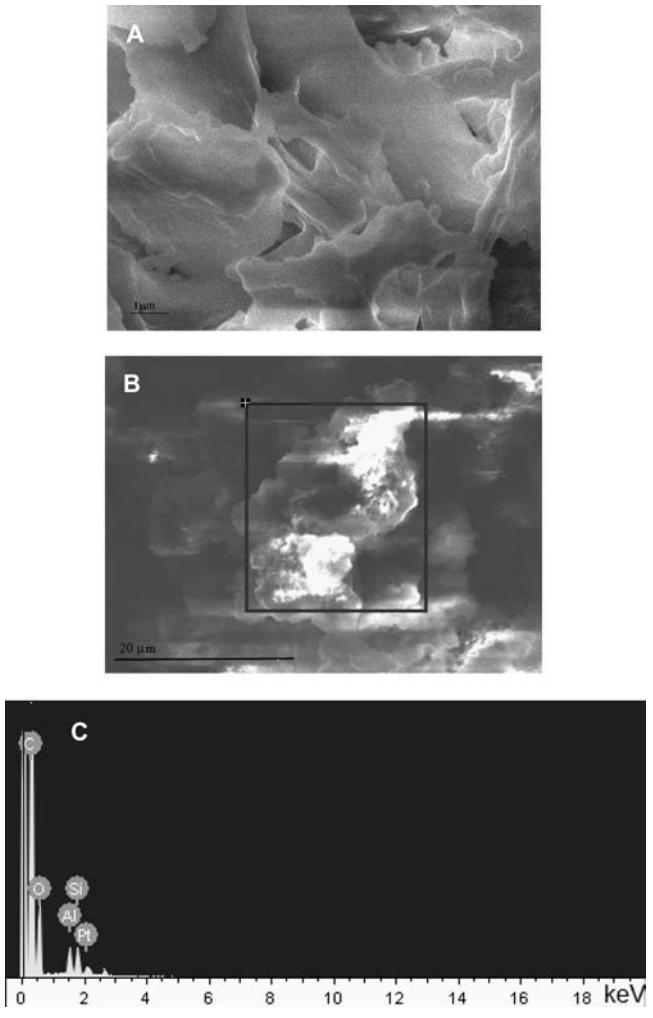

Figure 2. Scanning electron microscopic images of pure γ-PGA (A) and aluminum-adsorbed γ-PGA (B) along with energy dispersive X-ray spectra for aluminum-adsorbed γ-PGA (C). The conditions used for measurements are provided in the text.

dx.doi.org/10.1021/jf5011484 | J. Agric. Food Chem. 2014, 62, 4803–4811

adsorption under the experimental conditions studied.[14,15] The EDX analysis revealed the presence of carbon, oxygen, aluminum, platinum, and silicon at a weight percentage of 63.65, 29.53, 2.55, 2.29, and 1.98%, respectively, confirming adsorption of aluminum on γ-PGA. The presence of carbon and oxygen at high proportion may be attributed to γ-PGA, while the appearance of silicon and platinum peaks should be due to sample casting on silicon wafer and platinum coating steps carried out during sample preparation.

Aluminum Adsorption at Different pH. Given the wide variation in gastrointestinal pH (from highly acidic to slightly basic), an oral therapeutic drug undergoes interaction with varying pH conditions upon administration into the human body.[13,14,19] According to metal−solution chemistry, the variation in pH can affect the speciation of metal and stability of metal complexes.[13] Besides, for a multifunctional polymer like γ-PGA, pH can affect the dissociation ability of functional groups and structural conformation.[20] As mentioned before, the adsorption of aluminum by γ-PGA was studied as a function of different pH (1−7) (Figure 3), which showed an insignificant

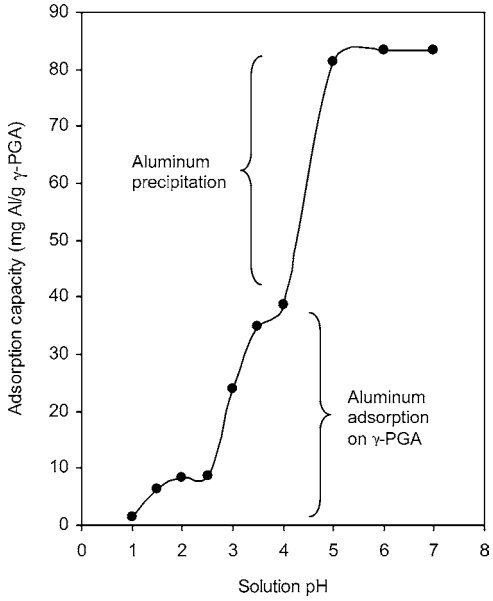

Figure 3. Influence of solution pH on aluminum adsorption by γ-PGA. Initial aluminum concentration, 50 mg/L; pH range, 1−7; γ-PGA dose, 0.6 g/L; temperature, 37 °C; shaking time, 2 h.

adsorption at pH 1, but climbed to 6.2−8.8 mg/g over the pH range 1.5−2.5 (stomach pH). However, a drastic increase in adsorption of aluminum did occur thereafter reaching a small plateau between pH 3.5 and 4. At pH > 4, a large increase in aluminum removal was mainly due to precipitation of aluminum rather than adsorption onto γ-PGA. This tendency can be attributed to the inherent characteristic of aluminum to precipitate as aluminum hydroxide ($Al(OH)_3$) through gradual formation of $Al(OH)^{2+}$ and $Al(OH)_2^{+}$.[3,7] As the maximum adsorption of aluminum on γ-PGA occurred in the pH range 3.5−4, all the subsequent studies were carried out after adjusting the aluminum solution to pH 4.

Upon raising the pH from 2.5 to 4, the adsorption of aluminum by γ-PGA reached 38.7 mg/g. Both solution pH and pH_{zpc} values are the critical factors responsible for the cation adsorption ability by materials rich in carboxyl groups.[13,14] Consequently, at pH < pH_{zpc} of γ-PGA (4.09),[14,15] the carboxyl groups in γ-PGA exist primarily in un-ionized form, thereby allowing only a low degree of metal adsorption at pH < 2.5. In addition, the γ-PGA's ability to form intramolecular hydrogen bonding because of helix conformation at acidic pH may also reduce active sites for cation adsorption.[14] Nevertheless, a more pronounced adsorption of aluminum by γ-PGA at pH > 2.5 may be due to gradual ionization of carboxyl groups in γ-PGA accompanied by a conformational transformation from helix to random coil. It is worth pointing out that when the solution pH is the same as pH_{zpc}, there is an equilibrium existence of 50% ionized and 50% un-ionized carboxyl groups in γ-PGA. Therefore, it is possible that some carboxyl groups may remain ionized even at pH < pH_{zpc}, resulting in a low degree of aluminum adsorption at pH ≤ 2.5. Additionally, the interaction between aluminum and γ-PGA at different pH levels may cause significant change in helix−coil transition thereby favoring aluminum adsorption by γ-PGA even at pH ≤ pH_{zpc}. The aluminum adsorption by γ-PGA can also be explained based on the Pearson's hard soft acid base (HSAB) principle,[14,21] which postulates that hard acids prefer to bind a hard base through ionic interaction, while soft acids prefer a soft base through covalent interaction. Accordingly, aluminum being a hard acid can interact with a hard base like carboxylate anions in γ-PGA through ionic interaction.

Although the adsorption of aluminum by γ-PGA was not practically feasible by in vitro study under physiological pH conditions ranging from 5.5 to 7.4, several in vivo studies have demonstrated an increased aluminum bioavailability during simultaneous administration of aluminum hydroxide and fruit juices or organic acids (citric, ascorbic, and glutamic acids).[7−10] It was also reported that aluminum-complexing dietary compounds in conjugation with gastric acid can solubilize aluminum cations through formation of soluble aluminum complex, thereby elevating aluminum absorption and bioavailability.[9,10] Moreover, in a study on in vitro adsorption of lead and cadmium by γ-PGA, Siao et al.[14] have shown a maximum adsorption in the pH ranging from 4 to 7, indicating that γ-PGA can bind with a metal cation in most of the physiological pH. Nonetheless, the maximum adsorption over a narrow pH range (pH 3.4−4) in this study should be due to tendency of aluminum to precipitate at pH > 4 rather than the inability of γ-PGA to bind aluminum. Moreover, as the pH_{zpc} of γ-PGA is 4.09, the adsorption capacity of aluminum by γ-PGA at pH 4 was due to only 50% ionized carboxyl groups in γ-PGA, which could greatly be enhanced at pH > 4 if the precipitation of aluminum is overcome by complexation with dietary ligands under in vivo gastrointestinal conditions as stated above. Therefore, irrespective of physiological pH, γ-PGA can still be used for aluminum adsorption under in vivo condition.

Aluminum Adsorption Kinetics. Studying the kinetics of aluminum adsorption on γ-PGA is vital for elucidating γ-PGA reactivity and assessing therapeutic efficiency as both the residence time and aluminum absorption in the human body depend on the rate of aluminum uptake.[13,14] Figure 4 illustrates the kinetics for adsorption of aluminum at two different concentrations (10 and 50 mg/L) with a rapid uptake of 81% for 10 mg/L and 96% for 50 mg/L being attained within 1 min and an equilibrium reached thereafter at 5 and 10 min, respectively. This fast adsorption characteristic of γ-PGA implies that the aluminum uptake is mainly caused by mass transfer onto γ-PGA surface with no intraparticle diffusion, which is advantageous for treatment of patients with acute aluminum intoxication. For a low aluminum concentration of

dx.doi.org/10.1021/jf5011484 | J. Agric. Food Chem. 2014, 62, 4803−4811

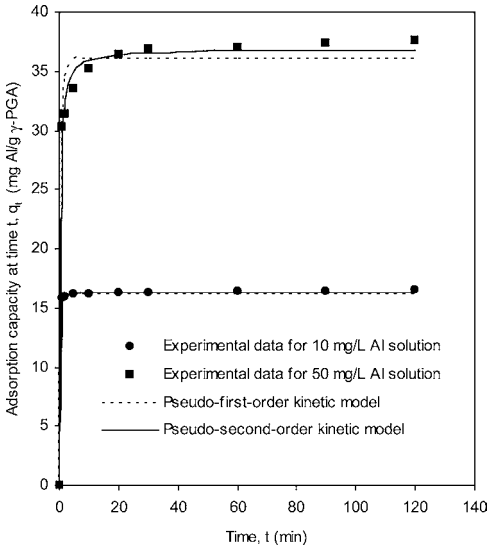

Figure 4. Kinetic profiles and their modeling for aluminum adsorption by γ-PGA. Initial aluminum concentration, 10 and 50 mg/L; pH, 4.0; γ-PGA dose, 0.6 g/L; temperature, 37 °C; shaking time intervals, 1, 2, 5, 10, 20, 30, 60, 90, and 120 min.

50 ppb, a comparable rapid kinetics of 90% and 70% aluminum adsorption within 5−10 min was shown for two different chelating resins iontosorb oxin and polyhydroxamic acid, respectively.[22] Nevertheless, a much slower adsorption rate of 300 min for 20 mg/L and 180 min for 50 mg/L was observed for aluminum uptake by chitosan[7] and date-pit activated carbon,[23] respectively. In order to determine the rate constant and adsorption capacity, the kinetic data were fitted with two classical kinetic models, namely, pseudo-first-order model (eq 1) and pseudo-second-order model (eq 2), and their nonlinear forms are shown below:[13,14,17]

$$q_t = q_e[1 - \exp(-k_1 t)] \quad (1)$$

$$q_t = \frac{t}{\frac{1}{k_2 q_e^2} + \frac{t}{q_e}} \quad (2)$$

where k_1 (L/min) and k_2 (g/mg·min) are the pseudo-first-order and pseudo-second-order rate constants, respectively. Based on error parameters, for 10 mg/L, both pseudo-first-order and pseudo-second order model precisely fitted the kinetic data, with r^2 and χ^2 being 0.998 and 0.024 for the former and 0.999 and 0.003 for the latter, whereas the pseudo-second-order model (r^2 = 0.994, χ^2 = 0.205) fitted the kinetic data for 50 mg/L better than the pseudo-first-order model (r^2 = 0.978, χ^2 = 0.741). This outcome revealed a dominant ion exchange mechanism involving carboxyl groups at low aluminum concentration.[14] On the contrary, at a higher aluminum concentration, the adsorption of aluminum onto γ-PGA may also involve chemical forces through participation of amide groups, as the pseudo-second-order model is usually applied to reactions involving valence forces via sharing or exchange of electrons.[13,14] The adsorption rate as determined by the pseudo-first-order and pseudo-second-order models were 15.142 L/min (k_1) and 1.587 g/mg·min (k_2) for 10 mg/L, respectively, while a relatively lower rate was observed for 50 mg/L (k_1 = 1.644 L/min, k_2 = 0.1018 g/mg·min). Likewise, an adsorption capacity of 16.35 mg/g for 10 mg/L and 36.89 mg/g for 50 mg/L was predicted by the pseudo-second-order model.

Adsorption Isotherms. Adsorption isotherms aid in elucidating the interaction behavior between aluminum and γ-PGA, adsorption affinity, adsorption mechanism, and maximum adsorption capacity, which is the key parameter used for comparative evaluation of materials applied as chelators or adsorbents for toxin removal.[13,14] Because of precipitation of aluminum at pH > 4, adsorption isotherms were developed at pH 4 in order to represent the gastrointestinal environment

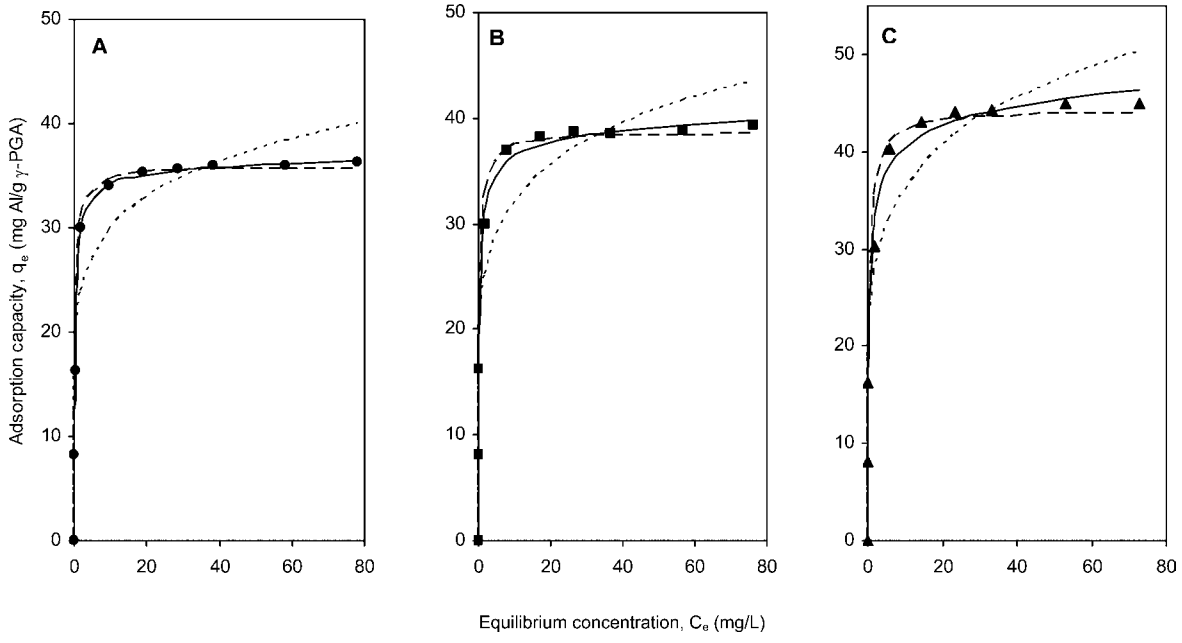

Figure 5. Adsorption isotherms for aluminum uptake by γ-PGA developed at 25 °C (A), 37 °C (B), and 50 °C (C). Initial aluminum concentration, 5−100 mg/L; pH, 4.0; γ-PGA dose, 0.6 g/L; shaking time, 2 h; (●), (■), and (▲) represent experimental data at 25, 37, and 50 °C, respectively. Modeling curves: (- - -), Freundlich isotherm; (− − −) Langmuir isotherm; (—), Redlich−Peterson isotherm.

dx.doi.org/10.1021/jf5011484 | J. Agric. Food Chem. 2014, 62, 4803−4811

(5.5−7.4), as precipitated aluminum can complex with several dietary constituents in the human body leading to formation of more soluble aluminum complex and eventual absorption,[7−10] as pointed out in a preceding section. Figure 5 illustrates the adsorption isotherms developed at three different temperatures (25, 37, and 50 °C) over a range of aluminum concentration (5−100 mg/L). The isotherm at 37 °C was developed to represent the physiological temperature, while both 25 and 50 °C were constructed to facilitate determination of thermodynamic parameters. Following a rise in aluminum level from 5 to 100 mg/L, the amount of aluminum adsorption increased from 8.18 to 36.23 mg/g, 8.19 to 39.39 mg/g, and 8.21 to 45.05 mg/g at 25, 37, and 50 °C, respectively (Figure 5), with an apparent elevation in adsorption at higher temperatures indicating an endothermic nature of the adsorption process. Comparison of the isotherm shapes with that reported by Giles et al.[24] revealed an H-type isotherm, which is an extreme case of L-type (Langmuir type), implying occurrence of chemical forces during aluminum adsorption by γ-PGA.[13] Moreover, such an isotherm shape represents a high adsorption capacity at low aluminum concentrations.[14]

Three classical isotherm models, namely, Freundlich (eq 3), Langmuir (eq 4), and Redlich−Peterson (eq 5), were employed to model the isotherm data and obtain some vital information on adsorption characteristics. The nonlinear form of these theoretical isotherm models can be represented as shown in eqs 3−5:[25−27]

$$q_e = K_F C_e^{1/n} \quad (3)$$

$$q_e = \frac{K_L C_e}{1 + K_e C_e} \quad (4)$$

$$q_e = \frac{K_R C_e}{1 + a_R C_e^{\alpha}} \quad (5)$$

where K_F (L^n mg^{1-n}/g) and n are the Freundlich constants denoting adsorption capacity and adsorption intensity, respectively; K_L (L/g) is a product of q_m (mg/g) and K_e (L/mg), representing maximum adsorption capacity and equilibrium constant or adsorption energy, respectively; and K_R, a_R, and α are the Redlich−Peterson constants. Of the three models fitted by the nonlinear regression method, both Langmuir and Redlich−Peterson models could more precisely describe the experimental data at all the three temperatures, as shown by high r^2 values and low χ^2 values compared to the Freundlich model (Figure 5 and Table 1). The best fit by Langmuir model revealed monolayer adsorption of aluminum on γ-PGA without precipitation of aluminum under the experimental conditions studied. The maximum adsorption capacity (q_m) values predicted by the Langmuir model were 35.85, 38.68, and 44.23 mg/g for aluminum adsorption by γ-PGA at 25, 37, and 50 °C, respectively, while the equilibrium adsorption constants were 3.275, 2.989, and 2.188 L/mg. Comparable q_m values of 45.45, 41.32, and 37.17 mg/g were reported for aluminum adsorption by chitosan at 30, 45, and 60 °C, respectively.[7] However, a very low q_m value was reported for several adsorbents including *Curcuma longa* (7.68 mg/g),[2] polyacrylonitrile powder and beads (0.09−0.82 mg/g),[28] date-pit activated carbon (5.83 mg/g),[23] and rice husk char (2.84 mg/g).[29]

Favorability of Aluminum Adsorption by γ-PGA. The adsorption intensity (n) obtained from the Freundlich model (6.1−7.1) ranged between 1 and 10, indicating favorable adsorption of aluminum by γ-PGA. Furthermore, based on the 4 idealized types of equilibrium behavior proposed by Hall et al.,[30] the behavior of each equilibrium type can be explained using a dimensionless equilibrium parameter or separation factor R_L, represented as $R_L = 1/(1 + bC_o)$ where b (L/mg) is the Langmuir constant. Accordingly, the R_L value indicates the shape of the isotherm to be either unfavorable ($R_L > 1$) or linear ($R_L = 1$) or favorable ($0 < R_L < 1$) or irreversible ($R_L = 0$).[20,30] Based on the equilibrium constant predicted by the Langmuir model, the R_L values were calculated to be from 0.003 to 0.058 at 25 °C, 0.003 to 0.063 at 37 °C, and 0.005 to 0.084 at 50 °C, suggesting that a favorable adsorption ($0 < R_L < 1$) of aluminum by γ-PGA occurred (Table 2).

Thermodynamic Parameters. To understand the thermodynamic aspects of aluminum adsorption by γ-PGA, the equilibrium constant (b) values obtained from the Langmuir modeling were fitted into the classical Van't Hoff equation (eq 6) and Gibbs free energy equation (eq 7) for determination of

Table 1. Predicted Isotherm Parameters for Aluminum Adsorption by PGA at Three Different Temperatures (25, 37, and 50 °C)[a]

	predicted isotherm parameters		
	25 °C	37 °C	50 °C
	Freundlich		
K_F (L^n mg^{1-n}/g)	21.68	22.87	24.89
n	0.14	0.15	0.16
r^2	0.842	0.857	0.879
χ^2	6.39	6.80	7.65
	Langmuir		
K_L (L/g)	117.41	115.61	96.76
K_e (L/mg)	3.275	2.989	2.188
r^2	0.997	0.988	0.975
χ^2	0.11	0.48	2.04
	Redlich−Peterson		
K_R (L/g)	129.79	138.55	141.15
a_R $(L/mg)^{\alpha}$	3.86	3.99	3.83
α	0.98	0.97	0.95
r^2	0.999	0.995	0.988
χ^2	0.04	0.20	0.55

[a]Isotherm model equations are provided in the text.

Table 2. Adsorption Favorability Data or Separation Factor (R_L) at Different Aluminum Concentrations and Temperatures

	adsorption favorability or separation factor (R_L)[a]		
aluminum concn (mg/L)	25 °C	37 °C	50 °C
5	0.058	0.063	0.084
10	0.030	0.032	0.044
20	0.015	0.016	0.022
30	0.010	0.011	0.015
40	0.008	0.008	0.011
50	0.006	0.007	0.009
60	0.005	0.006	0.008
80	0.004	0.004	0.006
100	0.003	0.003	0.005

[a]Equation for calculating separation factor (R_L) is provided in the text.

dx.doi.org/10.1021/jf5011484 | J. Agric. Food Chem. 2014, 62, 4803−4811

enthalpy change ($\Delta H°$), entropy change ($\Delta S°$), and free energy change ($\Delta G°$):[17]

$$\Delta G° = - RT \ln K_e \quad (6)$$

$$\ln K_e = - \frac{\Delta H°}{RT} + \frac{\Delta S°}{R} \quad (7)$$

where T is the absolute temperature (K), R is the universal gas constant (8.314 J/(mol K)), and K_e (L/mol) is the equilibrium constant. The negative $\Delta G°$ values of −11.10, −11.32, and −10.95 kJ/mol for 25, 37, and 50 °C, respectively, indicated the spontaneous nature of aluminum adsorption on γ-PGA. Both $\Delta H°$ and $\Delta S°$ can be deduced by plotting ln K_e versus $1/T$ (plot not shown), and the positive $\Delta H°$ value obtained (12.91 kJ/mol) confirmed the endothermic nature of aluminum adsorption. Likewise, the positive $\Delta S°$ (5.76 J/(mol K)) implied increased randomness (decreased orderliness) at the γ-PGA/aluminum solution interface. However, an opposite trend of negative $\Delta H°$ and $\Delta S°$ values were shown for aluminum adsorption by chitosan.[7]

Aluminum Adsorption at Different Ionic Strengths. Ionic strength in biological matrices like blood and urine vary widely when compared to that in most natural waters,[13,19] and therefore it is essential to study the impact of varying ionic strengths on aluminum adsorption by γ-PGA. More importantly, some ion-exchange resins currently employed as oral drugs for toxin removal undergo either swelling or shrinking depending on the ionic strength, ultimately hampering their therapeutic application.[13,19] The aluminum adsorption ability of γ-PGA was evaluated in the presence of varying ionic strengths (0.001−1 M) prepared using different concentrations of sodium acetate. The amount of aluminum adsorption in 0.001 M sodium acetate (38.77 mg/g) did not significantly change when compared to control without sodium acetate (38.67 mg/g). However, the adsorption capacity climbed to 47.12, 50.35, and 49.42 mg/g in 0.01, 0.1, and 1 M solution, respectively. This outcome implied that the varying ionic strengths might not reduce the aluminum adsorption ability of γ-PGA, but elevated its adsorption capacity instead.

Aluminum Adsorption As Affected by Essential Metals. Chelators currently employed in detoxification therapy not only bind the target metal but also remove significant amounts of essential minerals, thereby causing deficiency of essential minerals in the human body.[13,14,19] Consequently, the effect of five essential metals including potassium, calcium, zinc, iron, and copper was studied in a bisolute system incorporating a 1:1 mixture of aluminum:essential metal at four different concentrations (5, 25, 50, and 100 mg/L) (Figure 6). Though sodium is a biologically important essential metal, it was not used for evaluating the effect of essential metals, as sodium salts such as sodium sulfate and sodium chloride were already used in determining both effect of different ionic strengths and simulated gastrointestinal fluid in this study. However, another monovalent alkali metal, potassium, was used instead. Aluminum adsorption by γ-PGA in the presence of essential metals did not show any interference at 5 mg/L for all the essential metals except copper, which reduced the aluminum adsorption by 31.2% when compared to control. Nevertheless, when the concentration rose to 25 mg/L, the aluminum adsorption diminished by 4.4, 4.8, 15.3, 17.9, and 25.8% for potassium, calcium, zinc, iron, and copper, respectively (Figure 6). At 50 and 100 mg/L, the amount of aluminum adsorption by γ-PGA further dropped by 4.2 and 5.7% for potassium, 30.3 and 37.7% for calcium, 31.2 and 55.6% for zinc, 34.2 and 70.7% for iron, and 69.4 and 79.3% for copper, with the impact of essential metals on aluminum adsorption following the order copper > iron > zinc > calcium > potassium (Figure 6). As aluminum adsorption was shown previously to involve ionic interaction, this phenomenon can be explained based on comparison of the electronegativity values of these essential metal ions with aluminum. Among all the 5 metals, the copper, zinc, and iron possessing high electronegativity values of 1.75, 1.66, and 1.64 showed a larger impact on aluminum adsorption, as was only 1.47 for aluminum. Apparently, a lesser interfering effect shown by calcium and potassium may be due to their relatively low electronegativity values, which equaled 1.04 and 0.91, respectively. Nevertheless, by appropriate supplementation of essential metal ions, the loss of aluminum adsorption efficiency by γ-PGA could be prevented during in vivo application.

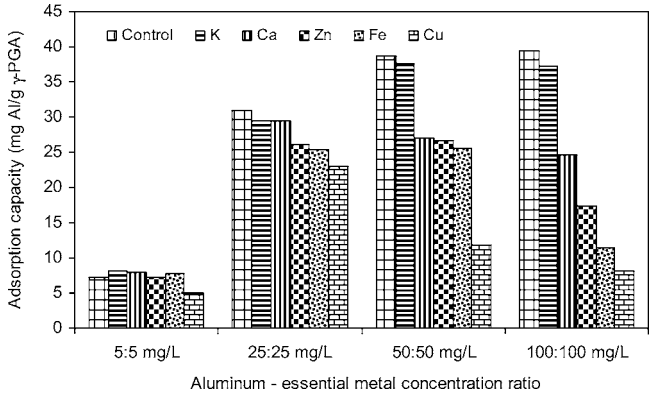

Figure 6. Influence of different essential metals on aluminum adsorption by γ-PGA. Initial aluminum:essential metal concentration, 5:5, 25:25, 50:50, and 100:100 mg/L; γ-PGA dose, 0.6 g/L; pH, 4.0; temperature, 37 °C; shaking time, 2 h.

Aluminum Adsorption from Simulated Gastrointestinal Fluid. In order to understand the effect of gastrointestinal environment, the aluminum adsorption capability of γ-PGA as affected by pH and different aluminum concentrations was determined in simulated GIF. Figure 7A shows the effect of solution pH on the aluminum adsorption efficiency by γ-PGA in GIF along with that in deionized water shown in dotted lines for comparison. A similar trend was observed for both GIF and deionized water, with the adsorption capacity exceeding at all pH levels (1−4) for the former. This outcome should be beneficial for in vivo application. Following a rise in the solution pH from 1 to 4, the adsorption capacity of aluminum from GIF soared from 5.43 to 50.23 mg/g, which was 73.7 to 23% higher than that for deionized water (Figure 7A). As GIF was rich in sodium ions (0.03 M), the high adsorption capacity of aluminum by γ-PGA in comparison with deionized water may be attributed to the extra mobility gained by aluminum ions through competition with sodium ions. Obviously, the ionic radius of sodium (97 pm) being higher than that of aluminum (51 pm) should compete effectively for the active sites on γ-PGA. Yet, when compared to monovalent sodium ions, the trivalent aluminum existing as $Al[(H_2O)_6]^{3+}$ at pH ≤ 4 should succeed in attaching onto γ-PGA through ionic interaction with carboxyl groups.

Adsorption isotherms were also developed over a range of aluminum concentration (5−100 mg/L) for determining aluminum adsorption capacity in GIF. Figure 7B depicts the

dx.doi.org/10.1021/jf5011484 | J. Agric. Food Chem. 2014, 62, 4803−4811

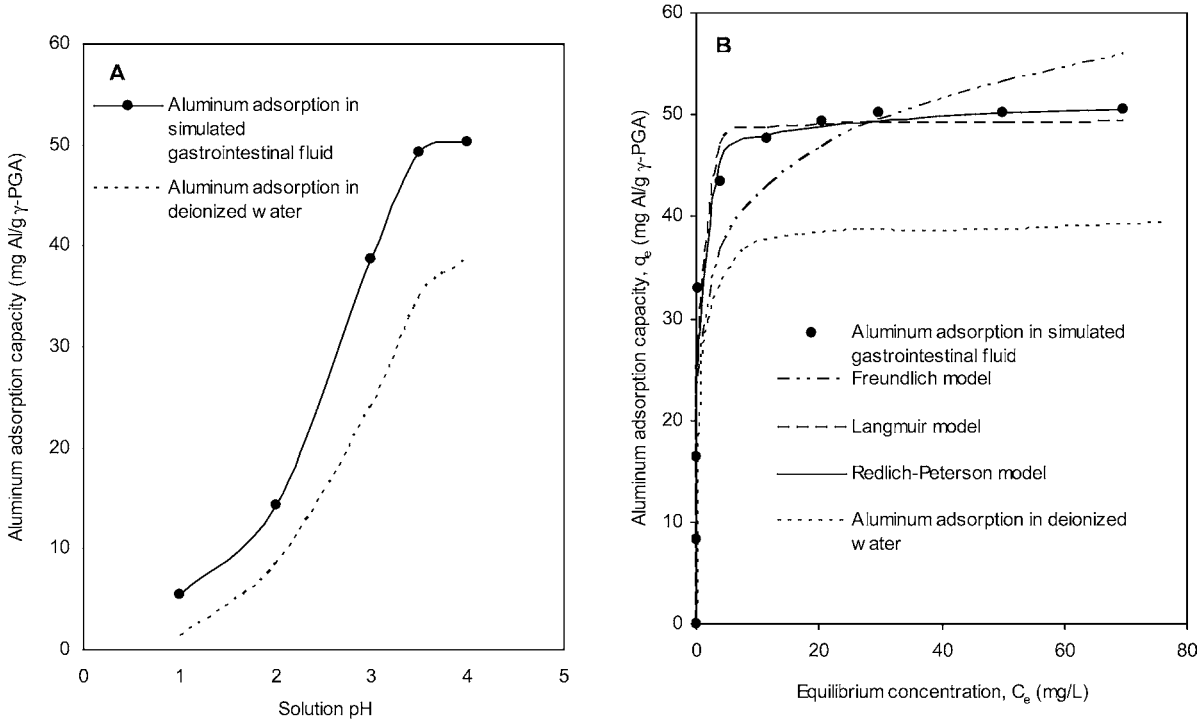

Figure 7. Influence of solution pH (A) and isotherms (B) for aluminum adsorption from simulated gastrointestinal fluid as compared to that from deionized water. (A) Initial aluminum concentration, 50 mg/L; pH range, 1−4; γ-PGA dose, 0.6 g/L; temperature, 37 °C; shaking time, 2 h. (B) Initial aluminum concentration, 5−100 mg/L; pH, 4.0; γ-PGA dose, 0.6 g/L; temperature, 37 °C.

aluminum adsorption isotherms obtained in GIF with dotted lines showing the trend in deionized water for comparison. Upon modeling of isotherm data, both Langmuir and Redlich−Peterson models were found to fit the isotherm data for GIF more precisely than the Freundlich model, with r^2 and χ^2 being 0.964 and 2.74 for the Langmuir and 0.967 and 2.80 for the Redlich−Peterson model (Figure 7B). The maximum adsorption capacity (q_m) and equilibrium constant (K_e) obtained from the Langmuir model were 49.43 mg/g and 5.394 L/mg, respectively. The isotherms developed for GIF showed a 22% increase in q_m value compared to that for deionized water.

Aluminum Release Study. To confirm the mechanism of aluminum adsorption by γ-PGA, the aluminum release from aluminum-adsorbed γ-PGA was studied as a function of different pH. Upon lowering the pH of deionized water from 4 to 1, the percentage of aluminum release rose from 0 to 98% (Figure 8). This trend was opposite to that observed for the effect of solution pH on aluminum adsorption by γ-PGA (Figure 1), suggesting that an ionic interaction occurred through exchange of hydrogen ions during aluminum adsorption onto γ-PGA.

In conclusion, this study demonstrated that the edible biopolymer poly(γ-glutamic acid) can be used as a safe detoxifying agent for aluminum. In vitro batch-mode adsorption experiments revealed that aluminum could be adsorbed by γ-PGA at an extremely fast rate, with maximum adsorption capacity as determined by the Langmuir nonlinear fit being 44.23 and 49.43 mg/g in aqueous solution and simulated gastrointestinal fluid at 37 °C, respectively. Ionic strength variation in different biological matrices did not alter aluminum adsorption capacity, while high electronegative essential metals like copper, iron, and zinc significantly reduced aluminum adsorption. Aluminum adsorption/release at different pH values indicated electrostatic interaction through exchange of hydrogen ions as a possible mechanism for aluminum adsorption by γ-PGA.

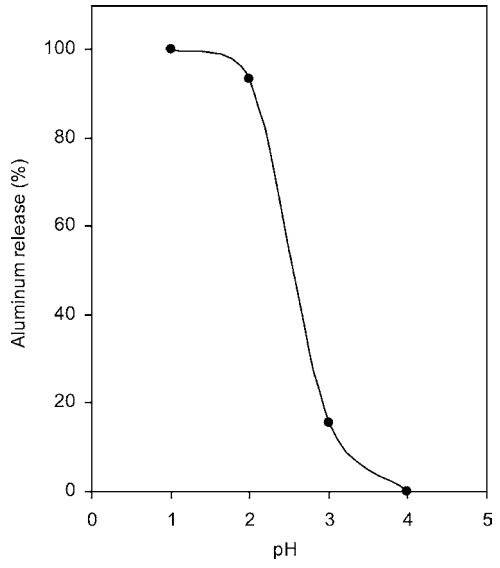

Figure 8. Influence of solution pH on aluminum release from aluminum-adsorbed γ-PGA. For adsorption study: initial aluminum concentration, 50 mg/L; γ-PGA dose, 0.6 g/L; shaking time, 1 h. For release study: release agents, deionized water adjusted to pH 1, 2, 3 and 4; shaking time, 30 min.

AUTHOR INFORMATION

Corresponding Author

*Tel: +886-2-29053626. Fax: +886-2-29051215. E-mail: 002622@mail.fju.edu.tw.

Notes

The authors declare no competing financial interest.

REFERENCES

(1) Lodeiro, P.; Gudina, A.; Herrero, L.; Herrero, R.; de Vicente, M. E. S. Aluminum removal from wastewater by refused beach cast seaweed. *J. Hazard. Mater.* **2010**, *178*, 861−866.

(2) Halim, A. A.; Ezani, E.; Othman, M. S.; Awang, N.; Ikram, M.; Ithnin, A. Adsorption study of aluminum onto *Curcuma longa*. *Aust. J. Basic Appl. Sci.* **2011**, *5*, 1170−1177.

(3) Aguilar, F.; Autrup, H.; Barlow, S.; Castle, L.; Crebelli, R.; Dekant, W.; Engel, K. H.; Gontard, N.; Gott, D.; Grilli, S.; Gurtler, R.; Larsen, J. C.; Leclercq, C.; Leblanc, J. C.; Malcata, F. X.; Mennes, W.; Milana, M. M. R.; Pratt, I.; Rietjens, P.; Tobback, P.; Toldra, F. Safety of aluminum from dietary intake. *Eur. Food Saf. Auth. J.* **2008**, *754*, 1−34.

(4) Bondy, S. C. Prolonged exposure to low levels of aluminum leads to changes associated with brain aging and neurodeneration. *Toxicology* **2014**, *315*, 1−7.

(5) Walton, J. R. Aluminum in hippocampal neurons from humans with Alzheimer's disease. *Neurotoxicology* **2006**, *27*, 385−394.

(6) Buratti, M.; Valla, C.; Pellegrino, F. M.; Rubino, A.; Colombi, A. Aluminum determination in biological fluids and dialysis concentrates via chelation with 8 hydroxyquinoline and solvent extraction/fluorimetry. *Anal. Biochem.* **2006**, *353*, 63−68.

(7) Septhum, C.; Rattanaphani, S.; Bremner, J. B.; Rattanaphani, V. An adsorption study of Al(III) ions onto chitosan. *J. Hazard. Mater.* **2007**, *148*, 185−191.

(8) Ecelbarger, C. A.; MacNeil, G. G.; Greger, J. L. Tissue aluminum accumulation and toxic consequences in rats chronically fed aluminum with and without citrate. *J. Agric. Food Chem.* **1994**, *42*, 2220−2224.

(9) Wu, X.; Li, J.; Hu, J. N.; Deng, Z. Y. The effects of glutamate and citrate on absorption and distribution of aluminum in rats. *Biol. Trace Elem. Res.* **2012**, *148*, 83−90.

(10) Domingo, J. L.; Gomez, M.; Llobet, J. M.; Corbella, J. Influence of some dietary constituents on aluminum absorption and retention in rats. *Kidney Int.* **1991**, *39*, 598−601.

(11) Shin, R. W.; Kruck, T. P.; Murayama, H.; Kitamoto, T. A novel trivalent cation chelator Feralax dissociates binding of aluminum and iron associated with hyperphosphorylated tau of Alzheimer's disease. *Brain Res.* **2003**, *961*, 139−146.

(12) McLachlan, D. R. C.; Dalton, A. J.; Kruck, T. P. A.; Bell, M. Y.; Smith, W. L.; Kalow, W.; Andrews, D. F. Intramuscular desferrioxamine in patients with Alzheimer's disease. *Lancet* **1991**, *337*, 1304−1308.

(13) Inbaraj, B. S.; Chen, B. H. In vitro removal of toxic heavy metals by poly(γ-glutamic acid)-coated superparamagnetic nanoparticles. *Int. J. Nanomed.* **2012**, *7*, 4419−4432.

(14) Siao, F. Y.; Lu, J. F.; Wang, J. S.; Inbaraj, B. S.; Chen, B. H. In vitro binding of heavy metals by an edible biopolymer poly(γ-glutamic acid). *J. Agric. Food Chem.* **2009**, *57*, 777−784.

(15) Ho, G. H.; Ho, T. I.; Hsieh, K. H.; Su, Y. C.; Lin, P. Y.; Yang, J.; Yang, K. H.; Yang, S. C. γ-Polyglutamic acid produced by *Bacillus subtilis* (natto): structural characteristics, chemical properties and biological functionalities. *J. Chin. Chem. Soc.* **2006**, *53*, 1363−1384.

(16) Shih, I. L.; Van, Y. T. The production of poly(γ-glutamic acid) from microorganisms and its various application. *Bioresour. Technol.* **2001**, *79*, 207−225.

(17) Inbaraj, B. S.; Wang, J. S.; Lu, J. F.; Siao, F. Y.; Chen, B. H. Adsorption of toxic mercury(II) by an extracellular biopolymer poly(γ-glutamic acid). *Bioresour. Technol.* **2009**, *100*, 200−207.

(18) Rizk, M.; Zakhari, N. A.; Toubar, S. S.; El Shabrawy, Y. Spectrophotometric determination of aluminum and copper ions using SPADNS. *Mikrochim. Acta* **1995**, *118*, 239−247.

(19) Yantasee, W.; Rutledge, R. D.; Chouyyok, W.; Sukwarotwat, V.; Orr, G.; Warner, C. L.; Warner, M. G.; Fryxell, G. E.; Wiacek, R. J.; Timchalk, C.; Addleman, R. S. Functionalized nanoporous silica for the removal of heavy metals from biological systems: adsorption and application. *ACS Appl. Mater. Interfaces* **2010**, *2*, 2749−2758.

(20) Inbaraj, B. S.; Chiu, C. P.; Chiu, J. T.; Ho, G. H.; Yang, J.; Chen, B. H. Effect of pH on binding of mutagenic heterocyclic amines by the natural biopolymer poly(γ-glutamic acid). *J. Agric. Food Chem.* **2006**, *54*, 6452−6459.

(21) Pearson, R. G. Hard and soft acids and bases. *J. Am. Chem. Soc.* **1963**, *85*, 3533−3539.

(22) Othman, M. N.; Abdullah, P. M. D.; Aziz, Y. F. A. Removal of aluminum from drinking water. *Sains Malays.* **2010**, *39*, 51−55.

(23) Al-Muhtaseb, S. A.; El-Naas, M. H.; Abdallah, S. Removal of aluminum from aqueous solutions by adsorption on date-pit and BDH activated carbons. *J. Hazard. Mater.* **2008**, *158*, 300−307.

(24) Giles, C. H.; MacEwan, T. H.; Nakhwa, S. N.; Smith, D. Studies in adsorption. Part XI. A system of classification of solution adsorption isotherms, and its use in diagnosis of adsorption mechanisms and in measurement of specific surface areas of solids. *J. Chem. Soc.* **1960**, *111*, 3973−3993.

(25) Freundlich, H. M. F. Über die adsorption in lösungen (Adsorption in solution). *Z. Phys. Chem.* **1906**, *57*, 384−470.

(26) Langmuir, I. The adsorption of gases on plane surfaces of glass, mica and platinum. *J. Am. Chem. Soc.* **1918**, *40*, 1361−1403.

(27) Redlich, O.; Peterson, D. L. A useful adsorption isotherm. *J. Phys. Chem.* **1959**, *63*, 1024−1026.

(28) Aly, Z.; Graulet, A.; Scales, N.; Hanley, T. Removal of aluminum from aqueous solutions using PAN-based adsorbents: characterization, kinetics, equilibrium and thermodynamic studies. *Environ. Sci. Pollut. Res.* **2014**, *21*, 3972−3986.

(29) Singh, T. S.; Parikh, B.; Pant, K. K. Investigation on the sorption of aluminum in drinking water by low-cost adsorbents. *Water SA* **2006**, *32*, 49−54.

(30) Hall, K. R.; Eagleton, L. C.; Acrivos, A.; Vermeulen, T. Pore and solid diffusion kinetics in fixed bed adsorption under constant pattern conditions. *Ind. Eng. Chem. Fundam.* **1966**, *5*, 212−219.

JOURNAL OF AGRICULTURAL AND FOOD CHEMISTRY

Article

pubs.acs.org/JAFC

Generic Characterization of Apolar Metabolites in Red Chili Peppers (*Capsicum frutescens* L.) by Orbitrap Mass Spectrometry.

Sebastiaan Bijttebier,*[,†,§] Kaouther Zhani,[‡,§] Els D'Hondt,[†] Bart Noten,[†] Nina Hermans,[§] Sandra Apers,[§] and Stefan Voorspoels[†]

[†]Business Unit Separation and Conversion Technology (SCT), Flemish Institute for Technological Research (VITO), Boeretang 200, 2400 Mol, Belgium

[‡]Department of Horticulture and Landscape, Sousse University, Higher Institute of Agronomy, 4042 Chott Mariem, Tunisia

[§]NatuRA, University of Antwerp, Universiteitsplein 1, 2610 Antwerp, Belgium

Supporting Information

ABSTRACT: The aim of the present study was to develop a generic analytical method for the identification and quantitation of apolar plant metabolites in biomass using liquid chromatography−photodiode array−accurate mass mass spectrometry (LC-PDA-amMS). During this study, a single generic sample preparation protocol was applied to extract apolar plant metabolites. Compound identification was performed using a single generic screening method for apolar compounds without the need for dedicated fractionation. Such a generic approach renders vast amounts of information and is virtually limited by only the solubility and detector response of the metabolites of interest. Method validation confirmed that this approach is applicable for quantitative purposes. Furthermore, an identification−quantitation strategy based on amMS and molar extinction coefficients was used for carotenoids, eliminating the need for reference standards for each carotenoid. To challenge the validated method, chili peppers (*Capsicum frutescens* L.) were analyzed to unravel their complex phytochemical composition (carotenoids, glycolipids, glycerolipids, capsaicinoids, lipid-soluble vitamins).

KEYWORDS: *LC-PDA-amMS, quantitation without reference standards, extinction coefficients, generic analysis of apolar plant metabolites, biomass composition, Capsicum frutescens L., carotenoids*

INTRODUCTION

Biomass such as algae and vegetables often contains natural components of high value including the so-called phytochemicals, such as antioxidants and essential oils, that are barely utilized from these resources today.[1,2] These natural products are thought to provide beneficial health effects and have an increasing sales market in the pharmaceutical, cosmetics, and food supplements industry.[3] Knowing the composition of these resources is thus an essential first step in a potential valorization process.

Because of the complexity of compound mixtures in biological samples, the usage of simple analytical instrumentation such as liquid chromatography−ultraviolet detection (LC-UV) has shifted toward more selective and more complex separation and detection systems such as ultrahigh-performance liquid chromatography−photodiode array−accurate mass mass spectrometry (UHPLC-PDA-amMS) instrumentation to achieve more definitive compound identification.[4] Accurate mass MS detectors allow the tentative identification of compounds without the use of analytical standards.[5] Because of the limited availability of analytical standards for plant metabolites, this utility has shown to be essential in natural products exploration.[6] Furthermore, modern high-end analytical instrumentation allows the detection of multiple compound classes, such as carotenoids, capsaicinoids, and glycolipids, in a single analysis, resulting in enormous time and consumables savings. To avoid compound discrimination during extraction, no cleanup steps should be used and the number of sample preparation steps should be limited as much as possible. Such a generic approach is virtually limited only by the solubility (extractability, chromatographic retention) and detector response (UV absorbance and ionization efficiency) of the compounds of interest. Furthermore, the use of a generic analytical screening application allows the setup of a compound database with specific chromatographic and spectrometric data. This database enables an effective dereplication during structure elucidation of the extract composition.[7]

The aim of the present study was to develop, optimize, and validate a generic analytical method for the identification and quantitation of apolar plant metabolites in biological matrices using UHPLC-PDA-amMS. Authentic standards of multiple phytochemical classes and various biological matrices were used to confirm and emphasize the generic character of the method. To challenge the validated method, the widely studied chili pepper matrix (*Capsicum frutescens* L.) was selected as it is known for its complex phytochemical composition (carotenoids, glycolipids, glycerolipids, capsaicinoids, lipid-soluble vitamins).[8−13] Finally, an identification−quantitation strategy based on the use of amMS data and extinction coefficients was applied for carotenoids, eliminating the need for reference standards for each carotenoid.

Received: January 17, 2014
Revised: April 23, 2014
Accepted: April 24, 2014
Published: April 24, 2014

ACS Publications © 2014 American Chemical Society

MATERIALS AND METHODS

Chemicals. LC-MS grade methanol, acetonitrile, and ethyl acetate were purchased from Biosolve (Valkenswaard, The Netherlands). Ultrapure water with a resistivity of 18.2 MΩ·cm at 25 °C was generated with a Millipore system. Dichloromethane for gas chromatography, *n*-hexane for gas chromatography, acetone for gas chromatography, sodium hydrogen carbonate, sodium hydroxide, and sodium chloride for analysis were purchased from Merck (Darmstadt, Germany). Ammonium acetate, (D-Ala^2)-leucine enkephalin, sand (quartz), and butylated hydroxytoluene were purchased from Sigma-Aldrich (Bornem, Belgium). Certified reference material BCR 485 consisting of freeze-dried mixed vegetables was bought from IRMM (Geel, Belgium). Commercially available mixtures to calibrate the mass spectrometer, that is, MSCAL5-1EA (caffeine, tetrapeptide "Met-Arg-Phe-Ala", Ultramark) for positive ion mode and MSCAL6-1EA (sodium dodecyl sulfate, taurocholic acid sodium salt, Ultramark) for negative ion mode, were purchased from Supelco (Bellefonte, PA, USA).

Lycopene, α-carotene, phytoene, lutein, zeaxanthin, tunaxanthin, astaxanthin dipalmitate, phytofluene, antheraxanthin, violaxanthin, canthaxanthin, and astaxanthin were purchased from Carotenature (Ostermundigen, Switzerland). β-Carotene, *trans*-β-apo-8′-carotenal, campesterol, stigmasterol, β-sitosterol, glyceryl trioleate, glyceryl dioleate, γ-tocopherol, α-tocopherol, phylloquinone, ergocalciferol, and cholecalciferol were purchased from Sigma-Aldrich. Glycerol dioleate and glycerol trioleate were obtained from Chem Service (West Chester, PA, USA). Monogalactosyldiacylglycerol with average MW 752.369 and digalactosyldiacylglycerol with average MW 926.767 were purchased from Avanti (Alabaster, AL. USA).

Preparation of Standard Solutions. Standard stock solutions and working solutions were prepared of each analyte separately at a concentration of approximately 200 μg/mL. Stock solutions of glyco- and glycerolipids were prepared in methanol. The stock solutions of sterols and lipid-soluble vitamins were prepared in methanol + 0.1% butylated hydroxytoluene. Stock solutions of carotenoids were prepared in dichloromethane + 0.1% butylated hydroxytoluene. Standard stock and working solutions were stored at −25 °C in the dark under an inert atmosphere (nitrogen). Dilutions of the stock solutions were prepared in dichloromethane + 0.1% butylated hydroxytoluene for analysis.

Sample Preparation. Red bell peppers (*Capsicum annuum*) and apples (*Malus domestica*) were bought in a local store. After removal of the stems and kernels, they were cut into pieces, frozen with liquid nitrogen, and immediately freeze-dried. After drying, they were milled and homogenized with a Grindomix GM 200 from Retsch (Haan, Germany) at 10000 rpm and stored in the dark under nitrogen at −25 °C.

Fruits of five chili pepper accessions (*Capsicum frutescens* L.), namely, 'Tebourba', 'Korba', 'Somâa', 'Awlad Haffouzz', and 'Souk jedid', were collected from plants cultivated in the experimental station of the Higher Institute of Agriculture, Chott Mariem, Tunisia. The peduncles of the peppers were removed, and the fruits were freeze-dried, milled, and stored at −25 °C until analysis.

Before sample preparation, the samples were allowed to equilibrate to room temperature. One gram of sample was mixed with 1 g of sodium hydrogen carbonate, spiked with *trans*-β-apo-8′-carotenal (internal standard), and mixed with sand. Ultrapure water was added until the sample was visually completely hydrated (approximately 3 mL, depending on the matrix). The mixture was kept in the dark under N_2 to allow swelling of the matrix for better analyte extraction. Afterward, the sample was mixed again with sand and loaded into a 33 mL accelerated solvent extraction (ASE) cell (Thermo Fisher Scientific, Bremen, Germany). The mixture was extracted three times (5 min static extraction) with 70:30 acetone/methanol + 0.1% butylated hydroxytoluene at 40 °C and 1050 psi, resulting in approximately 120 mL of sample extract. The three extracts were combined in a separation funnel, and 100 mL of 10% sodium chloride (aqueous) and 15 mL of hexane were added. The hexane phase was retained, and the polar phase was extracted twice more with 15 mL of hexane. The pooled hexane fractions were evaporated, dissolved in 10 mL of dichloromethane + 0.1% butylated hydroxytoluene, an aliquot was used for analysis, and the remaining extract was stored in the dark under nitrogen at −25 °C until further treatment.

For saponification 2 mL of 10% sodium hydroxide (in methanol) was added to 2 mL of dichloromethane extract and was consecutively shaken for 6 h at room temperature in the dark under an inert atmosphere. Afterward, the solution was washed five times with water to remove the alkali.[14] An aliquot of the saponified dichloromethane extract was used for analysis.

Instrumental Analysis. The analytical method was previously described[4] and is briefly summarized as follows. For analysis, 1.25 μL of extract was injected with a CTC PAL autosampler (CTC Analytics, Zwingen, Switzerland) on a 100 mm × 2.1 mm, 1.8 μm, Acquity UPLC HSS C18 SB column (Waters, Milford, MA, USA) and thermostatically (35 °C) eluted with an Accela quaternary solvent manager and a Hot Pocket column oven (Thermo Fisher Scientific, Bremen, Germany) with a chromatographic gradient. The mobile phase solvents consisted of 50:22.5:22.5:5 (v/v/v/v) water + 5 mM ammonium acetate/methanol/acetonitrile/ethyl acetate (A) and 50:50 (v/v) acetonitrile/ethyl acetate (B), and the gradient was set as follows (min/% A): 0.0/90, 0.1/90, 0.8/70, 20.0/9, 20.1/0, 20.4/0, 20.5/90, 23.0/90. For detection, an Exactive amMS (Thermo Fisher Scientific) was used in positive atmospheric pressure chemical ionization (APCI) mode. Full scan and all-ion fragmentation data were acquired with a scanning range of m/z 100−1400 at a resolution of 50000 full width at half-maximum (fwhm). The Accela PDA detector (Thermo Fisher Scientific) was set to scan from 190 to 800 nm.

RESULTS AND DISCUSSION

Method Validation. Carotenoids were chosen as model compounds for the optimization of a generic sample preparation and screening method for apolar plant metabolites. Carotenoids are apolar plant metabolites that can easily degrade or isomerize under the influence of light, oxygen, enzymes, heat, oxidants, and acid or alkaline conditions.[15] It can hence be assumed that if no isomerization or degradation occurs for carotenoids during sample preparation, most other apolar compounds should also be extracted without any artifact formation. The chromatographic gradient and MS settings were optimized on an UHPLC-PDA-amMS for a set of carotenoids representing the wide polarity range of carotenoids found in nature.[4] A validation study of the optimized method was performed for a range of compounds from several apolar metabolite classes (12 carotenoids, 5 lipid-soluble vitamins, 1 phytosterol) and different matrices. Furthermore, the extraction efficiency of other apolar plant metabolites (glycolipids, glycerolipids, steryl derivatives, chlorophyll) for which no commercial reference standards were available was investigated to confirm its generic character.

Dynamic Range and Sensitivity. High dynamic ranges (up to 4 orders of magnitude) with good linear fits were obtained in MS for most compound calibration curves. Because of the lower sensitivity of carotenoids in UV detection and the high cost of carotenoid standards, the dynamic ranges of the carotenoids were not tested to their full extent with PDA detection. However, it could be observed that smaller dynamic ranges were acquired for the very apolar carotenes in both MS and PDA, suggesting lower solubility to be the cause. Detection and quantitation limits are of less importance for valorization objectives as predominantly compounds with high concentrations are targeted.

Precision. The repeatability (intraday RSD) was obtained from the relative standard deviations (RSDs) of the recoveries from the spiking experiments. Because of the high price of

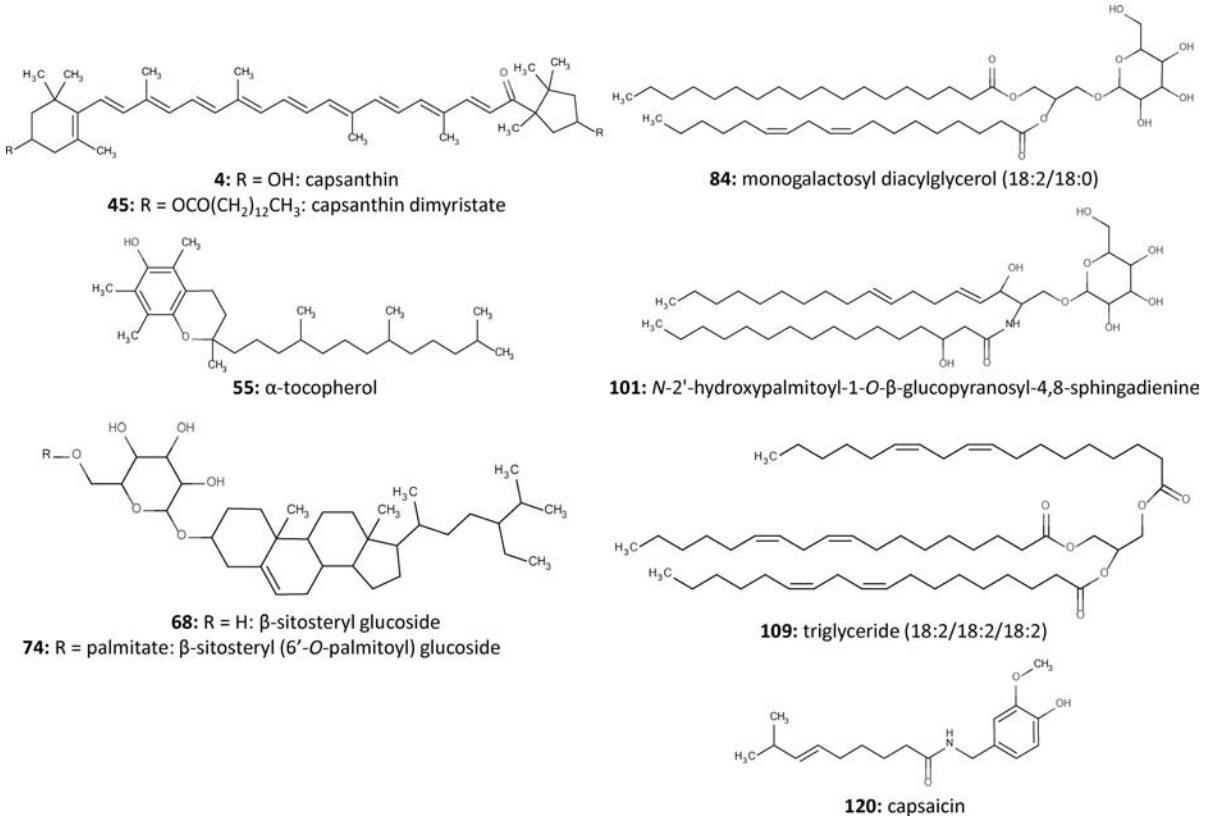

Figure 1. Representative structures of the different compound groups detected in chili peppers during this study.

analytical standards, it was chosen to obtain the intermediate precision (interday RSD) of the method with compounds natively present in red bell pepper (*Capsicum* variety). Five aliquots of freeze-dried pepper were extracted and analyzed the same day. This experiment was repeated for 3 days in total. Intraday RSDs ranged between 0.5 and 8.4% and interday RSDs between 0.0 and 6.0%.

Trueness. Certified reference material (CRM) is commercially available for only a very limited set of plant metabolites. Furthermore, reference standards are often not commercially available or very expensive for plant metabolites. Therefore, the trueness could only be assessed for a select set of compounds. A CRM of mixed vegetables, BCR 485 (consisting of sweet corn, tomatoes, and carrots), with certified concentration values for *all-trans-α-* and *β*-carotene, lutein, and lutein + zeaxanthin was extracted in triplicate. Values of 110 ± 8, 105 ± 3, 100.5 ± 2.7, and 94.5 ± 1.4% of the certified concentration values were found with MS, respectively, and 110.5 ± 2.5, 106.2 ± 1.1, 105 ± 4, and 101 ± 5% with PDA, respectively, with the uncertainties being the RSD of the three replicates. These results show good accuracy of the method for the quantitative determination of carotenoids natively present in biological matrices.

Spiking experiments were performed in triplicate on aliquots of freeze-dried apple (*M. domestica*) using an analytical standard mixture with 11 carotenoids, 6 lipid-soluble vitamins, and 1 phytosterol (concentrations ranging between 5.3 and 140 μg/g dw). The recoveries (*R* (%)) for all spiked compounds except violaxanthin ranged between 86 and 115% with MS detection, showing good accuracy. The slightly lower recoveries (74−87% in MS) found for violaxanthin can be attributed to epoxide rearrangements (which lead to large hypsochromic shifts in UV absorbance), catalyzed by the acids naturally present in the apple matrix.[16] Because of the low UV absorbance of phytosterols and lipid-soluble vitamins, only the recoveries of most of the spiked carotenoids could be calculated with PDA detection, showing similar values compared to the results calculated with MS.

Extraction Efficiency. Because of the lack of commercially available CRMs and reference standards, the conventional approach of method validation could be performed for only a select set of apolar plant metabolites. To investigate the extraction efficiency for a larger range of apolar plant metabolites, the two most critical steps in sample preparation were tested by exhaustive extraction of compounds naturally present in peppers. In a first experiment, an aliquot of freeze-dried red bell pepper was extracted five times with ASE followed by separate preparation of the obtained extracts. Assuming 100% extraction, the relative abundances of the compounds were calculated in the respective extracts. In a second experiment, the transfer of compounds to the hexane phase during liquid−liquid extraction was investigated by back-extracting the polar phase six times with hexane. After the first three hexane extracts had been pooled, an extra 240 mL of 10% sodium chloride solution was added to the polar phase. The polar phase was extracted three more times. The first two apolar extracts resulting from this second series of extractions were pooled. Subsequently, the three remaining extracts (consisting of three pooled, two pooled, and a single extract) were prepared separately for analysis. Again assuming 100% extraction, the relative abundances of the compounds were calculated in the respective extracts. The results showed that during the two most critical steps in the extraction procedure,

Table 1. Values for Maximum Absorbance, Precursor and Product Ions, and Retention Times of the Carotenoids Present in the Five Chili Pepper Accessions

compd	identity	mol formula	retention time (min)	max absorbance (nm)	MS mode	accurate mass of precursor ion	mass deviation (ppm)	in-source fragments	identification type
1	cucurbitaxanthin A	$C_{40}H_{56}O_3$	6.77	426, 449, 476	pos	585.43068	0.79	567.420	*a, b*
					neg	-	-	-	
2	cycloviolaxanthin	$C_{40}H_{56}O_4$	7.29	418, 443, 472	pos	601.42497	−0.28		*a, b*
					neg	-	-	-	
3	*cis*-capsanthin	$C_{40}H_{56}O_3$	7.77	467	pos	585.43029	0.12	567.419	*c*
					neg	584.42392	0.74	-	
4	*all-trans*-capsanthin	$C_{40}H_{56}O_3$	7.93	474	pos	585.43027	0.09	567.419, 549.409, 493.352, 475.35735, 461.342	*d*
					neg	584.42352	0.05	-	
5	*cis*-antheraxanthin	$C_{40}H_{56}O_3$	8.67	450, 472	pos	585.43029	0.12	567.419, 549.409, 493.352, 475.357 35	*a*
					neg	584.42385	0.62	-	
6	*all-trans*-zeaxanthin	$C4_0H_{56}O_2$	10.12	455, 481	pos	569.43546	0.26	551.425	*d*
					neg	568.42884	0.46	-	
7	*all-trans*-apo-carotenal	$C_{30}H_{40}O$	10.38	465	*pos*	417.31602	1.99	-	*d*
					neg	416.30875	0.70	-	
8	nigroxanthin	$C_{40}H_{54}O_2$	12.62	448, 478	pos	567.41995	0.51	-	*a, b*
					neg	-	-	-	
9	*β*-cryptoxanthin	$C_{40}H_{56}O$	13.61	456, 483	pos	553.44074	0.63	535.43	*a, b, c, e*
					neg	552.43436	1.27	-	
10	capsorubin-laurate (C12:0)	$C_{52}H_{78}O_5$	13.85	479	pos	783.59123	−1.24	583.414, 565.405	*b,e*
					neg	782.58620	0.93	-	
11	karpoxanthin-laurate (C12:0)	$C_{52}H_{80}O_5$	14.77	424, 448, 477	pos	785.60732	−0.67	767.597, 585.431, 567.420, 549.410, 475.357	*a, b,f*
					neg	784.60170	0.74	-	
12	capsorubin-myristate (C14:0)	$C_{54}H_{82}O_5$	15.01		pos	811.62242	−1.33	583.414, 565.405	*b, e*
					neg	810.61682	0.06	-	
13	*all-trans*-capsanthin-laurate (C12:0)	$C_{52}H_{78}O_4$	15.01	475	pos	767.59687	−0.55	749.587, 567.420	*c, e*
					neg	766.59080	0.31	-	
14	-	$C_{52}H_{76}O_4$	15.38	435, 465, 498	pos	765.58206	0.55	565.404	-
					neg	764.57505	0.18	672.513, 658.497, 564.397	

dx.doi.org/10.1021/jf500285g |J. Agric. Food Chem. 2014, 62, 4812−4831

Table 1. continued

compd	identity	mol formula	retention time (min)	max absorbance (nm)	MS mode	accurate mass of precursor ion	mass deviation (ppm)	in-source fragments	identification type
15	*all-trans*-capsanthin-laurate (C12:0)	$C_{52}H_{78}O_4$	15.72	474	pos	767.59639	−1.17	749.587, 567.420, 549.409	*c, e*
					neg	766.59059	0.04	674.528, 660.513, 566.413	
16	*cis*-capsanthin-laurate (C12:0)	$C_{52}H_{78}O_4$	15.85	463	pos	767.59704	−0.33	749.587, 567.420	*c*
					neg	766.59063	0.09	-	
17	*cis*-antheraxanthin-laurate (C12:0)	$C_{52}H_{78}O_4$	16.03	448, 478	pos	767.59672	−0.74	749.587, 567.420, 549.409	*c*
					neg	766.59051	−0.07	-	
18	*all-trans*-capsanthin-myristate (C14:0)	$C_{54}H_{82}O_4$	16.15	474	pos	795.62818	−0.52	777.617, 567.420, 549.409	*c, e*
					neg	794.62201	0.19	566.413, 227.202	
19	*all-trans*-β-carotene	$C_{40}H_{56}$	16.34	455, 482	pos	537.44556	0.15	457.384, 445.384	*d*
					neg	536.43894	0.35	-	
20	mutatoxanthin-laurate (C12:0)	$C_{52}H_{78}O_4$	16.45	405, 428, 457	pos	767.59653	−0.99	567.420	*b*
					neg	766.59097	0.53	-	
21	cucurbitaxanthin A-laurate (C12:0)	$C_{52}H_{78}O_4$	16.54	426, 451, 474	pos	767.59682	−0.61	749.587, 567.420, 549.409	*a, b*
					neg	766.59099	0.56	-	
22	*all-trans*-phytofluene	$C_{40}H_{62}$	16.66	334, 349, 369	pos	543.49255	0.22	-	*d*
					neg	-	-	-	
23	*all-trans*-capsanthin-myristate (C14:0)	$C_{54}H_{82}O_4$	16.83	473	pos	795.62760	−1.24	777.617, 567.420, 549.409	*c, e*
					neg	794.62178	−0.10	566.413, 227.202	
24	*cis*-antheraxanthin-myristate (C14:0)	$C_{54}H_{82}O_4$	17.05	450, 477	pos	795.62827	−0.40	777.617, 567.420, 549.409	*c*
					neg	794.62168	−0.23	-	
25	*all-trans*-phytoene	$C_{40}H_{64}$	17.08	276, 288, 297	pos	545.50774	−0.62	463.430	*d*
					neg	-	-	-	
26	*all-trans*-zeaxanthin-laurate (C12:0)	$C_{52}H_{78}O_3$	17.16	455, 483	pos	751.60171	−0.88	551.425	*c*
					neg	750.59539	−0.33	-	
27	*cis*-capsanthin-palmitate (C16:0)	$C_{56}H_{86}O_4$	17.21	463	pos	823.65929	−0.73	805.650, 567.420, 549.409	-
					neg	822.65320	0.05	566.413, 255.232	
28	*cis*-zeaxanthin-laurate (C12:0)	$C_{52}H_{78}O_3$	17.52	424, 447, 474	pos	751.60229	−0.11	-	-
					neg	750.59536	−0.37	-	

dx.doi.org/10.1021/jf500285g | J. Agric. Food Chem. 2014, 62, 4812−4831

Table 1. continued

compd	identity	mol formula	retention time (min)	max absorbance (nm)	MS mode	accurate mass of precursor ion	mass deviation (ppm)	in-source fragments	identification type
29	mutatoxanthin-myristate (C14:0)	$C_{54}H_{82}O_4$	17.54	405, 430, 456	pos	-	-	777.617, 567.420, 549.409	*b*
					neg	794.62109	−0.97	-	
30	*all-trans*-capsanthin-palmitate (C16:0)	$C_{56}H_{86}O_4$	17.83	472	pos	823.65985	−0.05	805.650, 567.420, 549.409	*e*
					neg	822.65301	−0.18	-	
31	*cis*-zeaxanthin-myristate (C14:0)	$C_{54}H_{82}O_3$	18.00	423, 447, 477	pos	779.63226	−1.81	551.425	*c*
					neg	778.62652	−0.54	-	
32	*all-trans*-zeaxanthin-myristate (C14:0)	$C_{54}H_{82}O_3$	18.16	454, 481	pos	779.63263	−1.33	761.622, 551.425	*c, e*
					neg	778.62677	−0.22	550.418	
33	*all-trans*-zeaxanthin-myristate (C14:0)	$C_{54}H_{82}O_3$	18.37	455, 479	pos	-	-	-	*c, e*
					neg	778.62666	−0.36	-	
34	-	-	18.44	473	pos	-	-	-	-
					neg	-	-	804.642 44	
35	-	$C_{58}H_{88}O_4$	18.58	434, 456	pos	-	-	-	-
					neg	848.66846	0.41	-	
36	*β*-cryptoxanthin-laurate (C12:0)	$C_{52}H_{78}O_2$	18.8	456, 482	pos	735.60815	0.94	535.430	*c, e*
					neg	734.60119	0.63	-	
37	*all-trans*-capsanthin-dilaurate (C12:0, C12:0)	$C_{64}H_{100}O_5$	19.12	476	pos	949.76483	0.51	749.587, 549.409	*e*
					neg	948.75682	−0.84	-	
38	*cis*-capsanthin-dilaurate (C12:0, C12:0)	$C_{64}H_{100}O_5$	19.32	463	pos	-	-	749.587, 549.409	-
					neg	948.75618	−1.52	-	
39	-	-	19.50	474	pos	-	-	-	-
					neg	-	-	-	
40	*β*-cryptoxanthin-myristate (C14:0)	$C_{54}H_{82}O_2$	19.56	455, 483	pos	-	-	535.430	*c, e*
					neg	762.63197	−0.08	-	
41	*all-trans*-capsanthin-laurate-myristate (C12:0, C14:0)	$C_{66}H_{104}O_5$	19.78	474	pos	977.79388	−1.81	749.587, 549.409	*c, e*
					neg	976.78806	−0.88	-	
42	*cis*-capsanthin-laurate-myristate (C12:0, C14:0)	$C_{66}H_{104}O_5$	19.97	463	pos	-	-	749.587, 549.409	-
					neg	976.78790	−1.04	-	

dx.doi.org/10.1021/jf500285g | J. Agric. Food Chem. 2014, 62, 4812−4831

Table 1. continued

compd	identity	mol formula	retention time (min)	max absorbance (nm)	MS mode	accurate mass of precursor ion	mass deviation (ppm)	in-source fragments	identification type
43	*cis*-capsanthin-laurate-myristate (C12:0, C14:0)	$C_{66}H_{104}O_5$	20.13	464	pos	-	-	749.587, 549.409	-
					neg	976.78853	−0.40	-	
44	*β*-cryptoxanthin-palmitate (C16:0)	$C_{56}H_{86}O_2$	20.25	457, 482	pos	-	-	-	*c*, *e*
					neg	790.66218	−1.45	-	
45	*all-trans*-capsanthin-dimyristate (C14:0, C14:0)	$C_{68}H_{108}O_5$	20.36	473	pos	1.005.82526	−1.68	777.617	*c*, *e*
					neg	1.004.81983	−0.39	776.611, 227.202	
46	*all-trans*-capsanthin-laurate-palmitate (C12:0, C16:0)	$C_{68}H_{108}O_5$	20.57	473	pos	-	-	805.650, 749.588, 549.409	*c*, *e*
					neg	1.004.81839	−1.82	776.611	
47	*cis*-capsanthin-dimyristate (C14:0, C14:0)	$C_{68}H_{108}O_5$	20.72	464	pos	-	-	777.617, 549.409	-
					neg	1.004.81860	−1.61	776.611	
48	*all-trans*-capsanthin-myristate-palmitate (C14:0, C16:0)	$C_{70}H_{112}O_5$	20.93	475	pos	-	-	805.648, 777.617, 549.409	-
					neg	1032.85050	−0.99	776.611, 548.4	
49	*cis*-capsanthin-myristate-palmitate (C14:0, C16:0)	$C_{70}H_{112}O_5$	21.10	464	pos	-	-	805.648, 777.617	-
					neg	1032.84970	−1.76	776.611	
50	*cis*-capsanthin-myristate-palmitate (C14:0, C16:0)	$C_{70}H_{112}O_5$	21.19	463	pos	-	-	805.648, 777.617, 549.409	-
					neg	1032.85057	−0.92	776.611, 548.4	
51	*all-trans*-capsanthin-dipalmitate (C16:0, C16:0)	$C_{72}H_{116}O_5$	21.33	473	pos	-	-	805.648, 549.409	*c*, *e*
					neg	1060.88213	−0.65	804.640, 255.233	
52	*all-trans*-zeaxanthin-laurate-myristate (C12:0- C14:0)	$C_{66}H_{104}O_4$	21.37	453, 480	pos	-	-	761.622, 733.591, 533.414	*c*, *e*
					neg	960.79331	−0.73	760.614, 732.584	
53	*all-trans*-zeaxanthin-dimyristate (C14:0- C14:0)	$C_{68}H_{108}O_4$	21.37	453, 480	pos	-	-	761.622, 533.414	*c*, *e*
					neg	988.82436	−0.96	760.614	

[a] *Dictionary of Natural Products*:[18] present in *Capsicum annuum*. [b] *Carotenoids Handbook*: present in *Capsicum annuum* and match with UV reference spectrum. [c] Identified by Giuffrida et al..[13] [d] Match with analytical standard. [e] Identified by Schweiggert et al.;[10] [f] Identified by Deli et al.[8]

dx.doi.org/10.1021/jf500285g | J. Agric. Food Chem. 2014, 62, 4812−4831

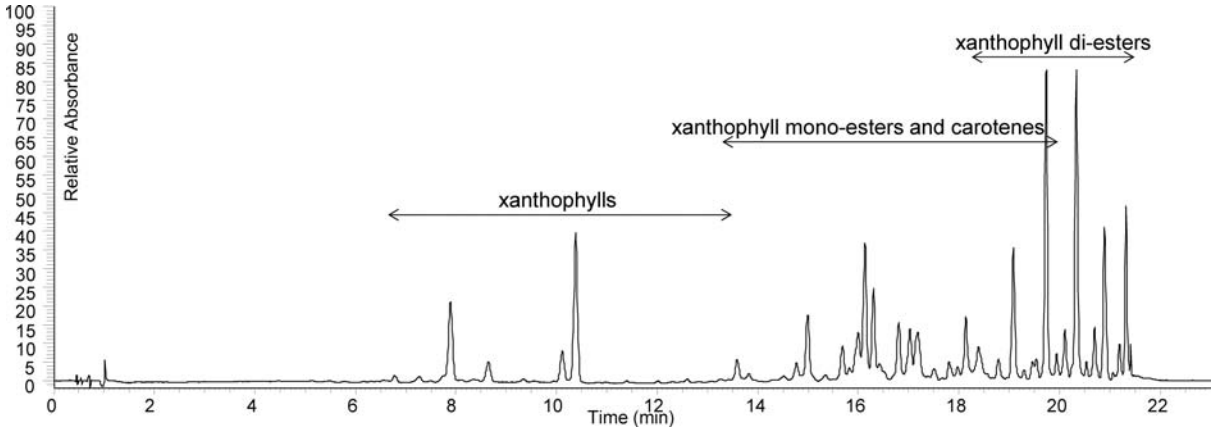

Figure 2. Chromatogram of the PDA signal at 470 nm depicts the elution profiles of the carotenoids present in the Korba chili pepper accession.

the greater part of compounds is extracted during the first three extractions (>90%).

Measurement Uncertainty. The results of the spiking experiments, CRM analysis, and intermediate precision were used to estimate the total expanded measurement uncertainty (U; $k = 2$). As not all compounds included during the spiking experiments were available for intermediate precision experiments, the intra- and interday RSDs of compounds of the same compound group were used to calculate U (e.g., for PDA analysis, the RSDs of β-carotene were applied for the calculation of U for α-carotene and lycopene). The obtained U values ranged between 10 and 26% (MS) and between 14 and 21% (PDA) for all compounds except violaxanthin, for which the U values were higher (44 and 59% for MS and PDA, respectively) as the bias of the lower R (%) obtained for violaxanthin was included in the calculation.

Identification Strategy. Identification of compounds is relatively easy when analytical standards are available. However, in natural products research, analytical standards are often very expensive or not commercially available. Therefore, identification is often based upon the available chromatographic and spectrometric information.[8−13] Carotenoids absorb UV light in a high-wavelength area (typical absorbance maxima at 400−500 nm) because of their conjugated system in the polyene backbone (e.g., molecular structures **4** and **45** in Figure 1).[17] PDA detectors are therefore very selective for the detection of carotenoids. However, the applicability of PDA detectors is limited as they are only useful for compounds that absorb UV or visible light and provide only very little structural information, which makes it impossible to identify unknown compounds with PDA spectra.[10] MS detectors are much more selective detectors than PDA detectors and can therefore facilitate the identification of plant metabolites. Orbitrap MS detectors can routinely generate mass spectra with a resolving power up to 140,000 at fwhm and obtain mass accuracies within 2 ppm (ppm), which enables the calculation of the most probable molecular formulas of the generated ions and fragments.[5] However, to date, even the most state-of-the-art MS detectors are often not capable of distinguishing between isomers, whereas PDA detectors in many cases are.[4,15] Furthermore, chromatography can be used to separate isomers before detection. The combination of orthogonal analytical techniques therefore provides a powerful tool for the identification of unknown compounds.

During this study carotenoids, steryl derivatives, glycolipids, glycerolipids, capsaicinoids, and lipid-soluble vitamins were tentatively identified in chili pepper samples. The information provided by the analysis alone is, however, not always enough for peak identification at an acceptable confidence level. Therefore, other sources of information such as in-house and commercial compound databases and peer-reviewed publications can give additional information for successful dereplication.[7] During this study, the *Dictionary of Natural Products*[18] and the *Carotenoids Handbook*[19] were consulted as commercial databases. Both of these databases give information on the occurrence of plant metabolites in nature. The *Carotenoids Handbook* also lists the UV absorbance spectra of most of the carotenoids known to exist in nature. These were used as reference spectra for comparison of experimental UV spectra if identification by amMS spectra resulted in several possible structures.

In the present study structures were assigned to unknown peaks only when both the mass/charge (m/z) ratios and molecular formulas of the ions were in agreement. PDA spectra often provided confirmation for the proposed structures when the reference information was available. Furthermore, the assigned identities often matched with their occurrence in chili peppers as described in the literature and databases. Figure 1 depicts the molecular structures of the identified plant metabolite classes. Tables 1 and 4 show the diagnostic amMS and PDA data used for compound identification in the chili pepper samples. These tables also specify the literature and databases used for confirmation of compound identity.

Carotenoids in Chili Peppers. *Identification of Carotenoids.* A wavelength of 470 nm is very specific to measure carotenoid absorbance. This wavelength was used to depict the carotenoids present in the 'Awlad Haffouzz' accession (Figure 2). The PDA chromatograms of the other four accessions appeared identical (not shown). All of the peaks in Figure 2 could be tentatively attributed to carotenoids as no chlorophyll peaks were detected (derived from the PDA profiles of the peaks). The greater part of PDA peaks in the chromatograms contained the same absorption profiles. As described previously,[10] carotenoid esterification with fatty acids does not affect the polyene backbone, and therefore esterification has virtually no effect on the absorption spectrum. The characteristic UV profiles of the nonesterified carotenoids, such as capsanthin, antheraxanthin, and zeaxanthin, can therefore also be used to locate their esters. Complementary to PDA detection, fatty acid esters of carotenoids easily fragment during MS ionization, and therefore information on the type of fatty acid moieties (number of carbons, number of double

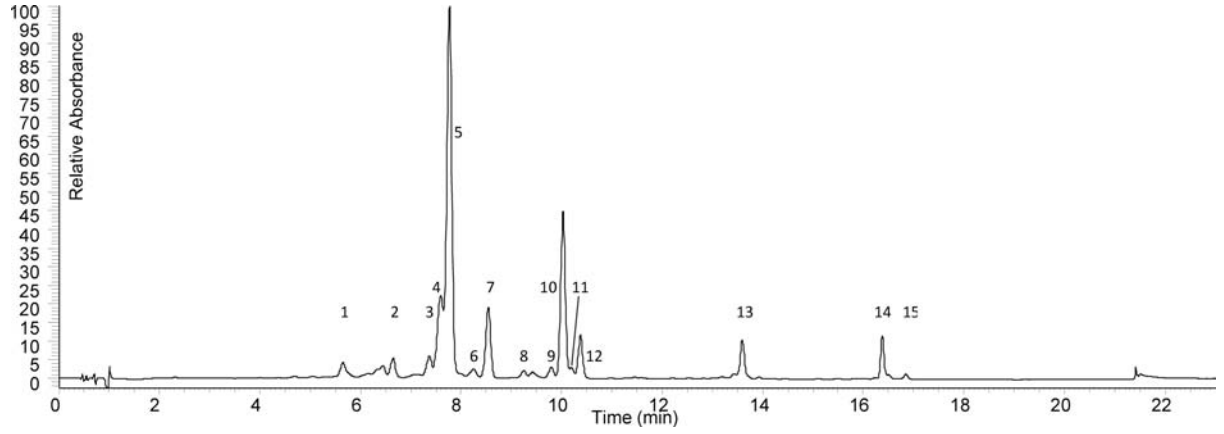

Figure 3. Chromatogram of the PDA signal at 470 nm depicts the elution profiles of the carotenoids present in the Korba chili pepper accession extract after 1 year of storage, after saponification. Peaks: 1, capsorubin; 2, cucurbitaxanthin A; 3, *cis*-capsanthin; 4, *cis*-capsanthin; 5, *trans*-capsanthin; 6, *cis*-antheraxanthin; 7, mutatoxanthin; 8, karpoxanthin; 9, *cis*-zeaxanthin; 10, *trans*-zeaxanthin; 11, *cis*-β-apo-8′-carotenal; 12, *trans*-β-apo-8′-carotenal; 13, β-cryptoxanthin; 14, *trans*-β-carotene; 15, *cis*-β-carotene.

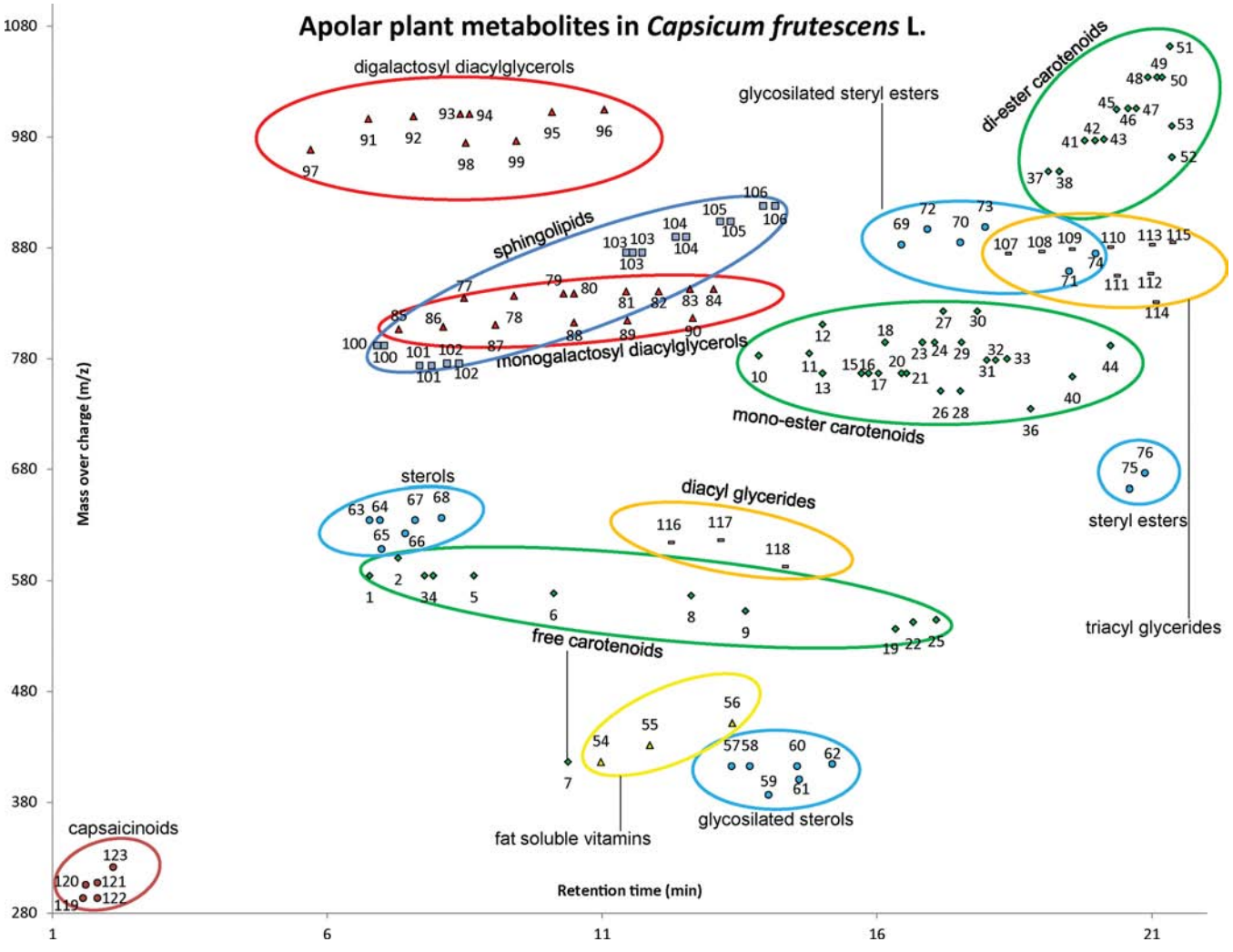

Figure 4. Correlation of the retention times and m/z values of the compounds identified in the chili peppers with the analytical screening method. The data labels match the compound numbers in Tables 1 and 4

bonds) can be obtained from full scan amMS spectra, as described earlier.[4,10,13] Most of the carotenoids in the chili pepper samples were esterified with laurate, myristate, and palmitate, and the major carotenoid present in the sample was capsanthin, in agreement with previuos findings.[10] Other studies[10,17,20] have shown that the *cis* isomers of carotenoids can be identified on the basis of a small hypsochromic shift (shorter wavelength) of the maximum absorbance values and a

dx.doi.org/10.1021/jf500285g | J. Agric. Food Chem. 2014, 62, 4812−4831

Table 2. Carotenoid Concentrations in the Five Chili Pepper Cultivars Calculated with Analytical Standards and Molar Extinction Coefficients

			concentration (μg/g dw)				
compd	identity	retention time (min)	'Awlad Haffouzz'	'Tebourba'	'Korba'	'Somâa'	'Souk jedid'
4	*all-trans*-capsanthin[a]	7.93	130 ± 20	70 ± 10	100 ± 20	100 ± 20	110 ± 20
5	*cis*-antheraxanthin[a,e]	8.67	27 ± 5	18 ± 3	22 ± 4	26 ± 5	24 ± 4
6	*all-trans*-zeaxanthin[a]	10.12	25 ± 5	13.0 ± 2.5	25 ± 5	9.0 ± 1.8	12.0 ± 2.3
19	β-carotene[a]	16.34	130 ± 20	120 ± 20	80 ± 10	100 ± 20	110 ± 20
22	*all-trans*-phytofluene[a]	16.66	27 ± 6	22 ± 5	17 ± 4	21 ± 4	20 ± 4
25	*all-trans*-phytoene[a]	17.08	90 ± 10	68 ± 9	48 ± 7	70 ± 10	58 ± 8
3	*cis*-capsanthin[f]	7.77					
12 + 13	capsorubin-myristate + capsanthin-laurate[b,g,h,i]	15.01	260 ± 50	220 ± 50	180 ± 40	310 ± 60	190 ± 40
15	*all-trans*-capsanthin-laurate[b,g]	15.72	70 ± 20	80 ± 20	70 ± 10	90 ± 20	50 ± 10
16	*cis*-capsanthin-laurate[f]	15.85					
17	*cis*-antheraxanthin-laurate[b,e,j]	16.03	70 ± 20	70 ± 20	70 ± 20	100 ± 20	60 ± 10
18	*all-trans*-capsanthin-myristate[b,g]	16.15	430 ± 90	390 ± 80	320 ± 70	540 ± 110	450 ± 90
23	*all-trans*-capsanthin-myristate[b,g]	16.83	120 ± 30	150 ± 30	120 ± 30	140 ± 30	110 ± 20
24	*cis*-antheraxanthin-myristate[b,e,j]	17.05	80 ± 20	80 ± 20	70 ± 10	80 ± 20	60 ± 10
26 + 27	*all-trans*-zeaxanthin-laurate + *cis*-capsanthin-palmitate[b,g,h,i]	17.16 + 17.21	160 ± 30	190 ± 40	160 ± 30	190 ± 40	200 ± 40
30	*all-trans*-capsanthin-palmitate[b,g]	17.83	60 ± 10	80 ± 20	50 ± 10	70 ± 10	60 ± 10
31	*cis*-zeaxanthin-myristate[b,k]	18	11.3 ± 2.3	19 ± 4	14 ± 2.8	13.4 ± 2.7	14.6 ± 2.9
32	*all-trans*-zeaxanthin-myristate[b,k]	18.16	80 ± 20	70 ± 10	90 ± 20	50 ± 10	37 ± 7
33	*all-trans*-zeaxanthin-myristate[b,k]	18.37	39 ± 7	50 ± 10	50 ± 10	70 ± 10	28 ± 5
37	*all-trans*-capsanthin-dilaurate[b,g]	19.12	380 ± 80	420 ± 90	330 ± 70	430 ± 90	210 ± 40
38	*cis*-capsanthin-dilaurate[b,g]	19.32	18 ± 4	13.8 ± 2.9	20 ± 4	19 ± 4	11.2 ± 2.4
41	*all-trans*-capsanthin-laurate-myristate[b,g]	19.78	700 ± 200	800 ± 200	700 ± 100	900 ± 200	500 ± 100
42	*cis*-capsanthin-laurate-myristate[b,g]	19.97	37 ± 8	27 ± 6	44 ± 9	50 ± 10	30 ± 10
43	*cis*-capsanthin-laurate-myristate[b,g]	20.13	120 ± 30	110 ± 20	120 ± 20	150 ± 30	80 ± 20
45	*all-trans*-capsanthin-dimyristate[b,g]	20.36	700 ± 100	800 ± 200	700 ± 100	800 ± 200	600 ± 100
46	*all-trans*-capsanthin-laurate-palmitate[b,g]	20.57	30 ± 6	25 ± 5	36 ± 8	42 ± 9	39 ± 8
47	*cis*-capsanthin-dimyristate[b,g]	20.72	120 ± 20	140 ± 30	130 ± 30	160 ± 30	110 ± 20
48	*all-trans*-capsanthin-myristate-palmitate[b,g]	20.93	370 ± 80	500 ± 100	400 ± 80	370 ± 80	330 ± 70
49	*cis*-capsanthin-myristate-palmitate[b,g]	21.1	17 ± 4	11.1 ± 2.3	12.6 ± 2.7	16 ± 3	21 ± 4
50	*cis*-capsanthin-myristate-palmitate[b,g]	21.19	70 ± 10	90 ± 20	80 ± 20	80 ± 20	80 ± 20
51	*all-trans*-capsanthin-dipalmitate[b,g]	21.33					
52 + 53	*all-trans*-zeaxanthin-dimyristate + *all-trans*-zeaxanthin-laurate-myristate[b,k]	21.37 + 21.37	80 ± 20	110 ± 20	120 ± 20	80 ± 10	60 ± 10
9	β-cryptoxanthin[c,k]	13.61	30 ± 10	29 ± 9	24 ± 7	26 ± 8	19 ± 6
10	capsorubin-laurate[c,g]	13.85	23 ± 7	22 ± 7	15 ± 5	30 ± 10	14 ± 4
36	β-cryptoxanthin-laurate[c,k]	18.8	28 ± 9	28 ± 9	24 ± 8	27 ± 9	12 ± 4
40	β-cryptoxanthin-myristate[c,k]	19.56	20 ± 6	28 ± 9	23 ± 7	18 ± 6	8 ± 2
44	β-cryptoxanthin-palmitate[c,k]	20.25	24 ± 8	36 ± 11	28 ± 9	31 ± 9	29 ± 9
1	cucurbitaxanthin A[d,k]	6.77	14 ± 5	8.4 ± 2.8	11 ± 4	14 ± 5	11 ± 4
2	cycloviolaxanthin[d,l]	7.29	11 ± 4	12 ± 4	6.4 ± 2.1	15 ± 5	10 ± 3
8	nigroxanthin[d,k]	12.62	7.4 ± 2.4	5.9 ± 1.9	4.7 ± 1.6	7.4 ± 2.4	3 ± 1
11	karpoxanthin-laurate[d,l]	14.77	30 ± 10	30 ± 10	30 ± 10	40 ± 10	20 ± 10
20 + 21	mutatoxanthin-laurate + cucurbitaxanthin A -laurate[d,h,k]	16.45 + 16.54	21 ± 7	20 ± 7	20 ± 7	22 ± 7	15 ± 5
28 + 29	*cis*-zeaxanthin-laurate + mutatoxanthin-myristate[d,h,k]	17.52 + 17.54	23 ± 5	24 ± 5	29 ± 6	27 ± 5	25 ± 5

[a]Carotenoid concentrations calculated with analytical standards and LC-amMS. [b]Quantitation with standards containing the same polyene backbone (the *U* (%) of zeaxanthin and capsanthin estimated during validation were used as uncertainties on the measurements of zeaxanthin and capsanthin esters, respectively). [c]Quantitation with the extinction coefficients (ε_{mol}) from the literature.[17] [d]Quantitation with the ε_{mol} from a compound with a similar polyene backbone. [e]Because antheraxanthin was not available as a reference standard at the time of validation, the average *U* (%) obtained from validation data was used as uncertainty for the measurement of antheraxanthin derivatives. [f]Too low intensity for quantitation. [g]Quantitated with capsanthin standard. [h]Peak overlap. [i]Predominantly capsanthin is present. [j]Quantitated with antheraxanthin standard. [k]Quantitated with zeaxanthin standard. [l]Quantitated with violaxantin standard.

characteristic peak around 330−350 nm. Several *cis*-carotenoids could be detected in the chili pepper samples, although in lesser amounts compared to their *trans* counterparts. It is generally known that absorbance maxima of carotenoids can shift depending on the diluent.[15] These shifts can be similar to or even greater than the shifts in maximum absorbances that occur during *trans* to *cis* isomerization of carotenoids.[15] The correct

dx.doi.org/10.1021/jf500285g | J. Agric. Food Chem. 2014, 62, 4812−4831

isomer form, *cis* or *all-trans*, was therefore attributed only when a reference standard of the compound of interest was available.

Table 1 shows the diagnostic amMS and PDA data used for carotenoid identification in the chili pepper samples. During positive APCI, carotenoids predominantly ionized to generate protonated molecules $[M + H]^+$, whereas predominantly radical molecular ions ($M^{\bullet -}$) were formed during negative APCI. A substantial amount of carotenoid product ions was detected due to in-source fragmentation, thereby providing additional structural information. Five of the 53 detected carotenoid peaks in the chili pepper accessions could be identified with reference standards. Forty-four unknown carotenoids could be tentatively identified on the basis of spectrophotometric and mass spectrometric data, chromatography, databases, and the literature. As the carotenoid content of different *Capsicum* varieties has been frequently reported, confirmation of identity was often obtained from comparison with the findings of other studies.[8,10,13] Four minor unknown carotenoids could not be assigned a tentative structure. These data show that the applied generic apolar screening method performs in the separation and identification of carotenoids as well as earlier reported methods that were optimized for the dedicated identification of carotenoids in chili peppers.[10,13]

To confirm the identity of the esterified carotenoids, the sample extracts were saponified. Due to circumstances, the saponification procedure was performed after 1 year of storage of the extracts in the dark, at −25 °C. Analysis of the extract before saponification revealed that no significant change had occurred in the carotenoid content during storage. The chromatogram of the saponified extract (Figure 3) shows the profile of the hydrolyzed carotenoids. The peaks of cucurbitaxanthin A (6.77 min), two *cis*-capsanthins (7.38 and 7.62 min), *all-trans*-capsanthin (7.78 min), *cis*-antheraxanthin (8.55 min), *all-trans*-zeaxanthin (10.05 min), and *β*-cryptoxanthin (13.61 min) augmented in the chromatogram of the saponified extract, which confirmed the presence of their esterified derivatives in the untreated extract (Figure 2). Furthermore, new peaks appeared in the saponified extract at 5.67, 8.26, 9.25, 9.82, 10.23, 13.61, and 16.88 min that could be identified as capsorubin, mutatoxanthin, karpoxanthin, *cis*-zeaxanthin, *cis*-*β*-apo-8′-carotenal, *β*-cryptoxanthin, and *cis*-*β*-carotene, respectively. Their free form was not detected before saponification, which confirms their presence as carotenoid esters in the untreated chili pepper extracts.

The three main maximum absorbance wavelengths of the isomers *all-trans*-lutein and *cis*-zeaxanthin are in close agreement and are only distinguishable in UV absorbance by a characteristic *cis* peak of *cis*-zeaxanthin. A *cis* peak was clearly detected in the PDA spectrum of peak 9 in the chromatograms of the saponified extracts (Figure 3), indicating the presence of *cis*-zeaxanthin. It has also been reported that zeaxanthin and lutein are distinguishable by in-source fragmentation in positive APCI mode by the relative heights of the $[M + H]^+$ and $[M + H - H_2O]^+$ peaks.[4] Comparison of the MS spectrum of peak 9 in Figure 3 showed close resemblance with that of a *trans*-zeaxanthin reference standard and differed from the spectrum of a *trans*-lutein reference standard. Peak 9 was therefore designated *cis*-zeaxanthin.

An overview of the chromatographic separation versus molecular mass of all the compounds identified in the chili pepper extracts during this study is given in Figure 4. Although most of the compounds were separated by chromatography, orthogonal detector selectivity remains essential for compound differentiation. This can in many cases not be achieved by PDA detection alone and highlights the added value of high-end instrumentation in this research field.

Quantitation of Carotenoids with Analytical Reference Standards. The concentrations of carotenoids for which an analytical standard was available were calculated with amMS (Table 2). The concentrations calculated with reference standards represent only a small fraction of the total number of carotenoids in the samples. Most of the xanthophylls in the samples appeared esterified, for which analytical standards are not commercially available.

Quantitation of Carotenoids with Extinction Coefficients. (a) Quantitation of Carotenoids Using Standards with the Same Polyene Backbone. In UV analysis, carotenoids can be quantitated by using reference standards having the same polyene backbone and thus extinction coefficient.[15] However, molar extinction coefficients (ε_{mol}) can be used for the calculation of the concentration expressed in weight units (e.g., μg/g) only when the molecular mass is known. To our knowledge earlier publications never used this quantification strategy in combination with amMS. Accurate mass MS enables the tentative identification of unknown carotenoids and therefore the designation of its polyene backbone and molecular weight. An LC-PDA-amMS configuration combined with the use of extinction coefficients should therefore allow unparalleled speed in the identification and quantification of unknown carotenoids. During this study, the majority of carotenoid esters, predominantly capsanthin esters, were quantitated with this procedure, that is, with a reference standard of free capsanthin (Table 2). The uncertainties represent the *U* of capsanthin estimated during method validation. Because UV absorbance profiles of carotenoids generally overlap, coeluting carotenoids could not be quantitated separately. In the few cases that coelution happened, the sum of both compounds was quantitated with the standard linked to the carotenoid with the highest contribution to the signal, as was judged from the PDA and MS spectra (Table 2).

To check the validity of quantitating carotenoid esters with standards containing the same polyene backbone, the total capsanthin content in the extracts without saponification (2100−3300 mg/kg dw) was compared to the free capsanthin concentration in the saponified extracts (2600−3800 mg/kg dw). The total capsanthin content in the extracts without saponification was calculated by conversion of the ester concentrations to free capsanthin concentrations followed by summation. The recoveries of the total capsanthin content in the extracts without saponification with respect to the capsanthin concentrations in the saponified extracts ranged between 83 and 87%, within the *U* of capsanthin (21%). These results demonstrate the suitability of using standards having the same polyene backbone as the analytes of interest for the quantitation of compounds for which no reference standards are available. The slightly lower concentrations obtained for the samples without saponification can be explained by the high density of peaks in the chromatograms, whereby the baseline is artificially elevated and integration is slightly biased. Care should, however, be taken when *all-trans*-carotenoids are used to quantitate *cis*-carotenoids, as extinction coefficients of *cis*-carotenoids are generally smaller.[21] Only small amounts of *cis* isomers were present in the chili pepper samples (4.5−6.0% for capsanthin). Higher percentages of *cis* isomers were detected (7.5−19% for capsanthin) in the saponified extracts. It is

Table 3. Concentrations of Fat-Soluble Vitamins and Free Phytosterols in the Chili Pepper Accessions, Calculated with Reference Standards

			concentration (μg/g dw)				
compd	identity	retention time (min)	'Awlad Haffouzz'	'Tebourba'	'Korba'	'Somâa'	'Souk jedid'
54	γ-tocopherol[a]	10.98	<100	<100	<100	<100	<100
55	α-tocopherol	11.87	500 ± 100	400 ± 100	400 ± 100	500 ± 100	400 ± 100
56	phylloquinone	13.37	1.55 ± 0.34	<0.7	1.11 ± 0.25	1.12 ± 0.25	1.01 ± 0.22
60	stigmasterol	14.55	80 ± 10	90 ± 10	90 ± 10	110 ± 10	100 ± 10
61	campesterol[b]	14.59	800 ± 100	500 ± 70	560 ± 70	580 ± 80	530 ± 70
62	β-sitosterol[b]	15.19	1300 ± 200	1100 ± 100	1100 ± 100	1100 ± 200	1000 ± 100

[a]Present, however, not quantifiable due to low intensity. [b]The measurement uncertainty of stigmasterol obtained with amMS was used.

generally known that saponification can induce the formation of artifacts,[15] although in this case *cis* isomer formation during 1 year of extract storage cannot be ruled out.

The shelf life of carotenoid esters in the pepper extracts was examined over a period of 1 year by correlating the concentrations of capsanthin esters in the extracts immediately after extraction (x) with the concentrations in the extracts after 1 year of storage (y). The capsanthin ester concentrations in solution did not decline over 1 year of storage ($y = 1.1629x - 21.895$). Furthermore, a coefficient of determination (R^2) of 0.9639 states a good fit between the measurements. These results indicate a long storage life for carotenoid esters in the extracts.

The above results demonstrate that the combination of amMS and PDA allows the identification and quantitation of esterified carotenoids without the need for individual standards for each and every carotenoid or for a saponification procedure.

(b) Quantitation with Extinction Coefficients from the Literature. A group of carotenoids, for which no reference standards with the same polyene backbone were available, could not be quantitated as described above. This group of carotenoids was quantitated with a carotenoid standard containing a different polyene backbone. To correct for the differences in absorbance between the standard and the carotenoid of interest, the calculated concentrations were subsequently converted to the concentration of the carotenoid of interest with the ε_{mol} values as tabulated[17] for 86 carotenoids. The results are shown in Table 2. The extinction coefficients reported[17] were compared to in-house experimentally determined extinction coefficients for four carotenoids and the deviations were 4.8, 22, 2.6, and 11% for α-carotene, β-carotene, lycopene, and zeaxanthin, respectively. These deviations were considered acceptable and confirmed that the ε_{mol} values from the literature can be used to estimate the concentrations of carotenoids for which no standards are available. The measurement uncertainty was estimated by combining the average U value obtained for carotenoids during method validation and the highest of the above-mentioned deviations between the experimentally determined and literature-described ε_{mol} values, resulting in an uncertainty of 31%. Carotenoids for which no extinction coefficients were available from the literature were quantitated in a similar manner, using the ε_{mol} values of carotenoids with an analogous polyene backbone (Table 2). The values of the listed extinction coefficients[17] differed up to a factor of 4 over the whole range of carotenoids, predominantly due to the very small and atypical conjugated system of phytoene, which results in a very low extinction coefficient. Carotenoids with similar polyene backbones have similar extinction coefficients, for example, 137,900 for zeaxanthin, 126,600 for β-carotene, 137,200 for antheraxanthin, 121,000 for capsanthin, and 132,000 for capsorubin. An additional uncertainty in the concentration is thus introduced by choosing an extinction coefficient of an analogous polyene backbone (estimated around 11%, corresponding to 2 × RSD of the above extinction coefficients). Combined with the average U value obtained for carotenoids during method validation and the highest of the above-mentioned deviations for the ε_{mol} values, this allowed the estimation of the measurement uncertainty at 33%. The combination of LC, amMS, and PDA thus allows the identification of unknown carotenoids and simultaneous estimation of their concentrations without the need for reference standards for each carotenoid.

(c) Comparison of the Carotenoids Content of the Different Accessions. As only one analysis was performed per chili pepper accession, the different peppers could not be compared using ANOVA. Pair-wise comparison resulted in good correlations ($R^2 \geq 0.90$). Only slightly lower concentrations were found for the 'Souk jedid' accession. The carotenoid profiles were thus very similar for the five chili pepper accessions.

Lipid-Soluble Vitamins and Phytosterol Derivatives in Chili Peppers. The generic method that was developed for carotenoids has a wider scope than first envisaged. Other compounds that are extracted and elute within the set chromatographic window can be analyzed. The lipid-soluble vitamins phylloquinone and α-tocopherol and phytosterols stigmasterol, campesterol, and β-sitosterol were identified and quantitated using MS and analytical standards (e.g., molecular structures **55**, **68**, and **74** in Figure 1; Tables 3 and 4). The concentrations of α-tocopherol were in line with the concentrations found previously.[12] Although γ-tocopherol was previously reported to be present in the seeds of chili peppers, it was detected only in small signal intensities during this study (most probably attributable to the difference in studied tissue), which prevented their quantitation.[22] As was found for the carotenoids, the concentrations for lipid-soluble vitamins and free phytosterols were very similar for the five studied cultivars.

It is known that phytosterols occur in plant tissues as the free alcohol, as fatty acid esters, as steryl glycosides, and as acylated steryl glycosides.[23] The free phytosterols thus represent only a fraction of the phytosterols in the chili peppers. Several steryl glucosides, acylated steryl glucosides, and acylated sterols were identified in the chili pepper extracts by amMS (Table 4 and Figure 4). The locations of the fatty acid double bonds could not be retrieved from the LC-MS data. However, the fatty acid composition of phytosterol derivatives in *Capsicum* oil, obtained by consecutive purifications and dedicated analytical methods, has been described in the literature and allowed for the correct fatty acid moiety assignment.[9,24] Most interestingly,

dx.doi.org/10.1021/jf500285g | J. Agric. Food Chem. 2014, 62, 4812−4831

Table 4. Values for Maximum Absorbance, Precursor and Product Ions, and Retention Times of Other Plant Metabolites Next to Carotenoids Identified in the Chili Pepper Accessions

compd	identity	mol formula	retention time (min)	max absorbance (nm)	MS mode	accurate mass of precursor ion	mass deviation (ppm)	in-source fragments and adducts	identification type
54	γ-tocopherol	$C_{28}H_{48}O_2$	10.98	297	pos	416.365 47	1.42	151.075, 401.342	*b*
					neg			150.068, 189.079	
55	α-tocopherol	$C_{29}H_{50}O_2$	11.87	293	pos	430.381 35	1.91	165.091, 431.388, 206.117, 182.117	*b*
					neg			414.350, 203.095, 164.084	
56	phylloquinone	$C_{31}H_{46}O_2$	13.37	263, 271, 330	pos	451.357 42	0.80	452.360	*b*
					neg	450.350 13	−0.44	451.353, 211.063	
57	Δ5- or Δ7-avenasterol	$C_{29}H_{48}O$	13.36		pos			395.369	*c*
					neg				
58	Δ5- or Δ7-avenasterol	$C_{29}H_{48}O$	13.69		pos			395.369, 255.210	*c*
					neg				
59	cholesterol	$C_{27}H_{46}O$	14.03		pos			369.352	*c*
					neg				
60	stigmasterol	$C_{29}H_{48}O$	14.55		pos			395.367, 311.273, 255.210	*b*
					neg				
61	campesterol	$C_{28}H_{48}O$	14.59		pos			383.367	*b*
					neg				
62	β-sitosterol	$C_{29}H_{50}O$	15.19		pos			397.382	*b*
					neg				
63	Δ5- or Δ7-avenasterol glucoside	$C_{35}H_{58}O_6$	6.77		pos			395.368	
					neg	633.43779[a]	0.95		
64	Δ5- or Δ7-avenasterol glucoside	$C_{35}H_{58}O_6$	6.96		pos			395.368	
					neg	633.43759[a]	0.63		
65	cholesterol glucoside	$C_{33}H_{56}O_6$	6.99		pos			369.352	
					neg	607.42098[a]	−0.92		
66	campesteryl glucoside	$C_{34}H_{58}O_6$	7.42		pos			383.367	*d*
					neg	561.415 34	−1.28	621.437[a]	
67	stigmasteryl glucoside	$C_{35}H_{58}O_6$	7.6		pos			395.368	*d*
					neg	633.4376[a]	0.65		

dx.doi.org/10.1021/jf500285g | J. Agric. Food Chem. 2014, 62, 4812−4831

Table 4. continued

compd	identity	mol formula	retention time (min)	max absorbance (nm)	MS mode	accurate mass of precursor ion	mass deviation (ppm)	in-source fragments and adducts	identification type
68	β-sitosteryl glucoside	$C_{35}H_{60}O_6$	8.08		pos			397.383	*d*
					neg	575.432 25	0.94	635.453[a]	
69	campesteryl (6′-*O*-linolenoyl) glucoside (C18:3)	$C_{52}H_{86}O_7$	16.45		pos			383.367	*d*
					neg	881.65187[a]	0.75		
70	campesteryl (6′-*O*-linoleoyl) glucoside (C18:2)	$C_{52}H_{88}O_7$	17.52		pos			383.367	*d*
					neg	883.66726[a]	0.45		
71	campesteryl (6′-*O*-palmitoyl) glucoside (C16:0)	$C_{50}H_{88}O_7$	19.5		pos			383.367	*d*
					neg	859.6671[a]	0.28		
72	β-sitosteryl (6′-*O*-linolenoyl) glucoside (C18:3)	$C_{53}H_{88}O_7$	16.92		pos			397.383	*d*
					neg	895.66669[a]	−0.19		
73	β-sitosteryl (6′-*O*-linoleoyl) glucoside (C18:2)	$C_{53}H_{90}O_7$	17.97		pos			397.383	*d*
					neg	897.68193[a]	−0.65		
74	β-sitosteryl (6′-*O*-palmitoyl) glucoside (C16:0)	$C_{51}H_{90}O_7$	19.98		pos			397.383	*d*
					neg	873.68167[a]	−0.96		
75	campesteryl linoleate (C18:2)	$C_{46}H_{78}O_2$	20.6		pos	663.607 42	−0.06	383.367	
					neg			279.232	
76	β-sitosteryl linoleate (C18:2)	$C_{47}H_{80}O_2$	20.88		pos	677.623 91	1.18	397.383	
					neg			279.232	
77	monogalactosyldiacylglycerol (18:3/18:3)	$C_{45}H_{74}O_{10}$	8.49		pos			613.482, 595.471	*d*
					neg	773.521 41	0.63	833.542,[a] 277.217	
78	monogalactosyldiacylglycerol (18:3/18:2)	$C_{45}H_{76}O_{10}$	9.4		pos			615.498, 597.488	*d*
					neg	775.536 83	0.34	835.557,[a] 277.217, 279.232	
79	monogalactosyldiacylglycerol (18:2/18:2)	$C_{45}H_{78}O_{10}$	10.3		pos			617.513, 599.503	*d*
					neg	777.552 77	0.71	837.573,[a] 279.232	
80	monogalactosyldiacylglycerol (18:3/18:1)	$C_{45}H_{78}O_{10}$	10.49		pos			617.51397, 599.503 36	*d*
					neg	777.552 67	0.15	837.573,[a] 277.217, 281.248	
81	monogalactosyldiacylglycerol (18:2/18:1)	$C_{45}H_{80}O_{10}$	11.44		pos				*d*
					neg	779.568 67	1.03	839.589,[a] 279.232, 281.248	
82	monogalactosyldiacylglycerol (18:3/18:0)	$C_{45}H_{80}O_{10}$	12.03		pos			619.529	*d*
					neg	779.568 16	0.37	839.589,[a] 277.217, 283.264	

dx.doi.org/10.1021/jf500285g | J. Agric. Food Chem. 2014, 62, 4812−4831

Table 4. continued

compd	identity	mol formula	retention time (min)	max absorbance (nm)	MS mode	accurate mass of precursor ion	mass deviation (ppm)	in-source fragments and adducts	identification type
83	monogalactosyldiacylglycerol (18:1/18:1)	$C_{45}H_{82}O_{10}$	12.6		pos				*d*
					neg	781.584 19	0.86	841.604[a]	
84	monogalactosyldiacylglycerol (18:2/18:0)	$C_{45}H_{82}O_{10}$	13.03		pos				*d*
					neg	781.584 07	0.70	841.604,[a] 279.233, 283.264	
85	monogalactosyldiacylglycerol (18:3/16:3)	$C_{43}H_{70}O_{10}$	7.3		pos			585.451, 567.440	*e*
					neg	745.489 99	0.50	805.510,[a] 277.217, 249.185	
86	monogalactosyldiacylglycerol (18:3/16:2)	$C_{43}H_{72}O_{10}$	8.11		pos			587.467, 569.457	*e*
					neg	747.506 02	1.00	807.526,[a] 277.217, 251.201	
87	monogalactosyldiacylglycerol (18:3/16:1)	$C_{43}H_{74}O_{10}$	9.06		pos			589.482, 571.472	*e*
					neg	749.520 88	−0.05	809.542,[a] 277.217, 253.217	
88	monogalactosyldiacylglycerol (18:3/16:0)	$C_{43}H_{76}O_{10}$	10.49		pos			591.498, 573.487	*e*
					neg	751.536 98	0.55	811.557,[a] 277.217, 255.233	
89	monogalactosyldiacylglycerol (18:2/16:0)	$C_{43}H_{78}O_{10}$	11.46		pos			575.503	*e*
					neg	753.553 01	1.05	813.573,[a] 279.232, 255.233	
90	monogalactosyldiacylglycerol (18:1/16:0)	$C_{43}H_{80}O_{10}$	12.65		pos				*e*
					neg	815.58935[a]	0.43	255.233	
91	digalactosyldiacylglycerol (18:3/18:3)	$C_{51}H_{84}O_{15}$	6.75		pos			613.481, 595.471	*e*
					neg	935.574 01	0.29	995.594,[a] 277.217	
92	digalactosyldiacylglycerol (18:3/18:2)	$C_{51}H_{86}O_{15}$	7.57		pos			615.498, 597.488	*e*
					neg	937.589 81	0.45	997.610,[a] 277.217, 279.232	
93	digalactosyldiacylglycerol (18:2/18:2)	$C_{51}H_{88}O_{15}$	8.42		pos			617.513, 599.503	*e*
					neg	939.605 51	0.49	999.626[a]	
94	digalactosyldiacylglycerol (18:3/18:1)	$C_{51}H_{88}O_{15}$	8.59		pos			617.513, 599.503	*e*
					neg	939.605 88	0.88	999.626[a]	
95	digalactosyldiacylglycerol (18:3/18:0)	$C_{51}H_{90}O_{15}$	10.09		pos			619.529, 601.518	*e*
					neg	941.620 55	−0.16	1001.641,[a] 277.217, 283.264	
96	digalactosyldiacylglycerol (18:2/18:0)	$C_{51}H_{92}O_{15}$	11.04		pos				*e*
					neg	943.635 47	−0.93	1003.657,[a] 283.264	

dx.doi.org/10.1021/jf500285g | J. Agric. Food Chem. 2014, 62, 4812−4831

Table 4. continued

compd	identity	mol formula	retention time (min)	max absorbance (nm)	MS mode	accurate mass of precursor ion	mass deviation (ppm)	in-source fragments and adducts	identification type
97	digalactosyldiacylglycerol (18:3/16:3)	$C_{49}H_{80}O_{15}$	5.7		pos			585.451, 567.440	*e*
					neg	907.542 86	0.46	967.563,[a] 277.217, 249.185	
98	digalactosyldiacylglycerol (18:3/16:0)	$C_{49}H_{86}O_{15}$	8.52		pos			591.498, 573.487	*e*
					neg	913.588 93	−0.50	973.610,[a] 277.217, 255.233	
99	digalactosyldiacylglycerol (18:2/16:0)	$C_{49}H_{88}O_{15}$	9.44		pos			575.503	*e*
					neg	915.605 16	0.12	975.626,[a] 279.232, 255.233	
100	*N*-2′-hydroxypalmitoyl-1-*O*-*β*-glucopyranosyl-4-hydroxy-8-sphingenine	$C_{40}H_{77}O_{10}N$	6.91, 7.04		pos	732.560 95	−1.46	714.550, 696.540, 570.509, 552.497, 272.258, 344.279, 326.269, 316.284, 308.258, 298.273, 280.263, 262.252	*d*
					neg	730.548 19	0.99	790.568,[a] 568.494, 550.484, 532.473, 271.227	
101	*N*-2′-hydroxypalmitoyl-1-*O*-*β*-glucopyranosyl-4,8-sphingadienine	$C_{40}H_{75}O_9N$	7.68, 7.90		pos			534.487, 516.477, 272.258, 280.263, 262.252	*d*
					neg	712.536 73	−0.25	772.557,[a] 550.484, 532.473, 514.462, 271.227	
102	*N*-2′-hydroxypalmitoyl-1-*O*-*β*-glucopyranosyl-8-sphingenine	$C_{40}H_{77}O_9N$	8.18, 8.40		pos			554.513, 536.503	*d*
					neg	714.553 41	1.19	774.574,[a] 552.500, 534.489, 516.478, 271.227	
103	*N*-2′-hydroxydocosanoyl-1-*O*-*β*-glucopyranosyl-4-hydroxy-8-sphingenine	$C_{46}H_{89}O_{10}N$	11.44, 11.56, 11.73		pos	816.6557	−0.27	798.645, 654.602, 636.592, 618.581, 356.351, 298.273, 280.263, 262.252	*d*
					neg	814.641 94	0.70	874.662,[a] 652.589, 634.578, 616.567	
104	*N*-2′-hydroxytricosanoyl-1-*O*-*β*-glucopyranosyl-4-hydroxy-8-sphingenine	$C_{47}H_{91}O_{10}N$	12.34, 12.53		pos	830.671 24	−0.40	812.660, 668.618, 650.607, 632.597, 298.273, 280.263	*d*
					neg	828.657 38	0.43	888.678,[a] 666.604, 630.583	
105	*N*-2′-hydroxytetracosanoyl-1-*O*-*β*-glucopyranosyl-4-hydroxy-8-sphingenine	$C_{48}H_{93}O_{10}N$	13.15, 13.34		pos	844.686 51	−0.84	826.676, 682.633, 664.623, 384.383, 646.613, 298.273, 280.263	*d*
					neg	842.672 66	−0.01	902.694,[a] 680.620, 662.609, 644.599	
106	*N*-2′-hydroxypentacosanoyl-1-*O*-*β*-glucopyranosyl-4-hydroxy-8-sphingenine	$C_{49}H_{95}O_{10}N$	13.93, 14.15		pos	858.702 18	−0.80	840.691, 696.649, 678.638, 660.628, 298.273, 280.263	*d*
					neg	856.688 78	0.54	916.710,[a] 694.636, 676.625, 658.614	
107	triacylglycerol (18:3,18:3,18:2)	$C_{57}H_{94}O_6$	18.34		pos	875.711 17	−1.31	597.486, 595.471	
					neg			277.217, 279.232	
108	triacylglycerol (18:3,18:2,18:2)	$C_{57}H_{96}O_6$	18.95		pos	877.726 41	−1.78	599.501, 597.486	
					neg			277.217, 279.232	
109	triacylglycerol (18:2,18:2,18:2)	$C_{57}H_{98}O_6$	19.5		pos	879.742 13	−1.69	599.502	
					neg			279.232	
110	triacylglycerol (18:2,18:2,18:1)	$C_{57}H_{100}O_6$	20.2		pos	881.758 19	−1.22	599.502, 601.517	
					neg			279.232, 281.248	

dx.doi.org/10.1021/jf500285g | J. Agric. Food Chem. 2014, 62, 4812−4831

Table 4. continued

compd	identity	mol formula	retention time (min)	max absorbance (nm)	MS mode	accurate mass of precursor ion	mass deviation (ppm)	in-source fragments and adducts	identification type
111	triacylglycerol (18:2,18:2,16:0)	$C_{55}H_{98}O_6$	20.32		pos	855.742 07	−1.81	599.502, 575.502	
					neg			279.232, 255.233	
112	triacylglycerol (18:2,18:1,16:0)	$C_{55}H_{100}O_6$	20.93		pos	857.758 03	−1.45	601.517, 577.518, 575.502	
					neg			279.232, 255.233, 281.248	
113	triacylglycerol (18:2,18:1,18:1)	$C_{57}H_{102}O_6$	20.96		pos	883.773 59	−1.50	601.518, 603.533	
					neg			279.232, 281.248	
114	triacylglycerol (18:1,16:0,16:0)	$C_{53}H_{98}O_6$	21.03		pos	831.7436	−0.02	575.503, 551.503	
					neg			255.233	
115	triacylglycerol (18:1,18:1,18:1)	$C_{57}H_{104}O_6$	21.33		pos	885.790 47	−0.11	603.534	
					neg			281.248	
116	diacylglycerol (18:3,18:2)	$C_{39}H_{66}O_5$	12.21		pos	615.497 74	−0.91	597.487, 335.258, 337.273	
					neg			277.217	
117	diacylglycerol (18:2,18:2)	$C_{39}H_{68}O_5$	13.11		pos	617.513 55	−0.65	599.503, 337.273	
					neg			279.233	
118	diacylglycerol (18:2,16:0)	$C_{37}H_{68}O_5$	14.28		pos	593.513 67	−0.47	575.502, 313.273, 337.273	
					neg			279.232, 255.233	
119	nordihydrocapsaicin	$C_{17}H_{27}O_3N$	1.56		pos	294.2065	0.44		*f*
					neg	292.1919	0.27		
120	capsaicin	$C_{18}H_{27}O_3N$	1.61	280	pos	306.206 24	−0.42		*f*
					neg	304.191 85	0.10	290.175	
121	dihydrocapsaicin	$C_{18}H_{29}O_3N$	1.82	279	pos	308.2219	−0.39		*f*
					neg	306.2075	0.10		
122	nonivamide	$C_{17}H_{27}O_3N$	1.82		pos				*f*
					neg	292.1921	0.96		
123	homodihydrocapsaicin	$C_{19}H_{31}O_3N$	2.11	279	pos	322.2378	0.40		*f*
					neg	320.2233	0.56		

[a]Acetate adduct formed in negative APCI mode. [b]Identification with analytical standard. [c]Identified by Matthäus et al.[24] [d]Identified by Yamauchi et al.[9] [e]Described by www.lipidmaps.org. [f]*Dictionary of Natural Products*:[18] present in *Capsicum annuum*.

dx.doi.org/10.1021/jf500285g | J. Agric. Food Chem. 2014, 62, 4812−4831

linoleic, linolenic, and palmitic acids were bound to the steryl and steryl glucoside moieties, corresponding to the results reported by Yamauchi et al.[9] This is different from the distribution of fatty acids bound to carotenoids (lauric, myristic, and palmitic acids) (Table 1). The elution order of the acylated steryl glucosides was predominantly influenced by the level of saturation of the fatty acid moieties, as the retention time increased in the order C18:3 < C18:2 < C16:0 (Figure 4).

Cholesterol, Δ5- and Δ7-avenasterol, and derivatives thereof were also tentatively identified by amMS, corresponding to the findings of Matthäus et al.[24] (Table 4). Due to the lack of reference standards for sterol derivatives and the complex relationship between detector response and concentration, the various molecular species could not be quantitated. Extinction coefficients could not be used as phytosterols were not detected by using PDA detection. An alkaline saponification procedure to assess the total concentration of phytosterols would require the use of both the free sterols and steryl glucosides, as the ether bonds of the steryl glucosides are stable during saponification.[25] Steryl glucoside bonds can otherwise be cleaved by acid hydrolysis.[26] During this study, it was chosen to calculate the relative abundances per group of the sterol derivatives (e.g., steryl glucosides) to enable quantitative comparison. This was achieved with the product ions corresponding to the m/z of the free sterol alcohols with the loss of water, found for all derivatives in positive APCI. Liengprayoon et al.[27] have previously reported this calculation strategy, with the hypothesis that the response to ionization is similar within a group of similar structures. Campesterol, β-sitosterol, and their derivatives were found to be the main phytosterols present in the five chili pepper accessions. The profiles of sterol derivatives were very similar between the samples; however, the total content did vary significantly between the samples for steryl glucosides and acylated steryl glucosides, being most abundant in the 'Awlad Haffouzz' and 'Souk jedid' accessions, respectively.

Yamauchi et al.[9] previously reported the detection of free phytosterols and phytosterol glucoside derivatives in chili pepper by performing consecutive prefractionations before analysis. During this study, a single generic sample preparation protocol was applied to extract all of the compounds reported in this paper. Subsequently, compound identification was performed using a single generic screening method for apolar compounds without the need for dedicated fractionation (Figure 4).

Monogalactosyldiacylglycerols and Digalactosyldiacylglycerols in Chili Peppers. In total, 23 monogalactosyldiacylglycerols and digalactosyldiacylglycerols were identified in the chili pepper accessions (e.g., molecular structure **84** in Figure 1; Table 4). Their identification was based on the ionization and in-source fragmentation pattern of a reference standard of monogalactosyldiacylglycerols and digalactosyldiacylglycerols. In positive APCI mode, predominantly product ions with the loss of the galactosyl moiety (and water) were found in the spectra. During negative APCI mode, predominantly acetate adducts were found. Differentiation between isomeric lipids containing different fatty acid moieties (e.g., C18:2/C18:2 and C18:1/C18:3) could be made by the fatty acid product ions obtained by in-source fragmentation in negative APCI mode. Almost all detected monogalactosyldiacylglycerols and digalactosyldiacylglycerols were separated with the generic chromatographic gradient. Faster elution was obtained for galactosyldiacylglycerol lipids with fatty acids of shorter chain length and/or a higher number of double bonds (Figure 4). The fatty acid moieties that were found to be part of the galactosyldiacylglycerol lipids consisted of C18:3, C18:2, C18:1, C18:0, C16:3, C16:2, C16:1, and C16:0, which corresponds with previous findings.[9]

Relative abundances were calculated for the monogalactosyldiacylglycerol and digalactosyldiacylglycerol families with the acetate adducts obtained in negative APCI mode. Monogalactosyldiacylglycerol (18:3/18:3), digalactosyldiacylglycerol (18:3/18:3), digalactosyldiacylglycerol (18:3/16:0), and digalactosyldiacylglycerol (18:3/18:0) were the most abundant galactosyl diacylglycerol lipids present in the chili pepper accessions, as previously found.[9] The profiles were very similar for the galactosyl diacylglycerol lipids between samples. However, the total content of monogalactosyldiacylglycerol and digalactosyldiacylglycerol per sample varied significantly, which showed to be highest in the 'Awlad Haffouzz' accession and lowest in the 'Souk jedid' and 'Tebourba' accessions, respectively.

Cerebrosides in Chili Peppers. Yamauchi et al.[9] identified seven molecular species of glucocerebrosides in *C. annuum* L. after HPLC purification to single compounds and consecutive NMR analysis. Owing to this work, these compounds were easily identified during the current study (e.g., molecular structure **101** in Figure 1; Table 4). The protonated molecules of these sphingolipids were detected together with several product ions such as the ceramide moiety, owing to the loss of the sugar moiety, and the α-hydroxy fatty acyl moieties, because of extensive in-source fragmentation during APCI positive mode.[9] Ionization in negative APCI mode rendered acetate adducts, deprotonated molecules, and ceramide product ions due to in-source fragmentation. For each of the identified compounds, two almost baseline separated peaks appeared in the chromatograms (Figure 4). A study reported by Whitaker et al.[28] showed that glucose is the only sugar present in the bell pepper cerebrosides and that both the 8-*cis* and 8-*trans* isomers of 4,8-sphingadienine and 8-sphingenine and the *cis*−*trans* isomers of 4-hydroxy-8-sphingenine are present in the fruits. The two isomeric peaks are explained by the respective *cis*- and *trans*-cerebrosides.

Relative abundances in MS detection were calculated for the cerebrosides by combining the chromatographic *cis*−*trans* peaks obtained for the acetate adducts in negative APCI mode. The profiles were very similar for the cerebrosides between the samples. The content per sample did vary significantly, which showed to be highest in the 'Awlad Haffouzz' accession and lowest in the 'Tebourba' accession.

Glycerolipids in Chili Peppers. Nine triglycerides and three diglycerides were identified in the chili pepper accessions (e.g., molecular structure **109** in Figure 1; Table 4). Their identification was based on the ionization and in-source fragmentation pattern of a glyceryl trioleate and glyceryl dioleate standard. As in most cases the order of the fatty acids bound to glycerol (i.e.*sn*-1, *sn*-2, or *sn*-3 position of the glycerol backbone) could not be deduced from the MS spectra, the lipids were noted as 'triglyceride (C18:2, C18:2, C16:0)" instead of "triglyceride (C18:2/C18:2/C16:0)" (Table 4). Predominantly triglycerides were present in the extracts. Faster elution was obtained with fatty acids of shorter chain length and/or a higher number of double bonds (Figure 4). The fatty acid moieties that were found to be part of the glycerolipids consisted of linolenic acid (C18:3), linoleic acid (C18:2), oleic acid (C18:1), and palmitic acid (C16:0), which is in line with

the fatty acid composition of the acylated steryl glucosides, the acylated sterols, monogalactosyldiacylglycerols, and digalactosyldiacylglycerols that were identified during this study.

Relative abundances in MS detection were calculated for the diglycerides and triglycerides with the protonated molecules obtained in positive APCI mode. The triglyceride with three linoleic acid moieties (C18:2, C18:2, C18:2) and diglyceride with two linoleic acid moieties (C18:2, C18:2) were most abundantly present in the chili pepper accessions. The profiles were very similar for the di- and triacylglycerides in the samples. However, the content did vary significantly and was highest in the 'Somâa' and 'Korba' accessions and lowest in the 'Awlad Haffouzz' and 'Souk jedid' accession for triglycerides and diglycerides, respectively.

Capsaicinoids in Chili Peppers. Five capsaicinoids, which are known to be present in high amounts in chili peppers, were identified with amMS. Because these compounds are relatively small and polar compared to the other studied compounds (molecular structure **120** in Figure 1), they partially coeluted within the first 3 min of the chromatographic gradient. The identities of nordihydrocapsaicin, capsaicin, dihydrocapsaicin, and nonivamide were later confirmed with their respective analytical standards (unpublished results). The profiles of the capsaicinoids were similar in the samples; however, the content did vary significantly, being lowest for 'Souk jedid' and highest in the 'Tebourba' and 'Korba' accessions.

During this study, a single generic sample preparation protocol was applied to extract all of the compounds reported in this paper. Subsequently, compound identification was performed using a single generic UHPLC-PDA-amMS screening method for apolar compounds without the need for dedicated fractionation. Method validation confirmed that the generic approach is applicable for quantitative purposes and is virtually limited only by the solubility and detector response of the metabolites of interest. It was shown that although most of the compounds were separated by chromatography, orthogonal detector selectivity remains essential for compound differentiation. This can in many cases not be achieved by PDA detection alone and highlights the added value of high-end instrumentation in this research field.

Second, an identification−quantitation strategy based on the use of LC-PDA-amMS and extinction coefficients was applied for carotenoids, enabling unparalleled speed in the identification and quantification of unknown carotenoids and eliminating the need for reference standards for each carotenoid. Finally, a case study on chili pepper fruits (*C. frutescens* L.) showed that carotenoids, steryl derivatives, glycolipids, glycerolipids, capsaicinoids, and lipid-soluble vitamins could be characterized simultaneously with the analytical platform. This system is thus a powerful tool to unravel the complex apolar phytochemicals composition of biomass, as it is useful not only as a fingerprinting method but also for the detailed profiling of individual components.

■ ASSOCIATED CONTENT

Supporting Information

Supplementary Tables 1−3. This material is available free of charge via the Internet at http://pubs.acs.org.

■ AUTHOR INFORMATION

Corresponding Author

*(S.B.) Phone: + 32 14 33 50 54. Fax: + 32 14 31 94 72. E-mail: sebastiaan.bijttebier@vito.be.

Notes

The authors declare no competing financial interest.

■ REFERENCES

(1) Cardozo, K. H. M.; Guaratini, T.; Barros, M. P.; Falcão, V. R.; Tonon, A. P.; Lopes, N. P.; Campos, S.; Torres, M. A.; Souza, A. O.; Colepicolo, P.; Pinto, E. Metabolites from algae with economical impact. *Comp. Biochem. Physiol.* **2007**, *146*, 60−78.

(2) O'Shea, N.; Arendt, E. K.; Gallagher, E. Dietary fibre and phytochemical characteristics of fruit and vegetable by-products and their recent applications as novel ingredients in food products. *Innovative Food Sci. Emerging Technol.* **2012**, *16*, 1−10.

(3) Frederici, F.; Fava, F.; Kalogerakis, N.; Mantzavinos, D. Valorisation of agro-industrial by products, effluents and waste: concept, opportunities and the case of olive mill wastewater. *J. Chem. Technol. Biotechnol.* **2009**, *84*, 895−900.

(4) Bijttebier, S. K. A.; D'Hondt, E.; Hermans, N.; Apers, S.; Voorspoels, S. Unravelling ionization and fragmentation pathways of carotenoids using orbitrap technology: a first step towards identification of unknowns. *J. Mass Spectrom.* **2013**, *48*, 740−754.

(5) Kind, T.; Fiehn, O. Metabolomic database annotations via query of elemental compositions: mass accuracy is insufficient even at less than 1 ppm. *BMC Bioinform.* **2006**, *7*, 234.

(6) Zhang, Y.; Xiao, S.; Sun, L.; Ge, Z.; Fang, F.; Zhang, W.; Wang, Y.; Cheng, Y. Rapid screening of bioactive compounds from natural products by integrating 5-channel parallel chromatography coupled with on-line mass spectrometry and microplate based assays. *Anal. Chim. Acta* **2013**, *777*, 49−56.

(7) El-Elimat, T.; Figueroa, M.; Ehrmann, B. M.; Cech, N. B.; Pearce, C. J.; Oberlies, N. H. High-resolution MS, MS/MS, and UV database of fungal secondary metabolites as a dereplication protocol for bioactive natural products. *J. Nat. Prod.* **2013**, *76* (9), 1709−1716.

(8) Deli, J.; Matus, Z.; Tóth, G. Carotenoid composition in the fruits of *Capsicum annuum* cv. szentesi kosszarvú during ripening. *J. Agric. Food Chem.* **1996**, *44*, 711−716.

(9) Yamauchi, R.; Aizawa, K.; Inakuma, T.; Kato, K. Analysis of molecular species of glycolipids in fruit pastes of red bell pepper (*Capsicum annuum* L.) by high-performance liquid chromatography-mass spectrometry. *J. Agric. Food Chem.* **2001**, *49*, 622−627.

(10) Schweiggert, U.; Kammerer, D. R.; Carle, R.; Schieber, A. Characterization of carotenoids and carotenoid esters in red pepper pods (*Capsicum annuum* L.) by high-performance liquid chromatography/atmospheric pressure chemical ionization mass spectrometry. *Rapid Commun. Mass Spectrom.* **2005**, *19*, 2617−2628.

(11) Topuz, A.; Ozdemir, F. Assessment of carotenoids, capsaicinoids and ascorbic acid composition of some selected pepper cultivars (*Capsicum annuum* L.) grown in Turkey. *J. Food Compos. Anal.* **2007**, *20*, 596−602.

(12) Wahyuni, Y.; Ballester, A.-R.; Sudarmonowati, E.; Bino, R. J.; Bovy, A. G. Metabolite biodiversity in pepper (*Capsicum*) fruits of thirty-two diverse accessions: variation in health-related compounds and implications for breeding. *Phytochemistry* **2011**, *72*, 1358−1370.

(13) Giuffrida, D.; Dugo, P.; Torre, G.; Bignardi, C.; Cavazza, A.; Corradini, C.; Dugo, G. Characterization of 12 *Capsicum* varieties by evaluation of their carotenoid profile and pungency determination. *Food Chem.* **2013**, *140*, 794−802.

(14) Rodriguez-Amaya, D. B. General procedure and sources of errors in carotenoid analysis. In *A Guide to Carotenoid Analysis in Food*, 1st ed.; ILSI Press: Washington, DC, USA, 2000; p 26.

(15) *Carotenoids: Isolation and Analysis*, 1st ed.; Britton, G., Liaaen-Jensen, S., Pfander, H., Eds.; Birkhäuser Verlag: Basel, Switzerland, 1994; Vol. 1A.

(16) Asai, A.; Terasaki, M.; Nagao, A. An epoxide−furanoid rearrangement of spinach neoxanthin occurs in the gastrointestinal tract of mice and *in vitro*: formation and cytostatic activity of neochrome stereoisomers. *J. Nutr.* **2004**, *134*, 2237−2243.

(17) *Carotenoids: Spectroscopy*, 1st ed.; Britton, G., Liaaen-Jensen, S., Pfander, H., Mercadante, A. Z., Egeland, E. S., Eds.; Birkhäuser Verlag: Basel, Switzerland, 1995; Vol. 1B.

(18) *Dictionary of Natural Products (DVD)*, version 2011; Taylor & Francis (Chapman and Hall/CRC): Boca Raton, FL, USA, 2011.
(19) *Carotenoids − Handbook*, 1st ed.; Britton, G., Liaaen-Jensen, S., Pfander, H., Mercadante, A. Z., Egeland, E. S., Eds.; Birkhäuser Verlag: Basel, Switzerland, 2004.
(20) Khoo, H.-E.; Prasad, K. N.; Kong, K.-W.; Jiang, Y.; Ismail, A. Carotenoids and their isomers: color pigments in fruits and vegetables. *Molecule* **2011**, *16*, 1710−1738.
(21) Britton, G.; Liaaen-Jensen, S.; Pfander, H. *E/Z* isomers and isomerization. In *Carotenoids, Vol. 4: Natural Functions*, 1st ed.; Birkhäuser Verlag: Basel, Switzerland, 2008; p 21.
(22) Osuna-García, J. A.; Wall, M. M.; Waddell, C. A. Endogenous levels of tocopherols and ascorbic acid during fruit ripening of New Mexican-type chile (*Capsicum annuum* L.) cultivars. *J. Agric. Food Chem.* **1998**, *46*, 5093−5096.
(23) Moreau, R. A.; Whitaker, B. D.; Hicks, K. B. Phytosterols, phytostanols, and their conjugates in foods: structural diversity, quantitative analysis, and health-promoting uses. *Prog. Lipid Res.* **2002**, *41*, 457−500.
(24) Matthäus, B.; Özcan, M. M. Chemical evaluation of some paprika (*Capsicum annuum* L.) seed oils. *Eur. J. Lipid Sci. Technol.* **2009**, *111*, 1249−1254.
(25) Phillips, K. M.; Ruggio, D. M.; Ashraf-Khorassani, M. Analysis of steryl glucosides in foods and dietary supplements by solid-phase extraction and gas chromatography. *J. Food Lipids* **2005**, *12*, 124−140.
(26) Kaloustian, J.; Alhanout, K.; Amiot-Carlin, M.-J.; Lairon, D.; Portugal, H.; Nicolay, A. Effect of water cooking on free phytosterol levels in beans and vegetables. *Food Chem.* **2008**, *107*, 1379−1386.
(27) Liengprayoon, S.; Sriroth, K.; Dubreucq, E.; Vaysse, L. Glycolipid composition of *Hevea brasiliensis latex*. *Phytochemistry* **2011**, *72*, 1902−1913.
(28) Whitaker, B. D. Cerebrosides in mature-green and red-ripe bell pepper and tomato fruits. *Phytochemistry* **1996**, *42*, 627−632.

JOURNAL OF AGRICULTURAL AND FOOD CHEMISTRY

Addition/Correction

pubs.acs.org/JAFC

Correction to Total Phospholipids in Edible Oils by In-Vial Solvent Extraction Coupled with FTIR Analysis

Xianghe Meng, Qin Ye, Qiuyue Pan, Yang Ding, Min Wei, Yun Liu,* and F. R. van de Voort*

J. Agric. Food Chem. **2014**, *62* (14), 3101−3107. DOI: 10.1021/jf404880v

The name of corresponding author van de Voort was presented incorrectly and is corrected above. Also, the postal code for his McGill University affiliation should be H9X 3V9.

Published: May 12, 2014

ACS Publications © 2014 American Chemical Society

JOURNAL OF AGRICULTURAL AND FOOD CHEMISTRY

Article

pubs.acs.org/JAFC

Synthesis of Nanopesticides by Encapsulating Pesticide Nanoparticles Using Functionalized Carbon Nanotubes and Application of New Nanocomposite for Plant Disease Treatment

Nahid Sarlak,*[,†] Asghar Taherifar,[†] and Fatemeh Salehi[§]

[†]Department of Chemistry, Faculty of Sciences, Lorestan University, Khorram Abad, Iran

[§]Department of Molecular Biology, Faculty of Biology, Tehran University, Tehran, Iran

ABSTRACT: Polymerization of citric acid onto the surface of oxidized multiwall carbon nanotubes led to MWCNT-*graft*-poly(citric acid) (MWCNT-*g*-PCA) hybrid materials. Because of the presence of conjugated citric acid branches, synthesized MWCNT-*g*-PCA hybrid materials were not only soluble in water but also able to trap water-soluble chemical species and metal ions. Trapping of pesticides such as zineb and mancozeb in aqueous solution by MWCNT-*g*-PCA hybrid materials led to encapsulated pesticide (EP) in the polycitric acid shell. Optimum conditions for encapsulation of zineb and mancozeb in hyperbranched polycitric acid such as pH, time of stirring, and temperature were investigated by the UV−vis spectroscopy method. Encapsulation of pesticides on CNT-*g*-PCA hybrid material was confirmed via TEM analysis. Experiments indicated that new the CNT-*g*-PCA-EP hybrid material in comparison with bulk pesticide had a superior toxic influence on *Alternaria alternata* fungi.

KEYWORDS: *zineb, mancozeb, pesticide, multiwalled carbon nanotubes, nanocomposite*

1. INTRODUCTION

Organic pesticides including insecticides and herbicides are widely used in agriculture because of their powerful biological activity.[1] Mancozeb and zineb were first introduced during the 1940s and widely used. Mancozeb as a pesticide protects many fruit, vegetable, nut, and agricultural crops against a wide range of fungal diseases. It is a grayish-yellow powder, and its chemical name is manganese ethylene bis(dithiocarbamate) (polymeric). Zineb is a light-colored powder or crystal the chemical name of which is zinc ethylene bis-(dithiocarbamate).[2−6] Figures 1a and 1b show the chemical structures of mancozeb and zineb molecules, respectively.

Encapsulation is a process of surrounding or enveloping one substance within another material on a very small scale. Another definition of encapsulation is the process by which a material is surrounded and protected from extraneous conditions that would otherwise break it down, yielding capsules ranging from less than one micrometer to several hundred micrometers in size.[7] Encapsulation can be achieved by several techniques with different purposes in mind. Encapsulation of materials may occur with the intention that the core material be confined within capsule walls for a specific period of time. Alternatively, core substances can be encapsulated so that the core material will be released either gradually through the capsule walls, known as controlled release or diffusion, or when external conditions activate the capsule walls to break, melt, or dissolve.[8] There are many applications for encapsulated materials in various fields such as agriculture, pharmaceuticals, foods, cosmetics and fragrances, textiles, paper, paints, coatings and adhesives, printing applications, and many other industries.

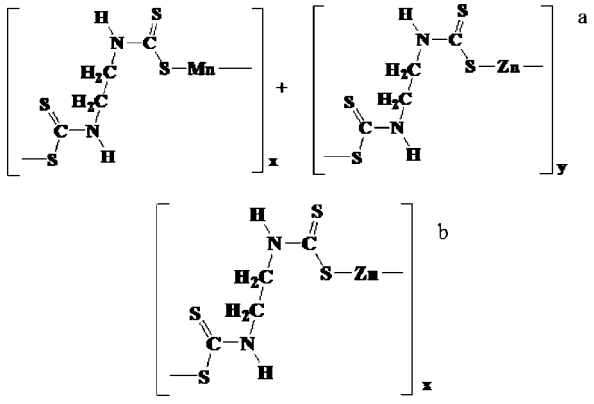

Figure 1. Structure of (a) mancozeb molecule and (b) zineb molecule.

Pesticides may be encapsulated to be released over time, allowing farmers to apply the pesticides less often rather than requiring very highly concentrated and perhaps toxic initial applications followed by repeated applications to battle the loss of efficacy due to leaching, evaporation, and degradation.[9] Protection of pesticides from full contact with the elements lessens the risk to the environment and those that might be exposed to the chemicals and provides a more efficient strategy for pest control.[10]

In the past decade, there has been increasing interest in the studies of polymer/CNT nanocomposites due to the unique combination of promising properties and construction of multifunctional structures of each component.[11] Previously

Received: May 6, 2013
Revised: April 12, 2014
Accepted: May 2, 2014
Published: May 15, 2014

ACS Publications © 2014 American Chemical Society

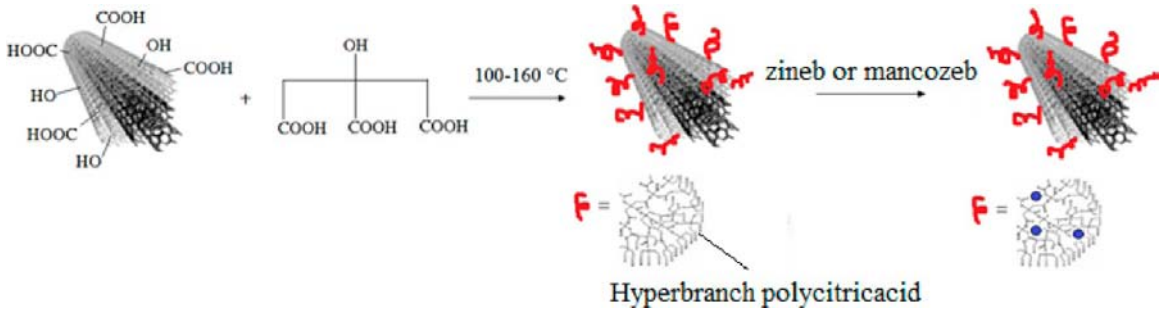

Figure 2. Synthetic scheme of CNT-*g*-PCA-EP.

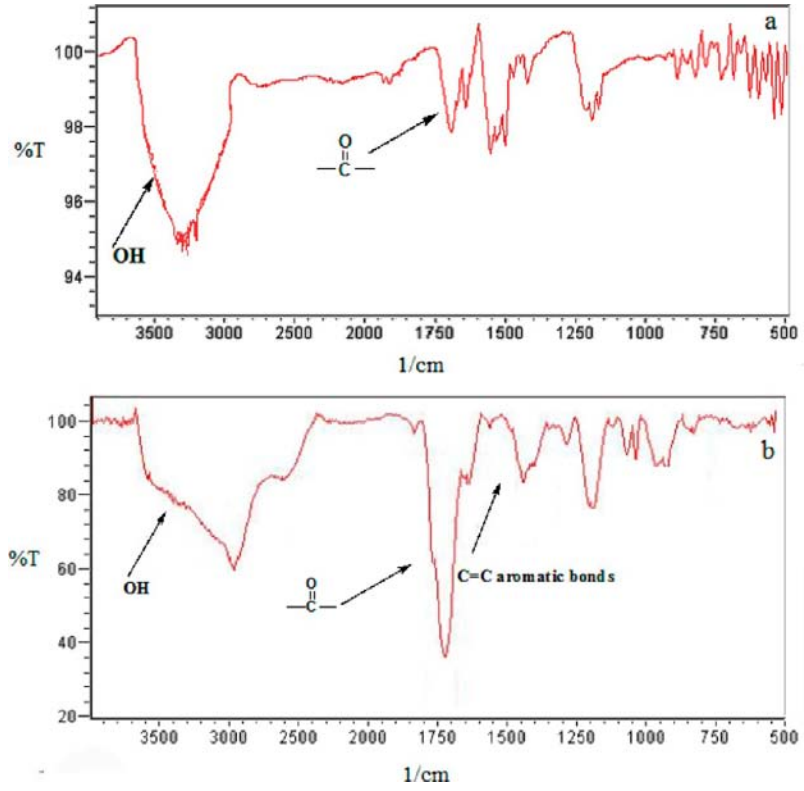

Figure 3. FTIR data for (a) MWCNT−COOH and (b) MWCNT-*g*-PCA hybrid material.

Trimnell et al.[12] investigated the encapsulation of pesticide within a starch−borate complex. In this work the starch, pesticide, and water were mixed and alkali was added to gelatinize the starch. Then the mixture was treated with boric acid.

In our study zineb and mancozeb were encapsulated into MWCNT-*g*-PCA hybrid material, which process leads to conversion of bulk pesticide to pesticide nanoparticles. Effective parameters in the encapsulation process, such as pH, temperature, and time of stirring, were optimized via the UV−vis spectroscopic method. The influence of encapsulated pesticide was studied on the malady *Alternaria alternate*, so, for this purpose, potato dextrose agar (PDA) was used as a growth medium. Results show that pesticide nanoparticles in contrast with bulk pesticide have extraordinary function. To the best of our knowledge, this paper is the first report about using water-soluble polymerized carbon nanotubes for encapsulation of pesticides and application the new nanopesticides in malady agent treatment.

In comparison with previous reports there are some novel and specific advantages as follows:

(a) Pesticide encapsulated into CNT-*g*-PCA hybrid material is more stable and effective than bulk pesticide.
(b) Pesticide usage will be decreased in agriculture.
(c) Water solubility of encapsulated pesticides will be increased.
(d) Multiwall carbon nanotubes will be dissolved in the water.

This product can be used extensively in several greenhouse and field studies and agriculture.

2. EXPERIMENTAL SECTION

2.1. Reagents. The MWCNT was purchased from Nutrino. The outer diameter of MWCNT was between 20−40 nm. Monohydrate citric acid, sulfuric and nitric acid, tetrahydrofuran, and cyclohexane were purchased from Merck. Pesticide standard was purchased from Delta Green South Corporation of Iran.

2.2. Apparatus. Fourier transform infrared (FT-IR) spectroscopic measurements were performed using a FT-IR spectrometer (Thermo

dx.doi.org/10.1021/jf404720d | J. Agric. Food Chem. 2014, 62, 4833−4838

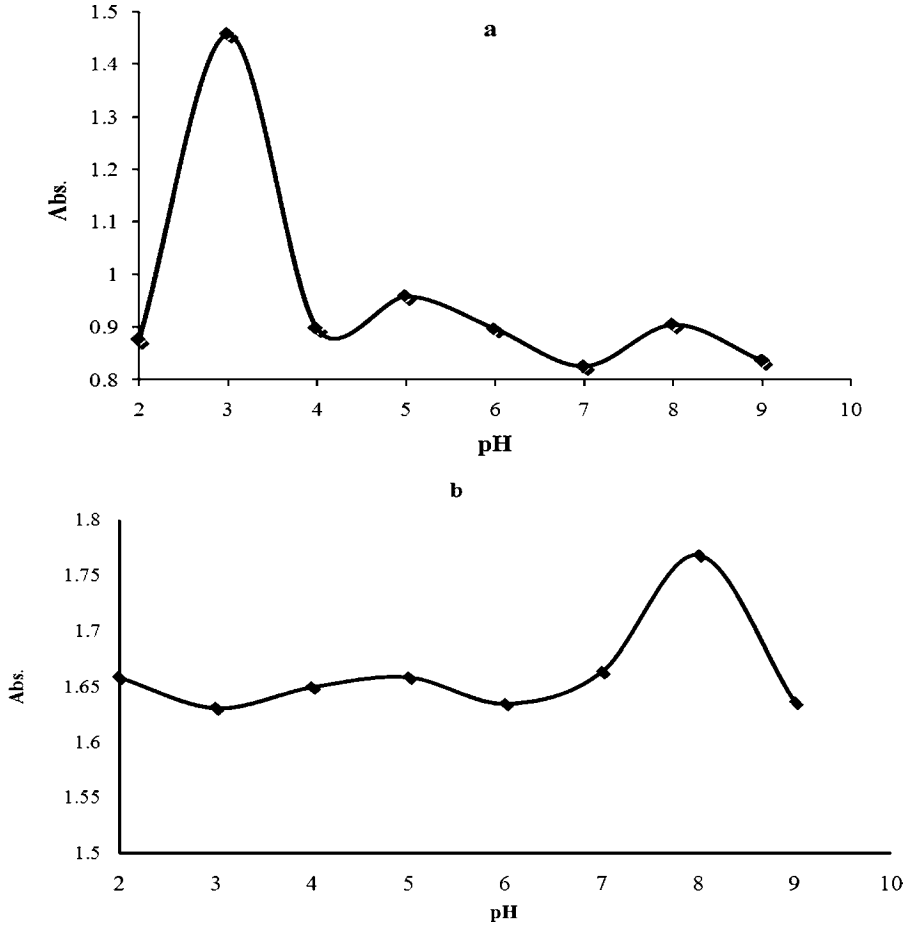

Figure 4. Effect of pH on the encapsulation of mancozeb (a) and zineb (b) with CNT-*g*-PCA.

Nicolet Magna-IR 560 spectroscope, USA). The FTIR spectra of acid modified CNTs and CNT-*g*-PCA were obtained in transmittance mode by placing a small amount of the materials in KBr pellets. The UV−vis measurements were obtained using a double beam spectrophotometer (Shimadzu 1650 UV−vis spectrophotometer, Japan) with 1 cm quartz cells. In order to well disperse pesticide in the polymeric shell of hybrid material, an ultrasonic bath (22 kHz) was used. The TEM study was carried out using a microscope operating at 100 kV. The samples for the TEM analysis were prepared by dilution of nanocomposite with distilled water. A drop of the suspension was applied onto a carbon-coated copper grid and was dried in air. A centrifuge (Eppendorf 5810) was used for separation of CNT-*g*-PCA-EP from pesticide molecules.

2.3. Preparation of MWCNT-*g*-PCA Hybrid Materials. MWCNTs were opened according to reported procedures in the literature.[13] Briefly, MWCNTs (2 g) were added to 40 mL of sulfuric and nitric acid mixture (3/1) in a reaction flask and refluxed for 24 h at 120 °C. The mixture was cooled and diluted with distilled water, and then it was filtrated and washed with distilled water until the pH reached 5; finally it was dried by vacuum oven. MWCNT-*g*-PCA hybrid materials were prepared according to the reported procedure.[14]

2.4. Preparation of MWCNT-*g*-PCA-EP. A water solution of MWCNT-*g*-PCA (39 mg/mL) with a mancozeb water solution (5.12×10^{-4} M) and also a water solution of MWCNT-*g*-PCA (28 mg/mL) with a zineb water solution (1.45×10^{-4} M) were mixed separately and placed in an ultrasonic bath for 10 min in order to well disperse pesticide nanoparticles in the polycitric acid shell. Then the mixtures were stirred for complete encapsulation of mancozeb and zineb into CNT-*g*-PCA for 35 and 80 min, respectively.

Encapsulated pesticide nanoparticles were purified by centrifugation. Pesticide molecules which were not reacted with CNT-*g*-PCA were separated from encapsulated pesticide nanoparticles using a centrifuge with rotating speed of 2000 rpm within 7 min. During the process of centrifugation the sample was separated into two phases, a pellet consisting of MWCNT-*g*-PCA-EP and a supernatant that was unreacted pesticide molecules. Then the supernatant was separated and discarded. Figure 2 shows the synthetic scheme of the CNT-*g*-PCA-EP.

2.5. Preparation of Potato Dextrose Agar (PDA) Medium. Usually for PDA medium preparation, 250 g of potatoes was boiled for 20 min and the sap of potato was taken. Afterward 20 g of dextrose agar was added to the sap under continuous stirring and slowly warmed until it was well dissolved. Then the medium was diluted to 1 L by warmed distilled water and autoclaved for 15 min at 121 °C and pressure 1.5 kg/cm^2. Finally PDA medium was chilled to 45 °C and was poured into a Petri dish.[15−17]

3. RESULTS AND DISCUSSION

3.1. Nanohybrid Characterization. The FTIR spectra shown in Figure 3 confirm the presence of functional groups in MWCNT−COOH and MWCNT-*g*-PCA hybrid materials. The carbonyl stretching frequency in MWCNT−COOH was seen at 1701 cm^{-1} (COOH); The 3200−3500 cm^{-1} band present in the MWCNT−COOH spectrum was attributed to the hydroxyl vibration of the carboxylic acid group attached through the opening. The peak around 1400−1500 cm^{-1} was assigned to the C═C stretching of the carbon skeleton. As shown in Figure 3b a broad absorbance band at 2600−3573 cm^{-1} was attributed to hydroxyl functional groups of grafted PCA. In this spectrum, a band of carbonyl groups of citric acid was seen at 1718 cm^{-1}. Also the C═C band of MWCNT appeared at 1400−1500 cm^{-1}.

dx.doi.org/10.1021/jf404720d | J. Agric. Food Chem. 2014, 62, 4833−4838

3.2. Optimization of Effective Parameters on Synthesis of CNT-*g*-PCA-EP. The effect of various parameters on encapsulation of pesticides into CNT-*g*-PCA was studied. Figure 4 shows the role of pH in the encapsulation of pesticides by MWCNT-*g*-PCA hybrid material. The maximum encapsulation of pesticide molecules into polymeric shell corresponds to maximum absorption in UV−vis spectra. Maximum encapsulation for mancozeb and zineb according to Figure 4 takes place at pH 3 and 8 respectively. Furthermore, temperature had no significant effect on the encapsulation reaction.

The required time for complete encapsulation of pesticides in CNT-*g*-PCA is very important. Figure 5 shows the effect of

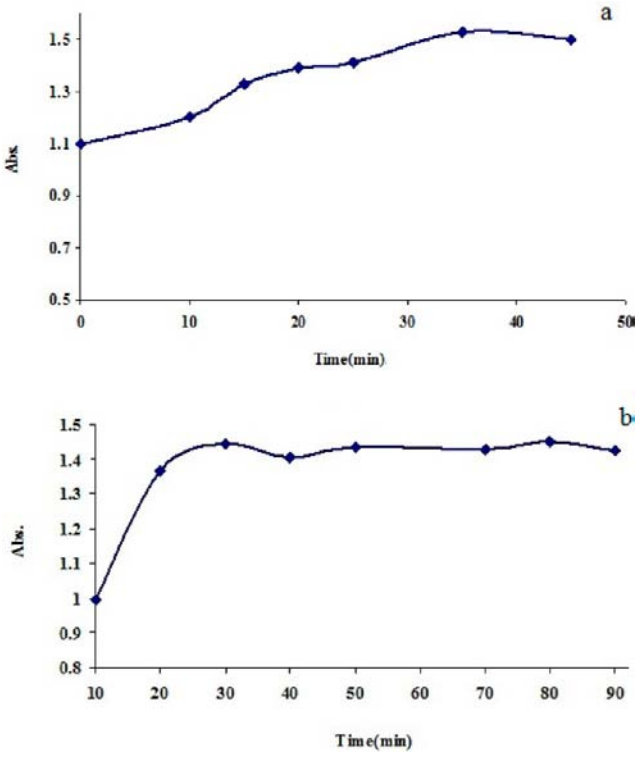

Figure 5. Effect of stirring time on encapsulation of pesticides into CNT-*g*-PCA hybrid material. Mancozeb (a) and zineb (b).

stirring time on the reaction between pesticides and CNT-*g*-PCA. As shown in Figure 5a,b with the addition of pesticide aqueous solutions to CNT-*g*-PCA the respective absorption peak increases. In other words, maximum encapsulation for mancozeb and zineb in hyperbranched polycitric acid shell takes place after 35 and 80 min, respectively.

Figure 6 shows the color change during the progress of the complexation reaction between zineb and CNT-*g*-PCA hybrid material under optimum conditions. As shown in Figure 6, the light yellow color of solution turned gradually to pale yellow after 2 h. The darkening of the solution continued and fixed after 8 h, which indicated that the encapsulation process was completed.

3.3. Encapsulation of the Pesticides by CNT-*g*-PCA: UV−Vis Study. The encapsulation of the zineb and mancozeb by polymeric shell of CNT-*g*-PCA was investigated spectrophtometrically. Figure 7a(iii),b(iii) shows the UV−vis spectra for encapsulated zineb and mancozeb by CNT-*g*-PCA respectively.

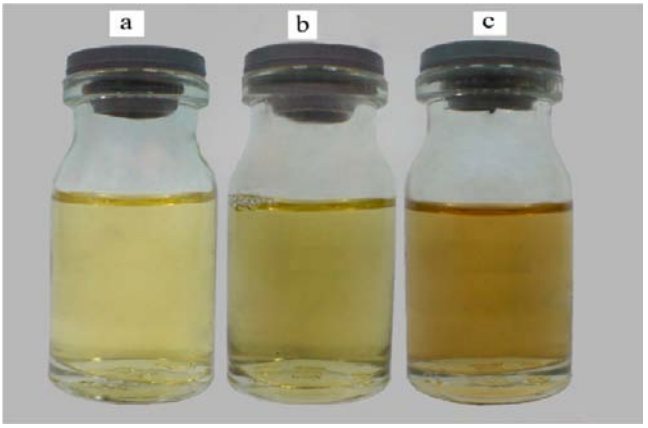

Figure 6. Color change during time progression of the encapsulation between pesticide zineb and MWCNT-*g*-PCA: (a) initial; (b) after 2 h; (c) after 8 h.

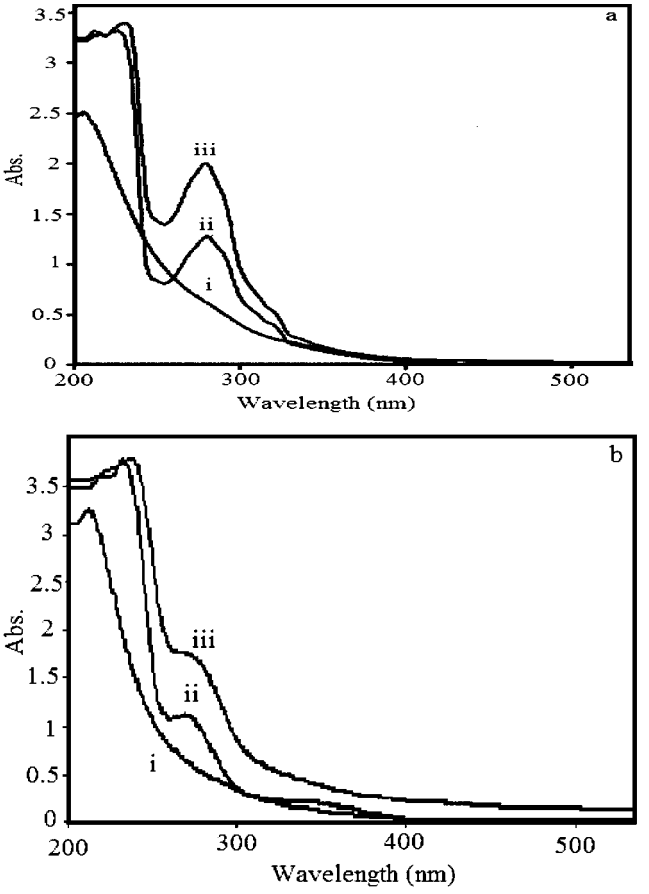

Figure 7. UV spectra for encapsulation of (a) zineb and (b) mancozeb by CNT-*g*-PCA: (i) aqueous solution of CNT-*g*-PCA; (ii) aqueous solution of pesticide; (iii) after addition of pesticide to CNT-*g*-PCA.

A simple route which clearly approves the encapsulation of pesticides in hyperbranched polycitric acid shell was attained with addition of various amounts of CNT-*g*-PCA to each pesticide and monitoring of the UV spectra. As shown in Figure 8, addition of CNT-*g*-PCA led to increasing the peak intensity while the fine structures of pesticide spectra follow the same pattern. These behaviors confirm the encapsulation of pesticides into polycitric acid hyperbranched shell.

dx.doi.org/10.1021/jf404720d | *J. Agric. Food Chem.* 2014, 62, 4833−4838

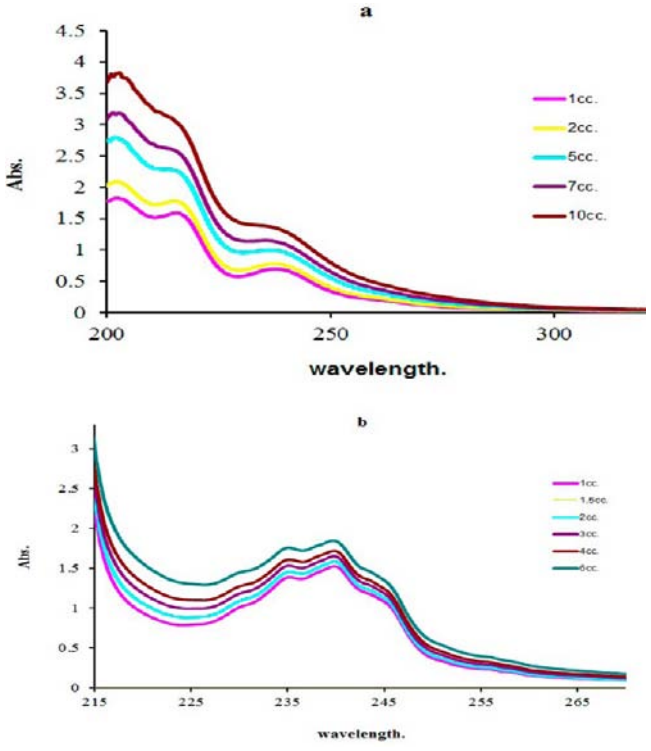

Figure 8. Addition of various amounts of a water solution of CNT-*g*-PCA to pesticides (a) mancozeb and (b) zineb.

3.4. TEM Images of Synthesized CNT-*g*-PCA-Pesticide. Finally encapsulation of pesticides by the CNT-*g*-PCA was confirmed by TEM analysis. Figure 9 shows TEM images of zineb and mancozeb encapsulation by the CNT-*g*-PCA hybrid material which clearly indicates polycitric acid (PCA) shell around CNTs and encapsulated pesticide nanoparticles.

3.5. Application of Encapsulated Zineb Nanoparticles on *Alternaria alternate* Fungi. Encapsulation of pesticide nanoparticles in hyperbranched polycitric acid results in the appearance of extraordinary characteristics. In this study, the influence of CNT-*g*-PCA-EP on the malady *Alternaria alternata* fungi was studied. For this purpose, potato dextrose agar (PDA) medium was used to grow the malady *Alternaria alternate*. Bulk and encapsulated zineb were added to the control medium, and their effects on growth of colonies were studied after 3 and 10 days (Figure 10). The results show that encapsulated zineb nanoparticles have more effect on growth restriction in comparison to the bulk zineb. This effect after 10 days reaches the maximum intensity. Probably this phenomenon is attributable to increases in the contact area which was formed between encapsulated pesticide and fungi.

3.6. Conclusion. In summary, mancozeb and zineb were successfully encapsulated into CNT-*g*-PCA hybrid material. Results showed that encapsulation of pesticides into hybrid material are dependent on pH and time of stirring but temperature has no significant effect on the encapsulation process. Experiments show that the optimum pH for encapsulation of mancozeb and zineb is 3 and 8 respectively.

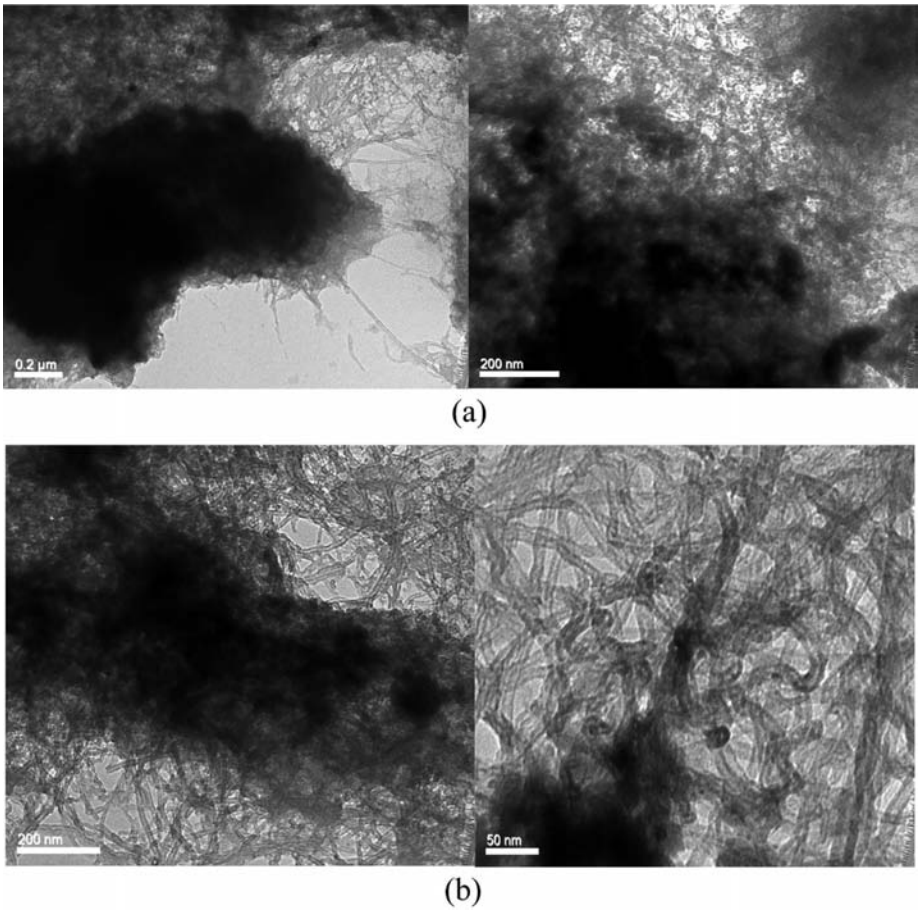

Figure 9. TEM images of encapsulation of zineb (a) and mancozeb (b) with MWCNT-*g*-PCA.

dx.doi.org/10.1021/jf404720d | *J. Agric. Food Chem.* 2014, 62, 4833−4838

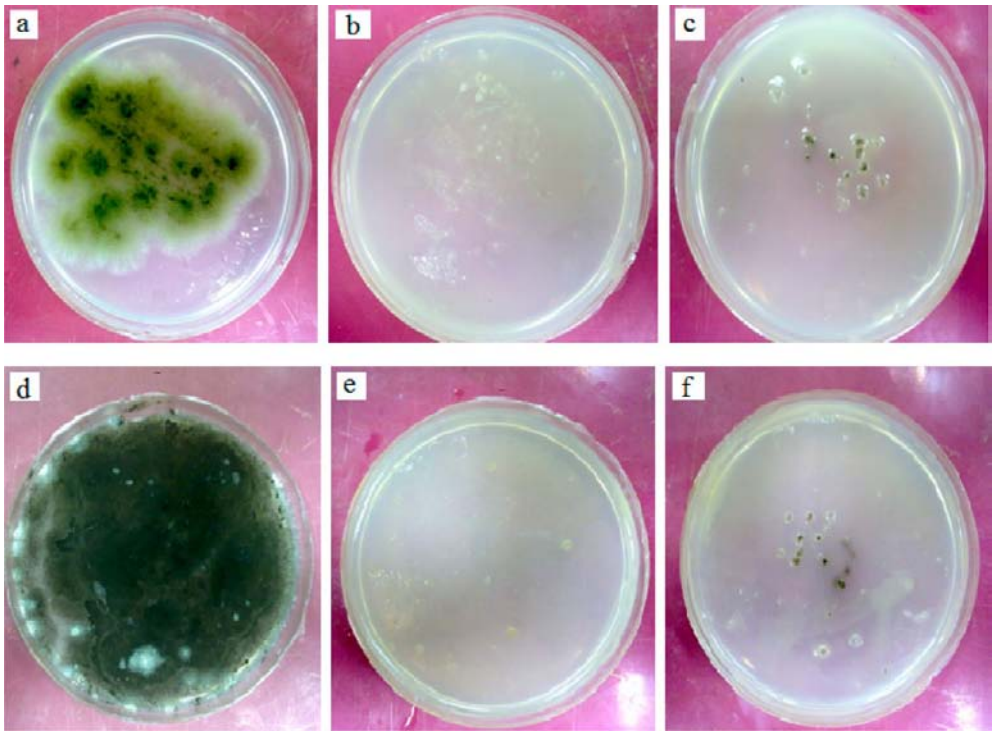

Figure 10. Influence of zineb encapsulation on *Alternaria alternate* fungi. Medium control (a and d), medium control with encapsulated zineb (b and e), and medium control with bulk zineb (c and f). Top, after 3 days; bottom, after 10 days.

Furthermore, the time of stirring for complete encapsulation of mancozeb and zineb was 35 and 80 min, respectively. As a result, in this work we could produce pesticide nanoparticles. So encapsulated zineb as pesticide nanoparticles in comparison with bulk zineb showed an extraordinary effect on the malady *Alternaria alternata* fungi, and its effect reached maximum after 10 days.

AUTHOR INFORMATION

Corresponding Author

*E-mail: sarlak.n@gmail.com.

Notes

The authors declare no competing financial interest.

REFERENCES

(1) Al-Degs, Y. S.; Al-Ghouti, M. A.; El-Sheikh, A. H. Simultaneous determination of pesticides at trace levels in water using multiwalled carbon nanotubes as solid-phase extractant and multivariate calibration. *J. Hazard. Mater.* **2009**, *169*, 128−135.

(2) Scher, H. B.Advances in Pesticide Formulation Technology. In *Advances in Pesticide Formulation Technology*; Scher, H. B., Ed.; American Chemical Society: Washington, DC, 1984; pp 1−7

(3) Matthews, G. A. Pests, Pesticides and Pest Management. In *Highlights In Environmental Research*; Mason, J., Ed.; Imperial College Press: London, **2000**; pp 165−189.

(4) Rijtema, P. E.; Groenendijk, P.; Kroes, J. G. Environmental Influences on Processes. In *Environmental Impact Of Land Use In Rural Regions*; Imperial College Press: London, 1999; pp 167−203.

(5) Tordoir, W. F. The Development of Safe Chemical Pesticides. In *Occupational Health In National Development*; World Scientific: 1994; pp 27−42.

(6) Honeycutt Richard, C.; Zweig, G.; Ragsdale, N.; Durham William, F. Preface, Introduction. In *Dermal Exposure Related to Pesticide Use*; American Chemical Society: Washington, DC, 1985; pp xi−xiv.

(7) Del Carmen Giménez-López, M.; Moro, F.; Torre, A. L.; Gómez-García, C. J.; Brown, P. D.; Slageren, J. V.; Khlobystov, A. N. Encapsulation of single-molecule magnets in carbon nanotubes. *Nat. Commun.* **2011**, *2*, 407.

(8) Doane, W. M. Encapsulation of pesticides in starch by extrusion. *Ind. Crops Prod.* **1992**, *1*, 83−87.

(9) Lewis, D. H.; Cowsar, D. R. Principles of Controlled Release Pesticides. In *Controlled Release Pesticides*; Scher, H. B., Ed.; American Chemical Society: Washington, DC, 1977; pp 1−16

(10) Ulbricht, H.; Hertel, T. Dynamics of C60 Encapsulation into Single-Wall Carbon Nanotubes. *J. Phys. Chem. B* **2003**, *107*, 14185−14190.

(11) Ajayan, P. M. Nanotubes from Carbon. *Chem. Rev.* **1999**, *99*, 1787−1800.

(12) Trimnell, D.; Shasha, B. S.; Wing, R. E.; Otey, F. H. Pesticide encapsulation using a starch−borate complex as wall material. *J. Appl. Polym. Sci.* **1982**, *27*, 3919−3928.

(13) Stobinski, L.; Lesiak, B.; Kövér, L.; Tóth, J.; Biniak, S.; Trykowski, G.; Judek, J. Multiwall carbon nanotubes purification and oxidation by nitric acid studied by the FTIR and electron spectroscopy methods. *J. Alloys Compd.* **2010**, *501*, 77−84.

(14) Adeli, M.; Bahari, A.; Hekmatara, H. Carbon Nanotube-graft-poly(citric acid) nanocomposites. *Nano* **2008**, *03*, 37−44.

(15) Kuo, C.-F.; Chyau, C.-C.; Wang, T.-S.; Li, C.-R.; Hu, T.-J. Enhanced Antioxidant and Anti-inflammatory Activities of Monascus pilosus Fermented Products by Addition of Turmeric to the Medium. *J. Agric. Food Chem.* **2009**, *57*, 11397−11405.

(16) Xu, M.-J.; Yang, Z.-L.; Liang, Z.-Z.; Zhou, S.-N. Construction of a Monascus purpureus Mutant Showing Lower Citrinin and Higher Pigment Production by Replacement of ctnA with pks1 without Using Vector and Resistance Gene. *J. Agric. Food Chem.* **2009**, *57*, 9764−9768.

(17) Zheng, Z.; Shetty, K. Solid-State Production of Beneficial Fungi on Apple Processing Wastes Using Glucosamine as the Indicator of Growth. *J. Agric. Food Chem.* **1998**, *46*, 783−787.

JOURNAL OF AGRICULTURAL AND FOOD CHEMISTRY

Article

pubs.acs.org/JAFC

Effects of Light-Emitting Diodes on Expression of Phenylpropanoid Biosynthetic Genes and Accumulation of Phenylpropanoids in *Fagopyrum tataricum* Sprouts

Aye Aye Thwe,[†,∥] Yeon Bok Kim,[†,∥] Xiaohua Li,[†] Jeong Min Seo,[‡] Sun-Ju Kim,[‡] Tastsuro Suzuki,[§] Sun-Ok Chung,*[,#] and Sang Un Park*[,†]

[†]Department of Crop Science, Chungnam National University, Daejeon 305-754, Korea

[‡]Department of Bio-Environmental Chemistry, Chungnam National University, Daejeon 305-764, Korea

[§]National Agriculture and Food Research Organization, Hokkaido Agricultural Research Center, Sapporo 062-8555, Japan

[#]Department of Biosystems Machinery Engineering, Chungnam National University, Daejeon 305-764, Korea

ABSTRACT: Buckwheat sprouts are a popular food item in many countries. The effects of light-emitting diodes (LEDs) on sprout growth and development, changes in mRNA transcription, and accumulation of phenylpropanoid compounds were studied in tartary buckwheat 'Hokkai T8' sprouts. The highest transcript levels were observed after 2 days of LED exposure for all genes, especially *FtPAL* and *FtF3′H*, which showed higher expression in sprouts grown under blue and white light than in those grown under red light. Catechin content in sprouts grown under red light increased dramatically throughout the 10 day time course. Maximum rutin content (43.37 mg/g dry weight (DW)) was observed in sprouts at 4 days after exposure (DAE) to blue light. Similarly, the highest cyanidin 3-*O*-rutinoside content (0.85 mg/g DW) was detected at 10 DAE to blue light. On the basis of these results, blue LED light is recommended as a light source for enhancing the content of phenolic compounds in tartary buckwheat sprouts.

KEYWORDS: *cyanidin, gene expression, light-emitting diode, phenolic compound, tartary buckwheat sprout*

INTRODUCTION

Plant products have been used as medicinal resources over the course of human history. These phytochemicals or non-nutritive substances possess disease-defensive properties.[1] Buckwheat (e.g., *Fagopyrum tataricum* L.), a pseudocereal, is recognized as a health food as it contains numerous medicinal compounds, especially rutin (quercetin-3-*O*-rutinoside), which is a major antioxidant.[2] Seed sprouts have been a part of the human diet for centuries in countries such as Japan, where they continue to be widely consumed. The interest in including fresh green sprouts in the diet has expanded across the world because of the health benefits they are thought to provide.[3]

Sprouts contain various substances (sulforaphane, sulforaphene, isothiocyanates, glucosinolates, enzymes, antioxidants, and vitamins) that can help in the prevention of cancer or provide therapeutic treatment against cancer.[4] In addition, sprouts contain much higher concentrations of some health-protecting phytochemicals than are found in the developed plant.[5] The most popular sprouts supplied in European and the Far Eastern markets are those of adzuki bean, alfalfa, broccoli, buckwheat, clover, mung bean, mustard, radish, red cabbage, and soybean.[4] Consumption of *Brassica* spp. sprouts has been shown to decrease the risk of cancer.[6,7] The use and application of foodstuffs that are rich in bioactive components can improve both food technologies and nutrition.[8] Buckwheat sprouts were first introduced and recommended as a new food source by Kim et al.,[9] who described them as having a soft and slightly crispy texture, attractive fragrance, and abundant nutrients. These authors also reported that rutin (quercetin-3-*O*-rutinoside), quericitrin (quercetin-3-*O*-rhamnoside), chlorogenic acid, and two unknown compounds were present in both buckwheat seeds and sprouts.[9]

Light-emitting diodes (LED) are artificial light sources that have many advantages for controlled-environment plant growth applications, including high energy-conversion efficiency, longer life, wavelength specificity, adjustable light intensity/quality, and low thermal energy output.[10,11] LED lights create specific wavelengths and a narrow bandwidth for plant growth compared with filters with broad-spectrum light sources.[12] Red light is crucial for the development of the photosynthetic apparatus as it can increase starch accumulation by inhibiting the translocation of photosynthates out of leaves.[13] Blue light is important for chloroplast development, chlorophyll formation, and stomata opening.[14] In addition, blue light plays a role in a wide range of plant processes such as phototropism, photomorphogenesis, stomatal opening, and photosynthesis.[15]

Flavonoid[16] and total flavonoid, polyphenol, and ascorbic acid contents have been examined in buckwheat sprouts.[17] The identification of flavonoids, accumulation of anthocyanin, and gene expression related to these compounds have been performed for tartary buckwheat sprouts under light or dark conditions.[18] On the basis of these studies, interest has developed in the ways in which gene expression patterns contribute to accumulation of specific flavonoid compounds in

Received: December 2, 2013
Revised: May 3, 2014
Accepted: May 5, 2014
Published: May 5, 2014

ACS Publications © 2014 American Chemical Society

dx.doi.org/10.1021/jf501335q | J. Agric. Food Chem. 2014, 62, 4839−4845

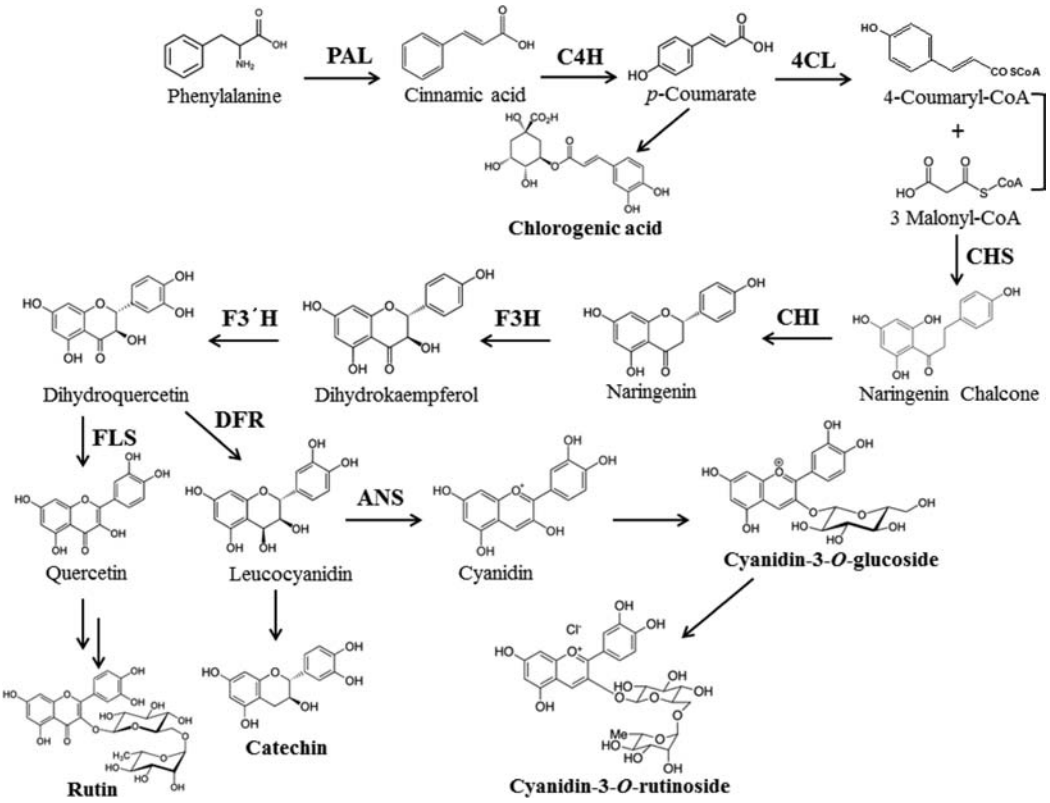

Figure 1. Schematic of the flavonoid pathway. PAL, phenylalanine ammonia-lyase; C4H, cinnamate 4-hydroxylase; 4CL, 4-coumaroyl-CoA ligase; CHS, chalcone synthase; CHI, chalcone isomerase; F3H, flavone 3-hydroxylase; FLS, flavonol synthase; F3′H, flavonoid 3′-hydroxylase; ANS, anthocyanidin synthase; DFR, dihydroflavonol-4 reductase. Bold letters indicate genes used and compounds analyzed in this study.

tartary buckwheat sprouts grown under LED light. Thus, this study aimed to characterize the growth response of tartary buckwheat sprouts 'Hokkai T8' to different LED light spectra (blue, red, and white) to better understand the regulation of expression of flavonoid biosynthetic pathway genes (Figure 1) and to investigate the effect of LEDs on accumulation of phenolic compounds in the sprouts.

MATERIALS AND METHODS

Chemical Reagents and Standards. The applied standards (caffeic acid, ferulic acid, gallic acid, 4-hydroxybenzoic acid, rutin, and quercetin) were purchased from Extrasynthese (Genay, France). Cyanidin-3-*O*-glucoside was purchased from Fujicco Co., Ltd. (Kobe, Japan) and cyanidin-3-*O*-rutinoside from ChromaDex, Inc. (Irvine, CA, USA). Formic acid and acetonitrile were obtained from commercial sources.

Sprouting Tartary Buckwheat Seeds. Tartary buckwheat cultivar 'Hokkai T8' was procured from Hokkaido Agricultural Research Center (Hokkaido, Japan). This cultivar was derived from a pure-line selection of the Russian cultivar 'Rotundatum'.[16] An incubator (B.O.D Incubator, HB-103, Han Baek Scientific Co., Korea) was used for germination. During incubation, seeds were checked every 24 h and watered as necessary. After 2 days of germination, the sprouts were grown in plastic pots containing vermiculite soil.

Initial sprouting was carried out to obtain uniform sprouted seeds for LED exposure using double-layered plastic pots (3 × 4 × 6 cm). The bottom of the inner pot contained small holes and was filled with a thin (approximately 3 cm) layer of vermiculite soil. The outer pot did not contain holes and was filled with approximately 30 mL of 0.05% (w/v) Bio Garden nutrient solution (6:5:8 N:P:K) for plant growth. Twenty-five sprouted seeds were sown in each plastic pot. There were three replications for each of three light conditions. The pots were covered with clean wrap (30 × 100 cm) that was pierced for aeration and were placed in the dark for another 2 days prior to LED exposure.

Sprout Development under LED. Sprouts (~2 cm) sown in 109 plastic pots containing vermiculite soil were exposed under different LEDs of red (wavelength, 660 nm), blue (470 nm), and white (380 nm) at a flux rate of 50 μmol $m^{-2}s^{-1}$ for a 16 h photoperiod. Sprouts were grown in an LED growth chamber at 25 °C and 70% humidity. LED exposure day was counted from the day started to exposure under LED. Then, sprouts were harvested at 2, 4, 6, 8, and 10 days after LED exposure (DAE). Pericarps were removed, and vermiculite soil attached to the root portion was carefully washed off under tap water. Then, sprout length (from the junction point of root and hypocotyl to the growing point) and fresh weight (including root portion) were immediately measured, and the sprouts were frozen in liquid nitrogen and stored at −80 °C until used.

Total RNA Extraction and cDNA Preparation. Total RNA was extracted from the different sprout samples using modified CTAB combined with total RNA extraction kit (Geneaid, Taiwan).[19] The quality of RNA was verified by demonstration of intact ribosomal bands following agarose gel electrophoresis in addition to the absorbance ratios (A_{260}/A_{280}) of 1.8−2.0 in a NanoVue Plus spectrophotometer (GE Healthcare Bio-Science Crop, USA). For cDNA synthesis, 1 μg of total RNA was reverse transcribed using oligo $d(T)_{20}$ and a Super-Script II First Strand Synthesis Kit (Life Technologies, Carlsbad, CA, USA) following the protocol of the supplier.

Quantitative Real-Time PCR Analysis for Gene Expression. To understand the contribution of phenylpropanoid biosynthesis-related genes to the content of anthocyanins and other phenolic compounds, qRT-PCR analysis of buckwheat sprouts was performed at 2, 4, 6, 8, and 10 DAE. Transcript levels of *FtPAL*, *FtC4H*, *Ft4CL*, *FtCHS*, *FtCHI*, *FtF3H*, *FtF3′H-1*, *FtF3′H-2*, *FtFLS-1*, *FtFLS-2*, *FtDFR*, and *FtANS* encoding phenylalanine ammonium-lyase (PAL), cinnamic acid 4-hydroxylase (C4H), 4-coumarate:CoA ligase (4CL), chalcone synthase (CHS), chalcone isomerase (CHI), flavanone-3-hydroxylase

Figure 2. *F. tataricum* 'Hokkai T8' sprout development at 2 days after exposure to LED light (blue, white, and red).

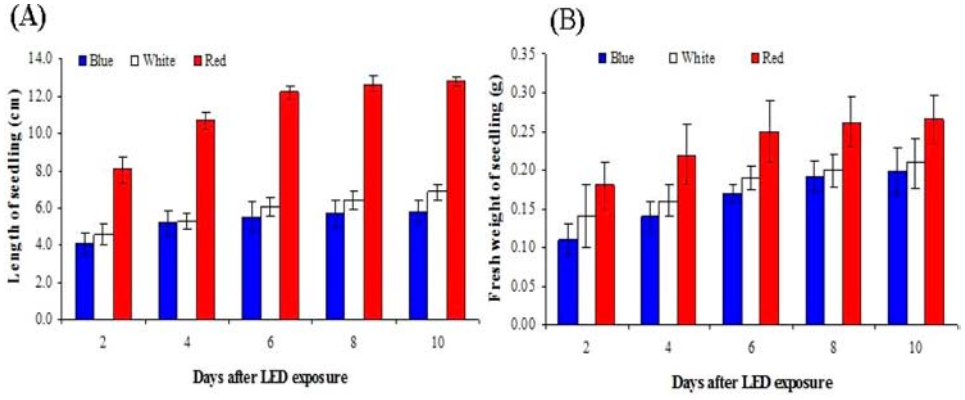

Figure 3. Growth of *F. tataricum* 'Hokkai T8' sprouts under LED light (blue, white, and red): (A) sprout length; (B) fresh weight from 2 to 10 days. Each value is the mean of three biological replicates ± standard deviation (SD).

(F3H), flavonoid-3′-hydroxylase (F3′H), flavonol synthase (FLS), dihydroflavonol reductase (DFR), and anthocyanin synthase (ANS), respectively, were analyzed relative to that of *Actin* (Genbank accession no. KC571237) as a housekeeping gene. Gene-specific primers are as follows: *FtActin* (F) 5′-GAGTTATGAGCTTCCTGA-TG-3′, *FtActin* (R) 5′-CCGCCACTCAACACAATGTT-3′. Gene expression results were evaluated as the mean of three replicates. Each PCR reaction (20 μL) contained 10 μL of SYBR green, 10 pmol of 0.5 μL primer (each), 5 μL of cDNA (diluted 1:19), and 4 μL of distilled water. The gene-specific primers used were designed as previously described by Li et al.[18] The thermal cycling conditions were 95 °C for 2 min followed by 95 °C for 30 s, 55 °C for 15 s, and 72 °C for 20 s for 40 cycles, and final extension occurred at 72 °C for 10 min.

Estimation of Phenolic Compounds and Anthocyanins by HPLC. Prior to extraction, sprout samples harvested at different days of LED exposure were powdered in liquid nitrogen by using a mortar and pestle. Then, 100 mg (dry weight) of powdered sample was extracted with 80% methanol and incubated for 1 h in a sonicator. Sample tubes were vortexed every 20 min during incubation and centrifuged at 14000 rpm for 5 min before getting the extract for further analysis by HPLC to estimate phenolic compounds content.

Quantification of Phenolic Compounds. The HPLC analysis of flavonoids was performed according to the system previously described by Li et al.[18] A Shimadzu class-VP HPLC system (Kyoto, Japan) equipped with a Capcell PAK ODS column (250 mm × 4.6 mm, 5 μm; Shiseido, Tokyo, Japan) was used. The mobile phase consisted of a mixture of (A) MeOH/water/acetic acid (5:92.5:2.5, v/v/v) and (B) MeOH/water/acetic acid (95:2.5:2.5, v/v/v). The initial mobile phase composition was 0% solvent B, followed by a linear gradient from 0 to 80% of solvent B over 48 min and then a hold at 0% solvent B for an additional 10 min. The column was maintained at 40 °C, the flow rate was 1.0 mL/min, the injection volume was 10 μL, and the eluted components were monitored at 350 nm. Different compounds were quantified on the basis of peak areas and calculated as equivalents of representative standard compounds.

Quantification of Anthocyanins. The anthocyanin filtrate was analyzed using an Agilent Technologies 1200 series HPLC (Agilent Technologies, Palo Alto, CA, USA) equipped with a Synergi 4 μ POLAR-RP 80A column (250 mm × 4.6 mm, i.d., particle size = 4 μm; Phenomenex, Torrance, CA, USA) equipped with a Security Guard Cartridges Kit AQ C18 column (4 mm × 3 mm, i.d.). The mobile phase consisted of a mixture of (A) water/formic acid (95:5, v/v) and (B) acetonitrile/formic acid (95:5, v/v). The gradient program was set as 0−8 min, 5−10% solvent B; 8−13 min, 10−13% solvent B; 13−15 min, 13% solvent B; 15−18 min, 13−15% solvent B; 18−25 min, 15% solvent B; 5% solvent B at 25.1 min; and finally 5% solvent B constant for 10 min (total = 35 min). Detection was performed at 520 nm wavelength, and the column oven temperature was at 40 °C. The flow rate was set at 1.0 mL/min, and the injection volume was 10 μL. Anthocyanin content was calculated by comparing HPLC peak area with that of authentic standards (cyanidin-3-*O*-glucoside and cyanidin-3-*O*-rutinoside).

RESULTS AND DISCUSSION

Effect of LEDs on Sprout Morphology. Normally, *F. tataricum* 'Hokkai T8' has a greenish hypocotyl color under

dx.doi.org/10.1021/jf501335q | J. Agric. Food Chem. 2014, 62, 4839−4845

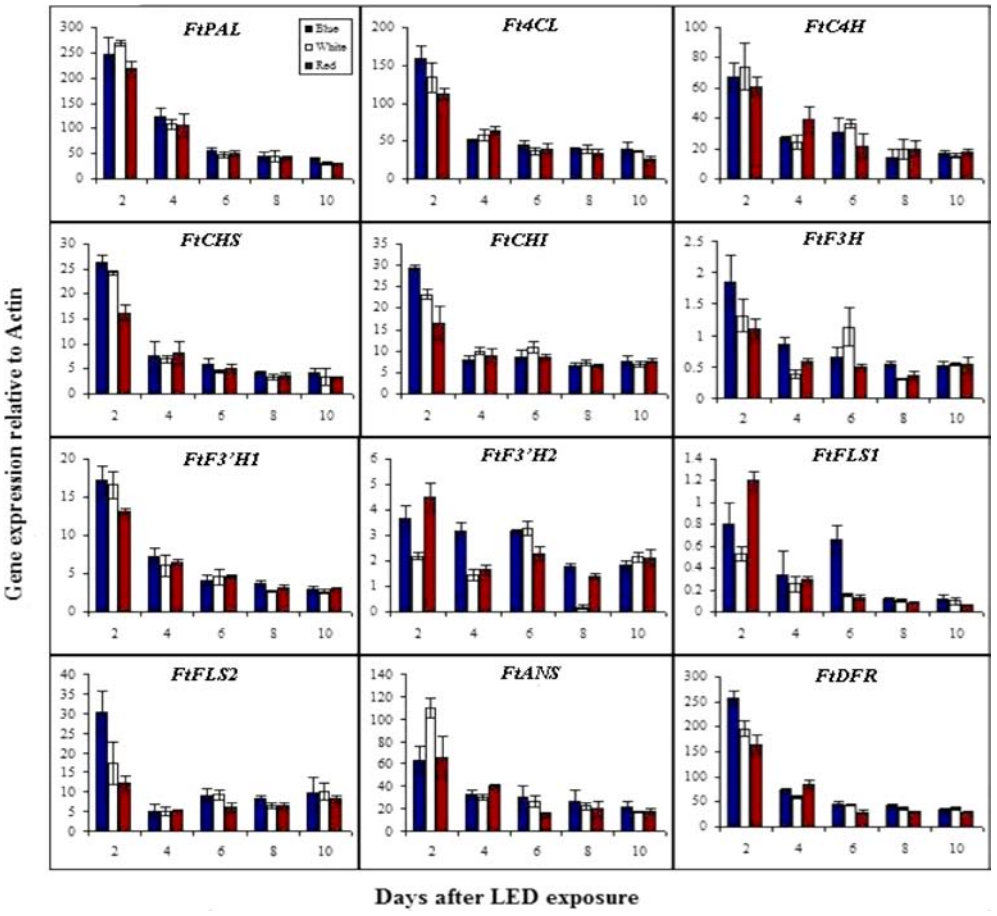

Figure 4. Expression levels of phenylpropanoid biosynthetic genes on *F. tataricum* 'Hokkai T8' sprouts grown under LED light. Transcript levels from three biological replicates were analyzed relative to that of *Actin*. Each value is the mean of three biological replicates ± SD.

light condition. Interestingly, a reddish appearance was observed in hypocotyls of blue- and white-LED-grown sprouts, and the color was more intense in sprouts grown under blue light. However, there were no color changes in sprouts grown under red LEDs (Figure 2). Light-induced color changes became apparent at 2 DAE. The red pigmentation is likely to have occurred as a result of sprouts' response to light stress after sudden transfer from dark to light (LED light) conditions. Light can advance metabolic changes during the different stages of germination.[20] These changes are most commonly due to anthocyanins, which are vacuolar flavonoids,[21] and anthocyanin (red) content is positively correlated with phenolics in several species.[22]

Sprout Length and Fresh Weight. Seedling length and fresh weight were greatly affected by different LEDs. Red light produced tall, spindly sprouts, whereas blue and white light resulted in shorter sprouts with stocky hypocotyls (Figure 2). Generally, seedling length and fresh weight of blue- and white-light-radiated seedlings were significantly less than those of red-light-radiated sprouts throughout the time course (from 2 to 10 DAE) of their development. Seedling length increased suddenly from approximately 2 cm prior to LED exposure (data not shown) to 4.0, 4.6, and 8.1 cm at 2 DAE in blue, white, and red light, respectively. Seedling length and fresh weight increased with time until 6 DAE in all sprouts under the respective light treatments (Figure 3A). Sprout length under red LEDs was almost double that under blue or white LEDs, which did not differ significantly during the observation period. Likewise, seedling fresh weight increased with time, and red-LED-grown sprouts attained greater fresh weight than sprouts grown under blue or white LEDs, consistent with their taller height (Figure 3B). However, there were no significant increases in seedling length and fresh weight beyond 6 DAE. These findings were consistent with those of McNellis and Deng,[23] who reported that blue light suppresses elongation and induces cotyledon expansion and that red light induces hypocotyl elongation and cotyledon expansion in *Arabidopsis* seedlings. Moreover, Miyashita et al.[24] revealed that red light significantly enhanced stalk elongation in pelargonium plantlets, whereas blue light inhibited elongation. After radiation for 4 days, red-light-radiated pea seedlings displayed significant increases in stem length and leaf area compared to a white light group.[25] In our study, morphological and growth parameters of seedlings, including hypocotyl color, length, and fresh weight, were controlled by light quality/intensity. Hence, LED light can be selectively utilized for plant growth by targeting the photomorphogenic pigments that are responsible for photoperception and triggering regeneration ability.[26] On the basis of the results presented here, we suggest that a sprouting period of 6 DAE would be best for achieving optimal biomass in buckwheat sprouts.

Phenylpropanoid Biosynthesis Gene Expression. Significant variability was observed in the expression levels of all pathway genes at 2 DAE in LED-exposed sprouts (Figure 4). The genes generally showed higher numbers of transcripts at 2 DAE compared with 4, 6, 8, and 10 DAE, when levels of gene

Table 1. Phenolic Compounds and Anthocyanin Accumulations in 'Hokkai T8' Sprouts under Different LED Lights

light type	days	catechin	chlorogenic acid	rutin	cyanidin 3-*O*-glucoside	cyanidin 3-*O*-rutinoside
blue	2	0.10 ± 0.01	2.89 ± 0.05	36.75 ± 0.48	0.08 ± 0.01	0.66 ± 0.01
	4	0.05 ± 0.02	3.65 ± 0.13	43.37 ± 1.56	0.08 ± 0.01	0.64 ± 0.09
	6	0.02 ± 0.01	3.48 ± 0.04	40.39 ± 0.34	0.05 ± 0.01	0.66 ± 0.09
	8	0.07 ± 0.00	3.15 ± 0.13	37.36 ± 1.65	0.07 ± 0.01	0.69 ± 0.10
	10	0.10 ± 0.01	3.05 ± 0.07	36.15 ± 0.67	0.08 ± 0.01	0.85 ± 0.05
white	2	0.09 ± 0.00	2.93 ± 0.07	38.00 ± 1.34	ND	0.51 ± 0.05
	4	0.09 ± 0.01	3.70 ± 0.06	41.39 ± 0.59	ND	0.24 ± 0.03
	6	0.03 ± 0.01	3.46 ± 0.26	40.61 ± 0.07	ND	0.34 ± 0.02
	8	0.02 ± 0.00	3.53 ± 0.03	39.79 ± 0.16	ND	0.23 ± 0.01
	10	0.02 ± 0.01	3.06 ± 0.01	36.68 ± 0.16	ND	0.30 ± 0.04
red	2	0.07 ± 0.03	2.65 ± 0.01	39.46 ± 0.47	ND	0.17 ± 0.04
	4	0.08 ± 0.01	2.76 ± 0.01	37.48 ± 0.15	ND	0.06 ± 0.02
	6	0.30 ± 0.03	2.59 ± 0.06	37.23 ± 0.32	ND	0.06 ± 0.02
	8	0.55 ± 0.00	2.58 ± 0.19	35.00 ± 2.56	ND	0.08 ± 0.03
	10	0.95 ± 0.05	2.54 ± 0.11	33.55 ± 2.44	ND	0.08 ± 0.01

expression did not differ substantially. Although gene expression peaked at 2 DAE, it decreased suddenly after 2 DAE and plateaued until 10 DAE. Similar gene expression patterns were observed for *FtPAL* and *FtF3′H*, where sprouts grown under blue and white LEDs, in which expression did not differ significantly, showed higher transcript levels than red-LED-grown sprouts at 2 DAE.

Transcript levels of *FtPAL* gene in blue-, white-, and red-light-grown sprouts were approximately 6.3-, 8.9-, and 6.9-fold higher at 2 DAE than those at 10 DAE. The PAL enzyme plays a key role in the biosynthesis of flavonoids by catalyzing the flux of primary metabolites into the flavonoid biosynthetic pathway.[27] Similar gene expression patterns were observed for *FtC4H*, *FtCHI*, *FtFLS-2*, and *FtANS*, where the relative abundance of transcript levels was higher in sprouts grown under blue LEDs than in those grown under white or red light. The *CHI* gene is required for the synthesis of naringenin from naringenin chalcone and has been considered essential for the biosynthesis of flavonoids.[28,29] Higher expression levels of *FtDFR* were also observed at 2 DAE, and white-light-grown sprouts had 1.7-fold greater transcript numbers than sprouts grown under blue or red light. In *FtANS*, blue-, white-, and red-LED-grown sprouts showed 7.4-, 5.2-, and 5.6-fold greater expression at 2 DAE compared with expression at 10 DAE. Higher transcript levels of *FtANS*, the gene responsible for anthocyanin accumulation, might be related to the reddish appearance of hypocotyls in blue- and white-LED-grown sprouts. Except for *FtF3′H-2*, the remaining genes showed relatively higher transcript levels in sprouts grown under blue or white LEDs than in sprouts grown under red light. Li et al.[30] reported that the expression levels of almost all flavonoid biosynthesis genes peaked within 4 DAE in common buckwheat sprouts grown under either light or dark conditions and gradually decreased thereafter.

Overall gene expression was highest at 2 DAE, after which it was down-regulated over the time. These results could be related to the sudden appearance of reddish coloration in hypocotyls at 2 DAE because of seedlings' response to light, which can cause metabolic changes during different stages of germination.[20] In addition, all of the genes were highly expressed at early stages of sprout development under all light treatments, and blue- and white-light-grown sprouts showed higher transcript levels than red-light-grown sprouts.

Accumulation of Phenolic Compounds and Anthocyanins in Sprouts. Phenolic compounds and anthocyanins were analyzed in 'Hokkai T8' sprouts grown under LED. Catechin content in sprouts grown under red LED light increased dramatically from 2 to 10 DAE (Table 1); the highest catechin content was detected at 10 DAE and was 9.6- and 43.1-fold higher, respectively, than that in sprouts grown under blue or white LED light. Rutin content in all sprouts was significantly greater than the content of other compounds, and there was no significant difference in rutin accumulation according to DAE. However, the maximum rutin content (43.37 mg/g dry weight (DW)) was observed at 4 DAE in sprouts under blue LED light and was higher than that observed under fluorescent light (30 mg/g DW at 4 days) in a previous study by Li et al.;[18] this indicates that the effects of LED and fluorescent light on rutin content in sprouts are comparable. Accumulation of chlorogenic acid was not significantly different between sprouts grown under blue or white LEDs, both of which showed higher chlorogenic acid content than sprouts grown under red light. Very small quantities (almost nondetectable) of caffeic acid, ferulic acid, and quercetin were present in the sprouts (data not shown).

Accumulation of two anthocyanins (cyanidin 3-*O*-glucoside and cyanidin 3-*O*-rutinoside) was also analyzed (Table 1). Cyanidin 3-*O*-glucoside was detected only in blue-LED-grown sprouts, and its content did not change significantly during sprout development. The cyanidin 3-*O*-rutinoside content of sprouts grown under blue LEDs at 10 DAE was 2.8- and 10.6-fold higher, respectively, than that in sprouts grown under white and red LEDs.

These results demonstrated that blue LED light enhances accumulation of anthocyanin compared with white or red LED light. Li et al.[18] reported that only cyanidin 3-*O*-rutinoside was detected in 'Hokkai T8' sprouts under light/dark conditions, and only in trace amounts. However, we detected cyanidin 3-*O*-glucoside in blue-LED-grown sprouts and cyanidin 3-*O*-rutinoside in sprouts grown under all LED light conditions. Cyanidin 3-*O*-rutinoside is the main compound that may contribute to the red color of tartary buckwheat sprouts.[31,32] Blue light induces the accumulation of anthocyanins, which

play a major role in antioxidant activity.[33] All of these reports help to explain the reddish hypocotyl appearance and anthocyanin detection in blue-LED-grown sprouts described in this study.

In recent years, it was suggested that consumption of anthocyanins is related to reduced risk of coronary heart disease and improvement of visual functions. The health benefits of anthocyanins have mainly antioxidant activity, anticancer property, and visual acuity enhancement.[31,34] Takeuchi[35] noted that petals of red-flowered buckwheat are used as materials in tea, juice, and alcohols after detoxification of fagopyrin in food processing. In addition, the presence of radical-scavenging activity was reported in common buckwheat,[36] and the change in DPPH radical-scavenging activity was similar to that of total flavonoid contents in buckwheat sprouts.[37]

In plants, secondary metabolites have been noted to act as warning signals, toxins, antifeedants, or precursors to physical defense systems.[38,39] Anthocyanins may serve both direct roles as chemical repellents and more indirect roles as visual signals to potential herbivores, displaying a strong metabolic investment in toxic or unpalatable chemicals.[40] Some anthocyanins have demonstrable antiviral, antibacterial, and fungicidal activities.[41,42] Karageorgou et al.[20] hypothesized that red leaf color is less easily perceived by folivorous insect photoreceptors or that red leaf color disables insect camouflage of plant parts against their backgrounds, in the undermining of insect crypsis, and in the mimicry of defensive structures. According to these results, anthocyanins may play an important role as visual signals.

We reported that the metabolomics and regulation of anthocyanin production in red-flowered (Gan-Chao) and white-flowered (Tanno) buckwheat cultivars were carried out through qRT-PCR, HPLC, and gas chromatography time-of-flight mass spectrometry.[43] Further studies that investigate the metabolomics and regulation of anthocyanin accumulation in 'Hokkai T8' tartary buckwheat after exposure to different LED light are required.

In conclusion, LED lights are effective for enhancing phenolic content, especially rutin and anthocyanin, in buckwheat sprouts. Our findings can have useful applications for commercial sprouting and biomass production for compound analysis and also as preliminary data for further experimentation with LED light.

AUTHOR INFORMATION

Corresponding Authors

*(S.-O.C.) Phone: +82-42-821-6712. Fax: +82-42-823-6246. E-mail: sochung@cnu.ac.kr.

*(S.U.P.) Phone: +82-42-821-5730. Fax: +82-42-822-2631. E-mail: supark@cnu.ac.kr.

Author Contributions

‖A.A.T. and Y.B.K. contributed equally to this work.

Funding

This work (K13101) was supported by the Korea Institute of Oriental Medicine (KIOM) grant funded by the Korean government.

Notes

The authors declare no competing financial interest.

ABBREVIATIONS USED

LED, light-emitting diodes; PAL, phenylalanine ammonium-lyase; C4H, cinnamic acid 4-hydroxylase; 4CL, 4-coumarate:-CoA ligase; CHS, chalcone synthase; CHI, chalcone isomerase; F3H, flavanone-3-hydroxylase; F3′H, flavonoid-3′-hydroxylase; FLS, flavonol synthase; DFR, dihydroflavonol reductase; ANS, anthocyanin synthase

REFERENCES

(1) Rajan, T.; Muthukrishnana, S. Characterization of phenolic compounds in *Pseudarthria viscida* root extract by HPLC and FT-IR analysis. *Asian J. Pharm. Clin. Res.* **2013**, *6*, 273−276.

(2) Morishita, T.; Yamaguchi, H.; Degi, K. The contribution of polyphenols to antioxidative activity in common buckwheat and tartary buckwheat grain. *Plant Prod. Sci.* **2007**, *10*, 99−104.

(3) Castro-Rosas, J.; Escartin, E. F. Survival and growth of *Vibrio cholerae* O1, *Salmonella typhi* and *Escherichia coli* O157:H7 in alfalfa sprouts. *J. Food Sci.* **2000**, *65*, 162−165.

(4) Márton, M.; Mándoki, Z.; Csapó-Kiss, Z.; Csapó, J. The role of sprouts in human nutrition. *Acta Univ. Sapientiae, Aliment.* **2010**, *3*, 81−117.

(5) Fernandez-Orozco, R.; Piskula, M. K.; Zielinski, H.; Kozlowska, H.; Frias, J.; Vidal-Valverde, C. Germination as a process to improve the antioxidant capacity of *Lupinus angustifolius* L. var. Zapaton. *Eur. Food Res. Technol.* **2006**, *223*, 495−502.

(6) Gill, C. I. R.; Haldar, S.; Porter, S.; Matthews, S.; Sullivan, S.; Coul-ter, J.; McGlynn, H.; Rowland, I. The effect of cruciferous and legumi-nous sprouts on genotoxicity, *in vitro* and *in vivo*. *Cancer Epidemiol. Biomarkers Prev.* **2004**, *13*, 1199−1205.

(7) Haddad, P. S.; Azar, G. A.; Groom, S.; Boivin, M. Natural health products, modulation of immune function and prevention of chronic disease. *Evidence-Based Complement Alternat. Med.* **2005**, *2*, 513−520.

(8) Schneeman, B. O. Emerging food technology and world health. *J. Food Sci.* **2004**, *69*, C123−C126.

(9) Kim, S. L.; Kim, S. K.; Park, C.-H. Introduction and nutritional evaluation of buckwheat sprouts as a new vegetable. *Food Res. Int.* **2004**, *37*, 319−327.

(10) Okamoto, K.; Yanagi, T.; Kondo, S. Growth and morphogenesis of lettuce seedlings raised under different combinations of red and blue light. *Acta Hortic.* **1997**, *435*, 149−157.

(11) Schuerger, A. C.; Brown, C. S.; Stryjewski, E. C. Anatomical features of pepper plants (*Capsicum annuum* L.) grown under red light emitting diodes supplemented with blue or far-red light. *Ann. Bot.* **1997**, *79*, 273−282.

(12) Masahumi, J.; Kazuhiro, S.; Fumiyuki, G.; Shin-nosuke, H.; Toshihiro, Y. Blue light-emitting diode light irradiation of seedlings improves seedling quality and growth after transplanting in red leaf lettuce. *HortScience* **2010**, *45*, 1809−1814.

(13) Saebo, A.; Krekling, T.; Appelgren, M. Light quality affects photosynthesis and leaf anatomy of birch plantlets *in vitro*. *Plant Cell Tiss. Org.* **1995**, *41*, 177−185.

(14) Senger, H. The effect of blue light on plants and micro-organisms. *Photochem. Photobiol.* **1982**, *35*, 911−920.

(15) Whitelam, G.; Halliday, K. *Light and Plant Developmen*; Blackwell Publishing: Oxford, UK, 2007

(16) Kim, S. J.; Zaidul, I. S. M.; Maeda, T.; Suzuki, T.; Hashimoto, N; Takigawa, S.; Takahiro, N.; Matsuura-Endo, C.; Yamauchi, H. A time-course study of flavonoids in the sprouts of tartary (*Fagopyrum tataricum* Gaertn.) buckwheats. *Sci. Hortic.* **2007**, *115*, 13−18.

(17) Caterina, B.; Camelia, V. Sprouted buckwheat an important vegetable source of antioxidants. *AUDJG−Food Technol.* **2012**, *36*, 53−60.

(18) Li, X.; Thwe, A. A.; Park, N. I.; Suzuki, T.; Kim, S. J.; Park, S. U. Accumulation of phenylpropanoids and correlated gene expression during the development of tartary buckwheat sprouts. *J. Agric. Food Chem.* **2012**, *60*, 5629−5635.

(19) Tuan, P. A.; Thwe, A. A.; Kim, J. K.; Kim, Y. B.; Lee, S.; Park, S. U. Molecular characterisation and the light−dark regulation of

carotenoid biosynthesis in sprouts of tartary buckwheat (*Fagopyrum tataricum* Gaertn.). *Food Chem.* **2013**, *141*, 3803−3812.
(20) Martín-Cabrejas, M. A.; Ariza, N.; Esteban, R.; Mollá, E.; Waldron, K.; López-Andréu, F. J. Effect of germination on the carbohydrate composition of the dietary fibre of peas (*Pisum sativum* L.). *J. Agric. Food Chem.* **2003**, *51*, 1254−1259.
(21) Archetti, M.; Döring, T. F.; Hagen, S. B.; Hughes, N. M.; Leather, S. R.; Lee, D. W.; Lev-Yadun, S.; Manetas, Y.; Ougham, H. J.; G, S. P.; Thomas, H. Unravelling the evolution of autumn colours: an interdisciplinary approach. *Trends Ecol. Evol.* **2009**, *24*, 166−173.
(22) Karageorgou, P.; Claus, B.; Yiannis, M. Red leaf color as a warning signal against insect herbivory: honest or mimetic? *FLORA* **2008**, *203*, 648−652.
(23) McNellis, T. W.; Deng, X. W. Light control of seedling morphogenetic pattern. *Plant Cell* **1995**, *7*, 1749−1761.
(24) Miyashita, Y.; Kimura, T.; Kitaya, Y.; Kubota, C.; Kozai, T. Effect of red light on the growth and morphology if potato plantlets *in vitro*: using light emitting diodes (LEDs) as a light source for micropropagation. *Acta Hortic.* **1997**, *418*, 169−173.
(25) Wu, M.-C.; Hou, C.-Y.; Jiang, C.-M.; Wang, Y.-T.; Wang, C.-Y.; Chen, H.-H.; Chang, H.-M. A novel approach of LED light radiation improves the antioxidant activity of pea seedlings. *Food Chem.* **2007**, *101*, 1753−1758.
(26) Lian, M. L.; Murthy, H. N.; Paek, K. Y. Effects of light emitting diodes (LEDs) on the *in vitro* induction and growth of bulblets of *Lilium* oriental hybrid Pesaro. *Sci. Hortic.* **2002**, *94*, 365−370.
(27) Chang, J.; Luo, J.; He, G. Regulation of polyphenols accumulation by combined overexpression/silencing key enzymes of phenylpropanoid pathway. *Acta Biochim. Biophys. Sin. (Shanghai)* **2009**, *41*, 123−130.
(28) Park, N. I.; Li, X.; Suzuki, T.; Kim, S. J.; Woo, S. H.; Park, C. H.; Park, S. U. Differential expression of anthocyanin biosynthetic genes and anthocyanin accumulation in tartary buckwheat cultivars 'Hokkai T8' and 'Hokkai T10'. *J. Agric. Food Chem.* **2011**, *56*, 2356−2361.
(29) Povero, G.; Gonzali, S.; Bassolino, L.; Mazzucato, A.; Perata, P. Transcriptional analysis in high-anthocyanin tomatoes reveals synergistic effect of Aft and atv genes. *J. Plant Physiol.* **2011**, *168*, 270−279.
(30) Li, X.; Park, N. I.; Xu, H.; Woo, S. H.; Park, C. H.; Park, S. U. Differential expression of flavonoid biosynthesis genes and accumulation of phenolic compounds in common buckwheat (*Fagopyrum esculentum*). *J. Agric. Food Chem.* **2010**, *58*, 12176−12181.
(31) Kim, S. J.; Maeda, T.; Sarker, M. Z. I.; Takigawa, S.; Matsuura-Endo, C.; Yamauchi, H.; Mukasa, Y.; Saito, K.; Hashimoto, N.; Noda, T.; Saito, T.; Suzuki, T. Identification of anthocyanins in the sprouts of buckwheat. *J. Agric. Food Chem.* **2007**, *55*, 6314−6318.
(32) Watanabe, M. An anthocyanin compound in buckwheat sprouts and its contribution to antioxidant capacity. *Biosci., Biotechnol., Biochem.* **2007**, *71*, 579−582.
(33) Duan, X. W.; Jiang, Y. M.; Su, X. G.; Zhang, Z. Q.; J, S. Antioxidant property of anthocyanins extracted from litchi (*Litchi chinenesis* Sonn.) fruit pericarp tissues in relation to their role in the pericarp browning. *Food Chem.* **2007**, *101*, 1382−1388.
(34) Matsumoto, H.; Inaba, H.; Kishi, M.; Tominaga, S.; Hirayama, M.; Tsuda, T. Orally administered delphinidin 3-rutinoside and cyanidin 3-rutinoside are directly absorbed in rats and humans and appear in the blood as the intact forms. *J. Agric. Food Chem.* **2001**, *49*, 1546−1551.
(35) Takeuche, K. A. A manufacturing process to produce buckwheat petals and seedling juice. Jpn. Patent 3771483, 2006.
(36) Watanabe, M.; Shimizu, H. Composition of flavonoid compounds in seedlings of tartary buckwheat. *Tohoku Agric. Res. (in Japanese)* **2004**, *57*, 267−268.
(37) Watanabe, M.; Ito, M. Effects of light on the content of phenolic compounds in buckwheat seedlings (in Japanese with English summary). *J. Jpn. Soc. Food Sci. Technol.* **2003**, *50*, 32−34.
(38) Bennett, R. N.; Wallsgrove, R. M. Secondary metabolites in plant defence mechanisms. *New Phytol.* **1994**, *127*, 617−633.
(39) Harborne, J. B. Biochemical plant ecology. In *Plant Biochemistry*; Dey, P. M., Harborne, J. B., Eds.; Academic Press: London, UK, 1997; pp 503−516.
(40) Lev-Yadun, S.; Gould, K. S. Role of anthocyanins in plant defence. *Anthocyanins* **2009**, 22−28.
(41) Konczak, I.; Zhang, W. Anthocyanins − more than nature's colours. *J. Biomed. Biotechnol.* **2004**, *2004*, 239−240.
(42) Wrolstad, R. E. Symposium 12: Interaction of natural colors with other ingredients. Anthocyanin pigments − bioactivity and coloring properties. *J. Food Sci.* **2004**, *69*, C419−C421.
(43) Kim, Y. B.; Park, S. Y.; Thwe, A. A.; Seo, J. M.; Suzuki, T.; Kim, S. J.; Kim, J. K.; Park, S. U. Metabolomic analysis and differential expression of anthocyanin biosynthetic genes in white- and red-flowered buckwheat cultivars (*Fagopyrum esculentum*). *J. Agric. Food Chem.* **2013**, *61*, 10525−10533.

JOURNAL OF AGRICULTURAL AND FOOD CHEMISTRY

Article

pubs.acs.org/JAFC

Accelerated Dissipation of the Herbicide Cycloxydim on Wax Films in the Presence of the Fungicide Chlorothalonil and under the Action of Solar Light

Shirin Monadjemi,[†] Alexandra ter Halle,[†,‡] and Claire Richard*[,†,‡]

[†]Institut de Chimie de Clermont-Ferrand, Clermont Université, B.P. 10448, 63000 Clermont-Ferrand, France

[‡]Equipe Photochimie CNRS, UMR 6296, ICCF, F-63171 Aubière, France

ABSTRACT: Photolysis is a known dissipation pathway of pesticides on leaves just after their spraying. This pathway may be affected by the residues of other pesticides. To illustrate this idea, this study investigated the mutual effect of two pesticides (chlorothalonil and cycloxydim) under simulated solar light. Cycloxydim was added at the agricultural rate (200 g ha^{-1}) and chlorothalonil at 1.3−10% of the rate (20−150 g ha^{-1}). These compounds were studied either pure or in their commercial formulation. Both analytical and kinetic data show that chlorothalonil significantly accelerates the decay of cycloxydim on wax films, promoting its oxidation, even at the lowest tested dose. Conversely, cycloxydim does not affect the fate of chlorothalonil. Moreover, the detection of oxidized forms of wax alkanes in the extracts demonstrates that chlorothalonil may have also a degrading effect on the leaves' constituents under the action of solar light.

KEYWORDS: *photolysis, sensitization, oxidation, pesticides, leaves surface*

INTRODUCTION

On foliage and under the action of sunlight, pesticides can undergo photodegradation.[1] Nevertheless, this route of dissipation is scarcely documented, although understanding its mechanism and evaluating its rate is of utmost importance for the improvement of pesticide formulations. Besides, photochemical reactions taking place on vegetation can follow specific pathways and lead to degradation products different from those observed in water, the most commonly studied medium. For example, it has been reported that the herbicides mesotrione and sulcotrione deposited on leaf models mainly undergo an intramolecular photocyclization when irradiated in a solar light simulator, whereas this process is very minor in aqueous solution.[2,3] Moreover, photochemical reaction rates of molecules in solution cannot be generalized to the solid state. For instance, the half-life of photolysis of the herbicide mesotrione is about 90 days in water against 8 h on leaf surface models.[2] Another poorly considered issue is the mutual potential effect that pesticides may have on each other when they are applied in a mixture. To improve crop protection, it is common to apply pesticides in mixtures or to use successively different pesticides during annual crop treatments. Mixing pesticides might have consequences on their photostability and thus influence their effectiveness. For example, it was shown that mesotrione and nicosulfuron herbicides show higher rates of photodegradation in a mixture than separately.[4]

In this work, we studied the fate of two pesticides in a mixture: the herbicide cycloxydim (*E* isomer, CD) and the fungicide chlorothalonil (CT) (Scheme 1). CD and CT are foliar pesticides that are both used for the control of tomato, asparagus, and pea crops; their presence altogether on crops is thus very likely. CD, on the one hand, is a systemic herbicide used for the control of grass weeds and the control of agricultural crops. In solution, photoisomerization of the C═N bond and cleavage of the oxime occur, leading to a rather fast loss of CD (*E* isomer).[5] Only a few data are, however, available on the photostability of this molecule on plants. A recent patent proposes to stabilize the cyclohexane oxime formulations by the addition of aromatic solvents such as toluene or benzene, epoxidized oil fatty acids, or more adjuvants.[6] This confirms that CD undergoes photodegradation on leaves. CD was shown also to react with singlet oxygen in acetonitrile.[7] CT, on the other hand, is a persistent fungicide. It is also a powerful sensitizer, which has the ability to produce singlet oxygen with a quantum yield close to 1 in alkanes.[8] Therefore, one might expect that CT is able to promote the photodegradation of CT. However, this enhancing effect of CT remains to be evidenced when both compounds are in the solid state. Moreover, its actual contribution to the CD photodissipation in simulated solar light and using commercial formulations has to be evaluated. Finally, the potential effect of CD on CT phototransformation is unknown so far. Comparative experi-

Scheme 1

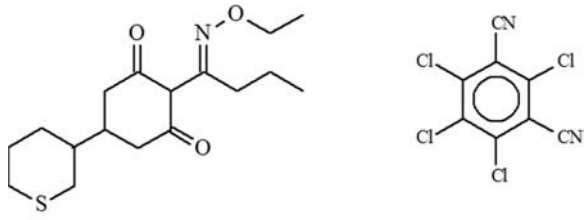

Cycloxydim (CD) Chlorothalonil (CT)

Received: February 24, 2014
Revised: May 9, 2014
Accepted: May 12, 2014
Published: May 12, 2014

ACS Publications © 2014 American Chemical Society

ments were conducted using phenalenone, a well-known singlet oxygen producer.[9]

EXPERIMENTAL PROCEDURES

Chemicals. All solvents and chemicals were used as received. CD (98%) and CT (99%) were obtained from Fluka (Saint-Quentin Fallavier, France). Commercial formulations of CD and CT, respectively Stratos Ultra (100 g L^{-1} of CD) and Fongil FL (500 g L^{-1} CT), were obtained from a regular agricultural shop. Phenalenone (97%) and paraffin wax (mp 70−80 °C) were both purchased from Aldrich (Saint-Quentin Fallavier, France). Water was purified using a Millipore Milli-Q system (Millipore αQ, resistivity = 18 MΩ cm^{-1}, DOC < 0.1 mg L^{-1}). Acetonitrile (99%, HPLC grade) was provided by Riedel de Haën (Saint-Quentin Fallavier, France).

Sample Preparation and Irradiation. Stock solutions of pure CD and CT (10^{-4} M) were prepared in acetonitrile and stored at 4 °C. Solutions of formulated CD (Stratos Ultra) and formulated CT (Fongil FL) were prepared in Milli-Q water just before use. The exact pesticide concentration was determined using a calibration curve established for the corresponding active ingredient in acetonitrile. Paraffin wax films were made by weighing 0.8 g of wax in each dish (3.2 cm diameter) and by heating them at 90 °C for wax melting and achieving film formation. Films were allowed to cool and ready for use. In all of the experiments, the surface concentration of CD was equal to 200 g ha^{-1}, this concentration corresponding to the recommended dose applications. In the set of experiments in which CD and CT were applied as nonformulated active ingredients, the surface concentration of CT was also chosen as 150 g ha^{-1}. When Stratos Ultra and Fongil FL formulations were used, the chosen CT concentrations were 20 and 150 g ha^{-1}. This choice aimed to mimic a situation in which CT traces are remaining on leaves when CD is applied. Actually, in the case of tomatoes, for instance, the recommended field application for CT is 1500 g ha^{-1}. We chose a situation in which 10 and 1.3% of CT are still present on the leaves when CD is applied. Acetonitrile solutions of pure CD and the CD + CT mixture were deposited on wax films as 1 mL volume. Stratos (diluted 125× in water) and a mixture of Stratos (diluted 125× in water) with Fongil (diluted 833× and 4550× in water) were applied as 10 droplets of 2 μL using a micropipet (Eppendorf). The solvent was allowed to evaporate overnight. After drying, 24 dishes (3 replicates for each sampling) were irradiated inside a Suntest CPS photosimulator (Atlas) equipped with a xenon lamp filtered below 290 nm (irradiance within the range of 290−800 nm). The intensity of the lamp was set at 400 W m^{-2} to simulate the sunlight average intensity in summer in France. Cold water (16 °C) was flowed through the bottom of the photosimulator to maintain the internal temperature as low as possible. Four dishes were taken after each selected irradiation times. For each, wax was rinsed using 1 mL of acetonitrile to recover remaining pesticides and photoproducts. These mixtures were further analyzed by UPLC and LC-MS. By this method, the recovery yields of CD and CT prior to irradiation were good (~95%). Mixtures of CD and phenalenone were also applied on wax films in acetonitrile. The same procedure as for CD + CT was used for photolytic tests.

Analyses. Absorption spectra were recorded using a Cary 3 UV−visible spectrometer (Varian). Solid state spectra were recorded using a DRA-CA-30I integrating sphere accessory (Varian) and a $BaSO_4$ reflectance standard (Spectralon). Acetonitrile solutions of CD (1 g L^{-1}) and CT (1 g L^{-1}) were deposited on quartz plates as 3 drops of 10 μL, and spectra were recorded after acetonitrile was completely evaporated. For the laser flash photolysis experiments, the apparatus consisted of a laser flash photolysis spectrometer from Applied Photophysics (LKS.60) equipped with a Quanta Ray GCR 130-01 Nd:YAG laser.[10] Solutions were deoxygenated by bubbling argon directly in the quartz cell. UPLC-UV analyses were performed using an Acquity Waters UPLC system equipped with a thermostated autosampler, a degasser, a pump, and a photodiode array detector. Chromatographic separation was performed on an Acquity UPLC BEH C18 column (2.1 mm × 50 mm, 1.7 μm). The operating temperature was maintained at 25 °C, and the sample volume injected was 6 μL. The flow rate was set at 0.5 mL min^{-1}, and elution was carried out in the gradient mode. The mobile phase composition started with 58% water (acidified with formic acid, 0.5‰ v/v) and 42% acetonitrile. The percentage of acetonitrile was increased linearly to 75% over 3 min and then kept constant during 0.5 min. The mobile phase was then returned to 42% acetonitrile in 0.5 min and kept for 0.5 min. Detection was set at 280 nm. CD and CT were monitored at 280 nm (retention times of 3.1 and 2.3 min, respectively). The MS system consisted of an LC/QTOF equipped with an orthogonal geometry Z-spray ion source (Waters/Micromass, Manchester, UK). A photodiode array detector, Waters Alliance 2695, system was used for UV detection. A volume of 25.0 μL was injected on a reversed-phase column (Xterra, Waters, C18, 3.5 μm, 100 mm × 2.1 mm). A flow rate of 0.2 mL min^{-1} was set. The binary solvent system used was composed of solvent A (acetonitrile) and solvent B (water acidified with 0.5‰ v/v formic acid). The gradient elution started with 5% A and reached 95% A in 15 min linearly. The gradient was held for 10 min and then decreased to 5% A in 10 min. The desolvation chamber and ion source block temperatures were set at 250 and 100 °C, respectively. N_2 was used as the nebulizer gas (35 L h^{-1}) and the desolvation gas (350 L h^{-1}). The electrospray interface was operating in positive ion mode. The capillary voltage was 3000 V; the sample cone and the extraction cone were set at 35 and 1 V, respectively. Data were acquired over the m/z 90−1000 range at a scan rate of 1 s per spectrum. The data recorded were processed with MassLynx (version 4.0).

RESULTS AND DISCUSSION

Phototransformation of Pure CD on Wax Films. The percentage of transmission of solid CD (12 kg ha^{-1}) between 500 and 250 nm is shown in Figure 1. Absorption of CD starts below 380 nm, meaning that, upon solar irradiation, CD can undergo direct photolysis. By extrapolating absorbances of Figure 1 to a dose of CD of 200 g ha^{-1}, one gets 0.0019 at 300 nm. Dark control experiments showed no CD decay on the time scale of the experiments, indicating that other phenomena such as volatilization, thermal degradation, or penetration into the wax are negligible. Pure CD undergoes fast photolysis on wax films at the recommended agricultural rate of 200 g ha^{-1}. The apparent first-order rate constant of phototransformation is 0.11 h^{-1} (see Figure 2).

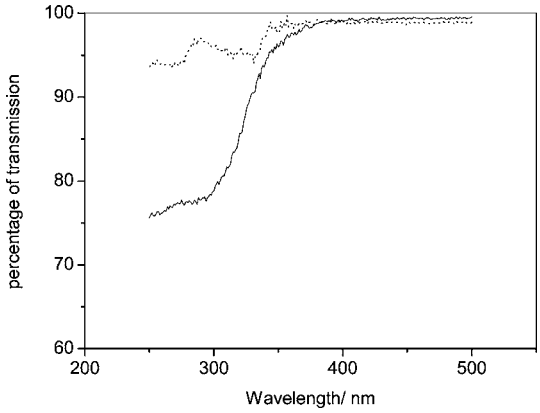

Figure 1. Transmission spectra of CD (12 kg ha^{-1}) (solid line) and CT (7 kg ha^{-1}) (dashed line) on quartz plates.

The typical chromatogram of irradiated CD is given in Figure 3a. CD in *E* form is eluted at 17.8 min and CD in *Z* form at 13.2 min. The *Z* form is very minor before and after irradiation. Thus, only the *E*-form peak variation was used for photodegradation rate determination. The small variation of the *Z*-form peak during irradiation indicates that photoisomerization

dx.doi.org/10.1021/jf500771s | J. Agric. Food Chem. 2014, 62, 4846−4851

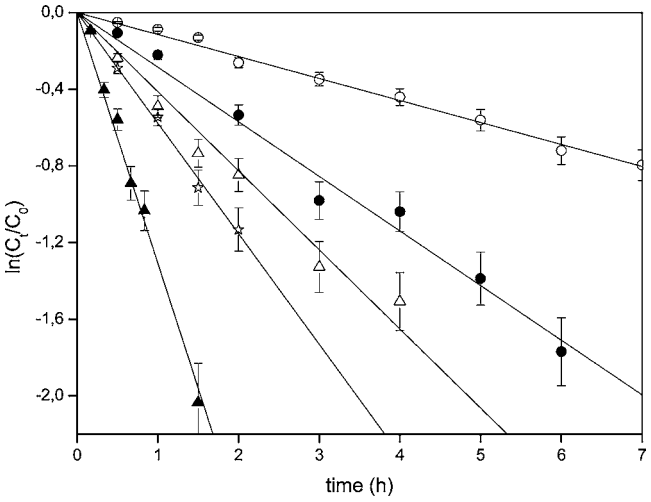

Figure 2. Decay of CD (200 g ha^{-1}) irradiated on paraffin wax in a solar simulator: CD alone (○, k = 0.11 ± 0.01 h^{-1}) and in the presence of CT at 150 g ha^{-1} (●, k = 0.30 ± 0.03 h^{-1}); Stratos alone (△, k = 0.41 ± 0.04 h^{-1}), in the presence of Fongil at 20 g ha^{-1} (☆, k = 0.58 ± 0.06 h^{-1}), and in the presence of Fongil at 150g ha^{-1}(▲, k = 1.3 ± 0.1h^{-1}).

is a minor process. Five other chromatographic peaks are detected, showing m/z at 298, 342, 282, and 358 u. Two peaks have the same m/z of 342 u. Using the exact mass measurement and MS/MS data (in the positive mode), we propose the elemental compositions given in Table 1 and the structures given in Scheme 2.

P_2, detected at 12.1 min, has gained O compared to CD. The oxidation can occur either on the sulfur atom or on the cyclohexane ring. Thanks to the MS/MS data, differentiation is possible. First, a fragment at m/z 101 u corresponding to the ion $C_5H_9S^+$ is detected in P_2 fragmentation pattern as in that of CD. This shows that the S atom is not oxidized. Second, the fragment at 324 u corresponding to the loss of water is in good accordance with the presence of an OH group on the cyclohexane ring, because the neighborhood of H atoms makes possible water elimination. The other fragments of P_2 show loss of C_2H_4O by cleavage of the N−O bond (m/z 298 u) and also subsequent loss of water (m/z 280 u).

P_3, detected at 13 min, gives a positive ion at m/z 282 u, resulting from the loss of C_2H_4O. The main fragments of the ion are at m/z 265 u (loss of NH_3), 254 u (loss of CO), and 182 u (loss of neutral C_5H_8S). Again, the fragment at 101 u

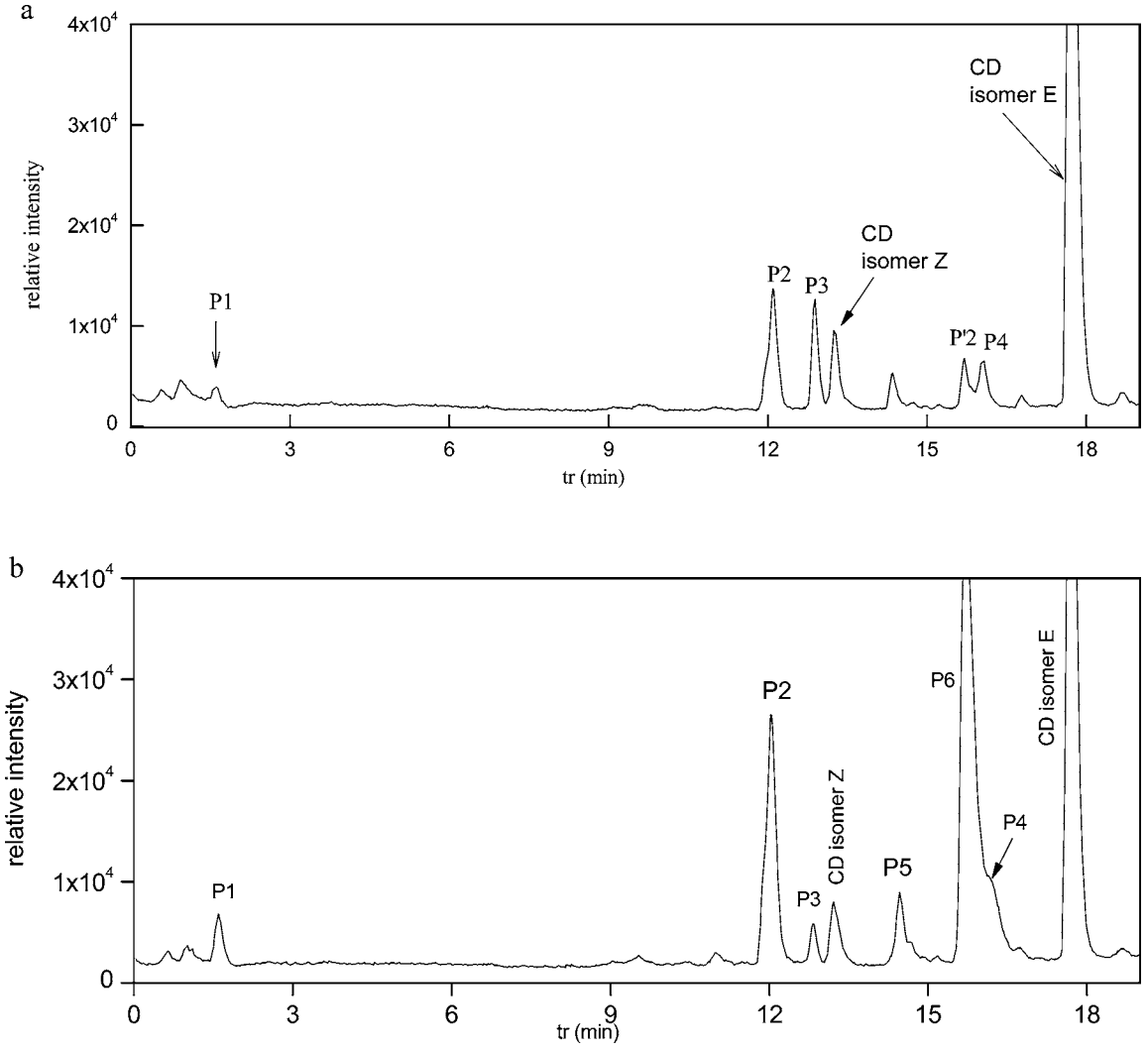

Figure 3. (a) TIC chromatogram in positive mode of the CD solution obtained by rinsing the 1-h-irradiated wax films by acetonitrile. (b) TIC chromatogram in positive mode of the solution used to rinse wax films after 30 min of irradiation of CD and CT mixture on pure wax films.

dx.doi.org/10.1021/jf500771s | J. Agric. Food Chem. 2014, 62, 4846−4851

Table 1. Fragmentation of CD and Main Photoproducts

protonated compound	measured m/z in u (ES+)	fragments in u (ES+)	elemental composition	error in ppm
$[CD + H]^+$	326.1792	280 $[M - C_2H_6O + H]^+$ 180 $[M - C_2H_6O - C_5H_8S + H]^+$ 101 $[C_5H_9S]^+$	$C_{17}H_{28}NO_3S$	0.4
$[P1 + H]^+$	298.1472	280 $[M - H_2O + H]^+$ 263 $[M - H_2O - NH_3 + H]^+$ 101 $[C_5H_9S]^+$	$C_{15}H_{24}NO_3S$	0.3
$[P2 + H]^+$ and $[P'2 + H]^+$	342.1741	324 $[M - H_2O + H]^+$ 298 $[M - C_2H_4O + H]^+$ 280 $[M - H_2O - C_2H_4O + H]^+$ 178 $[M - C_2H_4O - H_2O - C_5H_{10}S + H]^+$ 101 $[C_5H_9S]^+$	$C_{17}H_{28}NO_4S$	2.1
$[P3 + H]^+$	282.1530	265 $[M - NH_3 + H]^+$ 254 $[M - CO + H]^+$ 182 $[M - C_5H_8S + H]^+$ 101 $[C_5H_9S]^+$	$C_{15}H_{24}NO_2S$	2.8
$[P4 + H]^+$	358.1691	340 $[M - H_2O + H]^+$ 312 $[M - C_2H_6O + H]^+$ 296 $[M - H_2O - C_2H_4O + H]^+$ 215 $[M - C_2H_6O - C_4H_7N - CO + H]^+$ 197 $[M - C_2H_6O - C_4H_7N - CO - H_2O + H]^+$ 117 $[C_5H_9SO]^+$	$C_{17}H_{28}NO_5S$	2.3
$[P5 + H]^+$	341.3486	296 $[M - COOH + H]^+$	$C_{22}H_{45}O_2$	21.2
$[P6 + H]^+$	369.3805	324 $[M - COOH + H]^+$	$C_{24}H_{49}O_2$	21.2

Scheme 2

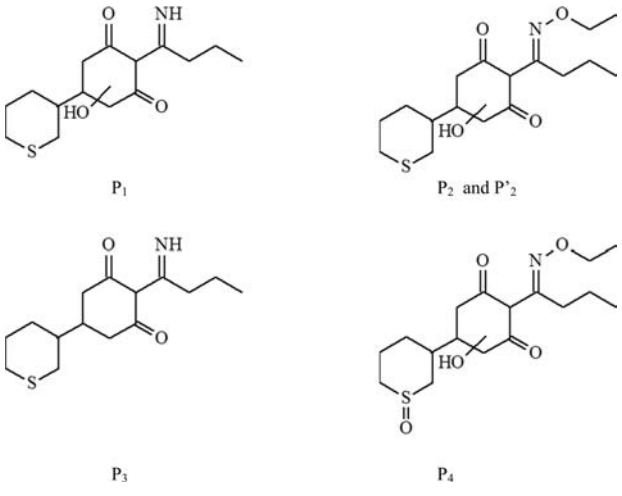

corresponding to $C_5H_9S^+$ is detected. P_3 is assigned to the imine.

P_2' (retention time at 15.7 min) is a minor photoproduct giving the same mass and fragmentation pattern as P_2. This is thus an isomer of P_2.

P_1, eluted at 1.6 min, has lost C_2H_4 compared to CD. Using data on the other photoproducts, this can be understood by the replacement of the ethoxyl group by H with the formation of the imine and oxidation with O addition. By MS/MS the main fragments are m/z 280, 263, and 101 u. The presence of a fragment at 101 u is again in accordance with oxidation of the cyclohexane ring.

P_4 with m/z 358 u is detected at 16.1 min. The $[P_4 + H]^+$ ion has two extra oxygen atoms compared to the $[CD + H]^+$ ion. Among fragments, the ion at m/z 117 u is detected. This ion corresponds to $[C_5H_9SO]^+$, and thus in P_4 the sulfur atom is oxidized. The second oxygen atom is on the cychohexane ring as indicated by the fragments at m/z 340 corresponding to the loss of water as observed for the other oxidized compounds.

Phototransformation of CD in the Presence of CT. As shown in Figure 1, CT absorbs solar light between 300 and 350 nm. On the basis of the transmission spectrum recorded at 7 kg ha^{-1}, one calculates that absorption of CT (200 g ha^{-1}) should be around 0.0012 at the maximum (340 nm) and 0.0006 at 300 nm. This means that CT absorbs solar light more weakly than CD when they are applied at the same dose.

In the presence of CT (150 g ha^{-1}), there is a marked increase of the rate of CD photolysis (Figure 2). The apparent first-order rate constant of phototransformation is equal to 0.3 ± 0.03 h^{-1}, thus 3-fold higher than for pure CD. On the contrary, the concentration of CT remains unchanged after 6 h of irradiation by considering a 5% error margin. The photolysis of pure CT was previously found to be quite slow (first-order rate constant of 0.065 $days^{-1}$ under continuous irradiation at 500 W m^{-2});[8] therefore, CD does not significantly affect its photoreactivity.

The phototransformations of CD and CT on wax film were also studied using commercial formulations, Stratos and Fongil, respectively. In this case, pesticide solutions were deposited as 2 μL droplets to better represent field conditions, and the surface concentration of CD was again fixed at 200 g ha^{-1}. Stratos alone disappears with a first-order rate constant of 0.4 ± 0.03 h^{-1} (Figure 2). In the presence of Fongil, the photodissipation

dx.doi.org/10.1021/jf500771s | J. Agric. Food Chem. 2014, 62, 4846−4851

of Stratos increases. When Fongil is added at 20 and 150 g ha^{-1}, the photodegradation rate constants of formulated CD are 0.6 ± 0.03 and 1.3 ± 0.03 h^{-1}, respectively. Thus, the photoreactivity of formulated CD is 1.5- and 3.2-fold higher, respectively. The same enhancement was measured when using the pure active ingredients; therefore, one can conclude that the accelerating effect is mainly due to the active ingredient CT and not the additives present in Fongil.

This experiment shows that the lowest level of Fongil, corresponding to a 70th of the recommended application dose on tomato crops, still has an impact on the photodissipation rate of CD. This result is amazing when one takes into account that the absorption of CT at this dose is very low compared to that of CD. CT is thus a very efficient sensitizer.

Typical HPLC-MS analysis of reactional mixtures is shown Figure 3b. In this case, six peaks are observed. On the basis of retention times and MS data, P_1, P_2, P_3, and P_4 correspond to the photoproducts identified in the case of pure CD. However, TIC data show that P_1 and P_2 are formed in much greater amount in the presence of CT than for pure CD. Two new photoproducts are also detected: P_5 and P_6. The chemical formulas of the respective ions $[P_5 + H]^+$ and $[P_6 + H]^+$ are $[C_{22}H_{44}O_2 + H]^+$ and $[C_{24}H_{48}O_2 + H]^+$, and the unique fragments are $[C_{21}H_{43} + H]^+$ and $[C_{23}H_{47}O_2 + H]^+$, respectively, demonstrating the loss of CO_2H radical in both cases. Clearly, these oxidation products do not arise either from CT or from CD, but from the wax that contains long-chain alkanes $C_{22}H_{44}$ and $C_{24}H_{48}$ as main constituents.[11] It must be pointed out that CT cannot be protonated and, consequently, cannot be detected by electrospray MS in the positive mode.

Phototransformation of CD in the Presence of Phenalenone. Experiments were repeated by replacing CT by phenalenone, a strong singlet oxygen sensitizer. To conduct the tests at the same molar concentration for phenalenone and CT, the surface concentration of P on wax films was set at 100 g ha^{-1}. Considering a 10% error margin, the apparent first-order rate constant of phototransformation of CD in the presence of P measured was 0.25 ± 0.03 h^{-1}, which is close to the rate constant measured for CD in the presence of CT at 150 g ha^{-1}. However, unlike CT, P disappeared rapidly during the irradiation. The same photoproducts as in the case of CD + CT mixtures were detected. Photoproducts P_5 and P_6 corresponding to the oxidation of the wax were also formed.

Laser-Flash Photolysis. When CD is irradiated in the presence of CT or phenalenone, it may disappear by reaction with singlet oxygen produced by the CT and phenalenone triplets[8,9] or be oxidized by the triplets themselves. The reactivity of CD with the triplet of phenalenone was reported elsewhere.[7] The reaction rate constant is $(9.6 \pm 1) \times 10^6$ M^{-1} s^{-1} in acetonitrile. Here, we measured the rate constant of reaction between the triplet of chlorothalonil and CD. To this end, acetonitrile solutions of CT were irradiated at 266 nm with the fourth harmonic of a Nd:YAG laser, and the triplet decay was monitored at 320 nm. In deoxygenated medium, the first-order rate constant for the triplet decay was equal to $(1 \pm 0.2) \times 10^5$ s^{-1}. In the presence of CD (5×10^{-5} M), the triplet decayed more quickly with an apparent first-order rate constant of $\sim 1.5 \times 10^5$ s^{-1}. In the reaction, the triplet of chlorothalonil is reduced into the radical anion that absorbs in the same wavelength range as the triplet.[12] As a consequence, the rate constant of reaction of CD with the triplet of chlorothalonil cannot be obtained accurately, but the experiment demonstrates that CD is oxidized by the triplet of chlorothalonil with a rate constant $\sim 10^9$ M^{-1} s^{-1}.

DISCUSSION

The photolysis of CD in solid form on wax films is very fast in simulated solar light. This reaction mainly leads to the imine by cleavage of the oxime function and to oxidation. Analytical data demonstrate that the oxidation takes place preferentially on the cyclohexane ring and not on the S atom. It must be stressed that the oxidation product is firmly identified for the first time. Traces of oxidized imine and doubly oxidized CD with one oxygen on the cyclohexane ring and another on the S atom are detected, too. The photoreactivity of CD is similar to that observed in acetonitrile.[13] In particular, photoisomerization of the *E* isomer into the *Z* isomer, which is observed in water but not in acetonitrile, does not occur in solid form. This means that the intramolecular hydrogen bond between the OH and the N detected in acetonitrile exists also in the solid.[13] When CD is formulated, the photoreactivity is faster, probably because of the better spreading of the molecules thanks to the formulation adjuvants. Photoproducts are the same as for pure CD; therefore, adjuvants do not affect photoreactivity.

CD is also phototransformed by sensitized reactions. At the chosen level of added CT that remains well below the rate applied in the field, the accelerating effect is very significant. CD photoproducts are the same as for pure CD, but their distribution is different. In particular, the oxidized imine and the photoproduct resulting from oxidation of the cyclohexane ring are formed in much greater amounts. This confirms that sensitized reactions induce oxidation.

The oxidation can imply two pathways: oxidation by singlet oxygen and oxidation by the sensitizer triplet itself. As the two routes probably give similar products, it is difficult at this stage to delineate the role of each of them in the CD photo-oxidation. The only indication is given by comparing the effects of CT and phenalenone. Both sensitizers photogenerate singlet oxygen with a yield close to 1.[8,9] As phenalenone is much more absorbing than CT within the wavelength range of 290−500 nm,[7] one might expect a much faster photodegradation of CD in the presence of phenalenone than of CT if singlet oxygen were the involved oxidant species. Actually, this is not the case as close rates of phototransformation are measured for both sensitizers. As far as the reactivity of CD with triplets is concerned, one found that the reaction rate constant is about 100-fold higher for triplet CT than for triplet phenalenone. This higher oxidant property of triplet CT may counterbalance a lower absorptivity and finally rationalize the close rates of phototransformation measured in the presence of both sensitizers. To sum up, data are consistent with an oxidation of CD by the sensitizer triplets as the main pathway of oxidation. This oxidation occurs on CD and on P_3, the main CD photoproduct (Scheme 3).

In the course of the reaction, the concentration of CT remains very stable, indicating that it is not measurably consumed, whereas phenalenone disappears quite rapidly. This difference may originate from the reactivity of the sensitizers' reduced radicals. Oxidation of CD by the triplets yields the reduced forms of sensitizers:

$$^3\mathrm{CT}^* + \mathrm{CD} \rightarrow \mathrm{CT}_{\mathrm{H}}^{\bullet} + \mathrm{CD}_{-\mathrm{H}}^{\bullet}$$

$$^3\mathrm{phenalenone}^* + \mathrm{CD} \rightarrow \mathrm{phenalenone}_{\mathrm{H}}^{\bullet} + \mathrm{CD}_{-\mathrm{H}}^{\bullet}$$

dx.doi.org/10.1021/jf500771s | J. Agric. Food Chem. 2014, 62, 4846−4851

Scheme 3

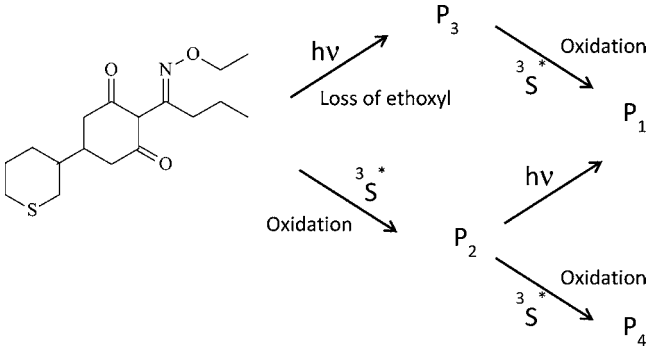

The nonconsumption of CT indicates that the radical $CT_H^{\bullet}$ gives the H atom back to oxygen, regenerating CT and producing $HO_2^{\bullet}$. From phenalenone, the hydroxylperinaphthenyl radical is expected to be formed. In solid medium, this radical is poorly reactive toward oxygen. It preferentially reacts by addition with other radicals; consequently, phenalenone is not regenerated.[14] This explains the disappearance of phenalenone and shows that, in the solid state, CT is a much better sensitizer than phenalenone.

The last but not the least interesting point here is the detection of oxidized long-chain alkanes. To our knowledge this is the first time it is shown that alkane wax constituents can be oxidized by a mild oxidation process involving light, oxygen, and an organic sensitizer. This implies that leaf constituents should be also subject to oxidation.

In conclusion, on leaf models, direct photolysis of cycloxydim leads to the loss of ethoxyl group and to the oxidation of the cyclohexane moiety. Applied at a dose 75-fold less than the recommended one, and although showing a weak absorptivity, chlorothalonil increases the phototransformation rate of cycloxydim through oxidation. Besides, chlorothalonil is also able to oxidize the wax components of the leaves. This exemplifies the necessity to test the photochemical reactivity of pesticides in mixtures. It is also worth noting that the sensitizers chlorothalonil and phenalenone do not have the same properties in the solid state. Chlorothalonil is quite stable during the irradiation experiment in the presence of cycloxydim, whereas phenalenone undergoes photodegradation.

AUTHOR INFORMATION

Corresponding Author

*(C.R.) E-mail: Claire.richard@univ-bpclermont.fr. Phone: +33 (0)4 73 40 71 42. Fax: +33 (0)4 73 40 77 00.

Notes

The authors declare no competing financial interest.

REFERENCES

(1) Katagi, T. Photodegradation of pesticides on plant and soil surfaces. *Rev. Environ. Contam. Toxicol.* **2004**, *182*, 1−195.

(2) Lavieille, D.; Ter Halle, A.; Richard, C. Understanding mesotrione photochemistry when applied on leaves. *Environ. Chem.* **2006**, *5*, 420−425.

(3) Ter Halle, A.; Drncova, D.; Richard, C. Phototransformation of the herbicide sulcotrione on maize cuticular wax. *Environ. Sci. Technol.* **2006**, *40*, 2989−2995.

(4) Ter Halle, A.; Lavieille, D.; Richard, C. The effect of mixing two herbicides mesotrione and nicosulfuron on their photochemical reactivity on cuticular wax film. *Chemosphere* **2010**, *79*, 482−487.

(5) *Metabolic Pathways of Agrochemicals*; Roberts, T. R., Ed.; Royal Society of Chemistry: Cambridge, UK, 1998.

(6) Stabilized herbicidal formulations and methods of use. U.S. Patent 2011/0015074 A1, Jan 20, 2011.

(7) Monadjemi, S.; Ter Halle, A.; Richard, C. Reactivity of cycloxydim toward singlet oxygen in solution and on wax film. *Chemosphere* **2012**, *89*, 269−273.

(8) Monadjemi, S.; El Roz, M.; Richard, C.; Ter Halle, A. Photoreduction of chlorothalonil fungicide on plant leaf models. *Environ. Sci. Technol.* **2011**, *45*, 9582−9589.

(9) Schmidt, R.; Tanielian, C.; Dunsbach, R.; Wolff, C. Phenalenone, a universal reference compound for the determination of quantum yields of singlet oxygen $O_2(^1\Delta_g)$ sensitization. J. *Photochem. Photobiol. A* **1994**, *19*, 11−17.

(10) Bonnichon, F.; Richard, C. Phototransformation of 3-hydroxybenzonitrile in water. *J. Photochem. Photobiol., A* **1998**, *119*, 25−32.

(11) Chastain, J. Unpublished results.

(12) Bouchama, S.; de Sainte-Claire, P.; Arzoumanian, E.; Oliveros, E.; Boulkamh, A.; Richard, C. Photoreactivity of the fungicide chlorothalonil in aqueous medium. *Environ. Sci.: Processes Impacts* **2014**, DOI: 10.1039/C3EM00537B.

(13) Monadjemi, S.; de Sainte-Claire, P.; Abrunhosa-Thomas, I.; Richard, C. Photolysis of cycloxydim, a cyclohexanedione oxime herbicide. Detection, characterization and reactivity of the iminyl radical. *Photochem. Photobiol. Sci.* **2013**, *12*, 2067−2075.

(14) Trivella, A.; Monadjemi, S.; Worrall, D. R.; Kirkpatrick, I.; Arzoumanian, E.; Richard, C. Perinaphthenone phototransformation in a model of leaf epicuticular waxes. *J. Photochem. Photobiol., B* **2014**, *130*, 93−101.

JOURNAL OF AGRICULTURAL AND FOOD CHEMISTRY

Article

pubs.acs.org/JAFC

Hydrolysis Reaction Mechanism in Atrazine Metabolism and Prediction of Its Metabolites' Toxicities

Jia Li, Jing Hu, Wenli Xu, Min Ling, and Jianhua Yao*

Shanghai Institute of Organic Chemistry, Chinese Academy of Sciences, Shanghai 200032, China

Supporting Information

ABSTRACT: Atrazine (ATR) is a widely used herbicide. There are several types of reactions in its metabolism. Herein, the mechanism of three paths of hydrolysis reactions in its metabolism and predictions of toxicities of its metabolites in the three paths will be presented. The calculation results by B3LYP (Becke, 3-parameter, Lee−Yang−Parr), one of the approaches in density functional theory, indicated that (1) there were three models in the three hydrolysis paths of ATR. The dissociation mechanisms of C(9/11)−N(8/10), C(4/6)−N(8/10), and C−Cl were dealkylation, deamination, and Cl substitution, respectively. (2) The energy barrier of C−Cl dissociation was lower. The dissociation was advantageous in dynamics and the primary reaction in the three hydrolysis paths. In these hydrolysis reactions, the different intermediates had different concentrations because of the impact of the reaction rate. (3) In addition, it was necessary to consider the solvent effect to investigate hydrolysis reaction. The conductor-like polarizable continuum model (CPCM) was used to simulate the hydrolysis reaction in bond length and energy barrier because of the solvent effect. Experimental or predictive results showed that atrazine and its metabolites in the three hydrolysis paths were carcinogenic.

KEYWORDS: *atrazine, density functional theory, hydrolysis reaction, solvent effect, prediction of toxicity*

INTRODUCTION

Atrazine (ATR; IUPAC name, 2-chloro-4-ethylamino-6-isopropylamine-s-triazine; CAS Registry No. 1912-24-9) is one of the triazine herbicides widely used in the United States.[1] Its chemical structure is shown in Figure 1. Its acute toxicity was at

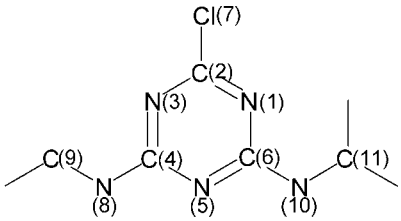

Figure 1. Structure of ATR.

a low level (rat, oral, LD_{50} = 2000 mg/kg), and AMES was negative,[2] Muntagenic (sperm from human) was positive.[3] It was carcinogenic by RTECS.[4] Its half-life depended on environmental fates. In the document reported by the U.S. EPA,[5] "Decision Documents for Atrazine", atrazine's overall half-life, water half-life, and sediment half-life were given as 608, 578, and 330 days, respectively.

Atrazine may act as an endocrine disrupter at sensitive stages in the developmental process and may subsequently significantly reduce the reproductive capacity of amphibians.[6] Therefore, the degradation rate and the properties of compounds generated in the degradation process should be attract attention.

Many works about ATR's metabolism have been reported: photolysis,[7] microbial degradation,[8,9] degradation in plants,[10] hydrolysis,[11−19] etc. All of these works focused on (1) the relationship between environmental fates and the metabolic rate of ATR and (2) metabolic processes in various environmental fates. Dr. Wen and his colleagues' showed that the salinity, pH, and temperature affected the degradation rate of ATR; the degradation of ATR in subsurface flow constructed wetland (SFCW) followed first-order kinetics, with a half-life of approximately 17.5 days.[13] Drs. Chu and Lin studied the relationship between four fates (pH, temperature, ATR concentration, and sunlight) and ATR degradation rate. The results showed that ATR's decomposition rate constant outdoors was slower in neutral pH and faster at extreme pH levels; the higher the ATR concentration was, the lower was the decomposition rate constant.[14]

Dr. Lin studied ATR degradation in selected plant species. The results showed that main product was ammeline (AMN) by N-dealkylation and hydrolysis in the metabolic process.[10] Dr. Cheney studied the degradation reaction of ATR on synthetic birnessite (δ-MnO_2). The result showed that hydrolysis of the C−Cl bond was primary in the metabolic process, and the main product was 2-hydroxy-4-ethylamino-6-isopropylamine-s-triazine (HA).[12] In other works about ATR degradation, HA is also the main product, and the hydrolysis of ATR was accelerated obviously in alkaline solution[15] or ultraviolet light.[16] Dr. Pelizzetti studied ATR degradation over TiO_2 particles under simulated solar light. The result showed that the final product, 2,4,6-trihydroxy-s-triazine (CA) was generated by photocatalytic hydrolysis via the intermediate AMN.[17]

Received: March 7, 2014
Revised: April 29, 2014
Accepted: May 7, 2014
Published: May 7, 2014

ACS Publications © 2014 American Chemical Society

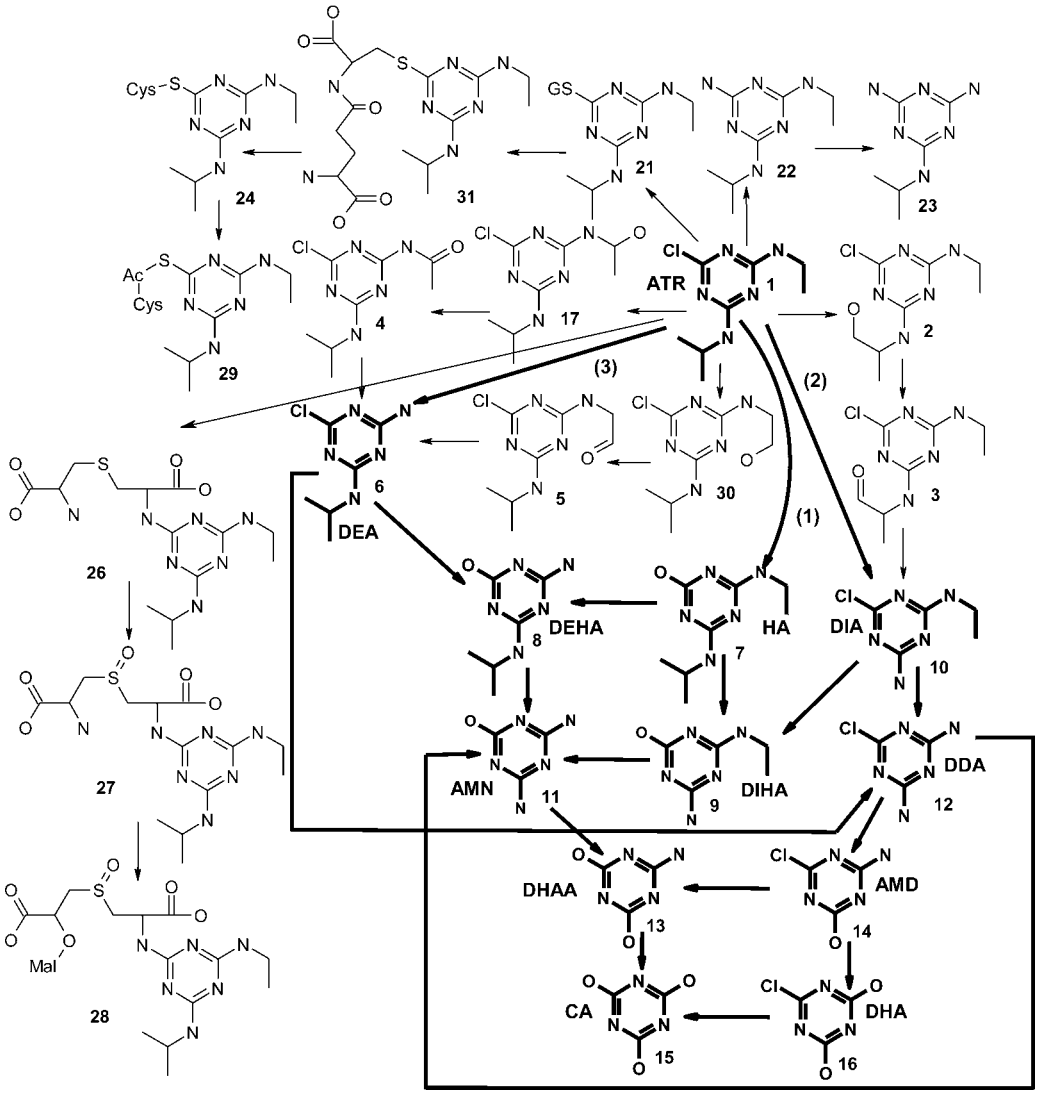

Figure 2. Metabolism pathways of ATR.

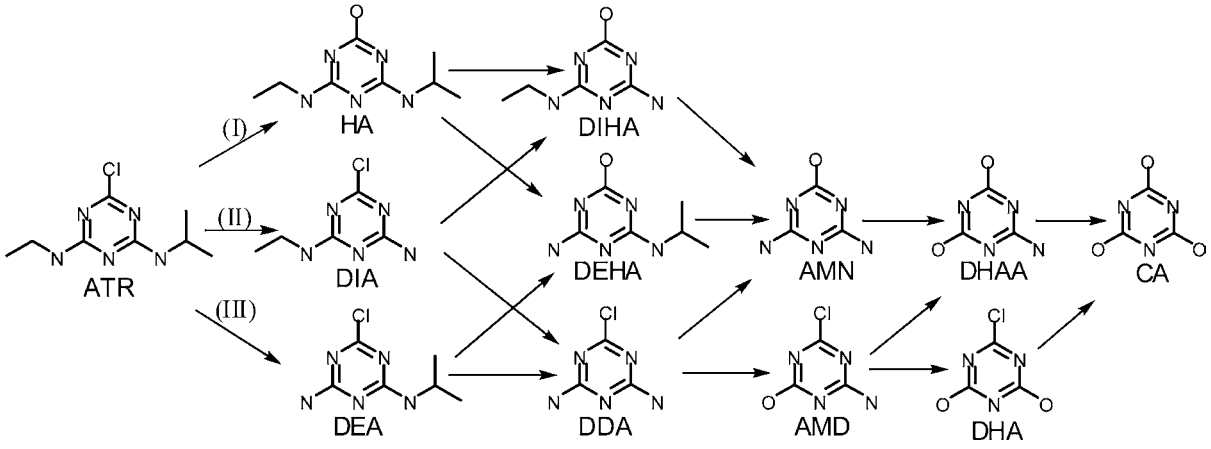

Figure 3. Part of the hydrolysis reactions in ATR metabolism (bold in Figure 2).

ATR's metabolism paths were summarized on the basis of publications[7−20] and are listed in Figure 2.

All reported studies of ATR's metabolism focused on its metabolites and metabolic conditions. Herein, the mechanism of hydrolysis reactions in three hydrolysis paths in ATR's metabolism (shown in Figure 3) was studied by B3LYP (Becke, 3-parameter, Lee−Yang−Parr)[21]/6-31++G(d, p),[22] one of the approaches in density functional theory (DFT). The calculation results explained three points related to the hydrolysis reactions in the three paths: (1) the mechanism of each hydrolysis

dx.doi.org/10.1021/jf501101q | J. Agric. Food Chem. 2014, 62, 4852−4863

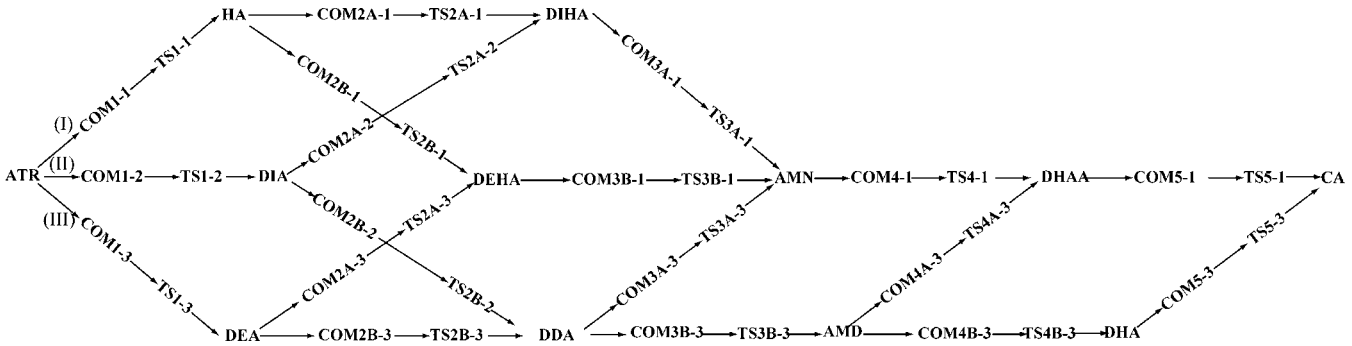

Figure 4. Hydrolysis reaction processes of ATR in the three hydrolysis paths.

reaction in the three paths; (2) the reaction path with the advantage of dynamics in the three paths and the influence of the advantage of dynamics on intermediate concentrations; and (3) in the calculation, the influence of the conductor-like polarizable continuum model (CPCM),[23] which was used to simulate the aqueous environments on the geometry and potential energy surface (PES) of hydrolysis reactions.

In this work, acute, mutagenic (AMES test)[24] and carcinogenic toxicities of ATR and its metabolites in Figure 3 were also predicted by three computer programs, CISOC-PSAT,[25] CISOC-PSMT,[26] and CISOC-PSCT,[27] respectively.

COMPUTATIONAL DETAILS

In this work, DFT calculations were performed with the Gaussian 09 program[28] using the B3LYP method and the 6-31++G(d,p) basis set. Equilibrium and transition state structures were fully optimized. For all calculated structures, harmonic vibration frequencies were calculated by numerical differentiation of the energy gradients. All structures were shown to be transition states (with one imaginary frequency) or stationary points (with no imaginary frequency). The vibrational zero point energy (ZPE) corrections were based on the corresponding frequency calculation. To analyze reaction path characters, the minimum energy path was followed in both directions (forward and backward) using the intrinsic reaction coordinate (IRC).[29] For all structures, natural bond orbital (NBO) analysis[30] was performed for further elucidation. In addition, CPCM was used to simulate the aqueous environments for interpreting the influence of the solvent effect. To gain insight into the various bond-breaking or bond-making processes in this reaction, an analysis of bond order[31−33] was carried out.

CISOC-PSAT is a program used to predict acute toxicity of an organic compound. The prediction results correspond to rat, oral and range of LD_{50}. CISOC-PSMT is a program to predict mutagenic toxicity (AMES test) of an organic compound. The prediction results correspond to mutagenicity in the test model: *Salmonella typhimurium*. CISOC-PSCT is a program to predict carcinogenic toxicity of an organic compound. The prediction results correspond to carcinogenicity in the test model: rat, oral.

RESULTS AND DISCUSSION

Atom Charge and Bond Length in This Hydrolysis Reaction. In principle, hydrolysis reactions of these groups connecting to C(2), N(8), and N(10) were able to occur. Therefore, three hydrolysis paths were observed (in Figure 3), and the reaction continued to hydrolyze the amino group connecting to C(4) and C(6). Their procedures are proposed in Figure 4. The structure parameters of the stationary points of the reactions are shown in Figure 5. Information about atomic charge of these first transition states in the three paths and the dissociation transition state of the amino group connecting to C(4) is shown in Figure 6.

In hydrolysis degradation shown in Figures 4 and 5, there were several steps in path I: (1) HA was formed. When one H_2O closed to N(1), the hydrogen bond complex COM1-1 was formed at first. The bond length of the hydrogen bond is 203.2 pm. (2) The O atom of H_2O attacked the C(2) to form the transition state TS1-1 with a four-membered ring (C(2)−O−H−Cl). In TS1-1, the bond length of C(2)−Cl increased from 176.1 to 227.5 pm and that of O−H in H_2O is elongated to 99.5 pm. The O and H atoms all closed to C(2)−Cl, and bond lengths of C(2)−O and Cl−H were 179.4 and 206.6 pm, respectively. (3) HA was generated via the transition state TS1-1. Meanwhile, one H_2O was consumed and one HCl was produced in the reaction. (4) The bond of C(11)−N(10) was hydrolyzed by H_2O. The complex COM2A-1 was formed by H_2O approaching the N(5) with the hydrogen bond. The hydrogen bond lengths of N(5)−H and O−H were 188.2 and 211.8 pm, respectively. In the transition state TS2A-1, there was a four-membered ring (N(10)−H−O−C(11)), and the C(11)−N(10) bond was elongated to 277.4 pm. The O−H bond in H_2O is slightly elongated to 103.5 pm, and C(11)−O and N(10)−H were generated in this reaction. DIHA was generated by the end of this reaction. On the other hand, the hydrolysis of C(9)−N(8) also occurred. DEHA was generated via COM2B-1 and TS2B-1. (5) DIHA was hydrolyzed to AMN. The complex COM3A-1 was formed when one H_2O closed to the C(9)−N(8); the transition state TS3A-1 was generated when a four-membered ring was formed (N(8)−H−O−C(9)). There was a difference between bond lengths of the four-membered ring in TS2A-1 and those in TS3A-1. By the end of this reaction, AMN, HCl, alcohol, and isopropanol were generated by three H_2O molecules consumed. (6) AMN was hydrolyzed to DHAA. The complex COM4-1 was formed when one H_2O closed to the amino groups connected to C(6), the transition state TS4-1 was generated when a four-membered ring was formed (N(10)−H−O−C(6)). By the end of this reaction, DHAA was generated. (7) DHAA was hydrolyzed to CA. The complex COM5-1 was formed when one H_2O closed to the amino groups connected to C(4), and the transition state TS5-1 was generated when a four-membered ring was formed (N(8)−H−O−C(4)). By the end of this reaction, CA was generated. The bond lengths of the four-membered ring in TS4-1 were a little different from those in TS5-1. We propose that the

dx.doi.org/10.1021/jf501101q | J. Agric. Food Chem. 2014, 62, 4852−4863

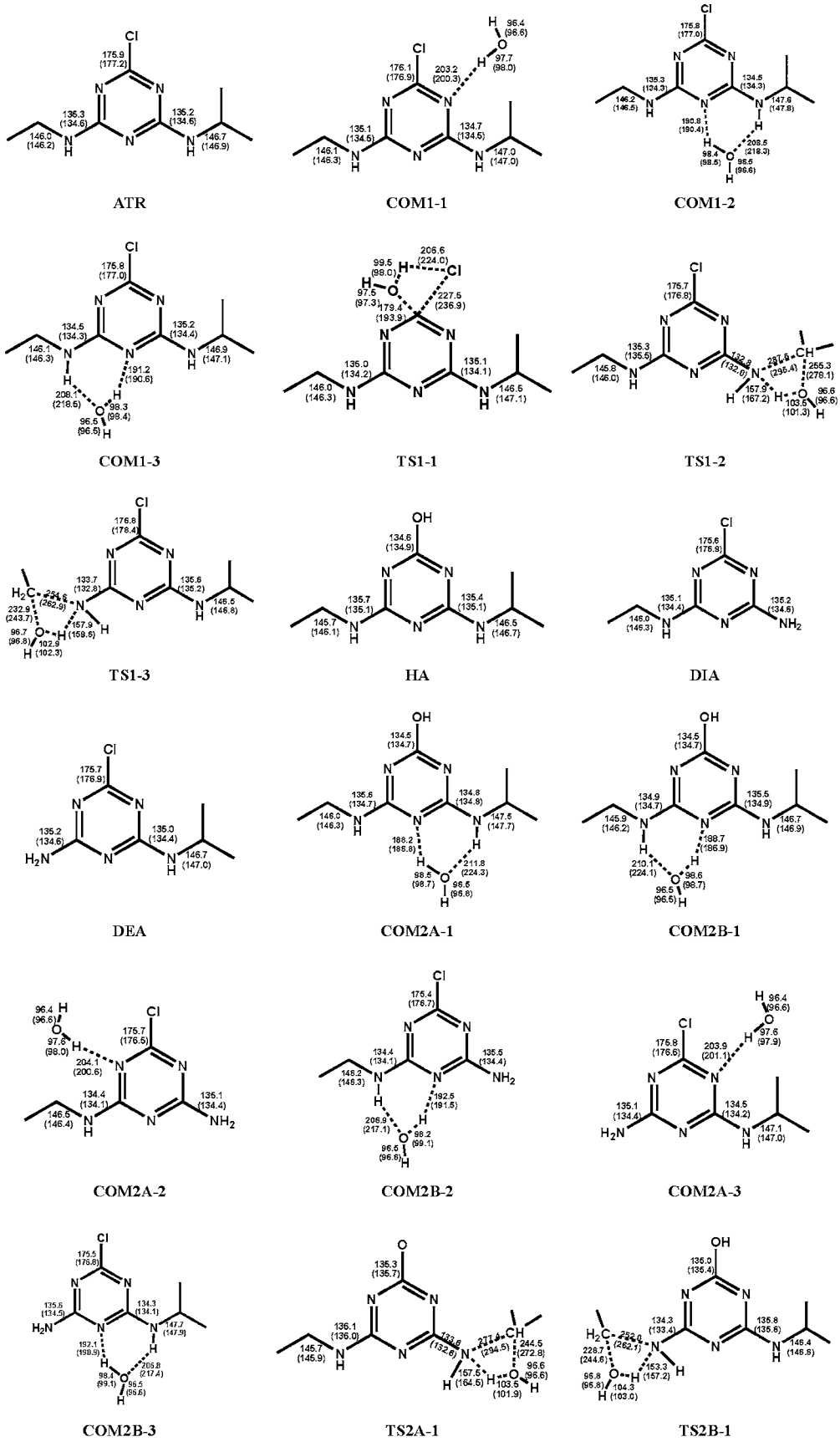

Figure 5. continued

dx.doi.org/10.1021/jf501101q | J. Agric. Food Chem. 2014, 62, 4852−4863

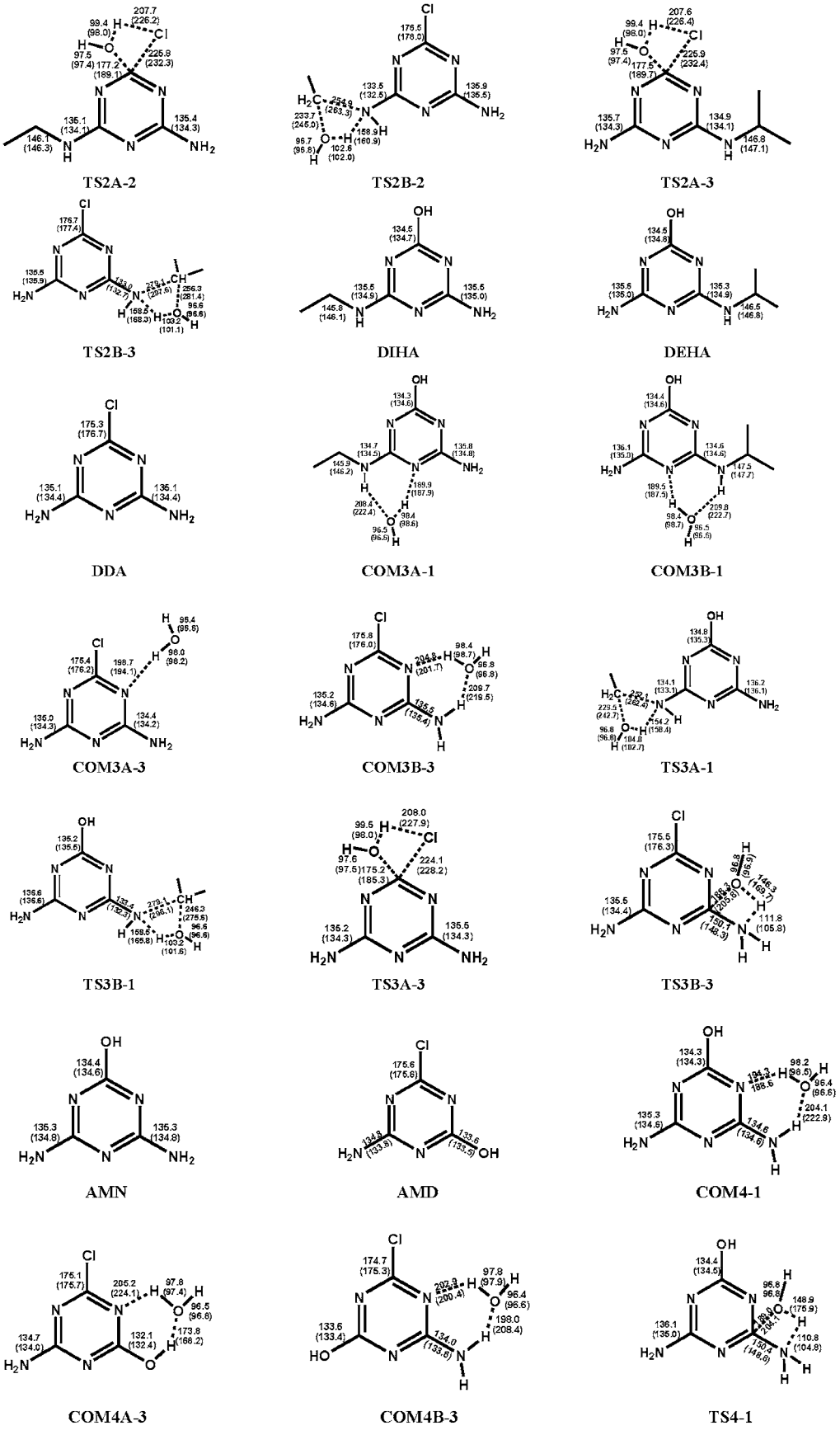

Figure 5. continued

dx.doi.org/10.1021/jf501101q | J. Agric. Food Chem. 2014, 62, 4852−4863

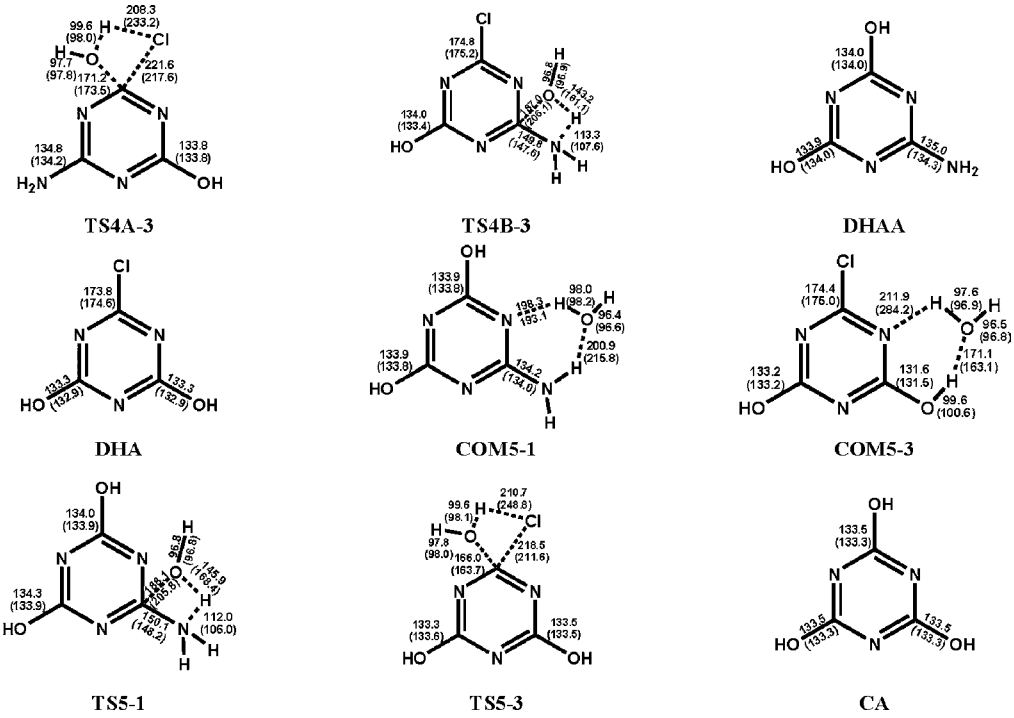

Figure 5. Optimized structures of the reactant, intermediates, transition states, and product in the hydrolysis reaction of ATR. The values in parentheses were calculated by CPCM. (Distance in pm.)

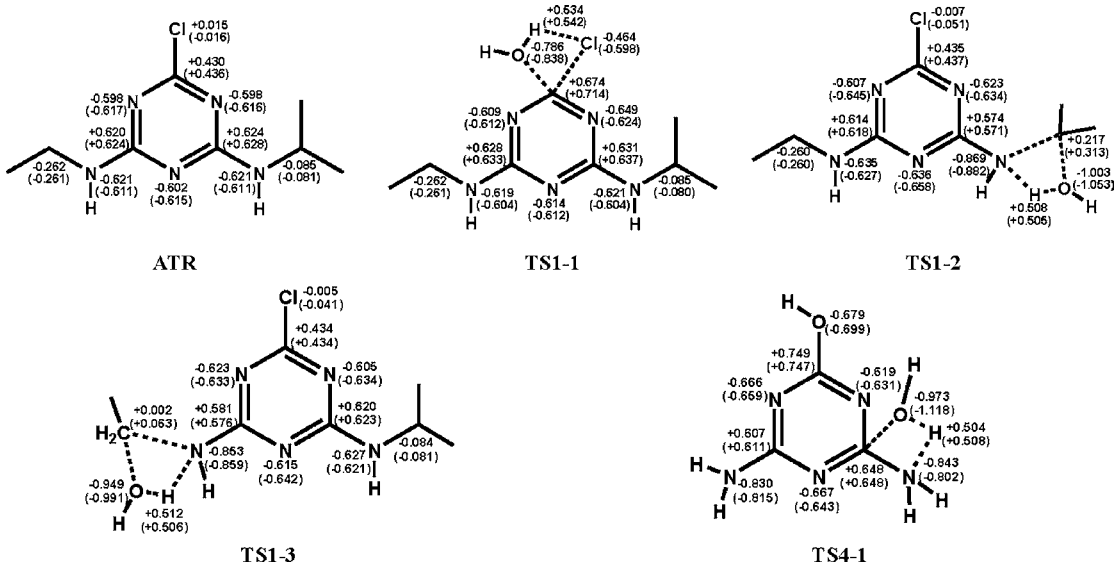

Figure 6. NBO analysis of ATR and transition states in paths. The values in parentheses were calculated by CPCM.

amino group and hydroxyl affected TS4-1 and TS5-1 slightly. In path I, the pH value of the reaction system was decreased.

Reactions in path II (shown in Figures 4 and 5) also included several steps: (1) DIA was formed. When one H_2O closed to N(10), the two hydrogen bond complex COM1-2 was formed at first. The bond lengths of the hydrogen bonds were 190.8 and 208.5 pm, respectively. (2) The O atom of H_2O attacked the C(11) to form the transition state TS1-2 with a four-membered ring (N(10)−H−O−C(11)). In TS1-2, the bond length of N(10)−C(11) increased from 147.6 to 287.6 pm, and that of O−H in H_2O was elongated to 103.5 pm. Bond lengths of C(11)−O and N(10)−H were 255.3 and 157.9 pm, respectively. DIA was generated via the transition state TS1-2. (3) DIA was degraded to DIHA or DDA. If C(2) was attacked by H_2O, a four-membered ring (C(2)−O−H−Cl) generated in the transition state TS2A-2. The bond length of C(2)−Cl was increased from 175.7 to 225.8 pm, and that of O−H in H_2O was elongated to 99.4 pm. DIHA was generated when H in H_2O was transferred. If C(9) was attacked by H_2O, a four-membered ring (C(9)−O−H−N(8)) generated in the transition state TS2B-2 via complex COM2B-2. The bond length of C(9)−N(8) was increased from 146.2 to 254.9 pm. DDA was generated from DIA.

dx.doi.org/10.1021/jf501101q | J. Agric. Food Chem. 2014, 62, 4852−4863

Table 1. Imaginary Frequencies (ν) of Transition States and Relative Energies (ΔE) Corrected by ZPVE of Reactants, Intermediates, Transition States, and Products[a]

compound	ΔE^b (kJ/mol)	ν^b (cm^{-1})	ΔE^c (kJ/mol)	ν (cm^{-1})[c]
ATR	0		0	
		Path I		
COM1-1	−18.2		−6.1	
TS1-1	167.4	−380.3*i*	157.2	−360.9*i*
HA	−42.7		−36.2	
COM2A-1	−59.1		−38.3	
TS2A-1	239.8	−334.6*i*	220.8	−215.8*i*
DIHA	−30.7		−23.2	
COM3A-1	−57.5		−36.6	
TS3A-1	281.5	−464.9*i*	276.9	−408.3*i*
COM2B-1	−70.8		−50.3	
TS2B-1	269.7	−469.2*i*	263.6	−413.9*i*
DEHA	−26.1		−16.4	
COM3B-1	−40.5		−16.9	
TS3B-1	257.4	−324.2*i*	240.2	−208.3*i*
AMN	−14.1		−3.2	
COM4-1	−45.6		−15.3	
TS4-1	211.7	−762.1*i*	209.4	−419.6*i*
DHAA	9.8		20.1	
COM5-1	−21.6		8.1	
TS5-1	232.4	−847.1*i*	230.9	−466.2*i*
		Path II		
COM1-2	−14.8		−0.9	
TS1-2	277.2	−320.5*i*	250.0	−195.9*i*
DIA	12.3		14.2	
COM2A-2	−6.2		7.5	
TS2A-2	181.6	−380.3*i*	174.0	−374.8*i*
COM2B-2	−12.8		2.6	
TS2B-2	319.9	−435.3*i*	308.8	−400.6*i*
		Path III		
COM1-3	−26.4		−12.6	
TS1-3	307.9	−441.0*i*	295.3	−408.3*i*
DEA	18.4		21.0	
COM2A-3	0.9		15.6	
TS2A-3	186.8	−397.6*i*	180.6	−373.4*i*
COM2B-3	4.5		21.0	
TS2B-3	298.1	−317.2*i*	269.4	−185.4*i*
DDA	31.7		36.8	
COM3A-3	1.9		25.5	
TS3A-3	201.8	−378.0*i*	197.5	−382.9*i*
COM3B-3	1.9		25.5	
TS3B-3	254.1	−836.5*i*	246.7	−448.3*i*
AMD	60.8		63.2	
COM4A-3	40.1		53.4	
TS4A-3	226.3	−342.8*i*	218.7	−301.6*i*
COM4B-3	30.9		52.8	
TS4B-3	280.8	−939.7*i*	312.2	−466.2*i*
DHA	93.5		95.1	
COM5-3	50.9		69.8	
TS5-3	257.9	−338.8*i*	252.4	−296.7*i*
CA	35.7		47.2	

[a]The other molecules in the reaction were considered. [b]The results in gas. [c]The results by CPCM.

Reactions in path III (shown in Figures 4 and 5) were similar to those in path II and included several steps: (1) C(9)−N(8) was hydrolyzed. DEA was generated via complex COM1-3 and transition state TS1-3 including a four-membered ring (C(9)−O−H−N(8)). (2) DEA was degraded into DEHA or DDA. If C(2) was attacked by H_2O, a four-membered ring (C(2)−O−H−Cl) generated in the transition state TS2A-3, and DEHA was generated. If N(10) was attacked by H_2O, a four-membered ring (C(11)−O−H−N(10)) was generated in the transition state TS2B-2 via complex COM2B-2. DDA was generated from DEA. (3) DDA was degraded into AMN or AMD. If N(1) was attacked by H_2O, a four-membered ring (C(2)−O−H−Cl) was generated in TS3A-3 via complex COM3A-3. AMN generated from DDA. If N(10) was attacked by H_2O, a four-membered ring (C(6)−O−H−Cl) was generated in TS3B-3 via complex COM3B-3. AMD generated from DDA. (4) AMD was degraded into DHAA or DHA. The complex COM4A-3 was formed when one H_2O closed to N(1), the transition state TS4A-3 was generated when a four-membered ring was formed (C(2)−O−H−Cl). By the end of this reaction, DHAA was generated. The complex COM4B-3 was formed when one H_2O closed to N(8), and the transition state TS4B-3 was generated when a four-membered ring was formed (C(4)−O−H−N(8)). By the end of this reaction, DHA was generated. (5) DHA was hydrolyzed to CA.

All results mentioned in the front were calculated in gaseous environments. In this work, the actual reaction process was in an aqueous environment. Therefore, the reactant, intermediates, transition states, and products were calculated by simulating the aqueous environment by CPCM. Some works reported that the solvent effect little influences compound structures.[34,35] From information shown in Figure 5, normal chemical bond lengths were slightly affected, about 1 pm, but the bond lengths in the center of the transition state were effected obviously, about 30 pm. Therefore, the solvent effect must necessarily be considered in the optimization of the geometry structure, especially for transition states in reactions.

In these hydrolysis reactions, the nucleophile H_2O attacked C(2), C(4), C(9), and C(11), respectively, to form corresponding transition states. As shown in Figure 6, the O atom in H_2O did not attack these C atoms directly, but formed complexes by the interaction of the hydrogen bond first. In the process of forming transition states, C(2), C(4), C(9), and C(11) lost electrons. In these corresponding transition states, the dissociated C atoms all had positive charges (+0.674/(+0.714) C(2), +0.648/(+0.648) C(4), +0.217/(+0.313) C(9), +0.002/(+0.063) C(11)), which were good for the nucleophilic reaction. The corresponding information in detail (calculated in gaseous) is in the Supporting Information.

Potential Energy Surface of Reaction. The imaginary frequencies of transition states in the reactions and relative energies corrected by ZPVE of reactant, intermediates, transition states, and product are listed in Table1. The potential energy surfaces of the reactions are shown in Figure 7. We can discern relative energies corrected by ZPVE of various compounds and transition states in reaction coordinates according to the information in Figure 7.

Information given in Table 1 and Figure 7 shows that system energy decreased about 20 kJ/mol with formation of complexes because the influence of the hydrogen bond was weak. In the reaction process, the energy barrier of the transition state was the key factor of the reaction rate. As shown in Figure 7, the energy barriers of the hydrolysis of the C(2)−Cl bond in three paths were 185.6, 187.8, 203.7, 187.7, 186.2, and 202.0 kJ/mol, respectively, and their vibrational frequencies were 380.3*i*, 380.3*i*, 378.0*i*, 397.6*i*, 342.8*i*, and 338.8*i*, respectively. The vibration mode was the swing of the Cl between the C(2) and

dx.doi.org/10.1021/jf501101q | J. Agric. Food Chem. 2014, 62, 4852−4863

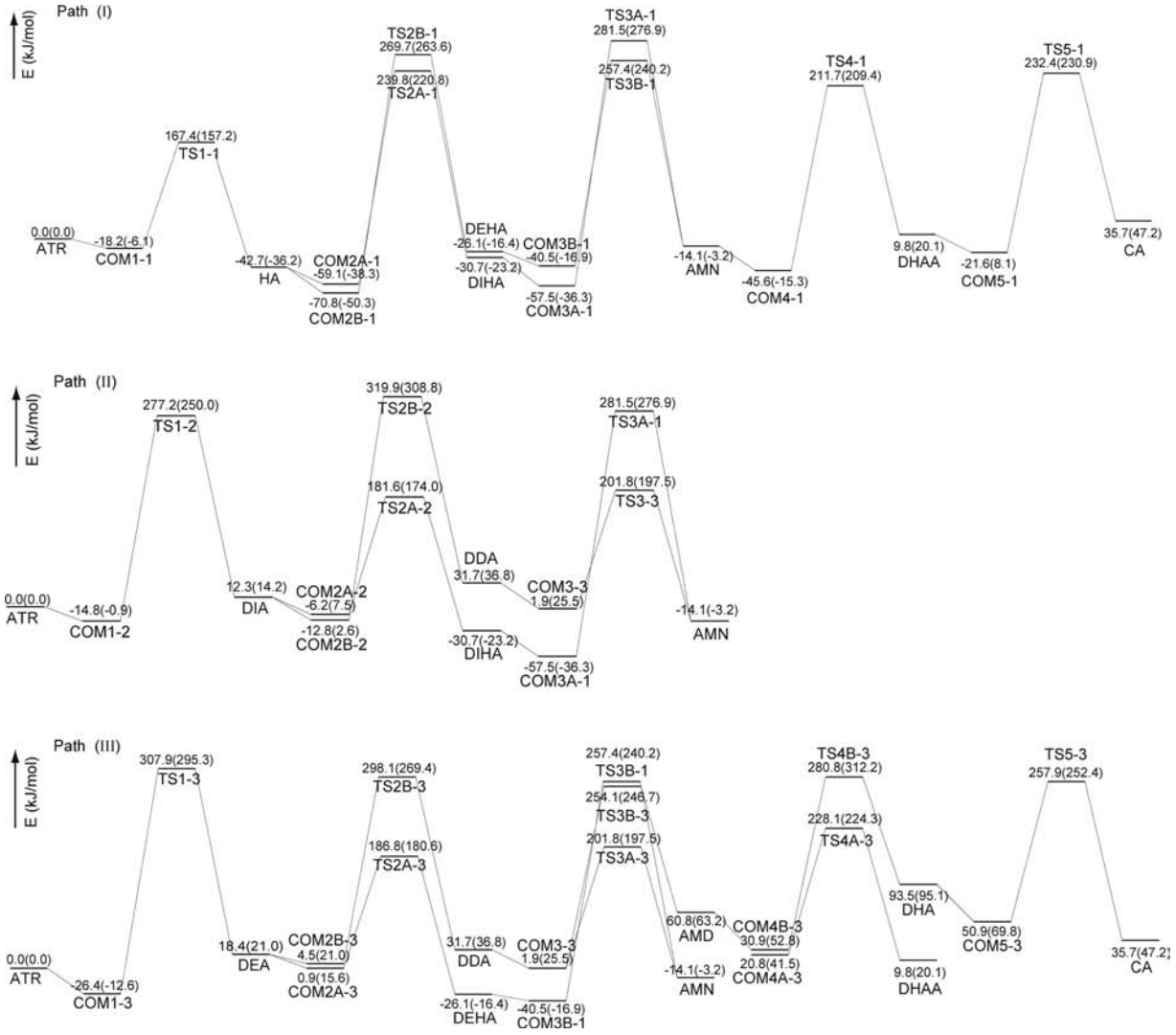

Figure 7. Potential energy profiles of ATR and its metabolites in the three paths.

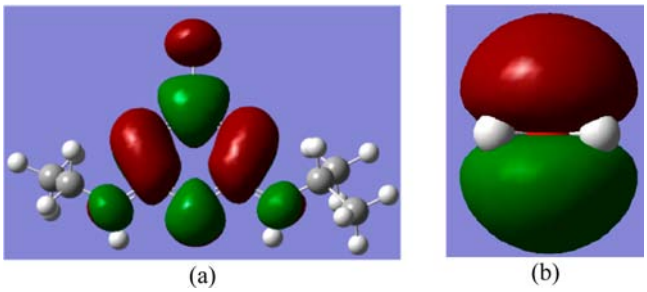

Figure 8. Schematic diagrams of (a) LUMO of ATR and (b) HOMO of H_2O.

H atom. The Cl was substituted in this step. The energy barriers of the hydrolysis of the bond of C(9)−N(8) were 340.5, 339.0, 332.7, and 334.3 kJ/mol. The energy barriers of the hydrolysis of the C(11)−N(10) were 298.9, 297.9, 292.0, and 293.6 kJ/mol. The vibrational frequencies of the C(9)−N(8) and C(11)−N(10) bonds were about 460*i* and 320*i*, respectively. Those vibration modes were all the swing of the H atom between N(8)/N(10) and the O atom, and the H atom was transferred in this step. For bonds of C(4)−N(8) and C(6)−N(10), those dissociation energy barriers were 256.3, 254.0, 256.0, and 257.2 kJ/mol, respectively, so the reaction energy barriers of the C(2)−Cl bond were obviously lower than those of the C−N bond. In this reaction, the hydrolysis reaction rate of ATR was slow because of higher reaction energy barriers.

In general, nucleophilic reactions are an interaction between the HOMO of a nucleophile and the LUMO of an electrophile. In this reaction system, there was an interaction between the HOMO of the nucleophile H_2O and the LUMO of ATR. The LUMO of ATR (the antibonding orbital of the C(2)−Cl bond) in Figure 8 shows that the bond of C(2)−Cl was elongated and dissociated by the interaction between the lone pair electrons of the nucleophile H_2O and the LUMO of ATR, so the bond of C(2)−Cl was dissociated previously by the nucleophile H_2O because of its lower energy barrier.

In principle, an energy barrier has an exponential relationship with the rate constant. The reaction energy barrier of the C(2)−Cl bond was about 110−150 kJ/mol lower than that of the C(9)−N(8) or C(11)−N(10) bond, and its reaction rate constant was obviously higher than that of the C(9)−N(8) or C(11)−N(10) bond. Therefore, there were obvious kinetics differences in the three paths. The hydrolysis of the C(2)−Cl

dx.doi.org/10.1021/jf501101q | J. Agric. Food Chem. 2014, 62, 4852−4863

Table 2. Wiberg Bond Orders (B_i), Percentage of Evolution of Bond Orders (E_v), and Synchronicity (S_y)

path	bond	B_i^{RC}[a]	B_i^{TS1}[b]	B_i^{INT}[c]	E_v	S_y
I	H−O	0.6961	0.6599	0	5.20	0.495
	H−Cl(7)	0.0022	0.0457	0.9113	4.78	
	C(2)—Cl(7)	1.0290	0.4062	0	39.48	
	C(2)—O	0.0011	0.3445	1.0520	32.68	
II	H−O	0.6757	0.6006	0	11.11	0.373
	H−N(10)	0.0007	0.1423	0.7853	18.05	
	C(11)—N(10)	0.9378	0.0865	0	90.77	
	C(11)—O	0.0005	0.0565	0.9118	6.15	
III	H−O	0.6761	0.5699	0	15.71	0.575
	H−N(8)	0.0006	0.1686	0.7840	21.44	
	C(9)—N(8)	0.9524	0.1999	0	79.01	
	C(9)—O	0.0005	0.2064	0.9176	22.45	

[a]The value for hydrogen bond complexes of the first step. [b]The value for transition states of the first step. [c]The value for intermediates of the first step.

bond was the easiest one in the three reactions: from ATR to HA, DIA, and DEA. In this hydrolysis reaction system (shown in Figure 3), the intermediate concentration in path I was the highest, such as HA in path I. The result corresponds to some experimental works.[12,15,16] The prediction will be beneficial to expand the study of pesticide effect on the environment from the pesticide compound to the possible intermediates.

The CPCM was used to simulate these reactions in aqueous state because of the solvent effect. The results showed that the dissociation energy barriers of the C(2)−Cl bond were 163.3, 166.5, 172.0, 159.6, 165.3, and 182.6 kJ/mol and lower than those in the gaseous state. Dissociation energy barriers of the C(9)−N(8) bond were 313.9, 313.2, 306.2, and 307.9 kJ/mol, respectively, and the dissociation energy barriers of the C(11)−N(10) bond were 259.1, 257.1, 250.9, and 248.4 kJ/mol. For the C(4)−N(8) and C(6)−N(10) bonds, the dissociation energy barriers were 224.7, 239.0, 221.2, and 259.4 kJ/mol. They were all lower than those in the gaseous state. It is necessary to consider the solvent effect in the study of potential energy surface in hydrolysis reactions.

Bond Order Analysis. To gain insight into the various transition states along with the reaction coordinate, an analysis of bond order was studied. The value of Wiberg bond order was calculated by NBO calculation. With regard to the reaction mechanism, synchronicity (S_y), proposed by Moyano et al.,[33] was used to represent the global nature of bond breaking/forming processes in the decomposition reaction and expressed by eq 1.

$$S_y = 1 - [\sum_{i=1}^{n} |(E_v)_i - (E_v)_{av}|/(E_v)_{av}]/(2n - 2) \quad (1)$$

In eq 1, n denotes the number of bonds directly involved in the reaction, and the percentage of evolution of bond orders $(E_v)_i$ is given by eq 2.

$$(E_v)_i = 100 \times [B_i^{TS} - B_i^{R}]/[B_i^{P} - B_i^{R}] \quad (2)$$

Superscipts TS, R, and P refer to the transition state, reactant, and product, respectively. The average $(E_v)_{av}$ is calculated by eq 3:

$$(E_v)_{av} = \frac{1}{n}\sum_{i=1}^{n} (E_v)_i \quad (3)$$

The information about Wiberg bond orders (B_i) and percentage of evolution of bond orders (E_v) of several bonds of the first step in paths I, II, and III are listed in Table 2. The synchronicity(S_y) of the first step in paths I, II, and III was calculated by eqs 1, 2 and 3, the values being 0.495, 0.373 and 0.575, respectively. The corresponding reactions can be viewed as very asynchronous processes according to S_y.

Toxicity of the Metabolites. The toxicities (experimental and prediction results) of ATR and a part of its metabolites are listed in Table 3.

The information listed in Table 3 shows that prediction results corresponded to experimental results if the experimental data were public. The prediction results showed that (1) carcinogenic toxicity of ATR and its metabolites was positive, (2) mutagenic toxicity (AMES test) of DHHA and CA was positive, and (3) acute toxicity of ATR and its metabolites was at middle or low toxic levels. These results explained ATR's harmful impact on the environment.

In this work, the mechanism of hydrolysis reactions in the metabolism of ATR was studied by the DFT B3LYP/6-31++g (d, p) method. It is necessary to use CPCM to simulate its aqueous system. The results showed the following: (1) The three degradation mechanisms corresponded to the three hydrolysis paths, dealkylation of C(9)−N(8) and C(11)−N(10) bonds by H transferred, deamination of C(4)−N(8) and C(6)−N(10) bond by H transferred, and dehalogenation of C(2)−Cl(7) bond by Cl substituted. (2) The hydrolysis reaction of ATR was prior to path I, and the C−Cl was dissociated first because its dissociation activation energy was lower than that of the C(9)−N(8) or C(11)−N(10) bond. (3) The concentrations of intermediates in the hydrolysis depended on reaction rate.

The results of toxicity prediction and experimental reports of ATR showed that it is carcinogenic. The prediction of its metabolites showed that they are carcinogenic. The results also showed that not only ATR but also it metabolites are harmful for the environment. We propose that we should evaluate the toxicity of not only candidates of pesticides but also their metabolites by in silico methods, which also could be employed before the candidates were synthesized or isolated and in the period of design.

Table 3. Toxicities of ATR and Its Metabolites

Compound	CAS	Acut Tox. Exp.[36,d]/Pred.[a]	Mutigenic Tox. Exp.[36,d]/Pred.[b]	Carcinogenic Tox. Exp.[36,d]/Pred.[c]
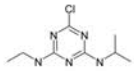 2-Chloro-4-ethylamino-6-isopropylamine-s-triazine (ATR)	1912-24-9	Rat , oral , LD_{50}=2000mg/kg /4.02	Negative /N	Positive/P
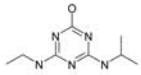 2-Hydroxy-4-ethylamino-6-isopropylamine-s-triazine (HA)	2163-68-0	NULL/4.21	Negative /N	NULL/P
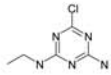 2-Chloro-4-ethylamino-6-amine-s-triazine (DIA)	1007-28-9	Rodent – rat, oral, TDLo.: 10mg/kg /3.93	Negative /N	NULL/P
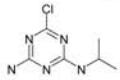 2-Chloro-4-amino-6-isopropylamine-s-triazine (DEA)	6190-65-4	NULL/3.98	Negative /N	NULL/P
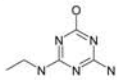 2-Hydroxy-4-ethylamino-6-amine-s-triazine (DIHA)	7313-54-4	NULL/4.12	NULL/N	NULL/P
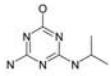 2-Hydroxy-4-amino-6-isopropylamine-s-triazine (DEHA)	19988-24-0	NULL/4.17	NULL/N	NULL/P
2-Chloro-4,6-diamine-s-triazine (DDA)	3397-62-4	Rat，unreported，TDLo: 800 mg/kg /3.89	Negative/N	NULL/P
2-Hydroxy-4,6-diamine-s-triazine (AMN)	645-92-1 (R)	NULL/4.08	NULL/ N	NULL/P
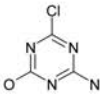 2-Chloro-4-amine-6-Hydroxy-s-triazine (AMD)	167939-59-5	NULL/4.05	NULL/ N	NULL/P
2,4-dihydroxy-6-amine-s-triazine (DHAA)	167613-80-1	NULL/4.20	NULL/ P	NULL/P

dx.doi.org/10.1021/jf501101q | J. Agric. Food Chem. 2014, 62, 4852−4863

Table 3. continued

Compound	CAS	Acut Tox. Exp.[36,d]/Pred.[a]	Mutigenic Tox. Exp.[36,d]/Pred.[b]	Carcinogenic Tox. Exp.[36,d]/Pred.[c]
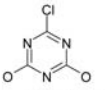 2-Chloro-4,6-dihydroxy-s-triazine (DHA)	135581-60-1	NULL/4.17	NULL/ N	NULL/P
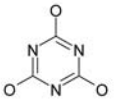 2,4,6-trihydroxy-s-triazine (CA) cyanuric acid	135581-61-2	NULL/4.28	NULL/ P	NULL/P

[a]Rat, oral, <2, LD_{50} < 1 mg/kg; ≥2 and <3, 1 ≤ LD_{50} < 50 mg/kg; ≥3 and <4, 50 ≤ LD_{50} < 500 mg/kg; ≥4 and <5, 500 ≤ LD_{50} < 5000 mg/kg; ≥5, LD_{50} ≥ 5000 mg/kg. [b]*Salmonella typhimurium*; P, positive; N, negative. [c]Rat, oral, *P*, probability of noncarcinogenicity is low. [d]Null, no experimental data.

■ ASSOCIATED CONTENT

Supporting Information

Information about NBO analysis of atrazine and some transition states (in gaseous) in the paths. This material is available free of charge via the Internet at http://pubs.acs.org.

■ AUTHOR INFORMATION

Corresponding Author

*(J.Y.) Mail: Shanghai Institute of Organic Chemistry, Chinese Academy of Sciences, 345 Lingling Road, Shanghai 200032, China. Phone: (86) 21-54925266. E-mail: yaojh@mail.sioc.ac.cn.

Funding

This work was supported by the National Natural Science Foundation of China (Nos. 21072216, 21302211) and MOST (2010CB126103).

Notes

The authors declare no competing financial interest.

■ ACKNOWLEDGMENTS

We thank the High Performance Computing and Data Center, Shanghai Advanced Research Institute, Chinese Academy of Sciences.

■ REFERENCES

(1) U.S. EPA. Toxicity and Exposure Assessment for Children's Health, Atrazine chemical summary, http://www.epa.gov/teach/chem_summ/Atrazine_summary.pdf (accessed Jan 3, 2014).

(2) De Veer, I.; Moriske, H. J.; Rueden, H. Photochemical decomposition of organic compounds in water after UV-irradiation: investigation of positive mutagenic effects. *Toxicol. Lett.* **1994**, *72* (1−3), 113−119.

(3) Betancourt, M.; Resendiz, A.; Casas, E.; Fierro, R. Effect of two insecticides and two herbicides on the porcine sperm motility patterns using computer assisted semen analysis (CASA) in vitro. *Reprod. Toxicol.* **2006**, *22* (3), 508−512.

(4) Hayes, W. J. Pesticides as endocrine-disrupting chemicals. In *Handbook of Pesticide Toxicology*, 3rd ed.; Krieger, R., Ed.; Elsevier: London, UK, 2010; Vol. 1, pp 558.

(5) U.S. Environmental Protection Agency. Decision documents for atrazine, http://www.epa.gov/oppsrrd1/REDs/atrazine_combined_docs.pdf (accessed Jan 3, 2014).

(6) Tavera-Mendoza, L.; Ruby, S.; Brousseau, P.; Fournier, M.; Cyr, D.; Marcogliese, D. Response of the amphibian tadpole (*Xenopus laevis*) to atrazine during sexual differentiation of the testis. *Toxical. Chem.* **2002**, *21* (3), 527−531.

(7) Prosen, H.; Zupančič-Kralj, L. Evaluation of photolysis and hydrolysis of atrazine and its first degradation products in the presence of humic acids. *Environ. Pollut.* **2005**, *133*, 517−529.

(8) Zhang, P.; Sun, H. W.; Yu, L.; Sun, T. H. Adsorption and catalytic hydrolysis of carbaryl and atrazine on pig manure-derived biochars: impact of structural properties of biochars. *J. Hazard. Mater.* **2013**, *244−245*, 217−224.

(9) Li, K. B.; Cheng, J. T.; Wang, X. F.; Zhou, Y.; Liu, W. P. Degradation of herbicides atrazine and bentazone applied alone and in combination in soils. *Pedosphere* **2008**, *18* (2), 265−272.

(10) Lin, C. H.; Lerch, R. N.; Kremer, R. J.; Harrett, H. E. Stimulated rhizodegradation of atrazine by selected plant species. *J. Environ. Qual.* **2011**, *40*, 1113−1121.

(11) Kuklenyik, Z.; Panuwet, P.; Jayatilaka, N. K.; Pirkle, J. L.; Calafat, A. M. Two-dimensional high performance liquid chromatography separation and tandem mass spectrometry detection of atrazine and its metabolic and hydrolysis products in urine. *J. Chromatogr., B* **2012**, *901*, 1−8.

(12) Shin, J. Y.; Cheney, M. A. Abiotic dealkylation and hydrolysis of atrazine by birnessite. *Environ. Toxicol. Chem.* **2005**, *24*, 1353−1360.

(13) Lin, T.; Wen, Y.; Jiang, L. Y.; Li, J. B.; Yang, S. L.; Zhou, Q. Study of atrazine degradation in subsurface flow constructed wetland under different salinity. *Chemosphere* **2008**, *72*, 122−128.

(14) Lin, K. Y.; Chu, W. Simulation and quantification of the natural decay of a typical endocrine disrupting chemical atrazine in an aquatic system. *J. Hazard. Mater.* **2011**, *192*, 1260−1266.

(15) Noblet, J. A.; Smith, L. A.; Suffet, I. H. Influence of natural dissolved organic matter, temperature, and mixing on the abiotic hydrolysis of triazine and organophosphate pesticieds. *J. Agric. Food Chem.* **1996**, *44* (11), 3685−3693.

(16) Chen, C.; Yang, S. G.; Guo, Y. P.; Sun, C.; Gu, C. G.; Xu, B. Photolytic destruction of endocrine disruptor atrazine in aqueous solution under UV irradiation: products and pathways. *J. Hazard. Mater.* **2009**, *172*, 675−684.

(17) Pelizzetti, E.; Minero, C.; Carlin, M.; Pramauro, E. Identification of photocatalytic degradation pathways of 2-Cl-s-triazine herbicides and detection of their decomposition intermediates. *Chemosphere* **1992**, *24* (7), 891−910.

(18) Konstantinou, I. K.; Zarkadis, A. K.; Albanis, T. A. Organic compound in the environment. *J. Environ. Qual.* **2001**, *30*, 121−130.

(19) Comber, S. D. W. Abiotic persistence of atrazine and simazine in water. *Pestic. Sci.* **1999**, *55*, 696−702.

(20) Atrazine. In *Metabolic Pathways of Agrochemicals, Part 1: Herbicides and Plant Growth Regulators*; Roberts, T. R., Huston, D. H., Lee, P. W., Nicholls, P. H., Plimmer, J. R, Eds.; Royal Society of Chemistry: Cambridge, UK, 1998; pp 629−635.

(21) (a) Perdew, J. P.; Yue, W. Accurate and simple density functional for the electronic exchange energy-generalized gradient approximation. *Phys. Rev. B* **1986**, *33* (12), 8800−8802. (b) Lee, C.;

Yang, W.; Parr, R. G. Development of the colle-salvetti correlation-energy formula into a functional of the electron-dentisy. *Phys. Rev. B* **1988**, *37* (2), 785−789.
(22) Ditchfield, R.; Hehre, W. J.; Pople, J. A. Self-consistent molecular-orbital methods extended Gaussian-type basis for molecular-orbital studies of organic molecules. *J. Chem. Phys.* **1971**, *54* (2), 724.
(23) Barone, V.; Cossi, M. Quantum calculation of molecular energies and energy gradients in solution by a conductor solvent model. *J. Phys. Chem. A* **1998**, *102* (11), 1995−2001.
(24) http://en.wikipedia.org/wiki/Ames_test (accessed Jan 25, 2014).
(25) Prediction System of Acute Toxicity (CISOC-PSAT) V1.0, Registration Number (China): 0232654 (software copyright).
(26) (a) Liao, Q.; Yao, J. H.; Yuan, S. G. Predication of mutagenic toxicity by combination of recursive partitioning and support vector machines. *Mol. Divers.* **2007**, *11*, 59−72. (b) Prediction System of Mutagenicity Toxicity (CISOC-PSMT), Registration Number (China): 042160 (software copyright).
(27) (a) Liao, Q.; Yao, J. H.; Li, F.; Yuan, S. G.; Doucet, J. P.; Panaye, A.; Fan, B. T. CISOC-PSCT: a predictive system for carcinogenic toxicity. *SAR QSAR Environ. Res.* **2004**, *3*, 217−235. (b) Prediction system of carcinogenic toxicity (CISOC-PSCT), Registration Number (China): 022239 (software copyright).
(28) Frisch, M. J.; Trucks, G. W.; et al. *Gaussian 09*, revision A.02; Gaussian Inc.: Wallingford, CT, USA, 2009.
(29) Deng, L.; Ziegler, T.; Fan, L. J. A combined density-functional and intrinsic reaction coordinate study on the ground-state energy surface of H_2CO. *J. Chem. Phys.* **1993**, *99* (5), 3823−3835.
(30) Reed, A. E.; Curtiss, L. A.; Weinhold, F. Intermolecular interactions from a natural bond orbital, donor-acceptor viewpoint. *Chem. Rev.* **1988**, *88* (6), 899−926.
(31) Xue, Y.; Kang, C. H.; Kim, C. K.; Lee, I. Theoretical studies on the gas-phase pyrolysis of 2-phenoxycarboxylic acids: an oniom approach. *J. Comput. Chem.* **2003**, *24*, 963−972.
(32) Xue, Y.; Kim, C. K.; Guo, Y.; Xie, D. Q.; Yan, G. S. DFT study and monte carlo simulation on proton transfers of 2-amino-2-oxazoline, 2-amino-2-thiazoline and 2-amino-2-imidazoline in the gas phase and in water. *J. Comput. Chem.* **2005**, *26*, 994−1005.
(33) Moyano, A.; Perica, M. A.; Valent, E. A theoretical study on the mechanism of the thermal and the acid-catalyzed decarboxylation of 2-oxetanones (*β*-lactones). *J. Org. Chem.* **1989**, *54* (3), 573−582.
(34) Jia, X. J.; Pan, X. M.; Wang, L. W.; Liu, Y.; Sun, H.; Su, Z. M.; Wang, R. S. Theoretical study of effect of solvent on the mechanism of reaction of pentafulvenone with hydrocyanic acid. *Chem. J. Chinese U.* **2008**, *29* (6), 1224−1227.
(35) Yi, G. Q.; Zeng, Y.; Xia, X. F.; Xue, Y.; Kim, C. K.; Yan, G. S. The substituent effects of the leaving groups on the aminolysis of phenyl acetates: DFT studies. *Chem. Phys.* **2008**, *345* (1), 73−81.
(36) MDL TOX database, http://accelrys.com/products/databases/bioactivity/toxicity.html (accessed Jan 20, 2014).

JOURNAL OF AGRICULTURAL AND FOOD CHEMISTRY

Article

pubs.acs.org/JAFC

Evaluation of the Combination of Dimethyl Disulfide and Dazomet as an Efficient Methyl Bromide Alternative for Cucumber Production in China

Liangang Mao,[†] Dongdong Yan,[†,‡] Qiuxia Wang,[†,‡] Yuan Li,[†,‡] Canbin Ouyang,[†,‡] Pengfei Liu,[†] Jin Shen,[†] Meixia Guo,[†,‡] and Aocheng Cao*[,†,‡]

[†]Department of Pesticides, Institute of Plant Protection, Chinese Academy of Agricultural Sciences, Ministry of Agriculture, Beijing 100193, People's Republic of China

[‡]State Key Laboratory for Biology of Plant Disease and Insect Pests, Beijing 100193, People's Republic of China

ABSTRACT: The combination of dimethyl disulfide (DMDS) and dazomet (DZ) is a potential alternative to methyl bromide (MB) for soil disinfestation. The efficacy of DMDS plus DZ in controlling key soilborne pests was evaluated in a laboratory study and in two commercial cucumber greenhouses. Laboratory studies found that all of the combinations had positive synergistic effects on root-knot nematodes, two key soilborne fungi, and two major weed seeds. Greenhouse trials revealed that the combination of DMDS and DZ (30 + 25 g m^{-2}) successfully suppressed *Meloidogyne* spp. root galling, sharply reduced the colony-forming units of *Fusarium* spp. and *Phytophthora* spp. on media, maintained high cucumber yields, and was not significantly different from MB or DMDS alone, but better than DZ alone. All of the chemical treatments provided significantly better results than the nontreated control. The results indicate that the combination of DMDS and DZ is an efficient MB alternative for cucumber production.

KEYWORDS: *soil fumigation, dimethyl disulfide, dazomet, root-knot nematode, soilborne fungi, weed control*

INTRODUCTION

Together with tomato (*Lycopersicon esculentum* Mill.) and pepper (*Capsicum annuum* Linn.), cucumber (*Cucumis sativus* L.) is one of the most important greenhouse crops in northern China. In the protected cultivation of cucumber, soilborne nematodes, fungi, and weeds exhibit a very strong yield-depressing potential. The main factors leading to high pest populations and crop losses are continuous cucumber−tomato rotations or the monocropping of cucumber and two cropping seasons per calendar year.[1,2] Methyl bromide (MB) has been widely used for preplant soil fumigation against soilborne nematodes, pathogens, and weeds in northern China. However, MB has to be totally phased out in China by January 1, 2015, due to the detrimental effects on stratospheric ozone.[3] The withdrawal of MB from use as an agricultural fumigant has prompted a good deal of research to find effective and economically acceptable alternatives.[4]

The current registered chemical MB alternatives for cucumber production in China are metham sodium (MNa), fosthiazate, abamectin, and calcium cyanamide (CC). 1,3-Dichloropropene (1,3-D),[5−8] dazomet (DZ),[7] MNa,[5,9] chloropicrin (Pic),[9] 1,3-D/DZ,[7] 1,3-D/Pic,[9] and others have also been tested as chemical alternatives to MB for cucumber production in China and other countries in the world.

Dimethyl disulfide (DMDS), which has been registered in the United States and other countries, appears to be highly efficient against various nematodes, including *Meloidogyne* spp., but is less effective on fungal pathogens.[10,11] DZ, a methyl isothiocyanate (MITC) generator, is highly effective at controlling a wide range of arthropods, soilborne fungi, nematodes, and weeds, but is less effective against bacteria and root-knot nematodes.[11] Therefore, the combination of DMDS and DZ could be useful as a broad-spectrum soil fumigant. There has been much information in the literature on combinations of 1,3-D and Pic,[9,10,12−15] MNa and Pic,[15] 1,3-D and DZ,[7,16] DMDS and Pic,[14] and other combinations as MB chemical alternatives. Little information, however, has been reported to date on the combination of DMDS and DZ. Previously, Van Wambeke et al. reported the synergistic activity of combinations of DMDS and Basamid (98% DZ) at reduced dose rates for broad-spectrum soil disinfestation in soil column experiments.[17]

The following work was initiated to determine and confirm the effects of the combination of DMDS and DZ on nematodes (*Meloidogyne* spp.), key soilborne fungi (*Fusarium* spp. and *Phytophthora* spp.), and weed seeds (*Abutilon theophrasti* and *Digitaria sanguinalis*) in laboratory studies. Two greenhouse trials were also designed to evaluate DMDS and DZ combinations as an MB alternative for cucumber production in China.

MATERIALS AND METHODS

Laboratory Studies. The efficacy of DMDS and DZ, singly and in combination, was studied in the laboratory. At the end of the cucumber crop growth period, soil samples were collected from the top 20 cm of a cucumber greenhouse in Tongzhou, Beijing, where the occurrence of nematodes and soilborne pathogens was severe. The soil was composed of 57.58% sand, 39.02% silt, and 3.40% clay, with an organic matter content of 32.20 g kg^{-1} soil and pH 7.26. The soil was sieved through a 2 mm mesh and then mixed together thoroughly. The soil moisture was 19.84% (w/w). Particle size analyses were performed using the pipet

Received: March 13, 2014
Revised: May 11, 2014
Accepted: May 12, 2014
Published: May 12, 2014

ACS Publications © 2014 American Chemical Society

Table 1. Soil Characteristics at the Experimental Sites

site, year	soil moisture (%)	pH (1:2.5)	organic matter (g kg^{-1})	N/NH_4^+ (mg kg^{-1})	N/NO_3^- (mg kg^{-1})	available K (mg kg^{-1})	available P (mg kg^{-1})	bulk density (g cm^{-3})
trial I, 2010	28.5	7.87	27.1	29.9	285.7	273.8	438.3	0.86
trial II, 2012	31.7	7.07	33	37.2	388.1	875.4	327.7	0.95

Table 2. Relevant Trial Dates and Some Other Details

site	cucumber cultivar	block area (m^2)	fumigant application	tarp removal	cucumber transplant	end of trial	preceding crop
trial I, 2010	No. 16 Zhongnong	3.2 × 5.7 = 18.24	Aug 5, 2010	Aug 27, 2010	Sept 5, 2010	Nov 25, 2010	tomato
trial II, 2012	No. 16 Zhongnong	3.2 × 5.6 = 17.92	July 27, 2012	Aug 17, 2012	Aug 28, 2012	Dec 3, 2012	tomato

method.[18] Organic carbon contents were determined by wet oxidation using the method of Walkley and Black.[19] The pH was measured in a 1:2.5 soil to H_2O extract. Soil moisture contents were measured by heating in a drying oven at 105 ± 5 °C until mass constancy was reached.[20]

Six hundred grams of soil was placed into 2.5 L desiccators. Ten *Abutilon theophrasti* seeds and 15 *Digitaria sanguinalis* seeds were buried at the depth of about 2 cm in each desiccator.[21] The following treatments were applied with three replicates: DMDS alone (20 or 40 mg active ingredient (ai) kg^{-1} soil), DZ alone (50 or 100 mg ai kg^{-1} soil), DMDS plus DZ (20 + 50, 20 + 100, 40 + 50, or 40 + 100 mg ai kg^{-1} soil), and nontreated control. DMDS was injected into the soil by pipet (Eppendorf, Germany) after sowing the weed seeds, and then the desiccators were immediately sealed with a cover. DZ was applied by mixing with soil, then the seeds were sown, and the vacuum dryer was immediately sealed with a cover. The desiccators were placed in incubators at 28 °C for 5 days. The desiccators were opened to release the residual fumigant for a day, and the weed height was then measured with a caliper. *Fusarium* spp. and *Phytophthora* spp. were isolated from the soil quantitatively according to methods described by Komada[22] and Masago et al.,[23] respectively. Root-knot nematodes (*Meloidogyne* spp.) were extracted from a 100 g subsample on the basis of methods described by Liu.[24]

Greenhouse Trials. In 2010 and 2012, two demonstration experiments were carried out in greenhouses growing cucumber on a commercial farm in Tongzhou, Beijing, which is an important production area for this vegetable. The farm has grown tomato and cucumber for more than 5 years and is facing problems caused by heavy infestations of root-knot nematode, soilborne fungi, and other pests. Details relevant to the experiments are given in Tables 1 and 2.

DMDS 99 TC (Shanghai Yuanji Chemical Co., Ltd., China, containing 99% DMDS), DZ 98 MG (Nantong Shizhuang Chemical Co., Ltd., China, a commercial product containing 98% DZ), and MB 98 TC (Changyi Chemical Plant, China, containing 98% MB and 2% chloropicrin) were used in this study. Polyethylene film (PE) (0.04 mm thick, from Baoding Baoshuo Plastic Co., Ltd., Hebei Province, China) was used as the soil mulch.

The treatments were designed as randomized blocks with three replicates (Table 3). MB as a reference treatment, DMDS alone, DZ alone, DMDS plus DZ, and nontreated control were tested. DMDS was applied by chisel injection at a rate of 60 g m^{-2}. DZ was applied by mixing with soil at a rate of 50 g m^{-2}. The DMDS plus DZ treatments were applied as follows: DZ was applied first by mixing with soil at a rate of 25 g m^{-2}, and then DMDS was applied by chemigation at a rate of 30 g m^{-2}. All of the above treatments were covered with PE film. MB was applied between a PE sheet and soil by the hot gas method at a rate of 40 g m^{-2}, and the PE sheet was left on the soil during the fumigation period.

Table 3. Experimental Program of the Greenhouse Trials

treatment[a]	rate (g ai m^{-2})	tarp type[b]	application method
DMDS 99 TC	60	PE	chisel injection
DZ 98 MG	50	PE	soil mixture
DMDS 99 TC + DZ 98 MG	30 + 25	PE	chemigation + soil mixture
MB 98 TC	40	PE	gas distribution
control	–	–	–

[a]DMDS, dimethyl disulfide; DZ, dazomet; MB, methyl bromide; TC, technical; MG, microgranule. [b]PE, polyethylene film.

Soil temperatures (at 15 cm depth) were monitored only in the plots of DMDS plus DZ treatments using a data logger (XR440 Pocket Data logger, Pace Scientific, America) for the period from fumigant application to tarp removal.

Soil fungus populations [colony-forming units (cfu) g^{-1} soil] were determined after fumigation from soil samples at the depth of 0−20 cm from the soil surface. Soil from each plot was sampled from three spots along the diagonal line in a plot. Root-knot nematode population densities in the soil were determined after fumigation from the depth of 0−20 cm. Soil from each plot was taken from three spots as above. Soil fungi and root-knot nematode populations were determined using the same methods as in the laboratory studies.

Cucumber plant height was evaluated at 4 weeks after transplant (WAT) (20 plants per plot). Root galls were assessed at the end of the trials (20 plants per plot). Plants were rated on a 0−4 scale: 0 = 0%, 1 = 1−25%, 2 = 26−50%, 3 = 51−75%, 4 = 76−100% roots galled.[4] Cucumber fruit yields were determined after each harvest and summed together at the end of the trials, and the farmer's income was calculated.

Statistical Analyses.[7] *Laboratory Studies.* Nematode mortality was calculated according to the equation

$$X = \frac{N_1}{N_1 + N_2} \times 100 \quad (1)$$

where X is nematode mortality (%), N_1 is the number of dead nematodes, and N_2 is the number of live nematodes. The numbers of dead and live nematodes were counted under a dissecting microscope. When nematodes were found to be still, they were touched with a dissecting needle lightly. If they did not move, we considered them dead. Otherwise, we considered them to be living.

Corrected nematode mortality was calculated according to the equation

$$Y = \frac{X_1 - X_2}{100 - X_2} \times 100 \quad (2)$$

where Y is the corrected nematode mortality (%), X_1 is the nematode mortality of treatments (%), and X_2 is the nematode mortality of the control (%).

The efficacy of controlling fungi or weed seeds was calculated according to the equation

$$Y = \frac{X_1 - X_2}{X_1} \times 100 \quad (3)$$

where Y is the control efficacy on fungi or weed seeds, X_1 is the fungal population or weed height in the control, and X_2 is the fungal population or weed height in treated plots.

The control efficacy of the combination of DMDS and DZ was calculated according to the following equation based on the method described by Colby:[25]

$$E_0 = X_1X_2/100 \quad (4)$$

E_0 is the expected control efficacy of the combination, X_1 is the actual measured control efficacy of the first fumigant, and X_2 is the actual measured control efficacy of the second fumigant. E is the actual measured control efficacy of the combination. If $E > E_0$, the combination was synergistic; if $E < E_0$, the combination was antagonistic.

Greenhouse Trials. The efficacy of controlling nematode or fungi was calculated according to eq 3.

The root galling index was calculated according to the equation

$$Y = \frac{R_1 + R_2 + \ldots + R_x}{r \times x} \times 100 \quad (5)$$

where Y is the root galling index, R_x is the root galling scale of the xth plant, r is the highest root galling scale, and x is the total number of plants.

Data were analyzed for ANOVA with SAS (SAS, version 8.0 for Windows). Data for soil fungal and nematode populations were transformed as necessary [square root transformations for small numbers (<100) and $\log_{10}$ for large numbers (>100) for statistical analyses], but all data are reported as nontransformed values. Significant differences among means were determined by Fisher's LSD test at $P = 0.05$.[26,27]

RESULTS

Laboratory Studies. *Root-Knot Nematodes.* All four tested rates of DMDS plus DZ combination treatments exhibited a positive synergistic efficacy on root-knot nematodes (Table 4), reducing the numbers of *Meloidogyne* spp. by at least 83.18%. The highest dose tested in our study (40 + 100 mg kg^{-1}) reduced *Meloidogyne* spp. by 93.85%.

Soilborne Fungi. The four tested rates of DMDS plus DZ also showed positive synergistic efficacy on *Fusarium* spp. and *Phytophthora* spp. (Table 4). The levels of *Fusarium* spp. and *Phytophthora* spp. were reduced by at least 91.67 and 88.29%, respectively.

Weed. The four rates of DMDS plus DZ were all synergistic on *Abutilon theophrasti* and *Digitaria sanguinalis* (Table 4), reducing the weed levels by at least 95.98 and 99.64%, respectively.

Greenhouse Trials. *Soil Temperature.* Soil temperatures (at 15 cm depth) during fumigation were similar during trial I (in 2010) and trial II (in 2012) (31.1−37.8 and 31.2−39.4 °C, respectively) in the DMDS plus DZ plots.

Root-Knot Nematodes. The untreated controls in trial I (in 2010) and trial II (in 2012) were heavily infested by *Meloidogyne* spp. (Table 5). *Meloidogyne* spp. levels were significantly higher in the untreated control compared to all fumigant treatments. However, the results of almost all of the fumigant treatments were not significantly different from each other. Nematode levels in all chemical treatments were statistically the same as with MB.

The chemical treatments reduced the nematode levels in trials I and II by at least 81.01 and 94.79%, respectively. The DMDS plus DZ combination treatment reduced the nematode levels by 84.46 and 95.83% in trials I and II, respectively; both results were not significantly different from the MB treatment, but significantly different from the untreated control.

Soilborne Fungi. The untreated controls were heavily infested by *Fusarium* spp. and *Phytophthora* spp. in both trials (Table 5). *Fusarium* spp. and *Phytophthora* spp. levels were significantly higher in the untreated control compared to all fumigant treatments (Table 5).

All chemical treatments, except for the DZ treatment, reduced *Fusarium* spp. by at least 90.15 and 95.38% in trials I and II, respectively (Table 5). The DMDS plus DZ treatments reduced *Phytophthora* spp. by at least 88.66 and 97.61% in trials I and II, respectively (Table 5). The results of the DMDS plus DZ

Table 4. Laboratory Studies on the Efficacy of DMDS and DZ Treatments on Root-Knot Nematodes, Soilborne Fungi, and Weed Seeds

		% corrected nematode mortality				% control efficacy on *Fusarium* spp.				% control efficacy on *Phytophthora* spp.				% control efficacy on *Abutilon theophrasti*				% control efficacy on *Digitaria sanguinalis*			
treatment[a]	rate (mg ai kg^{-1} soil)	E^b	$E_0{}^c$	$E - E_0$	CE[d]	E	E_0	$E - E_0$	CE	E	E_0	$E - E_0$	CE	E	E_0	$E - E_0$	CE	E	E_0	$E - E_0$	CE
DMDS	20	57.13				58.65				54.68				76.14				75.65			
DMDS	40	77.91				98.80				68.33				94.76				99.65			
DZ	50	52.57				47.60				62.58				99.34				64.49			
DZ	100	74.66				80.05				79.87				100.00				92.28			
DMDS + DZ	20 + 50	83.18	30.03	53.15	+	91.67	37.22	52.79	+	88.29	34.22	54.07	+	95.98	75.64	20.34	+	99.64	48.79	50.85	+
DMDS + DZ	20 + 100	88.14	42.65	45.49	+	95.46	48.02	47.20	+	90.70	43.67	47.03	+	100.00	76.14	23.86	+	100.00	69.81	30.19	+
DMDS + DZ	40 + 50	87.31	40.96	46.35	+	100.00	48.56	45.11	+	93.29	42.76	50.53	+	100.00	94.13	5.87	+	100.00	64.26	35.74	+
DMDS + DZ	40 + 100	93.85	58.17	35.68	+	100.00	62.65	36.79	+	96.69	54.58	42.11	+	100.00	94.76	5.24	+	100.00	91.96	8.04	+
control																					

[a]DMDS, dimethyl disulfide; DZ, dazomet. [b]E = actual measured control efficacy of the combination. [c]E_0 = expected control efficacy of the combination [d]CE, combined efficacy; if $E - E_0 > 0$, CE was expressed as +; if $E - E_0 < 0$, CE was expressed as −; if $E - E_0 = 0$, CE was expressed as ±.

dx.doi.org/10.1021/jf501255w | J. Agric. Food Chem. 2014, 62, 4864−4869

Table 5. Effects of Soil Fumigation on Numbers of *Meloidogyne* spp. Recovered from 100 g of Soil and Colony-Forming Units (cfu) of *Fusarium* spp. and *Phytophthora* spp. on Selective Media of 1 g from Soil after Fumigation

				Meloidogyne spp.		*Fusarium* spp.		*Phytophthora* spp.	
trial	treatment[a]	rate (g ai m^{-2})	tarp type[b]	no./100 g	% reduction	cfu/g	% reduction	cfu/g	% reduction
trial I, 2010	DMDS	60	PE	7b[c]	96.55	40bc[c]	90.15	1380bc[c]	72.69
	DZ	50	PE	37b	81.01	120b	70.44	1847b	63.45
	DMDS + DZ	30 + 25	PE	30b	84.46	27c	93.43	573 cd	88.66
	MB	40	PE	13b	93.09	0c	100	120d	97.63
	control	–	–	193a	–	407a	–	5053a	–
trial II, 2012	DMDS	60	PE	7b	97.92	7c	98.46	40c	99.47
	DZ	50	PE	17b	94.79	87b	79.98	2420b	67.91
	DMDS + DZ	30 + 25	PE	13b	95.83	20bc	95.38	180c	97.61
	MB	40	PE	33b	98.96	0c	100	7c	99.91
	control	–	–	320a	–	433a	–	7540a	–

[a]DMDS, dimethyl disulfide; DZ, dazomet; MB, methyl bromide. [b]PE, polyethylene film. [c]In each column, data are means of three replications. Means followed by the same letter are not different ($P = 0.05$) according to the LSD test.

Table 6. Effect of Fumigation Treatments on the First Yield of Cucumber

trial	date	price (¥ kg^{1-})	treatment[a]	rate (g ai m^{-2})	tarp type[b]	yield (kg m^{-2})
trial I, 2010	Oct 6, 2010	2.2	DMDS	60	PE	0.12ab[c]
			DZ	50	PE	0.15a
			DMDS + DZ	30 + 25	PE	0.08b
			MB	40	PE	0.13ab
			control	–	–	0.02c
trial II, 2012	Oct 1, 2012	3.2	DMDS	60	PE	0.26a
			DZ	50	PE	0.21a
			DMDS + DZ	30 + 25	PE	0.20a
			MB	40	PE	0.19a
			control	–	–	0.03b

[a]DMDS, dimethyl disulfide; DZ, dazomet; MB, methyl bromide. [b]PE, polyethylene film. [c]In the column, data are means of three replications. Means followed by the same letter are not different ($P = 0.05$) according to the LSD test.

Table 7. Effect of Fumigation Treatments on Cucumber Plant Height, Root Galling Index, Yield, and Income

trial	treatment[a]	rate (g ai m^{-2})	tarp type[b]	plant height[c] (cm)	root galling Index[d] (%)	yield[e] (kg m^{-2})	income[f] (¥ m^{-2})
trial I, 2010	DMDS	60	PE	152.6b[g]	0.00b[g]	5.04b[g]	11.10b[g]
	DZ	50	PE	139.0b	12.50b	4.52c	9.01c
	DMDS + DZ	30 + 25	PE	179.5a	0.00b	5.47b	11.50b
	MB	40	PE	170.2a	0.00b	6.95a	15.68a
	control	–	–	67.8c	72.50a	2.63d	5.86d
trial II, 2012	DMDS	60	PE	168.4bc	0.00b	6.31a	19.65a
	DZ	50	PE	157.5c	1.25b	4.94b	15.79b
	DMDS + DZ	30 + 25	PE	184.3ab	2.50b	6.59a	20.52a
	MB	40	PE	196.1a	0.00b	5.95a	18.33ab
	control	–	–	123.6d	36.25a	3.48c	11.01c

[a]DMDS, dimethyl disulfide; DZ, dazomet; MB, methyl bromide. [b]PE, polyethylene film; WAT, weeks after transplant. [c]Collected at 4 WAT. [d]Collected at the end of the trials. [e]Collected at each harvest time and summed together at the end of the trials. [f]Collected at each harvest time and accumulated together at the end of the trials. [g]In each column, data are means of three replications. Means followed by the same letter are not different ($P = 0.05$) according to the LSD test.

treatments and MB treatments were not significantly different (Table 5).

First Cucumber Fruit Yield. The first cucumber fruit yield varied with fumigation treatment (Table 6). Cucumbers grown in the untreated plots had the lowest first fruit yield (0.02 and 0.03 kg m^{-2}, respectively) in both greenhouse trials (Table 6). This was statistically different from the first yield of all chemical treatments. In trial I, plots treated with DZ had the highest yield (0.15 kg m^{-2}), although this was not statistically different from most of the other chemical treatments except for the combination, DMDS plus DZ (Table 6). In trial II the highest first cucumber fruit yield was in the DMDS plot (0.26 kg m^{-2}), but this was not statistically different from all of the other chemical treatments (Table 6).

Cucumber Plant Height, Root Galling Index, Plant Mortality, Yield, and Income. Fumigation treatments significantly

dx.doi.org/10.1021/jf501255w | J. Agric. Food Chem. 2014, 62, 4864−4869

affected cucumber plant height at 4 WAT (Table 7) in the two greenhouse trials. Cucumber height was significantly higher in all chemical treatments compared with the untreated control. In both trials, the highest cucumber height was observed in plots treated with the DMDS plus DZ and MB treatments. Plant heights in all DMDS plus DZ treatments were taller than those in plots where DMDS and DZ were used alone, except for DMDS treatment in trial II (Table 7).

Nematode infestation was evaluated at the end of the trials by calculating the root galling index. Cucumbers grown in the untreated plots had the highest root galling indices (72.50 and 36.25% in trials I and II, respectively). The root galling index of each fumigant treatment was significantly different from the untreated control; however, there were no significant differences among the chemical treatments (Table 7).

Cucumber yield varied with the fumigation treatment (Table 7). Cucumbers grown in the untreated plots had the lowest yields (2.63 and 3.48 kg m^{-2}, respectively, in trials I and II) compared to the chemical treatments. In trial I, the highest cucumber yield was observed in plots treated with MB (6.95 kg m^{-2}), followed by DMDS plus DZ, DMDS, and DZ. The DMDS plus DZ cucumber yield was statistically the same as that of DMDS alone, but significantly higher than that of DZ. In trial II, plots treated with DMDS plus DZ produced the highest yield (6.59 kg m^{-2}), which was not significantly different from the MB and DMDS treatments, but significantly higher than for DZ alone and the untreated control.

Similarly, the farmer's income from cucumber production differed with fumigation treatment (Table 7). Cucumbers grown in the untreated plots provided the lowest income in both trials (5.86 and 11.01 ¥ m^{-2}, respectively). In trial I, the plots treated with MB gave the highest income (15.68 ¥ m^{-2}), followed by DMDS plus DZ, DMDS, and DZ. The DMDS plus DZ yield was statistically the same as that of DMDS alone, but significantly higher than that of DZ. In trial II, the plots treated with DMDS plus DZ gave the highest income (20.52 ¥ m^{-2}) followed by those of DMDS, MB, DZ, and the untreated control and were statistically the same as that of DMDS and MB treatments, but significantly higher than those of other treatments.

DISCUSSION

It has been reported that no single chemical or nonchemical method can exhibit the efficacy of MB currently.[28] However, three major alternatives for preplant soil treatment (1,3-D/Pic, Pic, and MNa) either alone or in combination with other alternatives are proving as effective as MB in many situations and continue to be widely adopted as key alternatives in many applications.[14] On the basis of our greenhouse results, the combination of DMDS plus DZ was as effective as MB in terms of increasing cucumber yields and income.

Root-knot nematode control with DMDS has been demonstrated to be as good as with MB in China and elsewhere,[10,11,29] and our present laboratory studies and greenhouse trials both confirmed this. However, most DMDS formulations have poor activity against soilborne fungi and ordinary activity against weeds, and both factors were also confirmed in our laboratory studies and greenhouse trials. DMDS therefore requires additional herbicidal and fungicidal activity to improve the control of weeds and soilborne fungi. DZ, a granular MITC generator, was reported to effectively control various soilborne pests (fungi, nematodes, soil insects, and weeds).[30−32] Through our laboratory studies, we found that DZ had high activity against weeds and ordinary activity against nematodes and soilborne fungi. The combined use of DMDS and DZ for broad-spectrum soil fumigation, therefore, was at least theoretically feasible. Laboratory studies found that the four tested rates of DMDS plus DZ all had positive synergistic effects on root-knot nematodes (*Meloidogyne* spp.), two key soilborne fungi (*Fusarium* spp. and *Phytophthora* spp.), and two major weed seeds (*Digitaria sanguinalis* and *Abutilon theophrasti*). The specific synergistic mechanism of DMDS plus DZ was not clear to us; however, the above laboratory results gave a preliminary indication of the feasibility of their combined application and also confirmed the synergistic activity of combinations of DMDS plus DZ reported by Van Wambeke.[17] Our greenhouse trials revealed that the combination of DMDS plus DZ applied to the greenhouse at the rate of 30 + 25 g m^{-2} successfully suppressed *Meloidogyne* spp. root galling, sharply reduced the colony-forming units (cfu) of *Fusarium* spp. and *Phytophthora* spp. on media, maintained high cucumber yields, and was not significantly different from MB at the dose of 40 g m^{-2}. The results of DMDS plus DZ were statistically similar to those of DMDS alone (at the dose of 60 g m^{-2}), but better than those of DZ alone (at the dose of 50 g m^{-2}). The above greenhouse results also confirmed that the combination of DMDS plus DZ is a good alternative to MB.

The simultaneous application of MNa and halogenated fumigants (e.g., Pic and 1,3-D) was found to accelerate the degradation of halogenated fumigants, reducing their availability in soil.[33,34] However, the combined application of DMDS plus DZ did not exhibit degradation according to the positive synergistic effects observed from the different rates tested in our laboratory. It has been reported that relatively high application rates may possibly mask degradation;[4] however, both high and low rates were tested in our laboratory studies.

In both trials, DZ alone showed lower efficacy in controlling soilborne fungi (Table 5) and a lower yield and income than the other fumigant treatments (Table 7) and gave significantly lower results than the DMDS plus DZ combination treatment and the MB treatment. However, in both trials DZ provided a high first yield of cucumber (Table 6), although this was not significantly different from other chemical treatments. The reason could be attributed to a stronger initial plant vigor resulting from the DZ treatment, whereas the DMDS plus DZ and MB treatments produced a higher yield by the end of the season because they reduced more soilborne fungi, and this effect could also be seen in the plant height at the end of both trials (Table 7).

In summary, the fumigant combination of DMDS plus DZ was generally as effective as MB in terms of controlling the numbers of soilborne fungi and nematodes and increasing cucumber yields and farmers' income. However, more detailed work on its precise application method (formulations and so on) is necessary before the combination is recommended as an efficient MB alternative for cucumber production in China.

AUTHOR INFORMATION

Corresponding Author

*(C.A.) Mail: Department of Pesticides, Institute of Plant Protection, Chinese Academy of Agricultural Sciences, Beijing 100193, People's Republic of China. Phone: +8610-62815940. Fax: +8610-62894863. E-mail: caoac@vip.sina.com.

Funding

This research was supported by the Program on Substituted Technology for Methyl Bromide in China (Special Finance of Chinese Ministry of Agriculture, 2110402) and UNDIO Project on Phasing-out of Methyl Bromide in Agriculture Sector in China (TF/CPR-A/08/003).

Notes

The authors declare no competing financial interest.

■ ACKNOWLEDGMENTS

We thank Dr. Melanie Miller for editing the manuscript.

■ REFERENCES

(1) Giannakou, I.; Anastasiadis, I. Evaluation of chemical strategies as alternatives to methyl bromide for the control of root-knot nematodes in greenhouse cultivated crops. *Crop Prot.* **2005**, *24*, 499−506.

(2) Cao, A. Project background. In *Screening of the Alternatives to Methyl Bromide in Soil Fumigation in China*; Cao, A., Duan, X., Yuan, H., Eds.; China Agriculture University Press: Beijing, China, 2003; pp 1−8.

(3) Bell, C. H. Fumigation in the 21st century. *Crop Prot.* **2000**, *19*, 563−569.

(4) Desaeger, J. A.; Seebold, K. W.; Csinos, A. S. Effect of application timing and method on efficacy and phytotoxicity of 1,3-D, chloropicrin and metam-sodium combinations in squash plasticulture. *Pest Manage. Sci.* **2008**, *64*, 230−238.

(5) Giannakou, I. O.; Anastasiadis, I. Evaluation of chemical strategies as alternatives to methyl bromide for the control of root-knot nematodes in greenhouse cultivated crops. *Crop Prot.* **2005**, *24*, 499−506.

(6) Qiao, K.; Shi, X.; Wang, H.; Ji, X.; Wang, K. Managing root-knot nematodes and weeds with 1,3-dichloropropene as an alternative to methyl bromide in cucumber crops in China. *J. Agric. Food Chem.* **2011**, *59*, 2362−2367.

(7) Mao, L.; Wang, Q.; Yan, D.; Xie, H.; Li, Y.; Guo, M.; Cao, A. Evaluation of the combination of 1,3-dichloropropene and dazomet as an efficient alternative to methyl bromide for cucumber production in China. *Pest Manage. Sci.* **2012**, *68*, 602−609.

(8) Qiao, K.; Dong, S.; Wang, H.; Xia, X.; Ji, X.; Wang, K. Effectiveness of 1,3-dichloropropene as an alternative to methyl bromide in rotations of tomato (*Solanum lycopersicum*) and cucumber (*Cucumis sativus*) in China. *Crop Prot.* **2012**, *38*, 30−34.

(9) Gilreatha, J. P.; Nolingb, J. W.; Santosa, B. M. Methyl bromide alternatives for bell pepper (*Capsicum annuum*) and cucumber (*Cucumis sativus*) rotations. *Crop Prot.* **2004**, *23*, 347−35.

(10) Santos, B. M.; Lopez-Aranda, J. M.; Miranda, L.; Medina, J. J.; Soria, C.; de los Santos, B.; Romero, F.; Perez-Jimenez, R. M.; Talavera, M.; Fennimore, S. A. Methyl bromide alternatives for high tunnel strawberry production in southern Spain. *HortTechnology* **2009**, *19*, 187−192.

(11) De Cal, A.; Martinez-Treceño, A.; Lopez-Aranda, J. M.; Melgarejo, P. Chemical alternatives to methyl bromide in Spanish strawberry nurseries. *Plant Dis.* **2004**, *88*, 210−214.

(12) Gilreath, J.; Santos, B.; Busacca, J.; Egerjr, J.; Gilreath, P. Validating broadcast application of Telone C-35 complemented with chloropicrin and herbicides in commercial tomato farms. *Crop Prot.* **2006**, *25*, 79−82.

(13) Minuto, A.; Gullino, M.; Lamberti, F.; Daddabbo, T.; Tescari, E.; Ajwa, H.; Garibaldi, A. Application of an emulsifiable mixture of 1,3-dichloropropene and chloropicrin against root knot nematodes and soilborne fungi for greenhouse tomatoes in Italy. *Crop Prot.* **2006**, *25*, 1244−1252.

(14) UNEP. *Report of the Methyl Bromide Technical Options Committee, in 2010 Assessment*; United Nations Environment Programme: Nairobi, Kenya, 2010; pp 101−158.

(15) Santos, B. M.; Gilreath, J. P.; Motis, T. N.; Noling, J. W.; Jones, J. P.; Norton, J. A. Comparing methyl bromide alternatives for soilborne disease, nematode and weed management in fresh market tomato. *Crop Prot.* **2006**, *25*, 690−695.

(16) Van Wambeke, E. Combinations of reduced rates of 1,3-dichloropropene and dazomet as a broad spectrum soil fumigation strategy in view of methyl bromide replacement. *Commun. Agric. Appl. Biol. Sci.* **2007**, *72*, 61−70.

(17) Van Wambeke, E.; Ceustermans, A.; De Landtsheer, A.; Coosemans, J. Combinations of soil fumigants for methyl-bromide replacement. *Commun. Agric. Appl. Biol. Sci.* **2009**, *74*, 75−84.

(18) Schinner, F.; Öhlinger, R.; Kandeler, E.; Margesin, R. *Methods in Soil Biology*; Springer Verlag: Berlin, Germany, 1995; pp 386−389.

(19) Nelson, D. W.; Sommers, L. E. Total carbon, organic carbon and organic matter. In *Methods of Soil Analysis*; Page, A. L., Miller, R. H., Keency, O. R., Eds.; American Society of Agronomy: Madison, WI, USA, 1985; pp 539−576.

(20) Margesin, R.; Schinner, F. *Manual for Soil Analysis − Monitoring and Assessing Soil Bioremediation*; Springer Verlag: Berlin, Germany, 2005; pp 47−49.

(21) Klose, S.; Acosta-Martínez, V.; Ajwa, H. A. Microbial community composition and enzyme activities in a sandy loam soil after fumigation with methyl bromide or alternative biocides. *Soil Biol. Biochem.* **2006**, *38*, 1243−1254.

(22) Komada, H. Development of a selective medium for quantitative isolation of *Fusarium oxysporum* from natural soil. *Rev. Plant Prot. Res.* **1975**, *8*, 114−125.

(23) Masago, H.; Yoshikawa, M.; Fukada, M.; Nakanishi, N. Selective inhibition of *Pythium* spp. on a medium for direct isolation of *Phytophthora* spp. from soils and plants. *Phytopathology* **1977**, *67*, 425−428.

(24) Liu, W. *Plant Pathogenic Nematodes*; China Agriculture Press: Beijing, China, 2000; p 373.

(25) Colby, S. R. Calculating synergistic and antagonistic responses of herbicide combinations. *Weeds* **1967**, *15*, 20−22.

(26) Steel, R. G. D.; Torrie, J. H. *Principles and Procedures of Statistics*; McGraw-Hill Book: New York, 1960; p 481.

(27) Csinos, A. S.; Johnson, W. C.; Johnson, A. W.; Sumner, D. R.; McPherson, R. M.; Gitaitis, R. D. Alternative fumigants for methyl bromide in tobacco and pepper transplant production. *Crop Prot.* **1997**, *16*, 585−594.

(28) Yates, S. R.; Gan, J.; Papiernik, S. K.; Dungan, R.; Wang, D. Reducing fumigant emissions after soil application. *Phytopathology* **2002**, *92*, 1344−1348.

(29) Song, Z.; Wang, Q.; Guo, M.; Zhao, Y.; Cao, A. Assessment on dimethyl disulfide as a soil fumigant. *Agrochemicals* **2008**, *47*, 454−456.

(30) Saeed, I. A. M.; Rouse, D. I.; Harkin, J. M.; Smith, K. P. Effects of soil water content and soil temperature on efficacy of metham-sodium against *Verticillium dahliae*. *Plant Dis.* **1997**, *81*, 773−776.

(31) Di Primo, P. Accelerated degradation of metam-sodium and dazomet in soil: characterization and consequences for pathogen control. *Crop Prot.* **2003**, *22*, 635−646.

(32) Frick, A.; Zebarth, B. J.; Szeto, S. Y. Behavior of the soil fumigant methyl isothiocyanate in repacked soil columns. *J. Environ. Qual.* **1998**, *27*, 1158−1169.

(33) Guo, M.; Yates, S. R.; Papiernik, S. K.; Zheng, W. Incompatibility of metam sodium with halogenated fumigants. *Pest Manage. Sci.* **2005**, *61*, 467−476.

(34) Zheng, W.; Yates, S. R.; Guo, M.; Papiernik, S. K.; Kim, J. H. Transformation of chloropicrin and 1,3-dichloropropene by metam sodium in a combined application of fumigants. *J. Agric. Food Chem.* **2004**, *52*, 3002−3009.

JOURNAL OF AGRICULTURAL AND FOOD CHEMISTRY

Article

pubs.acs.org/JAFC

A Novel Single-Labeled Fluorescent Oligonucleotide Probe for Silver(I) Ion Detection in Water, Drugs, and Food

Liujiao Bian,*[,†] Xu Ji,[†] and Wei Hu[‡]

[†]College of Life Science, Northwest University, Xi'an, Shaanxi 710069, China

[‡]Emergency Department, Shaan'xi Provincial People's Hospital, Xi'an, Shaanxi 710068, China

Supporting Information

ABSTRACT: Due to the high toxicity of silver(I) ions, a method for the rapid, sensitive, and selective detection for silver(I) ions in water, pharmaceutical products, and food is of great importance. Herein, a novel single-labeled fluorescent oligonucleotide (OND) probe based on cytosine−Ag(I)−cytosine coordination and the inherent fluorescence quenching ability of the G-quadruplex is designed to detect silver(I) ions. The formation of a hairpin structure in the OND−Ag(I) complex brings the hexachloro fluorescein (HEX) labeled at the 5′-end of the OND probe close to the G-quadruplex located at the 3′-end of the OND probe, leading to a fluorescence quenching due to photoinduced electron transfer between HEX and the G-quadruplex. Through this method, silver(I) ions can be detected quantitatively, the linear response range is from 1 to 100 nmol/L with a detection limit of 50 pmol/L, and no obvious interference occurs with other metal ions with a 10-fold concentration. This assay is simple, sensitive, and selective, and it can be used to detect silver(I) ions in actual water, drug, and food samples.

KEYWORDS: *silver(I) ions, detection, fluorescent oligonucleotide probe, hexachloro fluorescein, G-quadruplex*

INTRODUCTION

Silver(I) ions are one of the most important bioactive cations. They exhibit low toxicity to living beings within the scope of the low concentration while high toxicity in high concentration range. For example, under a low concentration range, silver(I) ions have long been known to have strong inhibitory and bactericidal effects as well as a broad spectrum of antimicrobial activities. They have a microbicidal (germicidal and bacteriostatic) effect in drinking water, enabling it to be disinfected and conserved. The recommended and maximum quantities of silver(I) ions in drinking water are usually limited to a concentration of 100 μg/L. In both the United States (United States Environmental Protection Agency, secondary drinking water regulation) and Australia (National Health and Medical Research Council), the recommended value is 100 μg/L. In Germany (Current German Drinking Water Ordinance, TrinkwV 2001), the statutory limit is 100 or 80 μg/L depending on the treatment substances and disinfecting processes. Whereas in a high concentration area, a high dose of silver(I) ions has been found to be highly toxic to aquatic organisms and humans owing to the fact that silver(I) ions have a high affinity to sulfhydryl groups and amino groups and thereby form some harmful complexes with amino acids, nucleic acids, and other compounds in the body. For example, exposed to a high dose of silver nitrate, sodium/potassium ATPase, which regulates the level of potassium and sodium ions in fish and zooplankton, was seriously interfered with the silver(I) ions. In addition, silver(I) ions are the most common pollution cations and one of the main toxic substances in the field of agriculture and food. Through polluted water sources, such as river water for irrigation and lake or seawater for aquiculture, they can accumulate to the seed of crops and fruits and the body of aquatic organisms, and thereby enter the food chain of humans. Therefore, it is very important to monitor the content level of silver(I) ions in aquicolous ecosystems and the human food chain.[1,2]

To date, several methods including colorimetric analysis,[3] atomic absorption/emission spectroscopy,[4−7] inductively coupled plasma−mass spectrometry,[8,9] surface-enhanced Raman scattering,[10] ion-selective electrodes[11] and quantum dots,[12,13] and so forth[14] have been established to detect trace level of silver(I) ions in aqueous media, and a lot of efforts has also been made to develop fluorescent chemosensors, but there are only a few successful examples for silver(I) ion detection.[15−18] In view of the interaction between metal ions and nucleic acids, some oligonucleotide (OND)-based metal ion detection method had been established,[19−26] for example, on the basis of the fact that silver(I) ions are capable of coordinating cytosine bases (C) to form a stable C−Ag(I)−C complex, leading to the development of a silver(I) ion sensor.[27−32]

As illustrated in Scheme 1a, in the absence of Ag(I) ions, two separate C-rich ssDNA separately form a random coil. However, in the presence of Ag(I) ions, the Ag(I) ions bind directly to N3 of cytosine in place of the imino proton and bridge two cytosine residues in two separate C-rich ssDNA to form the C−Ag(I)−C complexes. By applying this principle, Tanaka et al. have developed a fluorescent C-rich OND probe for silver(I) ion detection with a fluorescent dye and a quencher at its 3′- and 5′-ends, respectively.[28] Qu et al.[33] and Fan et al.[34] separately developed a single-labeled fluorescent OND probe for silver(I) ion detection by employing a single-walled carbon nanotube or graphene as an extra nanoquencher.

Received: October 29, 2013
Revised: April 29, 2014
Accepted: May 1, 2014
Published: May 1, 2014

ACS Publications © 2014 American Chemical Society

Scheme 1. Schematic Illustration of the Formation of Cytosine−Ag(I)−Cytosine Complexes

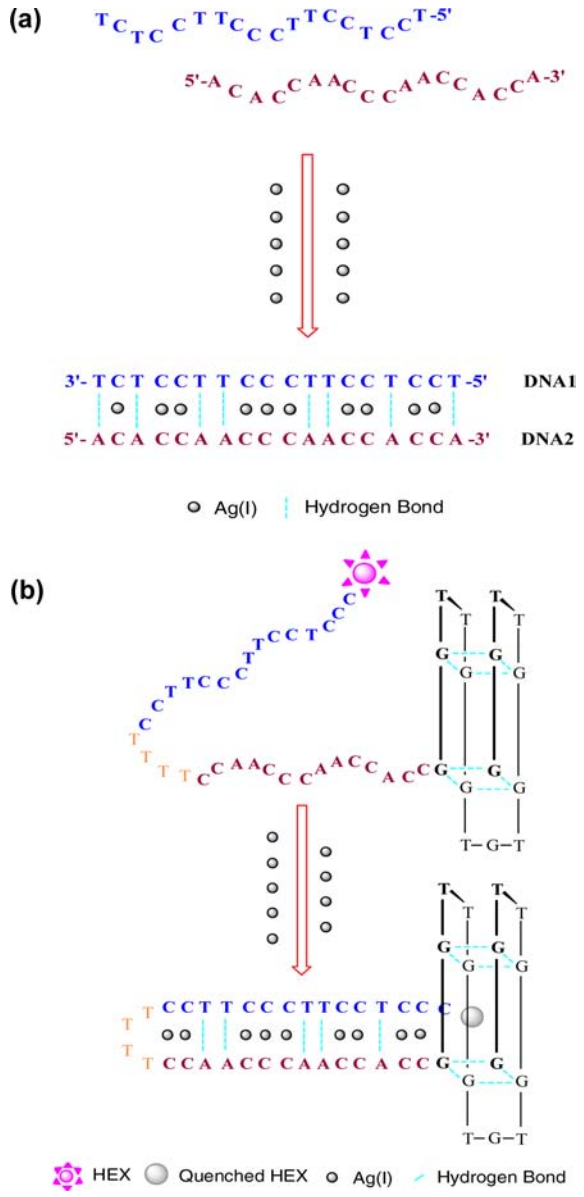

Sun et al. designed a single-labeled fluorescent OND probe for silver(I) ion detection based on the inherent quenching ability of deoxyguanosines,[35] and Luo et al. also developed a dual-output fluorescent DNA sensor for silver(I) ion and cysteine detection.[36]

Through intramolecular hydrogen-bonding interaction, a guanine base (G)-rich single-stranded DNA can form a specific secondary structure named the G-quadruplex that can serve as a very good electron donor and an extraordinary quencher for a variety of fluorescent groups due to its high density of guanosine stacking and low oxidation potential (1.25 V vs SCE).[37] Therefore, a resonant energy transfer or photoinduced electron transfer may take place between it and the fluorescent groups,[35,38] leading to the significant fluorescence quenching of the fluorescent groups in the excited state.[39]

In this work, we develop a novel single-labeled fluorescent OND probe for the sensitive and selective detection of silver(I) ions in aqueous solution based on the C−Ag(I)−C coordination and the inherent quenching ability of the G-quadruplex. In this fluorescent OND probe, a G-quadruplex (5′-GGTTGGTGTGGTTGG-3′) was designed to follow a C-rich OND (5′-CCCTCCTTCCCTTCCTTTTCCAACC-CAACCACC-3′) and a fluorescein-based dye, hexachloro fluorescein (HEX), was labeled at the 5′-end of the C-rich OND. In the presence of silver(I) ions, the C−Ag(I)−C coordination induced the labeled C-rich OND to fold into a hairpin structure that brings the fluorescent termini HEX close to the G-quadruplex, resulting in a significant fluorescence quenching of the fluorescent termini HEX owning to photoinduced electron transfer between HEX and the G-quadruplex.[40]

MATERIALS AND METHODS

Chemicals. The single-labeled fluorescent OND probe (5′-HEX-CCCTCCTTCCCT-TCCTTTTCCAACCCAACCACCGGTT-GGTGTGGTTGG-3′) was chemically synthesized by Takara Biotechnology Co. Ltd. (Dalian, China) and purified by high-performance liquid chromatography. DNA concentration was estimated by measuring the absorbance at 260 nm. 3-(*N*-Morpholino) propanesulfonic acid (MOPS) was purchased from Sigma−Aldrich Inc. (Shanghai, China). $AgNO_3$, $Ni(NO_3)_2$, $CoSO_4$, $CdSO_4$, $Cu(NO_3)_2$, $Hg(NO_3)_2$, $Mn(NO_3)_2$, $Ca(NO_3)_2$, $ZnSO_4$, $Pb(NO_3)_2$, $Mg(NO_3)_2$, $FeSO_4$, $Fe_2(SO_4)_3$, $NaNO_3$, KNO_3, KF, and $KClO_4$ were analytical grade without further purification. All the fluorescent OND probe solutions (20.0 nmol/L) and silver(I) ion solutions were prepared with 10.0 mmol/L MOPS buffer (containing 400.0 mmol/L $NaNO_3$ and 20.0 mmol/L KNO_3, pH 7.0) and stored in brown reagent bottles. The ultrapure water (18.2 MΩ·cm) was purified by a Millipore ultrapure water system.

Tap water and wastewater samples were separately taken from a household water pipe and wastewater storage tank in our laboratory. River water sample was collected from the Wei River near Xi'an. "Yin-Xin-Shuang" silver−zinc emulsion (approval no.: Henan health and diminish inflammation (2000) 0129, batch no.: 110606) and "Hong-Gao-Yao" red ointment (approval no.: Hubei pharmacy (2001) CX02-017, batch no.: 120425) are both typical ointment agents. "Bi-Luo-Chun" green tea (Tianfu Tea Industry Co., Ltd., batch no.: 20120812) and bean sprout were purchased from Walmart supermarket in Xi'an, China.

Fluorescence Emission Spectra. A 10 μL amount of 1.0 mmol/L fluorescent OND probe was first added to 490 μL of MOPS buffer and incubated at 95 °C for 10 min in order that the secondary structure of the OND was completely unwinded. Then, the mixed solution was naturally cooled down to 25 °C and was incubated overnight. The incubated solution was then transferred into a cuvette, and its fluorescent emission was scanned at 25 °C under the wavelength range 540−630 nm. The final solution contains 10.0 mmol/L MOPS, 400.0 mmol/L $NaNO_3$, and 20.0 mmol/L KNO_3 (pH 7.0), and its total volume is 500 μL. The concentration of the fluorescent OND probe is 20.0 nmol/L. After that, 1.0 μL of silver(I) ion solution with different concentrations was separately added to the above solution at 25 °C, and their fluorescent emissions were scanned under the same conditions. Fluorescent emission spectra were recorded on a Hitachi F-4500 fluorescence spectrophotometer (Hitachi Corporation, Japan). The instrument parameters were as follows: excitation wavelength, 520 nm; emission wavelength, 556 nm; excitation and emission slits, 10 nm; temperature, 25 °C.

Ultraviolet−Visible Absorbance Spectra. All the UV−visible (UV−vis) absorbance spectra were recorded on a Shimadzu UV-2450 spectrophotometer.

Detection of Silver(I) Ions. To verify the application of this method in actual samples, we determined the silver(I) ions in a tap water sample, a wastewater sample, a river water sample, two drug samples, and two food samples.

For the water sample detection, all the tap water, wastewater, and river water samples were filtered through a 0.22 μm membrane before testing. A 400 μL amount of MOPS buffer containing fluorescent

dx.doi.org/10.1021/jf404792z | J. Agric. Food Chem. 2014, 62, 4870−4877

OND probe was first incubated at 95 °C for 10 min in order that the secondary structure of the fluorescent OND probes was completely unwinded. Then, the solution was naturally cooled down to 25 °C and was incubated overnight. After that, 100 μL of different water samples were separately mixed with the incubated solution at 25 °C, and their fluorescence responses were monitored under the experimental conditions as described above. All of the final mixed solutions contain 10.0 mmol/L MOPS, 400.0 mmol/L $NaNO_3$, and 20.0 mmol/L KNO_3 (pH 7.0), and their total volumes are 500 μL. The final concentration of the fluorescent OND probe is 20.0 nmol/L, and the dilution factor is 4.0.

For the drug sample detection, about 1.0 g of the above silver−zinc cream or red ointment was accurately weighed and put in a small digestion flask, 4 mL of nitric acid was added to the digestion flask, and it was heated in order that the drug sample was fully digested. After complete digestion, the drug sample solution was transferred into a volumetric flask and diluted to 10 mL with MOPS buffer. Then, the digested sample was diluted to a proper proportion with MOPS buffer, and its fluorescence response was monitored under the test conditions as the determination of water samples.

For the tea and bean sprout sample detection, a porcelain crucible was first heated and cleaned for about 30 min on an electric furnace with a volume ratio of 1:4 hydrochloric acid solution; then, the porcelain crucible was rinsed three times with pure water and laid in a constant temperature box for drying. About 2.0 g of the tea or bean sprout sample was accurately weighed and put in the above porcelain crucible, the porcelain crucible was laid on an electric furnace making the sample be fully carbonized at low temperature until white smoke disappeared, and then, the porcelain crucible was placed into a muffle furnace at 520 °C for about 6 h in order that the sample was fully ashed. After that, it was cooled, 5 mL of 1:1 nitric acid solution was added to the porcelain crucible, and it was placed on a boiling water bath until the sample solution was fully dried. A 9 mL amount of distilled water and 1 mL of 2.0 mol/L nitric acid were added in the porcelain crucible, and it was heated at about 95 °C for 10 min. The sample solution was cooled and transferred into a 50 mL volumetric flask. The porcelain crucible was washed two times with MOPS buffer, the washes were collected into the volumetric flask, the sample solution was diluted to 50 mL with MOPS buffer, and it was mixed evenly. Finally, the sample solution was diluted to a proper proportion with MOPS buffer, and its fluorescence response was monitored under the experimental conditions as the determination of water samples.

RESULTS AND DISCUSSION

Fluorescence Quenching of the Fluorescent OND Probe. On the basis of the C−Ag(I)−C coordination and the inherent quenching ability of the G-quadruplex, a schematic diagram to illustrate the single-labeled fluorescent OND probe for silver(I) ion detection is shown in Scheme 1b. In the absence of silver(I) ions, the fluorescent HEX−OND probes form a random coil, which separates the fluorescent dye HEX and the G-quadruplex from each other, and hence, the fluorescent dye HEX exhibits strong fluorescence emission. However, in the presence of silver(I) ions, the silver-mediated base pairs are formed between cytosine residues in the fluorescent HEX−OND probes, leading to a hairpin structure. The fluorescent dye HEX and the G-quadruplex are close to each other upon formation of the hairpin structure, leading to the significant fluorescence quenching of the fluorescent dye HEX in the fluorescent HEX−OND probes.

Under the induction of different concentrations of silver(I) ions, the fluorescence quenching effect of the fluorescent HEX−OND probes was determined (Figure 1). In the absence of silver(I) ions, the fluorescent HEX−OND probes exhibit strong fluorescence emission at 556 nm, which can be attributed to the presence of the fluorescein-based dye HEX (curve a). When the molar ratios of Ag(I) to the HEX−OND probe increase from 5:1 (curve b) to 250:1 (curve d), the fluorescence quenching degree of the HEX−OND probes increases from 45% to 82%, indicating that the G-quadruplex at the 3′-end of the HEX−OND probe can quench the fluorescence of the fluorescent dye HEX labeled at the 5′-end of the HEX−OND probe. This observation also provides clear evidence to support the Ag(I)-induced formation of double helical structure.[25,33,35,36] In addition, a further experiment shows that there is no further decrease of the fluorescence intensity when the concentration of silver(I) ions is higher than 5 μmol/L, indicating the interaction between the HEX−OND probe and the silver(I) ions reaches a dynamic equilibrium.

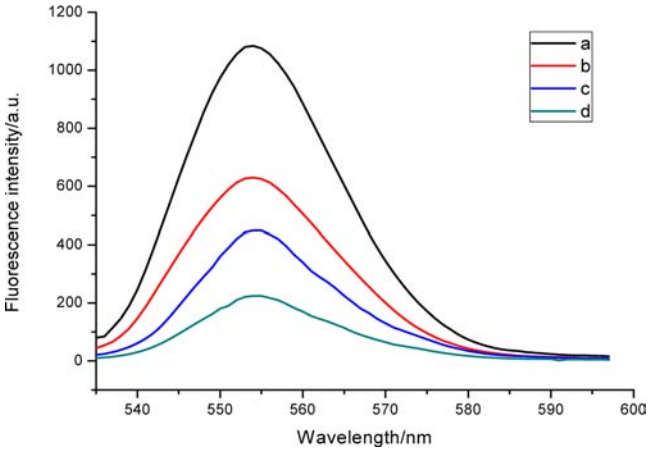

Figure 1. Fluorescence quenching of the HEX−OND probes under the induction of silver(I) ions. (a) HEX−OND probe (20.0 nmol/L); (b) HEX−OND probe (20.0 nmol/L) + Ag(I) (0.10 μmol/L); (c) HEX−OND probe (20.0 nmol/L) + Ag(I) (1.0 μmol/L); (d) HEX−OND probe (20.0 nmol/L) + Ag(I) (5.0 μmol/L). All measurements were performed in 10.0 mmol/L MOPS buffer (containing 400.0 mmol/L $NaNO_3$ and 20.0 mmol/L KNO_3, pH 7.0).

The analytical methods based on oligonucleotide probes modified with quenchers and fluorescent dyes required efficient quenching ability of quenchers. Although the fluorescence of fluorescent dyes could be quenched by the interaction between the dyes and guanosines, the quenching ability of guanosine itself was not enough to meet the need of a highly sensitive assay.[33,36] Therefore, as an effective way, the sensitivity can be improved by enhancing the quenching efficiency of the quenchers.

It has been reported that guanosine-rich tracts of nucleic acids could form four-stranded structure under appropriate condition of high sodium or potassium ionic strength. Four guanine bases can associate through Hoogsteen hydrogen bonding to form a square planar structure called a guanine tetrad, and two or more guanine tetrads can stack on top of each other to form a G-quadruplex. The quadruplex structure can be further stabilized by the presence of a cation, especially sodium or potassium, which sits in a central channel between each pair of tetrads.[41] As a structure with high density of guanosine stacking, the G-quadruplex has very good electron-donating property and extraordinary quenching ability. Therefore, it is used here as a convenient and robust tool to quench the fluorescence of fluorescent dyes.[42,43]

Fluorescence Quenching Mechanism. In order to further understand the quenching information in this Ag(I) detection method, the fluorescence spectra of HEX and UV−vis absorption spectra of HEX-labeled OND were investigated

dx.doi.org/10.1021/jf404792z | J. Agric. Food Chem. 2014, 62, 4870−4877

on addition of Ag(I) ions, and the results were listed as follows: First, by investigating the effect of Ag(I) on the HEX, it is found that the Ag(I) ions cannot quench the fluorescence of HEX under the same experimental conditions (Figure S1, Supporting Information). Second, in the presence of Ag(I) ions, no new absorption band occurred in the UV−vis absorption spectra of HEX-labeled OND, and almost no visible shift appeared in its maximum absorption (Figure S2, Supporting Information), which implied that there existed no ground-state complexes formed during the detection process.[40,44−46] Third, the absorption band of the HEX-labeled OND probe with the addition of Ag(I) ions ranging from 240 to 300 nm (Figure S2, Supporting Information) does not overlap with the emission spectra of HEX ranging from 530 to 580 nm (Figure 1), indicating the energy transfer could be neglected during the fluorescence quenching procedure.

Actually, it has been widely reported that the fluorescence of many fluorescent dyes including fluorescein and HEX that is a derivative of fluorescein are quenched by the interaction between the dyes and guanines, and this phenomenon is demonstrated to involve a photoinduced electron transfer mechanism.[35,36,40,47−49] For that reason, the fluorescence quenching in this work by the interaction between HEX and the G-quadruplex that is the guanosine stacking is also caused by the photoinduced electron transfer mechanism like the previously works mentioned.

Optimization of Detection Conditions. (i) pH. HEX belongs to a fluorescein-based dye. Although the fluorescence emission of HEX is relatively insensitive to pH compared with that of fluorescein, it can be still influenced by pH within a wider pH range. Therefore, we determined the fluorescence intensities of the HEX−OND probes and the OND−Ag(I) complexes over a pH range 4−10. As shown in Figure 2, a decreased pH leads to a decreased fluorescence intensity of the HEX−OND probes; meanwhile, as the silver(I) ions can form complex compounds or precipitates in alkaline conditions, when pH is higher than 7.0, the response of the HEX−OND probes to silver(I) ions becomes poorer and poorer with the increased pH. Therefore, all the experiments were performed in neutral condition.

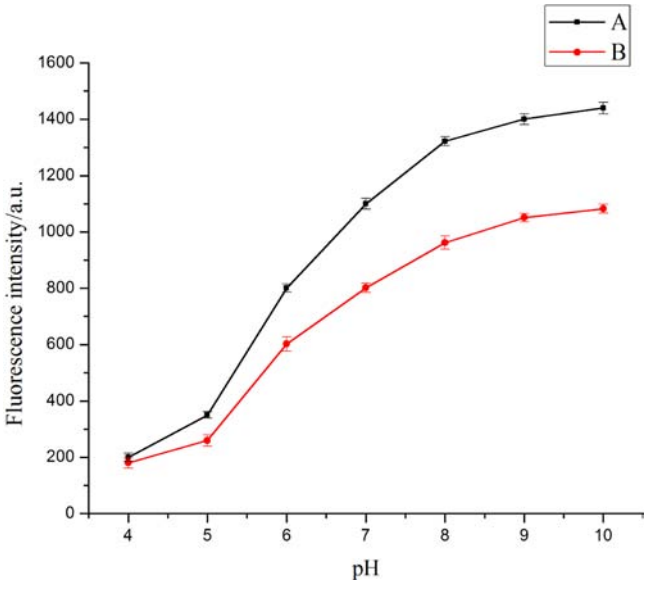

Figure 2. Fluorescence intensities of the HEX−OND probes and OND−Ag(I) complexes at different pH values. (A) HEX−OND probe (20.0 nmol/L); (B) HEX−OND probe (20.0 nmol/L) + Ag(I) (0.10 μmol/L). All measurements were performed in 10.0 mmol/L MOPS buffer (containing 400.0 mmol/L $NaNO_3$ and 20.0 mmol/L KNO_3) with different pH values.

(ii) Concentration of sodium nitrate. In the DNA hybridization system, ionic strength has an important influence on the stability and sensitivity of the molecular probes. Therefore, we further investigated the fluorescence quenching of the HEX−OND probes in the presence of 0.0−1.0 mol/L sodium nitrate (Figure 3). The quenching effect was evaluated with

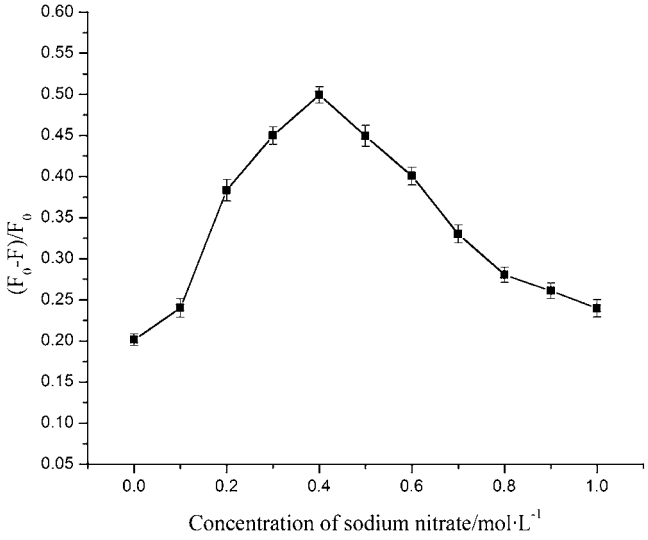

Figure 3. Fluorescence quenching extent of the HEX−OND probes in the presence of different concentrations of sodium nitrate. Concentrations of the HEX−OND probes and silver(I) ions were 20.0 nmol/L and 0.10 μmol/L, respectively. All measurements were performed in 10.0 mmol/L MOPS buffer (containing 20.0 mmol/L KNO_3, pH 7.0) with different concentrations of sodium nitrate ranging from 0.0 to 1.0 mol/L.

fluorescence quenching extent $(F_0 - F)/F_0$, where F_0 is the initial fluorescence intensity of the HEX−OND probes and F is the fluorescence intensity in the presence of 100.0 nmol/L silver(I) ions. The results show that, in the concentration of sodium nitrate ranging from 0 to 0.40 mol/L, the fluorescence quenching extents of the HEX−OND probes increase with the rising of the sodium nitrate concentrations, whereas under the concentration range 0.40−1.0 mol/L, they decrease as the concentrations of sodium nitrate increase. The highest fluorescence quenching extent (about 50%) occurs at 0.40 mol/L sodium nitrate. Therefore, we selected 0.40 mol/L as the optimum concentration of sodium nitrate.

(iii) Reaction time. In all of the above experiments, the measurement procedures were carried out right after the addition of the silver(I) ions into the HEX−OND probe solution, and the involvement of longer incubation times does not result in an observable increase in the fluorescence emission, indicating that the process of detection is very fast.

Establishment of Detection Method. (i) Sensitivity. To evaluate the sensitivity of this detection system, as shown in Figure 4, we further determined the fluorescence emission spectra of the HEX−OND probes in the presence of different concentrations of silver(I) ions ranging from 0.002 to 5 μmol/L under the above optimum condition. The results show that the fluorescence intensity of the HEX−OND probes is very

dx.doi.org/10.1021/jf404792z | J. Agric. Food Chem. 2014, 62, 4870−4877

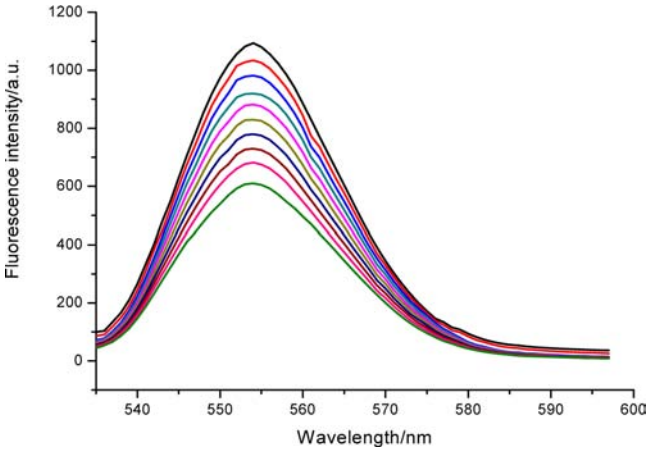

Figure 4. Fluorescence emission spectra of the HEX−OND probes in the presence of different concentrations of silver(I) ions. From top to bottom, the concentrations of silver(I) ions were 0, 0.002, 0.005, 0.008, 0.010, 0.020, 0.040, 0.060, 0.080, and 0.10 μmol/L, respectively. The concentration of the HEX−OND probe was 20.0 nmol/L. All measurements were performed in 10.0 mmol/L MOPS buffer (containing 400.0 mmol/L $NaNO_3$ and 20.0 mmol/L KNO_3, pH 7.0).

sensitive to silver(I) ions and steadily decreases as the concentrations of silver(I) ions increase from 0.002 to 5 μmol/L.

(ii) Selectivity. As shown in Figure 5a, b, the selectivity of the HEX−OND probes for Ag(I) detection was first examined with a variety of environmentally relevant metal ions including Mg(II), Mn(II), Ca(II), Cd(II), Cu(II), Hg(II), Zn(II), Fe(II), Co(II), Ni(II), Pb(II), and Fe (III) ions. Figure 5a shows the difference in the fluorescence intensity between the blank and solutions containing 1.0 μmol/L silver(I) ions and other metal ions, and Figure 5b shows the influence of these metal ions with a 10-fold concentration on the selectivity of the HEX−OND probes. The results show that, in the latter case, although the HEX−OND probes produce slightly bigger fluorescence difference than that observed at 1.0 μmol/L, the use of silver(I) ions still gives the best result. In addition, from Figure 5a, b, it can be also found that Co(II) ion is the most significant interference metal ion for Ag(I) detection. This may be due to the fact that Co(II) ion has strong binding ability with the guanine bases in DNA.[50] Then, the selectivity of the probes was examined with some environmentally relevant acid radical anions. In aqueous solution, free silver(I) ions exist mainly in the form of soluble nitrate. In addition to the limited kinds of anions, such as NO_3(I), F(I), and ClO_4(I), most of the anions, such as Cl(I), Br(I), I(I), S(II), SO_3(II), SO_4(II), CO_3(II), PO_4(III), C_2O_4(II), Ac(I), AsO_4(III), BrO_3(II), CN(I), and SCN(I), can combine with the free silver(I) ions to form insoluble or slightly soluble precipitates. Therefore, when the latter anions exist in solution, the fluorescence quenching process established in this work will not be performed due to the strong complexation of these anions to the silver(I) ions. Accordingly, here, we only examine the influence of NO_3(I), F(I), and ClO_4(I) on the selectivity of the fluorescent probe. Figure S3 (Supporting Information) shows the difference in the fluorescence intensities between the blank (no silver(I) ions) and the solution containing 1.0 μmol/L silver(I) ions and the influence of these anions with 10- and 100-fold concentrations to the silver(I) ions on the selectivity of the HEX−OND probes. The results showed that, in the presence of a high

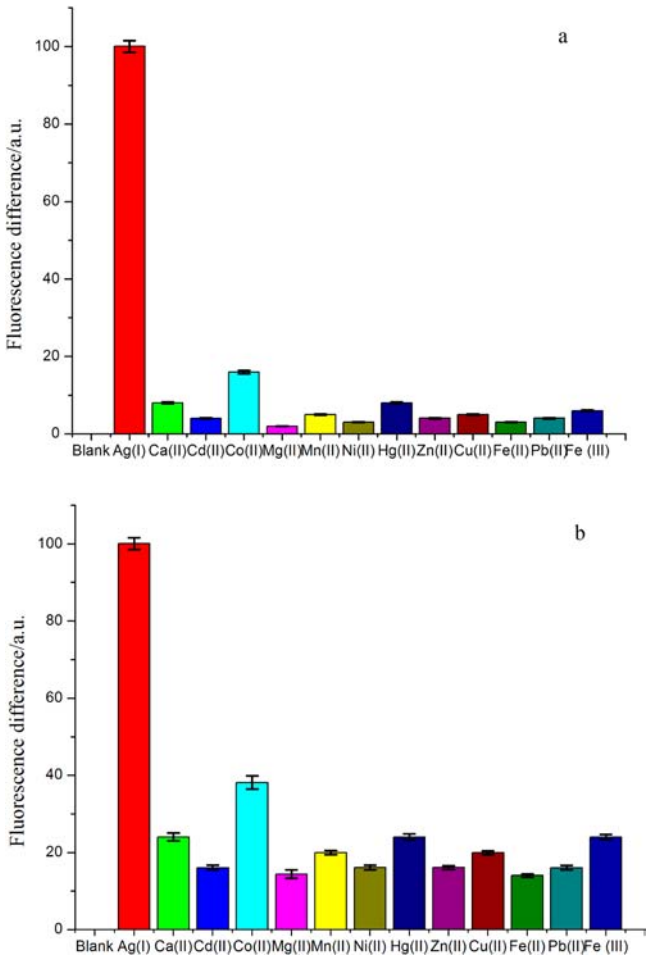

Figure 5. Difference in the fluorescence intensities between the blank and solutions containing different metal ions. (a) Concentration of all metal ions was 1.0 μmol/L; (b) concentrations of silver(I) ions and other metal ions were 1.0 and 10.0 μmol/L, respectively. The concentration of the HEX−OND probes was 20.0 nmol/L. All measurements were performed in 10.0 mmol/L MOPS buffer (containing 400.0 mmol/L $NaNO_3$ and 20.0 mmol/L KNO_3, pH 7.0).

concentration of NO_3(I), F(I), and ClO_4(I), the changes of the fluorescent signals were within 5%, indicating that the fluorescent probe has good selectivity to silver(I) ions too in this case.

(iii) Calibration curve. According to the fluorescence emission spectra of the HEX−OND probes in the presence of different concentrations of silver(I) ions, the plot of the fluorescence quenching extents $(F_0 - F)/F_0$ of the HEX−OND probes was created as the function of the concentrations of silver(I) ions (Figure 6) where F_0 and F are the fluorescence intensities of the HEX−OND probes at 556 nm in the absence and presence of different concentrations of silver(I) ions, respectively. The results show that a good linear relationship exists between the fluorescence quenching extents and the concentrations of silver(I) ions ranging from 1 to 100 nmol/L, and the equation of the calibration curve is shown as eq 1:

$$\frac{F_0 - F}{F_0} = 5.17 \cdot C_{Ag(I)} + 0.0025, \quad R^2 = 0.9999 \tag{1}$$

Through the parallel tests, it is known that the detection limit (3σ) is 50 pmol/L that is much higher than that of previous reported methods.

dx.doi.org/10.1021/jf404792z | J. Agric. Food Chem. 2014, 62, 4870−4877

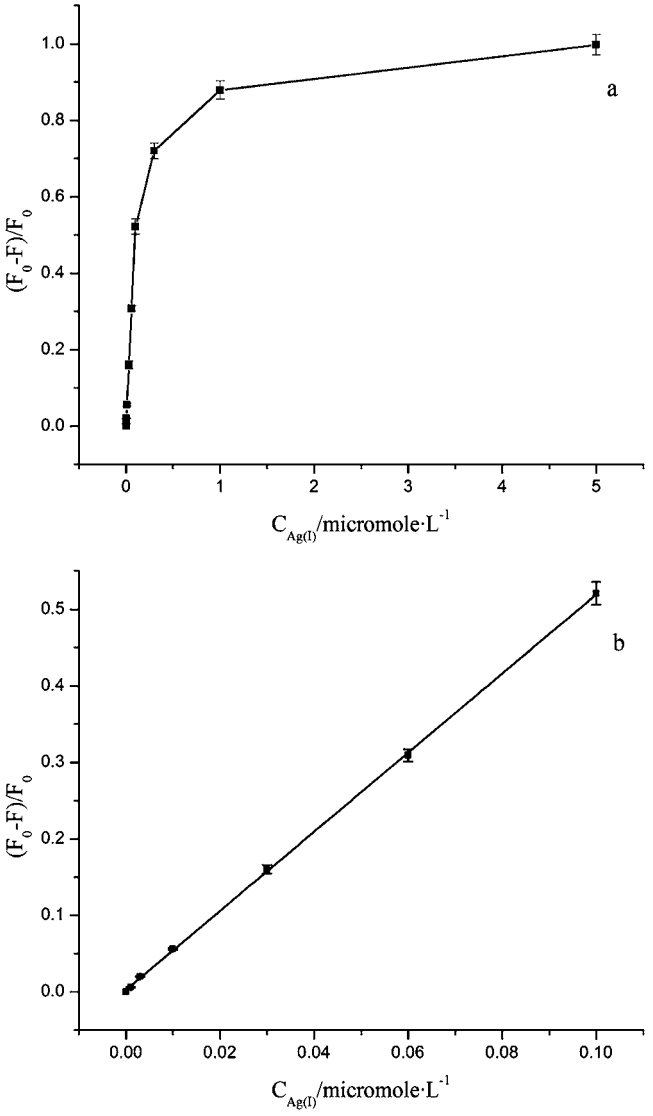

Figure 6. Fluorescence quenching extent $(F_0 - F)/F_0$ of the HEX–OND probes in the presence of different concentrations of silver(I) ions. (a) Concentration range of silver(I) ions was from 0.002 to 5.0 μmol/L; (b) concentration range of silver(I) ions was from 0.002 to 0.1 μmol/L. The concentration of the HEX–OND probe was 20.0 nmol/L. All measurements were performed in 10.0 mmol/L MOPS buffer (containing 400.0 mmol/L $NaNO_3$ and 20.0 mmol/L KNO_3, pH 7.0).

Detection of Silver(I) Ions. (i) Tap water and wastewater samples. For the silver(I) ion detection in tap water and wastewater samples, we carried out a standard addition experiment (Table 1). The results show that the recoveries are between 95% and 105% and all the relative standard deviations (RSD) are lower than 5% (n = 4), showing that this method can be used to detect silver(I) ions in tap water and wastewater samples with satisfaction.

(ii) River water sample. Wei River is a seriously polluted river near Xi 'an, and the content of silver(I) ions in it is at the level of micromoles. By means of the China National Standard (GB/T11908-1989, Cadion 2B spectrophotometry), inductively coupled plasma–atomic emission spectrometry (ICP-AES) and the single-labeled fluorescent OND probe established in this work, we separately determined the concentration of silver(I) ions in the Wei River water sample (Table 2). The results show that the detection result by this method is accurate and close to those determined by using the China National Standard and ICP-AES methods, and the relative deviation is 3.2% (n = 4).

Table 1. Determination Results of Silver(I) Ions in Tap Water and Wastewater Samples (n = 4)

	$c_{Ag(I)}$ (nmol/L)			
sample	detected	added	found	recovery (%)
tap water	24.0 ± 1.6	20.0	43.8 ± 2.0	95–104
	24.0 ± 1.6	50.0	72.0 ± 2.6	94–101
	24.0 ± 1.6	100.0	126.4 ± 3.4	99–105
wastewater	284.0 ± 6.4	200.0	486.0 ± 10.8	98–103
	284.0 ± 6.4	300.0	578.4 ± 14.2	97–101
	284.0 ± 6.4	400.0	682.2 ± 26.4	96–104

Table 2. Determination Results of Silver(I) Ions in the River Water Sample (n = 4)

sample	GB/T11908-1989 (μmol/L)	ICP-AES (μmol/L)	this method (μmol/L)	relative deviation (%)[a]
river water	0.30 ± 0.06	0.32 ± 0.06	0.32 ± 0.04	3.2

[a]The mean value determined by GB/T11908-1989 and ICP-AES.

(iii) Drug samples. "Yin-Xin-Shuang" silver–zinc emulsion and "Hong-Gao-Yao" red ointment are separately typical ointment agents. The former is made of 2% silver sulfadiazine and zinc sulfadiazine while the latter is a composite of silver sulfadiazine and the herbal ingredient salvia miltiorrhiza. Both of them have strong anti-inflammatory and antiseptic effects. By using atomic absorption spectroscopy (AAS) and the single-labeled fluorescent OND probe established in this work, we separately determined the concentrations of silver(I) ions in silver–zinc emulsion and red ointment samples (Table 3). The results again show that the detection result by this method is accurate and close to that determined by AAS, and the relative deviations are lower than 5% (n = 3).

Table 3. Determination Results of Silver(I) Ions in Drug Samples (n = 3)

sample	AAS (μmol/g)	this method (μmol/g)	relative deviation (%)
silver–zinc emulsion	55.8 ± 4.2	53.6 ± 5.4	−3.9
red ointment	60.4 ± 4.6	63.2 ± 5.6	+4.6

(iv) Tea and bean sprout samples. Through using ICP-AES and the single-labeled fluorescent OND probe designed in this work, we separately determined the concentrations of silver(I) ions in tea and bean sprout samples (Table 4). The results further demonstrated that the detection result by this method is accurate and close to that determined by ICP-AES, and the relative deviations are lower than 5% (n = 3).

Table 4. Determination Results of Silver(I) Ions in Tea and Bean Sprout Samples (n = 3)

sample	ICP-AES (μg/g)	this method (μg/g)	relative deviation (%)
tea	0.52 ± 0.08	0.51 ± 0.10	−3.7
bean sprouts	0.84 ± 1.02	0.81 ± 1.24	−3.6

dx.doi.org/10.1021/jf404792z | J. Agric. Food Chem. 2014, 62, 4870–4877

In conclusion, based on cytosine−Ag(I)−cytosine coordination and the inherent quenching ability of the G-quadruplex, a novel single-labeled HEX−OND probe is developed for Ag(I) detection. Compared with previous studies, this detection method provided several advantages, including simplicity, rapidity, and relative insensitivity to pH. In addition, the linear response range is 1−100 nmol/L with a detection limit of 50 pmol/L, and no obvious interference occurs with other metal ions with a 10-fold concentration increase, which indicates the sensitivity and selectivity are much higher than those of reported methods. Our design will provide a new method to help people to improve Ag(I) detection in water samples, pharmaceutical products, biological products, and food without the interference from other coexisting metal ions.

■ ASSOCIATED CONTENT

Supporting Information

Fluorescence spectra of HEX solution on addition of different concentrations of silver(I) ions; UV absorption spectra of the HEX−OND probes on addition of different concentrations of silver(I) ions; and difference in the fluorescence intensities in the presence of 10- and 100-fold concentrations of anions to the silver(I) ions. This material is available free of charge via the Internet at http://pubs.acs.org.

■ AUTHOR INFORMATION

Corresponding Author

*Phone/fax: +0086-29-88303446-221; e-mail: bianliujiao@sohu.com.

Funding

The study was financially supported by the National Natural Science Foundation of China (no. 21075097) and Key Program for Science and Technology Innovative Research Team of Shaanxi Province (no. 2013KCT-24).

Notes

The authors declare no competing financial interest.

■ REFERENCES

(1) Barriada, J. L.; Tappin, A. D.; Evans, E. H.; Achterberg, E. P. Dissolved silver measurements in seawater. *Trends Anal. Chem.* **2007**, *26*, 809−817.

(2) Ratte, H. T. Bioaccumulation and toxicity of silver compounds: A review. *Environ. Toxicol. Chem.* **1999**, *18*, 89−108.

(3) Liu, S.; Tian, J.; Wang, L.; Sun, X. Highly sensitive and selective colorimetric detection of Ag(I) ion using 3,3′,5,5′,-tetramethylbenzidine (TMB) as an indicator. *Sens. Actuators, B* **2012**, *165*, 44−47.

(4) Chakrapani, G.; Mahanta, P. L.; Murty, D. S. R.; Gomathy, B. Preconcentration of traces of gold, silver and palladium on activated carbon and its determination in geological samples by flame AAS after wet ashing. *Talanta* **2001**, *53*, 1139−1147.

(5) Pu, Q. S.; Sun, Q. Y.; Hu, Z. D.; Su, Z. X. Application of 2-mercaptobenzothiazole-modified silica on-line preconcentration and separation of silver for its atomic absorption spectrometric determination. *Analyst* **1998**, *123*, 239−243.

(6) Dadfarnia, S.; Haji Shabani, A. M.; Gohari, M. Trace enrichment and determination of silver by immobilized DDTC microcolumn and flow injection atomic absorption spectrometry. *Talanta* **2004**, *64*, 682−687.

(7) Sanchez-Pomales, G.; Mudalige, T.; Lim, J.; Linder, S. W. Rapid determination of silver in nanobased liquid dietary supplements using a portable X-ray fluorescence analyzer. *J. Agric. Food Chem.* **2013**, *61*, 7250−7257.

(8) Jitaru, P.; Tirez, K.; De Brucker, N. Panoramic analysis for monitoring trace metals in natural waters by ICP-MS. *At. Spectrosc.* **2003**, *24*, 1−10.

(9) Krachler, M.; Mohl, C.; Emons, H.; Shotyk, W. Analytical procedures for the determination of selected trace elements in peat and plant samples by inductively coupled plasma mass spectrometery. *Spectrochim. Acta, Part B* **2002**, *57*, 1277−1289.

(10) Tan, E.; Yin, P.; Lang, X.; Wang, X.; You, T.; Guo, L. Functionalized gold nanoparticles as nanosensor for sensitive and selective detection of silver ions and silver nanoparticles by surface-enhanced Raman scattering. *Analyst* **2012**, *137*, 3925−3928.

(11) Wygladacz, K.; Radu, A.; Xu, C.; Qin, Y.; Bakker, E. Fiber-optic microsensor array based on fluorescent bulk optode microspheres for the trace analysis of silver ions. *Anal. Chem.* **2005**, *77*, 4706−4712.

(12) Liang, J. G.; Ai, X. P.; He, Z. K.; Pang, D. W. Functionalized CdSe quantum dots as selective silver ion chemodosimeter. *Analyst* **2004**, *129*, 619−622.

(13) Chen, J. L.; Zhu, C. Q. Functionalized cadmium sulfide quantum dots as fluorescence probe for silver ion determination. *Anal. Chim. Acta* **2005**, *546*, 147−153.

(14) Zhang, Z.; Kong, F.; Vardhanabhuti, B.; Mustapha, A.; Lin, M. Detection of engineered silver nanoparticle contamination in pears. *J. Agric. Food Chem.* **2012**, *60*, 10762−10767.

(15) Chatterjee, A.; Santra, M.; Won, N.; Kim, S.; Kim, J. K.; Bin Kim, S.; Ahn, K. H. Selective fluorogenic and chromogenic probe for detection of silver ions and silver nanoparticles in aqueous media. *J. Am. Chem. Soc.* **2009**, *131*, 2040−2041.

(16) Yang, R. H.; Chan, W. H.; Lee, A. W. M.; Xia, P. F.; Zhang, H. K.; Li, K. A. Ratiometric fluorescent sensor for Ag+ with high selectivity and sensitivity. *J. Am. Chem. Soc.* **2003**, *125*, 2884−2885.

(17) Tharmaraj, V.; Devi, S.; Pitchumani, K. An intramolecular charge transfer (ICT) based chemosensor for silver ion using 4-methoxy-*N*-((thiophen-2-yl)methyl)benzenamine. *Analyst* **2012**, *137*, 5320−5324.

(18) Anand, T.; Sivaraman, G.; Anandh, P.; Chellappa, D.; Govindarajan, S. Colorimetric and turn-on fluorescence detection of Ag(I) ion. *Tetrahedron Lett.* **2014**, *55*, 671−675.

(19) Clever, G. H.; Kaul, C.; Carell, T. DNA-metal base pairs. *Angew. Chem., Int. Ed.* **2007**, *46*, 6226−6236.

(20) Okamoto, I.; Iwamoto, K.; Watanabe, Y.; Miyake, Y.; Ono, A. Metal-ion selectivity of chemically modified uracil pairs in DNA duplexes. *Angew. Chem., Int. Ed.* **2009**, *48*, 1648−1651.

(21) Liu, J.; Lu, Y. Rational design of "turn-on" allosteric DNAzyme catalytic beacons for aqueous mercury ions with ultrahigh sensitivity and selectivity. *Angew. Chem., Int. Ed.* **2007**, *46*, 7587−7590.

(22) Ono, A.; Togashi, H. Highly selective oligonucleotide-based sensor for mercury(II) in aqueous solutions. *Angew. Chem., Int. Ed.* **2004**, *43*, 4300−4302.

(23) Zhu, C. F.; Song, S. P.; Wang, L. H.; Long, Y. T.; Fan, C. H. Design of a gold nanoprobe for rapid and portable mercury detection with the naked eye. *Chem. Commun.* **2008**, 4885−4887.

(24) Li, D.; Song, S.; Fan, C. Target-responsive structures for nucleic acid sensors. *Acc. Chem. Res.* **2010**, *43*, 631−641.

(25) Wang, Y.; Geng, F.; Xu, H.; Qu, P.; Zhou, X.; Xu, M. A label-free oligonucleotide based thioflavin-T fluorescent switch for Ag^{+} detection with low background emission. *J. Fluoresc.* **2012**, *22*, 925−929.

(26) Yang, Q.; Li, F.; Huang, Y.; Xu, H.; Tang, L.; Wang, L.; Fan, C. Highly sensitive and selective detection of silver(I) in aqueous solution with silver(I)-specific DNA and Sybr Green I. *Analyst* **2013**, *138*, 2057−2060.

(27) Man, B. Y.; Chan, D. S.; Yang, H.; Ang, S. W.; Yang, F.; Yan, S. C.; Ho, C. M.; Wu, P.; Che, C. M.; Leung, C. H.; Ma, D. A selective G-quadruplex-based luminescent switch-on probe for the detection of nanomolar silver(i) ions in aqueous solution. *Chem. Commun.* **2010**, *46*, 8534−8536.

(28) Ono, A.; Cao, S.; Togashi, H.; Tashiro, M.; Fujimoto, T.; Machinami, T.; Oda, S.; Miyake, Y.; Okamoto, I.; Tanaka, Y. Specific interactions between silver(I) ions and cytosine-cytosine pairs in DNA duplexes. *Chem. Commun.* **2008**, 4825−4827.

(29) Li, T.; Shi, L. L.; Wang, E. K.; Dong, S. J. Silver-ion-mediated DNAzyme switch for the ultrasensitive and selective colorimetric

detection of aqueous Ag^+ and cysteine. *Chem.—Eur. J.* **2009**, *15*, 3347−3350.
(30) Lin, Y. H.; Tseng, W. L. Highly sensitive and selective detection of silver ions and silver nanoparticles in aqueous solution using an oligonucleotide-based fluorogenic probe. *Chem. Commun.* **2009**, 6619−6621.
(31) Freeman, R.; Finder, T.; Willner, I. Multiplexed analysis of Hg^{2+} and Ag^+ ions by nucleic acid functionalized CdSe/ZnS quantum dots and their use for logic gate operations. *Angew. Chem., Int. Ed.* **2009**, *48*, 7818−7821.
(32) Li, B. L.; Du, Y.; Dong, S. J. DNA based gold nanoparticles colorimetric sensors for sensitive and selective detection of Ag(I) ions. *Anal. Chim. Acta* **2009**, *644*, 78−82.
(33) Zhao, C.; Qu, K.; Song, Y.; Xu, C.; Ren, J.; Qu, X. A reusable DNA single-walled carbon-nanotube-based fluorescent sensor for highly sensitive and selective detection of Ag+ and cysteine in aqueous solutions. *Chem.—Eur. J.* **2010**, *16*, 8147−8154.
(34) Wen, Y. Q.; Xing, F. F.; He, S. J.; Song, S. P.; Wang, L. H.; Long, Y. T.; Li, D.; Fan, C. H. A graphene-based fluorescent nanoprobe for silver(I) ions detection by using graphene oxide and a silver-specific oligonucleotide. *Chem. Commun.* **2010**, *46*, 2596−2598.
(35) Wang, L.; Tian, J.; Li, H.; Zhang, Y.; Sun, X. A novel single-labeled fluorescent oligonucleotide probe for silver(I) ion detection based on the inherent quenching ability of deoxyguanosines. *Analyst* **2011**, *136*, 891−893.
(36) Xie, W. Y.; Huang, W. T.; Li, N. B.; Luo, H. Q. Silver(I) ions and cysteine detection based on photoinduced electron transfer mediated by cytosine-Ag(+)-cytosine base pairs. *Analyst* **2011**, *136*, 4130−4133.
(37) Fan, H. Y.; Shek, Y. L.; Amiri, A.; Dubins, D. N.; Heerklotz, H.; Macgregor, R. B., Jr.; Chalikian, T. V. Volumetric characterization of sodium-induced G-quadruplex formation. *J. Am. Chem. Soc.* **2011**, *133*, 4518−4526.
(38) Marras, S. A. E.; Kramer, F. R.; Tyagi, S. Efficiencies of fluorescence resonance energy transfer and contact-mediated quenching in oligonucleotide probes. *Nucleic Acid Res.* **2002**, *30*, e122.
(39) Seidel, C. A. M.; Schulz, A.; Sauer, M. H. M. Nucleobase-specific quenching of fluorescent dyes. 1. Nucleobase one-electron redox potentials and their correlation with static and dynamic quenching efficiencies. *J. Phys. Chem.* **1996**, *100*, 5541−5553.
(40) Torimura, M.; Kurata, S.; Yamada, K.; Yokomaku, T.; Kamagata, Y.; Kanagawa, T.; Kurane, R. Fluorescence-quenching phenomenon by photoinduced electron transfer between a fluorescent dye and a nucleotide base. *Anal. Sci.* **2001**, *17*, 155−160.
(41) Campbell, N. H.; Neidle, S. G-quadruplexes and metal ions. In *Interplay between Metal Ions and Nucleic Acids*; Sigel, A., Sigel, H., Sigel, R. K. O., Eds.; Springer: New York, 2012; Vol. *10*, Chapter 4, pp 119−1134.
(42) Kerwin, S. M. G-quadruplex DNA as a target for drug design. *Curr. Pharm. Des.* **2000**, *6*, 441−478.
(43) Davis, J. T. G-quartets 40 years later: From 5′-GMP to molecular biology and supramolecular chemistry. *Angew. Chem., Int. Ed.* **2004**, *43*, 668−698.
(44) Li, C.; Shen, T.; Chen, X.; Zhou, C.; Zhang, C.; Song, Q. Synthesis, characterization and properties of aza-BODIPY fluorescent dyes. *Chin. J. Org. Chem.* **2011**, *31*, 1440−1444.
(45) Hou, J.; Huo, L.; He, C.; Yang, C.; Li, Y. Synthesis and absorption spectra of poly(3-(phenylenevinyl)thiophene)s with conjugated side chains. *Macromolecules* **2006**, *39*, 594−603.
(46) Hou, J.; Tan, Z.; Yan, Y.; He, Y.; Yang, C.; Li, Y. Synthesis and photovoltaic properties of two-dimensional conjugated polythiophenes with bi(thienylenevinylene) side chains. *J. Am. Chem. Soc.* **2006**, *128*, 4911−4916.
(47) Walter, N. G.; Burke, J. M. Real-time monitoring of hairpin ribozyme kinetics through base-specific quenching of fluorescein-labeled substrates. *RNA* **1997**, *3*, 392−404.
(48) Fukui, K.; Tanaka, K.; Fujitsuka, M.; Watanabe, A.; Ito, O. Distance dependence of electron transfer in acridine-intercalated DNA. *J. Photochem. Photobiol., B* **1999**, *50*, 18−27.
(49) Jothikumar, N.; Hill, V. R. A novel photoinduced electron transfer (PET) primer technique for rapid real-time PCR detection of Cryptosporidium spp. *Biochem. Biophys. Res. Commun.* **2013**, *436*, 134−139.
(50) Gao, Y.; Sriram, M.; Wang, A. H. J. Crystallographic studies of metal ion-DNA interactions: Different binding modes of cobalt(II), copper(II) and barium(II) to N7 of guanines in Z-DNA and a drug-DNA complex. *Nucleic Acids Res.* **1993**, *21*, 4093−4101.

JOURNAL OF AGRICULTURAL AND FOOD CHEMISTRY

Article

pubs.acs.org/JAFC

UHPLC Quantification of Sotolon in White Wine

Mario Gabrielli, Daniela Fracassetti, and Antonio Tirelli*

DeFENS—Department of Food, Environmental and Nutritional Sciences, Università degli Studi di Milano, Via Giovanni Celoria 2, 20133 Milano, Italy

ABSTRACT: Sotolon (4,5-dimethyl-3-hydroxy-2,5-dihydrofuran-2-one) is a volatile compound involved in the atypical aging of dry white wine, causing an irreversible defect when it exceeds 7−8 μg L^{-1}, and it might be adopted as a chemical marker of oxidative aging. An easier and sensitive ultrahigh-pressure liquid chromatography method for its determination in white wine is reported. The sample preparation is based on the liquid/liquid extraction by dichloromethane and the purification by solid phase extraction of the redissolved dry sample. This method showed good linearity and intermediate repeatability (<0.7 μg L^{-1}), high recovery (>89.5%), and low detection limit (0.029 μg L^{-1}). This method was usefully applied to 30 Italian sparkling and still white wine samples, where sotolon was not detected in most of them and exceeded the perception threshold only in one sparkling wine (13 μg L^{-1}). The proposed method could be used to further investigate the aging/storage conditions and the chemical−physical parameters affecting its formation in wine.

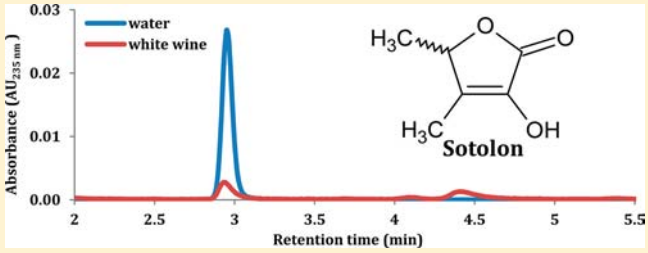

KEYWORDS: *sotolon, white wine, ultrahigh-pressure liquid chromatography, liquid/liquid extraction*

1. INTRODUCTION

Sotolon (4,5-dimethyl-3-hydroxy-2,5-dihydrofuran-2-one) is an odorous compound related to the oxidized character of wine.[1] Its flavor is usually described as curry, fenugreek, and old honey, and it is sought in oxidatively aged wines such as Madeira and Porto.[2,3] Sotolon's odor is considered a defect in young, dry, white wine, as it can decrease the intensity of the fruity and flowery flavor notes as well as the expected freshness character.[4] This defect is termed atypical aging.[1]

Sotolon is a thermolabile chiral lactone and it is stable in hydroalcoholic solution (14% ethanol v/v) at acid pH value. The chiral properties of carbon 5 in the furanic ring originate two optical isomers of sotolon with very different olfactory perception threshold: 5 and 89 μg L^{-1} in white wine for the *S* and *R* form, respectively. Since their quantitative ratio *S*/*R* can range from 1:3 to 3:1 in white wines,[5] perception threshold values up to 8 were proposed.

Detrimental amounts of sotolon in wine can rise through a number of chemical pathways mainly involving ethanal and 2-ketobutyric acid,[7] though other molecules can be involved through different chemical paths. Both hexoses and pentoses can give rise to sotolon formation via the Maillard reaction involving amino acids such as cysteine and 4-hydroxyisoleucine.[8] Sotolon formation can increase in wine containing threonine[9] and ascorbic acid,[7,10] as well as following exposure to high temperature[11] or oxygen[1] during aging or storage with oxidative aging in oak casks.[2]

The negative effect of sotolon on wine flavor and the wide number of chemical and physical factors affecting sotolon formation in wine have two important consequences on the role of this compound in wine evaluation. First, the role of wine compounds in sotolon formation should be better investigated. Second, the suitability of this off-flavor as a chemical marker of appropriate white wine aging and storage should be evaluated.

Several analytical methods were reported for sotolon quantification in water solution and wine. Nevertheless, the sensitivity of the analytical methods based on head space sampling technique (DHS and SPME) is negatively affected by both the low concentration in wine and the high boiling temperature (184 °C) of sotolon.[12,13] As a consequence, the chromatographic separation needs to be preceded by liquid/liquid extraction or solid-phase extraction (SPE) and concentration.[7,11] The analytical methods reported in the literature require long lasting sample extraction[14] and a substantial volume of sample and solvents,[7,15,16] leading to both long time and costly analysis.

This research aimed to develop an analytical method to assess sotolon by using ultrahigh-pressure liquid chromatography (UHPLC) coupled with UV detection. The availability of a fast, sensitive, and reliable analytical method could allow a better monitoring of the oxidative fate of white wine aging as well as a deeper knowledge of wine-making practices and wine compounds affecting sotolon formation.

2. MATERIALS AND METHODS

2.1. Chemicals and Reagents. Sotolon (purity exceeding 97%), methanol, ethanol, dichloromethane (DCM), heptane, chloroform, sodium chloride (NaCl), anhydrous sodium sulfate were purchased from Sigma-Aldrich (St. Louis, MO). Polyvinylpolypirrolidone (PVPP)

Received: January 29, 2014
Revised: April 28, 2014
Accepted: May 5, 2014
Published: May 5, 2014

ACS Publications © 2014 American Chemical Society

was purchased from Dal Cin (Sesto San Giovanni, Milan, Italy). All the chemicals were of analytical grade, at least.

HPLC grade water was obtained with a Milli-Q system (Millipore Filter Corp., Bedford, MA).

The synthetic wine contained 5 g L^{-1} tartaric acid in 12% ethanol/water solution (v/v), adjusted to pH 3.5 with 12 M sodium hydroxide (Sigma-Aldrich).

2.2. Commercial Wine Samples. Sotolon content was assessed in 18 Chardonnay sparkling wine samples (Brut-nature Champenoise method, 7 months in-bottle aging) produced in one single winery (Franciacorta area, Lombardy, Italy) according to the rational wine making conditions usually adopted to produce quality wine (PDO). Moreover, 12 commercial dry white wine samples purchased at the market and produced in Italy from three different grape cultivars (Chardonnay, Catarratto, and Trebbiano) in the vintages 2011−2012 were analyzed.

2.3. Sample Preparation Development. *2.3.1. Liquid/Liquid Extraction Trials.* A water solution containing sotolon (25 μg L^{-1}) was extracted by using different solvents: heptane, chloroform, and DCM. The solution (300 mL) was liquid/liquid extracted once with 100 mL of each solvent by stirring for 30 min. The organic phase was separated from the aqueous phase by a separatory funnel, to which about 2 g of anhydrous sodium sulfate was added before vacuum-drying. The dry material was dissolved in 2 mL of water and submitted to UHPLC separation.

Partition coefficient and extraction yield were calculated as follows

$$K = \frac{C_s}{C_a} = \frac{g_s V_a}{(g_0 - g_s)V_s} \quad (1)$$

$$g_s^n = \frac{KV_s\, g_0}{V_a + KV_s}\left(1 - \frac{KV_s}{V_a + KV_s}\right)^{n-1} \quad (2)$$

$$e_y^n = \frac{\sum_1^n g_s}{g_0} \quad (3)$$

where K is the partition coefficient, C_s is the concentration of analyte in the extraction solvent, C_a is the concentration of analyte in the water solution, g_s is mass of solute in the extraction solvent obtained with a single extraction step, g_0 is the overall mass of solute, V_s is the volume of extraction solvent, V_a is the volume of water solution, g_s^n is the mass of solute in the extraction solvent following to the nth extraction step, n is the number of extraction steps, and e_y^n is the overall extraction yield after the nth extraction step.

The influence of NaCl concentration on the partition coefficient was tested. Thirty milliliters of synthetic wine solution containing 1 mg L^{-1} sotolon were added with 20, 50, or 100 g L^{-1} NaCl. The solutions were extracted once with 30 mL of DCM (30 min shaking with a Griffin flask shaker) and prepared as described as above.

Moreover, the assessment of the extraction yield after 10, 20, 30, and 40 min of shaking under the above extraction conditions was carried out on synthetic wine solution (1 mg L^{-1} sotolon) added with 100 mg L^{-1} NaCl.

2.3.2. Sample Purification Trials. Three SPE resins were tested: C18, 360 mg (Waters, Milford, MA); polymer-based, 200 mg (Phenomenex, Torrence, CA); and in-lab packed PVPP, 50 mg. The SPE columns were conditioned by 5 mL of methanol and 5 mL of water and then loaded with 2 mL of sotolon (5 mg L^{-1} in water), and the unretained sample was collected. Then one or more aqueous solutions (2 mL each) prepared with increasing amounts of methanol (20, 40, 60, 80, 100% v/v) were sequentially passed through the column. The eluted fractions were separately collected and submitted to UHPLC separation. Trials were carried out by loading the extracted wine samples recovered with 5% and 10% methanol (v/v) on the PVPP column.

2.4. Sample Preparation. Three grams of NaCl was dissolved in 30 mL of wine in a 100 mL bottle and then 40 mL of DCM was added. The bottle was hermetically closed and shaken for 10 min with a wrist action stirrer (Griffin flask shaker). The mixture was centrifuged 5 min at 5000g and the DCM was separated by a separatory funnel and recovered. The solvent extraction procedure was carried out three times, and the three organic solvent fractions were jointly collected and to them were added about 2 g of anhydrous sodium sulfate in order to remove the dispersed water. The DCM was evaporated under vacuum and the dry material was dissolved with 2 mL of 5% methanol. The solution was loaded in a conditioned SPE column containing 50 mg of PVPP, and 2 mL of the purified sample was recovered.

2.5. Calibration Curves and Method Performances. Spiked white wine (young Chardonnay/Trebbiano) samples containing 2.36, 4.67, 11.7, and 23.4 μg L^{-1} of sotolon were prepared to assess the response linearity of the analytical method as well as its intermediate precision parameters. Each sample was submitted to three replicated determinations for three different days (nine determinations per sample). Standard water solutions containing sotolon (117, 219, and 438 μg L^{-1}) were submitted to triplicated UHPLC separations on three different days to assess the response linearity of water solutions. In order to assess the recovery parameters of the method, the response factors obtained were compared to the analytical response obtained by submitting spiked wine samples containing sotolon (7.8, 14.6, and 29.2 μg L^{-1}, equivalent to a 15× dilution factor compared to the water standard solutions) to triplicated determinations performed on three different days.

2.6. Limit of Detection and of Quantification. The LOD was calculated as indicated as follows

$$\mathrm{LOD} = a + 3s_{x/y} \quad (4)$$

where a is the intercept point of the regression line and $s_{x/y}$ is the standard deviation of the linear regression.

2.7. Ultrahigh-pressure liquid chromatography. The UHPLC separation was performed by an Acquity HClass UPLC (Waters, Milford, MA) system equipped with a photo diode array detector (2996 Waters). The column used was a Kinetex C18 (100 × 3 mm, 2.6 μm particle size, 100 Å pore size; Phenomenex, Torrence, CA). The chromatographic separation was carried out with an isocratic elution running 5% methanol for 4 min followed by column washing (100% methanol for 1 min) and column conditioning (4 min). The flow rate was 1 mL min^{-1} and the system pressure was 6700 psi. Sotolon was detected at 235 nm wavelength (detector sampling rate fixed as five points per second). The injection volume was 20 μL and the column was thermostated at 30 °C. All the samples were filtered through a 0.22 μm pore size PVDF membrane (Millipore, Billerica, MA) before injection.

2.8. Quantification of Sotolon. Sotolon was quantified in synthetic wine solutions and white wine samples by the external standard method. Chromatographic data acquisition and processing were performed by Empower 2 software (Waters).

2.9. Statistical Analysis. The equations of the calibration curves were assessed by the linear regression analysis. Differences between the calibration curve slopes obtained in aqueous solution and white wine were evaluated by the F-test ($P < 0.05$).

3. RESULTS AND DISCUSSION

3.1. Analytical Method Development. The general physical−chemical properties of sotolon were first evaluated in order to fulfill the analytical sensitivity required. The UV spectrum of sotolon in water standard solution (5 mg L^{-1}) showed one single peak having a maximum absorbance at 235 nm and a high molar extinction coefficient (ε° = 10 255 L cm^{-1} mol^{-1}). Preliminary UHPLC runs showed that sotolon concentrations in the range 60−90 μg L^{-1} (corresponding to 8−12-fold higher values than the perception threshold) were suitable to gain the required detection/quantification levels. Therefore, wine volume as low as 20−30 mL can be used for sotolon quantification. Such values are lower than the condition required in the previous literature.[1,10] In order to obtain the required concentration, a liquid/liquid extraction procedure was developed; therefore, sotolon extraction yield was evaluated by using heptane, chloroform, and DCM, which were previously

dx.doi.org/10.1021/jf500508m | J. Agric. Food Chem. 2014, 62, 4878−4883

employed.[15,16] The DCM showed an extraction yield 32% higher than that of chloroform, whereas heptane did not extract detectable amounts of sotolon (Table 1). Comparing the

Table 1. Sotolon Amounts (as peak area) and Corresponding Partition Coefficient Obtained from Water Solution (25 μg L^{-1} of sotolon) with Different Extraction Solvents

solvents	sotolon extracted (mV s)	partition coefficient
heptane	nd[a]	0
chloroform	32	0.81
dichloromethane	47	2.1

[a]Not detectable.

analytical responses (peak areas) obtained from sotolon in the water solution and the extracted sample, DCM showed the highest extraction yield (41%) corresponding to a partition coefficient exceeding 2.1 (Table 1). Moreover, DCM volumes ranging from 40 to 60 mL were calculated from the partition coefficient (see eqs 1, 2, and 3 reported in Materials and Methods) in order to inject quantifiable amounts of extracted sotolon (1.2−1.8 ng) and taking into account about 1 order of magnitude as the concentration factor for 30−40 mL of wine sample. Since sotolon amounts up to 68−76% were extracted by using solvent/wine volume ratios in the range from 1:1 to 2:1, three consecutive extractions were needed to obtain an overall extraction yield approaching 100%.

Higher extraction yield can be obtained by increasing the ionic strength of the aqueous solution;[17] therefore, different levels of NaCl (20, 50, and 100 g L^{-1}) were evaluated. As expected, the partition coefficient increased exponentially as the salt concentration increased (Table 2). The partition coefficient for

Table 2. Extraction Parameters of Sotolon Obtained with Different Amounts of Sodium Chloride in Synthetic Wine Solution (1 mg L^{-1} sotolon) Using Dichloromethane as Organic Solvent

sodium chloride (g L^{-1})	extraction yield (%)	partition coefficient
0	65.8	1.8
20	86.5	1.9
50	88.5	2.3
100	93.0	3.5

the salt-free synthetic wine solution was lower (K = 1.8) than the value obtained with the water solution (K = 2.1) owing to the solvent properties of ethanol. The highest NaCl content (100 g L^{-1}) doubled the partition coefficient and was also effective in decreasing the foaming during the liquid/liquid extraction.

The effect of the shaking time on the extraction was also investigated. Higher extraction yield was obtained in synthetic wine solution carrying out the shaking for less than 30 min. Up to 30% sotolon was lost following 30 min of shaking (Table 3) probably due to its degradation, which can occur in DCM.[18]

In spite of the extraction procedure, some interferences were eluted in the chromatographic run. Therefore, different SPE conditions were tested in order to improve the sample purification. Three different hydrophobic resins were tested with increasing methanol concentrations as eluting solvent. Sotolon has lower hydrophobic properties than other wine compounds capable of absorbing light at 235 nm wavelength, (e.g., polyphenols) owing to the lower molecular weight and the presence of a hydroxyl group in its molecular structure.

Table 3. Effect of the Shaking Time on the Sotolon Amount (as peak area ± uncertainty) Extracted from a Synthetic Wine Solution (1 mg L^{-1} sotolon) with Dichloromethane as Organic Solvent

shaking time (min)	peak area (mV s)
10	258 ± 6
20	294 ± 36
30	207 ± 2
40	222 ± 74

Therefore, the SPE conditions effective in retaining polyphenols and eluting sotolon were evaluated. Polymer and C18 resins showed high retentive properties, and sotolon was eluted with 60% and 40% methanol, respectively. Nevertheless, interfering compounds were still found in the chromatogram. A lower retention property was obtained with PVPP. More than 50% of sotolon was unretained by the resin and a further elution with 20% methanol was needed to complete the recovery (Table 4).

Table 4. Sotolon Recovery (%) Obtained with Different SPE Resins by Loading 2 mL of Extracted Wine Samples (5 mg L^{-1} sotolon) and Eluting with 2 mL for Each Solvent Tested[a]

methanol (%)	polymer (200 mg)	C18 (360 mg)	PVPP (50 mg)		
unretained sample	nd	0.4	56.0	56.0	56.0
5	–	–	–	31.2	–
10	–	–	–	–	34.4
20	0.1	37.7	43.2	–	–
40	29.4	54.1	0.6	–	–
60	69.9	0.5	tr	–	–
80	0.4	0.5	tr	–	–
100	0.1	nd	tr	–	–
cumulative	99.9	92.3	99.8	87.2	89.4

[a]Legend: tr: trace amount; nd: not detectable.

Sotolon recoveries up to 90% were found for the wine samples recovered in 5% and 10% methanol (v/v). The latter concentration allowed a sotolon recovery 2% higher, but 5% methanol was chosen since it allows an interference-free chromatographic separation (Figure 1). In order to avoid sample dilution due to the purification step, the dried sample was dissolved with 5% methanol before the SPE procedure. So 87% of the sotolon was recovered in the unretained sample without any further elution.

Finally, the wine samples were prepared using the following optimized analytical conditions: 30 mL of wine added with 100 g L^{-1} NaCl, three extraction steps with 40 mL of DCM and 10 min shaking each, vacuum drying, sample recovery with 2 mL of 5% methanol/water solution (v/v), SPE purification on PVPP resin, and UHPLC run. The chromatographic separation occurred with low-methanol content (5%) in very short time (2.9 min) due to the low hydrophobicity and molecular weight of sotolon. Moreover, this method was solvent-saving for both sample preparation[7,16] and chromatographic separation. No interfering chromatographic peak was found, and sotolon was obtained as a baseline-separated chromatographic peak (Figure 1).

The method performances were evaluated for the sotolon concentrations (up to 25−30 μg L^{-1}) usually reported in the literature for about white wine[1,11,19] and in agreement with its perception threshold (<8 μg L^{-1}). Therefore, sotolon levels up to 23 μg L^{-1} were evaluated in both water solution and white wine.

dx.doi.org/10.1021/jf500508m | J. Agric. Food Chem. 2014, 62, 4878−4883

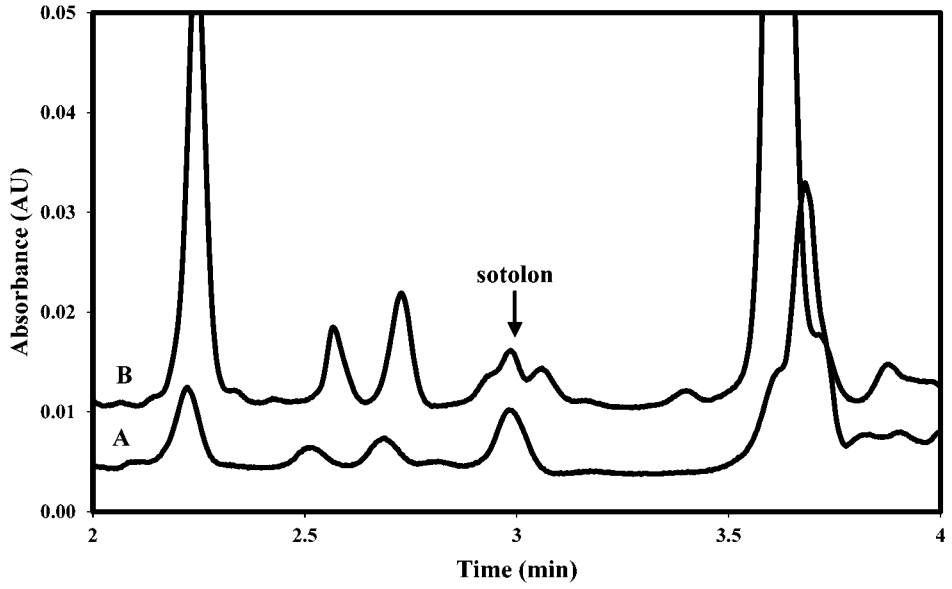

Figure 1. UHPLC separation of sotolon in white wine samples after SPE purification with PVPP by using methanol 5% (A) and 10% (B) as recovering solvent.

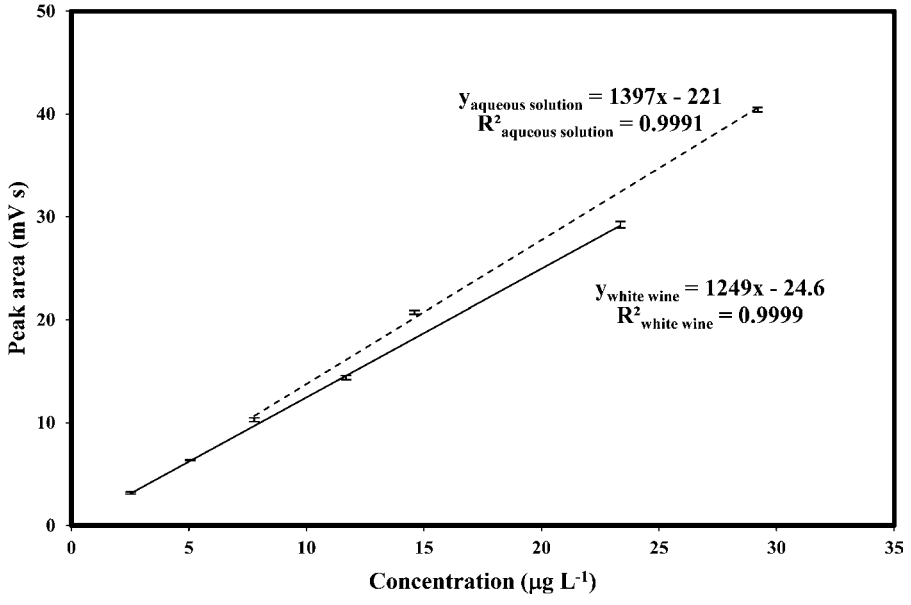

Figure 2. Calibration curves for sotolon in aqueous solution (dashed line) and white wine (solid line). Standard deviations are reported by vertical bars (n = 9).

The analytical method shows a linear response (R^2 > 0.999) in the whole range of concentrations tested with both the matrices (Figure 2), but a 10% lower response factor was calculated (as calibration curve slopes ratio) for the dry white wine compared to the corresponding water standard solution owing to the incomplete recovery of the SPE step. The calibration curves obtained are significantly different (p < 0.01), and a 10% higher sotolon amount in wine must be considered when water solutions are used as external standards.

Amounts as low as 2.5 μg L^{-1} were accurately quantifiable in wine, though with slightly higher precision values (Figure 2 and Table 5). The intermediate repeatability[20] were calculated for interday determinations; its values were close to 10% for sotolon levels as low as 2.3 μg L^{-1} and a mean value 3.1% was obtained for higher concentration values.

Table 5. Precision Parameters (n = 9) of Sotolon Quantification in White Wine[a]

concn added (μg L^{-1})	2.34	4.67	11.68	23.36
concn found (μg L^{-1}; mean value)	2.33	4.43	10.53	21.14
SD repeatability (μg L^{-1})	0.11	0.063	0.18	0.27
SD intermediate repeatability (μg L^{-1})	0.10	0.060	0.19	0.26
repeatability limit (μg L^{-1})	0.24	0.13	0.48	0.68
RSD (%)	3.36	0.85	1.36	1.08
av RSD (%)			1.66	

[a]Legend: SD, standard deviation (μg L^{-1}); RSD, relative standard deviation (%).

The LOD of sotolon in white wine was 0.029 μg L^{-1}, a value much lower than the perception threshold in white wine. It is lower than the LOD values reported by other researchers also

dx.doi.org/10.1021/jf500508m | J. Agric. Food Chem. 2014, 62, 4878−4883

considering the GC techniques.[1,3,6,13] The sotolon recovery was evaluated in spiked white wine and its values were 97.7%, 91.1%, and 89.5%, respectively, for sotolon concentrations of 7.78, 14.60, and 29.20 $\mu g\ L^{-1}$. Such values were higher than those previously reported.[6,19,21]

3.2. Quantification in Commercial White Wine. The proposed method was applied to the determination of sotolon in some commercial white wine samples (Brut-nature sparkling and still dry wines). In spite of the very low sugar content and the high CO_2 pressure occurring during bottle corking and storage, the highest sotolon levels (6 and 13 $\mu g\ L^{-1}$) were detected in two samples of sulfur dioxide-free and ascorbate-free sparkling wines (samples 11 and 12, respectively) stored for 7 months at 25 °C (Table 6). The role of sulfur dioxide in preventing sotolon formation is well-known,[1] even if other SO_2-free sparkling wine samples (e.g., samples 1 and 2 in Table 6) did not contain detectable amounts of sotolon. No perceptible concentrations of sotolon were found in two samples of still Catarratto dry wine (samples 19 and 20). No quantifiable or detectable amounts were obtained from the other 26 commercial samples of both sparkling wine and still wine. Such results are in agreement with other data reported in the literature[1,19,22,23] and highlight the need for deeper knowledge concerning the chemical, physical, and technological factors affecting sotolon formation in wine.

Table 6. Sotolon Amounts ($\mu g\ L^{-1}$) Detected in Commercial Samples of Brut-Nature Sparkling and Dry White Wine[a]

code	grape cultivar	vintage	description	sotolon
1	Chardonnay	2011	sparkling wine	nd
2	Chardonnay	2011	sparkling wine	nd
3	Chardonnay	2011	sparkling wine	nd
4	Chardonnay	2011	sparkling wine	nd
5	Chardonnay	2011	sparkling wine	nd
6	Chardonnay	2011	sparkling wine	nq
7	Chardonnay	2011	sparkling wine	nq
8	Chardonnay	2011	sparkling wine	nq
9	Chardonnay	2011	sparkling wine	nq
10	Chardonnay	2011	sparkling wine	nq
11	Chardonnay	2011	sparkling wine	6.4
12	Chardonnay	2011	sparkling wine	13.4
13	Chardonnay	2011	sparkling wine	nd
14	Chardonnay	2011	sparkling wine	nq
15	Chardonnay	2011	sparkling wine	nd
16	Chardonnay	2011	sparkling wine	nq
17	Chardonnay	2011	sparkling wine	nd
18	Chardonnay	2011	sparkling wine	n.q
19	Catarratto	2011	dry white wine	3.6
20	Catarratto	2011	dry white wine	3.0
21	Chardonnay/Trebbiano	2010	dry white wine	nd
22	Chardonnay/Trebbiano	2010	dry white wine	nd
23	Chardonnay/Trebbiano	2011	dry white wine	nd
24	Chardonnay/Trebbiano	2011	dry white wine	nd
25	Chardonnay/Trebbiano	2011	dry white wine	nd
26	Chardonnay/Trebbiano	2012	dry white wine	nd
27	Chardonnay/Trebbiano	2012	dry white wine	nd
28	Chardonnay/Trebbiano	2012	dry white wine	nd
29	Chardonnay/Trebbiano	2012	dry white wine	nd
30	Chardonnay/Trebbiano	2012	dry white wine	nd

[a]Legend: nd, not detectable; nq, not quantifiable.

The proposed analytical method provides a sample preparation procedure that is faster and easier-to-apply than those previously reported for the routine analyses of sotolon. It can be a suitable easy-to-apply analytical tool to investigate the formation of sotolon in either natural or synthetic wine systems. The sensitivity parameters above-described allow sotolon formation kinetics to be investigated at adequate concentration levels.

AUTHOR INFORMATION

Corresponding Author

*E-mail: antonio.tirelli@unimi.it. Phone: +390250316673. Fax: +390250316672.

Funding

This study was cofinanced by the postdoctoral fellow "Dote Ricerca": FSE, Regione Lombardia.

Notes

The authors declare no competing financial interest.

REFERENCES

(1) Lavigne, V.; Pons, A.; Darriet, P.; Dubourdieu, D. Changes in the sotolon content of dry white wines during barrel and bottle aging. *J. Agric. Food Chem.* **2008**, *56*, 2688−2693.

(2) Silva Ferreira, A. C.; Barbe, J. C.; Bertrand, A. Heterocyclic acetals from glycerol and acetaldehyde in Port wines: Evolution with aging. *J. Agric. Food Chem.* **2002**, *50*, 2560−2564.

(3) Camara, J. S.; Marques, J. C.; Alves, M. A.; Silva Ferreira, A. C. 3-Hydroxy-4,5-dimethyl-2(5*H*)-furanone levels in fortified Madeira wines: Relationship to sugar content. *J. Agric. Food Chem.* **2004**, *52*, 6765−6769.

(4) Silva Ferreira, A. C.; Barbe, J. C.; Bertrand, A. 3-Hydroxy-4,5-dimethyl-2(5*H*)-furanone: A key odorant of the typical aroma of oxidative aged Port wine. *J. Agric. Food Chem.* **2003**, *51*, 4356−4363.

(5) Pons, A.; Lavigne, V.; Landais, Y.; Darriet, P.; Dubourdieu, D. Distribution and organoleptic impact of sotolon enantiomers in dry white wines. *J. Agric. Food Chem.* **2008**, *56*, 1606−1610.

(6) Guichard, E.; Pham, T.T.; Etievant, P. Quantitative determination of sotolon in wines by high-performance liquid chromatography. *Chromatographia* **1993**, *37*, 539−542.

(7) Konig, T.; Gutsche, B.; Hartl, M.; Hubscher, R.; Schreier, P.; Schwab, W. 3-Hydroxy-4,5-dimethyl-2(5*H*)-furanone (sotolon) causing an off-flavor: Elucidation of its formation pathways during storage of citrus soft drinks. *J. Agric. Food Chem.* **1999**, *47*, 3288−3291.

(8) Hofmann, T.; Schieberle, P. Identification of potent aroma compounds in thermally treated mixtures of glucose/cysteine and rhamnose/cysteine using aroma extract dilution techniques. *J. Agric. Food Chem.* **1997**, *45*, 898−906.

(9) Pham, T. T.; Guichard, E.; Schlich, P.; Charpentier, C. Optimal conditions for the formation of sotolon from α-ketobutyric acid in the French "Vin Jaune". *J. Agric. Food Chem.* **1995**, *43*, 2616−2619.

(10) Pons, A.; Lavigne, V.; Landais, Y.; Darriet, P.; Dubourdieu, D. Identification of a sotolon pathway in dry white wines. *J. Agric. Food Chem.* **2010**, *58*, 7273−7279.

(11) Cutzach, I.; Chatonnet, P.; Dubourdieu, D. Study of the formation mechanisms of some volatile compounds during the aging of sweet fortified wines. *J. Agric. Food Chem.* **1999**, *47*, 2837−2846.

(12) Ferreira, V.; Ortega, L.; Escudero, A.; Cacho, J. A comparative study of the ability of different solvents and adsorbents to extract aroma compounds from alcoholic beverages. *J. Chromatogr. Sci.* **2000**, *38*, 469−476.

(13) Ferreira, V.; Jarauta, I.; Lopez, R.; Cacho, J. Quantitative determination of sotolon, maltol and free furaneol in wine by solid-phase extraction and gas chromatography−ion-trap mass spectrometry. *J. Chromatogr. A* **2003**, *1010*, 95−103.

(14) Escudero, A.; Cacho, J.; Ferreira, V. Isolation and identification of odorants generated in wine during its oxidation: A gas chromatography−olfactometric study. *Eur. Food Res. Technol.* **2000**, *211*, 105−110.

(15) Takahashi, K.; Tadenuma, M.; Sato, S. 3-Hydroxy-4,5-dimethyl-2(5*H*)-furanone, a brunt flavoring compound from aged sake. *Agr. Biol. Chem.* **1976**, *40*, 325−330.

(16) Schneider, R.; Baumes, R.; Bayonove, C.; Razungles, A. Volatile compounds involved in the aroma of sweet fortified wines (Vins Doux Naturels) from Grenache Noir. *J. Agric. Food Chem.* **1998**, *46*, 3230−3237.
(17) Xie, W.; Shiu, W.; Mackay, D. A review of the effect of salts on the solubility of organic compounds in seawater. *Mar. Environ. Res.* **1997**, *44*, 429−444.
(18) Martin, B.; Etievant, P.; Henry, R. The chemistry of sotolon: A key parameter for the study of a key component of flor Sherry wines. In *Flavor Science and Technology, 6th Weurman Symposium*; Bessière, Y., Thomas, A. F., Eds.; Wiley: New York, 1990; pp 53−56.
(19) Martin, B.; Etievant, P. Quantitative determination of solerone and sotolon in flor Sherries by two-dimensional-capillary GC. *J. High Res. Chromatogr.* **1991**, *14*, 133−135.
(20) *ISO 5725-1. Accuracy (Trueness and Precision) of Measurement Methods and Results. General Principles and Definitions*; ISO: Geneva, 1994.
(21) Bailly, S.; Jerkovic, V.; Meurée, A.; Timmermans, A.; Collin, S. Fate of key odorants in Sauternes wines through aging. *J. Agric. Food Chem.* **2009**, *57*, 8557−8563.
(22) Dagan, L.; Schneider, R.; Lepoutre, J. P.; Baumes, R. Stability of sotolon in acidic and basic aqueous solutions application to the synthesis of a deuterated analogue for its quantitative determination in wine. *Anal. Chim. Acta* **2006**, *563*, 365−374.
(23) Riberau-Gayon, P.; Glories, Y.; Maujean, A.; Dubourdieu, D. *Handbook of Enology, The Chemistry of Wine Stabilization and Treatments*, 2nd ed.; John Wiley & Sons Ltd: Chichester, UK, 2006; Vol. 2, pp 233−284.

identified at the mRNA level as one of the genes in the family of stress-induced, developmentally regulated soybean genes.[25] The physiological function of Gly m 4 is also still unknown. Gly m 4 is highly homologous with the birch pollen allergen Bet v 1.[24] The three-dimensional structures of recombinant Gly m 4 (rGlym 4) and Bet v 1 are nearly identical, thereby causing high cross-reactivity via the same IgE antibodies.[24] In a recent paper, our laboratory published a quantitative assay for the determination of endogenous intact Gly m 4 protein.[26] The endogenous Gly m 4 protein has 88.7% sequence homology with the theoretically predicted Gly m 4 sequence. The endogenous Gly m 4 protein belongs to the same stress-induced gene family as SAM 22 and H4 proteins.[26]

In this study, both HPS and Gly m 4 were isolated from soybean seeds. Following isolation, purification, and detailed characterization, a multiplexed 2DLC-based approach was developed for simultaneous quantification of the two proteins. The two orthogonal chromatographic dimensions used were strong anion exchange chromatography (SAX) and reversed phase chromatography (RPC) as the first and second dimensions, respectively. The advantage of using the 2DLC-based approach over single-dimension separation assays was the ability to completely resolve the protein of interest from other coeluting components and the ability to multiplex. The assay was evaluated for selectivity, linearity, sensitivity, and recovery and was used to determine the concentrations of Gly m 4 and HPS in different commercial soybean lines.

MATERIALS AND METHODS

Chemicals. The commercially available, non-transgenic soybean seeds were purchased from the following: H387 (lot JK1700) from Hoffman (Hoffmann, IL, USA); 363 (lot PS9-3633) from Phillips (Hope, KS, USA); William 82 (lot 9S-10-107) from Missouri Seed Foundation (Columbia, MO, USA); 3930 (lot S080184 GR01-596) from Croplan LC (St. Paul, MN, USA); C3884N (lot 1208294) from LG Seeds (Elmwood, IL, USA); pH-4396 (lot 01A (75148)) from Porter Hybrid (Wilmington, OH, USA); HS38C60 (lot SZ090151) from Hi Soy (Bloomington, IL, USA); 029311K (99915) (lot DSR-3590 029301K) from Dairyland/Precision Soya (West Bend, WI, USA); XP843-252 (lot 9E394N) from Brown Seed (Neoga, IL, USA); and Maverick (lot 8S-18-07) from Missouri Seed Foundation. Dithiothrietol (DTT), iodoacetamide (IAM), and E-64 enzyme inhibitor were purchased from Sigma (St. Louis, MO, USA). Sodium chloride, glycerol, LC-MS grade trifluoroacetic acid (TFA), HPLC grade isopropanol (IPA), tris buffer, hexanes, and acetonitrile (ACN) were purchased from Thermo Fisher Scientific (Waltham, MA, USA). A Steriflip disposable vacuum filtration system with a 0.22 μm membrane filter was purchased from Millipore (Billerica, MA, USA). Trypsin was obtained from Roche Applied Sciences (Indianapolis, IN, USA). For all analyses, Milli-Q (Millipore) deionized water was used.

Generation of HPS and Gly m 4 Reference Standards. Both HPS and Gly m 4 proteins were purified from a non-transgenic (Maverick) soybean line using similar conditions. Soybean kernels were first ground to a fine powder with a Robot Coupe grinder (model RSI 2Y-1, Robot Coupe USA, Inc.) using an equal amount of dry ice. This was followed by defatting the milled soybean seeds with hexanes (milled soybean seeds/*n*-hexanes, 1:0.19 g/mL) for 1 h at room temperature and subsequent removal of hexanes by centrifugation. The procedure was repeated two more times. The dry defatted seed material was distributed between 22 50-mL conical centrifuge tubes, with approximately 7 g of defatted soybean seeds in each tube. Allergens were extracted with 40% v/v IPA/water (seed/extraction buffer 1:5 g/mL) for 1 h at room temperature. Supernatant, containing residual fine flour particles, was filtered using a 0.45 μm filter membrane. The wet seed material was subjected to a second round of extraction with 40% v/v IPA/water, and the extract was subjected to filtration as before. The extracts were subsequently subjected to centrifugal separation at 20000*g* at 4 °C to remove the fine particles. Cold acetone precipitation of the extracted proteins was performed at −20 °C for 2 days (extract/acetone = 1:4). The resulting precipitate was subjected to centrifugal separation at 7200*g* for 15 min, and the supernatant was discarded. The protein precipitate was resolubilized in the solubilization buffer (0.1 M Na_2SO_4/0.2 M NaH_2PO_4/0.05% Tween-20/5% glycerol, pH 8). The purification of HPS and Gly m 4 from the resolubilized crude protein solutions was accomplished using reversed-phase HPLC in two steps: during the first step, HPS and Gly m 4 were crudely separated from each other and the other components in the extract; during the second step, each of the target components (HPS and Gly m 4) was purified to homogeneity. For both steps, reversed phase chromatography was performed using a linear gradient of buffer A (0.1% TFA in water) and buffer B (0.1% TFA in ACN) mobile phases on a Waters XBridge300 C4 250 × 4.6 mm column (Milford, MA, USA). During the first step, a linear gradient from 24 to 29% B was performed to crudely isolate HPS and a linear gradient from 36 to 39% B was performed to isolate Gly m 4. The HPS and Gly m 4 fractions were pooled, lyophilized to dryness, and reconstituted in 5% acetonitrile/0.1% TFA. The HPS-containing fraction was subjected to RP chromatographic separation using a linear gradient between 23 and 31% B over 40 min. HPS-containing fractions were pooled and lyophilized. The Gly m 4-containing fraction was subjected to RP chromatographic separation using a linear gradient between 35.5 and 45.5% B. The Gly m 4 fractions were pooled and lyophilized. The HPS fractions were resolubilized in dissolution buffer containing 100 mM Tris buffer at pH 8.5. For Gly m 4-containing fractions, 10 mM DTT was added to prevent dimerization of Gly m 4. For the generated reference standards, protein concentration was determined by quantitative amino acid analysis. The pooled fractions were aliquoted into vials and stored at −80 °C. Gly m 4 protein has one cysteine residue and, as mentioned, DTT was added to the reference standard to prevent dimerization. In contrast, the presence of DTT in the solvent results in a mixture of variably reduced and nonreduced species for HPS. Consequently, the two reference standards were resolubilized in different storage buffers and also analyzed separately to obtain their respective UV response factors prior to analysis of soybean extracts. The concentrations of HPS and Gly m 4 reference standards were determined by quantitative amino acid analysis based on the amino acid analyses method from Agilent Technologies.

Extraction of HPS and Gly m 4 from Soybean Seeds for 2DLC-UV/MS Assay. Milled ground soybean seeds, stored at −20 °C, were thawed at room temperature in a drybox containing Dry-Rite. Approximately 250 mg of milled soybean seeds was weighed, defatted using 1 mL of hexanes, and mixed at 1200 rpm for 1 h at 25 °C on a Thermomixer. The sample was centrifuged at 30130*g* for 5 min at 4 °C. The supernatant was discarded, and the procedure was repeated followed by removal of the residual hexane present in the defatted sample by evaporation for approximately 5 min. The resulting sample was resuspended in 1 mL of protein extraction buffer (40% v/v IPA/water fortified with enzyme inhibitor, E64 at 9.3 μM). This was followed by vortexing and overnight extraction (for 16 h) at 1200 rpm at 25 °C using a Thermomixer. Following extraction, the sample was centrifuged at 30130*g* for 30 min at 4 °C. The supernatant was transferred to a microfuge tube and subjected to additional centrifugation at 30130*g* for 5 min at 4 °C to remove residual particles. The extracts were then aliquoted for subsequent analyses by 2DLC-UV/MS analyses.

Conditions for 2DLC-UV/MS Assay. Two-dimensional liquid chromatography (2DLC) analyses with ultraviolet and mass spectrometric detection was performed in the heart-cutting mode as described previously.[26] The samples were injected as 10 μL injection volumes using a partial loop fill injection mode. A Propac SAX column (Thermo Scientific, Waltham, MA, USA) with dimensions of 250 mm × 4 mm and 5 μm particle size was used as the first-dimension column. A reversed phase Acquity BEH300 C4 column (Waters) at 70 °C with column dimensions of 100 mm × 2.1 mm and 1.7 μm particle size was used in the second dimension. The 2DLC method details are

presented in Table 1. The first-dimension window for elution of Gly m 4 and HPS reference standards was set before the analyses. The first-dimension cuts from respective time windows were diverted toward a 10 port valve containing two 5 mm × 2.1 mm Van Guard BEH300 C4 reversed phase (RP) trap cartridges (Waters). The proteins eluting between 2.2 and 6.0 min were trapped on the first RP trap cartridge, and the proteins eluting between 8.9 and 16.3 min were trapped on the second RP trap cartridge.

Table 1. Gradient Elution Conditions for First and Second Dimensions for Quantitation of HPS and Gly m 4 from Soybean Seeds Extracts

first dimension: SAX				second dimension: reversed phase			
SAX cuts: 2.2−6.0 and 8.9−16.3 min				temperature: 70 °C			
temperature: 30 °C				MPA2: 0.1% TFA in water			
MPA1: 10 mM Tris-HCl, pH 7.6				MPB2: 0.1% TFA in 90/10 2-propanol/acetonitrile			
MPB1: 10 mM Tris-HCl/1 M NaCl, pH 7.6				diode array detector wavelength: 215 nm			
VWD wavelength: 215 nm				bandwidth and slit width: 4 nm			
peak width: 0.2 min				peak width: 0.4 min			
time, min	flow rate, mL/min	% A1	% B1	time, min	flow rate, mL/min	% A2	% B2
initial	0.5	95	5	initial	0.3	86	14
20	0.5	75	25	8	0.3	86	14
21	1	75	25	38	0.3	80	20
26	1	0	100	41	0.3	40	60
31	1	95	5	44	0.3	74	26
36	1	95	5	49	0.3	74	26
37	0.1	95	5	59	0.3	65	35
63	0.1	95	5	62	0.3	40	60
64	0.5	95	5	65	0.3	86	14
				68	0.3	86	14

UV data were acquired using a variable-wavelength detector (Agilent) and a diode array detector (Agilent) for the first and second dimensions, respectively. A solution containing 7:25:68 v/v% of glycerol/acetonitrile/water was teed into the second-dimension effluent before mass spectrometric analysis. Positive-ion electrospray ionization (ESI) was performed on an Agilent 6538 mass spectrometer. The m/z scan range was 500−2500 amu, and the data were acquired at 1.32 spectra/s.

RESULTS AND DISCUSSION

Isolation and Characterization of HPS and Gly m 4 Allergens. HPS was isolated from soybean seeds using a 40% isopropanol solution on the basis of a previously published approach[26] with minor modifications. HPS elutes as two major isoforms; the main isoform (form II) consists of the complete amino acid sequence (1−80), whereas the minor isoform (Form I) is truncated at the N-termini (3−80). Truncation at the N-terminus has been attributed to the proteolytic activity in the soybean hulls and seeds. The reference standard was generated for the main isoform and was denoted as the HPS reference standard for quantification purposes. The HPS reference standard was characterized by reversed phase chromatographic analysis with UV (215 nm) and ESI-MS detection (Figure 1). The reference standard elutes as a single chromatographic peak with a retention time of 15.2 min. The transformed maximum entropy spectrum depicts intact masses for this peak at 8351.3 Da. The observed mass is within 0.006% of its theoretical average molecular mass. Further detailed characterization of the reference standard was carried out using peptide mass fingerprinting with successive in-solution proteolysis with trypsin/endoproteinase Asp-N and an in-solution limited trypsin proteolysis. The sequences were confirmed by ESI/LC/MS and tandem ESI/LC/MS/MS analyses. A summary of mass spectral data and assignments from ESI/LC/MS/MS analyses are presented in Table 2. On the basis of the application of multiple proteases, complete sequence coverage was obtained for the isolated HPS reference standard.

HPS has been interchangeably referred to as Gly m 1, a soybean allergen, in several papers. On the basis of one report, the two proteins are essentially the same protein but post-

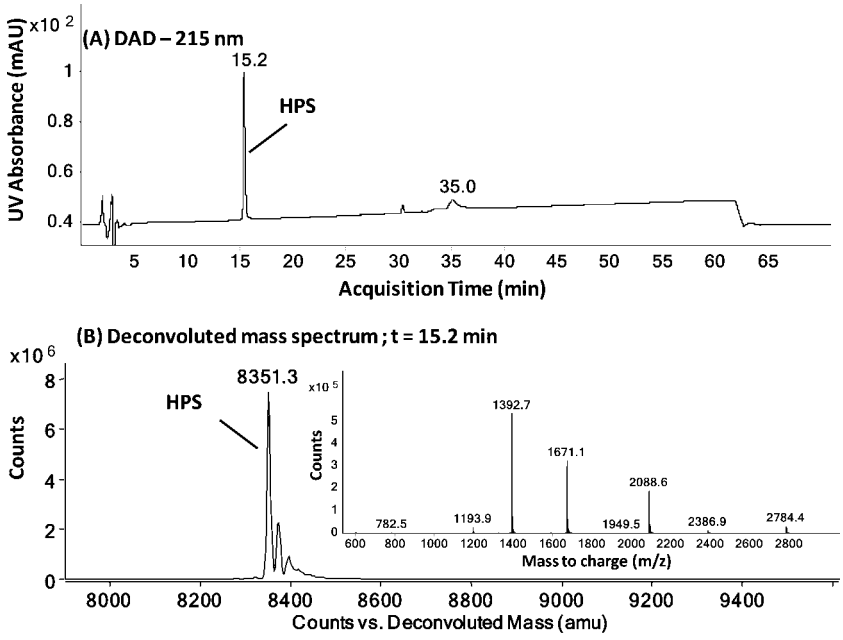

Figure 1. Characterization of reference HPS standard: (A) blank subtracted LC-UV (215 nm) chromatogram of intact reference HPS standard; (B) deconvoluted mass spectrum of reference HPS standard (inset, multiple charge envelope mass spectrum).

Table 2. Summary of Peptides Identified by LC-MS/MS Analysis of HPS Reference Standard Subjected to Successive Proteolytic Cleavage Using Trypsin and Endoproteinase AspN

sequence location	sequence	mass		delta ppm
		theor	exptl	
A(1−9)	ALITRPSCP	1013.5328	1013.5327	−0.1
A(1−25)	ALITRPSCPDLSICLNILGGSLGTV	2626.3823	2626.3807	−0.57
A(1−26)	ALITRPSCPDLSICLNILGGSLGTVD	2741.4092	2741.4068	−0.87
A(10−25)	DLSICLNILGGSLGTV	1630.8600	1630.8589	−0.67
A(10−26)	DLSICLNILGGSLGTVD	1745.8870	1745.8858	−0.66
A(26−36)	DDCCALIGGLG	1149.4794	1149.4791	−0.34
A(27−36)	DCCALIGGLG	1034.4525	1034.4519	−0.62
A(37−49)	DIEAIVCLCIQLR	1601.8269	1601.8252	−1.09
A(37−69)	DIEAIVCLCIQLRALGILNLNRNLQLILNSCGR	3835.0747	3835.0689	−1.51
A(50−58)	ALGILNLNR	982.5924	982.5919	−0.48
A(59−69)	NLQLILNSCGR	1286.6765	1286.6759	−0.45
A(70−79)	SYPSNATCPR	1151.5030	1151.5028	−0.18
A(70−80)	SYPSNATCPRT	1252.5506	1252.5500	−0.5

translationally processed in a different way.[22] Although there is a potential N-glycosylation site near the carboxyl terminus (aa 74−76), similar to other studies,[20] our laboratory did not detect the presence of glycosylation on the asparagine amino acid residue in HPS. The two purified HPS isoforms were subjected to isoelectric focusing. The p*I* of forms I and II were found to be 6.7 and 7.0, respectively (data not shown). No glycosylation was observed for either of the two isoforms of HPS. Further research is needed to unequivocally resolve whether glycosylation is indeed present on the Gly m 1 protein as stated in the literature.

The Gly m 4 reference standard was also generated from soybean seeds. Purification and detailed characterization of the Gly m 4 reference standard has been reported previously.[26] Similar to HPS, complete sequence coverage was also obtained for the Gly m 4 protein.

The concentrations of HPS and Gly m 4 reference standards were determined by quantitative amino acid analysis to be 770 and 402 μg/mL, respectively. Both HPS and Gly m 4 reference standards were diluted to the required concentration for 2DLC-UV/MS assay using 10 mM Tris, pH 8.5, buffer.

Method Development. The 2DLC-UV/MS-based Gly m 4 quantification method[26] was further expanded to accommodate quantitation of HPS in a single analysis. As aforementioned, the method consists of using a two-dimensional liquid chromatographic approach operating in the "heart-cutting" mode with strong anion exchange (SAX) chromatography and reversed phase chromatography in the first and second dimensions, respectively, followed by UV and mass spectrometric detection. The mass spectrometric confirmation for the absence of any coelution with HPS and Gly m 4 peaks during the separation of protein extracts was observed to be critical for ensuring that the required selectivity is achieved.

It was observed that HPS does not bind to the anion exchange column and elutes in the column void volume along with other nonretained proteins. The components eluting between 2.2 and 6.0 min were introduced into the second dimension. Careful method development was required in the second dimension to ensure the absence of any coelution. Figure 2 depicts the chromatographic separation achieved in the second dimension for the two major isoforms along with respective mass spectrometric characterization. As shown in Figure 2A, the optimized method has sufficient resolution to separate HPS isoforms from one another and from other components eluting from the heart-cut SAX chromatographic fraction. The raw mass spectra (Figures 2B,C) and the corresponding deconvoluted mass spectra (Figures 2D,E) further confirm the specificity of the developed 2DLC method.

In contrast, Gly m 4 elutes between 8.9 and 16.0 min during the linear salt gradient. Prior work from our laboratory has shown that the two isoforms of Gly m 4 elute in this window. The two isoforms were observed to have the same sequence but with slightly different anion exchange retention behavior, presumably due to different conformations. In this method, both of these isoforms were quantified as a single peak.

Several conditions were evaluated to optimize simultaneous extraction of the two allergenic proteins from soybean seeds. These included (i) selection of appropriate solvent, (ii) extraction time, and (iii) use of enzyme inhibitors. Once optimized for solvent, two different seed to solvent (w/v) ratios (1:4 and 1:7) were also evaluated.

The different solvents that were evaluated were 60% ethanol, 25% 2-propanol, 40% 2-propanol, and 55% 2-propanol. On the basis of the analyses, 40% 2-propanol extraction solvent was selected because of the maximum recovery obtained for both of the proteins. Of the two solvent ratios evaluated, the 1:4 ratio provided maximum extraction of the two proteins. Similarly, extraction times (2 h, 4 h, and overnight (16 h)) were compared to understand the level of recovery for the two proteins. On the basis of the analyses, overnight extraction (16 h) was selected. As reported previously, HPS elutes as two main isoforms during reversed phase chromatography along with other minor truncations. A number of enzyme inhibitors were evaluated to limit the truncations occurring during the extraction process. Of the different enzyme inhibitors evaluated, E-64, a cysteine protease inhibitor, was found to be critical in preventing further N-terminal truncation of HPS. Because the truncated version of HPS differs in only two neutral amino acids, an identical chromatographic response factor was assumed for the two isoforms, and quantitation was carried out using purified reference standard for HPS (form II). No truncations were observed for Gly m 4 in the presence or absence of E-64. A representative chromatographic and mass spectrometric profile obtained for the separation of soybean extracts is shown in Figure 3. The "heart-cuts" employed in the SAX dimension and the SAX chromatography profile are depicted in Figure 3A. The reversed-phase chromatography profiles for the first and second cuts are shown in Figure 3B.

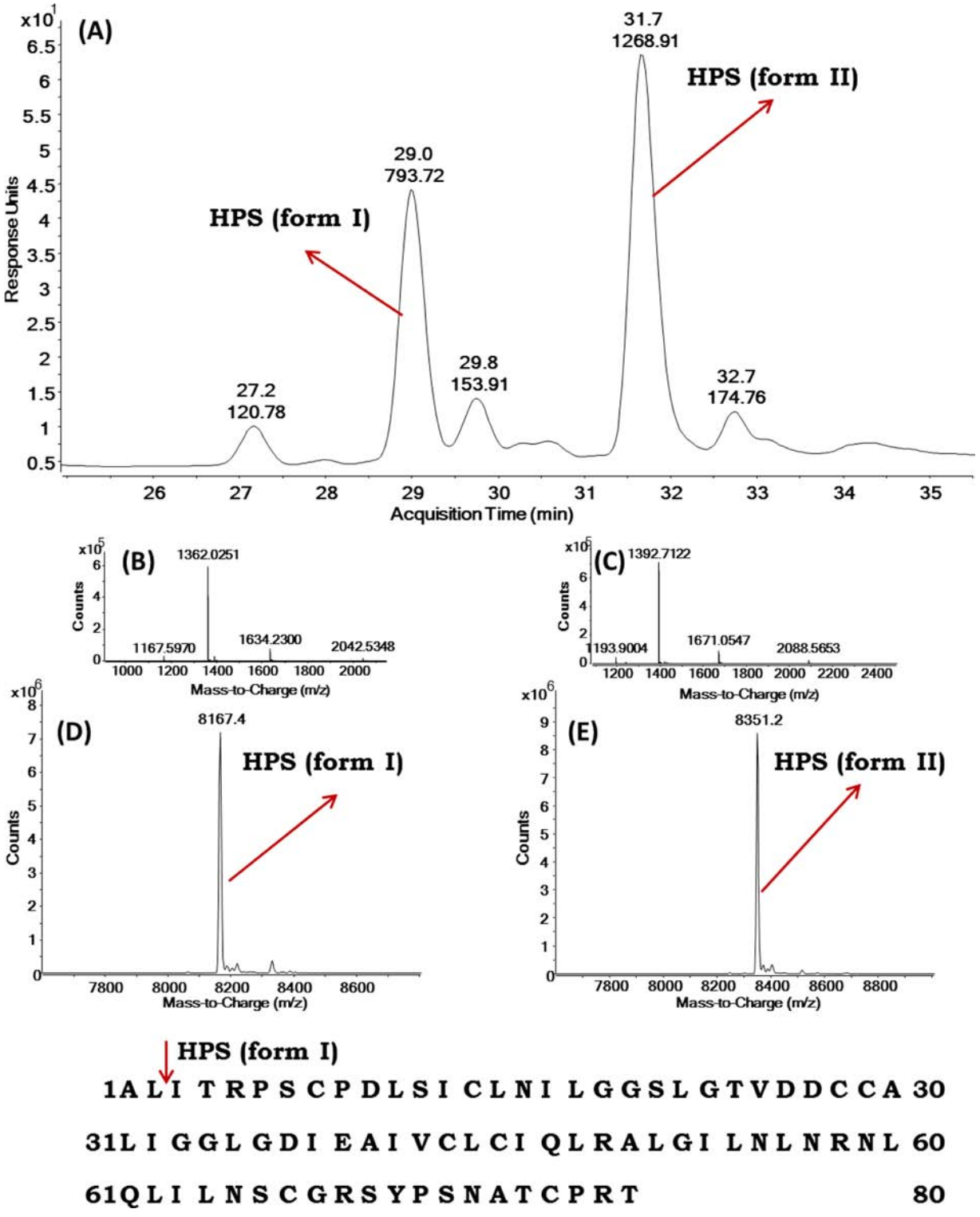

Figure 2. Representative (A) UV (215 nm) chromatogram from reversed-phased (second dimension) chromatography of soybean seed extract, (B) raw mass spectrum of HPS (form 1), (C) raw mass spectrum of HPS (form II), (D) deconvoluted mass spectrum of HPS (form I), and (E) deconvoluted mass spectrum of HPS (form II).

The deconvoluted mass spectra of HPS forms I and II and Gly m 4, shown in Figures 3C−3E, confirm the specificity of the 2DLC method.

Method Validation. Basal level of endogenous Gly m 4 and HPS was first determined in a control non-transgenic soybean sample for evaluating linearity and recovery of the 2DLC-UV/MS assay. The basal levels of endogenous HPS and Gly m 4 were observed to be 337.3 and 185.7 μg/g, respectively. Representative chromatograms from the second-dimension separation of protein extract at different HPS/Gly m 4 levels are presented in Figures 4A,B. The assay was observed to be linear over the evaluated range with R^2 values of 0.996 and 0.997 for HPS and Gly m 4, respectively. The evaluated linear ranges for HPS and Gly m 4 were from 11.9 to 599.8 μg/

dx.doi.org/10.1021/jf500087s | J. Agric. Food Chem. 2014, 62, 4884−4892

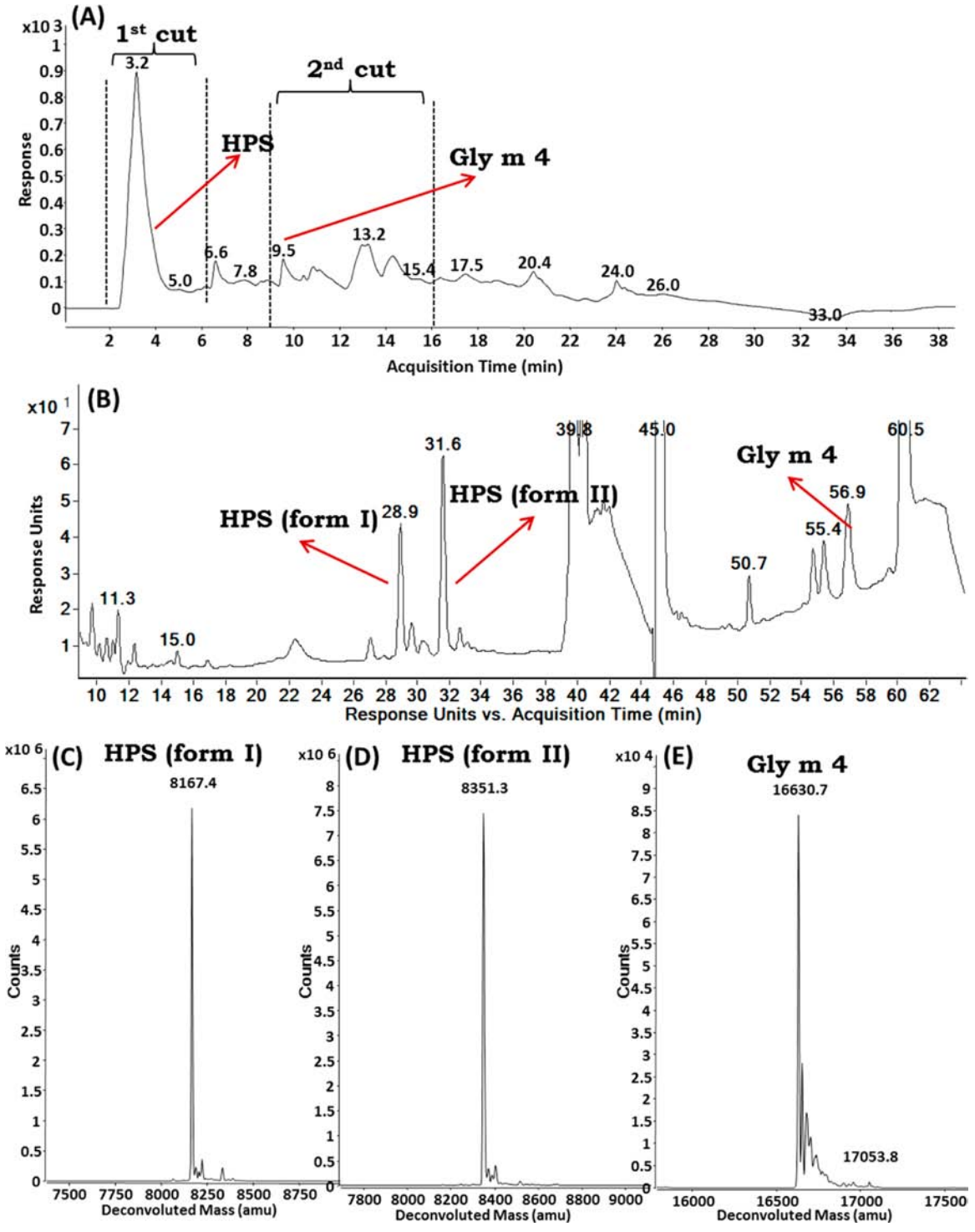

Figure 3. Representative 2DLC-UV/MS analyses of soybean extract from control soybean line: UV chromatograms (215 nm) from (A) first- and (B) second-dimension separations; (C) deconvoluted mass spectrum of component at retention time 28.9 min; (D) deconvoluted mass spectrum of component at retention time 31.6 min; (E) deconvoluted mass spectrum of component at retention time 56.9 min.

mL and from 6.9 to 355.1 μg/mL, respectively (Figure 4C,4D). The evaluated range was in the physiologically relevant range as also observed by the levels of these two allergens in the non-transgenic commercial lines.

Assay recovery (percent relative error, %RE) was also calculated for the two allergens in the respective linear range and is presented in Table 3. The recovery range (%RE) for HPS was observed to be from −1.1 to −13.7% with an average recovery of −4.8%. The recovery range (%RE) for Gly m 4 was observed to be from −3.5% to 15.2% with an average recovery of 5.6%. The validation results for assay intraday and interday precision (percent coefficient of variation, %CV) were calculated for the two allergens. The summarized results are presented in Table 4. Precision in the simultaneous measurement of two allergens at their intact level was measured by use of four different seed lines encompassing low, medium, and

dx.doi.org/10.1021/jf500087s | J. Agric. Food Chem. 2014, 62, 4884−4892

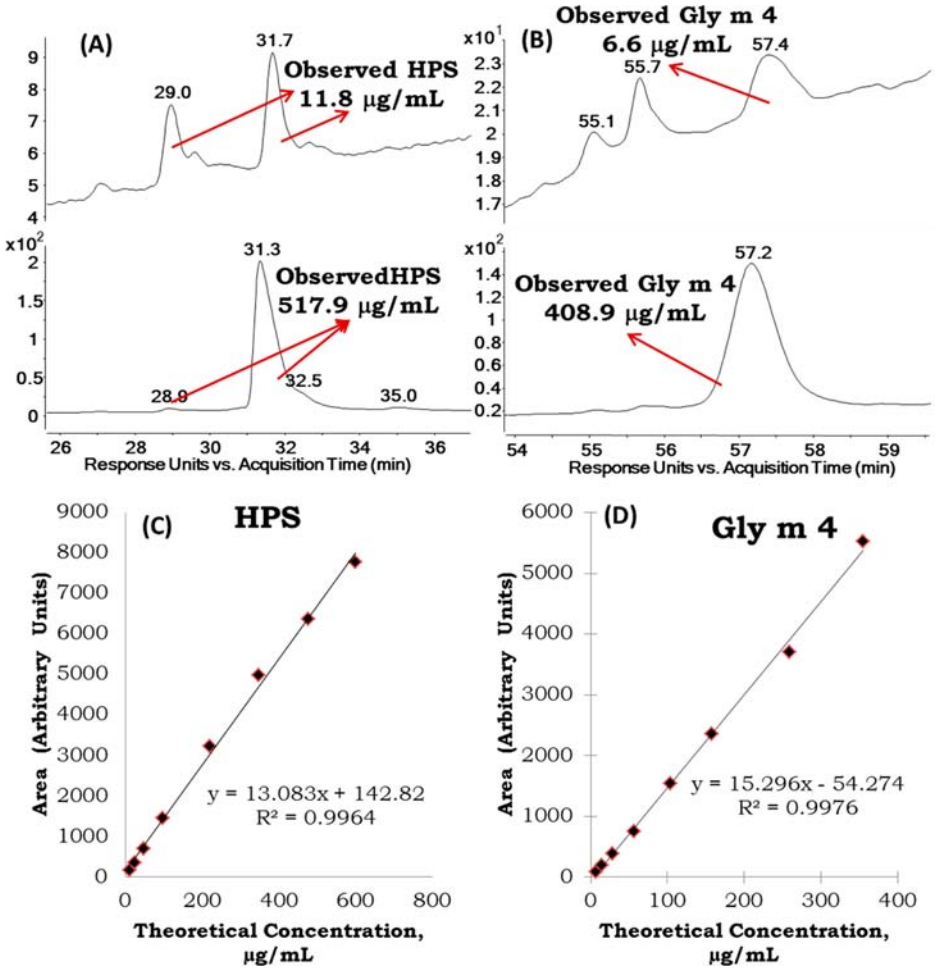

Figure 4. Second-dimension UV (215 nm) chromatograms obtained from the soybean seed kernel extracts spiked with HPS or Gly m 4 reference standards to obtain (A) HPS concentrations of 11.8 and 517.9 μg/mL and (B) Gly m 4 concentrations of 6.6 and 408.9 μg/mL; standard linearity curves for (C) HPS and (D) Gly m 4 over the ranges from 11.9 to 599.8 μg/mL and from 6.9 to 355.1 μg/mL, respectively.

Table 3. Multipoint Recovery of the 2DLC-UV Method for Quantification of HPS and Gly m 4 at Various Concentrations

HPS (μg/mL)			Gly m 4 (μg/mL)		
expected	observed	recovery (% RE)	expected	observed	recovery (% RE)
11.90	11.76	−1.14	6.9	6.6	−3.5
24.14	23.45	−2.84	13.9	14.3	3.1
48.50	46.83	−3.44	27.9	28.9	3.6
97.16	97.16	0.00	56.0	56.0	0.0
220.08	215.79	−1.95	103.4	113.8	10.1
347.59	332.10	−4.46	158.2	174.7	10.4
477.91	424.30	−11.22	258.6	274.7	6.2
599.87	517.88	−13.67	355.1	408.9	15.2
	av	−4.8		av	5.6

high levels of HPS and Gly m 4. For the 4 day validation study, the precision ranges (%CV) were observed to be 4.7−9.2% for HPS and 6.3−9.4% for Gly m 4 at the various allergen concentrations tested. The average precision over all the samples was found to be less than the average target precision of 15.0%.

The stability of the two allergens in seed extracts was evaluated at the autosampler temperature (5 °C) at different time intervals: 24, 47, and 69 h. For the three time intervals studied, compared with the initial time (~9 h), losses of 8.8, 3.6, and 17.1% were observed for HPS and losses of 12.4, 2.4, and 16.7% were observed for Gly m4. On the basis of the above data, the assay was determined to be stable for at least for 47 h when performed using an autosampler maintained at 5 °C.

The assay was also evaluated for its robustness with changes in column temperatures. The column temperature was systematically changed in each of the two dimensions, and the levels of Gly m 4 and HPS were compared with their levels observed with first- and second-dimension temperatures of 30 and 70 °C, respectively. Initially, the first-dimension column temperature was fixed at 30 °C, and the second-dimension column temperature was varied at two selected temperatures, 65 and 75 °C. The relative levels of HPS were observed to be 84 and 99.1%, respectively. Similarly, the relative levels of Gly m 4 were observed to be 96.1 and 106.2%, respectively. This was followed by maintaining the second-dimension temperature at 70 °C and setting the first-dimension temperatures of 27 and 33 °C. The relative levels of HPS were observed to be 103.8 and 98.7%, respectively, whereas the relative levels of Gly m 4 were observed to be 106.2 and 106.0%. The method was observed to be more sensitive to temperature changes in the second dimension. It is recommended to precisely control the assay temperatures in both dimensions.

dx.doi.org/10.1021/jf500087s | J. Agric. Food Chem. 2014, 62, 4884−4892

Table 4. Precision of the 2DLC-UV Method for Quantification of HPS and Gly m 4 from Soybean Extracts

		HPS			Gly m 4		
day		low	medium	high	low	medium	high
1	av μg/mL	51.0	74.4	124.1	53.3	92.1	150.6
	av μg/g	198.5	291.6	483.3	206.5	358.8	590.0
	SD	4.4	13.3	16.9	5.5	5.4	7.8
	%CV	2.2	4.6	3.5	2.7	1.5	1.3
2	av μg/mL	51.0	76.8	127.2	55.0	91.8	155.4
	av μg/g	188.6	284.2	470.1	204.3	339.5	574.8
	SD	1.8	5.5	5.0	6.6	4.1	9.9
	%CV	1.0	1.9	1.1	3.2	1.2	1.7
3	av μg/mL	47.1	69.9	119.6	59.0	98.5	148.1
	av μg/g	176.1	261.8	442.4	217.9	364.2	554.7
	SD	3.7	16.1	5.6	7.4	15.1	27.9
	%CV	2.1	6.2	1.3	3.4	4.2	5.0
4	av μg/mL	45.2	65.9	119.6	47.3	86.0	140.8
	av μg/g	168.0	243.1	439.2	173.9	315.9	519.4
	SD	3.7	8.7	5.7	9.1	5.0	7.9
	%CV	2.2	3.6	1.3	5.2	1.6	1.5
4 day av	av μg/mL	47.8	70.1	122.6	53.7	92.1	146.5
	av μg/g	180.8	265.5	458.8	200.7	344.6	554.7
	SD	15.8	24.5	21.4	18.8	21.9	35.3
	%CV	8.7	9.2	4.7	9.4	6.3	6.4

Carry-over present in samples that followed the highest respective HPS and Gly m 4 levels was observed to be 0.1 and 0.6%, respectively. This corresponded to 4.3 and 37.9% of the area of the lowest concentration of HPS and Gly m 4, respectively.

To evaluate extraction efficiency of Gly m 4 and HPS, two successive overnight extractions were carried out. The successive extraction did not yield additional Gly m 4 and HPS protein, suggesting complete extraction of the two proteins in the first extraction.

Simultaneous Analyses of HPS and Gly m 4 in Commercial Soybean Lines. The levels of HPS and Gly m 4 were quantified using this assay in 10 selected non-transgenic commercial lines. The concentrations of the two allergens were observed to be within respective validated linear ranges. The levels of HPS and Gly m 4 in each line are presented in Figure 5. On the basis of the analyses, various levels of HPS and Gly m 4 were observed in different commercial lines with no apparent trend. In most of the samples (7 of 11), Gly m 4 levels were observed to be higher than HPS levels. Significantly greater variability (648%) was observed in expression levels of HPS in the 10 commercial lines compared with variability in expression levels for Gly m 4 (212%). Further statistically designed and replicated studies need to be carried out to determine the source of this variation.

In conclusion, this study demonstrates the use of a 2DLC-UV/MS-based assay for the simultaneous quantification of two allergens of interest at their intact level. The ability to quantify more than one allergen in a single analysis expands the applicability of these assays. Throughput of the assay can be further improved by intelligent method development in either dimension and by using novel trapping approaches. The assay was successfully applied to understand levels of HPS and Gly m 4 in 10 non-transgenic commercial soybean lines. Further research is needed to understand the biovariability of these allergens, especially as a result of growing environment. Another important aspect to understand is the level at which each of these allergen elicits an allergenic response. Moreover, several methods are currently available to quantify proteins of interest. It will be critical to compare these methods to get consistency and understand the biases, if any, inherent within each of these quantitative methods.

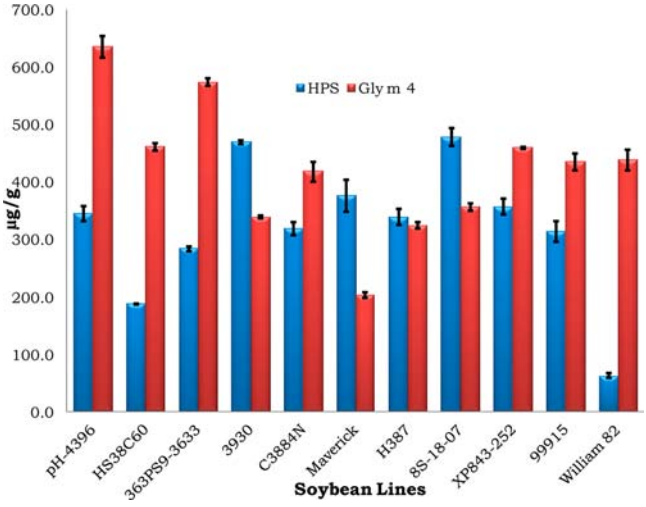

Figure 5. Determination of HPS and Gly m 4 levels in different commercially available soybean lines.

AUTHOR INFORMATION

Corresponding Author

*(S.J.) Phone: (989) 636-1533. Fax: (989) 638-6443. E-mail: sjulka@dow.com.

Notes

The authors declare no competing financial interest.

■ ACKNOWLEDGMENTS

We thank Rod Herman and Paul O'Connor for excellent technical review. We also thank Margaret Covington, Linda Singletary, and Shawna Embrey for their technical assistance and Michelle Mayes for sourcing and preparation of the ground soybean seeds.

■ REFERENCES

(1) Stevenson, S. E.; Houston, N. L.; Thelen, J. J. Evolution of seed allergen quantification − from antibodies to mass spectrometry. *Regul. Toxicol. Pharmacol.* **2010**, *58*, S36−S41.

(2) Natarajan, S.; Xu, C.; Cregan, P.; Caperna, T. J.; Garrett, W. M.; Luthria, D. Utility of proteomics techniques for assessing protein expression. *Regul. Toxicol. Pharmacol.* **2009**, *54*, S32−S36.

(3) Rouquié, D.; Capt, A.; Eby, W. H.; Sekar, V.; Hérouet-Guicheney, C. Investigation of endogenous soybean food allergens by using a 2-dimensional gel electrophoresis approach. *Regul. Toxicol. Pharmacol.* **2010**, *58*, S47−S53.

(4) Stevenson, S. E.; Woods, C. A.; Hong, B.; Kong, X.; Thelen, J. J.; Ladics, G. S. Environmental effects on allergen levels in commercially grown non-genetically modified soybeans: assessing variation across North America. *Front. Plant Sci.* **2012**, *3*, 1−13.

(5) Holzhauser, T.; Wackermann, O.; Ballmer-Weber, O. W.; Bindslev-Jensen, C.; Scibilia, J.; Perono-Garoffo, L.; Utsumi, S.; Poulsen, L. K.; Vieths, S. Soybean (*Glycine max*) allergy in Europe: Gly m 5 (β-conglycinin) and Gly m 6 (glycinin) are potential diagnostic markers for severe allergic reactions to soy. *J. Allergy Clin. Immunol.* **2009**, *123*, 452−458.

(6) IUIS Allergen Nomenclature Sub-Committee, http://www.allergen.org/search.php?allergensource=soy&searchsource=Search, April 7, 2014.

(7) Bando, N.; Tsuji, H.; Hiemori, M.; Yoshizumi, K.; Yamanishi, R.; Kimoto, M.; Ogawa, T. Quantitative analysis of Gly m Bd 28K in soybean products by a sandwich enzyme-linked immunosorbent assay. *J. Nutr. Sci. Vitaminol.* **1998**, *44*, 655−664.

(8) Liu, B.; Teng, D.; Wang, X.; Wang, J. Detection of the soybean allergenic protein *Gly m* Bd 28K by an indirect enzyme-linked immunosorbent assay. *J. Agric. Food Chem.* **2013**, *61*, 822−828.

(9) Batard, T.; Nony, E.; Hrabina, M.; Chabre, H.; Frati, F.; Moingeon, P. Advances in the quantification of relevant allergens in allergenic extracts. *Eur. Ann. Allergy Clin. Immunol.* **2013**, *45* (Suppl.2), 33−37.

(10) Picariello, G.; Mamone, G.; Addeo, F.; Ferranti, P. The frontiers of mass spectrometry-based techniques in food allergenomics. *J. Chromatogr., A* **2011**, *1218*, 7386−7398.

(11) Houston, N. L.; Lee, D.-G.; Stevenson, S. E.; Ladics, G. S.; Bannon, G. A.; McClain, S.; Privalle, L.; Stagg, N.; Herouet-Guicheney, C.; MacIntosh, S. C.; Thelen, J. J. Quantitation of soybean allergens using tandem mass spectrometry. *J. Proteome Res.* **2011**, *10*, 763−773.

(12) Seppala, U.; Dauly, C.; Robinson, S.; Hornshaw, M.; Larsen, J. N.; Ipsen, H. Absolute quantification of allergens from complex mixtures: a new sensitive tool for standardization of allergen extracts for specific immunotherapy. *J. Proteome Res.* **2011**, *10*, 2113−2122.

(13) Fenaille, F.; Nony, E.; Chabre, H.; Lautrette, A.; Couret, M.-N.; Batard, T.; Moingeon, P.; Ezan, E. Mass spectrometric investigation of molecular variability of grass pollen group 1 allergens. *J. Proteome Res.* **2009**, *8*, 4014−4027.

(14) Makawita, S.; Diamandis, E. P. The bottleneck in the cancer biomarker pipeline and protein quantification through mass spectrometry-based approaches: current strategies for candidate verification. *Clin. Chem.* **2010**, *56*, 212−222.

(15) Sherman, J.; McKay, M. J.; Ashman, K.; Molloy, M. P. How specific is my SRM? The issue of precursor and product ion redundancy. *Proteomics* **2009**, *9*, 1120−1123.

(16) Kuppannan, K.; Albers, D.; Schafer, B. W.; Dielman, D.; Young, S. A. Quantification and characterization of maize lipid transfer protein, a food allergen, by liquid chromatography with ultraviolet and mass spectrometric detection. *Anal. Chem.* **2011**, *83*, 516−524.

(17) Czerwenka, C.; Maier, I.; Potocnik, N.; Pittner, F.; Lindner, W. Absolute quantitation of α-lactoglobulin by protein liquid chromatography-mass spectrometry and its application to different milk products. *Anal. Chem.* **2007**, *79*, 5165−5172.

(18) Julka, S.; Folkenroth, J.; Young, S. A. Two dimensional liquid chromatography−ultraviolet/mass spectrometric (2DLC−UV/MS) analyses for quantitation of intact proteins in complex biological matrices. *J. Chromatogr., B* **2011**, *879*, 2057−2063.

(19) Gijzen, M.; Kuflu, K.; Moy, P. Gene amplification of the Hps locus in *Glycine max*. *BMC Plant Biol.* **2006**, *6*, 6.

(20) Odani, S.; Koide, T.; Ono, T.; Seto, T.; Tanaka, T. Soybean hydrophobic protein. Isolation, partial characterization and the complete primary structure. *Eur. J. Biochem.* **1987**, *162*, 485−491.

(21) Baud, F.; Pebay-Peyroula, E.; Cohen-Addad, C.; Odani, S.; Lehmann, M. S. Crystal structure of hydrophobic protein from soybean; a member of a new cysteine rich family. *J. Mol. Biol.* **1993**, *231*, 877−887.

(22) Gonzalez, R.; Varela, J.; Carreira, J.; Polo, F. Soybean hydrophobic protein and soybean hull allergy. *Lancet* **1995**, *346*, 48−49.

(23) Gijzen, M.; Miller, S. S.; Kuflu, K.; Buzzell, R. I.; Miki, B. L. A. Hydrophobic protein synthesized in the pod endocarp adheres to the seed surface. *Plant Physiol.* **1999**, *120*, 951−960.

(24) Berkner, H.; Neudecker, P.; Mittag, D.; Ballmer-Weber, B. K.; Schweimer, K.; Vieths, S.; Rosch, P. Cross-reactivity of pollen and food allergens: soybean Gly m 4 is a member of the Bet v 1 superfamily and closely resembles yellow lupine proteins. *Biosci. Rep.* **2009**, *29*, 183−192.

(25) Crowell, D. N.; John, M. E.; Russell, D.; Amasino, R. M. Characterization of a stress-induced, developmentally regulated gene family from soybean. *Plant Mol. Biol.* **1992**, *18*, 459−466.

(26) Julka, S.; Kuppannan, K.; Karnoup, A.; Dielman, D.; Schafer, B.; Young, S. A. Quantification of Gly m 4 protein, a major soybean allergen, by two-dimensional liquid chromatography with ultraviolet and mass spectrometry detection. *Anal. Chem.* **2012**, *84*, 10019−10030.

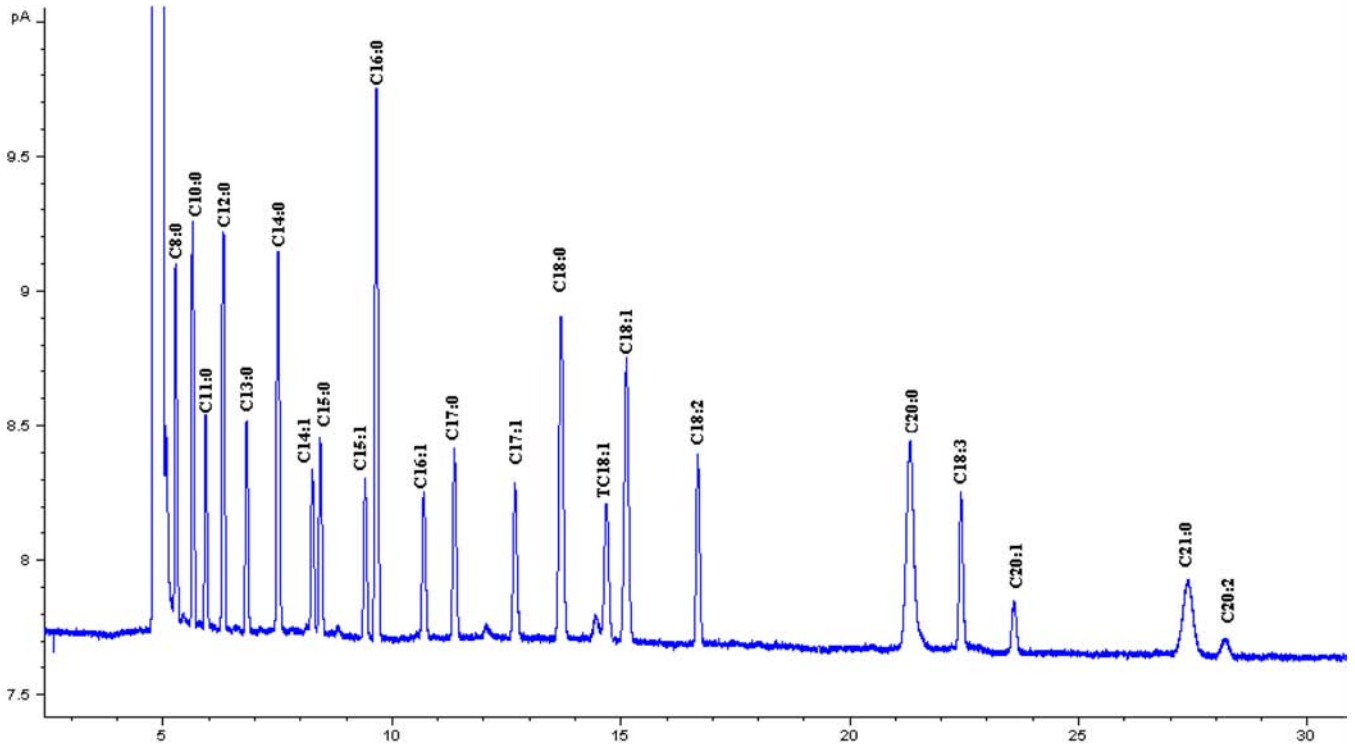

Figure 1. Gas chromatogram of standards solution containing the fatty acid methyl esters.

Table 1. Fatty Acid and Triglyceride Compositions of Extra-Virgin Olive Oil (EVOO), Soybean Oil (SO), and Mixtures of EVOO and SO[a]

	EVOO	SO	EVOO + 1% SO	EVOO + 2% SO	EVOO + 3% SO	EVOO + 4% SO	EVOO + 5% SO	EVOO + 10% SO
C16:0	15.82 ± 0.19	11.00 ± 0.13	15.59 ± 0.19	15.53 ± 0.19	15.49 ± 0.18	15.37 ± 0.18	15.30 ± 0.18	14.89 ± 0.18
C16:1	1.99 ± 0.02	0.10 ± 0.00	1.98 ± 0.02	1.98 ± 0.02	1.97 ± 0.02	1.95 ± 0.02	1.94 ± 0.02	1.91 ± 0.02
C17:0	0.04 ± 0.00	0.10 ± 0.00	0.05 ± 0.00	0.05 ± 0.00	0.05 ± 0.00	0.06 ± 0.00	0.06 ± 0.00	0.06 ± 0.00
C17:1	0.09 ± 0.00	0.05 ± 0.00	0.09 ± 0.00	0.09 ± 0.00	0.09 ± 0.00	0.08 ± 0.00	0.08 ± 0.00	0.08 ± 0.00
C18:0	2.18 ± 0.02	4.66 ± 0.06	2.24 ± 0.03	2.26 ± 0.03	2.29 ± 0.03	2.31 ± 0.02	2.34 ± 0.03	2.44 ± 0.03
C18:1	62.37 ± 0.76	21.83 ± 0.26	62.13 ± 0.76	61.75 ± 0.75	61.34 ± 0.75	61.12 ± 0.74	60.70 ± 0.74	59.07 ± 0.72
C18:2	16.21 ± 0.19	53.93 ± 0.66	16.60 ± 0.20	17.01 ± 0.20	17.44 ± 0.21	17.76 ± 0.21	17.91 ± 0.21	19.71 ± 0.24
C18:3	0.69 ± 0.01	7.77 ± 0.09	0.71 ± 0.01	0.72 ± 0.01	0.74 ± 0.01	0.76 ± 0.01	1.08 ± 0.01	1.25 ± 0.01
C20:0	0.41 ± 0.00	0.39 ± 0.00	0.41 ± 0.00	0.41 ± 0.00	0.40 ± 0.00	0.40 ± 0.00	0.40 ± 0.00	0 0.40 ± 0.00
C20:1	0.20 ± 0.00	0.17 ± 0.00	0.20 ± 0.00	0.20 ± 0.00	0.19 ± 0.00	0.19 ± 0.00	0.19 ± 0.00	0.19 ± 0.00
TC18:1	0.01 ± 0.00	0.04 ± 0.00	0.03 ± 0.00	0.03 ± 0.00	0.03 ± 0.00	0.03 ± 0.00	0.03 ± 0.00	0.03 ± 0.00
∑(TC18:2 + TC18:3)	0.02 ± 0.00	0.66 ± 0.01	0.04 ± 0.00	0.04 ± 0.00	0.06 ± 0.00	0.06 ± 0.00	0.08 ± 0.00	0.10 ± 0.00
LLL	0.49 ± 0.00	8.27 ± 0.10	0.54 ± 0.00	0.62 ± 0.00	0.90 ± 0.01	1.17 ± 0.01	1.24 ± 0.01	1.86 ± 0.02
ECN40 (LLLn)	0.00 ± 0.00	1.23 ± 0.01	0.27 ± 0.00	0.34 ± 0.00	0.41 ± 0.00	0.48 ± 0.00	0.70 ± 0.01	0.76 ± 0.01
ECN42	1.12 ± 0.01	8.58 ± 0.10	1.42 ± 0.02	1.57 ± 0.02	1.88 ± 0.02	2.08 ± 0.02	2.71 ± 0.03	3.59 ± 0.04
ECN44	10.03 ± 0.12	25.88 ± 0.31	10.15 ± 0.12	10.25 ± 0.12	10.46 ± 0.13	10.65 ± 0.13	10.70 ± 0.13	11.77 ± 0.14
ECN46	34.95 ± 0.42	31.96 ± 0.39	34.90 ± 0.43	34.86 ± 0.43	34.78 ± 0.42	34.74 ± 0.42	34.74 ± 0.42	34.04 ± 0.41
ECN48	50.14 ± 0.61	22.08 ± 0.27	49.49 ± 0.60	49.18 ± 0.60	48.62 ± 0.59	48.15 ± 0.59	47.24 ± 0.57	45.75 ± 0.56
ECN50	3.76 ± 0.04	10.27 ± 0.12	3.77 ± 0.05	3.80 ± 0.05	3.85 ± 0.04	3.90 ± 0.04	3.91 ± 0.04	4.09 ± 0.05
$ECN42_{theor}$	1.19 ± 0.01	24.00 ± 0.29	1.32 ± 0.02	1.43 ± 0.02	1.58 ± 0.02	1.67 ± 0.02	1.79 ± 0.02	1.82 ± 0.02
ΔECN42	0.07 ± 0.00	15.42 ± 0.19	0.10 ± 0.00	0.14 ± 0.00	0.30 ± 0.00	0.41 ± 0.00	0.93 ± 0.01	1.77 ± 0.02
ECN44 + ECN46	44.98 ± 0.54	57.84 ± 0.70	45.05 ± 0.55	45.11 ± 0.55	45.24 ± 0.55	45.39 ± 0.55	45.44 ± 0.55	45.81 ± 0.55
ECN46/LLL	71.32	3.86	64.62	56.22	38.64	29.69	28.01	18.30
(ECN44 + ECN46)/ LLL	91.79	6.99	83.42	72.75	50.26	38.79	36.64	24.62

[a]Each value represents the mean of four determinations of two successive crop seasons (n = 4; two different samples for each crop season).

With regard to GC, the International Union of Pure and Applied Chemistry (IUPAC) has adopted a method to resolve triglycerides according to the number of equal carbon atoms by gas−liquid chromatography (GLC).[24] However, the technique is

dx.doi.org/10.1021/jf500571n | J. Agric. Food Chem. 2014, 62, 4893−4904

Table 2. Fatty Acid and Triglyceride Compositions of Extra-Virgin Olive Oil (EVOO), Corn Oil (CO), and Mixtures of EVOO and CO[a]

	EVOO	CO	EVOO + 1% CO	EVOO + 2% CO	EVOO + 3% CO	EVOO + 4% CO	EVOO + 5% CO	EVOO + 10% CO
C16:0	15.82 ± 0.19	12.03 ± 0.14	15.83 ± 0.19	15.82 ± 0.19	15.80 ± 0.19	15.77 ± 0.19	15.60 ± 0.19	14.81 ± 0.18
C16:1	1.99 ± 0.02	0.13 ± 0.00	1.98 ± 0.02	1.98 ± 0.02	1.98 ± 0.02	1.97 ± 0.02	1.95 ± 0.02	1.90 ± 0.02
C17:0	0.04 ± 0.00	0.06 ± 0.00	0.04 ± 0.00	0.04 ± 0.00	0.04 ± 0.00	0.04 ± 0.00	0.04 ± 0.00	0.04 ± 0.00
C17:1	0.09 ± 0.00	0.03 ± 0.00	0.08 ± 0.00	0.08 ± 0.00	0.08 ± 0.00	0.08 ± 0.00	0.08 ± 0.00	0.08 ± 0.00
C18:0	2.18 ± 0.02	1.88 ± 0.02	2.18 ± 0.02	2.17 ± 0.02	2.17 ± 0.02	2.15 ± 0.02	2.15 ± 0.02	2.13 ± 0.02
C18:1	62.37 ± 0.76	28.48 ± 0.35	62.16 ± 0.76	61.87 ± 0.75	61.39 ± 0.75	60.78 ± 0.74	60.74 ± 0.74	59.52 ± 0.73
C18:2	16.21 ± 0.19	55.89 ± 0.68	16.42 ± 0.20	16.72 ± 0.20	17.23 ± 0.21	17.89 ± 0.22	18.11 ± 0.22	20.17 ± 0.24
C18:3	0.69 ± 0.01	0.88 ± 0.01	0.69 ± 0.01	0.70 ± 0.01	0.70 ± 0.01	0.71 ± 0.01	0.72 ± 0.01	0.74 ± 0.01
C20:0	0.41 ± 0.00	0.39 ± 0.00	0.41 ± 0.00	0.41 ± 0.00	0.40 ± 0.00	0.40 ± 0.00	0.40 ± 0.00	0.40 ± 0.00
C20:1	0.20 ± 0.00	0.23 ± 0.00	0.21 ± 0.00	0.21 ± 0.00	0.21 ± 0.00	0.21 ± 0.00	0.21 ± 0.00	0.21 ± 0.00
TC18:1	0.01 ± 0.00	0.05 ± 0.00	0.02 ± 0.00	0.04 ± 0.00	0.04 ± 0.00	0.04 ± 0.00	0.04 ± 0.00	0.11 ± 0.00
∑(TC18:2 + TC18:3)	0.02 ± 0.00	1.74 ± 0.02	0.05 ± 0.00	0.06 ± 0.00	0.07 ± 0.00	0.09 ± 0.00	0.10 ± 0.00	0.18 ± 0.00
LLL	0.49 ± 0.00	20.15 ± 0.24	0.52 ± 0.00	0.54 ± 0.00	0.90 ± 0.01	1.17 ± 0.01	1.24 ± 0.01	1.86 ± 0.02
ECN40 (LLLn)	0.00 ± 0.00	1.11 ± 0.01	0.11 ± 0.00	0.17 ± 0.00	0.24 ± 0.00	0.29 ± 0.00	0.36 ± 0.00	0.69 ± 0.01
ECN42	1.12 ± 0.01	20.63 ± 0.25	1.33 ± 0.01	1.38 ± 0.01	1.49 ± 0.02	1.86 ± 0.02	1.98 ± 0.02	2.87 ± 0.03
ECN44	10.03 ± 0.12	38.05 ± 0.46	10.24 ± 0.12	10.73 ± 0.13	11.16 ± 0.13	11.13 ± 0.13	11.67 ± 0.14	12.20 ± 0.15
ECN46	34.95 ± 0.42	27.94 ± 0.34	34.85 ± 0.43	34.83 ± 0.43	34.80 ± 0.43	34.77 ± 0.42	34.68 ± 0.42	34.22 ± 0.42
ECN48	50.14 ± 0.61	11.08 ± 0.13	49.72 ± 0.61	49.17 ± 0.60	48.58 ± 0.59	48.24 ± 0.59	47.60 ± 0.58	46.36 ± 0.56
ECN50	3.76 ± 0.04	1.19 ± 0.01	3.75 ± 0.04	3.72 ± 0.04	3.73 ± 0.04	3.71 ± 0.04	3.71 ± 0.04	3.66 ± 0.04
$ECN42_{theor}$	1.19 ± 0.01	18.39 ± 0.22	1.22 ± 0.01	1.23 ± 0.01	1.28 ± 0.01	1.36 ± 0.01	1.30 ± 0.01	1.61 ± 0.02
ΔECN42	0.07 ± 0.00	2.24 ± 0.03	0.11 ± 0.00	0.15 ± 0.00	0.21 ± 0.01	0.50 ± 0.01	0.68 ± 0.01	1.26 ± 0.01
ECN44 + ECN46	44.98 ± 0.54	65.99 ± 0.80	45.09 ± 0.55	45.56 ± 0.56	45.96 ± 0.56	45.90 ± 0.55	46.35 ± 0.56	46.42 ± 0.57
ECN46/LLL	71.32	1.38	67.01	64.50	38.66	29.71	27.96	18.39
(ECN44 + ECN46)/ LLL	91.79	3.27	86.71	84.37	51.06	39.23	37.37	24.95

[a]Each value represents the mean of four determinations of two successive crop seasons (n = 4; two different samples for each crop season).

Table 3. Fatty Acid and Triglyceride Compositions of Extra-Virgin Olive Oil (EVOO), Sunflower Oil (SfO), and Mixtures of EVOO and SfO[a]

	EVOO	SfO	EVOO + 1% SfO	EVOO + 2% SfO	EVOO + 3% SfO	EVOO + 4% SfO	EVOO + 5% SfO	EVOO + 10% SfO
C16:0	15.82 ± 0.19	6.53 ± 0.08	15.68 ± 0.19	15.56 ± 0.19	15.41 ± 0.18	15.15 ± 0.18	15.00 ± 0.18	14.72 ± 0.18
C16:1	1.99 ± 0.02	0.13 ± 0.00	1.99 ± 0.02	1.99 ± 0.02	1.99 ± 0.02	1.98 ± 0.02	1.98 ± 0.02	1.94 ± 0.02
C17:0	0.04 ± 0.00	0.04 ± 0.00	0.04 ± 0.00	0.04 ± 0.00	0.04 ± 0.00	0.04 ± 0.00	0.04 ± 0.00	0.04 ± 0.00
C17:1	0.09 ± 0.00	0.03 ± 0.00	0.09 ± 0.00	0.09 ± 0.00	0.09 ± 0.00	0.08 ± 0.00	0.08 ± 0.00	0.08 ± 0.00
C18:0	2.18 ± 0.02	3.64 ± 0.04	2.22 ± 0.03	2.24 ± 0.03	2.25 ± 0.02	2.26 ± 0.02	2.27 ± 0.02	2.33 ± 0.03
C18:1	62.37 ± 0.76	27.58 ± 0.33	61.91 ± 0.76	61.47 ± 0.75	61.23 ± 0.75	61.07 ± 0.74	60.82 ± 0.74	59.03 ± 0.72
C18:2	16.21 ± 0.19	61.54 ± 0.75	16.78 ± 0.20	17.35 ± 0.21	17.73 ± 0.21	18.17 ± 0.22	18.56 ± 0.23	20.67 ± 0.25
C18:3	0.69 ± 0.01	0.11 ± 0.00	0.68 ± 0.01	0.67 ± 0.01	0.67 ± 0.01	0.66 ± 0.01	0.66 ± 0.01	0.61 ± 0.00
C20:0	0.41 ± 0.00	0.26 ± 0.00	0.41 ± 0.00	0.40 ± 0.00	0.40 ± 0.00	0.40 ± 0.00	0.40 ± 0.00	0.39 ± 0.00
C20:1	0.20 ± 0.00	0.14 ± 0.00	0.20 ± 0.00	0.19 ± 0.00	0.19 ± 0.00	0.19 ± 0.00	0.19 ± 0.00	0.19 ± 0.00
TC18:1	0.01 ± 0.00	0.05 ± 0.00	0.02 ± 0.00	0.02 ± 0.00	0.02 ± 0.00	0.02 ± 0.00	0.02 ± 0.00	0.02 ± 0.00
∑(TC18:2 + TC18:3)	0.02 ± 0.00	0.73 ± 0.01	0.05 ± 0.00	0.05 ± 0.00	0.05 ± 0.00	0.06 ± 0.00	0.07 ± 0.00	0.15 ± 0.00
LLL	0.49 ± 0.00	23.79 ± 0.29	0.76 ± 0.01	1.04 ± 0.01	1.11 ± 0.01	1.45 ± 0.02	1.50 ± 0.02	2.46 ± 0.03
ECN40 (LLLn)	0.00 ± 0.00	0.21 ± 0.00	0.05 ± 0.00	0.06 ± 0.00	0.07 ± 0.00	0.07 ± 0.00	0.09 ± 0.00	0.11 ± 0.00
ECN42	1.12 ± 0.01	23.91 ± 0.29	1.26 ± 0.01	1.54 ± 0.02	1.84 ± 0.02	2.16 ± 0.02	2.32 ± 0.03	3.39 ± 0.04
ECN44	10.03 ± 0.12	35.66 ± 0.43	10.80 ± 0.13	10.97 ± 0.13	11.12 ± 0.14	11.35 ± 0.14	11.50 ± 0.14	13.00 ± 0.16
ECN46	34.95 ± 0.42	23.31 ± 0.28	34.76 ± 0.42	34.69 ± 0.42	34.52 ± 0.42	34.28 ± 0.41	34.07 ± 0.41	33.41 ± 0.40
ECN48	50.14 ± 0.61	14.61 ± 0.18	49.37 ± 0.60	48.99 ± 0.60	48.71 ± 0.59	48.42 ± 0.59	48.33 ± 0.59	46.47 ± 0.57
ECN50	3.76 ± 0.04	2.30 ± 0.03	3.76 ± 0.04	3.75 ± 0.04	3.74 ± 0.04	3.72 ± 0.04	3.69 ± 0.04	3.62 ± 0.04
$ECN42_{theor}$	1.19 ± 0.01	23.47 ± 0.28	1.28 ± 0.01	1.34 ± 0.01	1.40 ± 0.02	1.45 ± 0.02	1.50 ± 0.02	1.76 ± 0.02
ΔECN42	0.07 ± 0.00	0.44 ± 0.01	0.21 ± 0.00	0.29 ± 0.01	0.44 ± 0.00	0.72 ± 0.00	0.82 ± 0.01	1.64 ± 0.02
ECN44 + ECN46	44.98 ± 0.54	58.97 ± 0.71	45.56 ± 0.55	45.66 ± 0.55	45.64 ± 0.56	45.63 ± 0.55	45.57 ± 0.55	46.41 ± 0.56
ECN46/LLL	71.32	0.97	45.73	33.35	31.09	23.64	22.71	13.58
(ECN44 + ECN46)/ LLL	91.79	2.47	59.94	43.90	41.11	31.46	30.38	18.86

[a]Each value represents the mean of four determinations of two successive crop seasons (n = 4; two different samples for each crop season).

dx.doi.org/10.1021/jf500571n | J. Agric. Food Chem. 2014, 62, 4893−4904

Table 4. Sterol Composition (Percent) in Extra-Virgin Olive Oil (EVOO), Soybean Oil (SO), Corn Oil (CO), and Sunflower Oil (SfO) and Mixtures of EVOO with Different Percentages of Each Seed Oil (SO, CO, and SfO)[a]

	cholesterol	24-methylene cholesterol	campesterol	campestanol	stigmasterol	apparent β-sitosterol[b]	Δ7-stigmastenol	Δ7-avenasterol
EVOO	0.15 ± 0.00	0.12 ± 0.00	3.17 ± 0.03	0.07 ± 0.00	0.49 ± 0.00	94.94 ± 1.16	0.34 ± 0.00	0.72 ± 0.00
SO	0.41 ± 0.00	0.07 ± 0.00	19.95 ± 0.24	0.17 ± 0.00	17.61 ± 0.21	58.21 ± 0.71	2.31 ± 0.03	1.27 ± 0.01
EVOO + 1% SO	0.15 ± 0.00	0.12 ± 0.00	3.35 ± 0.04	0.07 ± 0.00	0.60 ± 0.00	94.62 ± 1.15	0.36 ± 0.00	0.73 ± 0.00
EVOO + 2% SO	0.16 ± 0.00	0.12 ± 0.00	3.54 ± 0.04	0.07 ± 0.00	0.69 ± 0.00	94.31 ± 1.15	0.37 ± 0.00	0.74 ± 0.00
EVOO + 3% SO	0.17 ± 0.00	0.11 ± 0.00	3.72 ± 0.04	0.08 ± 0.00	0.84 ± 0.01	93.95 ± 1.15	0.38 ± 0.00	0.75 ± 0.00
EVOO + 4% SO	0.17 ± 0.00	0.11 ± 0.00	3.90 ± 0.05	0.08 ± 0.00	1.11 ± 0.01	93.47 ± 1.14	0.40 ± 0.00	0.76 ± 0.00
EVOO + 5% SO	0.17 ± 0.00	0.11 ± 0.00	4.02 ± 0.05	0.08 ± 0.00	1.30 ± 0.02	93.11 ± 1.14	0.43 ± 0.00	0.78 ± 0.00
EVOO + 10% SO	0.19 ± 0.00	0.11 ± 0.00	6.17 ± 0.07	0.09 ± 0.00	2.81 ± 0.03	89.21 ± 1.09	0.59 ± 0.00	0.83 ± 0.01
CO	0.14 ± 0.00	0.12 ± 0.00	22.06 ± 0.27	0.05 ± 0.00	4.96 ± 0.06	70.50 ± 0.86	0.55 ± 0.00	1.62 ± 0.02
EVOO + 1% CO	0.15 ± 0.00	0.12 ± 0.00	3.27 ± 0.04	0.07 ± 0.00	0.52 ± 0.00	94.81 ± 1.16	0.34 ± 0.00	0.72 ± 0.00
EVOO + 2% CO	0.15 ± 0.00	0.12 ± 0.00	3.45 ± 0.04	0.06 ± 0.00	0.54 ± 0.00	94.61 ± 1.16	0.35 ± 0.00	0.72 ± 0.00
EVOO + 3% CO	0.15 ± 0.00	0.12 ± 0.00	3.70 ± 0.04	0.06 ± 0.00	0.66 ± 0.00	94.23 ± 1.15	0.35 ± 0.00	0.73 ± 0.00
EVOO + 4% CO	0.15 ± 0.00	0.11 ± 0.00	4.06 ± 0.05	0.06 ± 0.00	0.70 ± 0.00	93.82 ± 1.15	0.36 ± 0.00	0.74 ± 0.00
EVOO + 5% CO	0.15 ± 0.00	0.11 ± 0.00	4.24 ± 0.05	0.06 ± 0.00	0.74 ± 0.01	93.60 ± 1.14	0.36 ± 0.00	0.74 ± 0.00
EVOO + 10% CO	0.15 ± 0.00	0.11 ± 0.00	5.82 ± 0.07	0.06 ± 0.00	0.87 ± 0.01	91.86 ± 1.12	0.38 ± 0.00	0.75 ± 0.01
SfO	0.08 ± 0.00	0.08 ± 0.00	8.30 ± 0.10	0.08 ± 0.00	5.74 ± 0.07	61.24 ± 0.75	17.60 ± 0.21	6.88 ± 0.08
EVOO + 1% SfO	0.14 ± 0.00	0.12 ± 0.00	3.21 ± 0.04	0.07 ± 0.00	0.57 ± 0.00	94.60 ± 1.16	0.54 ± 0.00	0.75 ± 0.00
EVOO + 2% SfO	0.14 ± 0.00	0.12 ± 0.00	3.29 ± 0.04	0.07 ± 0.00	0.64 ± 0.00	94.05 ± 1.15	0.89 ± 0.01	0.80 ± 0.01
EVOO + 3% SfO	0.14 ± 0.00	0.11 ± 0.00	3.38 ± 0.04	0.07 ± 0.00	0.70 ± 0.00	93.70 ± 1.15	1.02 ± 0.01	0.88 ± 0.01
EVOO + 4% SfO	0.14 ± 0.00	0.11 ± 0.00	3.45 ± 0.04	0.07 ± 0.00	0.75 ± 0.01	93.36 ± 1.14	1.17 ± 0.01	0.95 ± 0.01
EVOO + 5% SfO	0.14 ± 0.00	0.11 ± 0.00	3.56 ± 0.04	0.07 ± 0.00	0.81 ± 0.01	92.89 ± 1.14	1.39 ± 0.02	1.03 ± 0.01
EVOO + 10% SfO	0.13 ± 0.00	0.11 ± 0.00	3.69 ± 0.05	0.07 ± 0.00	1.06 ± 0.01	91.62 ± 1.12	2.05 ± 0.02	1.27 ± 0.01

[a]Each value represents the mean of four determinations of two successive crop seasons ($n = 4$; two different samples for each crop season). [b][Δ5,23-Stigmastadienol + cholerosterol + β-sitosterol + sitostanol + Δ5-avenasterol + Δ5,24-stigmastadienol.

able to resolve triglycerides both by atom carbon number and by unsaturation using phenyl-methyl-silicone stationary phases.[25−27]

Sterols, which comprise a major portion of the unsaponifiable matter, are found in almost all fats and oils, and they are also characteristics of the genuineness of vegetable oils. Whereas sunflower, for example, contains significant levels of Δ7-stigmastenol, extra-virgin olive oil has high levels of β-sitosterol and Δ5-avenasterol, and soybean and corn oils have high levels of campesterol and stigmasterol. These apparent differences make them the most suitable for determining the botanical origin of oils and, hence, for detecting the adulteration of olive oil with other cheaper or lower quality vegetable oils.[28−30]

Many publications report the application of chemometrics such as the linear discriminant analysis (LDA) and other tools to find the best approach for the authenticity and traceability of extra-virgin olive oils.[31−35]

The utmost objective of the present research study is the detection of Chemlali EVOO adulteration with soybean, corn, and sunflower oils. For this purpose, analyses of fatty acid, sterol, and triacylglycerol profiles are performed using gas and liquid chromatography. This leads to the determination of the minimum detectable levels of vegetable oils (soybean, corn, and sunflower).

MATERIALS AND METHODS

Chemicals. Methanol (99.8%), diethyl ether (99.7%), ethanol (≥99.9%), *n*-heptane (99.0%), chloroform (99.1%), acetone (≥99.8%), and acetonitrile (≥99.9%) HPLC grade solvents were purchased from Riedel-de-Haen (Buchs SG, Switzerland). Potassium hydroxide (88.5%), pyridine (99.7%), hexamethyldisilazane (98.5%), and trimethylchlorosilazane (99.0%) were obtained from Sigma-Aldrich, Supelco (Bellefonte, PA, USA). FAME multistandards (>99.0%) were purchased from Sigma Chemical Co. (St. Louis, MO, USA).

Vegetable Oils. Four different extra-virgin olive oil samples were obtained from a Tunisian olive variety, which is the Chemlali cultivar harvested from the Sfax region (southern Tunisia) during two crop seasons (2011/2012 and 2012/2013) ($n = 4$; two different samples for each crop season).

The ripening degree was the same for the four Chemlali olive samples (maturation indices were 4.5). The olive samples were collected at the beginning of December from orchards in the same neighborhood carried out with the same cultural practices. The olive ripening index (RI) was determined according to the method developed by Boskou,[36] on the basis of the evaluation of the olive skin and pulp colors. RI values range from 0 (100% intense green skin) to 7 (100% purple flesh and black skin).

The pure soybean, corn, and sunflower oils, purchased from the local market in Tunisia and used as adulterants, were checked for their authenticity by classical tests such as iodine and refraction indices and other technical procedures, most of which are based on GC (fatty acid and sterol compositions), with some being based on HPLC (triglyceride composition). The different mixtures of extra-virgin olive oil with the aforementioned vegetable oils (at levels of 1, 2, 3, 4, 5, and 10% w/w) were prepared.

Analytical Methods. *Determination of Fatty Acid Composition.* The methyl esters for the determination of the *cis*- and *trans*-fatty acids by the use of capillary column GC were prepared according to a standard protocol (vigorous shaking of the solution of oil in *n*-heptane (0.1 g in 2 mL) with 0.2 mL of 2 N methanolic potassium hydroxide).[37,38] The GC analysis of FAMEs was performed on an AutoSystem gas chromatograph equipped with a FID detector (HP 6890N, Agilent (Palo Alto, CA, USA)). The column used was a capillary Agilent CP-Sil88 (cyanopropyl polysiloxane) (length = 50 m, i.d. = 0.25 mm, and film thickness = 0.20 μm), and the analysis conditions were as follows: the initial column temperature was settled at 165 °C for 25 min, then raised at a gradient of 5 °C/min to 195 °C;

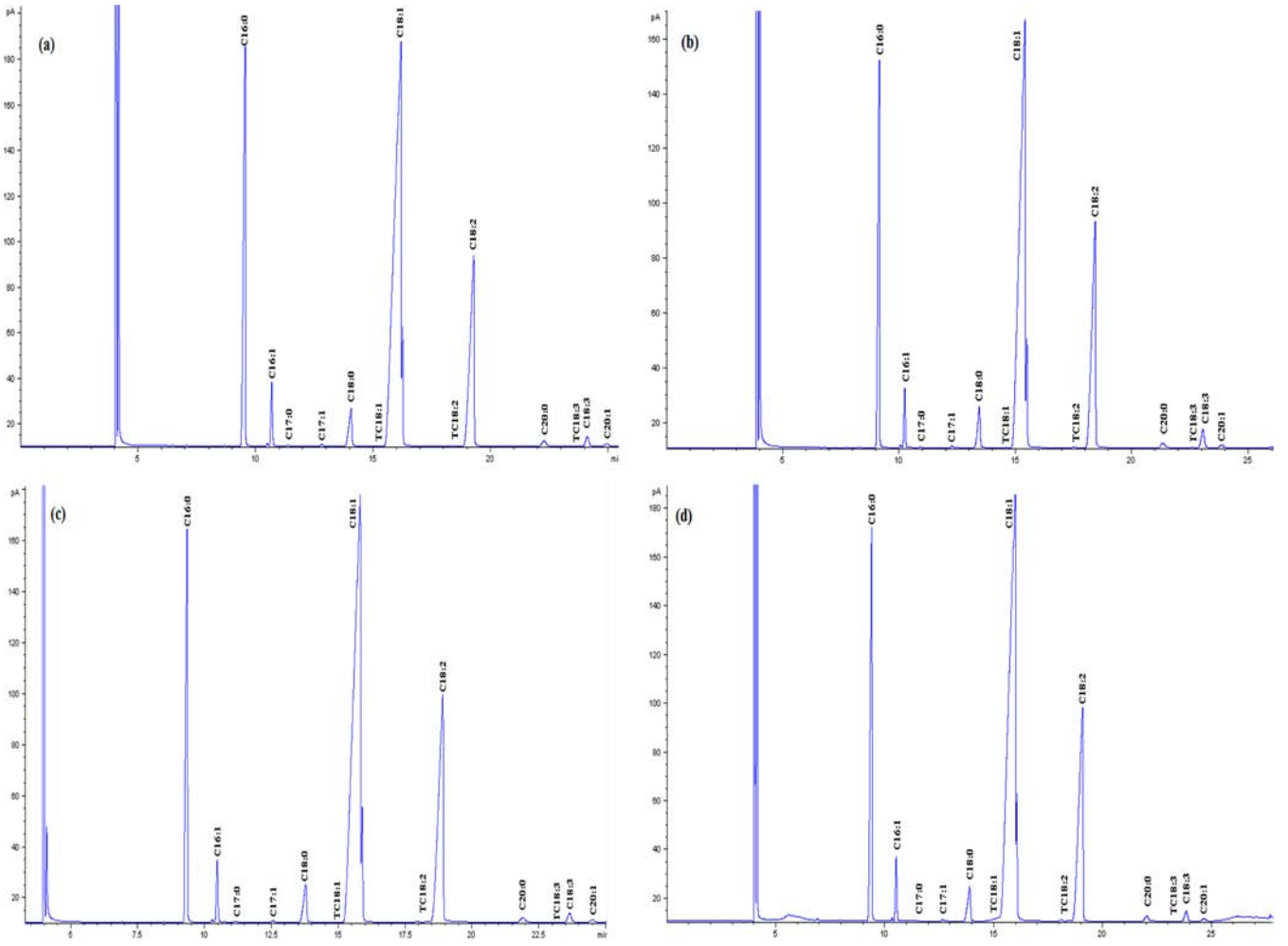

Figure 2. Gas chromatograms showing the FAMEs profiles of Chemlali EVOO (a) and binary mixtures containing 90% EVOO and 10% of either soybean (b), sunflower (c), or corn (d) oils using GC-FID.

the temperature of the injector and detector was set at 250 °C; helium was used as the carrier gas at a flow rate of 1 mL/min and 1:100 split ratio; the injection volume was 1 μL.

cis- and *trans*-FAMEs were identified through a comparison of their retention times versus pure standards analyzed under the same conditions. They were quantified according to their percentage area, obtained by the integration of the peaks (Figure 1). The results were expressed as the percentages of individual fatty acids in the lipid fraction. The 10 fatty acids (*cis*) considered in this study were palmitic (C16:0), hypogeic (C16:1n-9) + palmitoleic (C16:1n-7), margaric (C17:0), margaroleic (C17:1), stearic (C18:0), oleic (C18:1n-9) + *Z*-vaccenic (C18:1n-7), linoleic (C18:2), linolenic (C18:3), arachidic (C20:0), and gondoic (C20:1n-9) acids. The *trans*-fatty acid (TFA) content considered in this study included *trans*-octadecenoic (tC18:1), *trans*−*trans*-octadecadienoic (tt C18:2), *cis-trans*- and *trans-cis*-octadecadienoic [(ct + tc) C18:2], and *trans-cis-trans*-, *cis-cis-trans*-, *cis-trans-cis*-, and *trans-cis-cis*-octadecatrienoic [(tct + cct + ctc + tcc) C18:3] acids expressed as percentages of fatty acid methyl esters.

Determination of Triglyceride Composition. Five percent of the sample to be analyzed was prepared by weighing 0.25 ± 0.001 g into a 5 mL graduated flask and dissolved in 5 mL with acetone.[22] A HP1100 chromatograpic system from Agilent (Waldbronn, BW, Germany) equipped with a differential refractometer detector was employed. Next, the separation was carried out with a Spherisorb analytical column (250 × 4.6 mm, 5 μm particle size) from Supelco (Bellefonte, PA, USA). The optimized separation conditions were conducted by isocratic elution with a 60:40 acetone/acetonitrile mixture; column temperature, 30 °C; flow rate, 1.5 mL/min; and injection volume, 20 μL of the sample solution prepared as indicated above.

For the identification of TAGs, the retention times plotted in accordance with alternative reference chromatograms obtained from soybean oil, a 30:70 mixture of soybean oil/olive oil, and pure olive oil as described by COI.[22] It was assumed that the sum of the areas of the peaks corresponding to the various TAGs was equal to 100%, and the relative percentage of each TAG was calculated.

It is worthwhile noting that the theoretical value of ECN42 triacylglycerols was calculated by the computer program.

Determination of Sterol Composition. A mixture of each extra-virgin olive oil sample and vegetable oils (5 g) was dissolved by 50 mL of 2 N ethanolic potassium hydroxide solution, saponified, and extracted according to the official International Olive Oil Council (IOOC) method.[39] The unsaponifiable fraction was dissolved in chloroform, and approximately 20 mg was loaded on a basic silica TLC plate. The sterol and triterpene diol fraction was separated by elution with a mixture of hexane and diethyl ether 65:35 (v/v). The corresponding band was visualized under UV light after being sprayed with a 2,7-dichlorofluorescein in 0.2% ethanolic solution, than scraped off with a spatula, and extracted with chloroform. After the extract was evaporated to dryness, sterols and diols were converted to trimethylsilyl ethers by the addition of pyridine/hexamethyldisilazane/trimethylchlorosilane (9:3:1, v/v/v), left for 15 min, and then centrifuged. The analysis of sterols was performed on a 7890A Agilent gas chromatograph (Pudong, Shanghai, China) equipped with a flame ionization detector (FID). The column used was a capillary HP-5 (5% phenyl; 95% dimethylpolysiloxane) (length = 30 m, i.d. = 0.32 mm,

dx.doi.org/10.1021/jf500571n | J. Agric. Food Chem. 2014, 62, 4893−4904

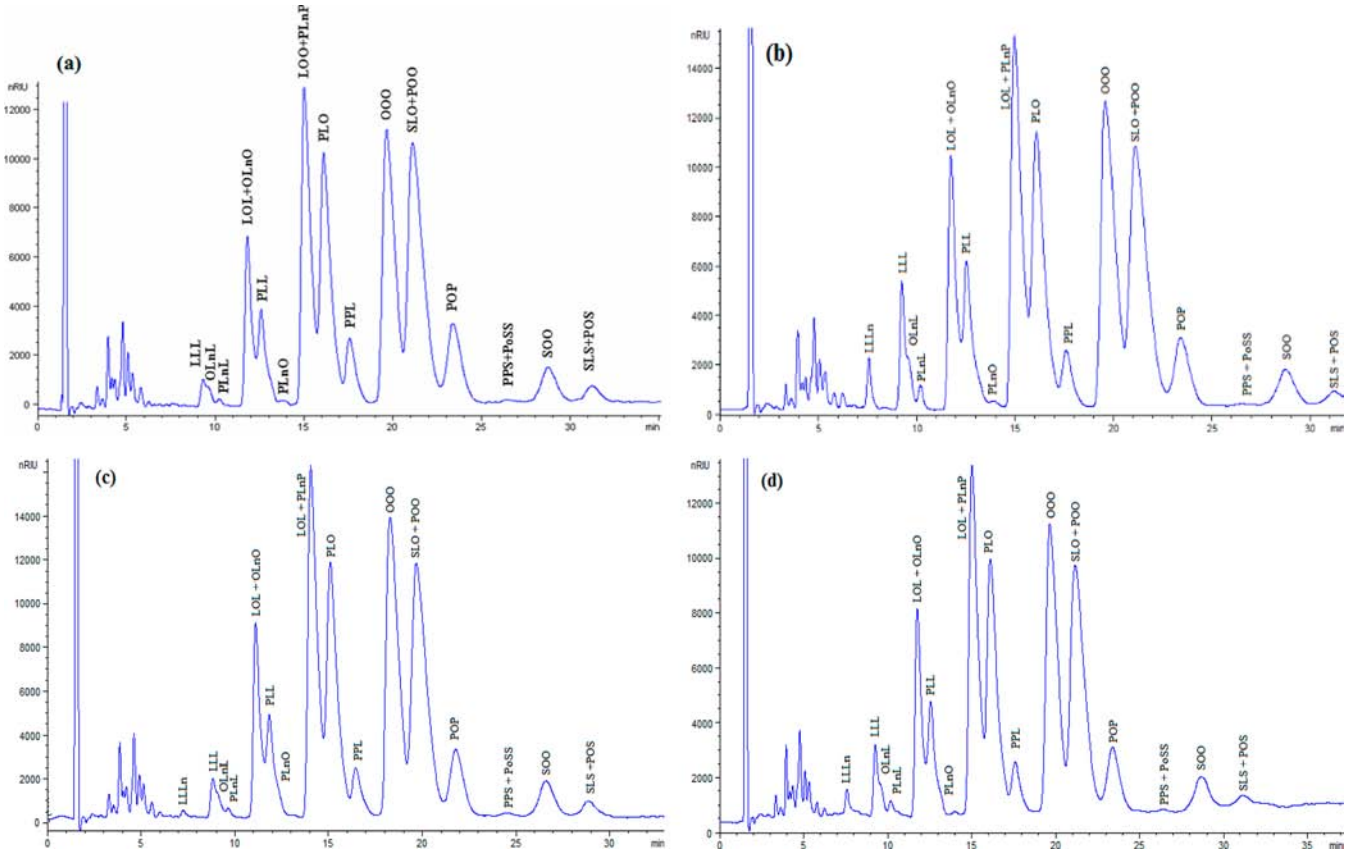

Figure 3. Chromatograms showing the TAGs profiles of Chemlali EVOO (a) and binary mixtures containing 90% EVOO and 10% of either soybean (b), sunflower (c), or corn (d) oils using HPLC-RID.

and film thickness = 0.25 μm), and the conditions for the analysis were as follows: the oven temperature was isothermal at 260 °C, the temperature of the injector was 280 °C, and the detector was set at 290 °C; helium was the carrier gas, with a flow through the column of 1 mL/min and a 1:50 split ratio, and the injection volume was 3 μL.

To identify the individual peaks of sterols, the determination of relative retention times (RRT) for sterols was carried out according to the majority compound of sterols (β-sistosterol), knowing that RRT (β-sistosterol) is equal to 1 as described by the COI.[40]

Statistical Analysis. The results were expressed as mean ± standard deviation (SD) of four measurements for the analytical determination. LDA was applied to discriminate Chemlali EVOO and the extra-virgin olive oils adulterated with different percentages of soybean, corn, and sunflower oils (1, 2, 3, 4, 5, and 10%) according to all of the parameters investigated. LDA plots were performed using SPSS Statistics 17.0 for Windows (SPSS Inc., 2008).

RESULTS AND DISCUSSION

Fatty Acid and Triglyceride Compositions in Vegetable Oils. The experimental results of fatty acid and triglyceride compositions in extra-virgin olive oil, soybean, corn, and sunflower oils are summarized in the Tables 1−3.

In the present research work, the fatty acid (FA) composition (%) of Chemlali extra-virgin olive oil was studied within the official limits established for olive oil referred to in the IOOC tade standard applied to olive oils and olive pomace oils.[7] The acid limits in olive oil are palmitic acid (C16:0), 7.50−20.00%; palmitoleic acid (C16:1), 0.30−3.50%; stearic acid (C18:0), 0.50−5.00%; oleic acid (C18:1), 55.00−83.00%; linoleic acid (C18:2), 3.50−21.00%; and linolenic acid (C18:3), ≤1.00%.

In the studied extra-virgin olive oil, the percentages of palmitic, oleic, linoleic, and linolenic acids are 15.82, 62.37, 16.21, and 0.69%, respectively. The vegetable oils, soybean, corn, and sunflower oils, exhibited considerably higher linoleic acid percentages than oleic acid percentages. Soybean oil had considerably high linolenic acid (7.77%). These differences, related to the linoleic and linolenic acid percentages, are depicted in Tables 1−3.

The detection of a triglyceride, which is not present in extra-virgin olive oil and has a number of equivalent carbons equal to 40 (LLLn), is an indicator of the presence of seed oil in olive oil. This result is in agreement with that reported by Rezanka et al.[41]

In all vegetable oils, the trilinolein (LLL) content was higher than that of the extra-virgin olive oil.[42] Actually, large differences pertaining to trilinolein contents between extra-virgin olive oil and soybean, corn, and sunflower oils, depicted in Tables 1−3, were observed.

The absolute value of the differences between theoretical and experimental ECN42 contents (ΔECN42) in all seed oils is higher than that in the extra-virgin olive oil. It ranges from 15.42 in soybean oil to 0.07 in extra-virgin olive oil. These differences are depicted in Tables 1−3.

According to the established limits, the ΔECN42 value must not exceed 0.20 in the case of edible virgin olive oil, 0.30 in the case of lampante olive oil, 0.50 in the case of olive pomace oil, and 0.60 in the case of crude olive pomace oil.

The above results reveal that there is a correlation between the linoleic acid percentage, trilinolein content, and ΔECN42. In other words, whereas soybean, corn, and sunflower oils have high linoleic acid percentages, high LLL contents, and high ΔECN42, extra-virgin olive oil exhibits low LLL content and

Table 5. Parameters Used for the Detection of Extra-Virgin Olive Oil (EVOO) Adulteration with Vegetable Oils

type of seed oil	parameter used for the detection of adulteration	COI threshold value	percentage of detectable seed oil exceeding the COI threshold value
soybean (SO)	C18:3	1%	EVOO + 5% SO (1.08%)
	ECN40	0	EVOO + 1% SO (0.27)
	ΔECN42	0.20	EVOO + 3% SO (0.30)
	campesterol	4%	EVOO + 10% SO (6.17%)
	Δ7-stigmastenol	0.50%	EVOO + 10% SO (0.59%)
	apparent β-sitosterol	93.00%	EVOO + 10% SO (89.21%)
	∑(TC18:2 + TC18:3)	0.05%	EVOO + 3% SO (0.06%)
corn (CO)	ECN40	0	EVOO + 1% CO (0.11)
	ΔECN42	0.20	EVOO + 3% CO (0.21)
	campesterol	4%	EVOO + 4% CO (4.06%)
	apparent β-sitosterol	93.00%	EVOO + 10% CO (91.86%)
	∑(TC18:2 + TC18:3)	0.05%	EVOO + 2% CO (0.06%)
sunflower (SfO)	ECN40	0	EVOO + 1% SfO (0.05)
	ΔECN42	0.20	EVOO + 1% SfO (0.21)
	Δ7-stigmastenol	0.50%	EVOO + 1% SfO (0.54%)
	apparent β-sitosterol	93.00%	EVOO + 5% SfO (92.89%)
	∑(TC18:2 + TC18:3)	0.05%	EVOO + 4% SfO (0.06%)

low ΔECN42. These results are in good agreement with literature data.[9]

Sterol Compositions in Vegetable Oils. Sterols are not only found in almost all fats and oils but also characteristic of the genuineness of vegetable oils. Indeed, the determination of the sterol composition of a vegetable oil is a very important criterion for identifying the botanical origin.

Sterol compositions (%) show higher contents in campesterol and stigmasterol in other vegetable oils compared to EVOO (Table 4). In fact, campesterol, which does not exceed 4.00% in EVOO, reaches values of 19.95, 22.06, and 8.30% in soybean, corn, and sunflower oils, respectively. Besides, stigmasterol, which always remains less than campesterol in EVOO, reaches values of 17.61, 4.96, and 5.74% in soybean, corn, and sunflower oils, respectively. Therefore, these two sterols could be used as an indicator of the adulteration of olive oil with vegetable oils. These results are in agreement with those reported by Al-Ismail et al.,[43] who suggested the presence of some refined vegetable oils in olive oil based on the sum of campesterol and stigmasterol percentages.

Moreover, sunflower oil has a high level of Δ7-stigmastenol (17.60%), whereas this sterol percentage in extra-virgin olive oil must not exceed 0.50%.

The model systems of corn, soybean, and sunflower oils at levels of 1, 2, 3, 4, 5, and 10% were prepared. These apparent differences, as shown in Table 4, make them the most suitable for the determination of the botanical origin of oils and therefore for the detection of the adulteration or contamination among vegetable oils.

Identification of EVOO Adulteration with Other Low-Cost Oils. This research study is meant to detect adulteration of EVOO by lower cost seed oils. Consequently, various blends of EVOO and soybean, corn, or sunflower oil were prepared and analyzed for fatty acid, triglyceride, and sterol compositions. The adulteration percentages ranged from 1 to 10% to determine a threshold of detection.

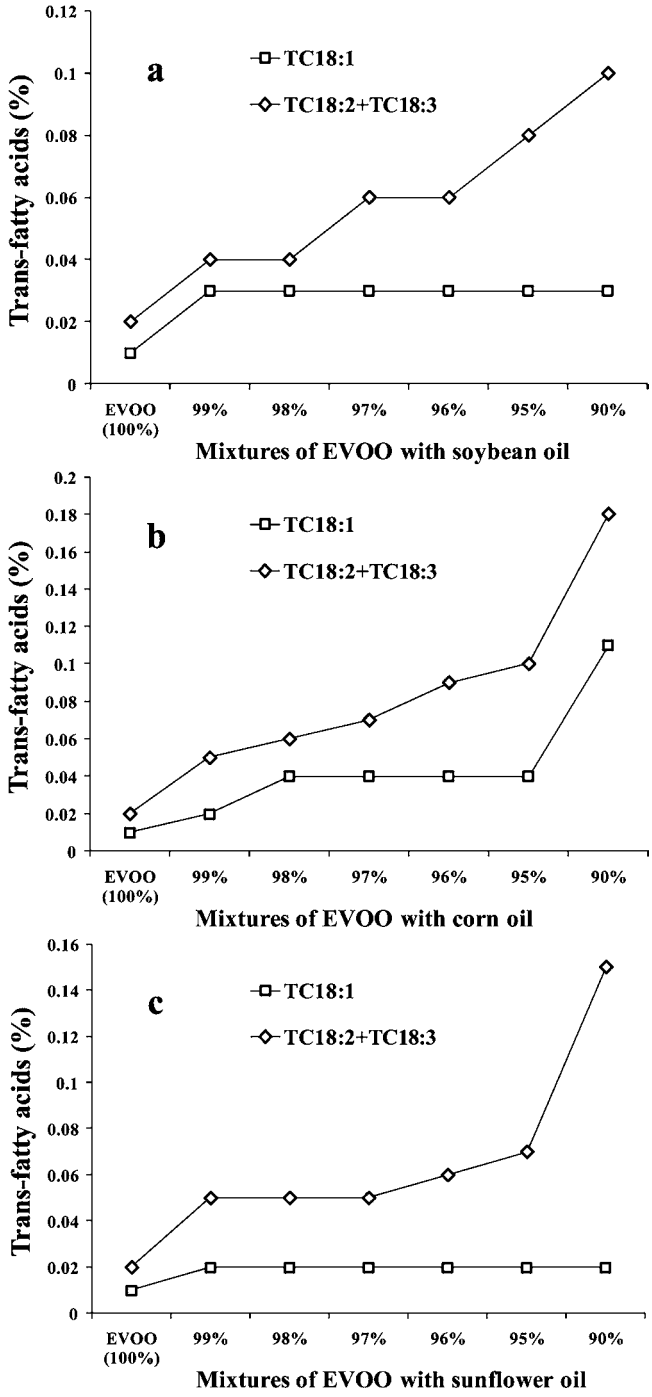

Figure 4. *trans*-Fatty acids of mixtures of extra-virgin olive oil (EVOO) with (a) soybean, (b) corn, and (c) sunflower oils. Each value represents the mean of four determinations of two successive crop seasons (n = 4; standard deviation < 0.001%).

Use of the Fatty Acid and Triglyceride Compositions for the Detection of Fraud. Fatty acid and TAG compositions of the adulterated extra-virgin olive oil mixed with 1−10% (w/w) quantities of soybean, corn, and sunflower oils are summarized in Tables 1−3 and Figures 2 and 3.

Taking into account the results presented in Tables 1−3, it could be concluded that the analysis of fatty acids does not produce satisfactory results with regard to the levels of adulteration investigated in this research study. The most effective

dx.doi.org/10.1021/jf500571n | J. Agric. Food Chem. 2014, 62, 4893−4904

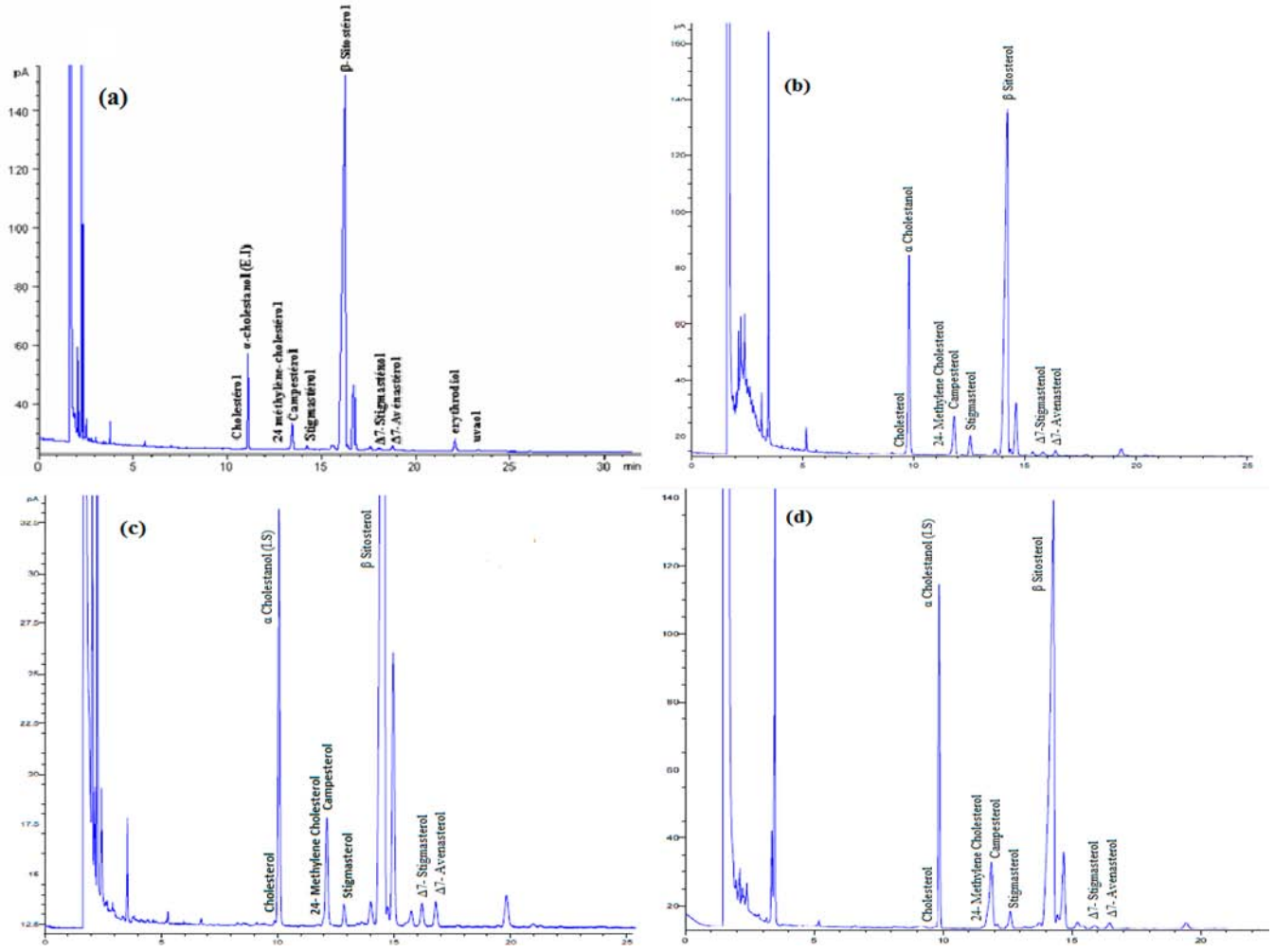

Figure 5. Typical gas chromatograms for sterols obtained in the analysis of Chemlali EVOO (a), EVOO adulterated with 10% soybean oil (b), EVOO adulterated with 10% sunflower oil (c), or EVOO adulterated with 10% corn oil (d).

parameters for the detection of adulteration are mentioned below.

The linolenic acid percentage could be used as a parameter for the detection of EVOO fraud with 5% of soybean oil as well as by the increase of *trans*-fatty acid contents with 3% of soybean oil, 2% of corn oil, and 4% of sunflower oil (Table 5 and Figure 4). None of the other fatty acids is effective for the detection of the added vegetable oil in an extra-virgin olive oil. Although the composition of fatty acids in the examined seed oils is different from that of olive oils, the fatty acids experiment could not be satisfactorily used as discriminatory parameters between olive oil and the respective vegetable oil in most cases.

According to Tables 1−3, it can be noted that the appearance of a specific triacylglycerol, normally not present in the olive oil, in oils adulterated with seed oils has a number of equivalent carbons equaling 40, known by LLLn. Thus, this triacylglycerol is an indicator of the presence of seed oil in extra-virgin olive oil.

Indeed, LLLn increases with the increase in the adulteration percentage of vegetable oils (from 1 to 10%). It ranges from 0.27 to 0.76% for the extra-virgin olive oil adulterated with soybean oil, from 0.11 to 0.69% for the extra-virgin olive oil adulterated with corn oil, and from 0.05 to 0.11% for the extra-virgin olive oil adulterated with sunflower oil. The adulteration with soybean oil produces a large increase of the areas of peak LLLn because the soybean oil is the only one rich in linolenic acid.

The addition of small quantities of seed oil can be identified in the extra-virgin olive oil by the determination of the rate of LLL because the three seed oils are rich in linoleic acid (C18:2). Similarly, the presence of soybean, sunflower, and corn oils was proven by an increase of the percentage of LLL and ECN42. The extra-virgin olive oils were adulterated by sunflower, corn, and soybean oils (from 1 to 10%). Having a content of LLL, they varied from 0.76 to 2.46% with sunflower oil, from 0.52 to 1.86% with corn oil, and from 0.54 to 1.86% with soybean oil. Besides, having a practical ECN42, they varied from 1.26 to 3.39% with sunflower oil, from 1.33 to 2.87% with corn oil, and from 1.42 to 3.59% with soybean oil. It is to be noted that olive oil is largely compared to the seed oils known by their highest linoleic acid percentages.

The use of the ΔECN42 proved to be more effective in detecting even low levels of adulteration of EVOO with most of the examined vegetable oils. According to the data on the fraudulent mixtures presented in Tables 1−3, the determination of the ΔECN42 can be used as a parameter for the detection of fraud of extra-virgin olive oils with each one of the studied seed oils: 1% of sunflower (0.21 > 0.20), 3% of soybean (0.30 > 0.20), and 3% of corn (0.21 > 0.20) (Table 5).

dx.doi.org/10.1021/jf500571n | J. Agric. Food Chem. 2014, 62, 4893−4904

This finding can be attributed to the fact that the ΔECN42 is a number calculated by the combination of fatty acids and triglyceride composition. Therefore, the difference in the composition of the triglycerides and the six fatty acids, taken into account for the calculation of the theoretical ECN42, between the initial samples and their mixtures can be expected. However, these differences do not have the expected effect on the values of the theoretical ECN42 and ΔECN42. A consequence of this is the complete lack of correlation between linoleic acid or LLL and ΔECN42 of vegetable oils and their admixtures with olive oil. These results are in agreement with those reported by Christopoulou et al.,[9] who claimed the parameter ΔECN42 is very useful and effective in the detection of adulteration of olive oils with vegetable oils.

Use of the Sterol Compositions for the Detection of Fraud. The composition of the sterol fraction of olive oil is a very useful parameter for detecting adulterations or to check authenticity, because it can be considered as a fingerprint.[44,45] The comparison between the extra-virgin olive oil and the studied seed oils reveals that there are high differences relating to sterol compositions as shown in Table 4 and Figure 5.

As stated below (Table 4), the profile of sterols is almost decisive in clarifying the contamination of some vegetable oils (EVOO) with other cheaper ones. Thus, the addition of 10% of soybean oil to EVOO can be detected by the increase of campesterol and Δ7-stigmastenol percentages, which exceed the maximum acceptable limits (6.17 > 4.00% and 0.59 > 0.50%, respectively) and also by the decrease of the apparent β-sitosterol (89.21 < 93.00%, minimal value limited by the COI).

The value of the Δ7-stigmastenol in sunflower oil is much higher (17.60%) than that in the EVOO (0.34%). This sterol is very effective for the detection of adulteration, even at the level of 1% of sunflower oil (0.54) in the extra-virgin olive oil. For example, a mixture consisting of 99% of EVOO (with 0.34% of Δ7-stigmastenol percentage) and 1% of sunflower oil (with 17.60% of Δ7-stigmastenol percentage) caused a significant increase in Δ7-stigmastenol percentage (from 0.34 to 0.54). In fact, the determined Δ7-stigmastenol percentage of the mixture was 0.54% of the total sterols (>0.50%, the maximum acceptable limit for Δ7-stigmastenol). Besides, the contamination of EVOO with 5% of sunflower oil could also be detected by the decrease of the apparent β-sitosterol (92.89% of total sterols). Similar results were reported by Aparicio and Aparicio-Ruíz.[8]

In addition, the adulteration of EVOO with 4% of corn oil increases the concentration of campesterol (4.06 > 4%), and falsification with 10% of corn oil decreases the concentration of apparent β-sitosterol (91.86% of the total sterols).

In the first conclusion, the parameters used for the detection of adulteration of extra-virgin olive oil with the studied seed oils as well as the percentages of detectable seed oil in extra-virgin olive oil mixtures are summarized in Table 5. It should be noted that the conclusions for the detection of fraud are drawn from the analyses performed on the samples examined in this research study. However, as has already been mentioned, the effectiveness of a parameter was based on the comparison of the determined value in each fraudulent sample with the maximum established limit of this parameter in EVOO. Consequently, the findings of this research study can be applied to the detection of adulteration of extra-virgin olive oil with the only reservation that the percentage of seed oil that is

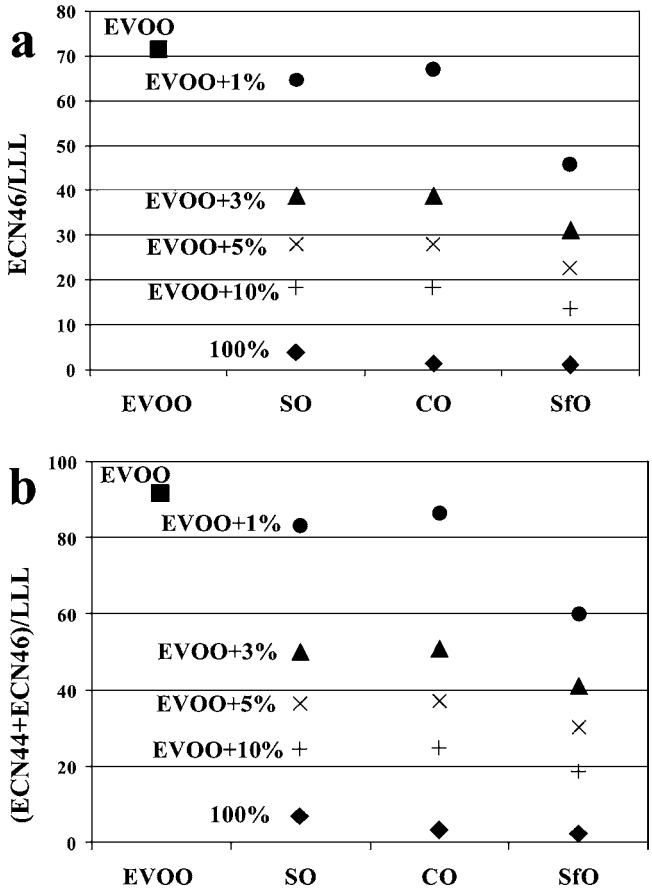

Figure 6. Values of the parameters ECN46/LLL (a) and (ECN44 + ECN46)/LLL (b) of Chemlali extra-virgin olive oil (EVOO), seed oils, and their mixtures: (■) 100% EVOO; (●) EVOO + 1% SO, CO, or SfO; (▲) EVOO + 3% SO, CO, or SfO; (×) EVOO + 5% SO, CO, or SfO; (+) EVOO + 10% SO, CO, or SfO; (◆) 100% SO, CO, or SfO. SO, soybean oil; CO, corn oil; SfO, sunflower oil.

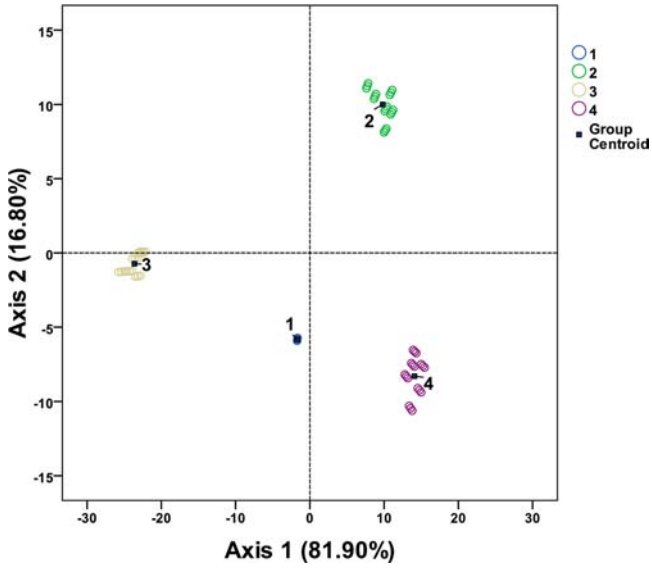

Figure 7. LDA score plot of pure extrav virgin olive oil (EVOO) and adulterated EVOO based on all of the analyses performed with four determinations: (1) EVOO; (2) EVOO + 1−10% of soybean oil; (3) EVOO + 1−10% of corn oil; (4) EVOO + 1−10% of sunflower oil.

dx.doi.org/10.1021/jf500571n | J. Agric. Food Chem. 2014, 62, 4893−4904

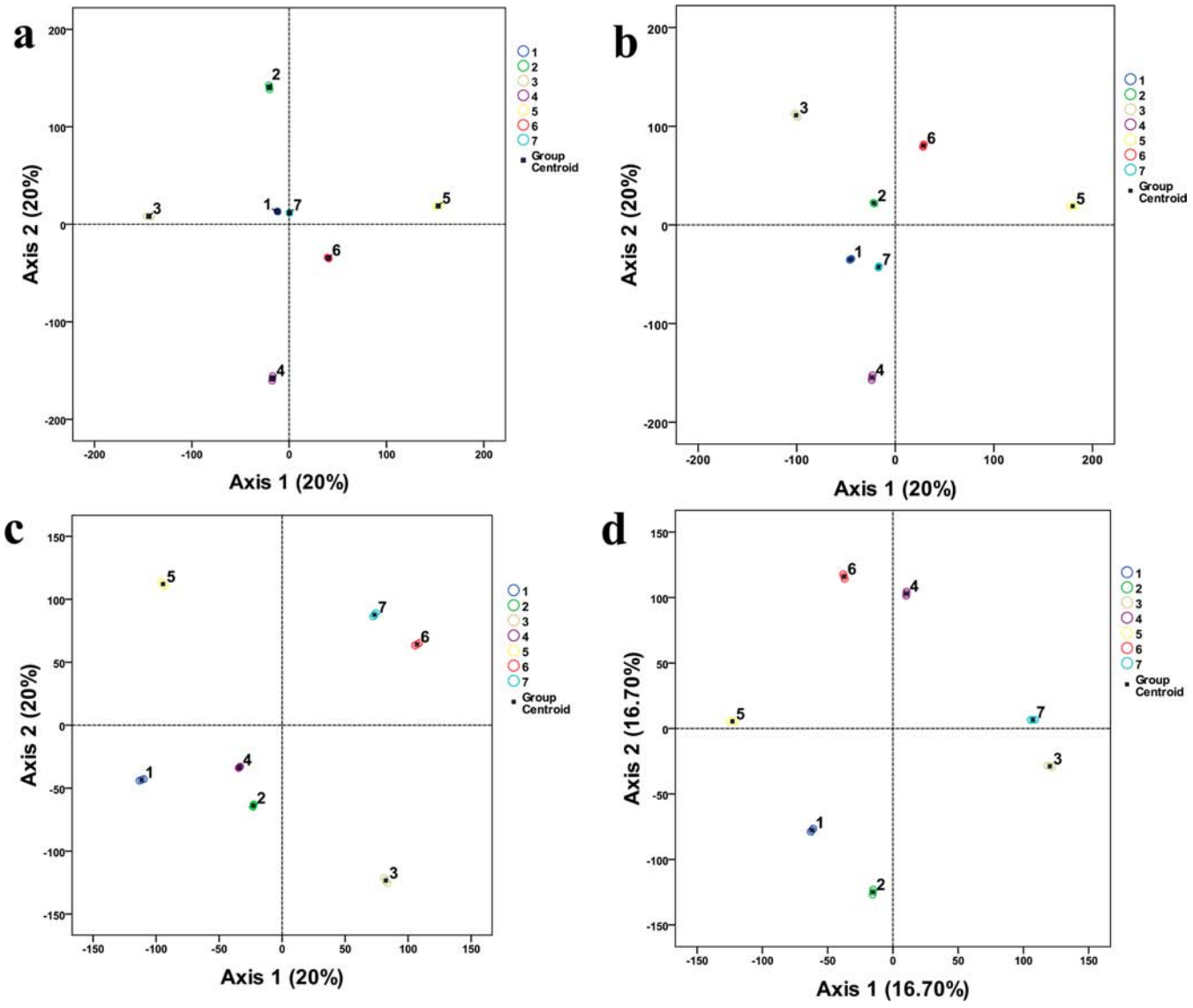

Figure 8. LDA score plot of pure extra-virgin olive oil (EVOO), pure seed oils, and adulterated EVOO at the same level based on all of the analyses performed with four determinations: (a) EVOO + 1% of seed oil; (b) EVOO + 2% of seed oil; (c) EVOO + 5% of seed oil; (d) EVOO + 10% of seed oil; (1) EVOO; (2) soybean oil; (3) corn oil; (4) sunflower oil; (5) EVOO + % of soybean oil; (6) EVOO + % of corn oil; (7) EVOO + % of sunflower oil.

detectable in olive oil mixtures may be somewhat different from that proposed in the present study. Overall, this table could be used as a simple guide for analysts working on EVOO analysis.

Use of Other Parameters for the Detection of Fraud. The parameters calculated by the triglycerides and reported in Tables 1−3 are ECN46/LLL and (ECN44 + ECN46)/LLL. Certain researchers have pointed out the importance of these factors in the detection of adulteration of extra-virgin olive oil with certain vegetable oils.[9,46]

These parameters are based on the low LLL content of the extra-virgin olive oil in comparison with that of the other vegetable oils such as soybean, corn, and sunflower oils. The similar ECN46 and ECN44 + ECN46 values of the extra-virgin olive oil are also compared with that of the studied seed oils. Then, the values of these parameters in the seed oils are much lower than that in the extra-virgin olive oil. Besides, the values of these parameters in the mixture of extra-virgin olive oil and sunflower oil (1%) were greatly lower than that in extra-virgin olive oil, whereas in the other mixtures of extra-virgin olive oil with soybean and corn oils, these values were much lower only at 3%. All of the mixtures in the other percentages (5 and 10%) of EVOO and each seed oil type were well separated as shown in Figure 6.

The use of the two parameters ECN46/LLL and (ECN44 + ECN46)/LLL is very effective in the detection of the seed oils in percentages <5% and produced very satisfactory results with regard to the studied vegetable oils, even in percentages lower than 3%, especially in the case of sunflower oil (1%). These results agree with the study performed by Christopoulou et al.,[9] which confirmed the effectiveness of these parameters for the detection of EVOO adulteration with vegetable oils in percentages lower than 5%.

Chemometric Analysis. LDA is probably the most frequently used supervised pattern recognition method. In principle, LDA determines linear discriminant functions, which maximize the ratio of between-class variance and minimize the ratio of within-class variance. It should be noted that, whereas the principal component analysis (PCA) selects a direction that

retains maximal structure among the data in a lower dimension, LDA selects a direction that achieves maximum separation among the given classes.[47]

Because the data structure analysis gave a good sample characterization, a classification model was built. LDA was applied to find a predictive classification model able to differentiate the pure extra-virgin olive oil and the adulterated olive oils.

The plot of the discriminant functions (Figure 7) obtained by LDA showed a clear discrimination between the Chemlali EVOO and the adulterated extra-virgin olive oils mixed with different percentages of soybean, corn, and sunflower oils (1, 2, 3, 4, 5, and 10%). Discriminant function 1, which was highly related to cholesterol, campestanol, stigmasterol, campesterol, Δ7-avenasterol, apparent β-sitosterol, Δ7-stigmastenol, ECN50, and C20:1, represents the function of minor compounds, already considered as a fingerprint for a specific oil. Discriminant function 2 is highly related to C17:0, $ECN42_{theor}$, LLLn, and C18:3.

In particular, by discriminant function 1 it was possible to discriminate Chemlali EVOO and the adulterated extra-virgin olive oils whatever the percentage of seed oil added (Figure 7). All samples were correctly discriminated using the two functions.

Application of LDA, after feature selection, was sufficient to differentiate Chemlali EVOO and all adulterated extra-virgin olive oils. The success was 100% in classification and close to 100% in prediction.

It is difficult to discriminate the adulterated EVOO with 1% of sunflower oil and the pure EVOO, whereas those adulterated with other vegetables oils are clearly separated at the same level (Figure 8a). The separation improves when the percentage of adulteration increases (Figure 8b–d).

Compared to classical methods, this new approach of using LDA application could represent an alternative and innovative tool for faster and cheaper evaluation of EVOO adulteration.

In conclusion, the present study has demonstrated that the threshold of the Chemlali extra-virgin olive oils adulteration by some cheaper vegetable oils such as soybean, corn, and sunflower oils was detected using gas chromatography in combination with liquid chromatography. According to these techniques, certain compounds found in the studied oils (triacylglycerols, trilinoleins, fatty acids, and sterols) are identified, analyzed, and used for the detection of the adulteration of extra-virgin olive oils. It should also be noted that this research work aims to facilitate the work of analysts by providing a simple guide for the detection of the adulteration of extra-virgin olive oil with the most common vegetable oils.

AUTHOR INFORMATION

Corresponding Author

*(M.B.) Phone: +216 98 667 581. Fax: +216 74 674 364. E-mail: mohamed.bouaziz@fsg.rnu.tn.

Funding

We thank the Ministére de l'Enseignement Supérieur et de la Recherche Scientifique and the Ministére de l'Agriculture (ONH-Sfax), Tunisia, for their support of this research work.

Notes

The authors declare no competing financial interest.

ACKNOWLEDGMENTS

We thank Leila Mahfoudhi, teacher of English at the Sfax Faculty of Science, for having proofread this paper.

ABBREVIATIONS USED

CO, corn oil; EC, equivalent carbon number; EVOO, extra-virgin olive oil; FAMEs, fatty acid methyl esters; GC, gas chromatography; GLC, gas–liquid chromatography; HPLC, high-performance liquid chromatography; IOOC, International Olive Oil Council; IUPAC, International Union of Pure and Applied Chemistry; LC-ESI-MS^2, liquid chromatography electrospray mass spectrometry; LDA, linear discriminant analysis; LLL, trilinolein; PCA, principal component analysis; SfO, sunflower oil; SO, soybean oil; TAGs, triacylglycerols

REFERENCES

(1) Issaoui, M.; Flamini, G.; Brahmi, F.; Dabbou, S.; Ben Hassine, K.; Taamali, A.; Chehab, H.; Ellouz, M.; Zarrouk, M.; Hammami, M. Effect of the growing area conditions on differentiation between Chemlali and Chétoui olive oils. *Food Chem.* **2010**, *119*, 220–225.

(2) Haddada, F. M.; Manaï, H.; Oueslati, I.; Daoud, D.; Sánchez, J.; Osorio, E.; Zarrouk, M. Fatty acid, triacylglycerol, and phytosterol composition in six Tunisian olive varieties. *J. Agric. Food Chem.* **2007**, *55*, 10941–10946.

(3) Tena, N.; Lazzez, A.; Aparicio-Ruiz, R.; García-González, D. L. Volatile compounds characterizing Tunisian Chemlali and Chétoui virgin olive oils. *J. Agric. Food Chem.* **2007**, *55*, 7852–7858.

(4) Ammar, S.; Zribi, A.; Gargouri, B.; Flamini, G.; Bouaziz, M. Effect of addition of olive leaves before fruits extraction process to some monovarietal Tunisian extra-virgin olive oils using chemometric analysis. *J. Agric. Food Chem.* **2014**, *62*, 251–263.

(5) Gargouri, B.; Zribi, A.; Bouaziz, M. Effect of containers on the quality of Chemlali olive oil during storage. *J. Food Sci. Technol.* **2014**, DOI: 10.1007/s13197-014-1273-2.

(6) Gargouri, B.; Ammar, S.; Zribi, A.; Ben Mansour, A.; Bouaziz, M. Effect of growing region on quality characteristics and phenolic compounds of Chemlali extra-virgin olive oils. *Acta Physiol. Plant.* **2013**, *35*, 2801–2812.

(7) International Olive Council, COI/T, 15/NC No. 3/Rev. 7. Trade standard applying to olive oils and olive-pomace oils, 2013.

(8) Aparicio, R.; Aparicio-Ruiz, R. Authentication of vegetable oils by chromatographic techniques. *J. Chromatogr., A* **2000**, *881*, 93–104.

(9) Christopoulou, E.; Lazaraki, M.; Komaitis, M.; Kaselimis, K. Effectiveness of determinations of fatty acids and triglycerides for the detection of adulteration of olive oils with vegetable oils. *Food Chem.* **2004**, *84*, 463–474.

(10) Gurdeniz, G.; Ozen, B. Detection of adulteration of extra-virgin olive oil by chemometric analysis of mid-infrared spectral data. *Food Chem.* **2009**, *116*, 519–525.

(11) Cordella, C.; Moussa, I.; Martel, A. C.; Sbirrazzuoli, N.; Lizzani-Cuvelier, L. Recent developments in food characterization and adulteration detection: technique-oriented perspectives. *J. Agric. Food Chem.* **2002**, *50*, 1751–1764.

(12) Škevin, D.; Kraljić, K.; Miletić, L.; Obranović, M.; Neđeral, S.; Petričević, S. Adulteration of Oblica virgin olive oil with edible sunflower and refined olive pomace oil. *Croatian J. Food Technol. Biotechnol. Nutr.* **2011**, *6*, 117–122.

(13) Frankel, E. N. Chemistry of extra-virgin olive oil: adulteration, oxidative stability, and antioxidants. *J. Agric. Food Chem.* **2010**, *58*, 5991–6006.

(14) Aparicio, R.; Aparicio-Ruíz, R. Authentication of vegetable oils by chromatographic techniques. *J. Chromatogr., A* **2000**, *881*, 93–104.

(15) Garcés, R.; Mancha, M. One-step lipid extraction and fatty acid methyl esters preparation from fresh plant tissues. *Anal. Biochem.* **1993**, *211*, 139–143.

(16) Zribi, A.; Gargouri, B.; Jabeur, H.; Rebaï, A.; Abdelhedi, R.; Bouaziz, M. Enrichment of pan-frying refined oils with olive leaf

phenolic-rich extract to extend the usage life. *Eur. J. Lipid Sci. Technol.* **2013**, *115*, 1443−1453.
(17) De la Mata-Espinosa, P.; Bosque-Sendra, J. M.; Bro, R.; Cuadros-Rodríguez, L. Olive oil quantification of edible vegetable oil blends using triacylglycerols chromatographic fingerprints and chemometric tools. *Talanta* **2011**, *85*, 177−182.
(18) Tsimidou, M.; Macrae, R. Authentication of virgin olive oils using principal component analysis of triglyceride and fatty acid profiles: Part 2 − Detection of adulteration with other vegetable oils. *Food Chem.* **1987**, *25*, 251−258.
(19) Fellatzarrouck, K.; Bouteiller, J. C.; Maurin, R. Detection of olive oil adulteration by HPLC in seed oils. *Rev. Fr. Corps Gras* **1988**, *35*, 383−386.
(20) García-González, D. L.; Viera, M.; Tena, N.; Aparicio, R. Evaluation of the methods based on triglycerides and sterols for the detection of hazelnut oil in olive oil. *Grasas Aceites* **2007**, *58*, 344−350.
(21) Cert, A.; Moreda, W. Algorithms for the detection of hazelnut oil in olive oil. *Grasas Aceites* **2000**, *51*, 143−149.
(22) International Olive Council, COI/T, 20/Doc. No. 20 Rev. 3. Determination of the difference between actual and theoretical content of triacylglycerols with ECN_{42}, 2010.
(23) Zeng, Y. X.; Araujo, P.; Du, Z. Y.; Nguyen, T. T.; Frøyland, L.; Grung, B. Elucidation of triacylglycerols in cod liver oil by liquid chromatography electrospray tandem ion-trap mass spectrometry. *Talanta* **2010**, *82*, 1261−1270.
(24) International Union of Pure and Applied Chemistry (IUPAC). Method 2.323. In *Standard Methods for the Analysis of Oils, Fats and Derivatives*, 7th ed.; Paquot, C., Hautfenne, A., Eds.; Blackwell: Oxford, UK, 1987.
(25) Antoniosi Filho, N. R.; Carrilho, E.; Langas, E. M. Quantitative analysis of soybean oil in olive oil by high-temperature capillary gas chromatography. *J. Am. Oil Chem. Soc.* **1993**, *70*, 1051−1053.
(26) Russo, M. V.; Goretti, G.; Soriero, A. Triglyceride analysis with microcapillary gas chromatography columns. *Ann. Chim.* **1996**, *86*, 281−291.
(27) Geeraert, E.; Sandra, P. Capillary GC of triglycerides in fats and oils using a high temperature phenylmethylsilicone stationary phase. Part II. The analysis of chocolate fats. *J. Am. Oil Chem. Soc.* **1987**, *64*, 100−105.
(28) Woodbury, S. E.; Evershed, R. P.; Rossel, J. B.; Griffith, R. E.; Farnell, P. Detection of vegetable oil adulteration using gas chromatography combustion/isotope ratio mass spectrometry. *Anal. Chem.* **1995**, *67*, 2685−2690.
(29) Galeano Diaz, T.; Duran Meras, I.; Sanchez Casas, J.; Alexendre Franco, M. F. Characterization of virgin olive oils according to its triglycerides and sterols composition by chemometric methods. *Food Control* **2005**, *16*, 339−347.
(30) Bohačenko, I.; Kopicová, Z. Detection of olive oils authenticity by determination of their sterol content using LC/GC. *Czech J. Food Sci.* **2001**, *19*, 97−103.
(31) Longobardi, F.; Ventrella, A.; Napoli, C.; Humpfer, E.; Schütz, B.; Schäfer, H.; Kontominas, M. G.; Sacco, A. Classification of olive oils according to geographical origin by using ^{1}H NMR fingerprinting combined with multivariate analysis. *Food Chem.* **2012**, *130*, 177−183.
(32) Román Falcó, I. P.; Grané Teruel, N.; Prats Moya, S.; Martín Carratalá, M. L. Kinetic study of olive oil degradation monitored by Fourier transform infrared spectrometry. Application to oil characterization. *J. Agric. Food Chem.* **2012**, 11800−11810.
(33) Bucci, R.; Magrí, A. D.; Magrí, A. L.; Marini, D.; Marini, F. Chemical authentication of extra-virgin olive oil varieties by supervised chemometric procedures. *J. Agric. Food Chem.* **2002**, *50*, 413−418.
(34) Pizarro, C.; Rodríguez-Tecedor, S.; Pérez-del-Notario, N.; Esteban-Díez, I.; González-Sáiz, J. M. Classification of Spanish extra-virgin olive oils by data fusion of visible spectroscopic fingerprints and chemical descriptors. *Food Chem.* **2013**, *138*, 915−922.
(35) Kalua, C. M.; Allen, M. S.; Bedgood, D. R., Jr.; Bishop, A. G.; Prenzler, P. D. Discrimination of olive oils and fruits into cultivars and maturity stages based on phenolic and volatile compounds. *J. Agric. Food Chem.* **2005**, *53*, 8054−8062.
(36) Boskou, D. *Olive Oil: Chemistry and Technology*; AOCS Press: Champaign, IL, USA, 1996; pp 85−127.
(37) International Olive Council, COI/T, 20/Doc. No. 24. Preparation of the fatty acid methyl esters from olive oil and olive pomace oil, 2001.
(38) International Olive Council, COI/T, 20/Doc. No. 17 Rev. 1. Determination of trans unsaturated fatty acids by capillary column gas chromatography, 2001.
(39) International Olive Council, COI/T, 20/Doc. No. 10 Rev. 1. Determination of the composition and content of sterols by capillary-column gas chromatography, 2001.
(40) International Olive Council, COI/ T, 20/ Doc. No. 30/Rev. 1. Determination of the composition and content of sterols and triterpene dialcohols by capillary column gas chromatography, 2013.
(41) Rezanka, T.; Rezanková, H. Characterization of fatty acids and triacylglycerols in vegetable oils by gas chromatography and statistical analysis. *Anal. Chim. Acta* **1999**, *398*, 253−261.
(42) Lerma-Garcia, M. J.; Lusardi, R.; Chiavaro, E.; Cerretani, L.; Bendini, A.; Ramis-Ramos, G.; Simo-Alfonso, E. F. Use of triacylglycerol profiles established by high performance liquid chromatography with ultraviolet−visible detection to predict the botanical origin of vegetable oils. *J. Chromatogr., A* **2011**, *1218*, 7521−7527.
(43) Al-Ismail, K. M.; Alsaed, A. K.; Ahmad, R.; Al-Dabbas, M. Detection of olive oil adulteration with some plant oils by GLC analysis of sterols using polar column. *Food Chem.* **2010**, *121*, 1255−1259.
(44) Cert, A.; Moreda, W.; Garcia-Moreno, J. Determination of sterols and triterpenic dialcohols in olive oils using HPLC separation and GC analysis. Standardization of the analytical method. *Grasas Aceites* **1997**, *48*, 207−218.
(45) Ballesteros, E.; Gallego, M.; Valcárcel, M. Simultaneous determination of sterols in edible oils by use of a continuous separation module coupled to a gas chromatograph. *Anal. Chim. Acta* **1995**, *308*, 253−260.
(46) Gigliotti, C.; Daghetta, A.; Sidoli, A. Indagine conoscitiva sul contenuto trigliceridico di oli extra vergini di oliva di varia provenienza. *Riv. Ital. Sostanze Grasse* **1993**, *70*, 483−489.
(47) Berrueta, L. A.; Alonso-Salces, R. M.; Heberger, K. Supervised pattern recognition in food analysis. *J. Chromatogr., A* **2007**, *1158*, 196−214.

antifungal effects of Cortex Pseudolaricis on mango anthracnose and other horticultural diseases has not been previously investigated. Our preliminarily experiments showed that ethanol extract from Cortex Pseudolaricis had a significant inhibitory activity against *C. gloeosporioides* (data not shown). Therefore, we further conducted a phytochemical study on the extract using a bioactivity-guided purification process, isolated and identified the main metabolites, and then evaluated their antifungal activity.

MATERIALS AND METHODS

General. The Cortex Pseudolaricis was collected in Yinzhou District, Ningbo City, Zhejiang Province of the People's Republic of China (29°46′6″E, 121°19′5″N) and identified by Associate Professor Jianyin Li from the Pharmacy Institute of Lanzhou University. The commercial fungicide carbendazim (nonformulated analytical grade, 98% purity) (Jiangsu Bailing Agrochemical Co., Ltd., China) was used as a positive control. *C. gloeosporioides* was obtained from Postharvest Pathology and Preservation Laboratory, Environment and Plant Protection Institute of Chinese Academy of Tropical Agricultural Science. It is carbendazim-sensitive and isolated from mango fruit. Analytical thin-layer chromatography (TLC) and preparative thin-layer chromatography (PTLC) were performed with silica gel plates using silica gel 60 GF254 (Qingdao Haiyang Chemical Co., Ltd.). Melting points were taken on a Kofler melting point apparatus and are uncorrected. Mass spectra were recorded on a Bruker Daltonics APEXII49e spectrometer with ESI source as ionization. ^{1}H and ^{13}C NMR spectra were recorded at 400 and 100 MHz on a Bruker AM-400 spectrometer using TMS as reference (Bruker Company, U.S.A.).

Isolation of Pseudolaric Acids. The Cortex Pseudolaricis (20 kg) was ground and percolated with 95% ethanol. After filtration and removal of the solvent, the ethanol extract was dissolved in 5 L of 5% $NaHCO_3$ solution to make a suspension and extracted with ethyl acetate to give a neutral ethyl acetate-soluble fraction. The aqueous solution was then treated with 5% HCl solution to about pH 6 and extracted with ethyl acetate again to afford an acidic ethyl acetate-soluble fraction. The acidic ethyl acetate-soluble fraction was subjected to silica gel column chromatography using a gradient solvent system of petrolumm-ethyl acetate (4:1), and then chloroform−methanol (10:1), and three major fractions, 1−3, were collected. Fraction 1 was then chromatographed sequentially over silica gel column using a solvent system of petroleum−ethyl acetate (4:1) to afford Pseudolaric acid A (**1**, PAA), a silica gel column petroleum−ethyl acetate (5:1), to afford Ethyl Pseudolaric acid B (**2**, EPAB). Fraction 2 was recrystallized from petroleumether−ethyl acetate (4:1) to afford pseudolaric acid B (**3**, PAB) (12.2 g). Fraction 3 was chromatographed sequentially over silica gel column using a solvent system of chloroform−methanol (20:1 to 1:1) to yield pseudolaric acid B—O-*β*-D-glucoside (**4**, PABG) (2.5 g).

Isolation of Other Compounds. The dried Cortex Pseudolaricis (20 kg) was ground and ultrasonically extracted with 95% ethanol. After filtration and removal of the solvent, the ethanol extract was dissolved in 5 L of 5% $NaHCO_3$ solution to make a suspension and immediately extracted with ethyl acetate to give a neutral ethyl acetate-soluble fraction. The aqueous solute was then treated with 5% HCl solution to about pH 2−3 and extracted with ethyl acetate again to afford an acidic ethyl acetate-soluble fraction (177g). The acidic ethyl acetate-soluble fraction was subjected to silica gel column chromatography using a gradient solvent system of petroleum−acetone (5:1−1:1), and three major fractions 1−3 were collected. The first of these fractions was then chromatographed sequentially over silica gel column using a solvent system of petroleum−acetone (3:1) to afford compound **5**. Fraction 2 was chromatographed sequentially over silica gel column using a gradient solvent system of petroleum−chloroform−acetone (5:2:2), and then petroleum−chloroform−acetone (5:1:2), and then petroleum−chloroform (1:1), to afford compounds **6**, **7**, and **8**, respectively.

*Pseudolaric Acid A (**1**).* White amorphous powder; mp 212−214 °C; ^{1}H NMR (400 MHz, $CDCl_3$) δ ppm: 7.28 (1H, brd, H-15), 6.57 (1H, dd, J = 10.8, 14.8 Hz, H-14), 5.94 (1H, d, J = 14.4 Hz, H-13), 5.58 (1H, m, H-8), 3.49 (1H, d, J = 3.6 Hz, H-3), 2.97(1H, dd, J = 8.4, 14.0 Hz, H-5), 2,46 (2H, d, J = 14.4 Hz, H-9), 2.24 (1H, m, H-5), 2.17 (3H, s, —COOC$\underline{H}_3$), 1.96 (3H, s, H-17), 1.88 (2H, d, J = 6.8 Hz, H-6), 1.82 (2H, d, J = 10.4 Hz, H-1), 1.80 (2H, m, H-2), 1.76 (3H, s, H-19), 1.60 (3H, s, H-12). ^{13}C NMR (400 MHz, $CDCl_3$) δ(ppm): 173.4 (C-2), 173.3 (C-18), 169.6 (—$\underline{C}OCH_3$), 144.9 (C-13), 139.2 (C-8), 138.8 (C-15), 127.6 (C-16), 123.1 (C-7), 121.5 (C-14), 90.6 (C-4), 83.2 (C-11), 55.3 (C-10), 49.0 (C-3), 33.2 (C-1), 30.6 (C-5), 28.3 (C-12), 27.2 (C-9), 26.7 (C-6), 26.5 (C-19), 24.3 (C-2), 21.7 (—CO$\underline{C}H_3$), 12.5 (C-17) ; ESI-MS m/z: 389 $[M + H]^+$.

*Ethyl Pseudolaric Acid B (**2**).* Yellow oily matter; ^{1}H NMR (400 MHz, $CDCl_3$) δ: 7.18 (1H, m, H-8), 7.13 (1H, d, J = 10.8 Hz, H-15), 6.51 (1H, dd, J = 7.2, 11.6 Hz, H-14), 5.85 (1H, d, J = 12.4 Hz, H-13), 4.22 (2H, q, J = 7.2 Hz, 18-OC$\underline{H}_2$CH$_3$), 3.72 (3H, s, —OC$\underline{H}_3$), 3.11 (1H, d, J = 8.4 Hz, H-3), 3.07 (1H, dd, J = 4.4, 11.2 Hz, H-5), 2.91 (1H, dd, J = 6.0, 13.6 Hz, H-6), 2.76 (1H, d, J = 8.8 Hz, H-9), 2.63 (1H, d, J = 15.2 Hz, H-9), 2.14 (3H, s, —COOC$\underline{H}_3$), 2.05 (1H, m, H-6), 1.96 (3H, s, H-17), 1.84−1.71 (5H, m, H-1,2,5), 1.60 (3H, s, H-12), 1.30 (3H, t, J = 8.4 Hz, 18-OCH$\underline{H}_2$C$\underline{H}_3$). ^{13}C NMR (400 MHz, $CDCl_3$) δ: 172.8 (C-18), 172.8 (C-20), 169.4(—$\underline{C}OCH_3$), 168.0 (C-19), 144.2 (C-13), 141.6 (C-8), 138.4 (C-15), 134.4 (C-7), 127.8 (C-16), 121.6 (C-14), 90.0 (C-4), 83.6 (C-11), 60.6 (18-O$\underline{C}$H$_2$CH$_3$), 55.1 (C-10), 51.9 (-O$\underline{C}$H$_3$), 49.2 (C-3), 33.2 (C-1), 30.6 (C-5), 28.3 (C-12), 27.6 (C-9), 24.2 (C-2), 21.6 (−CO$\underline{C}$H$_3$), 20.0 (C-6), 14.2 (18-OCH$\underline{H}_2$C$\underline{H}_3$), 12.5 (C-17) ; ESI-MS m/z: 483 $[M + Na]^+$.

*Pseudolaric Acid B (**3**).* Yellowish amorphous powder; mp 148−151 °C; ^{1}H NMR (400 MHz, $CDCl_3$) δ: 7.28 (1H, t, J = 15.6 Hz, H-15), 7.22 (1H, d, J = 7.6 Hz, H-8), 6.59 (1H, dd, J = 3.6, 11.6 Hz, H-14), 5.94 (1H, d, J = 15.2 Hz, H-13), 3.72 (3H, s, —OC$\underline{H}_3$), 3.11 (1H, d, J = 3.6 Hz, H-3), 3.07 (1H, dd, J = 5.6, 8.0 Hz, H-5), 2.87 (1H, dd, J = 6.0, 9.2 Hz, H-6), 2.76 (1H, dd, J = 8.8, 6.0 Hz, H-9), 2.63 (1H, m, H-9), 2.14 (3H, s, —COOC$\underline{H}_3$), 2.05 (1H, m, H-6), 1.96 (3H, s, H-17), 1.84−1.71 (5H, m, H-1,2,5), 1.60 (3H, s, H-12). ^{13}C NMR (400 MHz, $CDCl_3$) δ: 172.8 (C-18), 172.8 (C-20), 169.4 (—$\underline{C}OCH_3$), 168.0 (C-19), 144.2 (C-13), 141.6 (C-8), 138.4 (C-15), 134.4 (C-7), 127.8 (C-16), 12.16 (C-14), 90.0 (C-4), 83.6 (C-11), 55.1 (C-10), 51.9 (—O$\underline{C}H_3$), 49.2 (C-3), 33.2 (C-1), 30.6 (C-5), 28.3 (C-12), 27.6 (C-9), 24.2 (C-2), 21.6 (—CO$\underline{C}H_3$), 20.0 (C-6), 12.5 (C-17) ; ESI-MS m/z: 455 $[M + Na]^+$.

*Pseudolaric Acid B—O-β-D-Glucoside (**4**).* White powder; mp 109−113 °C; ^{1}H NMR (400 MHz, $CDCl_3$) δ: 7.31 (1H, t, J = 12.0 Hz, H-15), 7.26 (1H, d, J = 15.2 Hz, H-8), 6.39 (1H, dd, J = 4.0, 11.2 Hz, H-14), 6.06 (1H, d, J = 11.2 Hz, H-13), 4.92 (1H, d, J = 9.6 Hz, anomeric-H), 3.72 (3H, s, —OC$\underline{H}_3$), 3.25 (1H, d, J = 7.2 Hz, H-3), 3.04 (1H, dd, J = 5.6, 8.0 Hz, H-5), 2.87 (1H, dd, J = 6.0, 9.6 Hz, H-6), 2.74 (1H, dd, J = 9.2, 6.0 Hz, H-9), 2.59 (1H, m, H-9), 2.17 (3H, s, —COOC$\underline{H}_3$), 1.97 (1H, m, H-6), 1.89 (3H, s, H-17), 1.77−1.71 (5H, m, H-1,2,5), 1.57 (3H, s, H-12), 3.47−3.87 (sugar). ^{13}C NMR (400 MHz, $CDCl_3$) δ: 172.8 (C-18), 172.8 (C-20), 169.4 (—$\underline{C}OCH_3$), 168.0 (C-19), 144.2 (C-13), 141.6 (C-8), 138.4 (C-15), 134.4 (C-7), 127.8 (C-16), 121.6 (C-14), 90.0 (C-4), 83.6 (C-11), 55.1 (C-10), 51.9 (—O$\underline{C}H_3$), 49.2 (C-3), 33.2 (C-1), 30.6 (C-5), 28.3 (C-12), 27.6 (C-9), 24.2 (C-2), 21.6 (—CO$\underline{C}H_3$), 20.0 (C-6), 12.5 (C-17); ESI-MS m/z: 595 $[M + H]^+$, 617 $[M + Na]^+$.

*Piperonylic Acid (**5**).* White powder; mp 196−199 °C; ^{1}H NMR (400 MHz, DMSO-d_6) δ: 12.7 (1H, s, COO$\underline{H}$), 7.63(1H, dd, J = 1.2, 6.8 Hz, H-6), 7.34 (1H, d, J = 1.2 Hz, H-2), 6.97 (1H, d, J = 8.0 Hz, H-5), 6.02 (2H, s, O—C$\underline{H}_2$—O). ^{13}C NMR (400 MHz, DMSO-d_6) δ: 166.7 (C$\underline{O}$OH), 151.2 (C-4), 147.5 (C-3), 125.0 (C-6), 124.8 (C-1), 108.9 (C-2), 108.1 (C-5), 102.0 (O—$\underline{C}H_2$—O); ESI-MS m/z: 167 $[M + H]^+$, 205 $[M+K]^+$. $C_8H_6O_4$;

*Propionic Acid (**6**).* White crystals ; mp 130−132 °C; ^{1}H NMR (400 MHz, DMSO-d_6) δ: 11.9 (1H, s, COO$\underline{H}$), 2.16 (2H, t, J = 7.2 Hz, H-2), 1.46 (2H, t, J = 6.8 Hz, H-3), 1.23 (3H, s, H-4). ^{13}C NMR (400 MHz, DMSO-d_6) δ: 174.5 (C$\underline{O}$OH), 33.6 (C-2), 28.5 (C-3), 24.5 (C-4); ESI-MS m/z: 86 $[M + H]^+$.

dx.doi.org/10.1021/jf500968b | J. Agric. Food Chem. 2014, 62, 4905−4910

3-Hydroxy-4-methoxybenzoic Acid (7). White amorphous powder; mp 155−157 °C; ^{1}H NMR (400 MHz, DMSO-d_6) δ: 12.6 (1H, s, COOH), 7.54 (1H, dd, J = 1.6, 6.8 Hz, H-6), 7.43 (1H, d, J = 0.8 Hz, H-2), 7.01 (1H, d, J = 8.4 Hz, H-5), 6.10 (1H, d, J = 8.0 Hz, C-3—OH), 3.80 (3H, s, −O—CH$_3$). ^{13}C NMR (400 MHz, DMSO-d_6) δ: 167.2 (COOH), 152.7 (C-4), 148.4 (C-3), 125.0 (C-6), 123.2 (C-1), 111.9 (C-2), 108.9 (C-5), 55.7 (—O—CH$_3$); ESI-MS m/z: 169 [M + H]$^+$, 191 [M + Na]$^+$.

4-(3-Formyl-5-methoxyphenyl)butanoic Acid (8). White amorphous powder; mp: 99−102 °C; ^{1}H NMR (400 MHz, DMSO-d_6) δ: 12.3 (1H, s, COOH), 9.82 (1H, s, CHO), 7.41 (2H, t, J = 7.2 Hz, H-2, H-6), 6.83 (1H, d, J = 8.8 Hz, H-4), 3.79 (3H, s, O—CH$_3$), 3.34 (1H, s, H-9), 2.17 (1H, t, J = 7.6 Hz, H-7), 1.46 (1H, t, J = 6.8 Hz, H-7), 1.23 (2H, m, H-8), 1.15 (1H, dd, J = 6.4, 16.4 Hz, H-9). ^{13}C NMR (400 MHz, DMSO-d_6) δ: 174.5 (COOH), 167.3 (CHO), 151.1 (C-5), 147.3 (C-3), 123.5 (C-1), 121.7 (C-6), 115.1 (C-4), 112.7 (C-2), 55.6 (O—CH$_3$), 33.7 (C-7), 28.5 (C-9), 24.5 (C-8) ; ESI-MS m/z: 223 [M + H]$^+$, 245[M + Na]$^+$.

In Vitro Effect on Mycelial Growth of *C. gloeosporioides*. The effects of the compounds from Cortex Pseudolaricis on the mycelial growth against *C. gloeosporioides* were assessed using Poison Food Technique in solid media.[21] First, the compounds were dissolved in acetone and water containing Tween-80, then mixed with sterile molten potato dextrose agar to obtain final concentrations ranging from 0.3125 to 40.0 μg/mL. The PDA was poured into 9 cm Petri plates (15 mL) that were then inoculated with 4 mm plugs of *C. gloeosporioides*. Three replicate plates were used per treatment, and PDA containing a corresponding concentration of acetone in water as a normal growth control. After the fungal growth in the control had completely covered the Petri dishes, mycelial growth diameters were measured and inhibition percentages relative to the control with acetone were calculated using the formula from Agarwal:[22]

$$I(\%) = [(C - d) - (T - d)]/(C - d) \times 100$$

where d is diameter of the cut fungus (4 mm), I is the inhibition (%), and C and T are the average colony diameters of the mycelium of the control and treatment, respectively.

Spore Germination Assay. The inhibitory activity of compounds (**1**−**8**) on spore germination and germ-tube elongation of *C. gloeosporioides* were assessed by microscopic observation.[20] Spore suspensions (1 × 10^5 spores/mL) were prepared by seeding conidia in a 0.05% Tween 80 solution. The acetone solution of the test compounds was diluted with conidial suspension to obtain six different final concentrations of 0.5, 1, 5, 10, 20, and 40 μg/mL. Then, 30 μL of these cultures were removed to concave slide and incubated in a humidity chamber at 28 °C and 90% relative humidity. Three replicates were performed and conidial suspension containing a corresponding concentration of acetone in water was regarded as control. After incubation at 28 °C for 12 h, the number of germinated spores and the length of germ tubes were examined by counting and measuring approximately 100 conidia in each field of three randomly selected fields under a biological microscope photographic system at 400× magnification. The experiments were repeated three times.

In Vivo Trials on Mango Fruits. Mango fruit (*Mangifera indica*), cv. "Tai-Nong 1#"at the green mature stage were harvested from "Yangguang Farm" located in Sanya City, Hainan Province of China). The surface of the mango fruit was sterilized by immersion in 70% ethanol for 1 min and thereafter inflicting one wound (1 mm deep) in the middle of each fruit with a sterile needle. Then, 5 μL of spore suspension (10^4 spores/mL) of *C. gloeosporioides* were inoculated into wounded site. The inoculated fruit were incubated in a sterile box overnight at 28 °C prior to being dipped in the diluted compounds that were prepared by dissolution in 5 mL of 10% DMSO and then diluted with sterile distilled water to final concentrations of 50 and 100 μg/mL. The compound treatments were compared with carbendazim and 0.5% DMSO treatment that served as a negative control. The treated fruits were stored in a moisture chamber at 28 °C and 80% RH for 9 d. Disease developments were assessed by measuring the diameter of the anthracnose lesions on the mango fruit.[9] Each treatment consisted of 3 replicates with 10 fruits per replicate, and the experiment was repeated twice.

Scanning Electron Microscopy (SEM). SEM observations on the hyphae of *C. gloeosporioides* was conducted according to the method described by Feng et al.[23] A mycelial disk (4 mm diameter) was taken from the periphery of the colony grown on PDA medium containing 2.5 μg/mL (EC$_{80}$) of test compounds and incubated for 24−72 h at 28 °C. The youngest *C. gloeosporioides* hyphae were chosen from the margin of the mycelia, and the samples were routinely fixed in 2.5% glutaraldehyde (prepared previously with 0.1 mol/L phosphate buffer, pH 7.2) at 4 °C overnight, briefly postfixed for 2 h at 4 °C in 1% OsO_4 in the same buffer, and then dehydrated in a graded ethanol series, critical point dried, and gold coated. SEM observations were performed with an FEI Quanta 400 Thermal FE Environment Scanning Electron Microscope at an accelerating voltage of 20 kV.

Statistical Analyses. Data were presented as means and standard deviations. ANOVA was used to determine whether there were significant ($P < 0.05$) treatment effects between groups, and the means were compared using the Duncan's multiple range test. Differences among different treatments were analyzed using SAS version 9.13. Dose−response curves were analyzed using a four-parameter log−logistic model[24] using R software (version 2.15.2, R Foundation for Statistical Computing, Vienna, Austria) with the drc module.[25] Means and standard deviations were obtained using the raw data, and the EC$_{50}$ values were obtained from the parameters in the regression curves. The graphs were generated with Sigma Plot (version 11, Systat Software Inc., San Jose, CA, U.S.A.).

RESULTS

Structure Elucidation of the Bioactive Constitutes. Bioassay-guided separation of the components in the ethanol extract of the root bark of Cortex Pseudolaricis afforded eight major bioactive metabolites (Figure 1). All these compounds were purified by column chromatography, and their structures were characterized by ^{1}H NMR, ^{13}C NMR, and ESI-MS data,

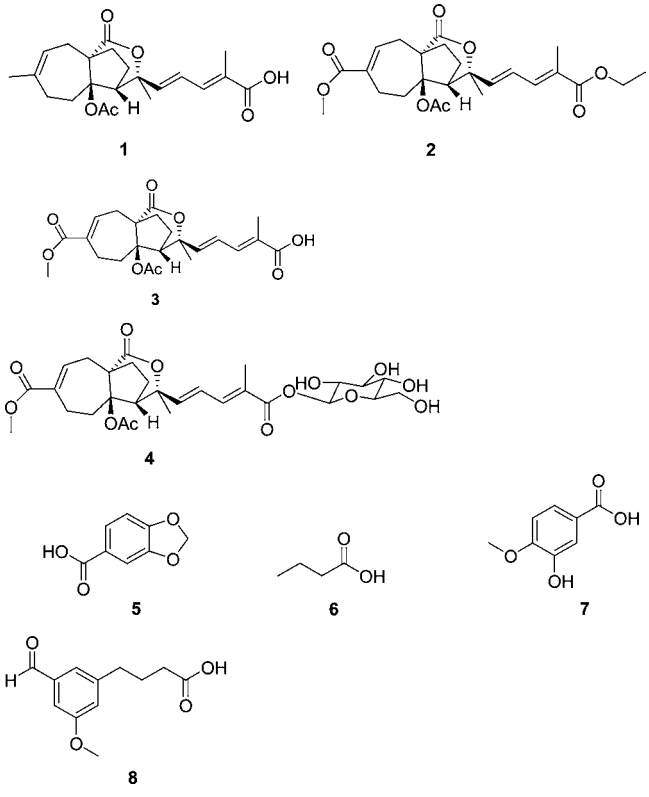

Figure 1. Chemical structures of compounds **1**−**8**.

dx.doi.org/10.1021/jf500968b | J. Agric. Food Chem. 2014, 62, 4905−4910

and their structures also were confirmed by direct comparison with previously reported spectroscopic data.[26,27] On the basis of the following data, the constituents were identified as pseudolaric acid A (1, PAA), ethyl pseudolaric acid B (2, EPAB), pseudolaric acid B (3, PAB), pseudolaric acid B—O-β-D-glucoside(4, PABG), piperonylic acid (5), propionic acid (6), 3-hydroxy-4-methoxybenzoic acid (7), and 4-(3-formyl-5-methoxyphenyl)butanoic acid (8).

Effects of Compounds on Mycelial Growth in Vitro. To evaluate the antifungal activity, the effects of the eight compounds on *C. gloeosporioides* mycelial growth on solid media were determined (Figure 2). The results showed that the

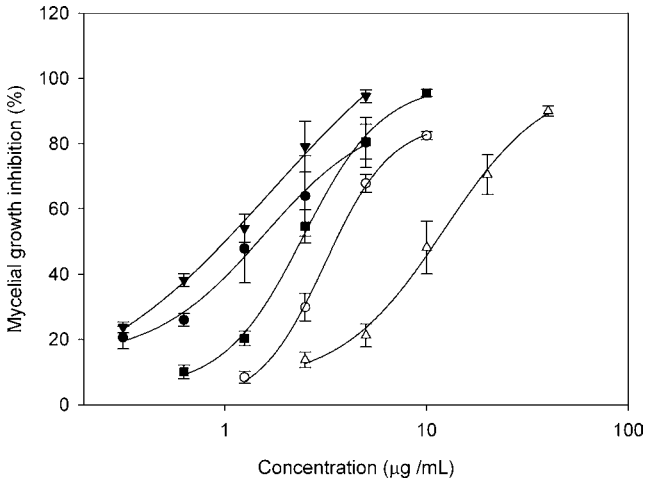

Figure 2. Dose−response curves of the test compounds on inhibition of *C. gloeosporioides* mycelial growth. ● = pseudolaric acid A; ○ = ethyl pseudolaric acid B; ▼ = pseudolaric acid B; △ = pseudolaric acid-O-β-D-glucoside; and ■ = commercial standard carbendazim.

PAB, PAA, EPAB, and PABG had high dose-dependent activities against the *C. gloeosporioides* mycelial growth with the EC_{50} value of 1.62, 3.7, 1.07, and 11.30 μg/mL, respectively. In particular, PAB and PAA showed a greater mycelial growth inhibition than that of carbendazim (2.37 μg/mL) (Figure 2). By contrast, compounds piperonylic acid, propionic acid, 3-hydroxy-4-methoxybenzoic acid, and 4-(3-formyl-5-methoxyphenyl) butanoic acid showed weaker inhibitory activity, whose mycelial growth inhibitions were all less than 30% at 40 μg/mL.

Effects of Compounds on Spore Germination and Germtube Elongation. PAB and PAA exhibited greater inhibition of spore germination and germ tube elongation than did the carbendazim standard (Table 1). PAB had an effective concentration of 50% (EC_{50}) value of of 3.80 μg/mL on spore germination and 0.75 μg/mL on germ tube elongation.

Effects of PAB on Control of *C. gloeosporioides* in Mango Fruit. The effects of four active compounds, including PAB, PAA, EPAB, and PABG, on the postharvest anthracnose of mango fruit were demonstrated in Figure 3. Results indicated that all the compounds tested at 50 and 100 μg/mL significantly suppressed lesion diameter of anthracnose in mango fruit inoculated with spore suspension of *C. gloeosporioides*. Smaller lesion development was achieved at higher concentrations of test compounds ($P < 0.05$). PAB treatment showed the greatest efficiency in controlling mango anthracnose, where the lesion diameters were 87.61% and 46.67% lower than those in control and carbendazim-treated fruit.

Table 1. EC_{50} Values (μg/mL) of Active Components from Cortex Pseudolaricis against Spore Germination and Germ Tube Elongation of *C. gloeosporioides*[a]

treatments	EC_{50} (95% FL)	
	spore germination	germ tube elongation
Pseudolaric acid A	5.69	1.14
ethyl Pseudolaric acid B	11.42	2.78
Pseudolaric acid B	3.80	0.75
Pseudolaric acid B—O-β-D-glucoside	23.57	6.35
piperonylic acid	>40	>40
propionic acid	>40	>40
3-hydroxy-4-methoxybenzoic acid	>40	>40
4-(3-formyl-5-methoxyphenyl)butanoic acid	>40	>40
carbendazim (98%)	21.34	2.04

[a] EC_{50} was determined by probit-log analysis. FL, fiducial limits.

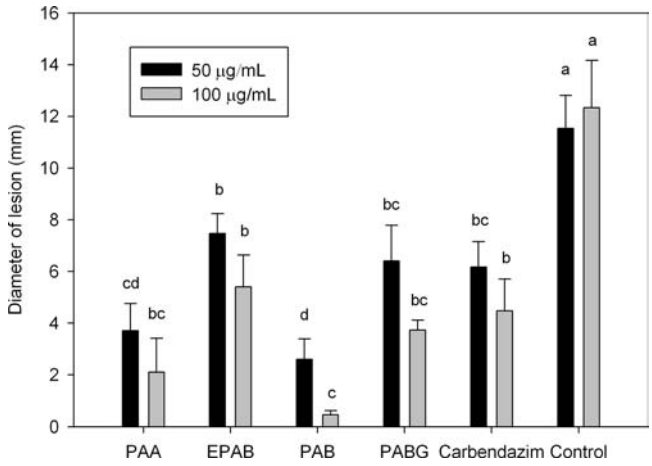

Figure 3. Efficacy of active components from Cortex Pseudolaricis in controlling anthracnose disease on mango fruits (Disease incidence was determined 9 days after inoculation). Each bar represents the mean of three independent experiments ± standard deviation. Different letters indicate that the means are significantly different at $P < 0.05$.

Changes in the Hyphae Morphology of *C. gloeosporioides*. To reveal the antifungal mechanism of PAB, the hyphae morphology of *C. gloeosporioides* treated with 2.4 μg/mL (EC_{80}) PAB was observed by scanning electron microscopy. *C. gloeosporioides* mycelium grown in PDA with 1% acetone (control) displayed characteristic morphology with lengthened, regular, homogeneous hyphae of constant diameter with smooth external surfaces and rounded apexes (Figure 4A,B). In the PAB treatment at 24 h, the hyphae morphology showed undulations along the hyphal border, a little swelling localized along the hyphae and at their extremities, and the formation of anomalous apex bifurcations (Figure 4C,D). Macroscopic morphologic alterations of *C. gloeosporioides* were more profound when the PAB treatment time was extended to 48 h. The apexes of *C. gloeosporioides* treated with PAB showed an irregular growth in dimension, with multiple ramifications in subapical expanded areas with an irregular shape (Figure 4E); several swellings of ovoidal or spherical shape were evident and were localized in the subterminal position near the apexes, or in the middle position along the hyphae (Figure 4F). Seventy-two hours after PAB treatment, hypha were distorted and collapsed (Figure 4G).

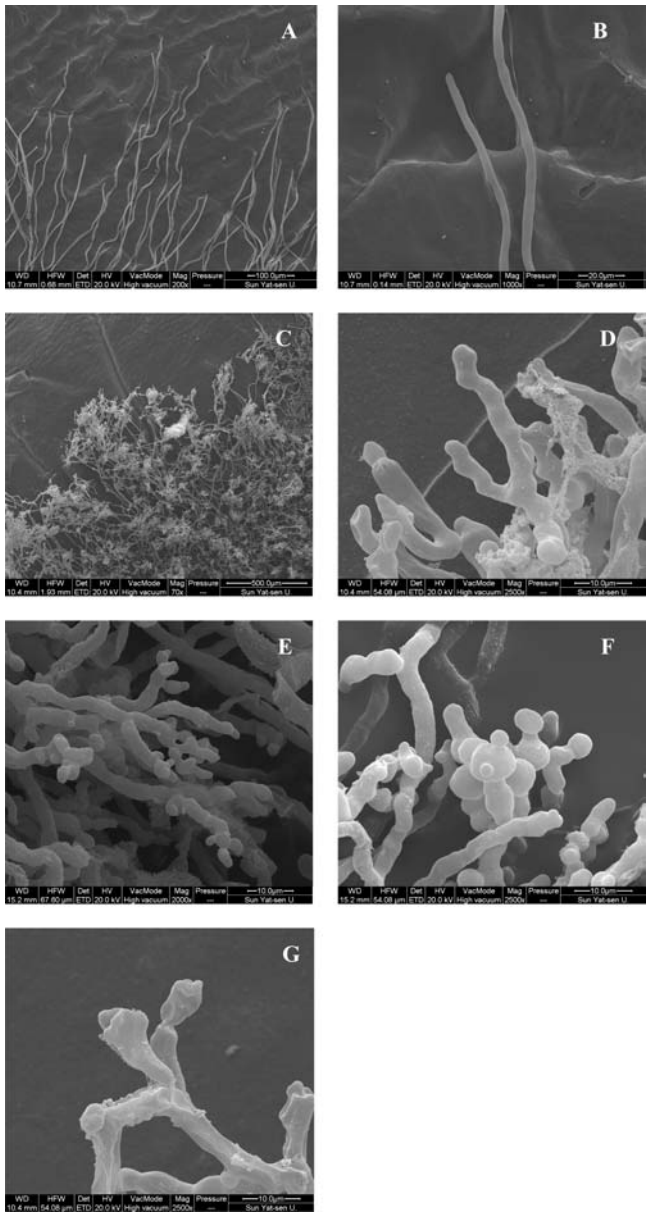

Figure 4. Scanning electron micrographs of the hyphae of *C. gloeosporioides* grown on PDA plates with or without PAB at 28 °C. (A, B) control (1% acetone); (C, D) PAB (24 h); (E, F) PAB (48 h), and (G) PAB (72 h).

DISCUSSION

In recent years, consumer demand for fresh fruits and vegetables without chemical residues has increased.[26] Susceptibility of anthracnose disease caused by *C. gloeosporioides* is one of the most serious problems affecting the mango industry worldwide. As alternatives to synthetic fungicides, the use of natural antifungal compounds isolated from plants to control mango anthracnose disease has been investigated, but few if any satisfactory compounds have been found.[9−13] The root bark of *P. kaempferi* has been successfully used in traditional Chinese medicine as an antifungal remedy and more recently, its major constituents have been isolated and characterized.[10,23,27] Although the antifungal activity and possible mechanisms of PAB against medical fungi have been well demonstrated, the effects of PAB and the pseudolaric acid analogues on plant phytopathogenic fungi were not documented. This is the first report on the potential agricultural use of these compounds isolated from Cortex Pseudolaricis against *C. gloeosporioides* in vitro and in vivo.

The present study evaluated the in vitro antifungal activity of eight compounds from the ethanol extracts of *Cortex Pseudolaricis* and their capability in controlling postharvest anthracnose. It was previously reported that pseudolaric acid analogues from Cortex Pseudolaricis were the active components.[27−29] Such observation was also supported by our study, in which pseudolaric acid analogues PAA, PAB, EPAB, and PABG, effectively suppressed *C. gloeosporioides* in mango fruit. PAB showed the strongest efficacy and had greater inhibitory activity than fungicide carbendazim. These results indicate that PAB has great potential to control postharvest mango anthracnose as a natural product based alternative to synthetic fungicides. Currently, natural PAA and PAB can only be obtained from the root bark of *P. kaempferi*. Recently, PAB was successfully achieved by manual synthesis in laboratory,[18] which could provide an ample supply of this compound and introduce a variety of novel structural modifications to the PAB molecule based on synthesis for structure activity relationships. Further studies need to be expanded to other important plant pathogenic fungi, and the indicated SAR need to be conducted on these compounds.

Research on the fungicidal mechanism of action for PAB is being carried out. Zhang et al. proposed that the mechanism of PAB could be unique and different from antibiotics with the known mechanisms of amphotericin B, nystatin, ketoconazole, and clotrimazole. It was been reported that PAB resulted in DNA damage and inhibited cell division.[30,31] Recently, Wong et al. showed that the antitumor activity of PAB could be associated with its ability to directly interact with tubulin and identified the microtubules as the molecular target of PAB.[18] In agricultural fungi, tubulin is one kind of important fungicide target. Both benzimidazole and zoxamide fungicides inhibit phytopathogenic fungus by binding to β-tubulin.[32,33] In our present study, PAB showed stronger inhibition of mycelial growth and germ tube elongation than spore germination. SEM images revealed that PAB treatments caused hyphal tip swelling, malformed branches, and swollen, distorted, concave-collapsed hyphae in *C. gloeosporioides*. Morphological changes induced by PAB are similar to those caused by tubulin inhibitors, such as benzimidazole fungicides.[34] Therefore, these findings suggest that PAB may have a similar function in inhibiting mycelial growth and germ-tube elongation in *C. gloeosporioides*.

AUTHOR INFORMATION

Corresponding Authors

*Phone: +86-898-66969260; fax: +86-898-66969211; e-mail: yqliu@lzu.edu.cn (Y.Q.L).

*Phone: +86-898-66969260; fax: +86-898-66969211; e-mail: feng8513@sina.com (G.F.).

Author Contributions

#These authors contributed equally to this work.

Notes

The authors declare no competing financial interest.

ACKNOWLEDGMENTS

This research was financially supported by the National Natural Science Foundation of China (31201538), Natural Science Foundation of Hainan Province of China (310086), Funda-

mental Research Fund for Central-level Nonprofit Research Institutes (1630042012002, Young Talents in Tropical Agriculture 2013hzs1J002), and the Fundamental Research Funds for the Central Universities (lzujbky-2013-69).

REFERENCES

(1) Kim, Y.; Brecht, J. K.; Talcott, S. T. Antioxidant phytochemical and fruit quality changes in mango (*Mangifera indica* L.) following hot water immersion and controlled atmosphere storage. *Food Chem.* **2007**, *105*, 1327−1334.

(2) Krishna, H.; Singh, S. K. Biotechnological advances in mango (*Mangifera indica* L.) and their future implication in crop improvement—A review. *Biotechnol. Adv.* **2007**, *25*, 223−243.

(3) Zhang, Z. K.; Yang, D. P.; Yang, B.; Gao, Z. Y.; Min, L.; Jiang, Y. M.; Hu, M. J. β-Aminobutyric acid induces resistance of mango fruit to postharvest anthracnose caused by *Colletotrichum gloeosporioides* and enhances activity of fruit defense mechanisms. *Sci. Hortic.* **2013**, *6*, 78−84.

(4) Dodd, J. C.; Prusky, D.; Jeffries, P. Fruit Diseases. In *The Mango: Botany, Production and Uses*; CAB International: Wallingford, 1997; p 257.

(5) Prior, C.; Elango, F.; Whitwell, A. Chemical Control of Colletotrichum Infection in Mangoes. In *Colletotrichum-Biology, Pathology and Control*; CAB International: Wallingford, 1992; p 326.

(6) Chung, W. H.; Chung, W. C.; Peng, M. T.; Yang, H. R.; Huang, J. W. Specific detection of benzimidazole resistance in *Colletotrichum gloeosporioides* from fruit crops by PCR-RFLP. *New Biotechnol.* **2010**, *27*, 17−24.

(7) Bacci, E.; Calamari, D.; Gaggi, C.; Fanelli, R.; Focardi, S.; Morosini, M. Organochlorine pesticide and PCB residues in plant foliage: (*Mangifera indica*) from West Africa. *Chemosphere* **1988**, *17*, 693−702.

(8) Filho, A. M.; dos Santos, F. N.; de Paula Pereira, P. A. Development, validation and application of a methodology based on solid-phase micro extraction followed by gas chromatography coupled to mass spectrometry (SPME/GC-MS) for the determination of pesticide residues in mangoes. *Talanta* **2010**, *81*, 346−354.

(9) Regnier, T.; du Plooy, W.; Combrinck, S.; Botha, B. Fungitoxicity of *Lippia scaberrima* essential oil and selected terpenoid components on two mango postharvest spoilage pathogens. *Postharvest Biol. Technol.* **2008**, *48*, 254−258.

(10) Crockett, S. L.; Poller, B.; Tabanca, N.; Pferschy-Wenzig, E. M.; Kunert, O.; Wedge, D. E.; Bucar, F. Bioactive xanthones from the roots of *Hypericum perforatum* (common St John's wort). *J. Sci. Food Agric.* **2011**, *91*, 428−34.

(11) Yenjit, P.; Issarakraisila, M.; Intana, W.; Chantrapromma, K. Fungicidal activity of compounds extracted from the pericarp of *Areca catechu* against *Colletotrichum gloeosporioides* in vitro and in mango fruit. *Postharvest Biol. Technol.* **2010**, *55*, 129−132.

(12) Kefialew, Y.; Ayalew, A. Postharvest biological control of anthracnose (*Colletotrichum gloeosporioides*) on mango (*Mangifera indica*). *Postharvest Biol. Technol.* **2008**, *50*, 8−11.

(13) Sergio, R. P. S.; Ernesto, O. C. C.; Esau, R. S. Screening of Yucatecan plant extracts to control *Colletotrichum gloeosporioides* and isolation of a new Pimarene from *Acacia pennatula*. *J. Agric. Food Chem.* **2005**, *7*, 2429−2432.

(14) Zhou, B. N.; Ying, B. P.; Song, G. Q.; Chen, Z. X.; Han, J.; Yan, Y. F. Pseudolaric Acids from *Pseudolarix kaempferi*. *Planta Med.* **1983**, *47*, 35−8.

(15) Li, E.; Clark, A. M.; Hufford, C. D. Antifungal evaluation of pseudolaric acid B, a major constituent of *Pseudolarix kaempferi*. *J. Nat. Prod.* **1995**, *58*, 57−67.

(16) Yang, S. P.; Dong, L.; Wang, Y.; Wu, Y.; Yue, J. M. Antifungal diterpenoids of *Pseudolarix kaempferi*, and their structure−activity relationship study. *Bioorg. Med. Chem.* **2003**, *11*, 4577−4584.

(17) Yang, S. P.; Yue, J. M. Two novel cytotoxic and anti-microbial triterpenoids from *Pseudolarix kaempferi*. *Bioorg. Med. Chem. Lett.* **2001**, *11*, 3119−3122.

(18) Wong, V. K. W.; Chiu, P.; Chung, S. S. M.; Chow, L. M. C.; Zhao, Y. Z.; Yang, B. B.; Ko, B. C. B. Pseudolaric acid B, a novel microtubule-destabilizing agent that circumvents multidrug resistance phenotype and exhibits antitumor activity in vivo. *Clin. Cancer Res.* **2005**, *11*, 6002−6011.

(19) Yang, S. P.; Cai, Y. J.; Zhang, B. L.; Tong, L. J.; Xie, H.; Wu, Y.; Lin, L. P.; Ding, J.; Yue, J. M. Structural modification of an angiogenesis inhibitor discovered from traditional chinese medicine and a structure-activity relationship study. *J. Med. Chem.* **2008**, *51*, 77−85.

(20) Chen, S. J.; Ding, W.; Yang, B.; Wu, X. B. Screening studies on fungistasis of ten traditional medicines. *Southwest China J. Agri Sci.* **2005**, *18*, 310−313 (in Chinese with English summary).

(21) Dhiangra, O. D.; Sinclair, J. B. Chemical control. *Basic Plant Pathology Methods*; CRC Press: Boca Raton, FL, 1986; p 227.

(22) Agarwal, M.; Walia, S.; Dhingra, S.; Khambay, B. P. S. Insect growth inhibition, antifeedant and antifungal activity of compounds isolated/derived from *Zingiber offcinale* Roscoe (ginger) rhizomes. *Pest Manag. Sci.* **2001**, *57*, 289−300.

(23) Feng, L. Y.; Wu, F. W.; Li, J.; Jiang, Y. M.; Duan, X. W. Antifungal activities of polyhexamethylene biguanide and polyhexamethylene guanide against the citrus sour rot pathogen *Geotrichum citriaurantii* in vitro and in vivo. *Postharvest Biol. Technol.* **2011**, *61*, 160−164.

(24) Seefeldt, S. S.; Jensen, J. E.; Fuerst, E. P. Log logistic analysis of herbicide dose-response relationships. *Weed Technol.* **1995**, *9*, 218−227.

(25) Ritz, C.; Streibig, J. C. Bioassay analysis using R. *J. Stat. Softw.* **2005**, *12*, 1−22.

(26) Schirra, M.; Aquino, S. D.; Cabras, P.; Angioni, A. Control of Postharvest Diseases of Fruit by Heat and Fungicides: Efficacy, Residue Levels, and Residue Persistence. *J. Agric. Food Chem.* **2011**, *59*, 8531−8542.

(27) Chen, G. F.; Li, Z. L.; Pan, D. J.; Tang, C. M.; He, X.; Xu, G. Y.; Chen, K.; Lee, K. H. The isolation and structural elucidation of four novel triterpene lactones, Peudolarolides A, B, C, and D, from *Pseudolarix kaempferi*. *J. Nat. Prod.* **1993**, *56*, 1114−1122.

(28) Yang, S. P.; Dong, L.; Wang, Y.; Wu, Y.; Yue, J. M. Antifungal diterpenoids of *Pseudolarix kaempferi*, and their structure−activity relationship study. *Bioorg. Med. Chem. Lett.* **2003**, *11*, 4577−4584.

(29) Li, E.; Clark, A. M.; Hufford, C. D. Antifungal evaluation of pseudolaric acid B, a major constituent of *Pseudolarix kaempferi*. *J. Nat. Prod.* **1995**, *58*, 57−67.

(30) Zhang, L.; Zhang, Y.; Zhou, Y. M.; An, S.; Zhou, Y. X.; Cheng, J. Expression profiling of the response of saccharomyces cerevisiae to 5-fluorocytosine using a DNA microarray. *Int. J. Antimicrob. Agents* **2002**, *20*, 444−450 (in Chinese with English summary).

(31) Zhang, L.; Zhang, Y.; Zhou, Y. M.; An, S.; Guo, D. A.; Zhou, Y. X.; Zeng, L. W.; Chen, G. J. Cluster analysis of yeast genome-wide expression patterns obtained by treating with different antifungal agents. *Prog. Biochem. Biophys.* **2002**, *29*, 538−542.

(32) Davidse, L. C.; Flach, W. Differential binding of methyl benzimidazol-2-yl carbamate to fungal tubulin as a mechanism of resistance to this antimitotic agent in mutant strains of *Aspergillus nidulans*. *J. Cell Biol.* **1977**, *72*, 174−193.

(33) Young, D. H.; Slawecki, R. A. Mode of action of zoxamide (RH-7281), a new oomycete fungicide. *Pestic. Biochem. Phys.* **2001**, *69*, 100−111.

(34) Hammerschlag, R. S.; Sisler, H. D. Benomyl and methyl-2-benzimidazolecarba-mate biochemical, cytological and chemical aspects of toxicity to *Ustilago maydis* and *Saccharomyces cerevisiae*. *Pestic. Biochem. Phys.* **1973**, *3*, 42−54.

MATERIALS AND METHODS

General. Aβ_{25-35}, *p*-CA, and UA were purchased from Sigma Chemical Co. (St. Louis, MO, USA). RPMI 1640 medium, phosphate-buffered saline (PBS), fetal bovine serum, donor equine serum, trypsin 0.25% solution, and penicillin/streptomycin solution were obtained from Hyclone Laboratories, Inc. (Logan, UT, USA). N_2 supplement and RPMI 1640 phenol red free medium were purchased Gibco BRL (Grand Island, NY, USA). Rabbit-antiphospho-iNOS, goat-antiphospho-COX-2, and goat-anti-β-actin were obtained from Santa Cruz Biotechnology, Inc. (Santa Cruz, CA, USA). Rabbit antiphospho-JNK, rabbit-antiphospho-ERK, rabbit-antiphospho-IκB-α, and rabbit-anti-phospho-p65 monoclonal antibodies were purchased from Cell Signaling Technology Inc. (Beverly, MA, USA). All other reagents used in this study were of the highest grade available.

Peptide Preparation and Cell Culture. Pheochromocytoma PC12 cells (ATCC CRL 1721) have been extensively used as an in vitro model system to study the mechanisms of neuronal toxicity.[18,19] PC12 cells were purchased from ATCC (Manassas, VA, USA). PC12 cells were maintained in RPMI 1640 supplemented with 10% heat-inactivated horse serum and 5% fetal bovine serum at 37 °C in a humidified atmosphere of 5% CO_2 and 95% air. All cells were cultured in serum-free medium for 16 h prior to sample treatment. Samples were added at indicated concentrations 1 h prior to Aβ_{25-35} treatment, and the cells were plated at a density of 2×10^6 cells/well.

The Aβ_{25-35} peptide used in this study preserves the toxicity of the full length Aβ and is widely used to model Aβ-induced neurodegeneration. The fragment Aβ_{25-35} has the central functional domain of the whole molecules Aβ that is required for neurotoxic effect.[20,21] Aβ_{25-35} was dissolved in DMSO at a concentration of 10 mM and stored at −20 °C. The stock solution was diluted with PBS to appropriate concentration and incubated for 48 h at 37 °C for aggregation prior to each experiment. Samples were dissolved in DMSO and further diluted with PBS. The final concentration of DMSO was adjusted to <0.01%, which was found to have no effect on the cell viability in our preliminary experiments (data not shown).

Western Blot Analysis. PC12 cells were incubated at 37 °C with 50 μM Aβ_{25-35} for 1 h for MAPKs family phosphorylation, for 4 h for NF-κB and I κB formation, and for 30 h for iNOS and COX-2 activation with or without pretreatment with samples. The treated cells were washed twice with cold PBS (pH 7.4) and harvested using a cell scraper. The cell pellets were resuspended in lysis buffer on ice for 1 h, and cell debris was removed by centrifugation at 13000 rpm for 10 min. Protein concentrations were determined by the BCA protein assay (Pierce, Rockford, IL, USA). Equal amounts of proteins were mixed with 4× Laemmli loading buffer and preheated at 95 °C for 5 min. The samples were then loaded onto a 10% SDS−polyacrylamide gel and transferred onto a PVDF membrane for 1 h with a semidry transfer system (Bio-Rad, Hercules, CA, USA). The membranes were blocked with 5% nonfat milk in PBST with 0.1% Tween 20 for 1 h at room temperature and then incubated overnight with anti-COX-2, anti-iNOS, antiphospho-p65, antiphospho-IκB-α, antiphospho-ERK1/2, antiphospho-JNK, and antiphospho-p38 antibodies diluted 1:1000 in blocking solution at 4 °C. After five washes with PBS containing Tween, the membrane was incubated with anti-goat or anti-rabbit immunoglobulin G horseradish peroxidase-conjugated secondary antibodies (diluted 1:1000) and visualized using Western blotting luminal reagents (Santa Cruz Biotechnology).

Statistical Analysis. All experiments were performed in triplicate. Data of each experiment showed the mean ± SD (n = 3). The values were compared with the control using analysis of variance followed by unpaired Student's t test.

RESULTS AND DISCUSSION

Protective Effect of *p*-CA and UA on Protein Expression of iNOS and COX-2 in Aβ_{25-35}-Induced PC12 Cells. The chemical structures of *p*-CA and UA are shown in Figure 1. Our previous study demonstrated that *p*-CA and UA exhibited predominant neuroprotective effects against

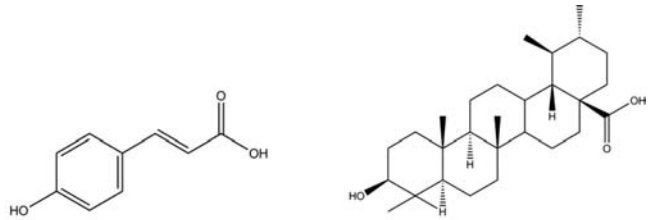

p-Coumaric acid (*p*-CA) Ursolic acid (UA)

Figure 1. Chemical structures of *p*-coumaric acid and ursolic acid.

Aβ_{25-35}-induced injury via attenuating cellular oxidative stress, suppressing capsase-3 activity, and thus inhibiting apoptosis.[17] Unlike *p*-CA, UA displayed adverse effects on cell viability at the higher concentration, and treatment of high concentration of UA showed neither protection nor exacerbation against Aβ_{25-35}-induced damage.[17] Thus, the experimental concentration limit of UA in the current study was adjusted to 20 μM, which did not affect cell viability. Concentration of UA (1, 10, and 20 μM) and *p*-CA (5, 25, and 50 μM) alone did not affect cell viability (data not shown). The concentration of 50 μM was used for determining Aβ_{25-35}-induced cell damage in the present experiments on the basis of our previous study.[17] To determine whether *p*-CA and UA can suppress inflammation, the inflammatory responses were induced in PC12 cells by Aβ_{25-35}. COX-2 and iNOS are well-known pro-inflammatory enzymes that play crucial roles in inflammatory responses.[22] As shown in Figure 2, Aβ_{25-35} significantly increased the expression of COX-2 and iNOS ($p < 0.01$ and $p < 0.001$, respectively) compared with the control without Aβ_{25-35} treatment. Cells pretreated with *p*-CA at 5 and 25 μM showed significantly reduced level of COX-2 expression in comparison to the Aβ_{25-35}-treated cells ($p < 0.05$). On the other hand, pretreatment of *p*-CA at 50 μM showed a somewhat weaker effect in COX-2 expression, which exerted neither positive nor negative effect against Aβ_{25-35}-induced inflammation. Each pretreatment of *p*-CA at 5, 25, and 50 μM strongly inhibited iNOS expression in a dose-dependent manner ($p < 0.01$). Even at 5 μM *p*-CA inhibited Aβ_{25-35}-induced iNOS expression. UA dose-dependently suppressed both iNOS and COX-2 levels. Even at 20 μM UA inhibited not only COX-2 expression but also iNOS expression to a level much lower than the control.

Protective Effect of *p*-CA and UA on Aβ_{25-35}-Induced Nuclear Translocation of NF-κB Subunit p65 and Phosphorylation of IκB in PC12 Cells. When binding with IκB, NF-κB is inactive in the cytosol. However, it becomes active via phosphorylation and degradation of IκB, and subsequent nuclear translocation of NF-κB is stimulated by Aβ.[23] NF-κB signaling regulates the expression of downstream NF-κB dependent gene products such as COX-2 and iNOS.[24] Because the expression levels of COX-2 and iNOS enzymes were reduced by *p*-CA and UA treatments, we further examined whether *p*-CA and UA could inhibit the nuclear translocation of NF-κB subunit p65 by using Western blot. It has been reported that phosphorylation of p65 affects the transcriptional activity of NF-κB.[25] As illustrated in Figure 3, the p-p65/p-IκB and β-actin ratios were significantly elevated by Aβ_{25-35} in PC12 cells ($p < 0.05$). UA exhibited significant and dose-dependent inhibition of p65 phosphorylation in comparison to the Aβ_{25-35}-stimulated control group ($p < 0.05$). *p*-CA also attenuated levels of p-p65 protein, however, somewhat lower than that of UA.

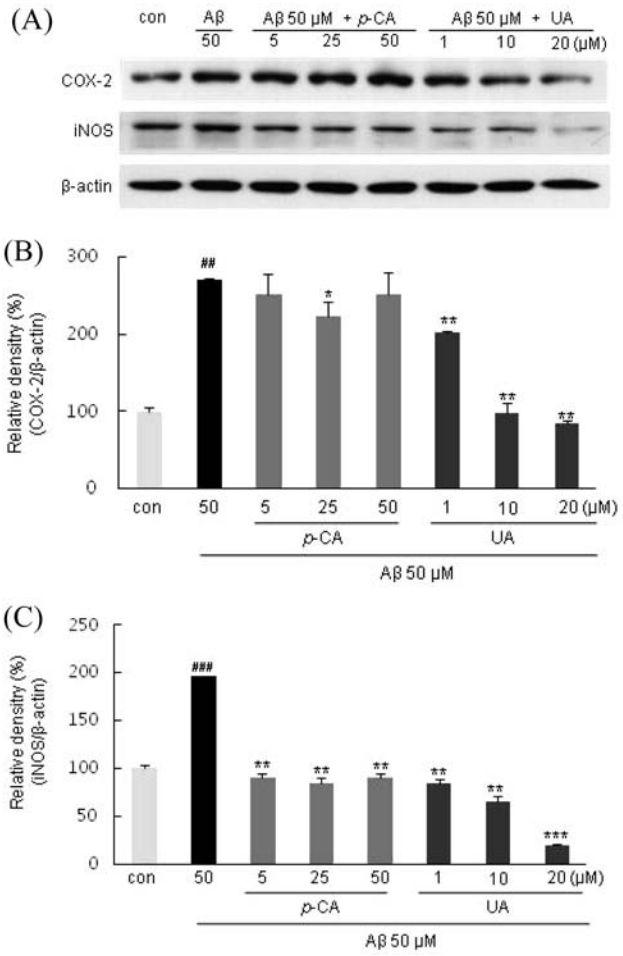

Figure 2. Effects of *p*-coumaric acid (*p*-CA) and ursolic acid (UA) on Aβ_{25-35}-induced iNOS and COX-2 expression in PC12 cells. The total lysates of the proteins were subjected to Western blot analysis, as described under Materials and Methods. Cells were pretreated with samples at the indicated concentrations for 1 h and then exposed to 50 μM Aβ_{25-35} for 30 h. The ratio of immunointensity between COX-2/iNOS and β-actin was calculated. Each bar represents the mean ± SD from three independent experiments. (###) $p < 0.001$ and (##) $p < 0.01$ versus control group. (***) $p < 0.001$, (**) $p < 0.01$, and (*) $p < 0.05$ versus the group treated with Aβ_{25-35} alone.

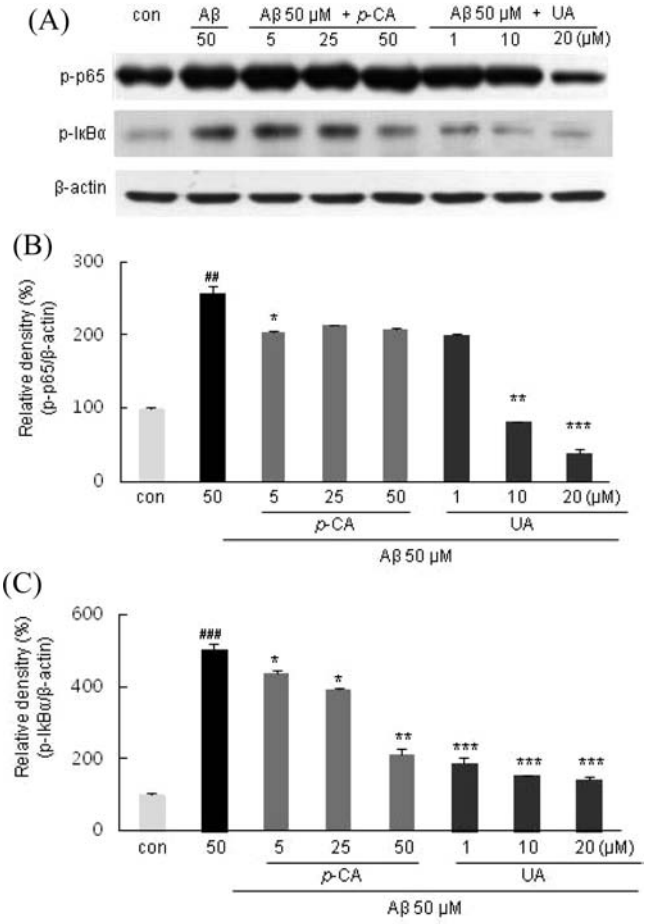

Figure 3. Effects of *p*-coumaric acid (*p*-CA) and ursolic acid (UA) against Aβ_{25-35}-induced phosphorylation of NF-κB subunit (p65) and degradation of IκB in PC12 cells. The total lysates of the proteins were subjected to Western blot analysis, as described under Materials and Methods. Cells were pretreated with the indicated concentrations of samples for 1 h and then exposed to 50 μM Aβ_{25-35} for 4 h. The ratio of immunointensity between the p-p65/IκB-α and β-actin was calculated. Each bar represents the mean ± SD from three independent experiments. (#) $p < 0.05$ versus control group. (**) $p < 0.01$ and (*) $p < 0.05$ versus the group treated with Aβ_{25-35} alone.

Protective Effect of *p*-CA and UA on MAPKs Phosphorylation in Aβ_{25-35}-Induced PC12 Cells. Because the activation of MAPKs family including ERK, JNK, and p38 is associated with the NF-κB activation and downstream inflammatory gene expression, we further investigated the activation of MAPKs.[26] The phosphorylation of p38, ERK, and JNK was significantly elevated when cells were treated with Aβ_{25-35} alone compared with the control (Figure 4). *p*-CA significantly suppressed ERK1/2 and JNK phosphorylation but relatively not that of p38 in response to Aβ_{25-35} treatment of PC12 cells. In particular, *p*-CA at a concentration of 25 μM strongly suppressed the phosphorylation of ERK1/2 and JNK even to levels much lower than that of the control. UA exclusively decreased the phosphorylation of p-38, JNK, and ERK in dose-dependent manners. In particular, the phosphorylation of ERK was markedly suppressed almost to its basal level when treated with 1 μM UA. In addition, 20 μM UA significantly reduced the phosphorylation of p38 and JNK even to a level much lower than the control. *p*-CA and UA comprehensively inhibited NF-κB activity, but the results of the upstream mechanisms were different.

A deleterious effect of Aβ against neuronal cells has been proved to be a critical cause of AD.[27] Aβ accumulation occurs at an early step in the AD cascade of events in cellular dysfunction through neuroinflammation.[28] The discovery of NF-κB as a key transcription factor in the inflammation provided a starting point that the suppression of NF-κB can be a promising therapeutic approach in inflammatory pathology such as arthritis, asthma, AD, and cancers.[29] Various researchers have proved that the activation of NF-κB is initiated by various stimuli including Aβ, ROS, and inflammatory cytokines.[23] Bioactive natural products have received much attention as predominant and promising sources in the development of novel therapeutic agents. Synthetic agents have not replaced natural products as essential substances, and many of the recently developed medicines are derived from natural sources. In addition, therapeutic properties of various natural substances with anti-inflammatory effects may result from their inhibition of NF-κB-dependent inflammation.[30]

dx.doi.org/10.1021/jf501314g | J. Agric. Food Chem. 2014, 62, 4911−4916

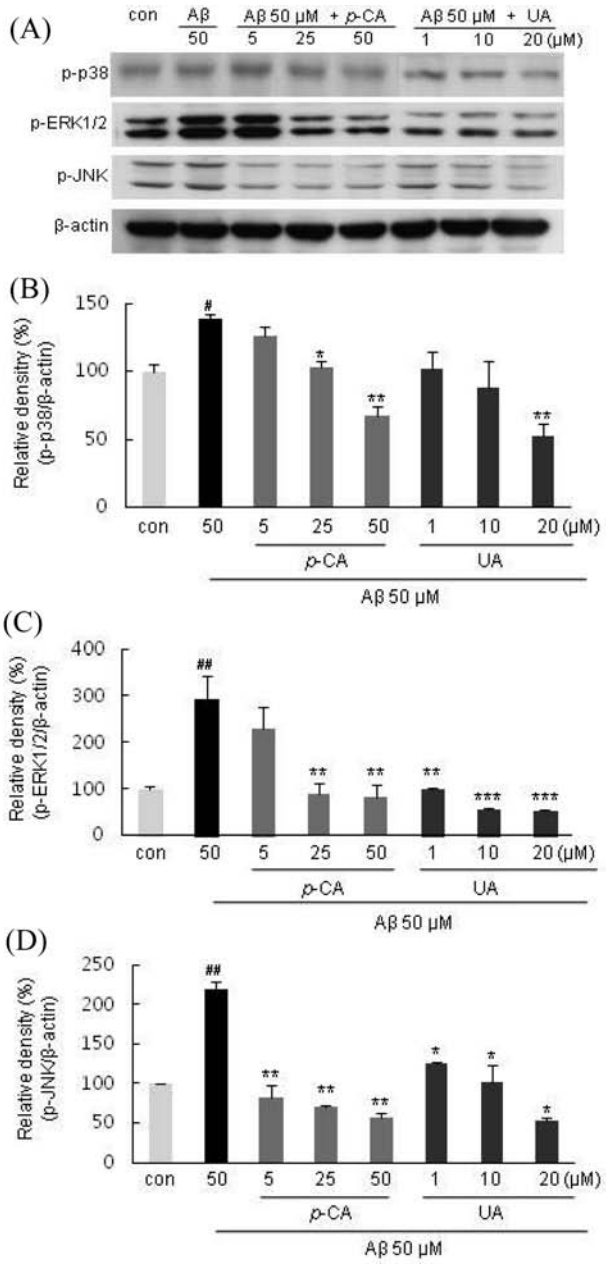

Figure 4. Effects of *p*-coumaric acid (*p*-CA) and ursolic acid (UA) against Aβ_{25-35}-induced phosphorylation of MAPKs in PC12 cells. The total lysates of the proteins were subjected to Western blot analysis, as described under Materials and Methods. Cells were pretreated with samples for 1 h and then exposed to 50 μM Aβ_{25-35} for 1 h. The ratio of immunointensity between the p-p38/ERK1/2/JNK and β-actin was calculated. Each bar represents the mean ± SD from three independent experiments. (**) $p < 0.01$ and (#) $p < 0.05$ versus control group. (**) $p < 0.01$ and (*) $p < 0.05$ versus the group treated with Aβ_{25-35} alone.

p-CA [3-(4-hydroxyphenyl)-2-propenoic acid], a ubiquitous intermediate metabolite in the synthesis of many polyphenols including flavonoids in plants, is widely found in fruits, vegetables, and cereals.[31] Previous investigators have shown that *p*-CA protected dextran sodium sulfate induced-intestinal inflammation through the suppression of COX-2 expression.[32] Apart from this, no report regarding the anti-inflammatory property of *p*-CA via suppression of the NF-κB pathway has been found so far.

UA (3β-hydroxyurs-12-en-28-oic acid) is a pentacyclic triterpene acid widely distributed in berries, flowers, and fruits. Previous research has demonstrated that UA inhibited LPS-induced inflammatory response through inhibition of NF-κB and iNOS expression in lung epithelial cells.[33] In addition, animal studies have shown that oral administration of UA (10 mg/kg·day) attenuated D-galactose-induced inflammatory response in the mouse prefrontal cortex through down-regulation of iNOS and COX-2 expression.[34] Another study has demonstrated that UA enhances collateral blood flow recovery through induction of neovascularization in a hind limb ischemia mouse model.[35]

The present study suggested for the first time that *p*-CA and UA isolated from CF efficiently suppressed the expression of iNOS and COX-2 in Aβ_{25-35}-treated PC12 cells. These inhibitions appeared to correlate with the inhibition of NF-κB activation as pretreating cells with *p*-CA and UA blocked the phosphorylation of the inhibitory subunit IκB. Similar inhibitory effects of UA on iNOS and COX-2 regulated by NF-κB inactivation have been observed in several different cell types including macrophages, platelets, and leukemic and cancer cells exposed to diverse oxidative or inflammatory stimuli.[36−38] Our results show that *p*-CA might exert its anti-inflammatory ability through inhibiting p38 and JNK pathways leading to NF-κB inactivation and thereby suppressing expressions of inflammatory target proteins including COX-2 and iNOS. On the other hand, UA may affect pro-inflammatory signaling through the inhibition of ERK, p38, and JNK, leading to NF-κB inactivation and thereby suppressing expressions of inflammatory target proteins including COX-2 and iNOS. Yeh et al. recently reported that UA suppressed migration of human breast cancer cells by reducing the level of JNK phosphorylation through inhibition of NF-κB.[39] For any compounds to exert direct neuroprotective actions they have to permeate the blood−brain barrier (BBB). UA has previously been found in the brain, which implied UA can cross the BBB.[40] Further studies regarding the BBB penetration by *p*-CA are needed. Our novel findings suggest that *p*-CA and UA have potential neuroprotective effects against Aβ_{25-35}-induced neurotoxicity through blocking iNOS and COX-2 via down-regulation of NF-κB and MAPKs pathways.

The results indicate that *p*-CA and UA derived from CF suppressed Aβ_{25-35}-stimulated expression of pro-inflammatory mediators such as iNOS and COX-2 in PC12 cells. Furthermore, *p*-CA and UA enhanced the inhibitory effects against inflammation via inactivation of both NF-κB and MAPKs signaling pathways. Even though PC12 cells display distinctive sensitivity to neurotoxicity and have been extensively used in the studies of Aβ-induced injury, they cannot thoroughly represent the primary cultured neurons. Therefore, further studies are required to concentrate on primary neurons and in vivo models. Taken together, these findings are the first to represent the anti-inflammatory effects of *p*-CA and UA against Aβ_{25-35} toxicity in PC12 cells, which may provide the pharmacological basis underlying the prevention of AD.

AUTHOR INFORMATION

Corresponding Author

*(M.J.) Phone: +82-51-200-7323. Fax: +82-51-200-7535. E-mail: mjun@dau.ac.kr.

Author Contributions

‖J.-H.Y. and K.Y. contributed equally to this work.

Funding

This research was supported by the Basic Science Research Program through the National Research Foundation (NRF) funded by the Ministry of Education, Science and Technology (2012-006723). This research was also partially supported by the Brain Busan 21 project in 2013.

Notes

The authors declare no competing financial interest.

■ ACKNOWLEDGMENTS

We are grateful to Y. Hwang for isolating and providing *p*-coumaric acid and ursolic acid from *Corni fructus*.

■ ABBREVIATIONS USED

AD, Alzheimer's disease; Aβ, β-amyloid; BACE1, β-secretase; NF-κB, nuclear factor κB; iNOS, inducible nitric oxide synthase; COX-2, cyclooxygenase-2; ILs, interleukins; TNF-α, tumor necrosis factor α; MAPKs, mitogen-activated protein kinase; ERK 1/2, extracellular signal regulated kinase 1/2; JNK, c-Jun NH_2-protein kinase; CF, *Corni fructus*; *p*-CA, *p*-coumaric acid; UA, ursolic acid; PBS, phosphate-buffered saline; PC12 cell, pheochromocytoma cell

■ REFERENCES

(1) Selkoe, D. J. Translating cell biology into therapeutic advances in Alzheimer's disease. *Nature* **1999**, *399*, A23−A31.

(2) Hardy, J. Amyloid the presenilins and Alzheimer's disease. *Trends Neurosci.* **1997**, *20*, 154−159.

(3) Szaingurten-Solodkin, I.; Hadad, N.; Levy, R. Regulatory role of cytosolic phospholipase A2α in NADPH oxidase activity and in inducible nitric oxide synthase induction by aggregated Aβ1-42 in microglia. *Glia* **2009**, *57*, 1727−1740.

(4) In't Veld, B. A.; Ruitenberg, A.; Hofman, A.; Launer, L. J.; Van Duijn, C. M.; Stijnen, T.; Breteler, M. M. B.; Stricker, B. H. C. Nonsteroidal anti-inflammatory drugs and the risk of Alzheimer's disease. *N. Engl. J. Med.* **2001**, *22*, 1515−1521.

(5) Kaltschmidt, B.; Uherek, M.; Volk, B.; Baeuerie, P. A.; Kaltschmidt, C. Transcription factor NF-κB is activated in primary neurons by amyloid β peptides and in neurons surrounding early plaques from patients with Alzheimer's disease. *Proc. Natl. Acad. Sci. U.S.A.* **1997**, *94*, 2642−2647.

(6) Yun, K. J.; Koh, D. J.; Kim, S. H.; Park, S. J.; Ryu, J. H.; Kim, D. G.; Lee, J. Y.; Lee, K. T. Anti-inflammatory effects of sinapic acid through the suppression of inducible nitric oxide synthase, cyclooxygase-2, and proinflammatory cytokines expressions via nuclear factor-κB inactivation. *J. Agric. Food Chem.* **2008**, *56*, 10265−10272.

(7) Tsai, S. J.; Lin, C. Y.; Mong, M. C.; Ho, M. W.; Yin, M. C. *S*-Ethyl cysteine and *S*-propyl cysteine alleviate β-amyloid induced cytotoxicity in nerve growth factor differentiated PC12 cells. *J. Agric. Food Chem.* **2010**, *58*, 7104−7108.

(8) Nolan, G. P.; Ghosh, S.; Liou, H. C.; Tempst, P.; Baltimore, D. DNA binding and IκB inhibition of the cloned p65 subunit of NF-κB, a rel-related polypeptide. *Cell* **1991**, *64*, 961−969.

(9) Saklatvala, J. Inflammatory signaling in cartilage: MAPK and NF-κB pathways in chondrocytes and the use of inhibitors for research into pathogenesis and therapy of osteoarthritis. *Drug Targets* **2007**, *8*, 305−313.

(10) Davis, R. The mitogen-activated protein kinase signal transduction pathway. *J. Biol. Chem.* **1993**, *268*, 14553−14556.

(11) Su, B.; Karin, M. Mitogen-activated protein kinase cascades and regulation of gene expression. *Curr. Opin. Immunol.* **1996**, *8*, 402−411.

(12) Ichijo, H. From receptors to stress-activated MAP kinases. *Oncogene* **1999**, *18*, 6087−6093.

(13) Hwang, D.; Jang, B. C.; Yu, G.; Boudreau, M. Expression of mitogen-inducible cyclooxygenase induced by lipopolysaccharide. *Biochem. Pharmacol.* **1997**, *54*, 87−96.

(14) Gao, D.; Li, N.; Li, Q.; Li, J.; Han, Z.; Fan, Y.; Liu, Z. Study of the extraction, purification and antidiabetic potential of ursolic acid from *Cornus officinalis* Sieb. et Zucc. *Therapy* **2008**, *5*, 697−705.

(15) Park, C. H.; Noh, J. S.; Tanaka, T.; Yokozawa, T. Effects of morroniside isolated from *Corni fructus* on renal lipids and inflammation in type 2 diabetic mice. *J. Pharm. Pharmacol.* **2010**, *62*, 374−380.

(16) Youn, K.; Jun, M. Effects of key compounds isolated from *Corni fructus* on BACE1 inhibition. *Phytother. Res.* **2012**, *26*, 1714−1718.

(17) Hong, S. Y.; Jeong, W. S.; Jun, M. Protective effects of the key compounds isolated from *Corni fructus* against β-amyloid-induced neurotoxicity in PC12 cells. *Molecules* **2012**, *17*, 10831−10845.

(18) Jang, J. H.; Surh, Y. J. Protective effects of resveratrol on hydrogen peroxide-induced apoptosis in rat pheochromocytoma (PC12) cells. *Mutat. Res.* **2001**, *496*, 181−190.

(19) Zhu, J. T.; Choi, R. C.; Chu, G. K.; Cheung, A. W.; Gao, Q. T.; Li, J.; Jiang, Z. Y.; Dong, T. T.; Tsim, K. W. Flavonoids possess neuroprotective effects on cultured pheochromocytoma PC12 cells: a comparison of different flavonoids in activating estrogenic effect and in preventing β-amyloid-induced cell death. *J. Agric. Food. Chem.* **2007**, *55*, 2438−2445.

(20) Qu, M.; Li, L.; Chen, C.; Li, M.; Pei, L.; Chu, F.; Yang, J.; Yu, Z.; Wang, D.; Zhou, Z. Protective effects of lycopene against amyloid β-induced neurotoxicity in cultured rat cortical neurons. *Neurosci. Lett.* **2011**, *505*, 286−290.

(21) Luo, S.; Lan, T.; Liao, W.; Zhao, M.; Yang, H. Genistein inhibits Aβ_{25-35}-induced neurotoxicity in PC12 cells via PKC signaling pathway. *Neurochem. Res.* **2012**, *37*, 2787−2794.

(22) Zhang, X.; Cao, J.; Zhong, L. Hydroxytyrosol inhibits pro-inflammatory cytokines, iNOS, and COX-2 expression in human monocytic cells. *Naunyn. Schmiedebergs Arch. Pharmacol.* **2009**, *379*, 581−586.

(23) Mattson, M. P.; Camandola, S. NFκB in neuronal plasticity and neurodegenerative disorders. *J. Clin. Invest.* **2001**, *107*, 247−254.

(24) Fang, M.; Wang, J.; Han, S.; Hu, Z.; Zhan, J.; Ling, S.; Rudd, J. A.; Geng, Y. Protective effects of ω-conotoxin on amyloid-β-induced damage in PC12 cells. *Toxicol. Lett.* **2011**, *206*, 325−338.

(25) Lentsch, A. B.; Ward, P. A. The NFκB/IκB system in acute inflammation. *Arch. Immunol. Ther. Exp. (Warsz.)* **2000**, *48*, 59−63.

(26) Lee, S. Y.; Lee, J. W.; Lee, H.; Yoo, H. S.; Yun, Y. P.; Oh, K. W.; Ha, T. Y.; Hong, J. T. Inhibitory effect of green tea extract on β-amyloid-induced PC12 cell death by inhibition of the activation of NFκB and ERK/p38 MAP kinase pathway through antioxidant mechanisms. *Mol. Brain Res.* **2005**, *140*, 45−54.

(27) Yan, S. D.; Zhu, H.; Fu, J.; Yan, S. F.; Roher, A.; Tourtellotte, W. W.; Rajavashisth, T.; Chen, X.; Godman, G. C.; Stern, D.; Schmidt, A. M. Amyloid-β peptide-receptor for advanced glycation end product interaction elicits neuronal expression of macrophage-colony stimulating factor: a proinflammatory pathway in Alzheimer's disease. *Proc. Natl. Acad. Sci. U.S.A.* **1997**, *94*, 5296−5301.

(28) Rosales-Corral, S.; Tan, D. X.; Reiter, R. J.; Valdivia-Velázquez, M.; Acosta-Martínez, J. P.; Ortiz, G. G. Kinetics of the neuro-inflammation-oxidative stress correlation in rat brain following the injection of fibrillar amyloid-β onto the hippocampus *in vivo*. *J. Neuroimmunol.* **2004**, *150*, 20−28.

(29) Chen, F.; Castranova, V.; Shi, X.; Demers, L. M. New insights into the role of nuclear factor-κB, aubiquitous transcription factor in the initiation of diseases. *Clin. Chem.* **1999**, *45*, 7−17.

(30) Heras, B.; Hortelano, S. Molecular basis of the anti-inflammatory effects of terpenoids. *Inflamm. Allergy Drug Targets* **2009**, *8*, 28−39.

(31) Luceri, C.; Giannini, L.; Lodovici, M.; Antonucci, E.; Abbate, R. *p*-Coumaric acid, a common dietary phenol, inhibits platelet activity *in vitro* and *in vivo*. *Br. J. Nutr.* **2007**, *97*, 458−463.

(32) Luceri, C.; Guglielmi, F.; Lodovici, M.; Giannini, L.; Messerini, L.; Dolara, P. Plant phenolic 4-coumaric acid protects against intestinal inflammation in rats. *Scand. J. Gastroenterol.* **2004**, *39*, 1128−1133.

(33) Lee, C. H.; Wu, S. L.; Chen, J. C.; Li, C. C.; Lo, H. Y.; Cheng, W. Y.; Lin, J. G.; Chang, Y. H.; Hsiang, C. Y.; Ho, T. Y. *Eriobotrya*

japonica leaf and its triterpenes inhibited lipopolysaccharide-induced cytokines and inducible enzyme production via the nuclear factor-κB signaling pathway in lung epithelial cells. *Am. J. Chin. Med.* **2008**, *36*, 1185−1198.

(34) Lu, J.; Wu, D.; Zheng, Y.; Hu, B.; Zhang, Z.; Ye, Q.; Liu, C.; Shan, Q.; Wang, Y. Ursolic acid attenuates D-galactose-induced inflammatory response in mouse prefrontal cortex through inhibiting AGEs/RAGE/ NFκB pathway activation. *Cereb. Cortex* **2010**, *20*, 2540−2548.

(35) Lee, A.; Chen, T. L.; Shih, C. M.; Huang, C. Y.; Tsao, N. W.; Chang, N. C.; Chen, Y. H.; Fong, T. H.; Lin, F. Y. Ursolic acid induces allograft inflammatory factor-1 expression via a nitric oxide-related mechanism and increases neovascularization. *J. Agric. Food Chem.* **2010**, *58* (24), 12941−12949.

(36) Najid, A.; Simon, A.; Cook, J.; Chable-Robinovitch, H.; Delage, C.; Chulia, A. J.; Rugaud, M. Characterization of ursolic acid as a lipoxygenase and cyclooxygenase inhibitor using macrophages, platelets and differentiated HL60 leukemic cells. *FEBS Lett.* **1992**, *299*, 213−217.

(37) Suh, N.; Honda, T.; Finlay, H. J.; Barchowsky, A.; Williams, C.; Benoit, N. E.; Xie, Q. W.; Nathan, C.; Gribble, G. W.; Sporn, M. B. Novel triterpenoids suppress inducible nitric oxide synthase (iNOS) and inducible cyclooxygenase (COX-2) in mouse macrophages. *Cancer Res.* **1998**, *58*, 717−723.

(38) Li, Y.; Xing, D.; Chen, Q.; Chen, W. R. Enhancement of chemotherapeutic agent-induced apoptosis by inhibition of NFκB using ursolic acid. *Int. J. Cancer* **2009**, *127*, 462−473.

(39) Yeh, C. T.; Wu, C. H.; Yen, G. C. Ursolic acid, a naturally occurring triterpenoid, suppresses migration and invasion of human breast cancer cells by modulating c-Jun N-terminal kinase, Akt and mammalian target of rapamycin signaling. *Mol. Nutr. Food Res.* **2010**, *54*, 1285−1295.

(40) Chen, Q.; Luo, S.; Zhang, Y. Development of a liquid chromatography-mass spectrometry method for the determination of ursolic acid in rat plasma and tissue: application to the pharmacokinetic and tissue distribution study. *Anal. Bioanal. Chem.* **2011**, *399*, 2877−2884.

role played by chemical characteristics on water dynamics within the pore system of the chars.

MATERIALS AND METHODS

Feedstock. The hydrochar and pyrochar samples were prepared by using poplar (*Populus* spp. L.) wood chips that were obtained from a dedicated short-rotation forest in the Po valley (Gadesco Pieve Delmona, $45°10^{I}13^{II}$ N, $10°06^{I}01^{II}$ E). The age of the forest at the time of harvest was 5 years. The characteristics of the biomass were already described in De Pasquale et al.[10]

Pyrochar and Hydrochar Preparation. Pyrochar was produced by using an industrial gasifier at the temperature of 1200 °C. All of the details about the gasifier and the pyrolitic conditions have been already reported in De Pasquale et al.[10] Hydrochar was obtained in a b.coal 2.0 reactor from Artec Biotechnology GmbH (Bad Königshofen, Germany) at 230 °C and 40 bar. Details about the procedure have been reported already in Wiedner et al.[24] Both pyrochar and hydrochar samples were 2 mm sieved with a stainless steel sieve and dried overnight in an oven set at 105 °C before each NMR analysis.

Specific Surface Area Measurement. Samples were first dried at 200 °C for 4.5 h and then stored in a desiccator. To retrieve the specific surface area by applying the Brunauer–Emmett–Teller (BET) five-point method, samples were degassed with N_2 at 200 °C for another hour and then measured in liquid N_2 (Quantachrome NOVA 4200 calibrated with BAM-PM-104) following DIN ISO 9277:2003-05. All measurements were done in triplicate. Specific surface areas of the pyrochar and the hydrochars were 54.6 ± 0.2 and 129 ± 2 $m^2\ g^{-1}$, respectively.

The poplar pyrochar surface area measured in this study was smaller than that already reported in De Pasquale et al.[10] (i.e., 98 ± 6 $m^2\ g^{-1}$). The difference can be explained by the different sample preparation used in De Pasquale et al.[10] prior to BET analysis. In fact, the BET investigations reported in De Pasquale et al.[10] have been conducted on agate–mortar ground samples. Pyrochar grinding reduces particle sizes, thereby increasing surface area values.

Evaluation of Pore Size Distribution from the Specific Surface Area Measurements. The nonlocal density functional theory (NLDFT) equilibration model[27] was applied to elaborate the isotherms (35 adsorption and 30 desorption points) of nitrogen adsorption experiments to achieve pore size distributions. Assumption of N_2 at −196 °C on carbon (slit-pore) was used. The cumulative pore volumes and surface areas for the micropore class (i.e., <2 nm, according to IUPAC classification) retrieved by the NLDFT model were 16.3 × 10^{-3} $cm^3\ g^{-1}$ and 29.4 $m^2\ g^{-1}$ for pyrochar, whereas they were 50.9 × 10^{-3} $cm^3\ g^{-1}$ and 93.3 $m^2\ g^{-1}$ for hydrochar. NLDFT surface area and pore volume for hydrochar were around 3 times higher than those for pyrochar, thereby evidencing that the number of pores in the former sample was larger than in the latter one. In particular, the surface/volume (S/V) ratios from NLDFT elaborations were $(S/V)_{pyrochar}$ = 1.80 × 10^9 m^{-1} and $(S/V)_{hydrochar}$ = 1.83 × 10^9 m^{-1}.

CP-TOSS ^{13}C NMR Spectra. Cross-polarization magic angle spinning (CPMAS) ^{13}C NMR measurements were performed on a Bruker Avance-II 400 spectrometer (Bruker Biospin, Milan, Italy) operating at 100.6 MHz on carbon-13 and equipped with a 4 mm standard-bore solid state probe. Samples were packed into 4 mm zirconia rotors with Kel-F caps, and the rotor spin rate was set at 5000 ± 2 Hz. A spectral width of 25252.52 Hz centered at 10061.78 Hz, an optimum contact time of 1 ms chosen after evaluation of variable contact time experiments, a recycle delay of 20 s, and 2K data points over an acquisition time of 35 ms were used. The spectra were acquired with the total suppression side bands (TOSS) sequence with a 50% RAMP to prevent artifacts in the spectra interpretation. A 4.1 μs ^{1}H 90° pulse with an attenuation level of −2.4 dB was applied. Spectra acquisition was achieved with Bruker Topspin 2.0. Data processing was done with MestRe-C software (version 4.9.9.9, Mestrelab Research, Santiago de Compostela, Spain). The free induction decays (FIDs) were transformed by applying first a 2K zero filling, then a line broadening of 100 Hz, and finally an automatic baseline correction with a third-order polynomial and Bernstein algorithm.

Fast Field Cycling (FFC) NMR Relaxometry. The 2 mm sieved and dried poplar pyrochar and hydrochar samples have been prepared as slurry for FFC NMR relaxometry investigations according to the procedure reported in Dunn et al.[28] The background theory of FFC NMR relaxometry has been already described in De Pasquale et al.[10] Moreover, more general environmental applications of FFC NMR relaxometry can be found in Conte and Alonzo.[29]

^{1}H NMR dispersion profiles (i.e., relaxation rates R_1 or $1/T_1$ vs proton Larmor frequencies) were acquired on a Stelar Spinmaster FFC2000 Relaxometer (Stelar s.r.l., Mede, PV, Italy) at temperatures of 25, 50, and 80 °C. The proton spins were polarized at a B_{POL} corresponding to the proton Larmor frequency (ω_L) of 24 MHz for a T_{POL} corresponding to about 5 times the T_1 estimated at this frequency. After each B_{POL} application, the magnetic field intensity (indicated as B_{RLX}) was systematically changed in the proton Larmor frequency ω_L comprised in the range 0.01–40 MHz. The period τ, during which B_{RLX} was applied, has been varied on 32 logarithmic spaced time sets, each of them adjusted at every relaxation field to optimize the sampling of the decay/recovery curves. FIDs were recorded following a single ^{1}H 90° pulse applied at B_{ACQ} corresponding to the proton Larmor frequency of 16 MHz. A time domain of 100 μs sampled with 512 points was applied. Field switching time was 3 ms, whereas spectrometer dead time was 15 μs. For all experiments, a recycle delay of 12 s was used. The NP sequence was applied when the relaxation magnetic fields were in the range of the proton Larmor frequencies between 40.0 and 9.0 MHz. The PP sequence was applied in the proton Larmor frequencies B_{RLX} range of 9.0–0.01 MHz.[30]

FFC NMR Data Processing. R_1 values were achieved by interpolating the ^{1}H magnetization decay/recovery curves at each B_{RLX} value (i.e., ^{1}H signal intensity vs τ) with the stretched exponential function (also known as the Kohlrausch–Williams–Watts function) reported in eq 1 after exportation of the experimental data to OriginPro 7.5 SR6 (version 7.5885, OriginLab Corp., Northampton, MA, USA). This equation provided the best fitting with the largest coefficients of determination ($R^2 > 0.998$). The choice of this function was due to the large sample heterogeneity resulting in a multi-exponential behavior of the decay/recovery curves.[29,31] This approach has the advantage that it is able to handle a wide range of behaviors within a single model. For this reason, assumptions about the number of exponentials to be used in modeling NMRD data are not necessary.

$$I(\tau) = I_0 \exp[-(\tau/T_1)^k] \quad (1)$$

In eq 1, $I(\tau)$ is the ^{1}H signal intensity at each fixed B_{RLX}, I_0 is the ^{1}H signal intensity at the thermal equilibrium, T_1 is the average proton spin–lattice relaxation time, and k is a heterogeneity parameter related to the stretching of the decay process. This function can be considered as a superposition of exponential contributions, thereby describing the likely physical picture of some distribution in T_1.

Relaxation data at the proton Larmor frequency of 40 MHz were evaluated by the inverse Laplace transformation through application of the UPEN algorithm (Alma Mater Studiorum, Università di Bologna, Italy)[32,33] with the aim to obtain the T_1 distributions at such magnetic field and, therefore, information on pore distribution and grain size. The choice of UPEN analyses only at 40 MHz was due to the larger NMR sensitivity at this frequency as compared to the other proton Larmor frequencies.[30]

RESULTS AND DISCUSSION

Hydrochar and Pyrochar Chemical Composition by CP-TOSS ^{13}C NMR Spectroscopy. The cross-polarization magic angle spinning with total suppression of side bands ^{13}C NMR spectra of the two samples studied here showed the more complex nature of hydrochar as compared to pyrochar (Figure 1). In particular, two main regions can be recognized in the hydrochar spectrum (Figure 1A). The first chemical shift

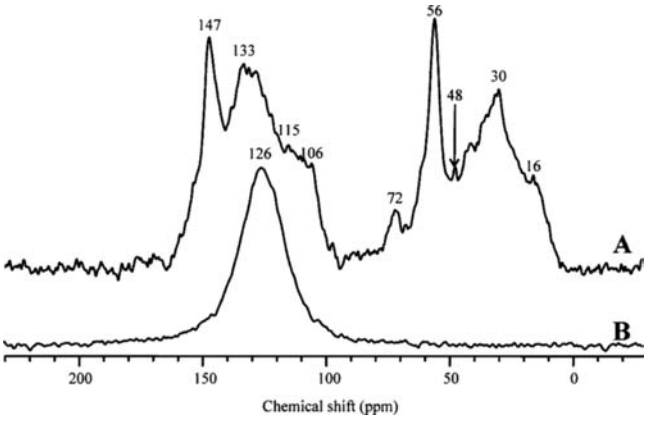

Figure 1. CP-TOSS ^{13}C NMR spectra of poplar hydrochar (A) and pyrochar (B).

interval between 0 and 80 ppm contains individual signals at 16, 30, 48, 56, and 72 ppm (Figure 1A). The first signal at 16 ppm can be attributed to methyl groups of terminating alkyl chains; the second one at 30 ppm is due to methylene groups in alkyl chains, whereas the signal at 48 ppm can be assigned to branched alkyl carbons; the signal at 56 ppm is assignable to methoxyl groups in lignin-like structures, and that at 72 ppm is due to carbons C2, C3, and C5 in the residual cellulose moiety from the poplar biomass.[24,34]

The second spectral region in Figure 1A occurred in the chemical shift interval between 90 and 160 ppm. The main signals recognized in this region are broad bands centered at 106, 115, 133, and 147 ppm. The signal at 106 ppm can be assigned to C1 in residual cellulose; that at 115 ppm is due to C5 in guaiacyl (G) and C3 and C6 in *p*-hydroxyphenyl groups; the signal at 133 ppm is due to the aromatic C−5/C−5′ in etherified 5−5 G units; finally, the signal at 147 ppm is assigned to C3 and C4 in etherified guaiacyl units.[24,34]

The spectrum reported in Figure 1B reveals only one broad band at 126 ppm, which can be assigned to polyaromatic systems.[10] The differences in the chemical composition of poplar hydrochar and pyrochar samples (Figure 1) can be explained by the different types of reactions occurring as either hydrothermal carbonization[24] or gasification[10] is applied. The hydrothermal carbonization used in this study consisted of a thermal degradation of the water-suspended biomass at high pressure and 230 °C by applying citric acid as catalyst.[24] During this process, carbohydrates in poplar biomass have been gradually transformed to aromatic and aliphatic structures, thereby providing a lignin-like material. However, the presence of signals at 56, 72, 106, 133, and 147 ppm (Figure 1A) indicates that the hydrothermal carbonization produced a carbonaceous material still containing oxygenated functionalities, but almost no polycondensed aromatic moieties as outlined in Wiedner et al.[24]

The sole aromatic signal in the CP-TOSS ^{13}C NMR spectrum of the poplar pyrochar (Figure 1B) is due to the diamagnetic currents produced by delocalized π-electrons in extended aromatic structures or graphite-like microcrystallites, which are generated by the high-temperature condensations as biomass feedstock is subjected to gasification.[10]

Effect of Pore Size on ^1H NMR T_1 Distributions. The 2 mm sieved poplar hydrochar and pyrochar samples were saturated with water and the slurry was analyzed by fast field cycling NMR relaxometry as indicated under Materials and Methods. Figure 2 reports the distributions of the longitudinal relaxation times (T_1), also referred to as relaxograms, at the

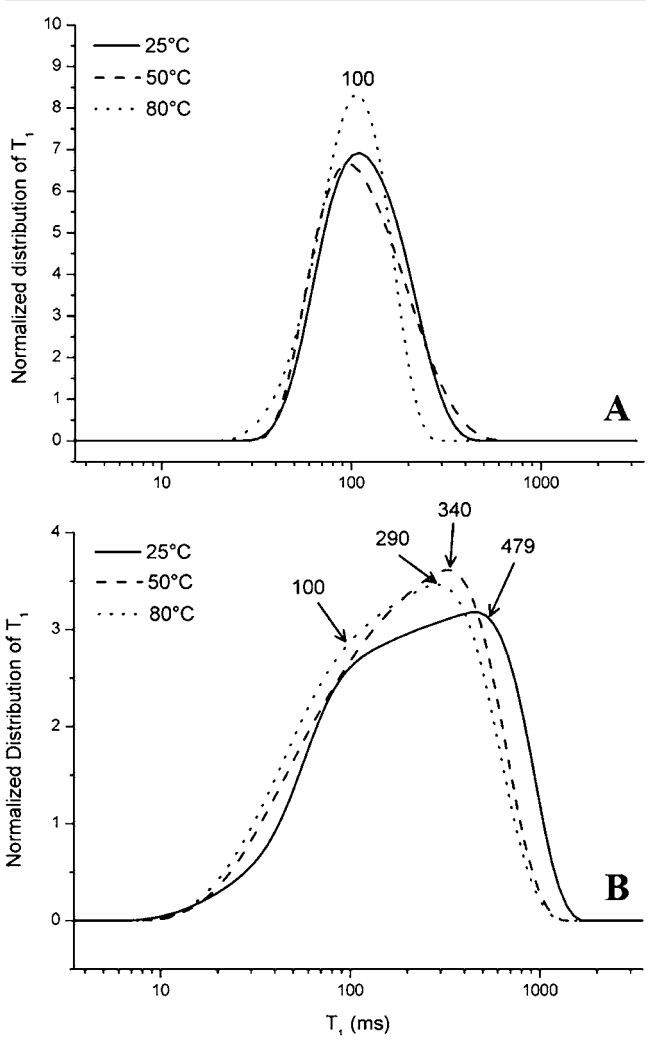

Figure 2. Relaxograms of poplar hydrochar (A) and pyrochar (B) acquired at the proton Larmor frequency of 40 MHz.

proton Larmor frequency of 40 MHz and three temperatures (25, 50, and 80 °C) as obtained by applying the inverse Laplace transformation of the relaxation data through the UPEN algorithm (see Materials and Methods).

Proton longitudinal relaxation times of water in porous media are affected by the collisions between the liquid state molecules and the walls of the porous boundaries.[35] In particular, longitudinal relaxation is dominated by the presence of a strong relaxation sink at the pore surface, which is imputable to the temporary adsorption of water on the solid surface.[36] Temporary adsorption can be achieved by formation of weak unconventional hydrogen bonds on the surface of pyrogenic char systems as already outlined in Conte et al.[26] and Conte and Alonzo.[29] However, as surficial polar groups are present, the weak unconventional H-bonds may turn toward stronger conventional ones, which may hook water molecules more strongly on the char surface. The effectiveness of the aforementioned relaxation sink depends on the ratio between the pore surface and the pore volume as well as on the diffusion rate across the pore.[37] In fact, space restriction in small-sized pores does not allow fast molecular mobility. As this condition

dx.doi.org/10.1021/jf5010034 | J. Agric. Food Chem. 2014, 62, 4917−4923

occurs, $^1H-^1H$ dipolar interactions become very efficient. Shorter relaxation times are, hence, retrieved.[35,37,38] Conversely, as pore size enlarges, molecular mobility increases and strength of dipolar interactions weakens. For this reason, longer relaxation times are expected.[35,37,38] As the number and size of the various pores present in a material is heterogeneous, water must diffuse through the differently sized pores, thereby providing a wide ensemble of longitudinal relaxation times that appear continuously distributed. The lowest limit of such an ensemble (the shortest T_1 value) is due to water moving into the smallest pores, whereas the highest limit (the longest T_1 value) is attributed to water moving into the largest pores. All T_1 values between the two limits are due to the dynamics of water inside pores having sizes lying between the two extremes.[29] According to the aforementioned mechanism, the differences observed at the same temperatures between the T_1 distributions reported in Figure 2 can be attributed to different pore size distributions present in the hydrochar and pyrochar samples. In particular, a homogeneous distribution of small-sized pores can be recognized in hydrochar rather than in pyrochar. The latter, in turn, is made by a less homogeneous distribution of pores, which are on average larger than in hydrochar. In fact, all of the hydrochar relaxograms showed a maximum centered at a T_1 value of around 100 ms regardless of the temperature used during the experiments (Figure 2A). Conversely, the relaxograms acquired for the water-saturated pyrochar span a larger interval of T_1 values (Figure 2B). Here a maximum at 100 ms independent of the applied temperature (similarly to the water-saturated hydrochar sample) can be observed. Moreover, second maxima centered at 479, 340, and 290 ms retrieved at 25, 50, and 80 °C, respectively, are also observed (Figure 2B). A wide distribution of T_1 values is included among the two longitudinal relaxation time limits in Figure 2B. We can identify water molecules relaxing at 100 ms in both carbonaceous samples as those restricted in the smallest sized pores; water molecules generating the maxima at 479 ms at 25 °C, 340 ms at 50 °C, and 290 ms at 80 °C as those tumbling in the largest pores; and, finally, water molecules relaxing in the intervals of 100−479 ms at 25 °C, 100−340 ms at 50 °C, and 100−290 ms at 80 °C as those occluded in transitional pores.

The aforementioned findings are supported by BET and NLDFT elaborations as reported under Materials and Methods. In fact, specific surface areas were 54.6 ± 0.2 and 129 ± 2 m^2 g^{-1} for pyrochar and hydrochar, respectively, thereby suggesting a larger volume of pores in the former than in the latter sample. On the other hand, NLDFT elaborations of isotherms obtained from nitrogen adsorption provided S/V ratios in the order $(S/V)_{pyrochar} < (S/V)_{hydrochar}$ (see Materials and Methods). It is well-known that the longitudinal relaxation rate $(1/T_1)$ is directly proportional to the S/V ratio[39] or by considering the reciprocal:

$$T_1 \propto \frac{V}{S}$$

Because $(S/V)_{pyrochar} < (S/V)_{hydrochar}$, it happens that $(V/S)_{pyrochar} > (V/S)_{hydrochar}$ and it is expected that the T_1 values for pyrochar must be longer than for hydrochar. The latter expectation has been evidenced in the experimental results shown in Figure 2 and discussed above.

It is interesting to note that the relaxogram reported in De Pasquale et al.[10] was obtained for the same pyrochar used in the present study. However, the T_1 distribution in De Pasquale et al.[10] revealed a larger pore size homogeneity than the relaxogram reported here in Figure 2B. This difference can be explained by considering that samples were prepared differently prior to the analysis. In fact, in the present study, we sieved the poplar pyrochar at <2 mm, whereas in De Pasquale et al.[10] the sample has been ground. As already outlined under Materials and Methods, sample grinding reduces pore size, thereby allowing larger surface area and more homogeneous pore size distribution.

Effect of Temperature on ^1H NMR T_1 Distributions. Longitudinal relaxation times are dependent not only on the pore size distribution, as outlined in the previous paragraph, but also on temperature variations.[29] In fact, it is well recognized that temperature increments accelerate molecular motions, thereby weakening the $^1H-^1H$ dipolar interactions responsible for the longitudinal relaxation of a liquid moving on the surface of porous materials.[40] When this condition occurs, an increase of T_1 values is expected because a longer time is needed for proton spin−lattice relaxation. However, it has been already shown that water retained in charred materials behaves diametrically, thereby suggesting that water dynamics is subjected to a slow-motion regime.[26] The latter is achieved when water molecules are hooked to the char surface via weak hydrogen bonds that may arise by the overlay of the electron-deficient orbitals of protons in water and the electron-rich orbitals in the organic and inorganic components of the charred system.[26] As temperature increases, the weak interactions, which allow water adhesion to the pore walls, oppose the 3D exchange with the bulk water (i.e., the replacement of water molecules hooked to the char surface with those appertaining to the bulk liquid).[40] For this reason, water preferentially diffuses more quickly within the channels connecting pores between one another through a two-dimensional (2D) motion (i.e., the diffusion of water molecules within the channels connecting either different surface pores or char surface with the interior part of the same material).[26,40] Due to the 2D surface diffusion just described, the water collision frequency with pore walls increases with temperature, thereby allowing an average residence time on pore walls longer than that retrieved at lower temperatures. Because of this, a shorter time for protons to relax is needed and lower T_1 values are achieved.[40] As a consequence, relaxograms, such as those in Figure 2, shrink as the temperature is increased. Moreover, it must be added that the larger the pore size, the more pronounced is the reduction of the relaxogram width and the reduction of the T_1 maxima. In fact, upon temperature increasing, water collision frequency in larger pores becomes higher than in the more spatially restricted ones. Because of this, the average time spent by water molecules on pore walls is higher in the transitional and largest pores than in the smallest pores. The latter is why the reduction of relaxogram widths is less pronounced in Figure 2A than in Figure 2B. Moreover, the same mechanism explains why the maximum at 100 ms due to water in the smallest pores either in hydrochar or in pyrochar is unaffected by temperature changes, whereas the T_1 maxima due to water in larger sized pores (T_1 >100 ms) shift toward shorter values.

Nuclear Magnetic Resonance Dispersion (NMRD) Profiles. Figure 3 shows the NMRD profiles (i.e., $R_1 = 1/T_1$ values vs ω_L) at 25, 50, and 80 °C for the water-saturated poplar hydrochar and pyrochar samples investigated here. In particular, the NMRD profiles of the former sample are all placed at faster longitudinal relaxation rates (Figure 3A) as compared to the NMRD profiles of the latter sample (Figure

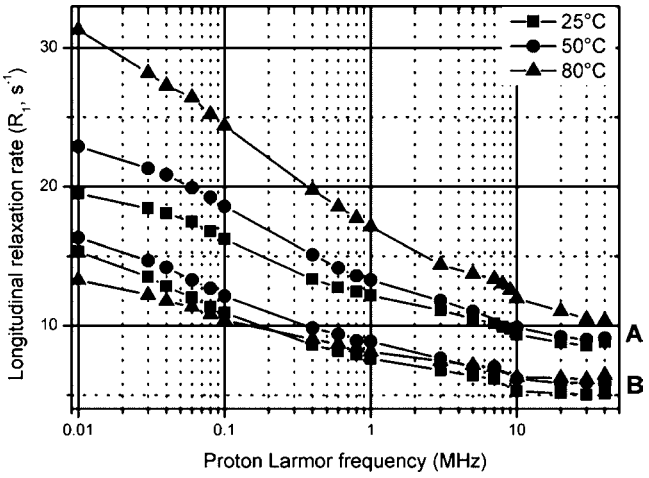

Figure 3. NMRD profiles of poplar hydrochar (A) and pyrochar (B).

3B). This is due to the differences in the surface areas between the two porous materials. In fact, $SSA_{hydrochar}$ was larger than $SSA_{pyrochar}$ (see above). The larger the surface area value, the smaller is the size of the pores. Restriction of water in small pores leads to stronger $^1H-^1H$ dipolar interactions, which, in turn, are the cause for the very efficient proton longitudinal relaxation in hydrochar (i.e., faster R_1 values) compared to pyrochar.[41]

It is worth noting that all of the NMRD profiles in Figure 3A are translated toward faster R_1 values in the whole range of proton Larmor frequencies as the temperature is increased. This behavior accords with that already described in Conte et al.,[26] thereby confirming the slow-motion regime also outlined in the previous paragraph. However, Conte et al.[26] reported that the slow-motion regime on the surface of char systems is due to nonconventional H-bonds arising by the overlay between the electron-deficient orbitals of protons in water and the electron-rich orbitals of the aromatic organic centers in the charred material. In the present study, we have reported that hydrothermal degradation did not remove all of the oxygen-containing functionalities (see above). For this reason, we cannot exclude participation of the more traditional O−H··· O bonds in the slow-motion regime observed for the hydrochar sample.

Figure 3B reveals that the NMRD profiles acquired for the pyrochar sample behaved similarly to the hydrochar only up to 50 °C. Conversely, an anomalous trend was observed at 80 °C. In fact, a slight increment of the R_1 values was retrieved between 40 and 10 MHz as the temperature was switched from 50 to 80 °C. Then the 80 °C NMRD profile crossed the one acquired at 50 °C as ω_L was set to 10 MHz and that retrieved at 25 °C as ω_L was switched to 0.2 MHz (Figure 3B). The H-bond-mediated slow-motion regime can explain the NMRD behavior up to 50 °C observed for the pyrochar sample (Figure 3B). However, as the temperature is raised to 80 °C, a chemical exchange with the bulk phase must be considered to account for the anomalous behavior reported in Figure 3B.[40]

The interesting feature that the temperature dependence of water dynamics in hydrochar is opposite than that observed in pyrochar can be explained only by considering the different pore size distribution in the two carbonaceous samples. In fact, as outlined above, the average pore size in hydrochar is smaller than in pyrochar. Water molecules are more tightly trapped in the former than in the latter material. For this reason, water can easily run toward the bulk liquid from pyrochar rather than from hydrochar surface as the temperature is increased to 80 °C.

The comparison among the temperature dependences of the NMRD profiles in Figure 3 and those in Conte et al.[26] supports the latter hypothesis on the role played by pore size in water exchange with the bulk solution. In fact, the pyrochar analyzed either in the present study or in Conte et al.[26] was obtained by the same gasification process.[10] However, whereas in Conte et al.[26] the pyrochar was ground in an agate mortar before NMRD investigations, here we have performed NMRD analyses after having sieved the same material to <2 mm. As a consequence, the surface area of the ground pyrochar[26] was larger than that used in the present study. As already noted above, larger surface area was associated with a more homogeneous pore size distribution made mainly by the smallest pores. Conversely, a more inhomogeneous distribution of pore size (with a larger contribution from transitional and larger pores) was identified in the porous charred material having a lower surface area. Hence, the more inhomogeneous pore size pyrochar used here revealed the anomalous temperature dependence behavior at 80 °C (Figure 3B) due to the higher number of larger pores, which make the exchange of surface water molecules with the bulk ones easier.

This paper reports high- and low-field NMR characterization of the physicochemical properties of hydrochar and pyrochar samples retrieved by applying either hydrothermal treatment or gasification to poplar forestry wastes. In particular, high-field NMR spectroscopy (i.e., CP-TOSS ^{13}C NMR) revealed that the thermal treatments produced two chemically different carbonaceous materials. Although poplar hydrochar appeared as a lignin-like material still containing oxygenated functionalities, poplar pyrochar emerged as a polyaromatic system where O-containing groups were not detected.

Notwithstanding the different chemical compositions, the mechanisms of water dynamics on the surface of poplar hydrochar and pyrochar were affected more by their physical characteristics rather than by their chemical peculiarities. In particular, isothermally 40 MHz acquired relaxograms revealed that water motion was more restricted in hydrochar than in pyrochar, thereby suggesting that the former sample included a larger number of small-sized pores than the latter one. On the other hand, the freer motion of water in pyrochar indicated a higher amount of transitional and very large pores.

Variable-temperature relaxometry experiments revealed that a 2D surface diffusion mechanism was the only force responsible for water motion in hydrochar up to the temperature of 80 °C. Surface diffusion was the predominating motion mechanism of water in pyrochar only up to 50 °C. Conversely, a 3D exchange with the bulk water appeared to interfere with the aforementioned 2D diffusion as the temperature was raised to 80 °C.

The differentiation between the 2D diffusion and the 3D exchange mechanisms was attributed to the different porosities in the charred materials. In fact, water constrained in small pores such as in hydrochar strongly interacts with the solid surfaces. For this reason, its fugacity toward the bulk liquid is inhibited in the whole temperature interval investigated here (25−80 °C). On the other hand, the larger pore sizes in poplar pyrochar prevent water exchange with the bulk solution only in a more restricted temperature interval (namely, 25−50 °C). As the temperature overcomes the limit of 50 °C, water surface

dx.doi.org/10.1021/jf5010034 | J. Agric. Food Chem. 2014, 62, 4917−4923

interactions become weaker and 3D exchange with the bulk liquid occurs.

Although in the present study the chemical composition of poplar hydrochar and pyrochar appeared of minor importance to the water dynamics, its contribution to the strength of water solid phase interactions is not yet clear. For this reason, more detailed studies on the effect of pore sizes and chemical composition of charred materials on water dynamics are urgently needed.

AUTHOR INFORMATION

Corresponding Author

*(P.C.) E-mail: pellegrino.conte@unipa.it. Phone: 0039 09123864673. Fax: 0039 091484035.

Present Address

§(U.M.H.) Soil Science and Biogeochemistry, University of Zurich, Winterthurerstrasse 190, 8057 Zürich, Switzerland.

Funding

We appreciate the support of COST action TD1107 (Biochar for sustainable resources management) for the Short-term Scientific Mission (STSM) for U.M.H.

Notes

The authors declare no competing financial interest.

ACKNOWLEDGMENTS

We are grateful to Centro Grandi Apparecchiature − UniNetLab of Università degli Studi di Palermo (http://www.unipa.it/cga/index.html) for having provided machine time at the high-field NMR spectrometer for the acquisition of the CP-TOSS ^{13}C NMR spectra. We acknowledge Dr. Alessandro Pozzi (AGT technologies) for providing the pyrochar sample.

REFERENCES

(1) Glaser, B.; Haumaier, L.; Guggenberger, G.; Zech, W. The "Terra Petra" phenomenon a model for sustainable agriculture in the humid tropics. *Naturwissenschaften* **2001**, *88* (1), 37−41, DOI: 10.1007/s001140000193.

(2) Mao, J. D.; Johnson, R. L.; Lehmann, J.; Olk, D. C.; Neves, E. G.; Thomson, M. L.; Schmidt-Rohr, K. Abundant and stable char residues in soils: implication for soil fertility and carbon sequestration. *Environ. Sci. Technol.* **2012**, *46*, 9571−9576.

(3) Mukherjee, A.; Lal, R. Biochar impacts on soil physical properties and greenhouse gas emissions. *Agronomy* **2013**, *3* (2), 313−339, DOI: 10.3390/agronomy3020313.

(4) Glaser, B.; Lehmann, J.; Zech, W. Ameliorating physical and chemical properties of highly weathered soils in the tropics with charcoal − a review. *Biol. Fert. Soils* **2002**, *35* (4), 219−230, DOI: 10.1007/s00374-002-0466-4.

(5) Vanderslice, N. C.; Marrero, T. R. Impact of bio-char on carbon dioxide in the atmosphere. In *Proceedings of the 2009 Midwest Section Conference of the American Society for Engineering Education*, 2009; available at http://www.asee.org/papers-and-publications/papers/section-proceedings/midwest/.

(6) Mohan, D.; Rajput, S.; Singh, V. K.; Steele, P. H.; Pittman, C. U., Jr. Modeling and evaluation of chromium remediation from water using low cost bio-char, a green adsorbent. *J. Hazard. Mater.* **2011**, *188* (1−3), 319−333, DOI: 10.1016/j.jhazmat.2011.01.127.

(7) Beesley, L.; Moreno-Jiménez, E.; Gomez-Eyles, J. L.; Harris, E.; Robinson, B.; Sizmur, T. A review of biochars' potential role in the remediation, revegetation and restoration of contaminated soils. *Environ. Pollut.* **2011**, *159* (12), 3269−3282, DOI: 10.1016/j.envpol.2011.07.023.

(8) Zhang, X.; Wang, H.; He, L.; Lu, K.; Sarmah, A.; Li, J.; Bolan, N. S.; Pei, J.; Huang, H. Using biochar for remediation of soils contaminated with heavy metals and organic pollutants. *Environ. Sci. Pollut. Res.* **2013**, *20* (12), DOI: 10.1007/s11356-013-1659-0.

(9) Lehmann, J.; Joseph, S. Biochar for environmental management: an introduction. In *Biochar for Environmental Management: Science and Technology*; Lehmann, J., Joseph, S., Eds.; Routledge: London, UK, 2009; pp 448.

(10) De Pasquale, C.; Marsala, V.; Berns, A. E.; Valagussa, M.; Pozzi, A.; Alonzo, G.; Conte, P. Fast field cycling NMR relaxometry characterization of biochars obtained from an industrial thermochemical process. *J. Soils Sediments* **2012**, *12* (8), 1211−1221, DOI: 10.1007/s11368-012-0489-x.

(11) Warnock, D. D.; Lehmann, J.; Kuyper, T. W.; Rilling, M. C. Mycorrhizal responses to biochar in soil − concepts and mechanisms. *Plant Soil* **2007**, *300* (1−2), 9−20, DOI: 10.1007/s11104-007-9391-5.

(12) Liang, B.; Lehmann, J.; Solomon, D.; Kinyangi, J.; Grossman, J.; O'Neill, B.; Skjemstad, J. O.; Thies, J.; Luizão, F. J.; Petersen, J.; Neves, E. G. Black carbon increases cation exchange capacity in soils. *Soil Sci. Soc. Am. J.* **2006**, *70* (5), 1719−1730, DOI: 10.2136/sssaj2005.0383.

(13) Thomas, S. C.; Frye, S.; Gale, N.; Garmon, M.; Launchbury, R.; Machado, N.; Melamed, S.; Murray, J.; Petroff, A.; Winsborough, C. Biochar mitigates negative effects of salt additions on two herbaceous plant species. *J. Environ. Manage.* **2013**, *129*, 62−68, DOI: 10.1016/j.jenvman.2013.05.057.

(14) Chan, K. Y.; Van Zwieten, L.; Meszaros, I.; Downie, A.; Joseph, S. Agronomic values of greenwaste biochar as a soil amendment. *Soil Res.* **2007**, *45* (8), 629−634, DOI: 10.1071/SR07109.

(15) Steinbeiss, S.; Gleixner, G.; Antonietti, M. Effect of biochar amendment on soil carbon balance and soil microbial activity. *Soil Biol. Biochem.* **2009**, *41* (6), 1301−1310, DOI: 10.1016/j.soilbio.2009.03.016.

(16) Novak, J. M.; Busscher, W. J.; Laird, D. L.; Ahmedna, M.; Watts, D. W.; Niandou, M. A. S. Impact of biochar amendment on fertility of a southeastern coastal plain soil. *Soil Sci.* **2009**, *174* (2), 105−112, DOI: 10.1097/SS.0b013e3181981d9a.

(17) Zimmerman, A. R.; Gao, B.; Ahn, M.-Y. Positive and negative carbon mineralization priming effects among a variety of biochar-amended soils. *Soil Biol. Biochem.* **2011**, *43* (6), 1169−1179, DOI: 10.1016/j.soilbio.2011.02.005.

(18) McClellan, T.; Deenik, J.; Uehara, G.; Antal, M. Effects of flashed carbonized macadamia nutshell charcoal on plant growth and soil chemical properties. *Am. Chem. Soc. Agron. Abstr.* **2007**.

(19) McLaughlin, H.; Anderson, P. S.; Shields F. E.; Reed, T. B. All biochars are not created equal, and how to tell them apart. *Proceedings, North American Biochar Conference, Boulder, Colorado*, 2009; www.biochar-international.org/sites/default/files/All-Biochars--Version2--Oct2009.pdf.

(20) McBeath, A. V.; Smernik, R. J. Variation in the degree of aromatic condensation of chars. *Org. Geochem.* **2009**, *40* (12), 1161−1168, DOI: 10.1016/j.orggeochem.2009.09.006.

(21) Cao, X.; Harris, W. Properties of dairy-manure-derived biochar pertinent to its potential use in remediation. *Bioresour. Technol.* **2010**, *101* (14), 5222−5228, DOI: 10.1016/j.biortech.2010.02.052.

(22) Knicker, H. Pyrogenic organic matter in soil: its origin and occurrence, its chemistry and survival in soil environments. *Quatern, Int.* **2011**, *243* (2), 251−263, DOI: 10.1016/j.quaint.2011.02.037.

(23) Schimmelpfennig, S.; Glaser, B. One step forward toward characterization: some important material properties to distinguish biochars. *J. Environ. Qual.* **2012**, *41*, 1001−1013, DOI: 10.2134/jeq2011.0146.

(24) Wiedner, K.; Naisse, C.; Rumpel, C.; Pozzi, A.; Wieczorek, P.; Glaser, B. Chemical modification of biomass residues during hydrothermal carbonization − what makes the difference, temperature or feedstock? *Org. Geochem.* **2013**, *54*, 91−100, DOI: 10.1016/j.orggeochem.2012.10.006.

(25) Zhao, L.; Cao, X.; Mašek, O.; Zimmerman, A. Heterogeneity of biochar properties as a function of feedstock sources and production temperatures. *J. Hazard. Mater.* **2013**, *256−257*, 1−9, DOI: 10.1016/j.jhazmat.2013.04.015.

(26) Conte, P.; Marsala, V.; De Pasquale, C.; Bubici, S.; Valagussa, M.; Pozzi, A.; Alonzo, G. Nature of water-biochar interface interactions. *GCB Bioenergy* **2013**, *5* (2), 116−121, DOI: 10.1111/gcbb.12009.
(27) Sing, K. The use of nitrogen adsorption for the characterization of porous materials. *Colloid Surf. A* **2001**, *187−188*, 3−9, DOI: 10.1016/S0927-7757(01)00612-4.
(28) Dunn, K. J.; Bergman, D. J.; Latorraca, G. A. *Handbook of Geographic Exploration−Seismic Exploration: Nuclear Magnetic Resonance Petrophysical and Logging Applications*; Elsevier Science: Oxford, UK, 2002.
(29) Conte, P.; Alonzo, G. Environmental NMR: fast-field-cycling relaxometry. *eMagRes* **2013**, 389−398, DOI: 10.1002/9780470034590.emrstm1330.
(30) Kimmich, R.; Anoardo, E. Fast-field-cycling NMR relaxometry. *Prog. Nucl. Magn. Reson. Spectrosc.* **2004**, *44*, 257−320, DOI: 10.1016/j.pnmrs.2004.03.002.
(31) Morozova-Roche, L. A.; Jones, J. A.; Noppe, W.; Dobson, C. M. Independent nucleation and heterogeneous assembly of structure during folding of equine lysozyme. *J. Mol. Biol.* **1999**, *289* (4), 1055−1073, DOI: 10.1006/jmbi.1999.2741.
(32) Borgia, G. C.; Brown, R. J. S.; Fantazzini, P. Uniform-penalty inversion of multiexponential decay data. *J. Magn. Reson.* **1998**, *132* (1), 65−77, DOI: 10.1006/jmre.1998.1387.
(33) Borgia, G. C.; Brown, R. J. S.; Fantazzini, P. Uniform-penalty inversion of multiexponential decay data: II. Data spacing, T_2 data, systematic data errors, and diagnostics. *J. Magn. Reson.* **2000**, *147* (2), 273−285, DOI: 10.1006/jmre.2000.2197.
(34) Almendros, G.; Martinez, A. T.; Gonzalez, A. E.; Gonzalez-Vila, F. J.; Fruend, R.; Luedemann, H.-D. CPMAS ^{13}C NMR study of lignin preparations from wheat straw transformed by five lignocellulose-degrading fungi. *J. Agric. Food Chem.* **1992**, *40* (7), 1297−1302, DOI: 10.1021/jf00019a043.
(35) Callaghan, P. T.; Coy, A. PGSE NMR and molecular translational motion in porous media. In *Nuclear Magnetic Resonance Probes of Molecula Dynamics*; Tycho, R., Ed.; Kluwer Academic Publishers: Dordrecht, The Netherlands, 1994; pp 551.
(36) Godward, J.; Gunning, P.; Hills, B. P. An NMR protocol for determining ice crystal size distributions during freezing and pore size distributions during freeze-drying. *Appl. Magn. Reson.* **1999**, *17* (4), 537−556, DOI: 10.1007/BF03162085.
(37) Browenstein, K. R.; Tarr, C. E. Importance of classical diffusion in NMR studies of water in biological cells. *Phys. Rev. A* **1979**, *19* (6), 2446−2454, DOI: 10.1103/PhysRevA.19.2446.
(38) Laudicina, V. A.; De Pasquale, C.; Conte, P.; Badalucco, L.; Alonzo, G.; Palazzolo, E. Effects of afforestation with four unmixed plant species on the soil−water interactions in a semiarid Mediterranean region (Sicily, Italy). *J. Soil Sediment* **2012**, *12* (8), 1222−1230, DOI: 10.1007/s11368-012-0522-0.
(39) Stingaciu, L. R.; Pohlmeier, A.; Blümler, P.; Weihermüller, L.; van Dusschoten, D.; Stapf, S.; Vereecken, H. Characterization of unsaturated porous media by high-field and low-field NMR relaxometry. *Water Resour. Res.* **2009**, *45* (8), DOI: 10.1029/2008WR007459.
(40) Korb, J.-P. Surface diffusion of liquids in disordered nanopores and materials: a field cycling relaxometry approach. In *Fluid Transport in Nanoporous Materials*; Conner, W. C., Fraissard, J., Eds.; Academic Press, Springer: Dordrecht, The Netherlands, 2006.
(41) Bakhmutov, V. I. Front matter. In *Practical NMR Relaxation for Chemists*; Wiley: Chichester, UK, 2004.

Table 1. Seed Sources, Pedigrees and Glutenin/Secalin Allele Identification of Triticale Cultivars and Breeding Lines

			Glutenin/Secalin alleles				
Cultivar	Breeding Agency[a]	Pedigree	*Glu-A1*	*Glu-B1*	*Glu-R1* (*Sec-3*)	*Glu-D1*	*Gli-R2* (*Sec-2*)
Berkshire	USYD, 2009	Yogui_1/Tapir//2*Fara_1/3/Erizo_11/ Yogui_3/5/Asad*2/Jun//Anoas_5/3/Sonni_6/4/Asad/Elk54// Erizo_10)	*a*	*a*	*c*		*a*
Bogong	UNE, 2008	H127	*c*	*f*	*c*		*a*
Canobolas	UNE, 2008	H 418	*c*	*f*	*c*		*a*
Chopper	AGT, 2010	TX93-19-2D-3[b]/Treat	*c*	*p*	*c*		*c*
Crackerjack	Heritage Seeds, 2003	Juanillo 159/4372	*a*	*f*	*c*		*c*
D12/Tatu	Norman Darvey, USYD	D12/Tatú	*c*	*f*	*c*		*a*
DH265	Adam Lukaszewski, UC, Riverside, U. S. A.	Unknown/Valdy	*c*	*av*		*d*	*c*
Endeavor	USYD, 2007	80469(II76-24)/II79-39E	*a*	*av*	*c*		*a*
Goanna	KC&ME, 2011	Treat/Tickit?	*c*	*f*	*c*		*c*
Hawkeye	AGT, 2007	POPP1_2/TX93-19-2[b]	*c*	*f*	*g*		*c*
Jaywick	AGT, 2007	BEAGLEB/2*RHINO_3//TX93-19-2[b]	*a*	*f*	*g*		*c*
Rufus	UNE, 2004	1181-196-12/Tahara-3	*c*	*p*	*c*		*c*
Tobruk	USYD, 2007	CHD982/3/ANSO/ARDI_3//ERIZO_7	*a*	*c*	?		*c*
Tuckerbox	KC&ME, 2010	Abacus/Tahara?	*c*	*f*	*c*		*c*
Vicuna	CIMMYT, 1992	IGUANA_4/CIVET	*a*	*b*	*c*		*a*
Yowie	KC&ME, 2010	Speedee	*c*	*p*	*c*		*c*
Yukuri	UNE, 2004	YOGUI/CMH79A.209	*a*	*f*	?		*a*

[a]Abbreviations: AGT = Australian Grain Technologies, SA, Australia; CIMMYT = International Maize and Wheat Improvement Center, Mexico; KC&ME = KV Cooper and MG Elleway, Farmers and Seedgrowers, SA, Australia; USYD = University of Sydney, NSW, Australia; UNE = University of New England, NSW, Australia. [b]TX93-19-2 is a sibling of Tickit and Speedee. [c]For more information on the alleles, see Table 2.

MATERIALS AND METHODS

Germplasm. The HMW glutenin and secalin composition was evaluated in 17 triticale genotypes (Berkshire, Bogong, Canobolas, Chopper, Crackerjack, D12/Tatu, DH265, Endeavor, Goanna, Hawkeye, Jaywick, Rufus, Tobruk, Tuckerbox, Vicuna, Yukuri, Yowie) from a diverse set of breeding programs and covering all triticale cultivars recommended for growing in Australia at the time, plus two breeding lines (Table 1). Pure seed of Berkshire, Chopper, Crackerjack, D12/Tatu, DH265, Endeavor, Tobruk, Tuckerbox, and Vicuna were sourced from the University of Sydney, NSW, Australia; Bogong and Canobolas were sourced from Robin Jessop at the University of New England, NSW, Australia; Goanna, Rufus, and Yowie were sourced from KV Cooper and MG Elleway, SA, Australia; and Yukuri was sourced from Seed Distributors, NSW, Australia. Crackerjack, Endeavor, Tobruk, and Tuckerbox and winter types, the remainder are spring types.

SDS-PAGE. Visualization of glutenin subunits was performed using SDS-PAGE based on previous methods used to characterized glutenins in Australian wheat cultivars.[15] The nongerm end of three grains were crushed individually with a pair of pliers and placed in 1.5 mL Eppendorf tubes. Nonsecaloglutenin proteins were removed by adding 200 μL of 50% (v/v) propan-1-ol, vortexing, and then incubating at 65 °C in a water bath for 30 min, with vortexing approximately every 7 min. Tubes were then centrifuged at 5000 rpm for 10 min, and supernatant was discarded. This process was repeated using only 5 min incubation time, repeated using distilled water and 5 min incubation, and then samples were oven-dried at 37 °C for 40 min to remove remaining liquid.

Extraction of secaloglutenins proceeded with vortexing and incubation of the pellet for 5.5 min at 95 °C in 150 μL of glutenin sample buffer (12.5% 0.5 M Tris−HCl at pH 6.8, 25% glycerol, 2% SDS (w/v), 0.001% bromophenol blue (w/v), and 2% mercaptoethanol). Samples were then centrifuged at 14 000 rpm for 2.5 min.

Extracted glutenins were fractionated in a vertical CBS-Scientific Dual Adjustable Mega-Gel kit (CBS-Scientific, CA, U. S. A.). The resolving gel contained 8% Acr/Bis, 24% 1.5 M Tris−HCl at pH 8.8, 0.1% SDS, 0.12% TEMED, and 0.06% APS. The stacking gel contained 4% Acr/Bis, 25% 0.5 M Tris−HCl at pH 6.8, 0.1% SDS, 0.3% TEMED, and 0.15% APS. Samples of 8 μL were resolved at 40 V overnight followed by 70 V for the final 4 h in electrode running buffer (0.3% Tris (w/v), 1.44% glycine (v/v), and 0.1% SDS (w/v)).

Gels were rinsed in water, stained in Coomassie blue solution (0.05% Coomassie blue G-250, 10% (w/v) phosphoric acid, 5% aluminum sulfate, and 20% methanol) for approximately 60 min with gentle agitation, destained in water for 33 h aided by paper towelling, and permanently stored between single layers of clear cellophane. Allele designations were defined by comparison to nine cultivars of *Triticum aestivum* (Bowie, Chinese Spring, Ellison, Federation, Gabo, QALBis, Sunco, Veery, Ventura), one cultivar of *Triticum durum* (Bellaroi), and three triticale checks (Sirius, Titan, Presto 1R.1D$_{5+10}$), for which the allele designations have been previously described.[5,16,17]

Field Trials. A subset of six triticale (Berkshire, Endeavor, Hawkeye, Jaywick, Tobruk, and Yukuri) and five wheat lines (hard wheats Ellison, Sunco, and Ventura, soft wheat QALBis, and durum wheat Bellaroi) were grown in duplicate plots under a completely randomized block design on John Pye farm at Greendale, NSW in 2009 (JP09) and at the Plant Breeding Institute, Narrabri, NSW in 2010 (NARR10). Unfortunately only one field plot of Sunco was able to be harvested at JP09. Triticale lines were selected based on their applicability to the two trial environments and to include both winter and spring types.

Sowing density for all lines was 60 kg/ha; plots were 3.75 m^2 at NARR10 and 4.68 m^2 at JP09. JP09 received 100 kg/ha of Starter 15 base dressing, 150 kg/ha urea at approximately 6 weeks followed by 2 L/ha Supa Trace and then a topdressing of Nitrophoska at 12 weeks. NARR10 received Granulock at sowing and 150 kg/ha urea at first irrigation. Both trials received limited irrigation.

Milling and Protein Content. Subsamples of approximately 50 g were ground on a Newport Scientific 600 Hammer Mill with 0.5 mm screen (Perten, Warriwood, NSW, Australia) for SDS-sedimentation testing. Subsamples of 50 g were also milled to white flour on a Quadrumat Junior Mill (Brabender, Duisburg, Germany) to determine flour protein content and mixograph parameters. Hard wheats were tempered to 15% moisture content and soft wheat (QALBis) plus all triticales to 13% (triticale is generally a soft grained species). Flour moisture and protein content were determined by NIR on an Inframatic 8100 PerCon (Perten, Hägersten, Sweden) that had been calibrated using a hard-grained wheat and is defined as proportion of moisture/protein of the flour. Wholegrain protein content and moisture content were assessed by near-infrared transmittance (NIT) on an Infratec 1241 Grain Analyzer (FOSS, Hillerød, Denmark) using triticale calibration TR260180 and wheat calibration WH002010. The proportion of grain protein that was retained in the main final commercial product (white flour) after the milling process ($P_{retained}$) is defined as

$$P_{retained} = 100 \times \frac{m_{flour}}{m_{total}}$$

where m_{total} is mass of protein in 100 g of grain, m_{flour} is mass of protein within the flour portion of 100 g of grain, and $P_{retained}$ is expressed as a percentage. Moisture content of grain and flour was standardized before calculation. Mass of protein within what would become the flour proportion of the total grain (m_{flour}) is expressed within the context of total grain weight from which it was sourced rather than as straight flour protein content to standardize the variable and hence allow determination of protein loss when milling grain to flour. The variable is defined as

$$m_{flour} = f_y \times m_{fp}$$

where f_y is flour yield and m_{fp} is the mass of protein in 100 g of flour. The difference between m_{flour} and total grain protein quantifies the amount removed as bran or pollard during milling. Thus, m_{fp} is not an exact measure of the mass of protein within the grain endosperm but rather the mass within flour that was able to be separated from bran during the milling process.

SDS-Sedimentation Test. The SDS-sedimentation height was assessed using a down-scaled version of AACC method 56-70.[18] Samples of 0.75 g wholemeal flour were added to 3 mL of 0.001% Bromophenol Blue solution (w/v) in 15 mL plastic tubes with screw-top lids, vortexed for 3 s, rested, and vortexed again before adding 9 mL of working solution (3.02% SDS w/v and 0.23% lactic acid w/v). Tubes were inverted 10 times, rested for 2 min, and then again inverted 10 times. Sediment height was read after 30 min and adjusted according to the height of the standard in each batch.

Mixographs. Mixing parameters from two replicates of each field plot were determined on a mixograph using a 10 g mixing bowl and 7 min evaluation time (National Manufacturing Co., Lincoln, Nebraska, U. S. A.). Immediately prior to mixing, 6 mL of deionized water was added to 10 g of flour. Graphs were analyzed using Mixsmart for Windows Version 1.0.404 and interpreted according to defined mixograph parameters.[19] In brief, these parameters are based on an arbitrary mixograph height scale from 0 to 100 (displayed as a percentage), plus peak time (displayed in minutes). Parameters of interest were time of peak (MPT), graph height at peak time (MPV), graph width at peak time (MPW), rate of dough breakdown (defined as the slope 1 min after peak time, RDB), and tail width at 6 min (MTW).

Statistical Analysis. Data were analyzed in Genstat v. Fourteen (VSN International, Hemel Hempstead, U. K.) with a 5% significance level. The influence of species and cultivar for all variates were analyzed using residual maximum likelihood (REML), with fixed-model terms defined as Species/Genotype and random model terms defined as Site/Block (or Site/Block/Replicate for SDS-sedimentation height). Grain protein (11% mb) and flour protein (11% mb) were analyzed on a natural log scale and SDS sedimentation on a square root scale with the distribution brought to a minimum of 1.[20] Flour protein was tested as a covariate for mixing parameters, and both grain and flour protein contents were tested as covariates for SDS-sedimentation height. Correlation between flour protein content and SDS-sedimentation was performed for both triticale and wheat in Genstat, also using a 5% significance level. Hard-grained lines Berkshire and Bellaroi were excluded from correlation analysis due to the different moisture absorption of hard grain flour.

RESULTS AND DISCUSSION

Glutenin and Secalin Classification. Despite sourcing cultivars from several breeding programs and including all cultivars recommended for sowing in the region at the time of the research, the triticale cultivars in this investigation displayed relatively little diversity in HMW glutenin profiles. This reflects the narrow source of background material: the majority are a cross between the cultivar Speedee or sibling TX93-19-2 with a CIMMYT parent or is a direct selection of CIMMYT origin (Table 1).

Only two alleles of *Glu-A1* were identified: *Glu-A1a* and *Glu-A1c* were present in 41.2% and 58.8% of the cultivars, respectively (Table 2). Six alleles were observed at the *Glu-B1* locus, with *Glu-B 1f* (13 + 16) found in 52% of lines (nine cultivars). *Glu-B 1f* is common in triticale.[5,11] Allele *Glu-B 1p* (23 + 18) is usually reported as *Glu-B1IV* in triticale owing to its original designation in durum wheat and relatively recent classification in bread wheat.[3,17]

Secalins encoded by *Glu-R1c* (6r+13r) were identified in 75% of lines surveyed (Table 2). *Glu-R1c* is the most common *Glu-R1* allele in triticale internationally, being found in 65.7% of European lines, 62.7% of French lines, and 71.4% of Portuguese lines.[3,5,10] An undefined set of rye HMW secalins was observed in Tobruk and Yukuri in the upper portion of the gel (Figure 1). These secalins may represent a new allele at *Glu-R1*; however, more extensive comparison to existing alleles found in both triticale and rye is required before a conclusion can be drawn.

Allele *Gli-R2c* (t1) was the most common of the 75K γ-secalins, being found in 59% of surveyed lines, but it was not as common as that documented in European triticales.[5] Only two of the four characterized alleles of 75K γ-secalins[5] were present among the tested cultivars; rare alleles *Gli-R2b* (d2) and *Gli-*

Table 2. Distribution of HMW Glutenin and Secalin Subunits and 75K γ-Secalins Amongst Tested Triticale Lines

allele	number of cultivars	proportion of total (%)
Glu-A1		
a = 1	7	41.2
c = null	10	58.8
Glu-B1		
a = 7	1	5.9
b = 7 + 8	1	5.9
c = 7 + 9	1	5.9
f = 13 + 16	9	52.9
p = 23 + 18	3	17.6
av = 7 + 18	2	11.8
Glu-R1 (***Sec-3***)[a]		
$c = 6^r + 13^r$	12	75.0
$g = 5.8^r$	2	12.5
$?^r$	2	12.5
Gli-R2 (***Sec-2***)		
a = *d*1	7	41.2
c = *t*1	10	58.8

[a]Translocation line DH265 was not included among total for *Glu-R1*

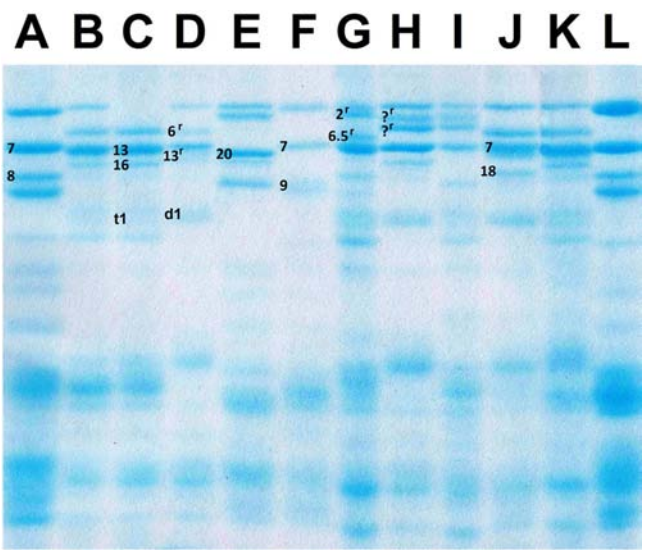

Figure 1. SDS-PAGE of selected Australian triticale cultivars with wheat standards (ws) and a triticale standard (ts): Lane A. Chinese Spring (ws); B. Jaywick; C. Hawkeye; D. Berkshire; E. Federation (ws); F. Bowie (ws); G. Titan (ts); H. Yukuri; I. Tobruk; J. Endeavor; K. Crackerjack; L. Sunco (ws). Glu-B1, GluR1 and Gli-R2 subunits are noted, including the unidentified Glu-R1 allele (Lane H).

R2d (null) were not observed. The null allele is likely the result of a 2*D*/2R translocation of CIMMYT origin.[10]

Some difficulty has been encountered with the identification and classification of glutenin subunits in triticale using SDS-PAGE. Currently the predominant nomenclature system for glutenin alleles in triticale follows that of wheat; however, the mobility of several secalins is identical to that of glutenins, particularly in the HMW range.[7] The overlap of bands on SDS-PAGE (as observed here) has led to conflicting glutenin characterization of the same cultivar, for example, Brzezinski and Lukaszewski[4] with Salmanowicz and Dylewicz.[7] Standards that are unique to triticale must be developed so that continued comparisons with wheat do not lead to misidentification of key alleles and to facilitate the development of linked DNA markers for manipulation of secaloglutenins in triticale improvement.

Furthermore, triticale cultivars are not necessarily uniform in their glutenin composition: heterogeneity in up to 41% of 139 cultivars has been reported.[4] Heterogeneity within cultivars is likely due to a combination of a lack of screening for glutenin alleles during the breeding process and a higher rate of allogamy in triticale compared to wheat.[13] No heterogeneity was observed among triticales evaluated in this study.

Because the small range in HMW glutenin diversity relative to the confounding influence of gliadins and LMW glutenins and the unknown effect of the secalins, no attempt was made to extrapolate the influence of individual HMW glutenin/secalin alleles on dough properties. The importance of gliadins and LMW (low molecular weight) glutenins in dough properties is well established both in durum[21] and in bread wheat;[22] however, practically no research has been published on the influence of individual secalin subunits in either rye or triticale. Furthermore, mixed polymers and oligomers are formed between secalins and glutenins: even the 40k-secalins of rye, which are usually monomeric, may be incorporated into polymeric gluten when expressed in wheat.[23] The HMW glutenins form an elastomeric network that acts as a "backbone" for the interactions of other proteins in addition to conferring strength and elasticity to dough.[1] Hence, the overall properties of the secalogluten network were investigated in a subset of triticale cultivars.

Protein Content and SDS-Sedimentation Height. Grain protein content greatly varied between environments and was on average 2.8% greater for triticale and 3.5% greater for wheat at JP09 (Table 3). No significant difference in grain protein content was detected between species ($P = 0.704$); however, triticale flour protein content (directly proportional to gluten/secalogluten content)[24] was significantly less than wheat ($P < 0.001$).

Furthermore, a significantly greater proportion of triticale protein was removed by the milling process compared to wheat ($P < 0.001$), most of which would have been in the outer aleurone layer and pericarp. After the milling process, triticale retained only 43.97% of its original grain protein content in the flour, whereas 53.55% of the protein was retained in wheat flour. Previous research has confirmed triticale stores a lower proportion of grain protein in flour/gluten compared to wheat.[11,24−26] This suggests triticale has a thicker seed coat. Milling yields and fiber content on the same set of cultivars as described here also provided evidence of thicker seed coat in triticale compared to wheat.[27,28] Note, however, variability existed between cultivars, for example, Tobruk retained significantly more protein following the milling process than all other triticale lines (Table 3). The environment did not have a notable effect on the proportion of protein retained following the milling process in either species, despite the higher average protein contents at JP09.

Storage of proportionately less protein in triticale flour compared to wheat has significant implications for both research and industry. First, research that reports triticale secalogluten strength based on wholegrain protein content, as opposed to flour protein content, should be interpreted with caution, particularly when comparing triticale to wheat. Triticale lines with similar wholegrain protein content to wheat lines are likely to have less flour protein content, and hence, the dough strengths cannot be equitably compared. Second, because the food industry requires a certain flour

dx.doi.org/10.1021/jf405138w | J. Agric. Food Chem. 2014, 62, 4924−4931

Table 3. Mean Protein Contents, Proportion of Protein Retained after Milling, SDS-Sedimentation Height, and Mixing Characteristics for a Subset of Triticale Lines Compared to Wheat Standards Grown in Two Environments

site	species	genotype	grain protein (11%mb)	flour protein (14%mb)	m_{flour} (g)[a]	$P_{retained}$ (%)[b]	SDS-sedimentation height (mm)	MPT (mins)	MPV	MPW	RDB	MTW
JP09	Triticale	Berkshire	14.1	13.8	6.1	43.2	36.1	2.4	75.5	23.3	−10.1	5.5
		Endeavor	14.1	10.9	6.3	44.9	40.6	3.3	61.2	17.6	−5.4	5.3
		Hawkeye	13.8	10.3	5.8	42	43.2	3.1	59.8	20.0	−1.5	11.2
		Jaywick	13.6	10.4	6.1	45.3	39.2	2.9	63.4	24.3	−5.8	6.8
		Tobruk	13.0	9.9	6.3	49	34.3	1.7	58.4	18.1	−6.4	5.5
		Yukuri	13.0	10.0	5.9	45.4	36.6	1.7	61.3	20.0	−10.8	3.6
	Wheat	Bellaroi	15.8	16.6	7.0	45.7	58.7	4.8	79.2	30.6	−1.9	28.0
		Ellison	14.3	13.4	8.0	57.2	79.1	4.3	74.6	26.2	−1.6	17.6
		Qalbis	12.8	10.6	6.2	49.1	51.8	2.6	76.4	22.5	−6.5	6.0
		Sunco	13.1	12.4	8.0	61.7	80.3	4.5	78.7	23.0	−4.2	13.2
		Ventura	13.5	13.0	8.4	59.2	79.2	3.9	83.2	25.7	−2.6	14.2
NARR10	Triticale	Berkshire	10.8	9.2	4.1	38.3	29.6	2.5	56.5	26.6	−3.0	8.7
		Endeavor	11.8	8.5	4.8	41	34.5	3.4	54.4	12.5	−4.0	5.1
		Hawkeye	10.5	7.2	4.1	39.3	34.5	3.5	51.3	30.2	−3.5	14.9
		Jaywick	10.5	8.0	4.7	44.7	33.5	4.0	51.0	14.9	−3.4	9.0
		Tobruk	9.8	7.4	4.8	49.9	31.7	1.5	44.6	14.9	−2.4	5.3
		Yukuri	11.3	8.8	5.1	44.6	32.7	1.9	58.7	19.0	−11.3	3.7
	Wheat	Bellaroi	11.2	11.0	4.9	44.8	47.8	6.0	63.1	31.4	−0.4	28.3
		Ellison	10.3	9.2	5.6	55.9	63.8	6.1	58.0	19.7	−2.4	20.3
		Qalbis	9.0	7.3	4.5	49.8	34.7	2.9	54.9	13.1	−4.9	6.4
		Sunco	11.0	9.9	6.2	56.9	64.7	4.0	70.1	26.4	0.4	18.1
		Ventura	10.9	10.0	5.9	55.2	58.1	3.6	71.0	25.4	−2.3	11.8

[a] m_{flour} is the mass of protein (in grams) within the flour portion of 100 g of grain. [b] $P_{retained}$ is the proportion (expressed as a percentage) of the original protein content that was retained in white flour after the milling process.

protein content to produce the variety of end products which consumers demand, millers should be aware that the appropriate content of wholegrain protein when purchasing a batch of grain will differ between triticale and wheat.

Significant differences in SDS-sedimentation height were detected between triticale cultivars ($P < 0.001$); Tobruk and Berkshire produced notably low SDS-sedimentation heights. SDS-sedimentation results of all triticale cultivars were significantly inferior to bread wheat ($P < 0.001$, Table 3), a result consistent with previous studies.[12] QALBis soft wheat produced significantly higher SDS-sedimentation height (43.2 mm) than triticale on average (35.5 mm) but significantly lower height than hard wheat cultivars (70.0 mm). This is reflective of its weak gluten and one of the reasons soft wheat is used for cakes and cookies. Triticale has been found to be suitable for products traditionally made from soft wheat.[29,30] However, to obtain satisfactory flat and loaf breads, most research suggests triticale must be blended with hard wheat.[26,31,32] The low SDS-sedimentation of Berkshire was likely from an interaction with grain hardness as Berkshire has a hardness comparable to durum wheat.[27]

The flour protein contents (indicative of gluten/secaloglutten) of the samples varied between sites, species and cultivars. Flour protein content was a highly significant predictor of sediment height in both wheat and triticale ($P < 0.001$; Figure 2). This trend was more substantial in wheat than triticale, reflecting decades of selection for combinations of glutenin alleles associated with high loaf volume in wheat improvement, in contrast to the narrow diversity and lack of selection pressure for HMW glutenin alleles in triticale. However, the trend was still apparent in triticale, where sediment height increased by 9.6% for every 1% increase in protein content (protein contents ranging from 6.5% to 15.8%). In a European study of four

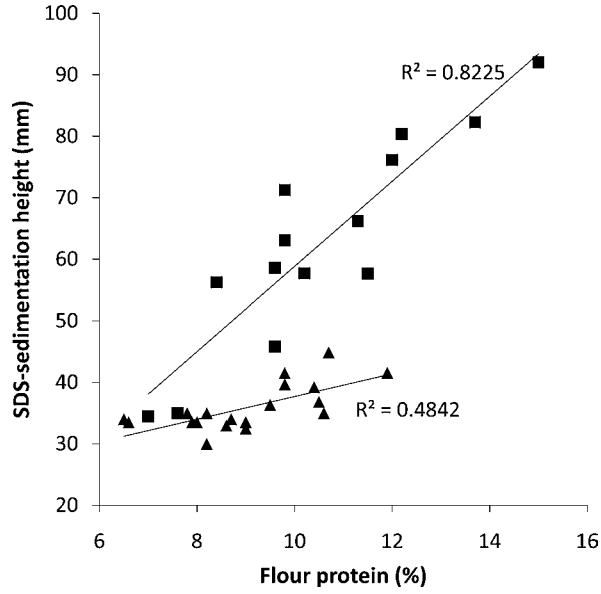

Figure 2. Relationship between SDS-sedimentation height and flour protein content in bread wheat samples (squares) and triticale samples (triangles). Each data point represents a field plot; lines represent best-fit linear trendlines.

triticale cultivars grown in four year-site environments, a significant correlation between SDS-sedimentation volume and protein content was observed.[33] Recalculation of the results revealed SDS-sedimentation volume increased by 20.3% for every 1% increase in protein content (protein content ranged from 10.9% to 17%). Similarly, recalculations from another study[32] also revealed a 25.5% increase (protein range from 5.0%

dx.doi.org/10.1021/jf405138w | J. Agric. Food Chem. 2014, 62, 4924−4931

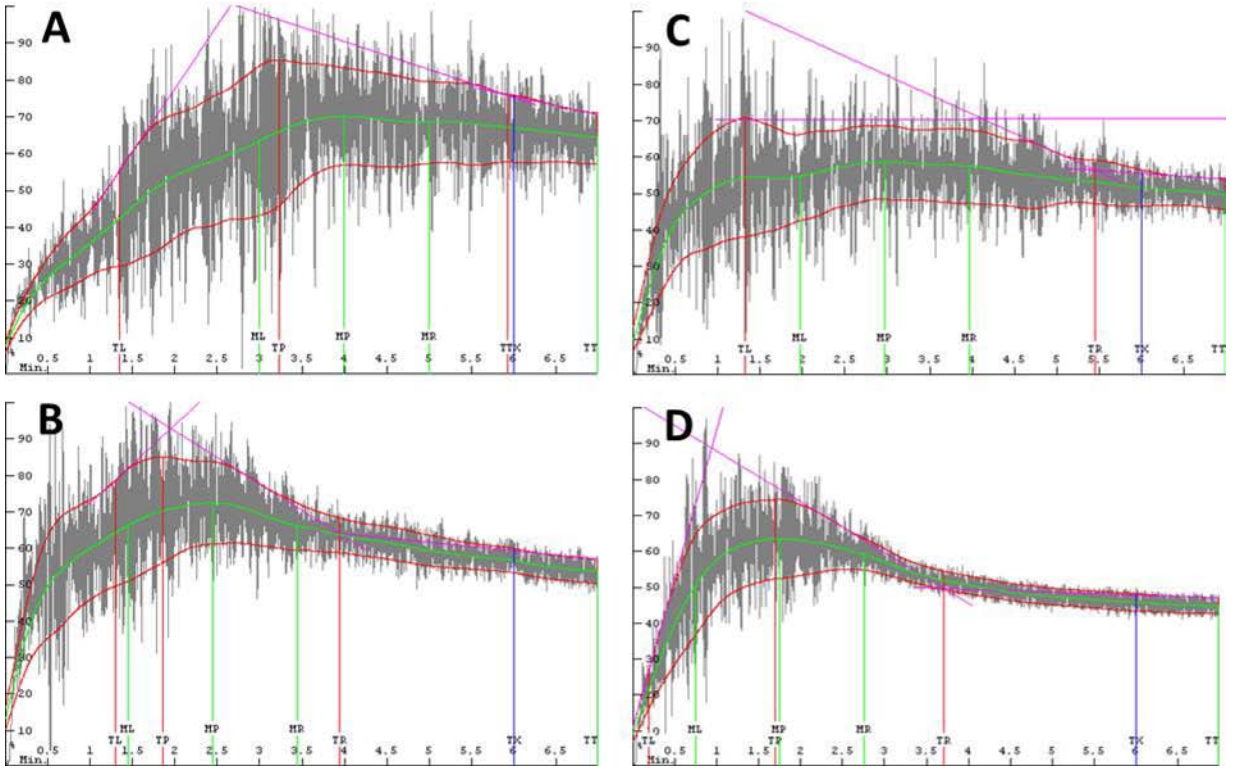

Figure 3. Mixographs of typical wheat and triticale lines from JP09. (A) Sunco bread wheat. (B) QALBis soft wheat. (C) Hawkeye triticale. (D) Tobruk triticale.

to 10.5%). The significance of flour protein content on dough properties in triticale has also been reported previously.[24,25]

The influence of flour protein content on SDS-sedimentation results illustrates the importance of comparing wheat and triticale samples with similar flour protein content. Several previous studies have drawn conclusions as to the strength of the triticale secalogluten network based on samples of widely different flour protein contents/gluten contents compared to wheat,[26,32,33] which is an inequitable comparison. It is particularly important to standardize the quantity of flour protein when attempting to ascertain the influence of the secalins on the strength of the secalogluten network. A set of four reconstituted triticale flours with identical gluten contents to two wheat standards found the triticale gluten had a comparable stretching value to wheat gluten.[25] Two of the four reconstituted triticale flours produced loaves of the same volume as the wheat standards. Extensibility has also been found to be highly correlated to both flour protein content and polymeric protein content in triticale (r = 0.96 and 0.97, respectively).[32] These results suggest that low polymeric protein content in triticale compared to wheat must be considered alongside polymeric protein quality and that the secalins are integrated into the hydrated polymeric protein network. The reduced response of triticale SDS-sedimentation height to increasing protein content compared to wheat confirms that secalogluten strength in triticale is not as high as gluten strength in wheat.

Mixing Parameters. Wheat mixing parameters were clearly superior to the mean of triticale flours evaluated from both sites (P = 0.01 or less for all parameters, Table 3). Triticale cultivars Berkshire, Tobruk, Yukuri, and to a lesser extent Endeavor and Jaywick, plus soft wheat cultivar QALBis, all exhibited a dramatic loss of dough strength and elasticity over time (Figure 3D). In several samples of low protein content, the dough collapsed completely and was wrapped around the sides of the mixing bowl. The influence of flour protein content was again apparent: flour protein content explained 62.5% of the variability in MPV in wheat samples and 84.1% in triticale samples. Several triticale lines produced the thin mixograph tails characteristic of high α-amylase activity (Figure 3D). Cultivars Endeavor, Hawkeye, and Jaywick are known to have high α-amylase activity;[28] however, this did not perfectly correlate with poor mixograph characteristics here.

All triticales exhibited a short mixing time and were in between (and not significantly different to) QALBis and Ventura, with the exception of Tobruk and Yukuri, which were significantly shorter (Table 3). The mixing time of Hawkeye was also very short; however, dough strength was maintained after reaching an early peak (Figure 3C). Short mixing times in triticale have been reported previously.[24,32] A standard volume of water was added to each sample to allow an even comparison between wheat and triticale cultivars and to clearly establish (and semiquantify) the inferiority of triticale compared to wheat. Future work should modify the water content of the dough relative to its protein content or use farinographs to accurately determine the water absorption of triticale lines.[18]

Nevertheless, some triticale cultivars displayed certain mixing parameters similar to the wheat checks. For example, no statistical difference was detected in MPW between most individual triticale and wheat cultivars, and Berkshire, Endeavor, Hawkeye, and Jaywick all had significantly later MPT than soft wheat QALBis. Other studies have also found certain triticale lines demonstrate similar dough strength to wheat standards despite inferior mixograph dough strength in triticale over-

dx.doi.org/10.1021/jf405138w | J. Agric. Food Chem. 2014, 62, 4924−4931

all.[32,34] Hawkeye did not reach the peak height of hard wheat; however, it maintained dough strength during mixing, had a wide mixograph profile (Figure 3C), and was the most suitable for end products requiring strong dough, for example, bread. Note that Hawkeye and Jaywick share similar pedigrees, polymeric storage protein profiles and flour protein contents; however, the SDS-sedimentation and mixograph results reveal different secalogluten strengths. This may be due to allelic differences in nonsecaloglutenin storage proteins, or low α-amylase activity in Hawkeye (although this appears unlikely).[28]

It is difficult to differentiate the influence on species from the influence of flour protein content when considering the inferior mixing properties of triticale compared to wheat. Flour protein content was a significant covariate in MPV ($P < 0.001$), RDB ($P < 0.001$), and MTW ($P = 0.015$). This illustrates the importance of G × E interactions and the role of agronomic practices in the production of milling-quality triticale, which has been largely overlooked in industry. Triticale often has lower protein content than bread wheat when grown under identical environmental conditions; this is due to a combination of higher yield and low (if any) selection pressure for high flour protein content during the breeding process. The effect of low flour protein was of particular significance for NARR10 results and was very apparent in both the SDS-sedimentation height and the mixographs. Agronomic interventions such as appropriate timing and rate of nitrogenous fertilizer application can improve grain storage protein accumulation.[35] Increasing the total gluten in triticale flour should be considered an important breeding aim in addition to optimizing the glutenin allele composition (indeed, the two are related).

The mixograph results imply that triticale dough should be treated differently to wheat in mechanized commercial systems due to its shorter mixing time. Nevertheless, the variation between triticale cultivars evaluated in this study suggests that dough properties can be significantly improved through targeted crossing and selection and appropriate agronomic practices, potentially to the level of bread wheat.

In summary, narrow diversity in HMW subunit expression was observed in the examined triticale cultivars; however there were still significant (statistical and commercial) differences in mixing parameters and SDS-sedimentation values. It is essential that wheat and triticale samples of similar flour (not grain) protein contents are used to assess gluten characteristics. Furthermore, it seems appropriate for the protein content of triticale flour be above 10% for both research and commercial purposes to allow the formation of an acceptable secalogluten network, as is recommended for wheat (Meiqin Lu, Pers. comm.). Provided the requirements for grain softness, flour color and α-amylase activity are met,[27,28] the results of this research suggest modern triticale is of appropriate gluten quality for use in cookies, cakes, and other products traditionally made from low-protein wheat.

AUTHOR INFORMATION

Corresponding Author

*E-mail: angela.pattison@sydney.edu.au. Phone: +61 2 6799 2200. Fax: +61 2 6799 2239.

Notes

The authors declare no competing financial interest.

ACKNOWLEDGMENTS

This work was funded by the Grains Research and Development Corporation. Thanks to Jeremy Roake and Jayne Onus for field and technical support and Katharine Cooper for pedigree information and help with manuscript preparation.

ABBREVIATIONS AND NOMENCLATURE

JP09, Greendale 2009 growing environment; NARR10, Narrabri 2010 growing environment; MPT, time of mixograph peak in minutes; MPV, mixograph height at peak time; MPW, mixograph width at peak time; MTW, tail width at 6 min; NIR, near-infrared reflectance; NIT, near-infrared transmittance; RDB, rate of dough breakdown (defined as the slope at 1 min after peak time); REML, residual maximum likelihood; Secaloglutenin, polymeric storage proteins of triticale, namely HMW glutenin from the 1A and 1B chromosomes, HMW secalin from the 1R chromosome, LMW glutenin from the 1A and 1B chromosomes, and 75k γ-secalin from the 2R chromosome; Secalogluten, the hydrated network of secaloglutenin protein including any incorporated monomeric units

REFERENCES

(1) Shewry, P. R.; Halford, N. G. Cereal seed storage proteins: structures, properties and role in grain utilization. *J. Exp. Bot.* **2001**, *53*, 947−958.

(2) Lukow, O. M.; Payne, P. I.; Tkachuk, R. The HMW glutenin subunit composition of Canadian wheat cultivars and their association with bread-making quality. *J. Sci. Food Agr.* **1989**, *46*, 451−460.

(3) Igrejas, G.; Guedes-Pinto, H.; Carnide, V.; Branlard, G. Seed storage protein diversity in triticale varieties commonly grown in Portugal. *Plant Breed.* **1999**, *118*, 303−306.

(4) Brzezinski, W.; Lukaszewski, A. J. Allelic variation at the Glu-1, Sec-2 and Sec-3 loci in winter triticale. In *Proceedings of the 4th International Triticale Symposium*; Juskiw, P., Ed.; International Triticale Association:Alberta, Canada, 1998; pp 266−283.

(5) Amiour, N.; Bouguennec, A.; Marcoz, C.; Sourdille, P.; Bourgoin, M.; Khelifi, D.; Branlard, G. Diversity of seven glutenin and secalin loci within triticale cultivars grown in Europe. *Euphytica* **2002**, *123*, 295−305.

(6) Tohver, M.; Kann, A.; That, R.; Mihhalevski, A.; Hakman, J. Quality of triticale cultivars suitable for growing and bread-making in northern conditions. *Food Chem.* **2005**, *89*, 125−132.

(7) Salmanowicz, B. P.; Dylewicz, M. Identification and characterization of high-molecular-weight glutenin genes in Polish triticale cultivars by PCR-based DNA markers. *J. Appl. Genet.* **2007**, *48*, 347−357.

(8) Vyhnanek, T.; Bednar, J. Polymorphism of prolamin proteins of the grain of triticale varieties certified in the Czech Republic. *Plant, Soil Environ.* **2005**, *51*, 151−155.

(9) Kozub, N. A.; Xynias, I. N.; Sozinov, I. A. Diversity in seed storage proteins in substituted hexaploid triticale cultivars (x *Triticosecale* Wittmack). *Cereal Res. Commun.* **2007**, *35*, 1469−1476.

(10) Bellil, I.; Bouguennec, A.; Khelifi, D. Diversity of seven glutenin and secalin loci within triticale cultivars grown in France. *Not. Bot. Horti. Agrobot. Cluj−Napoca* **2010**, *38*, 48−55.

(11) Peña, R. J.; Pfeiffer, W. H.; Amaya, A.; Zarco-Hernandez, J. High molecular weight glutenin subunit composition in relation to the bread making quality of spring triticale. In *Cereals International*; Martin, E. J., Wrigley, C. W., Eds; Royal Australian Chemical Institute: Brisbane, Australia, 1991; pp 436−440.

(12) McGoverin, C. M.; Snyders, F.; Muller, N.; Botes, W.; Fox, G.; Manley, M. A review of triticale uses and the effect of growth environment on grain quality. *J. Sci. Food Agr.* **2011**, *91*, 1155−1165.

(13) Varughese, G.; Pfeiffer, W. H.; Peña, R. J. Triticale: a successful alternative crop (Part 2). *Cereal Foods World* **1996**, *41*, 635−645.

(14) Dennett, A. L.; Cooper, K. V.; Trethowan, R. M. The genotypic and phenotypic interaction of wheat and rye storage proteins in primary triticale. *Euphytica* **2013**, *194*, 235−242.
(15) Appelbee, M. J. Quality potential of gluten proteins in hexaploid wheat and related species. Ph.D. Thesis, School of Agriculture, Food and Wine, University of Adelaide, Australia, 2007.
(16) Lukaszewski, A. J.; Curtis, C. A. Transfer of the Glu-D1 gene from the chromosome 1D to chromosome 1R in hexaploid triticale. *Plant Breed.* **1992**, *109*, 203−210.
(17) McIntosh, R. A.; Yamazaki, Y.; Dubcovsky, J.; Rogers, J.; Morris, C. F.; Somers, D. J.; Appels, R.; Devos, K. M. Catalogue of gene symbols for wheat. In *11th International Wheat Genetics Symposium*; Appels, R., Eastwood, R., Lagudah, E., Langridge, P., Mackay, M., McIntyre, L., Sharp, P., Eds.; Sydney University Press: Sydney, Australia, 2008.
(18) AACC. *Approved methods of the AACC*, 9th ed.; American Association of Cereal Chemists: St. Paul, MN, 1995.
(19) Bordes, J.; Branlard, G.; Oury, F. X.; Charmet, G.; Balfourier, F. Agronomic characteristics, grain quality and flour rheology of 372 bread wheats in a worldwide core collection. *J. Cereal Sci.* **2008**, *48*, 569−579.
(20) Osborne, J. Notes on the use of data transformations. *Practical Assessment, Research & Evaluation* **2012**, *8* (6), No. http://PAREonline.net/getvn.asp?v=8&n=6.
(21) Sissons, M. J.; Ames, N. P.; Hare, R. A.; Clarke, J. M. Relationship between glutenin subunit composition and gluten strength measurements in durum wheat. *J. Sci. Food Agr.* **2005**, *85*, 2445−2452.
(22) Meenakshi, S.; Khatkar, B. S. Structural and functional properties of wheat storage proteins: a review. *J. Food Sci. Technol.* **2005**, *42*, 455−471.
(23) Altpeter, F.; Popelka, J. C.; Wieser, H. Stable expression of 1Dx5 and 1Dy10 high-molecular-weight glutenin subunit genes in transgenic rye drastically increases the polymeric glutelin fraction in rye flour. *Plant Mol. Biol.* **2004**, *54*, 783−792.
(24) Macri, L. J.; Ballance, G. M.; Larter, E. N. Factors affecting the breadmaking potential of four secondary hexaploid triticales. *Cereal Chem.* **1986**, *63*, 263−267.
(25) Peña, R. J.; Ballance, G. M. Comparison of gluten quality in triticale: a fractionation-reconstitution study. *Cereal Chem.* **1987**, *64*, 128−132.
(26) Serna-Saldivar, S. O.; Guajardo-Flores, S.; Viesca-Rios, R. Potential of triticale as a substitute for wheat in flour tortilla production. *Cereal Chem.* **2004**, *81*, 220−225.
(27) Pattison, A. L.; Trethowan, R. M. Characteristics of modern triticale quality: commercially significant flour traits and cookie quality. *Crop Pasture Sci.* **2013**, *64*, 874−880.
(28) Dennett, A. L.; Wilkes, M. A.; Trethowan, R. M. Characteristics of modern triticale quality: the relationship between carbohydrate properties, α-amylase activity, and falling number. *Cereal Chem.* **2013**, *90*, 594−600.
(29) Leon, A. E.; Rubilol, A.; Anon, M. C. Use of triticale flours in cookies: quality factors. *Cereal Chem.* **1996**, *73*, 779−784.
(30) Oliete, B.; Perez, G. T.; Gomez, M.; Ribotta, P. D.; Moiraghi, M.; Leon, A. E. Use of wheat, triticale and rye flours in layer cake production. *Int. J. Food Sci. Technol.* **2010**, *45*, 697−706.
(31) Peña, R. J.; Amaya, A. Milling and breadmaking properties of wheat and triticale grain blends. *J. Sci. Food Agr.* **1992**, *60*, 483−487.
(32) Naeem, H. A.; Darvey, N. L.; Gras, P. W.; MacRitchie, F. Mixing properties, baking potential and functionality changes in storage proteins during dough development of triticale-wheat flour blends. *Cereal Chem.* **2002**, *79*, 332−339.
(33) Erekul, O.; Kōhn, W. Effect of weather and soil conditions on yield components and bread-making quality of winter wheat (*Triticum aestivum* L.) and winter triticale (*Triticosecale* Wittm.) varieties in north-east Germany. *J. Agron. Crop Sci.* **2006**, *192*, 452−464.
(34) Naik, H. R.; Sekhon, K. S.; Abbas Wani, A. Physicochemical and dough-handling characteristics of Indian wheat and triticale cultivars. *Food Sci. Technol. Int.* **2010**, *16*, 371−379.
(35) Johansson, E.; Prieto-Linde, M. L.; Gissen, C. Influences of weather, cultivar and fertiliser rate on grain protein polymer accumulation in field-grown winter wheat, and relations to grain water content and falling number. *J. Sci. Food Agr.* **2008**, *88*, 2011−2018.

Table 1. Range of Properties for the Samples Used

parameter	range of values
production areas	throughout Greece (i.e., Patras, Kalamata, Voiotia, Thessaloniki, Lesvos, Lamia, Volos, Tyrnavos, Komotini, Rhodes, Chalkidiki, Argos, Serres)
size of production	from big industry to local family run producers (9 of the 42 samples belong to the 30 most profitable Greek companies producing potable alcohol and spirits in 2006 and 2007 as judged by their gross income as published in Greek market literature)
packaging	bottled in 50, 100, 200, 300, 350, and 750 mL, sold by volume
price in 2013	2−4 €/200 mL, 6−12 €/750 mL in big supermarkets
consumption	4,000,000 bottles sold in Greece in 2010
percent of alcohol	37.5, 38, 40, 42, 45, 46%
type of alcohol	single distillation, double distillation
water source	tap water, well water, "river water"
water treatment	before and after mixing, no treatment
water treatment process[a]	deionization,[b] softening, membrane filtration, ion exchange, reverse osmosis, dechlorination
additives (according to labels on bottles and Web sites or commercials)	anise, and/or star anise, and/or fennel to be distilled, and in the case of geographical indications mastic and other aromatic seeds, plants or fruits

[a]Based on questionnaires answered by producers. [b]References 1 and 27.

MATERIALS AND METHODS

Samples. Most of the 42 samples were obtained from commercial shops. Some of the samples were provided by producers sealed in their commercial containers. Anethole was provided by one of the local producers. Alcohol was obtained from a local winery and ethanol from Merck. Deionized and distilled water samples were obtained from three different laboratories from the University of Patras. Deionized water (DI) was produced using a Dionel ion exchange system. Once-distilled and three-times-distilled water samples were produced using GFL and Jencons Autostills distillers, respectively. Tap water was obtained from the Patras municipal water supply system.

Conductivity and pH Measurements and Validation. Both conductivity and pH were measured using a Consort C862 instrument with Consort electrodes SK10B and SP10B, respectively. Conductivity standards from Hanna Instruments and Consort that corresponded to 84 and 147 μS/cm and to 1.413 and 12.88 mS/cm were used, respectively. Because the lower conductivity values to be measured were lower than the lower standard available, some samples of known conductivity were used to validate these low measurements. These "known samples" include samples having their conductivity measured by other instruments or by other investigators in the literature. pH standards were obtained from Metrohm Ltd. and Consort and were equal to 4.01, 7.0, and 10.0 at 25 °C. The known samples were also used to validate the pH measurements.

Measuring the pH with an electrode in the presence of high concentrations of solvents is problematic.[19] At 25 °C, it was found that in the presence of 40% ethanol the electrode would read the pH of a buffer solution approximately 0.7 point higher than its actual value in pure water. This value of 0.7 was used as a correction factor to correct pH solutions of the samples with ∼40% alcohol. For selected samples, the pH was additionally measured using pH indicator strips obtained from Macherey-Nagel.

Dilution Water Characteristic Measurements. For selected samples, additional physicochemical parameters were determined such as NO_3^-, NO_2^-, PO_4^{-3}, NH_4^+, total Fe, and carbonate hardness, using an Aquanal Fishwater Laboratory from Sigma-Aldrich.

Alcohol Characteristic Measurements. For selected samples, alcohol characteristics were determined. Methanol and ethanol percentages were determined on a Shimadzu GC-8A system consisting of a column packed with Porapac-S, N_2 as the carrier gas (20 mL/min), and a flame ionization detector. The injection port and detector temperatures were 210 °C, and the column temperature was 130 °C. Samples of 2 μL of each ouzo sample (1:4, 1:10, 1:20 dilutions) were injected directly in the column. The concentrations of the above compounds were determined by comparing the peak areas with those of standard solutions. Volatiles (acetaldehyde, ethanol, propanol-1, isobutyl alcohol, and amyl alcohols) were determined on a Shimadzu GC-8A system, with an 80/120 Carbopack B AW/6.6% Carbowax 20 M column, with N_2 as the carrier gas (20 mL/min) and a flame ionization detector. The injection port and detector temperatures were 210 °C, and the column temperature was set at 70−100 °C (rate at 5 °C/min). Samples of 4 μL of each ouzo sample were injected directly in the column. Two repetitions for each of two sample dilutions (1:10, 1:20) were used for each sample. Calculations were based on two different concentration standard solutions: (a) two different standards containing methanol and ethanol and (b) two different standards containing acetaldehyde, propanol-1, isobutul alcohol, ethyl acetate, and amyl alcohols. All samples were diluted with three-times-distilled water as in previous publications.[20,21]

RESULTS AND DISCUSSION

Sample Description. Table 1 presents a summary of the range of the different parameters of ouzo samples used in the present study. Almost 14% of the market was represented through the samples. The samples were produced in areas well spread out in the geographic region of Greece. Nine of the 42 samples belonged to the 30 most profitable (based on gross income in 2006 and 2007) Greek companies producing potable alcohol and spirits and not only ouzo. Samples packed in different size bottles or having different costs were tested. The percentage of the contained alcohol ranged from 37.5 to 46%. At least one ouzo sample was taken from ouzo labels containing up to six different alcohol percentages. In some cases, an alcohol percentage is represented by one label in the market. Most of the samples in the present study have 40% alcohol percentage, which is also the percentage found on the majority of the ouzo labels. Limited information on water treatment or on additives used was extracted from the labels on the bottles, the producers' Web sites, or personal contact with the producer. It seems that most producers that treat their dilution water use softening or deionization resins.

Conductivity and pH Measurement Validation. To validate the conductivity and pH measurements, known samples were tested, and the measurements are presented in Table 2. The values for the once-distilled water are different because the samples were produced in different laboratories. Also, the two values for the three-times-distilled water were obtained for water from the same laboratory but produced on different dates. The tap water results are consistent with the reports published by the local water supplier for the same sampling area (conductivity = 350 μS/cm, pH 7.7;[22]). Ethanol and anethole (the main flavor component of the anise essential

Table 2. Conductivity and pH Measurements for Some Known Samples and for Other Similar Drinks

sample	conductivity (μS/cm)	pH[a]
deionized water	17	5.6
once-distilled water	46, 36	5.6
three-times-distilled water	3.2, 3.5	5.4
tap water	311	7.5
ethanol	0.78	6.1 (6)
commercial alcohol	8.0	5.1
anethole	0.04	5.9
vodka 40%	4.3	7.6
tripouro 40% without anise	800	2.0
tsipouro 40% without anise	58	3.0
tsipouro 40% without anise	100	4.5
tsipouro 41% without anise	33	3.0
tsipouro 42% with anise	70	4.5
tsipouro house	516	2.0
raki 40%	163	6.0
tsikoudia 40%	126	2.5
zivania from Cyprus	130	6.5
sambuca from Italy 38%	30	7.5
sambuca from Italy 40%	24	5.0
sambuca from Italy 42%	14	8.0
grappa from Italy 40%	23	4.5

[a]pH value is not corrected; pH value in parentheses is measured with pH indicator strips.

oil), because they are organic substances, were not expected to contribute to the conductivity of ouzo, and this was evident by the measurement of the pure substances. Even the commercial alcohol sold for the preparation of homemade drinks, which is not highly purified, demonstrates a low conductivity. On the basis of literature data, the addition of alcohol in water causes the electrode to measure the pH higher than the theoretical pH value for the buffer solutions prepared.[19] However, as presented in Table 2, pure alcohol and anethole pH measurements, given by the electrode and verified by pH indicator strips, are mildly acidic. Vodka 40% is one of the vodka samples measured by Lachenmeier et al.,[9] and its conductivity was reported as 3.1 ± 0.4 μS/cm. The value measured in the present study (4.3 μS/cm) is within the 99.7% confidence interval of the values reported (1.9−4.3 μS/cm). On the basis of these findings the use of this conductivity meter was found appropriate for measuring the actual samples.

Conductivity and pH Measurements. As demonstrated in Table 2, conductivity in ouzo samples would be due to water because ethanol, which is the main constituent of ouzo, does not contribute to conductivity measurements. Conductivity values for all 42 samples ranged between 5.5 and 250 μS/cm, with an average value of 89 ± 70 μS/cm. Council Directive 98/83/EC[6] set a limit for water intended for human consumption of 2500 μS/cm. This value was too high for drinking water. Although all samples demonstrated low conductivity values, only 9 of 42 samples demonstrated conductivity values of <20 μS/cm. This value is indicated as a desirable value for dilution water conductivity in a study implementing hazard analysis and critical control points (HACCP) to a large-scale production line of Greek ouzo.[1] If the dilution of water with alcohol is considered (~60%), the conductivity value of the dilution water could be even higher than the conductivity value measured in the ouzo end-product.

It was attempted to find a trend for conductivity values. Two factors were examined: (a) alcohol degree and (b) geology of the production area (Figure 1). No trend is observed for

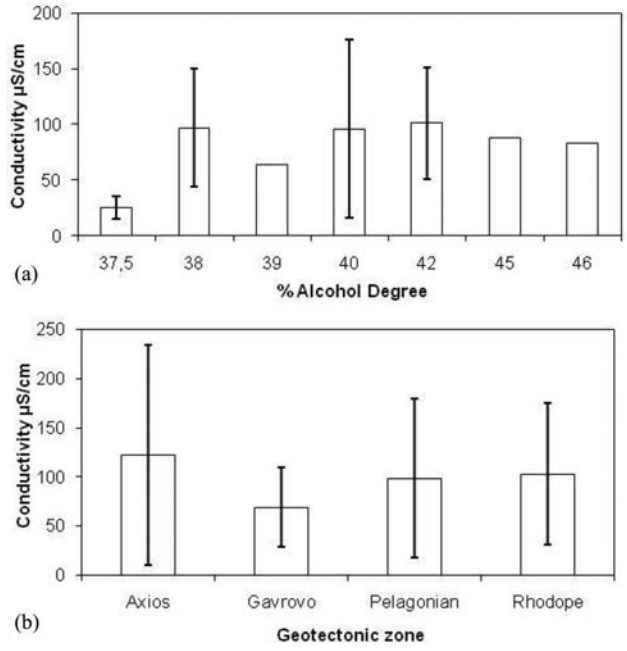

Figure 1. Conductivity measurements for all ouzo samples according to (a) alcohol degree and (b) the geology of the production area.

conductivity and alcohol degree of ouzo. For 37.5%, four samples were obtained from the same ouzo and, thus, the variability is due to differences during production. For 39, 45, and 46%, only one sample was tested. It seems that the conductivity ranges for all alcohol degrees are similar (Figure 1a), so the production of a stronger, or a lighter, ouzo does not prompt the producer to treat the dilution water before it is mixed with alcohol.

The geology of the production area was tested because it can affect the conductivity of the dilution water.[23] One would expect that in areas with hard water, producers would tend to treat the water before it is used in dilution. The geotectonic zone map of Greece presented in Demetriades[23] was used to identify the corresponding zones of each producer. Each zone corresponds to different lithology and, thus, different minerals diluted in water. The samples were grouped together on the basis of the geotectonic zones, and the average and standard deviation for the conductivity of each zone were calculated. As can be seen in Figure 1b, no trend can be identified between water treatment and water initial conductivity due to natural minerals. It seems that the quality of water that is selected (treated or not treated) is related to the producer quality goal for the final product as in other drinks such as beer and whiskey during previous years[7,8] and not to production problems as in vodka.[9] Additionally, water that does not include any harmful substances and, thus, not needing special treatment, is still abundant in most areas in Greece.[23]

Corrected pH values for all 42 samples range from 5.3 to 9.2, with a median value of 8. Most of these values are within the drinking water range from 6.5 to 9.5 (98/83/EC). The samples with low pH (~6) are the ones with low conductivity (<10 μS/cm). This suggests that deionization decreases dilution water pH. In addition, ethanol and anethole pH values are also <7

dx.doi.org/10.1021/jf501118e | J. Agric. Food Chem. 2014, 62, 4932−4937

Table 3. Conductivity and pH Measurements for Selected Ouzo Samples

sample	% alcohol	production scale[a]	conductivity (μS/cm)	pH[b]	special comments
1	40	large	169	6.5 (7)	high consumption (one of the five most consumed)
2	40	large	5.5	6.9 (6)	high consumption (one of the five most consumed)
3	40	large	162	8.3 (8)	private label
4	40	small	60	7.2 (7)	filtering after production
5	40	small	106	9.2 (9)	water softening
6	40	small	203	7.6 (7)	sold by volume double-distilled alcohol

[a]Large means it is one of the 15 most profitable Greek companies producing potable alcohol and spirits. [b]pH value is corrected; pH value in parentheses is measured with pH indicator strips.

Table 4. Dilution Water Characteristics for Selected Ouzo Samples

sample	NO_3^- (mg/L)	NO_2^- (mg/L)	PO_4^{-3} (mg/L)	NH_4^+ (mg/L)	total Fe (mg/L)	carbonate hardness (mg/L $CaCO_3$)
1	10	<0.02	1.2	<0.05	<0.05	54
2	10	<0.02	0.5	<0.05	0.05	0
3	10	<0.02	2.0	<0.05	<0.05	180
4	5	<0.02	0.5	<0.05	<0.05	71
5	3	0.05	1.2	<0.05	<0.05	270
6	10	<0.02	1.2	<0.05	<0.05	200
tap water[a]	5−10 (5.3)	<0.02 (0.006)	0.2 (N/A)[b]	0.1 (0.08)	<0.05 (10 μg/L)	230 (210)
98/83/EC[6]	<50	<0.5	(N/A)	<0.5	<0.2	(N/A)

[a]Values in parentheses from ref 24. [b]N/A, not available.

Table 5. Alcohol Characteristics for Selected Ouzo Samples

sample	ethanol (% v/v)	methanol (g/hL pa[a])	acetaldehyde (g/hL pa)	propanol-1 (g/hL pa)	isobutyl alcohol (g/hL pa)	amyl alcohols (g/hL pa)
1	41.2 ± 1.8	115 ± 23	21.4 ± 3.8	7.60 ± 0.95	8.00 ± 1.1	36.8 ± 10
2	38.4 ± 1.4	72 ± 13	27.8 ± 5.0	0.00 ± 0.00	0.25 ± 0.01	0.00 ± 0.00
3	39.5 ± 1.9	76 ± 14	46.8 ± 8.2	6.63 ± 0.33	5.33 ± 0.23	9.07 ± 9.70
4	38.9 ± 5.5	126 ± 23	29.8 ± 5.3	3.53 ± 0.18	3.35 ± 0.15	0.00 ± 0.00
5	40.0 ± 2.2	72 ± 15	29.5 ± 5.3	0.85 ± 0.04	0.00 ± 0.00	0.00 ± 0.00
6	38.4 ± 1.4	122 ± 22	30.8 ± 5.5	0.95 ± 0.04	1.09 ± 0.05	0.00 ± 0.00

[a]g/hL pa, grams per hectoliter of pure alcohol.

(Table 2) and, thus, their mixing with low-pH dilution water results in an end-product that is slightly acidic. The drinks with high pH values are from companies utilizing high-conductivity raw water, and they use softening or desalination, resulting into end-products that have both high conductivities (~100 μS/cm) and high pH values (~9). In all cases, final product pH is regulated by the addition of water.

Similar drinks from Greece, Cyprus, and Italy were tested in the same manner. As can be seen in Table 2, no trends can be observed for the conductivity values for the Greek drinks. Drinks from Italy demonstrate consistently low conductivity values, suggesting consistent water treatment for dilution water. The pH in most cases is acidic.

Qualitative Description of Selected Examples. To further explore the characteristics of the dilution water and the alcohol used, six samples were selected and their summary characteristics are presented in Table 3. Two samples from large-scale production lines having high and low conductivity values were selected. They both belong to the five ouzo brands most consumed. One company treats its water (sample 2) and the other one does not (sample 1). Another sample (sample 3) that comes from a large-scale production line but is a private-label product is made with untreated water. Two samples from two small companies from the same area are used. They both treat their water with different methods. One of these water treatment methods is successful (sample 4), whereas the other one is not successful, leading to high conductivity values and unusually high pH (sample 5). Another sample (sample 6) is from a small-scale production line that, although famous for using double-distilled alcohol, does not treat the dilution water.

Dilution Water Characteristics. A quick screening test was used to get further information on the dilution water characteristics. Again, the method was validated against local tap water, and the results for all characteristics are comparable to the values in the reports published by the local water supplier for the same sampling area[24] as seen in Table 4.

For all samples, the results suggest that good-quality dilution water has been used. Sample 2 is the one that seems to be treated through deionization. Sample 1, although having high conductivity, does not show as high hardness, suggesting that the presence of salt such as NaCl is possible. Sample 5 shows the lowest quality (high hardness and nitrites), suggesting that softening is not performed in an appropriate way.

Alcohol Characteristics. To test the hypothesis that a drink that was made with high-conductivity water may contain low-quality alcohol, the alcohol characteristics for the selected ouzo samples are presented in Table 5. It is obvious that ethanol percentage is as expected in accordance with the label. Methanol is a bit higher in samples 1, 4, and 6 compared to samples 2, 3, and 5. Several years ago, methanol concentration in ouzo samples was measured equal to 143 ± 20 mg/L, lower than the values measured in the present study.[25] However, even

dx.doi.org/10.1021/jf501118e | J. Agric. Food Chem. 2014, 62, 4932−4937

in the present study methanol concentration is lower than in other distilled drinks such as tsipouro or cognac[25] and the recommended values for similar type drinks.[12] In the current regulation, there are only specifications for methanol content in ethanol distillates that are only 20% v/v of the final product and, thus, the results are not directly comparable with the regulation limits.[4]

There are more than 20 volatile constituents identified in ouzo samples.[26] These constituents originate from the addition of flavorings. In the present study volatile compounds that are related to the quality of alcohol used are tested. For example, acetaldehyde is a direct alcoholic fermentation byproduct that increases with aging[11] and influences the aroma and quality of the drinks.[14] Acetaldehyde is found in comparable concentrations in all samples and is lower than the recommended values for similar types of drinks.[12] Propanol-1 is a bacterial spoilage index, and isobutyl alcohol is attributed to aging.[11] In all samples, propanol-1 concentration and isobutyl alcohol concentration are at similar levels. They are both higher in samples 1, 3, and 4 compared to samples 2, 5, and 6. Amyl alcohols contribute negatively to the aroma of the distillate.[11] Amyl alcohols are only found in samples 1 and 3, with the concentration in sample 1 higher than that in sample 3. Generally, all volatile constituents are present in concentrations lower than or within the range observed for all distilled alcoholic beverages, which is 50−2000 mg/L.[27]

On the basis of these observations, high consumption companies include the highest (sample 2) and lowest alcohol quality drinks (samples 1 and 3) among these six samples. The sample with the highest alcohol quality also demonstrates the lowest conductivity (sample 2). Small-scale companies demonstrate all ranges of conductivities, even though they use high-quality alcohol. One can suggest that a low conductivity value can be found in samples from large-scale companies and can be related to high-quality alcohol but not vice versa.

Ouzo is produced by many producers at different scales and with different philosophies. In all cases, water and alcohol qualities are high. There is definitely a trend that big-scale companies use deionized water and, thus, the alcohol quality is guaranteed. However, not all large-scale companies use deionized water. Water treatment and characteristics are not predictable and are subjective based on the goals of the producer. Ouzo production is not as massive as the production of other drinks such as vodka and can be considered highly local and diverse.

AUTHOR INFORMATION

Corresponding Author

*(H.K.K.) Phone: +30 2610 996728. E-mail: karapanagioti@upatras.gr.

Notes

The authors declare no competing financial interest.

ACKNOWLEDGMENTS

We thank I. D. Manariotis, J. Vakros, A. A. Koutinas, and A. Lycourghiotis, from the University of Patras, for helpful discussions and the companies Ioan. Pilavas, Tentoura Castro-G.P Hahalis Distillery, Babatzim Co. Winery and Distillery, Kosteas, Giannatsi, Ch. Pavlides Bros. S.A., Mavrakis, Tetteris Distillery, Karonis Distilleries, Kalogiannis-Koutsikos, Tsantali Vineyards-Wineries-Distilleries, and Rousali Bros S.A. Distillery for providing samples and information for this research.

REFERENCES

(1) Efstratiadis, M. M.; Arvanitoyannis, I. S. Implementation of HACCP to large scale line of Greek ouzo and brandy: a case study. *Food Control* **2000**, *11*, 19−30.

(2) Moutsatsou, A.; Chalarakis, E.; Zarangas, G. Influence of raw materials and distillation equipment on the heavy metal content of waste from an alcoholic anis-type beverage. *J. Hazard. Mater.* **2003**, *B96*, 53−64.

(3) Council Directive EC/110/2008 of 15 January (2008), a regulation on the definition, description, presentation, labeling, and the protection of geographical indications of spirit drinks and repealing Council Regulation (EEC) No. 1576/89.

(4) Council Regulation (EEC) No. 1576/89 of 29 May 1989 laying down general rules on the definition, description and presentation of spirit drinks.

(5) Council Directive 80/777/EEC of 15 July 1980 on the approximation of the laws of the Member States relating to the exploitation and marketing of natural mineral waters.

(6) Council Directive 98/83/EC of 3 November 1998 on the quality of water intended for human consumption.

(7) Cribb, S. J. Geology of beer. In *Encyclopedia of Geology*; Selley, R. C., Cocks, L. R. M., Plimer, I. R., Eds.; Elsevier Academic Press: Amsterdam, The Netherlands, 2005; pp 78−81.

(8) Cribb, S. J. Geology of whisky. In *Encyclopedia of Geology*; Selley, R. C., Cocks, L. R. M., Plimer, I. R., Eds.; Elsevier Academic Press: Amsterdam, The Netherlands, 2005; pp 82−85.

(9) Lachenmeier, D. W.; Schmidt, B.; Bretschneider, T. Rapid and mobile brand authentication of vodka using conductivity measurement. *Microchim. Acta* **2008**, *160*, 283−289.

(10) Platikanou, S.; Garcia, V.; Fonseca, I.; Rullán, E.; Devesa, R.; Tauler, R. Influence of minerals on the taste of bottled and tap water: a chemometric approach. *Water Res.* **2013**, *47*, 693−704.

(11) Apostolopoulou, A. A.; Flouros, A. I.; Demertzis, P. G.; Akrida-Demertzi, K. Differences in concentration of principal volatile constituents in traditional Greek distillates. *Food Control* **2005**, *16*, 157−164.

(12) Geroyiannaki, M.; Komaitis, M. E.; Stavrakas, D. E.; Polysiou, M.; Athanasopoulos, P. E.; Spanos, M. Evaluation of acetaldehyde and methanol in Greek traditional alcoholic beverages from varietal fermented grape pomaces (*Vitis vinifera* L.). *Food Control* **2007**, *18*, 988−995.

(13) Sádecká, J.; Tóthová, J.; Májek, P. Classification of brandies and wine distillates using front face fluorescence spectroscopy. *Food Chem.* **2009**, *117*, 491−498.

(14) López-Vázquez, C.; Orriols, I.; Perelló, M.-C.; de Revel, G. Determination of aldehydes as pentafluorobenzyl derivatives in grape pomace distillates by HS-SPME-GC/MS. *Food Chem.* **2012**, *130*, 1127−1133.

(15) Fotakis, C.; Christodouleas, D.; Kokkotou, K.; Zervou, M.; Zoumpoulakis, P.; Moulos, P.; Liouni, M.; Calokerinos, A. NMR metabolite profiling of Greek grape marc spirits. *Food Chem.* **2013**, *138*, 1837−1846.

(16) Lachenmeier, D. W.; Attig, R.; Frank, W.; Athanasakis, C. The use of ion chromatography to detect adulteration of vodka and rum. *Eur. Food Res. Technol.* **2003**, *218*, 105−110.

(17) Arbuzov, V. N.; Savchuk, S. A. Identification of vodkas by ion chromatography and gas chromatography. *J. Anal. Chem.* **2002**, *57*, 428−433 (translated from *Zh. Anal. Khim.* **2002**, *57*, 515−521.

(18) Lachenmeier, D. W.; Rehm, J. Is there a relationship between alcohol quality and health? *Alcohol Alcoholism* **2013**, *48*, 127−129.

(19) Mussini, T.; Covington, A. K.; Longhi, P.; Rondinini, S. Criteria for standardization of pH measurements in organic solvents and water + organic solvent mixtures of moderate to high permittivities. *Pure Appl. Chem.* **1985**, *57*, 865−876.

(20) Bekatorou, A.; Sarellas, A.; Ternan, N. G.; Mallouchos, A.; Komaitis, M.; Koutinas, A. A.; Kanellaki, M. Low-temperature brewing

using yeast immobilized on dried figs. *J. Agric. Food Chem.* **2002**, *50*, 7249−7257.
(21) Tsakiris, A.; Sipsas, V.; Bekatorou, A.; Mallouchos, A.; Koutinas, A. Red wine making by immobilized cells and influence on volatile composition. *J. Agric. Food Chem.* **2004**, *52*, 1357−1363.
(22) MEWSP (Municipal Enterprise for Water and Sewage of Patras), http://www.deyap.gr/news/?page_id=123 (in Greek; accessed 3/12/2013).
(23) Demetriades, A. General ground water geochemistry of Hellas using bottled water samples. *J. Geochem. Exploration* **2010**, *107*, 283−298.
(24) MEWSP (Municipal Enterprise for Water and Sewage of Patras), http://www.deyap.gr/news/?page_id=491 (in Greek; accessed 3/12/2013).
(25) Kana, K.; Kanellaki, M.; Papadimitriou, A.; Koutinas, A. A. Causes of and methods to reduce methanol content of Tsicoudia, Tsipouro and Ouzo. *Int. J. Food Sci. Technol.* **1991**, *26*, 241−247.
(26) Kontominas, M. G. Volatile constituents of Greek ouzo. *J. Agric. Food Chem.* **1986**, *34*, 847−849.
(27) Anli, R. T.; Bayram, M. Traditional aniseed-flavored spirit drinks. *Food Rev. Int.* **2010**, *26*, 246−269.

Table 1. Diversity in Ripening Time, Fruit Weight and Shape, and Ease of Peelability and Segmentation among Mandarin Varieties and Subgroups

variety	harvest date	time from blooming (weeks)	weight (g)	shape (hight/diameter)	peelability[a] (1−5)	segmentation[a] (1−5)
Common mandarin (*C. reticulata* Blanco)						
Rishon	23.10.12	29	138.1 ± 4.8	0.85 ± 0.02	3	3
Admoni	24.10.12	29	122.4 ± 2.9	0.83 ± 0.01	3	3
Michal	13.11.12	32	70.8 ± 1.3	0.84 ± 0.01	3	4
Tami	13.11.12	32	83.5 ± 2.2	0.85 ± 0.01	3	3
Fallglo	14.11.12	32	148.9 ± 3.4	0.76 ± 0.01	3	3
Hinanit	02.12.12	35	76.2 ± 1.8	0.81 ± 0.01	1	3
Lee	02.12.12	35	112.3 ± 1.9	0.84 ± 0.01	2	2
Fairchild	09.12.12	36	82.3 ± 2.2	0.85 ± 0.01	1	2
Idit	11.12.12	36	125.0 ± 3.3	0.68 ± 0.01	3	4
Merav	17.12.12	37	153.5 ± 4.3	0.77 ± 0.01	3	3
Vered	18.12.12	37	165.3 ± 6.1	0.71 ± 0.02	2	3
Dancy	27.12.12	38	98.8 ± 3.2	0.70 ± 0.01	4	4
Nova	27.12.12	38	123.6 ± 3.5	0.84 ± 0.01	2	2
Ponkan	27.12.12	38	114.0 ± 2.4	0.72 ± 0.01	5	5
Yifat	13.01.13	41	155.9 ± 2.3	0.75 ± 0.01	3	3
Nectar	13.01.13	41	99.3 ± 4.1	0.70 ± 0.01	3	4
Cami	13.01.13	41	121.9 ± 3.6	0.87 ± 0.01	3	2
Wilking	13.01.13	41	118.4 ± 3.3	0.73 ± 0.01	4	4
Ora	16.01.13	41	153.0 ± 3.7	0.74 ± 0.01	4	4
Winola	16.01.13	41	219.5 ± 5.5	0.70 ± 0.02	4	3
Yafit	16.01.13	41	127.9 ± 2.7	0.86 ± 0.01	3	3
Afourer	24.01.13	42	97.8 ± 3.5	0.70 ± 0.01	4	4
Orit	03.02.13	44	146.1 ± 3.5	0.75 ± 0.01	3	3
Odem	03.02.13	44	113.5 ± 3.6	0.76 ± 0.01	3	3
Nurit	04.02.13	44	185.1 ± 3.2	0.69 ± 0.01	1	3
Sigal	11.02.13	45	93.4 ± 1.9	0.66 ± 0.01	5	4
Fortune	19.02.13	46	150.8 ± 3.9	0.81 ± 0.02	3	3
Shani	19.02.13	46	117.9 ± 3.3	0.83 ± 0.01	3	3
Novel	04.03.13	48	167.5 ± 3.6	0.81 ± 0.01	3	3
Hadas	17.03.13	50	132.8 ± 4.9	0.78 ± 0.02	3	3
Clementine (*C. clementina* Hort. ex. Tan.)						
GPP	23.10.12	29	84.1 ± 1.9	0.79 ± 0.03	3	3
Nour	09.12.12	36	57.8 ± 1.5	0.87 ± 0.01	3	4
Tangor (*C. reticulata* × *C. sinensis*)						
Niva	26.11.12	34	109.9 ± 2.7	0.85 ± 0.01	1	2
Tacle	01.01.13	39	137.4 ± 7.1	0.76 ± 0.02	2	2
Temple	01.01.13	39	117.6 ± 2.9	0.80 ± 0.01	2	1
Kiyomi	04.02.13	44	187.2 ± 5.6	0.86 ± 0.01	3	1
Murcott	11.02.13	45	127.6 ± 3.2	0.75 ± 0.01	3	3
Tangelo (*C. reticulata* × *C. paradisi*)						
Orlando	27.12.12	38	155.3 ± 2.5	0.84 ± 0.01	1	2
Minneola	01.01.13	39	167.7 ± 6.9	0.89 ± 0.02	3	3
Satsuma (*C. unshiu* Marcovitch)						
Okitsu	16.10.12	28	134.6 ± 4.1	0.78 ± 0.01	5	5
Owari	23.10.12	29	95.1 ± 2.4	0.79 ± 0.01	5	5
Nucellar	31.10.12	30	93.4 ± 2.8	0.76 ± 0.01	5	5
Imamura	26.12.12	38	96.9 ± 3.1	0.71 ± 0.01	5	5
Mediterrenean (*C. deliciosa* Tenore)						
Avana	01.01.13	39	81.0 ± 3.5	0.69 ± 0.01	5	4
Tardivo	24.01.13	42	64.9 ± 3.0	0.78 ± 0.01	3	3
King (*C. nobilis* Loureiro)						
King	27.02.13	47	120.7 ± 3.7	0.80 ± 0.01	4	3

[a]Data are means of three evaluators' scores: 1 = very difficult, 5 = very easy.

Blanco), two clementines (*C. clementina* Hort. ex. Tan), five tangors (*C. reticulata* × *C. sinensis*), two tangelos (*C. reticulata* × *C. paradisi*), four satsumas (*C. unshiu* Marcovitch), two Mediterranean mandarins (*C. deliciosa* Tenore), and a King mandarin (*C. nobilis* Loureiro) (Table 1). Mandarin varieties not belonging purely to any specific subgroup, such as hybrids between different mandarin subgroups, were classified as common mandarins.

Fruit Weight, Shape, and Peel Thickness. Fruit weight was measured with a semianalytical scale (Citizen, Mumbai, India), and fruit height and diameter were measured with millimetric calipers.

dx.doi.org/10.1021/jf5002414 | J. Agric. Food Chem. 2014, 62, 4938−4946

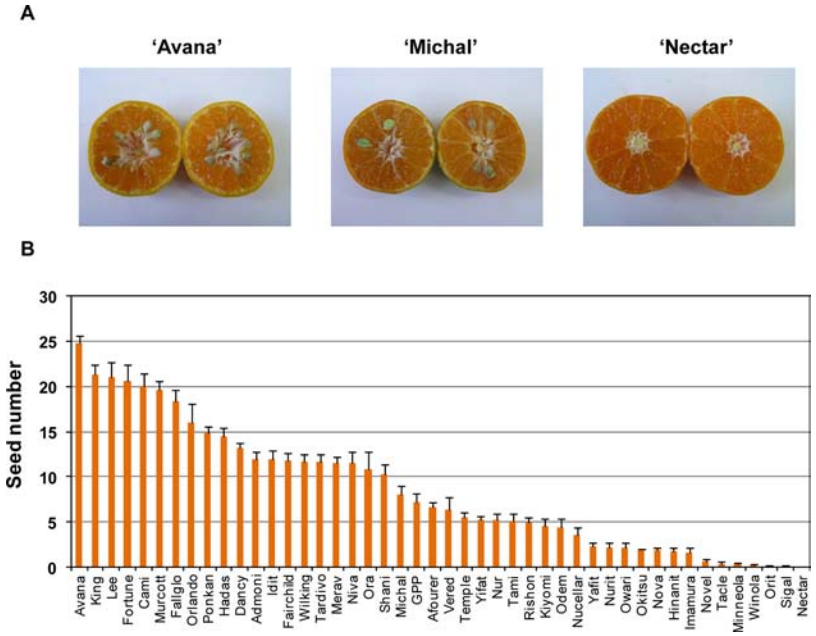

Figure 1. Diversity among mandarin varieties and subgroups in fruit seed number. (A) Photographs of 'Havana', 'Michal', and 'Nectar' mandarins containing high and moderate numbers and zero seeds, respectively. (B) Seed numbers of various mandarin varieties. Data are means ± SE of 10 fruit.

Thicknesses of the albedo (the inner white part of the peel), flavedo (the outer colored part of the peel), and the total peel were measured with a Leica MZ FLIII stereomicroscope (Leitz, Wetzlar, Germany) with the NIS-Elements Imaging software. All data are means ± SE of 10 fruit.

Seed Number and Peelability. The number of seeds per fruit was evaluated after cutting the fruit in half and extracting the juice with a hand extractor. Ease of peelability and segmentation were evaluated subjectively on a scale of 1 (very difficult) to 5 (very easy) by three laboratory personnel. The presented data are means ± SE of 10 fruit.

Color Measurement. Peel color was measured with a CR-310 Chroma Meter (Minolta, Tokyo, Japan), and the results are expressed as hue angle ($H°$), in which 0° represents red color, 45° orange, 90° yellow, and 120° green. Data are means ± SE of 10 fruit.

TSS, Acidity, and Vitamin C. Total soluble solids (TSS) content in the juice was determined with a PAL-1 digital refractometer (Atago, Tokyo, Japan), and acidity percentages were measured by titration to pH 8.3 against 0.1 M NaOH, with a CH-9101 automatic titrator (Metrohm, Herisau, Switzerland). Each measurement included four replications, each of juice collected from three different fruit (total of 12 fruit per measurement).

Vitamin C (ascorbic acid) content in the juice was determined by titration against 2,6-dichlorophenolindophenol, as described previously.[17] Ascorbic acid levels were determined by comparing the titration volumes of mandarin juices with those of 0.1% ascorbic acid (Sigma-Aldrich, St. Louis, MO, USA), and results are expressed as milligrams of ascorbic acid per 100 mL of juice. Each measurement included four replications, each of juice collected from three different fruit (total of 12 fruit per measurement).

Total Phenols and Flavonoids. Extraction of phenols and flavonoids was performed by stirring 1 mL of juice samples with 9 mL of 80% methanol for 30 min at room temperature, followed by centrifugation at 10000*g* for 10 min. Total phenolics were determined by the Folin−Ciocalteu method.[18] Briefly, the reaction mixtures included 0.2 mL of juice methanol extracts, 0.2 mL of Folin−Ciocalteu reagent, and 7 mL of 7% Na_2CO_3. The reaction mixtures were incubated for 90 min at room temperature, and the absorbance at 750 nm was measured by comparison with a prepared blank by means of a spectrophotometer. Total phenolic contents were expressed as gallic acid equivalents.

Total flavonoids were determined as described by Shin et al.[19] Briefly, the reaction mixtures included 1.0 mL of juice methanol extracts, 0.3 mL of 5% $NaNO_2$, and 0.3 mL of $AlCl_3$. The reaction mixtures were incubated for 10 min at room temperature, after which 2 mL of 1 N NaOH was added to stop the reaction, and the total volume was adjusted to 10 mL by adding double-distilled water. Flavonoid contents were measured by comparing the absorbance at 510 nm against that of a prepared blank, and the results were expressed as catechin equivalents. Total phenol and flavonoid contents are presented as means ± SE of four replications, each of juice collected from three different fruit (total of 12 fruit per measurement).

Total Carotenoid Content. Total carotenoids were extracted according to Lee and Castle.[20] In general, 1 mL of juice was homogenized with 2 mL of hexane/acetone/ethanol extraction solution (2:1:1 by volume) for 30 s and centrifuged for 5 min at 6500 rpm at 5 °C. Afterward, 100 mL of the colored top layer was diluted with 900 mL of hexane, and absorbance was measured at 450 nm with a spectrophotometer. Total carotenoid levels were calculated according to an equation provided by Schiedt and Liaaen-Jensen,[21] with a β-carotene extinction coefficient of $E^{1\%} = 2400$. Total carotenoid contents are presented as means ± SE of three replications, each of juice collected from three different fruit (total of 9 fruit per measurement).

Antioxidant Activity. Total antioxidant activity was determined by using the ABTS*$^+$ radical cation assay.[22] The reaction mixture included 1 mL of 75 μM $K_2O_8S_2$ and 150 μM 2,2′-azinobis(3-ethylbenzothiazoline-6-sulfonic acid) (ABTS*$^+$) dissolved in acetate buffer, pH = 4.3, and 10 μL of juice samples. The reaction mixtures were incubated for 15 min at room temperature. Afterward, total antioxidant activities of juice samples were compared with a 1 mM Trolox solution by determining the degree of disappearance of the blue color by comparing the absorbance at 734 nm against that of a prepared blank. Trolox equivalent (TE) was calculated according to the following formula:

$$\text{TE value (mM)} = (\text{Abs sample} - \text{Abs blank}) / (\text{Abs standard} - \text{Abs blank})$$

The results were expressed as Trolox equivalent antioxidant capacity (TEAC), calculated as

$$\text{TEAC (}\mu\text{M TE/g)} = (\text{TE} \times V)/(1000 \times M)$$

where V = sample volume and M = sample weight.

Antioxidant activity levels are presented as means ± SE of four replications, each of juice collected from three different fruit (total of 12 fruit per measurement).

Sensory Evaluations. Fruit sensory quality was tested on the day of harvest. The fruit were peeled and segments were separated, cut

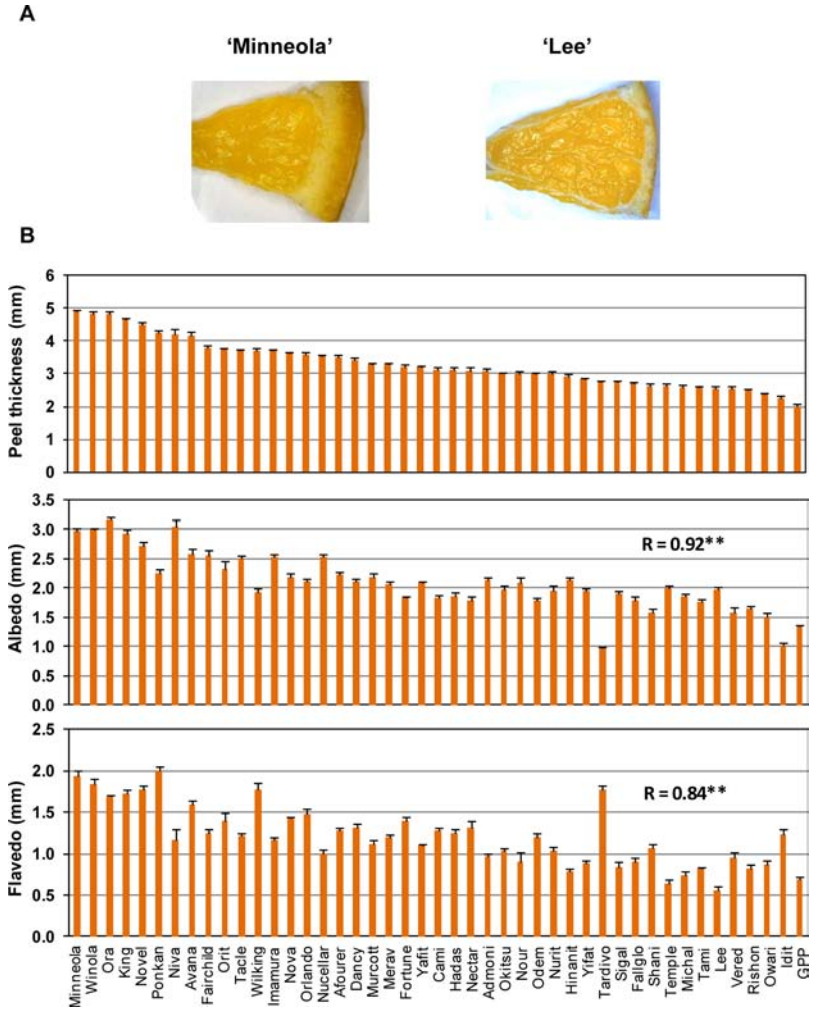

Figure 2. Diversity among mandarin varieties and subgroups in peel thickness. (A) Photographs of 'Minneola' and 'Lee' mandarins exhibiting thick and thin peel, respectively. (B) Total peel, albedo, and flavedo thicknesses of various mandarin varieties. Data are means ± SE of 10 fruit. Pearson correlation values were calculated and matched against total peel thickness; double asterisks (**) indicate significance at $P \leq 0.01$.

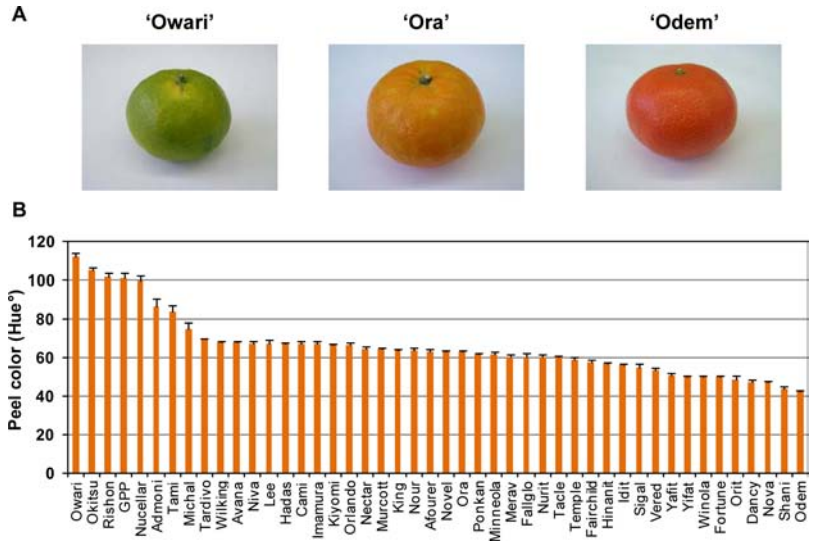

Figure 3. Diversity among mandarin varieties and subgroups in fruit color. (A) Photographs of 'Owari', 'Ora', and 'Odem' mandarins exhibiting green, orange, and reddish color, respectively. (B) Peel color of various mandarin varieties. Data are means ± SE of 10 fruit.

into halves, and placed into covered glass cups. Each sample comprised a mixture of cut segments prepared from five different fruit. Fruit taste was evaluated by a trained panel consisting of 10 members, five males and five females, aged 25 to 62, who routinely perform taste tests of

dx.doi.org/10.1021/jf5002414 | J. Agric. Food Chem. 2014, 62, 4938−4946

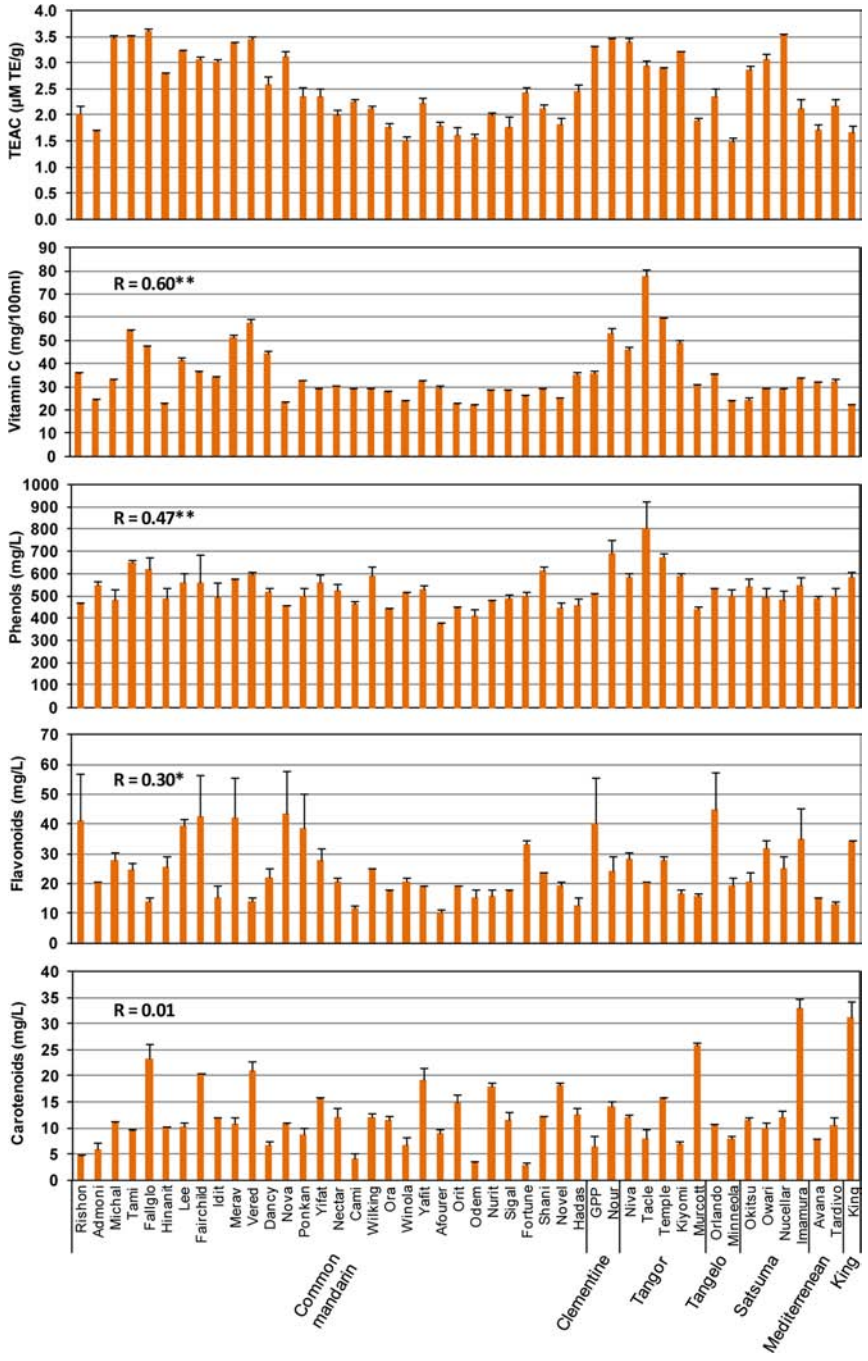

Figure 4. Diversity among mandarin varieties and subgroups in antioxidative activity and total vitamin C, phenols, flavonoids, and carotenoids levels. Data are means ± SE of four replications, each of juice from three different fruit. Pearson correlation values were calculated and matched against total antioxidant activity; single (*) and double (**) asterisks indicate significance at $P \leq 0.05$ and $P \leq 0.01$, respectively.

citrus fruit.[23,24] Each panelist assessed the taste attributes of the samples according to an unstructured 100 mm scale, on which the anchor points 'very weak' and 'very strong' for each attribute and/sensory data were recorded as distances (mm) from the origin. The samples were identified by means of randomly assigned three-digit codes. In addition, panelists were requested to rate overall fruit flavor preference on a scale of 1 to 9, where 1 = very bad and 9 = excellent.

Statistical Analysis. One-way analysis of variance (ANOVA) was applied with the Microsoft Office Excel program. Hierarchical clustering and heat-map analysis were performed with the Expander 4.1 software,[25] and Pearson correlations were calculated with the R software (http://www.r-project.org).

RESULTS

Diversity in Time of Ripening, Fruit Weight, Shape, and Peelability. We evaluated fruit-quality traits of 46 mandarin varieties within the Israeli *Citrus* breeding collection; they belonged to genetically differing natural subgroups, comprising 30 common mandarins (*C. reticulata* Blanco), two clementines (*C. clementina* Hort. ex. Tan), five tangors (*C. reticulata* × *C. sinensis*), two tangelos (*C. reticulata* × *C. paradisi*), four satsumas (*C. unshiu* Marcovitch), two Mediterranean mandarins (*C. deliciosa* Tenore), and one King mandarin (*C. nobilis* Loureiro) (Table 1). We observed great genetic variability in ripening time, which was spread over 6 months from October through March.

dx.doi.org/10.1021/jf5002414 | J. Agric. Food Chem. 2014, 62, 4938−4946

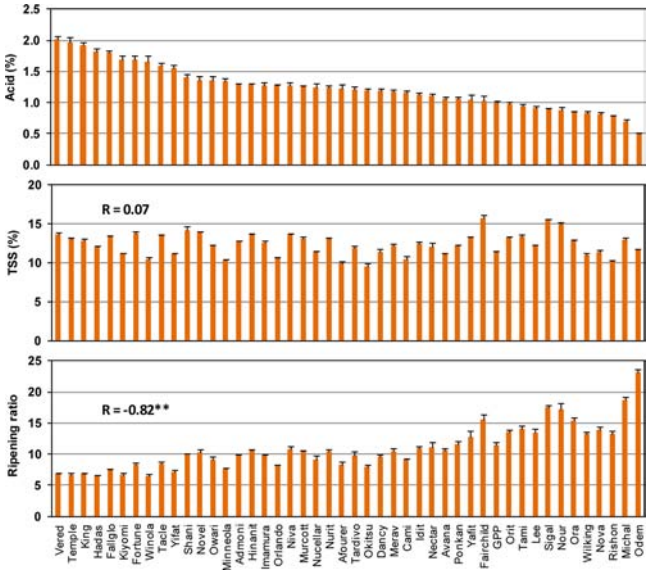

Figure 5. Diversity among mandarin varieties and subgroups in TSS and acidity contents and ripening ratios. Data are means ± SE of four replications, each of juice from three different fruit. Pearson correlation values were calculated and matched against acidity levels; double asterisks (**) indicate significance at $P \leq 0.01$.

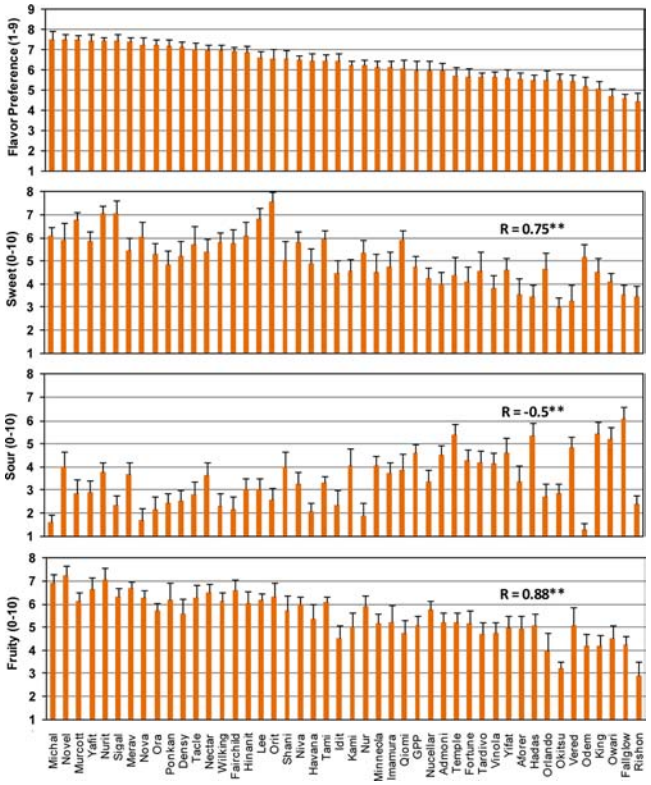

Figure 6. Diversity among mandarin varieties and subgroups in flavor preference and sensations of 'sweetness', 'sourness', and 'fruitiness'. Data are means ± SE of scores given by 10 trained testers. Pearson correlation values were calculated and matched against flavor preference scores; double asterisk (**) indicates significance at $P \leq 0.01$.

The earliest-ripening varieties, harvested in October, were the new Israeli breeding varieties 'Rishon' and 'Admoni', as well as the clementine 'GPP', and three satsumas, 'Okitsu', 'Owari', and 'Nucellar Satsuma' (Table 1). The latest-ripening varieties, harvested in March, were the common mandarins 'Novel' and 'Hadas' (Table 1).

There was also great genetic diversity in fruit weight: the variety with the largest fruit (219 g) was 'Winola', whereas the one with the smallest (58 g) was 'Nour' clementine (Table 1).

We further observed great variability in fruit shape, i.e., height/diameter ratio. Fruit of some varieties, including 'Minneola' tangelo, 'Kiyomi' tangor, 'Nour' clementine, and 'Cami' and 'Yafit' common mandarins, were nearly round, with height/diameter ratios above 0.85, whereas, in contrast, other varieties such as 'Sigal' were rather flat, with a height/diameter ratio of just 0.66 (Table 1).

Another important quality attribute of mandarins is ease of peelability and segment separation. We observed great variability in ease of peeling: some varieties, including all four satsumas, as well as 'Ponkan', 'Havana', and 'Sigal', were very easy to peel, whereas others, such as the 'Niva' tangor, 'Orlando' tangelo, and the common mandarins 'Fairchild', 'Hinanit', and 'Nurit', were very difficult to peel (Table 1). It was very easy to separate the segments of all four satsumas, as well as those of 'Ponkan', but very difficult to separate those of some others, especially the tangors 'Temple' and 'Kiyomi' (Table 1).

Diversity in Seed Number. The number of seeds per fruit is a very important quality trait, as consumers prefer seedless fruit, and we observed great variability in fruit seed number. Five varieties had an average of more than 20 seeds per fruit, with 'Avana' Mediterranean mandarin containing an average of 25 seeds per fruit (Figure 1). In contrast, seven mandarin varieties averaged ≤1 seed per fruit (Figure 1). Worth noticing is that the 'Nectar' common mandarin variety was obligatorily seedless, even under the unfavorable conditions of a mixed orchard with many pollinators (Figure 1).

Diversity in Peel Thickness. We observed substantial intervariety differences in peel thickness, which ranged from 2.0 to 5.9 mm (Figure 2). Furthermore, we observed significant correlations between overall peel thickness and thickness of the albedo ($R = 0.92$) and flavedo tissues ($R = 0.84$) (Figure 2). Most of the varieties that had a thick albedo also had a thick flavedo, and vice versa. However, some varieties differed in this respect. For example, the 'Tardivo' Mediterranean mandarin had a relatively thin albedo but a thick flavedo (Figure 2).

Diversity in Peel Color. The vast majority of mandarin varieties exhibited the typical mandarin orange color, with measurable hue angles between 50° and 70° (Figure 3). In contrast, the early ripening varieties, including 'Rishon' common mandarin, 'GPP' clementine, and three satsuma varieties, 'Okitsu', 'Owari', and 'Nucellar Satsuma', were harvested when their peel color was mostly green, with a persisting hue angle of ≥100° (Figure 3). Worth notice is that the 'Odem' and 'Shani' common mandarins had a unique deep reddish-orange color, with a hue angle of 40−45° (Figure 3).

Diversity in Fruit Nutritional Quality. The key nutritional components of citrus fruit that contribute to its overall antioxidative activity are vitamin C, phenols, flavonoids, and carotenoids. We observed significant variability among mandarin varieties and subgroups in their bioactive contents and total antioxidative activity. The total antioxidative activity ranged between 1.5 and 3.5 μM TE g^{-1} (Figure 4). Juice vitamin C levels were relatively high (i.e., between 45 and 60 mg per 100 mL) in most tangors as well as in a few common mandarin varieties, and the highest level (78 mg per 100 mL) was found in juice of 'Tacle' tangor (Figure 4). In contrast, juice from several common mandarin varieties, as well as 'Minneola' tangelo, 'Okitsu'

dx.doi.org/10.1021/jf5002414 | J. Agric. Food Chem. 2014, 62, 4938−4946

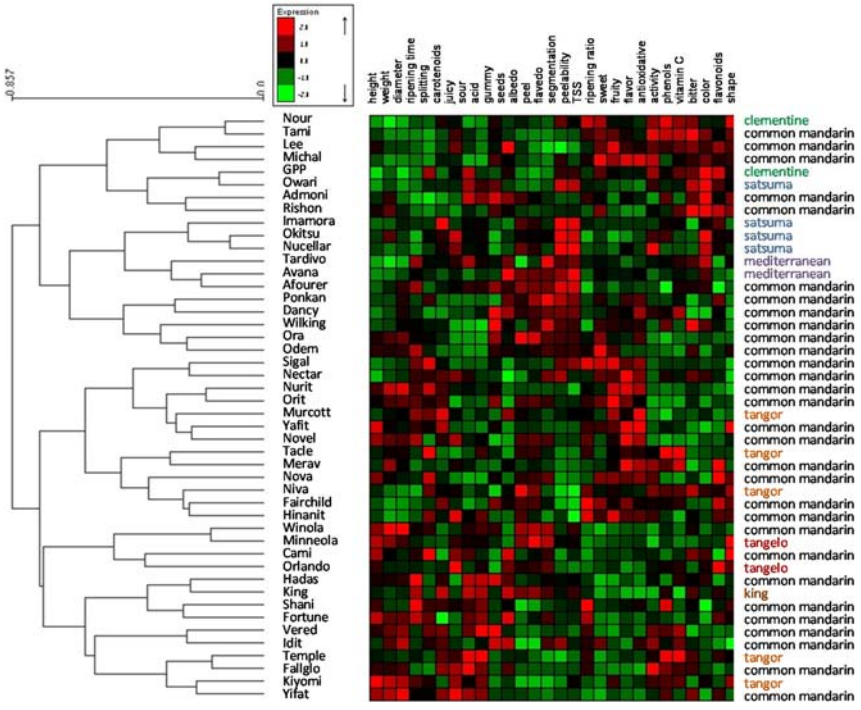

Figure 7. Hierarchical clustering of mandarin varieties and subgroups and heat-map analysis of fruit-quality traits. Red and green colors represents high and low levels, respectively. The units in the color scale are standard deviations. The various mandarin natural subgroups are listed in different colors at the right.

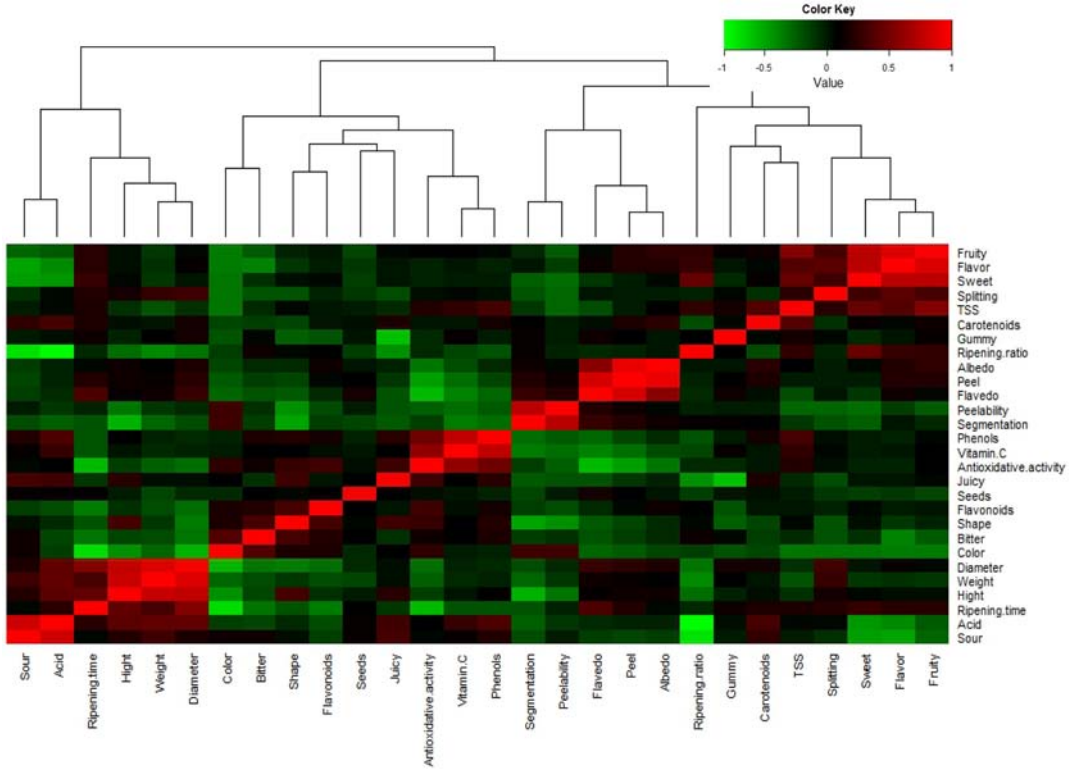

Figure 8. Hierarchical clustering and Pearson correlations among all fruit-quality traits. Red and green colors represent positive and negative correlations, respectively. Pearson correlations were calculated with the R software (http://www.r-project.org).

satsuma, and 'King' mandarin, contained relatively low vitamin C levels of 22−24 mg per 100 mL (Figure 4).

It was found that total phenol levels in mandarin juices ranged from just 375 mg L^{-1} in 'Afourer' common mandarin up to 804 mg L^{-1} in 'Tacle' tangor (Figure 4). Worth notice is that most tangors had relatively high phenol levels (Figure 4). We also observed wide variability among mandarin juices in their total flavonoid content, from just 10 mg L^{-1} in 'Afourer' common

dx.doi.org/10.1021/jf5002414 | J. Agric. Food Chem. 2014, 62, 4938−4946

mandarin up to 45 mg L^{-1} in 'Orlando' tangelo (Figure 4). However, we did not detect any clear differences among mandarin subgroups in their flavonoid contents.

We further observed wide genetic diversity among mandarin juices in their total carotenoid contents: the juices of some mandarin varieties, such as 'Fortune', were pale yellow in color and contained only 3 mg L^{-1}, whereas the juices of other varieties, such as 'King' mandarin and 'Imamura' satsuma, were dark orange in color and contained carotenoids at more than 30 mg L^{-1} (Figure 4).

Overall, we found R values of 0.60, 0.47, 0.30, and 0.01, respectively, for the correlations between total antioxidative activity of mandarin juices and vitamin C, phenol, flavonoid, and carotenoid levels. Thus, it seems that vitamin C provides the highest contribution to total antioxidant activity of mandarin fruit (Figure 4).

Diversity in Juice TSS, Acidity, and Flavor Perception. The taste of citrus fruit is principally governed by the levels of sugars and acids in the juice sacs, as well as the fruit ripening ratio. We observed remarkable differences among mandarins in their juice acidity levels, from as low as 0.5% in 'Odem' common mandarin to nearly 2.0% in 'Vered' common mandarin and 'Temple' tangor (Figure 5). The overall juice TSS levels ranged from as low as 9.6% in 'Okitsu' satsuma to 15.8% in 'Fairchild' common mandarin (Figure 5). These observed differences in juice TSS and acidity levels resulted in remarkable variability in fruit ripening ratios, from below 6.7 in the common mandarins 'Vered', 'Hadas', and 'Winola', the tangors 'Temple' and 'Kiyomi', and 'King' mandarins, up to 23 in 'Odem' common mandarin (Figure 5).

Overall, sensory analysis revealed wide genetic variability among mandarin flavor preferences, ranging from a relatively high score of 7.5 (on a 1−9 scale) for several common mandarin varieties such as 'Michal', down to scores below 5.0 for 'Owari' satsuma and 'Fallglo' and 'Rishon' common mandarins (Figure 6). In addition, descriptive sensory analysis tests conducted with the aid of a trained panel indicated differences among mandarins in their elicited sensations of 'sweetness', 'sourness', and 'fruitiness' (Figure 6). Furthermore, we observed significant positive correlations between flavor preference and perceptions of sweetness (R = 0.75) and fruitiness (R = 0.88) (Figure 6).

Hierarchical Clustering and Heat-Map Analysis. Hierarchical clustering of mandarin varieties and subgroups and heat-map analysis of fruit-quality traits demonstrated that the distinct mandarin varieties fell into two major subclusters: the first cluster included some common mandarins, satsumas, clementines, and Mediterranean mandarins; the second cluster included additional common mandarins, King mandarin, tangors, and tangelos (Figure 7). Furthermore, it can be seen that the different satsuma, clementine, Mediterranean mandarin, tangor, and tangelo varieties were clustered closely together, thus demonstrating the genetic diversity in fruit-quality traits among the various mandarin subgroups (Figure 7).

Hierarchical clustering and Pearson correlations among all of the 28 examined fruit-quality parameters demonstrated that the various quality attributes can be grouped into several subclusters (Figure 8). For example, it can be seen that peel traits, such as albedo, flavedo, and total peel thickness, were clustered together with ease of peelability and segment separation, which suggests that these traits are mutually related (Figure 8). Furthermore, many of the biochemical characteristics, including levels of vitamin C, phenols, and flavonoids, as well as total antioxidant activity, were also clustered together (Figure 8). Finally, it was found that flavor preference was clustered together with TSS levels and perceptions of 'sweetness' and 'fruitiness', whereas acidity and 'sourness' were clustered separately (Figure 8).

Table 2. Outlines of the Diversity Observed among Mandarin Varieties and Subgroups in Fruit-Quality Traits

	range of variability		
quality trait	lowest score	highest score	units
Physical Traits			
weight	57.8	219.5	g
height	39.2	68.3	mm
diameter	49.5	87.6	mm
shape	0.66	0.89	height/diameter ratio
peel color	42.4	112	$H°$
peel thickness	2.02	4.9	mm
albedo	0.98	3.15	mm
flavedo	0.56	2	mm
seed number	0	25	seeds/fruit
Physiological Traits			
ripening time	28	50	weeks after blooming
peelability	1	5	scale of 1−5
segmentation	1	5	scale of 1−5
splitting	0	3	scale of 0−3
Biochemical Composition			
antioxidative activity	1.5	3.6	μM TE g^{-1}
vitamin C	22.2	77.8	mg/100 mL
phenols	375	804	mg L^{-1}
flavonoids	10.4	44.9	mg L^{-1}
carotenoids	2.9	33.1	mg L^{-1}
Sensory Traits			
TSS	9.6	15.8	%
acid	0.5	2	%
ripening ratio	6.4	23.2	TSS/acid ratio
sweet	3	7.6	scale of 0−10
sour	1.3	6.1	scale of 0−10
bitter	0.1	1.7	scale of 0−10
gummy	0.9	4.1	scale of 0−10
juicy	4.9	7.9	scale of 0−10
fruity	2.9	7.2	scale of 0−10
flavor	4.4	7.5	scale of 1−9

DISCUSSION

A detailed phenotypic analysis study (phenomics) of fruit-quality traits is an obligatory requirement to enable designation of SNPs for marker-assisted breeding of new varieties with improved fruit-quality traits, as well as for selection of appropriate parents for future breeding programs.[12,13,26,27] In this respect, the present study provided the most comprehensive phenotypic analysis to date of fruit-quality traits among genetically distinct mandarin varieties and subgroups.

The data yielded by this study highlight the inclusive genetic diversity among mandarins, in their fruit-quality traits (Table 2). For example, ripening time can range from 28 to 50 weeks after blooming; fruit weight from 58 to 219 g; peel thickness from 2.0 to 4.9 mm; fruit shape from nearly round to flat; peelability from very easy to very difficult; and seed number from zero to 25 (Table 2). Regarding fruit nutritional attributes, we found that vitamin C levels ranged from 22 to 78 mg per 100 mL; phenols from 375 to 804 mg per 100 mL; flavonoids from 10 to 45 mg per 100 mL; and carotenoids from 3 to 33 mg per 100 mL (Table 2). Finally, TSS levels may range from 9.6% to 15.8%; acidity from

dx.doi.org/10.1021/jf5002414 | J. Agric. Food Chem. 2014, 62, 4938−4946

0.5% to 2.0%; and flavor preference from 4.4 through 7.5 on a 1−9 scale (Table 2).

These phenotypic analysis data are of great importance for citrus breeders worldwide, as they could assist in selection of appropriate varieties as putative parents in future breeding programs. For example, for breeding early-season varieties it would be preferable to choose 'Rishon', 'Admoni', or satsumas as putative parents, whereas for breeding late-season varieties it would be preferable to choose 'Hadas' (Table 1). In the case of breeding for high vitamin C content, it would be preferable to choose 'Tacle' tangor or other tangors as putative parents (Figure 4).

Regarding the genetic variability in fruit-quality traits among different natural mandarin subgroups, hierarchical clustering analysis revealed clear evolutionary differences among mandarins (Figure 7). For example, satsuma mandarins are early ripening, are very easy to peel, and contain few seeds, and their juice is deep orange in color and contains high carotenoid pigment contents (Table 1; Figures 1, 4). Clementines also ripen early and have relatively small fruit (Table 1). Tangors (orange × mandarin hybrids) are relatively difficult to peel, but have high vitamin C and phenol contents and high antioxidative activity levels (Table 1; Figure 4). Tangelos (grapefruit × mandarin hybrids) have a relatively thick peel (Figure 2), Mediterranean mandarins have many seeds (Figure 1), and King mandarin has many seeds and high carotenoid and acidity contents (Figures 1, 4, 5).

AUTHOR INFORMATION

Corresponding Author

*(R. Porat) Tel: 972-3-9683617. Fax: 972-3-9683622. E-mail: rporat@volcani.agri.gov.il.

Notes

This article is contribution no. 680/13 from the Agricultural Research Organization, Volcani Center, P.O. Box 6, Bet Dagan 50250, Israel.

The authors declare no competing financial interest.

REFERENCES

(1) United States Department of Agriculture. *Citrus: World Markets and Trade*; http://apps.fas.usda.gov/psdonline/circulars/citrus.pdf (accessed December 2013).

(2) Barkley, N. A.; Roose, M. L.; Krueger, R. R.; Federici, C. T. Assessing genetic diversity and population structure in a citrus germplasm collection utilizing simple sequence repeat markers (SSRs). *Theor. Appl. Genet.* **2006**, *112*, 1519−1531.

(3) Barret, H. C.; Rhodes, A. M. A numerical taxonomic study of affinity relationships in cultivated *Citrus* and its close relatives. *Syst. Bot.* **1976**, *1*, 105−136.

(4) Federici, C. T.; Fang, D. Q.; Scora, R. W.; Roose, M. L. Phylogenetic relationships within the genus *Citrus* (Rutaceae) and related genera as revealed by RFLP and RAPD analysis. *Theor. Appl. Genet.* **1998**, *96*, 812−822.

(5) Hodgson, R. W. Horticultural varieties of citrus. In *The Citrus Industry*, Vol. *1*; Reuther, W., Webber, H. J., Batchler, L. D., Eds.; University of California: Berkeley, CA, 1967; pp 431−588.

(6) Aleza, P.; Juarez, J.; Hernandez, M.; Pina, J. A.; Ollitrault, P.; Navarro, L. Recovery and characterization of a *Citrus clementina* Hort. ex Tan. 'Clemenules' haploid plant selected to establish the reference whole *Citrus* genome sequence. *BMC Plant Biol.* **2009**, *9*, 110.

(7) Tanaka, T. Fundamental discussion of citrus classification. *Stud. Citrolog.* **1977**, *14*, 1−6.

(8) Bermejo, A.; Cano, A. Analysis of nutritional constituents in twenty citrus cultivars from the Mediterranean area at different stages of ripening. *Food Nutr. Sci.* **2012**, *3*, 639−650.

(9) Cano, A.; Medina, A.; Bermejo, A. Bioactive compounds in different citrus varieties. Discrimination among cultivars. *J. Food Compos. Anal.* **2008**, *21*, 377−381.

(10) Gonzalez-Mas, M. C.; Rambla, J. L.; Alamar, M. C.; Gutierrez, A.; Granell, A. Comparative analysis of the volatile fraction of fruit juice from different citrus species. *PLoS One* **2011**, *6*.

(11) Goodner, K. L.; Rouseff, R. L.; Hofsommer, H. J. Orange, mandarin, and hybrid classification using multivariate statistics based on carotenoid profiles. *J. Agric. Food Chem.* **2001**, *49*, 1146−1150.

(12) Gmitter, F. G.; Chen, C.; Machado, M. A.; de Souza, A. A.; Ollitrault, P.; Froehlicher, Y.; Shimizu, T. Citrus genomics. *Tree Genet. Genome* **2012**, *8*, 611−626.

(13) Ollitrault, P.; Terol, J.; Garcia-Lor, A.; Berard, A.; Chauveau, A.; Froelicher, Y.; Belzile, C.; Morillon, R.; Navarro, L.; Brunel, D.; Talon, M. SNP mining in *C. clementina* BAC end sequences; transferability in the *Citrus* genus (Rutaceae), phylogenetic inferences and perspectives for genetic mapping. *BMC Genomics* **2012**, *13*.

(14) Schauer, N.; Semel, Y.; Roessner, U.; Gur, A.; Balbo, I.; Carrari, F.; Pleban, T.; Perez-Melis, A.; Bruedigam, C.; Kopka, J.; Willmitzer, L.; Zamir, D.; Fernie, A. R. Comprehensive metabolic profiling and phenotyping of interspecific introgression lines for tomato improvement. *Nat. Biotechnol.* **2006**, *24*, 447−454.

(15) White, J. W.; Andrade-Sanchez, P.; Gore, M. A.; Bronson, K. F.; Coffelt, T. A.; Conley, M. M.; Feldmann, K. A.; French, A. N.; Heun, J. T.; Hunsaker, D. J.; Jenks, M. A.; Kimball, B. A.; Roth, R. L.; Strand, R. J.; Thorp, K. R.; Wall, G. W.; Wang, G. Y. Field-based phenomics for plant genetics research. *Field Crop Res.* **2012**, *133*, 101−112.

(16) Furbank, R. T.; Tester, M. Phenomics−technologies to relieve the phenotyping bottleneck. *Trends Plant Sci.* **2011**, *16*, 635−644.

(17) Hiromi, K.; Kuwamoto, C.; Ohnishi, M. A rapid sensitive method for the determination of ascorbic acid in the excess of 2,6-dichlorophenolindophenol using a stopped-flow apparatus. *Anal. Biochem.* **1980**, *101*, 421−426.

(18) Singleton, V. L.; Orthofer, R.; Lamuela-Raventós, R. M. Analysis of total phenols and other oxidation substrates and antioxidants by means of Folin-Ciocalteu reagent. *Meth. Enzymol.* **1999**, *299*, 152−178.

(19) Shin, Y.; Liu, R. H.; Nock, J. F.; Holliday, D.; Watkins, C. B. Temperature and relative humidity effects on quality, total ascorbic acid, phenolics and flavonoid concentrations, and antioxidant activity of strawberry. *Postharv. Biol. Technol.* **2007**, *45*, 349−357.

(20) Lee, H. S.; Castle, W. S. Seasonal changes of carotenoid pigments and color in Hamlin, Earlygold, and Budd blood orange juices. *J. Agric. Food Chem.* **2001**, *49*, 877−882.

(21) Schiedt, K.; Liaaen-Jensen, S. *Carotenoids Vol. 1A: Isolation and Analysis*; Birkhauser: Basel, Switzerland, 1995.

(22) Miller, N. J.; Rice-Evans, C. A. Factors influencing the antioxidant activity determined by the ABTS(center dot+) radical cation assay. *Free Radical Res.* **1997**, *26*, 195−199.

(23) Benjamin, G.; Tietel, Z.; Porat, R. Effects of rootstock/scion combinations on the flavor of citrus fruit. *J. Agric. Food Chem.* **2013**, *61*, 11286−11294.

(24) Tietel, Z.; Lewinsohn, E.; Fallik, E.; Porat, R. Elucidating the roles of ethanol fermentation metabolism in causing off-flavors in mandarins. *J. Agric. Food Chem.* **2011**, *59*, 11779−11785.

(25) Shamir, R.; Sharan, R. Algorithmic approaches to clustering gene expression data. in *Current Topics in Computational Biology*; Jiang, T., Smith, T., Xu, Y., Zhang, M. Q., Eds.; MIT Press: Cambridge, MA, 2002; pp 269−299.

(26) DiStefano, G.; La Malfa, S.; Gentile, A.; Wu, S. B. EST-SNP genotyping of citrus species using high-resolution melting curve analysis. *Tree Genet. Genomes* **2013**, *9*, 1271−1281.

(27) Fujii, H.; Shimada, T.; Nonaka, K.; Kita, M.; Kuniga, T.; Endo, T.; Ikoma, Y.; Omura, M. High-throughput genotyping in citrus accessions using an SNP genotyping array. *Tree Genet. Genomes* **2013**, *9*, 145−153.

binding of coffee organics to familiar dissolved metal ions, Na^+, Mg^{2+}, and Ca^{2+}. We have selected five archetypal acids (**1**–**5**), caffeine (**6**), and eugenol (**7**) as representatives of the larger class of organic derivatives found in varying concentrations in roasted beans (Figure 1).[22] Of the five acids, lactic (**1**) and

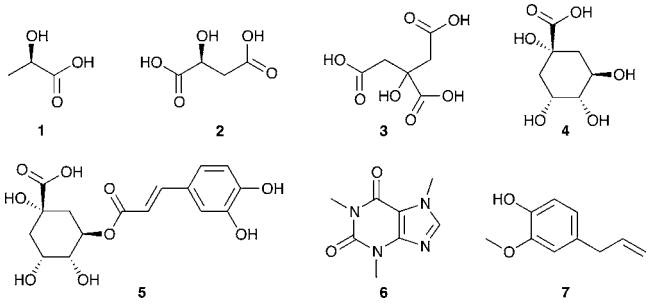

Figure 1. Seven compounds contained in roasted coffee, displaying a range of functionality. There are five carboxylic acids in increasing molecular weight: lactic acid (**1**), malic acid (**2**), citric acid (**3**), quinic acid (**4**), chlorogenic acid (**5**), an alkaloid, caffeine (**6**), and a flavor note, eugenol (**7**).

malic (**2**) acids embody sour notes, while citric acid (**3**) has an appealing sweet flavor. Quinic acid (**4**) and its larger derivative chlorogenic acid (**5**) are considered to taste pungent and unpalatable.[23,24] Caffeine (**6**) was included as an archetypal aromatic alkaloid (and is weakly basic, pK_a = 14),[25] while eugenol (**7**) is a delightful woody note found in coffee, wine, and whisky.[26,27] It should be noted that some acids exist as the potassium salt in the bean. As we will discuss later in this paper, K^+ displays significantly weaker binding to coffee constituents because it is both diffuse and singly charged. Here, we consider the acids in their free acid form, because the relative binding energies of the charge neutral molecules coordinating to ions represent the weakest possible interactions, highlighting the significance of the ionic species.

MATERIALS AND METHODS

All quantum-chemical calculations were performed using the FHI-aims quantum chemical package.[28] FHI-aims is an all-electron code that uses atomic-like orbitals numerically truncated for the inclusion of diffuse and polarization functions. The electronic wave functions are constructed using the combination of these numeric atom-centered basis functions. A converged "tight" basis was employed, which installs *d*, *f* and *g* functions on the O atoms, and scalar relativistic effects were included. Convergence criteria were set to 1×10^{-6} eV per system, corresponding to approximately 5×10^{-5} eV per atom. This criteria is comparatively high to other recent publications featuring similar methods.[29,30]

The thermodynamic relative binding energy of two compounds is defined by

$$E_T = E_{ab} - (E_a + E_b) \quad (1)$$

where the relative binding energy, E_T, is equal to the difference between the bound product, E_{ab}, and the individual components, E_a and E_b. These energies are relative to the molecular states, and thus the magnitude of these energies is only directly comparable within our experiment. Local structure optimizations were performed using the forces from the density functional, PBE (Perdew–Burke–Ernzerhof) exchange-correlation potential (V_{xc}^{KS}).[31] The PBE functional was selected for its desirable trade off between speed and qualitative energies. We tested other familiar hybrid exchange-correlation functionals such as PBE0 (Perdew–Burke–Ernzerhof with the inclusion of 25% Hartree–Fock exchange, 75% correlation) and B3LYP (Becke and Lee–Yang–Parr functional, common in organic chemistry modeling), and PBE produced the same trends in less than half the time.[32]

The consideration of the water interactions is important. There is a long-standing problem in computational modeling of water because it is unclear how many water molecules must be included before one is considering *liquid* water and not a collection of gaseous water molecules. Explicit water molecules severely increase computation time; to circumvent this problem, a familiar approximation is the inclusion of a polarizable continuum model (PCM) that mimics solvents through the application of a dielectric continuum, which acts to screen charges. The PCM (dielectric constant of H_2O, ϵ, = ca. 80) was tested for the calcium series and produced a consistent 30% decrease in relative binding energies. Given the linear nature of the adjustments using a PCM, we elected to exclude it to increase the speed and accessibility of these computations. We consider this acceptable, because values computed using PCM and explicit water are at the limitations of computational power today and still do not produce absolute energies but rather relative binding energies. As a result, our method is accessible and accurate, within the error of the methods and within the limitations of computational chemistry at the time of writing.

Furthermore, we would like to comment on the transferability of our methods to foreign systems. Following the aforementioned procedure, relative binding energies can be consistently calculated. In this case, we have neglected macroscopic variables, such as explicit water. This assumption is certainly not always applicable: this approximation yields poor results in, for instance, protein folding computations. However, there are many applications in which gas-phase computations may be informative, and we encourage the application of quantum mechanics to other chemical problems.[30]

RESULTS AND DISCUSSION

Dissolved cations interact with the nucleophilic motifs of solvated coffee constituents. This interaction may be understood with classical electrostatics:

$$U_r = \frac{(\mathbf{q}_i \cdot \mathbf{q}_s)}{r^2} \quad (2)$$

where the interaction energy U_r is proportional to the charge of both the ion and solute ($\mathbf{q}_i$ and $\mathbf{q}_s$) divided by the interatomic separation, r^2. With this considered, we would anticipate that the more localized charged species should interact more strongly with molecular multipoles. Upon geometry optimization, we recover an equilibrium local minimum energy structure, where the metal ions interact strongly with electron rich motifs. A representation of the equilibrium geometries of each ion–solute cluster is shown in Figure 2, with the notable bond lengths between metal ion and nucleophilic motif listed in Table 1.

The summary of the binding energies is shown in Figure 3, with H_2O-M^{n+} interaction included as a reference. The dissociation of metal-coordinated water is a process driven by entropy, however there is a thermodynamic competitive displacement of metal-coordinated water molecules by compounds **1**-**7**.[17] For coordination and interaction, the coffee compounds are thought to require a higher E_T than the H_2O-M^{n+}. This poses an interesting problem for Na^+ rich water: the binding of **6** and **7** are less favorable than water itself, suggesting that Na^+ does not facilitate extraction of caffeine or eugenol. The **1**-**5**-Na^+ interaction is of comparable energy to the H_2O–Na^+; the extraction of the five acids are not dramatically influenced by the presence of Na^+. First generation exchange filtration units featured a Ca^{2+}/Na^+ ion-exchange column: from our results, this only serves to decrease scale build up, at the deficit of extraction ability of some compounds.

dx.doi.org/10.1021/jf501687c | J. Agric. Food Chem. 2014, 62, 4947–4950

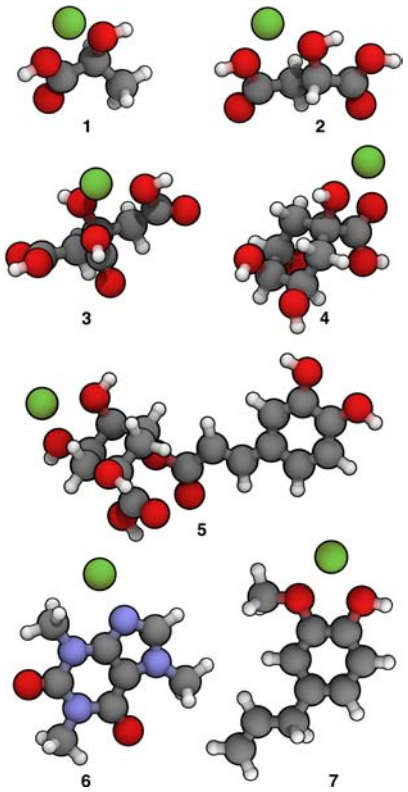

Figure 2. Equilibrium coordination environments of lactic (**1**), malic (**2**), citric (**3**), quinic (**4**), and chlorogenic acid (**5**), caffeine (**6**), and eugenol (**7**). Hydrogen, carbon, nitrogen, oxygen, and magnesium are shown in white, gunmetal, periwinkle, red and green, respectively.

Table 1. Interaction Lengths of Each Metal Ion to the Nearest/Most Nucleophilic Site, as Shown in Figure 2[a]

	1	2	3	4	5	6	7	H_2O
Ca^{2+}	2.21	2.19	2.23	2.15	2.22	2.22	2.21	2.20
Mg^{2+}	1.93	1.92	1.96	1.93	2.00	1.97	1.96	1.92
Na^{+}	2.25	2.26	2.25	2.24	2.24	2.28	2.24	2.23

[a]Distances are stated in Å.

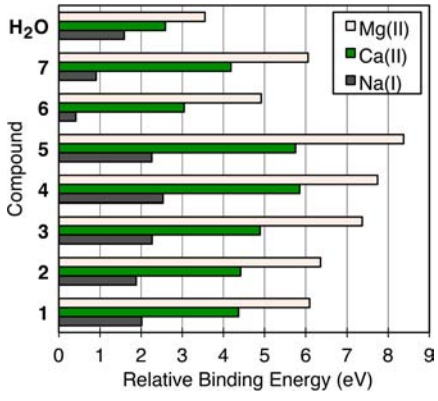

Figure 3. Gas phase binding energies of compounds **1**−**7** and H_2O to Na^{+}, Mg^{2+}, and Ca^{2+}, in gray, beige, and dark green, respectively.

The relative binding energy of (**1**−**7**)−Mg^{2+} is highest in all cases, with the E_T proportional to the charge density of compounds **1**−**7**. Mg^{2+}-rich water is paramount if increasing extraction yield is important. There is, however, a subtle but important increase in the relative binding energy of **1**−**3** relative to **4** and **5** to Mg^{2+} compared with Ca^{2+} (if only by approximately 5%). This is desirable, suggesting Mg^{2+}-rich water would bind to marginally more of the desirable flavors in coffee, although the macroscopic effects of this would be better probed experimentally. The high binding energies of the undesirable acids, **4** and **5**, is less pleasing. Relative to other ions, Mg^{2+} would significantly increase the extraction of these compounds, which may have implications for both the consumer's health and his enjoyment of the cup.[33,34] In this case, the importance of the dissolved carbonate and other bases are important. Bicarbonate/carbonate interacts strongly with **5** (pK_a = 2.66), neutralizing some of this less desirable acid, versus the interaction with the smaller acids, **1**−**3** (pK_a = 3.86, 3.40, and 3.14, respectively). This interaction is outside the scope of this article but is certainly important and is a direction we intend to explore in the future.

Similar binding trends are observed for Ca^{2+}; however, the relative binding energy is lower than that of Mg^{2+} in all cases. The binding energy of **6**−Ca^{2+} is comparable to H_2O−Ca^{2+}; this is the only instance in which one of the divalent cations interacts weakly with an electron-rich motif. This is not a surprising result as the electron density of caffeine is delocalized across the conjugated aromatic motif, resulting in low binding energies to all metal ions (in the case of Na^{+}, almost noninteractive). Considering the results from Table 1, the binding energies are evidently proportional to charge and inversely proportional to the ionic radii. Hence we do not need to explore the binding of K^{+} because it is anticipated that E_T is even lower than that of Na^{+}. Thus, the K^{+} found in the bean in the form of salts can be considered very weakly bound, if not labile (ions concerned in this paper would be anticipated to displace the K^{+}). This effect is amplified if the acids exist as the conjugate bases, and thus our study represents a conservative representation of the binding of coffee constituents to dissolved ions in water.

Based on our thermodynamic experiments, a compelling argument can be made for the favorable exchange of Ca^{2+} for Mg^{2+} to increase extraction yield, with no deficit to coffee flavor, and the additional benefit of removing the source of lime scale. We also emphasize the surprising result that Na^{+} binds weakly to most neutral compounds in coffee beans, suggesting that sodium rich water is of no benefit to the consumer, besides removing the source of scale build up. Thus, if the motivation is to extract the most coffee constituents (i.e., instant coffee), then Mg^{2+}-rich water is most suitable. If the motivation is to achieve the best balance of flavors for a given lighter roast coffee, then both Ca^{2+} and Mg^{2+} do a comparable job,[35] with Mg^{2+} having the added feature of preventing scale formation.

It should be noted that there is not one particular composition of water that produces consistently flavorsome extractions from *all* roasted coffee. Rather, there is water that has the most extracting ability (i.e., cation-rich), and the resultant flavor depends on the balance between both the cations in solution and the quantity of bicarbonate present (acting as a buffer). Furthermore, each bean is roasted to taste optimal when brewed with the water it was roasted to. We acknowledge this point, and emphasize that this work elucidates the important role that dissolved ions play in facilitating the extraction process.

AUTHOR INFORMATION

Corresponding Author

*E-mail: c.hendon@bath.ac.uk.

Notes

The authors declare no competing financial interest.

■ ACKNOWLEDGMENTS

We acknowledge Prof. A. Walsh for facilitating this research, K. Tobias Butler for rigorous corrections, and A. Thomas Murray for chemical insight. We also thank M. Gamwell, S. Stephenson, J. Gonzalez, P. Grosvenor-Attridge, and E. Russell for useful discussions. C.H.H is supported by Prof. A. Walsh, a Royal Society Research Fellow. This work benefited from access to both the University of Bath's High Performance Computing Facility and ARCHER, the UK's national high-performance computing service, which is funded by the Office of Science and Technology through EPSRC's High End Computing Programme (EP/L000202).

■ REFERENCES

(1) Johnston, W. R.; Frey, C. N. The volatile constituents of roasted coffee. *J. Am. Chem. Soc.* **1938**, *60*, 1624.
(2) Rhoades, J. W. Analysis of the Volatile Constituents of Coffee. *J. Agric. Food Chem.* **1960**, *8*, 136.
(3) Gianturco, M.; Giammarino, A.; Friedel, P. Volatile Constituents of Coffee-V. *Nature* **1966**, *210*, 1358.
(4) Bondarovich, H. A.; Friedel, P.; Krampl, V.; Renner, J. A.; Shephard, F. W.; Gianturco, M. A. Volatile constituents of coffee. Pyrazines and other compounds. *J. Agric. Food Chem.* **1967**, *15*, 1093.
(5) Müller, C.; Hofmann, T. Quantitative studies on the formation of phenol/2-furfurylthiol conjugates in coffee beverages toward the understanding of the molecular mechanisms of coffee aroma staling. *J. Agric. Food Chem.* **2007**, *55*, 4095.
(6) Hughes, E. B.; Smith, R. F. The volatile constituents of roasted coffee. *J. Soc. Chem. Ind.* **1949**, *68*, 322.
(7) Lyman, D. J.; Benck, R.; Dell, S.; Merle, S.; Murray-Wijelath, J. FTIR-ATR analysis of brewed coffee: effect of roasting conditions. *J. Agric. Food Chem.* **2003**, *51*, 3268.
(8) Navarini, L.; Rivetti, D. Water quality for Espresso coffee. *Food Chem.* **2010**, *122*, 424.
(9) Lockhart, E. E.; Tucker, C. L.; Merritt, M. C. The effect of water impurities on the flavor of brewed coffee. *J. Food Sci.* **1955**, *20*, 598.
(10) Pangborn, R. M.; Trabue, I. M.; Little, A. C. Analysis of coffee, tea and artificially flavoured drinks prepared from mineralised waters. *J. Food Sci.* **1971**, *36*, 355.
(11) Demichelis, R.; Raiteri, P.; Gale, J. D.; Quigley, D.; Gebauer, D. Stable prenucleation mineral clusters are liquid-like ionic polymers. *Nat. Commun.* **2011**, *2*, 590.
(12) The SCAE suggest that water with ≤300 ppm total dissolved solids is well-suited for the application. This seems to be vague based on the work we have proposed herein. A summary of the SCAE guidelines is provided in this link: http://tinyurl.com/onpcsms.
(13) The measurement of TDS is intrinsically flawed because the ionic mobilities are dependent on diffusion rates, coordinations spheres, and most importantly charge. As a result, the application of TDS for quantifying water components is certainly debatable.
(14) The impact of dissolved bicarbonate is problematic because both bicarbonate and water are polyprotic buffers. Regardless, water hardness is publically accessible information, an example of which is neatly summarized for the UK here: http://tinyurl.com/nowade8.
(15) http://www.brita.net.
(16) http://www.bwt-wam.com.
(17) Rodriguez-Cruz, S. Binding Energies of Hexahydrated Alkaline Earth Metal Ions, M^{2+} $(H_2O)_6$, M = Mg, Ca, Sr, Ba: Evidence of Isomeric Structures for Magnesium. *J. Am. Chem. Soc.* **1999**, *121*, 1986.
(18) Indeed, the formation of hydrated cages is an entropically driven process that pushes against the formation of local ordering of water around a hydrophic motif. However, the effect of dissolution is very small, because the electronic structure of water is not grossly affected by dissolved solids.
(19) Omta, A. W.; Kropman, M. F.; Woutersen, S.; Bakker, H. J. Negligible effect of ions on the hydrogen-bond structure in liquid water. *Science* **2003**, *301*, 347.
(20) Wernet, P.; Nordlund, D.; Bergmann, U.; Cavalleri, M.; Odelius, M.; Ogasawara, H.; Näslund, L. A.; Hirsch, T. K.; Ojamäe, L.; Glatzel, P.; Pettersson, L. G. M.; Nilsson, A. The structure of the first coordination shell in liquid water. *Science* **2004**, *304*, 995.
(21) Wang, W.; Zeng, P.; Long, X.; Huang, J.; Liu, Y.; Tan, B.; Sun, L. Methane storage in tea clathrates. *Chem. Commun.* **2014**, *50*, 1244.
(22) Stoffelsma, J.; Sipma, G.; Kettenes, D. K.; Pypker, J. New volatile components of roasted coffee. *J. Agric. Food Chem.* **1968**, *16*, 1000.
(23) Nagel, C. W.; Herrick, I. W.; Graber, W. R. Is Chlorogenic Acid Bitter? *J. Food Sci.* **1987**, *52*, 213.
(24) Moon, J.-K.; Yoo, H. S.; Shibamoto, T. Role of roasting conditions in the level of chlorogenic acid content in coffee beans: Correlation with coffee acidity. *J. Agric. Food Chem.* **2009**, *57*, 5365.
(25) Newton, D. W.; Kluza, R. B. pKa Values of Medicinal Compounds in Pharmacy Practice. *Ann. Pharmacother.* **1978**, *12*, 546.
(26) Arnaud, M. J. The metabolism of coffee constituents. *Coffee* **1988**, *3*, 33.
(27) Arapitsas, P.; Antonopoulos, A.; Stefanou, E.; Dourtoglou, V. Artificial aging of wines using oak chips. *Food Chem.* **2004**, *86*, 563.
(28) Blum, V.; Gehrke, R.; Hanke, F.; Havu, P.; Havu, V.; Ren, X.; Reuter, K.; Scheffler, M. Ab initio molecular simulations with numeric atom-centered orbitals. *Comput. Phys. Commun.* **2009**, *180*, 2175.
(29) Hendon, C. H.; Tiana, D.; Murray, A. T.; Carbery, D. R.; Walsh, A. Helical frontier orbitals of conjugated linear molecules. *Chem. Sci.* **2013**, *4*, 4278.
(30) Hendon, C. H.; Carbery, D. R.; Walsh, A. Three-electron two-centred bonds and the stabilisation of cationic sulfur radicals. *Chem. Sci.* **2014**, *5*, 1390.
(31) Perdew, J. P.; Burke, K.; Ernzerhof, M. Generalized Gradient Approximation Made Simple. *Phys. Rev. Lett.* **1996**, *77*, 3865.
(32) Adamo, C.; Barone, V. Toward reliable density functional methods without adjustable parameters: The PBE0 model. *J. Chem. Phys.* **1999**, *110*, 6158.
(33) Clifford, M. N. Chlorogenic acids and other cinnamates - nature, occurrence and dietary burden. *J. Sci. Food Agric.* **1999**, *372*, 362.
(34) Ludwig, I. A.; Clifford, M. N.; Lean, M. E. J.; Ashihara, H.; Crozier, A. Coffee: Biochemistry and potential impact on health. *Food Funct* **2014**, DOI: 10.1039/C4FO00042K.
(35) Indeed, the roast for Ca^{2+}-rich water is different from that of Mg^{2+}-rich water: the more powerful the extraction ability of water, the lighter the roast.

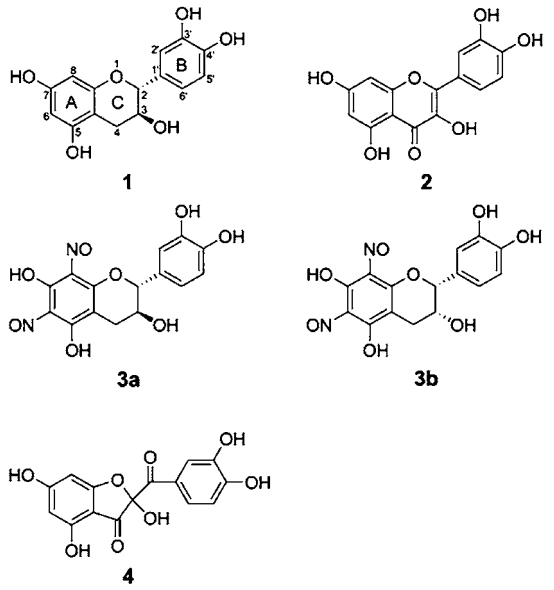

Figure 1. Compounds investigated in this study: (**1**) (+)-catechin, (**2**) quercetin, (**3a**) 6,8-dinitrosocatechin, (**3b**) 6,8-dinitrosoepicatechin, and (**4**) 2-(3,4-dihydroxybenzoyl)-2,4,6-trihydroxy-3(2*H*)-benzofuranone.

are taken into account, possible interactions between (+)-catechin and quercetin are discussed.

MATERIALS AND METHODS

Reagents. (+)-Catechin, (−)-epicatechin, and quercetin were obtained from Sigma-Aldrich Japan (Tokyo, Japan). 1-Hydroxy-2-oxo-3-(*N*-methyl-3-aminopropyl)-3-methyl-1-triazene (NOC 7) (purity > 90%) was from Dojindo (Kumamoto, Japan).

Apparatus. High-performance liquid chromatography (HPLC) was carried out using a Shimadzu LC-10AS pump combined with a SPD M10Avp photodiode array detector (Shimadzu Co., Kyoto, Japan). Atmospheric pressure chemical ionization (APCI) mass spectra were obtained with a Shimadzu LCMS QP8000α quadrupole mass spectrometer equipped with an APCI ion source. The deflector voltage of the mass spectrometer was maintained at +50 V for positive-mode measurement or at −50 V for negative-mode measurement. The sample was delivered into the ion source using an Ascentis express C18 column (15 cm × 2.1 mm inner diameter; particle size of 2 μm; Sigma-Aldrich Japan, Tokyo, Japan). The mobile phase was 35% methanol containing 0.2% formic acid, and the flow rate was 0.2 mL/min. Proton nuclear magnetic resonance (^{1}H NMR) spectra were recorded with an ECX-400P FT-NMR spectrometer (JEOL, Tokyo, Japan) with dimethyl sulfoxide-d_6 (DMSO-d_6) as the solvent and tetramethylsilane as the internal standard. ^{1}H NMR was performed at 399.78 MHz, and the ^{1}H−^{1}H chemical shift correlated technique was employed to assign ^{1}H shifts and couplings.

Isolation of 6,8-Dinitrosocatechin. (+)-Catechin (29 mg) in 100 mL of 50 mM KCl−HCl (pH 2.0), which was equivalent to 1 mM (+)-catechin, was reacted with 5 mM sodium nitrite for 5 min under anaerobic conditions, and then 5 mM ascorbic acid was added to terminate the reaction. The reaction products were extracted with 50 mL of ethyl acetate 5 times. Ethyl acetate extracts were combined and washed with 50 mL of 0.1% HCl twice. After water was removed from the ethyl acetate extract with anhydrous sodium sulfate, the solvent was removed *in vacuo* with a rotary evaporator, the residue was dissolved in 1.5 mL of methanol, and then the methanol solution was diluted with 1.5 mL of 0.2% formic acid to apply to a preparative HPLC column.

Preparative HPLC was performed using a Shim-pack PREP-ODS(H) kit (25 cm × 20 mm inner diameter; particle size of 5 μm; pore size of 10 nm; Shimadzu), and the volume of samples injected into the column was 0.9 mL. The mobile phases were mixtures of methanol and 0.2% formic acid. The concentration of methanol was increased stepwise as follows: 14, 20, 25, and 33% (v/v), and each mobile phase was flowed for 5, 15, 15, and 25 min, respectively. Their flow rate was 9 mL/min. Components separated by the preparative HPLC were detected at 210, 280, and 320 nm using the spectrophotometric detector. A peak supposed to be 6,8-dinitrosocatechin was eluted at about 7 min after changing the mobile phase to 25% methanol, and the peak component was collected. Methanol of the collected solution was removed *in vacuo*, and the residue was lyophilized. The yield was 27−35%. The above procedure was repeated 6 times, and about 50 mg of the lyophilizate was obtained.

Reactions of Nitrite with Quercetin, (+)-Catechin, and 6,8-Dinitrosocatechin. Interactions of quercetin with (+)-catechin or 6,8-dinitrosocatechin were studied in reaction mixtures (1 mL) that contained 0.1 mM (+)-catechin or 6,8-dinitrosocatechin and various concentrations of quercetin (0, 10, 30, or 100 μM) in 50 mM KCl−HCl (pH 2.0). When required, 2 mM ascorbic acid or 10 mM potassium thiocyanate was added to the above reaction mixtures. Reactions were initiated by the addition of 0.1 mM sodium nitrite. After incubation for defined periods, an aliquot (50 μL) of each reaction mixture was applied to a HPLC column to quantify (+)-catechin, dinitrosocatechin, quercetin, and their reaction products (see below).

Interactions between quercetin and (+)-catechin or 6,8-dinitrosocatechin were also studied under anaerobic conditions. The reaction mixture contained 50 μM (+)-catechin or 6,8-dinitrosocatechin and various concentrations of quercetin. Air of the reaction mixtures was removed by bubbling argon gas for 2 min, and then reactions were initiated by the addition of 0.25 mM sodium nitrite. After incubation for 1 min, 50 μL of the reaction mixture was applied to the HPLC column to quantify (+)-catechin, quercetin, dinitrosocatechin, and their reaction products (see below).

Analysis of Reaction Products by HPLC. Analytical HPLC was performed using a Shim-pack CLC-ODS column (15 cm × 6 mm inner diameter; particle size of 5 μm; Shimadzu). The mixture of methanol and 0.2% formic acid (1:2, v/v) was used to separate (+)-catechin (280 nm), 6,8-dinitrosocatechin (320 nm), and the oxidation product of quercetin (293 nm), when (+)-catechin and/or quercetin were reacted with nitrous acid. When 6,8-dinitrosocatechin was reacted with nitrous acid with and without quercetin, the mixture of methanol and 0.2% formic acid (2:5, v/v) was used as the mobile phase to detect the reaction products. The ratio of 2:1 (v/v) was used to detect quercetin (360 nm) in the above systems. The flow rate of the mobile phases was 1 mL/min. The concentration of each component was estimated from the area under the peak.

Measurements of •NO Production. Nitrite-induced •NO production was studied using a Clark-type electrode at 30 °C with a polarization voltage of −0.7 V.[24−26] The reaction mixture (2.0 mL) contained 50 μM (+)-catechin or 6,8-dinitrocatechin and various concentrations of quercetin in 50 mM KCl−HCl (pH 2.0). Reactions were initiated by the addition of 0.5 mM sodium nitrite after removing air from the reaction mixture by bubbling argon gas. The rate of •NO production was estimated from the slope.

Amounts of •NO produced in the above systems were calibrated by measuring •NO production in ascorbic acid/nitrous acid systems. In the ascorbic acid/nitrous acid system, one molecule of ascorbic acid produces two molecules of •NO under acidic conditions by the following reaction if the concentration of nitrous acid is more than 2 times that of ascorbic acid:[26,27]

$$\text{ascorbic acid} + 2HNO_2 \rightarrow \text{dehydroascorbic acid} + 2^{\bullet}NO + 2H_2O \quad (1)$$

The amount of •NO produced by the addition of 50 μM ascorbic acid in the presence of 0.5 mM sodium nitrite in 50 mM KCl−HCl (pH 2.0) was essentially the same as that of •NO produced by 50 μM NOC 7 in the same buffer, one molecule of which produces two molecules of

•NO,[28] indicating the usefulness of an ascorbic acid/nitrous acid system to calibrate the amounts of •NO produced.

Presentation of Data. Each experiment was repeated 3−8 times. Typical data or means with standard deviations (SDs) are presented in figures and tables. The statistical significance of the difference between groups was evaluated by Student's *t* test.

RESULTS AND DISCUSSION

Characterization of Isolated 6,8-Dinitrosocatechin. Liquid chromatography−mass spectrometry (LC−MS) analysis of the isolated dinitrosocatechin gave two peaks (**3a** and **3b**) (Figure 1) with retention times of 2.1 and 3.4 min, respectively. Their APCI mass spectra were the same. Compound **3a** at *m/z* (relative intensity, %): 123.1 (39), 270.1 (28), 285.1 (25, $[315.1 - NO]^+$), 286.1 (38), 315.1 (100, $[349.1 - (OH)_2]^+$), 331.1 (30, $[M - OH]^+$), and 349.1 (32, $[M + H]^+$) with positive-ion mode or at *m/z* 153.0 (43), 180.1 (72), 196.0 (98), 311.1 (52), 313.1 (97, $[347.1 - (OH)_2]^-$), 331.1 (46, $[M - OH]^+$), and 347.1 (100, $[M - H]^-$) with negative-ion mode. Compound **3b** at *m/z* (relative intensity, %): 123.1 (43), 270.0 (23), 285.1 (24, $[315.1 - NO]^+$), 286.1 (35), 315.1 (100, $[349.1 - (OH)_2]^+$), 331.1 (23, $[M - OH]^+$), and 349.1 (31, $[M + H]^+$) with positive-ion mode or *m/z* 153.0 (45), 180.1 (81), 196.0 (87), 311.1 (62), 313.1 (90, $[347.1 - (OH)_2]^-$), 331.1 (33, $[M - OH]^-$), and 347.1 (100, $[M - H]^-$) with negative-ion mode, suggesting that compounds **3a** and **3b** are dinitrosocatechin isomers. This was supported by the result that compound **3b** was produced when (−)-epicatechin was incubated with nitrite in 50 mM KCl−HCl (pH 2.0), the production of which was confirmed by the retention time and ultraviolet/visible (UV/vis) absorption spectrum. The mutual transformation of these dinitroso compounds has been reported.[15] Furthermore, each peak showed a fragment ion at *m/z* 123.1 with positive mode, corresponding to a B-ring fragment of catechin. This supports that the B ring of each compound is not modified.[15,29] The major fragment ion at *m/z* 196.0 with negative mode suggests that two NO groups could add to the A ring of catechins.

The chemicals structures of compounds **3a** and **3b** were supported by NMR data. ^{1}H NMR data indicated that isolated dinitrosocatechin was a mixture of 6,8-dinitrosocatechin and 6,8-dinitrosoepicatechin. ^{1}H NMR (DMSO-d_6) δ: 2.38 (dd, J = 7 and 18 Hz, 2/3H, H_c-4_{ax}), 2.50 (dd, J = 4 and 18 Hz, 2/3H, H_c-4_{eq}), 2.57 (m, 1/3H, H_e-4_{ax}), 2.67 (dd, J = 4 and 18 Hz, 1/3H, H_e-4_{eq}), 4.00 (m, 2/3H, H_c-3), 4.13 (m, 1/3H, H_e-3), 4.95 (d, J = 6 Hz, 2/3H, H_c-2), 5.07 (s, 1/3H, H_e-2), 5.34 (br s, 1H, 4-O*H*), 6.62 (dd, J = 1 and 8 Hz, 2/3H, H_c-6′), 6.63 (m, 1/3H, H_e-5′), 6.71 (s, 1/3H, H_e-6′), 6.72 (s, 2/3H, H_c-2′), 6.73 (d, J = 8 Hz, 2/3H, H_c-6′), 6.93 (s, 2/3H, H_e-2′), 8.92 (br s, 1H, O*H*), and 9.00 (br s, 1H, O*H*), where H_c is a proton signal from catechine and H_e is a proton signal from epicatechin. No signals assigned to H bound to C6 and C8 were detected, which were observed in (+)-catechin and (−)-epicatechin.[15,30] This supported that nitrosation took place on the C6 and C8 positions of the A ring. Nitrosation on the A ring is consistent with the previous reports, which concerned the nitrosation of epicatechin and epigallocatechiin gallate by nitrous acid.[15,16] The presence of 6,8-dinitrosocatechin (**3a**) and 6,8-dinitrosoepicatechin (**3b**) in the isolate was further supported by the order of elution, because catechin eluted earlier than epicatechin in reversed-phase columns.[31]

Reaction of (+)-Catechin with Nitrous Acid. When (+)-catechin (retention time of 5.4 min) was reacted with nitrite under the conditions of simulating the gastric lumen, a component with a retention time of 5.2 min was detected by analytical HPLC (top panels of Figure 2). The component had

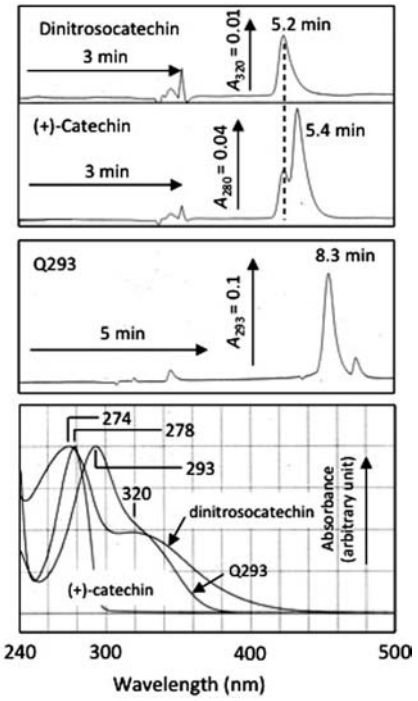

Figure 2. Formation of dinitrosocatechin and an oxidation product of quercetin, Q293. The reaction mixture that contained 0.1 mM sodium nitrite and 0.1 mM (+)-catechin or quercetin in 50 mM KCl−HCl (pH 2.0) was incubated for 5 min. (Top) (+)-Catechin and dinitrosocatechin. (Middle) Q293. (Bottom) Absorption spectrum of each peak in the mobile phase (methanol and 0.2% formic acid = 1:2, v/v).

an absorption peak at 274 nm with a shoulder at 320 nm (bottom panel of Figure 2). The retention time and absorption spectrum were identical to those of isolated 6,8-dinitrosocatechin under the conditions of Figure 2, and its formation increased with the increase in the concentration of sodium nitrite from 0 to 1 mM. It has been reported that dinitrosocatechin and dinitrosoprocyanidin B2 are formed when the methanol extract of apple fruit is incubated with acidified saliva (pH 2.0) that contains 0.4 mM nitrite.[32]

Figure 3A shows a time course of nitrite-induced formation of 6,8-dinitrosocatechin from (+)-catechin. The concentration increased nearly linearly during the incubation for 10 min. Figure 3A also shows a time course of (+)-catechin consumption. Because (+)-catechin was not completely separated from 6,8-dinitrosocatechin, the concentration of (+)-catechin was estimated by subtracting the area of 6,8-dinitrosocatechin at 280 nm, which was determined from the area of dinitrosocatechin at 320 nm, from the area of both components at 280 nm (Figure 2). Time courses of the formation of 6,8-dinitrosocatechin and the consumption of (+)-catechin indicate that the yield of 6,8-dinitrosocatechin was approximately 30% in molar ratio. The rate constant of (+)-catechin consumption was calculated from data of (+)-catechin consumed during 2 min of incubation, postulating that 1 mol of (+)-catechin reacted with 1 mol of nitrous acid, producing •NO and the (+)-catechin semiquinone radical as follows:

dx.doi.org/10.1021/jf500860s | J. Agric. Food Chem. 2014, 62, 4951−4959

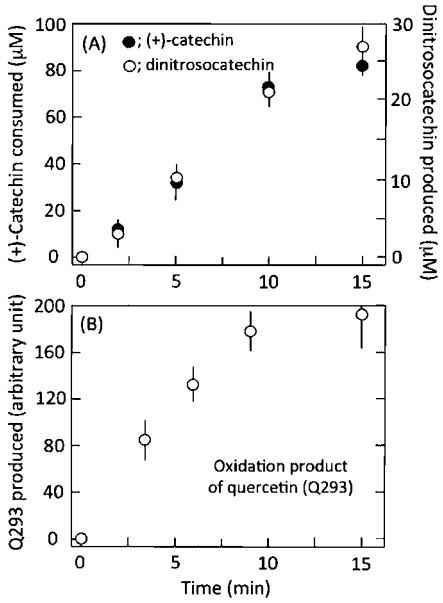

Figure 3. Time courses of the formation of reaction products of (+)-catechin and quercetin under aerobic conditions. The reaction mixture (1 mL) contained 0.1 mM (+)-catechin or 0.1 mM quercetin and 0.1 mM sodium nitrite in 50 mM KCl–HCl (pH 2.0). (A) Formation of dinitrosocatechin: (●) (+)-catechin consumption and (○) dinitrosocatechin formation. (B) Formation of the oxidation product of quercetin, Q293. Each data point represents the mean with SD (n = 3).

$$(+)\text{-catechin} + HNO_2 \rightarrow (+)\text{-catechin radical} + {}^{\bullet}NO + H_2O \quad (2)$$

The value was $(6.7 \pm 1.0) \times 10^2$ M^{-1} min^{-1} (n = 4). Nitrite-induced formation of the semiquinone radical of (+)-catechin has been reported under the conditions that simulate the gastric lumen,[14] and the unpaired electron is localized in the A ring of the (+)-catechin semiquinone radical.[23] The localization of the unpaired electron suggests that $^{\bullet}NO$ produced by reaction 2 can bind to the A ring of the semiquinone radical, generating mononitrosocatechin, and then mononitrosocatechin is oxidized in the A ring to react with $^{\bullet}NO$, generating 6,8-dinitrosocatechin as follows:

$$(+)\text{-catechin radical} + {}^{\bullet}NO \rightarrow NO\text{–catechin} \quad (3)$$

$$NO\text{–catechin} + HNO_2 \rightarrow NO\text{–catechin radical} + {}^{\bullet}NO + H_2O \quad (4)$$

$$NO\text{–catechin radical} + {}^{\bullet}NO \rightarrow diNO\text{–catechin} \quad (5)$$

In the above reactions, NO–catechin and diNO–catechin are mononitrosocatechin and 6,8-dinitrosocatechin, respectively. The formation of mononitrosocatechin in catechins/nitrous acid systems[15] and the reactions of $^{\bullet}NO$ with phenoxyl radicals[33] have been reported. Hypochlorous-acid-induced formation of 6,8-dichlorocatechins from catechins[34] supports the localization of unpaired electrons in the A ring of catechins. Panzella et al.[16] have reported the formation of 6,8-dinitroepigallocatechin-3-*O*-gallate in (−)-epigallocatechin-3-*O*-gallate/nitrous acid systems, and they proposed the reaction of epigallocatechin-gallate quinone with nitrous acid as the mechanism of 6,8-dinitrosoepicatechin-3-*O*-gallate formation. If $^{\bullet}NO$ was produced by reactions 2 and 4 under the conditions in Figure 3, namely, aerobic conditions, $^{\bullet}NO_2$ should be formed as follows ($k = 8.8 \times 10^6$ M^{-2} s^{-1}):[35]

$$2{}^{\bullet}NO + O_2 \rightarrow 2{}^{\bullet}NO_2 \quad (6)$$

$^{\bullet}NO_2$ may oxidize (+)-catechin and nitrosocatechins, producing their semiquinone radicals.

Oxidation of Quercetin by Nitrous Acid. The oxidation product of quercetin, which was referred to as Q293 in this study, had a retention time of 8.3 min in the mobile phase, and the absorption spectrum had a peak at 293 nm, with a shoulder around 320 nm (middle and bottom panels of Figure 2). We have reported the formation of the component in the acidic mixture of quercetin and nitrite[13] and determined its structure to be 2-(3,4-dihydroxybenzoyl)-2,4,6-trihydroxy-3(2*H*)-benzofuranone (**4**).[17] Figure 3B shows time courses of nitrite-induced formation of Q293 from 0.1 mM quercetin in 50 mM KCl–HCl (pH 2.0). The concentration of Q293 increased nearly linearly during incubation at least for 3 min, and the rate increased with the increase in the concentration of nitrite from 0 to 1 mM.

Reaction of Dinitrosocatechin with Nitrous Acid. Isolated 6,8-dinitrosocatechins (0.1 mM) were incubated with 0.1 mM nitrite for 5 min in 50 mM KCl–HCl (pH 2.0), and the reaction mixture was analyzed by HPLC (top panel of Figure 4). Two new components, P1 and P2, were detected, and their absorption peaks (270 nm) were shorter than those of compounds **3a** and **3b** (274 nm) (middle panel of Figure 4). The bottom panel of Figure 4 shows time courses of 6,8-dinitrosocatechin (**3a** plus **3b**) consumption and P1 and P2 formation. The formation of P1 slowed down more rapidly than that of P2, and the amount of P1 produced was smaller compared to that of P2, suggesting that P1 and P2 were formed from compounds **3b** and **3a**, respectively. The rate constant of the consumption of 6,8-dinitrosocatechin (**3a** plus **3b**) was calculated from the decrease in the concentration during 2 min of incubation. The value was $(6.5 \pm 2.5) \times 10^2$ M^{-1} min^{-1} (n = 4) under the postulation of the following reaction:

$$diNO\text{–catechin} + HNO_2 \rightarrow diNO\text{–catechin radicals} + {}^{\bullet}NO + H_2O \quad (7)$$

In addition to HNO_2, $^{\bullet}NO_2$ produced by reaction 6 can also oxidize dinitrosocatechins to the semiquinone radicals.

Because dinitrosocatechins have a catechol structure in the B ring, it is expected that the semiquinone radicals of dinitrocatechins are transformed to *o*-quinones by disproportionation. If components of P1 and P2 were quinones, the peaks should disappear by ascorbic acid.[36] In fact, when 2 mM ascorbic acid was added to the reaction mixture that had been incubated for 5 min under the conditions of Figure 4, peaks P1 and P2 disappeared, accompanying the increase in peak heights of compounds **3a** and **3b** to the original heights. This result supports the postulation that P1 and P2 are quinone forms of 6,8-dinitroscatechin and 6,8-dinitrosoepicatechin. Nitrous-acid-induced formation of quinone of dinitrosoepigallocatechin-3-*O*-gallate has been reported.[16]

o-Quinones of polyphenols, such as caffeic acid, chlorogenic acid, and rutin, react with thiocyanate at pH 2.0, producing thiocyanate conjugates, which are transformed to the oxathiolone derivatives by the addition of water and removal of ammonia.[37−39] Then, the effects of sodium thiocyanate on the formation of P1 and P2 were studied at pH 2.0.

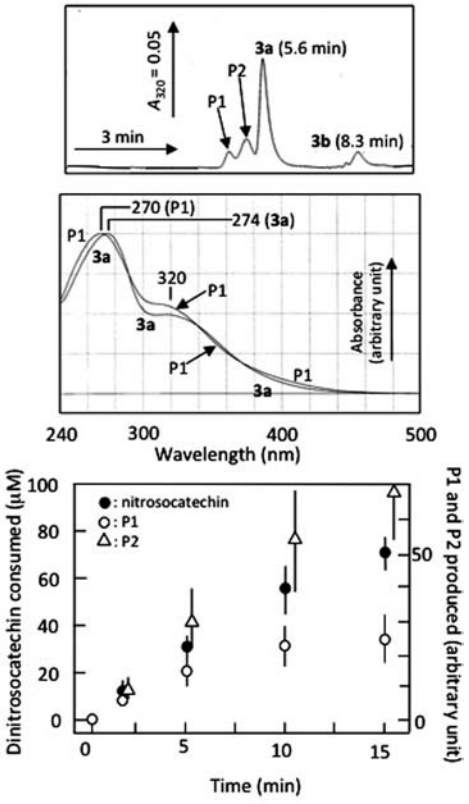

Figure 4. Reactions of dinitrosocatechin with nitrous acid. The reaction mixture (1 mL) contained 0.1 mM isolated dinitrosocatechin and 0.1 mM sodium nitrite in 50 mM KCl–HCl (pH 2.0). (Top) HPLC of reaction products of dinitrosocatechin at 5 min after initiation. Compound **3a**, 6,8-dinitrosocatechin; compound **3b**, 6,8-dinitrosoepicatechin; and P1 and P2, products of compounds **3b** and **3a**, respectively. Mobile phase, methanol and 0.2% formic acid = 2:5, v/v. (Middle) Absorption spectra of compound **3a** and P1 in the mobile phase. (Bottom) Time courses of (●) dinitrosocatechin (**3a** plus **3b**) consumption and (○) P1 and (△) P2 formation. Each data point represents the mean with SD (n = 3–4).

Thiocyanate (10 mM) suppressed the formation of P1 and P2 in the mixture that contained 0.1 mM dinitrosocatechin and 0.1 mM sodium nitrite in 50 mM KCl–HCl (pH 2.0). In addition, 2–10 mM thiocyanate decreased the concentration of P1 and P2 when added to a reaction mixture, in which P1 and P2 had been produced. These results further support that P1 and P2 were quinones. Two new components (retention times of 3.9 and 5.8 min) were produced in the dinitrosocatechin/thiocyanate/nitrous acid systems, and their molecular weights were estimated to be 405 by LC–MS, suggesting that the components were thiocyanate conjugates of 6,8-dinitrosocatechin and 6,8-dinitrosoepicatechin.

Interactions between (+)-Catechin and Quercetin. Figure 5 shows effects of 0.1 mM (+)-catechin on the formation of Q293 in the presence of various concentrations of quercetin. The formation of Q293 increased with the increase in the concentration of quercetin in the absence of (+)-catechin, when the concentration of Q293 was determined 2 min after the initiation of reactions (○). (+)-Catechin enhanced the production of Q293 independent of the quercetin concentration, and the enhancement in the presence of 10 and 30 μM quercetin was about 1.8-fold (□). The above result indicates that (+)-catechin can enhance the oxidation of quercetin. 6,8-Dinitrosocatechin was produced irrespective of

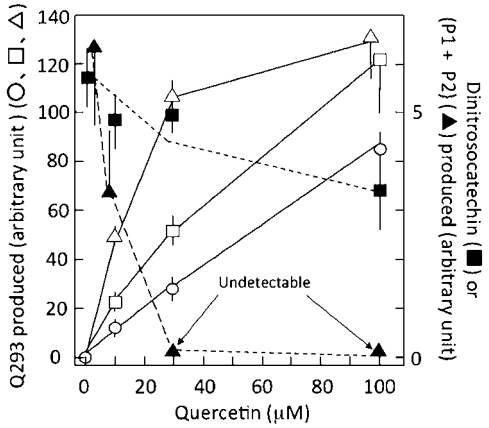

Figure 5. Interactions between quercetin and (+)-catechin or dinitrosocatechin. The reaction mixture (1 mL) that contained 0.1 mM sodium nitrite and 0.1 mM (+)-catechin or dinitrosocatechin in 50 mM KCl–HCl (pH 2.0) was incubated for 2 min. (Left vertical axis) Enhancement of Q293 production by catechin and dinitrosocatechin: (○) no addition, (□) (+)-catechin, (△) dinitrosocatechin. (Right vertical axis) Inhibition of the production of dinitrosocatechin and P1 + P2 by quercetin: (■) production of dinitrosocatechin from (+)-catechin and (▲) production of (P1 + P2) from dinitrosocatechin. Each data point represents the mean with SD (n = 3–4).

the presence and absence of quercetin, and 50 μM quercetin inhibited its production by about 60% (■). The concentration of (+)-catechin decreased during the formation of dinitrosocatechin, but the effects of quercetin on the decrease in the (+)-catechin concentration were unclear. The unclearness might be due to the small decrease in the (+)-catechin concentration during 2 min of incubation (see Figure 3) and/or quercetin-dependent preferential reduction of the mononitrosochatechin semiquinone radical rather than the (+)-catechin semiquinone radical for the inhibition of dinitrosocatechin formation.

The effects of (+)-catechin on the nitrous-acid-induced decrease in the concentration of quercetin are shown in Table 1. From the data in the absence of (+)-catechin, the rate constant of the reaction between quercetin and nitrous acid was calculated, postulating the following reaction:

$$\text{quercetin} + HNO_2 \rightarrow \text{quercetin radical} + {}^{\bullet}NO + H_2O \quad (8)$$

Table 1. Enhancement of Nitrite-Induced Quercetin Oxidation by (+)-Catechin and 6,8-Dinitrosocatechin[a]

	quercetin concentration after 2 min of incubation (μM)	
initial concentration of quercetin (μM)	10	30
no addition	7.7 ± 0.7 (n = 6)	19.6 ± 1.3 (n = 6)
(+)-catechin	3.3 ± 0.1 (n = 3)[b]	16.5 ± 1.8 (n = 3)[b]
6,8-dinitrosocatechin	2.9 ± 1.8 (n = 3)[b]	7.2 ± 2.3 (n = 3)[b]

[a]The reaction mixture (1 mL) that contained 0.1 mM sodium nitrite and 10 or 30 μM quercetin in 50 mM KCl–HCl (pH 2.0) in the presence and absence of 0.1 mM (+)-catechin or 6,8-dinitrosocatechin was incubated for 2 min. The quercetin concentration of the reaction mixture was determined by HPLC. Each data point represents the mean with SD (n = 3). [b]Significant differences in quercetin oxidation with and without the addition of (+)-catechin or 6,8-dinitrosocatechin (p < 0.05).

dx.doi.org/10.1021/jf500860s | J. Agric. Food Chem. 2014, 62, 4951–4959

Table 2. •NO Production in Nitrite/Quercetin Systems with and without (+)-Catechin or Dinitrosocatechin[a]

	rate of •NO production (μM/min)		
quercetin (μM)	no addition	+50 μM catechin	+50 μM diNO−CAT
0	0	16.7 ± 3.3 (n = 8)[b]	28.0 ± 3.3 (n = 6)
5	8.3 ± 3.1 (n = 4)	16.5 ± 3.7 (n = 4)[b,c]	39.0 ± 4.0 (n = 3)[c]
15	27.6 ± 5.3 (n = 4)	42.5 ± 9.1 (n = 4)[c]	63.3 ± 14.5 (n = 3)[c]
50	77.0 ± 9.6 (n = 8)	95.5 ± 14.9 (n = 3)[c]	132.7 ± 17.5 (n = 3)[c]

[a]The reaction mixture (2 mL) contained 0, 5, 15, or 50 μM quercetin in 50 mM KCl−HCl (pH 2.0) in the presence and absence of 50 μM (+)-catechin or dinitrosocatechin. Reactions were initiated by the addition of 0.5 mM sodium nitrite. Rates of •NO production were determined from the initial slopes. diNO−CAT = 6,8-dinitrosocatechin. Each data point represents the mean with SD. [b]No significant difference. [c]Significant differences in •NO production regarding the addition of the quercetin to catechin/nitrous acid or dinitrosocatechin/nitrous acid system (p < 0.05).

Table 3. Enhancement of Quercetin Consumption by (+)-Catechin and 6,8-Dinitrosocatechin under Anaerobic Conditions[a]

	concentration of quercetin (μM)			
	0	5	15	50
	(Decrease in the Quercetin Concentration, μM)			
no addition	0	2.5 ± 0.2	6.5 ± 0.4	21.1 ± 1.7
50 μM (+)-catechin	0	3.9 ± 0.4[b]	8.4 ± 0.8[b]	25.4 ± 1.6[b]
50 μM diNO−CAT	0	4.3 ± 1.1[b]	10.0 ± 0.3[b]	26.1 ± 0.6[b]
	(Formation of Q293, Arbitrary Units)			
no addition	0	17 ± 3	37 ± 6	83 ± 2
50 μM (+)-catechin	0	86 ± 2[b]	109 ± 11[b]	158 ± 9[b]
50 μM diNO−CAT	0	230 ± 5[b]	264 ± 9[b]	295 ± 9[b]
	(Formation of diNO−CAT, μM)			
50 μM (+)-catechin	3.4 ± 0.8	3.2 ± 0.4	2.7 ± 0.4[b]	2.3 ± 0.5[b]
	(Formation of P1 and P2, Arbitrary Units)			
50 μM diNO−CAT	14 ± 3	7 ± 2[b]	c	c

[a]The reaction mixture (2 mL) contained 0, 5, 15, or 50 μM quercetin in 50 mM KCl−HCl (pH 2.0) in the presence and absence of 50 μM (+)-catechin or dinitrosocatechin. Reactions were initiated by the addition of 0.25 mM sodium nitrite, and the concentrations of reactants and products were determined at 1 min after the initiation of reactions. diNO−CAT = 6,8-dinitrosocatechin. Each data point represents the mean with SD (n = 3−6). [b]Significant differences in the decrease and increase in concentrations of quercetin and Q293, respectively, in the absence and presence of catechin or dinitrosocatechin and significant differences in the formation of diNO−CAT and formation of P1 and P2 in relation to the absence of quercetin (p < 0.05). [c]Below detection.

The value was (15.0 ± 3.6) × 10^2 M^{-1} min^{-1} (n = 6), which was about 2.2-fold the rate constants of the reactions between nitrous acid and (+)-catechin and between nitrous acid and 6,8-dinitrosocatechin (see above). The decrease in the concentration of quercetin was enhanced by 0.1 mM (+)-catechin by about 2.9- and 1.5-fold when the initial concentrations of quercetin were 10 and 30 μM, respectively. The degree of the enhancement was somewhat greater than that of the enhancement of Q293 formation by 0.1 mM (+)-catechin. (+)-Catechin-dependent enhancement of the quercetin consumption in nitrous acid/quercetin systems was observed in a concentration range of nitrite from 0.05 to 0.7 mM, suggesting that interactions between (+)-catechin and quercetin can occur under the conditions of the gastric lumen. The results in Table 1 and Figure 5 indicate that semiquinone radicals produced by reactions 2 and 4 can oxidize quercetin, enhancing the production of Q293.

Interactions between Dinitrosocatechin and Quercetin. The effects of 0.1 mM 6,8-dinitrosocatechin on the formation of Q293 were also studied in the presence of various concentrations of quercetin (Figure 5). Dinitrosocatechin enhanced the formation of Q293, and the enhancement was about 4-fold in the presence of 10 and 30 μM quercetin (△). The production of P1 and P2 was effectively suppressed by quercetin, and 50% inhibition was observed at approximately 10 μM quercetin (▲). Table 1 shows the enhancement of nitrous-acid-induced oxidation of quercetin by 0.1 mM 6,8-dinitrosocatechin. The degrees of the enhancement were about 3.1- and 2.3-fold in the presence of 10 and 30 μM quercetin, respectively. The results in Table 1 and Figure 5 suggest that the dinitrosocatechin semiquinone radical generated by the reaction with nitrous acid (reaction 7) can oxidize quercetin, suppressing the formation of dinitrosocatechin quinones and enhancing the formation of Q293.

•NO Production under Anaerobic Conditions. Table 2 shows the rate of nitrous-acid-induced •NO production determined using a Clark-type electrode under anaerobic conditions. When 50 μM quercetin, (+)-catechin, or 6,8-dinitroscatechin was present in the reaction mixture, the rate of •NO production was in the order (+)-catechin < 6,8-dinitrosocatechin < quercetin. Such order of •NO production in a system simulating gastric lumen has been reported.[40] The faster •NO production in the presence of quercetin compared to the presence of dinitrosocatechin could be explained by the difference in their reaction rate with nitrous acid (see above), and the much slower •NO production in the presence of (+)-catechin might be due to the reaction of semiquinone radicals derived from (+)-catechin with •NO by reactions 3 and 5.

The rate of nitrous-acid-induced •NO production increased nearly linearly as a function of the quercetin concentration. In the presence of 50 μM (+)-catechin, however, quercetin did not increase the rate of •NO production as expected from the rate in the absence of (+)-catechin, when the concentration of

quercetin was 5 μM. In the presence of 15 and 50 μM quercetin, quercetin increased the rate of $^{\bullet}$NO production significantly. These results support the postulation that semiquinone radicals of (+)-catechin and mononitrosocatechin can react with not only quercetin but also $^{\bullet}$NO produced by quercetin/nitrous acid systems and suggest that the rate of $^{\bullet}$NO consumption was limited by the rate of production of semiquinone radicals of (+)-catechin and mononitrosocatechin by reactions 3 and 5. 6,8-Dinitrosocatechin (50 μM) increased $^{\bullet}$NO production almost additively or more than additively at every concentration of quercetin examined. The result indicates that the reaction of $^{\bullet}$NO with the semiquinone radical of 6,8-dinitrosocatechin will be slow or negligible, supporting the above conclusion that the radical will react rapidly with quercetin. Under the conditions of Table 2, N_2O_3 generated by reaction 9[41] appears not to contribute to the formation of dinitrosocatechin, because $^{\bullet}$NO production by reaction 9 was quite slow (less than 1 μM/min in the presence of 0.5 mM sodium nitrite).

$$2HNO_2 \leftrightarrows N_2O_3 + H_2O \leftrightarrows {}^{\bullet}NO + {}^{\bullet}NO_2 + H_2O \quad (9)$$

Nitrosonium cation (NO^+) formed by reaction 10[41] might not contribute significantly, either, to the formation of dinitrosocatechin.

$$HNO_2 + H^+ \leftrightarrows H_2NO_2{}^+ \leftrightarrows NO^+ + H_2O \quad (10)$$

If NO^+ contributed to the nitrosation, 5 μM quercetin should increase the rate of $^{\bullet}$NO production in the presence of (+)-catechin, effectively inhibiting the formation of dinitrosocatechin, because quercetin might reduce NO^+ to $^{\bullet}$NO.

Interactions between Quercetin and (+)-Catechin or Dinitrosocatechin under Anaerobic Conditions. The interactions between quercetin and (+)-catechin or 6,8-dinitrosocatechin were also studied under anaerobic conditions (Table 3). (+)-Catechin (50 μM) and 6,8-dinitrosocatechin (50 μM) enhanced a nitrous-acid-induced decrease in the concentration of quercetin and the formation of Q293, irrespective of the concentration of quercetin. The results indicate that quercetin also interacted with (+)-catechin and dinitrosocatechin under anaerobic conditions. The interaction between quercetin and (+)-catechin is supported by the suppression of nitrous-acid-induced formation of 6,8-dinitrosocatechin by quercetin, and the interaction between quercetin and dinitrosocatechin is supported by the suppression of P1 and P2 formation by quercetin. Although the concentrations of (+)-catechin decreased by about 4 μM during the incubation for 1 min, effects of quercetin on the decrease in the concentration were unclear, similar to under aerobic conditions, supporting the slower reaction of the (+)-catechin semiquinone radical with quercetin than with NO. From the data in Tables 1 and 3 and Figure 5, we could conclude that the interactions between quercetin and (+)-catechin or 6,8-dinitrosocatechin were possible under semi-anaerobic conditions, such as the gastric lumen.

Possibility of Interactions between Catechins and Quercetin in the Stomach. The reactions concerned in this study are summarized in Figure 6. The (+)-catechin semiquinone radical generated by the reaction of (+)-catechin with nitrous acid will react effectively with $^{\bullet}$NO, producing mononitrosocatechin. The reaction of the semiquinone radical with quercetin will not be rapid enough to suppress nitrous-acid-induced consumption of (+)-catechin (represented as broken lines). Mononitrosocatechin also reacts with nitrous acid, producing the semiquinone radical, which can react with both $^{\bullet}$NO and quercetin, producing dinitrosocatechin and the quercetin semiquinone radical, respectively. The quercetin semiquinone radical generated by the above reactions is rapidly transformed to Q293 via the quercetin quinone form.[12,42] Q293 has been reported to decompose to more stable 2,4,6-trihydroxyphenylglyoxylic acid and 3,4-dihydroxybenzoic acid by oxidation.[17] Dinitrosocatechin produced by the above reactions also reacts with nitrous acid producing $^{\bullet}$NO and the semiquinone radical that can be transformed to quinone by disproportionation.

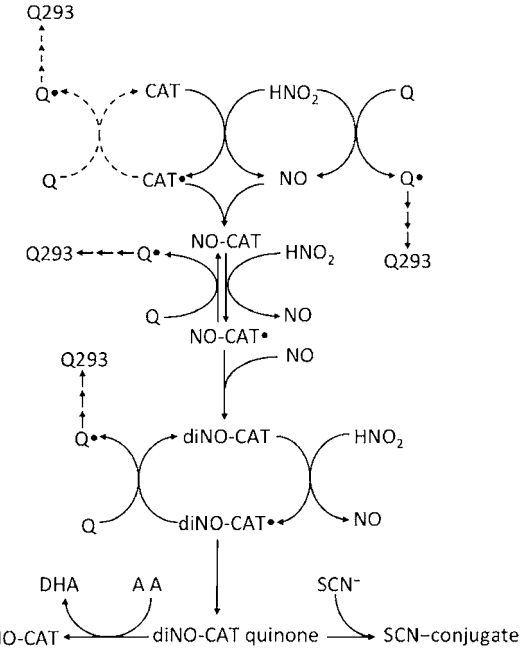

Figure 6. Possible interactions among quercetin, (+)-catechin, and 6,8-dinitrosocatechin. AA, ascorbic acid; DHA, dehydroascorbic acid; CAT and CAT$^{\bullet}$, (+)-catechin and its semiquinone radical; diNO−CAT and diNO−CAT$^{\bullet}$, 6,8-dinitrosocatechin and its semiquinone radical; diNO−CAT−quinone, quinone form of diNO−catechin; NO−CAT and NO−CAT$^{\bullet}$, mononitrosocatechin and its semiquinone radical, Q and Q$^{\bullet}$, quercetin and its semiquinone radical; Q293, an oxidation product of quercetin. Broken lines = slow reactions.

The molar ratios of (+)-catechin to quercetin glycosides were calculated to be about 0.7 and 0.5 in apple and buckwheat flour, respectively, and the ratios of (−)-epicatechin to quercetin glycosides were calculated to be about 3.2 and 3.5 in apple and buckwheat flour, respectively.[3,4] Because parts of quercetin glycosides from foods are hydrolyzed in the oral cavity, as described in the Introduction,[6−8] quercetin can coexist with (−)-epicatechin as well as (+)-catechin in gastric juice. There are no differences in the rate constants between (+)-catechin and (−)-epicatechin when these polyphenols react with superoxide anion radicals and singlet molecular oxygen,[23] and the antioxidant activity of (+)-catechin is equivalent to that of (−)-epicatechin when measured using the 2,2′-azino-bis(3-ethylbenzothiazoline-6-sulfonic acid cation radical ($ATBS^{\bullet+}$) as an oxidant.[43] Furthermore, 6,8-dinitorosoepicatechin produced in (−)-epicatechin/nitrous acid systems isomerizes to 6,8-dinitrosocatechin.[15] We can postulate from the results that (−)-epicatechin as well as (+)-catechin can interact with quercetin in the presence of nitrite under acidic conditions, as

dx.doi.org/10.1021/jf500860s | J. Agric. Food Chem. 2014, 62, 4951−4959

shown in Figure 6. The postulation was supported by the result that 0.1 mM (−)-epicatechin enhanced nitrite-induced oxidation of 10, 30, and 100 μM quercetin, increasing the formation of Q293 in 50 mM KCl−HCl (pH 2.0) under aerobic and anaerobic conditions.

It has been reported that (i) catechins can suppress nitrous-acid-induced *N*-nitrosodimethylamine formation from dimethylamine producing dinitrosocatechins and (ii) dinitrosocatechins induce toxic effects in Caco-2 cells, which are cultured colon carcinoma cells.[15] On the other hand, it is known that quinones are toxic because of their generation of reactive oxygen species and binding to DNA.[44] Thus, quercetin has an important function to prevent the formation of reactive quinone from the dinitrosocatechin semiquinone radical. In addition to quercetin, ascorbic acid in gastric juice may also prevent the formation of quinones by reducing corresponding radicals (not shown in Figure 6). If dinitrosocatechin quinone is produced in the stomach, ascorbic acid in gastric juice can reduce quinone to the mother compound and salivary thiocyanate can transform quinone to a stable thiocyanate conjugate.[37−39]

Although there are some systems to scavenge the quinones of dinitrosocatechins in the gastric lumen, it is beneficial if the formation of the quinones is prevented. Quercetin and ascorbic acid are candidates to prevent the formation of quinones in the gastric lumen. Thus, it seems to be favorable to ingest foods rich in components, which reduce semiquinone radicals derived from mononitrosocatechins and dinitrosocatechins, to prevent the formation of toxic quinones. In this way, the clarification of chemical interactions among polyphenols under the conditions simulating the stomach may be important to prepare foods that are beneficial for human health.

AUTHOR INFORMATION

Corresponding Author

*Telephone: +81-582-1131. Fax: +81-93-582-6000. E-mail: takahama@kyu-dent.ac.jp.

Funding

Part of this study was supported by Grants-in-Aid for Scientific Research (22500790 and 23500986) from the Ministry of Education and Science in Japan. Sonja Veljovic-Jovanovic and Filis Morina acknowledge the partial support from the Ministry of Education, Science, and Technological Development of the Republic of Serbia (III43010).

Notes

The authors declare no competing financial interest.

REFERENCES

(1) Hirota, S.; Shimoda, T.; Takahama, U. Tissue and spatial distribution of flavonol and peroxidase in onion bulbs and stability of flavonol glucosides during boiling of the scale. *J. Agric. Food Chem.* **1998**, *46*, 3497−3502.

(2) Takahama, U.; Yamauchi, R.; Hirota, S. Isolation and characterization of a cyanidin−catechin pigment from adzuki bean (*Vigna angularis*). *Food Chem.* **2013**, *141*, 282−288.

(3) Yoshida, K.; Kondo, T.; Ito, M.; Kondo, T. Analysis of polyphenols in water extract of red adzuki bean, *Vigna angularis*. *ITE Lett.* **2005**, *6*, 226−231.

(4) Danila, A. M.; Kotani, A.; Hakamata, H.; Kusu, F. Determination of rutin, catechin, epicatechin, and epicatechin gallate in buckwheat *Fagopyrum esculentum* Moench by micro-high-performance liquid chromatography with electrochemical detection. *J. Agric. Food Chem.* **2007**, *55*, 1139−1143.

(5) Bhagwat, S.; Haytowitz, D. B.; Holden, J. M. *USDA Database for the Flavonoid Content of Selected Foods, Release 3.1*; United States Department of Agriculture (USDA): Washington, D.C., 2013; http://www.ars.usda.gov/SP2UserFiles/Place/12354500/Data/Flav/Flav3-1.pdf.

(6) Hirota, S.; Nishioka, T.; Shimoda, T.; Miura, K.; Ansai, T.; Takahama, U. Quercetin glucosides are hydrolyzed to quercetin in human oral cavity to participate in peroxidase-dependent scavenging of hydrogen peroxide. *Food Sci. Technol. Res.* **2001**, *7*, 239−245.

(7) Browning, A. M.; Walle, U. K.; Walle, T. Flavonoid glycosides inhibit oral cancer proliferation—Role of cellular uptake and hydrolysis to the aglycones. *J. Pharm. Pharmacol.* **2005**, *57*, 1037−1041.

(8) Walle, T.; Browning, A. M.; Steed, L. L.; Reed, S. G.; Walle, U. K. Flavonoid glucosides are hydrolyzed and thus activated in the oral cavity in humans. *J. Nutr.* **2005**, *135*, 48−52.

(9) Pannala, A. S.; Mani, A. R.; Spencer, J. P. E.; Skinner, Y.; Bruckdorfer, K. R.; Moore, K. P.; Rice-Evans, C. A. The effect of dietary nitrate on salivary, plasma and urinary nitrate metabolism in humans. *Free Radical Biol. Med.* **2003**, *34*, 576−584.

(10) Vanýsek, P. *Electrochemical Series*; Issuu, Inc.: Palo Alto, CA, 2010; http://issuu.com/time-to-wake-up/docs/electrochemical_redox_potential.

(11) Janeiro, P.; Brett, A. M. O. Catechin electrochemical oxidation mechanism. *Anal. Chim. Acta* **2004**, *518*, 109−115.

(12) Brett, A. M. O.; Ghica, M.-E. Electrochemical oxidation of quercetin. *Electroanalysis* **2003**, *15*, 1745−1750.

(13) Takahama, U.; Oniki, T.; Hirota, S. Oxidation of quercetin by salivary components. Quercetin-dependent reduction of salivary nitrite under acidic conditions producing nitric oxide. *J. Agric. Food Chem.* **2002**, *50*, 4317−4322.

(14) Peri, L.; Pietraforte, D.; Scorza, G.; Napolitano, A.; Fogliano, V.; Minetti, M. Apples increase nitric oxide production by human saliva at the acidic pH of the stomach: A new biological function for polyphenols with a catechol group? *Free Radical Biol. Med.* **2005**, *39*, 668−681.

(15) Lee, S. Y. H.; Munerol, B.; Pollard, S.; Youdim, K. A.; Pannala, A. S.; Kuhnle, G. G. C.; Debnam, E. S.; Rice-Evans, C.; Spencer, J. P. E. The reaction of flavonols with nitrous acid protects against *N*-nitrosamine formation and leads to the formation of nitroso derivatives which inhibit cancer cell growth. *Free Radical Biol. Med.* **2006**, *40*, 323−334.

(16) Panzella, L.; Manini, P.; Napolitano, A.; d'Ischia, M. The acid-promoted reaction of the green tea polyphenol epigallocatechin gallate with nitrite ions. *Chem. Res. Toxicol.* **2005**, *18*, 722−729.

(17) Hirota, S.; Takahama, U.; Ly, T. N.; Yamauchi, R. Quercetin-dependent inhibition of nitration induced by peroxidase/H_2O_2/nitrite systems in human saliva and characterization of an oxidation product of quercetin formed during the inhibition. *J. Agric. Food Chem.* **2005**, *53*, 3265−3272.

(18) Benjamin, N.; O'Driscoll, F.; Dougall, H.; Duncan, C.; Smith, L.; Golden, M.; McKenzie, H. Stomach NO. *Nature* **1994**, *368*, 502.

(19) Xu, J.; Xu, X.; Verstraete, W. The bacteriacidal effect and chemical reactions of acidified nitrite under conditions simulating the stomach. *J. Appl. Microbiol.* **2001**, *90*, 523−529.

(20) Miyoshi, M.; Kasahara, E.; Park, A. M.; Hiramoto, K.; Minamiyama, Y.; Takemura, S.; Sato, E. F.; Inoue, M. Dietary nitrate inhibits stress-induced gastric mucosal injury in the rat. *Free Radical Res.* **2003**, *37*, 85−90.

(21) Björne, H. H.; Petersson, J.; Phillipson, M.; Weizberg, E.; Holm, L.; Lundberg, J. O. Nitrite in saliva increases gastric blood flow and mucuss thickness. *J. Clin. Invest.* **2004**, *113*, 106−114.

(22) Petersson, J.; Phillipson, M.; Jansson, E. A.; Patzak, A.; Lundberg, J. O. Dietary nitrate increase gastic blood flow and mucus defense. *Am. J. Physiol.: Gastrointest. Liver Physiol.* **2007**, *292*, G718−G724.

(23) Jovanovic, S. V.; Steenken, S.; Simic, M. G.; Hara, Y. Antioxidant properties of flavonoids: reduction potentials and electron transfer reactions of flavonoid radicals. In *Flavonoids in Health and Disease*;

Rice-Evans, C. A., Packer, L., Eds.; Marcel Dekker, Inc.: New York, 1998; pp 137−161.
(24) Zimmer, W.; Danneberg, G.; Bothe, H. Amperometric method for determining nitrous oxide in denitrification and in nitrogenase-catalyzed nitrous oxide reduction. *Curr. Micorbiol.* **1985**, *12*, 341−346.
(25) Volk, J.; Gorelik, S.; Granit, R.; Kohen, R.; Kanner, J. The dual function of nitrite under stomach conditions is modulated by reducing compounds. *Free Radical Biol. Med.* **2009**, *47*, 496−502.
(26) Takahama, U.; Hirota, S. Enhancement of iron(II)-dependent reduction of nitrite to nitric oxide by thiocyanate and accumulation of iron(II)/thiocyanate/nitric oxide complex under conditions simulating the mixture of saliva and gastric juice. *Chem. Res. Toxicol.* **2012**, *25*, 207−215.
(27) Licht, W. R.; Tannenbaum, S. R.; Deen, W. M. Effects of ascorbic acid and thiocyanate on nitrosation of proline in the dog stomach. *Carcinogenesis* **1988**, *9*, 365−372.
(28) Dojindo. *Dojindo Catalogue*, 29th ed.; Dojindo: Kumamoto, Japan, 2014; pp 38−40.
(29) Pollard, S. E.; Kuhnle, G. G. C.; Vauzour, D.; Vafeiadou, K.; Tzounis, X.; Whiteman, M.; Rice-Evans, C.; Spencer, J. P. E. The reaction of flavonoid metabolites with peroxynitrite. *Biochem. Biophys. Res. Commun.* **2006**, *350*, 960−968.
(30) Shen, C. C.; Chang, Y. S.; Ho, L. K. Nuclear magnetic resonance studies of 5,7-dihydroxyflavonoids. *Phytochemistry* **1993**, *34*, 843−845.
(31) Fossen, T.; Rayyan, S.; Andersen, Ø. M. Dimeric anthocyanidins from strawberry (*Fragaria ananasa*) consisting of pelargonidin 3-glucoside covalently linked to four flavan 3-ols. *Phytochemistry* **2004**, *65*, 1421−1428.
(32) Hirota, S.; Takahama, U. Reactions of apple fruit polyphenols with nitrite under the conditions of the gastric lumen: Generation of nitric oxide and formation of nitrosocatechins. *Food Sci. Technol. Res.* **2014**, *20*, 439−447.
(33) Gunther, M. P.; His, L. C.; Curtis, J. F.; Gierse, J. K.; Marnett, L. J.; Eling, T. E.; Mason, R. P. Nitric oxide trapping of the tyrosyl radical of prostaglandin H synthase-2 leads to tyrosine iminoxyl radical and nitrotyrosine formation. *J. Biol. Chem.* **1997**, *272*, 17086−17090.
(34) Kuruto-Niwa, R.; Ito, T.; Goto, H.; Nakamura, H.; Nozawa, R.; Terao, Y. Estrogenic activity of the chlorinated derivatives of estrogens and flavonoids using GFP expression system. *Environ. Toxicol. Pharmacol.* **2007**, *23*, 121−128.
(35) Wink, D. A.; Darbyshire, J. F.; Nims, R. W.; Saavedra, J. E.; Ford, P. C. Reactions of the bioregulatory agent nitric oxide in oxygenated aqueous media: Determination of the kinetics for oxidation and nitrosation by intermediates generated in the NO/O_2 reactions. *Chem. Res. Toxicol.* **1993**, *6*, 23−27.
(36) Issacs, N. S.; van Eldik, R. A mechanismtic study of the reaction of quinones by ascorbic acid. *J. Chem. Soc., Perkin Trans. 2* **1997**, 1465−1468.
(37) Takahama, U.; Tanaka, M.; Oniki, T.; Hirota, S.; Yamauchi, R. Formation of the thiocyanate conjugate of chlorogenic acid in coffee under acidic conditions in the presence of thiocyanate and nitrite: Possible occurrence in the stomach. *J. Agric. Food Chem.* **2007**, *55*, 4169−4176.
(38) Takahama, U.; Tanaka, M.; Hirota, S.; Yamauchi, R. Formation of an oxathiolone compound from rutin in acidic mixture of saliva and buckwheat dough: Possibility of its occurrence in the stomach. *Food Chem.* **2009**, *116*, 214−219.
(39) Takahama, U.; Tanaka, M.; Hirota, S. Formation of nitric oxide, ethyl nitrite and an oxathiolone derivative of caffeic acid in a mixture of saliva and white wine. *Free Radical Res.* **2010**, *44*, 293−303.
(40) Rocha, B. S.; Gago, B.; Barbosa, R. M.; Laranjinha, J. Dietary polyphenols generate nitric oxide from nitrite in the stomach and induce smooth muscle relaxation. *Toxicology* **2009**, *265*, 41−48.
(41) Oldreive, C.; Rice-Evans, C. The mechanism for nitration and nitrotyrosine formation in vitro and in vivo: Impact of diet. *Free Radical Res.* **2001**, *35*, 217−231.
(42) Timbola, A. K.; de Souza, C. D.; Giacomelli, C.; Spinelli, A. Electrochemical oxidation of quercetin in hydroalcoholic solution. *J. Braz. Chem. Soc.* **2006**, DOI: 10.1590/S0103-50532006000100020.
(43) Rice-Evans, C. A.; Miller, N. J. Structure−antioxidant activity relationship of flavonoids and isoflavonoids. In *Flavonoids in Health and Disease*; Rice-Evans, C. A., Packer, L., Eds.; Marcel Dekker, Inc.: New York, 1998; pp 199−219.
(44) Bolton, J. L.; Trush, M. A.; Penning, T. M.; Dryhurst, G.; Monks, T. J. Role of quinones in toxicology. *Chem. Res. Toxicol.* **2000**, *13*, 135−160.

Steinheim, Germany); sodium chloride (Carl Roth GmbH, Karlsruhe, Germany); β-ionone (Sigma-Aldrich, Steinheim, Germany); and NMR solvents (ARMAR Chemicals, Döttingen, Switzerland). Methanol and methyl *tert*-butyl ether as HPLC solvents were purchased from Sigma-Aldrich (HPLC grade ≥99.8%). All-*trans*-β-carotene (97% isomeric purity) was purchased from Sigma-Aldrich (Taufkirchen, Germany) and all-*trans*-lutein (95% isomeric purity) from Carl Roth GmbH.

Spinach Samples. Four different sets of spinach samples were considered during this study. In cooperation with the Leibniz Institute of Plant Biochemistry (Halle, Germany) a first set (varieties 'Bella' and 'Matador') was cultivated under greenhouse conditions from August to November 2012. A light period of 8 h was chosen to simulate short-day conditions. During this period a temperature of 22 °C and a relative humidity of 70% were adjusted. Electric illumination was performed by Cool Daylight lamps (Osram, 36 W/965). Temperature was regulated down to 15 °C during the dark phase (16 h) at the same humidity. Sampling started after 9 weeks (leaf size between 8 × 4 and 12 × 7 cm) and ended after 12 weeks of cultivation. In a second set spinach of both varieties was cultivated under field-grown conditions near Halle (Germany) at the same time. Additionally, spinach of the variety 'Matador' was cultivated during spring (from March to May) and summer (from June to August) in 2012. The other two sets were commercial samples from local markets and food stores. Altogether 37 samples of fresh spinach (origin Italy and Germany) and 43 samples of frozen spinach were collected. All samples were stored at −32 °C until processing.

Sample Preparation. Preparation of spinach was performed according to prior studies,[16] where the extraction method was adopted from Sadler et al.[17] Fresh or frozen material was cut into small slices first. Per sample about 15 g of spinach homogenate was filled into Falcon tubes and stored at −21 °C, followed by freeze-drying. Dry plant materials were extracted overnight with 150 mL of hexane/ethanol/acetone (2:1:1, v/v/v) containing 0.01% BHT by shaking with an orbital shaker (ca. 170 rpm) at room temperature under exclusion of light. For saponification of fatty compounds and an effective removal of interfering chlorophylls the organic extracts were treated with 15 mL of 10% methanolic potassium hydroxide solution and were shaken overnight at room temperature after saturation with argon to avoid oxidative degradation of carotenoids.[14,18] The alkaline extracts were washed five times with 60 mL of a 2% sodium chloride solution. Aliquots of the resulting carotenoid extracts (2 mL) were dried under argon and dissolved in 1 mL of mobile phase (methanol/MTBE, 50:50).

Sample preparation was performed under reduced light using amber glassware, and the temperature never exceeded 25 °C to avoid isomerization processes induced by light or temperature.

Analytical HPLC-UV and HPLC-DAD. The HPLC method was developed and optimized on the basis of studies of Fang et al.[19] A Jasco PU-2089 Plus quaternary gradient unit pump with a degasser and a Jasco AS-2055 Plus autosampler (Gross-Umstadt, Germany) were used. Elution of materials was monitored by a Jasco UV-2075 Plus UV-detector operating at 450 nm. For DAD analyses a Jasco MD-2015 Plus detector was used. Chromatographic separations were performed on a RP-C30 column (5 μm, 250 × 4.0 mm, YMC Europe, Dinslaken, Germany) connected to a C30 guard column (5 μm, 10 × 4.0 mm, YMC Europe) using a flow rate of 0.65 mL min^{-1}. Chosen column temperature was 20 °C. The mobile phase used consisted of methanol (solvent A) and methyl *tert*-butyl ether (solvent B). Samples were injected at 40% B (held for 5 min) followed by a gradient that changed to 52% B in 15 min. The gradient then changed to 100% B in 5 min (held for 10 min) and to 40% B in 5 min (held for 10 min).

Analytical HPLC-MS^2. A Jasco PU-2080 Plus quaternary gradient pump with degasser and a Jasco AS-2057 Plus autosampler were used. The RP-C30 column and HPLC gradient program used were the same as for HPLC-UV measurements. Elution of carotenoids was monitored by mass detection. The mass analyses were performed using an Applied Biosystems API 4000 quadrupole instrument (Applied Biosystems, Foster City, CA, USA) equipped with an API source using an atmospheric pressure chemical ionization (APCI, negative mode) interface. The LC system was connected directly to the probe of the mass spectrometer. Nitrogen was used as sheath and auxiliary gas. β-Carotene isomers were detected at 536.7 amu in Q1 (DP −60 V, no fragments in Q3).

Synthesis of Authentic β-Carotene Standards. In contrast to the literature 15-*cis*-β-carotene was synthesized via a C_{15} + C_{10} + C_{15} route.[20] Thus, C_{15}-Wittig salts were generated according to the method of Hengartner et al. using β-ionone as the starting compound instead of pseudoionone.[21] The central compound, 2,7-dimethylocta-2,6-dien-4-yne-1,8-dial, was assembled according to the method of Isler et al. and was directly coupled to the Wittig salts.[20] After Lindlar hydrogenation, the 15,15′-dehydro-β-carotene was transferred to 15-*cis*-β-carotene (ca. 27 mg) with an isomeric purity of 90% (HPLC-UV). 9-*cis*-β-Carotene was generated by coupling 9-*cis*-retinal and all-*trans*-retinyl-Wittig salt. First, the C_{20}-Wittig salt was generated according to the method of Britton et al. starting with commercially available all-*trans*-retinal (Sigma-Aldrich, Taufkirchen, Germany).[22] The second precursor, 9-*cis*-retinal, was obtained after reduction of 9-*cis*-retinyl ethyl ester, which was synthesized according to the literature.[23−26] Conventional Wittig condensation resulted in 20 mg of 9-*cis*-β-carotene with an isomeric purity of 71% (HPLC-UV). All structures were established by their NMR data (^{1}H; ^{13}C; H,H−COSY; HSQC; HMBC).

Irradiation Model Systems. Various model systems were established to simulate different light conditions during the cultivation of spinach. The influence of daylight on isomerization of carotenoids was simulated by irradiation of all-*trans*-β-carotene with a halogen lamp, thus mimicking field-growing conditions. On the other hand, different optical filters, which are impermeable below specific wavelengths, were interposed between standard solution and halogen lamp to imitate light conditions during greenhouse cultivation. A 550 nm filter was used to simulate illumination with a sodium vapor lamp, which is commonly used for cultivation in greenhouses, because natural sunlight does not suffice to harvest spinach during winter months. The wavelength spectrum of these lamps is optimized for photosynthesis; that is, they emit almost no light in the range of 250−550 nm. Growing spinach under greenhouse conditions without the use of additional sources of light was simulated by interposing a 420 nm filter. PE foils, PMMA sheets, or glass are typical materials that are used for cultivation in greenhouses. These materials cause a light permeability of <90%, which in cultivation depends additionally on the level of contamination, roof pitch, and deterioration. Light with wavelengths below 400 nm is efficiently blocked by these materials.[27] All-*trans*-β-carotene solutions (21 μM in hexane) were irradiated for defined periods of time (5, 10, 15, 20, 30, 60, 120, 180, and 240 min). Aliquots (500 μL) were dried afterward under argon stream. Residues were taken up in 400 μL of mobile phase (methanol/MTBE, 50:50) to adjust final concentrations to 26 μM (according to spinach samples) followed by HPLC-UV analyses. The isomeric composition was determined by integration of all identified β-carotene peaks first. Then the areas of the separate peaks were divided by the sum of all β-carotene values to express the percentage of the respective β-carotene concentration. Contents of β-carotene (including all isomers) were calculated on the basis of the external linear calibration of all-*trans*-β-carotene standard at its wavelength maximum of 450 nm.

Thermal Treatment. Concentrated all-*trans*-β-carotene solutions were stirred at 65 °C in amber glass vials, and aliquots of 500 μL were sampled after 5, 10, 15, 30, 60, 120, 180, and 240 min. HPLC-UV analyses were performed after the samples were dried and dissolved in mobile phase (400 μL). This experiment showed differences from photoinduced isomerization processes and allowed the exclusion of thermal-induced artifacts during the extraction method.

Blanching of Fresh Spinach. Fresh spinach leaves (ca. 5 g per sample) were immersed into boiling water for a period of 0.5, 1, 2, 3, 5, or 10 min. Treated samples were immediately quenched on ice water. Sample preparation was as described above.

Nuclear Magnetic Resonance Spectroscopy (NMR). NMR spectra were recorded on a Varian VXR 400 spectrometer operating at 400 MHz for ^{1}H and at 100 MHz for ^{13}C or on a Varian Unity Inova 500 instrument operating at 500 MHz for ^{1}H and at 125 MHz for ^{13}C, respectively.

Statistical Analysis. Analyses of carotenoid concentrations were performed in duplicate for each model system and resulted in coefficients of variation of <5%. All significance tests were performed by two-sample *t* test with a probability value of 99%. The Welch test was used alternatively in one case of differing standard deviations. The same probability value was selected. Confidence intervals were calculated with a probability value of 95%.

RESULTS AND DISCUSSION

Identification of β-Carotene Isomers. HPLC-UV analyses of spinach extracts led to the typical chromatograms shown in Figure 1. The identification was performed first by

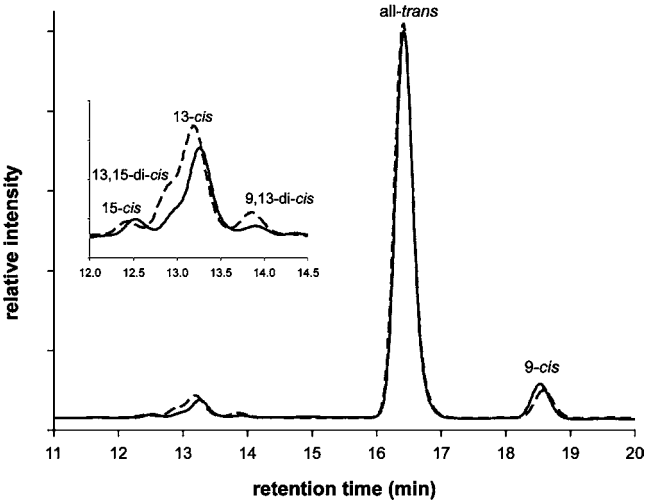

Figure 1. HPLC chromatograms of an authentic field-grown (solid line) and a greenhouse-grown (dashed line) spinach extract. Elution of β-carotene isomers (15-*cis*-β-carotene; 13,15-di-*cis*-β-carotene; 13-*cis*-β-carotene; 9,13-di-*cis*-β-carotene; all-*trans*-β-carotene; 9-*cis*-β-carotene) was monitored by UV detection at 450 nm.

LC/APCI-MS analyses. During negative ion APCI six peaks formed a pseudomolecular ion of *m/z* 536.7, thus verifying them as β-carotene isomers. Absolute configuration was verified by comparison of retention times using authentic references. Besides commercially available all-*trans*-β-carotene, independently synthesized 9-*cis*- and 15-*cis*-β-carotene were used. The remaining isomers were assigned on the basis of their spectral characteristics determined by HPLC-DAD analyses. *Q*-ratios (absorption at the subsidiary "*cis*-peak" divided by the absorption at λ_{max})[28,29] were formed and compared to the literature and thus allowed an identification of 13-*cis*-β-carotene.[30] As expected, our experiments gave the highest *Q*-ratio for 15-*cis*-β-carotene (0.61), followed by 13-*cis* (0.46), 9-*cis* (0.09), and all-*trans* (0.06). In addition, the HPLC elution pattern (Figure 1) was completely comparable to data of Strohschein et al., which identified the two remaining isomers as 13,15-di-*cis*- and 9,13-di-*cis*-β-carotene (exptl *Q*-ratio 0.42) using HPLC−NMR analyses.[31] The presented assignment using various approaches for the identification of β-carotene isomers allowed targeted analyses in the following studies.

Irradiation and Thermal Treatment Model Systems. Model system A simulated illumination conditions during field-grown cultivation. In this case a halogen lamp with a wavelength spectrum close to that of sunlight was used for irradiation (Figure 2A). All-*trans*-β-carotene underwent a strong degradation during the first 30 min of illumination, illustrated by a decrease starting from a concentration of 96.55 to 89.55%. After that, the degradation attenuated and almost reached equilibrium at 85.31%. 13-*cis*- and 15-*cis*-β-carotene showed opposite developments. Both isomers were formed in high yields during the first period of irradiation. 13-*cis*-β-Carotene rose from 2.39 to 6.96%, whereas 15-*cis* reached a concentration of 1.90% starting from 0.24%. Both isomers approximated equilibrium concentrations, too; however, a decrease was observed after full time of illumination (13-*cis*, 6.09%; and 15-*cis*, 1.66%). In contrast, an almost linear formation during the whole period of treatment was observed for 9-*cis*-β-carotene. Its concentration rose from 0.75 to 6.86% (ca. 1.5%/h); thus, 9-*cis* was the predominant *cis*-isomer after photoinduced isomerization. Interestingly, the formation of 9-*cis*-β-carotene was closely associated with degradation of 13-*cis*-β-carotene in the last period of irradiation, when all other isomers showed no appreciable changes anymore. Almost no change was observed for 9,13-di-*cis*-β-carotene, the concentration of which stayed unchanged at about 0.10%. Similar light-induced isomerization progress was observed by O'Neil et al. among others; that is, 13-*cis*- and dominantly 9-*cis*-β-carotene were formed after exposure to white light (24 h).[32] Further illumination yielded only a small increase of 9-*cis*, whereas 13-*cis* slightly decreased. Thus, the observed equilibrium for the 13-*cis* isomer is confirmed by the literature.[11,32]

In contrast, irradiation with limited-wavelength spectra using cutoff filters led to completely different isomerization progressions (Figure 2B,C). Model system B mimicked typical growing conditions under foils or plastic materials, which are impermeable for light under 400 nm. Thus, a 420 nm optical filter was interposed to simulate greenhouse-grown conditions. In comparison to model system A, the isomerization process was significantly suppressed, illustrated by a reduced decrease of all-*trans*-β-carotene to a concentration of just 90.08% (total loss of 6.91%). In the presence of energy-rich light a higher loss of 11.24% was observed before. Formations of 13-*cis*- and 15-*cis*-β-carotene were deferred, too. Their maximal concentrations of 6.00% (13-*cis*) and 1.50% (15-*cis*) were reached after 3 h to form equilibria. Slight decreases at the end of irradiation were detected as well. The concentration of 9-*cis*-β-carotene rose linearly to 2.47%, compared to 6.86% in model system A. Thus, the formation rate was almost 4 times higher in comparison to only 0.4%/h in model system B. The concentration of 9,13-di-*cis*-β-carotene showed no significant change during irradiation again. Although the degradation and formation of all isomers were extenuated, the pattern of isomerization was similar to that of model system A.

A 550 nm cutoff filter was used in model system C (Figure 2C) to simulate growing conditions under electric illumination. Commonly used sodium vapor lamps are designed especially for photosynthesis; that is, they emit only a wavelength range between 550 and 750 nm. Figure 2C illustrates that almost no isomerization occurred during this experiment. All-*trans*-β-carotene decreased to just 94.16%, that is, a total loss of 2.38% compared to 6.91% in model B or 11.24% in model A. 13-*cis*- and 15-*cis*-isomers were formed in only small amounts. Linear increases from 2.39 to 3.61% (13-*cis*) and from 0.24 to 0.60% (15-*cis*) were observed. Similar results were recorded for 9-*cis*-β-carotene, the concentration of which marginally rose to 1.27% starting at 0.75%. In contrast to both other models 9,13-di-*cis*-β-carotene was formed during this experiment. Here, its concentration increased significantly from 0.08 to 0.35%.

In addition, thermal treatment of β-carotene standard solutions was performed to exclude artifacts during extraction

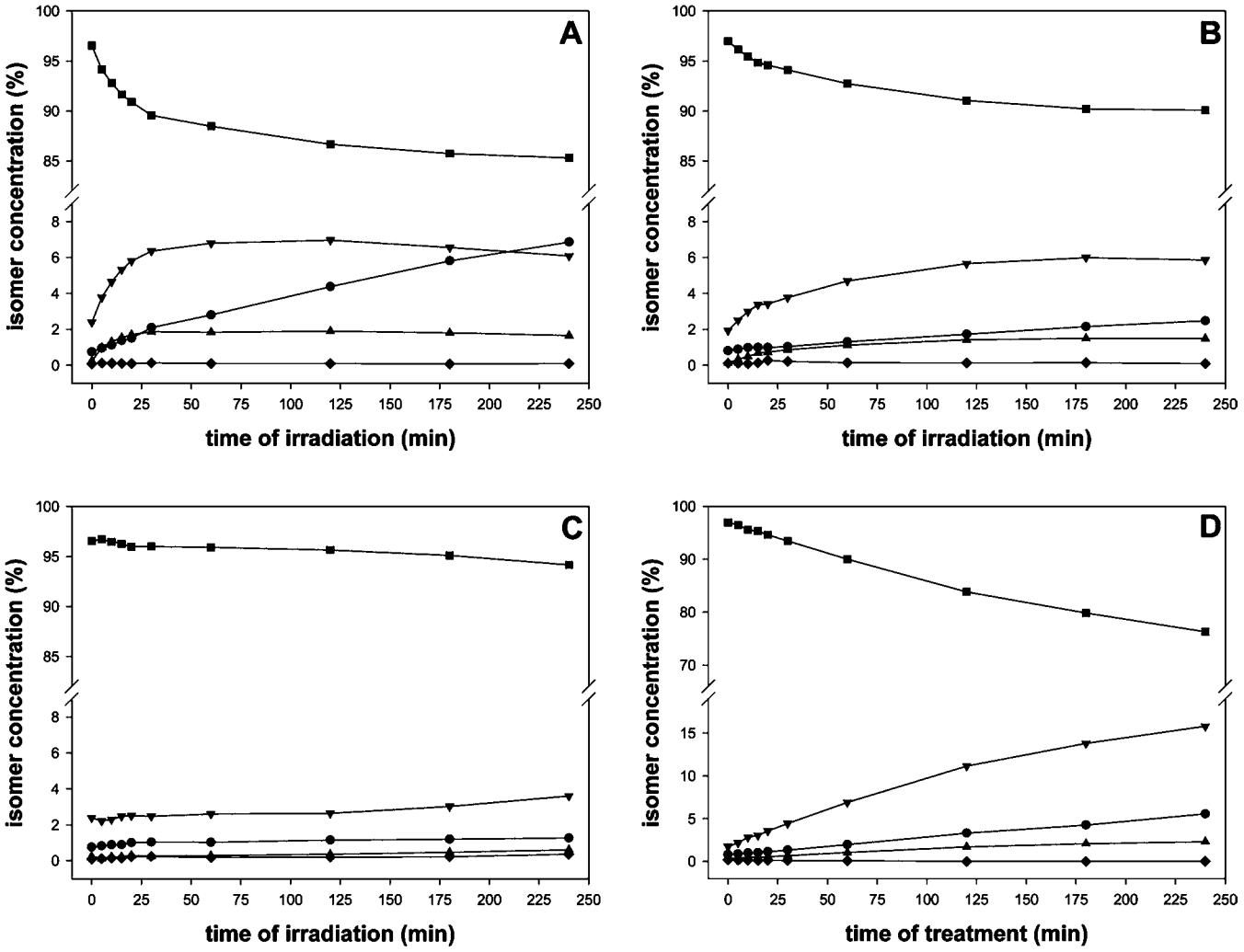

Figure 2. Concentrations of *β*-carotene isomers during irradiation with a halogen lamp over a period of 4 h using no filter (A), a 420 nm filter (B), a 550 nm filter (C), and thermal treatment at 65 °C (D), expressed as percentage of total *β*-carotene concentration (%): 15-*cis*-*β*-carotene (▲); 13-*cis*-*β*-carotene (▼); 9,13-di-*cis*-*β*-carotene (◆); all-*trans*-*β*-carotene (■); 9-*cis*-*β*-carotene (●).

and preparation for analyses. Simultaneous possible crossovers to photoinduced isomerization were clarified in this experiment. Thermal-triggered isomerization (Figure 2D) showed a similar pattern compared to model system B. All-*trans*-*β*-carotene was degraded from 96.97 to 76.31% and thus resulted in the highest decrease during all model systems (total loss of 20.66%). In parallel, 13-*cis*-*β*-carotene reached a concentration of 15.80% after 4 h of treatment at 65 °C, that is, nearly 3 times higher compared to model system A (6.09%). Furthermore, a linear increase was determined during heating with no equilibrium reached during the given time frame. Formation of 15-*cis*-*β*-carotene resulted in a similar progress. With a concentration of 2.31% the highest level of all systems was generated after thermal processing (compared to 1.66% in model A). 9-*cis*-*β*-Carotene was also formed during heating; however, its concentration rose to just 5.57% compared to 6.86% after irradiation in model system A. Interestingly, 9,13-di-*cis*-*β*-carotene was almost completely degraded after thermal treatment, when its concentration decreased to just 0.01%.

The results of all-*trans*-*β*-carotene model systems (Figure 2) were in line with theoretical studies on isomerization of *β*-carotene by Guo et al.[33] Compared to 13-*cis*- and 15-*cis*-*β*-carotene ($\Delta E^{\ddagger}$ = 9.1 and 9.7 kcal/mol (T_1)) the 9-*cis*-isomer has the highest barrier of activation energy ($\Delta E^{\ddagger}$ = 13.4 kcal/mol (T_1)). This means that its formation is preferred in the presence of energy-rich light.[33] Simultaneously, its high rotational barrier for reverse reaction leads to the highest stability within all *cis*-isomers and explains the linear formation during irradiation, whereas 13-*cis*-*β*-carotene was degraded after reaching a maximum (Figure 2A).[33] During irradiation in model systems B and C energy levels did not suffice to trigger the formation of hindered 9-*cis*-*β*-carotene up to that level. These studies provide an explanation for the curve progressions, too. On the one hand, 13-*cis*- and 15-*cis*-*β*-carotene represent the kinetically controlled products, because they were formed in high yields just at the beginning of irradiation. On the other hand, 9-*cis*-*β*-carotene was formed during the whole period of illumination associated with a decrease of 13-*cis* and 15-*cis* at the end of treatment, identifying 9-*cis*-*β*-carotene as the thermodynamically controlled product. Our experiments showed a formation of 9,13-di-*cis*-*β*-carotene during irradiation in model system C, whereas no formation was observed in model systems A and B. Accordingly, the barrier of activation energy has to be low to afford formation with energy-poor light. Otherwise, the isomer is characterized by a low rotational barrier for reisomerization processes, which

dx.doi.org/10.1021/jf501136g | J. Agric. Food Chem. 2014, 62, 4960−4967

explains constant concentrations during illumination with energy-rich light. During thermal processing the thermodynamic reaction product 9-*cis*-β-carotene was generated to a lesser extent compared to the daylight irradiation model, but higher than in model systems B and C. Similar observations were described in the literature; for example, Pott et al. showed increased levels of 9-*cis*-β-carotene in solar-dried mangoes, whereas conventionally dried mangoes contained high amounts of 13-*cis*-β-carotene.[10]

Thus, 9-*cis*-β-carotene and 9,13-di-*cis*-β-carotene were identified as potent markers for a possible differentiation of illumination conditions during cultivation of vegetables. In addition, 9,13-di-*cis* was not formed during thermal processing, which emphasizes its importance for a possible differentiation to photoinduced processes, whereas high levels of 13-*cis*- and 15-*cis*-isomers are useful parameters for the determination of thermal treatment of foods, as expected from the literature.[9−13] For example, Chandler et al. showed increased levels of 13-*cis*-β-carotene in various canned fruits and vegetables compared to fresh samples.[13]

Blanching of Fresh Spinach. Fresh spinach leafs were blanched in boiling water for defined periods of time. This experiment assigned the results of the above model systems to a complex matrix and was established to identify possible differences between untreated spinach and frozen commercial spinach, which is commonly blanched to inactivate enzymes and microorganisms.[34] Blanching of spinach resulted in a comparable pattern (Figure 3) to thermal incubation of all-

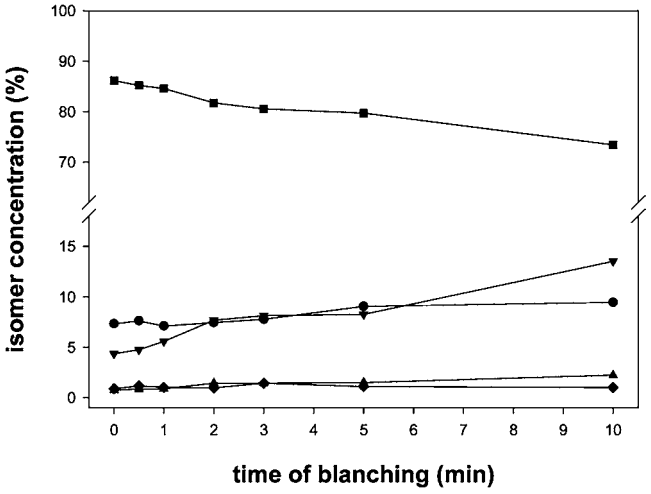

Figure 3. Concentrations of β-carotene isomers during blanching at 100 °C over a period of 10 min: 15-*cis*-β-carotene (▲); 13-*cis*-β-carotene (▼); 9,13-di-*cis*-β-carotene (◆); all-*trans*-β-carotene (■); 9-*cis*-β-carotene (●).

trans-β-carotene. The native all-*trans*-β-carotene concentration of 86.14% decreased to 73.43% during 10 min of blanching, whereas 13-*cis* (from 4.34 to 13.53%) was formed dominantly. A similar increase was found for 15-*cis*-β-carotene (from 0.71 to 2.22%) and 9-*cis*-β-carotene (from 7.32 to 9.44%), whereas 9,13-di-*cis*-β-carotene slightly rose from 0.87 to 0.99%. These results comply with observations in the thermal treatment model system and, thus, verify their validity for follow-up studies on authentic spinach samples. Lemmens et al. showed comparable results during the thermal processing of carrot puree, where 13-*cis* was dominantly formed and 9-*cis* resulted in a lower reaction rate constant.[11]

Isomeric Composition of Authentic and Commercial Spinach Samples. On the basis of the various model systems, four sets of spinach samples were analyzed with regard to their isomeric β-carotene pattern to identify possible differences caused by growing and processing conditions. All five β-carotene isomers showed significant differences compared to authentic field-grown and authentic greenhouse-grown spinach as depicted in Table 1 and Figure 4. In general, authentic field-grown spinach showed a higher *cis*-isomer concentration compared to authentic greenhouse-grown spinach, illustrated by a significantly lower concentration of all-*trans*-β-carotene (−1.28%). Simultaneously, significantly higher concentrations of 9-*cis*- (+1.03%), 13-*cis*- (+0.56%), and 15-*cis*-β-carotene (+0.27%) were determined. In contrast, 9,13-di-*cis*-β-carotene was the only isomer with a significantly lower concentration in field-grown spinach (0.25 ± 0.03%) compared to greenhouse-grown samples (0.76 ± 0.05%). Comparison of authentic field-grown and fresh commercial spinach led to two significant differences. Commercial spinach had a significantly lower concentration of all-*trans*-β-carotene (−1.10%) combined with a significantly higher level of 9-*cis*-β-carotene (+1.09%). A clear differentiation between authentic field-grown spinach and frozen commercial spinach was also possible; that is, five parameters with significant differences in the isomeric composition were observed. In this case 13-*cis*- and 15-*cis*-β-carotene showed significantly higher concentrations (13-*cis*, +0.98%; 15-*cis*, +0.22%), whereas all-*trans* (−0.49%), 9-*cis* (−0.48%), and 13,15-di-*cis* (−0.22%) resulted in significantly lower concentrations.

Table 1 shows that differences in the isomeric profile between authentic field- and greenhouse-grown spinach completely corresponded to model systems, where all relevant isomers (13-*cis*, 15-*cis*, 9-*cis*) reached higher concentrations during energy-rich irradiation. Additionally, 9,13-di-*cis*-β-carotene had a significantly lower concentration in authentic field-grown spinach (0.25 ± 0.03%) compared to authentic greenhouse-grown samples (0.76 ± 0.05%). This significant difference between both authentic groups is based on the limited stability of 9,13-di-*cis*-β-carotene in the presence of UV light as observed during the above model systems. On the basis of our experiments the most potent markers (9-*cis*- and 9,13-di-*cis*-β-carotene) were plotted in two dimensions in Figure 4 and led to a clear differentiation of authentic field- and greenhouse-grown spinach samples.

During analyses of both cultivated varieties 'Matador' and 'Bella' no significant differences were observed within the authentic groups; thus, no separation of samples was performed during plotting. Time of cultivation also led to no deviations within the groups.

A total of 37 fresh spinach samples available from local markets and food stores were then analyzed to prove the concept of differentiation of growing conditions for commercial spinach in open fields. Mean concentrations of the four above isomers showed no significant differences compared to authentic field-grown spinach, thus reflecting the typical cultivation of European spinach. In contrast, significant differences in all-*trans*- and 9-*cis*-β-carotene were determined compared to field-grown spinach. The mean concentration of all-*trans* was 1.10% lower, whereas 9-*cis* was 1.09% higher concentrated. This led to a separation in two subgroups of fresh spinach. One part indeed correlated to authentic field-grown spinach. The other set lay above the cluster of the authentic field-grown group, characterized by a strong increase in 9-*cis*-β-

Table 1. Mean Concentration (± Confidence Interval[a]) of All Analyzed β-Carotene Isomers Observed in Different Sets of Spinach Samples, Expressed as Percentage of Total β-Carotene

	authentic field-grown spinach (%) (n = 58)	authentic greenhouse-grown spinach (%) (n = 67)	fresh commercial spinach (%) (n = 37)	frozen commercial spinach (%) (n = 43)
15-*cis*	0.72 ± 0.04	0.45 ± 0.03#	0.64 ± 0.05	0.94 ± 0.05#
13,15-di-*cis*	0.80 ± 0.05	0.87 ± 0.05	0.75 ± 0.07	0.58 ± 0.06#
13-*cis*	4.37 ± 0.11	3.81 ± 0.11#	4.48 ± 0.12	5.35 ± 0.32*
9,13-di-*cis*	0.25 ± 0.03	0.76 ± 0.05#	0.28 ± 0.07	0.25 ± 0.04
all-*trans*	86.34 ± 0.21	87.62 ± 0.17#	85.24 ± 0.27#	85.85 ± 0.26#
9-*cis*	7.52 ± 0.14	6.49 ± 0.11#	8.61 ± 0.22#	7.04 ± 0.18#
μg/g FW (range)	41.90 (20.35−66.12)	64.55 (41.61−84.22)	44.93 (16.53−66.88)	34.00 (21.33−46.48)

[a]#, significant difference compared to authentic field-grown spinach calculated by t test (α = 0.01); *, significant difference compared to authentic field-grown spinach calculated by Welch test (α = 0.01).

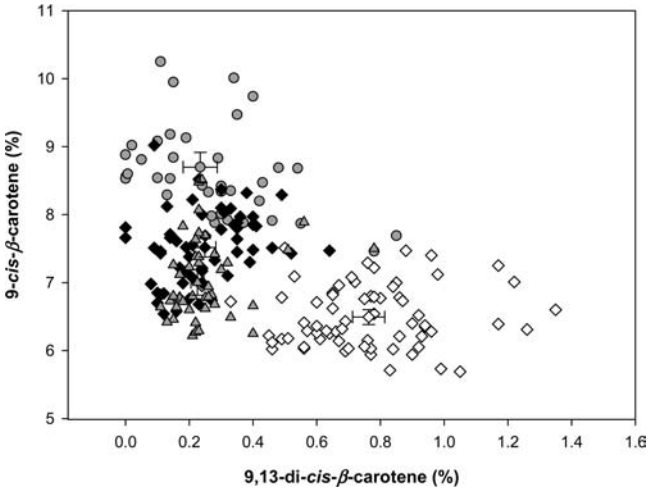

Figure 4. 9-*cis*- versus 9,13-di-*cis*-β-carotene concentrations of authentic field-grown (◆), authentic greenhouse-grown (◇), fresh commercial (gray circles), and frozen commercial (gray triangles) spinach samples, expressed as percentage of total β-carotene concentration (%).

carotene. These fresh spinach samples originated from Italy, where obviously not only higher sunlight intensity but also higher average temperatures lead to an increase of 9-*cis*. Moreover, 9-*cis* is known to be enzymatically formed from all-*trans* during biosynthesis of carlactones and strigolactones triggered by D27 isomerase.[35] This enzymatic activity might also be influenced by light conditions or the variety of spinach. Thus, 9,13-di-*cis*-β-carotene is clearly the stronger parameter for differentiation of field- and greenhouse-grown spinach as its concentration was just influenced by photoinduced processes, leading to 3 times lower concentrations in the presence of energy-rich UV light. Notably, three samples of fresh commercial spinach showed crossovers to authentic greenhouse-grown spinach caused by conspicuous 9,13-di-*cis*-β-carotene concentrations between 0.55 and 0.85%. This strongly suggested that these samples were cultivated in greenhouses. The purchase date (December 3, 2012; origin, Italy) further supported this hypothesis, because climatic conditions during November and December do not suffice for effective cultivation of spinach.

Furthermore, a total of 43 frozen spinach samples available from local food stores were analyzed for their isomeric composition. The mean concentration of 9,13-di-*cis*-β-carotene was in the same range compared to authentic field-grown and fresh commercial spinach. Unexpectedly, the concentration of 9-*cis*-β-carotene as a second marker for photoinduced isomerization was significantly lower than for the authentic field-grown set, but higher than for authentic greenhouse-grown samples. Still, two-dimensional plotting of 9-*cis*- and 9,13-di-*cis*-β-carotene allowed a clear assignment to authentic-field grown spinach, whereas almost no crossovers were observed to greenhouse-grown samples (Figure 4). This confirmed again that 9,13-di-*cis* is the stronger parameter for field-grown conditions and, in a broader sense, that commercial spinach is commonly cultivated under field-grown conditions in most European countries. Interestingly, three samples with unusually high concentrations of 9,13-di-*cis*-β-carotene (0.51−0.78%) compared to all other frozen samples overlapped to the greenhouse-grown set. According to the declaration, all three samples were produced in November 2012 with origin in Flanders, Belgium. In agreement with the literature, greenhouse cultivation is an intensive part of horticulture in the region of Flanders,[36] which for the present three samples was further supported by the date of production.

In addition, significantly higher concentrations of the identified thermal markers 13-*cis*- and 15-*cis*-β-carotene in parallel to a significantly lower concentration of all-*trans* were determined in frozen commercial spinach samples compared to both authentic-grown sets (Table 1). According to the above blanching model experiments and data from the literature, the increased concentrations must be attributed to thermal processing.[9,37] In general, frozen commercial spinach is blanched directly after harvest to inactivate enzymes and microorganisms that could influence quality or storage stability.[34] Obviously, the resulting isomeric composition allowed for a differentiation between frozen spinach and untreated fresh spinach samples based on two-dimensional plotting of 15-*cis*- and 13-*cis*-β-carotene concentrations (Figure 5). Although the mean concentration clearly differed from that of untreated fresh spinach samples, several crossovers were observed. This must be explained by considerable variations in temperature and duration of the industrial blanching processes. Nevertheless, this method seems to be applicable for a differentiation between blanched and untreated spinach. Comparable results were illustrated in the literature for blanched fruits and vegetables; for example, a 13-*cis*-β-carotene concentration of 15.3% was determined in canned spinach compared to just 8.8% in fresh samples by Chandler et al.[9,13]

In summary, on the basis of various model systems, 9-*cis*- and especially 9,13-di-*cis*-β-carotene were identified as potent markers for a differentiation of illumination conditions during cultivation, whereas 15-*cis*- and 13-*cis*-isomers were most characteristic for thermal processing as expected from the

dx.doi.org/10.1021/jf501136g | J. Agric. Food Chem. 2014, 62, 4960−4967

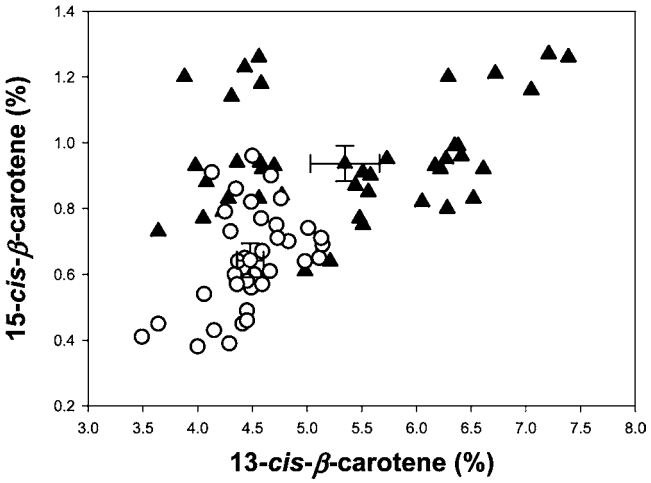

Figure 5. 15-*cis*- versus 13-*cis*-β-carotene concentrations of fresh (○) and frozen commercial (▲) spinach samples, expressed as percentage of total β-carotene concentration.

literature.[9−13] Results were successfully transferred to complex matrices and allowed a clear differentiation between authentic field- and greenhouse-grown spinach and additionally between blanched (frozen) and fresh spinach samples. The applicability to commercial spinach was proven and led to the putative identification of 6 greenhouse-grown samples of a total of 80 commercial samples. Further studies will show if the results on carotenoid isomerization can be transferred to other vegetables for authentication of growing and processing conditions.

■ ASSOCIATED CONTENT

Ⓢ Supporting Information

Additional experimental details. This material is available free of charge via the Internet at http://pubs.acs.org.

■ AUTHOR INFORMATION

Corresponding Author

*(M.A.G.) E-mail: marcus.glomb@chemie.uni-halle.de. Fax: ++049-345-5527341.

Notes

The authors declare no competing financial interest.

■ REFERENCES

(1) O'Neill, M. E.; Carroll, Y.; Corridan, B.; Olmedilla, B.; Granado, F.; Blanco, I.; van den Berg, H.; Hininger, I.; Rousell, A. M.; Chopra, M.; Southon, S.; Thurnham, D. I. A European carotenoid database to assess carotenoid intakes and its use in a five-country comparative study. *Br. J. Nutr.* **2001**, *85*, 499−507.

(2) Maiani, G.; Periago Caston, M. J.; Catasta, G.; Toti, E.; Goni Cambrodon, I.; Bysted, A.; Granado-Lorencio, F.; Olmedilla-Alonso, B.; Knuthsen, P.; Valoti, M.; Boehm, V.; Mayer-Miebach, E.; Behsnilian, D.; Schlemmer, U. Carotenoids: actual knowledge on food sources, intakes, stability and bioavailability and their protective role in humans. *Mol. Nutr. Food Res.* **2009**, *53*, 194−218.

(3) Krinsky, N. I. *The Antioxidant and Biological Properties of the Carotenoids*; New York Academy of Sciences: New York, 1998.

(4) Ma, L.; Dou, H. L.; Huang, Y. M.; Lu, X. R.; Xu, X. R.; Qian, F.; Zou, Z. Y.; Pang, H. L.; Dong, P. C.; Xiao, X.; Wang, X.; Sun, T. T.; Lin, X. M. Improvement of retinal function in early age-related macular degeneration after lutein and zeaxanthin supplementation: a randomized, double-masked, placebo-controlled trial. *Am. J. Ophthalmol.* **2012**, *154*, 625−634.

(5) Namitha, K. K.; Negi, P. S. Chemistry and biotechnology of carotenoids. *Crit. Rev. Food Sci. Nutr.* **2010**, *50*, 728−760.

(6) Singh, P.; Goyal, G. K. Dietary lycopene: its properties and anticarcinogenic effects. *Compr. Rev. Food Sci. Food Saf.* **2008**, *7*, 255−270.

(7) Schieber, A.; Carle, R. Occurrence of carotenoid cis-isomers in food: technological, analytical, and nutritional implications. *Trends Food Sci. Technol.* **2005**, *16*, 416−422.

(8) Courraud, J.; Berger, J.; Cristo, J. P.; Avallone, S. Stability and bioaccessibility of different forms of carotenoids and vitamin A during in vitro digestion. *Food Chem.* **2013**, *136*, 871−877.

(9) Marx, M.; Stuparic, M.; Schieber, A.; Carle, R. Effects of thermal processing on trans-cis-isomerization of β-carotene in carrot juices and carotene-containing preparations. *Food Chem.* **2003**, *83*, 609−617.

(10) Pott, I.; Marx, M.; Neidhart, S.; Mühlbauer, W.; Carle, R. Quantitative determination of β-carotene stereoisomers in fresh, dried, and solar-dried mangoes (*Mangifera indica* L.). *J. Agric. Food Chem.* **2003**, *51*, 4527−4531.

(11) Lemmens, L.; De, V. K.; Moelants Katlijn, R. N.; Colle Ines, J. P.; van Loey, A. M.; Hendrickx, M. E. β-Carotene isomerization kinetics during thermal treatments of carrot puree. *J. Agric. Food Chem.* **2010**, *58*, 6816−6824.

(12) Bengtsson, A.; Brackmann, C.; Enejder, A.; Alminger, M. L.; Svanberg, U. Effects of thermal processing on the in vitro bioaccessibility and microstructure of β-carotene in orange-fleshed sweet potato. *J. Agric. Food Chem.* **2010**, *58*, 11090−11096.

(13) Chandler, L. A.; Schwartz, S. J. HPLC separation of cis-trans carotene isomers in fresh and processed fruits and vegetables. *J. Food Sci.* **1987**, *52*, 669−672.

(14) Aman, R.; Schieber, A.; Carle, R. Effects of heating and illumination on trans-cis isomerization and degradation of β-carotene and lutein in isolated spinach chloroplasts. *J. Agric. Food Chem.* **2005**, *53*, 9512−9518.

(15) Reif, C.; Arrigoni, E.; Neuweiler, R.; Baumgartner, D.; Nystroem, L.; Hurrell, R. F. Effect of sulfur and nitrogen fertilization on the content of nutritionally relevant carotenoids in spinach (*Spinacia oleracea*). *J. Agric. Food Chem.* **2012**, *60*, 5819−5824.

(16) Heymann, T.; Raeke, J.; Glomb, M. A. Photoinduced isomerization of lycopene and application to tomato cultivation. *J. Agric. Food Chem.* **2013**, *61*, 11133−11139.

(17) Sadler, G.; Davis, J.; Dezman, D. Rapid extraction of lycopene and β-carotene from reconstituted tomato paste and pink grapefruit homogenates. *J. Food Sci.* **1990**, *55*, 1460−1461.

(18) Kimura, M.; Rodriguezamaya, D. B.; Godoy, H. T. Assessment of the saponification step in the quantitative-determination of carotenoids and provitamins-A. *Food Chem.* **1990**, *35*, 187−195.

(19) Fang, L.; Pajkovic, N.; Wang, Y.; Gu, C.; van Breemen, R. B. Quantitative analysis of lycopene isomers in human plasma using high-performance liquid chromatography-tandem mass spectrometry. *Anal. Chem.* **2003**, *75*, 812−817.

(20) Isler, O.; Gutmann, H.; Lindlar, H.; Montavon, M.; Ruegg, R.; Ryser, G.; Zeller, P. Syntheses in the carotenoid series. VI. Synthesis of crocetin dialdehyde and lycopene. *Helv. Chim. Acta* **1956**, *39*, 463−473.

(21) Hengartner, U.; Bernhard, K.; Meyer, K.; Englert, G.; Glinz, E. Synthesis, isolation, and NMR-spectroscopic characterization of fourteen (*Z*)-isomers of lycopene and of some acetylenic didehydro- and tetradehydrolycopenes. *Helv. Chim. Acta* **1992**, *75*, 1848−1865.

(22) Britton, G., Liaaen-Jensen, S., Pfander, H., Eds. *Carotenoids Vol. 2: Synthesis*; Birkhäuser Verlag: Basel, Switzlernad, 1996.

(23) Bennani, Y. L. An efficient and stereoselective synthesis of 9-*cis*-retinoic acid. *J. Org. Chem.* **1996**, *61*, 3542−3544.

(24) Negishi, E. I.; King, A. O.; Klima, W. L.; Patterson, W.; Silveira, A. Conversion of methyl ketones into terminal acetylenes and (E)-trisubstituted olefins of terpenoid origin. *J. Org. Chem.* **1980**, *45*, 2526−2528.

(25) Mata, E. G.; Thomas, E. J. Development of a synthesis of lankacidins − an investigation into 17-membered ring formation. *J. Chem. Soc., Perkin Trans. 1* **1995**, 785−799.

(26) Murray, R. E.; Zweifel, G. Preparation of phenyl cyanate and its utilization for the synthesis of α,β-unsaturated nitriles. *Synthesis–Stuttgart* **1980**, 150–151.
(27) Jansen, H.; Bachthaler, E.; Förster, E.; Scharpf, C. *Gärtnerischer Pflanzenbau*, 3rd ed.; Verlag Eugen Ulmer: Stuttgart, Germany, 1998.
(28) Lee, M. T.; Chen, B. H. Separation of lycopene and its cis isomers by liquid chromatography. *Chromatographia* **2001**, *54*, 613–617.
(29) Schierle, J.; Bretzel, W.; Buhler, I.; Faccin, N.; Hess, D.; Steiner, K.; Schuep, W. Content and isomeric ratio of lycopene in food and human blood plasma. *Food Chem.* **1997**, *59*, 459–465.
(30) Vecchi, M.; Englert, G.; Maurer, R.; Meduna, V. Separation and characterization of the cis-isomers of β,β-carotene. *Helv. Chim. Acta* **1981**, *64*, 2746–2758.
(31) Strohschein, S.; Pursch, M.; Handel, H.; Albert, K. Structure elucidation of β-carotene isomers by HPLC-NMR coupling using a C-30 bonded phase. *Fresenius' J. Anal. Chem.* **1997**, *357*, 498–502.
(32) O'Neil, C. A.; Schwartz, S. J. Photoisomerization of β-carotene by photosensitization with chlorophyll derivatives as sensitizers. *J. Agric. Food Chem.* **1995**, *43*, 631–635.
(33) Guo, W. H.; Tu, C. Y.; Hu, C. H. Cis-trans isomerizations of β-carotene and lycopene: a theoretical study. *J. Phys. Chem. B* **2008**, *112*, 12158–12167.
(34) Bahceci, K. S.; Serpen, A.; Gokmen, V.; Acar, J. Study of lipoxygenase and peroxidase as indicator enzymes in green beans: change of enzyme activity, ascorbic acid and chlorophylls during frozen storage. *J. Food Eng.* **2005**, *66*, 187–192.
(35) Alder, A.; Jamil, M.; Marzorati, M.; Bruno, M.; Vermathen, M.; Bigler, P.; Ghisla, S.; Bouwmeester, H.; Beyer, P.; Al-Babili, S. The path from β-carotene to carlactone, a strigolactone-like plant hormone. *Science* **2012**, *335*, 1348–1351.
(36) van den Bulck, N.; Coomans, M.; Wittemans, L.; Hanssens, J.; Steppe, K. Monitoring and energetic performance analysis of an innovative ventilation concept in a Belgian greenhouse. *Energy Buildings* **2013**, *57*, 51–57.
(37) Kuki, M.; Koyama, Y.; Nagae, H. Triplet-sensitized and thermal isomerization of all-trans, 7-cis, 9-cis, 13-cis and 15-cis isomers of β-carotene: configurational dependence of the quantum yield of isomerization via the T1 state. *J. Phys. Chem.* **1991**, *95*, 7171–7180.

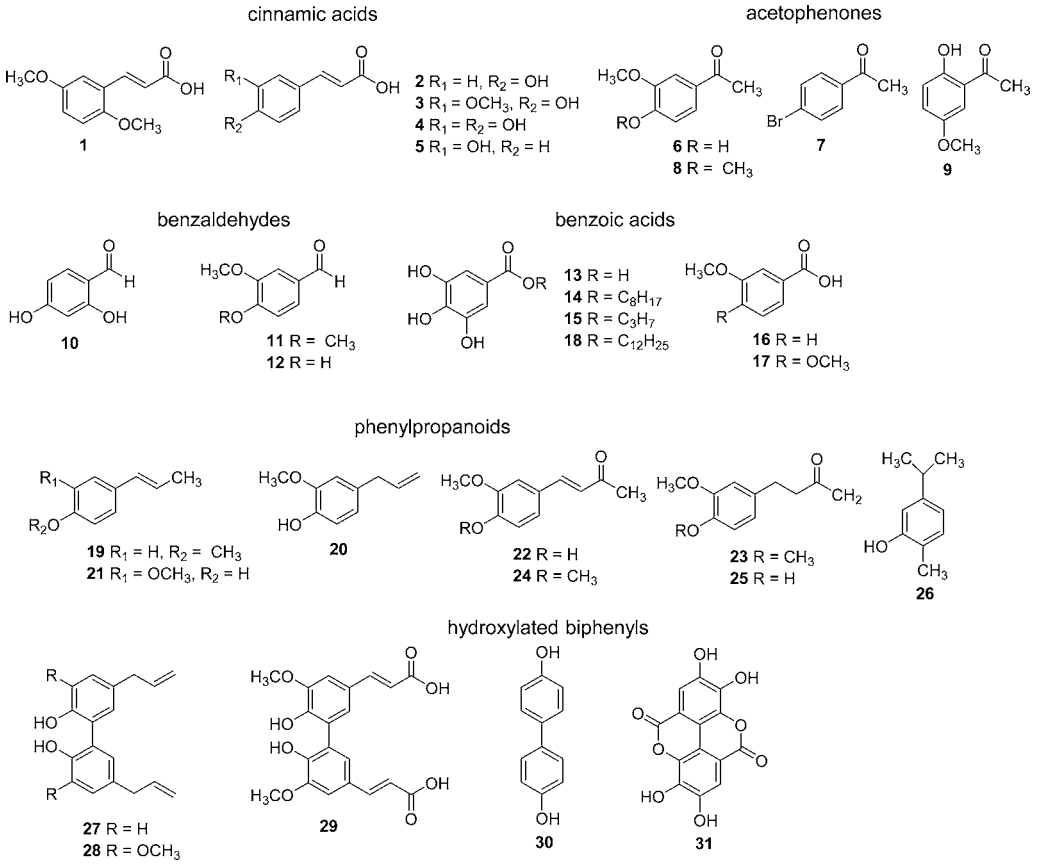

Figure 1. Chemical structures of studied compounds.

unsaturated chain are embedded in the aromatic ring.[15] Most of them are plant metabolites, generally present in food, spices, or food preservative or belonging to the generally recognized as safe (GRAS) list.[16]

The most abundant phenols extracted from maize grain pericarp and wheat bran are *trans*-ferulic acid and the corresponding dehydrodimers, namely, dehydrodiferulates.[13,14,17] Hydroxycinnamic acids are known to be major components of the primary cell wall of cereals.[13] The predominant feruloyl residues can also be dimerized under oxidative coupling mediated by peroxidases or form cross-links and/or dehydrodimers of ferulic acid that then lead to a reinforcement of the primary cell wall of the plant. Fungal esterases, which are overexpressed during growth on the host tissues, can release free forms of ferulic ester from cell wall tissues.[18] Once released, free ferulate may inhibit the ability of *Fusarium* to produce mycotoxins.

The objective of this study was to evaluate the inhibitory effect of a wide collection of natural and natural-like phenols and dimers on vegetative growth and mycotoxin *in vitro* production by a well-characterized 3-acetyl-4-deoxynivalenol producing strain of *F. culmorum*. We selected a series of compounds belonging to cinnamic acids, acetophenones, benzaldehydes, benzoic acids, phenylpropanoids, and hydroxylated biphenyls and compared their structural properties to the *in vitro* activity. A correlation between the inhibitory effect of the selected phenols and their lipophilicity, polarity, and antioxidant activity was also attempted.

MATERIALS AND METHODS

Fungal Strain and Culture Conditions. The highly virulent and well-characterized[1] strain ISPaVe MCf21 (synthetic strain INRA 117) of *F. culmorum* (W.G. Smith) Sacc., isolated in 1989 from triticale grown in Foggia, Apulia, southern Italy, was used in all of the experiments. Under *in vitro* conditions, *F. culmorum* MCf21 mainly produces 3-acetyl-4-deoxynivalenol (3-ADON) and, to a lesser extent, deoxynivalenol.[14,19] Strain cultures were set up on potato dextrose agar (PDA, at 25 °C in the dark). Short-term storage of PDA cultures was at 4 °C, while for long-term preservation, plugs of PDA cultures were stored in 50% aqueous glycerol at −80 °C.

For subsequent experiments, *F. culmorum* MCf 21 was grown in V8 vegetable juice for 7 days at 25 °C and 170 rpm. Cultures were filtered, and spores were collected by centrifugation, adjusted to 1×10^6 colony-forming units (CFU)/mL in sterile water, and used as inoculum for Vogel's liquid culture medium.[20]

All liquid and solid media were amended with streptomycin (50 μg/mL) and tetracycline (50 μg/mL), respectively, to prevent bacterial growth.

Tested Compounds (Figure 1 and Table 1). 2,5-Dimethoxycinnamic acid (**1**), 4-hydroxycinnamic acid (**2**), ferulic acid (**3**), caffeic acid (**4**), 3-hydroxycinnamic acid (**5**), apocynin (**6**), 4-bromoacetophenone (**7**), 3,4-dimethoxyacetophenone (**8**), 2-hydroxy-5-methoxyacetophenone (**9**), 2,4-dihydroxybenzaldehyde (**10**), veratraldehyde (**11**), vanillin (**12**), gallic acid (**13**), octyl gallate (**14**), propyl gallate (**15**), 3-methoxybenzoic acid (**16**), 3,4-dimethoxybenzoic acid (**17**), dodecyl gallate (**18**), *trans*-anethole (**19**), eugenol (**20**), isoeugenol (**21**), dehydrozingerone (**22**), Me-zingerone (**23**), Me-dehydrozingerone (**24**), zingerone (**25**), carvacrol (**26**), magnolol (**27**), dehydrodieugenol (eugenol dimer) (**28**), dehydrodiferulic acid (5,5′-diferulic acid dimer) (**29**), 4,4′-dihydroxybiphenyl (**30**), and ellagic acid (**31**) were selected and used with a purity >98%. Dehydrozingerone (**22**), Me-zingerone (**23**), Me-dehydrozingerone (**24**), dehydrodieugenol (**28**), and dehydrodiferulic acid (**29**) were prepared

dx.doi.org/10.1021/jf500647h | J. Agric. Food Chem. 2014, 62, 4969−4978

Table 1. Compounds Listed According to Lipophilicity and Their Value of Log *P*, Radical Scavenging Activity, and Antioxidant Activity

list of compounds according to the elution order by HPLC in reverse phase	log P^a	radical scavenging activity DPPH (TE[b]), EtOH abs, time = 30 min	ABTS (TEAC[c]), EtOH abs, time = 6 min
gallic acid (**13**)	0.47	3.20 ± 0.13	2.76 ± 0.07
caffeic acid (**4**)	1.15	1.53 ± 0.04	1.25 ± 0.08
vanillin (**12**)	1.26	0.029 ± 0.007	0.67 ± 0.12
2,4-dihydroxybenzaldehyde (**10**)	1.00	not determined	not determined
apocynin (**6**)	0.83	0.019 ± 0.002	0.41 ± 0.01
4-hydroxycinnamic acid (*p*-cumaric acid) (**2**)	1.54	no activity	1.08 ± 0.04
ellagic acid (**31**)	1.05	2.62 ± 0.02	3.05 ± 0.44
3,4-dimethoxybenzoic acid (**17**)	1.34	not determined	not determined
ferulic acid (**3**)	1.42	0.64 ± 0.04	1.45 ± 0.18
3-hydroxcinnamic acid (**5**)	1.54	not determined	not determined
3-methoxybenzoic acid (**16**)	1.46	not determined	not determined
veratraldehyde (**11**)	1.53	0.023 ± 0.03	0.05 ± 0.02
3,4-dimethoxyacetophenone (**8**)	1.09	not determined	not determined
zingerone (**25**)	1.95	0.38 ± 0.02	1.34 ± 0.08
propyl gallate (**15**)	1.51	5.20 ± 0.08	3.32 ± 0.10
dehydrozingerone (**22**)	1.27	0.60 ± 0.02	1.10 ± 0.02
4,4′-dihydroxybiphenyl (**30**)	2.93	not determined	not determined
Me-zingerone (**23**)	2.21	no activity	no activity
2,5-dimethoxycinnamic acid (**1**)	1.70	not determined	not determined
2-hydroxy-5-methoxyacetophenone (**9**)	0.83	not determined	not determined
Me-dehydrozingerone (**24**)	1.53	no activity	no activity
ferulic acid dimer (**29**)	2.47	0.85 ± 0.02	1.73 ± 0.03
eugenol (**20**)	2.57	028 ± 0.004	0.32 ± 0.01
4-bromoacetophenone (**7**)	2.51	no activity	no activity
isoeugenol (**21**)	2.52	0.58 ± 0.005	0.72 ± 0.03
carvacrol (**26**)	3.37	0.03 ± 0.006	0.29 ± 0.01
octyl gallate (**14**)	3.60	3.10 ± 0.048	3.00 ± 0.13
trans-anethole (**19**)	2.91	not determined	not determined
magnolol (**27**)	5.03	0.023 ± 0.008	0.55 ± 0.06
eugenol dimer (**28**)	4.78	0.83 ± 0.02	1.89 ± 0.02
dodecyl gallate (**18**)	5.27	2.99 ± 0.13	2.90 ± 0.10

[a]Log *P* = lipophilicity estimated by theoretical calculations, which express the partitioning of the phenols in a *n*-octanol/water system. [b]TE, Trolox equivalent; DPPH, 1,1′-diphenyl-2-picrylhydrazyl. [c]TEAC, Trolox equivalent antioxidant capacity; ABTS, 2,2-azinobis(3-ethylbenzothiazoline-6-sulfonic acid).

according to known procedures.[21−23] The other compounds were purchased from Sigma-Aldrich (Milan, Italy) and used as received. *β*-Cyclodextrin (*β*-CD, CAVAMAX W7 Pharma) was purchased from Wacker Chemie Italia (Peschiera Borromeo, Italy).

Amendment with Phenolic Inhibitors and Extraction of Type B Trichothecenes. Petri plates (60 mm diameter) containing 8 mL of Vogel's medium were amended with the compounds at different concentrations (ranging from 0.1 to 1.5 mM).

β-CD (3.0 mM) was added to the Vogel's medium to improve solubilization of phenolic compounds. The procedure was carried out in a way to exclude any stable inclusion of the compound into the *β*-CD cavity.

Each sample vial was sonicated at room temperature for 60 min and 60 Hz (Branson model 3510 OPTO-LAB). Sonicated media were inseminated with *F. culmorum* MCf 21 spore suspension to achieve a final concentration of 1×10^4 conidia/mL. Each compound was tested in triplicate, and cultures were incubated in the dark at 25 °C, without shaking. After 14 days of incubation, media and mycelia were collected for thin-layer chromatography (TLC) and liquid chromatography−mass spectrometry (LC−MS) analyses. Mycelia were separated from the medium by filtration through sterile filter paper, subsequently harvested from the filter papers with a sterile spatula, dried at 80 °C for 24 h, and weighed. Trichothecenes were extracted from 4 mL of harvested medium by adding 4 mL of ethyl acetate, followed by a shaking step at 150 rpm for 16−18 h at room temperature, and finally by recovering the organic phase. Each experiment was repeated at least 2 times.

LC−MS Analysis of Type B Trichothecenes. Quantitation was performed with reference to external calibration using type B trichothecene standards (Sigma-Aldrich, Milan, Italy). Quantitative determinations were carried out as described previously,[19] using a model HP 1100 liquid chromatography and mass spectrophotometric detector (Agilent Technologies, Palo Alto, CA).

Estimation of Lipophilicity and Polarity. Retention of a compound in reversed-phase liquid chromatography is governed by its lipophilicity and shows significant correlation with the *n*-octanol/water partition coefficient.[24] Lipophilicity of all phenols diluted in pure methanol was estimated by high-performance liquid chromatography (HPLC) on HP 1100 Agilent Technologies, Palo Alto, CA, using a 15 × 4.6 mm inner diameter, 3 μm, Luna RP-8 (Phenomenex, Torrance, CA), at temperature of 25 °C and with a flow of 0.4 mL/min, as reported in the literature.[25] Polarity of the compounds was estimated by TLC.

Radical Scavenging and Antioxidant Activity of Phenols. For each compound, a 5 mM stock solution was prepared in absolute ethanol. The radical scavenging activity of the compounds was determined *in vitro* [2,2-diphenyl-1-picrylhydrazyl (DPPH) and 2,2′-azino-bis(3-ethylbenzthiazoline-6-sulfonic acid) (ABTS)] by an electron paramagnetic resonance (EPR) spectrometer and ultraviolet/visible (UV/vis).

Table 2. *In Vitro* Effect of Different Phenolic Compounds (1.5 mM) on Vegetative Growth and 3-ADON Production by *F. culmorum* Strain ISPaVe MCf 21 (INRA 117)

treatment	dry fungal biomass (relative yield ± SE)[a]	3-ADON (relative yield ± SE)[b]
	Cinnamic Acids	
2,5-dimethoxycinnamic acid (**1**)	59 ± 4[c]	1[c]
	Acetophenones	
apocynin (**6**)	70 ± 5	1[c]
4′-bromoacetophenone (**7**)	67 ± 5	0[c]
	Benzaldehydes	
veratraldehyde (**11**)	88 ± 7	20 ± 6[c]
2,4-dihydroxybenzaldehyde (**10**)	25 ± 4[c]	20 ± 10[d]
	Benzoic Acids	
gallic acid (**13**)	78 ± 15	≤LOD[c,e]
	Hydroxylated Biphenyls	
magnolol (**27**)	0[c]	0[c]
	Phenylpropanoids	
trans-anethole (**19**)	81 ± 3	1 ± 1[c]
eugenol (**20**)	47 ± 3[c]	0[c]
isoeugenol (**21**)	47 ± 1[c]	≤LOD[c,e]
dehydrozingerone (**22**)	54 ± 1[c]	0[c]
Me-zingerone (**23**)	54 ± 4[c]	0[c]

[a]Dry fungal biomass values are expressed as mean percent values (±standard error) relative to their level in the control culture (31.2 ± 2.4 mg). [b]3-ADON yields are expressed as mean percent values (±standard error) relative to their level in the control culture (243 348 ± 42 326 ng/g of dry biomass). [c]Values are significantly different ($p < 0.01$) from the untreated control based on ANOVA followed by the Dunnett test. [d]Values are significantly different ($p < 0.05$) from the untreated control based on ANOVA followed by the Dunnett test. [e]Below the limit of detection.

Table 3. *In Vitro* Effect of Different Phenolic Compounds (1 mM) on Vegetative Growth and 3-ADON Production by *F. culmorum* Strain ISPaVe MCf 21 (INRA 117)

treatment	dry fungal biomass (relative yield ± SE)[a]	3-ADON (relative yield ± SE)[b]
	Cinnamic Acids	
4-hydroxycinnamic acid (**2**)	103 ± 15	16 ± 2[c]
ferulic acid (**3**)	111 ± 28	20 ± 10[c]
caffeic acid (**4**)	75 ± 1	3 ± 1[c]
3-hydroxycinnamic acid (**5**)	41 ± 10[c]	3 ± 1[c]
	Acetophenones	
apocynin (**6**)	66 ± 9	≤LOD[c,e]
4′-bromoacetophenone (**7**)	67 ± 2	1[c]
3,4-dimethoxyacetophenone (**8**)	67 ± 2	84 ± 20
2-hydroxy-5-methoxyacetophenone (**9**)	48 ± 3[d]	11 ± 5[c]
	Benzaldehydes	
2,4-dihydroxybenzaldehyde (**10**)	106 ± 40	80 ± 32
vanillin (**12**)	77 ± 2	30 ± 7[d]
	Benzoic Acids	
octyl gallate (**14**)	0[c]	0[c]
propyl gallate (**15**)	73 ± 1	12 ± 4[c]
	Hydroxylated Biphenyls	
magnolol (**27**)	9 ± 1[c]	2 ± 1[c]
eugenol dimer (**28**)	101 ± 5	224 ± 41[d]
4,4′-dihydroxybiphenyl (**30**)	59 ± 0	79 ± 9
ellagic acid (**31**)	79 ± 6	1[c]
	Phenylpropanoids	
eugenol (**20**)	119 ± 22	≤LOD[c,e]
isoeugenol (**21**)	135 ± 58	3 ± 1[c]
dehydrozingerone (**22**)	68 ± 2	16 ± 2[c]
Me-zingerone (**23**)	134 ± 60	3 ± 1[c]
Me-dehydrozingerone (**24**)	8 ± 2[c]	0[c]
carvacrol (**26**)	87 ± 26	1[c]

[a]Dry fungal biomass values are expressed as mean percent values (±standard error) relative to their level in the control culture (28.7 ± 2 mg). [b]3-ADON yields are expressed as mean percent values (±standard error) relative to their level in the control culture (182 982 ± 40 725 ng/g of dry biomass). [c]Values are significantly different ($p < 0.01$) from the untreated control based on ANOVA followed by the Dunnett test. [d]Values are significantly different ($p < 0.05$) from the untreated control based on ANOVA followed by the Dunnett test. [e]Below the limit of detection.

Table 4. *In Vitro* Effect of Different Phenolic Compounds (0.5 mM) on Vegetative Growth and 3-ADON Production by *F. culmorum* Strain ISPaVe MCf 21 (INRA 117)

treatment	dry fungal biomass (relative yield ± SE)[a]	3-ADON (relative yield ± SE)[b]
	Cinnamic Acids	
ferulic acid (**3**)	84 ± 1	45 ± 6[c]
	Acetophenones	
apocynin (**6**)	85 ± 5	17 ± 9[c]
	Benzoic Acids	
octyl gallate (**14**)	79 ± 1	106 ± 41
propyl gallate (**15**)	82 ± 3	17 ± 5[c]
3-methoxybenzoic acid (**16**)	92 ± 3	129 ± 10
3,4-dimethoxybenzoic acid (**17**)	85 ± 5	107 ± 11
dodecyl gallate (**18**)	115 ± 1[d]	91 ± 41
	Hydroxylated Biphenyls	
magnolol (**27**)	15 ± 12[c]	0[c]
eugenol dimer (**28**)	97 ± 4	451 ± 22[c]
ferulic acid dimer (**29**)	67 ± 16	68 ± 44
ellagic acid (**31**)	84 ± 3	101 ± 19
	Phenylpropanoids	
trans-anethole (**19**)	101 ± 3	57 ± 8[d]
dehydrozingerone (**22**)	72 ± 2	12 ± 1[c]
Me-zingerone (**23**)	86 ± 4	35 ± 14[d]
Me-dehydrozingerone (**24**)	72 ± 1	22 ± 11[c]
zingerone (**25**)	83 ± 6	33 ± 10[c]

[a]Dry fungal biomass values are expressed as mean percent values (±standard error) relative to their level in the control culture (26.3 ± 1.3 mg). [b]3-ADON yields are expressed as mean percent values (±standard error) relative to their level in the control culture (242 692 ± 41 029 ng/g of dry biomass). [c]Values are significantly different ($p < 0.01$) from the untreated control based on ANOVA followed by the Dunnett test. [d]Values are significantly different ($p < 0.05$) from the untreated control based on ANOVA followed by the Dunnett test.

Radical scavenging activity was determined by the DPPH method,[26] with few modifications. Briefly, 100 μL of a solution of 1.0 mM DPPH was mixed with 1900 μL of the appropriately diluted sample solution. The mixture was incubated in the dark for 30 min and subsequently analyzed by an EPR spectrophotometer. The antioxidant activity determination was carried out as reported previously.[27]

Statistical Analysis. Data on mycelium growth (milligrams of dry weight per Petri plate) and 3-acetyl-4-deoxynivalenol production (ng/mL) obtained from separate experiments were expressed as percent values of the relative control treatment and pooled to perform a one-way analysis of variance (ANOVA), followed by multiple comparisons by Dunnett test, using Minitab for Windows, release 16.1.

RESULTS AND DISCUSSION

Screening of Type B Trichothecene Inhibitors. In a first screening, performed at the concentration of 1.5 mM, representatives of each class of compounds were selected according to their functional and structural features (Table 2). The results obtained from the initial screening were used to design further assays at the lower 1.0 mM concentration (Table 3). When their concentration in the medium was reduced, it was possible to test other phenolic compounds that were not soluble at higher concentrations. On the basis of the results achieved at 1.0 mM, a limited set of compounds were further assayed at the concentration of 0.5 mM (Table 4) and 0.25 mM (Table 5), respectively. The strategy allowed us to investigate the efficacy of compounds that are poorly soluble in water and may inhibit mycotoxin *in vitro* production at low concentrations without affecting fungal growth.

Cinnamic Acids. Vegetative growth was reduced to 59% compared to the untreated control, and 3-acetyl-4-deoxynivalenol production was almost completely inhibited when *F. culmorum* was grown in the presence of 1.5 mM 2,5-dimethoxycinnamic acid (**1**) (Table 2). At the concentration of 1.0 mM, the *in vitro* production of 3-acetyl-4-deoxynivalenol was reduced to 16−20% without affecting fungal growth by 4-hydroxycinnamic acid (**2**) and ferulic acid (**3**) (Table 3), with the latter maintaining a significant inhibitory activity also at 0.5 mM (Table 4), as reported previously.[14] When tested at 1.0 mM, caffeic acid (**4**) caused almost complete 3-acetyl-4-deoxynivalenol inhibition but did not significantly affect mycelial growth. On the contrary, 3-hydroxycinnamic acid (**5**) reduced fungal growth to 41% and 3-acetyl-4-deoxynivalenol production to 3% with respect to the untreated control (Table 3).

Table 5. *In Vitro* Effect of Different Phenolic Compounds (0.25 mM) on Vegetative Growth and 3-ADON Production by *F. culmorum* Strain ISPaVe MCf 21 (INRA 117)

treatment	dry fungal biomass (relative yield ± SE)[a]	3-ADON (relative yield ± SE)[b]
dodecyl gallate (**18**)	78 ± 0	11 ± 1[c]
Me-dehydrozingerone (**24**)	94 ± 5	344 ± 71[c]
carvacrol (**26**)	99 ± 32	11 ± 3[c]
magnolol (**27**)	21 ± 2[d]	0[c]
ferulic acid dimer (**29**)	73 ± 6	33 ± 8[d]

[a]Dry fungal biomass values are expressed as mean percent values (±standard error) relative to their level in the control culture (25.3 ± 2.4 mg). [b]3-ADON yields are expressed as mean percent values (±standard error) relative to their level in the control culture (202 873 ± 66 153 ng/g of dry biomass). [c]Values are significantly different ($p < 0.01$) from the untreated control based on ANOVA followed by the Dunnett test. [d]Values are significantly different ($p < 0.05$) from the untreated control based on ANOVA followed by the Dunnett test.

Acetophenones. Fungal growth was slightly, albeit not significantly, reduced to 67−70% compared to the untreated control upon treatment with apocynin (**6**) or 4-bromo-

dx.doi.org/10.1021/jf500647h | J. Agric. Food Chem. 2014, 62, 4969−4978

acetophenone (**7**), resulting in complete inhibition of 3-acetyl-4-deoxynivalenol *in vitro* production when tested at 1.5 and at 1.0 mM (Tables 2 and 3), respectively. Apocynin (**6**) maintained its ability to significantly reduce 3-acetyl-4-deoxynivalenol at the lower concentration of 0.5 mM without affecting fungal growth (Table 4). When tested at 1.0 mM compounds, 3,4-dimethoxyacetophenone (**8**) and 2-hydroxy-5-methoxyacetophenone (**9**) caused 67 and 48% vegetative growth, respectively, whereas only acetophenone (**9**) induced a significant inhibition (11% compared to the untreated control) of 3-acetyl-4-deoxynivalenol production (Table 3).

Benzaldehydes. Fungicide activity (25% vegetative growth compared to the control) and 3-acetyl-4-deoxynivalenol inhibition (20% trichothecene production) were observed when 1.5 mM 2,4-dihydroxybenzaldehyde (**10**) was added to *F. culmorum* growth medium, whereas at the same concentration, veratraldehyde (**11**), a benzaldehyde with two phenolic −OH groups protected by methylation, reduced 3-acetyl-4-deoxynivalenol production to 20%, with no significant inhibition of mycelium growth (Table 2). The same effects were observed with vanillin (**12**) tested at 1.0 mM (Table 3).

Benzoic Acids. Gallic acid (**13**) was selected as a prototype of benzoic acids. The production of 3-acetyl-4-deoxynivalenol was below the limit of detection (<LOD), while fungal growth was only slightly inhibited when 1.5 mM gallic acid (**13**) was added to *F. culmorum* liquid culture (Table 2). A strong fungicidal activity was observed with octyl gallate (**14**) at the concentration of 1.0 mM, whereas at 0.5 mM, this compound had no effect on mycotoxin production nor vegetative growth (Tables 3 and 4). On the contrary, propyl gallate (**15**) displayed a good inhibitory effect on mycotoxin production, while having no significant influence on mycelium growth at both 1.0 mM (Table 3) and 0.5 mM (Table 4). Dodecyl gallate (**18**) displayed a contrasting behavior, as a significant increase of vegetative growth with no effect on mycotoxin production was observed at 0.5 mM (Table 4), whereas at 0.25 mM, the same compound reduced 3-acetyl-4-deoxynivalenol production to 11% compared to the untreated control, with no significant inhibition of mycelium development (Table 5). When tested at the concentration of 0.5 mM, 3-methoxybenzoic acid (**16**) and 3,4-dimethoxybenzoic acid (**17**) did not exhibit any significant activity on fungal growth or 3-acetyl-4-deoxynivalenol production.

Phenylpropanoids. A significant inhibition of 3-acetyl-4-deoxynivalenol biosynthesis or a mycotoxin concentration of <LOD were observed upon amendment of the substrate with 1.5 mM *trans*-anethole (**19**), eugenol (**20**), and isoeugenol (**21**), three phenylpropanoids with an unsaturated side chain (Table 2). Complete inhibition of 3-acetyl-4-deoxynivalenol *in vitro* production was also achieved at 1.0 mM for eugenol (**20**) and isoeugenol (**21**) without affecting mycelium growth (Table 3).

Dehydrozingerone (**22**) and Me-zingerone (**23**) caused 100% 3-acetyl-4-deoxynivalenol inhibition and 54% mycelium growth inhibition at 1.5 mM (Table 2). Dehydrozingerone (**22**) retained almost the same inhibitory activities toward trichothecene *in vitro* production and mycelium growth at both 1.0 and 0.5 mM. When tested at 1.0 mM, Me-zingerone (**23**) retained 3-acetyl-4-deoxynivalenol inhibitory activity with an apparent, albeit not significant, stimulation of vegetative growth, while inducing 35% of 3-acetyl-4-deoxynivalenol production compared to the untreated control at 0.5 mM (Tables 3 and 4).

Almost no fungal growth and complete inhibition of trichothecene production were observed when Me-dehydrozingerone (**24**) was added at 1.0 mM to liquid culture (Table 3). When its concentration in the medium was reduced to 0.5 mM, Me-dehydrozingerone (**24**) had no significant effect on fungal growth, whereas 3-acetyl-4-deoxynivalenol was reduced to 22% of the untreated control (Table 4). When tested at 0.25 mM, this compound behaved as a strong inducer of 3-acetyl-4-deoxynivalenol *in vitro* production (Table 5).

Only 33% 3-acetyl-4-deoxynivalenol production was detected with zingerone (**25**) tested at 0.5 mM without significantly affecting fungal growth (Table 4).

Almost complete 3-acetyl-4-deoxynivalenol inhibition, with no significant inhibition of fungal growth, was observed when carvacrol (**26**), an alkyl phenol, was added at 1.0 mM in the liquid medium (Table 3). At 0.25 mM, carvacrol (**26**) reduced 3-acetyl-4-deoxynivalenol production to 11% without affecting vegetative growth (Table 5). In the present work, the trichothecene inhibitory activity of carvacrol (**26**) was not concentration-dependent.

Hydroxylated Biphenyls. Magnolol (**27**), a symmetrical hydroxylated biphenyl with two free phenolic −OH groups and two side chains *para* to each other, displayed a marked fungicide activity when tested at 1.5 mM (Table 2). Despite not being perceivable, the progressive decline in its inhibitory effect on fungal growth as the dosage decreased to 1.0, 0.5, and 0.25 mM, this compound retained the capacity to inhibit 3-acetyl-4-deoxynivalenol production by the fungus even at the lowest concentration (Tables 3 and 5). Dehydrodieugenol (**28**), structurally equivalent to magnolol (**27**) but having a methoxyl group *ortho* to each phenolic −OH group, strongly induced 3-acetyl-4-deoxynivalenol overproduction, with no reduction of fungal growth at both 1.0 and 0.5 mM (Tables 3 and 5).

No significant inhibitory activity on vegetative growth or trichothecene *in vitro* production were observed upon amendment of the substrate with ferulic acid dimer **29** at 0.5 mM, whereas at 0.25 mM, a significant reduction of 3-acetyl-4-deoxynivalenol production was detected (Tables 4 and 5). This effect might be due to a different pH of the environment, which would influence the interactions between inhibitor and enzyme. Amendment with 4,4′-dihydroxylbiphenyl (**30**) produced a 40% reduction of the fungal growth, with no significant effect on 3-acetyl-4-deoxynivalenol production when tested at 1.0 mM (Table 3). Almost complete 3-acetyl-4-deoxynivalenol inhibition with no significant reduction of vegetative growth was observed with ellagic acid (**31**) tested at 1.0 mM (Table 3), while no significant effect was detected when the substrate was amended with 0.5 mM ellagic acid (**31**) (Table 4).

Antioxidant Activity and Lipophilicity. The cinnamic acids (**2**−**4**), which display poor lipophilic properties, presented radical scavenging and antioxidant activity comparable to that of Trolox (Table 1). No radical scavenging activity nor antioxidant activity were detected for acetophenones and aldehydes, whose lipophilicity values, estimated by a computational program (log *P*) and HPLC, differ significantly only for 4-Br-acetophenone (**7**) (Table 1).

Lipophilicity values of all benzoic acids analyzed are well-distributed in the list of compounds, ranging between 0.47 and 5.27 log *P* according to the trend observed by reverse-phase (RP)-HPLC (**13** < **17** < **16** < **15** < **14** < **18**). High radical scavenging and antioxidant activities were detected for gallic acid (**13**) and its esters, compounds **18**, **14**, and **15**, with the

latter being the best antioxidant among all compounds studied (Table 1).

With the exclusion of zingerone (**25**), all phenylpropanoids had no significant or no antioxidant activity compared to the other phenols (Table 1), despite most representatives of this class of compounds demonstrating a remarkable inhibitory activity toward 3-acetyl-4-deoxynivalenol production while allowing normal vegetative growth. Lipophilicity of the compounds determined by HPLC decreased in the following order: **19** > **26** > **21** > **20** > **24** > **23** > **22** > **25**. Approximately, the same trend was maintained in the score of lipophilicity estimated by theoretical calculations that ranged between 3.37 and 1.27 log *P*.

Both radical scavenging and antioxidant activities increased in the hydroxylated biphenyls with the following trend: **31** > **28** > **29** > **27**. Ellagic acid (**31**) showed radical scavenging and antioxidant activities more than doubled and tripled compared to Trolox units (Table 1). Although ellagic acid (**31**) is conformationally hindered, a large electronic delocalization occurs in the rings, hence providing strong radical scavenging and antioxidant activities.

TLC Chromatography. Mycotoxins cannot be detected under UV at 254 nm and are poorly detectable in common TLC visualization reagents.[28] Although a *F. culmorum* strain producing mainly 3-acetyl-4-deoxynivalenol has been used, a fast and reliable TLC detection protocol was optimized for the identification of five trichothecene mycotoxins (3-acetyl-4-deoxynivalenol, 15-acetyl-4-deoxynivalenol, nivalenol, deoxynivalenol, and fusarenone X) by a single chromatographic run.

In vitro assays indicated that 31 of the tested compounds belonging to the classes of cinnamic acids, acetophenones, benzaldehydes, benzoic acids, phenylpropanoids, and hydroxylated biphenyls are inhibitors of mycotoxin type B trichothecene (3-acetyl-4-deoxynivalenol) *in vitro* production by *F. culmorum* MCf 21 without significant reduction of fungal growth. Four compounds showed effective fungicidal activity, hence providing new opportunities for application in crop protection. In an attempt to improve bioavailability of the tested compounds, *β*-CD was added to the growth medium. Although previous studies have demonstrated a synergistic effect of *β*-CD on the antimicrobial activity of plant-derived phenols,[29] no significant effect was observed in the present study.

It is worth doing further comments on results achieved with some compounds. Carvacrol (**26**), whose fungicidal activity at 1.0 mM was previously demonstrated[30] turned out to be a good type B trichothecene inhibitor, whereas inhibition of fungal growth was determined only at higher concentrations (data not shown).

Zingerone (**25**) and dehydrozingerone (**22**), both constituents of *Zingiber officinale* and *Curcuma longa*, are structurally and biologically related to curcumin. Both compounds possess antioxidant, anti-inflammatory, and anti-tumor-promoting activities.[31,32] Recently, the *in vitro* inhibitory effect and fungicide activity of some curcumin derivatives were observed in *F. proliferatum*, a fumonisin B1 producer.[33] Fungitoxic properties of dehydrozingerone (**22**) and zingerone (**25**) were reported toward *F. oxysporum* and *Aspergillus* sp., respectively.[34,35] In our study, dehydrozingerone (**22**), zingerone (**25**), and its natural-like Me-zingerone (**23**) tested at 1.0 and 0.5 mM showed a strong inhibitory effect on trichothecene production by *F. culmorum*, without significantly affecting its vegetative growth *in vitro*. Protection of the phenolic −OH group of dehydrozingerone (**22**) (e.g., compound **24**) caused at differing concentrations a fungicidal effect, inhibition, or even overproduction of 3-acetyl-4-deoxynivalenol.

Recently, ferulic acid dimers were evaluated in *F. culmorum* liquid culture[14] based on the assumption that the inhibitory activity of ferulic acid should be attributed to the dimeric forms (hydroxylated biphenyls) rather than the single monomer. In the present study, other natural hydroxylated biphenyls were evaluated, such as the dimers of eugenol (**28**) and magnolol (**27**), two compounds with antioxidant, anti-inflammatory, and antimicrobial activities.[36,37] Eugenol dimer (**28**) caused a significant increase in trichothecene production by *F. culmorum*. This effect could be attributed to the phenolic −OH groups that, near the methoxyl group, would be embedded in a five-membered ring hydrogen bond rather than a seven-membered ring involving the two phenolic −OH groups. This conformation excludes or restricts intermolecular hydrogen bond interactions, thereby hampering a likely key factor in fungicide activity. Interestingly, in magnolol (**27**), structurally similar to eugenol dimer (**28**) but lacking methoxy groups in the *ortho* position to phenolic −OH groups, a concentration-dependent fungicide-like activity was observed. The presence of a free phenolic −OH group seems to improve fungicidal activity. The moderate inhibition of fungal growth displayed by biphenol (**30**) at 1.0 mM may be attributed to the *para* orientation of the two phenolic −OH groups, which would promote quinone formation on oxidation.

Apocynin (**6**), known for its antioxidant, antimicrobial, and anti-inflammatory activities,[38] displayed a concentration-dependent inhibitory effect on trichothecene biosynthesis. A five-membered ring hydrogen bond in compound **6** would prevent strong intermolecular interactions with phenolic −OH group. Because a series of halide acetophenones were designed and prepared as potential fungicides against different phytopathogenic fungi,[39] we postulated that 4-bromo-acetophenone (**7**) would be a good candidate. No phenolic −OH group is present in the structure of acetophenone (**7**); nevertheless, an electron-withdrawing bromo group located in the *para* position to the methyl ketone function makes the aromatic ring sufficiently electron-deficient. As expected, complete mycotoxin inhibition was observed, with only moderate reduction of fungal growth.

Esters of gallic acid have already been studied for their antioxidant and antimicrobial/fungicide activities, which depend upon the length of the chain.[40] This feature was confirmed in the present study, because when a long aliphatic chain is present, the trichothecene inhibitory effect or the fungicidal activity depends upon the concentration. The effect is likely influenced by aggregation phenomena, especially in the case of compounds with a longer aliphatic chain, such as compounds **14** and **18**. When the length of the alcoholic chain is shorter, as in compound **15**, strong and comparable inhibitory activity on trichothecene *in vitro* production was detected at both 1.0 and 0.5 mM.

As a general rule, the 4-substituted 2-methoxy phenol (e.g., compounds **3**, **6**, **11**, **20**, **21**, **22**, **25**, **28**, and **29**) is the most representative structural skeleton present in the tested compounds; less representative are units where hydroxylation, demethylation, and demethoxylation occur in the aromatic ring or in different positions. The structural skeleton is present in both monomer and dimer forms and is characterized by different electronic and steric features according to substituents in the *para* position to the phenolic −OH group. Phenolic

compounds bearing a methoxy group in the *ortho* position to phenolic −OH, namely, a guaiacyl unit, usually form an intramolecular hydrogen bond, which is energetically favorable.[41] The guaiacyl unit exhibits antioxidant proprieties because it acts as a H donor to scavenge radicals.[42] It is well-acknowledged that antioxidant activity of the guaiacyl unit acts as a free radical scavenger by H atom transfer from the phenolic OH group.[43,44] Phenoxy radicals formed from a guaiacyl moiety do not favor quinone formation, as happens when radicals are generated by a catechol moiety (e.g., compound **4**).

When the corresponding phenoxy radical $ArO^{\bullet}$ formed in guaiacyl moiety is also delocalized in the side chain *para* to the phenolic −OH group, the radical is easier to form, e.g., in compounds **3**, **4**, **22**, **25**, **28**, and **29**, as compared to eugenol (**20**), isoeugenol (**21**), vanillin (**12**), veratraldehyde (**11**), and apocynin (**6**), all having a less extended electronic conjugation. As a result, the antioxidant activity of compounds **6**, **11**, **12**, **20**, and **21** is lower than in compounds **3**, **4**, **22**, **28**, and **29**. Except for biphenyl (**28**), all compounds bearing a guaiacyl moiety caused a significant inhibition of mycotoxin production without affecting fungal growth. It is therefore reasonable to assume that the presence of a guaiacyl unit with an electron-withdrawing substituent in the *para* position may be a key structure in trichothecene inhibition.

The inhibitory activity of a guaiacyl unit, with a phenolic −OH methyl protected, was not strictly associated with the antioxidant activity in the present work (e.g., compounds **11**, **23**, and **24**).

In solution, the guaiacyl unit presenting an extended conjugation is expected to be in plane or to deviate only marginally from the plane. Consequently, any difference in the activity of the molecules should be correlated to electronic phenomena rather than steric effects. On the contrary, in dimer form (e.g., hydroxylated biphenyls), steric effects would strongly influence the molecular properties (e.g., capacity to form stable radicals, interaction with proteins, increased lipophilicity, Lewis acidity enhancement, and polarizability), mainly when the two phenolic −OH groups are *ortho* to the C−C bond of the two aromatic rings. Nonplanar arrangement of the four groups along the C−C coupling bond occurs, providing steric influence, even when free rotation around the C−C single bond is expected.[45] Therefore, a steric effect may drive the ability of hydroxylated biphenyls to inhibit mycotoxin production. In 2,2′-dihydroxybiphenyls lacking a guaicyl unit and being conformationally more flexible, such as magnolol (**27**), marked antifungal activity was observed also at 0.1 mM (data not shown).

The relative order to partitioning in the organic phase (lipophilicity, determined by RP-HPLC) is in agreement with that determined for the polarity of each compound, as determined by HPLC. In principle, the least polar compound should present higher partitioning in the lipid phase, and this behavior should reflect an inhibitory property. Nonetheless, fungal matrices are multi-component systems, where the medium can be considered as both lipidic and emulsion systems. Thus, correlating theoretical calculations and experimental data is not a straightforward approach. The balance among lipophilicity, antioxidant activity, and capacity to activate weak interactions with enzymes is a key factor to estimate a good phenolic mycotoxin inhibitor.[46,47]

In addition to the known inhibitory activity of ferulic acid (**3**) and its derivatives, common natural compounds, such as compounds **6**, **15**, **20**, **22**, **25**, and **26**, exhibited a strong inhibitory activity within the range of the tested concentrations. Although some of these compounds have already been known for their fungicidal or antimicrobial activity on different fungi, this is the first time such molecules have been evaluated as mycotoxin inhibitors in *F. culmorum*. It has not escaped our notice that the remarkable fungicide activity detected for magnolol (**27**) is worth further application in different fields. The inhibitory activity of selected compounds is being tested *in planta* to evaluate potential application for the control of *Fusarium* affecting wheat and other small grain cereals.

■ ASSOCIATED CONTENT

Supporting Information

Description of TLC and LC−MS methods, HPLC of the tested compounds in one chromatographic run, materials for detection of mycotoxins by TLC, estimation of lipophilicity (log *P*) of studied compounds, and detection of polarity of studied compounds by TLC. This material is available free of charge via the Internet at http://pubs.acs.org.

■ AUTHOR INFORMATION

Corresponding Author

*Telephone: +39-079-2841220. Fax: +39-079-2841299. E-mail: giovanna.delogu@icb.cnr.it.

Present Address

[§]Zahra Jahanshiri: Department of Mycology, Faculty of Medical Science, Tarbiat Modares University, Teheran 14115-331, Iran.

Funding

The authors acknowledge support by the Regione Autonoma della Sardegna (Legge Regionale 7 Agosto 2007, no. 7 "Promozione della Ricerca Scientifica e dell'Innovazione Tecnologica in Sardegna"), the Ministry of University and Research (PRIN 2011 "Cell Wall Determinants To Improve Durum Wheat Resistance to *Fusarium* Diseases"), and the University of Sassari (P.O.R. SARDEGNA F.S.E. 2007-2013-Obiettivo Competitività Regionale e Occupazione, Asse IV Capitale Umano, Linea di Attività l.3.1. "Identification of Natural and Natural-like Molecules Inhibiting Mycotoxin Biosynthesis by *Fusaria* Pathogen on Cereals").

Notes

The authors declare no competing financial interest.

■ ACKNOWLEDGMENTS

The authors thank Corrado Dimauro for assisting in statistical analysis.

■ REFERENCES

(1) Scherm, B.; Balmas, V.; Spanu, F.; Pani, G.; Delogu, G.; Pasquali, M.; Migheli, Q. *Fusarium culmorum*: Causal agent of foot and root rot and head blight on wheat. *Mol. Plant Pathol.* **2013**, *14*, 323−341.

(2) Lowe, R.; Jubault, M.; Canning, G.; Urban, M.; Hammond-Kosack, K. E. The induction of mycotoxins by trichothecene producing *Fusarium* species. In *Plant Fungal Pathogens—Methods in Molecular Biology*; Molton, M. D., Thomma, B. P. H. J., Eds.; Humana Press: New York, 2012; Vol. *835*, pp 439−455.

(3) Magan, N.; Aldred, D.; Mylona, K.; Lambert, R. J. W. Limiting mycotoxins in stored wheat. *Food Addit. Contam., Part A* **2010**, *27*, 644−650.

(4) Desmond, O. J.; Manners, J. M.; Stephens, A. E.; Maclean, D. J.; Schenk, P. M.; Gardiner, D. M.; Munn, A. L.; Kazan, K. The *Fusarium* mycotoxin deoxynivalenol elicits hydrogen peroxide production, programmed cell death and defence responses in wheat. *Mol. Plant Pathol.* **2008**, *9*, 435−445.

(5) Sudakin, D. L. Trichothecenes in the environment: Relevance to human health. *Toxicol. Lett.* **2003**, *143*, 97−107.
(6) Yang, G. H.; Jarvis, B. B.; Chung, Y. J.; Pestka, J. J. Apoptosis induction by the satratoxins and other trichothecene mycotoxins relationship to ERK, p8MAPK, and SAPK/JNK activation. *Toxicol. Appl. Pharmacol.* **2000**, *164*, 149−160.
(7) Chala, A.; Weinert, J.; Wolf, G. A. An integrated approach to the evaluation of the efficacy of fungicides against *Fusarium culmorum*, the cause of head blight of wheat. *J. Phytopathol.* **2003**, *151*, 673−678.
(8) Haidukowski, M.; Pascale, M.; Perrone, G.; Pancaldi, D.; Campagna, C.; Visconti, A. Effect of fungicides on the development of *Fusarium* head blight, yield and deoxynivalenol accumulation in wheat inoculated under field conditions with *Fusarium graminearum* and *Fusarium culmorum*. *J. Sci. Food Agric.* **2005**, *85*, 191−198.
(9) Jones, R. K. Assessments of *Fusarium* head blight of wheat and barley in response to fungicide treatment. *Plant Dis.* **2000**, *84*, 1021−1030.
(10) Paul, P. A.; Lipps, P. E.; Hershman, D. E.; McMullen, M. P.; Draper, M. A.; Madden, L. V. Efficacy of triazole-based fungicides for *Fusarium* head-blight and deoxynivalenol control in wheat: A multivariate meta-analysis. *Phytopathology* **2008**, *98*, 999−1011.
(11) Simpson, D. R.; Weston, G. E.; Turner, J. A.; Jennings, P.; Nicholson, P. Differential control of head blight pathogens of wheat by fungicides and consequences for mycotoxin contamination of grain. *Eur. J. Plant Pathol.* **2001**, *107*, 421−431.
(12) Picot, A.; Atanasova-Pébuchon, V.; Pons, S.; Marchegay, G.; Barreau, C.; Pinson Gadais, L.; Roucolle, J.; Daveau, F.; Caron, D.; Richard-Forget, F. Maize kernel antioxidants and their potential involvement in *Fusarium* ear rot resistance. *J. Agric. Food Chem.* **2013**, *61*, 3389−3395.
(13) Bakan, B.; Bily, A. C.; Melcion, D.; Cahagnier, B.; Regnault-Roger, C.; Philogène, B. J.; Richard-Molard, D. Possible role of plant phenolics in the production of trichothecenes by *Fusarium graminearum* strains on different fractions of maize kernels. *J. Agric. Food Chem.* **2003**, *51*, 2826−2831.
(14) Boutigny, A. L.; Atanasova-Penichon, V.; Benet, M.; Barreau, C.; Richard-Forget, F. Natural phenolic acids from wheat bran inhibit *Fusarium culmorum* trichothecene biosynthesis *in vitro* by repressing *Tri* gene expression. *Eur. J. Plant Pathol.* **2010**, *127*, 275−286.
(15) Kim, J. H.; Campbell, B. C.; Mahoney, N.; Chan, K. L.; Molyneux, R. J. Identification of phenolics for control of *Aspergillus flavus* using *Saccharomyces cerevisiae* in a model target-gene bioassay. *J. Agric. Food Chem.* **2004**, *52*, 7814−7821.
(16) Dambolena, J. S.; Lopez, A. C.; Meriles, J. M.; Rubinstein, H. R.; Zygadlo, J. A. Inhibitory effect of 10 natural phenolic compounds on *Fusarium verticilliodes*. A structure−property−activity relationship study. *Food Control* **2012**, *28*, 163−170.
(17) Kim, J. H.; Tsao, R.; Yang, R.; Cui, S. W. Phenolic acid profiles and antioxidant activities of wheat bran extracts and the effect of hydrolysis conditions. *Food Chem.* **2006**, *95*, 466−473.
(18) Balcerzak, M.; Harris, L. J.; Subramaniam, R.; Ouellet, T. The feruloyl esterase gene family of *Fusarium graminearum* is differentially regulated by aromatic compounds and hosts. *Fungal Biol.* **2012**, *116*, 478−488.
(19) Scherm, B.; Orrù, M.; Balmas, V.; Spanu, F.; Azara, E.; Delogu, G.; Hammond, T. M.; Keller, N. P.; Migheli, Q. Altered trichothecene biosynthesis in *TRI6*-silenced transformants of *Fusarium culmorum* influences the severity of crown and foot rot on durum wheat seedlings. *Mol. Plant Pathol.* **2011**, *12*, 759−771.
(20) Vogel, H. J. A convenient growth medium for *Neurospora* (Med N). *Microbiol. Genet. Bull.* **1956**, *13*, 42−43.
(21) De Faria Dias, A. An improved high yield synthesis of dehydrodieugenol. *Phytochemistry* **1988**, *27*, 3008−3009.
(22) Russel, W. R.; Scobbie, L.; Chesson, A. Structural modification of phenylpropanoid-derived compounds and the effects on their participation in redox processes. *Bioorg. Med. Chem.* **2005**, *13*, 2537−2546.
(23) Marchiani, A.; Mammi, S.; Siligardi, G.; Hussain, R.; Tessari, I.; Bubacco, L.; Delogu, G.; Fabbri, D.; Dettori, M. A.; Sanna, D.; Dedola, S.; Serra, P. A.; Ruzza, P. Small molecole interacting with α-synuclein: Antiaggregating and cytoprotective properties. *Amino Acids* **2013**, *45*, 327−338.
(24) Ponts, N.; Pinson-Gadais, L.; Boutigny, A.-L.; Barreau, C.; Richard-Forget, F. Cinnamic-derived acids significantly affect *Fusarium graminearum* growth and *in vitro* synthesis of type B trichothecenes. *Phytopathology* **2011**, *101*, 929−934.
(25) Bily, A. C.; Reid, L. M.; Savard, M. E.; Reddy, R.; Blackwell, B. A.; Campbell, C. M.; Krantis, A.; Durst, T.; Philogéne, B. J. R.; Arnason, J. T.; Regnault-Roger, C. Analysis of *Fusarium graminearum* mycotoxins in different biological matrices by LC/MS. *Mycopathologia* **2004**, *157*, 117−126.
(26) Sanna, D.; Delogu, G.; Mulas, M.; Schirra, M.; Fadda, A. Determination of free radical scavenging activity of plant extracts through DPPH assay: An EPR and UV−vis study. *Food Anal. Method* **2012**, *5*, 759−766.
(27) Re, R.; Pellegrini, N.; Proteggente, A.; Pannala, A.; Yang, M.; Rice-Evans, C. Antioxidant activity applying an improved ABTS radical cation decolorization assay. *Free Radical Biol. Med.* **1999**, *26*, 1231−1237.
(28) Trucksess, M. W.; Flood, M. T.; Mossoba, M. M.; Page, S. W. High-performance thin-layer chromatographic determination of deoxynivalenol, fusarenon-X, and nivalenol in barley, corn, and wheat. *J. Agric. Food Chem.* **1987**, *35*, 445−448.
(29) Liang, H.; Yuan, Q.; Vriesekoop, F.; Lv, F. Effects of cyclodextrins on the antimicrobial activity of plant-derived essential oil compounds. *Food Chem.* **2012**, *135*, 1020−1027.
(30) Dambolena, J. S.; Zygadlo, J. A.; Rubinstein, H. R. Antifumonisin activity of natural phenolic compounds A structure−property−activity relationship study. *Int. J. Food Microbiol.* **2011**, *145*, 140−146.
(31) Singh, G.; Kapoor, P. S.; Singh, P.; de Heluani, C. S.; de Lampasona, M. P.; Catalan, C. Chemistry, antioxidant and antimicrobial investigations on essential oil and oleoresins of *Zingiber officinale*. *Food Chem. Toxicol.* **2008**, *46*, 3295−3302.
(32) Marchiani, A.; Rozzo, C.; Fadda, A.; Delogu, G.; Ruzza, P. Curcumin and curcumin-like molecules: From spice to drugs. *Curr. Med. Chem.* **2014**, *21*, 204−222.
(33) Coma, V.; Portes, E.; Gardrat, C.; Richard-Forget, F.; Castellan, A. *In vitro* inhibitory effect of tetrahydrocurcuminoids on *Fusarium proliferatum* growth and fumonisin B1 biosynthesis. *Food Addit. Contam.* **2011**, *28*, 218−225.
(34) Kubra, I. R.; Murthy, P. S.; Rao, L. J. *In vitro* antifungal activity of dehydrozingerone and its fungitoxic properties. *J. Food Sci.* **2013**, *78*, M64−M69.
(35) Kim, J. H.; Mahoney, N.; Chan, K. L.; Molyneux, R. J.; Campbell, B. C. Controlling food-contaminating fungi by targeting their antioxidative stress-response system with natural phenolic compounds. *Appl. Microbiol. Biotechnol.* **2006**, *70*, 735−739.
(36) Choi, N. H.; Choi, G. J.; Min, B. S.; Jang, K. S.; Choi, Y. H.; Kang, M. S.; Park, M. S.; Choi, J. E.; Bae, B. K.; Kim, J. C. Effects of neolignans from the stem bark of *Magnolia obovata* on plant pathogenic fungi. *J. Appl. Microbiol.* **2009**, *106*, 2057−2063.
(37) Garcia-Cones, M. T.; Wilson, P. D.; Plumb, G. W.; Ralph, J.; Williamson, G. Antioxidant properties of 4,4′-dihydroxy−3,3′-dimethoxy-β,β′-bicinnamic acid (8−8-diferulic acid, non-cyclic form). *J. Sci. Food Agric.* **1999**, *79*, 379−384.
(38) Houser, K. R.; Johnson, D. K.; Ishmael, F. T. Anti-inflammatory effects of methoxyphenolic compounds on human airway cells. *J. Inflamm.* **2012**, 9−6.
(39) Ma, Y.-T.; Fan, H.-F.; Gao, Y.-Q.; Li, H.; Zhang, A.-L.; Gao, J.-M. Natural products as sources of new fungicides (I): Synthesis and antifungal activity of acetophenone derivatives against phytopathogenic fungi. *Chem. Biol. Drug Des.* **2013**, *81*, 545−552.
(40) Kubo, I.; Xiao, P.; Nihei, K.; Fujita, K.; Yamagiwa, Y.; Kamikawa, T. Molecular design of antifungal agents. *J. Agric. Food Chem.* **2002**, *50*, 3992−3998.

(41) Nenadis, N.; Zhang, H.; Tsimidou, M. Z.; Zhang, H. Y. Estimation of scavenging activity of phenolic compounds using the ABTS$^{\bullet+}$ assay. *J. Agric. Food Chem.* **2004**, *52*, 4669−4674.
(42) Priyadarsini, K. I.; Guha, S. N.; Rao, M. N. A. Physico-chemical properties and antioxidant activities of methoxy phenols. *Free Radical Biol. Med.* **1998**, *24*, 933−941.
(43) Litwinienko, G.; Ingold, K. U. Abnormal solvent effect on hydrogen atom abstraction. 2. Resolution of the curcumin antioxidant controversy. The role of sequential proton loss electron transfer. *J. Org. Chem.* **2004**, *69*, 5888−5896.
(44) Delomenède, M.; Bedos-Belval, F.; Duran, H.; Vindis, C.; Baltas, M.; Nègre-Salvayre, A. Development of novel antiatherogenic biaryls: Design, synthesis, and reactivity. *J. Med. Chem.* **2008**, *51*, 3171−3181.
(45) Amorati, R.; Lucarini, M.; Mugnaini, V.; Pedulli, F. Antioxidant activity of *o*-bisphenols: The role of intramolecular hydrogen bonding. *J. Org. Chem.* **2003**, *68*, 5198−5204.
(46) Bollina, V.; Kushalappa, A. C. *In vitro* inhibition of trichothecene biosynthesis in *Fusarium graminearum* by resistance-related endogenous metabolites identified in barley. *Mycology* **2011**, *2*, 291−296.
(47) Roleira, F. M. F.; Siquet, C.; Orrù, E.; Garrido, E. M.; Garrido, J.; Milhazes, N.; Podda, G.; Paiva-Martins, F.; Reis, S.; Carvalho, R. A.; Silva, E. J.; Borges, F. Lipophilic phenolic antioxidants: Correlation between antioxidant profile, partition coefficients and redox properties. *Bioorg. Med. Chem.* **2010**, *18*, 5816−5825.

polyphenols in tobacco leaves in 1977.[20] Snook et al.[21,22] made a good idea for improving above HPLC method and quantified seven polyphenols. In 1993, Achilli et al.[23] for the first time realized the separation of chlorogenic acid and rutin. The efforts of the separation of alkaloids and polyphenols are summarized in Table 1.

Table 1. Summarization of the Efforts on the Detection of Alkaloids and Polyphenols

year	author	target compound	separation mean
1962	Quin et al.[10]	alkaloids	GC with packed columns
1965	Massingill et al.[11]	alkaloids	GC with packed and capillary columns
2003	Cai et al.[12]	alkaloids	GC with megabore capillary column
1984	Sudan et al.[15]	alkaloids	reversed-phase HPLC
1985	Mousa et al.[13]	alkaloids	HPLC with electrochemical detection
1998	Sellergren et al.[14]	alkaloids	liquid−liquid extraction followed by reversed-phase HPLC using gradient elution
1999	Ciolino et al.[16−18]	alkaloids	reversed-phase ion-pair HPLC
1977	Court[20]	polyphenols	reversed-phase HPLC
1982	Snook et al.[21]	polyphenols	reversed-phase HPLC
1993	Achilli et al.[23]	polyphenols	reversed-phase HPLC

It is well recognized that chemical composition of tobacco is highly associated with the flavor of tobacco products and the risk of smoking.[24] Many methods have been developed to determine tobacco flavoring or harmful constitutions.[25−29] Currently, the chemical compositions of tobacco leaves have attracted a considerable amount of attention throughout the world.[30−33] In view of the fact that the unique combination of tobacco maturation stages and cultivation conditions result in unique secondary metabolites, comprehensive studies on the chemical constituents of tobacco sample of different origins harvested at different maturation stages might provide valuable information to identify superior cultivation condition and the appropriate time to harvest tobacco. However, to our knowledge, no such study was yet reported. In this study, a comprehensive high pressure liquid chromatography−photo-diode array-quadrupole time-of-flight mass spectrometry (HPLC−PDA-QTOF-MS) method was developed for the quantitative determination of the main polyphenols and alkaloids as well as qualitative profiling of other secondary metabolites in 12 batches of tobacco samples of three origins and four maturation stages. The reliability and adaptability of the method were verified by determination of linear range, recovery, and reproducibility with tobacco samples. We expect our work would provide a scientific basis and guidance for artificial cultivation and harvest of tobacco and, thereby, improve the quality of tobacco.

EXPERIMENTAL SECTION

Chemicals and Reagents. HPLC grade acetonitrile and methanol were purchased from Fisher Co. (Fisher Scientific, USA). Deionized water obtained from a Milli-Q water system (Milli-Pore Corp., Bedford, MA, USA) was used for sample preparation procedures and HPLC analyses. Other chemicals were of analytical grade. Eight reference compounds, namely nornicotine (**1**), neonicotine (**2**), anatabine (**3**), nicotine (**4**), myosmine (**5**), scopoletin (**6**), rutin (**7**), and quercetin (**8**) (Figure 1), were isolated and purified in our laboratory and were identified based on UV, IR, MS, ^{1}H NMR, and

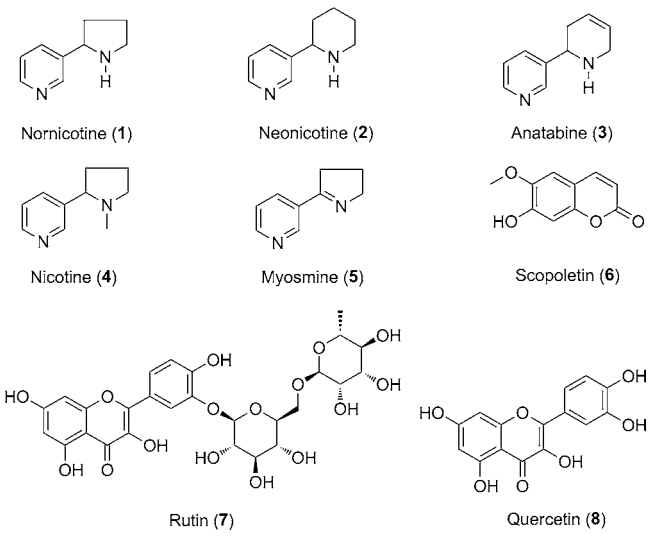

Figure 1. Chemical structures of reference compounds **1**−**8**.

^{13}C NMR analyses. The purity of these compounds was determined to be more than 98% by HPLC analysis. Among them, compounds **1**, **2**, **3**, **4**, and **5** are alkaloids, compounds **7** and **8** are polyphenols, and compound **6** is a coumarin.

Plant Material and Plantation Conditions. Seeds of a tobacco cultivar (*Nicotiana tabacum* "k326") were obtained from the Seed Center of Yunnan Academy of Tobacco (Yunnan, China). Seeds were planted and raised within a germination cabinet in 25 ± 1 °C. Thirty days after germination, the seedlings were transplanted into the pots (50 cm diameter × 50 cm deep). Soil for the potted plants was composed of the same red soil and humus (3:1). These plants were grown at three sites in China: Zhengzhou of Henan province (34°72′ N, 113°65′ E; elevation 110 m), Zunyi of Guizhou province (27°07′ N,106°88′ E; elevation 1000 m), and Jiangchuan of Yunnan province (24°17′ N,102°45′ E; elevation 1730 m). Each site had different temperature, humidity, and rainfall characteristics (Figure S-1 of the Supporting Information). Seedlings were transplanted between 23 April and 6 May of 2012. During the experiment, none of the plants experienced any water or nutrient stresses.

Tobacco leaf samples were collected from the three cultivation places at four maturities. The tobacco samples ZZ-T, ZZ-X, ZZ-C, and ZZ-C2 were collected from Zhengzhou, the samples ZY-T, ZY-X, ZY-C, and ZY-C2 were collected from Zunyi, and the JC-T, JC-X, JC-C, and JC-C2 samples were collected from Jiangchuan. Those sample names marked with -T, -X, -C, and -C2 suffixes represent they were harvested at 40 days (rosette stage), 60 days (squaring stage), 85 days (physiological maturation stage), and 100 days (harvest maturation stage) after transplantation, respectively.

Sample Preparation. The tobacco samples were sun dried on site right after collection and then fine-ground for further extraction. For HPLC analysis, an accurately weighted 1.0 g of the ground powder of each sample and 10 mL of methanol was added to a flask in an ultrasonic bath for 30 min. The extraction process was repeated three times. The extracted solutions were combined, filtered, and evaporated under vacuum. The residue was diluted to volume with methanol in a 25 mL volumetric flask. Then the solutions were filtered through a 0.22 μm PTFE syringe filter into HPLC vials for HPLC−PDA-MS analysis.

Trichloromethane was used to extract the fat-soluble components in the tobacco leaves. Then 1.0 g tobacco powder was introduced into a 25 mL flask, followed by the addition of 10 mL of trichloromethane. The extraction was performed under ultrasonication for 30 min. The mixture was filtered through a filter paper, and the solution was transferred to a 50 mL round-bottomed flask and evaporated to

Table 2. Fat-Soluble Compositions of Tobacco Samples from Three Different Origins Harvested at Four Maturation Stages by GC−MS

no.	t_R (min)	CAS	name	ZZ-T	ZZ-X	ZZ-C	ZZ-C2	ZY-T	ZY-X	ZY-C	ZY-C2	JC-T	JC-X	JC-C	JC-C2
1	3.31	000108-87-2	methylcyclohexane	13.94	23.43	15.74	20.19	26.56	15.30	22.05	14.19	16.70	15.74	16.51	14.93
2	3.45	001640-89-7	ethylcyclopentane	1.01	1.71	1.14	1.55	1.93	1.12	1.61	0.80	1.26	1.14	1.21	1.13
3	4.04	000108-88-3	toluene	0.82	1.04	0.91	1.07	1.58	0.91	1.33	0.80	0.66	0.96	0.84	0.77
4	6.42	000108-93-0	cyclohexanol	4.36	7.16	5.04	6.70	8.14	4.55	6.54	6.70	5.53	4.98	5.14	5.66
5	11.85	000054-11-5	nicotine	2.24	0.00	0.40	0.84	0.44	1.52	6.57	0.84	1.52	0.12	0.05	0.14
6	13.97	003076-04-8	2-propenoic acid, tridecyl ester	0.00	0.00	0.00	0.00	0.00	0.00	0.00	0.00	3.17	0.00	0.11	0.00
7	14.07	000139-08-2	tetradecyldimethylbenzylammonium chloride	0.00	0.00	0.00	0.00	0.00	0.00	0.00	0.00	3.18	0.00	0.14	0.00
8	14.42	000486-56-6	cotinine	0.07	0.00	0.08	0.00	0.00	0.28	0.11	0.00	1.53	0.00	0.10	0.00
9	15.27	000473-55-2	dihydropinene	3.40	5.03	4.56	2.36	2.64	3.11	0.00	0.18	5.78	2.52	2.90	3.96
10	15.79	056554-74-6	1,4-eicosadiene	0.00	1.33	0.41	0.66	0.00	0.00	0.00	2.36	1.63	0.32	0.41	1.10
11	16.87	000057-10-3	*n*-hexadecanoic acid	2.45	2.19	2.05	2.83	3.45	2.82	0.00	0.66	10.33	3.54	3.92	2.65
12	17.03	000473-55-2	dihydropinene	0.11	0.00	0.19	2.80	0.00	0.00	0.00	1.83	0.00	0.07	0.00	0.00
13	19.45	005208-51-5	[1*S*,3*S*,(+)]-1-methyl-3-isopropenyl-4-cyclohexene	1.35	0.00	0.61	0.09	0.00	0.80	0.70	2.80	1.54	0.25	0.55	0.16
14	19.98	000506-44-5	linolenic alcohol	2.42	1.23	1.44	0.73	2.26	2.75	1.77	0.09	4.63	1.31	2.51	1.25
15	20.32	000057-11-4	octadecanoic acid	1.22	0.10	0.69	0.75	0.43	1.15	0.91	0.73	1.12	0.52	0.73	0.49
16	20.68	000638-58-4	tetradecanamide	2.36	0.84	1.04	0.29	0.82	1.95	0.00	0.75	4.13	0.59	1.87	0.47
17	22.51	000077-94-2	butyl citrate	5.51	3.44	9.79	1.04	2.40	12.59	8.00	0.29	1.65	0.24	1.65	0.18
18	24.98	000301-02-0	oleamide	3.99	3.83	1.37	8.09	2.59	2.15	2.71	1.04	15.26	0.68	0.22	1.63
19	26.69	000119-47-1	2,2′-methylenebis(6-*tert*-butyl-4-methylphenol)	0.56	0.00	0.00	1.34	0.63	0.38	0.43	8.09	1.07	0.24	0.18	0.17
20	30.34	024468-13-1	2-ethylhexyl chloroformate	0.18	0.00	0.21	1.06	0.00	1.01	0.00	1.34	1.30	0.17	0.28	0.32
21	34.27	000593-49-7	heptacosane	1.83	1.71	2.32	2.32	1.46	1.31	1.95	1.06	1.49	2.52	2.16	2.10
22	36.94	000112-84-5	erucylamide	0.77	0.92	0.58	0.94	0.45	0.50	1.27	2.32	1.80	0.26	0.34	0.83
23	39.38	000593-45-3	octadecane	0.90	0.68	0.35	0.92	3.11	1.46	1.05	0.94	0.48	2.16	1.50	1.17
24	40.55	000630-03-5	nonacosane	2.58	2.37	3.14	3.76	3.22	2.04	3.04	0.92	0.49	4.17	3.69	4.23
25	42.24	000593-49-7	heptacosane	3.53	3.14	2.01	2.20	0.32	3.67	0.60	3.76	1.56	6.24	4.33	3.81
26	43.14	000593-45-3	triacontane	0.75	0.74	1.63	2.74	1.13	0.62	1.94	2.20	1.35	1.51	1.53	2.19
27	44.52	055470-98-9	10-heptyl-10-octylicosane	6.26	6.21	6.29	5.31	12.66	8.86	0.00	2.74	0.23	10.09	7.98	9.17
28	45.27	000646-31-1	tetracosane	10.43	9.35	12.69	11.25	10.61	8.33	17.89	5.31	0.36	15.13	15.70	18.40
29	46.06	101191-41-1	vitamin E	0.58	0.07	1.40	0.78	0.35	0.67	2.11	11.25	0.00	0.14	1.13	0.24
30	46.63	055470-98-9	1-triacontanol	7.55	8.51	5.87	4.26	0.00	5.95	0.00	0.78	0.30	8.34	6.37	7.37
31	47.06	055320-06-4	11-decylheneicosane	1.68	1.87	3.14	2.06	0.00	1.53	3.78	4.26	0.07	2.27	2.47	3.56
32	48.38	000297-35-8	cyclotriacontane	3.59	4.00	4.14	4.12	5.72	4.41	0.00	2.06	1.30	4.21	2.95	3.61
33	48.90	000630-03-5	nonacosane	6.75	6.52	6.73	6.09	1.43	5.80	8.31	4.12	0.52	7.96	6.38	7.43
34	49.87	000084-80-0	phytonadione	1.00	1.07	0.84	0.29	5.20	0.78	2.22	6.09	1.23	0.41	2.15	0.31

dx.doi.org/10.1021/jf5009204 | J. Agric. Food Chem. 2014, 62, 4979−4987

dryness at 45 °C under reduced pressure. The residue in the round-bottomed flask was dissolved in 2 mL of cyclohexane with ultrasonication. The solution was then filtered through a 0.22 μm PTFE syringe filter before GC-MS analysis.

GC−MS Analysis. The fat-soluble components were analyzed on an Agilent 7890A gas chromatograph (Agilent Technologies, Santa Clara, CA) coupled to an Agilent 5975C mass spectrometer. Helium was used as the carrier gas at a flow rate of 1 mL/min. The GC analyses were performed on a capillary column (30 m × 0.22 mm inner diameter × 1.00 μm d_f). The split ratio was 1:10. The oven temperature was held at 50 °C for 4 min, followed by a ramp of 15 °C/min to 140 °C, then increased to 200 °C at 30 °C/min, followed by a ramp of 2 °C/min to 250 °C and held for 2 min, and then increased to the final temperature of 290 °C at 5 °C/min for 10 min and the inlet was set to a temperature of 240 °C. Temperature of the interface, ion source and quadrapole of the mass spectrometer were set at 280, 230, and 150 °C, respectively. The mass range of m/z 50−700 was set for all GC-MS analyses. Compound identification was based on comparisons to mass spectra of authentic reference compounds by reference to the National Institute of Standards and Technology (NIST) library and published data.

HPLC−PDA-QTOF-MS Analysis. The HPLC analysis was performed on a Waters ACQUITY UPLC I Class system (Waters Corp., MA, USA), equipped with a binary solvent delivery system, a 48-vial autosampler, and a photodiode array detector (PDA). The separation of the main components was achieved on a TSK gel ODS-100Z column (150 mm × 4.6 mm, 3 μm). The mobile phases consisted of solvent A (deionized water with 10 mM ammonium acetate) and solvent B (acetonitrile). The gradient elution was applied at a flow rate of 1.2 mL/min as follows: 3% B (0−4 min), 3−10% B (4−8 min), 10% B (8−12 min), 10−15% B (12−16 min), 15% B (16−18 min), 15%−60% B (18−34 min), 60%−99% B (34−35 min), and 99% (35−37 min). The column and autosampler temperature were maintained at 60 and 15 °C, respectively. The injection volume was 5 μL, and the UV wavelength was set at 254 nm for the detection of **1**−**5**, and **8**. While for the detection of **6**, the UV wavelength of 340 nm was used.

Stock solutions containing eight reference compounds were prepared and diluted to appropriate concentrations for construction of calibration curves. Resulting solutions were filtered through 0.22 μm nylon syringe filters, and aliquots of 5 μL were injected in the chromatographic system for analyses. The standard solutions were analyzed in triplicate, and peak areas were used as an analytical signal. The calibration curves were constructed by plotting the peak areas versus the concentrations of standards.

The method was validated for linearity, sensitivity, repeatability, and accuracy. The limits of detection (LOD) and limits of quantification (LOQ) under the present conditions were determined at an S/N (signal-to-noise) of about 3 and 10, respectively. Intra- and interday variations were chosen to determine the precision of the developed assay. For intraday variability test, three different amounts (high, middle, and low level) of reference compounds were analyzed for six replicates within 1 day, while for interday variability tests, the same mixed standards were examined in duplicates in consecutive 3 days. Variations were expressed by the relative standard deviation (RSD) of the data. Recovery was used to evaluate the accuracy of the method. Three different amounts of the standard solutions were added to sample ZY-C2, and the recovery was measured in triplicate. For comparison, unspiked ZY-C2 sample was concurrently prepared and analyzed. The recovery was calculated as follows: recovery (%) = (amount found − amount original)/amount spiked × 100%. For the stability test, the sample solution was analyzed using the established method at 0, 2, 4, 6, 8, 10, and 12 h, respectively, the peak areas of eight analytes were recorded, and the RSD of peak areas at different times were calculated.

Mass spectrometric analysis was performed on a Synapt G2 QTOF-MS (HDMS, Waters, USA) operating in electrospray ionization (ESI) positive mode. The HPLC elution was split 3:1 using a flow splitting tee, resulting in flow rate of 0.3 mL/min to MS analysis. The mass spectrometer was operated with the following parameters: capillary voltage of 2.5 kV, cone voltage of 40 V, source temperature of 110 °C, desolvation temperature of 300 °C, and desolvation gas (N_2) flow of 700 L/h. The mass range was set at m/z 50−1000 with a scan time of 0.25 s and an interscan time of 0.02 s. LC−MS/MS analysis was performed by a collision energy ramp from 15 to 35 eV in the mass range of m/z 50−1000 in MS^E mode. To ensure the accuracy of the measured mass, leucine−enkephalin (with a reference mass at m/z 556.2771 in positive mode) was used as the lock-mass compound at a concentration of 500 pg/μL and a flow rate of 5 μL/min. The UPLC and Synapt G2 system operations were carried out using MassLynx 4.1 software (Waters, Manchester).

Statistical Analysis. Cluster analysis is a common technique for statistical data analysis which provides means for classifying a given set of objects into groups (clusters) in such a way that the similarities between objects could easily be determined. In this study, hierarchical cluster analysis (HCA) was performed to reveal the similarities between tobacco samples of different origins and maturities according to their fat-soluble constituents. The fat-soluble constituents of the 12 tobacco samples were subject to hierarchical cluster analysis based on the 34 most abundant fat-soluble constituents in the samples obtained by GC-MS. The percentage peak areas (PPAs) of these peaks in 12 batches of tobacco samples were used as variables for the HCA calculation. HCA was performed using Euclidean distance and average linkage without standardizing the variables. Statistical analysis was performed by Minitab for Windows, release 12 (Minitab Inc., State College, PA, USA).

RESULTS AND DISCUSSION

Influence of Origin and Maturity on the Fat-Soluble Composition. The fat-soluble composition is one of the important parameters to understand the variation among tobacco samples of different origins and maturities. More than 100 compounds were detected in 12 batches of tobacco samples through GC−MS analyses, and the percentage compositions of 34 most abundant compounds were tentatively identified and summarized in Table 2. Obvious variation can be found in fat-soluble composition among all samples. For instance, higher contents of cyclohexanol, butyl citrate, vitamin E, and cyclotriacontane were found in the Zhengzhou and Zunyi tobacco samples in comparison to those from Jiangchuan. However, Zunyi and Jiangchuan samples showed higher contents of phytonadione, octadecane, and linolenic alcohol, while the Zhengzhou and Jiangchuan tobacco samples had higher contents of heptacosane, 1-triacontanol, 11-decylheneicosane, tetracosane, dihydropinene, 10-heptyl-10-octylicosane, tetradecanamide, and nonacosane. During maturity, the 10-heptyl-10-octylicosane contents in Zhengzhou tobacco samples were almost constant (6.26, 6.21, 6.29, and 5.31% for ZZ-T, ZZ-X, ZZ-C, and ZZ-C2, respectively), while that of Zunyi tobacco samples showed significant reduction (12.66, 8.86, 0, and 2.74% for ZY-T, ZY-X, ZY-C, and ZY-C2, respectively). However, the Jiangchuan tobacco sample showed an approximate increased 10-heptyl-10-octylicosane content (0.23, 10.09, 7.98, and 9.17 for JC-T, JC-X, JC-C, and JC-C2, respectively) during maturity. In contrast to 10-heptyl-10-octylicosane content, the Zunyi tobacco samples showed the highest methylcyclohexane content (ZY-T with 26.56%) among all the tobacco samples, while the Zhengzhou tobacco sample showed the lowest methylcyclohexane content (ZZ-T with 13.94%). These results clearly demonstrated the influences of different origins from the same region and different regions on fat-soluble compositions during maturity. The GC-MS profile clearly shows that tobacco samples of all three origins harvested at rosette stage exhibited more fat-soluble components, while those harvested at harvest maturation stage exhibited the least

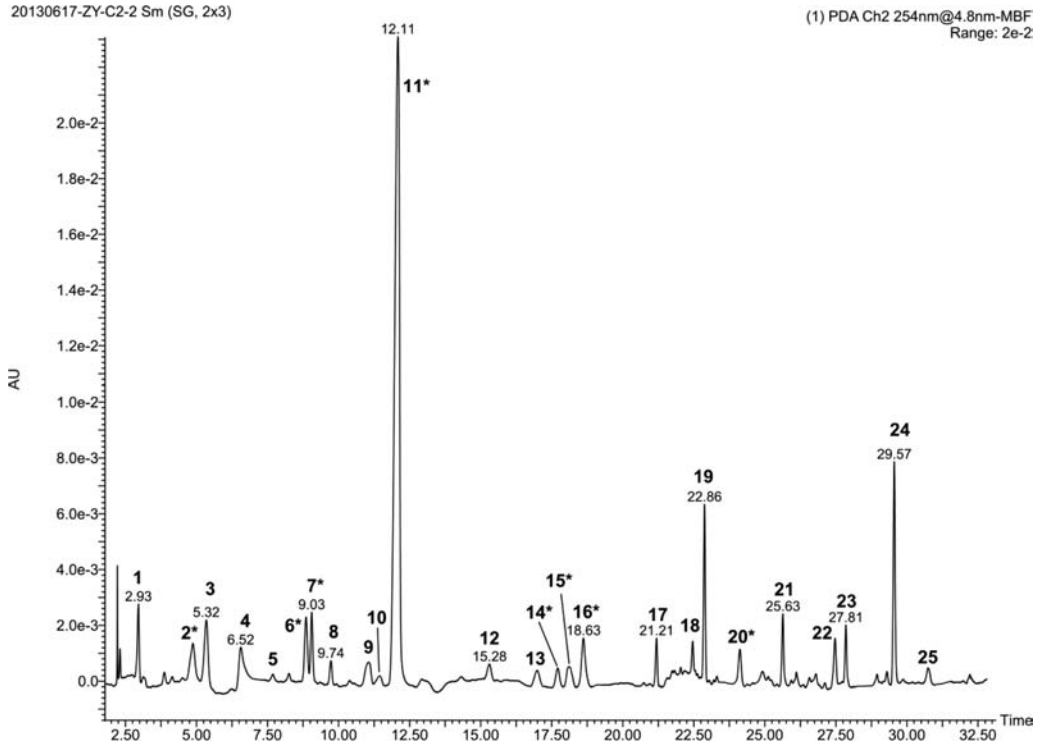

Figure 2. Chromatogram of a representative chromatogram of the tobacco samples (ZY-C2; detected at 254 nm). Peaks 2, 6, 7, 11, 14, 15, 16, and 20 were identified as reference standards **1**−**8**, and the tentative identification of the rest peaks can be found in Table 4.

Table 3. Retention Time, Regression Equation, Correlation Coefficient, Linearity Range, LOD, LOQ, Precision, Repeatability, and Recovery by HPLC−QTOF-MS for the Eight Analytes

							precision RSD (%)			
analyte	t_R (min)	calibration curve	r^2	linear range (μg/mL)	LOD (ng)	LOQ (ng)	intraday (n = 6)	interday (n = 6)	stability (RSD %, n = 6)	recovery (%)
nornicotine (**1**)	4.99	$y = 24.45x + 29.22$	0.9997	0.2−200	0.2	0.67	0.78	1.28	2.01	99.61
neonicotine (**2**)	8.27	$y = 21.54x - 37.84$	0.9999	0.2−200	0.2	0.67	0.52	0.70	0.94	98.90
anatabine (**3**)	9.09	$y = 20.11x - 75.47$	0.9995	0.2−200	1.0	3.3	0.94	1.35	0.40	100.71
nicotine (**4**)	12.02	$y = 14.70x - 35.84$	0.9996	0.5−200	1.4	4.5	1.34	3.01	1.75	99.51
myosmine (**5**)	18.35	$y = 34.83x - 24.06$	0.9997	0.5−200	1.0	3.2	0.41	0.75	3.67	99.31
scopoletin (**6**)	17.94	$y = 65.44x - 23.50$	0.9995	0.5−200	0.2	0.71	0.67	1.03	3.21	99.36
rutin (**7**)	18.82	$y = 44.89x - 88.48$	0.9995	0.5−200	1.5	4.9	2.62	3.66	0.39	98.40
quercetin (**8**)	24.87	$y = 81.45x - 368.88$	0.9990	0.5−200	0.5	1.6	3.04	3.46	1.01	101.22

fat-soluble components. The GC−MS profile of the fat-soluble components of the 12 batches of tobacco samples of three origins and four maturities is presented in Figures S-2−S-4 of the Supporting Information.

Validation of HPLC Method. All 12 batches of the tobacco sample were analyzed with the developed chromatographic condition, and the chromatogram of the eight standards and a representative chromatogram of the tobacco samples are illustrated in Figure 2. The chromatograms of the all the tobacco samples can be found in Figures S-4−S-6 of the Supporting Information.

The regression equation, correlation coefficient, linear range, LOD, LOQ, precision, repeatability, and recovery for the eight standards are summarized in Table 3. The correlation coefficient values (r^2 > 0.999) indicated appropriate correlations between the investigated compound concentrations and their peak area within the test ranges. The relative standard deviation (RSD) of peak area of each standard was within the range of 0.76−3.0% and 0.70−3.7% for intra- and interday repeatability and within 0.39−3.67% for stability. All the results demonstrated that the developed method is reproducible, precise, and stable. The spike recoveries were within the range of 98.8−102.7%, demonstrating superior performance of the method in both recovery and accuracy.

Variation in the Content of Alkaloids and Polyphenols between Samples of Different Origins during Maturity. Variation of the contents of nicotine and rutin in all tobacco samples is shown in Table 5. Of the five alkaloids and two polyphenols, nicotine and rutin showed the highest content in all tobacco samples, and thus nicotine and rutin were chosen as representative alkaloid and polyphenol compounds in the following discussion.

Affected by many factors such as growth conditions and leaf stalk position, the nicotine contents in tobacco varies from 1% to 3% of the total weight of tobacco.[34,35] Our results clearly showed that the nicotine content varied nearly 40-fold, ranging from 0.66 to 25.40 mg/g, in the tobacco samples of different origins and maturities (Table 5). As illustrated in Table 5,

dx.doi.org/10.1021/jf5009204 | J. Agric. Food Chem. 2014, 62, 4979−4987

Table 4. Identification of Main Chemical Constituents in ZY-C2 by HPLC-QTOF-MS (in ESI+ Mode; * Represents Reference Standards)

no.	t_R (min)	measured mass (m/z)	main fragment ions (relative intensity)	formula	exact mass	Δ (ppm)	tentative identification
1	2.93	136.0617	136.0617 (100), 119.0351 (51)	$C_5H_5N_5$	135.0545	−0.51	adenine
2*	5.22	149.1071	149.1071 (100), 132.0811 (37), 130.0649 (55), 117.0570 (23)	$C_9H_{12}N_2$	148.1000	−1.19	nornicotine (**1**)
3	5.32	179.1178	179.1178 (100), 132.0810 (65), 130.0649 (62), 117.0570 (43)	$C_{10}H_{14}N_2O$	178.1106	−0.43	nicotine-1′-*N*-oxide
4	6.52	251.1386	251.1386 (100), 234.1126 (55), 163.0391 (39),	$C_{13}H_{18}N_2O_3$	250.1317	−1.51	caffeoylputrescine (isomer 1)
5	7.63	325.1758	325.1758 (14), 163.1230 (100), 130.0653(15), 106.0650 (21)	$C_{17}H_{20}N_6O$	324.1699	−4.25	*N*-{2-[4-(2-pyrimidinyl)-1-piperazinyl]ethyl}-1,3-benzoxazol-2-amine
6*	8.52	163.1229	163.1229 (100), 146.0961 (30), 130.0645 (32), 118.0643 (61), 117.0572 (31)	$C_{10}H_{14}N_2$	162.1157	−0.47	neonicotine (**2**)
7*	9.03	161.1069	161.1069 (100), 144.0806 (42), 117.0571 (35)	$C_{10}H_{12}N_2$	160.1000	−2.35	anatabine (**3**)
8	9.74	251.1383	251.1383 (100), 234.1123 (46), 163.0388 (45)	$C_{13}H_{18}N_2O_3$	250.1317	−2.70	caffeoylputrescine (isomer 2)
9	11.01	177.1019	177.1019 (100), 159.0886 (8), 146.0598 (14), 120.0803 (10), 118.0643 (12),	$C_{10}H_{12}N_2O$	176.0950	−2.14	cotinine
10	11.44	193.0493	193.0498 (100), 178.0261 (82), 150.0310 (24), 135.0437 (80), 133.0284 (67), 122.0360 (18), 107.0489 (40)	$C_{10}H_8O_4$	192.0423	−1.44	herniarin
11*	12.11	163.1228	163.1228 (20), 132.0805 (52), 130.0648 (100), 120.0805 (10), 117.0571 (45), 106.0649 (15)	$C_{10}H_{14}N_2$	162.1157	−1.09	nicotine (**4**)
12	15.28	293.1493	293.1493 (100), 275.1373 (23), 227.1163 (11), 161.1069 (25), 132.0802 (21), 130.0651 (18),	$C_{15}H_{20}N_2O_4$	292.1423	−0.95	*rac-trans*-3′-hydroxymethylnicotine hemisuccinate
13	16.84	411.1993	411.1993 (100), 249.1581 (43)	$C_{22}H_{26}N_4O_4$	410.1954	−8.23	unknown
14*	17.63	193.0491	193.0491 (100), 178.0258 (82), 165.0549 (8), 150.0309 (21), 137.0595 (25), 133.0283 (65), 122.0362 (14), 105.0333 (10)	$C_{10}H_8O_4$	192.0423	−2.48	scopoletin (**5**)
15*	18.23	147.0914	147.0914 (100), 130.06567 (21), 117.0578 (35), 105.0453 (37), 104.0501 (15)	$C_9H_{10}N_2$	146.0844	−1.89	myosmine (**6**)
16*	18.63	611.1607	611.1607 (61), 465.1030 (44), 303.0501 (100)	$C_{27}H_{30}O_{16}$	610.1534	0.04	rutin (**7**)
17	21.21	314.1383	314.1383 (23), 238.1651 (11), 201.0461 (100), 135.0441 (27)	$C_{18}H_{19}NO_4$	313.1314	−1.20	feruloyltyramine
18	22.46	515.2611	515.2611 (13), 423.1979 (32), 303.0493 (43), 201.0461 (100)	$C_{29}H_{38}O_8$	514.2580	−8.12	unknown
19	22.86	191.1433	191.1433 (81), 175.1165 (36), 161.1071 (38), 135.0439 (100), 107.0487 (71)	$C_{13}H_{18}O$	190.1358	1.18	*β*-damascenone
20*	24.52	303.0497	303.0497 (63), 285.0391 (13), 257.0441 (31), 229.0491 (68), 201.0543 (35)	$C_{15}H_{10}O_7$	302.0426	−0.58	quercetin (**8**)
21	25.63	235.1441	235.1441 (13), 218.1174 (33), 161.1069 (100), 135.0442 (10)	$C_{13}H_{18}N_2O_2$	234.1368	0.10	*N*-Coumaroylputrescine
22	27.51	419.2039	419.2039 (100)	$C_{24}H_{26}N_4O_3$	418.2005	−9.27	unknown
23	27.81	497.3020	497.3020 (100), 466.2593 (10), 306.1596 (8), 161.1071 (35), 130.0651 (10)	$C_{29}H_{40}N_2O_5$	496.2937	2.06	1-(4-ethylphenyl)-*N*-{4-[(4-ethyl-1-piperazinyl)methyl]phenyl}-3,6-dimethyl-1*H*-pyrazolo[3,4-*b*]pyridine-4-carboxamide
24	29.57	276.1957	276.1957 (22), 234.1851 (100), 217.1581 (13), 177.1271 (9)	$C_{17}H_{25}NO_2$	275.1885	−0.28	1-(3-methoxybenzoyl)-2,2,6,6-tetramethylpiperidine
25	30.75	275.2115	275.2115 (100), 257.2007 (8), 149.1068 (63), 132.0803 (12)	$C_{17}H_{26}N_2O$	274.2045	−1.01	4-(1,2,4,4a,5,6-hexahydro-3*H*-pyrazino[1,2-*a*]quinolin-3-yl)-2-methyl-2-butanol

among tobacco samples, the content of nicotine showed certain trend along the maturation stages. The content of nicotine in tobacco samples of each origin harvested at rosette stage was in a medium level (except for ZZ-T, which showed the highest nicotine level among all the tobacco samples) and in a dramatic decrease to reach the lowest level at squaring stage, reached the highest level at physiological maturation stage, and then fell sharply at harvest maturation stage. For the Zhengzhou tobacco samples, the nicotine contents ranged from 5655.62 ± 230.88 to 25399.39 ± 308.95 μg/g. The highest nicotine content of 25399.39 ± 308.95 μg/g was found in the rosette stage sample (ZZ-T) and in a dramatic decrease to reach the lowest level (ZZ-X with 5655.62 ± 230.88 μg/g) at squaring stage. Subsequently, the nicotine level showed an upward trend and reached a higher level at the physiological maturation stage and then decreased at the harvest maturation stage. The lowest nicotine level of 660.16 ± 24.78 μg/g was detected in a Zunyi tobacco sample (ZY-X). For the Zunyi tobacco samples, the highest nicotine content of 12215.15 ± 122.95 μg/g was detected in the sample harvested at physiological maturation stage. Similar to the Zunyi tobacco samples, the highest nicotine level (21409.02 ± 176.10 μg/g) in the Jiangchuan tobacco sample was also observed in the sample collected at physiological maturation stage.

The rutin contents of the tobacco samples harvested at different maturation stages varied greatly. At rosette stage, the rutin content ranged from 103.86 ± 8.57 to 201.87 ± 9.16 μg/g, while those ranged from 87.42 ± 2.78 to 734.66 ± 27.42 μg/g at squaring stage. The rutin contents at physiological maturation stage ranged from 90.30 ± 4.80 to 725.93 ± 40.70 μg/g, while those ranged from 164.00 ± 5.08 to 243.44 ± 6.79 μg/g at harvest maturation stage. The highest level of rutin of 734.66 ± 27.42 μg/g was found in the Jiangchuan tobacco sample harvested at squaring stage (JC-X), which was more

dx.doi.org/10.1021/jf5009204 | J. Agric. Food Chem. 2014, 62, 4979−4987

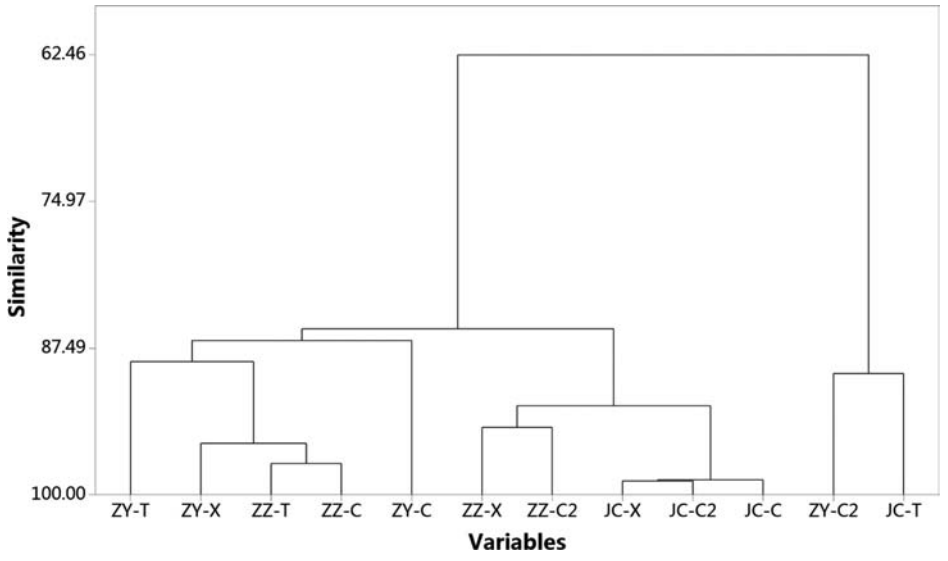

Figure 3. Dendrogram of hierarchical cluster analysis of 12 tobacco samples.

than 3-fold of that detected in the sample harvested at rosette stage (JC-T with 201.87 ± 9.16 μg/g). The lowest rutin content (ZY-X with 87.42 ± 2.78 μg/g) was detected in the Zunyi tobacco sample harvested at squaring stage, which was only approximately 70% amounts of that detected in the same origin harvest at harvest maturation stage (ZY-C2).

Among the Zhengzhou tobacco samples, the rutin content varied from 158.99 to 725.93 μg/g. The rutin content of the Zhengzhou tobacco samples harvested at physiological maturation stage was the highest (ZZ-C with 725.93 ± 40.70 μg/g) and was almost constant during rosette stage (ZZ-T with 186.28 ± 3.57 μg/g), squaring stage (ZZ-X with 158.99 ± 2.16 μg/g), and harvest maturation stage (ZZ-C2 with 164 ± 5.08 μg/g). For the Zunyi tobacco samples, the rutin contents varied from 87.42 ± 2.78 to 243.44 ± 6.79 μg/g. In the first three stages, the rutin contents did not vary with maturity (103.86 ± 8.57, 87.42 ± 2.78, 90.30 ± 4.80 μg/g for rosette stage, squaring stage, and physiological maturation stage, respectively). The maximum rutin content (ZY-C2 with 243.44 ± 6.79 μg/g) of the Zunyi tobacco samples was found at the harvest maturation stage. Compared to the tobacco samples from the other two origins, the Jiangchuan tobacco samples were found to have relatively high contents of rutin ranging from 201.87 ± 9.16 to 734.66 ± 27.42 μg/g. Generally, tobacco samples at the squaring stage had the highest level of rutin, which was about 3.5-fold over that measured in rosette stage.

Identification of the Main Constituents in Tobacco by HPLC-ESI-QTOF-MS. The difference of the chemical compositions is one of the important parameters to understand the variation among tobacco samples harvested from different origins and maturation stages. Unequivocal and tentative identification of the target compounds as well as the unknown constituents in the tobacco samples were performed by means of HPLC−ESI-QTOF-MS and MS/MS. Upon obtaining the data from MS and MS/MS analysis, a total of 25 compounds with relative high abundance were detected in 12 batches of the tobacco samples. Compounds at the retention times (t_R) of 5.0, 8.3, 9.1, 12.0, 17.9, 18.4, 18.8, and 24.9 min were unequivocally identified to be the reference compounds **1**−**8**, respectively. Other peaks were tentatively identified via searching for the precursor ion and fragmentation ions in MassBank Mass Spectral Database and literatures. We further performed empirical molecular formulas matching with those of the published compounds of tobacco in databases, such as PubMed of the U.S. National Library Medicine and the National Institutes of Health, SciFinder scholar of American Chemical Society, Chinese National Knowledge Infrastructure (CNKI) of Tsinghua University, and ChemSpider database when the precursor ion and fragmentation ions were not found in MassBank and literatures. When several empirical molecular formulas matched the same formula those isomeric compounds previously reported from tobacco would be preferentially selected as the putative ones. All the identified compounds in the tobacco samples were summarized in Table 4.

Statistical Analysis. To examine the change in similarity of fat-soluble compounds displayed in the 12 tobacco samples of different origins during maturity, a hierarchical cluster analysis based on the composition of major fat-soluble constituents was performed. The hierarchical cluster analysis is a multivariate procedure that allows the classification of variables into groups based on Euclidean distances between cases.[36] The dendogram of the 12 tobacco samples is shown in Figure 3. Two major clusters, viz., clusters 1 and 2, can be found in Figure 3. Cluster 1 was composed of 10 samples, while cluster 2 was composed of two samples. Cluster 1 formed two subclusters, viz., ZY-T, ZY-X, ZZ-T, and ZZ-C and ZZ-C2, JC-X, JC-C2, and JC-C. From the dendogram, it can be inferred that the tobacco samples of the same origin showed more similarity in the fat-soluble composition. The Jiangchuan tobacco sample showed more similarity during squaring stage, physiological maturation stage, and harvest maturation stage (i.e., JC-X, JC-C, and JC-C2). These clusters show that similarity mainly exists between samples of the same origin rather than different origins. In addition, it can be useful for farmers to choose the appropriate harvest stage of tobacco with desired content of components as well as to choose alternate origins with more similarity in the absence of a desired variety at the time of cultivation.

In conclusion, the presented study provided a comprehensive analysis in fat-soluble compositions as well as polar constituents in 12 batches of tobacco leaf samples of three origins at four maturations. The GC-MS analyses showed that tobacco samples harvested at rosette stage exhibited the most fat-

dx.doi.org/10.1021/jf5009204 | J. Agric. Food Chem. 2014, 62, 4979−4987

Table 5. Contents of Eight Reference Compounds in Each Tobacco Sample (μg/g)

no.	sample code	nornicotine	neonicotine	anatabine	nicotine	scopoletin	myosmine	rutin	quercetin
1	ZZ-T	175.30 ± 9.00	NQ	570.78 ± 18.11	25399.39 ± 308.95	NQ	101.73 ± 7.25	186.28 ± 3.57	156.91 ± 9.29
2	ZZ-X	45.79 ± 4.33	NQ	536.80 ± 28.25	5655.62 ± 230.88	112.59 ± 5.78	97.18 ± 4.16	158.99 ± 2.16	151.69 ± 3.60
3	ZZ-C	87.37 ± 6.06	NQ	433.20 ± 24.83	11737.14 ± 270.77	122.01 ± 7.34	267.53 ± 10.03	725.93 ± 40.70	125.60 ± 2.16
4	ZZ-C2	64.63 ± 4.27	NQ	260.82 ± 15.19	8326.26 ± 155.95	228.79 ± 6.55	64.64 ± 3.86	164.00 ± 5.08	146.58 ± 3.42
5	ZY-T	NQ	NQ	167.62 ± 15.37	1654.49 ± 34.52	36.41 ± 2.74	NQ	103.86 ± 8.57	NQ
6	ZY-X	NQ	NQ	601.86 ± 14.57	660.16 ± 24.78	37.58 ± 3.12	NQ	87.42 ± 2.78	170.11 ± 5.75
7	ZY-C	97.27 ± 5.41	94.68 ± 8.10	420.36 ± 8.99	12215.15 ± 122.95	338.52 ± 12.85	72.89 ± 4.59	90.30 ± 4.80	143.71 ± 10.61
8	ZY-C2	123.84 ± 6.62	89.96 ± 8.71	354.89 ± 18.65	8835.33 ± 215.52	124.95 ± 5.11	117.04 ± 10.70	243.44 ± 6.79	126.93 ± 1.38
9	JC-T	NQ	93.96 ± 10.14	179.60 ± 2.15	5070.59 ± 211.84	14.37 ± 3.32	NQ	201.87 ± 9.16	169.70 ± 8.12
10	JC-X	221.66 ± 11.58	98.08 ± 9.47	384.31 ± 18.11	12653.36 ± 241.26	99.66 ± 8.64	NQ	734.66 ± 27.42	169.29 ± 8.45
11	JC-C	126.56 ± 5.02	116.26 ± 4.08	850.91 ± 20.54	21409.02 ± 176.10	165.84 ± 10.52	80.91 ± 8.86	542.70 ± 33.01	149.54 ± 4.91
12	JC-C2	64.87 ± 3.85	92.66 ± 7.45	507.79 ± 13.84	10868.21 ± 263.04	94.36 ± 8.01	55.79 ± 6.82	237.33 ± 11.23	132.66 ± 1.69

soluble components, while those harvested at harvest maturation stage exhibited the least fat-soluble components. In addition to GC-MS analysis, an HPLC-QTOF-MS method was developed for the quantitative analyses of eight main compounds in tobacco including five alkaloids and two polyphenols. The nicotine contents varied greatly in the 12 tobacco samples. The Zhengzhou tobacco sample harvested at rosette stage was found to have the highest nicotine content (ZZ-T), and the lowest nicotine level was detected in Zunyi tobacco samples harvested at squaring stage (ZY-X). The highest level of rutin was found in the Jiangchuan tobacco sample harvested at squaring stage (JC-X), and the lowest rutin content was detected in the Zunyi tobacco sample harvested at squaring stage (ZY-X). In addition to quantitative analyses, the main compounds in the tobacco samples were also unequivocally or tentatively identified. The developed method provided a convenient approach which might be applied for rapid maturity evaluation, tobacco flavor identification, and also holds the potential for analysis of compounds present in other plants.

■ ASSOCIATED CONTENT

Ⓢ Supporting Information

The monthly average temperatures, total irradiances (average of 20 years), monthly average relative humidity, and monthly rainfall of May and June in 2012 in Zhengzhou, Zunyi, and Jiangchuan; GC-MS profile of fat-soluble compositions of tobacco samples planted in Zhengzhou, Zunyi, and Jiangchuan harvested at four maturities; HPLC-PDA (254 nm) profile of aroma composition of tobacco planted in Zhenzhou, Zunyi, and Jiangchuan harvested at four maturities. This material is available free of charge via the Internet at http://pubs.acs.org.

■ AUTHOR INFORMATION

Corresponding Authors

*For G.X: Phone: +86 871 5223058; Fax: +86 871 5215783; E-mail: xugang008@mail.kib.ac.cn.

*For Y.Z.: Phone: +86 28 85151902; Fax: +86 28 85223843; E-mail: zhouyan@cib.ac.cn.

Funding

This research was supported by the National Natural Science Foundation of China (21302180), Major Science and Technology Program (nos.110201101003-TS-03, 2011YN02 and 2011YN03), and a technological talents program of the Chinese Academy of Sciences granted to Dr. Y. Zhou.

Notes

The authors declare no competing financial interest.

■ REFERENCES

(1) Wallace, R. J. Antimicrobial properties of plant secondary metabolites. *Proc. Nutr. Soc.* **2004**, *63*, 621−629.

(2) Saitoh, F.; Noma, M.; Kawashima, N. The alkaloid contents of sixty *Nicotiana* species. *Phytochemistry* **1985**, *24*, 477−480.

(3) Sisson, V. A.; Severson, R. F. Alkaloid composition of the *Nicotiana* species. *Beitr. Tabakforsch. Int.* **1990**, *14*, 327−340.

(4) Snook, M. E.; Mason, P. F.; Sisson, V. A. Polyphenols in the *Nicotiana* species. *Tob. Sci.* **1986**, *30*, 43−49.

(5) Snook, M. E.; Johnson, A. W.; Severson, R. F.; Teng, Q.; White, R. A., Jr.; Sisson, V. A.; Jackson, D. M. Hydroxygeranyllinalool glycosides from tobacco exhibit antibiosis activity in the tobacco budworm [*Heliothis virescens* (F.)]. *J. Agric. Food Chem.* **1997**, *45*, 2299−2308.

(6) Andersen, R. A.; Fleming, P. D.; Burton, H. R.; Hamilton-Kemp, T. R.; Sutton, T. G. Nitrosated, Acylated, and Oxidized Pyridine Alkaloids during Storage of Smokeless Tobaccos: Effects of Moisture, Temperature, and Their Interactions. *J. Agric. Food Chem.* **1991**, *39*, 1280−1287.
(7) Jeffrey, R. N.; Tso, T. C. Qualitative Differences in the Alkaloid Fraction of Cured Tobaccos. *J. Agric. Food Chem.* **1955**, *3*, 680−682.
(8) Clark, M. S. G.; Rand, M. J.; Vanov, S. Comparison of Pharmacological Activity of Nicotine and Related Alkaloids Occurring in Cigarette Smoke. *Arch. Int. Pharmacodyn. Ther.* **1965**, *156*, 363−379.
(9) Ashton, H.; Marsh, V. R.; Millman, J. E.; Rawlins, M. D.; Stepney, R.; Telford, R.; Thomson, J. W. In *Electrophysiological Effects of Nicotine*;Remond, H., Izard, C., Eds.; Elsevier/North-Holland Biomedical Press: New York, 1979; p 159.
(10) Quin, L. D.; Pappas, N. A. Plant Nutrients and Regulators, Quantitative Determination of Individual Alkaloids in Tobacco by Gas Chromatography. *J. Agric. Food Chem.* **1962**, *10*, 79−82.
(11) Massingill, J. L.; Hodgkins, J. E. Gas Liquid Chromatography of Alkaloids Using Capillary Columns and Four Packed Columns. *Anal. Chem.* **1965**, *37*, 952−955.
(12) Cai, J. B.; Liu, B. Z.; Lin, P.; Su, Q. D. Fast analysis of nicotine related alkaloids in tobacco and cigarette smoke by megabore capillary gas chromatography. *J. Chromatogr., A* **2003**, *1017*, 187−193.
(13) Mousa, S.; Loon, G. R.; van Houdi, A. A.; Crooks, P. A. High-performance liquid chromatography with electrochemical detection of nicotine and *N*-methylnicotiniumion. *J. Chromatogr., A* **1985**, *347*, 405−410.
(14) Sellergren, B.; Zander, A.; Renner, T.; Swietlow, A. Rapid method for analysis of nicotine and nicotine-related substances in chewing gum formulations. *J. Chromatogr., A* **1998**, *829*, 143−152.
(15) Sudan, B. J. L.; Brouillard, C.; Strehler, C.; Strub, H.; Sterboul, J.; Sainte-Laudy, J. Determination of nicotine in allergenic extracts of tobacco leaf by high-performance liquid chromatography. *J. Chromatogr., A* **1984**, *288*, 415−422.
(16) Ciolino, L. A.; Turner, J. A.; McCauley, H. A.; Smallwood, A. W.; Yi, T. Y. Optimization study for the reversed-phase ion-pair liquid chromatographic determination of nicotine in commercial tobacco products. *J. Chromatogr., A* **1999**, *852*, 451−463.
(17) Ciolino, L. A.; McCauley, H. A.; Fraser, D. B.; Barnett, D. Y.; Yi, T. Y.; Turner, J. A. Reversed phase ion-pair liquid chromatographic determination of nicotine in commercial tobacco products. 1. Moist snuff. *J. Agric. Food Chem.* **1999**, *47*, 3706−3712.
(18) Ciolino, L. A.; Fraser, D. B.; Yi, T. Y.; Turner, J. A.; Barnett, D. Y.; McCauley, H. A. Reversed phase ion-pair liquid chromatographic determination of nicotine in commercial tobacco products. 2. Cigarettes. *J. Agric. Food Chem.* **1999**, *47*, 3713−3717.
(19) Bazinet, L.; DeGrandpré, Y.; Porter, A. Electromigration of tobacco polyphenols. *Sep. Purif. Technol.* **2005**, *41*, 101−107.
(20) Court, W. A. High-performance reversed-phase liquid chromatography of naturally occurring phenolic compounds. *J. Chromatogr., A* **1977**, *130*, 287−291.
(21) Snook, M. E.; Chortyk, O. T. An improved extraction-HPLC method for tobacco polyphenols. *Tob. Sci.* **1982**, *26*, 25−29.
(22) Zhao, R. F.; Li, F.; Hu, J. Rapid determination of polyphenols in cut tobacco by microwave-assisted extraction-ultrahigh performance liquid chromatography. *Anal. Methods* **2011**, *3*, 2421−2424.
(23) Achilli, G.; Cellerino, G. P.; Gamache, P. H. Identification and dertermination of phenolic constituents in natural beverages and plant extracts by means of a coulometric electrode array system. *J. Chromatogr., A* **1993**, *632*, 111−117.
(24) Thielen, A.; Klus, H.; Muller, L. Tobacco smoke: Unraveling a controversial subject. *Exp. Toxicol. Pathol.* **2008**, *60*, 141−156.
(25) Sha, Y. F.; Meng, J. R.; Zhang, Y. C.; Deng, C. H.; Wu, D. Determination of volatile organic acids in tobacco by single-drop microextraction with in-syringe derivatization followed by GC-MS. *J. Sep. Sci.* **2010**, *33*, 212−217.
(26) Zhu, X. L.; Gao, Y.; Chen, Z. Y.; Su, Q. D. Development of a Chromatographic Fingerprint of Tobacco Flavor by Use of GC and GC-MS. *Chromatographia* **2009**, *69*, 735−742.
(27) Ye, Q. Development of solid-phase microextraction followed by gas chromatography-mass spectrometry for rapid analysis of volatile organic chemicals in mainstream cigarette smoke. *J. Chromatogr., A* **2008**, *1213*, 239−244.
(28) Wu, J. C.; Joza, P.; Sharifi, M.; Rickert, W. S.; Lauterbach, J. H. Quantitative Method for the Analysis of Tobacco-Specific Nitrosamines in Cigarette Tobacco and Mainstream Cigarette Smoke by Use of Isotope Dilution Liquid Chromatography Tandem Mass Spectrometry. *Anal. Chem.* **2008**, *80*, 1341−1345.
(29) Mayer-Helm, B.; Hofbauer, L.; Muller, J. Method development for the determination of selected pesticides on tobacco by high-performance liquid chromatography-electrospray ionisation-tandem mass spectrometry. *Talanta* **2008**, *74*, 1184−1190.
(30) Crofcheck, C.; Loiselle, M.; Weekley, J.; Maiti, I.; Pattanaik, S.; Bummer, P. M.; Jayt, M. Histidine Tagged Protein Recovery from Tobacco Extract by Foam Fractionation. *Biotechnol. Prog.* **2003**, *19*, 680.
(31) Zhu, S. K.; Lu, X.; Dong, L.; Xing, J.; Su, X. L.; Kong, H. W.; Xu, G. W.; Wu, C. Y. Quantitative determination of compounds in tobacco essential oils by comprehensive two-dimensional gas chromatography coupled to time-of-flight mass spectrometry. *J. Chromatogr., A* **2005**, *1086*, 107−114.
(32) Li, H. F.; Zhong, K. J.; Lu, X.; Bai, C. M.; Huang, J. G.; Lu, H. L.; Ma, C. F.; Zhu, S. K.; Kong, H. W.; Zhao, M. Y.; Xie, J. P.; Niu, S.; Xu, G. W. Analysis of volatile and semi-volatile alkaline compounds in tobacco leaf by using comprehensive two-dimensional gas chromatography/time-of-flight mass spectrometry. *Acta. Chim. Sin.* **2006**, *64*, 1897−1903.
(33) Hegazy, M. E.; Hirata, T.; Abdet-Lateff, A.; El-Razek, M. H.; Mohamed, A. E.; Hassan, N. M.; Pare, P. W.; Mahmoud, A. A. *Z. Naturforsch. A* **2008**, *63*, 403.
(34) Gorrod, J. W.; Jacob, P., III, Eds. *Analytical Determination of Nicotine and Related Compounds and Their Metabolites*, 1st ed.; Elsevier: Amsterdam, 1999; p 285.
(35) Browne, C. L. *The Design of Cigarettes*; Hoechst Celanese Corp.: Charlotte, NC, 1990; pp 13−44.
(36) Wessa, P. *Free Statistics Software*, version 1.1.23-r7; Office for Research Development and Education, 2013; http://www.wessa.net/.

pears produced low levels of the ester ethyl 2,4-decadienoate (0.11%), which has a pear note and is prominent in other pear varieties.[12] Despite its low content of ethyl 2,4-decadienoate, 'Comice' is considered by some to be the best dessert pear variety due to its juicy, buttery texture and well-balanced flavor.[13] Aroma volatile production is regulated by ethylene biosynthesis and action in many climacteric fruit, as demonstrated through the use of the ethylene action inhibitor 1-methylcyclopropene (1-MCP) and the study of transgenic apples with suppressed ethylene biosynthesis.[14,15]

Taste is also a key factor of sensory quality. The balance of sweet and sour taste affects consumer acceptance of fruit.[16] Sugars (fructose, sorbitol, glucose, and sucrose) and acids (malic acid) are the compounds most influencing sweet and sour/tart taste in pears.[5] Consumer tests have shown that the acceptable range of sweet/sour balance as measured by soluble solids content/titratable acidity (SSC/TA) ratio in pear fruit is 2−4.[16]

Sensory descriptive analysis is a primary approach to investigate the important attributes of a product that people perceive.[18] The sensory descriptive analysis of 'Comice' pears after cold storage and ripening was compared with that of unripe pears.[1] Ripe 'Comice' pears had high levels of sweetness, cooked pear odor and flavor, softness, and juiciness, but low levels of grassy/green odor.

Instrumental fruit quality measurements are sometimes well correlated with sensory attributes. In one study,[20] the best correlations and predictions of sensory texture attributes in apples were between the penetrometer puncture test and crispness (r = 0.8) or juiciness (r = 0.7). In another study, compressive force using a Sinclair iQ System and Güss Fruit Texture measurements had a significant correlation with sensory perception of hardness in both apples (r = 0.78−0.83) and pears (r = 0.83).[17]

The relationships between volatile compound concentrations, SSC or TA, and sensory attributes have not been reported for pears. For apples, relationships between the main volatile compounds and sensory attributes were determined by Karlsen et al.[18] Butyl acetate, 2-methylbutyl acetate, hexyl acetate, and ethyl acetate were related to fruity and sweet sensory attributes, whereas ethyl butanoate, 1-butanol, ethanol, and α-farnesene were related to sour, bitter, and grassy attributes.[18] To predict sensory perception of acidity, TA was the best instrumental measurement in apple fruit (r = 0.86)[19] compared to individual acids, SSC/TA, Brim A (SSC − 10 × TA) or suspension pH (the pH of the macerate before the start of the titration). On the other hand, sensory sweetness was difficult to predict by any instrumental measurement in apple.[19]

In this study, we compare the effect of ethylene conditioning and cold (0 °C) or intermediate (10 °C) temperature conditioning on the sensory quality of 'Comice' pears as evaluated by descriptive sensory analysis. We also describe the relationship between the sensory attributes and instrumental measures of fruit quality. These parameters were measured as a function of firmness level for the various conditioning treatments.

MATERIALS AND METHODS

Fruit Source. Mature-green 'Comice' (*Pyrus communis* L.) pears were harvested at the average firmness of 43 N from a commercial orchard in Lake County, California, in midseason (September 15, 2010). The fruits were transported to the Postharvest Pilot Plant at the University of California, Davis, on the same day and visually sorted to eliminate defective fruits and to obtain fruits of uniform size and color for use in the experiments. The fruits were stored at 20 °C and >90% relative humidity prior to the initiation of treatments on the following day.

Conditioning Treatments. The pears were randomly divided into six groups (five conditioning treatment groups and one control, nonconditioned group) with 200−350 fruits per group. Three groups were exposed to different storage temperatures and times; 0 °C (low temperature) for 15 or 25 days and 10 °C (intermediate temperature) for 10 days with >90% relative humidity (RH). Two groups were exposed to 100 μL L^{-1} ethylene gas at 20 °C in two 300 L stainless steel tanks for 1 or 3 days. Humidified air (95% RH) containing 100 μL L^{-1} ethylene was passed through the tank at 4 L min^{-1} to keep CO_2 concentration <0.3 kPa. An additional group was held at 20 °C as a nonconditioned control. After the initial conditioning treatments, all groups were transferred to 20 °C for ripening until they softened to the firmness of 9 N (±2.50 N). Four single fruit replicates were chosen from each treatment group when the average fruit firmness (15 fruits measured randomly from each treatment) reached 27, 18, and 9 N (±4.00 N), and the firmness of the four fruits selected for instrumental and sensory evaluation were as close to 27, 18, or 9 N as possible. Portions of each individual fruit were used for analysis of skin color, firmness, cell wall polyuronides, volatile content, SSC, TA, and sensory evaluation by a trained panel as described below.

Ethylene Production. Ethylene production was measured every day or every other day on a subset of fruits from each treatment after fruit transfer to 20 °C and until the fruit began senescence. Five fruits were placed into a 3.8 L jar as one replicate with three replicates for each treatment. The jars were sealed for 10−30 min before a 10 mL headspace gas sample was collected and analyzed for ethylene concentration using a gas chromatograph (AGC series 400; Hach-Carle Co., Loveland, CO, USA) fitted with a 1 mL sample loop, a flame ionization detector (FID), and an alumina column. The oven temperature was 80 °C, and the carrier gas was N_2 at a flow rate of 37 mL min^{-1}.

Flesh Firmness. Fruit firmness was determined at harvest and was measured every day or every other day after transfer to 20 °C for ripening until the fruit softened to 9 N. For analysis, the skin was removed from an area ∼20 mm in diameter on opposite sides of the equatorial region of each pear. Firmness was measured on each side of the pear using a Güss FTA Penetrometer (Guss, Strand, Western Cape, South Africa) fitted with an 8 mm probe. The four fruits per replicate for each treatment and firmness stage were selected when the average firmness for each treatment reached 27, 18, or 9 N.

Soluble Solids Content and Titratable Acidity. Two wedge-shaped slices were cut from stem to blossom end from opposite sides of each pear used for sensory evaluation and juiced for SSC and TA determination. A few drops of juice were used to measure SSC by refractometry (Reichert AR6 Series, Depew, NY, USA), and 4 g of juice diluted in 20 mL of deionized water was used for determination of TA (as malic acid equivalents; pH 8.2 end point), using an automatic titrater (Radiometer TitraLab; Tim850 titration manager and SAC80 sample changer).

Cell Wall Polyuronides. Samples for cell wall polyuronide analyses were collected from each fruit used for sensory evaluation by cutting a wedge from stem to blossom end and frozen at −80 °C for 14−16 weeks before analysis. About 10 g of frozen pear flesh tissue (without peel or core) was collected from each single pear replicate and used for cell wall polyuronide determination. The percentage of water-soluble polyuronides (water-soluble polyuronides/total polyuronides × 100) was determined following the method of Ahmed and Labavitch.[20]

Cell Wall Extraction. Tissue samples (10 g) were boiled in 95% ethanol for 20 min followed by homogenization for 1 min (Polytron PT 10/35; Brinkmann/Kinematica, Westbury, NY, USA). The pellet was collected, and the supernatant was decanted following centrifugation at 1000g for 10 min. The pellet was resuspended in 80% ethanol and recentrifuged at the same speed. This washing cycle was repeated twice to ensure that the pellet was colorless. The pellet was then washed with acetone and dried under a fume hood for 1 day, yielding a crude cell wall extract. Next, the crude cell wall was suspended in dimethyl sulfoxide

(DMSO)/H_2O (9:1 v/v) and shaken at room temperature for 24 h to remove starch. The slurry was centrifuged (1000*g* for 10 min) and the DMSO discarded; the pellet was washed twice in 95% ethanol to remove all trace of DMSO and then washed twice in acetone. The solids were dried under a fume hood for 2−3 days. The alcohol-insoluble and starch-free cell wall material (CWM) was stored in a desiccator for subsequent analysis.

Total Polyuronide Preparation. Cell wall material was weighed (2−3 mg) into a test tube containing a magnetic stir bar. The sample was cooled in an ice−water bath before 1 mL of chilled concentrated sulfuric acid was added. The mixture was stirred gently for 5 min before another 1 mL of chilled, concentrated sulfuric acid was added with an additional 5 min of stirring. Distilled water (0.5 mL) was added dropwise into the mixture and stirred for 5 min followed by another 0.5 mL of dH_2O, and stirring was continued until dissolution was complete (about 1 h). An additional 7 mL of dH_2O was added to a total volume of 10 mL. This solution was ready to assay for uronic acids to determine the total polyuronides.

Water-Soluble Polyuronide (WSP) Preparation. Cell wall material was weighed (30 mg) into a test tube containing a stir bar. Distilled water (10 mL) was added to dissolve WSP in the sample. The sample was stirred for 2 h and then centrifuged at 11840*g* for 25 min. The supernatant was collected for uronic acid assay to determine WSP content.

Uronic Acid Assay. An aliquot (400 μL) of the total polyuronide solution or the WSP supernatant was added to a test tube and cooled in an ice water bath. An aliquot (2.4 mL) of chilled uronic acid reagent (4.767 g sodium tetraborate decahydrate/L concentrated sulfuric acid) was added and mixed. The mixture was heated in a 100 °C water bath for exactly 5 min. The sample was cooled immediately in an ice−water bath. A 1.4 mL aliquot was transferred to another test tube. A 20 μL aliquot of meta-phenyl phenol solution [0.15% (w/v) meta-phenyl phenol in 0.5% (w/v) NaOH] was added to the test tube. A blank sample was included that contained only 20 μL of 0.5% sodium hydroxide (NaOH). The reaction was allowed to continue for about 1 h at room temperature to ensure color stabilization. The color intensity of the sample was determined at 520 nm by spectrophotometry (UV-1601 UV−vis; Shimadzu Co., Columbia, MD, USA). A standard curve was generated using 0, 0.05, 0.10, 0.15, and 0.2 mg mL^{-1} uronic acid and used to calculate sample uronic acid content.

Volatile Compounds. Pear tissue samples for measurement of volatile content were collected from each fruit used for sensory evaluation, cutting a wedge from the stem to the blossom end. Samples were frozen at −80 °C for 18−20 weeks prior to analysis. Frozen pear tissue flesh (10 g, without peel or core) was placed in a test tube, and 10 mL of a saturated $CaCl_2$ solution was added to prevent enzymatic reactions. The mixture was homogenized (Polytron PT 10/35; Brinkmann/Kinematica, Westbury, NY, USA) at speed 4 for 1 min after warming to room temperature. An 8 mL aliquot of the puree was transferred to each of two 20 mL amber glass vials (Supelco Analytical, St. Louis, MO, USA) as two technical replicates. An aliquot (7 μL of a 0.1 mM solution) of 2-methylbutyl isovalerate (Sigma-Aldrich Inc., St. Louis, MO, USA) in methanol was added to each vial as an internal standard.

The volatiles were collected by headspace sorptive extraction (HSSE) and then analyzed by GC-MS (Agilent 7890A GC/5975CMSD; Santa Clara, CA, USA) equipped with a thermal desorption unit (TDU) and a cooled injection system (CIS) (Gerstel, GmbH & Co. KG). The headspace was sampled using a 10 mm magnetic stir bar (also known as Twister; Gerstel GmbH & Co. KG), coated with 24 μL of polydimethylsiloxane (PDMS). The bar, suspended above the sample in the vial, was exposed to the headspace for 1 h at room temperature, while the sample was stirred at 270 rpm, using a 15-position stir-plate (Gerstel GmbH & Co. KG). After exposure, the bars were placed onto the autosampler. The volatile compounds sorbed onto the PDMS coating were thermally desorbed into the TDU and then cryofocused prior to GC-MS analysis for separation and detection. For the thermal desorption, the following parameters were used: initial TDU temperature of 30 °C, then heated to 250 at 720 °C min^{-1} and held for 5 min; transfer line temperature at 280 °C. Simultaneously, the analytes were transferred into the PVT-injector, where they were cryogenically focused at −80 °C, using liquid nitrogen. Initial injection temperature was programmed at −80 °C and then heated to 280 °C at 12 °C min^{-1}. The inlet was operated in split mode (5:1). The GC was equipped with a DB-5MS capillary column (30 m × 0.25 mm; film thickness = 0.25 μm) (Agilent Technologies), injector temperature at 220 °C, and helium carrier gas flow rate of 1.2 mL min^{-1}. The oven temperature started at 40 °C, increased to 80 °C at a rate of 3 °C min^{-1}, and then increased to 180 °C at a rate of 5 °C min^{-1}. MS parameters were as follows: transfer line temperature of 230 °C, source temperature of 230 °C, quadrupole temperature of 150 °C, continuous scan range from m/z 30 to 300. Spectral deconvolution was performed with AMDIS software (version 2.69; NIST, Gaithersburg, MD, USA), and spectra were aligned and analyzed with Mass Profiler Professional (version 2.0; Agilent Technologies). The identity of volatile compounds was confirmed by matching retention time and mass spectra with those of authentic standards whenever possible. When authentic standards were not available, identification was performed by comparing the calculated retention index with published values and matching their spectra with those present in the NIST library (NIST 0.8). Volatile concentrations were calculated by comparing the integrated peak area of each compound with that of the internal standard (15.13 μg L^{-1} 2-methylbutyl isovalerate, final concentration) and are reported as micrograms per kilogram of fruit fresh weight.

Descriptive Sensory Evaluation. The sensory descriptive analysis of fruit samples from each treatment at 27, 18, and 9 N firmness levels was performed by a trained panel. Panelists were recruited on the University of California, Davis, campus and 9 were selected on the basis of interest and availability and trained during six training sessions of 1 h per session per day. Descriptive attributes for aroma, texture, and taste of pear and their definitions were developed during the first session (Table 1). During the training sessions, reference standards for the attributes were presented in 60 mL plastic cups with lids or 1 mL glass vials with caps (aroma attribute references). Refinement of the attributes was discussed among the panelists in two subsequent training sessions. In the following sessions, the panelists were exposed to different ripening stages of pear samples (firm and soft) to practice evaluating the attributes using an unstructured 10 cm line scale on a score sheet and to achieve consensus for how to define and rate the attributes. During the last training session, panelists practiced evaluating pear samples in the actual sensory booths, using automated data collection (Compusense Five software, Ontario, Canada). The final attributes consisted of five aroma, five texture, and two taste attributes (Table 1).

Four individual fruit replicates of each firmness stage were selected from each treatment immediately after their firmness was measured. A slice from each pear fruit, cut as a wedge from the stem to blossom end, and without peel or core, was presented to each panelist. Therefore, there were 4 replicates per judge and 44 replicates (9 judges × 4 fruit reps) per treatment. Each slice was placed in a plastic cup (118 mL with lid) and labeled with a random three-digit code, up to 30 min before tasting began. Pear slices were served with a cup of water and some unsalted saltine crackers as palate cleansers. Panelists were not required to expectorate the samples, but the size of the pear samples and number of samples was small and did not result in satiation. With different ripening rates driven by each treatment, the panelists usually tasted four or eight samples each day using a randomized complete block design for assessing the samples. Evaluation was performed in individual sensory booths under red light at room temperature (20 °C). Descriptions and definitions of pear attributes were posted, and related reference standards for aroma (orthonasal) and taste, as shown in Table 1, were available as references during the tasting. The panelists were asked to evaluate the pear attributes for aromas, textures, and tastes on an unstructured 10 cm line scale using the software program Compusense Five (Compusense).

Statistical Analysis. The data for each sensory attribute were analyzed across treatments at each firmness level (27, 18, and 9 N). Three-way analysis of variance (three-way ANOVA) was conducted to test the effects of treatment, panelists, replicates, and all two-way interactions for each sensory attribute using a pseudomixed model with

Table 1. Pear Attributes, Definitions, and Reference Standards for Sensory Descriptive Analysis of 'Comice' Pears

attribute (general category)	definition	reference standards (intensity on 10 cm line scale)
fruity (aroma)	sweet aromatic, characteristic of ripe fruit	Del Monte canned mixed fruit (peaches, pears, and pineapple) in extra light syrup (10)
apple (aroma)	aroma associated with fresh apple	'Fuji' apple (10)
pear (aroma)	aroma note associated with fresh pears	hexyl acetate high: 3% (v/v) in water (10) medium: 1.5% (v/v) in water (5)
fermented (aroma)	aroma associated with fermented fruits (sweet + alcohol)	high: hard pear cider with 4% alcohol (10) medium: regular apple cider (5)
green stem (aroma)	aroma associated with green wood stems; twiggy	*cis*-3-hexen-1-ol in diluted apple juice in water high: 0.1% (v/v) in 35% apple juice (10) medium: 0.01% (v/v) in 3% apple juice (5)
firmness (texture)	force required to bite completely through the sample (first bite/chew)	firm: 'Fuji' apple (9) medium: flesh of peeled zucchini (5) soft: banana (0.5)
crunchiness (texture)	amount of noise generated when chewing with the back teeth	high: 'Fuji' apple (9) medium: cucumber (5) low: banana (0.5)
juiciness (texture)	amount of wetness or juiciness released from the sample during the first three chews	high: orange (9) medium: 'Fuji' apple (5) low: banana (0.5)
butteriness (texture)	degree of smooth texture of the flesh with an absence of detectable particles, like butter	high: butter (10), milk chocolate (medium quality) (9) medium: apple sauce (5) low: corn meal (0.5)
fibrousness (texture)	presence of fibers that are continuous filaments or are in discrete elongated pieces in the sample	high: 'Tommy Atkins' mango (9) medium: squash/pumpkin (5) low: banana (1)
sweetness (taste)	basic taste on the tongue stimulated by sugar and high-potency sweeteners	Kern's canned pear nectar high: 67% (v/v) in water + 25 g of sugar (9) low: 67% (v/v) in water (1)
tartness (taste)	sour taste stimulated by acids	Kern's canned pear nectar high: 67% (v/v) in water + 0.5 g of citric acid (9) medium: 67% (v/v) in water (5)

the panelist by treatment interaction as denominator (SAS version 9.0, Cary, NC, USA). The analysis of variance was also done across firmness levels for each treatment using a pseudomixed model. The multiple least-squares means comparisons were carried out using Tukey's Studentized range test at $p < 0.05$.

The effects of treatments on volatile compound concentrations, SSC, TA, sugars, and acids were analyzed by analysis of variance (one-way ANOVA) for each firmness level (27, 18, and 9 N) (SAS version 9.0). Multiple least-squares means comparisons were done using Tukey's Studentized range test at $p < 0.05$.

Partial least-squares (PLS) regression analysis was performed to evaluate the relationships between sensory attributes (Y-variables) that were significantly different among the treatments and compositional data (X-variables) that were significantly different among the treatments using Unscrambler (version 9.2., CAMO A/S, Trondheim, Norway). Compositional data included WSP, volatile compounds, SSC, and TA.

RESULTS

Physiochemical Analysis. Firmness changes were monitored during pear ripening at 20 °C after conditioning treatment. Fruit conditioned with ethylene for 3 days or held at 10 °C for 10 days softened to 9 N within 4 days, followed by fruit held at 0 °C for 25 or 15 days, which softened to 9 N within 6 days, and fruit conditioned with ethylene for 1 day, which softened to 9 N within 10 days (Figure 1). Fruit held at 20 °C (nonconditioned control) did not soften to any of the targeted firmness stages, 27, 18, or 9 N, within 31 days (data not shown). As a result, the nonconditioned control fruits were not included in any subsequent evaluations. During softening, pear ethylene production was highest from fruit conditioned with exogenous ethylene for 3 days or held at 0 °C for 25 and 15 days (Figure 2). Fruit conditioned at 10 °C for 10 days or conditioned with

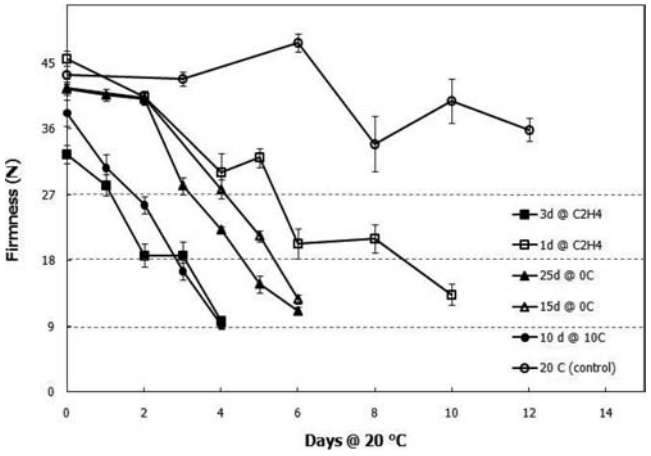

Figure 1. Changes in firmness (N) of 'Comice' pears at 20 °C after conditioning with C_2H_4 at 20 °C for 1 or 3 days or temperature conditioning at 0 °C for 15 or 25 days and at 10 °C for 10 days, and nonconditioned control at 20 °C. Vertical lines represent the standard error of the mean (n = 15).

ethylene for 1 days had similar levels of ethylene production, which were about half that of the highest level. The fruit from the control group had the lowest rate of ethylene production.

Sugar and acid content related to sweet and sour taste were estimated by SSC and TA, respectively. There were differences in SSC across treatments for fruit softened to 27 and 18 N ($p < 0.05$); there were no significant differences in SSC and TA among conditioning treatments when the fruit was softened to 9 N (data not shown). Fruit held at 0 °C for 15 days had the highest SSC at both 27 (15.4%) and 18 (14.0%) N firmness. Comparison of SSC across firmness levels revealed that fruit softened to 27 N had significantly higher SSC (14.2%) than fruit at 18 N (13.7%) and 9 N (13.6%). For TA, there were no significant differences across treatments within the same firmness levels or across firmness levels (data not shown). There were also no differences in the ratio of SSC/TA among treatments, but SSC/TA increased with fruit softening from 65.92 at 27 N to 71.57 at 9 N.

WSP content was not significantly different across conditioning treatments for each firmness level, but significantly increased with fruit softening from 27 to 18 to 9 N (from 17.9 to 26.2 to 38.1%) (data not shown).

Different conditioning treatments resulted in marked differences in pear aroma volatile profiles. Analysis of variance of 48 identified volatile compounds (Table 2) showed significant differences in the levels of 12 individual compounds, total alcohols, and total esters for the 27 N firmness stage; 18 compounds, total aldehydes, total alcohols, total esters, and total volatiles for the 18 N firmness stage; and 15 compounds, total aldehydes, total esters, and total volatiles for the 9 N firmness stage (Table 3). Within a conditioning treatment, the concentrations of many volatiles increased as firmness decreased. However, the magnitude of the increase in concentration of volatiles was dependent on the treatment (Table 3).

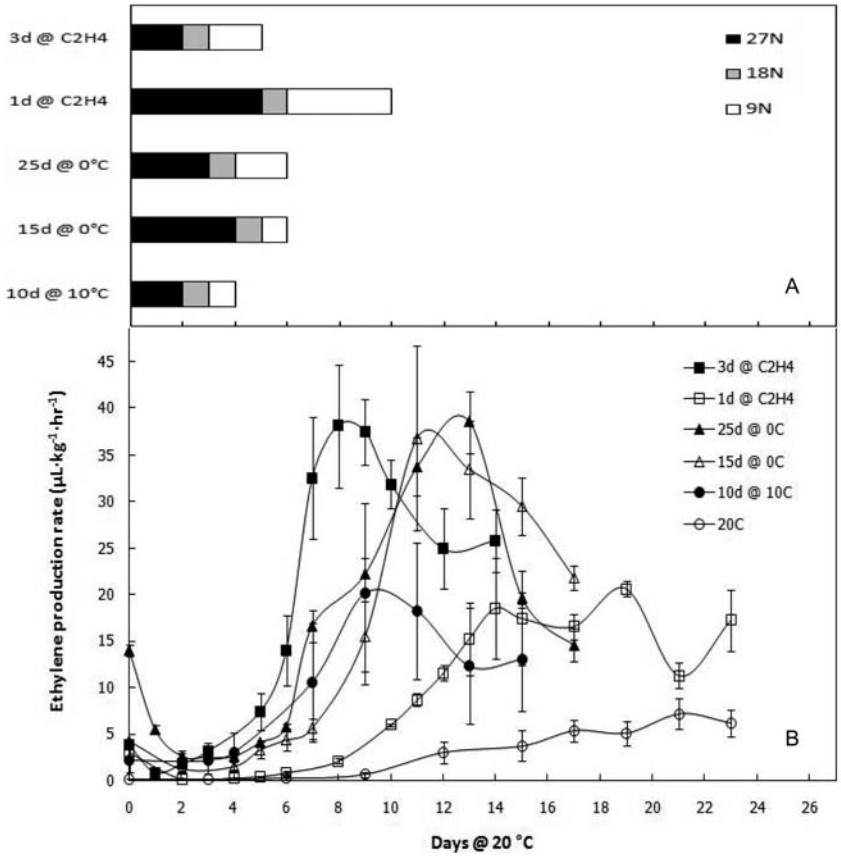

Figure 2. Days required to soften to 27, 18, and 9 N firmness (A) and changes in ethylene (C_2H_4) production (B) of 'Comice' pears at 20 °C after conditioning with C_2H_4 at 20 °C for 1 or 3 days or temperature conditioning at 0 °C for 15 or 25 days and at 10 °C for 10 days, and nonconditioned control at 20 °C. Vertical lines represent the standard error of the mean (n = 3).

Table 2. Volatiles in 'Comice' Pears by Headspace Sorptive Extraction and Gas Chromatography−Mass Spectrometry during Softening after Temperature or Ethylene Conditionings

compound class	peak	compound	RT[a] (min)	RI[b] (calcd)	RI[c] (std)	RI[d] (lit.)	MS[e]	pear refs[f]
aldehydes	2	butanal	2.05	596	600	595[g]	A, B	37
	6	pentanal	2.74	684	686	679[h]	A, B	37
	14	hexanal	4.26	800	800	801[i]	A, B	23, 38, 39
	17	(*E*)-2-hexenal	5.51	847	847	850[i]	A, B	23, 38, 39
	20	heptanal	6.98	902	901	902[i]	A, B	38
	32	nonanal	15.04	1104	1106	1104[i]	A, B	23, 38
	36	decanal	18.72	1205	1208	1205[i]	A, B	37
	38	2-decenal	20.51	1263	1265	1259[j]	A, B	
	44	dodecanal	24.69	1410	1412	1409[k]	A, B	
	46	tetradecanal	29.67	1614	1615	1611[l]	A, B	
	47	pentadecanal (tentative)[m]	31.94	1709		1711[n]	B	
alcohols	1	1-propanol	1.94	582	578	572[h]	A, B	12, 37
	3	2-methyl-1-propanol	2.23	619	622	606[o]	A, B	12, 23, 38
	4	1-butanol	2.49	652	654	657[r]	A, B	12, 23
	10	2-methyl-1-butanol	3.25	727	730	733[i]	A, B	12, 23, 37
	11	1-pentanol	3.74	762	761	761[i]	A, B	12, 23, 38
	18	1-hexanol	6.02	867	867	865[i]	A, B	12, 23, 38, 39
	24	1-heptanol	9.54	971	969	951[q]	A, B	12, 23, 39
	30	1-octanol	13.75	1073	1076	1070[i]	A, B	12, 23, 38, 39
esters	7	ethyl propanoate	2.91	703	705	692[q]	A, B	12, 39
	8	*n*-propyl acetate	2.93	704	706	707[i]	A, B	12, 23, 39
	9	methyl butanoate	3.04	712	714	717[s]	A, B	12, 39
	12	2-methylpropyl acetate	3.80	766	769	768[s]	A, B	12, 23, 39
	13	methyl 2-methylbutanoate	3.86	771	775	772[i]	A, B	23, 38
	15	butyl acetate	4.60	813	813	812[i]	A, B	12, 23, 38, 39
	16	ethyl 2-methylbutanoate	5.48	846	845	846[i]	A, B	12, 23, 38
	19	3-methylbutyl acetate	6.26	876	876	876[i]	A, B	12, 23, 38,
	21	butyl propanoate	7.26	910	907	907[i]	A, B	12, 37
	22	pentyl acetate	7.43	914	914	912[s]	A, B	12, 23, 39
	23	2-methylpropyl butanoate	8.92	954	954	953[i]	A, B	37
	24	ethyl hexanoate	10.67	1001	1001	999[s]	A, B	12, 23, 38, 39
	26	5-hexenyl acetate	10.90	1006	1004	1070[t]	A, B	23
	27	(*Z*)-3-hexenyl acetate	10.99	1008	1006	1004[s]	A, B	12, 37
	28	hexyl acetate	11.25	1015	1015	1011[i]	A, B	12, 23, 38, 39
	31	methyl benzoate	14.66	1095	1096	1091[n]	A, B	
	33	heptyl acetate	15.45	1115	1115	1111[i]	A, B	12, 39
	34	hexyl butanoate (tentative)	18.31	1193		1191[n]	B	12, 39
	35	ethyl octanoate	18.49	1198	1198	1194[i]	A, B	12, 23, 38
	37	octyl acetate	18.97	1213	1215	1213[i]	A, B	12, 23, 38, 39
	41	hexyl hexanoate	24.09	1387	1391	1369[q]	A, B	12, 39
	42	butyl octanoate	24.14	1389	1393	1393[n]	A, B	12
	43	ethyl decanoate	24.35	1397	1398	1398[u]	A, B	12
	45	ethyl (*E*,*Z*)-2,4-decadienoate	26.25	1471	1472	1457[p]	A, B	12, 23, 38, 39
ketones	5	2-pentanone	2.66	673	669	679[v]	A, B	
	40	1-(2,6,6-trimethyl-1,3-cyclohexadien-1-yl)-2-buten-1-one (*β*-damascenone)	24.03	1385	1381	1393[k]	A, B	
others	29	limonene	11.72	1026	1030	1029[i]	A, B	23, 38
	39	nonanoic acid (tentative)	20.97	1277		1280[n]	B	

[a]Retention time on DB-5MS column. [b]Retention indices calculated from C_8−C_{20} *n*-alkanes. [c]Retention indices calculated from authentic standards. [d]Retention indices reported in the literature. [e]Mass spectrometry ion comparisons, where A = match with authentic standard and B = match with library (NIST08). [f]References of compounds reported in pears. [g]Engel et al.[40] (HP-5). [h]Heydanek and McGorrin[41] (SE-30). [i]Beaulieu and Grimm[42] (DB-5). [j]Zoghbi et al.[44] (DB-5MS). [k]Hognadottir and Rouseff[45] (DB-5). [l]Adams[46] (DB-5). [m]Tentatively identified. [n]Pino et al.[47] (HP-5MS). [o]Shiota[23] (DB-1). [p]Riu-Aumatell et al.[38] (HP-5MS). [q]Takeoka et al.[39] (DB-1). [r]Habu et al.[48] (DB-1). [s]Beaulieu[49] (DB-5). [t]Shang et al.[50] (HP-5MS). [u]Ansorena et al.[51] (HP-5). [v]Jordan et al.[52] (HP-5).

dx.doi.org/10.1021/jf405047v | J. Agric. Food Chem. 2014, 62, 4988−5004

Table 3. Relative Concentration (μg kg^{-1} Fresh Weight Fruit) of Significant Volatiles in 'Comice' Pears Emitted during Softening after Temperature or Ethylene Conditionings[a]

peak	compound class and firmness level	compound	treatment: 3 days at C_2H_4			1 day at C_2H_4			25 days at 0 °C			15 days at 0 °C			10 days at 10 °C		
	aldehydes																
14	27 N	hexanal	118.77	a	A	101.38	a	A	83.40	a	B	94.83	a	B	83.14	a	A
	18 N		193.54	a	A	193.79	a	A	123.81	a	A	163.94	a	A	112.53	a	A
	9 N		178.57	ab	A	198.93	a	A	94.58	bc	AB	160.50	abc	A	76.76	c	A
17	27 N	(*E*)-2-hexenal	41.47	a	B	31.19	a	A	29.91	a	AB	32.81	a	A	28.48	a	A
	18 N		68.05	a	A	67.73	a	A	38.30	ab	A	48.85	ab	A	34.36	b	A
	9 N		49.20	ab	AB	67.63	a	A	24.10	b	B	40.70	ab	A	26.11	ab	A
20	27 N	heptanal	0.17	a	A	0.13	a	A	0.23	a	A	0.17	a	A	0.20	a	A
	18 N		0.08	ab	A	0.22	a	A	0.18	ab	A	0.11	ab	A	0.06	b	A
	9 N		0.22	a	A	0.13	a	A	0.07	a	A	0.07	a	A	0.07	a	A
	alcohols																
3	27 N	2-methyl-1-propanol	2.32	ab	A	2.52	a	A	1.37	bc	A	2.15	ab	A	0.83	c	B
	18 N		2.44	a	A	2.67	a	A	1.26	b	A	1.41	b	A	1.58	b	AB
	9 N		4.36	ab	A	7.04	a	A	2.20	b	A	2.55	b	A	2.80	ab	A
4	27 N	1-butanol	18.39	b	A	12.70	b	A	45.04	a	A	43.27	a	A	16.78	b	B
	18 N		19.01	bc	A	15.25	c	A	41.40	a	A	38.41	a	A	32.45	ab	AB
	9 N		32.21	ab	A	25.65	b	A	64.00	a	A	38.87	ab	A	34.78	ab	A
11	27 N	1-pentanol	0.83	ab	A	0.56	b	B	1.76	ab	A	2.21	a	A	0.55	b	A
	18 N		1.07	ab	A	0.52	b	B	1.35	ab	A	2.05	a	A	0.64	b	A
	9 N		1.57	a	A	1.94	a	A	3.48	a	A	1.51	a	A	0.06	a	A
18	27 N	1-hexanol	42.20	bc	B	10.92	c	B	105.71	a	A	71.73	ab	A	23.12	c	B
	18 N		25.05	c	B	33.12	bc	B	90.49	a	A	69.45	ab	A	61.46	ab	A
	9 N		107.75	a	A	90.16	a	A	118.58	a	A	69.98	a	A	77.37	a	A
24	27 N	1-heptanol	0.01	b	B	nd[b]	b	B	0.77	a	B	0.22	b	A	0.03	b	B
	18 N		0.04	a	B	0.08	a	B	0.48	a	B	0.41	a	A	0.68	a	AB
	9 N		1.60	a	A	1.31	a	A	1.95	a	A	0.56	a	A	1.38	a	A
30	27 N	1-octanol	0.01	b	A	0.01	b	A	0.58	a	A	0.05	b	A	0.04	b	A
	18 N		0.06	a	A	0.12	a	A	0.44	a	A	0.15	a	A	0.86	a	A
	9 N		1.98	a	A	1.03	a	A	0.59	a	A	0.11	a	A	1.75	a	A
	esters																
8	27 N	*n*-propyl acetate	0.10	ab	A	0.03	b	A	0.30	ab	A	0.17	ab	A	0.36	a	A
	18 N		0.45	b	A	0.25	b	A	0.30	b	A	0.48	b	A	2.08	a	A
	9 N		1.26	ab	A	0.50	b	A	1.02	ab	A	0.83	ab	A	5.48	a	A
15	27 N	butyl acetate	19.09	ab	B	3.77	b	B	89.87	ab	B	28.89	ab	B	104.32	a	B
	18 N		59.32	b	AB	40.99	b	AB	117.09	b	B	89.16	b	A	288.21	a	A
	9 N		147.28	bc	A	73.22	c	A	224.52	b	A	120.32	bc	A	403.55	a	A
19	27 N	3-methylbutyl	0.54	a	A	0.29	a	A	0.84	a	A	0.52	a	A	1.05	a	A
	18 N	acetate	0.28	b	A	0.36	b	A	0.36	b	A	0.30	b	A	1.27	a	A
	9 N		1.42	ab	A	1.08	b	A	0.69	b	A	0.56	b	A	3.38	a	A
21	27 N	butyl propanoate	nd	a	A	nd	a		nd	a	A	nd	a	A	0.00	a	A
	18 N		nd	b	A	nd	b		nd	b	A	0.04	ab	A	0.15	a	A
	9 N		0.18	a	A	nd	b		0.02	ab	A	nd	b	A	0.06	ab	A
22	27 N	pentyl acetate	1.54	b	B	1.79	ab	A	8.55	ab	B	2.19	ab	A	9.17	a	B
	18 N		3.77	b	B	4.34	b	A	10.31	b	B	8.95	b	A	32.65	a	A
	9 N		18.73	b	A	7.64	b	A	27.28	ab	A	11.34	b	A	41.58	a	A

dx.doi.org/10.1021/jf405047v | J. Agric. Food Chem. 2014, 62, 4988−5004

Table 3. continued

peak	compound class and firmness level	compound	treatment													
			3 days at C_2H_4			1 day at C_2H_4			25 days at 0 °C			15 days at 0 °C			10 days at 10 °C		
23	27 N	2-methylpropyl	2.05	a	A	0.56	a	A	0.65	a	A	0.08	a	A	3.79	a	A
	18 N	butanoate	0.38	a	A	1.13	a	A	0.17	a	A	0.12	a	A	2.97	a	A
	9 N		0.33	a	A	0.06	a	A	0.47	a	A	0.04	a	A	0.71	a	A
26	27 N	5-hexenyl acetate	0.11	a	A	nd	a		nd	a	A	nd	a	A	0.19	a	B
	18 N		nd	b	A	nd	b		0.02	b	A	nd	b	A	0.59	a	B
	9 N		0.01	b	A	nd	b		nd	b	A	nd	b	A	1.37	a	A
28	27 N	hexyl acetate	4.11	ab	A	0.83	b	A	32.68	a	A	4.16	ab	A	31.64	ab	B
	18 N		7.78	b	A	11.29	b	A	45.12	b	A	35.88	b	A	163.71	a	B
	9 N		109.99	b	A	28.97	b	A	90.77	b	A	33.56	b	A	412.10	a	A
33	27 N	heptyl acetate	nd	a	A	nd	a	A	0.01	a	A	nd	a	A	0.05	a	A
	18 N		nd	b	A	nd	b	A	nd	b	A	0.01	b	A	1.29	a	A
	9 N		0.63	b	A	0.03	b	A	0.21	b	A	nd	b	A	3.48	a	A
41	27 N	hexyl hexanoate	0.01	a	A	nd	a	A	0.04	a	A	0.03	a	A	0.04	a	B
	18 N		0.04	a	A	0.06	a	A	0.01	a	A	0.01	a	A	0.03	a	AB
	9 N		0.01	a	A	0.01	a	A	0.02	a	A	0.03	a	A	0.07	a	A
	27 N	total volatiles[c]	257.70	a	B	170.86	a	B	411.10	a	B	287.35	a	B	311.78	a	C
	18 N		387.07	b	AB	380.08	b	AB	478.25	b	AB	464.46	b	A	746.61	a	B
	9 N		664.97	b	A	515.92	b	A	661.24	b	A	487.22	b	A	1099.51	a	A
	27 N	total aldehydes[d]	163.25	a	A	135.35	a	A	120.40	a	B	130.49	a	A	114.60	a	A
	18 N		266.69	ab	A	267.72	a	A	168.66	ab	A	216.94	ab	A	151.70	b	A
	9 N		234.36	ab	A	272.19	a	A	123.75	b	B	205.16	ab	A	107.28	b	A
	27 N	total alcohols[e]	63.78	ab	AB	26.71	ab	B	155.28	a	A	119.72	ab	A	41.37	b	C
	18 N		47.67	c	B	51.75	c	B	135.43	a	A	111.94	ab	A	97.78	b	B
	9 N		149.53	a	A	131.51	a	A	190.95	a	A	114.90	a	A	118.25	a	A
	27 N	total esters[f]	30.45	ab	B	8.56	b	B	135.16	ab	B	36.81	ab	B	155.53	a	C
	18 N		72.51	b	AB	60.31	b	AB	173.85	b	B	135.38	b	AB	496.76	a	B
	9 N		280.84	b	A	111.79	b	A	346.24	b	A	167.05	b	A	873.82	a	A

[a]Within each row, values with the same lower case letter are not significantly different across treatments (Tukey: $p < 0.05$). Within each column, values with the same capital letter are not significantly different across firmness levels within each compound (Tukey: $p < 0.05$). [b]Not detected. [c]Total volatiles = sum of all compounds detected (all in Table 2). [d]Total aldehdyes = sum of all aldehydes shown in Table 2. [e]Total alcohols = sum of all alcohols shown in Table 2. [f]Total esters = sum of all esters shown in Table 2.

Descriptive Sensory Analysis. For fruit at the 27 N firmness level, an ANOVA using a pseudomixed model revealed that the sensory attributes of firmness, crunchiness, fibrousness, and tartness were significantly different across the different conditioning treatments ($p < 0.05$) (Table 4). The perception of firmness and crunchiness was highest for pears stored at 0 °C for 15 days, followed by pears stored at 0 °C for 25 days and pears stored at 10 °C for 10 days. Pears conditioned with ethylene for 3 and 1 days had the highest perceived fibrousness. Within the 27 N firmness group, pears conditioned with ethylene for 1 day also had the highest perceived tartness, whereas pears stored at 10 °C for 10 days were perceived as lowest in tartness (Table 4).

For fruit softened to 18 N firmness, crunchiness and fibrousness sensory attributes were significantly different across treatments as revealed by ANOVA ($p < 0.05$) (Table 4). Crunchiness was high in cold (0 °C) conditioned fruit, but low in ethylene conditioned fruit. However, ethylene conditioned fruits were perceived as the most fibrous.

For fruit softened to 9 N firmness, ANOVA showed significant differences among the treatments for fruity aroma, pear aroma, firmness, crunchiness, juiciness, and fibrousness sensory attributes ($p < 0.05$) (Table 4). Fruit conditioned at 10 °C for 10 days and at 0 °C for 25 days were highest in fruity aroma and pear aroma attributes. Fruit conditioned with ethylene for 1 day had the lowest perceived juiciness, but were not significantly different from fruit conditioned at 0 °C for 15 days. Fibrousness and firmness were highest in fruit conditioned with ethylene for 1 day, followed by fruit conditioned with ethylene for 3 days, and the latter were similar in fibrousness and firmness to fruit conditioned at 0 °C for 15 days (Table 4).

Relationship between Instrumental and Sensory Analysis. A partial least-squares (PLS) regression analysis showed the relationships and prediction of significant sensory attributes (*Y*-variable) by significant instrumental values (*X*-variable) at each firmness level. For pears with average firmness of 27 N, the first two latent vectors accounted for 95%

Table 4. Mean Sensory Score for Each Attribute in 'Comice' Pears during Softening after Temperature or Ethylene Conditioning[a]

		treatment														
attribute	firmness (N)	3 days at C_2H_4			1 days at C_2H_4			25 days at 0 °C			15 days at 0 °C			10 days at 10 °C		
fruity aroma	27	4.17	a	A	4.01	a	A	4.76	a	B	4.09	a	A	4.79	a	B
(sweet)	18	4.12	a	A	4.52	a	A	4.83	a	B	4.46	a	A	5.07	a	B
	9	4.94	bc	A	4.84	bc	A	5.59	ab	A	4.60	c	A	6.23	a	A
apple aroma	27	2.12	a	A	2.06	a	A	3.1	a	A	2.17	a	A	2.57	a	A
	18	2.03	a	A	2.07	a	A	2.59	a	A	2.46	a	A	3.19	a	A
	9	2.38	a	A	2.42	a	A	2.89	a	A	2.37	a	A	2.73	a	A
pear aroma	27	4.63	a	A	4.57	a	A	4.78	a	B	4.75	a	A	5.28	a	B
	18	4.56	a	A	4.98	a	A	5.29	a	B	5.42	a	A	4.91	a	B
	9	5.10	b	A	5.03	b	A	5.96	a	A	4.96	b	A	6.40	a	A
fermented aroma	27	1.64	a	B	1.94	a	A	1.59	a	A	1.81	a	A	1.43	a	B
	18	1.48	a	B	1.82	a	A	1.68	a	A	1.67	a	A	1.66	a	B
	9	2.38	a	A	2.47	a	A	2.11	a	A	2.15	a	A	2.80	a	A
green stem aroma	27	1.63	a	A	1.97	a	A	2.14	a	A	2.33	a	A	2.23	a	A
	18	2.46	a	A	2.41	a	A	2.37	a	A	2.25	a	A	2.13	a	A
	9	2.00	a	A	2.35	a	A	1.90	a	A	2.45	a	A	1.67	a	A
firmness	27	3.46	c	A	4.25	b	A	4.71	b	A	5.41	a	A	4.83	ab	A
	18	3.17	a	A	3.54	a	B	3.76	a	B	3.26	a	B	3.33	a	B
	9	2.25	ab	B	2.54	a	C	1.46	c	C	1.94	bc	C	1.70	c	C
crunchiness	27	2.55	b	A	2.96	b	A	3.91	a	A	4.24	a	A	3.81	a	A
	18	1.97	cd	B	1.92	d	B	3.11	a	B	2.81	ab	B	2.42	cb	B
	9	1.19	ab	C	1.56	a	B	1.04	b	C	1.32	ab	C	1.01	b	C
juiciness	27	2.10	a	C	2.91	a	C	3.22	a	C	2.89	a	C	2.82	a	B
	18	3.65	a	B	3.79	a	B	4.02	a	B	3.90	a	B	3.28	a	B
	9	6.52	a	A	5.77	b	A	6.96	a	A	6.34	ab	A	6.48	a	A
butteriness (texture)	27	3.52	a	C	4.00	a	B	4.19	a	B	3.82	a	B	3.43	a	C
	18	4.39	a	B	4.55	a	AB	4.34	a	B	4.35	a	B	4.12	a	B
	9	5.73	a	A	5.13	a	A	6.13	a	A	5.77	a	A	6.05	a	A
fibrousness	27	2.15	a	A	2.33	a	A	1.35	b	A	1.43	b	A	1.50	b	A
	18	2.19	ab	A	2.4	a	A	1.46	c	A	1.37	c	A	1.8	bc	A
	9	2.16	ab	A	2.26	a	A	1.44	c	A	1.49	bc	A	1.5	c	A
sweetness	27	3.01	a	B	3.54	a	C	4.03	a	B	3.59	a	C	3.58	a	B
	18	4.86	a	A	4.18	a	B	4.40	a	B	4.27	a	B	3.89	a	B
	9	5.18	a	A	5.34	a	A	6.03	a	A	5.66	a	A	5.64	a	A
tartness	27	3.78	bc	A	5.01	a	A	3.61	bc	A	3.99	b	A	3.07	c	A
	18	3.26	a	A	3.19	a	B	4.12	a	A	3.57	a	A	4.37	a	A
	9	4.61	a	A	3.58	a	B	3.97	a	A	3.34	a	A	3.91	a	A

[a]Within each row, values with the same lower case letter are not significantly different across treatments (Tukey: $p < 0.05$). Within each column, values with the same capital letter are not significantly different across firmness levels within each compound (Tukey: $p < 0.05$).

and 58% of the variance for the *X*- and *Y*-variables, respectively (Figure 3). The fibrousness sensory attribute characterized fruit conditioned with ethylene for 1 or 3 days and was negatively correlated with the volatile alcohols 1-octanol and 1-heptanol. Crunchiness and firmness sensory attributes had the strongest positive correlation with these alcohols, and these attributes were associated with fruit held at 0 °C for 25 days. In addition, 1-hexanol, 1-butanol, 1-pentanol, total alcohols, and SSC had the next strongest correlation with firmness and crunchiness, and this group of compounds was associated with fruit held at 0 °C for 25 and 15 days. The tartness sensory attribute was most strongly and positively associated with concentrations of 2-methyl-1-propanol; fruit conditioned with ethylene as well as fruit conditioned at 0 °C for 15 days were highest in both tartness perception and 2-methyl-1-propanol concentration. Fruit conditioned at 10 °C for 10 days had the highest levels of esters, but no sensory attributes were associated with these volatiles at this firmness stage.

dx.doi.org/10.1021/jf405047v | J. Agric. Food Chem. 2014, 62, 4988−5004

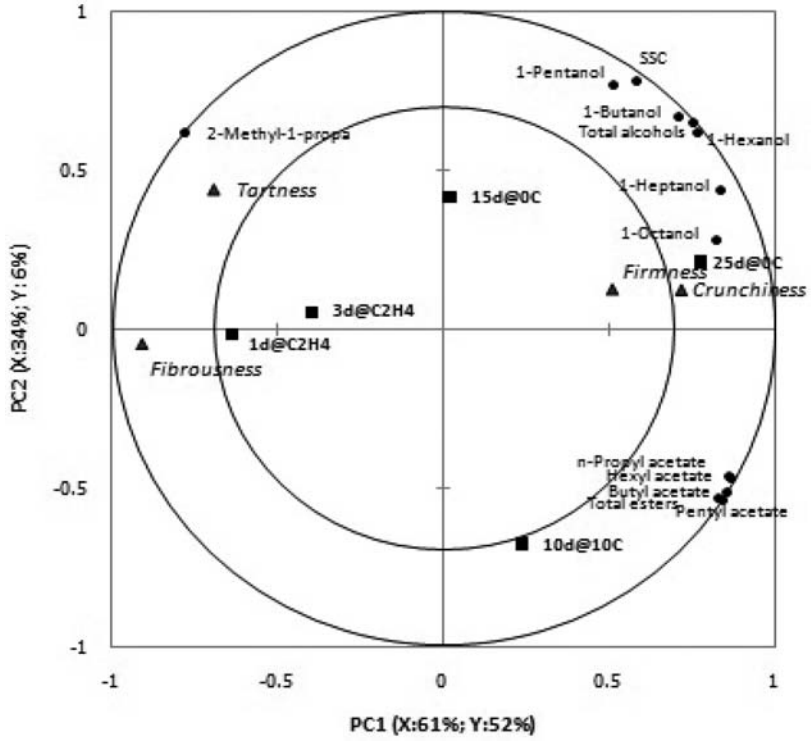

Figure 3. Partial least-squares (PLS) analysis of sensory attributes (*Y*-variable) and instrumental measurements (*X*-variable) of 'Comice' pears at 27 N on the conditioning treatments: (▲) sensory attributes; (●) chemical compounds; (■) conditioning treatments. 2-Methyl-1-propa = 2-methyl-1-propanol.

For pears with average firmness of 18 N, a PLS analysis showed that 92 and 97% of the variance for the *X*- and *Y*-variables was explained by the first two vectors, respectively (Figure 4). The crunchiness sensory attribute was strongly positively associated with high concentrations of 1-butanol, 1-hexanol, and total alcohols, followed by 1-pentanol. These volatiles and crunchiness perception were most associated with pears conditioned at 0 °C. On the opposite quadrant of the PLS map, fruits conditioned with ethylene were most closely associated with the fibrousness sensory attribute and with the concentration of 2-methyl-1-propanol. Pears conditioned with ethylene also had the highest levels of (*E*)-2-hexenal and total aldehydes and the lowest concentrations of esters. Esters, including propyl acetate, butyl acetate, 3-methylbutyl acetate, butyl propanoate, pentyl acetate, 5-hexenyl acetate, hexyl acetate, heptyl acetate, and total esters, as well as total volatiles were highest in pears conditioned at 10 °C.

For pears with average firmness of 9 N, the first two latent vectors accounted for 91 and 88% of the variance of the *X*- and *Y*-variables, respectively (Figure 5). Juiciness, pear aroma, and fruity aroma sensory attributes were negatively associated with fibrousness, firmness, and crunchiness attributes. Juiciness was most strongly correlated with concentrations of the alcohol 1-butanol and was associated with fruit held at 0 °C for 25 days. Pear aroma and fruity aroma were positively correlated with the acetate esters and the total ester concentration. Pentyl acetate had the strongest correlation with pear aroma, whereas butyl acetate had the strongest correlation with fruity aroma. These esters and aroma attributes were strongly positively associated with fruit held at 10 °C for 10 days and negatively associated with fruit held at 0 °C for 15 days. On the other hand, fibrousness and firmness had the strongest correlation with concentrations of 2-methyl-1-propanol, followed by (*E*)-2-hexenal. Crunchiness was highly associated with the concentration of hexanal and total aldehydes, followed by (*E*)-2-hexenal. These sensory attributes and volatile concentrations were most highly correlated with fruit conditioned with ethylene for 1 and 3 days.

Pearson correlation coefficients were also used to evaluate the relationships between sensory and instrumental measurements averaged across all treatments and firmness levels (Table 5). Many interesting correlations were found. For example, concentrations of hexanal and (*E*)-2-hexenal were positively correlated with green stem aroma and perception of fibrousness. Additionally, levels of (*E*)-2-hexenal were significantly negatively correlated with apple aroma intensity. Total aldehydes showed the same pattern of correlation as that of (*E*)-2-hexenal. The levels of the alcohols 1-propanol, 1-butanol, 1-hexanol, and 1-heptanol and the ester butyl acetate were positively correlated with fruity aroma, pear aroma, apple aroma, butteriness, juiciness, and sweetness perception. Propyl acetate, butyl acetate, pentyl acetate, and hexyl acetate were significantly and positively associated with fruity aroma, pear aroma, and butteriness. They were negatively correlated with firmness. Total esters and total volatiles displayed a correlation to sensory attributes similar to that of individual esters. For other analytical measurements, SSC was not significantly correlated with sweetness, whereas TA had a negative correlation with sweetness and a positive correlation with tartness. Moreover, the ratio of SSC/TA was negatively correlated with tartness. WSP levels displayed a very strong positive correlation with some texture (butteriness, juiciness) and some taste (sweetness) attributes, whereas WSP levels were negatively correlated with crunchiness and firmness. WSP levels were also positively correlated with fermented aroma, fruity aroma, and pear aroma (Table 5).

dx.doi.org/10.1021/jf405047v | *J. Agric. Food Chem.* 2014, 62, 4988−5004

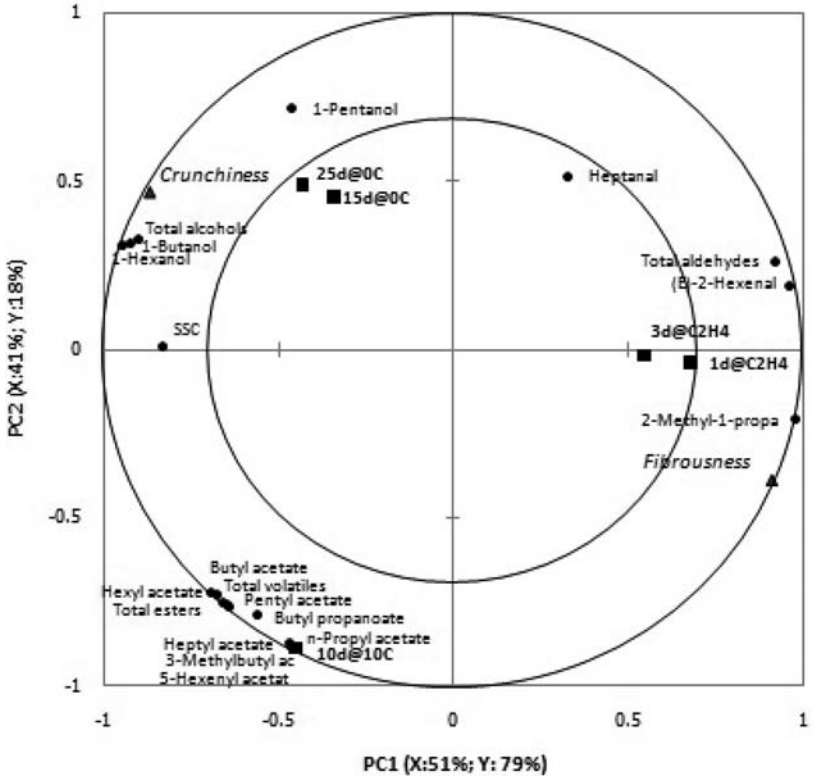

Figure 4. Partial least-squares (PLS) analysis of sensory attributes (*Y*-variable) and instrumental measurements (*X*-variable) of 'Comice' pears at 18 N on the conditioning treatments: (▲) sensory attributes; (●) chemical compounds; (■) conditioning treatments. 2-Methyl-1-propa = 2-methyl-1-propanol; 5-Hexenyl acetat = 5-hexenyl acetate; 3-Methylbutyl ac = 3-methylbutyl acetate.

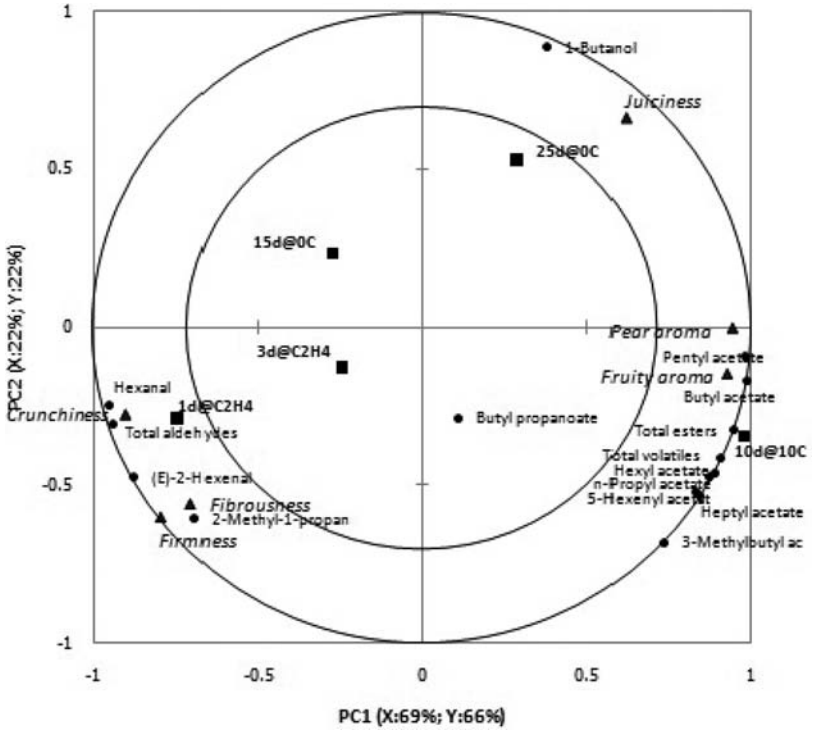

Figure 5. Partial least-squares (PLS) analysis of sensory attributes (*Y*-variable) and instrumental measurements (*X*-variable) of 'Comice' pears at 9 N on the conditioning treatments: (▲) sensory attributes; (●) chemical compounds; (■) conditioning treatments. 5-Hexenyl acetat = 5-hexenyl acetate; 3-Methylbutyl ac = 3-methylbutyl acetate; 2-methyl-1-propan = 2-methyl-1-propanol.

dx.doi.org/10.1021/jf405047v | *J. Agric. Food Chem.* 2014, 62, 4988−5004

Table 5. Pearson Correlation Coefficients between Sensory Attributes and Instrumental Values for 'Comice' Pears across All Treatments and Firmness Levels[a]

	aroma					texture					taste	
instrumental variable	fruity	apple	pear	fermented	green st[b]	firm	crunchy	juicy	buttery	fibrous	sweet	tart
aldehydes												
butanal	0.408	0.422	0.432	0.094	−0.045	−0.199	−0.043	0.367	0.356	**-0.519**	0.364	0.209
pentanal	−0.171	−0.162	−0.099	−0.236	**0.530**	0.046	0.040	−0.017	−0.025	0.067	0.109	−0.040
hexanal	−0.321	−0.492	−0.305	0.088	**0.534**	−0.314	−0.435	0.222	0.193	**0.583**	0.276	−0.275
(*E*)-2-hexenal	−0.379	**-0.538**	−0.374	−0.019	**0.524**	−0.134	−0.288	0.021	0.004	**0.657**	0.111	−0.375
heptanal	−0.332	−0.190	−0.348	−0.278	0.092	**0.573**	0.494	−0.377	−0.419	0.166	−0.482	−0.050
tetradecanal	0.508	0.165	**0.520**	**0.533**	−0.173	**-0.725**	**-0.653**	**0.701**	**0.678**	−0.074	**0.754**	−0.138
pentadecanal[c]	0.413	0.240	0.443	0.330	−0.191	**-0.559**	−0.483	**0.569**	**0.548**	−0.117	**0.584**	−0.033
alcohols												
1-propanol	**0.687**	**0.679**	**0.622**	0.417	−0.295	−0.441	−0.290	**0.563**	**0.570**	**-0.609**	**0.520**	0.166
2-methyl-1-propanol	0.089	−0.257	−0.030	**0.674**	0.025	−0.433	**-0.538**	0.492	0.441	**0.559**	0.437	0.095
1-butanol	0.468	**0.591**	0.485	0.197	−0.059	−0.292	−0.097	0.487	0.489	**-0.737**	0.491	0.102
2-hexanol	**-0.572**	−0.394	−0.506	−0.256	0.101	**0.702**	**0.623**	**-0.534**	−0.501	0.040	**-0.559**	0.006
1-hexanol	**0.551**	**0.572**	0.449	0.441	−0.119	−0.412	−0.266	**0.631**	**0.602**	−0.464	**0.571**	0.163
1-heptanol	**0.773**	**0.524**	**0.643**	**0.719**	−0.328	**-0.706**	**-0.622**	**0.852**	**0.828**	−0.202	**0.776**	0.252
1-octanol	**0.721**	0.407	0.511	**0.738**	−0.386	**-0.544**	**-0.541**	**0.653**	**0.641**	0.025	**0.535**	0.365
esters												
propyl propanoate	−0.176	0.253	−0.267	−0.339	0.014	**0.670**	**0.698**	−0.395	−0.407	−0.273	−0.411	0.078
n -propyl acetate	**0.820**	0.405	**0.723**	**0.647**	−0.484	**-0.529**	−0.495	0.497	**0.553**	−0.217	0.462	0.140
methyl butanoate	−0.283	−0.116	−0.253	−0.216	0.003	0.266	0.289	−0.252	−0.245	0.074	−0.208	**0.535**
methyl 2-methyl-butanoate	0.393	0.353	0.265	0.292	−0.272	−0.052	−0.028	0.065	0.101	−0.123	0.031	**0.659**
butyl acetate	**0.918**	**0.681**	**0.778**	0.511	−0.406	**-0.573**	−0.483	**0.554**	**0.583**	−0.386	**0.530**	0.148
ethyl 2-methyl-butanoate	0.139	0.324	0.006	−0.384	−0.291	0.286	0.259	−0.452	−0.461	−0.003	−0.492	−0.165
3-methylbutyl acetate	**0.813**	0.416	**0.668**	**0.679**	**-0.526**	−0.411	−0.392	0.461	0.478	−0.173	0.381	0.118
pentyl acetate	**0.914**	**0.687**	**0.762**	**0.536**	−0.450	**-0.601**	**-0.520**	**0.582**	**0.612**	−0.333	**0.535**	0.236
ethyl hexanoate	−0.294	0.088	−0.317	−0.467	−0.112	**0.762**	**0.786**	**-0.603**	**-0.626**	−0.258	**-0.628**	−0.133
5-hexenyl acetate	**0.714**	0.390	**0.615**	0.464	−0.513	−0.308	−0.284	0.220	0.278	−0.197	0.192	0.106
hexyl acetate	**0.859**	0.473	**0.756**	**0.632**	**-0.525**	−0.508	−0.462	0.491	**0.541**	−0.249	0.439	0.200
methyl benzoate	−0.277	0.086	−0.377	−0.390	−0.399	0.471	0.498	**-0.553**	**-0.518**	0.004	**-0.581**	0.000
heptyl acetate	**0.772**	0.382	**0.664**	**0.603**	**-0.532**	−0.428	−0.411	0.385	0.447	−0.163	0.336	0.207
ethyl octanoate	−0.167	0.159	−0.171	−0.451	0.035	**0.710**	**0.736**	−0.490	**-0.551**	−0.335	−0.502	−0.255
octyl acetate	**0.578**	0.324	0.443	0.272	**-0.547**	−0.184	−0.185	0.075	0.071	−0.069	−0.004	0.047
hexyl hexanoate[c]	0.456	0.177	0.394	0.127	0.007	−0.099	−0.157	0.131	0.211	−0.180	0.216	**-0.522**
butyl octanoate	0.271	0.127	0.173	0.007	0.171	−0.033	−0.103	0.038	0.107	−0.053	0.127	**-0.533**
ketone												
2-pentanone	−0.458	−0.271	−0.281	**-0.578**	0.264	**0.710**	**0.711**	**-0.629**	**-0.710**	−0.177	**-0.589**	−0.117
other												
nonanoic acid[c]	0.317	0.176	0.286	0.410	−0.004	−0.467	−0.427	**0.531**	0.461	0.062	**0.552**	−0.061
total aldehydes	−0.400	**-0.560**	−0.390	0.067	0.489	−0.248	−0.390	0.133	0.119	**0.676**	0.189	−0.213
total alcohols	0.491	**0.557**	0.420	0.420	−0.178	−0.352	−0.191	**0.584**	**0.564**	−0.509	**0.520**	0.267
total esters	**0.907**	**0.596**	**0.779**	**0.579**	−0.471	**-0.551**	−0.482	**0.533**	**0.573**	−0.323	0.494	0.181
total ketones	−0.450	0.002	**-0.620**	−0.409	−0.052	**0.765**	**0.683**	**-0.702**	**-0.688**	0.161	**-0.774**	0.318
total volatiles	**0.909**	**0.557**	**0.769**	**0.696**	−0.453	**-0.673**	**-0.612**	**0.661**	**0.696**	−0.229	**0.611**	0.235
SSC[d]	−0.136	0.210	−0.118	−0.145	−0.238	**0.532**	**0.625**	−0.357	−0.328	−0.466	−0.399	0.214
TA[e]	−0.413	−0.082	−0.501	−0.265	−0.382	0.399	0.369	−0.503	−0.497	0.267	**-0.588**	**0.657**
SSC/TA	0.401	0.134	0.505	0.270	0.299	−0.253	−0.201	0.409	0.430	−0.414	0.478	**-0.602**
WSP[f]	**0.662**	0.161	**0.599**	**0.783**	−0.052	**-0.928**	**-0.916**	**0.943**	**0.953**	0.024	**0.953**	−0.083

[a]Values in bold are significant at $p < 0.05$. [b]Green stem aroma. [c]Tentatively identified. [d]Soluble solids content. [e]Titratable acidity. [f]Water-soluble polyuronides.

DISCUSSION

Conditioning treatments effectively enhanced ripening of 'Comice' pears as compared to the nonconditioned group. Whereas the control fruit did not soften below 33 N within 31 days at 20 °C, all of the conditioned fruit softened to 13 N within 10 days, and all conditioning treatments except ethylene for 1 day were nearly full ripe (full ripe = 9 N[21]) after 6 days. However, different conditioning methods resulted in different rates of softening. The softening rate of fruit conditioned with ethylene for 3 days, at 10 °C for

dx.doi.org/10.1021/jf405047v | J. Agric. Food Chem. 2014, 62, 4988−5004

Table 6. Odor Description, Published Odor Thresholds, Relative Concentration, and Odor Units of Significant Volatile Compounds found in 'Comice' Pears at an Average Firmness of 9 N following Different Conditioning Treatments

class	compound	odor description	published odor threshold (μg/kg water)	rel concn (μg/kg)	odor units U_0[w]
alcohols	1-hexanol	green, grass, fruity, floral, nuts[r,x,y]	190,[g] 500,[b] 1100,[e] 2500,[d,h]	94.86[u]	0.04−0.50[u]
	1-butanol	fermented, fruity, medicinal, cheesy[ac]	500[b]	51.20[u]	0.10[u]
	1-octanol	green, floral, citrus[z]	110[f]	0.47[u]	0[u]
	1-pentanol	balsamic, sweet[aa]	1600,[g] 4000[i,j]	2.78[u]	0[u]
	1-heptanol	leafy green, fruity[aa]	3,[k] 100[g]	1.56[u]	0.02−0.52[u]
	2-methyl-1-propanol	balsamic, sweet (weaker than 1-pentanol)[aa]	7000[l,m]	5.63[v]	0[v]
aldehydes	hexanal	green, sour[r]	4.5,[k] 5[b,n] 5.8,[o] 9.2[p], 10.5,[q] 50,[r] 479[s]	159.15[v]	0.33−31.83[v]
	(*E*)-2-hexenal	green grass, almond, sweet, almond fruity, apple, plum, vegetable[r,z]	17,[bn] 123[s]	54.10[v]	0.44−3.18[v]
esters	butyl acetate	vanilla, sweet, fruity, pear,[x,y]	66[a,b]	322.84[t]	4.89[t]
	hexyl acetate	apple, pear, floral, banana[r,x,y]	2,[cb] 101,[d] 115[a]	329.68[t]	2.87−165[t]
	pentyl acetate	floral, fruity, banana[z]	5,[b] 38,[d] 43[a]	33.26[t]	0.77−6.65[t]
	propyl acetate	celery, fruity, pear, raspberry[z]	2000,[a] 4700[e]	4.39[t]	0[t]
	3-methylbutyl acetate	banana, sweet, fruity, pear[z]	2,[f] 3[d]	2.70[t]	0.90−1.35[t]
	heptyl acetate	green, waxy, fatty, citrus, aldehydic, winey, woody[aa]	420[a]	2.78[t]	0.01[t]
	ethyl 2-methylbutanoate	sweet, fruity, strawberry, melon, green, floral[z]	0.006,[f] 0.1[b]	1.03[t]	10−172[t]
	5-hexenyl acetate	coarse, harsh, herbaceous, ketonic estery, reminiscent of blue cheese[ab]			

[a]Takeoka et al.[53] [b]Flath et al.[54] [c]Buttery et al.[55] [d]Belitz et al.[56] [e]Etievant.[57] [f]Takeoka et al.[39] [g]Devos et al.[58] [h]Takeoka et al.[59] [i]Buttery et al.[60] [j]Buttery et al.[61] [k]Guadagni et al.[62] [l]Fazzalari.[63] [m]Salo.[64] [n]Buttery et al.[65] [o]Rychlik et al.[66] [p]Ahmed et al.[67] [q]Grosch et al.[68] [r]Larsen and Poll.[69] [s]Tandon et al.[70] Relative concentration given at 9 N firmness for the conditioning treatment that resulted in the highest concentration of the compound. [t]Relative concentration at 9 N of fruit conditioned at 10 °C for 10 days. [u]Relative concentration at 9 N of fruit conditioned at 0 °C for 25 days. [v]Relative concentration at 9 N of fruit conditioned with ethylene for 1 day. [w]U_0 = compound concentration divided by its odor threshold. [x]Rapparini et al.[71] [y]Chen et al.[72] [z]Beaulieu.[49] [aa]Good Scents Co.[73] [ab]Shiota.[23] [ac]El-Sayed.[74]

10 days, or at 0 °C for 25 days agrees with previously published results.[3]

The ability of the fruit to soften was related to their ethylene production rate, which varied by conditioning treatment. It was previously shown that treatments inducing a higher rate of ethylene biosynthesis resulted in more rapid and uniform softening.[22] In our study, the treatments that took less time to reach the climacteric peak produced more rapid softening. Fruit conditioned with ethylene for 3 days or conditioned at 10 °C for 10 days reached the climacteric peak and softened in the least amount of time, whereas fruit conditioned at 0 °C for 15 or 25 days or conditioned with ethylene for 1 day reached the climacteric peak later and softened more slowly.

The sensory profiles of 'Comice' pears within each firmness level evaluated were different for the various conditioning treatments. At 27 N, the fruits were still unripe and had fewer total volatiles, and the volatiles that were present were at low concentrations; however, once the fruit softened to 9 N firmness, the quantity and the number of different volatile compounds increased, causing many aroma attributes to become significantly different among the conditioning treatments.[23] Treatment at 10 °C for 10 days, followed closely by treatment at 0 °C for 25 days, produced fruit with the strongest fruity aroma and pear aroma, particularly once fruits softened to 9 N. As pears softened and ethylene production increased, the levels of many volatile compounds also increased, in particular, the major components of pear aroma, hexyl and butyl acetate, and total esters. This is consistent with previous studies highlighting a relationship between softening, ethylene production, and aroma volatile biosynthesis in climacteric fruit.[24−27] The volatile compound responsible for the characteristic aroma of 'Comice' pear, ethyl 2-methylbutanoate,[11] was detected in fruit from all treatments and softness stages, but no significant differences were found in ethyl 2-methylbutanoate levels among the conditioning treatments.

The five conditioning treatments resulted in marked differences in the aroma volatile profile. Regardless of the firmness level, the volatile composition of fruit conditioned at 10 °C for 10 days was dominated by esters, whereas ethylene treatments led to an aldehyde-rich volatile profile. The major esters of 'Comice' pear aroma (hexyl acetate and butyl acetate[12]) and other abundant esters that are found in most pear varieties (pentyl and propyl acetate) were highest in fruit conditioned at 10 °C for 10 days at all firmness levels. These compounds have sweet, fruity, floral, and pear notes (Table 6). In addition, other volatiles described as sweet and fruity were associated with fruit conditioned at 10 °C for 10 days, including heptyl acetate and 3-methylbutyl acetate in pears at both 18 and 9 N firmness and butyl propanoate in 9 N pears. Generally, many low boiling point esters increase when pear fruits ripen.[23] It is interesting that 5-hexenyl acetate, a less common fruit volatile previously detected only in 'La France' pear[23] and Chinese quince,[28] was found at significantly higher levels in fruit conditioned at 10 °C for 10 days. The odor of 5-hexenyl acetate is described as coarse, harsh, herbaceous, ketonic, estery, and reminiscent of blue cheese.[23] Similar to the results obtained in 'La France' pear,[23] its levels increased as the fruit softened.

Cold-temperature conditioning (0 °C) resulted in pears with relatively high levels of specific alcohols (1-butanol, 1-pentanol,

1-heptanol, 1-hexanol, 1-octanol) as compared to fruit from other conditioning treatments. These compounds have a sweet, green note except 1-butanol, which is described as fermented and fruity (Table 6). These alcohols described fruit conditioned at 0 °C and softened to 27 N; a reduced number of these compounds described fruit softened to 18 N, and only 1-butanol described fruit softened to 9 N firmness.

Our results showed that fruit conditioned at 10 °C for 10 days developed higher levels of volatiles in general and esters in particular at each ripeness stage evaluated, even though they had lower ethylene production at some firmness levels. The volatile composition of ripe fruit conditioned at 0 °C for 15 days was predominant in aldehydes, whereas fruits conditioned at 0 °C for 25 days were predominant in esters and alcohols. Fruit conditioned with ethylene for 1 or 3 days had high concentrations of aldehydes, but fruit conditioned with ethylene for 3 days also had high concentrations of esters. It appears that the longer treatments with ethylene or at 0 °C, both of which represent recommended treatments for maximum initiation of ripening, resulted in greater production of fruity esters. It will be interesting to further investigate gene expression and enzyme activities involved in alcohol formation (alcohol dehydrogenase, ADH) and ester formation (alcohol acyltransferase, ATT) in each conditioning treatment to determine how ADH and AAT are regulated in 'Comice' pears and the role of ethylene.

Most compounds detected in our study by headspace sorptive extraction (HSSE) have been previously detected in pears using other extraction techniques such as dynamic headspace concentration on carbon traps, simultaneous distillation and extraction, and solid phase microextraction (SPME). However, HSSE can be much more sensitive than those previous methods. Tienpont et al.[29] showed that HSSE was 100 times more sensitive than SPME, with high enrichment factors for highly volatile solutes. Limits of detection were on the order of 0.1 ppb in the full scan MS mode in Tienpont's study. Moreover, HSSE has a higher sensitivity than SPME for nonpolar and some medium polar compounds.[30,31] Using the dynamic headspace method, Lara et al.[32] detected ∼150 and ∼50 μg kg^{-1} butyl acetate and hexyl acetate, respectively, in 'Comice' pears after 2 months of storage at −1 °C and ripening. Suwanagul and Richardson[12] found butyl acetate and hexyl acetate in the amounts of ∼9 and ∼30 μg kg^{-1} 100 L^{-1}, respectively, after the fruits were stored at −1 °C for 3 months and softened. In our study using the HSSE technique, we detected much higher amounts of butyl acetate and hexyl acetate. Fruit conditioned at 0 °C for 25 days and softened to 9 N had 225 and 91 μg kg^{1-} of butyl acetate and hexyl acetate, respectively, whereas fruit conditioned at 10 °C for 10 days had more, with 404 and 412 μg kg^{-1}, respectively. Several compounds not previously identified in pears were detected in our samples, including four aldehydes (decanal, 2-decanal, tetrdecanal, and a tentative identification of pentadecanal), one ester (methyl benzoate), two ketones (2-pentanone, β-damascenone, and limonene) and nonanonic acid (tentative).

Even though the pears used in sensory testing were selected with an instrument (penetrometer) to have the same firmness, panelists perceived significant differences in firmness and crunchiness attributes among the various conditioning treatments. Crunchiness and firmness characterized cold-temperature treatments when the fruits were not fully ripe (27 and 18 N), whereas in 9 N fruit these attributes became prominent in fruit conditioned with ethylene. Juiciness was not significantly different among the various conditioning treatments in firmer fruit, but differences became apparent when the fruit softened to 9 N. At the softest firmness level, fruit that was cold conditioned at 0 °C for 25 days had the highest juiciness score. Fibrousness was consistently high in fruit conditioned with ethylene.

For sensory taste attributes, conditioning treatments did not differentially affect sweetness within any firmness level; however, differences in tartness could be perceived at 27 N, with fruits conditioned with ethylene for 1 day displaying the highest tartness score. Panelists perceived this difference in tartness of fruit conditioned with ethylene for 1 day, which the instrumental measurement (TA) did not detect. TA was significantly correlated to both sensory sweetness and tartness; however, SSC was not significantly related to either. The perception of tartness is influenced by the presence of both acids and sugars,[33] and there were significant differences in SSC in 27 N pears in our study. Aroma compounds can also affect perception of sweetness and sourness.

The instrumental parameters most significantly different (Tukey: $p < 0.05$) among the conditioning treatments were the volatile compounds. However, no significant differences in aroma attributes were perceived by the sensory panel in the firmest (27 N) pears, but differences were observed in 9 N pears. Pear aroma and fruity aroma sensory attributes were strongly correlated with esters, especially pentyl and butyl acetate. Butyl acetate is described as having sweet, vanilla, fruity, and pear notes, similar to pentyl acetate, which has sweet, floral, and banana notes (Table 6). The odor thresholds of these two compounds are low, and their odor units are among the highest of the statistically significant compounds in soft fruit conditioned at 10 °C for 10 days (Table 6). Therefore, butyl and pentyl acetate are likely important contributors to fruity aroma and pear aroma, which were predominant in fruit conditioned at 10 °C for 10 days. Hexyl acetate also exhibited a high odor unit value in soft (9 N) pears conditioned at 10 °C for 10 days; however, in our study, this compound showed weaker association with fruity aroma and pear aroma attributes than the other two compounds using both PLS and Pearson correlation analyses.

Ethyl 2-methylbutanoate has been reported as a characteristic aroma compound in 'Comice' pear.[11] Although the relative concentration of this compound detected in our pear samples was low, given its particularly low odor threshold, the odor unit was high and comparable to that of hexyl acetate in soft pears (9 N) conditioned at 10 °C for 10 days (Table 6). However, there were no significant differences in the concentrations of this compound across conditioning treatments or firmness levels tested. Interestingly, it also showed poor correlation to the sensory attributes in our study (Table 5), indicating that sensory evaluation may uncover additional predictors for characteristic aroma compounds in 'Comice' pears. Other compounds associated with the conditioning treatment at 10 °C for 10 days such as propyl acetate, heptyl acetate, octyl acetate, and 3-methylbutyl acetate may have less impact on aroma perception due to their very low odor units (Table 6). 5-Hexenyl acetate is not commonly found among fruit aroma volatiles; therefore, its odor threshold has not yet been evaluated, and we do not know how strong this compound's contribution is to aroma perception in pears.

Opposite to the sweet and fruity odor type compounds are the green-odor volatiles such as hexanal and (*E*)-2-hexenal. The concentration of these compounds was high in fruit conditioned with ethylene. Hexanal and (*E*)-2-hexenal may contribute to aroma perception in pears conditioned with ethylene at 9 N firmness due to their odor units >1 (Table 6).

Cold-temperature (0 °C) conditioning was associated with high concentrations of alcohols, including 1-butanol, 1-hexanol, 1-pentanol, 1-octanol, and 1-heptanol. These alcohols have a high odor threshold (Table 6), and their odor units in 9 N fruit held at 0 °C for 25 days (the conditioning treatment that resulted in the highest concentrations of these alcohols) were very low (<1). Therefore, these alcohols may be relatively small contributors to aroma in pear fruit conditioned at 0 °C. Esters may contribute more to the aroma of fruit held at 0 °C for 25 days, because this conditioning method also resulted in high production of esters, including butyl acetate and pentyl acetate, which have odor units >1. Hence, fruits conditioned at 0 °C for 25 days were predominant in fruity, pear aroma. However, each of the above assumptions is based on concentrations of volatile compounds calculated relative to the internal standard, and therefore more accurate quantification, along with aroma extract dilution analysis, and aroma reconstitution and omission experiments,[40] is needed to ascertain the precise contribution of each compound to pear aroma following each conditioning treatment.

Consumer studies have found that people like juicy and sweet pears with detectable pear flavor and aroma.[1,4,34] From the correlation table, the analytical variables (i.e., butyl acetate, pentyl acetate, hexyl acetate, propyl acetate, 3-methylbutyl acetate, 5-hexenyl acetate, heptyl acetate, 1-butanol, 1-hexanol, 1-hepatanol, 1-propanol, 1-octanol, total esters, total alcohols, total aroma, and WSP) all had similar positive correlations with sensory attributes including fruity aroma, pear aroma, apple aroma, fermented aroma, butteriness, juiciness, and sweetness; these compounds may therefore be indicators of ripeness associated with desired eating quality. The compounds having high correlation with fruity aroma ($r > 0.85$) and pear aroma ($r > 0.75$) were butyl acetate, pentyl acetate, and hexyl acetate. On the other hand, hexanal, (*E*)-2-hexenal, and pentanal were positively correlated with green stem aroma, an attribute that is generally undesirable in ripe pears.[1]

Water-soluble polyuronide content was the variable that best correlated with texture attributes generally associated with ripe fruit, such as butteriness ($r = 0.95$), juiciness ($r = 0.94$), and sweetness ($r = 0.95$), and was negatively correlated with firmness ($r = -0.93$) and crunchiness ($r = -0.92$). Our results are consistent with previous studies which showed that WSP levels increased as fruit softened[6] and that the fruits with higher WSP were more buttery and juicier than those with lower WSP.[6] Although there were significant differences in WSP among the firmness stages, the conditioning treatments did not affect WSP levels. This is interesting given the significant differences in perception of firmness, crunchiness, juiciness, and fibrousness that were detected among the conditioning treatments.

The present study found that SSC was not a good instrumental parameter for predicting sensory sweetness, confirming prior studies.[19,34,35] However, TA was a good parameter for predicting sensory sweetness and tartness, and SSC/TA was good for predicting sensory tartness. These results agree with previous studies.[19,36]

In conclusion, different conditioning treatments resulted in different sensory attributes of 'Comice' pears. The 10 °C for 10 day and 0 °C for 25 day treatments resulted in ripe fruit described as having fruity and pear aroma attributes that were associated with high ester content, especially butyl, pentyl, and hexyl acetate. These esters were much higher in fruit conditioned at 10 °C than at 0 °C. Fruity and pear aroma attributes were much lower in fruit conditioned at 0 °C for 15 days. Although treatment at 0 °C resulted in fruit with higher concentrations of alcohols, the odor units for these alcohols were low, and therefore their contribution to aroma perception is uncertain. Ester levels were also elevated in fruit conditioned at 0 °C for 25 days compared with other treatments, although not as high as in fruit conditioned at 10 °C. Ethylene treatments produced fruit described predominantly as fibrous in texture and having sweet, green aroma notes. The concentrations of hexanal and (*E*)-2-hexenal were high in fruit conditioned with ethylene for 1 day. When the same type of conditioning treatments were compared, fruit conditioned at 0 °C for 25 days had higher sweetness and juiciness scores than fruit conditioned at 0 °C for 15 days, and fruits conditioned with ethylene for 3 days were juicier than fruits conditioned with ethylene for 1 day. It is essential to determine whether the differences in sensory attributes observed among these conditioning treatments will influence consumer liking before the industry can determine the best conditioning treatment to use to maximize consumer satisfaction. This remains for a future study.

AUTHOR INFORMATION

Corresponding Author

*(E.J.M.) Phone: (530) 752-7512. Fax: (530) 752-6746. E-mail: ejmitcham@ucdavis.edu.

Present Address

¶(W.M.): Horticulture Research Institute, Department of Agriculture, Bangkok, Thailand.

Funding

This work was supported in part by a USDA Specialty Crops Grant (2009-51181-05783). Also, financial support from the Loyal Thai Government Scholarship is appreciated.

Notes

The authors declare no competing financial interest.

ACKNOWLEDGMENTS

We thank all of the members of the Mitcham laboratory group for their assistance.

ABBREVIATIONS USED

PLS, partial least-squares; SSC, soluble solids content; TA, titratable acidity; WSP, water-soluble polyuronides

REFERENCES

(1) Jaeger, S. R.; Lund, C. M.; Lau, K.; Harker, F. R. In search of the "ideal" pear (*Pyrus* spp.): results of a multidisciplinary exploration. *J. Food Sci.* **2003**, *68*, 1108−1117.

(2) Sugar, D.; Basile, S. Ethylene treatment promotes early ripening capacity in mature 'Comice' pears. *HortTechnology* **2006**, *16*, 89−91.

(3) Sugar, D.; Micham, E.; Kupferman, E. Re-thinking the chill requirement for pear ripening. Washington State University: Tree Fruit Research and Extension Center, postharvest information network, http://postharvest.tfrec.wsu.edu/REP2009B.pdf, 2009.

(4) Turner, J.; Bai, J.; Marin, A.; Colonna, A.; Theron, K. Consumer sensory evaluation of pear cultivars in the Pacific Northwest, USA. *Acta Hortic.* **2005**, *671*, 355−360.

(5) Eccher Zerbini, P. The quality of pear fruit. *Acta Hortic.* **2002**, *596*, 805−810.

(6) Murayama, H.; Takahashi, T.; Honda, R.; Fukushima, T. Cell wall changes in pear fruit softening on and off the tree. *Postharvest Biol. Technol.* **1998**, *14*, 143−149.

(7) Wang, C. Y.; Sams, C. E.; Gross, K. C. Ethylene, ACC, soluble polyuronide, and cell wall noncellulosic neutral sugar content in 'Eldorado' pears during cold storage and ripening. *J. Am. Soc. Hortic. Sci.* **1985**, *110*, 687−691.

(8) Spinardi, A.; Giovenzana, V.; Mignani, I. The effect of chilling and 1-MCP on quality attributes and physicochemical aspects of cell wall components of Passe-Crassane pears. *Adv. Plant Ethylene Res.* **2007**, *4*, 249−251.
(9) Jennings, W.; Sevenants, M. Volatile esters of Bartlett pear. III. *J. Food Sci.* **1964**, *29*, 158−163.
(10) Heinz, D. E.; Jennings, W. G. Volatile components of Bartlett pear. V. *J. Food Sci.* **1966**, *31*, 69−80.
(11) Rizzolo, A.; Cocucci, M.; Tagliabue, S.; Polesello, S. Gas chromatographic characterization of a pear aroma with parallel sniffing/FID, sniffing/PID and MS detection. In *Ninteenth International Symposium on Capillary Chromatography and Electrophoresis*, Annali I.V.T.P.A.: Wintergreen, VA, USA, 1998; Vol. 93.
(12) Suwanagul, A.; Richardson, D. Identification of headspace volatile compounds from different pear (*Pyrus communis* L.) varieties. *Acta Hortic.* **1998**, *475*, 605−624.
(13) Wrolstad, R. E.; Lombard, P. B.; Richardson, D. G. Chapter 5. The pear. In *Quality and Preservation of Fruits*; Eskin, N. A. M., Ed.;CRC Press: Boca Raton, FL, USA, 1991; pp 67−96.
(14) Dandekar, A. M.; Teo, G.; Defilippi, B. G.; Uratsu, S. L.; Passey, A. J.; Kader, A. A.; Stow, J. R.; Colgan, R. J.; James, D. J. Effect of down-regulation of ethylene biosynthesis on fruit flavor complex in apple fruit. *Transgenic Res.* **2004**, *13*, 373−384.
(15) Defilippi, B. G.; Dandekar, A. M.; Kader, A. A. Impact of suppression of ethylene action or biosynthesis on flavor metabolites in apple (*Malus domestica* Borkh) fruits. *J. Agric. Food Chem.* **2004**, *52*, 5694−5701.
(16) Kappel, F.; Hogue, E.; Fisher-Fleming, B. Sensory evaluation of pears. *Acta Hortic.* **1993**, *367*, 439−439.
(17) Chauvin, M. A.; Ross, C. F.; Pitts, M.; Kupferman, E.; Swanson, B. Relationship between instrumental and sensory determination of apple and pear texture. *J. Food Qual.* **2010**, *33*, 181−198.
(18) Karlsen, A. M.; Aaby, K.; Sivertsen, H.; Baardseth, P.; Ellekjaer, M. R. Instrumental and sensory analysis of fresh Norwegian and imported apples. *Food Qual. Pref.* **1999**, *10*, 305−314.
(19) Harker, F. R.; Marsh, K. B.; Young, H.; Murray, S. H.; Gunson, F. A.; Walker, S. B. Sensory interpretation of instrumental measurements. 2. Sweet and acid taste of apple fruit. *Postharvest Biol. Technol.* **2002**, *24*, 241−250.
(20) Ahmed, A. E. L. R.; Labavitch, J. M. A simplified method for accurate determination of cell wall uronide content. *J. Food Biochem.* **1978**, *1*, 361−365.
(21) Mitcham, E. J.; Mitchell, F. G. Conditioning and ripening of Bartlett pears. In *Pear Production and Handling Manual*,; Mitcham, E. J., Elkins, R. B., Eds.; University of California Agriculture and Natural Resources: Oakland, CA, USA, 2007; Vol. 3483, pp 179−181.
(22) Sfakiotakis, E.; Dilley, D. Induction of ethylene production in Bosc pears by postharvest cold stress. *HortScience* **1974**, *9*, 336−338.
(23) Shiota, H. Changes in the volatile composition of La France pear during maturation. *J. Sci. Food Agric.* **1990**, *52*, 421−429.
(24) Barry, C. S.; Giovannoni, J. J. Ethylene and fruit ripening. *J. Plant Growth Regul.* **2007**, *26*, 143−159.
(25) Defilippi, B. G.; Dandekar, A. M.; Kader, A. A. Relationship of ethylene biosynthesis to volatile production, related enzymes, and precursor availability in apple peel and flesh tissues. *J. Agric. Food Chem.* **2005**, *53*, 3133−3141.
(26) Flores, F.; Yahyaoui, E. F.; Billerbeck, G.; Romojaro, F.; Latche, A.; Bouzayen, M.; Pech, J. C.; Ambid, C. Role of ethylene in the biosynthetic pathway of aliphatic ester aroma volatiles in Charentais cantaloupe melons. *J. Exp. Bot.* **2002**, *53*, 201−206.
(27) Schaffer, R. J.; Friel, E. N.; Souleyre, E. J. F.; Bolitho, K.; Thodey, K.; Ledger, S.; Bowen, J. H.; Ma, J. H.; Nain, B.; Cohen, D.; Gleave, A. P.; Crowhurst, R. N.; Janssen, B. J.; Yao, J. L.; Newcomb, R. D. A genomics approach reveals that aroma production in apple is controlled by ethylene predominantly at the final step in each biosynthetic pathway. *Plant Physiol.* **2007**, *144*, 1899−1912.
(28) Mihara, S.; Tateba, H.; Nishimura, O.; Machii, Y.; Kishino, K. Volatile components of Chinese quince (*Pseudocydonia sinensis* Schneid). *J. Agric. Food Chem.* **1987**, *35*, 532−537.
(29) Tienpont, B.; David, F.; Bicchi, C.; Sandra, P. High capacity headspace sorptive extraction. *J. Microcolumn Sep.* **2000**, *12*, 577−584.
(30) Pfanncoch, E.; Whitecavage, J. Stir bar sorptive extraction capacity and competition effects, Gerstel Global, 2002.
(31) David, F.; Tienpont, B.; Sandra, P. Stir-bar sorptive extraction of trace organic compounds from aqueous matrices. *LC−GC Eur.* **2003** July 2−7.
(32) Lara, I.; Miro, R. M.; Fuentes, T.; Sayez, G.; Graell, J.; Lopez, M. L. Biosynthesis of volatile aroma compounds in pear fruit stored under long-term controlled-atmosphere conditions. *Postharvest Biol. Technol.* **2003**, *29*, 29−39.
(33) Savant, L.; McDaniel, M. R. Suppression of sourness: a comparative study involving mixtures of organic acids and sugars. *Perception Psychophys.* **2004**, *66*, 642−650.
(34) Kupferman, E.; Sater, C.; Walter, M.; Buchanan, N. *Conditioning Anjou Pears: Summary of Research Conducted by the WSU Tree Fruit Postharvest Laboratory*; Washington State University, http://postharvest.tfrec.wsu.edu, 2010.
(35) Predieri, S.; Gatti, E. Effects of cold storage and shelf-life on sensory quality and consumer acceptance of 'Abate Fetel' pears. *Postharvest Biol. Technol.* **2009**, *51*, 342−348.
(36) Echeverria, G.; Lara, I.; Fuentes, T.; Lopez, M. L.; Graell, J.; Puy, J. Assessment of relationships between sensory and instrumental quality of controlled atmosphere stored 'Fuji' apples by multivariate analysis. *J. Food Sci.* **2004**, *69*, S368−S375.
(37) Rapparini, F.; Predieri, S. Volatile constituents of 'Harrow' sweet pears by dinamic headspace technique. *Acta Hortic.* **2002**, *596*, 811−816.
(38) Riu-Aumatell, M.; Lopez-Tamames, E.; Buxaderas, S. Assessment of the volatile composition of juices of apricot, peach, and pear according to two pectolytic treatments. *J. Agric. Food Chem.* **2005**, *53*, 7837−7843.
(39) Takeoka, G. R.; Buttery, R. G.; Flath, R. A. Volatile constituents of Asian pear (*Pyrus serotina*). *J. Agric. Food Chem.* **1992**, *40*, 1925−1929.
(40) Engel, E.; Baty, C.; LeCorre, D.; Souchon, I.; Martin, N. Flavor-active compounds potentially implicated in cooked cauliflower acceptance. *J. Agric. Food Chem.* **2002**, *50*, 6459−6467.
(41) Heydanek, M. G.; McGorrin, R. J. Gas chromatography-mass spectroscopy investigations on the flavor chemistry of oat groats. *J. Agric. Food Chem.* **1981**, *29*, 950−954.
(42) Beaulieu, J. C.; Grimm, C. C. Identification of volatile compounds in cantaloupe at various developmental stages using solid phase microextraction. *J. Agric. Food Chem.* **2001**, *49*, 1345−1352.
(43) Hadaruga, N. G.; Hadaruga, D. I.; Paunescu, V.; Tatu, C.; Ordodi, V. L.; Bandur, G.; Lupea, A. X. Thermal stability of the linoleic acid/α- and β-cyclodextrin complexes. *Food Chem.* **2006**, *99*, 500−508.
(44) Zoghbi, M. G. B.; Andrade, E. H. A.; Maia, J. G. S. Volatile constituents from leaves and flowers of *Alpinia speciosa* K. Schum. and *A. purpurata* (Viell.) Schum. *Flavour Fragrance J.* **1999**, *14*, 411−414.
(45) Hognadottir, A.; Rouseff, R. L. Identification of aroma active compounds in orange essence oil using gas chromatography−olfactometry and gas chromatography−mass spectrometry. *J. Chromatogr., A* **2003**, *998*, 201−211.
(46) Adams, R. P. *Identification of Essential Oil Components by Gas Chromatography/Mass Spectrometry*; Allured Publishing: Carol Stream, IL, USA, 1995.
(47) Pino, J. A.; Mesa, J.; Munoz, Y.; Marti, M. P.; Marbot, R. Volatile components from mango (*Mangifera indica* L.) cultivars. *J. Agric. Food Chem.* **2005**, *53*, 2213−2223.
(48) Habu, T.; Flath, R. A.; Mon, T. R.; Morton, J. F. Volatile components of Rooibos tea (*Aspalathus linearis*). *J. Agric. Food Chem.* **1985**, *33*, 249−254.
(49) Beaulieu, J. C. Within-season volatile and quality differences in stored fresh-cut cantaloupe cultivars. *J. Agric. Food Chem.* **2005**, *53*, 8679−8687.
(50) Shang, C.; Hu, Y.; Deng, C.; Hu, K. Rapid determination of volatile constituents of *Michelia alba* flowers by gas chromatography-mass spectrometry with solid-phase microextraction. *J. Chromatogr., A* **2002**, *942*, 283−288.
(51) Ansorena, D.; Astiasarán, I.; Bello, J. Influence of the simultaneous addition of the protease flavourzyme and the lipase novozyme 677BG

on dry fermented sausage compounds extracted by SDE and analyzed by GC-MS. *J. Agric. Food Chem.* **2000**, *48*, 2395−2400.
(52) Jordán, M. J.; Goodner, K. L.; Shaw, P. E. Characterization of the aromatic profile in aqueous essence and fruit juice of yellow passion fruit (*Passiflora edulis* Sims F. Flavicarpa degner) by GC-MS and GC/O. *J. Agric. Food Chem.* **2002**, *50*, 1523−1528.
(53) Takeoka, G.; Buttery, R. G.; Ling, L. Odour thresholds of various branched and straight chain acetates. *Lebensm.−Wiss. -Technol.* **1996**, *29*, 677−680.
(54) Flath, R. A.; Black, D. R.; Guadagni, D. G.; McFadden, W. H.; Schultz, T. H. Identification and organoleptic evaluation of compounds in Delicious apple essence. *J. Agric. Food Chem.* **1967**, *15*, 29−35.
(55) Buttery, R. G.; Seifert, R. M.; Ling, L. C.; Soderstrom, E. L.; Ogawa, J. M.; Turnbaugh, J. G. Additional aroma components of honeydew melon. *J. Agric. Food Chem.* **1982**, *30*, 1208−1211.
(56) Belitz, H. D.; Grosch, W.; Schieberle, P. Aroma compounds. In *Food Chemistry*; Springer: Berlin, Germany, 2009; pp 340−402.
(57) Etievant, P. Wine. In *Volatile Compounds in Food and Beverages*; Maarse, H., Ed.; TNO-CIVO Food Analysis Institute: Zeist, The Netherlands, 1991; pp 486−546.
(58) Devos, M.; Patte, F.; Rouault, J.; Laffort, P.; Van Gemert, L. J. *Standardized Human Olfactory Thresholds*; IRL Press: Oxford, UK, 1990; p 165.
(59) Takeoka, G.; Flath, R. A.; Mon, T. R.; Teranishi, R.; Guentert, M. J. Volatile constituents of apricot (*Prunus armeniaca*). *J. Agric. Food Chem.* **1990**, *38*, 471−477.
(60) Buttery, R. G.; Turnbaugh, J. G.; Ling, L. C. Contribution of volatiles to rice aroma. *J. Agric. Food Chem.* **1988**, *36*, 1006−1009.
(61) Buttery, R. G.; Teranishi, R.; Ling, L. C.; Turnbaugh, J. G. Quantitative and sensory studies on tomato paste volatiles. *J. Agric. Food Chem.* **1990**, *38*, 336−340.
(62) Guadagni, D. G.; Buttery, R. G.; Okano, S. Odour thresholds of some organic compounds associated with food flavours. *J. Sci. Food Agric* **1963**, *14*, 761−765.
(63) Fazzalari, F. A. Compilation of odor and taste threshold values data. *ASTM Data Ser.* **1978**, *DS 48A*.
(64) Salo, B. P. Variability of odour thresholds for some compounds in alcoholic beverages. *J. Sci. Food Agric.* **1970**, *21*, 597−600.
(65) Buttery, R. G.; Teranishi, R.; Ling, L. C. Fresh tomato aroma volatiles: a quantitative study. *J. Agric. Food Chem.* **1987**, *35*, 540−544.
(66) Rychlik, M.; Schieberle, P.; Grosch, W. *Compilation of Odor Thresholds, Odor Qualities and Retention Indices of Key Food Odorants*; Deutsche Forschungsanstat fur Lebensmittelchemie and Instit fur Lebensmittelchemie der Technischen Universitat Munchen: Garching, Germany, 1998.
(67) Ahmed, E. M.; Dennison, R. A.; Dougherty, R. H.; Shaw, P. E. Flavor and odor thresholds in water of selected orange juice components. *J. Agric. Food Chem.* **1978**, *26*, 187−191.
(68) Grosch, W.; Zeiler-Hilgart, G.; Cerny, C.; Guth, H. Studies on the formation of odorants contributing to meat flavours. In *Progress in Flavour Precursor Studies*; Schreier, P., Winterhalter, P., Eds.; Allured: Carol Stream, IL, USA, 1993; pp 329−342.
(69) Larsen, M.; Poll, L. Odour thresholds of some important aroma compounds in strawberries. *Z. Lebensm. Forsch.* **1992**, *195*, 120−123.
(70) Tandon, K. S.; Baldwin, E. A.; Shewfelt, R. L. Aroma perception of individual volatile compounds in fresh tomatoes (*Lycopersicon esculentum*, Mill.) as affected by the medium of evaluation. *Postharvest Biol. Technol.* **2000**, *20*, 261−268.
(71) Rapparini, F.; Gatti, E.; Predieri, S.; Cavicchi, L. Effect of pear production system on volatile aroma constituents of fruits. *Acta Hortic.* **2008**, *800*, 1061−1068.
(72) Chen, J. L.; Yan, S.; Feng, Z.; Xiao, L.; Hu, X. S. Changes in the volatile compounds and chemical and physical properties of Yali pear (*Pyrus bertschneideri* Reld) during storage. *Food Chem.* **2006**, *97*, 248−255.
(73) Good Scents Co. Retrieved from http://www.thegoodscentscompany.com (Aug 2011).
(74) El-Sayed, A. M. The Pherobase: Database of Insect Pheromones and Semiochemicals, http://www.pherobase.com.

v/v). For aromatic reconstitutions, the various esters were added individually or blended together at the average concentrations found in red wines (Table 1),[32,33] to double-distilled ethanol and microfiltered water, to obtain an ethanol level of 12% (v/v) (pH adjusted to 3.5 with tartaric acid).[34]

Table 1. Composition of the Fruity Aromatic Reconstitutions Presented in the Olfactory Tests

compound	C (μg/L)
ethyl propanoate	150
ethyl butanoate	200
ethyl hexanoate	200
ethyl octanoate	200
ethyl 2-methylpropanoate	250
ethyl (2*R*)-2-hydroxy-4-methylpentanoate and ethyl (2*S*)-2-hydroxy-4-methylpentanoate (95:5, m/m)	400
ethyl 3-hydroxybutanoate	300
butyl acetate	10
hexyl acetate	2
methylpropyl acetate	50
methylbutyl acetate	250

GC-O Analysis of Reference Compounds. GC-O analyses were carried out to ensure that the high-purity reference compounds did not contain any odoriferous impurities and to ascertain that the compound considered was responsible for the odor properties identified. Olfactometry analyses were carried out using an HP-6890 gas chromatograph (Hewlett-Packard, Wilmington, DE, USA), equipped with a flame ionization detector (FID) and a sniffing port (ODO-I SGE, Ringwood, Australia), connected by a flow-splitter to the column exit. GC effluent was combined with humidified N_2 (Air Liquide, France) at the bottom of the glass-sniffing nose (SGE, Victoria, Australia) to avoid nasal dehydration. Samples containing <0.2 μL of each pure odorant were injected in splitless−split mode (injector temperature, 240 °C; splitless time, 30 s; split flow, 50 mL/min). The column was a BP20 (50 m × 0.22 mm i.d., film thickness = 0.25 μm, SGE, Ringwood, Australia). The oven was programmed at 40 °C for the first minute, and the temperature increased at a rate of 10 °C/min to a final isotherm at 220 °C for 10 min. The carrier gas was hydrogen 5.5 (Air Liquide, France) with a column head pressure of 15 psi.

1 Quantitation and Separation. Sample preparation was as optimized by Antalick et al.[33] The fiber (Supelco, Bellefonte, PA, USA) was coated with a 100 μm stationary phase polydimethylsiloxane film (PDMS-100). For the quantitative study, 20 μL of ethyl-d_5 butanoate, at about 200 mg/L in absolute ethanol, was added as an internal standard to 25 mL of the wine samples. A 10 mL sample of the mixture was placed in a 20 mL headspace vial, 3.5 g of sodium chloride was added, and the vial was tightly sealed with a PTFE-lined cap. The solution was homogenized in a vortex shaker and then loaded onto a Gerstel (Mülheim an der Ruhr, Germany) autosampling device. The program consisted of swirling the vial at 500 rpm at 40 °C for 2 min, then inserting the fiber into the headspace at 40 °C for 30 min as the solution was swirled again, and, finally, transferring the fiber to the injector for desorption at 250 °C for 15 min.

Gas chromatography analyses were carried out on an HP 6890N GC system coupled to an HP 5973 inert quadrupole mass spectrometer, equipped with a Gerstel MPS2 autosampler. Injections were in splitless mode, using a 2 mm i.d. nondeactivated direct linear (injector temperature, 200 °C; purge flow, 17.4 mL/min; interface temperature, 200 °C) and a Chiraldex B-DM column (40 m × 0.25 mm i.d., film thickness = 0.12 μm, Astec, Whippany, NJ, USA). Oven temperature was programmed at 30 °C for the first minute, raised to 60 °C at 2 °C/min, and, finally, increased at 4 °C/min to a final isotherm at 200 °C, maintained for 10 min. The carrier gas was helium Alphagaz 2 (Air Liquide, France) with a column head pressure of 15 psi. The mass spectrometer was operated in electron impact mode at 70 eV with selected ion monitoring (SIM), using seven characteristic ions: *m/z* 102 as quantifier and *m/z* 57, 85, 87, 74, 115, and 130 as qualifiers. **1a** and **1b** were characterized by comparing their linear retention indices and mass spectra with those of standards.

Calibration curves were evaluated in dilute alcohol solution (12%, v/v), using a representative range of average ester concentrations found in wines (linear range = 0.2−400 μg/L). The calibration curves were plotted as the relative peak areas (analyte versus the internal standard) as a function of the compound concentration. The functions are linear over the concentration range, presenting correlation coefficients of 0.9932 and 0.9955 for **1a** and **1b**, respectively. Repeatability was evaluated by relative standard deviation of 10 independent assays performed under the same analytical conditions over a short period of time. The relative standard deviation of the area ratios was <10% for both enantiomers, 7.6 and 6.8% for **1a** and **1b**, respectively. Detection and quantitation limits represent the average of 10 determinations at the lowest measurable peak area plus 3 and 10 times the standard deviation of this result, respectively. The limit of detection and limit of quantitation of both enantiomers were 0.2 and 0.6, respectively.

Recovery was also evaluated by adding **1a** and **1b** to a red wine with a low level of both enantiomers. Six different concentrations of **1a** and **1b** were spiked in the wine prior to extraction with dichloromethane (1, 5, 10, 50, 100, and 300 μg/L). The recovery was from 94 to 104% for both enantiomers.

Sensory Analyses. *General Conditions.* Sensory analyses were performed as described by Martin and de Revel.[35] Samples were evaluated at controlled room temperature (20 °C), in individual booths, using covered, black, ISO glasses (ISO 3591:1977),[36] containing about 50 mL of liquid, coded with three-digit random numbers. Sessions lasted approximately 5 min. Very recently Lytra et al.[34] evaluated the evolution of these 12 esters in dilute alcohol solution to assess the stability of the samples submitted to the panel. This evaluation demonstrated that the esters remained stable for the first 10 min. Consequently, the solutions presented to the panel were prepared every 10 min.

Sensory Panel. Panel 1 consisted of 22 judges, 10 males and 12 females, aged 28.4 ± 6.3 (mean ± SD) years. Panel 2 consisted of 8 judges, 2 males and 6 females, aged 27.3 ± 5.2 (mean ± SD) years. Panel 3 consisted of 18 judges, 8 males and 10 females, aged 29.3 ± 4.7 (mean ± SD) years. All panelists were research laboratory staff at ISVV, Bordeaux University, selected for their experience in assessing fruity aromas in red wines. They attended three sessions per week, for 4 weeks, each lasting 5 min. Fresh berry-fruit standards were presented (blueberry, blackberry, black currant, strawberry, cherry, and raspberry). Commercial jams, made from the same fruits, were presented directly as jammy fruit standards.

Discriminative Testing Methods. Olfactory thresholds were determined by panel 1 in dilute alcohol solution, using a three-alternative, forced-choice presentation (3-AFC) (NF ISO 13301:2002).[37] Each session consisted of 10 forced-choice tests. Each test contained one positive sample supplemented with increasing concentrations of the compound to be evaluated (Table 2). The olfactory thresholds of **1b** and the racemic mixture **1a** and **1b** (50:50, m/m) were measured.

The "olfactory thresholds" of specific mixtures were also established by panel 1. "Olfactory thresholds" of total aromatic reconstitution (TAR) excluding **1** were thus measured in two different matrices: dilute alcohol solution and dilute alcohol solution containing 50 μg/L **1b** (Table 2).

The results of all 3-AFC tests were statistically analyzed. The olfactory threshold was defined as the concentration at which the probability of detection was 50%. This statistical value was determined using an adaptation of the ASTM-E1432 method.[38] The concentration/response function is a psychometric function and fits a sigmoid curve ($y = 1/(1 + e^{(-\lambda x)})$). Detection probability was corrected using the chance factor ($P = (3p - 1)/2$, where p = proportion of correct responses for each concentration and P = proportion corrected by the chance effect, 1/3 for 3-AFC). Sigma Plot 8 (SYSTAT) software was used for graphic resolution and ANOVA transform for nonlinear regression.[39]

Table 2. Composition of Samples Subjected to Olfactory Threshold Determination in Different Matrices

compound tested	test concn (μg/L)	matrix
ethyl (2*R*)-2-methylbutanoate and ethyl (2*S*)-2-methylbutanoate (50/50, m/m)	0.5/1/2/4/8/16/32/64/128/256	dilute alcohol solution
ethyl (2*S*)-2-methylbutanoate	0.5/1/2/4/8/16/32/64/128/256	dilute alcohol solution
aromatic reconstitution	**aromatic reconstitution diluted in 50 mL of matrix (mL)**	**matrix**
fruity aromatic reconstitution excluding ethyl 2-methylbutanoate	0.1/0.2/0.4/0.8/1.6/3.1/6.3/12.5/25/50	dilute alcohol solution, dilute alcohol solution + 50 μg/L ethyl (2*S*)-2-methylbutanoate

A triangular test[40] was also performed, using two samples of aromatic reconstitutions in dilute alcohol solution. The first consisted of the fruity pool, consisting of all the esters excluding **1**, and the second contained the same fruity aromatic reconstitution supplemented with 50 μg/L **1b**. Three numbered samples were presented in random order, two identical and the third one different. Each judge had to identify the sample perceived as different in each test and give an answer, even if s/he was not sure. The results of this triangular test were statistically interpreted, according to the tables given in the literature,[35] on the basis of the binomial law corresponding to the distribution of answers in this type of test.

Descriptive Testing Methods. Descriptive analyses of the racemic mixture of **1** and the *S*-form alone were carried out by panel 2, using in both cases a concentration of 60 μg/L in dilute alcohol solution. Judges were asked to propose a maximum of three descriptors.

Panel 3 evaluated the sensory profiles of aromatic reconstitutions for overall aromatic intensity, red-berry-, black-berry-, fresh-, and jammy-fruit aroma intensity. Each sample was presented twice in each session. Two samples of aromatic reconstitutions in dilute alcohol solution were presented. The first consisted of the fruity pool, including all of the esters except **1**, and the second contained the same fruity aromatic reconstitution supplemented with 50 μg/L **1b**. For each sample, the subject rated the intensity of these descriptors on a 100 mm scale printed on paper, labeled "no odor perceived" on the left and "very intense" on the right.

Statistical data were analyzed using R analysis of variance (ANOVA) software: the homogeneity of variance was tested using Levene's test, and the normality of residuals was tested using the Shapiro–Wilk test. All descriptors were mean-centered per panelist and scaled to unit variance. The statistically significant level was 5% ($p < 0.05$).

RESULTS AND DISCUSSION

1 Enantiomer Distribution and Concentrations. The optical isomers of **1** were separated by chiral GC analysis on a β-cyclodextrin phase.

As previously observed, in the oldest wines, **1** levels were generally higher than those found in the youngest ones. The maximum concentration was 157 μg/L (Haut Médoc, 1988), and the minimum concentration was 3 μg/L (Pessac-Léognan, 2010), with an average concentration of about 50 μg/L. In light of these finding, it seems likely that only a few micrograms per liter of **1** was formed during alcoholic fermentation. Wine aging is marked by a gradual increase in **1** concentrations over time, stabilizing after about 5 years. These results corroborate those of Diaz-Maroto et al.,[41] who observed a tendency to **1** formation during wine aging. Other studies also reported that concentrations were higher in old red wines than in young red or white wines,[42] suggesting that it could be formed by esterification of the corresponding acid.

With regard to the enantiomeric distribution of **1**, the *S*-enantiomer was found almost exclusively in all wines studied. Generally, young red wines (2010) contained only the *S*-form, whereas very small amounts of the *R*-form were detected in aged red wines. The *R*-enantiomer is formed during storage, starting in the first year. Table 3 shows the enantiomeric distribution in the red wines studied. The highest **1a** levels were found in the oldest samples, with a maximum concentration of 1.3 μg/L (Médoc, 1985). The maximum enantiomeric ratio was 100% for the *S*-form (all 2010 vintage red wines). However, two wines (Pessac-Leognan) from young vintages contained particularly high **1a** ratios (2009 and 2008: 2.6 and 2.2%, respectively), but concentrations did not exceed 0.3 μg/L in either sample.

These findings are in agreement with data of previous studies on Dornfelder red wine, where analysis of **1**demonstrated that it occurred as its *S*-enantiomer in red wine, also identified as a key odorant.[29]

These results highlighted the importance of the *S*-enantiomeric form, in view of its relative abundance in red wines. According to Diaz-Maroto et al.,[41] ethyl esters of branched-chain fatty acids, such as **1b**, may be formed during alcoholic fermentation by *Saccharomyces cerevisiae* from the corresponding amino acid, L-isoleucine (2*S*,3*S*) in this case, through their transformation into α-oxo acids, which are decarboxylated to produce aldehydes, which are, in turn, oxidized to form the corresponding acids.

Our findings concerning the enantiomeric distribution of **1** are in agreement with previous investigations into its enantiomeric distribution in several fruits, which revealed that **1** occurred exclusively in the *S*-configuration.[6,10] More recent research found that the *S*-configuration represented at least 98% of **1**, with minute amounts of the *R*-form.[14,27,28]

Preliminary Verifications. GC-O analysis found parasite odors in some commercial odorant stimuli. These were eliminated, and new commercial products were purchased. Finally, all compounds used in this work were olfactively pure, as confirmed by the three judges who performed this analysis. Moreover, FID analysis confirmed the products' very high purity.

Olfactory Impact of 1 on Quantitative Odor Perception. The olfactory threshold of the racemic mixture of **1a** and

Table 3. Concentrations of Ethyl 2-Methylbutanoate Enantiomers

vintage	no. of wines analyzed	av concn **1**[a] (μg/L)	av concn **1a**[a] (μg/L)	av concn **1b**[a] (μg/L)	av ratio of **1a**:**1b**
1980–1990	6	103 ± 31.5	0.9 ± 0.3	102.1 ± 31.6	0.9:99.1 ± 0.4
1991–2000	10	95 ± 28.1	0.7 ± 0.2	94.3 ± 28.1	0.8:99.2 ± 0.3
2001–2009	14	38.3 ± 23.8	0.7 ± 0.1	38 ± 27.3	1.1:98.9 ± 0.6
2010	7	6.9 ± 3.2	0 ± 0	6.9 ± 3.2	0 ± 0

[a] ± standard deviation over average concentration.

dx.doi.org/10.1021/jf500670z | J. Agric. Food Chem. 2014, 62, 5005–5010

1b in dilute alcohol solution, determined by panel 1, was 2.60 μg/L, almost twice that of the *S*-form, which was 1.53 μg/L (confidence interval < 0.01) (Figure 1). These results match

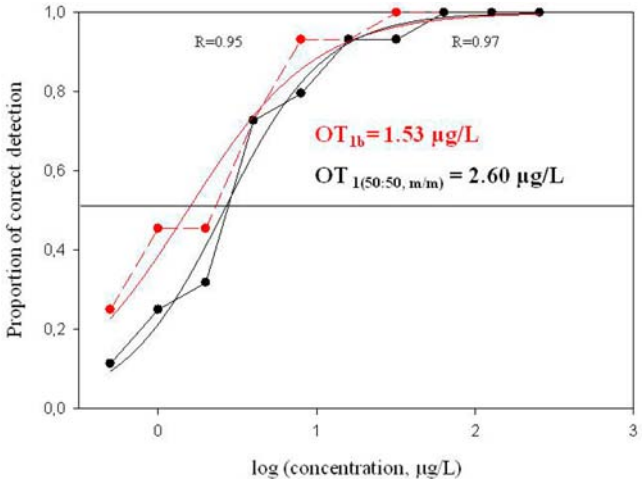

Figure 1. Detection probability of **1b** and the **1** racemic mixture (50:50, m/m) in dilute alcohol solution. OT, olfactory threshold. The curves are drawn according to a sigmoid function. **1**, ethyl 2-methylbutanoate; **1b**, ethyl (2*S*)-2-methylbutanoate.

those presented by Guth et al.,[27] who established the olfactory threshold of the racemic mixture in dilute alcohol solution (10%, v/v) at 1 μg/L. However, Ferreira et al.[43] referred to an olfactory threshold almost 7 times higher than our finding: 18 μg/L for **1** in synthetic wine model solution (11% v/v ethanol, 7 g/L glycerin, 5 g/L tartaric acid, pH adjusted to 3.4 with 1 M NaOH). In addition, both enantiomers have previously been studied in water: Amano et al.[44] mentioned an olfactory threshold of 10 μg/L for both enantiomers, whereas Takeoka et al.[6] referred to an olfactory threshold of 0.006 μg/L for the *S*-enantiomer, and, more recently, Buettner and Schieberle[14] determined the retronasal olfactory threshold of the *S*-enantiomer in water at 0.004 μg/L. The difference between our results and those found in the literature may be due to the fact that the olfactory threshold is extremely variable according to the matrix, experimental conditions (retronasal or orthonasal olfactory threshold, olfactory threshold determination method, etc.), and panel.[38,39,45]

As shown in Figure 2, the "olfactory threshold" of the fruity pool (excluding **1**), calculated by panel 1 in two different matrices, was 2.39 mL in dilute alcohol solution and 0.86 mL (diluted in 50 mL of each matrix) in dilute alcohol solution supplemented with 50 μg/L **1b** (confidence interval < 0.001).

These results, obtained using the average of the **1b** concentrations found in the red wines studied, detected by 98% of the panelists in dilute alcohol solution, confirmed the complexity of the matrix containing **1b**. Whereas a decrease in intensity is the most frequent effect of odor mixtures,[46] these data demonstrated that, despite the complexity of the matrix due to the suprathreshold concentration of **1b**, this compound enhanced the perception of fruity aromas. This effect may be explained by the fact that the fruity pool contained esters that were chemically and structurally similar to **1**.[47]

Organoleptic Impact of 1 on Qualitative Odor Perception. At concentrations perceived by the whole panel (60 μg/L), **1b** was mainly defined by fruity descriptors, such as green apple (Granny Smith) and strawberry, whereas a racemic

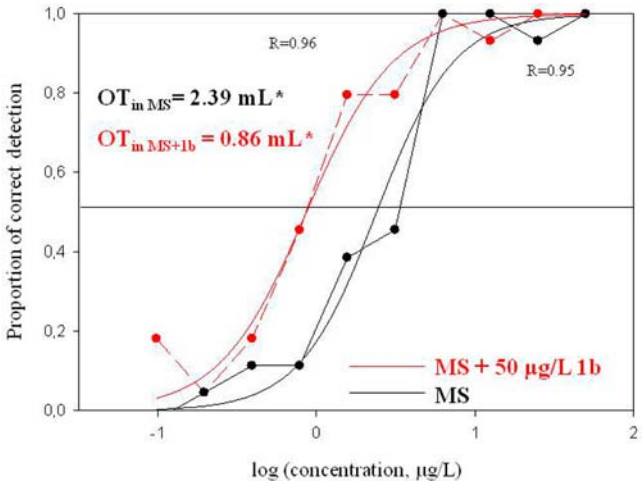

Figure 2. Effect of ethyl 2-methylbutanoate addition on the probability of detecting a fruity aromatic reconstitution. * Expressed in milliliters of fruity aromatic reconstitution diluted in 50 mL of matrix; **1**, ethyl 2-methylbutanoate; **1b**, ethyl (2*S*)-2-methylbutanoate; MS, model wine solution (dilute alcohol solution); OT, "olfactory threshold". The curves are drawn according to a sigmoid function.

mixture of **1a** and **1b** at the same concentration in dilute alcohol solution, also perceived by the whole panel (60 μg/L), was defined by an unspecific, irritating, fruity, solvent odor. Descriptors such us green apple for **1b** and an unspecific note for **1a** were previously mentioned in the literature by Amano et al.[44]

Before sensory analysis evaluation, the triangular test revealed that adding 50 μg/L **1b**, the average concentration found in red wines, to the fruity aromatic reconstitution, excluding **1**, was significantly perceived, confirming its impact in that fruity matrix. Later evaluations on a 100 mm scale of intensity revealed significant differences in black-berry-fruit intensity between the fruity aromatic reconstitution without **1** and that supplemented with 50 μg/L **1b** (Figure 3), whereas the average scores for red-berry-, fresh-, and jammy-fruit aroma descriptors were not modified by the addition of this ester. These results confirmed the sensory impact of 50 μg/L **1b**, suggesting that it contributed actively to the black-berry-fruit

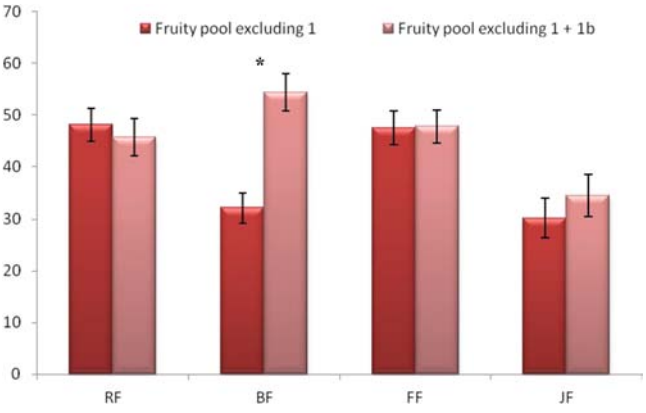

Figure 3. Mean intensities of aromatic descriptors of fruity aromatic reconstitutions prepared in dilute alcohol solution. *, $p < 0.05$; **1**, ethyl 2-methylbutanoate; **1b**, ethyl (2*S*)-2-methylbutanoate; RF, red-berry fruit; BF, black-berry fruit; FF, fresh fruit; JF, jammy fruit. Error bars indicate standard error deviation.

dx.doi.org/10.1021/jf500670z | J. Agric. Food Chem. 2014, 62, 5005−5010

nuances in the fruity matrix studied. The impact of **1** on qualitative odor perception was also demonstrated for complex mixtures of fruits, by Buettner and Schieberle[14] and Schieberle and Hofmann,[15] using omission tests, which revealed additive effects for the fruity aroma note. The qualitative contribution of **1b** was successfully demonstrated by Amano et al.,[44] who found that the *S*-enantiomer was an aroma-improving compound in food and drink, enhancing green and fresh notes.

Pineau et al.[32] demonstrated by addition tests that **1**, at a concentration of 40 μg/L, well below to its individual olfactory threshold in the wine matrices studied, contributed to black-berry-fruit aromas. The behavior of **1b** is similar to that of ethyl 2-hydroxy-4-methylpentanoate, as well as ethyl-3-hydroxybutanoate, ethyl propanoate, butyl acetate, and 2-methylpropyl acetate, compounds with similar chemical structures, recently described by Lytra et al.[34,48]

These experiments clarified current knowledge of this compound, particularly the relative abundance of its enantiomers. Taken together, these data revealed the importance of **1b**, due to its preponderance in all wines studied combined with its low olfactory threshold compared to that of the racemic mixture of **1a** and **1b**. In addition, the *S*-enantiomer, which was found almost exclusively in all wines studied, had a more pleasant, clearly fruity aroma than the racemic mixture of **1a** and **1b**, highlighting the real olfactory impact of this ester on the expression of fruity aroma.

Furthermore, the omission of **1b** from a complex matrix, such as an aromatic reconstitution of fruity esters, was clearly perceived. These findings also highlighted the indirect contribution of **1b** to red wine fruity esters aroma, showing that this ester enhanced perception of fruity character, particularly naturally enhancing black-berry-fruit aromas.

AUTHOR INFORMATION

Corresponding Author

*(J.-C.B.) Phone: +33 5 57 57 58 63. Fax: +33 5 57 57 58 13. E-mail: jean-christophe.barbe@agro-bordeaux.fr.

Funding

We thank the Bordeaux Wine Council (Conseil Interprofessionnel des Vins de Bordeaux, CIVB) for their financial support.

Notes

The authors declare no competing financial interest.

ACKNOWLEDGMENTS

We thank Château Luchey-Halde and Château Brane-Cantenac for providing wine samples.

REFERENCES

(1) Flath, R. A.; Black, D. R.; Guadagni, D. G.; McFadden, W. H.; Schultz, T. H. Identification and organoleptic evaluation of compounds in Delicious apple essence. *J. Agric. Food Chem.* **1967**, *15*, 29−35.

(2) Paillard, N. M. M. The flavour of apples, pears and quinces. In *Food FlaVours Part 3C. The FlaVour of Fruits*; Morton, I. D., Macleod, A. J., Eds.; Elsevier: Amsterdam, The Netherlands, 1990; pp 1−41.

(3) Fuhrmann, E.; Grosch, W. Character impact odorants of the apple cultivars Elstar and Cox orange. *Nahrung* **2002**, *46*, 187−193.

(4) Komthong, P.; Hayakawa, S.; Katoh, T.; Igura, N.; Shimoda, M. Determination of potent odorants in apple by headspace gas dilution analysis. *LWT* **2006**, *39*, 472−478.

(5) Elss, S.; Preston, C.; Hertzig, C.; Heckel, F.; Richling, E.; Schreier, P. Aroma profiles of pineapple fruit (*Ananas comosus* (L.) Merr.) and pineapple products. *Food Sci. Technol.* **2005**, *38*, 263−274.

(6) Takeoka, G. R.; Buttery, R. G.; Flath, R. A. Volatile constituents of Asian pear (*Pyrus serotina*). *J. Agric. Food Chem.* **1992**, *40*, 1925−1929.

(7) Lugemwa, F. N.; Lwande, W.; Bentley, M. D.; Mendel, M. J.; Randall-Alford, A. Volatiles of wild blueberry, *Vaccinium angustifolium*: possible attractants for the blueberry maggot fly, *Rhagoletis mendax*. *J. Agric. Food Chem.* **1989**, *37*, 232−233.

(8) Weenen, H.; Koolhaas, W. E.; Apriyantono, A. Sulfur-containing volatiles of durian fruits (*Durio zibethinus* Murr.). *J. Agric. Food Chem.* **1996**, *44*, 3291−3293.

(9) Franco, M. R. B.; Shibamoto, T. Volatile composition of some Brazilian fruits: umbu-caja (*Spondias citherea*), camu-camu (*Myrciaria dubia*), aracüa-boi (*Eugenia stipitata*), and cupuacüu (*Theobroma grandiflorium*). *J. Agric. Food Chem.* **2000**, *48*, 1263−1265.

(10) Reiners, J.; Grosch, W. Odorants of virgin olive oils with different flavor profiles. *J. Agric. Food Chem.* **1998**, *46*, 2754−2763.

(11) Baek, H. H.; Cadwallader, K. R.; Marroquin, E.; Silva, J. L. Identification of predominant aroma compounds in Muscatine grape juice. *J. Food Sci.* **1997**, *62*, 249−252.

(12) Buettner, A.; Schieberle, P. Characterization of the most odor active volatiles in fresh, hand-squeezed juice of grapefruit (*Citrus paradisi* MacFayden). *J. Agric. Food Chem.* **1999**, *47*, 5189−5193.

(13) Hinterholzer, A.; Schieberle, P. Identification of the most odor-active volatiles in fresh, hand-extracted juice of Valencia late oranges by odor dilution techniques. *Flavour Fragrance J.* **1998**, *13*, 49−55.

(14) Buettner, A.; Schieberle, P. Evaluation of aroma differences between hand-squeezed juices from Valencia late and Navel oranges by quantitation of key odorants and flavor reconstitution experiments. *J. Agric. Food Chem.* **2001**, *49*, 2387−2394.

(15) Schieberle, P.; Hofmann, T. Evaluation of the character impact odorants in fresh strawberry juice by quantitative measurements and sensory studies on model mixtures. *J. Agric. Food Chem.* **1997**, *45*, 227−232.

(16) Lasekan, O.; Buettner, A.; Christlbauer, C. Investigation of important odorants of palm wine (*Elaeis guineensis*). *Food Chem.* **2007**, *105*, 15−23.

(17) Fan, W.; Qian, M. C. Headspace solid-phase microextraction (HS-SPME) and gas chromatography-olfactometry dilution analysis of young and aged Chinese "Yanghe Daqu" liquors. *J. Agric. Food Chem.* **2005**, *53*, 7931−7938.

(18) Simpson, R. F.; Miller, G. C. Aroma composition of aged Riesling wine. *Vitis* **1983**, *22*, 51−63.

(19) Chrisholm, M. G.; Guiher, L. A.; Vonah, T. M.; Beaumont, J. L. Comparison of some French-American hybrid wines with White Riesling using gas chromatography-olfactometry. *Am. J. Enol. Vitic.* **1994**, *45*, 201−212.

(20) Schlich, P.; Moio, L. Correlation between flavour profiles and aromagrams of Chardonnay Burgundy wines. *Sci. Aliments.* **1994**, *14*, 609−615.

(21) Guth, H. Quantitation and sensory studies of character impact odorants of different white wine varieties. *J. Agric. Food Chem.* **1997**, *45*, 3027−3032.

(22) Ferreira, V.; Lopez, R.; Escudero, A.; Cacho, J. The aroma of grenache red wine: hierarchy and nature of its main odorants. *J. Sci. Food Agric.* **1998**, *77*, 259−267.

(23) Kotseridis, Y.; Baumes, R. Identification of impact odorants in Bordeaux red grape juice, in the commercial yeast used for its fermentation and in the produced wines. *J. Agric. Food Chem.* **2000**, *48*, 400−406.

(24) Marti, M. P.; Mestres, M.; Sala, C.; Busto, O.; Guasch, J. Solid phase microextraction and gas chromatography olfactometry analysis of successively diluted samples. A new approach of the aroma extract dilution analysis applied to the characterization of wine aroma. *J. Agric. Food Chem.* **2003**, *51*, 7861−7865.

(25) Gürbüz, O.; Rouseff, J. M.; Rouseff, R. L. Comparison of aroma volatiles in commercial Merlot and Cabernet Sauvignon wines using

gas chromatography-olfactomery and gas chromatography-mass spectrometry. *J. Agric. Food Chem.* **2006**, *54*, 3990−3996.
(26) Genovese, A.; Gambuti, A.; Piombino, P.; Moio, L. Sensory properties and aroma compounds of sweet Fiano wine. *Food Chem.* **2007**, *103*, 1228−1236.
(27) Mosandl, A. Authenticity assessment: a permanent challenge in food flavor and essential oil analysis. *J. Chromatogr. Sci.* **2004**, *42*, 440−449.
(28) Matich, A.; Rowan, D. Pathway analysis of branched-chain ester biosynthesis in apples using deuterium labeling and enantioselective gas chromatography-mass spectrometry. *J. Agric. Food Chem.* **2007**, *55*, 2727−2735.
(29) Frank, S.; Wollmann, N.; Schieberle, P.; Hofmann, T. Reconstitution of the flavor signature of Dornfelder red wine on the basis of the natural concentrations of its key aroma and taste compounds. *J. Agric. Food Chem.* **2011**, *59*, 8866−8874.
(30) Brenna, E.; Fuganti, C.; Serra, S. Enantioselective perception of chiral odorants. *Tetrahedron: Asymmetry* **2003**, *14*, 1−42.
(31) Lytra, G.; Tempere, S.; de Revel, G.; Barbe, J.-C. Distribution and organoleptic impact of ethyl 2-hydroxy-4-methylpentanoate enantiomers in wine. *J. Agric. Food Chem.* **2012**, *60*, 1503−1509.
(32) Pineau, B.; Barbe, J.-C.; Van Leeuwen, C.; Dubourdieu, D. Examples of perceptive interactions involved in specific "red- and black-berry" aromas in red wines. *J. Agric. Food Chem.* **2009**, *57*, 3702−3708.
(33) Antalick, G.; Perello, M. C.; de Revel, G. Development, validation and application of a specific method for the quantitative determination of wine esters by headspace-solid-phase micro-extraction−gas chromatography−mass spectrometry. *Food Chem.* **2010**, *121*, 236−1245.
(34) Lytra, G.; Tempere, S.; Le Floch, A.; de Revel, G.; Barbe, J.-C. Study of sensory interactions among red wine fruity esters in a model solution. *J. Agric. Food Chem.* **2013**, *61*, 8504−8513.
(35) Martin, N.; de Revel, G. Sensory evaluation: scientific bases and oenological applications. *J. Int. Sci. Vigne Vin* **1999**, No. Special Issue, 81−93.
(36) Sensory analysis − Apparatus − Wine-tasting glass. ISO 3591. In *Analyse Sensorielle*; AFNOR: Paris, France, 1977.
(37) Sensory analysis − Methodology − General guidance for measuring odour, flavour and test detection thresholds by a three-alternative forced-choice (3-AFC) procedure. ISO 13301. In *Analyse Sensorielle*; AFNOR: Paris, France, 2002.
(38) Cometto-Muñiz, J. E.; Abraham, M. H. Human olfactory detection of homologous *n*-alcohols measured via concentration − response functions. *Pharmacol., Biochem. Behav.* **2008**, *89*, 279−291.
(39) Tempere, S.; Cuzange, E.; Malak, J.; Bougeant, J. C.; de Revel, G.; Sicard, G. The training level of experts influences their ability to detect some wine key compounds. *Chemosens. Percept.* **2011**, *4*, 99−115.
(40) Sensory analysis − Methodology − Triangle test. NF EN ISO 4120. In *Analyse Sensorielle*; AFNOR: Paris, France, 2007.
(41) Diaz-Maroto, M. C.; Schneider, R.; Baumes, R. Formation pathways of ethyl esters of branched short-chain fatty acids during wine aging. *J. Agric. Food Chem.* **2005**, *53*, 3503−3509.
(42) Lopez, R.; Aznar, M.; Cacho, J.; Ferreira, V. Determination of minor and trace volatile compounds in wine by solid-phase extraction and gas chromatography with mass spectrometric detection. *J. Chromatogr., A* **2002**, *966*, 167−177.
(43) Ferreira, V.; Lopez, R.; Cacho, J. F. Quantitative determination of the odorants of young red wines from different grape varieties. *J. Sci. Food Agric.* **2000**, *80*, 1659−1667.
(44) Amano, A.; Tokoro, K.; Uchiumi, K. Method for improving flavor of food or drink. Takasago International Corp., Tokyo, Japan; U.S. Patent 5496580, 1996.
(45) Tempere, S.; Cuzange, E.; Bougeant, J. C.; de Revel, G.; Sicard, G. Explicit sensory training improves the olfactory sensitivity of wine experts. *Chemosens. Percept.* **2012**, *5*, 205−213.
(46) Derby, C. D.; Ache, B. W.; Kennel, E. W. Mixture suppression in olfaction: electrophysiological evaluation of the contribution of peripheral and central neural components. *Chem. Senses* **1985**, *10*, 301−316.
(47) Cometto-Muñiz, J. E.; Cain, W. S.; Abraham, M. H. Odor detection of single chemicals and binary mixtures. *Behav. Brain Res.* **2005**, *156*, 115−123.
(48) Lytra, G.; Tempere, S.; de Revel, G.; Barbe, J.-C. Impact of perceptive interactions on red wine fruity aroma. *J. Agric. Food Chem.* **2012**, *60*, 12260−12269.

DCCD, to detect ceftiofur residues in animal tissues.[12−23] DCCD is one of the ceftiofur metabolites that contribute to the concentration of ceftiofur residues as measured by the HPLC-UV method. Because DFC (including naturally derivatized forms, measured as DCA and referred to as "total DFC" in the following context) is the official marker residue designated for regulatory testing, we hypothesized that DCCD may be used as a surrogate marker residue if a quantitative relationship between DCCD and total DFC can be established.

In the past two decades, liquid chromatography−tandem mass spectrometry (LC-MS/MS) has become a predominant tool in the analysis of small molecular weight drugs and metabolites in biological samples.[14,16,20,21,23−26] It offers superior specificity to the conventional HPLC. By using d_3-cysteine-DCCD, an internal standard (IS) synthesized in our laboratory, we developed[15] a simple and quantitative LC-MS/MS method for detecting DCCD in bovine kidney. The method was quantitative because the labeled IS corrects for the matrix effect. We observed, however, a small degree (up to 1.5%) of deuterium-to-hydrogen conversion when d_3-cysteine-DCCD was exposed to kidney tissue, which presumably was due to thiol−disulfide exchange with endogenous non-deuterated cysteine in the sample matrix. Therefore, d_3-cysteine-DCCD can be added only after the SPE cleanup, and matrix-based calibration must be used to achieve quantitative results. Recently, a new IS (d_3-methoxy-DCCD) has become commercially available (see Materials and Methods). When spiked into extracts, the concentration of this compound is expected to be unaffected by the unavoidable interchange with endogenous cysteine.

Besides the target kidney tissue, other edible tissues are sometimes analyzed as alternatives in regulatory testing, especially if tolerance levels have been established in those tissues. Therefore, in addition to kidney, we are also interested in investigating bovine liver and muscle.

In summary, the goals of the present study are to (1) further improve the method for detecting DCCD in bovine kidney using the new IS (d_3-methoxy-DCCD), (2) establish the correlation in kidney between the HPLC regulatory method and the improved LC-MS/MS method, and (3) develop a quantitative LC-MS/MS method for DCCD in bovine liver and muscle.

MATERIALS AND METHODS

Reagents and Supplies. Ultrapure water was generated using a Milli-Q water purification system from Millipore (Danvers, MA, USA) to give resistivity ≥18 MΩ·cm^{-1} and was used for all references to water. Methanol (MeOH) and acetonitrile (MeCN) were high-purity grade from Burdick & Jackson (Muskegon, MI, USA). Formic acid was Optima grade for LC-MS from Fisher Scientific (Pittsburgh, PA, USA). All other chemicals were ACS grade reagents from Fisher Scientific. Strata X SPE columns (33 μm, 60 mg, 3 mL) were purchased from Phenomenex (Torrance, CA, USA). Amber glass vials (12 × 32 mm) with preslit PTFE/silicone septa for a LC-MS/MS autosampler were purchased from Waters (Milford, MA, USA).

Reference Standards. Reference standard materials of DCCD (96% chemical purity) and d_3-methoxy-DCCD (98.9% isotopic purity and 96% chemical purity) were purchased from Toronto Research Chemicals (Toronto, Canada). Working solutions of DCCD at 0.1, 0.2, 0.4, 0.6, 1.0, 2.0, 4.0, and 8.0 μg/mL were prepared in water as described previously.[15] Stock solutions of IS were prepared in water at approximately 0.4 mg/mL and diluted to 3.0 μg/mL for use as working solution. All standard solutions were stored at −80 °C until analysis.

Ceftiofur hydrochloride reference materials of various potencies were supplied by Pfizer Animal Health (Kalamazoo, MI, USA) for the regulatory HPLC-UV analysis. Stock solutions at 100 μg/mL (ceftiofur free acid equivalent) were prepared in phosphate buffer (pH 7.0) and stored at < −10 °C for up to 6 months. Serial dilutions of the ceftiofur stock solution with buffer to 10.0 and 1.0 μg/mL were prepared on the day of the HPLC analysis.

Bovine Tissue Samples. This study was approved by the Institutional Animal Care and Use Committee (IACUC) of the Office of Research under FDA/CVM, in accordance with the *Guide for the Care and Use of Laboratory Animals* provided by the National Research Council. Experiment animals (Holstein steer) were housed in climate-controlled facilities accredited by the Association for Assessment and Accreditation of Laboratory Animal Care International (AAALAC). Control kidney, liver, and muscle samples were obtained from either a local grocery store (later screened negative for ceftiofur residues by the LC-MS/MS methods described herein) or in-house reared steers with tracked records certifying that they were never treated with ceftiofur.

Dosing was performed at the FDA/CVM animal facility. The animal study was divided into three phases. Phase 1 was the plasma depletion of the drug, phase 2 was the washout period, and phase 3 was the incursion of tissues. Animals were dosed in phases 1 and 3. The drug used in the study was Naxcel (ceftiofur sodium; PBS Animal Health, Massillon, OH, USA). The administration route was intramuscular injection. Dosage was 2.2 mg/kg body weight at 24 h intervals for 5 days in both phases 1 and 3.

During phase 1, eight healthy animals were dosed and plasma samples were taken before dosing and at various time points after the last dose. Because there are no previous data on DCCD depletion in bovine kidney, phase 1 was partially intended to provide some guidance for tissue harvesting time. The results for this part of the study will be published elsewhere. Following the completion of phase 1, these animals went through a 2 week minimum washout period (phase 2), and plasma samples were analyzed again to make sure the drug had been depleted completely before phase 3 started. Seven of the eight animals were dosed a second time in phase 3 to harvest incursion tissue and plasma samples. Samples were obtained at 24, 30, 36, 48, 60, 64, and 76 h, respectively, after the last dose to obtain different concentrations in kidney. We anticipated a wide range of concentrations from below the tolerance to several times the tolerance. After removal of the fat tissue and outer layer of membrane, the whole kidneys, ∼500 g of liver (approximately equal portions from four different lobes), 50 mL of plasma, ∼500 g of muscle at the injection site, and ∼500 g at other muscle sites located remotely from the injection site [diaphragm and hind limb muscles (semimembranosus and semitendinosus)] were collected in the necropsy room and transported to the laboratory with dry ice. Kidney (whole) and liver (mixture of four lobes: left, right, caudate, and quadrate) were cut into ∼$^1/_4$ in. sections that were ground into a semiliquid mixture with a blender. The homogenized kidney or liver samples were stored at −80 °C after grinding. Muscles were cut into ∼$^1/_8$ in. sections and ground into a powdery mixture using a 1:3 ratio with dry ice. The powder was first placed in a −20 °C freezer for 24−48 h to sublimate the carbon dioxide; then it was stored at −80 °C. Tissue samples obtained from a steer 12 h after the last dose, as described in our previous study,[15] were also included in the present analysis.

Analysis of DCCD. *Calibration Standards.* To prepare 1 mL of the individual solvent-based calibration standards, 100 μL of the IS working solution was transferred into eight amber autosampler vials. Then 100 μL of each of the DCCD working standard solutions was added to the autosampler vials followed by 800 μL of water and vortex-mixed.

Kidney Extraction. The kidney extraction procedure is modified on the basis of our previous paper.[15] Briefly, 100 μL of IS working solution was added to approximately 0.4 ± 0.008 g of test and control samples (thawed to room temperature first) in 10 mL Falcon round-bottom polypropylene (PP) tubes (Fisher Scientific). Then 3.5 mL of 1% phosphate buffer (pH 6.2) was added to all samples. The samples were homogenized for 30 s using an Omni Prep homogenizer with

disposable plastic probes (Omni International, Marietta, GA, USA), followed by centrifugation (Thermo IEC, Centra GP-8R) at 4140*g* (standard gravity) at room temperature for 20 min. The supernatant was subjected to SPE cleanup. The SPE cartridges were conditioned sequentially with 2 mL of MeOH and 2 × 2 mL of water. Raw extracts were loaded onto the SPE cartridges and eluted under gravity. Cartridges were washed with 2 mL of water before the analyte and IS were eluted with 2 mL of MeCN/water (50:50, v/v) into graduated 15 mL PP centrifuge tubes. The eluate was evaporated under N_2 at 40 °C to 1 mL or slightly less than 1 mL. If necessary, water was added to bring the volume to the 1 mL mark. The samples were centrifuged at 4140*g* at room temperature for 10 min, and the supernatant was transferred into prelabeled autosampler vials. For samples that remained turbid after centrifugation, the extracts were filtered directly into the autosampler vials through 13 mm, 0.2 μm, PVDF syringe filters using a 3 mL disposable syringe.

Liver and Muscle Extraction. After the samples were thawed to room temperature, approximately 0.2 ± 0.01 g of test and control samples was weighed into 10 mL Falcon round-bottom PP tubes. Samples were centrifuged for 2 min at 200*g* to bring tissue to the bottom of the tubes. The IS working solution (100 μL) was added to each sample followed by 3 mL of 1% phosphate buffer. The samples were homogenized for 30 s followed by the addition of 3.5 mL of MeCN. The mixture was vortexed on a multitube vortexer (VWR, Bridgeport, NJ, USA) for 2 min. Samples were centrifuged at 4140*g* at room temperature for 20 min. The supernatant was decanted into 15 mL PP centrifuge tubes. Three milliliters of hexane was added to each tube, and the tubes were vortexed for 2 min. The samples were centrifuged at 4140*g* for 5 min. The top hexane layer was removed using a disposable pipet. The MeCN was evaporated under N_2 at 40 °C to a volume of 1.5 mL or slightly less than 1.5 mL to ensure that MeCN had been sufficiently removed. To each sample was added water to the 3.5 mL mark. The tubes were centrifuged again at 4140*g* for 5 min at room temperature. The supernatant was subjected to SPE cleanup in the same manner as the kidney supernatant.

LC-MS/MS Conditions. The LC-MS/MS system consisted of a Waters Acquity ultraperformance liquid chromatography (UPLC) system coupled with a Micromass Quattro Micro mass spectrometer (Milford, MA, USA). MassLynx V4.1 software and TargetLynx V4.1 software (Waters) were used for data acquisition, processing, and reporting.

LC Parameters. The UPLC system consisted of a temperature-controlled sample manager, a binary solvent manager, and a heated column compartment. Sample vials were kept at 10 °C in the autosampler. Chromatographic separation was performed using a Phenomenex Kinetex C18 column (50 mm × 2.1 mm, 2.6 μm particle size, 100 Å pore size), coupled to a SecurityGuard Ultra C18 cartridge for 2.1 mm i.d. columns (both from Phenomenex, Torrance, CA, USA). The column compartment temperature was kept at 30 °C. The gradient mobile phases (A, 0.1% formic acid in water; B, 0.1% formic acid in MeCN) were as follows: 0−1 min, 0% B; 1−4 min, 30% B; 4−4.1 min, ramped to 95% B and held for 2 min; 6.1−6.2 min, back to 0% B and then held for 1.8 min (the total run time was 8 min). The flow rate was 0.3 mL/min. The mobile phases should be used within 1 week after preparation. The injection volume was 10 μL in the full-loop mode. The typical injection sequence follows: one to three water blanks; one midlevel standard for checking the system; calibration standards; negative controls; fortified quality control samples (QC); incurred samples; QC to bracket the incurred samples; and repeat injection of the midlevel standard.

Mass Spectrometry. The mass spectrometer was equipped with an electrospray ionization (ESI) source operated in positive ion mode. The source-dependent operating parameters have been reported previously. The $[M + H]^+$ ions at m/z 548.8 and 552.1 were identified as the precursors for collision-induced dissociation (CID) for DCCD and the IS, respectively. The multiple reaction monitoring (MRM) transitions were m/z 548.8 → 183.0 (for quantitation) and m/z 548.8 → 241.0 (for confirmation) for DCCD and m/z 552.1 → 244.1 for IS. The cone voltage was 33 and 32 V for DCCD and IS, respectively; the collision energy was 30 eV for m/z 548.8 → 183.0 and 20 eV for both m/z 548.8 → 241.0 and 552.1 → 244.1.

Internal Standard Calibration. The internal standard calibration curve with $1/x^2$ weighting was constructed using a linear regression model: $y = mx + b$, where y is the ratio of the DCCD peak area to the IS peak area and x is the concentration of the standard in ng/g.

HPLC-UV Analysis. We basically followed the method as described in the literature.[6] Briefly, 10 g of homogenized kidney tissue was incubated with a solution of DTE that cleaves ceftiofur and desfuroylceftiofur-related metabolites from proteins or other sulfur-containing compounds, yielding a common unstable DFC moiety. DFC was reacted with iodoacetamide to yield the stable DCA derivative. The derivative was first extracted onto a C-18 SPE column. Further purification was performed on a strong anion exchange (SAX) extraction column, followed by cleanup using a strong cation exchange (SCX) column. The derivatized residues were then analyzed via gradient HPLC using a C-18 column with UV detection. Because a reference standard of DCA was not available, a six-point standard curve equivalent to 0.075, 0.25, 0.5, 2.5, 7.5, and 12.5 μg/g of ceftiofur free acid in bovine kidney was prepared daily by fortifying a buffer solution with various ceftiofur stock solutions (the literature method used a six-point curve equivalent to 0.05, 0.25, 0.5, 1.0, 5.0, and 10.0 μg/g in tissue). Then, these solutions were processed by this method to obtain DCA calibration standards. Negative control and QC samples fortified with ceftiofur at 0.1, 1.0, and 10.0 μg/g were included for daily quality assurance. The procedure has a limit of quantitation (LOQ, the lowest fortified concentration at which accuracy and precision were found to be acceptable) of 0.1 μg/g. The average recovery of the fortified controls must be ≥80% to accept the batch.

RESULTS AND DISCUSSION

Kidney Analyses. *LC-MS/MS Method Validation.* Three major changes were made in the modified procedure compared to the previously reported regulatory procedure.[15] The changes streamline the method and improve its efficiency, thereby reducing the burden on testing laboratories. First, the new IS, d_3-methoxy-DCCD, was added in the beginning of the extraction. We found no deuterium-to-hydrogen exchange during the extraction procedure. Second, the calibration standards (equivalent to 25−2000 ng/g in 0.4 g of kidney sample) were prepared in solvent (water) instead of matrix extracts. This change reduced the number of samples in each run by eight. Third, the ion transition monitored for the IS changed to m/z 552.1 → 244.1 because of the different locations of deuterium.

Three minor changes were also implemented using the modified procedure: (1) the final volume of the extract was 1 mL instead of 2 mL to increase the intensity of the signal, (2) the final extract was centrifuged instead of filtered before LC-MS/MS analysis to simplify the procedure, and (3) the guard column was changed to a SecurityGuard Ultra C18 cartridge from an in-line filter to improve the lifespan of the analytical column. The modified procedure was revalidated by assessing interday accuracy and precision (n = 2 per day × 3 days for each fortification level); the results are shown in Table 1. Other validation parameters such as extraction efficiency, matrix effect,

Table 1. Revalidation of the Kidney Procedure: Fortified Samples

fortification level (ng/g)	N	found (ng/g)	SD	CV (%)	accuracy (%)
50	6	52.0	4.9	9.5	103.9
250	6	243.4	18.8	7.7	97.3
1000	6	1052.5	35.7	3.4	105.2

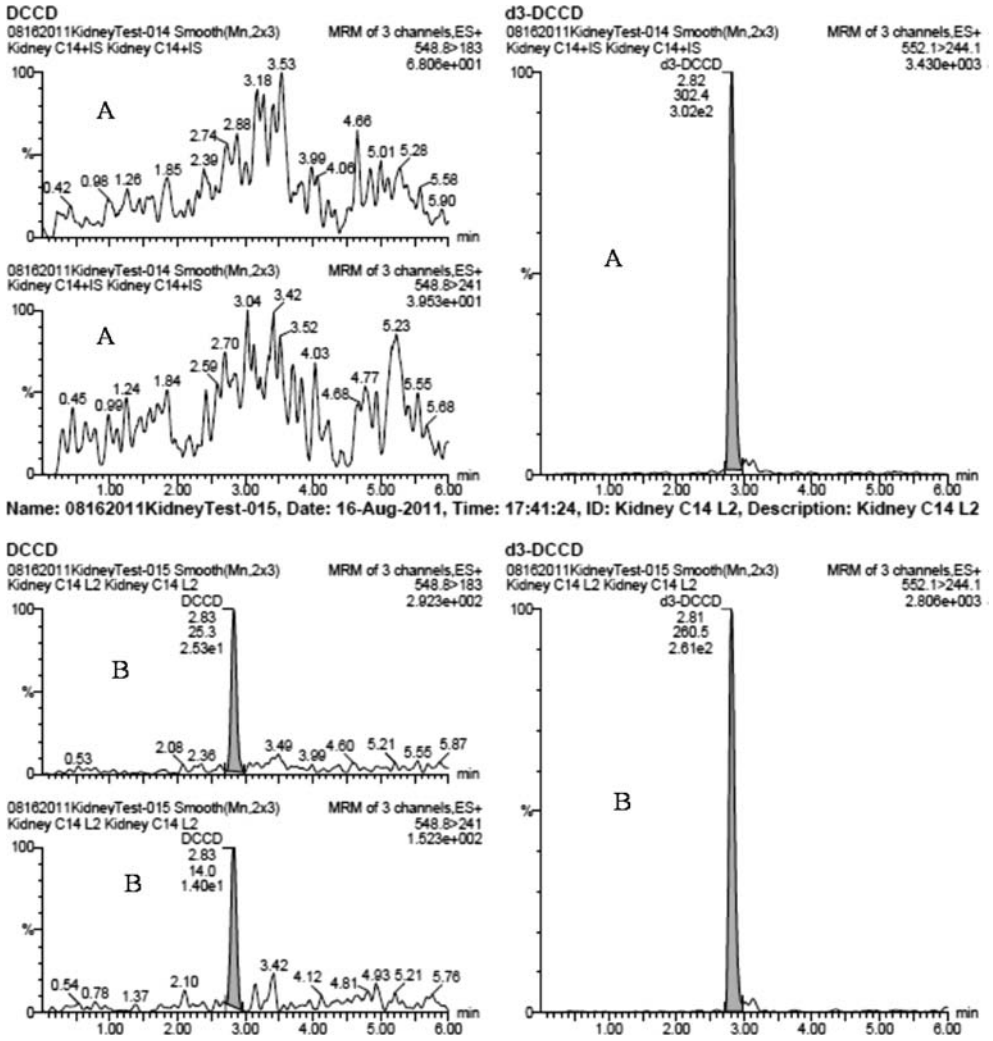

Figure 1. Typical LC-MS/MS chromatograms of DCCD and d_3-DCCD in bovine kidney tissue. First (left) and second (left) rows are quantitation and confirmation ions in a control sample (A), respectively; third (left) and fourth (left) are quantitation and confirmation ions in a control sample fortified with DCCD at 50 ng/g (B), respectively. The chromatograms on the right side are quantitation ions for d_3-DCCD in control (A) and fortified sample (B), respectively. DCCD, desfuroylceftiofur cysteine disulfide.

and matrix stability were reported previously and are not expected to change. Because a different IS was used in the modified procedure, we verified the stability of the final extract and found that changes in concentration were <15% when stored for 3 days at 10 °C or for 7 weeks at −20 °C.

The calibration curve was linear between 25 and 2000 ng/g. The interday accuracy ranged from 97 to 105%, and the interday precision ranged from 3.4 to 9.5%. The LOQ was 50 ng/g. In addition, we also reanalyzed the samples at two concentration levels that were analyzed previously.[15] The high-level kidney sample was obtained from a steer (steer A) 12 h after the last dose, and the low-level sample was obtained by diluting the high-level sample with a control kidney sample in a 1:3 ratio. The concentrations were 1338.9 ± 111.1 (N = 9) and 387.2 ± 25.0 (N = 9) by using the modified procedure compared to the original results of 1323.5 ± 143.6 (N = 9) and 406.3 ± 18.4 ng/g (N = 9). There was no statistically significant difference between the new and original results (two-tailed t test, $p > 0.05$). Figure 1 shows the typical LC-MS/MS chromatograms of DCCD in kidney samples.

Correlation between DCCD and Total DFC (DCA). The concentrations of the incurred kidney samples were measured in at least five replicates by both the LC-MS/MS and HPLC-UV methods, and the results are listed in Table 2. Steer A was reported previously; however, the kidney DCCD concentration listed in Table 2 was measured by the modified LC-MS/MS procedure as discussed above. Because the violative kidney tissues are sometimes reported to have very high ceftiofur

Table 2. Analytical Results by the Two Methods (N = 6 Other than Those Noted)

		DCA (ppm)			DCCD (ppm)		
steer	time (h)	mean	SD	CV%	mean	SD	CV%
A	12	2.55	0.114	4.5	1.34[a]	0.111	8.3
B	24	1.50	0.106	7.1	0.738	0.024	3.3
C	30	1.14[b]	0.071	6.3	0.405	0.021	5.1
D	36	0.785	0.036	4.5	0.329	0.010	3.1
E	48	0.438	0.015	3.4	0.143	0.011	7.8
F	60	0.527	0.056	10.7	0.147	0.006	4.3
G	64	0.430	0.008	1.9	0.119	0.007	6.2
H	76	0.391	0.051	13.1	0.0501	0.002	3.3

[a] N = 9. [b] N = 5 due to sample loss during the extraction.

residue levels,[27] analysis of a wide range of concentrations was deemed necessary to establish the relationship between the two methods and to show that the new method is useful in practice. The actual extractable total DFC (measured as DCA) concentration ranged from just below the tolerance (0.391 ppm) to ~6 times the tolerance level (2.55 ppm). DCCD concentrations ranged from 0.0501 to 1.34 ppm. The coefficient of variation (CV%) was 3.4−13.1% for total DFC and 3.1−8.3% for DCCD.

The linear relationship between DCCD and total DFC was evaluated using a measurement error model, which accounts for the fact that both variables are measured with error. The analytical software, Functional Relationship Estimation by Maximum Likelihood (FREML), was developed by the Analytical Methods Committee of the Royal Society of Chemistry.[28] Figure 2 shows the observed values and predicted

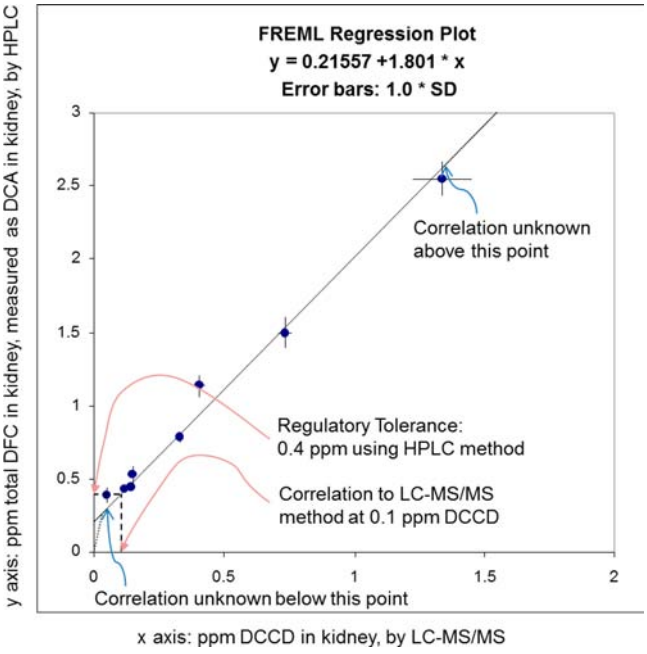

Figure 2. Correlation between the DCCD concentration by LC-MS/MS and the total DFC concentration measured as DCA by HPLC. DCCD, desfuroylceftiofur cysteine disulfide; DFC, desfuroylceftiofur; DCA, desfuroylceftiofur *S*-acetamide.

line with the DCCD concentrations on the *horizontal* axis and the total DFC concentrations on the *vertical* axis. The test for lack of fit is not significant ($p > 0.05$), and the model residuals did not display any pattern, an indication that the model is appropriate for describing the relationship between DCCD and total DFC. Figure 2 displays the linear relationship between DCCD and total DFC; for every unit increase in DCCD, there is a 1.8 unit increase in total DFC. On the basis of the relationship shown in Figure 2, when the kidney concentration of DCCD is 0.1 ppm, the predicted total DFC concentration would be around 0.4 ppm (tolerance level). Given adequate sample size at this level and establishment of a consistent correlation between the DCCD method and the official DFC method, a prediction interval for DCCD at the tolerance of 0.4 ppm can be estimated. Therefore, if a sample has a DCCD value below the lower prediction limit (or above the higher prediction limit), it can be confidently inferred that the corresponding total DFC level would be <0.4 ppm (or >0.4 ppm).

Figure 3 shows the relationship between the kidney concentration and sample harvesting time after the last dosing.

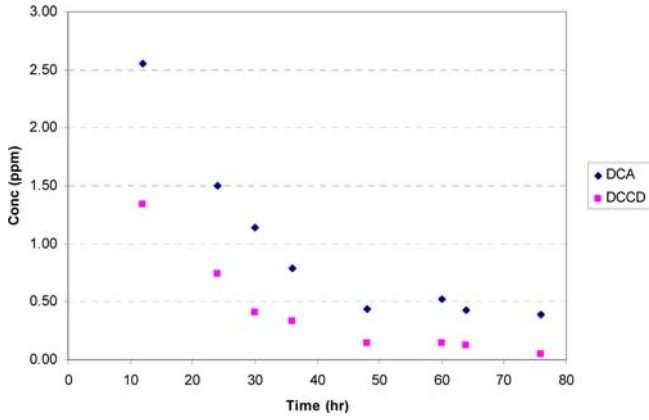

Figure 3. Kidney concentrations versus drug depletion time. DCCD, desfuroylceftiofur cysteine disulfide; DCA, desfuroylceftiofur *S*-acetamide.

From 12 to 48 h, the kidney concentrations were nearly inversely proportional to the harvesting time. By 48 h, the kidney total DFC concentration had already reached ~0.4 ppm. Therefore, we extended the harvesting time to achieve lower concentrations. Surprisingly, the next three animals harvested at 60, 64, and 76 h, respectively, showed a completely different depletion pattern for total DFC. The total DFC concentration first increased slightly at 60 h and then declined slowly. Even at 76 h, the total DFC concentration was still only slightly below 0.4 ppm. The DCCD depletion pattern paralleled total DFC except for the last time point, where it depleted more quickly (Figure 3). The total DFC depletion pattern observed in the present study is somewhat different from the data found in a residue depletion study reported in a Freedom of Information Act (FOIA) Summary[8] in support of a 4 day preslaughter withdrawal period for ceftiofur sodium. In this FOIA summary, cattle were dosed at the same dose level as in the present study, and total DFC was measured at 3, 24, 48, 72, 96, and 121 h after the last dose. Total DFC kidney concentrations showed a rapid decrease during the first 48 h and a nearly a 1-fold decrease every 24 h during the next 48 h. That study was specifically designed to investigate tissue depletion, and data were generated on the basis of multiple numbers of animals for each time point. Although our study was not designed as a tissue depletion study, similar depletion patterns between DCCD and total DFC support the use of DCCD as a surrogate for total DFC.

Berendsen et al.[12] summarized analytical methods for ceftiofur residues into three categories based on the targeted chemical entity: (1) ceftiofur, DFC (free form), or DCCD in biological matrices; (2) DCA derived from chemical conversion of all DFC derivatives, including protein-bound DFC; and (3) 2-amino-α-(methoxyamino)-4-thiazoleacetamide through ammonolysis. Although each of these approaches has its advantages and limitations, direct monitoring of the naturally occurring ceftiofur, DFC, or DCCD was considered inadequate for detecting ceftiofur's off-label use in poultry production. In poultry breast muscle, and possibly in bovine tissue as well, the combined yield of the three compounds listed above amounted

to only a small fraction of that acquired by either the DCA or the ammonolysis methods. Our result for DCCD in bovine kidney, however, shows that DCCD is present at a readily detectable concentration level compared to DCA (total DFC), and good correlation exists between the data generated by these two methods. For the regulatory application that this DCCD method was intended to address, the much simpler and higher throughput sample preparation procedure outweighs its weakness that not all DFC-related metabolites contribute to generating a single detection signal.

One of the advantages of a LC-MS/MS methodology is that the ion ratio can be used for structural confirmation along with the retention time and signal-to-noise ratio (S/N). For this study, we followed the confirmation criteria described in *FDA Guidance for Industry No. 118*[29] except we used a 2% acceptable range for retention time instead of 5% and an S/N ratio of 10 instead of 3. These changes made the confirmation process more stringent. The experimentally validated limit of confirmation (LOC) of the present LC-MS/MS procedure for DCCD in bovine kidney was 50 ng/g, the lowest fortified concentration at which all acceptance criteria were met. All incurred and fortified kidney samples passed confirmation. No false positives were observed. Therefore, the procedure described here for bovine kidney is valid for both determinative and confirmatory purposes.

Liver and Muscle Analyses. *Liver and Muscle Method Validation.* The procedure that worked well for kidney analysis was ineffective for liver and muscle. Liver showed more chemical interferences, and muscle formed a gel when homogenized in buffer. Therefore, we treated the initial buffer extract with acetonitrile and hexane to precipitate proteins and remove fats, respectively, as reported in previously published work.[16,20] After removal of the organic solvents by phase separation and evaporation, the aqueous extract was cleaned up by SPE. Because DCCD is very polar and hydrophilic, it is critical to remove all acetonitrile before the SPE to avoid loss of analyte due to weak retention of DCCD on the SPE sorbent. Extraction efficiency was measured by comparing the area ratio between prefortified and postfortified control samples. For liver, the overall extraction efficiencies of the sample preparation procedure were 81.7 ± 1.3% (N = 3), 74.4 ± 2.4% (N = 3), and 71.7 ± 8.3% (N = 3) at 100, 500, and 2000 ng/g, respectively. For muscle, the overall extraction efficiencies of the sample preparation procedure were 75.4 ± 5.8% (N = 3), 73.5 ± 7.3% (N = 3), and 71.8 ± 0.4% (N = 3) at 100, 500, and 2000 ng/g. The lower than 100% extraction efficiencies should not affect the quantitation because the labeled IS added in the beginning of the extraction was expected to track the analyte.

Despite extensive cleanup steps, significant matrix effects occurred for both liver and muscle extracts. The matrix effect was evaluated by the area ratio between the standards postfortified into the extracts of control samples and the standards in solvent (water) at 100, 500, and 2000 ng/g (N = 3 for each level). The average ratio was 1.23 for liver and 0.71 for muscle. This problem was again overcome by the use of the labeled IS, which provided satisfactory quantitation. Therefore, solvent-based calibration was used for quantitation. The curve was linear from 50 to 4000 ng/g. This range was chosen because of the much higher tolerances for cattle liver and muscle (2 and 1 ppm, respectively). The LOQ was 100 ng/g for both matrices. Tables 3 and 4 show the accuracy and precision in bovine liver and muscle. Figures 4 and 5 show the typical chromatograms in bovine liver and muscle matrices.

Table 3. Interday Accuracy and Precision in Bovine Liver

level (ng/g)	N	mean	SD	CV%	accuracy (%)
100	12	106.7	7.75	7.3	107
500	12	502.3	29.8	5.9	100
2000	12	2028.2	90.4	4.5	101

Table 4. Interday Accuracy and Precision in Bovine Muscle

level (ng/g)	N	mean	SD	CV%	accuracy (%)
100	12	97.3	10.7	11.0	97
500	12	499.1	28.9	5.8	100
2000	12	1984.9	98.3	5.0	99

Stability was also investigated during the method validation. The concentration of DCCD in bovine liver matrix decreased 16% after 12 months at −80 °C. An assessment of DCCD in incurred bovine muscle matrix was infeasible and unnecessary because concentrations are typically below the LOQ (see below). DCCD in the extract of bovine liver is stable for up to 48 h at 10 °C and for up to 19 days at −20 °C. DCCD in the extract of bovine muscle is stable for 72 h at 10 °C and for 35 days at −20 °C.

Liver and limb muscle samples were analyzed with validated methods except the limb muscle from steer G harvested at 64 h. Results are shown in Table 5. DCCD was found in all liver samples except the one collected at 76 h after the last dose. The liver DCCD concentrations peaked at 24 h at 573.2 ng/g, followed by a continuous decline in the next 24 h; increased at 60 h to 300.2 ng/g; and then decreased again rapidly. In contrast, the only muscle sample that contained a detectable but very low level of DCCD was the injection site muscle in steer A harvested at 12 h after the last dose.

In the aforementioned ceftiofur residue depletion study reported in the FOIA Summary,[8] ceftiofur marker residue (total DFC measured by the HPLC-UV method) in liver had a much lower concentration than the current tolerance level of 2 ppm set for bovine liver. The highest total DFC concentration in liver was 1.6 ppm at 3 h after the last dose. Total DFC concentration in liver showed a similar biphasic pattern to that of DCCD observed in our study, albeit the second peak was at 48 h, and the concentrations were below the LOQ (0.1 ppm) after 48 h. Total DFC at the injection site showed very high concentrations 3 h after the last dose, but the concentration fell below the 1 ppm tolerance level for bovine muscle quickly at approximately 24 h, although it remained detectable until 96 h. In muscle, total DFC was detectable 3 h after the last dose and diminished to below the LOQ within 24 h. In contrast to liver and muscle, the total DFC detection window in kidney was much wider (approximately 96 h), and the total DFC concentration was above the tolerance level of 0.4 ppm between 24 and 48 h. On the basis of these data and our own findings, we conclude that, although muscle is a common matrix for testing,[20,30−32] bovine muscle is unsuitable as the sole screening matrix for ceftiofur residues.

With regard to the confirmation of DCCD in liver samples, all fortified samples at 100, 500, and 2000 ng/g in acceptable batches were confirmed; 39 of a total of 45 replicates of incurred samples were confirmed. The six incurred samples that failed confirmation had concentrations between 100 and 150 ng/g. Therefore, the true LOC for the liver procedure is probably around 150 ng/g. We did not investigate this further, however, because we expect that the liver procedure will most

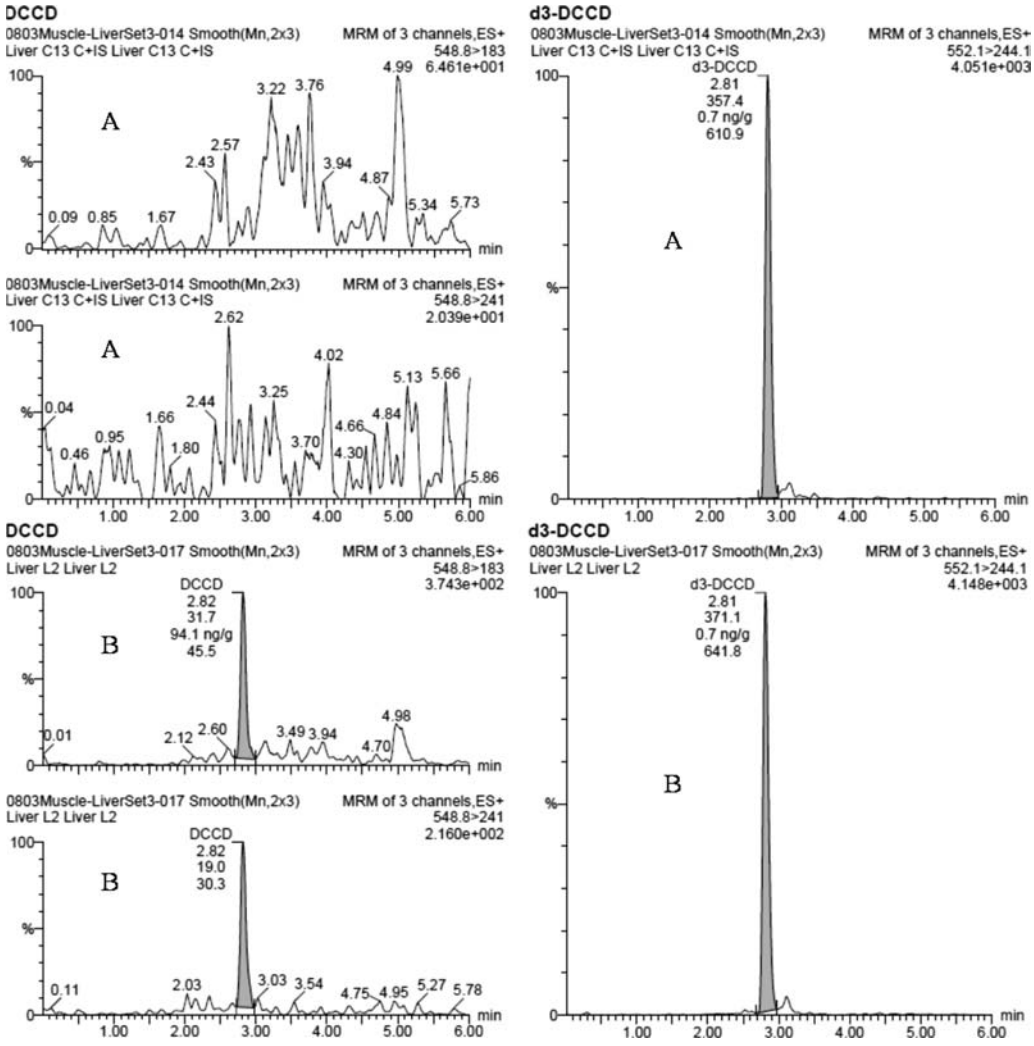

Figure 4. Typical LC-MS/MS chromatograms of DCCD and d_3-DCCD in bovine liver tissue. First (left) and second (left) rows are quantitation and confirmation ions in a control sample (A), respectively; third (left) and fourth (left) are quantitation and confirmation ions in a control sample fortified with DCCD at 100 ng/g (B), respectively. The chromatograms on the right side are quantitation ions for d_3-DCCD in control (A) and fortified sample (B), respectively. DCCD, desfuroylceftiofur cysteine disulfide.

likely be used for occasional ad hoc testing. Additionally, we did not investigate in detail confirmation of DCCD in bovine muscle because the procedure is unlikely to detect DCCD in bovine muscle samples.

Finally, because of the complex profile of ceftiofur's metabolites due to their chemically labile nature in the biological environment, proper selection of surrogate compounds in place of total DFC should match the specific animal species, the target tissue, and the intended regulatory purpose. In the work presented by Berendsen et al.,[12] DCCD was detectable (LOD 1 $\mu g/kg^{-1}$) in broiler breast muscle until at least 8 h postdosing, but at <24 h by extrapolation, with significant underestimation of total DFC. The ammonolysis approach was deemed more suitable for screening off-label use of cephalosporin antibiotics in poultry. Another ceftiofur in poultry study reported by Heinrich et al.,[33] however, reported that the parent compound, ceftiofur, could be detected for up to 28 days after a subcutaneous injection of Naxcel in the neck of a 1-day-old chicken (whole, including bones and feathers), but ceftiofur, DFC, and DCCD were undetectable in chicken muscle (20 days and older) or liver (16 days and older). Whether factors such as administration route and chicken age affect the relevance of a single metabolite's (or parent compound's) effectiveness as a surrogate marker or the applicability of particular analytical methods is unclear. Lastly, we noted a significant difference between the "DCFA method" (although no data were reported) and the "DCA method" used in the first example and the official method used in our work.

In conclusion, we report a simple and accurate LC-MS/MS method to detect and confirm DCCD in bovine kidney. DCCD may be used as a surrogate marker residue in regulatory testing on the basis of the quantitative relationship between DCCD and the official marker residue total DFC in bovine kidney. DCCD may also be used for ad hoc confirmatory analysis for bovine liver. Bovine muscle is not as suitable for screening or confirmation for ceftiofur residues if DCCD is the target analyte. As the two poultry studies mentioned above suggest, more work may be needed to substantiate the utility of DCCD for monitoring total DFC in targeted cattle tissues. Care must always be exercised when a correlation acquired under defined experimental conditions is extrapolated to other situations.

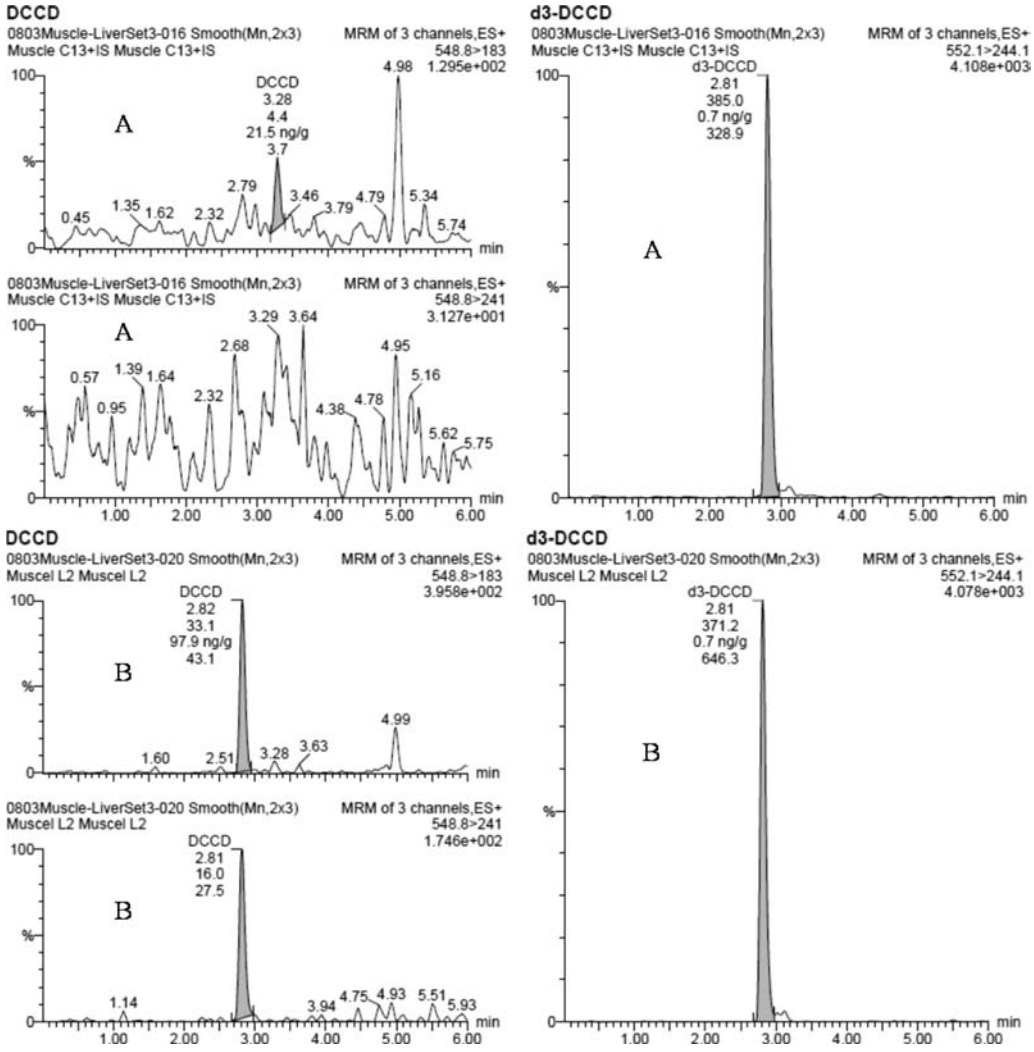

Figure 5. Typical LC-MS/MS chromatograms of DCCD and d3-DCCD in bovine muscle tissue. First (left) and second (left) rows are quantitation and confirmation ions in a control sample (A; peak at 3.28 min is incorrect assignment by software), respectively; third (left) and fourth (left) are quantitation and confirmation ions in a control sample fortified with DCCD at 100 ng/g (B), respectively. The chromatograms on the right side are quantitation ions for d_3-DCCD in control (A) and fortified sample (B), respectively. DCCD, desfuroylceftiofur cysteine disulfide.

Table 5. Levels (Mean ± SD) of DCCD in Bovine Tissues (N = 6 for All Quantifiable Values)

	animal							
	A	B	C	D	E	F	G	H
postdosing interval (h)	12	24	30	36	48	60	64	76
liver (ng/g)	513.7 ± 68.8	573.2 ± 61.7	294.8 ± 28.5	205.1 ± 37.2	110.7 ± 14.4	300.2 ± 17.4	120.2 ± 20.4	<LOQ
injection site muscle (ng/g)	<LOQ	ND[a]	ND	ND	ND	ND	ND	ND
muscle (ng/g)	ND	ND[b]	ND	ND	ND	ND	NA[c]	ND

[a]ND, not detected (level below LOQ). [b]Both diaphragm and hind limb muscles from this animal were analyzed. [c]NA, not analyzed.

AUTHOR INFORMATION

Corresponding Author

*(H.L.) E-mail: hui.li@fda.hhs.gov. Phone: (301) 210-4271. Fax: (301) 210-4689.

Present Addresses

[§](S.F.) Center for Tobacco Products, U.S. Food and Drug Administration, 9200 Corporate Blvd., Rockville, MD 20850, USA.

[⊥](V.L.) Center for Drug Evaluation and Research, U.S. Food and Drug Administration, 10903 New Hampshire Ave., Silver Spring, MD 20993, USA.

Notes

The information in this paper is not a formal dissemination of information by the U.S. Food and Drug Administration and does not represent the agency's position or policy.

The authors declare no competing financial interest.

ACKNOWLEDGMENTS

The authors thank Elizabeth Tall, Sharon Rasmussen, Scott Frobish, Mark McDonald, Steve Matthews, and Andrea Kuneski for technical assistance.

REFERENCES

(1) Office of the Federal Register National Archives and Records Administration. *Code of Federal Regulations, Title 21, Sections 522.313 and 526.313*, 2013.

(2) Office of the Federal Register National Archives and Records Administration. *Code of Federal Regulations, Title 21, Section 556.113*, 2013.

(3) U.S. Department of Agriculture, Food Safety and Inspection Service. *United States National Residue Program for Meat, Poultry, and Egg Product: 2010 Sample Results*, June 2012.

(4) Beconi-Barker, M. G.; Smith, E. B.; Olson, S. C.; Vidmar, T. J.; Martin, R. A.; Hornish, R. E. *An Overview of the Metabolism of Different Salts of Ceftiofur in Several Target Species*; American Chemical Society: Washington, DC, USA, 1997; p AGRO-033.

(5) Beconi-Barker, M. G.; Roof, R. D.; Vidmar, T. J.; Hornish, R. E.; Smith, E. B.; Gatchell, C. L.; Gilbertson, T. J. Ceftiofur sodium: absorption, distribution, metabolism, and excretion in target animals and its determination by high-performance liquid chromatography. In *Veterinary Drug Residues − Food Safety*; ACS Symposium Series 636; Moats, W. A., Medina, M. B., Eds.; American Chemical Society: Washington, DC, USA, 1996; pp 70−84.

(6) Beconi-Barker, M. G.; Roof, R. D.; Millerioux, L.; Kausche, F. M.; Vidmar, T. H.; Smith, E. B.; Callahan, J. K.; Hubbard, V. L.; Smith, G. A.; Gilbertson, T. J. Determination of ceftiofur and its desfuroylceftiofur-related metabolites in swine tissues by high-performance liquid chromatography. *J. Chromatogr. B: Biomed. Sci. Appl.* **1995**, *673*, 231−244.

(7) Hornish, R. E.; Hamlow, P. J.; Brown, S. A. Multilaboratory trial for determination of ceftiofur residues in bovine and swine kidney and muscle, and bovine milk. *J. AOAC Int.* **2003**, *86*, 30−38.

(8) U.S. Food and Drug Administration. *Freedom of Information Act Summary: Supplemental New Animal Drug Application for NADA 140−338 Naxcel Sterile Powder (Ceftiofur Sodium) to Establish a 4-Day Pre-Slaughter Withdrawal Period for Cattle* (date of approval: June 2, 2006).

(9) U.S. Department of Agriculture, Food Safety and Inspection Service. Determination for Ceftiofur-Related (DCA) Residues by HPLC. Effective Oct 1, 2012; http://www.fsis.usda.gov/wps/wcm/connect/b5d2670a-68d1-49df-af56-d75655c65e37/CLG-CEF1.pdf?MOD=AJPERES (accessed April 21, 2014).

(10) U.S. Food and Drug Administration. *Guidance for Industry No. 3: General Principles for Evaluating the Safety of Compounds Used in Food-Producing Animals*, July 25, 2006.

(11) U.S. Department of Agriculture, Food Safety and Inspection Service. *United States National Residue Program: 2010 Scheduled Sampling Plan*, January 2011.

(12) Berendsen, B. J.; Stolker, L. A.; Nielen, M. W. Assessment of liquid chromatography-tandem mass spectrometry approaches for the analysis of ceftiofur metabolites in poultry muscle. *Food Addit. Contam., Part A* **2012**, *29*, 197−207.

(13) Fagerquist, C. K.; Lightfield, A. R. Confirmatory analysis of β-lactam antibiotics in kidney tissue by liquid chromatography/electrospray ionization selective reaction monitoring ion trap tandem mass spectrometry. *Rapid Commun. Mass Spectrom.* **2003**, *17*, 660−671.

(14) Fagerquist, C. K.; Lightfield, A. R.; Lehotay, S. J. Confirmatory and quantitative analysis of β-lactam antibiotics in bovine kidney tissue by dispersive solid-phase extraction and liquid chromatography-tandem mass spectrometry. *Anal. Chem.* **2005**, *77*, 1473−1482.

(15) Feng, S.; Chattopadhaya, C.; Kijak, P.; Chiesa, O. A.; Tall, E. A. A determinative and confirmatory method for ceftiofur metabolite desfuroylceftiofur cysteine disulfide in bovine kidney by LC-MS/MS. *J. Chromatogr. B: Anal. Technol. Biomed. Life Sci.* **2012**, *898*, 62−68.

(16) Mastovska, K.; Lightfield, A. R. Streamlining methodology for the multiresidue analysis of β-lactam antibiotics in bovine kidney using liquid chromatography-tandem mass spectrometry. *J. Chromatogr., A* **2008**, *1202*, 118−123.

(17) Moats, W. A.; Romanowski, R. D.; Medina, M. B. Identification of β-lactam antibiotics in tissue samples containing unknown microbial inhibitors. *J. AOAC Int.* **1998**, *81*, 1135−1140.

(18) Moats, W. A.; Romanowski, R. D. Multiresidue determination of β-lactam antibiotics in milk and tissues with the aid of high-performance liquid chromatographic fractionation for clean up. *J. Chromatogr., A* **1998**, *812*, 237−247.

(19) Moats, W. A.; Buckley, S. A. Determination of free metabolites of ceftiofur in animal tissues with an automated liquid chromatographic cleanup. *J. AOAC Int.* **1998**, *81*, 709−713.

(20) Geis-Asteggiante, L.; Lehotay, S. J.; Lightfield, A. R.; Dutko, T.; Ng, C.; Bluhm, L. Ruggedness testing and validation of a practical analytical method for >100 veterinary drug residues in bovine muscle by ultra high performance liquid chromatography-tandem mass spectrometry. *J. Chromatogr., A* **2012**, *1258*, 43−54.

(21) Lehotay, S. J.; Lightfield, A. R.; Geis-Asteggiante, L.; Schneider, M. J.; Dutko, T.; Ng, C.; Bluhm, L.; Mastovska, K. Development and validation of a streamlined method designed to detect residues of 62 veterinary drugs in bovine kidney using ultra-high performance liquid chromatography-tandem mass spectrometry. *Drug Test Anal.* **2012**, *4* (S1), 75−90.

(22) Schneider, M. J.; Mastovska, K.; Lehotay, S. J.; Lightfield, A. R.; Kinsella, B.; Shultz, C. E. Comparison of screening methods for antibiotics in beef kidney juice and serum. *Anal. Chim. Acta* **2009**, *637*, 290−297.

(23) Schneider, M. J.; Lehotay, S. J.; Lightfield, A. R. Evaluation of a multi-class, multi-residue liquid chromatography-tandem mass spectrometry method for analysis of 120 veterinary drugs in bovine kidney. *Drug Test Anal.* **2012**, *4* (S1), 91−102.

(24) Lohne, J. J.; Andersen, W. C.; Casey, C. R.; Turnipseed, S. B.; Madson, M. R. Analysis of stilbene residues in aquacultured finfish using LC-MS/MS. *J. Agric. Food Chem.* **2013**, *61*, 2364−2370.

(25) Shelver, W. L.; Tell, L. A.; Wagner, S.; Wetzlich, S. E.; Baynes, R. E.; Riviere, J. E.; Smith, D. J. Comparison of ELISA and LC-MS/MS for the measurement of flunixin plasma concentrations in beef cattle after intravenous and subcutaneous administration. *J. Agric. Food Chem.* **2013**, *61*, 2679−2686.

(26) Wang, X.; Liu, Y.; Su, Y.; Yang, J.; Bian, K.; Wang, Z.; He, L. M. High-throughput screening and confirmation of 22 banned veterinary drugs in feedstuffs using LC-MS/MS and high-resolution Orbitrap mass spectrometry. *J. Agric. Food Chem.* **2014**, *62*, 516−527.

(27) U.S. Department of Agriculture, Food Safety and Inspection Service. *FSIS Residue Violation Information System: Weekly Residue Repeat Violator for Use by FSIS Inspection Program Personnel*, January 23, 2014.

(28) Analytical Methods Committee, Royal Society of Chemistry. *Fitting a linear functional relationship to data with error on both variables. AMC Technical Brief 10*, 2002.

(29) U.S. Food and Drug Administration. *Guidance for Industry No. 118: Mass Spectrometry for Confirmation of the Identity of Animal Drug Residues*, May 1, 2003.

(30) Hurtaud-Pessel, D.; Jagadeshwar-Reddy, T.; Verdon, E. Development of a new screening method for the detection of antibiotic residues in muscle tissues using liquid chromatography and high resolution mass spectrometry with a LC-LTQ-Orbitrap instrument. *Food Addit. Contam., Part A* **2011**, *28*, 1340−1351.

(31) Yamada, R.; Kozono, M.; Ohmori, T.; Morimatsu, F.; Kitayama, M. Simultaneous determination of residual veterinary drugs in bovine, porcine, and chicken muscle using liquid chromatography coupled with electrospray ionization tandem mass spectrometry. *Biosci., Biotechnol., Biochem.* **2006**, *70*, 54−65.

(32) Perez-Burgos, R.; Grzelak, E. M.; Gokce, G.; Saurina, J.; Barbosa, J.; Barron, D. Quechers methodologies as an alternative to solid phase extraction (SPE) for the determination and characterization of residues of cephalosporins in beef muscle using LC-MS/MS. *J. Chromatogr. B: Anal. Technol. Biomed. Life Sci.* **2012**, *899*, 57−65.

(33) Heinrich, K.; Chan, D.; Fussell, R. J.; Kay, J. F.; Sharman, M. Can the unauthorised use of ceftiofur be detected in poultry? *Food Addit. Contam., Part A* **2013**, *30*, 1733−1738.

as the stationary phase and a postcolumn reaction with 2,3,5-triphenyltetrazolium chloride. The resulting 1,3,5-triphenylformazans are detected photometrically at 480 nm, and in this case, free amino acids do not interfere with the quantitation.[6] Another approach follows the analysis of *N*-(2-furoylmethyl) amino acids formed by the controlled degradation of the Amadori products after acid hydrolysis, which can then be measured by either HPLC-UV or HPLC-MS, respectively.[7] High-performance cation or anion exchange chromatography in combination with either electrochemical detection[8] or tandem mass spectrometry[9] was recently used, but for electrochemical detection a special analytical equipment is required.

Most of the methods that have been developed so far use external calibration. However, quantitative data obtained by methods based on external calibration are difficult to correct for losses during extraction or degradation of the analyte, but such losses during workup can be completely compensated for by stable isotope dilution assays. There is only one study available on the quantitation of the Amadori product of lysine bound in a peptide using a stable isotope dilution assay.[10] Therefore, the aim of this study was to develop stable isotope dilution assays for seven Amadori compounds generated by a reaction of glucose with the amino acids valine, leucine, isoleucine, methionine, and phenylalanine as well as tyrosine and histidine. For this purpose, all seven unlabeled Amadori products as well as six carbon-13-labeled isotopologues were synthesized, and the new method was applied to the quantitation of the seven Amadori compounds in various food samples using LC-MS/MS.

MATERIALS AND METHODS

Materials. The following compounds were obtained from commercial sources: D-glucose (99.5%), malonic acid, *N*,*N*-dimethylformamide, and methanol (both Chromasolv) (Sigma-Aldrich, Steinheim, Germany); L-leucine, L-isoleucine, L-methionine, L-phenylalanine, L-valine, L-tyrosine, L-histidine (all for biochemistry), acetonitrile, and acetone (both Suprasolv) (Merck, Darmstadt, Germany); deuterium oxide (99.96% deuterium) (Euriso-top, Saint-Aubin Cedex, France); and [$^{13}C_6$]-D-glucose (99%) (Cambridge Isotope Laboratories, Andover, MA, USA).

Foods. Unroasted cocoa beans, 5 days fermented in wooden boxes, as well as roasted cocoa beans of the same batch (origin.. Sulawesi) were kindly provided by a food manufacturer. The green coffee beans (Arabica, Colombia) were supplied by Nestle PTC (Orbe, Switzerland). The beans were roasted in-house by means of a BRZ 4 drum roaster (Probat, Emmerich, Germany). The initial temperature of 185 °C was held for 3.5 min. Then, the air supply was opened, and the beans were roasted for another 2 min before cooling in the air stream of the collection chamber. Barley and wheat malt as well as wheat beer were obtained from a local brewery. The beer was produced from the same malt. Bell pepper and tomatoes were bought at a local market. The bell pepper powder was produced by drying of the vegetables in an oven at 50 °C for 7 days followed by grinding with a mill. Tomato powder was produced from fresh tomatoes by first shredding with a blender and then heating at 95 °C for 5 min followed by boiling for 3 h at 85−90 °C. The homogenized tomato paste was finally freeze-dried.

Syntheses of Amadori Rearrangement Products. D-Glucose (500 mg, 2.8 mmol) was dissolved in a 1:1 mixture of methanol/*N*,*N*-dimethylformamide (100 mL) and refluxed at 80 °C singly in the presence of each of the seven amino acids (3.8 mmol) with stirring for 3 h. Then, malonic acid (100 mg, 1.0 mmol) was added, and the mixture was refluxed for another 2 h at 90 °C until a light brownish color appeared. Undissolved components were filtered off, and the organic phase was concentrated to ∼5 mL by means of a rotary evaporator. The Amadori products were precipitated by the addition of cold acetone (45 mL) at −25 °C and, after centrifugation at 3500 rpm and 0 °C for 10 min, the precipitate was collected and the mother liquor was concentrated and treated again with cold acetone at −25 °C to gain a second portion of the target compound. The combined precipitates were dissolved in methanol (5 mL) at ∼45 °C and treated again with cold acetone (45 mL) at −25 °C before centrifugation. This step was repeated until the crystals were nearly white. The material was dried under vacuum in a desiccator overnight and then freeze-dried for 2 days. Yields varied between 8 and 40%. The products formed were assigned as 1-desoxyfructosyl amino acids using the following abbreviations, for example, Fru-Leu for the Amadori product from glucose and leucine, Fru-Phe for the Amadori product from glucose and phenylalanine, and so on.

Synthesis of the Carbon-13 [$^{13}C_6$]-Labeled Amadori Products. The respective carbon-13-labeled internal standards were synthesized using the same procedure but substituting glucose by [$^{13}C_6$]-glucose in the reaction with each of the amino acids. The assignment of the synthesized compounds was done by adding [$^{13}C_6$], for example, [$^{13}C_6$]-Fru-Phe for the carbon-13-labeled Amadori product synthesized from labeled glucose and phenylalanine.

HPLC-MS. The removal of glucose and the respective amino acid as well as byproducts was controlled by HPLC-MS using a combination of a P-4000 pump (Thermo Separation Products, Waltham, MA, USA), a 150 × 2 mm TSK Gel Amide-80 column (Tosoh Bioscience, Tokyo, Japan), and an ion trap MAT LCQ mass spectrometer (Finnigan, Bremen, Germany). Spectra were generated in the ESI$^+$ mode in parallel with UV detection at 210 nm.

Quantitative Nuclear Magnetic Resonance (qNMR) Spectroscopy. To cope with the amount of the remaining solvent and water in the labeled as well as unlabeled Amadori products, these were analyzed by quantitative NMR (qNMR).[11−13] Each analyte (100 mg) was dissolved in D_2O (Euriso-Top, Saarbrücken, Germany) in a 5 mL volumetric flask, and 600 μL of this stock solution was transferred into a 178 × 5 mm NMR tube (Norell, Landisville, NJ, USA) and analyzed using an AV III System (Bruker, Rheinstetten, Germany) at 400.13 MHz. The solutions were diluted with acetonitrile, placed in amber bottles, flushed with argon, and stored at −24 °C.

^{1}H NMR spectra were measured at 25 °C with a Bruker AV III system equipped with a 5 mm multinuclear observe probe head (BBFO, plus). The probe was tuned and matched with the sample in place, and the optimal 90° pulse width for the quantitation setup was investigated for every sample. The qNMR spectrum was determined by acquiring 16 scans with a relaxation delay of 40 s. Before Fourier transformation, the free induction decay was multiplied with a 0.3 Hz exponential line broadening factor and zero-filled. Phasing and integration of the peaks were done manually after automatic baseline correction. If necessary, the integrals were adjusted with the software functions SLOPE and BIAS. The concentration of each compound was calculated with the ERETIC 2 function of Topspin 3.0 (Bruker). Calibration of the qNMR was based on a solution of L-tyrosine of known concentration using the signal at 7.1 ppm (m, 2H). The signal of the methylene group at carbon-1 of the former glucose at 3.3 ppm (m, 2H) was used for the quantitation of the Amadori products Fru-Leu, Fru-Ile, Fru-Val, and Fru-Met. In the cases of Fru-Phe, Fru-Tyr, and Fru-His the aromatic protons were used for quantitation (Fru-Phe, 7.4 ppm, m; Fru-Tyr, 7.0 ppm, m; and Fru-His, 7.7 ppm, s) because the free amino acids were confirmed to be absent by HPLC measurements.

Isolation and Quantitation of Amadori Compounds in Foods. Either ground solid material (∼2 g) or beverages (∼20 mL) were exactly weighed in flasks and extracted with methanol (200 mL) after addition of the labeled internal standards. The mixtures were stirred for 1 h, then filtered and concentrated to ∼5 mL by means of a rotary evaporator. An extraction time of 1 h was needed for reproducible results, but a longer extraction did not change the results. To separate nonpolar substances, a 140 Å Strata C18-T SPE cartridge (1000 mg; volume, 6 mL) (Phenomenex, Aschaffenburg, Germany) was conditioned with methanol (10 mL). After application of the extract, the eluate (10 mL) was concentrated to dryness,

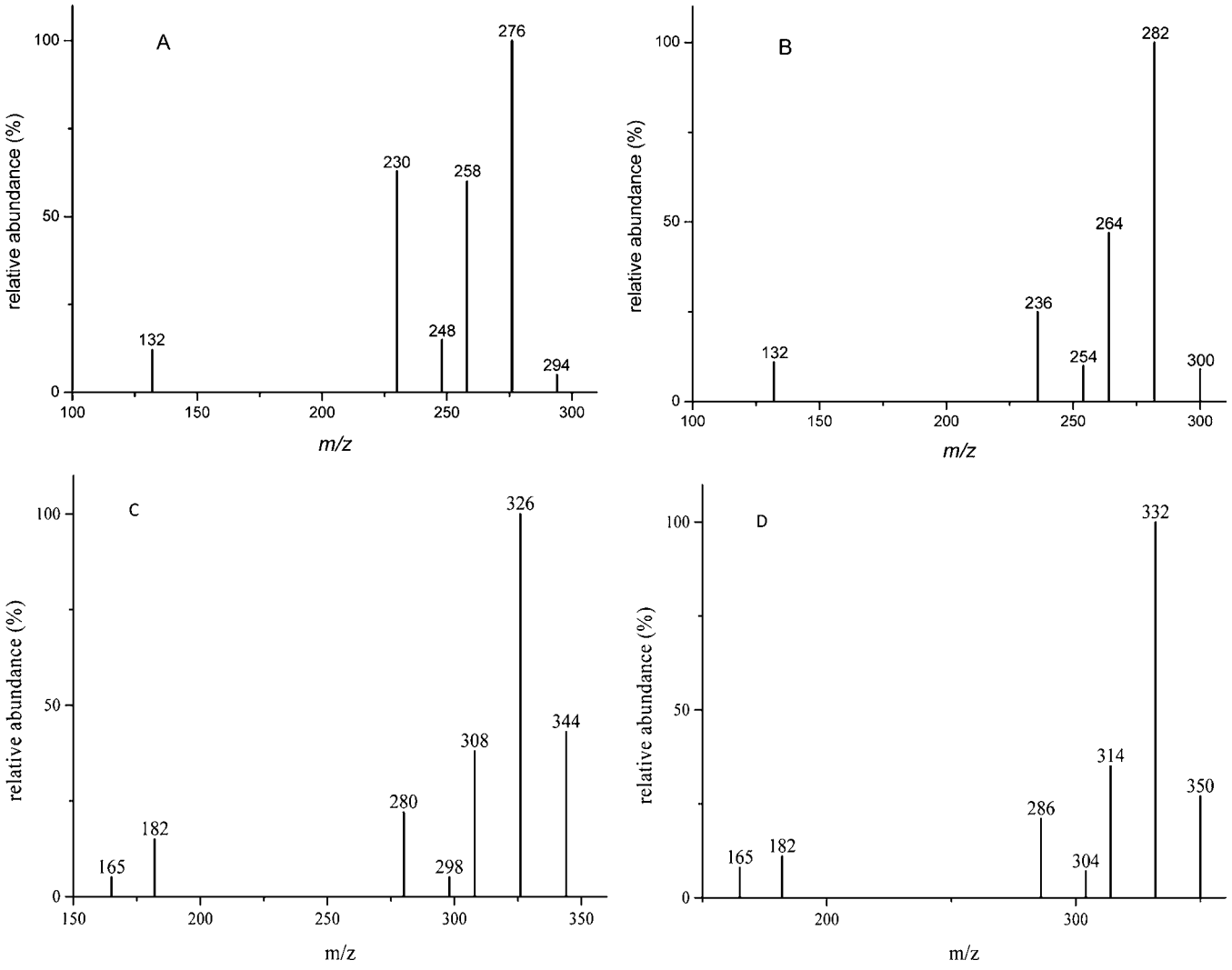

Figure 2. Mass spectra (ESI^+) of fructosyl leucine (Fru-Leu; A), [$^{13}C_6$]-fructosyl leucine (Fru-Leu; B), fructosyl tyrosine (Fru-Tyr; C), and [$^{13}C_6$]-fructosyl tyrosine (Fru-Tyr; D).

redissolved in acetonitrile (10 mL), and filtered through a Whatman Spartan 13/0.45 RC membrane filter (GE Healthcare, Wien, Austria).

HPLC-MS/MS. The samples were analyzed by LC-MS/MS using a Thermo Finnigan Quantum TSQ mass spectrometer (Finnigan, Bremen, Germany) connected to a 150 × 2 mm TSK Gel Amide 80 HPLC column (Tosoh Bioscience). Spectra were generated in the ESI-positive mode with selected reaction monitoring. The flow conditions were as follows: 0.2 mL/min acetonitrile/0.1% aqueous formic acid (9 + 1) for 3 min with a gradient to 0.1% aqueous formic acid/acetonitrile (9 + 1) within 12 min, then held for 5 min. The spray voltage was 3500 V, and the capillary temperature was 290 °C.

Determination of the Limit of Detection (LoD) and Limit of Quantitation (LoQ). Decreasing amounts of the synthesized, unlabeled Amadori products were added to either wheat starch or sunflower oil, respectively, and the mixtures were analyzed as described above for the food samples. The solutions were diluted until the analyte peaks were <3-fold the background noise (LoD) or 5-fold for LoQ.

Response Curves. Calibration curves were created from mixtures of each analyte and each labeled internal standard in ratios between 1:15 and 15:1 (by weight). To differentiate between Fru-Leu and Fru-Ile, first the sum of both was determined using [$^{13}C_6$]-Fru-Leu as the internal standard. Then, using a standard curve obtained by defined mixtures of Fru-Leu and Fru-Ile, the ratio of both isomers in the mixture was calculated by optimizing the collision energies for the intensities of the fragments m/z 88 and 144. At 31 eV, Fru-Leu showed an intensity of 94.7% for m/z 88 and only 5.3% intensity for m/z 144, whereas at 17 eV Fru-Ile showed an intensity of 5.9% for m/z 88 but 94.1% for m/z 144.[14] From these data, the ration of Fru-Leu and Fru-Ile in the total amount determined for both isomers could be determined.

RESULTS AND DISCUSSION

Syntheses. The general reaction route used in the synthesis of the 13 Amadori products from either glucose or [$^{13}C_6$]-glucose and the seven amino acids followed the formation pathway suggested for their formation in foods (Figure 1). Either glucose or labeled glucose, respectively, was singly reacted with each of the seven amino acids by refluxing in a mixture of methanol and dimethylformamide.[1] Smaller amounts of the educts were used, in particular because the expensive [$^{13}C_6$]-glucose was used to synthesize the isotopically labeled standards. For the analytes abbreviations were used to indicate the carbohydrate and the respective amino acid, for example, Fru-Leu to assign the Amadori reaction product from glucose and leucine, and [$^{13}C_6$]-Fru-Leu was used for the labeled isotopologue.

First, mass spectra in the ESI^+ mode were recorded. In panels A and B of Figure 2 the mass spectra of Fru-Leu and [$^{13}C_6$]-Fru-Leu are contrasted. The shift of the molecular ion m/z 294

dx.doi.org/10.1021/jf501464g | J. Agric. Food Chem. 2014, 62, 5020−5027

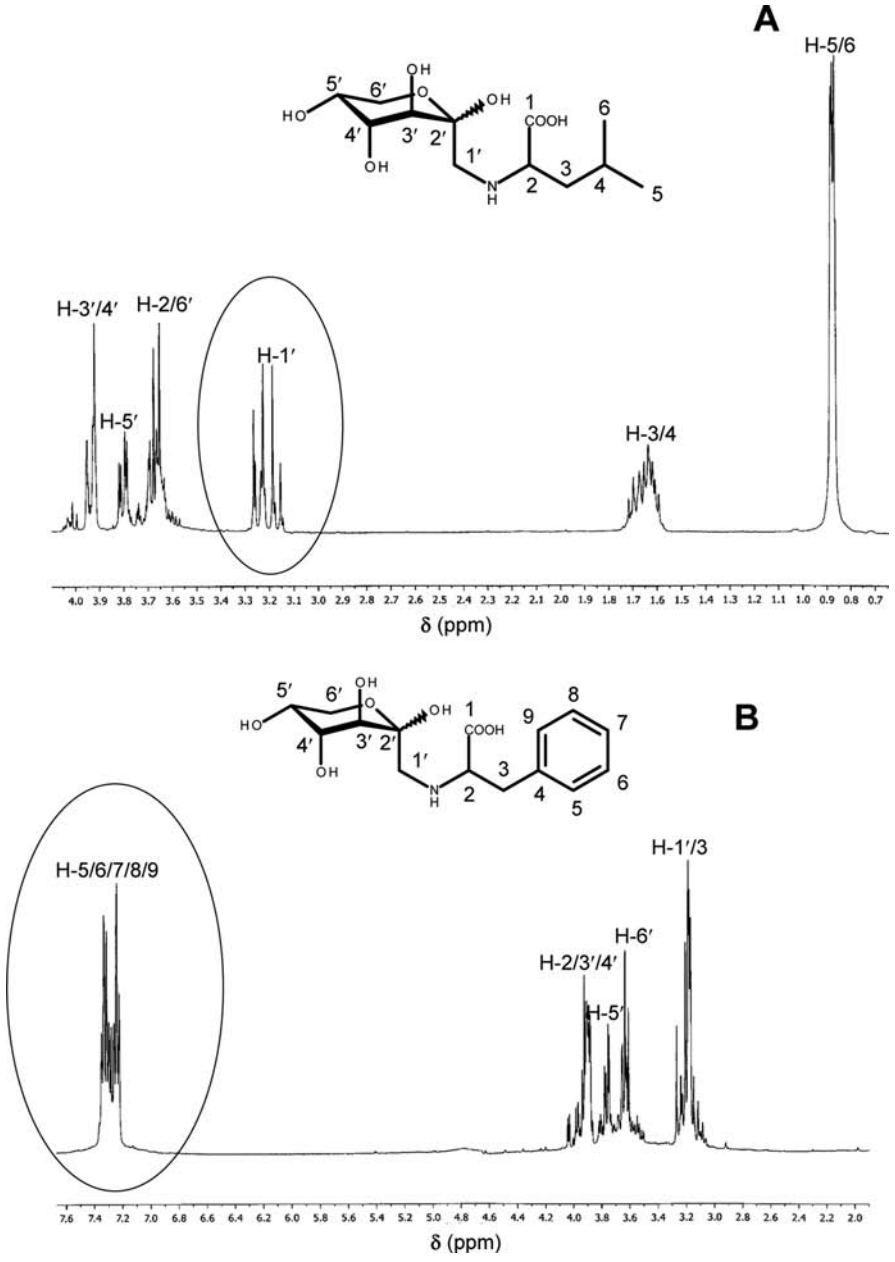

Figure 3. [1]H NMR spectra of fructosyl leucine (Fru-Leu; A) and fructosyl phenylalanine (Fru-Ph; B).

Table 1. ^{13}C NMR Data Obtained for Fructosyl Leucine (Fru-Leu) (100 MHz, D_2O, 300 K)

			HMBC	
carbon atom[a]	δ	HSQC	via ^{1}J (C,H)	via $^{2,3}J$ (C,H)
C(5/6)	21.3	CH_3	H–C(5/6)	H–C(4), H–C(3)
C(5/6)	22.0	CH_3	H–C(5/6)	H–C(4), H–C(3)
C(4)	24.7	CH	H–C(4)	H–C(2), H–C(3), H–C(5/6)
C(3)	39.3	CH_2	H–C(3)	H–C(2), H–C(4), H–C(5/6)
C(1′)	52.3	CH_2	H–C(1′)	H–C(3′)
C(2)	62.3	CH	H–C(2)	H–C(3), H–C(4)
C(6′)	64.0	CH_2	H–C(6′)	H–C(3′/4′), H–C(5′)
C(5′)	68.6	CH	H–C(5′)	H–C(3′/′, H–C(6′)
C(3′/4′)	69.2	CH	H–C(3′/4′)	H–C(5′), H–C(6′)
C(3′/4′)	70.0	CH	H–C(3′/4′)	H–C(5′), H–C(6′)
C(2′)	95.3			H–C(1′), H–C(3′/4′), H–C(6′)
C(1)	174.0			H–C(2), H–C(3)

[a]Numbering refers to Figure 3A.

dx.doi.org/10.1021/jf501464g | J. Agric. Food Chem. 2014, 62, 5020−5027

Table 2. ^{13}C NMR Data Obtained for Fructosyl Phenylalanine (Fru-Phe) (100 MHz, D_2O, 300 K)

			HMBC	
carbon atom[a]	δ	HSQC	via ^1J (C,H)	via $^{2,3}J$ (C,H)
C(3)	35.5	CH_2	H–C(3)	H–C(2), H–C(5/9)
C(1′)	52.7	CH_2	H–C(1′)	H–C(3′)
C(6′)	63.6	CH2	H–C(6′)	H–C(4′), H–C(5′)
C(2)	63.7	CH	H–C(2)	H–C(3)
C(5′)	68.6	CH	H–C(5′)	H–C(3′/4′), H–C(6′)
C(3′/4′)	69.5	CH	H–C(3′/4′)	H–C(5′), H–C(6′)
C(3′/4′)	70.1	CH	H–C(3′/4′)	H–C(5′), H–C(6′)
C(2′)	95.0			H–C(1′), H–C(3′/4′), H–C(6′)
C(7)	127.7	CH	H–C(7)	H–C(5), H–C(6), H–C(8), H–C(9)
C(5/9)/C(6/8)	129.1	CH	H–C(5/9)/H–C(6/8)	H–C(3), H–C(6), H–C(7), H–C(8)/ H–C(5), H–C(7), H–C(9)
C(5/9)/C(6/8)	129.5	CH	H–C(5/9)/ H–C(6/8)	H–C(3), H–C(6), H–C(7), H–C(8)/ H–C(5), H–C(7), H–C(9)
C(4)	134.5			H–C(3), H–C(5), H–C(9)
C(1)	172.3			H–C(2), H–C(3)

[a]Numbering refers to Figure 3B.

for Fru-Leu to m/z 300 for [$^{13}C_6$]-Fru-Leu clearly indicated the successful incorporation of six carbon atoms. Further fragment pairs (m/z 276 and 258; m/z 282 and 264) indicated a sequential elimination of two molecules of water. The same type of fragmentation was found for Fru-Tyr (Figure 2C) and [$^{13}C_6$]-Fru-Tyr (Figure 2D) as well as for the other four Amadori products and their labeled homologues.

For quantitation, the synthesized analytes had to be weighed. However, neither the Amadori compounds nor the labeled homologues could totally be freed from the solvent, for example, water and methanol. Therefore, to determine the correct concentrations in the reaction products, quantitative NMR experiments were performed. As shown in the ^1H NMR spectrum of Fru-Leu (Figure 3A), the hydrogen atoms of the methylene group at carbon 1′ are appropriate for the quantitation because these were exclusively present in the Amadori products, but not in glucose or in leucine, respectively (data not shown). For the Amadori products of the aromatic amino acids, signals of the hydrogen atoms at carbon 1′ were at the same position as the methylene protons of the amino acid (data not shown). Therefore, as shown for Fru-Phe, the sum of the hydrogens in the aromatic ring was used for qNMR (Figure 3B). In any case the absence of the free amino acid was checked by HPLC.

To precisely characterize the structure of the analytes, also ^{13}C NMR and two-dimensional NMR experiments were performed. As examples, the ^{13}C NMR data obtained for Fru-Leu are summarized in Table 1 and those for Fru-Phe in Table 2.

Method Development. For HPLC separation of the seven analytes, a gel permeation chromatography column was chosen, because the matrix effects were low and the chromatographic separation was better than with other columns tested. Although a clear separation was not achieved for all analytes (Figure 4), each Amadori compound could separately be quantitated using its molecular ion in the selected reaction monitoring mode. For identification and quantitation two mass transitions were used for each analyte and the respective labeled internal standard, respectively (Table 3). Because the molecular masses of Fru-Leu and Fru-Ile are identical, first, the sum of the concentrations of both compounds was determined by using [$^{13}C_6$]-Fru-Leu as the internal standard. At higher collision energies (Table 3), Fru-Leu had a much better tendency to form m/z 88, whereas m/z 144 was exclusively formed from

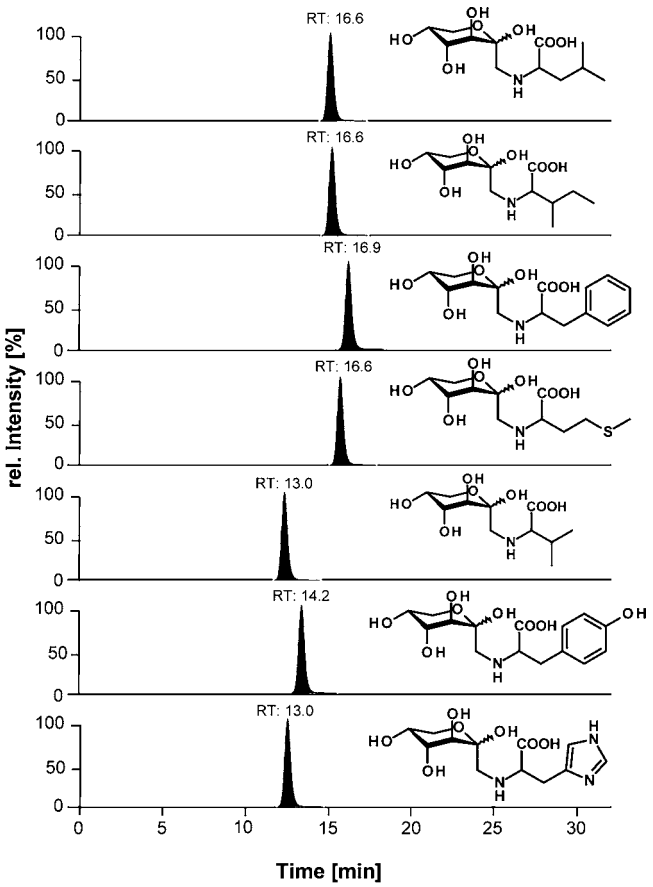

Figure 4. HPLC-MS/MS chromatograms obtained for the seven Amadori reaction products.

Fru-Ile.[14] By measuring defined mixtures of Fru-Leu and Fru-Ile, a calibration curve was created allowing the quantitation of both analytes by correlating the signal intensities m/z 88 and m/z 144 (Figure 5).

Method Validation. To determine the LoD and LoQ, mixtures of each analyte and the respective standard (1:1) were added in decreasing amounts to either wheat starch or sunflower oil as the matrix, respectively, and the samples were worked up as described for the food samples. Fru-Phe could be quantitated very sensitively down to 0.1 μg/kg in

dx.doi.org/10.1021/jf501464g | J. Agric. Food Chem. 2014, 62, 5020−5027

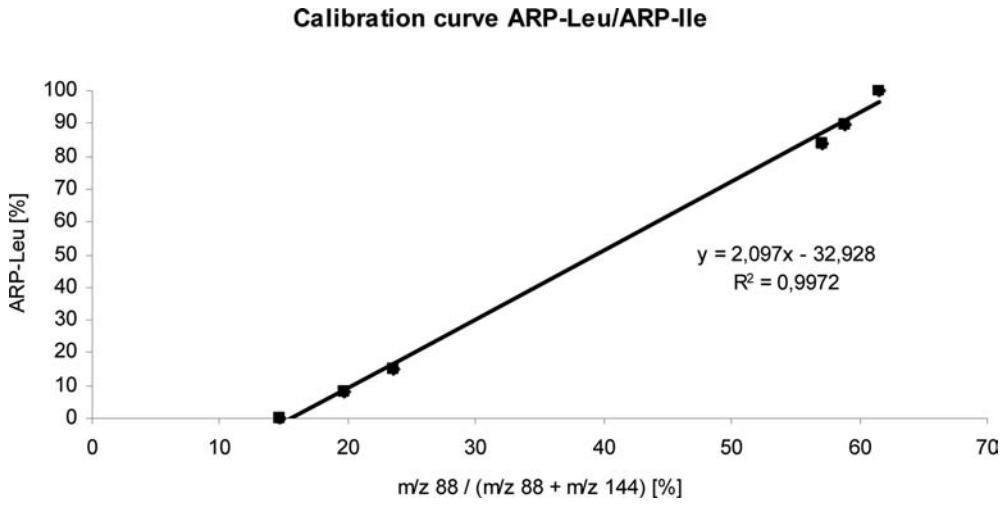

Figure 5. Calibration curve used in the differentiation of fructosyl leucine (Fru-Leu) and fructosyl isoleucine (Fru-Ile).

Table 3. Mass Spectrometric Parameters Used in the Quantitation of Seven Amadori Compounds

analyte	collision energy (eV)	first transition m/z	collision energy (eV)	second transition m/z
Fru-Leu	8	294 → 276	18	294 → 230
[$^{13}C_6$]-Fru-Leu	8	300 → 282	18	300 → 236
Fru-Leu/Fru-Ile[a]	17	294 → 144	31	294 → 88
Fru-Met	8	312 → 294	18	312 →248
[$^{13}C_6$]-Fru-Met	8	318 → 300	18	318 → 254
Fru-Phe	8	328 → 310	18	328 → 264
[$^{13}C_6$]-Fru-Phe	8	334 → 316	18	334 → 270
Fru-Tyr	8	344 → 326	16	344 → 280
[$^{13}C_6$]-Fru-Tyr	8	350 → 332	16	350 → 286
Fru-Val	8	280 → 262	16	280 → 216
[$^{13}C_6$]-Fru-Val	8	286 → 268	16	286 → 222
Fru-His	8	318 → 300	16	318 → 190
[$^{13}C_6$]-Fru-His	8	324 → 306	16	324 → 195

[a]Conditions used to separately quantitate both Amadori compounds in a mixture.

wheat starch or 0.2 μg/kg in sunflower oil, respectively; the LoQs of the other Amadori products were at 2−35 μg/kg and that of Fru-Met was at 50 μg/kg (Table 4). The reproducibility of the method can be derived from the data for the food samples given below.

Application to Foods. The amounts of some of the Amadori compounds have previously been determined in several foods, and a thermal treatment at lower temperatures was found to favor their generation, whereas, for example, roasting conditions led to their degradation. The new stable isotope dilution assays were, therefore, applied on foods, in which some of the Amadori compounds had previously been analyzed for by other methods (Table 5). First, the reproducibility of the data can nicely be seen from the analysis of the beer sample (sample 7) (Table 5). For this experiment, three samples of the same beer were separately worked up. The data showed no standard deviation for Fru-Val in the triplicate, values below 5% for Fru-Ile, Fru-Phe, and Fru-Tyr, whereas a bit higher values were measured for Fru-Leu and Fru-His. Quantitations in unroasted and roasted cocoa from the same batch (samples 1 and 2) (Table 5) showed quite high amounts of most Amadori products in the unroasted cocoa, with Fru-Val being at 342 mg/kg. After roasting of the beans, however, all analytes were significantly degraded, except Fru-Met. Also in unroasted coffee beans (sample 3) (Table 5), all seven analytes were present, but these were also degraded during roasting, except Fru-His, which was higher in the roasted coffee (sample 4) (Table 5). Two cereal malts (samples 5 and 6) (Table 5) also contained high amounts of the Amadori products, with Fru-Val predominating in wheat malt. During beer production obviously the Amadori compounds are degraded, but still significant amounts were found in the wheat beer (sample 7) (Table 5).

To study the influence of a drying process, bell pepper as well as tomatoes were slowly dried at lower temperatures or cooked under laboratory conditions. Drying of bell pepper led

Table 4. Limits of Detection (LoD) and Limits of Quantitation (LoQ) for Six Amadori Compounds in Two Model Matrices

	LoD (μg/kg)		LoQ (μg/kg)	
	sunflower oil	wheat starch	sunflower oil	wheat starch
Fru-His	6.4	14.5	10.7	24.2
Fru-Leu[a]	8.2	19.8	13.7	33.1
Fru-Met	30.1	33.7	50.1	56.2
Fru-Phe	0.2	0.1	0.3	0.1
Fru-Tyr	2.5	1.3	4.1	2.2
Fru-Val	21.1	20.9	35.1	34.8

[a]The same values were assumed for Fru-Ile.

dx.doi.org/10.1021/jf501464g | J. Agric. Food Chem. 2014, 62, 5020−5027

Table 5. Concentrations (Milligrams per Kilogram) of Seven Amadori Compounds in Selected Foods[a]

sample	food	Fru-Leu	Fru-Ile	Fru-Phe	Fru-Met	Fru-Val	Fru-His	Fru-Tyr
1	cocoa (unroasted)	152.00 ± 8%	104.00 ± 10%	104.00 ± 8%	2.33 ± 14%	342.00 ± 3%	27.20 ± 5%	73.00 ± 4%
2	cocoa (roasted)	6.47 ± 6%	5.38 ± 6%	3.99 ± 7%	1.34 ± 9%	19.00 ± 5%	0.62 ± 9%	3.04 ± 3%
3	coffee (green)	4.65 ± 14%	2.51 ± 5%	2.80 ± 29%	0.59 ± 14%	0.60 ± 5%	0.36 ± 23%	0.18 ± 16%
4	coffee (roasted)	0.81 ± 13%	0.87 ± 16%	0.09 ± 25%	<LoQ	<LoQ	15.33 ± 15%	<LoQ
5	barley malt	33.80 ± 8%	29.20 ± 7%	25.40 ± 12%	5.91 ± 16%	39.40 ± 12%	13.10 ± 15%	11.00 ± 15%
6	wheat malt	35.40 ± 14%	27.80 ± 14%	21.10 ± 12%	4.31 ± 6%	148.00 ± 6%	10.60 ± 10%	6.70 ± 5%
7	wheat beer	11.50 ± 8%	6.05 ± 2%	5.28 ± 1%	<LoQ	34.60 ± 0%	2.77 ± 10%	2.91 ± 4%
8	bell pepper	0.07 ± 14%	0.10 ± 2%	0.08 ± 2%	0.10 ± 2%	0.58 ± 20%	0.97 ± 21%	<LoQ
	(based on dry weight)	(0.70)	(1.00)	(0.80)	(1.00)	(5.80)	(9.70)	(<LoQ)
9	bell pepper powder	592.00 ± 2%	509.00 ± 3%	329.00 ± 8%	81.90 ± 5%	3460.00 ± 3%	405.00 ± 13%	210.00 ± 20%
10	tomato	0.16 ± 30%	0.12 ± 12%	0.19 ± 17%	<LoQ	<LoQ	0.57 ± 3%	<LoQ
	(based on dry weight)	(3.20)	(2.40)	(3.80)	(<LoQ)	(<LoQ)	(11.40)	(<LoQ)
11	tomato powder	9.60 ± 4%	9.30 ± 18%	22.60 ± 15%	<LoQ	10.60 ± 16%	45.00 ± 11%	7.96 ± 20%

[a]Data are mean values of triplicates (three separate workups). Standard deviation is given in %.

to a significant increase, leading, for example, to ∼3.5 g of Fru-Val in the dried compared to 5.8 mg/kg in the fresh sample (based on dry weight). The amounts were similar to those also reported before for bell pepper powder.[6] Drying and cooking of tomatoes showed the same behavior (samples 10 and 11) (Table 5). In particular, Fru-Val and Fru-Tyr, which were not detectable in the fresh tomatoes, increased to 10.6 or 7.96 mg/kg, respectively, after cooking. However, the literature data[6] were much higher, which was probably due to the drum-drying process applied in the previous study. However, to the best of our knowledge our results present the first data on Fru-His and Fru-Tyr in all food samples analyzed.

In conclusion, the newly developed stable isotope dilution assays for the quantitation of seven Amadori compounds by means of LC-MS/MS showed a very good peak to noise ratio with low matrix interferences and a good reproducibility even for foods low in analytes, such as unprocessed tomatoes or bell pepper. Thus, LC-MS/MS analysis in combination with a stable isotope dilution assay is suggested as a reliable approach for the fast and accurate quantitation of Amadori compounds in foods. The results further corroborate that their formation is probably favored when slow heating is applied in food drying, whereas roasting leads to their degradation. The fact that quite high amounts were also found in unprocessed foods, such as cocoa and green coffee beans, might suggest a formation pathway other than that shown in Figure 1. This idea is supported by an experiment showing that unfermented cocoa beans, when stored for 7 days at 60 °C in an oven, did not generate any Amadori compound (Pammer and Schieberle, unpublished data), whereas the fermented beans contained quite high amounts after 7 days at nearly the same temperature. Therefore, one could conclude that Amadori compounds may be formed during fermentation of cocoa beans by an enzymatic reaction. This, however, has to be confirmed in further studies.

■ ASSOCIATED CONTENT

Supporting Information

Figures S1−S6. This material is available free of charge via the Internet at http://pubs.acs.org.

■ AUTHOR INFORMATION

Corresponding Author

*(P.S.) Phone: +49 8161 71 2932. Fax: +49 8161 71 2970. E-mail: Peter.Schieberle@ch.tum.de.

Notes

The authors declare no competing financial interest.

■ ACKNOWLEDGMENTS

We gratefully acknowledge the technical assistance of Anita Herzner and Julia Bock. We thank Ines Otte and Sami Kaviani-Nejad for performing the LC-MS/MS measurements and Dr. Johanna Kreissl, and Dr. Oliver Frank for help with the qNMR experiments.

■ REFERENCES

(1) Hofmann, T.; Schieberle, P. Formation of aroma-active Strecker-aldehydes by a direct oxidative degradation of Amadori compounds. *J. Agric. Food Chem.* **2000**, *48*, 4301−4305.

(2) Beksan, E.; Schieberle, P.; Robert, F.; Blank, I.; Fay, L.; Schlichtherle-Cerny, H.; Hofmann, T. Synthesis and sensory characterization of novel umami-tasting glutamate glycoconjugates. *J. Agric. Food Chem.* **2003**, *51*, 5428−5436.

(3) Wittmann, R.; Eichner, K. Detection of Maillard products in malts, beers, and brewing colorants. *Z. Lebensm. Unters. Forsch.* **1989**, *188*, 212−220.

(4) Eichner, K.; Reutter, M.; Wittmann, R. Detection of Amadori compounds in heated foods. *ACS Symp. Ser.* **1994**, *No. 543*, 42−54.

(5) Ciner-Doruk, M.; Eichner, K. Formation and stability of Amadori compounds in dry foods (in German). *Z. Lebensm. Unters. Forsch.* **1979**, *168*, 9−20.

(6) Reutter, M.; Eichner, K. Separation and determination of Amadori compounds by high pressure liquid chromatography and post-column reaction. *Z. Lebensm. Unters. Forsch.* **1989**, *188*, 28−35.

(7) Schwietzke, U.; Malinowski, J.; Zerge, K.; Henle, T. Quantification of Amadori products in cheese. *Eur. Food Res. Technol.* **2011**, *233*, 243−251.

(8) Davidek, T.; Clety, N.; Devaud, S.; Robert, F.; Blank, I. Simultaneous quantitative analysis of Maillard reaction precursors and products by high performance anion exchange chromatography. *J. Agric. Food Chem.* **2003**, *51*, 7259−7265.

(9) Davidek, T.; Kraehenbuehl, K.; Devaud, S.; Robert, F.; Blank, I. Analysis of Amadori compounds by high-performance cation exchange chromatography coupled to tandem mass spectrometry. *Anal. Chem.* **2005**, *77*, 140−147.

(10) Vinale, F.; Fogliano, V.; Schieberle, P.; Hofmann, T. Development of a stable isotope dilution assay for an accurate

quantification of protein-bound N^{ε}-(1-deoxy-D-fructos-1-yl)-L-lysine using a ^{13}C-labeled internal standard. *J. Agric. Food Chem.* **1999**, *47*, 5084−5092.
(11) Korn, M.; Frank, O.; Hofmann, T.; Rychlik, M. Development of stable isotope dilution assays for ochratoxin A in blood sample. *Anal. Biochem.* **2011**, *419*, 88−94.
(12) Wider, G.; Dreier, L. Measuring protein concentrations by NMR spectroscopy. *J. Am. Chem. Soc.* **2006**, *128*, 2571−2576.
(13) Frank, O.; Kreissl, J.; Daschner, A.; Hofmann, T. Accurate determination of reference materials and natural isolates by means of quantitative ^{1}H NMR spectroscopy. *J. Agric. Food Chem.* **2014**, *62*, 2506−2515.
(14) Weigl, M. *Characterization of Key Aroma Compounds in Cocoa Liquor. Studies on Aroma Formation during Roasting of Cocoa Beans (in German)*. Ph.D. dissertation, TU Muenchen, 2006.

links and noncovalent links. Noncovalent interaction includes hydrogen bonding, hydrophobic bonding, and sometimes even ionic bonding. It occurs depending on the structure of polyphenols and various functional groups in proteins.[14−20] Noncovalent interaction could take place multisitely and multidentately due to the polarity of the polyphenol. Multisite interaction means that several phenolic compounds bound to one protein molecule, whereas multidentate interaction means that one phenolic compound bound to several protein sites or molecules. The type of interaction relies on the type and the molar ratio of both phenolic compound and protein.[21,22] Covalent interaction occurs through the interaction between oxidized phenolic substances and proteins.[23,24] Electrospray ionization (ESI) has been proven to be an effective tool to detect the weak associations of molecules in solutions such as receptor−ligand and protein−nucleic acid interaction.[25,26] A relatively well-developed way to determine the relative binding affinities of noncovalent complex has been established.[27,28] The mass spectrometry (MS) can reveal the noncovalent interaction strengths and qualitative information on the complex structure. Therefore, MS instrumentation was also used to detect and characterize soluble noncovalent complexes.[29]

In this study, the aim was to apply LC-ESI-MS to investigate the radical scavenging and other protein−phenolic interaction reactions between cloudberry ellagitannin and tryptic digests of β-Lg. Tryptic peptides of β-Lg have been used as a model to study protein−phenolic interactions. This simplified model enables the mechanistic investigations in more detail compared to those of a complicated protein. This model mimics possible reactions between proteins or peptides and plant phenolics during in vivo digestion but also in the food matrix as protein binding would affect polyphenol reactivity and influence its biological fate.

MATERIALS AND METHODS

Chromatographically purified and lyophilized β-Lg (variants A + B from bovine milk) was purchased from Sigma-Aldrich, Inc. (St. Louis, MO, U.S.A.). Sequencing-grade modified trypsin was obtained from Promega Corp./BioFellows (Madison, WI, U.S.A.). Of the reagents used in the analyses, ammonium bicarbonate, hydrogen peroxide (30% wt solution in water), and iron(III) chloride (reagent grade, 97%) were purchased from Sigma-Aldrich (Steinheim, Germany), whereas L(+)-ascorbic acid was a product of Merck (Darmstadt, Germany) and PIPES-buffer [piperazine-1,4-bis(2-ethanesulfonic acid)] from Fluka BioChemika (Buchs, Switzerland). Methanol, acetone, and acetonitrile were of HPLC grade and purchased from Rathburn (Walkerburn, Scotland). All other chemicals used in the analyses were supplied by J. T. Baker (Deventer, The Netherlands) or Sigma-Aldrich in either HPLC or reagent grade. The water used was always purified first by the Milli-Q system (Millipore Corp., Bedford, MA, U.S.A.). Fresh cloudberries (*Rubus chamaemorus*) were purchased from the local grocery.

Digestion and Fractionation of β-Lg Peptides. The in-liquid digestion of β-Lg was prepared using sequencing grade modified trypsin to obtain the cleavage to peptides which were later separated and collected using preparative HPLC according to the method described by Koivumäki et al.[8] In brief, 10 mg of β-Lg was dissolved in 50 mM ammonium bicarbonate buffer followed by addition of trypsin with a protease/protein ratio of 1:250. The protein digest was kept at 37 °C overnight, and thereafter the enzyme reaction was stopped by placing the digest in −20 °C. Isolation and fractionation of β-Lg peptides was carried out by using preparative HPLC and assigning the automated collection triggers for the corresponding m/z values of the theoretical peptides.

Isolation of Sanguiin H-6. Freeze-dried cloudberries (2 g, powder) were extracted with 70% acetone (2 × 20 mL) by accelerated solvent extraction (ASE) (Dionex, Sunnyvale, CA, U.S.A.). The extracts were evaporated to dryness and dissolved into Milli-Q water. Column (40 × 300 mm) chromatography with Amberlite XAD-7 was used for removal of sugars, organic acids, and phenolic acids eluting with 6% acetonitrile. A fraction containing flavonols, anthocyanins, and ellagitannins was collected using 100% acetonitrile. The dried polyphenol fraction dissolved into aq methanol (50%) was subject to further fractionation using a Sephadex LH-20 column (40 × 300 mm). The ellagitannin fraction was eluted with 70% acetone. An ellagitannin dimer, sanguiin H-6, was obtained from the ellagitannin fraction by using preparative-HPLC (Waters 2767 sample manager, Waters 2545 binary gradient module, and Waters system fluidic organizer) coupled with a Waters 2998 PDA and Waters ZQ single quadrupole mass spectrometer (Waters, Milford, MA, U.S.A.). The column was Develosil ODS-HG-5 column, 250 × 20 mm, 5 μm (Phenomenex, Torrance, CA, U.S.A.). The mobile phase consisted of 0.1% formic acid in water (solvent A) and 50% acetonitrile in water (solvent B). The elution condition was as follows: isocratic elution 0% B 0−2 min; linear gradient from 0% to 6% B, 2−8 min; from 6% to 10% B, 8−25 min; from 10% to 16% B, 25−40 min; isocratic 16% B 40−50 min; linear gradient from 16% to 64% B, 50−53 min; isocratic 64% B, 53−58 min; linear gradient from 64% to 0% B, 58−0 min. Injection volume was 1.0 mL. The flow (5.0 mL/min) was split 1:100 before the PDA and mass spectrometry (MS) detection. PDA scan range was 210−600 nm. Mass spectrometry (MS) was fitted with an ESI source and was operated in negative mode. The capillary voltage was 3.9 kV, cone 66.00 V, extractor 3.00, and RF lens 0.7 V. Source temperature was 120 °C, desolvation temperature 350 °C, cone gas flow 50 L/h, and desolvation gas flow 600 L/h. The scan range of the mass spectrometry was m/z 1200−2000. The m/z value 1869 (sanguiin H-6 $[M\text{-}H]^-$) was used as a trigger for the fraction collection. The system was controlled by Waters MassLynx software version 4.1 with FractionLynx (Waters).

The purity and identity of the isolated sanguiin H-6 was determined using the UHPLC-PDA-MS method outlined by Kähkönen et al.,[12] and the concentration was determined spectrophotometrically using the molar extinction coefficient $\varepsilon_{260\ nm}$ 72070 $M^{-1}cm^{-1}$ for sanguiin H-6 in methanol.[30] The concentration of isolated sanguiin H-6 was 254.3 μg/mL in methanol with a purity of 96%.

Oxidation of the Peptide Samples With and Without Sanguiin H-6. The three chosen peptides, LIVTQTMK, ALPMHIR and IPAVFK, were prepared into separate oxidation samples in triplicates, as well as both with and without the sanguiin H-6. The phenolic-to-peptide ratio was chosen to be 1000 μg of sanguiin H-6/g of peptide (molar ratio of 1:2000) according to pretesting done with LIVTQTMK, ALPMHIR, and IPAVFK. For further studies regarding the nature of the adduct between peptide and the ellagitannin, 162 mg sanguiin H-6/g of peptide (molar ratio of 1:12.5) was used with LIVTQTMK. After sanguiin H-6 was added to samples, H_2O_2 solution (final concentration 1 mM) was added into each sample just before the reaction in order to start the oxidation reactions. The samples were placed in an oven of +37 °C for 7 days with stirring on a magnetic tray. An aliquot of 200 μL of each sample was taken on

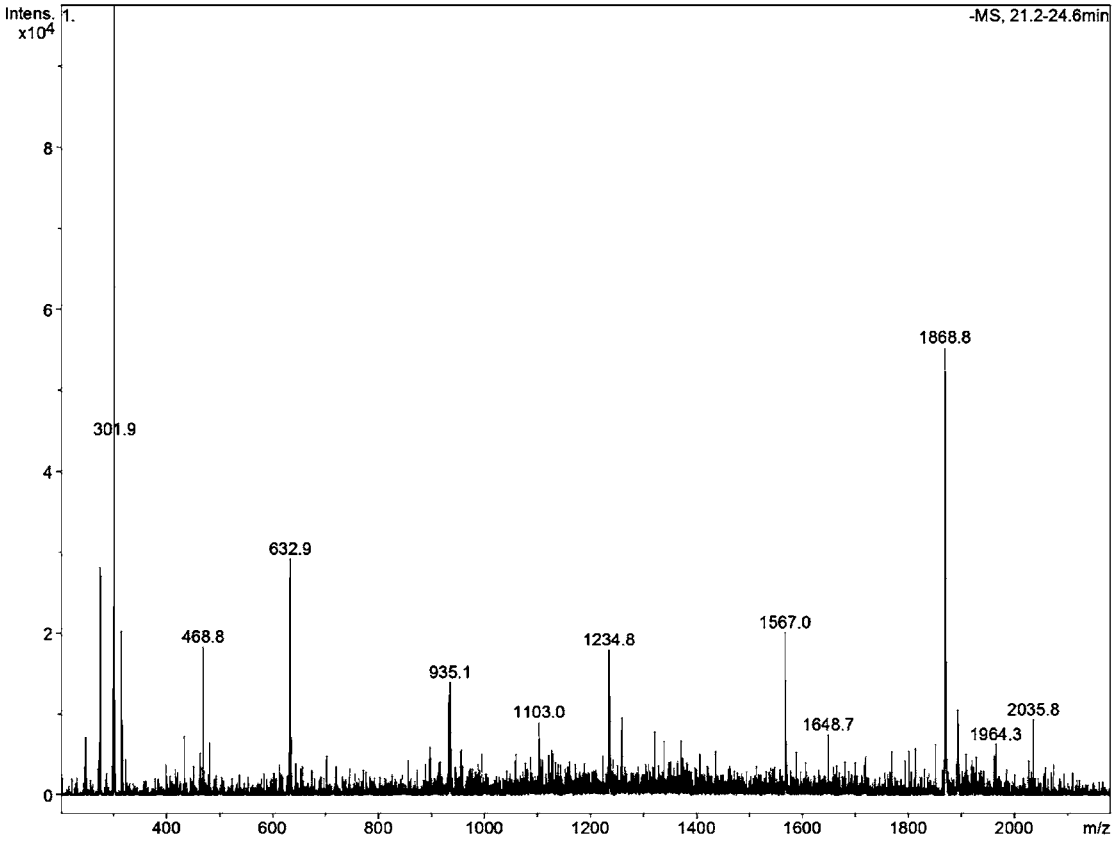

Figure 2. Full scan mass spectrum of isolated sanguiin H-6.

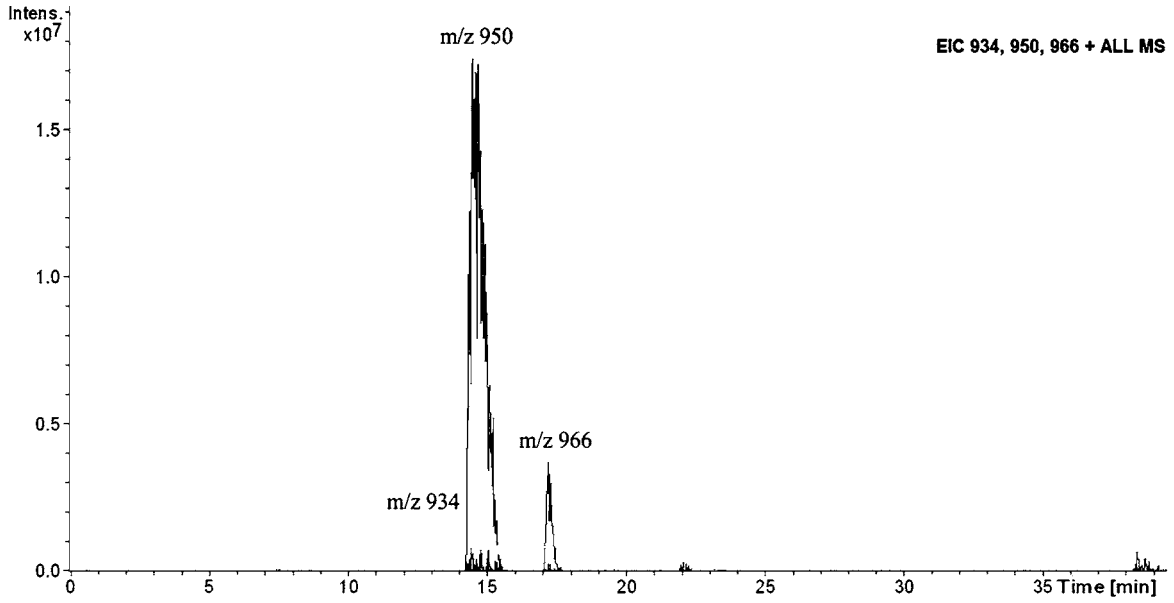

Figure 3. Extracted ion chromatograms (EIC) of the peptide LIVTQTMK ($[M + H]^+$ m/z 934), Met sulfoxide ([LIVTQTMK + O]) form of peptide LIVTQTMK, and Met sulfone ([LIVTQTMK + 2O]) form of peptide LIVTQTMK in positive mode by MS from day 0.

days 0, 1, 4, and 7 for analysis of reaction products. The sub samples were collected into Eppendorf tubes and immediately frozen at −20 °C until analysis.

Analysis of the Oxidation and Interaction Products by LC−MS. The LC−MS used in the analysis of all the oxidation samples was an Agilent 1100 HPLC including a binary pump, a degasser, an automated sample manager, a column heating unit and DAD, and fluorescence detectors (Agilent Technologies, Santa Clara, CA, U.S.A.), which were all connected to a Bruker Esquire quadrupole ion trap mass spectrometer (QIT-MS, Bremen, Germany) using ESI in both positive and negative mode. The column was a Waters XBridge BEH130 C18 (3.5 μm, 2.1 × 100 mm) together with a precolumn (both by Waters Corp., Wexford, Ireland). Injection volume was always 10 μL, and the column temperature was kept at +30 °C. Flow rate was 350 μL/min, and the eluents consisted of 0.1% formic acid in

dx.doi.org/10.1021/jf501190x | J. Agric. Food Chem. 2014, 62, 5028−5037

water (solvent A) and 0.1% formic acid in acetonitrile (solvent B). The diode array detector was set to record at 214 nm, and the fluorescence detector was set to 280 nm (Ex) and 350 nm (Em). The gradient used as well as all the MS-parameters for the positive mode were consistent with the method presented by Koivumäki et al.[8] Only in the negative mode the MS-parameters were optimized using peptides LIVTQTMK, ALPMHIR, and IPAVFK, and they were set to following: dry temperature +300 °C, dry gas 8.0 L/min, nebulizer 60.0 psi, capillary 3800 V, end plate offset −500, trap drive 102.5, capillary exit −178.5, lens-1 5.0, lens-2 60.0, and octopole rf amplitude 137.7 Vpp. For both positive and negative mode, the mass spectra were recorded in the full-scan mode over the m/z range of 200−2200 and analyzed by Bruker Daltonics Data Analysis software (Bremen, Germany).

Fragmentation of Sanguiin H-6 and Interaction Sample. Pure sanguiin H-6 sample and the sample with 162 mg of sanguiin H-6/g of peptide were also analyzed by LC-MS in negative mode. DAD and MS parameters were the same as mentioned previously, except that the nebulizer was changed to 70 psi. The m/z scan range of pure sanguiin H-6 sample was 200−2200, and it was 100−1200 for day 1 oxidation sample with 162 mg of sanguiin H-6/g of peptide.

Analysis of the Oxidation and Interaction Products by Sodium Dodecyl Sulfate Polyacrylamide Gel Electrophoresis (SDS-PAGE). Peptide and peptide-sanguiin H-6 complex (peptide-SH6) were analyzed with SDS-PAGE. Samples contained 10 μL of concentrated peptide or peptide-SH6 and 30 μL of sample buffer, which contained 12% SDS, 150 mM Tris/HCl pH 6.8, 0.05% bromophenol blue, and 30% glycerol, and they were incubated for 15 min at 37 °C and applied on gel wells.[30] The gels were Mini Protean Tris-Tricine Precast gels, 10−20% with 50 μL wells (Bio-Rad, Hercules, CA, U.S.A.). Molecular weight standard, 1.5 μL, was applied on two separate wells (Thermo Fisher, 10−170 kDa). Electrophoresis was performed using a Mini protean Electrophoresis system (Bio-Rad) at 20 °C as follows: maximum current throughout the run, 30 min at 30 V, 10 min at 60 and 100 V, until the electrophoresis was stopped. The anodic buffer was 1.0 M Tris and 0.225 M HCl at pH 8.9, and the cathodic buffer was 1.0 M Tris, 1.0 M Tricine, and 1.0% SDS at pH 8.25.[31] After the electrophoresis, the gel was fixed overnight in 30% ethanol, 0.5% acetic acid in deionized water and stained with silver.[32]

RESULTS AND DISCUSSION

MS Identification of Sanguiin H-6. A dimeric ellagitannin, sanguiin H-6, was isolated from cloudberry extracts and separated from the trimeric lambertianin C by using preparative HPLC. The isolated sanguiin H-6 was detected by MS in negative mode (Figure 2) with the fragmentation of m/z 1869. The fragment m/z 1869 of isolated sanguiin H-6 was further identified by MS/MS in negative mode. The retention time of m/z 1869 was around 23 min. These data are in accordance with earlier findings.[11,12] Hexahydroxydiphenoyl (HHDP), glucose, and galloyl groups are the basic functional groups contained in sanguiin H-6. The fragment ions of m/z 1567 (loss of HHDP), 1265 (loss of HHDP−HHDP), 1103 (loss of HHDP−HHDP-glu), and 933 (loss of HHDP−HHDP-glu-galloyl) are the characteristics for sanguiin H-6.[12] As the purity of isolated sanguiin H-6 was 96%, the rest of the extract contained peduculagin/casuarictin isomers because of the detection of m/z 1567, which was $[2M - H]^-$ of an ion m/z 783, potentillin/casuarictin due to $[M - H]^-$ at m/z 935, and its further fragmentation at m/z 633 was observed in the mass spectra of isolated sanguiin H-6 extracts (Figure 2).[33−35]

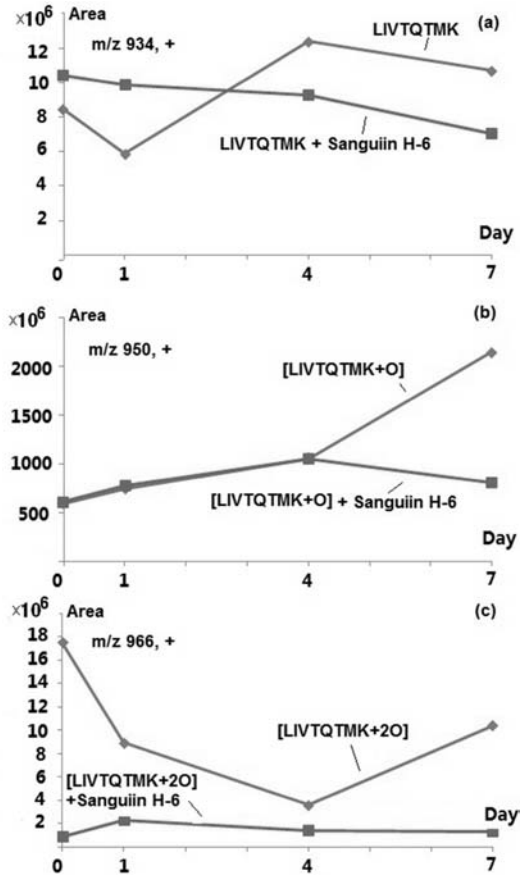

Figure 4. Changes of the amounts of peptide LIVTQTMK and its oxidation products in the samples with and without 1000 μg/g sanguiin H-6 and in positive mode detection (a) LIVTQTMK ($[M + H]^+$ m/z 934), (b) [LIVTQTMK + O] ($[M + H]^+$ m/z 950), and (c) [LIVTQTMK + 2O] ($[M + H]^+$ m/z 966).

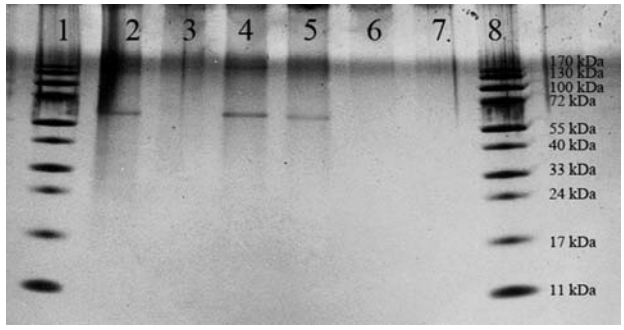

Figure 5. SDS PAGE gel with wells 1 and 8 for molar weight markers, well 2 with day 0 peptide LIVTQTMK, well 3 with day 7 peptide LIVTQTMK, wells 4 and 5 with replicate samples of day 7 peptide LIVTQTMK with high concentration (with 162 mg of sanguiin H-6/1 g of peptide) sanguiin H-6, and wells 6 and 7 empty.

Oxidation Products of Peptide LIVTQTMK and Its Interaction with Sanguiin H-6. Methionine sulfoxide (m/z 950) and methionine sulfone (m/z 966) forms of peptide LIVTQTMK were already observed in positive mode on day 0 (Figure 3), as previously reported by Koivumäki et al.[8] The amount of the unoxidized peptide LIVTQTMK (m/z 934) on day 0 was higher in the samples containing sanguiin H-6

dx.doi.org/10.1021/jf501190x | J. Agric. Food Chem. 2014, 62, 5028−5037

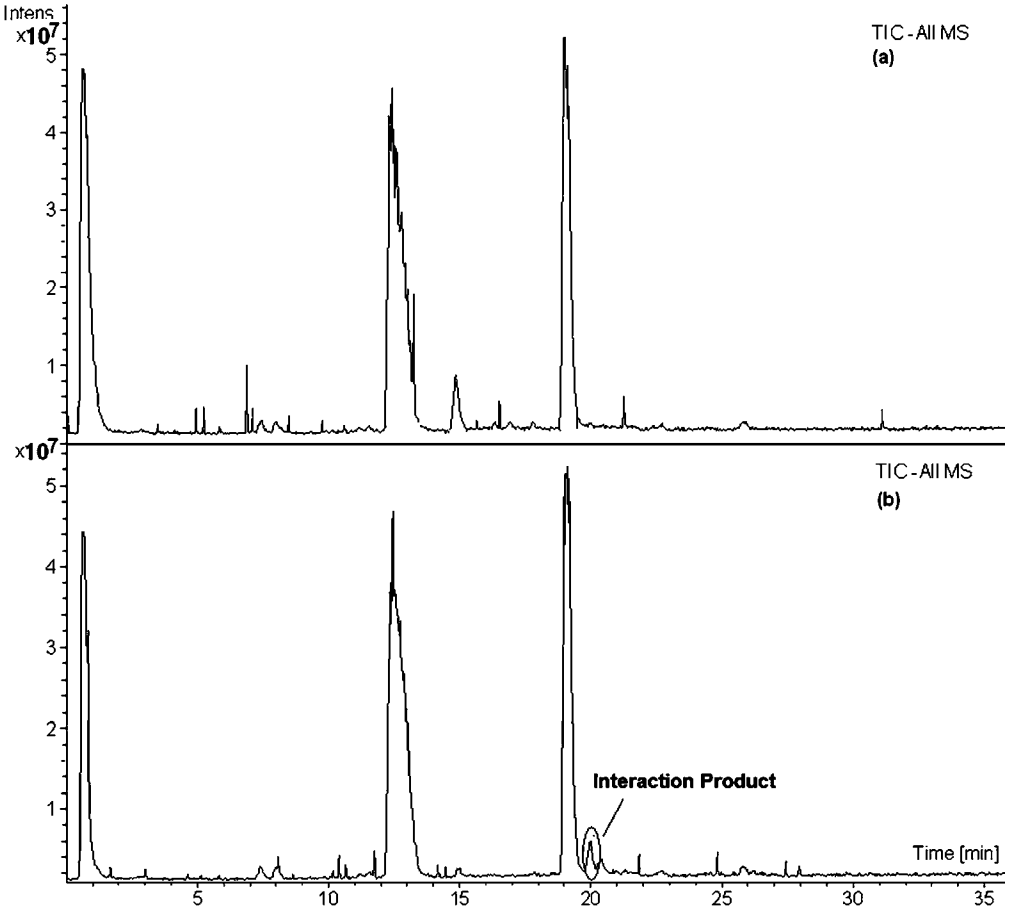

Figure 6. Day 0 LC-MS chromatograms in negative mode: (a) TIC of peptide LIVTQTMK without sanguiin H-6 and (b) TIC of peptide LIVTQTMK with 1000 μg/g of sanguiin H-6.

compared to the samples without sanguiin H-6 where the unoxidized peptide m/z 934 was not detectable (Figure 3). This may be due to the reduction of the methione sulfoxide form of peptide LIVTQTMK (by sanquiin H-6) back to the nonoxidized methionine residues in the peptide.[36] In the presence of sanquiin H-6, the unoxidized peptide m/z 934 continued to decrease (Figure 4a), which may be partly due to adduct formation as the amount of oxidized peptide forms did not increase (Figure 4 b, 4 c). In samples without sanguiin H-6 (Figure 4c), more of the methionine sulfone form of the peptide (m/z 966) was formed from methionine sulfoxide (m/z 950) because of further oxidation. For all the three ions (m/z 934, 950, 966), the trends of ion change were much less significant with sanguiin H-6 than for those without (Figure 4). This might indicate a significant slow scavenging step with sanguiin H-6 present, which maintained the stability of the sample system.[37] Rapid scavenging activity of sanguiin H-6 has earlier been seen toward lipid oxidation.[12] Sanguiin H-6 has been reported to donate an electron to highly reactive free radicals and to suppress the reactivity of the radical by delocalization of the unpaired electron on the phenolic ring.[38,39] Sanguiin H-6 might interact with protein through hydrogen bonding, hydrophobic bonding, or ionic bonding.[18−20,40,41] For example, for hydrogen bonding, the carbonyl functional groups of the amino acids or peptide backbone and the isolated phenolic hydroxyl group in the polyphenolic form a strong hydrogen bond during protein−polyphenol interaction.[15,42−45] It is postulated that when sanguiin H-6 interacts with ß-Lg with forming adducts this prevents the peptide from undergoing oxidation.

The gel electrophoresis showed the peptide LIVTQTMK on day 7 with replicate samples of sanguiin H-6 (well 4 and well 5), with two lines on both, one around 170 kDa and the other between 55 and 72 kDa (Figure 5). The peptide LIVTQTMK sample also displayed one line between 55 and 72 kDa on day 0 (well 2), but none was detected on day 7 with the oxidized peptide sample (well 3). Because the molar weight of peptide LIVTQTMK was less than 10 kDa (the cutoff of the gel), the peptide LIVTQTMK alone in the sample cannot be detected. It is assumed that the masses around 170 kDa and possibly also around 55−72 kDa might be due to the interaction products between sanguiin H-6 and peptide LIVTQTMK.

The interaction between peptide and sanguiin H-6 and the radical scavenging activity of sanguiin H-6 were observed by LC-MS in the negative mode. Normally, the peptide is detected in positive mode by LC-MS, whereas some of the phenolic compounds such as ellagitannins can only be perceived in negative mode.[12] The dimeric sanguiin H-6 with m/z of 1869 at $[M - H]^-$ in negative mode is shown in Figure 2. In the sample containing 1000 μg sanguiin H-6 per gram peptide LIVTQTMK, a new peak was found at retention time of 20 min compared with the sample without sanguiin H-6 on day 0 (Figure 6). The fragment ions m/z 1119 and m/z 997 that were detected on day 0 in negative mode may be the oxidation products of sanguiin H-6 fragments, which were m/z 1103 resulting in Δm = +16 amu (sanguiin H-6 loss of HHDP−HHDP-glu + O) and m/z 933

dx.doi.org/10.1021/jf501190x | J. Agric. Food Chem. 2014, 62, 5028−5037

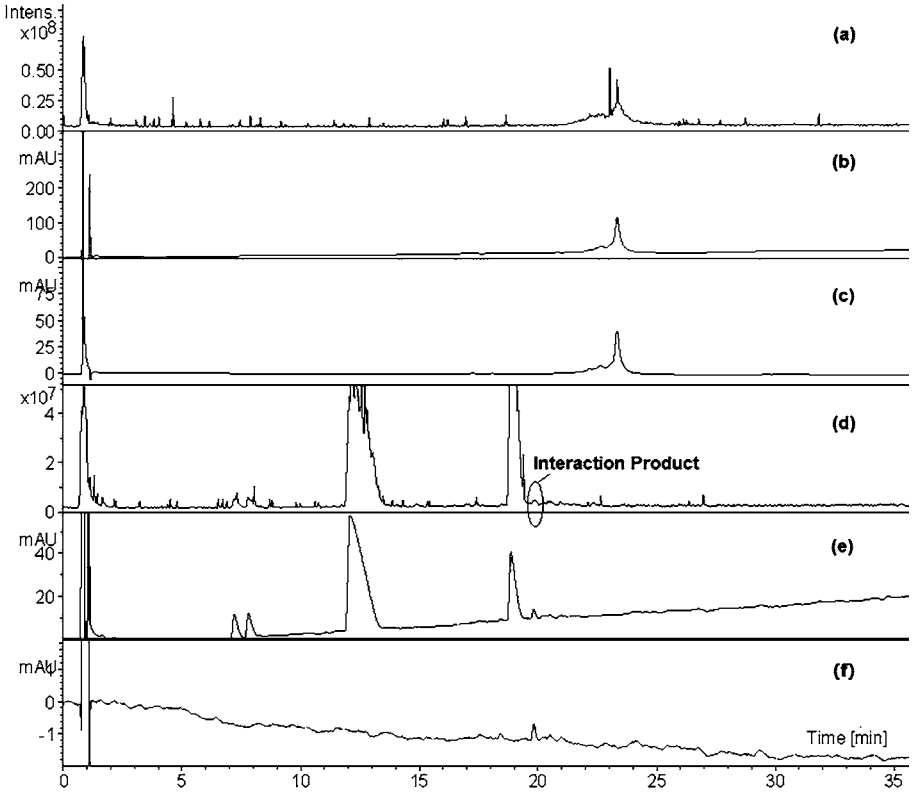

Figure 7. Sanguiin H-6 and interaction sample. (a) TIC of sanguiin H-6. (b) Chromatogram of sanguiin H-6 with UV detection at 210 nm. (c) Chromatogram of sanguiin H-6 with UV detection at 280 nm. (d) Day 0 TIC of peptide LIVTQTMK with a high concentration (with 162 mg of sanguiin H-6/1 g of peptide) of sanguiin H-6. (e) Chromatogram of peptide LIVTQTMK with a high concentration (with 162 mg of sanguiin H-6/1 g of peptide) of sanguiin H-6 with UV detection at 210 nm. (f) Chromatogram of peptide LIVTQTMK with a high concentration (with 162 mg of sanguiin H-6/1 g of peptide) of sanguiin H-6 with UV detection at 280 nm.

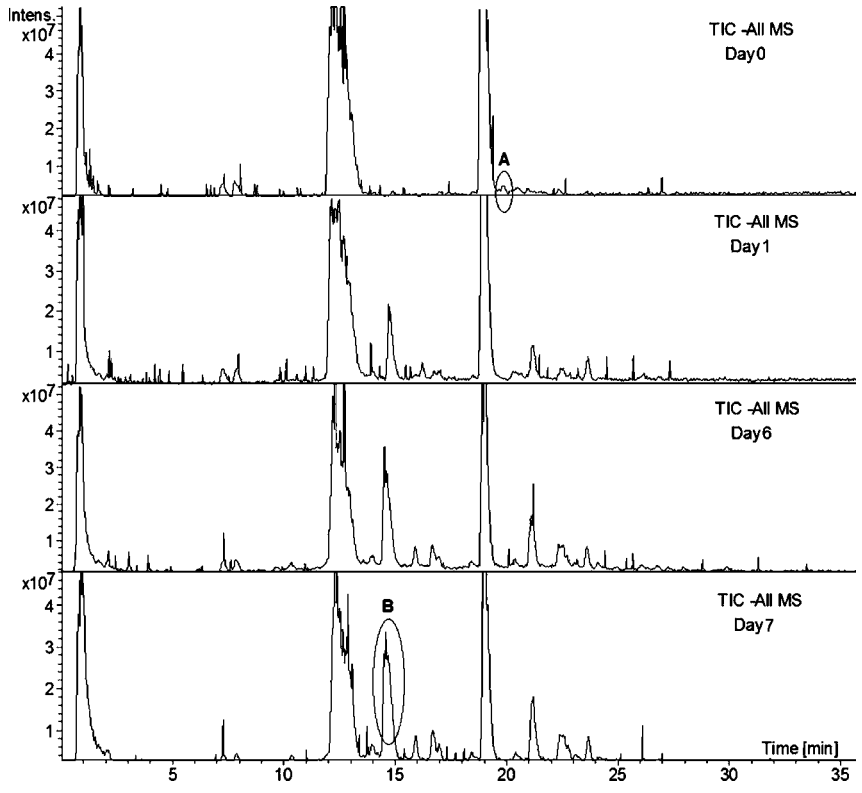

Figure 8. TIC of peptide LIVTQTMK with a high concentration (with 162 mg of sanguiin H-6/1 g of peptide) of sanguiin H-6 from days 0, 1, 6, and 7. Peaks A and B refer to interaction products.

dx.doi.org/10.1021/jf501190x | J. Agric. Food Chem. 2014, 62, 5028−5037

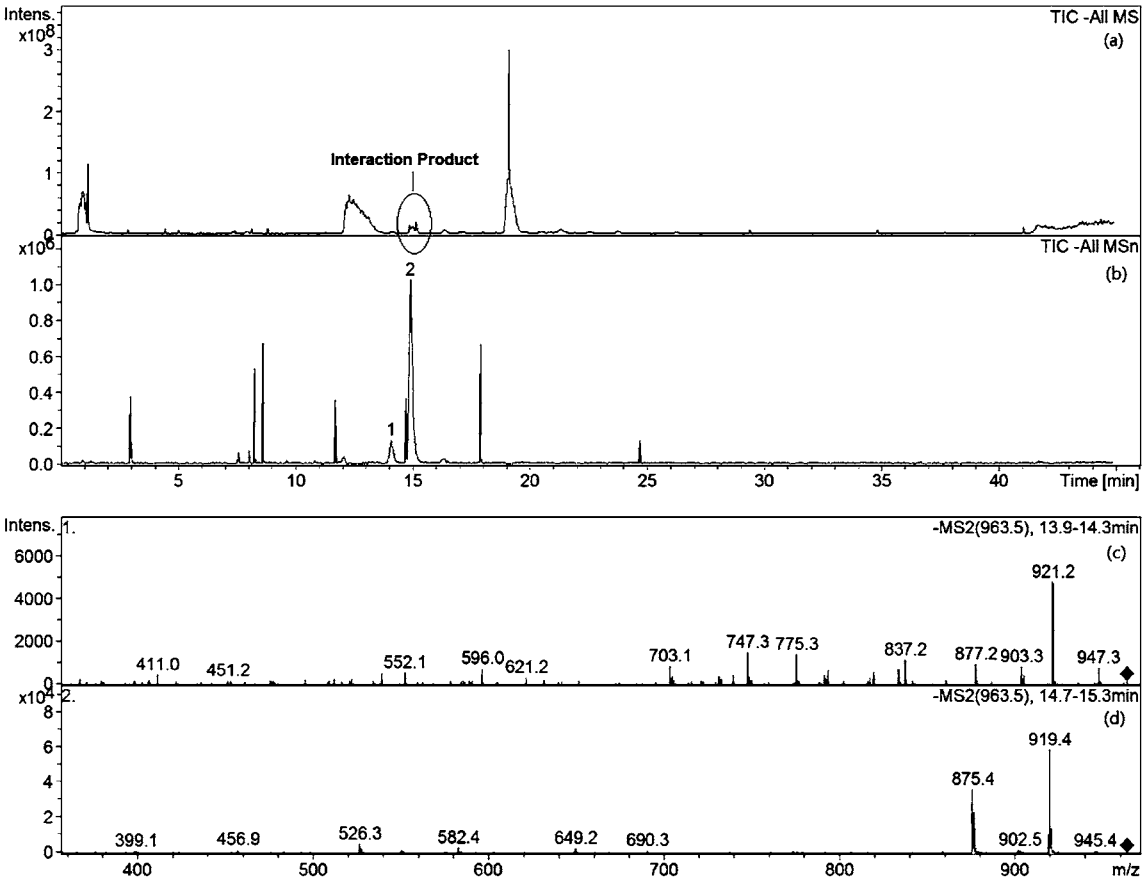

Figure 9. Peptide LIVTQTMK with a high concentration (with 162 mg of sanguiin H-6/1 g of peptide) from day 1 (a) TIC, (b) TIC of fragmentation of m/z 963.5, (c) MS/MS spectrum of peak 1, and (d) MS/MS spectrum of peak 2.

with +64 amu addition (sanguiin H-6 loss of HHDP−HHDP-glu-galloyl +4O). This suggests that the oxidation of sanguiin H-6 itself happened quite rapidly on day 0. The detection of ion m/z 963.5 and its extracted ion chromatogram reveal that the interaction product between oxidized peptide and oxidized ellagitannin monomer (casuarictin) with doubly charged ions was generated on day 0. Even though the intensity of m/z 963 was relatively low, m/z 963 is very likely to be the interaction product between peptide LIVTQTMK and sanguiin H-6.

The same peak indicating the formation of an interaction product was also detected at a retention time of 20 min (Figure 7d) in the samples containing a higher proportion of sanguiin H-6 to that of peptide (162 mg of sanguiin H-6/1 g of peptide). The peak of sanguiin H-6 (Figure 7a) was not detected on day 0 in the sample of sanguiin H-6 with peptide LIVTQTMK, whereas a new peak appearing at a retention time of 20 min (Figure 7d) was also detected both at 210 and 280 nm. This indicates the presence of both peptide bond and phenolic group, supporting the conclusion that the new peak is an interaction product of sanguiin H-6 and peptide LIVTQTMK. Other peaks (with retention times between 14 and 24 min, Figure 8) were found in the total ion chromatogram (TIC) in the samples with a higher concentration of sanguiin H-6 with peptide LIVTQTMK. The areas of these six peaks were increasing from day 0 to day 7. Peak A disappeared after day 1, which could indicate that further oxidation occurred. Peak B, around 15 min in Figure 8, seems to be the main interaction product with covalent bonding, as it was also identified in Figure 9. This figure also shows the $[M - H]^-$ m/z 963, which was further fragmented to m/z 919 and m/z 875. Compared to the MS/MS of peak 1 and 2 (Figure 10b), 877, 921, and m/z 947 in Figure 10c were 2 amu different compared with 875, 919, and m/z 945 in Figure 10d, which indicated there might be a double bond breakage. Furthermore, the 17 amu difference between m/z 921 and m/z 903 (Figure 9c), as well as m/z 902 and m/z 919 (Figure 9d), indicated that there might be an addition of ammonia. Lysine and methionine residues in peptide LIVTQTMK might be responsible for the interaction between peptide LIVTQTMK and sanguiin H-6. The interaction may occur owing to the hydrophoblic section in the side chain of lysine and methionine.[18,46−49] In addition, lysine has a positive charge near neutral pH, which makes it possible to interact with the carboxylate group or the aromatic ring of sanguiin H-6.

Oxidation Products of Peptide ALPMHIR and Its Interaction with Sanguiin H-6. Peptide ALPMHIR was detected with $[M + H]^+$ m/z 838 in positive mode and $[M - H]^-$ m/z 836 in negative mode by LC-MS. Met, His, and Pro present in peptide ALPMHIR are rather prone to be monoxidized, whereas Pro, Arg, and Met tend to be dioxidized.[2] [ALPMHIR + O] was observed to be the most prominent oxidation product formed during oxidation for 7 days, as earlier reported also by Koivumäki et al.[8] Similarly to peptide LIVTQTMK ($[M + H]^+$ m/z 934), during the oxidation process, the color of the peptide ALPMHIR ($[M + H]^+$ m/z 838) samples changed from transparent to lightly yellowish with tiny milky-white particles dissolving out from time to time. The precipitations were probably due to instable haze formed due to interaction between peptide and sanguiin H-6.

dx.doi.org/10.1021/jf501190x | J. Agric. Food Chem. 2014, 62, 5028−5037

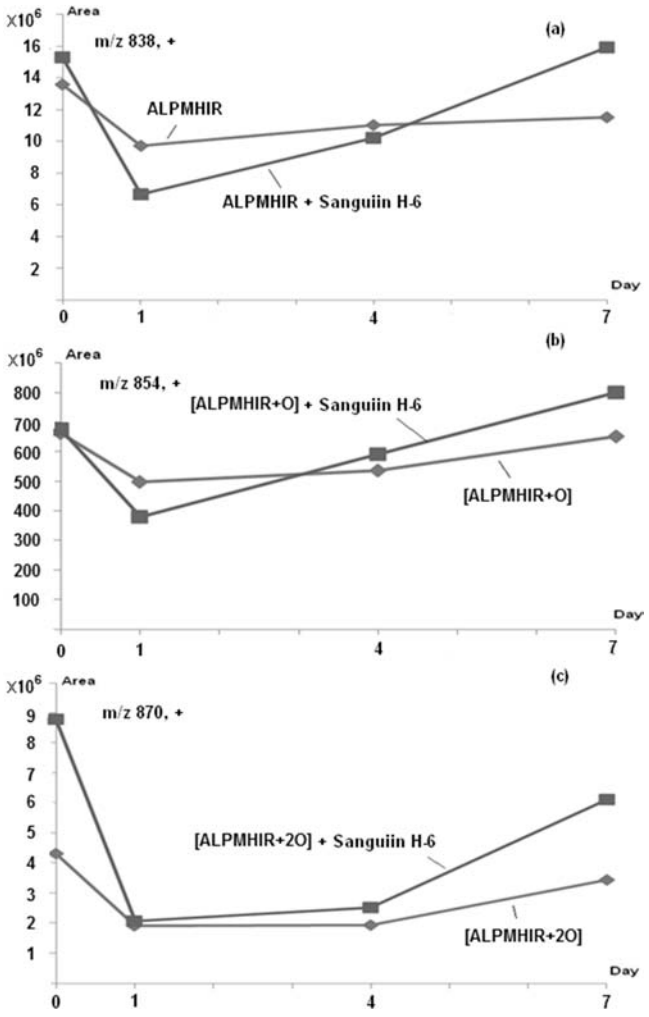

Figure 10. Changes in the amounts of peptide ALPMHIR and its oxidation products in the samples with and without 1000 μg/g sanguiin H-6 in positive mode detection in (a) ALPMHIR ($[M + H]^+$ m/z 838), (b) [ALPMHIR + O] ($[M + H]^+$ m/z 854), and (c) [ALPMHIR + 2O] ($[M + H]^+$ m/z 870).

The general trends of amounts for the peptide ALPMHIR ($[M + H]^+$ m/z 838) and its oxidation products ($[M + H]^+$ m/z 854 and $[M + H]^+$ m/z 870) were very analogous. They all decreased from day 0 to day 1 and increased through day 1 to day 7. The difference between the samples with and without sanguiin H-6 was that the changes of peptide and the amounts of its oxidation products were more stable without sanguiin H-6 than those with sanguiin H-6, thus contradicting the findings with peptide LIVTQTMK. Moreover, the rate of decline for the ion m/z 870 was faster than for the ions of m/z 838 and m/z 854 from day 0 to day 7 (Figure 10). On day 0, both monoxidized and dioxidized forms of peptide ALPMHIR (m/z 854 and m/z 870) were detected. The amount of unoxidized peptide ALPMHIR (m/z 838) was higher in the samples with sanguiin H-6 than without sanguiin H-6 because of the antioxidant or scavenging activity of sanguiin H-6 (Figure 10a). For [ALPMHIR + O], the amount in the sample with sanguiin H-6 was similar to that without sanguiin H-6 (Figure 10b). The reason might be that the oxidation of peptide ALPMHIR took place even more rapidly than the fast radical scavenging activity of sanguiin H-6. Therefore, the radical scavenging activity of sanguiin H-6 was not significant on day 0 for the very first oxidation step of peptide ALPMHIR. For the dioxidized form of peptide ALPMHIR (m/z 870), the amount of that in the samples with sanguiin H-6 was even higher (Figure 10c). This may be due to the dioxidation of proline, arginine, and methionine that occurred so rapidly and even faster than the scavenging activity of sanguiin H-6. Sanguiin H-6 may also have inhibited the further oxidation of dioxidized form of peptide ALPMHIR, and the amount of [ALPMHIR + 2O] was lower in the sample without sanguiin H-6, because many of them might be further oxidized. Contradictory to peptide LIVTQTMK, the sample without sanguiin H-6 was more stable than that with added sanguiin H-6 for peptide ALPMHIR. The reason might be the different amino acid composition of the peptides. Tannin presents both a fast and a significant slow scavenging step in the sample. Proline, methionine, histidine, lysine, and methionine are all capable to interact with sanguiin H-6. For example, proline residues could provide a hydrophobic binding site through pyrrolidine rings and may associate with aromatic rings in sanguiin H-6.[18,46−48] Therefore, besides oxidations on different residues, phenolic−protein interaction, antioxidant, and scavenging activity of sanguiin H-6 were occurring together in the sample with sanguiin H-6. Thus, the amount of interaction products was less stable. The tiny milky-white precipitation particles dissolved out from time to time were likely to be the haze due to the interaction between peptide ALPMHIR and sanguiin H-6 because the peptide ALPMHIR contains proline, which is usually rich in haze-forming proteins.[46] The haze was invisible to the eye until the formation of the polyphenol protein agglomeration precipitate. It was a less soluble entity most likely formed by the cross-linking of hydroxyl groups presented in polyphenol and protein molecules.[50] Therefore, the presence of haze also indicated the existence of unstable interaction products.

Oxidation Products of Peptide IPAVFK and Its Interaction with Sanguiin H-6. The peptide was detected at $[M + H]^+$ m/z 674 in positive mode and $[M - H]^-$ m/z 672 in negative mode by LC-MS. Phe (F) is known to be the most vulnerable residue to be oxidized due to its aromatic side chain.[51] However, peptide IPAVFK at $[M - H]^-$ m/z 672 was relatively stable and not easily and rapidly oxidized. There were no oxidation products significant enough to be quantified for peptide IPAVFK ($[M + H]^+$ m/z 674), as compared to the peptide LIVTQTMK ($[M + H]^+$ m/z 934) and the peptide ALPMHIR ($[M + H]^+$ m/z 838), in positive mode detection by MS.

Total ion chromatograms in Figure 11 were acquired from LC-ESI-MS in negative mode detection through oxidation day 0 to day 7. Two sets of samples were monitored, one is fractionated β-Lg peptide IPAVFK and the other is fractionated peptide IPAVFK with 1000 μg/g sanguiin H-6. When the peak integration was done by using the total ion chromatogram, several different analytes eluted simultaneously.

The amount of peptide IPAVFK did not change considerably in the samples with and without sanguiin H-6 on day 0. The same occurred also on day 7. Fewer peaks could be detected in the sample with sanguiin H-6 than without both on day 0 and day 7. The changes of peak areas of interaction products were not significant enough to be observed in the total ion chromatograms.

In negative mode, there were fewer peaks in the sample with sanguiin H-6 than that without. This may be because the scavenging activity of sanguiin H-6. Sanguiin H-6 interacted with other nontarget peptides and stabilized the reaction system. On day 7, unoxidized form of peptide IPAVFK ($[M - H]^-$ m/z 672) was still existing but slightly decreased as compared to day 0.

dx.doi.org/10.1021/jf501190x | J. Agric. Food Chem. 2014, 62, 5028−5037

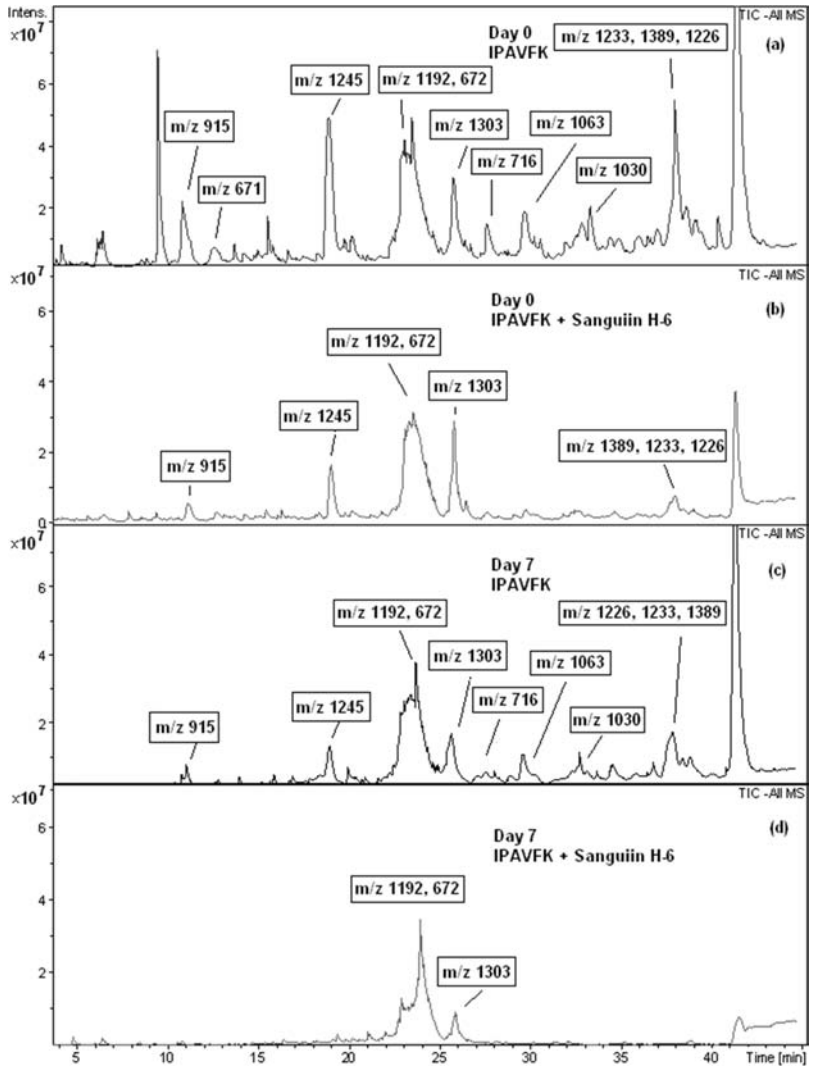

Figure 11. TIC of peptide IPAVFK with and without sanguiin H-6 in negative mode. (a) TIC of peptide IPAVFK without sanguiin H-6 on day 0. (b) TIC of peptide IPAVFK with 1000 μg/g of sanguiin H-6 on day 0. (c) TIC of peptide IPAVFK without sanguiin H-6 on day 7. (d) TIC of peptide IPAVFK with 1000 μg/g of sanguiin H-6 on day 7.

AUTHOR INFORMATION

Corresponding Author

*E-mail: Marina.Heinonen@helsinki.fi. Tel.: +358-2-941-58224.

Notes

The authors declare no competing financial interest.

REFERENCES

(1) Chicon, R. Hydrolysis under high hydrostatic pressure as a means to reduce the binding of beta-lactoglobulin to immunoglobulin E from human sera. *J. Food Prot.* **2008**, *71*, 1453−1459.

(2) Guedes, S.; Vitorino, R.; Domingues, M. R. M.; Amado, F.; Domingues, P. Oxidative modifications in glycated insulin. *Anal. Bioanal. Chem.* **2010**, *397*, 1985−1995.

(3) Berlett, B.; Stadtman, E. Protein oxidation in aging, disease, and oxidative stress. *J. Biol. Chem.* **1997**, *272*, 20313−20316.

(4) Elias, R. J.; McClements, D. J.; Decker, E. A. 2005. Antioxidant activity of cysteine, tryptophan and methionine residues in continuous phase beta-lactoglobulin in oil-in-water emulsions. *J. Agric. Food Chem.* **2005**, *53*, 10248−10253.

(5) Elias, R. J.; Bridgewater, J. D.; Vachet, R. W.; Waraho, T.; McClements, D. J.; Decker, E. A. Antioxidant mechanisms of enzymatic hydrolysates of beta-lactoglobulin in food lipid dispersions. *J. Agric. Food Chem.* **2006**, *54*, 9565−9572.

(6) Hernandez-Ledesma, B.; Davalos, A.; Bartolome, B.; Amigo, L. Preparation of antioxidant enzymatic hydrolysates from alpha-lactalbumin and from beta-lactoglobulin. Identification of active peptides by HPLC-MS/MS. *J. Agric. Food Chem.* **2005**, *53*, 588−593.

(7) Liu, H. C.; Chen, W. L.; Mao, S. J. T. Antioxidant nature of bovine milk beta-lactoglobulin. *J. Dairy Sci.* **2007**, *90*, 547−555.

(8) Koivumäki, T.; Gürbüz, G.; Poutanen, M.; Heinonen, M. A novel LC-MS application to investigate oxidation of peptides isolated from β-lactoglobulin. *J. Agric. Food Chem.* **2012**, *60*, 6799−6805.

(9) Viljanen, K.; Kivikari, R.; Heinonen, M. Protein−lipid interactions during liposome oxidation with added anthocyanin and other phenolic compounds. *J. Agric. Food Chem.* **2004**, *52*, 1104−1111.

(10) Viljanen, K.; Kylli, P.; Kivikari, R.; Heinonen, M. Inhibition of protein and lipid oxidation in liposomes by berry phenolics. *J. Agric. Food Chem.* **2004**, *52*, 7419−7424.

(11) McDougall, G.; Martinussen, I.; Stewart, D. Towards fruitful metabolomics: High throughput analyses of polyphenol composition in berries using direct infusion mass spectrometry. *J. Chromatogr.* **2008**, *871*, 362−369.

(12) Kähkönen, M.; Kylli, P.; Ollilainen, V.; Salminen, J. P.; Heinonen, M. Antioxidant activity of isolated ellagitannins from red raspberries and cloudberries. *J. Agric. Food Chem.* **2012**, *60*, 1167−1174.

(13) Loomis, W. D.; Battaile, J. Plant phenolic compounds and the isolation of plant enzymes. *Phytochemistry* **1966**, *5*, 423−438.

(14) Siebert, K. J.; Troukhanova, N. V.; Lynn, P. Y. Nature of polyphenol−protein interactions. *J. Agric. Food Chem.* **1996**, *44*, 80−85.
(15) Hagerman, A. E.; Rice, M. E. Mechanisms of protein precipitation for two tannins pentagalloyl glucose and epicatechin. *J. Agric. Food Chem.* **1998**, *46*, 2590−2595.
(16) Sarni-Manchado, P.; Cheynier, V.; Moutounet, M. Interactions of grape seed tannins with salivary proteins. *J. Agric. Food Chem.* **1999**, *47*, 42−47.
(17) Kroll, J.; Rawel, H. M.; Seidelmann, N. Physicochemical properties and susceptibility to proteolytic digestion of myoglobin-phenol derivatives. *J. Agric. Food Chem.* **2000**, *48*, 1580−1587.
(18) Suryaprakash, P.; Kumar, R. P.; Prakash, V. Thermodynamics of interaction of caffeic acid and quinic acid with multisubunit proteins. *Int. J. Biol. Macromol.* **2000**, *27*, 219−228.
(19) Rawel, H. M.; Rohn, S.; Kroll, J. Influence of a sugar moiety (rhamnosylglucoside) at 3-O position on the reactivity of quercetin with whey proteins. *Int. J. Biol. Macromol.* **2003**, *32*, 109−120.
(20) Simon, C.; Barathieu, K.; Laguerre, M.; Schmitter, J. M.; Fouquet, E.; Pianet, I.; Dufourc, E. J. Three-dimensional structure and dynamics of wine tannin-saliva protein complexes. A multitechnique approach. *Biochemistry* **2003**, *42*, 10385−10395.
(21) Ricardo da Silva, J. M.; Cheynier, V.; Souquet, J. M.; Moutounet, M.; Cabanis, J. C.; Bourzeix, M. Interaction of grape seed procyanidins with various proteins in relation to wine fining. *J. Sci. Food Agric.* **1991**, *57*, 111−125.
(22) Prigent, S. V. E.; Gruppen, H.; Visser, AJWG.; van Koningsveld, G. A.; de Jong, G. A. H.; Voragen, A. G. J. Effects of non-covalent interactions with 5-*O*-caffeoylquinic acid (chlorogenic acid) on the heat denaturation and solubility of globular proteins. *J. Agric. Food Chem.* **2003**, *51*, 5088−5095.
(23) Rawel, H. M.; Kroll, J.; Hohl, U. C. Model studies on reaction of plant phenols with whey proteins. *Nahrung* **2001**, *45*, 72−81.
(24) Rawel, H. M.; Kroll, J.; Rohn, S. Reactions of phenolic substances with lysozyme—physicochemical characterization and proteolytic digestion of the derivatives. *Food Chem.* **2001**, *72*, 59−71.
(25) Loo, J. A.; Hu, P.; McConnell, P.; Mueller, W. T.; Sawyer, T. K.; Thanabal, V. A study of Src SH2 domain protein−phosphopeptide binding interactions by electrospray ionization mass spectrometry. *J. Am. Soc. Mass Spectrom.* **1997**, *8*, 234−243.
(26) Pramanik, B. N.; Bartner, P. L.; Mirza, U. A.; Liu, Y. H.; Ganguly, A. K. Electrospray ionization mass spectrometry for the study of non-covalent complexes: an emerging technology. *J. Mass Spectrom.* **1998**, *33*, 911−920.
(27) Bligh, S. W. A.; Haley, T.; Lowe, P. N. Measurement of dissociation constants of inhibitors binding to Src SH2 domain protein by non-covalent electrospray ionization mass spectrometry. *J. Mol. Recognit.* **2003**, *16*, 139−147.
(28) Kapur, A.; Beck, J. L.; Brown, S. E.; Dixon, N. E.; Sheil, M. M. Use of electrospray ionisation mass spectrometry to study binding interactions between a replication terminator protein and DNA. *Protein Sci.* **2002**, *11*, 147−157.
(29) Sobott, F.; Benesch, J. L. P.; Vierling, E.; Robinson, C. V. Subunit exchange of multimeric protein complexes. Real-time monitoring of subunit exchange between small heat shock proteins by using electrospray mass spectrometry. *J. Biol. Chem.* **2002**, *277*, 38921−38929.
(30) Gasperotti, M.; Masuero, D.; Vrhovsek, U.; Guella, G.; Mattivi, F. Profiling and accurate quantification of *Rubus* ellagitannins and ellagic acid conjugates using direct UPLC-Q-TOF HDMS and HPLC-DAD analysis. *J. Agric. Food Chem.* **2010**, *58*, 4602−4616.
(31) Schägger, H. Tricine-SDS-PAGE. *Nat. Protoc.* **2006**, *1* (1), 16−22.
(32) O'Connel, K.; Stults, J. Identification of mouse liver proteins on two-dimensional electrophoresis gel by matrix-assisted laser desorption/ionization mass spectrometry of in situ enzymatic digests. *Electrophoresis* **1997**, *18*, 349−359.
(33) Moilanen, J.; Salminen, J.-P. Ecologically neglected tannins and their biologically relevant activity: chemical structures of plant ellagitannins reveal their in vitro oxidative activity at high pH. *Chemoecology* **2008**, *18*, 73−83.
(34) Salminen, J.-P.; Ossipov, V.; Loponen, J.; Haukioja, E.; Pihlaja, K. Seasonal variation in the content of hydrolysable tannins in leaves of *Betula pubescens*. *J. Chromatogr. A* **1999**, *864*, 283−291.
(35) Salminen, J.-P.; Ossipov, V.; Haukioja, E.; Pihlaja, K. Seasonal variation in the content of hydrolysable tannins in leaves of *Betula pubescens*. *Phytochemistry* **2001**, *57*, 15−22.
(36) Davies, M. J.; Fu, S.; Wang, H.; Dean, R. T. Stable markers of oxidative damage to proteins and their application in the study of human disease. *Free Radical Biol. Med.* **1999**, *27*, 1151−1163.
(37) Riedl, K. M.; Hagerman, A. E. Tannin−protein complexes as radical scavengers and radical sinks. *J. Agric. Food Chem.* **2001**, *49*, 4917−4923.
(38) Chimi, H.; Chillard, J.; Cillard, P.; Rahamani, M. Peroxyl and hydroxyl radical scavenging activity of some natural phenolic antioxidants. *J. Am. Oil Chem. Soc.* **1991**, *68*, 307−312.
(39) Husain, S. R.; Cillard, J.; Cillard, P. Hydroxyl radical scavenging activity of flavonoids. *Phytochemistry* **1987**, *26*, 2489−2491.
(40) Sarni-Manchado, P.; Cheynier, V.; Moutounet, M. Interactions of grape seed tannins with salivary proteins. *J. Agric. Food Chem.* **1999**, *47*, 42−47.
(41) Kroll, J.; Rawel, H. M.; Seidelmann, N. Physicochemical properties and susceptibility to proteolytic digestion of myoglobin-phenol derivatives. *J. Agric. Food Chem.* **2000**, *48*, 1580−1587.
(42) Van Buren, J. P.; Robinson, W. B. Formation of complexes between protein and tannic acid. *J. Agric. Food Chem.* **1969**, *17*, 772−777.
(43) Loomis, W. D. Overcoming problems of phenolics and quinones in the isolation of plant enzymes and organelles. *Methods Enzymol.* **1974**, *31*, 528−544.
(44) Hagerman, A. E.; Butler, L. G. The specificity of proanthocyanidin−protein interactions. *J. Biol. Chem.* **1981**, *256*, 4494−4497.
(45) De Freitas, V.; Mateus, N. Nephelometric study of salivary protein−tannin aggregates. *J. Sci. Food Agric.* **2001**, *82*, 113−119.
(46) Baxter, N. J.; Lilley, T. H.; Haslam, E.; Williamson, M. P. Multiple interactions between polyphenols and a salivary proline-rich protein repeat result in complexation and precipitation. *Biochemistry* **1997**, *36*, 5566−5577.
(47) Naurato, N.; Wong, P.; Lu, Y.; Wroblewski, K.; Bennick, A. Interaction of tannin with human salivary histatins. *J. Agric. Food Chem.* **1999**, *47*, 2229−2234.
(48) Charlton, A. J.; Haslam, E.; Williamson, M. P. Multiple conformations of the prolinerich protein/epigallocatechin gallate complex determined by time-averaged nuclear overhauser effect. *J. Am. Chem. Soc.* **2002**, *124*, 9899−9905.
(49) *Flavonoids: Chemistry, Biochemistry, and Applications* Andersen, O. M., Markham, K. R., Eds.; CRC Taylor & Francis: Boca Raton, FL, 2005; pp 443−470.
(50) *Beer: A quality perspective. Handbook of alcoholic beverages series*; Bamforth, C. W., Eds.; Elsevier: Oxford, U.K., 2009; pp 138−146.
(51) Hong, H. Role of aromatic side chains in the folding and thermodynamic stability of integral membrane proteins. *J. Am. Chem. Soc.* **2007**, *129*, 8320−8327.

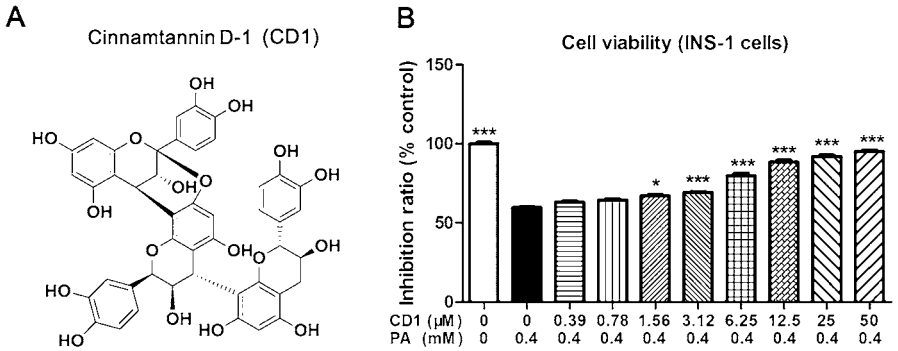

Figure 1. Cinnamtannin D-1 (CD1) protects INS-1 cells from PA-induced decrease in cell viability. (A) Chemical structure of CD1. (B) CD1 protection against PA-induced decreasing of cell viability in INS-1 cells. Cell viability was detected, and the results are shown as inhibition ratio (% of control). All data are expressed as the mean ± SE ($n = 6$). Asterisks denote significant difference versus the PA-treated alone group (∗, $p < 0.05$; ∗∗, $p < 0.01$; ∗∗∗, $p < 0.001$).

restoration of PA-injured insulin secretion in islets by CD1 was also observed.

MATERIALS AND METHODS

Materials and Reagents. All general reagents for cell culture were purchased from Hyclone, Shanghai, China; PA, bovine serum albumin (BSA), Hoechst 33342, 3-(4,5-dimethylthiazol-2-yl)-2,5-diphenyl tetrazolium bromide (MTT), and chloromethyl-2′,7′-dichlorodihydrofluorescein diacetate acetyl ester (CM-H_2DCFDA) were purchased from Sigma-Aldrich, Shanghai, China. A Total Nitric Oxide Assay Kit was obtained from Beyotime, Shanghai, China.

Source of CD1. CD1 (Figure 1A) was isolated from the bark of *C. tamala* as previously described.[17] The structure of CD1 was confirmed by mass spectrometry (MS) and nuclear magnetic resonance (NMR). The compound purity was approved by high-performance liquid chromatography (HPLC: column, Agilent Extend C18 column, 5 μm, 4.6 mm × 250 mm; solvent system, acetonitrile−0.2% acetic acid with gradient elution; flow rate, 1 mL/min; UV detection, 280 nm; Agilent 1200, Agilent Technologies, Santa Clara, CA, USA). CD1 was >95% pure.

Cell Culture and Mouse Pancreatic Islets Isolation. The INS-1 rat insulinoma cell line was cultured in Roswell Park Memorial Institute (RPMI)-1640 medium supplemented with 10% fetal bovine serum (FBS) and 50 μM β-mercaptoethanol. The MIN6 mouse insulinoma cell line was maintained in Dulbecco's modified Eagle medium (DMEM) containing 25 mM glucose, 10% FBS, and 50 μM β-mercaptoethanol. All cells at passage 10−15 were kept at 37 °C and 5% CO_2 in humidified air.

Pancreatic islets were isolated from 6-week-old male C57BL/6J mice (Slac, Shanghai, China). Briefly, the mice were anesthetized by chloral hydrate, and collagenase V (1 mg/mL concentration, Sigma-Aldrich, Shanghai, China) was injected into the pancreas through the common bile duct. The pancreas was quickly removed for digestion at 37 °C for 15 min. The intact islets were handpicked from the digest solution after multiple washes and maintained in RPMI-1640 medium supplemented with 10% FBS, 10000 units/mL penicillin, and 10000 mg/mL streptomycin with 11.1 mM glucose in a sterile cell incubator at 37 °C with 5% CO_2 infusion and humidified 95% air. The islets were used in the following experiments after 24 h of culture. All animal care and experiments were permitted by Institutional Animal Care and Use Committees of Shanghai Institute of Materia Medica.

Cell Viability Assay and Hoechst 33342 Staining. First, to investigate the effect of CD1 on cell viability in PA-treated pancreatic β-cells, INS-1 and MIN6 cells were seeded in 96-well plates. PA/BSA solution was prepared as previously described.[18] The cells were treated with different doses of CD1 in the presence or absence of 0.4 mM PA and incubated for 48 h. Cell viability was determined by MTT assay. Briefly, the cells were incubated with MTT regent (0.5 mg/mL) at 37 °C for 4 h, and the absorbency at a wavelength of 492 nm was measured by FlexStation 3 (Molecular Devices, Sunnyvale, CA, USA). The inhibition rates were calculated by comparison with the control group (treated with 0.5% BSA alone, 100%). In the H_2O_2-treated β-cell model, INS-1 or MIN6 cells were preincubated with CD1 for 4 h and exposed to 500 μM H_2O_2 for 1, 2, and 4 h, respectively. Then the cell viability was measured by MTT assay.

Hoechst 33342 staining was performed to evaluate the proportion of apoptotic cells. INS-1 cells were seeded in a 24-well plate on cover glasses. After incubation with different concentrations of CD1 in the presence/absence of 0.4 mM PA for 48 h, the cells were fixed in 4% paraformaldehyde and stained with Hoechst 33342. The photos were taken by fluorescence microscopy (DP70, Olympus, Japan), and the apoptotic ratio in each group was analyzed.

Determination of Cellular ROS and NO Production. After the INS-1 cells were preincubated with different concentrations of CD1 for 4 h, 10 μM CM-H_2DCFDA was added into cells to load fluorogenic probes at 37 °C for 30 min. Then the cells were incubated with or without 500 μM H_2O_2 for another 20 min. After removal of H_2O_2 and multiple washes, the ROS levels were assessed by determination of 2′,7′-dichlorofluorescein (DCF), which was converted from CM-H_2DCFDA through oxidation. The formation of fluorescent DCF in each well was observed by fluorescence microscopy or quantified at an excitation wavelength 488 nm and emission wavelength of 525 nm by FlexStation 3. To detect the effect of CD1 on PA-induced ROS production, the cells were treated with different concentrations of CD1 in the presence/absence of 0.4 mM PA for 48 h; after washes, the probe was loaded, and the ROS level in each group was detect by the fluorescence.

For further investigation of the effect of CD1 on PA-induced NO generation, INS-1 cells were treated with PA and different concentrations of CD1 for 48 h, and then aliquots of media from each treated group were collected. NO production was then immediately assessed by measuring the amount of nitrite in the supernatant using the Total NO Assay Kit (Beyotime) according to its instructions.

Western Blot Analysis and Immunofluorescence Assay. After the INS-1 cells were treated with CD1 in the presence/absence of PA for 48 h, proteins from each group were collected and the expression levels of cleaved caspase-3 and iNOS were detected using Western blot analysis as described previously.[19] The following primary antibodies and dilutions were used: rabbit anticleaved caspase-3 (Asp175, 1:1000), rabbit antiphospho-Nuclear Factor Kappa B (NFκB, Ser536, 1:1000), rabbit anti-NFκB (1:1000), rabbit antiphospho-c-Jun N-terminal kinase (JNK, Thr183/Tyr185, 1:1000), rabbit anti-JNK (1:1000), rabbit antiphospho-p38 (Thr180/Tyr182, 1:1000), rabbit anti-p38 (1:1000; all from Cell Signaling Technology, Danvers, MA, USA); rabbit anti-NOS2 (iNOS, Santa Cruz Biotechnology, Dallas, TX, USA, 1:500); and mouse anti-β-actin (Sigma-Aldrich, St. Louis, MO, USA, 1:10000). The secondary antibodies were anti-mouse IgG and anti-rabbit IgG (Jackson Laboratory, USA, 1:10000). The expression of protein was measured by optical density using ImageJ (National Institutes of Health, Bethesda, MD, USA).

For double-immunofluorescence staining of insulin and iNOS, INS-1 cells or primary cultured islets were grown on coverslips in a six-well

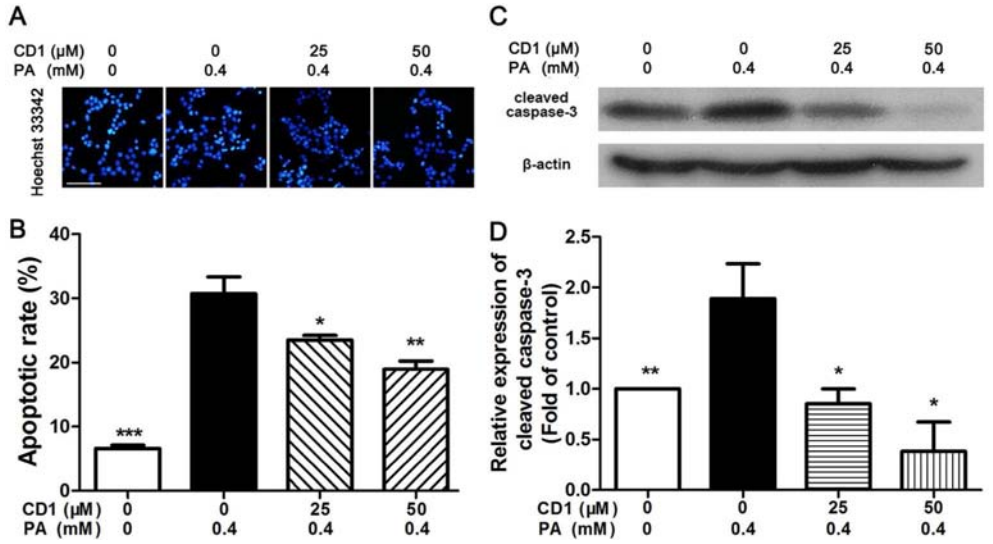

Figure 2. CD1 protects INS-1 β-cells from PA-induced apoptosis. (A) Representative fluorescent images of Hoechst 33342 staining in different treated INS-1 cells. Cells were treated with 0.5% BSA alone, 0.4 mM PA/0.5% BSA with or without 25 μM, and 50 μM CD1 for 48 h, and then Hoechst staining was performed. The brighter nuclei indicated Hoechst 33342-positive apoptotic cells. Scale bar = 50 μm and refers to all panels. (B) Statistical analysis of Hoechst 33342 staining showing the apoptotic rate in differently treated groups. The apoptotic rate was calculated as Hoechst 33342-positive nuclei divided by all nuclei ($n = 6$). (C) Western analysis of the effect of CD1 on the expression of cleaved caspase-3. (D) Histogram of the statistical results of Western blot analysis data. The optical density of each blot band of cleaved capsase-3 was determined and adjusted by the optical density of β-actin; the blots were performed for at least three independent experiments. All data are expressed as the mean ± SE. Asterisks denote significant difference versus the PA-treated alone group (*, $p < 0.05$; **, $p < 0.01$; ***, $p < 0.001$).

plate and then incubated with 0.5% BSA alone or PA/BSA or PA/BSA mixed with different concentrations of CD1 for 48 h. The immunofluorescence was performed as previously described.[20] Briefly, INS-1 cells or islets were fixed in 4% paraformaldehyde and incubated with primary antibodies (rabbit anti-insulin, Cell Signaling Technology, dilution 1:100; mouse anti-NOS2, Santa Cruz, dilution 1:100) overnight followed with secondary antibodies (Alexafluor 488-conjugated goat anti-rabbit IgG and Alexafluor 546-conjugated goat anti-mouse IgG, Invitrogen, dilution 1:400). Then the nuclei were stained with Hoechst 33342, and the coverslips were mounted and observed by confocal microscope (FV1200, Olympus, Japan). A terminal deoxynucleotidyl transferase dUTP nick end labeling (TUNEL) assay was carried out to evaluate the apoptotic cells in islets. After islets were treated with different concentrations of CD1 in the presence/absence of 0.4 mM PA, the apoptotic cells in islets were detected by TUNEL kit (Roche, USA) according to the manufacturer's instructions. Hoechst 33342 was used for visualization of nuclei. The rate of apoptosis was calculated as the number of TUNEL-positive cells divided by the area of each islet.

Determination of Glucose-Stimulated Insulin Secretion (GSIS). Islets of approximately the same size were plated in 24-well plates (10 islets per well) for insulin secretion studies. Islets were incubated with CD1 in the presence/absence of 0.4 mM PA for 48 h. Then the culture medium was removed, and cells or islets were washed and preincubated in Krebs−Ringer buffer (KRB; 135 mM NaCl, 3.6 mM KCl, 0.5 mM NaH_2PO_4, 0.5 mM $MgSO_4$, 1.5 mM $CaCl_2$, 2 mM $NaHCO_3$, 10 mM HEPES, and 0.1% w/v BSA, pH 7.4) without glucose for 1 h at 37 °C. Thereafter, the cells/islets were incubated in KRB containing 5 mM glucose for 1 h at 37 °C and then in 25 mM glucose for another 1 h. The supernatant was collected, and the insulin level was measured by using an insulin ELISA kit (Millipore, Bedford, MA, USA) according to its protocol.

Statistical Analysis. All data were expressed as the mean ± SE. The comparison of different groups was assessed by t test or one-way ANOVA analysis followed by Dunnett's test. Differences were considered statistically significant at $p < 0.05$.

RESULTS

CD1 Protects INS-1 β-Cells from PA-Induced Apoptosis. There was no cytotoxic effect of CD1 on pancreatic β-cell lines (Supporting Information Supplementary Figure 1A). To evaluate the protective effect of CD1 on PA-induced β-cell apoptosis, we first examined the protective effect of CD1 on cell viability in PA-treated INS-1 cells. It was shown that CD1 could dose-dependently increase cell viability in the presence of 0.4 mM PA in INS-1 cells (inhibitory rates were 95.2 ± 2.2% at 50 μM, 92.1 ± 2.1% at 25 μM, 88.4 ± 2.9% at 12.5 μM, 79.9 ± 3.9% at 6.25 μM, 69.3 ± 1.2% at 3.12 μM, and 67.1 ± 2.1% at 1.56 μM vs 59.7 ± 1.5% for the PA-treated alone group, Figure 1B), which suggested that CD1 could protect pancreatic β-cells from PA-induced decrease in cell viability.

To further evaluate whether the protective effect of CD1 on cell viability was associated with apoptosis, Hoechst 33342 staining was then performed to detect the apoptotic rate. In Hoechst 33342 staining, the nuclei of apoptotic cells visualized by fluorescence microscopy displayed a high condensed chromatin compared with normal cells.[21] Cells treated with 0.4 mM PA showed brighter nuclei with highly condensed DNA and nuclei shrinkage, whereas an obviously reduced apoptotic rate was observed in CD1 (25/50 μM) and PA cotreated INS-1 cells (Figure 2A,B). The activation of caspase-3 was identified as a key role in the execution of cell apoptosis. In this study, it was found that CD1 significantly reduced cleaved caspase-3 level in PA-treated cells at doses of both 25 and 50 μM compared with PA-treated alone group (Figure 2C,D). All of these data suggested that CD1 could protect β-cells from PA-induced apoptosis.

CD1 Attenuates PA-Induced ROS, NO Production, and iNOS Expression in INS-1 β-cells. We then investigated the effects of CD1 on some oxidative stress-associated markers in PA-induced β-cell apoptosis. By detecting DCF fluorescence, ROS generation was significantly decreased in CD1 and PA cotreated cells compared with PA-treated alone INS-1 cells (Figure 3A). Moreover, as shown in Figure 3B, total NO synthesis was obviously inhibited by CD1 in a dose-dependent manner. Increased expression of iNOS can lead to sustained

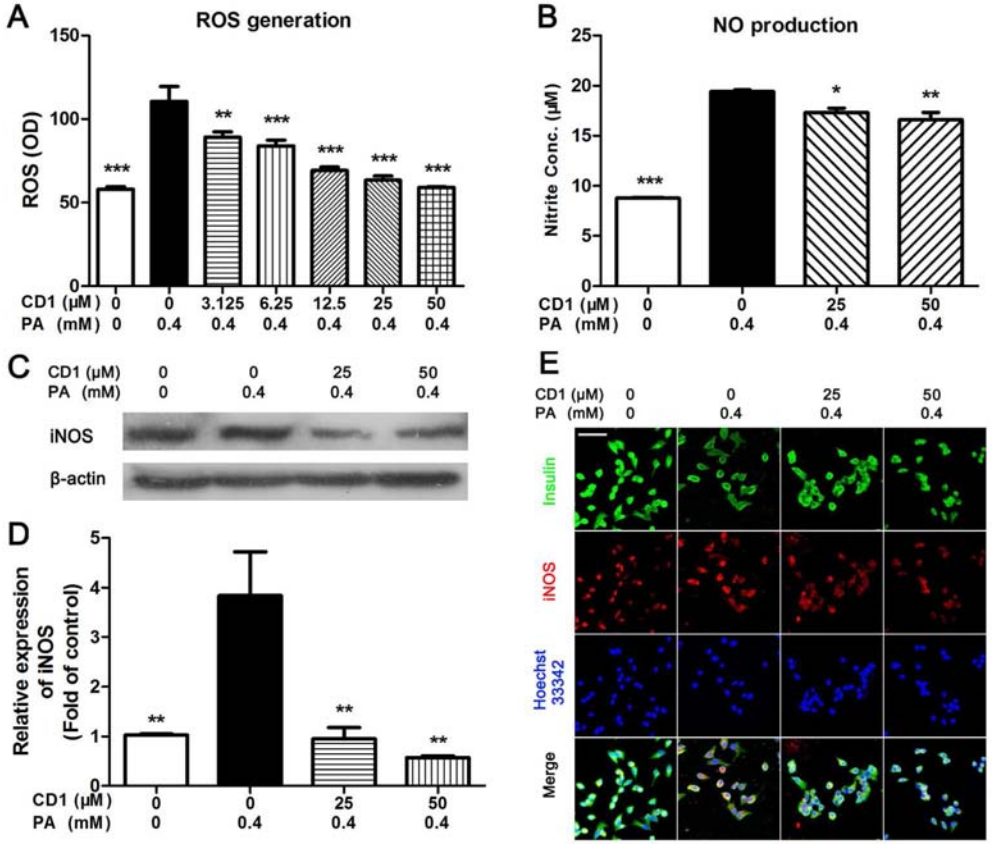

Figure 3. CD1 reduced PA-induced oxidative stress in INS-1 cells. (A) INS-1 cells were treated with different concentrations of CD1 in the presence/absence of 0.4 mM PA for 48 h. Quantified ROS production in the cells was detected ($n = 3$). (B) Cells were treated with different concentrations of CD1 in the presence/absence of 0.4 mM PA for 48 h. NO production was then detected ($n = 3$). (C) INS-1 cells were treated with 25 and 50 μM CD1 in the presence/absence of 0.4 mM PA for 48 h, and the expression levels of iNOS and β-actin were detected by Western blot analysis. (D) The optical density of each blot band of iNOS was determined and modified by the optical density of β-actin; the blots were performed for at least three independent experiments. (E) INS-1 cells were treated as above, and double immunofluorescence of insulin and iNOS was performed. Insulin was marked with green fluorescence, whereas iNOS was red; nuclei were stained by Hoechst 33342 (blue), and figures were merged. Scale bar = 50 μm and refers to all panels. This experiment was repeated at least three times. All data are expressed as the mean ± SE. Asterisks denote significant difference versus the PA-treated alone group (∗, $p < 0.05$; ∗∗, $p < 0.01$; ∗∗∗, $p < 0.001$).

elevation of NO, which was a major contributor in β-cell dysfunction and apoptosis.[22] Therefore, to investigate the expression level of iNOS in pancreatic β-cells, Western blot and immunofluorescence were performed in INS-1 β-cells and primary cultured islets. As expected, CD1 abolished the increasing expression level of iNOS induced by PA (Figure 3C,D). Double-immunofluorescence also showed that there were fewer iNOS-positive cells in CD1 and PA cotreated INS-1 cells than in PA-treated alone cells (Figure 3E), which was consistent with the results of Western blot analysis. Furthermore, to verify the effect of CD1 on iNOS expression in pancreatic β-cells, primary mouse islets were isolated and cultured for immunofluorescence staining. Compared with normal cultured islets, PA obviously increased iNOS expression. However, addition of 25 and 50 μM CD1 to culture medium could obviously suppress this deleterious effect (Figure 4A).

CD1 Decreases PA-Induced Apoptosis and Protects β-Cell Function against PA-Induced Impairment of GSIS in Isolated Mouse Islets. To further investigate whether CD1, an A-type proanthocyanidin trimer isolated from *C. tamala*, could reduce PA-induced apoptosis in primary cultured islets, TUNEL staining was carried out to detect the apoptotic cells by labeling DNA fragmentation.[23] After incubation with 0.4 mM PA for 48 h, the number of TUNEL-positive cells increased obviously in comparison with untreated islets. However, CD1 suppressed this pernicious effect significantly (Figure 4B,C).

It is known that chronic exposure to elevated levels of PA can induce β-cell apoptosis as well as impair β-cell insulin secretion. Therefore, the protective effect of CD1 against PA-induced impairment of insulin secretion in primary cultured islets was also investigated. It was found that PA-impaired GSIS function was partly restored by CD1 in a dose-dependent manner (Figure 4D). Together, results suggested that this compound could suppress PA-induced impairment of GSIS as it reduced the apoptosis of pancreatic β-cells.

CD1 Suppressed PA-Induced Phosphorylation of NFκB and JNK but Not p38 MAPKs. Multiple mechanisms are involved in PA-induced β-cell apoptosis, such as ER-stress, oxidative stress, and inflammatory effect. CD1 was involved as an antioxidant with the inhibitory activity against cyclooxygenase-2.[24] Therefore, in addition to iNOS, inhibition of other PA-activated pro-inflammatory gene expression in pancreatic β-cells might be associated with the protective effect of CD1. It was found that PA-induced phosphorylations of NFκB (Figure 5A,D) and JNK (Figure 5B,E) were significantly reduced in the presence of CD1. However, there was no obvious effect of CD1 on PA-activated p38 phosphorylation (Figure 5C,F).

dx.doi.org/10.1021/jf500387d | J. Agric. Food Chem. 2014, 62, 5038−5045

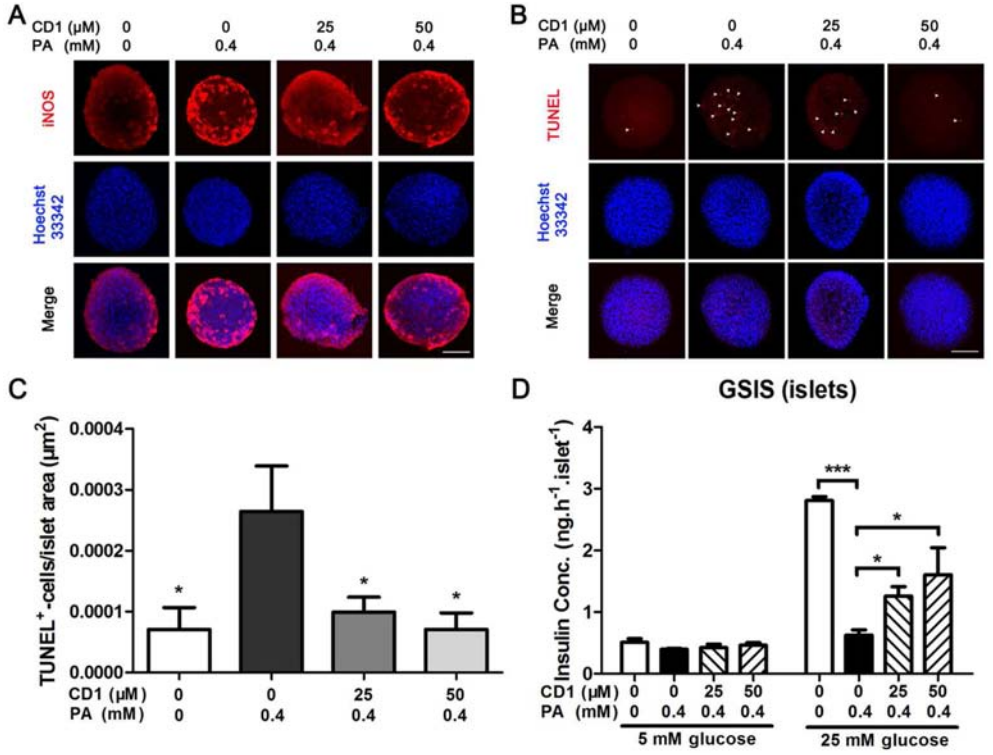

Figure 4. (A) CD1 affected iNOS expression in primary cultured islets. Islets were isolated and cultured with CD1 and PA for 48 h. Red fluorescence indicated iNOS expression, and Hoechst 33342 showed nuclei. The merged figures are shown in below. Scale bar = 50 μm and refers to all panels. (B) CD1 reduced cell apoptosis in PA-simulated primary cultured islets and restored PA-injured insulin secretion. After islets were treated with CD1 and PA, TUNEL staining was performed to investigate the apoptotic ratio of cells in primary cultured islets. TUNEL-positive nuclei were marked by red fluorescence. Representative TUNEL-positive cells are indicated by white arrows. All nuclei were stained with Hoechst 33342, which showed blue fluorescence. The merged figures are shown below. Scale bar = 50 μm and refers to all panels. (C) Histogram shows the number of TUNEL-positive cells modified by the area of each islet. At least 15 islets were analyzed in each group. (D) After treatment with CD1 and PA, isolated islets were incubated at 5 mM glucose and successive 25 mM. The supernatant was collected and used for insulin determination ($n = 3$). All data are shown as the mean ± SE. The statistics result showed significant difference versus the PA-treated alone group (*, $p < 0.05$; **, $p < 0.01$; ***, $p < 0.001$).

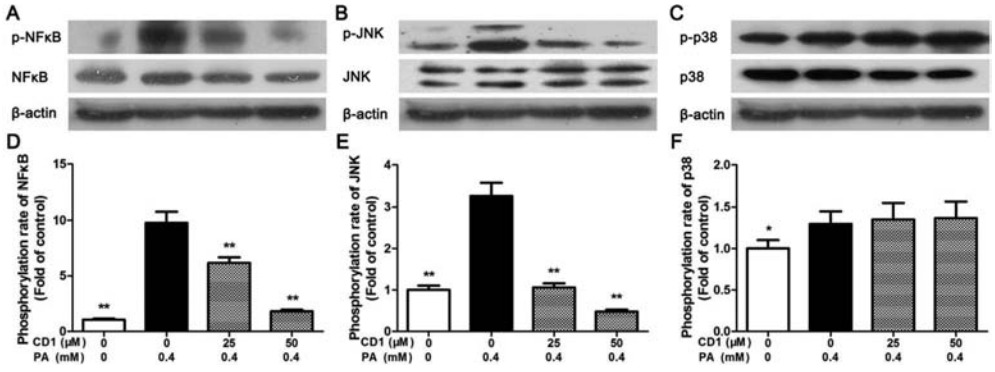

Figure 5. Western blot analysis of NFκB, JNK, and p38 phosphorylation. After the cells were treated with/without different concentrations of CD1 in the presence/absence of PA, the cell lysate was collected and followed phosphorylation proteins were detected. (A) The phosphorylation rate of NFκB was detected; β-actin was used as an internal. (B) The phosphorylation rate of JNK was detected; β-actin was used as an internal. (C) The phosphorylation rate of p38 was detected; β-actin was used as an internal. (D−F) The phosphorylation rate was measured by the expression of phosphorylated protein divided by total protein expression and adjusted by β-actin expression. All blots were repeated at least three times. The statistical data are expressed as the mean ± SE. Asterisks denote significant difference versus the PA-treated alone group (*, $p < 0.05$; **, $p < 0.01$).

DISCUSSION

Cinnamon exerts antidiabetic properties both in vitro and in vivo, and its antioxidative polyphenol components have been supposed to be the main contributor.[25,26] In a previous study, we have verified that *C. tamala* extracts exert antidiabetic effects and improve pancreas functions in a type 2 diabetic *db/db* mouse model.[17] As reported, the main components of extracts were A-type procyanidin trioligomers, including >43% CD1 and >23% CB1, one structural isomer of CD1.[17] A-type polymers were reported to reduce peroxide-induced pancreatic acinar cell injury,[27,28] generate insulin-like biological activity,[13] and improve insulin sensitivity in vivo.[29] However, as effective antioxidants[24] and the major components of antidiabetic natural products,[17] the effects of A-type polymers in *C. tamala* have not yet been

dx.doi.org/10.1021/jf500387d | J. Agric. Food Chem. 2014, 62, 5038−5045

explored on insulin-secreting β-cells. The present work focused on disclosing the mechanisms of the protective effects of CD1, one major A-type polymers in *C. tamala*. We demonstrated that CD1 could protect pancreatic β-cells from PA-induced apoptosis via attenuating oxidative stress in INS-1, MIN6 pancreatic β-cell line, and primary cultured murine islets. These findings also provide a new understanding of the mechanisms for the antidiabetic effects of procyanidin oligomers.

Many antioxidants have been reported to protect β-cells via their antioxidative activity.[30,31] Oxidative stress is involved in the pathobiology of T2D and its complications. During the development of T2D, high glucose and FFAs caused mitochondrial damage and overproduction of reactive species, such as ROS and RNS. These free radicals activate several stress-sensitive pathways including NF-κB, JNK/SAPK, and PKC, which lead to pancreatic β-cell death, insulin resistance, and impaired insulin secretion.[32] Combined with abnormal oxidation, oxidative stress leads to DNA damage, protein oxidationm and lipid peroxidation in various kinds of cells during T2D. We found that CD1 exhibited significant radical scavenging activity in INS-1 and MIN6 cells under oxidative stress condition induced by H_2O_2. Pretreatment with CD1 dose-dependently attenuated H_2O_2-induced decrease of cell viability in both INS-1 and MIN6 cells (Supporting Information Supplementary Figure 2A,B). The intracellular ROS level in each group was also detected. H_2O_2-induced ROS elevation was significantly reduced by pretreatment of CD1 in a dose-dependent manner (Supporting Information Supplementary Figure 2C,D). Therefore, CD1 might also reduce the elevated level of ROS and NO production induced by PA in β-cells.

Excessive and sustained generation of NO derived from iNOS plays a pivotal role in FFA-induced β-cell dysfunction and apoptosis.[33] Rachek et al. reported that elevated NO production induced by FFA could damage mitochondrial DNA and ultimately lead to apoptosis in INS-1 cells.[34] Meanwhile, evoked iNOS activity in pancreatic β-cells could lead to impairment of GSIS both in vivo and in vitro.[35,36] Therefore, inhibition of iNOS expression might reduce production of NO and exert a protective effect on β-cells. Hynes et al. demonstrated that inhibition of iNOS by lentiviral vector-based shRNA technology could protect β-cells from cytokine-induced apoptosis.[37] In this study, we found that CD1 could significantly suppress PA-induced ROS generation and NO production. PA-induced increase of iNOS expression level was also significantly inhibited by CD1 in both INS-1 cells and primary cultured islets. Similar results had also been confirmed on MIN6 β-cell line (Supporting Information Supplementary Figure 1C,D). Together the results suggested that the antioxidative activity might be one of the main mechanisms of the protective effect of CD1 on PA-injured β-cells.

Long-term exposure to FFAs results in increased β-oxidation and elevated reactive species levels in both islets[38] and β-cell lines.[39] Moreover, β-cell failure, including apoptosis and dysfunction, could be mediated obviously by oxidative stress in chronic exposure to elevated levels of FFAs in pancreatic islets.[40] Our experiments demonstrated that CD1 could significantly suppress PA-induced oxidative stress and subsequently reduced the apoptotic rate in PA-injured β-cells/islets. Together the results indicated that CD1 could protect pancreatic β-cells from PA-induced apoptosis.

As the compound showed great protective effect on cell viability and antiapoptosis in pancreatic β-cells cells, it was inferred that CD1 might have a protective effect on insulin secretion. In primary cultured islets, CD1 suppressed PA-induced impairment of GSIS. We speculated that the protective effect of CD1 on PA-treated islets could improve insulin secretion. Therefore, CD1 treatment may provide beneficial effects to the function of insulin secretion through its protective effect on pancreatic β-cells.

However, the underlying mechanism of the antioxidative effect of CD1 on pancreatic β-cells still needed further investigation. CD1 had been reported to act as an antioxidant with the inhibitory activity against cyclooxygenase-2,[24] and cyclooxygenase-2 could be regulated by an inflammatory-associated gene toll-like receptor-4 (TLR4).[41] Therefore, the expression of some downstream pro-inflammatory gene was detected in this study. We found that CD1 could significantly reduce PA-induced phosphorylation of NFκB and JNK. However, PA-activated p38 phosphorylation was not attenuated by CD1. Lee et al. had confirmed that JNK activation could be involved with TLR4 signaling pathway in palmitic acid-treated INS-1 cells and decrease inhibitory factor kappa B alpha (IκBα),[42] which was in accordance with our results. Therefore, the TLR4 pathway could at least associate with the protective effect of CD1 on pancreatic β-cells. In any case, further investigation on the effect mechanism of CD1 would still be necessary.

In conclusion, this study showed that CD1 protects pancreatic β-cells against PA-induced oxidative stress via its antioxidative properties. As the major component of *C. tamala*, CD1 could be the main active ingredient in *C. tamala* to possess antidiabetic activity and provide benefit for the protection of pancreatic β-cells during the development of T2D.

■ ASSOCIATED CONTENT

Supporting Information

Supplementary Figures 1 and 2. This material is available free of charge via the Internet at http://pubs.acs.org.

■ AUTHOR INFORMATION

Corresponding Authors

*(Y.L.) E-mail: ymlius@163.com.

*(H.W.) E-mail: hywang@mail.shcnc.ac.cn.

Author Contributions

‖T.W. and P.S. contributed equally to this work.

Funding

This work was supported by a grant from the National Nature Science Foundation of China (81072681), the National High Technology Research and Development Program of China ("863" Program, 2007AA02Z301), the State Key Program of Basic Research of China grant ("973" program, 2009CB918502), and the National Science and Technology Major Project (2012ZX09301001-001).

Notes

The authors declare no competing financial interest.

■ ACKNOWLEDGMENTS

We thank Professor S. Seino for his gift of MIN6 cells.

■ REFERENCES

(1) Itoh, Y.; Hinuma, S. GPR40, a free fatty acid receptor on pancreatic β-cells, regulates insulin secretion. *Hepatol. Res.* **2005**, *33*, 171−173.

(2) Robertson, R. P. β-Cell deterioration during diabetes: what's in the gun? *Trends Endocrinol. Metab.* **2009**, *20*, 388−393.

(3) Giacca, A.; Xiao, C.; Oprescu, A. I.; Carpentier, A. C.; Lewis, G. F. Lipid-induced pancreatic β-cell dysfunction: focus on in vivo studies. *Am. J. Physiol. Endocrinol. Metab.* **2011**, *300*, E255−E262.
(4) Sun, P.; Wang, T.; Zhou, Y.; Liu, H.; Jiang, H.; Zhu, W.; Wang, H. DC260126: a small-molecule antagonist of GPR40 that protects against pancreatic β-cells dysfunction in *db/db* mice. *PLoS One* **2013**, *8*, DOI: 10.1371/journal.pone.0066744.
(5) Lenzen, S.; Drinkgern, J.; Tiedge, M. Low antioxidant enzyme gene expression in pancreatic islets compared with various other mouse tissues. *Free Radical Biol. Med.* **1996**, *20*, 463−466.
(6) Lenzen, S. Oxidative stress: the vulnerable β-cell. *Biochem. Soc. Trans.* **2008**, *36*, 343−347.
(7) Lowell, B. B.; Shulman, G. I. Mitochondrial dysfunction and type 2 diabetes. *Science* **2005**, *307*, 384−387.
(8) Tanaka, Y.; Gleason, C. E.; Tran, P. O.; Harmon, J. S.; Robertson, R. P. Prevention of glucose toxicity in HIT-T15 cells and Zucker diabetic fatty rats by antioxidants. *Proc. Natl. Acad. Sci. U.S.A.* **1999**, *96*, 10857−10862.
(9) Youl, E.; Bardy, G.; Magous, R.; Cros, G.; Sejalon, F.; Virsolvy, A.; Richard, S.; Quignard, J. F.; Gross, R.; Petit, P.; Bataille, D.; Oiry, C. Quercetin potentiates insulin secretion and protects INS-1 pancreatic β-cells against oxidative damage via the ERK1/2 pathway. *Br. J. Pharmacol.* **2010**, *161*, 799−814.
(10) Johansen, J. S.; Harris, A. K.; Rychly, D. J.; Ergul, A. Oxidative stress and the use of antioxidants in diabetes: linking basic science to clinical practice. *Cardiovasc. Diabetol.* **2005**, *4*, 5.
(11) Khan, A.; Bryden, N. A.; Polansky, M. M.; Anderson, R. A. Insulin potentiating factor and chromium content of selected foods and spices. *Biol. Trace Elem. Res.* **1990**, *24*, 183−188.
(12) Rohdewald, P. A review of the French maritime pine bark extract (Pycnogenol), a herbal medication with a diverse clinical pharmacology. *Int. J. Clin. Pharmacol. Ther.* **2002**, *40*, 158−168.
(13) Anderson, R. A.; Broadhurst, C. L.; Polansky, M. M.; Schmidt, W. F.; Khan, A.; Flanagan, V. P.; Schoene, N. W.; Graves, D. J. Isolation and characterization of polyphenol type-A polymers from cinnamon with insulin-like biological activity. *J. Agric. Food Chem.* **2004**, *52*, 65−70.
(14) Schafer, A.; Hogger, P. Oligomeric procyanidins of French maritime pine bark extract (Pycnogenol) effectively inhibit α-glucosidase. *Diabetes Res. Clin. Pract.* **2007**, *77*, 41−46.
(15) Lu, Z.; Jia, Q.; Wang, R.; Wu, X.; Wu, Y.; Huang, C.; Li, Y. Hypoglycemic activities of A- and B-type procyanidin oligomer-rich extracts from different cinnamon barks. *Phytomedicine* **2011**, *18*, 298−302.
(16) Jia, Q.; Liu, X.; Wu, X.; Wang, R.; Hu, X.; Li, Y.; Huang, C. Hypoglycemic activity of a polyphenolic oligomer-rich extract of *Cinnamomum parthenoxylon* bark in normal and streptozotocin-induced diabetic rats. *Phytomedicine* **2009**, *16*, 744−750.
(17) Chen, L.; Sun, P.; Wang, T.; Chen, K.; Jia, Q.; Wang, H.; Li, Y. Diverse mechanisms of antidiabetic effects of the different procyanidin oligomer types of two different cinnamon species on *db/db* mice. *J. Agric. Food Chem.* **2012**, *60*, 9144−9150.
(18) Martinez, S. C.; Tanabe, K.; Cras-Meneur, C.; Abumrad, N. A.; Bernal-Mizrachi, E.; Permutt, M. A. Inhibition of Foxo1 protects pancreatic islet β-cells against fatty acid and endoplasmic reticulum stress-induced apoptosis. *Diabetes* **2008**, *57*, 846−859.
(19) Hu, H.; He, L. Y.; Gong, Z.; Li, N.; Lu, Y. N.; Zhai, Q. W.; Liu, H.; Jiang, H. L.; Zhu, W. L.; Wang, H. Y. A novel class of antagonists for the FFAs receptor GPR40. *Biochem. Biophys. Res. Commun.* **2009**, *390*, 557−563.
(20) Wu, J.; Sun, P.; Zhang, X.; Liu, H.; Jiang, H.; Zhu, W.; Wang, H. Inhibition of GPR40 protects MIN6 β-cells from palmitate-induced ER stress and apoptosis. *J. Cell Biochem* **2012**, *113*, 1152−1158.
(21) Zhang, A.; Zhang, J.; Sun, P.; Yao, C.; Su, C.; Sui, T.; Huang, H.; Cao, X.; Ge, Y. EIF2alpha and caspase-12 activation are involved in oxygen-glucose-serum deprivation/restoration-induced apoptosis of spinal cord astrocytes. *Neurosci. Lett.* **2010**, *478*, 32−36.
(22) Meidute Abaraviciene, S.; Lundquist, I.; Galvanovskis, J.; Flodgren, E.; Olde, B.; Salehi, A. Palmitate-induced β-cell dysfunction is associated with excessive NO production and is reversed by thiazolidinedione-mediated inhibition of GPR40 transduction mechanisms. *PLoS One* **2008**, *3*, DOI: 10.1371/journal.pone.0002182.
(23) Gavrieli, Y.; Sherman, Y.; Ben-Sasson, S. A. Identification of programmed cell death in situ via specific labeling of nuclear DNA fragmentation. *J. Cell Biol.* **1992**, *119*, 493−501.
(24) Killday, K. B.; Davey, M. H.; Glinski, J. A.; Duan, P.; Veluri, R.; Proni, G.; Daugherty, F. J.; Tempesta, M. S. Bioactive A-type proanthocyanidins from *Cinnamomum cassia*. *J. Nat. Prod.* **2011**, *74*, 1833−1841.
(25) Lee, J. S.; Jeon, S. M.; Park, E. M.; Huh, T. L.; Kwon, O. S.; Lee, M. K.; Choi, M. S. Cinnamate supplementation enhances hepatic lipid metabolism and antioxidant defense systems in high cholesterol-fed rats. *J. Med. Food* **2003**, *6*, 183−191.
(26) Verspohl, E. J.; Bauer, K.; Neddermann, E. Antidiabetic effect of *Cinnamomum cassia* and *Cinnamomum zeylanicum* in vivo and in vitro. *Phytother. Res.* **2005**, *19*, 203−206.
(27) Rivera-Barreno, R.; del Castillo-Vaquero, A.; Salido, G. M.; Gonzalez, A. Effect of cinnamtannin B-1 on cholecystokinin-8-evoked responses in mouse pancreatic acinar cells. *Clin. Exp. Pharmacol. Physiol.* **2010**, *37*, 980−988.
(28) Gonzalez, A.; Santofimia-Castano, P.; Rivera-Barreno, R.; Salido, G. M. Cinnamtannin B-1, a natural antioxidant that reduces the effects of H(2)O(2) on CCK-8-evoked responses in mouse pancreatic acinar cells. *J. Physiol. Biochem.* **2012**, *68*, 181−191.
(29) Roffey, B.; Atwal, A.; Kubow, S. Cinnamon water extracts increase glucose uptake but inhibit adiponectin secretion in 3T3-L1 adipose cells. *Mol. Nutr. Food Res.* **2006**, *50*, 739−745.
(30) Taniguchi, S.; Kang, L.; Kimura, T.; Niki, I. Hydrogen sulphide protects mouse pancreatic β-cells from cell death induced by oxidative stress, but not by endoplasmic reticulum stress. *Br. J. Pharmacol.* **2011**, *162*, 1171−1178.
(31) Kim, M. K.; Jung, H. S.; Yoon, C. S.; Ko, J. H.; Chun, H. J.; Kim, T. K.; Kwon, M. J.; Lee, S. H.; Koh, K. S.; Rhee, B. D.; Park, J. H. EGCG and quercetin protected INS-1 cells in oxidative stress via different mechanisms. *Front. Biosci. (Elite Ed.)* **2010**, *2*, 810−817.
(32) Evans, J. L.; Goldfine, I. D.; Maddux, B. A.; Grodsky, G. M. Are oxidative stress-activated signaling pathways mediators of insulin resistance and β-cell dysfunction? *Diabetes* **2003**, *52*, 1−8.
(33) Salehi, A.; Carlberg, M.; Henningson, R.; Lundquist, I. Islet constitutive nitric oxide synthase: biochemical determination and regulatory function. *Am. J. Physiol.* **1996**, *270*, C1634−C1641.
(34) Rachek, L. I.; Thornley, N. P.; Grishko, V. I.; LeDoux, S. P.; Wilson, G. L. Protection of INS-1 cells from free fatty acid-induced apoptosis by targeting hOGG1 to mitochondria. *Diabetes* **2006**, *55*, 1022−1028.
(35) Henningsson, R.; Salehi, A.; Lundquist, I. Role of nitric oxide synthase isoforms in glucose-stimulated insulin release. *Am. J. Physiol. Cell. Physiol.* **2002**, *283*, C296−C304.
(36) Takamura, T.; Kato, I.; Kimura, N.; Nakazawa, T.; Yonekura, H.; Takasawa, S.; Okamoto, H. Transgenic mice overexpressing type 2 nitric-oxide synthase in pancreatic β-cells develop insulin-dependent diabetes without insulitis. *J. Biol. Chem.* **1998**, *273*, 2493−2496.
(37) Hynes, S. O.; McCabe, C.; O'Brien, T. β-cell protection by inhibition of iNOS through lentiviral vector-based strategies. *Methods Mol. Biol.* **2011**, *704*, 153−168.
(38) Carlsson, C.; Borg, L. A.; Welsh, N. Sodium palmitate induces partial mitochondrial uncoupling and reactive oxygen species in rat pancreatic islets in vitro. *Endocrinology* **1999**, *140*, 3422−3428.
(39) Maestre, I.; Jordan, J.; Calvo, S.; Reig, J. A.; Cena, V.; Soria, B.; Prentki, M.; Roche, E. Mitochondrial dysfunction is involved in apoptosis induced by serum withdrawal and fatty acids in the β-cell line INS-1. *Endocrinology* **2003**, *144*, 335−345.
(40) Piro, S.; Anello, M.; Di Pietro, C.; Lizzio, M. N.; Patane, G.; Rabuazzo, A. M.; Vigneri, R.; Purrello, M.; Purrello, F. Chronic exposure to free fatty acids or high glucose induces apoptosis in rat pancreatic islets: possible role of oxidative stress. *Metabolism* **2002**, *51*, 1340−1347.
(41) Hirai, M.; Kobayashi, M.; Shimizu, N. Reduced tyrosine phosphorylation and nonresponsiveness to EGF-mediated cytotoxicity

in EGF receptor-hyperproducing UCVA-1 cells. *Cell Signal.* **1990**, *2*, 245−252.
(42) Lee, S. M.; Choi, S. E.; Lee, J. H.; Lee, J. J.; Jung, I. R.; Lee, S. J.; Lee, K. W.; Kang, Y. Involvement of the TLR4 (Toll-like receptor 4) signaling pathway in palmitate-induced INS-1 β-cell death. *Mol. Cell. Biochem.* **2011**, *354*, 207−217.

Japan). IR spectra were determined with a Nicolet 6700 FT-IR spectrophotometer (Madison, Wisconsin, USA). NMR spectra were obtained on Bruker Advance DRX-300, DRX-400 spectrometers (Rheinstetten, Germany) and the chemical shifts are given in δ (ppm) values with reference to TMS. The coupling constants (J values) are reported in Hz. HRMS were carried out on Waters Xevo G_2 Q-TOF mass spectrometer (Milford, Massachusetts, USA).

General Synthetic of Procedure CAPE Derivatives. *Method A for Compounds 1−4.* To a mixture of caffeic acid (1 mmol) in 10 mL anhydrous DME was added thionyl chloride (6 mmol) under nitrogen atmosphere. This mixture was heated to reflux for 12 h and then distilled under vacuum to remove the excess thionyl chloride completely. The intermediate was redissolved with 10 mL anhydrous DME, and to this solution was added alcohol (1 mmol). This mixture was heated to reflux for 4 h before evaporation. The residue was purified by column chromatography and/or recrystallization to give target compounds.

Modified Method A for Compounds 5−13. To a mixture of caffeic acid or its analogues (1 mmol) in 5−10 mL alcohol was added thionyl chloride (3−6 mmol) under nitrogen atmosphere. This mixture was heated slowly to 65 °C and stirred for 4 h. After distillation of most of alcohol under high vacuum the residue was purified by column chromatography and/or recrystallization to give target compounds.

Method B for Compounds 14 and 15. To a mixture of caffeic acid or its analogue (1 mmol), potassium carbonate (1.1 mmol) and 5 mL DMF was added benzyl bromide (1 mmol). This mixture was stirred at room temperature for 12 h. Fifteen mL water was added and the suspension was extracted with diethyl ether (10 mL × 3). The combined organic layer was washed with aqueous $NaHCO_3$ and brine, dried, evaporated and purified by recrystallization to give target compounds.

Method C for Compounds 16 and 17. A mixture of caffeic acid (1 mmol), phenethylamine/4-hydroxyphenethylamine (1 mmol), triethylamine (1.5 mmol) and 4 mL DMF were stirred at 0 °C for 10 min, to which was added a solution of BOP (1 mmol) in 4 mL DCM. After stirred for 30 min at 0 °C, the mixture was allowed to warm to room temperature and stirred for 20 h. Fifteen g crushed ice and 25 mL chloroform were added to the mixture, organic layer was separated and washed with 10% hydrochloric acid and brine, dried, evaporated and purified by column chromatography and recrystallization to give target compounds.

Method D for Compounds 18 and 19. A mixture of alcohol (10 mmol), meldrum's acid (12 mmol) and 40 mL 1, 4-dioxane was heated to reflux for 6 h before evaporation. The residue was purified by column chromatography to give the intermediate malonic acid mono ester. A mixture of malonic acid mono ester (5 mmol), 3,4-dihydroxybenzaldehyde/4-nitrobenzaldehyde (5 mmol), 5 mL pyridine and 0.5 mL piperidine was stirred for 15 h at room temperature before evaporation. The residue was redissolved with 50 mL ethyl acetate and washed with 5% hydrochloric acid, brine, dried, evaporated and purified column chromatography and recrystallization to give target compounds.

Caffeic Acid Cinnamyl Ester (1). The title compound was prepared according to method A as white powder (45 mg, 15.2% yield). mp 159−160 °C; IR (KBr) ν_{max} 3477, 3318, 1682, 1602, 1535, 1280, 1184 cm^{-1}; ^1H NMR (400 MHz, $CDCl_3$) δ 7.55 (1H, d, J = 16.0 Hz, H-β), 7.21−7.35 (5H, m, H-2′, 3′, 4′, 5′, 6′), 7.02 (1H, d, J = 1.2 Hz, H-2), 6.95 (1H, dd, J = 1.2, 8.0 Hz, H-6), 6.81 (1H, d, J = 8.0 Hz, H-5), 6.70 (1H, d, J = 16.0 Hz, H-γ'), 6.35 (1H, dt, J = 6.4, 16.0 Hz, H-β'), 6.31 (1H, d, J = 16.0 Hz, H-α), 4.79 (2H, d, J = 6.4 Hz, H-α'); HRESIMS $[M - H]^-$ m/z 295.0966 (Calcd for $C_{18}H_{15}O_4$, 295.0970).

Caffeic Acid Phenylpropyl Ester (2). The title compound was prepared according to method A as light yellow powder (47 mg, 15.8% yield). mp 121−123 °C; IR (KBr) ν_{max} 3491, 3338, 1683, 1603, 1535, 1278, 1183 cm^{-1}; ^1H NMR (300 MHz, DMSO-d_6) δ 9.56 (1H, s, −OH), 9.13 (1H, s, −OH), 7.45 (1H, d, J = 15.9 Hz, H-β), 7.15−7.30 (5H, m, H-2′, 3′, 4′, 5′, 6′), 7.03 (1H, d, J = 2.1 Hz, H-2), 6.98 (1H, dd, J = 2.1, 8.1 Hz, H-6), 6.75 (1H, d, J = 8.1 Hz, H-5), 6.24 (1H, d, J = 15.9 Hz, H-α), 4.09 (2H, t, J = 6.6 Hz, H-α'), 2.68 (2H, t, J = 6.6 Hz, H-γ'), 1.94 (2H, quintet, H-β'); HRESIMS $[M - H]^-$ m/z 297.1124 (Calcd for $C_{18}H_{17}O_4$, 297.1127).

Caffeic Acid 4-Hydroxyphenethyl Ester (3). The title compound was prepared according to method A as light yellow powder (60 mg, 20.0% yield). mp 153−155 °C; IR (KBr) ν_{max} 3495, 3266, 1698, 1605, 1513, 1283, 1204, 1170 cm^{-1}; ^1H NMR (400 MHz, $CDCl_3$) δ 7.89 (1H, d, J = 16.0 Hz, H-β), 7.46 (1H, d, J = 1.6 Hz, H-2), 7.40 (2H, d, J = 8.0 Hz, H-2′, 6′), 7.25 (2H, d, J = 8.0 Hz, H-3′, 5′), 7.16 (1H, dd, J = 1.6, 8.4 Hz, H-6), 7.00 (1H, d, J = 8.4 Hz, H-5), 6.55 (1H, d, J = 16.0 Hz, H-α), 3.87 (2H, t, J = 7.2 Hz, H-α'), 3.22 (2H, t, J = 7.2 Hz, H-β'); HRESIMS $[M - H]^-$ m/z 299.0916 (Calcd for $C_{17}H_{15}O_5$, 299.0919).

Caffeic Acid Nonyl Ester (4). The title compound was prepared according to method A as white powder (43 mg, 14.0% yield). mp 107−109 °C; IR (KBr) ν_{max} 3488, 3333, 1686, 1604, 1536, 1278, 1184 cm^{-1}; ^1H NMR (400 MHz, $CDCl_3$) δ 7.53 (1H, d, J = 16.0 Hz, H-β), 7.06 (1H, d, J = 2.0 Hz, H-2), 6.95 (1H, dd, J = 2.0, 8.0 Hz, H-6), 6.82 (1H, d, J = 8.0 Hz, H-5), 6.21 (1H, d, J = 16.0 Hz, H-α), 4.13 (2H, t, J = 6.8 Hz, H-1′), 1.63 (2H, m, H-2′), 1.20−1.32 (12H, m, H-3′-H-8′), 2.55 (3H, t, J = 6.8 Hz, H-9′); HRESIMS $[M - H]^-$ m/z 305.1739 (Calcd for $C_{18}H_{25}O_4$, 305.1753).

Ferulic Acid Phenethyl Ester (5). The title compound was prepared according to modified method A as light yellow gum (195 mg, 65.4% yield). IR (KBr) ν_{max} 3418, 1682, 1603, 1516, 1270, 1172 cm^{-1}; ^1H NMR (400 MHz, $CDCl_3$) δ 7.60 (1H, d, J = 16.0 Hz, H-β), 7.22−7.34 (5H, m, H-2′, 3′, 4′, 5′, 6′), 7.06 (1H, dd, J = 2.0, 8.4 Hz, H-6), 7.01 (1H, d, J = 2.0 Hz, H-2), 6.91 (1H, d, J = 8.4 Hz, H-5), 6.27 (1H, d, J = 16.0 Hz, H-α), 4.42 (2H, t, J = 7.2 Hz, H-α'), 3.91 (3H, s, 3−OCH_3), 3.02 (2H, t, J = 7.2 Hz, H-β'); HRESIMS $[M - H]^-$ m/z 297.1125 (Calcd for $C_{18}H_{17}O_4$, 297.1127).

Isoferulic Acid Phenethyl Ester (6). The title compound was prepared according to modified method A as white powder (202 mg, 67.7% yield). mp 79−81 °C; IR (KBr) ν_{max} 3384, 1686, 1600, 1262, 1184, 1165 cm^{-1}; ^1H NMR (400 MHz, $CDCl_3$) δ 7.58 (1H, d, J = 16.0 Hz, H-β), 7.22−7.34 (5H, m, H-2′, 3′, 4′, 5′, 6′), 7.13 (1H, d, J = 2.0 Hz, H-2), 7.01 (1H, dd, J = 2.0, 8.4 Hz, H-6), 6.83 (1H, d, J = 8.4 Hz, H-5), 6.27 (1H, d, J = 16.0 Hz, H-α), 4.41 (2H, t, J = 7.2 Hz, H-α'), 3.91 (3H, s, 3−OCH_3), 3.01 (2H, t, J = 7.2 Hz, H-β'); HRESIMS $[M - H]^-$ m/z 297.1120 (Calcd for $C_{18}H_{17}O_4$, 297.1127).

4-Methoxy Cinnamic Acid Phenethyl Ester (7). The title compound was prepared according to modified method A as light yellow gum (194 mg, 68.7% yield). IR (KBr) ν_{max} 2930, 1708, 1631, 1515, 1263, 1216, 1150 cm^{-1}; ^1H NMR (400 MHz, $CDCl_3$) δ 7.63 (1H, d, J = 16.0 Hz, H-β), 7.47 (2H, d, J = 8.8 Hz, H-2, 6), 7.24−7.32 (5H, m, H-2′, 3′, 4′, 5′, 6′), 6.90 (2H, d, J = 8.8 Hz, H-3, 5), 6.30 (1H, d, J = 16.0 Hz, H-α), 4.41 (2H, t, J = 7.2 Hz, H-α'), 3.83 (3H, s, 4−OCH_3), 3.02 (2H, t, J = 7.2 Hz, H-β'); HRESIMS $[M - H]^-$ m/z 281.1176 (Calcd for $C_{18}H_{17}O_3$, 281.1178)

3,4-Dimethoxycinnamic Acid Phenethyl Ester (8). The title compound was prepared according to modified method A as white powder (165 mg, 52.8% yield). mp 89−91 °C; IR (KBr) ν_{max} 2916, 2849, 1702, 1635, 1515, 1258, 1236, 1139 cm^{-1}; ^1H NMR (400 MHz, $CDCl_3$) δ 7.62 (1H, d, J = 16.0 Hz, H-β), 7.28 (5H, m, H-2′, 3′, 4′, 5′, 6′), 7.09 (1H, dd, J = 2.0, 8.4 Hz, H-6), 7.04 (1H, d, J = 2.0 Hz, H-2), 6.86 (1H, d, J = 8.4 Hz, H-5), 6.30 (1H, d, J = 16.0 Hz, H-α), 4.43 (2H, t, J = 7.2 Hz, H-α'), 3.90 (6H, s, 3, 4−OCH_3), 3.02 (2H, t, J = 7.2 Hz, H-β'); HRESIMS $[M - H]^-$ m/z 311.1300 (Calcd for $C_{19}H_{19}O_4$, 311.1283).

p-Coumaric Acid Phenethyl Ester (9). The title compound was prepared according to modified method A as white powder (157 mg, 58.5% yield). mp 90−92 °C; IR (KBr) ν_{max} 3279, 1681, 1631, 1582, 1515, 1278, 1206, 1170 cm^{-1}; ^1H NMR (400 MHz, $CDCl_3$) δ 7.62 (1H, d, J = 16.0 Hz, H-β), 7.39 (2H, d, J = 8.4 Hz, H-2, 6), 7.22−7.33 (5H, m, H-2′, 3′, 4′, 5′, 6′), 6.85 (2H, d, J = 8.8 Hz, H-3, 5), 6.27 (1H, d, J = 16.0 Hz, H-α), 4.42 (2H, t, J = 7.2 Hz, H-α'), 3.02 (2H, t, J = 7.2 Hz, H-β'); HRESIMS $[M - H]^-$ m/z 267.1016 (Calcd for $C_{17}H_{15}O_3$, 267.1021).

Cinnamic Acid Phenethyl Ester (10). The title compound was prepared according to modified method A as white powder (145 mg, 57.5% yield). mp 55−56 °C; IR (KBr) ν_{max} 1710, 1637, 1496, 1313,

1205, 1173 cm^{-1}; ^1H NMR (400 MHz, $CDCl_3$) δ 7.67 (1H, d, J = 16.0 Hz, H-β), 7.35−7.51 (5H, m, H-2, 3, 4, 5, 6), 7.21−7.33 (5H, m, H-2′, 3′, 4′, 5′, 6′), 6.42 (1H, d, J = 16.0 Hz, H-α), 4.42 (2H, t, J = 7.2 Hz, H-α'), 3.01 (2H, t, J = 7.2 Hz, H-β'); HRESIMS $[M - H]^-$ m/z 251.1067 (Calcd for $C_{17}H_{15}O_2$, 251.1072).

*Sinapic Acid Phenethyl Ester (**11**).* The title compound was prepared according to modified method A as light yellow oil (216 mg, 65.8% yield). IR (KBr) ν_{max} 3419, 1704, 1633, 1514, 1283, 1218, 1153 cm^{-1}; ^1H NMR (400 MHz, $CDCl_3$) δ 7.58 (1H, d, J = 16.0 Hz, H-β), 7.22−7.34 (5H, m, H-2′, 3′, 4′, 5′, 6′), 6.76 (2H, s, H-2, 6), 6.29 (1H, d, J = 16.0 Hz, H-α), 4.43 (2H, t, J = 7.2 Hz, H-α'), 3.91 (6H, s, 3, 5−OCH_3), 3.02 (2H, t, J = 7.2 Hz, H-β'); HRESIMS $[M - H]^-$ m/z 327.1228 (Calcd for $C_{19}H_{19}O_5$, 327.1232).

*Caffeic Acid 3-Bromophenethyl Ester (**12**).* The title compound was prepared according to modified method A as white powder (42 mg, 11.6% yield). mp 120−122 °C; IR (KBr) ν_{max} 3472, 3316, 1686, 1604, 1528, 1278, 1180 cm^{-1}; ^1H NMR (400 MHz, DMSO-d_6) δ 9.59 (1H, s), 9.12 (1H, s), 7.52 (1H, m, H-2′), 7.44 (1H, d, J = 16.0 Hz, H-β), 7.42 (1H, m, H-6′), 7.28 (2H, m, H-4′, 5′), 7.03 (1H, d, J = 2.0 Hz, H-2), 6.98 (1H, dd, J = 8.0, 2.0 Hz, H-6), 6.75 (1H, d, J = 8.0 Hz, H-5), 6.22 (1H, d, J = 16.0 Hz, H-α), 4.32 (2H, t, J = 6.8 Hz, H-α'), 2.95 (2H, t, J = 6.8 Hz, H-β'); ^{13}C NMR (100 MHz, DMSO-d_6) δ 166.4, 148.5, 145.6, 145.3, 141.1, 131.7, 130.5, 129.3, 128.1, 125.4, 121.6, 121.4, 115.7, 114.8, 113.7, 63.9, 34.0; HRESIMS $[M - H]^-$ m/z 361.0079 (Calcd for $C_{17}H_{14}O_4Br$, 361.0075).

*Caffeic Acid 2-Bromophenethyl Ester (**13**).* The title compound was prepared according to modified method A as white powder (68 mg, 18.7% yield). mp 137−139 °C; IR (KBr) ν_{max} 3465, 3301, 1694, 1607, 1529, 1280, 1188 cm^{-1}; ^1H NMR (400 MHz, DMSO-d_6) δ 9.59 (1H, s), 9.15 (1H, s), 7.61 (1H, dd, J = 7.6, 0.8 Hz, H-3′), 7.46 (1H, d, J = 16.0 Hz, H-β), 7.41 (1H, dd, J = 7.6, 1.6 Hz, H-6′), 7.34 (1H, dt, J = 7.6, 0.8 Hz, H-5′), 7.11 (1H, dt, J = 7.6, 1.6 Hz, H-4′), 7.04 (1H, d, J = 2.0 Hz, H-2), 6.98 (1H, dd, J = 8.0, 2.0 Hz, H-6), 6.76 (1H, d, J = 8.0 Hz, H-5), 6.22 (1H, d, J = 16.0 Hz, H-α), 4.34 (2H, t, J = 6.8 Hz, H-α'), 3.09 (2H, t, J = 6.8 Hz, H-β'); ^{13}C NMR (100 MHz, DMSO-d_6) δ 166.4, 148.5, 145.6, 145.3, 137.2, 132.6, 131.4, 128.8, 127.9, 125.4, 124.0, 121.4, 115.7, 114.8, 113.7, 62.7, 34.7; HRESIMS $[M - H]^-$ m/z 361.0073 (Calcd for $C_{17}H_{14}O_4Br$, 361.0075).

*Caffeic Acid Benzyl Ester (**14**).* The title compound was prepared according to method B as white powder (148 mg, 54.8% yield). mp 151−153 °C; IR (KBr) ν_{max} 3466, 3327, 1689, 1601, 1535, 1277, 1177 cm^{-1}; ^1H NMR (400 MHz, $CDCl_3$) δ 7.52 (1H, d, J = 16.0 Hz, H-β), 7.26−7.34 (5H, m, H-2′, 3′, 4′, 5′, 6′), 6.97 (1H, d, J = 1.2 Hz, H-2), 6.86 (1H, dd, J = 1.2, 8.0 Hz, H-6), 6.74 (1H, d, J = 8.0 Hz, H-5), 6.20 (1H, d, J = 16.0 Hz, H-α), 5.15 (2H, s, H-α'); HRESIMS $[M - H]^-$ m/z 269.0810 (Calcd for $C_{16}H_{13}O_4$, 269.0814).

*p-Coumaric Acid Benzyl Ester (**15**).* The title compound was prepared according to method B as white powder (213 mg, 83.8% yield). mp 90−92 °C; IR (KBr) ν_{max} 3401, 1691, 1599, 1517, 1279, 1203, 1170 cm^{-1}; ^1H NMR (400 MHz, $CDCl_3$) δ 7.60 (1H, d, J = 16.0 Hz, H-β), 7.34 (2H, d, J = 8.4 Hz, H-2, 6), 7.26−7.33 (5H, m, H-2′, 3′, 4′, 5′, 6′), 6.76 (2H, d, J = 8.4 Hz, H-3, 5), 6.27 (1H, d, J = 16.0 Hz, H-α), 5.18 (2H, s, H-α'); HRESIMS $[M - H]^-$ m/z 253.0860 (Calcd for $C_{16}H_{13}O_3$, 253.0865).

*Caffeic Acid Phenylacetamide (**16**).* The title compound was prepared according to method C as light yellow powder (81 mg, 28.6% yield). mp 153−155 °C; IR (KBr) ν_{max} 3488, 3346, 1649, 1602, 1551, 1326, 1287, 1189 cm^{-1}; ^1H NMR (400 MHz, $CDCl_3$) δ 7.34 (1H, d, J = 16.0 Hz, H-β), 7.13−7.24 (5H, m, H-2′, 3′, 4′, 5′, 6′), 6.93 (1H, d, J = 1.6 Hz, H-2), 6.82 (1H, dd, J = 1.6, 8.4 Hz, H-6), 6.71 (1H, d, J = 8.4 Hz, H-5), 6.16 (1H, d, J = 16.0 Hz, H-α), 3.48 (2H, t, J = 7.2 Hz, H-α'), 2.78 (2H, t, J = 7.2 Hz, H-β'); HRESIMS $[M - H]^-$ m/z 282.1125 (Calcd for $C_{17}H_{16}NO_3$, 282.1130).

*Caffeic Acid 4-Hydroxyphenylacetamide (**17**).* The title compound was prepared according to method C as light yellow powder (35 mg, 11.7% yield). mp 211−212 °C; IR (KBr) ν_{max} 3369, 1646, 1604, 1516, 1241 cm^{-1}; ^1H NMR (400 MHz, CD_3OD) δ 7.37 (1H, d, J = 15.6 Hz, H-β), 7.05 (2H, d, J = 8.4 Hz, H-2′, 6′), 6.99 (1H, d, J = 2.0 Hz, H-2), 6.89 (1H, dd, J = 2.0, 8.4 Hz, H-6), 6.75 (1H, d, J = 8.4 Hz, H-5), 6.70 (2H, d, J = 8.4 Hz, H-3′, 5′), 6.33 (1H, d, J = 15.6 Hz, H-α), 3.45 (2H, t, J = 7.2 Hz, H-α'), 2.74 (2H, t, J = 7.2 Hz, H-β'); HRESIMS $[M - H]^-$ m/z 298.1081 (Calcd for $C_{17}H_{16}NO_4$, 298.1079).

*Caffeic Acid 3,4-Dihydroxyphenethyl Ester (**18**).* The title compound was prepared according to method D as a white powder (648 mg, 41.0% yield for Knoevenagel condensation). mp 118−120 °C; IR (KBr) ν_{max} 3339, 1680, 1600, 1525, 1278, 1186 cm^{-1}; ^1H NMR (400 MHz, CD_3OD) δ 7.52 (1H, d, J = 16.0 Hz, H-β), 7.03 (1H, d, J = 2.0 Hz, H-2), 6.94 (1H, dd, J = 2.0, 8.0 Hz, H-6), 6.78 (1H, d, J = 8.0 Hz, H-5), 6.70 (1H, d, J = 2.0 Hz, H-2′), 6.70 (1H, d, J = 8.0 Hz, H-5′), 6.58 (1H, dd, J = 2.0, 8.0 Hz, H-6′), 4.29 (2H, t, J = 7.2 Hz, H-α'), 2.84 (2H, t, J = 7.2 Hz, H-β'); HRESIMS $[M - H]^-$ m/z 315.0862 (Calcd for $C_{17}H_{15}O_6$, 315.0869).

*Caffeic Acid 4-Nitrophenethyl Ester (**19**).* The title compound was prepared according to method D as a light yellow powder (305 mg, 18.5% yield for Knoevenagel condensation). mp 172−174 °C; IR (KBr) ν_{max} 3418, 1691, 1596, 1507, 1340, 1277, 1167 cm^{-1}; ^1H NMR (400 MHz, DMSO-d_6) δ 9.55 (1H, s), 9.11 (1H, s), 8.17 (2H, d, J = 8.8 Hz, H-2′, 6′), 7.58 (2H, d, J = 8.8 Hz, H-3′, 5′), 7.44 (1H, d, J = 16.0 Hz, H-β), 7.03 (1H, d, J = 2.0 Hz, H-2), 6.98 (1H, dd, J = 2.0, 8.0 Hz, H-6), 6.76 (1H, d, J = 8.0 Hz, H-5), 6.21 (1H, d, J = 16.0 Hz, H-α), 4.39 (2H, t, J = 6.4 Hz, H-α'), 3.11 (2H, t, J = 6.4 Hz, H-β'); ^{13}C NMR (100 MHz, DMSO-d_6) δ 166.4, 148.5, 146.7, 146.3, 145.6, 145.4, 130.2, 125.4, 123.4, 121.4, 115.7, 114.9, 113.6, 63.5, 34.2; HRESIMS $[M - H]^-$ m/z 328.0823 (Calcd for $C_{17}H_{14}NO_6$, 328.0821).

*Caffeic Acid 4-Aminophenethyl Ester (**20**).* A mixture of caffeic acid 4-nitrophenethyl ester (60 mg, 0.091 mmol), stannic chloride dihydrate (123 mg, 0.55 mmol) and 5 mL of ethanol was heated to reflux for 10 h before being cooled to room temperature. Ten milliliters of saturated Na_2CO_3 was added, and the suspension was extracted with ethyl acetate (10 mL × 3). The combined organic layer was dried, evaporated and purified by column chromatography to give the title compound as a light yellow powder (34 mg, 62.3% yield). mp 173−175 °C; IR (KBr) ν_{max} 3432, 1692, 1598, 1515, 1280, 1175 cm^{-1}; ^1H NMR (400 MHz, DMSO-d_6) δ 9.57 (1H, s), 9.12 (1H, s), 7.45 (1H, d, J = 16.0 Hz, H-β), 7.04 (1H, d, J = 2.0 Hz, H-2), 6.99 (1H, dd, J = 2.0, 8.0 Hz, H-6), 6.91 (2H, d, J = 8.4 Hz, H-2′, 6′), 6.76 (1H, d, J = 8.0 Hz, H-5), 6.50 (2H, d, J = 8.4 Hz, H-3′, 5′), 6.23 (1H, d, J = 16.0 Hz, H-α), 4.20 (2H, t, J = 7.2 Hz, H-α'), 2.75 (2H, t, J = 7.2 Hz, H-β'); ^{13}C NMR (100 MHz, DMSO-d_6) δ 167.0, 148.9, 147.5, 146.0, 145.5, 129.7, 126.0, 125.1, 121.8, 116.2, 115.3, 114.5, 65.4, 34.3; HRESIMS $[M - H]^-$ m/z 298.1075 (Calcd for $C_{17}H_{16}NO_4$, 298.1079).

*3,4-Dihydroxyphenyl Propionic Acid Phenethyl Ester (**21**).* To a solution of caffeic acid phenethyl ester (50 mg, 0.176 mmol) in 10 mL of ethyl acetate was added 10% Pd/C (5 mg) under nitrogen atmosphere. The reaction flask was vacuumed and backfilled with hydrogen and stirred at room temperature for 12 h. The mixture was filtered and evaporated to give the titled compound as yellow gum (50 mg, 99.4% yield). IR (KBr) ν_{max} 3400, 1709, 1605, 1519, 1352, 1282, 1192 cm^{-1}; ^1H NMR (400 MHz, $CDCl_3$) δ 7.18−7.30 (5H, m, H-2′, 3′, 4′, 5′, 6′), 6.74 (1H, d, J = 8.0 Hz, H-5), 6.63 (1H, d, J = 2.0 Hz, H-2), 6.57 (1H, dd, J = 2.0, 8.0 Hz, H-6), 4.28 (2H, t, J = 7.2 Hz, H-α'), 2.91 (2H, t, J = 7.2 Hz, H-β'), 2.79 (2H, t, J = 7.8 Hz, H-α), 2.55 (2H, t, J = 7.8 Hz, H-β); HRESIMS $[M - H]^-$ m/z 285.1120 (Calcd for $C_{17}H_{17}O_4$, 285.1127).

*Cytotoxicities of CAPE and Its Derivatives **1**-**21** in PC12 Cells.* Differentiated PC12 cells were maintained in DMEM medium supplemented with 1% L-glutamine and 10% fetal bovine serum at 37 °C under a humidified 5% CO_2 atmosphere. Each test compound with appropriate concentration was dissolved in DMSO and diluted with serum-free media. Before treatment, cells were seeded on a 96 well plate at the density of 5 × 10^3 cells/well and cultured for 24 h. Then the medium was changed and cells were treated with CAPE and its derivatives at 4 and 40 nM for 24 h, respectively. Then, 20 μL of MTT solution (final concentration, 0.5 mg/mL) were added to each well, and cells were incubated for 4 h. The resultant formazan product was dissolved by the addition of 150 μL of DMSO. The absorbance was measured at the wavelength of 570 nm using a Thermo Scientific

Scheme 1. Synthesis of CAPE Derivatives[a]

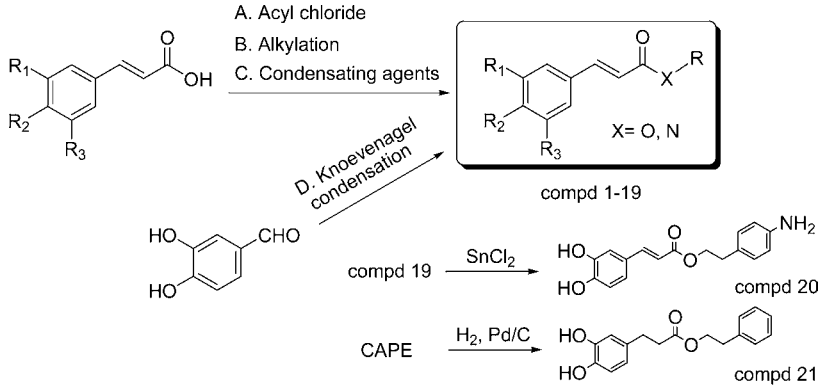

Compounds	R_1	R_2	R_3	R	X	Method
1	OH	OH	H	$C_6H_5CH{=}CHCH_2$	O	A
2	OH	OH	H	$C_6H_5CH_2CH_2CH_2$	O	A
3	OH	OH	H	4-OH-$C_6H_5CH_2CH_2$	O	A
4	OH	OH	H	n-nonyl	O	A
5	OCH_3	OH	H	$C_6H_5CH_2CH_2$	O	A
6	OH	OCH_3	H	$C_6H_5CH_2CH_2$	O	A
7	H	OCH_3	H	$C_6H_5CH_2CH_2$	O	A
8	OCH_3	OCH_3	H	$C_6H_5CH_2CH_2$	O	A
9	H	OH	H	$C_6H_5CH_2CH_2$	O	A
10	H	H	H	$C_6H_5CH_2CH_2$	O	A
11	OCH_3	OH	OCH_3	$C_6H_5CH_2CH_2$	O	A
12	OH	OH	H	3-Br-$C_6H_5CH_2CH_2$	O	A
13	OH	OH	H	2-Br-$C_6H_5CH_2CH_2$	O	A
14	OH	OH	H	$C_6H_5CH_2$	O	B
15	H	OH	H	$C_6H_5CH_2$	O	B
16	OH	OH	H	$C_6H_5CH_2CH_2$	N	C
17	OH	OH	H	4-OH-$C_6H_5CH_2CH_2$	N	C
18	OH	OH	H	3,4-di-OH-$C_6H_5CH_2CH_2$	O	D
19	OH	OH	H	4-NO_2-$C_6H_5CH_2CH_2$	O	D

[a]Reagents and conditions: Method A: (1) caffeic acid, $SOCl_2$, DME, reflux, 12 h, (2) acyl chloride of caffeic acid, alcohol, DME, reflux, 4 h; Modified method A: caffeic acid or its analogues, excess alcohol, $SOCl_2$, 65 °C, 4 h. Method B: caffeic acid or its analogues, benzyl bromide, K_2CO_3, DMF, RT, 12 h. Method C: caffeic acid, phenethylamines/4-hydroxyphenethylamine, triethylamine, BOP, DMF/DCM, 0 °C to RT, 20 h. Method D: (1) alcohol, meldrum's acid, 1,4-dioxane, reflux, 6 h; (2) malonic acid mono ester, 3,4-dihydroxybenzaldehyde/4-nitrobenzaldehyde, pyridine, piperidine, RT, 15 h. RT stands for ambient temperature.

Multiskan MK3 microplate reader (Waltham, MA, USA). Results were expressed as percentage of cell viability (%), assuming control cells as 100%. The cytotoxicities of CAPE and its derivatives in undifferentiated PC12 cells at 0.5, 5, 10, and 20 nM, respectively, were performed following a similar procedure, except that the culture media was changed to DMEM medium supplemented with 1% L-glutamine, 10% horse serum and 5% fetal bovine serum.

Cytoprotective Effects of CAPE and Its Derivatives 1–21 in PC12 Cells. Before treatment, differentiated PC12 cells were seeded on a 96 well plate at the density of 1×10^4 cells/well and cultured for 24 h. The medium was changed, and cells were pretreated for 6 h with 4 nM or 40 nM CAPE and its derivatives, respectively; then the cells were exposed to 200 μM H_2O_2 for another 24 h. Cell viability was determined using the MTT method as described above.

Neuritogenic Effects of CAPE and Its Derivatives 1–21 in PC12 Cells. Undifferentiated PC12 cells (5×10^4 cells/well) were seeded on poly-L-lysine-coated 12-well plates. NGF (Sigma-Aldrich, St. Louis, MO, USA) was dissolved in sterilized water and then diluted with serum-free media to the final concentration of 50 ng/mL. After 72 h of incubation with NGF, CAPE and its derivatives (0.5 nM or 10 nM), respectively, the neurite outgrowth of cells was observed by inverted microscope (OLYPUS IX71, Tokyo, Japan). Cells with one or more neurites whose lengths were greater than or equal to the length of one cell body were scored as positive. The number of neurite-bearing cells was counted in five randomly selected microscopic fields and expressed as a percentage of the total cells in the field. The neurite length was determined as the mean value for all identified neurite-bearing cells in a field (ImageJ software). At least 100 cells were selected for calculating the neurite length. Each experiment was conducted in triplicate.

Statistical Analysis. Data were reported as mean ± SD for triplicate determinations. Significant differences ($p < 0.05$ or $p < 0.01$) between the means of control and different treatment groups were analyzed by Dunnett's test using SPSS for Windows (version rel. 10.0.5, 1999, SPSS Inc., Chicago, IL).

RESULTS AND DISCUSSION

Synthesis of Caffeic Acid Phenethyl Ester Derivatives. Previous studies revealed that bioactivities of CAPE derivatives are mainly affected by the number of hydroxyl groups,[22,23] the methylation degree of the hydroxyl group,[24] the length of the ester moiety,[19] and the conjugate double bonds[25] in CAPE.

dx.doi.org/10.1021/jf500464k | J. Agric. Food Chem. 2014, 62, 5046–5053

These factors were the basis for designing the targeted compounds for the present study. In addition, selected electron-donating and -withdrawing groups were substituted on the benzene ring of the alcoholic moiety to alter the electronic density or provide additional binding sites.

As shown in Scheme 1, twenty-one CAPE derivatives (compounds **1**−**21**) were prepared, among which compounds **12**, **13** and **20** were first synthesized. Diverse methods were used for synthesis of these derivatives. We obtained caffeic acid esters (method A, compounds **1**−**4**) in 1,2-dichloroethane, which results in fewer side products compared to the frequently used 1,4-dioxane. Moreover, replacement of solvent with excess liquid alcohol lead to better yields of 50−70% in many cases (compounds **5**−**13**). Compounds **14** and **15** were conveniently obtained by alkylation (method B) with benzyl bromide in good yields and purities. Amide derivatives (compounds **16** and **17**) were synthesized by using a condensing agent such as BOP (method C). Some caffeate derivatives (compounds **18** and **19**) hardly unavailable by other methods were prepared by Knoevenagel condensation (method D). Reduction of compound **19** in the presence of stannous chloride gave compound **20** in high yield, and hydrogenation of CAPE afforded compound **21**.

Cytotoxicity of Caffeic Acid Phenethyl Ester Derivatives in PC12 Cells. CAPE and its derivatives were initially assayed for cytotoxic effects in differentiated PC12 cells (4 and 40 nM) and undifferentiated PC12 cells (0.5, 5, 10, and 20 nM), respectively. Differentiated and undifferentiated PC12 cells were incubated with these compounds for 24 h, respectively, and the extent of cell viability was determined using MTT assay. Cell viability less than 90% of control was considered toxic. The results demonstrated that CAPE and its derivatives were nontoxic in differentiated PC12 cells at 4 and 40 nM, respectively. While CAPE and its derivatives showed no toxicity at any tested concentrations except that compounds **4**, **12** and **13** have cytotoxicities at concentrations from 5 nM to 20 nM.

Caffeic Acid Phenethyl Ester Derivatives Protect PC12 Cells against H_2O_2-Induced Oxidative Stress. Reactive oxygen species (ROS) have been involved in the pathogenesis of many neurodegenerative diseases.[26] Hydroxyl radical is the most dangerous ROS and can be generated from H_2O_2 in the presence of transition metals including Fe and Cu. Hydroxyl radical can react rapidly with all types of intracellular biomolecules including lipids, DNA, and protein, eventually leading to cell death. Differentiated PC12 cells were reported to be more sensitive to oxidant stimulus than undifferentiated cells,[27] and be better for cytoprotective study. Thus, the cytoprotective activities of CAPE derivatives against H_2O_2-induced oxidative stress were evaluated on differentiated PC12 cells in the present study.

At the concentrations of 4 nM and 40 nM, all CAPE derivatives did not affect cell survival. Among the tested samples, 4 nM compounds **1** and **20** significantly increased the cell viability to 87.5% and 89.3%, respectively (Figure 1). Their cytoprotective activities were much better than those of the parent compound CAPE under the same concentrations. Compounds **3**, **4**, **12**, **13**, **15**, **16** and **19** showed similar protective capabilities to CAPE within the range of 62.9−81.1% at 4 nM, while compounds **1**−**4**, **6**, **7**, **9**, **10**, **12**, **13**, **16**, **19**, and **20** possessed equivalent protective effects as CAPE within the range 61.9−93.9% at 40 nM (Figure 1). Other CAPE derivatives demonstrated poorer activities against H_2O_2-indued cytotoxicity (data not shown).

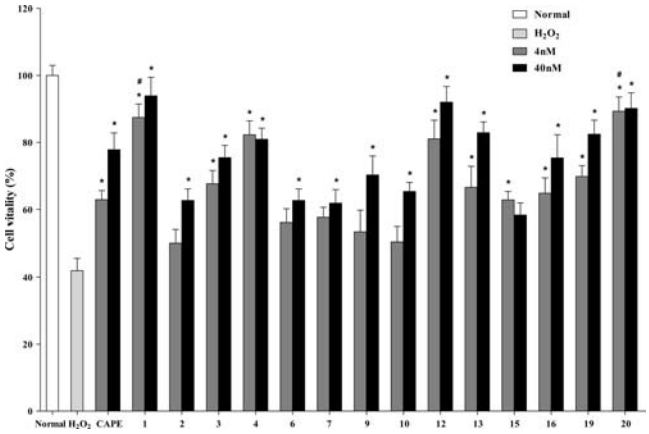

Figure 1. Cytoprotective effects of CAPE and selected CAPE derivatives in PC12 cells under H_2O_2-induced oxidative stress. Differentiated PC12 cells were treated with 4 nM, 40 nM CAPE and its derivatives for 6 h, respectively, and then the cells were exposed to 200 μM H_2O_2 for another 24 h. Cell viability was determined using the MTT method. The viability of normal cells was defined as 100%. Data are shown as mean ± SD (n = 3). (*) $p < 0.05$ compared to H_2O_2-treated group; (#) $p < 0.05$ compared to 4 nM CAPE group.

It is noteworthy that introduction of an amino group at C-4′ of the phenethyl ethanol moiety in CAPE could result in a more potent compound. Furthermore, a substitution of phenethyl ethanol with a cinnamyl group could more effectively suppress the toxicity induced by hydrogen peroxide. Our study also showed that the catechol group was not the crucial factor for the protective activities of CAPE derivatives on PC12 cells because compounds **14**, **17**, **18**, and **21** were inactive. Unexpectedly, caffeic acid 4-hydroxyphenethyl ester (**17**) and caffeic acid 3,4-dihydroxyphenethyl ester (**18**) poorly suppressed H_2O_2-induced cytotoxicity in PC12 cells. This phenomenon may be explained by their high hydrophilicities for additional phenolic hydroxyl on the phenethyl ethanol group, resulting in a poor permeability across the cellular membrane.

A series of catechol ring-fluorinated derivatives of CAPE and caffeic acid phenethyl amide (CAPA) were synthesized, respectively, and their cytoprotective effects were evaluated against menadione or H_2O_2-induced cytotoxicity in human umbilical vein endothelial cells (HUVEC).[24,28] One fluorinated derivative of CAPE and three fluorinated analogues of CAPA were found to possess similar cytoprotective activities with their parent compounds. Our results were well in accordance with these previous studies that CAPE derivatives could be considered as a new class of cytoprotective agents.

Caffeic Acid Phenethyl Ester Derivatives Induce Neurite Outgrowth of PC12 Cells. Nerve growth factor (NGF), showing benefits on the growth, differentiation and survival of neuronal cells, was expected to be a promising agent for the treatment of neurodegenerative diseases.[29] But the disadvantages of NGF such as inability to cross the blood−brain barrier and poor stability *in vivo*, drastically limited its application. As a result, discovery of small molecules from natural sources or their derivatives having neuritogenic ability is an alternative approach to prevent neurodegenerative diseases.[30,31]

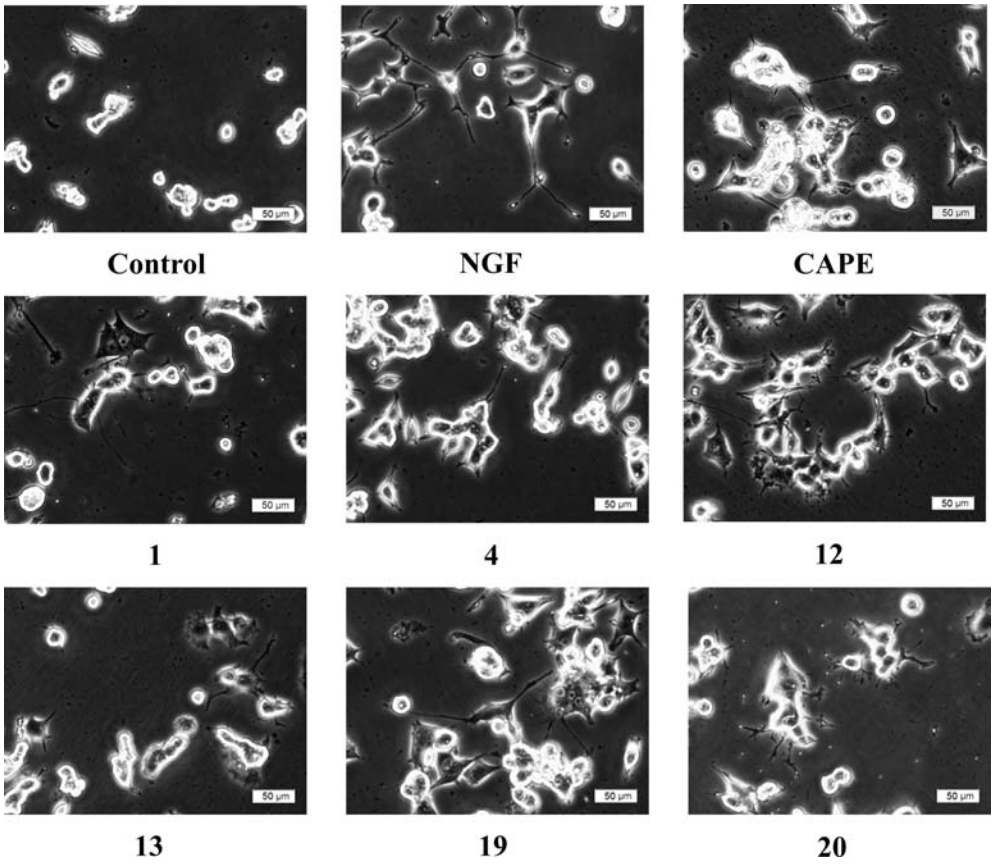

Figure 2. Morphology of PC12 cells treated with CAPE and its derivatives. Undifferentiated PC12 cells were seeded on poly-L-lysine-coated 12 well plates in DMEM medium (1% L-glutamine, 10% horse serum and 5% fetal bovine serum) for 24 h prior to treatment with NGF (50 ng/mL), CAPE (10 nM), and compounds **1** (0.5 nM), **4** (0.5 nM), **12** (0.5 nM), **13** (0.5 nM), **19** (10 nM), and **20** (10 nM) for an additional 72 h. Cell morphology was observed using inverted microscopy.

Undifferentiated PC12 cells are a useful model for the study of neuronal development *in vitro*, and they can be induced to differentiate into sympathetic-like neurons after exposure to NGF. The effects of CAPE derivatives **1**−**21** on the neurite outgrowth of undifferentiated PC12 cells were evaluated by morphological observations and a quantitative analysis of neurite-bearing cells and neurite length. Among the twenty-one CAPE derivatives, compounds **1**, **4**, **12** and **13** showed potential neuritogenic activities at 0.5 nM, while compounds **19** and **20** induced neurite outgrowth at 10 nM (Figure 2). As shown in Figure 3A, compounds **1**, **4**, **13**, **19** and **20** slightly increased the percent of neurite-bearing cells (<20%) and compound **12** modestly promoted the growth (>20%). The percent of neurite-bearing cells in groups treated with compounds **1**, **4**, **12**, **13**, **19** and **20** was significantly higher than the control. The average of neurite length for PC12 cells treated with compounds **1**, **4**, **12**, **13**, **19** and **20** was in the range of 25.1−37.0 μm, which was significantly higher than the control (18.4 μm) (Figure 3B). Specifically, 0.5 nM compound **12** markedly increased both the percentage of neurite bearing cells (21.5%) and the mean neurite length in those cells (37.0 μm) as compared with those in 10 nM CAPE (15.8% in numbers and 32.2 μm in length). Compounds **19** and **20** possessed similar neuritogenic activities as CAPE at 10 nM. These data suggested that the phenethyl alcohol group and its substitution were critical for maintaining or enhancing the neuritogenic activity of CAPE derivatives. Additional data are required for further structure−activity relationship analysis.

By comparison with the data from the literature,[30,31] the effective concentration of compounds **1**, **4**, **12** and **13** was much lower than that of natural products showing neuritogenic potential, and was comparable with that of tripchlorolide (10^{-10} M),[32] sargaquinoic acid (1.25−100 ng)[33] and catalpol (0.1−1 μg/mL),[34] geniposide (0.1−10 μg/mL),[34] and gardenoside (0.1−10 μg/mL).[34] Compounds **12** and **13** showed cytotoxicity against PC12 cells at 5 nM, which may be originated from the substitution of bromine atom on the aromatic ring. The cytotoxicity might be alleviated by the replacement of other halogen atoms such as fluorine (F) and chlorine (Cl) on the same position. Interestingly, we found that some compounds with significant cytoprotective activities also showed simulative effects on the neurite outgrowth of PC12 cells. These results indicated that the CAPE derivatives were promising candidates for reducing the risk of neurodegenerative diseases. To the best of our knowledge, this is the first report on neuritogenic activities of CAPE derivatives.

In conclusion, twenty-one CAPE derivatives with diverse substitution or carbon skeleton were synthesized. Among them, compounds **1** and **20** significantly protected the PC12 cells against H_2O_2-induced cytotoxicity. Meanwhile, compounds **1**, **4**, **12**, **13**, **19** and **20** remarkably induced the neurite outgrowth. Our study suggested that the presence of the caffeic acid group may be important for keeping the cytoprotective and neuritogenic activities, and the alcohol group and its substitution majorly affected the activities of CAPE derivatives. The results might promote the understanding of the health

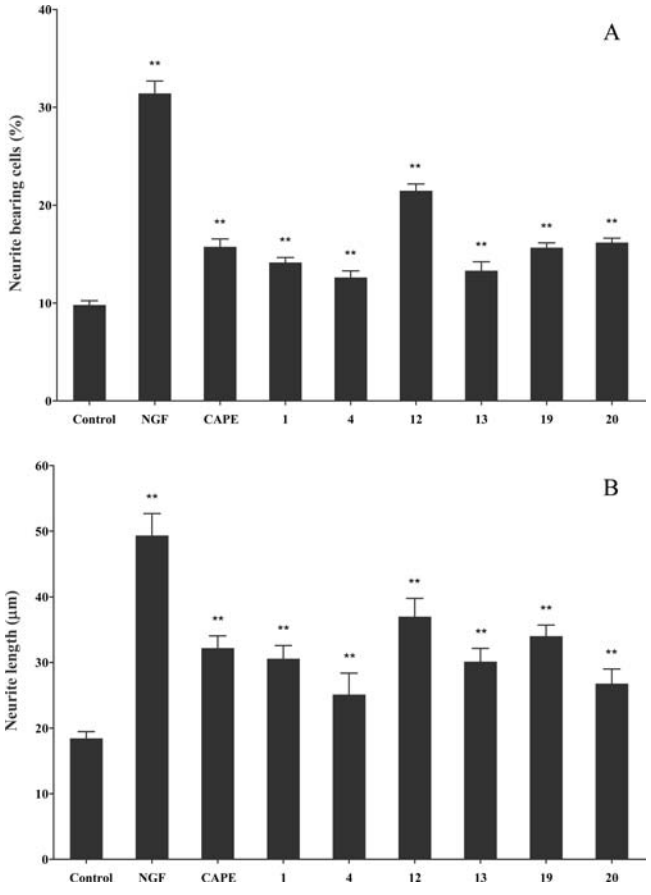

Figure 3. Effects of CAPE and its derivatives on neurite outgrowth in PC12 cells. Undifferentiated PC12 cells were treated with NGF (50 ng/mL), CAPE (10 nM), compounds **1** (0.5 nM), **4** (0.5 nM), **12** (0.5 nM), **13** (0.5 nM), **19** (10 nM) and **20** (10 nM) for 72 h to evaluate their neuritogenic effects, respectively. (A) Neurite bearing cells were counted under inverted microscopy in five random fields. (B) The average of neurite length for all identified neurite bearing cells was analyzed by ImageJ software. At least 100 cells were selected for calculating the neurite length. Data are expressed as mean ± SE (n = 3). (**) $p < 0.01$ represents significant differences compared with that of control.

benefits of CAPE and its derivatives, and may lead to the development of the functional food ingredients for the prevention of neurodegenerative diseases.

AUTHOR INFORMATION

Corresponding Author

*Tel: 86-21-34204041. Fax: 86-21-34204107. E-mail: hmshi@sjtu.edu.cn.

Author Contributions

‖H.S. and D.X. contributed equally to this work.

Funding

This research was supported by a special fund for agro-scientific research in the public interest (No. 201203069), the National High Technology Research and Development Program of China (Grant Nos. 2013AA102202; 2013AA102207), and a grant from the Opening Foundation of Zhejiang Provincial Top Key Discipline (Wenzhou University) (100061200125).

Notes

The authors declare no competing financial interest.

REFERENCES

(1) Butterfield, D. A.; Howard, B.; Yatin, S.; Koppal, T.; Drake, J.; Hensley, K.; Aksenov, M.; Aksenova, M.; Subramaniam, R.; Varadarajan, S.; Harris-White, M. E.; Pedigo, N. W.; Carney, J. M. Elevated oxidative stress in models of normal brain aging and Alzheimer's disease. *Life Sci.* **1999**, *65*, 1883−1892.

(2) Chu, Y. F.; Brown, P. H.; Lyle, B. J.; Chen, Y. M.; Black, R. M.; Williams, C. E.; Lin, Y. C.; Hsu, C. W.; Cheng, I. H. Roasted coffees high in lipophilic antioxidants and chlorogenic acid lactones are more neuroprotective than green coffees. *J. Agric. Food Chem.* **2009**, *57*, 9801−9808.

(3) Hwang, S. L.; Shih, P. H.; Yen, G. C. Neuroprotective effects of citrus flavonoids. *J. Agric. Food Chem.* **2012**, *60*, 877−885.

(4) Kano, Y.; Horie, N.; Doi, S.; Aramaki, F.; Maeda, H.; Hiragami, F.; Kawamura, K.; Motoda, H.; Koike, Y.; Akiyama, J.; Eguchi, S.; Hashimoto, K. Artepillin C derived from propolis induces neurite outgrowth in PC12m3 cells via ERK and p38 MAPK pathways. *Neurochem. Res.* **2008**, *33*, 1795−1803.

(5) Liao, K. K.; Wu, M. J.; Chen, P. Y.; Huang, S. W.; Chiu, S. J.; Ho, C. T.; Yen, J. H. Curcuminoids promote neurite outgrowth in PC12 cells through MAPK/ERK- and PKC-dependent pathways. *J. Agric. Food Chem.* **2012**, *60*, 433−443.

(6) Chuu, C. P.; Lin, H. P.; Ciaccio, M. F.; Kokontis, J. M.; Hause, R. J.; Hiipakka, R. A.; Liao, S. S.; Jones, R. B. Caffeic acid phenethyl ester suppresses the proliferation of human prostate cancer cells through inhibition of p70S6K and Akt signaling networks. *Cancer Prevention Res.* **2012**, *5*, 788−797.

(7) Lin, H. P.; Jiang, S. S.; Chuu, C. P. Caffeic acid phenethyl ester causes p21(Cip1) induction, akt signaling reduction, and growth inhibition in PC-3 human prostate cancer cells. *PLoS One* **2012**, *7*, e31286.

(8) Juman, S.; Yasui, N.; Ikeda, K.; Ueda, A.; Sakanaka, M.; Negishi, H.; Miki, T. Caffeic acid phenethyl ester suppresses the production of pro-inflammatory cytokines in hypertrophic adipocytes through lipopolysaccharide-stimulated macrophages. *Biol. Pharm. Bull.* **2012**, *35*, 1941−1946.

(9) Toyoda, T.; Tsukamoto, T.; Takasu, S.; Shi, L.; Hirano, N.; Ban, H.; Kumagai, T.; Tatematsu, M. Anti-inflammatory effects of caffeic acid phenethyl ester (CAPE), a nuclear factor-kappa B inhibitor, on *Helicobacter pylori*-induced gastritis in Mongolian gerbils. *Int. J. Cancer* **2009**, *125*, 1786−1795.

(10) Russo, A.; Longo, R.; Vanella, A. Antioxidant activity of propolis: role of caffeic acid phenethyl ester and galangin. *Fitoterapia* **2002**, *73*, S21−S29.

(11) Yang, H. S.; Dong, Y. Q.; Du, H. J.; Shi, H. M.; Peng, Y. H.; Li, X. B. Antioxidant compounds from propolis collected in Anhui, China. *Molecules* **2011**, *16*, 3444−3455.

(12) Park, J. H.; Lee, J. K.; Kim, H. S.; Chung, S. T.; Eom, J. H.; Kim, K. A.; Chung, S. J.; Paik, S. Y.; Oh, H. Y. Immunomodulatory effect of caffeic acid phenethyl ester in Balb/c mice. *Int. Immunopharmacol.* **2004**, *4*, 429−436.

(13) Tang, C. M.; Sojinu, O. S. Simultaneous determination of caffeic acid phenethyl ester and its metabolite caffeic acid in dog plasma using liquid chromatography tandem mass spectrometry. *Talanta* **2012**, *94*, 232−239.

(14) Celli, N.; Mariani, B.; Dragani, L. K.; Murzilli, S.; Rossi, C.; Rotilio, D. Development and validation of a liquid chromatographic-tandem mass spectrometric method for the determination of caffeic acid phenethyl ester in rat plasma and urine. *J. Chromatogr. B* **2004**, *810*, 129−136.

(15) Celli, N.; Dragani, L. K.; Murzilli, S.; Pagliani, T.; Poggi, A. In vitro and in vivo stability of caffeic acid phenethyl ester, a bioactive compound of propolis. *J. Agric. Food Chem.* **2007**, *55*, 3398−3407.

(16) Huang, Y. J.; Jin, M. H.; Pi, R. B.; Zhang, J. J.; Chen, M. H.; Ouyang, Y.; Liu, A. M.; Chao, X. J.; Liu, P. Q.; Liu, J.; Ramassamy, C.; Qin, J. Protective effects of caffeic acid and caffeic acid phenethyl ester against acrolein-induced neurotoxicity in HT22 mouse hippocampal cells. *Neurosci. Lett.* **2013**, *535*, 146−151.

(17) Kurauchi, Y.; Hisatsune, A.; Isohama, Y.; Mishima, S.; Katsuki, H. Caffeic acid phenethyl ester protects nigral dopaminergic neurons via dual mechanisms involving haem oxygenase-1 and brain-derived neurotrophic factor. *Br. J. Pharmacol.* **2012**, *166*, 1151−1168.
(18) Silva, R. B.; Santos, N. A. G.; Martins, N. M.; Ferreira, D. A. S.; Barbosa, F.; Souza, V. C. O.; Kinoshita, A.; Baffa, O.; Del-Bel, E.; Santos, A. C. Caffeic acid phenethyl ester protects against the dopaminergic neuronal loss induced by 6-hydroxydopamine in rats. *Neuroscience* **2013**, *233*, 86−94.
(19) Zhao, J.; Pati, S.; Redell, J. B.; Zhang, M.; Moore, A. N.; Dash, P. K. Caffeic acid phenethyl ester protects blood-brain barrier integrity and reduces contusion volume in rodent models of traumatic brain injury. *J. Neurotrauma* **2012**, *29*, 1209−1218.
(20) Shi, H. M.; Yang, H. S.; Zhang, X. W.; Sheng, Y.; Huang, H. Q.; Yu, L. L. Isolation and characterization of five glycerol esters from Wuhan propolis and their potential anti-inflammatory properties. *J. Agric. Food Chem.* **2012**, *60*, 10041−10047.
(21) Shi, H. M.; Yang, H. S.; Zhang, X. W.; Yu, L. L. Identification and quantification of phytochemical composition and anti-inflammatory and radical scavenging properties of methanolic extracts of Chinese propolis. *J. Agric. Food Chem.* **2012**, *60*, 12403−12410.
(22) Fiuza, S. M.; Gomes, C.; Teixeira, L. J.; da Cruz, M. T. G.; Cordeiro, M.; Milhazes, N.; Borges, F.; Marques, M. P. M. Phenolic acid derivatives with potential anticancer properties—a structure-activity relationship study. Part 1: Methyl, propyl and octyl esters of caffeic and gallic acids. *Bioorg. Med. Chem.* **2004**, *12*, 3581−3589.
(23) Son, S.; Lewis, B. A. Free radical scavenging and antioxidative activity of caffeic acid amide and ester analogues: Structure-activity relationship. *J. Agric. Food Chem.* **2002**, *50*, 468−472.
(24) Wang, X. Y.; Stavchansky, S.; Bowman, P. D.; Kerwin, S. M. Cytoprotective effect of caffeic acid phenethyl ester (CAPE) and catechol ring-fluorinated CAPE derivatives against menadione-induced oxidative stress in human endothelial cells. *Bioorg. Med. Chem.* **2006**, *14*, 4879−4887.
(25) Nagaoka, T.; Banskota, A. H.; Tezuka, Y.; Saiki, I.; Kadota, S. Selective antiproliferative activity of caffeic acid phenethyl ester analogues on highly liver-metastatic murine colon 26-L5 carcinoma cell line. *Bioorg. Med. Chem.* **2002**, *10*, 3351−3359.
(26) Barnham, K. J.; Masters, C. L.; Bush, A. I. Neurodegenerative diseases and oxidative stress. *Nat. Rev. Drug Discovery* **2004**, *3*, 205−214.
(27) Nouspikel, T. DNA repair in differentiated cells: Some new answers to old questions. *Neuroscience* **2007**, *145*, 1213−1221.
(28) Yang, J.; Marriner, G. A.; Wang, X. Y.; Bowman, P. D.; Kerwin, S. M.; Stavchansky, S. Synthesis of a series of caffeic acid phenethyl amide (CAPA) fluorinated derivatives: Comparison of cytoprotective effects to caffeic acid phenethyl ester (CAPE). *Bioorg. Med. Chem.* **2010**, *18*, 5032−5038.
(29) Levy, Y. S.; Gilgun-Sherki, Y.; Melamed, E.; Offen, D. Therapeutic potential of neurotrophic factors in neurodegenerative diseases. *Biodrugs* **2005**, *19*, 97−127.
(30) Tohda, C.; Kuboyama, T.; Komatsu, K. Search for natural products related to regeneration of the neuronal network. *Neurosignals* **2005**, *14*, 34−45.
(31) More, S. V.; Koppula, S.; Kim, I. S.; Kumar, H.; Kim, B. W.; Choi, D. K. The Role of Bioactive Compounds on the Promotion of Neurite Outgrowth. *Molecules* **2012**, *17*, 6728−6753.
(32) Li, F. Q.; Cheng, X. X.; Liang, X. B.; Wang, X. H.; Xue, B.; He, Q. H.; Wang, X. M.; Han, J. S. Neurotrophic and neuroprotective effects of tripchlorolide, an extract of Chinese herb *Tripterygium wilfordii* Hook F, on dopaminergic neurons. *Exp. Neurol.* **2003**, *179*, 28−37.
(33) Tsang, C. K.; Kamei, Y. Sargaquinoic acid supports the survival of neuronal PC 12D cells in a nerve growth factor-independent manner. *Eur. J. Pharmacol.* **2004**, *488*, 11−18.
(34) Yamazaki, M.; Chiba, K.; Mohri, T. Neuritogenesis effect of natural iridoid compounds on PC12h cells and its possible relation to signaling protein kinases. *Biol. Pharm. Bull.* **1996**, *19*, 791−795.

benefits in antiaging, as well as enhancements in vision and liver and kidney functions.[16,17] In recent years, goji has become increasingly popular in Europe and North America as a "superfruit" and botanical dietary supplement. The in vivo inhibitory activity of powdered *L. barbarum* (wolfberry) fruits when evaluated in an *N*-nitrosomethylbenzylamine-induced esophageal cancer model was reported recently in rats.[18] Other recent studies have indicated that goji berry extracts and *L. barbarum* polysaccharides possess a range of biological effects, including antiaging, antioxidant, antitumor, immunomodulatory, and cytoprotective activities.[17,19−21] The published chemical constituents of goji have been thoroughly reviewed, with the occurrence of pyrrole alkaloids well established.[16]

Due to the unexpected presence of the pyrrole alkaloids isolated, **1**−**4**, and their structural similarity to constituents found in goji berries,[12,13] as well as the recent report of contamination in commercial African mango samples,[9] the identity of the source material investigated came into question. The present study includes the bioactivity-guided isolation, identification, and biological evaluation of compounds **1**−**8** in addition to comparison of the commercial product with authentic African mango seeds and *L. barbarum* samples by chemotaxonomy using LC-MS and ^{1}H NMR fingerprinting as well as microscopic analysis.

MATERIALS AND METHODS

Instrumentation for Compound Isolation and Characterization. Optical rotations were measured using a PerkinElmer 343 automatic polarimeter (PerkinElmer, Waltham, MA, USA). UV spectra were collected on a Hitachi U-2910 spectrophotometer (Hitachi, Tokyo, Japan). IR spectra were obtained with a Nicolet 6700 FT-IR spectrometer (Thermo Scientific, Waltham, MA, USA). NMR spectroscopic data were recorded at room temperature on a Bruker Avance DRX-400 MHz spectrometer (Bruker, Billerica, MA, USA) using standard Bruker pulse sequences. High-resolution electrospray ionization mass spectra (HRESIMS) were obtained on a Micromass Q-Tof II (Micromass, Wythenshawe, UK) mass spectrometer operated in the positive-ion mode, with sodium iodide being used for mass calibration. Column chromatography was performed with Sephadex LH-20 (Supelco, Bellefonte, PA, USA) and 65 × 250 or 230 × 400 mesh silica gel (Sorbent Technologies, Atlanta, GA, USA). Analytical thin-layer chromatography (TLC) was conducted on precoated 250 μm thickness Partisil Si gel 60F_{254} glass plates. A 150 mm × 19 mm i.d., 5 μm, XBridge PrepC_{18} column with a 10 mm × 19 mm i.d. guard column of the same material (Waters, Milford, MA, USA) was used for semipreparative HPLC, along with a Hitachi system composed of an L-2130 prep pump, an L-2200 autosampler, and an L-2450 diode array detector (Hitachi, Tokyo, Japan).

Chemicals. All solvents used for chromatographic separations were purchased from Fisher Scientific (Fair Lawn, NJ, USA). 2′,7′-Dichlorodihydrofluorescein diacetate (H_2DCF-DA), esterase, ferrous sulfate ($FeSO_4$), hydrogen peroxide (H_2O_2), quercetin, dimethyl sulfoxide (DMSO), digitonin, EDTA, Trizma base, Tween 20, flavin adenine dinucleotide phosphate (FAD), glucose-6-phosphate (G-6-P), nicotinamide adenine dinucleotide phosphate (NADP), glucose-6-phosphate dehydrogenase (G-6-P-D), menadione, 3-(4,5-dimethylthiazol-2-yl)-2,5-diphenyltetrazolium bromide (MTT), bovine serum albumin (BSA), L-sulforaphane, and deuterated NMR solvents were purchased from Sigma-Aldrich (St. Louis, MO, USA). Cell culture media and supplements were obtained from Life Technologies, Inc. (Grand Island, NY, USA). Gallic acid, methyl gallate, and ellagic acid that served as standards for HPLC-PDA analysis were authentic samples isolated in previous studies and stored in a compound library at The Ohio State University.

Plant Material. The commercial sample labeled as powdered seeds of African mango (*I. gabonensis*), used for isolation, was obtained by Nature's Sunshine Products, Inc., from a manufacturer in the People's Republic of China. A representative sample (code OSUADK-CCP0024) was deposited in the Division of Medicinal Chemistry and Pharmacognosy, College of Pharmacy, The Ohio State University. An authentic sample of African mango seed powder, collected in Nigeria and imported by Nutralliance (Yorba Linda, CA, USA), was purchased by Nature's Sunshine Products, Inc. (code OSUADK-CCP0025; same repository). Three samples of authentic goji berries were obtained, two from the Ningxia province of People's Republic of China, by Nature's Sunshine, Inc., and another directly from a drug store in Chengdu, Sichuan, People's Republic of China (codes OSUADK-CCP0011, OSUADK-CCP0015, and OSUADK-CCP0026, respectively; same repository). The seeds of the last-mentioned product were separated manually from the fruit pulp. These five samples (OSUADK-CCP0024, OSUADK-CCP0026, OSUADK-CCP0015, OSUADK-CCP0011, and OSUADK-CCP0025) are referred to as products A−E, respectively, henceforth in this paper.

Extraction and Isolation. The commercial sample labeled as the powdered seeds of African mango (product A, 5 kg) was extracted by maceration with MeOH (3 × 10 L) at room temperature, for 3 days each. After filtration and evaporation of the solvent under reduced pressure, the combined crude methanol extract (ca. 1000 g) was suspended in H_2O (1 L) and then partitioned in turn with hexanes (3 × 1 L), $CHCl_3$ (3 × 1 L), EtOAc (3 × 1 L), and *n*-BuOH (3 × 1 L) to afford dried hexanes (40.1 g), $CHCl_3$ (5.0 g), EtOAc (6.5 g), *n*-BuOH (166.0 g), and H_2O-soluble (ca. 800 g) extracts. The $CHCl_3$-soluble extract showed activities in both hydroxyl radical-scavenging (ED_{50} 6.3 μg/mL) and QR induction (CD 12.4 μg/mL) assays and hence was selected for further fractionation. The $CHCl_3$-soluble extract was subjected initially to chromatography over a silica gel column, eluted with $CHCl_3$/MeOH (50:1 to pure MeOH, stepwise), to afford 12 fractions (fractions F01−F12). Fractions F01−F03 showed activity in either the hydroxyl radical-scavenging assay or the QR induction assay and were chosen for further purification.

Fraction F01 (ca. 890 mg) was chromatographed over an open C_{18} reversed-phase column, eluted with MeOH/H_2O (5:95 to pure MeOH, stepwise) to afford eight subfractions. Subfraction F0102 (ca. 400 mg, eluted by MeOH/H_2O 20:80) was subjected to passage over a Sephadex LH-20 column with MeOH/H_2O (20:80 to pure MeOH, stepwise) as the eluting solvent system to yield compound **8** (eluted by MeOH/H_2O 50:50; 3.0 mg) and a further subfraction F010211 (ca. 65 mg). Subfraction F010211 was separated by HPLC using a 150 mm × 19 mm i.d., 5 μm, XBridge PrepC_{18} column with a 10 mm × 19 mm i.d. guard column of the same material (Waters) and with CH_3CN/H_2O by isocratic elution (3:97; 8 mL/min) to afford compounds **5** (t_R 68.6 min; 5.7 mg) and **6** (t_R 55.0 min; 0.8 mg) and a further subfraction, F01021103 (ca. 40 mg, eluted with pure CH_3CN). F01021103 was purified further by HPLC on the same column with CH_3CN/H_2O (0.025% NH_4OH) isocratic elution (3:97; 8 mL/min) to obtain compound **2** (t_R 12.3 min; 4.5 mg).

Fractions F02 (ca. 180 mg) and F03 (ca. 120 mg) were subjected separately to Sephadex LH-20 column chromatography, eluted by MeOH/H_2O (50:50, 75:25, and pure MeOH) to remove pigments and afforded several subfractions. Subfraction F0203 (ca. 100 mg) was purified further by HPLC on the same XBridge PrepC_{18} column as above, by a gradient elution (A, CH_3CN; B, H_2O, 3−15% A over 70 min, 15−100% A from 70 to 85 min; 8 mL/min), to render the purification of compounds **1** (t_R 49.5 min; 4.8 mg), **3** (t_R 46.7 min; 1.3 mg), and **7** (t_R 16.5 min; 20.0 mg). Subfraction F0303 (ca. 80 mg) was also purified by HPLC on the same XBridge PrepC_{18} column, eluted by a CH_3CN/H_2O gradient (A, CH_3CN; B, H_2O, 3−15% A over 70 min, 15−100% A from 70 to 85 min; 8 mL/min), to yield compound **4** (t_R 22.7 min; 6.8 mg).

Methyl 2-[2-formyl-5-(hydroxymethyl)-1*H*-pyrrol-1-yl]-propanoate, 1, was isolated (ca. 0.0001% of dry weight) as a colorless resin: $[\alpha]^{20}_D$ +28.0 (*c* 0.1, MeOH); UV (MeOH) λ_{max} (log ε) 291 (4.09) nm; IR (film) ν_{max} 3424, 3120, 2946, 2850, 2803, 2727, 1749, 1655 cm^{-1}; ^{1}H NMR (400 MHz, CD_3OD) δ 9.31 (1H, s, CHO), 7.07 (1H, d, J = 4.0 Hz, H-3), 6.28 (1H, d, J = 4.0 Hz, H-4), 5.43 (1H, q, J = 7.0 Hz, H-1′), 4.63 (2H, ABq, $\Delta\nu$ = 8.1 Hz, J = 13.9 Hz, H-6), 3.67 (3H, s, OCH_3), 1.67 (3H, d, J = 7.0 Hz, CH_3); ^{13}C NMR (100 MHz,

CD_3OD) δ 180.5 (CHO), 172.5 (COO), 144.6 (C-5), 133.4 (C-2), 127.4 (C-3), 111.4 (C-4), 56.6 (C-6), 55.8 (C-1′), 52.8 (OCH_3), 18.0 (CH_3); HRESIMS m/z 234.0733 $[M + Na]^+$ (calcd for $C_{10}H_{13}NO_4Na$, 234.0742).

Evaluation of Hydroxyl Radical-Scavenging Activity. Hydroxyl radical-scavenging activity was tested according to the method previously reported.[22,23]

Evaluation of Quinone Reductase-Inducing Activity. The in vitro QR-inducing activity of the extracts, fractions, and pure isolates was assayed according to a previously published method.[24,25]

Microscopic Examination Procedure. The clean samples of products B−D were pulverized and passed through a no. 4 sieve to obtain fine granules. Products A and E were obtained as powders and thus passed through the sieve directly. The powdered materials of products A−E were each placed on a slide and stirred with a fine-pointed needle to distribute the powders evenly, followed by the application of 2 drops of clearing agent, Visikol (Phytosys LLC, New Brunswick, NJ, USA), and gentle heat until air bubbles moved to the edge of the slide. Two drops of diluted glycerin and a coverslip were added to the slide, followed by immediate observation under a Nikon Eclipse TE300 optical microscope (Nikon, Tokyo, Japan), along with an A01F881036 camera module (Roper Scientific, Trenton, NJ, USA) for digital imaging of the microscopic structures observed.

Sample Preparation and HPLC-PDA, LC-IT-MS, and ^{1}H NMR Fingerprinting Analysis. Each sample (3 g) was extracted with 10 mL of methanol by sonication at room temperature for 30 min. The methanol extracts were dried in vacuo (40 °C), followed by another ultrasonic extraction with 10 mL of chloroform at room temperature for 30 min, to obtain a chloroform-soluble extract of each sample, which was then dried in vacuo at 40 °C and stored at −20 °C before analysis. All analyses were completed within 24 h of extraction.

The HPLC-PDA analysis was performed using a 150 mm × 4.6 mm i.d., 5 μm, XBridge C_{18} analytical column (Waters), along with a Hitachi system composed of an L-2130 pump and an L-2450 diode array detector (Hitachi). The mobile phase consisted of 0.05% trifluoroacetic acid in water (A) and acetonitrile (B) using a gradient program of 3−20% B from 0 to 60 min and 20−100% B from 60 to 70 min. The mobile phase flow rate and the injection volume were 1 mL/min and 10 μL, respectively. The dried chloroform-soluble extract of each sample was dissolved in 1 mL of HPLC grade methanol, and filtered through a Fisher Scientific 13 mm syringe filter (0.2 μm) prior to injection. After comparison of the chromatograms of the chloroform-soluble extract solution recorded at wavelengths within 200−550 nm, it was found that 254 nm could best represent the profile of the analytes.

The LC-IT-MS analysis employed the same separation conditions and Xbridge C_{18} analytical column as used for the HPLC-PDA analysis mentioned above, on a Waters Alliance 2690 separation module. The injection volume was 10 μL. The mobile phase flow rate was maintained at 1 mL/min and was split approximately 50:1 postcolumn using a microsplitter valve (Upchurch Scientific, Oak Harbor, WA, USA) for the introduction to the ESI source. The electrospray ionization ion trap mass spectrometry (ESI-IT-MS) was performed on a Bruker dual funnel amaZon ETD ion trap mass spectrometer (Bremen, Germany) equipped with an orthogonal electrospray source operated in positive-ion mode. Sodium iodide was used for mass calibration for a calibration range of m/z 100−1000. Optimal ESI conditions were as follows: capillary voltage, 4500 V; source temperature, 250 °C; ESI drying gas (nitrogen), 4.0 L/min; and nebulizer, 10 psi. The ion trap was set to UltraScan mode with a target mass of m/z 500 pass ions from m/z 100 to 1000.

The ^{1}H NMR spectroscopic fingerprinting was conducted using the previously described chloroform-soluble extracts of products A−E. The samples were dissolved in 600 μL of $CDCl_3$, and spectra were measured at 300 K using a Bruker Avance-III HD400 spectrometer.

RESULTS AND DISCUSSION

Isolation, Structure Elucidation, and Biological Evaluation of the Constituents. The $CHCl_3$-soluble extract of product A (a commercial sample labeled as powdered seeds of African mango) was found to be the most potent among the hexanes-, $CHCl_3$-, EtOAc-, *n*-BuOH-, and H_2O-soluble extracts in the in vitro hydroxyl radical-scavenging (ED_{50}, concentration scavenging hydroxyl radical by 50%, 6.3 μg/mL) and QR induction (CD, concentration required to double QR activity, 12.4 μg/mL) assays. Therefore, it was selected for fractionation. Fractions F01−F03 of the $CHCl_3$-soluble extract showed hydroxyl radical-scavenging activity, with ED_{50} values of 3.3, 5.6, and 6.8 μg/mL, respectively. In addition, fractions F01 and F02 exhibited QR-inducing activity, with CD values of 6.9 and 10.2 μg/mL, respectively. Accordingly, fractions F01−F03 were used for further detailed purification. In this way, bioactivity-guided fractionation of product A led to the isolation of a new pyrrole alkaloid, **1**, and seven known compounds, **2**−**8**, as shown in Figure 1.

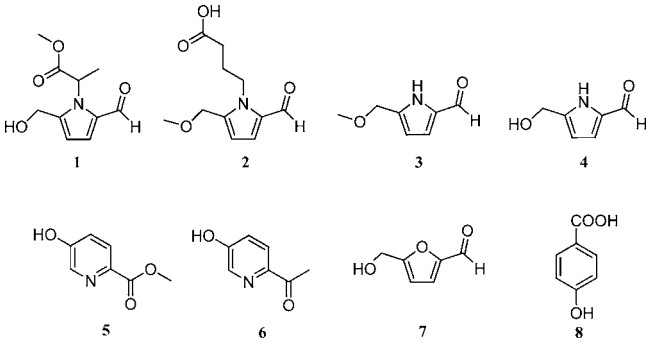

Figure 1. Structures of compounds isolated from a goji berry-contaminated commercial sample labeled African mango (*Irvingia gabonensis*).

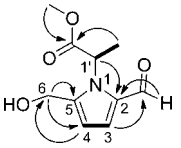

Figure 2. ^{1}H−^{1}H COSY (bold lines) and key HMBC (arrows) correlations of the new compound **1**.

Table 1. Hydroxyl Radical-Scavenging and Quinone Reductase-Inducing Activities of the Isolated Active Compounds 1, 2, and 6

	hydroxyl radical scavenging	QR induction		
compound[a]	ED_{50}[b] (μM)	CD[c] (μM)	IC_{50}[d] (μM)	CI[e]
1	16.7	43.1	>100	>2.3
2	11.9	2.4	>100	>42.6
6	>20	48.5	>100	>2.1
quercetin[f]	1.3			
L-sulforaphane[g]		0.77	16.7	21.7

[a]Compounds **3**−**5**, **7**, and **8** did not show hydroxyl radical-scavenging or QR-inducing activity at the concentrations tested. [b]ED_{50}, concentration scavenging hydroxyl radical by 50%. Compounds with ED_{50} values of <20 μM are considered active. [c]CD, concentration required to double QR activity. Compounds with CD values of <20, 20−100, and >100 μM are considered significantly active, weakly active, and inactive, respectively. [d]IC_{50}, concentration inhibiting cell growth by 50%. [e]CI, chemoprevention index (= IC_{50}/CD). [f]Positive control for hydroxyl radical-scavenging assay. [g]Positive control for QR induction assay.

dx.doi.org/10.1021/jf500802x | J. Agric. Food Chem. 2014, 62, 5054−5060

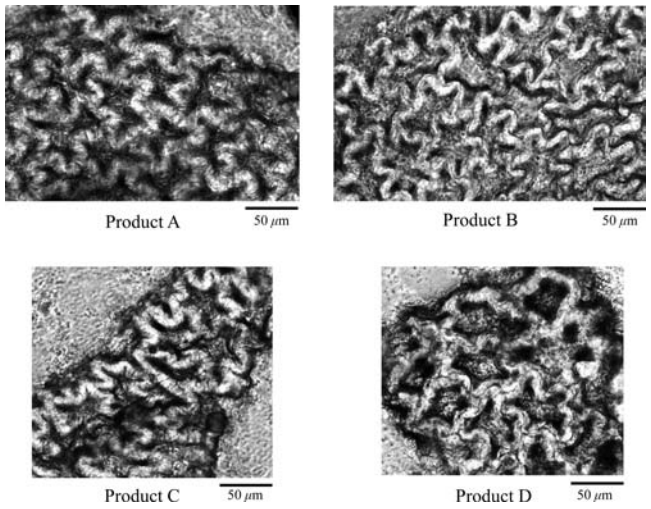

Figure 3. Microscopic structures of testa sclereids (stone cells) observed in products A–D.

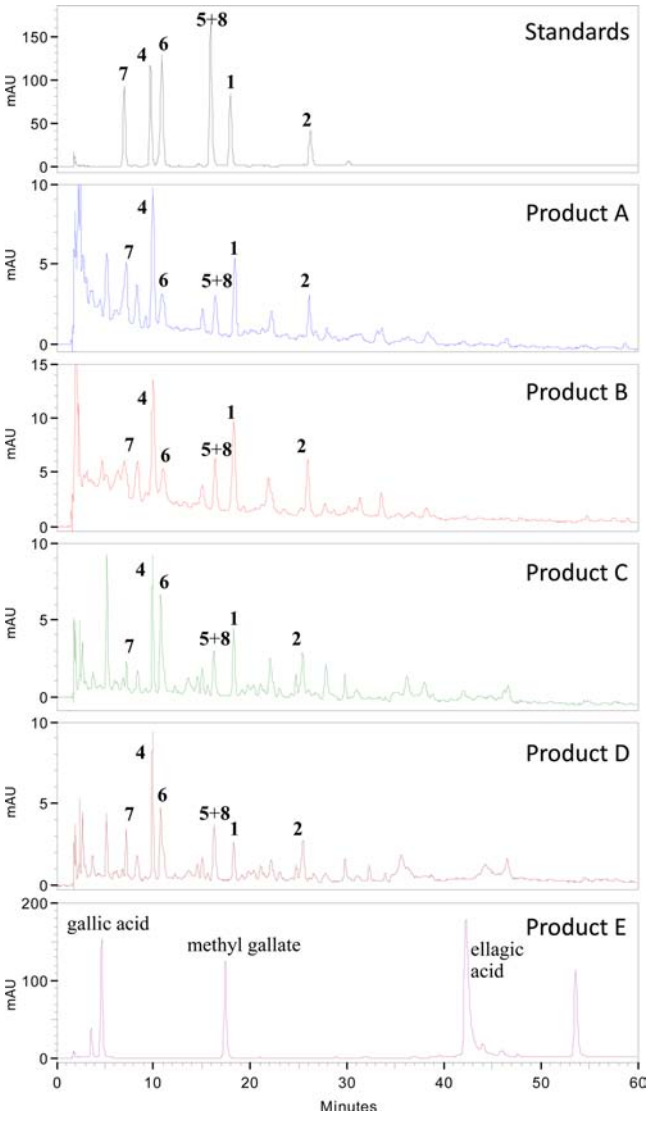

Figure 4. HPLC chromatograms (254 nm) of products A–E and standard compounds isolated from product A.

The new compound, **1**, was isolated as a colorless resin. The molecular formula was determined as $C_{10}H_{13}NO_4$ on the basis of the sodiated molecular ion peak in the HRESIMS. The IR spectrum showed absorptions of hydroxy (3424 cm^{-1}), ester carbonyl (1749 cm^{-1}), and conjugated aldehyde (2803, 2727, and 1655 cm^{-1}) groups. The UV spectrum of **1** exhibited a maximum absorption at 291 nm, which is characteristic of pyrrole 2-carbaldehyde.[13] The proton signal at δ_H 9.31 and the carbon signal at δ_C 180.5 correlated in the HSQC spectrum and indicated the presence of an aldehyde group. Two proton signals at δ_H 4.63 (2H, ABq, $\Delta\nu$ = 8.1 Hz, J = 13.9 Hz, H-6) resulted from a magnetically inequivalent oxygenated methylene group with geminal coupling. The HMBC correlation (Figure 2) of the methoxy group (δ_H 3.67, 3H, s, OCH_3) to the carbonyl at δ_C 172.5 revealed that this methoxy group forms an ester with this carbonyl. The quartet of H-1′ (δ_H 5.43, J = 7.0 Hz) and doublet of the methyl group (δ_H 1.67, J = 7.0 Hz), as well as their correlation in the COSY spectrum, clearly indicated the connection of the methyl group (δ_C 18.1) to C-1′ (δ_C 55.8). Furthermore, HMBC correlation of this methyl group (δ_H 1.67) to the ester carbonyl C-2′ (δ_C 172.5) suggested the connection of C-1′ (δ_C 55.8) to C-2′. The chemical shifts and coupling constants of the two protons at δ_H 7.07 (1H, d, J = 4.0 Hz, H-3) and δ_H 6.28 (1H, d, J = 4.0 Hz, H-4) implied the presence of a pyrrole ring. Moreover, the substitution pattern of the pyrrole ring should be 2,5- because a 2,3- or a 2,4-disubstituted pyrrole would have coupling constants of 1.3–2.9 or 2.3–3.2 Hz,[13] respectively. Also, the two carbons of the pyrrole ring at the lower field region (δ_C 144.6 and 133.4) were not present in the ^{13}C DEPT 135 spectrum, suggesting that C-2 and C-5 of this ring system are substituted (quaternary carbons). This was confirmed by the HMBC correlation of H-6 (δ_H 4.63) to C-4 (δ_C 111.4) and C-5 (δ_C 144.6), H-4 (δ_H 6.28) to C-6 (δ_C 56.6), H-3 (δ_H 7.07) to the aldehyde carbon (δ_C 180.5), and the aldehyde proton (δ_H 9.31) to C-2 (δ_C 133.4). In addition, the connection between C-1′ and N-1 was clearly indicated by the HMBC correlation of H-1′ (δ_H 5.43) to C-2 (δ_C 133.4). Therefore, the structure of **1** was established unambiguously as methyl 2-[2-formyl-5-(hydroxymethyl)-1*H*-pyrrol-1-yl]propanoate.

On the basis of the spectroscopic data measurements and the comparison of the data obtained with published values, the structures of the known compounds **2**–**8** were identified as 4-[formyl-5-(methoxymethyl)-1*H*-pyrrol-1-yl]butanoic acid, **2**,[13] 5-(methoxymethyl)-1*H*-pyrrole-2-carbaldehyde, **3**,[26] 5-(hydroxymethyl)-1*H*-pyrrole-2-carbaldehyde, **4**,[27,28] methyl-5-hydroxy-2-pyridinecarboxylate, **5**,[29] 5-hydroxy-2-pyridyl methyl ketone, **6**,[30] 5-hydroxymethyl-2-furancarbaldehyde, **7**,[31] and 4-hydroxybenzoic acid, **8**.[32]

In the present study, all of the isolates, **1**–**8**, were evaluated in vitro using the hydroxyl radical-scavenging and QR induction assays. The new compound, **1**, and the known pyrrole alkaloid, **2**, showed activities in both assays, as shown in Table 1. When the QR-inducing activities were compared among the structurally related pyrrole alkaloids, **1**–**4**, it was observed that **2**, containing a butanoic acid side chain at position N-1, exhibited the greatest potency (CD 2.4 μM); **1**, with a methyl propanoate substitution attached to N-1, showed much less potency (CD 43.1 μM), whereas **3** and **4**, each bearing no substituent to N-1, displayed no discernible activity (both CD >100 μM), suggesting that the length of the side chain at N-1 may significantly affect the QR-inducing activity of this type of compound.

dx.doi.org/10.1021/jf500802x | J. Agric. Food Chem. 2014, 62, 5054–5060

Table 2. LC-MS Data of Constituents Identified in a Representative Authentic Goji Berry Sample (Product C)

t_R (min)	UV λ_{max} (nm)	molecular formula	$[M + H]^+$	$[M + Na]^+$	identification
7.0	230, 284	$C_6H_6O_3$	127.1	149.1	compound **7**
9.7	254, 299	$C_6H_7NO_2$	126.1	148.1	compound **4**
10.9	217, 261, 294	$C_7H_7NO_2$	138.1	160.0	compound **6**
15.9	254, 285	$C_7H_6O_3$, $C_7H_7NO_3$	139.1, 154.1	161.1, 176.0	compounds **5** and **8**
18.0	258, 296	$C_{10}H_{13}NO_4$	212.1	234.1	compound **1**
26.2	258, 296	$C_{11}H_{15}NO_4$	226.1	248.1	compound **2**

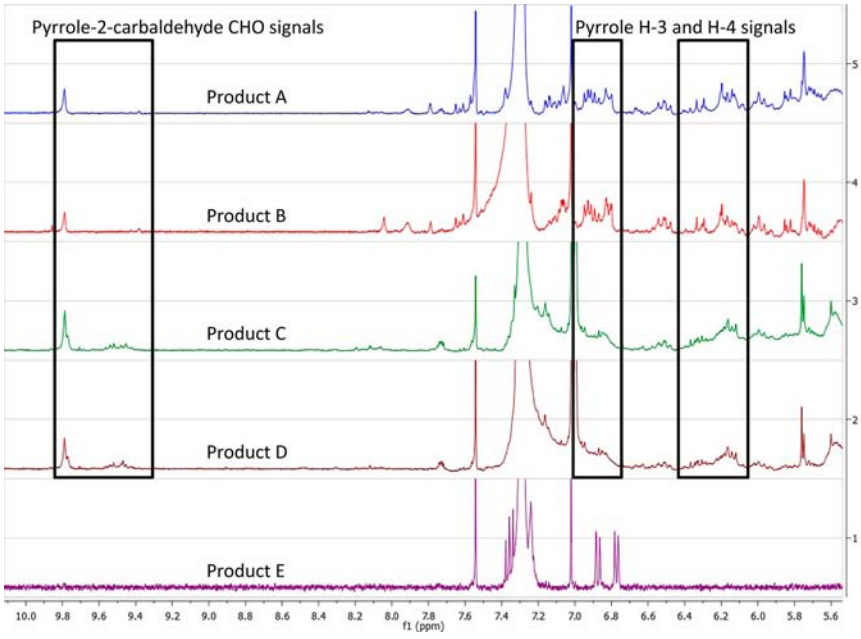

Figure 5. ^{1}H NMR fingerprinting (δ_H 5.5−10.1 ppm) of products A−E ($CDCl_3$, 400 MHz).

Pyrrole alkaloid **2** was initially isolated from goji berry (*L. chinense*).[13] Compounds **1**, **3**, and **4** are analogues of **2** and are also pyrrole alkaloids. In contrast, no alkaloid has been previously isolated or detected spectroscopically from African mango. In addition, both goji berry and African mango reportedly can be used as antiobesity medicinal plants.[33] Due to the unexpected presence of these pyrrole alkaloids and their structural similarity to and occurrence as constituents found in goji berries,[12,13] as well as the public concern and a recent report about frequent contamination in commercial African mango samples,[9] a comprehensive comparison of the commercial sample labeled as African mango seeds (product A) with authentic goji berry samples (products B−D) and African mango seeds (product E) was conducted via microscopic analysis as well as chemotaxonomy using LC-MS and ^{1}H NMR fingerprinting, as shown in the following sections.

Microscopic Examination. In the powders of products A−D, irregular polygonal testa sclereids (stone cells) were observed with thickened and curved walls as well as distinct striations in surface view (Figure 3), characteristic of the seeds of goji berry.[14] This microscopic feature was not found in the authentic sample of African mango seed powder (product E).

HPLC-PDA and LC-IT-MS Analysis. Products A−D shared very similar HPLC chromatograms, which differed significantly from that of product E (Figure 4). Compound **3** had been all consumed for bioassay and thus could not be used as a standard. However, compounds **1**, **2**, and **4**−**8** isolated from product A were present in the authentic goji berry samples (products B−D), as identified by comparison of the retention times, UV profiles, and mass spectra of the peaks with standard compounds that had been identified by NMR (Table 2). In contrast, the HPLC chromatogram of the authentic sample of African mango seeds (product E) was shown to be very different, containing gallic acid, methyl gallate, ellagic acid, and their derivatives as major constituents, as identified by the same analytical methods mentioned above. These substances have been previously detected in African mango.[8,9]

^{1}H NMR Fingerprinting. Visual inspection of the ^{1}H NMR spectra revealed that all samples tested contained triacylglycerols as major constituents. By comparison, however, products A−D each contained pyrrole alkaloids as minor constituents with characteristic signals at δ_H 6.0−6.4 ppm that were not observed in product E. The presence of signals in the region of δ_H 9.4−9.8 ppm can be attributed to the aldehyde functionality of the isolated pyrrole-2-carbaldehyde compounds and further distinguished the botanical identity of product A from product E. Additionally, the signals that were detected only in product E may be ascribed to the previously reported constituents of African mango, namely, methyl gallate, ellagic acid, or their derivatives.[8,9] The region of the NMR spectra pertinent to these comparisons is shown in Figure 5. The relative cleanness of the proton NMR spectrum of the authentic African mango seed extract suggests that ^{1}H NMR fingerprinting may be a useful tool for the future authentication and/or quality control of such samples.

Accordingly, chemotaxonomic examination by LC-IT-MS and ^{1}H NMR fingerprinting using authentic samples of goji berries and African mango suggested that there was evidence of

contamination, adulteration, and/or mislabeling of the commercial African mango sample evaluated (product A), in agreement with a concerning trend previously reported.[9] It is worth noting that goji berry from the same batch as product C was previously reported to exhibit in vivo inhibitory activity in a rat *N*-nitrosomethylbenzylamine (NMBA)-induced esophageal cancer model, and the detection of the in vitro active compounds **1**, **2**, and **6** in product C suggests that these compounds may possess potential in vivo cancer chemopreventive activity and hence merit further investigation.

■ ASSOCIATED CONTENT

Supporting Information

^{1}H NMR, ^{13}C NMR, ^{13}C DEPT 135, HSQC, HMBC, ^{1}H−^{1}H COSY, HRESIMS, and UV and IR spectra for compound **1**; HPLC-PDA and LC-IT-MS data for identification of the isolated compounds in the authentic goji berry and African mango samples; ^{1}H NMR fingerprinting of the $CHCl_3$-soluble extracts of products A−E, and protocols used to evaluate hydroxyl radical-scavenging and QR-inducing activity. This material is available free of charge via the Internet at http://pubs.acs.org.

■ AUTHOR INFORMATION

Corresponding Author

*(A.D.K.) Phone: (614) 247-8094. Fax: (614) 247-8119. E-mail: Kinghorn.4@osu.edu.

Funding

C.B.N. acknowledges financial support provided by ongoing predoctoral fellowships from the American Foundation for Pharmaceutical Education (AFPE) and an NIH Chemistry-Biology Interface Training Program (T32 GM008512).

Notes

The authors declare no competing financial interest.

■ ACKNOWLEDGMENTS

We thank John Fowble and Dr. Craig McElroy (College of Pharmacy, The Ohio State University) for facilitating the acquisition of NMR data and Nanette Kleinholz from the Mass Spectrometry and Proteomics Facility at The Ohio State University for the acquisition of LC-MS data.

■ REFERENCES

(1) Kuete, V.; Wabo, G. F.; Ngameni, B.; Mbaveng, A. T.; Metuno, R.; Etoa, F. X.; Ngadjui, B. T.; Beng, V. P.; Meyer, J. J.; Lall, N. Antimicrobial activity of the methanolic extract, fractions and compounds from the stem bark of *Irvingia gabonensis* (Ixonanthaceae). *J. Ethnopharmacol.* **2007**, *114*, 54−60.

(2) Donfack, J. H.; Fosto, G. W.; Ngameni, B.; Tsofack, F. N.; Tchoukoua, A.; Ambassa, P.; Abia, W.; Tchana, A. N.; Giardina, S.; Buonocore, D.; Finzi, P. V.; Vidari, G.; Marzatico, F.; Ngadjui, B. T.; Moundipa, P. F. In vitro hepatoprotective and antioxidant activities of the crude extract and isolated compounds from *Irvingia gabonensis*. *Asian J. Tradit. Med.* **2010**, *5*, 79−88.

(3) Okolo, C. O.; Johnson, P. B.; Abdurahman, E. M.; Abdu-Aguye, I.; Hussaini, I. M. Analgesic effect of *Irvingia gabonensis* stem bark extract. *J. Ethnopharmacol.* **1995**, *45*, 125−129.

(4) Agbor, G. A.; Oben, J. E.; Ngogang, J. Y.; Xinxing, C.; Vinson, J. A. Antioxidant capacity of some herbs/spices from Cameroon: a comparative study of two methods. *J. Agric. Food Chem.* **2005**, *53*, 6819−6824.

(5) Ngondi, J. L.; Oben, J. E.; Minka, S. R. The effect of *Irvingia gabonensis* seeds on body weight and blood lipids of obese subjects in Cameroon. *Lipids Health Dis.* **2005**, *4*, 12.

(6) Oben, J. E.; Ngondi, J. L.; Momo, C. N.; Agbor, G. A.; Sobgui, C. S. The use of a *Cissus quadrangularis*/*Irvingia gabonensis* combination in the management of weight loss: a double-blind placebo-controlled study. *Lipids Health Dis.* **2008**, *7*, 12.

(7) Ngondi, J. L.; Djiotsa, E. J.; Fossouo, Z.; Oben, J. Hypoglycaemic effect of the methanol extract of *Irvingia gabonensis* seeds on streptozotocin diabetic rats. *Virol. J.* **2006**, *3*, 74−77.

(8) Atawodi, S. E. Polyphenol content and in vitro antioxidant activity of methanol extract of seeds of *Irvingia gabonensis* Baill. of Nigerian origin. *Elec. J. Environ. Agric. Food Chem.* **2011**, *10*, 2314−2321.

(9) Sun, J.; Chen, P. Ultra high-performance liquid chromatography with high-resolution mass spectrometry analysis of African mango (*Irvingia gabonensis*) seeds, extract, and related dietary supplements. *J. Agric. Food Chem.* **2012**, *60*, 8703−8709.

(10) Cuendet, M.; Oteham, C. P.; Moon, R. C.; Pezzuto, J. M. Quinone reductase induction as a biomarker for cancer chemoprevention. *J. Nat. Prod.* **2006**, *69*, 460−463.

(11) Waris, G.; Ahsan, H. Reactive oxygen species: role in the development of cancer and various chronic conditions. *J. Carcinog.* **2006**, *5*, 14.

(12) Youn, U. J.; Kil, Y.; Nam, J.; Lee, Y.; Kim, J.; Lee, D.; Lee, J.; Seo, E. New pyrrole alkaloids with bulky *N*-alkyl side chains containing stereogenic centers from *Lycium chinense*. *Helv. Chim. Acta* **2013**, *96*, 1482−1487.

(13) Chin, Y. W.; Lim, S. W.; Kim, S. H.; Shin, D. Y.; Suh, Y. G.; Kim, Y. B.; Kim, Y. C.; Kim, J. Hepatoprotective pyrrole derivatives of *Lycium chinense* fruits. *Bioorg. Med. Chem. Lett.* **2003**, *13*, 79−81.

(14) American Herbal Pharmacopoeia. *Lycium chinense* Mill., *L. barbarum* L. In *Botanical Pharmacognosy − Microscopic Characterization of Botanical Medicines*; Upton, R., Graff, A., Jolliffe, G., Langer, R., Williamson, E., Eds.; CRC Press: Boca Raton, FL, USA, 2011; pp 468−470.

(15) Sze, S. C.; Song, J. X.; Wong, R. N.; Feng, Y. B.; Ng, T. B.; Tong, Y.; Zhang, K. Y. Application of SCAR (sequence characterized amplified region) analysis to authenticate *Lycium barbarum* (wolfberry) and its adulterants. *Biotechnol. Appl. Biochem.* **2008**, *51*, 15−21.

(16) Potterat, O. Goji (*Lycium barbarum* and *L. chinense*): phytochemistry, pharmacology and safety in the perspective of traditional uses and recent popularity. *Planta Med.* **2010**, *76*, 7−19.

(17) Chang, R. C.; So, K. F. Use of anti-aging herbal medicine, *Lycium barbarum*, against aging-associated diseases. What do we know so far? *Cell Mol. Neurobiol.* **2008**, *28*, 643−652.

(18) Stoner, G. D.; Wang, L. S.; Seguin, C.; Rocha, C.; Stoner, K.; Chiu, S.; Kinghorn, A. D. Multiple berry types prevent *N*-nitrosomethylbenzylamine-induced esophageal cancer in rats. *Pharm. Res.* **2010**, *27*, 1138−1145.

(19) Luo, Q.; Cai, Y.; Yan, J.; Sun, M.; Corke, H. Hypoglycemic and hypolipidemic effects and antioxidant activity of fruit extracts from *Lycium barbarum*. *Life Sci.* **2004**, *76*, 137−149.

(20) Amagase, H.; Farnsworth, N. R. A review of botanical characteristics, phytochemistry, clinical relevance in efficacy and safety of *Lycium barbarum* fruit (goji). *Food Res. Int.* **2011**, *44*, 1702−1717.

(21) Yu, M. S.; Ho, Y. S.; So, K. F.; Yuen, W. H.; Chang, R. C. Cytoprotective effects of *Lycium barbarum* against reducing stress on endoplasmic reticulum. *Int. J. Mol. Med.* **2006**, *17*, 1157−1161.

(22) LeBel, C. P.; Ischiropoulos, H.; Bondy, S. C. Evaluation of the probe 2′,7′-dichlorofluorescin as an indicator of reactive oxygen species formation and oxidative stress. *Chem. Res. Toxicol.* **1992**, *5*, 227−231.

(23) Chin, Y. W.; Chai, H. B.; Keller, W. J.; Kinghorn, A. D. Lignans and other constituents of the fruits of *Euterpe oleracea* (Açaí) with antioxidant and cytoprotective activities. *J. Agric. Food Chem.* **2008**, *56*, 7759−7764.

(24) Li, J.; Pan, L.; Deng, Y.; Munoz-Acuna, U.; Yuan, C.; Lai, H.; Chai, H.; Chagwedera, T. E.; Farnsworth, N. R.; Carcache de Blanco, E. J.; Li, C.; Soejarto, D. D.; Kinghorn, A. D. Sphenostylisins A-K: bioactive modified isoflavonoid constituents of the root bark of

Sphenostylis marginata ssp. *erecta*. *J. Org. Chem.* **2013**, *78*, 10166−10177.
(25) Prochaska, H. J.; Santamaria, A. B. Direct measurement of NAD(P)H:quinone reductase from cells cultured in microtiter wells: a screening assay for anticarcinogenic enzyme inducers. *Anal. Biochem.* **1988**, *169*, 328−336.
(26) Don, M. J.; Shen, C. C.; Lin, Y. L.; Syu, W. J.; Ding, Y. H.; Sun, C. M. Nitrogen-containing compounds from *Salvia miltiorrhiza*. *J. Nat. Prod.* **2005**, *68*, 1066−1070.
(27) Hiermann, A.; Kedwani, S.; Schramm, H. W.; Seger, C. A new pyrrole alkaloid from seeds of *Castanea sativa*. *Fitoterapia* **2002**, *73*, 22−27.
(28) Ahmed, F. R.; Cheung, K. M.; Toube, T. P.; Utley, J. H. P. Approaches to a cathodic route to polypyrrolylvinylenes. *J. Mater. Chem.* **1995**, *5*, 837−844.
(29) Wu, B.; Lin, W. H.; Gao, H. Y.; Kim, C. Antibacterial constituents of *Senecio cannabifolius* (II). *Chin. Tradit. Herbal Drugs* **2005**, *36*, 1447−1450.
(30) Olsson, K.; Pernemalm, P. A.; Theander, O. Formation of aromatic compounds from carbohydrates. VII. Reaction of D-glucose and glycine in slightly acidic, aqueous solution. *Acta Chem. Scand. B* **1978**, *B32*, 249−256.
(31) Pyo, M. K.; Jin, J. L.; Koo, Y. K.; Yun-Choi, H. S. Phenolic and furan type compounds isolated from *Gastrodia elata* and their anti-platelet effects. *Arch. Pharm. Res.* **2004**, *27*, 381−385.
(32) Rukachaisirikul, V.; Khamthong, N.; Sukpondma, Y.; Phongpaichit, S.; Hutadilok-Towatana, N.; Graidist, P.; Sakayaroj, J.; Kirtikara, K. Cyclohexene, diketopiperazine, lactone and phenol derivatives from the sea fan-derived fungi *Nigrospora* sp. PSU-F11 and PSU-F12. *Arch. Pharm. Res.* **2010**, *33*, 375−380.
(33) Hasani-Ranjbar, S.; Jouyandeh, Z.; Abdollahi, M. A systematic review of anti-obesity medicinal plants − an update. *J. Diabetes Metab. Disord.* **2013**, *12*, 28.

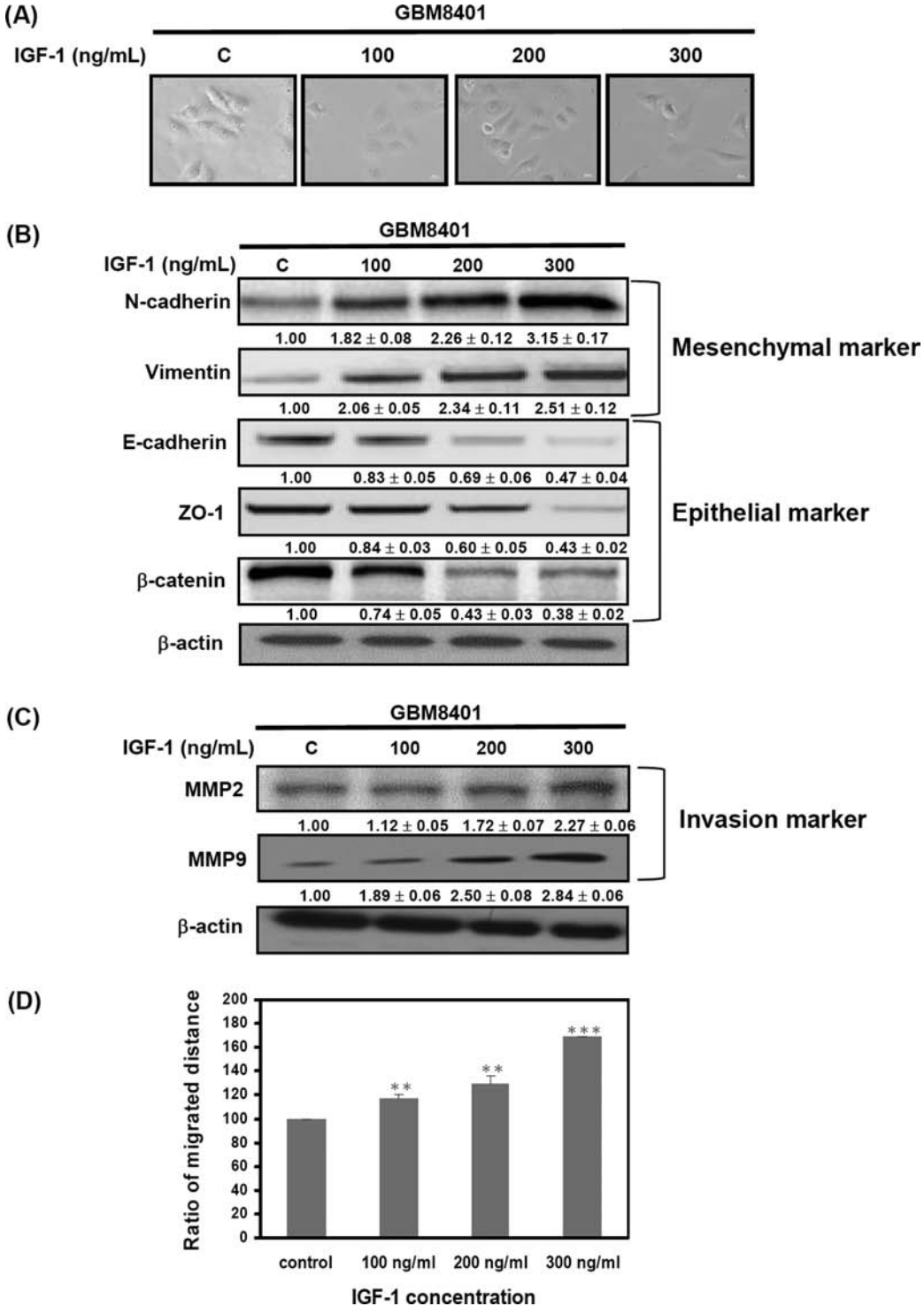

Figure 1. IGF-1-induced cell scattering and EMT in GBM8401 cells. GBM8401 cells were treated with DMSO (control) or increasing IGF-1 concentrations (100−300 ng/mL) for 24 h. (A) EMT was examined by phase contrast photomicrographs. (B) The cells were then harvested and lysed for the detection of N-cadherin, vimentin, E-cadherin, ZO-1, β-catenin, and β-actin. (C) The cells were then harvested and lysed for the detection of MMP-2, MMP-9, and β-actin. Western blot data presented are representative of those obtained in at least 3 separate experiments. Immunoblots were quantified, and the lower panel presents the average ± SD of three independent experiments. The value of the control cells was set to 1. (D) IGF-1-induced cell motility was determined by measuring the closure of wound. Data were plotted by mean ± SD ($n = 3$). The closure distance of the control cells was set to 100 (**, $p < 0.01$;***, $p < 0.001$).

Compared to normal brain tissue, IGF-1R is overexpressed in malignant GBM.[6] Recent studies suggested that IGF-1R activation, through autocrine or paracrine IGF-1 production, contributed to the proliferation and migration of GBM.[7]

Osthole, a coumarin derivative isolated from the fruit of *Cnidium monnieri* (L.) Cusson, has been widely used for the treatment of skin diseases and gynecopathy. Recently, osthole has taken considerable attention because of its broad spectrum of pharmacologic activities, including anti-inflammatory,[8,9] anti-

dx.doi.org/10.1021/jf501047g | J. Agric. Food Chem. 2014, 62, 5061−5071

allergic,[10] vasorelaxant,[11] antidiabetic,[12] and antitumor effects.[13] In addition, current studies demonstrated that osthole had neuroprotective effects on animal models of central nervous system (CNS) diseases, such as brain ischemia models,[14,15] and also in traumatic brain injury model.[16] However, the anti-GBM ability of osthole remains largely unknown.

A better understanding of the mechanisms behind the rapid growth of GBM may offer new therapeutic targets and improve outcome. IGF-1 activity has been closely examined in proliferative tissues for their relationship to change in cellular morphology associated with cancer progression. Therefore, the present study investigated whether IGF-1 could induce EMT in GBM cells. Since osthole has an ability to cross the blood−brain barrier and protect against brain injury, we further explore the potential of osthole in inhibiting the IGF-1-mediated EMT in GBM cells.

MATERIALS AND METHODS

Materials and Antibodies. Recombinant human IGF-1 was purchased from PeproTech, Inc. (Rocky Hill, NJ, USA). Osthole and PD98059 were purchased from Sigma Chemical Co. (St. Louis, MO, USA). LY294002 was purchased from Cayman Chemical Co. (Ann Arbor, Michigan, USA). Primary antibodies against IGF-1R, phospho-IGF-1R (Tyr 1135/1136), phospho-Akt (Ser 473), Akt, phospho-Erk1/2 (Thr 202/Tyr 204), Erk1/2, phospho-GSK3β (Ser 9), GSK3β, MMP-2, MMP-9, N-cadherin, vimentin, ZO-1, β-catenin, Snail, and E-cadherin were purchased from Cell Signaling Technology (Beverly, MA, USA). Antibody for β-actin was purchased from Sigma Chemical Co (St. Louis, MO, USA). Antibodies for ZEB1 and Twist were purchased from Santa Cruz Biotechnology (Santa Cruz, CA, USA). Anti-mouse and anti-rabbit antibodies conjugated to horseradish peroxidase were also obtained from Santa Cruz Biotechnology, Inc.

Cell Culture. HEK-293T cells were obtained from the American Type Culture Collection (Rockville, MD, USA). GBM8401 cells were obtained from Bioresources Collection and Research Center (Hsinchu, Taiwan). GBM8401 cells were cultured in RPMI1640 supplemented with 10% fetal bovine serum (FBS) and 1% penicillin−streptomycin. Cell culture materials were obtained from Invitrogen (Burlington, Ontario, Canada).

Morphology Observation. GBM8401 cells (2×10^4) were seeded in a 24-well plate and pretreated with the indicated concentrations of osthole for the appropriate time. IGF-1 was added to each well with indicated concentrations, and cells were then incubated for 24 h. A Nikon TE2000-U inverted microscope was used to take representative photographs at 200× magnification.

Western Blot Analysis. Western blot was done as described previously.[17] Briefly, cells (2×10^6) were treated with various agents as indicated in figure legends. After treatment, cells were placed on ice, washed with cold PBS, and lysed in the lysis buffer. Fifty micrograms of protein extract was loaded into sodium dodecyl sulfate polyacrylamide gels, and the separated proteins were transferred to nitrocellulose filters. The filters were probed with the appropriate primary antibody.

Cell Viability Studies. To evaluate the cell viability of osthole in GBM8401 cells, MTT assay was employed. GBM8401 cells at a density of 1×10^4 cells per well were exposed to osthole for 24 h. MTT solution (stock concentration: 5 mg/mL in PBS) was diluted to 500 μg/mL. Each well was treated with 100 μL of MTT working solution and incubated at 37 °C for 2 h. The optical density was measured using an ELISA reader at 570 nm wavelength.

Confocal Microscopy. After treatment, GBM8401 cells were fixed for 40 min with 4% paraformaldehyde in PBS at room temperature, permeabilized and blocked with 5% nonfat dry milk, 1% BSA, and 0.5% Triton X-100, and incubated overnight with anti-vimentin monoclonal antibody and then FITC-conjugated anti-mouse IgG antibody. DAPI staining was used to determine the nuclei. Cells were imaged with a Leica TCS SP2 Spectral Confocal System (Leica, Wetzlar, Germany).

Wound Healing Assay. 4.5×10^5 GBM8401 cells were plated on a 6-well plate to form a confluent monolayer in serum-containing medium. Before being scratched, the confluent monolayer was pretreated with the indicated concentrations of osthole for 2 h. A sterile 200 μL pipet tip was used to scratch the monolayers, followed by washing with PBS to remove cell debris. RPMI1640 containing 0.5% FBS, indicated concentrations of osthole, and 200 ng/mL IGF-1 were then added to each well for 24 h. A Nikon TE2000-U inverted microscope was used to measure ten random fields at 200× magnification. Data from three independent experiments were analyzed by GraphPad Prism 5 software.

RNA Isolation and Quantitative Real-Time PCR. RNA isolation was performed as previously described.[18] Briefly, total RNA was extracted according to the manufacturer's protocol (Qiagen, Germantown, MD, USA). The extracted RNA was purified on an RNeasy purification column (Qiagen) and treated with DNase I according to the manufacturer's protocol. Reverse transcriptase reactions were performed using a first-strand cDNA synthesis kit (Fermentas, Hanover, MD, USA). Quantitative real-time PCR was performed using StepOnePlus real-time PCR system (Applied Biosystems Inc., Foster City, CA, USA) on an ABI Prism 7500HT sequence detection system following the manufacturer's instructions. In quantitative real-time PCR experiments, GAPDH (glyceraldehyde 3-phosphate dehydrogenase) was applied as an internal control. Primers used for E-cadherin were as follows: 5′-TGCTCTTCCAGGAACCTCTGTG-3′ (forward) and 5′-GGTGACCACACTGATGACTCCTG-3′ (reverse).

Reporter Construct Generation and Dual-Luciferase Reporter Assay. The reporter constructs were performed as previously described.[18] For dual-luciferase reporter assay, 1×10^5 GBM8401 cells were plated onto 24-well plates 1 day before transfection and then transfected with reporter constructs by using Lipofectamine 2000 (Invitrogen, Carlsbad, CA, USA). After transient transfection, the GBM8401 cells were treated with osthole at various concentrations with or without IGF-1-stimulation. GBM8401 cells were lysed in the lysis buffer (Promega, Madison, WI, USA) and detected with dual luciferase assay kits (Promega).

Tranfection. One day before transfection, 2×10^5 GBM8401 cells without serum were plated in a 6 cm dish. Cells were grown to 90% confluence and transfected on the following day by Lipofectamine 2000 (Invitrogen, Carlsbad, CA, USA) and premixed plasmid DNA with OPTI-MEM (GIBCO, Carlsbad, CA, USA) for 5 min and then added to the dish. The transfection was completed after 24 h of incubation.

Statistical Analysis. All values were expressed as mean ± SD. The independent Student's *t*-test was used to compare the continuous variables between two groups, and the chi-squared test was applied for comparison of dichotomous variables. Asterisk indicates that the values were significantly different from the control (*, $P < 0.05$; **, $P < 0.01$; ***, $P < 0.001$).

RESULTS

IGF-1-Induced GBM8401 Cells Undergo EMT. To determine whether IGF-1 could initiate cell morphology changes, GBM8401 cells were treated with various concentrations (100−300 ng/mL) of IGF-1 for 24 h. GBM8401 cells maintained a classic cobblestone epithelial morphology; after exposure of GBM8401 cells to IGF-1, morphology was changed to fibroblast-like and the cell−cell contact was reduced (Figure 1A). GBM8401 cells were treated with various concentrations of IGF-1 for 24 h, and IGF-1 decreased the expression of epithelial phenotype markers, E-cadherin, ZO-1, and β-catenin in a dose-dependent manner (Figure 1B). Inversely, IGF-1 increased the expression of mesenchymal markers N-cadherin and vimentin in a dose-dependent manner (Figure 1B). Our results indicated that IGF-1 induced EMT in GBM cells. We also determined whether IGF-1 regulated MMP-2 and MMP-9 expressions related to invasion and metastasis. The expression of MMP-2 and MMP-9 was increased after IGF-1 treatment for 24 h (Figure 1C). Moreover, IGF-1 induced an increase in cell migration (Figure 1D).

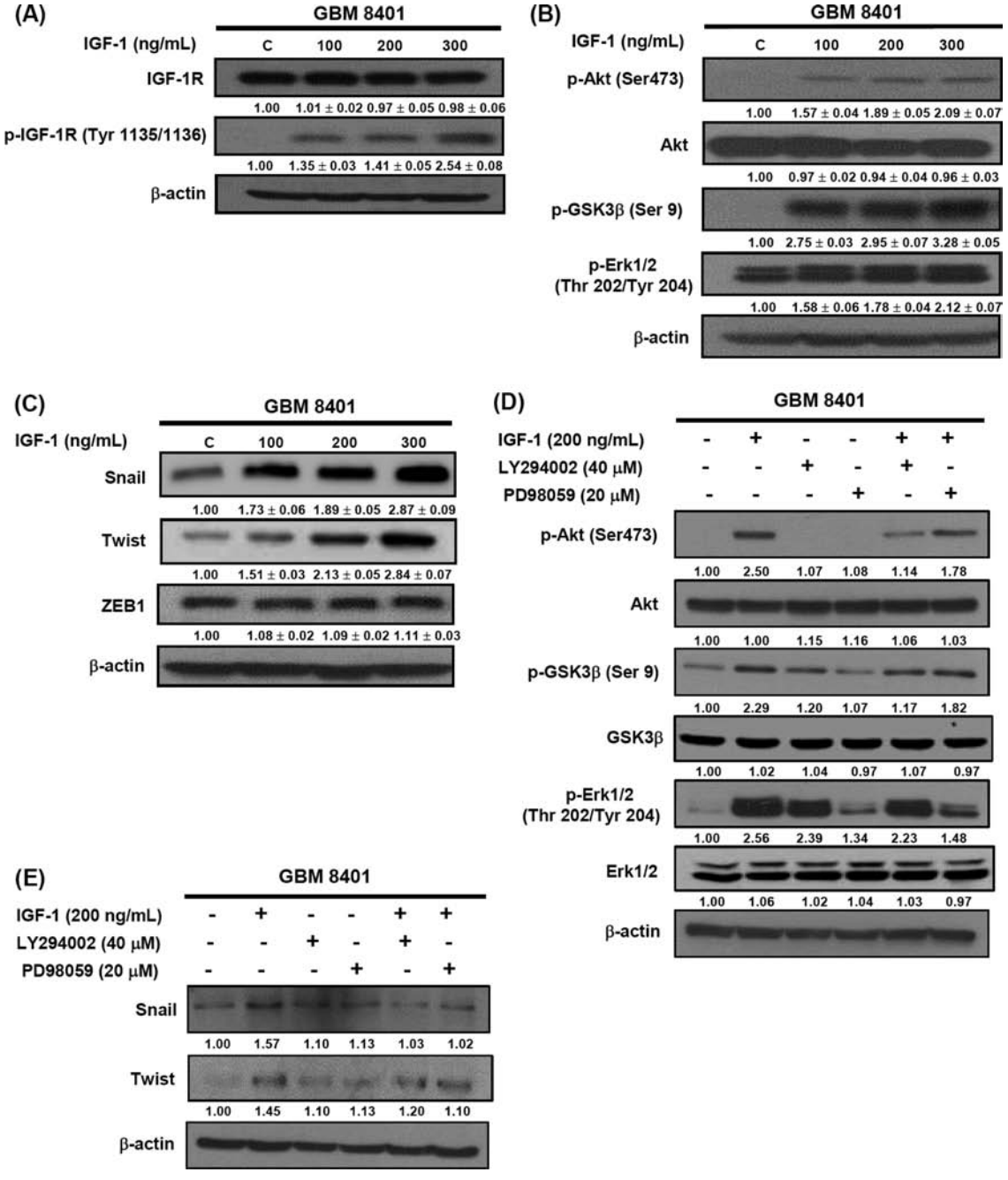

Figure 2. IGF-1 induced phosphorylation of Akt and Erk1/2 and Snail and Twist expression in GBM8401 cells. GBM8401 cells were treated with DMSO (control) or increasing IGF-1 concentrations (100−300 ng/mL) for 10 min. (A) The cells were then harvested and lysed for the detection of IGF-1R, p-IGF-1R, and β-actin. (B) The cells were then harvested and lysed for the detection of p-Akt, Akt, p-GSK3β, p-Erk1/2, and β-actin. (C) GBM8401 cells were treated with DMSO (control) or increasing IGF-1 concentrations (100−300 ng/mL) for 24 h. The cells were then harvested and lysed for the detection of Snail, Twist, ZEB1, and β-actin. (D) GBM8401 cells were pretreated with 40 μM LY294002 or 20 μM PD98059 for 2 h prior to with or without IGF-1 stimulation (200 ng/mL) for 10 min. The cells were then harvested and lysed for the detection of p-Akt, Akt, p-GSK3β, p-Erk1/2, and β-actin. (E) BM8401 cells were pretreated with 40 μM LY294002 or 20 μM PD98059 for 2 h prior to with or without IGF-1 stimulation (200 ng/mL) for 24 h. The cells were then harvested and lysed for the detection of Snail, Twist, and β-actin. Western blot data presented are representative of those obtained in at least 3 separate experiments. Immunoblots were quantified, and the value of the control cells was set to 1.

IGF-1-Induced EMT by Upregulating Snail and Twist in GBM8401 Cells. To investigate the ability of IGF-1-induced EMT through IGF-1R signaling, tyrosine phosphorylation of IGF-1R was examined in the presence of IGF-1. GBM8401 cells showed no detectable phosphorylation of IGF-1R when cells were cultured in a serum-free medium. In the presence of IGF-1, however, key tyrosine residues in the kinase domain of the β-subunit of IGF-1R became phosphorylated. There was no change in the amount of total IGF-1R as determined by immunoblotting (Figure 2A). We next determined the effect of IGF-1 on the key signaling molecules downstream of IGF-1R, Akt and Erk1/2. IGF-1 stimulation resulted in increased phosphorylation of Akt and Erk1/2 in comparison to serum-free condition (Figure 2B). Interestingly, IGF-1 stimulation also resulted in increased phosphorylation of GSK3β, the downstream of Akt, in a dose-dependent manner (Figure 2B). We next examined whether

dx.doi.org/10.1021/jf501047g | J. Agric. Food Chem. 2014, 62, 5061−5071

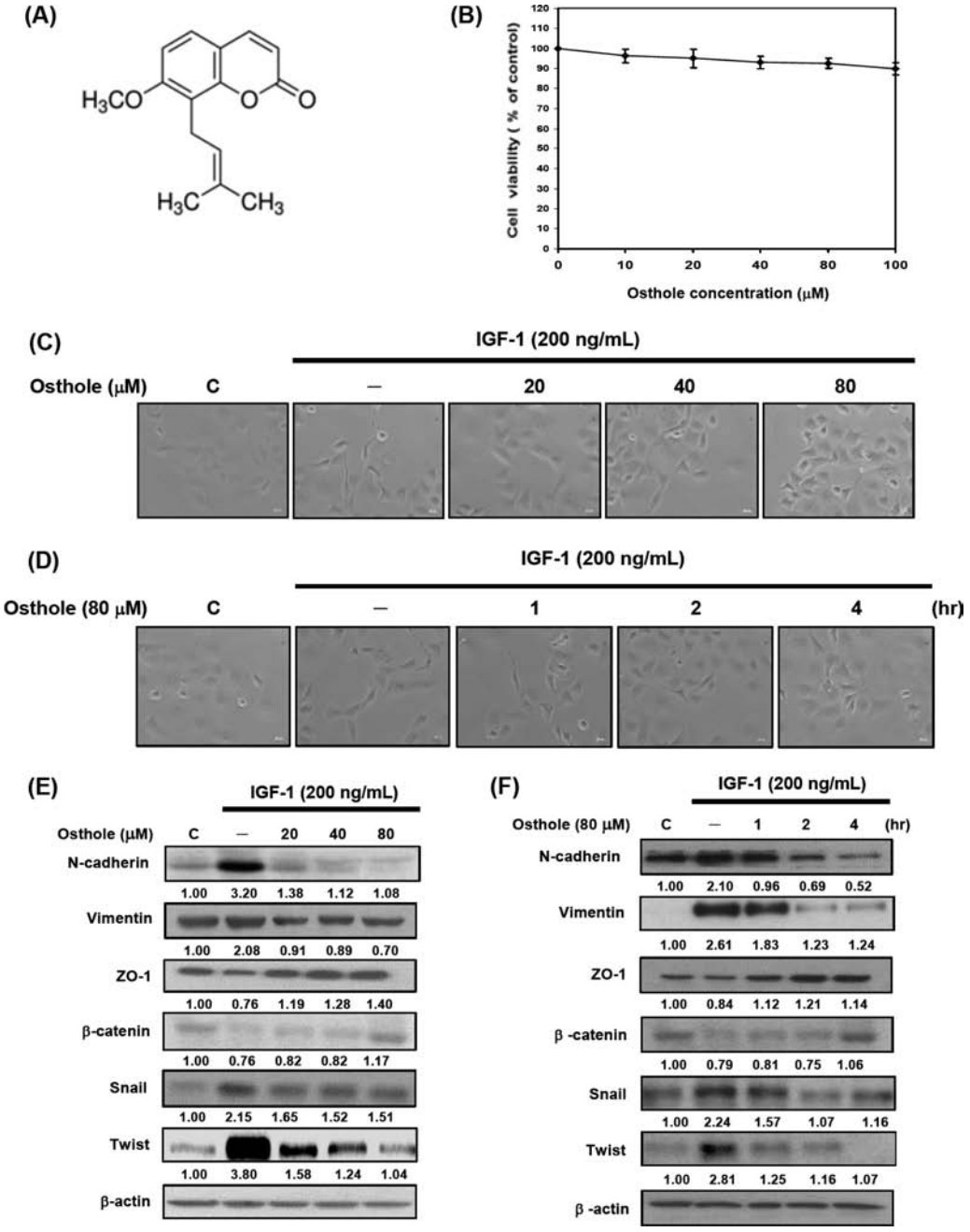

Figure 3. Osthole blocked IGF-1-induced cell scattering and EMT in GBM8401 cells. (A) Chemical structure of osthole. (B) GBM8401 cells were treated with increasing osthole concentrations (10−100 μM) for 24 h. The cell viability was then determined using MTT assay. This experiment was repeated three times. The data represented the mean ± SD. (C) GBM8401 cells were pretreated with DMSO (control) or increasing osthole concentrations (20−80 μM) for 2 h prior to IGF-1 stimulation (200 ng/mL) for 24 h. (D) GBM8401 cells were incubated with DMSO (control) or 80 μM osthole for 1, 2, or 4 h prior to IGF-1 stimulation (200 ng/mL). EMT was examined by phase contrast photomicrographs. (E) GBM8401 cells were pretreated with DMSO (control) or increasing osthole concentrations (20−80 μM) for 2 h prior to IGF-1 stimulation (200 ng/mL) for 24 h. The cells were then harvested and lysed for the detection of N-cadherin, vimentin, E-cadherin, ZO-1, β-catenin, Snail, Twist, and β-actin. (F) GBM8401 cells were incubated with DMSO (control) or 80 μM osthole for 1, 2, or 4 h prior to IGF-1 stimulation (200 ng/mL). The cells were then harvested and lysed for the detection of N-cadherin, vimentin, E-cadherin, ZO-1, β-catenin, Snail, Twist, and β-actin. Western blot data presented are representative of those obtained in at least 3 separate experiments. Immunoblots were quantified, and the value of the control cells was set to 1.

EMT-inducing regulators, Snail, Twist, and Zeb1, were involved in IGF-1-induced EMT. GBM8401 cells were treated with different concentrations of IGF-1, and Western blotting analysis showed that IGF-1 increased both Snail and Twist expressions, but not the ZEB1 expression (Figure 2C). In order to further confirm whether Akt and Erk1/2 were involved in IGF-1-mediated EMT, LY294002, a specific inhibitor of PI3K, and PD98059, a specific inhibitor of MAPK, were used to inhibit IGF-1-induced phosphorylation of Akt and Erk1/2 in GBM8401 cells. The results showed that IGF-1-induced phosphorylation of Akt and Erk1/2 (Figure 2D) and upregulation of Snail and Twist (Figure 2E) were significantly inhibited by pretreatment with 40 μM LY294002 or 20 μM PD98059. Taken together, IGF-1

dx.doi.org/10.1021/jf501047g | J. Agric. Food Chem. 2014, 62, 5061−5071

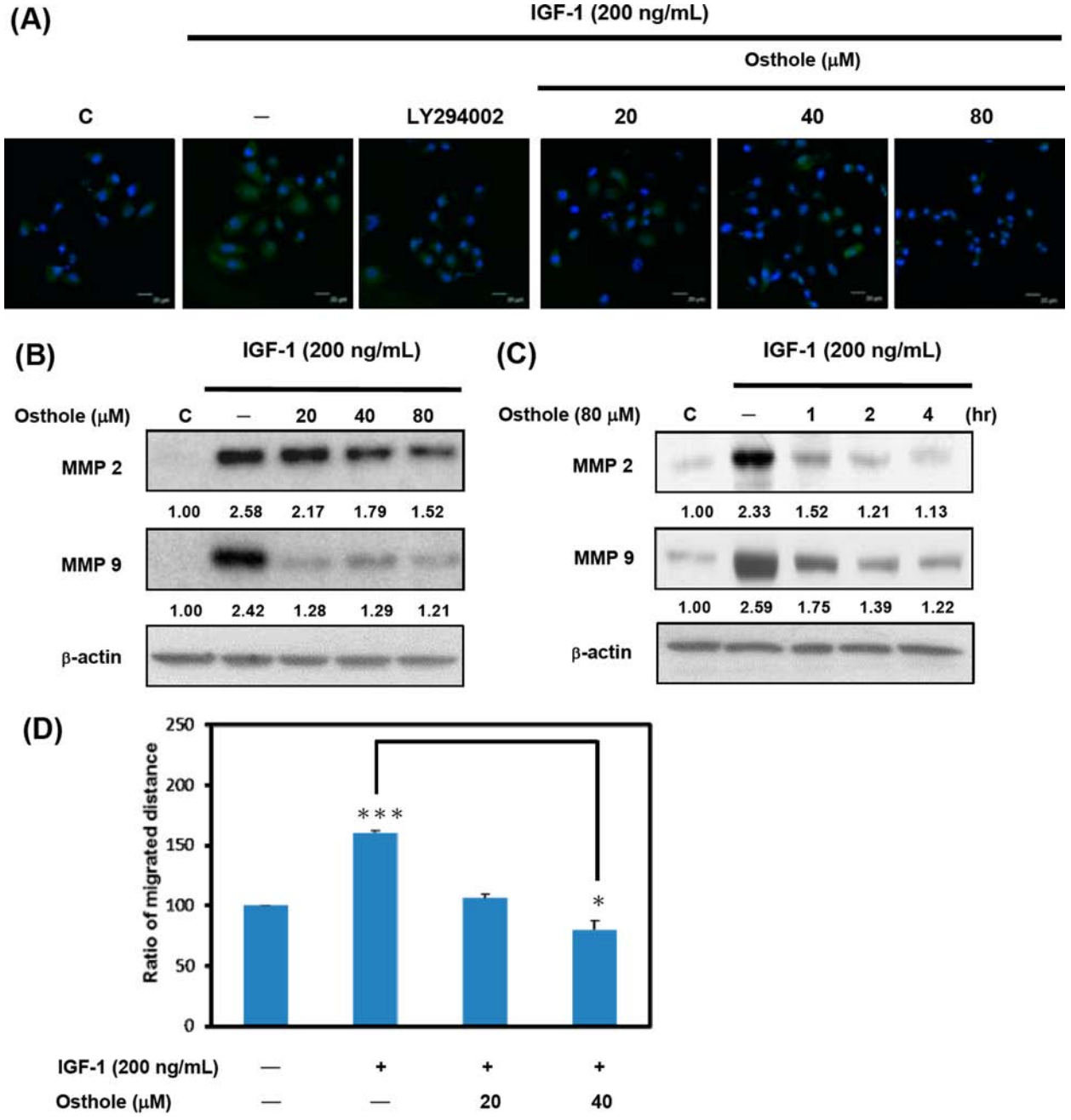

Figure 4. Osthole blocked IGF-1-induced cell migration in GBM8401 cells. (A) GBM8401 cells were pretreated with DMSO (control), 40 μM LY294002, or increasing osthole concentrations (20−80 μM) for 2 h prior to IGF-1 stimulation (200 ng/mL) for 24 h. Cells were fixed, permeabilized, and stained with anti-vimentin monoclonal antibody (green) and DAPI (blue). Cells were analyzed by confocal microscopy. (B) GBM8401 cells were pretreated with DMSO (control) or increasing osthole concentrations (20−80 μM) for 2 h prior to IGF-1 stimulation (200 ng/mL) for 24 h. The cells were then harvested and lysed for the detection of MMP-2, MMP-9, and β-actin. (C) GBM8401 cells were pretreated with DMSO (control) or 80 μM osthole for 1, 2, and 4 h prior to IGF-1 stimulation (200 ng/mL) for 24 h. The cells were then harvested and lysed for the detection of MMP-2, MMP-9, and β-actin. Western blot data presented are representative of those obtained in at least 3 separate experiments. Immunoblots were quantified, and the value of the control cells was set to 1. (D) GBM8401 cells were pretreated with DMSO (control) or increasing osthole concentrations (20, 40 μM) for 2 h prior to IGF-1 stimulation (200 ng/mL) for 24 h. IGF-1-induced cell motility was determined by measuring the closure of wound. Data were plotted by mean ± SD (n = 3). The closure distance of the control cells was set to 100. Osthole significantly inhibited IGF-1-induced cell motility (*, $p < 0.05$).

induced phosphorylation of Akt and Erk1/2 and expression of Snail and Twist leading to EMT induction.

Osthole Blocked IGF-1-Induced EMT in GBM8401 Cells. The activation of IGF-1 signaling significantly caused fibroblast-like morphology in GBM8401 cells. We next determined whether osthole (Figure 3A) could affect the IGF-1-induced fibroblast-like morphology, and GBM8401 cells were pretreated with osthole prior to stimulation with IGF-1. To ensure that osthole blocked IGF-1-induced fibroblast-like morphology was not due to inhibition of proliferation, we tested the cytotoxicity of osthole on GBM8401 cells. As shown in Figure 3B, osthole had no significant cytotoxicity on GBM8401 cells. GBM8401 cells were pretreated with osthole (20−80 μM) for 2 h prior to stimulation with IGF-1 (200 ng/mL) for 24 h. Osthole blocked

dx.doi.org/10.1021/jf501047g | J. Agric. Food Chem. 2014, 62, 5061−5071

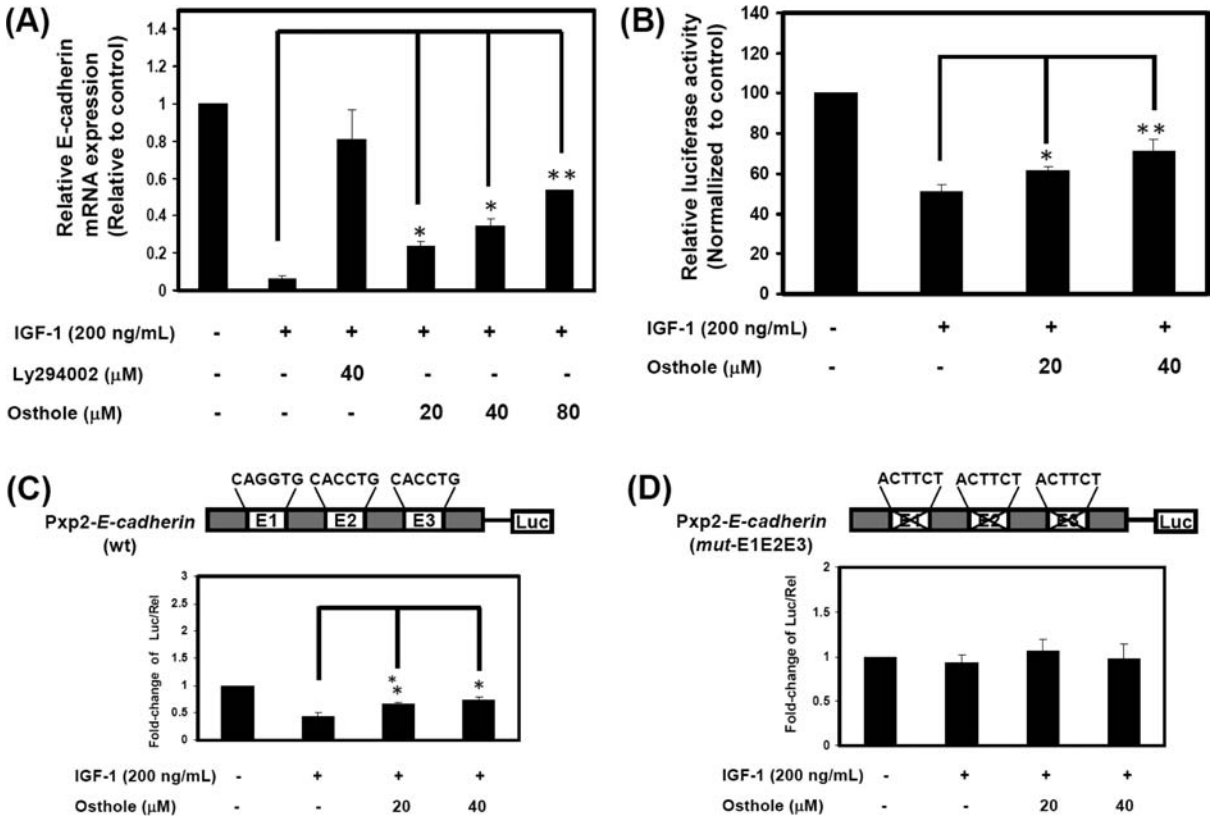

Figure 5. Osthole blocked IGF-1-induced EMT at transcriptional level. (A) GBM8401 cells were pretreated with DMSO (control), 40 μM LY294002, or increasing osthole concentrations (20−80 μM) for 2 h prior to IGF-1 stimulation (200 ng/mL) for 24 h. Quantitative real-time PCR was performed by the StepOnePlus real-time PCR system and GAPDH was applied as an internal control. Data were plotted by mean ± SD (n = 3). The value of control was set to 1. Asterisk, values significantly different from the IGF-1 stimulation. *, $p < 0.05$; **, $p < 0.01$. (B) After cotransfection with pRL-*CMV* and pXP2-*E-cadherin* in GBM8401 cells, cells were pretreated with DMSO (control) or increasing osthole concentrations (20, 40 μM) for 2 h prior to IGF-1 stimulation (200 ng/mL) for 24 h. *E-cadherin* promoter activity was analyzed by luciferase reporter assays. Data were plotted by mean ± SD (n = 3). The value of control was set to 1. Asterisk, values significantly different from the IGF-1 stimulation. *, $p < 0.05$; **, $p < 0.01$. (C) Top: schematic representation of the wild-type (pXP2-E-cadherin) *E-cadherin* promoter construct. E1, E2, and E3 indicate the E-boxes. Bottom: promoter-activity assay. HEK-293T cells were cotransfected with a promoter construct and the indicated vector. All cells were cotransfected with a plasmid that expressed *β-galactosidase,* and the luciferase activity values were normalized to the β-galactosidase activity. After cotransfection, the cells were pretreated with DMSO (control) or increasing osthole concentrations (20, 40 μM) for 2 h prior to IGF-1 stimulation (200 ng/mL) for 24 h. For each promoter, all values were standardized to the luciferase activity of the control; asterisks indicate $P < 0.05$, compared with the control cells. The data are shown as the means ± SD (n = 3). (D) Top: schematic representation of the mutated-E-boxes (pXP2-E-cadherin (*mut*-E1E2E3)) *E-cadherin* promoter construct. E1, E2, and E3 indicate the E-boxes. Bottom: promoter activity assay in HEK-293T cells under different transfection conditions. A vector expressing *β-galactosidase* was cotransfected to ensure the transfection efficiency and normalize the luciferase activity values. After cotransfection, the cells were pretreated with DMSO (control) or increasing osthole concentrations (20, 40 μM) for 2 h prior to IGF-1 stimulation (200 ng/mL) for 24 h. For each promoter, all values were standardized to the luciferase activity of the control. The data are shown as the means ± SD (n = 3).

IGF-1-induced fibroblast-like morphology in a dose-dependent fashion (Figure 3C). Moreover, we pretreated GBM8401 cells with 80 μM osthole for varying periods of time from 1 to 4 h prior to IGF-1 addition. An increase in inhibition of IGF-1-induced fibroblast-like morphology was observed beginning at 1 h of osthole pretreatment (Figure 3D). To further identify whether inhibition of IGF-1-induced fibroblast-like morphology in osthole treated GBM8401 cells resulted from inhibition of EMT, we examined the expression of EMT related proteins in GBM8401 cells. Pretreated GBM8401 cells with osthole significantly suppressed the IGF-1-induced upregulation of N-cadherin, vimentin, Snail, and Twist and downregulation of ZO-1 and β-catenin in a dose- and time-dependent manner (Figure 3E,F).

Osthole Blocked IGF-1-Induced Cell Migration by Downregulating MMP-2, and MMP-9 in GBM8401 Cells. To further examine that osthole suppressed the IGF-1-induced upregulation of vimentin, GBM8401 cells were imaged with confocal microscopy. As shown in Figure 4A, confocal microscopy with vimentin antibodies indicated that IGF-1 treatment resulted in upregulation of vimentin. Pretreatment with various concentrations of osthole for 2 h significantly suppressed the IGF-1-induced upregulation of vimentin in a dose-dependent manner (Figure 4A). IGF-1 has been shown previously to stimulate protease activity in many cell types.[19] To determine whether IGF-1 could stimulate metalloproteinase activity, GBM8401 cells were treated with 200 ng/mL IGF-1. IGF-1 stimulation resulted in increased expression of MMP-2 and MMP-9 compared to serum-free conditions (Figure 4B,C). Pretreatment with osthole significantly suppressed the IGF-1-induced upregulation of MMP-2 and MMP-9 in a dose- and time-dependent manner (Figure 4B,C). We next examined whether osthole inhibited IGF-1-induced cell migration by measuring the wound closure. Compared to GBM8401 cells treated with DMSO (control), IGF-1 significantly induced cell

dx.doi.org/10.1021/jf501047g | J. Agric. Food Chem. 2014, 62, 5061−5071

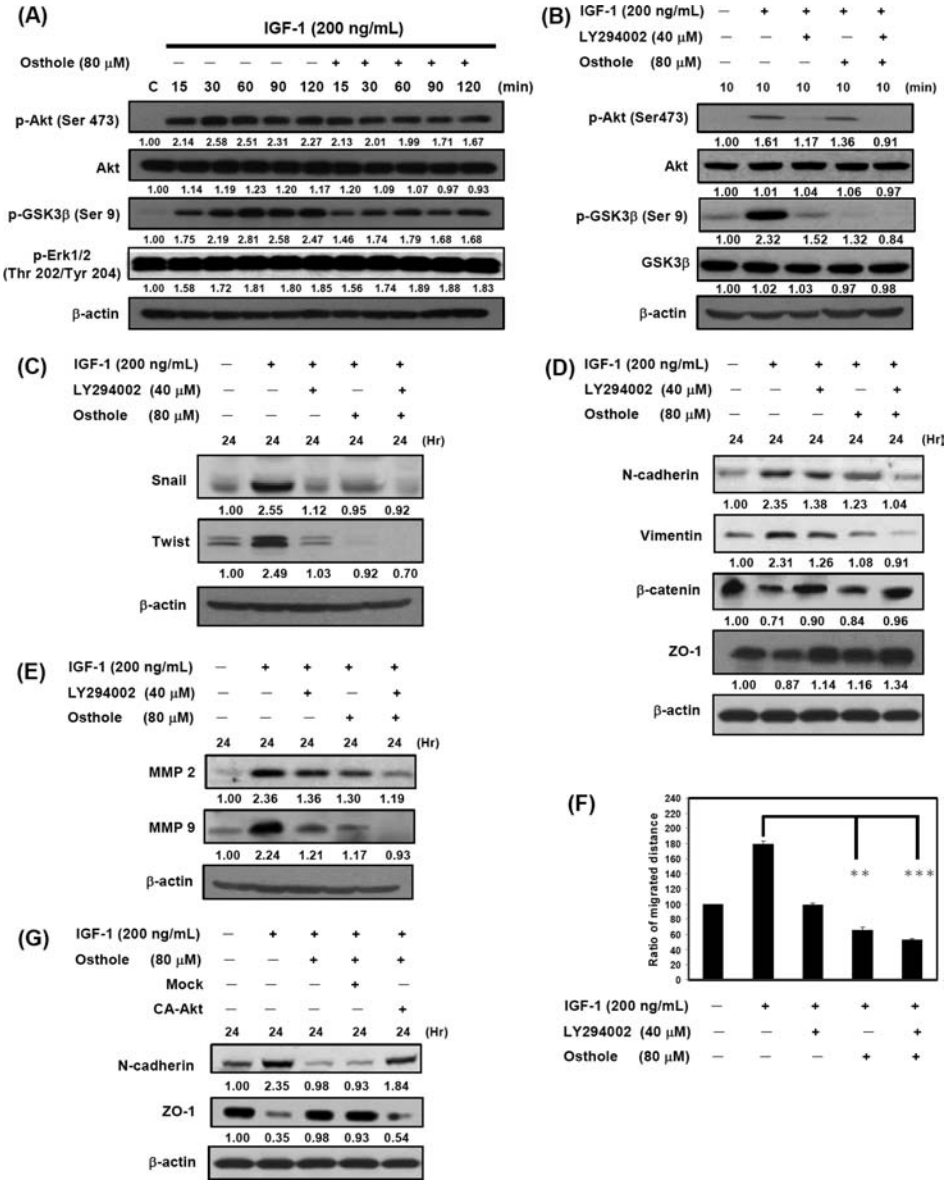

Figure 6. Osthole blocked IGF-1-induced Akt pathway in a time-dependent manner. (A) GBM8401 cells were preincubated in the presence or the absence of 80 μM osthole for 2 h prior to IGF-1 stimulation (200 ng/mL) for various times. The cells were then harvested and lysed for the detection of p-Akt, Akt, p-GSK3β, p-Erk1/2, and β-actin. (B) GBM8401 cells were pretreated with 80 μM osthole, or 40 μM LY294002, or a combination of 40 μM LY294002 and 80 μM osthole for 2 h and then treated with IGF-1 for 10 min. The cells were then harvested and lysed for the detection of p-Akt, p-GSK3β, and β-actin. GBM8401 cells were pretreated with 80 μM osthole, or 40 μM LY294002, or a combination of 40 μM LY294002 and 80 μM osthole for 2 h and then treated with IGF-1 for 24 h. (C) The cells were then harvested and lysed for the detection of Snail, Twist, and β-actin. (D) The cells were then harvested and lysed for the detection of N-cadherin, vimentin, β-catenin, ZO-1, and β-actin. (E) The cells were then harvested and lysed for the detection of MMP-2, MMP-9, and β-actin. (F) Cell motility was determined by measuring the closure of wound. Data were plotted by mean ± SD (n = 3). Osthole or a combination of LY294002 and osthole significantly inhibited IGF-1-induced cell motility (**, $p < 0.01$;***, $p < 0.001$). (G) GBM8401 cells were transfected with 50 nmol/L CA-Akt or mock. Twenty-four hours after transfection, preincubation was carried out in the presence or the absence of 80 μM osthole for 2 h prior to IGF-1 stimulation (200 ng/mL) for 24 h. The cells were then harvested and lysed for the detection of N-cadherin, ZO-1, and β-actin. Western blot data presented are representative of those obtained in at least three separate experiments. The values below the figures represent change in protein expression normalized to β-actin.

migration. Significantly, the IGF-1-induced cell migration was inhibited in the presence of osthole (Figure 4D).

Osthole Suppressed IGF-1 Inducible E-Cadherin Transcriptional Downregulation. We next determined whether pretreatment with osthole could inhibit IGF-1-induced downregulation of E-cadherin through transcriptional level. Real-time PCR analysis was performed to assess the effect of osthole on E-cadherin mRNA expression. As shown in Figure 5A, IGF-1-induced downregulation of E-cadherin mRNA was restored by pretreatment with osthole. Our luciferase assay indicated that IGF-1 inhibited *E-cadherin* promoter activity, and pretreatment with osthole significantly restored the IGF-1-repressed *E-cadherin* promoter activity in a dose-dependent manner (Figure 5B). Figure 2C indicates that IGF-1 induced Snail and Twist expression. Interestingly, Snail and Twist bind to the same elements in the *E-cadherin* promoter: three *E-boxes* with a core 5′-CACCTG-3′ sequence. We next investigated whether osthole suppressed the binding of Snail and Twist to these *E-boxes* and

dx.doi.org/10.1021/jf501047g | J. Agric. Food Chem. 2014, 62, 5061−5071

repressed the *E-cadherin* promoter. Promoter activity was analyzed by transfection of *E-cadherin* promoter containing three *E-boxes* constructed into HEK-293T cells. Our promoter-activity assay showed that IGF-1 inhibited *E-cadherin* promoter activity. Pretreatment with various concentrations of osthole restored the IGF-1-repressed *E-cadherin* promoter activity (Figure 5C). As shown in Figure 5D, mutation of all three *E-boxes* abrogated repression by IGF-1. Pretreatment with various concentrations of osthole was not able to restore the *E-boxes*-mutated *E-cadherin* promoter activity. These data suggest that osthole inhibits IGF-1-mediated EMT through transcriptional level.

Osthole Inhibited IGF-1-Induced EMT through Inhibiting PI3K/Akt Signaling Pathway. To determine whether osthole inhibited the key signaling molecules downstream of IGF-1R, Akt and Erk1/2, the phosphorylation of Akt and Erk1/2 was examined at various time points after adding IGF-1 (200 ng/mL) to GBM8401 cells. The phosphorylation of Akt and Erk1/2 was increased at 15 min after stimulation, and this effect lasted for at least 120 min (Figure 6A). Pretreatment with osthole (80 μM) for 2 h significantly suppressed the IGF-β-induced phosphorylation of Akt and GSK3β (Figure 6A). However, pretreatment with osthole was not able to suppress the IGF-β-induced phosphorylation of Erk1/2 (Figure 6A). We next investigated whether Akt was involved in osthole inhibited IGF-1-mediated EMT; PI3K inhibitor LY294002 was used. Our study showed that IGF-1-induced phosphorylation of Akt and GSK3β (Figure 6B), upregulation of Snail and Twist (Figure 6C), upregulation of N-cadherin and vimentin and downregulation of β-catenin and ZO-1 (Figure 6D), and upregulation of MMP-2 and MMP-9 (Figure 6E) were significantly inhibited by pretreatment with 40 μM LY294002. Interestingly, in the cotreatment of LY294002 (40 μM) and osthole (80 μM), IGF-1-induced phosphorylation of Akt and GSK3β (Figure 6B), upregulation of Snail and Twist (Figure 6C), upregulation of N-cadherin and vimentin and downregulation of β-catenin and ZO-1 (Figure 6D), and upregulation of MMP-2 and MMP-9 (Figure 6E) were more potent than pretreatment with LY294002 or osthole alone. We further confirmed whether Akt was involved in osthole inhibited IGF-1-mediated cell migration. Figure 6F showed that IGF-1-induced cell migration was significantly inhibited by pretreatment with 40 μM LY294002. In the cotreatment of LY294002 (40 μM) and osthole (80 μM), IGF-1-induced cell migration was more potent than pretreatment with LY294002 or osthole alone (Figure 6F). To assess whether Akt was involved in osthole inhibited IGF-1-mediated EMT, we performed Akt-overexpression experiment using constitutively active Akt (CA-Akt). The result showed that CA-Akt abolished the ability of osthole to suppress IGF-1-induced EMT (Figure 6G). Taken together, our data suggest that the inhibition of PI3K/Akt signaling pathway is involved in osthole inhibited IGF-1-mediated EMT, and cell migration in GBM8401 cells.

DISCUSSION

Recent studies indicated an important role for the IGF signaling pathway in the proliferation, progression, and antiapoptosis of GBM cells. For example, treatment of glioblastoma cells with IGF-1 increased cellular proliferation and migration.[20] Inhibition of IGF-1R by tyrosine kinase inhibitor inhibited GBM cell growth.[21] IGF-1R inhibition contributed to the growth suppression of primary cell lines derived from human high-grade gliomas.[22]

The EMT is crucial for the migration and invasion of many epithelial tumors. IGF-1 stimulation has been shown to promote dramatic neomorphic effects of an EMT and enhanced cell migration and invasion. For example, Graham et al. have clearly shown that aberrant expression of ZEB1 occurs in part due to IGF-1, and the activated ZEB1 is then able to promote epithelial prostate cancer cells to exhibit a mesenchymal phenotype.[23] Kim et al. found that overexpression of a constitutively activated IGF-1R was sufficient to cause human mammary epithelial cells to undergo an EMT which was associated with dramatically increased migration and invasion.[24] Moreover, overexpression of IGFBP4 in U343 glioma cells resulted in upregulation of molecules involved in tumor growth, EMT, and invasion.[25] Herein, we showed that IGF-1 treatment caused GBM8401 cells to lose their polygonal appearance and cell−cell contacts leading to the acquisition of an elongated, spindle-shaped morphology, suggesting that GBM8401 cells underwent EMT. Taken together, these data indicate that IGF-1 can initiate EMT in cancer cells and promote tumor cell metastasis. Moreover, targeting IGF-1 signaling in GBM may be a promising anticancer strategy.

There are several zinc finger transcription factors, including Snail, Twist, and ZEB1, which have been described as E-cadherin repressors. Herein, our Western blotting analysis showed that IGF-1 increased both the expressions of Snail and Twist, but not the ZEB1 expression. Mikheeva et al. revealed that Twist promoted invasion through mesenchymal changes in GBM.[26] Zhang et al. indicated that Snail promoted the migratory and invasive properties of glioma cells.[27] Taken together, these data show that expression of Snail and Twist is characteristic of mesenchymal tumor areas of GBM, suggesting that similar mechanisms involved in the EMT in epithelial neoplasms played a role in mesenchymal differentiation in GBM.

Following binding of IGF-1 to the extracellular subunits of the IGF-1R, it leads to the activation of at least 2 main pathways: first via RAS, RAF, and Erk1/2, and second via the PI3K and Akt signaling pathway. Our data suggest that Erk1/2 and Akt are upstream factors of Snail and Twist activation in GBM cells. IGF-1 has been shown to activate the Erk1/2 and Akt signaling pathways in various cancer cells, and we showed in GBM8401 cells that Snail and Twist expressions were Erk1/2 and Akt dependent. Pharmacologic inhibition of Erk1/2 and Akt signaling has been shown to decrease invasion or inhibit specific biochemical changes consistent with EMT.[28,29] Our results are consistent with previous reports, suggesting that Erk1/2- and Akt-dependent pathways are sufficient to maintain the mesenchymal phenotype.

Recent studies showed that osthole regulates the proliferation, apoptosis, and invasion in many cancer cells via multiple signaling pathways.[30,31] Moreover, osthole has essential roles in brain functions by protecting neurons, suggesting that osthole could penetrate the blood−brain barrier for the chemotherapy drugs of brain tumors.[14−16] In the present study, we first evaluated the effects of osthole on IGF-1 induced EMT in GBM8401 cells. The present study showed that IGF-1 induced EMT in GBM8401 cells and this process could be effectively blocked by osthole. Pretreatment with osthole blocks IGF-1-induced EMT, however, how osthole affects these changes remain to be determined.

To further delineate the molecular mechanism of osthole blocking IGF-1-induced EMT, related pathways were investigated. In the study, both Erk1/2 and PI3K/Akt signaling pathways were investigated in osthole-treated GBM8401 cells.

GBM8401 cells were pretreated with osthole and showed significant decrease of phospho-Akt but no obvious decrease of phospho-Erk1/2. Our previous studies showed that osthole suppresses fatty acid synthase expression in HER2-overexpressing breast cancer cells through modulating the Akt/mTOR pathway[31] and suppresses the hepatocyte growth factor (HGF)-induced epithelial−mesenchymal transition via repression of the c-Met/Akt/mTOR pathway in human breast cancer cells.[13] Ding et al. revealed that osthole inhibited the proliferation, promoted apoptosis, and inhibited cell migration/invasion in vitro in glioma cells through inhibiting both PI3K/Akt and MAPK signaling pathways.[32] Xu et al. showed that osthole induced G2/M arrest and apoptosis in lung cancer A549 cells by modulating the PI3K/Akt pathway.[33] Based on these findings, osthole may be an ideal inhibitor for PI3K/Akt signaling pathway.

AUTHOR INFORMATION

Corresponding Author

*Department of Biological Science and Technology, College of Life Sciences, China Medical University, No. 91 Hsueh-Shih Road, Taichung, Taiwan 40402. Tel: +886-4-2205-3366, ext 2509. Fax: +886-4-2203-1075. E-mail: tdway@mail.cmu.edu.tw.

Funding

This study was supported by the National Science Council of the Republic of China, Grant NSC 101-2320-B-039-031-MY3. Thanks are also due to support (in part) by a grant from the Department of Health (Taiwan), China Medical University Hospital Cancer Research Center of Excellence (DOH100-TD-C-111-005), and a grant from China Medical University (CMU101-N2-03). The authors would like to thank Prof. Mien-Chie Hung for generously providing the cDNA of CA-Akt.

Notes

The authors declare no competing financial interest.

ABBREVIATIONS USED

BBB, blood−brain barrier; EMT, epithelial−mesenchymal transition; MMPs, matrix metalloproteinases; IGF-1, insulin-like growth factor-1; IGF-1R, insulin-like growth factor-1 receptor; IGFBP, IGF binding protein; IRS, insulin receptor substrate; MTT, 3-(4,5-dimethylthiazol-2-yl)-2,5-diphenyltetrazolium bromide

REFERENCES

(1) Buckner, J. C. Factors influencing survival in high-grade gliomas. *Semin. Oncol.* **2003**, *30*, 10−14.

(2) Chen, Y. H.; Hung, M. C.; Shyu, W. C. Role of cancer stem cells in brain tumors. *Biomedicine* **2012**, *2*, 84−91.

(3) Kahlert, U. D.; Maciaczyk, D.; Doostkam, S.; Orr, B. A.; Simons, B.; Bogiel, T.; Reithmeier, T.; Prinz, M.; Schubert, J.; Niedermann, G.; Brabletz, T.; Eberhart, C. G.; Nikkhah, G.; Maciaczyk, J. Activation of canonical WNT/beta-catenin signaling enhances in vitro motility of glioblastoma cells by activation of ZEB1 and other activators of epithelial-to-mesenchymal transition. *Cancer Lett.* **2012**, *325*, 42−53.

(4) Nieto, M. A. Epithelial plasticity: a common theme in embryonic and cancer cells. *Science* **2013**, *342*, 1234850.

(5) LeRoith, D.; Roberts, C. T., Jr. The insulin-like growth factor system and cancer. *Cancer Lett.* **2003**, *195*, 127−137.

(6) Merrill, M. J.; Edwards, N. A. Insulin-like growth factor-1 receptors in human glial tumors. *J. Clin. Endocrinol. Metab.* **1990**, *71*, 199−209.

(7) Sinha, S.; Koul, N.; Dixit, D.; Sharma, V.; Sen, E. IGF-1 induced HIF-1α-TLR9 cross talk regulates inflammatory responses in glioma. *Cell. Signalling* **2011**, *23*, 1869−1875.

(8) Shi, Y.; Zhang, B.; Chen, X. J.; Xu, D. Q.; Wang, Y. X.; Dong, H. Y.; Ma, S. R.; Sun, R. H.; Hui, Y. P.; Li, Z. C. Osthole protects lipopolysaccharide-induced acute lung injury in mice by preventing down-regulation of angiotensin-converting enzyme 2. *Eur. J. Pharm. Sci.* **2013**, *48*, 819−824.

(9) Nakamura, T.; Kodama, N.; Arai, Y.; Kumamoto, T.; Higuchi, Y.; Chaichantipyuth, C.; Ishikawa, T.; Ueno, K.; Yano, S. Inhibitory effect of oxycoumarins isolated from the Thai medicinal plant Clausena guillauminii on the inflammation mediators, iNOS, TNF-alpha, and COX-2 expression in mouse macrophage RAW 264.7. *J. Nat. Med.* **2009**, *63*, 21−27.

(10) Matsuda, H.; Tomohiro, N.; Ido, Y.; Kubo, M. Anti-allergic effects of cnidii monnieri fructus (dried fruits of Cnidium monnieri) and its major component, osthol. *Biol. Pharm. Bull.* **2002**, *25*, 809−812.

(11) Yao, L.; Lu, P.; Li, Y.; Yang, L.; Feng, H.; Huang, Y.; Zhang, D.; Chen, J.; Zhu, D. Osthole relaxes pulmonary arteries through endothelial phosphatidylinositol 3-kinase/Akt-eNOS-NO signaling pathway in rats. *Eur. J. Pharmacol.* **2013**, *699*, 23−32.

(12) Liang, H. J.; Suk, F. M.; Wang, C. K.; Hung, L. F.; Liu, D. Z.; Chen, N. Q.; Chen, Y. C.; Chang, C. C.; Liang, Y. C. Osthole, a potential antidiabetic agent, alleviates hyperglycemia in db/db mice. *Chem.-Biol. Interact.* **2009**, *181*, 309−315.

(13) Hung, C. M.; Kuo, D. H.; Chou, C. H.; Su, Y. C.; Ho, C. T.; Way, T. D. Osthole suppresses hepatocyte growth factor (HGF)-induced epithelial-mesenchymal transition via repression of the c-Met/Akt/mTOR pathway in human breast cancer cells. *J. Agric. Food Chem.* **2011**, *59*, 9683−9690.

(14) Chao, X.; Zhou, J.; Chen, T.; Liu, W.; Dong, W.; Qu, Y.; Jiang, X.; Ji, X.; Zhen, H.; Fei, Z. Neuroprotective effect of osthole against acute ischemic stroke on middle cerebral ischemia occlusion in rats. *Brain Res.* **2010**, *1363*, 206−211.

(15) Chen, T.; Liu, W.; Chao, X.; Qu, Y.; Zhang, L.; Luo, P.; Xie, K.; Huo, J.; Fei, Z. Neuroprotective effect of osthole against oxygen and glucose deprivation in rat cortical neurons: involvement of mitogen-activated protein kinase pathway. *Neuroscience* **2011**, *183*, 203−211.

(16) He, Y.; Qu, S.; Wang, J.; He, X.; Lin, W.; Zhen, H.; Zhang, X. Neuroprotective effects of osthole pretreatment against traumatic brain injury in rats. *Brain Res.* **2012**, *1433*, 127−136.

(17) Hsu, S. C.; Lin, J. H.; Weng, S. W.; Chueh, F. S.; Yu, C. C.; Lu, K. W.; Wood, W. G.; Chung, J. G. Crude extract of Rheum palmatum inhibitsmigration and invasion of U-2 OS human osteosarcoma cells by suppression of matrix metalloproteinase-2 and -9. *BioMedicine* **2013**, *3*, 120−129.

(18) Way, T. D.; Huang, J. T.; Chou, C. H.; Huang, C. H.; Yang, M. H.; Ho, C. T. Emodin represses TWIST1-induced epithelial-mesenchymal transitions in head and neck squamous cell carcinoma cells by inhibiting the β-catenin and Akt pathways. *Eur. J. Cancer* **2014**, *50*, 366−378.

(19) Vincent-Salomon, A.; Thiery, J. P. Host microenvironment in breast cancer development: epithelial-mesenchymal transition in breast cancer development. *Breast Cancer Res.* **2003**, *5*, 101−106.

(20) Schlenska-Lange, A.; Knüpfer, H.; Lange, T. J.; Kiess, W.; Knüpfer, M. Cell proliferation and migration in glioblastoma multiforme cell lines are influenced by insulin like growth factor I in vitro. *Anticancer Res.* **2008**, *28*, 1055−1060.

(21) Yin, S.; Girnita, A.; Strömberg, T.; Khan, Z.; Andersson, S.; Zheng, H.; Ericsson, C.; Axelson, M.; Nistér, M.; Larsson, O.; Ekström, T. J.; Girnita, L. Targeting the insulin-like growth factor-1 receptor by picropodophyllin as a treatment option for glioblastoma. *Neuro-Oncology* **2010**, *12*, 19−27.

(22) Carapancea, M.; Cosaceanu, D.; Budiu, R.; Kwiecinska, A.; Tataranu, L.; Ciubotaru, V.; Alexandru, O.; Banita, M.; Pisoschi, C.; Bäcklund, M. L.; Lewensohn, R.; Dricu, A. Dual targeting of IGF-1R and PDGFR inhibits proliferation in high-grade gliomas cells and induces radiosensitivity in JNK-1 expressing cells. *J. Neurooncol.* **2007**, *85*, 245−254.

(23) Graham, T. R.; Zhau, H. E.; Odero-Marah, V. A.; Osunkoya, A. O.; Kimbro, K. S.; Tighiouart, M.; Liu, T.; Simons, J. W.; O'Regan, R. M. Insulin-like growth factor-I-dependent up-regulation of ZEB1 drives epithelial-to-mesenchymal transition in human prostate cancer cells. *Cancer Res.* **2008**, *68*, 2479−2488.

(24) Kim, H. J.; Litzenburger, B. C.; Cui, X.; Delgado, D. A.; Grabiner, B. C.; Lin, X.; Lewis, M. T.; Gottardis, M. M.; Wong, T. W.; Attar, R. M.; Carboni, J. M.; Lee, A. V. Constitutively active type I insulin-like growth factor receptor causes transformation and xenograft growth of immortalized mammary epithelial cells and is accompanied by an epithelial-to-mesenchymal transition mediated by NF-kappaB and snail. *Mol. Cell. Biol.* **2007**, *27*, 3165−3175.

(25) Praveen Kumar, V. R.; Sehgal, P.; Thota, B.; Patil, S.; Santosh, V.; Kondaiah, P. Insulin like growth factor binding protein 4 promotes GBM progression and regulates key factors involved in EMT and invasion. *J. Neurooncol.* **2014**, *116*, 455−464.

(26) Mikheeva, S. A.; Mikheev, A. M.; Petit, A.; Beyer, R.; Oxford, R. G.; Khorasani, L.; Maxwell, J. P.; Glackin, C. A.; Wakimoto, H.; González-Herrero, I.; Sánchez-García, I.; Silber, J. R.; Horner, P. J.; Rostomily, R. C. TWIST1 promotes invasion through mesenchymal change in human glioblastoma. *Mol. Cancer* **2010**, *9*, 194.

(27) Zhang, X.; Chen, T.; Zhang, J.; Mao, Q.; Li, S.; Xiong, W.; Qiu, Y.; Xie, Q.; Ge, J. Notch1 promotes glioma cell migration and invasion by stimulating β-catenin and NF-κB signaling via AKT activation. *Cancer Sci.* **2012**, *103*, 181−190.

(28) Buonato, J. M.; Lazzara, M. J. ERK1/2 Blockade Prevents Epithelial-Mesenchymal Transition in Lung Cancer Cells and Promotes Their Sensitivity to EGFR Inhibition. *Cancer Res.* **2014**, *74*, 309−319.

(29) Wang, Y.; Lin, Z.; Sun, L.; Fan, S.; Huang, Z.; Zhang, D.; Yang, Z.; Li, J.; Chen, W. Akt/Ezrin Tyr353/NF-κB pathway regulates EGF-induced EMT and metastasis in tongue squamous cell carcinoma. *Br. J. Cancer* **2014**, *110*, 695−705.

(30) Zhang, L.; Jiang, G.; Yao, F.; He, Y.; Liang, G.; Zhang, Y.; Hu, B.; Wu, Y.; Li, Y.; Liu, H. Growth inhibition and apoptosis induced by osthole, a natural coumarin, in hepatocellular carcinoma. *PLoS One* **2012**, *7*, e37865.

(31) Lin, V. C.; Chou, C. H.; Lin, Y. C.; Lin, J. N.; Yu, C. C.; Tang, C. H.; Lin, H. Y.; Way, T. D. Osthole suppresses fatty acid synthase expression in HER2-overexpressing breast cancer cells through modulating Akt/mTOR pathway. *J. Agric. Food Chem.* **2010**, *58*, 4786−4793.

(32) Ding, D.; Wei, S.; Song, Y.; Li, L.; Du, G.; Zhan, H.; Cao, Y. Osthole Exhibits Anti-Cancer Property in Rat Glioma Cells Through Inhibiting PI3K/Akt and MAPK Signaling Pathways. *Cell. Physiol. Biochem.* **2013**, *32*, 1751−1760.

(33) Xu, X.; Zhang, Y.; Qu, D.; Jiang, T.; Li, S. Osthole induces G2/M arrest and apoptosis in lung cancer A549 cells by modulating PI3K/Akt pathway. *J. Exp. Clin. Cancer Res.* **2011**, *30*, 33.

Table 1. Characterization and Proximate Composition of Atlantic Forest Fruit Pulps

fruit	pH	soluble solids (°Bx)	moisture (g/100g)	proteins[a] (g/100g)	lipids[a] (g/100g)	carbohydrates[a] (g/100g)	fibers[a] (g/100g)	ashes[a] (g/100g)	energetic values[a] (kcal/100g)
araça	4.3 ± 0.1	9.8 ± 0.1	85.5 ± 3.2	6.9 ± 0.1	1.4 ± 0.2	55.1 ± 3.4	31.0 ± 0.7	5.5 ± 0.2	260.7 ± 15.8
grumixama	4.2 ± 0.3	9.4 ± 0.1	90.8 ± 2.4	0.5 ± 0.1	n.d.[b]	82.6 ± 1.4	10.8 ± 0.5	5.4 ± 0.1	332.6 ± 8.7
jussara	5.6 ± 0.4	11.6 ± 0.1	88.7 ± 3.8	6.0 ± 0.3	29.2 ± 0.9	28.3 ± 3.5	28.3 ± 0.3	8.8 ± 0.8	400.0 ± 23.9
uvaia	3.7 ± 0.3	9.2 ± 0.2	91.0 ± 4.2	5.5 ± 0.8	2.2 ± 0.2	44.4 ± 5.5	42.2 ± 2.2	5.5 ± 0.9	213.3 ± 26.6

[a]Calculated values for dry basis. n = 3 samples. [b]n.d.: not detected.

ance liquid chromatography coupled to photodiode array and mass spectrometry detectors (HPLC-DAD-MS^n).

MATERIALS AND METHODS

Chemicals. HPLC-grade methanol, methyl *tert*-butyl ether (MTBE), acetonitrile, and formic acid were obtained from Merck (Darmstadt, Germany). The other reagents were all analytical grade and obtained from Labsynth (Diadema, Brazil). The samples and solvents were filtered through Millipore (Billerica, MA, USA) membranes (0.22 and 0.45 μm) before the HPLC analyses. The standards for all-*trans*-β-carotene (99.5%), all-*trans*-β-cryptoxanthin (99.0%), all-*trans*-lutein (98.0%), cyanidin 3-glucoside (98.9%), cyanidin 3-rutinoside (98.0%), and gallic acid (99%) were purchased from Sigma-Aldrich (Darmstadt, Germany). Standards of 9-*cis*- (99%), 13-*cis*- (98%), and 15-*cis*-β-carotene (97%) were provided by DSM Nutritional Products (Basel, Switzerland). The cyanidin 3-rhamnoside chloride (98%), cyanidin 3-sambubioside chloride (97%), and pelargonidin 3-glucoside chloride (98%) standards were obtained from Extrasynthése (Genay, France). The purity of these standards was determined by HPLC-DAD, and they were used as received.

Samples. The fruits were collected from the Atlantic Forest (Figure 1S). The samples of grumixama (*Eugenia brasiliensis* Lam.), jussara (*Euterpe edulis* Mart.), araça (*Psidium cattleianum* Sabine), and uvaia (*Eugenia pyriformis* Cambess) were obtained from Bello's farm, located in Paraibuna (latitude 23°23′10″ S and longitude 45°39′44″ W) in São Paulo State, Brazil. The fruits were harvested at ripe stage. They were part of batches sent to the fresh fruit market and were also used to obtain frozen pulp (farm produced). The fruits endured a selection and washing process before being pulped to remove any seeds or other inedible parts. The pulps were immediately frozen in farm and sent to the laboratory. The samples were stored at −40 °C until analysis. The harvest and sampling of the fruits were conducted between April and November of 2011. The fruit pulps were analyzed from a 3.0 kg single batch.

Characterization and Proximate Composition of Pulp. Each fruit pulp was thawed, homogenized, and characterized regarding pH and total soluble solids. The analyses of the moisture, protein (nitrogen conversion factor of 6.25 total protein), lipids, fiber, and ash contents were performed according to the official methods of AOAC.[16] The carbohydrate content of the samples was obtained using the difference between the total percentage of moisture, protein, lipids, fiber, and ash. The energy value was expressed in kcal/100 g and was calculated using the conversion factors of nutrients into energy (1 g of protein = 4 kcal, 1 g carbohydrate = 4 kcal, and 1 g of fat = 9 kcal). All analyses were performed in triplicate.

HPLC-DAD-MS^n Analysis of the Carotenoids, Anthocyanins, and Other Phenolic Compounds. The carotenoids, anthocyanins, and phenolic compounds were determined with a Shimadzu HPLC (Kyoto, Japan) equipped with quaternary pumps (model LC-20AD), a DAD detector (Shimadzu, model SPD-M20A), a degasser unit (DGU-20A5), and a Rheodyne injection valve with a 20 μL loop. The equipment was also connected in series to a mass spectrometer (Esquire 4000 model) from Bruker Daltonics (Bremen, Germany) with an ion-trap analyzer (MS^n), as well as APCI (atmospheric pressure chemical ionization) and ESI (electrospray ionization) sources.

The carotenoids were exhaustively extracted with acetone from 15 g of fruit pulp and transferred to petroleum ether/diethyl ether (2:1); the solution was saponified overnight at room temperature with 10% methanolic KOH, washed until alkali free, and concentrated to dryness.[17,18] The experimental conditions for the separation, identification, and quantification by HPLC-DAD-APCI-MS^2 were the same as previously described.[17]

The following parameters were utilized to identify the carotenoids: elution order on a C_{30} reversed phase column, cochromatography with standards, UV/visible spectral features (λ_{max}, spectral fine structure (%III/II), and *cis* peak intensity (%A_B/A_{II})), and MS spectrum characteristics compared to standards analyzed under the same conditions and data available in the literature.[18−21] In addition, the protonated molecule ($[M + H]^+$) was assigned and confirmed using second-order MS fragmentation. The carotenoids were quantified by HPLC-DAD using five-point analytical curves of all-*trans*-lutein (1.0−50.0 μg/mL), all-*trans*-β-cryptoxanthin (1.0−60 μg/mL), and all-*trans*-β-carotene (1.0−50 μg/mL). The limit of detection (LOD) was calculated using the parameters of each standard curve: LOD = 3.3 × SD/S, where SD is the standard deviation of the response and S is the slope of the curve. For the three analytical curves of carotenoids, R^2 = 0.99, the limit of detection was 0.1 μg/mL, and the limit of quantification was 0.5 μg/mL. The carotenoid concentration was expressed in μg/100 g of fresh matter (f.m.). All analyses were performed in triplicate.

The anthocyanins were extracted from the grumixama and jussara pulps (20 g) using 100 mL of 0.5% HCl in methanol overnight at 5 °C under darkness. The slurry was filtered, and the solids were washed with an additional 100 mL of 0.5% HCl in methanol at room temperature three times. The acidic methanol extracts were combined and concentrated in a rotary evaporator (T < 38 °C) to yield the crude extract. The crude extract was diluted with water containing 5% formic acid/methanol (85:15, v/v) immediately before analysis by HPLC-DAD-MS^2. The anthocyanin separation was carried out as previously described.[22]

The anthocyanins were identified based on the combined information provided by elution order in the C_{18} reversed phase column and cochromatography with standards, as well as UV−visible and mass spectra in comparison with the literature data.[22−25] The anthocyanins were quantified using the percentage of the area obtained during the HPLC-DAD-ESI-MS^2 analysis and the monomeric anthocyanin content. The monomeric anthocyanin content was evaluated using the pH-differential method, as described by Lee et al.[26] The concentration was expressed in mg cyanidin 3-glucoside/100 g fresh matter or mg cyanidin 3-rutinoside/100 g fresh matter according to the major anthocyanin identified. All analyses were performed in triplicate.

The other phenolic compounds were extracted from 20 g of frozen pulp with 100 mL of methanol/water (8:2 v/v) by agitation provided by a magnetic homogenizer (Tecnal, Piracicaba, Brazil) for 20 min. The slurry was filtered, and the solids were washed with an additional 50 mL of methanol/water (8:2) two times more and concentrated in a rotary evaporator (T < 38 °C) until methanol evaporation. The extract was used to determine the phenolic compounds by HPLC-DAD-ESI-MS^n, as previously described.[27] The phenolic compounds were tentatively identified based on the following information: elution order, retention time, and UV−visible and mass spectral features compared to those of the standards analyzed under the same conditions and the available literature data.[27−29] The phenolic compounds were quantified using a seven-point analytical curve of gallic acid (0.5−60 mg/mL). The analytical curve was linear (r^2 = 0.99); the limit of detection was 0.2 μg/mL, and the limit of

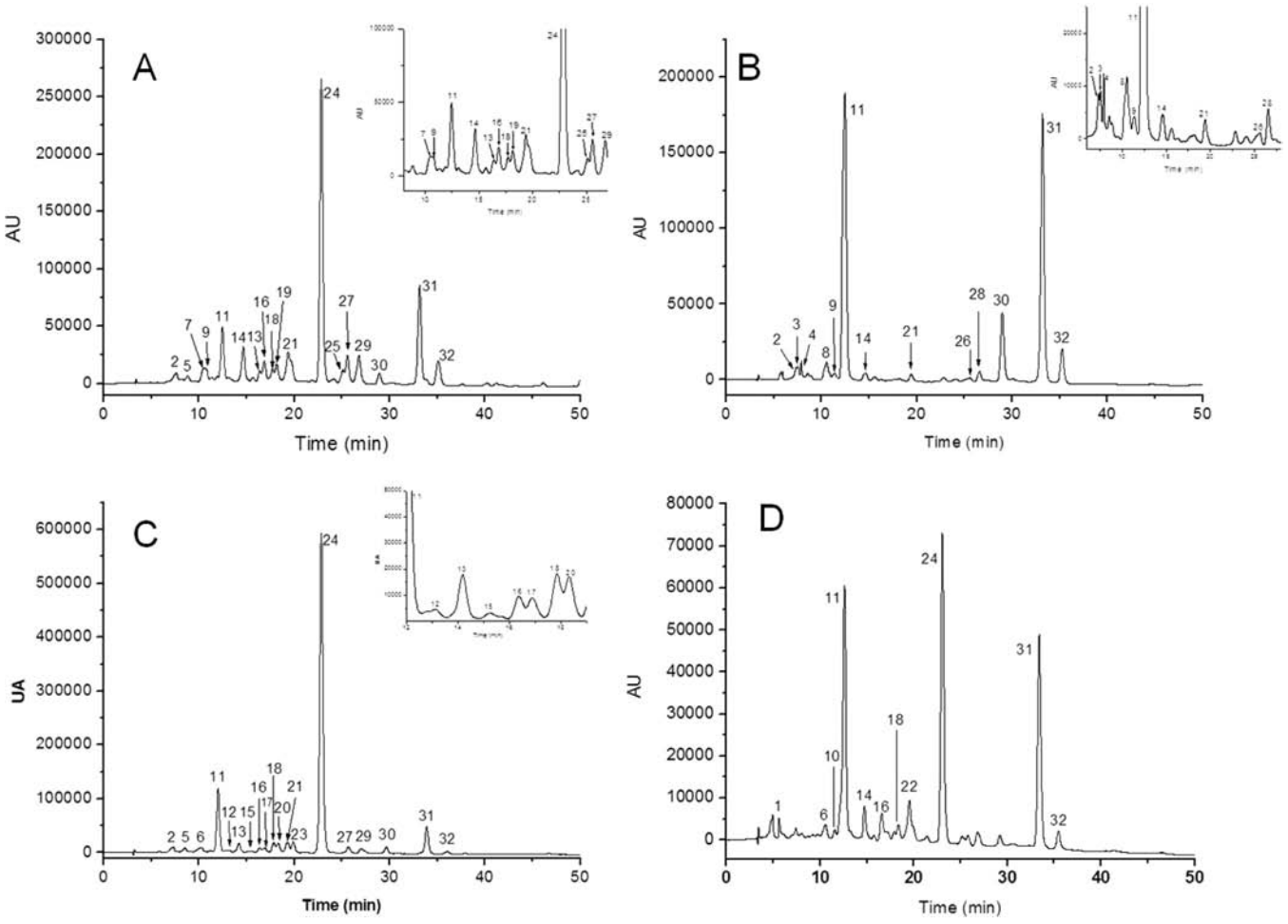

Figure 1. Chromatogram, obtained by HPLC-PDA-MS/MS, of the carotenoids from Atlantic Forest fruits: (A) uvaia, (B) jussara, (C) grumixama, and (D) araça. Chromatographic conditions: see text. Peak identification and characterization are given in Table 2. Processed at 450 nm.

quantification was 0.5 μg/mL as calculated using the parameters of the analytical curves (standard deviation and the slope). All analyses were performed in triplicate.

Statistical Analysis. The mean and standard deviation results related to the proximate composition and carotenoid and phenolic compound levels were calculated using the Microcal Origin 5.0 software.

RESULTS AND DISCUSSION

Characterization and Proximate Composition of the Fruit Pulp. The jussara fruit pulp had the highest pH (Table 1) and showed characteristics and chemical compositions similar to those of the established standards of identity and quality of açai.[30] Using the parameters of the Brazilian legislation, we might classify jussara as medium (type B) because the soluble solid content was between 11 and 14 degrees Brix. The levels of proteins, lipids, and carbohydrates of jussara, by dry weight, are consistent with the established legislation for açai pulp[30] (6.0 g protein/100 g; 20−60 g lipid/100 and 40 g total carbohydrates/100 g) since there is no current legislative regulation for jussara pulp. Moreover, our results show that the proximate composition of jussara from the state of São Paulo falls into the range of jussara samples obtained from five different regions in the state of Santa Catarina, Brazil.[11] However, the differences observed over the chemical composition of the pulp demonstrate that even jussara, which is native to the Atlantic Forest, is influenced by the soil, temperature, sunlight, and precipitation in the geographic location where the palms are grown.

The pulps under study were obtained from exotic fruits that have no current legislative regulation in Brazil, and only a few data for some fruits are available in the literature. The protein content of uvaia collected in the state of Rio Grande do Sul,[31] Brazil, was approximately 2.9 times higher than that measured in the present study, whereas soluble solid content (7.7°Bx)[11] was slightly lower than our results. In addition, the high fiber contents of these fruits are worth highlighting, particularly those from araça and jussara, because the consumption of a 100 g portion of fresh pulp of either fruit provides approximately 20% of the recommended daily intake of fiber, based on a 2000 kcal diet.

Carotenoid Composition. Figure 1 shows the chromatograms of the carotenoids from the four Atlantic Forest fruit pulps. The carotenoids separated from the jussara, grumixama, araça, and uvaia pulps were identified based on the combined information obtained from the chromatographic elution and UV−visible and mass spectral data (Table 2). Considering that a detailed description of carotenoid identification has already been reported,[18,22] only the most important aspects are discussed below.

As expected for the reversed phase columns, polar carotenoids with three and two hydroxyl groups, such as 9-*cis*-neoxanthin (peak 2) and all-*trans*-lutein (peak 11), eluted

Table 2. Chromatographic, UV−Vis, and Mass Spectroscopy Characteristics of Carotenoids from Atlantic Forest Fruit, Obtained from HPLC-DAD-MS/MS

peak[a]	carotenoid[b]	t_R (min)	λ_{max} (nm)[c]	% III/II	% A_B/II	$[M + H]^+$ (m/z)	MS/MS (m/z)
1	apocarotenoid	6.1	441	0	0	n.d.[d]	n.d.
2	9-*cis*-neoxanthin	7.3	327, 415, 438, 468	87	24	601	583, 565, 547, 509, 491, 221
3	mixture	7.6	327, 415, 438, 468	80	21	601	583, 565, 547, 509, 491, 221
4	13-*cis*-violaxanthin	7.9	326, 412, 435, 463	83	23	601	583, 565, 509, 491, 221
5	*all-trans*-neochrome	8.5	399, 421, 447	71	0	601	583, 565, 221
6	mixture	10.2	328, 402, 425, 447	33	50	585	n.d.
7	*cis*-antheraxanthin	10.5	328, 418, 440, 466	68	23	585	567, 549, 493, 221
8	*cis*-lutein	10.5	353, 328, 438, 464	53	34	569	551
9	9-*cis*-violaxanthin	11.4	328, 415, 435, 461	83	35	601	583, 565, 509, 491, 221
10	mixture	12.1	420, 445, 472	67	0	601	n.d.
11	*all-trans*-lutein	12.3	420, 444, 472	57	0	569	551, 533, 477, 459
12	mixture	13.1	402, 427, 448	n.c.[e]	n.c.	545	n.d.
13	5,6-epoxy-β-cryptoxanthin	14.2	421, 448, 474	40	0	569	551, 459, 221
14	*all-trans*-zeaxanthin	14.6	427, 450, 475	30	0	569	551, 533, 463
15	*cis*-lutein	15.2	353, 418, 439, 466	50	n.c.	n.d.	n.d.
16	5,8-epoxy-β-cryptoxanthin	16.3	401, 426, 453	75	0	569	551, 459, 221
17	15-*cis*-β-cryptoxanthin	16.9	335, 422, 447, 470	33	57	553	535, 495, 461
18	13-*cis*-β-cryptoxanthin or 13'-cis-β-cryptoxanthin	17.8	338, 418, 444, 470	23	50	553	535, 495, 461
19	phytoene	18.1	276, 286, 300	0	0	545	489, 435, 339
20	13-*cis*-β-cryptoxanthin or	18.3	336, 420, 444, 469	17	51	553	535, 495, 461
21	*all-trans*-zeinoxanthin	19.3	421, 447, 471	20	0	553	535, 495, 443
22	*all-trans*-α-cryptoxanthin	19.4	420, 444, 472	50	0	553	535, 461
23	not identified	19.9	405, 427, 452	50	0	569	551, 221
24	*all-trans*-β-cryptoxanthin	22.8	421, 450, 477	22	0	553	535, 497, 461
25	5,8-epoxy-β-carotene	25.1	408, 427, 452	66	0	553	535, 461, 205
26	15-*cis*-β-carotene	25.6	337, 420, 448, 471	15	61	537	444
27	9-*cis*-β-cryptoxanthin or 9'-cis-β-cryptoxanthin	25.7	339, 419, 446, 471	40	14	553	535, 497, 461
28	13-*cis*-β-carotene	26.5	335, 420, 444, 471	20	44	537	444
29	9-*cis*-β-cryptoxanthin or 9'-cis-β-cryptoxanthin	27.0	339, 420, 446, 471	37	17	553	535, 497, 461
30	*all-trans*-α-carotene	29.7	420, 445, 472	60	0	537	481, 444
31	*all-trans*-β-carotene	33.9	425, 451, 478	25	0	537	444
32	9-*cis*-β-carotene	36.0	338, 421, 447, 471	66	18	537	444

[a]Numbered according to the chromatograms shown in Figure 1. [b]Tentative identification based on UV−vis and mass spectra as well as relative HPLC retention times and published data. [c]Linear gradient of methanol/MTBE. [d]n.d.: not detected. [e]n.c.: not calculated.

before the monohydroxy carotenoids (all-*trans*-β-cryptoxanthin, peak 24). The carotenes, including the all-*trans*-α-carotene (peak 30) and all-*trans*-β-carotene (peak 31), were the last to elute under these conditions. The carotenoids with 5,6-epoxide and/or 5,8-furanoid groups located on the 3- or 3′-hydroxy β-rings, 9-*cis*-neoxanthin (peak 2), 13-*cis*-violaxanthin (peak 4), and 9-*cis*-violaxanthin (peak 9) showed UV−vis and mass spectra features similar to those reported in the literature.[18−21]

Although the all-*trans*-lutein (peak 11) and all-*trans*-zeaxanthin (peak 14) have the same chemical formula ($C_{40}H_{56}O_2$) and therefore identical protonated molecule $[M + H]^+$ at m/z 569, zeaxanthin possesses two β-rings, while lutein has one β-ring and one ε-ring. Therefore, one of the lutein hydroxyl groups is allylic to the double bond in the ε-ring and not conjugated with the polyene chain, resulting in 10 conjugated double bonds (c.d.b.). However, zeaxanthin has both double bonds in the β-ring conjugated to the polyene chain; consequently, its chromophore displays 11 c.d.b. Therefore, it is possible to distinguish these two compounds using their UV−visible and mass spectra. As expected, zeaxanthin showed λ_{max} values (427, 450, 475 nm) higher than those of lutein (420, 444, 472 nm). The mass spectrum of zeaxanthin showed a more intense protonated molecule peak ($[M + H]^+$) at m/z 569 compared to the fragment at m/z 551 $[M + H - 18]^+$, while the opposite was observed for lutein.[18,21,22]

Peak 24 was identified as all-*trans*-β-cryptoxanthin; the protonated molecule was detected at m/z 553 along with less intense fragments at m/z 535 $[M + H - 18]^+$ and 461 $[M + H - 92]^+$, generated from the loss of a hydroxyl group and toluene, respectively. The isomers 15-*cis*-β-cryptoxanthin (peak 17), 13- or 13′-*cis*-β-cryptoxanthin (peaks 18 and 20), and 9- or 9′-*cis*-β-cryptoxanthin (peaks 27 and 29) were tentatively identified by comparing their elution order and UV−vis characteristics with the literature data.[22] The fine spectral structure (%III/II) decreases and the intensity of the *cis*-peak (%A_B/A_{II}) increases as the *cis*-double bond gets closer to the center of the molecule. However, it was not possible to differentiate between the 13-*cis* and 13′-*cis* or between the 9-*cis* and 9′-*cis* isomers of β-cryptoxanthin because there are no data available in the literature reporting their elution order on a C_{30} column after assignment of the *cis*-double bond positions in the β-cryptoxanthin structure using nuclear magnetic resonance. All-*trans*-β-carotene (peak 31) and its *cis* isomers (15-*cis*- (peak 26), 13-*cis*- (peak 28), and 9-*cis*-β-carotene (peak 32)) were confirmed via coelution with authentic standards, as well as comparison of the UV−vis and mass spectral features with standards and literature data.[18,21,22]

dx.doi.org/10.1021/jf501211p | J. Agric. Food Chem. 2014, 62, 5072−5084

Table 3. Content of Carotenoids from Four Atlantic Forest Fruits

		concentration (μg/100 g fresh weight)[a]			
peak	carotenoid	grumixama	jussara	araça	uvaia
1	apocarotenoid	n.d.	n.d	1.9 ± 0.01	n.d.
2	9-*cis*-neoxanthin[b]	14.7 ± 8.6	13.2 ± 4.2	n.d.	22.8 ± 0.3
3	mixture[b]	n.d.	4.4 ± 2.9	n.d.	n.d.
4	13-*cis*-violaxanthin[b]	n.d.	6.5 ± 4.3	n.d.	n.d.
5	*all-trans*-neochrome[b]	3.2 ± 1.8	n.d.	n.d.	11.7 ± 1.8
6	mixture[b]	7.3 ± 2.0	n.d.	0.6 ± 0.1	n.d.
7	*cis*-antheraxanthin[b]	n.d.	n.d.	n.d.	22.1 ± 1.8
8	*cis*-lutein[b]	n.d.	12.6 ± 1.3	n.d.	n.d.
9	9-*cis*-violaxanthin[b]	n.d.	5.5 ± 0.4	n.d.	19.4 ± 7.6
10	mixture[b]	n.d.	n.d.	0.7 ± 0.1	n.d.
11	*all-trans*-lutein[b]	55.5 ± 12.89	292.7 ± 3.3	15.7 ± 3.8	86.0 ± 7.8
12	mixture[c]	1.1 ± 1.0	n.d.	n.d.	n.d.
13	5,6-epoxy-β-cryptoxanthin[c]	13.6 ± 1.1	n.d.	n.d.	24.3 ± 1.1
14	all-*trans*-zeaxanthin[c]	n.d.	5.4 ± 2.4	1.7 ± 0.4	56.0 ± 4.4
15	*cis*-lutein[b]	0.2 ± 0.01	n.d.	n.d.	n.d.
16	5,8-epoxyi-β-cryptoxanthin[c]	9.3 ± 1.6	n.d.	3.5 ± 0.9	36.5 ± 5.4
17	15-*cis*-β-cryptoxanthin[c]	14.4 ± 8.7	n.d.	n.d.	n.d.
18	13-*cis*-β-cryptoxanthin[c] or 13′-*cis*-β-cryptoxanthin[c]	26.8 ± 2.4	n.d.	n.d.	22.8 ± 2.4
19	phytoene[d]	n.d.	n.d.	0.6 ± 0.1	5.9 ± 0.5
20	13-*cis*-β-cryptoxanthin[c] or 13′-*cis*-β-cryptoxanthin[c]	9.5 ± 4.1	n.d	n.d	n.d
21	*all-trans*-zeinoxanthin[c]	7.4 ± 5.5	7.7 ± 0.4	n.d	78.4 ± 5.9
22	*all-trans*-α-cryptoxanthin[c]	n.d.	n.d.	3.6 ± 1.0	n.d.
23	not identified[c]	11.6 ± 1.3	n.d.	n.d.	n.d.
24	*all-trans*-β-cryptoxanthin[c]	286.7 ± 123.3	n.d.	26.4 ± 1.9	521.1 ± 18.6
25	5,8-epoxy-β-carotene[d]	n.d.	n.d.	n.d.	32.9 ± 1.9
26	15-*cis*-β-carotene[d]	n.d.	9.2 ± 0.3	n.d.	n.d.
27	9-*cis*-β-cryptoxanthin[c] or 9′-*cis*-β-cryptoxanthin[c]	7.1 ± 2.6	n.d.	n.d.	57.9 ± 1.3
28	13-*cis*-β-carotene[d]	n.d.	15.8 ± 1.9	n.d.	n.d.
29	9-*cis*-β-cryptoxanthin[c] or 9′-*cis*-β-cryptoxanthin[c]	6.2 ± 2.5	n.d.	n.d.	68.1 ± 0.01
30	*all-trans*-α-carotene[d]	4.2 ± 1.3	60.2 ± 6.0	n.d.	14.2 ± 1.2
31	*all-trans*-β-carotene[d]	31.1 ± 15.8	266.5 ± 41.5	20.0 ± 4.6	170.9 ± 11.3
32	9-*cis*-β-carotene[d]	5.3 ± 0.3	37.8 ± 3.5	3.0 ± 2.9	56.5 ± 3.0
	total carotenoids	515.2 ± 195.8	737.5 ± 72.8	77.7 ± 15.7	1306.6 ± 73.3
	vitamin A value (μg RAE/100 g)[e]	18.4 ± 7.7	27.8 ± 4.0	3.2 ± 0.7	53.6 ± 2.3

[a] n = 3 samples. n.d.: not detected. [b] The peaks were quantified as equivalent to all-*trans*-lutein. [c] The peaks were quantified as equivalent to all-*trans*-β-cryptoxanthin. [d] The peaks were quantified as equivalent to all-*trans*-β-carotene. [e] RAE: retinol activity equivalent.

According to Table 3, the total carotenoid content was highest in uvaia, followed by jussara and grumixama, and finally araça. The HPLC chromatogram separating the 18 carotenoids from uvaia is shown in Figure 1A. The all-*trans*-β-cryptoxanthin was the major carotenoid, representing 40% (m/m) of the total carotenoids content in this fruit pulp, followed by all-*trans*-β-carotene, which contributed 13% (m/m), in agreement with those reported in the literature for uvaia harvested in Rio Grande do Sul (South Brazil).[31] The levels of total carotenoids found in this study were lower than those previously reported (1700 μg/100 g fresh weight[32] for uvaia collected in Ceará (northwest region of Brazil)).

A typical HPLC-DAD chromatogram depicting the carotenoids from jussara is presented in Figure 1B, demonstrating the separation of 13 carotenoids on the C_{30} column. All-*trans*-lutein was the major carotenoid (39%, m/m) followed by all-*trans*-β-carotene (36%, m/m). The total carotenoid content found in the present study (737.5 μg/100 g) was 2.6 times lower than that found previously in jussara (1900 μg/100 g fresh matter) collected in Santa Catarina (South Brazil).[32] As far as we are concerned, this is the first report on the carotenoid profile of jussara.

Figure 1C shows the chromatogram of the carotenoids from grumixama, with 19 separated carotenoids, the principal ones being all-*trans*-β-cryptoxanthin (56%, m/m) and all-*trans*-lutein (11%). Studies regarding the carotenoid composition in grumixama were not found in the literature.

As observed in Figure 1D, 11 carotenoids from araça were separated on a C_{30} column, and nine were identified. The all-*trans*-β-cryptoxanthin was the major carotenoid, representing 34% of the total carotenoid content in this fruit, followed by all-*trans*-β-carotene and all-*trans*-lutein, corresponding to 26% and 20% of the total content, respectively. The other six minor carotenoids identified corresponded to 18.4% of the total content. This is the first report of the carotenoid composition of araça using mass spectrometry. In another study lutein has

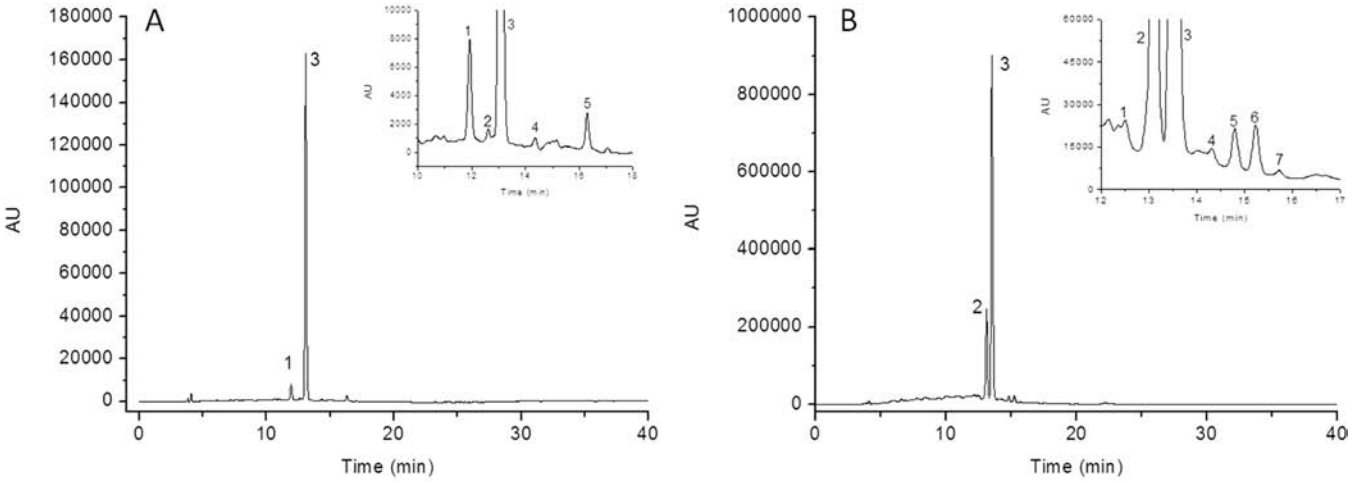

Figure 2. Chromatogram, obtained by HPLC-PDA-MS, of the anthocyanins from Atlantic Forest fruits: (A) grumixama and (B) jussara. Chromatographic conditions: see text. Peak identification and characterization are given in Table 4. Processed at 520 nm.

Table 4. Chromatographic and Spectroscopic Characteristics and Composition of Anthocyanins from Grumixama and Jussara, Obtained by HPLC-DAD-MS/MS

peak[a]	t_R (min)	λ_{max} (nm)[b]	$[M]^+$ (m/z)	MS/MS (m/z)	compound	concentration[c] (mg C3G/100 g)
Grumixama (*Eugenia brasiliensis*)						
1	11.9	228, 526	465	303 $[M + H - 162]^+$	delphinidin 3-glucoside	0.10 ± 0.01
2	12.6	270, 508	449	287 $[M + H - 162]^+$	cyanidin 3-galactoside	0.01 ± 0.001
3	13.1	280, 520	449	287 $[M + H - 162]^+$	cyanidin 3-glucoside	2.73 ± 0.02
4	14.3	271, 520	n.d.[d]	n.d.	n.i.[e]	0.01 ± 0.001
5	16.3	270, 518	491	287 $[M + H - 204]^+$	cyanidin 3-acetyl-hexoside	0.05 ± 0.004
monomeric anthocyanins (mg C3G/100 g)						2.90 ± 0.1
Jussara (*Euterpe edulis*)						
1	12.6	279, 521	581	449 $[M + H - 132]^+$, 287 $[M + H - 132 - 162]^+$	cyanidin 3,5-hexose pentose	1.43 ± 0.05
2	13.1	280, 520	449	287 $[M + H - 162]^+$	cyanidin 3-glucoside	47.93 ± 1.52
3	13.5	280, 522	595	449 $[M + H - 146]^+$, 287 $[M + H - 146 - 162]^+$	cyanidin 3-rutinoside	179.60 ± 5.77
4	14.5	278, 515	433	271 $[M + H - 162]^+$	pelargonidin 3-glucoside	1.66 ± 0.05
5	14.8	280, 509	579	433 $[M + H - 146]^+$, 271 $[M + H - 146 - 162]^+$	pelargonidin 3-rutinoside	2.87 ± 0.09
6	15.2	278, 522	609	463 $[M + H - 146]^+$, 301 $[M + H - 146 - 162]^+$	peonidin 3-rutinoside	3.59 ± 0.11
7	15.7	294, 524	433	287 $[M + H - 146]^+$	cyanidin 3-rhamnoside	0.30 ± 0.01
monomeric anthocyanins (mg C3R/100 g)						239.16 ± 7.6

[a]Peaks numbered according to Figure 2. [b]Linear gradient of water 5% v/v formic acid/methanol. C3G, cyanidin 3-glucoside; C3R, cyanidin 3-rutinoside. [c]Calculated using the percentage of the area and the content of monomeric anthocyanins. [d]n.d.: not detected. [e] n.i.: not identified.

been identified as the major carotenoid in araça (26.38 μg/g dry bases),[31] using only HPLC-DAD.

According to the classifications of good sources of carotenoids (low: 0−100 μg/100 g; moderate: 100−500 μg/100; high: 500−2000 μg/100 g; and very high: >2000 μg/100 g) proposed by Britton and Khachik,[33] uvaia and grumixama are high sources of carotenoids, particularly of β-cryptoxanthin (all-*trans* + *cis* isomers), while jussara is a moderate source of all-*trans*-lutein. However, araça is not a good source of carotenoids. Among the Atlantic Forest fruits evaluated in this study, the provitamin A activity value was higher in uvaia and jussara (Table 3). However, none of the fruits studied can be considered a good source of provitamin A compared with the Amazonian fruits[18] and acerola cultivar Olivier.[17]

Anthocyanin Composition. A typical chromatogram of the anthocyanins from grumixama is shown in Figure 2A, and their characteristics are presented in Table 4. The analysis performed by HPLC-DAD-MS/MS separated five anthocyanins. Peak 1 was identified as delphinidin 3-glucoside. This anthocyanin had a molecular ion at m/z 465 and a 303 u fragment related to the loss of a hexose; the identity of the hexose was assumed to be glucose according to the elution order.[24,25] Peaks 2 and 3 were identified as cyanidin 3-galactoside and cyanidin 3-glucoside, respectively. Both anthocyanins have a molecular ion at m/z 449 and a fragment at m/z 287 that is related to the loss of a hexose. This identification was confirmed using the elution order[24] and the coelution of peak 3 with a cyanidin 3-glucoside standard. The molecular ion and MS/MS fragments were not detected in peak 4, and thus this peak was not identified. Peak 5 exhibited a molecular ion at m/z 491, and in the MS/MS data, only a 287 u fragment ion was detected, indicating the presence of cyanidin after the loss of either an acetyl hexose or an oxalyl pentose moiety (204 u). Considering the occurrence of acylated anthocyanins in foods,[24,25] peak 5 was tentatively identified as cyanidin (acetyl)hexoside.

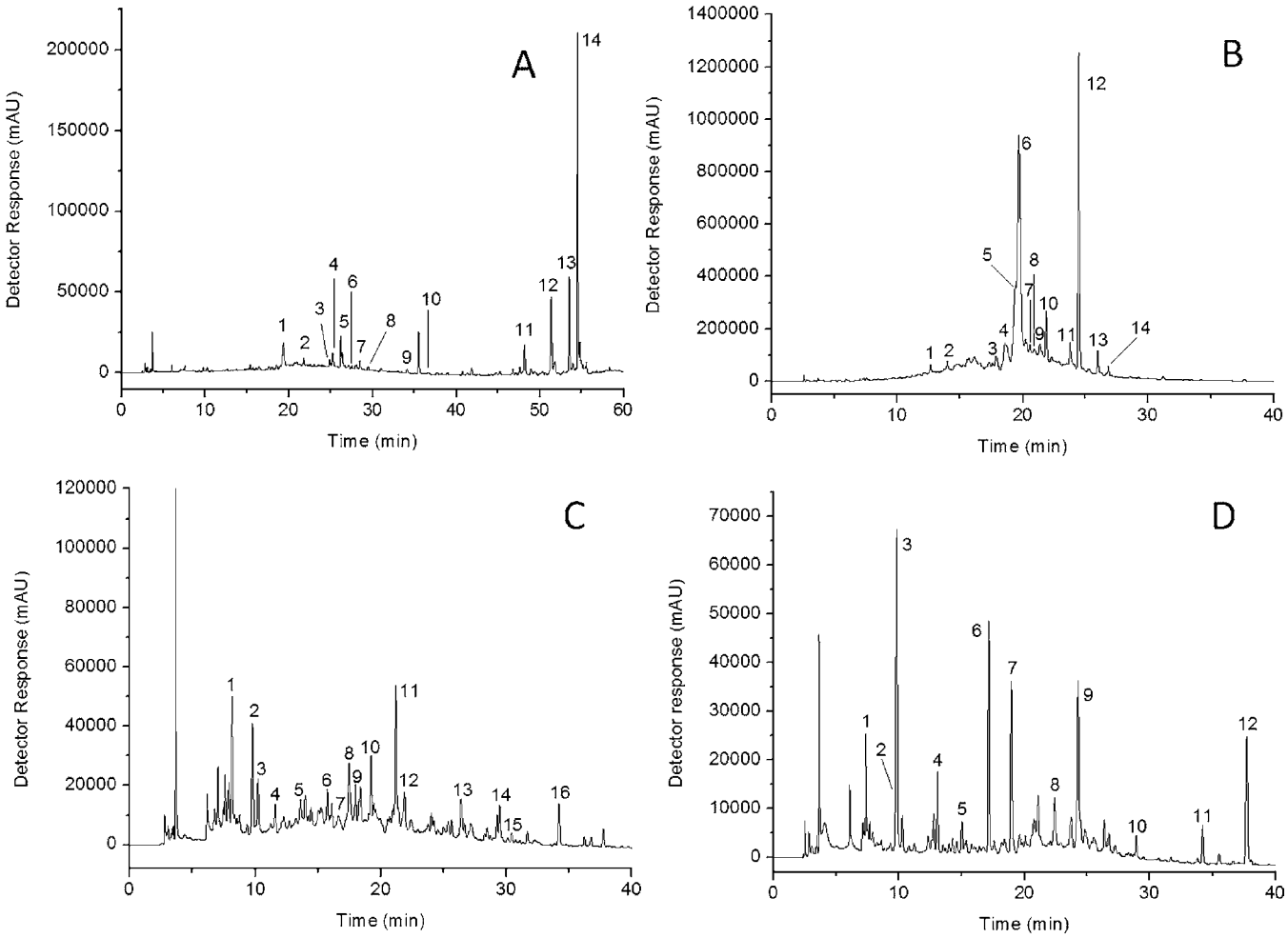

Figure 3. Chromatogram, obtained by HPLC-PDA-MS, of the phenolic compounds from Atlantic Forest fruits: (A) grumixama, (B) jussara, (C) araça, and (D) uvaia. Chromatographic conditions: see text. Peak identification and characterization are given in Tables 5 and 6. Processed at 280 nm.

The major anthocyanins found in grumixama were cyanidin 3-glucoside (94%) and delphinidin 3-glucoside (3.5%); the other anthocyanins (peaks 2, 4, and 5) were detected in amounts below 1.5%. These two major anthocyanins and cyanidin 3-galactoside are coincident with those reported in the literature;[13] however, cyanidin 3-acetylhexoside was not found by Flores et al.[13] and is therefore reported in grumixama for the first time. Cyanidin 3-arabinoside, delphinidin 3-pentoside, cyanidin 3-xiloside, malvidin 3-glucoside, and anthocyanidins delphinidin and cyanidin were detected in small amounts in grumixama by Flores et al.[13] but were not found in the present study. The monomeric anthocyanin level found in the present study was lower than that reported by Haminiuk et al.[14] for grumixama fruits collected in Brazil (266.34 ± 2.92 mg C3G/100 g).

The typical chromatogram of jussara shows the separation of seven anthocyanins (Figure 2B), and their characteristics are presented in Table 4. Peak 1 had a molecular ion peak at m/z 581, and two mass fragments were detected: one at m/z 449 related to the loss of one molecule of pentose ($[M - 132]^+$) and another at m/z 287 generated by elimination of one molecule of pentose plus one hexose ($[M - 132 - 162]^+$), furnishing a cyanidin aglycone with 287 u. Due to the presence of the fragment with 449 u, anthocyanin 1 was characterized as cyanidin 3,5-diglycosilated with a hexose and a pentose as the monosaccharides. However, the exact position of these two sugars could not be determined by MS. The identification as cyanidin 3-sambubioside could be excluded because two MS/MS fragments at m/z 287 and 449 were detected.[23]

In the mass spectrum of peak 2, the molecular ion was observed at m/z 449 with a fragment ion with 287 u ($[M - 162]^+$) by second-order MS, corresponding to the cyanidin moiety after hexose loss (162 u). The sugar moiety was confirmed to be glucose by coelution of peak 2 with the cyanidin 3-glucoside standard. Peak 3 showed a molecular ion at m/z 595 and two mass fragments with 287 and 449 u; the first corresponded to the cyanidin moiety after rutinose loss (308 u), and the fragment at m/z 449 resulted from the loss of deoxyhexose $[M - 146]^+$. The only disaccharide that showed fragmentation by MS/MS due to cleavage of the glycosidic bonds between the monosaccharides is rutinose, as previously described in the literature.[23−25] Cyanidin 3-rutinoside was definitively identified by coelution with a standard.

The mass spectrum of peak 4 showed a molecular ion at m/z 433 and an MS/MS fragment at m/z 271, corresponding to pelargonidin after the loss of a hexose. The identification of this anthocyanin was confirmed as pelargonidin 3-glucoside by coeluting peak 4 with the pelargonidin 3-glucoside standard. Peaks 5 and 6 were identified as pelargonidin 3-rutinoside and peonidin 3-rutinoside, respectively. The mass spectra of both

dx.doi.org/10.1021/jf501211p | J. Agric. Food Chem. 2014, 62, 5072−5084

Table 5. Chromatographic and Spectroscopic Characteristics and Content of Phenolic Compounds from Grumixama and Jussara, Obtained from HPLC-DAD-ESI-MS/MS

peak	t_R[a] (min)	phenolic compound[b]	λ_{max}[c] (nm)	$[M-H]^-$ (m/z)	MS/MS (m/z)	concentration[d] (mg GAE/100 g)
Grumixama						
1	19.3	cyanidin 3-glucoside	279, 518	447	285 $[M-H-162]^-$	5.0 ± 0.2
2	21.8	quercetin glucorunide	360	477	301 $[M-H-176]^-$	1.3 ± 0.04
3	24.8	quercetin galloyl-hexoside	360	615	463 $[M-H-152]^-$, 301 $[M-H-152-162]^-$	1.6 ± 0.02
4	25.2	quercetin deoxy-hexoside	361	447	301 $[M-H-146]^-$	1.2 ± 0.04
5	26.2	quercetin hexoside	355	463	301 $[M-H-162]^-$	6.7 ± 0.4
6	27.5	quercetin pentoside	353	433	301 $[M-H-132]^-$	2.8 ± 0.9
7	28.4	quercetin pentoside	352	433	301 $[M-H-132]^-$	6.6 ± 0.9
8	29.4	eriodictyol hexoside	285, 360	449	287 $[M-H-162]^-$, 151	0.8 ± 0.04
9	34.1	quercetin deoxyhexosyl-hexoside	353	609	463 $[M-H-146]^-$, 301$[M-H-162]^-$	1.4 ± 0.02
10	36.6	quercetin	365	301	273 $[M-H-28]^-$, 257 $[M-H-44]^-$, 229, 179, 151	10.7 ± 1.1
11	48.2	synapic acid dihexoside hydroxy benzoyl	277, 340	685	667 $[M-H-18]^-$, 461 $[M-H-224]^-$, 299 $[M-H-224-162]^-$, 137 $[M-H-224-162-162]^-$	7.2 ± 0.3
12	51.4	not identified	280, 335	699	681 $[M-H-18]^-$, 461 $[M-H-18-220]^-$, 299 $[M-H-18-220-162]^-$, 137 $[M-H-18-220-162-162]^-$	17.6 ± 1.0
13	53.5	gallic acid dihexoside sinapoyl	280, 330	699	493 $[M-H-206]^-$, 331 $[M-H-206-162]^-$, 169 $[M-H-206-162-162]^-$	19.6 ± 1.1
14	54.5	sinapic acid dihexoside benzoyl	282, 335	651	633 $[M-H-18]^-$, 427 $[M-H-224]^-$, 265 $[M-H-224-162]^-$, 103 $[M-H-224-162-162]^-$	62.8 ± 2.5
total phenolic						145.2 ± 8.6
Jussara						
1	12.6	gallic acid hexoside	280	331	169 $[M-H-162]^-$	1.7 ± 0.04
2	14.0	not identified	281	359	197 $[M-H-162]^-$	8.8 ± 0.4
3	17.8	apigenin dihexoside	279, 323	593	417 $[M-H-162]^-$, 269 $[M-H-162]^-$	11.06 ± 0.9
4	18.6	luteolin deoxyhexosyl-hexoside	281, 310	593	285 $[M-H-308]^-$	37.6 ± 1.9
5	19.4	cyanidin 3-glucoside	280, 517	447	285 $[M-H-162]^-$	51.4 ± 3.1
6	19.7	cyanidina 3-rutinoside	280, 518	593	575, 467, 299, 285 $[M-H-308]^-$	141.0 ± 8.5
7	20.6	apigenin hexoside	279, 325	431	269 $[M-H-162]^-$, 253, 225	13.2 ± 1.0
8	20.9	apigenin deoxyhexoside-hexoside	280, 328	577	269$[M-308]^-$, 253, 225	25.4 ± 1.5
9	21.3	chrysoeriol deoxyhexosyl-hexoside	280, 320	607	299 $[M-H-308]^-$, 285, 255, 239	22.5 ± 0.7
10	21.9	taxifolin hexoside	289, 330 (sh)	465	339, 303 $[M-H-162]^-$, 285, 151	13.3 ± 0.4
11	23.8	dihydroluteolin deoxyhexosyl-hexoside	281, 313	595	449 $[M-H-146]^-$, 287 $[M-H-308]^-$	12.7 ± 0.5
12	24.4	dihydrokaempferol hexoside	294, 335 (sh)	449	287 $[M-H-162]^-$, 269 $[M-H-162-18]^-$, 169, 151	66.4 ± 2.6
13	26.0	kaempferol deoxyhexosyl-hexoside	294, 335 (sh)	593	447 $[M-H-146]^-$, 285 $[M-H-308]^-$, 269	7.21 ± 0.9
14	26.8	dihydrokaempferol acetyl-hexoside	292, 333 (sh)	491	287 $[M-H-204]^-$, 269 $[M-H-204-18]^-$, 151	2.8 ± 0.01
total phenolic						415.1 ± 22.3

[a]Retention time on the C_{18} Synergi Hydro (4 μm) column. [b]Tentative identification based on UV–vis and mass spectra as well as relative HPLC retention times and published data. [c]Solvent: gradient of 0.5% formic acid in water and acetonitrile with 0.5% formic acid. [d]Peaks were quantified as equivalent to gallic acid.

anthocyanins showed the corresponding expected molecular ions (m/z 579 and 609, respectively) and two mass fragments after the loss of rhamnose and rutinose units, as verified in the MS/MS spectra. The molecular ion of peak 7 was found at m/z 433 with a fragment at m/z 287, indicating that the aglycone cyanidin was glycosylated with a deoxyhexose due to the loss of 146 u; this peak was identified as cyanidin 3-rhamnoside by coelution with the standard.

Cyanidin 3-glucoside (peak 2), cyanidin 3-rutinoside (peak 3), pelargonidin 3-glucoside (peak 4), pelargonidin 3-rutinoside (peak 5), and cyanidin 3-rhamnoside (peak 7) were also previously detected in jussara fruit.[12] In the present study cyanidin 3,5-diglycosilated with a hexose and a pentose was found instead of cyanidin 3-sambubioside;[12] our identification was confirmed by UV–vis and MS and the lack of coelution with the cyanidin 3-sambubioside standard. Peonidin 3-

dx.doi.org/10.1021/jf501211p | J. Agric. Food Chem. 2014, 62, 5072–5084

rutinoside (peak 6) was identified in jussara for the first time in the present study.

The monomeric anthocyanin content (239.16 ± 7.6 mg C3R/100 g) found in our jussara pulp was similar to the literature ranges for jussara pulps (192 mg/100 g f.m.[32] and 207 mg/100 g f.m. in jussara collected in region C in Santa Catarina State).[11] When compared to other fruits from the *Euterpe* genus, jussara showed a lower content of monomeric anthocyanins than those reported for açai (*Euterpe oleracea*) (282−303 mg C3G/100 g[23]). Similar to the results for jussara with 20% cyanidin 3-glucoside and 76% cyanidin 3-rutinoside, açai also shows large fractions of cyanidin 3-glucoside (12.5−13.2%) and cyanidin 3-rutinoside (86.8−87.5%).[23]

Profile of Phenolic Compounds. The HPLC-DAD-ESI$^-$-MS/MS method allowed for the separation and tentative identification of 14 phenolic compounds in the grumixama pulp (Figure 3A). Peak 1 was positively identified as cyanidin 3-glucoside based on coelution and comparison of the UV and mass spectral data with an authentic standard. Peaks 2−7, 9, and 10 belong to a series of quercetin derivatives (Table 5). All peaks exhibited λ_{max} values characteristic of flavonols, at 352−365 nm. Peaks 4, 5, 6, and 7 presented deprotonated molecules at m/z 447, 463, 433, and 433, respectively. In addition, the MS/MS fragmentation pattern obtained from these ions revealed the same fragment at m/z 301 corresponding to quercetin, suggesting neutral losses of the sugar moiety, deoxyhexose (loss of 146 u from $[M - H]^-$ in peak 4), hexose (loss of 162 u from $[M - H]^-$ in peak 5), and pentose (loss of 132 u from $[M - H]^-$ in peaks 6 and 7). Therefore, these peaks were identified as quercetin deoxyhexoside (peak 4), quercetin hexoside (peak 5), and quercetin pentoside (peaks 6 and 7). Peaks 2 and 3 show deprotonated molecules at m/z 477 and 615, respectively, and they showed MS/MS fragments at m/z 301 (loss of 176 u from $[M - H]^-$ in peak 2), as well as at m/z 463 and 301 (losses of 152 and 162 u from $[M - H]^-$ in peak 3). Consequently, these peaks were tentatively identified as quercetin glucuronide (peak 2) and quercetin galloylhexoside (peak 3). Due to the MS (m/z 609) and MS^2 (m/z 463, 301) data, quercetin deoxyhexosylhexose is presumptively identified as peak 9. Peak 10 was identified as quercetin (aglycone) based on coelution and comparison of the UV−vis and mass spectral data with an authentic standard. This peak presented a $[M - H]^-$ peak at m/z 301 and typical MS/MS fragmentation ions for quercetin at m/z 273 (loss of CO), 257 (loss of CO_2), and 229 (loss of CO + CO_2); the most interesting fragments concern the base peaks at m/z 179 and 151, due to a specific retro-Diels−Alder pathway leading to the $^{1,2}A^-$ and $^{1,3}A$ − CO.

Peaks 11, 13, and 14 were tentatively identified as sinapic acid derivatives, and peak 12 was not identified. Peak 11 was identified as sinapic acid dihexoside hydroxybenzoyl because of the deprotonated molecule at m/z 685 and MS/MS fragments at m/z 461 due to synapic acid loss (224 u) and at m/z 299 and 137 (loss of two hexose molecule). Peak 13 shows a $[M - H]^-$ peak at m/z 699 and MS/MS fragments at m/z 493, 331, and 169 after losing a sinapoyl group (206 u) and two hexose molecules, respectively. In addition the fragment at m/z 169 corresponded to gallic acid; consequently, these peaks were tentatively identified as gallic acid dihexoside sinapoyl. Sinapic acid dihexoside benzoyl (peak 14) was tentatively identified due to a deprotonated molecule at m/z 651 and MS/MS fragments at m/z 427, 265, and 103, suggesting losses of sinapic acid (224 u) and two hexose molecules.

The majority of the phenolic compounds in grumixama were sinapic acid derivatives (peaks 14 (43.2%) and 13 (13.5%)). The total phenolic compounds in grumixama comprised 145.2 ± 8.6 mg GAE/100 g fresh weight, while Haminuik et al.[14] reported a value of 25.98 ± 1.43 mg GAE/g dry basis. As far as we are concerned, this is the first report on the phenolic composition (except anthocyanins) from grumixama.

The HPLC chromatogram of the jussara extract is shown in Figure 3B. According to Table 5, 14 phenolic compounds were tentatively identified. The major phenolic compounds found in jussara include cyanidin 3-glucoside (peak 5), cyanidin 3-rutinoside (peak 6), and dihydrokaempferol hexoside (peak 12). Peaks 5 and 6 show their deprotonated molecule $[M - H]^-$ peaks at m/z 447 and 593, respectively. The MS/MS spectra of these compounds show fragments at m/z 285 for both peaks due to neutral hexose (peak 5) and rutinose losses (peak 6). This identification was confirmed in ESI positive mode during the anthocyanin analyses and by coelution with an authentic standard. Peak 12 was tentatively identified as dihydrokaempferol hexoside because the deprotonated molecule showed a $[M - H]^-$ peak at m/z 449 and MS/MS fragments at m/z 287 (loss of hexose molecule), corresponding to the dihydrokaempferol moiety, and at m/z 269 (loss of hexose molecule + H_2O). The fragment at m/z 269 (100%) was more intense than the fragment at m/z 287 (4%). The MS^3 spectra from the ion at m/z 287 showed typical flavanonol fragmentation. The fragments were detected at m/z 269 $[M - H - 18]^-$, m/z 243 $[M - H - 44]^-$, and m/z 215 $[M - H - 72]^-$, corresponding to the neutral losses of H_2O, CO_2, and CO + CO_2, respectively, and retro-Diels−Alder fragments were detected at m/z 151 ($^{1,3}A^-$) and 107 ($^{1,3}A^-$ − CO_2). Our MS data agree with those previously reported.[34,35]

Two other kaempferol derivatives are tentatively identified in jussara as peak 13 (kaempferol deoxyhexosylhexoside) and peak 14 (dihydrokaempferol acetylhexoside). Peak 13 shows a $[M - H]^-$ peak at m/z 593 and MS/MS fragments at m/z 447 and 285 after losing a deoxyhexose (146 u) and deoxyhexose + hexose unit (308 u), respectively. An MS^3-specific fragment (257, 243, 213, and 151) confirms the identity as kaempferol.[40] Peak 14 has a $[M - H]^-$ ion at m/z 491 and MS^2 ions at m/z 287 and 269, suggesting neutral losses of acetyl-hexose (204 u) and acetyl-hexose + H_2O (222 u). Peak 1 was tentatively identified as monogalloyl hexoside in jussara because of the deprotonated molecule at m/z 331, as well as the two MS^2 fragments at m/z 169, corresponding to the gallic acid moiety (loss of hexose) and m/z 125, corresponding to the consecutive losses of hexoside (162 u) and the CO_2 molecule (44 u). This fragmentation has been reported in *Caryocar villosum*[27] and jambolão.[36] Peak 2 was not identified; the deprotonated molecule had a m/z of 359, and the MS/MS fragment was at m/z 197, resulting from the loss of a hexose.

Five flavones were identified in jussara, three apigenin derivatives (peaks 3, 7, and 8), one luteolin derivative (peak 4), and one chrysoeriol derivative (peak 9). The flavones and their glycosides present two λ_{max} values at 320−370 and 250−280 nm due to their B-rings (cinnamoyl structure) and A-rings (benzoyl structure), respectively. The UV−vis spectra of the apigenin derivatives have λ_{max} values at 279 and 323−328 nm. Peaks 3, 7, and 8 were tentatively identified as apigenin dihexoside ($[M - H]^-$ at m/z 593), apigenin hexoside ($[M - H]^-$ at m/z 431), and apigenin deoxyhexosylhexoside ($[M - H]^-$ at m/z 577), respectively. All three compounds showed an MS^2 fragment at m/z 269 (apigenin moiety) as the most

Table 6. Chromatographic and Spectroscopic Characteristics and Content of Phenolic Compounds from Araça and Uvaia, Obtained from HPLC-DAD-ESI-MS/MS

peak	t_R[a] (min)	phenolic compound[b]	λ_{max}[c] (nm)	$[M-H]^-$ (m/z)	MS/MS (m/z)	concentration[d] (mg/100g)
Araça						
1	8.1	not identified	268	187	n.d.[e]	12.1 ± 0.6
2	9.8	gallic acid	271	169	125 $[M-H-44]^-$	12.2 ± 0.9
3	10.2	galloyl hexoside	277	331	271 $[M-H-60]^-$, 169 $[M-H-162]^-$, 125 $[M-H-44]^-$	7.4 ± 0.4
4	11.6	digalloyl hexoside	273	483	331 $[M-H-152]^-$, 313 $[M-H-170]^-$, 169	2.9 ± 0.2
5	13.6	di-HHDP hexoside	260	783	481 $[M-H-302]^-$, 301 $[M-H-482]^-$, 257	4.0 ± 0.7
6	15.7	di-HHDP hexoside isomer	260	783	481 $[M-H-302]^-$, 301 $[M-H-482]^-$, 257	3.9 ± 0.9
7	16.6	HHDP digalloyl hexoside	280	785	633 $[M-H-152]^-$, 615 $[M-H-169]^-$, 483 $[M-H-302]^-$, 301, 275, 249	2.3 ± 0.1
8	17.5	vanillic acid hexoside	260, 296	329	167$[M-H-162]^-$	8.1 ± 0.2
9	18.0	epicatechin epicatechin	278	579	289 $[M-H-290]^-$ MS^2 [289]: 271 $[M-H-18]^-$, 245 $[M-H-44]^-$, 205, 179	5.4 ± 0.1
10	19.2	HHDP digalloyl hexoside isomer	280	785	633 $[M-H-152]^-$, 615 $[M-H-169]^-$, 483 $[M-H-302]^-$, 301, 275, 249	5.9 ± 0.4
11	21.2	taxifolin hexoside	291, 347	465	303 $[M-H-162]^-$	11.7 ± 0.8
12	21.9	HHDP hexoside	279	481	301 $[M-H-180]^-$	5.7 ± 0.2
13	26.4	quercetin hexoside	353	463	301 $[M-H-162]^-$ MS^2 [301]: 273 $[M-H-28]^-$, 257 $[M-H-44]^-$, 229 $[M-H-72]^-$, 179, 151	6.4 ± 0.5
14	29.5	eriodictyol hexoside	289, 350	449	287 $[M-H-162]^-$, 181	4.0 ± 0.2
15	30.4	methyl ellagic acid hexoside	257, 373	491	329 $[M-H-162]^-$, 315 $[M-H-176]^-$, 301 $[M-H-190]^-$	5.2 ± 0.2
16	34.2	methyl ellagic acid pentoside	250, 370	461	315 $[M-H-146]^-$, 301$[M-H-160]^-$, MS^2[301]: 257 $[M-H-44]^-$, 229 $[M-H-72]^-$, 185	5.6 ± 0.1
total phenolics						103.1 ± 6.5
Uvaia						
1	7.3	galloyl hexoside	274	331	169 $[M-H-162]^-$, 125	5.1 ± 0.1
2	9.8	gallic acid	271	169	125 $[M-H-44]^-$	27.5 ± 1.2
3	10.2	galloyl hexoside isomer	277	331	169 $[M-H-162]^-$	1.8 ± 0.05
4	13.1	not identified	287	565	367 MS^2[367]: 247, 119	6.0 ± 0.4
5	15.0	dicaffeic acid	328	341	179 $[M-H-162]^-$, 281, 251 MS^2 [179]: 161 $[M-H-18]^-$, 135 $[M-H-44]^-$	2.0 ± 0.3
6	17.1	gallic acid derivative	292	415	367, 345, 331, 313, 169	14.8 ± 1.1
7	18.9	trigalloyl acid lactonized	292	451	313 $[M-H-138]^-$, 282 $[M-H-169]^-$, 169	13.8 ± 0.9
8	22.4	not identified	280	439	393, 379, 315	7.0 ± 0.3
9	24.3	galloyl-bis-HDDP hexoside	274	935	783 $[M-H-152]^-$, 633 $[M-H-302]^-$, 301	19.3 ± 1.5
10	28.9	quercetin deoxyhexoside	352	447	301 $[M-H-146]^-$	4.8 ± 0.1
11	34.2	not identified	276	263	219, 203, 153	2.8 ± 0.2
12	37.7	gallic acid derivative	276	347	329, 201, 169	11.0 ± 0.9
total phenolics						115.9 ± 7.1

[a]Retention time on the C_{18} Synergi Hydro (4 μm) column. [b]Tentative identification based on UV−vis and mass spectra as well as relative HPLC retention times and published data. [c]Solvent: gradient of 0.5% formic acid in water and acetonitrile with 0.5% formic acid. [d]Peaks were quantified as equivalent to gallic acid. [e]n.d.: not detected.

abundant ion, suggesting neutral losses of the sugar units. The MS^3 fragments from the ion at m/z 269 for peaks 3, 7, and 8 were not detected. Peak 4 was tentatively identified as luteolin deoxyhexosylhexoside according to the UV−vis spectra (λ_{max} at 273 nm (band II) and 323 nm (band I)) and MS fragmentation, leading to the luteolin aglycone at m/z 285 after loss of 146 u + 162 u (deoxyhexose and hexose moiety). The deprotonated molecule in peak 9 was observed at m/z 607, and the MS^2 fragment was detected at m/z 299, suggesting the loss of a rutinose unit. Chrysoeriol rutinoside (peak 9) and dihydroluteolin rutinoside (peak 11) were tentatively identified in jussara; both compounds showed a neutral loss of rutinose (308 u) from the deprotonated molecule at m/z 607 for peak 9 and at 595 for peak 11.

The three major phenolic compounds (peaks 5, 6, and 12) identified in jussara in this study were not reported in previous studies, but these compounds have been already identified in açai.[35,37] Previous studies have reported the presence of ferulic, gallic, protocatechuic, and coumaric acids, as well as catechin, epicatechin, and quercetin in jussara collected from the state of Santa Catarina, Brazil.[11] However, these compounds were not identified using mass spectrometry, which is currently the most suitable technique coupled to HPLC for identifying phenolic compounds in complex matrixes, such as fruit. Furthermore, we

dx.doi.org/10.1021/jf501211p | J. Agric. Food Chem. 2014, 62, 5072−5084

did not find the phenolic compounds reported by Da Silva Campelo Borges et al.[11] in our study.

The chromatograms of the phenolic compounds from araça and uvaia are shown in Figure 3C and D, respectively. Table 6 shows the chromatographic, UV−vis, and mass spectral data used to identify these compounds. Peak 2 from the phenolic compounds in araça (Figure 3C) and uvaia (Figure 3D) was identified as gallic acid because, in addition to presenting a maximum absorption in the UV−vis spectrum of 271 nm, the deprotonated molecule was detected at m/z 169 with a fragment in the MS^2 spectrum at m/z 125 due to neutral loss of 44 u (CO_2). The identification was confirmed by coelution with an authentic standard. Peaks 3 for araça and 1 and 3 of uvaia were identified as monogalloyl hexoside after they presented a deprotonated molecule at m/z 331 and three fragments in the MS^2 spectrum at m/z 271 after cross-ring fragmentation of the hexoside ring (M − H − 60) at m/z 169, corresponding to the gallic acid moiety, and at m/z 125 due to the decarboxylation of gallic acid (44 u). Notably, the existence and intensity of each fragment ion may be different for each galloyl hexoside peak, as well as for the other hydrolyzable tannins due to the presence of different isomeric forms in the same fruit.[15,38]

Peak 4 for araça showed a deprotonated molecule at m/z 483, as well as MS^2 fragments at m/z 331 due to loss of a galloyl group (152 u) and at m/z 313 due to loss of gallic acid (170 u). Furthermore, another isomer of digalloyl hexoside may have fragments at m/z 439 and 287; these signals are the result of the deprotonated molecule and the decarboxylation of a gallic acid linked to a hexoside (331 u). These fragmentation mechanisms were demonstrated by Meyers et al.[38] Peaks 5 and 6 for araça showed a UV−vis spectrum with a λ_{max} at 260 nm that is characteristic of dihexahydroxydiphenoyl hexoside (diHHDP-hexoside); furthermore, the two peaks showed a deprotonated molecule at m/z 783, yielding fragment ions at m/z 481 after the loss of a HHDP group, at m/z 301 after the loss of HHDP-hexoside group, and at m/z 257 after the decarboxylation of HHDP. Peaks 7 and 10 for araça showed UV−vis spectra with a λ_{max} at 280 nm and a deprotonated molecule at m/z 785, indicating the presence of HHDP-digalloyl-hexoside. In addition, the MS^2 spectra of these peaks showed fragments at m/z 633 after the loss of a galloyl residue (152 u), at m/z 615 after the loss of a gallic acid molecule, at m/z 483 due to loss of one HHDP group, and at m/z 301 after the loss of an HHDP hexoside molecule. Peak 12 for the araça sample was identified as HHDP-hexoside using the deprotonated molecule at m/z 481 and the MS^2 fragment at m/z 301, indicating the presence of HHDP. The gallic acid derivatives were identified based on literature data.[15,27,38]

In addition to the gallic acid derivatives, araça also contained quercetin hexoside (peak 13) and taxifolin hexoside (peak 11) in its phenolic fraction, presenting deprotonated molecules at m/z 463 and 465, respectively. The MS/MS spectra of these peaks showed fragments at m/z 301 (quercetin) and at m/z 303 (taxifolin), suggesting the loss of hexose units (162 u). Quercetin aglycone was identified and was confirmed using the MS^3 spectra: 273 $[M - H - CO]^-$, 257 $[M - H - CO_2]^-$, 229 $[M - H - CO - CO_2]^-$, 179 $[^{1,2}A]^-$, and 151 $[^{1,3}A]^-$. It was not possible to obtain an MS^3 spectrum from taxifolin, but the UV−vis absorption maxima at 291 and 347 nm helped to tentatively identify this compound. Peak 8 was tentatively identified as vanillic acid hexoside due to the presence of the deprotonated molecule at m/z 329 and the MS^2 fragment at m/z 167 after the loss of a neutral hexose. The UV−vis spectrum of this compound had λ_{max} at 260 and 296 nm, as well as the characteristic features of vanillic acid.

Peak 9 of araça was tentatively identified as the epicatechin−epicatechin dimer due to the protonated molecule at m/z 579 and the MS^2 fragment at m/z 289; the MS^3 spectrum of this fragment showed the characteristic configuration of an aglycone catechin with fragments at m/z 271 $[M - H - H_2O]^-$, 245 $[M - H - CO_2]^-$, 205 $[M - H - CO - CO_2]^-$, 179 $[^{1,2}A]^-$, and 151 $[^{1,3}A]^-$. Araça contained eriodictyol hexoside (peak 14) with a deprotonated molecular ion at m/z 449 and an MS^2 fragment at m/z 287 due to loss of a hexose. The MS^3 of the fragment at 287 was not obtained. Therefore, the identification of the aglycone was attempted. Peaks 15 and 16 were tentatively identified as ellagic acid derivatives (dimethyl ellagic acid hexoside and dimethyl ellagic acid pentoside) because both peaks showed characteristic fragments of methylated ellagic acid at m/z 315 and 313, respectively; at m/z 301, the ellagic acid was confirmed by the MS^3 spectrum of the fragment at 301 from peak 16.

Aside from peaks 1, 2, and 3, uvaia (Figure 3D) showed other derivatives of gallic acid in its phenolic composition. Peaks 6, 7, and 12 are gallic acid derivatives, but they have not been definitively identified. Peaks 7 and 9 were identified as lactonized trigalloyl acid and galloyl HHDP bis-hexoside, respectively. Peak 7 showed a deprotonated molecule at m/z 451 and MS^2 fragments at m/z 313, 282, and 169 that were attributed to galloyl and lactonized galloyl losses. Peak 9 was identified by the deprotonated molecule at m/z 935 and the MS^2 fragment at m/z 783 assigned to the loss of a galloyl group, as well as at m/z 633 due to loss of HHDP and at m/z 301 due to loss of HHDP-hexoside. The identification of this compound has already been reported in the phenolic composition of blackberries[39] and strawberries from Macedonia.[38]

Peak 5 in uvaia was identified as dicaffeic acid, with the deprotonated molecule at m/z 341 and an MS^2 fragment at m/z 179 due to the caffeoyl loss. Furthermore, the MS^3 spectrum at 179 u revealed fragments at m/z 161 and 135 attributed to water loss and decarboxylated caffeic acid, in accordance with the fragmentation pattern for dicaffeic acid proposed by Plazonić et al.[40] Peak 10 of uvaia presented a deprotonated molecule at m/z 447 and an MS^2 fragment at m/z 301 after the neutral loss of 146 u; this material was tentatively identified as quercetin deoxyhexoside. Peaks 4, 8, and 11 could not be identified.

The majority of the phenolic compounds in araça were gallic acid (peak 2, 12.24 ± 0.9 mg GAE/100 g fresh weight) and taxifolin hexoside (peak 12, 11.73 ± 0.8 mg GAE/100 g fresh weight). The total phenolic compounds in araça comprised 103.10 ± 6.5 mg GAE/100 g fresh weight, while Gordon et al.[15] reported a value of 754.4 ± 12.5 mg GAE/100 g dry weight. Although these authors have not quantified the compounds individually, the chromatogram revealed that the major compound was HHDP-digalloylglucoside.

Uvaia presented gallic acid (peak 2, 27.50 ± 1.2 mg GAE/100 g fresh weight) and galloyl HHDP-bis-hexoside (peak 7, 19.32 ± 1.5 mg GAE/100 g weight fresh) as the major phenolic compounds in the total 115.96 ± 7.15 mg GAE/100 g fresh weight. No data were found in the literature identifying the phenolic compounds in uvaia.

In conclusion, carotenoids and phenolic compounds were identified and quantified in four fruits from the Brazilian Atlantic Forest. In addition, jussara showed high levels of

phenolic compounds, primarily consisting of cyanidin 3-rutinoside, dihydrokaempferol hexoside, and cyanidin 3-glucoside. While the phenolic composition of jussara and grumixama was composed of several flavonoid glycosides, uvaia and araça presented mostly gallic acid derivatives. For the carotenoids, uvaia contained the highest concentrations. All-*trans*-β-Cryptoxanthin was the major carotenoid found in uvaia, grumixama, and araça, while all-*trans*-lutein was the major component in jussara. Therefore, these fruits are important as promising sources of bioactive compounds. Additionally, due to their nutritional value, high fiber content, and sweet taste, these four fruits from the Atlantic Forest can be used to supplement the diet of groups such as schoolchildren.

■ ASSOCIATED CONTENT

Supporting Information

Figure 1S shows the photographs of the fruits studied in this work. This material is available free of charge via the Internet at http://pubs.acs.org.

■ AUTHOR INFORMATION

Corresponding Author

*Tel: 55-13-3232-2569. E-mail: veriderosso@yahoo.com.

Funding

We thank the Brazilian Foundation FAPESP (Fundação de Amparo à Pesquisa do Estado de São Paulo) for financial support (process 2009/53884-8).

Notes

The authors declare no competing financial interest.

■ REFERENCES

(1) RBMA, Reserva da Biosfera da Mata Atlântica. Anuário da Mata Atlântica. Disponível em: www.rbma.org.br/anuariomataatlantica/mata_atlantica.php.

(2) APREMAVI, Associação de Preservação do meio Ambiente e da Vida. Muitas espécies da flora da Mata Atlântica são endêmicas e ameaçadas de extinção. Disponível em: http://www.apremavi.org.br/entrando-na-mata/flora/.

(3) Lorenzi, H. *Árvores Brasileiras, Manual de Identificação e Cultivo de Plantas Arbóreas Nativas do Brasil*; Instituto Plantarum de Estudos da Flora, 2002.

(4) Kriech, C. A.; Casanova, L.; Prochnow, M. Guia de Espécies. Disponível em www.apremavi.org.br/guia-de-especies. Accessed November 2, 2012.

(5) Maiochi, G. M. *Uvaia. Super dose de Vitamina C*. http://www.apremavi.org.br/noticias/apremavi/549/uvaia-super-dose-de-vitamina-c (accessed May 6, 2014).

(6) Temple, N. J. Antioxidant and disease: More questions than answers. *Nutr. Res. (N.Y.)* **2000**, *3*, 449−459.

(7) Willett, W. C. Balancing life-style and genomics research for disease prevention. *Science* **2002**, *296*, 695−698.

(8) Szajdek, A.; Borowska, E. J. Bioactive compounds and health-promoting properties of berry fruits: a review. *Plant Foods Hum. Nutr.* **2008**, *63*, 147−156.

(9) Seifried, H. E.; Anderson, D. E.; Fischer, E. I.; Milner, J. A. A review of the interaction among dietary antioxidants and reactive oxygen species. *J. Nutr. Biochem.* **2007**, *18*, 567−579.

(10) Halliwell, B.; Gutteridge, J. M. C. *Free Radicals in Biology and Medicine*, 4a ed.; OUP: Oxford, United States, 2007; pp 280−525.

(11) Da Silva Campelo Borges, G.; Vieira, F. G. K.; Copetti, C.; Gonzaga, L. V.; Zambiazi, R. C.; Mancini-Filho, J.; Fett, R. Chemical characterization, bioactive compounds, and antioxidant capacity of jussara (*Euterpe edulis*) fruit from the Atlantic Forest in southern Brazil. *Food Res. Int.* **2011**, *44*, 2128−2133.

(12) De Brito, E. S.; Araújo, M. C. P; Alves, R. E.; Carkeet, C.; Clevidence, B. A.; Novotny, J. A. Anthocyanins present in selected tropical fruits: acerola, jambolão, jussara, and guajiru. *J. Agric. Food Chem.* **2007**, *55*, 9389−9394.

(13) Flores, G.; Dastmalchi, K.; Paulino, S.; Whalen, K.; Dabo, A. J.; Reynertson, K. A.; Foronjy, R. F.; D'armiento, J. M.; Kennelly, E. J. Anthocyanins from *Eugenia brasilienis* edible fruits as potential therapeutics for COPD treatment. *Food Chem.* **2012**, *134*, 1256−1262.

(14) Haminiuk, C. W. I.; Plata-Oviedo, M. S. V.; Guedes, A. R.; Stafussa, A. P.; Bona, E.; Carpes, S. T. Chemical, antioxidant and antibacterial study of brazilian fruits. *Int. J. Food Sci. Technol.* **2011**, *46*, 1529−1537.

(15) Gordon, A.; Jungfer, E.; Da Silva, B. A.; Maia, J. G. S.; Marx, F. Phenolic constituents and antioxidant capacity of four underutilized fruits from the Amazon region. *J. Agric. Food Chem.* **2011**, *59*, 7688−7699.

(16) AOAC. *Official Methods of Analysis of the Association of Official Analytical Chemists*, 16th ed.; WA, 1997; Vol. 2, p 850.

(17) De Rosso, V. V.; Mercadante, A. Z. Carotenoid composition of two Brazilian genotypes of acerola (*Malpighia punicifolia* L.) from two harvests. *Food Res. Int.* **2005**, *38*, 1073−1077.

(18) De Rosso, V. V.; Mercadante, A. Z. Identification and quantification of carotenoids, by HPLC-PDA-MS^n, from amazonian fruits. *J. Agric. Food Chem.* **2007a**, *55*, 5062−5072.

(19) Britton, G.; Liaaen-Jensen, S.; Pfander, H. *Carotenoids Handbook*; Birkhäuser: Basel, Switzerland, 2004.

(20) Enzell, C. R.; Back, S. Mass Spectrometry. In *Carotenoids*. Vol. *1B*: Spectroscopy; Britton, G., Liaaen-Jensen, S., Pfander, H., Eds.; Birkhäuser: Basel, Switzerland, 1995; pp 261−320.

(21) Faria, A. F.; De Rosso, V. V.; Mercadante, A. Z. Carotenoid composition of jackfruit (*Artocarpus heterophyllus*), determined by HPLC-PDA-MS/MS. *Plant Foods Hum. Nutr.* **2009**, *64*, 108−115.

(22) De Rosso, V. V.; Mercadante, A. Z. HPLC-PDA-MS/MS of anthocyanins and carotenoids from dovyalis and tamarillo fruits. *J. Agric. Food Chem.* **2007b**, *55*, 9135−9141.

(23) De Rosso, V. V.; Hillebrand, S.; Montilla, E. C.; Bobbio, F. O.; Winterhalter, P.; Mercadante, A. Z. Determination of anthocyanins from acerola (*Malpighia emarginata* DC.) and açai (*Euterpe oleracea* Mart.) by HPLC-PDA-MS/MS. *J. Food Comp. Anal.* **2008**, *21*, 291−299.

(24) Wu, X.; Prior, R. L. Identification and characterization of anthocyanins by high-performance liquid chromatography−electrospray ionizations−tandem mass spectrometry in common foods in the United States: vegetables, nuts and grains. *J. Agric. Food Chem.* **2005a**, *53*, 3101−3113.

(25) Wu, X.; Prior, R. L. Systematic identifications and characterization of anthocyanins by HPLC-ESI-MS/MS in common foods in the United States: fruits and berries. *J. Agric. Food Chem.* **2005b**, *53*, 2589−2599.

(26) Lee, J.; Durst, R. W.; Wrolstad, R. E. Determination of total monomeric anthocyanin pigment content of fruit juices, beverages, natural colorants, and wines by the pH differential method: collaborative study. *J. AOAC Int.* **2005**, *88*, 1269−1278.

(27) Chisté, R. C.; Mercadante, A. Z. Identification and quantification, by HPLC-PDA-MS/MS of carotenoids and phenolic compounds from the Amazonian fruit *Caryocar villosum*. *J. Agric. Food Chem.* **2012**, *60*, 5884−5892.

(28) Faria, A. F.; Marques, M.; Mercadante, A. Z. Identification of bioactive compounds from jambolão (*Syzygium cumini*) and antioxidant capacity evaluation in different pH conditions. *Food Chem.* **2011**, *126*, 1571−1578.

(29) Ribeiro, J. C.; Antunes, L. M. G.; Aissa, A. F.; Darin, J. D. C.; De Rosso, V. V.; Mercadante, A. Z.; Bianchi, M. L. P. Evaluation of the genotoxic and antigenotoxic effects after acute and subacute treatments with açai pulp (*Euterpe oleracea* Mart) on mice using the erythrocytes micronucleus test and the comet assay. *Mutat. Res., Genet. Toxicol. Environ. Mutagen.* **2010**, *695*, 22−28.

(30) Brasil, Agência Nacional de Vigilância Sanitária. Padrão de Identidade e Qualidade Mínima da Polpa do Açaí. Instrução Normativa nº 01 de 07 de Janeiro de 2000.
(31) Pereira, M. C.; Steffens, R. S.; Jablonski, A.; Hertz, P. F.; Rios, A. de O.; Vizzotto, M.; Flôres, S. H. Characterization and antioxidant potential of Brazilian fruits from the Myrtaceae family. *J. Agric. Food Chem.* **2012**, *60*, 3061−3067.
(32) Rufino, M. S. M.; Alves, R. E.; de Brito, E. S.; Pérez-Jiménez, J.; Saura-Calixto, F.; Mancini-Filho, J. Bioactive compounds and antioxidant capacities of 18 non-traditional tropical fruits from Brazil. *Food Chem.* **2010**, *121*, 996−1002.
(33) Britton, G.; Khachik, F. Carotenoids in Food. In *Carotenoids: Nutrition and Health*; Britton, G., Liaaen-Jensen, S., Pfander, H., Eds.; Birkhäuser Basel: Boston, 2009; Vol. *5*, pp 45−66.
(34) Le Gall, G.-L.; Dupont, M. S.; Mellon, F. A.; Davis, A. L.; Collins, G. F.; Erhoeyen, M. E.; Colquhoun, I. J. Characterization and content of flavonoid glycosides in genetically modified tomato (*Lycopersicon esculentum*) fruits. *J. Agric. Food Chem.* **2003**, *51*, 2438−2446.
(35) Kang, J.; Thakali, K. M.; Xie, C.; Kondo, M.; Tong, Y.; Ou, B.; Jensen, G.; Medina, M. B.; Schauss, A. G.; Wu, X. Bioactivities of açaí (*Euterpe precatoria* Mart.) fruit pulp, superior antioxidant and anti-inflammatory properties to *Euterpe olerace* Mart. *Food Chem.* **2012**, *133*, 671−677.
(36) Meyers, K. J.; Swiecki, T. J.; Mitchell, A. E. Understanding the native Californian diet: identification of condensed and hydrolysable tannins in tanoak acorns (*Lithocarpus densiflorus*). *J. Agric. Food Chem.* **2006**, *54*, 7686−7691.
(37) Hager, T. J.; Howard, L. R.; Liyanage, R.; Lay, J. O.; Prior, R. L. Ellagitannin composition of blackberry determined by HPLC-ESI-MS and MALDI-TOF-MS. *J. Agric. Food Chem.* **2008**, *56*, 661−669.
(38) Kajdzanoska, M.; Gjamouski, V.; Stefova, M. HPLC-DAD-ESI-MS identification of phenolic compounds in cultivated strawberries from Macedonia. *Maced. J. Chem. Chem. Eng.* **2010**, *29*, 181−194.
(39) Fabre, N.; Rustan, I.; Hoffmann, E.; Quetin-Leclercq, J. Determination of flavone, flavonol, and flavanone aglycones by negative ion liquid chromatography electrospray ion trap mass spectrometry. *J. Am. Soc. Mass Spectrom.* **2001**, *12*, 707−715.
(40) Plazonic, A.; Bucar, F.; Males, Z.; Mornar, A.; Nigovic, B.; Kujundzic, N. Identification and quantification of flavonoids and phenolic acids in burr parsley (*Caucalis platycarpos* L.), using high-performance liquid chromatography with diode array detection and electrospray ionization mass spectrometry. *Molecules* **2009**, *14*, 2466−2490.

named teaghrelins in this study, were examined for the speculative biological activities via a food intake assay in rats as well as a biochemical assay detecting the stimulation of growth hormone secretion from rat primary anterior pituitary cells. Moreover, metabolites of teaghrelins were examined in bile of rats after intravenous (IV) injection.

MATERIALS AND METHODS

Chemicals and Materials. High-performance liquid chromatography (HPLC)-grade acetonitrile and methanol were purchased from Fisher Scientific (Fair Lawn, NJ). Acetic acid (99.7%) was obtained from J.T.Baker (Mallinckrodt Baker, Inc., Phillipsburg, NJ). Phosphoric acid (85%) was brought from Merck Millipore (Gibbstown, NJ). Purified water was afforded by a Millipore clear water purification system (Direct-Q, Millipore, Billerica, MA). Dulbecco's modified Eagle's medium (DMEM) and dialyzed fetal bovine serum were bought from Invitrogen (Carlsbad, CA). DNase I was obtained from Worthington Biochemical (Lakewood, NJ). GHRP-6 was purchased from GenWay Biotech, Inc. (San Diego, CA). Collagenase type I and [D-Arg^1,D-Phe^5,D-Trp^{7,9},Leu^{11}]-substance P were obtained from Sigma-Aldrich Co. (St. Louis, MO). Different oolong teas prepared from various cultivars (Tieguanyin, Chin-shin, Jin-xuan, Shy-jih-chuen, etc.) of tea plants (*Camellia sinensis*) were gifts or purchased from local manufacturers.

Preparation and HPLC Analysis of Tea Infusions. Tea infusions were prepared by adding 18 mL of boiling water to 1 g of various oolong teas. After 5 min, the brew was filtered through a 0.22 μm polyvinylidene difluoride (PVDF) membrane filter (Pall Corporation, Glen Cove, NY) and used for the following analysis. Chemical constituents in the tea infusions were analyzed on a liquid chromatography system coupled to a model 600E photodiode array detector (Waters Corporation, Milford, MA) and performed using a 250 × 4.6 mm inner diameter, 5 μm, C18 reversed-phase column (Waters Corporation, Milford, MA) as described previously.[19] The mobile phase consisted of (A) water containing 0.026% phosphoric acid and (B) acetonitrile. The gradient was as follows: 0−60 min, linearly gradient from 10 to 30% B; 61−70 min, 30% B; and 70−100 min, linear gradient from 30 to 10% B. The column was maintained at room temperature, and the injection volume was 5 μL at a flow rate of 1 mL/min. The ultraviolet (UV) absorbance detection wavelength was set at 280 nm.

Extraction and Isolation of Teaghrelins. Chin-shin oolong tea granules of 5 kg were powdered and extracted with 40 L of methanol 3 times (7 days for each time) at room temperature. Two unique acylated flavonoid tetraglycosides (termed teaghrelin-1 and teaghrelin-2 in this study), quercetin (3-*O*-[2^G-(*E*)-coumaroyl-3^G-*O*-β-D-glucosyl-3^R-*O*-β-D-glucosylrutinoside]) and kaempferol (3-*O*-[2^G-(*E*)-coumaroyl-3^G-*O*-β-D-glucosyl-3^R-*O*-β-D-glucosylrutinoside]), were first isolated from the methanol extract as a mixture preparation and then further separated to obtain their individual compounds according to the protocol as described previously.[20]

Animals. Male Sprague Dawley rats weighting 250−300 g were purchased from BioLASCO Taiwan Co., Ltd. (Taipei, Taiwan) and adapted for 1 week before use. Two animals were housed per cage and maintained in a controlled environment of 23 ± 2 °C, 60 ± 10% humidity, and 12 h light/dark cycle. The rats were fed with hard rodent chow pellets (Fwusow Industry Corporation, Taiwan) and purified water *ad libitum*. The animal experiments were approved by the Institutional Animal Care and Use Committee of the National Chung-Hsing University (IACUC Approval Number 102-92).

Food Intake Assay. The rats (n = 8) were fasted for 2 h with free access to drinking water and then orally administrated with aqueous solutions containing teaghrelins of 2.5 or 7.5 mg/kg. After oral administration for 2 h, rodent chow was supplied to rats and the net consumption (food intake) of each rat after feeding for 15 and 120 min was recorded to evaluate its appetite and total food consumption, respectively.

Primary Pituitary Cell Culture. Pituitary cells were isolated according to a modified enzymatic dispersion method developed by Yamazaki et al.[21] Briefly, Sprague Dawley male rats (n = 6) were anaesthetized with Zoletil 50 (40 mg/kg, IP; Virbac Laboratories, Carros, France), and the anterior pituitary glands were quickly removed after decapitation. The tissues were cut into small pieces and dispersed by incubations in DMEM containing 0.25% (w/v) collagenase type I for 60 min, 0.25% (w/v) trypsin for 15 min, and then DMEM containing 16 units of DNase I for 5 min. The dispersed anterior pituitary glands were passed through a 100 μm nylon cell strainer (BD Falcon, Franklin Lakes, NJ). Cells were finally suspended in DMEM containing 10% dialyzed fetal bovine serum. The yield of each anterior pituitary gland was approximately 1.5−2 × 10^6 cells.

Growth Hormone Secretion Assay. The anterior pituitary cells were seeded on a 96-well plate at a density of 4 × 10^4 cell/well and cultured at 37 °C under 5% CO_2 for 2 days prior to assay. The culture medium was removed, and cells were preincubated in serum-free DMEM for 90 min to stabilize basal hormone secretion. The medium was transferred to fresh DMEM containing teaghrelin-1 (from 10^{-9} to 10^{-4} M) or GHRP-6 (GHS-R1a agonist, 10^{-7} M), and cells were incubated for 15, 30, and 60 min at 37 °C under 5% CO_2. To test the effect of antagonist, the cells were incubated with a GHS-R1a antagonist, [D-Arg^1,D-Phe^5,D-Trp^{7,9},Leu^{11}]-substance P (0.5 μM), and then treated with DMEM containing teaghrelin-1 (10^{-5} M) or GHRP-6 (10^{-7} M) for 30 min. The medium was collected, and growth hormone secretion was assayed by a rat growth hormone enzyme-linked immunosorbent assay (ELISA) kit (EMD Millipore Corporation, Billerica, MA).

Bile Collection and Preparation. Male Sprague Dawley rats (n = 3) were fasted for 18 h and then anesthetized with Zoletil 50 (40 mg/kg, IP). The rats were kept alive at the period of surgery. All groups were treated with IV administration of normal saline containing teaghrelin-1 or teaghrelin-2 (30 mg/kg). Bile fistulas of the rats were cannulated with PE-20 polyethylene tubing for collection of bile. Bile was collected at 30 min intervals for 2.5 h after a single IV dosing. Bile samples of 200 μL were vortex-mixed with 2 volumes of methanol containing 0.1% phosphoric acid for 10 min and centrifuged at 10000g for 20 min at 4 °C. The supernatant was filtered by a 0.22 μm PVDF membrane filter (Pall Corporation) and used for the following analyses.

HPLC/UV and LC−MS^n Analyses of Bile Extraction. Bile metabolites were analyzed by a HPLC system (Waters Corp.) with a Syncronis C18 column (250 × 4.6 mm inner diameter, 5 μm) from Thermo Scientific (Waltham, MA). The HPLC mobile phase comprised (A) acetonitrile and (B) water containing 0.5% acetic acid. The gradient started at 5% solvent A and 95% solvent B, followed by a linearly increase of solvent A to 25% for 10 min, and raised to 30% for 30 min. Finally, the gradient was decreased to 5% A for 5 min. The sample injection volume was 20 μL with 1 mL/min flow rate at room temperature. The detection wavelength was set at 280 nm. Mass spectrometric analysis was performed on a LTQ linear ion trap tandem mass spectrometer (Thermo Electron, San Jose, CA) equipped with an electrospray ionization (ESI) interface and connected to a Surveyor LC system (Thermo Electron, San Jose, CA) with a 5 μL sample loop. The analytes were separated on a Waters Xterra-RP18 column (250 × 4.6 mm inner diameter, 5 μm). The tray temperature was set at 4 °C. The mobile phase comprised (A) acetonitrile and (B) water containing 0.5% acetic acid. The program for gradient elution started at 5% A, increased to 25% A in 10 min, and then changed to 30% A in 30 min. Subsequently, the gradient increased to 70% A in 1 min and was held for 8 min. Finally, the gradient went back to 5% A in 1 min and was held for 5 min. The flow rate was 1 mL/min. The mass spectra were obtained with negative ESI mode. The spray voltage was 4.5 kV, and the heated capillary temperature was at 300 °C. Flow rates of sheath gas, auxiliary gas, and sweep gas were 50, 13, and 3 arbitrary units, respectively. Data-dependent acquisition (DDA) was used to perform under automatic gain control conditions. The first scan was operated in full-scan mode ranging from m/z 150 to 1500. The other scans were set as the data-dependent MS^n scan using the high-purity helium (>99.99%) as the collision gas and the relative collision energy of 33−35%. Isolation width of the precursor ion was set to 2 Da. The MS/MS experiments of data-dependent acquisition were performed

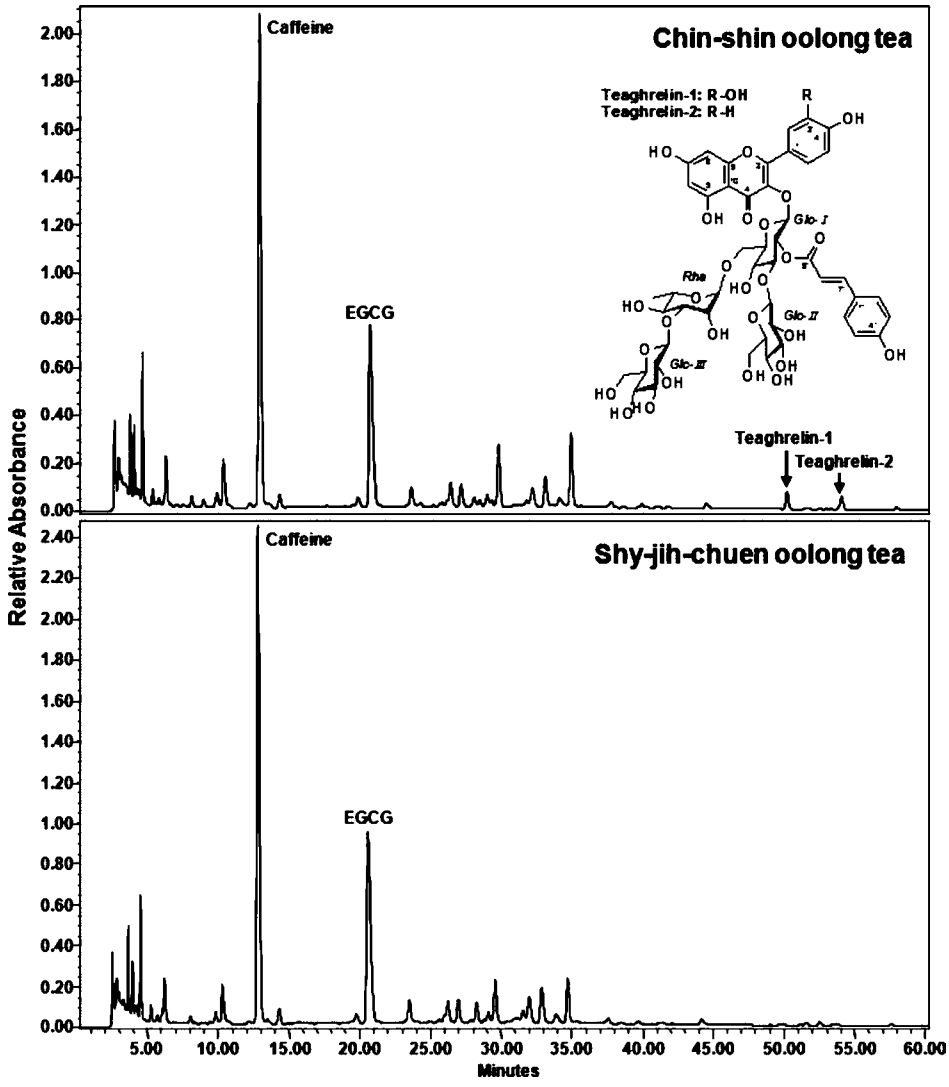

Figure 1. Comparison of the HPLC profiles of Chin-shin and Shy-jih-chuen oolong tea infusions. Two unique peaks, teaghrelin-1 and teaghrelin-2, in Chin-shin oolong tea were indicated by arrows, and their structures were shown on top of the peaks. Caffeine and the major catechin, epigallocatechin-3-gallate (EGCG), in both teas were labeled.

according to a previous scan. The highest intensity ion of the previous scan was chosen as the precursor ion for the successive MS/MS scans.

Statistical Analysis. The data were presented as mean values ± standard error of the mean (SEM). The differences were analyzed by one-way analysis of variance (ANOVA) followed by Duncan's post-hoc testing. Statistical calculations were performed by SigmaStat (version 3.5). A level of $p < 0.05$ was considered to be statistically significant.

RESULTS

Identification of Teaghrelins in Chin-shin Oolong Tea. To search for putative compounds responsible for the empirical effects (induction of hunger and acceleration of gastric emptying) of Chin-shin oolong tea, chemical compounds in the infusion of Chin-shin oolong tea were analyzed and compared to those of other oolong teas commonly found in Taiwan, as exemplified by Shy-jih-chuen oolong tea (Figure 1). Comparable patterns of chemical compounds, such as caffeine and catechins, were observed between Chin-shin oolong tea and Shy-jih-chuen oolong tea. Strikingly, two acylated flavonoid tetraglycosides whose structures were chemically determined by nuclear magnetic resonance (NMR) in our previous study were found relatively abundant in Chin-shin oolong tea.[20,22] Both compounds, tentatively named teaghrelin-1 and teaghrelin-2, were purified as a mixture or as their individual compounds and used for the following assays.

Effect of Teaghrelins on the Food Intake of Rats. In comparison to the control group, food intake of rats was significantly enhanced after ingestion with mixed teaghrelins (containing both teaghrelin-1 and teaghrelin-2) of 2.5 or 7.5 mg/kg (Figure 2A). The effect on the enhancement of food intake was more drastic after food supplied for 15 min than that after food supplied for 120 min. Apparently, ingestion of teaghrelins strongly induced the appetite of rats that ate relatively fast in the first 15 min, while the total food consumption accumulated for 120 min was only mildly increased in the long run. The appetite of rats induced by the ingestion with teaghrelins was also dose-dependent because a higher effect on the enhancement of food intake in the first 15 min was observed in rats ingested with 7.5 mg/kg of teaghrelins compared to those rats ingested with 2.5 mg/kg of teaghrelins. However, no statistical difference was observed for rats ingested with 2.5 and 7.5 mg/kg of teaghrelins with regard to their total food consumption accumulated for 120 min. Similar outcomes

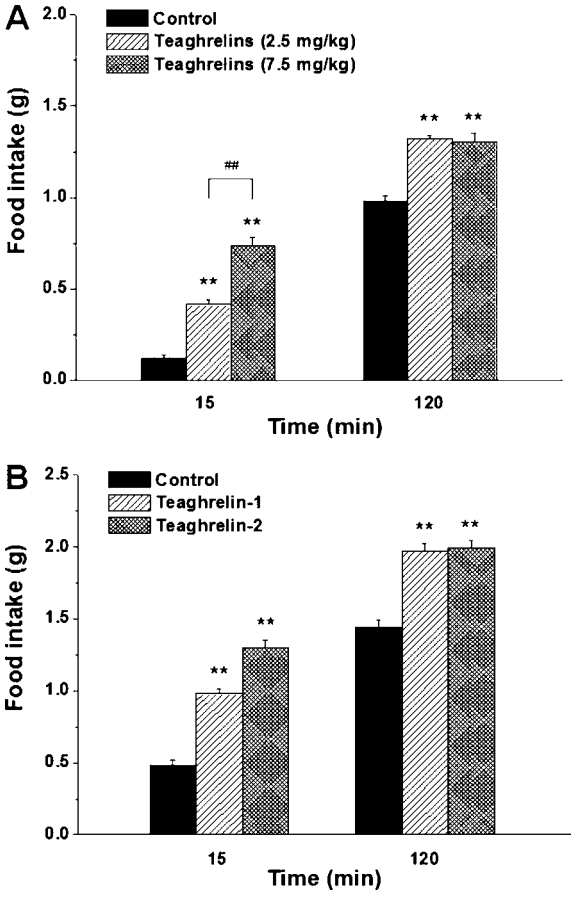

Figure 2. Effects of (A) mixed teaghrelins and (B) individual teaghrelin on food intake of rats. Mean cumulative values of food intake of rats 15 and 120 min after orally administration with mixed teaghrelins of 2.5 and 7.5 mg/kg as well as those with teaghrelin-1 or teaghrelin-2 of 7.5 mg/kg were recorded. Data were presented as means ± SEM with $n = 8$. Significance levels seen by one-way ANOVA were (**) $p < 0.001$ versus the control and (##) $p < 0.001$ significant differences between columns.

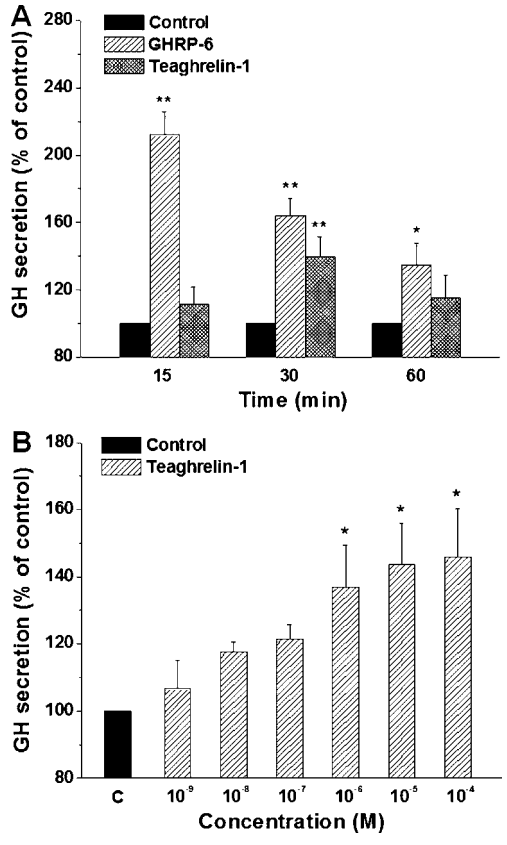

Figure 3. Effect of teaghrelin-1 administration on growth hormone (GH) secretion of pituitary cells. (A) GH secretion from rat primary pituitary cells was measured after incubation with medium (control), GHRP-6 (GHS-R1a agonist, 10^{-7} M), and teaghrelins-1 (10^{-5} M) for 15, 30, and 60 min. (B) GH secretion from rat primary anterior pituitary cells was observed by incubating with teaghrelin-1 of various concentrations for 30 min. Data were presented as means ± SEM with $n = 6$. Significance levels seen by one-way ANOVA were (*) $p < 0.05$ versus the control and (**) $p < 0.001$ versus the control.

and conclusion were obtained when 7.5 mg/kg of teaghrelin-1 and teaghrelin-2 were used in the same food intake assay, respectively (Figure 2B). Comparable effects on the enhancement of food intake were observed for both teaghrelins, and it was obvious that the minor structural difference in these two teaghrelins (one extra hydroxyl group at the 3′ position of teaghrelin-1) did not cause appreciable variation for their effects on hunger induction of rats.

Effect of Teaghrelin-1 on Growth Hormone Secretion of Rat Pituitary Cells. Stimulating growth hormone secretion of pituitary cells is a characteristic function of ghrelin. To evaluate if teaghrelins are also capable of stimulating the secretion of growth hormone, relatively abundant teaghrelin-1 is used to examine this characteristic function by incubating with primary rat anterior pituitary cells. Similar to GHRP-6, a synthetic analogue of ghrelin, teaghrelin-1 was able to stimulate the secretion of growth hormone from rat anterior pituitary cells (Figure 3A). In our assay conditions, the stimulatory effects of GHRP-6 and teaghrelin-1 on growth hormone secretion of rat pituitary cells were relatively high after treatment for 15 and 30 min, respectively. Treatment of teaghrelin-1 (from 10^{-9} to 10^{-4} M) for 30 min stimulated growth hormone secretion of the rat pituitary cells in a dose-

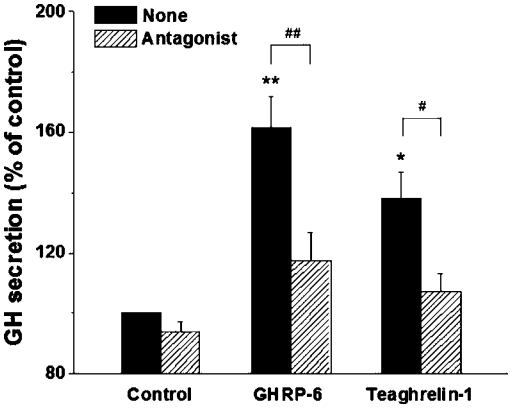

Figure 4. Effects of [D-Arg^1,D-Phe^5,D-Trp^{7,9},Leu^{11}]-substance P (GHS-R1a antagonist) on pituitary growth hormone (GH) secretion induced by GHRP-6 and teaghrelin-1. Rat primary anterior pituitary cells were incubated with GHRP-6 (10^{-7} M) and teaghrelin-1 (10^{-5} M) in the presence and absence of [D-Arg^1,D-Phe^5,D-Trp^{7,9},Leu^{11}]-substance P (0.5 μM) for 30 min. Data were presented as means ± SEM with $n = 6$. Significance levels seen by one-way ANOVA were (*) $p < 0.05$ versus the control, (**) $p < 0.001$ versus the control, (#) $p < 0.05$ significant differences between columns, and (##) $p < 0.001$ significant differences between columns.

dx.doi.org/10.1021/jf501425m | J. Agric. Food Chem. 2014, 62, 5085−5091

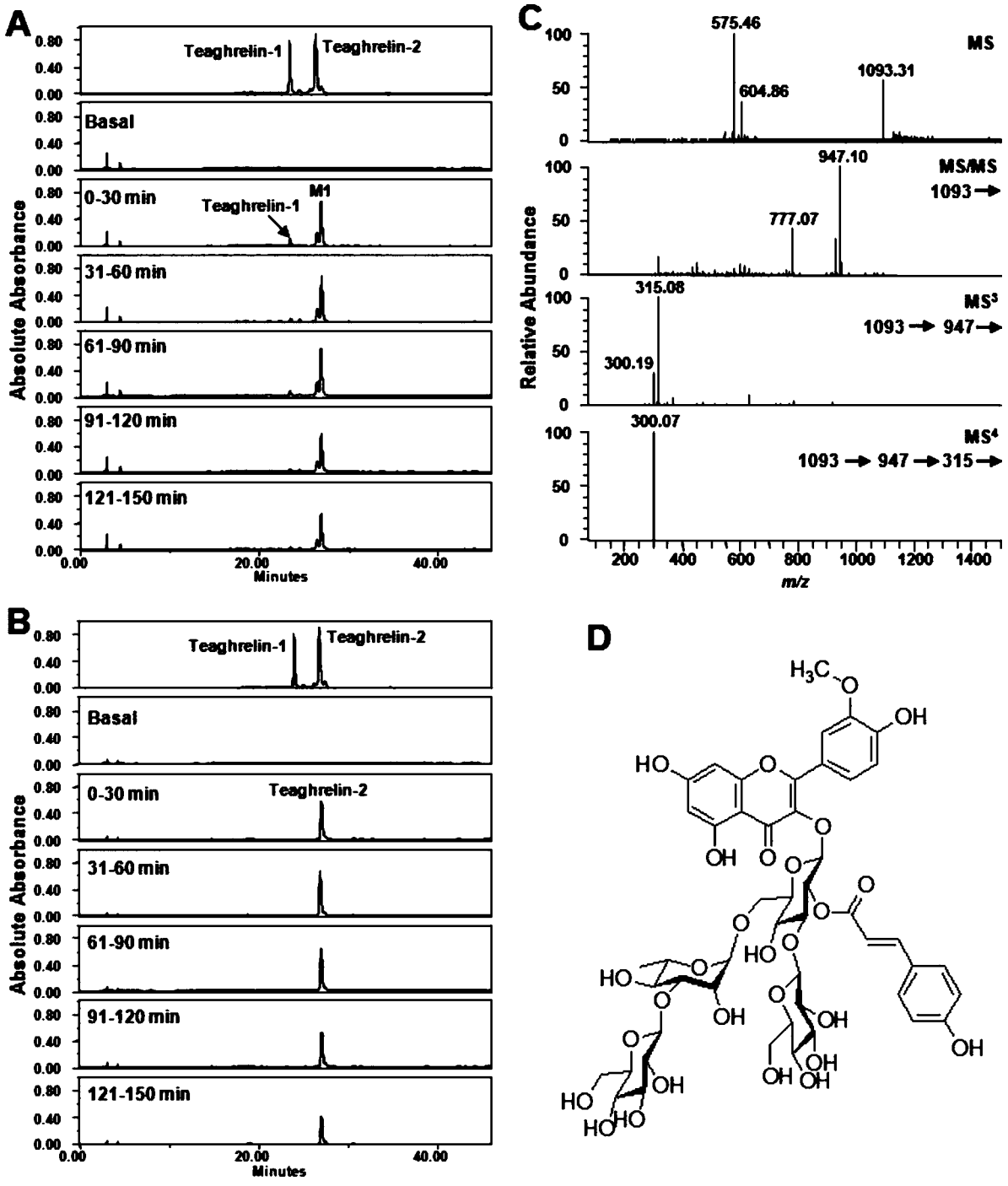

Figure 5. HPLC chromatograms of teaghrelins and bile metabolites in rats. Bile samples were collected from rats administrated with 30 mg/kg of (A) teaghrelin-1 and (B) teaghrelin-2 at different time intervals, basal, 0−30, 31−60, 61−90, 91−120, and 121−150 min. The samples were analyzed in a HPLC chromatogram by comparing to isolated teaghrelins as standards (teaghrelin-1 and teaghrelin-2 in the top panel). (C) Data-dependent MS^n spectra of teaghrelin-1 metabolite (M1). (D) Proposed chemical structure of M1.

dependent manner (Figure 3B). Moreover, both stimulatory effects of GHRP-6 and teaghrelin-1 on growth hormone secretion of the rat pituitary cells were inhibited by [D-Arg^1,D-Phe^5,D-$Trp^{7,9}$,Leu^{11}]-substance P, an antagonist of the ghrelin receptor (Figure 4). Taken together, teaghrelin-1 seems to be an agonist of the ghrelin receptor.

Identification of a Teaghrelin Metabolite in Rat Bile. To examine biliary metabolites, bile samples of three rats were collected every 30 min for 2.5 h after IV injection with 30 mg/kg of teaghrelin-1 and teaghrelin-2, respectively. Putative metabolites of teaghrelins were analyzed by LC−MS^n with data-dependent acquisition scan function. A major metabolite, M1, was detected after IV injection of teaghrelin-1 (Figure 5A). In contrast, teaghrelin-2 seemed to be unmodified in rat bile after IV injection (Figure 5B). The unmodified teaghrelin-2 in rat bile was also confirmed by mass spectroscopic analysis (data not shown). The structure of M1 was determined by multiple-stage mass spectra in the negative mode (Figure 5C). The deprotonated molecule of M1 at m/z 1093 was indicated in the full mass spectrum. The m/z 947 ion in the MS^2 spectrum was

dx.doi.org/10.1021/jf501425m | J. Agric. Food Chem. 2014, 62, 5085−5091

owing to the neutral loss of 146 Da identified as the *p*-coumaroyl moiety.[23] In the MS^3 spectrum, the fragment ion at *m*/*z* 315, produced from *m*/*z* 947 with the neutral loss of tetrasaccharide residue with 632 Da, was assigned as the monomethylated quercetin moiety of M1.[23] The fragment of *m*/*z* 300 was also found in the MS^3 spectrum and assigned as the $[M - H - CH_3^{\bullet}]^-$ fragment of the 3′-methyl quercetin.[24] The ion transition from *m*/*z* 315 to 300 observed in the MS^4 spectrum confirmed that the monomethylation occurred in the metabolite of teaghrelin-1. Altogether, M1 was proposed as 3′-methyl teaghrelin-1 (Figure 5D).

DISCUSSION

Two unique acylated flavonoid tetraglycosides (named teaghrelins in this study) previously identified in Chin-shin oolong tea were shown to be probably responsible for the empirical effects, such as hunger induction, of Chin-shin oolong tea presumably via the same molecular mechanism of the endogenous hunger hormone, ghrelin. Similar to ghrelin, teaghrelins are able to induce hunger sensation of rats as well as stimulate growth hormone secretion of rat primary anterior pituitary cells. The identification of teaghrelins in Chin-shin oolong tea seems to provide a scientific clue to resolve the mystery for the hunger experience strongly induced by Chin-shin oolong tea.

Several acylated flavonoid tetraglycosides with the same structural backbone but different hexosyl (at least, glucosyl, rhamnosyl, and arabinosyl) glycosides were detected in substantially low contents in various oolong teas, including Tieguanyin, Wuyi, Fenghuang, Gaoshan Shibi, Laocong Shuixian, and Baihao oolong teas, in our previous study.[23] These acylated flavonoid tetraglycosides are putatively regarded as different types of teaghrelins, and the presence of teaghrelins in variable oolong teas at a substantially low content presumably explains why many oolong teas are also able to induce hunger sensation, although not as strong as Chin-shin oolong tea. Moreover, it also explains why many green and black teas possess similar effects of hunger induction, because the same tea leaves, e.g., fresh leaves of Chin-shin tea plants, may be used to produce oolong tea as well as green and black teas.

Hepatic metabolism and biliary excretion mechanism are important for the pharmacological effects of drugs,[25] and thus, identification of drug metabolites in bile is helpful to realize the drug disposition for the preclinical study.[26] It has been shown that the most abundant compounds in tea, flavonoids, tend to be methylated in their *meta* (3′-*O*-) position of the catecholic moiety by catechol-*O*-methyltransferase, and the 3′-*O*-methyl derivatives are generally found as the major metabolites in bile.[27,28] Moreover, methylated flavonoids have been reported to possess better intestinal absorption and oral bioavailability than their unmethylated flavonoids.[29,30] Accordingly, a *meta*-O-methylated metabolite at the 3′ position of teaghrelin-1 was detected in rat bile after IV injection in this study. As expected, lacking a *meta* (3′-*O*-) position of the catecholic moiety, teaghrelin-2 was not methylated and remained unmodified in bile.

On the basis of the multiple biological activities of ghrelin, synthetic analogues (both peptidyl and non-peptidyl GHS-R1a agonists), such as GHRP-6, L-692,429, and MK-677, have been developed for the potential therapeutic applications of several diseases, e.g., gastrointestinal deficiency and anorexia.[31−34] In animal and human studies, ghrelin as well as its peptidyl analogues has a short biological half-life that limits its utility as a pharmacological agent.[35−37] In contrast, non-peptide oral ghrelin analogues have been found to possess better bioavailability.[31,34] However, oral ghrelin analogues, such as MK-677, lacked the efficacy for the treatment of gastrointestinal deficiency in elderly patients[38] and caused side effects in mild lower extremity edema and muscle pain, while the rise of appetite was maintained for a short period in healthy older people.[39] Moreover, TZP-101 and TZP-102, the macrocylic, peptidomimetic ghrelin receptor agonists, were reported to show no significant effect on diabetic gastroparesis treatment in the phase 2b program and caused minor adverse events, such as hyperglycemia, nausea, and diarrhea.[40−42] In a word, no synthetic oral agonists of the ghrelin receptor were satisfactory and approved for clinical application thus far. According to this study, teaghrelins extracted from oolong teas seem to be promising oral agonists of the ghrelin receptor, provided that they undergo necessary clinical trials.

AUTHOR INFORMATION

Corresponding Author

*Telephone: 886-4-22840328. Fax: 886-4-22853527. E-mail: tctzen@dragon.nchu.edu.tw.

Author Contributions

†Yuan-Hao Lo and Ying-Jie Chen contributed equally to this work.

Funding

The work was partly supported by grants to Jason T. C. Tzen of National Chung-Hsing University (NCHU-101D073, NCHU-102D604, NCHU-102S0503, and NSC 100-3114-B-005-001).

Notes

The authors declare no competing financial interest.

ACKNOWLEDGMENTS

The authors thank Jim-Fang Huang, Chao-Jie Lee, Maw-Song Lee, Kang-Sheng Fang, and Chien-Hong Chen for providing various oolong tea samples.

REFERENCES

(1) Vuong, Q. V. Epidemiological evidence linking tea consumption to human health: A review. *Crit. Rev. Food. Sci. Nutr.* **2014**, *54*, 523−536.

(2) Serafini, M.; Del Rio, D.; Yao, D. N.; Bettuzzi, S.; Peluso, I. Health benefits of tea. In *Herbal Medicine: Biomolecular and Clinical Aspects*, 2nd ed.; Benzie, I. F. F., Wachtel-Galor, S., Eds.; CRC Press (Taylor and Francis Group): Boca Raton, FL, 2011.

(3) Khan, N.; Mukhtar, H. Tea polyphenols for health promotion. *Life Sci.* **2007**, *81*, 519−533.

(4) Basu, A.; Sanchez, K.; Leyva, M. J.; Wu, M.; Betts, N. M.; Aston, C. E.; Lyons, T. J. Green tea supplementation affects body weight, lipids, and lipid peroxidation in obese subjects with metabolic syndrome. *J. Am. Coll. Nutr.* **2010**, *29*, 31−40.

(5) Haslam, E. Thoughts on thearubigins. *Phytochemistry* **2003**, *64*, 61−73.

(6) Kojima, M.; Hosoda, H.; Date, Y.; Nakazato, M.; Matsuo, H.; Kangawa, K. Ghrelin is a growth-hormone-releasing acylated peptide from stomach. *Nature* **1999**, *402*, 656−660.

(7) Sakata, I.; Nakamura, K.; Yamazaki, M.; Matsubara, M.; Hayashi, Y.; Kangawa, K.; Sakai, T. Ghrelin-producing cells exist as two types of cells, closed- and opened-type cells, in the rat gastrointestinal tract. *Peptides* **2002**, *23*, 531−536.

(8) Gutierrez, J. A.; Solenberg, P. J.; Perkins, D. R.; Willency, J. A.; Knierman, M. D.; Jin, Z.; Witcher, D. R.; Luo, S.; Onyia, J. E.; Hale, J.

E. Ghrelin octanoylation mediated by an orphan lipid transferase. *Proc. Natl. Acad. Sci. U. S. A.* **2008**, *105*, 6320−6325.
(9) Howard, A. D.; Feighner, S. D.; Cully, D. F.; Arena, J. P.; Liberator, P. A.; Rosenblum, C. I.; Hamelin, M.; Hreniuk, D. L.; Palyha, O. C.; Anderson, J.; Paress, P. S.; Diaz, C.; Chou, M.; Liu, K. K.; McKee, K. K.; Pong, S. S.; Chaung, L. Y.; Elbrecht, A.; Dashkevicz, M.; Heavens, R.; Rigby, M.; Sirinathsinghji, D. J. S.; Dean, D. C.; Melillo, D. G.; Patchett, A. A.; Nargund, R.; Griffin, P. R.; DeMartino, J. A.; Gupta, S. K.; Schaeffer, J. M.; Smith, R. G.; VanderPloeg, L. H. T. A receptor in pituitary and hypothalamus that functions in growth hormone release. *Science* **1996**, *273*, 974−977.
(10) Zigman, J. M.; Jones, J. E.; Lee, C. E.; Saper, C. B.; Elmquist, J. K. Expression of ghrelin receptor mRNA in the rat and the mouse brain. *J. Comp. Neurol.* **2006**, *494*, 528−548.
(11) Jia, Y. D.; Chen, X.; Tang, M.; Jiang, Z. Y. Expression of growth hormone secretagogue receptor type 1a in visceral vagal and spinal afferent parthways. *Shengli Xuebao* **2008**, *60*, 149−155.
(12) Hattori, N.; Saito, T.; Yagyu, T.; Jiang, B. H.; Kitagawa, K.; Inagaki, C. GH, GH receptor, GH secretagogue receptor, and ghrelin expression in human T cells, B cells, and neutrophils. *J. Clin. Endocrinol. Metab.* **2001**, *86*, 4284−4291.
(13) Gnanapavan, S.; Kola, B.; Bustin, S. A.; Morris, D. G.; McGee, P.; Fairclough, P.; Bhattacharya, S.; Carpenter, R.; Grossman, A. B.; Korbonits, M. The tissue distribution of the mRNA of ghrelin and subtypes of its receptor, GHS-R, in humans. *J. Clin. Endocrinol. Metab.* **2002**, *87*, 2988.
(14) Castaneda, T. R.; Tong, J.; Datta, R.; Culler, M.; Tschop, M. H. Ghrelin in the regulation of body weight and metabolism. *Front. Neuroendocrinol.* **2010**, *31*, 44−60.
(15) Kojima, M.; Kangawa, K. Structure and function of ghrelin. *Results. Probl. Cell Differ.* **2008**, *46*, 89−115.
(16) Kojima, M.; Kangawa, K. Ghrelin: Structure and function. *Physiol. Rev.* **2005**, *85*, 495−522.
(17) Broglio, F.; Gottero, C.; Benso, A.; Prodam, F.; Destefanis, S.; Gauna, C.; Maccario, M.; Deghenghi, R.; van der Lely, A. J.; Ghigo, E. Effects of ghrelin on the insulin and glycemic responses to glucose, arginine, or free fatty acids load in humans. *J. Clin. Endocrinol. Metab.* **2003**, *88*, 4268−4272.
(18) Ghigo, E.; Broglio, F.; Arvat, E.; Maccario, M.; Papotti, M.; Muccioli, G. Ghrelin: More than a natural GH secretagogue and/or an orexigenic factor. *Clin. Endocrinol. (Oxford, U. K.)* **2005**, *62*, 1−17.
(19) Chen, Y. J.; Kuo, P. C.; Yang, M. L.; Li, F. Y.; Tzen, J. T. C. Effects of baking and aging on the changes of phenolic and volatile compounds in the preparation of old Tieguanyin oolong teas. *Food. Res. Int.* **2013**, *53*, 732−743.
(20) Lee, V. S.; Chen, C. R.; Liao, Y. W.; Tzen, J. T. C.; Chang, C. I. Structural determination and DPPH radical-scavenging activity of two acylated flavonoid tetraglycosides in oolong tea (*Camellia sinensis*). *Chem. Pharm. Bull. (Tokyo)* **2008**, *56*, 851−853.
(21) Yamazaki, M.; Nakamura, K.; Kobayashi, H.; Matsubara, M.; Hayashi, Y.; Kangawa, K.; Sakai, T. Regulational effect of ghrelin on growth hormone secretion from perifused rat anterior pituitary cells. *J. Neuroendocrinol.* **2002**, *14*, 156−162.
(22) Lee, V. S.; Dou, J.; Chen, R. J.; Lin, R. S.; Lee, M. R.; Tzen, J. T. C. Massive accumulation of gallic acid and unique occurrence of myricetin, quercetin, and kaempferol in preparing old oolong tea. *J. Agric. Food Chem.* **2008**, *56*, 7950−7956.
(23) Dou, J.; Lee, V. S.; Tzen, J. T. C.; Lee, M. R. Rapid identification of acylated flavonol tetraglycosides in oolong teas using HPLC−MS^n. *Phytochem. Anal.* **2008**, *19*, 251−257.
(24) Ma, C.; Lv, H.; Zhang, X.; Chen, Z.; Shi, J.; Lu, M.; Lin, Z. Identification of regioisomers of methylated kaempferol and quercetin by ultra high performance liquid chromatography quadrupole time-of-flight (UHPLC-QTOF) tandem mass spectrometry combined with diagnostic fragmentation pattern analysis. *Anal. Chim. Acta* **2013**, *795*, 15−24.
(25) Ghibellini, G.; Leslie, E. M.; Brouwer, K. L. Methods to evaluate biliary excretion of drugs in humans: An updated review. *Mol. Pharmaceutics* **2006**, *3*, 198−211.
(26) Srinivas, N. R.; Mullangi, R. An overview of various validated HPLC and LC−MS/MS methods for quantitation of drugs in bile: Challenges and considerations. *Biomed. Chromatogr.* **2011**, *25*, 65−81.
(27) Blumberg, J. Introduction to the proceedings of the third international scientific symposium on tea and human health: Role of flavonoids in the diet. *J. Nutr.* **2003**, *133*, 3244S−3246S.
(28) Donovan, J. L.; Crespy, V.; Manach, C.; Morand, C.; Besson, C.; Scalbert, A.; Remesy, C. Catechin is metabolized by both the small intestine and liver of rats. *J. Nutr.* **2001**, *131*, 1753−1757.
(29) Walle, T. Methylation of dietary flavones increases their metabolic stability and chemopreventive effects. *Int. J. Mol. Sci.* **2009**, *10*, 5002−5019.
(30) Wen, X.; Walle, T. Methylated flavonoids have greatly improved intestinal absorption and metabolic stability. *Drug Metab. Dispos.* **2006**, *34*, 1786−1792.
(31) Moulin, A.; Ryan, J.; Martinez, J.; Fehrentz, J. A. Recent developments in ghrelin receptor ligands. *Chem. Med. Chem.* **2007**, *2*, 1242−1259.
(32) Mequinion, M.; Langlet, F.; Zgheib, S.; Dickson, S.; Dehouck, B.; Chauveau, C.; Viltart, O. Ghrelin: Central and peripheral implications in anorexia nervosa. *Front. Endocrinol.* **2013**, *4*, 15.
(33) Avau, B.; Carbone, F.; Tack, J.; Depoortere, I. Ghrelin signaling in the gut, its physiological properties, and therapeutic potential. *Neurogastroenterol. Motil.* **2013**, *25*, 720−732.
(34) Smith, R. G. Development of growth hormone secretagogues. *Endocr. Rev.* **2005**, *26*, 346−360.
(35) Akamizu, T.; Kangawa, K. Translational research on the clinical applications of ghrelin. *Endocr. J.* **2006**, *53*, 585−591.
(36) Hosoda, H.; Kangawa, K. Ghrelin measurement. *Nihon Rinsho* **2004**, *62* (Supplement 9), 354−356.
(37) Nagaya, N.; Kojima, M.; Uematsu, M.; Yamagishi, M.; Hosoda, H.; Oya, H.; Hayashi, Y.; Kangawa, K. Hemodynamic and hormonal effects of human ghrelin in healthy volunteers. *Am. J. Physiol.: Regul., Integr. Comp. Physiol.* **2001**, *280*, R1483−R1487.
(38) Bach, M. A.; Rockwood, K.; Zetterberg, C.; Thamsborg, G.; Hebert, R.; Devogelaer, J. P.; Christiansen, J. S.; Rizzoli, R.; Ochsner, J. L.; Beisaw, N.; Gluck, O.; Yu, L.; Schwab, T.; Farrington, J.; Taylor, A. M.; Ng, J.; Fuh, V.; Group, M. K. H. F. S. The effects of MK-0677, an oral growth hormone secretagogue, in patients with hip fracture. *J. Am. Geriatr. Soc.* **2004**, *52*, 516−523.
(39) Nass, R.; Pezzoli, S. S.; Oliveri, M. C.; Patrie, J. T.; Harrell, F. E., Jr.; Clasey, J. L.; Heymsfield, S. B.; Bach, M. A.; Vance, M. L.; Thorner, M. O. Effects of an oral ghrelin mimetic on body composition and clinical outcomes in healthy older adults: A randomized trial. *Ann. Int. Med.* **2008**, *149*, 601−611.
(40) Camilleri, M.; Acosta, A. A ghrelin agonist fails to show benefit in patients with diabetic gastroparesis: Let's not throw the baby out with the bath water. *Neurogastroenterol. Motil.* **2013**, *25*, 859−863.
(41) Ejskjaer, N.; Dimcevski, G.; Wo, J.; Hellstrom, P. M.; Gormsen, L. C.; Sarosiek, I.; Softeland, E.; Nowak, T.; Pezzullo, J. C.; Shaughnessy, L.; Kosutic, G.; McCallum, R. Safety and efficacy of ghrelin agonist TZP-101 in relieving symptoms in patients with diabetic gastroparesis: A randomized, placebo-controlled study. *Neurogastroenterol. Motil.* **2010**, *22*, 1069−e281.
(42) Ejskjaer, N.; Wo, J. M.; Esfandyari, T.; Mazen Jamal, M.; Dimcevski, G.; Tarnow, L.; Malik, R. A.; Hellstrom, P. M.; Mondou, E.; Quinn, J.; Rousseau, F.; McCallum, R. W. A phase 2a, randomized, double-blind 28-day study of TZP-102 a ghrelin receptor agonist for diabetic gastroparesis. *Neurogastroenterol. Motil.* **2013**, *25*, e140−e150.

p38 mitogen-activated protein are collectively known as stress-activated mitogen-activated protein kinases. JNK and p38 phosphorylate many known regulators of tumorigenesis, such as c-Jun, p53, Bax, Bcl-2, and Mcl-1. The activation of the p38 pathway has been shown to enhance the transcriptional activity of p53, leading to cell cycle arrest and apoptosis. JNK has also been shown to phosphorylate p53, activating transcription factor-2, c-Jun, and Elk-1 and regulating stability.[18,19] Activator protein 1 (AP-1) is a transcriptional factor which is composed of proteins belonging to the c-Fos, c-Jun, ATF, and ENDOG families, and it binds DNA at a site called a TRE and activates gene transcription. The regulation of c-Jun is complex and involves both increases in c-Jun protein levels and phosphorylation of JNK. Fos family proteins cannot form homodimers to bind a TRE in the absence of Jun.[20,21]

Polyphenol and anthocyanin-rich mulberry has been reported to have not only antiobesity, antidiabetic, antitumor, antioxidative, and anti-inflammatory effects but also neuro-, hepato-, and cardiovascular protective characteristics.[22−28] It has been reported that mulberry water extracts (MWEs) can inhibit the oxidation of low-density lipoprotein (LDL), thus preventing atherosclerosis.[29]

Our previous studies have shown that mulberry leaf extract (MLE) can inhibit atherosclerosis via effectively inhibiting proliferation and migration of VSMCs, and this inhibitory effect was attributed to the polyphenol component of MLE.[30,31] In the early stage of atherosclerosis, stimulating apoptosis of VSMCs and thus inhibiting VSMC proliferation and migration is an important process. To examine the effect of polyphenol-rich MWEs on the apoptosis of VSMCs and thus the prevention of atherosclerosis, we investigated the ability of MWEs to induce apoptosis and the underlying mechanism.

MATERIALS AND METHODS

Preparation of MWEs. MWEs were prepared from the fruit of *M. alba* L. (mulberry). Fresh mulberry fruit (500 g) was harvested and freeze-dried. Briefly, the dried fruit (100 g) was macerated, stirred with water (1000 mL), and centrifuged (6000 rpm, 10 min). The aqueous solution was lyophilized (−80 °C, 12 h) to obtain the MWEs and stored at −20 °C before use.

High-Performance Liquid Chromatography. The components of the MWEs were determined by high-performance liquid chromatography (HPLC) analysis using a Hewlett-Packard Vectra 436/33N system with a diode array detector.[32] The HPLC method employed a 5 μm RP-18 column (4.6 × 150 mm inner diameter). The MWEs were filtered through a 0.22 μm filter disk, and then 25 mg/mL of the MWEs was injected into the column. Chromatography was monitored at 280 nm, and UV spectra were collected to confirm peak purity. The mobile phase contained two solvents: A, 2% acetic acid/water; B, 0.5% acetic acid in water/acetonitrile. The total phenolic compound content in each extract was spectrophotometrically determined in accordance with the Folin−Ciocalteu procedure by reading the absorbance at 725 nm against a methanol blank. Briefly, samples (20 μL, with the addition of water to 1.6 mL) were introduced into test tubes, and then 100 μL of Folin−Ciocalteu reagent and 300 μL of sodium carbonate (20%) were added. The contents of the tubes were mixed and incubated at 40 °C for 40 min. Absorption at 725 nm was measured. The powders were then resuspended in distilled water and filtered through a 0.22 μm filter for use in cell cultures.

Animals and Diet. Thirty male New Zealand white rabbits (Da-Jung Animal Farm, Changhua, Taiwan), weighing 2000−2500 g were used. They were individually housed in metal cages in an air-conditioned room (22 ± 2 °C, 55 ± 5%, humidity), under a 12 h light/12 h dark cycle with free access to food and water. All experimental rabbits were randomly divided into five groups, each group containing six animals. Group I rabbits were fed with standard chow. Group II rabbits were fed with standard chow with 1% MWEs in the daily diet. Group III rabbits were fed with HCD diet (containing 95.7% standard Purina chow (Purina Mills, Inc.), 3% lard oil, and 1.3% cholesterol) for 10 weeks, to provoke an atherosclerotic process. Groups IV and V were fed with HCD plus 0.5% and 1.0% MWEs, respectively, in the daily diet. The selection of the MWEs dose was based on a suitable pharmacological dose for humans in a daily diet. During the 10 week feeding period, all of the animals were handled according to the guidelines of the Institutional Animal Care and Use Committee of Chung Shan Medical University for the care and use of laboratory animals. After 10 weeks, the rabbits were sacrificed by exsanguination after deep anesthesia with pentobarbital (30 mg/kg i.v.) via the marginal ear vein. Serum was stored at −80 °C prior to serum lipid analysis and measurement of serum values. The aortic arch and thoracic aortas were carefully removed to protect the endothelial lining, and the specimens were collected and freed of adhering soft tissue.

Evaluation of Atherosclerotic Lesions. Thoracic aortas were rapidly dissected, opened longitudinally, and stained with Sudan IV. Aortic arches were rapidly dissected and kept at −80 °C or in 10% neutral-buffer formalin. The sections of aortic arch were stained with hematoxylin and eosin or α-smooth muscle actin antibodies (Santa Cruz Biotechnology, Inc., CA). Immunohistochemistry was carried out to confirm the lesions. Experienced pathologists evaluated the presence of smooth muscle cells in the examined preparations.

Cell Cultures. Cell line A7r5, a rat thoracic aorta smooth muscle cell line, was obtained from ATCC (ATCC number: CRL-1444; Manassas, VA). The A7r5 cells were cultured in Dulbecco's modified Eagle's medium supplemented with 10% fetal bovine serum, 1% glutamine, 1% penicillin-streptomycin, and 1.5 g/L sodium bicarbonate (all from Gibco/BRL; Gaithersburg, MD). All cell cultures were maintained at 37 °C in a humidified atmosphere of 5% CO_2.

Cell-Cycle Analysis (Flow Cytometric Analysis). Cells synchronized at the G0 phase by serum starvation for 24 h were incubated in fresh serum-containing medium to allow for cell-cycle progression. At various time points after release from G0 arrest, the cells were analyzed by flow cytometry to determine cell-cycle distribution.[33] The cells were seeded in 10 cm dishes at a density of 10^7 cells/dish and cultured in normal or high glucose Dulbecco's modified Eagle's medium. The cells cultured in high glucose were treated with MWEs at various concentrations (0, 2.0, 4.0, 6.0, 8.0, and 10.0 mg/mL) at 37 °C for 48 h. At the end of treatment, they were collected, fixed in 1 mL of ice-cold 70% ethanol, incubated at −20 °C for at least 24 h, and centrifuged at 380 g for 5 min at room temperature. Cell pellets were treated with 1 mL of cold staining solution containing 20 μg/mL propidium iodide, 20 μg/mL RNase A, and 1% Triton X-100, and they were incubated for 15 min in darkness at room temperature. Subsequently, the samples were analyzed in a FACS Calibur system (version 2.0, BD Biosciences, Franklin Lakes, NJ) using CellQuest software. The extent of apoptosis was quantified by counting the fraction of

Table 1. Polyphenolic Compounds in the MWEs[a]

HPLC chromatogram assay	
polyphenolic compound	MWEs (%)
gallic acid	0.31 ± 0.05
protocatechuic acid	2.92 ± 0.45
catechin	0.54 ± 0.03
epigallocatechin gallate	2.68 ± 0.20
caffeic acid	1.10 ± 0.24
epicatechin	1.21 ± 0.17
p-coumaric acid	0.35 ± 0.04
rutin	3.22 ± 1.01
ferulic acid	0.27 ± 0.01
gossypin	0.26 ± 0.02
hesperetin	0.34 ± 0.10
resveratrol	0.35 ± 0.23
quercetin	0.50 ± 0.07
naringenin	0.52 ± 0.17
hydroxyflavin	0.58 ± 0.12
total	**15.13 ± 0.93**

[a]HPLC chromatograms of free polyphenols from MWEs (20 mg/mL). Quantitative assessment of the percentage of polyphenols in MWEs relative to the standards represents the average of three independent experiments.

cells with DNA content at the sub-G1 phase. The results were representative of at least three independent experiments.

DNA Fragmentation. A7r5 cells were pretreated with or without 20 nM pifithrin-α for 30 min before the addition of MWEs (1−5 mg/mL) for 48 h. The cells were detached by trypsin−EDTA, washed with phosphate buffered saline, and then subjected to genomic DNA extraction using a DNeasy Tissue Kit (QIAGEN) according to the manufacturer's instructions. DNA was separated by electrophoresis as previously described.[34]

P53, p38, JNK, ERK, PI3K, Caspase, and Fas-Ligand Inhibitor. Pifithrin-α, a p53 inhibitor, was purchased from Sigma (St. Louis, MO, U.S.A.), and diluted in dimethyl sulfoxide (DMSO). SB203580, a p38 inhibitor (Sigma, St. Louis, MO, U.S.A.), SP600125, a JNK inhibitor (Calbiochem-Novabiochem, San Diego, CA), PD98059, an ERK inhibitor (Sigma, St. Louis, MO, U.S.A.), wortmannin, a PI3K inhibitor (Sigma, St. Louis, MO, U.S.A.), and Z-VAD (OMe)-fluoromethyl ketone (FMK), a caspase inhibitor (Sigma, St. Louis, MO, U.S.A.) were diluted in DMSO. NOK-1 (sc-19681), a Fas-ligand (Fas-L) inhibitor (Santa Cruz Biotechnology, Santa Cruz, CA, U.S.A.), was diluted in phosphate-buffered saline. The cells were treated with different concentrations of the inhibitors (20 μM of SB203580, SP600125, or PD98059; 1 μM of wortmannin; 50 μM Z-VAD-FMK; or 5 μg/mL NOK-1) for 30 min followed by treatment with MWEs (3.0 mg/mL).

Transfection. A7r5 cells (3×10^5 cells/6-well dish) were pretransfected with dominant-negative (DN) JNK/p38 for 12 h. Liposome-mediated transfection was performed using LipofectAMINE Plus (Invitrogen).[35]

Extraction of Mitochondria Protein. Mitochondria were isolated with a mitochondria isolation kit according to the manufacturer's instructions by using a reagent-based method (cat. no. 89874; Pierce, Rockford).[36] After the indicated treatment of MWEs, we pelleted 2×10^7 cells by centrifuging the harvested cell suspension in a 2.0 mL microcentrifuge tube at ~850*g* for 2 min. Then, we carefully removed and discarded the supernatant. We added 800 μL of Mitochondria Isolation Reagent A, vortexed at medium speed for 5 s, and incubated the tube on ice for exactly 2 min. We added 10 μL of Mitochondria Isolation Reagent B and vortexed at maximum speed for 5 s. Then, we incubated the tube on ice for 5 min, vortexing at maximum speed every minute. We added 800 μL of Mitochondria Isolation Reagent C, and we centrifuged the tube at 700*g* for 10 min at 4 °C. We transferred the supernatant to a new, 2.0 mL tube and centrifuged at 12 000*g* for 15 min at 4 °C. Then, we transferred the supernatant (cytosol fraction) to a new tube. The pellet contained the isolated mitochondria.

Western Blot Analysis. For Western blot analysis,[37] we used specific antibodies to evaluate the expressions of p-JNK, p-p38, p-p53, p-Bad, Bad, Bcl-2, Mcl-1, p-Jun, Jun, Fos, activating transcription factor-2, cytochrome c, pro-caspase 3, cleavage-caspase 3, Fas-L, and C23 (all from Santa Cruz Biotechnology, Santa Cruz, CA, U.S.A.), p38, JNK, and p53 (Cell Signaling), and β-actin (Sigma, St. Louis, MO, U.S.A.). After the indicated treatment of MWEs (3.0 mg/mL) for 48 h, equal amounts of cell lysates (50 μg protein) were separated by electrophoresis on 8−12% SDS-PAGE and transferred to nitrocellulose membranes (Millipore, Bedford, MA, U.S.A.). The membranes were incubated with Tris-buffered saline containing 1% (W/V) nonfat-milk and 0.1% (V/V) Tween-20 for 1 h to block nonspecific binding, and they were then washed with Tween-20 for 30 min. Each membrane was incubated with the appropriate primary antibody for 2 h followed by horseradish peroxidase-conjugated second antibody (Sigma, St. Louis, MO, U.S.A.) for 1 h and developed by an ECL chemiluminescence kit (Millipore, Bedford, MA, U.S.A.), followed by analysis using AlphaImager Series 2200 software. The results were representative of at least three independent experiments.

4′, 6-Diamidino-2-phenylindole (DAPI) Staining. A7r5 cells (2×10^5 cells) were seeded in a 10 cm dish for 12 h and

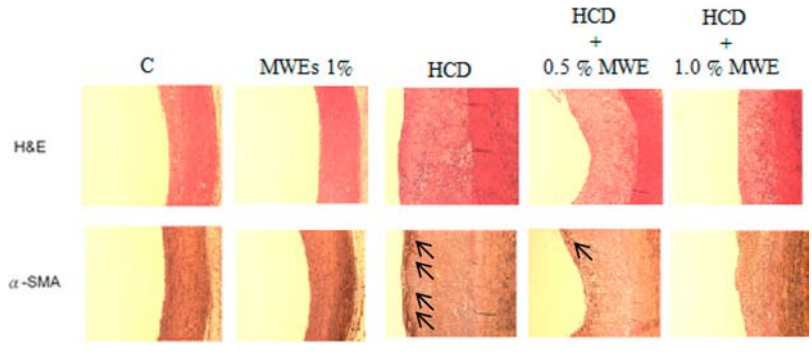

Figure 1. Histological analysis of a representative atherosclerotic lesion from HCD-fed rabbits treated for 10 weeks with MWEs.

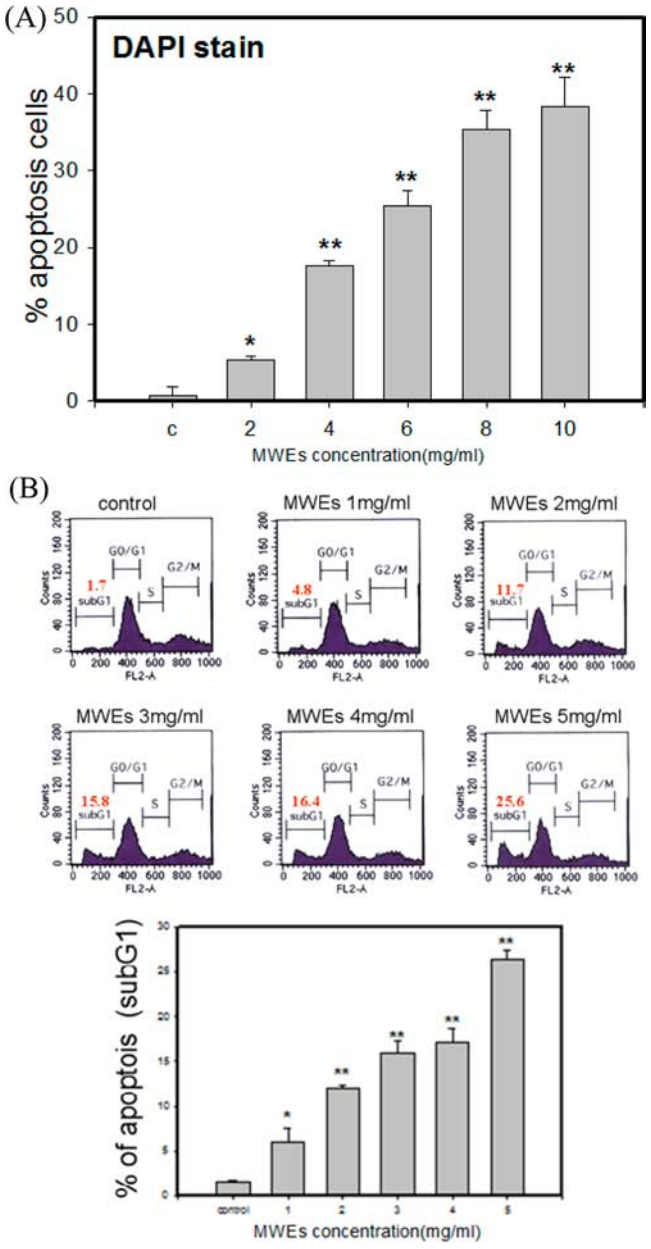

Figure 2. Effect of MWEs on the apoptosis of A7r5 cells. Cells were treated with or without MWEs (0−10 mg/mL) for 48 h, and then the apoptotic cells were stained by DAPI solution. (A) Apoptotic values were calculated as the percentage of apoptotic cells relative to the total number of cells in each random field (>100 cells). (B) Genomic DNA was analyzed by electrophoresis on 0.75% agarose gel and staining with ethidium bromide and then photographed under UV light. (C) Propidium-iodide-stained DNA histograms of the A7r5 cells were analyzed by flow cytometric analysis. Quantitative assessment of the percentage of cells in four phases represents the average of three independent experiments ± SD. *p < 0.001, **p < 0.0001 compared with the control.

then treated with MWEs (3 mg/mL) for 48 h. The A7r5 cells were fixed in 2−4% formaldehyde in phosphate-buffered saline for 30 min and then stained with DAPI (Sigma, St. Louis, MO, U.S.A.) to visualize nuclei.[38]

Statistical Analysis. The results are reported as the means and standard deviations of three independent experiments, and statistical comparisons were evaluated by one-way analysis of

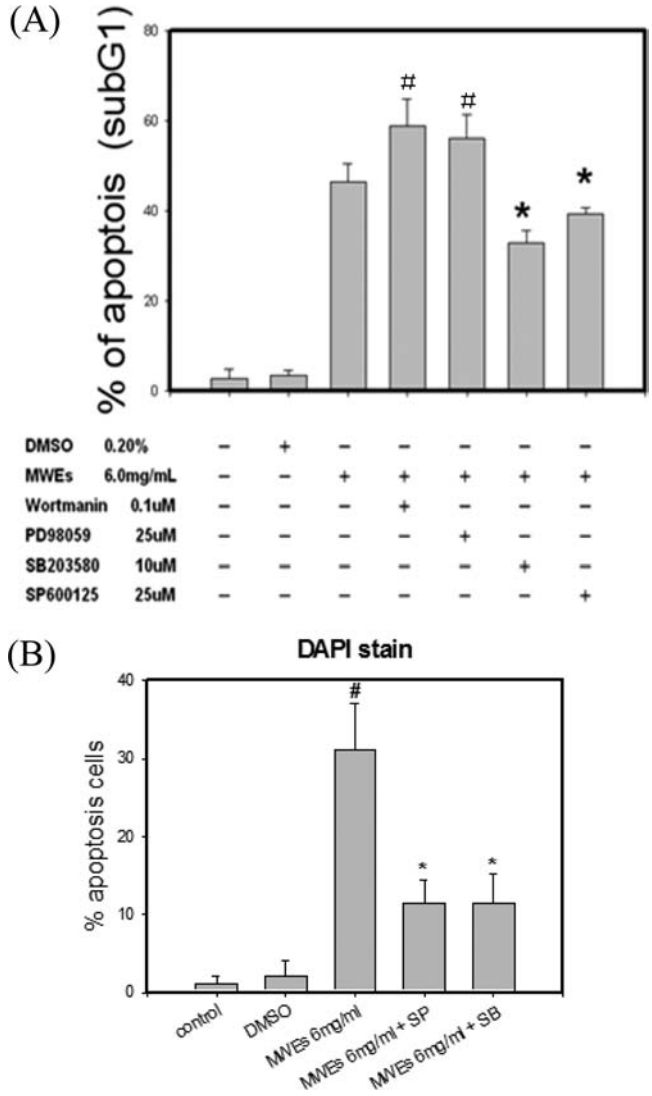

Figure 3. Effect of MAPK inhibitors on MWEs-induced apoptosis in A7r5 cells. Cultured cells were treated with or without 6.0 mg/mL of MWEs for 48 h and then treated in the absence or presence of various concentrations of wortmannin, PD98059, SP600125, and SB203580 for 30 min. Apoptosis was analyzed by (A) flow cytometry and (B) DAPI stain. Quantitative assessment of the percentage of A7r5 cells represents the average of three independent experiments. #p < 0.05, *p < 0.005 compared with MWEs only.

variance (ANOVA). A p-value less than 0.05 was considered to be statistically significant.

RESULTS

Polyphenolic Compounds of MWEs. The main constituents of MWEs have been identified as gallic acid (0.31%), protocatechuic acid (2.92%), catechin (0.54%), epigallocatechin gallate (2.68%), caffeic acid (1.10%), epicatechin (1.21%), p-coumaric acid (0.35%), rutin (3.22%), ferulic acid (0.27%), gossypin (0.26%), hesperetin (0.34%), resveratrol (0.35%), quercetin (0.50%), naringenin (0.52%), hydroxyflavin (0.58%), and unknown components without standards (Table 1).

MWEs Inhibited Proliferation of VSMCs via Stimulating Apoptosis. Histological analysis was performed on a representative atherosclerotic lesion from HCD-fed rabbits after treatment with MWEs for 10 weeks. Figure 1 shows that the MWEs dose-dependently inhibited HCD-fed-induced

dx.doi.org/10.1021/jf501466t | J. Agric. Food Chem. 2014, 62, 5092−5101

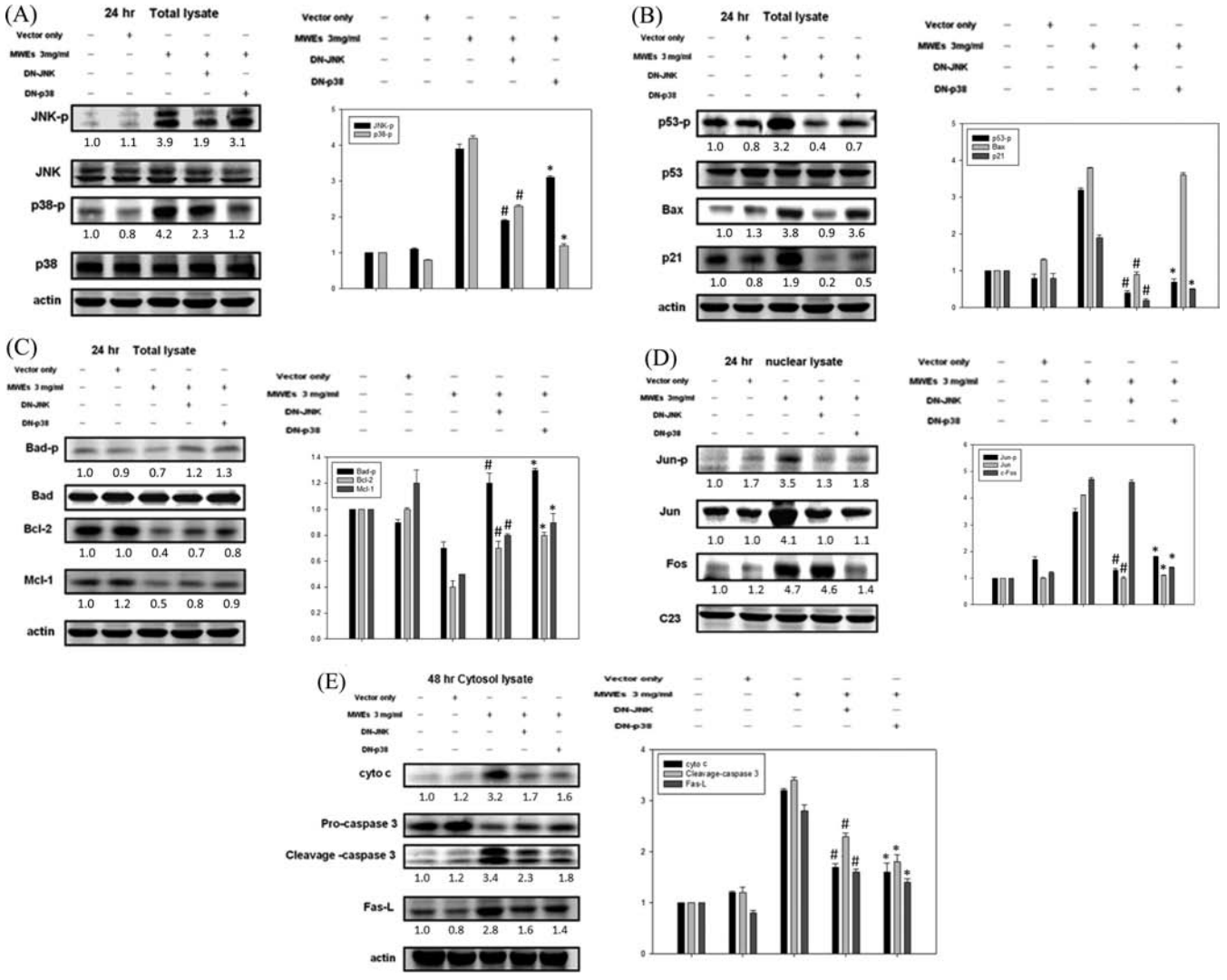

Figure 4. Effect of dominant-negative JNK/p38 on the related proteins of MWEs-induced apoptosis. A7r5 cells (5×10^5 cells/6-well dish) were pretransfected with dominant-negative JNK/p38 for 12 h and then were treated with MWEs (3.0 mg/mL) for 24 or 48 h. Cell lysates (50 μg) were prepared and subjected to Western blot analysis. Proteins were detected by (A) MAPK activation, (B) p53-signaling protein, (C) Bcl-2 family proteins, (D) nuclear transcriptional factors, and (E) caspase 3, FasL, and cytochrome c. β-actin was used for equal loading. $^{\#}p < 0.05$ compared with MWEs only, $^{*}p < 0.05$ compared with MWEs only. Beta-actin and C23 were used as internal standards.

intimal hyperplasia of vessel walls. In Figure 2, A7r5 cells were treated with or without MWEs (0−10 mg/mL) for the indicated times, and the apoptotic cells were stained by DAPI solution. As shown in Figure 2A, from the dose of 2 mg/mL, the MWEs effectively induced apoptosis of A7r5 VSMCs in a dose-dependent manner. DNA fragments in the A7r5 cells were then analyzed by electrophoresis on 0.75% agarose gel and staining with ethidium bromide. Propidium-iodide-stained DNA histograms of the A7r5 cells were analyzed by flow cytometry assay. DNA fragmentation of the A7r5 cells was increased as the dose of MWEs increased from 4 mg/mL (data not show). Flow cytometric analysis showed that the MWEs dose-dependently increased the percentage of apoptosis cells in the sub-G1 phase from the dose of 1 mg/mL (Figure 2B).

MWEs Induced Apoptosis via JNK/p38 Signaling Pathways. The A7r5 cultured cells were treated with or without 6.0 mg/mL of MWEs for 48 h in the absence or presence of wortmannin (PI3K inhibitor), PD98059 (ERK inhibitor), SB203580 (p38 inhibitor), and SP600125 (JNK inhibitor) for 30 min, and then the percentage of apoptotic cells in the sub-G1 phase was analyzed by flow cytometry and DAPI staining (Figure 3). The A7r5 cells (5×10^5 cells/6-well dish) were pretransfected with dominant-negative JNK/p38 (DN-JNK/DN-p38) for 12 h and then treated with MWEs (3.0 mg/mL) for 24 h. Total cell lysates (50 μg), nuclear lysates, and cytosol lysate were prepared and subjected to Western blot analysis. Proteins were detected by specific antibodies. In Figure 3A, the MWEs-induced apoptosis was significantly increased after treatment with inhibitors of PI3K and ERK. After inhibition of JNK and p38 with DN-JNK and DN-p38, the stimulatory effect of MWEs on apoptosis was reduced, and the MWE-induced increased DNA fragmentation was also reduced (data not show). As shown in Figure 4A, after treatment with the MWEs, the expressions of phosphorylation of JNK and p38 were significantly increased. However, these increased expressions decreased after treatment with DN-JNK and DN-p38. After treatment with the MWEs, the expressions of phosphorylation of p53, Bax, and p21 were increased (Figure 4B). The increased expressions of phosphorylated p53 and p21 after treatment with MWEs were significantly reduced

after treatment with the DN-JNK and DN-p38. The MWEs-induced increased expression of Bax was significantly reduced after inhibition of JNK but not changed after inhibition of p38. After treatment with the MWEs, the expressions of antiapoptosis proteins Bcl-2 and Mcl-1 were significantly decreased (Figure 4C). The decreased expressions of Bcl-2 and Mcl-1 after treatment with the MWEs were only partially recovered after treatment with the DN-JNK and DN-p38. After treatment with the MWEs, the expressions of Jun-p (phosphorylated Jun) and Fos in nuclei were increased (Figure 4D). Only the enhanced expression of Jun-p, but not Fos, was decreased after treatment with the DN-JNK. However, the enhanced expressions of Jun-p and Fos were decreased after treatment with the DN-p38. After treatment with the MWEs, the expressions of cytochrome c (cyto c), cleavage caspase-3 (activated caspase-3) and Fas-L in cytosol were all increased, and these increased expressions were all significantly reduced after treatment with the DN-JNK and DN-p38.

MWEs Induced Intrinsic and Extrinsic Pathways via the Up-Regulation of p53. The A7r5 cells were treated with or without 6.0 mg/mL of MWEs for 48 h in the absence or presence of 20 nM pifithrin-α (p53 inhibitor) for 30 min (Figure 5). After treatment with the MWEs, the percentage of apoptotic cells in the sub-G1 phase increased significantly (Figure 5A). After treatment with the p53 inhibitor, the percentage of apoptotic cells in the sub-G1 phase decreased significantly. The increase in DNA fragmentation after MWEs treatment was reduced after treatment with the p53 inhibitor (Figure 5B). The A7r5 cells were pretreated with or without 20 nM pifithrin-α for 30 min before the addition of the MWEs (3 mg/mL) for 24 h (Figure 6). Phospho-p53, p53, and Bax expressions were determined using a specific monoclonal antibody. After treatment with the MWEs, the expressions of phosphorylated p53 and Bax were enhanced, and these increased expressions of p53 and Bax were decreased after treatment with the p53 inhibitor (Figure 6A). After MWEs treatment, the expressions of p53 in the nuclei and mitochondria were all enhanced, and these increased expressions were reduced after treatment with the p53 inhibitor (Figure 6B). The MWEs-induced increased expression of phosphorylated JNK was decreased significantly after treatment with the p53 inhibitor (Figure 6C). However, the MWEs-induced increased expression of phosphorylated p38 was not affected after p53 inhibitor treatment. We then investigated the relationship between p53 and the downstream transcription factors of JNK and p38, including Jun, Fos, AIF, and ENDOG. The MWEs-induced increased expressions of p-Jun, AIF, and ENDOG were reduced significantly after treatment with the p53 inhibitor; however, the MWEs-induced increased expression of Fos was not affected after treatment with the p53 inhibitor (Figure 6D). The MWEs-induced decreased expressions of the antiapoptotic proteins Bcl-2 and Mcl-1 were recovered after treatment with the p53 inhibitor; however, the MWEs-induced decreased expression of phosphorylated Bad was not affected by treatment with the p53 inhibitor (Figure 6E). The MWEs-induced increased expressions of cytochrome c and activated caspase 3 from the mitochondria were decreased after treatment with the p53 inhibitor (Figure 6F). The MWEs-induced increased expression of Fas-L was also decreased after p53 inhibitor treatment.

Effect of Caspase Inhibitors on MWEs-Induced Apoptosis. A7r5 cultured cells were treated with or without 3.0 mg/mL of the MWEs for 48 h in the absence or presence of 5 μg/mL NOK-1 (Fas-L inhibitor) or 50 μM Z-VAD-FMK (caspase inhibitor) for 30 min (Figure 7). Apoptosis was analyzed by flow cytometry, and quantitative assessment of the percentage of A7r5 cells in the sub-G1 phase was completed. The increased number of MWEs-induced apoptotic cells in the sub-G1 phase were reduced after treatment with the inhibitors of Fas-L and caspase, and especially with the caspase inhibitor.

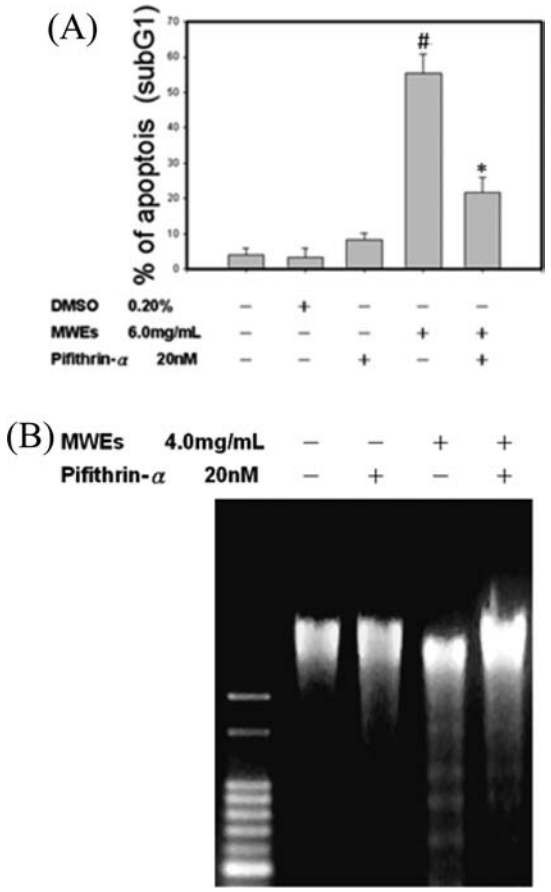

Figure 5. Effect of a p53 inhibitor on MWEs-induced apoptosis in A7r5 cells. Cultured cells were treated with or without MWEs (6.0 mg/mL) for 48 h in the absence or presence of 20 nM pifithrin-α for 30 min. (A) Apoptosis was analyzed by flow cytometry. (B) Genomic DNA was analyzed by electrophoresis on 0.75% agarose gel and staining with ethidium bromide and then photographed under UV light. The results are representative of the average of three independent experiments. $^{\#}p < 0.005$ compared with the control, $^{*}p < 0.005$ compared with MWEs only.

DISCUSSION

It has been reported that polyphenols have many biochemical activities. A previous study showed that MLE can inhibit the oxidation of LDL in rabbits and humans.[39] In addition, mulberry leaf polyphenols have been shown to possess an antiatherogenesis effect via inhibiting LDL oxidation and foam cell formation.[40] Our previous in vitro studies revealed the underlying mechanisms of polyphenol-rich MLE in the prevention of atherosclerosis via inhibiting proliferation and migration of VSMCs by way of up-regulating p53, inhibiting cyclin-dependent kinase, and blocking small GTPase, Akt/NF-κB signals. The inhibitory effect of MLE on the proliferation and migration of VSMCs has been attributed to the polyphenol component of MLE.[30,31] MWEs are rich in phenolic acids and

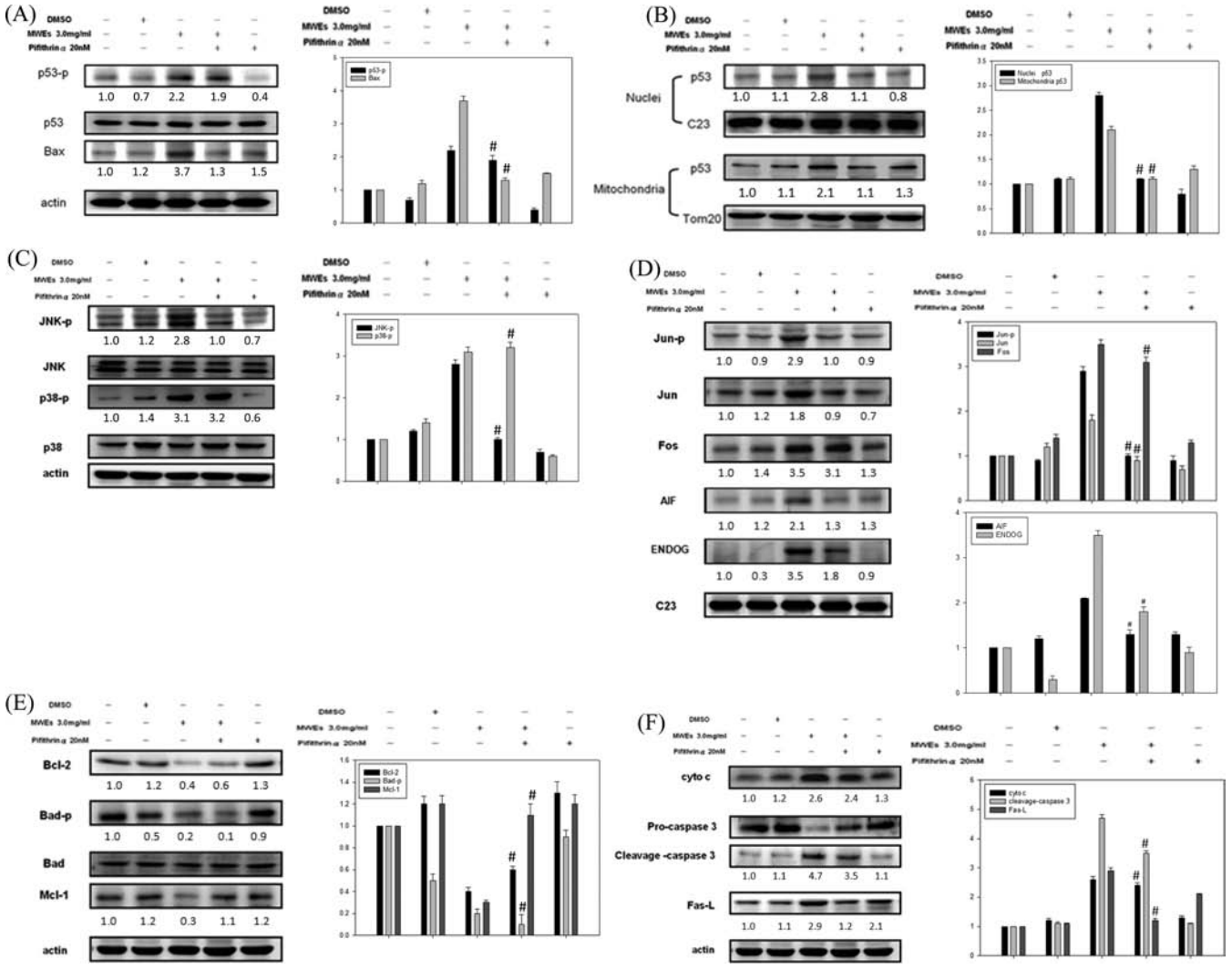

Figure 6. Effect of a p53 inhibitor on MWEs-induced p53 activation and expressions of related proteins in A7r5 cells. A7r5 cells were pretreated with or without 20 nM pifithrin-α for 30 min before the addition of MWEs at the indicated concentrations for 24 h. Fifty micrograms of total cell extracts was loaded per lane onto a 10% SDS-polyacrylamide gel and electro-blotted onto a nitrocellulose membrane. (A) p53 and Bax (B) p53 in nuclei and mitochondria extracts, (C) MAPK activation, (D) nuclear proteins, (E) Bcl-2 family protein, and (F) caspase 3, Fas-L, and cytochrome c. β-actin, C23, and Tom20 were used as internal controls. $^{\#}p < 0.05$ compared MWEs only and MWEs with pifithrin-α.

flavonoids, including gallic acid, caffeic acid, protocatechuic acid, catechin, epigallocatechin gallate, epicatechin, rutin, quercetin, and naringenin. Gallic acid has been reported to have a potential hypolipidemic effect on mice fed with a high-fat diet, as well as an ability to intervene in platelet−leukocyte interactions, thereby preventing atherosclerosis. Protocatechuic acid has also been reported to have an anti-inflammatory effect by inhibiting LDL oxidation. Flavones and catechins are the most powerful flavonoids that can protect against free radicals. Quercetin has been reported to inhibit the activity of xanthine oxidase, thereby reducing oxidative injury. Similarly, catechin, epicatechin, and epigallocatechin gallate have also been reported to have inhibitory effects on free radical production by inhibiting xanthine oxidase.[31] The supplementation of rutin was reported to promote the excretion of fecal sterols, thereby leading to a decreased absorption of dietary cholesterol as well as lower plasma and hepatic cholesterol.[41] Caffeic acid has been reported to inhibit PDGF-induced proliferation of vascular smooth muscle cells, thus to prevent atherosclerosis and restenosis.[42]

In the present in vivo and in vitro studies, we found that MWEs could effectively induce apoptosis of A7r5 VSMCs in a dose-dependent manner. As shown in Figure 3A, the MWEs-induced apoptosis was significantly increased after treatment with inhibitors of PI3K and ERK. This indicated that the mechanism of MWEs-induced apoptosis was less related to PI3K and ERK signaling. MWEs may inhibit VSMCs proliferation by way of inhibiting PI3K and ERK signaling with another unknown mechanism but not apoptosis. After treatment with inhibitors of p38 and JNK, the MWEs-induced increase in apoptosis was reduced, indicating that MWEs induce apoptosis via these two pathways. After treatment with DN-JNK and DN-p38, the increased expressions of JNK-p and p38-p by MWEs were reduced, which confirmed MWEs stimulate apoptosis via the JNK and p38 pathways. The increased expressions of phosphorylated-p53 and p21 after treatment with MWEs were significantly reduced after treatment with DN-JNK and DN-p38, indicating that JNK and p38 affect p53. The MWEs-induced increased expression of Bax was significantly reduced after treatment with DN-JNK but not changed after treatment with DN-p38, which indicates that JNK but not p38 affects the expression of Bax. The decreased expressions of the antiapoptosis proteins Bcl-2 and Mcl-1 after

dx.doi.org/10.1021/jf501466t | J. Agric. Food Chem. 2014, 62, 5092−5101

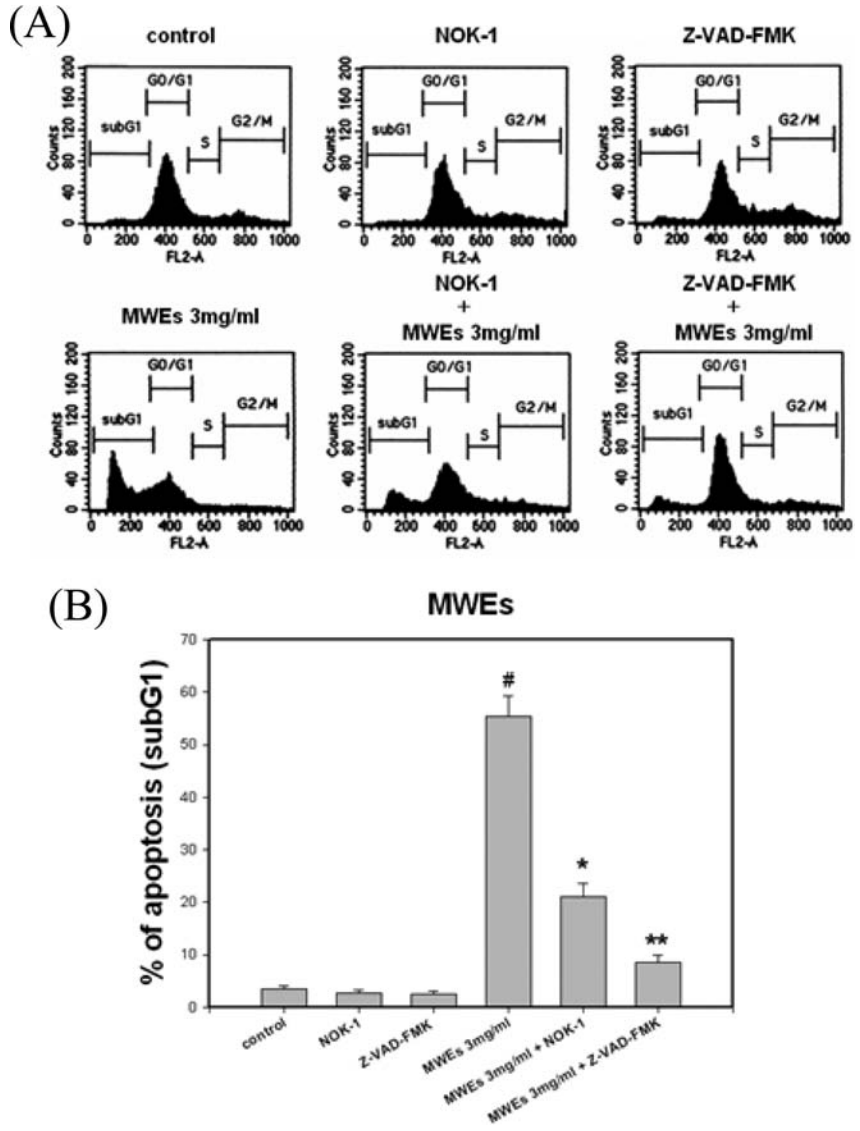

Figure 7. Effect of caspase inhibitors on MWEs-induced apoptosis in A7r5 cells. Cultured cells were treated with or without MWEs (3.0 mg/mL) for 48 h in the absence or presence of 5 μg/mL NOK-1 or 50 μM Z-VAD-FMK for 30 min. (A) Apoptosis was analyzed by flow cytometry. (B) Quantitative assessment of the percentage of A7r5 cells in the sub-G1 phase was done as indicated by propidium iodide (PI) and represents the average of three independent experiments. #p < 0.00001 compared with control, *p < 0.005, and **p < 0.0005 compared with MWEs only.

treatment with MWEs were only partially recovered after treatment with DN-JNK and DN-p38, suggesting that JNK and p38 affect the expressions of Bcl-2 and Mcl-1, but that there may still be other pathways regulating Bcl-2 and Mcl-1. Only the MWEs-induced enhanced expression of Jun-p, but not Fos, was decreased after treatment with DN-JNK. However, the MWEs-induced enhanced expressions of Jun-p and Fos were decreased after treatment with DN-p38, indicating that p38 is the key factor affecting transcription factors Jun and Fos and that JNK affects Jun. The MWEs-induced increased expressions of cytochrome c, cleavage caspase-3, and Fas-L in cytosol were all significantly reduced after treatment with DN-JNK and DN-p38, which confirmed the pathway by which MWEs activate p38 and JNK and then affect Fas-L and apoptosis. After treatment with a p53 inhibitor, the MWEs-induced increased apoptosis decreased significantly, indicating that MWEs induce apoptosis by way of p53. The MWEs-induced increased expression of Bax was decreased after treatment with a p53 inhibitor, indicating that the MWEs-induced apoptosis in mitochondria is related to p53. As shown in Figure 6B, after treatment with MWEs, the expressions of p53 in nuclei and mitochondria were enhanced, and these increased expressions were reduced again after treatment with a p53 inhibitor, indicating that MWEs affect the expressions of p53 in both nuclei and mitochondria. The MWEs-induced increased expression of phosphorylated JNK was decreased significantly after treatment with a p53 inhibitor. However, the MWEs-induced increased expression of phosphorylated p38 was not affected by treatment with a p53 inhibitor. These results indicate that p53 also affects MWEs-induced phosphorylation of JNK but not p38 phosphorylation. The MWEs-induced increased expressions of p-Jun, AIF, and ENDOG were reduced significantly after treatment with a p53 inhibitor; however, the MWEs-induced increased expression of Fos was not affected after treatment with a p53 inhibitor, indicating that p53 is upstream of Jun, AIF, and ENDOG but not Fos. The MWEs-induced decreased expressions of the antiapoptotic proteins Bcl-2 and Mcl-1 were recovered after treatment with a p53 inhibitor, however the MWEs-induced

dx.doi.org/10.1021/jf501466t | J. Agric. Food Chem. 2014, 62, 5092−5101

decreased expression of phosphorylated Bad was not affected by treatment with a p53 inhibitor. The MWEs-induced increased expressions of cytochrome c and activated caspase 3 from mitochondria were decreased after treatment with a p53 inhibitor. The MWEs-induced increased expression of Fas-L was also decreased after treatment with a p53 inhibitor. This indicates that MWEs affect apoptosis both in intrinsic mitochondria and extrinsic Fas-L pathways by way of p53. The increased number of apoptotic cells in the sub-G1 phase induced by the MWEs was reduced after treatment with the inhibitors of Fas ligand and caspase, indicating that MWEs induce apoptosis by way of both Fas-L and caspase pathways. In summary, MWEs first activate JNK/p38 and p53, which in turn activate the Fas-L and mitochondria pathways. This then causes mitochondria translocation of Bax as well as the reduction of Bcl-2, which triggers the cleavage of procaspases and finally results in apoptosis of VSMCs.

It is known that intimal hyperplasia is the main cause of restenosis after PCI. Stimulating apoptosis of VSMCs and thereby inhibiting VSMCs proliferation and migration is important for the prevention of atherosclerosis in the early stage, and this may be able to reduce the restenosis rate of PCI. The present study shows that MWEs can effectively stimulate the apoptosis of VSMCs by regulating both extrinsic and intrinsic pathways, thereby preventing atherosclerosis and intimal hyperplasia with restenosis after PCI. Our findings show that 0.5−1.0% of MWEs is effective to reduce HCD-fed-induced intimal hyperplasia in rabbits. Therefore, 2.5−5.0 g/day of MWEs for humans may be enough to prevent atherosclerosis.

AUTHOR INFORMATION

Corresponding Author

*E- mail: wcj@csmu.edu.tw. Fax: 886-4- 23248167. Tel.: 886-4-24730022 ext. 11670.

Author Contributions

#These authors contributed equally to this work and therefore share first authorship.

Funding

This study was supported by a grant (no. NSC99-2320-B-040-013-MY3) from the Ministry of Science and Technology, Taiwan.

Notes

The authors declare no competing financial interest.

ABBREVIATIONS

ATF-2: activating transcription factor-2; AP-1: activator protein 1; cyto c: cytochrome c; DAPI: 4′, 6-diamidino-2-phenylindole; DMSO: dimethyl sulfoxide; Fas-L: Fas ligand; HPLC: high-performance liquid chromatography; HCD-fed: high cholesterol diet fed; JNK: c-Jun N-terminal kinase; LDL: low-density lipoprotein; MLE: mulberry leaf extract; MWEs: mulberry water extracts; PCI: percutaneous coronary intervention; VSMCs: vascular smooth muscle cells

REFERENCES

(1) Stoneman, V. E.; Bennett, M. R. Role of apoptosis in atherosclerosis and its therapeutic implications. *Clinical Science* **2004**, *107*, 343−354.

(2) Sata, M.; Perlman, H.; Muruve, D. A.; Silver, M.; Ikebe, M.; Libermann, T. A.; Oettgen, P.; Walsh, K. Fas ligand gene transfer to the vessel wall inhibits neointima formation and overrides the adenovirus-mediated T cell response. *Proc. Natl. Acad. Sci. U. S. A.* **1998**, *95*, 1213−1217.

(3) Bennett, M. R. Apoptosis of vascular smooth muscle cells in vascular remodelling and atherosclerotic plaque rupture. *Cardiovascular research* **1999**, *41*, 361−368.

(4) Walsh, K.; Isner, J. M. Apoptosis in inflammatory−fibroproliferative disorders of the vessel wall. *Cardiovascular research* **2000**, *45*, 756−765.

(5) Ward, M. R.; Pasterkamp, G.; Yeung, A. C.; Borst, C. Arterial remodeling mechanisms and clinical implications. *Circulation* **2000**, *102*, 1186−1191.

(6) Pollman, M. J.; Hall, J. L.; Mann, M. J.; Zhang, L.; Gibbons, G. H. Inhibition of neointimal cell bcl-x expression induces apoptosis and regression of vascular disease. *Nature medicine* **1998**, *4*, 222−227.

(7) Wang, B. Y.; Ho, H. K. V.; Lin, P. S.; Schwarzacher, S. P.; Pollman, M. J.; Gibbons, G. H.; Tsao, P. S.; Cooke, J. P. Regression of atherosclerosis Role of nitric oxide and apoptosis. *Circulation* **1999**, *99*, 1236−1241.

(8) Pollman, M. J.; Hall, J. L.; Gibbons, G. H. Determinants of vascular smooth muscle cell apoptosis after balloon angioplasty injury influence of redox state and cell phenotype. *Circulation research* **1999**, *84*, 113−121.

(9) Bennett, M.; Macdonald, K.; Chan, S. W.; Luzio, J. P.; Simari, R.; Weissberg, P. Cell surface trafficking of Fas: a rapid mechanism of p53-mediated apoptosis. *Science* **1998**, *282*, 290−293.

(10) Toshiyuki, M.; Reed, J. C. Tumor suppressor p53 is a direct transcriptional activator of the human bax gene. *Cell* **1995**, *80*, 293−299.

(11) Miyashita, T.; Harigai, M.; Hanada, M.; Reed, J. C. Identification of a p53-dependent negative response element in the bcl-2 gene. *Cancer research* **1994**, *54*, 3131−3135.

(12) Bennett, M. R.; Macdonald, K.; Chan, S. W.; Boyle, J. J.; Weissberg, P. L. Cooperative interactions between RB and p53 regulate cell proliferation, cell senescence, and apoptosis in human vascular smooth muscle cells from atherosclerotic plaques. *Circulation research* **1998**, *82*, 704−712.

(13) Yonemitsu, Y.; Kaneda, Y.; Tanaka, S.; Nakashima, Y.; Komori, K.; Sugimachi, K.; Sueishi, K. Transfer of wild-type p53 gene effectively inhibits vascular smooth muscle cell proliferation in vitro and in vivo. *Circulation research* **1998**, *82*, 147−156.

(14) El-Deiry, W. S.; Tokino, T.; Velculescu, V. E.; Levy, D. B.; Parsons, R.; Trent, J. M.; Lin, D.; Mercer, W. E.; Kinzler, K. W.; Vogelstein, B. WAF1, a potential mediator of p53 tumor suppression. *Cell* **1993**, *75*, 817−825.

(15) Guevara, N. V.; Kim, H. S.; Antonova, E. I.; Chan, L. The absence of p53 accelerates atherosclerosis by increasing cell proliferation in vivo. *Nature medicine* **1999**, *5*, 335−339.

(16) Ihling, C.; Haendeler, J.; Menzel, G.; Hess, R. D.; Fraedrich, G.; Schaefer, H. E.; Zeiher, A. M. Co-expression of p53 and MDM2 in human atherosclerosis: implications for the regulation of cellularity of atherosclerotic lesions. *Journal of pathology* **1998**, *185*, 303−312.

(17) Haupt, Y.; Maya, R.; Kazaz, A.; Oren, M. Mdm2 promotes the rapid degradation of p53. *Nature* **1997**, *387*, 296−299.

(18) Whitmarsh, A.; Davis, R. Role of mitogen-activated protein kinase kinase 4 in cancer. *Oncogene* **2007**, *26*, 3172−3184.

(19) Chen, Y. R.; Wang, X.; Templeton, D.; Davis, R. J.; Tan, T. H. The role of c-Jun N-terminal kinase (JNK) in apoptosis induced by ultraviolet C and γ radiation duration of JNK activation may determine cell death and proliferation. *J. Biol. Chem.* **1996**, *271*, 31929−31936.

(20) Wisdom, R.; Johnson, R. S.; Moore, C. c-Jun regulates cell cycle progression and apoptosis by distinct mechanisms. *EMBO journal* **1999**, *18*, 188−197.

(21) Lenczowski, J. M.; Dominguez, L.; Eder, A. M.; King, L. B.; Zacharchuk, C. M.; Ashwell, J. D. Lack of a role for Jun kinase and AP-1 in Fas-induced apoptosis. *Molecular and cellular biology* **1997**, *17*, 170−181.

(22) Andallu, B.; Suryakantham, V.; Lakshmi Srikanthi, B.; Kesava Reddy, G. Effect of mulberry (Morus indica L.) therapy on plasma and erythrocyte membrane lipids in patients with type 2 diabetes. *Clin. Chim. Acta* **2001**, *314*, 47−53.

(23) Huang, H. P.; Shih, Y. W.; Chang, Y. C.; Hung, C. N.; Wang, C. J. Chemoinhibitory effect of mulberry anthocyanins on melanoma metastasis involved in the Ras/PI3K pathway. *Journal of agricultural and food chemistry* **2008**, *56*, 9286−9293.
(24) El-Beshbishy, H. A.; Singab, A. N. B.; Sinkkonen, J.; Pihlaja, K. Hypolipidemic and antioxidant effects of Morus alba L.(Egyptian mulberry) root bark fractions supplementation in cholesterol-fed rats. *Life sciences* **2006**, *78*, 2724−2733.
(25) Kimura, T.; Nakagawa, K.; Kubota, H.; Kojima, Y.; Goto, Y.; Yamagishi, K.; Oita, S.; Oikawa, S.; Miyazawa, T. Food-grade mulberry powder enriched with 1-deoxynojirimycin suppresses the elevation of postprandial blood glucose in humans. *Journal of agricultural and food chemistry* **2007**, *55*, 5869−5874.
(26) Isabelle, M.; Lee, B. L.; Ong, C. N.; Liu, X.; Huang, D. Peroxyl radical scavenging capacity, polyphenolics, and lipophilic antioxidant profiles of mulberry fruits cultivated in southern China. *Journal of agricultural and food chemistry* **2008**, *56*, 9410−9416.
(27) Huang, H.; Ou, T.; Wang, C. Mulberry (Sang Shèn Zǐ) and its Bioactive Compounds, the Chemoprevention Effects and Molecular Mechanisms In vitro and In vivo. *Journal of Traditional and Complementary Medicine* **2013**, *3*, 7.
(28) Peng, C. H.; Liu, L. K.; Chuang, C. M.; Chyau, C. C.; Huang, C. N.; Wang, C. J. Mulberry water extracts possess an anti-obesity effect and ability to inhibit hepatic lipogenesis and promote lipolysis. *Journal of agricultural and food chemistry* **2011**, *59*, 2663−2671.
(29) Chen, C. C.; Liu, L. K.; Hsu, J. D.; Huang, H. P.; Yang, M. Y.; Wang, C. J. Mulberry extract inhibits the development of atherosclerosis in cholesterol-fed rabbits. *Food chemistry* **2005**, *91*, 601−607.
(30) Chan, K. C.; Ho, H. H.; Huang, C. N.; Lin, M. C.; Chen, H. M.; Wang, C. J. Mulberry leaf extract inhibits vascular smooth muscle cell migration involving a block of small GTPase and Akt/NF-κB signals. *Journal of agricultural and food chemistry* **2009**, *57*, 9147−9153.
(31) Chan, K. C.; Ho, H. H.; Peng, C. H.; Lan, K. P.; Lin, M. C.; Chen, H. M.; Wang, C. J. Polyphenol-rich extract from mulberry leaf inhibits vascular smooth muscle cell proliferation involving upregulation of p53 and inhibition of cyclin-dependent kinase. *Journal of agricultural and food chemistry* **2010**, *58*, 2536−2542.
(32) Chang, Y. C.; Huang, K. X.; Huang, A. C.; Ho, Y. C.; Wang, C. J. Hibiscus anthocyanins-rich extract inhibited LDL oxidation and oxLDL-mediated macrophages apoptosis. *Food Chem. Toxicol.* **2006**, *44*, 1015−1023.
(33) Lo, C. W.; Huang, H. P.; Lin, H. M.; Chien, C. T.; Wang, C. J. Effect of Hibiscus anthocyanins-rich extract induces apoptosis of proliferating smooth muscle cell via activation of P38 MAPK and p53 pathway. *Molecular nutrition & food research* **2007**, *51*, 1452−1460.
(34) Lin, H. H.; Chen, J. H.; Kuo, W. H.; Wang, C. J. Chemopreventive properties of Hibiscus sabdariffa L. on human gastric carcinoma cells through apoptosis induction and JNK/p38 MAPK signaling activation. *Chemico-biological interactions* **2007**, *165*, 59−75.
(35) Mansouri, A.; Ridgway, L. D.; Korapati, A. L.; Zhang, Q.; Tian, L.; Wang, Y.; Siddik, Z. H.; Mills, G. B.; Claret, F. X. Sustained activation of JNK/p38 MAPK pathways in response to cisplatin leads to Fas ligand induction and cell death in ovarian carcinoma cells. *J. Biol. Chem.* **2003**, *278*, 19245−19256.
(36) She, H.; Yang, Q.; Shepherd, K.; Smith, Y.; Miller, G.; Testa, C.; Mao, Z. Direct regulation of complex I by mitochondrial MEF2D is disrupted in a mouse model of Parkinson disease and in human patients. *J. Clin. Invest.* **2011**, *121*, 930.
(37) Burnette, W. N. Western blotting": electrophoretic transfer of proteins from sodium dodecyl sulfate-polyacrylamide gels to unmodified nitrocellulose and radiographic detection with antibody and radioiodinated protein A. *Analytical biochemistry* **1981**, *112*, 195−203.
(38) Tarnowski, B. I.; Spinale, F. G.; Nicholson, J. H. DAPI as a useful stain for nuclear quantitation. *Biotechnic & histochemistry* **1991**, *66*, 296−302.
(39) Kojima, T.; Fujimoto, Y. Mulberry leaf extract inhibits the oxidative modification of rabbit and human low density lipoprotein. *Biological & pharmaceutical bulletin* **2000**, *23*, 1066−1071.
(40) Yang, M. Y.; Huang, C. N.; Chan, K. C.; Yang, Y. S.; Peng, C. H.; Wang, C. J. Mulberry leaf polyphenols possess antiatherogenesis effect via inhibiting LDL oxidation and foam cell formation. *Journal of agricultural and food chemistry* **2011**, *59*, 1985−1995.
(41) Park, S. Y.; Bok, S. H.; Jeon, S. M.; Park, Y. B.; Lee, S. J.; Jeong, T. S.; Choi, M. S. Effect of rutin and tannic acid supplements on cholesterol metabolism in rats. *Nutr. Res. (N.Y.)* **2002**, *22*, 283−295.
(42) Roos, T. U.; Heiss, E. H.; Schwaiberger, A. V.; Schachner, D.; Sroka, I. M.; Oberan, T.; Vollmar, A. M.; Dirsch, V. M. Caffeic acid phenethyl ester inhibits PDGF-induced proliferation of vascular smooth muscle cells via activation of p38 MAPK, HIF-1α, and heme oxygenase-1. *J. Nat. Prod.* **2011**, *74*, 352−356.

*bm*5 phenotype (five plants collected) and F2 × U740*bm*5 plants displaying a normal phenotype (five plants collected).

Samples were first roughly chopped, dried at 65 °C (ventilated oven) for 72 h and then ground with a hammer mill to pass through a 1 mm screen for further analyses. The milled samples were subjected to exhaustive extraction with water, then with ethanol in a Soxhlet apparatus. The recovered extractive-free samples were dried (65 °C) and used for the analyses of lignins and of cell-wall-linked ferulic and *p*-coumaric acids.

Dioxan lignin fractions were isolated from extractive-free U740 and U740*bm*5 stem samples according to a published procedure.[10]

Determination of Klason Lignin (KL). Extractive-free sample (approximately 300 mg weighed to the nearest 0.1 mg) was transferred to a 25 mL beaker, and a 72% (w/w) H_2SO_4 solution, which was prepared from concentrated 96% H_2SO_4 according to a published procedure,[11] was added (3 mL) while stirring with a small glass rod. The mixture was allowed to stand for 2 h at 20 ± 3 °C with rod stirring every 30 min. The content of the beaker was carefully transferred to a 250 mL round flask, and additional water was used to rinse the beaker and to dilute the acid to a final concentration of 5%. The solution was refluxed (sand bath) for 3 h and with occasional shaking. The cooled reaction mixture was quantitatively vacuum-filtered through a preweighed 60 mL porosity 1 filtering Pyrex crucible (Fischer Scientific, Illkirch, France) fitted with a type GF/A glass microfiber filter (Whatman-Fisher, Illkirch, France). The insoluble residue was washed free of acid with water and dried at 105 °C overnight. The KL content was calculated from the oven-dry weight of the residue. The crucible with residue was put in a muffle furnace at 550 °C overnight and then cooled before weighting to the nearest 0.1 mg. The KL content was corrected for the presence of acid-insoluble ash. All samples were assayed at least in triplicate.

Thioacidolysis and Subsequent Gas Chromatography−Mass Spectrometry (GC-MS) Analyses of the Lignin-Derived Monomers. The thioacidolysis reagent was prepared by adding 10 mL of ethanethiol and 2.5 mL of BF_3 etherate to a 100 mL volumetric flask containing 20 mL dioxane and then adjusting the final volume to 100 mL with dioxane. For each sample, 10 mg of extractive-free ground material was put into a 30 mL glass tube fitted with a Teflonlined screwcap, together with 7 mL of freshly prepared thioacidolysis reagent and 0.1 mL of internal standard solution (heinecosane C21, 2.5 mg/mL in CH_2Cl_2). The closed tubes were then heated for 4 h and at 100 °C (oil bath), with occasional gentle shaking. After tube cooling in ice water, 7 mL of 0.2 M $NaHCO_3$ was put into each tube to quench the excess BF_3 etherate. Then, 0.1 mL of HCl (6 M) solution was added to ensure that the pH of the reaction mixture was less than 3, before addition of 7 mL of dichloromethane extraction solvent and tube mixing. About half of the lower organic phase was carefully removed with a Pasteur pipet and dried over anhydrous sodium sulfate. The dried organic extract was then concentrated under reduced pressure to a final volume of about 1 mL. An aliquot of this solution (5 μL) was trimethylsilylated (TMS) with 100 μL of *N,O*-bis(trimethylsilyl)trifluoroacetamide and 10 μL of ACS-grade pyridine for 1 h at room temperature. The TMS sample was injected (1 μL) onto a GC-MS Varian 4000 instrument (Varian, Les Ulis, France) fitted with an autosampler, a splitless injector (280 °C), and an ion trap mass spectrometer operating in the electronic impact mode with a source at 220 °C, an interface at 280 °C, and a 50 to 650 *m*/*z* scanning range. The column used was a VF-1 ms 15 m × 0.25 mm i.d. polydimethylsiloxane capillary column (0.25 μm film thickness) (Agilent Technologies, Les Ulis, France) operated in the temperature program mode (from 45 to 180 °C at +30 °C/min, then 180 to 260 °C at +3 °C/min), with helium carrier gas at a 1.5 mL/min flow rate. The GC-MS determinations of the H, G, and S lignin-derived monomers were carried out on ion chromatograms respectively reconstructed at *m*/*z* 239, 269, and 299, as compared to the internal standard hydrocarbon evaluated on the ion chromatogram reconstructed at *m*/*z* (57 + 71 + 85).[12] In addition, the marker compound diagnostic for ferulic acid incorporation in lignins, referred to as the A_G marker,[13] was evaluated from ion chromatograms reconstructed at *m*/*z* 269. The evaluation of the frequency of free phenolic groups within the H, G, and S units was performed by the same thioacidolysis method applied to samples comprehensively permethylated according to a published procedure.[14]

Analysis of *p*-Coumaric Acid and Ferulic Acid Ester-Linked to the Cell Walls. *p*-Coumaric and ferulic acids linked to the cell walls by ester bonds were released by mild alkaline hydrolysis and then analyzed by high-performance liquid chromatography (HPLC) combined with photodiode array (PDA) detection, as previously described.[12,15]

Analysis of Arabinoxylan-Bound *p*-Coumaric and Ferulic Acids. The evaluation of *p*-coumaric and ferulic acids ester-linked to arabinose units was made according to a recently published mild acidolysis method[16] adapted from the trifluoroacetic acid hydrolysis developed earlier.[17,18] The 5-*O*-*p*-coumaroyl-L-arabinofuranose, **1**, and 5-*O*-feruloyl-L-arabinofuranose, **2**, compounds (α and β anomer mixture) (Figure 1) were analyzed by GC-MS of their TMS derivatives, as previously described.[16]

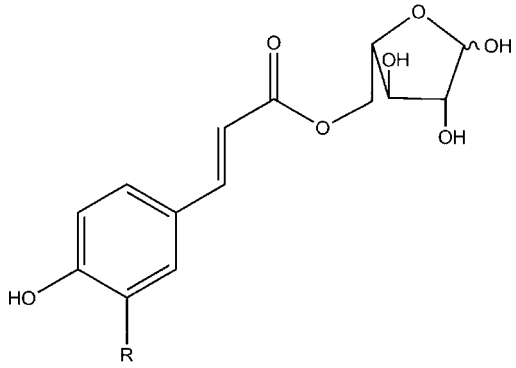

Figure 1. 5-*O*-*p*-coumaroyl-L-arabinofuranose, **1** (R = H), and 5-*O*-feruloyl-L-arabinofuranose, **2** (R = OMe), compounds (α and β anomer mixture) released by mild acidolysis of extractive-free maize samples.

RESULTS AND DISCUSSION

In the present work, we studied the cell wall phenolics (lignins and ester-linked *p*-hydroxycinnamic acids) in three different maize genetic backgrounds in order to reliably ascertain the effect of the *bm*5 mutation on these components. We thus analyzed mature stems from two inbred lines provided with the *bm*5 mutation (5803H*bm*5 and U740*bm*5) as compared to the corresponding controls (5803H and U740). In addition, we crossed the U740*bm*5 isogenic line with the INRA F2 line in

dx.doi.org/10.1021/jf5019998 | J. Agric. Food Chem. 2014, 62, 5102−5107

order to comparatively analyze F2 × U740*bm5* plants with the *bm* phenotype and F2 × U740*bm5* plants with a normal phenotype. Similar to other maize *bm* mutants,[1,2] the *bm5* plants analyzed herein displayed the brown-midrib phenotype together with the reduced Klason lignin (KL) (Table 1). In the three genetic backgrounds provided with the *bm5* mutation, the KL levels were reduced by 10−20% as compared to the corresponding controls.

Table 1. Compositional Analysis of Control (Ctrl) and *bm5* Extractive-Free Maize Samples[a]

maize samples	Klason lignin (wt %)	*p*-coumaric acid[b] (mg/g)	ferulic acid[b] (mg/g)
line 5803H[c]			
Ctrl	18.76 ± 0.55	26.19 ± 1.61	5.10 ± 0.22
bm5	15.11 ± 0.46[d]	19.53 ± 0.62[d]	5.94 ± 0.73
line U740[c]			
Ctrl	17.59 ± 0.59	29.98 ± 0.80	5.11 ± 0.12
bm5	15.62 ± 0.32[d]	23.76 ± 1.30[d]	6.91 ± 0.19[d]
F2 × U740*bm5*[e]			
no *bm* phenotype	16.32 ± 0.02	16.22 ± 0.23	4.49 ± 0.24
bm phenotype	14.30 ± 0.07[d]	11.50 ± 0.74[d]	6.37 ± 0.88[d]

[a]Data are means ± SD (n = 3 to 6). [b]Released by mild alkaline hydrolysis. [c]Stems of greenhouse-grown plants collected at the grain maturity stage. [d]Significantly different from control at $p < 0.01$ (Anova test). [e]Greenhouse-grown plants collected without ears and at the grain maturity stage.

Effect of the *bm5* Mutation on Levels of *p*-Coumarate Esters and Ferulate Esters in Lignified Cell Walls. The *bm5* mutation was found to significantly reduce the level of *p*-coumarate esters in the three *bm5* samples analyzed, which were decreased by 20−30% relative to the control values (Table 1). A reduced level of *p*-coumarate esters has also been found in *bm1* and *bm3* stems, whereas the level of *p*-coumarate esters is not affected by the *bm2* and *bm4* mutation.[1,19] The accretion of *p*-coumaric acid in maize cell walls has long been reported to parallel lignification because most maize *p*-coumarate esters are incorporated into lignins.[20,21] However, the fact that *p*-coumarate reduction by 20−30% exceeds the 10−20% reduction in lignin in *bm5* samples (Table 1) suggests that lignin *p*-coumaroylation is also affected by the *bm5* mutation. This hypothesis was confirmed by the analysis of purified dioxan lignin fractions isolated by acidolysis in refluxing dioxane/H_2O (9/1, v/v) containing 0.2 mol/L HCl for 30 min under nitrogen, a method which essentially preserves the *p*-coumarate esters linked to lignins. Although dioxan lignin fractions were recovered with a similarly high isolation yield from *bm5* and control extractive-free U740 stems (60% of the KL lignin level), the *bm5* dioxan lignin fraction contained about 10% less *p*-coumaric acid than the control dioxane lignin. *p*-Coumaric acid released by duplicate mild alkaline hydrolyses was 127.1 ± 1.5 mg/g from U740*bm5* dioxan lignin versus 140.9 ± 2.4 from U740 dioxan lignin. By contrast, the *p*-coumaroylation of maize arabinoxylans was not reduced by the *bm5* mutation as revealed by similar levels of 5-*O*-*p*-coumaroyl-L-arabinofuranose released by mild acidolysis of control and *bm5* samples (Table 2). It is noteworthy that the mild acidolysis method, run according to a recently published protocol,[16] provided the evidence that a weak but measurable amount of *p*-coumaric acid acylates maize arabinoxylans, whereas previous studies based on trifluoroacetic acid hydrolysis failed to provide such quantitation.[19,22] Taken together, these results suggest that the *bm5* mutation affects the content of *p*-coumarate esters linked to the cell walls by reducing both lignin level and lignin *p*-coumaroylation. According to literature,[23,24] both reductions could favorably affect the degradability of maize cell walls.

Table 2. Analyses of 5-*O*-*p*-Coumaroyl-L-Arabinofuranose, 1, and of 5-*O*- Feruloyl-L-Arabinofuranose, 2, Released by Mild Acidolysis of Control (Ctrl) and *bm5* Extractive-Free Maize Samples[a]

maize samples	**1** (mg/g)	**2** (mg/g)
line 5803H[b]		
Ctrl	0.10 ± 0.01	4.39 ± 0.20
bm5	0.16 ± 0.04	4.62 ± 0.34
line U740[b]		
Ctrl	0.27 ± 0.03	6.64 ± 0.12
bm5	0.32 ± 0.05	7.72 ± 0.10[c]
F2 × U740*bm5*[d]		
no *bm* phenotype	0.35 ± 0.06	3.70 ± 0.20
bm phenotype	0.48 ± 0.07	4.72 ± 0.41[c]

[a]Data are means ± SD (n = 3). [b]Stems of greenhouse-grown plants collected at the grain maturity stage. [c]Significantly different from control at $p < 0.05$ (Anova test). [d]Greenhouse-grown plants collected without ears and at the grain maturity stage.

As compared to control levels, mild alkaline hydrolysis released more ferulic acid from U740*bm5* and F2 × U740*bm5* samples provided with the *bm5* mutation (Table 1). Mild acidolysis consistently released more 5-*O*-feruloyl-L-arabinofuranose from the same *bm5* samples and relative to the controls (Table 2). It has been shown that measurable ferulate is reduced by lignification[1,25,26] as ferulate cross-links lignins to arabinoxylans not only at its *O*-4 position[27] but also in other bonding modes that resist alkaline hydrolysis.[25] Accordingly, the higher level of measurable ferulate esters observed for two *bm5* samples could originate from a higher ferulic acid incorporation into their arabinoxylans and/or from their reduced lignin content. The analysis of cell wall polysaccharides in control and *bm5* samples did not reveal any substantial change of the arabinose-to-xylose ratio, which suggests that the arabinoxylan substitution degree is not affected by the *bm5* mutation.

Unusually High Incorporation of Free Ferulic Acid in *bm5* Lignins as Revealed by Thioacidolysis. We then evaluated the impact of the *bm5* mutation on lignin structure by thioacidolysis. This method provides lignin-specific H, G, and S thioethylated monomers without any interference from ferulate and *p*-coumarate esters. In addition, the identification of minor, but diagnostic, unusual thioacidolysis monomers has provided major clues to the identification of lignin structural alterations induced by the mutation target gene.[5,28−30] On this basis, we performed an in-depth investigation of lignin-derived compounds released by thioacidolysis of extractive-free maize samples provided with the *bm5* mutation and as compared to control samples.

When calculated in μmol/gram of Klason lignin, the total yield of thioacidolysis monomers is a reflection of the frequency of lignin units only involved in 8-*O*-4 ether bonds.[4] This frequency is reduced by the *bm5* mutation as shown by lower thioacidolysis yield relative to the corresponding controls (Table 3). In addition, the relative percentage of H, G, and S thioacidolysis monomers was found to be strongly altered by

dx.doi.org/10.1021/jf5019998 | J. Agric. Food Chem. 2014, 62, 5102−5107

Table 3. Thioacidolysis Monomers Released from Extractive-Free Control and *bm*5 Maize Samples[a]

	H, G, and S main monomers (yield and % molar)				
maize samples	(H + G + S) yield (μmol/g lignin)[b]	% H	% G	% S	A_G yield (μmol/g lignin)[b]
line 5803H[c]					
Ctrl	882 ± 85	1.5 ± 0.4	43.8 ± 1.4	54.7 ± 1.3	0.25 ± 0.02
*bm*5	699 ± 31[d]	4.6 ± 0.3[d]	19.2 ± 0.7[d]	76.2 ± 0.7[d]	4.80 ± 0.11[d]
line U740[c]					
Ctrl	813 ± 14	1.7 ± 0.1	38.7 ± 1.1	59.6 ± 1.1	0.70 ± 0.15
*bm*5	586 ± 12[d]	3.6 ± 0.2[d]	21.0 ± 1.0[d]	75.4 ± 1.2[d]	3.81 ± 0.79[d]
F2 × U740*bm*5[e]					
no *bm* phenotype	602 ± 8	2.0 ± 0.3	49.8 ± 1.4	48.2 ± 1.7	0.47 ± 0.05
bm phenotype	485 ± 16[d]	4.7 ± 0.2[d]	27.6 ± 0.1[d]	67.7 ± 0.3[d]	3.77 ± 0.31[d]

[a]Data are means ± SD (n = 3). [b]Yield expressed in μmoles per gram of Klason lignin. [c]Stems of greenhouse-grown plants collected at the grain maturity stage. [d]Significantly different from control at $p < 0.05$ (Anova test). [e]Greenhouse-grown plants collected without ears and at the grain maturity stage.

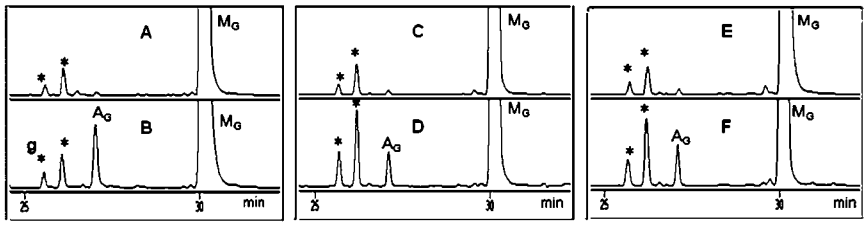

Figure 2. Partial GC-MS chromatograms reconstructed at m/z 269 of thioacidolysis monomers released from lignified cell walls of the following: (A) 5803H; (B) 5803H*bm*5; (C) U740; (D) U740*bm*5; (E) F2 × U740*bm*5 without bm phenotype; and (F) U740 × *bm*5 with bm phenotype. M_G: main guaiacyl monomers; A_G: marker for ferulic acid incorporation in lignins; * TMS derivatives of G-CHSEt-CHSET-COOH (G = guaiacyl ring), two diastereoisomers produced from thioacidolysis of ferulate esters.

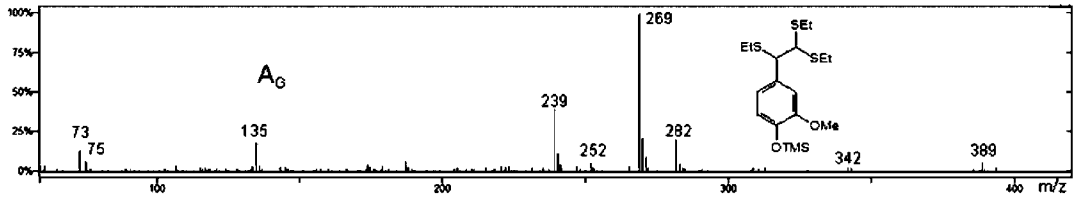

Figure 3. Mass spectrum of A_G TMS derivative ($M^{+\bullet}$ not visible, 389 ($M^{+\bullet}$-Me), 342 ($M^{+\bullet}$-EtSH), 282 (G-$(CSEt)_2$ with G = TMS guaiacyl ring), 269 (base peak, G-$CHSEt^+$), 135 ($CH(SEt)_2^+$), 75 (CH_2SEt^+), 73 (TMS^+).

the *bm*5 mutation, with a lower level of G monomers and a higher one of S or H monomers (Table 3). Beside these changes in conventional lignin-derived thioacidolysis monomers, we looked for the occurrence of unusual minor monomers. Not unexpectedly, there were neither increased 5-OH G monomers nor increased *p*-hydroxycinnamaldehyde-derived compounds, corroborating the fact that *bm*5 mutation does not affect the genes encoding the lignin-specific COMT or CAD enzymes. By contrast, 1,2,2-trithioethyl ethylguaiacol, the thioacidolysis A_G molecular marker reported to be diagnostic of the incorporation of free ferulic acid in the lignins from various cinnamoyl CoA reductase (CCR)-deficient angiosperms,[13,30,31] was systematically observed in noticeable amounts for the three genotypes provided with the *bm*5 mutation while detectable as a trace component on the GC-MS traces of control samples (Figure 2). This component could be unambiguously identified from the mass spectrum of its TMS derivative (Figure 3). It was released from samples provided with the *bm*5 mutation, with a yield accounting for 0.5−1% of the yield of the main (H + G + S) monomers, a level 5- to 20-fold higher than that from control samples (Table 3). Such an increase indicates that free ferulic acid has been incorporated into lignins at its 8 position and by *bis* 8-*O*-4 cross-coupling that induces the loss of its carboxylic group and the formation of an unusual acetal interunit bond.[9,13] This cross-coupling mode drastically contrasts with the more conventional cross-couplings of grass ferulate esters and lignin units involving mainly the ferulate *O*-4 position.[32] When subjected to thioacidolysis, ferulate esters with free or etherified *O*-4 positions only provide free ferulic acid together with its thioethylated addition products, but no A_G.[13] By contrast, A_G was released from CCR-deficient poplar, *Arabidopsis* or tobacco plants in 5- to 50-fold higher yield than from corresponding controls, a phenomenon diagnostic of ferulic acid incorporation into lignins.[13] From the three maize genotypes under examination that are provided with the *bm*5 mutation, A_G was recovered with similarly increased yields as compared to the control level.

Higher Frequency of Free-Phenolic G Units in the Lignins of Maize Provided with the *bm*5 Mutation. In addition to conventional thioacidolysis, we performed thioacidolysis following an exhaustive cell wall methylation.[4,14,33] In these conditions, thioacidolysis monomers methylated at C4 (HOMe, GOMe, and SOMe) originate from originally free-phenolic and methylatable H, G, or S parent structures, whereas monomers trimethylsilylated at C4 (HOTMS, GOTMS, and SOTMS) originate from originally etherified H, G, and S parent

dx.doi.org/10.1021/jf5019998 | J. Agric. Food Chem. 2014, 62, 5102−5107

Table 4. Percentage of Free Phenolic Groups in 8-*O*-4 Linked H, G, and S Lignin Units, as Determined by Thioacidolysis of Permethylated Samples[a]

maize samples	HOMe/(HOMe + HOTMS)[b](%)	GOMe/(GOMe + GOTMS)[b] (%)	SOMe/(SOMe + SOTMS)[b] (%)
line 5803H[c]			
Ctrl	82.5 ± 0.3	53.1 ± 0.3	8.3 ± 0.3
*bm*5	90.1 ± 0.3[d]	59.6 ± 1.2[d]	10.7 ± 0.3[d]
line U740[c]			
Ctrl	85.4 ± 2.7	55.1 ± 1.6	8.0 ± 0.3
*bm*5	87.8 ± 3.0	62.1 ± 1.4[d]	9.8 ± 0.2[d]
F2 × U740*bm*5[e]			
no *bm* phenotype	87.3 ± 0.3	48.1 ± 0.4	5.7 ± 0.4
bm phenotype	90.2 ± 0.1[d]	63.7 ± 0.5[d]	8.3 ± 0.3[d]

[a]Data are means ± SD (n = 2). [b]Monomers methylated at C4 (HOMe, GOMe, and SOMe) originate from free-phenolic parent structures, whereas monomers trimethylsilylated at C4 (HOTMS, GOTMS, and SOTMS) originate from etherified parent structures. [c]Stems of greenhouse-grown plants collected at the grain maturity stage. [d]Significantly different from control at $p < 0.01$ (Anova test). [e]Greenhouse-grown plants collected without ears and at the grain maturity stage.

structures. As shown in Table 4 and in agreement with previously published results,[4,33] the 8-*O*-4 linked H units were essentially free-phenolic units (i.e., 80−90% of H monomers were methylated at C4), whereas S units were prominently internal units etherified at C4 (only 6−8% could be methylated). G units displayed an intermediate behavior and, more importantly, the percentage of free-phenolic G units was substantially increased in the samples provided with the *bm*5 mutation. As already reported for maize samples,[4] the percentage of free-phenolic G units among the 8-*O*-4 linked G units was in the 50−55% range for the controls, whereas this percentage was in the 60−64% range for the samples with the *bm*5 mutation (Table 4). The same trend was observed for S units (Table 4). An increased frequency of free-phenolic G units relative to G units involved in 8-*O*-4 bonds has been already shown in the lignins of various CAD-deficient[4] and CCR-deficient plants.[13,30] Not unexpectedly, the thioacidolysis A_G molecular marker for ferulic acid incorporation into lignins was observed both as C4-OMe and C4-OTMS derivatives on the GC-MS traces of the TMS thioacidolysis reaction mixture obtained from permethylated samples provided with the *bm*5 mutation.

Introduction of Readily Cleavable Acetal Linkages into the Lignin Backbone by the *bm*5 Natural Mutation. In addition to the moderately reduced lignin content, the *bm*5 mutation induces substantial alterations in the structure of the lignins from the three maize *bm*5 genotypes analyzed herein. The most remarkable alteration, which is common to *bm*5 maize lignins and to the lignins from CCR-deficient plants,[13,30,31] is the increased frequency of *bis* 8-*O*-4 acetal linkages in the lignin polymers as revealed by the higher yield of the thioacidolysis-derived A_G marker. According to recent studies, these acetal bonds are produced by the incorporation of free ferulic acid into the lignin polymers through readily cleavable acetal linkages.[9,13] In recent years, research efforts have focused on redesigning lignin structure to make lignins more amenable to the chemical delignification pretreatments which are necessary for cost-effective production of cellulosic ethanol.[8,9,34] Such a structural redesigning can not only rely on elegant transgenic strategies as recently reported[35] but can also profit from spontaneous mutations like the *bm*5 maize mutation.

■ ASSOCIATED CONTENT

Supporting Information

GC-MS traces of 5-*O*-*p*-coumaroyl-L-arabinofuranose, **1**, and of 5-*O*-feruloyl- L-arabinofuranose, **2**, isomers released by acidolysis of extractive-free F2 × U740*bm*5 sample (α and β anomers analyzed as their TMS derivatives), and corresponding mass spectra (electronic impact 70 eV). GC-MS traces of thioacidolysis monomers from U740*bm*5 and from permethylated U740*bm*5 extractive-free samples. This material is available free of charge via the Internet at http://pubs.acs.org.

■ AUTHOR INFORMATION

Corresponding Author

*E-mail: catherine.lapierre@versailles.inra.fr. Fax: (33) (0)1-30-83-30-99. Tel.: (33)-(0)1-30-83-32-13.

Notes

The authors declare no competing financial interest.

■ ACKNOWLEDGMENTS

We very sincerely thank Dr. Paul Scott (Iowa State University), Dr. Thomas Lübberstedt (Iowa State University), and Dr. Marty Sachs (MGCSC, University of Illinois) for kindly providing the *bm*5 seeds in the U740 and 5803H genetic backgrounds. We thank Richard Chazal for performing the analysis of the composition of cell wall polysaccharides. This research was partially funded by the ANR Biomass for the Future program (BFF 2012−2019; http://www.biomassforthefuture.org/en/) and by the ANR MAGIC 2008−2012 program for financial support to A.L.

■ ABBREVIATIONS USED

CAD, cinnamyl alcohol dehydrogenase; COMT, caffeoyl-*O*-methyltransferase; CCR, cinnamoyl CoA reductase; G, guaiacyl; H, *p*-hydroxyphenyl; KL, Klason lignin; 5-OH G, 5-hydroxyguaiacyl; S, syringyl; TMS, trimethylsilylated

■ REFERENCES

(1) Barrière, Y.; Ralph, J.; Méchin, V.; Guillaumie, S.; Grabber, J. H.; Argillier, O.; Chabbert, B.; Lapierre, C. Genetic and molecular basis of grass cell wall biosynthesis and degradability. II. Lessons from *brown-midrib* mutants. *C. R. Biol.* **2004**, *327*, 847−860.

(2) Sattler, S. E.; Funnell-Harris, D. L.; Pedersen, J. F. *Brown midrib* mutations and their importance to the utilization of maize, sorghum, and pearl millet lignocellulosic tissues. *Plant Sci.* **2010**, *178*, 229−238.

(3) Tang, H. M.; Liu, S.; Hill-Skinner, S.; Wu, W.; Reed, D.; Yeh, C.-T.; Nettleton, D.; Schnable, P. S. The maize *brown midrib2* (*bm2*) gene encodes a methylenetetrahydrofolate reductase that contributes to lignin accumulation. *Plant J.* **2014**, *77*, 3806392.
(4) Lapierre, C. Determining lignin structure by chemical degradations. In *Lignin and lignans—Advances in Chemistry*; Heitner, C., Dimmel, D., Schmidt, J. A., Eds.; CRC Press, Taylor & Francis Group: Boca Raton, Florida, 2010; pp 11−48.
(5) Lapierre, C.; Tollier, M. T.; Monties, B. Occurrence of additional monomeric units in the lignins from internodes of a brown-midrib mutant of maize *bm3*. *C. R. Acad. Sci.* **1988**, *307*, 723−728.
(6) Ali, F.; Scott, P.; Bakht, J.; Chen, Y.; Lübberstedt, T. Identification of novel *brown midrib* genes in maize by tests of allelism. *Plant Breed.* **2010**, *129*, 724−726.
(7) Maize genetics and genomics database. URL (http://www.maizegdb.org/) (Accessed: 24 March 2014).
(8) Vanholme, R.; Morreel, K.; Ralph, J.; Boerjan, W. Lignin engineering. *Curr. Opin. Plant Biol.* **2008**, *11*, 278−285.
(9) Vanholme, R.; Morreel, K.; Darrah, C.; Oyarce, P.; Grabber, J. H.; Ralph, J.; Boerjan, W. Metabolic engineering of novel lignin in biomass crops. *New Phytol.* **2012**, *196*, 978−1000.
(10) Hibino, T.; Shibata, D.; Ito, T.; Tsuchiya, D.; Higuchi, T.; Pollet, B.; Lapierre, C. Chemical properties of lignin from *Aralia cordata*. *Phytochemistry* **1994**, *37*, 445−448.
(11) Dence, C. W. The determination of lignin. In *Methods in Lignin Chemistry*; Lin, S. Y., Dence, C. W., Eds.; Springer-Verlag: Berlin, Germany, 1992; pp 33−61.
(12) Bouvier d'Yvoire, M.; Bouchabke-Coussa, O.; Voorend, W.; Antelme, S.; Cézard, L.; Legée, F.; Lebris, P.; Legay, S.; Whitehead, C.; McQueen-Mason, S. J.; Gomez, L. D.; Jouanin, L.; Lapierre, C.; Sibout, R. Disrupting the cinnamyl alcohol dehydrogenase 1 gene (BdCAD1) leads to altered lignification and improved saccharification in *Brachypodium distachyon*. *Plant J.* **2013**, *73*, 496−508.
(13) Ralph, J.; Kim, H.; Lu, F.; Grabber, J. H.; Leplé, J.-C.; Berrio-Sierra, J.; Mir Derikvand, M.; Jouanin, L.; Boerjan, W.; Lapierre, C. Identification of the structure and origin of a thioacidolysis marker compound for ferulic acid incorporation into angiosperm lignins (and an indicator for cinnamoyl CoA reductase deficiency). *Plant J.* **2008**, *53*, 368−379.
(14) Pitre, F. E.; Pollet, B.; Lafarguette, F.; Cooke, J. E. K.; MacKay, J. J.; Lapierre, C. Effects of increased nitrogen supply on the lignification of poplar wood. *J. Agric. Food Chem.* **2007**, *55*, 10306−10314.
(15) Culhaoglu, T.; Zheng, D.; Méchin, V.; Baumberger, S. Adaptation of the Carrez procedure for the purification of ferulic and *p*-coumaric acids released from lignocellulosic biomass prior to LC/MS analysis. *J. Chromatogr. B* **2011**, *879*, 3017−3022.
(16) Petrick, D. L.; Karlen, S. D.; Cass, C. L.; Padmakshan, D.; Lu, F.; Liu, S.; Le Bris, P.; Antelme, S.; Santoro, N.; Wilkerson, C. G.; Sibout, R.; Lapierre, C.; Ralph, J.; Sedbrook, J. C. *p*-Coumaroyl-CoA:monolignol transferase (PMT) acts specifically in the lignin biosynthetic pathway in *Brachypodium distachyon*. *Plant J.* **2014**, *77*, 713−726.
(17) Brown, J. A.; Fry, S. C. The preparation and susceptibility to hydrolysis of novel *O*-galacturonoyl derivatives of carbohydrates. *Carbohydr. Res.* **1993**, *240*, 95−106.
(18) Saulnier, L.; Vigouroux, J.; Thibault, J. F. Isolation and partial characterization of feruloylated oligosaccharides from maize bran. *Carbohydr. Res.* **1995**, *272*, 241−253.
(19) Marita, J. M.; Vermerris, W.; Ralph, J.; Hatfield, R. D. Variations in the cell wall composition of maize *brown midrib* mutants. *J. Agric. Food Chem.* **2003**, *51*, 1313−1321.
(20) Ralph, J.; Hatfield, R. D.; Quideau, S.; Helm, R. F.; Grabber, J. H.; Jung, H. J. G. Pathway of *p*-coumaric acid incorporation into maize lignin as revealed by NMR. *J. Am. Chem. Soc.* **1994**, *116*, 9448−9456.
(21) Hatfield, R. D.; Marita, J. M.; Frost, K. Characterization of *p*-coumarate accumulation, *p*-coumaroyl transferase, and cell wall changes during the development of corn stems. *J. Sci. Food Agric.* **2008**, *88*, 2529−2537.
(22) Hatfield, R. D.; Chaptman, A. K. Comparing corn types for differences in cell wall characteristics and *p*-coumaroylation of lignin. *J. Agric. Food Chem.* **2009**, *57*, 4243−4249.
(23) Barrière, Y.; Thomas, J.; Denoue, D. QTL mapping for lignin content, lignin monomeric composition, *p*-hydroxycinnamate content, and cell wall digestibility in the maize recombinant inbred line progeny F838 × F286. *Plant Sci.* **2008**, *175*, 585−595.
(24) Zhang, Y.; Culhaoglu, T.; Pollet, B.; Melin, C.; Denoue, D.; Barrière, Y.; Baumberger, S.; Méchin, V. Impact of lignin structure and cell wall reticulation on maize cell wall degradability. *J. Agric. Food Chem.* **2011**, *59*, 10129−10135.
(25) Grabber, J. H.; Hatfield, R. D.; Ralph, J.; Zon, J.; Amrhein, N. Ferulate cross-linking in cell-walls isolated from maize cell-suspensions. *Phytochemistry* **1995**, *40*, 1077−1082.
(26) Grabber, J. H.; Ralph, J.; Lapierre, C.; Barrière, Y. Genetic and molecular basis of grass cell-wall degradability. I. Lignin−cell wall matrix interactions. *C. R. Biol.* **2004**, *327*, 455−465.
(27) Jacquet, G.; Pollet, B.; Lapierre, C. New ether-linked ferulic acid-coniferyl alcohol dimers identified in grass straws. *J. Agric. Food Chem.* **1995**, *43*, 2746−2751.
(28) Jouanin, L.; Goujon, T.; de Nadai, V.; Martin, M. T.; Mila, I.; Vallet, C.; Pollet, B.; Yoshinaga, A.; Chabbert, B.; Petit-Conil, M.; Lapierre, C. Lignification in transgenic poplars with extremely reduced caffeic acid *O*-methyltransferase activity. *Plant Physiol.* **2000**, *123*, 1363−1373.
(29) Kim, H.; Ralph, J.; Lu, F. C.; Pilate, G.; Leplé, J.-C.; Pollet, B.; Lapierre, C. Identification of the structure and origin of thioacidolysis marker compounds for cinnamyl alcohol dehydrogenase deficiency in angiosperms. *J. Biol. Chem.* **2002**, *277*, 47412−47419.
(30) Mir Derikvand, M.; Sierra, J. B.; Ruel, K.; Pollet, B.; Do, C.-T.; Thévenin, J.; Buffard, D.; Jouanin, L.; Lapierre, C. Redirection of the phenylpropanoid pathway to feruloyl malate in Arabidopsis mutants deficient for cinnamoyl-CoA reductase 1. *Planta* **2008**, *227*, 943−956.
(31) Leplé, J. C.; Dauwe, R.; Morreel, K.; Storme, V.; Lapierre, C.; Pollet, B.; Naumann, A.; Kang, K. Y.; Kim, H.; Ruel, K.; Lefebvre, A.; Joseleau, J. P.; Grima-Pettenati, J.; De Rycke, R.; Andersson-Gunneras, S.; Erban, A.; Fehrle, I.; Petit-Conil, M.; Kopka, J.; Polle, A.; Messens, E.; Sundberg, B.; Mansfield, S. D.; Ralph, J.; Pilate, G.; Boerjan, W. Downregulation of cinnamoyl-coenzyme a reductase in poplar: Multiple-level phenotyping reveals effects on cell wall polymer metabolism and structure. *Plant Cell* **2007**, *19*, 3669−3691.
(32) Grabber, J. H.; Ralph, J.; Hatfield, R. D. Model studies of ferulate-coniferyl alcohol cross-product formation in primary maize walls: Implications for lignification in grasses. *J. Agric. Food Chem.* **2002**, *50*, 6008−6016.
(33) Lapierre, C.; Monties, B.; Rolando, C. Thioacidolyses of diazomethane-methylated pine compression wood and wheat straw in situ lignins. *Holzforschung* **1988**, *42*, 409−411.
(34) Fu, C.; Mielenz, J. R.; Xiao, X.; Ge, Y.; Hamilton, C. Y.; Rodriguez, M.; Chen, F.; Foston, M.; Ragauskas, A.; Bouton, J.; Dixon, R. A.; Wang, Z.-Y. Genetic manipulation of lignin reduces recalcitrance and improves ethanol production from switchgrass. *Proc. Natl. Acad. Sci. USA* **2011**, *108*, 3803−3808.
(35) Wilkerson, C. G.; Mansfield, S. D.; Lu, F.; Withers, S.; Park, J.-Y.; Karlen, S. D.; Gonzales-Vigil, E.; Padmakshan, D.; Unda, F.; Rencoret, J.; Ralph, J. Monolignol ferulate transferase introduces chemically labile linkages into the lignin backbone. *Science* **2014**, *344*, 90−93.

Table 1. . Basic Chemical Profiles, Carbohydrate Chemical Profiles, and In Situ Rumen Digestibility of DM in Corn DDGS and Barley DDGS[a]

	corn DDGS coproducts from bioethanol processing				barley DDGS coproducts from beer-making					contrast				
item	1	2	3	4	5	6	7	SEM	*p* value	C_DDGS	B_DDGS	SEM	*p* value	differ estimate
Basic Chemical Profiles														
DM (g/kg)	893.7	942.9	905.3	896.6	917.6	927.5	943.2	0.17	<0.0001	907.6	935.3	0.15	<0.0001	11.84
ash (g/kg DM)	60.5	31.1	54.1	57.4	50.9	44.2	59.7	0.20	<0.0001	50.8	51.9	0.16	<0.0001	−4.26
OM (g/kg DM)	939.5	969.0	946.0	942.6	949.1	955.9	940.3	0.20	<0.0001	949.2	948.1	0.16	<0.0001	4.26
EE (g/kg DM)	77.5	154.0	74.7	65.9	82.6	150.0	35.0	1.5	<0.0001	90.9	92.5	1.08	<0.0001	24.01
Structural and Nonstructural Carbohydrate Profiles (g/kg DM)														
NDF	410.2	557.6	457.2	415.2	427.6	638.5	450.6	1.73	<0.0001	453.5	544.5	1.44	<0.0001	81.84
ADF	108.0	196.0	170.4	125.8	196.7	214.2	154.2	1.76	<0.0001	159.4	184.2	1.48	0.0016	7.35
ADL	18.9	40.0	27.0	18.4	21.2	79.4	23.9	1.60	<0.0001	25.1	51.6	1.03	<0.0001	14.53
hemicellulose	302.3	361.6	286.7	289.4	230.9	424.2	296.3	1.75	<0.0001	294.2	360.3	1.46	<0.0001	74.08
cellulose	89.1	156.0	143.4	107.4	175.4	134.9	130.3	3.12	<0.0001	134.3	132.6	2.39	0.0042	−10.69
Starch	38.8	63.5	32.4	30.0	18.9	14.4	62.9	1.14	<0.0001	36.7	38.7	0.95	<0.0001	17.97
CHO	541.9	490.9	544.2	597.9	517.8	562.8	619.0	1.75	<0.0001	536.9	590.9	0.71	0.0004	5.06
In Situ Rumen Digestibility of DM (%)														
R_DDM	56.75	28.65	51.12	57.09	46.00	46.11	56.89	0.859	<0.0001	47.92	51.50	0.043	0.0002	−3.639

[a]DM = dry matter; OM = organic matter; EE = ether extract; NDF = neutral detergent fiber; ADF = acid detergent fiber; ADL= acid detergent lignin; CHO = carbohydrate. Carbohydrate was calculated as CHO = 100 − EE − CP − Ash (NRC-2001). Hemicellulose = NDF − ADF (NRC-2001); cellulose = ADF − ADL (NRC-2001). R_DDM = in situ rumen digestibility od DM. C_DDGS = corn DDGS; B_DDGS = barley DDGS. SEM = pooled standard error of the mean. Means with the different letters in the same row are significantly different ($p < 0.05$).

dx.doi.org/10.1021/jf500711p | J. Agric. Food Chem. 2014, 62, 5108−5117

hypothesized that the changes in carbohydrate molecular structures were sensitive to different processing methods and interactively affect bioavailability in animals.

MATERIALS AND METHODS

Coproducts from Different Manufactures in China and Chemical Analysis. In this study, five kinds of corn DDGS and two kinds of barley DDGS were collected from 2012 to 2013 in China. They were numbered as "1, 2, 3, 4, 5, 6, and 7". Dry matter, ash, organic matter (OM), and ether extract (EE) were determined by using the procedure of AOAC (1990) method.[1] Neutral (NDF) and acid detergent fibers (ADF) and lignin (ADL) were determined using the filtration method.[11] For the starch content analysis, the samples were ground to 0.5 mm and measured using the Megazyme method.[12] The hemicellulose, cellulose, and carbohydrate (CHO) were calculated.[5,11]

Partitioning Carbohydrate Subfractions and Predict Values for Energy in Animals. The carbohydrate subfractions were partitioned by Cornell fraction system (CNCPS),[13,14] into CA fraction (CA = fast degradable), CB1 fraction (CB1 = medium degradable), CB2 fraction (CB2 = available cell wall), and CC fraction (CC = unfermentable fiber fraction).

Truly digestible fatty acid (tdFA), tdNDF, tdNFC, TDN, digestible ($DE_{1\times}$), metabolizable ($ME_{p3\times}$), net lactation ($NE_{lp3\times}$), net maintenance (NE_m), and net growth energy values (NE_g) were modeled[5,15,16]

In Situ Rumen Incubation. In situ nylon bag technique was used to estimate rumen digestibility of dry matter at 16 h with two nonlactating Holstein dairy cattle with a rumen cannula, housed at dairy research station in University of Saskatchewan (Saskatoon, Canada).[20,21] The detailed procedure was conducted according to previous published literature.[17−19] The animals were cared by following guidelines of the Canadian Council of Animal Care (CACC).[22]

Molecular Spectroscopy and Analyses on Carbohydrate Structure. The carbohydrate spectral features were studied at Professor Dr. Yu's molecular spectroscopy lab with JASCO FT/IR-4200 (Tokyo, Japan) in the University of Saskatchewan (Canada) following standard lab procedures.[23]

OMNIC 7.3 (Thermo-Nicolet, Madison, Wisconsin) software was used to analyze CHO molecular spectral data. The following chemical functional groups centered differently which are related to the CHO molecular structure were focused on (1) structural CHO (STCHO), (2) cellulosic compounds (CELC), and (3) total carbohydrate (CHO). The CHO spectral parameters (in terms of STCHO, CELC, and CHO peak intensity and their ratio) were obtained from publications.[24−28]

The univariate molecular spectral analysis was performed with OMNIC 7.3 (Thermo-Nicolet, Madison, Wisconsin) software. The STCHO peak, related to hemicellulose and cellulose, were in the region ca. 1507−1186 cm^{-1}, and three subpeaks in this region with peak height centering at ca. 1456, 1374, and 1240 cm^{-1}, respectively. The peak area region mainly associated with cellulose compounds was at ca. 1304−1186 cm^{-1}, and the cellulose compounds peak height centered at ca. 1240 cm^{-1}. For the CHO, the peak area region was at ca. 1217−907 cm^{-1}, and three subpeaks were also found in this region, with peak heights centered at ca. 1150, 1093, and 1037 cm^{-1}, respectively.

For multivariate molecular spectral analysis for CHO molecular structure, the CHO IR fingerprint data of different corn DDGS and barley DDGS were analyzed by cluster and principal component analyses using Statistics 8.0 software (StatSoft Inc., Tulsa, OK, U. S. A.) according to previous study.[24] These analyses were used to clarify and distinguish inherent carbohydrate structural difference and relationships among these kinds of DDGS samples within the regions of STCHO (ca. 1507−1186 cm^{-1}), cellulose compounds (ca. 1304−1186 cm^{-1}), and CHO (ca. 1217−907 cm^{-1}).

Statistical Analysis. *Basic Carbohydrate Chemical Profiles, Carbohydrate Subfractions, and Estimated Energy Studies.* All chemical composition, carbohydrate subfractions partitioned by CNCPS and estimated energy values data were analyzed by using the PROC MIXED procedure of Statistical Analysis System (SAS version 9.3, SAS Institute Inc., Cary, NC, U. S. A.).[29] The model was $Y_{ij} = \mu + F_i + e_{ij}$, where, Y_{ij} was measures ij; F_i was the feed source (i = 1−7). The comparison of corn based DDGS with barley based DDGS was carried out using Contrast statement in SAS.

In Situ Degradation. The model for the analysis was $Y_{ijk} = \mu + F_i + R_j + e_{ijk}$, where Y_{ijk} was an measure; F_i was the feed source (i = 1−7), as a fixed effect, R_j was the in situ experiment with two cows as a random effect. The comparison between corn DDGS and barley DDGS was carried out using Contrast statement in SAS.

Carbohydrate Molecular Structure Spectral Data Analysis. The FT/IR spectroscopic data were analyzed using a completely randomized design model $Y_{ij} = \mu + T_i + e_{ij}$, where Y_{ij} was measrue (STCHO peak area and three subpeak height and area, cellulose compounds peak area and peak height, CHO peak area and three subpeak height and area); T_i was the feed source (i = 1−7), as a fixed effect. The comparison between corn DDGS and barley DDGS was carried out using Contrast statement in SAS.

Correlation Analysis of CHO Molecular Spectral Profile with CHO Nutritional Profiles. The relationship between changes in CHO molecular structure spectral profile or functional groups and in CHO chemical and nutrients profiles (chemical composition, CHO fractions partitioned by CNCPS, in situ rumen degradation of DM) in the different types of Chinese DDGS were analyzed by using the PROC CORR procedure of SAS 9.2.[29] The assumption for correlation analysis was checked using Shapiro-Wilk method.

Significance was declared at $p < 0.5$. Differences among treatments were evaluated using Tukey-Karmer method; means with different letters were obtained with "pdmix800 SAS macro".[29]

RESULTS AND DISCUSSION

Difference in CHO Chemical Profiles and CHO Fractions among All DDGS Samples. The detailed CHO chemical profiles are presented in Table 1. Chemical feature differ among the DDGS samples. Our results showed that DM content in five kinds of corn DDGS and two kinds of barley DDGS was different ($p < 0.05$), and ash content in all DDGS samples also was different ($p < 0.05$). It might be explained by different plant location of original cereal grains, which produce the coproductions. Organic matter content in corn DDGS was similar (949 vs 956 g/kg DM) with previous study.[30] The content of EE showed differences ($p < 0.05$) among all DDGS samples. Corn DDGS was lower ($p < 0.05$) in NDF than barley DDGS (454 vs 545 g/kg DM), lower ($p < 0.05$) in ADF than

Table 2. Carbohydrate Fractions, Truly Digestible Nutrients, Energy Values, and In Situ Digestibility of DM in Corn DDGS and Barley DDGS[a]

	corn DDGS coproducts from bioethanol processing					barley ddgs Coproducts from beer-making				contrast				
item	1	2	3	4	5	6	7	SEM	p value	C-DDGS	B_DDGS	SEM	p value	estimate
Fractions of Carbohydrate Partitioned by CNCPS (g/kg CHO)														
CA	425.8	28.1	361.0	447.7	415.5	15.0	350.3	2.88	<0.0001	335.6	182.7	2.36	<0.0001	−195.54
CB1	38.8	63.5	32.4	30.0	18.9	14.6	62.9	1.15	<0.0001	36.7	38.8	0.95	<0.0001	18.01
CB2	452.0	712.9	489.8	446.4	467.4	628.3	494.2	8.78	<0.0001	513.7	561.3	5.67	<0.0001	98.54
CC	83.6	1956	116.9	76.0	98.4	338.2	92.7	7.68	<0.0001	114.1	215.5	4.84	<0.0001	78.19
Truly Digestible Nutrients and Total Digestible Nutrient (g/kg DM)														
tdNFC	246.8	44.1	213.7	271.3	220.5	18.5	250.7	1.59	<0.0001	199.3	134.6	1.33	<0.0001	−91.14
tdFA	67.5	144.0	64.7	55.9	72.6	140.0	25.0	1.50	<0.0001	80.9	82.5	1.08	<0.0001	24.01
tdNDF	170.7	240.1	188.9	180.9	168.5	252.1	213.1	3.96	<0.0001	189.8	232.6	3.32	<0.0001	38.50
$TDN_{1\times}$	807.8	853.6	772.1	790.9	803.4	752.8	733.4	2.79	<0.0001	805.6	743.1	2.31	0.0013	−13.17
Predicted Energy Values (Mcal/kg DM) (NRC-2001 Dairy and NRC-1996 Beef)														
$DE_{1\times}$	3.82b	4.01a	3.65d	3.71c	3.82b	3.49e	3.47e	0.0115	<0.0001	3.80	3.48	0.0096	<0.0001	−0.0785
$MEp_{3\times}$	2.82	2.94	2.74	2.76	2.83	2.67	2.64	0.0042	<0.0001	2.82	2.66	0.0033	<0.0001	−0.0035
$NEl_{p3\times}$	1.82	1.94	1.76	1.77	1.82	1.74	1.67	0.0038	<0.0001	1.82	1.71	0.0032	<0.0001	−0.0095
NE_m	2.38	2.56	2.24	2.29	2.38	2.13	2.08	0.0100	<0.0001	2.37	2.11	0.0084	0.0002	−0.0575
NE_g	1.66	1.81	1.55	1.59	1.66	1.46	1.41	0.0061	<0.0001	1.65	14.4	0.0058	0.002	−0.0490

[a]CNCPS = Cornell net carbohydrate and protein system; carbohydrate sub fractions using CNCPS include: CA = fraction of CHO that is instantaneously solubilized at time zero; CB1 = fraction of CHO that is rapidly degradable; CB2 = fraction of CHO that is slowly degradable; CC = fraction of CHO that is considered to be undegradable. tdNFC = total digestible nonfiber carbohydrate; tdFA = total digestible fatty acid; tdNDF = total digestible neural detergent fiber; TDN1× = total digestible nutrient at one times maintenance estimated for NRC dairy model 2001. $DE_{1\times}$ = digestible energy at one times maintenance estimated for NRC dairy model 2001; $ME_{p3\times}$ = metabolizable energy at production level of intake (3×) estimated from NRC dairy model 2001; $NE_{lp3\times}$ = net energy for lactation at production level of intake (3 ×) estimated from NRC dairy model 2001. NEm = net energy for maintenance estimated from NRC beef model 1996; NEg = net energy for growth estimated from NRC beef model 1996. C_DDGS = corn DDGS; B_DDGS = barley DDGS. SEM = pooled standard error of the mean. Means with the different letters in the same row are significantly different ($p < 0.05$).

dx.doi.org/10.1021/jf500711p | J. Agric. Food Chem. 2014, 62, 5108−5117

Table 3. Molecular Spectral Characteristics of Structure and Non-Structure Carbohydrate in Corn DDGS and Barley DDGS[†]

	corn DDGS (coproducts from bioethanol processing)					barley DDGS coproducts from beer-making				contrast				
item	1	2	3	4	5	6	7	SEM	*p* value	C_ DDGS	B_DDGS	SEM	*p* value	estimate
Structural Carbohydrate (STCHO) Spectral Profiles														
Cel_1_H	0.028	0.025	0.020	0.018	0.219	0.024	0.011	0.0008	<0.0001	0.062	0.018	0.0007	0.0253	0.0016
Cel_2_H	0.017	0.013	0.011	0.018	0.012	0.012	0.019	0.0006	<0.0001	0.014	0.016	0.0005	0.1967	−0.0007
Cel_3_H	0.012	0.018	0.010	0.026	0.011	0.016	0.013	0.0008	<0.0001	0.015	0.015	0.0007	<0.0001	−0.0045
Cel_He_A	4.035	3.028	2.485	6.082	2.015	3.459	3.125	0.1555	<0.0001	3.529	3.292	0.1302	<0.0001	−0.8222
Cellulosic Compounds (CELC) Profiles														
Cel_H	0.011	0.017	0.011	0.016	0.013	0.012	0.011	0.0008	<0.0001	0.014	0.012	0.0006	0.0052	−0.0019
Cel_A	0.857	0.847	0.568	1.661	0.395	0.594	0.551	0.0340	<0.0001	0.866	0.573	0.0287	<0.0001	−0.0344
Total Carbohydrate (CHO) Profiles														
CHO_1_H	0.081	0.038	0.059	0.027	0.043	0.022	0.030	0.0043	<0.0001	0.050	0.026	0.0036	0.0053	0.0106
CHO_2_H	0.201	0.096	0.133	0.098	0.100	0.085	0.084	0.0082	<0.0001	0.126	0.085	0.0069	0.0042	0.0207
CHO_3_H	0.153	0.120	0.147	0.153	0.114	0.116	0.122	0.0062	<0.0001	0.137	0.119	0.0052	0.7450	−0.0017
CHO_1_A	2.666	1.305	1.558	0.647	1.137	0.629	0.918	0.0940	<0.0001	1.463	0.774	0.0786	<0.0001	0.5235
CHO_2_A	11.018	4.746	5.610	5.969	4.212	4.069	3.876	0.4165	<0.0001	6.311	3.973	0.3488	0.0313	0.7735
CHO_3_A	9.526	9.179	12.879	9.251	9.723	9.599	9.739	0.5285	<0.0001	10.112	9.669	0.4426	0.1222	0.6962
CHO_A	23.21	15.23	20.059	15.87	15.08	14.30	14.53	0.876	<0.0001	17.89	14.42	0.734	0.0090	1.995
CHO Spectral Ratio Profiles														
RA_CH1_2	0.242	0.283	0.280	0.109	0.275	0.155	0.237	0.0096	<0.0001	0.238	0.196	0.0080	<0.0001	0.0473
RA_CH1_3	0.242	0.283	0.280	0.109	0.275	0.155	0.237	0.0096	<0.0001	0.238	0.196	0.0080	<0.0001	0.0473
RA_CH2_3	1.171	0.510	0.442	0.646	0.454	0.425	0.398	0.0433	<0.0001	0.645	0.412	0.0363	0.2872	0.0390
RH_CH1_2	0.40	0.39	0.440	0.284	0.432	0.256	0.358	0.0344	<0.0001	0.390	0.307	0.0288	0.6889	0.0116
RH_CH1_3	0.528	0.307	0.400	0.179	0.380	0.188	0.245	0.0259	<0.0001	0.359	0.217	0.0216	0.0164	0.0538
RH_CH2_3	1.171	0.510	0.442	0.646	0.454	0.425	0.398	0.0433	<0.0001	0.645	0.412	0.0363	0.2872	0.0390
RA_St_CH	0.174	0.201	0.123	0.383	0.135	0.244	0.215	0.0064	<0.0001	0.203	0.230	0.0053	<0.0001	−0.0674
RA_AI_CH	0.274	0.313	0.201	0.543	0.195	0.175	0.351	0.0119	<0.0001	0.305	0.263	0.0010	<0.0001	−0.1063

[†]Cel_1_H = STCHO 1st peak height, centered at ca. 1456 cm^{-1}; Cel_2_H = STCHO second peak height, centered at ca. 1374 cm^{-1}; Cel_3_H = STCHO third peak height, centered at ca. 1240 cm^{-1}; Cel_He_A = STCHO area, baseline ca. 1507−1186 cm^{-1}. Cel_H = Cellulosic compounds peak height, centered at ca. 1240 cm^{-1}; Cel_A = Cellulosic compounds area, baseline ca. 1304−1186 cm^{-1}. CHO_1_H = CHO 1st peak height, centered at ca. 1150 cm^{-1}; CHO_2_H = CHO second peak height, centered at ca. 1093 cm^{-1}; CHO_3_H = CHO third peak height, centered at ca. 1037 cm^{-1}; CHO_1_A = CHO 1st peak area; CHO_2_A = CHO second peak area; CHO_3_A = CHO third peak area; CHO_A = CHO area; CHO peak baseline and region were ca. 1217−907 cm^{-1}. RA_CH1_2 = ratio of CHO 1st peak area to second peak area; RA_CH1_3 = ratio of CHO 1st area to second peak area; RA_CH2_3 = ratio of peak second peak area to third peak are RH_CH1_2 = ratio of CHO 1st peak height to second peak height; RH_CH1_3 = ratio od CHO 1st height to third peak height; RH_CH2_3 = ratio of peak second height to third peak height; RA_St_CH = ratio of STCHO areat to CHO area; RA_AI_CH = ratio of amide I area to CHO area. Different ratios were calculated o n the basis of relevant spectral intensity data. C_DDGS = corn DDGS; B_DDGS = barley DDGS. SEM = pooled standard error of the mean. Means with the different letters in the same row are significantly different ($p < 0.05$).

dx.doi.org/10.1021/jf500711p | J. Agric. Food Chem. 2014, 62, 5108−5117

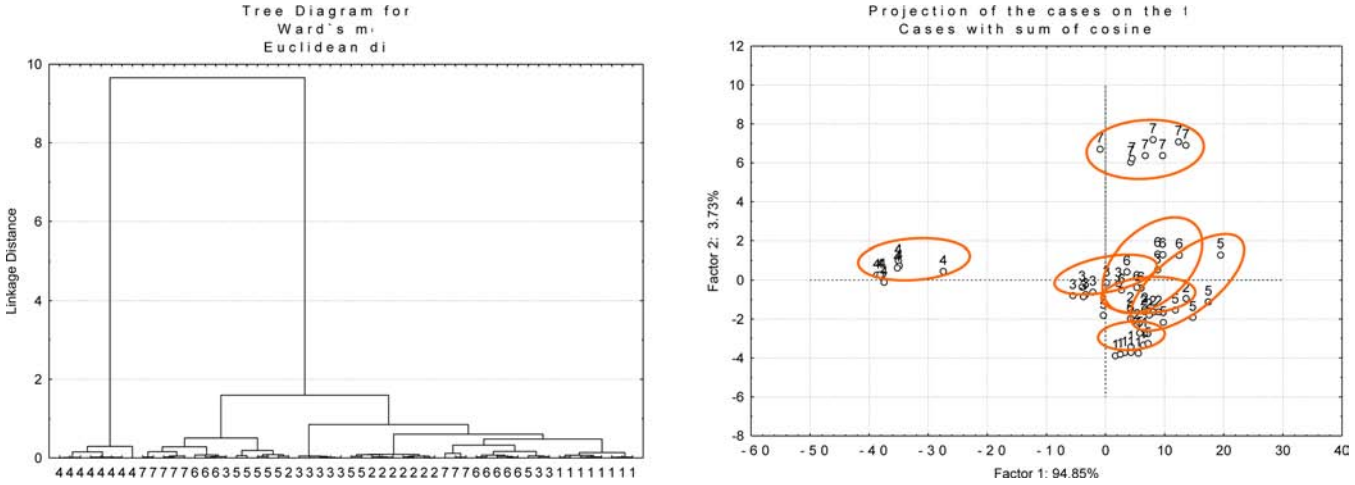

Figure 1. Multivariate molecular spectral analysis of STCHO (region: 1507−1186 cm^{-1}) CLA and PCA analysis.

barley DDGS (160 vs 184 g/kg DM), and lower ($p < 0.05$) in ADL than barley DDGS (25 vs 52 g/kg DM). Some residual starch in the Chinese DDGS samples indicated incompleted fermentation. However, the residual starch in the sample was not significantly different between two types of DDGS (37 vs 39 g/kg DM). The residual starch content in all seven DDGS samples was different ($p < 0.05$); cereal grain fermentation efficiency may account for the difference, which is associated with grain particle size, liquids temperature, and fermentation time in processing.

Carbohydrate subfractions, which were partitioned by CNCPS and included CA, CB1, CB2, and CC, are shown in Table 2. Compared with barley DDGS, corn DDGS was higher ($p < 0.05$) in the CA subfraction, lower ($p < 0.05$) in the CB2 subfraction and CC subfraction, similar in the CB1 subfraction. The CA subfraction content in corn DDGS in our result is much higher than the previous reported,[30] and the CA content in barley DDGS in our study is lower than previous study.[31]

Difference in Predicted Value for Energy in Animal from Corn DDGS and Barley DDGS. The NRC models are applied to predict the coproduct value of energy in animals, the results are presented in Table 2. Compared to barley DDGS, corn DDGS was lower ($p < 0.05$) in truly digestible FA and truly digestible NDF. Corn DDGS in our study was lower ($p < 0.05$) in TDN (806 vs 898 g/kg DM), lower ($p < 0.05$) in tdNDF (190 vs 221 g/kg DM), and higher ($p < 0.05$) in tdNFC (199 vs 85 g/kg DM) than corn DDGS in previous literature.[30] This may indicate that corn DDGS in our study is superior to those previous reported. In this study, the $DE_{1\times}$, $ME_{p3\times}$, $NE_{lp3\times}$, and NE_g in barley DDGS were not different from corn DDGS ($p > 0.05$).

Difference in In Situ Rumen Degradation. The effects of the DDGS types on in situ rumen degradability of DM (R_DDM) after 16 h rumen incubation are presented in Table 1. There are significant different ($p < 0.05$) in D_DM at 16 h incubation between corn DDGS and barley DDGS (R_DDM: 47.9−51.5%). Rumen degradability of DM at 24 and 48 h in the previous study were 65.8% and 81.8%, respectively.[30] There were no large quantities left after 24 h fermentation for the coproducts. In the lactating cow with typical levels of intake, little DM remains for 48 h. The samples were often stay in rumen for 12 to 18 h, and then the residue flows into the small intestine.[32]

Carbohydrate Molecular Structure Features in Different Type and Sources of DDGS. Absorbed IR intensity of carbohydrate and their spectral ratios in different type of DDGS are presented in Table 3. The carbohydrate-related molecular spectral groups or functional groups in our study are involved structural carbohydrate (STCHO), cellulose compounds (CELC), and total carbohydrate (CHO). For STCHO fraction, such as hemicellulose, cellulose and nonstructural carbohydrate, there were significantly different ($p < 0.05$) between corn DDGS and barley DDGS with regard to most of spectral profiles. The STCHO first and third peak heights as well as area absorbed intensities for corn DDGS were 0.062, 0.015, and 3.529 IR units and 0.018, 0.015, and 3.929 IR units for barley DDGS, respectively. The difference between the two type of DDGS may imply that the hemicellulose and cellulose compounds were higher ($p < 0.05$) in corn DDGS than in barley DDGS. However, no difference ($p > 0.05$) was observed between those two types of DDGS in STCHO second peak height. For CELC fraction, corn DDGS was significantly ($p < 0.05$) higher than barley DDGS in cellulose compound peak area (0.866 vs 0.573 IR unit). The absorption peak concentrate at ca. 1240 cm^{-1} within STCHO region (ca. 1507−1186 cm^{-1}), which was associated with CELC (baseline ca. 1304−1186 cm^{-1}), Compared to SCHO spectral parameters, corn DDGS was similar to barley DDGS in CELC peak height absorption intensities. These results are in good accordance with cellulose data showed in Table 1. CHO spectral intensities in terms of peak intensity area and three-subpeak area and height were significantly different ($p < 0.05$) in those two type of DDGS with regard to most of CHO spectral parameters. The above carbohydrate functional group ratios are associated with feed quality and nutritive values.[33,34]

In our study, parameters of ratio in terms of peak height and peak area showed significant difference ($p < 0.05$) between these two types of DDGS samples with regards to most of carbohydrate spectra. Corn DDGS had higher ($p < 0.05$) ratio values of CHO first peak to second and third peak area than barley DDGS (0.238 vs 0.196 IR unit). The ratio values of CHO first peak to third peak height in corn DDGS was higher ($p < 0.05$) than barley DDGS (0.359 vs 0.217 IR unit). The ratio of STCHO to CHO peak intensity area and amide I to CHO peak intensity area ratio were significantly different ($p < 0.05$) between corn DDGS and barley DDGS, the value of the peak area ratio was 0.203, 0.230, 0.305, and 0.263 IR unit,

dx.doi.org/10.1021/jf500711p | J. Agric. Food Chem. 2014, 62, 5108−5117

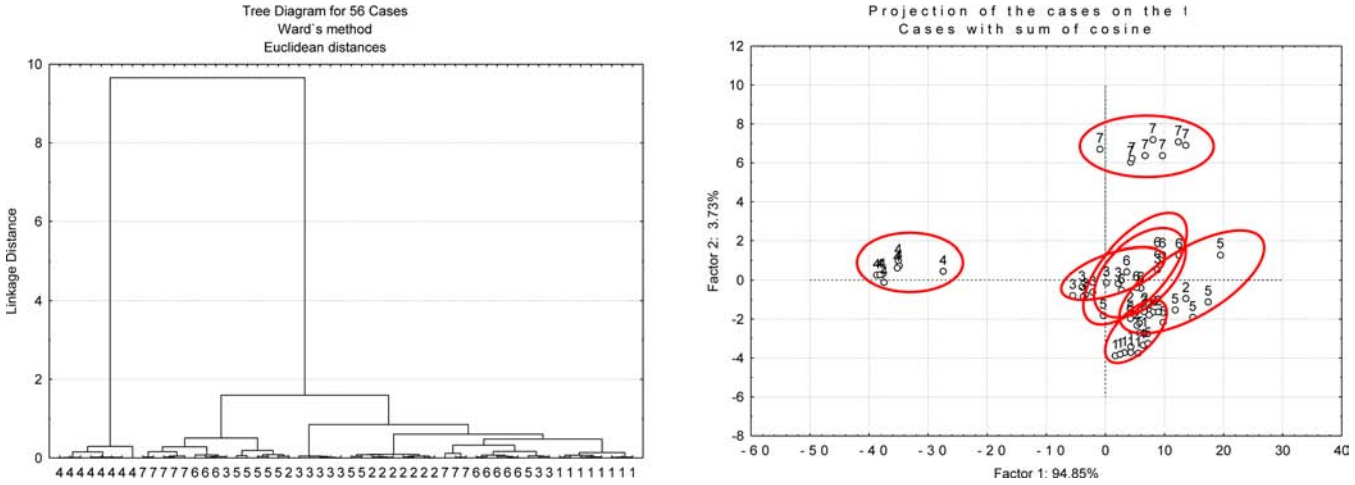

Figure 2. Multivariate molecular spectral analysis of cellulosic compounds (region: 1304−1186 cm^{-1}) CLA and PCA analysis.

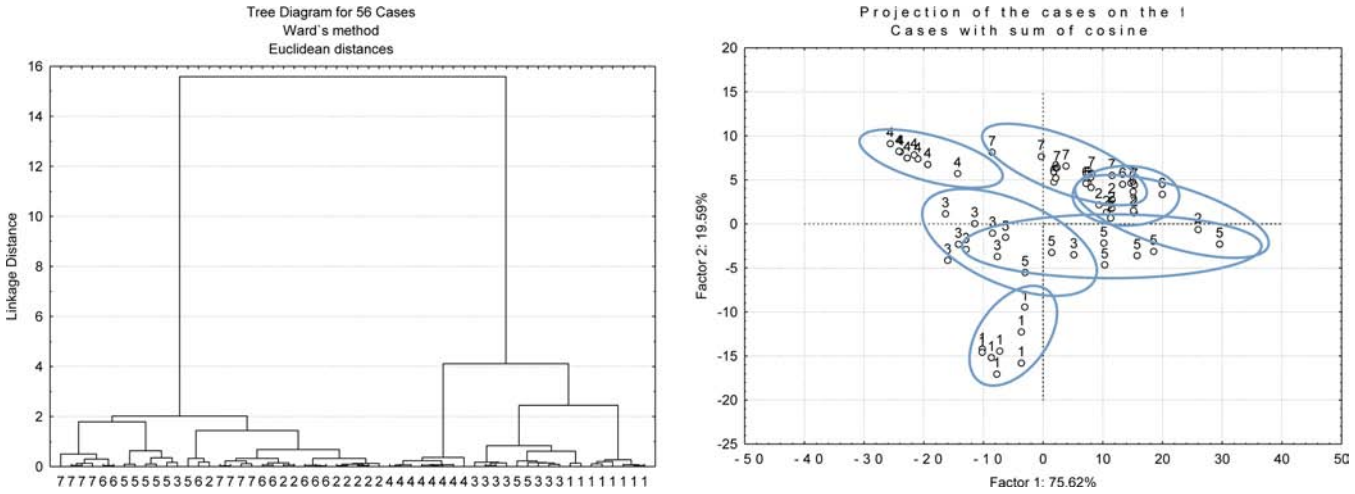

Figure 3. Multivariate molecular spectral analysis of total carbohydrate (region: 1217−907 cm^{-1}) CLA and PCA analysis.

respectively. This showed that the advanced molecular spectroscopic could reveal the real inherent molecular structure spectral profile. There was no published study of carbohydrate molecular structure in corn DDGS and barley DDGS, so the comparison of carbohydrate molecular spectral parameters between them could not be made. However, a previous study reported that the carbohydrate molecular (in terms of different component peaks and their ratio) ratio parameters were related to degradation rate and extend.[35] These molecular spectral profiles in those two types of DDGS are believed to highly relate feed quality.

Multivariate Molecular Spectral Analysis in the Fingerprint Region in Corn DDGS and Barley DDGS. The CLA and PCA analysis[23] were conducted on the entire spectral information within STCHO, CELC, and CHO region. The analysis results are showed in Figures 1−3. Figure 1 shows the result of CLA and PCA of carbohydrate molecular spectral in the fingerprint region ca. 1507−1184 cm^{-1}. The CLA indicated that the structures of carbohydrate (STCHO) were not fully separated except for the number 1 and 4 samples. Also, it was not distinguished from themselves except for the number 4 and 7 samples. The first and second principal components explained 94.85% and 3.73% of the total variance, respectively. Figure 2 shows the results of CLA and PCA analysis of cellulose compounds (CELC) molecular spectral in the fingerprint region ca. 1305−1184 cm^{-1}. The CLA showed that inherent structure makeup of five corn DDGS and two barley DDGS was not distinguished. The result of PCA analysis was similar to STCHO. Figure 3 showed the result of CLA and PCA analysis of total carbohydrate (CHO) molecular spectral in the fingerprint region ca. 1217−907 cm^{-1}. Carbohydrate structure makeup of five corn DDGS and two barley DDGS were not distinguished. The PCA showed that the first and second principal component were 75.62% and 19.59% of the total variance, respectively. These results illustrated that those DDGS samples were related to each other, although the molecular spectral structure of some DDGS samples were different.

Correlations between Carbohydrate Spectral Characteristics and Carbohydrate Nutritive Properties among Different Types and Sources of DDGS. The correlation results are presented in Table 4. The result showed that the molecular spectral intensity of STCHO and CELC peak area had no correlation ($p > 0.05$) with nutritive parameters in corn DDGS and barley DDGS, except for ADF. Negative correlation between STCHO peak area and ADF content with $R = -0.63$ ($p < 0.05$). CELC peak area had a negative correlation with ADF ($p < 0.05$) with $R = -0.57$. These results indicated that higher STCHO and CELC peak area are associated with lower ADF content in the corn DDGS and barley DDGS sample. It

dx.doi.org/10.1021/jf500711p | J. Agric. Food Chem. 2014, 62, 5108−5117

Table 4. Correlation between Carbohydrate Molecular Spectral Features and Carbohydrate Nutrient Profiles in Corn DDGS and Barley DDGS

	Cel_He_A		Cel_A		CHO_1_A		CHO_2_A		CHO_3_A		CHO_A	
item	correlation	p value	correlation	p value	correlation	p value	correlation	p value	correlation	p value	correlation	p value
Basic Chemical Profile												
DM	−0.48	0.083	−0.55	0.044	−0.53	0.051	−0.75	0.002	−0.19	0.526	−0.71	0.005
Ash	0.30	0.513	0.14	0.765	0.57	0.181	0.24	0.598	0.42	0.345	0.20	0.664
OM	−0.30	0.512	−0.14	0.764	−0.57	0.181	−0.24	0.599	−0.42	0.345	−0.20	0.668
EE	−0.17	0.557	−0.10	0.739	−0.18	0.538	−0.24	0.399	−0.23	0.435	−0.30	0.300
Structural Carbohydrate and Nonstructural Carbohydrate												
Starch	−0.06	0.834	0.04	0.895	0.11	0.701	−0.07	0.807	−0.17	0.568	−0.09	0.747
NDF	−0.21	0.472	−0.25	0.380	−0.44	0.118	−0.49	0.075	−0.15	0.608	−0.49	0.074
ADF	−0.63	0.016	−0.57	0.033	−0.54	0.048	−0.78	0.001	0.03	0.928	−0.65	0.013
ADL	−0.14	0.633	−0.26	0.373	−0.41	0.146	−0.39	0.165	−0.10	0.741	−0.40	0.161
Hemicellulose	0.12	0.793	0.01	0.980	−0.28	0.542	−0.23	0.618	−0.15	0.754	−0.23	0.621
Cellulose	−0.75	0.052	−0.58	0.169	−0.75	0.053	−0.39	0.389	−0.75	0.054	0.18	0.707
Total CHO	0.37	0.189	0.15	0.616	−0.27	0.354	−0.04	0.883	0.10	0.733	−0.04	0.884
CNSC	0.24	0.413	0.23	0.426	0.38	0.184	0.47	0.091	0.20	0.485	0.49	0.078
CHO Fractions Partitioned by CNCPS												
CA	0.24	0.404	0.23	0.437	0.36	0.203	0.47	0.088	0.22	0.450	0.49	0.074
CB1	−0.06	0.833	0.04	0.897	0.11	0.705	−0.07	0.803	−0.17	0.564	−0.10	0.742
CB2	−0.27	0.350	−0.18	0.549	−0.32	0.268	−0.48	0.085	−0.26	0.375	−0.50	0.068
CC	−0.17	0.553	−0.26	0.368	−0.39	0.171	−0.40	0.159	−0.12	0.695	−0.40	0.153
Truly Digestible Nutrients (g/kg DM)												
tdNFC	0.28	0.324	0.26	0.369	0.32	0.273	0.43	0.126	0.19	0.512	0.44	0.115
tdNDF	−0.13	0.656	−0.17	0.560	−0.50	0.071	−0.55	0.040	−0.21	0.482	−0.57	0.034
tdFA	−0.17	0.557	−0.10	0.739	−0.18	0.538	−0.24	0.399	−0.23	0.435	−0.30	0.300
TDN1x	−0.02	0.954	0.24	0.405	0.30	0.292	0.21	0.470	−0.28	0.332	0.10	0.743
Energy Value (NRC-2001 Dairy and NRC-1996 Beef)												
DE1x	−0.07	0.811	0.20	0.502	0.36	0.202	0.24	0.418	−0.24	0.408	0.14	0.629
MEp3x	−0.14	0.636	0.13	0.659	0.33	0.252	0.17	0.558	−0.24	0.416	0.09	0.757
NElp3x	−0.15	0.606	0.10	0.736	0.25	0.389	0.10	0.734	−0.27	0.347	0.01	0.970
NEm	−0.09	0.762	0.17	0.551	0.33	0.244	0.20	0.487	−0.26	0.375	0.11	0.718
NEg	−0.07	0.808	0.19	0.506	0.33	0.245	0.21	0.472	−0.25	0.392	0.11	0.697
In Situ DM Digestibility												
R_DDM	0.44	0.113	0.23	0.430	0.20	0.485	0.46	0.096	0.20	0.495	0.45	0.110

also indicated that STCHO and CELC could not be used as an indicator to predict nutrient profiles except for ADF in DDGS samples.

For the total CHO part, it also found that ADF had negative correlation with CHO first, second, and total peak area ($p < 0.05$) with $R = -0.54$, -0.78, and -0.65, respectively. However, there is no correlation ($p > 0.05$) with CHO third peak area. CHO first and total peak area had a negative correlation with truly digestible NDF (tdNDF) ($p < 0.05$) with $R = -0.55$ and -0.57, respectively. DM content in original corn DDGS and barley DDGS also had a negative with CHO second and total peak area ($p < 0.05$) with $R = -0.75$ and -0.71, respectively. However, no correlation ($p > 0.05$) was found between in situ digestibility of DM (R_DDM) and CHO second and total peak area. No correlation was found between all carbohydrate spectral parameters and energy values and carbohydrate subfractions partitioned by CNCPS. Our data of correlation between CHO spectral parameters and carbohydrate basic chemical profile and in situ digestible of DM were not consistent with a previous study; however, the results of relationship between all spectral intensities of CHO and energy values and carbohydrate subfractions were to some extent consistent with the previous report.[36] Further study with large range sample size is necessary to confirm whether carbohydrate structure spectral profiles could be used as a fast predictor of the nutritional values and to find which spectral of functional groups of carbohydrate are much more sensitive to the coproduct samples after the different processing.

In summary, different types and sources of DDGS from China in this study have different carbohydrate nutritional profiles and carbohydrate inherent structural makeup. According to the result of correlation analysis, ADF showed negative correlation with most of carbohydrate peak area (e.g., structural carbohydrate peak area, cellulose compounds peak area, and total carbohydrate first, second, and total peak area). CHO spectral parameters have no correlation with carbohydrate subfractions and energy values. Spectral intensities of CHO also showed no correlation with truly digestible nutrients except for truly digestible NDF (tdNDF). The results indicate that carbohydrate spectral profiles are highly associated with carbohydrate utilization in coproducts from biofuel and biobrewing processing. The results indicate that carbohydrate spectral profiles are highly associated with carbohydrate utilization in coproducts from biofuel and biobrewing processing.

AUTHOR INFORMATION

Corresponding Authors

*Peiqiang Yu. Tel: + 1 306 966 4132. Fax: + 1 306 966 4151. E-mail: peiqiang.yu@usask.ca.

*Xuewei Zhang. Tel: +86-22-23781297. E-mail: zhangxuewei63@163.com.

Funding

The current study was supported by the Thousand-Talent-People Program in Tianjin, the Ministry of Agriculture Strategic Feed Research Chair Program at the University of Saskatchewan, and the Natural Sciences and Engineering Research Council of Canada (NSERC- Individual Discovery). The scholarship was provided to L.C. for overseas training and research through the Thousand-Talent-People Program in Tianjin.

Notes

The authors declare no competing financial interest.

■ ACKNOWLEDGMENTS

The authors also thank the Department of Animal and Poultry Science at the University of Saskatchewan (Canada) for providing lab and animal research facilities to do this international collaborative feed research project, Jifei Ma for his support at Tianjin Agricultural University, Zhiyuan Niu, Hangshu Xin and Manji Sun for research and laboratory assistance.

■ REFERENCES

(1) AOAC. *Official Methods of Analysis*; Association of Analytical Chemists: Washington, DC, 1990.

(2) Ørskov, E. R.; McDonald, I. The estimation of protein degradability in the rumen from incubation measurements weighted according to rate of passage. *J. Agric. Sci.* **1979**, *92*, 499−503.

(3) Tamminga, S.; Van Straalen, W. M.; Subnel, A. P. J.; Meijer, R. G. M.; Steg, A.; Wever, C. J. G.; Blok, M. C. The Dutch protein evaluation system: the DVE/OEB-system. *Livest. Prod. Sci.* **1994**, *40*, 139−155.

(4) Gamage, I. H.; Yu, P. Short communication: Comparison of the newly developed DVE/OEB (2010) system and the National Research Council (2001) model in modeling metabolic characteristics of proteins in dairy cattle. *J. Dairy Sci.* **2013**, *96*, 5908−5913.

(5) NRC. *Nutrient Requirements of Dairy Cattle*, 7th revised ed.; National Academy of Sciences: Washington, DC, 2001.

(6) Yu, P.; Block, H. C.; Doiron, K. Understanding the differences in molecular conformation of carbohydrate and protein in endosperm tissues of grains with different biodegradation kinetics using advanced synchrotron technology. *Spectrochim. Acta, Part A: Mol. Biomol. Spectrosc.* **2009**, *71*, 1837−1844.

(7) Zhang, X.; Yu, P. Relationship of carbohydrate molecular spectroscopic features in combined feeds to carbohydrate utilization and availability in ruminants. *Spectrochim. Acta, Part A: Mol. Biomol. Spectrosc.* **2012**, *92*, 225−233.

(8) Zhang, X.; Yu, P. Differentiation of mixtures of co-product blend with barley grain based on Fourier transform infrared attenuated total reflection molecular spectroscopy: Carbohydrate molecular spectral profiles and nutritive characteristics in dairy cattle. *J. Dairy Sci.* **2012**, *95*, 6624−6634.

(9) Xin, H.; Falk, K. C.; Yu, P. Studies on Brassica carinata Seed. 2. Carbohydrate Molecular Structure in Relation to Carbohydrate Chemical Profile, Energy Values, and Biodegradation Characteristics. *J. Agric. Food Chem.* **2013**, *61*, 10127−10134.

(10) Yu, P. Short communication: Relationship of carbohydrate molecular spectroscopic features to carbohydrate nutrient profiles in co-products from bioethanol production. *J. Dairy Sci.* **2012**, *95*, 2091−2096.

(11) Van Soest, P. J.; Robertson, J. B.; Lewis, B. A. Methods for dietary fiber, neutral detergent fiber, and non-starch polysaccharides in relation to animal nutrition. *J. Dairy Sci.* **1991**, *74*, 3583−3597.

(12) McCleary, B. V.; Gibson, C. C.; Mugford, C. C. Measurements of total starch in cereal products by amylo-glucosidase alpha-amylase method: Collaborative study. *J. AOAC Int.* **1997**, *80*, 571−579.

(13) Sniffen, C. J.; O'Connor, J. D.; Van Soest, P. J.; Fox, D. G.; Russell, J. B. A net carbohydrate and protein system for evaluating cattle diets: II. Carbohydrate and protein availability. *J. Anim. Sci.* **1992**, *70*, 3562−3577.

(14) Chalupa, W.; Sniffen, C. J. Carbohydrate, protein and amino acid nutrition of lactating dairy cattle. In *Recent Advanced Animal Nutrition*; Nottingham University Press: Loughborough, U. K., 1994; 265−275.

(15) Weiss, W. P.; Conrad, H. R.; St Pierre, N. R. A theoretically-based model for predicting total digestible nutrient values of forages and concentrates. *Anim. Feed Sci. Technol.* **1992**, *39*, 95−110.

(16) NRC. *Nutrient Requirements of Beef Cattle*, 7th ed.; National Academy of Sciences: Washington, DC, 1996.

(17) McKinnon, J. J.; Olubobokun, J. A.; Mustafa, A.; Cohen, R. D. H.; Christensen, D. A.Influence of dry heat treatment of canola meal on site and extent of nutrient disappearance in ruminants. *Anim. Feed Sci. Technol.* **1995**, *56*, 243−252.

(18) Yu, P.; Goelema, J. O.; Tamminga, S. Using the DVE/OEB model to determine optimal conditions of pressure toasting on horse beans (Vicia faba) for the dairy feed industry. *Anim. Feed Sci. Technol.* **2000**, *86*, 165−176.

(19) Yu, P.; Meier, J. A.; Christensen, D. A.; Rossnagel, B. G.; McKinnon, J. J. Using the NRC-2001model and the DVE/OEB system to evaluation nutritive values of Harrington (malting-type) and Valier (feed-type) barley for ruminants. *Anim. Feed Sci. Technol.* **2003**, *107*, 45−60.

(20) Zhang, X.; Yu, P. molecular basis of protein structure in combined feeds (hulless barley with bioethanol coproduct of wheat dried distillers grains with solubles) in relation to protein rumen degradation kinetics and intestinal availability in dairy cattle. *J. Dairy Sci.* **2012**, *95*, 3363−3379.

(21) Nuez Ortín, W. G.; Yu, P. Modelling the metabolic characteristics of proteins in dairy cattle from co-products of bioethanol processing: comparison of the NRC 2001 model with the DVE/OEB system. *J. Sci. Food Agric.* **2011**, *91*, 405−411.

(22) CCAC, *Guide to the Care and Use of Experimental Animals*, 2nd ed.; Canadian Council of Animal Care: Ottawa, ON, Canada, 1993.

(23) Yu, P.; Damiran, D.; Azarfar, A.; Niu, Z. Detecting molecular features of spectra mainly associated with structural and non-structural carbohydrates in co-products from bioethanol production using DRIFT with uni- and multi- variate molecular spectral analyses. *Int. J. Mol. Sci.* **2011**, *12*, 1921−1935.

(24) Himmelsbach, D. S.; Khalili, S.; Akin, D. E. FT-IR micro-spectroscopic imaging of flax (Linum usitatissimum L.) stems. *Cell. Mol. Bio.* **1998**, *44*, 99−108.

(25) Wetzel, D. L.; Eilert, A. J.; Pietrzak, L. N.; Miller, S. S.; Sweat, J. A. Ultraspatially resolved synchrotron infrared microspectroscopy of plant tissue in situ. *Cell. Mol. Bio.* **1998**, *44*, 145−167.

(26) Wetzel, D. L. When molecular causes of wheat quality are known, molecular methods will supercede traditional methods. *Proc.—Int. Wheat Quality Conf. ,II*, Manhattan, Kansas, U. S. A., May **2001**; pp 1−20.

(27) Marinkovic, N. S., Chance, M. R. Synchotron Infared Microscopy. *Encyclopedia of Molecular Cell Biology and Molecular Medicine*, 2nd ed.; Meyers, R., Ed.; Wiley Inc.: Hoboken, NJ, 2006; Vol. *13*, pp 671−708.

(28) Yu, P.; Damiran, D.; Azarfar, A.; Niu, Z. Detecting molecular features of spectra mainly associated with structural and non-structural carbohydrates in co-products from bioethanol production using DRIFT with uni- and multi- variate molecular spectral analyses. *Int. J. Mol. Sci.* **2011**, *12*, 1921−1935.

(29) SAS Institute. *User's Guide Statistics*, Version 9.2; SAS Inst. Inc.: Cary, NC, 2005.

(30) Nuez Ortín, W. G.; Yu, P. Nutrient variation and availability of wheat DDGS, corn DDGS and blend DDGS from bioethanol plants. *J. Sci. Food Agric.* **2009**, *89*, 1754−1761.

(31) Mustafa, A. F.; Mckinnon, J. J.; Christensen, D. A. Chemical characterization and in situ nutrient degradability of wet distillers' grains derived from barley-based ethanol production. *Anim. Feed Sci. Technol.* **2000**, *83*, 301−311.
(32) Calsamiglia, S.; Stern, M. D. A three-step in vitro procedure for estimating intestinal digestion of protein in ruminants. *J. Anim. Sci.* **1995**, *73*, 1459−1465.
(33) Yu, P.; Christensen, C. R.; Christensen, D. A.; Marinkovic, N. S.; Miller, L. M. Chemical imaging of microstructure of plant tissues within cellular Dimension using Synchrotron infrared Microspectroscopy. *J. Agric. Food Chem.* **2003**, *51*, 6062−6067.
(34) Yu, P.; Christensen, C. R.; Christensen, D. A. Using Synchrotron Transmission FTIR Microspectroscopy as a Rapid, Direct and nondestructive Analytical Technique To Reveal Molecular Microstructural Chemical Features within tissue in grain Barley. *J. Agric. Food Chem.* **2004**, *52*, 1484−1494.
(35) Liu, N.; Yu, P. Characterize microchemical structure of seed endosperm within a cellular dimension among six barley varieties with distinct degradation kinetics, using ultraspatially resolved synchrotronbased infrared microspectroscopy. *J. Agric. Food Chem.* **2010**, *58*, 7801−7810.
(36) Zhang, X.; Yu, P. Relationship of carbohydrate molecular spectroscopic features in combined feeds to carbohydrate utilization and availability in ruminants. *Spectrochim. Acta, Part A: Mol. Biomol. Spectrosc.* **2012**, *92*, 225−233.

MATERIALS AND METHODS

Bacterial Strains, Plasmids, Enzymes, and Reagents. *L. plantarum* WCFS1 was kindly provided by M. Kleerebezem (NIZO Food Research, The Netherlands). *Escherichia coli* DH10B and *E. coli* BL21 (DE3) were used as transformation and expression hosts in the pURI3-Cter vector.[28] Plasmid pGro7 (TaKaRa) was used to overexpress GroES/GroEL chaperones. The *L. plantarum* strain was grown in MRS medium (Pronadisa, Spain) adjusted to pH 6.5 and incubated at 30 °C. The *E. coli* strains were cultured in Luria−Bertani (LB) medium at 37 °C with shaking at 200 rpm. When required, ampicillin, chloramphenicol, or arabinose were added to the medium at a concentration of 100 or 20 μg/mL or 2 mg/mL, respectively.

Plasmid DNA was extracted with a High Pure plasmid isolation kit (Roche). PCR product was purified with a QIAquick gel extraction kit (Quiagen). Oligonucleotides were purchased from Eurofins MWG Operon (Ebersberg, Germany). *Dpn*I and HS Prime Star DNA polymerase were obtained from TaKaRa. His-tagged protein was purified by a Talon Superflow resin (Clontech). All the *p*-nitrophenyl esters, isopropyl-β-D-thiogalactopyranoside (IPTG), ampicillin, chloramphenicol, and arabinose were obtained from Sigma (Madrid, Spain). All other chemicals were obtained from commercial suppliers.

Cloning of lp_1002 from *L. plantarum*. The gene encoding for a putative lipase/esterase (*lp_1002*) (gene ID 1063602) in *L. plantarum* WCFS1 was PCR-amplified by Prime Star HS DNA polymerase (TaKaRa) by using the primers 959 (5′-*TAACTTTAAGAAGGAGATATACATatg*caagttattaagcaaaaattaa) and 960 (5′-*GCTATTAATGATGATGATGATGATG*acgattatcagctagccattcaag) (the nucleotides pairing the expression vector sequence are indicated in italics, and the nucleotides pairing the *lp_1002* gene sequence are written in lowercase letters). The 795-bp purified PCR product was inserted into the pURI3-Cter vector using a restriction enzyme- and ligation-free cloning strategy.[28] The vector produced recombinant proteins having a six-histidine affinity tag in their C-termini. *E. coli* DH10B cells were transformed, recombinant plasmids were isolated, and those containing the correct insert were identified by restriction enzyme analysis, verified by DNA sequencing, and then transformed into *E. coli* BL21 (DE3) cells for expression.

Expression and Purification of Recombinant Lp_1002 Esterase. *E. coli* BL21(DE3) harboring pGro7 (TaKaRa), a vector overexpressing GroES/GroEL chaperones, was transformed with the recombinant plasmid pURI3-Cter-1002. *E. coli* was grown in LB medium containing 100 μg/mL ampicillin, 20 μg/mL chloramphenicol, and 2 mg/mL arabinose until an optical density at 600 nm of 0.4 was reached and then induced by adding isopropyl-β-D-thiogalactopyranoside (IPTG) at 0.4 mM final concentration. Following induction, the cells were grown at 22 °C for 20 h and collected by centrifugation (8000*g*, 15 min, 4 °C). The cells were resuspended in phosphate buffer (50 mM, pH 7) containing 300 mM NaCl. Crude extracts were prepared by French press lysis of the cell suspension (three times at 1,100 psi). The insoluble fraction of the lysate was removed by centrifugation at 47,000*g* for 30 min at 4 °C, and the supernatant was filtered through a 0.2 μm pore-size filter and then applied to a Talon Superflow resin (Clontech) equilibrated in phosphate buffer (50 mM, pH 7) containing 300 mM NaCl and 10 mM imidazole to improve the interaction specificity in the affinity chromatography step. The bound enzyme was eluted using 150 mM imidazole in the same buffer. The purity of the enzymes was determined by SDS-PAGE in Tris-glycine buffer. Protein concentration was measured according to the method of Bradford using a protein assay kit (Bio-Rad) with bovine serum albumin as the standard. Fractions containing the His6-tagged protein were pooled and analyzed for esterase activity.

Enzyme Assay. Esterase activity was determined by a spectrophotometric method described previously using *p*-nitrophenyl acetate (Sigma-Aldrich) as the substrate.[26] The rate of hydrolysis of *p*-nitrophenyl acetate for 10 min at 37 °C was measured in 50 mM sodium phosphate buffer pH 7.0 at 348 nm in a spectrophotometer (UVmini-1240 Shimadzu). The reaction was stopped by chilling on ice.

In order to carry out the reaction (1 mL), a stock solution of 25 mM of *p*-nitrophenyl acetate was prepared in acetonitrile/isopropanol (1:4, v/v)[29] and mixed with 50 mM sodium phosphate buffer (pH 7.0) to obtain a 1 mM substrate final concentration. Control reactions containing no enzyme were utilized to account for any spontaneous hydrolysis of the substrates tested. Enzyme assays were performed in triplicate. One unit of esterase activity was defined as the amount of enzyme required to release 1 μmol of *p*-nitrophenol per minute under standard reaction conditions

Substrate Specificity. The substrate specificity of Lp_1002 was determined by using different *p*-nitrophenyl esters of various chain lengths (Sigma-Aldrich) [*p*-nitrophenyl acetate (C2), *p*-nitrophenyl butyrate (C4), *p*-nitrophenyl caprylate (C8), *p*-nitrophenyl laurate (C12), *p*-nitrophenyl myristate (C14), and *p*-nitrophenyl palmitate (C16)] as substrates, as described previously.[22,26] A stock solution of each *p*-nitrophenyl ester was prepared in acetonitrile/isopropanol (1/4, v/v). Substrates were emulsified to a final concentration of 0.5 mM in 50 mM sodium phosphate buffer, pH 7.0, containing 1.1 mg/mL Arabic gum, and 4.4 mg/mL Triton X-100. The reaction mix consisted of 990 μL of emulsified substrate and 10 μL of enzyme solution (10 μg protein). Reactions were carried out at 37 °C in a spectrophotometer (UVmini-1240 Shimadzu) as described above.

The enzymatic substrate profile of purified protein was determined by using an ester library described previously.[30] *p*-Nitrophenol was used as pH indicator to monitor ester hydrolysis colorimetrically. The screening was performed in a 96-well Flat Bottom plate (Sarstedt) where each well contains a different substrate (1 mM) in acetonitrile (1%). A buffer/indicator solution containing 0.44 mM of *p*-nitrophenol in 1 mM sodium phosphate buffer pH 7.2 was used as pH indicator. Esterase solution (10 μg, 20 μL in 1 mM sodium phosphate buffer pH 7.2) was added to each well, and reactions were followed by measuring the decrease in absorbance at 410 nm for 2 h at 37 °C in a Synergy HT BioTek microplate spectrophotometer. Blanks without enzyme were carried out for each substrate, data were collected in triplicate, and the average activities were quantified. Results are shown as means ± standard deviations.

Effects of Temperature, pH, and Additives on Lp_1002 Esterase Activity. The effects of pH and temperature on the esterase activity of Lp_1002 were studied by using buffers of different pH ranging from 3 to 9. The buffers (100 mM) used were acetic acid−sodium acetate (pH 3−5), sodium phosphate (pH 6 to 7), Tris-HCl (pH 8), and glycine-NaOH (pH 9). The optimal temperature was assayed by incubating purified Lp_1002 esterase in 50 mM phosphate buffer (pH 7) at different temperatures (5, 20, 30, 37, 40, 45, 55, and 65 °C). For temperature stability measurements, the recombinant esterase was incubated in 50 mM phosphate buffer pH 7 at 20, 30, 37, 45, 55, and 65 °C for 5, 15, and 30 min and 1, 2, 4, 6, and 20 h. Aliquots were withdrawn at these incubation times to test the remaining activity at standard conditions. The nonheated enzyme was considered as control (100%). The analyses were performed in triplicate.

To study the effect of metals and ions on Lp_1002 esterase activity, the enzyme was incubated in the presence of the different additives at a final concentration of 1 mM for 5 min at room temperature. Then, the substrate was added, and the reaction mixture was incubated at 37 °C. The residual esterase activity was measured after the incubation of the purified enzyme with each additive. The additives analyzed were $MgCl_2$, KCl, $CaCl_2$, $HgCl_2$, $ZnCl_2$, $CuCl_2$, $NiCl_2$, $MnCl_2$, Triton-X-100, Tween 20, Tween 80, SDS, urea, EDTA, DMSO, cysteine, DTT, PMSF, DEPC, and β-mercaptoethanol. Esterase activity measured in the absence of any additive was taken as control (100%). Experiments were done in triplicate.

Effect of Wine Compounds on Lp_1002 Activity. The effect of the presence of compounds present during winemaking was assayed. The effect of ethanol on esterase activity was studied at ethanol concentrations ranging from 0 to 20% (v/v). Reaction mixtures were prepared as described for the temperature optimum experiments, but different volumes of ethanol were added, and the volume of the buffer was adjusted accordingly to maintain the final reaction volume. The reactions were preincubated for 5 min at room temperature, and the substrate (*p*-nitrophenyl acetate) was added. The effect of the presence of several organic acids was also studied. L-Malic, L-tartaric, DL-citric, and DL-lactic acids were assayed at concentrations ranging from 0 to 5 g/L.

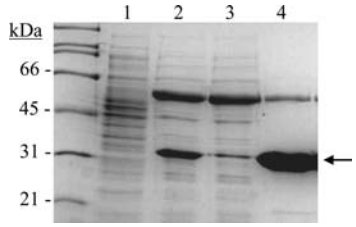

Figure 1. Purification of Lp_1002 esterase. SDS-PAGE analysis of the expression and purification of the His_6-Lp_1002 esterase. Analysis of soluble cell extracts of IPTG-induced *E. coli* BL21(DE3) (pURI3-Cter) (pGro7) (1) or *E. coli* BL21(DE3) (pURI3-Cter-1002) (pGro7) (2), flowthrough (3), or eluted protein after His affinity resin (4). The arrow indicated the overproduced and purified protein. The gel was stained with Coomassie blue. Molecular mass markers are located at the left (SDS-PAGE Standards, Bio-Rad).

Reaction mixtures were prepared by adding different volumes of the corresponding stock solution (25 g/L). Finally, the effect of sulfite was determined by adding sodium metabisulfite at concentrations ranging from 0 to 1 g/L. The reactions were done by adding different volumes of a 25 g/L stock solution. Reaction mixtures were preincubated for 5 min at room temperature before the enzyme was added. After the reaction, the absorbance was measured.

Statistical Analyses. The two-tailed Student́s *t* test performed using GraphPad InStat version 3.0 (GraphPad Software, San Diego, CA) was used to determine the differences between means. The data are representative means of at least three independent experiments.

RESULTS AND DISCUSSION

Production and Purification of Recombinant Lp_1002 Protein. Numerous open reading frames (ORF) encoding putative lipase/esterase proteins can be identified from the genomic information on complete *L. plantarum* genome sequences. Considering the *L. plantarum* WCFS1 genome (accession NC_004567), more than 20 ORF were annotated as putative esterases. The first two ORFs lipase/esterase have been already biochemically characterized, the feruloyl esterase Lp_0796[13,26] and the esterase Lp_0973.[22] The next ORF, annotated as putative esterase/lipase, is Lp_1002, present in all the available *L. plantarum* genome sequences, and predicted to

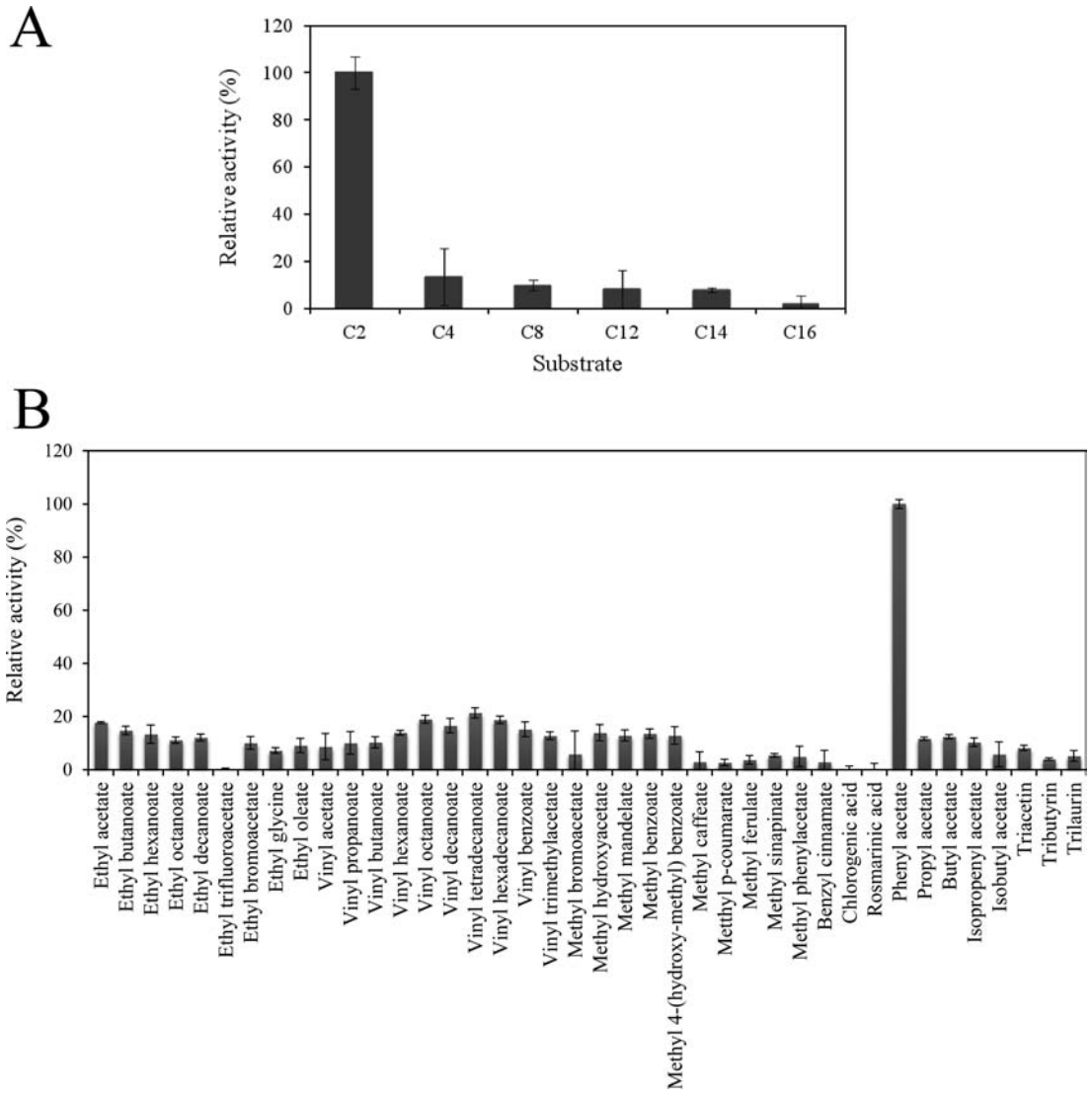

Figure 2. Substrate profile of Lp_1002 against chromogenic substrates (*p*-nitrophenyl esters) with different acyl chain lengths (C2, acetate; C4, butyrate; C8, caprylate; C12, laurate; C14, myristate; C16, palmitate) (A) or toward a general ester library (B). The relative activities obtained toward different substrates are shown. The error bars represent the standard deviation estimated from the three independent assays. The observed maximum activity was defined as 100%.

dx.doi.org/10.1021/jf500991m | J. Agric. Food Chem. 2014, 62, 5118−5125

```
LCA     -----------------MADDDILAKIQAGWAQTAARDKARYADERVPEDVHWETEYRYE 43
GOX     MNTRSLVLPELLPLLGEIPTVDLSAESLPAFRAGLEQTAGQSFLQAEDYPVTLERLNIPG 60
LPL     ------------------------------------------------------MQVIKQKL  8
PFL     ----------------------------------------MSTFVAKDGTQIYFKDW 17
                                                               :

LCA     NSADPQQTLNLYYPAKRRNATLPTVIDVHGGGWFYGDRNLN-RNYCRYLASQGYAVMGMG 102
GOX     TENAPPIRLLTVRPRKEATGPRRALLHLHGGGYFAGQPELTTTQLCQFAQELDCVVISPD 120
LPL     TATCAQLTGYLHQPDTNAHQTNLPAIIIVPGGSYTHIPVAQAESLAMAFAGHGYQAFYLE  68
PFL     GSGKPVLFSHGWLLDADMWEYQMEYLSSR-GYRTIAFDRRGFGRSDQPWTGNDYDTFADD  76
            .                   :    *                    .  .:

LCA     YRLLPDVDVR--GQIQDIFASLRWLSHFGPQRGFDLDHVLLTGDSAGGHLASLVACIQQS 160
GOX     YRLTPEHPFP--AAIEDAYTTLCWITRNADTLGIDPARIGLTGESAGGGLAAGLALLTRD 178
LPL     YTLLTDQQPLGLAPVLDLGRAVNLLRQHAAEWHIDPQQITPAGFSVGGHIVALYNDYWAT 128
PFL     IAQLIEHLDLKEVTLVGFSMGGGDVARYIARHGSAR----VAGLVLLGAVTPLFGQKPDY 132
             :        : .       : :              :*    * :..

LCA     EELQELFGVDRVN---FNFTLVALVCPVAEPGKLPEAAGDMSDMAAFYLDKLSGGDAALA 217
GOX     REGPALLFQNLIYPVLDDRTITGQPDASPVGGEFLWTRASNTFMWTALLNPVAPGSADVS 238
LPL     RVATELNVTPAMLK--PNNVVLGYPVISPLLG-FPKDDATLATWTPTPNELAADQHVNSD 185
PFL     PQGVPLDVFARFKT--ELLKDRAQFISDFNAPFYGINKGQVVSQGVQTQTLQIALLASLK 190
             *     .          .                .                .

LCA     DHLNFSQVAKDLKLPPFMLIGGQNDSFYLQSQALLEVFAADKVTYTTKLWPASAGPHLKH 277
GOX     PYAAPARATDLSDLPPVYLCVGALDLFLDEDLAYARRLIHQGISVELEIVPG-------- 290
LPL     NQPTFIWTTADDPIVP-----------ATNTLAYATALATAKIPYELHVFKHG-----PH 229
PFL     ATVDCVTAFAETDFRP-----------DMAKIDVPTLVIHGDGDQIVPFETTG---KVAA 236
               .     : *                    .          .

LCA     VFNVQHWEWPESIETNLAMLRQFDVLSKQHDEAEADEEDDL 318
GOX     --ACHIFDQTDTPVATRSIARRIDAMKRGFGL--------- 320
LPL     GLALANAQTAWKPDANQPHVAHWLTLALEWLADNR------ 264
PFL     ELIKGAELKVYKDAPHGFAVTHAQQLNEDLLAFLKR----- 272
                  .  .      :   :
```

Figure 3. Comparison of amino acid sequences of bacterial arylesterases from *Lactobacillus casei* (LCA), *Gluconobacter oxidans* (GOX), *Lactobacillus plantarum* (LPL), and *Pseudomonas fluorescens* (PFL). Multiple alignments were done using the program ClustalW2 after retrieval of sequences from BLAST homology searches. Residues that are identical (*), conserved (:), or semiconserved (.) in all sequences are indicated. Dashes indicated gaps introduced to maximize similarities.

encode a 260 amino acid sequence protein with a theoretical molecular mass of 28.7 kDa. The deduced amino acid sequence of Lp_1002 lacked a N-terminal secretion signal sequence, suggesting that this enzyme is located intracellularly. The amino acid sequence of Lp_1002 showed a 53% identity to *Lactobacillus brevis* and *Lactobacillus coryniformis* proteins, which are annotated as putative lipases/esterases (data not shown). The presence of the sequence conserved motif Gly-X-Ser-X-Gly, typical of serine hydrolases, suggests they belong to the α/β hydrolase superfamily of enzymes, which has been confirmed structurally since the atomic coordinates of Lp_1002 have been deposited at the Protein Data Bank by the Joint Center for Structural Genomics (PDB entry: 3bjr).

The *lp_1002* gene was cloned into the pURI3-Cter expression vector by a ligation-free cloning strategy described previously.[28] The vector incorporates the DNA sequence encoding a C-terminal hexa-histidine tail to create a His-tagged fusion enzyme for a further purification step. The integrity of the construct was confirmed by DNA sequencing. The *lp_1002* gene was expressed in *E. coli* under the control of an IPTG inducible promoter. Cell extracts were used to detect the presence of overproduced proteins by SDS-PAGE analysis. Whereas control cells containing the pURI3-Cter vector did not show protein overexpression, an overproduced protein with an apparent molecular mass around 28 kDa was present as inclusion bodies in the insoluble fraction. In order to produce Lp_1002 in a soluble form, plasmid pGro7, producing GroES/GroEL chaperones, was used. When pURI3-Cter-1002 and pGro7 plasmids were used simultaneously, Lp_1002 appeared in the intracellular soluble fraction of the cells (Figure 1). Since the cloning strategy would yield a His-tagged protein, *L. plantarum* Lp_1002 could be purified on an immobilized metal affinity chromatography (IMAC) resin. The recombinant protein was eluted from the resin at 150 mM imidazole and observed as a single band on SDS-PAGE (Figure 1), although some overproduced GroEL proteins were retained in the resin and eluted along Lp_1002. The eluted protein was dialyzed against 50 mM phosphate buffer (pH 7) containing 300 mM NaCl. Routinely about 20 mg of purified protein from 1-L culture was obtained. The calculated specific activity for the esterase Lp_1002 was 170 U/mg for *p*-nitrophenyl acetate.

As esterases and lipases could not be distinguished by sequence comparison, the activity of Lp_1002 against *p*-nitrophenyl esters possessing different acyl chain lengths was assayed. Lp_1002 showed activity only on short-acyl chain esters, exhibiting a clear preference for *p*-nitrophenyl acetate (Figure 2A), therefore confirming that Lp_1002 is a true esterase.

Substrate Profile and Biochemical Characterization of Lp_1002. Once the esterase activity of Lp_1002 was confirmed, it was biochemically characterized in further detail. To test the substrate range of esterases, an ester library was used.[30] This ester library consisted of esters that were chosen to identify acyl chain length preferences of the esterase and also the ability to hydrolyze charged substrates. From Figure 2B it

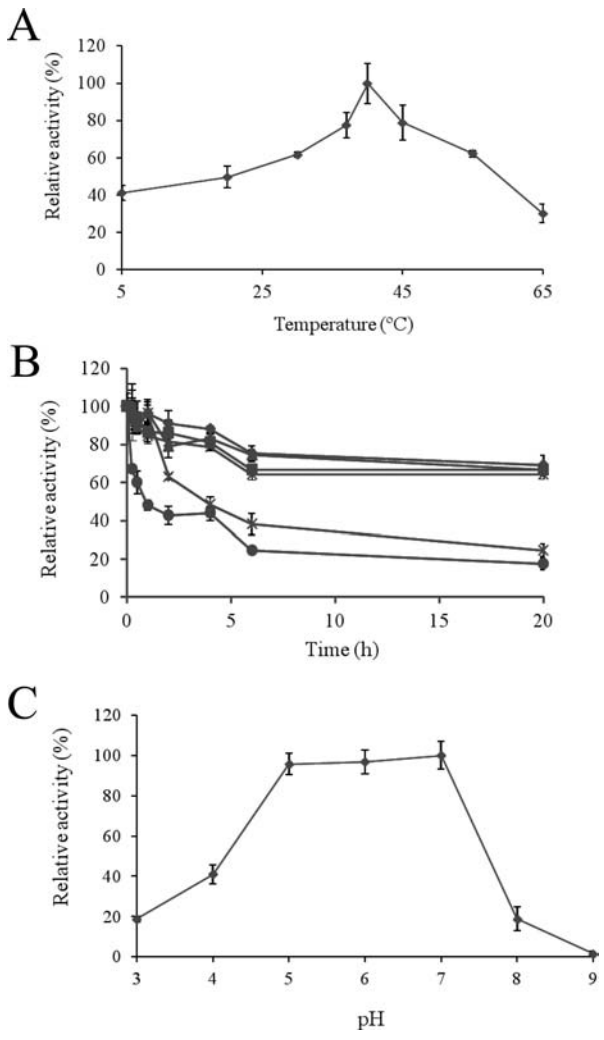

Figure 4. Biochemical properties of Lp_1002 esterase. (A) Relative activity of Lp_1002 versus temperature. (B) Thermal stability of Lp_1002 after preincubation at 22 °C (filled diamond), 30 °C (filled square), 37 °C (filled triangle), 45 °C (cross), 55 °C (star), and 65 °C (filled circle) in phosphate buffer (50 mM, pH 7); at indicated times, aliquots were withdrawn and analyzed as described in the Materials and Methods section. (C) Relative activity versus pH. The experiments were done in triplicate. The mean value and the standard error are shown. The observed maximum activity was defined as 100%.

Table 1. Effect of Additives on Lp_1002 Esterase Activity

additions (1 mM)	relative activity (%)
control	100
KCl	105
$HgCl_2$	14
$CaCl_2$	125
$MgCl_2$	80
$ZnCl_2$	58
$CuCl_2$	13
$NiCl_2$	23
$MnCl_2$	129
Tween 20	116
Tween 80	115
Triton-X-100	122
SDS	32
urea	97
DMSO	106
cysteine	117
DTT	92
β-mercaptoethanol	16
EDTA	98
PMSF	65
DEPC	105

can be deduced that Lp_1002 shows higher hydrolytic activity on phenyl acetate. Phenyl acetate is a commonly used substrate to identify bacterial arylesterases.[6] Among esterases, arylesterases are of biotechnological interest, since they are active not only toward aliphatic esters but also toward aromatic ones, modulating the ester profile of food substrates. Arylesterases were less understood that other esterases, especially carboxylesterases or lipases.[31] Until recently, most of the arylesterases reported were from mammalian sources, playing an important role in detoxification of organophosphorous compounds. In contrast, there are few reports on bacterial arylesterases, whose physiological function remains largely unknown. In addition, little is known about the genetic and biochemistry of bacterial arylesterases. Bacterial arylesterases have only been described from *Vibrio mimicus*,[32] *Agrobacterium radiobacter*,[33] *Acinetobacter* sp.,[34] *Pseudomonas fluorescens*,[35] and *Sulfolobus solfataricus*.[31] Among LAB, only arylesterases from *Lactobacillus helveticus*[9] and *Lactobacillus casei*[10] have been described. Finally, regarding wine-related bacteria, an arylesterase from *Gluconobacter oxidans* has been recently described.[36] As far as we know, Lp_1002 is the first arylesterase described in *L. plantarum* and in a wine LAB. Amino acid sequences of bacterial arylesterases showed less than 20% identity among them. The highest sequence identities detected were between Lp_1002 and *G. oxidans* (16% identity), *P. fluorescens* (16%), and *L. casei* (14%) arylesterases (Figure 3).

Bacterial arylesterases may be used for industrial purposes, especially considering the fact that they have broad substrate specificities.[32] In this regard, although to a lesser extent than phenyl acetate, Lp_1002 also hydrolyzes most of the substrates assayed (Figure 2B). Thus, Lp_1002 catalyzed the hydrolysis of small activated and small nonactivated esters with similar rates regardless of their size. Larger activated esters (e.g., vinyl decanoate) reacted similarly compared to larger nonactivated esters (e.g., ethyl decanoate). Regarding the acyl chain selectivity, Lp_1002 exhibited hydrolytic activity toward all the ethyl esters, vinyl esters, and methyl esters assayed, possessing varied chain length as well as an electron-withdrawing group (e.g., ethyl bromoacetate and ethyl glycine) or an hindered group (e.g., vinyl benzoate and vinyl trimethyl acetate). Considering the alcohol moiety selectivity, both acetates and butyrates were also hydrolyzed. From the 40 potential substrates assayed, only ethyl trifluoroacetate, chlorogenic acid, and rosmarinic acid were not hydrolyzed by Lp_1002.

The broad substrate range exhibited by Lp_1002 indicated its potential utility in wine fermentations. From the substrates included in the ester library, relevant aroma compounds such as ethyl acetate (pineapple aroma), ethyl butanoate (floral, fruity), ethyl hexanoate (green apple), ethyl octanoate (sweet soap), and ethyl decanoate (floral, soap) were hydrolyzed by Lp_1002.[3]

Other important biochemical properties of Lp_1002 have been characterized. Figure 4A shows that the optimal temperature for Lp_1002 activity against phenyl acetate is 40 °C, retaining 50% of its maximal activity at winemaking temperatures (15−25 °C). Moreover, Lp_1002 showed thermal stability since 70% of its maximal activity was observed after 20 h of incubation at 45 °C or below (Figure 4B).

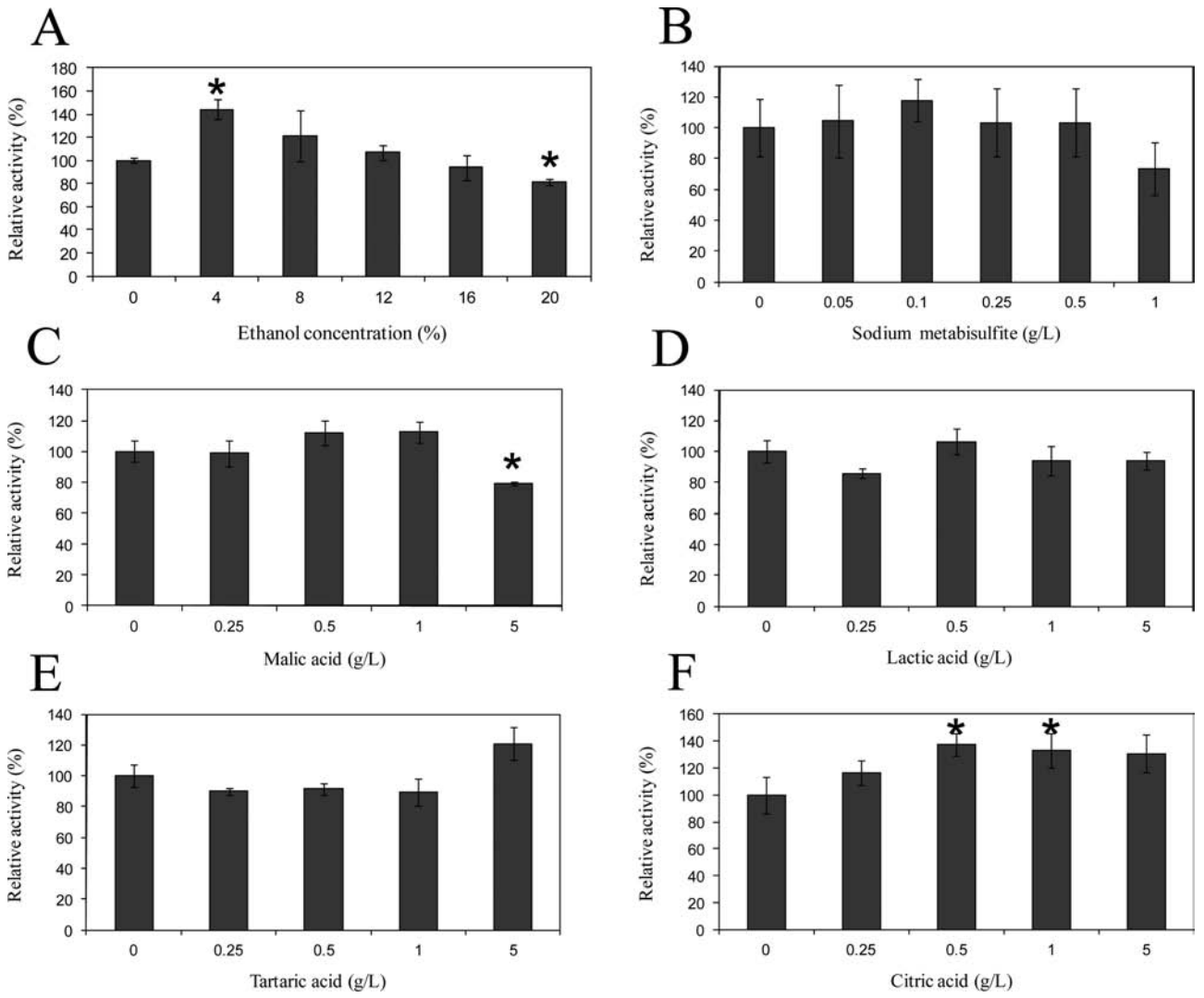

Figure 5. Activity of Lp_1002 esterase in the presence of compounds frequently found in wine. Relative activity of Lp_1002 after incubation in the presence of ethanol (A), sodium metabisulfite (B), malic acid (C), lactic acid (D), tartaric acid (E), and citric acid (F) at the concentrations indicated. The activity of the enzyme in the absence of the compound was defined as 100%. The experiments were done in triplicate. The mean value and the standard error are shown. Asterisks indicate a P value <0.05.

The optimal temperature shown by Lp_1002 is similar to the optimal temperatures exhibited by arylesterases from *P. fluorescens*,[30] *G. oxidans*,[23] and *L. helveticus*,[9] which are the arylesterases with the highest sequence similarity to Lp_1002. In addition, EstB28 and EstCOo8 esterases from a wine LAB, *O. oeni*, also showed optimal activity at 40 °C.[13,14]

Regarding the dependence on pH for Lp_1002 activity, Figure 4C showed that the protein was active between 3 and 8, exhibiting a broad optimal pH range (5 to 7). This result indicates that Lp_1002 shows a marked preference for acidic conditions when compared to other known bacterial arylesterases, which exhibited optimum pH values ranging from 7 to 9. However, acidic esterases were previously described for esterases from wine bacteria; thus, optimal pH around 5 was described for EstB28 and EstCOo8 from *O. oeni* and EstC34 from *L. hilgardii*.[13,14] At pH values commonly found in wines (pH 3−4), Lp_1002 still retained activity (20−40%), confirming its potential activity during winemaking.

The effect of some metal ions and additives on Lp_1002 activity was studied and is shown in Table 1. Esterase activity was significantly inhibited by Hg^{2+}, Cu^{2+}, and Ni^{2+} ions, as well as by β-mercaptoethanol. The enzymatic activity was increased by Mn^{2+} ion and by the detergents Tween-20 and Tween-80; contrarily, SDS inhibited 68% Lp_1002 activity. The increase in enzyme activity observed by nonionic detergents, and the decrease by an ionic detergent were previously described in an arylesterase isolated from goat rumen[37] and in a feruloyl esterase from *L. plantarum*.[26]

Effect of Wine Compounds on Lp_1002 Arylesterase Activity. The biochemical properties showed by Lp_1002 indicated that the enzyme could be defined as an arylesterase, potentially active at wine conditions. The observation that Lp_1002 is an intracellular protein indicates that cell lysis may be important for its release and the subsequent flavor formation during winemaking. Therefore, special attention should be paid to the effect of compounds that could affect Lp_1002 activity once it has been released to the media. With this aim, the influence of several compounds naturally present in wine fermentations, such as ethanol, sodium metabisulfite, and several organic acids, such as malic, lactic, tartaric, and citric acids, was studied.

Ethanol concentration is an important parameter during winemaking, since malolactic fermentation is often conducted

dx.doi.org/10.1021/jf500991m | J. Agric. Food Chem. 2014, 62, 5118−5125

after the completion of alcoholic fermentation, when the concentration of this compound in wine can exceed 12%.[38] For this reason, the influence of ethanol on the Lp_1002 arylesterase activity has been analyzed. Experiments were conducted with concentrations higher than those found in wines (up to 20%). Ethanol concentration up to 16% seem to increase Lp_1002 activity. The highest esterase activity was observed at the ethanol concentration 4% (Figure 5A). The activity of an esterase from the wine bacterium *O. oeni* was stimulated by 14% ethanol.[13]

In addition, sodium metabisulfite, a powerful antimicrobial commonly used in wine, did not inhibit the enzyme when present at concentrations commonly found in wine. Final levels of 0.1−0.2 g/L of metabisulfite are found in wines.[38] At wine concentrations, metabisulfite did not significantly affect Lp_1002 arylesterase activity (Figure 5B). In grape must there are several organic acids, such as malic acid (up to 8.6 g/L) or tartaric acid (up to 7.4 g/L). During vinification the concentration of these acids varies, and as a consequence of LAB metabolism, lactic acid appeared. In wines, concentrations of 5, 4, and 4 g/L (w/v) of malic, tartaric or lactic acid, respectively, could be found.[38] Esterase Lp_1002 retained high activity at wine concentrations of these organic acids (Figure 5C−F). Only 5 g/L malic acid concentrations inhibited 20% Lp_1002 activity (Figure 5C). The activity shown by Lp_1002 in the presence of wine compounds suggests that this arylesterase could play a role in modulating ester profiles during winemaking. The International Organization of Vine and Wine (OIV) recommends that side enzymatic activities which have a potential negative effect on wine should not be present in commercial enzyme preparations.[39] Therefore, the use of recombinant, pure, and widely biochemical characterized enzymes will avoid the negative side activities present on commercial preparations

In conclusion, in this work it is shown that Lp_1002 is the first arylesterase described in *L. plantarum* and in a wine LAB. This arylesterase showed a broad substrate range, being able to modify relevant compounds for wine aroma. Lp_1002 arylesterase showed high activity under conditions commonly found during winemaking, such as cold temperature, acid pH, the presence of ethanol, malic acid, tartaric acid, or sulphites. The biochemical characteristics shown by Lp_1002 from *L. plantarum* suggest that this arylesterase is a very promising enzyme during vinification

AUTHOR INFORMATION

Corresponding Author

*Tel: +34 91 5622900. Fax: +34 91 564 4853. E-mail: rmunoz@ifi.csic.es.

Funding

This work was financially supported by Grants AGL2011-22745 and BFU2010-17929 (MINECO), S2009/AGR-1469 (ALIBIRD) (Comunidad de Madrid), and RM2012-00004 (Inia). M.E.-T. is a recipient of a JAE predoctoral fellowship from the CSIC.

Notes

The authors declare no competing financial interest.

ACKNOWLEDGMENTS

The technical assistance of M.V.S. is greatly appreciated.

REFERENCES

(1) Styger, G.; Prior, B.; Bauer, F. F. Wine flavor and aroma. *J. Ind. Microbiol. Biotechnol.* **2011**, *38*, 1145−1159.

(2) Lambrechts, M. G.; Pretorius, I. S. Yeast and its importante to wine aroma: a review. *S. Afr. J. Enol. Vitic.* **2000**, *21*, 97−129.

(3) Bartowsky, E. J.; Pretorius, I. S. Microbial formation and modification of flavour and off-flavor compounds in wine. In *Biology of microorganisms on grapes, in must and in wine*; Köning, H., Unden, G., Frölich, J., Ed.; Springer: Heidelberg, Germany, 2008; pp 209−231.

(4) Bornscheuer, U. T. Microbial carboxyl esterases: classification, properties and application in biocatalysis. *FEMS Microbiol. Rev.* **2002**, *26*, 73−81.

(5) Chang, A.; Scheer, M.; Grote, A.; Schomburg, I.; Schomburg, D. BRENDA, AMENDA and FRENDA the enzyme information system: new content and tools in 2009. *Nucleic Acids Res.* **2009**, *37*, D588−592.

(6) Wang, L.; Mavisakalyan, V.; Tillier, E. R. M.; Clark, G. W.; Savchenko, A. V.; Yakunin, A. F.; Master, E. R. Mining bacterial genomes for novel arylesterase activity. *Microbiol. Biotechnol.* **2010**, *3*, 677−690.

(7) Sumby, K. M.; Grbin, P. R.; Jiranek, V.; et al. Microbial modulation or aromatic esters in wine: current knowledge and future prospects. *Food Chem.* **2010**, *121*, 1−16.

(8) Choi, Y. L.; Miguez, C. B.; Lee, B. H. Characterization and heterologous gene expression of a novel esterase from *Lactobacillus casei* CL96. *Appl. Environ. Microbiol.* **2004**, *70*, 3213−3221.

(9) Fenster, K. M.; Parkin, K. L.; Steele, J. L. Characterization of an arylesterase from *Lactobacillus helveticus* CNRZ32. *J. Appl. Microbiol.* **2000**, *88*, 572−583.

(10) Fenster, K. M.; Parkin, K. L.; Steele, J. L. Nucleotide sequencing, purification, and biochemical properties of an arylesterase from *Lactobacillus casei* LILA. *J. Dairy Sci.* **2003**, *86*, 2547−2557.

(11) Fernández, L.; Beerthuyzen, M. M.; Brown, J.; Siezen, R. J.; Coolbear, T.; Holland, R.; Kuipers, O. P. Cloning, characterization, controlled overexpression, and inactivation of the major tributyrin esterase gene of *Lactococcus lactis*. *Appl. Environ. Microbiol.* **2000**, *66*, 1360−1368.

(12) Davis, C. R.; Wibowo, D.; Eschenbruch, R.; Lee, T. H.; Fleet, G. H. Practical implications of malolactic fermentation: a review. *Am. J. Enol. Vitic.* **1985**, *36*, 290−301.

(13) Sumby, K. M.; Matthews, A. H.; Grbin, P. R.; Jiranek, V. Cloning and characterization of an intracellular esterase from the wine-associated lactic acid bacterium *Oenococcus oeni*. *Appl. Environ. Microbiol.* **2009**, *75*, 6729−6735.

(14) Sumby, K. M.; Grbin, P. R.; Jiranek, V. Characterization of EstCOo8 and EstC34, intracellular esterases, from the wine-associated lactic acid bacteria *Oenococcus oeni* and *Lactobacillus hilgardii*. *J. Appl. Microbiol.* **2012**, *114*, 413−422.

(15) Andersen, H. J.; Østdal, H.; Blom, H. Partial purification and characterization of a lipase from *Lactobacillus plantarum* MF32. *Food Chem.* **1995**, *53*, 369−373.

(16) Oterholm, A.; Witter, L. D.; Ordal, Z. J. Glycerol ester hydrolase activity of some lactic acid bacteria. *J. Dairy Sci.* **1967**, *50*, 954.

(17) Otherholm, A.; Ordal, Z. J.; Witter, L. D. Glycerol ester hydrolase activity of lactic acid bacteria. *Appl. Microbiol.* **1968**, *16*, 524−527.

(18) Gobbetti, M.; Fox, P. F.; Smacchi, E.; Stepaniak, L.; Damiani, P. Purification and characterization of a lipase from *Lactobacillus plantarum* 2739. *J. Food Biochem.* **1996**, *20*, 227−246.

(19) Gobbetti, M.; Fox, P. F.; Stepaniak, L. Isolation and characterization of a tributyrin esterase from *Lactobacillus plantarum* 2739. *J. Dairy Sci.* **1997**, *80*, 3099−3106.

(20) Silva Lopez, M. F.; Cunha, A. E.; Clemente, J. J.; Teixeira Carrondo, M. J.; Barreto Crespo, M. T. Influence of environmental factors on lipase production by *Lactobacillus plantarum*. *Appl. Microbiol. Biotechnol.* **1999**, *51*, 249−254.

(21) Silva Lopes, M. F.; Leitao, A. L.; Regalla, M.; Figueiredo Marques, J. J.; Teixeira Carrondo, M. J.; Barreto Crespo, M. T. Characterization of a highly thermostable extracellular lipase from *Lactobacillus plantarum*. *Int. J. Food Microbiol.* **2002**, *76*, 107−115.

(22) Navarro-González, I.; Sánchez-Ferrer, A.; García-Carmona, F. Overexpression, purification, and biochemical characterization of the

esterase Est0796 from *Lactobacillus plantarum* WCFS1. *Mol. Biotechnol.* **2013**, *54*, 651−660.
(23) Brod, F. C. A.; Vernal, J.; Bertoldo, J. B.; Terenzi, H.; Maisonnave Arisi, A. C. Cloning, expression, purification, and characterization of a novel esterase from *Lactobacillus plantarum*. *Mol. Biotechnol.* **2010**, *44*, 242−249.
(24) Oterholm, A.; Witter, L. D.; Ordal, Z. J. Purification and properties of an acetyl ester hydrolase (acetylesterase) from *Lactobacillus plantarum*. *J. Dairy Sci.* **1972**, *55*, 8−13.
(25) Benavente, R.; Esteban-Torres, M.; Acebrón, I.; de las Rivas, B.; Muñoz, R.; Mancheño, J. M. Structure, biochemical characterization and analysis of the pleomorphism of carboxylesterase Cest-2923 from *Lactobacillus plantarum* WCFS1. *FEBS J.* **2014**, DOI: 10.1111/febs.12569.
(26) Esteban-Torres, M.; Reverón, I.; Mancheño, J. M.; de las Rivas, B.; Muñoz, R. Characterization of a feruloyl esterase from *Lactobacillus plantarum*. *Appl. Environ. Microbiol.* **2013**, *79*, 5130−5136.
(27) Green, M. L.; Karp, P. D. A Bayesian method for identifying missing enzymes in predicted metabolic pathway databases. *BMC Bioinformatics* **2004**, *5*, 76.
(28) Curiel, J. A.; de las Rivas, B.; Mancheño, J. M.; Muñoz, R. The pURI family of expression vectors: a versatile set of ligation independent cloning plasmids for producing recombinant His-fusion proteins. *Protein Expr. Purif.* **2011**, *76*, 44−53.
(29) Glogauer, A.; Martini, V. P.; Faoro, H.; Couto, G. H.; Müller-Santos, M.; Monteiro, R. A.; Mitchel, D. A.; de Souza, E. M.; Pedrosa, O. F.; Krieger, N. Identification and characterization of a new true lípase isolated through metagenomic approach. *Microb. Cell Fact.* **2011**, *10*, 54.
(30) Lui, A. M. F.; Somers, N. A.; Kazlauskas, R. J.; Brush, T. S.; Zocher, T. S.; Enzelberger, M. M.; Bronscheuer, U. T.; Horsman, G. P.; Mezzetti, A.; Schmidt-Dannert, C.; Schmid, R. D. Mapping the substrate selectivity of new hydrolases using colorimetric screening lipases from *Bacillus thermocatenolatus* and *Ophiostoma piliferum*, esterases from *Pseudomonas fluorescens* and *Streptomyces diastatochromogenes*. *Tetrahedron: Asymmetry* **2001**, *12*, 545−556.
(31) Park, Y. J.; Yoon, S. J.; Lee, H. B. A novel thermostable arylesterase from the archaeon *Sulfolobus solfataricus* P1: purification, characterization, and expression. *J. Bacteriol.* **2008**, *190*, 8086−8095.
(32) Shaw, J. F.; Chang, R. C.; Chuang, K. H.; yen, Y. T.; Wang, Y. J.; Wang, F. G. Nucelotide sequence of a novel arylesterase gene from *Vibrio mimicus* and characterization of the enzyme expressed in *Escherichia coli*. *Biochem. J.* **1994**, *298*, 675−680.
(33) Sakai, Y.; Ayukawa, K.; Yurimoto, H.; Yamamoto, K.; Kato, N. A novel arylesterase active toward 7-aminocephalosporanic acid from *Agrobacterium radiobacter* IFO 12607: Purification and characterization. *J. Ferment. Bioeng.* **1998**, *85*, 58−62.
(34) Jones, R. M.; Collier, L. S.; Neidle, E. L.; Williams, P. A. *areABC* genes determine the catabolism of aryl esters in *Acinetobacter* sp. strain ADP1. *J. Bacteriol.* **1999**, *181*, 4568−4575.
(35) Cheeseman, J. D.; Tocilj, A.; Park, S.; Schrag, J.; Kazlauskas, R. J. Structure of an aryl esterase from *Pseudomonas fluorecens*. *Acta Crystallogr.* **2004**, *D60*, 1237−1243.
(36) Navarro-González, I.; Sánchez-Ferrer, A.; García-Carmona, F. Molecular characterization of a novel arylesterase from the wine-associated acetic acid bacterium *Gluconobacter oxidans* 621H. *J. Agric. Food Chem.* **2012**, *60*, 10789−10795.
(37) Wang, G.; Meng, K.; Luo, H.; Wang, Y.; Huang, H.; Shi, P.; Pan, X.; Yang, P.; Yao, B. Molecular cloning and characterization of a novel SGNH arylesterase from the goat rumen contents. *Appl. Micorbiol. Biotechnol.* **2011**, *91*, 1561−1570.
(38) Flanzy, C. *Enología: fundamentos científicos y tecnológicos*; Ediciones, A. M. V., Ed.; Mundi-Prensa: Madrid, 2000.
(39) Fia, G.; Canuti, V.; Rosi, I. Evaluation of potential side activities of commercial enzyme preparations used in winemaking. *Int. J. Food Sci. Technol.* **2014**, DOI: 10.1111/ijfs.12508.

MATERIALS AND METHODS

Strains, Plasmids, Media, and Materials. *L. plantarum* WCFS1, kindly provided by M. Kleerebezem (NIZO Food Research, Netherlands), was grown in MRS medium (Pronadisa, Spain) adjusted to pH 6.5, and incubated at 30 °C. This strain is a colony isolate of *L. plantarum* NCIMB 8826, which was isolated from human saliva. *Escherichia coli* DH10B was used as the host strain for all DNA manipulations. *E. coli* BL21 (DE3) was used for heterologous expression in the pURI3-TEV vector.[21] *E. coli* strains were cultured in Luria−Bertani (LB) medium at 37 °C with shaking at 200 rpm. When required, ampicillin and chloramphenicol were added to the medium at a concentration of 100 or 20 μg/mL, respectively.

Plasmid DNA was extracted by a High Pure Plasmid Isolation Kit (Roche). The polymerase chain reaction (PCR) product was purified with a QIAquick Gel Extraction Kit (Qiagen). Oligonucelotides were purchased from Eurofins MWG Operon (Ebersberg, Germany). *Dpn*I and HS Prime Star DNA polymerase were obtained from TaKaRa. His-tagged protein was purified by a Talon Superflow resin (Clontech).

Cloning of Lp_2631 Esterase Encoding Gene. Genomic DNA from *L. plantarum* WCFS1 was extracted. The gene encoding a putative lipase/esterase (*lp_2631*) in *L. plantarum* WCFS1 was amplified by PCR using the primers 569 (5′-*GGTGAAAACCTG-TATTTCCAGGGCat*ggtgcggacgaccaaatttggtg) and 570 (5′-*ATCGA-TAAGCTTAGTTAGCTATTATTA*tttaagaatgttggtctccaag) (the nucleotides pairing the expression vector sequence are indicated in italics, and the nucleotides pairing the *lp_2631* gene sequence are written in lowercase letters). Prime Star HS DNA polymerase (TaKaRa) was used for the PCR amplification. The 786 bp purified PCR product was inserted into the pURI3-TEV vector using a restriction enzyme- and ligation-free cloning strategy.[21] The vector produces recombinant proteins having a six-histidine affinity tag in their N termini. *E. coli* DH10B cells were transformed; recombinant plasmids were isolated; and those containing the correct insert were identified by size, verified by DNA sequencing, and then transformed into *E. coli* BL21 (DE3) cells for expression.

Expression and Purification of Lp_2631 Esterase. *E. coli* BL21 (DE3) harboring pGro7 (TaKaRa), a vector overexpressing GroES/GroEL chaperones, was transformed with the recombinant plasmid pURI3-TEV-2631. *E. coli* was grown in LB medium containing 100 μg/mL ampicillin, 20 μg/mL chloramphenicol, and 2 mg/mL arabinose, on a rotary shaker (200 rpm) at 37 °C until an optical density (OD) at 600 nm of 0.4 was reached. Isopropyl-β-D-thiogalactopyranoside (IPTG) was added to a final concentration of 0.4 mM, and protein induction was continued at 22 °C for 18 h.

The induced cells were harvested by centrifugation (8000*g* for 15 min at 4 °C), resuspended in phosphate buffer (50 mM, pH 7) containing 300 mM NaCl, and disrupted by French Press passages (3 times at 1100 psi). The insoluble fraction of the lysate was removed by centrifugation at 47000*g* for 30 min at 4 °C, and the supernatant was filtered through a 0.2 μm pore-size filter and then loaded onto a Talon Superflow resin (Clontech) equilibrated in phosphate buffer (50 mM, pH 7) containing 300 mM NaCl and 10 mM imidazole to improve the interaction specificity in the affinity chromatography step. The bound enzyme was eluted using McIlvaine buffer (100 mM, pH 5).[22] The purity of the enzyme was determined by sodium dodecyl sulfate−polyacrylamide gel electrophoresis (SDS−PAGE) in Tris−glycine buffer. Fractions containing the His_6-tagged protein were pooled and analyzed for esterase activity.

Enzyme Assay. Esterase activity was determined by a spectrophotometric method as described previously using *p*-nitrophenyl acetate (Sigma-Aldrich) as the substrate.[18]

Substrate Specificity. To investigate the substrate specificity of Lp_2631, activity was determined using different *p*-nitrophenyl esters of various chain lengths (Sigma-Aldrich), *p*-nitrophenyl acetate (C_2), *p*-nitrophenyl butyrate (C_4), *p*-nitrophenyl caprylate (C_8), *p*-nitrophenyl laurate (C_{12}), *p*-nitrophenyl myristate (C_{14}), and *p*-nitrophenyl palmitate (C_{16}), as substrates as described previously.[18,23]

Determination of Optimum pH, Temperature, and Thermostability. The effect of pH was studied by assaying esterase activity in a range of pH values from 3.0 to 9.0 as described previously.[18] The temperature effect was assayed in 50 mM sodium phosphate buffer (pH 7.0) at 5, 20, 30, 37, 40, 45, 55, and 65 °C for 10 min. For temperature stability measurements, the esterase was incubated in 50 mM sodium phosphate buffer (pH 7.0) at 22, 30, 37, 45, 55, and 65 °C for 5 min, 15 min, 30 min, 1 h, 2 h, 4 h, 6 h, and 20 h. After incubation, the residual activity was measured as described above.

Effects of Additives on Lp_2631 Esterase Activity. The effect of metal ions, surfactants, reductants, and inhibitors on the activity of the esterase was assayed by incubation of the enzyme in the presence of different additives at a final concentration of 1 mM for 5 min at room temperature. Then, the substrate was added, and the reaction was incubated at 20 °C.[18] The compounds analyzed were $MgCl_2$, KCl, $MnCl_2$, $CuCl_2$, $NiCl_2$, $CaCl_2$, $HgCl_2$, $ZnCl_2$, diethylpyrocarbonate (DEPC), cysteine, SDS, dithiothreitol (DTT), Triton X-100, urea, Tween 80, Tween 20, ethylenediaminetetracetic acid (EDTA), dimethyl sulfoxide (DMSO), phenylmethanesulfonyl fluoride (PMSF), and β-mercaptoethanol.

In addition, the effect of several compounds present in food fermentation was assayed. The effect of ethanol on esterase activity was studied at ethanol concentrations ranging from 0 to 20% (v/v). Reaction mixtures were prepared as described for the temperature optimum experiments; however, different volumes of ethanol were added, and the volume of the buffer was adjusted accordingly to maintain the final reaction volume (1 mL). The reactions were preincubated 5 min at room temperature, and the substrate (*p*-nitrophenyl acetate) was added. The effect of the presence of several organic acids was also studied. Malic, tartaric, citric, and lactic acids were assayed at concentrations ranging from 0 to 5 g/L. Reaction mixtures were prepared by adding different volumes of the corresponding stock solution (25 g/L) prepared in phosphate buffer (50 mM, pH 7.0). The effect of sulfite was determined by adding sodium metabisulfite at concentrations ranging from 0 to 1 g/L. The reactions were performed by adding different volumes of a 25 g/L stock solution. Finally, the effect of NaCl was determined by adding NaCl at concentrations ranging from 0 to 25% (v/v). Reaction mixtures were prepared as described for the temperature optimum experiments; however, different volumes of 25% NaCl solution were added, and the volume of the buffer was adjusted accordingly to maintain the final reaction volume. Reaction mixtures were preincubated for 5 min at room temperature before the enzyme was added. After the reaction, the absorbance was measured at 348 nm.

Statistical Analyses. Two-tailed Student's *t* test preformed using GraphPad InStat, version 3.0 (GraphPad Software, San Diego, CA), was used to determine the differences between means. The data are representative means of at least three independent experiments.

RESULTS AND DISCUSSION

Production and Characterization of Lp_2631 Esterase. LAB are used for the preservation of food raw materials, such as milk, meat, and vegetable or other plant materials. *L. plantarum* is a flexible and versatile species that is encountered in a variety of environmental niches, including some dairy, meat, and many vegetable or plant fermentations. The ecological flexibility of *L. plantarum* is reflected by the observation that this species has one of the largest genomes known among LAB.[10] This large genome codifies enzymatic activities, which could develop a fundamental role in food fermentations, such as cold-active esterases (also known as cold-adapted). When the published sequence of *L. plantarum* WCFS1 was analyzed, numerous open reading frames (ORFs) encoding putative esterases/lipases were found. Because it is not possible predict the biochemical function encoded by these *L. plantarum* ORFs, features found in cold-active esterases were searched. According to previous studies,[24−26] in comparison to mesophilic or themophilic esterases, cold-adapted enzymes

dx.doi.org/10.1021/jf501493z | J. Agric. Food Chem. 2014, 62, 5126−5132

revealed structural traits, such as a low ratio or Arg/(Arg + Lys), a low proportion of proline residues, or a high proportion of small residues (Gly and Ala). Among the putative esterases encoded by the *L. plantarum* WCFS1 genome, *lp_2631* encodes a protein that exhibits some of these structural features. Thus, when the amino acid composition of Lp_2631 was analyzed, the ratio of Arg/(Arg + Lys) was found to be 0.45, lower than that of other cold-adapted esterases: 0.50 in Est10 from *Psychrobacter pacifiensis*,[27] or 0.56 in rESt97 from a metagenomic library.[28] Also, the total percentage (20.31%) of small residues Gly (7.28%) and Ala (13.03%) is relatively high compared to the low proportion of Arg (3.45%) and Pro (5.75%). These characteristics of the primary structure may suggest that Lp_2631 could be a cold-active esterase.

Lp_2631 is predicted to encode a 261 amino acid protein, 42% identical to a putative esterase/lipase from *Lactobacillus sakei* and 35% identical to uncharacterized proteins from *Lactobacillus salivarius* or *Lactobacillus ruminis* (data not shown).

The *lp_2631* gene was cloned into the pURI3-TEV expression vector, and the recombinant plasmid obtained was transformed into *E. coli* BL21 (DE3). Cell extracts were used to detect the presence of overproduced proteins. SDS−PAGE analysis showed that there was one major band of protein, approximately 28 kDa, present as inclusion bodies in the insoluble fraction. To obtain Lp_2631 soluble, plasmid pGro7, producing GroES/GroEL chaperones, was used. When pURI3-TEV-2631 and pGro7 plasmids were used simultaneously, Lp_2631 appeared in the intracellular soluble fraction of the cells (Figure 1). The molecular weight of the overproduced

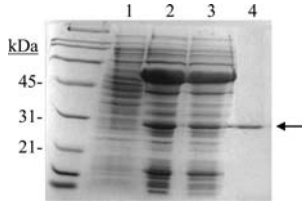

Figure 1. SDS−PAGE analysis of the purification of Lp_2631 esterase from *L. plantarum* WCFS1. Analysis by SDS−PAGE of soluble cell extracts of IPTG-induced *E. coli* BL21 (DE3) (pGro7) (pURI3-TEV) (1) or *E. coli* BL21 (DE3) (pGro7) (pURI3-TEV-2631) (2), flowthrough (3), or protein eluted after His affinity resin (4). The gel was stained with Coomassie blue. Molecular mass markers are located on the left (SDS−PAGE Standards, Bio-Rad).

protein was consistent with the theoretical one expected for Lp_2631. The recombinant protein was observed as a single band on SDS−PAGE (Figure 1). Routinely, about 8 mg of purified protein from a 1 L culture was obtained.

Lp_2631 protein purified by the affinity resin was biochemically characterized. Substrate specificity was determined using *p*-nitrophenyl-linked esters of various acyl chain lengths (C_2−C_{16}) at 20 °C (Figure 2). The enzyme was only active on substrates with a chain length up to C_4, with minimal activity detected with the longer chain lengths. This result indicated that Lp_2631 is an esterase and not a true lipase. This narrow substrate range displayed by Lp_2631 is similar to the substrate range described for a *L. plantarum* esterase described previously.[23]

The influence of pH, in the range of 3.0−9.0, on esterase activity was studied at 20 °C (Figure 3A). Although the enzyme showed activity at pH from 3.0 to 8.0, the highest activity was

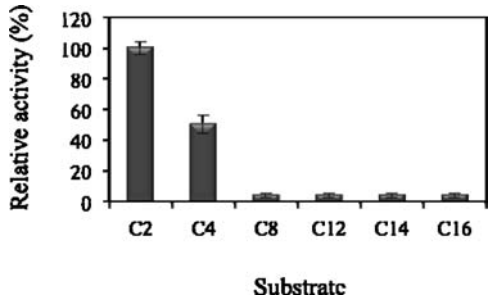

Figure 2. Substrate profile of Lp_2631 against chromogenic substrates (*p*-nitrophenyl esters) with different acyl chain lengths (C_2, acetate; C_4, butyrate; C_8, caprylate; C_{12}, laurate; C_{14}, myristate; and C_{16}, palmitate). The figure displays the relative specificities obtained toward different substrates, and lines on top of each bar represent the standard deviations estimated from three independent assays. The observed maximum activity was defined as 100%.

observed at pH 6.5. Similar to the substrate range, only the esterase described previously by Brod et al. exhibited an optimal pH range of 6.0−6.5. Apart from both of these esterases, the *L. plantarum* esterases described thus far showed higher optimum pH, pH 7 for Lp_2923[29] and a feruloyl esterase[18] and pH 8 for Lp_0796.[30] LAB-fermented food products are characterized by a low pH. For example, a final pH around 5.5 could be found in meat fermentations; at this pH, Lp_2631 still exhibited 40% of its maximal activity.

The influence of the temperature on enzymatic activity was determined (Figure 3B). Maximal activity was observed at 20 °C, confirming previous structural data of Lp_2631, suggesting that this esterase could be a cold-adapted protein. As far as we know, Lp_2631 is the first esterase from *L. plantarum* exhibiting such functional features. In fact, other *L. plantarum* esterases show higher optimal temperatures, such as 30 °C for Lp_2923,[29] 35 °C for Lp_0796,[30] or 40 °C for Lp_0973.[31] More interestingly, Lp_2631 showed more than 90% activity at 5 °C and decreases to 30% at 30 °C. A similar behavior has been described in cold-active esterases described from non-LAB or metagenomic libraries.[31−35] Lp_2631 is the first esterase described from LAB that shows higher activity at refrigeration temperatures. This is an important property in food fermentations; e.g., during the ripening of a fermented meat product in the traditional manufacturing process, temperatures can be as low as 15 °C. Moreover, esterase activity could be important even at meat storage temperatures (3 and 7.5 °C).[33]

The available data regarding psychrophilic enzymes pointed out that the high specific activity at low temperatures is often associated with a low thermostability, which make them inclined to lose their activity at moderate and even high temperatures.[24] Low-temperature activity has been generally associated with low conformational stability. To assess the thermostability of Lp_2631, the enzyme was preincubated at different temperatures for different time intervals, before assaying the residual activity. Figure 3C shows that Lp_2631 was fairly stable under room temperatures. The enzyme retained up to 80% activity after incubation for 20 h at 20 °C. The enzyme showed 50% of its maximal activity after 4 h of incubation at 30 or 37 °C or 40% after 2 h at 45−65 °C. Therefore, esterase Lp_2631 not only showed high activity levels at low temperature but also exhibited higher thermostability when compared to other cold-active enzymes, e.g., the low-temperature lipase from psychrotopic *Pseudomonas* sp. strain KB700A.[36] In fact, other cold-adapted esterases are also

dx.doi.org/10.1021/jf501493z | J. Agric. Food Chem. 2014, 62, 5126−5132

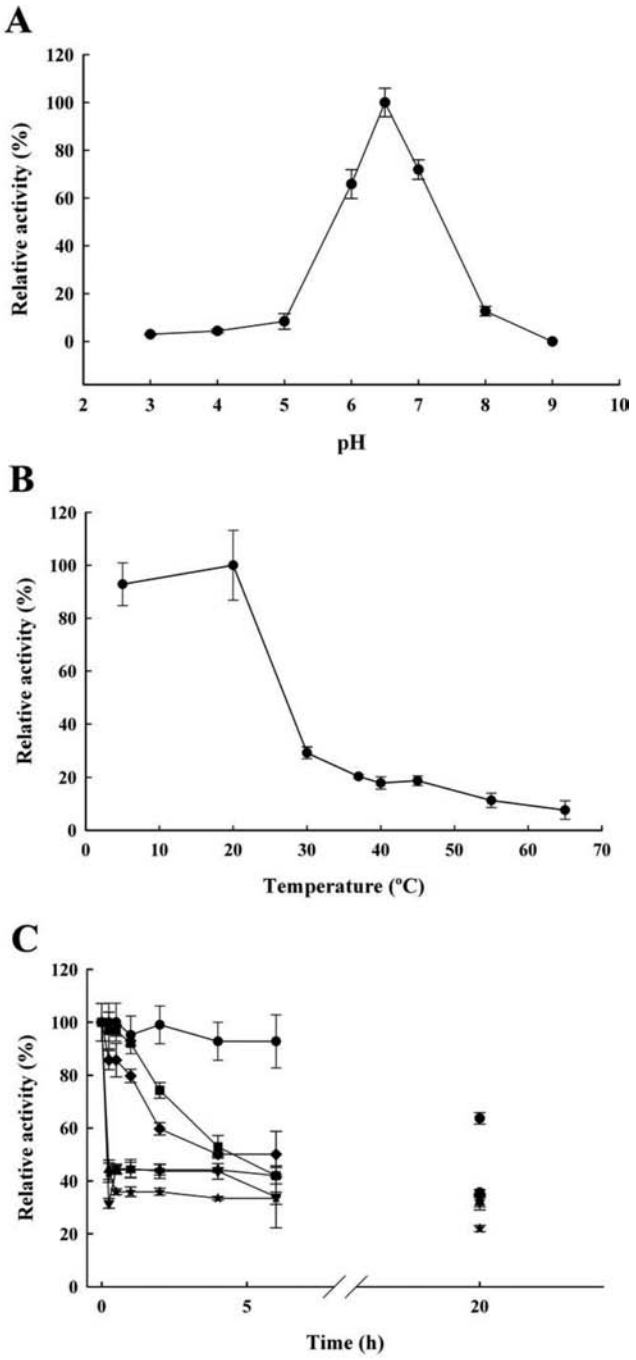

Figure 3. Biochemical properties of Lp_2631 esterase. (A) pH activity profile of Lp_2631. (B) Temperature–activity profile of Lp_2631. (C) Thermal stability profile for Lp_2631 after preincubation at 22 °C (●), 30 °C (■), 37 °C (◆), 45 °C (▲), 55 °C (▼), and 65 °C (★) in phosphate buffer (50 mM, pH 7) at indicated times. Aliquots were withdrawn and analyzed as described in the Materials and Methods. The experiments were performed in triplicate. The mean value and standard error are shown. The percentage of residual activity was calculated by comparing to unincubated enzyme.

fairly stable.[37] Although high catalytic activity at a low temperature tends to be associated with thermosensitivity, directed evolution studies to improve the thermostability of cold-adapted enzymes revealed that, as in Lp_2631, there is not a strict correlation.[19]

The effects of several ions, surfactants, reductants, and inhibitors on Lp_2631 activity are shown in Figure 4. In

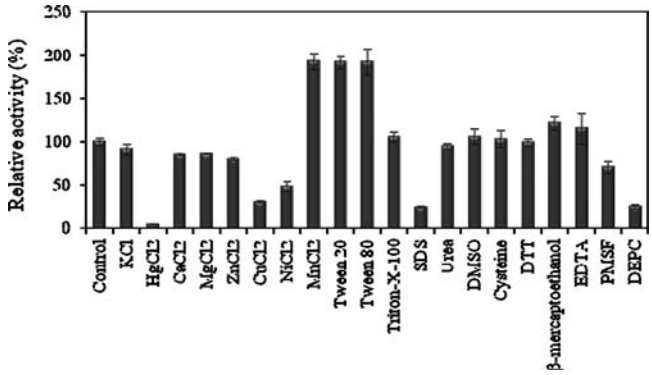

Figure 4. Effects of additives on Lp_2631 esterase activity. Relative activity of Lp_2631 after incubation with 1 mM concentration of different additives. The activity of the enzyme in the absence of additives was defined as 100%. The experiments were performed in triplicate. The mean value and standard error are shown.

comparison to the enzyme incubated in 50 mM phosphate buffer at pH 7, the enzymatic activity was increased 2-fold by the detergents Tween 20 and Tween 80, and in contrast, SDS greatly inhibited Lp_2631. The increase in enzyme activity observed by non-ionic detergents and the decrease by ionic detergent were previously described in a feruloyl esterase from *L. plantarum*[16] and in the cold-active lipase EML1 from a deep-sea sediment metagenome.[38] With regard to metal ions, only Mn^{2+} increases activity, while Ni^{2+}, Cu^{2+}, and Hg^{2+} significantly inhibited esterase activity. Inactivation by Hg^{2+} ions has previously been described in other *L. plantarum* esterases, such a feruloyl esterase[18] and a lipase purified from *L. plantarum* 2739.[14] Normally, the esterase activity of hydrolases does not require cofactors, such as metals. On the contrary, the inhibitory effects of some of then are observed and explained in terms of covalent modification of catalytic residues (such as the covalent modification of thiol groups by Hg^{2+}). The effects of other metals on esterase activity (either activating or inhibiting the enzyme) have also been reported;[29] however, the molecular mechanisms underlying these effects have not been determined, and most likely, they are unspecific. The enzyme was also partially inactivated by PMSF and DEPC, confirming the involvement of a serine and a histidine at the active site of the enzyme.

Activity of Lp_2631 in the Presence of Compounds Found in Food Fermentations. Also important, to understand the role of Lp_2631 esterase activity during food processing is the study of compounds present in food fermentation media that could affect its activity. Food processing subjects microorganisms and their enzymes to adverse environmental conditions (such as osmotic stress, toxic compounds, and ethanol), which affect their survival and technological performances. Because of its industrial relevance, a better understanding of the influence of compounds present in food fermentations is important. The influence on Lp_2631 activity of several compounds naturally present in food fermentations, such as ethanol, malic acid, tartaric acid, and sodium metabisulfite in winemaking, NaCl in cheese and meat fermentations, and lactic acid as a main product resulting for LAB fermentation, was also studied.

The ethanol concentration is an important compound during winemaking, because malolactic fermentation is often conducted after the completion of alcoholic fermentation, when the ethanol concentration of wine can exceed 12%.[39] For this

dx.doi.org/10.1021/jf501493z | J. Agric. Food Chem. 2014, 62, 5126–5132

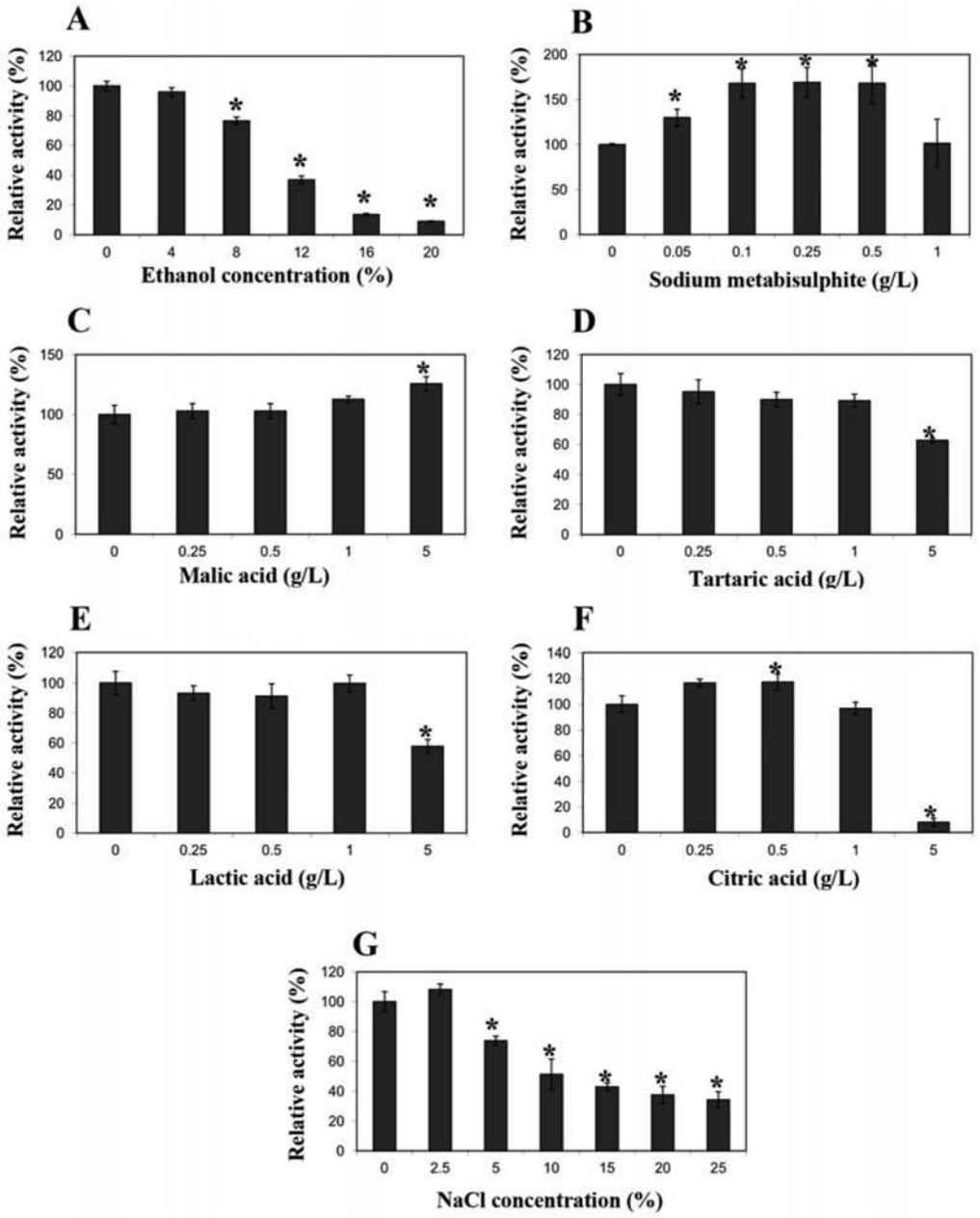

Figure 5. Activity of Lp_2631 esterase in the presence of compounds found in food fermentations. Relative activity of Lp_2631 after incubation in the presence of compounds present in food fermentation media, such ethanol (A), sodium metabisulfite (B), malic acid (C), tartaric acid (D), lactic acid (E), citric acid (F), and NaCl (G) at the concentrations indicated. The activity of the enzyme in the absence of the compound was defined as 100%. The experiments were performed in triplicate. The mean value and standard error are shown. Asterisks indicate a p value < 0.05.

reason, the influence of ethanol on the Lp_2631 esterase activity has been analyzed. Experiments were conducted with concentrations higher than those found in wines (up to 20%). The highest esterase activity was observed in the absence of ethanol; however, at wine ethanol concentrations (12%), Lp_2631 exhibited 40% of its maximal activity (Figure 5A). A different ethanol effect was observed in an esterase from the wine bacterium *Oenococcus oeni* because it was stimulated by 14% ethanol, producing a 49% activity increase.[22]

In addition, sodium metabisulfite, a powerful antimicrobial commonly used in wine, did not inhibit the enzyme when present at concentrations commonly found in wine. Final levels of 0.1−0.2 g/L of metabisulfite are found in wines.[39] At wine concentrations, metabisulfite increases up to 70% esterase activity (Figure 5B). Again, Lp_2631 esterase showed a different behavior than *O. oeni* esterase, which was partially inhibted in the presence of metabisulfite.[22] In grape must, there are several organic acids, such as malic acid (up to 8.6 g/L) or tartaric acid (up to 7.4 g/L). During vinification, the concentration of these acids varies, and as a consequence of LAB metabolism, lactic acid appeared. In wines, concentrations of 5, 4, and 4 g/L malic, tartaric, or lactic acid, respectively, could be found.[39] Esterase Lp_2631 showed activity at wine concentrations of these organic acids. Malic acid concentrations up to 5 g/L increased esterase activity (Figure 5C); however, esterase was partially inhibited by tartaric and lactic acids at wine concentrations (panels D and E of Figure 5). Lp_2631 activity was not affected by concentrations of citric acid usually

dx.doi.org/10.1021/jf501493z | J. Agric. Food Chem. 2014, 62, 5126−5132

found in grape musts or wines, with a maximum of 0.90 and 0.88 g/L, respectively.[37]

L. plantarum strains are active in fermented foods, such as milk or meat fermentations, in which salt or citric or lactic acid are present.[40] Under cheese-ripening conditions (4% NaCl), Lp_2631 was only partially inhibited, retaining 74% of its maximal activity at 5% (Figure 5G). Citric and lactic acids showed a similar behavior, with both acids inhibiting Lp_2631 activity at 5 g/L, whereas at 1 g/L, the enzyme keeps full activity. At cheese concentrations (50 mg/100 g),[41] citric acid did not inhibit Lp_2631 activity. The activity shown by Lp_2631 suggests that this esterase could play a role in modulating ester profiles during cheese ripening.

The obtained results indicated that Lp_2631 is an esterase, which retains activity under conditions commonly found in food fermentations, such as cold temperature and the presence of salt, ethanol, organic acids, or antimicrobials. The main disadvantage for the use of Lp_2631 in food fermentations is its narrow pH profile under standard reaction conditions. Further assays need to be performed under combined conditions to know the effect of the simultaneous presence of different factors on Lp_2631 activity.

In conclusion, in the present study, the cold-active esterase, namely, Lp_2631 from *L. plantarum*, an industrially important LAB species, which can be found in numerous fermented foods, was purified and biochemically characterized. Lp_2631 is a cold-active esterase that exhibited maximum activity at 20 °C and, more importantly, retains more than 90% activity at refrigeration temperatures. In addition, esterase Lp_2631 not only showed good activity at low temperatures but also had good thermostability compared to other cold-active enzymes. On the basis of the findings reported in this study, it appears that Lp_2631 will retain adequate activity under food fermentation conditions.

AUTHOR INFORMATION

Corresponding Author

*Telephone: +34-91-5622900. Fax: +34-91-5644853. E-mail: r.munoz@csic.es.

Funding

This work was financially supported by Grants AGL2011-22745 and BFU2010-17929 (MINECO), S2009/AGR-1469 (ALIBIRD) (Comunidad de Madrid), and RM2012-00004 (INIA). María Esteban-Torres is a recipient of a JAE predoctoral fellowship from the CSIC.

Notes

The authors declare no competing financial interest.

ACKNOWLEDGMENTS

The assistance of J. M. Barcenilla and M. V. Santamaría is greatly appreciated.

REFERENCES

(1) McFeeters, R. F. Fermentation microorganisms and flavour changes in fermented foods. *J. Food Sci.* **2004**, *69*, 35−37.

(2) Park, Y. C.; Shaffer, C. E. H.; Bennett, G. N. Microbial formation of esters. *Appl. Microbiol. Biotechnol.* **2009**, *85*, 13−25.

(3) Bornscheuer, U. T. Microbial carboxyl esterases: Classification, properties and application in biocatalysis. *FEMS Microbiol. Rev.* **2002**, *26*, 73−81.

(4) Flores, M.; Toldrá, F. Micorbial enzymatic activities for improved fermented meats. *Trends Food Sci. Technol.* **2011**, *22*, 81−90.

(5) Montel, M. C.; Masson, F.; Talon, R. Bacterial role in flavour development. *Meat Sci.* **1998**, *49*, S111−S123.

(6) Silva Lopes, M. F.; Leitao, A. L.; Regalla, M.; Figueiredo Marques, J. J.; Teixeira Carrondo, M. J.; Barreto Crespo, M. T. Characterization of a highly thermostable extracellular lípase from *Lactobacillus plantarum*. *Int. J. Food Microbiol.* **2002**, *76*, 107−115.

(7) Antalick, G.; Perello, M.-C.; de Revel, G. Characterization of fruity aroma modifications in red wines during malolactic fermentation. *J. Agric. Food Chem.* **2012**, *60*, 12371−12383.

(8) Cao, M.; Fonseca, L. M.; Schoenfuss, T. C.; Rankin, S. A. Homogenization and lipase treatment of milk and resulting methyl ketone generation in blue cheese. *J. Agric. Food Chem.* **2014**, DOI: 10.1021/jf4048786.

(9) Castillo, I.; Requena, T.; Fernández de Palencia, P.; Fontecha, J.; Gobbetti, M. Isolation and characterization of an intracellular esterase from *Lactobacillus casei* subps. *casei* IFLP731. *J. Appl. Microbiol.* **1999**, *86*, 653−659.

(10) Kleerebezem, M.; Boekhorst, J.; van Kranenburg, R.; Molenaar, D.; Kuipers, O. P.; Leer, R.; Tarchini, R.; Peters, S. A.; Sandbrink, H. M.; Fiers, M. W. E. J.; Stiekema, W.; Klein Lankhorst, R. M.; Bron, P. A.; Hoffer, S. M.; Nierop Groot, M. N.; Kerkhoven, R.; de Vries, M.; Ursing, B.; de Vos, W. M.; Siezen, R. J. Complete genome sequence of *Lactobacillus plantarum* WCFS1. *Proc. Natl. Acad. Sci. U. S. A.* **2003**, *100*, 1990−1995.

(11) Andersen, H. J.; Østdal, H.; Blom, H. Partial purification and characterization of a lipase from *Lactobacillus plantarum* MF32. *Food Chem.* **1995**, *53*, 369−373.

(12) Oterholm, A.; Witter, L. D.; Ordal, Z. J. Glycerol ester hydrolase activity of some lactic acid bacteria. *J. Dairy Sci.* **1967**, *50*, 954.

(13) Otherholm, A.; Ordal, Z. J.; Witter, L. D. Glycerol ester hydrolase activity of lactic acid bacteria. *Appl. Microbiol.* **1968**, *16*, 524−527.

(14) Gobbetti, M.; Fox, P. F.; Smacchi, E.; Stepaniak, L.; Damiani, P. Purification and characterization of a lipase from *Lactobacillus plantarum* 2739. *J. Food Biochem.* **1996**, *20*, 227−246.

(15) Gobbetti, M.; Fox, P. F.; Stepaniak, L. Isolation and characterization of a tributyrin esterase from *Lactobacillus plantarum* 2739. *J. Dairy Sci.* **1997**, *80*, 3099−3106.

(16) Silva Lopez, M. F.; Cunha, A. E.; Clemente, J. J.; Teixeira Carrondo, M. J.; Barreto Crespo, M. T. Influence of environmental factors on lípase production by *Lactobacillus plantarum*. *Appl. Microbiol. Biotechnol.* **1999**, *51*, 249−254.

(17) Oterholm, A.; Witter, L. D.; Ordal, Z. J. Purification and properties of an acetyl ester hydrolase (acetylesterase) from *Lactobacillus plantarum*. *J. Dairy Sci.* **1972**, *55*, 8−13.

(18) Esteban-Torres, M.; Reverón, I.; Mancheño, J. M.; de las Rivas, B.; Muñoz, R. Characterization of a feruloyl esterase from *Lactobacillus plantarum*. *Appl. Environ. Microbiol.* **2013**, *79*, 5130−5136.

(19) Wintrode, P. L.; Miyazaki, K.; Arnold, F. H. Cold adaptation of a mesophilic subtilisin-like protease by laboratory evolution. *J. Biol. Chem.* **2000**, *275*, 31635−31640.

(20) Tutino, M. L.; Parrilli, E.; De Santi, C.; Guiliani, M.; Marino, G.; de Pascale, D. Cold-adapted esterases and lipases: A biodiversity still under-exploited. *Curr. Chem. Biol.* **2010**, *4*, 74−83.

(21) Curiel, J. A.; de las Rivas, B.; Mancheño, J. M.; Muñoz, R. The pURI family of expression vectors: A versatile set of ligation independent cloning plasmids for producing recombinant His-fusion proteins. *Protein Expression Purif.* **2011**, *76*, 44−53.

(22) Sumby, K. M.; Matthews, A. H.; Grbin, P. R.; Jiranek, V. Cloning and characterization of an intracellular esterase from the wine-associated lactic acid bacterium *Oenococcus oeni*. *Appl. Environ. Microbiol.* **2009**, *75*, 6729−6735.

(23) Brod, F. C. A.; Vernal, J.; Bertoldo, J. B.; Terenzi, H.; Maisonnave Arisi, A. C. Cloning, expression, purification, and characterization of a novel esterase from *Lactobacillus plantarum*. *Mol. Biotechnol.* **2010**, *44*, 242−249.

(24) Feller, G.; Gerday, C. Psychrophilic enzymes: Molecular basis of cold adaptation. *Cell. Mol. Life Sci.* **1997**, *53*, 830−841.

(25) Feller, G.; Gerday, C. Psychrophilic enzymes: Hot topics in cold adaptation. *Nat. Rev. Microbiol.* **2003**, *1*, 200−208.
(26) Siddiqui, K. S.; Cavicchioli, R. Cold-adapted enzymes. *Annu. Rev. Biochem.* **2006**, *75*, 403−433.
(27) Wu, G.; Wu, G.; Zhan, T.; Shao, Z.; Liu, Z. Characterization of a cold-adapted and salt-tolerant esterase from a psychrotrophic bacterium *Psychrobacter pacificensis*. *Extremophiles* **2013**, *17*, 809−819.
(28) Fu, J.; Leiros, H. K.-S.; Pascale, D.; Johnson, K. A.; Blencke, H.-M.; Landfald, B. Functionak and structural studies of a novel cold-adapted esterase from an Arctic intertidal metagenomic library. *Appl. Microbiol. Biotechnol.* **2012**, *97*, 3965−3978.
(29) Benavente, R.; Esteban-Torres, M.; Acebrón, I.; de las Rivas, B.; Muñoz, R.; Mancheño, J. M. Structure, biochemical characterization and analysis of the pleomorphism of carboxylesterase Cest-2923 from *Lactobacillus plantarum* WCFS1. *FEBS J.* **2013**, *280*, 6658−6671.
(30) Navarro-González, I.; Sánchez-Ferrer, A.; García-Carmona, F. Overexpression, purification, and biochemical characterization of the esterase Est0796 from *Lactobacillus plantarum* WCFS1. *Mol. Biotechnol.* **2013**, *54*, 651−660.
(31) Ko, K. C.; Rim, S. O.; Han, Y.; Shin, B. S.; Kim, G. J.; Choi, J. H.; Song, J. J. Identification and characterization of anovel cold-adapted esterase from a metagenomic library on mountain soil. *J. Ind. Microbiol. Biotechnol.* **2012**, *39*, 681−689.
(32) Novototskaya-Vlasova, K.; Petroskaya, L.; Yakimov, S.; Gilichinsky, D. Cloning, purification, and characterization of a cold-adpated esterase produced by *Psychrobacter cryohalolentis* K5T from Siberian cryopeg. *FEMS Microbiol. Ecol.* **2012**, *82*, 367−375.
(33) Zhang, S.; Wu, G.; Liu, Z.; Shao, Z.; Liu, Z. Characterization of EstB, a novel cold-active and organic solvent-tolerant esterase from marine microorganism *Alcanivorax dieselolei* B-5(T). *Extremophiles* **2014**, *18*, 251−259.
(34) Park, S.-Y.; Kim, J.-Y.; Bae, J.-H.; Hou, C. T.; Kim, H.-R. Optimization of culture conditions for production of a novel cold-active lipase from *Pichia lynferdii* NRRL Y-7723. *J. Agric. Food Chem.* **2013**, *61*, 882−886.
(35) Papon, M.; Talon, R. Factors affecting growth and lipase production by meat lactobacilli strains and *Brochothrix thermosphacta*. *J. Appl. Bacteriol.* **1988**, *64*, 107−115.
(36) Rashid, N.; Shimada, Y.; Ezaki, S.; Atomi, H.; Imanaka, T. Low-temperature lipase from psychrotrophic *Pseudomonas* sp. strain KB700A. *Appl. Environ. Microbiol.* **2001**, *67*, 4064−4069.
(37) Soror, S. H.; Verma, V.; Rao, R.; Rasool, S.; Koul, S.; Qazi, G. N.; Cullum, J. A cold-active esterase of *Streptomyces coelicolor* A3(2): From genome sequence to enzyme activity. *J. Ind. Microbiol. Biotechnol.* **2007**, *34*, 525−531.
(38) Jeon, J. H.; Kim, J.-T.; Kim, Y. J.; Kim, H. K.; Lee, H. S.; Kang, S. G.; Kim, S. J.; Lee, J. H. Cloning and characterization of anew cold-active lipase from a deep-sea sediment metagenome. *Appl. Microbiol. Biotechnol.* **2008**, *81*, 865−874.
(39) Flanzy, C. *Enología: Fundamentos Científicos y Tecnológicos*; Mundi-Prensa: Madrid, Spain, 2000.
(40) Ammor, M. S.; Mayo, B. Selection criteria for lactic acid bacteria to be used as functional starter cultures in dry sausage production: An update. *Meat Sci.* **2007**, *76*, 138−146.
(41) Güler, Z. Profiles of organic acid and volatile compounds in acid-type cheeses containing herbs and spices (surk cheese). *Int. J. Food Prop.* **2014**, *17*, 1379−1392.

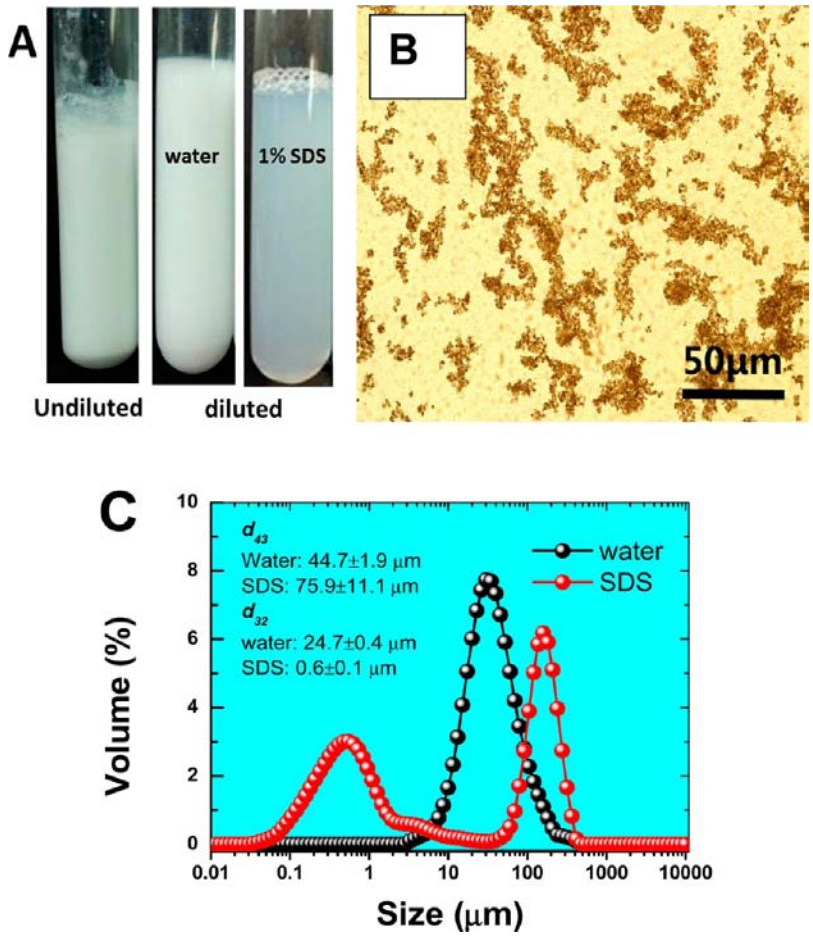

Figure 1. (A) Visual observations of undiluted and diluted phytosterol colloidal dispersions, obtained at a protein concentration of 0.05% (w/v) and organic phase fraction of 0.5. The dispersion was diluted by 5-fold volume of water or 1% SDS. (B) Typical light microscopic image of the phytosterol colloidal dispersion. (C) Volume-average droplet size distribution profiles of the corresponding dispersion, with water or SDS solution as the dispersing solvent.

Thus, the present work was undertaken to develop phytosterol into a kind of Pickering-like stabilizer. To achieve this, we first successfully prepared a kinetically stable phytosterol colloidal dispersion, using an emulsification process using whey protein as the emulsifier, followed by a solvent displacement/or evaporation. Instead of Tween series (e.g., Tween 20), whey protein was applied as the emulsifier, because of the safety consideration. Then, the obtained colloidal dispersion was applied to form emulsions, at varying solid concentrations (in the phytosterol dispersion; in the range of 0.1−3.0%, w/v) and oil fractions (ø; 0.2−0.6). The emulsion characterization was carried out by visual and confocal laser scanning microscopy (CLSM) observations. Interestingly, we found that, at high solid concentrations and/or ø values, gel-like emulsions using the phytosterol-based particles as the Pickering stabilizers could be formulated.

MATERIALS AND METHODS

Materials. Phytosterol with a total content of >95% (dry basis), consisting of β-sitosterol (~40%), compsterol (15−30%), stigmasterol (15−30%), and brassicasterol (<10%), was obtained from Xi'an Healthful Biotechnology Co., Ltd. (China). A commercial whey protein concentrate (WPC80) was purchased from New Zealand Milk Products (NZMP, Fonterra Co-operative Group Limited, New Zealand), whose composition was 78.1% protein, 6.67% fat, 4.83% moisture, and less than 3% ash (dry basis). Soy oil was purchased from a local supermarket in Guangzhou (China). Nile Red was obtained from Sigma-Aldrich (Sigma Chemical Co., St. Louis, MO). All other chemicals used were of analytical grade.

Preparation of Phytosterol Colloidal Dispersion. The phytosterol colloidal particles were synthesized on the basis of an anti-solvent precipitation method.[21,22] The synthesis process basically consisted of two steps: first, phytosterols are fully dissolved in organic solvent (100% ethanol in the present work), and then, the organic phase was dispersed in an aqueous phase with an emulsifier; and second, the organic phase in the resultant dispersion was removed by rotary evaporation. Phytosterol (1.2%, w/v) in 100% ethanol was applied as the organic solvent, while a concentration (0.05%, w/v) of WPC solution in 10 mM phosphate buffer (pH 7.0) was applied as the aqueous phase. Sodium azide (0.02%, w/v) was applied as an antimicrobial agent for the aqueous phase. The organic phase (100 mL) was fast (added using a syringe without a needle within 2 min) and mixed with the aqueous phase (100 mL), under vigorous mixing conditions (at a rate of 8000 rpm) using a high-speed dispersing unit (model IKA Ultra-Turrax T25 basic, IKA 190 Works, Inc., Wilmington, NC). After complete mixing of the organic phase with the aqueous phase, the dispersion was further stirred at the same rate for an additional 2 min. Then, a turbid dispersion with a milky color was formed. At last, the ethanol in the resultant dispersion was removed, until the dispersion was concentrated by approximately 4-fold. The total solid concentration (c) of the final dispersion containing colloidal particles was precisely adjusted to 3% (w/v), with the same phosphate buffer.

Phytosterol Colloidal Particle Characterization. *Particle Size Distribution and Volume- and Surface-Averaged Size ($d_{4,3}$ and $d_{3,2}$).*

dx.doi.org/10.1021/jf404930c | J. Agric. Food Chem. 2014, 62, 5133−5141

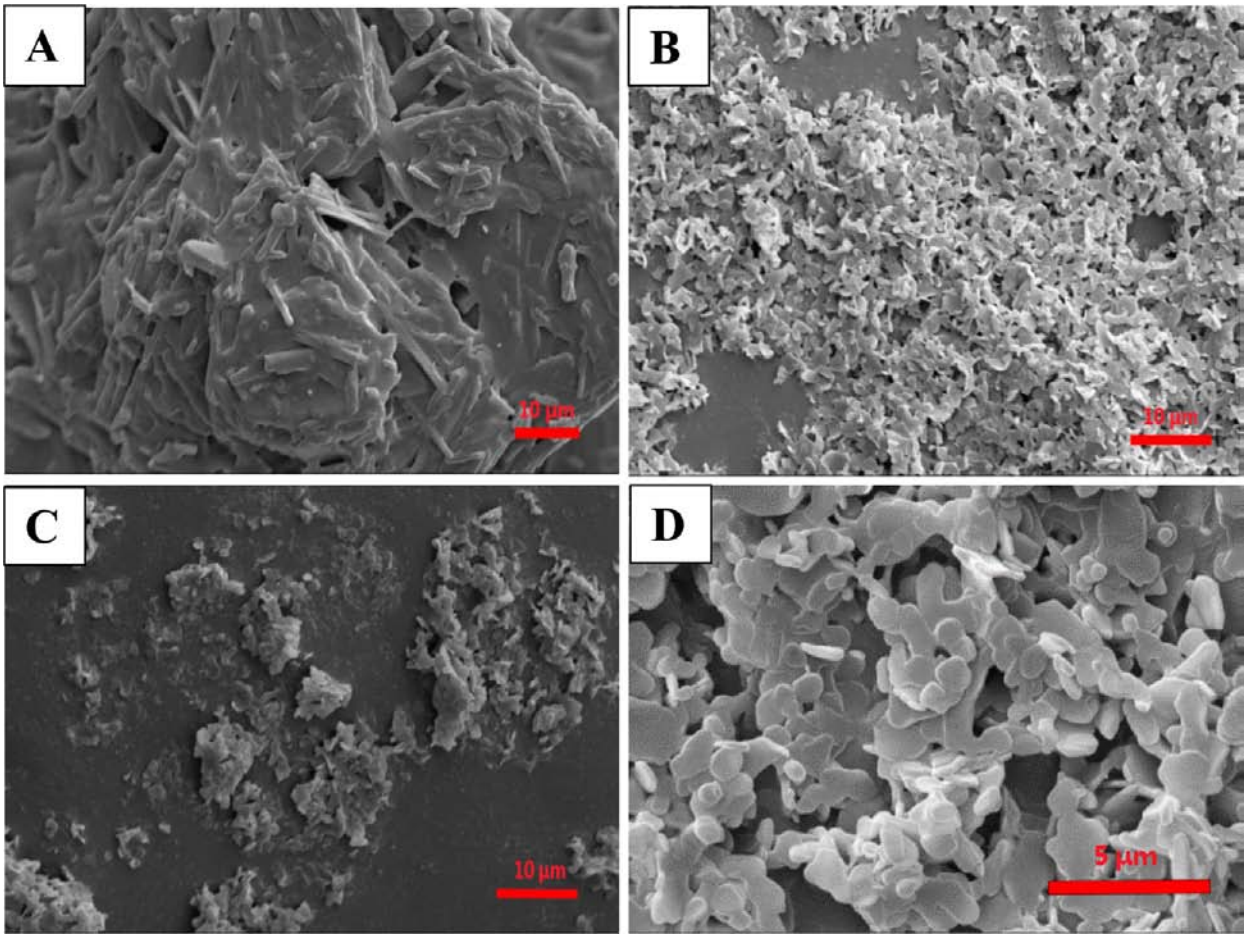

Figure 2. SEM micrographs of (A) original phytosterol and phytosterol colloidal dispersion (B and D) untreated or (C) treated by homogenization. The dispersion was prepared according to the same process as described in the caption of Figure 1.

The size distribution and $d_{4,3}$ (or $d_{3,2}$) of particles in fresh phytosterol preparations (see the above) were measured using a Malvern MasterSizer 2000 (Malvern Instruments, Ltd., Malvern, Worcestershire, U.K.). The pH 7.0 phosphate buffer was used as the diluting solvent. The relative refractive index was taken as the value of 1.095, which was calculated by the refractive index of the phytosterol particle (1.456) dividing by that of the continuous phases (1.33). The determinations were performed on separate samples at least in duplicate, with the means and standard deviation reported.

Microstructure. Light microscopy (LM) and scanning electron microscopy (SEM) were used to characterize the morphology of colloidal particles in the phytosterol preparation. For the LM observation, a drop of the dispersion was directly deposited on a microscope slide. The specimens for the SEM observation were prepared by drying a drop of the dispersion on the SEM stub using conductive double-side adhesive tape. After drying, the specimens were coated with gold and examined using a Zeiss EVO 18 scanning electron microscope (Carl Zeiss SMT, Oberkochen, Germany) at an accelerating voltage of 10 kV.

Preparation of Phytosterol Colloidal Particle-Stabilized Emulsions. For all emulsions, the phytosterol colloidal particle dispersion with a c of 3.0% (w/v) was applied. If necessary, the dispersion was diluted with the same phosphate buffer (pH 7.0) to an appropriate solid concentration up to 0.1% (w/v). To prepare an emulsion (with a constant total volume of 6 mL), a certain volume of the phytosterol preparation (dependent upon ϕ) was poured into a glass vial and a predetermined volume of soybean oil was slowly added to the dispersion while mixing with an Ultra Turrax homogenizer with a dispersing head operating at 13 500 rpm for 2 min. After all of the oil was added, the emulsion was further homogenized at the same rate for an additional 1 min. The last obtained emulsions were stored at 4 °C.

Emulsion Characterization. *Microstructure.* The microstructure of the emulsions was examined by CLSM, using the same microscope and process as described in our previous work.[23]

Drop Test and Conductivity Measurement. The type of the emulsions, formed at ϕ = 0.3−0.6, was evaluated by the dropt test and conductivity, immediately after the preparation. The droplet test was performed by dispersing a small portion of emulsions into either 10 mM phosphate buffer (pH 7.0) or pure oil, under the conditions with or without vortexing for 10 s. The conductivity measurement was conducted using a DDS-307 conductivity meter (Leici Co., China) at 25 °C, with means and standard deviations of two replicates on separate samples reported.

Droplet Size Analysis from Microscopy. The emulsion droplet size was manually measured over 100 droplets from the CLSM image using the microscopic image analysis software (Nano Measurer 1.2.5, Fudan University, China). The average droplet size was presented in terms of the volume mean diameter, $d_{4,3}$ $(=\sum n_i d_i^4 / \sum n_i d_i^3$, where i is the number of droplets with diameter d_i).[24]

Rheological Property. The flow behavior and dynamic oscillatory measurement of the formed gel-like emulsions were performed at 25 °C using a HAAKE RS600 rheometer (Thermo Electron Co., Waltham, MA) between two parallel plates (d = 27.83 mm) with a gap of 1.0 mm. The equipment was driven through the RheoWin 3 data manager (Thermo Electron Co., Waltham, MA). For the steady shear measurement, the shear rate was increased in the range of 0.1−100 s^{-1}, and apparent viscosity (η) was recorded with the shear rate increasing. For dynamic oscillation measurement, the frequency sweep was performed at 25 °C with the frequency ranging from 1 to 100 rad/s (all of the measurements were conducted within the linear viscoelastic region). The elastic (G') and loss (G'') moduli as a

function of the frequency were recorded. All determinations were conducted on separate samples at least in duplicate.

RESULTS AND DISCUSSION

Characterization of Phytosterol Colloidal Dispersions. The obtained phytosterol colloidal dispersion at c = 3.0% (w/v), with a WPC concentration of 0.12% (w/v) and a phytosterol concentration of 2.88% (w/v), was milky and turbid, and aggregation could be observed on the wall of the container (Figure 1A, undiluted). The aggregated state of phytosterol colloidal particles could be well-observed in the LM observation (Figure 1B). When the dispersion was diluted with water by 5-fold, the aggregation seemed to be greatly reduced and the diluted dispersion was still milky but homogeneous. When the dispersion was diluted with 1% sodium dodecyl sulfate (SDS) by 5-fold, the turbidity of the dispersion considerably decreased, as compared to that with water, and in this case, the dispersion even became a bit translucent (Figure 1A). The observations indicated that most of the phytosterol colloidal particles in the dispersion were in the aggregated form and the weak interparticle hydrophobic interactions seemed to play a role in the aggregation.

The detailed morphology of the colloidal particles in the dispersion was further evaluated by SEM. The untreated phytosterol sample exhibited a typical needle-like crystal morphology (Figure 2A), which well agrees with the previous observations.[16,18] In contrast, most of the phytosterol colloidal particles in the dispersion exhibited morphology of stacked platelet-like sheets (panels B and D of Figure 2). The morphology of these colloidal particles is completely different from that of phytosterol nanodispersions, formed with small-molecular-weight emulsifiers (e.g., Tween 20) using a similar preparation process,[20,25] where the particles were basically present in the regularly spherical form. The morphology is also completely different from that of phytosterol crystals in an emulsion stabilized by a series of Tween group emulsifiers,[16] where the corresponding crystals exhibited a needle-like morphology. The differences in morphology might be due to the differences in the extent of crystallization of phytosterols that occurred during the evaporation of organic solvents as well as the amount of crystals per particle. The application of whey proteins to coat the phytosterol particles might to a certain extent inhibit the crystallization of the free phytosterol molecules. Taking the particle size data together (Figure 1), it can be reasonably proposed that the phytosterol colloidal particles were the flocs of platelet-like phytosterol crystals, with a kind of fractal network.

Phytosterol Colloidal Particle-Stabilized Emulsions. *Visual Observation and Phase Diagram.* Figure 3 shows the photographs of all of the emulsions, formed at varying c (0–3.0%, w/v) and $ø$ (0–0.6) values, after storage periods of 1 and 3 days. In the absence of the oil phase, the homogenization process caused instability of the aqueous dispersions and there were sediments at the bottom of the vessel as well as some kind of sticky "creams" at the top of the vessel (Figure 3, first column). The extent of instability seemed to increase with increasing c from 0.1 to 3.0%. The observations are in accordance with the SEM observations at c = 3.0% (w/v), showing that, after the homogenization, most of the colloidal particles became more clustered (panels B and C of Figure 2). Thus, the colloidal particle structure in the dispersion could be disrupted by the mechanical agitation during the homogenization.

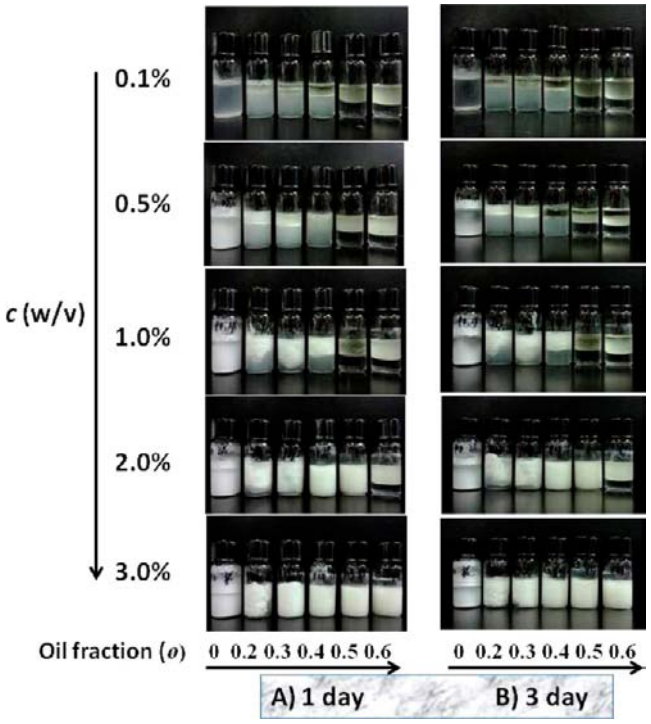

Figure 3. Photographs of emulsions stabilized with different solid concentrations (0.1–3.0%, w/v) of phytosterol colloidal particles at various oil fractions of 0–0.6. The photographs were taken 1 or 3 days after the preparation.

As expected, the morphology of the emulsions stabilized by the colloidal particles changed with the applied c and $ø$ (Figure 3). At c = 0.1 or 0.5%, the formed emulsions fast phase-separated over the whole test $ø$ range and a macroscopic oil phase was observed after longer storage periods and at higher $ø$, indicating that the amount of colloidal particles was not enough to stabilize the emulsions. However, it can still be observed that, at high $ø$ values above 0.4, most of the colloidal particles were absent from the aqueous phase (because the bottom layer was transparent), suggesting that the phytosterol colloidal particles were hydrophobic in nature and tended to be dispersed in the organic phase. When c was increased up to 1.0%, some "cotton fiber"-like aggregates were formed in the top phase for the emulsions at low $ø$ values of <0.4, while at higher $ø$ values, a phase separation with a macroscopic oil phase was still observed (Figure 3). In this case, a strong emulsion-gel material for the top phase was interestingly obtained at $ø$ = 0.4, which could be put upside down without leaking out the aqueous phase (Figure 4A, left). When c was further increased up to 3%, a homogeneous and turbid emulsion-gel-phase material, without phase separation, could be formed at appropriate $ø$ values. For example, at c = 2.0%, a homogeneous emulsion gel was formed at $ø$ = 0.4 or 0.5, while at $ø$ = 0.6, the emulsion-gel material was formed in the top phase. Whereas in the situation at c = 3.0%, the emulsion-gel structure could be observed over a much larger $ø$ range (0.3–0.6) and a typical morphology of the formed emulsion gel at $ø$ = 0.6 is illustrated in Figure 4A (right).

Figure 4B summarizes the phase diagram of all of the emulsions after 1 day of storage. At a low $ø$ value of 0.2, a serious aggregation occurred at c values of 1.0–3.0%, with a higher extent observed at higher c values, while at c values of <1.0%, a macroscopic oil phase could be observed (Figure 3A).

dx.doi.org/10.1021/jf404930c | J. Agric. Food Chem. 2014, 62, 5133–5141

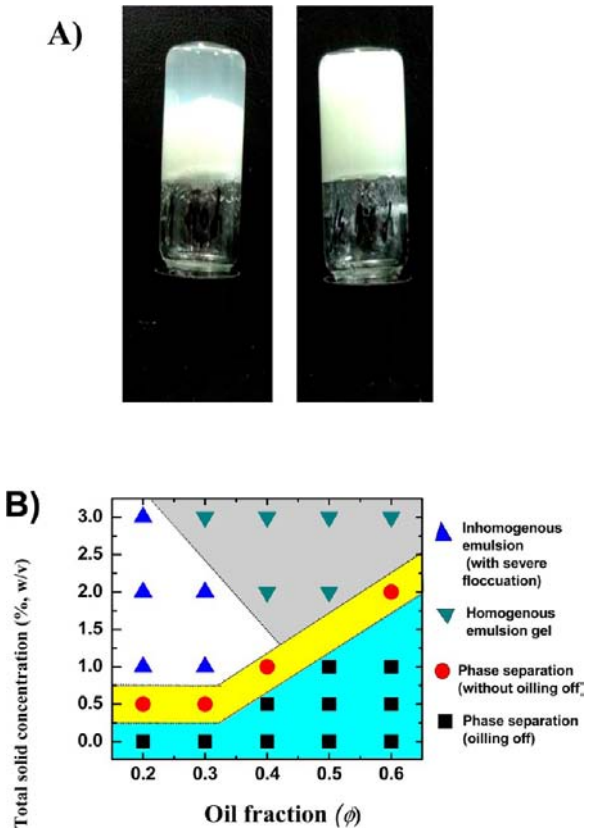

Figure 4. (A) Photograms of the emulsions formed at c = 1.0% and ϕ = 0.4 (left) or at c = 3.0% and ϕ = 0.6 (right), which were put upside down. (B) Phase diagram of the emulsions stabilized by the phytosterol colloidal particles at different solid concentrations of 0.0−3.0% (w/v) and oil fractions of 0.2−0.6.

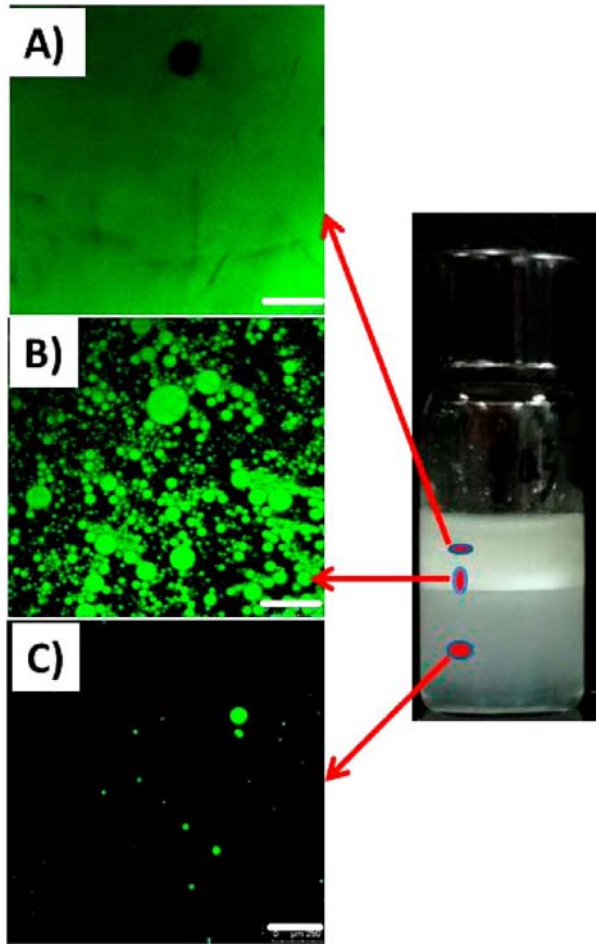

Figure 5. CLSM images of the different parts of the phytosterol colloid particle-stabilized emulsion at c = 0.5% and ϕ = 0.3 after a storage of 3 days: (A) macroscopic oil phase (upper layer), (B) middle emulsion phase, and (C) bottom aqueous phase. The bars represent 250 μm in scale.

In this case, the colloidal particle-coated oil droplets seriously flocculated to exhibit a "cotton fiber"-like morphology. The flocculated droplets remained on the top of the aqueous phase. On the other hand, at a high ϕ value of 0.6, it can be observed that a macroscopic separation occurred at c values up to 2.0% (w/v), with all of the colloidal particles incorporated in the upper phase (oil phase) (Figure 3A, last column). Interestingly, within the upper phase, a new phase separation occurred, with the extent decreasing upon the increase in c. In this situation, when c was increased up to 3.0% (w/v), no distinct phase separation was observed and, instead, a homogeneous emulsion-gel network was formed throughout the whole emulsion (Figures 3A and 4B). A similar emulsion-gel material could be observed at higher c (e.g., 2.0% or above) and ϕ (at least 0.3) values (Figure 4B).

Microstructure of the Emulsions [Inversion from O/W to Water-in-Oil (W/O) Type]. The microstructure of the phytosterol colloidal particle-stabilized emulsions, formed at different c or ϕ values, was evaluated using the CLSM technique in combination with light microscopic observation. The oil phase was dyed using Nile Blue A, which shows a green color in the CLSM images. In the emulsions, where the amount of the colloidal particles was distinctly not enough to stabilize the droplet interface, e.g., at low c values of <1.0% (w/v), a phase separation with a macroscopic oil phase occurred (Figure 3). Figure 5 shows typical CLSM observations for the emulsion at c = 0.5% and ϕ = 0.3 after 3 days of storage. In this case, the CLSM images of different parts of the emulsion (upper or bottom phase) were provided. The CLSM image for the bulk part of the upper phase of the emulsion was basically green, while that for the bottom part was black (panels A and C of Figure 5), confirming the occurrence of phase separation (with a macroscopic oil phase). However, in the vicinity of the border of the two phases, a droplet-flocculated microstructure of an O/W emulsion could be still observed (Figure 5B). This observation suggests that, at a low c value and a relatively high ϕ value (e.g., 0.3), an O/W type of emulsion stabilized by the phytosterol colloidal particles was formed, although the emulsion was unstable against coalescence, flocculation, and even creaming.

When c was increased up to 3.0%, a homogeneous emulsion-gel material with no phase separation was formed at ϕ values of 0.3−0.6 (Figure 3A). Accordingly, in the CLSM images of these gel-like emulsions, the oil phase (with green color) became the continuous phase, while the aqueous phase with black color (undyed) was relatively even dispersed in the system (Figure 6, upper row). This observation indicated that all of these emulsions were basically W/O type in nature. In this case, it can be still observed that the microstructure of the dispersed phase considerably changed with the applied ϕ (Figure 6, upper row). For the emulsion at ϕ = 0.3, the aqueous phase with a homogeneous and globular droplet morphology was relatively

dx.doi.org/10.1021/jf404930c | J. Agric. Food Chem. 2014, 62, 5133−5141

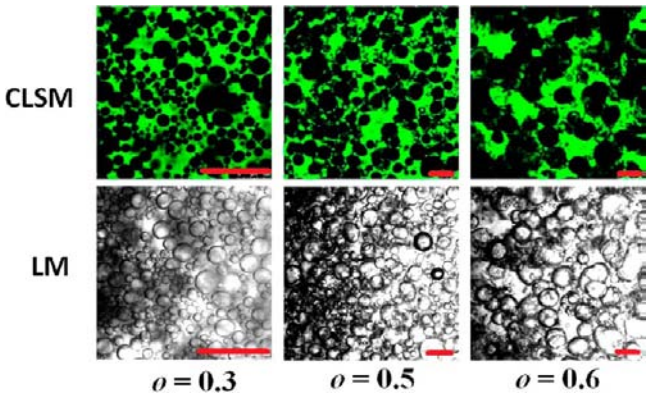

Figure 6. CLSM (upper row) and LM (bottom row) images of the phytosterol colloidal particle-stabilized emulsions at a constant c of 3.0% (w/v) and different ø values of 0.3−0.6 after a storage of 3 days. The bars represent 200 μm in scale.

dispersed in the continuous oil phase, while in the cases at ø = 0.5 or 0.6, the morphology of the dispersed phase became more uneven and irregular with greater droplet flocculation and the emulsions were more like the oil-in-water-in-oil (O/W/O) type in nature (relative to that at ø = 0.3; Figure 6, upper row). The formation of the complex O/W/O colloidal structure led to a distinct increase for the volume of dispersed droplets, thus strengthening the gel network. On the other hand, the CLSM and LM observations also interestingly showed that, in the emulsions at ø = 0.5 or 0.6, there were plenty of emulsified oil droplets with much smaller sizes stabilizing the colloidal structure of dispersed droplets (Figure 6). In a recent work, Ye and others[26] reported that nanoemulsion droplets stabilized by micellar casein could be applied as an emulsifier to stabilize W/O emulsions, through being adsorbed at the interface. This interesting finding implies that, in the present work, a small portion of oil droplets coated with the phytosterol colloidal particles or whey proteins, initially formed during the emulsification, might stabilize the dispersed aqueous droplets in the system.

To ascertain the transition of the emulsion type, we visually evaluated the dispersion of the formed gel-like emulsions at a constant c value of 3.0% (w/v) and varying ø values of 0.3−0.6 in water or oil, as displayed in Figure 7. All of the emulsions remained at the top of the water and could not be dispersed in water, while they could be well-dispersed in oil, under vortexing conditions. After vortexing, a turbid and homogeneous dispersion was formed for each case, confirming that the gel-like emulsions were the W/O type in nature. This can be further confirmed by the conductivity measurement of the emulsions, where the conductivity of the gel-like emulsions progressively decreased from 6.7 ± 1.5 to 1.5 ± 0.7 μs/cm, as ø increased from 0.3 to 0.6 (data not shown). The magnitude of conductivity values for these emulsions was considerably lower than that of the aqueous phase (~2270 μs/cm), with the latter basically comparable to those previously reported.[27]

Emulsion Size. In the present work, the droplet size of the emulsions, especially for those formed at low c values, was difficult to measure, because of their instability, e.g., against flocculation, creaming, and phase separation. In contrast, the gel-like emulsions formed in the present work (Figure 4) were relatively stable against creaming and phase separation, thus providing a possibility to evaluate the c dependence of the droplet size of the emulsions (although the emulsions were the

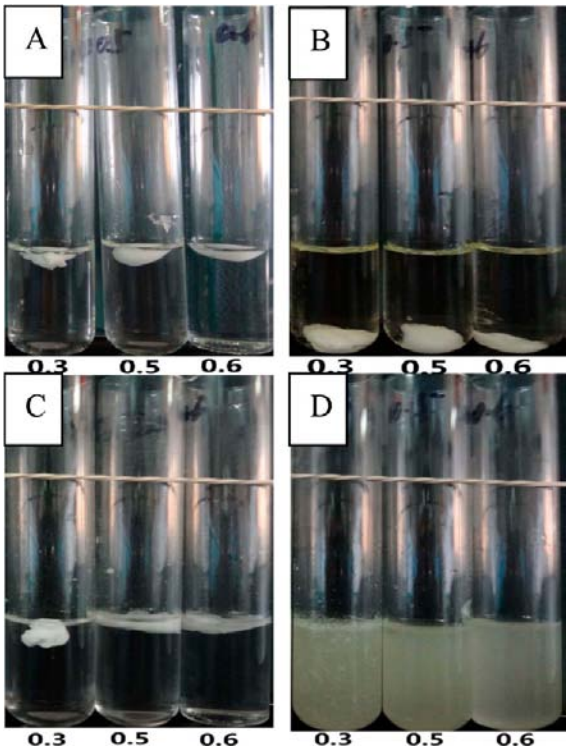

Figure 7. Visual observations for the dispersion of the phytosterol colloidal particle-stabilized emulsions (at c = 3%, w/v, and ø = 0.3−0.6) in (A and C) 10 mM phosphate buffer (pH 7.0) or (B and D) oil under conditions (A and B) without and (C and D) with vortexing for 10 s.

W/O type in nature). Figure 8 shows the influence of the solid content/oil ratio on the droplet size of these gel-like emulsions,

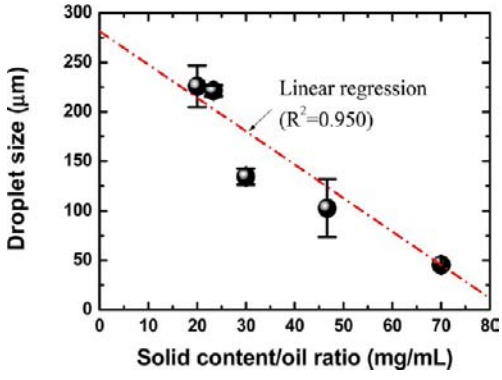

Figure 8. Droplet size values of the gel-like emulsions formed at varying c values and at ø = 0.3−0.6, as a function of the total solid content/oil ratios (mg/mL). The droplet size ($d_{4,3}$) of droplets was obtained by analyzing the CLSM images of the emulsions using an image analysis software. Each data is the mean and standard deviation of duplicate measurements on separate samples.

formed at varying c values and at ø = 0.3−0.6, by analyzing their CLSM images using the Nanomeasurer software. As expected, the approximately calculated droplet diameter progressively reduced from around 230 to 50 μm as the solid content/oil ratio increased from 20 to 70 mg/mL (Figure 8). This observation basically reconciles with the general consensus that the droplet size of Pickering emulsions stabilized by solid particles is negatively related to the particle concentration,

because at higher particle concentrations, more particles help to stabilize the smaller oil droplets produced during the emulsification.[28−30]

Rheological Characterization of Gel-like Emulsions. All of the gel-like emulsions, formed at c = 3.0% and three specific $ø$ values of 0.3, 0.5, and 0.6, exhibited a distinct shear-thinning behavior at high shear rates above 0.1 s^{-1}, with η progressively decreasing with increasing shear rate (Figure 9A). This

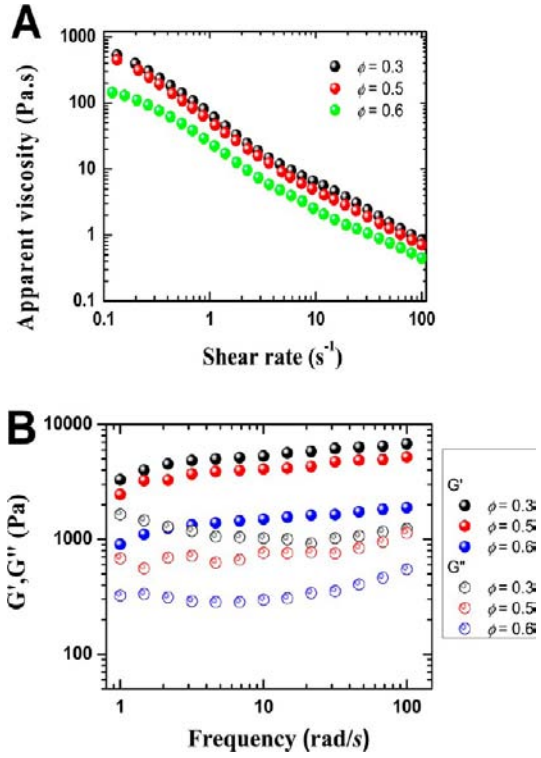

Figure 9. Dependence of (A) apparent viscosity (η) and (B) storage moduli upon the shear rate and frequency, respectively, of the gel-like emulsions stabilized by the phytosterol colloidal particles at c = 3.0% and $ø$ values of 0.3−0.6. G', storage modulus; G'', loss modulus.

phenomenon is a typical flow behavior of weakly flocculated colloidal dispersions, including oil-in-water emulsions,[31−33] which corresponds to the deflocculation of droplets in the system upon shearing. Among all of the emulsions, G' at any test frequency was considerably higher than G'' (Figure 9B), indicating a predominantly elastic gel-like behavior. Furthermore, G' persistently increased with the frequency, while G'' was relatively less dependent upon the applied frequency at low frequencies (e.g., <20 rad/s) (Figure 9B). A similar observation was reported in gel-like O/W emulsions stabilized by proteins.[33−35] Similar to the situation in heat-induced gels of proteins,[36] the present observations suggest that the gel-like network might be maintained through non-covalent "physical" cross-links in nature.

For these emulsions, η (or the moduli) at any test point progressively decreased with increasing $ø$ from 0.3 to 0.6 (panels A and B of Figure 9), indicating weakening in the gel strength or stiffness. The observation is well in accordance with the fact that the volume of the dispersed aqueous phase progressively declined upon the increase in $ø$, further confirming that these gel-like emulsions were mainly the W/O type in nature. The weakening effect of decreasing the volume of the dispersed phase on the gel stiffness has also been observed in the gel-like O/W emulsions stabilized by the proteins.[33,34]

Supposed Mechanism for the Formation of Phytosterol Colloidal Particle-Stabilized Emulsions. Besides the whey proteins, free phytosterol molecules, such as stigmasterol and β-sitosterol, have been confirmed to have a high ability to reduce interfacial tension.[37] This allows these colloidal particles to migrate to the interface of the droplets in the emulsions, and as a consequence, a kind of phytosterol colloidal particle-stabilized emulsion can be formed. Because a small portion of WPC [e.g., approximately 0.12% (w/v) at the maximal c of 3.0%, w/v] was applied to coat and stabilize the phytosterol particles, the possibility should be excluded that the applied WPC rather than the colloidal particles might largely contribute to the stabilization of the emulsions. To exclude this possibility, we evaluated and compared the stability of the emulsions stabilized by the phytosterol colloidal particles or WPC alone (in both cases, the WPC concentration was comparable), according to the method by Timgren et al.[30] Sudan III was applied to indicate the stability of the emulsions stabilized by WPC alone. If the emulsions are not stable, e.g., against coalescence and oiling off, they will exhibit a bright red color or would still exhibit a milky morphology. The results indicated that, at a constant concentration of WPC (0.125%), increasing the oil fraction from 0.2 to 0.6 progressively decreased the stability of the emulsions stabilized by WPC alone, while at a fixed oil fraction (0.3), increasing the concentration of WPC progressively increased the stability (see Figure S1 of the Supporting Information, upper row). In contrast, the situation for the emulsions stabilized by the colloidal particles (at a comparable concentration of WPC) is completely different. In this situation, at a fixed total solid content of 3% (w/v), increasing the oil fraction (increasing the solid content at a fixed oil fraction) progressively favored the formation of more homogeneous and stable (against creaming and phase separation) emulsions (see Figure S1 of the Supporting Information, bottom row). The observations clearly confirmed that the amount of WPC alone up to 0.12% (w/v) was not enough to fully stabilize the emulsions and the stabilization of the emulsions was thus mainly due to the action of the WPC-coated phytosterol particles.

Another point is worth mentioning that these phytosterol colloidal particles, especially after the homogenization, were mainly hydrophobic in nature, which is consistent with the fact that the phytosterols are much more soluble in the oil phase than in the water phase.[38,39] During emulsification together with the oil phase, these colloidal particles would be preferentially adsorbed to the oil−water interface, stabilizing the emulsions. The colloidal particles, initially adsorbed at the interface, might locate in a close proximity and associate with one another. Besides the strong lateral interactions between individual adsorbed colloidal particles, the interdroplet interactions between the adsorbed particles on different oil droplets were also strong, which might greatly facilitate the droplet flocculation in the emulsions. Furthermore, these adsorbed colloidal particles would further migrate toward the oil phase, upon storage of the emulsions, because of their high insolubility in water and much better solubility in oil.[16] As result, the extent of adsorption at the interface and migration between the different phases as well as the interdroplet attractive interactions, which were largely dependent upon the applied c and/or $ø$, would produce a significant influence on the

dx.doi.org/10.1021/jf404930c | J. Agric. Food Chem. 2014, 62, 5133−5141

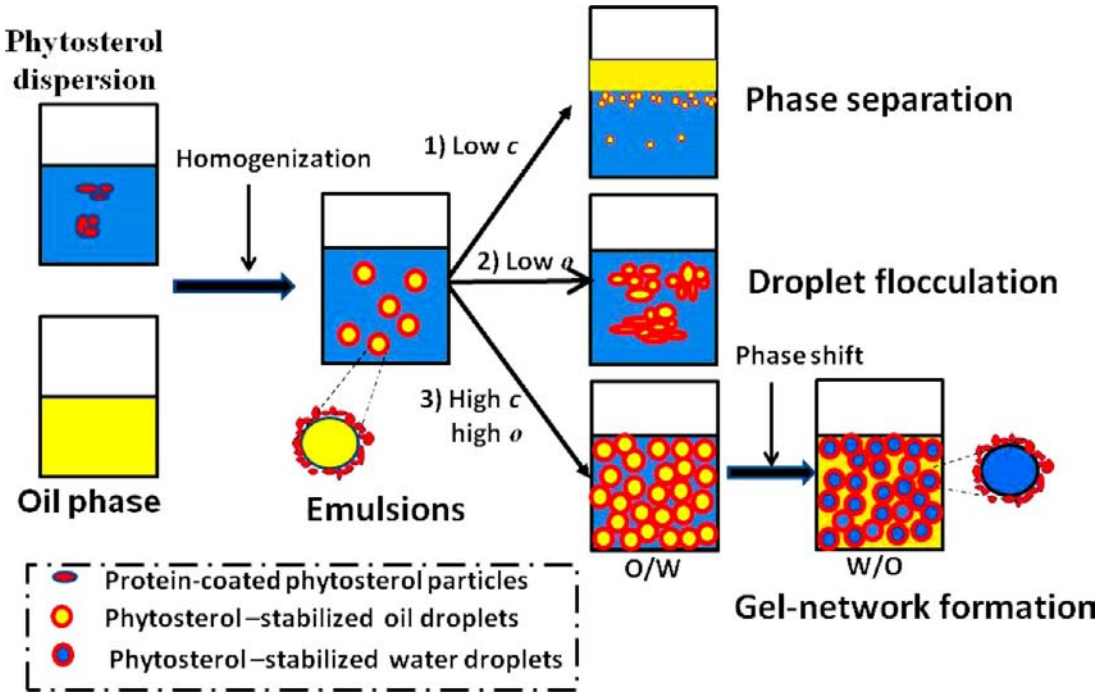

Figure 10. Supposed mechanism for the formation and instability of the emulsions stabilized by the phytosterol colloidal particles.

type, properties, and stability of the correspondingly formed emulsions.

If the droplet flocculation in the emulsions that is favored by increasing the volume of dispersed phase aand the enhancement of interdroplet attractive interactions are high enough, the instability of the emulsions will happen fast. In the present work, what kinds of instability of the emulsions occurred highly depended upon the magnitude of c and/or ϕ values. Thus, there were approximately several situations of instability of the emulsions occurring, depending upon the applied c and/or ϕ values. For example, at low c values (e.g., 0.1−0.5%, w/v), the emulsions were easily susceptible to severe coalescence and even oiling off, when the ϕ was above 0.3 (Figure 3), because of the shortage of colloidal particles to stabilize the emulsions. Once the amount of colloidal particles was enough to fully cover the interface newly created during the emulsification, the droplet flocculation might dominate the whole instability of the emulsions (rather than the instability against coalescence and phase separation). Especially when both the c and ϕ values are high enough, the droplet flocculation will lead to formation of a kind of self-supporting gel-like emulsion, such as at c = 3.0% and ϕ above 0.2 (Figure 3). The flocculation-induced gel network formation has been similarly proposed for the emulsions stabilized by denatured whey protein or soy proteins.[34,35]

At c = 3.0% (w/v), it can be interestingly observed that the type of emulsions changed from the O/W (at ϕ < 0.3) to W/O (ϕ = 0.3 or above) type (Figures 3 and 6), implying that the emulsions at high ϕ values might suffer a phase inversion from the O/W to W/O type. In this case, we tend to hypothesize that the initially formed emulsions were basically the O/W type in nature. The initially adsorbed colloidal particles at the oil−water interface are kinetically unstable, and they may gradually migrate from the aqueous side of the interface to the other side (oil phase), upon the storage of these emulsions. When the migration of the colloidal particles occurs to a certain extent, the interface between initially individual oil droplets fuses and, concomitantly, the initially coated oil droplets are released. As a result, a phase inversion occurs for these emulsions. A schematic representation for the formation and instability of the phytosterol colloidal particle-stabilized emulsions is illustrated in Figure 10.

In conclusion, water-insoluble phytosterols have been successfully developed into a kind of colloidal particle stabilizer for the emulsions. The properties and stability of the emulsions stabilized by these colloidal particles were highly dependent upon the applied c and ϕ. If both c and ϕ were appropriately high, a kind of self-supporting gel-like emulsion could be formulated. The emulsions could change from the O/W to W/O type, with ϕ increasing from 0.2 to 0.6 (especially at high c values, e.g., 3.0%, w/v). The elaborated Pickering emulsions with a gel-like structure could be applied as a novel delivery system for the unmodified phytosterol and other water- or lipid-soluble active ingredients. However, further research is needed to elaborate a kind of phytosterol colloidal particle at the nanoscale to be effective Pickering emulsion stabilizers.

■ ASSOCIATED CONTENT

Supporting Information

Visual observations of the emulsions stabilized by the phytosterol colloidal particles (bottom row) or WPC alone at comparable protein concentrations (to that in the colloidal particle dispersions; upper row) after 1 day of preparation (Figure S1). This material is available free of charge via the Internet at http://pubs.acs.org.

■ AUTHOR INFORMATION

Corresponding Author

*Fax: 086-20-87114263. E-mail: chtang@scut.edu.cn.

Funding

This work is supported by the National Natural Science Foundation (NNSF) of China (31171632 and 31130042) and

the Program for New Century Excellent Talents in University (NCET-10-0398).

Notes

The authors declare no competing financial interest.

■ ACKNOWLEDGMENTS

The authors are very grateful to Junguo Fu for performing some of the experiments.

■ REFERENCES

(1) Dickinson, E. Use of nanoparticles and microparticles in the formation and stabilization of food emulsions. *Trend. Food Sci. Technol.* **2012**, *24*, 4−12.
(2) Frelichowska, J.; Bolzinger, M.-A.; Pelletier, J.; Valour, J.-P.; Chevalier, Y. Topical delivery of lipothilic drugs from o/w Pickering emulsions. *Int. J. Pharm.* **2009**, *371*, 56−63.
(3) Kargar, M.; Spyropoulos, F.; Norton, I. T. Microstructural design to reduce lipid oxidation in oil-in-water emulsions. *Procedia Food Sci.* **2011**, *1*, 104−108.
(4) Karger, M.; Fayazmanesh, K.; Alavi, M.; Spyropoulos, F.; Norton, I. T. Investigation into the potential ability of Pickering emulsions (food-grade particles) to enhance the oxidative stability of oil-in-water emulsions. *J. Colloid Interface Sci.* **2012**, *366*, 209−215.
(5) Simovic, S.; Prestidge, C. A. Nanoparticle layers controlling drug release from emulsions. *Eur. J. Pharm. Biopharm.* **2007**, *67*, 39−47.
(6) Tzoumaki, M. V.; Moschakis, T.; Scholten, E.; Biliaderis, C. G. *In vitro* lipid digestion of chitin nanocrystal stabilized o/w emulsions. *Food Function* **2013**, *4*, 121−129.
(7) Tzoumaki, M. V.; Moschakis, T.; Kiosseoglou, V.; Biliaderis, C. G. Oil-in-water emulsions stabilized by chitin nanocrystal particles. *Food Hydrocolloids* **2011**, *25*, 1521−1529.
(8) de Folter, J. W.; van Ruijven, M. W. M.; Velikov, K. P. Oil-in-water Pickering emulsions stabilized by colloidal particles from water-insoluble protein zein. *Soft Matter* **2012**, *8*, 6807−6815.
(9) Rayner, M.; Timgren, A.; Sjöö, M.; Dejmek, P. Quinoa starch granules: A candidate for stabilising food-grade Pickering emulsions. *J. Sci. Food Agric.* **2010**, *92*, 1841−1847.
(10) Tan, Y.; Xu, K.; Liu, C.; Li, Y.; Lu, C.; Wang, P. Fabrication of starch-based nanospheres to stabilize pickering emulsions. *Carbohydr. Polym.* **2012**, *88*, 1358−1363.
(11) Luo, Z.; Murray, B. S.; Ross, A.-L.; Povey, M. J. W.; Morgan, M. R. A.; Day, A. J. Effects of pH on the ability of flavonoids to act as Pickering emulsion stabilizers. *Colloids Surf., B* **2012**, *92*, 84−90.
(12) Luo, Z.; Murray, B. S.; Yusoff, A.; Morgan, M. R. A.; Povey, M. J. W.; Day, A. J. Particle-stabilizing effects of flavonoids at the oil−water interface. *J. Agric. Food Chem.* **2011**, *59*, 2636−2645.
(13) Gupta, R.; Rousseau, D. Surface-active solid lipid nanoparticles as Pickering stabilizers for oil-in-water emulsions. *Food Function* **2012**, *3*, 302−311.
(14) Liu, F.; Tang, C. H. Soy protein nanoparticle aggregates as Pickering stabilizers for oil-in-water emulsions. *J. Agric. Food Chem.* **2013**, *61*, 8888−8898.
(15) Kamal-Eldin, A.; Moazzami, A. Plant sterols and stanols as cholesterol-lowering ingredients in functional foods. *Recent Pat. Food, Nutr. Agric.* **2009**, *1*, 1−14.
(16) Engel, R.; Schubert, H. Formulation of phytosterols in emulsions for increased dose response in functional foods. *Innovative Food Sci. Emerging Technol.* **2005**, *6*, 233−237.
(17) MacKay, D. S.; Jones, P. J. H. Phytosterols in human nutrition: Type, formulation, delivery, and physiological function. *Eur. J. Lipid Technol.* **2011**, *113*, 1427−1432.
(18) Rozner, S.; Garti, N. The activity and adsorption relationship of cholesterol and phytosterols. *Colloids Surf., A* **2006**, *282*−*283*, 435−456.
(19) Leong, W. F.; Che Man, Y. B.; Lai, O. M.; Long, K.; Misran, M.; Tan, C. P. Optimization of processing parameters for the preparation of phytosterol microemulsions by the solvent displacement method. *J. Agric. Food Chem.* **2009**, *57*, 8426−8433.
(20) Leong, W. F.; Lai, O. M.; Long, K.; Che Man, Y. B.; Misran, M.; Tan, C. P. Preparation and characterisation of water-soluble phytosterol nanodisperions. *Food Chem.* **2011**, *129*, 77−83.
(21) Rossi, L.; Sacanna, S.; Velikov, K. P. Cholesteric colloidal liquid crystals from phytosterol rod-like particles. *Soft Matter* **2010**, *7*, 64−67.
(22) Rossi, L.; ten Hoorn, J. W. S.; Melnikov, S. M.; Velikov, K. P. Colloidal phytosterols: Synthesis, characterization and bioaccessibility. *Soft Matter* **2010**, *6*, 928−936.
(23) Liu, F.; Tang, C. H. Emulsifying properties of soy protein nanoparticles: Influence of protein concentration and/or emulsification process. *J. Agric. Food Chem.* **2014**, *62*, 2644−2654.
(24) Li, C.; Sun, P.; Yang, C. Emulsion stabilized by starch nanocrystals. *Starch/Staerke* **2012**, *64*, 497−502.
(25) Leong, W. F.; Che Man, Y.; Lai, O. M.; Long, K.; Nakajima, M.; Tan, C. P. Effect of sucrose fatty acid esters on the particle characteristics and flow properties of phytosterol nanodisperions. *J. Food Eng.* **2011**, *104*, 63−69.
(26) Ye, A.; Zhu, X.; Singh, H. Oil-in-water emulsion system stabilized by protein-coated nanoemulsion droplets. *Langmuir* **2013**, *29*, 14403−14410.
(27) Binks, B. P.; Isa, L.; Tyowua, A. T. Direct measurement of contact angles of silica particles in relation to double inversion of pickering emulsions. *Langmuir* **2013**, *29*, 4923−4927.
(28) Binks, B. P.; Whitby, C. P. Silica particle-stabilized emulsions of silicone oil and water: Aspects of emulsification. *Langmuir* **2004**, *20*, 1130−1137.
(29) Marku, D.; Wahlgren, M.; Rayner, M.; Sjöö, M.; Timgren, A. Characterization of starch Pickering emulsions for potential applications in topical formulations. *Int. J. Pharm.* **2012**, *428*, 1−7.
(30) Timgren, A.; Rayner, M.; Dejmek, P.; Marku, D.; Sjöö, M. Emulsion stabilizing capacity of intact starch granules modified by heat treatment or octenyl succinic anhydride. *Food Sci. Nutr.* **2013**, *1*, 157−171.
(31) Boutin, C.; Giroux, H. J.; Paquin, P.; Britten, M. Characterization and acid-induced gelation of butter oil emulsions produced from heated whey protein dispersions. *Int. Dairy J.* **2007**, *17*, 696−703.
(32) Demetriades, K.; McClements, D. J. Influences of pH and heating on physicochemical properties of whey protein-stabilized emulsions containing nonionic surfactant. *J. Agric. Food Chem.* **1998**, *46*, 3936−3942.
(33) Manoi, K.; Rizvi, S. S. H. Emulsification mechanisms and characterizations of cold, gel-like emulsions produced from texturized whey protein concentrate. *Food Hydrocolloids* **2009**, *23*, 1837−1847.
(34) Liu, F.; Tang, C. H. Cold, gel-like whey protein emulsions by microfluidisation emulsification: Rheological properties and microstructures. *Food Chem.* **2011**, *127*, 1641−1647.
(35) Tang, C. H.; Liu, F. Cold, gel-like soy protein emulsions by microfluidization: Emulsion characteristics, rheological and microstructural properties, and gelling mechanism. *Food Hydrocolloids* **2013**, *30*, 61−72.
(36) Dickinson, E.; Yamamoto, Y. Rheology of milk protein gels and protein-stabilized emulsion gels cross-linked with transglutaminase. *J. Agric. Food Chem.* **1996**, *44*, 1371−1377.
(37) Cercaci, L.; Rodriguez-Estrada, M. T.; Lercker, G.; Decker, E. A. Phytosterol oxidation in oil-in-water emulsions and bulk oil. *Food Chem.* **2007**, *102*, 161−167.
(38) Engel, R.; Knorr, D. Production of liquid, water-dispersible phytosterol formulations for increased dose response in food systems. *Eng. Life Sci.* **2004**, *4*, 374−377.
(39) Izadi, Z.; Nasirpour, A.; Garousi, G. Optimization of phytosterols dispersion in an oil/water emulsion using mixture design approach. *J. Dispersion Sci. Technol.* **2012**, *33*, 1715−1722.

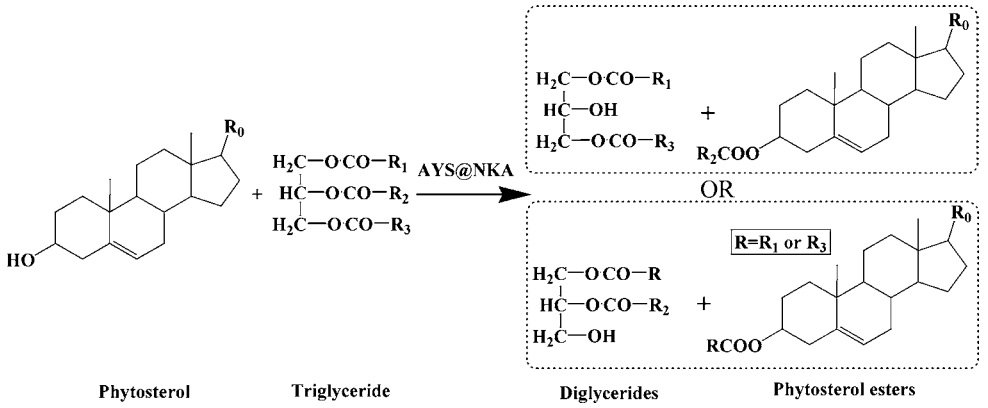

Figure 1. Preparation scheme of functional oil rich in both phytosterol esters and diglycerides using AYS@NKA as the biocatalyst.

the intermediate chemical compounds would save time and resources.[21] The main objective of this study is to develop a novel functional oil rich in both phytosterol esters and diglycerides with one-pot enzymatic esterification. Lipase immobilized on porous cross-linked polystyrene resin beads (NKA) was prepared, characterized, and used as the biocatalyst. The transesterification activity of immobilized lipase was compared with that of the free lipase. Then, a rapid and convenient method was proposed for the enzymatic transesterification of phytosterols with different vegetable oils to produce functional oils in one pot. The physiochemical properties of four kinds of functional oils with phytosterol esters and diglycerides as well as the different fatty acid (FA) compositions were also determined. As far as we are aware, a method related to producing functional oils containing both phytosterol esters and diglycerides with controllable FA composition has not been reported yet.

EXPERIMENTAL PROCEDURES

Reagents and Chemicals. The porous cross-linked polystyrene resin beads (NKA, 200−220 Å) used for preparing the immobilized lipase were obtained from the Chemical Plant of NanKai University (Tianjin, China). Ethanol, 2-propanol, acetonitrile, iso-octane, *n*-hexane, *tert*-amyl alcohol, cyclohexane, anhydrous disodium phosphate, molecular sieves (3 Å), and other solvents were all purchased from Sinopharm Chemical Reagent (Shanghai, China). 2-Propanol and acetonitrile were of chromatographic pure grade, and other reagents were of analytical reagent grade. Purified water was obtained with a Millipore water purification equipment (Boston, MA, USA). Thin layer chromatography (TLC) silica gel 60 glass plates were purchased from Merck (Darmstadt, Germany).

Lipase PS (*Burkholderia cepacia* lyophilized powder) and AYS (*Candida rugsa*, lyophilized powder) was purchased from Amano Enzyme Inc. (Tokyo, Japan). Novozym 435 (*Candida antarctica*), Lipozyme TL IM (*Thermomyces lanuginosus*), and Lipozyme RM IM (*Rhizomucor miehei*) were purchased from Novozymes A/S (Bagsværd, Denmark). Phytosterols (*β*-sitosterol (89.0%), campesterol (8.9%), stigmasterol (2.1%)) were purchased from Vita-Solar Biotechnology Co., Ltd. (Xi'an, China). Refined and bleached sunflower oil, rapeseed oil, corn oil, and linseed oil, which were used as the source of triglycerides, were purchased from the supermarket. Diglyceride and monoglyceride standards were purchased from Larodan Fine Chemicals (Malmö, Sweden). Phytosterol ester standard (97%) was purchased from BASF (China) Co., Ltd. (Shanghai, China).

Immobilization of Lipase AYS on the NKA Beads. The immobilized lipase AYS was prepared as proposed by Yan et al. with some modification.[22] First, 20.0 g of NKA beads was prewetted with 40 mL of ethanol. Then immobilization of lipase AYS on the NKA beads via adsorption was studied in phosphate buffer (400 mL, 100 mM, pH 7.0). The initial concentration of lipase was kept at 0.5−7.0 mg/mL in buffer solution. The immobilization experiment was conducted at 30 °C for 8 h with continuous stirring. After immobilization, the NKA beads were separated from the lipase solution and then washed with buffer solution three times and then washed with acetone twice. The resulting immobilized lipase (designated AYS@NKA) was lyophilized and stored at 4 °C prior to use. The amount of immobilized lipase was obtained by using the equation

$$Q = [(C_0 - C)V]/M \quad (1)$$

where Q is the amount of lipase immobilized onto NKA (mg/g), C_0 and C are the concentrations of the lipase in the solutions before and after immobilization, respectively (mg/mL), V is the volume of the aqueous solution (mL), and M is the mass of the beads (g). The amounts of protein in the medium and wash solutions were determined according to the Bradford method.[23] Nitrogen sorption experiments were carried out at 77 K using Gemini V2380 surface area and pore size analyzer (Micromeritics, Norcross, GA, USA).

One-Pot Enzymatic Synthesis of Functional Oil. The following esterification conditions were used: phytosterols (50−150 mmol/L), triglycerides such as sunflower oil, corn oil, rapeseed oil, or linseed oil (80−640 mmol/L), lipase (free AYS, AYS@NKA, 10−40 mg/mL), and solvent (hexane, iso-octane, etc., 10 mL) were added into an Erlenmeyer flask. The solvent had, in advance, been dehydrated with 15% (w/w) molecular sieves 3 Å for at least 24 h.

The vial was placed in a shaking incubator at 45−60 °C with a shaking speed of 180 rpm for a certain time. The reaction bioconversion was monitored periodically by HPLC to confirm production. The bioconversion was calculated from the ratio between the measured concentration of phytosterol esters and the expected concentration assuming complete reaction. Standard solution calibration curves were used to quantify target analytes, as it was found that no matrix effect was present. Calibration curves for phytosterol esters and diglycerides were obtained by dissolving standard substances with mobile phase in different concentrations, and results were detected and recorded on the HPLC-PDA detection. The reaction lasted for a certain time, and the relevant samples (50 μL) were withdrawn from the reaction mixture at relevant time intervals and diluted to 1 mL with the mobile phase for the analytical monitoring of the reaction. The transesterification of phytosterols might occur at either sn-1,3 or sn-2 position of triglyceride; thus, the products including diglycerides and phytosterol esters might be several possibilities (see Figure 1).

Following the lipase-catalyzed esterification, immobilized lipase and molecular sieves were filtered from the mixture. Functional oil was prepared after rotary evaporation to remove reaction solvent.

Isolation and Analysis of Functional Ingredients in the Functional Oil. High-performance liquid chromatography (HPLC) analysis was performed on an LC-6A Prominence instrument (Shimadzu, Japan) equipped with a photodiode array (PDA) detector. An Inertsil ODS-SP column (5 μm, 250 mm × 4.6 mm) purchased

dx.doi.org/10.1021/jf500744n | J. Agric. Food Chem. 2014, 62, 5142−5148

from GL Science Inc. (Tokyo, Japan) was adopted to separate and detect the targeted products. Injection volume was 10 μL. The mobile phase was acetonitrile/2-propanol (65:35, v/v). Column temperature was 40 °C, and flow rate was 1.0 mL/min. Detection was carried out by PDA at 205 nm.

A 50 μL aliquot of the reaction product was taken from the reaction system and isolated by thin layer chromatography (TLC) plates with hexane/acetic ether/acetic acid (88:12:1, v/v/v) as the developing solvent.[24,25] First, products were diluted with the developing solvent and spotted on TLC plates repeatedly (>10 times), with standard substances of phytosterol ester and diglyceride as references. Then development was carried out in the developing solvent, and the spots were visualized by iodine vapor and exposure in an oven set at 60 °C for 5 min. Ten bands corresponding to diglycerides and phytosterol esters were scraped off and collected, respectively.

Fatty Acid Composition Analysis. The fatty acid compositions of the triglycerides, diglycerides, and phytosterol esters were further confirmed by gas chromatography (GC) analysis. First, the fatty acid methyl esters (FAMEs) were prepared from diglycerides, triglycerides, and phytosterol esters according to "Animal and Vegetable Fats and Oils Preparation of FAMEs" (GB/T 17376, ISO 5509:2000, IDT) with some modification. Briefly, 100 μL of sodium methylate solution (0.5 M in methanol) and 2.5 mL of hexane were added to 0.2 g of triglyceride or a certain amount of other targets (diglycerides or phytosterol esters; each needs 10 bands collected from TLC) and then reacted for 10 min in the shaker at 55 °C. The FAMEs were extracted twice with 20 mL of hexane, and after 10 min of centrifugation, the supernatant FAMEs were concentrated with nitrogen before being preserved for GC analysis.

The fatty acid compositions of the diglycerides, triglycerides, and phytosterol esters in the products were analyzed by GC. An Agilent 7890 series gas chromatograph (Hewlett-Packard Co., Avondale, PA, USA), equipped with a flame ionization detector (FID) and a fused silica capillary column (DB-5 HT, 30.0 m × 320 μm × 0.25 μm, Agilent Technologies, Palo Alto, CA, USA) was used. The injection volume was 1 μL at a split ratio of 80:1. The carrier gas was nitrogen, and the nitrogen flow rate was 1.5 mL/min in constant flow rate mode. The flow rates of hydrogen and air were 40 and 400 mL/min, respectively, and the makeup gas was also nitrogen at a flow rate of 41.5 mL/min. The injector and detector temperatures were maintained at 250 and 300 °C, respectively. The oven temperature was held at 210 °C for 9.0 min, then increased to 250 °C at a rate of 20 °C/min, and held at 250 °C for 5 min. The fatty acid compositions of the diglycerides, triglycerides, and phytosterol esters in the products were compared with the standard substances of different fatty acids and confirmed by the retention time. The proportion of each fatty acid could be calculated by the ratio of peak area assigned to corresponding fatty acid in the GC profile.

Physiochemical Properties of Functional Oils from Different Triglyceride Sources. The peroxide value (PV) and acid value (AV) were determined according to the National Standard of the People's Republic of China (PRC) (GB/T 5538, ISO 3960:2001, IDT; GB/T 5530, ISO 660:1996, IDT).[26]

The conjugated diene (CD) value was determined as reported previously.[27] Briefly, the sample was dissolved in 50 mL of cyclohexane and the optical density (1 cm light path) recorded at 234 nm against a cyclohexane blank. The conjugated diene value was calculated according to the equation

$$\mathrm{CD\ (mmol/kg\ of\ oil)} = \frac{AV}{\varepsilon bm} \times 100 \quad (2)$$

where A is the absorbance at 234 nm of the test sample, V is the constant volume, ε is the molar absorption coefficient, 26000 L/(mol·cm), b is the thickness of the absorption cell, and m is the sample mass.

RESULTS AND DISCUSSION

Preparation and Characterization of the AYS@NKA. Five enzymes including lipase PS, lipase AYS, Novozym 435, Lipozyme TL IM, and Lipozyme RM IM were selected as the biocatalyst for transesterification of phytosterol with triglyceride. Lipase AYS was the most effective among the enzymes tested (conversion >52%). Thus, lipase AYS was selected for the following experiments. To take advantage of high specific surface area and ideal porous structure, NKA beads were used as a support matrix to immobilize lipase AYS.

However, it is difficult for the enzyme solution to access the inner surface of the NKA bead pores because of the highly hydrophobic nature of these surfaces. When prewetted with ethanol, the NKA beads were perfectly suspended in the enzyme solution, which could help the lipase reach the internal of the hydrophobic pores. The presence of ethanol may also contribute to a rearrangement of the secondary structure involving a higher accessibility of some hydrophobic side chains, which could increase the activity of noncovalently immobilized lipase.[28] Furthermore, the catalytic activity of soluble lipase in the presence of 10% ethanol concentrations could not have been negatively affected.[28] Thus, ethanol (10%, v/v) was added and acted as an intermediate between the lipase solution and the NKA beads in this experiment.

The AYS@NKA was characterized by measuring the texture parameters of samples using a Brunauer−Emmett−Teller (BET) treatment of the N_2 sorption isotherm data. It can be found that the surface area and pore volume of NKA are 562 m^2/g and 0.66 cm^3/g, respectively. After lipase absorption, the NKA beads have a lower surface area (501 m^2/g) and a lower pore volume (0.63 cm^3/g). The decrease of surface area and pore volume values of NKA after absorption indicated that the lipase AYS has been absorbed on the NKA surface and partly occupied the NKA surface pores.

To evaluate the loading capacity of the carrier, 20 g of NKA beads was loaded with 400 mL of different initial lipase concentrations ranging from 0.5 to 7.0 mg/mL. The adsorbed AYS amount increased with increasing initial AYS amount until 6.5 mg/mL and reached a maximum value of 51.2 mg/g, which was higher than that of lipase immobilized on magnetic microspheres (48.1 mg/g) and a fibrous polymer (44.7 mg/g).[23,29] The result shows that the macroporous resin NKA beads have excellent adsorption properties and allow the adsorption of a high amount of AYS with high activity.

Activity and Thermal Stability of Free AYS and AYS@NKA. The catalytic activity and thermal stability of free AYS and AYS@NKA during the transesterification reaction were evaluated. As shown in Figure 2, almost no formation of phytosterol esters occurred in the absence of AYS. Under the temperature of 50 °C, the conversion of phytosterol esters increased rapidly during the first 12 h and reached a relatively high conversion (92.4%) with AYS@NKA, whereas the conversions of phytosterol esters reached only 68.6% after 24 h of reaction using free AYS as the catalyst. These facts indicated that the immobilized AYS@NKA showed much higher catalytic activity than that of free AYS, especially at the first 12 h. The high catalytic activity of the immobilized AYS@NKA might be ascribed to the better dispersion effect as well as the higher mass transfer rate of the immobilized AYS@NKA in the reaction system compared with that of the free AYS, which might easily become aggregated in the reaction system.

The conversion of phytosterol esters catalyzed by free AYS in 60 °C showed a sharp decrease compared with that in 50 °C, which might be because the higher temperature would inhibit the activity of lipase AYS. In contrast, AYS@NKA retained most of its initial activity, and the conversion was 87.2% under the same conditions, proving enhanced thermostability for this

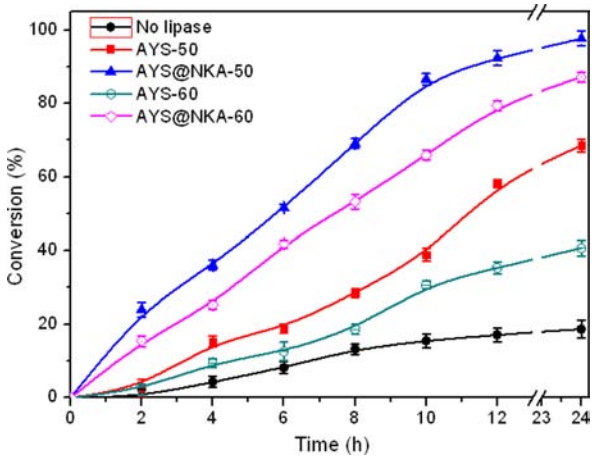

Figure 2. Activity and thermal stability of AYS@NKA and free AYS. Each experiment from Figures 2−6 was duplicated three times. The standard deviations are shown as error bars in each figure.

composite material. This is attributed to the stabilizing effect of the AYS immobilized on the NKA surface, which prevents extensive structural changes typical of thermal denaturation. The ability to retain enzyme activity at high temperatures provides several processing advantages, such as improved substrate solubility.

Optimization of Enzymatic Transesterification Conditions. Generally speaking, the kind of organic solvent is a key factor for enzymatic transesterification, because it affects not only the activity and stability of enzymes but also the solubility of substrates. The more hydrophobic solvent used, the greater activity and stability the lipase exhibited. Taking the whole into consideration, *n*-hexane, iso-octane, cyclohexane, and *tert*-amyl alcohol, which show different log *P* values, were chosen as solvents for the esterification reaction. As shown in Table 1, the

Table 1. Effects of Organic Solvents on Conversion of Enzymatic Transesterification[a]

solvent	log *P*	conversion (%)
n-hexane	3.2	95.2
iso-octane	4.5	89.7
cyclohexane	3.5	75.4
tert-amyl alcohol	1.2	80.6

[a]Reaction conditions: 80 mmol/mL phytosterols, 1:2 molar ratio of phytosterols to sunflower oil, 25 mg/mL AYS@NKA in solvent, 180 rpm, and 50 °C.

reaction in hexane exhibits the highest conversion after 12 h among the four solvents. As is known to all, the conversion is affected by both the solubility of substrates and solvent polarity. The highest conversion in hexane might ascribed to the compromise of the solubility of substrates and solvent polarity.

The effect of the substrate concentration on the conversion of phytosterol esters was evaluated. The molar ratio of phytosterols to sunflower oil was 1:2. As shown in Figure 3, it was observed that increasing the concentration of phytosterols from 50 to 150 mmol/L led to a continued decrease in the conversion. Some of the phytosterols were not soluble in the solvent at higher concentration, which was responsible for the lower conversion. In addition, an increase in phytosterols and triglyceride concentration may change the catalytic environment and the active site of AYS@NKA to some

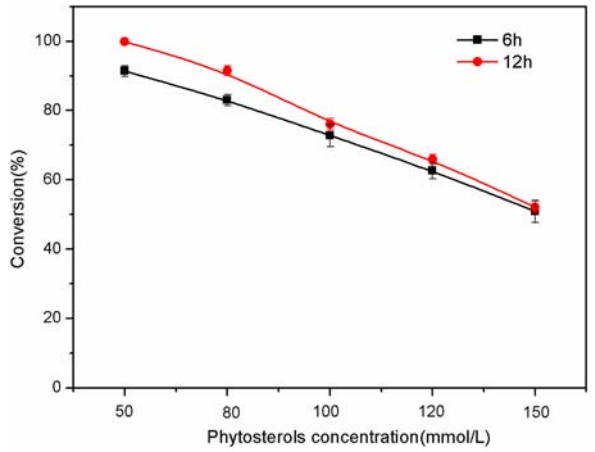

Figure 3. Effect of phytosterol concentration on the conversion of phytosterol esters in lipase-catalyzed reaction. Reaction conditions: 1:2 molar ratio of phytosterols to sunflower oil, 25 mg/mL AYS@NKA in hexane, 180 rpm, and 50 °C.

extent.[29] With phytosterol concentrations of 50 and 80 mmol/L, the phytosterol esters reached relatively high conversions, 99.8 and 91.5% after 12 h, respectively. Considering both the conversion and the economical aspect of the process, a relatively higher phytosterol concentration of 80 mmol/L was selected for the subsequent experiment.

The effect of the molar ratio of phytosterols to triglycerides on the conversion of phytosterol esters was evaluated. The molar ratio of phytosterols to sunflower oil was 1:1−1:8. With the molar ratio of phytosterols to sunflower oil increasing from 1:1 to 1:8, as shown in Figure 4, the conversions increased from

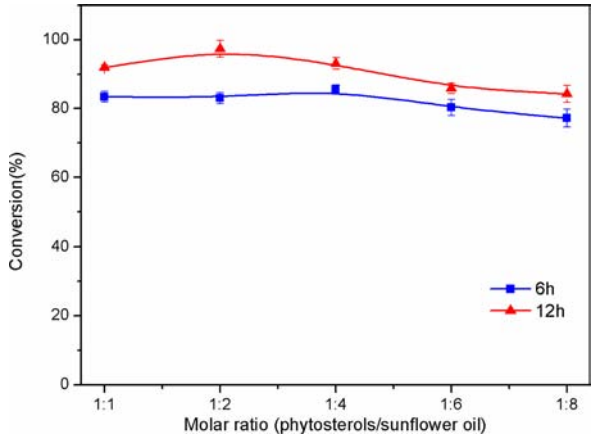

Figure 4. Effect of molar ratio of phytosterols to triglycerides on the conversion of phytosterol esters in lipase-catalyzed reaction. The phytosterol concentration was 80 mmol/L. Other conditions were the same as described in Figure 3.

91.8 to 97.4% and then decreased to 84.3%. This might due to the fact that an increase in triglyceride molar ratio may not only change the catalytic environment and the active site of AYS@NKA but also increase the viscosity of the reaction solvent and thus decrease the mass transfer rate.[30] Considering the extent of esterification and economical aspect of the process, the mole ratio of 1:2 was selected for the subsequent experiment.

The influence of the AYS@NKA load on the conversion of phytosterol esters was evaluated with a 1:2 phytosterols to sunflower oil molar ratio and an 80 mmol/L phytosterol

dx.doi.org/10.1021/jf500744n | J. Agric. Food Chem. 2014, 62, 5142−5148

concentration using various amounts of AYS@NKA from 0 to 40 mg/mL. The content of phytosterol esters was very low (18.7%) in the absence of AYS@NKA (See Figure 2). From Figure 5, it observed that with the amount of AYS@NKA

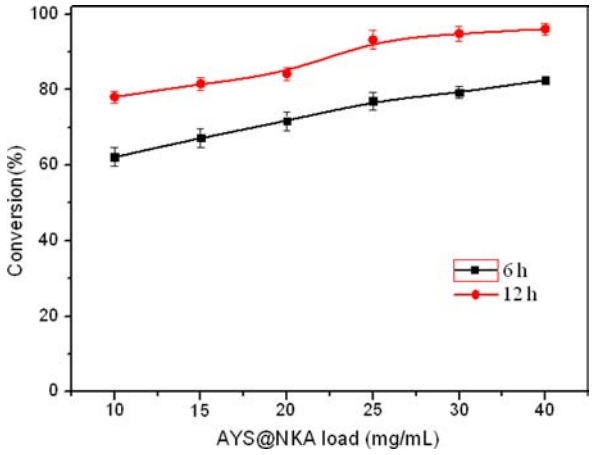

Figure 5. Effect of AYS@NKA load on the conversion of phytosterol esters in lipase-catalyzed reaction. Reaction conditions: 80 mmol/L phytosterols, 1:4 of the molar ratio of phytosterols to sunflower oil, hexane, 180 rpm, and 50 °C.

loaded increasing from 10 mg/mL to 40 mg/mL, the conversion increased from 78.1 to 96.1%. A good synthesis method should consider the conversion and economical interest of the reaction, in other words, use less AYS@NKA to obtain a satisfactory transesterification ratio. Using a minimal amount of AYS@NKA such as 10 mg/mL would be economically attractive, but conversion of phytosterols reached only 78.1% after 12 h. Increasing the amount of AYS@NKA loaded led to better production of phytosterol esters. The formation of the phytosterol esters was much higher with a 25 mg/mL AYS@NKA load and reached a 93.2% conversion after 12 h of reaction. Considering both the conversion and the economical aspects of the process, 25 mg/mL AYS@NKA was selected for the subsequent experiment.

The effect of temperature on the conversion of phytosterol esters was evaluated. The temperature ranged from 40 to 60 °C. As the reaction temperature increased from 40 to 60 °C, as shown in Figure 6, the conversion of phytosterol esters increased from 78.7 to 97.4% and then decreased to 79.2%. The highest conversion was achieved when the temperature was 50 °C. As the temperature was up to 60 °C, the conversion showed an obvious decrease (79.2%), and the energy consumption was high as well. Thus, 50 °C was selected as the reaction temperature for the subsequent experiment, which yielded an excellent conversion as well as energy savings.

Synthesis of Functional Oils with Different Vegetable Oils. Under the optimized conditions, the transesterification of phytosterols with four vegetable oils including sunflower oil, corn oil, rapeseed oil, and linseed oil was investigated. As listed in Table 2, the transesterification ratios of phytosterols with four vegetables oils were between 92.1 and 100.2%. The results suggest that AYS@NKA could be used to catalyze the transesterification of phytosterols with different acyl donors with relatively high conversion. This might be ascribed to the fact that lipases prefer to adsorb on hydrophobic supports, involving the adsorption of the hydrophobic areas surrounding the active center and leaving the active site fully exposed to the

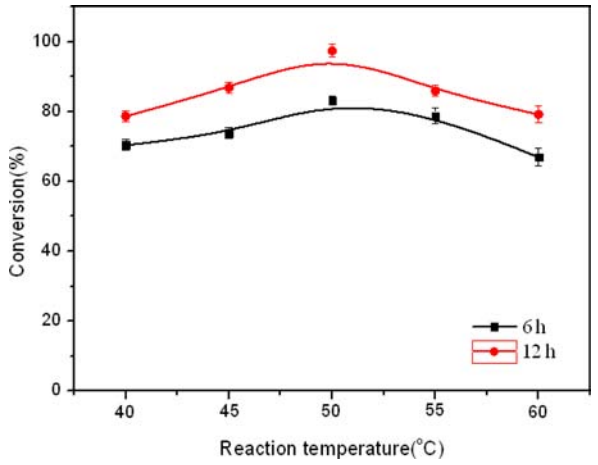

Figure 6. Effect of reaction temperature on the conversion of phytosterol esters in lipase-catalyzed reaction. Reaction conditions: 80 mmol/L phytosterols, 1:4 molar ratio of phytosterols to sunflower oil, hexane, and 180 rpm.

reaction medium.[31] HPLC analysis results showed that the peaks of two functional ingredients including phytosterol esters and diglycerides were observed in two functional oils obviously (Figuer 7). The peaks of phytosterol in functional oils were almost disappeared, which prove that the enzymatic transesterification ratio was quite high (>92.1%). As listed in Table 2, the contents of functional ingredients in four different functional oils were in the ranges of 10.4−12.5% for diglycerides and 20.2−25.1% for phytosterol esters, respectively.

Table 2 also lists the FA profile of the original vegetable oils (four kinds of triglycerides) and phytosterol esters and diglycerides produced. Four vegetable oils, which cover a wide range of oleic, linoleic, and linolenic acid values, were used as the sources of different acyl donors. Analysis of the FA composition of vegetable oils, phytosterol esters, and diglycerides by GC showed that almost all of the FAs present in the vegetable oils were incorporated into the corresponding phytosterol esters and diglycerides. In other words, the developed method could produce functional oils rich in both phytosterol esters and diglycerides with controllable FA composition by modulating the initial acyl donors with the wanted FA composition.

Physiochemical Properties of Functional Oils Prepared from Different Vegetable Oils. The physiochemical properties of functional oils prepared from different vegetable oils are shown in Table 3. The PV and CD values were low, which showed that few products of peroxidation were produced, a benefit of the mild reaction conditions. The AV and PV values were less than 1.0 mg KOH/g and 2.1 mmol/kg, respectively, which agree with the standards of sunflower oil, rapeseed oil, corn oil, and linseed oil of China (GB10464-2003, GB1536-2004, GB19111-2003, GB8235-2008) as well as the cold pressed oils standards of the Codex Alimentarius Commission (CAC) and thus could be used as the functional lipid alone or as the fat-soluble additive in vegetable oils.

Conclusion. In conclusion, a rapid and convenient esterification method using immobilized AYS@NKA as catalyst was developed to synthesize novel functional oils rich in both phytosterol esters and diglycerides in high yield under mild conditions. Furthermore, the developed method could produce phytosterol esters and diglycerides with controllable FA

Table 2. Fatty Acid Profile of the Phytosterol Esters (PE) and Diglycerides (DG) in Functional Oils Corresponding to Different Vegetable Oils as the Acyl Donors[a]

			fatty acid composition (%, w/w)					
product		content (%)	C16:0	C18:0	C18:1	C18:2	C18:3	conversion (%)
sunflower oil			6.4	3.4	30.4	59.8	0	
functional oil 1	PE	25.1	6.9	2.4	29.4	61.3	0	98.9
	DG	12.3	5.3	5.4	32.4	56.9	0	
corn oil			13.0	1.7	31.1	54.2	0	
functional oil 2	PE	20.2	13.5	2.6	24.8	59.1	0	96.5
	DG	10.4	12.0	0	42.7	45.3	0	
rapeseed oil			4.9	1.9	64.9	20.9	7.4	
functional oil 3	PE	24.1	4.2	2.6	64.8	20.3	8.1	92.1
	DG	12.5	6.9	0	65.2	22.5	5.5	
linseed oil			5.2	3.2	18.1	16.3	57.2	
functional oil 4	PE	22.3	7.4	4.5	14.5	15.3	58.3	100.2
	DG	11.2	0	0	26.8	18.7	54.6	

[a]Values are the average of analysis from triplicate sets. Functional oils 1−4 were obtained by transesterification of phytosterols with triglycerides from sunflower oil, corn oil, rapeseed oil, and linseed oil, respectively. Contents of PE and DG were short for the content of phytosterol esters and diglycerides in different kinds of functional oils. Reaction conditions: 80 mmol/L phytosterols, 1:2 molar ratio of phytosterols to triglycerides, *n*-hexane, 180 rpm, and 50 °C.

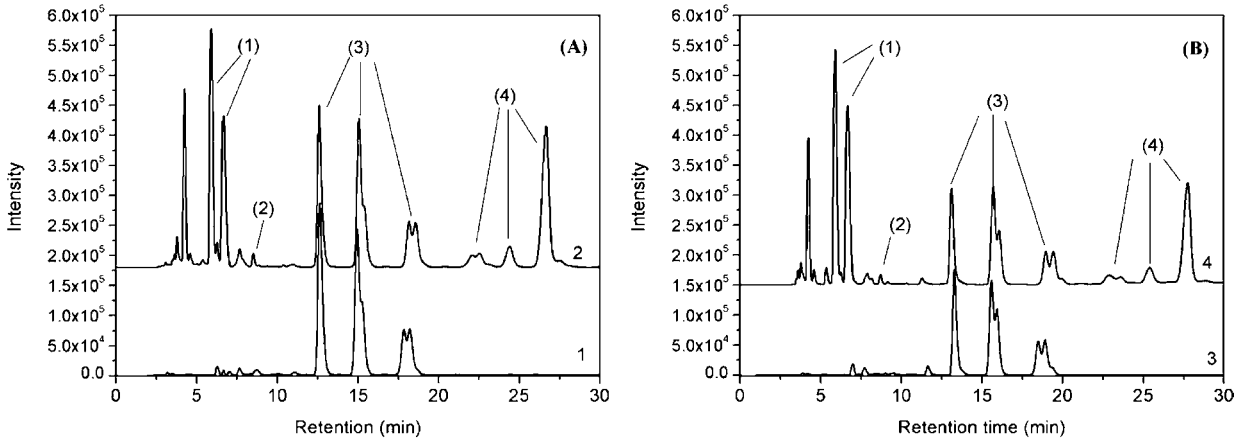

Figure 7. Liquid chromatograms of sunflower oil (A1), corn oil (B3), and responding functional oils (A2, B4). Peaks: (1) diglycerides; (2) phytosterols; (3) triglycerides; (4) phytosterol esters.

Table 3. Physiochemical Properties of Four Vegetables and Corresponding Functional Oils

product	PV[a] (mmol/kg)	AV[a] (mg of KOH/g)	CD[a] (mmol/kg)
sunflower oil	1.6	0.8	1.93
functional oil 1	1.6	0.9	1.87
corn oil	1.5	0.5	1.47
functional oil 2	1.8	0.7	1.62
rapeseed oil	1.5	0.6	1.96
functional oil 3	1.7	0.8	1.95
linseed oil	1.8	0.7	1.72
functional oil 4	2.1	1.0	1.69

[a]PV, AV, and CD are abbreviations for peroxide value, acid value, and conjugated diene value, respectively. Functional oils 1−4 are the same as those described in Table 2.

composition by modulating the initial acyl donors with the wanted FA composition. The physiochemical properties of four prepared functional oils were found to be closely related to the FA composition of the corresponding triglycerides. These findings could promote the wide application of the novel functional oils produced by the food grade process in different formulations of functional foods.

AUTHOR INFORMATION

Corresponding Author

*(F.-H.H.) Phone: +86-27-86827874. Fax: +86-27-86815916. E-mail: jiagongzx@oilcrops.cn.

Author Contributions

‖M.-M.Z. and Q.H. contributed equally to this work.

Funding

This work was supported by the National Science Foundation of China (NSFC-31371843, 31101353), the Director Fund of Oil Crops Research Institute (1610172014006), the Open Foundation of Hubei Key Laboratory of Lipid Chemistry and Nutrition (2012003), and the Foundation for Modern Agro-industry Technology Research System (CARS-13).

Notes

The authors declare no competing financial interest.

REFERENCES

(1) Chen, Z. Y.; Ma, K. Y.; Liang, Y. T.; Peng, C.; Zuo, Y. Y. Role and classification of cholesterol-lowering functional foods. *J. Funct. Food* **2011**, *3* (2), 61−69.

(2) Kim, B. H.; Akoh, C. C. Modeling and optimization of lipase-catalyzed synthesis of phytosteryl esters of oleic acid by response surface methodology. *Food Chem.* **2007**, *102* (1), 336−342.

(3) Weber, N.; Weitkamp, P.; Mukherjee, K. D. Cholesterol-lowering food additives: lipase-catalysed preparation of phytosterol and phytostanol esters. *Food Res. Int.* **2002**, *35* (2−3), 177−181.

(4) Maki, K. C.; Davidson, M. H.; Tsushima, R.; Matsuo, N.; Tokimitsu, I.; Umporowicz, D. M.; Dicklin, M. R.; Foster, G. S.; Ingram, K. A.; Anderson, B. D. Consumption of diacylglycerol oil as part of a reducedenergy diet enhances loss of body weight and fat in comparison with consumption of a triacylglycerol control oil. *Am. J. Clin. Nutr.* **2002**, *76* (6), 1230−1236.

(5) Kamphuis, M. M.; Saris, W. H.; Westerterp-Plantenga, M. S. The effect of addition of linoleic acid on food intake regulation in linoleic acid tasters and linoleic acid non-tasters. *Br. J. Nutr.* **2003**, *90* (1), 199−206.

(6) Watanabe, H.; Tokimitsu, I. Digestion and absorption of diacylglycerol. In *Diacylglycerol Oil*; Katsuragi, Y., Yasukawa, T., Matsuo, N., Flickinger, B. D., Toimitsu, I., Matlok, M. G., Eds.; American Oil Chemists' Society: Champaign, IL, USA, 2004; pp 30−45.

(7) Guo, Z.; Sun, Y. Solvent-free production of 1,3-diglyceride of CLA: strategy consideration and protocol design. *Food Chem.* **2007**, *100* (3), 1076−1084.

(8) Morita, O.; Soni, M. G. Safety assessment of diacylglycerol oil as an edible oil: a review of the published literature. *Food Chem. Toxicol.* **2009**, *47* (1), 9−21.

(9) Watanabe, T.; Shimizu, M.; Sugiura, M.; Sato, M.; Kohori, J.; Yamada, N.; Nakanishi, K. Optimization of reaction conditions for the production of DAG using immobilized 1,3-regiospecific lipase lipozyme RM IM. *J. Am. Oil Chem. Soc.* **2003**, *80* (12), 1201−1207.

(10) Zhao, Y. J.; Liu, J. F.; Deng, L.; Wang, F.; Tan, T. W. Optimization of *Candida* sp.99−125 lipase catalyzed esterification for synthesis of monoglyceride and diglyceride in solvent-free system. *J. Mol. Catal. B: Enzym.* **2011**, *72* (3), 157−162.

(11) Ziv, E.; Patlas, N.; Kalman, R.; Pelled, D.; Herzog, Y.; Dror, T.; Cohen, T. A high oleic sunflower oil fatty acid esters of plant sterols mixed with dietary diacylglycerol reduces plasma insulin and body fat accumulation in *Psammomys obesus*. *Lipids Health Dis.* **2009**, *8* (1), 42−50.

(12) Duan, Z. Q.; Wei Du, W.; Liu, D. H. Improved synthesis of 1,3-diolein by Novozym 435-mediated esterification of monoolein with oleic acid. *J. Mol. Catal. B: Enzym.* **2013**, *89* (1), 1−5.

(13) Torrelo, G.; Torres, C. F.; Senórans, F. J.; Blanco, R. M.; Reglero, G. Solvent-free preparation of phytosteryl esters with fatty acids from butterfat in equimolecular conditions in the presence of a lipase from *Candida rugosa*. *J. Chem. Technol. Biotechnol.* **2009**, *84* (5), 745−750.

(14) Zheng, M. M.; Wang, L.; Huang, F. H.; Dong, L.; Guo, P. M.; Deng, Q. C.; Li, W. L.; Zheng, C. Ultrasonic pretreatment for lipase-catalyed synthesis of phytosterol esters with different acyl donors. *Ultrason. Sonochem.* **2012**, *19* (5), 1015−1020.

(15) Vu, P. L.; Shin, J. A.; Lim, C. H.; Lee, K. T. Lipase-catalyzed production of phytosteryl esters and their crystallization behavior in corn oil. *Food Res. Int.* **2004**, *37* (2), 175−180.

(16) Liu, N.; Wang, Y.; Zhao, Q. Z.; Zhang, Q. L.; Zhao, M. M. Fast synthesis of 1,3-DAG by Lecitase® Ultra-catalyzed esterification in solvent-free system. *Eur. J. Lipid Sci. Technol.* **2011**, *113* (8), 973−979.

(17) Song, Z. H.; Liu, Y. F.; Jin, Q. Z.; Li, L.; Wang, X. G.; Huang, J. H.; Liu, R. J. Lipase-catalyzed preparation of diacylglycerol-enriched oil from high-acid rice bran oil in solvent-free system. *Appl. Biochem. Biotechnol.* **2012**, *168* (2), 364−374.

(18) Lucente Fregolente, P. B.; Pinto, G. M.; Wolf-Maciel, M. R.; Maciel Filho, R. Monoglyceride and diglyceride production through lipase-catalyzed glycerolysis and molecular distillation. *Appl. Biochem. Biotechnol.* **2010**, *160* (7), 1879−1887.

(19) Dizge, N.; Aydiner, C.; Imer, D. Y.; Bayramoglu, M.; Tanriseven, A.; Keskinler, B. Biodiesel production from sunflower, soybean and waste cooking oils by transesterification using lipase immobilized onto a novel microporous polymer. *Bioresour. Technol.* **2009**, *100* (6), 1983−1991.

(20) Zheng, M. M.; Lu, Y.; Huang, F. H.; Wang, L.; Guo, P. M.; Feng, Y. Q.; Deng, Q. C. Lipase immobilization on hyper-cross-linked polymer-coated silica for biocatalytic synthesis of phytosterol esters with controllable fatty acid composition. *J. Agric. Food Chem.* **2013**, *61* (1), 231−237.

(21) Climent, M. J.; Corma, A.; Iborra, S. Heterogeneous catalysts for the one-pot synthesis of chemicals and fine chemicals. *Chem. Rev.* **2011**, *111* (2), 1072−1133.

(22) Liu, T.; Liu, Y.; Wang, X. F.; Li, Q.; Wang, J. K.; Yan, Y. J. Improving catalytic performance of *Burkholderia cepacia* lipase immobilized on macroporous resin NKA. *J. Mol. Catal. B: Enzym.* **2011**, *71* (1−2), 45−50.

(23) Arica, M. Y.; Soydogan, H.; Bayramoglu, G. Reversible immobilization of *Candida rugosa* lipase on fibrous polymer grafted and sulfonated p(HEMA/EGDMA) beads. *Bioprocess Biosyst. Eng.* **2010**, *33* (2), 227−236.

(24) Zou, X. Q.; Huang, J. H.; Jin, Q. Z.; Liu, Y. F.; Tao, G. J.; Cheong, L. Z.; Wang, X. G. Preparation of human milk fat substitutes from palm stearin with arachidonic and docosahexaenoic acid: combination of enzymatic and physical methods. *J. Agric. Food Chem.* **2012**, *60* (37), 9415−9423.

(25) Yen, C. L. E.; Monetti, M.; Burrj, B. J.; Farese, R. V. J. The triacylglycerol synthesis enzyme DGATl also catalyzes the synthesis of diacylglycerols, waxes, and retinyl esters. *J. Lipid Res.* **2005**, *46*, 1502−1511.

(26) Laubli, M. W.; Bruttel, P. A. Determination of the oxidative stability of fats and oils. *J. Am. Oil Chem. Soc.* **1986**, *63* (6), 792−795.

(27) Weber, J.; Bochi, V. C.; Ribeiro, C. P.; Victório, A. M.; Emanuelli, T. Effect of different cooking methods on the oxidation, proximate and fatty acid composition of silver catfish fillets. *Food Chem.* **2008**, *106* (1), 140−146.

(28) Blanco, R. M.; Terreros, P.; Muñoz, N.; Serra, E. Ethanol improves lipase immobilization on a hydrophobic support. *J. Mol. Catal. B: Enzym.* **2007**, *47* (1−2), 13−20.

(29) Yong, Y.; Bai, Y. X.; Li, Y. F.; Lin, L.; Cui, Y. J.; Xia, C. G. Characterization of *Candida rugosa* lipase immobilized onto magnetic microspheres with hydrophilicity. *Process Biochem.* **2008**, *43* (11), 1179−1185.

(30) Zheng, M. M.; Dong, L.; Lu, Y.; Guo, P. M.; Deng, Q. C.; Li, W. L.; Feng, Y. Q.; Huang, F. H. Immobilization of *Candida rugosa* lipase on magnetic poly(allyl glycidyl ether-co-ethylene glycol dimethacrylate) polymer microsphere for synthesis of phytosterol esters of unsaturated fatty acids. *J. Mol. Catal. B: Enzym.* **2012**, *74* (1−2), 16−23.

(31) Mateo, C.; Palomo, J. M.; Fernandez-Lorente, G.; Guisan, J. M.; Fernandez-Lafuente, R. Improvement of enzyme activity, stability and selectivity via immobilization techniques. *Enzyme Microb. Technol.* **2007**, *40* (6), 1451−1463.

Scheme 2. Revised Mechanism of Oxygen Reduction Coupled to Catechol Oxidation Mediated by Fe Redox Cycling; Participation of Sulfite in Regenerating the Catechol and Removing Hydrogen Peroxide

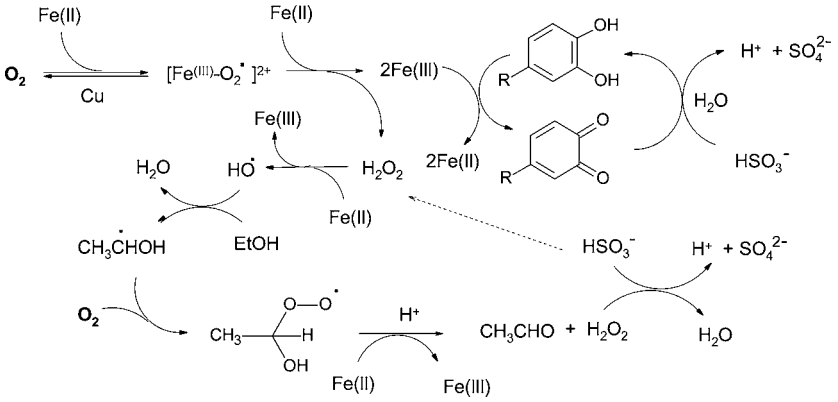

which is presumably formed in very small amounts.[16,20] Importantly, sulfite also reacts rapidly with hydrogen peroxide and so prevents ethanol oxidation.[15]

For some time it was accepted that sulfite simply reacted with oxygen, but it is now apparent that its action is far more complex. As with polyphenols, oxygen cannot react directly with sulfite. It requires the catalytic intervention of Fe. Sulfite is first oxidized by Fe(III) to the sulfite radical ($SO_3^{\bullet-}$), which then reacts rapidly with oxygen to produce the peroxomonosulfate radical ($SO_5^{\bullet-}$). This radical is a stronger oxidant capable of oxidizing sulfite directly to generate further sulfite radicals and so continue the chain reaction.[21−23] Sulfate radicals ($SO_4^{\bullet-}$) are also produced. These radicals are very powerful oxidants of similar oxidizing capability to hydroxyl radicals and so will also oxidize ethanol to acetaldehyde.[15] Far from being a reductant, sulfite alone will generate a highly oxidizing system in the presence of oxygen. Similarly, polyphenols alone produce a powerful oxidant by generating hydrogen peroxide. It has been proposed that polyphenols and sulfite complement each other, in that polyphenols would prevent sulfite oxidation by intercepting peroxomonosulfate radicals, whereas sulfite reduces quinones back to polyphenols and removes any hydrogen peroxide that is produced.[16] However, more recent results have confirmed that sulfite autoxidation is so slow that it is unlikely to occur in wine conditions.[18] In any event, under ideal conditions when a catechol is oxidized in model wine, the SO_2:O_2 molar reaction ratio is 2:1, one mole of SO_2 reacting with the quinone and the other with the hydrogen peroxide. However, in real wine the ratio may be less than 2:1, and this has been ascribed to substances that compete with sulfite for quinones.[20]

In addition to the above reactions, sulfite forms nonvolatile adducts with carbonyl compounds,[24] such as acetaldehyde, phenylacetaldehyde, and methional, produced during the winemaking process, which otherwise would produce unpleasant (oxidized) aromas.[25] Importantly, SO_2 also prevents microbial growth both directly as molecular SO_2 and indirectly as sulfite,[24,26] by preventing the growth of aerobic bacteria by facilitating polyphenol oxidation, so removing oxygen.[18]

A detailed examination of wine oxidation, therefore, reveals the key involvement of iron throughout the process. It is proposed that the ability of Fe to redox cycle is made possible by its co-ordination to tartaric and malic acids, which determine the reduction potential of the Fe(III)/Fe(II) couple in relation to that of the oxygen and catechol couples.[18,27] In this paper the importance of tartaric and malic acids is demonstrated by comparing the mechanism of catechol oxidation in tartrate, malate, and acetate model wines at pH 3.6. Acetic acid coordinates less strongly with Fe(III) than the diacids and so should raise the reduction potential of the Fe couple.

MATERIALS AND METHODS

Materials. Water (Emsure, Fe ≤ 1 μg/L, Cu ≤ 0.4 μg/L; E. Merck, Darmstadt, Germany), Cu(II) sulfate pentahydrate, Fe(III) chloride hexahydrate, sodium hydroxide, L-(+)-tartaric acid (BDH AnalaR grade), L-(−)-malic acid, acetic acid (BDH, GPR), and ethanol (96% GPR grade) were obtained from VWR International (Lutherworth, UK). 4-Methylcatechol (4-MeC, 95+%) and Fe(II) sulfate heptahydrate (99+% ACS reagent) were obtained from Sigma-Aldrich (Poole, Dorset, UK), and potassium metabisulfite (Kadifit) was from Erbslöh Geisenheim AG (Geisenheim, Germany). UV−vis spectra were taken with a Jenway 7315 spectrometer (Keison Products, Chelmsford, UK)

Preparation of Model Wine Solutions. L-(+)-Tartaric acid (5.0 g, 3.33×10^{-2} mol/L), L-(−)-malic acid (4.46 g, 3.33×10^{-2} mol/L), and acetic acid (3.81 mL, 6.66×10^{-2} mol/L) were each dissolved in water (∼800 mL) in a 1 L volumetric flask. Ethanol was added to give a 12% (v/v) final concentration, and the pH was increased to 3.60 with 2.5 N sodium hydroxide; also, water was added progressively to the mark as the required pH was approached.

Solutions of $FeSO_4$, $FeCl_3$, 4-MeC, and $K_2S_2O_5$ were freshly made up in water and (+)-catechin in 1:1 H_2O/EtOH by volume before use and added in small volumes (25−200 μL) to the model wines as required.

Reaction of Fe(II) with Oxygen in Tartrate and Acetate Model Wine. Fe(II) (20 mg/L) was added to the model wine (3 × 20 mL) containing Cu(II) (0.3 mg/L). The resulting solutions were immediately transferred to three 100 mL bottles fitted with screw caps, stored in the dark, and shaken periodically to maintain air saturation. Fe(III) concentration was determined from the absorbance at 334 nm in triplicate.

Oxidation of 4-MeC in Model Wines. 4-MeC (1.0 g/L) was added to model wines (500 mL) containing Cu(II) (0.15 mg/L), followed by SO_2 (∼60 mg/L) and Fe(II) (5.0 mg/L). Initial free SO_2 concentration was determined in duplicate, and the resulting solution was immediately divided between three 500 mL stoppered flasks, stored in the dark with periodic shaking to maintain air saturation. Oxidation was followed by measuring SO_2 concentration in triplicate on the basis of a 2:1 SO_2/O_2 molar reaction ratio.

Spectroscopic Measurements. Spectra were taken using 10 mm quartz cuvettes against a model wine blank. The small notch that was observed in spectra at ∼248 nm coincided with a sharp increase in absorbance of the model wine. It was, therefore, assumed that it was due to a large decrease in light transmission through the instrument, and spectra at lower wavelengths were not taken to be reliable. Fe(III) calibration curves were obtained by dissolving $FeCl_3$ hexahydrate (48.4 mg) in 10 mL of model wine; 50−400 μL of this solution was then

dx.doi.org/10.1021/jf5007402 | J. Agric. Food Chem. 2014, 62, 5149−5155

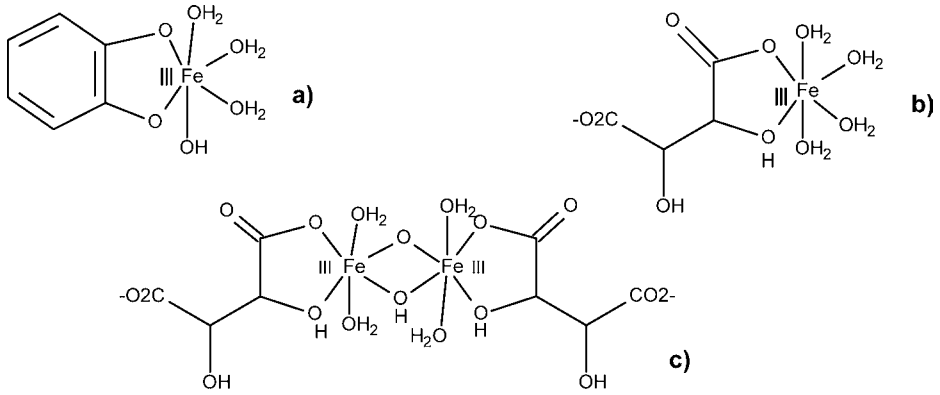

Figure 1. Proposed structures Fe complexes: (a) Fe(III)−catecholate complex;[29,30] (b) Fe(III)−tartrate monomer; (c) Fe(III)−tartrate dimer at wine pH.[31,32]

diluted to 20 mL with model wine to give the calibration standards. Such solutions were stable for at least 9 h when stored in the dark.

Measurement of SO_2. Free SO_2 concentration was measured with the modified Ripper procedure, using potassium iodate and starch−KI.[28]

When measurements were taken in triplicate, mean values (±SD) were calculated and figures drawn using Excel software (Microsoft, Redmond, WA, USA). Where error bars denoting ± SD are not shown, they were smaller than the data point symbol dimensions. Experiments were conducted at ambient temperature (18.5−20.5 °C).

RESULTS AND DISCUSSION

In the absence of stronger competing ligands such as tartaric acid, catechol forms a 1:1 complex, $[Fe(L^{2-})(H_2O)_4]^+$, with Fe(III) at pH 2−3, which exhibits two broad absorption bands at 429 and 700 nm, ε_{max} = 880 and 1000, respectively.[29,30] Bound water molecules in the complex are rendered more acidic, and one is likely to deprotonate to give $[Fe(L^{2-})(OH^-)(H_2O)_3]$ at wine pH, where LH_2 stands for the catechol (Figure 1a).[30] However, the complex is unstable and decomposes over ∼24 h to a mixture of Fe(II) and quinone,[29] which in turn decomposes further.[27] Fe(II) does not form a catecholate complex below pH ∼7.[29] Fe(III) coordinates strongly with tartaric acid, forming a monomeric complex $Fe(L^{2-})^+$ at low pH (Figure 1b), with an absorption maximum at 346 nm, where LH_2 is tartaric acid and L^{2-} is where both carboxyl groups are ionized. Above pH 2 the dimeric complex, $[Fe_2(L^{2-})_2(-3H^+)]^-$, is formed, becoming the dominant species at pH ∼3.5 (Figure 1c), which has a less pronounced absorption maximum that is shifted to 335 nm. At pH 5 the analogous trimer, $[Fe_3(L^{2-})_3(-6H^+)]^{3-}$ is produced, which displays no clear maximum but a flat shoulder at ∼300 nm.[31,32] The exact structure of these complexes has not been established. However, the water molecules attached to two Fe(III) are the most acidic, and the dioxygen olate bridge system is drawn here to explain the loss of the three protons on dimerization (Figure 1c).[33] Fe(II) binds much more weakly with tartaric acid to form a monomeric complex.[31] The greater affinity of tartaric acid for Fe(III) displaces the redox equilibrium toward Fe(III), making it a weaker oxidant and hence Fe(II) a stronger reductant.[18] Consequently, the reduction potential of the Fe(III)/Fe(II) couple was found to be lowered to 385 mV by cyclic voltammetry in model wine pH 3.3.[18] This value was the same as found in aqueous tartaric acid.[34] Because the reduction potential was found to decrease by 130 mV per pH unit increase in the wine pH range,[34] it should be 345 mV at pH 3.6, which places it well below that of the O_2/H_2O_2 couple ($E_{3.6}$ = 565 mV).[18,27] As a result, Fe(II) is rapidly oxidized to Fe(III) in air-saturated model wine containing a small amount of Cu(II) (Figure 2). In contrast,

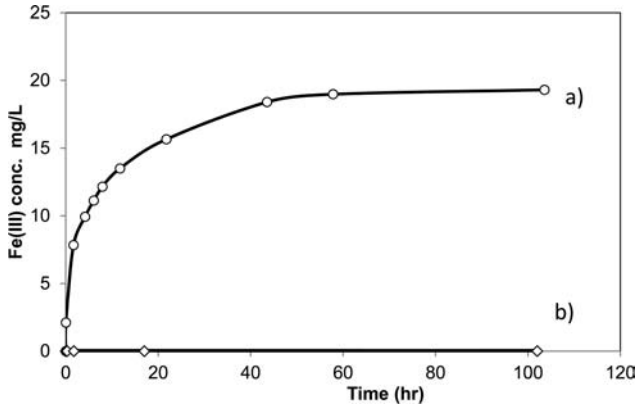

Figure 2. Oxidation of Fe(II) (20 mg/L, 3.58 × 10^{-4} mol/L) at pH 3.6 in model wines saturated with aerial oxygen in the presence of Cu(II) (0.3 mg/L): (a) tartrate model wine; (b) acetate model wine.

under the same conditions, Fe(II) failed to reduce oxygen in the acetate model wine (Figure 2), which is consistent with an increase in the reduction potential of the Fe(III)/Fe(II) couple. The reduction potential of the Fe(III)/Fe(II) couple in aqueous $NaClO_4/H_2SO_4$, where Fe(III) and Fe(II) exist as the hexaaquo complexes, $[Fe(H_2O)_6]^{3+}$ and $[Fe(H_2O)_6]^{2+}$, was found to be 687 mV at pH 3.3 by cyclic voltammetry, which also places it above that of the oxygen couple. Consequently, Fe(II) was also found not to reduce oxygen in this system.[18] Raising the reduction potential even further by adding 2,2′-bipyridyl to tartrate model wine has the same effect.[18] Inhibition of oxidation has also been demonstrated by electron paramagnetic resonance spectroscopy, where addition of 2,2′-bipyridyl as well as FerroZine to the tartrate model wine and real wine prevented the production of 1-hydroxyethyl radicals.[35]

It is also apparent that the reduction potential of the Fe couple is lowered to well below that of the quinone/4-MeC couple ($E_{3.6}$ = 577 mV) and, as observed previously at higher tartaric acid concentration,[18] Fe(III) is no longer able to oxidize 4-MeC at wine pH. When Fe(III) is added as $FeCl_3$ to tartrate model wine, a weak absorption band (λ_{max} = 335 nm, ε_{max} = 2050) (Figure 3, curve a) is observed, which can be ascribed to the dimer (Figure 1c). When 4-MeC is added, the resulting

dx.doi.org/10.1021/jf5007402 | J. Agric. Food Chem. 2014, 62, 5149−5155

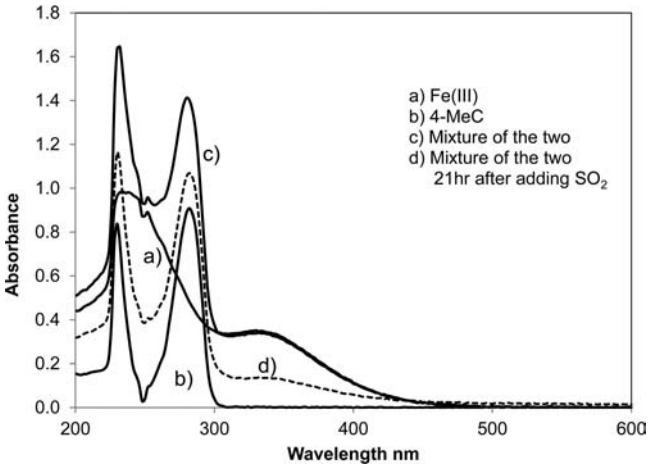

Figure 3. UV−vis spectra in tartrate model wine: (a) Fe(III) (10 mg/L, 1.79×10^{-4} mol/L); (b) 4-MeC (44.5 mg/L, 3.58×10^{-4} mol/L); (c) spectrum taken immediately after mixing the two; (d) spectrum 21 h after mixing the two with the addition of SO_2 (32 mg/L, 5.0×10^{-4} mol/L).

spectrum is the sum of the two individual spectra (curve a plus b) and remains unchanged for at least 4 days (curve c). Not only is the catechol unable to reduce Fe(III), but it is also too weak a ligand to compete with tartaric acid for Fe(III) at the relative concentration used in this experiment, as the absorbance due to the Fe(III)−tartrate dimer at 335 nm remains unchanged over many days. (+)-Catechin and gallic acid behaved similarly and were not oxidized by Fe(III) in the same system (Supporting Information Figures SI 1 and SI 2). However, with pyrogallol, which is a stronger reductant, addition of Fe(III) caused a steady increase in absorbance in the 300−350 nm range, presumably due to oxidation products as the reaction mixture progressively yellowed. This spectral change overlapped with the Fe(III) absorption band, and it was not possible to follow the extent of reduction (Supporting Information Figure SI 3). Previously, it had been shown by monitoring oxygen uptake that, in contrast to (+)-catechin, pyrogallol is oxidized in model wine without sulfite assistance.[17] The importance of reduction potentials in polyphenol oxidation is illustrated by the addition of FerroZine to model wine. This Fe(II) selective ligand raises the reduction potential of the Fe couple to such an extent that Fe(III) is then able very rapidly to oxidize catechols.[18,19]

It has been shown that when (+)-catechin is exposed to oxygen in tartrate model wine, enough oxygen is taken up to oxidize the initial Fe(II) that is present but oxidation proceeds no further. However, oxygen uptake continues when sulfite is added.[17] The rate of oxidation in model systems containing sulfite increases with increasing Fe and catechol concentration, and it is, therefore, concluded that sulfite functions by promoting catechol oxidation, drawing forward the thermodynamically unfavorable reaction by reacting with the quinone.[16,20] It has also been shown that, although 4-MeC does not reduce Fe(III) in tartrate model wine, it does so in the presence of sulfite.[18] This is a key reaction as it allows the metal to redox-cycle, and the effect is also seen in the above experiment. Addition of sulfite to a nonreacting mixture of 4-MeC and Fe(III) results in the reduction of Fe(III); the concentration of Fe(III) stabilizes from 10 to 3.4 mg/L after 21 h (Figure 3, curve d). It has been found that sulfite alone does not reduce Fe(III) in tartrate model wine, or at least the reaction is extremely slow.[18]

Fe(III) is reported to form a trimeric complex in acetate buffer at pH 1.9−3.31,[31] and addition of Fe(III) as $FeCl_3$ to acetate model wine gave a similar absorbance curve as in the tartrate model wine (Figure 4, curve a; λ_{max} = 334−338 nm,

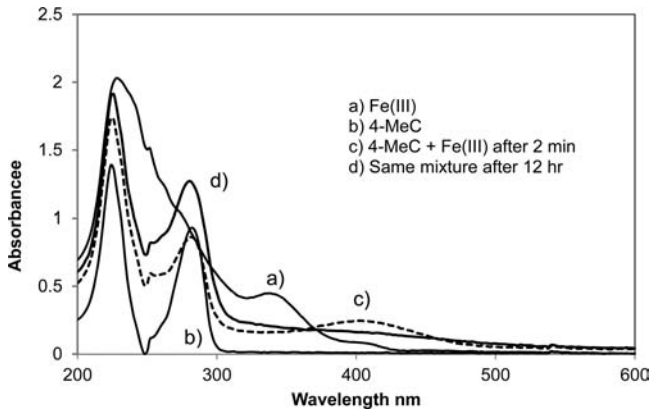

Figure 4. UV−vis spectra in acetate model wine: (a) Fe(III) (20 mg/L, 3.58×10^{-4} mol/L); (b) 4-MeC (44.5 mg/L, 3.58×10^{-4} mol/L); (c) spectrum taken 2 min after mixing the two; (d) spectrum of the same mixture taken after 12 h.

ε_{max} = 1273) but with a slight shoulder at ∼400 nm. However, catechols interacted very differently with Fe(III) in the acetate system. Addition of 4-MeC (Figure 4, curve b) resulted in an immediate loss of absorption at ∼335 nm and formation of a new broad absorption band at ∼400 nm, ε_{max} = 690 (curve c). It is proposed that this absorption is due to the formation of the catecholate complex (Figure 1a) discussed above, as the catechol is now capable of competing with the weaker monodentate acetate ligand. As previously reported, this absorption band faded over 12 h, and it is concluded that electron transfer within the complex results in the reduction of Fe(III) by the catechol.[29,30] (+)-Catechin was found to behave similarly in this system. Addition of (+)-catechin (3.58×10^{-4} mol/L) to Fe(III) (1.79×10^{-4} mol/L) in acetate model wine instantly abolished the absorption band at 334 nm due to the Fe(III)−acetate complex with the formation of a blue-green Fe(III)−(+)-catechin complex, with broad absorption maxima at ∼426 and ∼700 nm. The color progressively changed to green over 1.3 h, with intensification of the broad absorption band at ∼426 nm, which shifted to ∼392 nm over 31 h, as the catechin is oxidized (Supporting Information Figure SI 4).

Sulfite was also found to affect oxidation in the acetate model wine but in a different manner. Although Fe(II) does not react with oxygen in this system (Figure 2), it does so on addition of sulfite. Addition of an equimolar amount of sulfite to a solution of Fe(II) (20 mg/L, 3.58×10^{-4} mol/L) in air-saturated acetate model wine resulted in a steady increase in absorbance at 336 nm as Fe(III) was produced, 8.6 mg/L after 106 min (Figure 5). Under the same conditions sulfite alone did not reduce Fe(III) over 17.5 h. These results were unexpected as sulfite is generally viewed as a reductant rather than facilitating Fe(II) oxidation. Perhaps sulfite is able to coordinate with Fe(III)/Fe(II) in the presence of acetate and lower the reduction potential of the couple so that it may reduce oxygen. However, as in tartrate model wine, Fe(II) is very rapidly oxidized by H_2O_2. From the absorbance at 338 nm it was shown that all of the Fe(II) (3.58×10^{-4} mol/L) was oxidized within 1 min in

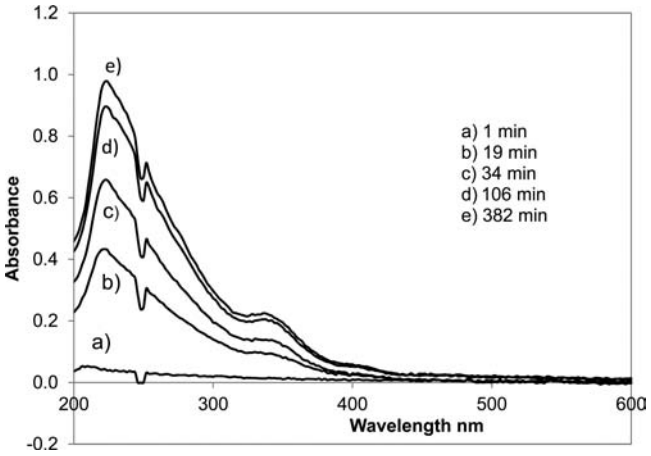

Figure 5. UV−vis spectra in air-saturated acetate model wine: oxidation of Fe(II) (20 mg/L, 3.58×10^{-4} mol/L) at times indicated after addition of SO_2 (22.9 mg/L, 3.58×10^{-4} mol/L).

acetate model wine upon the addition of H_2O_2 (5.1×10^{-4} mol/L). It is concluded, therefore, that the Fenton reaction would proceed in this as in the tartrate model system.

Malic acid has a similar chelating ability with Fe(III) as tartaric acid, forming similar polynuclear complexes at wine pH.[36] Below pH 2.6 the mononuclear complex, $[(Fe\ (L^{2-})]^{+}$, is formed, which exhibits a weak absorption maximum at 241 nm, similar to that of the corresponding tartrate complex. However, in the wine pH range the dinuclear, $[Fe_2\ (L^{2-})_3(-H^{+})_2]^{2-}$, and trinuclear, $[Fe_3(L^{2-})_5(-H^{+})_4]^{5-}$, complexes are both formed, which differ from the tartrate complexes in that the Fe(III)/ligand ratios are no longer 1:1.[36] No absorption maximum is observed in the 330−350 nm range, absorbance increasing steadily without inflection (Figure 6, curve a). Like tartaric acid,

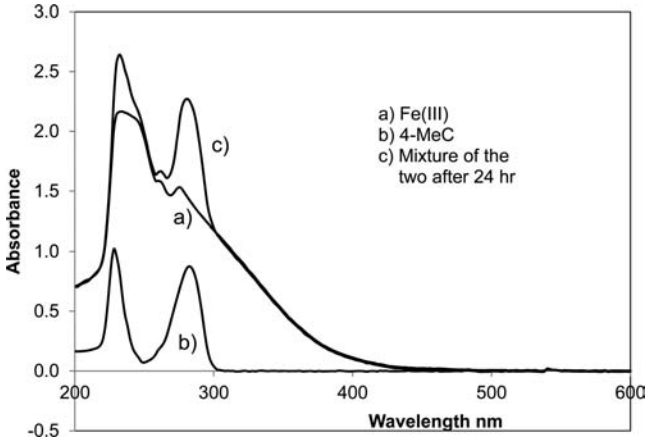

Figure 6. UV−vis spectra in malate model wine: (a) Fe(III) (20 mg/L, 3.58×10^{-4} mol/L); (b) 4-MeC (44.5 mg/L, 3.58×10^{-4} mol/L); (c) spectrum taken 24 h after mixing the two.

malic acid coordinates only weakly with Fe(II), both acids being hard ligands that bind preferentially to Fe(III). Consequently, they should modify the catalytic activity of the Fe(III)/Fe(II) couple in a similar manner.

When $FeCl_3$ was added to 4-MeC in malate model wine, the same result is obtained as in the tartrate system. The resultant spectrum (Figure 6, curve c) was the sum of that for Fe(III) and 4-MeC, and no change was discernible for 24 h. As in the tartrate system, Fe(III) did not oxidize the model catechol nor was the catechol able to coordinate with Fe(III) to a detectable extent. Furthermore, when Fe(II) was added to air-saturated malate model wine containing a small amount of Cu(II), Fe(II) was rapidly oxidized. From the absorbance measured at 350 nm it was estimated that 94% had been oxidized to Fe(III) over 15 h (Figure 7).

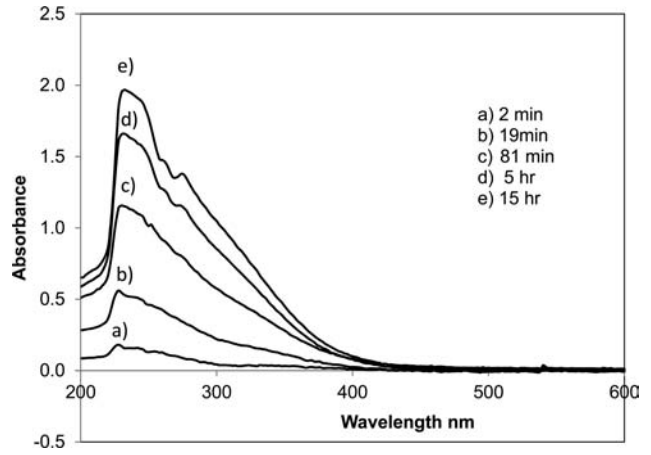

Figure 7. UV−vis spectra in air-saturated malate model wine: spectra at times indicated after adding Fe(II) (20 mg/L, 3.58×10^{-4} mol/L) to model wine containing Cu(II) (0.3 mg/L).

As discussed above, the oxidation of catechols is dependent on the ability of Fe to redox cycle, that is, the reaction of Fe(II) with oxygen to generate Fe(III) and the ability of Fe(III) in turn to oxidize catechols to regenerate Fe(II). Having compared both halves of the cycle in tartrate and acetate model wines, the overall rates of 4-MeC oxidation were compared in the two systems in the presence of sulfite (Figure 8). In the tartrate model system sulfite reacts with the hydrogen

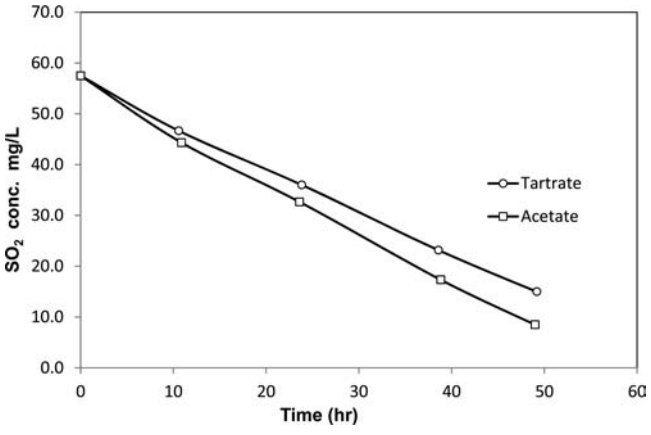

Figure 8. Free SO_2 concentration during the oxidation of 4-MeC (1.0 g/L) in acetate and tartrate model wine maintained at air saturation containing Fe(II) (5.0 mg/L) and Cu(II) (0.15 mg/L).

peroxide that is generated as oxygen is reduced and the quinone as the catechol is oxidized, resulting in a 2:1 molar reaction ratio as discussed in the Introduction.[15,16,20] The rate of reaction was found to be independent of SO_2 concentration, as it remained constant over a wide SO_2 concentration range. It is concluded that its rate of reaction with the above oxidation products is fast relative to that of oxidation, which is dependent on oxygen and catechol concentrations. Oxygen concentration

dx.doi.org/10.1021/jf5007402 | J. Agric. Food Chem. 2014, 62, 5149−5155

was held constant as the model wines were maintained at air saturation, and catechol concentration changes little as it is in substantial molar excess and is in part regenerated as oxidation proceeds. In the above studies it was shown that Fe(II) is oxidized in acetate model wine, which presumably generates hydrogen peroxide. It was also demonstrated that the catechol/Fe(III) complex is unstable, spectral changes being consistent with formation of the quinone.[29] It is, therefore, assumed that SO_2 will react with the hydrogen peroxide and quinone as in the tartrate system, also resulting in a 2:1 molar reaction ratio in acetate model wine. As can be seen, the rates of reaction are both linear, with rate in the tartrate model system a little slower. However, on the basis of the above results, it would have been a mistake to assume that the underlying mechanisms are the same. In the tartrate case, Fe(II) reacts directly with oxygen, but the oxidation of the catechol requires sulfite assistance. In the acetate system the reverse operates. Fe(III) reacts unaided with the catechol; it is Fe(II) oxidation that requires sulfite assistance.

Previous studies have provided strong evidence that polyphenol oxidation in wine is dependent on Fe catalysis, in which electrons are transferred from the polyphenol to oxygen by the intermediate redox cycling of the Fe(III)/Fe(II) couple.[15,16] The overall rate of reaction will be dependent on either the rate of reaction of Fe(II) with oxygen or the rate of reduction of Fe(III) by the polyphenol, whichever is slower. As discussed above, the rates of these reactions should depend on the reduction potential of the Fe(III)/Fe(II) couple relative to that of the oxygen and polyphenol couples.[18] Therefore, tartaric and malic acids do not just provide an acidic environment but also determine the catalytic activity of the Fe redox couple. It would not be valid to base mechanistic arguments on standard reduction potentials, which are determined at pH 0. The reduction potential of the oxygen and polyphenol couples is pH dependent, decreasing linearly by 59 mV per unit increase in pH, one proton adding to neutralize the negative charge as each electron is introduced in the reduction step.[27] Both Fe(III) and Fe(II) form octahedral complexes, and the reduction potential of the couple will depend on the relative affinity of ligands for the two oxidation states. The structure of the complexes may also be pH dependent, such as in the case of Fe, by determining the degree of "polymerization". The pH will also determine the extent to which ligands forming the complex are protonated, so altering the charge surrounding metal ions. Therefore, the reduction potential of the metal couple may not be simply deduced. These findings should apply to other model systems designed to study oxidation in foods and other beverages. Consequently, not only should pH be considered, but metal ligands mimicking those present in the system being studied should be incorporated.

Studies in model wine have proved very helpful for exploring the catalytic function of Fe and Cu and the mechanism of action of sulfite in real wine. These present model wine studies should be no less relevant. In white wine tartaric and malic acids are present in very large molar excess compared to any polyphenol that might coordinate with Fe and so will be the dominant Fe ligands. In red wines, with higher polyphenol and lower acid concentrations, it is possible that polyphenols could compete effectively with tartaric acid for Fe(III). However, as hard ligands, which also favor co-ordination to Fe(III) relative to Fe(II), polyphenols would lower the reduction potential of the Fe(III)/Fe(II) couple in a similar manner to the acid.[18] Such co-ordination would, therefore, also facilitate Fe(II) autoxidation and, by binding directly to Fe(III), could facilitate polyphenol oxidation. It is possible, therefore, that the mechanisms of oxidation of white and red wines may differ slightly. As concluded in the present study, the ligand would determine the catalytic activity of the metal.

■ ASSOCIATED CONTENT

Supporting Information

Additional figures. This material is available free of charge via the Internet at http://pubs.acs.org.

■ AUTHOR INFORMATION

Corresponding Author

*Phone: 44 1304 812 530. E-mail: jdanilewicz@btconnect.com.

Notes

The authors declare no competing financial interest.

■ REFERENCES

(1) Ugliano, M.; Kwiatkowski, M.; Vidal, S.; Capone, D.; Siebert, T.; Dieval, J.-B.; Aagaard, O.; Waters, E. J. Evolution of 3-mercaptohexanol, hydrogen sulfide, and methyl mercaptan during bottle storage of Sauvignon blanc wines. Effect of glutathione, copper, oxygen exposure, and closure-derived oxygen. *J. Agric. Food Chem.* **2011**, *59*, 2564−2572.

(2) Nguyen, D.-D.; Nicolau, L.; Dykes, S. I.; Kilmartin, P. A. Influence of microoxygenation on reductive sulphur off-odors and color development in a Cabernet Sauvignon wine. *Am, J. Enol. Vitic.* **2010**, *61*, 457−464.

(3) Ugliano, M.; Dieval, J.-B.; Siebert, T.; Kwiatkowski, M.; Aagaard, O.; Vidal, S.; Waters, E. J. Oxygen consumption and development of volatile sulfur compounds during bottle aging of Shiraz wines. Influence of pre- and postbottling controlled oxygen exposure. *J. Agric. Food Chem.* **2012**, *60*, 8561−8670.

(4) Danilewicz, J. C. Review of the reaction mechanisms of oxygen and proposed intermediate reduction products in wine: central role of iron and copper. *Am. J. Enol. Vitic.* **2003**, *54*, 73−85.

(5) Waterhouse, A. L.; Laurie, V. F. Oxidation of wine phenolics: a critical evaluation and hypotheses. *Am. J. Enol. Vitic.* **2006**, *57*, 306−313.

(6) du Toit, W. J.; Marias, J.; Pretorius, I. S.; du Toit, M. Oxygen in must and wine. *S. Afr. J. Enol. Vitic.* **2006**, *27*, 76−94.

(7) Li, H.; Guo, A.; Wang, H. Mechanism of oxidative browning of wine. *Food Chem.* **2008**, *108*, 1−13.

(8) Nikolantonaki, M.; Chichuc, I.; Teissedre, P.-L.; Darriet, P. Reactivity of volatile thiols with polyphenols in a wine-model medium: impact of oxygen, iron, and sulfur dioxide. *Anal. Chim. Acta* **2010**, *660*, 102−109.

(9) Nikolantonaki, M.; Waterhouse, A. L. A method to quantify quinone reaction rates with wine relevant nucleophiles: a key to the understanding of oxidative loss of varietal thiols. *J. Agric. Food Chem.* **2012**, *60*, 8484−8491.

(10) Saucier, C.; Bourgeois, G.; Vitry, C.; Roux, D.; Glories, Y. Characterization of (+)-catechin-acetaldehyde polymers: a model for colloidal state in wine polyphenols. *J. Agric. Food Chem.* **1997**, *45*, 1045−1049.

(11) Es-Safi, N.-E.; Fulcrand, H.; Cheynier, V.; Moutounet, M. Competition between (+)-catechin and (−)-epicatechin in acetaldehyde polymerization of flavanols. *J. Agric. Food Chem.* **1999**, *47*, 2088−2095.

(12) Es-Safi, N.-E.; Fulcrand, H.; Cheynier, V.; Moutounet, M. Studies on the acetaldehyde-induced condensation of (−)-epicatechin and malvidin 3-*O*-glucoside in a model solution system. *J. Agric. Food Chem.* **1999**, *47*, 2096−2102.

(13) Singleton, V. L. Oxygen with phenols and related reactions in musts, wines, and model systems: observations and practical implications. *Am. J. Enol. Vitic.* **1987**, *38*, 69−77.

(14) Singleton, V. L.; Trousdale, E.; Zaya, J. Oxidation of wines. 1. Young white wines periodically exposed to air. *Am. J. Enol. Vitic.* **1979**, *30*, 49−54.
(15) Danilewicz, J. C. Interaction of sulfur dioxide, polyphenols, and oxygen in a wine-model system: central role of iron and copper. *Am. J. Enol. Vitic.* **2007**, *58*, 53−60.
(16) Danilewicz, J. C.; Wallbridge, P. J. Further studies on the mechanism of interaction of polyphenols, oxygen and sulfite in wine. *Am. J. Enol. Vitic.* **2010**, *61*, 166−175.
(17) Danilewicz, J. C. Mechanism of autoxidation of polyphenols and participation of sulfite in wine: key role of iron. *Am. J. Enol. Vitic.* **2011**, *62*, 319−328.
(18) Danilewicz, J. C. Reactions involving iron in mediating catechol oxidation in model wine. *Am. J. Enol. Vitic.* **2013**, *64*, 316−324.
(19) Elias, R. J.; Waterhouse, A. L. Controlling the Fenton reaction in wine. *J. Agric. Food Chem.* **2010**, *58*, 1699−1707.
(20) Danilewicz, J. C.; Seccombe, J. T.; Whelan, J. Mechanism of interaction of polyphenols, oxygen, and sulfur dioxide in model wine and wine. *Am. J. Enol. Vitic.* **2008**, *59*, 128−136.
(21) Brandt, C.; Fábián, I.; van Eldik, R. Kinetics and mechanism of the iron(III)-catalysed autoxidation of sulfur(IV) oxides in aqueous solution. Evidence for the redox cycling of iron in the presence of oxygen and modelling of the overall reaction mechanism. *Inorg. Chem.* **1994**, *33*, 687−701.
(22) Brandt, C.; van Eldik, R. Transition metal-catalyzed oxidation of sulfur(IV) oxides. Atmospheric-relevant processes and mechanisms. *Chem. Rev.* **1995**, *95*, 119−190.
(23) Connick, R. E.; Zhang, Y.-X.; Lee, S.; Adamic, R.; Chieng, P. Kinetics and mechanism of the oxidation of HSO_3^- by O_2. 1. The uncatalyzed reaction. *Inorg. Chem.* **1995**, *34*, 4543−4553.
(24) Boulton, R. B.; Singleton, V. L.; Bisson, L. F.; Kunkee, R. E. The role of sulfur dioxide in wine. In *Principles and Practices of Winemaking*; Chapman and Hall: New York, 1996; pp 448−473.
(25) Balboa-Lagunero, T.; Arroyo, T.; Cabellos, J. M.; Aznar, M. Sensory and olfactometric profiles of red wines after natural and forced oxidation processes. *Am. J. Enol. Vitic.* **2011**, *62*, 527−535.
(26) Ribéreau-Gayon, P.; Dubourdieu, D.; Donèche, B.; Lonvaud, A. The use of sulfur dioxide in must and wine treatment. In *Handbook of Enology: The Microbiology of Wine and Vinifications*; Wiley: Chichester, UK, 2000; Vol. 1, pp 179−197.
(27) Danilewicz, J. C. Review of oxidative processes in wine and value of reduction potentials in enology. *Am. J. Enol. Vitic.* **2012**, *63*, 1−10.
(28) Ough, C. S.; Amerine, M. A. *Methods for Analysis of Musts and Wines*, 2nd ed.; Wiley: New York, 1988; pp 230−231.
(29) Powell, H. K. J.; Taylor, M. C. Interactions of iron(II) and iron(III) with gallic acid and its homologues: a potentiometric and spectrophotometric study. *Aust. J. Chem.* **1982**, *35*, 739−756.
(30) Sever, M. J.; Wilker, J. J. Visible absorption spectra of metal-catecholate and metal-tironate complexes. *J. R. Soc. Chem., Dalton Trans.* **2004**, 1061−1072.
(31) Timberlake, C. F. Iron-tartrate complexes. *J. Chem. Soc.* **1964**, 1229−1240.
(32) Yokoi, H.; Mitani, T.; Mori, Y.; Kawata, S. Complex formation between iron(III) and tartaric and citric acids in a wide pH range 1 to 13 as studied by magnetic susceptibility measurements. *Chem. Lett.* **1994**, 281−284.
(33) Kurtz, D. M., Jr. Oxo- and hydroxo-bridged diiron complexes: a chemical perspective on a biological unit. *Chem. Rev.* **1990**, *90*, 585−606.
(34) Green, R. W.; Parkins, G. M. Complexes of iron with d-tartaric and meso-tartaric acids. *J. Phys. Chem.* **1961**, *65*, 1658−1659.
(35) Kreitman, G. Y.; Cantu, A.; Waterhouse, A. L.; Elias, R. J. Effects of metal chelators on the oxidative stability of model wine. *J. Agric. Food Chem.* **2013**, *61*, 9480−9487.
(36) Timberlake, C. F. Iron-malate and iron-citrate complexes. *J. Chem. Soc.* **1964**, 5078−5085.

centrifuged to remove insoluble substances and was adjusted to pH 8.0 by 1 M Tris-HCl (pH 8.0) and 1 N HCl. The solution was then run through a DEAE-Sepharose FF column (buffered with 20 mM Tris-HCl buffer, pH 8.0, ⌀ 2.6 × 30 cm) and eluted with the same buffer followed by 0.14 M NaCl in the same buffer and a linear NaCl concentration gradient of 0.14−0.5 M, again in the same buffer. The eluted fraction was subjected to 55% saturated ammonium sulfate fractionation. The precipitate fraction was separated from the supernatant fraction, desalted by dialysis against deionized water, and lyophilized to obtain purified emu TENP.

Deglycosylation of TENP. Specific cleavage of *N*-glycan moieties (*N*-acetylglucosamine−asparagine bonds) present in TENP was carried out using glycopeptidase F (Takara-Bio Inc., Otsu, Japan). After denaturation by boiling for 3 min in buffer containing 0.5% SDS and 0.75% β-mercaptoethanol, the sample was subjected to digestion with glycopeptidase F at 37 °C overnight.

SDS-PAGE. SDS-PAGE was performed using 12.5 or 15% polyacrylamide gel according to the method of Laemmli.[10] The sample solution was mixed with an equal volume of loading buffer prior to heat treatment. The resulting sample was run on a SDS-PAGE gel. After electrophoresis, the gels were stained with 0.025% Coomassie Brilliant Blue R-250 (CBB) in an aqueous solution of 50% methanol and 10% acetic acid. The stained gels were washed using an aqueous solution of 25% methanol and 10% acetic acid, followed by water.

cDNA Cloning of Emu TENP. Total RNA was extracted from emu tissues using the TRI Reagent (Molecular Research Center, Inc., Cincinnati, OH, USA), and first-strand cDNA was synthesized using SuperScript III First-Strand Synthesis SuperMix and oligo-dT (20) primer (Invitrogen Co., Carlsbad, CA, USA). The first-strand cDNA was used for subsequent PCR amplifications of emu TENP cDNA with Ex *Taq* DNA polymerase (Takara Bio Inc., Shiga, Japan). For the cloning of emu TENP cDNA, primers were designed on the basis of the nucleotide sequence of chicken TENP (GenBank ID NM_205026). Sequences of the primers are listed in Table 1.

Table 1. Primers Used in This Study

name	sequence (5′ → 3′)	use
TENP-7F	CCTGGCTTTGTCCGAGCA	cloning
TENP-5R	CCCACATTGGAGGCAGCCA	cloning
TENP-8F	CTACTACACCAGCCTCTTCCTC	cloning
TENP-16R	GTTACAATCCATCCTCCTTC	cloning
TENP-10F	ACAGCAAACAGAAAAGGCAG	cloning
TENP-12R	GACGGTGAGGAAGAGCTTCA	RT-PCR
TENP-15F	CGGACAAGGAGATTGATGTCG	RT-PCR
bact-13F	GTGACCTGACAGACTACCT	RT-PCR
bact-14R	CAGGAAGGATGGCTGGAAGAG	RT-PCR

At first, emu TENP cDNA fragment was amplified from magnum cDNA using the primers TENP-7F and TENP-5R. Next, the primers TENP-8F based on the emu TENP cDNA fragment and TENP-16 based on the chicken TENP were used for amplification of the fragment containing a start codon of emu TENP cDNA. Also, the reverse primer TENP-12R based on the emu TENP cDNA fragment and the forward primer TENP-10F based on the sequence of chicken TENP cDNA were used for amplification of the fragment containing a stop codon of emu TENP cDNA. All amplified fragments were cloned into pCR2.1-TOPO (Invitrogen) and sequenced.

DNA Sequencing. Nucleotide sequences of cloned DNAs in pCR2.1-TOPO were analyzed by Macrogen Japan Co. (Tokyo, Japan). T7 promoter primer and M13 reverse primer (Invitrogen) were used as sequencing primers. The resultant nucleotide sequence data were assembled using the ATGC program (Genetyx Corp., Tokyo, Japan) and analyzed by using the NCBI nucleotide BLAST program.

Reverse Transcription Polymerase Chain Reaction (RT-PCR). For tissue expression profiling of emu TENP mRNA, the primer set composed of TENP-15F/TENP-12R and emu magnum cDNA were used for RT-PCR analysis. Sequences of the primers are listed in Table 1. PCR amplification was performed with Ex *Taq* DNA polymerase (Takara Bio) at 94 °C for 30 s followed by 35 cycles at 94 °C for 30 s, 55 °C for 30 s, and 72 °C for 45 s. To calibrate the cDNA concentration between samples, the β-actin gene was amplified as a housekeeping gene using a primer set of bact-13F/bact-14R, as determined by the same program. Amplicon sizes were confirmed by agarose gel electrophoresis with ethidium bromide staining.

Phylogenetic Tree Analysis. The amino acid sequences of TENP and other BPI superfamily proteins were obtained from the NCBI GenBank database as indicated in Figure 3. The ClustalW 1.81 multiple sequence alignment program was used for the alignments of protein sequences of various BPI superfamily proteins and emu ovotransferrin (DDBJ ID AB455549), determination of amino acid substitution, and construction of the neighbor-joining phylogenetic tree. Bootstrap analysis was replicated 1000 times to evaluate the phylogenetic tree topology.[11]

Antibacterial Assay. *Escherichia coli* TOP10, *Salmonella* Typhimurium TA1535/pSK1002, *Micrococcus luteus* NRIC1094, and *Bacillus subtilis* NRIC1016 were used for antibacterial assay. The antibacterial activity of TENP was measured using the method described by Wellman-Labadie et al.[12] with some modifications. Overnight bacterial cultures were grown to the log phase in nutrient broth (for all bacteria except *E. coli*) or in LB broth (for *E. coli*), then centrifuged, washed, and resuspended in 10 mM sodium phosphate buffer (pH 7.4). TENP dissolved in the same buffer or in homogenized egg white samples was added to an equal volume of bacterial suspension diluted to 0.02 at $OD_{675\ nm}$ to give 5−200 μM final TENP concentration and then incubated for 1 h at 37 °C. After incubation, a serial dilution of the sample was plated onto nutrient agar or LB agar and incubated at 37 °C until distinct colonies could be counted (18−36 h). All assays were performed in triplicate, and the antibacterial activity was represented as the percentage of reduced bacterial cell (colony) number compared with controls consisting of microbes incubated alone.

RESULTS AND DISCUSSION

Primary Structure of TENP. In a previous study, we detected and identified TENP by amino acid sequencing of its N-terminus and found that TENP was one of the major proteins in emu egg white.[2] Here we designed a gene-specific primer set for emu TENP based on the sequence of chicken TENP and successfully cloned and sequenced the 1356 bp sequence of TENP precursor cDNA, containing an ORF encoding for a 46 kDa mature protein (Figure 1). A signal peptide cleavage site of emu TENP (indicated in Figure 1) was previously identified by N-terminal amino acid sequencing of the purified protein.[4] The results were in accordance with the prediction obtained from the SignalP program using the emu TENP precursor sequence. They were also in agreement with that of the chicken TENP (HG007958) proposed by Whenham et al.,[8] but different from that published by Yan and Wang[7] (AF029841), as shown in Figure 2. Our results indicate that the emu TENP sequence is 6 amino acids longer than that of chicken TENP (HG007958) at the C-terminus and has 1 amino acid insertion at position 123 (Figure 2). The predicted N-glycosylation site and the number of cysteine residues were conserved features of both TENPs of emu and chicken. A consensus proline-rich region was found in the midsection (amino acid position 209−220 in emu) of both sequences. It was previously reported that human BPI consists of two domains of similar size that are connected by a proline-rich linker of 21 residues including 6 prolines.[13] Upon phylogenetic analysis of the inferred amino acid sequence, results showed that emu TENP belongs to the BPI/LBP/PLUNC superfamily together with other avian TENPs but distinct from other BPI-related proteins[14] such as BPI-like 1

dx.doi.org/10.1021/jf5008117 | J. Agric. Food Chem. 2014, 62, 5156−5162

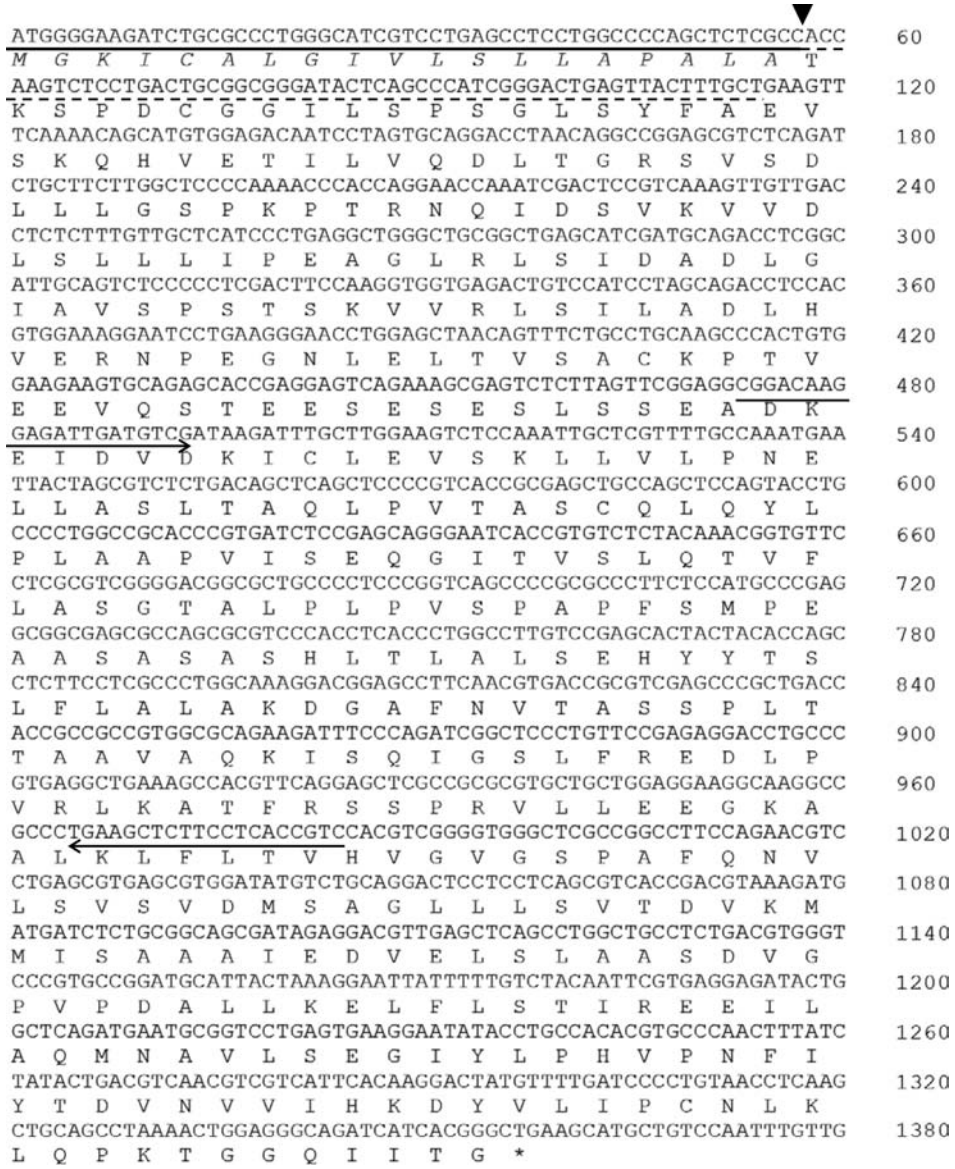

Figure 1. Nucleotide and deduced amino acid sequences of emu TENP. Signal peptide sequence is indicated by a bold underline. The amino acids determined by direct sequencing in a previous paper[2] are indicated by a dashed line. A signal cleavage site is indicated by an inverted triangle. This sequence will appear in the DDBJ database under the accession number AB556937. Arrows indicate locations of the primers for RT-PCR.

(BPIL1) and ovocalyxin-36 (OCX-36) (Figure 3). OCX-36 is an eggshell protein that is secreted during shell formation and found in the basal shell and associated membranes[15] and also eggshell cuticle.[16] Upon BLAST search for emu TENP, chicken TENP sequence was found to be identical to the protein previously known as chicken ovoglobulin G2 (sequence ID AB219158). Ovoglobulin G2 has three different polymorphic forms, AA, AB, and BB, with the majority being of the BB type.[17] Although ovoglobulin G2 is well documented for its presence in chicken egg white,[18] its biological function in egg white remains unknown. On the basis of amino acid sequence similarity with BPI and in relation to its bactericidal domain, chicken TENP was predicted to exert bactericidal activity similar to that of BPI protein. It is well established that BPI is an essential component of the innate immune system repertoire against Gram-negative bacterial infections.[19] Antibacterial activity and LPS-binding capacity of chicken OCX-36 were recently reported.[20] The phylogeny represented in Figure 3 suggests that avian TENPs, including emu TENP, are orthologous to mammalian BPIL1s, as previously suggested by Gautron et al.[14]

Gene Expression of TENP in Emu Tissues. The chicken egg is formed in the reproductive system composed of the ovary and the oviduct, and the egg white is produced in the magnum, a specific region of the oviduct.[21] To confirm whether TENP mRNA is expressed in the magnum, RT-PCR analysis of the magnum and the ovary of female egg-laying emus was performed. As expected, the TENP gene was highly amplified from the emu magnum, but was hardly detected in the ovary, as shown in Figure 4. Yan and Wang[7] reported the transient expression of chicken TENP gene in embryonic retina and brain tissues during the early developmental stages. Recently, a strong expression of the TENP gene was reported in the chicken magnum.[22] Whenham et al.[8] revealed that the expression of TENP gene is largely confined to the magnum of the oviduct of adult chicken and is controlled by gonadal steroids as a typically egg-specific gene. It is predicted that the emu TENP gene is also specifically expressed in the magnum of

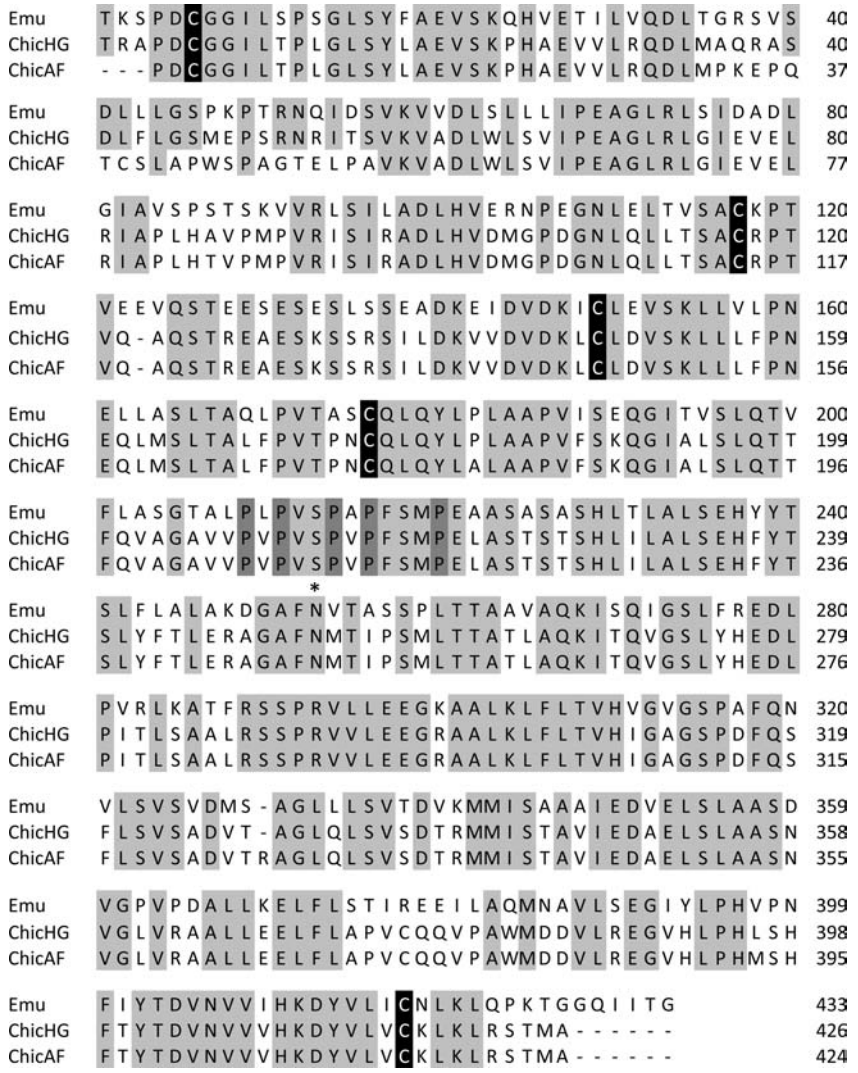

Figure 2. Alignment of amino acid sequences of emu and chicken TENPs [GenBank ID HG007958 (ChicHG) and AF029841 (ChicAF)]. Consensus sequences are highlighted in gray. Consensus cysteine residues are highlighted in black, whereas proline-rich regions are indicated by a dark gray background. The asterisk indicates a potential N-glycosylation site.

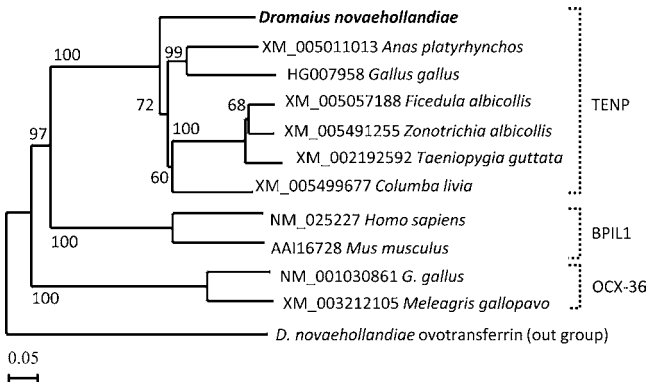

Figure 3. Phylogenetic analysis of TENPs and BPI/LBP/PLUNC-related proteins based on amino acid sequences. The accession numbers of the proteins used in this analysis are indicated. Numbers at the nodes represent bootstrap proportions (%) from 1000 replicates.

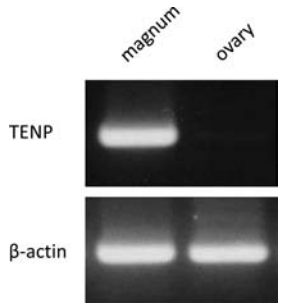

Figure 4. RT-PCR analysis of expression of TENP gene in emu magnum and ovary.

laying emus, as is the case in chickens. It would thus be of great interest to investigate the tissue distribution and regulation of TENP gene expression in each region of the emu oviduct including the magnum, the white isthmus, and the uterus, to further understand the abundance of TENP in the emu egg white in relation to its gene expression profiles.

Purification and Identification of TENP from Emu Egg White. Emu egg white preparation was separated into three peaks on DEAE-Sepharose FF column with NaCl elution. As determined by SDS-PAGE analysis, peaks P1 and P2 contained mainly an 80 kDa protein and a 100 kDa protein, respectively (Figure 5B). These peaks were further characterized by

dx.doi.org/10.1021/jf5008117 | J. Agric. Food Chem. 2014, 62, 5156−5162

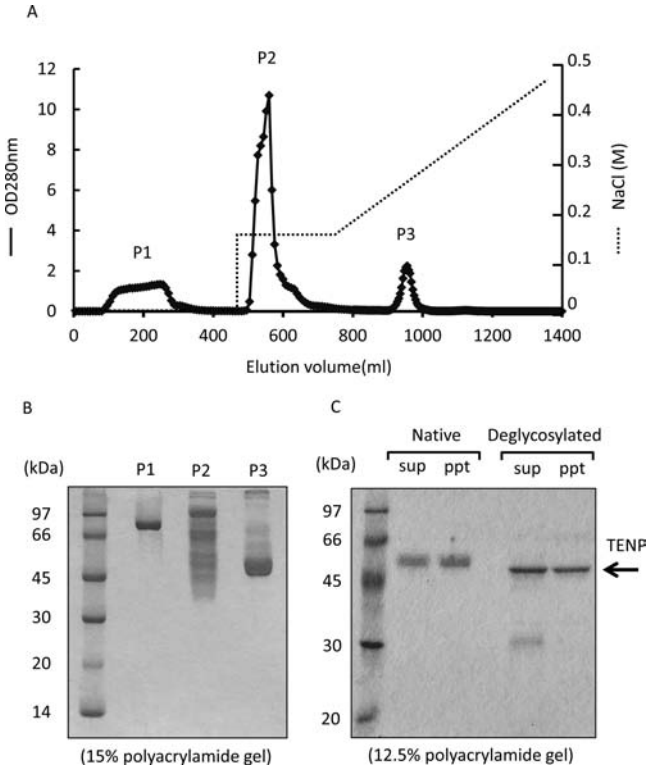

Figure 5. (A) Separation of emu egg white on DEAE-Sepharose column. (B) SDS-PAGE of DEAE peaks. (C) SDS-PAGE of deglycosylated samples from ammonium sulfate fractions (sup, supernatant; ppt, precipitate) of P3. Deglycosylation was carried out using glycopeptidase F.

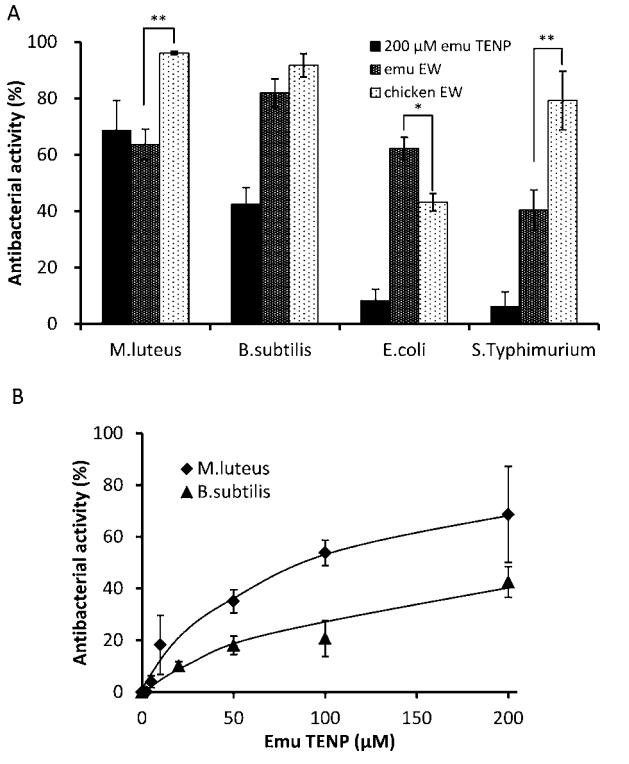

Figure 6. (A) Antibacterial activity of emu and chicken egg whites (EW) versus emu TENP. (B) Antibacterial activity of emu TENP against *M. luteus* and *B. subtilis*. M. luteus, *Micrococcus luteus* NRIC1094; B. subtilis, *Bacillus subtilis* NRIC1016; *E. coli*, *Escherichia coli* TOP10; S. Typhimurium, *Salmonella* Typhimurium TA1535/pSK1002. The results are represented as the average values obtained from three independent experiments. (∗) $p < 0.05$; (∗∗)$p < 0.01$.

separation (data not shown) and identified as ovotransferrin and ovalbumin, respectively, as previously described in our studies.[4] P3 contained mainly a 50 kDa protein, which was further separated by a 55% saturated ammonium sulfate fractionation. Resultant supernatant (sup) and precipitate (ppt) fractions both showed a single band on SDS-PAGE, as indicated in Figure 5C. However, after deglycosylation the sup fraction revealed another protein of 30 kDa. We reported in our previous study that emu egg albumen contained a riboflavin-binding protein of 50 kDa, which showed a 30 kDa band after deglycosylation.[23] A 50 kDa protein, reduced in size after deglycosylation, of the ppt fraction was identified as TENP by protein sequencing and we thereby concluded that emu TENP is an N-glycosylated protein as predicted from its amino acid sequence. The deglycosylation also confirmed that the ppt fraction was not contaminated with RBP. Thus, purified TENP migrating as a single band on SDS-PAGE was obtained from the ppt fraction and used for further testing on antimicrobial activity.

Antimicrobial Activity of Emu TENP. It is well-known that chicken egg white significantly reduces growth of bacteria;[12] more particularly, Gram-positive bacteria are sensitive to a bacteriolytic enzyme, lysozyme, in the egg white. As represented in Figure 6A, chicken egg white exhibited antibacterial activity against Gram-positive bacteria including *M. luteus* and *B. subtilis*. Similarly, emu egg white exhibited antibacterial activity against Gram-positive bacteria. However, it has been reported that emu egg white hardly contains lysozyme, so lytic activity is not detected in emu egg white.[5] It is now widely recognized that the avian egg holds a number of antimicrobial proteins, not only ovotransferrin and lysozyme, but also defensin peptides, protease inhibitors, and novel unidentified proteins.[2] Therefore, the existence of bactericidal proteins against Gram-positive bacteria, other than well-established substances, was expected in emu egg white. Emu TENP (0.2 mM) purified from emu egg white reduced the growth of Gram-positive bacteria, especially *M. luteus*, but substantively failed to affect the growth of Gram-negative bacteria including *E. coli* and *S.* Typhimurium. The final concentration of TENP present in the bacterial suspension mixed with emu egg white was estimated to be approximately 0.15 mM on the basis of the 16% estimated level of TENP[4] present in 8.9% of total protein in egg white.[1] The antibacterial activities of emu TENP against *M. luteus* and *B. subtilis* increased as a function of TENP concentration, as shown in Figure 6B. The protein purity of the TENP sample was evaluated by SDS-PAGE; however, further confirmation is required to rule out any concern with contaminants that may affect its antibacterial activity. Human[24] and oyster[25] BPIs exert antimicrobial activities against *Pseudomonas aeruginosa* and *E. coli*, respectively. On the basis of its structural similarity with BPI, it was expected that TENP would exhibit a bactericidal activity spectrum similar to that of BPI against Gram-negative bacteria. Surprisingly, emu TENP was found not to affect Gram-negative bacteria but caused bactericidal effects against Gram-positive bacteria. These results suggest a contribution of TENP to the antibacterial activity of emu egg white against Gram-positive bacteria such as *M. luteus* and *B. subtilis*. OCX-36, a member of the BPI superfamily, which is an abundant

dx.doi.org/10.1021/jf5008117 | J. Agric. Food Chem. 2014, 62, 5156−5162

component of chicken egg shell membrane, was recently investigated for its antimicrobial activity and was found to be effective against *Staphylococcus aureus* but not against Gram-negative bacteria such as *P. aeruginosa*, *E. coli* and *S.* Typhimurium.[21] The avian eggshell protects the embryo against entry of micro-organisms.[26] OCX-36 was suggested to play an innate role in the protection of the egg.[21] Defensins constitute a large number of cationic antibacterial peptides.[27] Avian β-defensin 11 was purified from chicken egg vitelline membrane and exhibited antimicrobial activity toward both Gram-positive and Gram-negative bacteria.[28] In emu egg, an ovocalyxin-17 (OC-17)-like protein, a member of the C-type lectin-like proteins, was named dromaiocalcin and represents a dominant protein in the eggshell matrix.[29] Because chicken OC-17 is a bactericidal protein,[30] dromaiocalcin is also expected to play an important role in the protection of the emu egg. In a previous study by Wellman-Labadie et al., species differences in the antibacterial activity of egg albumen were observed between Galliformes and Anseriformies and were attributed to the concentrations of ovotransferrin and lysozyme.[12] Because ovotransferrin is present in emu egg white[4] in a remarkably abundant amount, it was suggested that ovotransferrin was the main contributor to the antibacterial activity of emu egg white, whereas TENP was only partially involved, for example, against *M. luteus*.

In this study, we examined for the first time the bioactivity of TENP and found that emu TENP is a novel antibacterial protein but exerts a different spectrum of action compared to BPI, despite their structural similarity. Because TENP is contained abundantly in emu egg white, emu TENP might play a role, even partially, in the defense system against bacterial infection of the egg white. Further investigations on the antimicrobial action of TENP is required to elucidate the natural defense system present in emu egg white, with a particular focus on the role of ovotransferrin, the most abundant protein in emu egg white.

AUTHOR INFORMATION

Corresponding Author

*(K.M.) Phone/fax: +81-3-5477-2748. E-mail: maehashi@nodai.ac.jp.

Funding

This work was financially supported by the Kieikai Research Foundation.

Notes

The authors declare no competing financial interest.

ACKNOWLEDGMENTS

We thank Ms. Yuki Yoshida for her technical assistance.

REFERENCES

(1) Takeuchi, J.; Nagashima, T. Chemical and physical characterization of *Dromaius novaehollandiae* (emu) eggs. *Food Sci. Technol. Res.* **2010**, *16*, 149−156.

(2) Wellman-Labadie, O.; Picman, J.; Hincke, M. T. Avian antimicrobial proteins: structure, distribution and activity. *Worlds Poult. Sci. J.* **2007**, *63*, 421−438.

(3) Mine, Y.; Yang, M. Recent advances in the understanding of egg allergens: basic, industrial, and clinical perspectives. *J. Agric. Food Chem.* **2008**, *56*, 4874−4900.

(4) Maehashi, K.; Matano, M.; Irisawa, T.; Uchino, M.; Itagaki, Y.; Takano, K.; Kashiwagi, Y.; Watanabe, T. Primary structure of potential allergenic proteins in emu (*Dromaius novaehollandiae*) egg white. *J. Agric. Food Chem.* **2010**, *58*, 12530−12536.

(5) Maehashi, K.; Matano, M.; Irisawa, T.; Uchino, M.; Kashiwagi, Y.; Watanabe, T. Molecular characterization of goose- and chicken-type lysozymes in emu (*Dromaius novaehollandiae*): evidence for extremely low lysozyme levels in emu egg white. *Gene* **2012**, *492*, 244−249.

(6) Guerin-Dubiard, C.; Pasco, M.; Molle, D.; Desert, C.; Croguennec, T.; Nau, F. Proteomic analysis of hen egg white. *J. Agric. Food Chem.* **2006**, *54*, 3901−3910.

(7) Yan, R.-T.; Wang, S.-Z. Identification and characterization of tenp, a gene transiently expressed before overt cell differentiation during neurogenesis. *J. Neurobiol.* **1998**, *34*, 319−328.

(8) Whenham, N.; Wilson, P. W.; Bain, M. M.; Stevenson, L.; Dunn, I. C. Compaative biology and expression of TENP, an egg protein related to the bacterial permeability-increasing family of proteins. *Gene* **2014**, *538*, 99−108.

(9) Takeuchi, J.; Maehashi, K.; Yasutake, Y.; Muramatsu, Y.; Miyata, K.; Watanabe, T.; Nagashima, T. Properties of emu (*Dromaius novaehollandiae*) albumen proteins. *Food Res. Int.* **2012**, *49*, 567−571.

(10) Laemmli, U. K. Cleavage of structural proteins during the assembly of the head of bacteriophage T4. *Nature* **1970**, *227*, 680−685.

(11) Felsenstein, J. Confidence limits on phylogenies: an approach using the bootstrap. *Evolution* **1985**, *39*, 783−79.

(12) Wellman-Labadie, O.; Picman, J.; Hincke, M. T. Comparative antibacterial activity of avian egg white protein extracts. *Br. Poult. Sci.* **2008**, *49*, 125−132.

(13) Beamer, L. J.; Carroll, S. F.; Eisenberg, D. Crystal structure of human BPI and two bound phospholipids at 2.4 angstrom resolution. *Science* **1997**, *276*, 1861−1864.

(14) Gautron, J.; Rehault-Godbert, S.; Pascal, G.; Nys, Y.; Hincke, M. T. Ovocalyxin-36 and other LBP/BPI/PLUNC-like proteins as molecular actors of the mechanisms of the avian egg natural defenses. *Biochem. Soc. Trans.* **2011**, *39*, 971−976.

(15) Gautron, J.; Murayama, E.; Morisson, M.; Mckee, M. D.; Rehault, S.; Labas, V.; Belghazi, M.; Vidal, M.-L.; Nys, Y.; Hincke, M. T. Cloning of ovocalxin-36, a novel chicken eggshell protein related to lipopolysaccharide-binding proteins, bactericidal permeability-increasing proteins, and Plunc family proteins. *J. Biol. Chem.* **2007**, *282*, 5273−5286.

(16) Rose-Martel, M.; Du, J.; Hincke, M. T. Proteomic analysis provides new insight into the chicken eggshell cuticle. *J. Proteomics* **2012**, *75*, 2697−2706.

(17) Myint, S.-L.; Shimogiri, T.; Kawabe, K.; Hashiguchi, T.; Maeda, Y.; Okamoto, S. Characteristics of seven Japanese native chicken breeds based on egg white protein polymorphisms. *Asian−Aust. J. Anim. Sci.* **2010**, *23*, 1137−1144.

(18) Forsythe, R. H.; Foster, J. F. Egg white proteins. I. Electrophoretic studies on whole white. *J. Biol. Chem.* **1950**, *184*, 377−384.

(19) Weiss, J. Bactericidal/permeability-increasing protein (BPI) and lipopolysaccharide-binding protein (LBP): structure, function and regulation in host defence against Gram-negative bacteria. *Biochem. Soc. Trans.* **2003**, *31*, 785−790.

(20) Cordeiro, C. M. M.; Esmail, H.; Ansah, G.; Hincke, M. T. Ovocalyxin-36 is a pattern recognition protein in chicken eggshell membranes. *PLoS One* **2013**, *8*, DOI: 10.1371/journal.pone.0084112.

(21) Jonchere, V.; Rehault-Godbert, S.; Hennequet-Antier, C.; Cabau, C.; Sibut, V.; Cogburn, L. A.; Nys, Y.; Gautron, J. Gene expression profiling to identify eggshell proteins involved in physical defense of the chicken egg. *BMC Genomics* **2010**, *11*, 57.

(22) Chiang, S.-C.; Veldhuizen, E. J. A.; Barnes, F. A.; Craven, C. J. Identification and characterisation of the BPI/LBP/PLUNC-like gene repertoire in chickens reveals the absence of a LBP gene. *Dev. Comp. Immunol.* **2011**, *35*, 285−295.

(23) Maehashi, K.; Matano, M.; Uchino, M.; Yamamoto, Y.; Takano, K.; Watanabe, T. The primary structure of a novel riboflavin-binding protein of emu (*Dromaius novaehollandiae*). *Comp. Biochem. Physiol. Part B* **2009**, *153*, 95−100.

(24) Aichele, D.; Schunare, M.; Saake, M.; Rollinghoff, M.; Gessner, A. Expression and antimicrobial function of bactericidal permiability-increasing protein in cystic fibrosis patients. *Infect. Immun.* **2006**, *74*, 4708−4714.
(25) Gonzalez, M.; Gueguen, Y.; Destoumieux-Garzon, D.; Romestand, B.; Fievet, J.; Pugniere, M.; Roquet, F.; Escoubas, J.-M.; Vandenbulcke, F.; Levy, O.; Saune, L.; Bulet, P.; Bachere, E. Evidence of a bactericidal permeability increasing protein in an inverterbrate, the *Crassostrea gigas Cg*-BPI. *Proc. Natl. Acad. Sci. U.S.A.* **2007**, *45*, 17759−17764.
(26) Rose, M. L. H.; Hincke, M. T. Protein constituents of the eggshell: eggshell-specific matrix proteins. *Cell. Mol. Life Sci.* **2009**, *66*, 2707−2719.
(27) Xiao, Y.; Hughes, A. L.; Ando, J.; Matsuda, Y.; Cheng, J.-F.; Skinner-Noble, D.; Zhang, G. A genome-wide screen identifies a single β-defensin gene cluster in the chicken: implications for the origin and evolution of mammalian defensins. *BMC Genomics* **2004**, *5*, 56.
(28) Herve-Grepinet, V.; Rehault-Godbert, S.; Labas, V.; Magallon, T.; Derache, C.; Lavergne, M.; Gautron, J.; Lalmanach, A.-C.; Nys, Y. Purification and characterization of afffvian β-defensin 11, an antimicrobial peptide of the hen egg. *Antimicrob. Agents Chemother.* **2010**, *54*, 4401−4408.
(29) Mann, K. Identification of the major proteins of the organic matrix of emu (*Dromaius novaehollandiae*) and rhea (*Rhea americana*) eggshell calcified layer. *Br. Poult. Sci.* **2004**, *45*, 483−490.
(30) Wellman-Labadie, O.; Lakshminarayanan, R.; Hincke, M. T. antimicrobial properties of avian eggshell-specific C-type lectin-like proteins. *FEBS Lett.* **2008**, *582*, 699−704.

electrospun fibers after heat treatment. Thermal processing will generally reduce the α-helix structure, and increase the intermolecular antiparallel β-sheet form of protein secondary structure, which induces protein conformational changes.[12] Hence, the protein secondary structure of the heat-cured electrospun fibers was investigated using a vibrational spectroscopy technique such as ATR-FTIR. Overall, the objectives of this work were to evaluate the effect of heat treatment on the physicochemical properties of the electrospun fibers, and to characterize the extent of denaturation along with the degree of cross-linking on heat-cured Ze and Ze-GA electrospun fibers using ATR-FTIR, SS-NMR, and gel permeation chromatography (GPC). Other physicochemical properties, namely, the color properties, surface hydrophobicity, morphology, and release performance of the heat-cured electrospun fibers, were also determined in this work.

MATERIALS AND METHODS

Materials. Zein (Z 3625) and *N*-methyl-2-pyrrolidone (NMP, HPLC grade) were purchased from Sigma-Aldrich (St. Louis, MO, USA). The zein powder was used without further purification. Ethanol (ACS grade) was purchased from ECP Ltd. (Auckland, New Zealand). Milli-Q water (18 MΩ cm, Millipore, Bedford, MA, USA) was used for preparation of all solutions.

Electrospinning Process. The zein and gallic acid incorporated zein solutions were prepared and electrospun as described in our previous studies.[10,11] Briefly, zein solution was prepared at a concentration of 25 wt % by dissolving zein powder in 80 wt % ethanol aqueous solutions under constant stirring using a magnetic stirrer at room temperature (approximately 21 to 24 °C). Zein electrospun fibers containing various amounts of gallic acid in the solid fibers were prepared by first dissolving gallic acid in 80 wt % ethanol aqueous solutions, followed by dissolving zein powder to obtain 25 wt % zein solutions. The final content for the gallic acid in the solid fibers was 5 and 10 wt %, meaning gallic acid to zein weight ratio of 1:19 and 1:9 in the final dry electrospun fibers, respectively. These electrospun fibers were designated as Ze (for pure zein with no gallic acid incorporation), Ze-GA 5%, and Ze-GA 10%, respectively. The solutions were placed in 5 mL syringes that were driven by a syringe pump (Cole Parmer 74900 series, Vernon Hills, IL, USA) to give a solution feed rate of 0.8 mL h^{-1}. The positive electrode of a direct current power supply (high voltage power supply series 230, Bertan, Hicksville, NY, USA) was connected to a 20 gauge needle (i.d. of 0.61 mm) of a syringe and the negative terminal to a grounded collector. The applied voltage was 16 kV with a distance between needle tip and collector of 13 cm. Finally, the as-spun electrospun fibers were heat-cured in a laboratory oven at 150 °C for 24 h.

Scanning Electron Microscopy (SEM). The morphology of the fibers was examined using a Philips XL 30S FEG (Philips, Eindhoven, The Netherlands) scanning electron microscope, after sputter coating the samples with platinum under vacuum for 5 min at 5 to 10 mA using a Quorum Q150R-S sputter coater (Quorum Technologies Ltd., Ashford, Kent, U.K.) to reduce electron charging effects. The fiber diameter was measured as the average diameter with UTHSCSA image tool (IT) for windows, version 3.00 (University of Texas Health Science Center, San Antonio, TX, USA) from over 60 randomly selected fibers.

Color Measurement. Instrumental color analyses of the heat-cured Ze and Ze-GA fiber mats after heat curing were determined using a CR300 colorimeter (Minolta, Osaka, Japan) to provide background information on their optical properties. L^* value describes lightness, where $L^* = 0$ is black and $L^* = 100$ is close to white; a negative a^* represents greenness, and a positive a^* is redness; a negative b^* indicates blueness, while a positive b^* is yellowness. Measurements were made directly on the fiber mats after calibrating the instrument using a standard white calibration plate ($L^* = 96.86$, $a^* = -0.02$, and $b^* = 1.99$). The measurements were carried out in triplicate.

Water Contact Angle. The wettability of the electrospun fibers was determined by using the sessile drop method. Each of the electrospun fiber mats (thickness was approximately 77 μm) was carefully peeled off from the aluminum foil and was mounted on the lifting stage connected to a KSV CAM 100 contact angle goniometer (KSV Instrument Ltd., Finland). A droplet (approximately 5 μL) of distilled water was placed on the fiber surface with a microsyringe. The tangent line at the point of contact of the water droplet with the fiber surface was captured and measured immediately using the CAM 100 computer simulation software at room temperature (approximately 22 °C). The contact angle for each sample was taken as the average of 10 different measurements in order to get a reliable value.

Release Assay. The release characteristics of gallic acid from the heat-cured Ze-GA electrospun fibers were determined by a modification of total immersion method by Tungprapa et al.[13] in Milli-Q water. Briefly, 20 mg of the electrospun fiber mat was submerged in 40 mL of Milli-Q water at 23 °C under gentle stirring. An aliquot of 50 μL of the solution was withdrawn at specified time intervals, ranging between 0 and 360 min and diluted with 450 μL of Milli-Q water. The sample solutions were filtered through a cellulose acetate 0.45 μm (Phenomenex, Torrance, CA, USA) syringe filter before analysis by high performance liquid chromatography (HPLC). The amount of the released gallic acid was quantified by HPLC using a Phenomenex Luna C18 column (250 mm × i.d. 4.6 mm, 5 μm particle size) according to the previously published method by Neo et al.[14] Briefly, isocratic elution was carried out with a mobile phase consisting of water/methanol (82:18 v/v) containing 2% (v/v) acetic acid, at a flow rate of 1 mL min^{-1}. A diode array detector was used for the detection of gallic acid, and the HPLC profiles were obtained at 280 nm. The injection volume for all samples was 20 μL. Identification of gallic acid was based on retention times in comparison with standards. The concentration of the gallic acid was calculated using peak area and the calibration curves obtained from the gallic acid standard solutions. The morphology of heat-cured electrospun fibers after the release assay was determined using SEM, as described in the aforementioned section.

Gel Permeation Chromatography (GPC). The molecular characteristics of the electrospun fiber mats were investigated using gel permeation chromatography (GPC). The GPC system consisted of a Waters 515 HPLC pump (Waters Inc., Milford, MA, USA), a Rheodyne manual injector (Rheodyne, Cotati, CA, USA) fitted with 200 μL injection loop, a Phenomenex Degassex DG-4400 online degasser (Phenomenex, Torrance, CA, USA), two PolyPore columns (300 mm × 7.5 mm with mixed pore sizes) from Polymer Laboratories/Varian Inc. (Amherst, MA, USA) with a PolyPore guard, a multiangle laser light scattering (MALLS) detector (632.8 nm, DAWN DSP, Wyatt Technology, Santa Barbara, CA, USA), and a Shimadzu RID-10A refractive index (RI) detector (Shimadzu, Kyoto, Japan), and the columns were thermostated at 40 °C using a Waters column oven (Waters Inc., Milford, MA, USA). The electrospun fiber mats were dissolved in 5 mL of *N*-methyl-2-pyrrolidone (NMP) separately after constant stirring using a magnetic stirrer until complete solubility. The prepared concentration for each sample was 5 mg mL^{-1}. The samples were filtered through 13 mm 0.45 μm polytetrafluoroethylene (PTFE) syringe filters (Grace, Deerfield, IL, USA) before injection onto the column set. A 100% NMP was used as the mobile phase, which had been filtered by 0.2 μm PTFE membrane filter (Supelco, Bellefonte, PA, USA). The flow rate was 0.2 mL min^{-1}, and the pump pressure was approximately 950 psi. Six poly(methyl methacrylate) (PMMA) standards (EasyCal Kit, Polymer Laboratories, U.K.) were dissolved in the same mobile phase at 2 mg mL^{-1}. The 29960 g mol^{-1} standard peak was used to normalize the light scattering detectors. Data acquisition and processing were performed using the ASTRA 4.0 software (Wyatt Technology, Santa Barbara, CA, USA). The specific RI increment value (dn/dc) was determined by assuming 100% mass recovery for non-heat-cured Ze solution of accurately known concentration in NMP, and was found to be 0.056 mL g^{-1}. The molecular weight and root-mean-square radius of gyration for each electrospun fiber mat were calculated with a first-

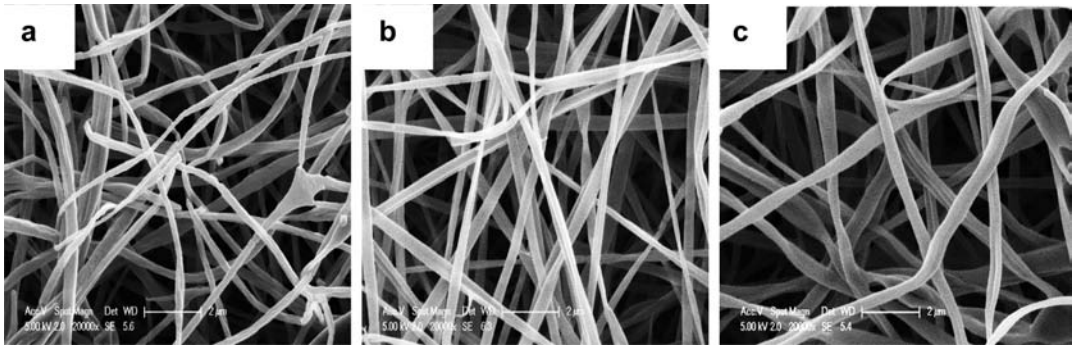

Figure 1. SEM images of heat-cured Ze and Ze-GA electrospun fibers at 2 μm scale bar: (a) Ze, (b) Ze-GA 5%, (c) Ze-GA 10%.

order Debye fit. Four of the 18 detector signals were excluded for the data processing due to poor signal-to-noise ratio.

Attenuated Total Reflectance Fourier Transform Infrared (ATR-FTIR) Spectroscopy. The chemical interaction and compositional analysis of the electrospun fiber mats were examined using ATR-FTIR spectroscopy. The ATR-FTIR spectra were recorded on a Thermo Electron NICOLET 8700 FTIR spectrophotometer using the Smart Orbit ATR accessory with diamond crystal, single bounce at 45° (Thermo Electron Corporation, Waltham, MA, USA) over the wavenumber region of 700 to 3600 cm^{-1}. Interferograms were averaged for 32 scans at 4 cm^{-1} resolution. The measurements were carried out in triplicate. Second derivative spectra (Savitsky−Golay derivative) were obtained using the OMNIC 5.0 spectroscopic software (Nicolet Instrument Corp., Madison, WI) to determine the component peak positions. Next, fitting of the component bands was carried out for the 1300 to 1730 cm^{-1} region using the OMNIC 5.0 spectroscopic software, and a Gaussian/Lorentzian function was used for the fitted curves. The composition of the protein secondary components was determined semiquantitatively through the relative peak heights of each component. Fitting was not limited to the amide I region (1600 to 1700 cm^{-1}) in order to overcome the possible errors due to overlapping components from the other regions. All the given fits converged with the original spectra.

^{13}C Solid State Nuclear Magnetic Resonance (SS-NMR). Structural analysis of the electrospun fiber mats was conducted using SS-NMR. CPMAS NMR experiments were performed at a ^{13}C frequency of 75.47 MHz using a Bruker Avance 300 spectrometer (Bruker BioSpin GmbH, Germany). The magic angle was adjusted by maximizing the sidebands of ^{79}Br signal of a KBr sample. The electrospun fiber mats were packed in zirconium oxide 7 mm rotors with airtight Kel-F caps. The sample rotation frequency was 7000 ± 1 Hz, and the free induction decays were acquired with a spectral width of 40 kHz. The ^{1}H 90° pulse was 4.2 μs, 1 ms contact time, using a recycle delay of 2 s to avoid signal loss through saturation. The number of scans for the CPMAS experiments was 4000 to 5000. The spectra were externally referenced using polycrystalline adamantane (38.48 ppm relative to tetramethylsilane (TMS, 0 ppm)) as suggested by Morcombe and Zilm.[15] All experiments are performed at room temperature (approximately 21 to 24 °C).

Statistical Analysis. Statistical analysis was performed using MINITAB 13.0 software (Minitab Inc., State College, PA, USA). The data were compared using analysis of variance (ANOVA) at 5% significance level. All values are reported as means of three determinations, and the results were expressed as mean values ± standard deviation.

RESULTS AND DISCUSSION

Morphological and Color Properties of the Fiber Mats. The microstructures of the heat-cured Ze and Ze-GA electrospun fibers using SEM are shown in Figure 1. The heat-cured fibers exhibited distorted and flattened structures. They generally retained their morphological integrity as continuous randomly oriented cylindrical fibers, and the average diameter of the heat-cured electrospun fibers was in the range from 357 to 519 nm.

Color values of the electrospun fiber mats are presented as L^*, a^*, and b^* values as shown in Table 1. The average color values of heat-cured Ze and Ze-GA electrospun fiber mats were found to be between 91.31 and 94.68 for L^*, 0.25 and 1.32 for a^*, and 8.64 and 10.28 for b^*. The heat-cured electrospun fibers became significantly darker, redder, and more yellowish with the increasing amount of gallic acid loaded, as evidenced by their lower L^* and greater a^* and b^* values as shown in Table 1. Interestingly, the heat-cured electrospun fibers were also found to be more yellowish than the non-heat-cured electrospun fibers. The average color values of non-heat-cured Ze and Ze-GA electrospun fiber mats were reported to be between 0.90 and 2.51 for b^* in our previous study (Table 1).[11] These observations are in agreement with other reported studies on heat-treated protein films.[2,8,16] Overall, the color values of the heat-cured Ze-GA electrospun fibers mats were significantly different ($P < 0.05$) from those of the non-heat-cured fiber mats in terms of lightness, yellowness, and redness. The browning reaction of zein protein during high temperature processing is suggested to be due to isopeptide bond formation between the amine, $-NH_2$ side chain of lysine or arginine with the carboxyl −COOH containing side chains or amide group of glutamic acid, aspartic acid, glutamine, and asparagine, through the liberation of water and ammonia.[17,18] These reactions are also reported to be responsible for the formation of cross-linking bonds. Other than that, Reddy et al.[19] also reported that

Table 1. Reflectance (Hunter L^*, a^*, b^*) Values of Heat-Cured Ze and Ze-GA Electrospun Fibers

GA content (wt % in solid fibers)	L^*	a^*	b^*
	Non-Heat-Cured[a]		
0	96.488 ± 0.55 a	0.034 ± 0.08 d	1.368 ± 0.99 h
5	94.805 ± 1.32 b	0.178 ± 0.06 de	0.895 ± 0.25 h
10	95.680 ± 0.80 ab	0.187 ± 0.12 de	2.512 ± 0.59 i
	Heat-Cured		
0	94.683 ± 0.48 b	0.253 ± 0.06 e	8.643 ± 0.57 j
5	92.850 ± 0.54 c	0.663 ± 0.17 f	8.883 ± 0.58 jk
10	91.310 ± 0.28 c	1.315 ± 0.05 g	10.282 ± 0.05 k

[a]The reflectance values for non-heat-cured electrospun fibers were extracted from the previously published data (Neo et al., 2013).[11] Data are displayed as means ± standard deviation of three replications. Means in each column bearing different letters are significantly different ($P < 0.05$).

dx.doi.org/10.1021/jf500841m | J. Agric. Food Chem. 2014, 62, 5163−5172

the dehydration of the carboxylic acids at high temperature that forms an unsaturated acid would cause yellowness of the cross-linked material. Hence, the greater yellowness of Ze-GA electrospun fiber mats suggested the potential chemical interactions of the carboxylic group of gallic acid with the zein amino acids.

Water Contact Angle of the Heat-Cured Electrospun Fiber Mats. The wettability of the heat-cured electrospun fiber was determined using the water contact angle upon the surface of the fiber mats. A large contact angle ($\theta > 65°$) generally implies a hydrophobic surface, while a small contact angle ($\theta < 65°$) suggests a hydrophilic surface.[20] The wettability of the non-heat-cured Ze and Ze-GA electrospun fibers was very high, judging by the fact that the water droplets spread instantly into the non-heat-cured fiber matrices. Hence, no contact angle value could be measured for the non-heat-cured fibers during the experiments. All heat-cured Ze and Ze-GA electrospun fiber mats exhibited a contact angle of approximately 110° in the first 10 s, indicating the variation of the surface properties after the heat-curing process (Figure 2). The contact angle gradually

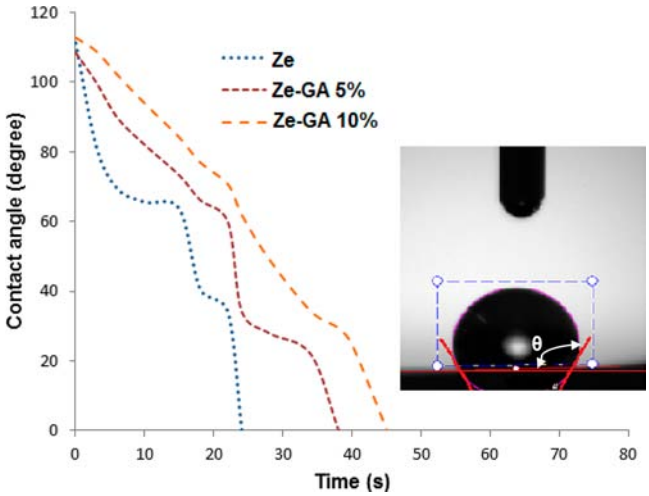

Figure 2. Plot of contact angle of heat-cured electrospun fiber mats as a function of time.

decreases with time, and a complete spreading of the water droplets is observed for all the heat-cured fiber mats within 50 s. Tang et al.[21] suggested that heat treatment will induce the unfolding of proteins, which consequently will uncover some of the hydrophobic functional groups of the protein that were originally buried in the interior of the molecules. Hence, the differences in the wettability among the electrospun fiber mats might be due to the alterations in the protein structure after the heat-curing process. Interestingly, the wettability of the heat-cured electrospun fiber mats decreased with the increase in gallic acid content. Thus, it is prudent to assume there was significant chemical bonding between gallic acid and zein protein after the heat-curing process, which have modified the chemical properties of zein.

Release Performance of the Loaded Gallic Acid. The release curves of gallic acid from the heat-cured Ze-GA electrospun fiber mats in water at 23 °C for 6 h are shown in Figure 3. The electrospun fibers with different gallic acid loadings displayed comparable gradual release trends. In our previous study,[11] we showed a rapid release performance of the loaded gallic acid from the non-heat-cured Ze-GA fiber mats that increased with an increase in gallic acid content. However, it was obvious in this study that the release performance of gallic acid was inhibited after the heat-curing process as compared to the non-heat-cured Ze-GA fibers reported in our previous studies. Figure 3 shows that, in heat-cured fiber mats, only approximately 60% release of gallic acid was detected after 6 h of immersion in water at 23 °C, while in the non-heat-cured sample the release was over 80% within 1 h. Interestingly, it was noticed that the release rate of the gallic acid decreased with the increasing content of loaded gallic acid. Heat-cured Ze-GA 5% and Ze-GA 10% demonstrated gallic acid release percentages of 53% and 48%, respectively, at the end of 2 h of immersion in water.

The zein electrospun fibers normally demonstrate excessive swelling in aqueous medium due to hydrophobic interactions among the zein molecules.[22] The morphology of the heat-cured electrospun fibers was examined after the release assay, in order to determine the effect of soaking in water. Figure 4 shows the Ze electrospun fibers after immersion in water for 6 h. The number of junction pores of the soaked Ze fiber mat was reduced, and the high surface area-to-mass ratios of the electrospun fiber mats were compromised. Figure 4b,c indicates a swollen fiber network of heat-cured Ze-GA electrospun fiber mats. The fiber diameter was found to range from 531 to 657 nm for the heat-cured and soaked Ze-GA fibers. In contrast to Ze electrospun fibers that lost the fiber structure, heat-cured Ze-GA fiber mats retained their fibrous structure after immersion in water. Figure 4c evidently shows that Ze-GA 10% maintains better fiber morphology and greater water stability as compared to Ze-GA 5%. It could be deduced that cross-linking reactions have occurred between the gallic acid reactive sites and zein protein to form linkages during the heat-curing process. The rapid release performance of gallic acid seen in non-heat-cured Ze-GA electrospun fiber mats had been decelerated in the heat-cured fibers, which might be due to the chemical bonding between gallic acid and zein after heating.

Molecular Characteristics of the Electrospun Fibers Using Gel Permeation Chromatography (GPC). Figure 5 shows the elution profile of the electrospun fiber mats in the GPC from the RI detector. The non-heat-cured electrospun fiber mats eluted from the column in one peak with a maxima at around 9 mL. A progressive shift toward smaller elution volumes was observed for the heat-cured electrospun fiber mats. These results suggest the formation of higher molecular weight components with non-heat-cured electrospun fiber mats. The relevant molecular parameters for the electrospun fiber mats are tabulated in Table 2 and include molecular mass averages, polydispersity indices (weight-average molecular weight/number-average molecular weight, M_w/M_n), and molecular radii (expressed as the root-mean-squared radius of gyration, R_g). All the electrospun fiber mats are showing polydispersity indices greater than 1.0, indicating a broad range of molecular masses. The polydispersity of the non-heat-cured electrospun fiber mats decreased with increasing gallic acid content, but variations were noted among the heat-cured electrospun fiber mats. It is important to note that both the heat-cured and non-heat-cured Ze-GA 5% fiber mats generally exhibited higher radii of gyration and molecular weight compared with the other electrospun fiber mats studied. Figure 5 shows a small peak (indicated by an arrow) eluting before the primary component of heat-cured Ze-GA 5% fiber mats, suggesting the possible formation of higher molecular weight aggregates after the heat-curing process. As a result, the heat-

dx.doi.org/10.1021/jf500841m | J. Agric. Food Chem. 2014, 62, 5163−5172

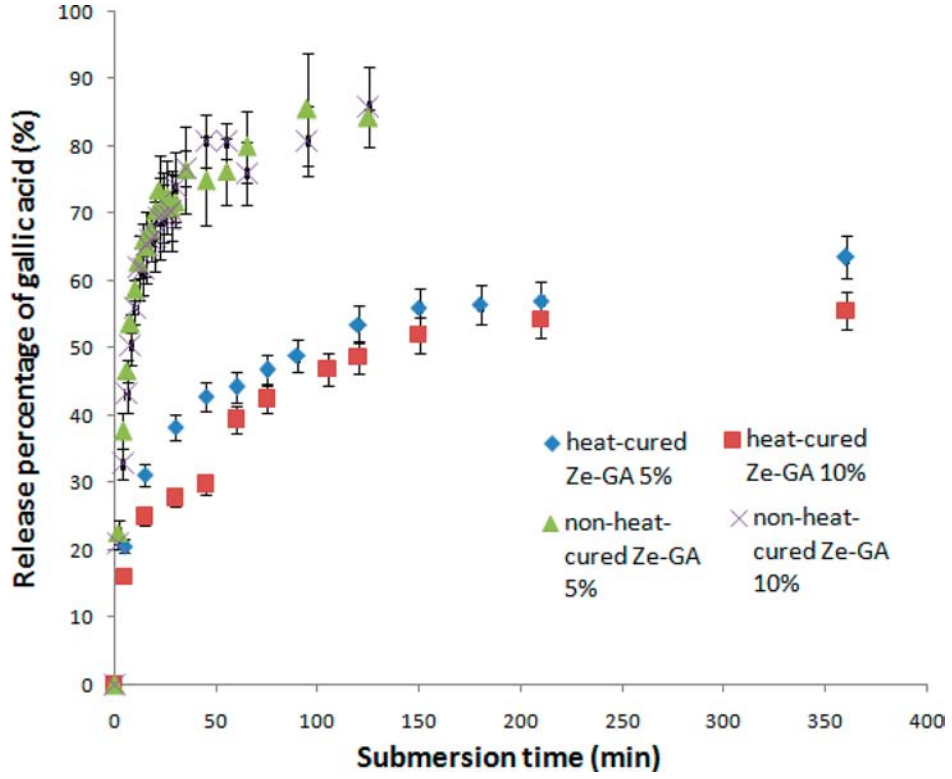

Figure 3. Release percentage of gallic acid (%) from heat-cured Ze-GA electrospun fibers in a hydrophilic model (Milli-Q water) at 23 °C over time. The release percentage of gallic acid for non-heat-cured electrospun fibers is from the previously published data (Neo et al., 2013).[11]

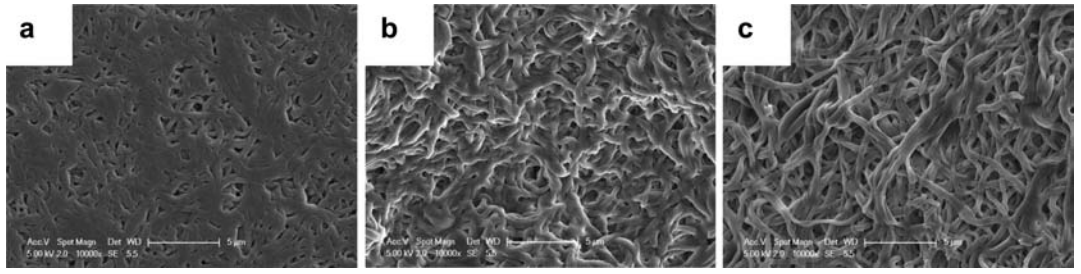

Figure 4. SEM images (at 5 μm scale bar) of Ze and heat-cured Ze-GA electrospun fibers after immersion in water for 6 h: (a) Ze, (b) Ze-GA 5%, (c) Ze-GA 10%.

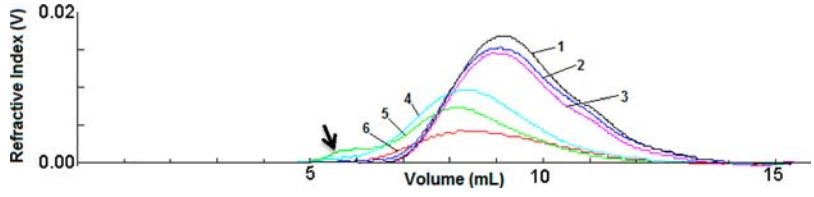

Figure 5. GPC elution profile of the electrospun fiber mats: (1) Ze, (2) Ze-GA 5%, (3) Ze-GA 10%, (4) heat-cured Ze, (5) heat-cured Ze-GA 5%, (6) heat-cured Ze-GA 10%. Arrow indicates a small peak eluting before the primary component of heat-cured Ze-GA 5% fiber mats.

cured Ze-GA 5% fiber mats exhibited the highest polydispersity and molecular weight among the electrospun fiber mats, with number-average (M_n), weight-average (M_w), and *z*-average (M_z) molecular weight of 1.497×10^6 g mol^{-1}, 6.586×10^6 g mol^{-1}, and 4.451×10^7g mol^{-1}, respectively and a polydispersity of 4.40. Interestingly, the heat-cured Ze-GA 10% shows the lowest molecular weight and also the lowest polydispersity compared with the other heat-cured fibers. This might be due to the nonstoichiometry in mixing that occurs in the Ze-GA 10% system that requires further investigation. Also shown in Table 2 are the R_g values (R_n, R_w, R_z) of the electrospun fiber mats. The radii of gyration for the non-heat-cured electrospun fiber mats ranged from 51.3 to 63.5 nm, whereas the radii of gyration for the heat-cured-electrospun fiber mats ranged from 62.6 to 67.5 nm as shown in Table 2. The nonmajor change in radii of gyration between heat-cured and non-heat-cured fibers suggested that the zein protein still exists in the globular form after the heat-curing process. Yet, the generally larger hydrodynamic radius observed in heat-cured electrospun fiber mats implies the formation of larger

dx.doi.org/10.1021/jf500841m | J. Agric. Food Chem. 2014, 62, 5163−5172

Table 2. Relevant Molecular Parameters of the Electrospun Fiber Mats[a]

	non-heat-cured			heat-cured		
params	Ze	Ze-GA 5%	Ze-GA 10%	Ze	Ze-GA 5%	Ze-GA 10%
M_n (g mol^{-1})	3.667×10^4	7.651×10^4	5.906×10^4	2.888×10^5	1.497×10^6	3.376×10^5
M_w (g mol^{-1})	7.690×10^4	1.513×10^5	7.769×10^4	7.399×10^5	6.586×10^6	5.703×10^5
M_z (g mol^{-1})	3.993×10^5	4.686×10^5	1.168×10^5	4.767×10^6	4.451×10^7	1.498×10^6
M_w/M_n (polydispersity index)	2.097 ± 0.023	1.978 ± 0.014	1.315 ± 0.010	2.562 ± 0.020	4.401 ± 0.024	1.689 ± 0.012
R_n (nm)	51.3	59.6	55.4	65.2	66.3	62.6
R_w (nm)	52.8	61.2	56.1	65.7	66.6	63.0
R_z (nm)	57.3	63.5	57.2	67.2	67.5	63.8

[a] M_n, M_w, and M_z are the abbreviations for number-average molecular weight, weight-average molecular weight, and z-average molecular weight, respectively. R_n, R_w, and R_z are the abbreviations for number-average mean square radius, weight-average mean square radius, and z-average mean square radius, respectively.

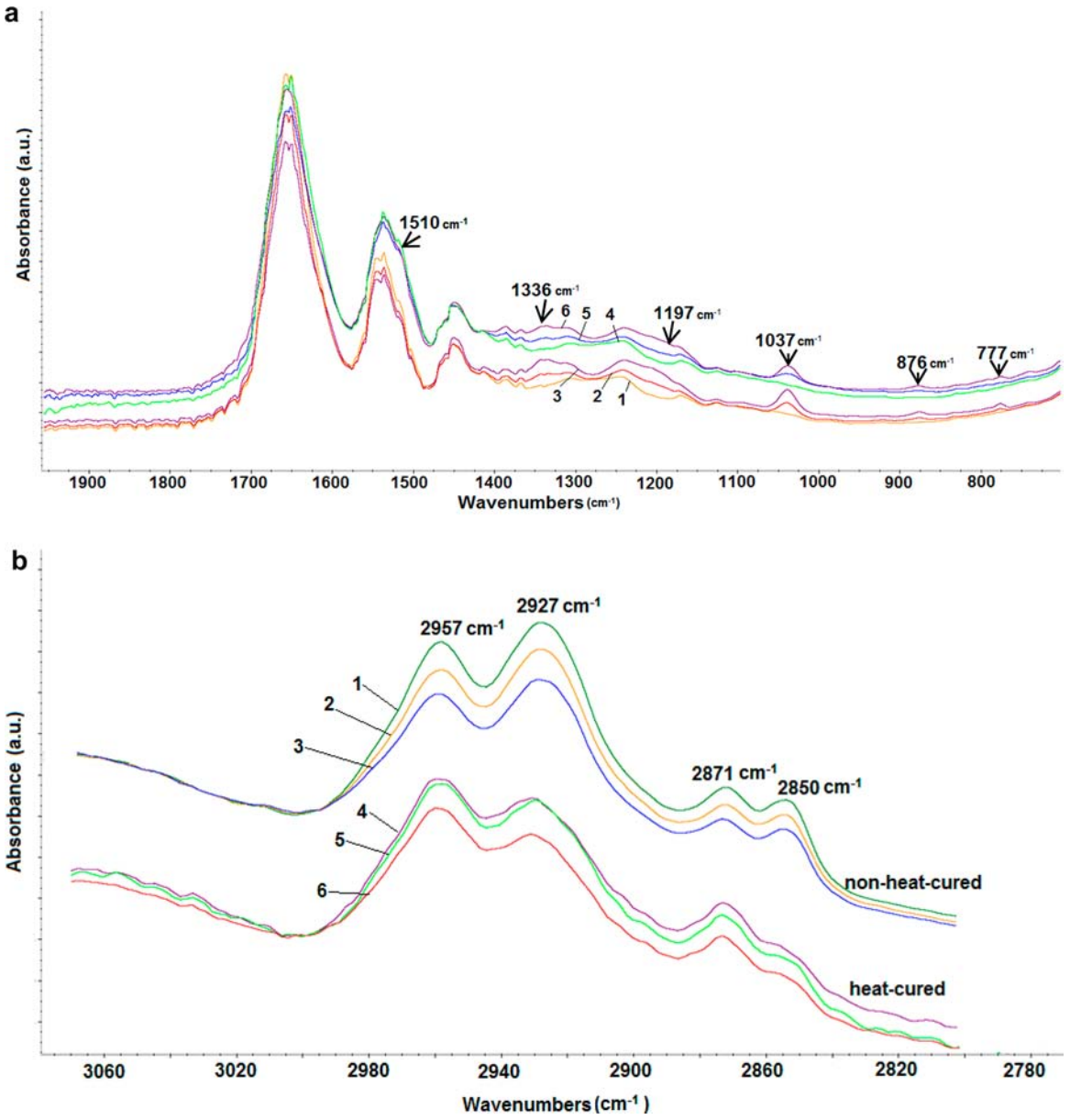

Figure 6. (a) Amide I and amide II region for the electrospun fibers; the arrow indicates the appearance of a shoulder at 1510 cm^{-1} region. (b) C−H stretching vibrations of aliphatic groups. (1) Ze, (2) Ze-GA 5%, (3) Ze-GA 10%, (4) heat-cured Ze, (5) heat-cured Ze-GA 5%, (6) heat-cured Ze-GA 10%.

aggregates or extended protein conformation by cross-linking after the heat-curing process. The chemical nature of the cross-linking process might be inferred as the formation of amide cross-links between amine and carboxyl groups as suggested by

dx.doi.org/10.1021/jf500841m | J. Agric. Food Chem. 2014, 62, 5163−5172

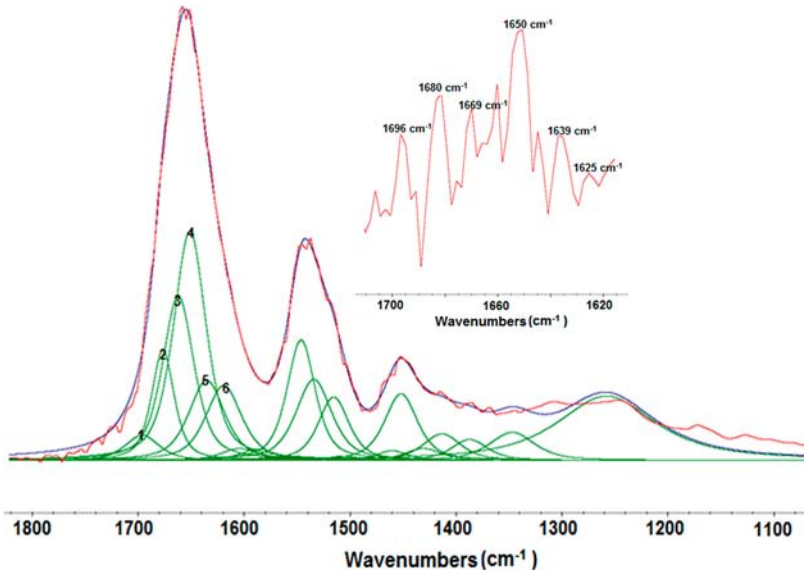

Figure 7. Curve-fitted ATR-FTIR spectra for the 1300 to 1730 cm^{-1} region for non-heat-cured Ze electrospun fiber mats. The original spectra were curve fitted based on the number of peak components and positions identified from the second derivatives. Components are numbered (1−6) for the amide I region and are given in green. Inset is the second-derivative spectrum showing the bands associated with the secondary structure of zein protein. Peaks (1) inter/anti parallel β-sheet (1696 cm^{-1}), (2) β-sheet (1680 cm^{-1}), (3) β-turn (1669 cm^{-1}), (4) α-helix (1650 cm^{-1}), (5) random coil (1639 cm^{-1}), (6) β-sheet (1625 cm^{-1}). The fits (blue) overlay the original spectra.

Gorham et al.[1] and Rombouts et al.[23] in collagen and wheat gluten. Overall, all the electrospun fiber mats have shown high molecular weight after the heat-curing process, which may imply thermal polymerization of the zein protein.

Compositional Analysis of the Electrospun Fiber Mats. Figure 6 shows the normalized ATR-FTIR spectra of the electrospun fiber mats. Compared with the Ze electrospun fibers (spectra 1 and 4), all the Ze-GA fibers (spectra 2, 3, 5, and 6) demonstrated new peaks at 1336 cm^{-1}, 1197 cm^{-1}, 1037 cm^{-1}, 876 cm^{-1}, and 777 cm^{-1}, which confirms the presence of gallic acid.[10] The heat-cured Ze-GA fibers demonstrated similar ATR-FTIR spectra to their non-heat-cured counterparts as shown in Figure 6a. However, differences in intensity for the bands of heat-cured and non-heat-cured fibers were observed in the amide II band at 1530 cm^{-1} (Figure 6a) and the CH_2 stretch modes at bands 2927 and 2850 cm^{-1} (Figure 6b). The heat-cured electrospun fibers generally showed peak shifting to near 1525 cm^{-1} from approximately 1530 cm^{-1} for the non-heat-cured fibers. Figure 6a indicates broadening of the amide II bands and the presence of a shoulder at approximately 1510 cm^{-1} (indicated by an arrow in Figure 6a). The amide II mode is predominantly an −NH bending vibration coupled to −CN stretching vibration.[24] Pelton and McLean[25] suggested that bands between 1510 and 1530 cm^{-1} indicate the presence of β-sheet structures; the shoulder at 1510 cm^{-1} in this study is thus evidence of the presence of new intermolecular bonding in the heat-cured electrospun fibers. On the other hand, significant reductions in the bands at 2927 and 2850 cm^{-1} were observed for all the heat-cured fibers as shown in Figure 6b, which are attributed to the CH_2 stretching vibrations. These results show the substantial influence of the heat-curing process on the aliphatic group of zein protein, especially the methylene groups as shown in Figure 6b. Overall, the broadening of amide II band and the loss of methylene groups implies the potential formation of new isopeptide bonding in the zein electrospun fiber mats due to heat curing.

The correlation between protein secondary structure and the frequency in the ATR-FTIR spectra for the amide II band is proposed to be less straightforward than those for the amide I vibrations.[24] Hence, analysis of the amide I region was used to further investigate the secondary structural changes upon the heat-curing process. The amide I band is mainly due to stretching vibrations of the carbonyl group, and hence represents the secondary structure of the proteins well.[3] To study the structural changes of zein, the band positions of the overlapping components corresponding to different secondary structures were determined from the secondary derivative spectra, and then fitted to the amide I band using curve fitting. The band positions of six major bands thus determined in the amide I band are shown in the inset in Figure 7. Resolution of the amide I peak into these six bands was performed using the Peak resolve curve fitting function of the OMNIC 5.0 spectroscopic software, following the method of Forato et al.[26] and Georget et al.[27] The six band components thus identified in this study were the inter/antiparallel β-sheet at 1696 cm^{-1}, β-sheet at 1680 cm^{-1}, β-turn at 1669 cm^{-1}, α-helix at 1650 cm^{-1}, random coil at 1639 cm^{-1}, and intermolecular β-sheets at 1625 cm^{-1}. Estimation of the secondary structural content was based on the band component areas as shown in Figure 7. The assigned component areas are tabulated in Table 3. All the electrospun fiber mats exhibited characteristics of α-helix rich protein that shows a strong vibrational mode at around 1650 cm^{-1}. The amount of α-helix content calculated from the ATR-FTIR spectra ranged from 34.3 to 45.1% for all the electrospun fibers. This result is in agreement with the observations of other studies that suggested α-helix content of approximately 43% in solid state zein.[26] The high content of α-helix structure in zein is generally associated with α-zein that accounts for more than 80% of total zein. Nevertheless, Table 3 shows that non-heat-cured Ze-GA fibers have higher β-turn content (22.9% and 24.6% for Ze-GA 5% and Ze-GA 10%, respectively) as compared to non-heat-cured Ze fibers (18.7%). The secondary structure content of the heat-cured Ze

dx.doi.org/10.1021/jf500841m | J. Agric. Food Chem. 2014, 62, 5163−5172

Table 3. Assignment of Components Fitted to the Amide I Region of the ATR-FTIR Spectra for the Electrospun Fiber Mats[a]

	assigned component area (%)					
	non-heat-cured			heat-cured		
component	Ze	Ze-GA 5%	Ze-GA 10%	Ze	Ze-GA 5%	Ze-GA 10%
inter/antiparallel β-sheet (1696 cm^{-1})	1.98	0.35	0.25	0	0	0.74
β-sheet (1680 cm^{-1})	12.79	14.40	13.18	14.06	14.54	14.50
β-turn (1669 cm^{-1})	18.67	22.93	24.63	22.50	20.44	17.59
α-helix (1650 cm^{-1})	39.16	34.52	35.83	34.28	42.54	45.14
random coil (1639 cm^{-1})	15.30	17.69	13.80	20.06	9.31	8.74
β-sheet (1625 cm^{-1})	12.10	10.11	12.31	9.10	13.17	13.29
total β-sheet content	26.87	24.86	25.74	23.16	27.71	28.53

[a]The amide I peak deconvolution using OMNIC 5.0 spectroscopic software was carried out according to Forato et al.[26] and Georget et al.[27]

electrospun fibers was 34.3% α-helix, 23.2% of total β-sheets, 22.5% of β-turn, and 20.1% of random coil as shown Table 3. The results exhibited a slight decrease in α-helix and β-sheet content, and a slight increase in β-turn and random coil content for heat-cured Ze compared with the non-heat-cured Ze electrospun fibers. These results suggest an increase of the "disordered phase (or lack of defined structure)" of zein protein after heat treatment, as α-helix and β-sheets are generally considered as "ordered phases", while β-turns and random coil are "disordered phases" as suggested by Oliviero et al.[28] The reduction of α-helix content after heating has also been observed in other protein films such as gelatin and wheat gluten,[12] yet it is important to note that α-helix structure in zein protein is linked by rigid structures that are generally stable.[29] The considerable changes in the α-helix content between the heat-cured and non-heat-cured fibers support this statement. Interestingly, the heat-cured Ze-GA fibers have exhibited higher α-helix content and total β-sheets content at the expense of β-turn and random coil as shown in Table 3. The random coil content of heat-cured Ze-GA fibers is 9.3% and 8.7% for Ze-GA 5% and Ze-GA 10%, respectively. The increase in β-sheet content of heat-cured Ze-GA fibers at 1696 cm^{-1}, 1680 cm^{-1}, and 1625 cm^{-1} (Table 3 and Figure 7 inset) indicates an extensive inter- and intramolecular bonding after the heat-curing process. This result corresponds well with the observation of amide II band broadening as demonstrated previously. The secondary structural component changes of the protein as determined for the electrospun fiber mats indicate the covalent cross-linking of protein during heat treatment. The results also suggest the potential of the heat-curing as a post-electrospinning treatment of proteinaceous materials as a method to modify their functional properties.

Assignment of ^{13}C Peaks. Solid-state NMR has been used to generate information related to molecules of proteins using $^{13}C-^{1}H$ cross-polarization.[30] SS-NMR chemical shifts can be used to elucidate the protein conformation since the internal rotation around the peptide bonds is usually fixed.[31] In zein, glutamine, glutamic acid, tyrosine, histidine, arginine, aspartic acid, asparagine, threonine, serine, and cysteine are the amino acids which contain potential reactive side groups.[32] It is a challenge to assign specific amino acid sites in the zein ^{13}C NMR spectrum due to line broadening and the considerable overlap of peaks. Nevertheless, the ^{13}C NMR resonances can be assigned on the basis of previous reports.[26,32,33] The solid state CPMAS spectra of the electrospun fiber mats are presented in Figure 8. Zein shows resonance signals of the carbonyl carbons,

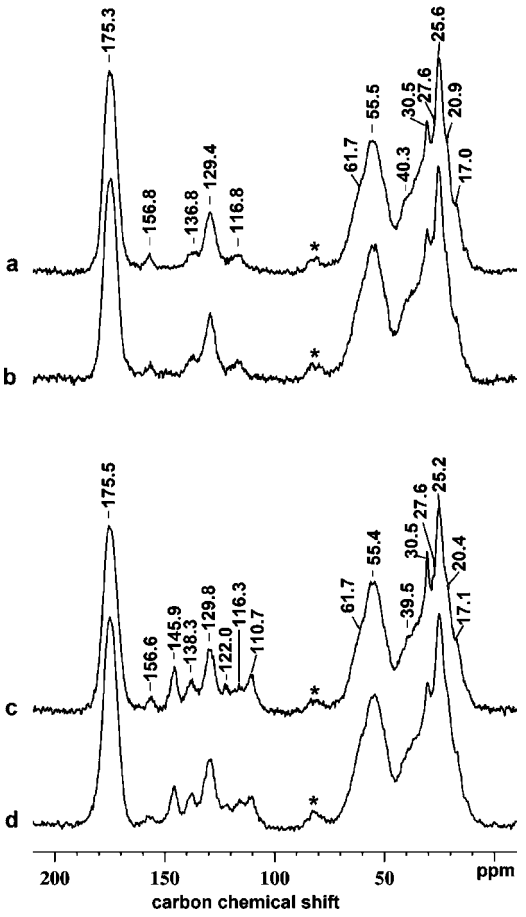

Figure 8. ^{13}C CPMAS NMR spectra of the electrospun fiber mats: (a) non-heat-cured Ze, (b) heat-cured Ze, (c) non-heat-cured Ze-GA 10%, and (d) heat-cured Ze-GA 10%. The asterisks denote spinning sidebands.

aromatic side chains, α-carbons, and carbons of the amino acid aliphatic side chains at about 175, 100 to 140, 45 to 70, and 15 to 45 ppm, respectively (Figure 8a,b), which is in accordance with the findings of Forato et al.[26] Out of the potential reactive side groups in zein suggested by Wu et al.,[32] only those from tyrosine at 156.8, 129.4, and 116.8 ppm and histidine at 136.8 ppm show relatively resolved peaks (Figure 8a,b). Figure 8c,d demonstrates that the ^{13}C NMR spectra of Ze-GA 10% fibers have exhibited new resonance signals in the aromatic carbon region between 100 to 140 ppm. This observation is in agreement with the literature that suggested ^{13}C NMR chemical shifts for gallic acid between 110 and 169 ppm.[34] The carbonyl chemical shifts at the resonance 170 to 178 ppm region are generally sensitive to the protein conformations.[26,35] The SS-NMR characteristics obtained from this region should represent the protein behavior. Figure 8 shows that all the electrospun

dx.doi.org/10.1021/jf500841m | J. Agric. Food Chem. 2014, 62, 5163−5172

fiber mats have exhibited strong resonance at 175 ppm, indicating high α-helix content that is in accordance with the ATR-FTIR peak assignments. Other than the presence of new resonance signals at the aromatic carbon region, ^{13}C NMR spectrum for non-heat-cured Ze-GA 10% also revealed changes in resonance intensity at 30.5 ppm, which indicates the resonance for amino acid aliphatic side chains (Figure 8c,d). Even though the ^{13}C NMR chemical shift spectra of the heat-cured and non-heat-cured electrospun fiber mats look similar, the relative differences observed on the resonance intensities of the electrospun fibers implied possible structural changes after the heat-curing process, which is in line with ATR-FTIR data. Specifically, the cross-polarization experiment relies on magnetization transfer from abundant (^1H) to the rare spin system (^{13}C). This process is dependent on dipolar interactions between nuclear spins making it very sensitive to structural and dynamic aspects of the local environment. Further studies using relaxation and spin-diffusion experiments will need to be conducted in the future, in order to provide information on the rigidity and the spatial distribution of microscopic domain sizes for various components in the electrospun fiber systems.

In summary, the heat-curing process has shown prominent modification on the physicochemical properties of the Ze and Ze-GA electrospun fibers. Thermal treatments had also induced color changes on the electrospun fiber mats. Interestingly, the changes increased with the increase in gallic acid content, which implied that chemical interactions had taken place between zein and gallic acid. The morphology of the heat-cured fibers was found to be flattened and the fiber diameters were enlarged and the hydrophobicity of the electrospun fiber surface was found to have increased after the heat-curing process. In addition, Ze-GA fibers showed slow but constant release of gallic acid in water over time. An improved morphological stability of Ze-GA fibers was observed after immersion in water at 23 °C for 6 h. It was also found that the molecular weight of Ze and Ze-GA fiber mats increased tremendously after the heat-curing process. Changes in the amide II bands and CH_2 stretch modes were observed in the heat-cured electrospun fiber mats as indicated by the ATR-FTIR spectra. All the electrospun fiber mats exhibited characteristic of α-helix rich protein. The α-helix and β-sheet contents of Ze-GA fibers were found to increase at the expense of β-turn and random coil after the heat-curing process. No major chemical shifts were observed among the ^{13}C NMR spectra, yet the difference in the resonance intensities among the electrospun fibers implied the presence of different chemical environment between the electrospun fiber systems before and after heat curing. Current studies provide a base for further assessment of the thermal treatment of protein based electrospun fibers. Further studies on the elucidation of Ze and Ze-GA structure are essential to complement the investigation. The new properties exhibited by the heat-cured gallic acid loaded zein electrospun fibers will offer potential to develop new protein based nanostructured electrospun fibers for food packaging or food-contact materials with enhanced properties.

AUTHOR INFORMATION

Corresponding Author

*Tel: +64 9 3737599. Fax: +64 9 3737422. E-mail: conradperera@gmail.com.

Funding

Yun Ping Neo is supported by a University of Auckland Doctoral Scholarship.

Notes

The authors declare no competing financial interest.

REFERENCES

(1) Gorham, S. D.; Light, N. D.; Diamond, A. M.; Willins, M. J.; Bailey, A. J.; Wess, T. J.; Leslie, N. J. Effect of chemical modifications on the susceptibility of collagen to proteolysis. II. Dehydrothermal crosslinking. *Int. J. Biol. Macromol.* **1992**, *14*, 129−138.

(2) Miller, K. S.; Chiang, M. T.; Krochta, J. M. Heat curing of whey protein films. *J. Food Sci.* **1997**, *62*, 1189−1193.

(3) Mangavel, C.; Barbot, J.; Popineau, Y.; Guéguen, J. Evolution of wheat gliadins conformation during film formation: A Fourier transform infrared study. *J. Agric. Food Chem.* **2001**, *49*, 867−872.

(4) Rangavajhyala, N.; Ghorpade, V.; Hanna, M. Solubility and molecular properties of heat-cured soy protein films. *J. Agric. Food Chem.* **1997**, *45*, 4204−4208.

(5) Vachon, C.; Yu, H. L.; Yefsah, R.; Alain, R.; St-Gelais, D.; Lacroix, M. Mechanical and structural properties of milk protein edible films cross-linked by heating and γ-irradiation. *J. Agric. Food Chem.* **2000**, *48*, 3202−3209.

(6) Hurrell, R. F.; Carpenter, K. J.; Sinclair, W. J.; Otterburn, M. S.; Asquith, R. S. Mechanisms of heat damage in proteins. 7. The significance lysine-containing isopeptides and of lanthionine in heated proteins. *Br. J. Nutr.* **1976**, *35*, 383−395.

(7) Shimada, K.; Cheftel, J. C. Sulfhydryl group/disulfide bond interchange reactions during heat-induced gelation of whey protein isolate. *J. Agric. Food Chem.* **1989**, *37*, 161−168.

(8) Denavi, G.; Tapia-Blácido, D. R.; Añón, M. C.; Sobral, P. J. A.; Mauri, A. N.; Menegalli, F. C. Effects of drying conditions on some physical properties of soy protein films. *J. Food Eng.* **2009**, *90*, 341−349.

(9) Neo, Y. P.; Ray, S.; Easteal, A. J.; Nikolaidis, M. G.; Quek, S. Y. Influence of solution and processing parameters towards the fabrication of electrospun zein fibers with sub-micron diameter. *J. Food Eng.* **2012**, *109*, 645−651.

(10) Neo, Y. P.; Ray, S.; Jin, J.; Gizdavic-Nikolaidis, M.; Nieuwoudt, M. K.; Liu, D.; Quek, S. Y. Encapsulation of food grade antioxidant in natural biopolymer by electrospinning technique: A physicochemical study based on zein−gallic acid system. *Food Chem.* **2013**, *136*, 1013−1021.

(11) Neo, Y. P.; Swift, S.; Ray, S.; Gizdavic-Nikolaidis, M.; Jin, J.; Perera, C. O. Evaluation of gallic acid loaded zein sub-micron electrospun fibre mats as novel active packaging materials. *Food Chem.* **2013**, *141*, 3192−3200.

(12) Bonwell, E. S.; Wetzel, D. L. Innovative FT-IR imaging of protein film secondary structure before and after heat treatment. *J. Agric. Food Chem.* **2009**, *57*, 10067−10072.

(13) Tungprapa, S.; Jangchud, I.; Supaphol, P. Release characteristics of four model drugs from drug-loaded electrospun cellulose acetate fiber mats. *Polymer* **2007**, *48*, 5030−5041.

(14) Neo, Y.-P.; Ariffin, A.; Tan, C.-P.; Tan, Y.-A. Phenolic acid analysis and antioxidant activity assessment of oil palm (E. guineensis) fruit extracts. *Food Chem.* **2010**, *122*, 353−359.

(15) Morcombe, C. R.; Zilm, K. W. Chemical shift referencing in MAS solid state NMR. *J. Magn. Reson.* **2003**, *162*, 479−486.

(16) Kim, K. M.; Weller, C. L.; Hanna, M. A.; Gennadios, A. Heat curing of soy protein films at atmospheric and sub-atmospheric conditions. *J. Food Sci.* **2002**, *67*, 708−713.

(17) Mecham, D. K.; Olcott, H. S. Effect of dry heat on proteins. *Ind. Eng. Chem.* **1947**, *39*, 1023−1027.

(18) Senoz, E.; Wool, R. P.; McChalicher, C. W. J.; Hong, C. K. Physical and chemical changes in feather keratin during pyrolysis. *Polym. Degrad. Stab.* **2012**, *97*, 297−307.

(19) Reddy, N.; Li, Y.; Yang, Y. Wet cross-linking gliadin fibers with citric acid and a quantitative relationship between cross-linking conditions and mechanical properties. *J. Agric. Food Chem.* **2008**, *57*, 90−98.

(20) Vogler, E. A. Structure and reactivity of water at biomaterial surfaces. *Adv. Colloid Interface Sci.* **1998**, *74*, 69−117.

(21) Tang, C.-H.; Xiao, M.-L.; Chen, Z.; Yang, X.-Q.; Yin, S.-W. Properties of cast films of vicilin-rich protein isolates from Phaseolus legumes: Influence of heat curing. *LWT—Food Sci. Technol.* **2009**, *42*, 1659−1666.
(22) Wang, Y.; Chen, L. Fabrication and characterization of novel assembled prolamin protein nanofabrics with improved stability, mechanical property and release profiles. *J. Mater. Chem.* **2012**, *22*, 21592−21601.
(23) Rombouts, I.; Lagrain, B.; Brunnbauer, M.; Koehler, P.; Brijs, K.; Delcour, J. A. Identification of isopeptide bonds in heat-treated wheat gluten peptides. *J. Agric. Food Chem.* **2011**, *59*, 1236−1243.
(24) Barth, A.; Zscherp, C. What vibrations tell us about proteins. *Q. Rev. Biophys.* **2002**, *35*, 369−430.
(25) Pelton, J. T.; McLean, L. R. Spectroscopic methods for analysis of protein secondary structure. *Anal. Biochem.* **2000**, *277*, 167−176.
(26) Forato, L. A.; Bicudo, T. D. C.; Colnago, L. A. Conformation of α zeins in solid state by Fourier transform IR. *Biopolymers* **2003**, *72*, 421−426.
(27) Georget, D. M. R.; Barker, S. A.; Belton, P. S. A study on maize proteins as a potential new tablet excipient. *Eur. J. Pharm. Biopharm.* **2008**, *69*, 718−726.
(28) Oliviero, M.; Verdolotti, L.; Di Maio, E.; Aurilia, M.; Iannace, S. Effect of supramolecular structures on thermoplastic zein-lignin bionanocomposites. *J. Agric. Food Chem.* **2011**, *59*, 10062−10070.
(29) Tatham, A. S.; Field, J. M.; Morris, V. J.; I'Anson, K. J.; Cardle, L.; Dufton, M. J.; Shewry, P. R. Solution conformational analysis of the alpha-zein proteins of maize. *J. Biol. Chem.* **1993**, *268*, 26253−26259.
(30) Duodu, K. G.; Tang, H.; Grant, A.; Wellner, N.; Belton, P. S.; Taylor, J. R. N. FTIR and solid state 13C NMR spectroscopy of proteins of wet cooked and popped sorghum and maize. *J. Cereal Sci.* **2001**, *33*, 261−269.
(31) Ando, I.; Kameda, T.; Asakawa, N.; Kuroki, S.; Kurosu, H. Structure of peptides and polypeptides in the solid state as elucidated by NMR chemical shift. *J. Mol. Struct.* **1998**, *441*, 213−230.
(32) Wu, Q.; Yoshino, T.; Sakabe, H.; Zhang, H.; Isobe, S. Chemical modification of zein by bifunctional polycaprolactone (PCL). *Polymer* **2003**, *44*, 3909−3919.
(33) Augustine, M. E.; Baianu, I. C. High-resolution carbon-13 nuclear magnetic resonance studies of maize proteins. *J. Cereal Sci.* **1986**, *4*, 371−378.
(34) Wawer, I.; Zielinska, A. ^{13}C-CP-MAS-NMR studies of flavonoids. I. Solid-state conformation of quercetin, quercetin 5′-sulphonic acid and some simple polyphenols. *Solid State Nucl. Magn. Reson.* **1997**, *10*, 33−38.
(35) Yoshimizu, H.; Ando, I. Conformational characterization of wool keratin and S-(carboxymethyl)kerateine in the solid state by carbon-13 CP/MAS NMR spectroscopy. *Macromolecules* **1990**, *23*, 2908−2912.

public associated with improved nutritional properties, which led to increasing demand for organic vegetables.[15] However, there is a need for better scientific data to prove whether the hypotheses like "organic tomatoes contain more health-promoting compounds" or "some tomato cultivars are more suitable for cultivation in organic conditions than others" are true. Oliveira et al.[16] have found significantly higher content of vitamin C, soluble solids, and total phenolics in organically cultivated tomato fruits. At the same time, the authors also state that the dimensions of organic fruits were smaller. Rembialkowska[17] has shown in a review article that organic plant products contain more vitamin C, phenolic compounds, and minerals (Fe, Mg, P). Similar conclusions, pointed out by Hunter et al.,[18] showed higher contents of micronutrients in organic vegetables, cereals, and legumes. The higher contents of phenolic compounds in organic agricultural crops has also been confirmed by Brandt et al.,[19] Lima and Vianello,[20] and Lairon.[21] However, opposing views have been reported by Rosen[22] and Dangour et al.,[23] according to whom there is no difference in the chemical composition of organic and conventional food. Many factors may determine the level of secondary plant metabolites, polyphenols, and antioxidants in the plant food. Some factors depend on the cultivation conditions, plant genetics, agricultural practices, meteorological factors, soil fertility, pest-related factors, harvest time, and maturity of the crops.[24]

The aim of this study was to determine the differences in polyphenols contents, antioxidant capacities, and total phenolic contents in four tomato cultivars grown in organic and conventional conditions; to get more information about the polyphenolic composition and their antioxidant capacity in fruits of tomato cultivars bred in Estonia; and to evaluate the influence of cultivars, cultivation systems, and weather conditions in the growing years.

MATERIALS AND METHODS

Plant Material. The experiment was carried out in three consecutive years (2008−2010). Plants of four tomato cultivars were grown at the Jõgeva Plant Breeding Institute (58°44′N, 26°24′E), in two unheated plastic greenhouses, one for conventional and another for organic cultivation. Greenhouses with similar size and construction were located next to each other. Soil at the site was classified as a soddy−podzolic sandy loam. Every autumn soil was fertilized with cattle manure (60 t ha^{-1}) and enriched with peat (40 t ha^{-1}) incorporated into soil. For basic fertilization, the conventional experimental area was fertilized with a compound fertilizers including 90 kg ha^{-1} N, 60 kg ha^{-1} P, and 170 kg ha^{-1} K (plus other macro- and micronutrients).The seeds were sown in the heated greenhouse in March, transplanted twice, and planted in the middle of May in unheated greenhouses in double rows, six plants per plot, three replications per cultivar in different parts of greenhouses. Substrate for conventionally cultivated seedlings and transplants was a peat-based mixture fertilized with 2 kg m^{-3} PeatCare 11−25−24 (Kemira GrowHow) and 0.5 kg m^{-3} magnesium sulfate, mixed with dolomite lime (7 kg m^{-3}). Substrate for organically cultivated seedlings and transplants was peat mixed with dolomite lime (7 kg m^{-3}) and enriched with chicken manure pellets (1 L of pellets per 50 L of peat).

During the growing period, once or twice a week the plants were irrigated through tubes installed in the soil. The conventional experimental area was fertilized with 50 kg ha^{-1} N and 60 kg ha^{-1} K. The organic experimental area was fertilized with humic acids solution (fertilizer Humistar diluted by 1:50), resulting in a total supply of 0.6 kg ha^{-1} K, and with fermented nettle infusion 1:5 three times during the growing period. Tomatoes were grown without any pesticides in the organic and conventional area. Red-ripe tomato fruits were harvested in the beginning of September. Six fruits per replication of Maike, Malle F1, and Valve and 20 fruits of Gartenfreude were harvested. Fruits equal in size and ripeness were carefully selected to form the best representative samples for each cultivar.

Four tomato cultivars, Maike, Malle F1, Valve, and Gartenfreude, were selected for the tests. The first three cultivars have been bred in Estonia, at the Jõgeva Plant Breeding Institute (registered as new cultivars in 2003, 2004, 2003, respectively). In the previous years these cultivars have shown good results in yields and disease resistance. All the cultivars are early ripening type; the first fruits ripen within 105−115 days after germination, and the ripe fruits have red color. Maike is a determinate (with limited growth) cultivar with multibranched bunch and round, smooth fruits with average weight of 60−65 g. Malle F1 is an indeterminate (with unlimited growth) cultivar with uniform, medium-sized, slightly flattened fruits weighing about 80−90 g. Valve is a semideterminate cultivar with a single or multibranched bunch and with round or slightly elongated fruits weighing about 95 g. Gartenfreude is an indeterminate, cherry-type, high-yield cultivar with round-shaped fruits that are 2 cm in diameter and of an average weight of 15−20 g.

Weather Conditions in the Years 2008−2010. In the early summer of 2008 (May, June), the weather was warm, dry, and windy with very low relative air humidity. The end of June and all of July and August were rainy and cool. September was cloudy and the total sum of active air temperature (>10 °C) was 155 °C, which is 59 °C lower than the long period average (LPA, 80 years).

In 2009, the second half of May was cold and rainy, and low temperatures (even frosts) at night did not support plant growth. The first half of June was unusually warm (over 29 °C), but the second half was cold and very rainy (120−240% of normal). In the beginning of July, the temperature varied a lot, from 29 °C at daytime to frosts at night. August was cooler and rainier than usual; inversely, September was extremely warm with a total sum of active air temperature of 329 °C (LPA, 218 °C) with little rain.

May 2010 was extraordinarily warm, but temperatures in June were below the average level. Inversely, July and half of August were extremely warm. Weather favored the plant species that require a lot of heat. In the second half of August and in September, the temperatures dropped but still remained higher than average (the total sum of active air temperature was 241 °C, which was 23 °C more than the LPA).[25]

Sample Preparation and Extraction. Organically and conventionally grown tomato fruits, three samples of each cultivar, were taken to the laboratory and kept at room temperature overnight. The next day tomato fruits were washed, dried, sliced into segments, and divided into three groups: for hot air-drying at 45 °C in a ventilated drier Binder FED 53 (Binder GmbH, Tuttlingen, Germany), homogenization, and freeze-drying for previous and further experiments. In this study, the air-dried material was ground into fine powder using a Foss Knifetec 1095 (Foss Tecator, Höganäs, Sweden) laboratory mill, passed through a sieve, and additionally ground in a mortar. Samples were extracted without hydrolysis of glycosides. For extraction, 0.5 g of tomato powder was weighed and 5 mL of 80% (v/v) aqueous methanol (Romil Ltd., Cambridge, UK) was added. The samples were placed into a Biosan Multi RS 60 (BioSan, Riga, Latvia) rotator for 5 h and left at room temperature overnight. The next day the samples were centrifuged at 20 °C at 3220*g* for 10 min using an Eppendorf 5810 R (Eppendorf AG, Hamburg, Germany) centrifuge, and supernatant was poured into another tube. The samples were re-extracted with an additional 5 mL of 80% (v/v) aqueous methanol. After centrifugation, two supernatants were mixed and filtered through a 0.45 μm syringe filter, 20 μL of (0.8 mg mL^{-1}) daidzein methanol solution as internal standard was added, and samples were stored at −40 °C prior the chromatographic analysis.

Chromatographic Analysis. Single phenolic compounds were detected, identified, and quantified using tandem liquid chromatography with diode array detection−mass spectrometry (HPLC-DAD−ESI-MS/MS) in the negative ion mode at an Agilent 1100 Series (Agilent Technologies, Santa Cruz, CA) system, consisting of a binary pump, vacuum degasser, autosampler, thermostated column department, diode array detector, and ion trap analyzer with electrospray ionization (ESI). For the separation of compounds, a reversed-phase

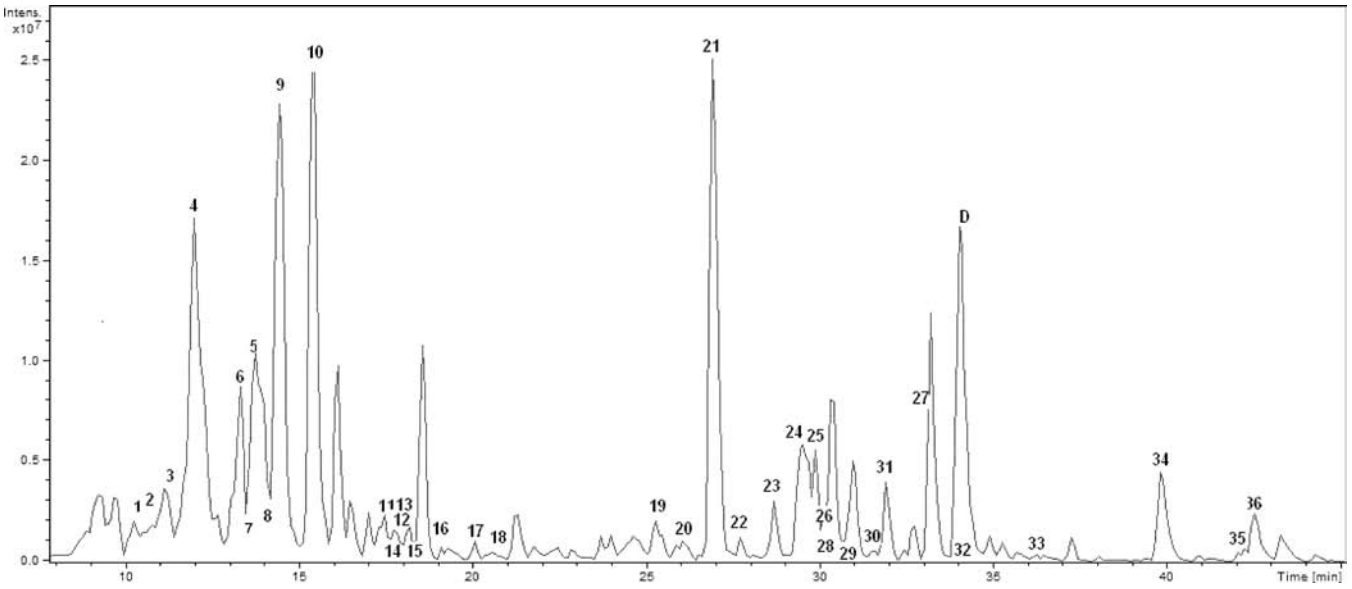

Figure 1. Phenolic compounds identified by HPLC−MS/MS in tomato fruit in negative ionization mode. MS-base peak chromatogram of the conventionally grown cultivar Gartenfreude (2010). Peak numbers designate identified compounds: **1**, **2**, **3**, **4**, and **5**, caffeic acid hexosides; **6**, homovanillic acid hexoside; **7**, caffeic acid; **8**, *p*-coumaroyl hexoside; **9**, chlorogenic (3-caffeoylquinic) acid; **10**, cryptochlorogenic (4-caffeoylquinic) acid; **11**, neochlorogenic (5-caffeoylquinic) acid; **12** and **13**, apigenin hexosides; **14**, *p*-coumaric acid; **15**, naringenin dihexoside; **16**, rutin hexoside; **17**, apigenin acetylhexoside; **18**, ferulic acid; **19**, eriodictyol hexoside; **20**, quercetin dihexoside; **21**, quercetin rutinoside (rutin); **22**, kaempferol rutinoside pentoside; **23**, phloretin dihexoside; **24**, naringenin glucoside; **25**, dicaffeoylquinic acid I; **26**, dicaffeoylquinic acid II; **27**, dicaffeoylquinic acid III; **28**, kaempferol rutinoside; **29**, naringin; **30**, caffeic acid derivative; **31**, dihydrocaffeic acid dihexoside; **32**, eriodictyol; **33**, quercetin; **34**, naringenin; **35** tricaffeoylquinic acid; **36**, naringenin chalcone; **D**, daidzein (internal standard).

(RP) Zorbax 300SB-C18 column (2.1 × 150 mm, 5 μm; Agilent Technologies) was used. The mobile phase gradient was formed of 0.1% formic acid (Fluka Chemie GmbH) (solvent A) and acetonitrile (Romil Ltd., Cambridge, UK) (solvent B), and stepwise gradient elution program was from 1% solvent B up to 28% in 1−45 min, in 45−55 min solvent B concentration was raised up to 95% and remained there for 5 min. Subsequently, the solvent B content was decreased to the initial conditions and for 13 min the column was re-equilibrated. The total run time was 73 min. The column flow was 0.3 mL min^{-1} and the thermostat was regulated at 35 °C. The injection volume of samples was 4 μL. The conditions of MS/MS detection were as follows: m/z interval, 50−1000 amu; target mass, 400 amu; number of fragmented ions, two; maximal collection time, 100 ms; compound stability, 100%; drying gas (N_2 from agenerator) speed, 10 L min^{-1}; gas temperature, 350 °C; gas pressure 30 psi; collision gas (He) pressure, 6×10^{-6} mbar. Data were collected and analyzed by an Agilent 2D ChemStation Software with a ChemStation Spectral SW module. Phenolic compounds were tentatively identified by their retention time, mass to charge ratio (m/z), UV spectra, and MS fragmentation spectra reported in the literature. Eight commercially available standards: caffeic acid, chlorogenic acid, *p*-coumaric acid, ferulic acid, rutin, naringin, quercetin, and naringenin (Sigma-Aldrich Chemie GmbH, Steinheim, Germany) were used to confirm the identification.

Determination of Total Phenolic Content. The content of total phenolics was determined spectrophotometrically with the Folin−Ciocalteau reagent (Sigma-Aldrich Chemie GmbH, Steinheim, Germany) according to the method described by Waterhouse.[26] The absorbance was measured at 765 nm using an AnalyticJena Specord 200 spectrophotometer (AnalyticJena AG). Gallic acid (Sigma-Aldrich Chemie GmbH, Steinheim, Germany) was used as the standard, and the results were expressed as gallic acid equivalent (GAE) milligrams per gram of dry matter.

Antioxidant Capacity Assay. The DPPH (2,2-diphenyl-1-picrylhydrazyl) free radical scavenging assay was performed according to the method described by Helmja et al.[27] and Lee et al.[28] with some modifications. The absorbance was measured at 515 nm using an AnalyticJena Specord 200 spectrophotometer (AnalyticJena AG). A solution of DPPH (Sigma-Aldrich Chemie GmbH, Steinheim, Germany) in methanol (23.7 mg L^{-1}) was freshly prepared, 100 μL of tested extracts was mixed with 3900 μL of DPPH solution, and the absorbance results were recorded immediately after mixing and after every 10 min during a 60 min period until a steady state of the reaction was registered. The reference cuvette (blank) contained 80% (v/v) aqueous methanol. The percentage inhibition was calculated by the formula:

$$\%\text{inhibition} = [(\text{Abs}_0 - \text{Abs}_{\text{sample,60min}})/\text{Abs}_0] \times 100$$

As a reference compound and a positive control, *tert*-butyl-1-hydroxytoluene (BHT, Sigma-Aldrich Chemie GmbH, Steinheim, Germany) was used. The results were expressed as millimole of BHT equivalents per gram of dry matter.

Statistical Analysis. Four tomato cultivars grown conventionally and organically were analyzed in triplicate. MS extracted ion chromatogram (EIC) peak areas were used in statistical analyses to compare the polyphenols contents of organically and conventionally cultivated tomato fruits. The principal component analysis was applied to find the common patterns in single phenolic compounds. Two- and three-way ANOVA was applied to test the statistical significance of cultivar, year, and cultivation method effect on single polyphenols, on the total content of polyphenols evaluated as a sum of contents of single polyphenols, and on the total phenolic content and antioxidant capacity. Pearson correlation analysis was used to estimate the relationships between single polyphenols, total phenolic content, and antioxidant capacity. All statistical analyses were conducted using R statistical software (version 2.14.1) and STATISTICA software (version 10.0). All image manipulations were done using R statistical software, open source Inkscape Vector Graphics Editor (version 0.48.3.1), and MS Excel 2010.

RESULTS AND DISCUSSION

Several previous studies have compared[29−32] qualitative characteristics in relation to different tomato cultivars and growing conditions. In our study, we focused on identified phenolic acids and flavonoids reported by Helmja et al.,[27] Moco

dx.doi.org/10.1021/jf500792k | J. Agric. Food Chem. 2014, 62, 5173−5180

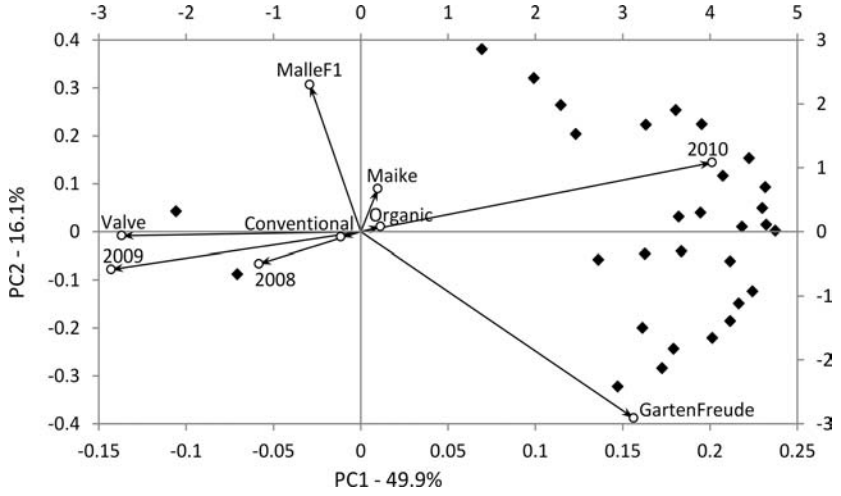

Figure 2. Principal component analysis (PCA) biplot expressing the relation of the first two principal components with polyphenols (black rhombus according to the primary axes) and average scores by cultivars, years, and cultivation methods (arrows according to the secondary axes).

et al.,[33] Martínez-Valverde et al.,[34] Gómez-Romero et al.,[3] and Slimestad and Verheul.[35] Differently, in sample preparation we did not use hydrolysis, and therefore, the main identified compounds are glycosylated. Six identified aglycons, which showed very low levels, were excluded from the statistical analysis.

Single Polyphenols. Kähkönen et al.[36] reported that synthesis of phenolic compounds in plants is greatly influenced by the internal factors like genetics, nutrients, and enzymes, as well as by the external factors like sunlight, temperature, and humidity. Since in our experiment the greenhouses were situated close to each other, the same degree of illumination, hours of daylight, temperature, and humidity for all plants could be expected.

When analyzing the chemical constitution of tomato fruits, particular attention was paid to polyphenols, which are naturally present in plants, fruits, berries, and vegetables. In tomatoes, polyphenols comprise basically phenolic acids and flavonoids, and 36 phenolic compounds (numbered peaks in Figure 1) were identified tentatively or by comparison with authentic standards. Unmarked peaks in Figure 1 may belong to other classes of compounds (e.g., amino acids, fatty acids) eluting at the same retention time as phenolic acids and flavonoids. Some compounds had several peaks or isomers that eluted at different retention times. Following the list of phenolic compounds described by Gómez-Romero et al.,[3] there were several compounds in our cultivars that we could not detect, or it was not possible to identify them by fragmentation because of their very low contents.

In our samples, phenylacetic acids were represented by homovanillic acid, and hydroxycinnamic acids that formed the main phenolic acids subgroup were represented by caffeic, chlorogenic, *p*-coumaric and caffeoylquinic acids and their derivatives. Mattila and Kumpulainen[37] reported that the most common hydroxycinnamic acid derivatives frequently occur in tomatoes as simple esters with quinic acid or glucose. Chlorogenic acids and related compounds are the main phenolic compounds besides flavonoids in tomatoes. Chlorogenic acids are good antioxidants, but they may be also responsible for a somewhat astringent taste of tomato fruits.[35]

Identified flavonoid glycosides belong to the subgroups of flavones (apigenin), flavonols (quercetin, kaempferol), flavanones (eriodictyol, naringenin), dihydrochalcones (phloretin), and chalcones (naringenin chalcone). Caffeic acid hexoside, chlorogenic acid, and quercetin rutinoside (rutin) were the main phenolic constituents in our tested tomato fruits.

Chalcones and dihydrochalcones are precursors in the flavonoids biosynthesis pathway and are widely investigated for their chemopreventive and antitumor activity,[38] but there is limited knowledge about their contents in tomatoes. In 2008, Slimestad et al.[39] described for the first time a compound representing dihydrochalcones in tomatoes, phloretin dihexoside, as dihydrochalconaringenin (phloretin) 3′,5′-di-C-*β*-glucopyranoside and confirmed the structure by NMR. A powerful antioxidant but unstable naringenin chalcone has been found in great amounts in fresh tomatoes,[39] but in our study we found quite low amounts of naringenin chalcone. Most probably, during sample drying at 50 °C and the extraction procedure this polyphenol was converted into other compounds.

Principal Component Analysis (PCA). The principal component analysis of the whole data set shows that the most common pattern in phenolic compounds reflects the differences between years (Figure 2). All detected compounds except apigenin hexosides (black rhombus on the left side of Figure 2) show the higher values for the year 2010 and lower values for 2008 and 2009. The second principal component mainly distinguishes the cultivars Malle F1 and Maike from Gartenfreude. The difference between cultivation methods is only fractional.

On the basis of the results, we need to bring out the fact that some phenolic compounds had higher concentrations only in one cultivar in all three years either in conventional or organic fruits, e.g., eriodictyol hexose in cultivar Maike organic fruits and in cultivar Valve conventional fruits. Obviously, these compounds were more influenced by cultivation mode than by weather conditions. In all three years, but only in one cultivar, Maike had four compounds with higher concentrations for the organic fruits and five compounds (out of 30) for conventionally grown fruits. Cultivar Malle F1 showed higher concentrations for 17 compounds in organic fruits and none of the compounds in the conventional fruits. Cultivar Gartenfreude had six compounds with higher concentrations in favor of the organic and four in the conventional cultivation method. Cultivar Valve had higher contents of two compounds in

dx.doi.org/10.1021/jf500792k | J. Agric. Food Chem. 2014, 62, 5173−5180

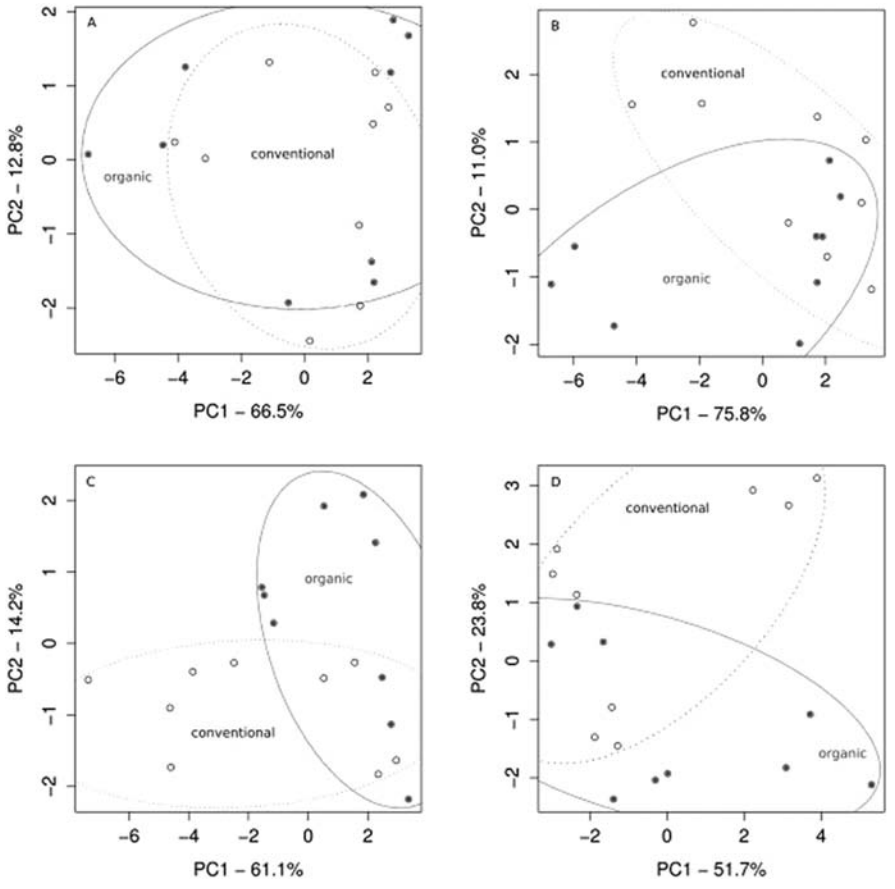

Figure 3. Biplots of principal component analysis (PCA) scores expressing the differentiation of polyphenols in organically and conventionally grown tomato cultivars: Maike (A), Malle F1 (B), Valve (C), and Gartenfreude (D).

organically grown fruits and eight compounds in conventionally grown fruits.

When the PCA was applied separately to all four studied tomato cultivars, these otherwise minor differences between cultivation methods could easily be observed (Figure 3). It is interesting to note that the effect of the cultivation method was cultivar dependent. When differences between the organic and conventionally grown Malle F1 were clearly distinguishable on the PCA biplot, the phenolic composition of cultivar Maike showed no difference.

Impact of Cultivars on the Content of Polyphenols. While using three-way ANOVA analysis we observed that the content of almost all polyphenols, except one isomer of apigenin hexoside and caffeic acid hexoside, was statistically significantly affected by cultivar ($P < 0.001$). Fruits of cultivar Gartenfreude had the highest contents of 19 compounds out of 30, while the fruits of cultivar Valve had the lowest contents of 18 compounds out of 30. The total content of polyphenols of cultivar Gartenfreude was the highest but had no statistically significant differences from Maike and Malle F1. Cultivar Valve differed from other cultivars Gartenfreude ($P < 0.001$), Maike ($P < 0.05$), and Malle F1 ($P < 0.05$), having the lowest total content of polyphenols. Martínez-Valverde et al.[34] also concluded that the concentration of various phenolic compounds as well as the antioxidant capacity was significantly influenced by the tomato cultivar.

In our study, all identified compounds were found in all tested cultivars in lower or higher amounts. It is essential to mention that in all three consecutive years and in both cultivation modes an extremely low amount of apigenin acetylhexoside was found in fruits of cultivars Gartenfreude and Valve ($P < 0.001$), compared with cultivars Maike and Malle F1. Also Gómez-Romero et al.[3] found that the presence of apigenin acetylhexoside was greatly cultivar-dependent.

Impact of the Growing Year on the Content of Polyphenols. While assessing the influence of the year we can report that the content of all polyphenols was affected by the year ($P < 0.001$). Hallmann[32] also pointed out that growing season has a large impact on the variability of content of phenolic compounds. As the weather conditions varied between the years greatly, it also impacted the content of polyphenols, and all three years were significantly different. The levels of detected compounds (except apigenin hexosides) as well as the total content of polyphenols in all cultivars were the highest in 2010 ($P < 0.001$) due to very good weather conditions in September and the lowest levels were in 2009 ($P < 0.001$), which can be explained by the cold and rainy weather during the harvesting period. Despite the fact that the growing period in 2008 was rainy and suitable for spreading gray mold, the percentage of damaged fruits in all cultivars was low. We suppose that the cultivars themselves had good resistance characteristics or the suitable concentration of phenolic compounds, with higher content in 2008 compared with year 2009.

Impact of Cultivation Method on the Content of Polyphenols. In the current study under these growing conditions the cultivation method had generally minor impact on the content of phenolic compounds (Figure 2). We found

dx.doi.org/10.1021/jf500792k | J. Agric. Food Chem. 2014, 62, 5173−5180

that some compounds had higher content in all cultivars only in one year. In 2008, the higher contents of naringenin chalcone ($P < 0.01$), naringenin glucoside ($P < 0.001$), phloretin dihexoside ($P < 0.05$), and neochlorogenic acid ($P < 0.05$) were found in all organic fruits and quercetin dihexoside ($P < 0.05$) in conventional fruits.

In 2010, the same findings were observed for caffeic acid derivative ($P < 0.05$), dihydrocaffeic acid dihexoside ($P < 0.01$), phloretin dihexoside ($P < 0.05$), apigenin acetylhexoside ($P < 0.01$), chlorogenic acid ($P < 0.05$), *p*-coumaroyl hexoside ($P < 0.05$), homovanillic acid hexoside ($P = 0.01$), caffeic acid hexoside I ($P < 0.05$). The exception is naringenin dihexoside, which was found in higher content in conventionally grown fruits ($P < 0.01$).

Considering the effects of cultivar and year with three-way ANOVA, we found that there still exist several compounds showing statistically significant differences between cultivation methods generally. We can highlight three compounds (with statistical significance $P < 0.001$), phloretin dihexoside, caffeic acid hexoside I, and apigenin acetylhexoside, whose contents were higher in the organic fruits irrespective of years and cultivars. The results are displayed as a volcano plot (Figure 4).

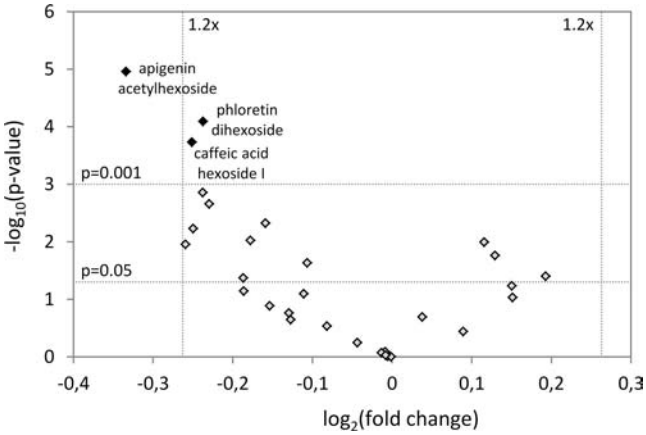

Figure 4. A volcano plot, where the *X*-axis represents the difference between organic and conventional cultivation methods and the *Y*-axis represents the statistical significance of the difference evaluated according to the three-way ANOVA considering effects of cultivar, year, and cultivation method. Every individual compound is displayed as a point. Negative values on the *X*-axis represent compounds that accumulate better under organic practices and vice versa. Statistically significantly ($P < 0.001$) different compounds are presented with names.

Comparing organic and conventional fruits of different cultivars grown in 2008−2010, organically cultivated cultivars Gartenfreude and Malle F1 had statistically significantly higher total contents of polyphenols than the organically cultivated cultivar Valve ($P < 0.01$, $P < 0.05$, respectively). Contrary, fruits of the cultivar Valve had the best results in the conventional growing system. This finding can be used in selection of tomato cultivars for cultivation systems.

Total Phenolics Content. Different methods can be used to determine the antioxidant capacity. In our study we used total phenolics assay by the Folin−Ciocalteu reagent and free radical scavenging method with DPPH. Both methods are the most frequently used techniques based on electron transfer from the antioxidant and color change of the oxidant in the reaction.[40]

The means and standard deviations of triple analysis are shown in Table 1. The total phenolic contents were the highest in conventional Gartenfreude in 2010 and the lowest in organic Maike in the same year, ranging from 5.70 to 8.54 mg GAE g^{-1} DW, respectively. Compared with others, cultivar Gartenfreude had higher content of total phenolics in all three years ($P < 0.001$). Comparing total phenolics contents in organic or conventional fruits of cultivars Maike, Gartenfreude, and Valve, there was no statistically significant difference in growing systems. Statistically higher total phenolics content was found only for cultivar Malle F1 in 2008 in conventional cultivation and in 2010 in the organic system ($P < 0.005$ and $P < 0.05$, respectively). According to the three-way ANOVA, the total phenolics contents were affected only by cultivar ($P < 0.001$).

Free Radical Scavenging Capacity. Antioxidant capacity results, presented in Table 1, show the highest DPPH radical scavenging capacity in three consecutive years ($P < 0.001$) in fruits of the cherry-type cultivar Gartenfreude. These results can be explained by the highest levels of several polyphenols and other compounds having high antioxidant capacity. None of the cultivars showed higher radical scavenging results either in organic or conventional system in all three years. Obviously, the antioxidant capacity of tomato extracts is not clearly influenced by cultivation mode, although the results were slightly in favor of the conventional cultivation. In the three year experiment, the free radical scavenging capacity depended first of all on cultivar ($P < 0.001$). The descending order of cultivars by the antioxidant capacity was again Gartenfreude, Malle F1, Maike, and Valve. Although in the organic fruits of cultivar Malle F1 17 polyphenols had higher contents in all three years, the radical scavenging tests did not confirm better results in favor of organic fruits of this cultivar. Polyphenols provide only part of the total antioxidant capacity and the remaining is the result of lycopene, vitamin C and other compounds.

Nevertheless, a strong positive correlation between total phenolics content and free radical scavenging capacity with $r = 0.80$ ($P < 0.001$) shows the leading role of polyphenols in the overall scavenging effect. The polyphenols having the strongest statistically significant ($P < 0.001$) positive correlation with free radical scavenging capacity of tomato samples were rutin hexoside ($r = 0.75$), dihydrocaffeic acid dihexoside ($r = 0.72$), eriodictyol hexoside ($r = 0.64$), homovanillic acid hexoside ($r = 0.61$), naringenin glucoside ($r = 0.59$), caffeic acid hexoside II ($r = 0.59$), phloretin dihexoside ($r = 0.53$), and dicaffeoylquinic acids ($r = 0.53$).

In summary, it was found that the growing year and cultivar had a major impact on the variations in the content of individual polyphenols, total phenolic contents, and free radical scavenging capacity of tomato fruits. The cultivation method, organic or conventional, affected some of the polyphenolic constituents of tomato fruits, but the direction of the effect was usually dependent on the cultivar. The contents of several polyphenols in single years were significantly influenced by the cultivation system. Especially three of them, apigenin acetylhexoside, phloretin dihexoside, and caffeic acid hexoside I, were positively influenced by the organic cultivation method in the fruits of all cultivars in all three years.

The results indicate that the cherry-type tomato Gartenfreude clearly differed from the other cultivars, having the highest free radical scavenging capacity, total phenolics, and several individual polyphenols contents. This phenomenon can be explained by smaller dimensions of the fruits of this cultivar

Table 1. Total Phenolics Content (mg GAE g^{-1} DW) and Antioxidant Capacity (mmol BHT equiv g^{-1} DW) of Four Tomato Cultivars Grown in Organic and Conventional Conditions in 2008−2010[a]

	Maike		Malle F1		Gartenfreude		Valve	
	organic	conventional	organic	conventional	organic	conventional	organic	conventional
2008								
total phenolics	6.17 ± 0.33	6.23 ± 0.27	6.55 ± 0.04	6.95 ± 0.09	8.06 ± 0.57	8.21 ± 0.1	6.68 ± 0.25	6.26 ± 0.19
	ns		$P < 0.005$		ns		ns	
antioxidant capacity	66 ± 6.6	67 ± 6.3	52 ± 3.9	64 ± 5.5	98 ± 3.3	101 ± 6.4	58 ± 3.3	56 ± 5.6
	ns		$P < 0.05$		ns		ns	
2009								
total phenolics	6.39 ± 0.6	6.70 ± 0.47	7.17 ± 0.39	7.44 ± 0.21	8.07 ± 0.67	7.55 ± 0.14	5.8 ± 0.45	6.8 ± 0.86
	ns		ns		ns		ns	
antioxidant capacity	47 ± 5.1	66 ± 10.6	54 ± 6.4	57 ± 2.6	81 ± 5.8	76 ± 6.1	38 ± 2.6	51 ± 8.7
	$P = 0.05$		ns		ns		ns	
2010								
total phenolics	5.7 ± 0.49	6.35 ± 0.63	7.69 ± 0.28	6.51 ± 0.47	7.15 ± 0.9	8.54 ± 0.1	6.04 ± 0.27	6.84 ± 0.47
	ns		$P < 0.05$		ns		ns	
antioxidant capacity	50 ± 12.9	48 ± 11.5	75 ± 7.5	52 ± 12.8	75 ± 6.3	86 ± 7.4	45 ± 9.7	64 ± 7.3
	ns		$P = 0.05$		ns		$P = 0.05$	

[a]ns, statistically not significant.

and accumulation of the polyphenols mainly in the peel. The cultivars Malle F1 and Gartenfreude showed higher overall polyphenols content when grown organically. These cultivars are evidently more reasonable for organic cultivation; cultivar Valve, on the contrary, is more appropriate for conventional cultivation, accumulating more phenolic compounds under these cultivation conditions. For the cultivar Maike, the weather conditions in growing years affected the chemical composition more than the cultivation method.

AUTHOR INFORMATION

Corresponding Author

*Phone +372 731 3921. Fax +372 731 3432. E-mail: dea.anton@emu.ee.

Funding

This study was supported by the Estonian Scientific Council Grant No. 9315 and European Social Fund's Doctoral Studies and Internationalization Programme DoRa, which is carried out by Foundation Archimedes.

Notes

The authors declare no competing financial interest.

REFERENCES

(1) Gülçin, I. Antioxidant activity of food constituents: An overview. *Arch. Toxicol.* **2012**, *86*, 345−391.

(2) FAOSTAT 2011; http://faostat.fao.org (accessed July 24, 2013).

(3) Gómez-Romero, M.; Segura-Carretero, A.; Fernández-Gutiérrez, A. Metabolite profiling and quantification of phenolic compounds in methanol extracts of tomato fruit. *Phytochemistry* **2010**, *71*, 1848−1864.

(4) Slimestad, R.; Verheul, M. J. Content of chalconaringenin and chlorogenic acid in cherry tomatoes is strongly reduced during postharvest ripening. *J. Agric. Food Chem.* **2005**, *53*, 7251−7256.

(5) Dixon, R. A.; Palva, N. L. Stress-induced phenylpropanoid metabolism. *Plant Cell* **1995**, *7*, 1085−1097.

(6) Manach, C.; Scalbert, A.; Morand, C.; Rémésy, C.; Jiménez, L. Polyphenols: Food sources and bioavailability. *Am. J. Clin. Nutr.* **2004**, *79*, 727−47.

(7) Krause, M.; Galensa, R. Analysis of enantiomeric flavanones in plant extracts by high-performance liquid chromatography on a cellulose triacetate based chiral stationary phase. *Chromatographia* **1991**, *32*, 69−72.

(8) Slimestad, R.; Verheul, M. Properties of chalconaringenin and rutin isolated from cherry tomatoes. *J. Agric. Food Chem.* **2011**, *59*, 3180−3185.

(9) Hunt, G. M.; Baker, E. A. Phenolic constituents of tomato fruit cuticles. *Phytochemistry* **1980**, *19*, 1415−1419.

(10) Minoggio, M.; Bramati, L.; Simonetti, P.; Gardana, C.; Iemoli, L.; Santangelo, E.; Mauri, P. L.; Spigno, P.; Soressi, G. P.; Pietta, P. G. Polyphenol pattern and antioxidant activity of different tomato lines and cultivars. *Ann. Nutr. Metab.* **2003**, *47*, 64−69.

(11) Guidi, L.; Lorefice, G.; Pardossi, A.; Malorgio, F.; Tognoni, F.; Soldatini, G. F. Growth and photosynthesis of *Lycopersicon esculentum* (L.) plants as affected by nitrogen deficiency. *Biol. Plant.* **1998**, *40*, 235−244.

(12) Miller, N. J.; Ruiz−Larrea, M. B. Flavonoids and other plant phenols in the diet: Their significance as antioxidants. *J. Nutr. Envir. Med.* **2002**, *12*, 39−51.

(13) González-Gallego, J.; Sánchez-Campos, S.; Tuñón, M. J. Anti-inflammatory properties of dietary flavonoids. *Nutr. Hosp.* **2007**, *22*, 287−293.

(14) Grassi, D.; Desideri, G.; Ferri, C. Flavonoids: Antioxidants against atherosclerosis. *Nutrients* **2010**, *2*, 889−902.

(15) Raigón, M. D.; Rodríguez-Burruezo, A.; Prohens, J. Effects of organic and conventional cultivation methods on composition of eggplant fruits. *J. Agric. Food Chem.* **2010**, *58*, 6833−6840.

(16) Oliveira, A. B.; Moura, C. F. H.; Gomes-Filho, E.; Marco, C. A.; Urban, L.; Miranda, M. R. A. The impact of organic farming on quality of tomatoes is associated to increased oxidative stress during fruit development. *PLoS One* **2013**, *8* (2), e56354.

(17) Rembiałkowska, E. Review: Quality of plant products from organic agriculture. *J. Sci. Food Agric.* **2007**, *87*, 2757−2762.

(18) Hunter, D.; Foster, M.; McArthur, J. O.; Ojha, R.; Petocz, P.; Samman, S. Evaluation of the micronutrient composition of plant foods produced by organic and conventional agricultural methods. *Crit. Rev. Food Sci. Nutr.* **2011**, *51*, 571−582.

(19) Brandt, K.; Leifert, C.; Sanderson, R.; Seal, C. J. Agroecosystem management and nutritional quality of plant foods: The case of organic fruits and vegetables. *Crit. Rev. Plant. Sci.* **2011**, *30*, 177−197.

(20) Lima, G. P. P.; Vianello, F. Review on the main differences between organic and conventional plant-based foods. *IJFST* **2011**, *46*, 1−13.

(21) Lairon, D. Nutritional quality and safety of organic food. A review. *Agron. Sustainable Dev.* **2010**, *30*, 33−41.

(22) Rosen, J. D. A review of the nutrition claims made by proponents of organic food. *Compr. Rev. Food Sci. Food Saf.* **2010**, *9*, 270−277.

(23) Dangour, A. D.; Lock, K.; Hayter, A.; Aikenhead, A.; Allen, E.; Uauy, R. Nutrition-related health effects of organic foods: A systematic review. *Am. J. Clin. Nutr.* **2010**, *92*, 203−210.
(24) Benbrook, C. *Elevating Antioxidant Levels in Food through Organic Farming and Food Processing. An Organic Center State of Science Review*; 2005; http://organic.insightd.net/reportfiles/Antioxidant_SSR.pdf; (accessed July 28, 2013).
(25) Valdmaa, U.; Keppart, L. Agricultural sector review, 2008, 2009, 2010. www.agri.ee (accessed July 10, 2013).
(26) Waterhouse, A. L. Determnation of Total Phenolics. *Current Protocols in Food Analytical Chemistry*; Wrolstad, R. E., Ed.; Wiley: New York, 2001; pp I.1.1−1.1.8.
(27) Helmja, K.; Vaher, M.; Püssa, T.; Raudsepp, P.; Kaljurand, M. Evaluation of antioxidative capability of the tomato (*Solanum lycopersicum*) skin constituents by capillary electrophoresis and high-performance liquid chromatography. *Electrophoresis* **2008**, *29*, 3980−3988.
(28) Lee, J. H.; Renita, M.; Fioritto, R. J., St; Martin, S. K.; Schwartz, S. J.; Vodovotz, Y. Isoflavone characterisation and antioxidant activity of Ohio soybeans. *J. Agric. Food Chem.* **2004**, *52*, 2647−2651.
(29) Mitchell, A. E.; Hong, Y. J.; Koh, E.; Barrett, D. M.; Bryant, D. E.; Denison, R. F.; Kaffka, S. Ten-year comparison of the influence of organic and conventional crop management practices on the content of flavonoids in tomatoes. *J. Agric. Food Chem.* **2007**, *55* (15), 6154−6159.
(30) Chassy, A. W.; Bui, L.; Renaud, E. N. C.; Van Horn, M.; Mitchell, A. E. Three-year comparison of the content of antioxidant microconstituents and several quality characteristics in organic and conventionally managed tomatoes and bell peppers. *J. Agric. Food Chem.* **2006**, *54*, 8244−8252.
(31) Caris-Veyrat, C.; Amiot, M. J.; Tyssandier, V.; Grasselly, D.; Buret, M.; Mikolajczak, M.; Guilland, J. C.; Bouteloup-Demange, C.; Borel, P. Influence of organic versus conventional agricultural practice on the antioxidant microconstituent content of tomatoes and derived purees; consequences on antioxidant plasma status in humans. *J. Agric. Food Chem.* **2004**, *52*, 6503−6509.
(32) Hallmann, E. The influence of organic and conventional cultivation systems on the nutritional value and content of bioactive compounds in selected tomato types. *J. Sci. Food Agric.* **2012**, *92*, 2840−2848.
(33) Moco, S.; Bino, R. J.; Vorst, O.; Verhoeven, H. A.; de Groot, J.; van Beek, T. A.; Vervoort, J.; Ric de Vos, C. H. A liquid chromatography−mass spectrometry-based metabolome database for tomato. *Plant Physiol.* **2006**, *141*, 1205−1218.
(34) Martínez-Valverde, I.; Periago, M. J.; Provan, G.; Chesson, A. Phenolic compounds, lycopene and antioxidant activity in commercial varieties of tomato (*Lycopersicum esculentum*). *J. Sci. Food Agric.* **2002**, *82*, 323−330.
(35) Slimestad, R.; Verheul, M. Review of flavonoids and other phenolics from fruits of different tomato (*Lycopersicon esculentum* Mill.) cultivars. *J. Sci. Food Agric.* **2009**, *89*, 1255−1270.
(36) Kähkonen, M. P.; Hopia, A. I.; Vuorela, H. J.; Rauha, J. P.; Pihlaja, K.; Kujala, T. S.; Heinonen, M. Antioxidant activity of plant extracts containing phenolic compounds. *J. Agric. Food Chem.* **1999**, *47*, 3954−3962.
(37) Mattila, P.; Kumpulainen, J. Determination of free and total phenolic acids in plant-derived foods by HPLC with diode-array detection. *J. Agric. Food Chem.* **2002**, *50*, 3660−3667.
(38) Szliszka, E.; Czuba, Z. P.; Mazur, B.; Paradysz, A.; Krol, W. Chalcones and dihydrochalcones augment TRAIL-mediated apoptosis in prostate cancer cells. *Molecules* **2010**, *15*, 5336−5353.
(39) Slimestad, R.; Fossen, T.; Verheul, M. J. The flavonoids of tomatoes. *J. Agric. Food Chem.* **2008**, *56*, 2436−2441.
(40) Huang, D.; Ou, B.; Prior, R. L. The chemistry behind antioxidant capacity assays. *J. Agric. Food Chem.* **2005**, *53*, 1841−1856.

Table 1. Oligonucleotide Primers Used in This Study

primer	sequence[a] (5′−3′)
NAGF	TCCGCTATTGATTGCAATTGAYCARGARAAYG
NAGR	TTYGTRAARGGACCCGTACCTCTGTGATG
NAG5′GSP	ATCGCTACGTTTCTCGCTGCTGT
NAG5′NGSP	CGCCCCCAGCGCCATGTTGCC
NAG3′GSP	ATGGGCCTGGCTCAAGTTGAAG
NAG3′NGSP	AGGCTATCAACGAGGAAAAGTTG
NAGBamHF	TAATCGCGGATCCACGGTCGGTAACGATGACAATCTAGAC
NAGNotR	ATAAGAATGCGGCCGCAAAGTGACCAAGGCGGTAACTTCTC

[a]R = A/G, Y = C/T; restriction sites incorporated into the primers are underlined.

Restriction endonucleases and DNA polymerase LA *Taq* were purchased from TaKaRa Corporation (Japan). DNA polymerase *Pfu* was obtained from Promega (Madison, WI). T4 DNA ligase was purchased from New England Biolabs (Ipswich, MA). *p*-Nitrophenol (*p*NP), *p*-nitrophenyl *β*-gluopyranoside (*p*NP-Glu), *p*-nitrophenyl *β*-galactopyranoside (*p*NP-Gal), *p*-nitrophenyl *β*-*N*-acetylglucosaminide (*p*NP-GlcNAc), and *p*-nitrophenyl *β*-*N*-acetylgalactosaminide (*p*NP-GalNAc) were obtained from Sigma Chemical Co. (St. Louis, MO). All other chemicals used in this study were of analytical grade unless otherwise stated.

Cloning of Full-Length cDNA of a GlcNAcase and Sequence Analysis. DNA manipulations were performed as described by Sambrook and Russell.[30] Genomic DNA was isolated from *R. miehei* CAU432 mycelia by the CTAB method.[31] Total RNA was isolated by use of the Trizol kit (Invitrogen, Carlsbad, CA), and mRNAs were purified by use of the Oligotex mRNA midi kit (Qiagen, Germany). For mycelia collection, *R. miehei* CAU432 was cultivated at 50 °C for 2 days in the medium containing (grams per liter) glucose 10, tryptone 10, yeast extract 10, $MgSO_4·7H_2O$ 0.3, $FeSO_4$ 0.3, and $CaCl_2$ 0.3, and then the fungal mycelia were collected by centrifugation (5000*g*, 10 min) and washed twice with sterilized water at 4 °C.

Genomic DNA of *R. miehei* CAU432 was used as template for subsequent polymerase chain reaction (PCR) amplification. To clone the GlcNAcase gene, degenerate primers NAGF and NAGR (Table 1) were designed on the basis of conserved amino acid sequences IAVDQENG and KHFPGHGDT derived from other known GH family 3 GlcNAcases' sequences by use of the CODEHOP algorithm.[32] PCR conditions were as follows: a hot start at 94 °C for 5 min; 20 cycles of 94 °C for 30 s, 65−45 °C for 30 s, and 72 °C for 1 min; followed by 20 cycles of 94 °C for 30 s, 55 °C for 30 s, and 72 °C for 1 min. Target amplifications were TA cloned into pMD18-T vector and sequenced.

On the basis of partial sequence information, the SMART RACE cDNA amplification kit (Clontech) was used to clone both 5′ and 3′ ends of the cDNA. For the 5′ RACE, the PCR was performed with primers NAG5′GSP and UPM, which was followed by a nested PCR using nested gene-specific primer NAG5′NGSP and NUP (Table 1). For the 3′ RACE, primers NAG3′GSP and UPM were used, followed by a nested PCR using the nested gene-specific primer NAG3′NGSP and NUP (Table 1). The PCR conditions for RACE were as follows: a hot start at 94 °C for 5 min; followed by 30 cycles of 30 s at 94 °C, 30 s at 60 °C, and 1 min at 72 °C; and finally 10 min at 72 °C. All products were purified, TA cloned, and sequenced. Compiled nucleotide sequences were subjected to BLAST analysis. The GlcNAcase (RmNag) cDNA sequence from *R. miehei* CAU432 was deposited in the GenBank nucleotide sequence database under accession number KC357713.

Nucleotide sequence and its deduced amino acid sequence were analyzed by use of DNAMAN 6.0 software (LynnonBiosoft). Protein sequence was analyzed by SignalP 4.0 server (http://www.cbs.dtu.dk/services/SignalP/) and Motif Scan (http://myhits.isb-sib.ch/cgi-bin/motif_scan). BLAST analysis was performed at NCBI server (http://blast.ncbi.nlm.nih.gov/Blast.cgi). Amino acid sequence alignment was performed by use of the ClustalW2.0 program (http://www.ebi.ac.uk/Tools/clustalw2/index.html).

Heterologous Expression of GlcNAcase Gene in *E. coli*. The amplified gene (*RmNag*) products were digested with *Bam*HI and *Not*I. The resulting fragments were cloned into *Bam*HI/*Not*I-digested pET28a(+) expression vector, and the recombinant plasmids were transformed into *E. coli* BL21(DE3) for protein expression. *E. coli* BL21(DE3) cells transformed with *RmNag* were inoculated into LB medium (containing 50 *μ*g/mL kanamycin) and cultured at 37 °C on a rotary shaker (200 rpm) until the optical density OD_{600} reached about 0.8−1.0. Then isopropyl *β*-D-thiogalactopyranoside (IPTG) was added to the culture to a final concentration of 1 mM, and the culture was continuously grown at 30 °C for 12 h.

Purification of Recombinant GlcNAcase. The cells were centrifuged, suspended in 50 mM phosphate buffer (pH 7.4), and disrupted by ultrasonication. Cell debris was removed by centrifugation at 10000*g* for 10 min. The supernatant was loaded onto a nickel−iminodiacetic acid (Ni-IDA) column (1× 5 cm) (GE Life Sciences) pre-equilibrated with 50 mM phosphate buffer (pH 7.4) containing 500 mM NaCl and 20 mM imidazole. The bonded proteins were then eluted by 50 mM phosphate buffer (pH 7.4) containing 500 mM NaCl and 50 mM imidazole, followed by 50 mM phosphate buffer (pH 7.4) containing 500 mM NaCl and 200 mM imidazole at a flow rate of 1 mL/min. The fractions were monitored by enzyme activity assay, and the purity of enzyme was checked by sodium dodecyl sulfate−polyacrylamide gel electrophoresis (SDS−PAGE). The purified GlcNAcase (RmNag) was used for further studies.

Enzyme Assay and Protein Determination. GlcNAcase activity was determined spectrophotometrically with *p*NP-GlcNAc as the substrate. A 200 *μ*L assay mixture containing 50 *μ*L of enzyme solution, 100 *μ*L of *p*NP-GlcNAc (2 mM), and 50 *μ*L of 200 mM phosphate buffer (pH 6.5) was incubated at 50 °C for 10 min. The reaction was terminated by the addition of 200 *μ*L of 0.5 M NaOH solution, and then the amount of *p*NP released was determined by measuring the absorbance at 410 nm. One unit of enzyme activity was defined as the amount of enzyme required to liberate 1 *μ*mol of *p*NP/min under the assay conditions.

Protein concentration was determined by Lowry method[33] with bovine serum albumin (BSA) as the standard. Specific activity was expressed as units per milligram of protein.

SDS−PAGE and Molecular Mass Determination. SDS−PAGE was performed according to the method of Laemmli et al.[34] with 12.5% (w/v) separating gel and 4.5% stacking gel. Protein bands were visualized by Coomassie brilliant blue R-250 staining. The molecular mass of the GlcNAcase was calibrated by use of a low molecular weight calibration kit (TakaRa, Japan) containing phosphorylase *b* (97.0 kDa), bovine serum albumin (66.0 kDa), ovalbumin (45.0 kDa), carbonic anhydrase (30.0 kDa), trypsin inhibitor (20.1 kDa), and *α*-lactalbumin (14.4 kDa).

The native molecular mass of the purified RmNag was determined on a Superdex-300 (GE Life Science) gel-filtration column (1.0 × 40 cm). The purified enzyme was loaded onto the column and eluted with 20 mM phosphate buffer (pH 6.5) at a flow rate of 0.3 mL/min. The calibration standard proteins used were catalase (247.0 kDa), alcohol dehydrogenase (150.0 kDa), phosphorylase *b* (97.2 kDa), fetuin (from fetal calf serum, 68.0 kDa), and albumin (from chicken egg white, 45.0 kDa).

Effect of pH and Temperature on Activity and Stability of Purified GlcNAcase. The effect of pH on the enzyme activity was determined in different buffers (50 mM) within pH 4.5−10.5. The buffers used were citrate (pH 4.5−6.0), 2-(*N*-morpholino)-ethanesulfonic acid (MES) (pH 5.5−6.5), phosphate (pH 6.0−8.0),

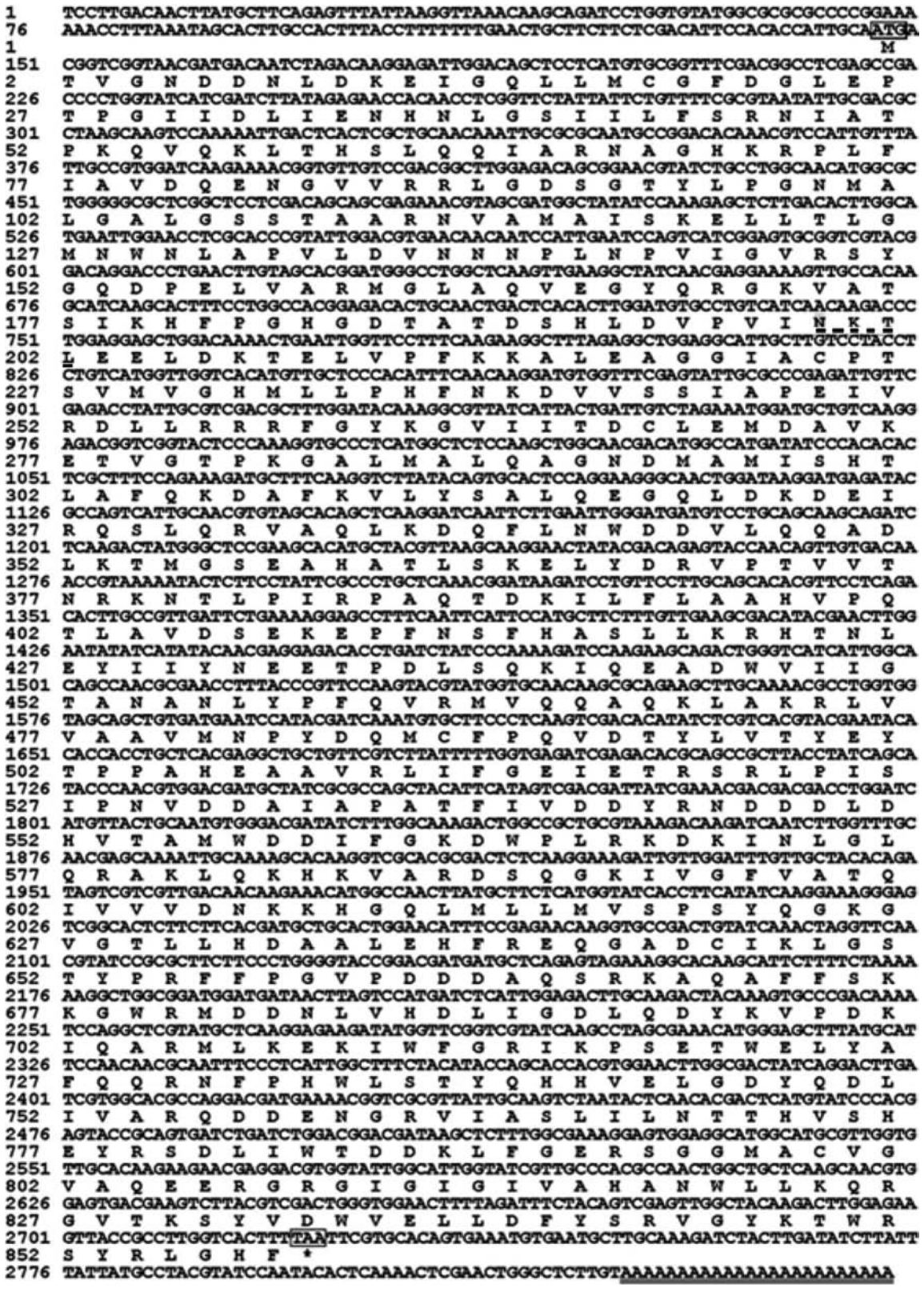

Figure 1. Nucleotide and deduced amino acid sequences of GlcNAcase (RmNag) from *R. miehei* containing the ORF and 5′ and 3′ flanking regions. The translational initiation codon ATG is boxed in frame. The termination codon, TAA, is boxed and marked by an asterisk (*). A poly(A+) tail is double-underlined. The N-linked glycosylation site is marked by a dotted line.

Tris-HCl (pH 7.5−9.0), and glycine−NaOH (8.5−10.5). For pH stability, the purified enzyme was incubated in different buffers mentioned above at 30 °C for 30 min, and the residual activities were measured at 50 °C in 50 mM phosphate buffer (pH 6.5).

The optimal temperature of RmNag was examined in the temperature range 25−65 °C in 50 mM phosphate buffers (pH 6.5). To determine the thermostability, the enzyme was incubated at different temperatures for 30 min, and the residual activities were measured at 50 °C in 50 mM phosphate

dx.doi.org/10.1021/jf500912b | J. Agric. Food Chem. 2014, 62, 5181−5190

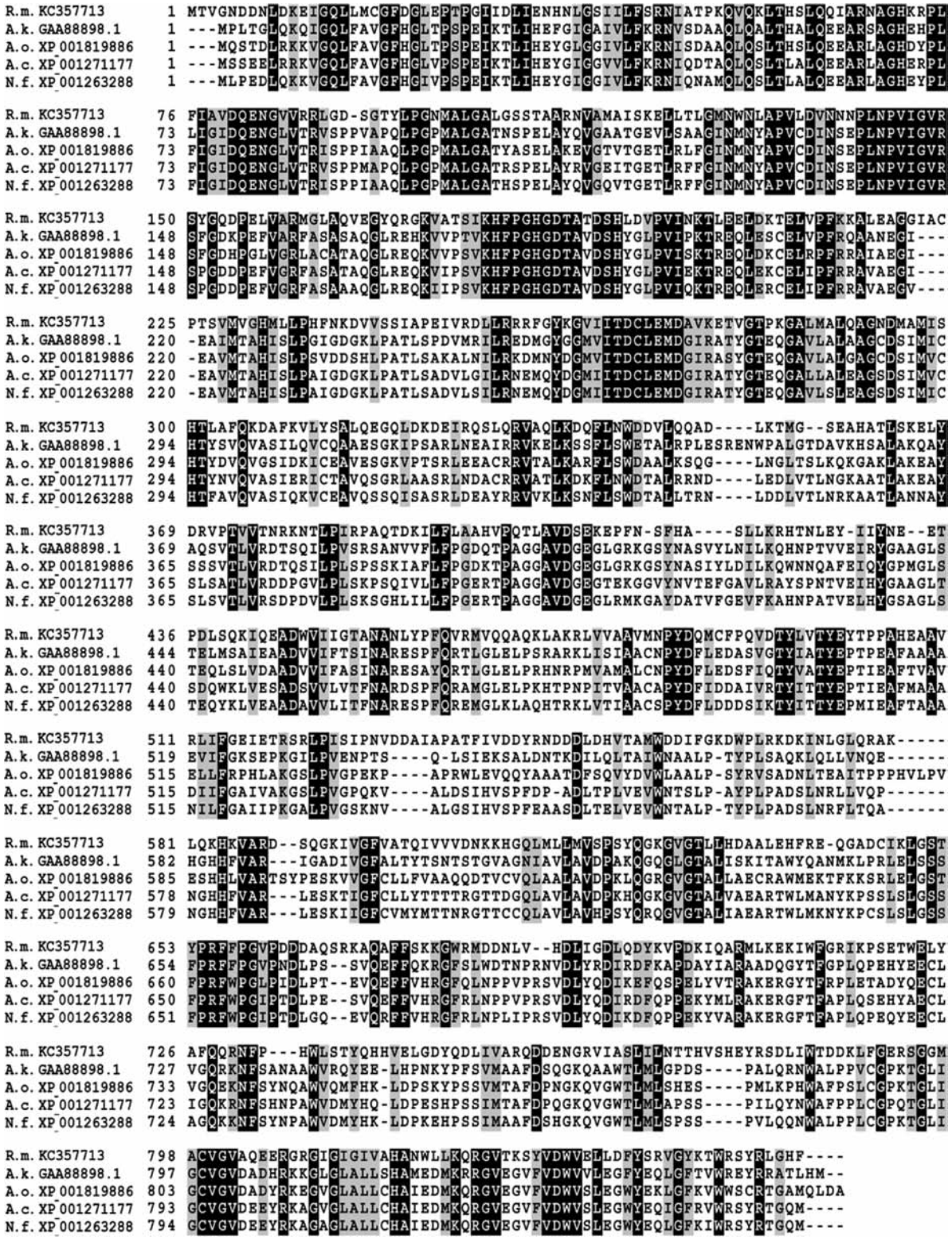

Figure 2. Multiple alignment of amino acid sequences for RmNag and other putative fungal GlcNAcases. Numbers on the left are the residue numbers of the first amino acid in each line. Abbreviations and accession numbers of those GlcNAcases are as follows: *Rhizomucor miehei* CAU432 (R.m. KC357713), *Rhizopus delemar* RA 99-880 (R.d. EIE86479), *Aspergillus kawachii* IFO 4308 (A.k. GAA88898.1), *Aspergillus oryzae* RIB40 (A.o. XP_001819886.2), *Aspergillus clavatus* NRRL 1 (A.c. XP_001271177.1), and *Neosartorya fischeri* NRRL 181 (N.f. XP_001263288.1). Identical residues are shaded in black and conserved residues are shaded in gray.

buffer (pH 6.5). For thermal denaturing half-lives of RmNag, the enzyme was incubated at different temperatures (40, 45, and 50 °C) for 4 h, and then the residual activities of the samples withdrawn at different time intervals were measured in 50 mM phosphate buffer (pH 6.5) at 50 °C.

The effect of metal ions and agents on GlcNAcase activity was determined by incubating the enzyme in 50 mM phosphate buffer (pH 6.5) with various metal ions and reagents (1 mM) at 30 °C for 30 min. The residual activities were then measured by standard enzyme assay.

Substrate Specificity and Kinetic Parameters. The substrate specificity of RmNag was determined by measuring the enzyme activity with various substrates including polysaccharides (1% w/v) such as chitin, chitosan, barley glucan, lichenin, laminarin, carboxymethylcellulose, birchwood xylan, and pullulan; *N*-acetyl chitooligosaccharides (1% w/v) with degrees of polymerization (DP) of 2−5; and *p*NP derivatives (1 mM) such as *p*NP-Gal, *p*NP-Glu, and *p*NP-GalNAG in 50 mM phosphate buffer (pH 6.5) at 50 °C for 10 min. The released reducing sugars from polysaccharides were determined by the dinitrosalicylic acid (DNS) method[35] with glucose as the standard. The released GlcNAc from *N*-acetyl chitooligosaccharides was estimated by HPLC on an Agilent series 1200 system (Agilent) equipped with a Cosmosil column. The oven temperature was set at 45 °C, and acetonitrile/water (3:1) solution was used as mobile phase (1 mL/min). The released *p*NP was measured at 410 nm. One unit of enzyme activity was defined as the amount of enzyme required to release 1 μmol of reducing sugar or GlcNAc or *p*NP per minute under the above conditions.

The kinetic parameters of RmNag toward *p*NP-GlcNAc were determined by measuring the enzyme activities with different substrate concentrations in 50 mM sodium phosphate buffer (pH 6.5). The constant kinetic parameters of K_m and V_{max} were calculated by use of GraFit software.

Hydrolytic Property of Purified GlcNAcase. Hydrolysis of *N*-acetyl chitooligosaccharides $(GlcNAc)_{2-5}$ by the purified RmNag was performed by incubating 1 mL of 1% (w/v) various substrates dissolved in 50 mM phosphate buffer (pH 6.5) with 2 units of purified enzyme at 30 °C for 4 h. Samples were withdrawn at different time intervals, terminated by boiling for 5 min, and then qualitatively analyzed by thin-layer chromatography (TLC). For TLC analysis, samples (2 μL) were applied to a Merck silica gel 60 plate with *n*-butyl alcohol/acetate/water (2:1:1 v/v/v) as developing solution. The plate was first sprayed with solution I [12.5% (w/v) KOH dissolved in ethanol and 1% (v/v) acetyl acetone dissolved in *n*-butyl alcohol at a ratio of 1:20 (v/v)] and dried, then sprayed with solution II [3.33% (w/v) dimethylaminobenzaldehyde dissolved in a solution of ethanol/HCl/1-butanol (6:6:1 v/v/v)]. The compounds separated on the TLC plate were visualized by heating at 130 °C for a few minutes.

Tolerance of Purified GlcNAcase to GlcNAc. The extent of GlcNAc inhibition on GlcNAcase activity was determined by incubation of 50 μL of enzyme solution, 100 μL of *p*NP-GlcNAc prepared in distilled water, 50 μL of 200 mM phosphate buffer (pH 6.5), and various amounts of GlcNAc with a final concentration of 1−20 mM at 50 °C for 10 min. Then the GlcNAcase activities were determined according to the standard enzyme assay. K_i was calculated by nonlinear regression fit of Michaelis−Menten with GraphPad Prism software.

RESULTS

Cloning of GlcNAcase Gene from *R. miehei*. A partial gene fragment was obtained by PCR with degenerate primers NAGF and NAGR (Table 1). Complete cDNA sequence of the GlcNAcase (designated as RmNag) was obtained by the rapid amplification of complementary DNA ends (RACE) method. The 2849-bp RmNag cDNA sequence contains an open reading frame (ORF) of 2577 bp encoding 858 amino acids, a 146-bp 5′ untranslated region (UTR), and a 126-bp 3′ UTR, and no intron was found in the coding region (Figure 1). The mature protein has a predicted molecular mass of 96.1 kDa and a theoretical p*I* of 6.73. No potential signal peptide was detected in the *N*-terminal region of the gene. One potential N-glycosylation site was identified in the amino acid sequence of the mature protein at residues 199−202. The RmNag cDNA sequence has been submitted to NCBI GenBank under accession number KC357713.

RmNag showed low similarities to those of putative GH family 3 GlcNAcases from fungi, such as *Aspergillus clavatus* NRRL 1 (37%, XP_001271177.1), *Neosartorya fischeri* NRRL 181 (37%, XP_001263288.1), *Aspergillus kawachii* IFO 4308 (36%, GAA88898.1) and *Aspergillus oryzae* RIB40 (35%, XP_001819886.2), and very low similarities to those of other known bacterial GlcNAcases. Multiple sequence alignment of RmNag with other GH family 3 GlcNAcases in the GenBank database is indicated in Figure 2. A typical amino acid sequence, KHFPGHGDTxxDSH, that is highly conserved among GH family 3 GlcNAcases[19] was found in RmNag.

Expression and Purification of Recombinant RmNag. The RmNag gene was successfully expressed in *E. coli* BL21 as a soluble intracellular enzyme. The recombinant RmNag was purified to apparent homogeneity by Ni-IDA chromatography with purification of 7.9-fold and recovery yield of 45.8% (Table 2).

Table 2. Purification Summary for Recombinant GlcNAcase (RmNag) from *R. miehei*

purification step	total activity[a] (units)	protein (mg)	specific activity (units/mg)	purification factor (*x*-fold)	recovery (%)
culture supernatant	278.6	103.2	2.7	1	100
Ni-IDA agarose	127.6	6.0	21.2	7.9	45.8

[a]Enzyme reactions were carried out at 50 °C in 50 mM phosphate buffer (pH 6.5) for 10 min.

The specific activity of the enzyme increased from 2.7 to 21.2 units/mg (Table 2). The molecular mass of the purified RmNag was determined to be 96 kDa on SDS−PAGE (Figure 3) while

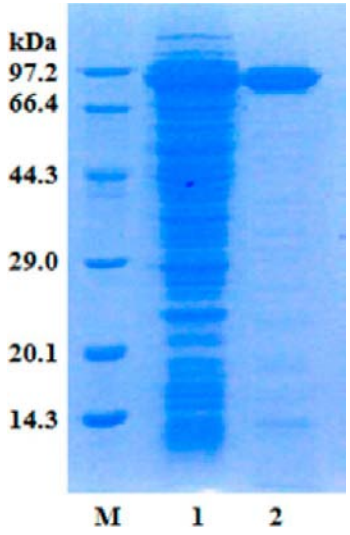

Figure 3. SDS−PAGE analysis of proteins during the purification process of recombinant GlcNAcase (RmNag) from *R. miehei*. Lane M, low molecular mass standard proteins; lane 1, crude enzyme; lane 2, after Ni-IDA column.

determined to be 200.8 kDa by Superdex-300 gel-filtration chromatography (data not shown), indicating that the enzyme was a homodimer.

Effect of pH and Temperature on Enzyme Activity and Stability of RmNag. The optimal pH of RmNag was found to be pH 6.5 in 50 mM phosphate buffer (Figure 4A). At pH 6.0−7.0, the enzyme showed relatively high activity, with more than 80% of the maximum activity retained, while a rapid decline was observed at pH below 5.5 or above 7.5 (Figure 4A). The enzyme was stable in the pH range 6.0−8.0, since more than 80% enzyme activity was remained after 30 min incubation in various buffers

dx.doi.org/10.1021/jf500912b | J. Agric. Food Chem. 2014, 62, 5181−5190

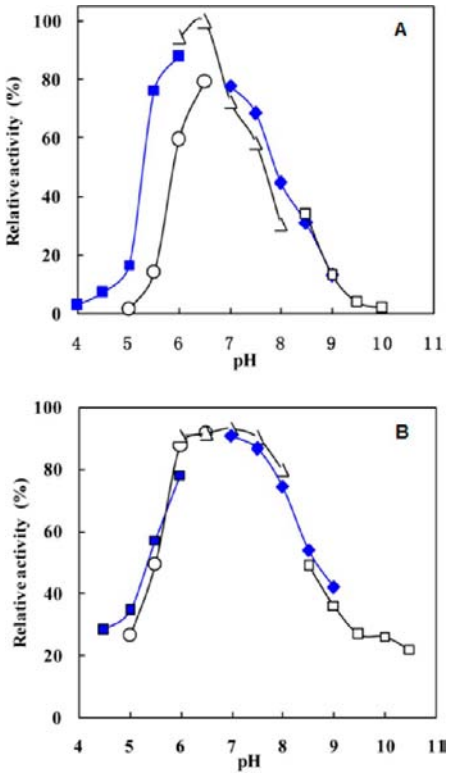

Figure 4. (A) Optimal pH and (B) pH stability of purified RmNag. The influence of pH on GlcNAcase activity was determined at 50 °C with 50 mM different buffers. Residual activities were measured after the enzyme was incubated at 30 °C for 30 min over various pH ranges. Buffers used: (■) citrate, (●) MES, (▲) phosphate, (◆) Tris-HCl, and (□) glycine−NaOH.

(Figure 4B). RmNag was most active at 50 °C and showed a relatively wide range of optimal temperature at 40−55 °C, having more than 80% of its maximum activity (Figure 5A). The enzyme was stable up to 45 °C, as more than 90% of its activity was retained (Figure 5B). The thermal denaturing half-lives of RmNag at 40, 45, and 50 °C were determined to be 1190, 494, and 42 min, respectively (Figure 5C). The enzyme activity was markedly inhibited by more than 30% in the presence of 1 mM Ag^{+}, Cu^{2+}, Zn^{2+}, Co^{2+}, Hg^{2+}, and SDS, while no obvious effect was observed for Ba^{2+}, K^{+}, Na^{+}, and some other metal ions (Table 3).

Substrate Specificity and Kinetic Parameters of Purified RmNag. The specificity of RmNag for various substrates is presented in Table 4. Among the tested chromogenic substrates, RmNag efficiently hydrolyzed only *p*NP-GlcNAc, with specific activity of 21.2 units/mg, and could hardly hydrolyze *p*NP-GalNAc (0.2 unit/mg). The enzyme showed no activity on the tested polysaccharides. Among the tested *N*-acetyl chitooligosaccharides, RmNag exhibited the highest activity toward $(GlcNAc)_3$, followed by $(GlcNAc)_2$, $(GlcNAc)_4$, and $(GlcNAc)_5$ (Table 4).

The Michaelis−Menten constant K_m and V_{max} values of RmNag toward *p*NP-GlcNAc were determined to be 0.13 mM and 49.3 μmol·min^{-1}·mg^{-1}, respectively.

Hydrolytic Properties of Purified RmNag on *N*-acetyl Chitooligosaccharides. The hydrolytic pattern of RmNag on *N*-acetyl chitooligosaccharides was analyzed by TLC (Figure 6). It can be seen that RmNag efficiently hydrolyzed all chitin oligomers tested (DP 2−5), yielding GlcNAc as the end product, and in the hydrolysis process, the enzyme cleaves one GlcNAc at a time until all the intermediates were converted to GlcNAc (Figure 6).

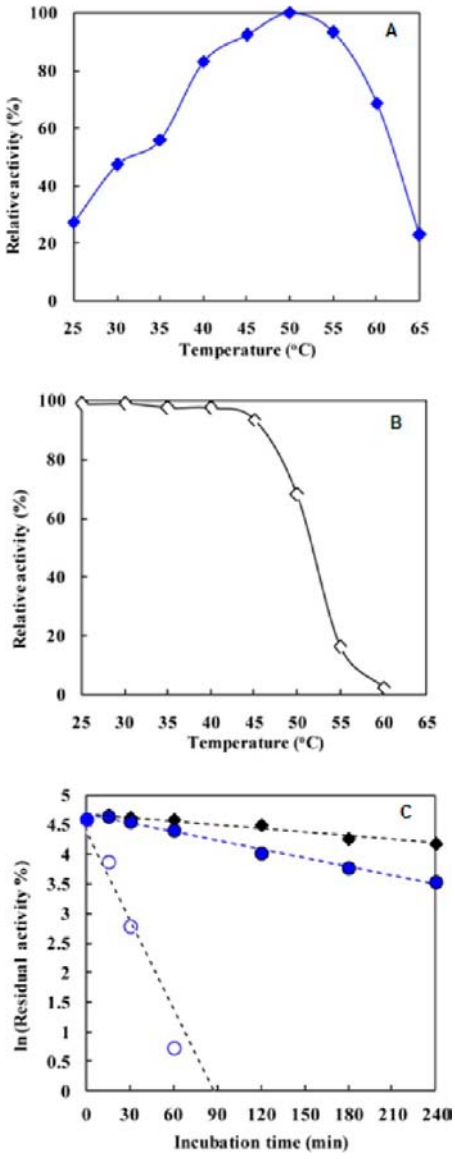

Figure 5. (A) Optimal temperature, (B) thermostability, and (C) thermal denaturing half-life of purified RmNag. The temperature profile was measured at different temperatures in 50 mM phosphate (pH 6.5). For determination of thermostability, residual activity of the treated enzyme was measured according to the standard assay after a 30 min preincubation at different temperatures. For thermal denaturing half-life, the enzyme was incubated at (◆) 40, (●) 45, and (○) 50 °C.

These results suggested that the enzyme was an exo-type enzyme acting on the nonreducing end of the substrate to release GlcNAc one by one.

Tolerance of RmNag to GlcNAc. The effect of various concentrations of GlcNAc on GlcNAcase activity was studied (data not shown). The enzyme activity of RmNag was inhibited by 49.9% in the presence of 9 mM GlcNAc. RmNag was competitively inhibited by GlcNAc with a K_i value of 9.68 mM.

DISCUSSION

GlcNAcases play important roles in chitin degradation, as well as in the cell wall recycling process of bacteria. To date, a number of GlcNAcases have been identified, gene cloned, and characterized from a wide variety of organisms, including bacteria, plants, insects, and animals.[4,9,11,15] Nevertheless, there is only scant information on GlcNAcases from fungi[15,24,25] and no report on

Table 3. Effect of Metal Ions and Reagents on Activity of RmNag

metal ion or reagent (1 mM)	specific activity[a] (units/mg)	relative activity (%)
control	21.1	100
Fe^{3+}	18.2	86.1
Cr^{2+}	13.5	63.8
Ag^{+}	0.2	0.8
Cu^{2+}	0.2	0.7
Ni^{2+}	13.8	65.2
Mg^{2+}	17.5	83.0
Sn^{2+}	12.0	56.7
Zn^{2+}	2.7	12.8
Mn^{2+}	20.7	98.2
Co^{2+}	4.8	22.5
Ba^{2+}	21.5	102
Hg^{2+}	2.5	11.8
K^{+}	22.4	106
Na^{+}	21.4	101
SDS	0.3	1.4
EDTA	14.3	67.6
β-mercaptoethanol	18.5	87.5

[a]Activity was determined at 50 °C in 50 mM phosphate buffer (pH 6.5) for 10 min.

Table 4. Substrate Specificity of Purified RmNag

substrate	specific activity[a] (units/mg)	relative activity (%)
*p*NP-GlcNAc	21.2	100
*p*NP-GalNAc	0.2	0.7
$(GlcNAc)_2$	1.06[b]	5.0
$(GlcNAc)_3$	1.11	5.2
$(GlcNAc)_4$	0.88	4.1
$(GlcNAc)_5$	0.68	3.2

[a]Specific activities toward *N*-acetyl chitooligosaccharides were determined by measuring the released GlcNAc by HPLC. Reactions were performed in 50 mM phosphate buffer (pH 6.5) at 50 °C for 10 min. [b]Specific activity was divided by 2, as the hydrolysis of 1 mol of $(GlcNAc)_2$ can release 2 mol of GlcNAc.

fungal GlcNAcases belonging to GH family 3. Here, to the best of our knowledge, is the first report on a fungal GlcNAcase belonging to GH family 3.

GlcNAcases have been classified into three GH families, 3, 20, and 84, in the CAZy database on the basis of their amino acid sequence similarities.[26] GH families 3 and 84 GlcNAcases are mainly distributed in various bacteria and metazoan cells, respectively, while GH family 20 GlcNAcases are versatile enzymes mainly abundant in fungi and insects.[36] Analysis of the nucleotide sequence of *RmNag* indicated that the deduced amino acid sequence contained a typical motif, KHFPGHGDTxxDSH (KHFPGHGDTMVDSH) (Figure 1), which is highly conserved among GH family 3 GlcNAcases.[19] Besides, multiple amino acid sequence alignment revealed that RmNag showed the highest identity with a putative GH family 3 GlcNAcase from *A. clavatus* NRRL 1 (Figure 2). These results suggest that RmNag should be a novel member of GH family 3 GlcNAcases. Hence it may represent the first fungal GH family 3 GlcNAcase.

The molecular masses of most reported bacterial GH family 3 GlcNAcases are mainly distributed in the range 36–89 kDa,[11,18,20,23] while those of fungal GlcNAcases (GH family 20) are somewhat higher, mainly above 70 kDa, such as the enzymes from *Trichoderma harzianum* P1 (72 kDa),[17] *Lentinula edodes* (79 kDa),[4] *T. harzianum* (150 kDa)[16] and *P. oxalicum* (160 kDa).[24] The denatured molecular mass of RmNag in the present study was estimated to be 96.1 kDa on SDS–PAGE (Figure 3), while the native molecular mass was determined to be 200.8 kDa by gel filtration, indicating the enzyme is a homodimer. This is distinct from most known bacterial GH3 GlcNAcases but similar to the GlcNAcases from two fungi: *P. oxalicum*[24] and *T. harzianum*.[16]

RmNag was most active at pH 6.5 and was stable within pH 6.0–8.0 (Figure 4). The optimal pH is similar to that of most other reported GlcNAcases in the range 6.0–7.0.[9,13,15,23] RmNag was most active at 50 °C (Figure 5). The GH family 20 GlcNAcases from *C. paraputrificus*[12] and *L. edodes*[4] are also most active at 50 °C. However, the optimal temperature of RmNag is lower than that of the GH family 3 enzymes from thermophilic bacteria *S. thermoviolaceus* (60 °C)[5] and *T. maritima* (65–75 °C).[23] It is worth noting that RmNag exhibited a wide range of temperature optimum at 40–55 °C and was stable up to 45 °C, with a thermal denaturing half-life of 494 min (Figure 5).

Generally, GH family 3 GlcNAcases have broad substrate specificity, while GH family 20 GlcNAcases exhibit strict substrate specificity.[19,37] However, the differences of GlcNAcases from each other still exist, even within the same GH family.[13] RmNag showed the highest activity toward *p*NP-GlcNAc among the tested *p*NP drivatives and appeared to have the highest activity against $(GlcNAc)_3$ (the activities for $GlcNAc_2$ and $GlcNAc_3$ are almost the same) among tested *N*-acetyl chitooligosaccharides (Table 4). This property is similar to fungal GH family 20 GlcNAcases, which have the highest catalytic efficiency for $(GlcNAc)_2$ among natural substrates and do not hydrolyze or hardly hydrolyze long-chain chitomaterials,[4] but is different from most other reported bacterial GH family 3 GlcNAcases. For example, the specific activity of NagA, a GH family 3 GlcNAcase from *S. thermoviolaceus*, increased with the DP of the *N*-acetyl chitooligosaccharides substrates.[5] GlcNAcase from *S. thermophilum* showed much lower specific activity for *p*NP-GlcNAc than for *N*-acetyl chitooligosaccharides substrates (DP 2–5).[20] It appears that the GlcNAcases reported to date possess two major types of substrate specificity. The first type of enzymes prefers to hydrolyze *N*-acetyl chitobiose, while the other type of enzymes favors chitooligomers (DP 3–6) over *N*-acetyl chitobiose. However, GlcNAcases from both GH families 3 and 20 are randomly distributed in the two types from this classification aspect. GlcNAcases from *T. harzianum*,[16] *S. thermophilum*,[20] and *L. edodes*[4] belong to the first type, while GlcNAcases from *S. thermoviolaceus*[5] and *V. harveyi*[9] are classified into the second type. RmNag belongs to neither of the two types of GlcNAcase, but it is closer to the first type as it exhibited almost equal highest activities for $(GlcNAc)_3$ and $(GlcNAc)_2$ and low activities for $(GlcNAc)_4$ and $(GlcNAc)_5$ (Table 4). Many GlcNAcases are also called *N*-acetylhexosaminidases as they showed high activity toward *p*NP-GalNAc.[4,20,21,23] However, RmNag showed a trace amount of activity for *p*NP-GalNAc. The GlcNAcase from *S. thermoviolaceus* also showed no activity for *p*NP-GalNAc.[5] RmNag exhibited no activity toward chitin polymers, which is in accordance with most other reported GH family 3 GlcNAcases.[5,23] However, there are still a few GlcNAcases showing chitin-degrading ability in both GH families 3 and 20.[4,9,13] Thus, RmNag exhibited unique enzymatic properties with respect to all the reported GlcNAcases.

Degradation pattern of RmNag toward *N*-acetyl chitooligosaccharides was analyzed by TLC. RmNag hydrolyzed chitin oligomers (DP 2–5), yielding GlcNAc as the sole end product

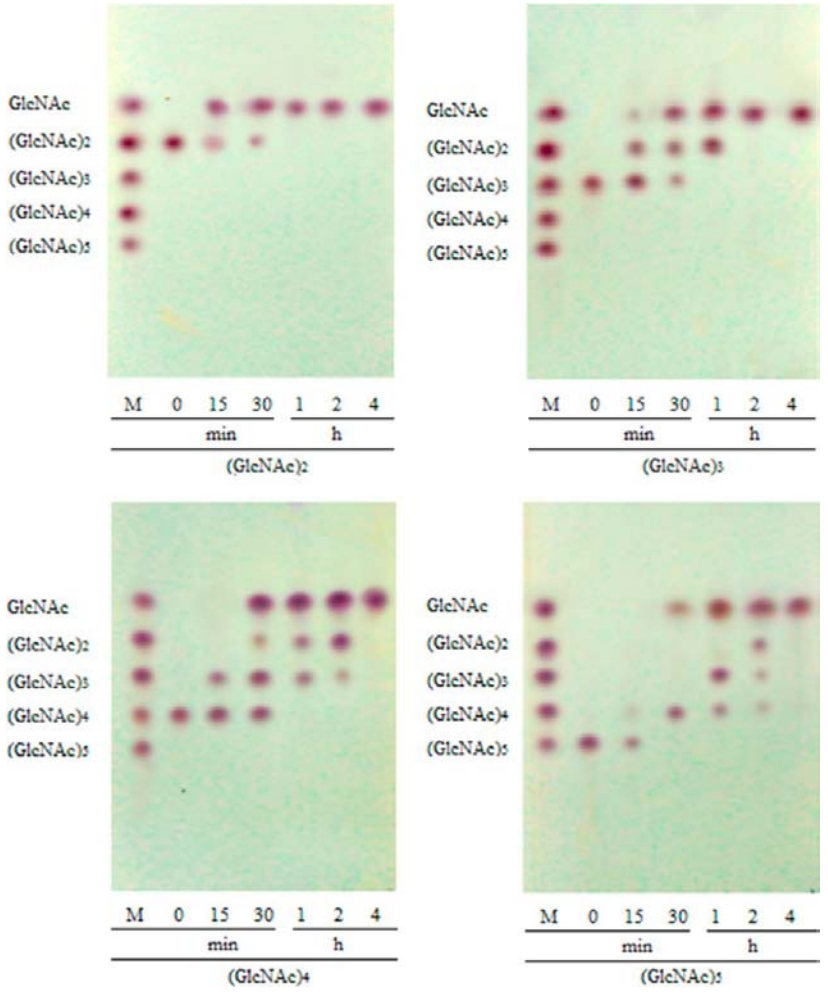

Figure 6. TLC analysis of hydrolytic products of *N*-acetyl chitooligosaccharides by purified RmNag. Reactions were performed in 50 mM phosphate buffer (pH 6.5) at 30 °C for various times.

(Figure 6). During the hydrolytic reaction, all substrates were hydrolyzed exolytically, that is, $(GlcNAc)_n$ ($n < 5$) was first converted to $(GlcNAc)_{n-1}$ and equivalent amount of GlcNAc, and then the intermediate product $(GlcNAc)_{n-1}$ was further converted to $GlcNAc_{n-2}$ and equivalent amount of GlcNAc, and the reaction continued until all the intermediate products were converted to the final end product GlcNAc (Figure 6). These results clearly indicated that RmNag released GlcNAc from the nonreducing end of the substrate and exhibited an exo-type cleavage mechanism. Similar results were also reported for the GlcNAcases from *A. hydrophila*,[21] *T. maritima*,[23] and *V. harveyi*,[9] which belong to GH families 20, 3, and 20, respectively.

High concentration of GlcNAc tolerance is an advantage for GlcNAcases in the complete enzymatic hydrolysis of chitin. However, most reported GlcNAcases are inhibited by their hydrolysis product (GlcNAc), with K_i values ranging from 0.2 to 2 mM.[12,18] The enzyme in the present study exhibited relatively high tolerance to GlcNAc, with a K_i value of 9.68 mM, which is much higher than that of the GlcNAcases from *V. furnissii* (K_i = 0.21 mM),[18] *A. oryzae* (K_i = 1.6 mM),[38] *T. harzianum* (K_i = 1.6 mM),[39] and *Spodoptera frugiperda* (K_i = 2.0 mM).[12] GlcNAcase from *Trichinella spiralis* was also GlcNAc-tolerant, with a K_i value of 15.75 mM, which represents the highest tolerance to GlcNAc.[40] The high GlcNAc tolerance is an attractive feature, which may enable the enzyme great potential in chitin conversion industry, especially for biofuel production.

In conclusion, this study reported the gene cloning, expression, and biochemical characterization of the first fungal GH family 3 GlcNAcase. The recombinant enzyme exhibited maximal activity at pH 6.5 and 50 °C. It hydrolyzed *N*-acetyl chitooligosaccharides to yield mainly GlcNAc as the only final product, and it exhibited relative high GlcNAc tolerance with a K_i value of 9.68 mM. These excellent properties may enable the enzyme to have great potential in industry.

AUTHOR INFORMATION

Corresponding Author

*Phone +86 10 62737689; fax +86 10 82388508; e-mail zhqjiang@cau.edu.cn.

Funding

This work was supported by grants from the National Science Fund for Distinguished Young Scholars (31325021) and National Natural Science Foundation of China (Project 31101238).

Notes

The authors declare no competing financial interest.

REFERENCES

(1) Tharanathan, R. N.; Kittur, F. S. Chitin: The undisputed biomolecule of great potential. *Crit. Rev. Food Sci. Nutr.* **2003**, *43*, 61−87.

(2) Da Silva, L. C. A.; Honorato, T. L.; Franco, T. T.; Rodrigues, S. Optimization of chitosanase production by *Trichoderma koningii* sp.

under solid-state fermentation. *Food Bioprocess. Technol.* **2012**, *5*, 1564−1572.
(3) Sweeney, M. D.; Xu, F. Biomass converting enzymes as industrial biocatalysts for fuels and chemicals: Recent developments. *Catalysts* **2012**, *2*, 244−263.
(4) Konno, N.; Takahashi, H.; Nakajima, M.; Takeda, T.; Sakamoto, Y. Characterization of *β-N*-acetylhexosamidase (LeHex20A), a member of glycoside hydrolase family 20, from *Lentinula edodes* (shiitake mushroom). *AMB Express* **2012**, *2*, 29.
(5) Tsujibo, H.; Hatano, N.; Mikami, T.; Hirasawa, A.; Miyamoto, K.; Inamori, Y. A novel *β-N*-acetylhexoosaminidase from *Streptomyces thermoviolaceus* OPC-520: Gene cloning, expression, and assignment to family 3 of the glycosyl hydrolases. *Appl. Environ. Microbiol.* **1988**, *64*, 2920−2924.
(6) Horsch, M.; Mayer, C.; Sennhauser, U.; Rast, D. M. *β-N*-Acetylhexosamidases: A target for the design of antifungal agents. *Pharmacol. Therapeut.* **1997**, *76*, 187−218.
(7) Zhuravleva, N. V.; Luk'yanov, P. A.; Pivkin, M. V. *N*-Acetyl-*β*-D-hexosamidase secreted by the marine fungus *Phoma glomerata*. *Appl. Biochem. Microbiol.* **2004**, *40*, 448−453.
(8) Zeng, X.; Sun, Y.; Ye, H.; Liu, J.; Uzawa, H. Synthesis of *p*-nitrophenyl sulfated disaccharides with *β*-D-(6-sulfo)-GlcNAc units using *β-N*-acetylhexosaminidase from *Aspergillus oryzae* in a transglycosylation reaction. *Biotechnol. Lett.* **2007**, *29*, 1105−1110.
(9) Suginta, W.; Chuenark, D.; Mizuhara, M.; Fukamizo, T. Novel *β-N*-acetylglucosamidases from *Vibrio harveyi* 650: Cloning, expression, enzymatic properties, and subsite identification. *BMC Biochem.* **2010**, *11*, 40.
(10) Votsch, W.; Templin, M. F. Characterization of a *β-N*-acetylhexosaminidase of *Escherichia coli* and elucidation of its role in muropeptide recycling and *β*-lactamase induction. *J. Biol. Chem.* **2000**, *275*, 39032−39038.
(11) Gomes, J. E., Jr.; Souza, D. S. L.; Nascimento, R. M.; Lima, A. L. M.; Melo, J. A. T.; Rocha, T. L.; Miller, R. N. G.; Franco, O. L.; Grossi-de-Sa, M. F.; Abreu, L. R. D. Purification and characterization of liver-derived *β-N*-acetylhexosaminidase from marine mammal *Sotalia fluviatilis*. *Protein J.* **2010**, *29*, 188−194.
(12) Tomiya, N.; Narang, S.; Park, J.; Abdul-Rahman, B.; Choi, O.; Singh, S.; Hiratake, J.; Sakata, K.; Betenbaugh, M. J.; Palter, K. B.; Lee, Y. C. Purification, characterization, and cloning of a *Spodoptera frugiperda* Sf9 *β-N*-acetylhexosamidase that hydrolyzes terminal *β-N*-acetylglucosamine on the *N*-glycan core. *J. Biol. Chem.* **2006**, *28*, 19545−19560.
(13) Li, H.; Morimoto, K.; Katagiri, N.; Kimura, T.; Sakka, K.; Lun, S.; Ohmiya, K. A novel *β-N*-acetylglucosaminidase of *Clostridium paraputrificum* M-21 with high activity on chitobiose. *Appl. Microbiol. Biotechnol.* **2002**, *60*, 420−427.
(14) Ferrara, M. C.; Cobucci-Ponzano, B.; Carpentieri, A.; Henrissat, B.; Rossi, M.; Amoresano, A.; Moracci, M. The identification and molecular characterization of the first archaeal bifunctional exo-*β*-glucosidase/N-acetyl-*β*-glucosaminidase demonstrate that family GH116 is made of three functionally distinct subfamilies. *Biochim. Biophys. Acta* **2014**, *1840*, 367−377.
(15) Sanon, A.; Tournaire-Arellano, C.; Younes El Hage, S.; Bories, C.; Caujolle, R.; Loiseau, P. M. *N*-Acetyl-*β*-D-glucosamidase from *Trichomonas vaginalis*: Substrate specificity and activity of inhibitors. *Biomed. Pharmacother.* **2005**, *59*, 245−248.
(16) Koga, K.; Iwamoto, Y.; Sakamoto, H.; Hatano, K.; Sano, M.; Kato, I. Purification and characterization of *β-N*-acetylhexoosaminidase from *Trichoderma harzianum*. *Agric. Biol. Chem.* **1991**, *55*, 2871−2823.
(17) Peterbauer, C. K.; Lorito, M.; Hayes, C. K.; Harman, G. E.; Kubicek, C. P. Molecular cloning and expression of the nag1 gene (*N*-acetyl-*β*-D-glucosaminidase-encoding gene) from *Trichoderma harzianum* P1. *Curr. Genet.* **1996**, *30*, 325−331.
(18) Chitlaru, E.; Roseman, S. Molecular cloning and characterization of a novel *β-N*-acetylhexoosaminidase from *Vibrio furnissii*. *J. Biol. Chem.* **1996**, *271*, 33433−33439.
(19) Mayer, C.; Vocadlo, D. J.; Mah, M.; Rupitz, K.; Stoll, D.; Warren, R. A. J.; Withers, S. G. Characterization of a *β-N*-acetylhexoosaminidase and a *β-N*-acetylglucosaminidase/*β*-glucosidase from *Cellulomonas fimi*. *FEMS J.* **2006**, *273*, 2929−2941.
(20) Ogawa, M.; Kitagawa, M.; Tanaka, H.; Ueda, K.; Watsuji, T.; Beppu, T.; Kondo, A.; Kawachi, R.; Oku, T.; Nishio, T. A *β-N*-acetylhexoosaminidase from *Symbiobacterium thermophilum*: Gene cloning, overexpression, purification and characterization. *Enzyme Microbiol. Technol.* **2006**, *38*, 457−464.
(21) Lan, X.; Zhang, X.; Kodaira, R.; Zhou, Z.; Shimosaka, M. Gene cloning, expression, and characterization of a second *β-N*-acetylhexoosaminidase from the chitinolytic bacterium *Aeromonas hydrophila* strain SUWA-9. *Biosci. Biotechnol. Biochem.* **2008**, *72*, 492−498.
(22) Sumida, T.; Ishii, R.; Yanagisawa, T.; Yokoyama, S.; Ito, M. Molecular cloning and crystal structural analysis of a novel *β-N*-acetylhexoosaminidase from *Paenibacillus* sp. TS12 capable of degrading glycosphingolipids. *J. Mol. Biol.* **2009**, *392*, 87−99.
(23) Choi, K. H.; Seo, J. Y.; Park, K. M.; Park, C. S.; Cha, J. Characterization of glycosyl hydrolase family 3 *β-N*-acetylglucosaminidases from *Thermotoga maritima* and *Thermotoga neapolitana*. *J. Biosci. Bioeng.* **2009**, *108*, 455−459.
(24) Ryslava, H.; Kalendova, A.; Doubnerova, V.; Skocdopol, P.; Kumar, V.; Kukacka, Z.; Pompach, P.; Vaněk, O.; Slámová, K.; Bojarová, P.; Kulik, N.; Ettrich, R.; Křen, V.; Bezouška, K. Enzymatic characterization and molecular modeling of an evolutionarily interesting fungal *β-N*-acetylhexoosaminidase. *FEBS J.* **2011**, *278*, 2469−2484.
(25) Slámová, K.; Kulik, N.; Fiala, M.; Krejzová-Hofmeisterová, J.; Ettrich, R.; Křen, V. Expression, characterization and homology modeling of a novel eukaryotic GH84 *β-N*-acetylglucosaminidase from *Penicillium chrysogenum*. *Protein Expression Purif.* **2014**, *95*, 204−210.
(26) Cantarel, B. L.; Coutinho, P. M.; Rancurel, C.; Bernard, T.; Lombard, V.; Henrissat, B. The Carbohydrate-Active enZymes database (CAZy): An expert resource for glycogenomics. *Nucleic Acids Res.* **2009**, *37*, 233−238.
(27) Maheshwari, R.; Bharadwaj, G.; Bhat, M. K. Thermophilic fungi: Their physilology and enzymes. *Microbiol. Mol. Biol. Rev.* **2000**, *64*, 461−488.
(28) Katrolia, P.; Jia, H.; Yan, Q.; Song, S.; Jiang, Z.; Xu, H. Characterization of a protease-resistant *α*-galactosidase from the thermophilic fungus *Rhizomucor miehei* and its application in removal of raffinose family oligosaccharides. *Bioresour. Technol.* **2012**, *110*, 578−586.
(29) Tang, Y.; Yang, S.; Yan, Q.; Cui, J.; Jiang, Z. High-level production, purification and characterization of a novel (lichenase) from the thermophilic *Rhizomucor miehei* with high specific activity. *J. Agric. Food Chem.* **2012**, *60*, 2354−2361.
(30) Sambrook, J.; Russell, D. W. *Molecular Cloning: A Laboratory Manual*, 2nd ed.; Cold Spring Harbor Laboratory: Cold Spring Harbor, NY, 2001.
(31) Lodhi, M. A.; Ye, G. N.; Weeden, N. F.; Reisch, B. I. A simple and efficient method for DNA extractions from grape vine cultivars and *Vitis* species. *Plant Mol. Biol. Rep.* **1994**, *12*, 6−13.
(32) Rose, T. M.; Henikoff, J. G.; Henikoff, S. CODEHOP (COnsensus-DEgenerate Hybrid Oligonucleotide Primer) PCR primer design. *Nucleic Acids Res.* **2003**, *31*, 3763−3766.
(33) Lowry, O. H.; Rosebrough, N. J.; Farr, A. L.; Randall, R. J. Protein measurement with the folin phenol reagent. *J. Biol. Chem.* **1951**, *193*, 265−275.
(34) Laemmli, U. K. Cleavage of structural proteins during the assembly of the head of bacteriophage T4. *Nature* **1970**, *227*, 680−685.
(35) Miller, G. L. Use of dinitrosalicylic acid reagent for determination of reducing sugar. *Anal. Chem.* **1959**, *31*, 426−428.
(36) Liu, T.; Yan, J.; Yang, Q. Comparative biochemistry of GH3, GH20 and GH84 *β-N*-acetyl-D-hexosaminidases and recent progress in selective inhibitor discovery. *Curr. Drug Targets* **2012**, *13*, 512−525.
(37) Lee, R. C.; Hrmova, M.; Burton, R. A.; Lahnstein, J.; Fincher, G. B. Bifunctional family 3 glycoside hydrolases from barley with *α*-L-arabinofuranosidase and *β*-D-xylosidase activity. Characterization, primary structures, and COOH-terminal processing. *J. Biol. Chem.* **2003**, *278*, 5377−5387.

(38) Rajnochova, E.; Dvorakova, J.; Hun kova, Z.; Kren, V. Reverse hydrolysis catalysed by *β*-*N*-acetylhexosaminidase from *Aspergillus oryzae*. *Biotechnol. Lett.* **1997**, *19*, 869−872.
(39) Nieder, V.; Kutzer, M.; Kren, V.; Gallego, R. G.; Kamerling, J. P.; Elling, L. Screening and characterization of *β*-*N*-acetylhexosaminidases for the synthesis of nucleotide-activated disaccharides. *Enzyme Microb. Technol.* **2004**, *34*, 407−414.
(40) Bruce, A. F.; Gounaris, K. Characterisation of a secreted *N*-acetyl-*β*-hexosaminidase from *Trichinella spiralis*. *Mol. Biochem. Parasitol.* **2006**, *145*, 84−93.

using a commercial gas-fired roaster (IMSA, Lima, Peru). Batch size was 4.5 kg approximately Three roasting conditions were applied to obtain the corresponding degrees of roasted kernels: lightly roasted (75−81 °C × 9 min), medium roasted (83−86 °C × 10 min), and highly roasted (99−102 °C × 10 min). The light roasting conditions correspond to the minimum roasting level that eliminates the astringent flavor. Weight loss during roasting ranged from ∼5.5−6.6%. After roasting, the kernels were immediately cooled with the built-in fan of the roaster.

Oil Extraction, Clarification and High Temperature Storage. Oil extraction was achieved by pressing the kernels the following day after roasting. The unroasted and the three roasted samples were pressed with a laboratory Komet expeller (IBG Monforts GmbH, Monchengladbach, Germany). The press temperature of 100−110 °C was measured by inserting a thermocouple in the cake mass that emerged from the expeller. The extracted oil with fine suspended solids was immediately placed in amber glass bottles (0.5 L) and filled to the top to minimize headspace. The bottles were stored in the dark and under refrigeration (5 °C) until clarification by centrifugation. The nonclarified oil yield increased with roasting temperature with values of ∼42, 49, and 65% by weight for lightly, medium and highly roasted samples, respectively.

Oil samples were clarified by centrifuging at 29 000*g* for 15 min in a laboratory centrifuge Beckman Model J2−21 (Fullerton, CA, U.S.A.). The clarified samples were placed in amber glass bottles (120 mL) and flushed with nitrogen and stored in the dark under refrigeration at 5 °C until testing time.

For high temperature storage studies, oil samples (50g) were placed in 100 mL beakers (in triplicate) and stored in an oven at 60 °C in the dark for 30 days. Samples were analyzed for peroxide value, *p*-anisidine, tocopherols, and fatty acid profile at 0, 8, 18, and 30 days of accelerated storage while antioxidant capacity, by measuring total phenols and DPPH, were done on samples at days zero and 30. All analyses were performed in triplicate.

Peroxide Value and *p*-Anisidine Value. The peroxide value was determined using the AOCS Cd 8−53 official method.[9] This method determines all substances in the oil that oxidize potassium iodide (KI) under test conditions. The assumption is that these substances are peroxides or similar compounds that resulted from lipid oxidation. Results are expressed as peroxide milliequivalents/1000 g oil. The *p*-anisidine value was determined using the AOCS Cd 18−90 official method.[9] This method quantifies the amount of aldehydes (especially, 2-alkenals and 2,4-dienals) present in the oil through the reaction between aldehydes and *p*-anisidine in an acetic solution. Absorbance was measured at 350 nm with an 8452A photodiode array spectrophotometer (Hewlett-Packard, Palo Alto, CA).

Antioxidant Capacity. Two methods were used to measure antioxidant capacity: Total phenols and DPPH assay. Previously, phenolic extracts, to be used for both methods, were prepared from oil samples. Phenolic extracts were prepared according to a procedure by Ninfali and others[10] with some modifications: 0.5 g oil were diluted in 25 mL 80% methanol−water and vortexed for 1 min, then stirred using a gyratory shaker model G2 (New Brunswick Scientific Co., Inc., NJ) at 200 rpm × 1 h. The mixture was centrifuged (29 000*g* × 15 min) using a Beckman Model J2−21 centrifuge (Fullerton, CA, U.S.A.) and an 8 mL aliquot of supernatant was taken. The solvent of the supernatant was removed using a rotovapor and then a laboratory freeze-dryer FTS Systems Inc. (Stone Ridge, NY) for ∼8 h. The solid residue was redissolved in 500 μL methanol (900 μL for samples from intensely roasted seeds). These extracts were used for total phenols and DPPH analyses.

Total Phenols Using the Folin Assay. A procedure was used based on the method by Swain and Hillis.[11] Four milliliters of distilled water was added to a 250 μL aliquot of phenolic extract and mixed for 30 s in a vortex. Folin-Ciocalteu reagent (250 μL) was added and allowed to react for exactly 3 min. Then 500 μL 1N Na_2CO_3 solution was added, and the mixture was allowed to react in the dark for 2 h, after which absorbance was read at 725 nm in a spectrophotometer. Chlorogenic acid was used as standard and results were expressed as mg chlorogenic acid/g oil.

DPPH (2,2-Diphenyl-1-picrylhydrazyl) Assay. This analysis was based on the method used by Thaipong and others.[12] In this method, antioxidant activity was determined using DPPH as free radical. The procedure is as follows: A 150 μL aliquot of phenolic extract and 2.85 mL of DPPH solution were mixed. After a 24-h period of incubation in the dark, the absorbance was measured at 515 nm with a spectrophotometer. A blank was prepared using methanol instead of phenolic extract. A linear standard curve was built using trolox as the reference reactant in a range from 25 to 800 μM. Antioxidant capacity was expressed as μg trolox equivalents/g oil. A higher trolox equivalent is indicative of a greater antioxidant potential or reducing power.

Tocopherol Content. Sample preparation to be analyzed by chromatography was based on the method used by Rodas-Mendoza and others,[13] which is described briefly. A 0.5 g oil sample was diluted in 2 mL methanol and mixed for 1 min, afterward, 500 μL hexane was added and mixed in a vortex. The mixture was then centrifuged (2500*g* × 10 min) and a 1 mL aliquot of supernatant was removed and filtered with a PTFE filter (pore size 0.2 μm) before 20 μL volume injection into the HPLC. The samples were run using a Waters Millennium 3.2 software (Milford, MA, U.S.A.). The HPLC system was equipped with a binary pump system (Waters 515, Milford, MA, U.S.A.), an autoinjector (Waters 717 plus, Milford, MA, U.S.A.), a photodiode array (PDA) detector (Waters 996, Milford, MA, U.S.A.), and a column heater (SpectraPhysics SP8792, San Jose, CA, U.S.A.). The column used was a Tracer Spherisorb ODS2 C_{18}, 250 × 4.6 mm (i.d.), particle size 5 μm (Tracer Analitica, Barcelona, Spain) protected by a column guard of the same composition (Waters Corp., Milford MA, U.S.A.). Methanol was used as the mobile phase, and elution took place at a flow rate of 1 mL/min. The column temperature was kept at 50 °C. Detection was done at 295 nm. Chromatographic peaks were identified by comparing sample retention times with those of standards, and quantification was achieved by external standardization.

Fatty Acid Profile. Sample preparation for GC analysis was based on the method used by Misir and others.[14] This method consisted in the formation of methyl esters of fatty acids from the corresponding fatty acids. The procedure used is as follows: 0.15 g of oil was diluted in 3 mL of diethyl ether in a test tube to which 0.2 mL of 20% tetramethylammonium hydroxide was added. The mixture was stirred for 2 min and allowed for phase separation. One drop of thymol blue indicator was added, followed by dropwise addition of 0.5 N HCl methanol solution until the color changed from blue to yellow. Finally, 0.5 mL methanol was added to make the samples homogeneous.

The chromatographic method used was that described by Misir and others.[14] The fatty acid methyl esters were analyzed with a Varian CP 3800 gas chromatograph (Palo Alto CA, U.S.A.) equipped with a Varian CP 8200 automatic injector and a flame ionization detector (FID). A Varian FAME fused silica capillary column (100 m × 0.25 mm, i.d.) (Varian CP-Select). The oven temperature had the following program: 0−30 min at 185 °C and 30−45 min at 235 °C, with increments of 20 °C/min. The FID temperature was 270 °C. The flow rates of helium, air, and hydrogen were 1.6, 300, and 35 mL/min.

Statistics. Results are reported as mean values of three replicates and their corresponding confidence intervals at a 95% confidence level ($p < 0.05$).

RESULTS AND DISCUSSION

Roasting Process Effect on Sensorial Characteristics of Kernel and Oil. The varying degrees of roasting of Sacha-inchi seeds resulted in changes in seed color and kernel taste. The color changed from cream in unroasted kernels to light brown—similar to roasted peanuts—in lightly roasted Sacha-inchi kernels, to brown and dark brown, in medium and highly roasted kernels, respectively (Figure 1). The typical astringent taste of unroasted kernels disappeared with roasting; lightly roasted kernels had no astringent taste but rather a slightly sweet taste; medium roasted kernels had no sweet taste but rather a slightly burnt taste; highly roasted kernels had a bitter and burnt taste. The color of Sacha-inchi oil from lightly

roasted seeds did not differ visually from that of unroasted seeds. However, oil from medium and highly roasted seeds exhibited darker oils (Figure 2).

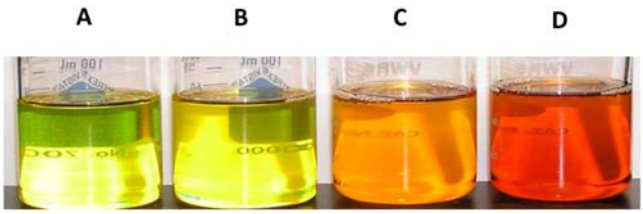

Figure 2. Visual appearance of Sacha-inchi oil samples at day 0 from unroasted (A), slightly roasted (B), medium-roasted (C), and highly roasted seeds (D).

Roasting Process Effect on Oil Oxidation, Composition and Antioxidant Activity. *Peroxide Value.* Oil peroxide value (PV) did not follow a distinct trend with seed roasting (Table 1). Oil from unroasted seeds gave a value of 0.57 mEq/kg oil. PV increased with light and medium roasting to 3.35 and 4.09, respectively; and then decreased with high roasting to 0.5 mEq/kg oil. As a comparison, flaxseed oil had a PV of 0.47. All these values are below the maximum acceptable PV value of 15 set by the Codex Alimentarius[15] for nonrefined oils.

According to the lipid oxidation theory, hydroperoxides begin to form at the initial stages of oxidation until reaching a maximum, and then decline at the latter stages of oxidation because of decomposition to secondary products (aldehydes, ketones, etc.). In light of the results obtained, one might be tempted to suggest that oils from lightly and medium roasted seeds are on the ascending hydroperoxide curve, and therefore, on the initial stages of oxidation; whereas, oils from highly roasted seeds are on the descending hydroperoxide curve, and therefore, on the latter stages of oxidation. However, an alternative explanation would be that roasting produced two opposing effects. On the one hand, it might have favored lipid oxidation, which is reflected in an increase in PV; but on the other hand, it could have favored production of phenolic compounds with potent free radical scavenging abilities, especially in highly roasted seeds (as will be explained later), which resulted in low PV in oils from highly roasted seeds.

These results differ from those of Yoshida,[4] who studied the effect of roasting seeds on sesame oil, where PV is reported to increase with roasting intensity, especially when roasting temperature surpasses 200 °C. Alternatively, Yoshida and Takagi[5] observed an increase in PV in roasted sesame seeds compared to unroasted seeds; however, no PV differences were detected between roasting temperatures in the range 160−220 °C. It is important to keep in mind that different roasting temperatures may have different oxidation and transformation processes reflected in peroxides and aldehydes with completely different behaviors, thus the need to elucidate the specific compounds formed.

p-Anisidine Value. Results for *p*-anisidine showed a well-defined trend in relation to roasting intensity (Table 1). The highest value corresponded to Sacha-inchi oil from the highly roasted seeds, 12.32, followed by medium roasted, slightly roasted, and unroasted seed oils, 9.40, 3.72, and 0.43, respectively, whereas the *p*-anisidine value obtained for flaxseed oil was zero. These results indicate that oil from seeds subjected to increased roasting show increasing amounts of secondary compounds of oxidation as a result of decomposition of hydroperoxides. This is in agreement with the results obtained on sesame seed oil by Yoshida[4] and by Yoshida and Takagi.[5]

In relation to the increased *p*-anisidine values and low PV observed before in highly roasted seed oil, we surmise that early in the roasting process, kinetics favors hydroperoxide scission into secondary oxidation products; whereas, in the latter part of the roasting process, kinetics favors the reaction of the antioxidant compounds generated with hydroperoxides.

Total Phenols. Oils from unroasted and lightly roasted seeds exhibited similar total phenol values, 2.32 and 2.55 mg chlorogenic acid/100g oil, respectively (Table 1). However, total phenol values increased with roasting intensity; thus, oils from lightly, medium, and highly roasted seeds had total phenol values of 2.55, 6.31, and 13.85 mg/100g oil (Table 1). These results could suggest that as roasting intensity increases, the formation of phenolic compounds, with stronger antioxidant capacities, is favored. Phenolic compounds have antioxidant properties, which can be increased by specific changes in the ring substitution groups.[16] An example of changes in phenols with roasting that lead to the formation of phenols with more potent reducing capacities is the conversion of sinapic acid into vinylsyringol (canolol) in rapeseed (canola).[7,8] Total phenol values can be correlated with oil color: the higher the phenol value, the darker the oil color (Figure 2).

DPPH Assay. Roasting increased the antioxidant capacity of Sacha-inchi oil as measured by DPPH. Roasting intensity increased DPPH values further. The values obtained were 18.2, 23.8, 47.6, and 95.0 μg TE/g oil for oils from unroasted, slightly, medium, and highly roasted seeds, respectively (Table 1). These results suggest that roasting of Sacha-inchi seeds increases the antioxidant capacity of the corresponding oils, with roasting intensity further increasing the antioxidant capacity. As mentioned in the previous section, this could be

Table 1. Roasting Effects on Sacha-Inchi Oil Oxidation, Antioxidant Capacity, Tocopherol Content and Fatty Acid Profile at Day 0[a]

					tocopherol content (mg/100g oil)	
oil sample	peroxide value (meq/kg oil)	*p*-anisidine value	total phenols (mg/100g oil)	DPPH (μg trolox equiv/g oil)	γ	δ
from unroasted seeds	0.57 ± 0.01	0.43 ± 0.04	2.32 ± 0.06	18.2 ± 1.3	70.6 ± 0.27	12.6 ± 0.1
lightly roasted seeds	3.35 ± 0.04	3.72 ± 0.06	2.55 ± 0.18	23.8 ± 1.4	65.5 ± 0.18	12.5 ± 0.02
medium roasted seeds	4.09 ± 0.02	9.40 ± 0.1	6.31 ± 0.32	47.6 ± 1.5	64.4 ± 0.28	12.3 ± 0.07
highly roasted seeds	0.50 ± 0.01	12.32 ± 0.31	13.81 ± 0.23	95.0 ± 2.8	66.2 ± 0.32	12.3 ± 0.07
commercial flaxseed	0.47 ± 0.02	0	3.79 ± 0.32	17.5 ± 1.7	19.9 ± 1.0	0.1 ± 0

[a]The ± values indicate the 95% confidence interval for the respective mean.

dx.doi.org/10.1021/jf500936j | J. Agric. Food Chem. 2014, 62, 5191−5197

Table 2. Changes in Fatty Acid Profile of Sacha-inchi Oils from Unroasted and Roasted Seeds during High-Temperature Storage at 60 °C for 30 Days[a]

	%				
oil sample	16:0	18:0	18:1	18:2	18:3
			day 0		
unroasted	4.7 ± 0.2	3.3 ± 0.1	8.9 ± 0.1	34.1 ± 0.1	48.2 ± 0.4
lightly roasted	4.8 ± 0.3	3.2 ± 0.1	8.2 ± 0.3	34.2 ± 0.2	48.8 ± 0.45
medium roasted	5.0 ± 0.3	3.2 ± 0.1	8.3 ± 0.2	34.3 ± 0.2	48.4 ± 0.2
highly roasted	4.7 ± 0.1	3.1 ± 0	8.4 ± 0	34.3 ± 0.1	48.1 ± 0.2
flaxseed	5.3 ± 0.1	3.6 ± 0	15.8 ± 0	16.6 ± 0.0	57.5 ± 0.1
			day 8		
unroasted	4.7 ± 0.2	3.3 ± 0	9.3 ± 0	34.6 ± 0.1	47.2 ± 0
lightly roasted	4.8 ± 0.2	3.1 ± 0	8.7 ± 0.1	34.7 ± 0.2	47.7 ± 0.1
medium roasted	4.7 ± 0.1	3.1 ± 0	8.6 ± 0	34.7 ± 0.1	47.6 ± 0.1
highly roasted	5.0 ± 0.3	3.1 ± 0	8.4 ± 0	34.5 ± 0.1	48.0 ± 0.1
flaxseed	5.4 ± 0	3.7 ± 0	15.9 ± 0	16.7 ± 0	57.2 ± 0.1
			day 18		
unroasted	5.0 ± 0.1	3.5 ± 0.1	9.1 ± 0.1	34.2 ± 0.3	47.2 ± 0.2
lightly roasted	5.2 ± 0.4	3.3 ± 0.1	8.6 ± 0.3	34.5 ± 0.3	47.6 ± 0.3
medium roasted	4.9 ± 0.1	3.2 ± 0	8.8 ± 0	34.8 ± 0	47.2 ± 0.1
highly roasted	4.9 ± 0.2	3.2 ± 0	8.6 ± 0	34.6 ± 0	47.6 ± 0.1
flaxseed	6.4 ± 0.2	3.8 ± 0.2	16.2 ± 0.1	17.1 ± 0.5	56.2 ± 0.4
			day 30		
unroasted	5.1 ± 0.2	3.6 ± 0	10.1 ± 0.1	35.1 ± 0.1	44.3 ± 0.4
lightly roasted	5.1 ± 0	3.4 ± 0	9.4 ± 0	35.1 ± 0.1	45.5 ± 0.1
medium roasted	5.2 ± 0	3.4 ± 0	9.3 ± 0	35.3 ± 0	45.5 ± 0.1
highly roasted	5.1 ± 0.1	3.3 ± 0	9.2 ± 0.1	35.1 ± 0.2	45.7 ± 0.1
flaxseed	6.7 ± 0.2	4.6 ± 0.1	19.3 ± 0.1	17.2 ± 0.1	50.0 ± 0.3

[a]The ± values indicate the 95% confidence interval for the respective mean.

due to the formation of phenolic compounds with more potent antioxidant capacities. However, Maillard reaction products, which form during roasting of seeds, are also known to possess antioxidant capacities.[16] Furthermore, the formation of oxidative products with reducing power like aldehydes,[17] as reflected by the increase in *p*-anisidine in the present study could also have contributed partially to the observed increase in antioxidant capacity.

Tocopherol Content. Sacha-inchi oil, variety Pinto Recodo, showed a high tocopherol content, compared to flaxseed oil (Table 1). Only γ- and δ-tocopherols were detected in Sacha-inchi oil, 70.6 and 12.6 mg/100g oil, respectively. Oil from roasted seeds had a slightly lower γ-tocopherol content than oil from unroasted seeds; whereas, δ-tocopherols were unaffected by roasting. Oils from seeds roasted to different degrees had similar tocopherol contents (Table 1). These results indicate that only γ-tocopherols were slightly affected by roasting, however, no further decrease in content was detected by increasing roasting intensity.

Fatty Acid Profile. The fatty acid profile of Sacha-inchi is shown in Table 2 (day 0). The most abundant fatty acid corresponds to α-linolenic acid (18:3), 48.2%; followed by linoleic acid (18:2), 34.1%; oleic acid (18:1), 8.9%; palmitic acid (16:0), 4.7%; and stearic acid (18:0), 3.3%. These results confirm the high content of α-linolenic acid in Sacha-inchi oil reported previously by Hamaker and others.[2] However, the α-linolenic acid content of flaxseed oil obtained in our study is ~57.5% (Table 2, day 0).

It is worth noting the very low content of saturated fatty acids (8.0%) and the very high content of unsaturated fatty acids (91.2%) of Sacha-inchi oil. As a reference, flaxseed oil had 8.9% saturated and 89.9% unsaturated fatty acids. Roasting did not have any major effect on the fatty acid profile of Sacha-inchi oil, which is in agreement with previous results obtained for other oilseeds.[3−5]

High Temperature Storage and Roasting Intensity Effect on Oil Stability. *Peroxide Value.* The PV of all oil samples increased continuously during storage at 60 °C for 30 days (Figure 3). Sacha-inchi oils from roasted seeds had lower PV than that from unroasted seeds during storage, especially at the end of the storage period (30 days). Roasting intensity slowed down the PV rate of increase of oils during storage, although at the end of the storage period (30 days) the difference in PV between the oils from the lightly and the

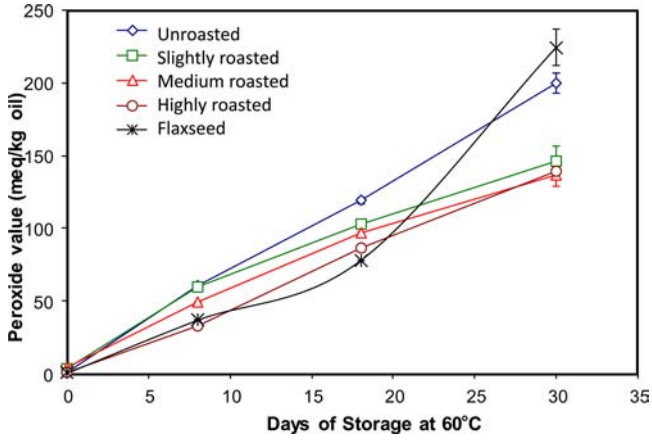

Figure 3. Peroxide values of Sacha-inchi oil unroasted and roasted samples during high-temperature storage at 60 °C for 30 days. Bars for each mean value indicate the 95% confidence interval.

dx.doi.org/10.1021/jf500936j | J. Agric. Food Chem. 2014, 62, 5191−5197

highly roasted seeds was not significant. The explanation for the lower peroxide content in Sacha-inchi oil from roasted seeds during storage, compared to that from unroasted seeds, seems to be due to the antioxidative protection of the phenolic compounds formed during roasting. Although residual lipoxygenase activity could have been a factor in the oxidation of oil from unroasted seeds, it is unlikely, because the temperature reached at the expeller for the unroasted seeds was around 110 °C. It has been previously shown that this temperature would be high enough to inactivate lipoxygenase.[18]

p-Anisidine Value. All Sacha-inchi oil samples showed an increase of *p*-anisidine values during high temperature storage (Figure 4). These values increased rapidly up to day 18, and

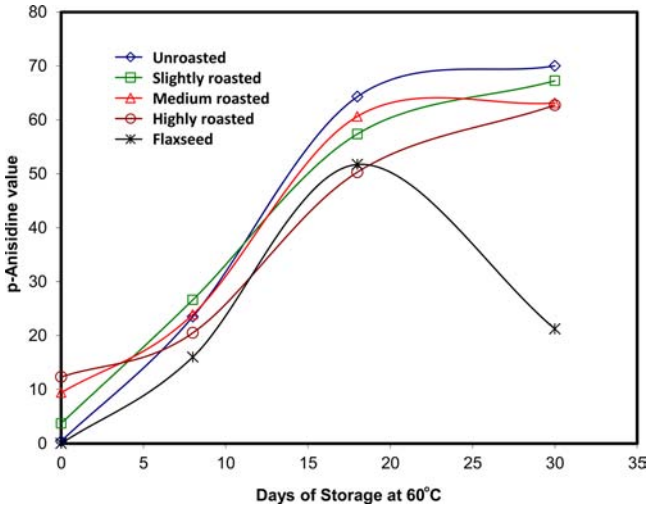

Figure 4. *p*-Anisidine values of Sacha-inchi oil unroasted and roasted samples during high-temperature storage at 60 °C for 30 days. Confidence intervals (95%) are so small that bars do not appear.

from there up to day 30, the increase in *p*-anisidine values slowed down. Prior to high-temperature storage, Sacha-inchi oil from unroasted seeds showed lower *p*-anisidine values than oil from roasted seeds. However, during and at the end of the storage period, the reverse is true, indicating that in oils from roasted seeds, *p*-anisidine values increase at a slower rate than in oil from unroasted seeds during storage (Figure 4).

The higher resistance to oxidation of oils from roasted seeds could be attributed to the formation of phenolic compounds with higher antioxidant activity, during the roasting process, possibly derived from precursor compounds with lower antioxidant activity, such as was observed in sesame and canola oil.[5−8] Maillard reaction products with antioxidant properties, generated during roasting, may also contribute to the higher stability of oil to oxidation.[16,19−21]

Total Phenols and DPPH Antioxidant Assays. Sacha-inchi oil samples from unroasted and lightly roasted seeds increased their antioxidant capacity—measured as total phenols and DPPH—during the high-temperature storage period. However, the antioxidant capacity decreased in oils from medium and highly roasted seeds, especially from the latter (Figures 5 and 6). We surmise that this increase in antioxidant activity in unroasted and lightly roasted oils during storage would be associated with the formation of oxidative products with reducing power as reported previously for aldehydes.[17] Alternatively, the decrease in antioxidant activity in medium and highly roasted oils could be due to reactions taking place

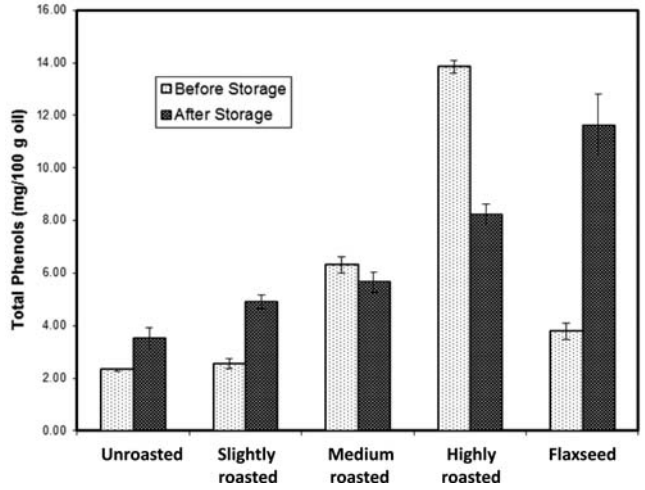

Figure 5. Total phenol values of Sacha-inchi oil unroasted and roasted samples during high-temperature storage at 60 °C for 30 days. Bars for each mean value indicate the 95% confidence interval.

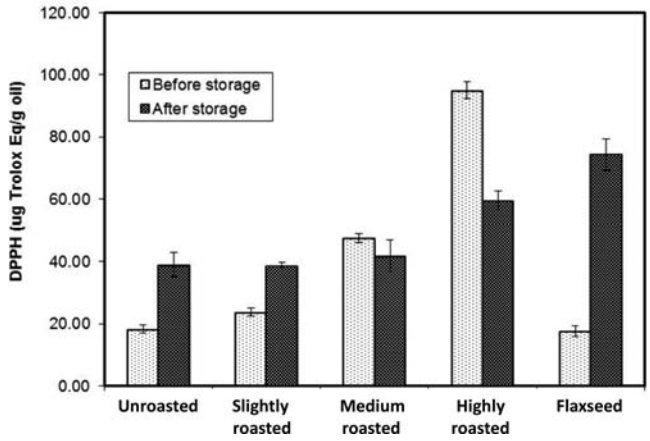

Figure 6. DPPH antioxidant activity of Sacha-inchi oil unroasted and roasted samples during high-temperature storage at 60 °C for 30 days. Bars for each mean value indicate the 95% confidence interval.

between phenols and hydroperoxides and possibly through partial regeneration reactions of oxidized tocopherols.[22] This is in agreement with the observation that roasting reduces the formation of hydroperoxides and the loss of tocopherols during storage (Figures 3, 7). It is worth noting that total phenols and DPPH exhibited the same trend in all samples.

Tocopherol Content. Tocopherol content (both γ- and δ-tocopherol) was notably reduced during storage at high temperatures in all oil samples (Figure 7). However, tocopherol degradation rate was slower in oils from roasted seeds compared to oil from unroasted seeds; moreover, tocopherol degradation rate was slower in oil samples from more intensely roasted Sacha-inchi seeds (Figure 7). This lower degradation rate of tocopherols in Sacha-inchi oil from roasted seeds seems to result from additional protection from oxidation due to roasting; specifically, higher antioxidant capacity stemming from the formation of compounds with higher antioxidant properties during roasting of seeds.

Fatty Acid Profile. Slight changes in the fatty acid profile of all Sacha-inchi oil samples were observed during the high-temperature storage period (30 days) (Table 2). There is a slight trend for the α-linolenic acid relative content to decrease,

dx.doi.org/10.1021/jf500936j | J. Agric. Food Chem. 2014, 62, 5191−5197

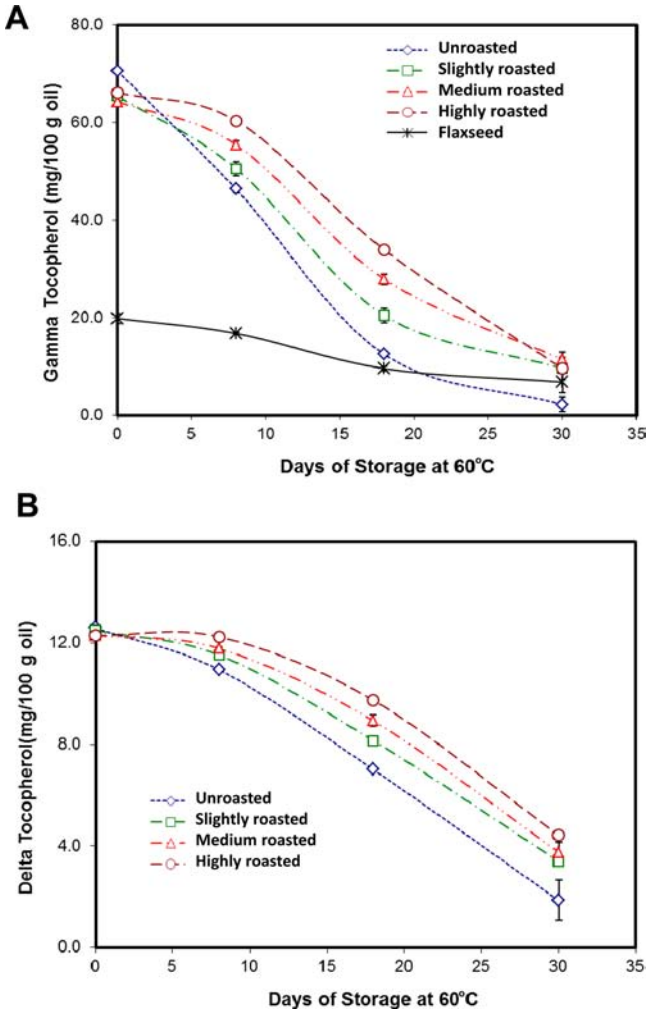

Figure 7. Tocopherol content of Sacha-inchi oil unroasted and roasted samples during high-temperature storage at 60 °C for 30 days. (A) γ-tocopherol and (B) δ-tocopherol. Bars for each mean value indicate the 95% confidence interval.

while the percentage of all other fatty acids (linoleic, oleic, palmitic, and stearic acids) showed a slight increasing trend. From these results, it can be inferred that the most unsaturated fatty acid, α-linolenic acid, was the fatty acid most susceptible to oxidation during high-temperature storage. This is in agreement with the fact that the higher the unsaturation of a fatty acid the more readily it is oxidized.[23]

In conclusion, the roasting process of Sacha-inchi seeds caused a slight increase of the oxidation indicators, such as the peroxide value and *p*-anisidine value of the oil; however, it also increased the antioxidant capacity of the oil as expressed by total phenols and DPPH, which seemed to provide some protection to the oil against oxidation during its storage at high temperatures. During storage stability studies, oils from roasted seeds exhibited lower oxidation and higher tocopherol content compared to oil from unroasted seeds. The intensity of roasting had an important effect in enhancing the protection against oxidation during storage. The fatty acid profile was not affected by roasting. In general, we have shown in this study that roasting favors the stability of Sacha-inchi oil and is recommended for extending its shelf life. Further studies are needed to elucidate the specific compounds formed due to oxidation as well as to characterize the formation of Maillard reaction products or new phenolic compounds formed during seed roasting that seem to favor the oil protection.

AUTHOR INFORMATION

Corresponding Author

*Phone: +(511) 317-1000; e-mail: fcisneros@usil.edu.pe.

Funding

We thank the financial support from CONCYTEC, Peru (Contract 142-2006-OAJ).

Notes

The authors declare no competing financial interest.

ACKNOWLEDGMENTS

We are thankful to Mr. Dante Cachique who kindly donated the Sacha-inchi seeds, and to Mr. Gaston Vizcarra for allowing the use of his expeller.

REFERENCES

(1) Guillen, M. D.; Ruiz, A.; Cabo, N.; Chirinos, R.; Pascual, G. Characterization of Sacha Inchi (*Plukenetia volubilis* L.) Oil by FTIR Spectroscopy and H NMR Comparison with Linseed Oil. *J. Am. Oil Chem. Soc.* **2003**, *80*, 755−762.

(2) Hamaker, B. R.; Valles, C.; Gilman, R.; Hardmeier, R. M.; Clark, D.; García, H. H.; Gonzales, A. E.; Kohlstad, I.; Castro, M.; Valdivia, R.; Rodríguez, T.; Lescano, M. Amino acid and fatty acid profiles of the inca peanut (*Plukenetia volubilis*). *Cereal Chem.* **1992**, *69*, 461−463.

(3) Lee, Y.-C.; Kim, I.-H.; Chang, J.; Rhee, Y.-K.; Oh, H.-I.; Park, H.-K. Chemical composition and oxidative stability of safflower oil prepared with expeller from safflower seeds roasted at different temperature. *J. Food Sci.* **2004**, *69*, C33−C38.

(4) Yoshida, H. Composition and quality characteristics of sesame seed (*Sesamum indicum*) oil roasted at different temperatures in an electric oven. *J. Sci. Food Agric.* **1994**, *65*, 331−335.

(5) Yoshida, H.; Takagi, S. Effects of seed roasting temperature and time on the quality characteristics of sesame (*Sesamum indicum*) oil. *J. Sci. Food Agric.* **1997**, *75*, 19−26.

(6) Yen, G.-C.; Shyu, S.-L. Oxidative stability of sesame oil prepared from sesame seed with different roasting temperatures. *Food Chem.* **1989**, *31*, 215−224.

(7) Wakamatsu, D.; Morimura, S.; Sawa, T.; Kida, K.; Nakai, C.; Maeda, H. Isolation, identification, and structure of a potent alkyl radical scavenger in crude canola oil, canolol. *Biosci. Biotechnol. Biochem.* **2005**, *69*, 1568−1574.

(8) Spielmeyer, A.; Wagner, A.; Jahreis, G. Influence of thermal treatment of rapeseed on the canolol content. *Food Chem.* **2009**, *112*, 944−948.

(9) American Oil Chemists' Society (AOCS). *Official Methods and Recommended Practices*, 5th ed.; AOCS Press: Champaign, IL, 1998.

(10) Ninfali, P.; Bacchiocca, M.; Biagiotti, E.; Servili, M.; Montedoro, G. Validation of the ORAC parameter as a new index of quality and stability of virgin olive oil. *J. Am. Oil Chem. Soc.* **2002**, *79*, 977−982.

(11) Swain, T.; Hillis, W. E. The phenolic constituents of *Prunus domestica*. I—The quantitative analysis of phenolic constituents. *J. Sci. Food Agric.* **1959**, *10*, 63−68.

(12) Thaipong, K.; Boonprakob, U.; Crosby, K.; Cisneros-Zevallos, L.; Byrne, D. Comparison of ABTS, DPPH, FRAP and ORAC assays for estimating antioxidant activity from guava fruit extracts. *J. Food Comp. Anal.* **2006**, *19*, 669−675.

(13) Rodas-Mendoza, B.; Morera-Pons, S.; Castellote-Bargalló, A. I.; López-Sabater, M. C. Rapid determination by reversed-phase high-performance liquid chromatography of vitamin A and E in infant formulas. *J. Chromatogr. A* **2003**, *1018*, 197−202.

(14) Misir, R.; Loarveld, B.; Blair, R. Evaluation of a rapid method for preparation of fatty acid methyl esters for analysis by gas-liquid chromatography. *J. Chromatogr.* **1985**, *331*, 141−148.

(15) Codex Alimentarius Commission. *The Codex Alimentarius. Volume 8: Fats, Oils and Related Products*, 2nd ed.; Joint FAO/WHO Food Standards Programme; Rome, Italy, 2001.
(16) Reische, D. W.; Lillard, D. A.; Eitenmiller, R. R. Antioxidants. In *Food Lipids*,2nd ed.;Akoh, C. C; Min, D. B., Ed.; Marcel Dekker, Inc.: New York, 2002.
(17) Jeong, M. K.; Yeo, J.; Jang, E. Y.; Kim, M.-J. Aldehydes from oxidized lipids can react with 2,2-diphenyl-1-picrylhydrazyl (DPPH) free radicals in isooctane systems. *J. Am. Oil Chem. Soc.* **2012**, *89*, 1831−1838.
(18) Lhu, S.; Riaz, M. N.; Lusas, E. W. Effect of different extrusion temperatures and moisture content on lipoxygenase inactivation and protein solubility in soybeans. *J. Agric. Food Chem.* **1996**, *44*, 3315−3318.
(19) Beckel, R. W.; Waller, G. R. Antioxidative arginine-xylose Maillard reaction products: Condition for synthesis. *J. Food Sci.* **1983**, *48*, 996−997.
(20) Elizade, B. E.; Bressa, F.; Rosa, M. D. Antioxidative action of Maillard reaction volatiles: Influence of Maillard solution browning level. *J. Am. Oil Chem. Soc.* **1992**, *69*, 331−334.
(21) Jung, M. Y.; Bock, J. Y.; Baik, S. O.; Lee, T. K. Effects of roasting on pyrazine contents and oxidative stability of red pepper seed oil prior to its extraction. *J. Agric. Food Chem.* **1999**, *47*, 1700−1704.
(22) Decker, E. A. Antioxidant Mechanisms. In *Food Lipids*, 2nd ed.;Akoh, C. C, Min, D. B., Eds.; Marcel Dekker, Inc.: New York NY, USA, 2002.
(23) Choe, E.; Min, D. B. Mechanisms and factors of edible oil oxidation. *Comp. Rev. Food Sci. Food Safety* **2006**, *5*, 169−186.

including borate precipitation and reconstitution of vegetable protein. CE−SDS with UV detection was used to detect soy protein in milk powder. The limit of detection (LOD) for soy was about 10% w/w, unless tetraborate precipitation is used, which can lower the LOD to 1% soy.[18]

MS and HPLC−MS have been successfully used to detect adulteration of food. Matrix-assisted laser desorption ionization-time-of-flight (MALDI-TOF) mass spectrometry detected adulteration of ewe's milk with 5% cow's milk.[19] MALDI-TOF detected adulteration of fresh cow's milk with powdered milk at the 1% level using a targeted, proteomics method.[20] Quadrupole-time-of-flight MS (Q-TOF-MS) coupled to HPLC was used to detect 5% soy and pea protein added to SMP in a nontargeted approach, but the method required a borate buffer enrichment step and specialized proprietary software for data analysis.[21,22] The MS-based methods are sensitive and accurate but require extensive sample pretreatment in the case of peptide marker methods, which require protein digestion and borate buffer enrichment.

Amino acid analysis with a standard amino acid analyzer has been used to detect adulteration of SMP by whey proteins.[23] An immunochemical sensor was developed to detect soy, pea, and soluble wheat proteins in milk powders added at 1−5% levels using affinity-purified monoclonal antibodies.[24]

Near-Infrared (NIR) spectroscopy combined with chemometric data analysis is a widely used technique for food authentication and has been applied to dairy products.[25,26] NIR is a simple and fast technique but requires extensive data processing with multivariate techniques to extract useful information from the broad and overlapped spectral features.

Ultrahigh-performance liquid chromatography with UV detection (UHPLC−UV) is a method that provides more discriminating features in the form of sharper, more resolved features (peaks) than NIR.[27] However, the variable axis of UHPLC−UV (retention time) is not as reproducible as NIR (wavelength) due to typical drift and changes in HPLC conditions over time. Software alignment of the UHPLC retention time axis could improve peak alignment and enable UHPLC−UV to be an effective fingerprinting tool for food adulteration detection.

In this study, our objective was to develop a simple, nontargeted UHPLC−UV method for detection of adulteration of SMP by foreign-protein-containing substances using a simple procedure aimed at minimizing sample preparation time. The simplicity of this procedure derives from the data analysis by comparing chromatographic profiles as fingerprints. The fingerprint approach considers the overall pattern of the chromatogram and eliminates the need for protein standards and calibration curves to quantify individual peaks.

MATERIALS AND METHODS

Reagents. Water, acetonitrile, methanol, and formic acid for UHPLC were Optima LCMS grade from Fisher Scientific, (Fairlawn, NJ). Trifluoroacetic acid (Fluka LCMS TFA), sodium citrate tribasic dihydrate, guanidine hydrochloride, and dithiothreitol were all greater than 98% purity from Sigma (St Louis, MO).

Samples. All samples of SMP and protein adulterants were obtained by USP, Rockville, MD, and provided to our laboratory. Medium-heat skim milk powder lot S-085 (32.44% protein) and lot S-094 (32.44% protein) were from sources in the United States. Skim milk powder lot S-095 (32.7% protein) was from a New Zealand source. Soy protein isolate (SPI) lot A-027 (86.95% protein) was from China. Pea protein isolate (PPI) lot A-011 (84% protein), brown rice protein concentrate (BRP) lot A-017 (90.1% protein), and lightly hydrolyzed wheat protein (HWPI) lot A-028 (82.7% protein) were from the United States.

Sample Preparation. Samples were prepared for UHPLC analysis following a procedure based on that of Bordin et al.[28] SMP aliquots of 50.0 ± 0.5 mg were weighed into a 15 mL polypropylene tube, and 10 mL of denaturing buffer (6 M guanidine HCl, 20 mM dithiothreitol, 5 mM trisodium citrate, pH 7) was added to samples. The tubes were immediately vortexed for approximately 30 s and shaken to disperse the SMP. The samples were shaken on a model 2010 Geno-Grinder (Spex Sample Prep, Metuchen, NJ) for 15 min at 1000 rpm. If necessary, the samples were sonicated at room temperature and shaken again on a Geno-grinder to ensure complete dissolution of the SMP. Aliquots of 0.5 mL from the 5 mg/mL samples were further diluted with 1.0 mL of denaturing buffer to produce samples with nominal SMP concentrations of 1.67 mg/mL in microcentrifuge tubes. The samples were vortexed and placed in a refrigerator at 4−8 °C for a minimum of 30 min. Samples were checked for precipitation and then centrifuged at 12 000 rpm for 10 min at 10 °C. Some samples (brown rice protein) required filtering with 0.2 μm polyvinylidene difluoride (PVDF) syringe tip filters. Approximately 1 mL of the samples was transferred to autosampler vials for UHPLC−UV analysis.

Stock solutions (5 mg/mL) of the potential adulterant proteins were prepared as described above for SMP. Volumes of the adulterant stock solution were added to the 5 mg/mL SMP stock to produce the desired level of adulterant in the SMP sample. The percent weight of adulteration is based on the actual weight of materials blended, not on the percentages of protein in SMP and the adulterant protein substances. For example, to make a 1% mixture of adulterated SMP, 100 μL of the adulterant 5 mg/mL stock solution was transferred into a 15 mL polypropylene tube containing 9900 μL of the 5 mg/mL SMP stock solution. The sample was shaken on a Geno-Grinder for 15 min at 1000 rpm. The adulterated SMP sample solution was then processed as described above by further dilution, refrigeration, centrifugation, and transfer to autosampler vial for UHPLC analysis. Five samples of SMP S-085 were prepared and injected multiple times, resulting in 18 chromatograms, and two samples of SMP S-094 and S-095 were prepared and injected twice, for a total of 26 authentic SMP chromatograms. Two preparations of each SPI-adulterated were made and injected four times resulting in eight replicate chromatograms of SPI-adulterated SMP. Single preparations of the PPI-, BRP-, and HWPI-adulterated SMP were made and injected two times, resulting in two replicate chromatograms for each protein adulterant material. The UHPLC sample analysis was initially conducted with authentic SMP S-085 and the adulterated samples of SMP S-085. In a second set of sample analysis, SMP S-085, S-094, and S-095 were chromatographed to provide a larger set of authentic SMP samples. Two samples of each SMP lot were prepared, and each was injected in duplicate to provide four replicate chromatograms. These two sets of samples are identified as sets 1 and 2.

UHPLC Instrumentation. An Acquity UHPLC system from Waters (Milford, MA) equipped with Acquity Sample Manager Module and with e-Lambda PDA wavelength range 190−800 nm with 1.5 μL titanium flow cell was used for UHPLC analysis. The column was a BEH C4 (150 × 2.1 mm, 1.7 um packing) and the guard column was a Vanguard (BEH C4) from Waters. The Acquity Sample Manager module was temperature-controlled, and the sample loop volume was 10 μL. The chromatographic data system was Masslynx from Waters.

RP-HPLC−UV Analysis. Mobile phase A was water + 0.1% TFA. Mobile phase B was acetonitrile + 0.1% TFA. The sample manager weak flush solvent was 10/90 acetonitrile/water, and the strong flush solvent methanol + 0.1% formic acid was used to flush the sample loop after injection. The sample compartment temperature was 10 °C, and the inject volume was 7.5 μL in partial loop needle overflow mode. The mobile phase gradient is shown in Table 1. Column temperature was maintained at 50 °C. The PDA collected 210−800 nm spectra at a sampling rate of 5 Hz, resolution of 1.2 nm, and filter time constant of 0.4 s. The 215 nm wavelength was used for data analysis. Sample sets typically consisted of 14−20 injections. The column was flushed with methanol followed by 70/30 acetonitrile/water (column storage

Table 1. Solvent Program for the UHPLC Method

time (min)	flow (mL/min)	% A	% B
0.0	0.2	70	30
5.0	0.2	70	30
40.0	0.2	50	50
45.0	0.2	50	50
45.1	0.2	20	80
50.0	0.2	20	80
50.1	0.3	70	30
55.0	0.3	70	30

solvent) after each sample set. A few conditioning injections of dilution buffer and SMP samples were made prior to collection of chromatograms for inclusion into the sets for statistical analysis. These injections were made to ensure that retention times were stabilized.

Chromatographic data were collected 300 times a minute for 32 min (from 3 to 35 min) to provide a profile of 9600 points. The result was a final sample matrix that consisted of 82 samples (rows) by 9600 variables (chromatographic profile), including 26 nonadulterated samples and 56 adulterated samples. The chromatographic conditions were chosen after an initial method development period in which parameters such as solvent strength, gradient steepness, flow rate, and temperature were investigated. The conditions used for sample analysis provided a good compromise between resolution, sensitivity, and run time.

Data Formatting For Statistical Analysis. The 0−3 min retention window was excluded, since it gave a very large off-scale "solvent front" peak. Peak retention time (t_R) drift was compensated for by software alignment of chromatograms. Since pure protein standards were not employed in this work, alignment of the independent variable (time) axis is critical to ensure meaningful statistical comparisons and classification of samples as authentic or adulterated without peak integration. Then the raw chromatographic data (3−35 min window) from the data system was copied as a time−intensity list into ASCII format and pasted into a calculation spread sheet (Excel, Microsoft, Redmond WA). The chromatogram data table was imported into Pirouette (Infometrix, Bothell, WA), and the file was saved in a CDF format. The CDF chromatograms of authentic SMP and mixed SMP were aligned to a target SMP chromatogram using correlation-optimized warping (COW) (Lineup, Infometrix, Bothell, WA), and the correlation of the peak profiles was improved to greater than 0.9 in most cases using a warp factor of 10 and segment size of 30 or 60. The target is the standard to which all other sample chromatograms in the set are aligned. In this study a total of 82 chromatograms comprised the data set. The sampling rate of 5 Hz over the elution window of 3−35 min gave a data matrix with 9600 time point variables. The target for alignment was an authentic SMP sample with peaks in the approximate center of the observed range of drift. Aligned files were then copied and combined into a Pirouette table.

Statistical Analysis. *Point-by-Point Data Analysis.* A nontargeted "threshold" classification approach using classical statistics was developed and investigated for its capability to discriminate between nonadulterated SMPs and those adulterated with plant proteins. The threshold classification is based on a t test at each data point as described by Yuk et al.[29] Retention-time-aligned chromatographic files were transferred from Pirouette to Excel, and baseline normalization was performed in Excel to improve the reproducibility of SMP chromatographic fingerprints on the vertical axis (UV response). The baselines were normalized at T = 35 min, where no UV-absorbing analytes eluted at the end of the chromatographic profile. The mean UV intensity at T = 35 min of all chromatograms was subtracted from each data point to perform the normalization. The 99% confidence interval boundaries at each point in the chromatographic profile for nonadulterated SMP were generated by calculating the mean ± 3SD (standard deviations) for all nonadulterated sample chromatograms in the data set. The chromatographic profiles of each adulterated and nonadulterated sample were then compared point-by-point to the 99% confidence boundaries for nonadulterated SMP. The total number of chromatographic points falling outside the 99% confidence boundary was then calculated. A "threshold" was chosen for classification of profiles as nonadulterated or adulterated, corresponding to the total number of chromatographic points that fell outside the 99% confidence.

Chemometric Analysis. Data were analyzed using principal component analysis (PCA) and soft independent modeling of class analogy (SIMCA) using both Pirouette (Infometrix, Bothell, WA) and Solo (eigenvector Research, Inc., Wenatchee, WA). Pretreatment for both PCA and SIMCA consisted of normalization and mean-shifting of the chromatograms to align the data from separate experiments (see below).

Mean-Shifted Chromatograms. Draper et al.[30] have described "mean intensity shifting" as a preprocessing means of removing bias or drift between batches of data collected over long intervals. In this report, we used "mean-shifted chromatograms" to remove differences in the chromatographic profiles that occurred between experiments (see Table 2). For the first experiment, the mean chromatogram was based on only the 14 runs of the pure SMP (S085), and in the second experiment the mean chromatogram was based on the 12 runs of S085, S094, and S095. In each case, the chromatograms were normalized prior to mean shifting. Subtraction of the mean chromatograms from the pure samples provided residuals at each point that were randomly distributed around the means. Subtraction of the mean chromatogram from the adulterated SMP samples provided residuals that were not random but showed systematic deviations due to chemical differences.

Table 2. SMP Standard Lot and Adulterant Sample Set List

			replicates	
standard lot	adulterant	%	set 1	set 2
S085			14	4
S094				4
S095				4
S085	SPI	0.5	8	
S085	SPI	1.0	8	
S085	SPI	3.0	8	
S085	SPI	10.0	8	
S085	PPI	0.5	2	
S085	PPI	1.0	2	
S085	PPI	3.0	2	
S085	PPI	10.0	2	
S085	HWPI	0.5	2	
S085	HWPI	1.0	2	
S085	HWPI	3.0	2	
S085	HWPI	10.0	2	
S085	BRP	0.5	2	
S085	BRP	1.0	2	
S085	BRP	3.0	2	
S085	BRP	10.0	2	

PCA. Data matrices consisting of 82 samples by 9600 variables (full chromatograms) or smaller intervals (e.g., 82 samples by 5100−5500 variables, the optimum region determined by visual comparison of the nonadulterated SMP and SMP adulterated with 10% SPI) were submitted to PCA. Preprocessing of the data consisted of mean-shifting the chromatograms, applying mean scatter correction to vertically align the spectra, and normalizing the intensities of each sample (sum of squares of intensities = 1.0).

SIMCA. There are many options available for chemometric treatment of a large data set. In general, PCA is used as an exploratory method to visually look for patterns and SIMCA is a modeling method for classifying samples as authentic or nonauthentic (adulterated). This treatment was recently used to detect adulterated *Ginkgo biloba* supplements.[31] SIMCA was used to establish the confidence level for

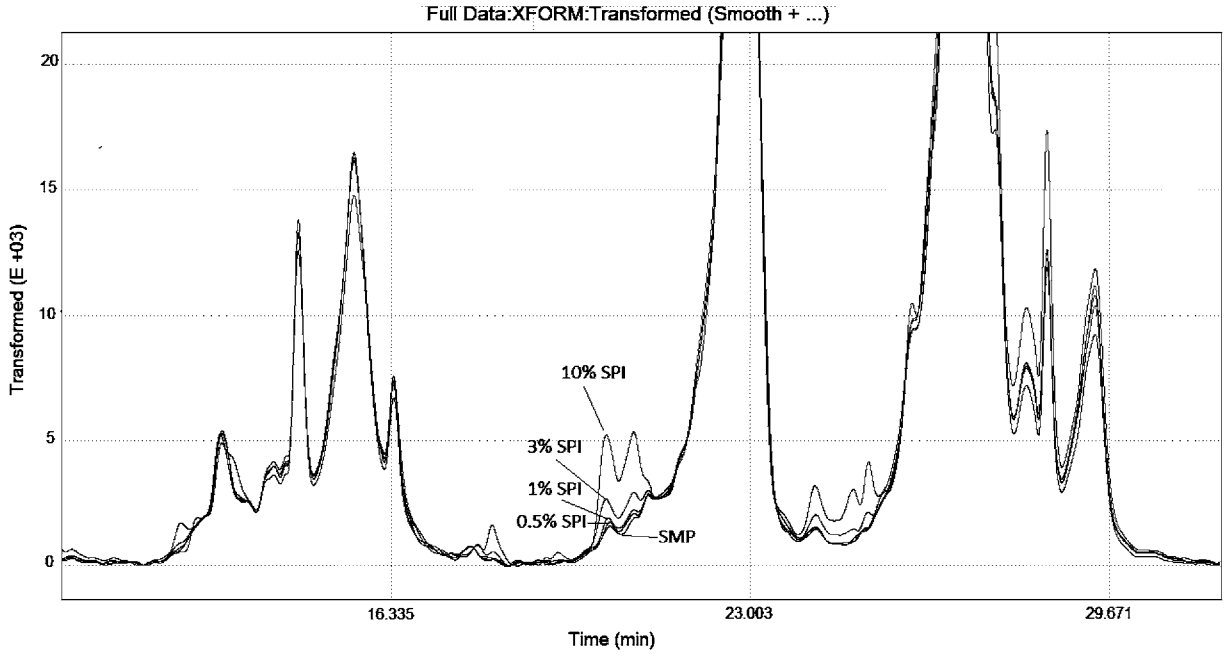

Figure 1. Chromatographic profiles (215 nm) of SMP and SMP mixed with 0.5, 1, 3, and 10% SPI.

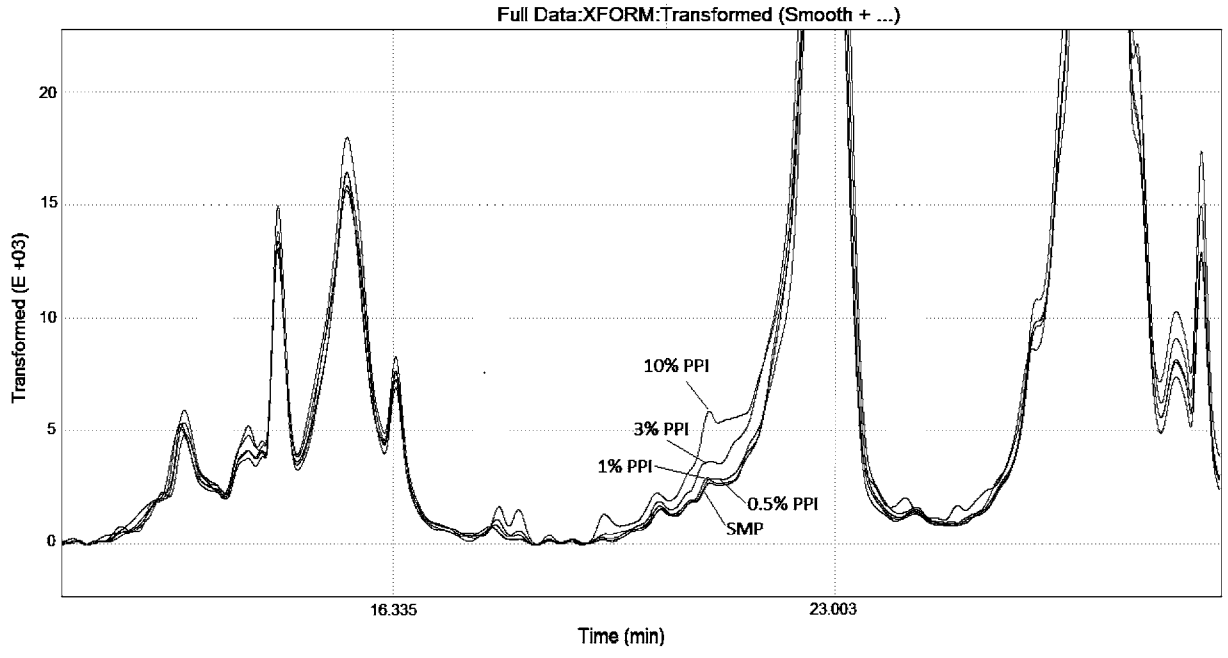

Figure 2. Chromatographic profiles (215 nm) of SMP and SMP mixed with 0.5, 1, 3, and 10% PPI.

detection of protein adulterants in SMP in this study. A single PCA model was constructed on the basis of the nonadulterated SMPs to establish the model boundaries. The Hotelling T^2 residual describes the sample variance accounted for by the model, and the Q residual describes the remaining variance, i.e., the variance not accounted for by the model. Consequently, the Q residual is a good indicator of adulteration if the sample lies outside the 95% confidence limit (or any other predetermined limit).[32]

RESULTS AND DISCUSSION

Chromatographic Profiles. Figure 1 shows overlaid chromatograms of an authentic SMP sample and SMP adulterated with SPI. At the 3% and 10% SPI levels, additional peaks are clearly visible in the SMP chromatographic profile at the 20 and 24 min marks. The visual difference is not as readily observable at the 1% and 0.5% SPI levels, and a statistical treatment of the chromatograms is needed to see if the lower levels of adulteration can be detected with confidence. Figure 2 shows overlaid chromatograms of an authentic SMP sample and SMP adulterated with PPI. The presence of additional peaks at the 21 min mark are visible for the 3 and 10% PPI-adulterated samples. Figure 3 shows overlaid chromatograms of an authentic SMP sample and SMP adulterated with BRP. The presence of additional peaks at the 31 min mark are visible at 3 and 10% adulteration level. At the 0.5% and 1.0% adulteration levels the presence of the additional peaks is hard to visualize and a statistical treatment is clearly necessary to identify SMP

dx.doi.org/10.1021/jf404924x | J. Agric. Food Chem. 2014, 62, 5198−5206

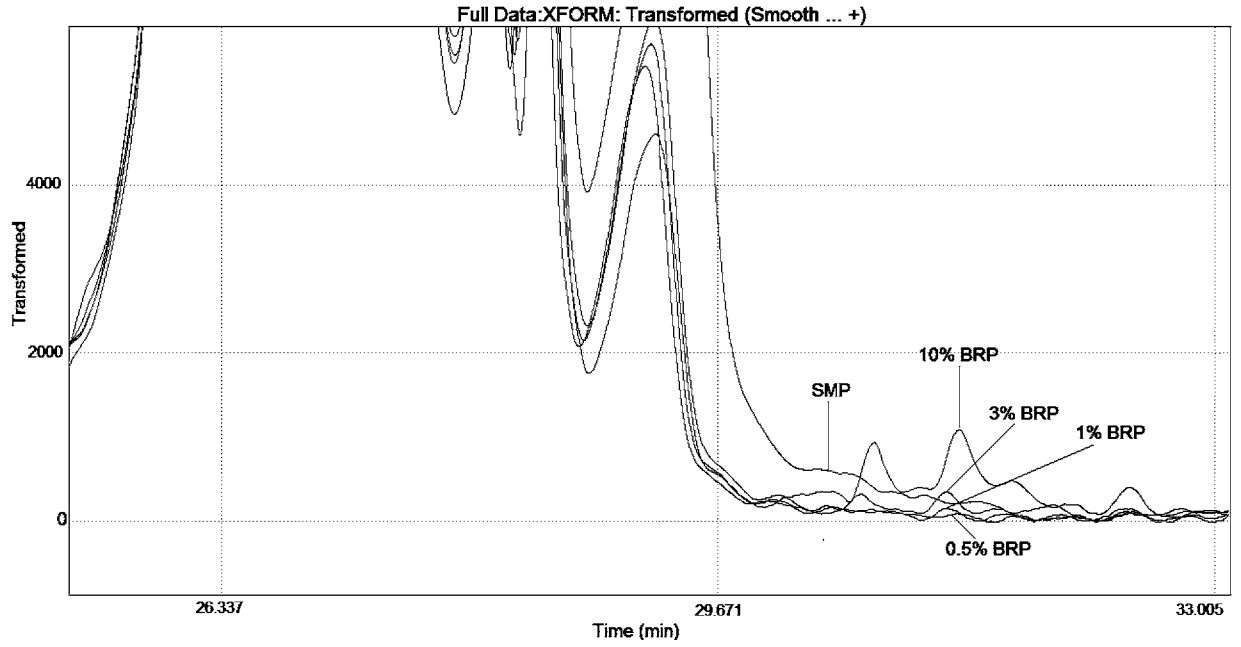

Figure 3. Chromatographic profiles (215 nm) of SMP and SMP mixed with 0.5, 1, 3, and 10% BRP.

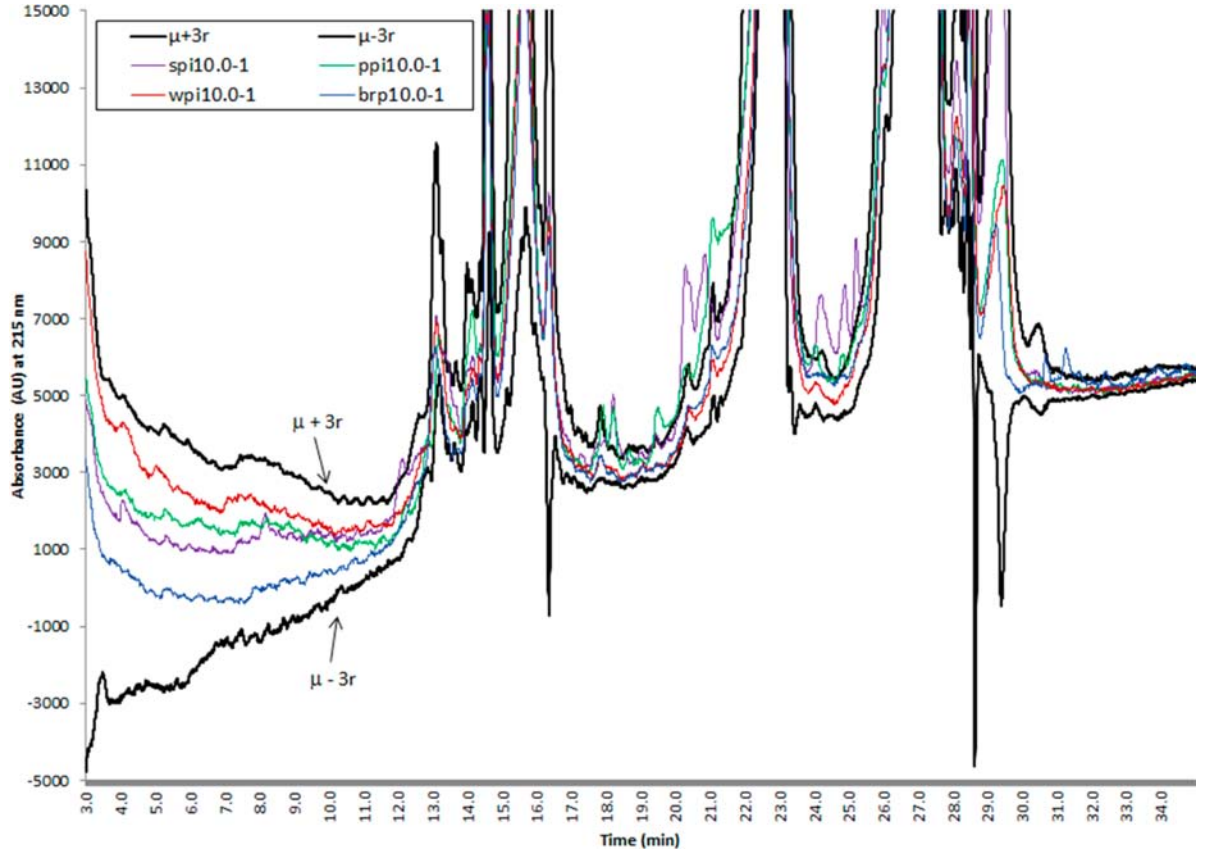

Figure 4. The 99% confidence interval of mean authentic SMP chromatogram (black lines) and chromatograms of 10% adulterated SMP samples: SPI (purple), PPI (green), BRP (blue), HWPI (red).

contaminated with these proteins at levels below 3%. The HWPI-adulterated SMP samples produced chromatograms that were visibly identical to the pure SMP samples (data not shown). Chromatograms of the pure adulterant protein materials are shown in the Supporting Information (Figure S1).

Point-by-Point *t* Test Data Analysis. After vertical alignment, the 99% confidence interval boundaries were determined at each point in the chromatogram by calculating the mean ± 3SD for all 26 nonadulterated chromatograms in the data set. Figure 4 shows chromatograms of 10% w/w blends of each model adulterant overlaid on the 99% confidence

Table 3. Identification of Samples as Nonadulterated or Adulterated versus Threshold with Point-by-Point *t* Test[a]

		25[b]		50[b]		100[b]		200[b]	
sample	adulterant (%)	NEG[c]	POS[c]	NEG	POS	NEG	POS	NEG	POS
SMP	0.0	22	**4**	23	**3**	25	**1**	26	0
SMP + SPI	0.5	**6**	2	**7**	1	**8**	0	**8**	0
SMP + SPI	1.0	**3**	5	**4**	4	**8**	0	**8**	0
SMP + SPI	3.0	0	8	0	8	0	8	0	8
SMP + SPI	10.0	0	8	0	8	0	8	0	8
SMP + PPI	0.5	**2**	0	**2**	0	**2**	0	**2**	0
SMP + PPI	1.0	0	2	0	2	**2**	0	**2**	0
SMP + PPI	3.0	0	2	0	2	**1**	1	**2**	0
SMP + PPI	10.0	0	2	0	2	0	2	0	2
SMP + BRP	0.5	**1**	1	**1**	**1**	**2**	0	**2**	0
SMP + BRP	1.0	**2**	0	**2**	0	**2**	0	**2**	0
SMP + BRP	3.0	**1**	1	**2**	0	**2**	0	**2**	0
SMP + BRP	10.0	0	2	0	2	0	2	0	2
SMP + HWPI	0.5	**1**	1	**1**	1	**2**	0	**2**	0
SMP + HWPI	1.0	**2**	0	**2**	0	**2**	0	**2**	0
SMP + HWPI	3.0	**2**	0	**2**	0	**2**	0	**2**	0
SMP + HWPI	10.0	0	2	**1**	1	**2**	0	**2**	0

[a]Bold values indicate incorrect classification. [b]Threshold is number of data points exceeding the mean ± 3SD boundary. [c]NEG = nonadulterated, POS = adulterated.

interval (mean ± 3SD) boundaries for nonadulterated SMP (dotted lines). Figure 4 demonstrates that all tested adulterants at the 10% spike level, except hydrolyzed wheat protein, exhibit clear chromatographic features that fall outside the 99% confidence boundaries for nonadulterated SMP that should enable correct classification of these samples as adulterated.

A threshold value was established for classification of samples as nonadulterated or adulterated. The threshold was the minimum number of data points in a chromatogram that had to exceed the 99% confidence limits before a sample was classified as adulterated. Table 3 shows the results for this approach based on entire chromatograms (3−35 min window) for 56 adulterant-spiked samples preprocessed using the same retention time and baseline alignment as used for the authentic SMP samples. Four different thresholds from 25 to 200 chromatographic points (0.26−2% of chromatographic points) were investigated. A sample was classified as adulterated if the number of points falling outside the 99% limit exceeded the threshold. Because the test is searching for adulterated samples, a positive result is defined as a sample that exceeds the threshold. In Table 3 there are two distinct trends: the number of "positive" results (samples identified as adulterated) increases as the threshold is decreased, and the number of positive results increases as the level of adulteration increases.

Table 3 makes it clear that the number of false positives (a nonadulterated sample is identified as adulterated, a type I error) and false negatives (an adulterated sample is identified as nonadulterated, a type II error) is dependent on the threshold. For example, if the threshold is 25, then 4 of the authentic SMP samples were identified as adulterated (false positives). With the same 25 point threshold, 6 of the SMP samples adulterated with 0.5% SPI were identified as nonadulterated (false negatives). The number of false positives decreases as the threshold increases and the number of false negatives decreases as the level of adulteration increases. It can be seen that each threshold represents a compromise, the number of false positives for the nonadulterated SMPs balanced against the number of false negatives for the adulterated SMPs

The "detection capability" value can be defined as an estimate of the lowest adulterant spike levels that could be classified as adulterated with 0% false positive classification rate (i.e., no adulterated samples were classified as nonadulterated) based on the data analyzed. There were no misclassifications (false positives) of authentic SMP at the 200 point threshold. Using this strict criteria, the detection capabilities were 3.0% for SPI, 10% for PPI, 10% for BRP, and greater than 10% for HWPI.

The better detection capabilities for PPI and SPI compared to BRP and HWPI can be explained on the basis of the respective fingerprint profiles of each adulterant. SPI and PPI both exhibited more chromatographic profile features compared to BRP and HWPI (Supporting Information). There was a very large peak observed in the void region of the chromatogram, approximately 1.0−2.5 min. This region was not evaluated for differences between chromatograms but would be expected to contain the nonretained species such as amino acids. Therefore, only the 3−35 min retention window was evaluated and processed for this statistical comparison.

Multivariate Data Analysis. Initially, PCA was applied to the full chromatograms (9600 data points) of the authentic samples and SPI adulterated samples from set 1. The PCA score plot showed poor discrimination between the authentic and adulterated samples (data not shown). Only the 10% SPI was clearly separated from the cluster of authentic samples. This observation was also supported by a SIMCA model (data not shown).

Visual examination of Figure 1 shows that there are two regions (20.0−21.3 and 28.0−29.5 min) where there are distinct differences between the SMP and SPI chromatographic profiles. PCA score plots of just the data from 20.0−21.3 min showed a clear separation of the 1%, 3%, and 10% adulterated samples from the authentic samples (Figure 5A). Supporting results were obtained with SIMCA (Figure 5B). All samples with 10% SPI fell above the 95% confidence limit and were judged to be adulterated. Seven of the eight samples with 1% SPI and six of the eight samples with 0.5% SPI were judged to be adulterated.

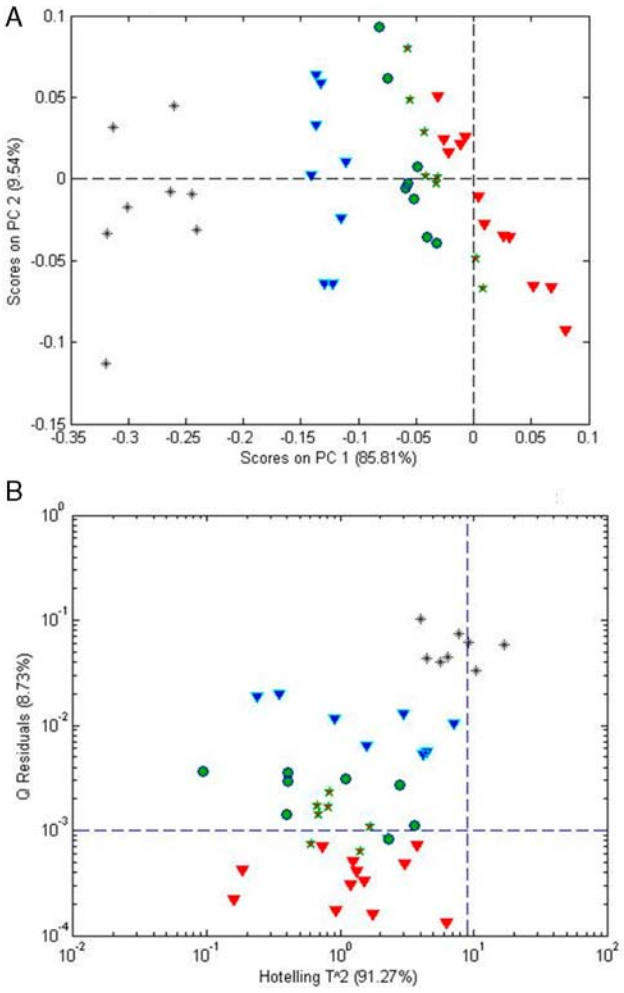

Figure 5. (A). PCA score plot of non-adulterated and SPI-adulterated SMP samples from Set 1: red triangles = SMP lot S085; green stars = 0.5% SPI; green circles = 1.0% SPI; blue triangles = 3.0% SPI; black asterisks = 10% SPI. (B) SIMCA plot of Q-Residuals versus samples for non-adulterated and SPI-adulterated SMP samples from Set 1: red triangles = SMP lot S085; green stars = 0.5% SPI; green circles = 1.0% SPI; blue triangles = 3.0% SPI; black asterisks = 10% SPI.

PCA of SMP samples adulterated with PPI produced results similar to those adulterated with SPI (data not shown). Poor discrimination was observed using the full chromatogram, but the same selected time interval (20.0−21.3 min; see Figure 2) produced improved separation. SIMCA identified 100% of the samples with 10% and 3% PPI as adulterated but was unable to detect adulteration at the 1% or 0.5% level. PCA of SMP samples adulterated with HWPI and BRP failed to reveal any adulteration using the full chromatogram or any selected time interval (data not shown). Additional lots of SMP were analyzed in a second analytical set, experiment 2, to provide a broader range of authentic SMP to model.

PCA of the combined data from sets 1 and 2 showed distinct differences between the authentic samples (Supporting Information, Figure S2). In fact, the authentic and adulterated (with SPI) samples from set 1 were more similar than the authentic samples from sets 1 and 2. This is particularly revealing since the authentic sample from set 1 (S085) was repeated in set 2. SIMCA based on the nonadulterated SMP from set 1 (S085) showed that the nonadulterated SMPs from set 2 (S085, S094, and S095) were well outside the 95% confidence limit (Supporting Information, Figure S3). These results were observed for both the full chromatogram and the 20.0−21.3 min range. It was apparent that there was a major shift in the chromatograms between the two experiments.

The disparity in the chromatograms was minimized by mean-shifting the data (see Materials and Methods). Briefly, the mean chromatogram for the nonadulterated SMPs of each experiment (sets 1 and 2) was subtracted from all the samples of that experiment. Thus, the basic chromatographic shape was removed from the data, leaving randomly distributed residuals for the nonadulterated SMPs. Only the systematic bias of the adulterated samples provided nonrandom residuals. After mean-shifting sets 1 and 2, the PCA scores of the authentic samples were well-aligned (Supporting Information, Figure S4), and SIMCA showed that both sets of authentic samples fell within the 95% confidence limit (Supporting Information, Figure S5).

Figure 6 shows PCA and SIMCA plots after all the authentic samples from both data sets have been combined into one model and labeled identically. The plot shows adulteration with SPI examined over the 20.0−21.3 min interval. Figure 6A clearly shows that there is no difference in the authentic SMPs from sets 1 and 2. All but the 0.5% SPI samples appear well-separated from the authentic SMPs. This is also shown in the Q residuals plot for SIMCA in Figure 6B. Six of the eight samples with 1% SPI and four of the eight samples with 0.5% SPI are judged to be adulterated.

For the combined data sets, SIMCA identified all of the samples with 10% and 3% PPI as adulterated using the chromatographic region between 20.0 and 21.3 min. One of the two samples with 1% PPI was judged adulterated and none of the 0.5% PPI samples were determined to be adulterated. None of the samples containing HWPI or BRP were judged to be adulterated, either examining the full chromatogram or an isolated region.

In general, the results obtained by multivariate analysis were very similar to those obtained using point-by-point analysis. This is expected since both methods examine deviations of the chromatographic signal with respect to the analytical variance. Multivariate analysis of the entire chromatogram is less sensitive to changes in chromatographic features than a point-by-point analysis, since the variance of the whole chromatogram, even for random noise, accumulates with the square root of the number of data points. Thus, the variance for the 9600 data points of the full chromatogram is roughly 100 times greater than seen using a point-by-point analysis. The point-by-point analysis can detect much smaller changes in the chromatogram but is also more subject to random variations. Consider that 1% of the data will fall above the 99% confidence limit. For 9600 points, that is 96 possible false positives. However, the data are not totally random, they are correlated with their near neighbors since the chromatographic peaks have a finite width. Possibly the best strategy is achieved by using point-by-point analysis to identify a selected region for application of multivariate analysis. This process of feature selection is warranted when an unknown test material can be compared to an authentic material.

Experimental Factors. The chromatographic data for the two experiments, which occurred 6 months apart, suggest that additional sample analysis will be required to verify the utility of UHPLC fingerprinting with chemometric data treatment. The change in protein peak retention times is relatively small over a given run of consecutive samples and time-axis shifts are easily

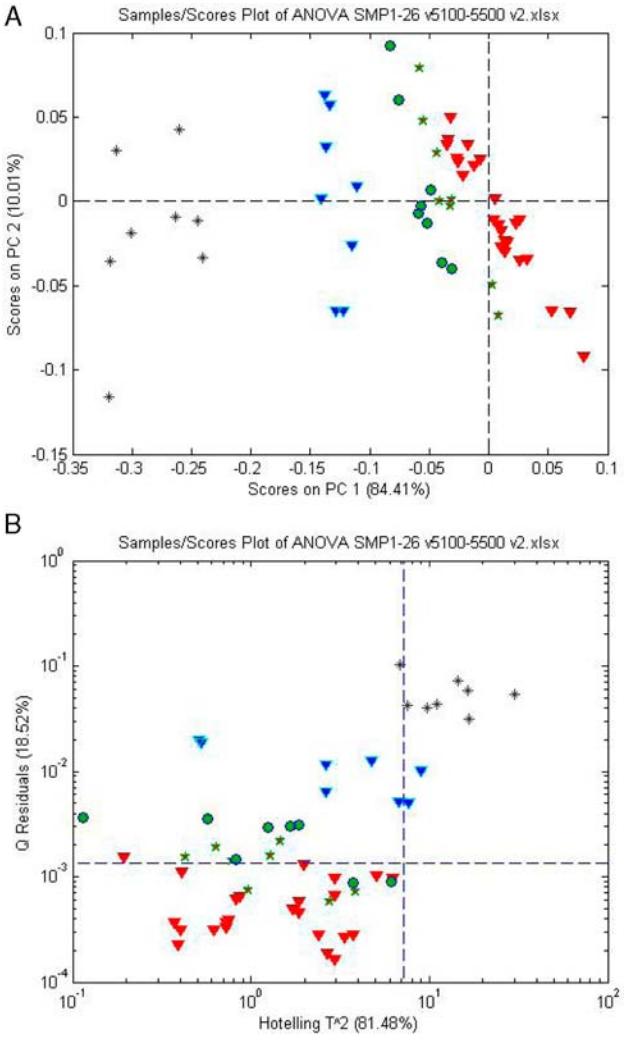

Figure 6. (A). PCA score plot of non-adulterated and SPI-adulterated SMP samples from Set 1 and 2 combined: red triangles = SMP lots S085, S094, and S095; green stars = 0.5% SPI; green circles = 1.0% SPI; blue triangles = 3.0% SPI; black asterisks = 10% SPI. (B) SIMCA plot of Q-Residuals versus samples for non-adulterated and SPI-adulterated SMP samples from Set 1 and 2 combined: red triangles = SMP lots S085, S094, and S095; green stars = 0.5% SPI; green circles = 1.0% SPI; blue triangles = 3.0% SPI; black asterisks = 10% SPI.

aligned by the COW software. Dealing with the peak intensity changes over time and between batches is more difficult. The variance in the SMP peak intensities is fairly high for the major peaks. Normalization of the chromatograms is likely to reduce or change adulterant peak height along with SMP peak height and lead to error in estimation of the adulterant peak intensity. Regions of the SMP chromatogram that show the least variance (show relatively flat baselines) should be selected for statistical analysis. This allows detection of prominent adulterant peaks that elute in selected retention windows for best probability.

Chromatograms of the SMP proteins were evaluated at 215 and 280 nm. The profiles appeared to have very similar signal-to-noise (S/N) ratios. The 215 nm wavelength produced higher absolute intensities for the protein peaks, so it was chosen as the wavelength for data processing. The S/N with UHPLC–UV systems is negatively impacted by TFA in the mobile phase. TFA is a known to induce baseline noise due to its strong absorbance at the low-UV wavelengths needed to detect proteins.[33]

In summary, the potential of single wavelength UHPLC to classify SMP as pure versus adulterated by foreign proteins is demonstrated. Feature-rich protein adulterants, such as SPI and PPI, present in SMP at approximately at or above 3% w/w produce observable additional peaks in the nominal SMP UHPLC profile. The UHPLC–UV fingerprinting technique shows the ability to differentiate SMP from SMP adulterated with SPI at 3% w/w from point-by-point *t* test comparison of chromatograms. With SIMCA analysis after mean-shifting the profiles it was possible to incorporate samples from different experiments and to differentiate all SPI-adulterated samples in the range from 1.0 to 10.0% at 95% confidence level. A larger sample set including SMP from more sources is needed to confirm and validate the procedure.

■ ASSOCIATED CONTENT

Ⓢ Supporting Information

Figure S1 shows chromatograms of individual test substances (a) skim milk powder, (b) pea protein isolate, (c) soy protein isolate, (d) brown rice protein powder, and (e) hydrolyzed wheat protein isolate. Figures S2–S5 show additional chemometric analysis of the SMP samples adulterated with SPI. This material is available free of charge via the Internet at http://pubs.acs.org.

■ AUTHOR INFORMATION

Corresponding Author

*Telephone: 708-924-0615. Fax: 708-924-0690. E-mail: joseph.jablonski@fda.hhs.gov.

Notes

The authors declare no competing financial interest.

■ REFERENCES

(1) USDA. Nonfat Dry Milk Production and Consumption: Summary For Selected Countries; http://www.fas.usda.gov/psdonline/circulars/dairy.pdf (accessed 8/28/2012).

(2) Codex Standard for Milk Powders and Cream Powder (CSX_07e.pdf from http://www.codexalimentarius.org/standards/list-of-standards/en/?no_cache=1) (accessed 10/13/2012).

(3) DeVries J. 2009. U.S. Pharmacopeia's Food Ingredients Intentional Adulterants Advisory Panel. Presented at USP's 2009 Food Ingredients Stakeholder Forum. http://www.usp.org/pdf/EN/stakeholderForums/foodAdditives/Aug2009/2009-08-04FISFPresentationspdf.pdf (slides 80–91).

(4) United States Code, 2010 Edition, Title 21-Food and Drugs, Chapter 9-Federal Food, Drug, and Cosmetic Act, Subchapter IV-Food, Sec 342-Adulterated Food.

(5) Moore, J. C.; Spink, J.; Lipp, M. Development and Application of a Database of Food Ingredient Fraud and Economically Motivated Adulteration from 1980 to 2010. *J. Food Sci.* **2012**, *4*, R118–R126.

(6) Xin, H.; Stone, R. Tainted Milk Scandal: Chinese Probe Unmasks High-Tech Adulteration with Melamine. *Science* **2008**, *322*, 1310–1311.

(7) Better Coordination Could Enhance Efforts To Address Economic Adulteration and Protect the Public Health. United States Government Accountability Office, GAO-12-46, October 2011.

(8) *Modern Techniques for Food Authentication*, 1st ed.; Sun, D.-W., Ed.; Academic Press: Burlington, MA, 2008.

(9) Cordella, C.; Moussa, I.; Martel, A.-C.; Sbirrazuoli, N.; Lizzani-Cuvelier, L. Recent Developments in Food Characterizaation and Adulteration Detection: Technique-Oriented Perspectives. *J. Agric. Food Chem.* **2002**, *50*, 1751–1764.

(10) Lavine, B. K.; Workman, J. Chemometrics. *Anal. Chem.* **2010**, *82*, 4699−4711.
(11) Visser, S. J.; Slangern, C. J.; Rollema, H. S. Phenotyping of Bovine Milk Proteins by Reversed-Phase High-Performance Liquid Chromatography. *J. Chromatogr.* **1991**, *548*, 361−370.
(12) Rodrigues, N.; Ortiz, M. C.; Sarabia, L.; Gredilla, E. Analysis of Protein Chromatographic Profiles Joint to Partial Least Squares to Detect Adulterations in Milk Mixtures and Cheeses. *Talanta* **2008**, *81*, 255−264.
(13) Veloso, A. C. A.; Teixeira, N.; Ferreira, I.; MP, L. V. O. Separation and Quantification of the Major Casein Fractions by Reverse-Phase High-performance Liquid Chromatography and Urea−Polyacrylamide Gel Electrophoresis Detection of Milk Adulterations. *J. Chromatogr. A* **2002**, *967*, 209−218.
(14) Johnson, P.; Philo, R.; Watson, A.; Mills, E. N. C. Rapid Fingerprinting of Milk Thermal Processing History by Intact Mass Spectrometry with Nondenaturing Chromatography. *J. Agric. Food Chem.* **2011**, *59*, 12420−12427.
(15) Dziuba, J.; Nalecz, D.; Minkiewicz, P.; Dziuba, B. Identification and Determination of Milk and Soybean Protein Preparations Using Enzymatic Hydrolysis Follwed by Chromatgraphy and Chemometrical Data Analysis. *Anal. Chim. Acta* **2004**, *521*, 17−24.
(16) Commission Regulation (EEC) No. 2426/90 of 21 August, 1990, amending Regulation (EEC) No. 1725/79 on the rules for granting aid to skimmed milk processed into compound feedingstuffs and skimmed-milk powder intended in particular for feed for calves.
(17) Manso, M. A.; Cattaneo, T. M.; Barzghi, S.; Olieman, C.; López-Fandino, R. Determination of Vegetal Proteins in Milk Powder by Sodium Dodecyl Sulfate−Capillary Gel Electrophoresis: Interlaboratory Study. *J. AOAC, Intl* **2002**, *85*, 1090−1095.
(18) López-Tapia, J.; Garcia-Risco, M. R.; Manso, M. A.; López-Fandino, R. Detection of the Presence of Soya Protein in Milk by Sodium Docdecyl Sulfate Capillary Electrophoresis. *J. Chromatogr. A* **1999**, *836*, 153−160.
(19) Cozzolino, R.; Passalacqua, S.; Salemi, S.; Malvagna, P.; Spina, E.; Garozzo, D. Identification of Adulteration in Milk by Matrix-Assisted Laser Desorption Time-of-Flight Mass Spectrometry. *J. Mass Spectrom.* **2001**, *36*, 1031−1037.
(20) Calvano, C. D.; Monopoli, A.; Loizzo, P.; Faccia, M.; Zambonin, Z. G. A Proteomic Approach Based on MALDI-TOF MS To Detect Powdered Milk in Fresh Cow Milk. *J. Agric. Food Chem.* **2013**, *61*, 1609−1617.
(21) Luykx, D. M. A. M.; Cordewener, J. H. G.; Ferranti, P.; Frankhuizen, R.; Bremer, M. G. E. G.; Hooijerink, H.; America, A. H. P. Identification of Plant Proteins in Adulterated Skimmed Milk Powder by High-Performance Liquid Chromatography-Mass Spectrometry. *J. of Chromatogr.A* **2007**, *1164*, 189−197.
(22) Cordewener, J. H. G.; Luykx, D.M.AM.; Frankhuizen, R.; Bremer, M. G. E. G.; Hooijerink, H.; America, A. H. P. Untargeted LC-Q-TOF Mass Spectrometry Method for the Detection of Adulteration in Skimmed-Milk Powder. *J. Sep. Sci.* **2009**, *32*, 1216−1223.
(23) Greenberg, R.; Dower, H. J. Detection of Added Whey Protein Concentrate in Nonfat Dry Milk by Amino Acid Analysis. *J. Agric. Food Chem.* **1986**, *34*, 30−32.
(24) Hasnoot, W.; Olieman, K.; Cazmemier, G.; Verheijen, R. Direct Biosensor Immunoassays for the Detection of Nonmilk Proteins in Milk Powder. *J. Agric. Food Chem.* **2001**, *49*, 5201−5206.
(25) *Near-Infrared Spectroscopy in Food Science and Technology*; Ozaki, Y., McClure, W. F., Christy, A. A., Eds.; John Wiley & Sons: Hoboken, NJ, 2007; Chapter 8.4.
(26) Maraboli, A. M.; Cattaneo, T. M. P.; Giangiacomo, R. Detection of Vegetable Proteins from Soy, Pea and Wheat Isolates in Milk Powder by Near Infrared Spectroscopy. *J. Near Infrared Spectrosc.* **2002**, *10*, 63−60.
(27) CFR PART 211—Current Good Manufacturing Practice for Finished Pharmaceuticals Subpart I—Laboratory Controls, Sec. 211.165 Testing and Release for Distribution.http://www.accessdata.fda.gov/scripts/cdrh/cfdocs/cfCFR/CFRSearch.cfm?fr=211.165 (accessed 04/22/2013).
(28) Bordin, G.; Raposo, F. C.; de la, Calle B.; Rodriguez, A. R. Identification of Major Bovine Milk Proteins by Liquid Chromatography. *J. Chromatogr. A* **2001**, *928*, 63−76.
(29) Yuk, J.; McIntyre, K. K. L.; RFischer, C.; Hicks, J.; Colson, K. L.; Lui, C.; Brown, D.; Arnason, J. T. Distinguishing Ontario ginseng landraces and ginseng species using NMR-based metabolomics. *Anal. Bioanal, Chem.* **2013**, *13*, 4499−4509.
(30) Draper, J.; Lloyd, A. J.; Goodacre, R.; Beckman, M. Flow Infusion Electrospray Ionization Mass Spectrometry for High Throughput, Non-Targeted Metabolite Fingerprinting: A Review. *Metabolomics* **2013**, *9*, S4−S29.
(31) Harnly, J. M.; Luthria, D.; Chen, P. Detection of Adulterated Ginkgo Biloba Supplements using Chromatographic and Spectral Fingerprints. *J. AOAC, Int.* **2012**, *95*, 1579−1587.
(32) Brereton, R. G. *Chemometrics for Pattern Recognition*; John Wiley & Sons, West Sussex, UK, 2009; ISBN 978-0-470-98725-4.
(33) Choikhet, K., Glatz, B. Rozing, G. The Physiochemical Causes of Baseline Disturbances in HPLC. Part I—TFA-Containing Eluents. *LC-GC Eur.* February 2003.http://www.chromatographyonline.com/lcgc/data/articlestandard//lcgceurope/052003/45019/article.pdf (accessed 10/15/2012).

Table 1. Sample Weight (kg) and Concentrations of *n*-3 LCPUFAs (mg/100 g Edible Part) and MeHg (μg/kg Edible Part) in Marine Fish from Zhoushan[a]

scientific name	sample wt		*n*-3 DPA		EPA + DHA		MeHg	
	mean	std	mean	std	mean	std	mean	std
Trichiurus lepturus	0.92	0.14	54.4	11.5	590.7	57.2	22.8	3.1
Larimichthys polyactis	0.53	0.07	40.3	6.1	758.9	110.8	15.9	2.7
Pampus argenteus	0.65	0.08	19.6	4.8	175.6	28.8	18.8	2.7
Collichthys lucidus	0.92	0.13	5.5	6.5	181.3	37.1	12.2	0.8
Hapaloyenys mucronatus	1.08	0.17	88.7	25.6	358.0	105.8	56.3	4.1
Pampus chinensis	1.00	0.13	71.6	12.3	470.3	93.2	22.4	3.7
Cynoglossus robustus	0.92	0.10	32.7	5.5	228.0	37.3	27.2	13.1
Muraenesox bagio	1.13	0.16	87.0	15.2	836.4	175.7	34.8	6.0
Conger myriaster	1.08	0.15	130.8	21.9	893.8	124.0	40.6	5.2
Nibea albiflora	1.20	0.12	55.1	17.4	413.4	73.0	36.2	3.2
Sebastiscus marmoratus	1.00	0.16	41.6	10.3	448.9	98.6	39.6	7.2
Thamnaconus modestus	1.33	0.17	4.4	5.9	137.2	40.1	17.2	2.0
Scomber japonicus	1.13	0.15	84.8	11.0	1251.4	146.5	16.4	1.9
Scomberomorus niphonius	1.08	0.13	34.6	7.7	520.9	94.0	27.4	2.7
Ilisha elongata	1.37	0.15	58.4	5.8	733.1	42.8	36.5	6.7
Argyrosomus argentatus	1.20	0.11	18.0	4.8	205.4	41.4	62.7	3.1
Miichthys miiuy	1.03	0.08	23.9	15.0	453.6	60.3	16.2	1.7
Scoliodon sorrakowah	2.33	0.28	6.1	1.3	75.5	12.7	166.6	29.4
Sparus macrocephalus	1.09	0.10	135.7	29.6	678.8	142.0	30.5	3.8
Harpadon nehereus	1.13	0.10	1.6	2.5	189.7	32.5	14.1	4.4
Arius sinensis	0.97	0.12	71.0	27.6	533.7	172.5	58.4	4.8
Raja porosa	1.08	0.12	18.2	4.3	123.6	36.8	47.6	4.7
Mugil cephalus	1.10	0.13	84.5	106.8	266.3	268.0	7.7	5.3
Lateolabrax maculatus	1.23	0.19	92.5	24.5	858.5	230.3	21.0	2.8
Trachinotus ovatus	0.87	0.11	199.8	22.5	891.0	110.8	24.1	4.6
Hexagrammos otakii	1.13	0.14	10.1	1.8	379.8	24.6	20.6	1.8
Oplegnathus fasciatus	1.07	0.13	84.4	12.8	469.8	20.6	27.7	5.7
Rhabdosargus sarba	1.00	0.13	100.1	15.8	568.1	96.8	48.0	3.8
Seriola quinqueradiata	0.97	0.14	7.0	4.7	96.0	4.2	28.6	1.3
Auxis thazard	1.03	0.12	81.5	11.5	2458.2	395.1	122.8	4.9
Coilia nasus	0.93	0.14	112.9	28.5	1186.2	142.7	14.9	7.8

[a]The data of *n*-3 DPA, EPA, and DHA of all studied species[26] and the mean of MeHg concentration of majority studied species[27] could be obtained from Chinese published articles.

for regional specific assessment.[18] The concentrations of specific fatty acids and total mercury in some Chinese marine/freshwater fish were reported,[12,19] but there are clear location differences in MeHg concentrations and species differences in DHA concentrations in marine fish,[20] and there is little information on assessment of net neurodevelopmental effect via maternal marine fish consumption in China. In response to this public health concern, we calculated and integrated benefits of DHA and risks of MeHg caused by maternal consumption of some edible marine fish farmed or grown in Zhoushan, southeast China, to assess the net neurodevelopmental effect of these species according to the aforementioned FAO/WHO approach.

MATERIALS AND METHODS

Samples Collection and Preparation. Common edible marine fish were collected between September and October 2011 from Zhoushan archipelago, which is a major fish farming area in southeast China. A total of thirty-one species (6 samples/species, 1 individual fish/sample) were purchased from local piers or traditional markets. All fish samples were farmed or grew locally and were medium-sized (Table 1). Scientific names have been used to represent the species in this article.

Edible parts of samples were prepared by collectors. The processed filet of each sample was homogenized and expressed directly into a separate plastic container, and was frozen immediately at −20 °C for further analysis.

Sample Analysis. Total lipids were extracted from 2 g of thawed sample by 50 mL of chloroform−methanol (2:1, by volume[21]). The preparation of fatty acid methyl esters (FAME) was operated according to a method described previously.[22] FAME was analyzed by gas chromatography. Heneicosanoic acid was used as internal standard.

MeHg was extracted from 1 g of thawed sample, and the concentrations of MeHg were analyzed by a method published previously.[23]

Methodology of Assessment of Net Neurodevelopmental Effect. The benefit−risk assessment approach developed by FAO/WHO[18] was used. Equations for quantitative integration which focus on net IQ point gain are listed as follows, and the meanings of all parameters in eqs 1 and 2 are available in a published brochure:[18]

$$\text{IQ point loss} = [\text{MeHg}] \times 100(x/7) \div 60 \times 9.3 \times (-0.18 \text{ or } -0.7) \quad (1)$$

where −0.18 is the central estimate of IQ points gained per microgram per gram of hair mercury gained, and −0.7 is the upper-bound estimate of IQ points gained per microgram per gram of hair mercury gained.[18] In our study we choose −0.7 for the reason of more conservative assessment.

dx.doi.org/10.1021/jf500343w | J. Agric. Food Chem. 2014, 62, 5207−5213

Table 2. Change of IQ Points via Common and Extreme Maternal Consumption Scenarios

	common consumption scenario						extreme consumption scenario					
	IQ gain		IQ loss		net IQ gain		IQ gain		IQ loss		net IQ gain	
scientific name	mean	std	mean	std	mean	std	mean	std	mean	std	mean	std
Trichiurus lepturus	4.0	0.4	0.1	0.0	3.9	0.4	5.8	0.0	0.2	0.0	5.6	0.0
Larimichthys polyactis	5.0	0.7	0.0	0.0	5.0	0.7	5.8	0.0	0.1	0.0	5.7	0.0
Pampus argenteus	1.2	0.2	0.1	0.0	1.1	0.2	3.0	0.5	0.1	0.0	2.9	0.5
Collichthys lucidus	1.2	0.2	0.0	0.0	1.2	0.2	3.1	0.6	0.1	0.0	3.0	0.6
Hapaloyenys mucronatus	2.4	0.7	0.2	0.0	2.2	0.7	5.3	0.7	0.4	0.0	4.9	0.6
Pampus chinensis	3.2	0.6	0.1	0.0	3.1	0.6	5.8	0.0	0.2	0.0	5.6	0.0
Cynoglossus robustus	1.5	0.2	0.1	0.0	1.5	0.3	3.9	0.6	0.2	0.1	3.7	0.7
Muraenesox bagio	5.2	0.9	0.1	0.0	5.1	0.9	5.8	0.0	0.2	0.0	5.6	0.0
Conger myriaster	5.6	0.4	0.1	0.0	5.5	0.4	5.8	0.0	0.3	0.0	5.5	0.0
Nibea albiflora	2.8	0.5	0.1	0.0	2.7	0.5	5.7	0.2	0.3	0.0	5.5	0.2
Sebastiscus marmoratus	3.0	0.7	0.1	0.0	2.9	0.7	5.7	0.2	0.3	0.1	5.4	0.2
Thamnaconus modestus	0.9	0.3	0.0	0.0	0.9	0.3	2.4	0.7	0.1	0.0	2.2	0.7
Scomber japonicus	5.8	0.0	0.0	0.0	5.8	0.0	5.8	0.0	0.1	0.0	5.7	0.0
Scomberomorus niphonius	3.5	0.6	0.1	0.0	3.4	0.6	5.8	0.0	0.2	0.0	5.6	0.0
Ilisha elongata	4.9	0.3	0.1	0.0	4.8	0.3	5.8	0.0	0.3	0.0	5.5	0.0
Argyrosomus argentatus	1.4	0.3	0.2	0.0	1.2	0.3	3.5	0.7	0.4	0.0	3.1	0.7
Miichthys miiuy	3.0	0.4	0.0	0.0	3.0	0.4	5.8	0.0	0.1	0.0	5.7	0.0
Scoliodon sorrakowah	0.5	0.1	0.5	0.1	0.1	0.1	1.3	0.2	1.2	0.2	0.1	0.3
Sparus macrocephalus	4.5	0.9	0.1	0.0	4.4	0.9	5.8	0.0	0.2	0.0	5.6	0.0
Harpadon nehereus	1.3	0.2	0.0	0.0	1.2	0.2	3.3	0.6	0.1	0.0	3.2	0.6
Arius sinensis	3.6	1.2	0.2	0.0	3.4	1.2	5.6	0.6	0.4	0.0	5.2	0.5
Raja porosa	0.8	0.2	0.1	0.0	0.7	0.2	2.1	0.6	0.3	0.0	1.8	0.6
Mugil cephalus	1.8	1.8	0.0	0.0	1.8	1.8	3.0	2.2	0.1	0.0	3.0	2.2
Lateolabrax maculatus	5.2	0.7	0.1	0.0	5.1	0.7	5.8	0.0	0.1	0.0	5.7	0.0
Trachinotus ovatus	5.7	0.3	0.1	0.0	5.6	0.3	5.8	0.0	0.2	0.0	5.6	0.0
Hexagrammos otakii	2.5	0.2	0.1	0.0	2.5	0.2	5.8	0.0	0.1	0.0	5.7	0.0
Oplegnathus fasciatus	3.1	0.1	0.1	0.0	3.1	0.1	5.8	0.0	0.2	0.0	5.6	0.0
Rhabdosargus sarba	3.8	0.6	0.1	0.0	3.7	0.6	5.8	0.0	0.3	0.0	5.5	0.0
Seriola quinqueradiata	0.6	0.0	0.1	0.0	0.6	0.0	1.7	0.1	0.2	0.0	1.5	0.1
Auxis thazard	5.8	0.0	0.3	0.0	5.5	0.0	5.8	0.0	0.9	0.0	4.9	0.0
Coilia nasus	5.8	0.0	0.0	0.0	5.8	0.0	5.8	0.0	0.1	0.1	5.7	0.1

$$\text{IQ point gain} = [\text{EPA} + \text{DHA}] \times 100 \times 0.67 \times (x/7) \times 0.04 \quad (2)$$

The maximum IQ gain from maternal consumption of EPA plus DHA was estimated at 5.8 points, with no further benefits with increasing consumption thereafter.[18]

Combining eqs 1 and 2 then gives a relationship between net IQ point gain and specific species consumption due to MeHg and *n*-3 LCPUFA intake:

$$\text{net IQ point gain} = \{[\text{EPA} + \text{DHA}] \times 2.68 \div 7 - [\text{MeHg}] \times 1.55\}x \quad (3)$$

where [EPA + DHA] is the total concentration of EPA plus DHA in fish (mg/g); MeHg] is the concentration of methylmercury in fish (μg/g); and x is the number of maternal servings of fish per week (100 g/serving).

We estimated maternal intake of EPA plus DHA and MeHg from specific species consumption by two possible consumption patterns. According to "2002 China National Nutrition and Health Survey" (2002 CNNHS), the mean value of fish intake (including marine fish and freshwater fish) in China was 24.8 g/standard man-day (i.e., about 175 g/week of fish consumption), but coastal Chinese appear to have much higher consumption of aquatic foods, especially marine fish. According to data from "2007 Chinese Total Diet Study", people who live in Fujian province, which is a coastal province of southeast China, had the highest marine fish consumption among all studied provinces in China (64.47 g/day, i.e., about 450 g/week of marine fish consumption).[24] Therefore, 175 and 450 g/week of filet consumption were applied in equations, respectively, to represent the maternal common and extreme consumption scenarios of specific species.

The joint FAO/WHO expert committee on food additives (JECFA) has established a provisional tolerable weekly intake (PTWI) of 1.6 μg/kg bw for MeHg.[25] In our study, 60 kg was considered to be the body weight of a pregnant woman/mother,[18,25] in order to determine if the calculated results of maternal weekly MeHg intake exceeded the PTWI.

We used probabilistic computation to represent uncertainty of sample variations, if the calculated results of the FAO/WHO deterministic approach could not provide a clear dietary recommendation for some species. Monte Carlo simulation was applied in probabilistic computation for these species to generate probabilistic distribution for the net neurodevelopmental effect caused by quantified uncertainties.

There would be an optimal number of weekly servings (i.e., "optimal x") of specific species for neurodevelopment according to eq 3, because the maximum positive effect from intake of EPA plus DHA is definite (5.8 points[18]). The "optimal x" of specific species could be determined by the relationship between the value of "net IQ point gain" and x, on the premise that the "[EPA + DHA]" and "[MeHg]" were known in eq 3. If the value of "net IQ point gain" increases with the increment of x in eq 3, then the "optimal x" of the species would be the value of x, by which the calculated result of "IQ point gain" equals 5.8 points in eq 2; if the value of "net IQ point gain" decreases with the increment of x in eq 3, then the "optimal x" of the species would be zero, that is, no recommended consumption of the species.

Statistical Analysis. Data are expressed as mean and standard deviation. Pearson correlation analysis was used to assess relationships

between concentrations of total lipids and MeHg, and between concentrations of EPA plus DHA and MeHg. A value for $p < 0.05$ was considered to indicate statistical significance. All data analysis (including Monte Carlo simulation) was carried out by Statistical Analysis System 9.1 (SAS Institute Inc., Cary, NC, U.S.).

RESULTS

The concentrations of total lipids, main LCPUFAs (in the form of mean and standard deviation), and MeHg (in form of mean) of species could be obtained from Chinese published articles.[26,27] The standard deviation of MeHg of all species was never published before this article. The mean concentrations of EPA plus DHA (in the form of mg/100 g edible part) of all species ranged from 75.5 (*Scoliodon sorrakowah*) to 2458.2 (*Auxis thazard*); the mean concentrations of MeHg (in the form of μg/kg edible part) of all species ranged from 7.7 (*Mugil cephalus*) to 166.6 (*Scoliodon sorrakowah*). It is noteworthy that the concentrations of *n*-3 LCPUFAs of all species would increase by about 10% if *n*-3 LCPUFAs included *n*-3 docosapentaenoic acid (*n*-3 DPA) (Table 1).

Obviously, the largest exposure of MeHg in this study would be found in extreme scenario consumers when they consumed the species with the highest concentration of MeHg (*Scoliodon sorrakowah*). The intake amount of MeHg in this maternal group (1.68 μg/kg bw/week) was slightly higher than the PTWI, when mean plus 1.96 standard deviations was considered to be the extreme MeHg concentration of the species. The extreme consumption scenario of other species and the common consumption scenario of all species could not result in a weekly MeHg intake over 1.0 μg/kg bw.

Except for *Scoliodon sorrakowah*, both 175 and 450 g of other species weekly maternal consumption would result in a positive neurodevelopmental effect in terms of change of net IQ points (Table 2). *Scoliodon sorrakowah* would cause an unclear neurodevelopmental effect via both consumption scenarios: the calculated results of two samples belonging to this species showed negative net IQ point gain (−0.108 points and −0.076 points via common consumption scenario, −0.278 points and −0.195 points via extreme consumption scenario, respectively), and the net IQ point gain via both consumption scenarios of the other four samples belonging to this species were positive but the values were less than 0.5 points.

Both consumption scenarios of *Scoliodon sorrakowah* would result in a net beneficial neurodevelopmental effect according to probabilistic computation based on 10000 times simulated sampling (Table 3).

Table 3. Results of Probabilistic Computation for *Scoliodon sorrakowah*

scenario	sample size	times of simulated sampling	mean of net IQ point gain	lower 95% CI for mean	upper 95% CI for mean
common	6	10000	0.0545	0.0536	0.0554
extreme	6	10000	0.1401	0.1377	0.1425

Net IQ point gain decreases with the increment of weekly servings of the two aforementioned samples belonging to *Scoliodon sorrakowah*. Therefore, the optimal weekly consumption (or "the optimal *x*") of this species is zero for the reason of more conservative assessment. The optimal weekly consumption (g) of other species ranged from 63.0 (*Auxis thazard*) to 1580.7 (*Seriola quinqueradiata*). The maximum IQ point gain via other species optimal consumption ranged from 4.9 (*Raja porosa*) to 5.8 (*Coilia nasus*), and optimal weekly consumption of all species does not cause a PTWI-exceeded MeHg exposure (Table 4).

Table 4. Weekly Optimal Maternal Consumption (g) and the Maximum IQ Point Gain and MeHg Exposure (μg/kg bw/week) via Weekly Optimal Consumption of Specific Species

	weekly optimal consumption		max. IQ point gain		MeHg exposure	
scientific name	mean	std	mean	std	mean	std
Trichiurus lepturus	258.4	23.8	5.7	0.0	0.1	0.0
Larimichthys polyactis	203.2	29.8	5.8	0.0	0.1	0.0
Pampus argenteus	881.8	141.6	5.5	0.1	0.3	0.1
Collichthys lucidus	870.1	206.8	5.6	0.0	0.2	0.0
Hapaloyenys mucronatus	453.2	125.2	5.4	0.1	0.4	0.1
Pampus chinensis	333.4	68.7	5.7	0.0	0.1	0.0
Cynoglossus robustus	680.1	117.5	5.5	0.2	0.3	0.2
Muraenesox bagio	189.0	44.9	5.7	0.0	0.1	0.0
Conger myriaster	172.3	24.4	5.7	0.0	0.1	0.0
Nibea albiflora	377.2	73.7	5.6	0.0	0.2	0.1
Sebastiscus marmoratus	351.4	79.1	5.6	0.1	0.2	0.1
Thamnaconus modestus	1173.7	291.0	5.5	0.1	0.3	0.1
Scomber japonicus	122.4	13.9	5.8	0.0	0.0	0.0
Scomberomorus niphonius	299.4	57.7	5.7	0.0	0.1	0.0
Ilisha elongata	207.2	11.8	5.7	0.0	0.1	0.0
Argyrosomus argentatus	758.3	126.0	5.1	0.1	0.8	0.1
Miichthys miiuy	339.1	46.4	5.7	0.0	0.1	0.0
Scoliodon sorrakowah	0.0	0.0	0.0	0.0	0.0	0.0
Sparus macrocephalus	231.5	48.3	5.7	0.0	0.1	0.0
Harpadon nehereus	821.1	158.3	5.6	0.0	0.2	0.1
Arius sinensis	320.0	140.4	5.5	0.1	0.3	0.1
Raja porosa	1297.6	296.7	4.9	0.2	1.0	0.2
Mugil cephalus	1175.5	733.9	5.7	0.1	0.1	0.1
Lateolabrax maculatus	187.0	47.9	5.7	0.0	0.1	0.0
Trachinotus ovatus	172.0	19.4	5.7	0.0	0.1	0.0
Hexagrammos otakii	400.2	23.9	5.7	0.0	0.1	0.0
Oplegnathus fasciatus	323.0	14.1	5.7	0.0	0.1	0.0
Rhabdosargus sarba	272.8	43.4	5.6	0.0	0.2	0.0
Seriola quinqueradiata	1580.7	67.9	5.1	0.0	0.8	0.0
Auxis thazard	63.0	10.0	5.7	0.0	0.1	0.0
Coilia nasus	129.3	15.9	5.8	0.0	0.0	0.0

There was a positive relationship between concentrations of total lipids and specific *n*-3 LCPUFAs (*n*-3 DPA, EPA, and DHA),[26] but no relationship between concentrations of total lipids and MeHg ($r = 0.011$, $p = 0.880$). There was also a positive relationship between concentrations of EPA plus DHA and MeHg in the studied samples, though the relationship appeared to be moderate ($r = 0.200$, $p = 0.006$).

DISCUSSION

We have presented results on a benefit−risk assessment based on fish samples collected from a major fish farming area in southeast China, and found that there would be neurodevelopmental benefits when almost all species were consumed at either the common or extreme consumption scenario. As Zhoushan archipelago is a main fishing ground in China and it provides aquatic foods to the whole country, our results are likely applicable to a majority of the population in China.

IQ score was also applied as a common metric in other studies which focused on risk−benefit analysis on child neurodevelopment, but methodologies of quantitative integra-

tion of net IQ point change varied.[28−30] The physiologically based pharmacokinetic (PBPK) model and several epidemiological studies were applied by Zeilmaker et al. to estimate the relationship between maternal DHA/MeHg intake via specific species consumption and change of IQ score.[28] The results of their study indicated that the adverse effect of MeHg outweighed the beneficial effect of DHA in a majority of studied species (about 30 species), except a few oily fish species. Our results are more optimistic, partially because of the generally lower concentration of MeHg in species of our study (the ranges of MeHg concentration were 7.7−166.6 μg/kg in 31 species of our study and 0.011−0.829 mg/kg in 31 species of their study, respectively). Moreover, maternal fish consumption in that study was considered as 100 g/day, which is relatively higher than the actual intake amount in Chinese maternal population. Net IQ loss/gain calculated based on quality adjusted life year (QALY) required some basic information on the target population, for example, number of births to women in a specific age group,[29,30] which was difficult to obtain in some instances. "Visual response memory points" (VRM) was applied as a "tentative" common metric to assess in utero neurodevelopmental health end point by risk−benefit index (RBI) equation,[31] but the results of wild fish consumption in Alaska calculated by the VRM-RBI equation indicated that it is "difficult to craft consistent consumption advice" because net effects of consumption of many species varied significantly among regions or studies within the same region.[32] A minimum ratio of DHA intake to mercury exposure ("de minimus", 17 mg of DHA to 1 μg of MeHg) was calculated according to the women's minimum daily recommended intake of DHA (100 mg) and the reference dose for MeHg (RfD, 0.1 μg/kg bw/d, proposed by the US Environmental Protection Agency).[33] When the ratio of DHA to MeHg in one species was higher than "de minimus", a woman would meet the daily recommended intake for DHA while not exceeding the RfD for MeHg.[33] There was application of this ratio to "illustrate which species may be most beneficial for consumption".[20] The upper limit for MeHg intake proposed by US Environmental Protection Agency appeared to be more conservative than by JECFA: according to the PTWI for MeHg, "de minimus" would be about 7.3 mg of DHA to 1 μg of MeHg. In consideration of different characteristics of studies mentioned above, we considered that the FAO/WHO approach would be most suitable for our data. We did not find a report about net neurodevelopmental effect of Western Pacific species consumption assessed by the FAO/WHO deterministic approach before this study.

Consumption of fish at high trophic level would cause a significant negative neurodevelopmental effect, because of bioaccumulation of MeHg.[28] That is in accordance with our data: the species with the highest MeHg concentration in our study (*Scoliodon sorrakowah*) would be the top species in the local food pyramid. *Scoliodon sorrakowah* also has the lowest EPA plus DHA concentration in our studied species. All of these would be reason why consumption of this species would have the lowest net IQ point gain. Though the results of probabilistic computation for this species were positive, we still do not consider that its consumption scenarios deserve to be recommended. After all, there were samples of this species that showed negative results, while all samples of other species can provide a net beneficial outcome according to deterministic computation, which indicates that there would be more risk when a sample of *Scoliodon sorrakowah* was consumed; in other words, negative net IQ gain would be more likely to occur via both consumption scenarios of this species, at least compared with both consumption scenarios of other species. Moreover, the positive results of *Scoliodon sorrakowah* consumption scenarios obtained by probabilistic computation almost equal zero, which indicates that the net neurodevelopmental benefit of consumption scenarios of this species would be negligible.

Though the net IQ point gain via optimal weekly consumption is maximal according to the FAO/WHO deterministic approach, it appears that the application of common or extreme consumption scenario is more practical than of optimal weekly consumption, because filet consumption of the two scenarios is quantitative, which means that recommendation of common or extreme consumption scenario is more feasible than of optimal weekly consumption, in addition to *Scoliodon sorrakowah*.

In most instances, *n*-3 LCPUFAs refer to EPA and DHA, and according to FAO/WHO expert consultation, "EPA plus DHA data were used to represent LCn3PUFAs, because it was considered that the evidence in the literature was most robust for these specific fatty acids".[18] That means some other *n*-3 LCPUFAs and their beneficial effects would be omitted, for example, *n*-3 DPA, which would exert neuroprotective effects according to animal study and could be a precursor to synthesize DHA in vivo.[34] Our results showed that concentration of *n*-3 DPA provided about 10% of concentration of EPA plus DHA, which indicated that there would be underestimation about beneficial neurodevelopmental effect caused by both consumption scenarios when *n*-3 DPA in samples was ignored. However, the dose−response relationship between *n*-3 DPA and its biological effects would be uncertain, because "*n*-3 DPA has not been extensively studied".[34] Alpha linolenic acid (ALA) is the primary member of the *n*-3 PUFAs family, which is rich in some kinds of culinary oil such as rapeseed oil and soybean oil. ALA also could be a precursor to synthesize DHA in vivo.[35] Study about fish-eaters and non-fish-eaters (including meat-eaters, vegetarians, and vegans) showed that intake of *n*-3 LCPUFAs was much higher in fish-eaters but the differences of EPA and DHA concentrations in plasma of different dietary groups were "considerably smaller", because precursor−product ratio of ALA to *n*-3 LCPUFAs would be greater in non-fish-eaters.[36] Moreover, young women seem to be fairly efficient at converting ALA to DHA, compared with men.[37] The efficient conversion capability of young women would be an important physiological compensative mechanism for meeting the development of fetus and neonate during pregnancy and lactation. Indeed, the high consumption of ALA-rich culinary oil such as rapeseed oil or soybean-salad oil by pregnant women in some regions of China could be a reason why the DHA concentrations of colostrum in these regions with different aquatic food consumption are more similar than the aquatic food consumption difference would indicate they might be.[22] Consumption of culinary oil in the Chinese dietary pattern tends to be relatively high (data from 2002 CNNHS showed that a Chinese metropolitan consumed about 44 g of culinary oil per day), and ALA-rich vegetable oil seemed to be the main culinary oil in many regions of China according to 2002 CNNHS. Therefore, we consider that methodologies about assessment of neurodevelopment caused by maternal fish consumption would refer to the potential benefit of other *n*-3 LCPUFAs and the endogenous production of EPA and DHA to a greater extent, which would contribute to revise the

beneficial effects caused by marine fish derived EPA and DHA intake in assessment.

Our analysis about net neurodevelopmental effect could be part of risk−benefit assessment of fish consumption. Besides neurodevelopmental benefit, *n*-3 LCPUFAs were also known as a beneficial factor to the adult cardiovascular system[38] and immune system.[39] Moreover, fish contain other contaminants, such as dioxin-like compounds (DLCs), which would cause cancers[40] and diabetes[41] and also be neurotoxic.[42] The FAO/WHO expert consultation also proposed equations to assess net change of mortality caused by DLCs and *n*-3 LCPUFA intake via fish consumption.[18] A further risk−benefit assessment which refers to the net change of mortality would be considered if the DLC data of samples could be obtained.

Besides IQ point change, there are still some other end points which were applied to assess adverse neurodevelopmental effect caused by prenatal MeHg exposure in cohort studies from Faroe Islands[13,43] and Seychelles.[44−46] Findings showed that impacts of prenatal MeHg exposure on these end points varied, but there would be little information about the impact of *n*-3 LCPUFAs on them, and they are not regarded as common metrics by which risks and benefits could be compared at present. However, a sustained concern on these end points would be worth considering.

Even though the consumption amount of the general population was used to estimate the consumption amount of pregnant women/mothers, the error would not be significant as the majority of Chinese pregnant women/mothers usually share foods with their family members.[11,22] There would be a high concentration of *n*-3 LCPUFAs in some species of shellfish,[18] but the consumption mean of shellfish in the Chinese dietary pattern (4.8 g/standard man-day, according to 2002 CNNHS) would be negligible when compared with fish, though high consumption of shellfish was found in a few regions of China.[24] Therefore, shellfish samples were not considered in our study.

In summary, the current study indicates that there was no recommendation of maternal consumption scenarios of *Scoliodon sorrakowah*. Common and extreme maternal consumption scenarios of other studied species from Zhoushan would be beneficial to neurodevelopment, and both consumption scenarios of other species would deserve to be recommended according to calculated results of the FAO/WHO assessment approach. The MeHg exposure via optimal weekly consumption of all studied species would not exceed the PTWI. More factors would deserve to be considered in future analysis.

AUTHOR INFORMATION

Corresponding Authors

*(X.S.) Tel: 86-10-87776914. E-mail: shangxh2002@aliyun.com.

*(Y.W.) Tel: 86-10-67779118. E-mail: wuyongning@cfsa.net.cn.

Funding

This study was financially supported by the National Nature Science of Foundation of China (No. 81172675) and National Key Basic Research Program of China (No. 2012CB720804). Professor Jian Zhang from National Institute of Nutrition and Food Safety, China CDC, provided assistance in concentration analysis of fatty acids. Zhongjun Dun from Guangdong CDC provided assistance in probabilistic computation. Professor Shenglong Zhao from Zhejiang Ocean University provided assistance in species identification. Professor Linmao Ma from China CDC provided assistance in use of SAS software. We thank all sample-collectors from Zhoushan CDC.

Notes

The authors declare no competing financial interest.

REFERENCES

(1) Salem, N., Jr.; Litman, B.; Kim, H. Y.; Gawrisch, K. Mechanisms of action of docosahexaenoic acid in the nervous system. *Lipids* **2001**, *36*, 945−959.

(2) Koletzko, B.; Lien, E.; Agostoni, C.; Böhles, H.; Campoy, C.; Cetin, I.; Decsi, T.; Dudenhausen, J. W.; Dupont, C.; Forsyth, S.; Hoesli, I.; Holzgreve, W.; Lapillonne, A.; Putet, G.; Secher, N. J.; Symonds, M.; Szajewska, H.; Willatts, P.; Uauy, R. The roles of long-chain polyunsaturated fatty acids in pregnancy, lactation and infancy: review of current knowledge and consensus recommendations. *J. Perinat. Med.* **2008**, *36*, 5−14.

(3) Smithers, L. G.; Gibson, R. A.; Makrides, M. Maternal supplementation with docosahexaenoic acid during pregnancy does not affect early visual development in the infant: a randomized controlled trial. *Am. J. Clin. Nutr.* **2011**, *93*, 1293−1299.

(4) Brémond-Gignac, D.; Copin, H.; Lapillonne, A.; Milazzo, S. Visual development in infants: physiological and pathological mechanisms. *Curr. Opin. Ophthalmol.* **2011**, *22* (Suppl.), S1−S8.

(5) Dutta-Roy, A. K. Transport mechanisms for long-chain polyunsaturated fatty acids in the human placenta. *Am. J. Clin. Nutr.* **2000**, *71*, 315s−322s.

(6) Krauss-Etschmann, S.; Shadid, R.; Campoy, C.; Hoster, E.; Demmelmair, H.; Jiménez, M.; Gil, A.; Rivero, M.; Veszprémi, B.; Decsi, T.; Koletzko, B. V. Effects of fish-oil and folate supplementation of pregnant women on maternal and fetal plasma concentrations of docosahexaenoic acid and eicosapentaenoic acid: a European randomized multicenter trial. *Am. J. Clin. Nutr.* **2007**, *85*, 1392−1400.

(7) Harris, W. S.; Connor, W. E.; Lindsey, S. Will dietary omega-3 fatty acids change the composition of human milk? *Am. J. Clin. Nutr.* **1984**, *40*, 780−785.

(8) Helland, I. B.; Smith, L.; Saarem, K.; Saugstad, O. D.; Drevon, C. A. Maternal supplementation with very-long-chain n-3 fatty acids during pregnancy and lactation augments children's IQ at 4 years of age. *Pediatrics* **2003**, *111*, e39−e44.

(9) Colombo, J.; Kannass, K. N.; Shaddy, D. J.; Kundurthi, S.; Maikranz, J. M.; Anderson, C. J.; Blaga, O. M.; Carlson, S. E. Maternal DHA and the development of attention in infancy and toddlerhood. *Child Dev.* **2004**, *75*, 1254−1267.

(10) Hibbeln, J. R.; Davis, J. M.; Steer, C.; Emmett, P.; Rogers, I.; Williams, C.; Golding, J. Maternal seafood consumption in pregnancy and neurodevelopmental outcomes in childhood (ALSPAC study): an observational cohort study. *Lancet* **2007**, *369*, 578−585.

(11) Zhang, J.; Wang, Y.; Meng, L.; Wang, C.; Zhao, W.; Chen, J.; Ghebremeskel, K.; Crawford, M. A. Maternal and neonatal plasma n-3 and n-6 fatty acids of pregnant women and neonates from three regions of China with contrasting dietary patterns. *Asia Pac. J. Clin. Nutr.* **2009**, *18*, 377−388.

(12) Li, P.; Feng, X.; Liang, P.; Chan, H. M.; Yan, H.; Chen, L. Mercury in the seafood and human exposure in coastal area of Guangdong province, south China. *Environ. Toxicol. Chem.* **2013**, *32*, 541−547.

(13) Grandjean, P.; Weihe, P.; White, R. F.; Debes, F.; Araki, S.; Yokoyama, Y.; Murata, K.; Sørensen, N.; Dahl, R.; Jørgensen, P. J. Cognitive deficit in 7-year-old children with prenatal exposure to methylmercury. *Neurotoxicol. Teratol.* **1997**, *19*, 417−428.

(14) Choi, A. L.; Grandjean, P. Methylmercury exposure and health effects in humans. *Environ. Chem.* **2008**, *5*, 112−120.

(15) Oken, E.; Radesky, J. S.; Wright, R. O.; Bellinger, D. C.; Amarasiriwardena, C. J.; Kleinmann, K. P.; Hu, H.; Gillman, M. W. Maternal fish intake during pregnancy, blood mercury levels, and child cognition at age 3 years in a US cohort. *Am. J. Epidemiol.* **2008**, *167*, 1171−1181.

(16) Jensen, T. K.; Grandjean, P.; Jørgensen, E. B.; White, R. F.; Debes, F.; Weihe, P. Effects of breast feeding on neuropsychological development in a community with methylmercury exposure from seafood. *J. Exposure Anal. Environ. Epidemiol.* **2005**, *15*, 423−430.
(17) Laird, B. D.; Goncharov, A. B.; Egeland, G. M.; Chan, H. M. Dietary advice on Inuit traditional food use needs to balance benefits and risks of mercury, selenium, and n3 fatty acids. *J. Nutr.* **2013**, *143*, 923−930.
(18) FAO/WHO. *Report of the joint FAO/WHO expert consultation on the risks and benefits of fish consumption*; Food and Agriculture Organization of the United Nations: Rome; and World Health Organization: Geneva, 2011; 50 pp.
(19) Du, Z. Y.; Zhang, J.; Wang, C.; Li, L.; Man, Q.; Lundebye, A. K.; Frøyland, L. Risk-benefit evaluation of fish from Chinese markets: nutrients and contaminants in 24 fish species from five big cities and related assessment for human health. *Sci. Total Environ.* **2012**, *416*, 187−199.
(20) Mahaffey, K. R.; Sunderland, E. M.; Chan, H. M.; Choi, A. L.; Grandjean, P.; Mariën, K.; Oken, E.; Sakamoto, M.; Schoeny, R.; Weihe, P.; Yan, C. H.; Yasutake, A. Balancing the benefits of n-3 polyunsaturated fatty acids and the risks of methylmercury exposure from fish consumption. *Nutr. Rev.* **2011**, *69*, 493−508.
(21) Folch, J.; Lees, M.; Sloane Stanley, G. H. A simple method for the isolation and purification of total lipides from animal tissues. *J. Biol. Chem.* **1957**, *226*, 497−509.
(22) Gao, Y. X.; Zhang, J.; Wang, C.; Li, L.; Man, Q.; Song, P.; Meng, L.; Lie, Ø.; Frøyland, L. The fatty acids composition of colostrum in three geographic regions of China. *Asia Pac. J. Clin. Nutr.* **2013**, *22*, 276−282.
(23) Houserová, P.; Matejícek, D.; Kubán, V.; Pavlícková, J.; Komárek, J. Liquid chromatographic cold vapour atomic fluorescence spectrometric determination of mercury species. *J. Sep. Sci.* **2006**, *29*, 248−255.
(24) Shang, X. H.; Li, X. W.; Zhang, L.; Zhao, Y. F.; Wu, Y. N. Estimation of methylmercury intake from the 2007 Chinese Total Diet Study. *Food. Addit. Contam. B* **2010**, *3*, 236−245.
(25) Watzl, B.; Gelencser, E.; Hoekstra, J.; Kulling, S.; Lydeking-Olsen, E.; Rowland, I.; Schilter, B.; van Klaveren, J.; Chiodini, A. Application of the BRAFO-tiered approach for benefit-risk assessment to case studies on natural foods. *Food Chem. Toxicol.* **2012**, *50*, S699−S709.
(26) Gao, Y. X.; Yue, B.; Yu, X.; He, J.; Shang, X.; Li, X.; Wu, Y. Fatty acid composition of edible marine fish in Zhoushan, Zhejiang Province. *Zhonghua Yufang Yixue Zazhi* **2013**, *47*, 552−555 (in Chinese).
(27) He, J.-l. Analysis of methylmercury residue in seafish from Zhoushan area. *Chin. J. Health Lab. Technol.* **2013**, *23*, 971−972 (in Chinese).
(28) Zeilmaker, M. J.; Hoekstra, J.; van Eijkeren, J. C.; de Jong, N.; Hart, A.; kennedy, M.; Owen, H.; Gunnlaugsdottir, H. Fish consumption during child bearing age: a quantitative risk-benefit analysis on neurodevelopment. *Food Chem. Toxicol.* **2013**, *54*, 30−34.
(29) Cohen, J. T.; Bellinger, D. C.; Connor, W. E.; Kris-Etherton, P. M.; Lawrence, R. S.; Savitz, D. A.; Shaywitz, B. A.; Teutsch, S. M.; Gray, G. M. A quantitative risk−benefit analysis of changes in population fish consumption. *Am. J. Prev. Med.* **2005**, *29*, 325−334.
(30) Guevel, M.; Sirot, V.; Volatier, J.; Leblanc, J. A risk-benefit analysis of French high consumption: a QALY approach. *Risk Anal.* **2008**, *28*, 37−48.
(31) Ginsberg, G. L.; Toal, B. F. Quantitative approach for incorporating methylmercury risks and omega-3 fatty acid benefits in developing species-specific fish consumption advice. *Environ. Health Perspect.* **2009**, *117*, 267−275.
(32) Loring, P. A.; Duffy, L. K.; Murray, M. S. A risk-benefit analysis of wild fish consumption for various species in Alaska reveals shortcomings in data and monitoring needs. *Sci. Total Environ.* **2010**, *408*, 4532−4541.
(33) Tsuchiya, A.; Hardy, J.; Burbacher, T. M.; Faustman, E. M.; Mariën, K. Fish intake guidelines: incorporating n-3 fatty acid intake and contaminant exposure in the Korean and Japanese communities. *Am. J. Clin. Nutr.* **2008**, *87*, 1867−1875.
(34) Kaur, G.; Cameron-Smith, D.; Garg, M.; Sinclair, A. J. Docosapentaenoic acid (22:5n-3): a review of its biological effects. *Prog. Lipid Res.* **2011**, *50*, 28−34.
(35) Sprecher, H.; Luthria, D. L.; Mohammed, B. S.; Baykousheva, S. P. Reevaluation of the pathways for the biosynthesis of polyunsaturated fatty acids. *J. Lipid Res.* **1995**, *36*, 2471−2477.
(36) Welch, A. A.; Shakya-Shrestha, S.; Lentjes, M. A. H.; Wareham, N. J.; Khaw, K. T. Dietary intake and status of n-3 polyunsaturated fatty acids in a population of fish-eating and non-fish-eating meat-eaters, vegetarians, and vegans and the precursor-product ratio of α-linolenic acid to long-chain n-3 polyunsaturated fatty acids: results from the EPIC-Norfolk cohort. *Am. J. Clin. Nutr.* **2010**, *92*, 1040−1051.
(37) Bakewell, L.; Burdge, G. C.; Calder, P. C. Polyunsaturated fatty acid concentrations in young men and women consuming their habitual diets. *Br. J. Nutr.* **2006**, *96*, 93−99.
(38) Mozaffarian, D.; Rimm, E. B. Fish intake, contaminants, and human health evaluating the risks and the benefits. *JAMA* **2006**, *296*, 1885−1899.
(39) Calder, P. C. n-3 Polyunsaturated fatty acids, inflammation, and inflammatory diseases. *Am. J. Clin. Nutr.* **2006**, *83* (Suppl.), 1505S−1519S.
(40) Kogevinas, M. Human health effects of dioxins: cancer, reproductive and endocrine system effects. *Hum. Reprod. Update* **2001**, *7*, 331−339.
(41) Lee, D. H.; Lee, I. K.; Song, K.; Steffes, M.; Toscano, W.; Baker, B. A.; Jacobs, D. R., Jr. A strong dose-response relation between serum concentrations of persistent organic pollutants and diabetes results from the national health and examination survey 1999−2002. *Diabetes Care* **2006**, *29*, 1638−1644.
(42) Jacobson, J. L.; Jacobson, S. W. Prenatal exposure to polychlorinated biphenyls and attention at school age. *J. Pediatr.* **2003**, *143*, 780−788.
(43) Debes, F.; Budtz-Jørgensen, E.; Weihe, P.; White, R. F.; Grandjean, P. Impact of prenatal methylmercury exposure on neurobehavioral function at age 14 years. *Neurotoxicol. Teratol.* **2006**, *28*, 536−547.
(44) Davidson, P. W.; Myers, G. J.; Cox, C.; Axtell, C.; Shamlaye, C.; Sloane-Reeves, J.; Cernichiari, E.; Needham, L.; Choi, A.; Wang, Y.; Berlin, M.; Clarkson, T. W. Effects of prenatal and postnatal methylmercury exposure from fish consumption on neurodevelopment: outcomes at 66 months of age in the Seychelles Child Development Study. *JAMA* **1998**, *280*, 701−707.
(45) Myers, G. J.; Davidson, P. W.; Cox, C.; Shamlaye, C. F.; Palumbo, D.; Cernichiari, E.; Sloane-Reeves, J.; Wilding, G. E.; Kost, J.; Huang, L. S.; Clarkson, T. W. Prenatal methylmercury exposure from ocean fish consumption in the Seychelles child development study. *Lancet* **2003**, *361*, 1686−1692.
(46) Davidson, P. W.; Cory-Slechta, D. A.; Thurston, S. W.; Huang, L. S.; Shamlaye, C. F.; Gunzler, D.; Watson, G.; van Wijngaarden, E.; Zareba, G.; Klein, J. D.; Clarkson, T. W.; Strain, J. J.; Myers, G. J. Fish consumption and prenatal methylmercury exposure: cognitive and behavioral outcomes in the main cohort at 17 years from the Seychelles Child Development Study. *Neurotoxicology* **2011**, *32*, 711−717.

Paulo, Brazil). Poly(ethylene glycol) (PEG) was obtained from Isofar Ltd.a. (Duque de Caxias, Brazil). Difco Laboratories (Detroit, MI, USA) supplied bacteriological peptone.

Essential Oil Concentrations. The concentrations of clove bud and oregano essential oils to be incorporated into the antimicrobial films were determined by diffusion through solid medium in cavity-containing plates[29] against *Aspergillus niger* (ATCC 16404) and *Penicillium* sp. (ATCC 2147), common spoilage fungi in bakery products. Aliquots of 100 μL of fungal suspension ($(8.0 \pm 1.4) \times 10^5$ CFU mL^{-1}) were spread onto solidified PDA in 90 mm diameter Petri dishes. A 6 mm diameter cavity was made in the PDA with a sterilized borer at the midpoint of each dish. Cavities were filled with 50 μL of essential oil aqueous solutions at concentrations of 40, 20, 10, 5, 2.5, 1.25, and 0 (control) mg mL^{-1}. An aqueous stock solution comprising 4% (w/v) of clove bud or oregano essential oil, 1.6% (w/v) of Tween 80, and 0.2% (w/v) of PEG was 2 times serially diluted in sterilized distilled water to achieve the mentioned concentrations. Plates were sealed and incubated at 25 ± 2 °C for 5 days before inhibition haloes around cavities were measured to the nearest 0.01 mm with a digital caliper from Mitutoyo Manufacturing (Tokyo, Japan). Six plates were prepared for every essential oil concentration and fungus, three for each repetition.

Emulsification. Coarse oil-in-water emulsions were formed by mixing clove bud or oregano essential oil (at the concentration determined in the previous item), 3% (w/v) of Tween 80, and double-distilled water at 1000 rpm for 5 min. An ultrasonicator (model DES500) from Unique Group (Indaiatuba, Brazil) was used to prepare nanoemulsions by ultrasonicating the coarse emulsions at 20 kHz (frequency) and 400 W (nominal power input) for 10 min.

Droplet Size and Polydispersity Index (PdI). The mean droplet diameter and the PdI were determined through light scattering in a Nanophox from Sypatec GmbH (Clausthal-Zellerfels, Germany) after emulsion samples had been diluted in double-distilled water to $^1/_{10}$ of their initial concentration to avoid multiple scattering effect. Droplet size was indicated by the *Z*-average, which measures the scattering intensity-weighed mean diameter of the droplets present in an emulsion.

Film Casting. To emulsions were added 2% (w/v) of methylcellulose, as the polymeric matrix, and 0.2% (w/v) of PEG, as a plasticizer to improve film handling. The resulting film-forming solution was gently homogenized for 30 min at 6 rpm, rested for 2 h to eliminate air bubbles, cast onto glass plates, and allowed to dry at 25 ± 2 °C overnight. Control films were produced likewise except for the essential oil concentration, which was zero for comparison purposes. Table 1 shows the compositions of all film-forming solutions. For sliced bread shelf life evaluation, the films were cast directly onto the metalized layer of metalized polypropylene sheets, selected for their low gas transmission rates.[11]

Table 1. Compositions of Aqueous Film-Forming Solutions

film	MC[a] (%)	PEG[b] (%)	OEO[c] (%)	CBEO[d] (%)	Tween 80 (%)	emulsification
CF	2.0	0.2			3.0	mixing
RCF	2.0	0.2		4.0	3.0	mixing
NCF	2.0	0.2		4.0	3.0	ultrasound
ROF	2.0	0.2	4.0		3.0	mixing
NOF	2.0	0.2	4.0		3.0	ultrasound

[a]MC, methylcellulose. [b]PEG, poly(ethylene glycol). [c]OEO, oregano essential oil. [d]CBEO, clove bud essential oil.

Scanning Electron Microscopy (SEM). Films were characterized as to their morphologies through SEM images taken in a tabletop microscope (model TM3000) from Hitachi High Technologies America, Inc. (Schaumburg, IL, USA) operating with an accelerating voltage of 15 kV and at a magnification of 10000×.

Mechanical Properties. At least seven films from each treatment were shaped into 100 mm × 25 mm test strips according to ASTM D882-12. Their thicknesses were measured to the nearest 0.001 mm in five random positions with a digital micrometer from Mitutoyo Manufacturing (Tokyo, Japan). Films' tensile strength (TS), elastic modulus (EM), and elongation at break (EB) were determined in a universal testing machine (model 3367) from Instron Corp. (Canton, MA, USA), fitted with a 1 kN load cell and set to stretch the film strips from an initial gauge length of 50 mm at 50 mm min^{-1}. TS was calculated by dividing the highest load that a film strip withstood prior to breakage by its initial cross-sectional area. EM was given by the relationship between stress and strain at the initial slope of the chart. EB was calculated by dividing the deformation of a film strip right before breaking by its initial length and multiplying by 100 to be expressed as percentage.

Bread Storage. Preservative-free bread slices (18.98 ± 0.95 g) were bought at a local bakery in Viçosa, MG, Brazil. They were placed, two by two, inside methylcellulose film/metalized polypropylene bags, which were sealed and stored at 25 ± 2 °C in an effort to simulate usual commercialization conditions of bakery products. The storage system with two slices also aimed at reproducing the typical distribution of sandwiches due to convenience reasons. Preservative-free slices packaged alongside essential oil-free films were used as control (C−). Bread slices with an added commercial antifungal comprising sorbic acid, calcium propionate, ethanol, and grain alcohol were packed likewise, except for the absence of the inner layer (methylcellulose film) of the package system (C+). This antifungal mixture is used in the sliced bread sold at the bakery, and this evaluation allowed the comparison of the shelf life extension provided by the films developed here and by the commercially applied preservation method that advertises a shelf life of 7 days for this product. Table 2 summarizes the components of each storage set.

Table 2. Components Present (+) or Absent (−) in Each Sliced Bread Storage System

treatment	preservative	film	essential oil	emulsion
C−	−	CF	−	−
RC	−	RCF	clove bud	coarse
NC	−	NCF	clove bud	nano
RO	−	ROF	oregano	coarse
NO	−	NOF	oregano	nano
C+	+	−	−	−

Microbiological Evaluation. Counts of yeasts and molds, microorganisms that are known to spoil bakery products in a short period of time, were monitored after 0, 5, 10, and 15 days of storage. Bread slices (25 ± 0.2 g) were randomly and aseptically sampled, diluted in 225 mL of 0.1% (w/v) bacteriological peptone solutions, and homogenized for 2 min in a stomacher from ITR Ltd.a. (Esteio, Brazil). Serial 10-fold dilutions (10^{-1}–10^{-4}) were prepared and inoculated in Petrifilm plates from 3 M do Brasil Ltd.a. (Sumaré, Brazil), specific for counting yeasts and molds. The plates were incubated at 25 ± 2 °C for 5 days before counts of yeasts and molds were reported as colony-forming units per gram of sliced bread, in a logarithm scale (log CFU g^{-1}).

Statistical Analysis. All data were submitted to one-way analysis of variance (ANOVA) followed by Tukey's test at the 5% of probability level in statistical software (version 9.1) from SAS Institute Inc. (Cary, NC, USA).

RESULTS AND DISCUSSION

Essential Oil Concentrations. Table 3 shows the inhibition halo values of *Penicillium* sp. and *A. niger* for each essential oil concentration. No inhibition halo was recorded at concentrations lower than 20 mg mL^{-1}, regardless of the microorganisms and essential oil. The largest ($p < 0.05$) inhibition halo of *A. niger* and *Penicillium* sp. was provided by clove bud and oregano essential oils at 40 mg mL^{-1} (Table 3). Thus, 40 mg mL^{-1} was the concentration used for film

Table 3. Inhibition Haloes of *Aspergillus niger* or *Penicillium* sp. after 5 Days at 25 ± 2 °C, As Affected by Clove Bud or Oregano Essential Oil Concentration

	clove bud essential oil		oregano essential oil	
concn (mg mL^{-1})	*Aspergillus niger*	*Penicillium* sp.	*Aspergillus niger*	*Penicillium* sp.
40.0	34.43 ± 2.10 a	30.71 ± 3.50 a	29.24 ± 1.20 a	27.59 ± 2.05 a
20.0	15.93 ± 10.20 b	13.10 ± 12.25 a	15.85 ± 12.44 b	9.72 ± 10.77 b
10.0	0.00 ± 0.00 c	0.00 ± 0.00 b	0.00 ± 0.00 c	0.00 ± 0.00 c
5.00	0.00 ± 0.00 c	0.00 ± 0.00 b	0.00 ± 0.00 c	0.00 ± 0.00 c
2.50	0.00 ± 0.00 c	0.00 ± 0.00 b	0.00 ± 0.00 c	0.00 ± 0.00 c
1.25	0.00 ± 0.00 c	0.00 ± 0.00 b	0.00 ± 0.00 c	0.00 ± 0.00 c
0.00	0.00 ± 0.00 c	0.00 ± 0.00 b	0.00 ± 0.00 c	0.00 ± 0.00 c

production. The antimicrobial activities of the essential oils from oregano and clove bud against several foodborne pathogenic and spoilage microorganisms, including fungi from *Aspergillus* and *Penicillium* genera, have been widely reported.[11,30−34]

Droplet Size and Polydispersity Index. The mean diameters and PdI values obtained for droplets of both clove bud and oregano essential oils in coarse emulsions and nanoemulsions are shown in Table 4. Coarse emulsions produced at low mixing speed had droplets with diameters of a couple of micrometers, which is in accordance with the values (1−20 μm) previously reported in the literature.[21] The formation of a coarse emulsion prior to a high-energy process improves both droplet size reduction and polydispersity of the resulting emulsion.[35]

Table 4. Droplet Diameters and Polydispersity Index (PdI) Values of Aqueous Coarse Emulsions and Nanoemulsions of Clove Bud and Oregano Essential Oils

essential oil	emulsion	droplet diameter[a] (nm)	PdI
clove bud	coarse	1999.03 ± 1856.82 a	0.863
	nano	250.43 ± 100.67 b	0.162
oregano	coarse	1313.38 ± 1302.41 a	0.983
	nano	180.59 ± 84.76 b	0.220

[a]Mean values ± standard deviations followed by different letters are significantly different ($p < 0.05$).

Coarse emulsion droplets were remarkably larger ($p < 0.05$) than those present in nanoemulsions (Table 4), regardless of the essential oil used. Droplet breakdown is a nonspontaneous process that requires enough energy input to enhance droplet interfacial area by overcoming its surface free energy,[21] and the low-speed process used for coarse emulsion preparation did not provide the required energy to reduce droplet size to the nanoscale. Ultrasonication, however, created thoroughly disruptive forces resulting from an intense acoustic field, leading to rapid formation and collapse of microbubbles at the droplet interface.[36] The collapse of microbubbles, known as cavitation, induced turbulence and shock waves that disrupted droplets to the nanoscale level.[35,37,38] The type of essential oil did not affect ($p > 0.05$) droplet size either in coarse emulsions or in nanoemulsions (Table 4).

Another remarkable difference between the coarse emulsions and nanoemulsions produced here was the PdI. Coarse emulsions had PdI values close to unity (Table 4), indicating a multimodal, wide droplet size distribution. Nanoemulsions, however, had a narrow size distribution as indicated by low PdI values. This difference is attributable to the increased energy input of ultrasonication when compared to the low-speed mixing used in coarse emulsification, given that droplets tend to assume an equilibrium diameter as the energy input increases, leading to a more uniform emulsion having reduced PdI values.[21,25]

Scanning Electron Microscopy. SEM images aimed at confirming that droplet aggregation and coalescence did not take place during film drying and that droplet diameters remained stable in the final films. Figure 1 shows typical SEM micrographs of the methylcellulose films. As expected, the essential oil-free film showed a homogeneous surface without any droplets (Figure 1A). Contrastingly, droplets are easily

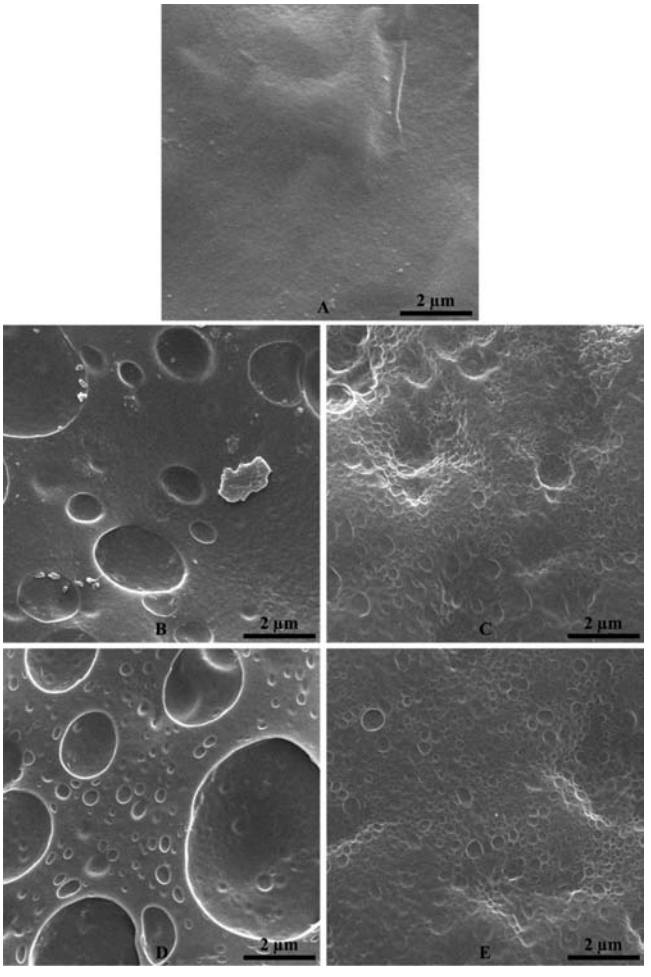

Figure 1. Typical SEM micrographs of methylcellulose films (A) with added clove bud or oregano coarse emulsions (B and D, respectively) or nanoemulsions (C and E, respectively).

Table 5. Mechanical Properties of Methylcellulose Films Incorporated or Not with Clove Bud or Oregano Essential Oil Coarse Emulsions or Nanoemulsions

essential oil	emulsion	TS[a] (MPa)	EM[a] (MPa)	EB[a] (%)
		5.40 ± 1.13 a	118.86 ± 24.53 a	20.46 ± 2.71 a
clove bud	coarse	6.07 ± 1.11 a	53.97 ± 8.71 b	40.29 ± 4.53 b
	nano	6.11 ± 1.26 a	56.79 ± 16.58 b	56.61 ± 5.59 c
oregano	coarse	8.05 ± 1.45 a	104.21 ± 4.15 a	34.08 ± 5.17 b
	nano	7.61 ± 1.32 a	72.94 ± 10.97 b	54.77 ± 1.66 c

[a]Mean values ± standard deviations followed by different letters within the same column are significantly different ($p < 0.05$).

observed in the emulsified films. Methylcellulose films with added coarse emulsions (Figure 1B,D) presented much larger droplets and a more heterogeneous size distribution profile than films with added nanoemulsions (Figure 1C,E), regardless of essential oil type. This validates the droplet diameter and PdI values obtained through light scattering (Table 4) and also indicates that the emulsion remained stable with regard to droplet diameter during film polymerization at the tested conditions.

Mechanical Properties. The mechanical attributes tensile strength (TS), elastic modulus (EM), and elongation at break (EB) of the films produced here are summarized in Table 5. The essential oils added to methylcellulose films had a plasticizing effect, as suggested by reduced ($p < 0.05$) EM and increased ($p < 0.05$) EB when compared to those of essential oil-free films. However, TS was not affected ($p > 0.05$) by the addition of essential oils. Similarly to our results, essential oils have been widely reported to weaken the intermolecular interactions between polymeric chains, resulting in less rigid and more extensible and flexible films.[19,39−44] The reduction in droplet size led to an even more remarkable plasticizing effect, because smaller droplets increased ($p < 0.05$) the EB and reduced ($p < 0.05$) the EM of the methylcellulose films. The addition of clove bud essential oil nanodroplets provided almost a 3-fold increase in EB and a 2-fold decrease in EM when compared to control films. Oregano essential oil showed a similar behavior.

Microbiological Evaluation. The counts of yeasts and molds throughout the storage of sliced bread are illustrated in Figure 2. At the very beginning of the storage period, the counts of yeasts and molds did not differ ($p > 0.05$) among the different treatments because no time was available for microbial development, even in C− in which neither synthetic preservatives nor antimicrobial films had been used. As expected, there was a trend of increasing counts of yeasts and molds during storage, regardless of treatment. Different storage conditions (Table 2), however, led to different survival patterns.

After 5 days, the counts in all treatments were not different ($p > 0.05$), except in slices packaged alongside clove bud nanoemulsion films (NC), which showed counts lower ($p < 0.05$) than the other treatments. The synthetic antifungal present in C+ worked just as well as the antimicrobial films until day 5, but the emulsified films were more efficient ($p < 0.05$) in lessening microbial growth at all further analysis times. At 10 days of storage, the essential oil-free treatments (C− and C+) allowed greater ($p < 0.05$) growth of yeasts and molds when compared to the treatments that included antimicrobial films. This suggests that neither the essential oil-free film (C−) nor the synthetic preservative (C+) was effective in preventing microbial development after 10 days of storage at 25 ± 2 °C,

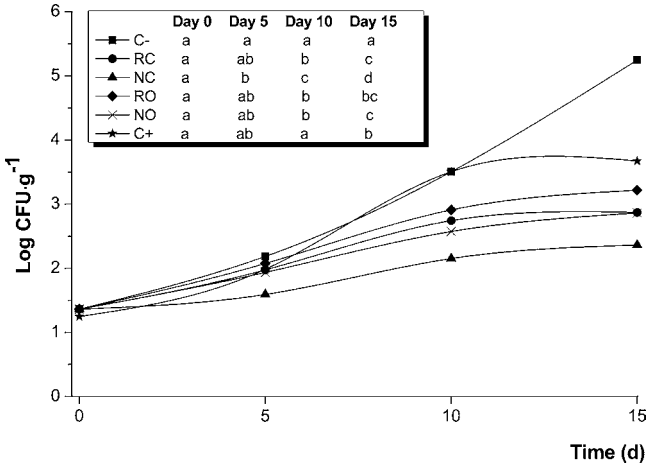

Figure 2. Counts of yeasts and molds in bread slices containing (C+) or not (C−) synthetic antifungal and packaged alongside methylcellulose films incorporated with clove bud and oregano essential oils coarse emulsions (RC and RO, respectively) or nanoemulsions (NC and NO, respectively), throughout 15 days of storage at 25 ± 2 °C. In the table, different letters within the same column indicate different means ($p < 0.05$).

conditions that simulate conventional commercialization practices of bakery products. At 15 days of storage, C− bread showed the greatest ($p < 0.05$) count of yeasts and molds, followed by C+ and then antimicrobial film-containing treatments. This corroborates the hypothesis that clove bud and oregano essential oils are effective in lessening microbial development in food matrices, even when compared to the commercial antimicrobial technique currently used (C+).

Overall, clove bud and oregano essential oils within the same droplet diameter range displayed similar ($p > 0.05$) antimicrobial activities against yeasts and molds, although clove bud nanodroplets were more effective ($p < 0.05$) than oregano nanodroplets at days 10 and 15. The antifungal activities of clove bud and oregano essential oils are related to their major phenolic constituents eugenol and carvacrol (Figure 3), respectively.[45] These phenols interact with and alter the

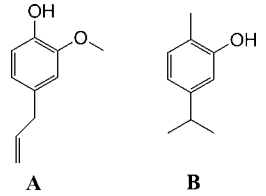

Figure 3. Chemical structures of eugenol (A) and carvacrol (B).

dx.doi.org/10.1021/jf501055f | J. Agric. Food Chem. 2014, 62, 5214−5219

permeability of cell membranes, leading to leakage of cell contents, which are essential to microorganism survival.[46] The similarity observed here is also attributable to the presence of hydroxyl groups (Figure 3) and delocalized electrons.[47,48] The delocalized electrons allow proton release from the hydroxyl groups in a way that the proton gradient through cell membrane is reduced. The reduced proton gradient, along with the resulting depletion of the ATP pool, kills microbial cells.[45]

Droplet size reduction from a few micrometers to a few hundreds of nanometers improved ($p < 0.05$) the antimicrobial properties of the clove bud essential oil-containing films (Figure 2). Although this difference was not significant ($p > 0.05$) for oregano essential oil, there is a clear trend of decreasing the counts of yeasts and molds by smaller droplets. This observation is attributable to the increased bioavailability of nonpolar bioactive compounds encapsulated in smaller droplets, which possess a higher surface-to-volume ratio and are able to more easily penetrate cell membranes.[22,26] This improvement in antimicrobial properties of nanoemulsified films provided by reduced droplet diameters had already been reported for cinnamaldehyde emulsions, but in laboratory medium.[25]

In summary, emulsion films were successfully produced with plant essential oils that displayed antimicrobial activity against spoilage fungi in bakery products. Ultrasonication was effective in reducing droplet diameter and in narrowing droplet size distribution. Both essential oils acted as plasticizers in methylcellulose films, as well as provided them with antimicrobial activity against yeasts and molds in sliced bread. Droplet size reduction was shown to increase both plasticizing and antimicrobial behaviors of essential oils. The antimicrobial films developed here improved sliced bread shelf life, even when compared to the commercial antifungal agent that is currently used in bakeries. The improvement of antimicrobial properties of an essential oil simply by reducing its droplet size has clear implications for food preservation, as lower preservative contents may be used to deliver the same antimicrobial efficiency if encapsulated in smaller particles. Future works are needed to validate the efficiency of the system proposed here in prolonging the shelf life of different food products and to study its impacts on product acceptance by consumers as well as to assess the feasibility of scaling up this system to a large-scale food production scenario.

AUTHOR INFORMATION

Corresponding Author

*(N.F.F.S.) Phone: +55 31 3891 1796. E-mail: nfsoares@ufv.br.

Present Addresses

[†](C.G.O.) National Nanotechnology Laboratory for Agribusiness, EMBRAPA-CNPDIA, Rua XV de Novembro 1452, São Carlos, SP 13560-970, Brazil, and PPG-CEM, Department of Materials Engineering, Federal University of São Carlos, Rod. Washington Luis, km 235, São Carlos, SP 13565-905, Brazil.

[§](S.F.O.P.) Department of Rural and Animal Technology, Southwest Bahia State University, Praça Primavera 40, Itapetinga, BA 45700-000, Brazil.

Funding

This work was supported by the National Council for Scientific and Technological Development/CNPq (Grant 800184/2011-4).

Notes

The authors declare no competing financial interest.

ABBREVIATIONS USED

PDA, potato dextrose agar; PdI, polydispersity index; SEM, scanning electron microscopy; TS, tensile strength; EM, elastic modulus; EB, elongation at break; CFU, colony-forming units; PEG, poly(ethylene glycol)

REFERENCES

(1) Burt, S. Essential oils: their antibacterial properties and potential applications in foods − a review. *Int. J. Food Microbiol.* **2004**, *94* (3), 223−253.

(2) Tiwari, B. K.; Valdramidis, V. P.; O' Donnell, C. P.; Muthukumarappan, K.; Bourke, P.; Cullen, P. J. Application of natural antimicrobials for food preservation. *J. Agric. Food Chem.* **2009**, *57* (14), 5987−6000.

(3) Lang, G.; Buchbauer, G. A review on recent research results (2008−2010) on essential oils as antimicrobials and antifungals. A review. *Flavour Fragrance J.* **2012**, *27* (1), 13−39.

(4) Soares, N. F. F.; Pires, A. C. S.; Camilloto, G. P.; Santiago-Silva, P.; Espitia, P. J.; Silva, W. A. Recent patents on active packaging for food application. *Recent Pat. Food, Nutr. Agric.* **2009**, *1* (2), 171−178.

(5) Espitia, P. J. P.; Du, W.-X.; Avena-Bustillos, R. J.; Soares, N. F. F.; McHugh, T. H. Edible films from pectin: physical-mechanical and antimicrobial properties − a review. *Food Hydrocolloids* **2014**, *35*, 287−296.

(6) López, P.; Sánchez, C.; Batlle, R.; Nerín, C. Development of flexible antimicrobial films using essential oils as active agents. *J. Agric. Food Chem.* **2007**, *55* (21), 8814−8824.

(7) Silveira, M. F. A.; Soares, N. F. F.; Geraldine, R. M.; Andrade, N. J.; Gonçalves, M. P. J. Antimicrobial efficiency and sorbic acid migration from active films into pastry dough. *Packag. Technol. Sci.* **2007**, *20* (4), 287−292.

(8) Espitia, P. J. P.; Soares, N. F. F.; Botti, L. C. M.; Melo, N. R.; Pereira, O. L.; Silva, W. A. Assessment of the efficiency of essential oils in the preservation of postharvest papaya in an antimicrobial packaging system. *Braz. J. Food Technol.* **2012**, *15* (4), 333−342.

(9) Gonçalves, M. P. J. C.; Pires, A. C. S.; Soares, N. F. F.; Araújo, E. A. Use of allyl isothiocyanate sachet to preserve cottage cheese. *J. Foodservice* **2009**, *20* (6), 275−279.

(10) Otoni, C. G.; Soares, N. F. F.; Silva, W. A.; Medeiros, E. A. A.; Baffa Junior, J. C. Use of allyl isothiocyanate-containing sachets to reduce *Aspergillus flavus* sporulation in peanuts. *Packag. Technol. Sci.* **2014**, DOI: 10.1002/pts.2063.

(11) Passarinho, A. T. P.; Dias, N. F.; Camilloto, G. P.; Cruz, R. S.; Otoni, C. G.; Moraes, A. R. F.; Soares, N. F. F. Sliced bread preservation through oregano essential oil-containing sachet. *J. Food Process Eng.* **2014**, *37* (1), 53−62.

(12) Pires, A. C. S.; Soares, N. F. F.; Andrade, N. J.; Silva, L. H. M.; Camilloto, G. P.; Bernardes, P. C. Increased presevation of sliced mozzarella cheese by antimibrobial sachet incorporated with allyl isothiocyanate. *Braz. J. Microbiol.* **2009**, *40* (4), 1002−1008.

(13) Bitencourt, R. G.; Possas, A. M. M.; Camilloto, G. P.; Cruz, R. S.; Otoni, C. G.; Soares, N. F. F. Antimicrobial and aromatic edible coating on fresh-cut pineapple preservation. *Cienc. Rural* **2014**, in press (DOI not yet released).

(14) Durango, A. M.; Soares, N. F. F.; Andrade, N. J. Microbiological evaluation of an edible antimicrobial coating on minimally processed carrots. *Food Control* **2006**, *17* (5), 336−341.

(15) Geraldine, R. M.; Soares, N. F. F.; Botrel, D. A.; Gonçalves, L. A. Characterization and effect of edible coatings on minimally processed garlic quality. *Carbohydr. Polym.* **2008**, *72* (3), 403−409.

(16) Soares, N. F. F.; Silva, D. F. P.; Camilloto, G. P.; Oliveira, C. P.; Pinheiro, N. M.; Medeiros, E. A. A. Antimicrobial edible coating in post-harvest conservation of guava. *Rev. Bras. Frutic.* **2011**, *33*, 281−289.
(17) Du, W.-X.; Olsen, C. W.; Avena-Bustillos, R. J.; McHugh, T. H.; Levin, C. E.; Friedman, M. Storage stability and antibacterial activity against *Escherichia coli* O157:H7 of carvacrol in edible apple films made by two different casting methods. *J. Agric. Food Chem.* **2008**, *56* (9), 3082−3088.
(18) Du, W.-X.; Olsen, C. W.; Avena-Bustillos, R. J.; McHugh, T. H.; Levin, C. E.; Friedman, M. Antibacterial activity against *E. coli* O157:H7, physical properties, and storage stability of novel carvacrol-containing edible tomato films. *J. Food Sci.* **2008**, *73* (7), M378−M383.
(19) Du, W.-X.; Olsen, C. W.; Avena-Bustillos, R. J.; McHugh, T. H.; Levin, C. E.; Friedman, M. Effects of allspice, cinnamon, and clove bud essential oils in edible apple films on physical properties and antimicrobial activities. *J. Food Sci.* **2009**, *74* (7), M372−M378.
(20) Du, W.-X.; Olsen, C. W.; Avena-Bustillos, R. J.; McHugh, T. H.; Levin, C. E.; Mandrell, R.; Friedman, M. Antibacterial effects of allspice, garlic, and oregano essential oils in tomato films determined by overlay and vapor-phase methods. *J. Food Sci.* **2009**, *74* (7), M390−M397.
(21) Abbas, S.; Hayat, K.; Karangwa, E.; Bashari, M.; Zhang, X. An overview of ultrasound-assisted food-grade nanoemulsions. *Food Eng. Rev.* **2013**, *5* (3), 139−157.
(22) Huang, Q.; Yu, H.; Ru, Q. Bioavailability and delivery of nutraceuticals using nanotechnology. *J. Food Sci.* **2010**, *75* (1), R50−R57.
(23) Fryd, M. M.; Mason, T. G. Advanced nanoemulsions. *Annu. Rev. Phys. Chem.* **2012**, *63*, 493−518.
(24) Solans, C.; Solé, I. Nano-emulsions: formation by low-energy methods. *Curr. Opin. Colloid Interface Sci.* **2012**, *17* (5), 246−254.
(25) Otoni, C. G.; Moura, M. R. de Aouada, F. A.; Camilloto, G. P.; Cruz, R. S.; Lorevice, M. V.; Soares, N. de F. F.; Mattoso, L. H. C. Antimicrobial and physical-mechanical properties of pectin/papaya puree/cinnamaldehyde nanoemulsion edible composite films. *Food Hydrocolloids* **2014**, *41*, 188−194.
(26) Acosta, E. Bioavailability of nanoparticles in nutrient and nutraceutical delivery. *Curr. Opin. Colloid Interface Sci.* **2009**, *14* (1), 3−15.
(27) Donsì, F.; Annunziata, M.; Sessa, M.; Ferrari, G. Nano-encapsulation of essential oils to enhance their antimicrobial activity in foods. *LWT − Food Sci. Technol.* **2011**, *44* (9), 1908−1914.
(28) Salvia-Trujillo, L.; Rojas-Graü, M. A.; Soliva-Fortuny, R.; Martín-Belloso, O. Impact of microfluidization or ultrasound processing on the antimicrobial activity against *Escherichia coli* of lemongrass oil-loaded nanoemulsions. *Food Control* **2014**, *37*, 292−297.
(29) Cleeland, L.; Squires, E. Evaluation of new antimicrobials *in vitro* and experimental animal infections. In *Antibiotics in Laboratory Medicine*; Lorian, V. M. D., Ed.; Williams & Wilkins: Baltimore, MD, USA, 1991; pp 739−788.
(30) Carmo, E. S.; Lima, E. O.; Souza, E. L. The potential of *Origanum vulgare* L. (Lamiaceae) essential oil in inhibiting the growth of some food-related *Aspergillus* species. *Braz. J. Microbiol.* **2008**, *39*, 362−367.
(31) Dorman, H. J. D.; Deans, S. G. Antimicrobial agents from plants: antibacterial activity of plant volatile oils. *J. Appl. Microbiol.* **2000**, *88* (2), 308−316.
(32) Elgayyar, M.; Draughon, F. A.; Golden, D. A.; Mount, J. R. Antimicrobial activity of essential oils from plants against selected pathogenic and saprophytic microorganisms. *J. Food Prot.* **2001**, *64* (7), 1019−1024.
(33) Pinto, E.; Vale-Silva, L.; Cavaleiro, C.; Salgueiro, L. Antifungal activity of the clove essential oil from *Syzygium aromaticum* on *Candida*, *Aspergillus* and dermatophyte species. *J. Med. Microbiol.* **2009**, *58* (11), 1454−1462.
(34) Rana, I. S.; Rana, A. S.; Rajak, R. C. Evaluation of antifungal activity in essential oil of the *Syzygium aromaticum* (L.) by extraction, purification and analysis of its main component eugenol. *Braz. J. Microbiol.* **2011**, *42* (4), 1269−1277.
(35) Tang, S. Y.; Shridharan, P.; Sivakumar, M. Impact of process parameters in the generation of novel aspirin nanoemulsions − comparative studies between ultrasound cavitation and microfluidizer. *Ultrason. Sonochem.* **2013**, *20* (1), 485−497.
(36) Mason, T. G.; Wilking, J. N.; Meleson, K.; Chang, C. B.; Graves, S. M. Nanoemulsions: formation, structure, and physical properties. *J. Phys.: Condens. Matter* **2006**, *18* (41), R635.
(37) Kentish, S.; Wooster, T. J.; Ashokkumar, M.; Balachandran, S.; Mawson, R.; Simons, L. The use of ultrasonics for nanoemulsion preparation. *Innovative Food Sci. Emerging Technol.* **2008**, *9* (2), 170−175.
(38) Li, P.-H.; Chiang, B.-H. Process optimization and stability of d-limonene-in-water nanoemulsions prepared by ultrasonic emulsification using response surface methodology. *Ultrason. Sonochem.* **2012**, *19* (1), 192−197.
(39) Bilbao-Sáinz, C.; Avena-Bustillos, R. J.; Wood, D. F.; Williams, T. G.; McHugh, T. H. Nanoemulsions prepared by a low-energy emulsification method applied to edible films. *J. Agric. Food Chem.* **2010**, *58* (22), 11932−11938.
(40) Hosseini, M. H.; Razavi, S. H.; Mousavi, M. A. Antimicrobial, physical and mechanical properties of chitosan-based films incorporated with thyme, clove and cinnamon essential oils. *J. Food Process. Preserv.* **2009**, *33* (6), 727−743.
(41) Quezada Gallo, J.-A.; Debeaufort, F.; Callegarin, F.; Voilley, A. Lipid hydrophobicity, physical state and distribution effects on the properties of emulsion-based edible films. *J. Membr. Sci.* **2000**, *180* (1), 37−46.
(42) Rojas-Graü, M. A.; Raybaudi-Massilia, R. M.; Soliva-Fortuny, R. C.; Avena-Bustillos, R. J.; McHugh, T. H.; Martín-Belloso, O. Apple puree-alginate edible coating as carrier of antimicrobial agents to prolong shelf-life of fresh-cut apples. *Postharvest Biol. Technol.* **2007**, *45* (2), 254−264.
(43) Zivanovic, S.; Chi, S.; Draughon, A. F. Antimicrobial activity of chitosan films enriched with essential oils. *J. Food Sci.* **2005**, *70* (1), M45−M51.
(44) Zúñiga, R. N.; Skurtys, O.; Osorio, F.; Aguilera, J. M.; Pedreschi, F. Physical properties of emulsion-based hydroxypropyl methylcellulose films: effect of their microstructure. *Carbohydr. Polym.* **2012**, *90* (2), 1147−1158.
(45) Ben Arfa, A.; Combes, S.; Preziosi-Belloy, L.; Gontard, N.; Chalier, P. Antimicrobial activity of carvacrol related to its chemical structure. *Lett. Appl. Microbiol.* **2006**, *43* (2), 149−154.
(46) Lambert, R. J. W.; Skandamis, P. N.; Coote, P. J.; Nychas, G.-J. E. A study of the minimum inhibitory concentration and mode of action of oregano essential oil, thymol and carvacrol. *J. Appl. Microbiol.* **2001**, *91* (3), 453−462.
(47) Bajpai, V. K.; Baek, K.-H.; Kang, S. C. Control of *Salmonella* in foods by using essential oils: A review. *Food Res. Int.* **2012**, *45* (2), 722−734.
(48) Ultee, A.; Bennik, M. H. J.; Moezelaar, R. The phenolic hydroxyl group of carvacrol is essential for action against the food-borne pathogen *Bacillus cereus*. *Appl. Environ. Microbiol.* **2002**, *68* (4), 1561−1568.

demonstrate the development of an easy, effective, and sensitive MISPE protocol for OTA determination in wine matrices.

EXPERIMENTAL PROCEDURES

Materials. Ochratoxin A standard solution at a concentration of 10 μg/mL in acetonitrile (standard Oekanal) was supplied by Sigma (Milano, Italy) and was stored at −20 °C. The imprinted polymer was prepared by using as template a mimic of OTA, *N*-(4-chloro-1-hydroxy-2-naphthoylamido)-L-phenylalanine, **2** (Figure 1), according to the published literature.[23−25] Acetonitrile and methanol (HPLC gradient grade), ethanol (95% v/v), tetrahydrofuran, and acetone were supplied by VWR International (Milano, Italy).

Citric acid monohydrate, potassium chloride, sodium chloride, sodium hydrogen carbonate, tartaric acid, acetic acid, and poly-(ethylene glycol) 8000 were all of analytical grade and were supplied by Sigma.

A citrate−tartrate buffer (named "hydroalcoholic citrate−tartrate buffer") was prepared by mixing 30 mM citric acid, 0.5 mM tartaric acid, and 8 mM potassium chloride and titrating at pH 3.2 with 0.1 M NaOH. It was mixed with ethanol to obtain a final buffer composition containing 10% v/v of ethanol. It was used to simulate the wine matrix as previously described.[26] All of the buffered solutions were filtered after preparation on 0.22 μm nylon membrane from Alltech Italia (Milano, Italy) and preserved at 4 °C until use. The water for buffer preparation was deionized on mixed ion exchange columns, and it was ultrapurified in a Purelab Prima System from Elga (Marlow, UK) for HPLC eluents.

The real sample matrices were constituted by 18 red wines provided with Protected Designation of Origin label, from different Italian regions and produced in the years 2005−2012. Blank wine samples certified to be free from OTA contamination were kindly provided by Neotron SpA (Modena, Italy).

The commercial immunoaffinity columns were OchraTest from VICAM (Watertown, MA, USA). Solid phase extraction (SPE) was performed with a VacMaster-10 sample processing manifold, equipped with a vacuum control valve and PTFE cartridge adapters (VWR International).

HPLC Method. Reversed phase HPLC analysis was used for OTA determination after SPE in accordance with the literature.[11] A LaChrom Elite HPLC system composed of programmable binary pump L-2130, autosampler L-2200, UV detector L-2400, and fluorescence detector L-2480 and provided with EZChrom Elite software for instrumental programming, data acquisition, and data processing was from Merck-Hitachi (Milano, Italy).

The column used was a 250 mm × 4.6 mm i.d., 5 μm, Li-Chrospher 100 RP-18 (Merck, Milano, Italy). The mobile phase was composed of acetonitrile/water/acetic acid 40:59:1 v/v/v, and the elution was performed in isocratic conditions at a flow rate of 0.5 mL/min. The sample volume injected was 10 μL, and OTA was detected by setting the excitation wavelength at 333 nm and the emission wavelength at 460 nm. In these instrumental conditions OTA retention time is 20.3 ± 0.1 min.

Reference standard solutions of OTA at concentrations of 5, 3, 2, 1, 0.75, 0.5, 0.25, and 0.1 ng/mL were prepared both in the eluent solution for the external calibration method and in blank wine sample for the standard addition method and immediately analyzed three times consecutively, and peak areas were plotted against concentration. A calibration curve was drawn using a weighted linear regression (weight = 1/conc).

Optimization of MISPE Protocol. All of the SPE experiments were made in 3 mL polypropylene SPE cartridges, packed with 250 mg of OTA-imprinted imprinted polymer. All measurements were performed in triplicate so that the analyte recoveries were evaluated as the averages of the repeated measures to estimate the method repeatability. Different experiments of loading, washing, and elutions were performed to optimize the extraction procedure. Before each experiment, the stationary phase was conditioned with 5 volumes of hydroalcoholic citrate−tartrate buffer.

To measure the MISPE cartridge loading capacity, 1 mL of 250 ng/mL standard solution of OTA in hydroalcoholic citrate−tartrate buffer was loaded by applying the vacuum. The eluate was analyzed by HPLC. After the sample loading, the cartridge was washed with 5 mL of methanol/acetic acid 9:1 v/v to remove OTA.

To investigate the effect of different washing solutions on removal of the mycotoxin from the cartridge, 1 mL of OTA solution at the concentration of 25 ng/mL in hydroalcoholic citrate−tartrate buffer was loaded and a vacuum was applied to facilitate the passage of the sample through the cartridge bed. After sample loading, air was passed through the columns for 5 min. Then, the cartridges were sequentially washed with 1 mL of water containing increasing amounts of organic solvent (0, 10, 20, 30, 40, 50, 60, 70, 80, 90, and 100% v/v). The organic solvents investigated for elution were acetonitrile, methanol, tetrahydrofuran, and acetone. A final wash with 5 mL of methanol/acetic acid 9:1 v/v was performed to completely remove the mycotoxin from the stationary phase.

To investigate the effect of different elution conditions, 1 mL of OTA solution at the concentration of 25 ng/mL in hydroalcoholic citrate−tartrate buffer was loaded and the vacuum was applied. Thereafter, air was passed through the columns for 5 min and a washing step with 1 mL of deionized water was performed. The cartridge was then sequentially washed with 1 mL of acetonitrile containing increasing amounts of acetic acid (1, 2 and 5% v/v) by drying the stationary phase after each addition. The different aliquots were recovered and analyzed by HPLC to measure OTA concentration. A final washing step with 5 mL of methanol/acetic acid 9:1 v/v was performed to remove all compounds still bound.

MISPE of Real Samples. The MISPE protocol was evaluated on wine samples. The analytical performance of the MISPE extraction protocol was compared with those obtained with commercial immunoaffinity columns. All of the experiments were performed in triplicate as in the previous protocol optimization with OTA standards.

Preliminary wine treatment was performed in accordance with the literature.[11] Tannins were precipitated by diluting the red wine samples 1:2 v/v with a 1% v/v aqueous solution of PEG 8000, incubated at 4 °C overnight, centrifuged at 8000 rpm for 15 min, and filtered on 0.22 μm polypropylene membranes.

Extraction of OTA from wine samples was performed by loading 2 mL of pretreated wine sample on the cartridge and applying a vacuum. Afterward, the cartridge was washed with 1 mL of the following solutions: (1) water/acetone 4:1 v/v; (2) water/acetonitrile 4:1 v/v; (3) water/tetrahydrofuran 4:1 v/v. The OTA elution was then performed with 2 mL of acetonitrile/acetic acid 49:1 v/v, as optimized in the MISPE protocol with OTA standards. A final wash of the stationary phase was performed with 5 mL of methanol/acetic acid 9:1 v/v. To investigate the minimum volume capable of washing away the retained interferents when loading volumes >1 mL were applied, a set of additional experiments were performed by loading 10 mL of pretreated wine sample, and subsequent washing steps were performed by using increasing amounts of washing solution (2, 3, 4, and 5 mL).

Recovery of OTA from red wine samples was performed on 2 mL of pretreated wine samples spiked with 0.25, 0.5, 1, 2, and 5 ng/mL of OTA. Then, samples were extracted according to the optimized protocol above-described. The peak areas measured by the external calibration method allowed the determination of OTA recovery.

Preconcentration of OTA from red wine samples was performed on pretreated wine samples (2, 5, 10, and 20 mL) spiked with amounts of OTA to final mycotoxin concentrations of 2, 0.8, 0.4, and 0.2 ng/mL. In this way, an ochratoxin amount equal to 4 ng was added to each volume and loaded into the MISPE cartridge. The wine samples were then extracted and analyzed.

IAC Procedure. Pretreated wine samples (10 mL) were loaded on the IAC column and passed through it at a flow rate of about 1 drop/s without allowing the column to dry. The column was washed with 5 mL of a 2.5% m/v aqueous solution of sodium chloride, 0.5% m/v sodium hydrogen carbonate, pH 8.1, and then with 5 mL of water, allowing the column to dry by passing air through it. OTA elution was performed with 2 mL of methanol, and the eluate was evaporated under a gentle stream of dry nitrogen. OTA was redissolved in 0.25

mL of HPLC mobile phase, sonicated for 5 min, and immediately analyzed.

RESULTS AND DISCUSSION

The high selectivity toward OTA of a molecular imprinted polymer obtained by a thermal polymerization of methacrylic acid as functional monomer and ethylene glycol dimethacrylate as cross-linker in the presence of *N*-(4-chloro-1-hydroxy-2-naphthoylamido)-L-phenylalanine as mimic template has been previously described.[23−25] The present work starts from these results to develop a solid phase extraction procedure tailored for red wines as real matrices. To this purpose, we first investigated the behavior of the imprinted polymer in loading and recovery of the analyte and in removing the interfering substances. Once the optimal operating conditions were defined by using a standard solution of OTA, the experimental work concerned the refining of the extraction protocol on Italian red wines.

Development of MISPE Protocol. A MISPE protocol was developed by using OTA standard solutions diluted in a hydro-organic buffer containing ethanol, the so-called hydroalcoholic citrate−tartrate buffer, that has previously been shown to mimic real wine samples.[26]

The assessment of the loading capacity of the MISPE cartridge allowed us to define how much mycotoxin could be loaded on the stationary phase without a detectable amount of OTA in the flow-through. The loading of 250 ng of ochratoxin A, a very high amount compared to the maximum permitted level in wine samples, allowed us to verify that no target compound was unretained in the loading step.

The washing step removed interfering substances from the MISPE cartridge retaining at the same time the target analyte. Thus, these experiments aimed to evaluate the capability of water−organic solvent mixtures to keep loaded OTA bound to the MISPE cartridge. The considered organic solvents have different polarities, although they are all water-soluble, allowing their use in aqueous mixture at variable percentages. Figure 2 shows the different trends obtained with different water−organic solvent mixtures. All of the profiles show a maximum

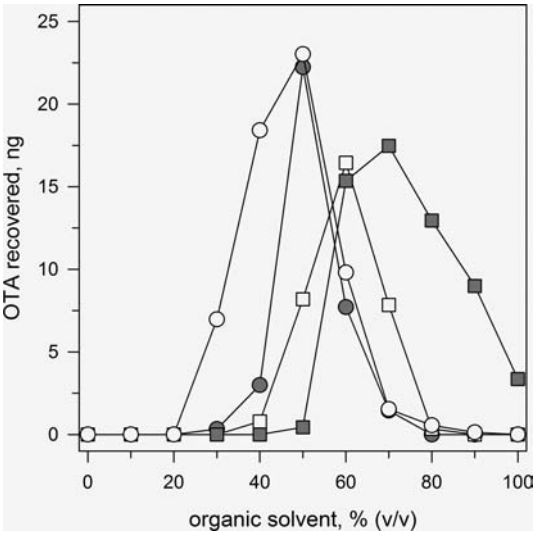

Figure 2. Recovery profiles of OTA in the cartridge washing step as a function of different water−organic solvent mixtures: acetonitrile (open circle); tetrahydrofuran (solid circle); acetone (open square); methanol (solid square).

OTA elution at a given solvent percentage that is related to the solvent elution strength following the order acetonitrile ∼ tetrahydrofuran > acetone > methanol. These results allowed us to make some preliminary considerations about the kind of organic solvent and its relative percentage useful for both washing and elution steps of OTA in the MISPE protocol. However, the final choice was dependent on the results obtained for real samples by considering that the properties of the organic solvent could also affect the selectivity of the extraction protocol.

The recovery of OTA was performed in experimental conditions minimizing the required volume, that is, the target analyte dilution. The organic solvents that more efficiently eluted the mycotoxin were acetonitrile and tetrahydrofuran, although the best choice for chromatographic analysis reasons was acetonitrile. As a consequence, this solvent was tested in elution experiments, also with the addition of variable amounts of acetic acid as hydrogen bond disruptor. Figure 3 summarizes

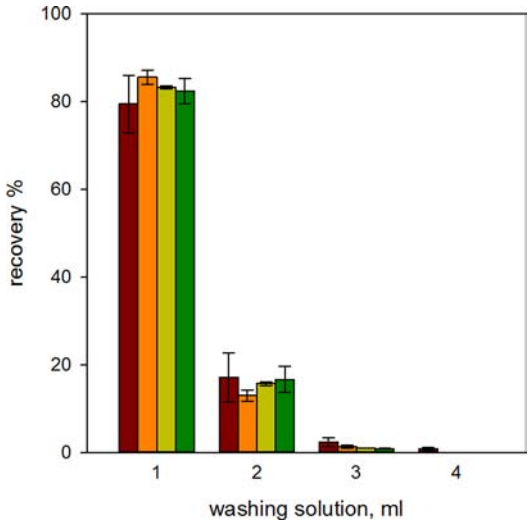

Figure 3. Recovery of eluted OTA by using acetonitrile with increasing percentages of acetic acid: acetonitrile (red bar); acetonitrile + 1% v/v acetic acid (orange bar); acetonitrile + 2% v/v acetic acid (pale green bar); acetonitrile + 5% v/v acetic acid (dark green bar).

the results obtained in terms of recovered percentages of OTA: the use of acetic acid allowed the quantitative recovery of OTA (>99%) in 2 mL. As a consequence, OTA elution was performed with 2 mL of acetonitrile/acetic acid 98:2 v/v.

Refining the MISPE Protocol on Real Wine Samples. The MISPE protocol developed in the previous section was then applied to different wine samples for a further improvement in the presence of real matrices. Therefore, after the preliminary wine treatment, the washing solution composition was refined, considering again several washing mixtures by using an OTA-negative certified wine sample.

The choice of the tested washing solutions was made on the basis of the experimental results reported in Figure 2, where acetonitrile and tetrahydrofuran seemed to be the strongest eluents, followed by acetone. Hydro-organic mixtures (water/solvent 80:20 v/v) were tested to refine the ability to wash away the interfering matrices from the MISPE cartridge while minimally affecting OTA retention. The comparison of chromatographic profiles obtained by the analysis of pretreated red wine samples, loaded and recovered from the MISPE cartridge by using three different washing solutions, showed

dx.doi.org/10.1021/jf5010995 | J. Agric. Food Chem. 2014, 62, 5220−5225

that the difference in the chromatograms mainly concerned the analytical signals in the first 5 min, far from the peak corresponding to OTA. Thus, a 2 mL washing solution made of water/acetonitrile 4:1 v/v was chosen as appropriate to remove matrix interferents.

The minimum volume capable of washing away the retained interferents even in the case of loading volumes >1 mL was further investigated. This step was useful to preconcentrate the target analyte. No significant differences were observed, confirming that all potentially interfering substances were easily removed from the MISPE cartridge even with large sample volumes. Thus, a minimum volume of 2 mL was then considered as the best choice.

Choice of HPLC Method Calibration. The complexity and the variety of the wine matrix pose a question about what kind of HPLC calibration is more suitable for OTA determination. In fact, if the matrix effect is completely eliminated by the optimized MISPE extraction, then it would be possible to use external calibrators, whereas if a matrix effect is present, the addition standard method should be preferred. However, it should be noted that this last approach is more cumbersome because it requires different calibrations for different matrices and so is less practicable.

To compare the two approaches, the analytical signals (i.e., peak areas) obtained from wine samples spiked with OTA in the concentration range of 0.25−5 ng/mL were used to set up a standard addition plot (LoD, 0.080 ng/mL; LoQ, 0.285 ng/mL) and read on the external calibration plot described under Optimization of MISPE Protocol (LoD, 0.075 ng/mL; LoQ, 0.225 ng/mL). In this way, added concentrations were plotted versus found concentrations. The goodness of fit (r^2_{adj} = 0.9857, SEE = 0.2167) highlights that the matrix effect is well compensated so that we chose the calibration plot based on the use of external standards for OTA determination in red wines combined with the optimized MISPE extraction above-described.

The recovery and preconcentration tests were performed on an OTA-certified negative red wine according to the optimized MISPE protocol. The experimental results show the overall good performance of the MISPE column. In the concentration range of 0.25−5 ng/mL of OTA, the recoveries lie between 92 and 110%, and a substantial independence of these values from loaded analyte concentration can be observed. When increasing volumes of wine (2−20 mL) containing a fixed amount of OTA are loaded, a satisfying target analyte recovery, between 88 and 102%, was obtained, allowing a 10-fold increase of the method sensitivity with respect to the initially optimized MISPE protocol. Hence, this condition leads to a preconcentration factor of 5 taking into account the initial untreated wine.

MISPE of Real Samples. Finally, to evaluate the effect of the matrix variability, the MISPE protocol was applied to 17 red wine samples of different types and from several regions of Italy. A HPLC chromatogram of a wine sample eluted by the MISPE cartridge is shown in Figure 4. The amounts of OTA found by MISPE-HPLC and determined on 20 mL of pretreated wine samples were compared with those obtained by the conventional IAC-HPLC procedure. The obtained results (Table 1) show a good agreement between the two extraction methods fit (r^2_{adj} = 0.9817, SEE = 0.0262) (Figure 5) without any bias effect due to different geographic origin of wines. Therefore, the MISPE procedure can be considered a reliable alternative to the conventional IAC protocol. Although the preconcentration factor is more reduced for MISPE with respect to IAC, the cleanup procedure is simple and capable of successfully eliminating most of the matrix effects. Moreover, the combination of the MISPE with the sensitive fluorescence detection allows OTA determination well below the legal limit of 2 ng/mL.

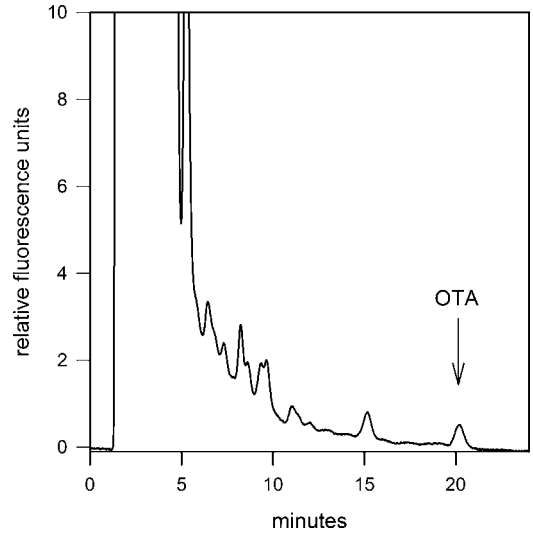

Figure 4. HPLC chromatogram of red wine sample (Novello 2012) obtained by MISPE.

Table 1. OTA Determination in Italian Red Wines[a]

wine denomination	region of provenience	OTA by MISPE, ng/mL	OTA by IAC, ng/mL
Aglianico (2005)	Campania	0.377 ± 0.049	0.301 ± 0.041
Aglianico (2009)	Campania	0.451 ± 0.054	0.428 ± 0.045
Barbera d'Asti (2010)	Piedmont	0.437 ± 0.055	0.413 ± 0.051
Barbera d'Asti (2012)	Piedmont	0.941 ± 0.095	0.886 ± 0.089
Birbet (2011)	Piedmont	0.271 ± 0.046	0.200 ± 0.019
Bonarda (2011)	Piedmont	0.182 ± 0.022	0.179 ± 0.024
Freisa d'Asti (2011)	Piedmont	0.197 ± 0.029	0.194 ± 0.031
Freisa di Chieri (2011)	Piedmont	<LOD	<LOD
Mastro (2011)	Campania	0.388 ± 0.045	0.312 ± 0.036
Merlot (2011)	Veneto	0.589 ± 0.074	0.544 ± 0.065
Montepulciano (2012)	Tuscany	0.171 ± 0.023	0.165 ± 0.021
Nebbiolo (2009)	Piedmont	0.200 ± 0.019	0.189 ± 0.017
Nero d'Avola (2011)	Sicily	0.294 ± 0.032	0.255 ± 0.026
Novello (2012)	Piedmont	0.548 ± 0.069	0.538 ± 0.062
Primitivo di Manduria (2009)	Apulia	0.492 ± 0.051	0.482 ± 0.047
Rouchè (2011)	Piedmont	0.212 ± 0.027	0.199 ± 0.025
Salento (2011)	Apulia	0.434 ± 0.049	0.423 ± 0.051

[a]Comparison between results by MISPE and by IAC. Each result was the average of three replicates.

In conclusion, we have developed a MISPE protocol for the extraction and preconcentration for HPLC analysis of OTA in red wine samples. The molecularly imprinted polymer, prepared through a mimic template approach, was used for the preparation of a MISPE stationary phase. The assessment of a SPE protocol indicates that a careful choice of both the washing and eluting conditions allows the optimization of a reliable MISPE extraction protocol, selective for the mycotoxin and capable of preconcentrating the analyte well below the

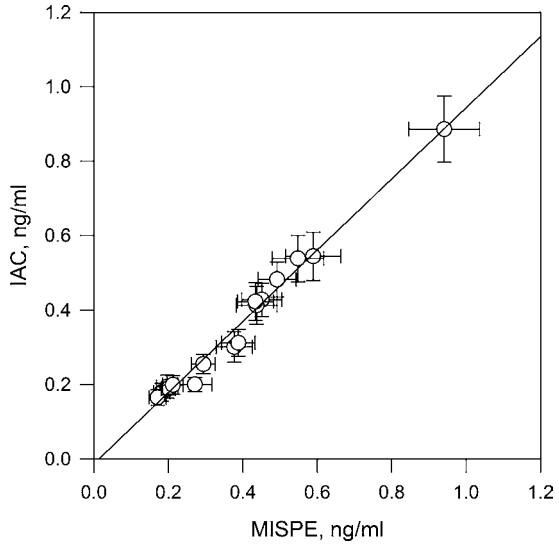

Figure 5. Comparison of OTA detemination in wine samples by IAC versus MISPE.

maximum permitted levels. Recoveries performed on different Italian red wine samples spiked with OTA showed good reproducibility and agreement with those obtained by the IAC method, demonstrating the potentiality of this procedure to substitute for the current IAC-HPLC protocol.

■ ASSOCIATED CONTENT

Supporting Information

Tables 1SI–3SI. This material is available free of charge via the Internet at http://pubs.acs.org.

■ AUTHOR INFORMATION

Corresponding Author

*(C.G.) Phone: +39 011 6705252. Fax: +39 011 6705242. E-mail: cristina.giovannoli@unito.it.

Notes

The authors declare no competing financial interest.

■ ABBREVIATIONS USED

IAC, immunoaffinity chromatography; LoD, limit of detection; LoQ, limit of quantification; MISPE, molecularly imprinted solid phase extraction; PEG 8000, poly(ethylene glycol) 8000; PTFE, polytetrafluoroethylene; r^2_{adj}, adjusted regression coefficient; SEE, standard estimate of error; SPE, solid phase extraction

■ REFERENCES

(1) Poland, A. E.; Nesheim, S.; Friedman, L. Ochratoxin A: a review. *Pure Appl. Chem.* **1992**, *64*, 1029–1046.

(2) Pfohl-Leszkowicz, A.; Mandeville, R. A. Ochratoxin A: an overview on toxicity and carcinogenicity in animals and humans. *Mol. Nutr. Food Res.* **2007**, *51*, 61–99.

(3) Duarte, S. C.; Peña, A.; Lino, C. M. A review on ochratoxin A occurrence and effects of processing of cereal and cereal derived food products. *Food Microbiol.* **2010**, *27*, 187–198.

(4) Magan, N.; Aldred, D.; Mylona, K.; Lambert, R. J. W. Limiting mycotoxins in stored wheat. *Food Addit. Contam. A* **2012**, *27*, 644–650.

(5) Duarte, S. C.; Lino, C. M.; Peña, A. Ochratoxin A in feed of food-producing animals: an undesirable mycotoxin with health and performance effects. *Vet. Microbiol.* **2011**, *154*, 1–13.

(6) Kabak, B. The fate of mycotoxins during thermal food processing. *J. Sci. Food Agric.* **2009**, *89*, 549–554.

(7) Bertuzzi, T.; Rastelli, S.; Mulazzi, A.; Donadini, G.; Pietri, A. Mycotoxin occurrence in beer produced in several European countries. *Food Control* **2011**, *22*, 2059–2064.

(8) Anli, E.; Bayram, M. Ochratoxin A in wines. *Food Rev. Int.* **2009**, *25*, 214–232.

(9) Copetti, M. V.; Pereira, J. L.; Iamanaka, B. T.; Pitt, J. I.; Taniwaki, M. H. Ochratoxigenic fungi and ochratoxin A in cocoa during farm processing. *Int. J. Food Microbiol.* **2010**, *143*, 67–70.

(10) Commission of the European Communities (CEC). Commission Regulation (EC) No. 1881/2006 of 19 December 2006 setting maximum levels for certain contaminants in foodstuffs. *Off. J. Eur. Union* **2006**, *L 364*, 5–24.

(11) Visconti, A.; Pascale, M.; Centonze, G. Determination of ochratoxin A in wine and beer by immunoaffinity column cleanup and liquid chromatographic analysis with fluorometric detection: collaborative study. *J. AOAC Int.* **2001**, *84*, 1818–1827.

(12) Zollner, P.; Mayer-Helm, B. Trace mycotoxin analysis in complex biological and food matrices by liquid chromatography-atmospheric pressure ionisation mass spectrometry. *J. Chromatogr., A* **2006**, *1136*, 123–169.

(13) Sforza, S.; Dall'Asta, C.; Marchelli, R. Recent advances in mycotoxin determination in food and feed by hyphenated chromatographic techniques/mass spectrometry. *Mass Spectrom. Rev.* **2006**, *25*, 54–76.

(14) Zheng, M. Z.; Richard, J. L.; Binder, J. A review of rapid methods for the analysis of mycotoxins. *Mycopathologia* **2006**, *161*, 261–273.

(15) Anfossi, L.; Baggiani, C.; Giovannoli, C.; D'Arco, G.; Giraudi, G. Lateral-flow immunoassays for mycotoxins and phycotoxins: a review. *Anal. Bioanal. Chem.* **2013**, *405*, 467–480.

(16) Scott, P. M.; Trucksess, M. W. Application of immunoaffinity columns to mycotoxin analysis. *J. AOAC Int.* **1997**, *80*, 941–949.

(17) Baggiani, C.; Anfossi, L.; Giovannoli, C. Molecularly imprinted polymers as synthetic receptors for the analysis of myco- and phycotoxins. *Analyst* **2008**, *133*, 719–730.

(18) Maier, N. M.; Buttinger, G.; Welhartizki, S.; Gavioli, E.; Lindner, W. Molecularly imprinted polymer-assisted sample clean-up of ochratoxin A from red wine: merits and limitations. *J. Chromatogr., B* **2004**, *804*, 103–111.

(19) Yu, J. C. C.; Krushkova, S.; Lai, E. P. C.; Dabek-Zlotorzynska, E. Molecularly-imprinted polypyrrole-modified stainless steel frits for selective solid phase preconcentration of ochratoxin A. *Anal. Bioanal. Chem.* **2005**, *382*, 1534–1540.

(20) Yu, J. C. C.; Lai, E. P. C. Molecularly imprinted polypyrrole modified carbon nanotubes on stainless steel frit for selective micro solid phase pre-concentration of ochratoxin A. *React. Funct. Polym.* **2006**, *66*, 702–711.

(21) Yu, J. C. C.; Lai, E. P. C. Determination of ochratoxin A in red wines by multiple pulsed elutions from molecularly imprinted polypyrrole. *Food Chem.* **2007**, *105*, 301–310.

(22) Cao, J. L.; Kong, W. J.; Zhou, S. J.; Yin, L. H.; Wan, L.; Yang, M. H. Molecularly imprinted polymer-based solid phase clean-up for analysis of ochratoxin A in beer, red wine, and grape juice. *J. Sep. Sci.* **2013**, *36*, 1291–1297.

(23) Baggiani, C.; Biagioli, F.; Anfossi, L.; Giovannoli, C.; Passini, C.; Giraudi, G. Effect of the mimic structure on the molecular recognition properties of molecularly imprinted polymers for ochratoxin A prepared by a fragmental approach. *React. Funct. Polym.* **2013**, *73*, 833–837.

(24) Baggiani, C.; Giraudi, G.; Vanni, A. A molecular imprinted polymer with recognition properties towards the carcinogenic mycotoxin ochratoxin A. *Bioseparation* **2001**, *10*, 389–394.

(25) Jodlbauer, J.; Maier, N. M.; Lindner, W. Towards ochratoxin A selective molecularly imprinted polymers for solid-phase extraction. *J. Chromatogr., A* **2002**, *945*, 45–63.

(26) Baggiani, C.; Baravalle, P.; Giraudi, G.; Tozzi, C. Molecularly imprinted solid-phase extraction method for the high-performance

liquid chromatographic analysis of fungicide Pyrimethanil in wine. *J. Chromatogr., A* **2007**, *1141*, 158−164.

and quantities of mycotoxins and plant defense compounds in plant tissue (i.e., zealexins, fatty acid-derived oxylipins).

MATERIALS AND METHODS

Chemicals. Authentic standards for 3-hexen-1-ol, heptan-2-ol, 1-octen-3-ol, octan-3-one, and octan-3-ol were purchased from Sigma-Aldrich, Munich, Germany. β-Macrocarpene and β-bisabolene were produced using recombinant TPS6. The enzyme was heterologously expressed in *Escherichia coli*, purified, and incubated with the substrate farnesyl pyrophosphate. Enzyme products were collected from the headspace of the assay using SPME. Heterologous expression, enzyme assays, and product analysis were carried out as described earlier.[12] α-Selinene and β-selinene were identified using celery (*Apium graveolens*) seed oil (Carl Roth, Karlsruhe, Germany).[14]

Plant Material and Growth Conditions. Experiments were performed on two corn varieties, including the commercial hybrid variety Ronaldinio (obtained from KWS Saat AG, Einbeck, Germany) and the dwarf corn variety GaspeFlint landrace (originally collected in Quebec, Canada, provided by Prof. Dr. J. Schirawski, RWTH Aachen University, Germany).

Corn was grown under greenhouse conditions at 26 ± 5 °C with a 16 h photoperiod (6600 lx at ear height) and a relative humidity of 58%. Corn seeds were sown in a soil mix consisting of 30% sand (<2 mm particle size granularity) and 70% commercial plant substrate (Fruhstorfer Erde, Typ T25, HAWITA Group, Vechta, Germany). After 21 days of growth, the hybrid corn plants were separated, and single plants were transferred to plastic pots (18 × 18 × 25 cm). Dwarf corn seedlings were sown and raised in plastic pots (11 × 11 × 12 cm). Plants were irrigated with tap water as required. After 1 month of growth, plants were supplemented weekly with a macronutrient fertilizer (N:P:K = 15:10:15) dissolved in the irrigation water.

Fungal Strains. Hybrid corn ears were inoculated with two strains of *Fusarium graminearum* (FG1 and FG2), two strains of *Fusarium verticillioides* (FV1 and FV2), and one strain of *Fusarium subglutinans* (FSUB). FG1 is a nivalenol (NIV) chemotype strain, and FG2 is a deoxynivalenol (DON) chemotype strain. Infection of dwarf corn ears included one strain each for *F. graminearum* (FG1), *F. verticillioides* (FV1), and *Fusarium avenaceum* (FA). The sources of fungal material and abbreviations used in this study are described in the Supporting Information (Table S1). These strains/species of *Fusarium* were selected for their different abilities to infect corn and also because of their ability to produce different mycotoxins.

Fungal spores were produced under sterile conditions in liquid mung bean medium following a modified protocol.[15] Modifications included an additional initial cultivation step for 5 days at 28 °C to enhance final spore concentration. Final cultures were filtered through cotton wool and were centrifuged at 7000*g* for 5 min. The supernatant was discarded, and spores were suspended in glycerol (15% v/v, Carl Roth, Karlsruhe, Germany). Suspensions were mixed gently, and the spores were counted with a Thoma chamber (0.0025 mm^2). Spore suspensions were stored at −70 °C, and germination tests were regularly performed on potato dextrose agar (PDA, Carl Roth, Karlsruhe, Germany) to assess viability.

Inoculation of Corn Ears. Commercial corn ears of the hybrid variety were inoculated with fungal strains FG1, FG2, FV1, FV2, and FSUB. Ears of the dwarf corn variety were inoculated with FG1, FV1, and FA only. A summary of the treatments and parameters monitored for each treatment is provided in Table 1. The harvested spores were suspended in autoclaved tap water containing the detergent Tween 20 (0.14%, Applichem, Darmstadt, Germany), which prevented clumping. For inoculation of hybrid corn ears, the spore concentration was 10^6 mL^{-1} for *F. verticillioides* and *F. subglutinans* and 10^5 mL^{-1} for *F. graminearum* (the latter species is more aggressive than the other two species). Each hybrid corn ear was treated with 1.0 mL of inoculum, and control plants were treated with 1.0 mL of water containing 0.14% Tween 20. For inoculation of dwarf corn ears, the spore concentration was 10^5 mL^{-1} for *F. graminearum* and 2×10^5 mL^{-1} for *F. verticillioides* and *F. avenaceum*. Because the ears of dwarf corn are small, only 0.5 mL of inoculum was injected per ear, and control plants were treated with 0.5 mL of water containing 0.14% Tween 20. Hybrid and dwarf corn ears were inoculated by injecting the spore suspension into the silk channel at the main flowering stage (BBCH 65).[16,17]

Table 1. Overview of *Fusarium* Species and Strains Used To Inoculate Hybrid Corn and Dwarf Corn, Timing of Sample Collection, and Variables Measured[a]

		hybrid maize		dwarf maize
maize ears treated with	abbreviation for treatment	maize ears at milk ripeness (~24 dpi)	maize ears at 4, 8, 12, 16, 20, and 24 dpi	maize ears at milk ripeness (~14 dpi)
noninfected control	CONT	SPME, OLS, oxylipins; DS; DNA; mycotoxins		SPME, zealexins, GEA; DS; DNA
F. graminearum strain 1	FG1	SPME, OLS, oxylipins; DS; DNA; mycotoxins		SPME, zealexins, GEA; DS; DNA
F. graminearum strain 2	FG2	SPME, OLS, oxylipins; DS; DNA; mycotoxins	SPME; DS; DNA	
F. verticilloides strain 1	FV1	SPME, OLS, oxylipins; DS; DNA; mycotoxins	SPME; DS; DNA	SPME, zealexins, GEA; DS; DNA
F. verticilloides strain 2	FV2	SPME, OLS, oxylipins; DS; DNA; mycotoxins		
F. subglutinans	FSUB	SPME, OLS, oxylipins; DS; DNA; mycotoxins		
F. avenaceum	FA			SPME, zealexins, GEA; DS; DNA

[a]Volatiles were sampled by solid phase microextraction (SPME) and by open-loop stripping (OLS). For hybrid corn and SPME and OLS at 24 days postinoculation (dpi), n = 4 ears/treatment. For hybrid corn and SPME in the time series (4−24 dpi), n = 3. For dwarf corn at 14 dpi, n = 6. Nonvolatile defense compounds were quantified in hybrid corn (oxylipins, n = 4) and dwarf corn (zealexins n = 4−6) along with gene expression analysis of *tps6/11* (GEA, n = 4−6). Mycotoxins were quantitied in hybrid corn ears at 24 pdi (n = 4). Disease severity (DS) was evaluated visually on dehusked corn ears, and fungal biomass (as indicated by DNA) was quantitied by RT-PCR.

Collection of Plant Material for Chemical and Molecular Analysis. Hybrid corn and dwarf corn ears were harvested at the early milk ripeness maturity stage, BBCH 73,[17] which was 24 days postinoculation (dpi) for hybrid corn and 14 dpi for dwarf corn. Hybrid corn was also harvested at 4, 8, 12, 16, 20, and 24 dpi (Table 1). Corn ears were dehusked, and disease severity was visually estimated as the percentage of affected/infected surface (from 0 to 100%). Afterward, corn ears were cut longitudinally into halves. Immediately after harvest, corn ears were placed on ice and within 30 min frozen at −20 °C (samples for SPME, mycotoxin, oxylipin, and qPCR analysis) or shock frozen in liquid N_2 (samples for zealexin quantitation and gene expression analysis). Handling of the samples on ice or with liquid N_2 was performed to ensure that the profiles of secondary metabolites measured in this study were attributed to *Fusarium* infection and not to the damage of the ears induced by cutting. Additionally, to validate the results obtained by SPME on cut material, volatiles were also sampled from undamaged infected and uninfected corn ears on live plants (see Collection of Volatiles by Open-Loop Stripping).

dx.doi.org/10.1021/jf500560f | J. Agric. Food Chem. 2014, 62, 5226−5236

From the cut corn ears, a 2.0 g quantity of kernels from the tip of the first half was transferred to an SPME vial, which was sealed airtight and stored at −20 °C for subsequent volatile analysis. Kernels from the second half were used for further chemical and molecular analysis. Hybrid corn material from the second half was susequently freeze-dried and ground with a ball mill (Retsch, Haan, Germany). Subsamples of homogenized material were used for fungal biomass quantitation by quantitative real-time PCR and for the analysis of mycotoxins and oxylipins (Table 1). Dwarf corn material from the second half was homogenized in liquid nitrogen immediately after cutting and used for fungal biomass quantitation by quantitative real-time PCR, for gene expression analysis, and for the detection of zealexins (Table 1).

Collection of Volatiles by SPME. Samples (2.0 g of corn kernels) were enclosed in 20 mL SPME vials (VWR, Darmstadt, Germany) that had screw caps containing a silicone/polytetrafluoroethylene (PTFE) septum (1.3 mm, VWR). The samples were extracted by SPME using a polydimethylsiloxane divinylbenzene (PDMS-DVB) fiber (65 μm coating thickness, Supelco, purchased from Sigma-Aldrich, Taufkirchen, Germany). The SPME fiber was conditioned according to the manufacturer's instruction before extraction. Before extraction, the samples, which were initially frozen at −20 °C, were allowed to equilibrate to room temperature for 3 h and were then incubated at 40 °C for 25 min. Headspace SPME was then carried out for 10 min at 40 °C, resulting in equilibrium extraction. The fiber was immediately injected into the GC inlet (heated to 260 °C) for VOC desorption and chromatographic analysis. Blank runs using empty SPME vials were regularly performed to check for carry-over effects.

Collection of Volatiles by Open-Loop Stripping (OLS). Because SPME was used on frozen and cut corn kernels, OLS was used as another, independent volatile-sampling technique to validate the SPME results. Specifically this was done to ensure that the volatiles identified by SPME were not artifacts due to cutting or freezing the samples. In the OLS setup used here, volatiles were collected from live corn ears on intact plants. The maturity stage of the corn ears was the same as that of the ears subjected to SPME; that is, the ears were at the main flowering stage (BBCH 65[17]). Corn ears were enclosed in commercial, polyester cooking bags (50 cm adjusted length, Toppits, Minden, Germany), and air was circulated in the bags with a flow of 1.5 L min^{-1} to carry/strip the volatiles away using an N86KT.18 pull pump equipped with a PTFE-coated membrane (VWR). Incoming air was precleaned on steam-activated charcoal pellets (1 mm diameter, Sigma-Aldrich) to minimize background signal. Volatiles from corn ears were trapped in a glass cartridge containing a 1.5 mg activated charcoal filter (from D. Graenicher, Daumazan sur Arize, France), and extraction was performed for 24 h to exclude diurnal variations. The quantity of 1.5 mg of activated charcoal was sufficient to trap all volatiles emitted from corn ears within 24 h, and no trap saturation or volatile breakthrough was observed (this was validated by sampling the volatiles of a *Fusarium*-infected corn ear using three cartridges in a row). Blank runs were performed with empty bags to determine the background signal of the system. Pump, bags, volatile trap, and precleaning cartridge were all connected using silicon tubing.

After extraction of the volatiles, traps were rinsed with 100 μL of dichloromethane spiked with 8 μg mL^{-1} nonyl acetate (FCC grade, Sigma-Aldrich) as an internal standard. A 2 μL volume was used for volatile analysis by gas chromatography coupled to mass spectrometry (GC-MS). Because cartridges were used many times, they were cleaned/reconditionned between each run by rinsing them three times with dichloromethane and three times with *n*-pentane. Organic solvents were then removed by vacuum for 2 min. This reconditioning step was performed to make sure that no volatile contamination was carried over from one sampling to the next.

Gas Chromatography–Mass Spectrometry (GC-MS) Conditions for Volatile Profiling. An Agilent 6890 gas chromatograph that was coupled with an Agilent 5973 mass selective detector (Agilent, Waldbronn, Germany) and equipped with an autosampler for SPME vials (PAL Combi, CTC Analytics AG, Zwingen, Switzerland) was used to analyze the SPME samples and extracts of OLS. The GC was equipped with a capillary HP-5MS column (0.25 mm nominal diameter × 30 m length × 0.25 μm film thickness, Agilent). Conditions were as follows: inlet pressure, 48.5 kPa; helium flow, 19 mL min^{-1}; injector, 250 °C; transfer line, 260 °C; and electron energy, 70 eV. The GC was programmed as follows: 40 °C (2 min isothermic), increasing at 3.2 °C min^{-1} to 140 °C followed by 80 °C min^{-1} to 250 °C (3.38 min isothermic) and operated in splitless mode; carrier gas (helium), 1 mL min^{-1}. The scan range was between 40 and 450 atomic mass units.

Comparison of SPME and OLS Extraction Methods. Without proper calibration, SPME is considered at best semiquantitative. Furthermore, because SPME is a nonexhaustive extraction method, matrix effects cannot be ruled out. To estimate possible matrix effects, we compared results obtained with SPME (no standard) and OLS (internal standard) on the same samples. For this purpose, kernels of hybrid corn ears were collected at 24 dpi with FG1 and homogenized in a mortar. A 5 g quantity of the fresh material from the mortar was distributed to each of three replicates of SPME vials and glass Petri dishes. HS-SPME was conducted as described before in 20 mL SPME vials. For OLS, the glass Petri dishes containing the homogenized kernels were placed in polyester bags; volatiles were trapped by flushing the bags for 4 h and were collected as described before for live corn ears.

Mycotoxin Extraction and Analysis. For each sample of homogenized corn flour, a 500 mg quantity was transferred to a 15 mL centrifuge tube. The material in the tube was then mixed with 5 mL of extraction solvent (methanol/isopropanol/water/acetic acid, 79:5:15:1, v/v/v/v, Carl Roth), followed by an overnight extraction on a rotary shaker (170 rpm) and centrifugation at 7000*g* for 10 min. A 1.0 mL volume of the clear supernatant was evaporated to dryness under vacuum at 35 °C, redissolved in 500 μL of methanol/water (1:1, v/v), and defatted with cyclohexane. Mycotoxin content was determined by HPLC-MS/MS using the instrument, columns, and methods previously described for trichothecenes[18] and for zearalenone and fumonisins.[19,20]

Quantitation of Fungal DNA. DNA was extracted from 100 mg samples of corn ear material following a protocol described earlier.[21] DNA quality was checked by agarose electrophoresis. Standards were produced in noncontaminated corn matrix spiked with pure fungal DNA. DNA extraction from fungal mycelium was conducted as described in ref 21, but an additional phenol extraction step was included and DNA concentration was determined by densitometry. Real-time PCR with species-specific primers was used to determine fungal biomass in plant tissue according to protocols published for *F. graminearum*[21] and *F. verticillioides*.[22] *F. subglutinans* and *F. avenaceum* were quantified with the aid of species-specific primers described elsewhere[23,24] using a reaction mixture consisting of 16 mM $(NH_4)_2SO_4$, 67 mM Tris-HCl pH 9.0, 0.3 μM each primer, 0.1× SYBR Green I (Invitrogen, Karlsruhe, Germany), 1 u/50 μL BIOTaq DNA polymerase (Bioline, Lückenwalde, Germany), 0.1 mM dNTP, and $MgCl_2$ (3.5 mM for *F. subglutinans* and 2 mM for *F. avenaceum*). The following thermocycler program was used: initial denaturation for 2 min/94 °C followed by 34 cycles of 30 s/94 °C, 30 s/64 °C (*F. subglutinans*) or 25 s/62 °C (*F. avenaceum*) and 40 s/72 °C (*F. subglutinans*) or 30 s/72 °C (*F. avenaceum*). The final extension was carried out for 5 min at 72 °C.

Gene Expression Analysis of Terpene Synthase Genes *tps6/11*. Total RNA was extracted from 100 mg samples of fresh matter (ground with a mortar and pestle in liquid nitrogen) using the RNeasy Plant Mini Kit (Quiagen, Hilden, Germany). The quality and quantity of RNA were assessed by gel electrophoresis (1.2% (w/v) agarose gels).

DNase digestion was carried out, followed by the synthesis of cDNA using Super Script III polymerase (Invitrogen, Karlsruhe, Germany). Each volume was diluted 2:1 (v/v). Amplification of DNA was accomplished for each candidate primer pair using Phusion High-Fidelity DNA-Polymerase (Biozym, Hessisch Oldendorf, Germany). PCR products were purified with the QIAquick PCR Purification Kit (Quiagen). The DNA fragments were ligated in the pCRBlunt II-TOPO vector (Invitrogen) following the manufacturer's instructions. The vector was transformed in competent cells of *Escherichia coli*

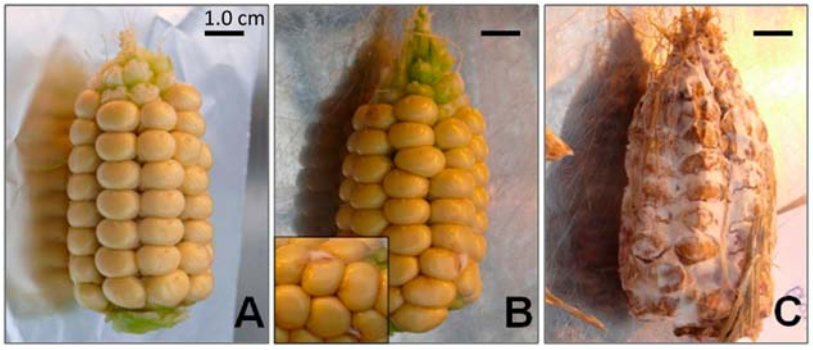

Figure 1. Photographs showing typical symptoms of *Fusarium* infection on corn ears. The representative dwarf corn ears were at the milk ripeness maturation stage and had been inoculated 14 days earlier with (A) water as a control treatment (no symptoms), (B) *F. verticillioides* (inset illustrates mycelium of *F. verticilllioides* on single kernels), and (C) *F. graminearum* (the whole ear is heavily colonized). Infection symptoms for hybrid corn ears were comparable.

(TOP10, Invitrogen). Colony PCR was carried out to identify successfully transformed colonies. Plasmid DNA was extracted from the *E. coli* cultures with the NucleoSpin Plasmid Kit (Macherey-Nagel, Dueren, Germany). Extracted plasmids were sequenced to confirm correct insert sequence. Quantitative real-time PCR was carried out for a housekeeping gene[25] (putative APT1a for adenine phosphoribosyltransferase 1; primer forward HG5:5′-AGGCGTTCCGTGACACCATC-3′, primer reverse HG6:5′-CTGGCAACTTCTTCGGCTTCC-3′) and candidate genes (*tps6/11*, QRT5:5′-TGGTAATTTGGACTTAGTTTCACG-3′; QRT6:5′-CACTGTCTCTCCATGAATCCTC-3′) using Brilliant III Ultra-Fast qPCR master mix (Stratagene, La Jolla, CA, USA). Because of the high sequence similarity, only one primer pair was used for the amplification of both *tps6* and *tps11*. Primer specificity was confirmed by agarose gel electrophoresis, melting curve analysis, standard curve analysis, and sequence verification of cloned PCR amplicons (see above). ROX was used as a reference dye. The following PCR conditions were applied for all reactions: initial incubation at 95 °C for 3 min followed by 40 cycles of amplification (95 °C for 20 s, 60 °C for 20 s). Plate reads were taken during the annealing and the extension step of each cycle. Data for the melting curves were recorded at the end of cycling from 55 to 95 °C.

All samples were run on the same PCR machine (MxPro-Mx3000P, Stratagene, Agilent Technologies, USA) in an optical 96-well plate. Five biological replicates were analyzed as triplicates in the qRT-PCR for each of the three treatments. Data for the relative quantity to calibrator average (dRn) were exported from the MXPro software.

Detection of Oxylipins and Zealexins. Aliquots of freeze-dried hybrid corn material, corresponding to 2 g of fresh weight, were extracted as described earlier.[26] Extraction was performed with the internal standard (6*Z*,9*Z*,11*E*,13*S*)-13-hydroxy-6,9,11-octadecatrienoic acid (13γ-HOT), and extracts were methylated with trimethylsilyldiazomethane (2 M in hexane, Sigma-Aldrich). Hydroxyl fatty acids were purified by reverse phase HPLC using an ET250/2 Nucleosil 120-5 C18 column (Macherey-Nagel) as described earlier.[26] The eluate fraction was collected between 8.0 and 13.5 min, evaporated to dryness, and redissolved in 2 μL of acetonitrile. After the addition of 2 μL of *N*,*O*-bis(trimethylsilyl)trifluoroacetamide (Sigma-Aldrich), analysis was carried out with the GC-MS system as described earlier for the volatile profiling. Standard curves were constructed by plotting ion intensities versus concentrations of known hydroxyl fatty acids. For determination of the recovery of the hydroxyl fatty acids, 13γ-HOT was used.

For zealexin analysis, a 100 mg quantity of fresh dwarf corn ear material was transferred to a 2 mL reaction tube. Samples were extracted without an internal standard, derivatized, and identified as described by others.[13,27] Samples (1 μL) were injected into an GC-MS system as described earlier for the volatile profiling. Conditions were as follows: inlet pressure, 52.5 kPa; helium flow, 11 mL min^{-1}; injector, 260 °C; transfer line, 260 °C; and electron energy, 70 eV. The GC was programmed as follows: 50 °C (1 min isothermic), increasing at 10.0 °C min^{-1} to 260 °C (15 min isothermic), and operated in split mode (split ratio of 7:1); carrier gas (helium), 1 mL min^{-1}. Tentative identification of zealaxins A1 and A3 was based on mass spectral data.[13]

Data Processing, Relative Quantitation of Volatiles, and Statistical Analysis. Chromatograms of OLS and SPME samples were integrated automatically using Agilent MSD ChemStation software (version D.01.02.16, June 15, 2004, Agilent). Integration parameters were set to initial area reject = 1, initial peak width = 0.02, shoulder detection = OFF, and initial threshold =14. Kovat's retention indices (KI) were calculated on the basis of a homologous series of *n*-alkanes.[28] Peaks in different samples corresponding to the same volatile were realigned manually using an RT shift of maximum ±0.1 min. This low RT shift was appropriate because of the good resolution of the chromatograms and the low temporal shift among peaks. Two separate data matrices, including aligned retention times and corresponding integrated peak areas for all samples, were constructed, one for the SPME/GC-MS data set and one for the OLS/GC-MS data set. Relative quantitation was performed to be able to compare the concentration of each volatile among samples as follows: peak areas of the SPME/GC-MS data were normalized to the total ion current (TIC), whereas OLS/GC-MS peak areas were normalized to the peak area of the internal standard. Background signals (empty vial/empty bag sample) were subtracted from the corresponding matrices. Because our aim was to identify volatiles for which occurrence/concentration was affected by fungal infection, relative quantitation was appropriate because it allows comparison of the concentration of specific volatiles among samples. No absolute quantitation of volatiles was performed.

A nonparametric Kruskal–Wallis test[29] was used to identify those volatiles for which concentrations significantly differed between control and individual *Fusarium* infection treatments. This was performed on the SPME-GC/MS data of hybrid corn at 24 dpi. The Kruskal–Wallis test is included in the package "pgirmess: data analysis in ecology" for R (version 2.14.2; this recent version is available at http://cran.r-project.org/web/packages/pgirmess/index.html). Volatiles that significantly differed between one or more infection treatments and the healthy controls were considered as infection markers.

Markers were identified by calculation of retention indices (KI), when possible by injection of authentic standards, and by comparison of their MS fragmentation patterns with those available in mass spectral libraries, including NIST 08 (National Institute of Standards and Technology, Gaithersburg, MD, USA), the Adams library,[30] and the Wiley Registry of Mass Spectral Data.[31] Appropriate parametric and nonparametric statistical tests were used for statistics. The exact statistical tests are described in the captions.

RESULTS AND DISCUSSION

Specific Volatiles Are Induced/Repressed in *Fusarium*-Infected Corn Ears. In a first experiment, SPME volatile

Table 2. Volatiles Identified as Markers of *Fusarium* Infection in Hybrid Maize[a]

				peak area (% TIC)																
volatile	ID[b]	OLS	KI	control			*F. gramin*_1			*F. gramin*_2			*F. sub.*			*F. verticill*_1			*F. verticill*_1		
3-hexen-1-ol	a		856	0.53	±	0.30							0.19	±	0.14	0.24	±	0.14	0.02	±	0.02
heptan-2-ol	a		904	1.61	±	0.60	**0.20**	±	**0.18**	**0.02**	±	**0.02**	0.20	±	0.07	0.52	±	0.33	0.22	±	0.14
1-octen-3-ol	a		978	0.22	±	0.07	0.39	±	0.08	**0.89**	±	**0.29**	0.17	±	0.06	0.07	±	0.07	0.07	±	0.04
octan-3-one	a		985				**0.62**	±	**0.35**	**0.52**	±	**0.13**	0.13	±	0.13	**1.21**	±	**0.50**	**1.24**	±	**0.43**
octan-3-ol	a		993				0.07	±	0.07							**0.14**	±	**0.12**	**0.08**	±	**0.04**
(+)-cycloisosativene	b	+	1375	0.92	±	0.36	**0.10**	±	**0.04**	**0.04**	±	**0.04**	0.44	±	0.14	0.32	±	0.13	0.12	±	0.07
α-ylangene	b	+	1380	0.38	±	0.13	**0.02**	±	**0.02**				0.22	±	0.06	0.17	±	0.07	0.07	±	0.04
(+)-aromadendrene	b		1410				**0.37**	±	**0.08**	**0.09**	±	**0.03**									
longifolene	b	+	1412				0.47	±	0.68	**0.76**	±	**0.18**									
unidentified SQT	b	+	1418	0.10	±	0.01	**0.42**	±	**0.12**	**0.26**	±	**0.06**	0.09	±	0.01	0.03	±	0.02	0.07	±	0.01
unidentified SQT	b		1442				**0.40**	±	**0.10**	**0.14**	±	**0.03**									
unidentified SQT	b		1445				**0.71**	±	**0.18**	**0.16**	±	**0.03**									
(*E*)-β-farnesene	b	+	1477				**0.22**	±	**0.07**	**0.11**	±	**0.06**	**0.14**	±	**0.10**						
unidentified SQT	b		1485				**0.27**	±	**0.05**	**0.07**	±	**0.03**									
unidentified SQT	b		1488				**0.26**	±	**0.07**	**0.14**	±	**0.02**	0.02	±	0.02						
β-selinene	a	+	1499				**3.03**	±	**2.05**	**1.51**	±	**0.91**	**5.89**	±	**3.27**	**1.86**	±	**0.97**	**0.54**	±	**0.42**
α-selinene	a	+	1509				**1.33**	±	**0.83**	**0.24**	±	**0.17**	**1.24**	±	**0.69**	**0.41**	±	**0.23**	0.14	±	0.14
β-macrocarpene	a	+	1517				**9.69**	±	**2.54**	**5.64**	±	**0.44**	**0.97**	±	**0.61**	**0.42**	±	**0.15**	0.19	±	0.04
β-bisabolene	a		1525				**1.99**	±	**0.63**	**1.26**	±	**0.49**	**0.64**	±	**0.47**	**0.26**	±	**0.14**	0.04	±	0.04
trichodiene	b	+	1533				**1.47**	±	**0.52**	**0.81**	±	**0.25**									
unidentified SQT	b		1547				**0.12**	±	**0.07**	**0.23**	±	**0.07**	0.04	±	0.04						
no ID	b		1603	0.05	±	0.05	0.02	±	0.01	**0.17**	±	**0.01**	**0.38**	±	**0.09**	0.14	±	0.05	0.15	±	0.03

[a]Volatiles identified as markers of *Fusarium* infection in hybrid corn. Overview of volatile markers for Fusarium infection of hybrid corn ears at milk ripeness stage (24 dpi). Values are peak areas (± SE) normalized to TIC (% TIC). KI = calculated Kovats indices; Compounds were fully identified (**a**) based on the comparison of their MS fragmentation patterns to the NIST and Adams MS libraries, comparison of their KI to the values listed in literature, and comparison of their retention times to those of authentic standards. If no authenthic standards were available (**b**), compounds were *tentatively identified* based only on MS data and KI. Values in bold significantly differed from the control treatment (uninfected corn ears) ($p < 0.05$ according to the Kruskal-Wallis test.[29] + Indicates that infection marker occurrence was confirmed by open loop-stripping (OLS) using charcoal cartridges. [b]ID refers to the mode of identification. Volatiles a were identified on the basis of MS, KI, and authentic standards. Compounds b were tentatively identified on the basis of MS and KI only.

dx.doi.org/10.1021/jf500560f | J. Agric. Food Chem. 2014, 62, 5226−5236

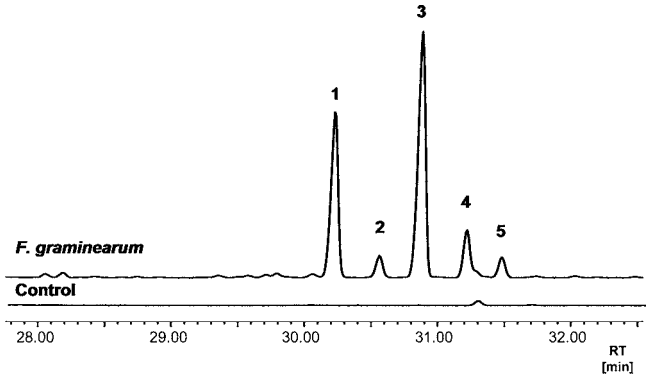

Figure 2. Major sesquiterpene volatiles induced in corn ears following fungal infection. Stacked chromatograms (TIC from SPME-GC/MS) of volatile profiles from ears inoculated with water (control) or *F. graminearum*. The profile for *F. graminearum*-infected ears illustrates the *de novo* synthesis of the defined and main VOC markers for infection: (1) *β*-selinene; (2) *α*-selinene; (3) *β*-macrocarpene; (4) *β*-bisabolene; (5) trichodiene (only in *F. graminearum* infection).

profiles of *Fusarium*-infected hybrid and dwarf corn ears were compared to the profiles of healthy hybrid and dwarf corn ears at the milk ripeness maturation stage. Under the experimental conditions of this study, milk ripeness was reached in hybrid corn at 24 dpi and in dwarf corn at 14 dpi. Photographs of uninfected and *Fusarium*-infected corn ears at the milk ripeness maturation stage are provided in Figure 1. Statistical analysis of the profiles revealed that the concentrations of 22 volatiles significantly differed between the infected and the uninfected ears. Infection markers included volatiles that were emitted at significantly higher or lower concentrations from infected than from healthy ears or that were detected only from infected ears. Nine infection markers were identified using authentic standards, MS fragmentation patterns, and Kovats retention indices, whereas 13 other markers were tentatively identified only on the basis of their MS fragmentation patterns and Kovats retention indices (Table 2). Infection markers comprised C_6–C_8 volatiles, including alcohols, a ketone, terpenoids, and unidentified volatiles (Table 2). The mass spectra of six unidentified markers were characterized as having

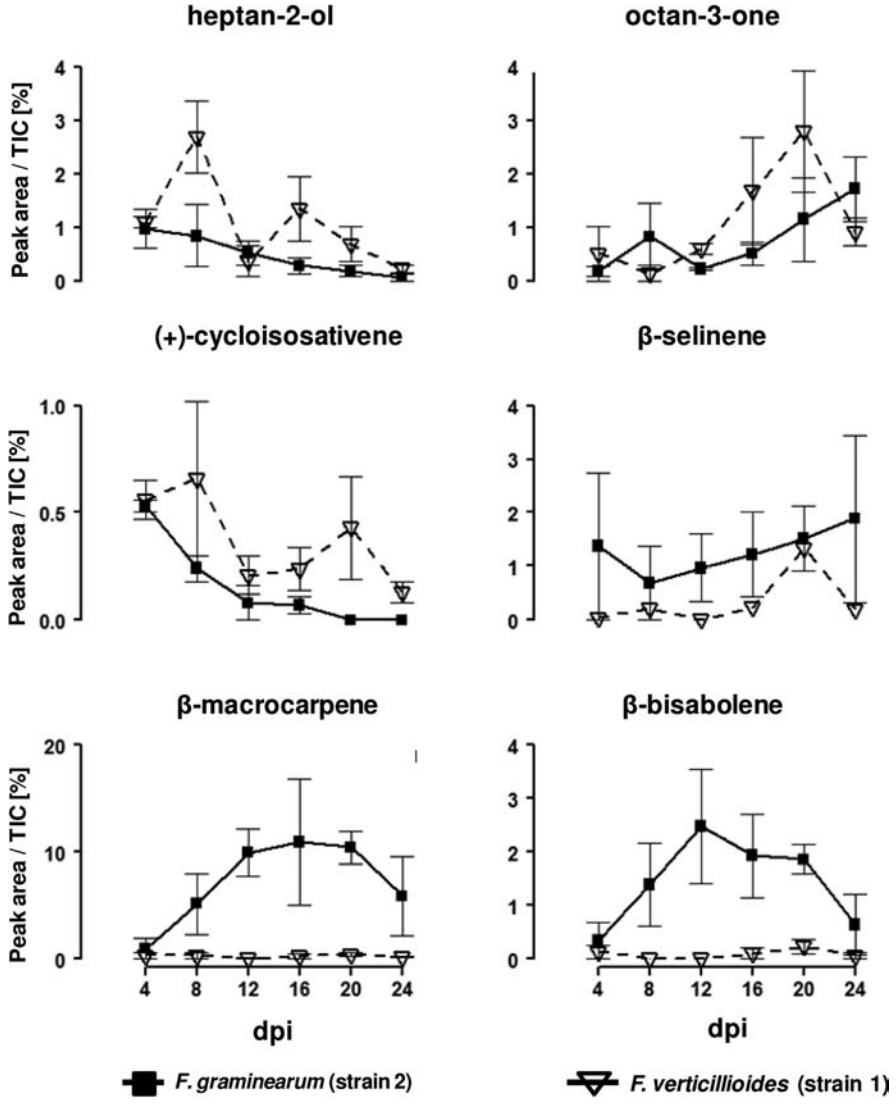

Figure 3. Emission of six selected volatile markers over time from *Fusarium*-infected hybrid corn. The abbreviation dpi refers to days postinoculation with *F. graminearum* (FG2) and *F. verticillioides* (FV1). Relative quantities of volatiles, as determined by SPME/GC-MS, are reported as mean peak areas (± standard error, n = 3) normalized by total ion chromatogram (TIC).

dx.doi.org/10.1021/jf500560f | J. Agric. Food Chem. 2014, 62, 5226–5236

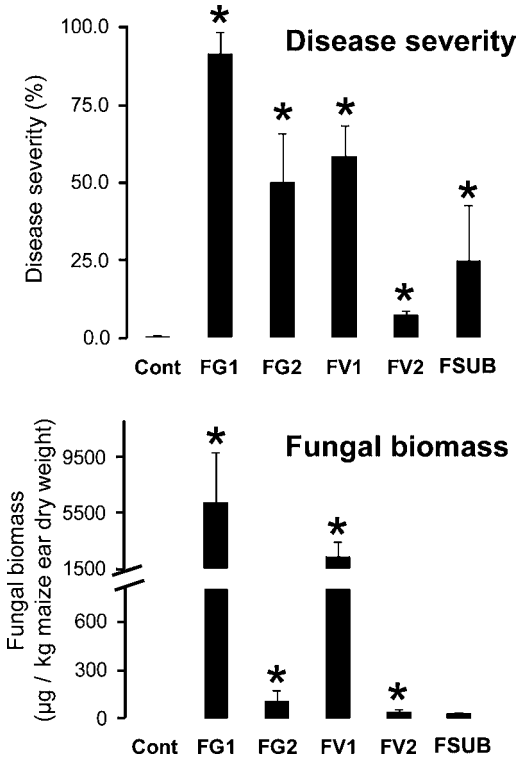

Figure 4. Disease severity and quantity of fungal DNA in hybrid corn ears inoculated with water (Cont), *F. graminearum* (strains FG1 and FG2), *F. verticillioides* (strains FV1 and FV2), or *F. subglutinans* (strain FSUB). Values are means + SE for two replicates for FSUB biomass and for theee to four replicates for all other treatments. The asterisk indicates statistical differences from control treatment ($p < 0.05$, Mann–Whitney *U* test).

Table 3. Myxotoxins in *Fusarium*-Infected Hybrid Corn Ears[a]

	mg toxin kg^{-1} dry weight ± standard error				
treatment	DON	ZEN	NIV	FB1	FB2
control					
FG1			>50[b]		
FG2	>50[b]	0.55 ± 0.45			
FV1				>10[b]	>10[b]
FV2				1.07 ± 0.45	0.51 ± 0.22
FSUB					

[a]Influence of inoculation with *Fusarium* strains on the formation of the mycotoxins deoxynivalenol (DON), zearalenone (ZEN), nivalenol (NIV), and fumonisins B1 and B2 (FB1, FB2) in hybrid corn ears at 24 dpi. [b]Concentration exeeds range of detection (trichothecenes, >50 mg kg^{-1}; fumonisins, >10 mg kg^{-1}).

a parent ion with *m/z* 204 and typical daughter ions having *m/z* values of 189 and 93 (Supporting Information Figure S1). On the basis of these properties, the six unidentified markers were tentatively assigned as sesquiterpenoids (SQTs).

Sesquiterpenoids represented the major class of infection markers, and five sesquiterpenes, including β-selinene, α-selinene, β-macrocarpene, β-bisabolene, and trichodiene, were dominant in the chromatograms (Figure 2). Trichodiene was emitted only by ears infected with FG1 and FG2, whereas β-selinene, α-selinene, β-macrocarpene, and β-bisabolene were emitted by ears infected with all *Fusarium* species/strains tested. Healthy hybrid corn ears released high levels of (+)-cycloisosativene and α-ylangene. These volatile sesquiterpenoids were absent or at low concentration in the headspace of *Fusarium*-infected samples. Most infection markers, including alcohols and major sesquiterpenoids that were detected from infected hybrid corn, were also detected from infected dwarf corn (not shown).

The majority of sesquiterpenoids identified in this study as infection markers have been previously described as herbivore-induced corn volatiles[32−34] and are consequently most likely derived from the plant. Nevertheless, *Fusarium* also has the ability to produce the sesquiterpenoid β-bisabolene,[35] and a mixed fungal and plant origin for the latter volatile cannot be ruled out. Interestingly, some of the major (defined as TIC normalized peak area in Table 2 >1.00%) volatile infection markers detected in *Fusarium*-infected corn ears (β-macrocarpene and β-bisabolene) appear to be minor or undetectable infection markers in corn leaves, stems, and roots,[11,36] where they might be fully transformed to nonvolatile zealexins involved in plant defense.[36] Other major infection markers included the sesquiterpenoids α- and β-selinene, which are known components of celery oil.[14] Both compounds have been reported to be involved in defense against pathogens and insects in plants other than corn[37,38] and might have a similar role in corn.

Infection Markers Are Detectable before Infection Symptoms Appear on Dehusked Corn. A second experiment was performed to investigate how quickly volatile infection markers were detectable after inoculation. This experiment was performed by sampling *F. graminearum* (strain FG2)- or *F. verticillioides* (strain FV1)-infected ears every 4 days, from 4 to 24 dpi. The earliest time point of 4 dpi was selected because at this time almost no infection symptoms are evident on ears that have not been dehusked. SPME/GC-MS analysis revealed that the majority of infection markers identified at 24 dpi (Table 2) were already detectable between 4 and 8 dpi (see Figure 3 for selected markers and the Supporting Information (Figure S2) for a heatmap of all markers). The induction of the major SQT markers β-macrocarpene and β-bisabolene was clearly the strongest with the most aggressive *Fusarium* species (*F. graminearum*, Figures 3 and 4A). Some volatiles, such as heptan-2-ol and (+)-cycloisosativene, decreased in concentration over time (i.e., after infection with *F. graminearum*), whereas others, such as octan-3-one, β-selinene, β-macrocarpene, and β-bisabolene, increased over time and reached a maximum at 16−24 dpi (Figure 3 and Supporting Information Figure S2).

Because most volatile markers were detectable at a very early stage of infection, they could be used for the early, nondestructive detection of fungal infection in the field (patent application, University of Goettingen, Germany, DE 101012204237.7). Sensitive portable devices such as ion mobility spectrometers (IMS) could be used for detection of infected ears in the field or during postharvest processes (i.e., storage, transport, or feed production). In the field, distinguishing healthy from infected corn plants might help guide decisions concerning the application of fungicides. In postharvest processes, infected corn ears might be separated from healthy ones and used for applications where mycotoxins are not a concern (i.e., for the production of biofuels).

Sesquiterpenoid Infection Markers Are Also Detectable from Corn Ears on Live Plants. SPME and OLS were used to capture the volatiles emitted by corn ears. SPME was performed on cut and frozen ears, whereas OLS was carried out

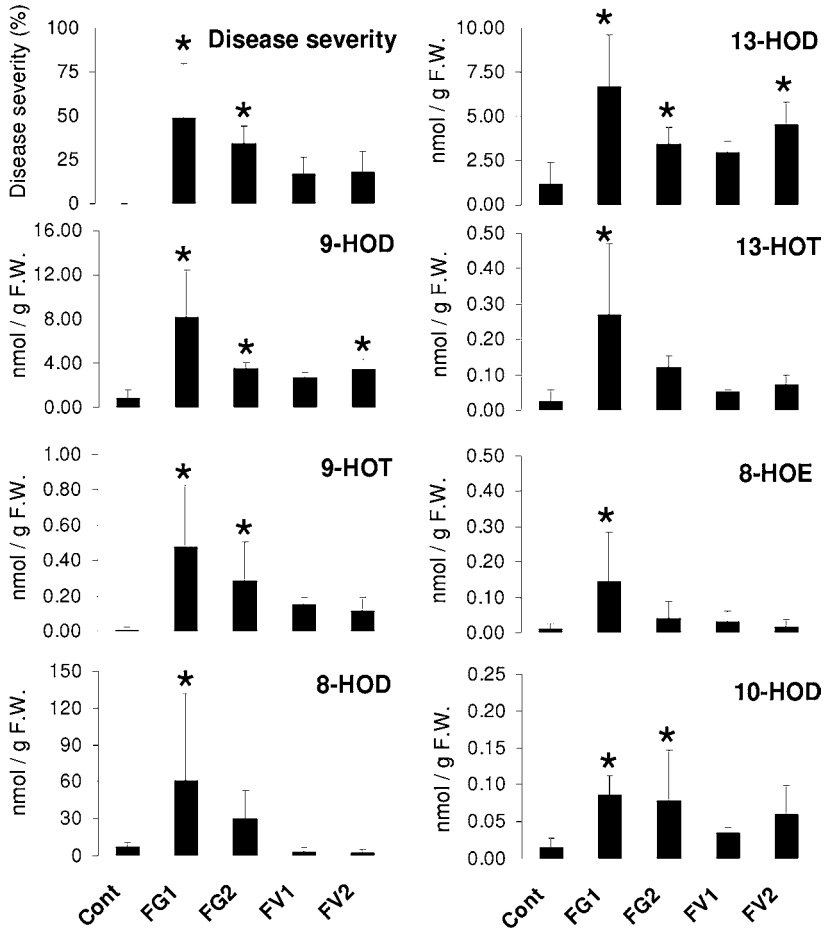

Figure 5. Disease severity and fatty acids in *Fusarium*-infected hybrid corn ears at 24 dpi. 13-HOD, (9*Z*,12*Z*)-8-hydroxy-9,12-octadecadienoic acid; 9-HOD, (10*E*,12*Z*)-9-hydroxy-10,12-octadecadienoic acid; 8-HOD, (9*Z*,12*Z*)-8-hydroxy-9,12-octadecadienoic acid; 13-HOT, (9*Z*,11*E*,15*Z*)-13-hydroxy-9,11,15-octadecatrienoic acid; 9-HOT, (10*E*,12*Z*,15*Z*)-9-hydroxy-10,12,15- octadecatrienoic acid; 8-HOE, (9*Z*)-8-hydroxy-9-octadecenoic acid; 10-HOD, (8*E*,12*Z*)-10-hydroxy-8,12-octadecadienoic acid. The asterisk indicates statistical differences from control treatment ($p < 0.05$, Dunnet test). See Figure 4 caption for explanation of strain abbreviations. F.W. = fresh weight.

on both cut and frozen ears as well as undamaged ears attached to live plants. One advantage of SPME compared to OLS is that SPME requires minimal sample preparation; quantitation, however, is more difficult with SPME than with OLS. SPME (no internal standard) and OLS (nonyl acetate as internal standard) were used here for relative quantitation of volatiles.

First both OLS and SPME techniques were compared on the same frozen material (equal aliquots *F. graminearum*-infected corn ears). Considering the major sesquiterpenoids identified in this study, the results obtained with SPME and OLS were highly correlated ($R^2 = 0.998$) (Supporting Information Figure S3). This indicates that even without the use of an internal standard, the SPME data generated here can be used for relative quantitation. OLS was further performed on live corn ears that were undamaged through cutting to ascertain that the markers identified by SPME were not an artifact due to cutting or freezing. SPME (frozen and cut ears) and OLS (live and undamaged ears) gave similar results for most but not all sesquiterpenoids, whereas C_6 and C_8 alcohols were identified only by SPME (Table 2 and Supporting Information Table S2). These differences might be explained by the fact that many short-chain alcohols are poorly retained on the activated carbon[39] in the OLS traps, whereas they are better retained on polymers such as the PDMS-DVB used here for SPME.[40] Another reason might be that the freezing and cutting of the SPME samples might have released enzymes/substrates that would not colocalize in live plants. Despite these differences, both methods confirmed that sesquiterpenoids were major markers of *Fusarium* infection of corn ears (Table 2).

Disease Severity Is Correlated with the Amount of Fungal DNA in Corn Ears. Disease severity, the percentage of the ears showing infection symptoms, was visually assessed for dehusked hybrid corn ears at the milk ripeness stage after inoculation with single *Fusarium* strains (Figure 4A). Strain FG1 was the most aggressive (>90% disease severity), FV2 and FSUB were the least aggressive (<25% disease severity), and FG2 and FV1 were intermediate (Figure 4A). Fungal biomass (as indicated by fungal DNA) (Figure 4B) was correlated with disease severity ($R^2 = 0.75$, $p = 0.026$). DNA quantity was much lower with FG2, FV2, and FSUB than with FG1 and was intermediate with FV1. Despite the low DNA level, FG2 induced average disease symptoms, confirming the high aggressiveness of *F. graminearum* compared to other *Fusarium* species. In a time series, corn ears were inoculated with either FV1 or FG2, and disease severity was assessed every 4 days, from 4 to 24 dpi. Disease severity for both *Fusarium* species averaged about 10% at 4 dpi and increased to 50 − 70% at 20 dpi (Supporting Information Figure S4).

Mycotoxins, Oxylipins, and Zealexins in *Fusarium*-Infected Corn Ears. An overview of mycotoxin concentrations

dx.doi.org/10.1021/jf500560f | J. Agric. Food Chem. 2014, 62, 5226−5236

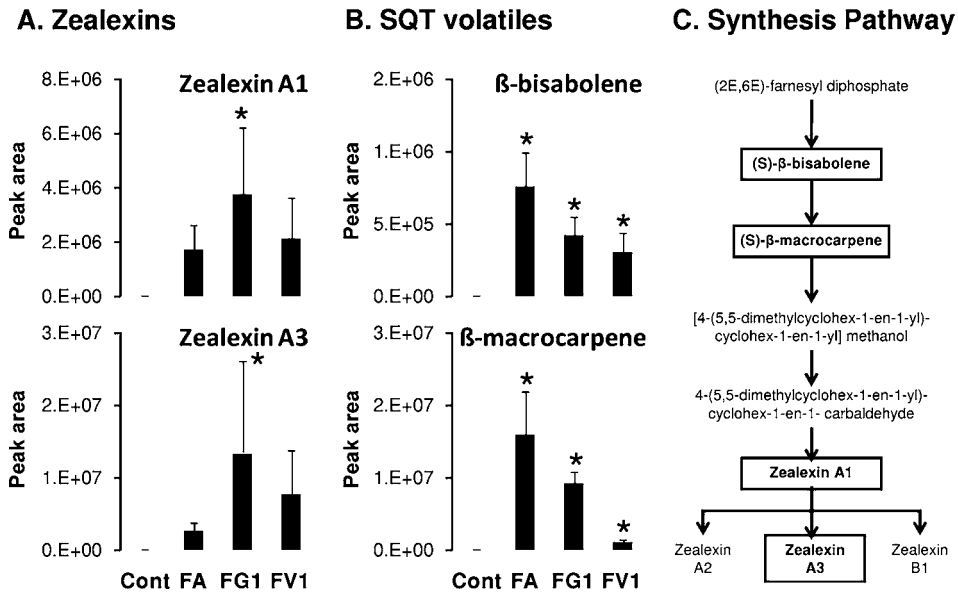

Figure 6. Zealexins and their volatile intermediates in *Fusarium*-infected dwarf corn ears at 14 dpi: (A) induction of zealexins A1 and A3 and (B) their volatile precursors (bisabolene and macrocarpene) after inoculation with water (Cont), strain FA of *F. avenaceum*, strain FG1 of *F. graminearum*, or strain FV1 of *F. verticillioides*. Values are mean peak area of TIC ± SE (n = 3 to 6). The asterisk indicates statistical differences from control treatment (p < 0.05, Mann–Whitney U test). (C) Zealexin biosynthetic pathway (modified from http://pmn.plantcyc.org/PLANT/NEW-IMAGE?type=PATHWAY&object=PWY-6888).

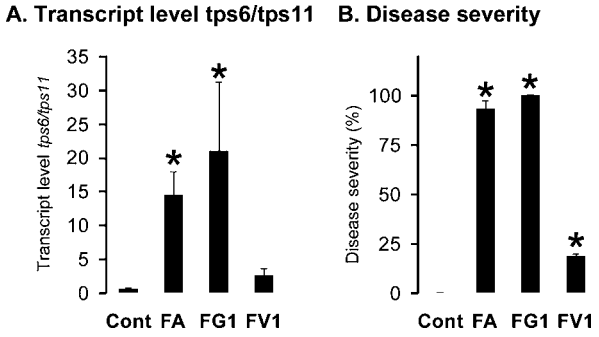

Figure 7. Gene expression and disease severity in dwarf maize ears at milk ripeness (14 dpi). Values are means ± SE for three to four replicate per treatment. The asterisk indicates difference from control treatment (p < 0.05, Mann–Whitney U test). Note that transcript levels of *tps6/tps11* were normalized to the expression level of a housekeeping gene, which was stable in Cont, FA, and FV1 but which was reduced in FG. This reduction might reflect either RNA degradation (i.e., due to fungal infection) or the fact that an important share of the total RNA in the FG samples was of fungal origin.

in hybrid corn ears at 24 dpi is provided in Table 3. FG1 produced NIV and FG2 produced DON at concentrations >50 mg kg^{-1}. Zearalenone (ZEN) was irregularly produced by *F. graminearum* strain 2 (FG2). Both *F. verticillioides* strains produced fumonisins B1 and B2, but FV1 produced much larger quantities of these mycotoxins than FV2 (Table 3).

In time series with FG2 and FV1, DON was detectable at 4 dpi, whereas fumonisin FB1 was detectable only at 16 dpi (Supporting Information Figure S5). The relationship between emission of volatile markers and mycotoxin concentration over time is also presented in the Supporting Information (Figure S5). The relative quantity of trichodiene, which is the volatile precursor of trichothecenes, showed roughly the same pattern as DON production until 20 dpi (the correlation $R^2_{4-20dpi}$ = 0.43). The correlation became nonsignificant at 24 dpi ($R^2_{4-24dpi}$ = 0.02). The emission of octan-3-one, a common fungal volatile, was most abundant in *F. verticillioides*-treated corn and showed a slight correlation with FB1 (R^2 = 0.25).

Oxidized fatty acids, so-called oxylipins, and zealexins were induced at different levels in infected corn ears depending on which *Fusarium* species was used as inoculum (Figure 5). In hybrid corn ears, oxidized fatty acids (8/9/10/13-hydroxy octadecadienoic acid (8/9/10/13-HOD) and 9/13-hydroxy octadecatrienoicacid (9/13-HOT)) as well as 8-hydroxy-(9Z)-octadecenoic acid (8-HOE) were all induced by the most aggressive *F. graminearum* strain (FG1), whereas only some of the oxylipins were induced by the other *Fusarium* species/strains. The number of oxylipins significantly induced upon infection was highly correlated with disease severity (R^2 = 0.78, p = 0.019, see also Figure 5).

The zealexin biosynthetic pathway was investigated in dwarf corn ears. Compounds tentatively identified as zealexins A1 and A3, which are nonvolatile sesquiterpenoids derived from β-bisabolene and β-macrocarpene, were induced in dwarf corn ears upon *Fusarium* infection. Their relative concentrations in corn ears infected with different *Fusarium* species are shown in Figure 6 along with the concentrations of their volatile precursors. Relative to their expression in uninfected corn ears, the terpene synthase genes *tps6* and *tps11* were up-regulated in the aggressive strain FA and FG1 (disease severity >90%), whereas a slight yet not significant increase was detected in FV (disease severity <20%) (Figure 7). In the case of FG1 (disease severity >90%), an up-regulation in *tps6/11* gene expression was also observed, but the expression of the housekeeping gene was reduced compared to uninfected plants. Possible explanations for this reduction are that RNA was degraded (i.e., due to fungal infection) or that a substantial proportion of the total RNA in the FG1 samples was of fungal origin. Both cases, however, should influence target genes and housekeeping genes at the same level. Overall, disease severity and expression levels of *tps6/tps11* were correlated (R^2 = 0.35, p = 0.006).

The up-regulation of zealexins A1 and A3 as well as of the terpene synthase genes *tps6/11* indicates that β-macrocarpene and β-bisabolene, known to be fully transformed into nonvolatile zealexins in corn leaves, stems, and roots,[12,36] are also partially transformed into zealexins in corn ears. However, the massive amounts of β-macrocarpene and β-bisabolene released by corn ears suggest that these volatiles might be further involved in direct plant defense or possibly in communication with neighboring plants (i.e., defense priming).[41]

Some of the fatty acid-derived volatiles (i.e., oxylipins[42]) identified in this study as infection marker volatiles are commonly produced by fungi and plants. Their source (fungal vs plant) can be determined by their different biosynthetic origins. Plants oxidize polyunsaturated fatty acids from membranes via the so-called lipoxygenase or oxylipin pathway, leading to the formation of green leaf volatiles such as 3-hexen-1-ol via 13-H(P)OT as an intermediate (13-H(P)OT is the hydroperoxyl derivative of 13-HOT) (Figure 5).[43] These green leaf volatiles (C_6 volatiles) play a role in priming neighboring corn plants against insect attack.[44] In addition, 13-H(P)OT may serve as a substrate for the formation of the phytohormone jasmonic acid, which is a master regulator of plant reaction against wounding and necrotrophic pathogens.[45] In contrast, fungi oxidize the same substrates by a different enzyme family called psi-factor producing oxygenases.[46] In fungi, 10-H(P)OD serves as the intermediate for the formation of C_8 volatiles. Moreover, 8- and 10-H(P)OD regulate sexual reproduction and mycotoxin formation in ascomycetes.[47,48] Indeed, the latter oxylipins were induced by *Fusarium* infection in the current study (Figure 5). Interestingly, the concept that oxylipins regulate mycotoxin formation is supported by the combined accumulation of the mycotoxin fumonisin B1 and octan-3-one.[49] Similarly, levels of thrichodiene, which is a known volatile precursor of thricothecenes in *F. graminearum*,[50] were correlated with DON concentrations (Supporting Information Figure S5), again indicating a fungal origin.

In summary, the volatile markers identified here might be used to discriminate healthy from *Fusarium*-infected corn ears. Unlike most existing techniques for detecting fungal infection in plants, volatile detection is nondestructive. If combined with the right technology, the markers identified in this study might be used for the management of corn fields and postharvest facilities.

■ ASSOCIATED CONTENT

Supporting Information

Figures S1-S5 and Tables S1 and S2. This material is available free of charge via the Internet at http://pubs.acs.org.

■ AUTHOR INFORMATION

Corresponding Author

*(R.S.) E-mail: richard.splivallo@a3.epfl.ch. Fax: +49 551/391 2919. Phone: +49 551/393 3963.

Author Contributions

P.K. wrote the proposal and secured funding. E.-M.B., R.S., and P.K. drafted the manuscript with input from all other coauthors. E.-M.B. handled all fungal and plant material, preformed corn ear infections, and monitored disease severity. E.-M.B., with guidance from R.S., carried out volatiles sampling by SPME, by OLS-GC/MS, zealexins extraction and quantitation and data analysis. E.-M.B., with guidance from P.K., extracted DNA for fungal biomass quantitation by RT-PCR, RNA for gene expression analysis, and mycotoxins for quantitation by HPLC-MS. E.-M.B., S.I., and T.K. analyzed the gene expression of *tps6/11*. I.F. and C.H. quantitied oxylipins. E.-M.B. analyzed and processed all data. E.-M.B. and R.S. performed the statistics.

Funding

Funding for part of this research was provided by the German Federal Ministry of Education and Research (BMBF) within the framework of the project MykoSensExpert.

Notes

The authors declare the following competing financial interest(s): EMB, RS and PK have applied for a patent describing the use of the volatile markers discovered in this study for identifying fungal infection in maize (patent application, University of Goettingen, Germany, DE 101012204237.7). The other author(s) declare that they have no competing interests.

■ ACKNOWLEDGMENTS

Katharina Döll and Philip Kössler are gratefully acknowledged for running the mycotoxin analysis on the HPLC-MS. We are thankful to J. Schirawski (RWTH Aachen University, Germany) for providing the seeds of dwarf-corn, to A. Prodi (University of Bologna, Italy) for *Fusarium* strain FV2, and to T. Miedaner (University of Hohenheim, Germany) for *Fusarium* strain FG1.

■ REFERENCES

(1) D'Mello, J. P. F.; Placinta, C. M.; Macdonald, A. M. C. *Fusarium* mycotoxins: a review of global implications for animal health, welfare and productivity. *Anim. Feed Sci. Technol.* **1999**, *80*, 183−205.

(2) Vogelgsang, S.; Hecker, A.; Musa, T.; Dorn, B.; Forrer, H.-R. On-farm experiments over 5 years in a grain maize/winter wheat rotation: effect of maize residue treatments on *Fusarium graminearum* infection and deoxynivalenol contamination in wheat. *Mycotoxin Res.* **2011**, *27*, 81−96.

(3) Desjardins, A. E. *Fusarium Mycotoxins: Chemistry, Genetics, and Biology*; American Phytopathological Society: St. Paul, MN, USA, 2006.

(4) Brandfass, C.; Karlovsky, P. Simultaneous detection of *Fusarium culmorum* and *F. graminearum* in plant material by duplex PCR with melting curve analysis. *BMC Microbiol.* **2006**, *6*, 4.

(5) Perkowski, J.; Buśko, M.; Chmielewski, J.; Góral, T.; Tyrakowska, B. Content of trichodiene and analysis of fungal volatiles (electronic nose) in wheat and triticale grain naturally infected and inoculated with *Fusarium culmorum*. *Int. J. Food Microbiol.* **2008**, *126*, 127−134.

(6) Dicke, M.; Baldwin, I. T. The evolutionary context for herbivore-induced plant volatiles: beyond the "cry for help". *Trends Plant Sci.* **2010**, *15*, 167−175.

(7) Holopainen, J. K.; Gershenzon, J. Multiple stress factors and the emission of plant VOCs. *Trends Plant Sci.* **2010**, *15*, 176−184.

(8) Schnee, C.; Koellner, T. G.; Held, M.; Turlings, T. C. J.; Gershenzon, J.; Degenhardt, J. The products of a single maize sesquiterpene synthase form a volatile defense signal that attracts natural enemies of maize herbivores. *Proc. Natl. Acad. Sci. U.S.A.* **2006**, *103*, 1129−1134.

(9) Christensen, S. A.; Nemchenko, A.; Borrego, E.; Murray, I.; Sobhy, I. S.; Bosak, L.; DeBlasio, S.; Erb, M.; Robert, C. A. M.; Vaughn, K. A.; Herrfurth, C.; Tumlinson, J.; Feussner, I.; Jackson, D.; Turlings, T. C. J.; Engelberth, J.; Nansen, C.; Meeley, R.; Kolomiets, M. V. The maize lipoxygenase, ZmLOX10, mediates green leaf volatile, jasmonate and herbivore-induced plant volatile production for defense against insect attack. *Plant J.* **2013**, *74*, 59−73.

(10) Rasmann, S.; Kollner, T. G.; Degenhardt, J.; Hiltpold, I.; Toepfer, S.; Kuhlmann, U.; Gershenzon, J.; Turlings, T. C. J. Recruitment of entomopathogenic nematodes by insect-damaged maize roots. *Nature* **2005**, *434*, 732−737.
(11) Koellner, T. G.; Held, M.; Lenk, C.; Hiltpold, I.; Turlings, T. C. J.; Gershenzon, J.; Degenhardt, J. A maize (*E*)-caryophyllene synthase implicated in indirect defense responses against herbivores is not expressed in most American maize varieties. *Plant Cell Online* **2008**, *20*, 482−494.
(12) Koellner, T. G.; Schnee, C.; Li, S.; Svatoš, A.; Schneider, B.; Gershenzon, J.; Degenhardt, J. Protonation of a neutral (*S*)-bisabolene intermediate is involved in (*S*)-macrocarpene formation by the maize sesquiterpene synthases TPS6 and TPS11. *J. Biol. Chem.* **2008**, *283*, 20779−20788.
(13) Huffaker, A.; Kaplan, F.; Vaughan, M. M.; Dafoe, N. J.; Ni, X.; Rocca, J. R.; Alborn, H. T.; Teal, P. E. A.; Schmelz, E. A. Novel acidic sesquiterpenoids constitute a dominant class of pathogen-induced phytoalexins in maize. *Plant Physiol.* **2011**, *156*, 2082−2097.
(14) Joulain, D.; König, W. A. *The Atlas of Spectral Data of Sesquiterpene Hydrocarbons*; E.B.-Verlag Dr. Brandt: Berlin, Germany, 1998.
(15) Bai, G. H. Variation in *Fusarium graminearum* and cultivar resistance to wheat scab. *Plant Dis.* **1996**, *80*, 975.
(16) Reid, L. M.; Hamilton, R. l.; Mather, D. E. Effect of macroconidial suspension volume and concentration on expression of resistance to *Fusarium graminearum* in maize. *Plant Dis.* **1995**, *79*, 461−466.
(17) Zadoks, J. C.; Chang, T. T.; Konzak, C. F. A decimal code for the growth stages of cereals. *Weed Res.* **1974**, *14*, 415−421.
(18) Adejumo, T. O.; Hettwer, U.; Karlovsky, P. Occurrence of *Fusarium* species and trichothecenes in Nigerian maize. *Int. J. Food Microbiol.* **2007**, *116*, 350−357.
(19) Adejumo, T. O.; Hettwer, U.; Karlovsky, P. Survey of maize from south-western Nigeria for zearalenone, α- and β-zearalenols, fumonisin B1 and enniatins produced by *Fusarium* species. *Food Addit. Contam.* **2007**, *24*, 993−1000.
(20) Visentin, I.; Montis, V.; Döll, K.; Alabouvette, C.; Tamietti, G.; Karlovsky, P.; Cardinale, F. Transcription of genes in the biosynthetic pathway for fumonisin mycotoxins is epigenetically and differentially regulated in the fungal maize pathogen *Fusarium verticillioides*. *Eukaryotic Cell* **2012**, *11*, 252−259.
(21) Brandfass, C.; Karlovsky, P. Upscaled CTAB-based DNA extraction and real-time PCR assays for *Fusarium culmorum* and *F. graminearum* DNA in plant material with reduced sampling error. *Int. J. Mol. Sci.* **2008**, *9*, 2306−2321.
(22) Nutz, S.; Doll, K.; Karlovsky, P. Determination of the LOQ in real-time PCR by receiver operating characteristic curve analysis: application to qPCR assays for *Fusarium verticillioides* and *F. proliferatum*. *Anal. Bioanal. Chem.* **2011**, *401*, 717−726.
(23) Mulè, G.; Susca, A.; Stea, G.; Moretti, A. Specific detection of the toxigenic species *Fusarium proliferatum* and *F. oxysporum* from asparagus plants using primers based on calmodulin gene sequences. *FEMS Microbiol. Lett.* **2004**, *230*, 235−240.
(24) Turner, A. S.; Lees, A. K.; Rezanoor, H. N.; Nicholson, P. Refinement of PCR-detection of *Fusarium avenaceum* and evidence from DNA marker studies for phenetic relatedness to *Fusarium tricinctum*. *Plant Pathol.* **1998**, *47*, 278−288.
(25) Kollner, T. G.; Lenk, C.; Zhao, N.; Seidl-Adams, I.; Gershenzon, J.; Chen, F.; Degenhardt, J. Herbivore-induced SABATH methyltransferases of maize that methylate anthranilic acid using *S*-adenosyl-L-methionine1[W]. *Plant Physiol.* **2010**, *153*, 1795−1807.
(26) Goebel, C.; Feussner, I.; Rosahl, S. Lipid peroxidation during the hypersensitive response in potato in the absence of 9-lipoxygenases. *J. Biol. Chem.* **2003**, *278*, 52834−52840.
(27) Schmelz, E. A.; Engelberth, J.; Tumlinson, J. H.; Block, A.; Alborn, H. T. The use of vapor phase extraction in metabolic profiling of phytohormones and other metabolites. *Plant J.* **2004**, *39*, 790−808.
(28) Alencar, J. W.; Craveiro, A. A.; Matos, F. J. A. Kovats' indices as a preselection routine in mass spectra library searches of volatiles. *J. Nat. Prod.* **1984**, *47*, 890−892.
(29) Siegel, S.; Castellan, N. J., Jr. *Nonparametric Statistics for the Behavioral Sciences*, 2nd ed.; McGraw-Hill: New York, 1988.
(30) Adams, R. P. *Identification of Essential Oil Components by Gas Chromatography/Mass Spectroscopy*; Allured Publishing: Carol Stream, IL, USA, 2007.
(31) *Wiley Registry of Mass Spectral Data*; Wiley: New York, 2006.
(32) Turlings, T. C. J.; Tumlinson, J. H.; Lewis, W. J. Exploitation of herbivore-induced plant odors by host-seeking parasitic wasps. *Science* **1990**, *250*, 1251−1253.
(33) Degen, T.; Dillmann, C.; Marion-Poll, F.; Turlings, T. C. J. High genetic variability of herbivore-induced volatile emission within a broad range of maize inbred lines. *Plant Physiol.* **2004**, *135*, 1928−1938.
(34) Köllner, T. G.; Schnee, C.; Gershenzon, J.; Degenhardt, J. The sesquiterpene hydrocarbons of maize (*Zea mays*) form five groups with distinct developmental and organ-specific distributions. *Phytochemistry* **2004**, *65*, 1895−1902.
(35) Dickschat, J. S.; Brock, N. L.; Citron, C. A.; Tudzynski, B. Biosynthesis of sesquiterpenes by the fungus *Fusarium verticillioides*. *ChemBioChem* **2011**, *12*, 2088−2095.
(36) Huffaker, A.; Kaplan, F.; Vaughan, M. M.; Dafoe, N. J.; Ni, X.; Rocca, J. R.; Alborn, H. T.; Teal, P. E. A.; Schmelz, E. A. Novel acidic sesquiterpenoids constitute a dominant class of pathogen-induced phytoalexins in maize. *Plant Physiol.* **2011**, *156*, 2082−2097.
(37) Tuetun, B.; Choochote, W.; Pongpaibul, Y.; Junkum, A.; Kanjanapothi, D.; Chaithong, U.; Jitpakdi, A.; Riyong, D.; Pitasawat, B. Celery-based topical repellents as a potential natural alternative for personal protection against mosquitoes. *Parasitol. Res.* **2008**, *104*, 107−115.
(38) Momin, R. A.; Ramsewak, R. S.; Nair, M. G. Bioactive compounds and 1,3-di[(*cis*)-9 octadecenoyl]-2-[(*cis*,*cis*)-9,12-octadecadienoyl]glycerol from *Apium graveolens* L. seeds. *J. Agric. Food Chem.* **2000**, *48*, 3785−3788.
(39) Harper, M. Sorbent trapping of volatile organic compounds from air. *J. Chromatogr., A* **2000**, *885*, 129−151.
(40) Snow, N. H. Solid-phase micro-extraction of drugs from biological matrices. *J. Chromatogr., A* **2000**, *885*, 445−455.
(41) Piesik, D.; Lemńczyk, G.; Skoczek, A.; Lamparski, R.; Bocianowski, J.; Kotwica, K.; Delaney, K. J. *Fusarium* infection in maize: volatile induction of infected and neighboring uninfected plants has the potential to attract a pest cereal leaf beetle, *Oulema melanopus*. *J. Plant Physiol.* **2011**, *168*, 1534−1542.
(42) Christensen, S. A.; Kolomiets, M. V. The lipid language of plant-fungal interactions. *Fungal Genet. Biol.* **2011**, *48*, 4−14.
(43) Stumpe, M.; Feussner, I. Formation of oxylipins by CYP74 enzymes. *Phytochem. Rev.* **2006**, *5*, 347−357.
(44) Howe, G. A.; Jander, G. Plant immunity to insect herbivores. *Annu. Rev. Plant. Biol.* **2008**, *59*, 41−66.
(45) Wasternack, C.; Hause, B. Jasmonates: biosynthesis, perception, signal transduction and action in plant stress response, growth and development. An update to the 2007 review in *Annals of Botany*. *Ann. Bot.* **2013**, *111*, 1021−1058.
(46) Brodhun, F.; Feussner, I. Oxylipins in fungi. *FEBS J.* **2011**, *278*, 1047−1063.
(47) Tsitsigiannis, D. I.; Keller, N. P. Oxylipins as developmental and host-fungal communication signals. *Trends Microbiol.* **2007**, *15*, 109−118.
(48) Shwab, E. K.; Keller, N. P. Regulation of secondary metabolite production in filamentous Ascomycetes. *Mycol. Res.* **2008**, *112*, 225−230.
(49) Brodhun, F.; Schneider, S.; Göbel, C.; Hornung, E.; Feussner, I. PpoC from *Aspergillus nidulans* is a fusion protein with only one active haem. *Biochem. J.* **2010**, *425*, 553−565.
(50) Jeleń, H. H.; Latus-Ziętkiewicz, D.; Wąsowicz, E.; Kamiński, E. Trichodiene as a volatile marker for trichothecenes biosynthesis. *J. Microbiol. Methods* **1997**, *31*, 45−49.

focused on global gene expression profiling with Affymetrix GeneChip Yeast Genome 2.0 arrays. To be able to correlate PYR-triggered transcriptional responses with the yeast outcome at the phenotypic level, we first examined the fungicide concentration-dependent effects on the growth of a yeast population. Then, gene expression profiles representing the yeast global response to two exposure conditions eliciting sublethal effects of increasing magnitude from 20% to 50% inhibition of growth rate were examined. Molecular indicators of PYR toxicity were identified in the yeast, and insights into mechanisms involved in response to PYR inhibitory effects revealed from the microarray data are discussed in the context of their potential relevance for wine yeasts and other relevant eukaryotes, particularly when PYR is misused or applied under extreme agricultural practices.

MATERIALS AND METHODS

Yeast Strain, Culture Conditions, and Growth Experiments with Pyrimethanil (PYR). *Saccharomyces cerevisiae* strain BY4741 (Mat*a, his3Δ1, leu2Δ0, met15Δ0, ura3Δ0*) (Euroscarf collection) was batch-cultured at 30 °C with orbital agitation (250 rpm) in MMB basal medium (pH 6.5) that contained, per liter: 1.7 g of Yeast Nitrogen Base without amino acids or NH_4^+ (Difco Laboratories, Detroit, MI, US), 20 g of glucose, 2.65 g of $(NH_4)_2SO_4$ (both from Merck, Darmstadt, GE), 20 mg of histidine, 20 mg of methionine, 60 mg of leucine, 20 mg of uracil (all from Sigma, SP).[22] Pyrimethanil (Pestanal) was purchased from Sigma-Aldrich (Seelze, GE). Examination of its effects in the yeast growth curve was carried out as described elsewhere.[22] Briefly, standardized exponential yeast cultures grown in MMB medium, with optical density at 640 nm (OD_{640nm}) equal to 0.25 ± 0.05, were supplemented with adequate volumes of a stock solution of PYR (55000 mg/L, in dimethyl sulfoxide) to obtain fungicide concentrations up to 150 mg/L (slightly above the aqueous solubility limit of 121 mg/L, 20 °C). Final dimethyl sulfoxide in all cultures including control (CT) without added PYR was equal to 0.2% (v/v).[22] Cell suspensions were immediately incubated at 30 °C with orbital agitation (250 rpm), and yeast growth was monitored by measuring over-time culture OD_{640nm}. The culture specific growth rate and the percentage of inhibition of growth rate by PYR were estimated as described elsewhere.[22] At least three independent growth experiments were carried out for each test concentration.

Exposure Experiments and RNA Preparation. Exponential yeast cell suspensions in MMB medium (OD_{640nm} = 0.25 ± 0.05) were supplemented with 10, 20, or 110 mg/L of PYR, or nonsupplemented with the fungicide (CT cells), as described above (the latter three for DNA microarray analysis, and all four for qRT-PCR analysis). After a 2 h incubation period at 30 °C and 250 rpm, cells were harvested by centrifugation (10000 rpm, 5 min, 4 °C), immediately frozen in liquid nitrogen, and stored at −80 °C. Total RNA isolation (hot-phenol method) and further examination of RNA concentration, purity, and integrity were performed as described before.[22]

DNA Microarray Analysis. Independent biological triplicates for each exposure condition (indicated above) and CT cells were processed and analyzed. For each biological replicate, 100 ng of total RNA was processed for use on Affymetrix GeneChip Yeast Genome 2.0 Arrays (Santa Clara, CA, US), according to the manufacturer's GeneChip 3′ IVT Express kit user manual. Further details on RNA processing and on array hybridization, washes, and double-stain protocols (FS450_0003; GeneChip HWS kit, Affymetrix) performed on an Affymetrix GeneChip Fluidics Station 450 are described elsewhere.[22] Arrays were scanned on an Affymetrix GeneChip scanner 3000 7G. Analysis of the nine scanned arrays for quality control and Absent/Present calls using Affymetrix Expression Console software, and with DNA-Chip Analyzer (dChip 2010; Wong Lab, Stanford, CA, US), for normalization and gene expression calculations, were performed as described elsewhere.[22] Genes were considered as differentially expressed if the 90% lower confidence bound of the fold change (hereafter designated as lbFC) between the PYR treatments and the baseline (for CT cells) was above 1.2, with a median false discovery rate (FDR) <5%, as described before.[22] Microarray data are deposited in the Gene Expression Omnibus (GEO) repository under accession number GSE53126.

Interpretation of Gene Expression Profiles. Annotations for the 5716 *S. cerevisiae* transcripts represented on the DNA microarrays were obtained from Affymetrix.[25] Functional description of the genes is also available in *Saccharomyces* Genome Database (SGD)[26] and in MIPS Functional Catalogue Database (FunCatDB).[27] Functional clustering of the differentially expressed genes in the microarray data sets was performed using the hypergeometric-distribution-based FunSpec bioinformatics tool[28] and the hierarchically structured Functional Distribution of Gene Lists tool of the MIPS FunCatDB.[27] Similar results were obtained with both tools unless otherwise indicated. Enrichment of a functional category, compared with gene frequency in the entire yeast genome, was considered whenever the respective p value was <0.01. Search for proteins of diverse fungi and higher eukaryotes with potential sequence homology to yeast proteins encoded by genes differentially expressed in response to PYR was performed in the National Center for Biotechnology Information database using the BLASTP algorithm, as described elsewhere.[22]

Real-Time Quantitative Reverse Transcriptase PCR (qRT-PCR). To confirm microarray data and potential indicators of PYR toxicity in the yeast, modifications in the transcript levels of selected genes upon PYR exposure were assessed based on the two-step SYBRGreen I dye assay in a 7500 Real-Time PCR system (Applied Biosystems, Carlsbad, CA, US) as described elsewhere.[22] Briefly, specific primers for the selected genes were designed using Primer Express Software, and primer sequences are available in Table S1 in the Supporting Information. Independent biological triplicates for each PYR exposure condition and CT cells were processed and analyzed (indicated above). Treatment of total RNA samples with TURBO DNA-free Kit (Ambion, Life technologies Europe BV, Porto, P), spectrophotometric assessment of purity and quantity, and further processing of samples, including reverse transcription (using Applied Biosystem's TaqMan Reverse Transcription reagents kit), PCR steps (using Life Technologie's Power SYBRGreen PCR Master Mix), and control assays, were carried out as described elsewhere.[22] Relative quantification of fold changes (FC) in gene transcription was performed by the $\Delta\Delta C_T$ method according to the Applied Biosystems Expression Analysis Technical Manual instructions. *ACT1* mRNA level was used as internal control. Normalized FC values are relative to CT cells (set as 1). Data reported are average values of at least three gene expression determinations from the independent triplicates. Statistical analysis of FC values to identify differences in relation to CT and between exposure treatments was based on one-way analysis of variance (ANOVA), followed by the post hoc Tukey honest significant difference multiple comparison test for unequal sample size, using Statistica 7.0 software (StatSoft, Inc., Tulsa, OK, US).

RESULTS AND DISCUSSION

Effect of PYR on Yeast Growth. Exposure of a yeast growing population to PYR concentrations equal or higher than 5 mg/L (up to 150 mg/L) affected its growth curve. For each fungicide concentration the yeast population continued exponential growth without a significant lag-phase lengthening, but the specific growth rate was reduced in a concentration-dependent manner (Figure 1, and data not shown). Based on these data, the PYR concentrations leading to 10%, 20%, and 50% inhibition of *S. cerevisiae* BY4741 growth rate (hereafter designated as IC10, IC20, and IC50, respectively) under the experimental conditions used were estimated approximately equal to 10, 20, and 110 mg/L, respectively (Figure 1).

Concentrations close to the lowest values herein found toxic for the yeast (e.g., between 5 and 10 mg/L) have been detected in must from grapes treated with PYR under extreme agricultural practices,[1,4,5] and were associated with alterations on the course and final outcome (e.g., aromatic composition,

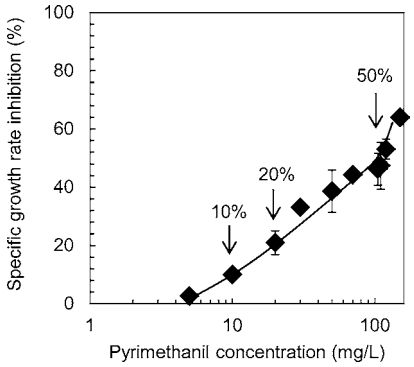

Figure 1. Effect of exposure of an exponentially growing population of *S. cerevisiae* BY4741 to increasing concentrations of pyrimethanil supplemented to the growth medium. The results, expressed as the percentage of inhibition of the yeast specific growth rate compared with control growth in fungicide absence, are means ± SD.

volatile acidity) of spontaneous and inoculated wine fermentations.[6,7] On the other hand, for example, the PYR IC20 value estimated is of an order of magnitude similar to that of the concentrations reported as cytotoxic toward the yeast antiandrogen test system (EC20 ~ 33 mg/L)[8] or inhibiting ATP production in human neuronal and glial cell lines (IC50 ~ 9 mg/L).[9] In the environmental context also, they are relatively close to or moderately higher than levels of concern reported for nontarget freshwater primary producers (e.g., chronic EC50 ~ 23.1 mg/L for *Scenedesmus acutus*, or chronic EC50 ~ 46.1 mg/L for *Lemna minor*)[15,16] or organisms in higher trophic levels (e.g., chronic EC50 = 1.18 mg/L or acute LC50 = 2.9 mg/L for *Daphnia magna*, and acute LC50 = 10.6 mg/L for fish).[16]

Since we intended to get relevant information on modifications that PYR might trigger on yeast transcriptome and that could be associated with its effects at a higher level of biological organization (e.g., growth inhibition), we chose 20 and 110 mg/L as test concentrations for the assessment of the global gene expression changes in the yeast in response to PYR challenge. The IC20 exposure condition would allow transcriptional insights associated with moderate phenotypic effects to be obtained without a substantial deterioration on cellular function, thus representing presumably a transient cellular response.[22,24] On the other hand, the IC50 was chosen to represent a higher challenge, thus eliciting a stronger and more informative transcriptional response in the yeast cells.[24]

Outline of PYR Transcriptional Response. Overall, a total of 1677 genes (about 28% of the yeast genome) showed significant changes in expression levels (777 upregulated; 900 downregulated) following yeast exposure to both PYR concentrations considered altogether, compared with CT cells not challenged with the fungicide (Figure 2A). The genes found differentially expressed in the IC50-stressed cells (~72% of the total) were considerably more in number (3.3-fold) than those in the IC20-exposed cells (Figure 2A, and Table S2 in the Supporting Information), and this increment was slightly above the one in growth inhibition (2.5-fold). Most of the IC20-responsive genes (88% or 63% of up- or downregulated, respectively) were also present in the data set of genes differentially expressed by the IC50 of PYR (Figure 2A, Table S2 in the Supporting Information). In general, for the majority of these genes with expression modified in both exposure conditions, the lower-bound of fold change values (relative to CT cells) were lower in the IC20-challenged cells compared to the IC50 ones (Table 1, Tables S3 and S4 in the Supporting Information). This is consistent with the different stress intensity sensed by the yeast cells.[22,24] In all data sets, about 80% of the differentially expressed genes have known or inferred biological functions, the rest being uncharacterized open reading frames.

To interpret biological relevance of gene expression profiles in the PYR-stressed cells, functional clustering of the induced or repressed genes in the microarray data sets (complete lists in Tables S2, S3 and S4 of the Supporting Information) was analyzed for significance compared to the entire yeast genome. The main functional categories significantly enriched ($p < 0.01$) with genes differentially expressed by both the IC20 and the IC50 of PYR (186 upregulated; 167 downregulated) (Figure 2A) were in general coincident with those found when the complete IC20 data set was analyzed, and they are summarized in Figure 2B. Significantly, besides these over-represented functional categories common to the IC20 and IC50 exposures (Figure 2B), a number of additional ones were involved in the response to the IC50 only (Figure 2C, Table S5 in the Supporting Information), and this difference was far more notable for the data sets of repressed genes (Table S5 in the Supporting Information). Overall, results thus suggest that there were clearly higher numbers and diversity of over-represented functional categories in the yeast in response to the IC50 compared to the IC20, which may be associated with the stronger deleterious effect of the fungicide at the phenotypic level.

Effects of PYR on Metabolism Related Genes. From functional clustering analysis of microarray data sets, it became evident that a core transcriptional response elicited by both concentrations of PYR involved upregulation of genes related to amino acid metabolism, mostly focused on biosynthesis of arginine (~5.6% or 1.4% of the IC20 or IC50 complete data sets, respectively) and metabolism of the sulfur amino acids methionine, cysteine, and the nonprotein one homocysteine (overall, ~3.8 or 1.8%, respectively) (Figure 2 and Table S5A in the Supporting Information). A particularly relevant finding seems the increased expression of the whole set of genes assigned to biosynthesis of arginine (from *ARG1* to *ARG11*, and *CPA1/CPA2*) in the microarray data (Table 1). Significantly, the modifications in transcription of these genes were confirmed by qRT-PCR measurements in cells subjected to increasing growth-inhibitory concentrations of PYR in independent exposure experiments (Figure 3A). Concretely, this set of PYR-responsive genes comprised the four involved in the biosynthesis of ornithine (a precursor of arginine biosynthesis) from glutamate in the mitochondrion, *ARG11* (also named *ORT1*) encoding the mitochondrial inner membrane that exports ornithine into the cytosol, the three genes involved in the interconversion of ornithine, citrulline and arginine in the cytosol (known as urea cycle), and *CPA1* and *CPA2* that encode the two subunits of the cytosolic carbamoyl-phosphate synthase catalyzing formation of carbamoyl-phosphate (precursor of citrulline) from glutamine[29] (Figure 4). These data suggest that the fungicide may somehow affect arginine and ornithine metabolism and/or their cellular compartmentation[29] in the yeast. It seems less likely that the reported increases in transcription of *ARG* and *CPA* genes might be associated with a situation of amino acid limitation or imbalance[30] due to lowering in metabolism rate in the PYR-stressed cells; indeed, microarray data did not support such an all-inclusive transcriptional modification in any other of the amino acid metabolism categories also enriched with PYR-induced genes

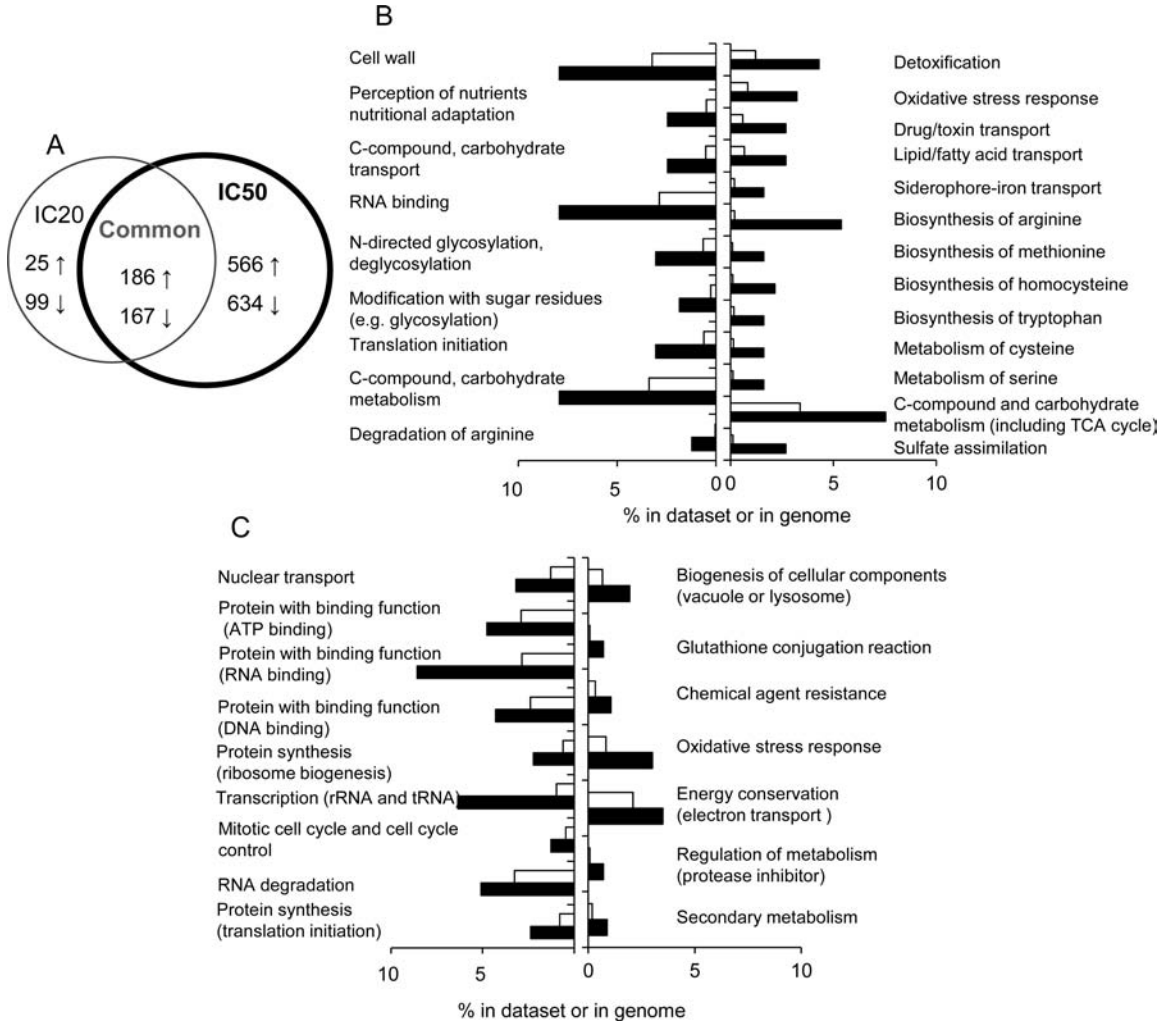

Figure 2. Categorization of gene expression profiles in *S. cerevisiae* BY4741 cells upon 2 h exposure to the 20%-inhibitory (IC20; 20 mg/L) and/or the 50%-inhibitory concentrations (IC50; 110 mg/L) of pyrimethanil. (A) Venn diagrams illustrate the distribution and overlap of the data sets of genes differentially expressed (↑ = induced; ↓ = repressed) on exposure to the IC20 or the IC50 of pyrimethanil compared with its absence. (B, C) Functional clustering of the genes with expression increased (right panel) or decreased (left panel) (B) by both PYR concentrations (IC20 and IC50 common), or (C) uniquely by the IC50. Only the classes found to be statistically over-represented in each data set (black) compared with the frequency in the yeast genome (white) ($p < 0.01$) are represented.

(namely, biosynthesis of sulfur amino acids, of serine, or of tryptophan), but on the contrary only a few genes of these pathways were in general affected (Table 1, and Table S5 in the Supporting Information). Besides, none of the genes encoding regulators (e.g., *GCN* or *GCD*) of the general amino acid control system[30] were found induced in the microarray data sets (Tables S3 and S4 in the Supporting Information); this system coregulates yeast transcription of arginine's and at least 11 other amino acid biosynthesis pathways in response to amino acid limitation.[30] Additionally, the fact that transcription of *CAR1* (encodes arginase; Figure 4) was not significantly modified, as confirmed by qRT-PCR (Figure 3A), and *CAR2* (mediates further ornithine catabolism; Figure 4) was repressed (Table 1 and Figure 3A) suggests that PYR-stressed cells may have sufficient levels of nitrogen source available for their physiological needs.[29,30] Based in the herein reported transcriptional evidence, we propose that this response may reflect a novel aspect of PYR mode of action in the yeast. To the best of our knowledge, the mode of action of PYR was not assigned before to arginine or ornithine metabolism either in yeast or in target phytopathogenic fungi.[10,12] But, in a transcriptional profile analysis upon exposure to the closely related structural analogue cyprodinil, *S. cerevisiae*'s *ARG1*, *ARG3*, *ARG5,6*, and *ARG8* were also reported to be upregulated.[23]

Most of the proteins encoded by these arginine metabolism genes were found to share significant amino acid sequence homology and conserved function with proteins of *B. cinerea*[10] and *Penicillium digitatum*,[12] and (except for Arg7p, Arg2p, and Arg5,6p) of species representative of nontarget higher eukaryotes that might be exposed to PYR residues via contaminated foodstuffs[4,9] or in the environment[8,14−16] (Figure 5, and data not shown). Arginine and its associated metabolites (e.g., citrulline and ornithine) are known to have important biological roles, as precursors of proteins, polyamines, and nitric oxide, in fungi,[31,32] plants,[33] mammals,[34] and fish,[35] and have been associated with freeze tolerance in the yeast[36] and oxidative stress response in diverse eukaryotes.[31,33,34] Imbalance in arginine metabolism and/or availability can have repercussions on dysfunction/disease states and affect early stages of development in mammals[34] or fish.[35] Yeast's *CAR2*, *ARG1*, *ARG3*, and *ORT1* are also homologues of human disease-related genes.[19,37] Further studies are thus required to clarify the mechanisms underlying PYR interference with yeast arginine gene transcription and to

Table 1. Selected Differentially Expressed Genes and Over-Represented Functional Categories on *S. cerevisiae* Transcriptome upon Cells' Exposure to the IC20 or the IC50 of Pyrimethanil

gene name[a]	function	lbFC[b] IC20	lbFC[b] IC50
	Biosynthesis of Arginine[c]		
ARG2	first step in biosynthesis of arginine precursor L-ornithine (mitochondrial)	1.3	1.4
ARG5,6	second and third steps in L-ornithine biosynthesis (mitochondrial)	2.8	3.3
ARG8	fourth step in the biosynthesis of L-ornithine (mitochondrial)	2.7	3.0
ARG7	fifth step of arginine precursor L-ornithine biosynthesis (mitochondrial)	1.5	1.7
ARG11	ornithine transporter in the inner mitochondrial membrane	1.8	1.9
ARG3	ornithine carbamoyltransferase; sixth step in arginine biosynthesis	2.4	2.5
CPA1	small subunit of carbamoyl phosphate synthetase	1.6	1.8
CPA2	large subunit of carbamoyl phosphate synthetase	1.5	1.6
ARG1	argininosuccinate synthetase	1.4	1.4
ARG4	argininosuccinate lyase; final step in the arginine biosynthesis pathway	1.6	2.1
	Degradation of Arginine		
CAR1	arginase; first step of arginine degradation	−1.2	−1.9
CAR2	L-ornithine transaminase; second step of arginine degradation	−2.2	−2.2
	Metabolism of Sulfur Amino Acids (Methionine, Cysteine, Homocysteine)		
MET28	transcriptional activator in the regulation of sulfur metabolism	2.7	9.9
MET32	transcriptional regulation of the methionine biosynthetic genes	1.3	2.0
STR2	cystathionine gamma-synthase, converts cysteine into cystathionine	1.3	2.2
STR3	cystathionine beta-lyase, converts cystathionine into homocysteine	4.1	12.7
SAM4	*S*-adenosylmethionine-homocysteine methyltransferase	1.3	1.4
MHT1	*S*-methylmethionine-homocysteine methyltransferase	ne[d]	1.5
MET2	L-homoserine-*O*-acetyltransferase (methionine biosynthetic pathway)	1.5	2.6
ADI1	acireductone dioxygenease (methionine salvage pathway)	1.6	1.8
	Sulfate Assimilation		
MET16[e]	3′-phosphoadenylsulfate reductase (reduced thioredoxin as cosubstrate)	1.7	2.4
MET5[e]	sulfite reductase beta subunit	1.8	2.3
MET10[e]	assimilatory sulfite reductase alpha subunit	2.2	3.3
MET3	ATP sulfurylase (first step of intracellular sulfate activation)	ne	1.6
MET14	adenylylsulfate kinase	1.4	2.2
MET22	dephosphorylates intermediates of the sulfate assimilation pathway	1.3	1.6
	Energy Metabolism (Electron Transport; TCA Cycle; Fatty Acid β-Oxidation)		
CYB2	cytochrome b2 (L-lactate cytochrome-*c* oxidoreductase)	1.3	2.5
CIT2	citrate synthase (condensation of acetyl coenzyme A and oxaloacetate)	1.4	1.5
CIT3	dual specificity mitochondrial citrate and methylcitrate synthase	1.3	1.5
COX5B	subunit Vb of cytochrome *c* oxidase	1.2	1.5
COX12	subunit VIb of cytochrome *c* oxidase	ne	1.3
CRC1	mitochondrial inner membrane carnitine transporter	1.8	2.5
RSB1	putative integral membrane transporter or flippase of sphingoid LCB	7.2	46.2
RTA1	integral membrane protein (fungal lipid-translocation exporter family)	2.6	19.3
PDR16	phosphatidylinositol transfer protein controlled by the regulator Pdr1p	1.6	4.3
ICT1	lysophosphatidic acid acyltransferase	1.4	5.3
	Cell Rescue and Defense/Detoxification/Related to Pleiotropic Drug Resistance (PDR)		
SNQ2[f]	plasma membrane ATP-binding cassette (ABC) transporter	1.8	4.3
PDR5[f]	plasma membrane ABC transporter; regulated by Pdr1p and Pdr3p	1.5	2.4
PDR10[f]	plasma membrane ABC transporter; regulated by Pdr1p and Pdr3p	ne	2.9
PDR15[f]	plasma membrane ABC transporter; regulated by Pdr1p, Pdr3p, Pdr8p	ne	9.6
YLR346c	regulation by transcription factors involved in PDR	2.2	34.6
PDR1	zinc cluster protein regulator of the PDR network	ne	1.3
PDR3	transcriptional activator of the PDR network	ne	4.8
YOR1[f]	plasma membrane ABC transporter	1.2	4.3
AZR1	plasma membrane transporter of the major facilitator superfamily	1.2	6.1
	Cell Rescue and Defense/Oxidative Stress Response		
GRE2	NADPH-dependent methylglyoxal reductase; general stress response	1.5	8.2
POS5	mitochondrial NADH kinase	1.4	1.9
MXR1	methionine-*S*-sulfoxide reductase; protects iron−sulfur clusters	1.7	2.1
MXR2	methionine-*R*-sulfoxide reductase; protects iron−sulfur clusters	ne	1.4
HMX1	heme-binding peroxidase, endoplasmic reticulum localized	ne	1.8
GPX2	membrane-located phospholipid hydroperoxide glutathione peroxidase	ne	1.7
TSA2	stress inducible cytoplasmic thioredoxin-dependent peroxidase	ne	2.2
PRX1	mitochondrial peroxiredoxin with thioredoxin peroxidase activity	ne	1.7
DOT5	nuclear thiol peroxidase	ne	1.3
TRX2	cytoplasmic thioredoxin isoenzyme; part of thioredoxin system	ne	1.4
TRX3	mitochondrial thioredoxin	ne	1.6
	Detoxification by Modification/Glutathione Conjugation Reaction		
GTO2[g]	omega class glutathione transferase	ne	2.3
GTT1[g]	endoplasmic reticulum associated glutathione *S*-transferase	ne	1.9
GTT2[g]	glutathione *S*-transferase	ne	1.3
GRX1[g]	glutathione-dependent disulfide oxidoreductase	ne	1.6
GRX2[g]	glutaredoxin; involved in maintaining redox state of target proteins	ne	1.5
	Cell Rescue and Defense/Others		
HSP12	plasma membrane localized 12 kDa heat shock protein	1.5	10.6
HSP26	small heat shock protein with chaperone activity	1.6	6.1
HSP31	possible chaperone and cysteine protease	1.6	2.5
HSP32	possible chaperone and cysteine protease	1.4	2.6
YGP1	cell wall-related secretory glycoprotein; induced by nutrient deprivation	1.9	3.8

dx.doi.org/10.1021/jf5007775 | J. Agric. Food Chem. 2014, 62, 5237−5247

Table 1. continued

gene name[a]	function	lbFC[b] IC20	lbFC[b] IC50
	Miscellaneous/Related to Volatile Acid Production		
AAD10	aryl-alcohol dehydrogenase (degradation of aromatic compounds)	1.8	1.7
PLB2	lysophospholipase B involved in phospholipid metabolism	−1.2	−1.5
EEB1	acyl-coenzymeA:ethanol *O*-acyltransferase	−1.7	−2.0
ATF2	alcohol acetyltransferase; forms volatile esters during fermentation	−1.8	−1.8
ALD4	mitochondrial aldehyde dehydrogenase	−1.5	−1.3
ALD6	cytosolic aldehyde dehydrogenase	−1.4	−1.2
ADH5	alcohol dehydrogenase isoenzyme V	1.3	1.6
PHD1	transcriptional activator (metabolic regulation; pseudohyphal growth)	−1.4	−1.4
SOK2	nuclear protein (negatively regulates pseudohyphal differentiation)	ne	1.3
STE12	transcription factor (mitogen-activated protein kinase signaling cascade)	−1.3	−1.7

[a]Genes belong to the indicated functional categories statistically over-represented ($p < 0.01$), unless they are included in the miscellaneous group. Genes underlined were selected for further examination of transcriptional changes by qRT-PCR. [b]Lower bound of fold change (lbFC) of transcript levels of the selected genes in microarray data sets following exposure to pyrimethanil IC20 or IC50 compared to CT cells not exposed to the fungicide. [c]Subheadings in the table represent categories. [d]Not significantly differentially expressed in microarray experiments. [e]Also in categories methionine and homocysteine metabolism. [f]Also in category drug/toxin transport. [g]Also in category oxidative stress response.

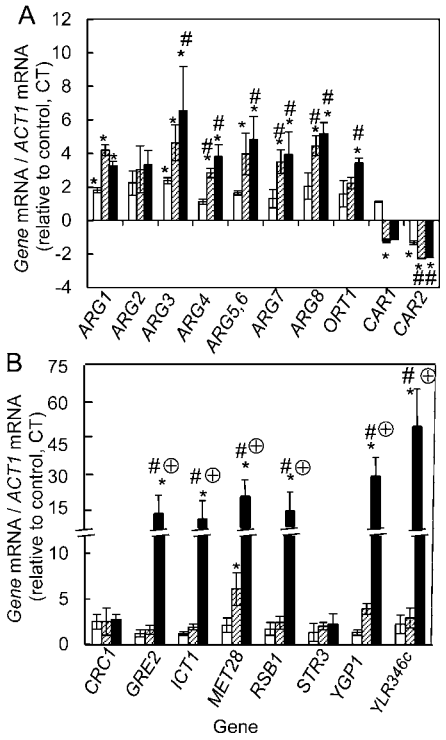

Figure 3. Normalized gene expression modification profiles obtained by qRT-PCR for the indicated genes selected as PYR-responsive from microarray data sets. Relative values of gene mRNA/*ACT1* mRNA were determined for (A) the genes involved in arginine metabolism and (B) genes involved in other functions, in *S. cerevisiae* BY4741 cells exposed during 2 h to pyrimethanil concentrations that exerted 10% (white), 20% (hashmarks), or 50% (black) growth inhibition, compared to control (CT) cells incubated in fungicide absence. Results are expressed as means ± SD; *, #, and ⊕ indicate mean statistically different ($p < 0.05$) from CT cells and from the ones exposed to the 10%- and the 20%-inhibitory concentrations, respectively.

elucidate the actual role of arginine pathway and metabolites in the ambit of PYR mode of action in yeast, mycelial fungi, and other relevant eukaryotes.

After PYR exposure, the genes encoding Str2p and Str3p (cystathionine γ-synthase and cystathionine β-lyase, respectively) (Figure 4) were also upregulated (Table 1, Figure 3B); they catalyze conversion of cysteine into homocysteine via the trans-sulfuration pathway.[38] Homocysteine is an essential intermediate in the biosynthesis of methionine and *S*-adenosyl methionine (AdoMet), the end-product of the sulfur amino acid biosynthesis pathway in diverse organisms.[38,39] A related gene also significantly upregulated in the microarray data and confirmed by qRT-PCR was *MET28* (Table 1, Figure 3B); it encodes a positive regulator of *MET* genes when endogenous AdoMet is low.[38] In addition, genes encoding Sam4p and Mht1p (reported to play major roles in AdoMet recycling and maintenance of equilibrium between its levels and methionine),[39] Met32p (regulator of sulfur amino acid metabolism in combination with Met28p),[38] Met2p (catalyzes the first step of methionine biosynthetic pathway),[38] and several genes of the sulfur assimilation pathway[38] were induced by PYR (Table 1, Figure 4). Proteins were found in phytopathogenic fungi that share homology with yeast Str2p, Str3p, and Sam4p, but not with Met28p (Figure 5, and data not shown). The increased expression of *STR2*, *STR3*, *SAM4*, *MET28*, and *MET32* is consistent with the idea that PYR may affect homocysteine and methionine metabolism in the yeast cells. This insight seems particularly interesting in the context of PYR mode of action because it is still not clear whether methionine metabolism and cystathionine β-lyase or cystathionine γ-synthase are anilinopyrimidine primary targets in *B. cinerea* and other phytopathogenic fungi.[10,12]

In the yeast and other eukaryotes, major consumption of AdoMet is as a methyl donor in the synthesis of major macromolecules and of essential metabolites such as polyamines.[32,34,38] A link appears to exist also between arginine metabolism and polyamine biosynthesis via the common intermediate metabolite ornithine[32,34] (Figure 4). However, we detected no induction of the genes involved in the polyamine biosynthesis pathway (e.g., from *SPE1* to *SPE4*)[32] (Figure 4), and the ones encoding the Spe1p regulators *OAZ1* and *MEU1*[32] were differentially expressed in opposite directions in the PYR-challenged cells (Tables S3 and S4, in the Supporting Information). Nevertheless, we speculate that the transcriptional alterations triggered by PYR in the genes of arginine, methionine, and homocysteine pathways (Figure 4) would allow intracellular arginine, ornithine, and/or AdoMet to be kept at appropriate levels for their essential cellular roles in the stressed cells, including for instance formation of polyamines and macromolecule turnover.[31−34,38,39] For example, spermine is a precursor of coenzyme-A via β-alanine and pantothenate (Figure 4), and three genes (*FMS1*, *CAB1*, and *CAB2*) encoding enzymes of this pathway were also induced by PYR (Tables S3 and S4, in the Supporting Information). It is worth noting that polyamines have been proposed as biomarkers of insecticide effects related to embryonic malformation in tadpoles and frogs.[40] A protective role of AdoMet against acid stress in the yeast was also reported.[41]

dx.doi.org/10.1021/jf5007775 | J. Agric. Food Chem. 2014, 62, 5237−5247

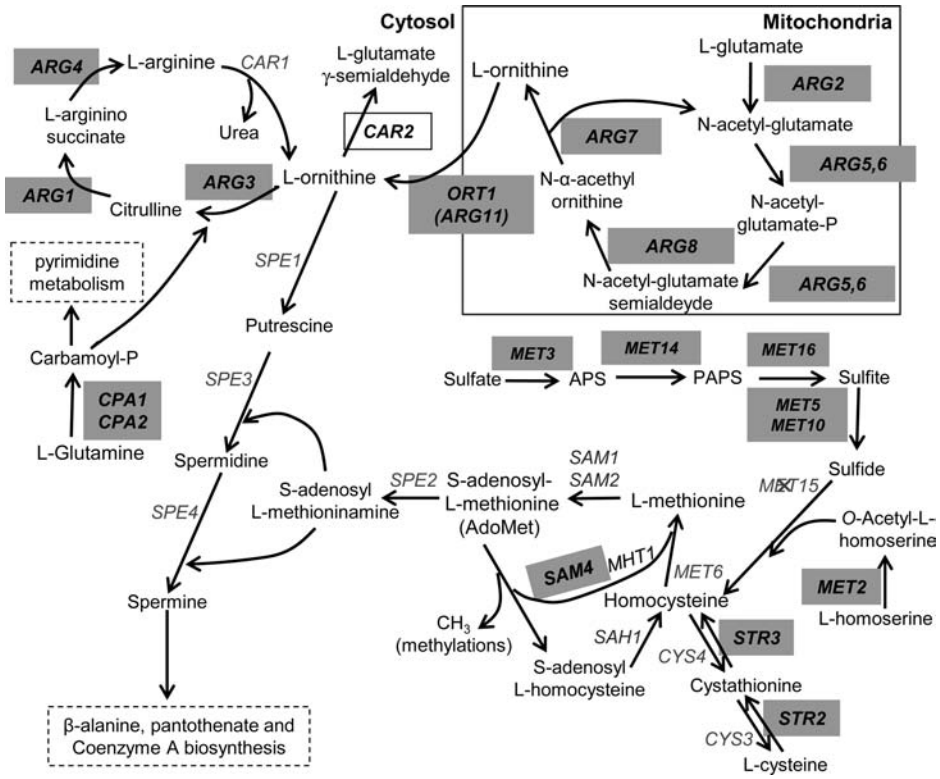

Figure 4. Biochemical steps and corresponding genes involved in the pathways of L-arginine/L-ornithine biosynthesis, sulfur amino acid metabolism, and polyamine biosynthesis in *S. cerevisiae* (adapted from published literature[29,32,38,39] and from the "arginine biosynthesis pathway", the "methionine salvage pathway", and the "polyamine pathway" in SGD[26]). The genes induced (gray box) or repressed (white box) as a result of cells' exposure to the IC20 and the IC50 of pyrimethanil are indicated. APS = 5′-adenylylsulfate; PAPS = 3′-phospho-5′-adenylylsulfate; × means gene eliminated in the auxotrophic strain BY4741.

Effects on Genes Related to Volatile Acid Production. A number of yeast genes that are relevant in the context of production of volatile aroma impact compounds during alcoholic fermentation[42−44] were also transcriptionally modified by PYR. They were, concretely, *AAD10* (overexpression in wine *S. cerevisiae* strains influence levels of propionic, valeric, hexanoic, and decanoic acids, ethyl caprylate, isobutanol, and 2-phenyl ethanol, in the end of fermentation);[42] *PLB2* (a determinant of octanoic and decanoic acid and ethyl ester production);[44] *EEB1* (key gene in synthesis of medium-chain fatty acid ethyl esters and respective acids);[42,44] *ATF2*, *ALD4*, and *ALD6* (expression levels influence formation of diverse volatile aroma impact products);[42] and *STE12*, *PHD1*, *YAP6*, and *SOK2* (encode transcriptional factors that showed variable expression patterns in different industrial wine yeast strains that produce diverse aroma profiles)[43] (more detail in Table 1). The whole picture of the specific roles of these yeast genes is not fully characterized, and it is well-known that laboratory and industrial yeast strains are highly diverse in this respect.[42−44] However, these results point to potential interference of PYR in the network of pathways that influence the patterns of volatile aroma compounds during alcoholic fermentation (e.g., fatty acid and amino acid metabolism, lipid and sterol biosynthesis) in the yeast,[42−44] thus possibly imparting variable organoleptic properties and influencing the quality of the final wine, at least in worst-case situations associated with fungicide misuse.[4,6,7]

Alterations on Genes Related to Stress Response. As expectable for transcriptional responses initiated in response to growing chemical challenges in the yeast,[18,22,24] a significant number of gene expression alterations related to cell rescue, defense, and detoxification increased considerably in cells exposed to the IC50 of PYR compared with the IC20s (Table 1, and Table S5 in the Supporting Information). It may correspond to enhanced requirements for reprogramming gene expression in order to maintain cellular homeostasis under sublethal PYR stress before more detrimental effects and cell deterioration may be activated.[22,24] Among them, a number of genes within the over-represented categories RNA degradation, transcription, ribosome biogenesis, translation initiation, protein synthesis, and mitotic cell cycle control were repressed (Figure 2C, and Table S5 in the Supporting Information). This type of transcriptional response is considered to help the cell to safeguard energy while adapting to the new challenging conditions.[24] Consistently, the number of upregulated genes in over-represented categories related to TCA cycle and membrane-associated electron transport/energy conservation increased from the IC20 to the IC50 PYR-stressed cells (Figure 2, Table 1, and Table S5 in the Supporting Information). They may contribute to provide energy for the function of ATP-depleting processes presumably involved in cells' protection against stress (e.g., drug transport, iron homeostasis/siderophore-iron transport, detoxification).[22,24] In the context of potential energy expenses in the PYR-stressed cells, it seems relevant that activity of the "ornithine carbamoyltransferase-carbamoyl phosphate synthetase couple"[29] encoded by the upregulated *ARG3*, *CPA1*, and *CPA2* genes (Figure 4) is an important ATP consumer in eukaryotic cells,[29] as are the presumably PYR-affected AdoMet synthesis and sulfate assimilation pathways (Figure 4) in the yeast.[38,39] Other major consumers of cellular energy include putative multidrug/pleiotropic active transmembrane transporters[45,46] encoded by

dx.doi.org/10.1021/jf5007775 | J. Agric. Food Chem. 2014, 62, 5237−5247

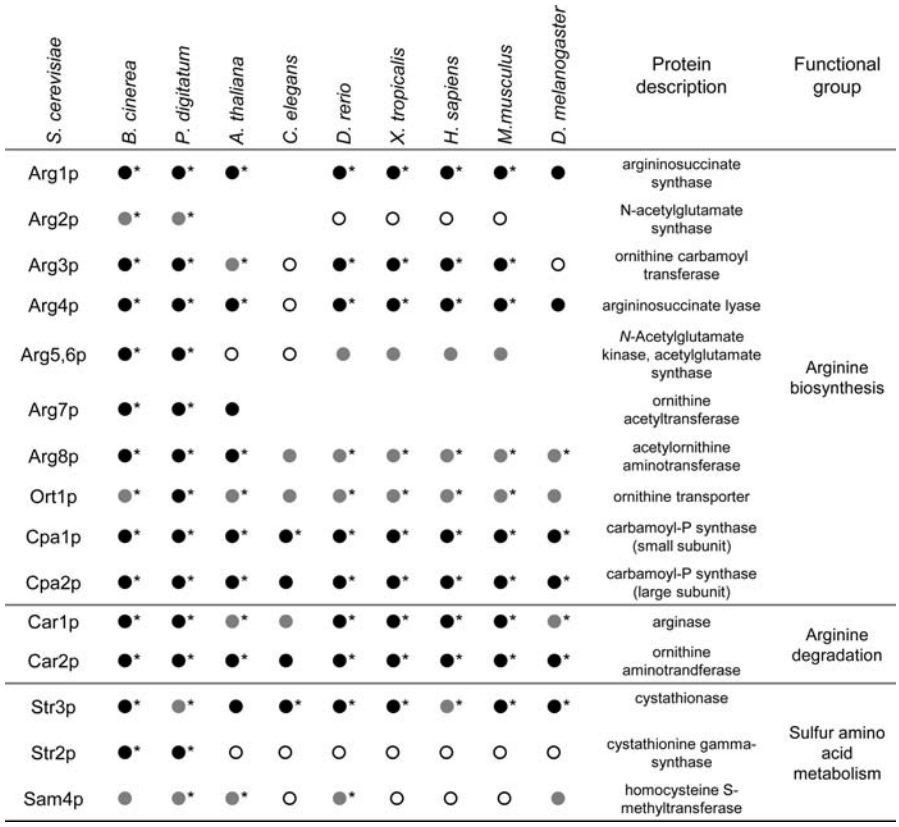

Figure 5. Homology between yeast proteins encoded by selected pyrimethanil-responsive genes and proteins from the phytopathogenic fungi *Botrytis cynerea* and *Penicillium digitatum* and from higher eukaryotes that are representative of ecologically relevant organisms (namely, *Arabidopsis thaliana*, *Caenorhabditis elegans*, *Danio rerio*, *Drosophila melanogaster*, *Homo sapiens*, *Mus musculus*, and *Xenopus tropicalis*). Symbols provide information on the best similarity hit of each query protein, as follows: (black) score ≥ 200 bits and identity ≥ 40%; (gray) 90 ≤ score < 200 bits and 22% ≤ identity < 40%; (white) 35 ≤ score < 90 bits and/or 20% ≤ identity < 22%; (empty space) homologue absent. On the right side, the description of the conserved gene product indicated with an * is shown, as well as the respective functional group.

genes also induced due to PYR stress and enriched in the over-represented functional category "detoxification" (detailed in Table 1). In addition, *RSB1* and the closely related *RTA1*[47] were also strongly induced because of PYR exposure (Table 1, Figure 3B). Their encoded transmembrane proteins may play roles in hampering accumulation of aberrant metabolites and presumably also of xenobiotics in the cytoplasm.[47] These gene expression modifications suggest a possible contribution of export of the intact and/or the biotransformed fungicide molecule from the cytosol among the PYR detoxification processes, as proposed for other xenobiotics.[20,45,46] It is worth noting that five genes encoding enzymes that can act as glutathione-*S*-transferases in the yeast (e.g., *GTT1*, *GTT2*, *GTO2*, *GRX1*, *GRX2*),[48] with presumable roles in xenobiotic detoxification,[18,20,48] were also among the PYR-responsive genes (Table 1). As far as we are aware, there is no report of conjugation reactions of PYR in the yeast. In rats, evidence of biotransformation of the structurally analogue cyprodinil that culminated in formation and excretion of sulfate-conjugated metabolites, were reported.[49] A high level of functional conservation exist within multidrug resistance mechanisms among eukaryotes.[21,45,46] The actual role of multidrug resistance in response of field strains of phytopathogenic fungi to PYR and other fungicides is of utmost importance.[10−12]

Also significantly over-represented in the transcriptome of PYR stressed cells were several upregulated genes that encode cytosolic and/or mitochondrial glutathione (GSH)-dependent glutaredoxins and thioredoxins, thioredoxin-dependent methionine-*S*-sulfoxide reductases, thioredoxin- or GSH-dependent peroxidases, in different locations, and a number of glutathione-*S*-transferases with dual roles (Figure 2; more detail in Table 1). They are known to have critical roles in defense against oxidative stress and regulation of the redox state of protein sulfydryl groups that is essential for many cell functions.[48] It is worth noting that genes encoding enzymes more typically specialized in reactive oxygen species (ROS) detoxification, like superoxide dismutases, catalases, or other peroxidases,[18,24,48] were apparently not induced following PYR exposure (Tables S3 and S4 in the Supporting Information). However, possible increases by PYR of ROS flux cannot be ruled out, associated for instance with electron flow disruption, as proposed with respect to PYR detrimental effects on ATP yield in neuronal cell lines (presumably linked with neurotoxicity)[9] or on chlorophyll production and photosynthesis in the aquatic primary producer *Lemna minor*.[15] Given the type of antioxidant response genes herein detected (Table 1), which encode enzymes where GSH is the major redox donor,[48] we hypothesize PYR-stressed cells possibly experiencing enhanced endogenous GSH depletion. It might for instance be due to modulation of the redox state of protein sulfur amino acids, because methionine and cysteine are major targets for protein oxidation,[48] and/or with GSH-dependent conjugation reactions of PYR molecule mediated by glutathione-*S*-transferases (Table 1) in xenobiotic detoxification.[48] Other genes that may be relevant in the context of cell response and adaptation to PYR stress were strongly induced, like those encoding the cytosolic Gre2p (Table 1, Figure 3B) and the heat-shock

proteins with chaperone activity (*HSP26*, *HSP31*) or involved in maintenance of membrane organization under stress conditions (*HSP12*) (Table 1). These genes, but not *HSP31*, were also induced in *S. cerevisiae* on exposure to the anilinopyrimidine cyprodinil,[23] and are typically associated with general stress response in the yeast.[24]

This analysis of potential effects of PYR in the yeast is restricted to transcriptional response, and further information on post-transcriptional and translational control of the gene products and on physiological performance is necessary to gain a complete picture. Nevertheless, the transcriptional modifications discussed above allowed novel questions to be raised over PYR mode of action, for instance whether the arginine pathway may be a specific target, whether PYR may act as pro-oxidant, whether interplay may exist between arginine, polyamines, methionine, and AdoMet metabolism and antioxidant defense[31−34,38] and PYR may interfere on it, or what yeast processes influencing volatile aroma product formation during wine fermentations may be impacted by PYR residues. These insights deserve further in-depth studies in relevant wine yeast strains and phytopathogenic fungi to gain better understanding of PYR action, with possible repercussions on control of fungicide resistance in target fungi[10−12] and in enology.[4,6,42−44] In this respect, it is noteworthy that, besides PYR,[4,6,7] other new fungicides that may be used alone or together with anilinopyrimidine fungicides to treat vineyards, and whose residues can persist in grapes, have been reported to alter wine yeast biosynthesis of volatile products that contribute to the wines' sensorial properties.[50,51] In the (eco)toxicological context, we are aware that there are differences in xenobiotic susceptibility across species and a discrepancy exists between the fungicide concentrations herein used and those usually found in aquatic compartments under regulatory agricultural practices (e.g., <22−90 μg/L in vineyards).[14−16] Despite that, we propose that the transcriptional insights gained in this work may contribute to assist planning of toxicological studies in nontarget and experimentally less accessible eukaryotes, to predict potential adverse side effects of bioavailable PYR, particularly with respect to irregular scenarios of fungicide misuse in agricultural fields[1,4−6] or accidental spills. For example, possible exposure of useful microbiota and/or higher eukaryotes from ecosystems to fungicide residues in contaminated soil, water, and sediments[14−16] in agricultural or adjacent regions, and/or of humans due to consumption of fruit, vegetable, and wine products[1,4,5,8,9] or occupational activities,[52] may be of toxicological concern.

Molecular Indicators of Toxicity. Several experimental advantages that contribute to lower costs and time in chemical toxicity testing have been attributed to yeast-based assays.[18,21,22] However, assays relying solely on phenotypic end points[21] often lack sensitivity and provide no mechanistic information. Therefore, we also examined the possible suitability of several PYR-responsive genes as indicators of toxicity in the yeast. Of the 20 genes selected for confirmation of transcription modification by PYR using qRT-PCR (Table S1 in the Supporting Information), five involved in the main affected metabolic pathways (e.g., *ARG3*, *ARG4*, *ARG5,6*, *ARG8*, and *MET28*) displayed consistent transcription variation profiles that correlated well with the concentration-dependent inhibition of yeast growth by the fungicide (Figure 3A,B). Moreover, for example, modifications in their expression between 4.0- and 6.1-fold (depending on the gene) compared with CT cells were detected in cells exposed to a PYR concentration that inhibited growth by only 20% (Figure 3). This suggests that measuring transcriptional changes of these genes is more sensitive than the phenotypic end point based on effects in yeast growth. Therefore, they could be interesting for instance to incorporate in yeast-based cellular reporters or biosensors for purposes of biomonitoring or preliminary screening of fungicide toxicity, in line with the 3Rs attempt to "reduce, refine, and replace" animal models in toxicity testing.[17,21]

■ ASSOCIATED CONTENT

Ⓢ Supporting Information

Tables containing the primer sets for qRT-PCR of selected genes (Table S1), the lists of yeast genes differentially expressed in the microarray data sets upon yeast exposure to the IC20 and/or the IC50 of PYR and Venn comparative analysis (Table S2), the complete lists, fold-change values, and functions of the genes differentially expressed on exposure to the IC20 (Table S3) or the IC50 (Table S4) of PYR, and the complete list of functional categories over-represented within the microarray data sets (Tables S5). This material is available free of charge via the Internet at http://pubs.acs.org.

■ AUTHOR INFORMATION

Corresponding Author

*Tel: +351-218419380. Fax: +351-218419199. E-mail: cristina.viegas@tecnico.ulisboa.pt.

Funding

Research was supported by European Funds for Regional Development—FEDER through the Competitiveness Factors Operational Programme—COMPETE and National Funds through Foundation for Science and Technology, Portugal (Contracts PTDC/AMB/64230/2006, PTDC/AAC-AMB/111317/2009, PEst-OE/EQB/LA0023/2011, and fellowship SFRH/BD/60933/2009 for F.N.G.).

Notes

The authors declare no competing financial interest.

■ ABBREVIATIONS USED

AdoMet, *S*-adenosylmethionine; BLASTP, protein basic local alignment search tool; GSH, glutathione; EC20 or EC50, 20%- or 50%-effective concentration; IC10, IC20, or IC50, 10%-, 20%-, or 50%-inhibitory concentration; LC50, median-lethal concentration; MIPS, Munich Information Center for Protein Sequences; OD_{640nm}, optical density measured at 640 nm; PYR, pyrimethanil; qRT-PCR, real-time quantitative reverse transcriptase polymerase chain reaction; ROS, reactive oxygen species; TCA, tricarboxylic acids

■ REFERENCES

(1) Vaquero-Fernández, L.; Sanz-Asensio, J.; Fernández-Zurbano, P.; Lopez-Alonso, M.; Martínez-Soria, M.-T. Determination of fungicide pyrimethanil in grapes, must, fermenting must and wine. *J. Sci. Food. Agric.* **2013**, *93*, 1960−1966.

(2) European Food Safety Authority (EFSA). Review of the existing maximum residue levels (MRLs) for pyrimethanil according to Article 12 of Regulation (EC) No 396/2005. *EFSA J.* **2011**, *9* (11), 2454 [65 pp].

(3) Menard, C.; Heraud, F.; Nougadere, A.; Volatier, J.-L.; Leblanc, J.-C. Relevance of integrating agricultural practices in pesticide dietary intake indicator. *Food Chem. Toxicol.* **2008**, *46*, 3240−3253.

(4) Cabras, P.; Angioni, A. Pesticide residues in grapes, wine, and their processing products. *J. Agric. Food Chem.* **2000**, *48*, 967−973.

(5) Fernández, M. J.; Oliva, J.; Barba, A.; Câmara, M. A. Fungicide dissipation curves in winemaking processes with and without maceration step. *J. Agric. Food Chem.* **2005**, *53*, 804−811.
(6) Bizaj, E.; Cus, F.; Raspor, P. Removal of pyrimethanil and fenhexamid from *Saccharomyces cerevisiae* liquid cultures. *Food Technol. Biotechnol.* **2011**, *49*, 474−480.
(7) Garcia, M. A.; Oliva, J.; Barba, A.; Câmara, M. A.; Pardo, F.; Díaz-Plaza, E. M. Effect of fungicide residues on the aromatic composition of white wine inoculated with three *Saccharomyces cerevisiae* strains. *J. Agric. Food Chem.* **2004**, *52*, 1241−1247.
(8) Orton, F.; Rosivatz, E.; Scholze, M.; Kortenkamp, A. Widely used pesticides with previously unknown endocrine activity revealed as *in vitro* antiandrogens. *Environ. Health Perspect.* **2011**, *119*, 794−800.
(9) Coleman, M. D.; Neil, J. D. O.; Woehrling, E. K.; Ndunge, O. B. A.; Hill, E. J.; Menache, A.; Reiss, C. J. A preliminary investigation into the impact of a pesticide combination on human neuronal and glial cell lines *in vitro*. *PloS One* **2012**, *7* (8), e42768.
(10) Walker, A.-S.; Micoud, A.; Rémuson, F.; Grosman, J.; Gredt, M.; Leroux, P. French vineyards provide information that opens ways for effective resistance management of *Botrytis cinerea* (grey mould). *Pest Manage. Sci.* **2013**, *69*, 667−678.
(11) Andrade, A. C.; Sorbo, G. D.; van Nistelrooy, J. G. M.; de Waard, M. A. The ABC transporter AtrB from *Aspergillus nidulans* mediates resistance to all major classes of fungicides and some natural toxic compounds. *Microbiology* **2000**, *156*, 1987−1997.
(12) Kanetis, L.; Förster, H.; Jones, C. A.; Borkovich, K. A.; Adaskaveg, J. E. Characterization of genetic and biochemical mechanisms of fludioxonil and pyrimethanil resistance in field isolates of *Penicillium digitatum*. *Phytopathology* **2008**, *98*, 205−214.
(13) Milling, R. J.; Richardson, C. J. Mode of action of the anilino-pyrimidine fungcide pyrimethanil. 2. Effects on enzyme secretion in *Botrytis cinerea*. *Pestic. Sci.* **1995**, *45*, 43−48.
(14) Stamatis, N.; Hela, D.; Konstantinou, I. Occurrence and removal of fungicides in municipal sewage treatment plant. *J. Hazard. Mater.* **2010**, *175*, 829−835.
(15) Verdisson, S.; Couderchet, M.; Vernet, G. Effects of procymidone, fludioxonil and pyrimethanil on two non-target aquatic plants. *Chemosphere* **2001**, *44*, 467−474.
(16) Seeland, A.; Oehlmann, J.; Müller, R. Aquatic ecotoxicity of the fungicide pyrimethanil: effect profile under optimal and thermal stress conditions. *Environ. Pollut.* **2012**, *168*, 161−169.
(17) Robbens, J.; van der Ven, K.; Maras, M.; Blust, R.; de Coen, W. Ecotoxicological risk assessment using DNA chips and cellular reporters. *Trends Biotechnol.* **2007**, *25*, 460−466.
(18) Yasokawa, D.; Iwahashi, H. Toxicogenomics using yeast DNA microarrays. *J. Biosci. Bioeng.* **2010**, *110*, 511−522.
(19) Foury, F. Human genetic diseases: a cross-talk between man and yeast. *Gene* **1997**, *195*, 1−10.
(20) dos Santos, S. C.; Teixeira, M. C.; Cabrito, T. R.; Sá-Correia, I. Yeast toxicogenomics: Genome-wide responses to chemical stresses with impact in environmental health, pharmacology, and biotechnology. *Front. Genet.* **2012**, *3* (63), 1−17.
(21) Papaefthimiou, C.; Cabral, M. D. G.; Mixailidou, C.; Viegas, C. A.; Sá-Correia, I.; Theophilidis, G. Comparison of two screening bioassays, based on the frog sciatic nerve and yeast cells, for the assessment of herbicide toxicity. *Environ. Toxicol. Chem.* **2004**, *23*, 1211−1218.
(22) Gil, F. N.; Gonçalves, A. C.; Jacinto, M. J.; Becker, J. D.; Viegas, C. A. Transcriptional profiling in *Saccharomyces cerevisiae* relevant for predicting alachlor mechanisms of toxicity. *Environ. Toxicol. Chem.* **2011**, *30*, 2506−2518.
(23) Kagan, I. A.; Michel, A.; Prause, A.; Scheffler, B. E.; Pace, P.; Duke, S. O. Gene transcription profiles of *Saccharomyces cerevisiae* after treatment with plant protection fungicides that inhibit ergosterol biosynthesis. *Pestic. Biochem. Physiol.* **2005**, *82*, 133−153.
(24) Gasch, A. P.; Werner-Washburne, M. The genomics of yeast responses to environmental stress and starvation. *Funct. Integr. Genomics* **2002**, *2*, 181−192.
(25) Affymetrix database, URL (http://www.affymetrix.com) (November 2009).
(26) Cherry, J. M.; Hong, E. L.; Amundsen, C.; Balakrishnan, R.; Binkley, G.; Chan, E. T.; Christie, K. R.; Costanzo, M. C.; Dwight, S. S.; Engel, S. R.; Fisk, D. G.; Hirschman, J. E.; Hitz, B. C.; Karra, K.; Krieger, C. J.; Miyasato, S. R.; Nash, R. S.; Park, J.; Skrzypek, M. S.; Simison, M.; Weng, S.; Wong, E. D. *Saccharomyces* Genome Database: the genomics resource of budding yeast. *Nucleic Acids Res.* **2012**, *40* (Database issue), D700−705.
(27) Ruepp, A.; Zollner, A.; Maier, D.; Albermann, K.; Hani, J.; Mokrejs, M.; Tetko, I.; Güldener, U.; Mannhaupt, G.; Münsterkötter, M.; Mewes, H. W. The FunCat, a functional annotation scheme for systematic classification of proteins from whole genomes. *Nucleic Acids Res.* **2004**, *32*, 5539−5545.
(28) Robinson, M. D.; Grigull, J.; Mohammad, N.; Hughes, T. R. FunSpec: a web-based cluster interpreter for yeast. *BMC Bioinf.* **2002**, *3*, 35−39.
(29) Jauniaux, J. C.; Urrestarazu, L. A.; Wiame, J. M. Arginine metabolism in *Saccharomyces cerevisiae*: subcellular localization of the enzymes. *J. Bacteriol.* **1978**, *133*, 1096−1107.
(30) Hinnebusch, A. G. General and pathway-specific regulatory mechanisms controlling the synthesis of amino acid biosynthetic enzymes in *Saccharomyces cerevisiae*. In *The molecular and cellular biology of the yeast Saccharomyces*, 1st ed.; Jones, E. W., Pringle, J. R., Broach, J. R., Eds.; Cold Spring Harbor Laboratory Press: New York, 1992; pp 319−414.
(31) Nishimura, A.; Kotani, T.; Sasano, Y.; Takagi, H. An antioxidative mechanism mediated by the yeast N-acetyltransferase Mpr1: oxidative stress-induced arginine synthesis and its physiological role. *FEMS Yeast Res.* **2010**, *10*, 687−698.
(32) Valdés-Santiago, L.; Cervantes-Chávez, J. A.; León-Ramírez, C. G.; Ruiz-Herrera, J. Polyamine metabolism in fungi with emphasis on phytopathogenic species. *J. Amino Acids* **2012**, DOI: 10.1155/2012/837932.
(33) Shi, H.; Ye, T.; Chen, F.; Cheng, Z.; Wang, Y.; Yang, P.; Chan, Z. Manipulation of arginase expression modulates abiotic stress tolerance in *Arabidopsis*: effect on arginine metabolism and ROS accumulation. *J. Exp. Bot.* **2013**, *64*, 1367−1379.
(34) Wu, G.; Bazer, F. W.; Davis, T. A.; Kim, S. W.; Li, P.; Rhoads, J. M.; Satterfield, M. C.; Smith, S. B.; Spencer, T. E.; Yin, Y. Arginine metabolism and nutrition in growth, health and disease. *Amino Acids* **2009**, *37*, 153−168.
(35) Capiotti, K. M.; Fazenda, L.; Nazario, L. R.; Menezes, F. P.; Kist, L. W.; Bogo, M. R.; Bonan, C. D. Arginine exposure alters ectonucleotidase activities and morphology of zebrafish larvae (*Danio rerio*). *Int. J. Dev. Neurosci.* **2013**, *31*, 75−81.
(36) Shima, J.; Sakata-Tsuda, Y.; Suzuki, Y.; Nakajima, R.; Watanabe, H.; Kawamoto, S.; Takano, H. Disruption of the *CAR1* gene encoding arginase enhances freeze tolerance of the commercial baker's yeast *Saccharomyces cerevisiae*. *Appl. Environ. Microbiol.* **2003**, *69*, 715−718.
(37) Camacho, J. A.; Obie, C.; Biery, B.; Goodman, B. K.; Hu, C. A.; Almashanu, S.; Steel, G.; Casey, R.; Lambert, M.; Mitchell, G. A.; Valle, D. Hyperornithinaemia-hyperammonaemia-homocitrullinuria syndrome is caused by mutations in a gene encoding a mitochondrial ornithine transporter. *Nat. Genet.* **1999**, *22*, 151−158.
(38) Thomas, D.; Surdin-Kerjan, Y. Metabolism of sulphur amino acids in *Saccharomyces cerevisiae*. *Microbiol. Mol. Biol. Rev.* **1997**, *61*, 503−532.
(39) Thomas, D.; Becker, A.; Surdin-Kerjan, Y. Reverse methionine biosynthesis from *S*-Adenosylmethionine in eukaryotic cells. *J. Biol. Chem.* **2000**, *62*, 40718−40724.
(40) Sottomayor, V.; Lascano, C.; de D'Angelo, A. M. P.; Venturino, A. Developmental and polyamine metabolism alterations in *Rhinella arenarum* embryos exposed to the organophosphate chlorpyrifos. *Environ. Toxicol. Chem.* **2012**, *31*, 2052−2058.
(41) Malakar, D.; Dey, A.; Basu, A.; Ghosh, A. K. Antiapoptotic role of S-adenosyl-L-methionine against hydrochloric acid induced cell death in *Saccharomyces cerevisiae*. *Biochim. Biophys. Acta* **2008**, *1780*, 937−947.

(42) Rossouw, D.; Næs, T.; Bauer, F. F. Linking gene regulation and the exo-metabolome: A comparative transcriptomics approach to identify genes that impact on the production of volatile aroma compounds in yeast. *BMC Genomics* **2008**, *9*, 530−547.
(43) Rossouw, D.; Jacobson, D.; Bauer, F. F. Transcriptional Regulation and the Diversification of Metabolism in Wine Yeast Strains. *Genetics* **2012**, *190*, 251−261.
(44) Steyer, D.; Ambroset, C.; Brion, C.; Claudel, P.; Delobel, P.; Sanchez, I.; Erny, V.; Blondin, B.; Karst, F.; Legras, J.-L. QTL mapping of the production of wine aroma compounds by yeast. *BMC Genomics* **2012**, *13*, 573−587.
(45) Paumi, C. M.; Chuck, M.; Snider, J.; Stagljar, I.; Michaelis, S. ABC transporters in *Saccharomyces cerevisiae* and their interactors: New technology advances the biology of the ABCC (MRP) subfamily. *Microbiol. Mol. Biol. Rev.* **2009**, *73*, 577−593.
(46) Sá-Correia, I.; Santos, S. C.; Teixeira, M. C.; Cabrito, T. R.; Mira, N. P. Drug:H antiporters in chemical stress response in yeast. *Trends Microbiol.* **2008**, *17*, 22−31.
(47) Manente, M.; Ghislain, M. The lipid-translocating exporter family and membrane phospholipid homeostasis in yeast. *FEMS Yeast Res.* **2009**, *9*, 673−687.
(48) Herrero, E.; Ros, J.; Bellí, G.; Cabiscol, E. Redox control and oxidative stress in yeast cells. *Biochim. Biophys. Acta* **2008**, *1780*, 1217−1235.
(49) Müller, T.; Thanei, P.; Mücke, W.; Kriemler, H.-P.; Winkler, T. The sex-specific sulfation of the major metabolite of the novel fungicide cyprodinil in the rat. *Pestic. Sci.* **1999**, *55*, 566−614.
(50) González-Rodriguez, R. M.; Noguerol-Pato, R.; González-Barreiro, C.; Cancho-Grande, B.; Simal-Gandára, J. Application of new fungicides under good agricultural practices and their effects on the volatile profile of white wines. *Food Res. Int.* **2011**, *44*, 397−403.
(51) Gonzalez-Álvarez, M.; Noguerol-Pato, R.; González-Barreiro, C.; Cancho-Grande, B.; Simal-Gandára, J. Changes on the sensorial attributes of white wines with the application of new anti-mildew fungicides under critical agricultural practices. *Food Chem.* **2012**, *130* (1), 139−146.
(52) Schummer, C.; Salquèbre, G.; Briand, O.; Millet, M.; Appenzeller, B. M. R. Determination of farm workers' exposure to pesticides by hair analysis. *Toxicol. Lett.* **2012**, *210*, 203−210.

Plant Material. Soybeans seeds (*Glycine max* (L.) Merr.) were supplied from the Botanical Garden in Lublin. The plants were germinated from seeds on wet filter paper in a thermostat-controlled chamber. After 7 days, the seedlings were transferred into Hoagland's nutrient solution for 3 days, and then the growth medium was removed. The composition of Hoagland's solution was modified by addition of Sr^{2+} ions to obtain appropriate concentrations (0.5, 1.0, 1.5, 2.0, 2.5, and 3.0 mM). Additionally, iron citrate was removed and $Mg(NO_3)_2{\cdot}6H_2O$ instead of $MgSO_4{\cdot}7H_2O$ was used in order to avoid precipitation of insoluble strontium salt.

Twenty plants for each concentration of Sr were grown in modified Hoagland's medium for another 14 days at a day/night cycle of 16/8 h and 24/17 °C, respectively, relative humidity 60−70%, and photosynthetic photon flux density of 150 μmol/m^2 s. The nutrient solution with Sr^{2+} ions was changed every 3 days. After harvest, the plants were separated into roots and shoots and accurately weighed. Some material was frozen in liquid nitrogen and stored at −80 °C prior to analysis of the content of chlorophylls and carotenoids.

Atomic Absorption Spectrometry (AAS) Procedure. Fresh roots were washed with deionized water three times to remove Sr^{2+}adsorbed on the surface. Five roots and two shoots were taken per replication. The plant material was dried at 80 °C to constant weight and pulverized. The shoots and roots were accurately weighed (0.5 and 0.3 g respectively) and mineralized in a microwave-assisted high-pressure digestion closed system (UniClever BM-1, 350 W, Plazmotronika, Poznań, Poland) with the use of a mixture containing 4 mL of 65% nitric acid and 10 mL of deionized water. The mineralization parameters were as follows: the power of the microwave generator at 60%, 80%, and 100% during 10, 15, and 20 min, respectively. The mineralizates were weighed. Sr^{2+} contents were determined by flame atomic absorption spectrometry (High-Resolution Continuum Source atomic absorption spectrometer ContrAA 700, Analytik Jena AG, Germany). A xenon lamp working in an optimized Hot-Spot-Mode and a CCD array detector (185−900 nm) with high quantum efficiency and increased UV-sensitivity were employed. The measurements were performed at λ = 460.733 nm, and the concentration range of strontium for the calibration curve was from 0 to 20 mg/L (n = 5). The validation parameters obtained were as follows: correlation coefficient R = 0.9999, the value of characteristic concentration for 1% of absorbance was 0.04513 mg/L, calibration equation $y = (-0.0001968 + 0.0580274)/(1 + 0.0201765x)$, and precision expressed as relative standard deviation (% RSD) 0.7−2.9%.

Chlorophyll and Carotenoid Analysis. Chlorophyll *a* (Chl*a*), chlorophyll *b* (Chl*b*), and carotenoids (Car) were extracted with 80% acetone, and their contents were spectrophotometrically determined (Shimadzu UV 160A) at λ = 663, λ = 646, and λ = 470 nm, respectively. The concentrations (mg/g) were calculated according to Wellburn.[25]

Statistical Analysis. Statistical analysis was conducted using the STATISTICA ver.10 (StatSoft, Inc., USA) program. Data was analyzed by ANOVA, and the significances of differences were examined using Fisher's LSD test. The statistical confidence was set at p = 0.05.

RESULTS AND DISCUSSION

Phytoextraction of metals is a common effect which may be used for phytoremediation of soil contaminated by toxic elements or radionuclides[26] or for biofortification with microelements, for instance essential for plant physiology.[27] Here we present the results of the influence of strontium fertilization on accumulation of the metal in *Glycine max*. Our research may be useful to obtain phytoestrogen-containing vegetable products or herbal formulations enriched with strontium to alleviate the risk of osteoporosis effects for postmenopausal women.

In our investigations, hydroponic cultivation was employed to ensure controlled conditions of the plant culture; otherwise, such components of soil as other ions could influence the uptake of strontium.

Table 1. Content of Strontium in Different Parts of *Glycine max* Treated with Various Sr Concentrations (±SD)[a]

	content of Sr (mg/kg) DW	
concn of Sr in medium (mM)	shoot (n = 10)	root (n = 4)
0.5	175.06 ± 10.21	18.40 ± 1.97
1	351.06 ± 17.12	37.39 ± 2.61
1.5	673.85 ± 31.19	85.20 ± 4.20
2	885.80 ± 40.05	111.26 ± 5.11
2.5	1014.85 ± 50.43	147.20 ± 7.07
3	1246.13 ± 65.63	180.22 ± 9.94

[a]The concentration of Sr in control was below the limit of detection.

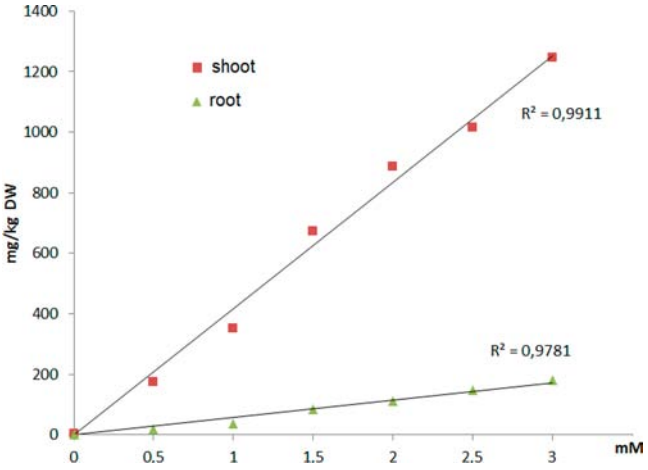

Figure 1. Linear correlation between of the strontium content in the growth medium and its content in dry weight of *Glycine max*.

Table 2. Strontium Distribution and Uptake by *Glycine max* Treated with Various Sr Concentrations (±SD)[a]

	BCF					
Sr concn in medium (mM)	shoot (S/M)		root (R/M)		TF (S/R)	
0.5	3.97	±0.10 a	0.42	±0.010 a	9.45	±0.32 a
1	4.01	±0.11 a	0.43	±0.010 a	9.39	±0.33 a
1.5	5.13	±0.16 b	0.65	±0.017 b	7.91	±0.29 b
2	5.06	±0.17 b	0.64	±0.020 b	7.96	±0.24 b
2.5	4.63	±0.11 c	0.67	±0.014 bc	6.89	±0.31 c
3	4.74	±0.18 bc	0.69	±0.012 c	6.91	±0.23 c

[a]Values followed by the same letters were not significantly different (p < 0.05).

Accumulation and Translocation of Strontium in soy. The accumulation of strontium in plants strongly depends on its concentration in the growth medium and the type of biota. Its content may vary from a few to even more than 2000 ppm.[23] Moreover, differences in the amount of strontium between above-ground and under-ground plant parts have been observed,[28−30] with higher concentrations generally present in shoot.[23,31] As our experiments showed, soy has a pronounced tendency toward accumulation of Sr^{2+} in shoots. Its content ranged from 87.4% to 90.4% of the total amount of the ions in the plants (Table 1). A positive linear correlation (R^2 > 0.98) between the amount of strontium in the growth medium and its content in the plant was also observed (Figure 1).

dx.doi.org/10.1021/jf501257r | J. Agric. Food Chem. 2014, 62, 5248−5252

Table 3. Effect of Treatment with Various Concentrations of Strontium on *Glycine max* Biomass (n = 20)[a]

	FW				DW			
	shoot		root		shoot		root	
concn (mM)	g	SD	g	SD	g	SD	g	SD
0	1.924	±0.096 ab	1.518	±0.091 ab	0.312	±0.019 a	0.092	±0.006 a
0.5	1.990	±0.109 ac	1.570	±0.099 a	0.318	±0.020 ab	0.092	±0.006 a
1	2.160	±0.109 cd	1.595	±0.096 a	0.324	±0.022 ac	0.097	±0.007 a
1.5	2.298	±0.110 d	1.862	±0.112 d	0.358	±0.023 bc	0.113	±0.007 c
2	2.121	±0.109 ad	1.356	±0.081 bc	0.303	±0.021 ad	0.090	±0.006 a
2.5	1.756	±0.093 be	1.271	±0.076 c	0.287	±0.017 ae	0.074	±0.004 b
3	1.735	±0.089 e	1.265	±0.076 c	0.274	±0.016 de	0.072	±0.004 b

[a]The values followed by the same letters were not significantly different (p < 0.05).

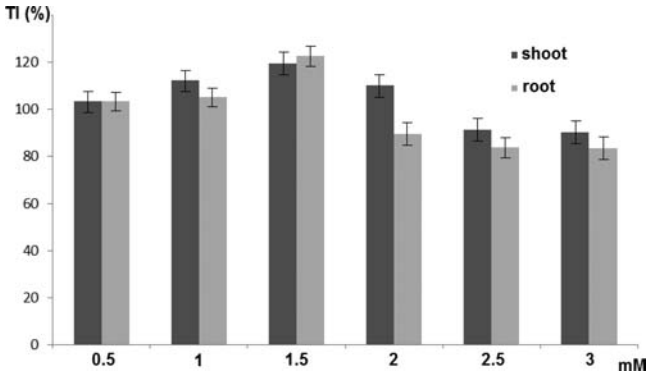

Figure 2. Tolerance index for the shoots and roots of *Glycine max* to different concentrations of strontium.

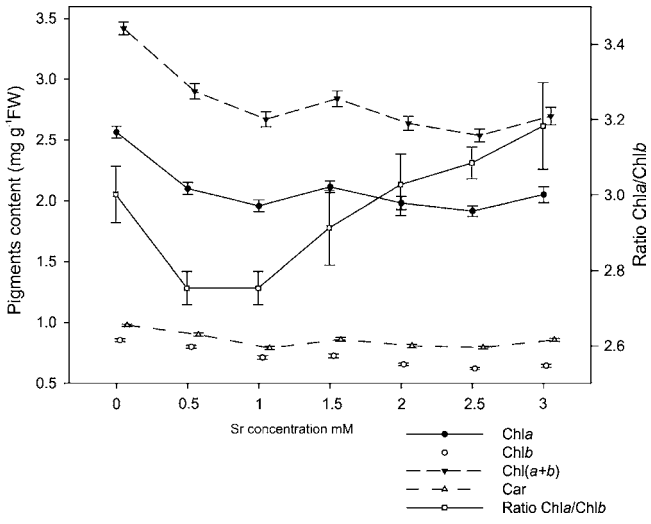

Figure 3. Effect of different strontium concentrations on the content of chlorophyll *a* (Chl*a*), chlorophyll *b* (Chl*b*), and carotenoids (Car) and on the chlorophyll *a*/*b* ratio in *Glycine max*.

The ability to accumulate a metal from the medium can be estimated by the bioconcentration factor (BCF), expressed as the ratio of the ion content in plant (*S*, shoot, or *R*, root) to its concentration in the environment (*M*, medium). The tendency toward translocation of a metal in the plant can be described by the transfer factor (TF), which is defined as the ratio of the ion content in shoots to roots.[32] The calculated BCF and TF values are presented in Table 2.

The TF for strontium content in the shoots was 6.89−9.39 times higher than in the roots, which proves that Sr^{2+} are effectively transferred to the above parts of the plants and accumulated therein. The active transport from the roots to shoots decreased at higher concentrations and resulted in lower values of TF.

As it can be seen in Table 2, the BCF depends on the content of the metal in the medium. The BCF for the roots was increased for all the investigated concentrations of strontium; however, it reached the highest value at 1.5−2 mM of Sr^{2+} for the shoots (BCF = 5.13−5.06). A value of the BCF higher than 1 indicates that soy has a strong capacity to absorb strontium.[29]

Effect of Strontium on Soy Growth. The average fresh (FW) and dry (DW) weight of biomass, of both the root and the shoot, obtained after 24 days of cultivation (including 14 days of treatment with various concentrations of strontium) and the weight of the control cultivated without strontium addition are shown in Table 3.

At concentrations up to 1.5 mM, strontium stimulated plant growth by approximately 19.42% FW (14.70% DW) and 22.62% FW (22.66% DW) for the shoots and roots, respectively (Table 3). However, toxic effects occurred at concentrations higher than 2 mM. The total amount of fresh and dry weight at concentration 3 mM was lower by approximately 12.84−14.37%, in comparison to the control.

A similar tendency was observed by Moyen and Roblin[29] for hydroponic cultivation of maize. This study on maize showed that the moisture content remained at a constant level; the FW/water ratio was from 1.13 to 1.14.

Table 4. Coefficient of Correlation between the Indexes of *Glycine max* and the Strontium Treatment (n = 10)

correlation coeff	Sr content in plant	FW	DW	chlorophyll content	chlorophyll *a*/*b* ratio	carotene content
			Concentration Range 0−1.5 mM			
Sr content in medium	0.969	0.867	0.801	−0.544	−0.124	−0.382
Sr content in plant		0.961	0.918	−0.558	−0.133	−0.395
			Concentration Range 1.5−3.0 mM			
Sr content in medium	0.9930	−0.861	−0.840	−0.294	0.986	−0.010
Sr content in plant		−0.834	−0.822	−0.255	0.994	−0.004

dx.doi.org/10.1021/jf501257r | J. Agric. Food Chem. 2014, 62, 5248−5252

The tolerance index (TI) is commonly used to quantify tolerance of plant organs to metals. It is calculated from the formula: TI = ($FW_{S\ or\ R}/FW_{control}$) 100%. As can be seen in Figure 2, the concentration of strontium in the range 0.5−1.5 mM turned out to be nontoxic.

This finding may be explained by the physical and chemical similarity of strontium to calcium, which is an essential component for plant growth and can be partially replaced by Sr^{2+}.[33] The TI for the roots was significantly lower than that for the shoots at the higher concentration of strontium. Inhibition of root growth is one of the fastest physiological reactions to stress.[34,35]

Effect of Strontium on the Content of Plant Pigments. It has been reported that strontium significantly affected the content of plant pigments depending on its amount and time of exposure.[29,33] Figure 3 shows changes in the chlorophyll *a*, *b*, and carotene content after 24 days of cultivation (including 14 days of treatment with the increasing concentrations of strontium).

The total amount of plant pigments decreased at the 0.5 mM concentration of strontium, in comparison to plants without Sr. However, the changes in the plant pigments were not correlated with the metal concentration. The differences were not significant ($p > 0.05$). In comparison to the control, a decrease in the chlorophyll *a*/*b* ratio was observed. This finding may be explained by greater sensitivity of Chl*a* than Chl*b* to strontium.

The present data showed a positive correlation between the Sr concentration in the media and Sr content in plants. Sr concentrations up to 1.5 mM stimulated plant growth; however, at a higher concentration, a negative correlation between concentration and fresh and dry weight was observed (Table 4).

Soy has a relatively high ability (BCF >1) to accumulate strontium, which may be useful to obtain phytoestrogen-containing vegetable products or herbal formulations for prevention postmenopausal osteoporosis. In vivo and in vitro studies showed high efficiency of strontium salts in osteoporosis therapy and lack of their toxicity in animals and human.[36] Our further investigations will focus on examining the activity and toxicity of extracts from soy enriched with strontium.

AUTHOR INFORMATION

Corresponding Author

*Tel/fax: +48 81 5357350. E-mail: i.sowa@umlub.pl.

Notes

The authors declare no competing financial interest.

REFERENCES

(1) Alezandro, M. R.; Granato, D.; Lajolo, F. M.; Genovese, M. I. Nutritional aspects of second generation soy foods. *J. Agric. Food Chem.* **2011**, *59*, 5490−5497.

(2) Jiao, Z.; Si, X.; Zhang, Z.; Li, G.; Cai, Z. Compositional study of different soybean (Glycine max L.) varieties by 1H NMR spectroscopy, chromatographic and spectrometric techniques. *Food Chem.* **2012**, *135*, 285−291.

(3) Song, J.; Liu, Ch.; Li, D.; Gu, Z. Evaluation of sugar, free amino acid, and organic acid compositions of different varieties of vegetable soybean (Glycine max (L.) Merr). *Ind. Crop Prod.* **2013**, *50*, 743−749.

(4) Mebrahtu, T.; Mohamed, A.; Wang, C. Y.; Andebrhan, T. Analysis of Isoflavone Contents in Vegetable Soybeans. *Plant Food Hum. Nutr.* **2004**, *59*, 55−61.

(5) Yoshida, H.; Hirakawa, Y.; Murakami, Ch.; Mizushina, Y.; Yamade, T. Variation in the content of tocopherols and distribution of fatty acids within soya bean seeds (Glycine max L.). *J. Food Compos. Anal.* **2003**, *16*, 429−440.

(6) Şensöz, S.; Kaynar, I. Bio-oil production from soybean (Glycine max L.); fuel properties of Bio-oil. *Ind. Crop Prod.* **2006**, *23*, 99−105.

(7) Messina, M. Legumes and soybeans: overview of their nutritional profiles and health effects. *Am. J. Clin. Nutr.* **1999**, *70*, 439−450.

(8) Lee, Y. B.; Lee, H. J.; Kim, C. H.; Lee, S. B.; Sohn, H. S. Soy Isoflavones and Soyasaponins: Characteristics and Physiological Functions. *Agric. Chem. Biotechnol.* **2005**, *48*, 49−57.

(9) Wu, A. H.; Yu, M. C.; Tseng, C. C.; Pike, M. C. Epidemiology of soy exposures and breast cancer risk. *Br. J. Cancer* **2008**, *98*, 9−14.

(10) Ahn-Jarvis, J. H.; Riedl, K. M.; Schwartz, S. J.; Vodovotz, Y. Design and Selection of Soy Breads Used for Evaluating Isoflavone Bioavailability in Clinical Trials. *J. Agric. Food Chem.* **2013**, *61*, 3111−3120.

(11) Prakash, D.; Upadhyay, G.; Singh, B. N.; Singh, H. B. Antioxidant and free radical-scavenging activities of seeds and agri-wastes of some varieties of soybean (Glycine max). *Food Chem.* **2007**, *104*, 783−790.

(12) Silva, L. R.; Pereira, M. J.; Azevedo, J.; Gonçalves, R. F.; Valentão, P.; Guedes de Pinho, P.; Andrade, P. B. Glycine max (L.) Merr., Vigna radiata L. and Medicago sativa L. sprouts: A natural source of bioactive compounds. *Food Res. Int.* **2013**, *50*, 167−175.

(13) Zieliński, H. Contribution of Low Molecular Weight Antioxidants to the Antioxidant Screen of Germinated Soybean Seeds. *Plant Food Hum. Nutr.* **2003**, *58*, 1−20.

(14) Wildman, R. E. C. Handbook of nutraceuticals and functional foods. In: Hendrich, S.; Murphy, P. A. *Isoflavones*; CRC Press: Boca Raton, FL, 2006; pp 23−54.

(15) Cornwell, T.; Cohick, W.; Raskin, I. Dietary phytoestrogens and health. *Phytochemistry* **2004**, *65*, 995−1016.

(16) Booth, N. L.; Overk, C. R.; Yao, P.; Totura, S.; Deng, Y.; Hedayat, A. S.; Bolton, J. L.; Pauli, G. F.; Farnsworth, N. R. Seasonal variation of red clover (*Trifolium pratense* L., Fabaceae) isoflavones and estrogenic activity. *J. Agric. Food Chem.* **2006**, *54*, 1277−1282.

(17) Taku, K.; Melby, M. K.; Nishi, N.; Omori, T.; Kurzer, M. S. Soy isoflavones for osteoporosis: An evidence-based approach. *Maturitas* **2011**, *70*, 333−338.

(18) Marquis, P.; Roux, C.; De la Loge, C.; Diaz-Curiel, M.; Cormier, C.; Isaia, G.; Badurski, J.; Wark, J.; Meunier, P. J. Strontium ranelate prevents quality of life impairment in post-menopausal women with established vertebral osteoporosis. *Osteoporosis Int.* **2008**, *19*, 503−510.

(19) Rizzoli, R.; Boonen, S.; Brandi, M. L.; Burlet, N.; Delmas, P.; Reginster, J. Y. The role of calcium and vitamin D in the management of osteoporosis. *Bone* **2008**, *42*, 246−249.

(20) Marie, P. J. Strontium ranelate: a novel mode of action optimizing bone formation and resorption. *Osteoporosis Int.* **2005**, *16*, 7−10.

(21) Marie, P. J.; Felsenberg, D.; Brandi, M. L. How strontium ranelate, via opposite effects on bone resorption and formation, prevents osteoporosis. *Osteoporosis Int.* **2011**, *22*, 1659−1667.

(22) Stepan, J. J. Strontium ranelate: in search for the mechanism of action. *J. Bone Miner. Metab.* **2013**, *31*, 606−612.

(23) Kabata-Pendias, A. *Trace Elements in Soils and Plants*, 4th ed.; CRC Press: Boca Raton, FL, 2010; pp 135−146.

(24) Eapen, S.; Singh, S.; Thorat, V.; Kaushik, C. P.; Raj, K.; D'Souza, S. F. Phytoremediation of radiostrontium (90Sr) and radiocesium (137Cs) using giant milky weed (*Calotropis gigantea* R.Br.) plants. *Chemosphere* **2006**, *65*, 2071−2073.

(25) Wellburn, A. R. The spectral determination of chlorophylls a and b, as well as total carotenoids, using various solvents with spectrophotometers of different resolution. *J. Plant Physiol.* **1994**, *144*, 307−313.

(26) Singh, S.; Eapen, S.; Thorat, V.; Kaushik, C. P.; Raj, K.; D'Souza, S. F. Phytoremediation of 137cesium and 90strontium from solutions and low-level nuclear waste by Vetiveria zizanoides. *Ecotoxicol. Environ. Saf.* **2008**, *69*, 306−311.

(27) Zhang, H.; Yang, H.; Wang, Y.; Gao, Y.; Zhang, L. The response of ginseng grown on farmland to foliar-applied iron, zinc, manganese and copper. *Ind. Crop Prod.* **2013**, *45*, 388−394.
(28) Sasmaz, A.; Sasmaz, M. The phytoremediation potential for strontium of indigenous plants growing in a mining area. *Environ. Exp. Bot.* **2009**, *67*, 139−144.
(29) Moyen, C.; Roblin, G. Uptake and translocation of strontium in hydroponically grown maize plants, and subsequent effects on tissue ion content, growth and chlorophyll a/b ratio: comparison with Ca effects. *Environ. Exp. Bot.* **2010**, *68*, 247−257.
(30) Wang, D.; Wen, F.; Xu, C.; Tang, Y.; Luo, X. The uptake of Cs and Sr from soil to radish (Raphanus sativus L.) - potential for phytoextraction and remediation of contaminated soils. *J. Environ. Radioact.* **2012**, *110*, 78−83.
(31) Bonanno, G. Trace element accumulation and distribution in the organs of *Phragmites australis* (common reed) and biomonitoring applications. *Ecotoxicol. Environ. Saf.* **2011**, *74*, 1057−1064.
(32) Tsukada, H.; Takeda, A.; Takahashi, T.; Hasegawa, H.; Hisamatsu, S.; Inaba, J. Uptake and distribution of 90Sr and stable Sr in rice plants. *J. Environ. Radioact.* **2005**, *81*, 221−231.
(33) Chen, M.; Tang, Y. L.; Ao, J.; Wang, D. Effects of strontium on photosynthetic characteristics of oilseed rape seedlings. *Russ. J. Plant Physiol.* **2012**, *59*, 772−780.
(34) Schützendübel, A.; Schwanz, P.; Teichmann, T.; Gross, K.; Langenfeld-Heyser, R.; Godbold, D.; Polle, A. Cadmium induced changes in antioxidative systems, hydrogen peroxide content, and differentiation in scots pine roots. *Plant Physiol.* **2001**, *127*, 887−898.
(35) Drążkiewicz, M.; Baszyński, T. Growth parameters and photosynthetic pigments in leaf segments of Zea mays exposed to cadmium, as related to protection mechanisms. *J. Plant Physiol.* **2005**, *162*, 1013−1021.
(36) Cianferotti, L.; D'Asta, F.; Brandi, M. L. A review on strontium ranelate long-term antifracture efficacy in the treatment of postmenopausal osteoporosis. *Ther. Adv. Musculoskeletal Dis.* **2013**, *5* (3), 127−139.

Herein, we reported the first fluorometric assay for NO_2 absorbance capacity (abbreviated as NO_2 AC) of antioxidants by taking advantage of the novel NO_2-selective probe reported by our group previously, using diethylamine NONOate (DEANO) as the NO_2 source.[17] The chemical mechanisms behind NO_2 scavenging by phenolic compounds were deduced from the reaction products formed as revealed by liquid chromatography−mass spectrometry (LC−MS) and secondary mass, using epicatechin (EC) and gallic acid as examples. Through measuring the antioxidant capacity of flavanols and related polyphenolic compounds as well as characterization of the reaction products, the structure−activity relationship was established, which provides a rational explanation on the good correlation of peroxyl radical scavenging activity and NO_2 scavenging activity.

EXPERIMENTAL SECTION

Materials and Instruments. All experiments were performed with reagents of analytical grade or high-performance liquid chromatography (HPLC) grade. Chemicals were purchased from Sigma-Aldrich Chemical Co. (Singapore) and used without further purification. A NO_2-selective fluorescent probe, a sulforhodamine-B-containing nickel(II) dithiocarbamate complex, was prepared according to our previous reported method.[17] Fluorescence measurements were gathered using a Synergy HT microplate fluorescence reader from Bio-Tek Instruments, Inc. (Winooski, VT), installed with KC4 software. The fluorescence spectrum was obtained on a PerkinElmer LS55 fluorometer with a slit width at 10 nm for both excitation and emission. Ultraviolet−visible (UV−vis) spectroscopic studies were obtained on a Shimadzu UV-1601 UV−vis spectrophotometer accompanied by a quartz cell and installed with UVProbe software. HPLC analysis was performed on a Waters 2695 HPLC system equipped with an Alliance 2659 separation module and a Waters 2996 photodiode array (PDA) detector (Milford, MA) and installed with an Empower program. A C18 reverse-phase column (Waters Atlantis T3, 6 μm, 4.6 × 150 mm) was used throughout this study. The photodiode array (PDA) acquisition wavelength range was set at 210−700 nm. LC−MS spectra were acquired using a Bruker Amazon ion trap mass spectrometer (Billerica, MA) equipped with an electrospray ionization (ESI) source and a Dionex ultimate 3000RS HPLC system (Bannockburn, IL), installed with Chameleon, Hystar, and Trapcontrol software. The heated capillary and spray voltage were maintained at 200 °C and 4.5 kV, respectively. Nitrogen was operated at 80 psi for sheath gas flow rate and 20 psi for auxiliary gas flow rate. The full-scan mass spectra from m/z 70 to 1000 were obtained in negative-ion mode with a scan speed of 1 scan per second.

Construction of the Dose Response Curve for DEANO. NO_2 probe stock solution was diluted in methanol to a final concentration of 3 μM. A series of concentrations of DEANO (0, 200, 400, 500, 600, 700, 800, 900, and 1000 μM) was obtained by dilution with sodium hydroxide solution and mixed with phosphate buffer and probe solutions in a ratio of 1:1:8 to a final volume of 3.0 mL. The fluorescence intensities were measured 5 min after the addition of DEANO stock solutions on the fluorescent spectrometer (see Figure S2A of the Supporting Information). The data in Figure S2B of the Supporting Information was obtained using the microplate reader. Preparations of reagents followed the above procedure but were mixed to a final volume of 200 μL in each well of the 96-well microplate. Fluorescence intensities were monitored over a period of 10 min.

Experimental Procedure for Nitrogen Dioxide Radical Absorbance Capacity Assay (NO_2 AC). NO_2 probe solution (4.3 μM) was prepared in methanol, and DEANO (8.0 mM) was completely dissolved in sodium hydroxide solution (10 mM, pH 12) and kept in an ice bath. Stock solutions of phenolic compounds were diluted with methanol to 10, 20, 30, and 40 μM working solutions. Fluorescent probe (140 μL), sample (20 μL in methanol), phosphate buffer (10 mM, 20 μL), and DEANO solution (20 μL) were pipetted and mixed in individual wells of a 96-well flat-bottom microplate. In the resulting reaction solution, the fluorescent probe concentration is 3.0 μM, the DEANO concentration is 0.80 mM, the phosphate buffer concentration is 1.0 mM, and the methanol concentration is 80%. Fluorescence intensity of each well was immediately monitored upon addition of DEANO solution every minute for 15 min with excitation wavelength of 540 nm and emission wavelength of 590 nm at 37 °C. Before each reading, the microplate was shaken for 4 s at low intensity to ensure sample homogeneity. Methanol control (20 μL) was conducted in parallel for each of the samples on the same microplate as a blank.

Data Processing (NO_2 AC Value). With a half life of 2 min, DEANO decomposes to give NO when dissolved in psychological pH medium at 37 °C.[18] Under aerobic ambient conditions, NO undergoes autoxidation, generating NO_2.[9,19,20]

$$2\,{}^{\bullet}NO + O_2 \rightarrow 2\,{}^{\bullet}NO_2 \tag{1}$$

NO_2 produced will either react with the fluorescent probe (P) or be scavenged by an antioxidant (AH). There exists competition between them for the constant flux of NO_2 (R_i).[21]

$$P + {}^{\bullet}NO_2 \xrightarrow{k_p} \text{fluorescent products} \tag{2}$$

$$AH + {}^{\bullet}NO_2 \xrightarrow{k_{AH}} A^{\bullet} + NO_2^{-} + H^{+} \tag{3}$$

The radical $A^{\bullet}$ can further react with NO_2 to form an adduct, as we have shown in the mechanistic study (*vide infra*). The radical coupling reaction is not likely to be a rate-limiting step. For the initial reaction, reaction 3 is dominant because the antioxidant concentration is at its highest. Therefore, the rate of probe oxidation can be expressed by the following equation:

$$V = -\frac{d[P]}{dt} = \frac{k_p[P]R_i}{k_p[P] + k_{AH}[AH]} \tag{4}$$

In the absence of antioxidant ([AH] = 0), the uninhibited reaction rate is

$$V_0 = R_i \tag{5}$$

From eqs 4 and 5, the following relation between the fluorescence increase rates in the absence (V_0) and presence (V) of an antioxidant can be drawn

$$\frac{V_0}{V} = 1 + \frac{k_{AH}[AH]}{k_p[P]} \tag{6}$$

The plot of V_0/V against [AH] will yield a linear function with an intercept at (0, 1) and a slope of $k_{AH}/k_p[P]$. With reference to Figure 1A, a tangent at the second minute was plotted on each kinetic curve to obtain the initial fluorescence increase rates for each concentration. The V_0/V values are plotted against their corresponding [AH], as expressed in Figure 1B. Under the experimental conditions, the probe concentration [P] is constant at the initial reaction stage; thus, $k_p[P]$ is a constant. Therefore, the k_{AH} value can be obtained from the slope and is the NO_2 AC value as

$$k_{AH} = S_{AH}k_p[P] \tag{7}$$

where S_{AH} is the slope for the antioxidant (AH). However, to obtain the absolute values for k_{AH}, k_p needs to be determined. If a reference standard can be used, there is no need to obtain the absolute k_{AH} values for comparison of relative NO_2 scavenging activity. We selected one of the most common flavanols, EC, as a reference standard to compare to samples. Therefore

$$S_{EC} = k_{EC}/(k_p[P]) \tag{8}$$

$$\therefore k_{EC} = S_{EC}k_p[P] \tag{9}$$

Normalizing k_{AH} with k_{EC}, we have

dx.doi.org/10.1021/jf5001925 | J. Agric. Food Chem. 2014, 62, 5253−5258

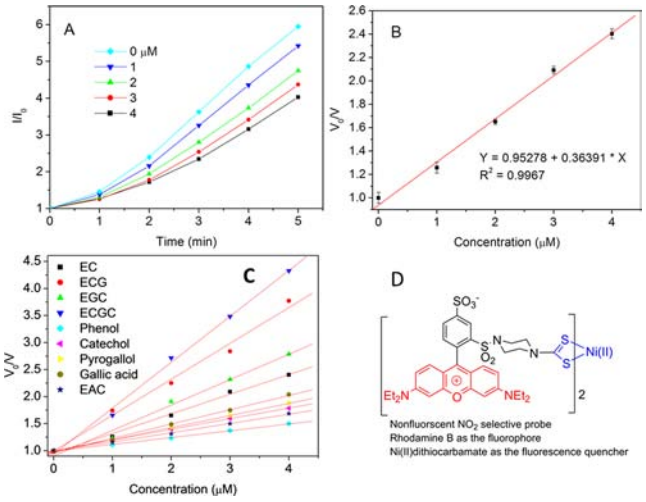

Figure 1. (A) Increments of fluorescence intensity of the probe (3 μM) against time after the addition of DEANO (800 μM) and EC at different concentrations. (B) V_0/V as a function of the concentration of EC. (C) Dose responses of V_0/V versus different concentrations of selected antioxidants. (D) Molecular structure of the fluorescent probe that is selective to NO_2 detection.

$$\text{NO}_2\text{ AC value of AH} = \frac{k_{\text{AH}}}{k_{\text{EC}}} = \frac{S_{\text{AH}}k_{\text{p}}[\text{P}]}{S_{\text{EC}}k_{\text{p}}[\text{P}]} = \frac{S_{\text{AH}}}{S_{\text{EC}}} \quad (10)$$

On the basis of eq 10, k_{AH} can be obtained because k_{EC} was measured recently as 1.0×10^8 M^{-1} s^{-1} by a pulse radiolysis study.[21,22] For convenience sake, epicatechin equivalency (ECE) is used to express the NO_2 AC. For single compounds, the concentrations used were the same, and the NO_2 AC values for polyphenolic compounds are dimensionless. The NO_2 AC value for EC is defined as 1 because it is the reference. For samples that are composed of mixtures of antioxidants, the unit of NO_2 AC will be micromoles of ECE per gram (for solid) or micromoles of EC equivalents per liter for liquid samples, such as fruit juices.

Preparation of NO_2 Gas. NO_2 gas was prepared by adding concentrated nitric acid dropwise to copper wire and collected in a dry round-bottom flask with phosphorus pentoxide inside. The flask was sealed and kept in a dark and cool place. NO_2 gas at certain concentrations was prepared by diluting pure NO_2 with argon. Caution: The highly toxic NO_2 gas should be used with extreme caution and handled only in relative small quantities in a well-ventilated fume hood.

Preparation of NO Gas and Its Reaction with EC. Reaction of sodium nitrite and ascorbic acid was reported to give NO gas.[23] Sodium nitrite (2.87 g) was dissolved in deionized water, and ascorbic acid (3.67 g) were accurately weighed. EC (3 mg/mL) was prepared by dissolution in methanol. All reagents were placed in the airtight setup, and then the system was flushed with argon gas for 30 min to ensure an inert environment, so that there would be absence of NO autoxidation. Aqueous $NaNO_2$ solution in the buret was then released in a dropwise manner to react with ascorbic acid placed in the round-bottom flask for generation of NO gas. Approximately 1 L of NO gas was generated and passed through concentrated NaOH (4 M) first to remove acidic gas before NO is bubbled to EC solution. There was no visible color change for the EC solution after 6 min. The resulting EC solution was flushed with argon for 0.5 h to remove any NO in the solution and analyzed by HPLC.

HPLC and LC–MS Studies of the Reaction Product. The reaction products between NO_2 and EC (2.0 mg/mL) in methanol were analyzed by HPLC with a detection wavelength from 210 to 700 nm. The mobile phases were water (solvent A) and methanol (solvent B). The sample (10 μL) was injected into the HPLC system with the column equilibrated with 60% solvent A. Gradient elution was used and programmed to obtain a linear increase in the solvent A ratio from 60 to 0% in 60 min at a flow rate of 0.2 mL/min. The column was equilibrated to 60% A in 10 min prior to the next run. The above was also performed for the analysis of the reaction product from EC and NO. The LC conditions for LC–MS analysis were similar to those mentioned above, except with 5 μL of sample injected and detection wavelengths at 280 and 350 nm. The same procedure was used for analysis of product between gallic acid and NO_2.

RESULTS AND DISCUSSION

Fluorescent Approach for Quantification of NO_2 Scavenging Activity. Here, we present an accurate and highly efficient assay to assess antioxidant capacity against NO_2, monitoring competitive reaction kinetics between an introduced antioxidant and probe. In this assay, we applied our newly developed, NO_2-selective "turn on" fluorescent probe containing $(\text{dithiocarbamato})_2\text{Ni}^{\text{II}}$ as a fluorescence quencher and NO_2 reaction center.[17] The fluorescence of the rhodamine fluorophore was quenched by $(\text{dithiocarbamato})_2\text{Ni}^{\text{II}}$ via photo-induced electron transfer. The fluorescence "turn on" is caused by oxidation of the complex by NO_2 that triggered release of oxidized ligands.[17] This probe demonstrated good selectivity because NO_2 is the only radical that can turn on the fluorescence, while other common ROS, such as ClO^-, H_2O_2, $ONOO^-$, O_2^-, NO, $HO^\bullet$, and $ROO^\bullet$, could not.[17] Furthermore, it is evident that this probe is photostable and the antioxidants examined will not influence the fluorescence (see Figure S1 of the Supporting Information); therefore, this probe was suitably used for monitoring the NO_2 scavenging activity of antioxidants. DEANO was proven to be a good NO_2 source in oxygenated solution to establish the dose–response curve for the NO_2 fluorescent probe, yielding the identical products as NO_2 gas after reacting with the probe.[17] There exists a good linear relationship between the fluorescence intensity ratio and the concentration of DEANO (see Figure S2B of the Supporting Information), and 800 μM was selected for use in the assay. It should be pointed out that DEANO or other similar NO donors have been applied in the investigation of NO scavenging activity of polyphenolic compounds. However, we found that NO does not react with EC under air-free conditions. It is likely that the reaction is due to other RNS with polyphenolic compounds. Characterization of the reaction products showed that NO_2 is the species responsible for the reaction. Our results highlighted the importance of eliminating oxygen when one intended to measure NO scavenging activity.

We took advantage of the sensitive NO_2 fluorescent probe as a reporting reaction in a competitive reaction system, where generated NO_2 reacts with probe and antioxidants, which protect the probe from being oxidized, as shown by a reduced rate fluorescence intensity change (Figure 1A). The initial fluorescence increase rates in the presence of different amounts of antioxidants were determined from the plot. V_0/V versus the antioxidant concentrations yield excellent linear curves (panels B and C of Figure 1). The slopes of the curves for different antioxidants were normalized with that of EC and shown in Table 1. The rate constants of the compounds with NO_2 can be readily obtained by multiplying the NO_2 AC values with k_{EC}, which is quantified as 1×10^8 M^{-1} s^{-1}.[22] Therefore, our assay provides a rapid and sensitive method to quantify NO_2 scavenging activity. Our results are in good agreement with the rate constants of epigallocatechin gallate (EGCG) and gallic acids measured using pulse radiolysis methods, which shown

dx.doi.org/10.1021/jf5001925 | J. Agric. Food Chem. 2014, 62, 5253–5258

Table 1. NO_2 AC Values (EC Equivalents) of Phenolic Compounds

phenolic compounds	slope ($k_{AH}/k_p[P]$)	NO_2 AC value (S_{AH}/S_{EC})
EC (standard)	0.36	1.00 ± 0.08
ECG	0.67	1.83 ± 0.10
EGC	0.47	1.29 ± 0.04
EGCG	0.85	2.33 ± 0.03
phenol	0.13	0.35 ± 0.03
catechol	0.20	0.54 ± 0.02
pyrogallol	0.22	0.62 ± 0.01
gallic acid	0.26	0.73 ± 0.02
EAC	0.17	0.47 ± 0.05

that EGCG has a rate constant of 2.3 times larger than that of EC and the rate constant for gallic acid is half that of EC.[22,22]

Structure and Activity Relationship of NO_2 Scavenging Activity of Flavanols. We have quantified the NO_2 scavenging activity of five common flavanols, including epiafzelechin (EAC), EC, epigallocatechin (EGC), epicatechin gallate (ECG), and EGCG (Figure 2), and four compounds of

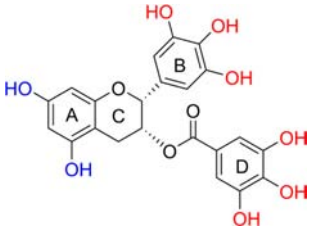

Figure 2. Structure of EGCG, indicating four ring numbers. The OH groups in red are responsible for its NO_2 scavenging activity, while those in blue contribute little.

structural relevance to flavanols. They are phenol, catechol, pyrogallol, and gallic acid. From the data, a few observations are remarkable: (1) The scavenging potential of these nine compounds against the NO_2 radical are in the order of phenol < EAC < catechol < pyrogallol < gallic acid < EC < EGC < ECG < EGCG. (2) For the flavanols, the one with the most phenolic hydroxyl groups exhibits the greatest scavenging activity. A similar trend is observed for phenol, catechol, and pyrogallol. (3) The flavanols are seen to exert a greater antioxidant effect than their model phenolic compounds, such as catechol and phenol.

From these observations, we can conclude that the *ortho*-dihydroxyl groups are an important structural feature for high NO_2 scavenging activity, while the *meta*-OH units in the A ring of the flavanols have little contribution in NO_2 scavenging activity. The galloyl ester unit in EGC and EGCG further enhance the NO_2 scavenging activity in comparison to EC and EGC, yet the addition of one more *ortho*-OH group in the B ring of flavanol has much less effect on NO_2 scavenging activity (by comparing EC to EGC).

Reaction Products and Mechanisms of Catechin/Gallic Acid with NO_2. It is commonly known that the B and D rings (galloyl) of the flavanols are responsible for their radical scavenging activity (Figure 2).[22,24,25] To shed some light on the NO_2 scavenging activity, we characterized the reaction products of NO_2 with EC by HPLC and LC–MS/MS. The HPLC chromatograms of the reaction products are shown in Figure 3B. EC (R_t = 18.4 min) reacted with NO_2 generated three isomeric products with a retention time at 29.8, 31.8, and

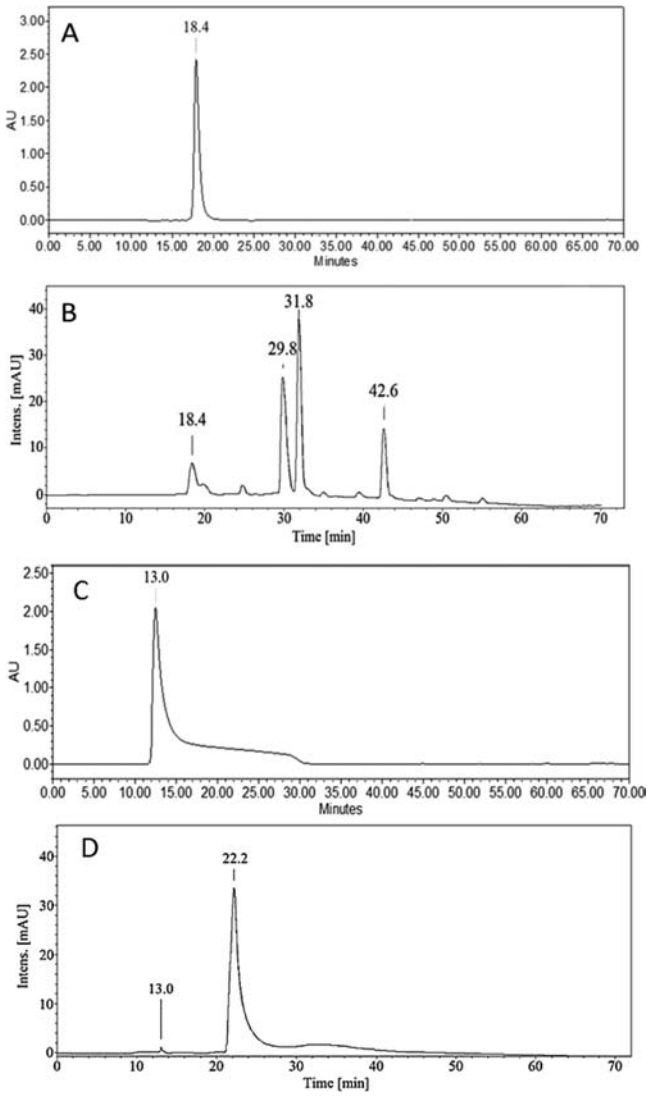

Figure 3. (A) HPLC profile of pure EC, recorded at 280 nm. (B) LC–MS LC profile of EC and its oxidized product with NO_2, recorded at 350 nm. The ESI (anionic mode)–MS of the three products has m/z of 334, and they give the same MS^2 pattern with major peaks at m/z of 124.8, 164.7, and 287.8. (C) HPLC profile of pure gallic acid, recorded at 280 nm. (D) LC–MS LC profile of gallic acid and its oxidized product with NO_2, recorded at 350 nm. The ESI (anionic mode)–MS of the product has m/z of 169.7, and it gives the MS^2 pattern with a peak at m/z of 124.2.

42.6 min, respectively, with m/z 334.0 ($[M - H]^-$) and m/z 669.0 ($[2M - H]^-$). Fragmentation of MS^2 for m/z 334.0 gave rise to peaks with m/z of 287.8, 124.8, and 164.7. The m/z 287.8 peak corresponds to the loss of NO_2 (molecular weight of 46) from the molecular ion, while the m/z 124.8 and m/z 164.7 ions were formed from the characteristic heterocyclic ring fragmentation (see Figure S3 of the Supporting Information).[26,27] This fragmentation pattern indicates that NO_2 is not attached in the A ring. The phenoxyl radical derived by hydrogen atom abstraction from the B-ring OH groups of EC is delocalized among three resonance structures.[28] The combination of the radical with NO_2 will lead to three isomers observed by LC–MS (Scheme 2). The nitrated B ring absorbs light at a longer wavelength at the visible light range as the solution color turned from colorless to light yellow, and the UV–vis spectra of the products gave rise to multiple bands centered at 350 nm

Scheme 2. Proposed Mechanism for NO_2 Radical Scavenging by EC and Gallic Acid[a]

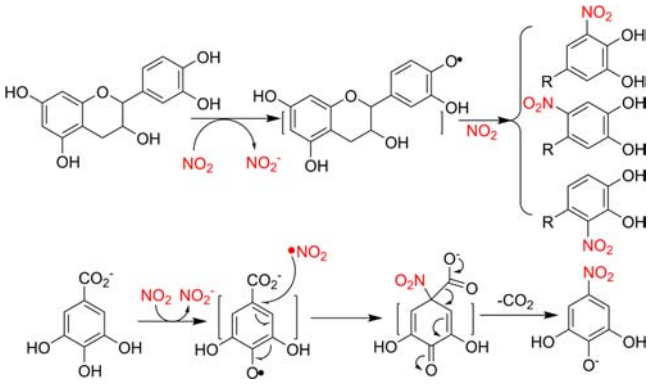

[a]R = moiety of A and C rings of EC.

and stretched to 400 nm (see Figure S4A of the Supporting Information).

The reaction between gallic acid and NO_2 gave rise to an unusual product with an UV−vis absorption maximum at 350 nm, indicating a NO_2 adduct with phenyl (Figure 3D). The mass spectrum shows peaks at m/z 170 and 341, which fit that of nitrogallol (molecular weight of 171) and its dimer (molecular weight of 342). We proposed that the reaction happens via two steps (Scheme 2): first, hydrogen atom abstraction (or electron transfer followed by the loss of a proton) by NO_2 resulted in a phenolic radical, and second, NO_2 would attack carbon at the *para* position of the phenol radical to give a ketone intermediate. Subsequent decarboxylation resulted in the observed product, 4-nitrogallol. The molecular weight of the product is only 1 unit more than that of gallic acid and can be deceptive to assign its structure at the first sight. MS^2 of gallic acid and that of nitrogallol give rise to the same fragment gallol anion at m/z 125. The structure of nitrogallol requires further confirmation by preparative-scale synthesis, infared spectroscopy, and X-ray crystallographic data. Overall, the mechanistic study using EC and gallic acid validate the conclusion made by several other researchers that the radical scavenging by catechin will produce a phenoxyl radical localized on the B or D ring (represented by gallic acid, a common moiety for the D ring).[20,23,24]

UV−vis spectroscopic analyses on the products between EC and NO_2 and those of EC and DEANO under normal aerobic conditions produced the same spectra (see Figure S4A of the Supporting Information), showing product absorbance peaks from 300 to 400 nm. However, as a NO donor, DEANO does not release NO_2 directly but releases NO, which is also a radical species. To figure out whether phenolic compounds scavenge NO_2 directly or scavenge NO to prevent NO_2 generation, UV−vis spectroscopic analyses for the reaction between EC and NO gas and that of EC with DEANO (under deaerated conditions) were performed. As demonstrated in Figure S4B of the Supporting Information, no change was found, in comparison to the EC spectra. This observation is reaffirmed by HPLC analysis (see Figure S5 of the Supporting Information), which exhibited only a single absorption peak for EC (R_t = 18 min), suggesting that there was no reaction between EC and NO.

ECG and EGCG contain an additional gallate moiety (D ring) compared to EC and EGC, respectively. The gallate group enhanced the NO_2 scavenging activity of ECG (NO_2 AC value of 1.83 ± 0.10) and EGCG (NO_2 AC value of 2.33 ± 0.03) by about twice that of EC (1.00 ± 0.08) and EGC (1.29 ± 0.04), respectively. This correlates well with ECG and EGCG having twice the number of catechol/pyrogallol moieties compared to EC and EGC, respectively. These results are in agreement with the notion that the NO_2 scavenging effect is attributed to the *ortho* OH groups in the B and D rings.[24] The bimolecular rate constants of NO_2 and EC, EGCG, and gallic acid were quantified by a pulse radiolysis method to be 1.0×10^8, 2.3×10^8, and 5.3×10^7 M^{-1} s^{-1}, respectively.[22,21] The NO_2 scavenging activity measured using our method is in good agreement with these values. Using reaction rate constants to determine NO_2 AC values is accurate but technically complicated. It should be pointed out that the linearity range is not very large between the concentration of antioxidants and the rate changes. This may limit its application to food sample measurements when, particularly, their antioxidant activity is unknown. For application of this method to a large amount of samples, end point readings would be more convenient in providing IC_{50} for comparison of the NO_2 scavenging activity of different samples.

Under air-saturated conditions, NO is reported to react with oxygen as the dominant pathway to give NO_2. The kinetic analysis of the NO oxidation reaction in the presence of thiols and amine was identical to that obtained for the autoxidation of NO.[29] Nitrosylation of thiols only occurs under oxygenated conditions. Therefore, NO_2 is responsible for the reaction. In agreement with this pioneering work, we have demonstrated that NO failed to react with EC even with 30 min at room temperature with a large excess of NO. In the presence of oxygen, EC is nitrosylated by NO_2. Because of the strong oxidative power of NO_2 and its relevancy of NO_2 formation as a result of endogenously formed NO, the scavenging activity of NO_2 (and not NO) is an important but neglected aspect of antioxidants.

Our assay overcomes the technical hurdle to quantify the NO_2 scavenging capacity of dietary antioxidants, including flavanols. Given the fact that there are a wide range of ROS/RNS that are important to biological systems, different antioxidant capacity assays are needed to comprehensively evaluate antioxidant activity. These reactive oxygen species and their related scavenging capacity assays include peroxyl radicals ($ROO^•$) in the $ORAC_{FL}$ assay,[30] hydroxyl radical (M^{II}/H_2O_2) averting capacity assay,[31] superoxide anion absorbance capacity assay (SORAC assay),[32] NO_2 AC, peroxynitrite ($ONOO^-$) absorbance capacity assay, hypochlorous acid absorbance capacity assay, and singlet oxygen absorbance capacity assay. Because these ROS/RNS species have different reactivity patterns, it is essential to use different methods to quantify their scavenging activity. This is only possible with validated and convenient assays in place.

■ ASSOCIATED CONTENT

Ⓢ Supporting Information

Fluorescent probe (3 μM) demonstrating excellent photostability and antioxidants examined having little influence on fluorescence (Figure S1), (A) increments of the fluorescence intensity of the fluorescent probe (3 μM) after the addition of DEANO at different concentrations and (B) dose response of the fluorescence intensity of the fluorescent probe (3 μM) obtained 2 min after the addition of DEANO (Figure S2), ESI(−)−MS/MS fragmentation pattern for EC (Figure S3), (A) UV−vis spectrum showing the EC absorption peak at 280 nm and product peaks (300−400 nm) from the reaction of EC

dx.doi.org/10.1021/jf5001925 | J. Agric. Food Chem. 2014, 62, 5253−5258

with NO_2 gas and (B) UV−vis spectrum showing only the EC absorption peak observed at 280 nm for the reaction between EC and NO gas or DEANO in degassed solution (Figure S4), and HPLC profile for the reaction mixture of EC with NO in degassed solution (Figure S5). This material is available free of charge via the Internet at http://pubs.acs.org.

AUTHOR INFORMATION

Corresponding Authors

*E-mail: shwang@iim.ac.cn.

*Telephone: 65-6516-8821. Fax: 65-6775-7895. E-mail: chmhdj@nus.edu.sg.

Funding

Dejian Huang thanks the Agency of Science, Technology and Research (A*STAR) of Singapore for financial support (Grant 112 177 0036). Dejian Huang and Suhua Wang thank the National Natural Science Foundation of China for a grant (Grant 21228702).

Notes

The authors declare no competing financial interest.

REFERENCES

(1) Olsen, L. F.; Issinger, O. G.; Guerra, B. The Yin and Yang of redox regulation. *Redox Rep.* **2013**, *18*, 245−252.

(2) Ray, P. D.; Huang, B. W.; Tsuji, Y. Reactive oxygen species (ROS) homeostasis and redox regulation in cellular signaling. *Cell. Signalling* **2012**, *24*, 981−990.

(3) Jomova, K.; Valko, M. Health protective effects of carotenoids and their interactions with other biological antioxidants. *Eur. J. Med. Chem.* **2013**, *70*, 102−110.

(4) Prior, R. L. Fruits and vegetables in the prevention of cellular oxidative damage. *Am. J. Clin. Nutr.* **2003**, *78*, 570S−578S.

(5) Shahidi, F. C. A. Millet grain phenolics and their role in disease risk reduction and health promotion: A review. *J. Funct. Foods* **2013**, *5*, 570−581.

(6) Huang, D.; Ou, B.; Prior, R. L. The chemistry behind antioxidant capacity assays. *J. Agric. Food Chem.* **2005**, *53*, 1841−1856.

(7) Pryor, W. A.; Houk, K. N.; Foote, C. S.; Fukuto, J. M.; Ignarro, L. J.; Squadrito, G. L.; Davies, K. J. A. Free radical biology and medicine: It's a gas, man! *Am. J. Physiol.: Regul., Integr. Comp. Physiol.* **2006**, *291*, R491−R511.

(8) Bascom, R. P. A.; C, D. A.; Devlin, R.; Dockery, D. W.; Frampton, M. W.; Lambert, W.; Samet, J. M.; Speizer, F. E.; Utell, M. Health effects of outdoor air pollution. Committee of the Environmental and Occupational Health Assembly of the American Thoracic Society. *Am. J. Respir. Crit. Care Med.* **1996**, *153*, 3−50.

(9) Augusto, O.; Bonini, M. G.; Amanso, A. M.; Linares, E.; Santos, C. C. X.; De Menezes, S. l. L. Nitrogen dioxide and carbonate radical anion: Two emerging radicals in biology. *Free Radical Biol. Med.* **2002**, *32*, 841−859.

(10) Bian, K.; Gao, Z.; Weisbrodt, N.; Murad, F. The nature of heme/iron-induced protein tyrosine nitration. *Proc. Natl. Acad. Sci. U. S. A.* **2003**, *100*, 5712−5717.

(11) Kirsch, M.; Korth, H. G.; Sustmann, R.; de Groot, H. The pathobiochemistry of nitrogen dioxide. *Biol. Chem.* **2002**, *383*, 389−399.

(12) Moore, J.; Yin, J.-J.; Yu, L. Novel fluorometri assay for hydroxyl radical scavenging capacity (HOSC) estimation. *J. Agric. Food Chem.* **2006**, *54*, 617−626.

(13) Cheng, Z.; Moore, J.; Yu, L. A high-throughput relative DPPH radical scavenging capacity (RDSC) assay. *J. Agric. Food Chem.* **2006**, *54*, 7429−7436.

(14) Verhagen, J. V.; Guido R, M. M.; Haenen, G. R. M. M.; Bast, A. Nitric oxide radical scavenging by wines. *J. Agric. Food Chem.* **1996**, *44*, 3733−3734.

(15) Moncada, S.; Higgs, A. Mechanisms of disease—The l-arginine nitric-oxide pathway. *N. Engl. J. Med.* **1993**, *329*, 2002−2012.

(16) Kirsch, M.; Korth, H.-G.; Sustmann, R.; de Groot, H. The pathobiochemistry of nitrogen dioxide. *Biol. Chem.* **2002**, *383*, 389−399.

(17) Yan, Y.; Krishnakumar, S.; Yu, H.; Ramishetti, S.; Deng, L. W.; Wang, S.; Huang, L.; Huang, D. Nickel(II) dithiocarbamate complexes containing sulforhodamine B as fluorescent probes for selective detection of nitrogen dioxide. *J. Am. Chem. Soc.* **2013**, *135*, 5312−5315.

(18) Maragos, C. M.; Morley, D.; Wink, D. A.; Dunams, T. M.; Saavedra, J. E.; Hoffman, A.; Bove, A. A.; Isaac, L.; Hrabie, J. A.; Keefer, L. K. Complexes of •NO with nucleophiles as agents for the controlled biological release of nitric oxide. Vasorelaxant effects. *J. Med. Chem.* **1991**, *34*, 3242−3247.

(19) Schmidt, K.; Desch, W.; Klatt, P.; Kukovetz, W. R.; Mayer, B. Release of nitric oxide from donors with known half-life: A mathematical model for calculating nitric oxide concentrations in aerobic solutions. *Naunyn-Schmiedeberg's Arch. Pharmacol.* **1997**, *355*, 457−462.

(20) Ignarro, L. J.; Fukuto, J. M.; Griscavage, J. M.; Rogers, N. E.; Byrns, R. E. Oxidation of nitric oxide in aqueous solution to nitrite but not nitrate: Comparison with enzymatically formed nitric oxide from L-arginine. *Proc. Natl. Acad. Sci. U. S. A.* **1993**, *90*, 8103−8107.

(21) Miao, J. L.; W, W. F.; Pan, J. X.; Lu, C. Y.; Li, R. Q.; Yao, S. D. The scavenging reactions of nitrogen dioxide radical and carbonate radical by tea polyphenol derivatives: A pulse radiolysis study. *Radiat. Phys. Chem.* **2001**, *60*, 163−168.

(22) Gebicki, J. L.; M, P.; Stawowska, K.; Gebicka, L. Pulse radiolysis study of the reactions of catechins with nitrogen dioxide. *Radiat. Phys. Chem.* **2012**, *81*, 1881−1884.

(23) Kuroiwa, Y.; Yamada, M.; Matsui, K.; Okamura, T.; Ishii, Y.; Masumura, K.; Tasaki, M.; Umemura, T.; Mitsumori, K.; Nohmi, T.; Hirose, M.; Nishikawa, A. Induces oxidative DNA damage-associated mutagenicity in vitro, but lacks initiation activity in rat forestomach epithelium. *Toxicol. Sci.* **2008**, *104*, 274−282.

(24) Senba, Y.; Nishishita, T.; Saito, K.; Yoshioka, H.; Yoshioka, H. Stopped-flow and spectrophotometric study on radical scavenging by tea catechins and the model compounds. *Chem. Pharm. Bull.* **1999**, *47*, 1369−1374.

(25) Jovanovic, S. V.; Hara, Y.; Steenken, S.; Simic, M. G. Antioxidant potential of gallocatechins. A pulse radiolysis and laser photolysis study. *J. Am. Chem. Soc.* **1995**, *117*, 9881−9888.

(26) Delphine Callemien, S. C. Use of RP-HPLC-ESI(−)-MS/MS to differentiate various proanthocyanidin isomers in lager beer extracts. *J. Am. Soc. Brew. Chem.* **2008**, *66*, 109−115.

(27) Delcambre, A.; Saucier, C. Identification of new flavan-3-ol monoglycosides by UHPLC-ESI-Q-TOF in grapes and wine. *J. Mass Spectrom.* **2012**, *47*, 727−736.

(28) Sang, S.; Tian, S.; Wang, H.; Stark, R. E.; Rosen, R. T.; Yang, C. S.; Ho, C. T. Chemical studies of the antioxidant mechanism of tea catechins: Radical reaction products of epicatechin with peroxyl radicals. *Bioorg. Med. Chem.* **2003**, *11*, 3371−3378.

(29) Golsstein, S. C. G. Mechanism of the nitrosation of thiols and amines by oxygenated NO solutions: The nature of the nitrosating intermediates. *J. Am. Chem. Soc.* **1996**, *118*, 3419−3425.

(30) Huang, D.; O, B.; Hampsch-Woodill, M.; Flanagan, J. A.; Prior, R. L. High-throughput assay of oxygen radical absorbance capacity (ORAC) using a multichannel liquid handling system coupled with a microplate fluorescence reader in 96-well format. *J. Agric. Food Chem.* **2002**, *50*, 4437−4444.

(31) Ou, B.; Hampsch-Woodill, M.; Flanagan, J.; Deemer, E. K.; Prior, R. L.; Huang, D. Novel fluorometric assay for hydroxyl radical prevention capacity using fluorescein as the probe. *J. Agric. Food Chem.* **2002**, *50*, 2772−2777.

(32) Zhang, L.; Huang, D.; Kondo, M.; Fan, E.; Ji, H.; Kou, Y.; Ou, B. Novel high-throughput assay for antioxidant capacity against superoxide anion. *J. Agric. Food Chem.* **2009**, *57*, 2661−2667.

perfluoroalkyl chains) has not always been achieved. For difficult separations unusual stationary phases or mobile phase components have been used and in many cases successfully. Using fluorinated stationary phases[21−23] or methylpiperidine as eluent modifier,[24] separation of PFNA and PFOS has been achieved successfully. In addition, a number of publications show the separation of PFNA and PFOS with C_{18} stationary phases from different manufacturers; however, variations in eluent compositions and stationary phases make it difficult to systematically analyze the retention mechanisms of those compounds on the basis of literature data.[25,26]

From a mass spectrometric point of view PFOS displays some other inconvenient aspects when compared with perfluorinated carboxylic acids of similar chain length. In the MS/MS regime it has a relatively low fragmentation yield and, as a consequence, a low S/N ratio. In the case of PFOS an MRM "transition" 499 → 499 (i.e., monitoring the non-fragmented parent) has been proposed.[27] However, the problem of accuracy remains, because in this case it has also been shown that certain steroidic bile acids present in fish samples have the same nominal m/z ratio of 499 with a similar fragmentation pattern and a retention time close to that of the PFOS and therefore may strongly affect the peak area of PFOS.[22,27]

The selection of eluent additives in LC-MS is limited by the volatility requirement. Fluorinated alcohols are volatile compounds of weak to medium acidity and are neutral in protonated form. These properties make them a potentially promising class of compounds to be used as weak acids for preparing buffers of pH value above 7 for use in LC-MS.

1,1,1,3,3,3-Hexafluoro-2-propanol (HFIP, pK_a = 9.3)[24] has been used as an additive to the LC mobile phase in several studies.[28−35] The suitability of fluoroalcohols, HFIP and 1,1,1,3,3,3-hexafluoro-2-methyl-2-propanol (HFTB, pK_a = 9.6)[36], as buffer additives at concentration levels from 1 to 10 mM has been studied, and application for separation of antibiotics−fluoroquinolones and sulfonamides is demonstrated.[37,38] It turned out that mobile phases with perfluorinated alcohols provide retention mechanisms that differ from the ones traditionally observed with regular eluent modifiers for C_{18} stationary phases.[38]

Alternatively, a promising group of stationary phases that have been successfully applied in pharmaceutical and drug analysis are fluorinated (pentafluorophenyl and pentafluorophenylpropyl) stationary phases.[39−41] Fluorinated stationary phases are associated with various interaction mechanisms improving retention and chromatographic resolution. Most similar to common stationary phases are perfluorinated alkyl chains, for example, C_8F_{17}, used for their alternative retention in several applications for separating polar molecules,[42,43] especially halogenated analytes,[44−47] but also for aromatic polycyclic hydrocarbons due to the interactions between π-electrons of analytes and C−F dipole of the stationary phase.[46,48] The performance of fluorinated columns has improved in recent years with respect to their pH stability and column lifetime. Additionally, stationary phase bleeding is reduced, allowing the use of these stationary phases also in MS applications. The retention of all analytes has been reported to be overall lower on the fluorinated stationary phase than on C_{18}.[47] Therefore, the retention of PFCs using a fluorinated stationary phase and fluoroalcohols with a regular C_{18} stationary phase is of interest.

The focus of this work is the LC-ESI-MS analysis of PFOA, PFNA, and PFOS in raw fish samples using a different approach for chromatographic separation and signal improvement: replacement of common eluent buffers (ammonium acetate) with a polyfluorinated alcohol−ammonia buffer.[34,36]

MATERIALS AND METHODS

Instrumentation for Sample Preparation and Analysis. For primary sample homogenization a Retsch Grindomix GM 200 homogenizer was used. A Heidolph 900 DIAX homogenizer was used during the PFC extraction step, and a centrifuge Eppendorf 5430R was used during sample preparation. Chromatographic separation of the analytes was carried out on a Waters 2695 series chromatograph (Waters, Milford, MA, USA) equipped with a binary pump, degasser, autosampler, and column thermostat. Detection and quantification of analytes was carried out with a QuattroMicro triple-quadrupole mass spectrometer (Micromass, Manchester, UK). Tested analytical columns were Epic FO LB (150 mm × 3.0 mm, 3 μm) and YMC Triart C18 columns (150 mm × 3 mm, 3 μm). Preliminary tests for chromatographic separation were performed with an Agilent 1290 series UHPLC (Agilent) and a J-320 mass spectrometer (Varian).

Chemicals. PFOA, PFNA, potassium perfluorooctanesulfonate standards, HFIP, HFTB, and anhydrous $MgSO_4$ were purchased from Sigma (St. Louis, MO, USA). Acetonitrile and methanol were obtained from J. T. Baker (Deventer, The Netherlands), formic acid and ammonium hydroxide were from Riedel-de-Haën, and ammonium acetate was from Fluka (Buchs, Germany). All solvents were of reagent grade or higher quality. Water was purified in-house using a Milli-Q Advantage A10 system from Millipore (Bedford, MA, USA).

Standard and Buffer Solutions. Calibration solutions were prepared in methanol so that the concentrations were in the range of 0.5−500 ng/mL. Spiking solutions were prepared in acetonitrile at concentrations of 7.5, 75, and 750 ng/mL; in that case the analyte concentrations in samples were 1.0, 10, and 100 μg/kg, respectively. Solvent A (see below) was prepared by dissolving 0.965 g of HFTB in 1 L of Milli-Q water, and the pH was adjusted to 10.0 by adding a concentrated solution of ammonium hydroxide.

Sample Preparation. The fish samples were purchased from local markets and delivered to the laboratory on the same day for homogenization. Samples included the most common fish species available on the Estonian market (Table 1). The initial amount of sample was typically >1 kg. Upon arrival, the fish samples were cleaned of skin, intestines, and bones. Edible parts of fish (muscle and fat tissue) were homogenized with a Retsch Grindomix GM 200 at 2000 rpm for 4 min. Homogeneous samples were stored in a freezer at −20 °C until analysis. Further sample preparation was carried out using a modified "Quick, Easy, Cheap, Effective, Rugged, and Safe" protocol (QuEChERS), essentially as described in ref 49. As a modification, the cleanup step with dispersive SPE was omitted, because there was no need for it due to the already low matrix effects. In addition, the use of HFTB/HFIP increased analyte signal intensity and reduced matrix effects.

Homogenized fish tissue was weighed (7.5 g) into a 50 mL polypropylene (PP) tube, and 10 mL of water was added. The sample was then additionally homogenized during 1 min with a Heidolph Diax 900 homogenizer at 18000 rpm. Fifteen milliliters of acetonitrile was added to the tubes, and the tubes were shaken by hand for 10 s. A preweighed mixture of salts (6 g of anhydrous $MgSO_4$ and 1.5 g of NaCl) was then added to the samples, and the tubes were shaken vigorously by hand for 1 min and for 1 min on a vortex-mixer. Samples were then centrifuged at 7000 rpm for 15 min. Twelve milliliters of clear supernatant was transferred into a 15 mL PP tube containing 1.8 g of anhydrous $MgSO_4$. Tubes were shaken once more for 1 min by hand and on a vortex mixer and then centrifuged at 7000 rpm for 15 min. Eight milliliters of supernatant was transferred into a 15 mL glass vial and evaporated to dryness under a stream of nitrogen at 40 °C. The dry residue was dissolved in 1 mL of methanol. The final extract was filtered through a 0.45 μm regenerated cellulose syringe filter into a chromatographic vial.

dx.doi.org/10.1021/jf5007243 | J. Agric. Food Chem. 2014, 62, 5259−5268

Table 1. Analyzed Fish Samples

sample	scientific name	place of origin	content of PFAAs (μg/kg)		
			PFOA	PFNA	PFOS
pike	*Esox lucius*	river Emajõgi	<LOD	<LOD	<LOD
ide	*Leuciscus Idus*	lake Lämmijärv	<LOD	<LOD	0.54
European perch	*Perca fluviatilis*	Baltic Sea	<LOD	0.28	1.68
		lake Võrtsjärv	<LOD	<LOD	<LOD
Baltic herring	*Clupea harengus membras*	Baltic Sea	<LOD	<LOD	<LOD
European whitefish	*Coregonus lavaretus*	Baltic Sea	<LOD	0.16	<LOD
vimba bream	*Vimba vimba*	Baltic Sea	<LOD	0.63	1.26
common bream	*Abramis brama*	river Emajõgi	<LOD	0.4	0.76
European flounder	*Platichthys flesus*	Baltic Sea	<LOD	<LOD	<LOD
European plaice	*Pleuronectes platessa*	Norway	<LOD	0.24	0.34
Atlantic salmon	*Salmo salar*	Norway	<LOD	<LOD	<LOD
		Norway	<LOD	<LOD	<LOD
pike-perch	*Sander lucioperca*	river Emajõgi	<LOD	0.6	<LOD
		lake Võrtsjärv	<LOD	<LOD	<LOD
common carp	*Cyprinus carpio*	Härjanurme fish farm (Estonia)	<LOD	<LOD	<LOD
rainbow trout	*Oncorhynchus mykiss*	Karilatsi fish farm (Estonia)	<LOD	<LOD	<LOD
		Härjanurme fish farm (Estonia)	<LOD	<LOD	<LOD
Crucian carp	*Carassius carassius*	Baltic sea	<LOD	0.17	1.11
African sharptooth catfish	*Clarias gariepinus*	Sõmerpalu fish farm (Estonia)	<LOD	<LOD	<LOD
European sprat	*Sprattus sprattus*	Baltic Sea	<LOD	<LOD	1.2

Chromatographic and Mass Spectrometric Conditions. Analytes were separated on a YMC Triart C_{18} column (150 mm × 3 mm, 3 μm). This stationary phase was used because of its good retention properties and excellent stability toward pH in the range from 1 to 12.[50] The mobile phase was composed of 5 mM HFTB (pH adjusted to 10 with saturated aqueous ammonia) (solvent A) and methanol (solvent B). Gradient elution at a flow rate 0.3 mL/min started at 20% methanol for 1 min and was raised to 50% within 4 min, then the methanol concentration was slowly raised to 65% by the 18th minute, and after that the methanol concentration was raised to 100% within 0.3 min. Methanol concentration was kept at 100% for 5 min, lowered to 10% in 1 min, and equilibrated at 20% for 5 min. The column temperature was set to 40 °C, and the injection volume was 10 μL. ESI-MS/MS measurements were performed in negative MRM detection mode. The first quadrupole was set to the m/z of the deprotonated $[M - H]^-$ ions of the analytes: m/z 413 (PFOA), 463 (PFNA), 499 (PFOS). Mass spectrometer parameters for ESI-MS/MS were as follows: desolvation gas (N_2) flow rate, 300 L/h, and temperature, 350 °C; source temperature, 135 °C; cone gas flow rate, 50 L/h; capillary voltage, −3 kV; cone voltage, 10 V. Fragmentation of deprotonated analyte molecules was performed with argon gas. Detected fragment ions and fragmentation parameters were as follows: PFOA, m/z 369, 169 (E_{coll} 10 and 15 eV); PFNA, m/z 419 and 219 (E_{coll} 10 and 15 eV); PFOS, m/z 99, 80 (E_{coll} 45 eV). LC and MS instruments were controlled by MassLynx 4.1 software (Waters). Data analysis was carried out using QuanLynx 2 software (Waters).

Validation of the Method. Validation of the method was performed according to the FDA Guidance for Industry Bioanalytical Method Validation.[51] Partial validation was performed, and estimation of process efficiency, matrix effects, sample preparation recovery, limit of detection (LOD), limit of quantification (LOQ), accuracy, precision, and measurement uncertainty were carried out.

RESULTS AND DISCUSSION

Retention Mechanism and MS Signal Improvement. Separations of structurally similar perfluorinated compounds on C_{18} stationary phases have been problematic in several previous studies.[10,17−20]

In this study the retentions of the analytes on the C_{18} stationary phase were similar using 0.1% formic acid (pH 2.6) and MeCN in eluent, and separation between the three analytes was not achieved. Asymmetrical and wide peaks eluted with 82% of MeCN.

However, the previous studies indicate separation of PFOA, PFNA, and PFOS using perfluorinated stationary phase,[21] and retention of fluorinated compounds is enhanced on fluorous stationary phases.[47] The separation of PFOA, PFNA, and PFOS was studied using an alkyl perfluorinated stationary phase. Fluorinated analytes' retention on the fluorinated stationary phase is mainly influenced by the amount on fluorine atoms in the analyte molecule.[47] The number of fluorine atoms in PFOA molecule is 15; on the other hand, PFNA and PFOS have equally similar 17 fluorine atoms in the molecule.

To achieve advanced separation for analytes, a fluorinated stationary phase was tested in this work. An Epic FO LB (150 mm × 3.0 mm, 3 μm) column meant for separating fluorinated compounds demonstrated significant column bleed and contaminated the source very quickly. In addition, separation of PFNA and PFOS was not observed (Figure 1). Because the Epic FO LB column showed inadequate separation of compounds and significant source contamination was observed, and in addition the column maximum pH range was 8, further attempts were made with a C_{18} stationary phase using 5 mM ammonium acetate at higher pH values (pH 9 and 10) as a component of eluent.

Therefore, the change in eluent pH was made and 5 mM ammonium acetate (pH 10) was used for elution. Increased eluent pH with the C_{18} column (YMC Triart C18) led to better peak shape on the chromatogram, but the analysis of PFNA and PFOS was still problematic due to the low S/N ratio (Figure 2).

To enhance separation of analytes on the C_{18} stationary phase, alternative eluent components were used: 5 mM HFIP and 5 mM HFTB at the same pH as ammonium acetate (pH 10).

The resolution, assessed as the R_s values, of the analyzed compounds using 5 mM HFTB was slightly better at pH 10 (Figure 3) compared to ammonium acetate and HFIP buffer. However, the used MeOH content at the retention time of the

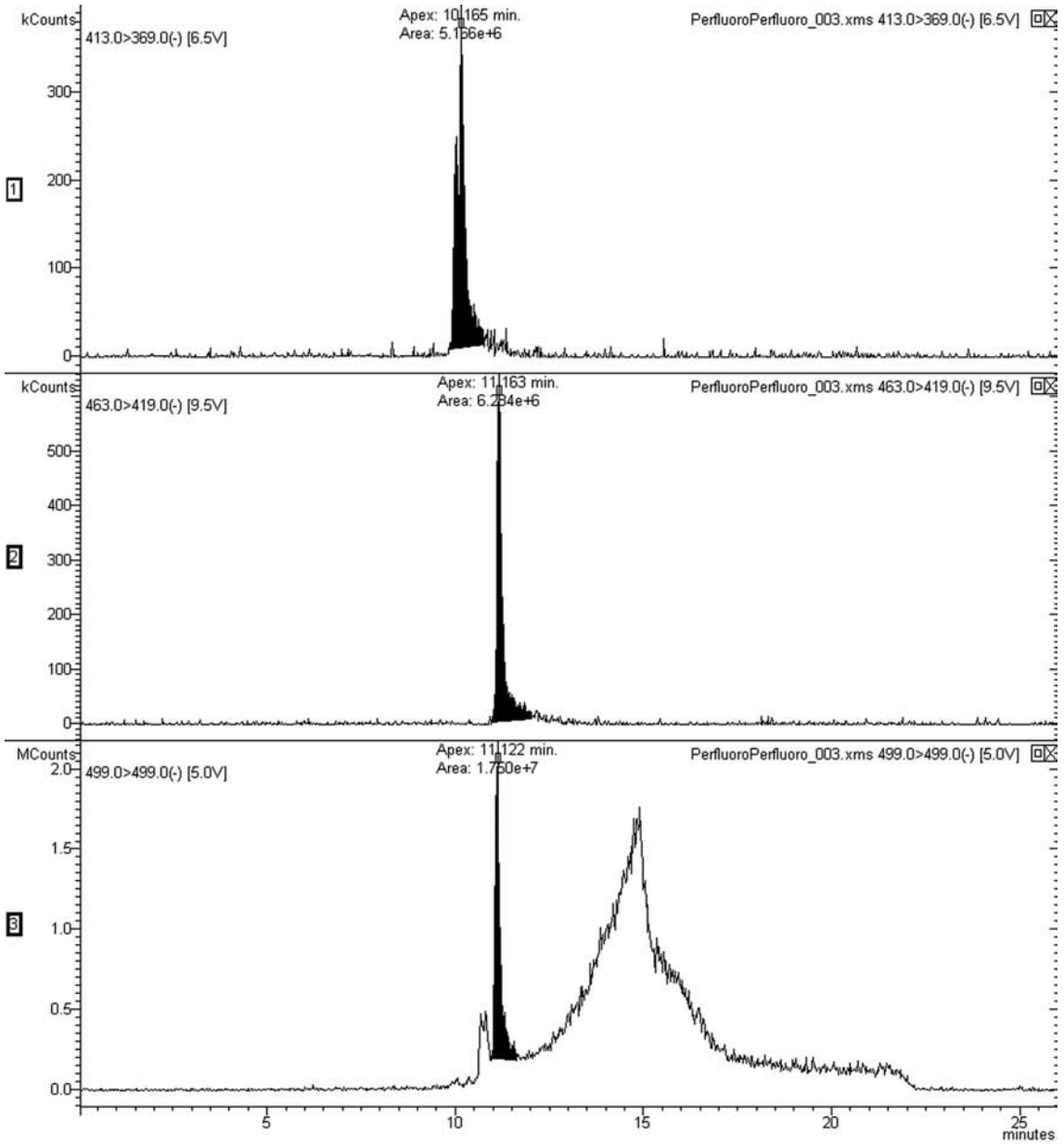

Figure 1. Separation of PFOA, PFNA, and PFOS achieved with fluorinated stationary phase using an Agilent 1290 UHPLC with a J-320 mass spectrometer.

analyte was different; with HFTB the MeOH content was in the range of 62−63%, and with ammonium acetate the content was in the range of 83−84%.

Thus, the use of polyfluorinated alcohols can enhance the separation of fluorinated compounds, leading to alternative selectivity due to the fluoroalcohol competition over the C_{18} stationary phase surface. Fluoroalcohols tend to "stick" on the C_{18} surface, covering the surface with a fluorous layer and shifting the stationary phase properties nearer to a fluorinated stationary phase. This enhances the separation of PFAAs. On the other hand, the stationary phase has a negative charge on its surface due to the negatively charged HFTB molecules at pH 10. PFOS and PFNA are deprotonated at pH 10, and the two anions are rather similar by their size and charge distribution. As a difference, however, the negative charge on the PFOS anion is more efficiently delocalized over the larger SO_3^- moiety than is possible in the PFNA anion's smaller CO_2^- moiety. This leads to more efficient solvation of the carboxylate center by water molecules than of the sulfonate center.[52,53] The negative charge localization in the PFNA anion leads to two consequences: (1) it is better solvated by the polar mobile phase and is thus less forced out of the mobile phase and (2) possibly the repulsion between the partially negatively charged stationary phase surface and the PFNA anion is stronger than the repulsion between the stationary phase and the PFOS anion, leading to decreased retention of the PFNA anion on the stationary phase, compared to the PFOS anion. This difference between the anions of PFNA and PFOS is small, however, and therefore their retention times are still very similar. In addition, their retention can be decreased due to the competition of buffer additive and analytes for the stationary phase surface.

Even though the MeOH content of eluent was lower at the analyte's retention time using 5 mM HFTB as additive, significant signal improvement (by 2−8 times in peak area) was

dx.doi.org/10.1021/jf5007243 | J. Agric. Food Chem. 2014, 62, 5259−5268

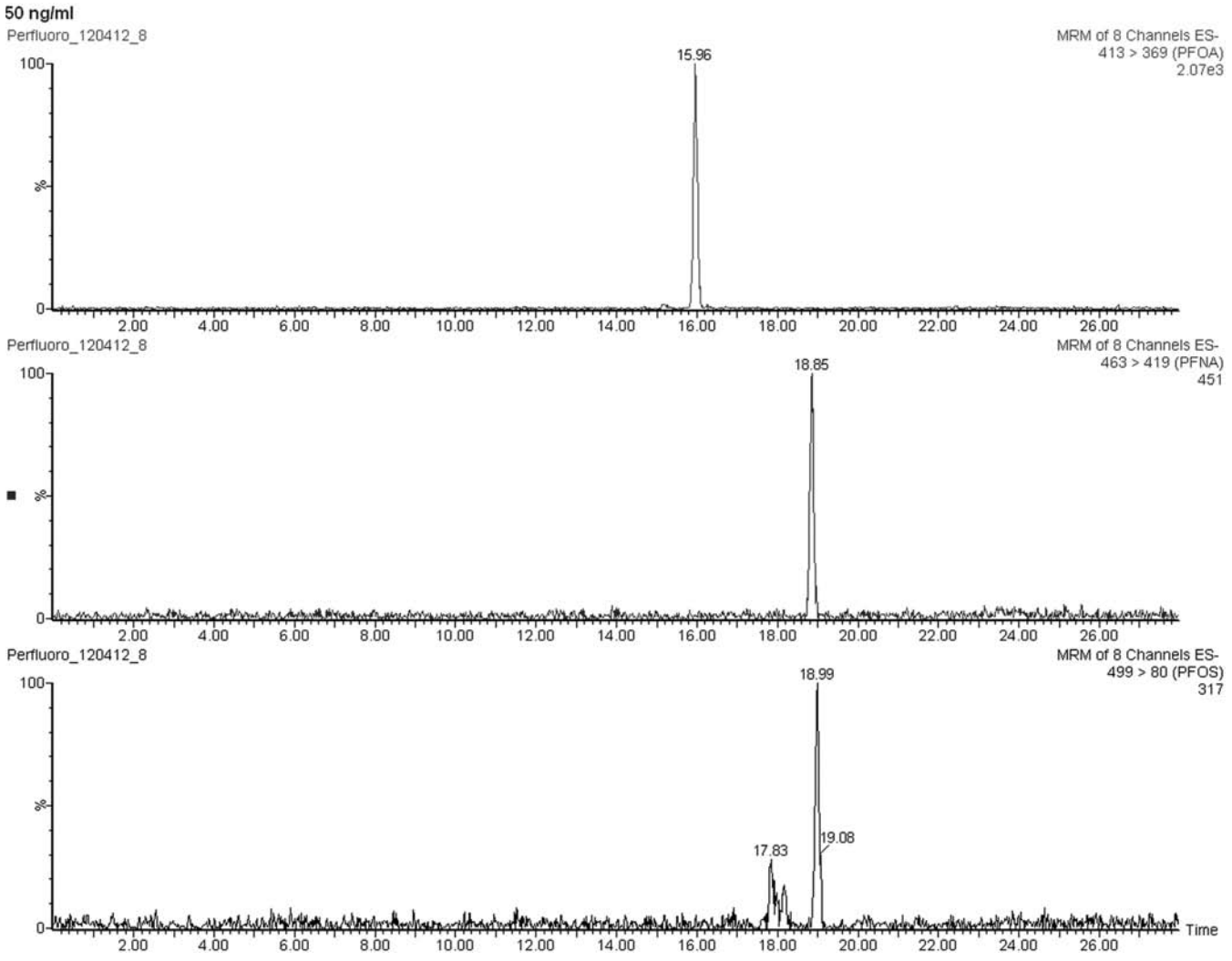

Figure 2. Chromatographic separation of PFOA, PFNA, and PFOS using 5 mM ammonium acetate at pH 10. The R_s between PFNA and PFOS is 0.7.

observed when using HFTB as eluent component when compared to the ammonium acetate at low analyte concentrations (10 ng/mL) (Figure 4).

Method Validation. For the calibration graph solutions, appropriate dilutions from working standard in the concentration range of 1−600 ng/mL (n = 14) for PFOA, PFNA, and PFOS were made in MeOH. The overall range was divided into three independent narrower calibration ranges: 1−15 ng/mL (n = 5), 15−110 ng/mL (n = 6), and 110−600 ng/mL (n = 5). The calibration graphs showed adequate linearity in the narrower concentration ranges ($r^2 \geq 0.9902$). An unweighted linear regression analysis of representative calibration curves resulted in slopes of 17.3 (PFOA), 18.2 (PFNA), and 4.0 (PFOS) in the lower concentration region and of 13.5 (PFOA), 14.3 (PFNA), and 2.5 (PFOS) in the higher concentration region. The intercepts of the calibration curves were taken into account for PFOA (50.6), PFNA (5.9), and PFOS (1.1) in the lower concentration range and for PFOA (499.6), PFNA (600.6), and for PFOS (186) in the higher concentration range.

Spiking experiments for method validation were performed so that concentrations in samples corresponded to 1, 10, and 100 μg/kg. Samples were spiked before the second homogenization step with 1 mL of spiking solutions with different concentrations (7.5, 75, and 750 ng/mL) and mixed thoroughly. After homogenization, 14 mL of acetonitrile was added and the procedure was continued as described above.

The average process efficiency (including sample preparation recovery and matrix effect) for the studied compounds was in the range of 99−116% and exceptionally 115−143% for PFOS in the low concentration range. The matrix effects were evaluated using post extraction spiking (salmon extract) and a signal-enhancing effect was determined: up to 120−141% for PFOA, 136−178% for PFNA, and 132−189% for PFOS. The recovery rates were estimated over the calibration range and were in the ranges of 88−133% for PFOA, 85−108% for PFNA, and 70−98% for PFOS.

The LOQ and LOD were estimated (as 10 and 3.3 times the standard deviation, respectively) from six replicate analyses of unspiked and pre-extraction spiked salmon samples (Figure 5).

Method accuracy and precision were estimated from the spiked salmon samples at the three concentrations of 1, 10, and 100 μg/kg. Accuracy was estimated as the closeness of mean test results obtained by the method to the true concentration value of the analyte and ranged from 2 to 9% for all analytes at high, medium, and low concentrations.

Precision was estimated as coefficient of variation (CV) at three concentration levels and is presented in Table 2.

dx.doi.org/10.1021/jf5007243 | J. Agric. Food Chem. 2014, 62, 5259−5268

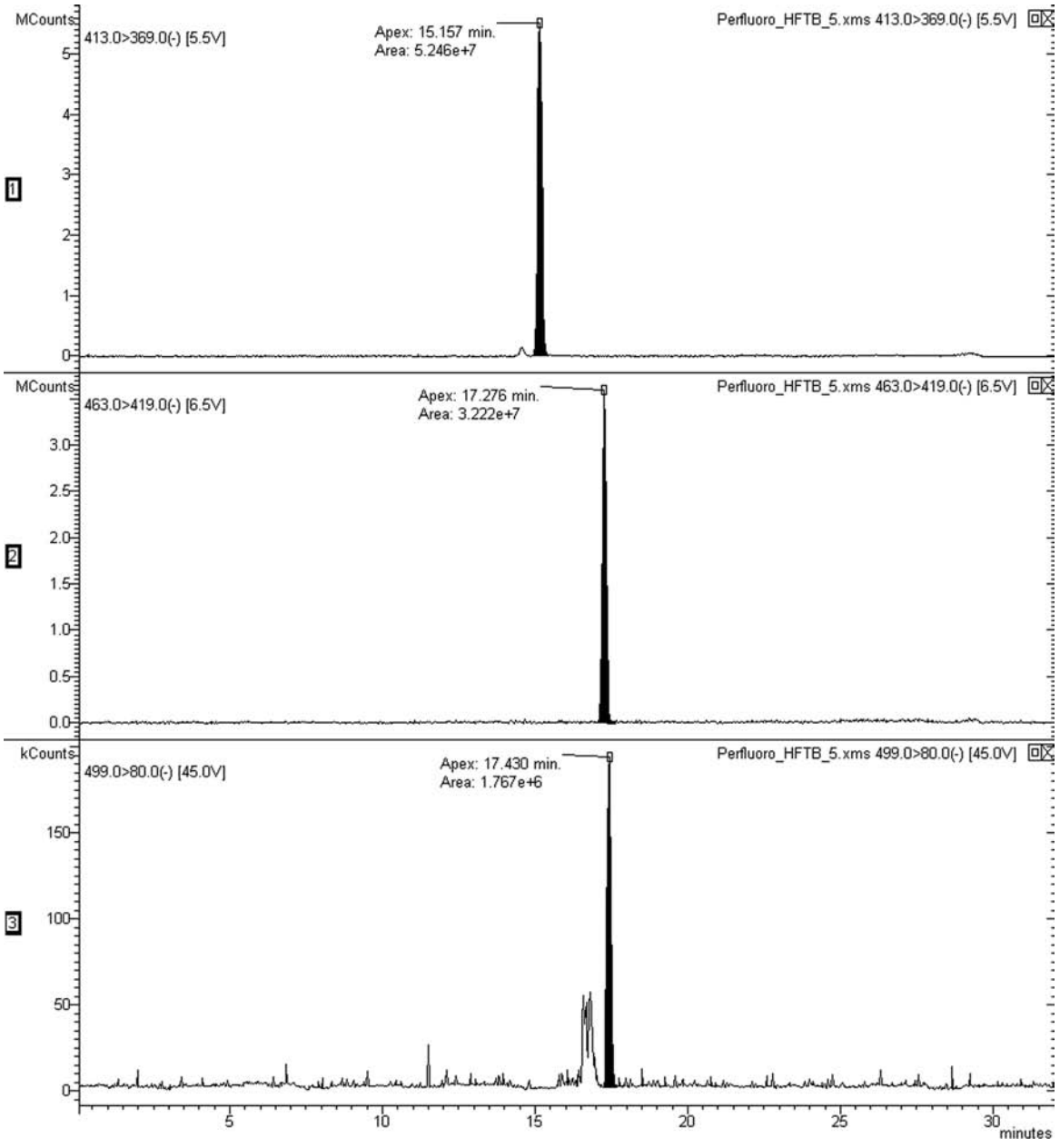

Figure 3. Standard solution analyzed using an Agilent 1290 UHPLC with a J-320 MS and 5 mM HFTB as eluent component. The R_s between PFNA and PFOS is 1.1.

It has been stressed that due to the Teflon tubing of chromatographic systems a significant contamination of PFAAs might occur and therefore a trapping column has been used, which catches PFAAs originating from tubing.[49] In this work a trapping column was not used and blank injections were monitored constantly to determine the extent of contamination, and the average area of blank injection peaks within sequences was subtracted from standard and sample chromatograms.

Method Application to Fish Samples. For practical application this method was transferred to a different LC-MS system, validated for the Estonian Health Board Tartu laboratory, and tested on number of samples available in Estonia.

Of the 20 analyzed samples, 7 originated from the Baltic sea, 3 from Norway, 4 from fresh water fish farms, and 6 from fresh waters of Estonia. All of the samples were analyzed twice on two separate days. The content of PFOA remained below the LOD in all samples. PFNA was found to be present at low concentrations in seven samples, and in two cases the content exceeded the LOQ. PFOS was found to be present in six samples, and the concentration exceeded the LOQ in three samples (see Table 1).

Due to the low salinity of the Baltic Sea many species that usually live in fresh water can also be found in marine water. The obtained results for the fish samples from the Baltic Sea are comparable with previous studies.[54] PFC bioaccumulation in organisms has increased significantly, and the research conducted in the Baltic Sea area has focused on analyzing fish, predatory mammals, and birds. The concentrations of PFAAs is significantly higher in mammals and birds.[55,56]

PFOS is one of the core indicators for the Baltic Marine Environment Protetction Commission (HELCOM), and its levels in fish livers and muscle have been analyzed overa long

dx.doi.org/10.1021/jf5007243 | J. Agric. Food Chem. 2014, 62, 5259−5268

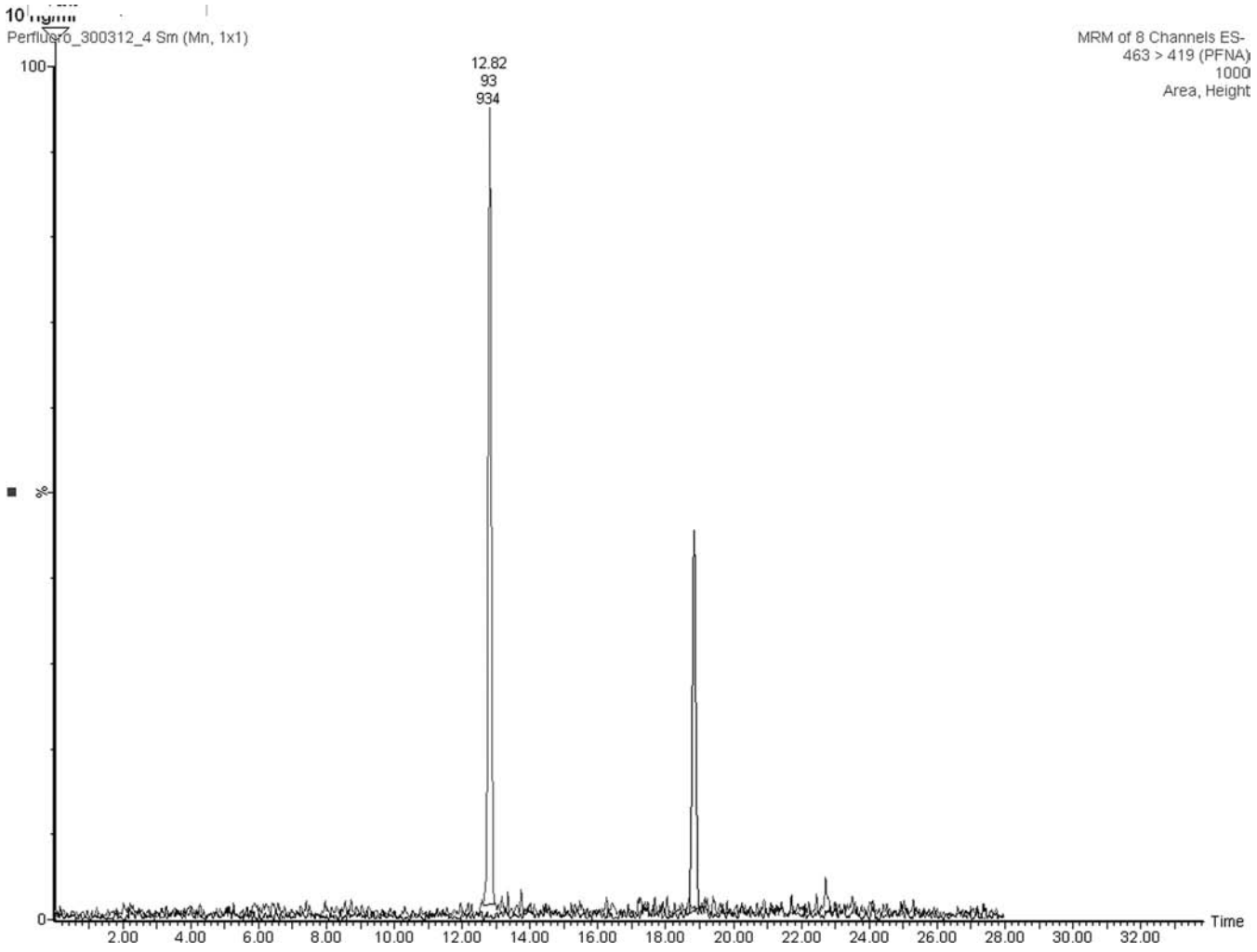

Figure 4. Overlaid PFNA signals obtained by injecting a 10 ng/mL solution under the same chromatographic gradient and mass spectrometric conditions as in the cases of HFTB (t_r = 12.82 min) and ammonium acetate (t_r = 18.85 min) buffer additive.

period of time. Concentrations of PFOS have been dependent on the species of fish and catching area, showing elevated levels of PFOS from parts of the Baltic Sea where industrial activity is more intense.[56]

In 2010 Hradkova et al. analyzed the contents of PFOA, PFOS, and perfluorooctane sulfonamide in canned fish products available in Czech Republic and found that most contaminated samples originated from the Baltic Sea.[58] Their study showed also that concentrations of PFOS and PFOA vary to a great extent despite the similarities between samples; one particular type of sample originating from the same country (sardines in oil) contained PFOS from below the LOQ (0.3 μg/kg) to 12.8 μg/kg and PFOA from below the LOQ (0.2 μg/kg) to 5.1 μg/kg of PFOA, which is supposedly related to the catch site.[57] Similar variations of PFOS and PFOA contents were also shown by Lacina et al. in the case of canned cod liver originating from the Baltic Sea.[49]

In the current work, similarly to previous studies, PFOS was found to be in higher content than other PFAAs. However, the content of PFOS was higher in fish samples originating from the Baltic Sea than compared with fresh water. Obtained results are diverse compared with previous studies.[54,59] This can be explained by a lower population density and the lack of intense industrial activity in Estonia compared with Germany and Sweden.

QuEChERS-type sample preparation with cleanup has proven to be a reliable method on many occasions when different types of contaminants such as pesticides, acrylamide, and mycotoxins have been analyzed in food samples.[60−62] Sample preparation is fast and simple and removes unwanted sample components such as fats, proteins, and starch from the extract.

Conclusions. This work describes an alternative method for LC-MS/MS analysis of perfluorinated compounds in fish using a novel eluent additive. The method uses simplified sample treatment but still provides sufficient LC selectivity and enhanced signal intensities for analytes. An important factor for achieving this is applying polyfluorinated alcohol (HFTB) in the chromatographic separation. Brief monitoring of Estonian fresh and marine water fish was carried out, and the content of PFAAs was low.

AUTHOR INFORMATION

Corresponding Author

*E-mail: karin.kipper@gmail.com. Fax: +372 737 5264. Phone: +372 566 675 04.

Funding

This work was supported by Grant 8572 from the Estonian Science foundation, by Institutional Funding IUT20-14

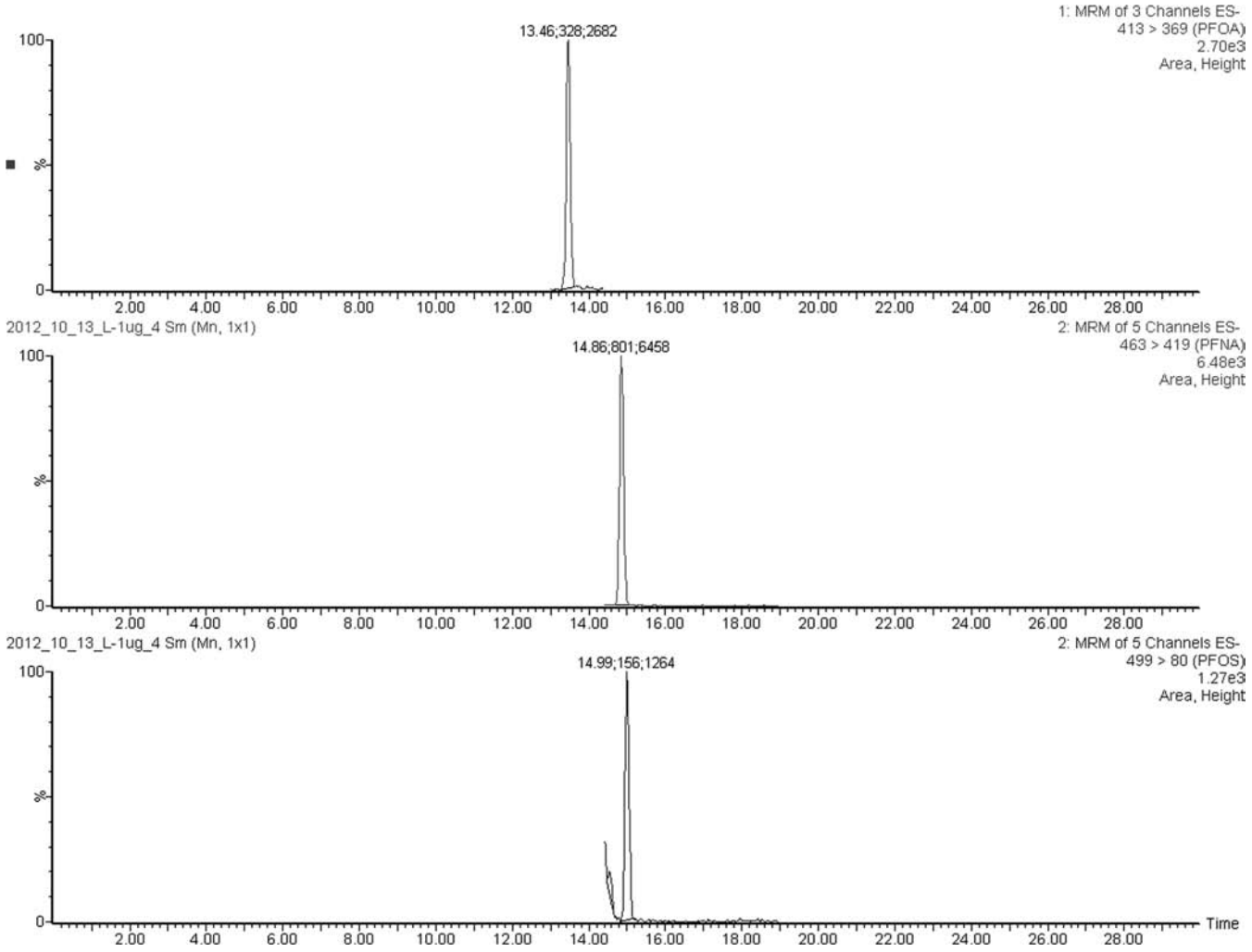

Figure 5. Salmon spiked at 1 μg/kg concentration level.

Table 2. Overview of Validation Results at Three Different Spiking Levels

spiking level (μg/kg)	method parameters[a]	PFOA	PFNA	PFOS
1	CV %	6.8	4.2	8.4
	LOD (μg/kg)	0.26	0.16	0.38
	LOQ (μg/kg)	0.77	0.48	1.14
	u_{rel} (%, k = 2)	13.6	8.4	16.8
10	CV %	5.3	5.9	3.2
100	CV %	2.4	3.8	1.9

[a]In all cases five replicate measurements were made.

(TLOKT14014I) from the Estonian Ministry of Education and Science, and by the Estonian Ministry of Agriculture (under the state project "Agricultural applied research and development in 2009−2014").

Notes

The authors declare no competing financial interest.

REFERENCES

(1) Perfluoroalkylated substances in food: occurrence and dietary exposure. *EFSA J.* **2012**, *10*, 2743.

(2) Ohmori, K.; Kudo, N.; Katayama, K.; Kawashima, Y. Comparison of the toxicokinetics between perfluorocarboxylic acids with different carbon chain length. *Toxicology* **2003**, *184*, 135−140.

(3) Tian, M. P.; Peng, S. Y.; Martin, F. L.; Zhang, J.; Liu, L. P.; Wang, Z. L.; Dong, S. J.; Shen, H. Q. Perfluorooctanoic acid induces gene promoter hypermethylation of glutathione-S-transferase Pi in human liver L02 cells. *Toxicology* **2012**, *296*, 48−55.

(4) Berthiaume, J.; Wallace, K. B. Perfluorooctanoate, perfluorooctanesulfonate, and *N*-ethyl perfluorooctanesulfonamido ethanol; peroxisome proliferation and mitochondrial biogenesis. *Toxicol. Lett.* **2002**, *129*, 23−32.

(5) Perfluorooctane sulfonate (PFOS), perfluorooctanoic acid (PFOA) and their salts. *EFSA J.* **2008**, *653*, 2−131.

(6) Yoo, H.; Washington, J. W.; Jenkins, T. M.; Ellington, J. J. Quantitative determination of perfluorochemicals and fluorotelomer alcohols in plants from biosolid-amended fields using LC/MS/MS and GC/MS. *Environ. Sci. Technol.* **2011**, *45*, 7985−7990.

(7) Lv, G.; Wang, L.; Liu, S.; Li, S. Determination of perfluorinated compounds in packaging materials and textiles using pressurized liquid extraction with gas chromatography-mass spectrometry. *Anal. Sci.* **2009**, *25*, 425−429.

(8) Dufkova, V.; Cabala, R.; Maradova, D.; Sticha, M. A fast derivatization procedure for gas chromatographic analysis of perfluorinated organic acids. *J. Chromatogr., A* **2009**, *1216*, 8659−8664.

(9) Llorca, M.; Farre, M.; Pico, Y.; Barcelo, D. Development and validation of a pressurized liquid extraction liquid chromatography-tandem mass spectrometry method for perfluorinated compounds determination in fish. *J. Chromatogr., A* **2009**, *1216*, 7195−7204.

(10) Llorca, M.; Farre, M.; Pico, Y.; Barcelo, D. Analysis of perfluorinated compounds in sewage sludge by pressurized solvent

extraction followed by liquid chromatography-mass spectrometry. *Chemosphere* **2011**, *1218*, 4840−4846.
(11) Haug, L. S.; Thomsen, C.; Becher, G. A sensitive method for determination of a broad range of perfluorinated compounds in serum suitable for large-scale human biomonitoring. *J. Chromatogr., A* **2009**, *1216*, 385−393.
(12) Kato, K.; Wong, L. Y.; Basden, B. J.; Calafat, A. M. Effect of temperature and duration of storage on the stability of polyfluoroalkyl chemicals in human serum. *Chemosphere* **2013**, *91*, 115−117.
(13) Kruve, A.; Leito, I. Comparison of different methods aiming to account for/overcome matrix effects in LC/ESI/MS on the example of pesticide analyses. *Anal. Methods* **2013**, *5*, 3035−3044.
(14) Burns, D. C.; Ellis, D. A.; Li, H.; Mcmurdo, C. J.; Webster, E. Experimental pK(a) determination for perfluorooctanoic acid (PFOA) and the potential impact of pK(a) concentration dependence on laboratory-measured partitioning phenomena and environmental modeling. *Environ. Sci. Technol.* **2008**, *42*, 9283−9288.
(15) Goss, K.-U.; Arp, H. P. H. Comment on experimental pK(a) determination for perfluorooctanoic acid (PFOA) and the potential impact of pK(a) concentration dependence on laboratory-measured partitioning phenomena and envrionmental modeling. *Environ. Sci. Technol.* **2009**, *43*, 5150−5151.
(16) Kunleda, H.; Shinoda, K. Krafft points, critical micelle concentrations, surface tension, and solubilizing power of aqueous solutions of fluorinated surfactants. *J. Phys. Chem.* **1968**, *80*, 2468−2470.
(17) Villaverde-de-Sáa, E.; Racamonde, I.; Quintana, J. B.; Rodil, R.; Cela, R. Ion-pair sorptive extraction of perfluorinated compounds from water with low-cost polymeric materials: polyethersulfone vs polydimethylsiloxane. *Anal. Chim. Acta* **2012**, *740*, 50−57.
(18) Vestergren, R.; Berger, U.; Glynn, A.; Cousins, I. T. Dietary exposure to perfluoroalkyl acids for the Swedish population in 1999, 2005 and 2010. *Environ. Int.* **2012**, *49*, 120−127.
(19) Onghena, M.; Moliner-Martinez, Y.; Picó, Y.; Campíns-Falcó, P.; Barceló, D. Analysis of 18 perfluorinated compounds in river waters: Comparison of high performance liquid chromatography−tandem mass spectrometry, ultra-high-performance liquid chromatography−tandem mass spectrometry and capillary liquid chromatography−mass spectrometry. *J. Chromatogr., A* **2012**, *1244*, 88−97.
(20) Li, J.; Guo, F.; Wang, Y.; Liu, J.; Cai, Z.; Zhang, J.; Zhao, Y.; Wu, Y. Development of extraction methods for the analysis of perfluorinated compounds in human hair and nail by high performance liquid chromatography tandem mass spectrometry. *J. Chromatogr., A* **2012**, *1219*, 54−60.
(21) Benskin, J. P.; Ikonomou, M. G.; Woudneh, M. B.; Cosgrove, J. R. Rapid characterization of perfluoralkyl carboxylate, sulfonate, and sulfonamide isomers by high-performance liquid chromatography−tandem mass spectrometry. *J. Chromatogr., A* **2012**, *1247*, 165−170.
(22) Reiner, J. L.; Nakayama, S. F.; Delinsky, A. D.; Strynar, M. J.; Lindstrom, A. B. Method development and measurement of perfluorinated compounds in U.S. chicken eggs. *Environ. Sci. Technol.* **2011**, *45*, 7949−7949.
(23) Ballesteros-Gómez, A.; Rubio, S.; van Leeuwen, S. Tetrahydrofuran−water extraction, in-line clean-up and selective liquid chromatography/tandem mass spectrometry for the quantitation of perfluorinated compounds in food at the low picogram per gram level. *J. Chromatogr., A* **2010**, *1217*, 5913−5921.
(24) Ullah, S.; Alsberg, T.; Berger, U. Simultaneous determination of perfluoroalkyl phosphonates, carboxylates, and sulfonates in drinking water. *J. Chromatogr., A* **2011**, *1218*, 6388−6395.
(25) Nakata, A.; Saito, K.; Iwasaki, Y.; Ito, R.; Kishi, R.; Nakazawa, H. Determination of perfluorinated compounds in human milk and evaluation of their transition from maternal plasma. *Bunseki Kagaku* **2009**, *58*, 653−659.
(26) Wang, L.; Sun, H.; Yang, L.; He, C.; Wu, W.; Sun, S. Liquid chromatography/mass spectrometry analysis of perfluoroalkyl carboxylic acids and perfluorooctanesulfonate in bivalve shells: extraction method optimization. *J. Chromatogr., A* **2010**, *1217*, 436−442.
(27) Kadar, H.; Veyrand, B.; Antignac, J. P.; Durand, S.; Monteau, F.; Le Bizec, B. Comparative study of low- versus high-resolution liquid chromatography-mass spectrometric strategies for measuring perfluorinated contaminants in fish. *Food Addit. Contam. A* **2011**, *28*, 1261−1273.
(28) Apffel, A.; Chakel, J.; Fischer, S.; Lichtenwalter, K.; Hancock, W. New procedure for the use of high-performance liquid chromatography electrospray ionization mass spectrometry for the analysis of nucleotides and oligonucleotides. *J. Chromatogr., A* **1997**, *777*, 3−21.
(29) Apffel, A.; Chakel, J.; Fischer, S.; Lichtenwalter, K.; Hancock, W. Analysis of oligonucleotides by HPLC-electrospray ionization mass spectrometry. *Anal. Chem.* **1997**, *69*, 1320−1325.
(30) Huber, C. G.; Oberacher, H. Analysis of nucleic acids by on-line liquid chromatography-mass spectrometry. *Mass Spectrom. Rev.* **2001**, *20*, 310−343.
(31) Gilar, M.; Fountain, K. J.; Budman, Y.; Neue, U. D.; Yardley, K. R.; Rainville, P. D.; Russell, R. J.; Gebler, J. C. Ion-pair reversed-phase high-performance liquid chromatography analysis of oligonucleotides: retention prediction. *J. Chromatogr., A* **2002**, *958*, 167−182.
(32) Beverly, M.; Hartsough, K.; Machemer, L.; Pavco, P.; Lockridge, J. Liquid chromatography electrospray ionization mass spectrometry analysis of the ocular metabolites from a short interfering RNA duplex. *J. Chromatogr., B* **2006**, *835*, 62−70.
(33) Zhang, G.; Lin, J.; Srinivasan, K.; Kavetskaia, O.; Duncan, J. N. Strategies for bioanalysis of an oligonucleotide class macromolecule from rat plasma using liquid chromatography-tandem mass spectrometry. *Anal. Chem.* **2007**, *79*, 3416−3424.
(34) Zou, Y.; Tiller, P.; Chen, I. W.; Beverly, M.; Hochman, J. Metabolite identification of small interfering RNA duplex by high-resolution accurate mass spectrometry. *Rapid Commun. Mass Spectrom.* **2008**, *22*, 1871−1881.
(35) Doneanu, C. E.; Chen, W. B.; Gebler, J. C. Analysis of oligosaccharides derived from heparin by ion-pair reversed-phase chromatography/mass spectrometry. *Anal. Chem.* **2009**, *81*, 3485−3499.
(36) Serjeant, E. P.; Dempsey, B. *Ionization Constants of Organic Acids in Aqueous Solution*; IUPAC Chemical Data Series 23; Pergamon Press: Oxford, UK, 1979.
(37) Kipper, K.; Herodes, K.; Leito, I.; Nei, L. Two fluoroalcohols as components of basic buffers for liquid chromatography electrospray ionization mass spectrometric determination of antibiotic residues. *Analyst* **2011**, *136*, 4587−4594.
(38) Kipper, K.; Herodes, K.; Leito, I. Fluoroalcohols as novel buffer components for basic buffer solutions for liquid chromatography electrospray ionization mass spectrometry: retention mechanisms. *J. Chromatogr., A* **2011**, *1218*, 8175−8180.
(39) Dailly, E.; Bouquie, R.; Deslandes, G.; Jolliet, P.; Le Floch, R. A liquid chromatography assay for a quantification of doripenem, ertapenem, imipenem, meropenem concentrations in human plasma: application to a clinical pharmacokinetic study. *J. Chromatogr., B* **2011**, *879*, 1137−1142.
(40) Needham, S. R.; Jeanville, P. M.; Brown, P. R.; Estape, E. S. Performance of a pentafluorophenylpropyl stationary phase for the electrospray ionization high-performance liquid chromatography-mass spectrometry-mass spectrometry assay of cocaine and its metabolite ecgonine methyl ester in human urine. *J. Chromatogr., B* **2000**, *748*, 77−87.
(41) Bell, D. S.; Cramer, H. M.; Jones, A. D. Rational method development strategies on a fluorinated liquid chromatography stationary phase: mobile phase ion concentration and temperature effects on the separation of ephedrine alkaloids. *J. Chromatogr., A* **2005**, *1095*, 113−118.
(42) Jinno, K.; Nakamura, H. Retention characteristics of fluorinated bonded silica phase in reversed-phase liquid-chromatography. *Chromatographia* **1994**, *39*, 285−293.
(43) Euerby, M. R.; McKeown, A. P.; Petersson, P. Chromatographic classification and comparison of commercially available perfluorinated stationary phases for reversed-phase liquid chromatography using principal component analysis. *J. Sep. Sci.* **2003**, *26*, 295−306.

(44) Obayashi, M.; Kosugi, T.; Yamazaki, J.; Matsumoto, Y.; Matsumoto, M. Determination of concentrations of flecainide in human serum by high-performance liquid chromatography on a fluorocarbon-bonded silica gel column. *J. Chromatogr., B* **1999**, *726*, 219−223.
(45) Glatz, H.; Blay, C.; Engelhardt, H.; Bannwarth, W. New fluorous reversed phase silica gels for HPLC separations of perfluorinated compounds. *Chromatographia* **2004**, *49*, 567−570.
(46) De Miguel, I.; Roueche, A.; Betbeder, D. W. Separation of dipalmitoyl phosphatidyl choline, cholesterol and their degradation products by high-performance liquid chromatography on a perfluorinated stationary bonded phase. *J. Chromatogr., A* **1999**, *840*, 31−38.
(47) Gladysz, J. A.; Curran, D. P.; Horvath, I. T. *Handbook of Florous Chemistry*; Wiley-VCH: Weinheim, Germany, 2004; pp 101−127.
(48) Yamamoto, F. M.; Rokushika, S. Retention properties of the fluorinated bonded phase on liquid chromatography of aromatic hydrocarbons. *J. Chromatogr., A* **2000**, *898*, 141−151.
(49) Lacina, O.; Hradkova, P.; Pulkrabova, J.; Hajslova, J. Simple, high throughput ultra-high performance liquid chromatography/tandem mass spectrometry trace analysis of perfluorinated alkylated substances in food of animal origin: milk and fish. *J. Chromatogr., A* **2011**, *1218*, 4312−4321.
(50) YMC Europe GMBH, YMC-Triart C18 versatile hybrid silica based (U)HPLC columns (Broschure), http://www.ymc-europe.com/ymceurope/files/literature/YMC-Triart-C18_Hybrid-AQ_LQ.pdf (accessed May 2014).
(51) FDA: U.S. Department of Health and Human Services Food and Drug Administration Center of Drug Evaluation and Research (CDER) Center for Veterinarity Medicine (CVM) (2001). Guidance for Industry Bioanalytical Method Validation (accessed December 2012).
(52) Marcus, Y.; Kamlet, M. J.; Taft, R. W. Linear solvation energy relationships − standard molar gibbs free-energies and enthalpies of transfer of ions from water into nonaqueous solvents. *J. Phys. Chem.* **1988**, *92*, 3613−3622.
(53) Raamat, E.; Kaupmees, K.; Ovsjannikov, G.; Trummal, A.; Kutt, A.; Saame, J.; Koppel, I.; Kaljurand, I.; Lipping, L.; Rodima, T.; Pihl, V.; Koppel, I. A.; Leito, I. Acidities of strong neutral Bronsted acids in different media. *J. Phys. Org. Chem.* **2013**, *26*, 162−170.
(54) Berger, U.; Glynn, A.; Holmström, K. E.; Berglund, M.; Ankarberg, E. H.; Törnkvist, A. Fish consumption as a source of human exposure to perfluorinated alkyl substances in Sweden − analysis of edible fish from Lake Vättern and the Baltic Sea. *Chemosphere* **2009**, *76*, 799−804.
(55) Lilja, K.; Norström, K.; Remberger, M.; Kaj, L.; Egelrud, L.; Junedahl, E. Borström-Lunden Report: Screening of selected hazardous substances in the eastern Baltic marine environment, 2009, Swedish Environmental Research Institute, B1874, http://www3.ivl.se/rapporter/pdf/B1874.pdf (accessed May 2014).
(56) Kannan, K.; Corsolini, S.; Falandysz, J.; Oehme, G.; Focardi, S.; Giesy, J. P. Perfluorooctanesulfonate and related fluorinated hydrocarbons in marine mammals, fishes, and birds from coasts of the Baltic and the Mediterranean Seas. *Environ. Sci. Technol.* **2002**, *36*, 3210−3216.
(57) HELCOM, Core Indicator of Hazardous substances Perfluorooctane Sulphonate (PFOS). HELCOM 2013, http://helcom.fi/Core%20Indicators/HELCOM-CoreIndicator_Perfluorooctane_sulphonate.pdf (accessed May 2014).
(58) Hradkova, P.; Poustka, J.; Hlouskova, V.; Pulkrabova, J.; Tomaniova, M.; Hajslova, J. Perfluorinated compounds: occurrence of emerging food contaminants in canned fish and seafood products. *Czech J. Food Sci.* **2010**, *28*, 333−342.
(59) Schuetze, A.; Heberer, T.; Effkemann, S.; Juergensen, S. Occurrence and assessment of perfluorinated chemicals in wild fish from northern Germany. *Chemosphere* **2010**, *78*, 647−652.
(60) Anastassiades, M.; Lehotay, S. J.; Stajnbaher, D.; Schenck, F. J. Fast and easy multiresidue method employing acetonitrile extraction/partitioning and "dispersive solid-phase extraction" for the determination of pesticide residues in produce. *J. AOAC Int.* **2003**, *86*, 412−413.
(61) Ferreira, I.; Fernandes, J. O.; Cunha, S. C. Optimization and validation of a method based in a QuEChERS procedure and gas chromatography-mass spectrometry for the determination of multimycotoxins in popcorn. *Food Control* **2012**, *27*, 188−193.
(62) Mastovska, K.; Lehotay, S. J. Rapid sample preparation method for LC-MS/MS or GC-MS analysis of acrylamide in various food matrices. *J. Agric. Food Chem.* **2006**, *54*, 7001−7008.

MATERIALS AND METHODS

Reagents, Materials, and Apparatus. HA, HIS, tyramine (TYR), phenylethylamine (PEA), 3-mercaptopropyltriethoxysilane (MPTES), and tetraethoxysilane (TEOS) were supplied by Sigma-Aldrich (St. Louis, MO, USA). Polyvinyl chloride (PVC, M_w = 8000) and dichloromethane (DCM) were obtained from Alfa Aesar (Tianjin, China). Methanol, acetonitrile, NaH_2PO_4, Na_2HPO_4, and other reagents were purchased from Tianjin No. 1 Chemical Reagent Factory (Tianjin, China). All chemicals were analytical reagent grade. Cans of sardines, mackerel, saury, tuna, salmon, and Spanish mackerel for sample analysis were purchased from a local market.

Phosphate-buffered saline (PBS; pH 7.6) was prepared by mixing 0.2 M NaH_2PO_4 with 0.2 M Na_2HPO_4 (1:4 v/v).

Frequency change (Δf, Hz) was recorded using a QCM (QCM-922, Princeton Applied Research, Princeton, NJ, USA) equipped with a quartz crystal resonator (AT-cut, 9 MHz, platinum electrode (0.196 cm^2, 100 Å), Princeton Applied Research) and Teflon holder (Princeton Applied Research). The quartz crystal was positioned in the Teflon holder to ensure that only one side of the Pt electrode was in contact with the solution. The holder was placed vertically in a static detection cell to minimize any gravity-induced precipitation on the crystal surface. A magnetic stirrer (HJ-6A, Jin Tan Sheng Lan Instrument Co., Jiang Su, China) was used throughout the experiments to ensure homogeneous and complete interaction between agents. UV spectrophotometer (Cary 50-Bio, Varian, Palo Alto, CA, USA) was used to evaluate the ability of the MIP to adsorb the analyte. The morphology of the modified quartz crystals was investigated by scanning electron microscopy (SEM, SU1510, Hitachi, Tokyo, Japan). An HPLC analyzer (LC-10ATVP, Shimadzu, Kyoto, Japan) was used to validate the results obtained for real samples using the HA-MIP QCM sensor.

Sol–Gel Synthesis of HA-MIP. A novel HA-imprinted polymer was synthesized through hydrolytic cross-linking of silanol groups using a sol–gel process as follows: HA (0.10 g) was dissolved in methanol (5.0 mL) and mixed with MPTES (0.5 mL) in a 25 mL round-bottomed flask. After 30 min, TEOS (1.09 mL) and 0.1 M $NH_3{\cdot}H_2O$ (0.5 mL) were added and the mixture was incubated at 55 °C in a water bath for 12 h. The product was filtered and then aged in a vacuum oven at 60 °C for 10 h. After protonation in a mixture of CH_3OH and 1.0 M HCl (4:1 v/v, 100 mL) for 4 h, the solid product was collected by vacuum filtration and rinsed with deionized distilled water until the eluent reached neutral pH. Then, the product was dried in a vacuum oven at 60 °C until constant weight was obtained. The original template was removed by Soxhlet extraction in a mixture of methanol and acetic acid (9:1 v/v, 300 mL) until no HA was detected by UV absorbance measurement at 210 nm. The obtained polymer was dried in a vacuum oven at 60 °C and stored hermetically until further use. All solutions were mixed by gentle magnetic stirring to ensure homogeneous distribution and complete interaction between agents. Nonimprinted polymer (NIP) was also prepared in a manner identical to that used to synthesize MIP, except that the template was omitted.

Adsorption of HA-MIP. HA-MIP (20.0 mg) was mixed with PBS (5.0 mL, pH = 7.6) containing different concentrations of HA (10, 20, 30, 40, 60, 80, 100, and 120 mg L^{-1}) in polypropylene centrifuge tubes. After vigorous shaking at 150 rpm for 2 h and centrifugation at 4500*g* for 10 min, the amount of unbound HA in each supernatant was determined by UV absorbance measurement at 210 nm. The adsorption capacity (Q, mg·g^{-1}) of HA-MIP was calculated as follows:

$$Q = (C_i - C_f) \times V/W \quad (1)$$

where C_i and C_f are the initial and final concentration of analyte in solution, respectively (mg L^{-1}), V is the volume of solution (L), and W is the mass of polymer (g).

Scatchard analysis of binding isotherms was used to evaluate the binding capacity of HA-MIP for the template. The relevant equation is

$$Q/C = (-Q + Q_{max})/K_d \quad (2)$$

where C is the initial concentration of analyte in solution (mg L^{-1}), Q is the adsorption capacity at adsorption equilibrium (mg·g^{-1}), K_d is the equilibrium disassociation constant at the binding site (mg L^{-1}), and Q_{max} is the saturated adsorption capacity (mg·g^{-1}).[25−27]

The NIP was also tested using the above procedure. Mean adsorption values obtained from triplicate measurements of MIP and NIP were determined and compared.

Modification of a Quartz Crystal Surface with HA-MIP. Before modification, the quartz crystal electrode surface was cleaned in piranha solution (30% H_2O_2:98% H_2SO_4; 1:3 v/v) for 2 min to remove possible residual chemicals, and thoroughly rinsed with deionized water. HA-MIP or NIP (48.50 mg) was suspended in PVC-DCM (0.7 wt % solution). After ultrasonication to obtain a homogeneous solution, 5.0 μL of the mixture was carefully dispensed onto the immobilized quartz crystal surface. The modified quartz crystal was dried (30 min, 25 °C) and stored at room temperature in a vacuum chamber before use. Figure 1 outlines the processes of HA-MIP sensor construction and adsorption.

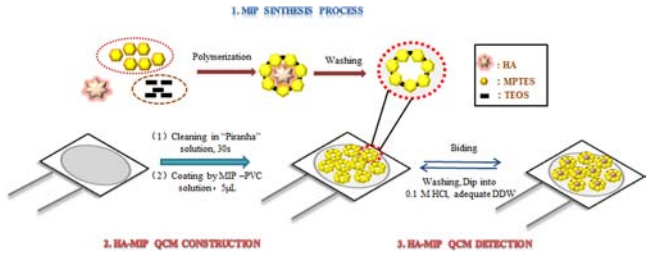

Figure 1. HA-MIP sensor construction and adsorption.

QCM Sensor Detection. After anchoring of the prepared quartz crystal into the Teflon holder, the assembled HA-MIP QCM sensor was immersed in PBS (20.0 mL) at room temperature. A steady resonant frequency (f_0, Δf < 1.0 Hz) was obtained after equilibration for 5 min. A small aliquot of analyte solution was injected into the solution. After equilibration for 5 min, a stable frequency change caused by analyte binding was obtained and recorded. After each test, the MIP-modified quartz crystal was washed with 0.1 M HCl and deionized water until the frequency recovered to f_0 and the crystal could be reused. Throughout the entire testing process, the solution was stirred at 240 rpm to accelerate the transmission of analyte. Analyses were performed in triplicate, and the average value of the obtained frequency shift (Δf, Hz) was used to calculate the mass of HA adsorbed onto the crystal surface according to the Sauerbrey equation:[28]

$$\Delta f = -2.26 \times 10^{-6} \Delta m f_0^{\,2}/A \quad (3)$$

where f_0 is the original frequency of the quartz crystal (Hz), Δm is the mass change (g), and A is the surface area of the electrode (cm^2).

For comparison, the NIP-modified QCM sensor was also tested using the same procedure.

Sample Preparation for HA-MIP QCM Sensor Analysis. Sample slurry (1.0 g) was mixed with $HClO_4$ (10.0 mL, 0.4 M) to induce protein precipitation. After homogenization for 15 min, the mixture was centrifuged. The collected supernatant was extracted with *n*-hexane (2:1 v/v) for further fat separation; the *n*-hexane supernatant was discarded. The defatting procedure was repeated twice, and then the product was dried using a rotary evaporator at 45 °C. The residue was redissolved in PBS (20.0 mL, pH = 7.6) and analyzed using the HA-MIP QCM sensor.

For the recovery test, slurries of sardine, mackerel, or saury were spiked with HA at 25, 100, and 400 μg kg^{-1}; the procedure used to extract HA was the same as that described above.

Sample Pretreatment for HPLC Analysis. HPLC was used to confirm the accuracy of the developed sensor. The procedure up until rotary evaporation was the same as described above; the residue was then reconstituted with $HClO_4$ (4.0 mL, 0.4 M) and derivatized as described in previous literature[29] with slight modification. The

dx.doi.org/10.1021/jf501092u | J. Agric. Food Chem. 2014, 62, 5269−5274

redissolved solution (1.0 mL) was placed in a 5 mL brown volumetric flask. NaOH (200 μL, 2.0 M), saturated $NaHCO_3$ (300 μL), and dansyl chloride (4.0 mL, 0.02 M) were added in succession. After incubation at 60 °C for 30 min, $NH_3{\cdot}H_2O$ solution (100.0 μL, 25 wt %) was added to remove excess dansyl chloride. Each solution was adjusted to 5.0 mL with acetonitrile and filtered through a 0.22 μm filter before HPLC analysis.

HPLC Analysis. In HPLC analysis, an analytical octadecylsilyl-3 column (4.6 × 250 mm, 5 μm particle size, Shimadzu) was used with acetonitrile:water (65:35 v/v) as the mobile phase at a flow rate of 1.0 mL min^{-1}. The injection volume and detection wavelength were 20 μL and 254 nm, respectively. All spectral and chromatographic data were obtained and processed using Class-VP software.

RESULTS AND DISCUSSION

Adsorption of HA-MIP. The abilities of the prepared MIP and reference NIP to adsorb HA were evaluated in PBS (pH = 7.6) containing different concentrations of HA. The adsorption isotherms of the polymers were obtained and assessed by Scatchard analysis (Figure 2). As shown in Figure 2A, with

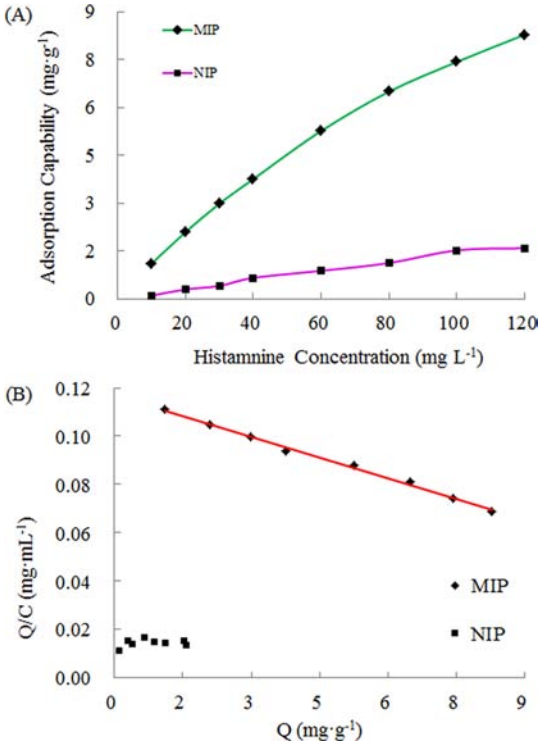

Figure 2. (A) Binding isotherms and (B) Scatchard plots of MIP and NIP for HA.

increasing HA concentration, the adsorption capacities (Q, mg·g^{-1}) of both the MIP and NIP increased. At an HA concentration of 120 mg L^{-1}, Q of MIP (8.28 mg·g^{-1}) was 5.2 times that of NIP (1.60 mg·g^{-1}), indicating that MIP has a markedly greater ability than NIP to adsorb HA. The Scatchard plot in Figure 2B reveals that a good linear relationship between Q/C and Q (mg·g^{-1}) was obtained of $Q/C = -0.0057Q + 0.1169$, with a correlation coefficient of 0.9964. K_d and Q_{max} calculated using this model were 175.44 mg L^{-1} and 20.51 mg·g^{-1}, respectively, suggesting that the MIP has a high affinity for HA. These results also demonstrate that recognition sites or cavities (presumably based on the acid−base pair resulting from the reaction between $-NH_2$ of HA and −SH of MPTES) form in the MIP; these would play an important role in the selective recognition of HA by the MIP. The nonlinearity of the Scatchard model plot for the NIP (Figure 2B) was caused by the disordered arrangement of recognition sites in the NIP system resulting from the lack of template during the polymerization process. The lower adsorption of HA by the NIP compared with that by the MIP could be attributed to the lack of specific binding sites within the polymer matrix.

Optimization of the PVC:HA-MIP Ratio. In this experiment, PVC was chosen as the matrix material to immobilize the prepared HA-MIP particles on the quartz crystal, because the recognition sites of a MIP encapsulated in PVC are easily accessible to the template[30] and the solubility of PVC in DCM could enhance the processability of the insoluble MIP.[31] The PVC:HA-MIP ratio used to modify the quartz crystal surface affected the capability of the prepared HA-MIP QCM sensor. Although more PVC could enhance the attachment of MIP particles, the amount of MIP immobilized on the surface of the quartz crystal was decreased, reducing the sensitivity and specificity of the modified sensor. Therefore, to ensure maximum and steady adsorption of HA on the quartz crystal surface, the amount of MIP used should be as large as possible while still effective adhering to the crystal. In this work, frequency changes (Δf) of HA-MIP QCM sensors prepared using PVC-DCM solutions (0.7 wt %) containing various ratios of PVC to MIP (PVC:MIP = 1:1, 1:2, 1:3, 1:4, 1:5, and 1:6 m/m) were compared at the same HA concentration (4.45×10^{-2} mg L^{-1}). Δf increased with the ratio of PVC to MIP until it reached 1:5. Adding further MIP (1:6) caused Δf to decrease sharply. Based on these results, a ratio of PVC to MIP of 1:5 was chosen for modification of the QCM sensor.

Morphological Characterization. SEM was used to evaluate the morphology of the HA-MIP-modified quartz crystal surface (Figure 3). Figure 3A shows that the layer containing MIP was completely adhered to the transducer surface, with a relatively uniform dispersion of polymer particles. Compared with the bare electrode (Figure 3B), the modified one possessed a much rougher surface, which provided a larger surface area for the specific adsorption of the target molecule.

Influence of Test Solution pH on QCM Detection. In the process of HA recognition, the HA-MIP QCM sensor selectively recognizes HA through the acid−base interaction between the immobilized −SH groups of the sensor and $-NH_2$ group of HA; the latter is affected by the adsorption microenvironment, particularly pH. Therefore, it is necessary to optimize the pH of the test solution so that the analyte readily adsorbs onto the prepared sensor. HA solutions (4.45×10^{-2} mg L^{-1}) with different pH ranging from 6.0 to 8.8 were prepared in PBS for frequency analysis. Δf increased slowly for pH 6.0−6.8, before reaching a peak at pH 7.6; it then decreased continuously as the solution pH value increased beyond 7.6. This phenomenon might be attributed to the competition between the abundant H^+ and −SH to react with $-NH_2$ of HA under acidic conditions. The interaction between HA and MPTES would be decreased by the abundance of OH^- groups when the pH exceeded 7.6. Therefore, the optimum pH of the test solution was 7.6, which was used in further tests to guarantee excellent recognition ability of the developed QCM sensor.

Evaluation of Binding Performance. The frequency responses of the MIP and NIP QCM sensors for HA were compared in solutions with HA concentrations ranging from 0.11×10^{-2} to 6.67×10^{-2} mg L^{-1} to evaluate their specific

dx.doi.org/10.1021/jf501092u | J. Agric. Food Chem. 2014, 62, 5269−5274

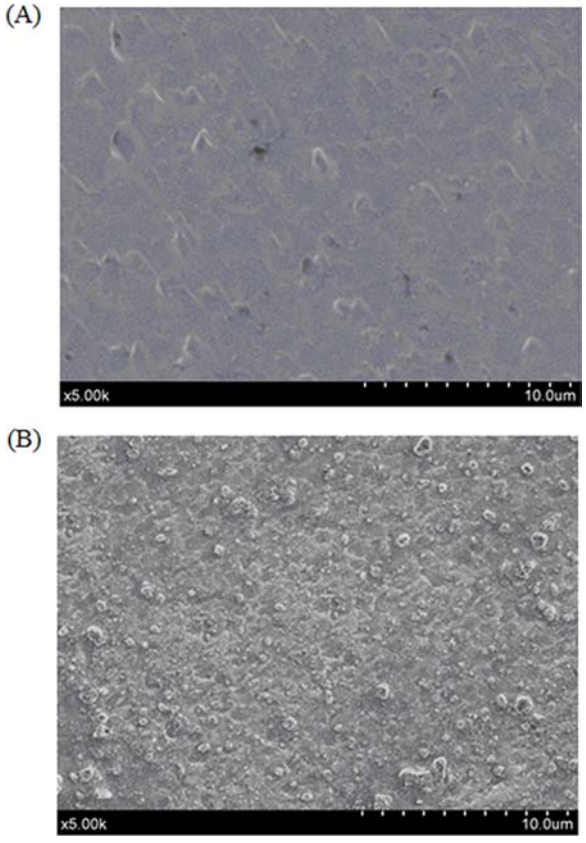

Figure 3. SEM images of the surface of a quartz crystal (A) before and (B) after HA-MIP modification.

adsorptive capability; the results are presented in Figure 4. Δf increased with HA concentration for both modified sensors. At

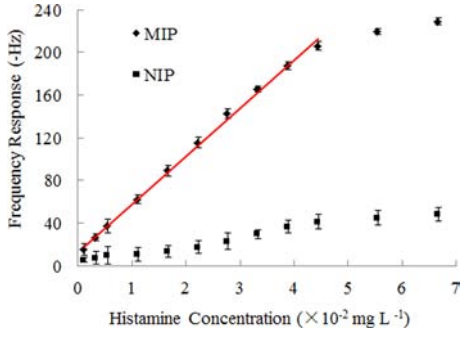

Figure 4. Frequency responses of MIP and NIP QCM sensors in solutions containing different concentrations of HA.

any particular concentration, the HA-MIP QCM sensor showed a larger frequency response than the NIP one, demonstrating the differential binding capability of the MIP sensor for HA. At an HA concentration of 6.67×10^{-2} mg L^{-1}, the frequency change for the MIP sensor was −229.0 Hz, about 5 times that of the NIP one (−45.0 Hz). This might be caused by imprinting the MIP with HA, which caused cavities that specifically fit HA in terms of spatial structure and functional groups to form during polymerization. The frequency response tended to equilibrate at HA concentrations above 6.67×10^{-2} mg L^{-1}, because the MIP became saturated with adsorbed HA. The small response of the NIP-modified QCM sensor is attributed to nonspecific adsorption of HA.

Good linearity of the relationship of frequency change with concentration was obtained for HA concentrations from 0.11×10^{-2} to 4.45×10^{-2} mg L^{-1} (correlation coefficient = 0.9978). The calculated detection limit (S/N = 3) of the MIP QCM sensor for HA was 7.49×10^{-4} mg kg^{-1}, which is lower than that for HA by HPLC (0.054 mg kg^{-1}).[6]

A PVC-modified QCM sensor did not show any detectable frequency response to HA at selected concentrations, indicating that PVC used to immobilize the MIP on the electrode surface did not affect the specific recognition of HA by the proposed sensor.

Kinetic and Selectivity Experiments. The adsorption kinetics of the developed sensor were tested in PBS containing HA (4.45×10^{-2} mg L^{-1}, pH = 7.6) under continuous stirring. A steady frequency response (−206.1 Hz) was obtained within 10 min, indicating that the HA-MIP QCM sensor could achieve adsorption equilibrium in a short period, which would be helpful for rapid detection of HA.

The selectivity (or specificity) of the prepared QCM sensor is another important parameter to evaluate. For this purpose, different concentrations (0.11×10^{-2} to 4.45×10^{-2} mg L^{-1}) of TYR, HIS, and PEA (Figure 5A), which are structurally

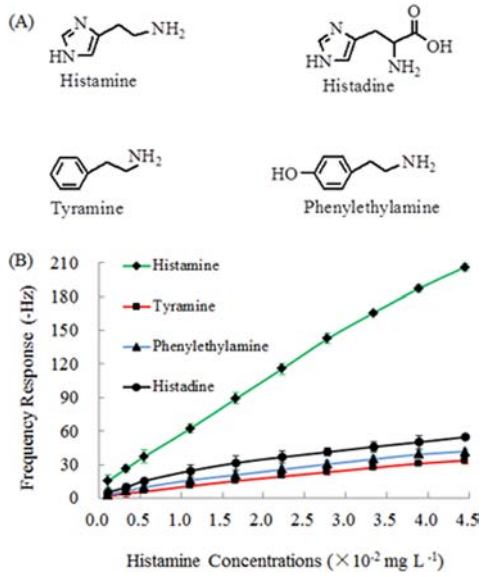

Figure 5. (A) Chemical structures of HA, HIS, TYR, and PEA. (B) Selectivity of the HA-MIP QCM sensor for different analytes.

similar to HA, in PBS (pH = 7.6) were tested with the HA-MIP QCM sensor. The selectivity coefficient (SC), defined as $\alpha_{HA}/\alpha_{analyte}$, where α is the slope of the analyte calibration curve, was used to assess the selectivity of the HA-MIP QCM sensor for HA. The detection results illustrated in Figure 5B reveal much weaker frequency responses for HIS, TYR, and PEA than for HA with SC of 4.18, 6.43, and 5.17, respectively, indicating that the developed sensor has excellent selectivity and specificity for HA. This selectivity results from the tuned cavities of the HA-MIP that are complementary to HA in size, shape, and functional groups.

Reproducibility and Stability. The reproducibility and stability of the developed QCM are important for successful HA detection. Therefore, the same HA-MIP QCM sensor was used to evaluate the frequency change in PBS containing HA (4.45×10^{-2} mg L^{-1}, pH = 7.6) 7 times continuously. After each test, the imprinted sensor was washed with 0.1 M HCl and

dx.doi.org/10.1021/jf501092u | J. Agric. Food Chem. 2014, 62, 5269−5274

deionized water sequentially until the resonance frequency reached its original value. The frequency change during repeated testing decreased slightly from 206.1 to 196.3 Hz; this loss of just 4.8% confirmed the good recyclability and stability of the MIP QCM sensor for HA detection. The stability of the HA-MIP QCM sensor over a long period of time was also demonstrated. After hermetic storage at room temperature for 6 months, the average frequency shift of the quartz crystal was 195.0 Hz, which is only 5.4% less than the initial frequency shift of 206.1 Hz. This result further confirms the excellent stability of the developed QCM sensor, which suggests that the MIP is also highly stable.

Recovery Test. Samples of canned sardines, saury, and mackerel were spiked with HA at three levels (25, 100, and 400 $\mu g\ kg^{-1}$). The HA concentration of each sample was detected 3 times under the same conditions. The relative standard deviation (RSD, %) of the repeated measurements was calculated to determine the precision of the method; the results are listed in Table 1. The overall precision ranged from 0.3 to 4.4%, and the recovery values were also good, ranging from 93.2 to 100.4%, suggesting that results obtained using the HA-MIP QCM sensor were both accurate and reproducible.

Table 1. Recoveries of HA from Spiked Food Samples Determined by the HA-MIP QCM Sensor (n = 3)

sample	orig concn ($\mu g\ kg^{-1}$), mean ± SD	spiked concn ($\mu g\ kg^{-1}$)	detected concn ($\mu g\ kg^{-1}$), mean ± SD	RSD (%)	recovery (%)
canned sardines	67.7 ± 0.1	25	92.8 ± 1.9	2.0	100.4
		100	167.1 ± 2.5	1.5	99.4
		400	446.8 ± 2.6	0.6	94.8
canned saury	55.2 ± 0.5	25	79.8 ± 3.5	4.4	98.4
		100	148.4 ± 2.1	1.4	93.2
		400	429.3 ± 1.1	0.3	93.5
canned mackerel	102.7 ± 0.3	25	127.9 ± 1.1	0.9	100.2
		100	200.8 ± 1.4	0.7	99.1
		400	494.6 ± 3.5	0.7	98.4

Actual Sample Analysis. Using the established sample pretreatment method, the concentration of HA in six different samples (canned sardines, mackerel, saury, tuna, salmon, and Spanish mackerel) was measured by the HA-MIP QCM sensor. The results of these measurements are shown in Table 2.

HPLC Validation. Traditional HPLC was used to validate the results obtained using the HA-MIP QCM sensor. The concentration of HA in six different samples (canned sardines, mackerel, saury, tuna, salmon, and Spanish mackerel) was determined by HPLC. The results of both methods were recorded, and the regression equation was calculated to be $y = 1.0086x - 0.0214$ with a correlation coefficient of 0.9965, signifying the accuracy of the HA-MIP QCM sensor.

Table 2. Content of HA in Samples Detected by the HA-MIP QCM Sensor and HPLC (n = 3)

	HA-MIP QCM sensor		HPLC	
sample	detected concn ($\mu g\ kg^{-1}$), mean ± SD	RSD (%)	detected concn ($\mu g\ kg^{-1}$), mean ± SD	RSD (%)
canned sardines	76.7 ± 1.5	2.0	67.7 ± 0.1	0.1
canned tuna	299.0 ± 1.6	0.5	278.4 ± 0.5	0.2
canned salmon	669.4 ± 3.9	0.6	666.3 ± 1.2	0.2
canned mackerel	111.5 ± 1.7	1.5	102.7 ± 0.3	0.3
canned Spanish mackerel	463.8 ± 2.5	0.5	427.6 ± 0.7	0.2
canned saury	91.4 ± 2.6	2.8	55.2 ± 0.5	0.9

Compared with HPLC, the developed QCM sensor enhanced HA detection efficiency greatly because it is sensitive, easy to operate, stable for more than 6 months, and portable for field analysis, and it does not require pre- or postcolumn derivation. The results show that the MIP-based QCM sensor can be used for accurate HA detection in food samples.

AUTHOR INFORMATION

Corresponding Author

*Tel: +86 22 60601456. Fax: +86 22 60601332. E-mail: s.wang@tust.edu.cn.

Funding

This work was supported by the Ministry of Science and Technology of the People's Republic of China (Project No. 2011AA100807), China Postdoctoral Science Foundation (Project No. 2013M540210), and the Program for Changjiang Scholars and Innovative Research Team in University (IRT1166).

Notes

The authors declare no competing financial interest.

REFERENCES

(1) Hungerford, J. M. Scombroid poisoning: a review. *Toxicon* **2010**, *56*, 231−243.

(2) Phuvasate, S.; Su, Y. C. Effects of electrolyzed oxidizing water and ice treatments on reducing histamine-producing bacteria on fish skin and food contact surface. *Food Control* **2010**, *21*, 286−291.

(3) Švarc-Gajić, J.; Stojanović, Z. Determination of histamine in cheese by chronopotentiometry on a thin film mercury electrode. *Food Chem.* **2010**, *124*, 1172−1176.

(4) Scombrotoxin (histamine) formation. In *Fish and fisheries products hazards and controls guidance*; Center for Food Safety and Applied Nutrition, Office of Seafood, Food and Drug Administration: Washington, DC, 2001; pp 83−102.

(5) Jadidi-Niaragh, F.; Mirshafiey, A. Histamine and histamine receptors in pathogenesis and treatment of multiple sclerosis. *Neuropharmacology* **2010**, *59*, 180−189.

(6) Tang, T.; Qian, K.; Shi, T. U.; Wang, F.; Li, J. Q.; Cao, Y. S.; Hu, Q. B. Monitoring the contents of biogenic amines in sufu by HPLC with SPE and pre-column derivatization. *Food Control* **2011**, *22*, 1203−1208.

(7) Zhai, H. L.; Yang, X. Q.; Li, L. H.; Xia, G. B.; Cen, J. W.; Huang, H.; Hao, S. X. Biogenic amines in commercial fish and fish products sold in southern China. *Food Control* **2012**, *25*, 303−308.

(8) Jia, S.; Kang, Y. P.; Park, J. H.; Lee, J.; Kwon, S. W. Determination of biogenic amines in Bokbunja (*Rubus coreanus* Miq.) wines using a novel ultra-performance liquid chromatography coupled with quadrupole-time of flight mass spectrometry. *Food Chem.* **2012**, *132*, 1185−1190.

(9) Muscarella, M.; Lo Magro, S.; Campaniello, M.; Antonio, A.; Stacchini, P. Survey of histamine levels in fresh fish and fish products collected in Puglia (Italy) by ELISA and HPLC with fluorimetric detection. *Food Control* **2012**, *31*, 211−217.

(10) Pérez, S.; Bartrolí, J.; Fàbregas, E. Amperometric biosensor for the determination of histamine in fish samples. *Food Chem.* **2013**, *141*, 4066−4072.

(11) Özkütük, E. B.; Diltemiz, S. E.; Özalp, E.; Özalp, E.; Say, R.; Ersöz, A. Ligand exchange based paraoxon imprınted QCM sensor. *Mater. Sci. Eng.: C* **2012**, *33*, 938−942.

(12) Hauptmann, P. Resonant sensors and applications. *Sens. Actuators, A* **1991**, *26*, 371−377.
(13) Escuderos, M. E.; Sánchez, S.; Jiménez, A. Virgin olive oil sensory evaluation by an artificial olfactory system, based on Quartz Crystal Microbalance (QCM) sensors. *Sens. Actuators, B* **2010**, *147*, 159−164.
(14) Sener, G.; Ozgur, E.; Yılmaz, E.; Uzun, L.; Say, R.; Denizli, A. Quartz crystal microbalance based nanosensor for lysozyme detection with lysozyme imprinted nanoparticles. *Biosens. Bioelectron.* **2010**, *26*, 815−821.
(15) Hussain, M.; Iqbal, N.; Lieberzeit, P. A. Acidic and basic polymers for molecularly imprinted folic acid sensors-QCM studies with thin films and nanoparticles. *Sens. Actuators, B* **2012**, *176*, 1090−1095.
(16) Vasapollo, G.; Sole, R. D.; Mergola, L.; Lazzoi, M. R.; Scardino, A.; Scorrano, S.; Mele, G. Molecularly imprinted polymers: present and future prospective. *Int. J. Mol. Sci.* **2011**, *12*, 5908−5945.
(17) Zhang, H. Q.; Ye, L.; Mosbach, K. Non-covalent molecular imprinting with emphasis on its application in separation and drug development. *J. Mol. Recognit.* **2006**, *19*, 248−259.
(18) Alexander, C.; Andersson, H. S.; Andersson, L. I.; Ansell, R. J.; Kirsch, N.; Nicholls, I. A.; O'Mahony, J.; Whitcombe, M. J. Molecular imprinting science and technology: a survey of the literature for the years up to and including 2003. *J. Mol. Recognit.* **2006**, *19*, 106−180.
(19) Horemans, F.; Alenus, J.; Bongaers, E.; Weustenraed, A.; Thoelen, R.; Duchateau, J.; Lutsen, L.; Vanderzande, D.; Wagner, P.; Cleij, T. J. MIP-based sensor platforms for the detection of histamine in the nano-and micromolar range in aqueous media. *Sens. Actuators, B* **2010**, *148*, 392−398.
(20) Tamayo, F. G.; Casillas, J. L.; Martin-Esteban, A. Highly selective fenuron-imprinted polymer with a homogeneous binding site distribution prepared by precipitation polymerisation and its application to the clean-up of fenuron in plant samples. *Anal. Chim. Acta* **2003**, *482*, 165−173.
(21) Cummins, W.; Duggan, P.; McLoughlin, P. A comparative study of the potential of acrylic and sol−gel polymers for molecular imprinting. *Anal. Chim. Acta* **2005**, *542*, 52−60.
(22) Fang, G. Z.; Tan, J.; Yan, X. P. An ion-imprinted functionalized silica gel sorbent prepared by a surface imprinting technique combined with a sol-gel process for selective solid-phase extraction of cadmium (II). *Anal. Chem.* **2005**, *77*, 1734−1739.
(23) Olwill, A.; Hughes, H.; O'Riordain, M.; McLoughlin, P. The use of molecularly imprinted sol−gels in pharmaceutical separations. *Biosens. Bioelectron.* **2004**, *20*, 1045−1050.
(24) Su, P. G.; Hung, F. C.; Lin, P. H. Fabrication, characterization and sensing properties of Cu (II) ion imprinted sol−gel thin film on QCM. *Mater. Chem. Phys.* **2012**, *135*, 130−136.
(25) Mohajeri, S. A.; Ebrahimi, S. A. Preparation and characterization of a lamotrigine imprinted polymer and its application for drug assay in human serum. *J. Sep. Sci.* **2008**, *31*, 3595−3602.
(26) Yin, X. Y.; Liu, Q. S.; Jiang, Y. F.; Luo, Y. M. Development of andrographolide molecularly imprinted polymer for solid-phase extraction. *Spectrochim. Acta, Part A* **2011**, *79*, 191−196.
(27) Scatchard, G. The attractions of proteins for small molecules and ions. *Ann. N.Y. Acad. Sci.* **1949**, *51*, 660−672.
(28) Sauerbrey, G. Verwendung von Schwingquarzen zur Wägung dünner Schichten und zur Mikrowägung. *Z. Phys.* **1959**, *155*, 206−222.
(29) Mey, E. D.; Drabik-Markiewicz, G.; Maere, H. D.; Peeters, M.-C.; Derdelinckx, G.; Paelinck, H.; Kowalska, T. Dabsyl derivatisation as an alternative for dansylation in the detection of biogenic amines in fermented meat products by reversed phase high performance liquid chromatography. *Food Chem.* **2012**, *130*, 1017−1023.
(30) Chronakis, I. S.; Jakob, A.; Hagström, B.; Ye, L. Encapsulation and selective recognition of molecularly imprinted theophylline and 17β-estradiol nanoparticles within electrospun polymer nanofibers. *Langmuir* **2006**, *22*, 8960−8965.
(31) Matsuguchi, M.; Uno, T. Molecular imprinting strategy for solvent molecules and its application for QCM-based VOC vapor sensing. *Sens. Actuators, B* **2006**, *113*, 94−99.

Table 1. Chemical Structures of Studied ILs

ILs	Cations	Anions
1-dodecyl-3-methylimidazolium chloride	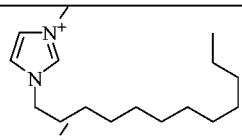	Cl^-
1-dodecyl-3-methylimidazolium bromide	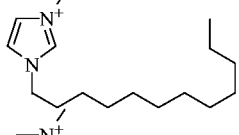	Br^-
1-dodecyl-3-methylimidazolium trifluoromethanesulfonate	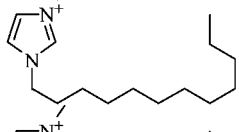	$CF_3SO_3^-$
1 -dodecyl-3-methylimidazolium nitrate	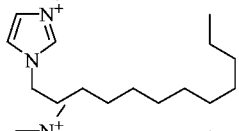	NO_3^-
1-dodecyl-3-methylimidazolium hydrogen sulfate	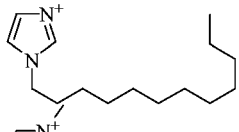	HSO_3^-
1-ethyl-3-methylimidazolium bromide	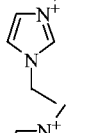	Br^-
1-hexyl-3-methylimidazolium bromide	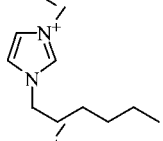	Br^-
1-butyl-3-methylimidazolium methanesulfonate	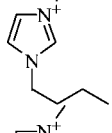	$CH_3SO_3^-$
1-butyl-3-methylimidazolium tetrafluoroborate	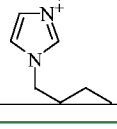	BF_4^-

solvent extraction is common, popular, and yet with unavoidable disadvantages, for example, contamination to the environment and human health. Until now, IL-based one-step micellar extraction has not been applied for the analysis of multiclass compounds in sample preparation, and no work has been reported on the use of IL-micelles for the extraction of hydrophobic and hydrophilic components from food samples.

Hawthorn is well-known as both a fruit and food supplement in Europe and China. Recent studies have demonstrated that hawthorn fruits were mainly used in the treatment of indigestion, hyperlipidemia, hypertension, abdominal pain, and amenorrhea for many years.[20] Several analytical methods including high-performance liquid chromatography (HPLC),[21] capillary electrophoresis (CE),[22] and liquid chromatography–mass spectrometry (LC-MS)[23] have been reported to analyze the bioactive constituents, especially phenolic compounds, of this fruit. However, to date, there are no studies related to the utilization of a sub 2 μm particle size column-based LC system for the separation of hawthorn samples, especially coupled with Q-TOF/MS.

In the current study, an IL-based one-step micellar extraction followed by UHPLC-Q-TOF/MS was established and further applied for the determination of multiclass phenolic compounds (protocatechuic acid, chlorogenic acid, epicatechin, hyperoside, isoquercitrin, quercetin) in hawthorn fruits. The effects of various experimental parameters, such as selection of ILs and surfactant concentration, as well as extraction time, were investigated systematically. The proposed method is environmentally friendly with good repeatability and is expected to have wider utilization instead of organic solvents in the future.

MATERIALS AND METHODS

Reagents and Samples. The ionic liquids tested in the present study, including 1-ethyl-3-methylimidazolium bromide ([emin]Br), 1-hexyl-3-methylimidazolium bromide ([hmin]Br), 1-butyl-3-methylimidazolium methanesulfonate ([bmim]SO_3), 1-butyl-3-methylimidazolium tetrafluoroborate ([bmin]BF_4), 1-dodecyl-3-methylimidazolium chloride ([C_{12}mim]Cl), 1-dodecyl-3-methylimidazolium bromide ([C_{12}mim]Br), 1-dodecyl-3-methylimidazolium trifluoromethanesulfonate ([C_{12}mim]CF_3SO_3), 1 -dodecyl-3-methylimidazolium nitrate ([C_{12}mim]NO_3), and 1-dodecyl-3-methylimidazolium hydrogen sulfate ([C_{12}mim]HSO_3), were purchased from Chengjie Chemical Co. Ltd. (Shanghai, China) and used without further purification (Table 1). HPLC grade methanol and acetonitrile were obtained from Sigma-Aldrich, Inc. (St. Louis, MO, USA). All other chemicals were of

dx.doi.org/10.1021/jf501171w | J. Agric. Food Chem. 2014, 62, 5275−5280

analytical grade (Aladdin Reagent Inc., Shanghai, China), and ultrapure water (Milli-Q system) was used throughout.

Analytical standards of protocatechuic acid (1), chlorogenic acid (2), epicatechin (3), hyperoside (4), isoquercitrin (5), and quercetin (6) were provided by Shanghai Winherb Medical Technology Co., Ltd. (Shanghai, China). The hawthorn fruits were obtained from a local drugstore in Hangzhou, China.

Preparation of Sample Solution. One gram of accurately weighed hawthorn fruit was extracted with 20 mL of various solvents (ionic liquids, water, or methanol) by ultrasonication for 40 min. The suspension was then filtered through a 0.2 μm disposable membrane filter and stored at room temperature before injection.

Instrumental Conditions. Chromatographic analysis was performed on a modular Agilent UHPLC system (Agilent 1290 Infinity LC, Agilent Technologies, Santa Clara, CA, USA) equipped with a vacuum degasser, a binary solvent delivery system, a thermostated autosampler, and a thermostabilized compartment. An Agilent Zorbax Extend-C_{18} column (2.1 mm × 50 mm, 1.8 μm) was used for separation at a room temperature of 35 °C. The mobile phase was a mixture of acetonitrile (A) and water with 0.1% formic acid (B) using a gradient elution of 10−15% A at 0−2.5 min, 15−15% A at 2.5−3.0 min, 15−40% A at 3.0−6.0 min, and 40−100% A at 6.0−7.0 min, with an equilibrium time of 5 min. The injection volume was 1 μL, and the flow rate was set at 0.4 mL/min.

This UHPLC system was connected to a 6530 Q-TOF/MS (Agilent Technologies) equipped with a dual ESI source, operating in the negative ion mode, using the following operation conditions: nebulizer pressure, 45 psig; drying gas, 12 L/min; gas temperature, 350 °C; capillary voltage, 3500 V; fragmentor voltage, 175 V; skimmer voltage, 65 V; octopole RF, 750 V. The data recorded were controlled by MassHunter software (version B 05.00 Qualitative Analysis), and the mass range was recorded in the range m/z 100−2000.

RESULTS AND DISCUSSION

Optimization of IL-Based Micellar Extraction. To obtain the highest extraction ratios for the investigated analytes, some parameters of micellar extraction such as type of IL, concentration of IL, and extraction time were explored systematically.

Selection of ILs. The structures of ILs have great impacts on their physical and chemical properties, such as density, viscosity, and solubility, which might greatly affect the micellar extraction yield of target compounds.[24] To find the optimal IL and evaluate its performance in the micellar extraction of six analytes of hawthorn fruit, 1-dodecyl-3-methylimidazolium type ILs with different anions were tested using protocatechuic acid, chlorogenic acid, epicatechin, hyperoside, isoquercitrin, and quercetin as model compounds. In this study, five long-chain ILs including $[C_{12}mim]Cl$, $[C_{12}mim]Br$, $[C_{12}mim]CF_3SO_3$, $[C_{12}mim]NO_3$, and $[C_{12}mim]HSO_3$ were compared as extraction solvents. These ILs have the same hydrocarbon chain length but different hydrophilic groups, presenting varied properties by different amphiphilic molecular structure. All five IL surfactants were found to be water-soluble and could enhance water miscibility of solutes. Actually, compared with traditional cationic surfactants, the investigated ILs with long chains were demonstrated to have significantly lower CMC values, which means these ILs more easily formed ionic surfactants. Figure 1 indicates that when the other conditions were constant, the anions of ILs strongly affected the extraction yield of the compounds of interest. Moreover, it shows that the extraction yields of hydrophobic and hydrophilic compounds were largely anion-dependent, which was consistent with a previous paper.[25] As shown in Figure 1E, $[C_{12}mim]Cl$ exhibited the highest extraction yields for all investigated analytes, especially for analytes 1 and 2 compared with other ILs. It was

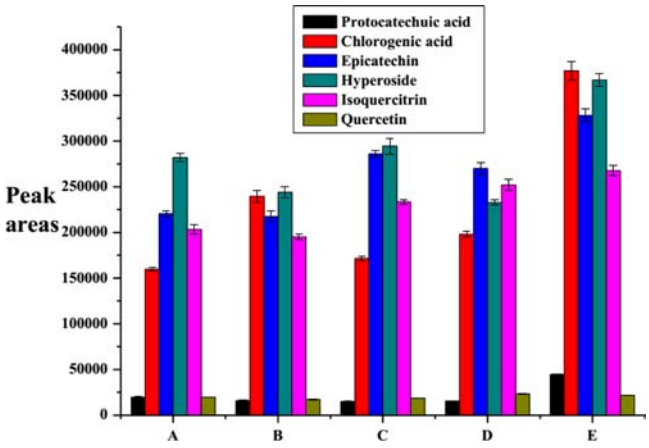

Figure 1. Impact of type of IL on extraction efficiency: (A) $[C_{12}mim]Br$; (B) $[C_{12}mim]CF_3SO_3$; (C) $[C_{12}mim]NO_3$; (D) $[C_{12}mim]HSO_3$; (E) $[C_{12}mim]Cl$. Extraction conditions: 1.0 g of dried hawthorn samples was mixed with 20 mL of different ionic liquids and then extracted for 40 min at 100 W ultrasonic power. Analytes: protocatechuic acid, chlorogenic acid, epicatechin, hyperoside, isoquercitrin, quercetin.

supposed that the two analytes had stronger interactions with the tested IL, giving rise to higher dissolubility in plant cells. With regard to analyte 6, however, these five ILs had no significant effect on the extraction yield with an extraction time of 40 min. These results suggested that the micellar extraction was a complex result of distinct multiple interactions including the viscosity of sample solution and solvent, solubilities of analytes in ILs, the diffusion coefficient, partition coefficient of the solutes, etc. Thus, $[C_{12}mim]Cl$ was selected as extraction solvent in the subsequent experiments.

Optimization of Surfactant Concentration and Extraction Time. In previous studies, it was shown that the surfactant concentration was an essential factor which could influence the extraction efficiency of target analytes.[25] In this study, the effect of $[C_{12}mim]Cl$ concentration on the extraction of multiclass polar compounds from hawthorn fruit was examined in the range of 50−250 mM, and the results are exhibited in Figure 2. The extraction yields of six analytes were found to increase with the rising surfactant concentration until 150 mM as the maximum and then decrease when the surfactant concentration went higher. The first part of the positive correlation phenomenon was attributed to the higher

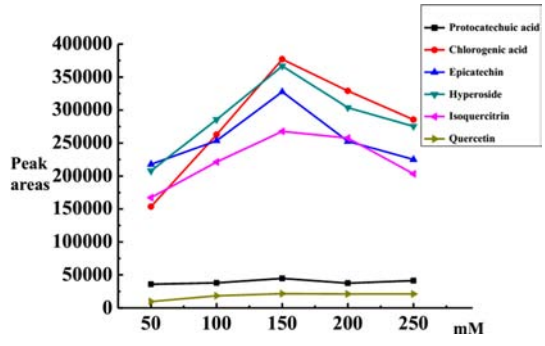

Figure 2. Effect of $[C_{12}mim]Cl$ concentrations on the extraction yields of target ingredients. One gram of dried samples was mixed with 50−250 mM $[C_{12}mim]Cl$ and then extracted for 40 min at 100 W ultrasonic power. Other conditions were as in Figure 1.

dx.doi.org/10.1021/jf501171w | J. Agric. Food Chem. 2014, 62, 5275−5280

$[C_{12}mim]Cl$ concentration exhibiting greater solvency, resulting in higher rates of analytes transferring to the extraction solvent. After a certain concentration, more $[C_{12}mim]Cl$ would be dissolved into the sample solution, which possibly reduced the molecular interaction of solvent and compounds, giving rising to a decreased solubility of investigated analytes. Thus, the negative correlation phenomenon was observed for analytes 2, 3, 4, and 5 when extracted by higher concentrations of ILs after 150 mM. On the other hand, the extraction efficiency for analytes 1 and 6 rarely changed when the hawthorn sample was extracted. This was probably due to the chemical structures of the two compounds, which made their distribution between the micellar phase and the aqueous phase insensitive to the IL concentration. Considering the extraction efficiency, the optimized concentration of 150 mM $[C_{12}mim]Cl$ was adopted in the following experiments.

Generally, extraction time was an important factor usually studied in the conventional extraction process, which could affect the effectiveness of extraction of analytes. In micelle-assisted extraction, the effects of extraction time were evaluated in the range of 20−80 min employing 150 mM $[C_{12}mim]Cl$. Results showed the chromatographic peak areas increased almost linearly when the extraction time went up from 20 to 40 min for all analytes. With longer extraction times, the extraction efficiency decreased on the contrary (data not shown). Therefore, the extraction time was set to 40 min in the following study.

Comparison of Different Extraction Methods. To compare the efficiencies of micellar-based and conventional solvent extractions, water, several ILs with the short alkyl chains, and methanol were used to extract six analytes from hawthorn fruit in the present study. It can be observed from Figure 3F that water exhibited much higher extraction yields for

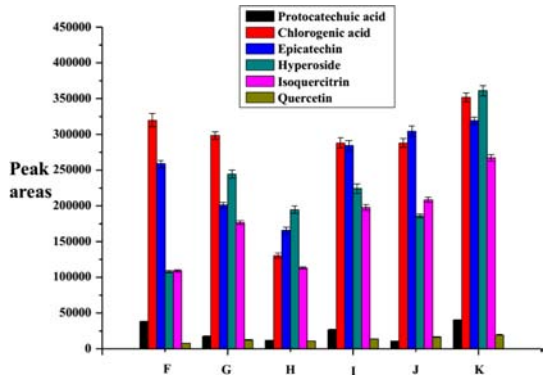

Figure 3. Comparison of different extraction methods: (F) water; (G) [emin]Br; (H) [hmin]Br; (I) $[bmim]SO_3$; (J) $[bmin]BF_4$; (K) methanol. Other conditions were as in Figure 1.

the hydrophilic components than the hydrophobic ones, indicating itself to be an unsuitable extraction solvent for multiclass polar compounds. When the short-chain ILs (Figure 3G−J) were used as extraction solvents, the yields of hydrophobic compounds were distinctly higher than that of water solvent, and yet lower than that of micellar-based or methanol extraction. In the case of hydrophilic analytes, the change of peak areas resulted from the dissolving of the IL drop in sample solutions. As seen in Figure 3, the analytes extracted by methanol presented much higher yields than those by water and short-chain ILs. In addition, the results shown in Figures 1 and 3 indicated that, as extraction solvents, the micellar solution and methanol had no significant difference in the extraction of target analytes from hawthorn fruit. In other words, the long-chain ILs could be an alternative solvent to replace toxic organic solvents. Moreover, IL micelle was a rapid and effective means for simultaneous extraction of hydrophilic and hydrophobic compounds from foods.

Performance of UHPLC-Q-TOF/MS. Electrospray ionization (ESI) is a soft ionization technique used widely for the analysis of various analytes ranging from small organic molecules to biomolecules of hundreds of kilodaltons.[26] Generally, the sensitivity is often low in the positive or negative ion mode when the analyte of interest is prepared along with the matrix in involatile salts. In this study, it was fortunate to find that the IL matrix provided similar signal intensities compared to commonly used methanol solvent. The results indicated that no significant signal suppression occurred for the six tested analytes and, thus, matrix effect could be neglected in the experiment.

To achieve a good separation for multiple ingredient determination, several mobile phase systems including methanol−water, methanol−0.1% formic acid, acetonitrile−water, and acetonitrile−0.1% formic acid were investigated. The result demonstrated that the optimal MS separation of six compounds detected in negative ion mode was achieved by using a gradient elution with 0.1% formic acid−water and acetonitrile at 0.4 mL/min in 6 min (Figure 4). Different columns including an Agilent Zorbax Extend-C_{18} column (2.1 mm × 50 mm, 1.8 μm), a Zorbax Eclipse XDB-C_{18} column (2.1

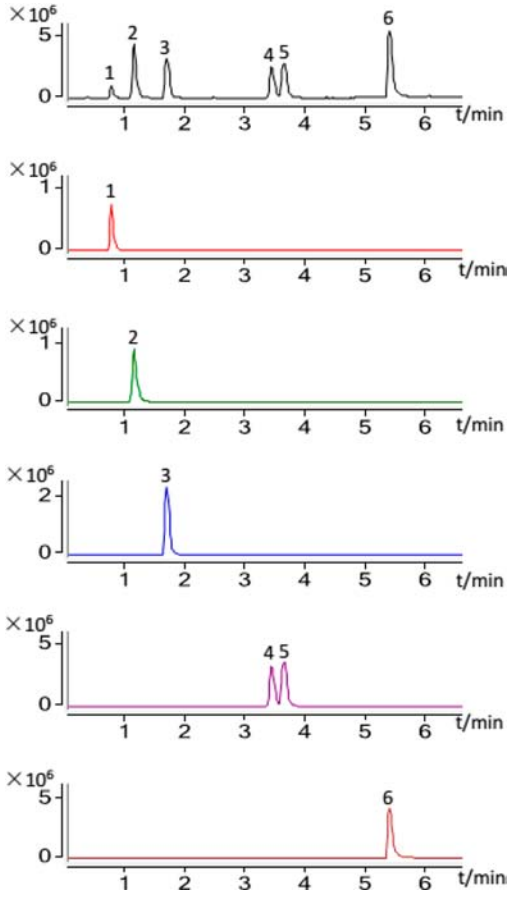

Figure 4. TIC of standard solution determined by UHPLC-Q-TOF/MS.

dx.doi.org/10.1021/jf501171w | J. Agric. Food Chem. 2014, 62, 5275−5280

Table 2. Linear Regression Data, Precision, and Limits of Detection (LODs) of the Investigated Compounds

			precision (RSD%)				
			intraday(n = 6)		interday(n = 3)		
analyte	calibration curve	r^2	peak area	retention time	peak area	retention time	LOD (μg/mL)
protocatechuic acid	y = 35202x + 17221	0.9970	3.28	0.51	5.22	0.74	0.0047
chlorogenic acid	y = 64075x + 11624	0.9995	1.37	0.45	3.31	0.46	0.0038
epicatechin	y = 157405x + 47530	0.9984	2.15	0.42	2.36	0.45	0.0054
hyperoside	y = 116331x + 16155	0.9995	1.97	0.22	4.68	0.33	0.0033
isoquercitrin	y = 150086x + 14966	0.9999	2.61	0.26	4.00	0.44	0.0048
quercetin	y = 278146x + 388804	0.9934	2.63	0.10	3.03	0.26	0.0030

Table 3. Retention Time, Detected Mass, Collision Energy, MS/MS Data, and Content of Analytes

analyte	retention time (min)	detected mass (m/z)	collision energy (V)	MS/MS			content (mg/g)
protocatechuic acid	0.760	154.0178	10	112.9848	110.0326	109.0290	0.0203
chlorogenic acid	1.144	354.0689	10	315.7659	264.9461	191.0568	0.3727
epicatechin	1.677	290.0536	25	247.6703	144.8024	112.9854	0.3081
hyperoside	3.412	464.0874	25	343.0467	300.0269	271.0236	0.1743
isoquercitrin	3.629	464.0867	20	343.0459	300.0269	151.0035	0.0870
quercetin	5.380	302.0350	20	229.0457	151.0038	107.0144	0.0186

mm × 50 mm, 1.8 μm), and a Zorbax StableBond-C_{18} column (2.1 mm × 50 mm, 1.8 μm) were also investigated. It was found that the Zorbax Extend-C_{18} column at a temperature of 40 °C was suitable to separate the constituents present in hawthorn fruit. ESI parameters also played major effects in the signal response and peak shape measured for $[M - H]^-$ ions of analytes. As a result, higher signal intensity was observed in negative mode at the following conditions: capillary voltage, 3500 V; nebulization gas flow rate, 12 L/min at a temperature of 350 °C; nebulizer, 45 psig; and fragmentor, 175 V.

Method Evaluation. To evaluate the proposed micellar extraction method for simultaneous determination of multiclass polar compounds in hawthorn fruits, linearity, precision, limits of detection (LODs), repeatability, and recovery were determined under the optimized conditions. Linearity was investigated at seven different concentration levels ranging from 0.1 to 40 μg/mL for the six analytes. Results shown in Table 2 indicate that good linearity of all target compounds was obtained with correlation coefficients (r^2) ranging from 0.9934 to 0.9999. The intraday precision was examined by analyzing six determinations within 1 day, and interday precision was determined within consecutive 3 days among a middle concentration of linear range. As shown in Table 2, the intra- and interday variations regarding peak areas and retention time were less than 3.3% (n = 6) and 5.3% (n = 3) for all analytes, respectively, which indicated that the developed method had good precision. The sensitivity of the proposed method was evaluated by determining the LODs at low concentration levels giving a signal-to-noise ratio of 3. The LODs ranged from 0.0030 to 0.0054 μg/mL for all analytes (Table 2). Accredited repeatability was achieved by relative standard deviations (RSDs, n = 5) between 2.1 and 4.3% for the determination of five repeated extractions of hawthorn fruit samples. Recoveries were studied by standard addition method for the accuracy evaluation of the proposed method. Each target compound was added at concentrations ca. 0.5, 1, and 1.5 times the observed concentration in hawthorn fruit samples and then determined by UHPLC-Q-TOF/MS. Results manifested that the recovery values were from 89.3 to 106% for the six analytes with RSDs lower than 5.5%. Considering all validation results, the newly developed method was accurate and reliable for detecting analytes in hawthorn fruit samples.

Analysis of Real Samples. The proposed method was applied to the analysis of target compounds in hawthorn samples collected from the local drugstore in China. All analytes 1−6 produced abundant $[M - H]^-$ ions as the base peaks in negative ESI-MS spectra because $[M - H]^-$ provided better sensitivity compared with the other protonation states. The $[M - H]^-$ ions were selected as the precursor ions to produce MS/MS spectra at optimal collision energies (Table 3). In the current research, all of the compounds could be easily identified by their retention time, characteristic accurate masses (error < 5 ppm), and fragment ions (Table 3). Typical LC-MS chromatograms demonstrating the separation of six analytes are shown in Figure 4. The contents of the targeted compounds were found to be different in hawthorn fruit sample (Table 3). The analytical results manifested that the micellar extraction was a precise and reliable method, which could be substituted for the conventional methanol extraction to detect multiclass polar compounds in the complex samples.

In conclusion, a new method of IL-based micellar extraction coupled with UHPLC-Q-TOF/MS has been developed for the determination of multiclass polar compounds in hawthorn fruit samples. The optimum micellar extraction conditions were 150 mM $[C_{12}mim]Cl$, a solid−liquid ratio of 1:20 (g/mL), and an ultrasonication time of 40 min under ultrasonic power of 100 W. Compared to conventional extraction techniques, the developed method provided higher extraction yields and reduced the consumption of volatile organic solvent. More important, the IL-based extraction technique was not only reliable by its good repeatability and precision but also environmentally friendly. This green sample preparation approach is bound to have much wider applications in dealing with food samples.

AUTHOR INFORMATION

Corresponding Author

*(J.C.) Phone: +86-571-28867909. Fax: +86-571-28867909. E-mail: caojun91@163.com.

Funding

This study was supported by the General Program of National Natural Science Foundation of China (No. 81274065), Changjiang Scholars and Innovative Research Team in Chinese University (IRT 1231), Scientific Research Foundation of Hangzhou Normal University (2011QDL33), and the new-shoot Talents Program of Zhejiang province (2013R421044).

Notes

The authors declare no competing financial interest.

REFERENCES

(1) Wang, J. H.; Cheng, D. H.; Chen, X. W.; Du, Z.; Fang, Z. L. Direct extraction of double-stranded DNA into ionic liquid 1-butyl-3-methylimidazolium hexafluorophosphate and its quantification. *Anal. Chem.* **2007**, *79*, 620−625.

(2) Du, F. Y.; Xiao, X. H.; Luo, X. J.; Li, G. K. Application of ionic liquids in the microwave-assisted extraction of polyphenolic compounds from medicinal plants. *Talanta* **2009**, *78*, 1177−1184.

(3) Li, T. H.; Joshi, M. D.; Ronning, D. R.; Anderson, J. L. Ionic liquids as solvents for in situ dispersive liquid-liquid microextraction of DNA. *J. Chromatogr., A* **2013**, *1272*, 8−14.

(4) Padró, J. M.; Marsón, M. E.; Mastrantonio, G. E.; Altcheh, J.; García-Bournissen, F.; Reta, M. Development of an ionic liquid-based dispersive liquid-liquid microextraction method for the determination of nifurtimox and benznidazole in human plasma. *Talanta* **2013**, *107*, 95−102.

(5) Zhao, Q. C.; Wajert, J. C.; Anderson, J. L. Polymeric ionic liquids as CO_2 selective sorbent coatings for solid-phase microextraction. *Anal. Chem.* **2010**, *82*, 707−713.

(6) Sarafraz-Yazdi, A.; Vatani, H. A solid phase microextraction coating based on ionic liquid sol-gel technique for determination of benzene, toluene, ethylbenzene and *o*-xylene in water samples using gas chromatography flame ionization detector. *J. Chromatogr., A* **2013**, *1300*, 104−111.

(7) Freire, M. G.; Neves, C. M. S. S.; Marrucho, I. M.; Lopes, J. N. C.; Rebelo, L. P. N.; Coutinho, J. A. P. High-performance extraction of alkaloids using aqueous two-phase systems with ionic liquids. *Green Chem.* **2010**, *12*, 1715−1718.

(8) Romero, L.; Osorio Grisales, J.; Reta, M. Comparison between phase-transfer and cloud-point methodologies for the micellar extraction of biogenic amines. *Talanta* **2010**, *81*, 1431−1437.

(9) Kumar, S.; Hemavathi, A. B.; Hebbar, H. U. Affinity based reverse micellar extraction and purification of bromelain from pineapple (*Ananas comosus* L. Merryl) waste. *Process Biochem.* **2011**, *46*, 1216−1220.

(10) Yao, C.; Pino, V.; Anderson, J. L. Utilization of solid-phase microextraction-high-performance liquid chromatography in the determination of aromatic analyte partitioning to imidazolium-based ionic liquid micelles. *J. Chromatogr, A* **2009**, *1216*, 948−955.

(11) Cao, J.; Li, P.; Yi, L. Ionic liquids coated multi-walled carbon nanotubes as a novel pseudostationary phase in electrokinetic chromatography. *J. Chromatogr., A* **2011**, *1218*, 9428−9434.

(12) Pino, V.; Anderson, J. L.; Ayala, J. H.; González, V.; Afonso, A. M. The ionic liquid 1-hexadecyl-3-methylimidazolium bromide as novel extracting system for polycyclic aromatic hydrocarbons contained in sediments using focused microwave-assisted extraction. *J. Chromatogr., A* **2008**, *1182*, 145−152.

(13) Wu, K. K.; Zhang, Q. L.; Liu, Q.; Tang, F.; Long, Y. M.; Yao, S. Z. Ionic liquid surfactant-mediated ultrasonic-assisted extraction coupled to HPLC: application to analysis of tanshinones in *Salvia miltiorrhiza* Bunge. *J. Sep. Sci.* **2009**, *32*, 4220−4226.

(14) Glauser, G.; Veyrat, N.; Rochat, B.; Wolfender, J. L.; Turlings, T. C. J. Ultra-high pressure liquid chromatography-mass spectrometry for plant metabolomics: a systematic comparison of high-resolution quadrupole-time-of-flight and single stage Orbitrap mass spectrometers. *J. Chromatogr., A* **2013**, *1292*, 151−159.

(15) Li, S. L.; Shen, H.; Zhu, L. Y.; Xu, J.; Jia, X. B.; Zhang, H. M.; Lin, G.; Cai, H.; Cai, B. C.; Chen, S. L.; Xu, H. X. Ultra-high-performance liquid chromatography-quadrupole/time of flight mass spectrometry based chemical profiling approach to rapidly reveal chemical transformation of sulfur-fumigated medicinal herbs, a case study on white ginseng. *J. Chromatogr., A* **2012**, *1231*, 31−45.

(16) Cao, J.; Li, P.; Chen, J.; Tan, T.; Dai, H. B. Enhanced separation of compound Xueshuantong capsule using functionalized carbon nanotubes with cationic surfactant solutions in MEEKC. *Electrophoresis* **2013**, *34*, 324−330.

(17) Lou, S.; Di, D. L. Synthesis of resins with ionic liquids for purification of flavonoids from *Hippophae rhamnoides* L. leaves. *J. Agric. Food Chem.* **2012**, *60*, 6546−6558.

(18) Natale, D.; Gibis, M.; Rodriguez-Estrada, M. T.; Weiss, J. Inhibitory effect of liposomal solutions of grape seed extract on the formation of heterocyclic aromatic amines. *J. Agric. Food Chem.* **2014**, *62*, 279−287.

(19) Castro-Puyana, M.; García-Cañas, V.; Simó, C.; Cifuentes, A. Recent advances in the application of capillary electromigration methods for food analysis and foodomics. *Electrophoresis* **2012**, *33*, 147−167.

(20) Liu, P. Z.; Kallio, H.; Yang, B. R. Phenolic compounds in hawthorn (*Crataegus grayana*) fruits and leaves and changes during fruit ripening. *J. Agric. Food Chem.* **2011**, *59*, 11141−11149.

(21) Zhou, Y. C.; Kong, W. J.; Li, Y.; Logrieco, A. F.; Xu, J.; Yang, M. H. A new solid-phase extraction and HPLC method for determination of patulin in apple products and hawthorn juice in China. *J. Sep. Sci.* **2012**, *35*, 641−649.

(22) Urbonavičiūtė, A.; Jakštas, V.; Kornyšova, O.; Janulis, V.; Maruška, A. Capillary electrophoretic analysis of flavonoids in single-styled hawthorn (*Crataegus monogyna* Jacq.) ethanolic extracts. *J. Chromatogr., A* **2006**, *1112*, 339−344.

(23) Liu, P. Z.; Kallio, H.; Lü, D. G.; Zhou, C. S.; Yang, B. R. Quantitative analysis of phenolic compounds in Chinese hawthorn (*Crataegus* spp.) fruits by high performance liquid chromatography-electrospray ionisation mass spectrometry. *Food Chem.* **2011**, *127*, 1370−1377.

(24) Sun, P.; Armstrong, D. W. Ionic liquids in analytical chemistry. *Anal. Chim. Acta* **2010**, *661*, 1−16.

(25) Pino, V.; Germán-Hernández, M.; Martín-Pérez, A.; Anderson, J. L. Ionic liquid-based surfactants in separation science. *Sep. Sci. Technol.* **2012**, *47*, 264−276.

(26) Luo, L. P.; Shen, L. M.; Sun, F.; Ma, Z. J. Immunoprecipitation coupled with HPLC-MS/MS to discover the aromatase ligands from *Glycyrrhiza uralensis*. *Food Chem.* **2013**, *138*, 315−320.

and seed of different tomato cultivars from Sinaloa, Mexico, to take advantage of these byproducts to enrich animal or human food and have ecological and economic benefits, reducing tomato agricultural and industrial wastes.

MATERIALS AND METHODS

Chemicals and Reagents. HPLC grade acetonitrile and methanol were purchased from Karal (Leon, Gto., Mexico). Minimal glucose agar and Oxoid nutrient broth were bought from Oxoid Microbiology Products (Thermo Fisher Scientific, New York, NY, USA). Solvents and other reagents, including the phenolic standards (gallic acid, caffeic acid, ferulic acid, *p*-coumaric acid, *o*-coumaric acid, (+)-catechin hydrate, quercetin anhydrous, rutin hydrate, kaempferol, isorhamnetin, and myricetin) were ACS grade solvents or reactives and pure grade standards (Sigma Chemical Co., St. Louis MO, USA).

Biological Material. Organically grown tomatoes, cultivated in Sinaloa (a state in northwestern Mexico) during the autumn/winter 2010−2011 season, of four varieties (saladette, bola, grape, and cherry) were collected (20 kg/cultivar) in the breaker stage (USDA, 1991) during the morning and within the period from December 17, 2010, to January 23, 2011. Collected tomato materials were transported to the laboratory and stored at 20 °C until they reached the red stage (last stage in the color scale). Commercial saladette tomatoes (20 kg) were bought in a local market to get simulated industrial byproducts; saladette tomatoes are the main material used for the regional tomato-processing industry to produce tomato paste.

Color Analysis. The color of ripe tomatoes was measured with a chroma meter CR-400 (Konica Minolta Sensing, Inc., Japan); 10 whole fruits of each type were evaluated in five points, three equidistant equatorial points and two axial. Chroma and a^*/b^* data were calculated from L^*, a^*, and b^* CIELab parameters, using a white standard CR-A43.

Sample Processing. For the chemical analysis, the peel and seeds of all tomato types were manually separated from the pulp, frozen (−20 °C)m and freeze-dried (Labconco Co., Kansas City, MO, US). The simulated commercial tomato byproducts were prepared as suggested by an engineer from a local processor in the tomato industry (personal communication); ripe saladette tomato (20 kg) was cut into cubes of 2 cm^3, ground in a conventional blender until juice appearance, and heated at 80 °C during 1 h in an aluminum pot with constant stirring to get the higher yield of juice. The mixture was filtered with a gauze swab, juice was discarded, and the remnants of peel and seeds were manually separated, frozen at −20 °C, and freeze-dried. Dried byproducts were ground in a laboratory mill (Thomas Wiley, Thomas Scientific, Swedesboro, NJ, USA) until we had a fine flour (80 mesh size) and stored (4 °C/protected from light) until analyses. Three biological replicates of each variety of tomato were processed.

Proximal Composition Analysis. Proximal composition was determined by the following methods described in the AOAC (2005) standard methodologies:[18] 930.15 for humidity; weight difference method 942.05 for ashes; 976.05 for total nitrogen; 976.05 for total lipids; and 978.10 for total crude fiber. All quantifications were conducted in triplicate.

Preparation of the Methanolic Extract. Peel and seed flour were extracted as described by Ferreres et al.[10] with some modifications. Samples (0.5 g) were suspended in 5 mL of methanol in 15 mL plastic tubes, sonicated during 1 h (mixed with a vortex every 10 min), transferred into 125 mL Erlenmeyer flasks, and made up to 20 mL with methanol. Then, samples were incubated for 22 h (25 °C/darkness/220 rpm) and centrifuged at 1409*g*/3 min in a rotor J600R2004 (Solbat S.A. de C.V., Puebla de Zaragoza, Mexico), the supernatant was decanted and stored at −20 °C, and the pellet was re-extracted by adding 20 mL of methanol and following the previously described steps. After re-extraction, both supernatants were combined and concentrated to dryness at 37 °C in a rotary evaporator (Yamato, Santa Clara, CA, USA). The extract were reconstituted with 3 mL of methanol, filtered through 0.22 μm Durapore syringe filters (Millipore, Carrigtwohill, Co. Cork, Ireland), and kept stored at −20 °C until use (this was called the methanolic crude extract). Each tomato sample was made in triplicate.

Total Polyphenol Content. The total polyphenol content of crude methanolic extract was quantified using the Folin−Ciocalteu spectrophotometric method, according to Nurmi et al.,[19] with modifications made by Ramírez-Mares et al.[20] Briefly, methanolic crude extract was dissolved in methanol (1:30 p/v), and 100 μL of the solution was mixed with 1 mL of 0.5 N Folin−Ciocalteu's phenol reagent and 2 mL of a 20% (w/v) Na_2CO_3 solution; the mixture was allowed to stand for 15 min at darkness, and the absorbance was measured at 734 nm. Gallic acid (GA) and (+)-catechin hydrate (CAT) were used to prepare calibration curves, and results were reported as milligrams of gallic acid equivalents per gram of flour (mg GAE/g) or catechin equivalents (mg CE/g). Groups of phenolic compounds were quantitated by spectrophotometry[21] at 320 nm for tartaric esters of phenolic acids and at 404 nm for flavonoids in a Thermo Spectronic Genesys 2 spectrophotometer (Thermo Fisher Scientific). Results of groups of phenolic compounds were expressed as caffeic acid or quercetin equivalents per gram of peel or seed flour, for phenolic tartaric esters or flavonoids, respectively.

Antioxidant Activity. The antioxidant activity of crude methanolic extracts was measured by the DPPH,[22] ABTS,[23] and ORAC[24] methods. DPPH and ABTS are free stable oxidative radicals, and we measured spectrophotometrically their decrease in absorbance (as the effect of the phenolic compounds presents in the samples). In the ABTS method, the $ABTS^{\bullet+}$ radical was chemically prepared (7 mM in methanol); the ABTS reagent was mixed with potassium persulfate (2.45 mM), incubated during 16 h at room temperature, and diluted with methanol to get an absorbance value of 0.70 ± 0.02 at 734 nm. To measure the antioxidant activity, 10 μL of the concentrated methanol crude extract (controls or standard) was mixed with 1000 μL of $ABTS^{\bullet+}$ and vortexed gently during 20 s, and the absorbance at 734 nm was registered.

For the DPPH assay, the radical (125 μM in methanol) was daily prepared and kept at 4 °C/darkness. Assay was done in a 96-well microplate; 20 μL of the concentrated methanol crude extract (controls or standard) was mixed with 200 μL of DPPH solution, and absorbance (515 nm) was read at 0, 10, 20, 30, 40, 50, 60, 70, 80, and 90 min with a DTX 880 multimode detector (Beckman Coulter, Brea, CA, USA). Trolox standard curve was constructed at 30 min.

For the Oxygen radical absorbance capacity (ORAC) (performed fluorometrically) assay,[24] analysis was done at 37 °C in pH 7.4, 75 mM phosphate buffer, peroxyl radical was generated using AAPH (70 mM), and fluorescein (87 μM) was the substrate. Twenty-five microliters of diluted (1:100) sample (control or standard) was mixed with 200 μL of fluorescein and 50 μL of AAPH, and the decrease of fluorescence was calculated in a DTX 880 multimode detector, using the following conditions: excitation wavelength of 485 nm and emission wavelength of 530 nm; 76 cycles were read, every 2 min. In all cases we report antioxidant activity as Trolox equivalents, a standard curve was prepared with a correlation coefficient up to R = 0.99, and the equivalents were calculated as micromole equivalents of Trolox per 100 g of flour. Three independent experiments were conducted in each assay.

Profile of Phenolics by HPLC-DAD. The HPLC profile of phenolics in the methanolic crude extract was established with a Dionex UltiMate 3000 liquid chromatograph, equipped with a titanium quaternary pump (LPG-3400AB), an autosampler (WPS-3000TBPL), a column oven, and a photodiode array detector DAD-3000(RS) (scan range 190−800 nm and scan speed 2 nm/s) from Thermo Scientific. Separation was carried out using an analytical column Acclaim 120 A (C18, 5 μm, 120 Å, 4.6 × 250 mm), from Dionex (Thermo Fisher Scientific), at ambient temperature. Elution was done with a gradient of two solvents: water acidified with acetic acid (pH 2.8) (A) and acetonitrile (B). The gradient for phenolic acids[25] was 100% phase A, 6% phase B, from 0 to 8 min; from 6 to 12% B from 8 to 14 min; from 12 to 20% B from 14 to 18 min; from 20 to 35% B from 18 to 24 min, from 35 to 95% B from 24 to 27 min; from 95 to 100% B from 27 to 30 min; and from 100% B to 100% A in 10 min. The fixed wavelengths were 260, 270, 275, 280, 285, 290, 295, and 300 nm.

dx.doi.org/10.1021/jf5012374 | J. Agric. Food Chem. 2014, 62, 5281−5289

Table 1. Parameters of Color of Whole Tomato Fruits from Several Varieties Cultivated in Northwestern Mexico ($X \pm$ SD, $n = 10$)[a]

tomato type	L^*	a^*	b^*	chroma	a^*/b^*
cherry	31.4 ± 1.45 b	13.8 ± 1.64 ab	11.2 ± 1.29 b	17.5 ± 3.72 a	1.24 ± 0.17 a
grape	34.2 ± 1.58 a	17.2 ± 1.50 a	13.0 ± 0.96 ab	21.6 ± 1.36 a	1.32 ± 0.15 a
bola	36.7 ± 1.30 a	15.9 ± 1.74 a	15.1 ± 0.96 a	20.1 ± 3.14 a	1.05 ± 0.13 ab
saladette	35.6 ± 1.36 a	15.9 ± 1.35 a	15.0 ± 0.92 a	19.4 ± 4.03 a	1.06 ± 0.09 ab
byproducts	34.8 ± 1.80 a	17.5 ± 2.60 a	12.9 ± 2.10 ab	18.2 ± 4.40 a	1.37 ± 0.11 a

[a]Values marked by the same letter within the same column are not statistically significantly different (multiple-range test; Tukey, $p \leq 0.05$).

The gradient for the elution of flavonoids was 100% A, 10% B, from 0 to 2.5 min, from 10 to 12% B from 2.5 to 6 min; from 12 to 23% B from 6 to 18 min; from 23 to 35% B from 18 to 24 min; from 35 to 95% B from 24 to 27 min; from 95 to 100% B from 27 to 30 min; and from 100% B to 100% A in 10 min; 260 and 342 nm were the fixed wavelengths for flavonoids. The flow rate was 0.5 mL/min. The injection volume was 10 μL. Chromatographic peaks were identified by comparing the retention times and UV−visible absorption of pure standards (i.e., gallic, caffeic, ferulic, *p*-coumaric, and *o*-coumaric acids; and flavonoids (+)-catechin hydrate, quercetin, rutin hydrate, kaempferol, isorhamnetin, and myricetin). A standard curve was constructed with the mix of all phenolic acids and another with the mix of all flavonoids. Each sample was injected three times. The data were processed using Chromeleon 7.0 software (Dionex, Thermo Fisher Scientific).

Antimutagenic Activity Test. The antimutagenicity of the methanolic crude extracts was determined, the extracts were concentrated to dryness under a nitrogen flow, and the solid extract was resuspended in sterilized DMSO. The antimutagenic activity was done by the microsuspension assay using YG1024 *Salmonella typhimurium* as tester strain and 1-nitropyrene as mutagen, according to the method of Santos-Cervantes et al.[26] A dose−response curve of mutagen and different sample concentrations was constructed. An aliquot (10 μL) of resuspended extract was homogenized with the components of the incubation mix, including 1-nitropyrene. A mix of bacteria plus mutagen was used as a positive control of mutation reversion. The capacity of tomato seed or peel extracts to prevent the action of 1-nitropyrene against the cells was measured with the follow equation:

$$\%\ \text{antimutagenic activity} = [(\text{His}^+\ \text{revertants of positive control plate} - \text{His}^+\ \text{revertants of sample test plate}) / \text{His}^+\ \text{revertants of positive control plate}] \times 100$$

Statistical Analysis. A totally random experimental design was used to evaluate the color parameters and a factorial design 5 × 2 for the chemical and antimutagenic analysis; the first factor was tomato type, and the second one was the anatomic part of the tomato fruit. ANOVA analysis and a multiple-ranges test (Tukey, $p \leq 0.05$) were done with the SAS 7.0 statistic program (SAS Institute Inc., Cary, NC, USA). A correlation test between total phenolics/individual phenolic content and antioxidant or antimutagenic activity was done through SAS 7.0 using the Pearson's correlation coefficient option. Three biological replicates and at least two independent experiments were performed.

RESULTS AND DISCUSSION

Color and Proximal Composition. Maturity stage was not significantly different among tomato varieties considered in this study. Tomato color was uniform inter- and intratomato varieties, as indicated by the low variability of the color parameters (L^*, a^*, b^*, chroma, and a^*/b^* values) and their statistical similarity (Table 1). The ripeness stage for these tomatoes corresponded with that accepted for marketing.[27]

The proximal composition of peel and seed of all tomato types can be observed in Figure 1. All measured parameters

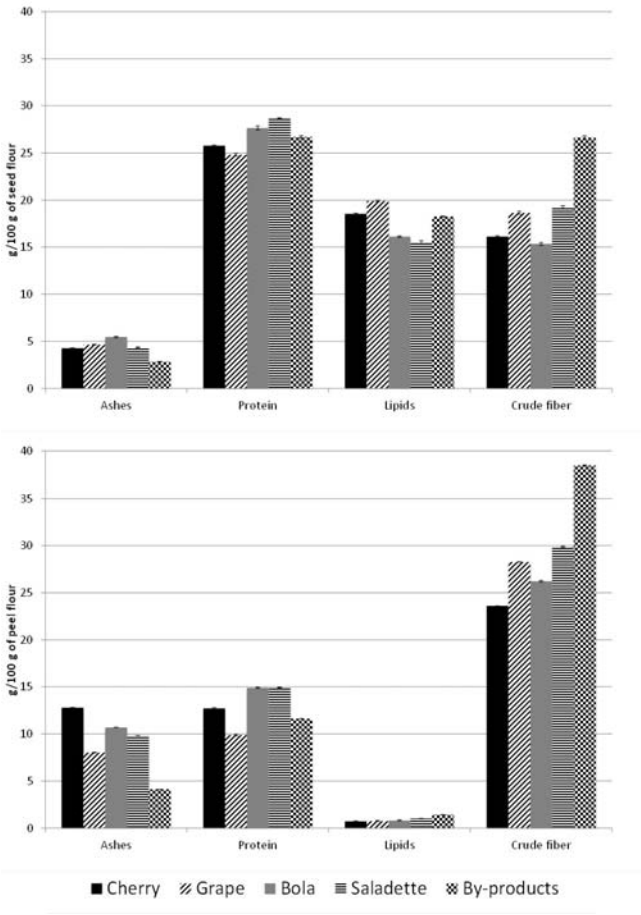

Figure 1. Proximal composition of flour from peel (A) and seeds (B) of different tomato types and tomato byproducts. Data are the average of three replicates ± standard deviation. Statistical analysis of proximal composition is not shown in this figure, but significant differences between treatments were observed.

were higher than the average values previously reported for whole tomato fruit,[28] except total lipids in peel,[6] and were closer than those reported for seed and peel from tomato pomace.[11,29] Notable protein content was found in all seed samples, >24 g/100 g, closer than that reported by Fuentes et al. for tomato seed from pomace.[29] saladette type had the highest protein percentage (28.7 g/100 g of flour), and a high ash content was quantified in the majority of tomato types (6.7 g/100 g of flour, on average); the mentioned parameter was superior to that reported by different authors in flour of

dx.doi.org/10.1021/jf5012374 | J. Agric. Food Chem. 2014, 62, 5281−5289

tomato byproducts (5 g/100 g of flour).[5,6,29] Crude fiber of seed plus peel of each tomato type was superior that previously reported for tomato pomace.[28] The byproducts contained the highest fiber content (38.5 g/100 g of flour) ($p \leq 0.05$). This effect could be the result of the heat process, as it has been previously reported in other vegetables that insoluble dietary fiber increased as a result of a cooking process.[30] Total lipids in peel correspond to 3% of the proximal composition and are represented by waxes, mainly.[15] In seeds, total lipids represented up to 15 g/100 g of flour, and in the case of grape tomato seeds, these compounds reached 20 g/100 g of flour; it could be important to analyze the fatty acid profile and other hydrophobic compounds as phytosterols to determine a potential commercial use. Analysis of variance (ANOVA) showed that all proximal composition parameters were affected by tomato type, the part of the fruit analyzed (peel or seed), and the interaction of both factors.

High protein and total fiber contents found in our samples suggest that the peel or seed of tomato dry flour can be used as a source of those substances to enrich animal or human food.

Total Phenolic Content, Groups of Phenolic Compounds, and Antioxidant Capacity. Crude methanolic extracts showed levels of phenolic content (Table 2) comparable with those of other fruits recognized for their phenolic content, such as kiwi and grapes.[31] The ranges were from 71.6 to 351.6 mg equiv gallic acid (GA)/100 g peel flour samples (208.2 mg equiv GA/100 g flour, on average) and from 67.3 to 121.8 mg equiv GA/100 g seed flour (95.2 mg equiv GA/100 g flour, on average); these values were superior to those reported for peel and seed from several tomato varieties and tomato byproducts.[17,28] In the case of the total phenolic content expressed as milligram equivalents of (+) catechin (CAT), data ranged between 464.3 and 1824.1 mg equiv oCAT/100 g peel flour samples (1136.8 mg equiv CAT/100 g flour, on average) and between 438.3 and 682.8 mg equiv CAT/100 g seed flour (569.4 mg equiv CAT/100 g, on average) in seed samples and were superior to thosee previously reported by George et al. in tomato peel.[32] There were found statistically significant differences ($p \leq 0.05$) due to the interaction of tomato type and part of the fruit and the notable presence of a higher amount of phenolic compounds in peel flour than in seed flour, as has been reported by Chandra et al.[17] Grape peel flour was the material with the best total phenolic content in both ways of expressing phenolic concentration (351.6 mg equiv GA/100 g flour and 1824.1 mg equiv CAT/100 g flour), whereas byproduct seed flour showed the lowest phenolic content (67.3 mg equiv GA/100 g flour and 464.3 mg equiv CAT/100 g flour) than saladette (byproducts were produced from a saladette tomato type); perhaps this decrease in phenolic content could be due to the heat processing.[33] In addition, phenolics oxidation could have occurred during homogenization of the fresh fruit due to polyphenol oxidase,[33] but the total phenolic concentration in byproducts remains attractive for their use as a source of phenolic compounds. Sagdic et al.[34] in 2011 reported the content of total phenolic compounds in byproducts from grape fruit; our data obtained in cherry and grape tomato peel flours were comparable to those reported by these authors. Differences in the phenolic content for effect of tomato genotype have been reported;[17,32] the highest amount of phenolic compounds found in cherry and grape tomato types could be due to these genotypes being less genetically manipulated than saladette and bola, and it is known that

Table 2. Total Phenolic Content, Groups of Phenolics, and Antioxidant Capacity of Methanolic Extracts from Peel or Seed Flour of Different Tomato Varieties ($X \pm SD$/100 g, $n = 3$)[a]

		total phenols[b]				groups of phenolics[c]				antioxidant capacity (μmol equiv Trolox[h])					
						tartaric esters		flavonoids							
sample	tomato type	mg equiv GA[d]		mg equiv CAT[e]		mg equiv CA[f]		mg equiv QUER[g]		ABTS		DPPH		ORAC	
peel	cherry	266.3 ± 13.6	b	1481.8 ± 36.6	b	11.2 ± 0.3	b	218.3 ± 37.7	b	209.2 ± 31.6	b	171.0 ± 10.1	ab	2812.6 ± 235.9	b
	grape	351.6 ± 12.7	a	1824.1 ± 68.7	a	16.9 ± 0.1	a	572.2 ± 174.4	a	405.7 ± 29.7	a	181.4 ± 20.2	a	4131.7 ± 86.8	a
	bola	157.8 ± 19.5	d	922.6 ± 34.6	c	8.9 ± 0.8	d	225.8 ± 37.2	b	201.4 ± 29.0	b	155.5 ± 20.2	ab	1899.6 ± 57.0	bcd
	saladette	192.8 ± 0.2	c	991.3 ± 34.5	c	10.2 ± 0.1	c	216.5 ± 55.0	b	196.3 ± 16.2	b	168.9 ± 19.5	ab	2188.6 ± 110.7	bc
	byproducts	71.6 ± 2.7	g	464.3 ± 6.7	fg	3.1 ± 0.5	g	83.7 ± 1.0	c	47.9 ± 5.0	e	51.4 ± 10.2	d	705.3 ± 20.3	f
seed	cherry	121.8 ± 3.5	e	682.8 ± 16.7	d	6.3 ± 0.5	e	60.1 ± 10.4	c	85.0 ± 6.8	cd	92.4 ± 17.7	cd	1404.7 ± 238.7	cdef
	grape	113.3 ± 4.9	e	648.8 ± 24.2	de	6.3 ± 0.3	e	69.2 ± 8.3	c	139.6 ± 1.1	c	156.2 ± 17.4	ab	1825.0 ± 375.4	cde
	bola	99.6 ± 2.1	f	589.9 ± 10.1	e	4.8 ± 0.8	f	53.1 ± 5.0	c	49.4 ± 1.2	e	118.8 ± 5.2	bc	1213.7 ± 20.0	cdef
	saladette	73.8 ± 9.8	g	486.7 ± 11.6	f	3.3 ± 0.9	g	57.0 ± 8.5	c	67.4 ± 4.2	de	92.4 ± 17.6	cd	1146.5 ± 218.5	def
	byproducts	67.3 ± 0.3	h	438.8 ± 6.7	g	3.2 ± 0.4	g	50.0 ± 23.4	c	35.1 ± 8.1	e	83.6 ± 6.8	cd	1028.3 ± 78.9	ef

[a]Values marked by the same letter within the same column are not statistically significantly different (multiple-range test; Tukey, $p \leq 0.05$). [b]Total phenols were quantified with the Folin–Ciocalteu method. [c]Group of phenolics were determined by direct measurement according to Oomah et al.[21] [d]mg equivalents of gallic acid (GA) per 100 g of sample. [e]mg equivalents of (+) catechin (CAT) per 100 g of sample. [f]mg equivalents of caffeic acid (CA) per 100 g of sample. [g]mg equivalents of quercetin (QUER) per 100 g of sample. [h]μmol equivalents of Trolox per 100 g of sample.

dx.doi.org/10.1021/jf5012374 | J. Agric. Food Chem. 2014, 62, 5281–5289

crops that have been largely genetically improved show reduced concentration of some metabolites, even phenolic compounds.[35] The amount of the different phenolic groups can be observed in Table 1. The major group was flavonoids, ranging from 83.7 mg/100 g flour in byproducts to 572.2 mg/100 g of grape tomato peel flour; in the case of seed samples, flavonoids were quantified from 50.0 to 69.2 mg/100 g in byproducts and grape tomato flour, respectively. On the other hand, phenolic tartaric esters ranged from 3.1 to 16.9 mg/100 g for byproducts and cherry tomato peel flours, respectively; meanwhile in seeds a decrease in content until 2.6 times ranged from 3.2 to 6.3 mg/100 g for byproducts and grape tomato seed, respectively. In the same way as happened with total phenolic content, flavonoid and ester phenolics concentrations were higher in the peel flour than in seed flour, in most of cases. Statistically significant differences ($p \leq 0.05$) were observed between treatments. We observed that approximately 60% of total phenolic content corresponded to flavonoids and 30% to phenolic acids, in the same way that has been found in several samples.[36] Oomah et al.[21] reported levels of flavonols similar to those that we found in tomato peel in hull fractions and residues from red and green lentils, but this previous study was done with acetone and hot water extracts, and the proportion of phenolic compounds extracted varies widely according to the extraction solvent, so our results and those reported previously are not completely comparable.

Antioxidant activity was determined with three methodologies, ABTS, DPPH, and ORAC, and results were expressed as micromole equivalents of Trolox per 100 g of flour (peel or seed) in all cases. Peel samples showed the best results in all cases. ABTS and DPPH methodologies have a similar chemical makeup, but the data obtained with these two methods were different between the same samples. ABTS measured a more major antioxidant activity than DPPH in the peel samples of all evaluated genotypes except in byproducts, in which case there was no significant difference ($p \leq 0.05$) in the antioxidant activity due to the radical used (ABTS or DPPH). In contrast, in seed samples, the DPPH methodology showed the best results in all genotypes. Due to the previously described behavior, it can be inferred that the qualities of the extracted compounds are different between peel and seed samples because both extracts reacted differently on the same free radical, as observed before.[37] The best results were obtained in grape tomato genotype, again. This sample showed 405.7 μmol equiv Trolox/100 g flour by ABTS and 181.4 μmol equiv Trolox/100 g flour by DPPH in peel and 139.6 μmol equiv Trolox/100 g flour by ABTS and 156.2 μmol equiv Trolox/100 g flour with DPPH methodology in seed sample. Antioxidant activity determined by ABTS was superior to that previously reported in aqueous extracts from tomato plants and yellow cherry whole tomato fruits.[2,32]

Antioxidant capacity calculated with ORAC methodology was significantly higher than those quantified with ABTS and DPPH methodologies ($p \leq 0.05$); values were in the range between 705.3 and 4131.7 μmol equiv Trolox/100 g of flour in peel samples and from 1028.3 to 1825.0 μmol equiv Trolox/100 g flour in the case of seed samples. In both cases the lowest activity corresponded to byproducts. The highest activity was measured in grape tomato type ($p \leq 0.05$). Despite this, the antioxidant activity of the byproducts remained at high levels.[21,37] Several studies have shown that ORAC methodology is more adequate to quantify antioxidant activity, due to its resemblance to a biological process in vivo, regarding the peroxyl free radicals. It is, however, desirable that our results were validated through an in vivo antioxidant activity methodology, reducing confounding factors that affect the action of phenolic compounds over free radicals. The ORAC methodology does not take into account those factors; thus, further studies are required.[38] There was observed an influence of the tomato type, as has been reported before by Chandra et al.,[17] the part of the fruit analyzed, and the interaction of these two factors on the antioxidant activity measured by the three methodologies used.

Correlations analysis (Pearson, SAS 7.0) between total phenolic and antioxidant activity and between groups of phenolic compounds and antioxidant activity were done (data not shown). We calculated R values >0.8 in all cases except when we correlated flavonoids with antioxidant activity determined by the DPPH method. R values >0.8 are considered higher. It has been reported that not all extractable compounds that can be measured as total phenols or belonging to a phenolic group may have the capacity to act against a free radical used in a particular methodology to determine antioxidant activity (scavenging activity, mainly); this may be due to structural aspects or steric impediments of the different compounds that are present in the extract.[34,39]

Phenolic Compounds Profile by HPLC-DAD. Results of phenolic compounds profile by HPLC-DAD of each tomato sample (peel and seed flour) are summarized in Table 3, and Figure 2 shows the chromatograms obtained in the peel of grape tomato type. We have identified and quantified 16 compounds in total, 8 phenolic acids and 8 flavonoids. It is interesting that byproducts did not always present the lowest concentration of individual phenolic compounds, but the trend was to diminish the content of the evaluated compounds in byproducts, perhaps by the heat-processing effect,[29] as has been mentioned above. Flavonoids were found in higher concentration than phenolic acids in all tomato types (as happened in phenolic groups evaluation). The most abundant phenolic acids were caffeic acid, in concordance with that reported before in whole red tomato fruit,[40] followed by vanillic, ferulic, sinapic, and chlorogenic acids; in the case of flavonoids, the most concentrated were quercetin-3-β-O-glycoside, rutin, isorhamnetin, and kaempferol. Rutin (and its diverse chemical drivatives) is localized in the last steps of the phenolic biosynthesis route and is related to a commercially mature stage of fruits.[41] The content of all phenolic acids and flavonoids determined by HPLC-DAD, in our samples, was 3−5 times greater than that evaluated with the total phenolic methodology (Folin−Ciocalteu). There are diverse reports about the individual content of phenolic compounds in tomato fruits and seeds generated as byproduct, including an effort to characterize tomato metabolome, from a mix of 96 cultivars from the Iberian peninsula; these works were done by HPLC and HPLC coupled to mass spectrometry.[2,11,12,29,42] The main phenolic compounds found in tomato in previous studies (caffeic, ferulic, p-coumaric, and sinapic acids, rutin, quercetin, and kaempferol) are almost the same as those found in our work and were present in comparable levels to those reported by other authors. There have been reported attractive phenolic compounds such as caffeic, ferulic, and chlorogenic acids and rutin in tomato industrialized products (tomato juices and ketchup) in important levels, and we observed the presence of these phenolics in our byproduct samples. Therefore, we can mention that these compounds remain after a heat or cooking process.[11]

Table 3. Profile of Phenolic Compounds, Phenolics Acids, and Flavonoids in the Peel and Seed of Different Tomato Types Cultivated in Northwestern Mexico ($X \pm$ SD, $n = 3$)[a]

			mg/100 g DW[b]																	
			caffeic acid		vanillic acid		ferulic acid		sinapic acid		chlorogenic acid		*p*-coumaric acid		*trans*-cinnamic acid		gallic acid		total
phenolic acid	peel	cherry	5.11 ± 1.24	cd	1.57 ± 0.11	d	1.36 ± 0.05	e	2.66 ± 0.80	cde	3.24 ± 0.72	a	1.52 ± 0.29	b	0.23 ± 0.05	de	0.00 ± 0.00	d	15.7
		grape	22.06 ± 3.24	a	7.02 ± 0.74	b	3.32 ± 0.27	b	4.22 ± 0.17	a	2.01 ± 0.15	b	1.54 ± 0.56	b	2.42 ± 0.28	b	0.72 ± 0.18	b	43.3
		bola	7.85 ± 0.00	bc	11.27 ± 0.50	a	1.60 ± 0.02	e	3.45 ± 0.32	abc	1.52 ± 0.15	b	1.57 ± 0.15	b	0.87 ± 0.03	c	0.95 ± 0.13	ab	29.1
		saladette	10.51 ± 0.38	b	3.07 ± 0.18	c	4.56 ± 0.22	a	2.77 ± 0.06	bcd	0.41 ± 0.10	c	0.64 ± 0.04	c	0.22 ± 0.06	de	0.00 ± 0.00	d	22.2
		byproducts	1.05 ± 0.17	e	0.00 ± 0.00	e	3.67 ± 0.24	b	0.00 ± 0.00	f	0.10 ± 0.01	c	1.36 ± 0.06	bc	0.56 ± 0.01	cd	0.00 ± 0.00	d	6.7
	seeds	cherry	2.19 ± 0.17	de	0.00 ± 0.00	e	1.67 ± 0.00	e	2.11 ± 0.04	de	1.41 ± 0.08	b	0.79 ± 0.00	bc	0.72 ± 0.04	c	0.00 ± 0.00	d	8.9
		grape	1.67 ± 0.16	e	0.00 ± 0.00	e	4.31 ± 0.17	a	1.82 ± 0.15	e	0.61 ± 0.04	c	3.96 ± 0.15	a	0.16 ± 0.01	e	0.11 ± 0.01	d	12.6
		bola	2.13 ± 0.03	de	0.00 ± 0.00	e	2.75 ± 0.11	c	3.56 ± 0.15	ab	0.29 ± 0.07	c	1.31 ± 0.27	bc	0.83 ± 0.03	c	1.17 ± 0.22	a	12.0
		saladette	0.95 ± 0.04	e	2.01 ± 0.27	d	2.19 ± 0.09	d	2.87 ± 0.18	bcd	0.10 ± 0.02	c	0.90 ± 0.21	bc	0.10 ± 0.00	e	0.40 ± 0.00	c	9.5
		byproducts	1.95 ± 0.04	de	0.00 ± 0.00	e	2.20 ± 0.03	d	3.08 ± 0.28	cd	0.05 ± 0.01	c	1.58 ± 0.44	b	3.01 ± 0.31	a	0.00 ± 0.00	d	11.9

			mg/100 g DW[b]																	
			quercetin-3-*O*-*β*-glucoside		rutin		isorhamnetin		kaempferol		naringenin		quercetin		apigenin		myricetin		total
flavonoids	peel	cherry	15.12 ± 2.04	d	4.56 ± 0.49	e	2.65 ± 0.11	b	1.06 ± 0.20	cd	0.00 ± 0.00	d	2.58 ± 0.18	a	1.34 ± 0.03	a	0.16 ± 0.00	c	27.5
		grape	47.99 ± 2.71	a	14.19 ± 0.17	b	3.17 ± 0.12	a	3.74 ± 0.58	a	4.86 ± 0.39	a	2.08 ± 0.22	b	0.82 ± 0.04	b	0.50 ± 0.16	abc	77.4
		bola	18.30 ± 0.05	c	11.85 ± 0.41	c	3.16 ± 0.05	a	3.70 ± 0.49	a	2.52 ± 0.36	b	0.19 ± 0.01	e	0.95 ± 0.04	b	0.54 ± 0.03	abc	40.9
		saladette	25.24 ± 0.23	b	20.09 ± 0.13	a	1.03 ± 0.03	d	2.04 ± 0.07	b	1.66 ± 0.09	c	1.48 ± 0.30	c	1.55 ± 0.23	a	0.66 ± 0.05	ab	53.8
		byproducts	4.47 ± 0.10	e	5.95 ± 0.12	d	0.89 ± 0.01	d	0.33 ± 0.01	ed	0.00 ± 0.00	d	0.04 ± 0.00	e	0.23 ± 0.03	c	0.33 ± 0.02	bc	12.2
	seeds	cherry	3.94 ± 0.07	e	2.76 ± 0.58	fg	0.56 ± 0.00	e	1.10 ± 0.01	c	0.35 ± 0.06	d	0.28 ± 0.01	e	0.00 ± 0.00	d	0.29 ± 0.04	bc	9.3
		grape	2.61 ± 0.14	e	3.53 ± 1.10	ef	0.00 ± 0.00	g	2.01 ± 0.22	b	0.00 ± 0.00	d	0.90 ± 0.20	d	0.00 ± 0.00	d	0.88 ± 0.39	a	9.9
		bola	3.23 ± 0.01	e	2.68 ± 0.00	fg	0.34 ± 0.02	f	0.00 ± 0.00	e	0.34 ± 0.03	d	0.17 ± 0.04	e	0.00 ± 0.00	d	0.34 ± 0.03	bc	7.1
		saladette	3.37 ± 0.03	e	2.94 ± 0.09	fg	0.00 ± 0.00	g	0.46 ± 0.01	cde	0.00 ± 0.00	d	0.31 ± 0.02	c	0.00 ± 0.00	d	0.34 ± 0.03	bc	7.4
		byproducts	2.68 ± 0.16	e	2.06 ± 0.15	g	1.36 ± 0.06	c	0.00 ± 0.00	e	0.16 ± 0.01	d	0.08 ± 0.03	e	0.00 ± 0.00	d	0.34 ± 0.04	bc	6.7

[a]Values marked by the same letter within the same column are statistically significantly different between treatments (multiple-range test; Tukey, $p \leq 0.05$). [b]Dry weight.

dx.doi.org/10.1021/jf5012374 | J. Agric. Food Chem. 2014, 62, 5281−5289

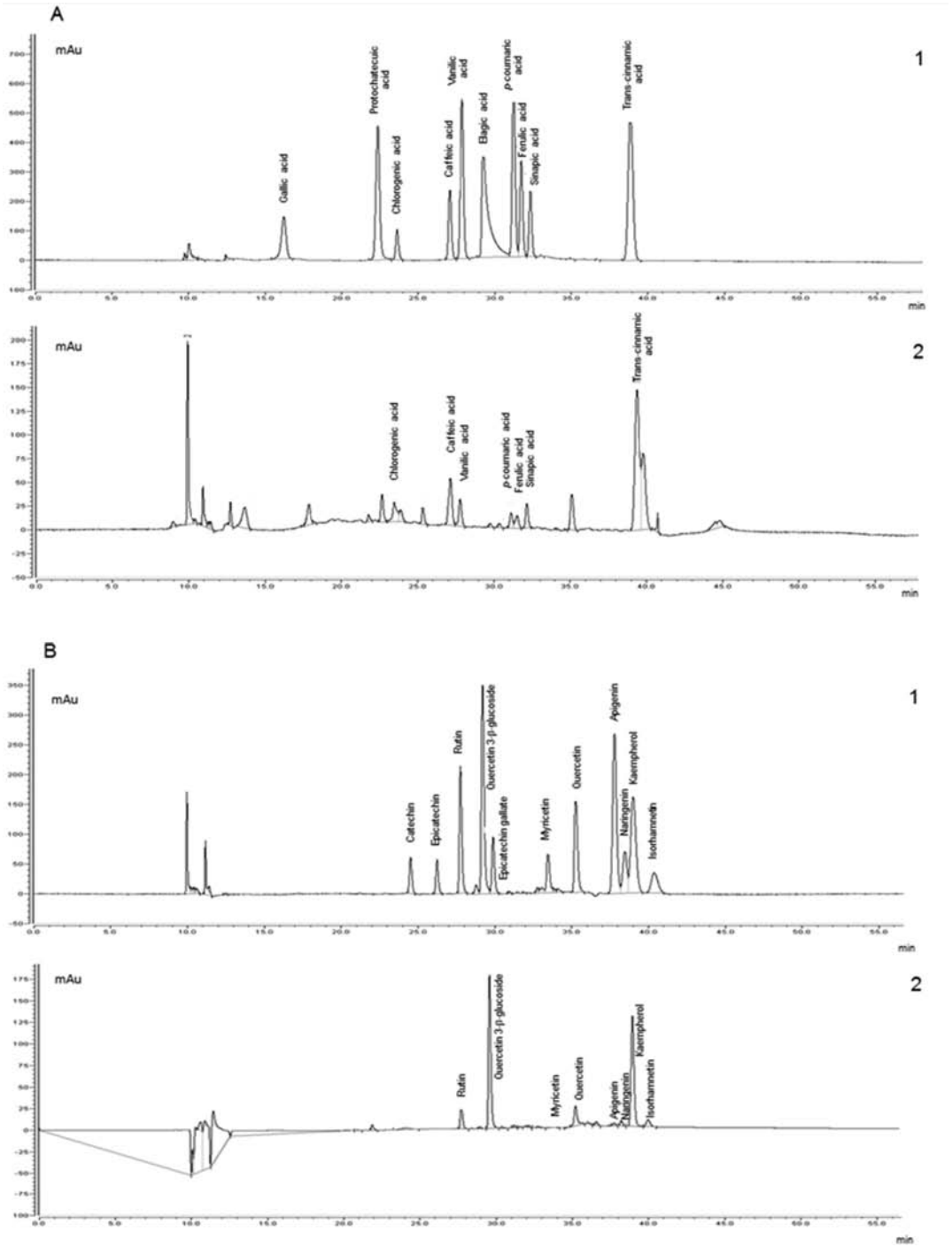

Figure 2. HPLC-DAD chromatograms of phenolic compound standards and phenolics and flavonoids determined in a methanolic extract from the peel of grape tomato. (A1) Phenolic acids standard mix, absorbance at 260 nm, labeled peaks in order from left to right are gallic, protocatechuic, chlorogenic, caffeic, vanillic, ellagic, *p*-coumaric, ferulic, sinapic, and *trans*-cinnamic. (A2) Phenolic acids detected in grape tomato peel methanolic extract at 260 nm (retention times): 23.7 min = chlorogenic acid, 27.1 min = caffeic acid, 27.9 min = vanillic acid, 31.3 min = *p*-coumaric acid, 31.8 min = ferulic acid, 32.3 min = sinapic acid, and 38.9 min = *trans*-cinnamic acid; other signals unknown. (B1) Flavonoids standard mix, absorbance at 360 nm, labeled peaks from left to right are catechin, epicatechin, rutin, quercetin 3-β-glucoside, epicatechin gallate, myricetin, quercetin, apigenin, naringenin, kaempferol, and isorhamnetin. (B2) Flavonoids found in grape tomato peel methanolic extract, main signals detected at 360 nm, retention times of the identified compounds are 27.7 min = rutin, 29.1 min = quercetin 3-β-glucoside, 33.3 min = myricetin, 35.1 min = quercetin, 37.9 min = apigenin, 38.4 min = naringenin, 39.0 min = kaempferol, and 40.1 min = isorhamnetin; other signals unknown.

Attractive biological activities have been reported in the phenolic compounds found in the higher concentrations in this work; that is, ferulic and sinapic acids have been correlated with antioxidant and anti-inflammatory activities and act as chemoprotector agents, if they are frequently consumed in the diet;[43] rutin and quercetin are able to suppress mutagenesis and have antitumoral capacity.[43]

Mathematical correlation analysis (data not shown) revealed that the compounds that showed the highest level of correlations (R = 0.8) with antioxidant activity were those that were detected

dx.doi.org/10.1021/jf5012374 | J. Agric. Food Chem. 2014, 62, 5281−5289

in high levels, but only quercetin-3-β-*O*-glycoside, quercetin, and naringenin showed correlation with antioxidant activity evaluated with at least two methodologies. The high correlations found between individual phenolic concentrations and antioxidant activity, in many cases, suggest that the antioxidant activity determined in this work could be given by the action of the quantified phenolic compounds or by the interaction between the different compounds present in the extract, although further studies are necessary to prove this.

Antimutagenic Activity Test. Antimutagenic activity, expressed as percentage of mutagenic inhibition, as a response to methanolic tomato peel and seed extracts was determined (Figure 3). A dose−response curve using 0.0, 5.0, 10.0, 20.0, 30.0, and 40.0 mg/mL of solid extract (using seed saladette tomato type extract) was constructed; no differences in the percentage of mutagenic inhibition were obtained at concentrations ≥20 mg/mL; for that reason, the following experiments were done at 20 mg/mL extract concentration. There were no statistically significant differences ($p \leq 0.05$) between peel and seed flours, except for byproduct flours, where peel samples had a higher antimutagenic activity than seed samples. Percentages of mutagenic inhibition were between 40 and 60%; peel extracts from byproducts showed an antimutagenic activity greater than those of bola and saladette tomato types and very similar to the activities determined in cherry and grape tomato genotypes. We suggested that the heat process did not affect compounds, which conferred the antimutagenic activity. Bunkova et al.[44] reported in antimutagenic studies made with green tea (using TA98 *S. typhimurium* strain) that the percentage of mutagenic inhibition between 40 and 60% represents an antimutagenic activity from moderate to strong.

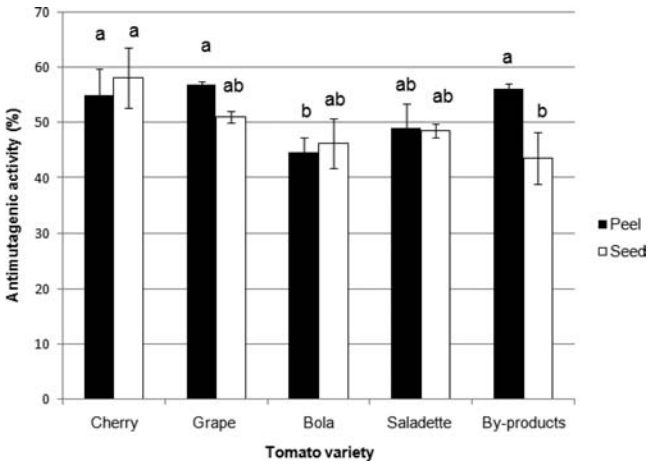

Figure 3. Antimutagenic activity of methanolic extracts (20 mg solid extract/mL) from peel and seed flour from different tomato types. Values are the mean of three replicates of two independent experiments. Different letters indicate statistically significant difference between treatments (multiple-range test; Tukey, $p \leq 0.05$).

Correlation analyses between total phenolic content and antimutagenic activity and between groups of phenolic compounds and antioxidant activity and also profile of individual phenolic compounds (by HPLC-DAD) and antimutagenicity were done. We were not able to obtain a strong linear, second- or third-grade correlation between all evaluated parameters and the percentage of antimutagenicity. In relation to this negative correlation, it could be that the antimutagenic activity observed results from the action of several compounds (or their interactions), some of them not identified with the used methodology. More work is needed to determine which compounds impart the antimutagenic activity observed in our extracts and their mechanisms of action.

Finally, we can affirm that methanolic extracts from peel and seed of several tomato types cultivated in northwestern Mexico, including industrial byproducts, can be a potential source of compounds with attractive antioxidant and antimutagenic activities. These extracts could be utilized as nutraceutical ingredients in animal or human food or as nutritional supplements. For this reason, further studies are needed to complete the metabolite characterization of these materials and to realize in vivo assays.

AUTHOR INFORMATION

Corresponding Author

*(S.M.-G.) Phone: +52-(687)87-29626. Fax: +52-(687)87-29625. E-mail: smedinam@ipn.mx.

Notes

The authors declare no competing financial interest.

ACKNOWLEDGMENTS

We give special acknowledgment to farmers from Guasave and Culiacán, Sinaloa, for providing the biological material and to Basilio Heredia and Rosalva Carolina Valdez Agramón for technical facilities.

REFERENCES

(1) SIAP. Servicio de información agroalimentaria y pesquera, Secretaría de agricultura, ganadería desarrollo rural, pesca y alimentación de México, 2010; http://www.siap.sagarpa.gob.mx (Jan 2013).

(2) Vallverdú-Queralt, A.; Arranz-Martinez, S.; Medina-Remon, A.; Casals-Ribes, I.; Lamuela- Raventós, R. M. Changes in phenolic content of tomato products during storage. *J. Agric. Food Chem.* **2011**, *59*, 9358−9365.

(3) García, H. E. J.; Hernández, I.; Tarango, L. A.; Torres, M. E.; Becerra, J. J.; Pastor, F. J.; Martínez, O.; Valverde, A.; García, J. P.; Espinoza, A.; Talavera, D.; Cedillo, I.; Quero, A. R.; Amante, A.; Rössel, D.; Ortiz, L.; Tiscareño, A. B. Colegio de Postgraduados-Campus SLP, FUNDACIÓN PRODUCE SLP. Estudio de la trayectoria y prospectiva de los mercados de jitomate, 2003; http://www.cofupro.org.mx/cofupro/Publicacion/Archivos/penit32.pdf) (May 2013).

(4) Stefanon, B.; Sgorlon, S.; Gabai, G. Usefulness of nutraceutics in controlling oxidative stress in dairy cows around parturition. *Vet. Res. Commun.* **2005**, *29*, 387−390.

(5) Del Valle, M.; Cámara, M.; Torija, M. E. Chemical characterization of tomato pomace. *J. Sci. Food Agric.* **2006**, *86*, 1232−1236.

(6) Silva, V. M.; García, L. A. Uso de sub productos industriales de tomate en el enriquecimiento de harina de maíz con fibra dietética y proteína para la elaboración de arepas. *Agron. Tropical.* **2004**, *54*, 145−159.

(7) Strati, I. F.; Oreopoulou, V. Effect of extraction parameters on the carotenoid recovery from tomato waste. *Int. J. Food Sci. Technol.* **2011**, *46*, 23−29.

(8) Vagi, E.; Simándi, B.; Vásárhelyiné, K.; Daood, H.; Kéry, A.; Doleschall, F.; Nagy, B. Supercritical carbon dioxide extraction of carotenoids, tocopherols and sitosterols from industrial tomato by-products. *J. Supercrit. Fluids.* **2009**, *40*, 218−226.

(9) Kotíková, Z.; Lachman, J.; Hejtmánková, A.; Hejtmánková, K. Determination of antioxidant activity and antioxidant content in tomato varieties and evaluation of mutual interactions between antioxidants. *Food Sci. Technol.* **2011**, *44*, 1703−1710.

(10) Ferreres, F.; Taveira, M.; Pereira, D. M.; Valentão, P.; Andrade, P. Tomato (*Lycopersicum esculentum*) seeds: new flavonols and cytotoxic effect. *J. Agric. Food Chem.* **2010**, *58*, 2854−2861.
(11) Lavelli, V.; Kerr, W.; Sri Harsha, P. S. C. Phytochemical stability in dried tomato pulp and peel as affected by moisture properties. *J. Agric. Food Chem.* **2012**, *61*, 700−707.
(12) Gómez-Romero, M.; Segura-Carretero, A.; Fernández-Gutiérrez, A. Metabolite profiling and quantification of phenolic compounds in methanol extracts of tomato fruit. *Phytochemistry* **2010**, *71*, 1848−1864.
(13) Migliori, C.; Di Cesare, L. F.; Lo Scalzo, R.; Campanelli, G.; Ferrari, V. Effects of organic farming and genotype on alimentary and nutraceutical parameters in tomato fruits. *J. Sci. Food Agric.* **2012**, *92*, 2833−2839.
(14) Taveira, M.; Silva, R. L.; Vale-Silva, L. A.; Pinto, E.; Valentão, P.; Ferreres, F.; Guedes de Pinho, P.; Andrade, P. B. *Lycopersicum esculentum* seeds: an industrial byproduct as an antimicrobial agent. *J. Agric. Food Chem.* **2010**, *58*, 9529−9536.
(15) Capanoglu, E.; Beekwilder, J.; Boyacioglu, D.; De Vos, R. C. H.; Hall, R. D. The effect of industrial food processing on potentially health-beneficial tomato antioxidants. *Crit. Rev. Food Sci. Nutr.* **2010**, *50*, 919−930.
(16) Shahidi, F. Nutraceuticals and functional foods: whole versus processed foods. *Trends Food Sci.Technol.* **2009**, *20*, 376−387.
(17) Chandra, H. M.; Shanmugaraj, B. M.; Srinivasan, B.; Ramalingam, S. Influence of genotypic variations and antioxidant properties in different fractions of tomato. *J. Food Sci.* **2012**, *77*, C1174−C1178.
(18) AOAC. *Official Methods of Analysis*, 17th ed.; Association of Official Analytical Chemists: Arlington, VA, USA, 2002.
(19) Nurmi, K.; Ossipov, V.; Haukioja, E.; Pihlaja, K. Variation of total phenolic content and individual low-molecular-weight phenolics in foliage of mountain birch trees (*Betulapubescens* ssp. *tortuosa*). *J. Chem. Ecol.* **1996**, *22*, 2023−2040.
(20) Ramirez-Mares, M. V.; Chandra, S.; de Mejia, E. G. *In vitro* chemopreventive activity of *Camellia sinensis*, *Ilex paraguariensis* and *Ardisia compressa* tea extracts and selected polyphenols. *Mutat. Res.* **2004**, *554*, 53−65.
(21) Oomah, B. D.; Caspar, F.; Malcolmson, L. J.; Bellido, A.-S. Phenolics and antioxidant activity of lentil and pea hulls. *Food Res. Int.* **2011**, *44*, 436−441.
(22) Cardador-Martínez, A.; Loarca-Piña, G.; Oomah, B. D. Antioxidant activity in common beans (*Phaseolus vulgaris* L.). *J. Agric. Food Chem.* **2002**, *24*, 6975−6980.
(23) Rojano, B.; Gaviria, C.; Gil, M.; Saenz, J.; Schinella, G.; Tournier, H. Actividad antioxidante del isoespintanol en diferentes medios. *Vitae* **2008**, *5*, 173−181.
(24) Prior, R. L.; Hoang, H.; Gu, L.; Wu, X.; Bacchiocca, M.; Howard, L.; Hampsch-Woodill, M.; Huang, D.; Ou, B.; Jacob, R. Assays for hydrophilic and lipophilic antioxidant capacity (oxygen radical absorbance capacity (ORAC-FL) of plasma and other biological and food samples. *J. Agric. Food Chem.* **2003**, *51*, 3273−3279.
(25) Graham, M. Y.; Graham, T. L. Rapid accumulation of anionic peroxidases and phenolic polymers in soybean cotyledon tissues following treatment with *Phytophthora megasperma* f. sp. *glycinea* wall glucan. *Plant Physiol.* **1991**, *97*, 1445−1455.
(26) Santos-Cervantes, M. E.; Ibarra-Zazueta, M. E.; Loarca-Piña, G.; Paredes-López, O.; Delgado Vargas, F. Antioxidant and antimutagenic activities of *Randia echinocarpa* fruit. *Plants Foods Hum. Nutr.* **2007**, *62*, 71−77.
(27) Zapata, L.; Gerard, L.; Davies, C.; Oliva, L.; Schvab, M. Correlación matemática de índices de color del tomate con parámetros texturales y concentración de carotenoides. *Cienc., Docencia Tecnol.* **2007**, *18*, 207−226.
(28) Choi, S.-H.; Kim, H.-R.; Kim, H.-J.; Lee, I.-S.; Kozukue, N.; Levin, C. E.; Friedman, M. Free aminoacids and phenolic contents and antioxidative and cancer cell-inhibiting activities of extracts of 11 greenhouse-grown tomato varieties and 13 tomato-based foods. *J. Agric. Food Chem.* **2011**, *59*, 12801−12814.
(29) Fuentes, E.; Carle, R.; Astudillo, L.; Guzmán, L.; Gutiérrez, M.; Carrasco, G.; Palomo, I. Antioxidant and antiplatelet activities in extracts from green and fully ripe tomato fruits (*Solanum lycopersicum*) and pomace from industrial tomato processing. *Evidence-Based Complement. Alternat. Med.* **2013**, DOI: 10.1155/2013/867578.
(30) Khanum, F.; Siddalinga Swamy, M.; Sudarshana Krishna, K. R.; Santhanam, K.; Viswanathan, K. R. Dietary fiber content of commonly fresh and cooked vegetables consumed in India. *Plant Foods Hum. Nutr.* **2000**, *55*, 207−218.
(31) Ros Berruezo, G.; Periago Castón, M. J.; Pérez Conesa, D. Legumbres, verduras y productos hortícolas. In *Tratado de Nutrición. Tomo II. Composición y Calidad Nutritiva de los Alimentos*, 2nd ed.; Gil, A., Ed.; Ed.ial Médica Panamericana: Madrid, Spain, 2010; p 176.
(32) George, B.; Kaur, Ch.; Khurdiya, D. S.; Kapoor, H. C. Antioxidants in tomato (*Lycopersicum esculentum*) as a function of genotype. *Food Chem.* **2004**, *84*, 45−51.
(33) Chipurura, B.; Muchuweti, M.; Manditseraa, F. Effects of thermal treatment on the phenolic content and antioxidant activity of some vegetables. *Asian J. Clin. Nutr.* **2010**, *2*, 93−100.
(34) Sagdic, O.; Ozturk, I.; Ozkan, G.; Yetim, H.; Ekici, L.; Yilmaz, M. T. RP-HPLC-DAD analysis of phenolic compounds in pomace extracts from five grape cultivars: evaluation of their antioxidant, antiradical and antifungal activities in orange and apple juices. *Food Chem.* **2011**, *126*, 1749−1758.
(35) Prohens, J.; Whitaker, B. D.; Vilanova, S.; Hurtado, M.; Blasco, M.; Plazas, M.; Gramazio, P.; Stommel, J. R. Genetic diversity in morphological characters and phenolic acid content resulting from an interspecific cross between eggplant (*Solanum melongena*) and its wild antecesor (*S. incanum*). *Ann. Appl. Biol.* **2013**, *162*, 242−257.
(36) Nichenametla, S. N.; Taruscio, T. G.; Barney, D. L.; Exon, J. H. A review of the effects and mechanisms of polyphenolics in cancer. *Crit. Rev. Food Sci. Nutr.* **2006**, *46*, 161−183.
(37) Awika, J. M.; Rooney, L. W.; Wu, X.; Prior, R. L.; Cisneros-Zevallos, L. Screening methods to measure antioxidant activity of sorghum (*Sorghum bicolor*) and sorghum products. *J. Agric. Food Chem.* **2003**, *23*, 6657−6662.
(38) Wood, L. G.; Gibson, P. G.; Garg, M. L. A review of the methodology for assessing *in vivo* antioxidant capacity. *J. Sci. Food Agric.* **2006**, *86*, 2057−2066.
(39) Singleton, V.; Orthofer, R.; Lamuela-Raventos, R. M. Analysis of total phenols and other oxidation substrates and antioxidants by means of Folin-Ciocalteu reagent. *Methods Enzymol.* **1999**, *299*, 152−175.
(40) Barros, L.; Dueñas, M.; Pinela, J.; Carvalho, A. M.; Santos Buelga, C.; Ferreira, I. C. F. R. Characterization and quantification of phenolic compounds in four tomato (*Lycopersicon esculentum* L.) farmers varieties in northeastern Portugal homegardens. *Plants Foods Hum Nutr.* **2012**, *67*, 229−234.
(41) Giuntini, D.; Lazzeri, V.; Calvenzani, V.; Dall'Asta, C.; Galaverna, G.; Tonelli, C.; Petroni, K.; Ranieri, A. Flavonoid profiling and biosynthetic gene expression in flesh and peel of two tomato genotypes grown under UV-B-depleted conditions during ripening. *J. Agric. Food Chem.* **2008**, *56*, 5905−5915.
(42) Olijima, Y.; Suda, K.; Suzuki, T.; Aoki, K.; Shibata, D. Metabolite profiling of chalcones and flavanones in tomato fruit. *J. Jpn. Soc. Hortic. Sci.* **2008**, *77*, 94−102.
(43) Han, X.; Shen, T.; Lou, H. Dietary polyphenols and their biological significance. *Int. J. Mol. Sci.* **2007**, *8*, 950−988.
(44) Bunkova, R.; Marova, I.; Nemec, M. Antimutagenic properties of green tea. *Plant Foods Hum. Nutr.* **2005**, *60*, 25−29(5).

investigated the intestinal cell permeability of hydroxycinnamic acids in a Caco-2 cell transport model.

MATERIALS AND METHODS

Samples and Chemicals. α-Amylase, pepsin, pancreatin, pancreatic lipase, and bile extract were purchased from Sigma-Aldrich for simulated digestion. All cell culture reagents, including Dulbecco's modified Eagle's medium (DMEM), fetal bovine serum, 1 M 4-(2-hydroxyethyl)-1-piperazineethanesulfonic acid (HEPES), phosphate-buffereds saline (PBS), 100× penicillin and streptomysin, and trypsin/EDTA, were obtained from Gibco (Carlsbad, CA). Hank's balanced salt solution (HBSS) and 100× nonessential amino acids were purchased from Sigma-Aldrich. Transwell permeable polycarbonate inserts (0.4 μm) and 12-well cell culture plates were obtained from Corning Inc. Solvents used for HPLC were purchased from Fisher Scientific (Springfield, NJ). Unless indicated, all other chemicals were supplied by Sigma-Aldrich. The standard for quantitative analysis, chlorogenic acid, was purchased from Aldrich Chemical Co. (St. Louis, MO). Caftaric acid, chicoric acid, luteolin-7-*O*-glucuronide, and 3,5-DCQA were purified from *C. denticulatum* by open column chromatography and semipreparative HPLC. Chemical structures were confirmed by ^{1}H and ^{13}C nuclear magnetic resonance data by comparison with the references.[16,20,21]

Sample Preparation. The whole plants of *C. denticulatum* were collected at the Wild Vegetable Experiment Station, Pyeongchang, Korea, in June 2012. For simulated digestion, the whole plants of *C. denticulatum* were dried at room temperature and ground to a powder before being used. All extracts were filtered (0.45 μm, 13 mm, syringe filter GHP, Smartpor) and analyzed in the HPLC system. All experiments were conducted in triplicate.

***In Vitro* Simulated Digestion.** Simulated digestion was performed according to the method described by Garrett et al.[22] with minor modifications. To simulate *in vitro* digestion, digestive steps were conducted sequentially. Briefly, *C. denticulatum* powder (1 g) was homogenized in 10 mL of saline solution containing 120 mM NaCl, 5 mM KCl, and 6 mM $CaCl_2$ (pH 5.5). Then, 1000 units of α-amylase was added, and the pH was adjusted to 6.5. After the saline solution had been added to a volume of 12.5 mL, the samples were incubated at 37 °C for 5 min in a shaking water bath (Lab companion, Jeio Tech, Korea) at 95 rpm for the simulated oral phase of digestion. To mimic the gastric phase of human digestion, the pH of the sample was acidified to 2.2 with HCl and 0.5 mL of a porcine pepsin solution (0.075 g/mL in 0.1 N HCl) was added. The samples were suspended in a saline solution to a volume of 15 mL and incubated at 37 °C for 2 h in a shaking water bath at 95 rpm. To simulate the intestinal phase more accurately and specifically, that phase was separated into three intestinal parts (duodenum, jejunum, and ileum) and simulated sequentially. In the duodenum part, 250 mg of bile extract, 0.5 mL of pancreatic lipase (0.01 g/mL of 0.1 M sodium bicarbonate), and 0.5 mL of pancreatin (0.08 g/mL saline) were added and the pH was increased to 4.0 by adding 1 M sodium bicarbonate. Samples were incubated for 30 min at 37 °C (final volume of 20 mL). In the jejunum part, the pH was adjusted to 5.5 and the sample incubated for 90 min at 37 °C (final volume of 22.5 mL). Finally, the pH was adjusted to 7.0 and the sample incubated for 300 min at 37 °C (final volume of 25 mL) to mimic the ileum part. At the end of each digestion, digestates (100 μL) were collected and added to aqueous ethanol [1:1 (v/v)] to determine the bioaccessibility of hydroxycinnamic acids. To measure the digestive stability of hydroxycinnamic acids, digestates of each intestinal phase were added to ethanol (25 mL) and extracted by sonication for 1 h. After the mixtures had been centrifuged at 12300*g* for 10 min, their supernatants were collected and filtered through a 0.45 μm GHP filter prior to HPLC analysis.

Transport of Hydroxycinnamic Acids via a Caco-2 Cell Monolayer. Caco-2 cells (HTB-37, American Type Culture Collection, Rockville, MD) were maintained for cellular transport experiments, according to the method of Hubatsch et al.[23] For the experiments, cells were seeded at a density of 3×10^5 cells/cm^2 on the tissue culture-treated polycarbonate filter in 12-transwell plates. The cultures were grown for 21−29 days to obtain a differentiated intestinal cell monolayer. Transepithelial electrical resistance (TEER) measurements were taken twice weekly using a Millipore Millicell-ERS system (Millipore Corp., Bedford, MA) to ensure the monolayer was intact. Once the TEER values reached 600−800 Ω/cm^2, the monolayer was used for transport study.

To initiate the transport experiments, the culture media in the donor and receiving compartments were carefully aspirated, and the cells were rinsed with prewarmed transport medium [HBSS supplemented with 25 mM HEPES (pH 7.4)]. Following a 30 min equilibration with the transport medium at 37 °C, the cells were incubated with each hydroxycinnamic acid for 2 h for transport studies. The transport studies were performed in both directions as follows. For apical-to-basolateral (a-to-b) transport, 1.2 mL of transport medium was added in the basolateral part, 0.45 mL of each hydroxycinnamic acid (2 mM) dissolved in the transport medium was added in the apical part, and 0.05 mL of the sample (C_0) was immediately withdrawn into a collection tube. After 2 h, 0.6 mL of basolateral transport medium was withdrawn for the analysis and replenished with an equal volume of fresh transport medium. For basolateral-to-apical (b-to-a) transport, 1.25 mL of each hydroxycinnamic acid dissolved in the transport solution was added in the basolateral part and a 0.05 mL sample was immediately withdrawn, followed by 0.4 mL of transport medium being added in the apical part; 0.2 mL of apical transport medium was withdrawn after 2 h and replenished with the same volume of fresh transport medium. The TEER values were measured after the experiment to confirm the cell integrity status. All of the collected samples were added to the same volume of 0.6% formic acid in acetonitrile to increase the stability of hydroxycinnamic acids prior to liquid chromatography−MS analysis. The apparent permeability coefficient (P_{app}) was calculated as

$$P_{app} = \frac{\partial Q}{AC_0\,\partial t}$$

where $\partial Q/\partial t$ is the permeability rate, A is the surface area of the membrane filter, and C_0 is the initial concentration in the donor compartment (the apical compartment in the a-to-b transport study and the basolateral compartment in the b-to-a transport study).

HPLC Analysis. HPLC was used for the quantitative analysis of hydroxycinnamic acids in *C. denticulatum* during simulated digestion. The HPLC system consisted of an Agilent Series 1200 liquid chromatography system with a G1379B vacuum degasser, a G1312A binary pump, a G1329A autosampler, a G1316A column oven, a G1315B diode array detector (DAD), and ChemStation (version B.02.01, Agilent, Waldbronn, Germany). The separation was undertaken with a Shiseido Capcell pak MG II C18 column (4.6 mm × 250 mm, 5 μm). The mobile phase consisted of 0.3% formic acid in water (solvent A) and 0.3% formic acid in acetonitrile (solvent B) with the following conditions: 82:18 [A:B (v/v)] isocratic mode for 30 min. The flow rate was 1.0 mL/min, and the oven temperature was set at 35 °C. Detection was conducted at 330 nm, and the injection volume of the standards and extracts was 10 μL.

HPLC−PDA−MS Analysis. HPLC−PDA−MS analysis was used for the identification of major compounds in *C. denticulatum* and the quantitative analysis of hydroxycinnamic acids during the intestinal Caco-2 cell permeability test. All analyses were performed using a Thermo HPLC−PDA−MS system (Thermo Fisher Scientific Inc., San Jose, CA) equipped with an ACCELA photodiode array detector, an autosampler, a quarternary pump, and an LCQ FLEET ion trap mass spectrometer with an electrospray ionization source. Thermo Xcalibur (version 2.1) was used for data acquisition and processing. The mobile phase was the same as that previously described in the HPLC analysis section. A Waters Acquity BEH C18 column (3.0 mm × 100 mm, 1.7 μm) was used. The gradient mode was as follows: from 0 to 10 min, initial mobile phase solvent A/B [90:10 (v/v)]; from 10 to 45 min, 70:30 linear gradient and reconditioning steps to initial condition for 15 min. The flow rate was 150 μL/min, and detection was conducted at 330 nm. The injection volume of samples was 10 μL. The mass spectrometer conditions were as follows: negative ion mode; mass

dx.doi.org/10.1021/jf500319h | J. Agric. Food Chem. 2014, 62, 5290−5295

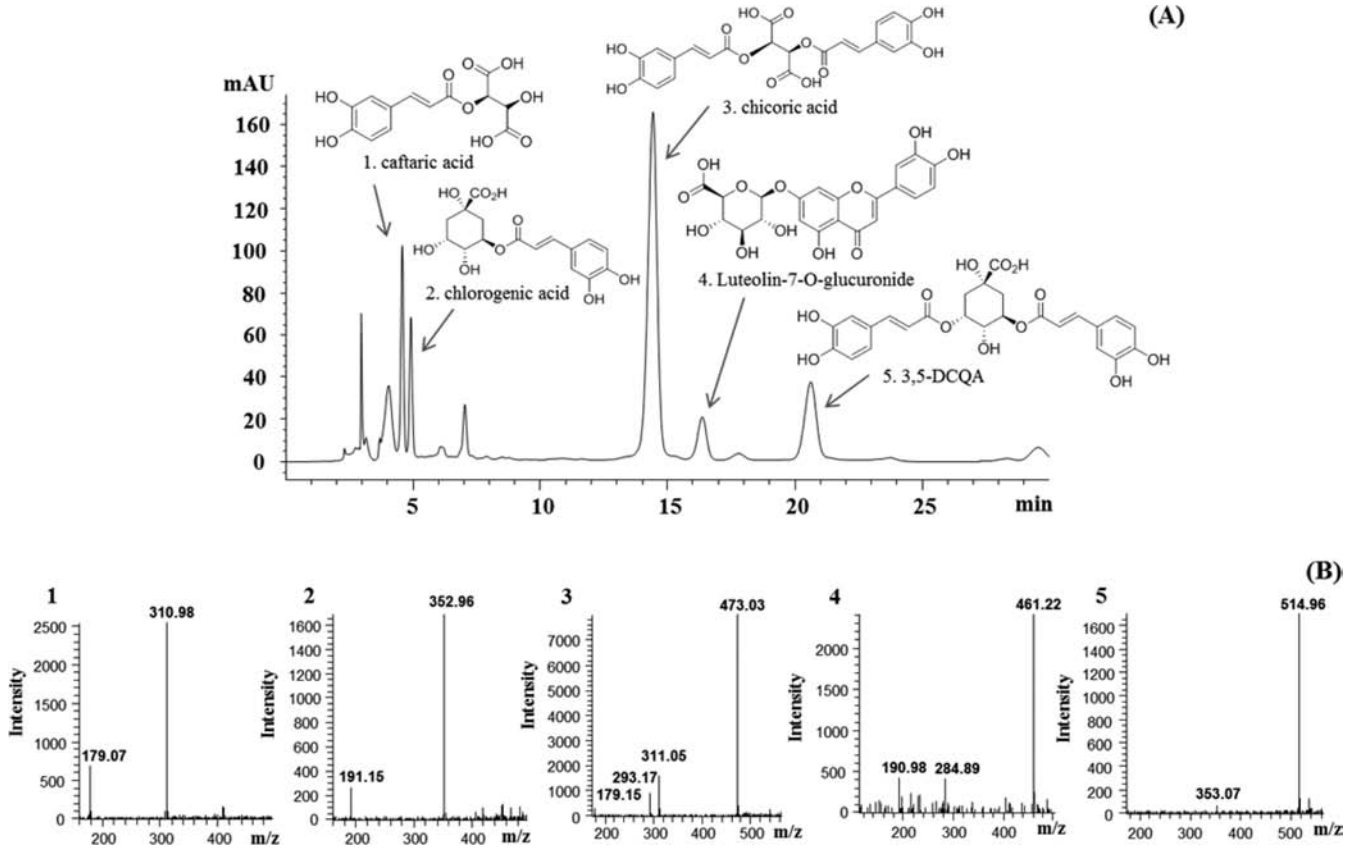

Figure 1. (A) HPLC chromatogram of *C. denticulatum* extracts and structures of four hydroxycinnamic acids and one flavonoid and (B) ESI-MS spectra of five compounds.

Table 1. Calibration Curve, Precision, LOD, and LOQ of Five Compounds in *C. denticulatum*

	calibration curve		precision, RSD (%)				
compound	regressive equation	r^2	linear range (μg/mL)	intraday (n = 3)	interday (n = 3)	LOD (μg/mL)	LOQ (μg/mL)
caftaric acid	$y = 25.399x - 9.299$	0.9997	3.90625−125	0.09	0.12	0.82	2.48
chlorogenic acid	$y = 24.963x - 12.613$	0.9999	7.8125−62.5	0.55	0.56	0.90	2.74
chicoric acid	$y = 32.962x - 42.775$	1.0000	3.90625−1000	2.39	1.73	0.93	2.83
luteolin-7-*O*-glucuronide	$y = 16.006x + 7.051$	0.9998	3.90625−62.5	0.36	0.97	0.13	0.39
3,5-DCQA	$y = 29.750x + 73.041$	0.9999	3.90625−500	0.44	0.11	0.22	0.66

range, m/z 100−1000; capillary voltage, −7.0 V; tube lens, −45 V; sheath gas flow rate (N_2), 50 arbitrary units; auxiliary gas flow rate (N_2), 12 arbitrary units; capillary temperature, 350 °C.

Data Analysis. A minimum of three independent observations were made in each experiment. All data are expressed as means ± the standard error of the mean (SEM). Statistical comparisons between the experimental groups and the control group were performed using the Student's t test. The Student−Newman−Keuls test was performed to separate the means of experimental groups when significant differences ($P < 0.05$) occurred. Statistical analyses were performed using GraphPad Prism version 5.

RESULTS AND DISCUSSION

Identification and Quantitative Analysis of Hydroxycinnamic Acids in *C. denticulatum*. The aqueous ethanol extracts of *C. denticulatum* were injected into the HPLC system. Following separation, five major compounds were detected in their HPLC profiles with a DAD chromatogram (Figure 1A). HPLC−ESI-MS was used to identify the four hydroxycinnamic acids and one flavonoid, and the mass spectra of the five compounds are shown in Figure 1B. Peak 1 showed $[M - H]^-$ ions at m/z 311, and fragmentation in the MS experiment produced a caffeic acid (m/z 179) as a prominent fragment. Peak 1 appeared to be caftaric acid. Peak 2 was identified as chlorogenic acid by mass spectra. Fragmentation of the $[M - H]^-$ ion at m/z 353 was characterized by the loss of a caffeic acid moiety, resulting in a product ion at m/z 191. Peak 3 showed $[M - H]^-$ ions at m/z 473. The fragmentation of peak 3 produced a product ion at m/z 311 (loss of a caffeoyl moiety) and m/z 293 (loss of the caffeic acid and an additional loss of water). Peak 3 was assigned to chicoric acid. Peak 4 showed $[M - H]^-$ ions at m/z 461 and another characteristic fragment at m/z 285 of the aglycone, corresponding to the loss of a glucuronide moiety. Therefore, peak 4 was assigned to luteolin-7-*O*-glucuronide following a comparison against the reference compound. Peak 5 showed $[M - H]^-$ ions at m/z 515 and a product ion at m/z 353 after the loss of one caffeic acid. This fragment is typical of dicaffeoylquinic acid. Peak 5 was identified as 3,5-DCQA through comparison with an authentic compound. Five compounds were identified as caftaric acid, chlorogenic acid, chicoric acid, luteolin-7-*O*-glucuronide, and 3,5-DCQA by comparing their MS data with references[24,25] and

dx.doi.org/10.1021/jf500319h | J. Agric. Food Chem. 2014, 62, 5290−5295

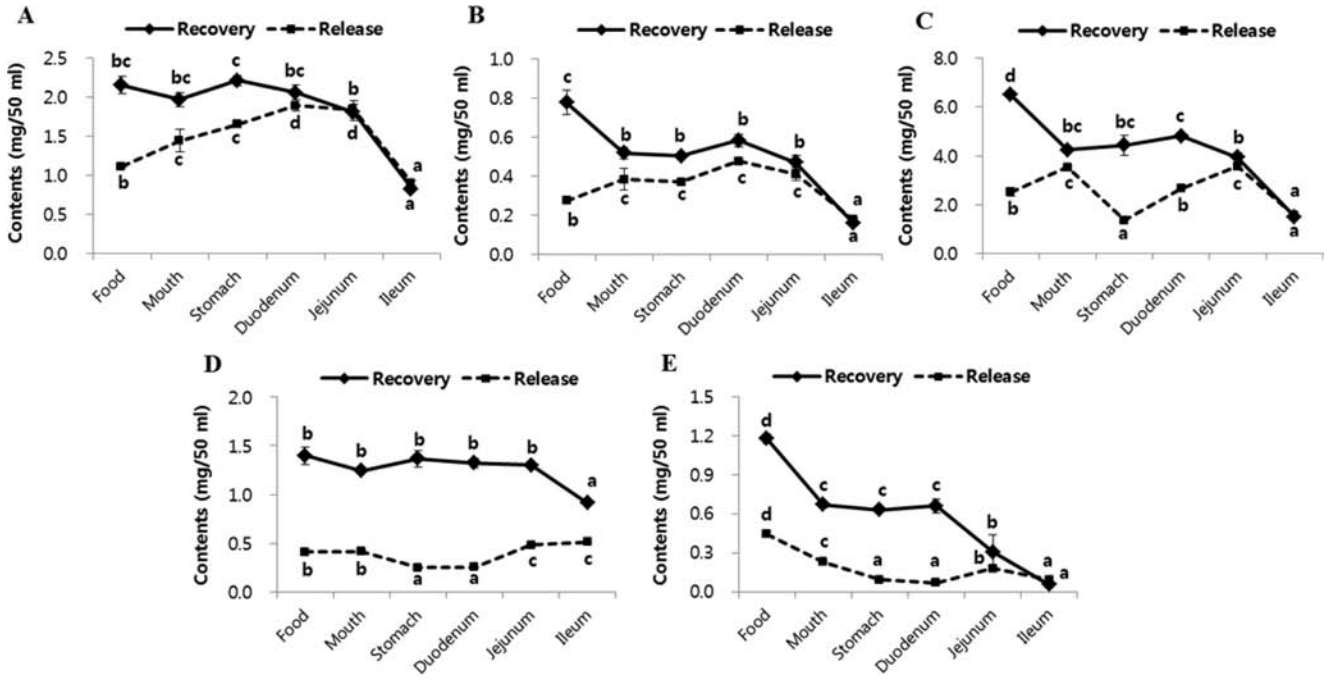

Figure 2. Digestive stability (◆, solid line) and release (■, dotted line) of four hydroxycinnamic acids and one flavonoid during simulated digestion: (A) caftaric acid, (B) chlorogenic acid, (C) chicoric acid, (D) luteolin-7-*O*-glucuronide, and (E) 3,5-DCQA. A different letter for each digestive stage indicates significant differences ($P < 0.05$) between the treatment means of each compound's recovery or release.

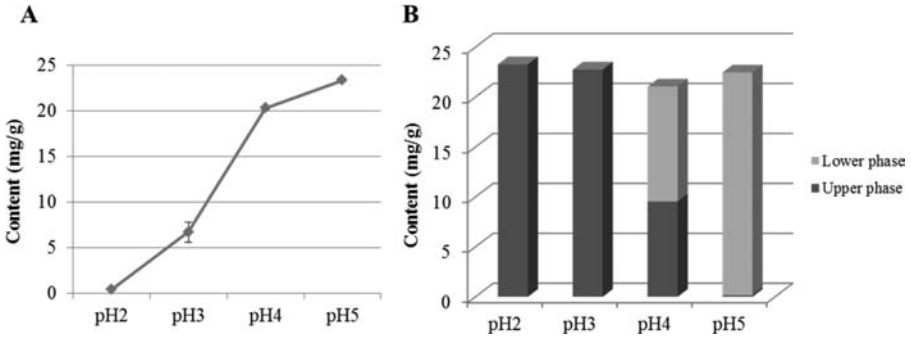

Figure 3. (A) Content of soluble chicoric acid at various pH values in the absence of gastric enzymes and (B) solvent partition of the digestate at various pH values to evaluate insoluble chicoric acid under each condition (upper phase, ethyl acetate; lower phase, aqueous fraction).

co-injections of authentic standards. Five concentrations of each standard compound were injected in triplicate to establish the calibration curves. As shown in Table 1, the limits of detection (LOD) and quantification (LOQ) for each standard were determined at the standard deviation (SD) of the response and the slope with values of ∼3.3 and ∼10, respectively. Intra- and interday variability was determined three times each day and on three separate days. Variations are indicated by the relative standard deviations (RSDs).

Digestive Stability and Bioaccessibility of Hydroxycinnamic Acids in *C. denticulatum* during Simulated Digestion. The contents of hydroxycinnamic acids in *C. denticulatum* were measured by HPLC to evaluate the digestive stability and bioaccessibility of the major compounds (Figure 2). The stability of each compound was checked by measuring the amount of compound remaining after each digestion step. Values for chlorogenic acid, chicoric acid, and 3,5-DCQA remained at 66.6, 65.1, and 57.0%, respectively, during the initial digestion phase from food to the mouth, while the value for caftaric acid decreased only slightly throughout the digestion phase from the mouth to the jejunum, indicating that caftaric acid was stable under general digestive conditions compared with chlorogenic acid, chicoric acid, and 3,5-DCQA. Values for caftaric acid, chlorogenic acid, and chicoric acid remained at 38.2, 20.4, and 23.1%, respectively, after harsh digestion in the ileum at pH 7.0 for 5 h. The value for 3,5-DCQA was also markedly degraded after simulated digestion and remained at only 5.1% in the soluble fraction of the ileum phase. Unlike the four hydroxycinnamic acids, luteolin-7-*O*-glucuronide was stable and was preserved after total simulated digestion (residual percentage, 65.3%). The degradation of caftaric acid, chlorogenic acid, chicoric acid, and 3,5-DCQA might be dependent on the pH, and the stability of these compounds tends to be decreased under higher-pH conditions (pH >6.0).[26]

Bioaccessibility is defined as the relative amount of phytochemicals "released" from a complex food matrix during digestion, which could potentially also be available for absorption.[27] Five compounds were released from their food matrices during simulated digestion, and the digestates of the

Table 2. Apparent Permeability Coefficients (P_{app}) of Hydroxycinnamic Acids in the Caco-2 Model

compound	$P_{app\ A\ to\ B}$ ($\times 10^{-6}$ cm/s)[a]	$P_{app\ B\ to\ A}$ ($\times 10^{-6}$ cm/s)[b]	$P_{app\ A\ to\ B}/P_{app\ B\ to\ A}$[c]
caftaric acid	0.119 ± 0.010	2.197 ± 0.075	0.054
chlorogenic acid	0.046 ± 0.006	0.839 ± 0.174	0.055
chicoric acid	0.038 ± 0.004	3.502 ± 0.188	0.011
luteolin-7-*O*-glucuronide	ND[d]	7.850 ± 0.265	ND[d]
3,5-DCQA	0.025 ± 0.003	4.337 ± 0.211	0.006

[a]$P_{app\ A\ to\ B}$, transport of the compounds from the apical to basolateral compartment. [b]$P_{app\ B\ to\ A}$, transport from the basolateral to apical compartment. [c]The $P_{app\ A\ to\ B}/P_{app\ B\ to\ A}$ ratio is the ratio of $P_{app\ A\ to\ B}$ to $P_{app\ B\ to\ A}$. Data are means ± SEM (n = 3−6). [d]No detection.

soluble fraction were available for uptake by absorptive epithelial cells.[28] Because of their hydrophilic properties, 1.12, 0.28, and 2.52 mg of caftaric acid, chlorogenic acid, and chicoric acid, respectively, were released from the food matrix. A significant increase appeared in the bioaccessibility of caftaric acid (87.8%) and chlorogenic acid (61.3%) during simulated digestion (Figure 2A,B). More than 60% of caftaric and chlorogenic acid was released in the stomach and duodenum phase. However, the bioaccessibility of chicoric acid was very low through the mouth and stomach step, which suddenly underwent a change in pH from 6.5 to 2.2 (Figure 2C). Because of the pH change, chicoric acid (stomach phase, 1.36 mg) was aggregated during digestion and was insoluble in the digestate. The solubility of chicoric acid was shown at various pH values in the absence of gastric enzymes (Figure 3A) and was low at pH 2 and 3 compared to that at pH 4 and 5. This result may explain why the result in Figure 2C was obtained. The additional experiment was conducted using the solvent partition of chicoric acid from the digestate to evaluate the insoluble chicoric acid at various pH values (Figure 3B). The lower phase (aqueous fraction) and upper phase (ethyl acetate fraction) were analyzed by HPLC to evaluate the chicoric acid content. Chicoric acid, which was insoluble at pH <3, was more soluble when the pH increased. The bioaccessibility of chicoric acid recovered to 2.66 and 3.56 mg during the intestinal digestion phase. In the case of 3,5-DCQA, it was markedly degraded during simulated digestion, and only 8% of 3,5-DCQA remained in the digestate. Caftaric acid, chlorogenic acid, chicoric acid, and 3,5-DCQA were degraded during ileum intestinal digestion. The stability of these compounds may be affected by the pH and digestion time during the ileum phase. These results highlight how four hydroxycinnamic acids were bioaccessible during the simulated stomach and upper parts of intestinal digestion and were available for absorption in the duodenum and jejunum phase. Our results are similar to those of Lafay et al.,[19] showing that the absorption percentage of chlorogenic acid in the small intestine was only 8% using the *in situ* perfusion model. The release of luteolin-7-*O*-glucuronide after simulated digestion is shown in Figure 2D. The luteolin-7-*O*-glucuronide was released slightly during small intestinal digestion, and the bioaccessibility of luteolin-7-*O*-glucuronide was stable with pH conditions and solubility.

Permeability of Hydroxycinnamic Acids in Intestinal Cells. A cell permeability study for the four hydroxycinnamic acids and one flavonoid was performed using a Caco-2 cell monolayer. Both a-to-b and b-to-a directional transport were evaluated, as shown in Table 2. Transport of the hydroxycinnamic acids from a to b ranged from 0.025×10^{-6} to 0.119×10^{-6} cm/s, indicating the extremely low cell permeability of hydroxycinnamic acids. However, the P_{app} for b-to-a flux of hydroxycinnamic acids was $>10^{-6}$ cm/s, except for that of chlorogenic acid (0.839×10^{-6} cm/s). In particular, there were significant differences between the $P_{app\ B\ to\ A}$ of each hydroxycinnamic acid, and the ratio of $P_{app\ A\ to\ B}$ to $P_{app\ B\ to\ A}$ was approximately 5−9 times higher in chlorogenic acid and caftaric acid than in chicoric acid and 3,5-DCQA. According to previous sudies,[29,30] chlorogenic acid was not well absorbed in the Caco-2 cell transport model, rat chronic absorption study, or human clinical study. The ratio of $P_{app\ A\ to\ B}$ to $P_{app\ B\ to\ A}$ of caftaric acid, chicoric acid, and 3,5-DCQA was even lower than that of chlorogenic acid. This result indicates that some efflux mechanisms may exist with hydroxycinnamic acids in their transport across the Caco-2 cell monolayer. Luteolin-7-*O*-glucuronide, which was the most stable compound among the five main components from *C. denticulatum* during simulated digestion, has a $P_{app\ B\ to\ A}$ far higher than those of four hydroxycinnamic acids. This agreed well with other studies that demonstrated that flavonoid glycosides such as luteolin-7-*O*-glucuronide were poorly absorbed in Caco-2 cells because of the active extrusion of P-glycoprotein.[31−33] Interestingly, chicoric acid is most abundant in *C. denticulatum*, followed by caftaric acid, 3,5-DCQA, and chlorogenic acid. However, caftaric acid and chlorogenic acid might be more important hydroxycinnamic acids in humans when considering their entire bioavailability such as their digestive stability, their efficiency of release from the food matrix, and their intestinal absorption. Further research using *in vivo* rat models and clinical studies will be required to clarify the bioavailability of these hydroxycinnamic acids.

In conclusion, this study shows that hydroxycinnamic acids from *C. denticulatum* were rapidly accessible in the stomach and duodenum phase, maximizing the possibility of absorption in intestinal Caco-2 cells. However, the intestinal cell permeability of hydroxycinnamic acids indicated that some efflux mechanisms might exist with hydroxycinnamic acids in their transport across the Caco-2 cell monolayer. The digestive stabilities of hydroxycinnamic acids from *C. denticulatum* were markedly low after simulated digestion and remained minimal in the soluble fraction of the ileum phase. Further, *in vivo* rat models and human clinical studies are needed to clarify the bioavailability of hydroxycinnamic acids.

AUTHOR INFORMATION

Corresponding Author

*Telephone: +82-33-650-3652. Fax: +82-33-650-3679. E-mail: cheolpan@gmail.com.

Funding

This work was supported by a KIST intramural research grant (2Z04220).

Notes

The authors declare no competing financial interest.

■ ACKNOWLEDGMENTS

We thank the Wild Vegetable Experiment Station (Pyeongchang, Korea) for supplying the cultivated *C. denticulatum*.

■ ABBREVIATIONS USED

3,5-DCQA, 3,5-dicaffeoylquinic acid; TEER, transepithelial electrical resistance; DAD, diode array detector; SEM, standard error of the mean; LOD, limit of detection; LOQ, limit of quantification; RSD, relative standard deviation

■ REFERENCES

(1) Hermann, K. Flavonols and flavones in food plants: A review. *J. Food Technol.* **1976**, *11*, 433−438.
(2) Kuhnau, J. The flavonoids. A class of semi-essential food components: Their role in human nutrition. *World Rev. Nutr. Diet.* **1976**, *24*, 117−191.
(3) Winter, M.; Herrmann, K. Esters and glucosides of hydroxycinnamic acids in vegetables. *J. Agric. Food Chem.* **1986**, *34*, 616−620.
(4) Radtke, J.; Linseisen, L.; Wolfram, G. Phenolsäurezufuhr Erwachsener in einem bayerischen Teikollektiv der Nationalen Verzehrssudie. *Z. Ernährungswiss* **1998**, *37*, 190−197.
(5) Clifford, M. N. Chlorogenic acids and other cinnamates: Nature, occurrence and dietary prevention. *J. Food Sci. Agric.* **2000**, *80*, 1118−1125.
(6) Singleton, V. L.; Zaya, J.; Trousdale, E. K. Caftaric and coutaric acid in fruit of *Vitis*. *Phytochemistry* **1986**, *25*, 2127−2133.
(7) Scarpati, M. L.; Oriente, G. Chicoric acid (dicaffeyltartic acid): Its isolation from chicory (*Cichorium intybus*) and synthesis. *Tetrahedron* **1958**, *4*, 43−48.
(8) Molgaard, P.; Johnsen, S.; Christensen, P.; Cornett, C. HPLC method validated for the simultaneous analysis of cichoric acid and alkamides in *Echinacea purpurea* plants and products. *J. Agric. Food Chem.* **2003**, *51*, 6922−6933.
(9) Anna, S.; Janusz, M.; Agnieszka, S.; Wanda, K. Caffeic acid derivatives from a hairy root culture of *Lactuca virosa*. *Acta Physiol. Plant.* **2012**, *34*, 291−298.
(10) Lau, F. C.; Shukitt-Hale, B.; Joseph, J. A. Effects of Concord grape juice on cognitive and motor deficits in aging. *Nutrition* **2006**, *22*, 295−302.
(11) Zafra-Stone, S.; Yasmin, T.; Bagchi, M.; Chatterjee, A.; Vinson, J. A.; Bagchi, D. Berry anthocyanins as novel antioxidants in human health and disease prevention. *Mol. Nutr. Food Res.* **2007**, *51*, 675−683.
(12) Puupponen-Pimia, R.; Nohynek, L.; Alakomi, H. L.; Oksman-Caldentey, K. M. Bioactive berry compounds: Novel tools against human pathogens. *Appl. Microbiol. Biotechnol.* **2005**, *67*, 8−18.
(13) Ohwi, J. *Flora of Japan*; Smithsonian Institute Press: Washington, DC, 1984.
(14) Yun, J. H.; Lee, S. B.; Lee, H. J.; Kim, C. Y.; Kim, M. A.; Sohn, Y. C.; Nho, C. W. Bifunctional induction of the QR and CYP1A1 by youngiasides via Nrf2-ARE and AhR-XRE pathways. *Biol. Pharm. Bull.* **2010**, *33*, 1650−1657.
(15) Kang, K.; Jho, E. H.; Lee, H. J.; Oidovsambuu, S.; Yun, J. H.; Kim, C. Y.; Yoo, J.; Kim, Y.; Kim, J. H.; Ahn, S. Y.; Nho, C. W. *Youngia denticulate* protects against oxidative damage induced by *tert*-butylhydroperoxide in HepG2 cells. *J. Med. Food* **2011**, *14*, 1198−1207.
(16) Maeda, G.; Takara, K.; Wada, K.; Oki, T.; Masuda, M.; Ichiba, T.; Chuda, Y.; Ono, H.; Suda, I. Evaluation of antioxidant activity of vegetables from Okinawa prefecture and determination of some antioxidative compounds. *Food Sci. Technol. Res.* **2006**, *12*, 8−14.
(17) Olthof, M. R.; Hollman, P. C. H.; Katan, M. B. Chlorogenic acid and caffeic acid are absorbed in humans. *J. Nutr.* **2001**, *131*, 66−71.
(18) Azuma, K.; Ippoushi, K.; Nakayama, M.; Ito, H.; Higashio, H.; Terao, J. Absorption of chlorogenic acid and caffeic acid in rats after oral administration. *J. Agric. Food Chem.* **2000**, *48*, 5496−5500.
(19) Lafay, S.; Morand, C.; Manach, C.; Besson, C.; Scalbert, A. Absorption and metabolism of caffeic acid and chlorogenic acid in the small intestine of rats. *Br. J. Nutr.* **2006**, *96*, 1−8.
(20) Goetz, G.; Fkyerat, A.; Metatis, N.; Kunz, M.; Tabacchi, R.; Pezet, R.; Pont, V. Resistance factors to grey mould in grape berries: Identification of some phenolics inhibitors of *Botrytis cinerea* stilbene oxidase. *Phytochemistry* **1999**, *52*, 759−767.
(21) Carnat, A.; Heitz, A.; Fraisse, D.; Carnat, A.; Lamaison, J. Major dicaffeoylquinic acids from *Artemisia vulgaris*. *Fitoterapia* **2000**, *71*, 587−589.
(22) Garrett, D. A.; Failla, M. L.; Sarama, R. J. Development of an *in vitro* digestion method to assess carotenoid bioavailability from meals. *J. Agric. Food Chem.* **1999**, *47*, 4301−4309.
(23) Hubatsch, I.; Ragnarsson, E. G. E.; Artursson, P. Determination of drug permeability and prediction of drug absorption in Caco-2 monolayers. *Nat. Protoc.* **2007**, *2*, 2111−2119.
(24) Schütz, K.; Kammerer, D. R.; Carle, R.; Schieber, A. Characterization of phenolic acids and flavonoids in dandelion (*Taraxacum officinale* WEB. ex WIGG.) root and herb by high-performance liquid chromatography/electrospray ionization mass spectrometry. *Rapid Commun. Mass Spectrom.* **2005**, *19*, 179−186.
(25) Alexandru, L.; Pizzale, L.; Conte, L.; Barge, A.; Cravotto, G. Microwave-assisted extraction of edible *Cicerbita alpine* shoots and its LC-MS phenolic profile. *J. Sci. Food Agric.* **2013**, *93*, 2676−2682.
(26) Takenaka, M.; Nagata, T.; Yoshida, M. Stability and bioavailability of antioxidants in garland (*Chrysanthemum coronarium* L.). *Biosci., Biotechnol., Biochem.* **2000**, *64*, 2689−2691.
(27) Mandalari, G.; Faulks, R. M.; Rich, G. T.; Lo Turco, V.; Picout, D. R.; Lo Curto, R. B. Release of protein, lipid, and vitamin E from almond seeds during digestion. *J. Agric. Food Chem.* **2008**, *56*, 3409−3416.
(28) Ferruzzi, M. G. The influence of beverage composition on delivery of phenolic compounds from coffee and tea. *Physiol. Behav.* **2010**, *100*, 33−41.
(29) Renouf, M.; Marmet, C.; Giuffrida, F.; Lepage, M.; Barron, D.; Beaumont, M.; Williamson, G.; Dionisi, F. Dose-response plasma appearance of coffee chlorogenic and phenolic acids in adults. *Mol. Nutr. Food Res.* **2014**, *58*, 301−309.
(30) Dupas, C.; Marsset Baglieri, A.; Ordonaud, C.; Tomé, D.; Maillard, M.-N. Chlorogenic acid is poorly absorbed, independently of the food matrix: A Caco-2 cells and rat chronic absorption study. *Mol. Nutr. Food Res.* **2006**, *50*, 1053−1060.
(31) Tian, X.; Yang, X.; Wang, K.; Yang, X. The Efflux of Flavonoids Morin, Isorhamnetin-3-*O*-Rutinoside and diosmetin-7-*O*-*β*-D-xylopyranosyl-(1−6)-*β*-d-glucopyranoside in the human intestinal cell line Caco-2. *Pharm. Res.* **2006**, *23*, 1721−1728.
(32) Tian, X.; Yang, X.-W.; Yang, X.; Wang, K. Studies of intestinal permeability of 36 flavonoids using Caco-2 cell monolayer model. *Int. J. Pharm.* **2009**, *367*, 58−64.
(33) Walle, T. Absorption and metabolism of flavonoids. *Free Radical Biol. Med.* **2004**, *36*, 829−837.

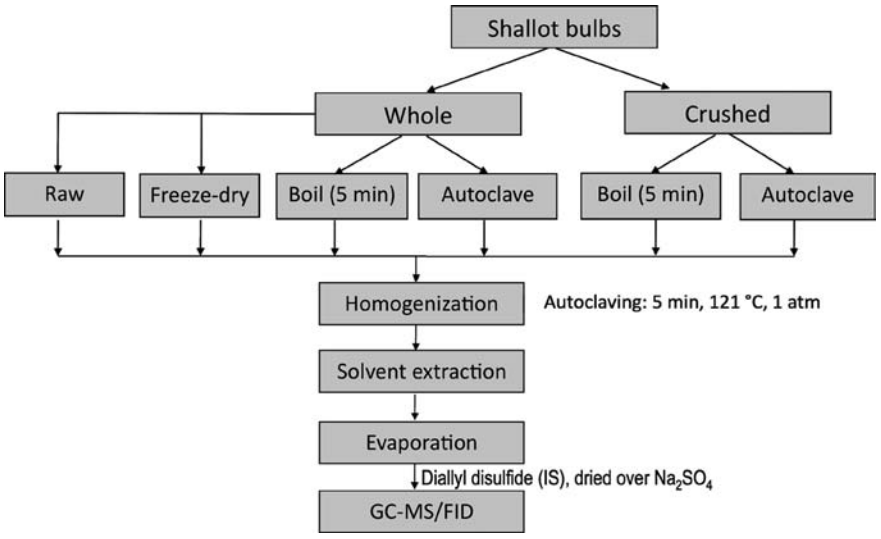

Figure 1. Overview of the processing treatments evaluated in the present study.

Enterprise (Singapore) while citric acid was from Avantor Performance Materials (USA).

Processing of Shallot before Extraction. Shallots from Vietnam were purchased from a local fruit and vegetable wholesale center in Singapore in July 2013. Shallot bulbs were immediately frozen (−20 °C) until further processing. Shallots were sorted out according to their physical qualities (e.g., size), and the first thin layer of the skin was peeled off using a knife. The peeled shallots were then washed with deionized water and wiped dried with sanitary paper towels. To evaluate the effect of the processing conditions on the enzyme-mediated production of organosulfides, 5 kg of shallot bulbs were divided into 3 portions and processed by different methods. The bulbs of portion 1 were crushed and homogenized using a Philips HR2001 food processor, and incubated at room temperature for 30 min in a shaker. Portion 2 was directly subjected to the processing treatments as described below. Portion 3 was freeze-dried. Triplicate samples coming from portions 1 and 2 were boiled for 5 min. The homogenates/bulbs and the heating medium (water) were collected and subjected to solvent extraction as described below. The remaining samples from portions 1 and 2 were subjected to autoclaving (1 atm, 121 °C, 5 min) using a Hiclave HV-50 autoclave (Hirayama Manufacturing Corp., Japan). Portion 3 samples were either freeze-dried using an Advantage Plus ES-53 VirTis freeze-dryer for 72 h (−50 °C, under a vacuum of 180 mTorr) or ground immediately without any pretreatment. After each treatment, homogenates or the whole bulbs were further crushed and homogenized followed by solvent extraction, as described in the following section. Tested samples were assigned as whole-boiled (WB), whole-autoclaved (WA), crushed-boiled (CB), crushed-autoclaved (CA), and freeze-dried (FD). The entire experiment was carried out in triplicate. Figure 1 gives an overview of the processing conditions tested.

Effect of pH Adjustment. A 3 kg portion of bulb samples from the same batch was allotted for the pH adjustment experiment. Freshly peeled shallot bulbs (200 g) were crushed and homogenized with an equal amount of deionized water for 1 min in a commercial blender. The homogenate was then placed on a shaker at room temperature for 30 min to allow the alliinase-mediated polysulfide formation to take place, after which the pH was immediately adjusted to 3.0, 7.0, and 9.0 using food grade citric acid (3.0 M) or sodium carbonate (2.0 M) solutions. A pH 5.0 experiment was not performed because the pH of homogenized shallot was about 5.35. The resulting pH-adjusted homogenates were incubated at room temperature (22 ± 2 °C) for 90 min in a shaker followed by solvent extraction. Three solvent extractions for each pH level, including control (pH not adjusted) were carried out to give three replicates.

Solvent Extracted Shallot Oil. Shallot bulbs (200 g) were crushed and homogenized with an equal amount of deionized water and incubated with shaking at room temperature. After 30 min of incubation, shallot homogenates were quantitatively transferred into a 1-L flask and extracted (at room temperature with shaking) with diethyl ether (200 mL) spiked with 0.1 mL of 10,000 ppm of diallyl disulfide in dichloromethane as internal standard. Extraction was repeated two more times. The combined ether extracts were concentrated using a rotary evaporator at 30 °C under vacuum. The pungent oil recovered was dried over anhydrous Na_2SO_4 and stored at (−20 °C) until further analysis.

Hydrodistillation of Shallot Oil. A portion of the shallots coming from the same batch was subjected to hydrodistillation. Preparation of the homogenate was carried out as described above. After standing for 30 min, the homogenate was placed in a 500 mL round-bottom flask and charged to a distillation apparatus and immediately subjected to hydrodistillation for 3 h. The milky distillate was extracted 3 times with diethyl ether spiked with the same amount of internal standard in dichloromethane. Diethyl ether extracts were then concentrated using a rotary evaporator and dried over anhydrous Na_2SO_4. The shallot oil obtained was kept at −20 °C until further analysis.

GC and GC-MS/FID Analyses. A portion (100 μL) of the oil recovered was diluted with dichloromethane to 1.0 mL and filtered through a Sartorius Minisart polytetrafluoroethylene (PTFE) membrane (0.45 μm) into a GC-vial. The gas chromatographic analyses were performed with an Agilent 7890A gas chromatography system equipped with a fused silica DB-5MS (30 m × 0.25 mm i.d., 0.25 μm film thickness) column. Injector and transfer line temperatures were 250 and 270 °C, respectively. The initial temperature was 50 °C (3 min), raised to 150 °C (3 min) at the rate of 3 °C/min and further ramped to 250 °C (5 min) at 25 °C/min. Helium (99.999%) was the carrier gas with a flow rate of 1 mL/min. Samples of 1.0 μL were injected using an autosampler (Agilent 7683B) at a 1:5 split ratio. For GC-MS detection, the GC system was interfaced with an Agilent 5975C MS unit operated under the EI mode (70 eV) with an ion source temperature of 200 °C at a mass range of 40.0−500.0. Carrier gas was helium (99.99%) at a flow rate of 1 mL/min.

GC-FID analysis of the hydrodistilled oil and lipophilic extracts was performed using a Varian CP 3800 GC system equipped with a SUPELCO fused silica capillary column (30 m × 0.25 mm I.D., film thickness = 0.25 μm). Carrier gas was helium (99.99%) at a flow rate of 1 mL/min and an injector temperature of 250 °C. The GC conditions were similar as described above. Diluted samples of 1.0 μL were injected manually. The components were identified by matching their retention times with those of the compounds identified by GC-MS.

Identification and Quantification of Organosulfides. Identification of compounds was based on comparison of their mass spectra with those of the National Institute of Standards and Technology

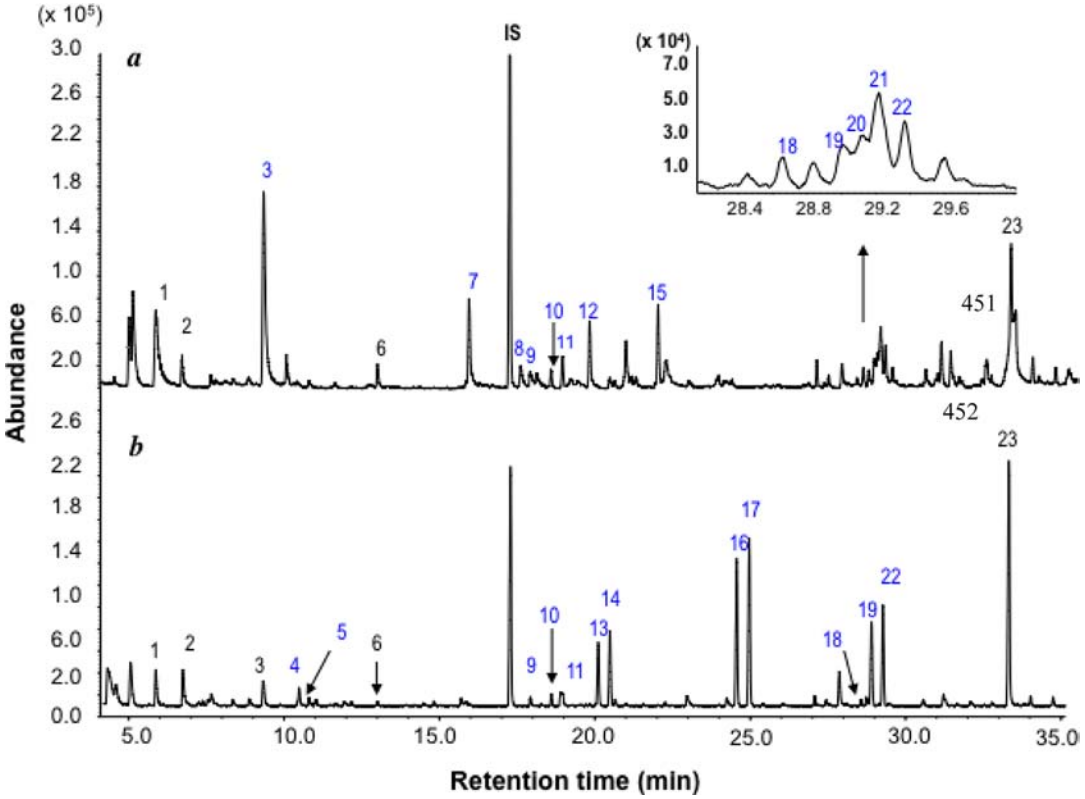

Figure 2. Typical GC chromatograms of organosulfides in (a) solvent extracted and (b) hydrodistilled shallot oil. Peak numbers correspond to the peaks listed in the first column of Table 1. The analytical conditions are described in the text. Peak numbers in blue indicate organosulfides.

(NIST 0.5a) database library of the GC/MS system and by comparing mass spectra with either those of available authentic compounds or published data.11[11,17] When neither a good library match nor published information was available, the identification was established by interpreting the fragmentation pattern of mass spectra. The relative GC peak area of each ion spectrum was calculated against the internal standard and was used to obtain the concentration of each compound expressed in ppm. The relative response factors (RRFs) were measured under the same conditions using the available standard compounds and were calculated as RRF = $(C_{compound}A_{IS})/(C_{IS}A_{compound})$, where $C_{compound}$ and $A_{compound}$ were the concentration and corresponding GC peak area of the compound, C_{IS} and A_{IS} were the concentration and GC peak area of the internal standard.[18] The RRFs of the commercially unavailable compounds were assumed to be 1.0.

Statistical Analysis. Results were expressed as means ± standard deviations (SD) of three separate experiments. Differences between the concentration of organosulfides in solvent extracted and hydrodistilled shallot oil were analyzed by Student's t test ($p < 0.05$). The effect of pH and processing conditions on the yield of organosulfides was analyzed by ANOVA ($p < 0.05$) using OriginPro 8 (OriginLab, USA). Posthoc analysis using Tukey's test was carried out to determine significant differences among the means ($p < 0.05$).

RESULTS AND DISCUSSION

Organosulfide Profiles of Solvent Extracted vs Hydrodistilled Shallot Oil. Shallot oil was obtained by hydrodistillation and extraction using anhydrous diethyl ether. Yellowish oil with pungent odor was obtained at a yield of 0.3−0.5%. The typical GC profile of the oil constituents identified in the solvent extracts and hydrodistilled oil is shown in Figure 2. The solvent extracted samples have more peaks in comparison with hydrodistilled oils. Among them, 14 peaks were identified as sulfur-containing compounds, accounting for 76.47% of the total number of volatile components. Table 1 lists the identified compounds along with their mass spectral characteristics, chemical structures, and GC retention times.

For the solvent extracted oil (Figure 2a), peaks 9 and 11 were acyclic organosulfides identified as trans or cis isomers of propyl-1-propenyl disulfide based on the similarity of their mass fragmentations to those reported in the literature.[19] The other disulfide identified was dipropyl disulfide (peak 10). Three trisulfides were detected as dipropyl trisulfide (peak 18) and cis/trans propyl-1-propenyl trisulfide (peak 20 and 21) based on the comparison of their mass spectra with the mass spectral data of Wu et al.[11] and Sinha et al.[17d] Cyclic organosulfides identified include 3,4-dimethylthiophene (peak 3), cis/trans 2-ethyl-3-methylthiophane (peak 7 and 8), 3-ethyl-1,2-dithi-5-ene (peak 12), and 3-ethyl-1,2-dithi-4-ene (peak 15). A number of nonsulfur flavor compounds were also identified as 2-methyl-2-pentenal (peak 1), *n*-hexanal (peak 2), 2-pentylfuran (peak 6), and 2-hexyl-5-methyl-3(2H)-furanone (peak 23). They are decomposition products fatty acids except 2-methyl-2-pentenal, which was previously reported in solvent extracts of Welsh onions and scallions[17c] and suggested to be the decomposition product of the onion lachrymatory factor (LF).[20] 2-Hexyl-5-methyl-3(2H)-furanone has previously been detected in shallot.[11]

The hydrodistilled oil (Figure 2b) contains two acyclic disulfides, methyl propyl disulfide and methyl 1-propenyl disulfide (peaks 4 and 5, respectively), which are not found in solvent extracted oil. On the other hand, cis and trans propyl-1-propenyl trisulfide (peaks 20 and 21) were not detected in hydrodistilled oil but were present in the solvent extracted oil. Four additional peaks not present in solvent extracted oil were identified as cis/trans 3,5-dimethyl-1,2,4-trithiolane (peaks 13

Table 1. Identity and Mass Spectral Data of Sulfur-Containing and Other Volatile Compounds in Shallot Oil

No[a]	Retention time (min)	Compound	Chemical structures	*m/z* (%)[b]	Identification[c]
1	5.77	Hexanal	$C_5H_{11}CHO$	41 (100), 56 (85), 44 (66), 57 (60), 43 (52), 82 (39), 72 (39)	MS
2	6.65	2-methyl-2-pentenal	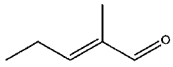	98 (100), 41 (79), 69 (53), 55 (40), 83 (33), 53 (18), 43 (11)	MS, STD, Ref 18, Ref 24
3	9.31	3,4-dimethyl thiophene	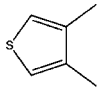	111 (100), 112 (77), 97 (72), 130 (65), 101 (52), 45 (30), 67 (25)	MS, STD, Ref 11
4	10.39	methyl propyl disulfide	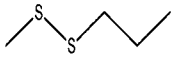	122 (100), 80 (89), 45 (26), 64 (19), 79 (14), 43 (13), 124 (13)	MS, Ref 19, 20
5	10.71	methyl 1-propenyl disulfide	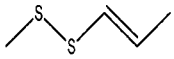	120 (100), 45 (45), 72 (31), 75 (25), 80 (19), 71 (17), 73 (16)	MS, Ref 11, 19, 20
6	12.93	2-pentyl furan	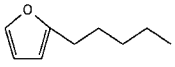	81 (100), 82 (24), 138 (16), 53 (17), 43 (16), 44 (7), 95 (6)	MS
7	15.96	(cis/trans)-2-ethyl-3-methylthiophane	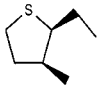	130 (100), 101 (87), 45 (61), 97 (55), 67 (52), 111 (47), 69 (45)	MS, MS-I
8	17.63	(cis/trans)-2-ethyl-3-methylthiophane		130 (100), 101 (96), 45 (89), 69 (74), 67 (63), 115 (58), 111 (56)	MS, MS-I
9	17.83	cis propyl 1-propenyl disulfide	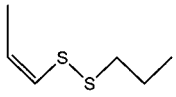	148 (100), 106 (82), 45 (41), 41 (35), 73 (22), 72 (23), 74 (21)	MS-I, Ref 17, 19, 20
10	18.51	dipropyl disulfide	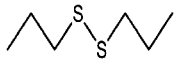	148 (100), 43 (83), 150 (83), 106 (64), 108 (60), 41 (48), 45 (41)	MS, STD
11	19.46	(trans) propyl 1-propenyl disulfide	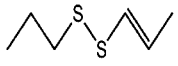	41 (100), 148 (90), 106 (69), 45 (63), 43 (62), 64 (39), 66 (26)	MS, MS-I, Ref 17, 19, 20
12	19.85	3-ethyl-1,2-dithi-5-ene	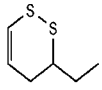	113 (100), 111 (52), 97 (44), 112 (36), 146 (27), 79 (22), 98 (16)	MS, MS-I, Ref 19, 20
13	20.01	(cis) 3,5-dimethyl-1,2,4-trithiolane	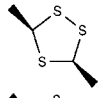	152 (100), 59 (75), 92 (57), 64 (49), 88 (42), 60 (37), 45 (34)	MS, MS-I, Ref 26, 28
14	20.39	(trans) 3,5-dimethyl-1,2,4-trithiolane	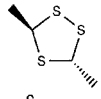	152 (100), 59 (78), 92 (60), 64 (49), 88 (42), 60 (41), 45 (35)	MS, MS-I, Ref 26, 28
15	22.05	3-ethyl-1,2-dithi-4-ene	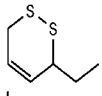	113 (100), 111 (43), 97 (40), 112 (29), 146 (27), 79 (20), 98 (17)	MS, MS-I, Ref 19, 20
16	24.56	(cis) ethyl 1-propenyl trisulfide	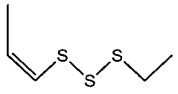	166 (100), 45 (46), 59 (45), 60 (45), 69 (41), 102 (34), 64 (31)	MS, Ref 27
17	24.97	(trans) ethyl 1-propenyl trisulfide	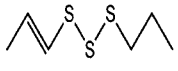	166 (100), 45 (47), 59 (45), 60 (43), 69 (40), 102 (36), 64 (32)	MS, Ref 27
18	28.57	dipropyl trisulfide	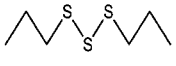	182 (100), 75 (80), 43 (54), 41 (36), 98 (13), 45 (13), 184 (13)	MS, STD
19	28.9	(cis) 3,5-diethyl-1,2,4-trithiolane	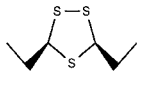	180 (100), 74 (70), 41 (60), 45 (59), 106 (51), 73 (48), 115 (41)	MS, MS-I, Ref 26, 28

[a]Refers to peaks in Figure 1. [b]Determined with an Agilent 7890A quadruple mass spectrometer (Agilent, CA, USA), DB-5MS (30 m × 0.25 mm i.d., 0.25 μm film thickness) column, *m/z* with relative intensity in parentheses, decreasing order. [c]Identification method: MS = mass spectrum compared to NIST 0.5a database library; STD = comparison with standard compound; MS-I = mass spectral interpretation.

dx.doi.org/10.1021/jf500739n | J. Agric. Food Chem. 2014, 62, 5296−5304

and 14) and cis/trans ethyl 1-propenyl trisulfide (peaks 16 and 17), respectively. Formation of the isomers of 3,5-dimethyl-1,2,4-trithiolane may be due to thermal decomposition of cysteine,[21] while peaks 16 and 17 (m/z = 166) were assigned as isomeric forms of ethyl 1-propenyl trisulfide.[22] Peaks 19 and 22, identified as cis/trans 3,5-diethyl-1,2,4-trithiolane, showed notably larger peak areas and good peak separation in hydrodistilled oil.[21] 3,5-Dimethyl-1,2,4-trithiolane has previously been identified in diethyl ether and ethyl acetate extracts of garlic.[23] The relative abundance of sulfur-containing compounds from *Alliums* may vary according to the method of isolation. Kuo and Ho[19] found that methylene chloride extracts of Welsh onions and scallions contained 30 volatile components, including 7 sulfur-containing compounds that were not found in the hydrodistilled oils of the same plants.[24]

A comparison of the organosulfide concentrations (Table 2) in solvent extracted and hydrodistilled oil showed that the solvent extracted one had significantly higher total organosulfides content (266.82 ppm) as compared to hydrodistilled oil (97.81 ppm). In solvent extracted oil, the major cyclic organosulfides were 3,4-dimethylthiophene (58.39 ppm), cis/trans 2-ethyl-3-methylthiophane (68.88 ppm), 3-ethyl-1,2-dithi-4-ene (23.66 ppm), and 3-ethyl-1,2-dithi-5-ene (20.54 ppm). The major linear organosulfides were cis/trans propyl 1-propenyl disulfide (37.75 ppm), cis/trans propyl 1-propenyl trisulfide (27.19 ppm), and dipropyl trisulfide (22.95 ppm). In the hydrodistilled oil, the predominant organosulfides include cis/trans ethyl 1-propenyl trisulfide (41.17 ppm), cis/trans 3,5-diethyl-1,2,4-trithiolane (23.06 ppm), and cis/trans 3,5-dimethyl-1,2,4-trithiolane (19.71 ppm). In terms of the cyclic organosulfide components, trans 2-ethyl-3-methylthiophane, 3-ethyl-1,2-dithi-4-ene, and 3-ethyl-1,2-dithi-5-ene, which were major organosulfides in solvent extracts, were not detected in hydrodistilled oils. Similarly, a significantly ($p < 0.05$) lower amount of 3,4-dimethylthiophene was observed in hydrodistilled oil (3.67 ppm) as compared to those of the solvent extracts. It is remarkable that four isomeric cyclic polysulfides (cis/trans 3,5-dimethyl-1,2,4-trithiolane and cis/trans 3,5-diethyl-1,2,4-trithiolane) predominated in the hydrodistilled oils.

Hydrodistilled oil had significantly lower ($p < 0.05$) concentrations of acyclic polysulfides (95 ppm) as compared to the solvent extracted counterpart (51 ppm). Notable changes in the acyclic polysulfides include reduced amounts of cis/trans propyl 1-propenyl disulfide (1.88 ppm) and dipropyl disulfide (1.15 ppm) in hydrodistilled oil from 37.75 and 22.95 ppm, respectively, in solvent extracted oil. This is in agreement with the literature report that alkyl-1-propenyl disulfides may decompose into saturated disulfides upon heating.[1]

Table 2. Comparison of Organosulfides Obtained from Solvent Extracted and Hydrodistilled Shallot Oil[a]

compd	solvent extracted (mg/kg)	hydrodistilled oil (mg/kg)
Acyclic polysulfides		
methyl propyl disulfide	n.d.	2.53 ± 0.20
methyl 1-propenyl disulfide	n.d.	2.37 ± 0.54
cis/trans propyl 1-propenyl disulfide	37.75 ± 3.54 a	1.88 ± 0.06 b
dipropyl disulfide	7.45 ± 0.28 a	2.27 ± 0.18 b
dipropyl trisulfide	22.95 ± 3.56 a	1.15 ± 0.39 b
cis/trans propyl 1-propenyl trisulfide	27.19 ± 3.85	n.d.
cis/trans-ethyl 1-propenyl trisulfide	tr	41.17 ± 5.04
Total acyclic polysulfides	95.34 ± 3.80 a	51.37 ± 5.35 b
Cyclic polysulfides		
3,4-dimethylthiophene	58.39 ± 4.98 a	3.67 ± 0.41 b
cis/trans-2-ethyl-3-methylthiophane	68.88 ± 12.66	n.d.
3-ethyl-1,2-dithi-5-ene	20.54 ± 3.74	n.d.
3-ethyl-1,2-dithi-4-ene	23.66 ± 3.89	n.d.
(cis/trans) 3,5-dimethyl-1,2,4-trithiolane	n.d.	19.71 ± 3.00
(cis/trans) 3,5-diethyl-1,2,4-trithiolane	n.d.	23.06 ± 3.05
Total cyclic polysulfides	113.09 ± 5.02 a	46.44 ± 13.66 b
Total polysulfides	266.82 ± 12.55 a	97.81 ± 24.37 b

[a]Data are expressed as means ± SD, and the difference among treatments was analyzed by Student's t test at a level of significance p < 0.05. Values across rows without a common letter are significantly different.. n.d.: not detected; tr: trace amount.

Effect of pH on the Organosulfide Profiles of Shallot Oil. Media acidity is an important factor in transformation of organosulfides in *Alliums* because thiols (RSH) and sulfenic acid (RS(O)H) are weak acids. Therefore, we examined the effect of pH on organsulfide profiles and the results are shown in Figure 3. It is clear that the total acyclic disulfides were favored at basic conditions (pH 9.0, 87.99 ppm). Dipropyl disulfide increased 2-fold at pH 9.0 compared to that in control. Methyl propyl disulfide and cis/trans methyl 1-propenyl disulfide were detected only at pH 9.0 (Table 3). On the other hand, total acyclic trisulfides have the highest concentration at pH 3.0 (83.01 ppm) as compared to control (50.14 ppm), pH 7.0 (20.67 ppm), and pH 9.0 (41.37 ppm). Significantly reduced concentrations of individual trisulfides were also observed (Table 3) upon increase of pH values. In terms of total cyclic organosulfides, the highest concentration was observed at pH 3.0 (299.68 ppm), much higher than the sample treated at pH 9.0 (80 ppm). In particular, the concentration of 3,4-dimethylthiophene was 8 times higher (193 ppm) at pH 3.0 compared to that at pH 9.0 (23.35 ppm). Similarly, 3-ethyl-1,2-dithi-4-ene and 3-ethyl-1,2-dithi-5-ene showed significantly higher ($p < 0.05$) concentrations at pH

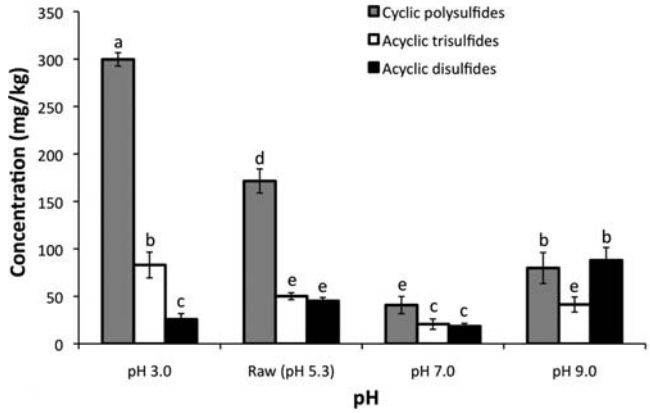

Figure 3. Effect of pH on the polysulfides in hydrodistilled shallot oil. Data are expressed as means ± SD, and the difference among treatments was analyzed by Tukey's test at a level of significance $p < 0.05$. Bar graphs without a common letter differ significantly.

dx.doi.org/10.1021/jf500739n | J. Agric. Food Chem. 2014, 62, 5296−5304

Table 3. Effect of pH on the Individual Organosulfide of Shallot[a]

compd	control (pH 5.35)	pH 3.0	pH 7.0	pH 9.0
Acyclic organosulfides				
dipropyl disulfide	7.45 ± 0.28 a	7.55 ± 1.52 a	4.88 ± 0.93 a	16.67 ± 2.45 b
cis/trans propyl 1-propenyl disulfide	37.75 ± 3.54 b	18.23 ± 2.25 a	13.62 ± 1.02 a	37.51 ± 3.27 b
dipropyl trisulfide	22.95 ± 3.56 a	17.69 ± 3.35 a	4.52 ± 0.28 b	8.45 ± 2.15 b
cis/trans propyl 1-propenyl trisulfide	27.19 ± 2.85 a	63.22 ± 4.45 b	16.15 ± 1.07 c	43.39 ± 3.96 d
methyl propyl disulfide	n.d.	n.d.	n.d.	9.13 ± 1.88
methyl 1-propenyl disulfide	n.d.	n.d.	n.d.	24.68 ± 3.56
Cyclic organosulfides				
cis/trans-2-ethyl-3-methylthiophane	68.88 ± 4.67 a	42.95 ± 3.23 b	17.72 ± 2.52 c	15.85 ± 2.93 c
3-ethyl-1,2-dithi-5-ene	20.54 ± 1.74 a	29.77 ± 2.13 a	1.53 ± 0.15 b	18.59 ± 3.10 b
3-ethyl-1,2-dithi-4-ene	23.66 ± 2.89 a	34.34 ± 3.20 b	2.14 ± 0.54 c	22.02 ± 2.56 a
3,4-dimethylthiophene	58.39 ± 4.98 a	192.61 ± 32.16 b	19.39 ± 3.30 c	23.35 ± 3.70 c

[a]Data are expressed as means ± SD and the difference among treatments was analyzed by Tukey's test at a level of significance $p < 0.05$. Values across rows without a common letter are significantly different. n.d.: not detected.

Table 4. Effect of Processing Methods on the Individual Organosulfide of Shallot

	processing method (mg/kg w.b.)[a]					
compd	raw	freeze-dried	crush-boiled	crushed-autoclaved	whole-boiled	whole-autoclave
Acyclic organosulfides						
dipropyl disulfide	7.45 ± 0.28 a	10.02 ± 0.91 a	3.01 ± 0.48 b	2.47 ± 0.41 b	n.d.	0.97 ± 0.17 b
cis/trans propyl 1-propenyl disulfide	37.75 ± 3.54 a	23.84 ± 3.59 b	11.38 ± 2.59 b	11.50 ± 1.80 b	1.24 ± 0.18 c	0.60 ± 0.12 c
dipropyl trisulfide	22.95 ± 3.56 a	14.97 ± 0.57 a	4.90 ± 0.68 b	6.21 ± 1.23 b	1.05 ± 0.67 c	1.07 ± 0.12 c
cis/trans propyl 1-propenyl trisulfide	27.19 ± 3.85 a	24.63 ± 2.33 a	5.14 ± 1.23 b	6.38 ± 0.49 b	0.24 ± 0.15 c	1.17 ± 0.15 c
Cyclic organosulfides						
cis/trans-2-ethyl-3-methylthiophane	68.88 ± 12.66 a	60.55 ± 7.88 a	20.02 ± 0.25 b	9.08 ± 0.86 c	1.59 ± 0.07 d	1.84 ± 0.13 d
3-ethyl-1,2-dithi-5-ene	20.54 ± 3.74 a	9.46 ± 1.98 b	2.17 ± 0.42 c	2.38 ± 0.67 c	n.d.	0.18 ± 0.06 c
3-ethyl-1,2-dithi-4-ene	23.66 ± 3.89 a	19.61 ± 5.39 a	2.47 ± 1.08 b	5.05 ± 0.28 b	0.09 ± 0.02 c	n.d.
3,4-dimethylthiophene	58.39 ± 4.98 a	48.48 ± 9.36 a	19.29 ± 4.06 b	11.47 ± 1.26 b	n.d.	n.d.

[a]Data are expressed as means ± SD, and the difference among treatments was analyzed by Tukey's test at a level of significance $p < 0.05$. Values across rows without a common letter differ significantly. n.d.: not detected.

3.0 as compared to control and pH 9.0 and 7.0. Finally, cis- and trans-2-ethyl-3-methylthiophane were significantly higher at pH 3.0 (42.95 ppm) compared to pH 7.0 (17.72 ppm) and pH 9.0 (15.85 ppm) but showed the highest concentration at pH 5.3 (68.88 ppm).

In general, acyclic disulfides were favored at basic pH (9.0) whereas acyclic trisulfide formation is favored at weakly acidic pH (5.3) and pH 3.0. On the other hand, cyclic sulfides were highest at pH 3.0. The trends we observed were consistent with a literature report on garlic oil.[25] Our results were also in agreement with a literature report that formation of methyl allyl disulfide and methyl propyl disulfide was favored at pH 9.0 while that of diallyl trisulfide and methyl allyl trisulfide was favored in the neutral or weak acidic pH range.[26] Optimal formations of trisulfides at pH 5.0 or neutral pH could be due to their stability in this pH range rather than at other pH values.[27] The unstable intermediates that are formed after alliinase catalyzed conversion of ACSO may decompose easier into disulfides at pH 9.0, explaining the notable increases of these compounds at this pH.[24]

Effect of Processing Methods on Organosulfides. We further examined different ways of processing, nonthermal and thermal methods, and evaluated their effects on the organosulfide profiles of shallot. Freeze-drying is a nonthermal method for food preservation and is recognized for retaining the quality and health-promoting attributes of onions.[28] We freeze-dried some shallots and extracted the organosulfides using solvent extraction and analyzed the organosulfide profile. Our results show that the ratio of acyclic to cyclic organosulfides in raw (35.7:64.3) remained essentially the same as that of freeze-dried samples (34.7:63.3), although changes in the concentrations of some of the individual polysulfides were observed (Table 4). In freeze-dried shallots, cis/trans propyl 1-propenyl disulfide (23.84 ppm) and dipropyl trisulfide (14.97 ppm) decreased significantly ($p < 0.05$) as compared to raw extracts (37.75 and 22.95 ppm, respectively). Moreover, the total cyclic organosulfides of the freeze-dried sample (138.11 ppm) significantly decreased as compared to the raw one (171.48 ppm), but this reduction was mainly due to the loss of 3-ethyl-1,2-dithi-5-ene. Only slight differences were observed in the levels of cis/trans 2-ethyl-3-methylthiophane, 3-ethyl-1,2-dithi-4-ene, and 3,4-dimethylthiophene between raw and freeze-dried samples. In general, although the total organosulfide content of freeze-dried samples (211.57 ppm) decreased significantly ($p < 0.05$) as compared to those of raw shallots (266.82 ppm), most of the organosulfides remained essentially the same except a few acyclic and cyclic polysulfides, which may have evaporated out during the freeze-drying process. Colina-Coca et al.[27] found that freeze-drying retained ACSO in diced onions. Their result may indicate that the organosulfides of onions can be maintained after the freeze-drying process. In another study, Colina-Coca et al.[28] found that dipropyl disulfide and dipropyl trisulfide significantly ($p < 0.05$) decreased in freeze-dried onions (*Allium cepa* L. var. cepa, "Recas") as compared to diced onions. Our results are in agreement with this except for dipropyl disulfide.

dx.doi.org/10.1021/jf500739n | J. Agric. Food Chem. 2014, 62, 5296−5304

The typical GC chromatograms of shallot oils treated by thermal and freeze-dried processing methods are shown in Figure 4. GC-FID quantification revealed significant changes (p < 0.05) in the concentrations of the individual organosulfide as a result of the different processing methods evaluated. It is apparent that thermal treatments significantly (p < 0.05) reduced the contents of total organosulfides (Figure 5). Boiling (100 °C) and autoclaving (121 °C) temperatures will inactivate the thermal-labile alliinase (80% inactivation at 50 °C for 10 min).[29] Consequently, individual polysulfides dramatically decreased or were completely lost after the heat treatment. In the case of crushed and boiled shallots and crushed and autoclaved samples, the homogenates were allowed to stand for 30 min after crushing before heat treatment was applied. Thus, alliinase shall have sufficient time to react with ACSOs. This treatment is responsible for significantly higher (p < 0.05) organosulfides of crush-boiled and crushed-autoclaved samples as compared to the whole shallots treated in the same manner. Notably lower organosulfide contents of crushed boiled and autoclaved samples suggested that the thiosulfinates or polysulfides in shallot are thermally degraded to nonvolatile compounds. Thiosulfinates showed sensitivity to heat in a time- and intensity-dependent manner.[12] It was suggested that a short heat treatment (boiling for 6 min) did not reduce the *in vitro* antiplatelet activity (IVAA) of onion extract; however, increasing the temperature and heating time resulted in complete loss of activity.

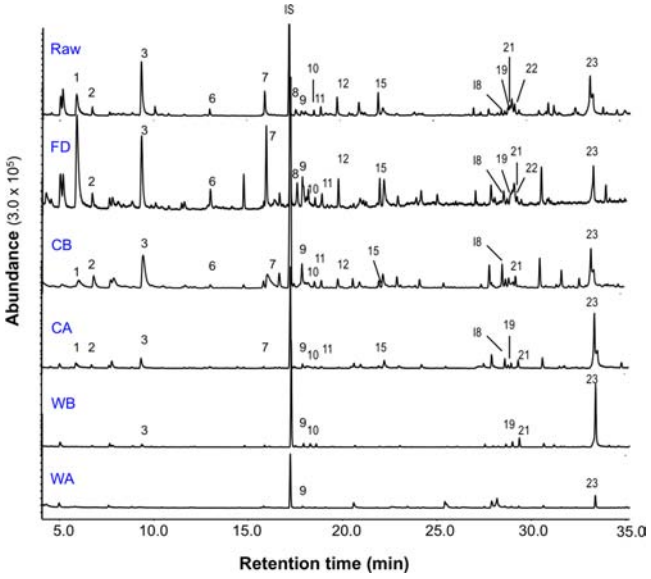

Figure 4. GC chromatograms of organosulfides in (a) raw, (b) freeze-dried (FD), (c) crushed-boiled (CB), (d) crushed-autoclaved (CA), (e) whole-boiled (WB), and (f) whole-autoclaved (WA) shallot. The analytical conditions are described in the text.

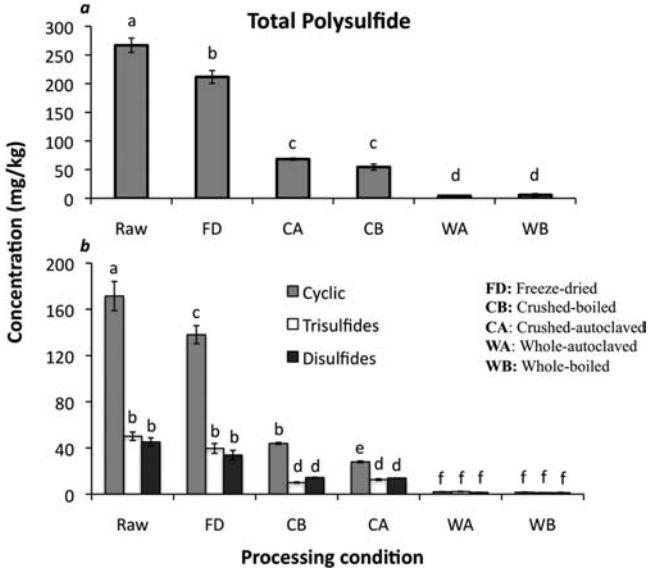

Figure 5. Effect of processing on the (a) total polysulfide content and (b) polysulfide distribution profile of shallot. Data are expressed as means ± SD, and the difference among treatments was analyzed by Tukey's test at a level of significance p < 0.05. Bar graphs without a common letter differ significantly.

Another study demonstrated that although in general degradation of thiosulfinates in onions (*Allium cepa* L.) was affected by heating, the extent to which these antiplatelet agents are destroyed varied depending upon the method (whole, quarters, crushed) of sample preparation.[13] Moreover, the effect of domestic cooking on allicin and pyruvate levels as estimators of the IVAA of cooked garlic extracts was investigated.[16] Oven-heating (200 °C) and boiling for 3 min or less resulted in similar antiplatelet activity as that of the raw extracts; however, crushed garlic subjected to 6 min of boiling or oven heating retained some antiplatelet activity as compared to the uncrushed samples, which completely lost their IVAA. The allicin and pyruvate contents of crushed and uncrushed garlic showed similar trends in IVAA in both cooking methods, suggesting that the thiosulfinates in garlic (mainly allicin) are responsible for the antiaggregatory response.[16] Concordant with the findings of these studies, our results suggest that, in order to allow formation of organosulfides and their retention after processing, shallot should be crushed prior to cooking under mild heat. Intense heating may not only result in the degradation of thiosulfinates. Significant reduction in the polysulfide contents of shallots as an effect of thermal treatment has also been reported.[11]

GC-MS is suggested by Block et al. to be an analytical tool of choice for analysis of volatile organosulfides.[15] In our study, we obtained distilled and diethyl ether extracts after allowing sufficient reaction time to ensure formation of polysulfides. The weakly polar solvents (e.g., diethyl ether and hexane) used favor extraction of polysulfides. In addition, the oil distillate obtained shall not contain thiosulfinates, as these compounds decompose readily to polysulfides during the distillation step.

Block et al. analyzed *Allium* homogenate extracts for their thiosulfinates content. They suggested that there is a serious problem in artifact formation when using GC-based analysis of *Allium* flavorants due to the sensitivity of thiosulfinates to the high temperature conditions during GC analysis.[15] The focus of their study was on the detection of thiosulfinates from *Allium* homogenates while the present study deals with the polysulfides that are present after isolating the lipophilic extracts and distilled oils in shallots that were subjected to different processing conditions and oil isolation methods.

In summary, we have demonstrated that thermal processing by boiling and autoclaving results in significant loss in the cyclic and acyclic organosulfides of shallot while freeze-drying retains the majority of organosulfides. Although freeze-drying resulted

in a significant decrease in the total polysulfide content, this reduction was only attributed to a few organosulfides while the majority of the organosulfides remained the same. In light of the goal of isolating optimal amounts of organic polysulfides with potential H_2S-releasing activity, direct extraction is the preferred method and freeze-drying is a good alternative. Adjusting pH prior to solvent extraction alters the amounts of organosulfides in shallot, with trisulfides showing the highest concentrations at weakly acidic (pH 5.0) to acidic pH (3.0) while disulfides were highest at pH 9.0. It should be pointed out that organic polysulfides that are present only in hydrodistilled oil may be of interest as potential H_2S donors and that the H_2S donating activity of the different oils obtained demands further evaluation using biological models such as cell-line and experimental animal.

AUTHOR INFORMATION

Corresponding Author

*Tel: 65-6516-8821. Fax: 65-6775-7895. E-mail: chmhdj@nus.edu.sg.

Funding

The authors thank the Agency of Science, Technology and Research (A*Star) of Singapore for financial support (Grant Number: 112 177 0036) and the support of a Jiangsu Province Grant to NUSRI for Food Science and Technology (platform 2).

Notes

The authors declare no competing financial interest.

REFERENCES

(1) Block, E. The organosulfur chemistry of the genus *Allium*—Implications for the organic chemistry of sulfur. *Angew. Chem., Int. Ed. Engl.* **1992**, *31*, 1135−1178.

(2) Predmore, B. L.; Kondo, K.; Bhushan, S.; Zlatopolsky, M. A.; King, A. L.; Aragon, J. P.; Bennett Grinsfelder, D.; Condit, M. E.; Lefer, D. J. The polysulfide diallyl trisulfide protects the ischemic myocardium by preservation of endogenous hydrogen sulfide and increasing nitric oxide bioavailability. *Am. J. Physiol. Heart Circ. Physiol.* **2012**, *302*, H2410−H2418.

(3) Benavides, G. A.; Squadrito, G. L.; Mills, R. W.; Patel, H. D.; Isbell, T. S.; Patel, R. P.; Darley-Usmar, V. M.; Doeller, J. E.; Kraus, D. W. Hydrogen sulfide mediates the vasoactivity of garlic. *Proc. Natl. Acad. Sci. U.S.A.* **2007**, *104*, 17977−17982.

(4) Shin, C. C.; Moore, P. K.; Zhu, Y. Z. S-allylcysteine mediates cardioprotection in an acute myocardial infarction rat model via a hydrogen sulfide-mediated pathway. *Am. J. Physiol. Heart Circ. Physiol.* **2007**, *293*, H2693−H2701.

(5) Coletta, C.; Papapetropoulos, A.; Erdelyi, K.; Olah, G.; Módis, K.; Panopoulos, P.; Asimakopoulou, A.; Gerö, D.; Sharina, I.; Martin, E.; Szabo, C. Hydrogen sulfide and nitric oxide are mutually dependent in the regulation of angiogenesis and endothelium-dependent vasorelaxation. *Proc. Natl. Acad. Sci. U.S.A.* **2012**, *109*, 9161−9166.

(6) Zhu, Y. Z.; Zhong, J. W.; Ho, P.; Yoke, Y. L.; Yi, C. Z.; Shan, H. H.; Chee, S. T.; Whiteman, M.; Lu, J.; Moore, P. K. Hydrogen sulfide and its possible roles in myocardial ischemia in experimental rats. *J. Appl. Physiol.* **2007**, *102*, 261−268.

(7) Whiteman, M.; Le Trionnaire, S. L.; Chopra, M.; Fox, B.; Whatmore, J. Emerging role of hydrogen sulfide in health and disease: Critical appraisal of biomarkers and pharmacological tools. *Clin. Sci.* **2011**, *121*, 459−488.

(8) Vu, H. Q.; El-Sayed, M. A.; Ito, S. I.; Yamauchi, N.; Shigyo, M. Discovery of a new source of resistance to Fusarium oxysporum, cause of Fusarium wilt in *Allium fistulosum*, located on chromosome 2 of *Allium cepa* Aggregatum group. *Genome* **2012**, *55*, 797−807.

(9) Wongmekiat, O.; Leelarugrayub, N.; Thamprasert, K. Beneficial effect of shallot (*Allium ascalonicum* L.) extract on cyclosporine nephrotoxicity in rats. *Food Chem. Toxicol.* **2008**, *46*, 1844−1850.

(10) Phuong, P. T. M.; Isshiki, S.; Tashiro, Y. Genetic variation of shallot (*Allium cepa* L. Aggregatum Group) in Vietnam. *J. Jpn. Soc. Hort. Sci.* **2006**, *75*, 236−242.

(11) Wu, J. L.; Chou, C. C.; Chen, M. H.; Wu, C. M. Volatile flavor compounds from shallots. *J. Food Sci.* **1982**, *47*, 606−608.

(12) Cavagnaro, P. F.; Sance, M. M.; Galmarini, C. R. Effect of heating on onion (*Allium cepa* L.) antiplatelet activity and pungency sensory perception. *Food Sci. Technol. Int.* **2007**, *13*, 447−453.

(13) Cavagnaro, P. F.; Galmarini, C. R. Effect of processing and cooking conditions on onion (*Allium cepa* L.) induced antiplatelet activity and thiosulfinate content. *J. Agric. Food Chem.* **2012**, *60*, 8731−8737.

(14) Hansen, E. A.; Folts, J. D.; Goldman, I. L. Steam-cooking rapidly destroys and reverses onion-induced antiplatelet activity. *Nutr. J.* **2012**, *11*, 1−8.

(15) Block, E.; Putman, D.; Zhao, S. H. *Allium* chemistry: GC-MS analysis of thiosulfinates and related compounds from onion, leek, scallion, shallot, chive, and chinese chive. *J. Agric. Food Chem.* **1992**, *40*, 2431−2438.

(16) Cavagnaro, P. F.; Camargo, A.; Galmarini, C. R.; Simon, P. W. Effect of cooking on garlic (*Allium sativum* L.) antiplatelet activity and thiosulfinates content. *J. Agric. Food Chem.* **2007**, *55*, 1280−1288.

(17) (a) Boelens, M. Volatile flavor compounds from onion. *J. Agric. Food. Chem.* **1971**, *19*, 984−991. (b) Schreyen, L.; Dirinck, P.; Van Wassenhove, F.; Schamp, N. Volatile flavor components of leek. *J. Agric. Food Chem.* **1976**, *24*, 336−341. (c) Kallio, H.; Salorinne, L. Comparison of onion varieties by headspace gas chromatography-mass spectrometry. *J. Agric. Food Chem.* **1990**, *38*, 1560−1564. (d) Sinha, N. K. Supercritical carbon dioxide extraction of onion. Flavors and their analysis by gas chromatography-mass spectrometry. *J. Agric. Food Chem.* **1992**, *40*, 842−845. (e) Hanum, T.; Sinha, N. K.; Guyer, D. E.; Cash, J. N. Pyruvate and flavor development in macerated onions (*Allium cepa* L.) by γ-glutamyl transpeptidase and exogenous C-S lyase. *Food Chem.* **1995**, *54*, 183−188. (f) Pino, J. A.; Fuentes, V.; Correa, M. T. Volatile constituents of Chinese chive (*Allium tuberosum* Rottl. ex Sprengel) and rakkyo (*Allium chinense* G. Don). *J. Agric. Food Chem.* **2001**, *49*, 1328−1330. (g) Yabuki, Y.; Mukaida, Y.; Saito, Y.; Oshima, K.; Takahashi, T.; Muroi, E.; Hashimoto, K.; Uda, Y. Characterisation of volatile sulphur-containing compounds generated in crushed leaves of Chinese chive (*Allium tuberosum* Rottler). *Food Chem.* **2010**, *120*, 343−348.

(18) Cheong, M. W.; Zhu, D.; Sng, J.; Liu, S. Q.; Zhou, W.; Curran, P.; Yu, B. Characterisation of calamansi (*Citrus microcarpa*). Part II: Volatiles, physicochemical properties and non-volatiles in the juice. *Food Chem.* **2012**, *134*, 696−703.

(19) Kuo, M. C.; Ho, C. T. Volatile constituents of the solvent extracts of welsh onions (*Allium fistulosum* L. variety maichuon) and scallions (*Allium fistulosum* L. variety caespitosum). *J. Agric. Food Chem.* **1992**, *40*, 1906−1910.

(20) Mondy, N.; Duplat, D.; Christides, J. P.; Arnault, I.; Auger, J. Aroma analysis of fresh and preserved onions and leek by dual solid-phase microextraction-liquid extraction and gas chromatography-mass spectrometry. *J. Chromatogr., A* **2002**, *963*, 89−93.

(21) Yu, A. N.; Tan, Z. W.; Wang, F. S. Mechanism of formation of sulphur aroma compounds from L-ascorbic acid and L-cysteine during the Maillard reaction. *Food Chem.* **2012**, *132*, 1316−1323.

(22) Sass-Kiss, A.; Petru-Turza, M.; Szarfoldi-Szalma, I.; Pino, J.; Rosaldo, A. Investigation on the volatile oil of Mako onions. *Nahrung* **1989**, *33*, 413−421.

(23) Kimbaris, A. C.; Siatis, N. G.; Daferera, D. J.; Tarantilis, P. A.; Pappas, C. S.; Polissiou, M. G. Comparison of distillation and ultrasound-assisted extraction methods for the isolation of sensitive aroma compounds from garlic (*Allium sativum*). *Ultrason. Sonochem.* **2006**, *13*, 54−60.

(24) Kuo, M. C.; Ho, C.-T. Volatile constituents of the hydrodistilled oils of Welsh onions (*Allium fistulosum* L. variety Caepistusom). *J. Agric. Food Chem.* **1992**, *40*, 111−117.
(25) Huang, T. C.; Teng, K. C.; Liou, Y. Y.; Ho, C. T.; Liu, H. J.; Chuang, K. P. Diallyl disulphide, but not diallyl sulphide, increases leucocyte function-associated antigen-1 expression and cellular adhesion in monocytes. *Food Chem.* **2010**, *120*, 113−120.
(26) Yu, T. H.; Wu, C. M.; Chen, S. Y. Effects of pH adjustment and heat treatment on the stability and the formation of volatile compounds of garlic. *J. Agric. Food Chem.* **1989**, *37*, 730−734.
(27) Colina-Coca, C.; Ancos, B.; Sánchez-Moreno, C. Nutritional composition of processed onion: S-Alk(en)yl-L-cysteine sulfoxides, organic acids, sugars, minerals, and vitamin C. *Food Bioprocess. Technol.* **2014**, *7*, 289−298.
(28) Colina-Coca, C.; González-Peña, D.; Vega, E.; de Ancos, B.; Sánchez-Moreno, C. Novel approach for the determination of volatile compounds in processed onion by headspace gas chromatography-mass spectrometry (HS GC-MS). *Talanta* **2013**, *103*, 137−144.
(29) Jansen, H.; Muller, B.; Knobloch, K. Characterization of an Alliin lyase preparation from garlic (*Allium sativum*). *Planta Med.* **1989**, *55*, 434−439.

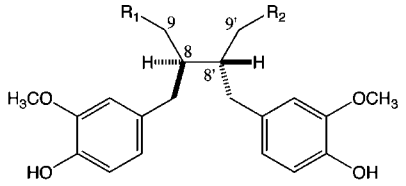

1: R_1 = OH, R_2 = OH ((8*R*,8′*R*)-Secoisolariciresinol, SECO)

3: R_1 = H, R_2 = H ((8*R*,8′*R*)-dihydroguaiaretic acid, (8*R*,8′*R*)-DGA)

6: R_1= R_2 = OAc, **7**: R_1 = R_2 = OCH_3, **8**: R_1 = R_2 = CN

9: R_1 = OH, R_2 = H, **10**: R_1 = OAc, R_2 = H, **11**: R_1 = OCH_3, R_2 = H

12: R_1 = F, R_2 = H, **13**: R_1 = $CH_3(CH_2)_3$, R_2 = H

14: R_1 = $(CH_3)_2CH$, R_2 = H, **15**: R_1 = $(CH_3)_2N$, R_2 = H

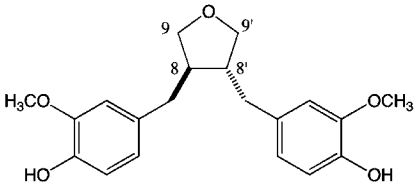

(8*R*,8′*R*)-9,9′-anhydrosecoisolariciresinol (**2**)

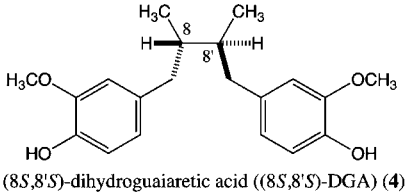

(8*S*,8′*S*)-dihydroguaiaretic acid ((8*S*,8′*S*)-DGA) (**4**)

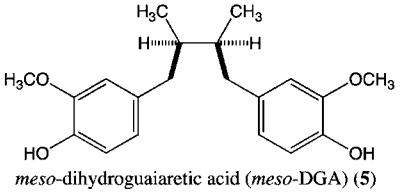

meso-dihydroguaiaretic acid (*meso*-DGA) (**5**)

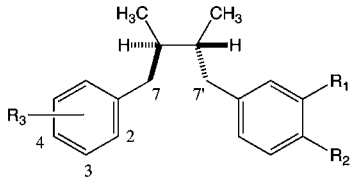

16-42: R_1 = OCH_3, R_2 = OH

16: R_3 = H, **17**: R_3 = 2-OH, **18**: R_3 = 2-OCH_3, **19**: R_3 = 2-$O(CH_2)_3CH_3$

20: R_3 = 2-CH_3, **21**: R_3 = 2-F, **22**: R_3 = 2-Cl, **23**: R_3 = 3-OH, **24**: R_3 = 3-OCH_3

25: R_3 = 3-$O(CH_2)_3CH_3$, **26**: R_3 = 3-CH_3, **27**: R_3 = 3-F, **28**: R_3 = 3-Cl

29: R_3 = 4-OH, **30**: R_3 = 4-OCH_3, **31**: R_3 = 4-$O(CH_2)_3CH_3$, **32**: R_3 = 4-CH_3

33: R_3 = 4-F, **34**: R_3 = 4-Cl, **35**: R_3 = 3,4-OH, **36**: R_3 = 3,5-OH, **37**: R_3 = 3,4-OCH_3

38: R_3 = 3-OH-4-OCH_3, **39**: R_3 = 3-OCH_2CH_3-4-OH, **40**: R_3 = 3,4-OCH_2O

41: R_3 = 3,5-OCH_3-4-OH, **42**: R_3 = 3,4,5-OH

43: R_1 = OH, R_2 = OH, R_3 = 3,4,5-OH

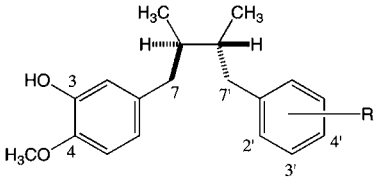

44: R = H, **45**: R = 2′-OH, **46**: R = 2′-OCH_3, **47**: R = 2′-OCH_2CH_3

48: R = 2′-$O(CH_2)_3CH_3$, **49**: R = 2′-$OCH(CH_3)_2$, **50:** R = 2′-CH_3

51: R = 2′-F, **52**: R = 3′-OH, **53**: R = 3′-OCH_3, **54**: R = 3′-CH_3

55: R = 3′-F, **56**: R = 4′-OH, **57**: R = 4′-OCH_3, **58**: R = 4′-CH_3

59: R = 4′-F

Figure 1. Butane-type lignans and their derivatives.

measured with a Horiba SEPA-200 instrument. NMR data were obtained with a JNM-ECS400 spectrometer, using tetramethylsilane and trifluoroacetic acid as a standard (0 ppm) for ^{1}H NMR and (−76.5 ppm) for ^{19}F-NMR, respectively. EIMS data were measured with a JMS-MS700 V spectrometer. The synthetic methods are described in Supporting Information. The numbering of compounds follows the nomenclature of lignans.[19]

*(8R,8′R)-4,4′-Dihydroxy-3,3′-dimethoxylignane-9,9′-diyl diacetate (**6**).* Colorless crystals; mp 108−110 °C; $[\alpha]_D^{25}$ −30 (*c* 1.3, $CHCl_3$); ^{1}H NMR (400 MHz, $CDCl_3$) δ 2.07 (6H, s), 2.07−2.11 (2H, overlapped), 2.61 (4H, m), 3.78 (6H, s), 4.03 (2H, dd, *J* = 11.4, 5.7 Hz), 4.20 (2H, dd, *J* = 11.4, 5.9 Hz), 5.62 (2H, br. s), 6.47 (2H, d, *J* = 2.0 Hz), 6.55 (2H, dd, *J* = 8.0, 2.0 Hz), 6.79 (2H, d, *J* = 8.0 Hz); ^{13}C NMR (100 MHz, $CDCl_3$) δ 21.0, 35.1, 39.6, 55.8, 64.5, 111.2, 114.2, 121.7, 131.5, 144.0, 146.5, 171.1; MS (EI) *m*/*z* 446 (M^+, 42), 189 (19), 137 (100); HRMS (EI) *m*/*z* calcd for $C_{24}H_{30}O_8$ 446.1941, found 446.1940.

*(8R,8′R)- 3,3′,9,9′-Tetramethoxy-4,4′-lignanediol (**7**).* Colorless oil; $[\alpha]_D^{25}$ −27 (*c* 1.1, $CHCl_3$); ^{1}H NMR (400 MHz, $CDCl_3$) δ 2.01 (2H, m), 2.61 (4H, d, *J* = 7.3 Hz), 3.28 (2H, dd, *J* = 9.5, 5.4 Hz), 3.30 (6H, s), 3.35 (2H, dd, *J* = 9.5, 5.4 Hz), 3.76 (6H, s), 5.58 (2H, s), 6.51 (2H, d, *J* = 1.9 Hz), 6.59 (2H, dd, *J* = 7.9, 1.9 Hz), 6.78 (2H, d, *J* = 7.9 Hz); ^{13}C NMR (100 MHz, $CDCl_3$) δ 35.1, 40.6, 55.7, 58.7, 72.7, 111.3, 113.9, 121.9, 132.9, 143.6, 146.4; MS (EI) *m*/*z* 390 (M^+, 41), 358 (21), 189 (32), 137 (100); HRMS (EI) *m*/*z* calcd for $C_{22}H_{30}O_6$ 390.2043, found 390.2050.

*(8R,8′R)-4,4′-Dihydroxy-3,3′-dimethoxy-9a,9′a-dihomolignane-9a,9′a- dinitrile (**8**).* Colorless oil; $[\alpha]_D^{25}$ +40 (*c* 0.5, $CHCl_3$); ^{1}H NMR (400 MHz, $CDCl_3$) δ 2.24 (2H, m), 2.36−2.38 (4H, m), 2.57 (2H, dd, *J* = 14.0, 9.4 Hz), 2.98 (2H, dd, *J* = 14.0, 5.0 Hz), 3.88 (6H, s), 5.58 (2H, s), 6.64 (2H, d, *J* = 1.9 Hz), 6.66 (2H, dd, *J* = 7.9, 1.9 Hz), 6.87 (2H, d, *J* = 7.9 Hz); ^{13}C NMR (100 MHz, $CDCl_3$) δ 19.0, 36.3, 39.3, 56.0, 111.0, 114.7, 118.1, 121.7, 129.6, 144.7, 146.9; EIMS *m*/*z* 380 (M^+, 43), 137 (100), 122 (12); HRMS (EI) *m*/*z* calcd for $C_{22}H_{24}O_4N_2$ 380.1737, found 380.1739.

*(8R,8′R)-3,3′-Dimethoxy-4,4′,9-liganetriol (**9**).* Colorless oil; $[\alpha]_D^{25}$ −24 (*c* 1.0, $CHCl_3$); ^{1}H NMR (400 MHz, $CDCl_3$) δ 0.90 (3H, d, *J* = 6.9 Hz), 1.40−1.70 (1H, br), 1.77 (1H, m), 1.88 (1H, dq, *J* = 6.9, 3.3 Hz), 2.39 (1H, dd, *J* = 13.8, 8.1 Hz), 2.53 (1H, dd, *J* = 13.8, 7.6 Hz), 2.65 (1H, dd, *J* = 13.8,

dx.doi.org/10.1021/jf5010572 | J. Agric. Food Chem. 2014, 62, 5305−5315

Scheme 1. Syntheses of 9- and 9′-Derivatives of (8*R*,8′*R*)-Dihydroguaiaretic Acid

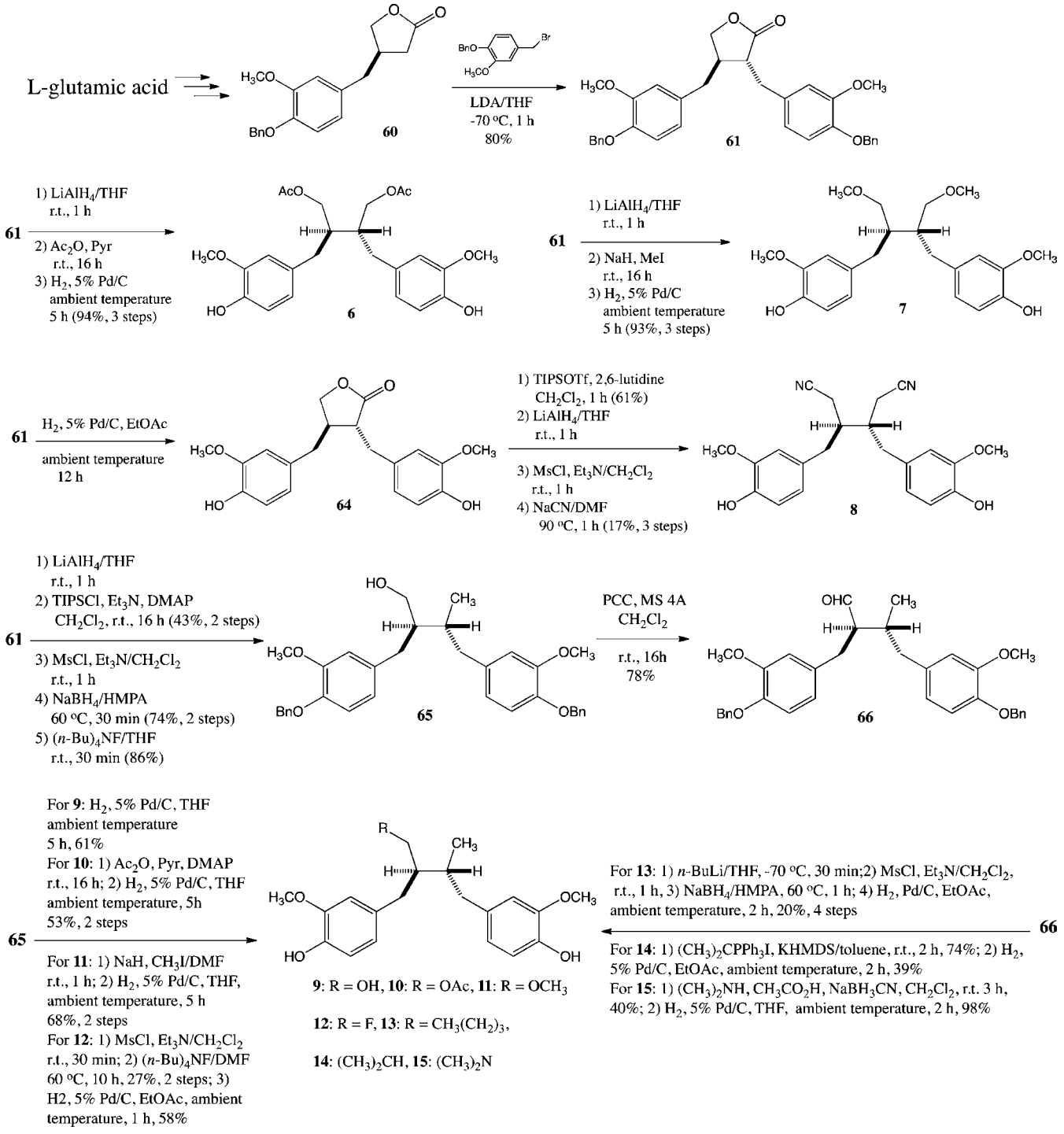

7.0 Hz), 2.67 (1H, dd, *J* = 13.8, 7.5 Hz), 3.57 (1H, dd, *J* = 10.9, 6.6 Hz), 3.72 (1H, dd, *J* = 10.9, 5.3 Hz), 3.77 (3H, s), 3.78 (3H, s), 5.64 (2H, br s), 6.50 (1H, d, *J* = 1.9 Hz), 6.54 (1H, d, *J* = 1.9 Hz), 6.57 (1H, dd, *J* = 8.0, 1.8 Hz), 6.61 (1H, dd, *J* = 8.0, 1.8 Hz), 6.78 (1H, d, *J* = 8.0 Hz), 6.80 (1H, d, *J* = 8.0 Hz); ^{13}C NMR (100 MHz, $CDCl_3$) δ 15.6, 35.0, 35.3, 40.5, 45.8, 55.75, 55.78, 63.0, 111.29, 111.34, 114.0, 114.1, 121.67, 121.71, 132.9, 133.2, 143.6, 143.7, 146.4, 146.5; MS (EI) *m*/*z* 346 (M^+, 11), 137 (100), 122 (14); HRMS (EI) *m*/*z* calcd for $C_{20}H_{26}O_5$ 346.17808, found 346.17811.

(8R,8′R)-3,3′-Dimethoxy-4,4′-dihydroxyligan-9-yl acetate (***10***). Colorless oil; $[\alpha]_D^{25}$ −28 (*c* 0.8, $CHCl_3$); ^{1}H NMR (400 MHz, $CDCl_3$) δ 0.91 (3H, d, *J* = 7.1 Hz), 1.83 (1H, dq, *J* = 7.1, 3.1 Hz), 1.94 (1H, m), 2.06 (3H, s), 2.40 (1H, dd, *J* = 13.7, 7.8 Hz), 2.52 (1H, dd, *J* = 13.9, 8.2 Hz), 2.61 (1H, dd, *J* = 13.7, 6.9 Hz), 2.62 (1H, dd, *J* = 13.9, 6.5 Hz), 3.78 (3H, s), 3.79 (3H, s), 4.00 (1H, dd, *J* = 11.2, 6.7 Hz), 4.19 (1H, dd, *J* = 11.2, 5.8 Hz), 5.53 (1H, s), 5.55 (1H, s), 6.47−6.48 (2H, m), 6.55 (1H, dd, *J* = 8.0, 2.0 Hz), 6.57 (1H, dd, *J* = 7.9, 1.9 Hz), 6.79 (1H, d, *J* = 8.0 Hz), 6.80 (1H, d, *J* = 7.9 Hz); ^{13}C NMR (100 MHz, $CDCl_3$) δ 15.2, 21.1, 35.0, 35.4, 40.6, 41.9, 55.7, 55.8,

dx.doi.org/10.1021/jf5010572 | J. Agric. Food Chem. 2014, 62, 5305−5315

64.7, 111.2, 111.3, 114.0, 114.1, 121.7, 132.2, 132.9, 143.7, 143.8, 146.3, 146.4, 171.3; MS (EI) m/z 388 (M^+, 25), 137 (100); HRMS (EI) m/z calcd for $C_{22}H_{28}O_6$ 388.1886, found 388.1885.

*(8R,8′R)-3,3′,9-Trimethoxy-4,4′-liganediol (**11**).* Colorless oil; $[\alpha]_D^{25}$ −30 (c 1.0, $CHCl_3$); ^{1}H NMR (400 MHz, $CDCl_3$) δ 0.87 (3H, d, J = 6.9 Hz), 1.80−1.88 (2H, m), 2.36 (1H, dd, J = 13.8, 7.8 Hz), 2.49 (1H, dd, J = 13.8, 7.7 Hz), 2.65 (1H, dd, J = 13.8, 7.1 Hz), 2.66 (1H, dd, J = 13.8, 7.0 Hz), 3.25 (1H, dd, J = 9.4, 6.2 Hz), 3.32 (3H, s), 3.40 (1H, dd, J = 9.4, 5.3 Hz), 3.765 (3H, s), 3.772 (3H, s), 5.53 (1H, s), 5.55 (1H, s), 6.48 (1H, d, J = 1.9 Hz), 6.52 (1H, d, J = 1.9 Hz), 6.57 (1H, dd, J = 8.1, 1.9 Hz), 6.59 (1H, dd, J = 8.1, 1.9 Hz), 6.77 (1H, d, J = 8.1 Hz), 6.79 (1H, d, J = 8.1 Hz); ^{13}C NMR (100 MHz, $CDCl_3$) δ 15.4, 34.8, 35.3, 40.7, 43.3, 55.70, 55.74, 58.8, 72.9, 111.28, 111.32, 113.9, 121.79, 121.80, 133.0, 133.4, 143.5, 143.6, 146.3, 146.4; MS (EI) m/z 360 (M^+, 14), 137 (100), 122 (14); HRMS (EI) m/z calcd for $C_{21}H_{28}O_5$ 360.1937, found 360.1929.

*(8R,8′R)-9-Fluoro-3,3′-dimethoxy-4,4′-lignanediol (**12**).* Colorless oil; $[\alpha]_D^{25}$ +20 (c 0.2, $CHCl_3$); ^{1}H NMR (400 MHz, $CDCl_3$) δ 0.94 (3H, d, J = 6.8 Hz), 1.85−1.98 (2H, m), 2.43 (1H, dd, J = 13.8, 7.6 Hz), 2.56 (1H, dd, J = 13.6, 7.4 Hz), 2.62−2.69 (2H, m), 3.798 (3H, s), 3.803 (3H, s), 4.45 (2H, m), 5.46 (1H, s), 5.48 (1H, s), 6.49 (1H, br s), 6.51 (1H, br s), 6.58 (1H, br d, J = 8.1 Hz), 6.60 (1H, br d, J = 7.7 Hz), 6.79 (1H, dd, J = 7.7, 1.2 Hz), 6.81 (1H, dd, J = 8.1, 1.2 Hz); ^{13}C NMR (100 MHz, $CDCl_3$) δ 15.5, 34.3, 34.8 (d, J = 77.8 Hz), 40.9, 43.8 (d, J = 17.2 Hz), 55.7, 55.8, 84.0 (d, J = 167.7 Hz), 111.15, 111.21, 113.9, 114.0, 121.7, 132.0, 132.8, 143.6, 143.8, 146.3, 146.4; ^{19}F NMR (376 MHz, $CDCl_3$) δ −226.4; MS (EI) m/z (%) 348 (M^+, 57), 137 (100); HRMS (EI) m/z calcd for $C_{20}H_{25}O_4F$ 348.1737, found 348.1728.

*(8R,8′R)-3,3′-Dimethoxy-9a,9b,9c,9d-tetrahomolignane-4,4′-diol (**13**).* Colorless oil; $[\alpha]_D^{25}$ −37 (c 0.9, $CHCl_3$); ^{1}H NMR (400 MHz, $CDCl_3$) δ 0.83 (3H, d, J = 6.9 Hz), 0.89 (3H, t, J = 7.2 Hz), 1.10 (1H, m), 1.24−1.44 (7H, m), 1.49 (1H, m), 1.73 (1H, dq, J = 6.9, 2.3 Hz), 2.33 (1H, dd, J = 13.7, 2.4 Hz), 2.35 (1H, dd, J = 13.7, 4.1 Hz), 2.47 (1H, dd, J = 13.7, 7.8 Hz), 2.57 (1H, dd, J = 13.7, 5.9 Hz), 3.75 (3H, s), 3.77 (3H, s), 5.49 (2H, s), 6.41 (1H, d, J = 1.8 Hz), 6.44 (1H, d, J = 1.8 Hz), 6.51 (1H, dd, J = 8.0, 1.9 Hz), 6.55 (1H, dd, J = 8.0, 1.9 Hz), 6.77 (1H, d, J = 8.0 Hz), 6.78 (1H, d, J = 8.0 Hz); ^{13}C NMR (100 MHz, $CDCl_3$) δ 14.1, 14.8, 22.7, 27.7, 28.9, 32.4, 35.4, 37.5, 40.3, 42.3, 55.65, 55.73, 111.19, 111.24, 113.79, 113.83, 121.69, 121.73, 133.7, 133.8, 143.4, 146.2, 146.3; MS (EI) m/z 386 (M^+, 49), 137 (100); HRMS (EI) m/z calcd for $C_{24}H_{34}O_4$ 386.2458, found 386.2449.

*(8R,8′R)-3,3′-Dimethoxy-9a,9b,9b-trihomoligane-4,4′-diol (**14**).* Colorless crystals; mp 70−71 °C; $[\alpha]_D^{25}$ −41 (c 0.4, $CHCl_3$); ^{1}H NMR (400 MHz, $CDCl_3$) δ 0.83 (3H, d, J = 6.9 Hz), 0.84 (3H, d, J = 6.5 Hz), 0.89 (3H, d, J = 6.6 Hz), 1.08 (1H, ddd, J = 18.2, 4.9, 4.9 Hz), 1.18 (1H, ddd, J = 18.2, 3.9, 3.9 Hz), 1.58−1.66 (2H, m), 1.75 (1H, dq, J = 6.6, 2.2 Hz), 2.31 (1H, dd, J = 14.0, 9.6 Hz), 2.34 (1H, dd, J = 14.0, 6.8 Hz), 2.43 (1H, dd, J = 13.8, 8.0 Hz), 2.56 (1H, dd, J = 13.8, 5.4 Hz), 3.74 (3H, s), 3.77 (3H, s), 5.44 (1H, s), 5.45 (1H, s), 6.40 (1H, d, J = 1.9 Hz), 6.43 (1H, d, J = 1.9 Hz), 6.51 (1H, dd, J = 8.0, 1.9 Hz), 6.55 (1H, dd, J = 8.0, 1.9 Hz), 6.76 (1H, d, J = 8.0 Hz), 6.78 (1H, d, J = 8.0 Hz); ^{13}C NMR (100 MHz, $CDCl_3$) δ 14.6, 22.3, 24.0, 25.5, 35.1, 37.6, 38.4, 39.6, 40.2, 55.6, 55.7, 111.16, 111.21, 113.7, 113.8, 121.7, 121.8, 133.6, 133.8, 143.4, 146.2, 146.3; MS (EI) m/z 372 (M^+, 33), 137 (100), 122 (13); HRMS (EI) m/z calcd for $C_{23}H_{32}O_4$ 372.2302, found 372.2305.

*(8R,8′R)-9-(N,N-Dimethylamino)-3,3′-dimethoxylignane-4,4′-diol (**15**).* Colorless oil; $[\alpha]_D^{25}$ −59 (c 0.4, $CHCl_3$); ^{1}H NMR (400 MHz, $CDCl_3$) δ 0.85 (3H, d, J = 7.0 Hz), 1.71 (1H, m), 1.86 (1H, dq, J = 7.0, 2.3 Hz), 2.15−2.24 (2H, overlapped), 2.20 (6H, s), 2.33 (1H, dd, J = 13.8, 9.7 Hz), 2.39 (1H, dd, J = 13.7, 7.1 Hz), 2.49 (1H, dd, J = 13.7, 8.4 Hz), 2.77 (1H, dd, J = 13.8, 5.1 Hz), 3.71 (3H, s), 3.76 (3H, s), 6.39 (1H, d, J = 1.8 Hz), 6.46 (1H, d, J = 1.8 Hz), 6.51 (1H, dd, J = 8.0, 1.8 Hz), 6.55 (1H, dd, J = 8.0, 1.8 Hz), 6.74 (1H, d, J = 8.0 Hz), 6.77 (1H, d, J = 8.0 Hz); ^{13}C NMR (100 MHz, $CDCl_3$) δ 14.8, 33.9, 36.3, 40.0, 40.2, 46.2, 55.6, 55.7, 60.1, 111.1, 111.3, 113.7, 113.8, 121.7, 121.8, 133.3, 133.5, 143.49, 143.54, 146.3; MS (EI) m/z 373 (M^+, 100), 164 (20), 137 (43); HRMS (EI) m/z calcd for $C_{22}H_{31}O_4N$ 373.2254, found 373.2260.

*(8R,8′R)-2-Butoxy-3′-methoxy-4′-lignanol (**19**).* Colorless oil; $[\alpha]_D^{25}$ −42 (c 0.8, $CHCl_3$); ^{1}H NMR (400 MHz, $CDCl_3$) δ 0.81 (3H, d, J = 6.9 Hz), 0.85 (3H, d, J = 6.7 Hz), 0.96 (3H, t, J = 7.4 Hz), 1.46 (2H, m), 1.68 (2H, m), 1.75 (1H, m), 1.85 (1H, m), 2.35 (1H, dd, J = 13.6, 8.4 Hz), 2.38 (1H, dd, J = 12.9, 8.2 Hz), 2.57 (1H, dd, J = 13.6, 6.8 Hz), 2.69 (1H, dd, J = 12.9, 6.2 Hz), 3.78−3.84 (1H, overlapped), 3.80 (3H, s), 3.90 (1H, m), 5.43 (1H, s), 6.53 (1H, d, J = 1.8 Hz), 6.58 (1H, dd, J = 7.9, 1.8 Hz), 6.78 (2H, br d, J = 7.9 Hz), 6.82 (1H, dd, J = 7.7, 7.3, 1.4 Hz), 7.03 (1H, dd, J = 7.3, 1.5 Hz), 7.12 (1H, ddd, J = 7.8, 7.7, 1.8 Hz); ^{13}C NMR (100 MHz, $CDCl_3$) δ 13.9, 14.1, 14.2, 19.4, 31.5, 35.9, 36.1, 38.6, 41.1, 55.8, 67.3, 110.9, 111.3, 113.9, 119.8, 121.6, 126.8, 130.2, 130.8, 133.9, 143.4, 146.2, 157.2; MS (EI) m/z 356 (M^+, 88), 163 (34), 137 (81), 107 (29), 59 (100); HRMS (EI) m/z calcd for $C_{23}H_{32}O_3$ 356.2351, found 356.2340.

*(8R,8′R)-3-Butoxy-3′-methoxy-4′-lignanol (**25**).* Colorless oil; $[\alpha]_D^{25}$ −28 (c 0.6, $CHCl_3$); ^{1}H NMR (400 MHz, $CDCl_3$) δ 0.83 (6H, d, J = 6.7 Hz), 0.98 (3H, t, J = 7.4 Hz), 1.49 (2H, m), 1.72−1.82 (4H, m), 2.37 (1H, dd, J = 13.6, 8.1 Hz), 2.41 (1H, dd, J = 13.5, 8.1 Hz), 2.55 (1H, dd, J = 13.6, 6.7 Hz), 2.59 (1H, dd, J = 13.5, 6.7 Hz), 3.82 (3H, s), 3.91 (2H, t, J = 6.5 Hz), 5.45 (1H, s), 6.54 (1H, d, J = 1.7 Hz), 6.59 (1H, dd, J = 8.1, 1.7 Hz), 6.63 (1H, m), 6.67 (1H, br d, J = 7.5 Hz), 6.70 (1H, m), 6.80 (1H, d, J = 8.1 Hz), 7.14 (1H, dd, J = 7.8, 7.8 Hz); ^{13}C NMR (100 MHz, $CDCl_3$) δ 13.9, 14.0, 19.3, 31.5, 37.6, 37.9, 41.1, 41.5, 55.8, 67.5, 111.3, 111.5, 113.9, 115.3, 121.3, 121.6, 128.9, 133.5, 143.3, 143.5, 146.2, 159.0; MS (EI) m/z 356 (M^+, 23), 164 (62), 137 (100), 107 (74), 58 (62); HRMS (EI) m/z calcd for $C_{23}H_{32}O_3$ 356.2351, found 356.2342.

*(8R,8′R)-4-Butoxy-3′-methoxy-4′-lignanol (**31**).* Colorless oil; $[\alpha]_D^{25}$ −18 (c 0.7, $CHCl_3$); ^{1}H NMR (400 MHz, $CDCl_3$) δ 0.81 (3H, d, J = 6.8 Hz), 0.82 (3H, d, J = 6.8 Hz), 0.98 (3H, t, J = 7.3 Hz), 1.49 (2H, m), 1.70−1.79 (4H, m), 2.36 (1H, dd, J = 13.6, 3.2 Hz), 2.38 (1H, dd, J = 13.5, 3.2 Hz), 2.55 (1H, dd, J = 13.5, 3.5 Hz), 2.56 (1H, dd, J = 13.6, 3.5 Hz), 3.82 (3H, s), 3.93 (2H, t, J = 6.5 Hz), 5.46 (1H, s), 6.54 (1H, d, J = 1.8 Hz), 6.57 (1H, dd, J = 8.1, 1.8 Hz), 6.78 (2H, d, J = 8.5 Hz), 6.80 (1H, d, J = 8.1 Hz), 6.98 (2H, d, J = 8.5 Hz); ^{13}C NMR (100 MHz, $CDCl_3$) δ 13.9, 19.3, 31.5, 37.86, 37.91, 40.5, 41.1, 55.8, 67.7, 111.3, 113.9, 114.1, 121.6, 129.8, 133.5, 133.6, 143.5, 146.2, 157.2; MS (EI) m/z 356 (M^+, 12), 208 (39), 137 (99), 107 (74), 58 (100); HRMS (EI) m/z calcd for $C_{23}H_{32}O_3$ 356.2351, found 356.2341.

*(8R,8′R)-4-Methoxy-3-lignanol (**44**).* Colorless oil; $[\alpha]_D^{25}$ −24 (c 0.5, $CHCl_3$); ^{1}H NMR (400 MHz, $CDCl_3$) δ 0.81 (3H, d, J = 6.7 Hz), 0.82 (3H, d, J = 6.7 Hz), 1.75−1.83 (2H, m),

dx.doi.org/10.1021/jf5010572 | J. Agric. Food Chem. 2014, 62, 5305−5315

2.33 (1H, dd, J = 13.5, 5.6 Hz), 2.41 (1H, dd, J = 13.5, 8.7 Hz), 2.57 (1H, dd, J = 13.5, 6.1 Hz), 2.65 (1H, dd, J = 13.5, 6.0 Hz), 3.86 (3H, s), 5.54 (1H, s), 6.56 (1H, dd, J = 8.1, 1.9 Hz), 6.69 (1H, d, J = 1.9 Hz), 6.73 (1H, d, J = 8.1 Hz), 7.10 (2H, d, J = 7.3 Hz), 7.16 (1H, dd, J = 7.3, 7.3 Hz), 7.23−7.27 (2H, m); ^{13}C NMR (100 MHz, $CDCl_3$) δ 13.9, 14.0, 38.2, 38.3, 40.7, 41.4, 56.0, 110.4, 115.1, 120.3, 125.6, 128.1, 129.0, 135.0, 141.7, 144.5, 145.2; MS (EI) m/z 284 (M^+, 69), 137 (100), 101 (75), 91 (30); HRMS (EI) m/z calcd for $C_{19}H_{24}O_2$ 284.1776, found 284.1768.

(8R,8′R)-4-Methoxy-2′,3-lignanediol (**45**). Colorless oil; $[\alpha]_D^{25}$ −30 (c 0.4, $CHCl_3$); ^{1}H NMR (400 MHz, $CDCl_3$) δ 0.83 (3H, d, J = 6.5 Hz), 0.85 (3H, d, J = 6.6 Hz), 1.79 (1H, m), 1.87 (1H, m), 2.34 (1H, dd, J = 13.6, 8.7 Hz), 2.42 (1H, dd, J = 13.6, 8.9 Hz), 2.58 (1H, dd, J = 13.6, 6.2 Hz), 2.67 (1H, dd, J = 13.6, 5.9 Hz), 3.85 (3H, s), 4.78 (1H, s), 5.58 (1H, s), 6.58 (1H, dd, J = 8.1, 2.1 Hz), 6.70−6.74 (3H, m), 6.83 (1H, ddd, J = 7.4, 7.3, 0.9 Hz), 7.03 (1H, dd, J = 7.6, 1.5 Hz), 7.07 (1H, d, J = 7.7, 1.7 Hz); ^{13}C NMR (100 MHz, $CDCl_3$) δ 14.1, 35.4, 36.6, 38.6, 40.7, 56.0, 110.4, 115.1, 115.2, 120.4, 120.5, 127.0, 127.5, 131.1, 135.0, 144.5, 145.1, 153.6; MS (EI) m/z 300 (M^+, 90), 137 (100), 107 (27); HRMS (EI) m/z calcd for $C_{19}H_{24}O_3$ 300.1725; found 300.1730.

(8R,8′R)-2′,4-Methoxy-3-lignanol (**46**). Colorless oil; $[\alpha]_D^{25}$ −32 (c 0.4, $CHCl_3$); ^{1}H NMR (400 MHz, $CDCl_3$) δ 0.81 (3H, d, J = 6.2 Hz), 0.82 (3H, d, J = 6.1 Hz), 1.76 (1H, m), 1.84 (1H, m), 2.33 (1H, dd, J = 13.6, 8.6 Hz), 2.39 (1H, dd, J = 13.2, 8.7 Hz), 2.57 (1H, dd, J = 13.6, 6.4 Hz), 2.69 (1H, dd, J = 13.2, 5.8 Hz), 3.74 (3H, s), 3.85 (3H, s), 5.52 (1H, s), 6.57 (1H, dd, J = 8.2, 2.0 Hz), 6.69 (1H, d, J = 2.0 Hz), 6.73 (1H, d, J = 8.2 Hz), 6.81 (1H, br d, J = 8.1 Hz), 6.85 (1H, ddd, J = 7.6, 7.3, 1.0 Hz), 7.04 (1H, dd, J = 7.3, 1.7 Hz), 7.15 (1H, ddd, J = 7.8, 7.6, 1.7 Hz); ^{13}C NMR (100 MHz, $CDCl_3$) δ 14.06, 14.12, 35.7, 36.3, 38.6, 40.7, 55.1, 56.0, 110.2, 110.3, 115.1, 120.0, 120.4, 126.8, 130.2, 130.6, 135.3, 144.5, 145.2, 157.6; MS (EI) m/z 314 (M^+, 100), 137 (88), 121 (45); HRMS (EI) m/z calcd for $C_{20}H_{26}O_3$ 314.1882, found 314.1891.

(8R,8′R)-2′-Ethoxy-4-methoxy-3-lignanol (**47**). Colorless oil; $[\alpha]_D^{25}$ −28 (c 0.5, $CHCl_3$); ^{1}H NMR (400 MHz, $CDCl_3$) δ 0.80 (3H, d, J = 6.9 Hz), 0.85 (3H, d, J = 6.7 Hz), 1.33 (3H, t, J = 7.0 Hz), 1.75 (1H, m), 1.85 (1H, m), 2.32 (1H, dd, J = 13.6, 8.6 Hz), 2.35 (1H, dd, J = 13.1, 8.7 Hz), 2.58 (1H, dd, J = 13.6, 6.4 Hz), 2.73 (1H, dd, J = 13.1, 5.6 Hz), 3.85 (3H, s), 3.95 (2H, m), 5.51 (1H, s), 6.57 (1H, dd, J = 8.2, 2.1 Hz), 6.68 (1H, d, J = 2.1 Hz), 6.72 (1H, d, J = 8.2 Hz), 6.79 (1H, d, J = 8.0 Hz), 6.83 (1H, dd, J = 7.4, 7.4 Hz), 7.04 (1H, dd, J = 7.4, 1.7 Hz), 7.13 (1H, ddd, J = 7.4, 7.4, 1.7 Hz); ^{13}C NMR (100 MHz, $CDCl_3$) δ 14.2, 14.3, 14.9, 35.8, 36.4, 38.8, 40.6, 56.0, 63.2, 110.3, 111.0, 115.1, 119.9, 120.3, 126.7, 130.3, 130.8, 135.4, 144.5, 145.2, 157.0; MS (EI) m/z 328 (M^+, 78), 137 (100), 135 (54); HRMS (EI) m/z calcd for $C_{21}H_{28}O_3$ 328.2038, found 328.2020.

(8R,8′R)-2′-Butoxy-4-methoxy-3-lignanol (**48**). Colorless oil; $[\alpha]_D^{25}$ −17 (c 0.5, $CHCl_3$); ^{1}H NMR (400 MHz, $CDCl_3$) δ 0.80 (3H, d, J = 6.8 Hz), 0.84 (3H, d, J = 6.8 Hz), 0.97 (3H, t, J = 7.4 Hz), 1.48 (2H, m), 1.71 (2H, m), 1.76 (1H, m), 1.86 (1H, m), 2.30 (1H, dd, J = 13.5, 8.9 Hz), 2.36 (1H, dd, J = 13.0, 8.9 Hz), 2.59 (1H, dd, J = 13.5, 6.1 Hz), 2.72 (1H, dd, J = 13.0, 5.6 Hz), 3.86 (3H, s), 3.89 (2H, m), 5.51 (1H, s), 6.57 (1H, dd, J = 8.1, 2.0 Hz), 6.68 (1H, d, J = 2.0 Hz), 6.72 (1H, d, J = 8.1 Hz), 6.79 (1H, d, J = 8.2 Hz), 6.84 (1H, d, J = 7.3 Hz), 7.04 (1H, dd, J = 7.3, 1.4 Hz), 7.13 (1H, ddd, J = 7.8, 7.7, 1.4 Hz); ^{13}C NMR (100 MHz, $CDCl_3$) δ 13.9, 14.1, 19.4, 31.5, 35.8, 36.6, 38.9, 40.7, 56.0, 67.3, 110.3, 110.9, 115.1, 119.8, 120.3, 126.7, 130.2, 130.8, 135.4, 144.5, 145.2, 157.1; MS (EI) m/z 356 (M^+, 61), 208 (33), 163 (20), 137 (100), 107 (26); HRMS (EI) m/z calcd for $C_{23}H_{32}O_3$ 356.2351, found 356.2347.

(8R,8′R)-2′-Isopropoxy-4-methoxy-3-lignanol (**49**). Colorless oil; $[\alpha]_D^{25}$ −26 (c 0.4, $CHCl_3$); ^{1}H NMR (400 MHz, $CDCl_3$) δ 0.79 (3H, d, J = 6.5 Hz), 0.85 (3H, d, J = 6.8 Hz), 1.24 (3H, d, J = 5.9 Hz), 1.26 (3H, d, J = 6.0 Hz), 1.75−1.88 (2H, m), 2.30 (1H, dd, J = 13.0, 8.7 Hz), 2.32 (1H, dd, J = 13.5, 8.6 Hz), 2.58 (1H, dd, J = 13.5, 6.4 Hz), 2.72 (1H, dd, J = 13.0, 5.2 Hz), 3.85 (3H, s), 4.48 (1H, m), 5.52 (1H, s), 6.57 (1H, dd, J = 8.1, 2.0 Hz), 6.69 (1H, d, J = 2.0 Hz), 6.72 (1H, d, J = 8.1 Hz), 6.78−6.82 (2H, m), 7.04 (1H, dd, J = 7.4, 1.7 Hz), 7.11 (1H, ddd, J = 7.8, 7.1, 1.7 Hz); ^{13}C NMR (100 MHz, $CDCl_3$) δ 14.0, 14.3, 22.0, 22.1, 36.0, 36.4, 39.0, 40.7, 56.0, 69.2, 110.3, 112.3, 115.1, 119.6, 120.3, 126.6, 131.00, 131.04, 135.4, 144.5, 145.2, 155.7; MS (EI) m/z 342 (M^+, 92), 137 (100), 107 (50); HRMS (EI) m/z calcd for $C_{22}H_{30}O_3$ 342.2195, found 342.2177.

(8R,8′R)-4-Methoxy-2′-methyl-3-lignanol (**50**). Colorless oil; $[\alpha]_D^{25}$ −36 (c 0.4, $CHCl_3$); ^{1}H NMR (400 MHz, $CDCl_3$) δ 0.81 (3H, d, J = 6.6 Hz), 0.87 (3H, d, J = 6.8 Hz), 1.73−1.85 (2H, m), 2.21 (3H, s), 2.35 (1H, dd, J = 13.5, 8.3 Hz), 2.39 (1H, dd, J = 13.5, 9.1 Hz), 2.56 (1H, dd, J = 13.5, 6.6 Hz), 2.65 (1H, dd, J = 13.5, 5.2 Hz), 3.85 (3H, s), 5.53 (1H, s), 6.57 (1H, dd, J = 8.1, 2.2 Hz), 6.69 (1H, d, J = 2.2 Hz), 6.73 (1H, d, J = 8.1 Hz), 7.03 (1H, m), 7.07−7.12 (3H, m); ^{13}C NMR (100 MHz, $CDCl_3$) δ 13.7, 14.3, 19.4, 36.5, 38.8, 39.0, 40.6, 56.0, 110.4, 115.1, 120.3, 125.5, 125.7, 129.9, 130.1, 135.0, 136.2, 139.8, 144.6, 145.2; EIMS m/z (%) 298 (M^+, 82), 137 (100), 105 (21); HRMS (EI) m/z calcd for $C_{20}H_{26}O_2$ 298.1933, found 298.1932.

(8R,8′R)-2′-Fluoro-4-methoxy-3-lignanol (**51**). Colorless oil; $[\alpha]_D^{25}$ −37 (c 0.4, $CHCl_3$); ^{1}H NMR (400 MHz, $CDCl_3$) δ 0.83 (3H, d, J = 6.8 Hz), 0.84 (3H, d, J = 6.7 Hz), 1.77 (1H, m), 1.83 (1H, m), 2.32 (1H, dd, J = 13.5, 8.9 Hz), 2.46 (1H, dd, J = 13.5, 8.9 Hz), 2.58 (1H, dd, J = 13.5, 5.9 Hz), 2.69 (1H, dd, J = 13.5, 6.0 Hz), 3.86 (3H, s), 5.54 (1H, s), 6.57 (1H, dd, J = 8.1, 1.9 Hz), 6.68 (1H, d, J = 1.9 Hz), 6.73 (1H, d, J = 8.1 Hz), 6.97 (1H, br d, J = 8.8 Hz), 7.02 (1H, dd, J = 7.3, 6.6 Hz), 7.08 (1H, dd, J = 7.4, 1.6 Hz), 7.14 (1H, m); ^{13}C NMR (100 MHz, $CDCl_3$) δ 13.97, 13.99, 34.1, 37.4, 38.5, 40.7, 56.0, 110.4, 115.09, 115.10 (d, J = 22.3 Hz), 120.3, 123.7 (d, J = 3.7 Hz), 127.3 (d, J = 7.9 Hz), 128.5 (d, J = 15.9 Hz), 131.3 (d, J = 4.8 Hz), 134.9, 144.6, 145.2, 161.3 (d, J = 244.3 Hz); ^{19}F NMR (376 MHz, $CDCl_3$) δ −119.1; MS (EI) m/z 302 (M^+, 90), 137 (100); HRMS (EI) m/z calcd for $C_{19}H_{23}O_2F$ 302.1682, found 302.1680.

(8R,8′R)-4-Methoxy-3,3′-lignanediol (**52**). Colorless oil; $[\alpha]_D^{25}$ −19 (c 0.5, $CHCl_3$); ^{1}H NMR (400 MHz, $CDCl_3$) δ 0.80 (3H, d, J = 6.7 Hz), 0.81 (3H, d, J = 6.7 Hz), 1.73−1.81 (2H, m), 2.36 (1H, dd, J = 13.5, 8.5 Hz), 2.38 (1H, dd, J = 13.5, 8.6 Hz), 2.52 (1H, dd, J = 13.4, 6.5 Hz), 2.57 (1H, dd, J = 13.4, 6.4 Hz), 3.86 (3H, s), 4.90−5.40 (1H, br), 5.65 (1H, br s), 6.54 (1H, dd, J = 2.1, 1.7 Hz), 6.58 (1H, dd, J = 8.2, 2.1 Hz), 6.64−6.69 (3H, m), 6.74 (1H, d, J = 8.2 Hz), 7.11 (1H, dd, J = 7.8, 7.8 Hz); ^{13}C NMR (100 MHz, $CDCl_3$) δ 13.8, 13.9, 37.1, 37.6, 40.6, 41.1, 56.0, 110.4, 112.7, 115.1, 115.8, 120.6, 121.6, 129.2, 134.9, 143.5, 144.6, 145.0, 155.4; MS (EI) m/z 300 (M^+, 91), 137 (100); HRMS (EI) m/z calcd for $C_{19}H_{24}O_3$ 300.1725, found 300.1733.

dx.doi.org/10.1021/jf5010572 | J. Agric. Food Chem. 2014, 62, 5305−5315

Table 1. Cytotoxic Activities of (8*R*,8′*R*)-Secoisolariciresinol (1), (8*R*,8′*R*)-9,9′-Anhydrosecoisolariciresinol (2), All Stereoisomers of Dihydroguaiaretic Acid (3−5), and 9-,9′-Derivatives of (8*R*,8′*R*)-Dihydroguaiaretic Acid 6−15 against HL-60 and HeLa Cells (IC_{50} ± SD, n = 3)

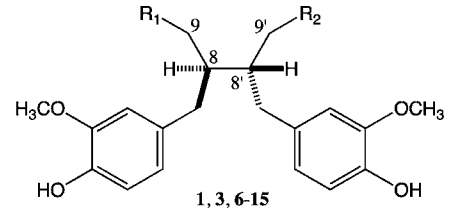

1, 3, 6-15

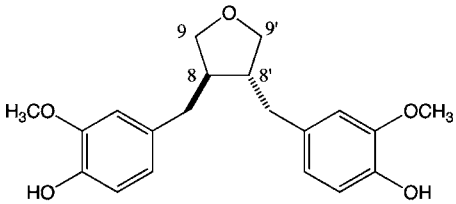

(8*R*,8′*R*)-9,9′-anhydrosecoisolariciresinol (**2**)

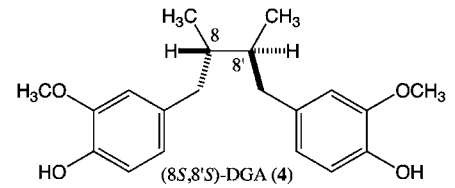

(8*S*,8′*S*)-DGA (**4**)

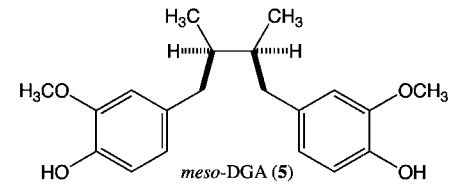

meso-DGA (**5**)

No	R_1	R_2	HL-60 IC_{50} (μM) ± SD	HeLa IC_{50} (μM) ± SD
1: (8*R*,8′*R*)-SECO	OH	OH	> 100 (8% inhibition)	>100 (33% inhibition)
2 : (8*R*,8′*R*)-9,9′-anhydro-SECO	—O—		>100 (23% inhibition)	>100 (35% inhibition)
3: (8*R*,8′*R*)-DGA	H	H	25.7 ± 0.9	21.7 ± 4.1
4: (8*S*,8′*S*)-DGA			24.0 ± 1.6	31.9 ± 3.9
5: *meso*-DGA			27.7 ± 3.3	40.6 ± 1.1
6	OAc	OAc	77.8 ± 0.8	80.1 ± 3.5
7	OCH_3	OCH_3	25.3 ± 1.1	24.2 ± 0.7
8	CN	CN	>100 (39% inhibition)	>100 (45% inhibition)
9	OH	H	79.3 ± 11	97.7 ± 4.8
10	OAc	H	20.7 ± 1.5	43.0 ± 1.6
11	OCH_3	H	15.1 ± 3.1	19.9 ± 3.9
12	F	H	33.5 ± 1.8	28.6 ± 1.5
13	$CH_3(CH_2)_3$	H	6.4 ± 0.3	6.0 ± 0.4
14	$(CH_3)_2CH$	H	6.6 ± 1.3	8.0 ± 1.2
15	$(CH_3)_2N$	H	>100 (23% inhibition)	>100 (41% inhibition)

*(8R,8′R)-3′,4-Methoxy-3-lignanol (**53**).* Colorless oil; $[\alpha]_D^{25}$ −25 (*c* 0.6, $CHCl_3$); ^{1}H NMR (400 MHz, $CDCl_3$) δ 0.82 (6H, d, *J* = 6.8 Hz), 1.73−1.84 (2H, m), 2.33 (1H, dd, *J* = 13.6, 8.5 Hz), 2.39 (1H, dd, *J* = 13.4, 8.6 Hz), 2.56 (1H, dd, *J* = 13.6, 6.3 Hz), 2.62 (1H, dd, *J* = 13.4, 6.2 Hz), 3.78 (3H, s), 3.86 (3H, s), 5.55 (1H, s), 6.56 (1H, dd, *J* = 8.2, 1.9 Hz), 6.65 (1H, m), 6.68−6.74 (4H, m), 7.16 (1H, dd, *J* = 7.9, 7.8 Hz); ^{13}C NMR (100 MHz, $CDCl_3$) δ 14.0, 38.0, 38.2, 40.7, 41.5, 55.1, 56.0, 110.4, 110.9, 114.6, 115.1, 120.3, 121.5, 129.0, 135.0, 143.3, 144.6, 145.2, 159.4; MS (EI) *m*/*z* 314 (M^+, 100), 137 (96), 122 (37); HRMS (EI) *m*/*z* calcd for $C_{20}H_{26}O_3$ 314.1882, found 314.1890.

*(8R,8′R)-4-Methoxy-3′-methyl-3-lignanol (**54**).* Colorless oil; $[\alpha]_D^{25}$ −26 (*c* 0.6, $CHCl_3$); ^{1}H NMR (400 MHz, $CDCl_3$) δ 0.81 (3H, d, *J* = 6.6 Hz), 0.82 (3H, d, *J* = 6.7 Hz), 1.73−1.84 (2H, m), 2.30−2.35 (1H, overlapped), 2.31 (3H, s), 2.37 (1H, dd, *J* = 13.4, 8.6 Hz), 2.57 (1H, dd, *J* = 13.4, 6.0 Hz), 2.61 (1H, dd, *J* = 13.4, 6.0 Hz), 3.86 (3H, s), 5.54 (1H, s), 6.57 (1H, dd, *J* = 8.2, 1.9 Hz), 6.69 (1H, d, *J* = 1.9 Hz), 6.73 (1H, d, *J* = 8.2 Hz), 6.90 (1H, br d, *J* = 7.2 Hz), 6.91 (1H, br s), 6.98 (1H, br d, *J* = 7.5 Hz), 7.14 (1H, dd, *J* = 7.5, 7.1 Hz); ^{13}C NMR (100 MHz, $CDCl_3$) δ 14.0, 21.4, 38.0, 38.3, 40.7, 41.3, 56.0, 110.3, 115.1, 120.3, 126.0, 126.3, 128.0, 129.8, 135.0, 137.6, 141.6, 144.5, 145.2; MS (EI) *m*/*z* 298 (M^+, 25), 137 (100); HRMS (EI) *m*/*z* calcd for $C_{20}H_{26}O_2$ 298.1933, found 298.1929.

*(8R,8′R)-3′-Fluoro-4-methoxy-3-lignanol (**55**).* Colorless oil; $[\alpha]_D^{25}$ −26 (*c* 0.5, $CHCl_3$); ^{1}H NMR (400 MHz, $CDCl_3$) δ 0.815 (3H, d, *J* = 6.8 Hz), 0.821 (3H, d, *J* = 6.7 H), 1.72−1.83 (2H, m), 2.34 (1H, dd, *J* = 13.5, 8.5 Hz), 2.41 (1H, dd, *J* = 13.5, 8.6 Hz), 2.55 (1H, dd, *J* = 13.5, 6.4 Hz), 2.64 (1H, dd, *J* = 13.5, 6.3 Hz), 3.87 (3H, s), 5.54 (1H, s), 6.56 (1H, d, *J* = 8.1, 2.1 Hz), 6.68 (1H, d, *J* = 2.1 Hz), 6.74 (1H, d, *J* = 8.1 Hz), 6.79 (1H, ddd, *J* = 10.0, 2.1, 1.7 Hz), 6.83−6.89 (2H, m), 7.20 (1H, ddd, *J* = 7.8, 7.7, 6.3 Hz): ^{13}C NMR (100 MHz, $CDCl_3$) δ 13.9, 14.0, 37.9, 38.2, 40.7, 41.2, 56.0, 110.4, 112.5 (d, *J* = 20.8 Hz), 115.1, 115.7 (d, *J* = 21.0 Hz), 120.3, 124.7, 129.4 (d, *J* = 8.5 Hz), 134.8, 144.3 (d, *J* = 7.1 Hz), 144.6, 145.3, 162.8 (d, *J* = 245.3 Hz); ^{19}F NMR (376 MHz, $CDCl_3$) δ −115.2; MS (EI) *m*/*z* 302 (M^+, 74), 137 (100); HRMS (EI) *m*/*z* calcd for $C_{19}H_{23}FO_2$ 302.1682, found 302.1682.

*(8R,8′R)-4-Methoxy-3,4′-lignanediol (**56**).* Colorless oil; $[\alpha]_D^{25}$ −21 (*c* 0.5, $CHCl_3$); ^{1}H NMR ($CDCl_3$) δ 0.797 (3H, d, *J* = 6.5 Hz), 0.801 (3H, d, *J* = 6.7 Hz), 1.70−1.78 (2H, m), 2.32 (1H, dd, *J* = 13.5, 8.9 Hz), 2.35 (1H, dd, *J* = 13.5, 8.9 Hz), 2.55 (1H, dd, *J* = 13.5, 6.7 Hz), 2.56 (1H, dd, *J* = 13.5, 6.7 Hz), 3.86 (3H, s), 4.77 (1H, s), 5.56 (1H, s), 6.57 (1H, dd, *J* = 8.1, 2.0 Hz), 6.68 (1H, d, *J* = 2.0 Hz), 6.72 (2H, d, *J* = 8.5 Hz), 6.74 (1H, d, *J* = 8.1 Hz), 6.95 (2H, d, *J* = 8.5 Hz); ^{13}C NMR (100 MHz, $CDCl_3$) δ 13.9, 38.1, 38.3, 40.5, 40.8, 56.0, 110.4, 115.0, 115.1, 120.4, 130.0, 133.9, 135.0, 144.5, 145.2, 153.4; MS (EI) *m*/*z* 300 (M^+, 95), 137 (100), 107 (35); HRMS (EI) *m*/*z* calcd for $C_{19}H_{24}O_3$ 300.1725, found 300.1731.

*(8R,8′R)-4,4′-Methoxy-3-lignanol (**57**).* Colorless oil; $[\alpha]_D^{25}$ −22 (*c* 0.8, $CHCl_3$); ^{1}H NMR (400 MHz, $CDCl_3$) δ 0.80 (3H, d, *J* = 6.7 Hz), 0.81 (3H, d, *J* = 6.5 Hz), 1.75 (2H, m), 2.32

dx.doi.org/10.1021/jf5010572 | J. Agric. Food Chem. 2014, 62, 5305−5315

Table 2. Cytotoxic Activities of 7-Aryl Derivatives of (8*R*,8′*R*)-Dihydroguaiaretic Acid against HL-60 and HeLa Cells (IC_{50} ± SD, n = 3)

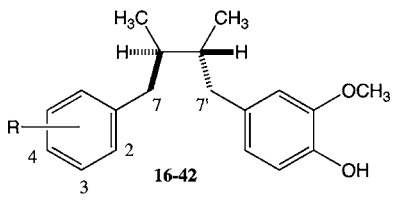

16-42

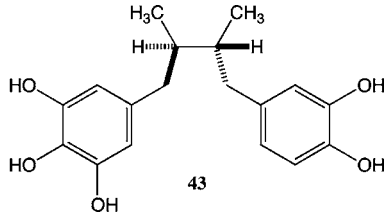

43

no.	R	HL-60 IC_{50} (μM) ± SD	HeLa IC_{50} (μM) ± SD	no.	R	HL-60 IC_{50} (μM) ± SD	HeLa IC_{50} (μM) ± SD
16	H	10.3 ± 2.4	31.8 ± 1.5	**30**	4-OCH_3	12.5 ± 1.5	27.6 ± 2.6
17	2-OH	9.6 ± 2.7	9.3 ± 2.0	**31**	4-$O(CH_2)_3CH_3$	6.6 ± 1.9	10.7 ± 1.1
18	2-OCH_3	6.3 ± 0.2	24.4 ± 0.5	**32**	4-CH_3	16.1 ± 2.0	17.5 ± 2.5
19	2-$O(CH_2)_3CH_3$	7.2 ± 2.4	9.3 ± 0.3	**33**	4-F	13.4 ± 2.5	19.1 ± 0.3
20	2-CH_3	5.9 ± 1.5	17.3 ± 0.4	**34**	4-Cl	10.6 ± 2.5	18.3 ± 0.4
21	2-F	13.5 ± 0.8	18.7 ± 0.3	**35**	3,4-OH	5.9 ± 0.2	13.6 ± 1.1
22	2-Cl	10.0 ± 0.5	18.5 ± 0.7	**36**	3,5-OH	10.8 ± 0.6	7.6 ± 1.0
23	3-OH	26.1 ± 3.4	26.5 ± 2.1	**37**	3,4-OCH_3	31.9 ± 3.5	30.5 ± 1.9
24	3-OCH_3	27.1 ± 3.3	24.3 ± 0.4	**38**	3-OH-4-OCH_3	8.7 ± 1.2	7.5 ± 0.5
25	3-$O(CH_2)_3CH_3$	7.5 ± 2.2	10.6 ± 1.4	**39**	3-OCH_2CH_3-4-OH	7.3 ± 1.9	27.9 ± 2.8
26	3-CH_3	15.9 ± 2.9	18.7 ± 0.4	**40**	3,4-OCH_2O	28.6 ± 1.9	32.7 ± 2.5
27	3-F	11.0 ± 0.1	17.9 ± 1.1	**41**	3,5-OCH_3-4-OH	9.0 ± 3.6	6.8 ± 0.5
28	3-Cl	9.1 ± 2.6	17.0 ± 1.8	**42**	3,4,5-OH	12.6 ± 1.0	34.9 ± 2.4
29	4-OH	5.9 ± 0.5	10.8 ± 0.8	**43**		28.9 ± 1.7	>100 (36% inhibition)

(1H, dd, J = 13.6, 8.5 Hz), 2.36 (1H, dd, J = 13.6, 8.5 Hz), 2.55 (1H, dd, J = 13.6, 5.9 Hz), 2.59 (1H, dd, J = 13.6, 5.9 Hz), 3.79 (3H, s), 3.86 (3H, s), 5.55 (1H, s), 6.57 (1H, dd, J = 8.1, 2.0 Hz), 6.69 (1H, d, J = 2.0 Hz), 6.73 (1H, d, J = 8.1 Hz), 6.80 (2H, d, J = 8.6 Hz), 7.01 (2H, d, J = 8.6 Hz); ^{13}C NMR (100 MHz, $CDCl_3$) δ 13.9, 38.2, 38.3, 40.5, 40.8, 55.2, 56.0, 110.4, 113.5, 115.1, 120.3, 129.8, 133.7, 135.0, 144.5, 145.2, 157.6; MS (EI) m/z 314 (M^+, 89), 137 (75), 121 (100), 101 (28); HRMS (EI) m/z calcd for $C_{20}H_{26}O_3$ 314.1882, found 314.1885.

*(8R,8′R)-4-Methoxy-4′-methyl-3-lignanol (**58**).* Colorless oil; $[\alpha]_D^{25}$ −23 (c 0.5, $CHCl_3$); ^{1}H NMR (400 MHz, $CDCl_3$) δ 0.80 (3H, d, J = 6.7 Hz), 0.81 (3H, d, J = 6.7 Hz), 1.77 (2H, m), 2.29−2.35 (1H, overlapped), 2.31 (3H, s), 2.37 (1H, dd, J = 13.3, 8.5 Hz), 2.56 (1H, dd, J = 13.3, 5.9 Hz), 2.61 (1H, dd, J = 13.3, 5.7 Hz), 3.85 (3H, s), 5.55 (1H, s), 6.57 (1H, dd, J = 8.2, 1.9 Hz), 6.69 (1H, d, J = 1.9 Hz), 6.73 (1H, d, J = 8.2 Hz), 6.99 (2H, d, J = 7.9 Hz), 7.06 (2H, d, J = 7.9 Hz); ^{13}C NMR (100 MHz, $CDCl_3$) δ 13.9, 21.0, 38.2, 38.3, 40.8, 41.0, 56.0, 110.3, 115.1, 120.3, 128.8, 128.9, 134.9, 135.0, 138.5, 144.5, 145.2; MS (EI) m/z 298 (M^+, 58), 137 (100), 105 (41); HRMS (EI) m/z calcd for $C_{20}H_{26}O_2$ 298.1933, found 298.1930.

*(8R,8′R)-4′-Fluoro-4-methoxy-3-lignanol (**59**).* Colorless oil; $[\alpha]_D^{25}$ −26 (c 0.6, $CHCl_3$); ^{1}H NMR (400 MHz, $CDCl_3$) δ 0.80 (3H, d, J = 6.7 Hz), 0.81 (3H, d, J = 6.5 Hz), 1.70−1.78 (2H, m), 2.33 (1H, dd, J = 13.5, 8.3 Hz), 2.38 (1H, dd, J = 13.5, 8.4 Hz), 2.54 (1H, dd, J = 13.5, 6.1 Hz), 2.60 (1H, dd, J = 13.5, 6.1 Hz), 3.86 (3H, s), 5.54 (1H, s), 6.55 (1H, dd, J = 8.2, 2.0 Hz), 6.68 (1H, d, J = 2.0 Hz), 6.73 (1H, d, J = 8.2 Hz), 6.93 (2H, m), 7.03 (2H, m); ^{13}C NMR (100 MHz, $CDCl_3$) δ 13.8, 13.9, 38.1, 38.2, 40.6, 40.7, 56.0, 110.4, 114.8 (d, J = 21.1 Hz), 115.1, 120.3, 130.2 (d, J = 7.8 Hz), 134.9, 137.2 (d, J = 3.0 Hz), 144.6, 145.2, 161.1 (d, J = 242.6); ^{19}F NMR (376 MHz, $CDCl_3$) δ −119.1; MS (EI) m/z 302 (M^+, 92), 137 (100); HRMS (EI) m/z calcd for $C_{19}H_{23}FO_2$ 302.1682, found 302.1679.

Cytotoxic Assay. Human cervical carcinoma cell line HeLa cells and human promyelocytic leukemia cell line HL-60 cells were obtained from American Type Culture Collection (Manassas, VA). Colon 26 colon adenocarcinoma cells derived from BALB/c mouse were kindly provided by the Institute of Development, Aging and Cancer, Tohoku University (Sendai, Japan). Vero cells (JCRB0111) were purchased from JCRB Cell Banks. These cells were cultured in the DMEM medium (Sigma, St. Louis, MO) supplemented with 10% fetal bovine serum (FBS) at 37 °C in a humidified atmosphere of 5% CO_2. HeLa, Colon 26, and Vero cells were inoculated in 96-well culture plates at 2.0 × 10^4 cells/well suspended in the DMEM medium, and HL-60 cells were inoculated in 96-well culture plates at 1.0 × 10^4 cells/well suspended in RPMI1640 with FBS and various concentrations of different compounds. After cultivation for 48 h, the cell viability was assessed by a WST-8 reduction assay (Dojin Laboratories, Japan). The WST-8 reduction activity of the cells is presented as the ratio of cell activity. Briefly, a WST-8 solution was added to the culture medium at 10% concentration and incubated for 1 h at 37 °C prior to colorimetry at 450 nm. The single cytotoxic assay was performed in triplicate.

RESULTS AND DISCUSSION

Syntheses of Derivatives. As shown in Scheme 1, 9- and 9′-derivatives of (8*R*,8′*R*)-DGA **6**−**15** were synthesized from dibenzyloxymatairesinol **61**. The aromatic derivatives **16**−**59** were synthesized by the previously described method[15] with modification.

Cytotoxic Activities of 9- and 9′-Derivatives against HL-60 and HeLa Cells. Table 1 shows the cytotoxic activity of dietary (8*R*,8′*R*)-secoisolariciresinol (SECO) (**1**) and its 9 and 9′-derivatives against HL-60 and HeLa cells. (8*R*,8′*R*)-SECO (**1**) and (8*R*,8′*R*)-9,9′-anhydrosecoisolariciresinol (**2**), which is a metabolite from (−)-(8*R*,8′*R*)-SECO, did not show the remarkable activity at 100 μM, suggesting that the oxidations at

dx.doi.org/10.1021/jf5010572 | J. Agric. Food Chem. 2014, 62, 5305−5315

Table 3. Cytotoxic Activities of (8*R*,8′*R*)-7-(3-Hydroxy-4-methoxyphenyl)-7′-aryl Dihydroguaiaretic Acid Derivatives against HL-60 and HeLa Cells (IC_{50} ± SD, n = 3)

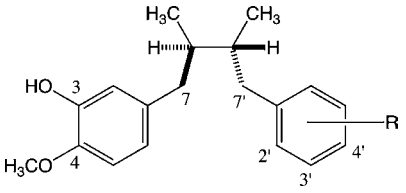

no.	R	HL-60 IC_{50} (μM) ± SD	HeLa IC_{50} (μM) ± SD
44	H	8.2 ± 1.8	9.5 ± 1.3
45	2′-OH	3.5 ± 0.6	3.8 ± 1.1
46	2′-OCH_3	1.6 ± 0.2	2.6 ± 0.6
47	2′-OCH_2CH_3	0.8 ± 0.4	1.7 ± 0.6
48	2′-$O(CH_2)_3CH_3$	7.2 ± 0.4	6.7 ± 1.2
49	2′-$OCH(CH_3)_2$	3.8 ± 0.3	4.3 ± 1.0
50	2′-CH_3	2.7 ± 0.04	4.7 ± 1.3
51	2-F	3.7 ± 0.8	4.8 ± 0.6
52	3′-OH	8.7 ± 0.6	9.7 ± 0.7
53	3′-OCH_3	7.1 ± 1.2	6.2 ± 1.0
54	3′-CH_3	5.9 ± 0.3	5.1 ± 0.5
55	3′-F	9.5 ± 0.6	9.5 ± 0.2
56	4′-OH	4.3 ± 0.4	9.8 ± 1.3
57	4′-OCH_3	4.5 ± 1.2	5.4 ± 1.5
58	4′-CH_3	5.3 ± 1.3	5.9 ± 1.1
59	4′-F	5.8 ± 0.7	9.9 ± 0.3

9- and 9′-positions on the butane chain are disadvantageous for the activity. This fact was ascertained by the examination using dihydroguaiaretic acids (DGA) **3**−**5**, whose 9- and 9′-positions were reduced. All stereoisomers of dihydroguaiaretic acids exhibited the almost same level of activities (IC_{50} = 22−41 μM). The stereochemistry of 8 and 8′-positions did not affect the activity. The activity of 9, 9′-acetoxy derivative **6** was 2−3-fold less potent than DGA stereoisomers, and the activity of 9, 9′-nitrile derivative **8** was very weak (IC_{50} > 100 μM); however, a similar level of activity to DGA stereoisomers was observed in 9, 9′-methoxy derivative **7**. Compared with inactive tetrahydrofuran structure **2**, the disadvantage of the ring structure was suggested. Even if the oxygen atoms are present at 9- and 9′-positions, the methoxy derivative kept the activity. For further research on the 9-position, the activities of 9-derivatives of (8*R*,8′*R*)-DGA **9**−**15** were tested. Compared with inactive (−)-(8*R*,8′*R*)- SECO (**1**), 9′-dehydroxy SECO **9** showed the weak activity (IC_{50} = 79−98 μM). The activities of 9-acetoxy and 9-methoxy DGA derivative **10** and **11** were the same level as those of all stereoisomers of DGA **3**−**5**, 9,9′-acetoxy **6**, and 9,9′-methoxy **7** derivative. On the other hand, 9-alkyl DGA derivative **13** and **14** displayed 3−4-fold higher activity than that of (8*R*,8′*R*)-DGA (**3**). The activity level of 9-butyl DGA **13** and 9-isopropyl DGA **14** was similar, indicating the importance of higher hydrophobic structure for the higher activity. Because 9-fluoro derivative **12** showed comparable activity to that of (8*R*,8′*R*)-DGA (**3**), the activity would not be affected by an electron-withdrawing atom. The activity of basic derivative, 9-dimethylamino DGA derivative **15**, was very low. The relationship between cytotoxic activity and 9-, 9′-structure of butane-type lignan containing dietary secoisolariciresinol became clear. The higher hydrophobic compounds exhibited higher activity.

Cytotoxic Activities of 7-Aryl Derivatives against HL-60 and HeLa Cells. As a next step, the effect of the substituent

Table 4. Cytotoxic Activities of 3, 38, and 47 against Colon 26 and Vero Cells (IC_{50}± SD, n = 3)

Compounds	Colon 26 IC_{50} (μM) ± SD	Vero IC_{50} (μM) ± SD	HL-60 IC_{50} (μM) ± SD	HeLa IC_{50} (μM) ± SD
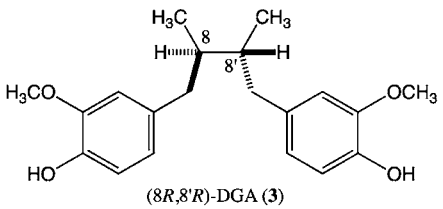 (8*R*,8′*R*)-DGA (**3**)	32.3 ± 4.4	35.7 ± 1.8	25.7 ± 0.9 (Table 1)	21.7 ± 4.1 (Table 1)
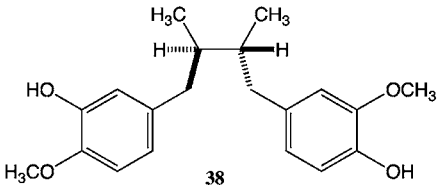 **38**	17.4 ± 0.8	28.7 ± 4.0	8.7 ± 1.2 (Table 2)	7.5 ± 0.5 (Table 2)
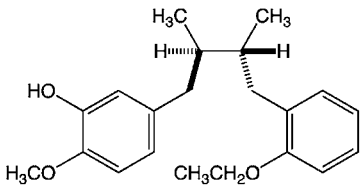 **47**	6.9 ± 1.4	10.2 ± 2.2	0.8 ± 0.4 (Table 3)	1.7 ± 0.6 (Table 3)

dx.doi.org/10.1021/jf5010572 | J. Agric. Food Chem. 2014, 62, 5305−5315

of the aromatic ring on the activity was examined. Table 2 shows the activities of 7-derivatives of (8*R*,8′*R*)-DGA. Without a substituent on the 7-aromatic ring, derivative **16** showed 2.6-fold higher activity than (8*R*,8′*R*)-DGA (**3**) against HL-60 cells and similar activity to **3** against HeLa cells. It could be assumed that the 3-methoxy group and 4-hydroxy group of **3** do not play an important role to keep 10−30 μM of IC_{50} values. As for 2-substituted derivatives **17**−**22**, all derivatives showed 2−4-fold higher activity than that of (8*R*,8′*R*)-DGA (**3**) against HL-60 cells. The activities of 2-methoxy derivative **18**, 2-butoxy derivative **19**, and 2-methyl derivative **20** bearing an electron donor group were about 2-fold higher than those of hydrophilic 2-hydroxy derivative **17** and 2-halo derivative **21** and **22** bearing an electron-withdrawing group, suggesting that the hydrophobic and electron donor substituents on the 2-position are favorable for higher activity against HL-60 cells. Because the activity of 2-butoxy derivative **19** was similar to that of 2-methoxy derivative **18** against HL-60 cells, the length of alkoxy group would not affect the activity. Against HeLa cells, hydrophilic 2-hydroxy derivative **17** and 2-butoxy derivative **19** bearing a longer alkoxy group exhibited 2-fold higher activity than that of (8*R*,8′*R*)-DGA (**3**). On the other hand, the same level of activities as that of (8*R*,8′*R*)-DGA (**3**) were observed in 2-methoxy derivative **18**, 2-methyl derivative **20**, and 2-halo derivative **21** and **22**. The 2-hydroxy derivative **17** and 2-butoxy derivative **19** showed higher activity than (8*R*,8′*R*)-DGA (**3**) against both cells. The effect of 3-substituent was also examined. It was shown that the activities of 3-hydroxy derivative **23** and 3-methoxy derivative **24** were similar to that of (8*R*,8′*R*)-DGA (**3**) against both HL-60 and HeLa cells. The more hydrophobic derivatives, 3-butoxy derivative **25**, 3-methyl derivative **26**, 3-fluoro derivative **27**, and 3-chloro derivative **28** were 2−3-fold more effective than (8*R*,8′*R*)-DGA (**3**) against HL-60 cells. Against HeLa cells, the activity level of 3-methyl derivative **26**, 3-fluoro derivative **27**, and 3-chloro derivative **28** was almost the same as that of (8*R*,8′*R*)-DGA (**3**); however, 3-butoxy derivative **25** exhibited 2-fold more potent activity than (8*R*,8′*R*)-DGA (**3**). The 3-butoxy derivative **25** bearing a longer and hydrophobic group displayed the highest activity among the 3-substituted derivatives against both cells. In the case of the 4-position, 4-hydroxy derivative **29** and 4-butoxy derivative **31** were 4-fold more potent and 4-methoxy derivative **30** and 4-halide derivative **33** and **34** were 2-fold more potent than that of (8*R*,8′*R*)-DGA (**3**) against HL-60 cells. Against HeLa cells, 2-fold higher activities than that of (8*R*,8′*R*)-DGA (**3**) were observed in 4-hydroxy derivative **29** and 4-butoxy derivative **31**. The activities of 4-methyl derivative **32** against HL-60 and HeLa cells and 4-methoxy derivative **30** and 4-halide derivative **33** and **34** against HeLa cells were similar to that of (8*R*,8′*R*)-DGA (**3**). The phenolic derivative and longer alkoxy derivative were more effective at the 4-position as well as the 2-position against both cells. The activities of all monosubstituted derivatives are not less potent than that of (8*R*,8′*R*)-DGA (**3**). Especially, the IC_{50} values of 2-hydroxy derivative **17** and 2-butoxy derivative **19** were less than 10 μM against both HL-60 and HeLa cells. The activities of disubstituted compounds **35**−**40** were also compared. The 3,4-dihydroxy derivative **35** was 5-fold more potent against HL-60 cells and 2-fold more potent against HeLa cells than 3,4-dimethoxy derivative **37** and 3,4-methylenedioxy derivative **40**, whose activities were similar to that of (8*R*,8′*R*)-DGA (**3**). The 3,5-dihydroxy derivative **36** showed 3-fold and 4-fold higher activity against HL-60 cells and HeLa cells, respectively, than 3,4-dimethoxy derivative **37**. These facts mean that the hydrophilic disubstituted compound is advantageous for higher activity. The longer-chain derivative, 3-ethoxy-4-hydroxy derivative **39** enhanced the activity, showing 4-fold higher activity than (8*R*,8′*R*)-DGA (**3**) against HL-60 cells; however, similar activity to (8*R*,8′*R*)-DGA (**3**) was observed against HeLa cells. It is noteworthy that 3-hydroxy-4-methoxy derivative **38**, in which the positions of substituents are exchanged from that of natural DGA, showed 3-fold more potent activity than (8*R*,8′*R*)-DGA (**3**) against both cells. The positions of the hydrophobic and hydrophilic group affected the activity. The addition of a methoxy group to the 5-position of (8*R*,8′*R*)-DGA (**3**) enhanced the activity. The activity of 3,5-methoxy-4-hydroxy derivative **41** was 3-fold more potent than (8*R*,8′*R*)-DGA (**3**) against both cells. Compared with HeLa cells, HL-60 cells were more sensitive to more hydrophilic DGA derivatives. The activity of 3,4,5-hydroxy derivative **42** and pentahydroxy derivative **43** was 2-fold higher and comparable to (8*R*,8′*R*)-DGA (**3**), respectively. On the other hand, against HeLa cells, the activities of 3,4,5-hydroxy derivative **42** and pentahydroxy derivative **43** were similar to and much lower than (8*R*,8′*R*)-DGA (**3**), respectively. The position and the number of hydrophobic and hydrophilic groups affected the activity. The 7-(3-hydroxy-4-methoxy)-7′-(3-methoxy-4- hydroxy) derivative **38** showed less than 9 μM IC_{50} value against both cells.

Cytotoxic Activities of 7′-Aryl Derivatives against HL-60 and HeLa Cells. With the results of the cytotoxic experiment on 7-aryl derivatives, we selected 3-hydroxy-4-methoxyphenyl group as an aryl group for 7-position to detect the effect of the 7′-aryl group on the activity. The cytotoxic activities of 7-(3-hydroxy-4-methoxyphenyl)-7′-aryl derivatives **44**−**59** were evaluated. The activity of 7′-phenyl derivative **44** was comparable to that of 7′-(3-methoxy-4-hydroxyphenyl) derivative **38**. The presence of substituent on 7′-aryl group is not necessary to exhibit the activity level of **38**. Introduction of the substituent to the 2′-position of **44** enhanced the activity against both cells. The 2′-hydroxy derivative **45** and 2′-F derivative **51** showed 2-fold higher activity, and 2′-methoxy derivative **46** and 2′-methyl derivative **50** were 5-fold and 3-fold more potent, respectively, than **38** against HL-60 cells. These facts mean that the electron donor substituent is more effective than the hydrophilic and electron-withdrawing substituent on the 2′-position. The activity of 2′-ethoxy derivative **47** was 2-fold potent than 2′-methoxy derivative, showing the highest activity among 2′-derivatives; however, the longer and bulky substituent at the 2′-position decreased activity. The butoxy **48** and isopropoxy **49** derivative exhibited 2−4-fold less potent activity than that of the 2′-methoxy derivative. Against HeLa cells, 2′-ethoxy derivative **47** was also most effective among the 2′-derivatives, showing 4-fold higher activity than **38**. The shorter alkoxy derivative **46** and longer and bulker alkoxy derivative **48** and **49** showed weaker activity than that of 2′-ethoxy derivative **47** against HeLa cells as well as against HL-60 cells. The activities of 2′-methyl derivative **50**, 2′-fluoro derivative **51**, and 2′-hydroxy derivative **45** were 1.6−2-fold higher than that of **38** against HeLa cells. The 3′- and 4′-derivatives **52**−**59** showed comparable activity to **38** against both cells except for 4′-hydroxy derivative **56** and 4′-methoxy derivative **57**, which were 1.6-fold more potent than **38** against HL-60 cells. The presence of substituent on 2′-position of 7-(3-hydroxy-4-methoxyphenyl)-7′-aryl derivatives was important for the higher activity. 7-(3-Hydroxy-4-methoxyphenyl)-7′-(2′-

dx.doi.org/10.1021/jf5010572 | J. Agric. Food Chem. 2014, 62, 5305−5315

ethoxyphenyl) derivative **47** showed the most potent activity against both cells in this research. The shorter and longer alkoxy group at the 2′-position decreased activity (Table 3).

Cytotoxic Activity against Colon 26 and Vero Cells. Finally, the natural (8*R*,8′*R*)-DGA (**3**) and the higher active derivatives **38** and **47** against HL-60 and HeLa cells were applied to cytotoxic assay against colon 26 as colorectal cancer cells and Vero cells as normal cells (Table 4). Although the activities against colon 26 cells were weaker than against HL-60 and HeLa cells, these derivatives were also effective. Especially, the IC_{50} value of compounds **47** against colon 26 was less than 10 μM. Theses derivatives were also effective against Vero cells; however, their activities were weaker than against HL-60 and HeLa cells. The activity of derivative **38** was 3-fold less active, and derivative **47** showed 4−8.5-fold less activity against Vero cells than against HL-60 and HeLa cells, respectively. The most specific activity against cancer cells was observed in derivative **47**.

In conclusion, we clarified the structure-cytotoxic activity relationship of butane-type lignan containing dietary lignan, secoisolariciresinol, for the first time. The hydroxy groups on 9- and 9′-positions of secoisolariciresinol are disadvantageous for the activity. This fact was confirmed by the appearance of activity of 9- and 9′-reductive type lignan, dihydroguaiaretic acid (DGA), whose all stereoisomers showed same level of activities. In the course of the evaluation of activities of the derivatives, 9-butyl (8*R*,8′*R*)-DGA derivative **13**, 7-(2-hydroxyphenyl) (8*R*,8′*R*)-DGA derivative **17**, 7-(2-butoxyphenyl) (8*R*,8′*R*)- DGA derivative **19**, 7-(3,5-dimethoxy-4-hydroxy (8*R*,8′*R*)-DGA derivative **41**, and 7-(3-hydroxy-4-methoxyphenyl) (8*R*,8′*R*)-DGA derivative **38** showed 2−4-fold higher activity than (8*R*,8′*R*)-DGA (**3**). Finally, 7-(3-hydroxy-4-methoxyphenyl)-7′-(2′-ethoxyphenyl) DGA derivative **47** showed highest cytotoxic activity in this research, showing 32-fold and 13-fold higher activity against HL-60 cells (IC_{50} = 0.8 μM) and HeLa cells (IC_{50} = 1.7 μM), respectively, than (8*R*,8′*R*)-DGA (**3**). This derivative **47** was also effective against colon 26 cells. Although (8*R*,8′*R*)-9,9′-anhydrosecoisolariciresinol (**2**), which is a candidate for metabolite of dietary secoisolariciresinol, did not show the cytotoxic activity in this research, the higher cytotoxic active dihydroguaiaretic acid (DGA) derivative was prepared as a new lead compound, whose main chemical structure is same as that of dietary secoisolariciresinol. Since there is a possibility that dietary lignan derivatives will be detected as a metabolite, the study on structure−activity relationship of lignan should be promoted to examine the effect of dietary lignan on health and safety. This result would contribute to development of newer lead compounds of medicine based on natural dietary compounds.

■ ASSOCIATED CONTENT

Supporting Information

Supplementary data includes melting points and both NMR and MS data for investigated compounds. Supporting Information also includes additional details for compound syntheses. This material is available free of charge via the Internet at http://pubs.acs.org.

■ AUTHOR INFORMATION

Corresponding Author

*E-mail: syamauch@agr.ehime-u.ac.jp. Fax: +81-89-977-4364. Tel.: +81-89-946-9846.

Funding

We are grateful to Marutomo Co. for financial support.

Notes

The authors declare no competing financial interest.

■ ACKNOWLEDGMENTS

Part of this study was performed at INCS (Johoku station) of Ehime University. Our thanks to the president of Ehime University for supporting this project.

■ REFERENCES

(1) Penalvo, J. L.; Adlercreutz, H.; Uehara, M.; Ristimaki, A.; Watanabe, S. Lignan content of selected foods from Japan. *J. Agric. Food Chem.* **2008**, *56*, 401−409.

(2) Ayres, D. C.; Loike, J. D. Biological and clinical properties of podophyllotoxin and other lignans. *Lignans*; Cambridge University Press: Cambridge, U.K., 1990; pp 85−112.

(3) Osawa, T. Phenolic antioxidants on dietary plants as antimutagens. In *Phenolic compounds in food and their effects on health II, antioxidants and cancer prevention*; Huang, M.-T, Ho, C.-T, Lee, C. Y., Eds.; American Chemical Society: Washington, DC, 1992; pp 135−149.

(4) Kawahara, S.; Iwata, I.; Fujita, E.; Yamawaki, M.; Nishiwaki, H.; Sugahara, T.; Yamauchi, S.; Akiyama, K.; Kishida, T. IgE-suppressive activity of (−)-matairesinol and its structure-activity relationship. *Biosci. Biotechnol. Biochem.* **2010**, *74*, 1878−1883.

(5) Yamawaki, M.; Nishi, K.; Nishimoto, S.; Yamauchi, S.; Akiyama, K.; Kishida, T.; Maruyama, M.; Nishiwaki, H.; Sugahara, T. Immunomodulatory effect of (−)-matairesinol in vivo and ex vivo. *Biosci. Biotechnol. Biochem.* **2011**, *75*, 859−863.

(6) Tominaga, S.; Sugahara, T.; Nishimoto, S.; Yamawaki, M.; Nakashima, Y.; Kishida, T.; Akiyama, K.; Maruyama, M.; Yamauchi, S. *Biosci. Biotechnol. Biochem.* **2009**, *73*, 35−39.

(7) Yamauchi, S.; Kishida, T.; Sugahara, T.; Yamawaki, M.; Nishimoto, S.; Shinomiya, Y.; Yamamoto, T. Inhibition of the discoloration of yellowtail dark muscle by lignan. *Biosci. Biotechnol. Biochem.* **2009**, *73*, 1718−1721.

(8) Yamauchi, S.; Kawahara, S.; Wukirsari, T.; Nishiwaki, H.; Nishi, K.; Sugahara, T.; Akiyama, K.; Kishida, T. Structure−cytotoxic activity relationship of sesquilignan, morinol A. *Bioorg. Med. Chem. Lett.* **2013**, *23*, 4923−4930.

(9) Niemeyer, H. B.; Honig, D. M.; Kulling, S. E.; Metzler, M. Studies on the metabolism of the plant lignans secoisolariciresinol and matairesinol. *J. Agric. Food Chem.* **2003**, *51*, 6317−6325.

(10) Struijs, K.; Vincken, J.-P; Gruppen, H. Bacterial conversion of secoisolariciresinol and anhydrosecoisolariciresinol. *J. Appl. Microbiol.* **2009**, *107*, 308−317.

(11) Ho, S. S. H.; Go, M. L. Restraining the flexibility of the central linker in terameprocol results in constrained analogs with improved growth inhibitory activity. *Bioorg. Med. Chem. Lett.* **2013**, *23*, 6127−6133.

(12) Mansoor, T. A.; Ramalho, R. M.; Rodrigues, C. M. P.; Ferreira, M.-J. U. Dibenzylbutane- and butyrolactone-type lignans as apoptosis inducers in human hepatoma HuH-7 cells. *Phytother. Res.* **2012**, *26*, 692−696.

(13) Yamauchi, S.; Sugahara, T.; Matsugi, J.; Someya, T.; Masuda, T.; Kishida, T.; Akiyama, K.; Maruyama, M. Effect of the benzylic structure of lignan on antioxidant activity. *Biosci. Biotechnol. Biochem.* **2007**, *71*, 2283−2290.

(14) Yamauchi, S.; Hayashi, Y.; Nakashima, Y.; Kirikihira, T.; Yamada, K.; Masuda, T. Effect of benzylic oxygen on the antioxidant activity of phenolic lignans. *J. Nat. Prod.* **2005**, *68*, 1459−1470.

(15) Yamauchi, S.; Masuda, T.; Sugahara, T.; Kawaguchi, Y.; Ohuchi, M.; Someya, T.; Akiyama, J.; Tominaga, S. *Biosci. Biotechnol. Biochem.* **2008**, *72*, 2981−2986.

(16) Kawaguchi, Y.; Yamauchi, S.; Masuda, K.; Nishiwaki, H.; Akiyama, K.; Maruyama, M.; Sugahara, T.; Kishida, T.; Koba, Y.

Antimicrobial activity of stereoisomers of butane-type lignans. *Biosci. Biotechnol. Biochem.* **2009**, *73*, 1806−1810.
(17) Nishiwaki, H.; Hasebe, A.; Kawaguchi, Y.; Akamatsu, M.; Shuto, Y.; Yamauchi, S. Larvicidal activity of (−)-dihydroguaiaretic acid derivatives against Culex pipiens. *Biosci. Biotechnol. Biochem.* **2011**, *75*, 1735−1739.
(18) Hasebe, A.; Nishiwaki, H.; Akiyama, K.; Sugahara, T.; Kishida, T.; Yamauchi, S. Quantitative structure−activity relationship analysis of antifungal (+)-dihydroguaiaretic acid using 7-phenyl derivatives. *J. Agric. Food Chem.* **2013**, *61*, 8548−8555.
(19) Moss, G. P. Nomenclature of lignans and neolignans (IUPAC recommendations 2000). *Pure Appl. Chem.* **2000**, *72*, 1493−1523.

concentrations of $LFP_{91\text{-}3}A2$ for 24 h. The cell pellets were washed with PBS after centrifugation and having supernatant removed, and they were stained with annexin V-FITC and PI in binding buffer according to the manufacturer's protocol. Cells were incubated at room temperature for 15 min in the dark, and flow cytometry was conducted using emission filters of 525 and 575 nm within 10 min, respectively.

Transmission Electron Microscope. For conventional transmission electron microscopy, the sample was postfixed with 1% buffered osmium at 4 °C for 2 h, dehydrated by an ethanol series and embedded in EPON 812. The semithin sections were stained by 1% Toluidine blue dye (TB) .

Statistical Analysis. All data are expressed as mean ± SD. Statistical analysis was evaluated by one-way analysis of variance (Anova), and calculations were done by the SPSS/Win 13.0 software. $P < 0.05$ was considered as the statistically significant difference.

RESULTS

Purification of $LFP_{91\text{-}3}A2$. The *Lentinula edodes* $C_{91\text{-}3}$ mycelium fermentative liquid extract from $(NH_4)_2SO_4$ precipitation (95% saturation) was applied on the DEAE−cellulose column. Four peaks (A, B, C and D) were eluted (Figure 1), and peak A ($LFP_{91\text{-}3}A2$) showed distinctive biological activity and then was subjected to a Sephacryl S-200 HR column in the next step; two peaks were obtained from the Sephacryl S-200 HR column, and the biological activity was largely confined to the fraction peak A2 ($LPF_{91\text{-}3}A2$) (Figure 1). The homogeneity of purified $LFP_{91\text{-}3}A2$ checked by SDS−PAGES appeared as a single band with a molecular mass of 26 kDa (Figure 1). At the same time, a single peak with the same molecular mass was obtained upon rechromatography on Superdex 75. The protein gel did not stain with the periodic acid-Schiff (PAS) reagent after being subjected to glycoprotein staining.

Polysaccharides isolated from mushrooms are best known for their antitumor macromolecules both *in vitro* and *in vivo*; some are already used in clinical cancer treatment.[7,8] Recently, various protein compounds, such as polysaccharide−peptides and polysaccharide−protein complexes, have been proven to possess effective antitumor activities;[9] however, only a few reports about proteins from mushroom have been identified and even fewer characterized, although mushrooms are an abounding source of diverse proteins. SDS-PAGE results and PAS negatively demonstrated that the $LPF_{91\text{-}3}A2$ is a pure protein without any polysaccharide conjugates.

Mushrooms contain a large number of biologically active proteins and peptides. The general protocol for isolating and purifying the target bioactive protein in a pure form consists of several steps.[10,11] In our study, two-step serial gel chromatography and ion exchange chromatography to isolate and purify protein $LPF_{91\text{-}3}A2$ proved to be simpler and more rapid than the frequently used protocol for separating protein from mushroom.

Assay of Antiproliferative Activity of $LPF_{91\text{-}3}A2$ on Tumor Cell Lines in Vitro. The cytotoxicity of $LFP_{91\text{-}3}A2$ on tumor cells and normal cells was examined in vitro by using the MTT microculture assay. H22, S180, A549 and the chick embryo fibroblasts growth proliferation were investigated after different incubation periods with different concentrations of $LPF_{91\text{-}3}A2$ (Figure 2). H22 and A549 cell growth were pressed in a dose-dependent manner which responded to increasing concentrations of $LPF_{91\text{-}3}A2$ (5−15 μg/mL). S180 growth also proliferated by $LFP_{91\text{-}3}A2$; although it had low significance in contrast to the other tumor cell lines, the difference was

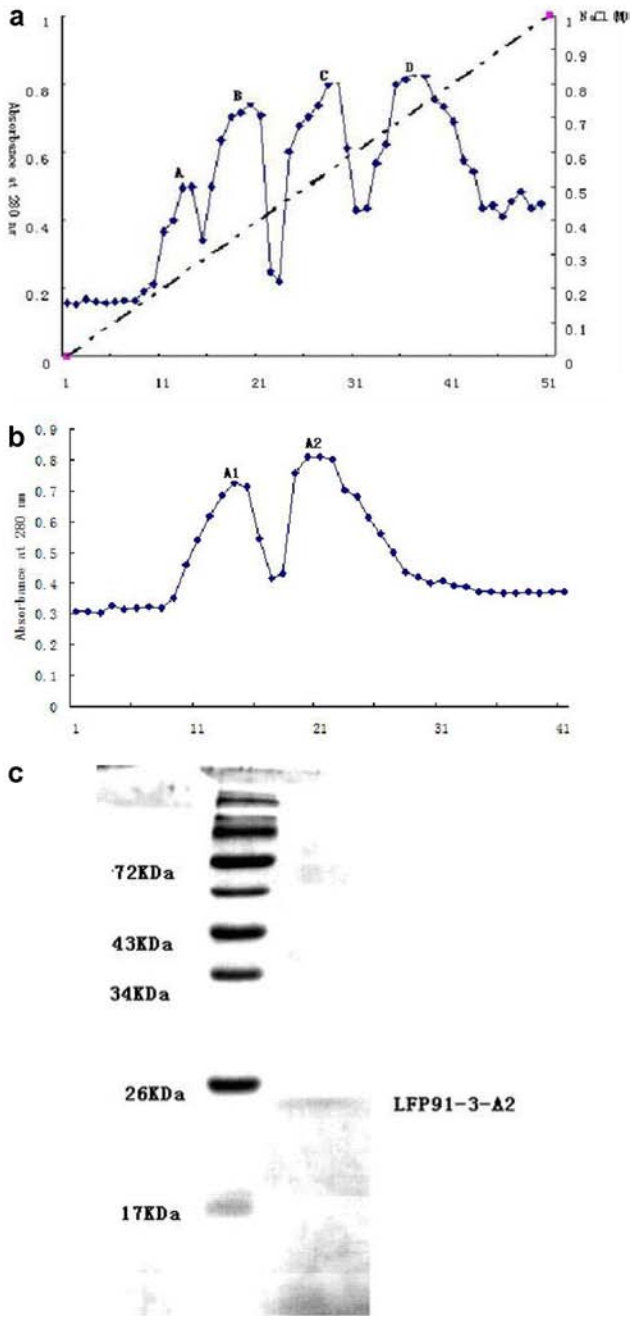

Figure 1. (a) Ion exchange chromatography on DEAE-cellulose of the mycelium fermentative liquid extract of *Lentinula edodes* C91-3. Adsorbed fraction A showed prominent biological activity. (b) Gel filtration on a Sephacryl S-200 HR column of peak A. Two peaks were obtained, and biological activity was largely confined to fraction peak A2. (c) SDS-PAGE of LFP91-3A2. Left lane: Amersham Biosciences molecular mass markers. Right lane: LFP91-3A2. Samples were electrophoresced on a 15% gel and stained with silver.

significant compared with the negative control groups ($p < 0.05$). H22 cells had a more insignificant inhibition rate after being treated with $LPF_{91\text{-}3}A2$, so this lineage was used to test exact the proliferation mechanism further. The growth of the chick embryo fibroblasts was not suppressed at given concentrations of $LFP_{91\text{-}3}A2$, and the difference was not significant compared with the negative control groups. The tumor cells were also inhibited by 5 μg/mL of DDP but with no more pronounced effects compared with the groups treated

dx.doi.org/10.1021/jf500316f | J. Agric. Food Chem. 2014, 62, 5316−5320

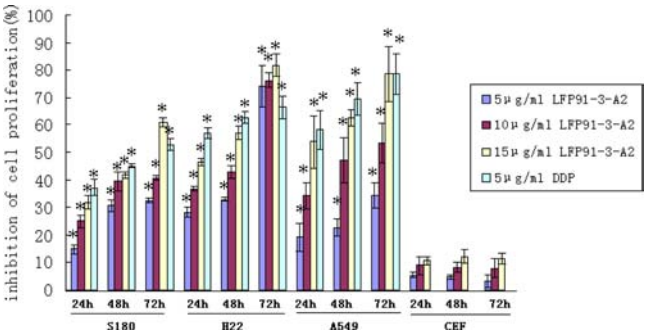

Figure 2. Effect of $LFP_{91\text{-}3}A2$ on viability of cell lines S180, H22, A549 and the normal chick embryo fibroblasts (CEF). The cytotoxicity of $LFP_{91\text{-}3}A2$ on the tumor lines S180, H22, A549 and against the normal chick embryo fibroblasts was performed by MTT reduction assay. The test cells were treated with different concentrations of $LFP_{91\text{-}3}A2$ (5−15 μg/mL) for 24, 48, and 72 h of culture in microplates. 5 μg/mL of DDP was used as positive control. Results represent the mean ± SD (standard deviation) of three experiments run in three replicates. *p < 0.001 compared to control.

with different concentrations of $LPF_{91\text{-}3}A2$ under the same conditions. Our findings revealed that $LFP_{91\text{-}3}A2$ suppressed tumor cells remarkably without side effects on the normal cells. This is particularly important, since many traditional chemotherapeutic agents and ratios exhibit severe toxicity against the normal cells, causing undesirable side effects and thus limiting their application in the clinical field.[10,12]

For further characterization, $LPF_{91\text{-}3}A2$ induced tumor cell death was analyzed by flow cytomery after staining H22 cells with annexin V-FITC/PI. As shown in Figure 3, the early and late apoptosis rates of the cells which were incubated for 24 h were significantly higher compared with those of the control group at 5, 10 and 15 μg/mL of $LPF_{91\text{-}3}A2$, and it induced H22 cell apoptosis in a dose-dependent manner. All the experiments were repeated three times and obtained similar results.

Although the MTT and the flow cytometry assay results present strong evidence that $LFP_{91\text{-}3}A2$ could activate the apoptotic pathway in tumor cells, the morphological characteristics in apoptosis need to be observed by transmission electron microscopy to consolidate the results of cytotoxicity tests. Morphological changes of the H22 cells were observed after treatment by 5 μg/mL of $LFP_{91\text{-}3}A2$ in 24 h. Transmission electron microscopy observation showed that H22 cells had the early changes of apoptosis, such as cell shrinkage, floating of the cell bodies and microvilli disappearance, nuclear chromatin condensation and formation of a crescent clump, which are the typical morphological appearance of apoptosis (Figure 4a). After treatment with 15 μg/mL of $LFP_{91\text{-}3}A2$, chromatin was condensed strongly, forming a high-density area, and the apoptotic body was observed in the H22 cell (Figure 4b). The morphological changes in $LFP_{91\text{-}3}A2$ treated tumor cells observed by transmission electron microscopy gave further evidence of the antitumor activity.

The antitumor activities of polysaccharides and polysaccharide−protein complexes from *Lentinula edodes* are considered dependent on activation of the host immune system rather than direct cytotoxic effects on the cancer cells.[13−15] Recently, a few studies demonstrated that polysaccharide from *Lentinula edodes* inhibited tumor cell proliferation not only by enhancing the host immunity but also by directly inducing tumor cell apoptosis.[11,16,17] $LPF_{91\text{-}3}A2$ showed direct cytotoxic and cell growth inhibitory effects without being accompanied by

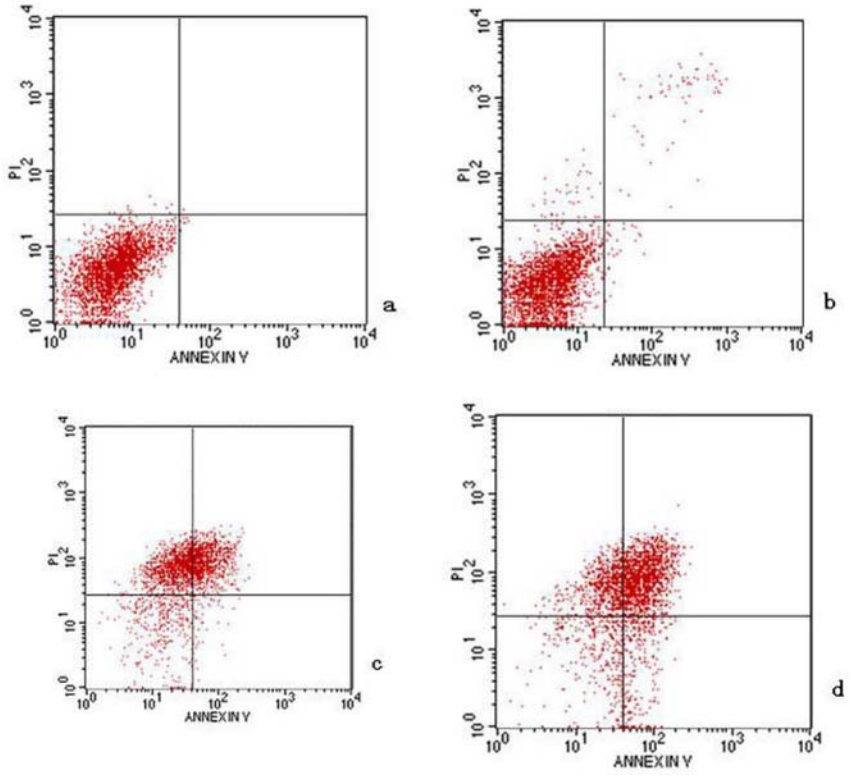

Figure 3. Assessment of apoptosis using flow cytometry with Annexin V-FITC/PI staining, showing the dot-plot graph of H22cells: (a) control group; (b) H22 treated with 5 μg/mL of LFP91-3A2; (c) H22 treated with 10 μg/mL of $LFP_{91\text{-}3}A2$; (d) H22 treated with 15 μg/mL of LFP91-3A2.

dx.doi.org/10.1021/jf500316f | J. Agric. Food Chem. 2014, 62, 5316−5320

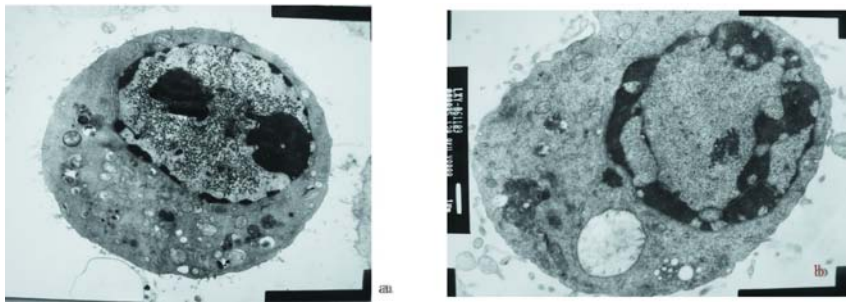

Figure 4. Tumor cell apoptosis morphology examined by transmission electron microscopy. (A, left) Native control. (B, right) The short microvilli disappeared and chromatin was condensed strongly, forming a high-density area.

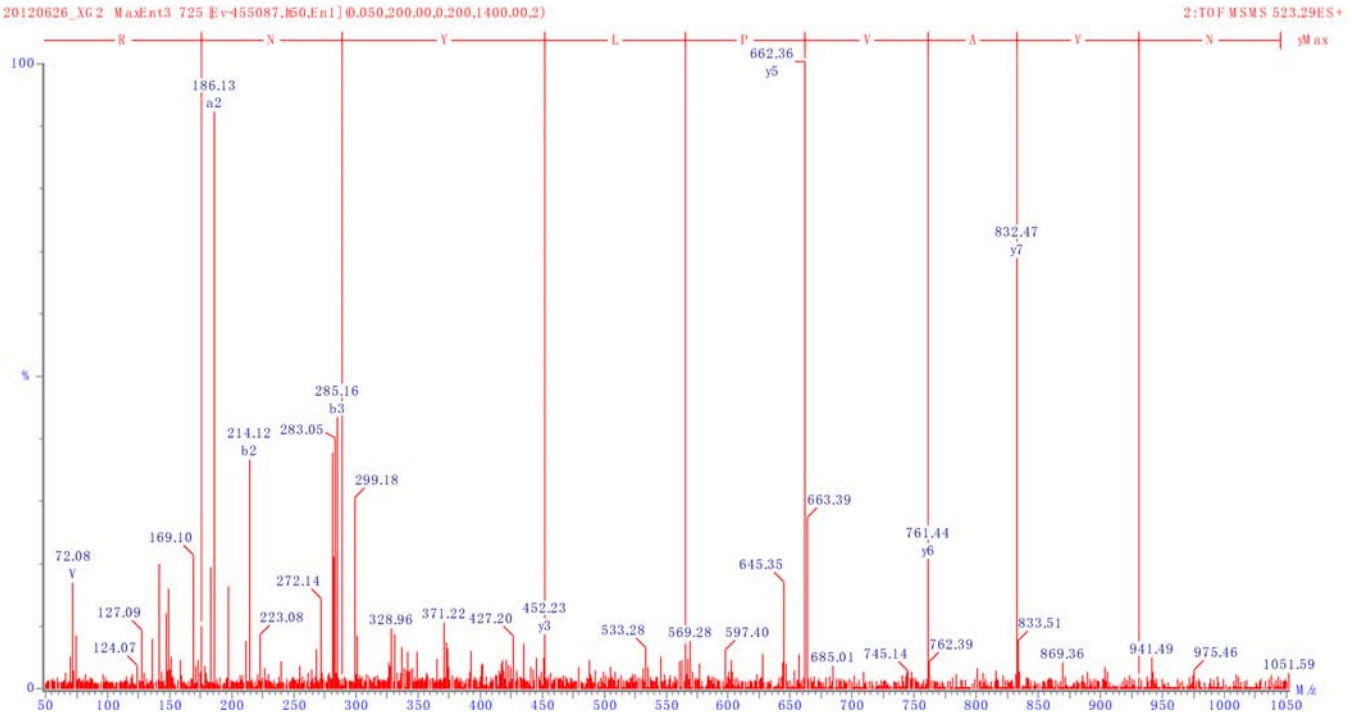

Figure 5. Peptide fragments of $LFP_{91\text{-}3}A2$ generated by trypsin cleavage analysis by MS/MS.

stimulating the immune system, which is distinct from extracts previously mentioned.

Mass Spectrometric Identification of Novel Proteins. The purified sample of $LPF_{91\text{-}3}A2$ was excised, digested by trypure in-gel and characterized by matrix assisted laser desorption/ionization/time of flight (MALDI-TOF) MS. Using the Mascot search engine (http://www.matrixscience.com), the MALDI-TOF data obtained from $LPF_{91\text{-}3}A2$ was matched significantly with adenylate kinase isoenzyme2 mitochondrial [*Harpengnathos saltalor*](gil307198091). The score of mascot search matching was 85, and sequence coverage was 27%. Adenylate kinase isoenzyme2 is localized in the space of mitochondrial intermembrane and plays a role in mediating a novel intrinsic apoptotic pathway that may be involved in tumorigenesis processes. Adenylate kinase isoenzyme2 is released from mitochondria during the early phase of the apoptotic process.[18,19] The antitumor activity of $LFP_{91\text{-}3}A2$ was supposed to be related to the similar molecular structure with adenylate kinase isoenzyme2. Three peptide fragments generated from $LFP_{91\text{-}3}A2$ by trypsin cleavage were subjected to MS/MS analysis for sequencing (Figure 5). The amino acid sequences were (a) NVAVPLYNR, (b) SDGANGLLTK and (c) NKYEDELNKR. However, the BLAST searches in several databases of de novo amino acid sequences derived from analysis of the 26 kDa band failed to identify any homologous proteins.[20] The paucity of related fungi protein amino acid sequences in accessible databases may be the reason why we found no homologous proteins from mushroom. In order to well know the properties of $LPF_{91\text{-}3}A2$, we leveraged Solexa sequencing technology in de novo assembly of *Lentinula edodes* $C_{91\text{-}3}$ transcriptome and obtained 28,923 unigene sequences including 18,120 unigenes with a coding sequence.[6] Based on this gene information, we can obtain deep insight into the medical function, especially antitumor activity at the protein level in *Lentinula edodes*.

The present study was carried out to purify and characterize active antitumor protein $LPF_{91\text{-}3}A2$ from the mycelium fermentative liquid extract of *Lentinula edodes* $C_{91\text{-}3}$. $LPF_{91\text{-}3}A2$ was isolated and purified to homogeneity after $(NH_4)_2SO_4$ precipitation and two steps of chromatography analysis. SDS-PAGE results are in accordance with MALDI/MS analysis, which show an approximate molecular weight of 26 kDa. The role of protein molecules from natural resources in drug and toxin-induced apoptosis is not clearly defined. In fact, very little

dx.doi.org/10.1021/jf500316f | J. Agric. Food Chem. 2014, 62, 5316−5320

information is available in the literature about this regard. A few articles, published recently, revealed that some protein molecules from various plant sources possess activities like those of our protein, although these reports do not describe any mechanism of protective action or structural features of the active principles.[21−23] In this study, we isolated and partially characterized antitumor protein $LFP_{91\text{-}3}A2$ from *Lentinula edodes* $C_{91\text{-}3}$ However, the identities and detailed characteristic properties of $LFP_{91\text{-}3}A2$ remain unknown up to now. Further studies are needed such as molecular properties, gene clone, expression and characterization of $LFP_{91\text{-}3}A2$. All these experiments are now under investigation in our laboratory based on the transcriptome sequence.[24] These antitumor studies would be helpful for its potential medical application in the future.

AUTHOR INFORMATION

Corresponding Author

*Tel.:0411 86110007. Fax: 0411 86110007. E-mail address: huangminchao@163.com.

Notes

The authors declare no competing financial interest.

REFERENCES

(1) Watanabe, A.; Kobayashi, M.; Hayashi, S.; Kodama, D.; Isoda, K.; Kondoh, M.; Kawase, M.; Tamesada, M.; Yagi, K. Protection against D-galactosamine-induced acute liver injury by oral administration of extracts from Lentinus edodes mycelia. *Biol. Pharm. Bull.* **2006**, *29*, 1651−4.

(2) Lee, H. H.; Lee, J. S.; Cho, J. Y.; Kim, Y. E.; Hong, E. K. Study on immunostimulating activity of macrophage treated with purified polysaccharides from liquid culture and fruiting body of Lentinus edodes. *J. Microbiol. Biotechnol.* **2009**, *19*, 566−72.

(3) Bisen, P. S.; Baghel, R. K.; Sanodiya, B. S.; Thakur, G. S.; Prasad, G. B. Lentinus edodes: a macrofungus with pharmacological activities. *Curr. Med. Chem.* **2010**, *17*, 2419−2430.

(4) Takehara, M.; Mori, K.; Kuida, K.; Hanawa, M. A. Antitumor effect of virus-like particles from Lentinus edodes (Shiitake) on Ehrlich ascites carcinoma in mice. *Arch. Virol.* **1981**, *68*, 297−301.

(5) Enman, J.; Hodge, D.; Berglund, K. A.; Rova, U. Production of the bioactive compound eritadenine by submerged cultivation of shiitake (Lentinus edodes) mycelia. *J. Agric. Food Chem.* **2008**, *56*, 2609−12.

(6) Zhong, M.; Liu, B.; Wang, X.; Liu, L.; Lun, Y.; Li, X.; Ning, A.; Cao, J.; Huang, M. De novo characterization of Lentinula edodes C91-3 transcriptome by deep Solexa sequencing. *Biochem. Biophys. Res. Commun.* **2012**, *431*, 111−115.

(7) Lindequist, U.; Niedermeyer, T. H.; Julich, W. D. The pharmacological potential of mushrooms. *Evidence-based complementary and alternative medicine: eCAM* **2005**, *2*, 285−99.

(8) Wasser, S. P. Current findings, future trends, and unsolved problems in studies of medicinal mushrooms. *Appl. Microbiol. Biotechnol.* **2011**, *89*, 1323−32.

(9) Erjavec, J.; Kos, J.; Ravnikar, M.; Dreo, T.; Sabotic, J. Proteins of higher fungi—from forest to application. *Trends Biotechnol.* **2012**, *30*, 259−73.

(10) Newman, D.; Cragg, G. Natural products from marine invertebrates and microbes as modulators of antitumor targets. *Curr. Drug Targets* **2006**, 279−304.

(11) Xu, X.; Yan, H.; Chen, J.; Zhang, X. Bioactive proteins from mushrooms. *Biotechnol. Adv.* **2011**, *29*, 667−674.

(12) Ren, R. Mechanisms of BCR-ABL in the pathogenesis of chronic myelogenous leukaemia. *Nat. Rev. Cancer* **2005**, *5*, 172−83.

(13) Wasser, S. Medicinal mushrooms as a source of antitumor and immunomodulating polysaccharides. *Appl. Microbiol. Biotechnol.* **2002**, *60*, 258−274.

(14) Lull, C.; Wichers, H.; Savelkoul, H. Antiinflammatory and immunomodulating properties of fungal metabolites. *Mediators Inflamm.* **2005**, 63−80.

(15) Lo, T. C.; Hsu, F. M.; Chang, C. A.; Cheng, J. C. Branched α-(1,4) glucans from Lentinula edodes (L10) in combination with radiation enhance cytotoxic effect on human lung adenocarcinoma through the Toll-like receptor 4 mediated induction of THP-1. *J. Agric. Food Chem.* **2011**, *59*, 11997−12005.

(16) Israilides, C.; Kletsas, D.; Arapoglou, D.; Philippoussis, A.; Pratsinis, H.; Ebringerova, A.; Hribalova, V.; Harding, S. E. In vitro cytostatic and immunomodulatory properties of the medicinal mushroom Lentinula edodes. *Phytomed.: Int. J. Phytother. Phytopharmacol.* **2008**, *15*, 512−9.

(17) Yukawa, H.; Ishikawa, S.; Kawanishi, T.; Tamesada, M.; Tomi, H. Direct cytotoxicity of Lentinula edodes mycelia extract on human hepatocellular carcinoma cell line. *Biol. Pharm. Bull.* **2012**, *35*, 1014−21.

(18) Kohler, C.; Gahm, A.; Noma, T.; Nakazawa, A.; Orrenius, S.; Zhivotovsky, B. Release of adenylate kinase 2 from the mitochondrial intermembrane space during apoptosis. *FEBS Lett.* **1999**, *447*, 10−2.

(19) Lee, H.; Pyo, J.; Oh, Y.; Kim, H.; Hong, S.; Jeon, Y.; Kim, H.; Cho, D.; Woo, H.; Song, S.; Nam, J.; Kim, H.; Kim, K.; Jung, Y. AK2 activates a novel apoptotic pathway through formation of a complex with FADD and caspase-10. *Nat. Cell Biol.* **2007**, 1303−1310.

(20) Au, C. H.; Wong, M. C.; Bao, D.; Zhang, M.; Song, C.; Song, W.; Law, P. T.; Kues, U.; Kwan, H. S. The genetic structure of the A mating-type locus of Lentinula edodes. *Gene* **2014**, *535*, 184−90.

(21) Tsoi, A. Y.; Ng, T. B.; Fong, W. P. Antioxidative effect of a chymotrypsin inhibitor from Momordica cochinchinensis (Cucurbitaceae) seeds in a primary rat hepatocyte culture. *J. Peptide Sci.* **2005**, *11*, 665−8.

(22) Lee, S.; Oh, P.; Ko, J.; Lim, K.; Lim, K. Protective effect of glycoprotein isolated from Ulmus davidiana Nakai on carbon tetrachloride-induced mouse liver injury. *J. Pharm. Pharmacol.* **2006**, *58*, 143−152.

(23) Oh, P.; Lim, K. Plant originated glycoprotein has anti-oxidative and anti-inflammatory effects on dextran sulfate sodium-induced colitis in mouse. *J. Biomed. Sci.* **2006**, *13*, 549−560.

(24) Liu, B.; Zhong, M.; Lun, Y.; Wang, X.; Sun, W.; Li, X.; Ning, A.; Cao, J.; Zhang, W.; Liu, L.; Huang, M. A Novel Apoptosis Correlated Molecule: Expression and Characterization of Protein Latcripin-1 from Lentinula edodes C(91-3). *Int. J. Mol. Sci.* **2012**, *13*, 6246−65.

(25) Laemmli, U. K. Cleavage of structural proteins during the assembly of the head of bacteriophage T4. *Nature* **1970**, *227*, 680−685.

AC were found, including polysaccharide, maleic/succinic acid derivatives, triterpenoids, benzenoids, and benzoquinone derivatives.[7,8] Recent studies have various biological activities of AC, including antioxidant, anti-inflammation, liver fibrosis, antimetastasis, vasorelaxation, immunomodulation, and anticancer activities.[9−11] In addition, different fermentation processes have been conducted in either liquid or solid states of *A. camphorata* mycelium. Ergostatrien-3β-ol (EK100), a triterpenoid isolated from the liquid fermentation of *A. camphorata* mycelia, was demonstrated to exhibit significant anti-inflammatory and hepatoprotective bioactivity in vitro.[9,12] However, this study investigated whether oral treatment of MAC could attenuate ALI induced by LPS in vivo and explored the molecular mechanism of this regulatory pathway. The results demonstrated that MAC may protect against LPS-induced lung injury in mice and possibly exert its activity through the regulation of antioxidant enzyme activity, NF-κB, and MAPKs signaling pathways.

MATERIALS AND METHODS

Chemicals. LPS (*Escherichia coli* 055:B5) and dexamethasone (Dex) were obtained from Sigma (St. Louis, MO, USA). TNF-α, IL-1β, and IL-6 were obtained from Biosource International Inc. (Camarillo, CA, USA). The polyclonal antibodies against iNOS, COX-2, NF-κB, IκB-α, ERK, JNK, p38, p-ERK, p-JNK, p-p38, and β-actin were purchased from Abcam (Cambridge, UK). Polyvinylidene fluoride transfer membranes (Immobilon P) were from Millipore Corp. (Bedford, MA, USA).

Plant Material. The powder of AC of the submerged whole broth (batch MZ-247) was obtained from Biotechnology Center of Grape King Inc. (Chung-Li City, Taiwan). The preparative processes were all of commercial security.

Fingerprint Chromatogram of MAC Extracts by HPLC. The chromatographic system consisted of a quaternary gradient pump (SFD 2100), a C-18 column (4.6 i.d. × 250 mm; TSK gel column, ODS-80TM; 5 μm particles, Merck), and an S-3210 photodiode array detector (PDA) (Schambeck SFD GmbH, Bad Honnef, Germany). The samples were detected with H_2O (solvent A) and 100% methanol (solvent B) at 280 nm. The solvent gradient started with solvent A (10%) for 0 min and then linearly increased to solvent B (100%) for another 120 min. This linear gradient was followed by a solvent B elution until 180 min. The flow rate was 0.6 mL/min, and the injection volumes of standards and samples were 10 μL. Identification of EK100 was based on retention time and UV spectra by comparison with standards.

Animals. All animal procedures adhered to the NIH *Guide to the Care and Use of Laboratory Animals*. All tests were conducted under the guidelines of the International Association for the Study of Pain (IASP). Male imprinting control region (ICR) mice (6 weeks old) were obtained from the BioLASCO Taiwan Co., Ltd. The animals were kept in isolation for at least 1 week before the experiment with the temperature maintained within 22−23 °C. Mice were given ad libitum access to food and water.

LPS-Induced Acute Lung Injury in Mice. ALI was induced by intratracheal administration of LPS as previously described.[13] Fifty-four mice were randomly divided into six groups, the control group and five treatment groups. Normal mice were given 50 μL of normal saline without LPS. LPS (1.0 g/kg; 50 μL/per mouse) was administered intravenously to induce lung injury. MAC [25, 50, and 100 mg/kg; distilled water dissolved with 0.5% carboxymethyl cellulose (CMC)], dexamethasone (DEX; 10 mg/kg), or vehicle (PBS) was administered orally 1 h before 50 μL of LPS intratracheal (I.T.) instillation.

Lung tissue samples were collected for Western blot assay, MPO assays, and antioxidant enzyme (SOD) activity assays. In these studies, bronchoalveolar lavage fluid (BALF) was collected for protein concentration assay (Bio-Rad, Hercules, CA, USA) and leukocyte infiltration assessment. The BALF samples were centrifuged (700*g* for 10 min at 4 °C) and their supernatants were frozen at −80 °C for protein and cytokine ELISA. The cell pellets were resuspended in PBS (1 mL) and the total cell counts were determined using a hemocytometer in the BALF. Lung tissues from mice were collected but not subjected to BALF collection and then stored at −80 °C for further experiments.

Histopathological Analysis. At 6 h after treatment with LPS, mice were euthanized and lung tissues were harvested and fixed in 4% paraformaldehyde. For light microscopic examination, the lung tissue was dehydrated, then paraffin embedded, and sliced. After hematoxylin and eosin (H&E) staining of lung tissue slices, pathological changes were observed.

Measurement of Myeloperoxidase (MPO) Activity. The MPO activity was determined to assess neutrophil accumulation, and it was measured as described previously.[14] The lung tissues were homogenized in 80 mM phosphate buffer, pH 5.4, and then homogenate was centrifuged (12000*g* for 15 min, at 4 °C). Ten microliters of sample was added to 290 μL of 50 mM potassium phosphate buffer (pH 6.0) containing 0.167 mg/mL *o*-dianisidine chloride and 0.0005% H_2O_2 as a substrate. Oxidized *o*-dianisidine was determined by spectrophotometry ($OD_{460\ nm}$) (Molecular Devices, Sunnyvale, CA, USA). MPO content was expressed as relative MPO activity ($OD_{460\ nm}$/mg protein of lung tissue).

Lung Wet-to-Dry Weight (W/D) Ratio. The lung tissues were excised, immediately weighed, and then placed in an oven at 80 °C for 48 h to obtain the "dry" weight. The W/D ratio was then calculated.

Measurement of BALF TNF-α, IL-1β, and IL-6 by an Enzyme-Linked Immunosorbent Assay (ELISA). The concentrations of cytokine levels of TNF-α, IL-1β, and IL-6 in the BALF were measured by ELISA using commercially available reagents according to the manufacturer's instruction (Biosource International Inc.). TNF-α, IL-1β, and IL-6 were determined from a standard curve.

Measurement of Nitric Oxide/Nitrite. Nitrite and nitrate could have a role by producing NO. The nitrite level was determined by the Griess reagent in BALF.[15] One hundred microliters was applied to 96-well plates, followed by 100 μL of Griess reagent. The Griess reagent was prepared by mixing equal amounts of 0.1% *N*-1-naphthylethylenediamine dihydrochloride and 1% sulfanilamide. Absorbance at 540 nm was measured after 10 min of incubation at room temperature using a microplate reader (Molecular Devices). A standard curve was plotted with the concentration of sodium nitrite.

Total SOD activity Measurements. Total SOD activity was determined by an indirect method involving the reduction of cytochrome *c*.[16] For the cytochrome *c* reaction, the SOD mediated inhibition of ferricytochrome *c* reduction in the presence of a superoxide anion generating system (xanthine/xanthine oxidase) was determined by monitoring the change in absorbance at 550 nm. One SOD enzyme unit was defined as the amount of enzyme that causes a 50% inhibition.

Western Blot Analysis. Lung tissues were homogenized in the protein extract solution and protease inhibitors and centrifuged at 12000*g* for 20 min. The supernatants were frozen at −20 °C until use. The amount of protein (50 μg) from the supernatant was resolved on 10% SDS-PAGE and transferred onto nitrocellulose membranes. The membrane was incubated with an appropriate dilution of specific primary antibodies (anti-iNOS, anti-COX-2, anti-COX-2, anti-IκBα, and anti-NF-κB) followed by appropriate horseradish peroxidase-conjugated (Sigma), goat anti-mouse, or anti-rabbit IgG. The bands were detected by enhanced chemiluminescence (ECL) by using hyperfilm and ECL reagent (Thermo). Band intensity on scanned films was quantified using Kodak Molecular Imaging software (version 4.0.5, Eastman Kodak Co., Rochester, NY, USA) and expressed as relative intensity compared with the control group.

Statistical Analysis. Data are expressed as the mean ± standard error of the mean (SEM). Statistical analyses were performed by one-way analysis of variance (ANOVA followed by Scheffe's multiple-range tests). The levels of statistical significance are expressed as (*) $p < 0.05$, (**) $p < 0.01$, and (***) $p < 0.001$.

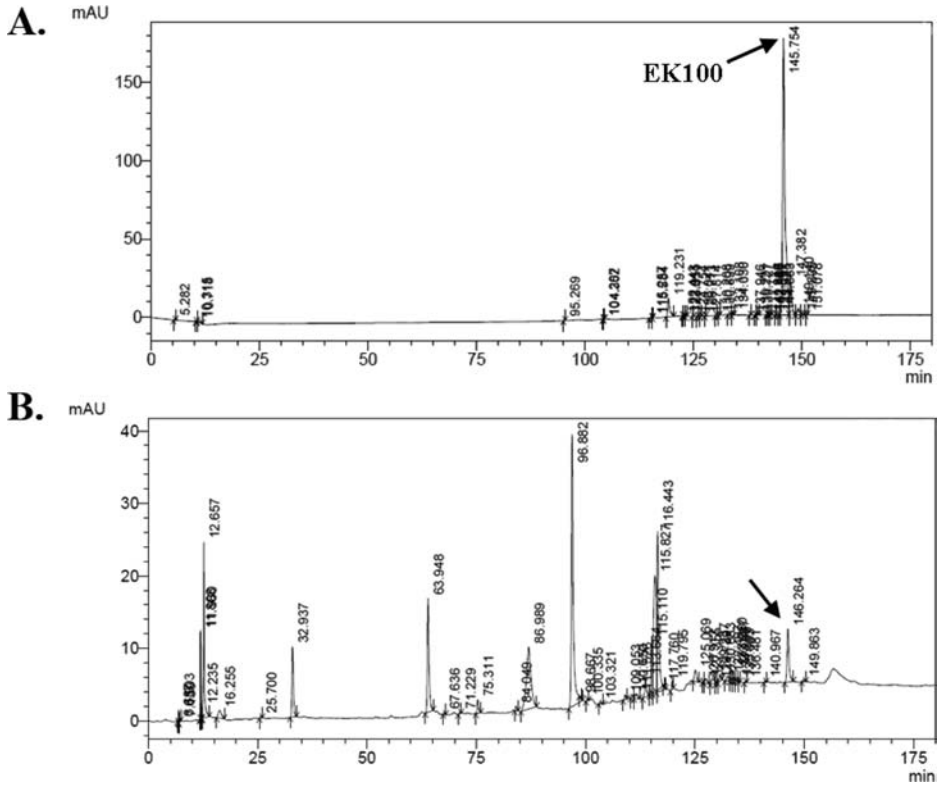

Figure 1. HPLC analysis of the compound identification of EK100 (retention time = 145.75 min) (A) and MAC (methanol extract of *Antrodia camphorata*) (B). Total volume of 20 μL was loaded into the HPLC column to measure the relative content of ST1 in MAC extract according to the concentration of standard compounds.

RESULTS

Fingerprint Chromatogram of MAC by HPLC. The fingerprint chromatogram of MAC was established for the quality control of the liquid fermentation of *A. camphorata* mycelia. The structure of ergostatrien-3β-ol (EK100) was elucidated by its retention time, UV absorbance of purified standards, and comparison with the literature.[17] Figure 1 shows the predominant constituents identified as EK100.

MAC Reduces LPS-Induced Lung Injury in Vivo. To evaluate the LPS-induced lung injury after MAC treatment, we observed the histological changes of lungs in the different groups. In the control group, no obvious histological alteration was found in lung tissues (Figure 2). In the LPS-induced lung injury group H&E staining evidenced a large number of infiltrations of inflammatory cells, lung tissue damage, and marked alveolar wall edema. These pathological changes were improved by treatment with MAC (25, 50, and 100 mg/kg) and DEX (10 mg/kg), suggesting that MAC could protect against histological changes in the LPS-induced ALI model.

Effects of MAC on Inflammatory Cell Count and MPO Activity on LPS-Induced ALI in Mice. Six hours after LPS-induced ALI, the total cell numbers in the BALF increased compared with the control group, significantly ($p < 0.001$). MAC (100 mg/kg) and DEX (10 mg/kg) significantly also decreased the number of total cells ($p < 0.001$) compared to LPS-induced ALI mice (Figure 3A).

Polymorphonuclear leukocyte (PMN) infiltration plays a central role in inflammation, and it is also a major cause of tissue damage. MPO activity can be considered a good indicator of lipid peroxidation in lung tissues. As Figure 3B shows, the intratracheal instillation of LPS increased MPO activities (0.41 ± 0.04 OD $_{460\ nm}$/mg protein) in mouse lung tissues, significantly ($p < 0.001$). Pretreatment with MAC (25, 50, 100 mg/kg) decreased MPO activity to 0.23 ± 0.03, 0.27 ± 0.04, and 0.32 ± 0.02 OD $_{460\ nm}$/mg protein, respectively, and DEX decreased it to 0.26 ± 0.02 OD$_{460\ nm}$/mg protein. These data indicated that MAC prevented excessive infiltration of neutrophils into the lung tissues in LPS-induced ALI mice.

MAC Attenuates the Lung Wet-to-Dry Ratio and Protein Concentration Induced in LPS-Induced ALI Mice. To assess lung edema, we determined the lung water content in ALI mice 6 h after LPS treatment. LPS challenge increased the lung vascular permeability, as shown by the lung W/D ratio as compared to the control group, significantly. Therefore, we further investigated the W/D ratios and protein concentrations of different groups, and as shown in Figure 4, the W/D ratio and protein concentration expanded in the LPS group compared with the control group and the pretreatment with MAC (100 mg/kg) and DEX ameliorated the W/D ratio and protein concentration compared with the LPS group. These results indicated that MAC could suppress lung edema in LPS-induced ALI mice.

Effect of MAC on Anti-inflammatory Cytokines in Lung Tissues of LPS-Induced ALI mice. LPS-induced ALI is related to the various pro-inflammatory cytokines. In this study, the levels of pro-inflammatory cytokines (NO, TNF-α, IL-1β, and IL-6) in BALF were measured 6 h after LPS instillation. As shown in Figure 5, the pro-inflammatory cytokine NO, TNF-α, IL-1β, and IL-6 levels of LPS-induced ALI mice in the BALF were improved compared to those in the control group, significantly ($p < 0.001$). MAC (100 mg/kg) and DEX significantly reduced NO, TNF-α, IL-1β, and IL-6 production compared to the LPS-induced ALI group.

dx.doi.org/10.1021/jf405113g | J. Agric. Food Chem. 2014, 62, 5321−5329

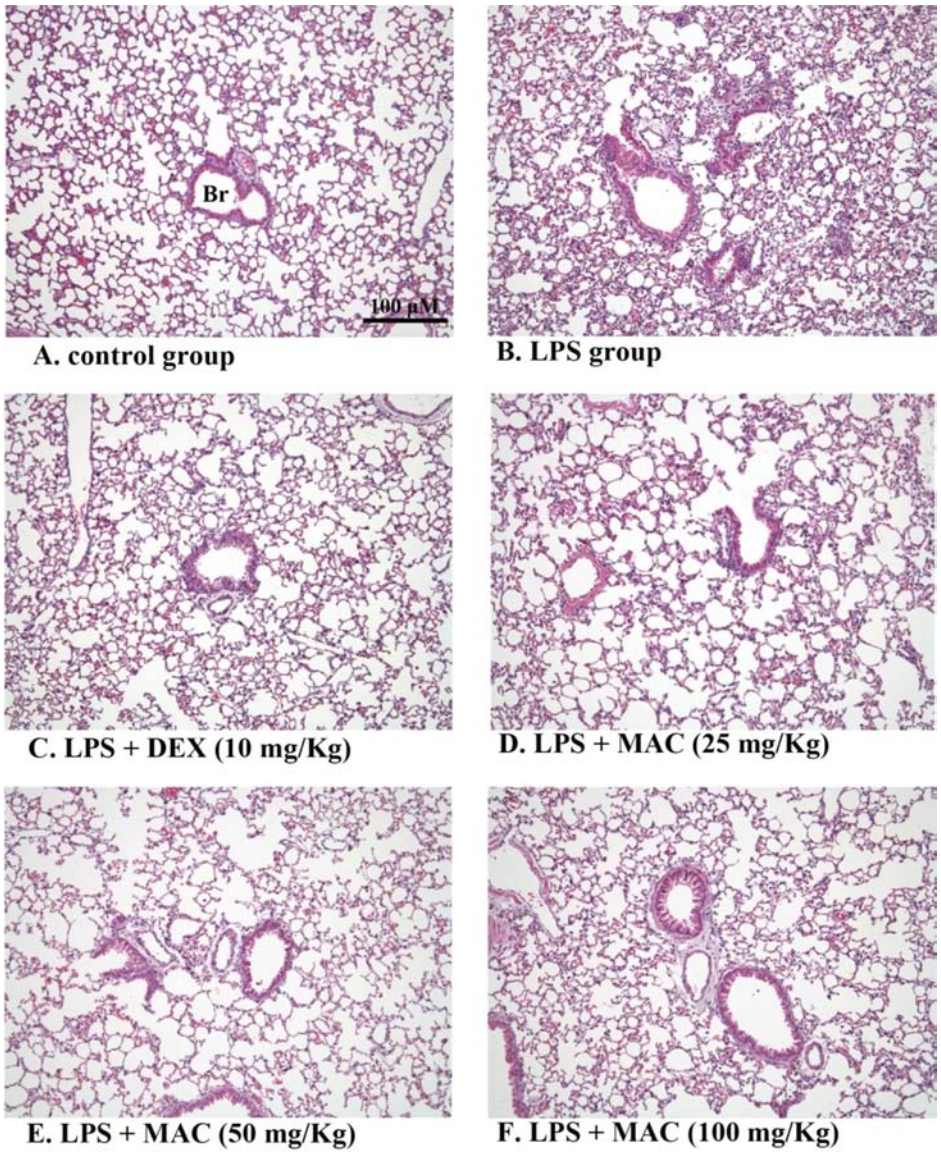

Figure 2. Effects of MAC on lung histopathological changes in LPS-induced ALI mice. Mice were killed at 6 h after LPS stimulation. The left lungs were excised and embedded in 10% formalin and sectioned, followed by H&E staining; magnification ×100. Images are representative of three experiments. Br, bronchi; DEX, dexamethasone.

Effects of MAC Protect against Oxidative Stress in LPS-Induced ALI Mice. Oxidative stress may lead to apoptosis and lung injury. SODs are a class of enzymes that can acting as the chief ROS scavenging enzyme, and the activity of SODs has decreased in some reports of LPS-induced ALI mice. The data presented demonstrated that the pretreatment with MAC (100 mg/kg) and DEX increased SOD activity in mice as compared to the LPS-induced ALI group (Figure 6). Therefore, in this study, we demonstrated that MAC might be attributed to its antioxidant enzyme activities in the inflammatory response og LPS-induced ALI mice.

Effects of MAC on iNOS and COX-2 Protein Expressions in LPS-Induced ALI Mice. To investigate possible mechanisms of whether the level of NO was due to regulated iNOS and COX-2 protein expressions, the effects were studied by Western blot in the LPS-induced ALI. The results showed that the pretreatment with MAC (100 mg/kg) for 6 h inhibited iNOS and COX-2 protein expression in lung tissues of LPS-induced ALI mice (Figure 7A).

Effect of MAC on NF-κB and IκBα Inactivation in LPS-Induced ALI Mice. NF-κB is activated by a variety of stimuli including LPS, TNFα, and IL-1β. The effect of MAC on NF-κB expression in lung tissue of LPS-induced ALI mice was assessed by Western blot. In this study, Figure 7B shows that LPS-induced IκBα and NF-κB degradation was inhibited by pretreatment with MAC in LPS-induced ALI mice. The signal of NF-κB inhibition is regulated by interaction with inhibitory IκBα proteins. Overall, our findings provide support that the NF-κB inhibitor IκBα contains a functional nuclear export signal.

Effect of MAC on MAPK Signaling Pathway in LPS-Induced ALI Mice. To examine the mechanisms of the LPS-induced ALI mice, we investigated the effect of MAC on the MAPKs signal pathway. As shown in Figure 8, MAPKs were activated in LPS-induced ALI. Furthermore, MAC (100 mg/kg) and DEX dramatically inhibited the phosphorylation of ERK, JNK, and p38 protein expressions. These results

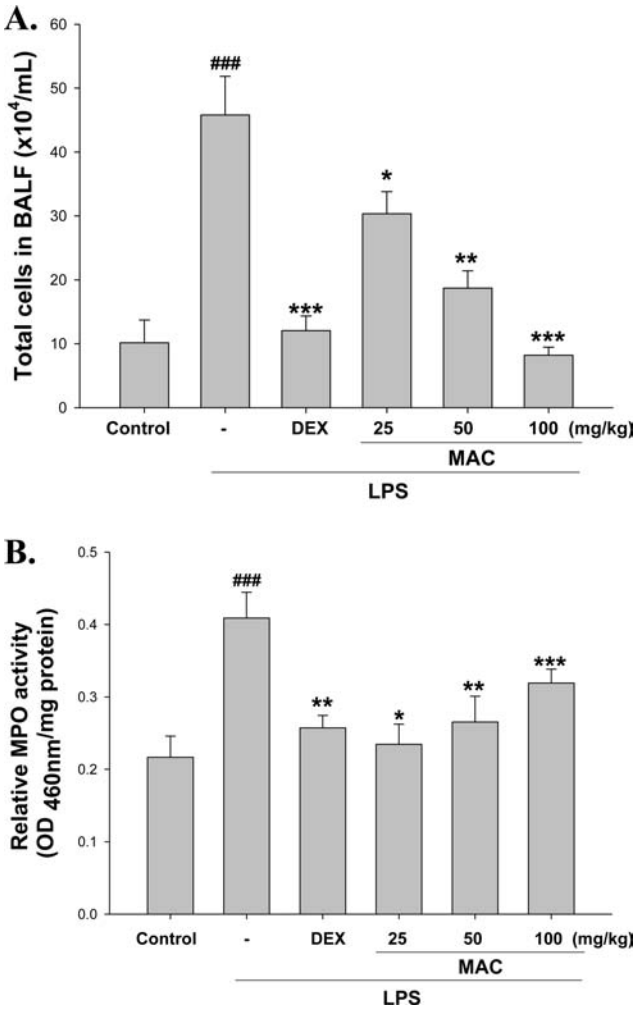

Figure 3. Effects of MAC on the number of total cells in the BALF of LPS-induced ALI mice: (A) number of total cells; (B) myeloperoxidase activity (MPO) performed at 6 h after LPS challenge. Its activity reflects the neutrophil infiltration in the lungs. Cell counts were performed with a hemocytometer. Each value represents the mean ± SEM. (###) $p < 0.001$ as compared with the control group; (*) $p < 0.05$, (**) $p < 0.01$, and (***) $p < 0.001$ as compared with the LPS group (one-way ANOVA followed by Scheffe's multiple-range test).

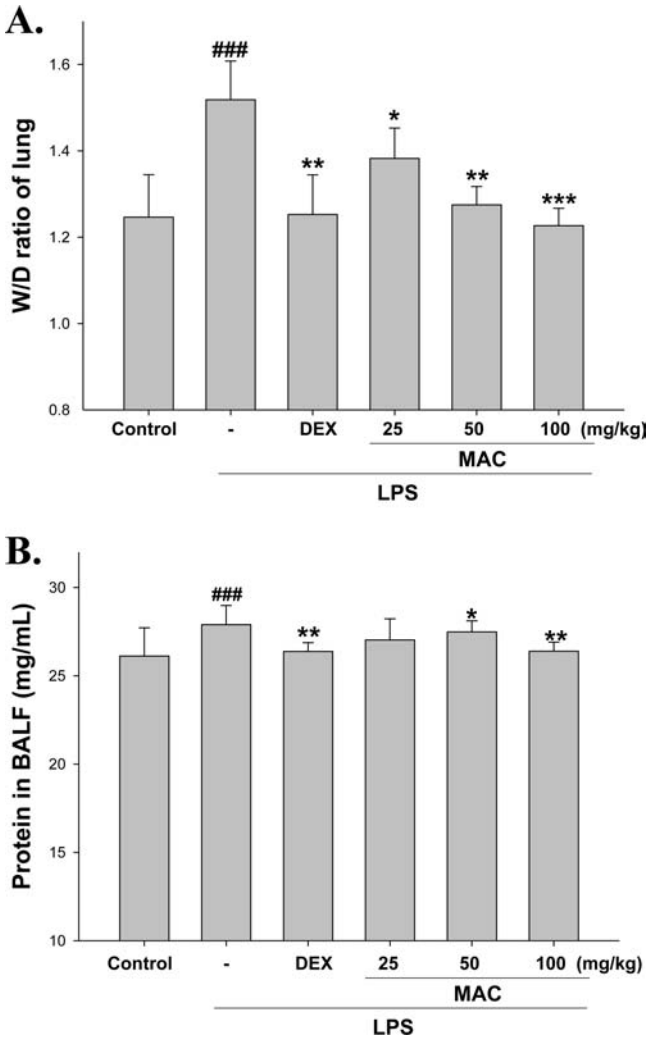

Figure 4. Effects of MAC on the lung W/D ratio and total protein level in the BALF of LPS-induced ALI mice. Mice were given MAC (25, 50, or 100 mg/kg) 1 h prior to an intratracheal (I.T.) instillation administration of LPS. The lung W/D ratio (A) and total protein concentration in the BALF (B) were determined 6 h after the LPS challenge. Each value represents the mean ± SEM. (###) $p < 0.001$ as compared with the control group; (**) $p < 0.01$ and (***) $p < 0.001$ as compared with the LPS group (one-way ANOVA followed by Scheffe's multiple-range test).

demonstrated that MAC inhibited the activity of MAPK pathways in LPS-induced ALI.

DISCUSSION

In this study, these data are the first to demonstrate the anti-inflammatory activity of MAC in LPS-induced mice ALI. In our experiment, we used this model to determine whether MAC could prevent ALI induced by LPS intranasal instillation. The MAC has been reported to exhibit anti-inflammatory properties in vitro and in vivo.[18] Thus, this study is the first to investigate the effects of MAC inhibition on NF-κB and MAPK activation occurring together with IκBα degradation in a mouse model of LPS-induced ALI.

ALI/ARDS are diseases of multifactorial etiology by acute respiratory failure that cause acute lung tissue edema, lung injury, and inflammatory responses. Multiple clinical studies have reported the development of ALI associated with sepsis, pulmonary injury from pneumonia and aspiration, aspiration of gastric contents, and pulmonary injury from trauma.[19] ALI has added to the understanding of the epidemiology and pathogenesis, but the reason for the morbidity and mortality in critically ill patients is unclear.[20] Administration of LPS-induced ALI in mice has been used to study the pathophysiological and biological pathways.[21] Intratracheal or intranasal bacterial products such as LPS administration trigger the optimal ALI, which is characterized by increased capillary permeability, hemorrhage, intra-alveolar and interstitial edema, and an influx of inflammatory cells into the lung. Currently, DEX, a strong synthetic glucocorticoid, is the most used anti-inflammatory and antioxidative drug in the clinical treatment of ALI because it regulates an efficient decrease of inflammation.[22] Therefore, in this study, the anti-inflammatory effect of DEX was a positive control in LPS-induced mice ALI.

Lung edema is one of the important features of ALI.[23] Furthermore, we investigated the lung W/D ratio and protein concentration in the BALF to quantify the magnitude of lung edema. Here, we found that MAC decreased the lung W/D

dx.doi.org/10.1021/jf405113g | J. Agric. Food Chem. 2014, 62, 5321−5329

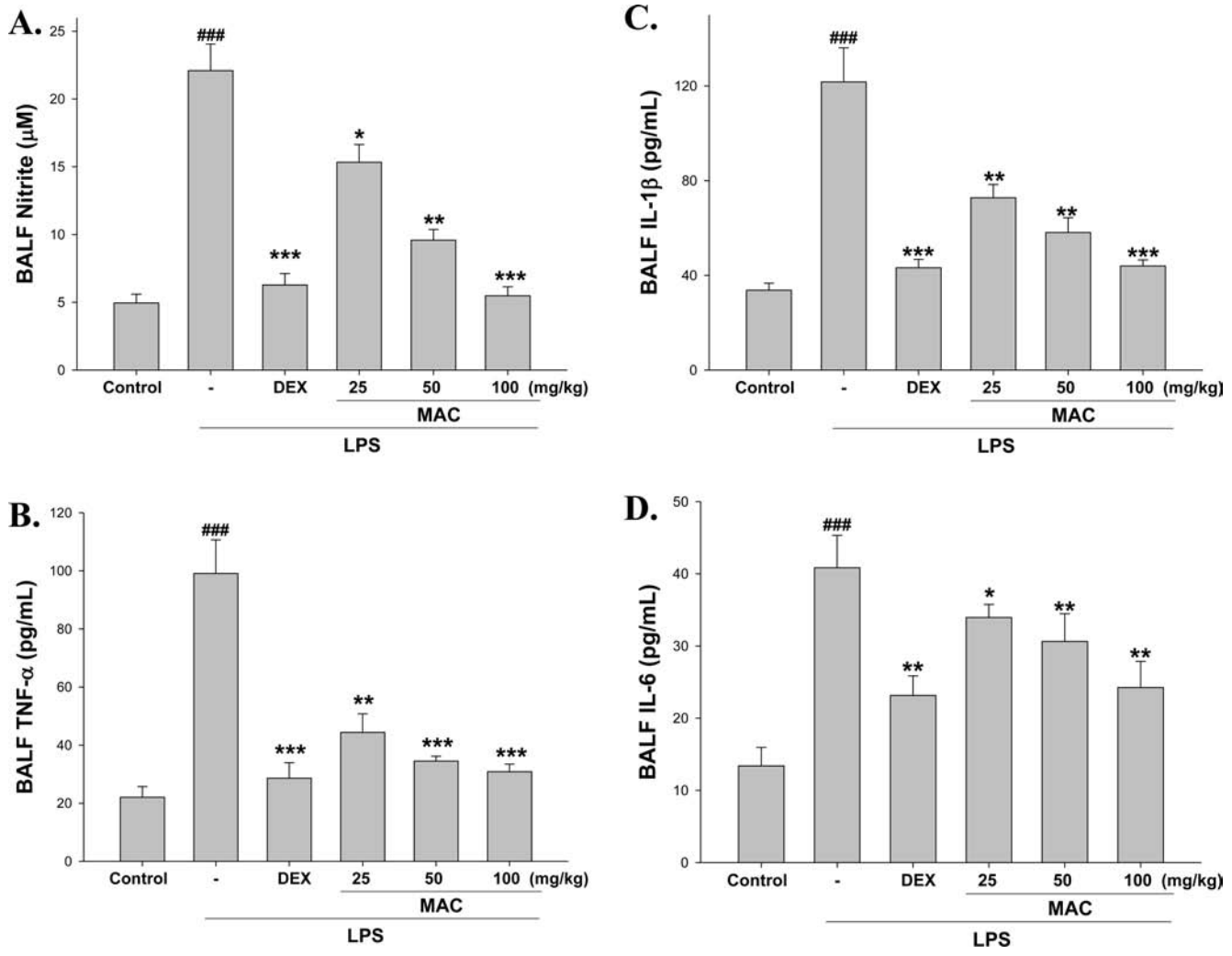

Figure 5. Effect of MAC on NO, TNF-α, IL-1β, and IL-6 expression from mice with ALI. Mice were given MAC (25, 50, or 100 mg/kg) by intraperitoneal injection 1 h before challenge with LPS. BALF was collected at 6 h following LPS challenge to analyze the inflammatory cytokines NO (A), TNF-α (B), IL-1β (C), and IL-6 (D). Each value represents the mean ± SEM. (###) $p < 0.001$ as compared with the control group; (**) $p < 0.01$ and (***) $p < 0.001$ as compared with the LPS group (one-way ANOVA followed by Scheffe's multiple-range test).

ratio after pretreatment 1 h before mice were subjected to LPS-induced ALI. In addition, we also evaluated that lung sections were stained by H&E staining and analyzed by light microscopy after pretreatment with MAC in LPS-induced mice. This result identified the inhibition of MAC or DEX in LPS-induced pulmonary edema and inflammation by lung morphological examination.

In vivo the I.T. administration of LPS is a well-known model for the induction of lung inflammation.[23] Leukocytes move within 1 h to the lung tissue and are replaced by monocytes and macrophages cells and influence the level of inflammatory reaction.

Neutrophil infiltration associated with a LPS-induced inflammatory reaction and the free radical productions from neutrophils have potent antimicrobial activity in acute infections consisting of oxidants, proteinases, and cationic peptides that lead to lung injury.[24] In this study, we found that total numbers of cells and the expressed of MPO activity in neutrophils were decreased after pretreatment with MAC in LPS-induced mice and were relative to the oxidative stress, and free radicals may intensify inflammatory reaction.[25] In this regard, it has been proposed that oxidative stress may be related with corticosteroid resistance and increased the severe inflammatory response, including ALI/ARDS. LPS-induced mouse ALI is characterized by neutrophil infiltration in lung tissues that reduced SOD activity and increased MPO activity.[26] It was supposed that LPS-induced mouse ALI stimulates the neutrophil to migrate into the BALF, and LPS induced pro-inflammatory mediator expressions.[4] This paper suggests that MAC potently inhibited the neutrophil infiltration, MPO activity, and edema formation and increased the SOD activity. LPS-induced mouse ALI displays some characteristics such as neutrophil accumulation, pro-inflammatory cytokine production, and lung injury. The levels of pro-inflammatory cytokines such as TNF-α, IL-1β, and IL-6 can be used to evaluate lung injury and inflammatory level.[27] Our previous studies also have reported that MAC can decrease iNOS and COX-2 protein expression in vitro and in vivo.[18] In this experiment, we found that pretreatment with MAC reduced the TNF-α, IL-1β, and IL-6 expressions in BALF. These results indicate that MAC could effectively improve the LPS-induced ALI in mice.

NO acts as a second messenger with multiple functions, including neural activity, blood flow, and pain modulation.[28] Excessive levels of NO produced from iNOS lead to a reaction

dx.doi.org/10.1021/jf405113g | J. Agric. Food Chem. 2014, 62, 5321−5329

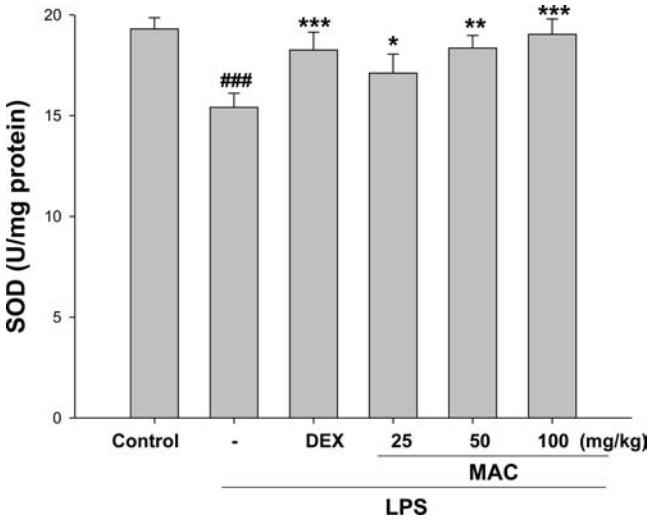

Figure 6. Effects of MAC on SOD activity in lungs from mice with ALI. Lung homogenates were prepared for measuring SOD activity. Each value represents the mean ± SEM. (###) $p < 0.001$ as compared with the control group; (**) $p < 0.01$ and (***) $p < 0.001$ as compared with the LPS group (one-way ANOVA followed by Scheffe's multiple-range test).

of NO with superoxide to create $ONOO^-$. $ONOO^-$ formation represents one of the major mechanisms of acute lung injury, including substantial oxidative/nitrative stress, destruction of cellular constituents, and induction of cell apoptosis and necrosis.[29]

Transcription factor NF-κB plays a critical role that controls multiple key cellular processes. Members of the NF-κB family include p50 and p65 heterodimers. The translocation of NF-κB p65 is related to cancer, inflammation, and acute immune response.[26] Inhibition of the NF-κB pathway has been shown to recover septic dysfunction and inhibit the expression of pro-inflammatory cytokines, including TNF-α, IL-1β, and IL-6.[30] The results from the present study show that pretreatment with MAC inhibits the degradation of IκBα and NF-κB in the LPS-induced mouse ALI.

MAPK families (ERK, JNK, and p38) play an important role in regulating cytokine release and signal transduction pathways. JNK and p38 MAP kinase have been reported to identify regulatory pro-inflammatory cytokines (such as IL-1 and TNF-α).[29] MAPK pathways (ERK, p38, and JNK) have been demonstrated as participating in LPS-induced mouse ALI.[31] In addition, p38 regulated the LPS-induced NF-κB activation by blocking neutrophil infiltration into the lung in LPS-induced mouse ALI.[2] In this study, pretreatment of MAC inhibited LPS-induced phosphorylation of MAPKs (ERK, JNK, and p38). Thus, it is possible that the inhibition of pro-inflammatory (TNF-α, IL-1β, and IL-6) expressions by pretreatment with MAC occurs through pathways that inhibit the phosphorylation of MAPKs and IκB activation in LPS-induced acute lung injury.

The fruiting body and mycelium of AC are well-known as a traditional medicine for many diseases. The anti-inflammatory

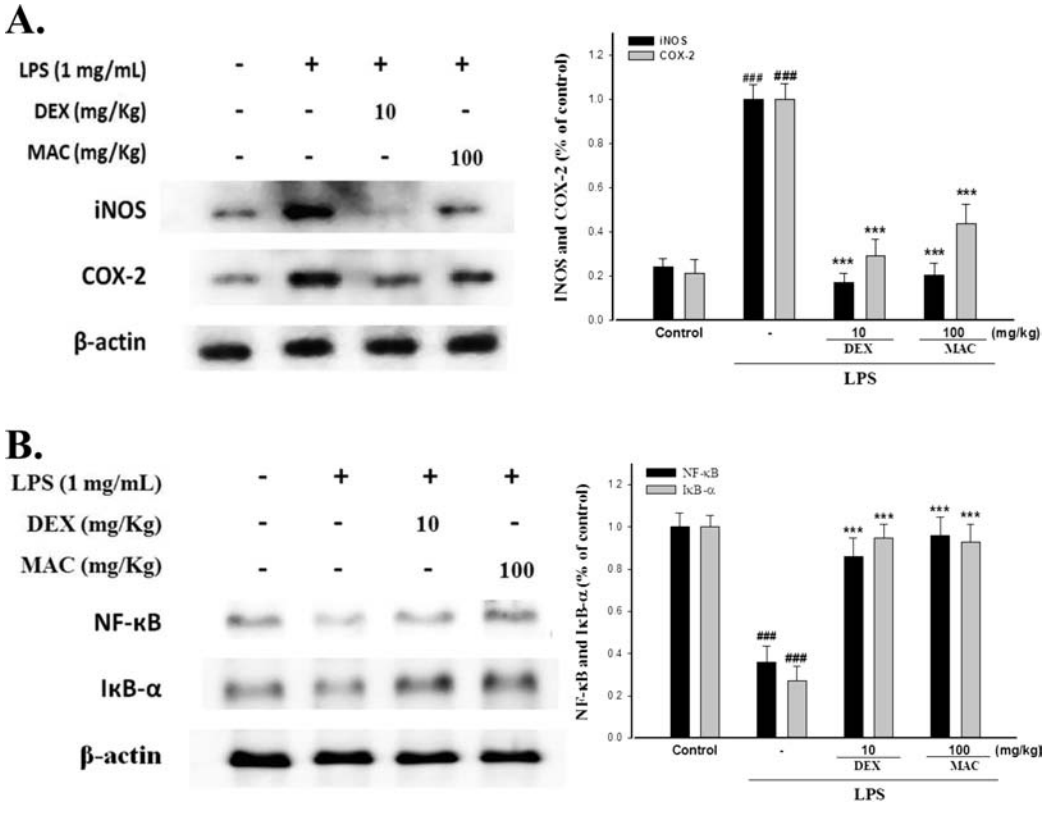

Figure 7. Inhibition of iNOS, COX-2 (A), IκBα, and NF-κB (B) protein expression by MAC in LPS-induced ALI mice. Tissues suspended were then prepared and subjected to Western blotting by using an antibody specific for iNOS, COX-2, IκBα, and NF-κB. β-Actin was used as an internal control. A representative Western blot from two separate experiments is shown. (###) Compared with sample of control group. Data represent the mean ± SD for the three different experiments performed in triplicate. (***) $p < 0.001$ compared with the LPS-alone group (one-way ANOVA followed by Scheffe's multiple-range test).

dx.doi.org/10.1021/jf405113g | J. Agric. Food Chem. 2014, 62, 5321−5329

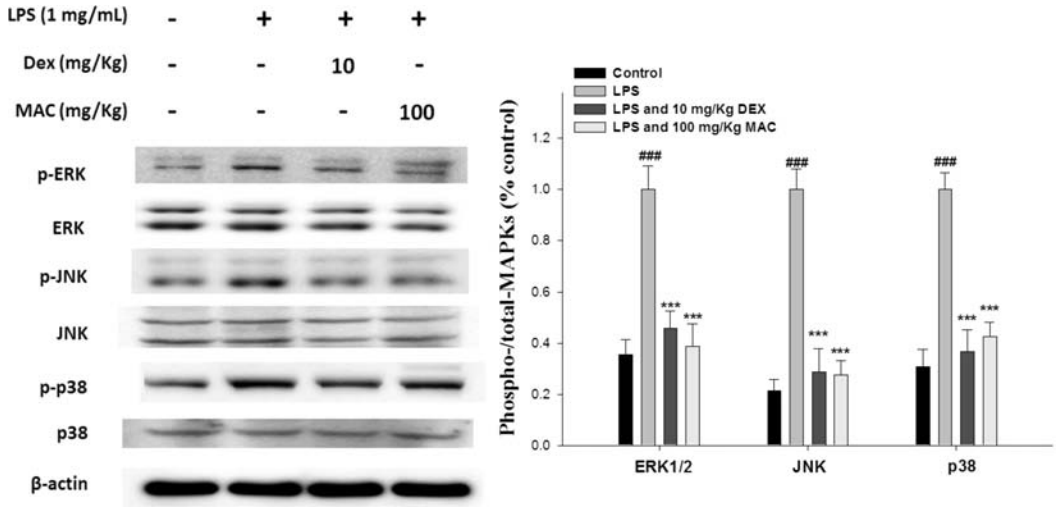

Figure 8. Effects of MAC on LPS-induced phosphorylation of MAPK in LPS-induced ALI mice. Mice were pretreated with different concentrations of MAC for 1 h and stimulated with LPS. Cellular proteins from the lungs were used for the detection of phosphorylated or total forms of three MAPK molecules, ERK, p38, and JNK. A representative Western blot from two separate experiments is shown. (###) Compared with sample of control group. Data represent the mean ± SD for the three different experiments performed in triplicate. (***) $p < 0.001$ compared with the LPS-alone group (one-way ANOVA followed by Scheffe's multiple-range test).

activity of *A. camphorata* mycelium contributed to prevent inflammatory disease through repression of iNOS and COX-2 protein expression.[18,28] Eburicoic acid and dehydroeburicoic acid, an active ingredient from solid-state culture of AC, were evaluated for anti-inflammatory and hepatoprotective effects.[10,11] In our previous paper, we showed that ergostatrien-3β-ol (EK100) had analgesic, anti-inflammatory,[9] and hepatoprotective[12] activities. Thus, we used EK100 to evaluate the quality of *A. camphorata* mycelium using high-performance liquid chromatography in this study. Antrocamphin A, antcin A, antcin B, and eburicol from AC have anti-inflammatory activity by inhibition of *N*-formylmethionylleucylphenylalanine (fMLP)-induced superoxide anion generation.[32]

In summary, our study shows protective effects of MAC on LPS-induced mouse ALI. MAC pretreatment reduced lung histological changes, lung edema, and leukocyte infiltration in lungs, changed the wet/dry ratio in the lung tissue, and inhibited the release of inflammatory mediators in the BALF. These data suggested that MAC was proposed as a novel therapeutic strategy for inflammatory diseases through inhibition of the NF-κB pathway by directly blocking phosphorylation and degradation of inhibitory IκBα via inhibition of MAPK-responsive signaling pathways. Thus, MAC exerts an anti-inflammatory effect in rodents, and more research needs to be done before a clinical trial of this drug can be realized.

AUTHOR INFORMATION

Corresponding Authors

*(S.-S.H.) Phone: +886 4 22053366, ext 5127. Fax: +886 4 22083362. E-mail: sshuang@mail.cmu.edu.tw.

*(Y.-H.K.) Phone: +886 4 22071693. Fax: +886 4 22071693. E-mail: kuoyh@mail.cmu.edu.tw.

Author Contributions

‖G.-J.H. and J.-S.D. contributed equally to this work.

Funding

The authors want to thank the financial supports from the National Science Council (NSC101-2313-B-039-002-MY3, NSC 102-2320-B-031-022-, and NSC 102-2320-B-468-004-), China Medical University (CMU) (CMU100-ASIA-15 and CMU101-AWARD-08), Asia University (100-ASIA-15), and CMU under the Aim for Top University Plan of the Ministry of Education, Taiwan, and the Department of Health Clinical Trial and Research Center of Excellent (DOH102-TD-C-111-004), Taiwan.

Notes

The authors declare no competing financial interest.

REFERENCES

(1) Tunceroglu, H.; Shah, A.; Porhomayon, J.; Nader, N. D. Biomarkers of lung injury in critical care medicine: past, present, and future. *Immunol, Invest.* **2013**, *42*, 247−261.

(2) Chu, X.; Ci, X.; Wei, M.; Yang, X.; Cao, Q.; Guan, M.; Li, H.; Deng, Y.; Feng, H.; Deng, X. Licochalcone a inhibits lipopolysaccharide-induced inflammatory response in vitro and in vivo. *J. Agric. Food Chem.* **2012**, *60*, 3947−3954.

(3) Liu, L.; Xiong, H.; Ping, J.; Ju, Y.; Zhang, X. *Taraxacum officinale* protects against lipopolysaccharide-induced acute lung injury in mice. *J. Ethnopharmacol.* **2010**, *130*, 392−397.

(4) Wei, M.; Chu, X.; Jiang, L.; Yang, X.; Cai, Q.; Zheng, C.; Ci, X.; Guan, M.; Liu, J.; Deng, X. Protocatechuic acid attenuates lipolysaccharide-induced acute lung injury. *Inflammation* **2012**, *35*, 1169−1178.

(5) Liu, Y.; Wu, H.; Nie, Y. C.; Chen, J. L.; Su, W. W.; Li, P. B. Naringin attenuates acute lung injury in LPS-treated mice by inhibiting NF-κB pathway. *Int. Immunopharmacol.* **2011**, *11*, 1606−1612.

(6) Liaw, C. C.; Chen, Y. C.; Huang, G. J.; Tsai, Y. C.; Chien, S. C.; Wu, J. H.; Wang, S. Y.; Chao, L. K.; Sung, P. J.; Huang, H. C.; Kuo, Y. H. Anti-inflammatory lanostanoids and lactone derivatives from *Antrodia camphorata*. *J. Nat. Prod.* **2013**, *76*, 489−494.

(7) Chen, Y. C.; Chiu, H. L.; Chao, C. Y.; Lin, W. H.; Chao, L. K.; Huang, G. J.; Kuo, Y. H. New anti-inflammatory aromatic components from *Antrodia camphorata*. *Int. J. Mol. Sci.* **2013**, *14*, 4629−4639.

(8) Hsieh, Y. H.; Chu, F. H.; Wang, Y. S.; Chien, S. C.; Chang, S. T.; Shaw, J. F.; Chen, C. Y.; Hsiao, W. W.; Kuo, Y. H.; Wang, S. Y. Antrocamphin A, an anti-inflammatory principal from the fruiting body of *Taiwanofungus camphoratus*, and its mechanisms. *J. Agric. Food Chem.* **2010**, *58*, 3153−3158.

(9) Huang, G. J.; Huang, S. S.; Lin, S. S.; Shao, Y. Y.; Chen, C. C.; Hou, W. C.; Kuo, Y. H. Analgesic effects and the mechanisms of anti-inflammation of ergostatrien-3β-ol from *Antrodia camphorata* sub-

merged whole broth in mice. *J. Agric. Food Chem.* **2010**, *58*, 7445−7452.
(10) Deng, J. S.; Huang, S. S.; Lin, T. H.; Lee, M. M.; Kuo, C. C.; Sung, P. J.; Hou, W. C.; Huang, G. J.; Kuo, Y. H. Analgesic and anti-inflammatory bioactivities of eburicoic acid and dehydroeburicoic acid isolated from *Antrodia camphorata* on the inflammatory mediator expression in mice. *J. Agric. Food Chem.* **2013**, *61*, 5064−5071.
(11) Huang, G. J.; Deng, J. S.; Huang, S. S.; Lee, C. Y.; Hou, W. C.; Wang, S. Y.; Sung, P. J.; Kuo, Y. H. Hepatoprotective effects of eburicoic acid and dehydroeburicoic acid from *Antrodia camphorata* in a mouse model of acute hepatic injury. *Food Chem.* **2013**, *141*, 3020−3027.
(12) Huang, G. J.; Deng, J. S.; Huang, S. S.; Lin, S. S.; Shao, Y. Y.; Chen, C. C.; Hou, W. C.; Kuo, Y. H. Protective effects of antrosterol against carbon tetrachloride-induced acute liver injury in mice. *Food Chem.* **2012**, *132*, 709−716.
(13) Sun, J.; Chi, G.; Soromou, L. W.; Chen, N.; Guan, M.; Wu, Q.; Wang, D.; Li, H. Preventive effect of imperatorin on acute lung injury induced by lipopolysaccharide in mice. *Int. Immunopharmacol.* **2012**, *14*, 369−374.
(14) Bani, D.; Masini, E.; Bello, M. G.; Bigazzi, M.; Sacchi, T. B. Relaxin protects against myocardial injury caused by ischemia and reperfusion in rat heart. *Am. J. Pathol.* **1998**, *152*, 1367−1376.
(15) Sheu, M. J.; Deng, J. S.; Huang, M. H.; Wu, C. H.; Huang, S. S.; Huang, G. J. Antioxidant and anti-inflammatory properties of *Dichondra repens* Forst. and its reference compounds. *Food Chem.* **2012**, *132*, 1010−1018.
(16) Flohe, L.; Otting, F. Superoxide dismutase assays. *Methods Enzymol.* **1984**, *105*, 93−104.
(17) Shao, Y. Y.; Chen, C. C.; Wang, H. Y.; Chiu, H. L.; Hseu, T. H.; Kuo, Y. H. Chemical constituents of *Antrodia camphorata* submerged whole broth. *Nat. Prod. Res.* **2008**, *22*, 1151−1157.
(18) Wen, C. L.; Chang, C. C.; Huang, S. S.; Kuo, C. L.; Hsu, S. L.; Deng, J. S.; Huang, G. J. Anti-inflammatory effects of methanol extract of *Antrodia cinnamomea* mycelia both *in vitro* and *in vivo*. *J. Ethnopharmacol.* **2011**, *137*, 575−584.
(19) Matthay, M. A.; Zimmerman, G. A. Acute lung injury and the acute respiratory distress syndrome: four decades of inquiry into pathogenesis and rational management. *Am. J. Respir. Cell Mol. Biol.* **2005**, *33*, 319−327.
(20) Johnson, E. R.; Matthay, M. A. Acute lung injury: epidemiology, pathogenesis, and treatment. *J. Aerosol Med. Pulm. Drug Delivery* **2010**, *23*, 243−252.
(21) Philippakis, G. E.; Lazaris, A. C.; Papathomas, T. G.; Zissis, C.; Agrogiannis, G.; Thomopoulou, G.; Nonni, A.; Xiromeritis, K.; Nikolopoulou-Stamati, P.; Bramis, J.; Patsouris, E.; Perrea, D.; Bellenis, I. Adrenaline attenuates the acute lung injury after intratracheal lipopolysaccharide instillation: an experimental study. *Inhal. Toxicol.* **2008**, *20*, 445−453.
(22) Azoulay, É.; Canet, E.; Raffoux, E.; Lengliné, E.; Lemiale, V.; Vincent, F.; de Labarthe, A.; Seguin, A.; Boissel, N.; Dombret, H.; Schlemmer, B. Dexamethasone in patients with acute lung injury from acute monocytic leukaemia. *Eur. Respir. J.* **2012**, *39*, 648−653.
(23) Zhang, S.; Rahman, M.; Zhang, S.; Song, L.; Herwald, H.; Thorlacius, H. Targeting rac1 signaling inhibits streptococcal m1 protein-induced CXC chemokine formation, neutrophil infiltration and lung injury. *PLoS One* **2013**, *8*, No. e71080.
(24) Lin, Y. C.; Lai, Y. S.; Chou, T. C. The protective effect of α-lipoic acid in lipopolysaccharide-induced acute lung injury is mediated by heme oxygenase-1. *Evidence-Based Complement. Alternat. Med.* **2013**, *2013*, No. 590363.
(25) El-Sayed, N. S.; Mahran, L. G.; Khattab, M. M. Tempol, a membrane-permeable radical scavenger, ameliorates lipopolysaccharide-induced acute lung injury in mice: a key role for superoxide anion. *Eur. J. Pharmacol.* **2011**, *663*, 68−73.
(26) Yang, R.; Yang, L.; Shen, X.; Cheng, W.; Zhao, B.; Ali, K. H.; Qian, Z.; Ji, H. Suppression of NF-κB pathway by crocetin contributes to attenuation of lipopolysaccharide-induced acute lung injury in mice. *Eur. J. Pharmacol.* **2012**, *674*, 391−396.
(27) Ni, Y. F.; Kuai, J. K.; Lu, Z. F.; Yang, G. D.; Fu, H. Y.; Wang, J.; Tian, F.; Yan, X. L.; Zhao, Y. C.; Wang, Y. J.; Jiang, T. Glycyrrhizin treatment is associated with attenuation of lipopolysaccharide-induced acute lung injury by inhibiting cyclooxygenase-2 and inducible nitric oxide synthase expression. *J. Surg. Res.* **2011**, *165*, e29−e35.
(28) Hseu, Y. C.; Wu, F. Y.; Wu, J. J.; Chen, J. Y.; Chang, W. H.; Lu, F. J.; Lai, Y. C.; Yang, H. L. Antiinflammatory potential of *Antrodia camphorata* through inhibition of iNOS, COX-2 and cytokines via the NF-κB pathway. *Int. Immunopharmacol.* **2005**, *5*, 1914−1925.
(29) Kosaka, J.; Morimatsu, H.; Takahashi, T.; Shimizu, H.; Kawanishi, S.; Omori, E.; Endo, Y.; Tamaki, N.; Morita, M.; Morita, K. Effects of biliverdin administration on acute lung injury induced by hemorrhagic shock and resuscitation in rats. *PLoS One* **2013**, *8*, No. e63606.
(30) Kang, P.; Kim, K. Y.; Lee, H. S.; Min, S. S.; Seol, G. H. Anti-inflammatory effects of anethole in lipopolysaccharide-induced acute lung injury in mice. *Life Sci.* **2013**, *93*, 955−961.
(31) Chi, G.; Wei, M.; Xie, X.; Soromou, L. W.; Liu, F.; Zhao, S. Suppression of MAPK and NF-κB pathways by limonene contributes to attenuation of lipopolysaccharide-induced inflammatory responses in acute lung injury. *Inflammation* **2013**, *36*, 501−511.
(32) Chen, J. J.; Lin, W. J.; Liao, C. H.; Shieh, P. C. Anti-inflammatory benzenoids from *Antrodia camphorata*. *J. Nat. Prod.* **2007**, *70*, 989−992.

beginning of the study. During the interview, each subject was asked, item-by-item, whether they usually ate each food and, if so, how much they usually ate. For this purpose, three different serving sizes of each cooked food were presented in pictures to the participants so that they could choose from up to seven serving sizes (from "less than the small one" to "more than the large one"). For some of the foods consumed, amounts were recorded in household units, by volume, or by measuring with a ruler. Information was also collected about the cooking practices, number and amount of ingredients used in each recipe (e.g., type of oil used, type of milk), and other relevant information for the study, such as the consumption of skin in fruit. Furthermore, variability in the consumption of some foods, especially fruits and vegetables, according to the season was taken into account. Methodological issues concerning dietary assessment have been detailed elsewhere.[19] The consumption of foods was converted into energy intake using the nutrient Food Composition Tables developed by the Centro de Enseñanza Superior de Nutrición Humana y Dietética.[20] The intake of nonstarch dietary fiber, soluble (pectin and hemicellulose) and insoluble types (pectin, hemicellulose, Klason lignin, and cellulose), in the sample was determined using the Marlett et al. food composition tables.[21] These authors used the enzymatic–chemical method developed by Theander et al.,[22] by which pectin content is determined using a colorimetric assay, cellulose and hemicellulose are determined by high-performance liquid chromatography (HPLC), and Klason lignin is estimated as the insoluble material after a Saeman acid hydrolysis.[23] Resistant starch intake was calculated using the tables published by Roberts et al., which collect information from eight scientific publications,[24] and the consumption of polyphenols in the sample was obtained using the Phenol-Explorer Database, which contains information mainly determined by HPLC, gas chromatography (GC), and capillary electrophoresis (CE) from more than 1300 publications.[25]

Microbiological Analyses. Each volunteer was asked to provide a single fecal sample immediately after the interview for nutrition assessment. Fecal samples were immediately frozen at −80 °C and stored until further analyses. One gram of fecal sample was employed for DNA extraction by using the QIAamp DNA stool mini kit (Qiagen, Hilden, Germany) as previously described.[26] Quantification of different bacterial populations (*Akkermansia*, *Bacteroides*, *Bifidobacterium*, *Blautia coccoides* group, *Clostridium leptum* group, and *Lactobacillus* group) in feces was performed with a 7500 Fast Real Time PCR System (Applied Biosystems, Foster City, CA, USA) using SYBR Green PCR Master Mix (Applied Biosystems) as previously described.[27]

Statistical Analysis. Statistical analysis was performed using SPSS version 19.0 (SPSS Inc., Chicago, IL, USA). Goodness of fit to normal distribution was analyzed with the Kolmogorov–Smirnov test. For descriptive purposes, mean values were presented on untransformed variables. Multiple linear regression analysis was used to investigate the correlations between the intake of fibers and polyphenols and fecal levels of the studied microorganisms. We also introduced age and energy intake as covariates in the models. Because the fibers and polyphenols significantly related to microbiota are usually present in the same foods, multiple stepwise regression models were carried out to explore whether their association with microbial groups remained with independence of covariates and other related variables included in the model. The statistical parameters employed were β (standardized regression coefficient) and R^2 (coefficient of multiple determinations). The conventional probability value (0.05) for significance was used in the interpretation of results. Considering the standard deviation of the microbial levels and the standard deviation of the regression errors, we could reject the null hypothesis with an estimated probability around 0.97 and a type I error probability of 0.05 for all models in which the slope of the line is above 0.3 [calculated using the software PS: Power and Sample Size Calculation version 3.0.43 (Vanderlbilt University, Nashville, TN, USA)].

RESULTS

General characteristics of the studied human sample are described in Table 1. Results showed that in the diet of the participants the consumption of dairy products, fruits and vegetables, and cereals prevailed, with a moderate intake of meat, fish, and seafood. Tables 2 and 3 present the mean intakes of nonstarch and resistant starch dietary fibers (types and subtypes) and polyphenols (classes and subclasses), respectively, together with their respective association with intestinal microbial groups. With regard to the fibers, soluble pectin was negatively associated with *B. coccoides* and *C. leptum*. This latter microbial group, which includes important intestinal microorganisms such as *Faecalibacterium prausnitzii* and several *Ruminococcus* species, was also inversely associated with insoluble pectin. On the contrary, a positive association was found between *Akkermansia* and *B. coccoides* levels and resistant starch. *Lactobacillus* was also positively associated with soluble fiber, hemicellulose (soluble and insoluble), cellulose, and resistant starch. From all of the evaluated polyphenols, only flavanone intake was found to be negatively associated with both *B. coccoides* and *C. leptum* groups.

To explore these associations, the main food sources of the fibers and polyphenols significantly associated with microbiota were calculated (Figure 1). Orange consumption was found as the top contributor to insoluble hemicellulose, pectin (soluble and insoluble), cellulose, and flavanone intake, whereas white

Table 1. General Characteristics of the Human Sample (n = 38)

	$X \pm$ SD	P_5–P_{95}[a]
energy (kcal/day)	1928.20 ± 554.56	1040.26–3313.48
food groups (g/day)		
oils and fats[b]	25.33 ± 10.73	10.00–50.5
alcoholic beverages[c]	138.69 ± 170.14	0.00–507.18
nonalcoholic beverages[d]	110.00 ± 125.40	0.00–334.68
meats and derived products[e]	107.38 ± 58.25	34.15–211.29
cereals and derived products[f]	175.32 ± 125.67	30.75–385.76
fruits and derived products[g]	408.61 ± 295.32	134.55–1038.70
eggs[h]	15.70 ± 10.77	0.66–44.00
dairy products[i]	503.21 ± 254.53	38.81–816.74
legumes[j]	19.61 ± 22.66	0.00–69.89
fish and seafood[k]	75.40 ± 48.16	9.74–175.86
vegetables and root crops[l]	257.60 ± 186.37	1.37–528.56
dietary fiber (nonstarch polysaccharides) (g/day)	18.18 ± 7.07	8.11–29.21
resistant starch (g/day)	5.07 ± 2.99	1.37 ± 10.22
total polyphenols (mg/day)	2341.33 ± 1057.68	1180.66–5480.55
microbial groups (log no. cells/g of feces)		
Akkermansia	6.57 ± 1.84	4.09–9.39
B. coccoides	9.32 ± 0.79	7.55–10.46
C. leptum	8.06 ± 0.68	6.96–9.22
Bacteroides	7.45 ± 1.65	4.00–9.54
Bifidobacterium	9.26 ± 1.36	5.52–10.46
Lactobacillus	5.77 ± 1.28	4.00–9.54

[a]5th and 95th percentiles. [b]Oils, margarine, and butter. [c]Distilled beverages, beer, cider, liquors, and wines. [d]Coffee, cocoa, infusions, soft drinks, and canned juices. [e]Fresh white and red meat, sausages, and ham. [f]Breakfast cereals, biscuits, grains and flours, breads, pasta, and pastries. [g]Fresh, dried, and canned fruit. [h]Chicken eggs. [i]Milk, ice cream, dairy desserts, cheese, yogurt, and fermented milks. [j]Fresh, dried, and canned legumes. [k]Fresh lean and fat fish, fresh crustaceans and mollusks, and canned seafood. [l]Fresh and canned mushrooms, vegetables, and potatoes.

dx.doi.org/10.1021/jf501546a | J. Agric. Food Chem. 2014, 62, 5330–5336

Table 2. Daily Intake of Types and Subtypes of Nonstarch Dietary Fiber and Resistant Starch and Its Association with the Quantification of Microbial Groups (Log No. Cells per Gram Feces) (n = 38)

		Akkermansia[a]		*B. coccoides*[a]		*C. leptum*[a]		*Bacteroides*[a]		*Bifidobacterium*[a]		*Lactobacillus*[a]	
	intake (g/day), $X \pm$ SD	R^2	β	R^2	β	R^2	β	R^2	β	R^2	β	R^2	β
dietary fiber (NSP)													
soluble fiber	3.28 ± 1.41	0.018	0.012	0.061	−0.205	0.034	0.030	0.022	0.053	0.091	0.218	**0.173**	**0.481***
hemicellulose	1.97 ± 0.97	0.032	−0.189	0.062	0.217	0.137	0.486	0.021	0.010	0.143	0.409	**0.443**	**0.924***
pectin	1.21 ± 0.73	0.052	0.191	**0.173**	**−0.408***	**0.141**	**−0.369***	0.023	0.053	0.084	−0.135	0.105	−0.215
insoluble fiber	14.90 ± 5.76	0.028	−0.125	0.046	−0.091	0.034	−0.029	0.023	−0.065	0.071	0.054	0.139	0.369
cellulose	5.40 ± 2.00	0.028	−0.124	0.043	0.055	0.036	0.071	0.025	−0.084	0.080	0.134	**0.190**	**0.459***
hemicellulose	4.57 ± 1.90	0.036	−0.167	0.044	0.067	0.036	0.071	0.034	−0.149	0.071	0.057	**0.182**	**0.437***
pectin	2.49 ± 1.45	0.031	0.117	**0.174**	**−0.408***	0.132	−0.353	0.021	0.020	0.074	−0.078	0.087	−0.152
Klason lignin	2.44 ± 1.24	0.056	−0.257	0.048	0.107	0.074	0.276	0.024	0.069	0.075	0.100	0.174	0.442
resistant starch		**0.174**	**0.397***	**0.162**	**0.404***	0.069	0.262	0.022	−0.037	0.127	0.228	**0.226**	**0.429***

[a]Based on multiple regression analysis adjusted by age and energy intake. β, standardized regression coefficient; R^2, coefficient of multiple determinations. *, $p \leq 0.05$.

Table 3. Daily Intake of Classes and Subclasses of Polyphenols and Its Association with the Quantification of Microbial Groups (Log No. Cells per Gram Feces) (n = 38)

		Akkermansia[a]		*B. coccoides*[a]		*C. leptum*[a]		*Bacteroides*[a]		*Bifidobacterium*[a]		*Lactobacillus*[a]	
	intake (mg/day), $X \pm$ SD	R^2	β	R^2	β	R^2	β	R^2	β	R^2	β	R^2	β
flavonoids	480.97 ± 281.48	0.055	−0.182	0.158	−0.399*	0.086	−0.299	0.021	0.015	0.092	−0.108	0.129	−0.270
anthocyanins	28.44 ± 43.16	0.050	−0.087	0.033	−0.107	0.011	−0.034	0.024	−0.052	0.084	−0.050	0.107	−0.202
dihydrochalcones	2.95 ± 2.76	0.044	0.036	0.023	0.035	0.021	0.109	0.050	0.173	0.109	0.167	0.067	−0.006
dihydroflavonols	3.51 ± 4.43	0.047	0.071	0.033	−0.109	0.011	−0.040	0.109	−0.304	0.083	0.041	0.071	−0.069
flavanols	232.57 ± 189.02	0.054	0.110	0.035	−0.117	0.011	−0.036	0.024	0.050	0.082	−0.024	0.074	−0.088
flavanones	157.07 ± 169.74	0.094	0.235	0.244	−0.559*	0.214	−0.536*	0.024	0.018	0.129	−0.256	0.157	−0.356
flavones	4.34 ± 5.17	0.048	0.078	0.115	−0.355	0.115	−0.377	0.024	0.059	0.082	−0.027	0.141	−0.316
flavonols	52.09 ± 42.77	0.076	−0.184	0.022	−0.021	0.012	0.050	0.035	−0.116	0.145	0.252	0.077	0.099
phenolic acids	164.33 ± 164.47	0.090	0.218	0.040	−0.135	0.014	−0.065	0.040	0.139	0.098	0.129	0.078	−0.104
hydroxybenzoic	17.04 ± 26.29	0.059	−0.129	0.028	−0.079	0.010	−0.016	0.021	0.016	0.085	−0.056	0.102	−0.190
hydroxycinnamic	147.15 ± 153.64	0.107	0.255	0.039	−0.131	0.014	−0.067	0.042	0.146	0.103	0.0148	0.073	−0.080
hydroxyphenylacetic	0.15 ± 0.16	0.069	−0.169	0.028	−0.081	0.010	−0.021	0.097	−0.283	0.084	0.043	0.067	0.021
lignans	1.00 ± 0.38	0.048	−0.094	0.048	0.195	0.035	0.191	0.034	−0.133	0.082	0.000	0.154	0.352
stilbenes	2.30 ± 2.84	0.046	0.063	0.033	−0.111	0.011	−0.041	0.104	−0.294	0.083	0.035	0.073	−0.080
other polyphenols	0.41 ± 0.48	0.053	−0.110	0.034	0.113	0.014	0.067	0.068	−0.225	0.090	−0.094	0.078	0.107

[a]Based on multiple regression analysis adjusted by age and energy intake. β, standardized regression coefficient; R^2, coefficient of multiple determinations. *, $p \leq 0.05$.

dx.doi.org/10.1021/jf501546a | J. Agric. Food Chem. 2014, 62, 5330−5336

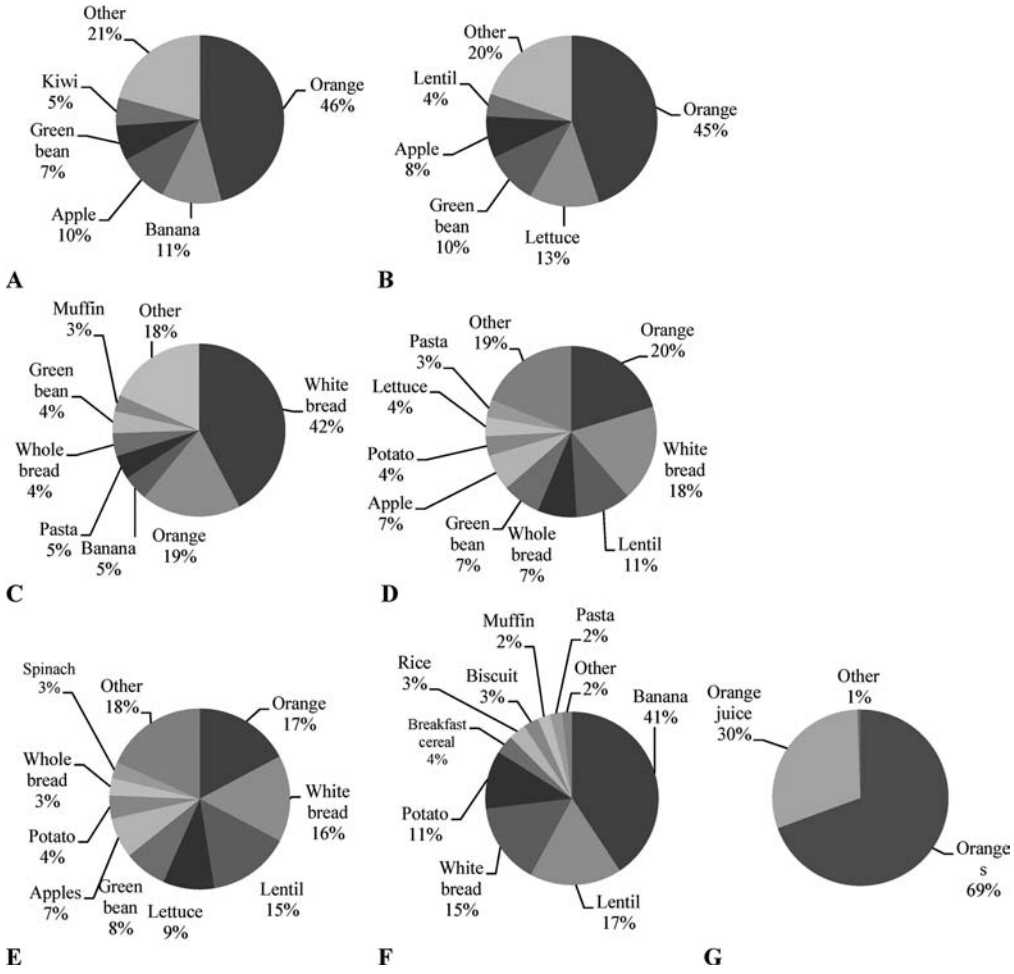

Figure 1. Food sources of pectin (soluble and insoluble), hemicellulose (soluble and insoluble), cellulose, resistant starch and flavanones in the sample: (A) soluble pectin; (B) insoluble pectin; (C) soluble hemicellulose; (D) insoluble hemicellulose; (E) cellulose; (F) resistant starch; (G) flavanone.

Table 4. Combined Effect of Fibers, Polyphenols, and Their Food Sources on Fecal Levels of Microbial Groups (Log No. Cells per Gram Feces) (n = 38)[a]

	B. coccoides[b]			*C. leptum*[b]			*Lactobacillus*[b]		
model	variable	R^2	β	variable	R^2	β	variable	R^2	β
1[c]	–[1]			flavanone	0.121	−0.348*	hemicellulose I		0.819**
	resistant starch[2]	0.134	0.366*				resistant starch		0.316*
							energy	0.520	−0.389*
2[d]	orange[1]		−0.532*	orange	0.131	−0.362*	white bread	0.266	0.515**
	energy	0.244	0.389*						
	pasta[2]	0.110	0.331*						

[a]No results are presented for *Akkermansia* because neither resistant starch nor any of its food sources persisted in the models. [b]Based on multiple stepwise regression analysis adjusted by age and energy intake. Hemicellulose I, insoluble hemicellulose; β, standardized regression coefficient; R^2, coefficient of multiple determinations. *, $p \leq 0.05$; **, $p \leq 0.001$. [c]Model 1 (fibers and polyphenols): *C. coccoides* [1](age; energy; soluble and insoluble pectin and flavanone intakes) and [2](age; energy; and resistant starch intake), *C. leptum* (age; energy; soluble pectin and flavanone intakes), *Lactobacillus* (age; energy; soluble fiber, soluble and insoluble hemicellulose, cellulose, and resistant starch intakes). [d]Model 2 (food sources): *B. coccoides* [1](age; energy; orange, orange juice, lentils, apple, lettuce, green bean, kiwi, and banana intakes) and [2](age; energy; banana, lentil, white bread, potato, breakfast cereal, biscuit, muffin, and pasta intakes), *C. leptum* (age; energy; orange, orange juice, kiwi, green bean, apple, and banana intakes), *Lactobacillus* (age; energy; orange, white bread and whole bread, lentil, lettuce, green bean, apple, potato, spinach, pasta, banana, muffin, breakfast cereal, rice, and biscuit intakes).

bread was the main food source of soluble hemicellulose and banana was the main supplier of resistant starch.

Multiple stepwise linear regression analyses were carried out to explore the association between the fibers, polyphenols, or any of their food sources and the microbiota (Table 4). These dietary components and foodstuffs are highly correlated. Therefore, to avoid findings that can be explained by any other highly correlated variable, fibers and polyphenols which appeared in our study as significantly associated with microbiota were placed in a model at the same time. The same approach was used to explore

the association between food sources and microbial groups. *B. coccoides* levels were negatively associated with orange intake and positively with resistant starch from pasta; *C. leptum* variation was explained, in part, by the intake of flavanones from oranges, whereas *Lactobacillus* was associated with insoluble hemicellulose and resistant starch from white bread.

DISCUSSION

Most research about diet and intestinal microbiota has been traditionally focused on the effect of single food components (usually soluble fibers) acting as prebiotics to promote the growth of some beneficial bacterial groups, such as *Lactobacillus* or *Bifidobacterium*. To the best of our knowledge, this is the first attempt to analyze the impact of the consumption of different types of fibers, together with polyphenols and their dietary sources, on the fecal microbiota, within the context of a regular diet in healthy adults.

The detection of a direct association between dietary fibers provided by white bread and the levels of *Lactobacillus*, as well as the identification of an inverse association between flavanones and pectins from orange and *B. coccoides* and *C. leptum*, confirms the complexity of the diet−microbiota interrelationship.

Previous studies indicated that pectin evades digestion by human digestive enzymes and reaches the colon, where it is metabolized by several microbial groups, then favoring their growth.[28] However, in the present study we have found an inverse association between pectin intake and fecal levels of *B. coccoides* and *C. leptum*, which include important groups such as *Lachnospira*, *Ruminococcus*, or *Faecalibacterium*. Because this result was unexpected, we checked the possibility that part of this effect of pectin may be due to its interaction with other components present in the same foods,[18] as is the case of flavanones. It has been recently suggested that the absorption of flavanones takes place in both the small and large bowels, being compounds with a reduced bioavailability.[29] Also, processing of flavanone-rich foods, such as citrus fruits, can lead to the precipitation of these flavonoids by combination with pectins or other macromolecules,[30] resulting in compounds with less bioavailability than the original ones.[31] Therefore, given that an appreciable amount of polyphenols passes the small intestine in tandem with dietary fiber[32,33] and the high grade of correlation between their intake, some authors have suggested that both compounds should be approached together.[34] In accordance with this, pectin and flavanone intake in our sample were highly correlated ($r = 0.734$; data not shown); oranges were identified as the main contributor to the intake of both dietary compounds, accounting for aproximately 45 and 69% of pectin and flavanone intake, respectively. The inclusion of both pectins and flavanones, together, in a linear regression model revealed that only flavanone intake persists as a predictor of *C. leptum* levels. Therefore, it seems plausible that the inverse association previously reported for pectins may be actually due to their interaction with flavanones. Although no information is currently available on the effect of flavanones on *Clostridium*, in vitro experiments conducted by other authors have demonstrated the antimicrobial activity of some flavanones and their metabolites.[35,36] This antimicrobial activity may be involved in the inverse association with the levels of *B. coccoides* and *C. leptum* groups observed in the present study.

In terms of food consumption, probably the most novel finding of our study was the positive association between the intake of white bread and *Lactobacillus* levels. This genus has been traditionally considered, together with *Bifidobacteria*, as the target of prebiotic action.[37−39] To date, the prebiotic effect of cereals has been traditionally attributed to whole-grain foods[40,41] because of their high fiber content. However, our results reveal that the consumption of refined grains, often undervalued in this regard, could beneficially modulate intestinal microbiota. These data are of great interest because refined foods are the cereals more consumed in Western societies (white bread consumption in our sample was 105.68 ± 117.06 g/day). Consistent with this, some authors have also found, in human intervention studies, higher levels of *Lactobacillus* in control subjects that had eaten white bread,[42] thus supporting our results. The hemicellulose content in white bread, which represents about 25.8% of total hemicellulose intake in the sample, could be the basis of the prebiotic effect observed in our study, being consistent with the direct association found between this type of fiber and *Lactobacillus*. In this sense, previous results have demonstrated the ability of arabinoxylans, one of the main cereal hemicelluloses, to positively modulate some beneficial intestinal bacterial groups.[43,44] Moreover, other components present in white bread could underlie this association, as is the case of resistant starch, directly associated with *Lactobacillus* levels. However, it is important to consider that determining the amount of this compound originating from foods is difficult, because it depends on several factors that are not well standardized in nutritional studies, such as food structure and processing, as well as consumer-related factors, such as mastication.[24] Also, it might be possible that the association between white bread and *Lactobacillus* could be mediated by other foods usually consumed with bread, although we have not found such an association between any of these foodstuffs and *Lactobacillus* in our study (data not shown). The association found between the intake of pasta and *B. coccoides* levels is noteworthy, because the amount of this foodstuff in the diet of the participants is low (9.62 ± 7.92 g/day) and provides only 2% of total resistant starch intake. Nevertheless, our results could be due to the high content of resistant starch in pasta, being one of its main sources in countries where this food is more frequently consumed.[45]

Finally, the lack of effect of polyphenol and fiber intake on the fecal levels of other microorganisms, such as *Bacteroides* group, including *Prevotella* or *Bifidobacterium*, evidenced in our work, does not support the associations previously reported in intervention studies.[46,47] At this point, it should be considered that the intake of polyphenols in our sample could be insufficient to influence certain members of the intestinal microbiota and that the mean fiber intake of this study is below the recommended value of 16−24 g/day for nonstarch polysaccharides,[48] 47.4% of the sample being under the acceptable intake of fiber. Some factors related to the content of fibers and polyphenols in foods (plant variety, degree of maturity, or cooking, storage, and processing practices) are not considered in food composition tables and, consequently, are not taken into account in nutritional studies. Also, polyphenols are compounds showing a high variability in their bioavailability, strongly influenced by factors such as food matrix, food processing, and microbial metabolism. In addition, although the limited sample size and high interindividual variability do not allow firm conclusions to be established, our study highlights the complex diet−microbiota interactions and the importance of considering the diet as a whole, rather than isolated components, on such interactions.

In conclusion, our results provide further evidence regarding the relationship between components of a regular diet and fecal

microbiota in healthy adults. The identification of an association between the intake of regular foods, such as oranges or white bread, and certain microbial groups emphasizes the requirement of future research focused on diet rather than on isolated compounds.

AUTHOR INFORMATION

Corresponding Author

*(S.G.) Phone: +34 985 10 42 09. Fax: +34 985 10 35 34. E-mail: soniagsolares@uniovi.es.

Funding

This work was funded by Biopolis SL. within the framework of the e-CENIT Project SENIFOOD from the Spanish Ministry of Science and Innovation.

Notes

The authors declare no competing financial interest.

ACKNOWLEDGMENTS

We express our greatest gratitude to all of the volunteers participating in the study.

ABBREVIATIONS USED

CE, capillary electrophoresis; FFQ, food frequency questionnaire; GC, gas chromatography; HPLC, high-performance liquid chromatography; PCR, polymerase chain reaction

REFERENCES

(1) Eckburg, P. B.; Bik, E. M.; Bernstein, C. N.; Purdom, E.; Dethlefsen, L.; Sargent, M.; Gill, S. R.; Nelson, K. E.; Relman, D. A. Diversity of the human intestinal microbial flora. *Science* **2005**, *308*, 1635−1638.

(2) Yatsunenko, T.; Rey, F. E.; Manary, M. J.; Trehan, I.; Dominguez-Bello, M. G.; Contreras, M.; Magris, M.; Hidalgo, G.; Baldassano, R. N.; Anokhin, A. P.; Heath, A. C.; Warner, B.; Reeder, J.; Kuczynski, J.; Caporaso, J. G.; Lozupone, C. A.; Lauber, C.; Clemente, J. C.; Knights, D.; Knight, R.; Gordon, J. I. Human gut microbiome viewed across age and geography. *Nature* **2012**, *486*, 222−227.

(3) Bosscher, D.; Breynaert, A.; Pieters, L.; Hermans, N. Food-based strategies to modulate the composition of the intestinal microbiota and their associated health effects. *J. Physiol. Pharmacol.* **2009**, *60*, 5−11.

(4) Khan, M. T.; Duncan, S. H.; Stams, A. J.; van Dijl, J. M.; Flint, H. J.; Harmsen, H. J. The gut anaerobe *Faecalibacterium prausnitzii* uses an extracellular electron shuttle to grow at oxic-anoxic interphases. *ISME J.* **2012**, *6*, 1578−1585.

(5) Sokol, H.; Pigneur, B.; Watterlot, L.; Lakhdari, O.; Bermudez-Humaran, L. G.; Gratadoux, J. J.; Blugeon, S.; Bridonneau, C.; Furet, J. P.; Corthier, G.; Grangette, C.; Vasquez, N.; Pochart, P.; Trugnan, G.; Thomas, G.; Blottiere, H. M.; Dore, J.; Marteau, P.; Seksik, P.; Langella, P. *Faecalibacterium prausnitzii* is an anti-inflammatory commensal bacterium identified by gut microbiota analysis of Crohn disease patients. *Proc. Natl. Acad. Sci. U.S.A.* **2008**, *105*, 16731−16736.

(6) Cuervo, A.; Arboleya, S.; Gueimonde, M.; González, S. Microbiota modulation by diet in humans. Prebiotics, fibres and other compounds. *Agro Food Ind. Hi-Tech* **2012**, *23*, 23−26.

(7) Petry, N.; Egli, I.; Chassard, C.; Lacroix, C.; Hurrell, R. Inulin modifies the bifidobacteria population, fecal lactate concentration, and fecal pH but does not influence iron absorption in women with low iron status. *Am. J. Clin. Nutr.* **2012**, *96*, 325−331.

(8) Yang, J.; Martinez, I.; Walter, J.; Keshavarzian, A.; Rose, D.J. *In vitro* characterization of the impact of selected dietary fibers on fecal microbiota composition and short chain fatty acid production. *Anaerobe* **2013**, *23*, 74−81.

(9) Yen, C. H.; Kuo, Y. W.; Tseng, Y. H.; Lee, M. C.; Chen, H. L. Beneficial effects of fructo-oligosaccharides supplementation on fecal bifidobacteria and index of peroxidation status in constipated nursing-home residents − a placebo-controlled, diet-controlled trial. *Nutrition* **2011**, *27*, 323−328.

(10) Clavel, T.; Fallani, M.; Lepage, P.; Levenez, F.; Mathey, J.; Rochet, V.; Serezat, M.; Sutren, M.; Henderson, G.; Bennetau-Pelissero, C.; Tondu, F.; Blaut, M.; Dore, J.; Coxam, V. Isoflavones and functional foods alter the dominant intestinal microbiota in postmenopausal women. *J. Nutr.* **2005**, *135*, 2786−2792.

(11) Tzounis, X.; Vulevic, J.; Kuhnle, G. G.; George, T.; Leonczak, J.; Gibson, G. R.; Kwik-Uribe, C.; Spencer, J. P. Flavanol monomer-induced changes to the human faecal microflora. *Br. J. Nutr.* **2008**, *99*, 782−792.

(12) Hervert-Hernández, D.; Goni, I. Dietary polyphenols and human gut microbiota: a review. *Food Rev. Int.* **2011**, *27*, 154−169.

(13) Queipo-Ortuño, M. I.; Boto-Ordoñez, M.; Murri, M.; Gómez-Zumaquero, J. M.; Clemente-Postigo, M.; Estruch, R.; Cardona, D. F.; Andres-Lacueva, C.; Tinahones, F. J. Influence of red wine polyphenols and ethanol on the gut microbiota ecology and biochemical biomarkers. *Am. J. Clin. Nutr.* **2012**, *95*, 1323−1334.

(14) Lee, H. C.; Jenner, A. M.; Low, C. S.; Lee, Y. K. Effect of tea phenolics and their aromatic fecal bacterial metabolites on intestinal microbiota. *Res. Microbiol.* **2006**, *157*, 876−884.

(15) Massot-Cladera, M.; Pérez-Berezo, T.; Franch, A.; Castell, M.; Pérez-Cano, F. J. Cocoa modulatory effect on rat faecal microbiota and colonic crosstalk. *Arch. Biochem. Biophys.* **2012**, *527*, 105−112.

(16) Guglielmetti, S.; Fracassetti, D.; Taverniti, V.; Del Bo, C.; Vendrame, S.; Klimis-Zacas, D.; Arioli, S.; Riso, P.; Porrini, M. Differential modulation of human intestinal *Bifidobacterium* populations after consumption of a wild blueberry (*Vaccinium angustifolium*) drink. *J. Agric. Food Chem.* **2013**, *61*, 8134−8140.

(17) Vendrame, S.; Guglielmetti, S.; Riso, P.; Arioli, S.; Klimis-Zacas, D.; Porrini, M. Six-week consumption of a wild blueberry powder drink increases bifidobacteria in the human gut. *J. Agric. Food Chem.* **2011**, *59*, 12815−12820.

(18) Tabernero, M.; Venema, K.; Maathuis, A. J.; Saura-Calixto, F. D. Metabolite production during in vitro colonic fermentation of dietary fiber: analysis and comparison of two European diets. *J. Agric. Food Chem.* **2011**, *59*, 8968−8975.

(19) Cuervo, A.; Salazar, N.; Ruas-Madiedo, P.; Gueimonde, M.; González, S. Fibers from regular diet are directly associated with fecal shor-chain fatty acid concentrations in the elderly. *Nutr. Res. (N.Y.)* **2013**, *33*, 811−816.

(20) Centro de Enseñanza Superior de Nutrición Humana y Dietética (CESNID). *Tablas de Composición de Alimentos por Medidas Caseras de Consumo Habitual en España*; McGraw-Hill, Publicaciones y Ediciones de la Universidad de Barcelona: Barcelona, Spain, 2008.

(21) Marlett, J. A.; Cheung, T. F. Database and quick methods of assessing typical dietary fiber intakes using data for 228 commonly consumed foods. *J. Am. Diet. Assoc.* **1997**, *97*, 1139−1151.

(22) Theander, O.; Westerlund, E. A. Studies on dietary fiber, 3: improved procedures for analysis of dietary fiber. *J. Agric. Food Chem.* **1986**, *34*, 330−336.

(23) Saeman, J. F. Kinetics of wood saccharification: hydrolysis of cellulose and decomposition of sugars in dilute acid at high temperature. *Ind. Eng. Chem.* **1945**, *37*, 43−52.

(24) Roberts, J.; Jones, G. P.; Rutsihauser, I.; Birkett, A.; Gibbons, C. Resistant starch in the Australian diet. *Nutr. Diet.* **2004**, *61*, 98−104.

(25) Neveu, V.; Perez-Jiménez, J.; Vos, F.; Crespy, V.; du Chaffaut, L.; Mennen, L.; Knox, C.; Eisner, R.; Cruz, J.; Wishart, D.; Scalbert, A. Phenol-Explorer: an online comprehensive database on polyphenol contents in foods. *Database (Oxford)* **2010**, bap024.

(26) Gueimonde, M.; Tölkkö, S.; Korpimäki, T.; Salminen, S. New realtime quantitative PCR procedure for quantification of bifidobacteria in human fecal samples. *Appl. Environ. Microbiol.* **2004**, *70*, 4165−4169.

(27) Salazar, N.; López, P.; Valdés, L.; Margolles, A.; Suárez, A.; Patterson, A. M.; Cuervo, A.; de los Reyes-Gavilán, C. G.; Ruas-Madiedo, P.; González, S.; Gueimonde, M. Microbial targets for the development of functional foods accordingly with nutritional and immune parameters altered in the elderly. *J. Am. Coll. Nutr.* **2013**, *32*, 399−406.

(28) Shinohara, K.; Ohashi, Y.; Kawasumi, K.; Terada, A.; Fujisawa, T. Effect of apple intake on fecal microbiota and metabolites in humans. *Anaerobe* **2010**, *16*, 510−515.
(29) Borges, G.; Lean, M. E.; Roberts, S. A.; Crozier, A. Bioavailability of dietary (poly)phenols: a study with ileostomists to discriminate between absorption in small and large intestine. *Food Funct.* **2013**, *4*, 754−762.
(30) Baker, R.; Cameron, R. Clouds of citrus juice and juice drink. *Food Technol.* **1999**, *53*, 64−69.
(31) Gil-Izquierdo, A.; Gil, M. I.; Ferreres, F.; Tomas-Barberan, F. A. In vitro availability of flavonoids and other phenolics in orange juice. *J. Agric. Food Chem.* **2001**, *49*, 1035−1041.
(32) Arranz, S.; Silvan, J. M.; Saura-Calixto, F. Nonextractable polyphenols, usually ignored, are the major part of dietary polyphenols: a study on the Spanish diet. *Mol. Nutr. Food Res.* **2010**, *54*, 1646−1658.
(33) Mainai, G.; Periago, M. J.; Catasta, G.; Toti, E.; Goñi, I.; Bysted, A.; Granado-Lorencio, F.; Olmedilla, B.; Knuthsen, P.; Valoti, M.; Böhm, V.; Mayer, E.; Behsnilian, D.; Schelemer, U. Carotenoids: actual knowledge on food sources, intakes, stability and bioavailability and their protective role in humans. *Mol. Nutr. Food Res.* **2009**, *53*, 194−218.
(34) Saura-Calixto, F. Dietary fiber as a carrier of dietary antioxidants: an essential physiological function. *J. Agric. Food Chem.* **2011**, *59*, 43−49.
(35) Celiz, G.; Audisio, M. C.; Daz, M. Antimicrobial properties of prunin, a citric flavanone glucoside, and its prunin 6″-*O*-lauroyl ester. *J. Appl. Microbiol.* **2010**, *109*, 1450−1457.
(36) Mazimba, O.; Masesane, I. B.; Majinda, R. R. A flavanone and antimicrobial activities of the constituents of extracts from *Mundulea sericea*. *Nat. Prod. Res.* **2012**, *26*, 1817−1823.
(37) Christensen, H. R.; Frokiaer, H.; Pestka, J. J. Lactobacilli differentially modulate expression of cytokines and maturation surface markers in murine dendritic cells. *J. Immunol.* **2002**, *168*, 171−178.
(38) Hedin, C.; Whelan, K.; Lindsay, J. O. Evidence for the use of probiotics and prebiotics in inflammatory bowel disease: a review of clinical trials. *Proc. Nutr. Soc.* **2007**, *66*, 307−315.
(39) Rafter, J.; Bennett, M.; Caderni, G.; Clune, Y.; Hughes, R.; Karlsson, P. C.; Klinder, A.; O'Riordan, M.; O'Sullivan, G. C.; Pool-Zobel, B.; Rechkemmer, G.; Roller, M.; Rowland, I.; Salvadori, M.; Thijs, H.; Van Loo, J.; Watzl, B.; Collins, J. K. Dietary synbiotics reduce cancer risk factors in polypectomized and colon cancer patients. *Am. J. Clin. Nutr.* **2007**, *85*, 488−496.
(40) Costabile, A.; Klinder, A.; Fava, F.; Napolitano, A.; Fogliano, V.; Leonard, C.; Gibson, G. R.; Tuohy, K. M. Whole-grain wheat breakfast cereal has a prebiotic effect on the human gut microbiota: a double-blind, placebo-controlled, crossover study. *Br. J. Nutr.* **2008**, *99*, 110−120.
(41) Langkamp-Henken, B.; Nieves, C., Jr.; Culpepper, T.; Radford, A.; Girard, S. A.; Hughes, C.; Christman, M. C.; Mai, V.; Dahl, W. J.; Boileau, T.; Jonnalagadda, S. S.; Thielecke, F. Fecal lactic acid bacteria increased in adolescents randomized to whole-grain but not refined-grain foods, whereas inflammatory cytokine production decreased equally with both interventions. *J. Nutr.* **2012**, *142*, 2025−2032.
(42) Walton, G. E.; Lu, C.; Trogh, I.; Arnaut, F.; Gibson, G. R. A randomised, double-blind, placebo controlled cross-over study to determine the gastrointestinal effects of consumption of arabinoxylan-oligosaccharides enriched bread in healthy volunteers. *Nutr. J.* **2012**, *11*, 36.
(43) Neyrinck, A. M.; Possemiers, S.; Druart, C.; Van de Wiele, T.; De Backer, F.; Cani, P. D.; Larondelle, Y.; Delzenne, N. M. Prebiotic effects of wheat arabinoxylan related to the increase in bifidobacteria, *Roseburia* and *Bacteroides/Prevotella* in diet-induced obese mice. *PLoS One* **2011**, *6*, No. e20944.
(44) Van den Abbeele, P.; Gerard, P.; Rabot, S.; Bruneau, A.; El Aidy, S.; Derrien, M.; Kleerebezem, M.; Zoetendal, E. G.; Smidt, H.; Verstraete, W.; Van de Wiele, T.; Possemiers, S. Arabinoxylans and inulin differentially modulate the mucosal and luminal gut microbiota and mucin-degradation in humanized rats. *Environ. Microbiol.* **2011**, *13*, 2667−2680.
(45) Brighenti, F.; Casiraghi, M. C.; Baggio, C. Resistant starch in the Italian diet. *Br. J. Nutr.* **1998**, *80*, 333−341.
(46) Jung, C. M.; Heinze, T. M.; Schnackenberg, L. K.; Mullis, L. B.; Elkins, S. A.; Elkins, C. A.; Steele, R. S.; Sutherland, J. B. Interaction of dietary resveratrol with animal-associated bacteria. *FEMS Microbiol. Lett.* **2009**, *297*, 266−273.
(47) Rodríguez Vaquero, M. J.; Alberto, M. R.; Manca de Nadra, M. C. Antibacterial effect of phenolic compounds from different wines. *Food Control* **2007**, *18*, 93−101.
(48) Nishida, C.; Uauy, P.; Kumanyika, S. The Joint WHO/FAO Expert Consultation on diet, nutrition and prevention of chronic diseases: process, product and policy. *Public Health Nutr.* **2004**, *7*, 245−250.

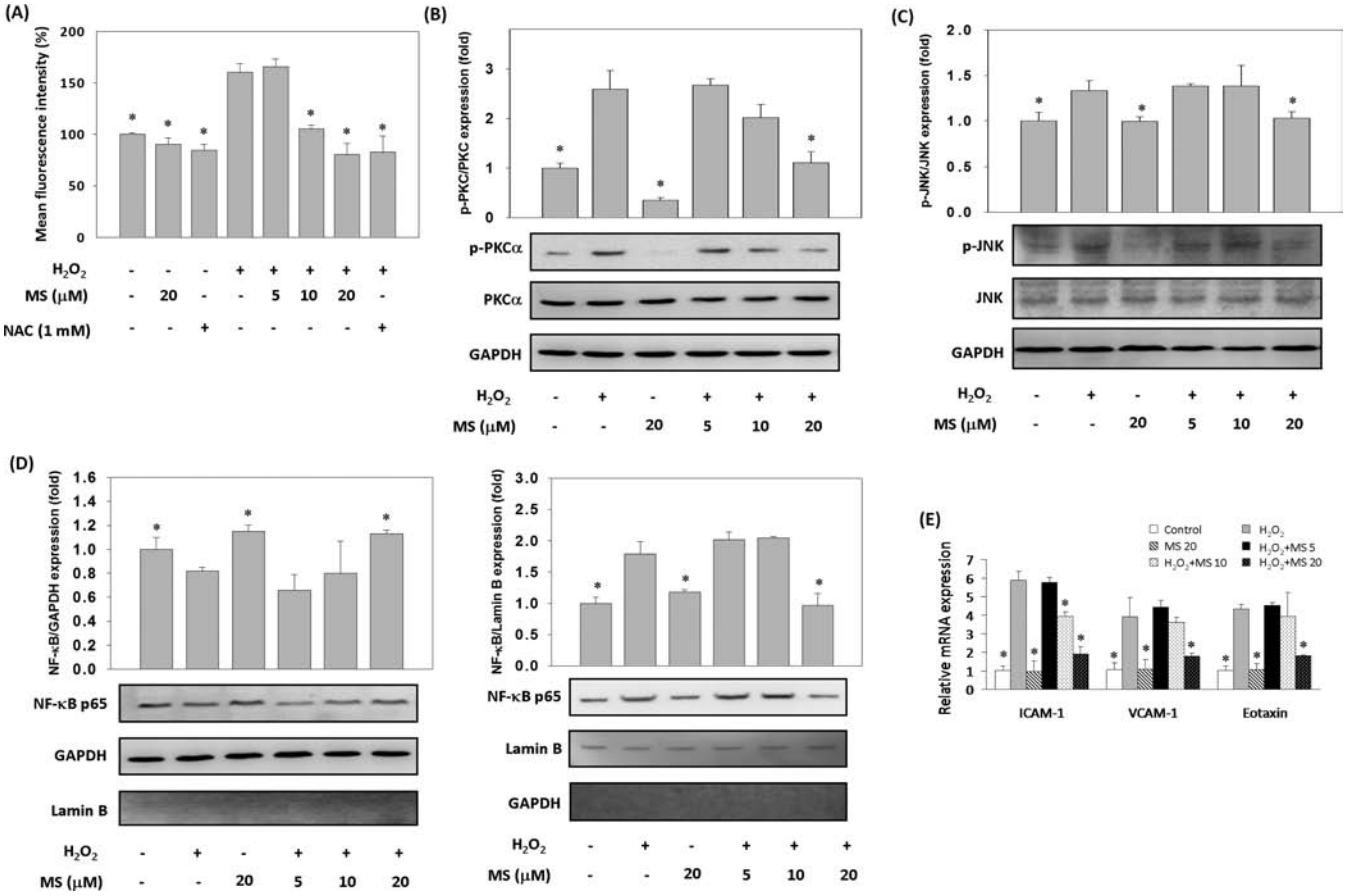

Figure 1. MS attenuated H_2O_2-induced lung oxidative damage in airway epithelial cells. A549 cells were treated with H_2O_2 and different concentrations of MS for 12 h. (A) Effect of H_2O_2 and/or MS on intracellular ROS levels in A549 cells. MS significantly attenuated H_2O_2-mediated ROS generation. (B–D) Western blot analysis of protein extracts obtained from A549 cells. Cells were lysed and immunoblotted with antibodies against (B) phosphorylated-PKC, (C) phosphorylated-JNK, (D) cytosol NF-κB, and nuclear NF-κB. Each protein was normalized with total (B) PKC, (C) JNK, (D) GAPDH, and Lamin B. MS reduced PKC and JNK phosphorylation as well as NF-κB translocation caused by H_2O_2. (E) Real-time PCR analysis of adhesion molecules expression in cells. GAPDH was used as a control. MS decreased ICAM-1, VCAM-1, and eotaxin mRNA expression induced by H_2O_2. Results are expressed as the mean ± SD ($n = 3$). (∗) Significantly different from the H_2O_2 treatment alone group at $p < 0.05$. H_2O_2, hydrogen peroxide (400 μM); MS, monascin; NAC, *N*-acetylcysteine (1 mM); ROS, reactive oxygen species; PKC, protein kinase C; JNK, c-Jun NH_2-terminal kinase; NF-κB, nuclear factor-κB; ICAM-1, intercellular adhesion molecule-1; VCAM-1, vascular cell adhesion molecule-1.

ties, MS may have potential to improve lung inflammation by regulating the oxidative stress pathway.

MATERIALS AND METHODS

Chemicals and Reagents. 2,7-Dichlorodihydrofluorescein diacetate (DCFH-DA), D-glucose, hydrogen peroxide (H_2O_2), *N*-acetylcysteine (NAC), *tert*-butylhydroquinone (tBHQ), and trypsin were purchased from Sigma Chemical Co. (St. Louis, MO, USA). Fetal bovine serum (FBS) was purchased from Life Technologies (Carlsbad, CA, USA). Dimethyl sulfoxide (DMSO) was purchased from Wako Pure Chemical Industries (Saitama, Japan). Ham's F-12K medium was purchased from HyClone Laboratories (Logan, UT, USA). Sodium dodecyl sulfate (SDS) was purchased from Merck (Darmstadt, Germany). The Bio-Rad protein assay dye was from Bio-Rad Laboratories (Hercules, CA, USA). PPAR-γ antagonist GW9662 was purchased from Cayman Chemical Co. (Ann Arbor, MI, USA).

Monascin Purification. MS (Supporting Information Supplemental Figure 1) was obtained as previously described,[14] which was identified by nuclear magnetic resonance (NMR, Varian Gemini, 200 MHz, FT-NMR, Varian Inc., Palo Alto, CA, USA) and electrospray ionization-mass spectrometry (ESI-MS, FinniganMAT LCQ, Thermo Electron Co., Waltham, MA, USA) analysis.

Cell Culture. Human lung adenocarcinoma epithelial cell line A549 was obtained from the Bioresource Collection and Research Center (BCRC 60430; Food Industry Research and Development Institute, Hsinchu, Taiwan). Cells were maintained in Ham's F-12K medium supplemented with 10% FBS, streptomycin (100 mg/mL), and penicillin (100 U/mL) in a 5% CO_2 incubator at 37 °C. All experiments were performed when cells were 80–90% confluent.

Determination of ROS Level. The assay for oxidative stress was monitored by the measurement of ROS.[10] A549 cells were collected and stained with 10 μM DCFH-DA prior to incubation for 30 min at 37 °C. ROS level was analyzed by FACS (Becton-Dickinson Lmmunocytometery Systems, San Jose, CA, USA).

Immunoblot Analysis. A549 cells were lysed, and the cell lysates were centrifuged (10000*g* for 10 min) to recover the supernatant. The supernatant was taken as the cell extract. The protein concentration in the cell extract was 50 μg and was determined using a Bio-Rad protein assay kit. The samples were subjected to 10% SDS–polyacrylamide gel electrophoresis (PAGE). The protein spots were electrotransferred to a polyvinyldiene difluoride (PVDF) membrane. The membrane was incubated with block buffer and then probed with primary antibody overnight at 4 °C. The membrane was washed and shaken in a solution of HRP-linked anti-rabbit IgG secondary antibody. The expressions of proteins were detected by enhanced chemiluminescent (ECL) reagent (Millipore, Billerica, MA, USA).

Nuclear and Cytosol Protein Extraction. Cells were collected for nuclear protein extraction according to the fractionation kit protocol supplied from BioVision (Mountain View, CA, USA). Briefly,

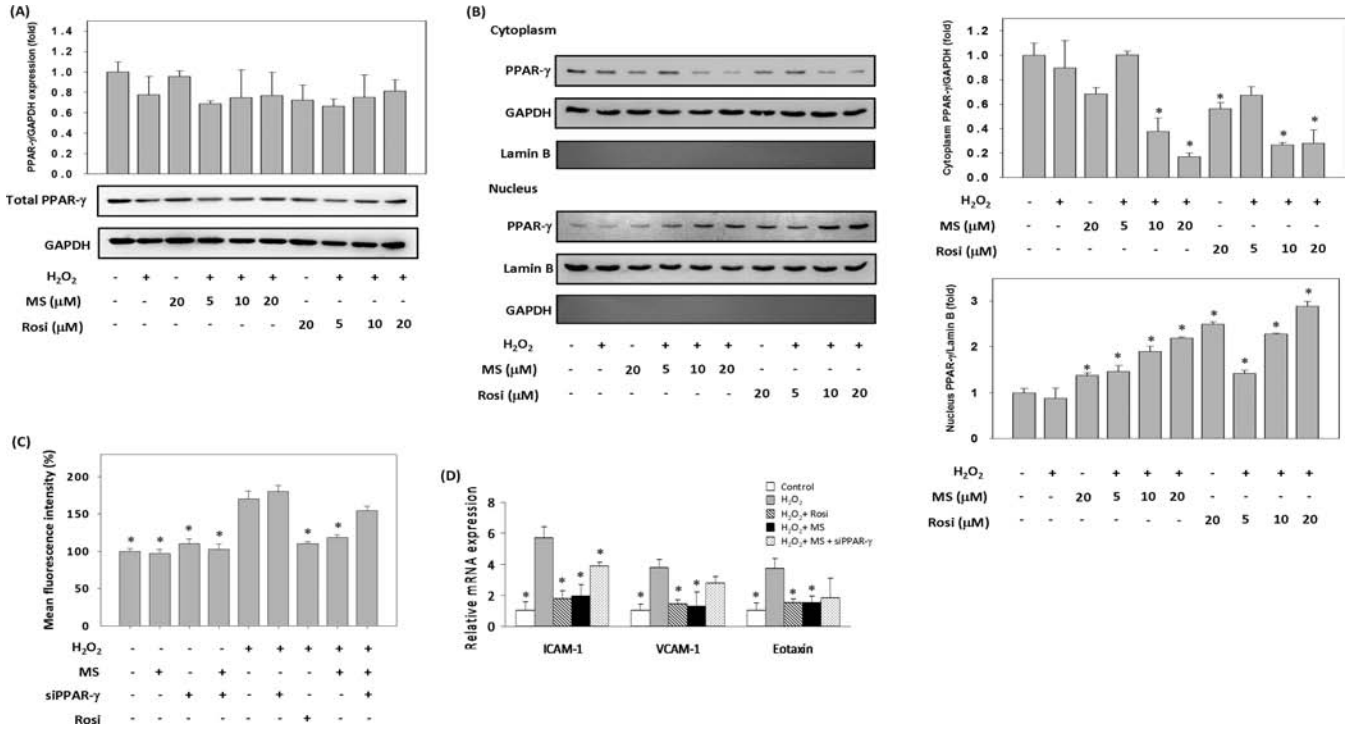

Figure 2. MS ameliorated lung oxidative and inflammatory injury through PPAR-γ regulation in airway epithelial cells. A549 cells were treated with H_2O_2 and different concentrations of MS for 12 h. (A, B) Western blot analysis of protein extracts obtained from A549 cells. Each protein was normalized with GAPDH or Lamin B. MS elevated PPAR-γ expression and promoted PPAR-γ translocation from cytoplasm to the nucleus. (C) Intracellular ROS levels in A549 cells. MS and Rosi significantly reduced H_2O_2-mediated ROS generation, whereas ROS level was restored by siPPAR-γ. (D) Real-time PCR analysis of adhesion molecules expression in cells. GAPDH was used as a control. The inhibitory effect of MS on adhesion molecules expression was abolished by siPPAR-γ. Results are expressed as the mean ± SD (n = 3). (∗) Significantly different from the H_2O_2 treatment alone group at $p < 0.05$. H_2O_2, hydrogen peroxide (400 μM); MS, monascin (20 μM); Rosi, rosiglitazone (20 μM); siPPAR-γ, siRNA against PPAR-γ (50 nM); ICAM-1, intercellular adhesion molecule-1; VCAM-1, vascular cell adhesion molecule-1.

cells were harvested and added to 200 μL of cytosol extraction buffer containing dithiothreitol (DTT) and protease inhibitors. After vortexing and 10 min of incubation on ice, the extracts were centrifuged at 16000g for 5 min at 4 °C, and the supernatant was removed to separate the cytoplasmic fraction from nuclei. The nuclei pellets were then further added to 100 μL of nuclei extraction buffer, vortexed, and set on ice every 10 min for 40 min. After centrifuging, the supernatant nuclear extracts were stored at −80 °C for future use. The protein concentration of the cell extract was determined using a Bio-Rad protein assay kit.

RNA Preparation and Real-Time PCR. Total RNA was isolated using Trizol (Life Technologies) according to the manufacturer's instructions. cDNA from 3 μg of RNA was generated using a SuperScript III First-Strand Synthesis System for RT-PCR (Life Technologies) according to the manufacturer's instructions. The reverse transcription product was diluted in water, and a volume corresponding to 30 ng of original RNA was used for real-time PCR. Real-time PCR amplification and detection were performed using the SYBR Green qPCR SuperMix-UDG with ROX (Life Technologies) in a fluorescence thermal cycler (StepOne Real-Time PCR System, Life Technologies) according to the manufacturer's protocol. All amplifications were conducted within the linear range of the assay, normalized to respective GAPDH levels using SPSS version 17.0 (SPSS Institute, Inc., Chicago, IL, USA).

Transfection of Cells with Small Interfering RNA (siRNA). PPAR-γ and Nrf-2 siRNA were purchased from Santa Cruz Biotechnology Inc. (Burlingame, CA, USA), and specific siRNA was transfected into A549 cells by lipofectamine RNAiMAX reagent (Invitrogen, Carlsbad, CA, USA).

PPAR-γ and Nrf-2 Luciferase Assay. The specific PPAR-γ reporter assay was carried out in A549 cells according to the previous study.[19] The plasmid was designed by Blossom Biotechnologies Inc. (Taipei, Taiwan). In addition, we used a DNA fragment containing three copies of the ARE4 elements from the GCL gene (5′-CCC GTG ACT CAG CGC TCC GTG ACT CAG CGC TCC GTG ACT CAG CGC T-3′), which was subcloned into a pGL3-promoter vector to construct pGL3-ARE4-Luc. A549 cells were transiently transfected with a DNA mixture containing 2 μg of pGL3-ARE4-Luc and 0.5 μg of control plasmid pRL-TK (Promega, Madison, WI, USA) using the lipofectamine-2000 transfection reagent in serum-free medium (Invitrogen). After treatment with samples for various times, luciferase activity was conducted utilizing the Dual-Luciferase Reporter Assay System (Promega). Luciferase activity of pRL-TK was used to normalize the transfection efficiency.

PPAR-γ DNA Binding Assay. Nuclear extracts were prepared from A549 cells by means of a commercially available kit and performed according to the instructions of the manufacturer. The binding activities of the PPAR-γ were measured by using specific transcription factor assay kits (Panomics, Redwood City, CA, USA). Oligonucleotides encoding for the human PPAR-γ consensus binding site were bound to microtiter plates. The binding of activated PPAR-γ-heterodimers, in the prepared nuclear extracts, to the immobilized DNA was revealed by incubation with PPAR-γ specific antibody using ELISA technology. Optical density was determined at 450 nm.

Statistical Analysis. The statistical significance was determined by one-way analysis of variance (ANOVA) using the general linear model procedure of SPSS software (SPSS Institute, Inc.), followed by ANOVA with Duncan's test. The results were considered to be statistically significant if the p value was <0.05. Data are presented as the mean ± SD or SEM.

RESULTS

MS Attenuates Oxidative Stress-Induced Lung Inflammation in A549 Cells. The endogenous levels of ROS in

dx.doi.org/10.1021/jf501373a | J. Agric. Food Chem. 2014, 62, 5337−5344

A549 cells were quantified. We found clear induction of ROS production for 160.2% in the group treated with 400 μM hydrogen peroxide (H_2O_2) compared to the control group, as expected (Figure 1A). MS decreased the ROS level in H_2O_2-induced cells in a dose-dependent manner ($p < 0.05$), whereas MS treatment alone did not influence ROS production. Antioxidant *N*-acetylcysteine (NAC) (1 mM) was used as a positive control group, which reduced the production of ROS to a level similar to that of the control and MS-treated group (Figure 1A).

ROS stimulates phosphorylation of protein kinase C (p-PKC), leading to the activation of NF-κB.[20] ROS and other oxidative stress factors also promote phosphorylation of c-Jun NH_2-terminal kinase (JNK), a member of the mitogen-activated protein kinase (MAPK) family that activates transcription factors such as NF-κB and activator protein (AP)-1.[21] As shown in Figure 1, 400 μM H_2O_2 induced phosphorylation of PKCα (Figure 1B) and JNK (Figure 1C), but this was blocked by treatment with 20 μM MS. Likewise, H_2O_2 activated NF-κB translocation from the cytoplasm to the nucleus; however, treatment with MS prevented the NF-κB translocation (Figure 1D).

Leukocytes are recruited into tissues by adhesion molecules and chemokines. Adhesion molecule expression is induced in the endothelium or epithelium by several mediators, including cytokines or ROS, in a variety of chronic inflammatory conditions.[22] Figure 1E shows that whereas H_2O_2 increased mRNA expression of various adhesion molecules, treatment with 20 μM MS attenuated this effect ($p < 0.05$).

MS Ameliorates Lung Oxidative Inflammation through PPAR-γ Regulation. The mechanism underlying the antioxidative and anti-inflammatory effects of PPAR-γ in multiple tissues has been under investigation. It has been shown that PPAR-γ antagonizes signal transducing kinases and transcriptional regulators such as AP-1, nuclear factor of activated T cell, and NF-κB.[23] PPAR-γ also represses inflammatory mediators such as cytokines, chemokine receptors, and adhesion molecules.[24,25] A known PPAR-γ agonist, rosiglitazone (Rosi), was used as a positive control group. Our results indicate that there was no significant difference for the total PPAR-γ protein level in each group (Figure 2A). After treatment with H_2O_2 and MS/Rosi for 12 h, the translocation of PPAR-γ from the cytoplasm to the nucleus was increased (Figure 2B). Notably, 20 μM MS or Rosi treatment alone also promoted PPAR-γ translocation.

We next determined if there was a relationship between the MS-induced inhibition of ROS generation and adhesion molecule expression and its effect on the expression of PPAR-γ. The PPAR-γ antagonist GW9662 (10 μM) was added to A549 cells treated with H_2O_2 (400 μM) and/or MS/Rosi (20 μM). As previously observed in Figure 1, the H_2O_2-induced ROS generation, JNK and PKCα activation, and increase in adhesion molecule expression were inhibited by MS treatment. However, the inhibitory effect of MS on oxidative damage was abated by addition of the PPAR-γ antagonist (Supporting Information Supplemental Figure 2).

Next, we used siRNA against PPAR-γ (siPPAR-γ) to verify that the regulation of MS during lung oxidative injury was mediated by PPAR-γ. Specific siRNA for PPAR-γ was transfected into A549 cells, and PPAR-γ protein levels were decreased after treatment with siRNA for 48 and 72 h (Supporting Information Supplemental Figure 3). Hence, 48 h was chosen for the further experiments. Our results show that although MS or siPPAR-γ treatment alone did not change the ROS level, both Rosi and MS (20 μM) decreased ROS generation compared to the H_2O_2-induced group, but the ROS level was restored when cells were treated with both MS and siPPAR-γ (Figure 2C). Moreover, the inhibitory effect of MS on adhesion molecule expression was clearly abolished by siPPAR-γ in both mRNA and protein levels (Figure 2D and Supporting Information Supplemental Figure 4). These results provide further evidence indicating that the effect of MS on oxidative damage in epithelial cells was partly mediated by PPAR-γ.

To further elucidate that MS may act as PPAR-γ activator, we first wonder whether MS promotes PPAR-γ activity. The specificity of MS for the PPAR response element (PPRE) sequences was then determined by transfecting A549 cells with the luciferase reporter construct harboring this element. At 24 h following transfection, MS was applied, and enhanced luciferase activity was observed and analyzed. The data presented in Figure 3A clearly indicate that 20 μM MS enhanced luciferase activity at 2.38-fold compared with the control group for 12 h, whereas 20 μM pioglitazone (Pio) and Rosi enhanced the activity at 1.69- and 2.95-fold, respectively ($p < 0.05$).

A DNA binding assay was performed to confirm that MS has the ability to bind to PPAR-γ. We first investigated PPAR-γ expression after MS treatment for 2, 4, 8, and 12 h. After treatment with 20 μM MS for 4 h, the translocation of PPAR-γ from the cytoplasm to the nucleus was increased, with the most prominent translocation at 8 and 12 h of treatment (Supporting Information Supplemental Figure 5). We next examined the effect of MS on the DNA binding activity of PPAR-γ. As shown in panels B and C of Figure 3, treatment with 20 μM MS significantly elevated PPAR-γ binding to DNA at 8 and 12 h after treatment, and 20 μM Rosi clearly elevated PPAR-γ binding to DNA at 4, 8, and 12 h after treatment, whereas 400 μM H_2O_2 decreased the binding activity after 24 h of treatment when compared with the control group. Moreover, MS and Rosi still significantly increased PPAR-γ binding activity in H_2O_2-treated cells at 8 and 12 h.

MS Elevates Nrf-2 Translocation in A549 Cells. The transcription factor Nrf-2 is involved in lung defense against oxidative injury.[12] Nrf-2 plays a critical part in basal activity and coordinated induction of genes encoding heme oxygenase-1 (HO-1).[26] We found that MS accelerated the translocation of Nrf-2 from the cytoplasm to the nucleus in a dose-dependent manner in H_2O_2-induced cells. Moreover, translocation of Nrf-2 to the nucleus was markedly increased in the MS treatment alone group ($p < 0.05$). However, Rosi did not have the ability to promote Nrf-2 translocation. Furthermore, the expression of HO-1, a downstream molecule of Nrf-2, also increased following either MS treatment alone or MS treatment combined with H_2O_2 (Figure 4A,B).

We then investigated Nrf-2 expression after MS treatment for 2, 4, 8, and 12 h. After treatment with 20 μM MS for 4 h, the translocation of Nrf-2 from the cytoplasm to the nucleus was increased, with the most prominent translocation at 8 and 12 h of treatment (Supporting Information Supplemental Figure 6). Figure 4C reveals that 20 μM MS significantly promoted luciferase activity at 1.70-fold compared with the control group at 12 h ($p < 0.05$). However, treatment with Rosi did not enhance luciferase activity compared with the control group. tBHQ was used as a positive control group, which enhanced luciferase activity at 2.11-fold.

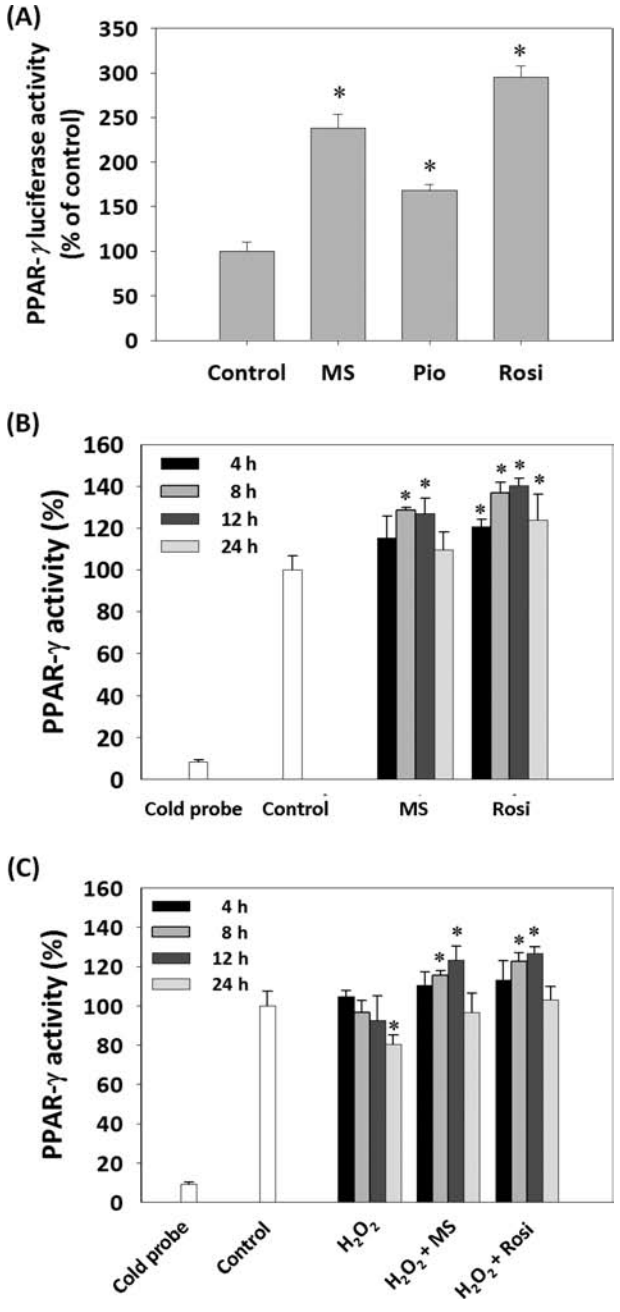

Figure 3. MS promoted PPAR-γ activity in A549 cells. (A) Luciferase assay. The specificity of MS for the PPAR-γ sequences was determined by transfecting A549 cells with the luciferase reporter construct harboring this element. At 24 h following transfection, MS was applied and enhanced luciferase activity was observed and analyzed. MS enhanced luciferase activity at 2.38-fold compared with the control group for 12 h, whereas Pio and Rosi were 1.69- and 2.95-fold, respectively. Pio and Rosi were used as positive control groups. (*) Significantly different from the H_2O_2 treatment alone group at $p < 0.05$. (B, C) DNA binding acitivity. A549 cells were treated with 20 μM of MS alone or combined with H_2O_2 for 4, 8, 12, and 24 h: (B) MS significantly elevated PPAR-γ binding to DNA for 8 and 12 h treatment; (C) H_2O_2 attenuated this binding activity compared to the control group after 24 h of treatment. MS significantly recovered the alleviation of PPAR-γ binding activity caused by H_2O_2 treatment at 8 and 12 h. Results are expressed as the mean ± SEM (n = 3). (*) Significantly different from the control group at $p < 0.05$. MS, monascin (20 μM); Pio, pioglitazone (20 μM); Rosi, rosiglitazone (20 μM); H_2O_2, hydrogen peroxide (400 μM).

DISCUSSION

Lung inflammation is central to the pathogenesis of airway disorders, and oxidative stress has been shown to be related to the pathogenesis of inflammatory lung diseases.[2,3] Oxidative stress is caused by a large variety of free oxygen radicals, including superoxide anion, hydroxyl radicals, and oxygen derivatives such as hydrogen peroxide, hypochlorous acid, peroxynitrite, and ozone; collectively, these are referred to as ROS.[2] ROS are important in the pathogenesis of various lung disorders, such as asthma, chronic obstructive pulmonary disease, and acute lung injury. ROS can beget endothelial barrier dysfunction, with subsequent increased permeability to inflammatory cells.[2,4] Using A549 human lung epithelial cells, we have identified several protein targets involved in modulating the expression of adhesion molecules that are affected by both H_2O_2-induced oxidative stress and MS treatment.

H_2O_2 is one of the most abundant ROS in aerobic biological systems and has been widely used to induce oxidative stress in cellular systems in vitro. H_2O_2 was chosen to induce injury because airway disorder is associated with chronic oxidative stress. In addition, patients with asthma demonstrate increased production of ROS, including H_2O_2, which is released in relatively large amounts by activated leucocytes during the process of lung inflammation in asthma.[27] ROS cause oxidative stress and activate p-PKC, which is a kinase that stimulates the inflammatory cascade, as well as transcription factors such as NF-κB.[20] NF-κB controls many adhesion molecules and cytokines in the epithelium and is an important signaling module for the synthesis of mediators such as cytokines and adhesion molecules in the processes of chronic airways diseases. The expression of these molecules will further amplify inflammation by recruiting monocytes and facilitating their binding to and migration through the endothelium.

In addition to NF-κB activation, JNK is also activated by environmental insults, such as ROS and inflammatory stimuli.[28] JNK regulates the transcription of inflammatory genes, leading to the activation or coactivation of redox-sensitive transcription factors such as NF-κB and AP-1. Activation of JNK is implicated in the synthesis of pro-inflammatory cytokines and plays a role in cellular responses in the pulmonary epithelium. In this study, we found that MS attenuated oxidative stress-induced ROS generation, and we considered that this may be mediated by PKCα and JNK inactivation and reduced the translocation of NF-κB from the cytoplasm to the nucleus (Figure 1), indicating that MS has the potential to protect airway epithelial cells against oxidative injury.

PPARs inhibit the phosphorylation of JNK by interacting with the JNK-responsive region of c-Jun and other transcriptional coactivators such as p65 and cAMP-responsive element-binding protein-binding protein (CBP). Activation of PPARs represses both c-Jun- and p65-induced transcription of the human IL-6 promoter and further suppresses the inflammatory gene response.[29] In the present study, we demonstrated that MS decreased the abundance of adhesion molecules by elevating the expression of PPAR-γ, and this was confirmed using a PPAR-γ antagonist and siRNA against PPAR-γ. Furthermore, luciferase assay and DNA binding activity were used to affirm that the protective effect of MS on epithelial cells may be due to its ability to promote PPAR-γ binding to DNA, thereby enhancing the transcription of anti-inflammatory and antioxidant genes, and inhibition of NF-κB translocation by MS

dx.doi.org/10.1021/jf501373a | J. Agric. Food Chem. 2014, 62, 5337−5344

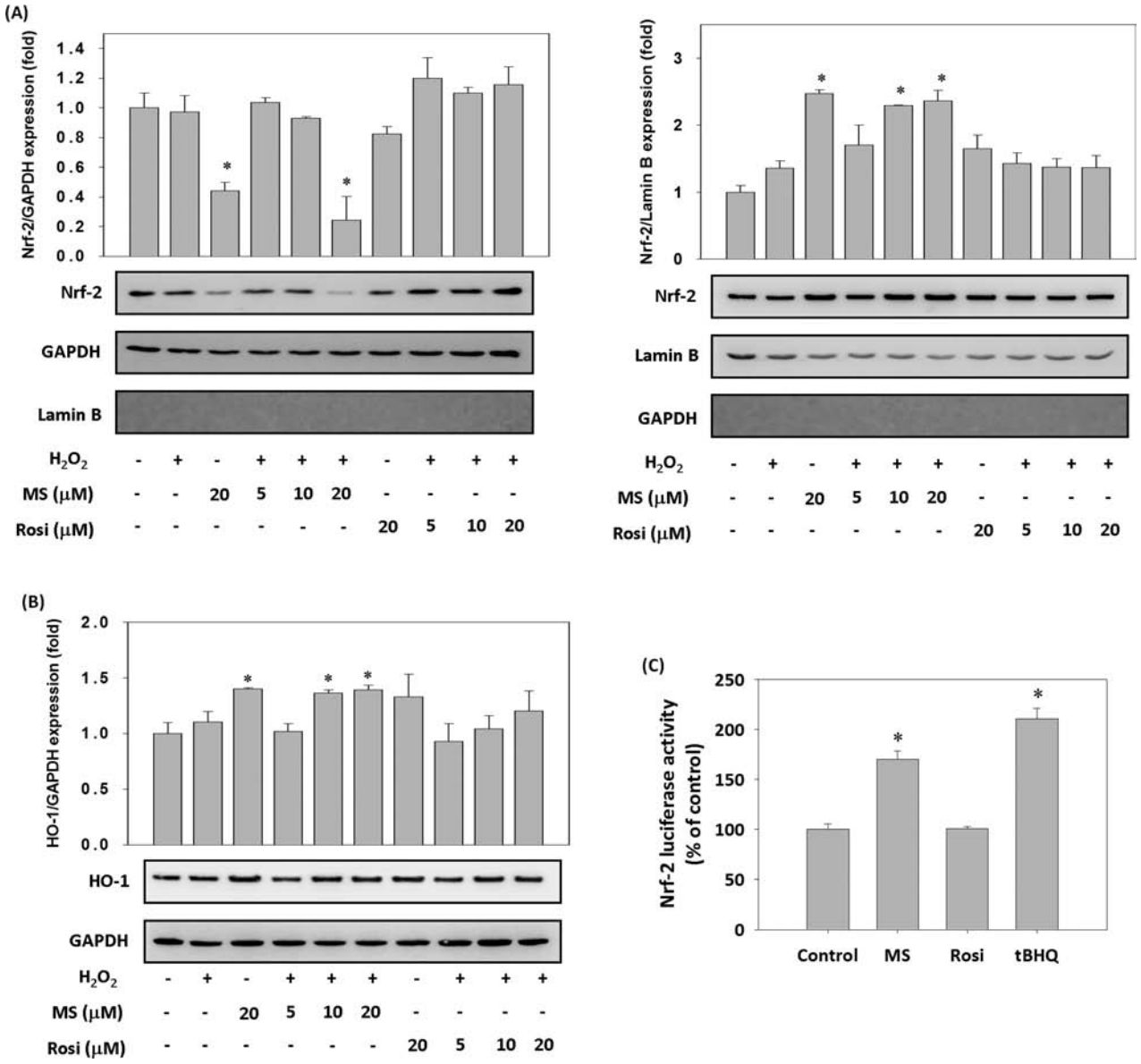

Figure 4. MS activated Nrf-2 in A549 cells. Western blot analysis of Nrf-2 and HO-1 in A549 cells. (A) MS up-regulated Nrf-2 translocation and (B) HO-1 expression. A549 cells were treated with H_2O_2 and different concentrations of MS for 12 h. (∗) Significantly different from the H_2O_2 treatment alone group at $p < 0.05$. (C) Luciferase assay. The specificity of MS for the ARE sequences was determined by transfecting A549 cells with the luciferase reporter construct harboring this element. At 24 h following transfection, MS was applied and enhanced luciferase activity was observed and analyzed. MS enhanced luciferase activity at 1.70-fold compared with the control group for 12 h, whereas Rosi and tBHQ were 1.00- and 2.11-fold, respectively. Results are expressed as the mean ± SEM ($n = 3$). (∗) Significantly different from the control group at $p < 0.05$. H_2O_2, hydrogen peroxide (400 μM); MS, monascin (20 μM); Rosi, rosiglitazone (20 μM); tBHQ, *tert*-butylhydroquinone (50 μM).

may also be involved. Consequently, MS treatment was sufficient to ameliorate the increase in adhesion molecule expression induced by H_2O_2.

PPAR-γ enhances the transcription of anti-inflammatory and antioxidant genes, including Nrf-2. The Nrf-2-mediated cellular antioxidant and anti-inflammatory effects play a crucial role in the defense against oxidative stress. The activation of Nrf-2 and up-regulation of the downstream enzymes provides vascular protection during oxidative stress and inhibits inflammatory responses via suppression of the NF-κB pathway and expression of adhesion molecules such as ICAM-1 and VCAM-1.[30] Our results suggest that MS promoted the translocation of Nrf-2 and increased Nrf-2 activity, thereby elevating the level of the antioxidant HO-1.

Pharmacological agents that enhance lung antioxidant levels have been extensively investigated in airway disease. Some compounds such as phenols, flavonoids, isothiocyanates, diterpenes, and sulforaphane have phenolic hydroxyl groups and have been used to mediate antioxidative gene expression through the ARE either via the disruption of Nrf-2-keap1 complexes or via the activation of the transcriptional complex of Nrf-2.[31] Growing evidence suggests that the activation of Nrf-2 signaling contributes to the health benefits of natural compounds including curcumin, resveratrol, epicatechin, glucoraphanin, and isothiocyanate that have been reported in the treatment of lung,[32] neurological,[33] and cardiovascular diseases.[34] PPAR-γ is also a novel target for chronic inflammatory lung diseases due to its anti-inflammatory

dx.doi.org/10.1021/jf501373a | J. Agric. Food Chem. 2014, 62, 5337−5344

capacity. The above compounds such as resveratrol and curcumin have been demonstrated to prevent lung diseases, obesity, or other metabolic diseases via PPAR-γ activation.[35−39] Our group previously demonstrated that pigment MS derived from *Monascus* increases PPAR-γ mRNA expression and prevents PPAR-γ phosphorylation, thereby increasing the uptake of the deoxyglucose analogue 2-NBDG to exhibit antidiabetic activity in C2C12 myotubes.[40] The primary aim of the current study was to evaluate the therapeutic potential of MS against lung epithelial cell oxidative damage. Our results reveal that MS prevented oxidative stress-induced adhesion molecule expression in epithelial cells through PPAR-γ translocation and inhibited NF-κB translocation, leading to a decrease in the expression of inflammatory mediators. However, this regulatory ability was abolished by PPAR-γ antagonist GW9662 and siRNA against PPAR-γ, implying that MS has the potential to modulate PPAR-γ activity. Our results also indicate that MS elevated antioxidant enzyme expression via Nrf-2 activation. We further demonstrated this hypothesis by using luciferase and a DNA binding assay, which suggest that MS may be a novel PPAR-γ agonist and Nrf-2 activator.

Our research group has previously found that MS could act as a PPAR-γ activator to attenuate carboxymethyllysine-induced fibrosis in hepatic stellate cells[41] and inflammation in monocytes[42] and inhibit Th2 cytokine production in T cells.[43] Moreover, we have shown that MS prevented type 2 diabetes in methylglyoxal-treated Wistar rats via PPAR-γ and Nrf-2 activation.[44] In our data, similarly, MS activated PPAR-γ and Nrf-2 in the lung cells, which means that MS has the ability to improve inflammation- and oxidative stress-associated diseases through PPAR-γ- and/or Nrf-2-dependent pathways. It is worth noting that this is the first study to point out that MS has the ability to bind to PPAR-γ using a DNA binding activity assay.

Our findings hypothesize that MS may act as a novel PPAR-γ agonist to inhibit NF-κB translocation and further avoid adhesion molecules expression, which accelerated immune cells infiltration (Figure 5). MS also activated Nrf-2 and downstream antioxidant enzymes to attenuate lung oxidative inflammation. MS can regulate PPAR-γ and Nrf-2, and therefore MS has a stronger ability in lung protection than rosiglitazone, which is a known synthetic PPAR-γ ligand. Taken together, MS could regulate PPAR-γ and Nrf-2 activities, and both of these two transcription factors are involved in protecting the lung during airway disease. Hence, MS may regulate the oxidative stress pathway to improve lung inflammation.

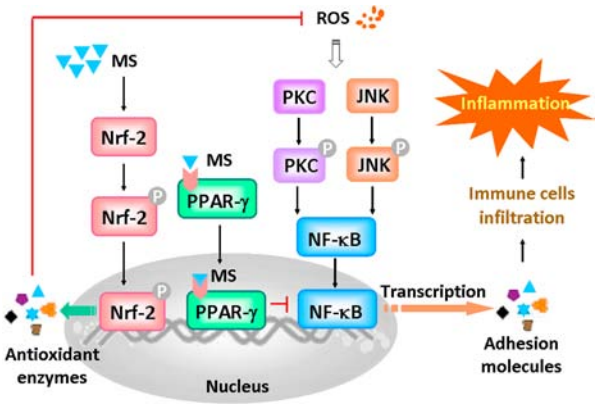

Figure 5. Proposed mechanism of MS-mediated amelioration of oxidative stress-induced lung inflammation. MS prevented oxidative stress-induced lung inflammation in epithelial cells through PPAR-γ translocation, which further inhibited NF-κB translocation and avoided adhesion molecule expression that accelerates immune cell infiltration. MS also activated Nrf-2 via phosphorylation and downstream antioxidant enzymes to attenuate lung oxidative injury.

■ ASSOCIATED CONTENT

Supporting Information

Additional methods and figures. This material is available free of charge via the Internet at http://pubs.acs.org.

■ AUTHOR INFORMATION

Corresponding Author

*(T.-M.P.) Phone: +886-2-33664519, ext. 10. Fax: +886-2-33663838. E-mail: tmpan@ntu.edu.tw.

Funding

We express our gratitude to the National Science Council, ROC, for supporting this research work (NSC101-2313-B-002-060) and subsidiary.

Notes

The authors declare no competing financial interest.

■ REFERENCES

(1) Holgate, S. T. The airway epithelium is central to the pathogenesis of asthma. *Allergol. Int.* **2008**, *57*, 1−10.

(2) Andreadis, A. A.; Hazen, S. L.; Comhair, S. A.; Erzurum, S. C. Oxidative and nitrosative events in asthma. *Free Radical Biol. Med.* **2003**, *35*, 213−225.

(3) Barnes, P. J. New concepts in the pathogenesis of bronchial hyperresponsiveness and asthma. *J. Allergy Clin. Immunol.* **1989**, *83*, 1013−1026.

(4) Rahman, I.; MacNee, W. Oxidative stress and regulation of glutathione in lung inflammation. *Eur. Respir. J.* **2000**, *16*, 534−554.

(5) MacNee, W. Oxidants/antioxidants and COPD. *Chest* **2000**, *117*, 303−317.

(6) Fireman, P. Understanding asthma pathophysiology. *Allergy Asthma Proc.* **2003**, *4*, 79−83.

(7) Kips, J. C. Cytokine in asthma. *Eur. Respir. J. Suppl.* **2001**, *34*, 24−33.

(8) Kensler, T. W.; Wakabayashi, N.; Biswal, S. Cell survival responses to environmental stresses via the keap1-Nrf2-ARE pathway. *Annu. Rev. Pharmacol. Toxicol.* **2007**, *47*, 89−116.

(9) Cho, H. Y.; Reddy, S. P.; Debiase, A.; Yamamoto, M.; Kleeberger, S. R. Gene expression profiling of NRF2-mediated protection against oxidative injury. *Free Radical Biol. Med.* **2005**, *38*, 325−343.

(10) Standiford, T. J.; Keshamouni, V. G.; Reddy, R. C. Peroxisome proliferator-activated receptor-γ as a regulator of lung inflammation and repair. *Proc. Am. Thorac. Soc.* **2005**, *2*, 226−231.

(11) Malur, A.; McCoy, A. J.; Arce, S.; Barna, B. P.; Kavuru, M. S.; Malur, A. G.; Thomassen, M. J. Deletion of PPAR gamma in alveolar macrophages is associated with a Th-1 pulmonary inflammatory response. *J. Immunol.* **2009**, *182*, 5816−5822.

(12) Cho, H. Y.; Gladwell, W.; Wang, X.; Chorley, B.; Bell, D.; Reddy, S. P.; Kleeberger, S. R. Nrf2-regulated PPARγ expression is critical to protection against acute lung injury in mice. *Am. J. Respir. Crit. Care Med.* **2010**, *182*, 170−182.

(13) Su, N. W.; Lin, Y. L.; Lee, M. H.; Ho, C. Y. Ankaflavin from *Monascus* fermented red rice exhibits selective cytotoxic effect and induces cell death on Hep G2 cells. *J. Agric. Food Chem.* **2005**, *53*, 1949−1954.

(14) Akihisa, T.; Tokuda, H.; Yasukawa, K.; Ukiya, M.; Kiyota, A.; Sakamoto, N.; Suzuki, T.; Tanabe, N.; Nishino, H. Azaphilones, furanoisophthalides, and amino acids from the extracts of *Monascus*

pilosus-fermented rice (red-mold rice) and their chemopreventive effects. *J. Agric. Food Chem.* **2005**, *53*, 562−565.
(15) Lin, C. P.; Lin, Y. L.; Huang, P. H.; Tsai, H. S.; Chen, Y. H. Inhibition of endothelial adhesion molecule expression by *Monascus purpureus*-fermented rice metabolites, monacolin K, ankaflavin, and monascin. *J. Sci. Food Agric.* **2011**, *91*, 1751−1758.
(16) Jou, P. C.; Ho, B. Y.; Hsu, Y. W.; Pan, T. M. The effect of *Monascus* secondary polyketide metabolites, monascin and ankaflavin, on adipogenesis and lipolysis activity in 3T3-L1. *J. Agric. Food Chem.* **2010**, *58*, 12703−12709.
(17) Lee, C. L.; Kung, Y. H.; Wu, C. L.; Hsu, Y. W.; Pan, T. M. Monascin and ankaflavin act novel hypolipidemic and high density lipoprotein cholesterol-raising agents in red mold dioscorea. *J. Agric. Food Chem.* **2010**, *58*, 9013−9019.
(18) Hsu, W. H.; Lee, B. H.; Huang, Y. C.; Hsu, Y. W.; Pan, T. M. Ankaflavin and monascin regulate endothelial adhesion molecules and endothelial NO synthase (eNOS) expression induced by tumor necrosis factor-α (TNF-α) in human umbilical vein endothelial cells (HUVECs). *J. Agric. Food Chem.* **2012**, *60*, 1666−1672.
(19) Kimura, H.; Li, X.; Torii, K.; Okada, T.; Takahashi, N.; Fujii, H.; Ishihara, S.; Yoshida, H. A natural PPAR-gamma agonist, 15-deoxy-delta 12,14-prostaglandin J2, may act as an enhancer of PAI-1 in human proximal renal tubular cells under hypoxic and inflammatory conditions. *Nephrol. Dial. Transplant* **2008**, *23*, 2496−2503.
(20) Moscat, J.; Diaz-Meco, M. T.; Rennert, P. NF-κB activation by protein kinase C isoforms and B cell function (review). *EMBO Rep.* **2003**, *4*, 31−36.
(21) Persinger, R. L.; Poynter, M. E.; Ckless, K.; Janssen-Heininger, Y. M. Molecular mechanisms of nitrogen dioxide induced epithelial injury in the lung. *Mol. Cell. Biochem.* **2002**, *234*−*235*, 71−80.
(22) Cassie, S.; Masterson, M. F.; Polukoshko, A.; Viskovic, M. M.; Tibbles, L. A. Ischemia/reperfusion induces the recruitment of leukocytes from whole blood under flow conditions. *Free Radical Biol. Med.* **2004**, *36*, 1102−1111.
(23) Su, C. G.; Wen, X.; Bailey, S. T.; Jiang, W.; Rangwala, S. M.; Keilbaugh, S. A.; Flanigan, A.; Murthy, S.; Lazar, M. A.; Wu, G. D. A novel therapy for colitis utilizing PPAR-gamma ligands to inhibit the epithelial inflammatory response. *J. Clin. Invest.* **1999**, *104*, 383−389.
(24) Crosby, M. B.; Svenson, J.; Gilkeson, G. S.; Nowling, T. K. A novel PPAR response element in the murine iNOS promoter. *Mol. Immunol.* **2005**, *42*, 1303−1310.
(25) Dubuquoy, L.; Bourdon, C.; Peuchmaur, M.; Leibowitz, M. D.; Nutten, S.; Colombel, J. F.; Auwerx, J.; Desreumaux, P. Peroxisome proliferator activated receptor (PPAR) gamma: a new target for the treatment of inflammatory bowel disease. *Gastroenterol. Clin. Biol.* **2000**, *24*, 719−724.
(26) Li, W.; Khor, T. O.; Xu, C.; Shen, G.; Jeong, W. S.; Yu, S.; Kong, A. N. Activation of Nrf2-antioxidant signaling attenuates NF-κB-inflammatory response and elicits apoptosis. *Biochem. Pharmacol.* **2008**, *76*, 1485−1489.
(27) Chin, J. E.; Hatfield, C. A.; Winterrowd, G. E.; Brashler, J. R.; Vonderfecht, S. L.; Fidler, S. F.; Griffin, R. L.; Kolbasa, K. P.; Krzesicki, R. F.; Sly, L. M.; Staite, N. D.; Richards, I. M. Airway recruitment of leukocytes in mice is dependent on α4-integrins and vascular cell adhesion molecule-1. *Am. J. Physiol. Lung Cell Mol. Physiol.* **1997**, *272*, 219−229.
(28) Davis, R. J. Signal transduction by the JNK group of MAP kinases. *Cell* **2000**, *103*, 239−252.
(29) Delerive, P.; De Boscher, K.; Besnard, S.; Vanden Berghe, W.; Peters, J. M.; Gonzalez, F. J.; Fruchart, J. C.; Tedgui, A.; Haegeman, G.; Staels, B. Peroxisome proliferator-activated receptor a negatively regulates the vascular inflammatory gene response by negative cross-talk with transcription factors NF-κB and AP-1. *J. Biol. Chem.* **1999**, *274*, 32048−32054.
(30) Hurttila, H.; Koponen, J. K.; Kansanen, E.; Jyrkkanen, H. K.; Kivelä, A.; Kylätie, R.; Ylä-Herttuala, S.; Levonen, A. L. Oxidative stress-inducible lentiviral vectors for gene therapy. *Gene Ther.* **2008**, *15*, 1271−1279.
(31) Surh, Y. J.; Kundu, J. K.; Na, H. K. Nrf2 as a master redox switch in turning on the cellular signaling involved in the induction of cytoprotective genes by some chemopreventive phytochemicals. *Planta Med.* **2008**, *74*, 1526−1539.
(32) Niso-Santano, M.; González-Polo, R. A.; Bravo-San Pedro, J. M.; Gómez-Sánchez, R.; Lastres-Becker, I.; Ortiz-Ortiz, M. A.; Soler, G.; Morán, J. M.; Cuadrado, A.; Fuentes, J. M. Activation of apoptosis signal-regulating kinase 1 is a key factor in paraquat-induced cell death: modulation by the Nrf2/Trx axis. *Free Radical Biol. Med.* **2010**, *48*, 1370−1381.
(33) Shah, Z. A.; Li, R. C.; Ahmad, A. S.; Kensler, T. W.; Yamamoto, M.; Biswal, S.; Doré, S. The flavanol (−)-epicatechin prevents stroke damage through the Nrf2/HO1 pathway. *J. Cereb. Blood Flow Metab.* **2010**, *30*, 1951−1961.
(34) Mann, G. E.; Bonacasa, B.; Ishii, T.; Siow, R. C. Targeting the redox sensitive Nrf2-Keap1 defense pathway in cardiovascular disease: protection afforded by dietary isoflavones. *Curr. Opin. Pharmacol.* **2009**, *9*, 139−145.
(35) Shehzad, A.; Ha, T.; Subhan, F.; Lee, Y. S. New mechanisms and the anti-inflammatory role of curcumin in obesity and obesity-related metabolic diseases. *Eur. J. Nutr.* **2011**, *50*, 151−161.
(36) Zhang, Y.; Luo, Z.; Ma, L.; Xu, Q.; Yang, Q.; Si, L. Resveratrol prevents the impairment of advanced glycosylation end products (AGE) on macrophage lipid homeostasis by suppressing the receptor for AGE via peroxisome proliferator-activated receptor gamma activation. *Int. J. Mol. Med.* **2010**, *25*, 729−734.
(37) Chen, F.; Zhou, X.; Lin, Y.; Jing, C.; Yang, T.; Ji, Y.; Sun, Y.; Han, X. Resveratrol prevents interleukin-1β-induced dysfunction of pancreatic β-cells. *J. Biomed. Res.* **2010**, *24*, 381−388.
(38) Voloshyna, I.; Hai, O.; Littlefield, M. J.; Carsons, S.; Reiss, A. B. Resveratrol mediates anti-atherogenic effects on cholesterol flux in human macrophages and endothelium via PPARγ and adenosine. *Eur. J. Pharmacol.* **2013**, *698*, 299−309.
(39) Zhang, H. Y.; Du, Z. X.; Meng, X. Resveratrol prevents TNFα-induced suppression of adiponectin expression via PPARγ activation in 3T3-L1 adipocytes. *Clin. Exp. Med.* **2013**, *13*, 193−199.
(40) Lee, B. H.; Hsu, W. H.; Liao, T. H.; Pan, T. M. The *Monascus* metabolite monascin against TNF-α-induced insulin resistance via suppressing PPAR-γ phosphorylation in C2C12 myotubes. *Food Chem. Toxicol.* **2011**, *49*, 2609−2617.
(41) Hsu, W. H.; Lee, B. H.; Hsu, Y. W.; Pan, T. M. Peroxisome proliferator-activated receptor-γ activators monascin and rosiglitazone attenuate carboxymethyllysine-induced fibrosis in hepatic stellate cells through regulating the oxidative stress pathway but independent of the receptor for advanced glycation end products signaling. *J. Agric. Food Chem.* **2013**, *61*, 6873−6879.
(42) Hsu, W. H.; Lee, B. H.; Liao, T. H.; Hsu, Y. W.; Pan, T. M. *Monascus*-fermented metabolite monascin suppresses inflammation via PPAR-γ regulation and JNK inactivation in THP-1 monocytes. *Food Chem. Toxicol.* **2012**, *50*, 1178−1186.
(43) Hsu, W. H.; Lee, B. H.; Hsu, Y. W.; Pan, T. M. Inhibition of Th2 cytokine production in T cells by monascin via PPAR-γ activation. *J. Agric. Food Chem.* **2013**, *61*, 8126−8133.
(44) Hsu, W. H.; Lee, B. H.; Chang, Y. Y.; Hsu, Y. W.; Pan, T. M. A novel natural Nrf2 activator with PPARγ-agonist (monascin) attenuates the toxicity of methylglyoxal and hyperglycemia. *Toxicol. Appl. Pharmacol.* **2013**, *272*, 842−851.

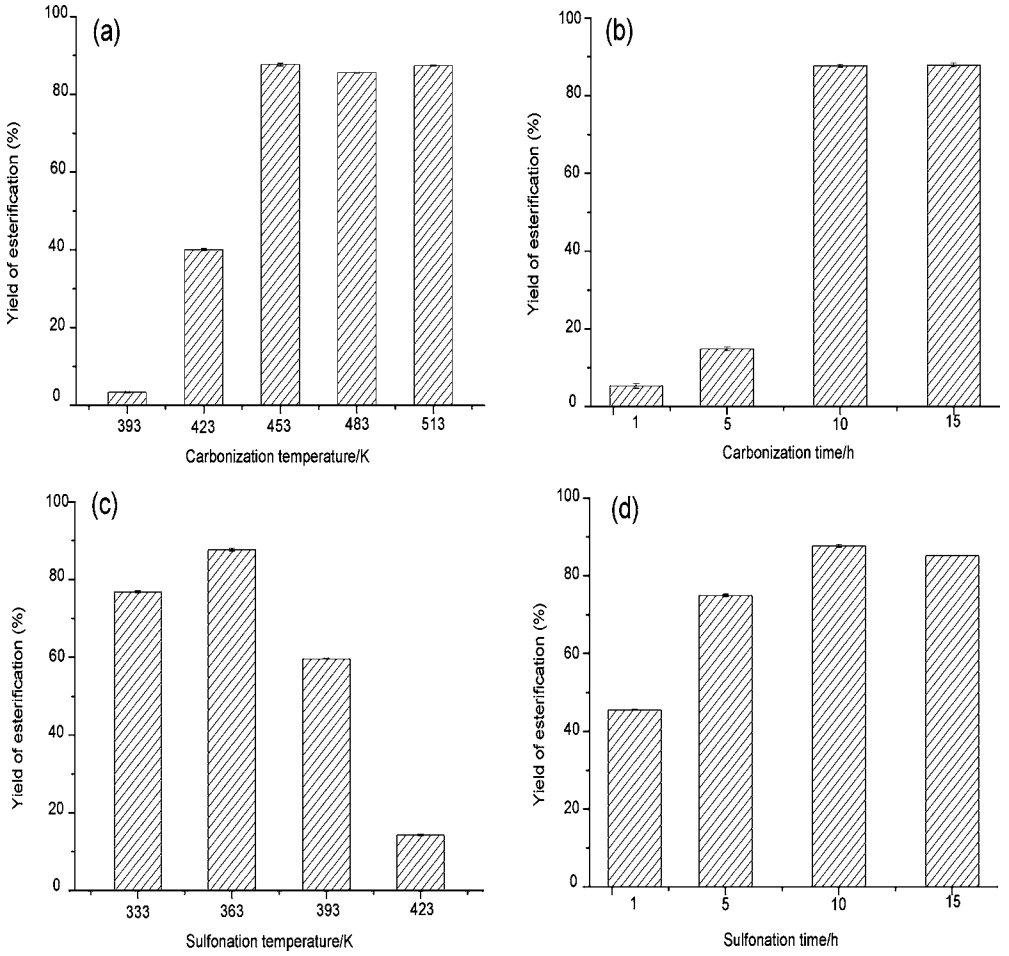

Figure 1. (a) Effect of the carbonization temperature on esterification activity of the corncob-derived solid acid. Preparation conditions: HTC at 393−513 K for 10 h, followed by sulfonation at 363 K for 10 h. (b) Effect of the carbonization time on esterification activity of the corncob-derived solid acid. Preparation conditions: HTC at 453 K for 1−15 h, followed by sulfonation at 363 K for 10 h. (c) Effect of the sulfonation temperature on esterification activity of the corncob-derived solid acid. Preparation conditions: HTC at 453 K for 10 h, followed by sulfonation at 333−423 K for 10 h. (d) Effect of the sulfonation time on esterification activity of the corncob-derived solid acid. Preparation conditions: HTC at 453 K for 10 h, followed by sulfonation at 363 K for 1−15 h. Esterification reaction conditions: ratio of methanol/oleic acid of 10 (for a typical experiment, 10 g of oleic acid and 11.34 g of methanol were added), 10% catalyst (on the basis of the mass of oleic acid), 353 K, 300 rpm, and 2 h.

its structure−function relationship was investigated with scanning electron microscopy (SEM), Fourier transform infrared spectroscopy (FTIR), X-ray diffraction (XRD), elemental analysis (EA), and ^{13}C solid-state nuclear magnetic resonance (NMR).

MATERIALS AND METHODS

Material. Corncob was provided by the maize base of Anhui Agricultural University, Hefei, China, milled into powder, and dried at 378 K for 24 h. All of the reagents and chemicals were purchased from Sinopharm Chemical Reagent Co., and the acid value of oleic acid used in the esterification was 196 mg of KOH/g.

Preparation of the Novel Carbon-Based Solid Acid. The catalysts were prepared by a low-temperature hydrothermal method under a range of conditions. In a typical preparation, the corncob powder was pretreated at first by ultrasonic wave and dilute alkali and then 5 g of corncob powder and 40 mL of water were maintained in a sealed, Teflon-lined autoclave at a specific temperature (393−513 K) for 1−15 h. After cooling to room temperature, the resulting material was washed with pure water several times and oven-dried at 378 K for 10 h. Then, 5 g of the above dried powder was heated in 25 mL of concentrated H_2SO_4 to introduce SO_3H groups under hydrothermal conditions. After sulfonation of the mixture for 1−15 h at a specific temperature (333−423 K), the mixture was cooled to room temperature and the black precipitate was filtered and washed repeatedly with hot distilled water (>353 K) until the washing liquid was neutral. Finally, the black solid was oven-dried at 378 K for 24 h.

Catalytic Activity of the Catalysts. The esterification reaction system contained 10 g of oleic acid and 11.34 g of methanol, with the ratio of methanol/oleic acid of 10 and 10 wt % catalyst loading based on the mass of oleic acid. The reaction system was conducted at 353 K and 300 rpm for 2 h. The yield of the esterification was determined according to the changes of the acid value in the oil phase and calculated as follows:

$$\text{ester yield}\ (\%) = (AV_0 - AV_1/AV_0) \times 100\% \quad (1)$$

where AV_0 and AV_1 are the acid values of the oleic acid and products, respectively.

Analysis Methods. The morphology of the solid acid was analyzed using SEM (Sirion 200, FEI Electron Optics Company, Hillsboro, OR) coupled with energy-dispersive X-ray (EDX, INCA Energy, U.K.). FTIR spectra were recorded on a Bruker Vector 33 FTIR spectrometer in the range of 4000−500 cm^{-1} with a resolution of 4 cm^{-1}. The XRD was performed using a Rigaku D/MAX β power X-ray diffractometer using Cu Kα radiation (λ = 0.184 15 nm) at 30 kV and 30 mA in the scanning angle of 3−60° at a scanning speed of 10°/min. EA was performed on an Elementar Vario Micro Cube. ^{13}C cross-polarization/total sideband suppression (CP/TOSS) NMR spectra were measured at room temperature using a Bruker Avance III 400

dx.doi.org/10.1021/jf500490m | J. Agric. Food Chem. 2014, 62, 5345−5353

spectrometer at a ^{13}C Larmor frequency of 100 MHz. A Bruker magic angle spinning (MAS) probe head was used with a 4 mm zirconia rotor. The spinning rate of the sample was 5 kHz. Sub-spectra for non-protonated and mobile carbon groups were obtained by combining the ^{13}C CP/TOSS sequence with a 40 μs dipolar dephasing.

Reusability of the Corncob-Derived Solid Acid Catalyst. To assess the catalytic stability of the corncob-derived solid acid, the reusability of the catalyst was investigated for the esterification of oleic acid and methanol. The reaction was conducted under the same conditions mentioned above for 8 cycles (2 h of reaction time per cycle). After each reaction cycle, the catalyst was recovered by filtration and washed with methanol or *n*-hexane until no methyl oleate was detected in the washing. The catalyst was then dried for the removal of the organic solvent and water under vacuum at 378 K for 2 h before reuse.

RESULTS AND DISCUSSION

The catalytic activities of the resulting corncob-derived solid acids were investigated by the esterification of oleic acid with methanol. Different preparation variables have different influences on the esterification activity of the synthesized catalysts (Figure 1). Within the tested range of 393−513 K, the HTC temperature greatly influenced the activity of the catalysts (Figure 1a). In comparison to the samples carbonized below 453 K, the resulting solid acids prepared at higher temperatures (453−513 K) were more active, with greater methyl oleate yields of nearly 90%. Similarly, increasing the carbonization time to 10 h resulted in an obvious increase in the catalytic activity of corncob-derived catalysts (Figure 1b). This may be attributed to the higher OH density in the samples carbonized at lower temperatures or in shorter times; these conditions allow for more water from esterification to be absorbed on the surface of the resulting catalyst, which can poison the acid sides and hinder the relatively hydrophobic reactants from accessing the catalyst.[23,24] In addition, samples carbonized at lower temperatures or in shorter times are less rigid; their aromatic and SO_3H groups will be leached out at high reaction temperatures or when higher fatty acids are used as reactants, resulting in a rapid deactivation of the catalyst. Therefore, taking both energy efficiency and time into consideration, 453 K and 10 h were selected as the suitable carbonization conditions for subsequent experiments.

Panels c and d of Figure 1 show the influences of the sulfonation temperature and time on the performance of the catalyst, respectively. After carbonization at 453 K for 10 h, the catalytic activity of the solid acid is largely dependent upon the sulfonation temperature. The catalyst sulfonated at 363 K displayed the highest esterification activity; the catalytic activity then dropped markedly with increasing temperature from 363 to 423 K (Figure 1c). This may be because the further carbonization by H_2SO_4 during sulfonation at higher temperatures generated a more rigid catalyst with a lower SO_3H density, which was confirmed in the structural characterization and elemental analysis. As shown in Figure 1d, 10 h was determined to be the optimal sulfonation time for the prepared catalyst. At this sulfonation time, the density of SO_3H groups at the suitable sulfonation temperature of 363 K reached a plateau, which is consistent with previous reports.[25]

Within the tested range, the optimal preparation conditions for the most effective catalyst are found to be HTC at 453 K for 10 h, followed by hydrothermal sulfonation at 363 K for 10 h. Under these conditions, a relatively high yield of methyl oleate (nearly 90%) was reached by catalysis with the corncob-derived solid acid after only 2 h of esterification. The structural differences in the catalysts prepared under different conditions will be discussed.

Figure 2 illustrates the morphologies of the corncob powders, the pretreated corncob, and the hydrothermal carbon

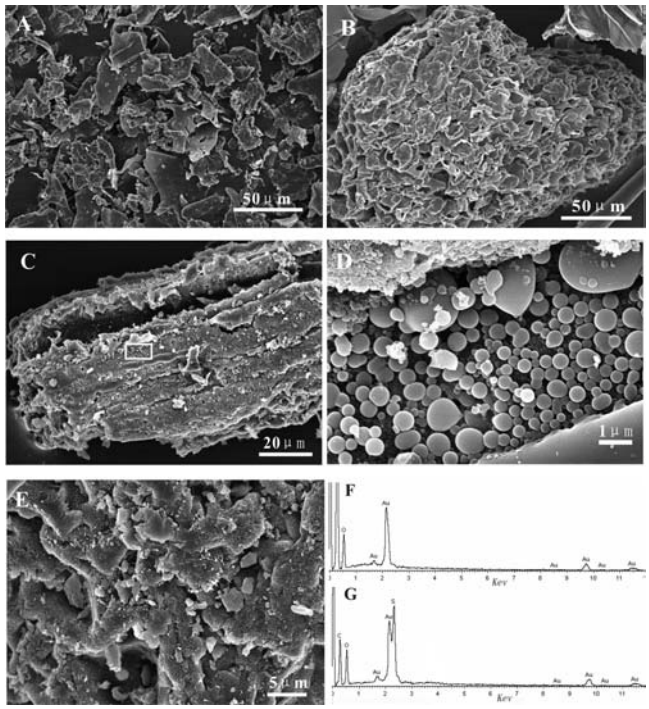

Figure 2. Field emission scanning electron microscopy (FESEM) images of the corncob powder (A) before and (B) after ultrasonic-assisted alkali pretreatment, (C and D) FESEM images of hydrothermal carbon materials obtained from carbonization at 453 K for 10 h, (E) FESEM images of the solid acid obtained from carbonization at 453 K for 10 h, followed by sulfonation at 363 K for 10 h. (F and G) Corresponding EDS spectra of the hydrothermal carbon material before and after sulfonation.

samples before and after sulfonation. In comparison to the raw material (Figure 2A), the pretreated corncob had a relatively rough surface and a distinctly looser structure with more pores, attributed to the swelling effect of the alkaline solution. A remarkable morphological transformation of corncob can be observed in panels C and D of Figure 2. When hydrothermally treated at 453 K, the fibrous corncob network was disrupted and carbon spheres with an average diameter of 400 nm started forming, indicating that the carbonization of corncob indeed occurred in the hydrothermal process. After sulfonation, the solid acid derived from corncob showed a completely different morphology (Figure 2E). By the further oxidation effect of H_2SO_4 and the intercalation of SO_3H groups, the spherical particles disappeared and aggregated to form irregular particles with highly granular surfaces. The S of the SO_3H groups can be observed in the EDX spectra after sulfonation (panels F and G of Figure 2).

Figure 3 shows the FTIR spectra of the carbon precursors derived from corncob and the catalysts prepared under different conditions. According to the spectra shown in Figure 3a, the carbonized samples produced at 393−513 K (Figure 3a) contained both aromatic and aliphatic hydrocarbons, as indicated by the peaks at approximately 2899 cm^{-1} (aliphatic C−H stretching) and 894 cm^{-1} (aromatic C−H bending).[18,19] The peaks assigned to OH and C−O near 3314 and 1037

dx.doi.org/10.1021/jf500490m | J. Agric. Food Chem. 2014, 62, 5345−5353

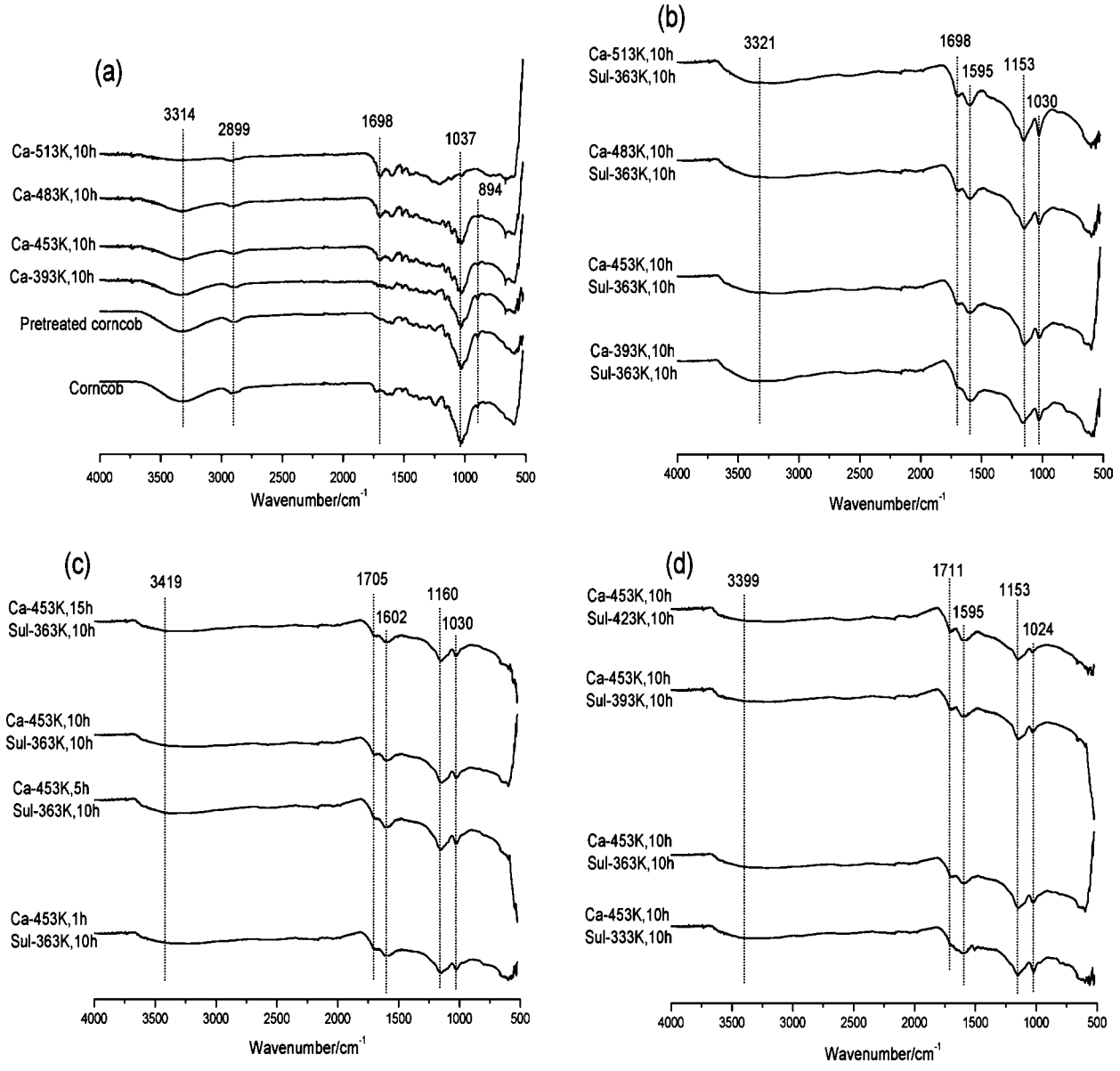

Figure 3. FTIR spectra of the carbon precursors and the catalysts prepared under various conditions. (a) Spectra of the carbon precursors hydrothermally carbonized at different temperatures (393−513 K) for 10 h (corncob and pretreated corncob are also shown as controls). (b) Spectra of the catalysts prepared at different carbonization temperatures (393−513 K) for 10 h, followed by sulfonation at 363 K for 10 h. (c) Spectra of the catalysts prepared under carbonization at 453 K for 1−15 h, followed by sulfonation at 363 K for 10 h. (d) Spectra of the catalysts prepared under carbonization at 453 K for 10 h, followed by sulfonation at different temperatures (333−423 K) for 10 h.

cm^{-1},[26] respectively, became weaker as the carbonization temperature increased, while the C═O peak at approximately 1698 cm^{-1} was enhanced. This suggests that incomplete carbonization reactions occurred at hydrothermal conditions, resulting in structural changes in the carbon precursors. The structural changes could also be clearly observed in the SEM images (panels c and d of Figure 3). This result is consistent with previous studies of the HTC of cellulose and waste biomass.[21] In comparison to the carbonized samples, the most obvious changes after sulfonation were the appearance of peaks at approximately 1030 and 1153 cm^{-1}, which are identified as the O═S═O symmetric stretching and SO_3 stretching modes in SO_3H, respectively (panels b−d of Figure 3). This can be further confirmed by EA, detailed below. In addition, the C═C peak intensity at approximately 1595 cm^{-1} was significantly enhanced, and the aliphatic C−H peak (2899 cm^{-1}) diminished after sulfonation. All of these observations indicate that the sulfonation process not only introduced SO_3H groups into the solid acid but also led to the further carbonization of the carbon precursors, which was also demonstrated by the color change of the samples from brown to black after sulfonation.

The peak intensities because of C═O and SO_3H were enhanced, while that for the OH group was significantly decreased, when the hydrothermal temperature was above 393 K (Figure 3b). Similarly, catalysts prepared at lower carbonization times (below 10 h) contained more OH groups (Figure 3c). This could partially explain why the catalysts carbonized at 393 K or in shorter times (below 10 h) had much lower catalytic activities, because greater water absorption by the OH groups during esterification can easily poison the acid sides of the catalysts and reduce the catalyst activity.[23,27] The C═O and SO_3H peak intensities were strongly dependent upon the

dx.doi.org/10.1021/jf500490m | J. Agric. Food Chem. 2014, 62, 5345−5353

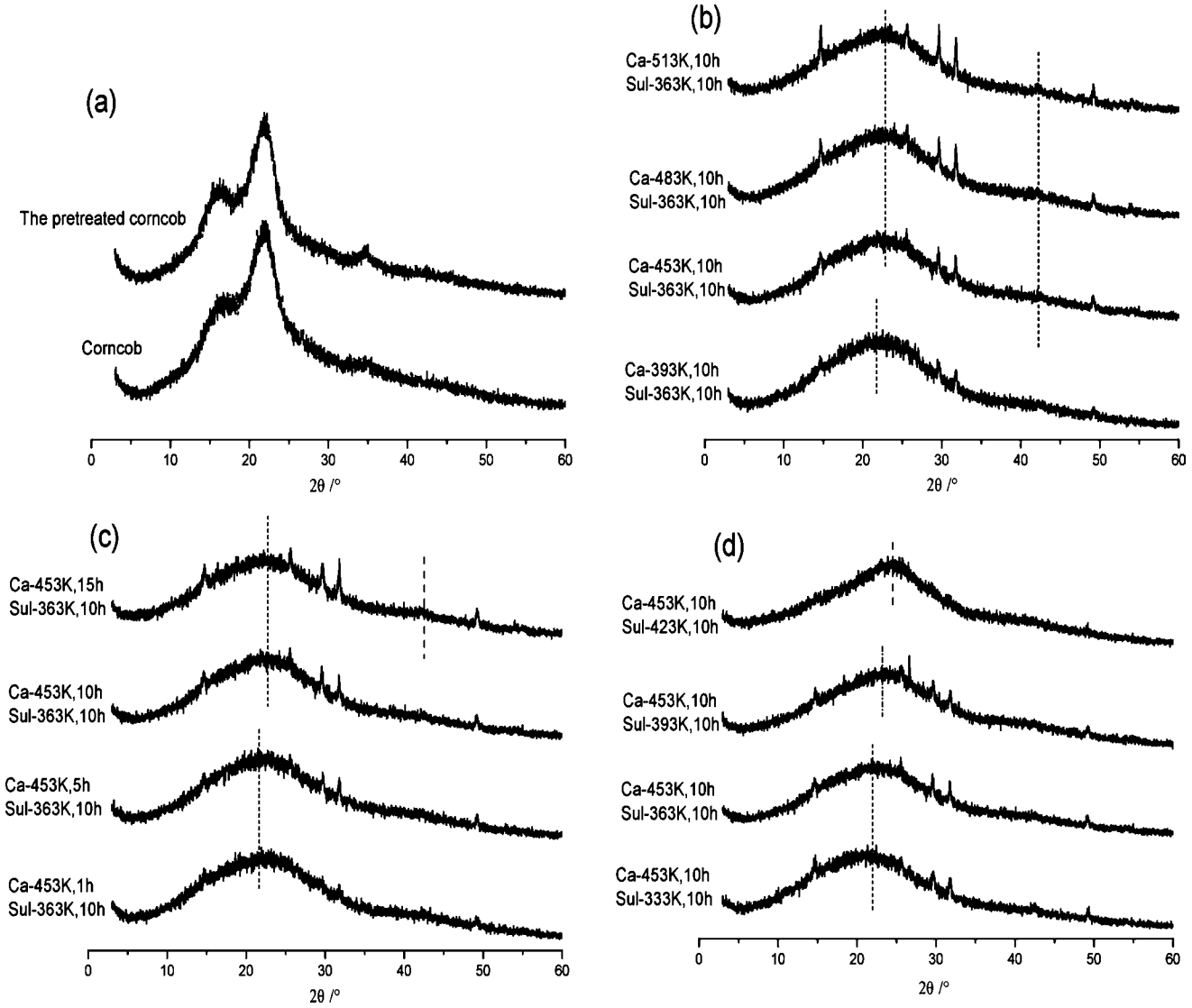

Figure 4. XRD patterns of the catalysts prepared under various conditions. (a) Catalysts prepared with carbonization at different temperatures (393−513 K) for 10 h, followed by sulfonation at 363 K for 10 h (corncob and pretreated corncob are also shown). (b) Catalysts prepared with carbonization at 453 K for different times (1−15 h), followed by sulfonation at 363 K for 10 h. (c) Catalysts prepared with carbonization at 453 K for 10 h, followed by sulfonation at different temperatures (333−423 K) for 10 h.

sulfonation temperature (Figure 3d). The FTIR spectra of catalysts sulfonated for different times showed only slight differences (data not shown), indicating that the sulfonation time was less important in determining catalytic activity than the other variables. This result is in agreement with the esterification results (Figure 1d).

Figure 4 illustrates the XRD patterns of the raw material, pretreated corncob, and catalysts prepared under different conditions. In comparison to the raw material, the characteristic peaks of pretreated corncob became more obvious, indicating that pretreatment removed impurities without destroying the "core" structure of corncob (Figure 4a). All of the XRD patterns of the corncob-derived catalysts exhibited a broad diffraction peak (2θ = 15−30°) attributable to amorphous carbon composed of polycyclic aromatic carbon sheets oriented in a considerably random fashion.[8,28] With an increasing carbonization temperature, time, and sulfonation temperature, the amorphous carbon diffraction peak became more obvious and shifted to higher angles (panels b−d of Figure 4), indicating the production of a more carbonized structure composed of large carbon sheets. Simultaneously, the weak diffraction peak (2θ = 40−45°) became more visible as well. This suggests that further carbonization during sulfonation yields a graphite-like carbon structure in the catalysts. Noticeably, when the carbonized sample was sulfonated at 423 K, the broad diffraction peak at 2θ = −30° became sharp and moved to a higher angle because of the formation of a more carbonized and rigid structure, which would prevent large molecular reactants from coming into contact with the SO_3H groups.[28] This also contributed to a lower SO_3H content in the catalyst, which is consistent with the result of EA and the limited esterification activity of the catalyst.

EA was employed to estimate the S content of the catalysts prepared under different conditions. The SO_3H density was calculated from the S content because all S atoms were present as SO_3H groups. The S contents in the raw material and pretreated corncob are not shown in Table 1 because both of them contained little S, as illustrated by EDX (Figure 2). As seen in Table 1, the density of SO_3H contained in various

dx.doi.org/10.1021/jf500490m | J. Agric. Food Chem. 2014, 62, 5345−5353

Table 1. S Content and SO_3H Density of Catalysts Prepared under Various Conditions

sample[a]	S content[b] (wt %)	SO_3H density[c] (mmol/g)
Ca-393 K, 10 h−Sul-363 K, 10 h	2.26	0.70
Ca-423 K, 10 h−Sul-363 K, 10 h	3.81	1.19
Ca-453 K, 10 h−Sul-363 K, 10 h	4.93	1.54
Ca-483 K, 10 h−Sul-363 K, 10 h	4.63	1.45
Ca-513 K, 10 h−Sul-363 K, 10 h	4.67	1.46
Ca-453 K, 1 h−Sul-363 K, 10 h	3.56	1.11
Ca-453 K, 5 h−Sul-363 K, 10 h	3.99	1.25
Ca-453 K, 15 h−Sul-363 K, 10 h	4.33	1.35
Ca-453 K, 10 h−Sul-333 K, 10 h	3.96	1.24
Ca-453 K, 10 h−Sul-393 K, 10 h	3.56	1.11
Ca-453 K, 10 h−Sul-423 K, 10 h	2.21	0.69
Ca-453 K, 10 h−Sul-363 K, 1 h	4.35	1.36
Ca-453 K, 10 h−Sul-363 K, 5 h	4.45	1.39
Ca-453 K, 10 h−Sul-363 K, 15 h	4.83	1.51

[a]The solid acid samples prepared at various conditions are denoted with different abbreviations. For example, Ca-393 K,10 h−Sul-363 K,10 h indicates that the catalyst was prepared by carbonization at 393 K for 10 h, followed by sulfonation at 363 K for 10 h. [b]The S content was estimated by EA. [c]The density of SO_3H groups was calculated from the S content.

catalysts ranged from 0.69 to 1.54 mmol/g and largely depended upon the preparation conditions.

The SO_3H density was dramatically enhanced (from 0.7 to 1.54 mmol/g) as the HTC temperature increased from 393 to 453 K, whereas it showed a slight decline (from 1.54 to 1.46 mmol/g) when the temperature exceeded 453 K. This may be because the sulfonation of the sample carbonized at 453 K resulted in amorphous carbon composed of small aromatic carbon sheets, to which the SO_3H group can be easily bonded. In contrast, the carbon precursors carbonized at low temperatures (below 453 K) had higher densities of aliphatic C−H and lower densities of cyclic aromatic hydrocarbons, which would be oxidized by the consumption of H_2SO_4 in the sulfonation process and, thus, reduce the SO_3H density in the catalyst. On the other hand, the sulfonation of the samples carbonized at high temperatures (above 453 K) resulted in increased sp^2-hybridized cross-linking among the carbon sheets, which can be shown by the decreasing amounts of phenolic OH and COOH groups in NMR spectra (Figure 5a).[25,29,30] As a result, this would prevent the intercalation of SO_3H groups into the carbon sheets and limit reactant access to SO_3H groups. Similar effects on SO_3H density were observed for carbonization time and sulfonation temperature. Although they had the same SO_3H density of 1.11 mmol/g, the catalyst Ca-453 K, 10 h-Sul-393 K, 10 h exhibited a much higher esterification activity than Ca-453 K, 1 h-Sul-363 K, 10 h (panels b and c of Figure 1). This could be explained by the distinct difference in the OH density of these two catalysts, which can be observed in the NMR spectra (panels b and c of Figure 5), because a higher water absorption by the OH group in the esterification reaction can easily poison the acid sides of the catalysts and, thus, reduce the catalyst activity.

Figure 5 displays the spectra of ^{13}C CP/TOSS and ^{13}C CP/TOSS with dipolar dephasing (DD) of the raw corncob, with its carbon precursors (Figure 5a) and the catalysts (panels b−d of Figure 5) prepared under different conditions. ^{13}C CP/TOSS spectra provided semi-quantitative structural information for all carbon sites, and DD spectra selected the signals of non-protonated carbons and carbons of mobile groups, such as CCH_3 groups. In Figure 5a, the spectrum of raw corncob was shown as a reference to evaluate the structural changes of the carbon precursor carbonized at different hydrothermal temperatures (393−513 K). The ^{13}C CP/TOSS spectrum of raw corncob is dominated by cellulose signals from 60 to 110 ppm. Signals in much lower abundances are seen for lignin (110−160 ppm) and hemicellulose [$-OC(=O)-CH_3$ at approximately 20 ppm and approximately 175 ppm]. Most of these carbon signals arose from protonated carbons and were selectively dephased in the DD spectrum (Figure 5a). The carbon precursor obtained at 393 K had a spectrum similar to that of raw corncob, indicating that nearly no structural changes occurred at the low temperature. Note that the signals associated with hemicellulose were less visible. Major spectral changes occurred as the hydrothermal temperature increased from 453 to 513 K. The signals for aliphatic groups (0−60 ppm) and aromatic groups (110−180 ppm) were enhanced in ^{13}C CP/TOSS spectra. At 513 K, the signals associated with cellulose disappeared; the spectrum was composed of the signals from mostly non-protonated polycyclic aromatic carbons (130 ppm), phenolic OH/aromatic C−O−C (153 ppm), and nonpolar alkyl carbons (0−60 ppm). Carbons of mobile groups, such as CCH_3 (22 ppm) and OCH_3 (57 ppm), also became more abundant. This indicates the initial formation of aromatic carbon sheets and other altered lignin residues at 453 K, as observed with FTIR and SEM.

Panels b−d of Figure 5 show the spectra of the solid acid catalysts prepared by the hydrothermal sulfonation of carbon precursors under different conditions: carbonization temperature from 393 to 513 K (Figure 5b), carbonization time from 1 to 15 h (Figure 5c), and sulfonation temperature from 333 to 423 K (Figure 5d). In comparison to the spectra of carbon precursors before sulfonation (Figure 5a), those of solid acids produced by hydrothermal sulfonation lost cellulose signals and were composed primarily of signals from mostly non-protonated aromatic carbons (130 ppm), phenolic OH/aromatic C−O−C (153 ppm), and nonpolar alkyl carbons (0−60 ppm). Signals from COOR carbons (178 ppm) and ketone carbons (approximately 200 ppm) were also present.[25,28,31] The aromatic C−O signals became gradually less abundant in the solid acids prepared from higher temperature carbon precursors. Furthermore, the aliphatic carbon peaks of the solid acid (0−60 ppm) were markedly reduced in intensity compared to those of the carbon precursor carbonized at 513 K (Figure 5a). All of these results revealed that the structure of the carbon precursor was further modified by H_2SO_4 during sulfonation, possibly leading to the development of polycyclic aromatic sheets in the solid acid.[8,25,29,30] According to panels b−d of Figure 5, the strong suppression of the aliphatic C signals after DD indicated that most of the sp^3-hybridized carbons were protonated, except of mobile carbons of CCH_3 and OCH_3. In addition, the peak because of aromatic carbon-bearing SO_3H groups could not be distinguished in the spectra of the sulfonated samples because the broad aromatic carbon (130 ppm) and aromatic C−O (150 ppm) peaks obscure the $Ar-SO_3H$ (140 ppm) peak.[25,29,30]

A remarkable reduction in the aromatic C−O peak intensity and an enhancement of the aromatic carbon peak with an increasing carbonization temperature from 393 to 513 K were observed in the CP/TOSS and DD spectra of the solid acids (Figure 5b). This might result from enhanced cross-linking between the carbon sheets at high temperatures, which would

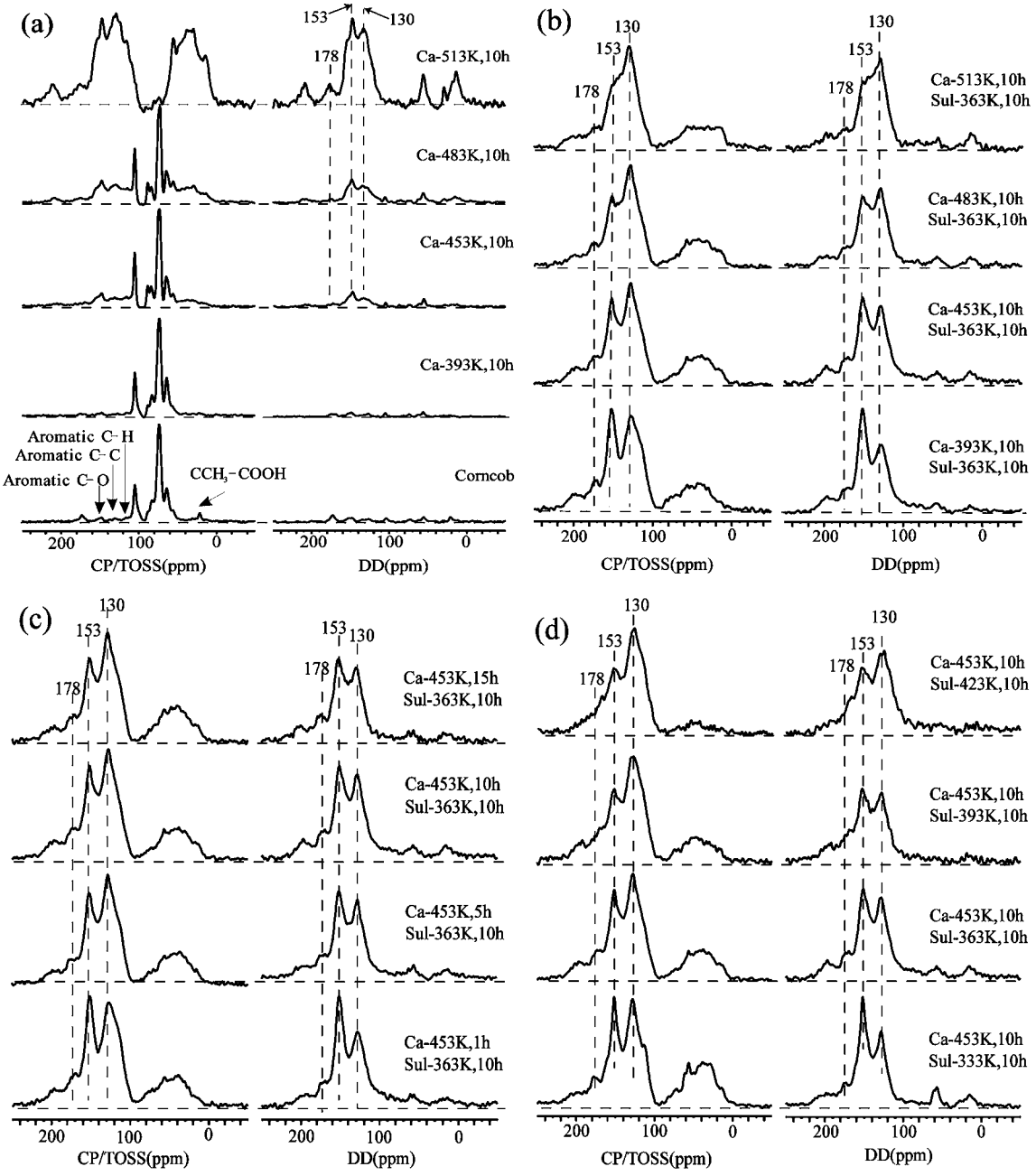

Figure 5. Spectra of ^{13}C CP/TOSS and corresponding ^{13}C CP/TOSS with DD. (a) Spectra of raw corncob and carbon precursors hydrothermally carbonized at different temperatures (393−513 K). (b) Spectra of corncob-derived solid acids prepared at different carbonization temperatures (393−513 K). (c) Spectra of corncob-derived solid acids prepared with different carbonization times (1−15 h). (d) Spectra of corncob-derived solid acids prepared at different sulfonation temperatures (333−423 K).

prevent the incorporation of reactants in the carbon bulk and hinder reactant access to SO_3H groups.[5,25] As a result, the aggregation of small carbon sheets with high cross-linking would decrease the reactivity of SO_3H groups, partially explaining the relatively low esterification activity of solid acids carbonized above 453 K. Figure 5b also shows that the catalyst prepared at 393 K had the highest content of aromatic C−O, such as phenolic OH groups, which caused its inefficiency in the esterification reaction, as mentioned before. Therefore, the sample carbonized at 453 K had the highest catalytic activity. As expected, the changes in peaks corresponding to the aromatic C−O groups and aromatic carbons in panels c and d of Figure 5 were similar to those seen in Figure 5b, as a result of the varying carbonization time from 1 to 15 h and the sulfonation temperature from 333 to 423 K, respectively. When the sulfonation temperature was above 363 K, however, the resonances of aliphatic carbon and COO groups significantly decreased (Figure 5d). At the same time, the COO peak shifted to 170 ppm because of the reduction in aliphatic carbon intensity. This result reveals that the concentrated H_2SO_4 acted as not only a sulfonating reagent but also a strong oxidant during sulfonation at high temperatures (above 363 K). This probably generated a prominent reduction in catalytic activity by contributing to a rigid catalyst structure with fewer SO_3H groups. In addition, it should be noted that the catalytic activity of the solid acids may

dx.doi.org/10.1021/jf500490m | J. Agric. Food Chem. 2014, 62, 5345−5353

not simply depend upon the synergetic combination of their structure and their functional groups, as suggested by previous studies.[1,31] The catalytic activity also depends upon the functional groups (such as SO_3H, COOH, and phenolic OH) being bonded to the carbon sheet in adequate amounts and, more importantly, in proper proportions.

To evaluate the catalytic performance of the new catalyst, a comparative study was performed using different catalysts for the esterification of oleic acid with methanol at 353 K to form methyl oleate. The same amount of catalyst was used in all cases. The catalysts tested were concentrated H_2SO_4, Amberlyst-15, niobic acid, and corncob-derived solid acid. As shown in Table 2, no methyl oleate was detected when the reaction was conducted for 24 h in the absence of catalysts, implying the critical role of the catalyst in this esterification reaction. The corncob-based solid acid possessed a high catalytic activity, with an 89.2% esterification yield after only 2 h. The yields of Amberlyst-15 and niobic acid after 2 h were 68.8 and 29.6%, respectively. The synergetic effect of three different functional groups (SO_3H, COOH, and phenolic OH groups) in the corncob-derived solid acid may be the main reason for its high catalytic activity compared to the conventional catalysts (niobic acid and Amberlyst-15), which contain only one functional group.[28,31] Although its catalytic activity was a little lower than that of concentrated H_2SO_4 (95.4% for 2 h), the corncob-derived solid acid can be easily recovered and reused at the end of each step. Additionally, the corncob-derived solid acid can prevent corrosion, which normally occurs in the presence of H_2SO_4, and can be successfully prepared from biomass by hydrothermal methods, providing a holistic and green approach to biomass conversion. In this regard, the corncob-derived solid acid prepared by the hydrothermal method is more promising and competitive.

Table 2. Comparison of the Esterification Yield of Oleic Acid with Methanol Catalyzed by Various Catalysts[a]

catalyst	reaction time (h)	yield of methyl oleate (%)
control (no catalyst)	24	
corncob-based solid acid	2	89.2
Amberlyst-15	2	68.8
niobic acid	2	29.6
concentrated H_2SO_4	2	95.4

[a]Reaction conditions: ratio of methanol/oleic acid of 10 (for a typical experiment, 10 g of oleic acid and 11.34 g of methanol were added), 353 K, 2 h, 300 rpm, and 10 wt % catalyst loading based on the mass of oleic acid.

The recycling performance of the corncob-derived solid acid catalyst was also investigated using the esterification reaction of oleic acid with methanol. Between each cycle of the reaction, methanol and *n*-hexane were employed as washing solvents to recovery the catalyst. As shown in Figure 6, the catalytic activity of the corncob-derived solid acid was maintained with a 66% conversion for methanol washing and a 75% conversion with *n*-hexane washing after 8 cycles of reuse. As reported by Mo et al.,[32] sulfonated catalysts were deactivated during the washing procedure mainly because of the leaching of polycyclic aromatic hydrocarbons containing $-SO_3H$ groups because these hydrocarbons are not completely insoluble in common solvents. Therefore, the different recycling performances of the corncob-derived solid acids in methanol and *n*-hexane might result from the varying solubilities of the polycyclic aromatic hydrocarbons in the different washing solvents. Although the deactivation of the catalytic activity was noticed in the case of carbon-based solid acid,[33−35] the corncob-derived catalyst prepared in this work still gave a satisfactory yield of methyl oleate after 8 cycles, indicating the high stability of the catalyst.

To the best of our knowledge, this is the first report of the synthesis of carbon-based solid acids from lignocellulosic biomass employing a hydrothermal method. The high catalytic activity of the corn-derived catalyst obtained under optimal hydrothermal conditions (453 K carbonization for 10 h and 363 K sulfonation for 10 h) can be attributed to the synergetic combination of the specific structure (polycyclic aromatic carbon sheets) and three functional groups (SO_3H, COOH, and phenolic OH groups) in adequate amounts. This work

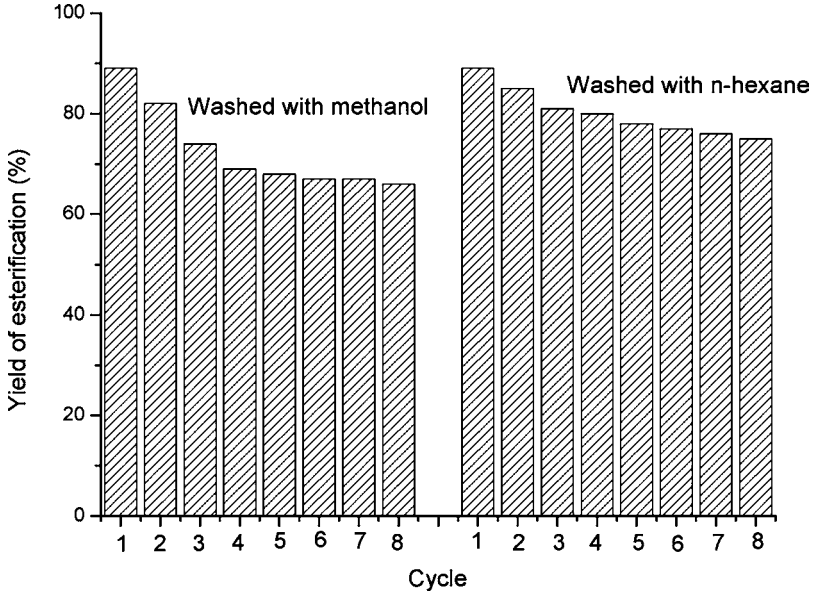

Figure 6. Reusability of the novel corncob-derived solid acid (prepared under the optimized conditions). Reaction conditions for each cycle: molar ratio of methanol/oleic acid of 10 (10 g of oleic acid and 11.34 g of methanol), 353 K, 300 rpm, and 2 h of reaction time per cycle.

dx.doi.org/10.1021/jf500490m | J. Agric. Food Chem. 2014, 62, 5345−5353

provides a simple and energy-efficient method to synthesize carbon-based catalysts from lignocellulosic biomass and develops a holistic and green approach to biomass conversion and environmental protection.

AUTHOR INFORMATION

Corresponding Author

*Telephone: +86-551-65786021. Fax: +86-551-65786021. E-mail: zhusuwen@126.com.

Funding

This work was financially supported by the Natural Science Foundation of Higher Education Institutes of Anhui Province, China (Grant KJ2014A073).

Notes

The authors declare no competing financial interest.

†Huan Ma and Jiabao Li contributed equally to this work.

ACKNOWLEDGMENTS

The authors thank Prof. Hong Wang at the Chinese Academy of Agriculture Sciences for help with the NMR test. The authors also thank Dr. Peirong Chen for providing the facilities for FTIR.

REFERENCES

(1) Hara, M. Biomass conversion by a solid acid catalyst. *Energy Environ. Sci.* **2010**, *3*, 601−607.

(2) Rinaldi, R.; Schüth, F. Design of solid catalysts for the conversion of biomass. *Energy Environ. Sci.* **2009**, *2*, 610−626.

(3) Yang, F.; Liu, Q.; Bai, X.; Du, Y. Conversion of biomass into 5-hydroxymethylfurfural using solid acid catalyst. *Bioresour. Technol.* **2011**, *102*, 3424−3429.

(4) Jiang, Y.; Li, X.; Cao, Q.; Mu, X. Acid functionalized, highly dispersed carbonaceous spheres: An effective solid acid for hydrolysis of polysaccharides. *J. Nanopart. Res.* **2010**, *13*, 463−469.

(5) Lou, W. Y.; Guo, Q.; Chen, W. J.; Zong, M. H.; Wu, H.; Smith, T. J. A highly active bagasse-derived solid acid catalyst with properties suitable for production of biodiesel. *ChemSusChem* **2012**, *5*, 1533−1541.

(6) Huang, Y.-B.; Fu, Y. Hydrolysis of cellulose to glucose by solid acid catalysts. *Green Chem.* **2013**, *15*, 1095−1111.

(7) Hara, M.; Yoshida, T.; Takagaki, A.; Takata, T.; Kondo, J. N.; Hayashi, S.; Domen, K. A carbon material as a strong protonic acid. *Angew. Chem., Int. Ed.* **2004**, *43*, 2955−2958.

(8) Hara, M. Biodiesel production by amorphous carbon bearing SO_3H, COOH and phenolic OH groups, a solid Brønsted acid catalyst. *Top. Catal.* **2010**, *53*, 805−810.

(9) Suganuma, S.; Nakajima, K.; Kitano, M.; Yamaguchi, D.; Kato, H.; Hayashi, S. Hydrolysis of cellulose by amorphous carbon bearing SO_3H, COOH, and OH groups. *J. Am. Chem. Soc.* **2008**, *130*, 12787−12793.

(10) Xiao, H.; Guo, Y.; Liang, X.; Qi, C. One-step synthesis of a novel carbon-based strong acid catalyst through hydrothermal carbonization. *Monatsh. Chem.* **2010**, *141*, 929−932.

(11) Song, X.-l.; Fu, X.-b.; Zhang, C.-w.; Huang, W.-y.; Zhu, Y.; Yang, J.; Zhang, Y.-m. Preparation of a novel carbon based solid acid catalyst for biodiesel production via a sustainable route. *Catal. Lett.* **2012**, *142*, 869−874.

(12) Zong, M.-H.; Duan, Z.-Q.; Lou, W.-Y.; Smith, T. J.; Wu, H. Preparation of a sugar catalyst and its use for highly efficient production of biodiesel. *Green Chem.* **2007**, *9*, 434−437.

(13) Berge, N. D.; Ro, K. S.; Mao, J.; Flora, J. R.; Chappell, M. A.; Bae, S. Hydrothermal carbonization of municipal waste streams. *Environ. Sci. Technol.* **2011**, *45*, 5696−5703.

(14) Libra, J. A.; Ro, K. S.; Kammann, C.; Funke, A.; Berge, N. D.; Neubauer, Y.; Titirici, M.-M.; Fühner, C.; Bens, O.; Kern, J. Hydrothermal carbonization of biomass residuals: A comparative review of the chemistry, processes and applications of wet and dry pyrolysis. *Biofuels* **2011**, *2*, 71−106.

(15) Funke, A.; Ziegler, F. Hydrothermal carbonization of biomass: A summary and discussion of chemical mechanisms for process engineering. *Biofuels, Bioprod. Biorefin.* **2010**, *4*, 160−177.

(16) Kubo, S.; Demir-Cakan, R.; Zhao, L.; White, R. J.; Titirici, M. M. Porous carbohydrate-based materials via hard templating. *ChemSusChem* **2010**, *3*, 188−194.

(17) Hu, B.; Wang, K.; Wu, L.; Yu, S. H.; Antonietti, M.; Titirici, M. M. Engineering carbon materials from the hydrothermal carbonization process of biomass. *Adv. Mater.* **2010**, *22*, 813−828.

(18) Sevilla, M.; Fuertes, A. B. Chemical and structural properties of carbonaceous products obtained by hydrothermal carbonization of saccharides. *Chem.—Eur. J.* **2009**, *15*, 4195−4203.

(19) Sevilla, M.; Fuertes, A. B. The production of carbon materials by hydrothermal carbonization of cellulose. *Carbon* **2009**, *47*, 2281−2289.

(20) Falco, C.; Baccile, N.; Titirici, M.-M. Morphological and structural differences between glucose, cellulose and lignocellulosic biomass derived hydrothermal carbons. *Green Chem.* **2011**, *13*, 3273−3281.

(21) Aydıncak, K.; Yumak, T.; Sınağ, A.; Esen, B. Synthesis and characterization of carbonaceous materials from saccharides (glucose and lactose) and two waste biomasses by hydrothermal carbonization. *Ind. Eng. Chem. Res.* **2012**, *51*, 9145−9152.

(22) Titirici, M.-M.; White, R. J.; Falco, C.; Sevilla, M. Black perspectives for a green future: Hydrothermal carbons for environment protection and energy storage. *Energy Environ. Sci.* **2012**, *5*, 6796−6822.

(23) Liu, F.; Kong, W.; Qi, C.; Zhu, L.; Xiao, F.-S. Design and synthesis of mesoporous polymer-based solid acid catalysts with excellent hydrophobicity and extraordinary catalytic activity. *ACS Catal.* **2012**, *2*, 565−572.

(24) Morales, G.; Athens, G.; Chmelka, B. F.; van Grieken, R.; Melero, J. A. Aqueous-sensitive reaction sites in sulfonic acid-functionalized mesoporous silicas. *J. Catal.* **2008**, *254*, 205−217.

(25) Nakajima, K.; Hara, M. Amorphous carbon with SO_3H groups as a solid Brønsted acid catalyst. *ACS Catal.* **2012**, *2*, 1296−1304.

(26) Okuhara, T. Water-tolerant solid acid catalysts. *Chem. Rev.* **2002**, *102*, 3641−3666.

(27) Ishimaru, K.; Hata, T.; Bronsveld, P.; Meier, D.; Imamura, Y. Spectroscopic analysis of carbonization behavior of wood, cellulose and lignin. *J. Mater. Sci.* **2006**, *42*, 122−129.

(28) Okamura, M.; Takagaki, A.; Toda, M.; Kondo, J. N.; Domen, K.; Tatsumi, T.; Hara, M.; Hayashi, S. Acid-catalyzed reactions on flexible polycyclic aromatic carbon in amorphous carbon. *Chem. Mater.* **2006**, *18*, 3039−3045.

(29) Suganuma, S.; Nakajima, K.; Kitano, M.; Kato, H.; Tamura, A.; Kondo, H.; Yanagawa, S.; Hayashi, S.; Hara, M. SO_3H-bearing mesoporous carbon with highly selective catalysis. *Microporous Mesoporous Mater.* **2011**, *143*, 443−450.

(30) Suganuma, S.; Nakajima, K.; Kitano, M.; Yamaguchi, D.; Kato, H.; Hayashi, S.; Hara, M. Synthesis and acid catalysis of cellulose-derived carbon-based solid acid. *Solid State Sci.* **2010**, *12*, 1029−1034.

(31) Toda, M.; Takagaki, A.; Okamura, M.; Kondo, J. N.; Hayashi, S.; Domen, K.; Hara, M. Default green chemistry: Biodiesel made with sugar catalyst. *Nature* **2005**, *438*, 178−178.

(32) Mo, X.; López, D. E.; Suwannakarn, K.; Liu, Y.; Lotero, E.; Goodwin, J. G., Jr.; Lu, C. Activation and deactivation characteristics of sulfonated carbon catalysts. *J. Catal.* **2008**, *254*, 332−338.

(33) Van de Vyver, S.; Peng, L.; Geboers, J.; Schepers, H.; de Clippel, F.; Gommes, C. J.; Goderis, B.; Jacobs, P. A.; Sels, B. F. Sulfonated silica/carbon nanocomposites as novel catalysts for hydrolysis of cellulose to glucose. *Green Chem.* **2010**, *12*, 1560−1563.

(34) Tian, X.; Su, F.; Zhao, X. Sulfonated polypyrrole nanospheres as a solid acid catalyst. *Green Chem.* **2008**, *10*, 951−956.

(35) Shu, Q.; Gao, J.; Nawaz, Z.; Liao, Y.; Wang, D.; Wang, J. Synthesis of biodiesel from waste vegetable oil with large amounts of free fatty acids using a carbon-based solid acid catalyst. *Appl. Energy* **2010**, *87*, 2589−2596.

purification.[18−21] Recently, several enzymes, such as *Yarrowia lipolytica* lipases, *Candida antarctica* lipase B, and *Enterobacter* sp. FMB-1 sucrose isomerase, have been successfully immobilized onto the yeast cell surface, and their potential as biocatalysts for industrial applications has been investigated.[17,21,22]

In the present study, the phospholipase D gene (*pld*) cloned from *Streptomyces chromofuscus* was efficiently expressed on the cell surface of *P. pastoris* GS115 with FS as anchor protein. The enzymatic properties of the displayed PLD (dPLD) were systematically investigated. Importantly, the dPLD was successfully applied in the PS production so as to assess its potential in industrial applications.

MATERIALS AND METHODS

Chemicals and Enzymes. Choline oxidase (EC 1.1.3.17 from *Alcaligenes* sp.), peroxidase (EC 1.11.1.7 from horseradish), PC, PS, and PA were purchased from Sigma-Aldrich Co. (St. Louis, MO, USA). DNA modifying enzymes, such as restriction endonucleases, T4 DNA ligase, and La Tap DNA polymerase were purchased from Takara Co. (Dalian, China).

Strains, Media, and Vectors. *S. chromofuscus* AS 4.331 used for amplifying the PLD gene was purchased from China General Microbiological Culture Collection Center and was used to amplify the PLD gene. *E. coli* DH5α [F$^-$ φ80*lac*ZΔM15 Δ(*lac*ZYA-*arg*F) U169 *rec*A1 *end*A1 *hsd*R17 (r_k-, m_k+) *pho*A *sup*E44 λ^- *thi*-1 *gyr*A96 *rel*A1] was purchased from Takara Biotechnology Co. Ltd. and used as a host for general gene manipulation. *P. pastoris* GS115 [*his*4] and the pKFS vector were kind gifts from Professor Ying Lin (South China University of Technology). *P. pastoris* GS115 was employed as a host for the expression of the yeast cell display vector. Yeast extract−peptone−dextrose (YPD), buffered glycerol complex (BMGY), and buffered minimal methanol (BMMY) media were prepared according to the instructions of the Original *Pichia* Expression Kit (Invitrogen, USA).

The FS anchor sequence was amplified and inserted into the vector pPIC9K without signal peptide, resulting in recombinant plasmid designated pKFS. The pKFS vector was employed as the yeast cell surface display vector. Heterologous PLD was displayed on the *P. pastoris* cell surface by fusion with FS via the N-terminal anchor system, which adhered to the cell surface via noncovalent interactions with the mannan chain of the cell wall.[22]

Construction of the PLD Expression Plasmid. The PLD gene was amplified from genomic DNA of *S. chromofuscus* using the following primers: P1 5′-ccg<u>acgcgt</u>*tacccatacgacgtcccagactacgct*gccgaccaggcgcccgccttcct-3′ and P2 5′-ccg<u>gaattc</u>cctacacggggtcgtaggtgcgc-3′. (Recognition sites of *Mlu*I and *Eco*RI are underlined, and the HA tag sequence is shown in italics.) The amplified fragment was digested with *Mlu*I and *Eco*RI and subsequently cloned into the pKFS vector to generate the plasmid pKFS-*pld*. To construct the codon-optimized PLD gene (*pldh*), the rare codon used in the PLD sequence was replaced according to the preferred codon usage of *P. pastoris*. The synthesized *pldh* (Sangon Co., Ltd., Shanghai, China) was cloned into the pKFS vector to generate the plasmid pKFS-*pldh*. All plasmids were confirmed by sequencing.

Yeast Transformation of pKFS-*pld* and pKFS-*pldh*. Recombinant plasmids (pKFS-*pld* and pKFS-*pldh*) were transformed into *P. pastoris* GS115 cells using electroporation according to the instructions provided with the Original Pichia Expression Kit. The pKFS vector without the PLD gene insertion was transformed into *P. pastoris* GS115 (GS115/pKFS) as control. Transformation was performed according to the manufacturer's instructions. Ten micrograms of plasmid DNA linearized by *Sal*I was mixed with 80 μL of electrocompetent cells and subjected to electroporation at 1500 V (25 μF, 5 ms, BTX ECM399). Next, 1 mL of 1 M ice-cold sorbitol was added to the cuvette immediately after pulse discharge. Subsequently, 200 μL aliquots were plated in MD medium containing 13.4 g/L yeast nitrogen base (YNB) without amino acids, 20 g/L glucose, 4×10^{-4} g/L biotin, and 15 g/L agar. The *P. pastoris* transformants harboring pKFS-*pld* (GS115/pKFS-*pld*) and pKFS-*pldh* (GS115/pKFS-*pldh*) were selected by incubation at 30 °C for 48 h on MD plates.

Immunofluorescence Assay and Enzyme Assay. The transformants were precultured in YPD medium at 30 °C for 12 h and used to inoculate 50 mL of BMGY medium (13.4 g/L YNB, 10 g/L yeast extract, 20 g/L peptone, 20 g/L glycerol, and 4×10^{-4} g/L biotin) in a 250 mL shake flask at an initial OD_{600} value of 0.2. After incubation for 24 h, the cells were harvested by centrifugation at 4500 rpm for 10 min and resuspended in BMMY medium (13.4 g/L YNB, 10 g/L yeast extract, 20 g/L peptone, and 4×10^{-4} g/L biotin) containing 5 g/L methanol. To maintain the induction of the fusion protein, methanol was added to the culture every 24 h to a final concentration of 5 g/L, and the cells were incubated for 8 days at 30 °C with agitation (250 rpm).

An immunofluorescence assay was performed using a mouse monoclonal antihemagglutinin (HA) tag and a fluorescein isothiocyante (FITC)-conjugated goat anti-mouse IgG. Yeast cells were harvested and washed with phosphate-buffered saline (PBS, 10 mM, pH 7.4) containing 1 mg/mL bovine serum albumin (BSA), and then the cells were incubated with the mouse monoclonal antihemagglutinin (HA) tag in a dilution of 1:100 in PBS for 30 min on ice, washed twice with PBS containing 1 mg/mL BSA, and mixed with FITC-conjugated goat anti-mouse IgG diluted 1:200 on ice for 30 min. After a washing with PBS, the cells were observed with a fluorescence microscope.

The induced cells were harvested by centrifugation and washed twice with deionized water and lyophilized for activity assays.[22] The PLD activity in this study, represented as the hydrolytic activity due to its convenience of determination, was determined according to the method of Uhm et al. with minor modifications.[23] The PLD hydrolytic activity was determined by measuring the amount of choline released from the substrate PC. The cells were resuspended in 10 mM Tris-HCl (pH 8.0) at a concentration of 100 mg dry cells/mL. The reaction was initiated by adding 100 μL of cell solution to 10 mM Tris-HCl (pH 8.0) containing 10 mM $CaCl_2$, 20 mM TX-100, and 10 mM PC in a final volume of 1.5 mL at 37 °C for 10 min and was terminated by adding 0.5 mL of a solution containing 1 M Tris-HCl (pH 8.0) and 0.5 M ethylenediaminetetraacetic acid (EDTA). The reaction mixture was boiled for 5 min to completely arrest the reaction and then subsequently centrifuged at 6000 rpm for 5 min and mixed with 2 mL of 10 mM Tris-HCl (pH 8.0) containing 1 unit of choline oxidase, 1 unit of peroxidase, 0.4 mg of 4-aminoantipyrine, and 0.2 mg of phenol. The solution was then incubated for 20 min at 37 °C. The absorbance of the resulting mixture was measured spectrophotometrically at 500 nm.

One unit (U) of hydrolysis activity of PLD was defined as the amount of enzyme that produced 1 μmol of choline per minute under these assay conditions.

Enzyme Characterization. The optimal temperatures of the dPLD and secreted PLD (sPLD) were assayed by incubating the reaction mixture at various temperatures ranging from 30 to 65 °C in 50 mM sodium acetate buffer (pH 8.0). The thermostability of the enzyme was determined by incubating the enzyme at various temperatures ranging from 20 to 65 °C at pH 8.0 for 1 h. The remaining activity was then measured under standard conditions.

Optimum pH values for the two forms of PLD were determined by measuring the hydrolytic activity with 1 mM PC as the substrate in the pH range of 4.0−6.0 using 50 mM sodium acetate buffer, in the pH range of 7.0−8.0 using 50 mM potassium phosphate buffer, and in the pH range of 9.0−11.0 using 50 mM Tris-HCl buffer at 37 °C. The stability of PLD at various pH values was determined by preincubating the PLD in solutions at various pH values, ranging from 4.0 to 11.0, at 25 °C for 1 h. The residual activity was then quantified under standard assay conditions.

Organic Solvent Stability of the Enzyme. In this study, the conversion of PC to PS was performed in biphasic systems consisting of water-insoluble organic solvent. Diethyl ether was used as the organic solvent for the production of PS by dPLD as our previous studies demonstrated its suitability for sPLD-mediated reactions (data

dx.doi.org/10.1021/jf405836x | J. Agric. Food Chem. 2014, 62, 5354−5360

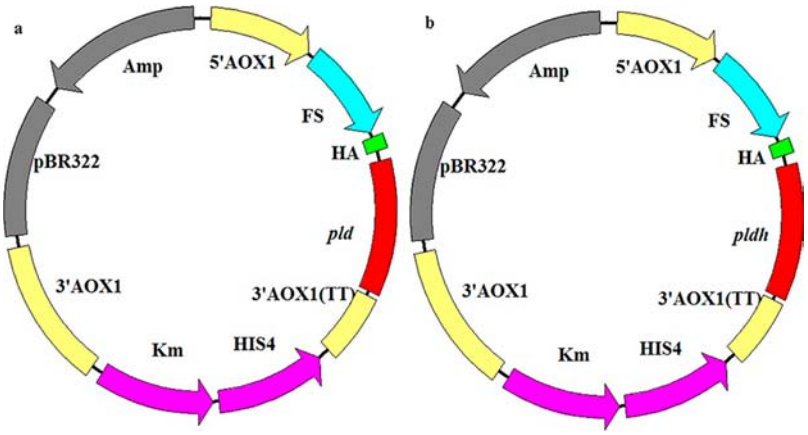

Figure 1. Schematic diagram of (a) plasmid pKFS-*pld* and (b) plasmid pKFS-*pldh* encoding the PLD protein.

not shown). To determine the effect of diethyl ether on the activity of dPLD, 5 mL of the enzyme preparation (containing 40 U of dPLD) was added to 5 mL of diethyl ether in a final concentration of 50% and incubated at 37 °C for specific times at a rotor speed of 200 rpm. The residual enzymatic activity of dPLD was then determined under standard assay conditions.

Conversion of PC to PS. To obtain the optimum dPLD-catalyzed transphosphatidylation conditions, the reaction was carried out in biphasic systems with various volume ratios between buffer and organic solvent (2.0:1.0, 1.5:1.0, 1.0:1.0, 1.0:1.5, 1.0:2.0), in which PC (0.05, 0.1, 0.15, 0.2, 0.25, 0.3 M) was dissolved in the organic solvent phase (diethyl ether), whereas dPLD (1.0, 1.5, 2.0, 2.5, 3.0, 3.5, 4.0 U/mL) and serine (0.5, 1.0, 1.5, 2.0, 2.5, 3.0, 3.5 M) were dissolved in 0.2 M sodium acetate buffer phase (containing 0.1 M $CaCl_2$). The mixture was stirred vigorously at different reaction temperatures (20, 30, 40, 50, 60, 70 °C) and pH values (3.5, 4.0, 4.5, 5.0, 5.5, 6.0) for 6, 8, 10, 12, 14, or 16 h with different rotor speeds (200, 300, 400, 500, 600, 700 rpm) to obtain a homogeneous emulsion. The optimum sPLD (from *S. chromofuscus*)-catalyzed transphosphatidylation conditions was obtained as control. The amount of biotransformation reaction products was determined using HPLC. The transphosphatidylation conversion rate (%) of PC to PS was defined as the percentage of PS obtained compared with the initial PC.

Recycling of the dPLD. The repeated use of dPLD was investigated on the basis of the optimal reaction conditions. After one cycle of reaction finished, The yeast cells were harvested, washed with 0.2 M sodium acetate buffer (pH 4.5), and used for the next batch under the same conditions. Recyclability of dPLD was evaluated by the conversion rate (%) of PS in each batch.

High-Performance Liquid Chromatography (HPLC) Analysis. The phospholipids PC, PS, and PA in the reaction mixture were analyzed via high-pressure liquid chromatography using an Agilent 1200 Infinity HPLC (Palo Alto, CA, USA) equipped with an Agilent 1260 Infinity diode array detector (wavelength = 205 nm). The column (purchased from Waters, Milford, MA, USA) was a μPorasil 10 μm 125 Å (3.9 × 300 mm), which was maintained at 25 °C. The eluting solvent was acetonitrile/methanol/85% phosphoric acid (100:8:0.8, v/v) with the flow rate of 1.0 mL/min. Prior to sampling, the agitation was stopped, and the reaction mixture was left undisturbed until the two phases were completely separated. After solvent evaporation, the fraction residue was redissolved in normal hexane/isopropanol (70:30, v/v), and 10 μL of a solution containing phospholipids was directly injected into the HPLC column. The relative concentrations of phospholipids were estimated from the peak area of the integrator. Each phospholipid peak was determined via the elution retention time using a standard phospholipid solution.

RESULTS AND DISCUSSION

Comparison of Wild-Type *pld* and *pldh*. The *S. chromofuscus* PLD possesses unusual codons compared with condon usage of *P. pastoris*. It has been shown that a correlation existed between the codon bias of a gene and its expression levels in a given organism. Codon optimization has been shown to be effective for maximizing the production of heterologous proteins in yeast.[24,25] Thus, consistent with the codon usage frequency of *P. pastoris* using the statistical method, the *pld* codons were optimized. The synthesized 1533 bp *pldh* showed 74% homology with the wild-type *pld*. Compared with the *pld*, the synthesized *pldh* contains 404 nucleotide variations, involving 396 of 511 codons. Meanwhile, the overall GC content of the synthesized *pldh* was reduced to 49.38 from 72.02%.

Construction of Yeast Strains for the Cell Surface Display of PLD. Yeast surface display is a powerful technique that is used to engineer proteins with enhanced affinity, specificity, stability, and catalytic activity. Several studies have successfully employed engineered yeast cells to display lipases on their surfaces as biocatalysts such as *C. antarctica* lipase B, *Rhizopus oryzae* lipase, and *Rhizomucor miehei* lipase.[22,26,27]

In this study, the yeast surface display system of *P. pastoris* was employed to immobilize PLD. The *pld* and *pldh* were ligated into the expression vector pKFS of *P. pastoris* to generate the plasmids pKFS-*pld* and pKFS-*pldh* (Figure 1). The recombinant plasmids were then linearized by *Sal*I and electroporated into *P. pastoris* GS115 to obtain the pKFS-*pld*/GS115 and pKFS-*pldh*/GS115, in which the recombinant PLD was displayed on the yeast cell surface by FS and its secretion signal peptide.

Localization of dPLD in *P. pastoris* and dPLD Activity Assay. To examine whether the dPLD was indeed displayed on the surface of *P. pastoris*, the cells that displayed PLD on GS115/pKFS-*pld* and GS115/pKFS-*pldh* were examined by immunofluorescence microscopy. As shown in Figure 2, the cells containing the recombinant vectors pKFS-*pld* and pKFS-*pldh* were labeled with green fluorescence on the surface, whereas the control cells containing pKFS were not fluorescent. This observation confirmed that dPLD was successfully displayed on the cell surface of the yeast.

Following induction, the activity of the *P. pastoris* cells that displayed PLD on GS115/pKFS-*pld* and GS115/pKFS-*pldh* and the culture supernatant were examined. As shown in Figure 3, the activity of PLD displayed on GS115/pKFS-*pldh* was higher compared to the PLD displayed on GS115/pKFS-*pld* after induction, whereas the activity of the culture supernatant was negligible. Meanwhile, the activity of PLD displayed on

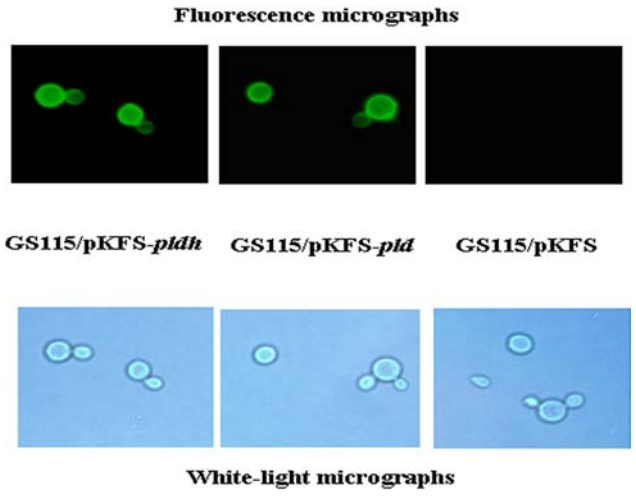

Figure 2. Immunofluorescent labeling of PLD on the cell surface of *Pichia pastoris* cells harboring the plasmids pKFS-*pld* and pKFS-*pldh*. The cells were immunologically labeled with the anti-HA antibody as the first antibody and FITC-conjugated anti-IgG as the second antibody. Control cells (GS115/pKFS) showed no fluorescence.

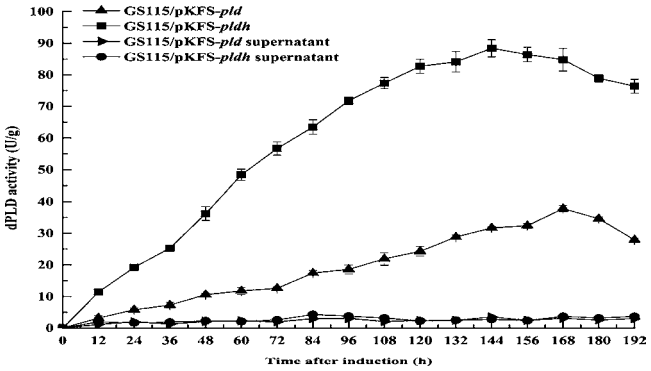

Figure 3. Activity of dPLD expressed on the surface of recombinant *Pichia pastoris* harboring pKFS-*pld* and supernatant at different induction times. Activity of dPLD expressed on the surface of recombinant *Pichia pastoris* harboring pKFS-*pldh* and supernatant at different induction times. The activity of dPLD on the surface of *P. pastoris* and supernatant was determined by sampling 10 mL of the fermentation broth and assaying the activity of cells and supernatant. The data points represent the mean ± SD (error bars) of three independent experiments.

GS115/pKFS-*pldh* reached a maximum of 88.4 U/g after 144 h of culture, which was 2.8 times that of PLD displayed on GS115/pKFS-*pld*. These results demonstrated that the PLD was all firmly immobilized on the yeast cell surface and the production of PLD was improved by codon optimization of *pld*.

Characterization of the dPLD. The enzymatic characteristics of dPLD were determined and compared with those of sPLD from *S. chromofuscus*. The optimum temperature for activity was increased after the enzyme was displayed on the yeast surface. The sPLD showed the highest activity at 50 °C, whereas the dPLD showed a maximum activity at 55 °C. At a temperature of 65 °C, the sPLD was nearly inactive, whereas the dPLD maintained >90% of its optimal activity (Figure 4a). The stability of the enzyme was determined by incubating the enzyme at various temperatures, ranging from 20 to 65 °C, for 1 h. As shown in Figure 4b, the residual enzyme activity of the dPLD was 72.3% after incubation at 60 °C for 1 h, whereas the sPLD lost >80% of its initial activity. Moreover, after 1 h of

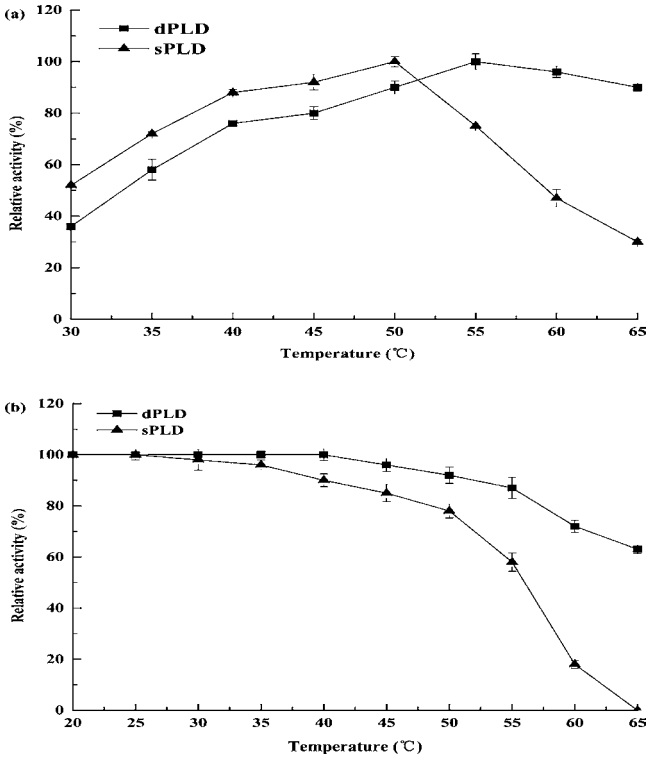

Figure 4. (a) Effects of temperature on PLD. Influence of temperature on dPLD and sPLD activity was investigated by assaying the activity from 30 to 65 °C in 50 mM sodium acetate buffer (pH 8.0). (b) Effects of temperature on PLD stability. Thermostability of the dPLD and sPLD was studied by incubation at various temperatures ranging from 20 to 65 °C at pH 8.0 for 1 h. The residual activity was then measured under standard conditions. The data points represent the mean ± SD of three replicates.

incubation at 65 °C, the sPLD had no detectable activity, whereas the remaining dPLD activity was 63.0%. On the basis of these results, dPLD was active over a broader temperature ranges and had a higher thermostability than sPLD, which is beneficial to industrial applications.

The activity of dPLD and sPLD at different pH values is shown in Figure 5a. The sPLD exhibited an optimal pH value at pH 7.0, whereas the dPLD had a maximum activity at pH 6.0. Interestingly, the dPLD maintained high activity at all pH ranges studied, whereas the sPLD showed dramatically decreased activity by moving 1 pH unit away from the optimal pH value. This might be related to the higher stability of the dPLD. Importantly, the yeast surface display also greatly enhanced the stability of the enzyme at the highest pH (11.0) and lowest pH (4.0) values studied (Figure 5b). Although the sPLD could not withstand incubation at pH 4.0 for 1 h, the dPLD retained >70% activity. These results suggested that the pH stability of the dPLD was significantly improved by immobilization on the yeast cell surface. Thus, dPLD showed the property of acid stability, which might serve as a basis for further application in industry.

Tolerance of PLD Activity to Organic Solvents. The synthesis of PS by PLD is usually performed in biphasic systems consisting of water-insoluble diethyl ether. The tolerance of PLD to diethyl ether was investigated by determining the stability of the enzyme in diethyl ether at 37 °C for 60 h. The activity of sPLD showed a rapid decline, whereas that of dPLD was maintained. Compared with the

dx.doi.org/10.1021/jf405836x | J. Agric. Food Chem. 2014, 62, 5354−5360

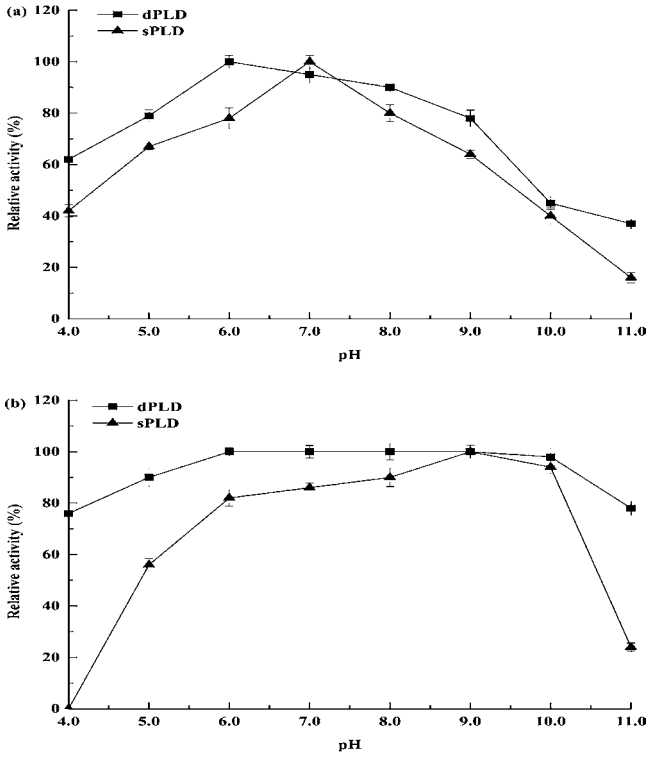

Figure 5. (a) Effects of pH on PLD. Optimal pH was determined by assaying the dPLD and sPLD at various pH values (pH 4.0−6.0, 50 mM sodium acetate buffer; pH 7.0−8.0, 50 mM potassium phosphate buffer; pH 9.0−11.0, 50 mM Tris-HCl buffer), at a temperature of 37 °C. (b) Effects of pH on PLD stability. Influence of pH on stability of dPLD and sPLD was determined by preincubating the PLD in solutions at various pH values, ranging from 4.0 to 11.0, at 25 °C for 1 h. The residual activity was then measured under standard conditions. The data points represent the mean ± SD of three replicates.

sPLD, which retained only 12.4% of its initial activity after incubation for 30 h, dPLD could maintain 63.1% residual activity (Figure 6). After 40 h of incubation, the sPLD showed no detectable activity, whereas the remnant dPLD activity was 53.8%.

When PLD was displayed on the cell surface of *P. pastoris*, the stability of dPLD in organic solvents was significantly enhanced, which was beneficial to the application of PLD in the synthesis of PS.

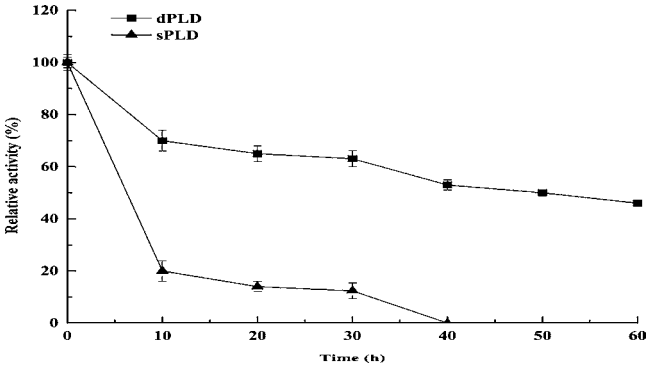

Figure 6. Effect of diethyl ether at a concentration of 50% (v/v) (5 mL of diethyl ether/5 mL of enzyme liquid) on dPLD and sPLD activities. The time course of the remaining PLD activity was assayed under previously described standard conditions. The data points represent the mean ± SD of three replicates.

Conversion of PC to PS. In this enzymatic reaction, several factors, including the volume ratios between buffer and organic solvent, PC concentrations, dPLD concentrations, serine concentrations, pH value, reaction temperature, reaction time, and rotor speed, can affect PS yield. In view of this, the effects of these parameters on the reaction were assayed to maximize PS yield.

The conversion rate of PC catalyzed by dPLD was compared with those of sPLD. Under optimum conditions (buffer/diethyl ether ratio 1.0:1.0, 0.1 M PC, 3.0 U/mL dPLD, 2.0 M serine, pH 4.5, 40 °C, rotor speed 600 rpm), 67.5% of PC in the reaction system could be converted by dPLD within 10 h, whereas the sPLD could convert 86.7% of PC in its optimum reaction conditions (data not shown). These results indicated that the dPLD on the surface of *P. pastoris* had the correct spatial configuration and could convert PC to PS with high efficiency. The dPLD had several advantages through display PLD on the yeast cell surface. By standard fermentation, dPLD could be readily produced as a yeast whole cell biocatalyst; thus, no further work was required to either purify or immobilize the enzymes. Furthermore, when compared with sPLD, dPLD exhibited favorable thermostability, acid stability, and organic solvent tolerance.

Operational Stability of dPLD. In industrial applications, recycling of PLD is required to reduce the production costs. Thus, the operational stability of dPLD was examined. The dPLD whole cells were recovered by centrifugation after each batch reaction, followed by washing with 0.2 M sodium acetate buffer (pH 4.5), and then added to fresh reactants. The result showed that the conversion rate of PS was >50% after seven batches (Figure 7), indicating that the dPLD whole cell biocatalyst exhibits a relatively good operational stability and that it is particularly suitable for conversion of PC to PS.

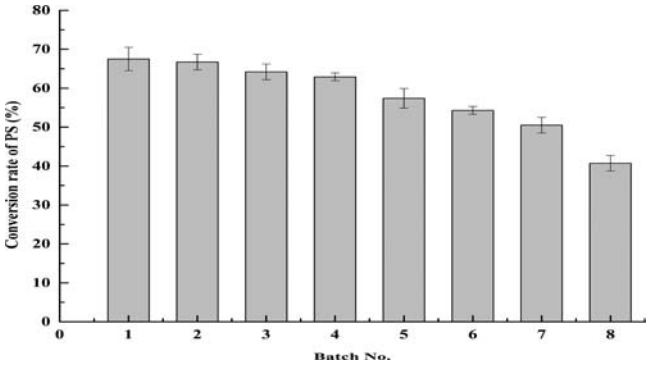

Figure 7. Investigation of repeated use of dPLD. After one cycle of reaction finished, the yeast cells were harvested, washed with 0.2 M sodium acetate buffer (pH 4.5), and used for the next batch under the same conditions. The conversion rate of PS in each detected batch (from the first to the eighth batch) was calculated. The data points represent the mean ± SD of three replicates.

The yeast cell surface display is a convenient method for preparing soluble, correctly folded recombinant proteins with native activity. Recently, several studies have successfully used yeast cells displaying recombinant proteins on their surfaces as whole cell biocatalysts, such as lipase from the fungus *Geotrichum* sp. for enriching eicosapentaenoic acid and docosahexaenoic acid in fish oil[28] and linoleic acid isomerase

from *Propionibacterium acnes* for bioconversion of linoleic acid to conjugated linoleic acids.[29] Here we report successful PLD display on the cell surface of *P. pastoris*. Previous studies on the enzymatic synthesis of PS involved the use of sPLD. For instance, sPLD from *Actinomadura* sp. was used for PS synthesis using a bile salt mixed micelle system, achieving a transphosphatidylation conversion rate of 57% after 24 h.[30] PS synthesis with the conversion rate up to 88% was also documented using the sPLD from *Streptomyces racemochromogenes*.[31] However, PLD-associated costs are still a major limiting factor for a sPLD-based process for efficient commercial PS production. In this study, we have demonstrated that the dPLD on the surface of *P. pastoris* converted 67.5% of PC to PS within 10 h. Although the PS yield was relatively lower compared with some of the sPLD-based process, the conversion rate of PS remained >50% after seven batches. Moreover, the thermostability, acid stability, and organic solvent tolerance of the dPLD were significantly enhanced compared with the sPLD. Considering the relatively high cost of sPLD, PLD-displaying whole cell biocatalysts might be particularly suitable for cost-effective PS production.

AUTHOR INFORMATION

Corresponding Author

*(F.L.) Mail: College of Biotechnology, Tianjin University of Science and Technology, No. 29 13th Avenue, Tianjin Economic and Technological Development Area, Tianjin 300457, China. Phone: 086 + 022 + 60601958. Fax: 086 + 022 + 60602298. E-mail: lfp@tust.edu.cn.

Funding

This work was supported by the National High-Tech Research and Development Plan ("863" Plan) (2013AA102106-07), the Tianjin Research Program of Application Foundation and Advanced Technology (14JCYBJC23800), the program for Changjiang Scholars and Innovative Research Team in University (IRT1166), and the National Natural Science Fund (31101219) of China.

Notes

The authors declare no competing financial interest.

ACKNOWLEDGMENTS

We are grateful to Professor Ying Lin (South China University of Technology) for providing technical assistance.

ABBREVIATIONS USED

PLD, phospholipase D; dPLD, displayed phospholipase D; sPLD, secreted phospholipase D; PC, phosphatidylcholine; PS, phosphatidylserine; PA, phosphatidic acid; *pld*, phospholipase D gene; *pldh*, codon-optimized phospholipase D gene; YPD, yeast extract−peptone−dextrose; BMGY, buffered glycerol complex; BMMY, buffered minimal methanol; YNB, yeast nitrogen base; EDTA, ethylenediaminetetraacetic acid

REFERENCES

(1) Leiros, I.; McSweeney, S.; Hough, E. The reaction mechanism of phospholipase D from *Streptomyces* sp. strain PMF snapshots along the reaction pathway reveal a pentacoordinate reaction intermediate and an unexpected final product. *J. Mol. Biol.* **2004**, *339*, 805−820.

(2) Kato-Kataoka, A.; Sakai, M.; Ebina, R.; Nonaka, C.; Asano, T.; Miyamori, T. Soybean-derived phosphatidylserine improves memory function of the elderly Japanese subjects with memory complaints. *J. Clin. Biochem. Nutr.* **2010**, *47*, 246−255.

(3) Claro, F. T.; Patti, C. L.; Abilio, V. C.; Filho, R. F.; Silva, R. H. Bovine brain phosphatidylserine attenuates scopolamine induced amnesia in mice. *Prog. Neuro−psychopharmacol. Biol. Psychiatry* **2006**, *30*, 881−886.

(4) Hirayama, S.; Masuda, Y.; Rabeler, R. Effect of phosphatidylserine administration on symptoms of attention-deficit/hyperactivity disorder in children. *Agro Food Ind. Hi-Tech.* **2006**, *17*, 16−20.

(5) Starks, M. A.; Starks, S. L.; Kingsley, M.; Purpura, M.; Jager, R. The effects of phosphatidylserine on endocrine response to moderate intensity exercise. *J. Int. Soc. Sports Nutr.* **2008**, *5*, 5−11.

(6) Ogino, C.; Negi, Y.; Matsumiya, Y.; Nakaoka, K.; Kondo, A.; Kuroda, S. Purification, characterization, and sequence determination of phospholipase D secreted by *Streptoverticillium cinnamoneum*. *J. Biochem.* **1999**, *125*, 263−269.

(7) Hatanaka, T.; Negishi, T.; Kubota-Akizawa, M.; Hagishita1, T. Purification, characterization, cloning and sequencing of phospholipase D from *Streptomyces septatus* TH-2. *Enzyme Microb. Technol.* **2002**, *31*, 233−241.

(8) Servi, S. Phospholipases as synthetic catalysts. *Top. Curr. Chem.* **1999**, *200*, 127−158.

(9) Chiaki, O.; Yukinari, N.; Hidenori, D.; Masayuki, K.; Akihiko, K.; Shun'ichi, K.; Katsuyuki, T.; Nobuaki, S.; Hideki, F. Identification of novel membrane-bound phospholipase D from *Streptoverticillium cinnamoneum*, possessing only hydrolytic activity. *Biochim. Biophys. Acta* **2001**, *1530*, 23−31.

(10) Chiaki, O.; Shunichi, K.; Shinji, T.; Akihiko, K.; Nobuaki, S.; Katsuyuki, T.; Hideki, F. Phospholipase D from *Streptoverticillium cinnamoneum*: protein engineering and application for phospholipid production. *J. Mol. Catal. B−Enzym.* **2003**, *23*, 107−115.

(11) Alexandra, L.; Johanna, M.; Ines, S.; Regina, S.; Helge, K. B.; Renate, U. Two highly homologous phospholipase D isoenzymes from *Papaver somniferum* L. with different transphosphatidylation potential. *Biochim. Biophys. Acta* **2005**, *1737*, 94−101.

(12) Tadashi, H.; Tomofumi, N.; Megumi, K.; Tairo, H. Study on thermostability of phospholipase D from *Streptomyces* sp. *Biochim. Biophys. Acta* **2002**, *1598*, 156−164.

(13) Wang, X. M. Multiple forms of phospholipase D in plants: the gene family, catalytic and regulatory properties, and cellular functions. *Prog. Lipid Res.* **2000**, *39*, 109−149.

(14) Sahyun, H.; Hiroyuki, H.; Akinori, O. Molecular cloning of a phospholipase D gene from *Aspergillus nidulans* and characterization of its deletion mutants. *FEMS Microbiol. Lett.* **2003**, *224*, 231−237.

(15) Masashi, H. k.; Tatuya, S.; Teruyuki, K.; Yoshikazu, I.; Koretaro, T. Conversion to docosahexaenoic acid-containing phosphatidylserine from squid skin lecithin by phospholipase D-mediated transphosphatidylation. *J. Agric. Food Chem.* **2000**, *48*, 4550−4554.

(16) Nemanja, M.; Aleksandra, N.; Katja, L. Immobilization of biocatalysts for enzymatic polymerizations: possibilities, advantages, applications. *Bioresour. Technol.* **2012**, *115*, 126−135.

(17) Lee, G. Y.; Jung, J. H.; Seo, D. H.; Hansin, J.; Ha, S. J.; Cha, J.; Kim, Y. S.; Park, C. S. Isomaltulose production via yeast surface display of sucrose isomerase from *Enterobacter* sp. FMB-1 on *Saccharomyces cerevisiae*. *Bioresour. Technol.* **2011**, *102*, 9179−9184.

(18) Ueda, M.; Tanaka, A. Cell surface engineering of yeast: construction of arming yeast with biocatalyst. *J. Biosci. Bioeng.* **2000**, *90*, 125−136.

(19) Tanaka, T.; Yamada, R.; Ogino, C.; Kondo, A. Recent developments in yeast cell surface display toward extended applications in biotechnology. *Appl. Microbiol. Biotechnol.* **2012**, *95*, 577−591.

(20) Li, P. Z.; Anumanthan, A.; Gao, X. G.; Ilangovan, K.; Suzara, V. V.; Düzgüneş, N.; Renugopalakrishnan, V. Expression of recombinant proteins in *Pichia pastoris*. *Appl. Biochem. Biotechnol.* **2007**, *142*, 105−124.

(21) Jiang, Z. B.; Song, H. T.; Gupta, N.; Ma, L. X.; Wu, Z. B. Cell surface display of functionally active lipases from *Yarrowia lipolytica* in *Pichia pastoris*. *Protein Express. Purif.* **2007**, *56*, 35−39.

(22) Su, G. D.; Huang, D. F.; Han, S. Y.; Zheng, S. P.; Lin, Y. Display of *Candida antarctica* lipase B on *Pichia pastoris* and its application to

flavor ester synthesis. *Appl. Microbiol. Biotechnol.* **2010**, *86*, 1493−1501.
(23) Uhm, T. B.; Li, T.; Bao, J.; Chung, G.; Ryu, D. D. Y. Analysis of phospholipase D gene from *Streptoverticillium reticulum* and the effect of biochemical properties of substrates on phospholipase D activity. *Enzyme Microb. Technol.* **2005**, *37*, 641−647.
(24) Graham, S.; Francis, Y. M. C. Synonymous codon usage bias and the expression of human glucocerebrosidase in the methylotrophic yeast, *Pichia pastoris*. *Protein Express. Purif.* **2002**, *26*, 96−105.
(25) Chang, S.-W.; Lee, G.-C.; Shaw, J.-F. Codon optimization of *Candida rugosa lip*1 for improving expression in *Pichia patoris* and biochemical characterization of the purified recombinant LIP1 lipase. *J. Agric. Food Chem.* **2006**, *54*, 815−822.
(26) Tanino, T.; Fukuda, H.; Kondo, A. Construction of a *Pichia pastoris* cell-surface display system using Flo1p anchor system. *Biotechnol. Prog.* **2006**, *22*, 989−993.
(27) Han, Z. L.; Han, S. Y.; Zheng, S. P.; Lin, Y. Enhancing thermostability of a *Rhizomucor miehei* lipase by engineering a disulfide bond and displaying on the yeast cell surface. *Appl. Microbiol. Biotechnol.* **2009**, *85*, 117−126.
(28) Pan, X. X.; Xu, L.; Zhang, Y.; Xiao, X.; Wang, X. F.; Liu, Y.; Zhang, H. J.; Yan, Y. J. Efficient display of active *Geotrichum* sp. lipase on *Pichia pastoris* cell wall and its application as a whole-cell biocatalyst to enrich EPA and DHA in fish oil. *J. Agric. Food Chem.* **2012**, *60*, 9673−9679.
(29) Farmani, J.; Roohvand, F.; Safari, M.; Aghasadeghi, M. R.; Razavi, S. H.; Motevalli, F. Cell surface display of *Propionibacterium acnes* linoleic acid isomerase by *Pichia pastoris*. *Rom. Biotechnol. Lett.* **2013**, *18*, 8307−8316.
(30) Pinsollea, A.; Roy, P.; Buré, C.; Thienpont, A.; Cansell, M. Enzymatic synthesis of phosphatidylserine using bile salt mixed micelles. *Colloid Surf. B* **2013**, *106*, 191−197.
(31) Chen, S.; Xu, L.; Li, Y.; Hao, N.; Yan, M. Bioconversion of phosphatidylserine by phospholipase D from *Streptomyces racemochromogenes* in a microaqueous water-immiscible organic solvent. *Biosci. Biotechnol.* **2013**, *77*, 1939−1941.
(32) Tanino, T.; Fukuda, H.; Kondo, A. Construction of a *Pichia pastoris* cell-surface display system using Flo1p anchor system. *Biotechnol. Prog.* **2006**, *22*, 989−993.
(33) Liang, X. X.; Wang, B. B.; Sun, Y. F.; Lin, Y.; Han, S. Y.; Zheng, S. P.; Cui, T. B. Quantitative evaluation of *Candida antarctica* lipase B displayed on the cell surface of a *Pichia pastoris* based on an FS anchor system. *Biotechnol. Lett.* **2013**, *35*, 367−374.

and genotype. However, reports on the genetic analysis of the genotype by environment interaction effects for the polyphenol content and antioxidant capacity in whole grain rice have been rare.

Twenty rice accessions including cultivars, germplasm lines, and landraces were introduced from the OryzaSNP project[20] and used in this study. These rice materials have been well sequenced and have been used in the genetic diversity analyses for root growth and drought avoidance responses,[20−22] water uptake,[23] biomass traits,[24] and nutritional components of cooked rice.[25] This panel has also been used to identify genes and genetic pathways that are critical to biomass traits[24] and nutritional components in cooked rice.[25] While in this study, the set was planted in the winter season of year 2011 and 2012 in Hainan province (South China), and the objectives were to investigate the genotype, environment, and genotype × environment effects for the polyphenol and antioxidant capacity traits. In addition, we identified single nucleotide polymorphism (SNP) loci that were strongly associated with these traits using the association mapping approach.

MATERIAL AND METHODS

Rice Materials. Twenty rice accessions (*Oryza sativa* L.) including cultivars, germplasm lines, and landraces were introduced from the OryzaSNP project (http://www.oryzasnp.org/),[20] and these included 5 genotypes with red pericarp and 15 with white. All the accessions were planted in 2 years in Lingshui, Hainan province, China. Ten rows with six plants per row were planted for each accession in the field with two replications per year. The seeds were sowed in early December of 2010 and 2011, managed using nutrient and pest control procedures to ensure the production in this area, and harvested in April of 2011 and 2012, respectively. Hereafter, 2 years (environments) are denoted 2011 and 2012 for when the grain was harvested.

The grains were air-dried to a moisture content of about 12%, stored at room temperature for 2 months and then at 4 °C in the dark, until all the grain materials were obtained. The samples were dehulled on a Satake Rice Machine (Satake Co., Tokyo, Japan) and milled to pass through a 100 mesh sieve on a Cyclone sample mill (UDY Corporation, Fort Collins, CO, U.S.A.).

Chemicals. Analytical grade methanol, hexane, and sulfuric acid were purchased from Sinopharm (Sinopharm Chemistry Reagent Co., Ltd., Shanghai, China). Sodium carbonate, aluminum chloride, sodium nitrite, potassium peroxydisulfate, sodium hydroxide, and vanillin were purchased from BBI (Toronto, ON, Canada). Folin−Ciocalteu reagent, gallic acid, catechin, DPPH (1,1- diphenyl-2-picrylhydrazyl radical, Trolox (6-hydroxy-2,5,7,8-tetramethylchroman-2-carboxylic acid), and ABTS (2,2-azino-bis-(3-ethylbenzothiazoline-6-sulfonic acid) diammonium salt) were purchased from Sigma (St. Louis, MO, U.S.A.).

Extraction. Before extraction, 0.5 g of whole grain flour was defatted twice with 10 mL of hexane, and the mixture was shaken on an oscillator at 250 rpm (HZ-9210K Desktop frozen oscillator, Jiangsu, China) for 30 min at room temperature. After centrifuging at 10 000*g* (Sorvall ST16R, Thermo Scientific, Osterode, Germany) for 10 min, the residue was dried at room temperature in a fume hood and then extracted with 10 mL of 80% methanol twice. After shaking at 250 rpm for 45 min per extraction, the mixture was centrifuged at 10 000*g* for 15 min. The supernatants of each duplicate extraction were collected and combined together, and they were stored at −20 °C for further analysis. Duplicate extractions were carried out for each sample.

Determination of Total Phenolic Content (TPC). TPC was determined using the method of Folin−Ciocalteu assay[26] modified by Shen et al.[8] Appropriately diluted sample extracts or standard solutions (200 μL) were mixed thoroughly with 1.5 mL of 10-fold-diluted Folin−Ciocalteu reagent. After incubating for about 5 min, 1.5 mL of saturated sodium carbonate (75 g/L) was subsequently added to the mixture. After reacting for 2 h at room temperature in dark, the absorbance of the resulting blue color was measured by a spectrophotometer (UNICAM UV300, Thermo scientific, England, Britain) at 725 nm. TPC was expressed as milligrams of gallic acid equivalent per 100 g of rice flour (mg GAE/100 g). Duplicate determinations were conducted for each extract.

Determination of Total Flavonoid Content (TFC). TFC was assayed using a colorimetric method with minor modifications.[8,27] In short, 150 μL of 5% $NaNO_2$ was mixed with 500 μL of the appropriately sample diluted extracts or standard solutions in 15 mL polypropylene tubes and then incubated for 5 min. After adding 150 μL of 10% $AlCl_3{\cdot}6H_2O$ and allowing 5 min of reaction time, 1 mL NaOH (1 M) and then 3 mL ddH_2O were added. Before measuring the absorbance at 510 nm, the contents were thoroughly mixed and reacted for about 10 min. TFC was expressed as milligrams of catechin equivalent per 100 g of rice flour (mg CAE/100 g). Duplicate determinations were conducted for each extract.

Determination of Total Proanthocyanidin Content (TPAC). TPAC was measured by the method of vanillin assay with slight modifications.[28] Two solutions were prepared before measurement: (A) 1% vanillin solution in methanol; (B) sulfuric acid/methanol solution (1:4, V/V). Appropriately diluted sample extracts or standard solutions (0.6 mL) were added to 1.5 mL of solution A and mixed thoroughly. They were then allowed to react with 1.5 mL of solution B for 20 min in a 30 °C water bath. The absorbance was measured at 500 nm. In order to eliminate interferences (e.g., anthocyanins, which are present mainly in black rice), samples treated with 100% methanol instead of solution A were used as blank. TPAC was expressed as mg catechin equivalent per 100 g sample (mg CAE/100 g). Duplicate determinations were conducted for each extract.

Determination of DPPH Radical Scavenging Activity. The DPPH assay was conducted as described before.[29] The DPPH working solution (100 μmol/L) was prepared by using methanol. Appropriately diluted extracts or standards (200 μL) were mixed with 3 mL of DPPH solution. The absorbance was measured at 517 nm after incubating for 45 min in the dark. The DPPH scavenging activity (%) of both samples and standard (Trolox) was calculated as follows:

$$\text{DPPH\%} = (1 - A_{\text{sample}}/A_{\text{control}})\,100\%$$

The results were expressed as Trolox equivalent DPPH radical scavenging activity per 100 g of sample (μmol TE/100 g). Duplicate determinations were conducted for each extract.

Determination of $ABTS^{\bullet+}$ Radical Scavenging Activity. Total antioxidant capacity was carried out using a spectrophotometer by the improved $ABTS^{\bullet+}$ radical cation method, as described previously.[8,30] The aqueous $ABTS^{\bullet+}$ stock solution was prepared using 7 mM ABTS and 2.45 mM potassium peroxydisulfate (V/V = 2:1) and agitated overnight. The $ABTS^{\bullet+}$ working solution was diluted by methanol to adjust the

Table 1. Mean Square Values from Analysis of Variance for TPC, TFC, TPAC, ACA, and ACD from 20 Rice Varieties Grown in 2 Years[a]

source	df	TPC	TFC	TPAC	ACA	ACD
genotype	19	157929.0***	49746.8***	18576.7***	14361644.6***	9911461.7***
year	1	6581.2***	627.8***	173.2***	599947.5***	288264.1***
year × genotype	19	2501.9***	501.3***	353.5***	223167.1***	129792.5***

[a]*** indicates the significant level at 0.001. TPC: total phenolic content; TFC: total flavonoid content; TPAC: total proanthocyanidins content; ACD: antioxidant capacity (DPPH); ACA: antioxidant capacity ($ABTS^{\bullet+}$).

Table 2. TPC, TFC, TPAC, ACA, and ACD of 20 Rice Varieties in 2011 and 2012

		2011					2012				
genotype	color	TPC[b]	TFC[c]	TPAC[c]	ACA[d]	ACD[d]	TPC[b]	TFC[c]	TPAC[c]	ACA[d]	ACD[d]
Azucena	white	39.8	19.1	0	230.8	119.7	47.9	23.7	0	280.6	155.7
Dom Sufid	white	42.1	21.3	0	225.8	117.5	40.6	23.1	0	267.8	139
Dular	white	42.2	22.3	0	253.8	167.7	44	23.3	0	304.4	169
IR64-21	white	53	20.2	0	329	205.6	53.1	22.5	0	329	210.6
M202	white	63.7	23.6	0	380.4	236.6	65.9	26.9	0	416.5	246.6
Minghui63	white	50.1	26.6	0	288.5	161.8	59.5	31.8	0	344.2	206.7
Moroberekan	white	45.5	24.1	0	285.5	137.2	50.4	26.4	0	322.3	160.4
N22	white	46.9	23.1	0	309.5	140.7	48.8	25.6	0	308	169.2
Nipponbare	white	59	23.8	0	318.2	171.8	64.9	22	0	392.2	223.5
Sadu-Cho	white	45.7	21.6	0	260.3	147.5	47.9	21.3	0	351.5	182.8
SHZ-2	white	55.8	18.6	0	329.6	212.1	58.4	20.3	0	408.1	257
Swarna	white	49	21.7	0	266.7	171.4	48.9	20.7	0	359.4	188.2
Tainung67	white	55.8	24.7	0	313.6	182.1	65.7	26.3	0	431.9	255.8
Zhenshan97B	white	61.6	22.3	0	396.3	234.9	56.9	23.1	0	392.6	222.3
Cypress	white	59.8	22.6	0	409.7	233	66.3	23.9	0	490.7	272.6
FR13A	red	539.5	304	171.8	5004.3	4155.9	477.3	258	128.2	4487.7	3567.6
LTH	red	430.7	238.6	122.6	3852.7	3197.3	497.3	263.9	130.5	4317.5	3875.2
Pokkali	red	450.6	251.7	123.8	3914.4	3402.6	637.5	333	190.4	5914	4726.5
Aswina	red	257.6	152	49.1	2449.4	1834.7	280	152.2	56	2661.9	2029.7
Rayada	red	562.1	327.7	206.3	5514.5	4329.4	662.1	353.9	227.3	6016.3	4702.3
	mean	150.5	80.5	33.7	1266.7	978	168.7	86.1	36.6	1439.8	1098
	LSD[a]	13.9	7	3.9	161	167.2	14.1	9.7	9	172.6	90

[a]LSD: least significant difference ($P < 0.05$). [b]The results are presented as mg of gallic acid equivalent/100 g of rice. [c]The results are presented as mg of catechin equivalent/100 g of rice. [d]The results are presented as μmol of Trolox equivalent/100 g of rice.

absorbance to 0.700 ± 0.020 at 734 nm. Appropriately diluted extracts or standard solution (0.1 mL) were mixed with $ABTS^{\bullet+}$ working solution (3.9 mL) and reacted for about 6 min before measuring the absorbance at 734 nm. Results were expressed as μmol of Trolox equivalent antioxidant capacity per 100 g of rice flour (μmol TEAC/100 g). Duplicate determinations were conducted for each extract.

Statistical Analysis. All the chemical parameters were measured at least in duplicate. Data analyses were performed with the SAS program version 8 (SAS Institute Inc., Cary, NC, U.S.A.). Analysis of variance (ANOVA) was carried out to determine genotypic and environmental variation among the parameters using the general linear model procedure (Proc glm). Means of different genotypes and environments were determined using Proc means, followed by Tukey multiple comparison tests at $P < 0.05$. Correlation analysis among the parameters in (or between) the two environments were conducted by Proc corr procedure.

Genotype Data and Association Mapping. The publically available genotype data were downloaded from the Gramene Web site (http://www.gramene.org/) on March 10, 2013. During downloading, we first removed the reference genome data, and we then filtered sites with the following parameters: minimum count was 16 out of 20 sequences, and minimum frequency was set at 0.25. Finally, a total of 32 655 SNPs distributed in 12 chromosomes were downloaded.[31]

The population structure (Q) among the 20 rice accessions was performed using the software package STRUCTURE version 2.2.[32] The optimum number of populations was three.[31] Principle component analysis (PCA) was calculated and input into association mapping, which was performed with GAPIT.[33] To avoid the probability of spurious association between markers and traits, six models (i.e., ANOVA, K (Kinship), P (PCA), Q (structure), P + K, Q + K) were compared with GAPIT,[33] and the best model for each trait was chosen according to the Bayesian information criterion (BIC) value. The results with the best model were presented at the significance level of $P < 0.005$.

RESULTS

Analysis of Variations for Nutritional Parameters. ANOVA indicated that TPC, TFC, TPAC, ACA, and ACD differed dramatically among 20 genotypes. The genotypic variance accounted for 94.56%, 97.78%, 97.24%, 94.58%, and 95.95% of the total variation, respectively (Table 1). Effects of year were significant, with all traits slightly higher in 2012 than in 2011 harvested seed (Table 1; Table 2). In addition, G ×

Table 3. Correlation Analysis of TPC, TFC, TPAC, ACA, and ACD in 2 Years[a]

	TPC	TFC	TPAC	ACA	ACD
TPC	**0.979*****	0.999***	0.992***	0.998***	0.999***
TFC	0.999***	**0.982*****	0.991***	0.998***	0.998***
TPAC	0.989***	0.990***	**0.965*****	0.992***	0.990***
ACA	0.998***	0.999***	0.989***	**0.975*****	0.997***
ACD	0.999***	0.999***	0.986***	0.998***	**0.978*****

[a]*** indicate significance at 0.001 levels; below diagonal: 2011; above diagonal: 2012; in diagonal: 2011 and 2012.

year were also significant ($P < 0.001$), although in total they explained less than 5% of the total variance (Table 1).

The selected rice materials had different phytochemicals and antioxidant activities (Table 2). The average TPAC, TPC, TFC, and ACD levels were similar in the 2 years. However, ACA differed significantly ($P < 0.05$) between the 2 years with the average values of 1266.7 in 2011 and 1439.8 in 2012 (Table 2). TPAC was only detected in red rice, so it was not surprising that red rice had higher TPC, TFC, ACA, and ACD than white rice. Among the red rice, Rayada was significantly high for TPAC, TPC, TFC, ACA, and ACD. Conversely, Aswina was consistently low, and LTH, Pokkali, and FRI3A were almost the same. Among the white rice, the TPC, TFC, ACA, and ACD ranged from 39.8 to 63.7 mg GAE/100 g, from 18.6 to 26.6 mg CAE/100 g, from 225.8 to 409.7 μmol TE/100 g, and from 117.5 to 236.6 μmol TE/100 g, respectively, in 2011, and ranged from 40.6 to 66.3 mg GAE/100 g, from 20.3 to 31.8 mg CAE/100 g, from 267.8 to 490.7 μmol TE/100 g, and from 139.0 to 272.6 μmol TE/100 g, respectively, in 2012. The ranges of ACA and ACD between 2 years were different in white and red rice. For ACA and ACD of white rice, there were about 1 and 0.5 μm TEAC/g differences across 2 years, whereas for that of red rice, there were 20 and 10 μm TEAC/g differences due to environmental effects.

Correlation Analysis. The correlation coefficients among TPAC, TPC, TFC, ACA, and ACD of 20 genotypes in 2 years are listed in Table 3. The correlations among TPAC, TPC, TFC, ACA, and ACD were at the significant level of 0.001. The correlation coefficients between 2 years were more than 0.96 ($P < 0.001$), also suggesting that these traits were quite stable across different planting years.

Association Mapping. Given the distinct population structure among three subspecies (*indica*, *japonica*, and *aus*) of the 20 rice accessions,[20] the optimal model was first chosen according to BIC values using GAPIT.[33] Six models (i.e., ANOVA, K (kinship), P (PCA with the principal components ranging from 1 to 3), Q (structure), P + K, and Q + K) were compared (Supplementary Table 1). For TPC, the Q model was the best for the 2011 data, and ANOVA was the best for the 2012 data. For the traits of TFC, TPAC, and ACA, the P2 was the best model for the 2011 data, and ANOVA was the best for the 2012 data. For ACD, the K model was the best one in both years' data (Supplementary Table 1). Then, the strong association signals were identified with the best model at $P < 0.005$, discarding all but the most significant signals for each parameter if there was an excess of strong associations (Table 4). Manhattan plots of association mapping results are shown in Figure 1. In the year of 2011, there were more peaks for the TFC, TPAC, ACA, and ACD than those in 2012.

In total, we identified 23 unique loci for TPC, TFC, TPAC, ACA, and ACD in the 2 years, and they were mainly located on chromosomes 1, 4, 6, and 12 (Figure 2). The locus at 34 679 495 bp on chromosome 1 and the locus at 27 875 425bp on chromosome 4 were associated with TPC, TFC, ACA, and ACD in the 2 years. The locus at 11 522 358 bp on chromosome 1, the locus at 5 416 397 bp on chromosome 2, the locus at 1 585 914 bp on chromosome 3, and the locus at 27 240 579 bp on chromosome 6 were associated with TFC, TPAC, ACA, and ACD in the year of 2011, but no such associations were found in 2012. On the contrary, the locus at 25 206 526 bp on chromosome 12 was significantly associated with TFC, TPAC, ACA, and ACD in the year of 2012, but it was not detected in 2011.

TPC was mainly affected by genotype, and the same significant association signals on chromosome 1, 4, and 12 were identified in 2 years. The minor allele frequencies of qPC1, qPC12, and qPC4 were 0.20, 0.25, and 0.20, respectively, with the former two having negative effects and the latter one having positive effects in both years.

The QTLs of qFC1-2 and qFC4 on chromosome 1 and 4, respectively, were significantly associated with TFC in both years. Both alleles had the same minor allele frequencies of 0.20. When the major allele (T) of qFC1-2 was replaced by the minor allele (C), TFC decreased by 129.30 mg CAE/100 g in 2011 and decreased by 116.90 mg CAE/100 g in 2012. However, the change from major allele (C) to minor allele (T) of qFC4 caused the increase of the TFC in the 2 years. The QTLs of qFC1-1, qFC2, qFC3, and qFC6 located on chromosome 1, 2, 3, and 6, respectively, were only detected in 2011, whereas the QTLs of qFC5 and qFC12 were only detected in 2012.

The QTLs for TPAC were mainly located on chromosome 1, 4, 6, and 7 with more QTLs detected in 2011 than detected in 2012. The QTLs of qPAC4/qPAC4-3 and qPAC12-2 were almost at the same position as qPC4/qFC4 and qPC12/qFC12, respectively. qPAC1-1, qPAC2-2, qPAC3, and qPAC6-2 were allelic to qFC1-1, qFC2, qFC3, qFC6 for TFC. Two groups of QTLs had the same minor allele frequency and P value in 2011: (1) qPAC2-1, qPAC7-1, qPAC7-2, qPAC7-3, qPAC8, and qPAC11; (2) qPAC1-2, qPAC1-3, qPAC4-1, qPAC4-2, qPAC4-3, qPAC6-3, and qPAC6-4. These loci were clearly derived from the linkage disequilibrium in the same chromosome (i.e., chromosome 4 and 7) or from different chromosomes. In 2012, there were only three significant signals associated with TPAC (qPAC1, qPAC4, qPAC12-2).

The antioxidant capacity was measured with two methods: $ABTS^{\bullet+}$ and DPPH radical scavenging capacities. The significant association signals with the two methods were almost the same except that the qACA5 was detected only in 2012 for the ABTS. qACA3/qACD3 had the highest signals in Manhattan plots in 2011 by ABTS and DPPH (Figure 1). The QTLs of qACA1-2/qACD1-2 and qACA4/qACD4 on chromosome 1 and 4, respectively, were detected in 2 years. The QTLs of qACA1-1/qACD1-1, qACA2/qACD2, and qACA6/qACD6 were detected only in 2011, whereas qACA12/qACD12 was detected only in 2012.

Table 4. Significantly Associated QTLs for TPC, TFC, TPAC, ACA, and ACD Detected in 2 Years by Association Mapping

trait	year	QTL	chromosome	position (bp)	major allele	minor allele	minor allele frequency	*P* value	effect
TPC	2011	qPC1	1	34 679 495	T	C	0.20	2.05×10^{-3}	−209.14
		qPC4	4	27 875 425	C	T	0.20	2.30×10^{-3}	181.93
		qPC12	12	25 206 526	T	A	0.25	3.24×10^{-3}	−175.16
	2012	qPC1	1	34 679 495	T	C	0.20	2.24×10^{-3}	−213.51
		qPC4	4	27 875 425	C	T	0.20	2.03×10^{-3}	216.17
		qPC12	12	25 206 526	T	A	0.25	2.93×10^{-3}	−190.86
TFC	2011	qFC1-1	1	11 522 358	C	T	0.45	4.53×10^{-3}	−111.41
		qFC1-2	1	34 679 495	T	C	0.20	4.09×10^{-3}	−129.93
		qFC2	2	5 416 397	G	T	0.40	4.05×10^{-3}	−118.28
		qFC3	3	1 585 914	T	A	0.45	2.43×10^{-3}	163.77
		qFC4	4	27 875 425	C	T	0.20	3.90×10^{-3}	101.21
		qFC6	6	27 240 579	A	G	0.35	4.50×10^{-3}	147.67
	2012	qFC1-2	1	34 679 495	T	C	0.20	2.04×10^{-3}	−116.90
		qFC4	4	27 875 425	C	T	0.20	2.03×10^{-3}	116.91
		qFC5	5	26 712 196	A	G	0.25	4.67×10^{-3}	98.23
		qFC12	12	25 206 526	T	A	0.25	2.67×10^{-3}	−104.50
TPAC	2011	qPAC1-1	1	11 522 358	C	T	0.45	3.79×10^{-3}	−68.24
		qPAC1-2	1	14 757 889	C	T	0.45	4.87×10^{-3}	96.06
		qPAC1-3	1	41 712 845	A	T	0.45	4.87×10^{-3}	96.06
		qPAC2-1	2	34 701 916	C	T	0.50	4.96×10^{-3}	−100.16
		qPAC2-2	2	5 416 397	G	T	0.40	3.63×10^{-3}	−71.73
		qPAC3	3	1 585 914	T	A	0.45	1.90×10^{-3}	100.97
		qPAC4-1	4	19 373 019	G	T	0.45	4.87×10^{-3}	96.06
		qPAC4-2	4	23 417 930	A	G	0.45	4.87×10^{-3}	96.06
		qPAC4-3	4	28 192 972	C	T	0.45	4.87×10^{-3}	96.06
		qPAC6-1	6	23 929 475	G	A	0.45	4.67×10^{-3}	65.74
		qPAC6-2	6	27 240 579	A	G	0.35	4.00×10^{-3}	89.66
		qPAC6-3	6	8 723 274	C	T	0.45	4.87×10^{-3}	96.06
		qPAC6-4	6	14 391 022	C	G	0.45	4.87×10^{-3}	96.06
		qPAC7-1	7	17 424 069	G	A	0.50	4.96×10^{-3}	100.16
		qPAC7-2	7	25 566 351	G	T	0.50	4.96×10^{-3}	100.16
		qPAC7-3	7	7 473 184	G	A	0.50	4.96×10^{-3}	−100.16
		qPAC8	8	21 040 886	C	T	0.50	4.96×10^{-3}	−100.16
		qPAC9	9	16 181 486	T	G	0.45	3.58×10^{-3}	86.91
		qPAC11	11	8 416 957	C	A	0.50	4.96×10^{-3}	−100.16
		qPAC12-1	12	3 878 067	C	T	0.45	4.78×10^{-3}	−76.21
	2012	qPAC1	1	34 679 495	T	C	0.20	2.63×10^{-3}	−69.91
		qPAC4	4	27 875 425	C	T	0.20	2.63×10^{-3}	69.91
		qPAC12-2	12	25 206 526	T	A	0.25	3.49×10^{-3}	−62.31
ACA	2011	qACA1-1	1	11 522 358	C	T	0.45	4.61×10^{-3}	−1838.54
		qACA1-2	1	34 679 495	T	C	0.20	4.36×10^{-3}	−2129.19
		qACA2	2	5 416 397	G	T	0.40	3.76×10^{-3}	−1976.60
		qACA3	3	1 585 914	T	A	0.45	2.12×10^{-3}	2757.63
		qACA4	4	27 875 425	C	T	0.20	3.95×10^{-3}	1671.00
		qACA6	6	27 240 579	A	G	0.35	4.16×10^{-3}	2469.73
	2012	qACA1-2	1	34 679 495	T	C	0.20	1.98×10^{-3}	−2042.25
		qACA4	4	27 875 425	C	T	0.20	1.78×10^{-3}	2068.24
		qACA5	5	26 712 196	A	G	0.25	4.51×10^{-3}	1717.90
		qACA12	12	25 206 526	T	A	0.25	2.62×10^{-3}	−1823.09
ACD	2011	qACD1-1	1	11 522 358	C	T	0.45	4.24×10^{-3}	−1566.70
		qACD1-2	1	34 679 495	T	C	0.20	4.29×10^{-3}	−1797.67
		qACD2	2	5 416 397	G	T	0.40	4.14×10^{-3}	−1624.66
		qACD3	3	1 585 914	T	A	0.45	2.44×10^{-3}	2280.93
		qACD4	4	27 875 425	C	T	0.20	4.16×10^{-3}	1397.49
		qACD6	6	27 240 579	A	G	0.35	4.97×10^{-3}	2027.55
	2012	qACD1-2	1	34 679 495	T	C	0.20	2.18×10^{-3}	−1678.88
		qACD4	4	27 875 425	C	T	0.20	2.08×10^{-3}	1675.74
		qACD12	12	25 206 526	T	A	0.25	2.94×10^{-3}	−1490.07

dx.doi.org/10.1021/jf500951e | J. Agric. Food Chem. 2014, 62, 5361−5368

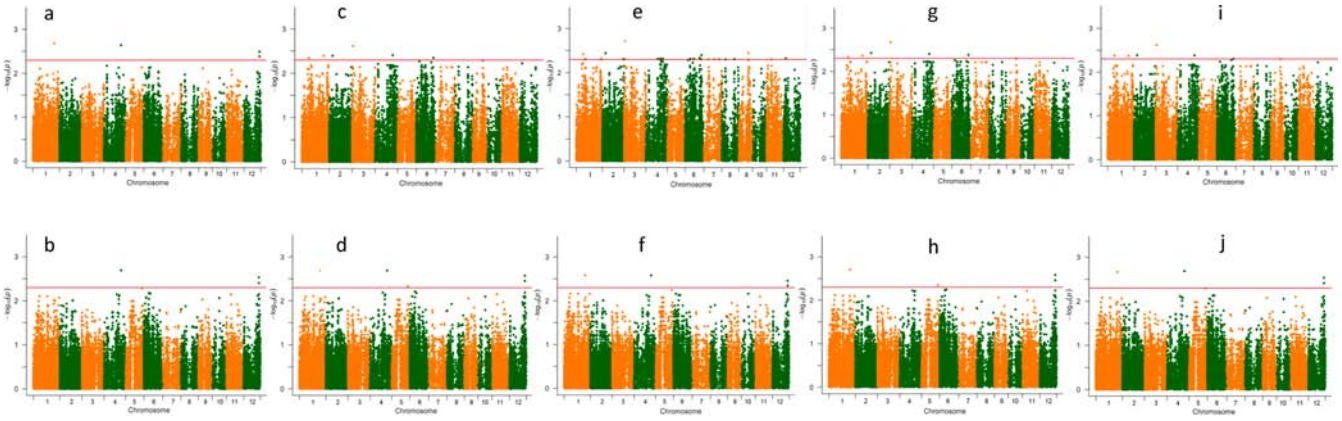

Figure 1. Manhattan plots of the association mapping of polyphenol and antioxidant capacity traits in 2 years. TPC (a, 2011; b, 2012), TFC (c, 2011; d, 2012), TPAC (e, 2011; f, 2012), ACA (g, 2011; h, 2012), and ACD (i, 2011; j, 2012).

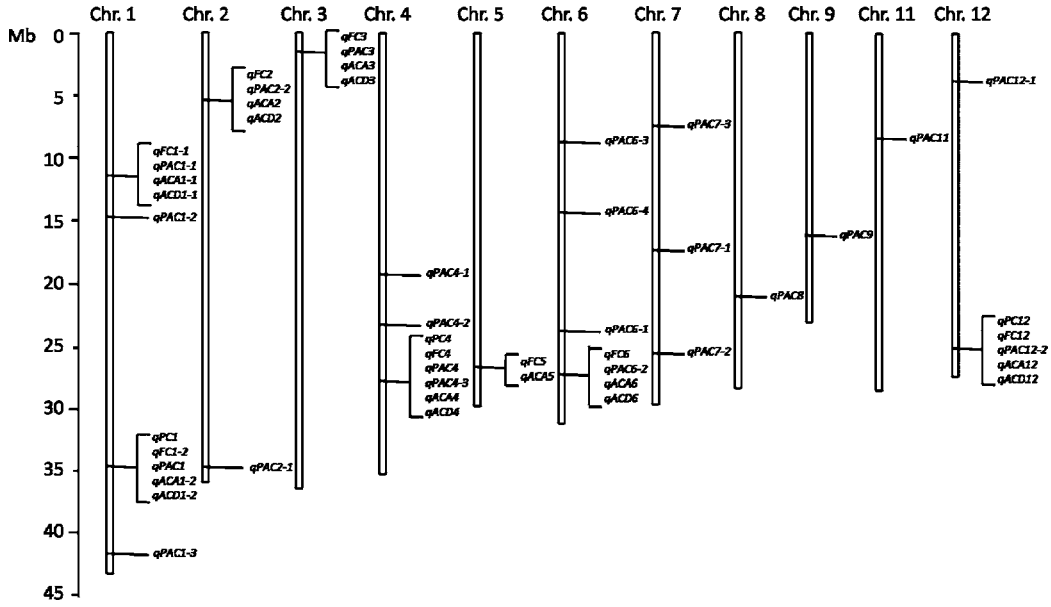

Figure 2. Positions of QTLs in rice chromosomes detected by association study.

DISCUSSION

The 20 rices in this study have been widely used in genetic diversity and genetic mapping studies.[21−25] Genomic regions and SNPs have been identified for biomass traits[24] and nutritional components in cooked rice.[25] In this study, the 20 rices have been used to study the genetic diversity in the polyphenols and antioxidant capacity traits of whole grain rice (Table 2). Total phenolic, flavonoid, proanthocyanidin contents, and total antioxidant capacity of rice grain are affected by heredity as well as environment (Table 1). An ANOVA showed that TPC, TFC, TPAC, ACA, and ACD are mainly affected by genotype, which indicated that the content of polyphenols and the antioxidant capacity of rice grain were controlled by certain genes (Table 1). The high correlation between 2 years also suggested that these traits are quite stable across different years and genotypes (Table 3). The high correlations found among these five traits may be due to pleiotropy or genetic linkage. Plant breeders could either improve correlated traits simultaneously or reduce undesirable side effects when improving only one of the correlated traits.[34]

Red-pericarp grain accumulates proanthocyanidin,[5] which had significantly higher TPC, TFC, and antioxidant capacity than white rice (Table 2). The color of red rice is controlled by two loci, brown pericarp and seed coat (*Rc*) and red pericarp and seed coat (*Rd*), which are located on chromosome 7 and 1, respectively.[9] *Rc* encodes a transacting regulatory factor with a bHLH motif, and *Rd* encodes a DFR protein which is a key enzyme in the biosynthesis of proanthocyanidin.[9,10] These two loci present together will produce red seed color, whereas the absence of *Rc* or *Rd* will produce no phenotype or brown seed color.[9] Association mapping with 416 rice accessions including red rice and black rice showed that *Rc* and *Ra* were the main effect loci associated with TPC, TFC, and antioxidant capacity.[14] Genetic analysis with a double haploid population derived from a cross between *japonica* and weedy rice showed that pericarp color was associated with the major genes of *Rc* and *Rd*.[13] One QTL identified in this study, qPAC7-3 (7 473 184 bp) was significantly associated with TPAC, which is near to *Rc* (6 061 890−6 068 318 bp). The signal was only detected in 2011 but not in 2012, indicating that environment affected TPAC. Three QTLs on the chromosome 1 were associated with TPAC, but none of them were near to the *DFR* locus at the 25 382 714 bp position. *Rd*, as a structural gene, should express in red-pericarp rice. No detectable QTL signal for

dx.doi.org/10.1021/jf500951e | J. Agric. Food Chem. 2014, 62, 5361−5368

TPAC at the *DFR* locus might be due to the small population and few red rice involved. It also might be due to other QTLs flanking this locus but showing an opposite effect.

One locus at the position of 27 875 425 bp on chromosome 4 was significant for all five traits. It is very close to the *Ra* gene (27 764 248−27 770 504 bp). Previous study also identified the *Ra* locus for these traits by association mapping with 416 rice accessions including red rice and black rice.[14] The color of black rice is controlled by two loci, *Pb* (*Prp-b*) and *Pp* (*Prp-a*), located on chromosome 4 and 1, respectively.[12] Wang and Shu suggested that the *Ra* gene may be the *Pb* gene and that the purple pericarp characteristic of rice is caused by two bases deletion (GT) within exon 7 of the *Ra*.[35] However, there is no black rice in this study. It is plausible that other genes or regulatory factors nearby may affect polyphenol biosynthesis, such as *Plw-OsB1* and *Plw-OsB2*.[36]

In addition to the loci which colocate at the major genes, we also identified other QTLs that associated with rice polyphenol and antioxidant capacity traits. The QTL cluster on chromosome 1, qFC1-1/qPAC1-1/qACA1-1/qACD1-1, was around the QTL detected for antioxidant capacity by linkage mapping in a double haploid population.[15] qPC1/qFC1-2/qACA1-2/qACD1-2 could be detected in the 2 years, so it might be a new important locus affecting the nutritional quality of the whole grain. Similarly, qPC12/qFC12/qPAC12-2/qACA12/qACD12 and qPAC2-1 were nearby the QTLs detected for TPC and TFC by linkage mapping.[15]

In conclusion, we conducted an association study for polyphenol contents and antioxidant capacity traits among 20 rice accessions. With 32 655 SNPs, a total of 23 unique loci have been identified using the best model selected from ANOVA, K, P, Q, P + K, and Q + K models. The peak signals at five loci (qPAC7-3, qPC4, qPC12, qFC1-1, and qPAC2-1) were very close to previously identified genes or QTLs. Among these five loci, qPAC7-3 was near to *Rc*, and qPC4 was near to *Ra*. The qPC1/qFC1-2/qACA1-1/qACD1-1 cluster could be detected in the two environments. However, the loci of qFC1-1/qPAC1-1/qACA1-1/qACD1-1, qFC2/qPAC2-2/qACA2/qACD2, qFC3/qPAC3/qACA3/qACD3, qFC6/qPAC6-2/qACA6/qACD6, and qFC12/qPAC12-2/qACA12/qACD12 were easily affected by environment, and were only detected in one year. Results of the present study demonstrated that association mapping in rice is an effective method to find more potential loci for polyphenol and antioxidant capacity traits. The loci could be further finely tagged with candidate genes and applied in maker-assisted selection to improve the polyphenol and antioxidant capacity traits in whole grain rice. Functional studies of the candidate genes are also needed to reveal their connections to the known phenotypes (i.e., polyphenol content and antioxidant activities) at the molecular biological levels.

■ ASSOCIATED CONTENT

Supporting Information

Supplementary Table 1. Bayesian information criterion (BIC) value (the larger the better) for the choice of the best model for each polyphenol and antioxidant capacity trait for association mapping. This material is available free of charge via the Internet at http://pubs.acs.org.

■ AUTHOR INFORMATION

Corresponding Author

*E-mail: jsbao@zju.edu.cn. Fax: +86-571-86971421. Tel.: +86-571-86971932.

Funding

This work was financially supported by the Special Fund for Agro-Scientific Research in the Public Interest (no. 201103007) from the Ministry of Agriculture.

Notes

The authors declare no competing financial interest.

■ ACKNOWLEDGMENTS

We thank Dr. Kenneth L. McNally of the International Rice Research Institute for providing the rice materials used in this study.

■ ABBREVIATIONS USED

ACA,antioxidant capacity measured with $ABTS^{\bullet+}$; ACD,antioxidant capacity measured with DPPH; ANOVA,analysis of variance; QTL,quantitative trait locus; SNP,single nucleotide polymorphism; TFC,total flavonoid content; TPAC,total proanthocyanidins content; TPC,total phenolic content

■ REFERENCES

(1) Slavin, J. Whole grains and human health. *Nutr. Res. Rev.* **2004**, *17*, 99−100.

(2) Liu, R. H. Whole grain phytochemicals and health. *J. Cereal Sci.* **2007**, *46*, 207−219.

(3) U.S. Department of Agriculture. Department of Health and Human Services. Nutrition and Your Health: Dietary Guidelines for Americans. Washington, DC, 2005 (http://www.health.gov/dietaryguidelines/dga2005/document/).

(4) U.S. Department of Agriculture; Department of Health and Human Services. Nutrition and Your Health: Dietary Guidelines for Americans. Washington, DC, 2010 (http://www.cnpp.usda.gov/dietaryguidelines.htm).

(5) Gunaratne, A.; Wu, K.; Li, D.; Bentota, A.; Corke, H.; Cai, Y. Z. Antioxidant activity and nutritional quality of traditional red-grained rice varieties containing proanthocyanidins. *Food Chem.* **2013**, *138*, 1153−1161.

(6) Min, B.; Gu, L. W.; McClung, A. M.; Bergman, C. J.; Chen, M. H. Free and bound total phenolic concentrations, antioxidant capacities, and profiles of proanthocyanidins and anthocyanins in whole grain rice (*Oryza sativa* L.) of different bran colours. *Food Chem.* **2012**, *133*, 715−722.

(7) Shao, Y. F.; Xu, F. F.; Sun, X.; Bao, J. S.; Beta, T. Phenolic acids, anthocyanins, and antioxidant capacity in rice (*Oryza sativa* L.) grains at four stages of development after flowering. *Food Chem.* **2014**, *143*, 90−96.

(8) Shen, Y.; Jin, L.; Xiao, P.; Lu, Y.; Bao, J. S. Total phenolics, flavonoids, antioxidant capacity in rice grain and their relations to grain color, size, and weight. *J. Cereal Sci.* **2009**, *49*, 106−111.

(9) Sweeney, M. T.; Thomson, M. J.; Pfeil, B. E.; McCouch, S. R. Caught red-handed: *Rc* encodes a basic helix−loop−helix protein conditioning red pericarp in rice. *Plant Cell* **2006**, *18*, 283−294.

(10) Furukawa, T.; Maekawa, M.; Oki, T.; Suda, I.; Iida, S.; Shimada, H.; Takamure, I.; Kadowaki, K. I. The Rc and Rd genes are involved in proanthocyanidin synthesis in rice pericarp. *Plant J.* **2007**, *49*, 91−102.

(11) Gu, X. Y.; Foley, M. E.; Horvath, D. P.; Anderson, J. V.; Feng, J.; Zhang, L.; Mowry, C. R.; Ye, H.; Suttle, J. C.; Kadowaki, K.; Chen, Z. Association between seed dormancy and pericarp color is controlled by a pleiotropic gene that regulates abscisic acid and flavonoid synthesis in weedy red rice. *Genetics* **2011**, *189*, 1515−1524.

(12) Yoshimura, A.; Ideta, O.; Iwata, N. Linkage map of phenotype and RFLP markers in rice. *Plant Mol. Biol.* **1997**, *35*, 49−60.

(13) Bres-Patry, C.; Lorieux, M.; Clément, G.; Bangratz, M.; Ghesquière, A. Heredity and genetic mapping od domestication-related traits in a temperate *japonica* weedy rice. *Theor. Appl. Genet.* **2001**, *102*, 118−126.
(14) Shao, Y. F.; Jin, L.; Zhang, G.; Lu, Y.; Shen, Y.; Bao, J. S. Association mapping of grain color, phenolic content, flavonoid content and antioxidant capacity in dehulled rice. *Theor. Appl. Genet.* **2011**, *122*, 1005−1016.
(15) Jin, L.; Xiao, P.; Lu, Y.; Shao, Y. F.; Shen, Y.; Bao, J. S. Quantitative trait loci for brown rice color, phenolics, flavonoid contents, and antioxidant capacity in rice grain. *Cereal Chem.* **2009**, *86*, 609−615.
(16) Zhu, C.; Gore, M.; Buckler, E. S.; Yu, J. Status and prospects of association mapping in plants. *Plant Genome* **2008**, *1*, 5−20.
(17) Mpofu, A.; Sapirstein, H. D.; Beta, T. Genotype and environment variation in phenolic content, phenoliv acid composition, and antioxidant activity of hard spring wheat. *J. Agric. Food Chem.* **2006**, *54*, 1265−1270.
(18) Yu, L.; Haley, S.; Perret, J.; Harris, M. Comparison of wheat flours grown at different locations for their antioxidant properties. *Food Chem.* **2004**, *86*, 11−16.
(19) Bellato, S.; Ciccoritti, R.; Del Frate, V.; Sgrulletta, D.; Carbone, K. Influence of genotype and environment on the content of 5-n alkylresorcinols, total phenols and on the antiradical activity of whole durum wheat grains. *J. Cereal Sci.* **2006**, *57*, 162−269.
(20) McNally, K. L.; Childs, K. L.; Bohnert, R.; Davidson, R. M.; Zhao, K.; Ulat, V. J.; Zeller, G.; Clark, R. M.; Hoen, D. R.; Bureau, T. E.; Stokowski, R.; Ballinger, D. G.; Frazer, K. A.; Cox, D. R.; Padhukasahasram, B.; Bustamante, C. D.; Weigel, D.; Mackill, D. J.; Bruskiewich, R. M.; Rätsch, G.; Buell, C. R.; Leung, H.; Leach, J. E. Genomewide SNP variation reveals relationships among landraces and modern varieties of rice. *Proc. Natl. Acad. Sci. U.S.A.* **2009**, *106*, 12273−12278.
(21) Henry, A.; Gowda, V. R.; Torres, R. O.; McNally, K. L.; Serraj, R. Variation in root system architecture and drought response in rice (*Oryza sativa*): Phenotyping of the OryzaSNP panel in rainfed lowland fields. *Field Crops Res.* **2011**, *120*, 205−214.
(22) Shrestha, R.; Al-Shugeairy, Z.; Al-Ogaidi, F.; Munasinghe, M.; Radermacher, M.; Vandenhirtz, J.; Price, A. H. Comparing simple root phenotyping methods on a core set of rice genotypes. *Plant Biol.* **2014**, *16*, 632−642.
(23) Gowda, V. R.; Henry, A.; Vadez, V.; Shashidhar, H. E.; Serraj, R. Water uptake dynamics under progressive drought stress in diverse accessions of the OryzaSNP panel of rice (*Oryza sativa*). *Funct. Plant Biol.* **2012**, *39*, 402−411.
(24) Jahn, C. E.; Mckay, J. K.; Mauleon, R.; Stephens, J.; McNally, K. L.; Bush, D. R.; Leung, H.; Leach, J. E. Genetic variation in biomass traits among 20 diverse rice varieties. *Plant Physiol.* **2011**, *155*, 157−168.
(25) Heuberger, A. L.; Lewis, M. R.; Chen, M. H.; Brick, M. A.; Leach, J. E.; Ryan, E. P. Metabolomic and functional genomic analyses reveal varietal differences in bioactive compounds of cooked rice. *PLoS One* **2010**, *5* (9), e12915.
(26) Singleton, V. L.; Orthofer, R.; Lamuela-Raventos, R. M. Analysis of total phenols and other oxidation substrate and antioxidants by means of Folin-Ciocalteu reagent. *Methods Enzymol.* **1999**, *299*, 152−178.
(27) Jia, Z.; Tang, M.; Wu, J. The determination of flavnoid contents in mulberry and their scavenging effects on superoxide radicals. *Food Chem.* **1999**, *64*, 555−559.
(28) Sun, B.; Ricardo-da-Silva, J. M.; Spranger, I. Critical factors of vanillin assay for catechins and proanthocyanidins. *J. Agric. Food Chem.* **1998**, *46*, 4267−4274.
(29) Brand-Williams, W.; Cuvelier, M. E.; Berset, C. Use of a free radical method to evaluate antioxidant activity. *LWT-Food Sci. Technol.* **1994**, *28*, 25−30.
(30) Re, R.; Pellegrini, N.; Proteggente, A.; Pannala, A.; Yang, M.; Rice-Evans, C. Antioxidant activity applying an improved ABTS radical cationdecolorization assay. *Free Radical Biol. Med.* **1999**, *26*, 1231−1237.
(31) Xu, F. F.; Tang, F. F.; Shao, Y. F.; Chen, Y. L.; Tong, C.; Bao, J. S. Genotype × environment interactions for agronomic traits of rice revealed by genome-wide association mapping. *Rice Sci.* **2014**, *21*, 133−141.
(32) Pritchard, J. K.; Stephens, M.; Donnelly, P. Inference of population structure using multilocus genotype data. *Genetics* **2000**, *155*, 945−959.
(33) Lipka, A. E.; Tian, F.; Wang, Q.; Peiffer, J.; Li, M.; Bradbury, P. J.; Gore, M. A.; Buckler, E. S.; Zhang, Z. GAPIT: genome association and prediction integrated tool. *Bioinformatics* **2012**, *28*, 2397−2399.
(34) Chen, Y.; Lübberstedt, T. Molecular basis of trait correlations. *Trends Plant Sci.* **2010**, *15*, 454−461.
(35) Wang, C. X.; Shu, Q. Y. Fine mapping and candidate gene analysis of purple pericarp gene Pb in rice (*Oryza sativa* L.). *Chin. Sci. Bull.* **2007**, *52*, 3097−3104.
(36) Sakamoto, W.; Ohmori, T.; Kageyama, K.; Miyazaki, C.; Saito, A.; Murata, M.; Noda, K.; Maekawa, M. The *Purple leaf* (*Pl*) locus of rice: The Pl^{w} allele has a complex organization and includes two genes encoding basic helix-loop-helix proteins involved in anthocyanin biosynthesis. *Plant Cell Physiol.* **2001**, *42*, 982−991.

amylases.[5,16,17] This could mean that the required diastatic power for sufficient starch degradation in rice malt could be lower than in barley malt. One of these amylolytic enzymes is limit dextrinase, a debranching enzyme which catalyzes the hydrolysis of the α-1,6-glucosidic linkages in starch and related oligosaccharides and exhibits activity levels in rice several-fold higher than in barley malt.[6,13] Another enzyme, α-glucosidase, shows high activity in rice malt and an optimum temperature of 55 °C, while in barley malt its activity is low and the optimum temperature is 35−40 °C. Above 50 °C in barley malt the enzyme is inactivated very rapidly.[18] Evidently the same enzyme can have different features in different cereals. But the suitability of rice malt for brewing depends not only on its enzymatic activity but also on an adequate gelatinization of the starch in a temperature range where the amylolytic enzymes are still active; otherwise the amylolytic enzymes cannot degrade the starch to fermentable sugars and dextrins. This gelatinization temperature is quite high for unmalted cereals, in the case of barley 70−80 °C, but it can be lowered, according to Narziß and Back,[4] up to 20 °C in the presence of enzymes. It depends on the malting conditions. So the high gelatinization temperature of rice (65−85 °C) should also be lowered after maltation. But there is no knowledge about the real optimal temperature range of the amylolytic enzymes of rice malt, which can differ from that of barley malt. Moreover Keßler[18] notes that the starch granules are already attacked by enzymes during germination, and therefore the starch can be also hydrolyzed below the gelatinization temperature. Therefore, the main objective was to verify the complete saccharification of the rice malt starch during mashing with the iodine test, because in this case gelatinization occurred and enough endogenous malt enzymes were present. And, given that the overall enzymatic activity of the rice malt depends on the malting conditions,[3,9,12] a key aspect of the study was to find the optimal malting parameters.

2. EXPERIMENTAL SECTION

2.1. Rice Samples. Ten paddy-rice varieties of *O. sativa* L. cultivated in Italy were examined. Eight belong to the subspecies japonica, Centauro, Creso, Selenio, Karnak, Arborio, Vialone Nano, Crono, and Balilla (respective amylose contents by percent: 16.3, 18.0, 18.1, 20.9, 17.3, 22.8, 16.4, 18.5),[19] and two to the subspecies indica, Sirio and Libero (respective amylose contents: 26.5 and 23.0).[19] Furthermore, three different samples of the Centauro variety were studied that differed in harvest year and origin.

2.2. Rice Analysis. The following quality attributes of the paddy-rice grains were determined in duplicate using the Analytica-EBC methods:[20] grain moisture (%), EBC method 3.2; thousand kernel weight (TKW, g), EBC method 3.4; total protein content (% dry matter (DM)), EBC method 3.3.1 (total $N \times 5.95$); the germinative energy and water sensitivity, modified EBC method 3.6.2 (germination temperature, 28 °C).

2.3. Micromalting. An automatic micromalting system from Custom Laboratory Products (Keith, Scotland), containing a steep and germination unit separate from the kilning unit, was used as previously described.[21]

2.4. Malting Procedure. *2.4.1. Steeping and Germination.* Three malting trials were performed. The first trial was performed by steeping the rice samples continuously in water at 28 °C for 47 h (steeping/germination A); the second, at 22 °C for 73 h (steeping/germination B). The third trial (steeping/germination C) was done under improved conditions (Figure 1). The total steeping and germination time for all trials was 8 days.

2.4.2. Kilning. Two kilning programs were tested with the green malt produced in trial steeping/germination B, one for 21 h at 50 °C (kilning program 1) and the other for 21 h at 50 °C, then 3 h at 72 °C, and finally 3 h at 82 °C (kilning program 2).

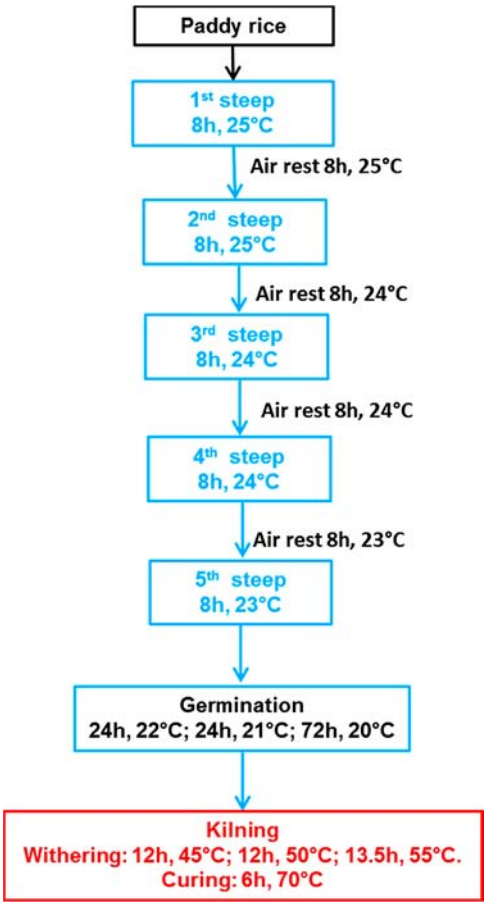

Figure 1. Improved malting conditions (steeping/germination C).

An improved kilning program was tested with the green malt produced in trial steeping/germination C (kilning program 3) (Figure 1).

2.5. Malt Quality. *2.5.1. Rice Malt Analysis.* Rice malt quality was assessed in duplicate using the following Analytica-EBC methods:[20] moisture content (%), EBC method 4.2; extract yield (% DM), iodine test/saccharification rate time (min), and filtration rate, EBC method 4.5.1, modified EBC method 4.5.1 (changing the temperature rests to 30 min at 45 °C, 30 min at 64 °C, and 30 min at 74 °C); colored malt extract, EBC method 5.5; total nitrogen content (% DM), EBC method 4.3.1; soluble nitrogen content (mg/L), soluble nitrogen content (% DM) as a portion of total nitrogen content (% DM), and Kolbach index, EBC method 4.9.1; free amino nitrogen content (FAN; mg/L), EBC method 4.10; viscosity (mPa s at 20 °C and 8.6 °P (from the Plato scale)), EBC method 4.8; apparent final attenuation (%), EBC method 4.11.1; diastatic power (Windisch−Kolbach units (WK)), EBC method 4.12; pH, EBC method 8.17; malt color, EBC method 4.7.1.

The activity of α-amylase, β-amylase, and limit dextrinase of malted rice was determined using the Megazyme Assay Kits.

The dimethyl sulfide (DMS) concentration was determined in the static headspace using a gas chromatograph equipped with a mass spectrometer coupled with an autosampler after sample preparation. DMS precursors were calculated as the difference between total and free DMS.[22]

Aspartic acid, glutamic acid, serine, threonine, arginine, histamine, methionine, valine, leucine, isoleucine, lysine, glycine, alanine, tyrosine, and phenylalanine were determined in rice malt worts by high-performance liquid chromatography (HPLC) quantifying the fluorescence of the orthophtaldialdehyde (OPA)/mercaptoethanol derivatives.[23,24]

dx.doi.org/10.1021/jf501462a | J. Agric. Food Chem. 2014, 62, 5369−5377

Table 1. Rice Grain Quality Attributes[a]

variety	subspecies	crop year	origin	moisture (%)	TKW (g)	germinative energy (%)	water sensitivity (%)	total protein (g/(100 g of DM))
Creso	*japonica*	2010	Sardinia	12.6a	26.6a	93a	91ad	8.51a
Selenio	*japonica*	2010	North Italy	13.6b	21.2bc	90a	90ad	6.31b
Karnak	*japonica*	2010	North Italy	11.9c	31.2d	77b	67b	7.32c
Arborio	*japonica*	2010	North Italy	13.2d	36.3e	87a	69b	9.52d
Vialone nano	*japonica*	2010	North Italy	11e	29.5f	63c	54c	9.40d
Centauro 1	*japonica*	2010	Sardinia	12.6a	23.3g	92a	91ad	8.87e
Sirio	*indica*	2010	Sardinia	12.8f	20.2bh	96a	93d	8.63a
Crono	*japonica*	2010	Sardinia	14g	21.8c	90a	87ad	9.16f
Libero	*indica*	2010	Sardinia	13.5bh	19.1g	94a	96d	9.58d
Centauro 2	*japonica*	2011	Sardinia	14.1g	21.3bc	90a	81a	8.51a
Centauro 3	*japonica*	2011	North Italy	13.4h	25.4a	93a	92d	7.62g
Balilla	*japonica*	2011	North Italy	13i	21.7c	90a	90ad	7.44g

[a] $n = 2$ repetition; TKW = thousand kernel weight; DM = dry matter. Values in the same column followed by a different letter are statistically different ($p \leq 0.05$).

Table 2. Optimization of the Malting Conditions[a]

	steeping/germination B and kilning 1[b]		steeping/germination B and kilning 2[c]		steeping/germination C and kilning 3[d]	
rice malt	diastatic power (WK)	moisture (%)	diastatic power (WK)	moisture (%)	diastatic power (WK)	moisture (%)
Creso	78a	6.7a′	56b	4.3b′	n.t.	n.t.
Centauro 1	42a	6.1a′	34b	4.3b′	42a	4.6c′
Sirio	118a	6.7a′	89b	4.4b′	n.t.	n.t.
Libero	n.t.	n.t.	69	4.6	n.t.	n.t.
Crono	n.t.	n.t.	5	4.5	n.t.	n.t.

[a] $n = 2$ repetitions; n.t. = not tested. Values in the same row followed by a different letter are statistically different ($p \leq 0.05$). [b]Steeping/germination B and kilning 1: 22 °C for 73 h (steeping)/22 °C for 120 h (germination) and 21 h at 50 °C (kilning1). [c]Steeping/germination B and kilning 2: 22 °C for 73 h (steeping)/22 °C for 120 h (germination) and 21 h at 50 °C, 3 h at 72 °C, and 3 h at 82 °C (kilning2). [d]Steeping/germination C and kilning 3: see Figure 1.

The carbohydrate concentration in rice malt worts was determined by HPLC coupled with evaporative light scattering detector (ELSD) as reported by Floridi et al.[25]

2.5.2. Mashing Tests To Improve Saccharification and FAN Content. The following mashing tests were utilized: 1, EBC method 4.5.1; 2, EBC method 4.5.1 with the addition of 10 mL of an aqueous solution of $CaCl_2 \cdot 2H_2O$ at a concentration of 22 g/L; 3, rice malt with acrospires and rootlets applying the EBC method 4.5.1 with the addition of 10 mL of an aqueous solution of $CaCl_2 \cdot 2H_2O$ at a concentration of 22 g/L; 4, EBC method 4.5.1 with modified temperature rests (30 min at 45 °C, 30 min at 64 °C, and 30 min at 74 °C); 5, EBC method 4.5.1 with modified temperature rests and the addition of 10 mL of an aqueous solution of $CaCl_2 \cdot 2H_2O$ at a concentration of 22 g/L; 6, EBC method 4.5.1 with modified temperature rests and the addition of 0.144 mL of lactic acid at a concentration of 80% (v/v).

2.6. Statistical Analysis. Statistical analysis was performed using SigmaPlot Software (version 11.0; Systat Software, Inc., San Jose, CA, USA). Comparisons of the different matrices were made by one-way repeated measures analysis of variance, and the results were further analyzed using the Holm-Sidak test and the Tukey test.

3. RESULTS AND DISCUSSION

The rice grain quality attributes of the different samples are reported in Table 1. The moisture content of the rice samples (11.0−14.1%) permitted their storage at low temperatures without pretreatment. The total protein content was in a range of 7.3−9.6% (w/w) and were higher in comparison to the values found in the literature for rice (5.8−7.7% (w/w));[26] however they were still low compared to brewing barley (10.5−11.5% (w/w)).[27] The protein content in brewing is very important for foam stability, taste, and yeast nutrition during fermentation, so the Selenio sample was excluded from malting because of its very low protein content of 6.3%. Of all rice varieties, Karnak, Arborio, and Vialone Nano showed higher TKW values, but they were lower than typical TKW values of barley (38−40 g).[28] The germinative energy gives information about the proportion of grains that will germinate under the conditions of a specified test,[29] and the corresponding EBC method (method 3.6.2) requires a germination temperature of 20 °C. In this study the germination temperature was set at 28 °C which is more appropriate for rice. The resulting values for the rice varieties Crono, Creso, Selenio, Centauro 1, Sirio, Libero, Centauro 2, Centauro 3, and Balilla were below 96%, which is a minimum for commercial brewing malt, but enough to try a pilot malting. They showed no water sensitivity. All of the samples with a good high germinative energy germinated on the third day. This indicates that kernel processing should be homogeneous during malting.[28] On the other hand, the varieties Karnak, Arborio and Vialone Nano have an inadequate germinative energy (77, 87, and 63%, respectively) and were water sensitive (67, 69, and 54%, respectively). Because these last values were likely due to the presence of mold, these samples were excluded from malting.

Three steeping/germination trials were done. Steeping/germination A and steeping/germination B were characterized by long and unusual steeping times, in order to favor the water uptake and solubilize any inhibitors for germination, the hull features of rice and barley being different. The steeping/germination A was performed with the varieties Creso, Centauro 1, and Sirio by steeping the rice continuously in water at 28 °C for 47 h to achieve 42−44% water uptake after

dx.doi.org/10.1021/jf501462a | J. Agric. Food Chem. 2014, 62, 5369−5377

Table 3. Quality Attributes of Centauro 1 Rice Malt Wort Obtained with Congress Mash[a]

	mashing test 1[b]	mashing test 2[c]	mashing test 3[d]
fine extract (% DM)	72.3a	72.7a	71.7a
saccharification time (min)	>60′	50	50
pH	5.96a	5.61a	5.76b
color (EBC-U)	2.0a	1.7a	1.8a
total nitrogen (g/(100 g of DM))	1.34a	1.34a	1.43b
soluble nitrogen (mg/L at 8.6 °P)	450a	482ab	506b
Kolbach index (%)	27.4a	29.5a	28.5a
viscosity (mPa s at 8.6 °P)	n.t.	1.40a	1.48b
free amino nitrogen (mg/L at 8.6 °P)	146a	148a	166b
fermentability (%)	n.t.	73.2a	71.2b

[a]n = 2 repetitions; DM = dry matter; n.t. = not tested. Values in the same row followed by a different letter are statistically different ($p \leq 0.05$). [b]Mashing test 1: A-EBC method 4.5.1. [c]Mashing test 2: A-EBC method 4.5.1 with the addition of $CaCl_2$ aqueous solution. [d]Mashing test 3: A-EBC method 4.5.1 with the addition of $CaCl_2$ aqueous solution, acrospires and rootlets.

steeping, which is necessary for good rice endosperm modification.[6] The resulting water uptake was 39, 40, and 38% for Creso, Centauro 1, and Sirio, respectively. After 8 days of steeping/germination there was clearly the odor of a mold infestation. To avoid a microbiological hazard, another trial (steeping/germination B) with a lower germination temperature of 22 °C was conducted with continuous steeping for 73 h. The longer steeping time was used to compensate for the lower water temperature. According to Kunze,[27] the warmer the steeping water the faster the water is taken up, and vice versa. In this case, the water uptake was 40, 39, and 38% for Creso, Centauro 1, and Sirio respectively and there was no evident mold formation. The green malts of steeping/germination B were kilned at 50 °C for 21 h (kilning program 1), and the diastatic power was analyzed. As expected, the diastatic power values were not very high: 78, 42, and 118 WK respectively for Creso, Centauro 1, and Sirio (Table 2). This is in strong contrast with pale barley malt, which normally contains 240−260 WK.[27] The moisture content was 6.7, 6.1, and 6.7% respectively for Creso, Centauro 1, and Sirio. These relative high moisture contents do not guarantee a stable final malt, so the malting was repeated using kilning program 2 with higher temperatures (21 h, 50 °C; 3 h, 72 °C; and 3 h, 82 °C) to achieve less than 5% moisture, an increased aroma, and less undesirable flavors. With this approach a lower moisture content was achieved, but the diastatic power was decreased to 56, 34, and 86 WK for Creso, Centauro 1, and Sirio. The same conditions (steeping/germination B and kilning program 2) were also tested on Libero and Crono, where Crono showed no diastatic power and Libero was in the same range of the other tested rices.

It was also important to explore if rice malt starch underwent an adequate gelatinization. For this purpose the Analytica EBC method 5.5 was applied. In this method, the Congress mash is made with 25 g of rice malt and 25 g of standard malt, and the amylases of the added standard malt compensate for the poor enzyme content of the rice malts. Consequently complete saccharification depends only on the complete gelatinization, and it was possible to eliminate the rice malt varieties which did not gelatinize under the conditions of the Congress wort. Then we could improve the mashing conditions ($CaCl_2$, lactic acid) for the enzymes, being sure that at least gelatinization occurred. Only the variety Centauro 1 had saccharified after 15 min. The other varieties showed a dark blue color still after 60 min by the iodine test. Therefore, only the rice malt Centauro 1 was used for the subsequent tests.

To increase the water absorption, another steeping and germination trial (steeping/germination C) was performed only with Centauro 1 by alternating steeping and drying periods every 8 h at 25 °C, and then decreasing the germination temperature to 20 °C (Figure 1). The water uptake of Centauro 1 was 42%. After 8 days of steeping and germination the malt did not show any evidence of mold and had a good smell and appearance.

The kilning program was improved to better protect the enzymes of the green malt during kilning (kilning program 3). Rice's hull is likely why paddy-rice absorbs water slowly and it dries also slowly for this reason; therefore the withering time was extended to 37.5 h to bring the water content to 10−12% before a higher temperature is used, because the enzymes tolerate dry heat better than wet heat.[27] The first drying step at 45 °C was introduced in order to extend the time for cytolysis.[29] Lastly a moderate final temperature of 70 °C for 6 h was selected. The diastatic power of the resulting Centauro 1 malt was 42 WK, which was equal to the value obtained with the kilning program 1, and also a moisture content of <5% was achieved (Table 2).

Thus, the optimized malting program was established: germination C and kilning program 3. The malt from Centauro 1 was analyzed with mashing test 1, mashing test 2, and mashing test 3 for the saccharification rate, speed of filtration, pH, color, viscosity, soluble nitrogen content, and free amino nitrogen content of the laboratory wort. These are all quality attributes used for evaluating the potential of a brewing malt. Table 3 shows the results. Mashing test 1 did not yield a positive saccharification. The reason seemed the low enzyme content; therefore a $CaCl_2$ solution was added to protect the few enzymes present in the malt (mashing test 2).[30] After 50 min the saccharification was completed. Another benefit was the soluble nitrogen content of mashing test 2 (482 mg/L). It was slightly higher compared to mashing test 1 (450 mg/L); however compared to barley malt both values were still low.[27]To improve the soluble nitrogen content, mashing test 3 was performed on a sample of rice malt without removing the acrospires and rootlets after kilning. During germination acrospires and rootlets grow out of the rice's hull, unlike in barley where only the rootlets grow outside. That means for rice that the acrospires will be eliminated after malting together with the rootlets during processing and the rice malt, which is already poor in protein, will lose additional protein.[24] As Table 3 shows, the soluble nitrogen content in mashing test 3 was increased.

All FAN values were surprisingly high compared to barley malt wort in relation to the soluble nitrogen content. Normally in a good brewing malt the FAN content is around 22% of the soluble nitrogen.[4] In this case it was 32, 31, and 33% respectively for mashing tests 1, 2, and 3. This could be an overstimation that depends on the method for FAN determination, which is a color reaction with ninhydrin. The test is a cumulative method for the estimation of amino acids, ammonia, and the terminal α-amino groups of the peptides and proteins,[24] where the individual amino acids give different color intensities,[31] and for this the comparison between barley malt and rice malt could be less significant. There was no difference in the FAN values of mashing test 1 and mashing test 2, but in mashing test 3 the FAN value was increased.

The fine extracts were nearly the same for the three trials and showed very good results considering the fact that the hull accounts for up to 20% of the kernel's mass and contributes less to the extract.[1]

The optimized malting program was repeated with Centauro 2 and Centauro 3, but surprisingly, the results of mashing test 2 and Analytica EBC method 5.5 revealed an incomplete saccharification (data not shown). The color of the iodine test remained light blue instead of yellow. The reason for that could be a slightly higher gelatinization temperature of Centauro 2 and Centauro 3, because the values of the diastatic power of all three rice malts were nearly the same: 42, 44, and 31 WK respectively for Centauro 1, Centauro 2, and Centauro 3. According to Narziß and Back,[6] the gelatinization temperature depends on the variety and cultivation area and particularly on the climate during the crop year. Therefore, the final congress temperature of 70 °C did not permit a complete gelatinization, and a new mashing program tailored specifically for rice malt was developed. The conditions of this new standardized mashing program correspond to the typical EBC Congress Mash but with different temperature rests (Figure 2): 30 min at 45 °C, 30 min at 64 °C and 30 min at 74 °C (mashing test 4). In mashing test 5 this test was performed with the aqueous solution of $CaCl_2$ while in mashing test 6 the $CaCl_2$ was replaced with lactic acid to lower the pH of the mash and to determine if the improved saccharification was due to a lower pH or the presence of calcium or chloride ions. The results are shown in Table 4. Centauro 2 and Centauro 3 saccharified completely without the use of exogenous enzymes in 20 min after reaching 74 °C with the addition of an aqueous solution of $CaCl_2$ as well as with the addition of lactic acid. Therefore, the improved saccharification in tests 5 and 6 was probably due to the lower pH value. The very low value of the diastatic power could not be decisive for assessing good saccharification, but there should be other important amylolytic enzymes in rice malt such as limit dextrinase,[14] pullulanase,[17]

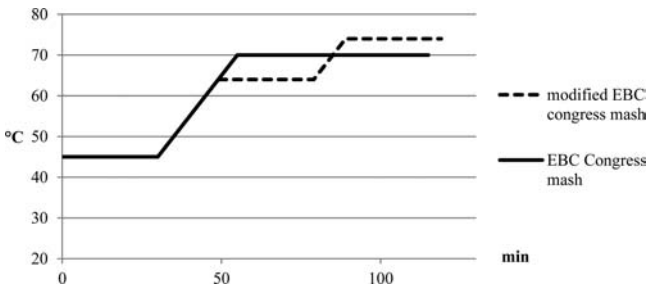

Figure 2. Mashing Programs.

Table 4. Quality Attributes of Centauro 2, Centauro 3, and Balilla Rice Malt Wort Obtained with Modified Congress Mash[a]

	Centauro 2			Centauro 3			Balilla		
	mashing test 4[b]	mashing test 5[c]	mashing test 6[d]	mashing test 4[b]	mashing test 5[c]	mashing test 6[d]	mashing test 4[b]	mashing test 5[c]	mashing test 6[d]
fine extract (% DM)	73.3a	72.8a	73.5a	73.4a′	73.7a′	74.7a′	75.9a″	76.6ab″	77.2b″
filtration time (min)	>60	>60	>60	>60	>60	>60	>60	>60	>60
saccharification time (min)	n.s.	20	20	n.s.	25	25	30	20	20
pH	5.98a	5.58b	5.38c	5.99a′	5.63b′	5.45b′	5.95a″	5.62b″	5.51b″
color (EBC-U)	2.3a	2.1a	2.2a	2.0a′	1.8a′	1.8a′	2.7a″	2.4b″	2.5b″
soluble nitrogen (mg/L at 8.6 °P)	453a	499b	569c	425a′	468b′	541c′	450a″	470b″	518c″
Kolbach index (%)	28a	31a	35a	29a′	32a′	36b′	34a″	36a″	40a″
viscosity (mPa s at 8.6 °P)	1.55a	1.41b	1.47ab	1.53a′	1.40b′	1.44b′	1.62a″	1.49b″	1.51b″
free amino nitrogen (mg/L at 8.6 °P)	126a	134a	146b	116a′	125a′	141b′	131a″	135a″	142a″
fermentability (%)	74.6a	77.1ab	80.6b	68.9a′	70.3a′	75.0a′	85.2a″	84.4a″	87.9a″

[a] $n = 2$ technological repetitions; n.s. = no saccharification; EBC-U = European brewing convention unit; DM = dry matter. Values in the same row followed by a different letter are statistically different ($p \leq 0.05$). [b]Mashing test 4: EBC method 4.5.1. with modified temperature rests (30 min at 45 °C, 30 min at 64 °C, and 30 min at 74 °C). [c]Mashing test 5: EBC method 4.5.1 with modified temperature rests and the addition of an aqueous solution of $CaCl_2$. [d]Mashing test 6: EBC method 4.5.1 with modified temperature rests and the addition of lactic acid aqueous solution.

dx.doi.org/10.1021/jf501462a | J. Agric. Food Chem. 2014, 62, 5369−5377

and α-glucosidase[18] that significantly contribute to the degradation of the rice malt starch. The filtration time of the laboratory worts last more than an hour despite rice wort's low viscosity. The cause may be the cooling of the wort after the laboratory mashing process to 20 °C where the pectin begins to form a gel, and this could hinder the filtration; however this should not be a problem in beer production where the filtration is carried out at 78 °C.

Soluble protein increased in both samples from mashing test 4 to mashing test 5 to mashing test 6. There was also a positive correlation with the FAN values. Compared to Centauro 3, Centauro 2 displayed higher rice malt quality values probably due to its higher total protein content in the crude rice (Tables 1and 5) that could provide more soluble nitrogen and FAN but could also imply a greater protein enzyme endowment. For every sample the fine extract of mashing tests 4, 5, and 6 was nearly the same; meanwhile the viscosity decreased with the addition of $CaCl_2$ and lactic acid, but for all tests it was in an acceptable range.

Table 5. Starch Degrading Enzymes in Rice Malt as Mean and Standard Deviation[a]

	Centauro 2	Balilla
limit dextrinase (U/(malt kg))	6940 ± 21	6129 ± 25
α-amylase (Ceralpha (U/g))	47.4 ± 1.1	48.3 ± 0.1
β-amylase (Betamyl-3 (U/g))	3.8 ± 0.3	8.4 ± 0.2

[a] n = 2 repetitions.

The optimized malting and mashing trials were repeated again using the variety Balilla which has similar characteristics (subspecies *japonica*, 16−18% amylose content) as Centauro. This variety gave even better results than Centauro (Table 4) in spite of the low diastatic power of 34 WK. The saccharification occurred also without the addition of $CaCl_2$ or lactic acid after 30 min. The fermentability, extract content, FAN, soluble nitrogen, and Kolbach Index were all higher than those of Centauro 2 and 3.

The α- and β-amylases as well as limit-dextrinase content of the rice malts Centauro 2 and Balilla were analyzed (Table 5). The α- and β-amylase values are very low and correspond to the very low diastatic power; meanwhile the results of the limit-dextrinase activity was 6940 and 6129 U/(malt kg) for Centauro 3 and Balilla, respectively, which is much higher than in barley malt (200−400 U/(malt kg));[5] so limit dextrinase is certainly one of the supplemental enzymes that contribute to the degradation of the rice malt starch in conjunction with α- and β-amylases. Table 6 shows the sugar profiles of the laboratory rice malt worts. All of the rice malt worts from the different mashing programs produced a wide range of sugar spectra which are characterized by the greater amount of glucose than maltose highlighting the different trend with respect to barley malt wort and could be due to the presence of different enzymes. The data also differed from the results obtained by Agu et al. in 2012[8] perhaps of a different malting and mashing process. Table 7 reports the amino acid profile of the rice malt worts. Histidine and arginine are the amino acids present in major amount. The amino acid profile of the samples did not change a lot between the different mashing programs and varieties. The total amino acid concentration of the rice malt worts is in the range of a barley malt Congress wort[28] even if the total nitrogen content is lower than a barley malt wort. This confirmed the high FAN values. The DMS

Table 6. Sugar Profile of Rice Malt Worts[a]

	Centauro 2			Centauro 3			Balilla		
	mashing test 4[b]	mashing test 5[c]	mashing test 6[d]	mashing test 4[b]	mashing test 5[c]	mashing test 6[d]	mashing test 4[b]	mashing test 5[c]	mashing test 6[d]
fructose	0.56a	0.36b	0.82c	0.61a′	0.45a′	0.46a′	0.58a″	0.48a″	0.59a″
glucose	28.94a	34.64b	44.81c	36.54a′	34.05a′	34.63a′	30.15a″	32.76a″	33.21a″
sucrose	0.22a	0.45b	0.37c	0.54a′	0.19b′	0.19b′	0.19a″	0.14b″	0.12b″
maltose	17.54a	24.32b	38.96c	15.76a′	32.10b′	32.64b′	30.59a″	30.57a″	34.74a″
maltriose	7.74a	3.88b	5.90c	4.58a′	4.61a′	4.69a′	4.65a″	4.46a″	4.59a″
maltotetraose	7.44a	8.61b	6.11c	8.24a′	7.94a′	8.08a′	6.53a″	6.57a″	3.00b″
maltopentaose	3.14a	4.17b	1.00c	5.31a′	2.21b′	2.25b′	2.49a″	2.20a″	0.01b″
maltohexaose	8.08a	8.99b	0.34c	6.29a′	3.17b′	3.23b′	3.44a″	2.71a″	0.01b″

[a] n = 2 technological repetitions. Values in the same row followed by a different letter are statistically different ($p \leq 0.05$). [b]Mashing test 4: EBC method 4.5.1. with modified temperature rests (30 min at 45 °C, 30 min at 64 °C, and 30 min at 74 °C). [c]Mashing test 5: EBC method 4.5.1 with modified temperature rests and the addition of an aqueous solution of $CaCl_2$. [d]Mashing test 6: EBC method 4.5.1 with modified temperature rests and the addition of lactic acid aqueous solution.

dx.doi.org/10.1021/jf501462a | J. Agric. Food Chem. 2014, 62, 5369−5377

Table 7. Amino Acid Profiles of Rice Malt Worts (mg/L)[a]

	Centauro 2			Centauro 3			Balilla		
	mashing test 4[b]	mashing test 5[c]	mashing test 6[d]	mashing test 4[b]	mashing test 5[c]	mashing test 6[d]	mashing test 4[b]	mashing test 5[c]	mashing test 6[d]
group A									
aspartic acid	52a	47b	51a	50a′	42b′	41b′	50a″	45b″	46b″
glutamic acid	54a	49b	67c	54a′	41b′	50c′	46a″	43b″	46a″
serine	57a	55b	62c	61a′	57b′	56b′	65a″	59b″	57c″
arginine	140a	148b	177c	134a′	142b′	137c′	136a″	136a″	151b″
treonine	39a	38a	49b	38a′	34b′	36b′	39a″	35b″	39a″
lysine	90a	96b	113c	89a′	93b′	100c′	96a″	97a″	94b″
group B									
histidine	190a	191a	206b	184a′	180b′	175c′	185a″	177b″	176b″
methionine	24a	21a	29b	42a′	42a′	25b′	25a″	26a″	47b″
valine	87a	88a	101b	87a′	89b′	82c′	94a″	90b″	95a″
leucine	43a	41b	47c	41a′	45b′	38c′	51a″	48b″	49b″
isoleucine	83a	86b	118c	81a′	93b′	88c′	100a″	100a″	110b″
group C									
alanine	55a	55a	65b	56a′	62b′	53c′	67a″	66a″	67a″
tyrosine	97a	85c	105c	93a′	101b′	86c′	96a″	91b″	99a″
phenylalanine	78a	80a	97b	79a′	82b′	78c′	86a″	86a″	91b″
glycine	31a	28a	38b	44a′	31b′	38c′	40a″	37b″	42c″
total	1119a	1107b	1324c	1131a′	1134a′	1082b′	1175a″	1135b″	1209c″

[a] $n = 2$ technological repetitions. Values in the same row followed by a different letter are statistically different ($p \leq 0.05$). [b] Mashing test 4: EBC method 4.5.1. with modified temperature rests (30 min at 45 °C, 30 min at 64 °C and 30 min at 74 °C). [c] Mashing test 5: EBC method 4.5.1 with modified temperature rests and the addition of an aqueous solution of $CaCl_2$. [d] Mashing test 6: EBC method 4.5.1 with modified temperature rests and the addition of lactic acid aqueous solution.

dx.doi.org/10.1021/jf501462a | J. Agric. Food Chem. 2014, 62, 5369−5377

values (free, total, and precursor) for Centauro 2 and Balilla were determined (Table 8). They were higher than the accepted values for a commercial barley malt (5−6 mg/kg) and could be due to the high germination temperatures and the relatively low curing temperature.[32]

Table 8. Dimethyl Sulfide (Total, Free, and Precursor) Of Rice Malts (mg/kg)[a]

rice malt	total DMS	free DMS	DMS-P
Centauro 2	17.15 ± 0.74	3.66 ± 0.01	13.50 ± 0.74
Balilla	12.70 ± 0.69	2.52 ± 0.07	10.18 ± 0.70

[a] $n = 2$ repetitions.

In conclusion, a malting program to produce rice malt for brewing was developed and 10 rice varieties were screened. Probably due to the resistant hull of paddy-rice, five steeping steps were necessary to achieve at least 42% of steeping-out moisture, and a long-time kilning program was developed with a particular drying step at 45 °C for 12 h to impair the degradation of the cell walls. Another 12 h at 50 °C and 13.5 h at 55 °C dried the malt enough to protect the enzymes from the following heat (6 h at 70 °C). But this curing temperature and time were not enough to eliminate the high DMS values found in the rice malt. It was shown that the amount of the endogenous rice malt enzymes is high enough to saccharify the rice malt starch and that their optimal temperature and pH conditions are different from those of barley malt. So the conventional Congress mash (mashing test 1) was slightly changed. With different temperature rests and the addition of $CaCl_2$ and lactic acid a complete saccharification of the rice malt starch was achieved. Balilla and Centauro of the subspecies *japonica* are the most suitable varieties for the production of an all-rice malt beer. The addition of lactic acid also yielded higher soluble nitrogen and FAN contents and enhanced fermentability. In the case of the Balilla rice malt, the saccharification occurred also without the addition of $CaCl_2$ and lactic acid. The soluble nitrogen and FAN values of rice malt wort can be increased by incorporating the acrospires and rootlets during mashing. Work is in progress for brewing an all-rice beer with the malt obtained from this study.

AUTHOR INFORMATION

Corresponding Author

*Tel.: +39 075 585 7926. E-mail: ombretta.marconi@unipg.it.

Funding

We thank the Italian Ministry of Agricultural, Food and Forestry Policies for financial support of the project CERSUOM.

Notes

The authors declare no competing financial interest.

ACKNOWLEDGMENTS

We are grateful to Dr. Simona Floridi for the analytical support.

REFERENCES

(1) FAO. *Rice Market Monitor*, Vol. *XVI* (Issue No. 1), Food and Agriculture Organization of the United Nations: Rome, Italy, 2013; pp 2 and 14, www.fao.org/docrep/017/aq144e/aq144e.pdf (accessed September 2013).

(2) Italian breeds online. http://www.agraria.org/coltivazionierbacee/riso.htm (accessed September 2013).

(3) Ceppi, E. L. M.; Brenna, O. V. Brewing with rice malt-—Agluten-free alternative. *J. Inst. Brew* **2010**, *116*, 275−279.

(4) Narziß, L.; Back, W. Die Bierbrauerei: Band 2: Die Technologie der Würzebereitung; John Wiley & Sons: Weinheim, Germany, 2012.

(5) Taylor, J. R. N.; Dlamini, B. C.; Kruger, J. 125th Anniversary Review: The science of the tropical cereals sorghum, maize and rice in relation to lager beer brewing. *J. Inst. Brew.* **2013**, *119*, 1−14.

(6) Narziß, L.; Back, W. Die Bierbrauerei: Band 1: Die Technologie der Malzbereitung; John Wiley & Sons: Weinheim, Germany, 2012.

(7) Adebowale, A. A.; Sanni, S. A.; Karim, O. R.; Ojoawo, J. A. Malting characteristics of Ofada rice: Chemical end sensory qualities of malt from Ofada rice grains. *Int. Food Res. J.* **2010**, *17*, 83−88.

(8) Agu, R.; Yukihiro, C.; Goodfellow, V.; MacKinlay, J.; Brosnan, J.; Bringhurst, T.; Jack, F.; Macdonald Harrison, B.; Pearson, S.; Bryce, J. H. Effect of germination temperatures on proteolysis of the gluten-free rice and buckwheat during malting and mashing. *J. Agric. Food Chem.* **2012**, *60*, 10147−10154.

(9) Ceppi, E. L. M.; Brenna, O. V. Experimental studies to obtain rice malt. *J. Agric. Food Chem.* **2010**, *58*, 7701−7707.

(10) Kongkaew, A.; Usansa, U.; Wanapu, C. Optimisation of wort production from rice malt using enzymes and barley malt. *Afr. J. Biotechnol.* **2012**, *11*, 9941−9949.

(11) Owusu-Mensah, E.; Oduro, I.; Sarfo, K. J. Steeping: A way of improving the malting of rice grain. *J. Food Biochem.* **2011**, *35*, 80−91.

(12) Usansa, U.; Sampong, N.; Wanapu, C.; Boonkerd, N.; Teaumroong, N. The influences of steeping duration and temperature on the α- and β-amylase activities of six thai rice malt cultivars (*Oryza sativa* L. indica). *J. Inst. Brew.* **2009**, *115*, 140−147.

(13) Usansa, U.; Burberg, F.; Geiger, E.; Black, W.; Chokchai, W.; Arendt, E. K.; Kreisz, S.; Boonkerd, N.; Teamuroong, N.; Zarnkow, M. Optimization of malting conditions for two black rice varieties, black non-waxy rice and black waxy rice (*Oryza sativa* L. indica). *J. Inst. Brew.* **2011**, *117*, 39−46.

(14) Dziedzoave, N. T.; Graffham, A. J.; Westby, A.; Komlaga, G. Comparative assessment of amylolytic and cellulolytic enzyme activity of malts prepared from tropical cereals. *Food Control* **2010**, *21*, 1349−1353.

(15) Bunzel, M.; Steinhart, H. Ballaststoffe aus Pflanzenzellwänden. *Ernaehr.-Umsch.* **2003**, *50* (12), 469−475.

(16) Nakai, H.; Ito, T.; Hayashi, M.; Kamiya, K.; Yamamoto, T.; Matsubara, K.; Kim, Y. M.; Jintanart, W.; Okuyama, M.; Mori, H.; Chiba, S.; Sano, Y.; Kimura, A. Multiple forms of alpha-glucosidase in rice seeds (*Oryza sativa* L., var Nipponbare). *Biochemistry* **2007**, *89*, 49−62.

(17) Yamasaki, Y.; Nakashima, S.; Konno, H. Pullulanase from rice endosperm. *Acta Biochim. Polym.* **2008**, *3*, 507−510.

(18) Keßler, M.; Zarnkow, M.; Kreisz, S.; Back, W. Gelatinisation properties of different cereals and pseudocereals. *Monatsschr. Brauwiss.* **2005**, *Sep./Oct.*, 82−88.

(19) Ente Nazionale Risi, http://www.enterisi.it (accessed September 2013).

(20) European Brewery Convention. *Analytica-EBC*, 5th ed.; Fachverlag Hans Carl: Nürnberg, Germany, 2007.

(21) Mayer, H.; Marconi, O.; Perretti, G.; Sensidoni, M.; Fantozzi, P. Investigation on suitability of hulled wheats for malting and brewing. *J. Am. Soc. Brew. Chem.* **2011**, *69*, 116−120.

(22) Stafisso, A.; Marconi, O.; Perretti, G.; Fantozzi, P. Determination of dimethyl sulphide in brewery samples by headspace gas chromatography mass spectrometry (HS-GC/MS). *Ital. J. Food Sci.* **2011**, *23*, 19−27.

(23) Lookhart, G. L.; Jones, B. High performance liquid chromatography analysis of amino acids at the picomole level. *Cereal Chem.* **1985**, *62*, 97−102.

(24) Marconi, O.; Mayer, H.; Chiacchieroni, F.; Ricci, E.; Perretti, G.; Fantozzi, P. The influence of glumes on malting and brewing of hulled wheats. *J. Am. Soc. Brew. Chem.* **2013**, *71*, 41−48.

(25) Floridi, S.; Miniati, E.; Montanari, L.; Fantozzi, P. Carbohydrate determination in wort and beer by HPLC-ELSD. *Monatsschr. Brauwiss.* **2001**, *9/10*, 209−215.

(26) Bienvenido O. J. *Rice in human nutrition*; Food and Agriculture Organization of the United Nations: Rome, Italy, 1993; Chapter 3, http://www.fao.org/docrep/t0567e/T0567E08.htm#Grossnutrientcomposition (accessed September 2013).
(27) Kunze, W. Raw materials. *Technology Brewing and Malting*; VLB: Berlin, 2004; pp 32−49.
(28) *Mitteleuropäische Brautechnische Analysenkommission. Brautechnische Analysenmethoden Rohstoffe*; MEBAK: Freising-Weihenstephan, Germany, 2006.
(29) Briggs, D. E. The selection and purchase of grain. *Malts and malting*; Blackie Academic & Professional: London, 1998; p 265.
(30) Montanari, L.; Mayer, H.; Marconi, O.; Fantozzi, P. Minerals in Beer. In *Beer in Health and Disease Prevention*; Preedy, V. R., Ed.; Elsevier: Amsterdam, 2009; Chapter 34, pp 359−365.
(31) Friedman, M. Applications of the ninhydrin reaction for analysis of aminoacids, peptides, and proteins to agricultural and biomedical sciences. *J. Agric. Food Chem.* **2004**, *52*, 385−406.
(32) Anness, B. J.; Bamforth, C. W. Dimethylsulphide—A Review. *J. Inst. Brew.* **1982**, *88*, 244−252.

consensus has been established regarding the impact of MLF or bacteria strains on the intensity of the fruity aroma. The lack of fundamental data on aromatic markers of red wine fruity notes and the dearth of concomitant biochemical, chemical, and sensory studies are probably two of the reasons why the impact of yeast and bacteria strains on fruity flavor in Bordeaux red wines has remained elusive.

This study aims at evaluating the formation and evolution of yeast- and LAB-derived volatile compounds during wine aging. In particular, we assessed the influence of three active dry *Saccharomyces cerevisiae* yeast strains and two commercial *Oenococcus oeni* strains on ester levels and organoleptic characteristics from the end of AF until 12 months of aging. Ester levels were quantified using a HS-SPME-GC/MS method developed by Antalick et al.[15] in our laboratory. Sensory analyses were also carried out to highlight the influence of the interaction of these microorganisms on the aroma profile of wines produced in conditions of "macro-vinification" and in industrial-scale winemaking conditions. To our knowledge, this is the first report evaluating the effect of both yeast and LAB strains on ester levels as assessed by sensory analysis in aged Bordeaux red wines.

MATERIALS AND METHODS

Yeast and Bacteria Strains and Nutrient Composition. The yeasts strains *Saccharomyces cerevisiae,* Actiflore cerevisiae (522D), Zymaflore FX10 (Laffort Oenologie, Floirac, France) and Excellence XR (Lamothe-Abiet, Canéjan, France) and the bacterial strains *Oenococcus oeni*, Lactoenos 450 PreAc, and Lactoenos B28 PreAc (Laffort Oenologie, Floirac, France) used were commercially dried preparations. Controls of the implantation of yeast commercial starter cultures were performed by PCR at the SARCO laboratory (Laffort Oenologie, Floirac, France) (data not shown). Controls of the implantation of bacterial commercial starter cultures were performed by the Microflora laboratory (Univ. Bordeaux, France) based on a method developed by Claisse and Lonvaud−Funel[29] (data not shown).

Yeast nutrient Superstart/Dynastart (Laffort Oenologie, Floirac, France) is approximately composed of 45% proteins, 35% carbohydrates, 7% total nitrogen, and 6% minerals. Energizer bacterial nutrient (Laffort Oenologie, Floirac, France) contains approximately 55% proteins, 20% carbohydrates, 9% total nitrogen, and 7% lipids.

Winemaking. Complete experimentation on the 2011 Bordeaux appellation vintage was performed in the Laffort Wine Experimental Center (WEC) located in the "Graves de Vayres" area. Cabernet Sauvignon grapes were harvested by hand, destemmed, crushed, and homogeneously distributed into nine 2 hL stainless steel tanks (150 kg of grapes in each). A sample of each batch was analyzed before AF for sugar and nitrogen content, total acidity, and pH (Table 1). Grape must was treated by addition of Lafase Fruit enzyme (Laffort Oenologie, Floirac, 3 g/100 kg) containing pectinase (6700 PGNU/g). Yeast assimilable nitrogen in musts was corrected to around 210 mg N/L. AF was conducted at 19−22 °C and initiated by inoculation with rehydrated dry yeast. The yeast nutrient Superstart/Dynastart was added during rehydration of active dried yeast, according to the manufacturer's recommendations. AF was performed using three different yeast strains in triplicate. Implantation controls were performed for each tank at the middle of AF (density close to 1.040). At completion of AF (<0.2 g/L glucose/fructose), wine composition was analyzed (sugar and malic acid content, total acidity, total SO_2 content, pH, and alcohol content) (Table 1). Samples were collected for volatile compound analysis in a 0.75 L glass bottle and stored at 10 °C for 1 week after addition of 5 g/hL SO_2. Wines were then decanted and frozen at −18 °C before being analyzed.

Each 2 hL tank was divided into two stainless steel barrels of 30 L for MLF. Bacterial cells were rehydrated with Energizer bacterial nutrient according to the manufacturer's instructions and inoculated into wines at the recommended rate. For the entire duration of MLF, the malic acid concentration was measured once a week to monitor the bacterial metabolism. At the end of MLF (<0.1 g/L malic acid), 50 g/hL of SO_2 were added. Samples were collected like those after AF to assess chemical composition (Table 1) and volatile compounds. Wines were drained into 20 L stainless steel barrels for 3 months of aging. After 3 months, they were sampled in a 0.75 L glass bottle for chemical and volatile analysis, and were decanted and frozen like those after AF and MLF. Sub-batches (3 × 20 L) of each wine were racked and mixed to ensure homogeneity. Wines were bottled in two 0.75 L glass bottles for sensory analysis and then evaluated. The rest of the wine was stored in a 30 L stainless steel barrel for 3 more months of aging. SO_2 content was measured and adjusted if necessary. After the sixth month of aging, the wines were bottled and frozen for those destined for analysis or analyzed immediately for the purpose of sensory analysis. Some of the wines were also bottled in 1.5 L glass bottles and stored at 10 °C for one year of aging. These wines were then analyzed like the others with chemical and sensory analysis.

The same experimentation was also performed during the 2012 vintage. Cabernet Sauvignon grapes harvested for the WEC 2012 experimentation were thermovinified, (i.e., heated at 70 °C for 6 h). The complete experimental design is shown Figure 1.

Two other experimentations were also performed in 2012 on two other Bordeaux region sites, Vineyard A (V-A) with Cabernet Sauvignon grapes and Vineyard B (V-B) with Merlot grapes in order to observe yeast/LAB interactions at industrial-scale winemaking during 2012. AF in Vineyard A was performed in one 65 hL stainless steel tank with 522D or FX10 strains and was performed in one 120 hL stainless steel tank with 522D or XR strains in Vineyard B (Table 2). For both experimentations, MLF and storage were achieved in plastic food barrels of 30 and 20 L, respectively. Only MLF and the first 3 months of aging were performed in triplicate. These experimentations were stopped after six months of aging.

Chemicals. Deuterated compounds ethyl butyrate-4,4,4-d_3 (>99%), ethyl hexanoate-d_{11} (>98%), ethyl octanoate-d_{15} (>98%), and ethyl *trans*-cinnamate-d_5 (phenyl-d_5) (>99%) were obtained from Cluzeau (Sainte Foy la Grande, France). Ethanol (≥99.9%) was obtained from Merck (Damstadt, Germany) and sodium chloride (norma pure) from VWR (Fontenay-sous-Bois, France).

Standard Chemical Analysis. The standard chemical parameters of wines (as total acidity, sugar, malic acid, yeast assimilable nitrogen, SO_2 contents, pH, and alcohol) were analyzed by SARCO laboratory (Laffort Oenologie, Floirac, France) which has been accredited by COFRAC since 1995 (NF EN ISO 17025, accreditation no. 1-0588). Analyses were carried out using the official methods or those recommended by the International Organization of Viticulture and Wine.

Sensory Analysis. Sensory analyses were performed as described by Martin and de Revel.[30] Samples (about 50 mL) were poured into clear INAO wine glasses (NF V09-110, 1971), labeled with random three-digit codes and covered with half of a plastic Petri dish. Evaluations were performed in a dedicated room (ISO 8589:2007) equipped with individual booths to prevent communication between assessors, under normal daylight, and at room temperature (around 20 °C). All the 20 panelists were from research laboratory staff at ISVV, Bordeaux University, or from the Laffort Company and had previous experience with the sensory evaluation of wines. Analyses were carried out by orthonasal and gustative evaluations.

Napping positioning and ultraflash profiling[31] were used to evaluate WEC wines for the 2011 vintage after 3, 6 and 12 months of aging. The six wines were simultaneously presented to each judge in random order. They had to position the six glasses on a sheet of paper (40 × 60 cm) in such a way that two wines were very near if they were globally perceived similar and that two wines were distant from one another if they seemed different, on the basis of their own criteria. After Napping, judges were asked to enrich their tablecloth by adding a few terms to describe the wines or groups of wine. They were encouraged to choose specific descriptors of each wine or groups of wine they had previously separated.

Table 1. Main Technological Parameters of the Different Musts and Wines after Alcoholic and Malolactic Fermentations

wine	yeast strain	bacteria strain	reducing sugar (g/L)	D-glucose + D-fructose (g/L)	alcoholic degree (% v/v)	pH	total acidity (g/L H_2SO_4)	volatile acidity (g/L acetic acid)	YAN (mg N/L)[a]	total sulfur dioxide (mg/L)	free sulfur dioxide (mg/L)	malic acid (g/L)
must												
WEC 2011	NA[b]	NA	218	NQ[c]	NQ	3.48	3.38	NQ	100	55	NQ	NQ
WEC 2012	NA	NA	207	NQ	NQ	3.59	4.31	NQ	129	42	NQ	NQ
V-A 2012	NA	NA	216	NQ	NQ	3.60	2.87	NQ	94	56	NQ	NQ
V-B 2012	NA	NA	199	NQ	NQ	3.50	3.66	NQ	95	58	NQ	NQ
after alcoholic fermentation												
WEC 2011	XR	NA	1.1	nd[d]	12.9	3.53	4.81	0.07	NQ	27	4	2.27
WEC 2011	522D	NA	1.0	nd	12.8	3.53	4.77	0.07	NQ	29	4	2.07
WEC 2011	FX10	NA	1.1	nd	13.1	3.50	4.92	0.09	NQ	30	5	2.22
WEC 2012	XR	NA	1.0	0.01	11.9	3.64	4.93	0.19	NQ	23	5	3.25
WEC 2012	522D	NA	0.7	0.01	11.9	3.65	4.85	0.23	NQ	22	4	3.08
WEC 2012	FX10	NA	0.8	0.01	11.9	3.66	5.00	0.29	NQ	23	4	3.41
V-A 2012	522D	NA	1.0	0.09	13.1	3.59	4.47	0.15	NQ	8	nd	1.66
V-A 2012	FX10	NA	1.1	0.12	13.0	3.60	4.75	0.22	NQ	7	nd	2.16
V-B 2012	XR	NA	1.2	0.06	13.0	3.64	4.26	0.20	NQ	6	nd	2.19
V-B 2012	522D	NA	1.2	0.07	13.1	3.57	4.27	0.16	NQ	3	nd	2.04
after malolactic fermentation												
WEC 2011	XR	B28	1.0	nd	13.2	3.68	3.40	0.29	NQ	41	30	0.01
WEC 2011	522D	B28	1.0	nd	13.2	3.67	3.43	0.23	NQ	43	28	0.01
WEC 2011	FX10	B28	0.9	nd	13.2	3.60	3.56	0.30	NQ	42	30	0.01
WEC 2011	XR	450	1.1	nd	13.2	3.64	3.51	0.13	NQ	33	20	0.01
WEC 2011	522D	450	1.0	nd	13.2	3.64	3.54	0.09	NQ	39	25	0.01
WEC 2011	FX10	450	1.0	nd	13.1	3.59	3.67	0.16	NQ	29	21	0.01
WEC 2012	XR	B28	0.8	0.09	12.1	3.81	2.83	0.37	NQ	52	31	0.01
WEC 2012	522D	B28	0.8	0.09	12.1	3.82	2.84	0.44	NQ	46	29	0.01
WEC 2012	FX10	B28	0.9	0.14	12.2	3.81	2.95	0.50	NQ	45	29	0.01
WEC 2012	XR	450	0.8	0.11	12.1	3.79	2.86	0.28	NQ	69	37	0.01
WEC 2012	522D	450	0.8	0.12	12.1	3.81	2.84	0.35	NQ	61	34	0.01
WEC 2012	FX10	450	0.9	0.13	12.1	3.79	2.95	0.39	NQ	60	35	0.01
V-A 2012	522D	B28	1.3	0.12	13.2	3.70	3.42	0.23	NQ	32	18	0.01
V-A 2012	FX10	B28	1.3	0.14	13.1	3.71	3.53	0.35	NQ	32	17	0.01
V-A 2012	522D	450	1.3	0.10	13.2	3.70	3.60	0.20	NQ	31	18	0.01
V-A 2012	FX10	450	1.3	0.14	13.1	3.71	3.57	0.28	NQ	29	18	0.01
V-B 2012	XR	B28	1.1	0.01	13.0	3.69	3.25	0.31	NQ	60	33	0.01
V-B 2012	522D	B28	1.1	0.01	13.1	3.68	3.25	0.30	NQ	70	36	0.01

dx.doi.org/10.1021/jf500707e | J. Agric. Food Chem. 2014, 62, 5378−5389

Table 1. continued

wine	yeast strain	bacteria strain	reducing sugar (g/L)	D-glucose + D-fructose (g/L)	alcoholic degree (% v/v)	pH	total acidity (g/L H_2SO_4)	volatile acidity (g/L acetic acid)	YAN (mg N/L)[a]	total sulfur dioxide (mg/L)	free sulfur dioxide (mg/L)	malic acid (g/L)
after malolactic fermentation												
V-B 2012	XR	450	1.2	0.04	13.0	3.67	3.27	0.23	NQ	39	20	0.01
V-B 2012	522D	450	1.2	0.04	13.1	3.67	3.26	0.21	NQ	34	17	0.01

[a]YAN: Yeast Assimilable Nitrogen. [b]NA: Not Applicable. [c]NQ: Not Quantified. [d]nd: not detectable.

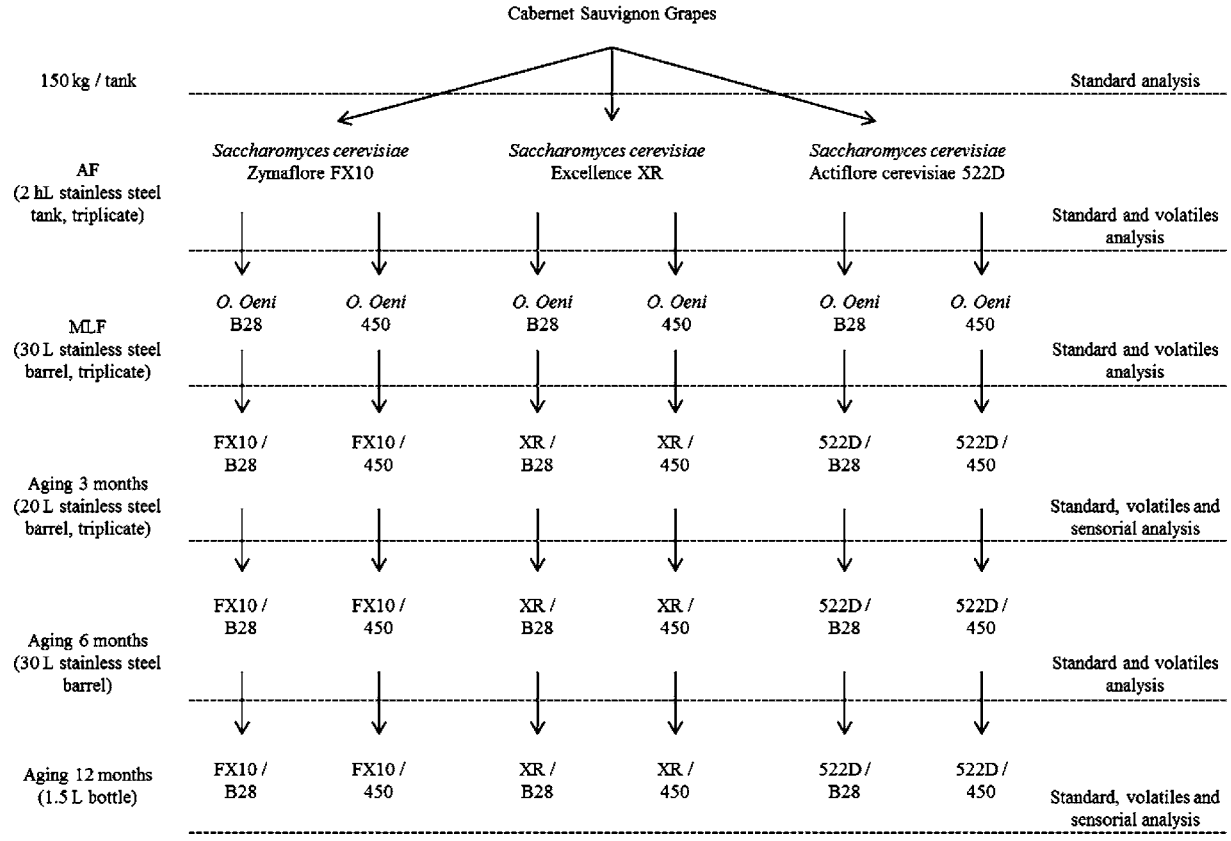

Figure 1. Experimental design in wine experimental center (WEC) for vintages 2011 and 2012.

Ranking tests (ISO 8587:2006) were used for 2012 vintage wines. To evaluate the influence of an experimental factor on the perceived fruitiness in wine, the samples were presented simultaneously to the panel. The members were asked to order each of the 4 (V-A or V-B wines) or 6 samples (WEC wines) according to its fruitiness, from the least to the most. Equal ranking was not allowed.

Finally, comparison profiles (ISO 13299:2003) were used on both 2011 and 2012 vintages, to compare the aroma profiles of wines of the same age (3, 6 and 12 months of aging). A list of five odorant descriptive terms was previously proposed. The odorant terms chosen were based on the fruity aroma ("fermentation aroma", "fresh fruit", and "cooked fruit") and overall aroma potentially having a masking impact on the fruity aroma ("vegetal" and "smoked/toasted"). The panelists evaluated the intensity of the five attributes on a discontinuous scale from 0 to 7.

Statistical Analyses Applied to Sensory Analysis. Results obtained from comparison profiles and ranking tests were statistically interpreted according to the norms published by the international organization for standardization (ISO).

Results from Napping were processed by Multiple Factor Analysis (MFA) as by Pagès.[31] Vocabulary generated with ultraflash profiling was treated as described by Perrin et al.[32]

The second test implemented here consisted in a ranking test with no preordained order, so the Friedman test was applied. For each assessor, a value between 1 and 4 was attributed to each sample, depending on the response of the assessor (1 for samples designated as the least intense, 4 for the most intense). The sums of the ranks were obtained for each sample, then parameter F was calculated using Friedman test specifications and compared with a χ^2 value in order to determine whether the result of the test was significant ($F \geq \chi^2$) or not ($F < \chi^2$).

Statistical significance of data from the comparison profile was evaluated with a three-way analysis of variance (yeast, bacteria, and yeast/bacteria interaction). To compensate for idiosyncratic scale usage, attribute ratings were normalized to obtain equal means and standard deviations for each subject. ANOVA was analyzed by a Duncan *post hoc* test to confirm differences between groups.

Statistical analyses (ANOVA and Duncan's *post hoc* tests) were performed using XL-STAT (Addinsoft, Paris, France), whereas graphical representations of MFA were performed using R v2.15.0 (R Development Core Team 2009, Vienna, Austria, R Foundation for Statistical Computing).

Esters Quantification by HS-SPME-GC/MS Analyses. Each wine sample from the same winemaking step was analyzed at the same time after defrosting. Analyses were performed in triplicate.

The method developed and validated by Antalick et al.[15] was used to quantify 32 esters: ethyl fatty acid esters, acetates of higher alcohol, ethyl branched acid esters, isoamyl esters, methyl esters, ethyl

cinnamates, and some other esters (Table 3). A mixture of ethyl butyrate-4,4,4-d_3, ethyl hexanoate-d_{11}, ethyl octanoate-d_{15}, and ethyl *trans*-cinnamate-d_5 (phenyl-d_5) at about 200 mg/L in ethanol was used as internal standard. In accordance with this method, 20 μL of internal standard solution was added to 25 mL of wine. An aliquot of 10 mL of this wine was introduced into a 20 mL standard headspace vial filled with 3.5 g of sodium chloride. The samples were extracted by HS-SPME and analyzed by GC/MS. The fiber used was polydimethylsiloxane 100 μm (PDMS-100) (Supelco, Bellefonte, PA, U.S.A.). They were conditioned before use, as recommended by the manufacturer. Quantification was performed with calibration curves built in red wines.

Statistical Analysis for Esters Quantifications. Volatile compound concentrations (micrograms per liter) were expressed as mean ± standard deviation. The effects of yeast and LAB strains on each variable were tested by two-way analysis of variance (yeast strain, LAB strain and yeast*LAB strain interactions). ANOVA was followed by a Duncan *post hoc* test to identify differences between groups using a 95% confidence interval.

To obtain a general overview of the data, a PCA was performed from ester concentrations (32 esters). We sought whether the different factors (sampling time, vintage, yeast/LAB couples) allowed clear clustering of the data. Since the matrix effect was considerable, the data were standardized independently, i.e., the data were mean-centered and scaled for each vintage in order to reveal the impact of the other factors. PCA was run using the ade4, car, and plotrix packages from the R program.

Statistical analyses (ANOVA and Duncan's *post hoc* tests) and graphical representations were performed using R v2.15.0 (R Development Core Team 2009, Vienna, Austria, R Foundation for Statistical Computing).

RESULTS AND DISCUSSION

First Approach for Characterizing the Impact of Yeast/Bacteria Couples on Red Wine Aromatic Profiles. Napping is one of the best sensory tests to evaluate global aroma and taste.[32] It permits the global characterization of wines and allows each judge to build his/her representation based on sensory dimensions he/she considers important. Representations of attributes and wines from the 2011 vintage after 3 and 12 months of aging are presented in Figure 2. The most frequently used descriptors to define the aroma of these wines belonged to the lexical field of fruit (fruity, fresh fruits, cooked fruits, red fruits, black fruits, fermentation aroma), as expected for young Bordeaux red wines. Other descriptors used to qualify these wines were "smoked", "toasted", and "vegetal".

Figure 2b for 3 months aged wines and Figure 2d for 12 months aged wines show the projection of the sensory variables on the plane formed by Principal Components 1 and 2 (58% of the total variance) and by PC 2 and 3 (45% of the total variance), respectively. For wines after 3 months of aging, the first component (36%) is defined by the smoked/toasted descriptor, whereas the second component (22%) is mainly characterized by fruity descriptors (fruity, red fruits, fermentation aroma, cooked fruits). The second component (24%) of Figure 2d (wines aged 12 months) highlights the contrast between the fresh fruits on one side and the smoked and toasted descriptor on the other, positioning the latter aromas as a potential mask of fruity aroma. The third axis (21%) opposes "fruity" (red and cooked fruits, fermentation aroma, fruity) and "pleasant mouthfeel" terms to the vegetal attribute.

Projections of wines after 3 and 12 months of aging in the bidimensional plot are presented in Figure 2a,c. As shown, samples were scattered over the map, principally according to the "fruity" vector: in both cases, the trained panel perceived FX10s and XRs wines as being fruitier than 522D fermented wines. Moreover, wines were also separated according to the bacteria strain: samples fermented with the 450 *O. oeni* strain appeared more smoked and toasted in wines after 3 months of aging than the wines where the B28 strain performed MLF. After 12 months of aging, a separation of wines regarding to the bacteria strain were also observed (axis 1, 24.5%, data not shown), but no correlation with none descriptors could be established to confirm 3 months aging results.

According to these initial results obtained with wines at two different steps of aging, the differences observed between wines seemed to be correlated with yeast strain. Most descriptors used for discriminating wines refer to fruity notes. This suggests that yeast strains could be the predominant factor involved in the modulation of fruity aroma, which is not surprising in young wines (after 3 and 12 months of aging). Nevertheless, a bacterial strain effect was also observed, to a lesser extent, and seemed to be linked to smoked/toasted descriptors. The development of these notes during MLF has already been observed by Antalick et al.[19] and could play a role in the masking of the perception of fruity aroma. They also hypothesized that interactions between yeast and LAB could play a key role in the modification of aroma in wine during MLF, but at this point, the hypothesis of an effect of the yeast/LAB association on the fruity aroma of red wines seemed less probable.

Impact of Yeast and Bacterial Strain on Fruity Aroma Perception. Descriptors associated with fruity notes were proposed by each judge during the Napping tests to characterize a wine or group of wines. Thus, a ranking test and comparison profile were performed with wines from the 2012 vintage to investigate the impact of the choice of yeast and LAB strains on fruity aroma perception.

Table 2. Experimentations Implemented[a]

sites	vintage	volume* (hL)	grape cultivars	yeast	bacteria
WEC	2011	2	Cabernet Sauvignon	522D, FX10, XR	450, B28
WEC	2012	2	Cabernet Sauvignon**	522D, FX10, XR	450, B28
vineyard A (V-A)	2012	65	Cabernet Sauvignon	522D, FX10	450, B28
vineyard B (V-B)	2012	120	Merlot	522D, XR	450, B28

[a]Volume* correspond to the volume of stainless steel tank used for AF; ** thermovinification.

First, each taster had to assign 1 point to the least fruity wine and 4 (V-A, V-B) or 6 points (WEC) to the fruitiest one. The sum of the ranks was calculated for each modality from each experiment. Statistical analysis was significant at 1% (Table 4) with wines in the WEC experiment, which means that the tasters were able to distinguish different strains according to their fruity perception. Moreover, the highest sum of ranks was observed for the associations FX10/B28 and FX10/450, followed by 522D/B28 and 522D/450, and XR/B28 and XR/450. Results were in agreement with those of the Napping tests. Furthermore, they were similar to those obtained in Vineyard A and in Vineyard B in the Bordeaux region with two different grape cultivars in real conditions of winemaking. The Friedman test was significant at 0.1% with wines from the V-A

Table 3. Esters Quantified

aroma compound	abbreviation	aroma compound	abbreviation
ethyl fatty acid esters (EFAE)		*methyl fatty acid esters*	
ethyl propanoate	C2C3	methyl butyrate	C1C4
ethyl butyrate	C2C4	methyl hexanoate	C1C6
ethyl hexanoate	C2C6	methyl octanoate	C1C8
ethyl octanoate	C2C8	methyl decanoate	C1C10
ethyl decanoate	C2C10	*isoamyl esters of fatty acid*	
ethyl dodecanoate	C2C12	isoamyl butyrate	iC5C4
ethyl branched acid esters (EBAE)		isoamyl hexanoate	iC5C6
ethyl isobutyrate	C2iC4	isoamyl octanoate	iC5C8
ethyl 2-methylbutyrate	C2 2-mC4	*ethyl acid esters with odd number of carbon*	
ethyl isovalerate	C2iC5	ethyl valerate	C2C5
ethyl phenylacetate	C2PhC2	ethyl heptanoate	C2C7
acetates of higher alcohols (AHA)		ethyl nonanoate	C2C9
propyl acetate	C3C2	*cinnamates and minor esters*	
isobutyl actetate	iC4C2	ethyl cinnamate	C2Cin
butyl acetate	C4C2	ethyl dihydrocinnamate	C2dhCinn
isoamyl acetate	iC5C2	ethyl *trans* 2-hexanoate	C2hex
hexyl acetate	C6C2	isobutyl hexanoate	iC4C6
octyl acetate	C8C2	methyl *trans*-geranate	C1ger
2-phenylethyl acetate	2-PhC2C2		

essay and significant at 5% with V-B wines (Table 4). The highest sum of ranks for V-A wines was observed with the associations FX10/B28 and FX10/450, followed by 522D/450, and finally 522D/B28. Results with wines from V-B confirmed that wines inoculated with the 522D yeast strain appeared less fruity, since the highest sum of ranks was observed for XR/B28, XR/450, 522D/B28 ,and then 522D/450. These results observed in 3 different wines, made in "macro-vinification" or in real winemaking conditions confirmed the impact of the yeast strain on fruity aroma in Bordeaux red wines, despite a potential matrix effect (different region, grape cultivars or winemaking process).

Next, each judge had to attribute a score for each modality from 0 to 7 for 5 descriptors potentially involved in the modulation of fruity aroma (Figure 3). Statistical analyses confirmed that the judges differentiated wines inoculated with yeast strain FX10 from the others. Indeed, for WEC wines (Figure 3a), the FX10/450 association appeared significantly different from the others with "fermentation aroma" notes ($P < 0.01$). Wines fermented with yeast strain FX10 also seemed to be different from the other wines and were described as having more "fresh fruit" notes (yeast effect: $P < 0.01$). Alternatively, wines inoculated with yeasts XR or 522D were described as less fruity and more vegetal (yeast effect: $P < 0.05$) than FX10 wines. A bacterial strain effect was also observed for "fresh fruit" notes, indicating that wines fermented with B28 LAB seemed more fruity than those with the 450 strain (LAB effect: $P < 0.01$). Similar results were observed in wineries, especially in Vineyard A (Figure 3b), where both FX10/450 and FX10/B28 wines were described as fruitier than 522D/450 and 522D/B28 wines, thereby confirming the results from the ranking test. In contrast, the two latter wines appeared more smoked and toasted than the others (yeast effect: $P < 0.01$). Finally, results obtained with Vineyard B wines (Figure 3c) were less clear, perhaps indicating a less significant difference between yeasts XR and 522D. This is consistent with observations made with wines from WEC, where differences were perceived only between FX10 and XR wines and FX10 and 522D wines, but where no significant difference was observed between wines inoculated with XR or 522D.

In this study, the yeast strain appears to be a dominant factor involved in the modulation of fruity notes in Bordeaux red wines. Wines inoculated with FX10 were perceived as fruitier, regardless of the vintage or grape cultivar, after 3 and 12 months of aging. These findings highlight the persistence of a yeast strain effect on fruity aroma over time. The impact of bacterial strains is not as clear.

There is known to be a decrease in fruity notes further to an intensification of the lactic aroma after MLF,[33] mainly due to the increase in diacetyl levels. However, no reference was made to lactic or buttery notes during the Napping test to characterize the differences between wines. It seems unlikely that diacetyl is responsible for the modulation of fruity aroma. Recent studies highlight the difficulty to perceive lactic notes in very young wines,[19,22] probably because of interactions between diacetyl and sulfur dioxide.[33] The olfactory mask of smoked notes over the fruity aroma described by Antalick et al.[19] could also explain differences observed between wines. The bacterial effect observed mostly with the Napping test could be due to sulfur compounds such as hydrogen sulfide or dimethyl sulfide synthesized by certain LAB strains with toasted notes.[34,35] However, the link between bacterial strain and these notes is not clear, and other compounds with reduction notes might be involved. Finally, the question is which aromatic compounds could be responsible for the differences observed. Esters are considered to be the primary source of fruity aroma.[36] They are mainly synthesized by yeast during alcoholic fermentation but LAB can modulate their concentration during MLF close to their perception threshold. These variations could explain the differences observed during sensory tests.

Overview of Changes in Ester Composition Due to Yeast/Bacteria Associations over Time. The PCA scores plot and corresponding loadings plot in Figure 4 provide an overview of ester profiles associated with the metabolic activity of the six associations from the end of AF to 12 months of aging in WEC 2011 and 2012 wines.

Separation along the first axis (48.3% of the total variance) was due to an effect of sampling time. Samples taken at the same time (AF11 and AF12, MLF1 and MLF12, and so on) overlapped and were situated toward the first axis in chronological order, with clear separations between AF, MLF samples, and those collected during wine aging. Indeed, samples after AF for both vintages are positioned to the left of the scores plot and are strongly correlated with esters with long carbon chains such as ethyl decanoate, ethyl octanoate, ethyl hexanoate, octyl acetate, hexyl acetate, and methyl decanoate. This indicates that samples after AF have high levels of these esters. MLF11 and MLF12 samples are positioned toward the left of the scores plot and associated with a lesser extent with long carbon chain esters, indicating lower concentrations in post MFL wines than in post AF wines. Samples after 3, 6, and 12 months of aging are positioned toward the right of the scores plot. Separation between the three aging times is less prominent but the chronology still seems to be respected. They are inversely correlated to long carbon chain esters, indicating lower concentrations than post MLF and post AF wines. This is in accordance with other studies that highlighting the decrease in EFAE and AHA concentrations during wine aging.[37,38] Wine aging samples (12m12, 6m12, 3m12, and to a lesser extent 6m11 and 3m11) are correlated with ethyl branched acid esters (C2iC4, C2–

dx.doi.org/10.1021/jf500707e | J. Agric. Food Chem. 2014, 62, 5378−5389

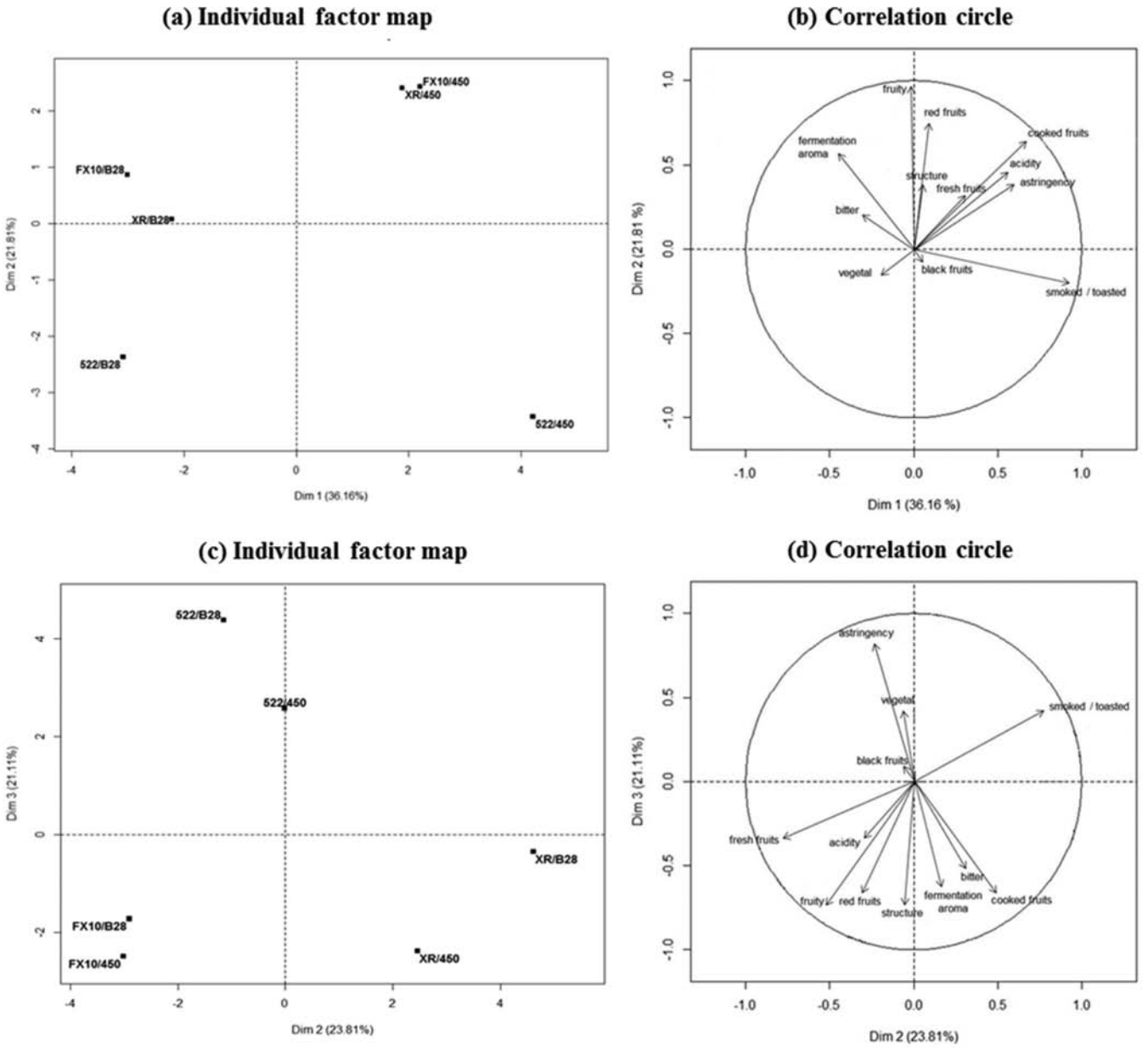

Figure 2. Wines representation (a, c) and characterization (b, d) emerging from Napping combined with Ultra-Flash Profiling (MFA, plane 1−2 and 2−3), realized with wines after 3 months (a, b) and 12 months (c, d) of aging, 2011 vintage.

Table 4. Ranking of Perceived Fruitiness in Wines after 3 Months of Aging in Vintage 2012

		strains and sums of ranks							
wine	no.	XR/B28	XR/450	FX10/B28	FX10/450	522D/B28	522D/450	F[a]	results[b]
WEC	22	72	53	95	94	76	72	16.10	significant at 1%
vineyard A	24			75	72	39	54	21.15	significant at 0.1%
vineyard B	18	59	44			42	35	10.2	significant at 5%

[a] F was calculated as described in ISO 8587:2006 for Friedman test. $F = (12 \times \sum_p^{i=1} R_i^2)/(n \times p \times (p+1)) - 3 \times n \times (p+1)$ with n represents the number of tasters, p represents the number of modalities and R_i represents the sum of the ranks for the modality i. [b] With six modalities (WEC), the test was significant at 5% when $F > 11.07$, at 1% when $F > 15.09$ and at 0.1% when $F > 20.52$. With four modalities (V-A, V-B), the test was significant at 5% when $F > 7.81$, at 1% when $F > 11.34$ and at 0.1% when $F > 16.27$.

2mC4, and C2iC5), indicating higher levels in these samples than in MLF11, MLF12, AF11, and AF12, and therefore an increase in the concentration of EBAE during wine aging.[39,40]

The second axis (11.6% of the total variance) seems to separate samples with regard to the yeast strain. Samples inoculated with strain 522D (represented with circles in Figure 4) are positioned toward the bottom of the scores plot and are associated with propyl acetate, 2-phenylethyl acetate, ethyl propanoate, ethyl phenylacetate, and methyl butanoate. Wines fermented with strain FX10 (represented by squares) tend to

dx.doi.org/10.1021/jf500707e | J. Agric. Food Chem. 2014, 62, 5378−5389

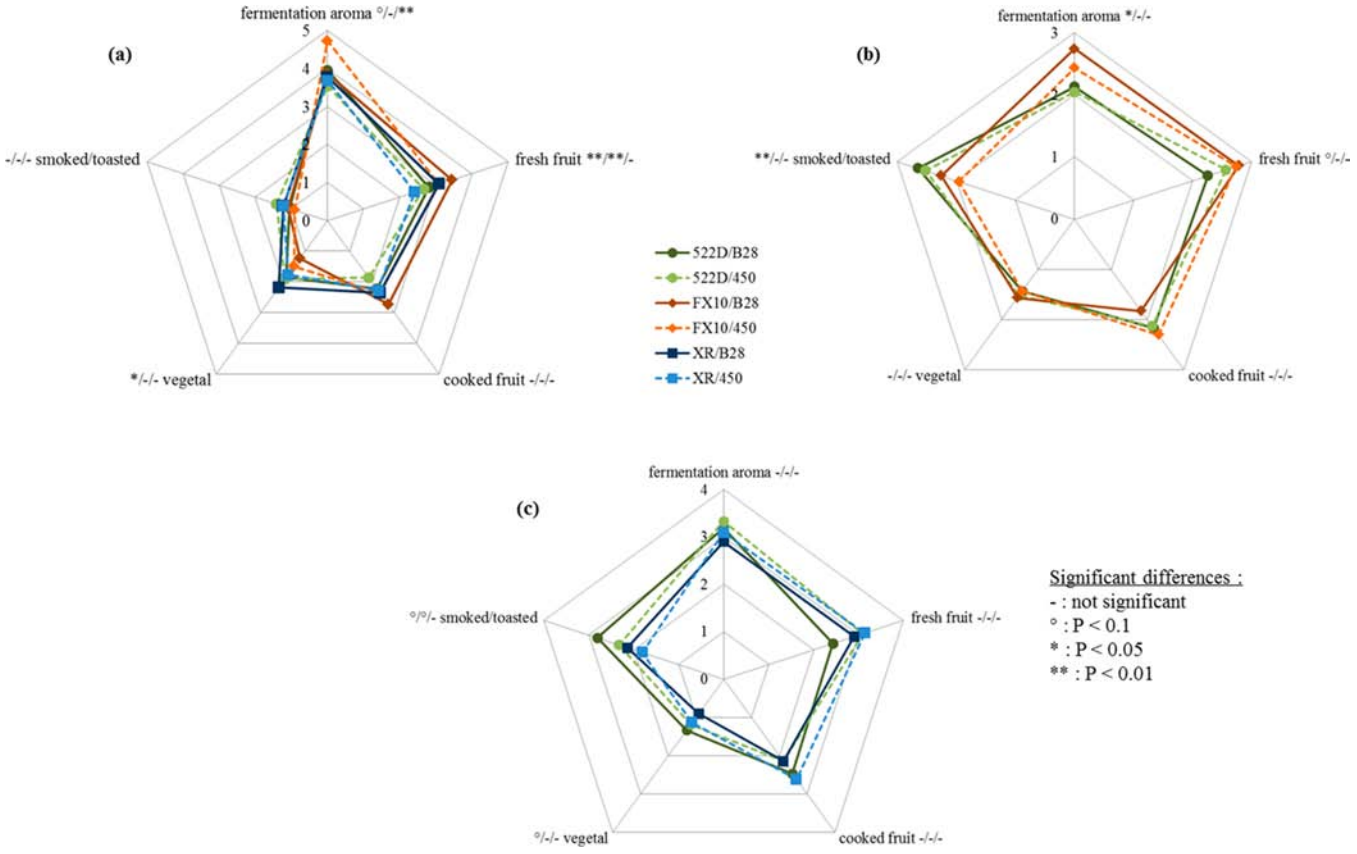

Figure 3. Mean sensory descriptor values for WEC (a), Vineyard A (b), and Vineyard B (c) red wines after 3 months of aging made in 2012 vintage with six yeast/bacteria couples. Significant differences are indicated with asterisks (yeast strain effect/LAB strain effect/yeast × LAB interaction effect).

cluster in the middle of the scores plot, whereas XR samples (denoted with diamonds) are positioned toward the top of the scores plot and are inversely correlated to almost all esters, indicating that the levels of esters in these samples are lower than in FX10 and 522D samples. Interestingly, samples inoculated with the same yeast overlap in the scores plot regardless of bacteria strain. The synthesis of esters by yeast has been known for decades, whereas the impact of bacteria is still controversial. Evidence exists of esterase activity in *O. oeni*[41,42] and several reports have shown changes in ester concentrations in wines after MLF with *O. oeni*. However, no consensus has been established, since these variations differ between studies.[19,43,44] In the present study, the impact of bacterial metabolism on ester concentrations seems very limited compared to that of yeast, which seems to be the predominant factor.

Ester Profiles and Link with Sensory Analysis. Significance levels of a yeast effect calculated with the Analyses of Variance on the different wines are presented Table 5. Significant effect of yeast strain was observed for all esters in all wines at almost each step of winemaking. Quantitative data of the 32 esters analyzed in the experimental wines are summarized in Figure 5, while the entire data collected are available in the Supporting Information (SI, Tables S1−S4). In terms of valuable contribution to the fruity aroma of red wines, three subfamilies of esters can be highlighted: ethyl fatty acid esters (EFAE), acetates of higher alcohols (AHA), and ethyl branched acid esters (EBAE).[3,19] All esters from the same family generally presented the same pattern, so we assumed that total concentration in esters in each family would be a good representation.

Changes in ethyl fatty acid esters depended on both matrix and yeast strain. FX10 yeast strain tended to produce significantly higher EFAE concentrations in WEC 2012 and Vineyard A wines, in accordance with the sensory results. However, Napping tests in the WEC on 2011 wines clearly differentiated 522D wines from FX10 and XR wines, which were described as fruitier, whereas chemical analysis demonstrated higher EFAE levels in 522D wines after 3 and 12 months. Similar results were observed with Vineyard B wines, fermented with Merlot grapes, which were described as fruitier when inoculated with XR than with 522D, even though the latter synthesized more EFAE. A recent study suggested that precursor availability rather than the expression level of genes responsible of ethyl ester synthesis is the limiting factor in esters production.[45] In other words, matrix effect could be the predominant factor responsible for the modulation of ethyl ester levels, and it appears that EFAE might not explain yeast differences observed during sensory analyses. Similar observations were made with acetates of higher alcohols, which were found in comparable concentrations in wines inoculated with 522D and FX10 as in wines from WEC 2011, WEC 2012, and V-A, while their aromatic profiles were significantly different. Finally, 522D also significantly synthesized more ethyl branched acid esters than XR and FX10 in all wines analyzed in this study. Overall, wines fermented with yeast strains FX10 and 522D had roughly the same profile in terms of ester levels, but 522D wines appeared less fruity. These observations are not

dx.doi.org/10.1021/jf500707e | J. Agric. Food Chem. 2014, 62, 5378−5389

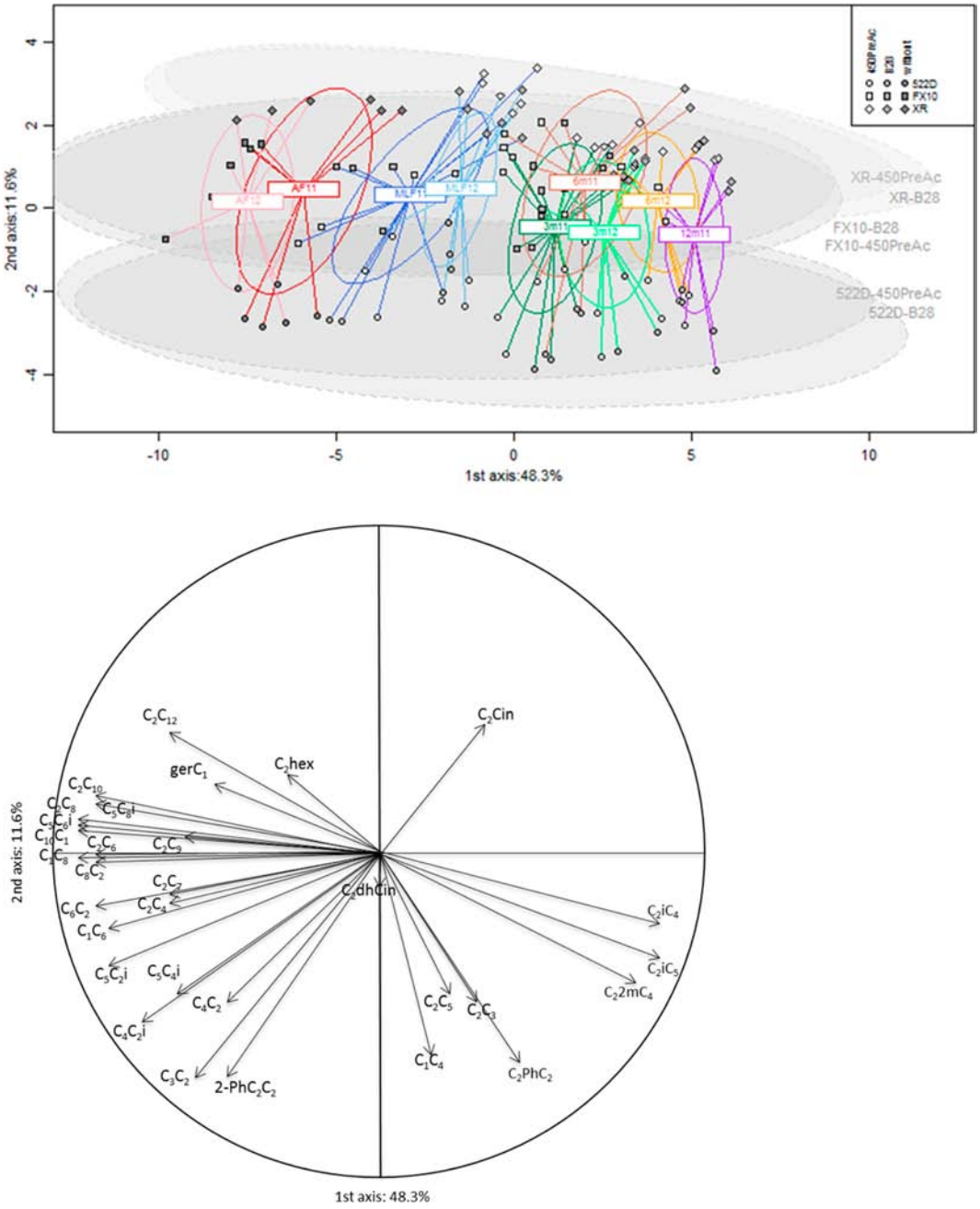

Figure 4. Principal Component Analysis (PCA) providing a visual overview of changes in the esters composition over the time in WEC wines from 2011 (AF11 to 12m11) and 2012 (AF12 to 6m12) vintages: after Alcoholic Fermentation (AF), Malolactic Fermentation (MLF), 3, 6, and 12 months of aging (3m, 6m, 12m). The data were mean-centered and scaled for each vintage in order to decrease the matrix impact and to reveal the impact of the other factors. Yeasts strains are represented by circle (522D), square (FX10), and diamond (XR); empty geometric shapes represent 450 LAB strain and full ones are for B28 LAB strain. Abbreviations of esters in the correlation circle are listed in Table 3.

as surprising and confirm results from other studies investigating fruity aroma in red wine over the past decade. In fact, wine consists of a highly complex mixture of volatiles, but only a few of these compounds are known to contribute directly to wine aroma.[46,47] However, the perception of flavors is not the result of a single dominant compound, but rather stems from the result of interactions between a multitude of volatiles.[48] Thus, no key aromatic compounds responsible for fruity aroma in Bordeaux red wines have yet been identified, although several studies highlight the indirect potential role of a certain number of compounds. Moreover, Ferreira et al.[49] suggested that the concentrations of compounds from the same chemical family had a cumulative effect, resulting in a perception of their overall fruity character. Pineau et al.[3] highlighted the importance of esters and acetates in the red- and blackberry aroma, which was confirmed subsequently.[4,14] They also demonstrated in dearomatized wines that very small variations in ester levels can be perceived by a panelist, even at concentrations far below their olfactory threshold, and that this can affect the perception of fruity aroma. Ester profiles of 522D and FX10 strains may look quite similar, but small variations in the concentration of only a few esters could cause a flavor profile to be perceived completely differently. However, the study of minor esters as isoamyl esters, methyl esters, or ethyl

dx.doi.org/10.1021/jf500707e | J. Agric. Food Chem. 2014, 62, 5378−5389

Table 5. Significance Level in the Analysis of Variance for Yeast Effect on the Different Esters Quantified[a]

	WEC 2011					WEC 2012				vineyard A				vineyard B		
	after AF	after MLF	after 3 months	after 6 months	after 12 months	after AF	after MLF	after 3 months	after 6 months	after AF	after MLF	after 3 months	after 6 months	after AF	after MLF	after 3 months
ethyl fatty acid esters (EFAE)																
C2C3	***	***	***	***	***	***	***	***	***	***	***	***	***	**	***	***
C2C4	NS	***	**	***	NS	*	***	***	***	**	**	***	*	NS	***	***
C2C6	**	*	*	NS	NS	***	***	***	***	***	***	***	***	***	***	***
C2C8	NS	***	**	*	*	***	***	***	***	***	***	***	***	***	***	***
C2C10	NS	NS	**	**	**	***	NS	***	***	**	***	***	***	***	***	***
C2C12	***	NS	***	**	***	***	*	***	**	***	NS	NS	***	***	***	**
EFAE sum	**	***	***	**	**	***	**	***	***	***	*	*	*	**	***	***
ethyl branched acid esters (EBAE)																
C2iC4	**	***	NS	NS	NS	***	***	***	***	**	***	***	***	*	**	NS
C2 2-mC4	***	***	***	***	***	***	***	***	***	***	***	***	***	**	***	***
C2iC5	***	**	***	***	*	***	***	***	***	***	***	***	***	*	NS	NS
C2PhC2	***	***	***	***	***	***	***	***	***	**	***	***	***	***	***	***
EBAE sum	***	***	*	**	**	**	***	***	***	***	***	***	***	NS	**	*
acetate of higher alcohols (AHA)																
C3C2	**	***	***	***	***	***	***	***	***	NS	**	***	NS	***	***	***
iC4C2	***	***	***	**	***	***	***	***	***	NS	*	***	NS	***	***	**
C4C2	***	***	*	**	NS	***	***	***	***	NS	**	***	NS	***	***	***
iC5C2	**	***	**	**	***	***	***	***	***	NS	NS	*	*	***	***	***
C6C2	***	NS	NS	*	*	**	***	***	***	**	***	***	***	***	***	***
C8C2	*	**	***	**	NS	***	***	***	***	NS	***	NS	NS	NS	NS	*
2-PhC2C2	***	***	***	**	***	***	***	***	***	***	***	***	***	***	***	***
AHA sum	**	***	***	***	***	**	***	***	***	NS	NS	NS	NS	**	***	***
methyl fatty acid esters																
C1C4	***	***	***	***	***	NS	NS	NS	***	NS	NS	*	*	***	*	***
C1C6	***	***	***	*	**	***	***	***	***	NS	NS	*	*	***	***	***
C1C8	*	***	**	**	**	***	***	***	***	**	***	***	NS	***	***	***
C1C10	NS	**	***	***	***	***	*	***	*	**	***	***	NS	***	***	*
ethyl acid esters with odd number of carbon																
C2C5	***	*	***	***	**	NS	***	***	**	**	***	***	*	***	*	***
C2C7	*	***	***	***	***	***	***	***	***	**	***	***	***	***	***	***
C2C9	***	NS	***	*	**	***	***	***	*	***	**	***	*	***	***	***
isoamyl esters of fatty acid																
iC5C4	NS	***	***	**	**	***	***	***	***	*	NS	**	NS	***	***	***
iC5C6	NS	*	**	*	***	*	***	***	***	NS	NS	NS	***	***	***	***
iC5C8	NS	NS	**	**	**	**	***	**	NS	**	***	***	***	***	***	***
cinnamates and minor esters																
C2hex	NS	NS	**	**	*	***	***	***	***	NS	NS	NS	NS	***	***	***
iC4C6	**	**	***	**	NS	NS	NS	***	***	NS	***	***	**	*	NS	NS
C1ger	***	*	***	NS	***	***	***	***	***	NS	NS	**	**	*	**	NS
C2dhCinn	*	NS	**	NS	*	***	***	***	***	*	***	***	***	***	***	***
C2 Cin	*	NS	***	**	**	***	NS	*	***	NS	***	***	**	***	***	***

[a]*, **, *** indicate significance at $p < 0.05$, $p < 0.01$, $p < 0.001$, respectively; NS: non significant differences.

cinnamates also failed to establish a link with fruity aroma perception (available in SI Table S5).

Other interactions involving volatile compounds from other families could also be responsible for the modulation of fruity aroma. Empirical observations have shown that the addition of copper sulfate in Cabernet Sauvignon or Merlot wines leads to a significant decrease in the perception of fruity flavor. This suggests the contribution of sulfur-derivative compounds and especially odorous thiols in the development of the aromatic complexity of red wines. Varietal compounds revealed by yeast during AF such as mercaptans present in Cabernet Sauvignon and Merlot wines may participate in the toasted and blackcurrant nuances of these wine aromas.[50,51] Small variations in the release of these powerful odoriferous volatile compounds due to yeast strain during AF may be sufficient to modulate the aromatic expression of wines.

In summary, sensory analyses of wines from different Bordeaux appellations at different fermentation and aging times allowed the impact of both yeast and bacteria strain on fruity aroma to be investigated. The perception of fruity notes in Bordeaux red wines was particularly impacted by the yeast strain, while bacterial strain had little impact on the modulation of fruity aroma. Ester profiles alone cannot account for the differences in the perception of fruity notes, despite their important role. Yeast strains also had a large impact on ester composition in wines, to such an extent that significant differences detectable at the end of alcoholic fermentation were unaffected by MLF and aging. The impact of these micro-

dx.doi.org/10.1021/jf500707e | J. Agric. Food Chem. 2014, 62, 5378−5389

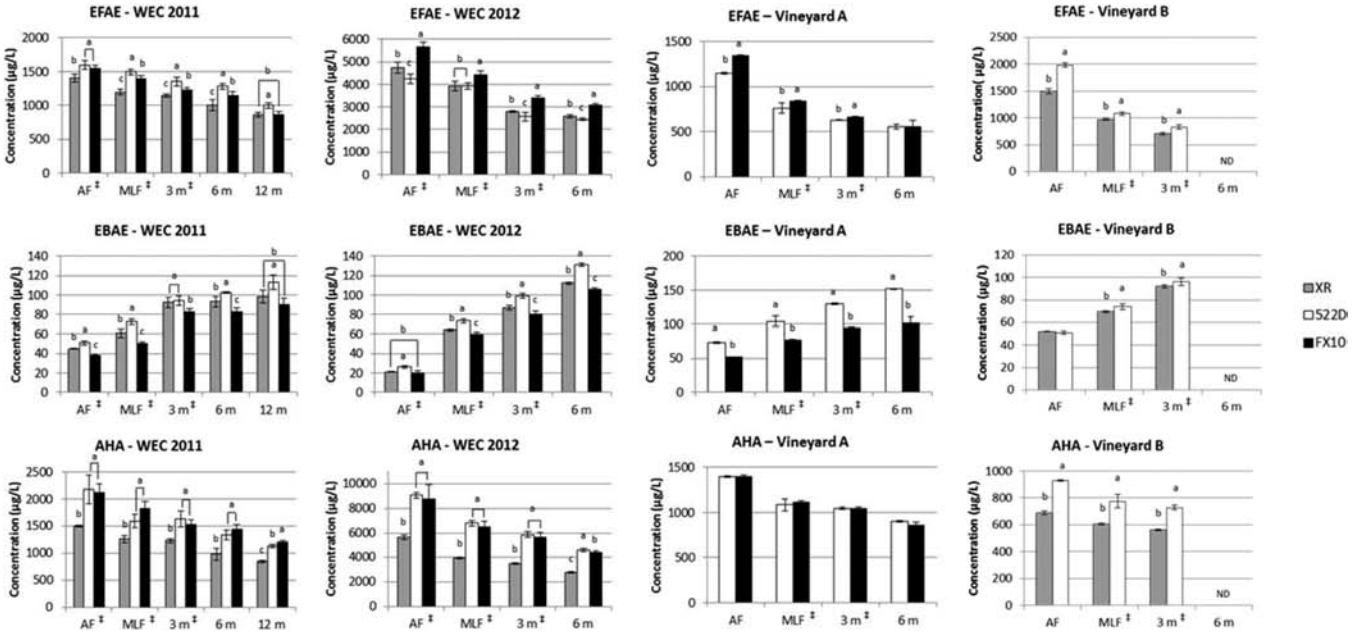

Figure 5. Sum of mean concentrations with standard deviations (micrograms per liter) of esters after alcoholic fermentation (AF), malolactic fermentation (MLF), 3, 6, and 12 months of aging (3m, 6m, 12m) in wines from WEC 2011, WEC 2012, Vineyard A (V-A) and Vineyard B (V-B). Esters were grouped in families described in Table 3 regarding yeast strains. Samples with biological triplicates were injected twice each. For samples which were not triplicated, three injections were carried out. Different alphabetical letters indicate significant differences. EFAE: Ethyl Fatty Acid Esters; EBAE: Ethyl Branched Acid Esters; AHA: Acetates of Higher Alcohols; ND: No Data; the ‡ indicates biological triplicates.

organisms on the concentration of other compounds involved in the modulation of fruity notes should lead to better correlation between sensory and chemical analyses. Henceforth, winemakers have a sensory parameter choosing industrial yeast strains and no longer need to rely only on kinetic and technical specifications.

■ ASSOCIATED CONTENT

Supporting Information

Mean concentrations with standard deviations (micrograms per liter) after AF, MLF, 3, 6, and 12 months of aging in WEC 2011, WEC 2012, Vineyard A, and Vineyard B wines for each yeast strain are presented in Tables S1, S2, S3, and S4 respectively. Results of Duncan *post hoc* tests for yeast effect on the different esters quantified are presented in Table S5. Indicated groups represent yeasts which had synthesized the most esters after AF, 3 months, and 12 months (only for WEC 2011 wines) of aging. This material is available free of charge via the Internet at http://pubs.acs.org.

■ AUTHOR INFORMATION

Corresponding Author

*Tel.: (33) 5 57 57 58 44; fax: (33) 5 57 57 58 13; e-mail: marine.gammacurta@u-bordeaux.fr.

Notes

The authors declare no competing financial interest.

■ ACKNOWLEDGMENTS

We thank Château Latour-Martillac, Château Goudichaud, and Union des Producteurs de Saint-Emilion for providing wine samples.

■ REFERENCES

(1) Peynaud, E. In *Connaissance et Travail du Vin*; Dunod Ed.: Paris, France, 1981.

(2) Pineau, B.; Barbe, J.-C.; Leeuwen, C. V.; Dubourdieu, D. Olfactory specificity of red-and black-berry fruit aromas in red wines and contribution to the red Bordeaux wine concept. *J. Int. Sci. Vigne Vin* **2010**, *44*, 39−49.

(3) Pineau, B.; Barbe, J.-C.; Van Leeuwen, C.; Dubourdieu, D. Examples of Perceptive Interactions Involved in Specific "Red-" and "Black-Berry" Aromas in Red Wines. *J. Agric. Food Chem.* **2009**, *57*, 3702−3708.

(4) Lytra, G.; Tempere, S.; De Revel, G.; Barbe, J.-C. Impact of Perceptive Interactions on Red Wine Fruity Aroma. *J. Agric. Food Chem.* **2012**, *60*, 12260−12269.

(5) Escudero, A.; Campo, E.; Fariña, L.; Cacho, J.; Ferreira, V. Analytical Characterization of the Aroma of Five Premium Red Wines. Insights into the Role of Odor Families and the Concept of Fruitiness of Wines. *J. Agric. Food Chem.* **2007**, *55*, 4501−4510.

(6) Pineau, B.; Barbe, J.-C.; Van Leeuwen, C.; Dubourdieu, D. Which Impact for β-Damascenone on Red Wines Aroma? *J. Agric. Food Chem.* **2007**, *55*, 4103−4108.

(7) Loscos, N.; Hernandez-Orte, P.; Cacho, J.; Ferreira, V. Release and Formation of Varietal Aroma Compounds during Alcoholic Fermentation from Nonfloral Grape Odorless Flavor Precursors Fractions. *J. Agric. Food Chem.* **2007**, *55*, 6674−6684.

(8) Tominaga, T.; Blanchard, L.; Darriet, P.; Dubourdieu, D. A Powerful Aromatic Volatile Thiol, 2-Furanmethanethiol, Exhibiting Roast Coffee Aroma in Wines Made from Several *Vitis vinifera* Grape Varieties. *J. Agric. Food Chem.* **2000**, *48*, 1799−1802.

(9) Blanchard, L.; Tominaga, T.; Dubourdieu, D. Formation of Furfurylthiol Exhibiting a Strong Coffee Aroma during Oak Barrel Fermentation from Furfural Released by Toasted Staves. *J. Agric. Food Chem.* **2001**, *49*, 4833−4835.

(10) Anocibar Beloqui, A.; Kotseridis, Y.; Bertrand, A. Determination of the content of dimethyl sulphide in some red wines. *J. Int. Sci. Vigne Vin* **1996**, *30*, 167−170.

(11) Ebeler, S. E. Analytical chemistry: Unlocking the secrets of wine flavor. *Food Rev. Int.* **2001**, *17*, 45−64.

(12) Ferreira, V.; López, R.; Cacho, J. F. Quantitative Determination of the Odorants of Young Red Wines from Different Grape Varieties. *J. Sci. Food Agric.* **2000**, *80*, 1659−1667.

(13) Jiang, B.; Xi, Z.; Luo, M.; Zhang, Z. Comparison on aroma compounds in Cabernet Sauvignon and Merlot wines from four wine grape-growing regions in China. *Food Res. Int.* **2013**, *51*, 482−489.
(14) Falcao, L. D.; Lytra, G.; Darriet, P.; Barbe, J.-C. Identification of ethyl 2-hydroxy-4-methylpentanoate in red wines, a compound involved in blackberry aroma. *Food Chem.* **2012**, *132*, 230−236.
(15) Antalick, G.; Perello, M. C.; de Revel, G. Development, validation and application of a specific method for the quantitative determination of wine esters by headspace-solid-phase micro-extraction-gas chromatography−mass spectrometry. *Food Chem.* **2010**, *121*, 1236−1245.
(16) Vilanova, M.; et al. Assimilable nitrogen utilisation and production of volatile and non-volatile compounds in chemically defined medium by *Saccharomyces cerevisiae* wine yeasts. *Appl. Microbiol. Biotechnol.* **2007**, *77*, 145−157.
(17) Mateo, J. J.; Jiminez, M.; Huerta, T.; Pastor, A. Contribution of different yeasts isolated from musts of Monastrell grapes to the aroma of wine. *Int. J. Food Microbiol.* **1991**, *14*, 153−160.
(18) Molina, A. M.; et al. Differential synthesis of fermentative aroma compounds of two related commercial wine yeast strains. *Food Chem.* **2009**, *117*, 189−195.
(19) Antalick, G.; Perello, M. C.; de Revel, G. Characterization of Fruity Aroma Modifications in Red Wines during Malolactic Fermentation. *J. Agric. Food Chem.* **2012**, *60*, 12371−12383.
(20) Malherbe, S.; Tredoux, A. G. J.; Nieuwoudt, H. H.; Toit, M. Comparative metabolic profiling to investigate the contribution of *O. oeni* MLF starter cultures to red wine composition. *J. Ind. Microbiol. Biotechnol.* **2011**, *39*, 477−494.
(21) Vestner, J.; et al. Investigation of the Volatile Composition of Pinotage Wines Fermented with Different Malolactic Starter Cultures Using Comprehensive Two-Dimensional Gas Chromatography Coupled to Time-of-Flight Mass Spectrometry (GC×GC-TOF-MS). *J. Agric. Food Chem.* **2011**, *59*, 12732−12744.
(22) Ruiz, P.; Izquierdo, P. M.; Seseña, S.; García, E.; Palop, M. L. Malolactic Fermentation and secondary metabolite production by *Oenoccocus oeni* strains in low pH wines. *J. Food Sci.* **2012**, *77*, M579−M585.
(23) Henick-Kling, T.; Edinger, W.; Daniel, P.; Monk, P. Selective effects of sulfur dioxide and yeast starter culture addition on indigenous yeast populations and sensory characteristics of wine. *J. Appl. Microbiol.* **1998**, *84*, 865−876.
(24) Egli, C. M.; Edinger, W. D.; Mitrakul, C. M.; Henick-Kling, T. Dynamics of indigenous and inoculated yeast populations and their effect on the sensory character of Riesling and Chardonnay wines. *J. Appl. Microbiol.* **1998**, *85*, 779−789.
(25) Dubourdieu, D.; Tominaga, T.; Masneuf, I.; des Gachons, C. P.; Murat, M. L. The role of yeasts in grape flavor development during fermentation: The example of Sauvignon blanc. *Am. J. Enol. Vitic.* **2006**, *57*, 81−88.
(26) Takush, D. G.; Osborne, J. P. Impact of yeast on the aroma and flavour of Oregon Pinot Noir wine: Yeast and wine aroma. *Aust. J. Grape Wine Res.* **2012**, *18*, 131−137.
(27) Holt, H.; et al. Influence of yeast strain on Shiraz wine quality indicators. *Int. J. Food Microbiol.* **2013**, *165*, 302−311.
(28) Álvarez-Pérez, J. M.; et al. Sensory and chemical characterisation of the aroma of Prieto Picudo rosé wines: The differential role of autochthonous yeast strains on aroma profiles. *Food Chem.* **2012**, *133*, 284−292.
(29) Claisse, O.; Lonvaud-Funel, A. Development of a multilocus variable number of tandem repeat typing method for *Oenococcus oeni*. *Food Microbiol.* **2012**, *30*, 340−347.
(30) Martin, N.; de Revel, G. Sensory evaluation: Scientific bases and oenological applications. *J. Int. Sci. Vigne Vin* **1999**, *33*, 81−93.
(31) Pagès, J. Collection and analysis of perceived product inter-distances using multiple factor analysis: Application to the study of 10 white wines from the Loire Valley. *Food Qual. Prefer.* **2005**, *16*, 642−649.
(32) Perrin, L.; et al. Comparison of three sensory methods for use with the Napping procedure: Case of ten wines from Loire valley. *Food Qual. Prefer.* **2008**, *19*, 1−11.
(33) Bartowsky, E. J.; Henschke, P. A. The "buttery" attribute of wine—Diacetyl—Desirability, spoilage and beyond. *Int. J. Food Microbiol.* **2004**, *96*, 235−252.
(34) Pripis-Nicolau, L.; De Revel, G.; Bertrand, A.; Lonvaud-Funel, A. Methionine catabolism and production of volatile sulphur compounds by *Œnococcus œni*. *J. Appl. Microbiol.* **2004**, *96*, 1176−1184.
(35) Vallet, A.; Lucas, P.; Lonvaud-Funel, A.; De Revel, G. Pathways that produce volatile sulphur compounds from methionine in *Oenococcus oeni*. *J. Appl. Microbiol.* **2008**, *104*, 1833−1840.
(36) Sumby, K. M.; Grbin, P. R.; Jiranek, V. Microbial modulation of aromatic esters in wine: Current knowledge and future prospects. *Food Chem.* **2010**, *121*, 1−16.
(37) Marais, J.; Pool, H. J. Effect of storage time and temperature on the volatile composition and quality of dry white table wines. *Vitis* **1980**, 151−154.
(38) Ramey, D.; Ough, C. S. Volatile Ester Hydrolisys or Formation during Storage of Model Solutions of Wine. *J. Agric. Food Chem.* **1980**, 928−934.
(39) Ferreira, V.; Aznar, M.; López, R.; Cacho, J. Quantitative Gas Chromatography−Olfactometry Carried out at Different Dilutions of an Extract. Key Differences in the Odor Profiles of Four High-Quality Spanish Aged Red Wines. *J. Agric. Food Chem.* **2001**, *49*, 4818−4824.
(40) Díaz-Maroto, M. C.; Schneider, R.; Baumes, R. Formation Pathways of Ethyl Esters of Branched Short-Chain Fatty Acids during Wine Aging. *J. Agric. Food Chem.* **2005**, *53*, 3503−3509.
(41) Sumby, K. M.; Matthews, A. H.; Grbin, P. R.; Jiranek, V. Cloning and characterization of an intracellular esterase from the wine-associated lactic acid bacterium *Oenococcus oeni*. *Appl. Environ. Microbiol.* **2009**, *75*, 6729−6735.
(42) Sumby, K. M.; Grbin, P. R.; Jiranek, V. Characterization of EstCOo8 and EstC34, intracellular esterases, from the wine-associated lactic acid bacteria *Oenococcus oeni* and *Lactobacillus hilgardii*. *J. Appl. Microbiol.* **2013**, *114*, 413−422.
(43) Boido, E.; et al. The effect of bacterial strain and aging on the secondary volatile metabolites produced during malolactic fermentation of Tannat red wine. *J. Agric. Food Chem.* **2009**, *57*, 6271−6278.
(44) Costello, P. J.; Francis, I. L.; Bartowsky, E. J. Variations in the effect of malolactic fermentation on the chemical and sensory properties of Cabernet Sauvignon wine: Interactive influences of *Oenococcus oeni* strain and wine matrix composition: Malolactic fermentation in Cabernet Sauvignon wine. *Aust. J. Grape Wine Res.* **2012**, *18*, 287−301.
(45) Saerens, S. M. G.; et al. The *Saccharomyces cerevisiae* EHT1 and EEB1 genes encode novel enzymes with medium-chain fatty acid ethyl ester synthesis and hydrolysis capacity. *J. Biol. Chem.* **2006**, *281*, 4446−4456.
(46) Mestres, M.; Busto, O.; Guasch, J. Analysis of organic sulfur compounds in wine aroma. *J. Chromatogr. A* **2000**, *881*, 569−581.
(47) Ortega-Heras, M.; González-SanJosé, M. L.; Beltrán, S. Aroma composition of wine studied by different extraction methods. *Anal. Chim. Acta* **2002**, *458*, 85−93.
(48) Francis, I. L.; Newton, J. L. Determining wine aroma from compositional data. *Aust. J. Grape Wine Res.* **2005**, *11*, 114−126.
(49) Ferreira, V.; López, R.; Escudero, A.; Cacho, J. F. The aroma of Grenache red wine: Hierarchy and nature of its main odorants. *J. Sci. Food Agric.* **1998**, *77*, 259−267.
(50) Bouchilloux, P.; Darriet, P.; Henry, R.; Lavigne-Cruège, V.; Dubourdieu, D. Identification of Volatile and Powerful Odorous Thiols in Bordeaux Red Wine Varieties. *J. Agric. Food Chem.* **1998**, *46*, 3095−3099.
(51) Rigou, P.; Triay, A.; Razungles, A. Influence of volatile thiols in the development of blackcurrant aroma in red wine. *Food Chem.* **2014**, *142*, 242−248.

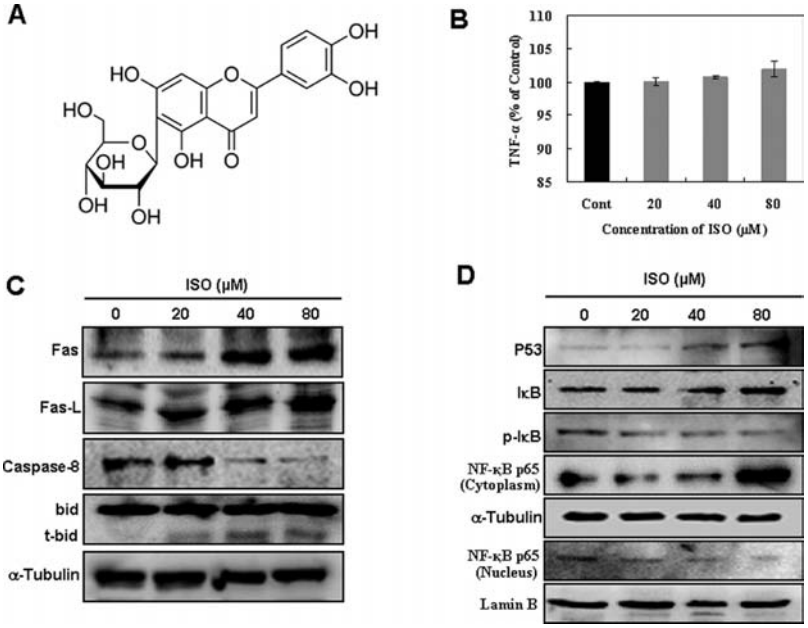

Figure 1. ISO induces apoptosis in HepG2 cells. (A) Chemical structure of ISO. (B) HepG2 cells were treated with ISO at the indicated concentrations for 24 h. The levels of TNF-α in the supernatant was measured using an ELISA assay kit, the results are shown as the mean ± standard deviation (SD) of nine separate experiments. Representative immunoblots for (C) Fas, FasL, caspase-8, and Bid and (D) p53, IκB, p-IκB, and NF-κB are shown. α-Tubulin and lamin B were used as internal controls.

In the present study, we investigated the mechanisms by which ISO affects autophagy in HepG2 cells and demonstrated the interplays between apoptosis and autophagy induced by ISO in HepG2 cells.

MATERIALS AND METHODS

Reagents and Antibodies. ISO (purity of ≥98%) was purchased from Forever Biotechnology, Ltd. (Shanghai, China). RPMI-1640 cell cultures, fetal bovine serum (FBS), and the BCA protein kit were purchased from Thermo Fisher (Shanghai, China). 3-(4,5-Dimethylthiazol-2-yl)-2,5-diphenyltetrazoliunbromide (MTT) (purity of ≥93%) was obtained from Wolsen Biotechnology, Ltd. (Xian, China). *N*-Acetyl-L-cysteine (NAC) (purity of ≥99%), pyrrolidinedithiocarbamic acid (purity of ≥99%), 3-methyladenine, rapamycin (purity of ≥95%), and pifithrin-α (purity of ≥95%) were purchased from Sigma. Acridine orange (AO), LY294002 (purity of ≥98%), and ZVAD-fmk were provided by Beyotime Institute of Biotechnology (Jiangsu, China).

Antibodies against Bcl-2 (SC-492), Bax (SC-493), cytochrome *c* (SC-7159), caspase-8 (SC-56070), FasL (SC-6237), α-tubulin (SC-5286), lamin B (SC-6216), and horseradish-peroxidase-conjugated secondary antibodies were purchased from Santa Cruz Biotechnology (Santa Cruz, CA). Beclin-1 (1353R) and cleaved caspase-3 (p17) (BS7004) were obtained from Abcam (Hong Kong) and Bioworld Technology, Inc. (Louis Park, MN). Nuclear factor (NF)-κB p65 (8242), IκB (9242), p-IκB (Ser32/36) (9246), poly(ADP-ribose) polymerase (PARP) (9542), LC3A/B (4108), p53 (9282), Fas (8023), p-Akt (Ser473) (9271), and Akt (9272) polyclonal antibodies were purchased from Cell Signaling Technology Company (Shanghai, China). An enzyme-linked immunosorbent assay (ELISA) kit for TNF-α was obtained from the Xinle Biology Technology (Shanghai, China). All other chemicals made in China were of analytical grade.

Cell Culture and Treatment. Human hepatoblastoma HepG2 cells were obtained from the Fourth Military Medical University (Xian, China) and cultured in RPMI-1640 medium with 10% FBS and 1% penicillin/streptomycin at 37 °C in a humidified incubator (5% CO_2 and 95% air). For the ISO treatment, ISO was dissolved in dimethyl sulfoxide (DMSO) and further diluted to final concentrations with serum-free culture medium.

Measurement of Cell Viability. Cell viability was determined using the MTT assay. Cells were seeded at a density of 1×10^6 cells/mL in 96-well polystyrene culture plates at 37 °C with 5% (v/v) CO_2 for 1 day. After 24 h of incubation, 100 μL of medium was removed from each well and 100 μL aliquots of different concentrations of ISO were added to the cells and incubated for 24 h. Subsequently, 100 μL of 0.5% (w/v) MTT dissolved in phosphate-buffered saline was added to each well and incubated for 4 h. The formazan crystals formed by live cells were solubilized with 100 μL of DMSO, and absorbance at 490 nm was measured with a microplate reader (Bio-Rad Laboratories, Ltd., China). Cell viability was expressed as a percentage of the control (untreated cells).

Measurement of TNF-α. Cells were treated with ISO for 24 h. The levels of TNF-α in the culture medium were measured using an ELISA kit according to the instructions of the manufacturer.

Detection of Autophagic Vacuoles by AO. Autophagy is the process of sequestering cytoplasmic proteins into the lytic component and is characterized by the formation and promotion of acidic vesicular organelles, as described previously. AO was always used to detect the acidic cellular compartment, which emits bright red fluorescence in acidic autophagic vacuole vesicles, but green fluoresces in the cytoplasm and nucleus. After treatment, cells were incubated with 1 μg/mL AO for 15 min. Then, the AO was removed and observed using a fluorescence microscopy (Olympus Optical Co., Ltd., Tokyo, Japan).

Observation and Quantification of Monodansylcadaverine (MDC) Staining. MDC staining was introduced to analyze autophagy induction in cells. After treatment, cells were rinsed with phosphate-buffered saline (PBS) and stained with 50 m/L MDC at 37 °C for 1 h. Finally, cells were washed with PBS, and the cellular fluorescence changes were observed using fluorescence microscopy (Olympus Optical Co., Ltd., Tokyo, Japan), and the MDC fluorescent intensity changes were determined by the microplate reader with excitation light at 488 nm and emission light at 530 and 650 nm (Molecular Devices Co., Sunnyvale, CA).

Transmission Electron Microscopy (TEM). HepG2 cells were treated with ISO, and then the cell pellets were fixed with a 0.1 M PBS solution containing 2.5% glutaraldehyde for 12 h. They were then washed with 0.1 M PBS, embedded in 2% agarose gel, and postfixed in 4% osmium tetroxide solution for 1 h. Next, the examples were

dx.doi.org/10.1021/jf500903g | J. Agric. Food Chem. 2014, 62, 5390−5400

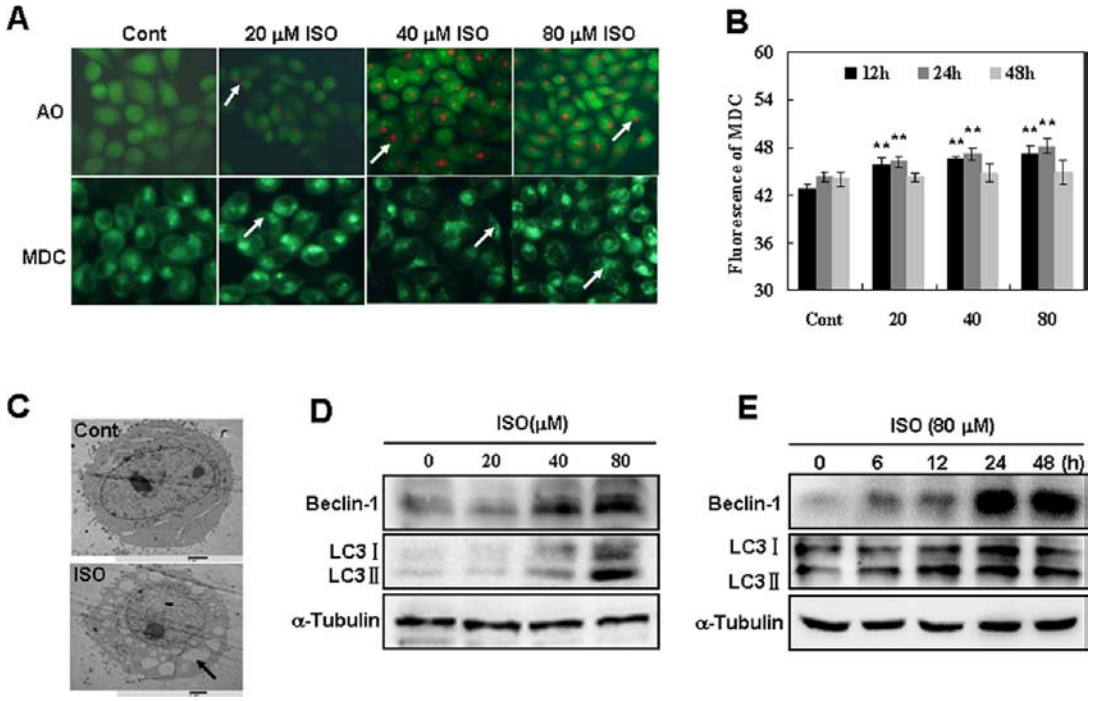

Figure 2. ISO induces autophagy in HepG2 cells. (A) Cells were seeded at a density of 1×10^5 cells/mL in 96-well polystyrene culture plates at 37 °C with 5% (v/v) CO_2 for 1 day. Then, cells were incubated with variable concentrations of ISO for 24 h, then exposed to AO and MDC, and observed by fluorescent microscopy. Arrows indicated the cells containing autophagic vacuoles. (B) Cells were incubated with variable concentrations of ISO for 12, 24, and 48 h, respectively, and were determined by the microplate reader of MDC staining at the emission wavelength of 525 nm. The results are shown as the mean ± SD of nine separate experiments. (**) $p < 0.01$ versus the corresponding control. (C) TEM shows the ultrastructure of cells treated with 80 μM ISO for 24 h. Arrows indicate autophagosomes, including residual digested material and empty vacuoles. (D) Cells were incubated with variable concentrations of ISO for 24 h, and (E) cells were treated with ISO at 80 μM for 0, 6, 12, 24, and 48 h before collection and lysis, respectively. Beclin-1 and LC3 were assessed by western blot analysis, and α-tubulin was used as an internal control.

desiccated with a range of ethanol concentrations and embedded in epoxy resin. The resin was polymerized at 30 °C for 24 h and 60 °C for 48 h, respectively. Ultrathin sections obtained with an ultramicrotome were stained with uranyl acetate and lead citrate and examined under TEM (HT7700, Hitachi, Japan).

Measurement of Mitochondrial Membrane Potential (MMP) by JC-1. The MMP was measured using the mitochondria-specific lipophilic cationic fluorescence dye JC-1. As a monomer, JC-1 is capable of selectively entering the mitochondria. Under normal conditions, JC-1 aggregates within the mitochondria and emits red fluorescence, but when the MMP collapses during apoptosis, JC-1 emits green fluorescence. The ratio of red/green JC-1 fluorescence reflects the change in MMP. Cells were seeded into 96-well polystyrene culture plates. After treatment, medium was removed from each well and 100 μL of 5 μg/mL JC-1 was added to the cells for 1 h. Finally, cells were washed twice with PBS and then quantitatively analyzed by a microplate reader (Molecular Devices Co., Sunnyvale, CA).

Detection of Intracellular Reactive Oxygen Species (ROS) Production. Cellular ROS was measured with 2′,7′-dichlorodihydrofluorescein diacetate (H_2DCFDA, Sigma). This dye is a stable nonpolar compound that diffuses readily into cells and yields DCFH. Intracellular ROS in the presence of peroxidase changes DCFH to the highly fluorescent compound DCF. Thus, the fluorescent intensity is proportional to the amount of ROS produced by the cells. After treatment, 10 μM H_2DCFDA was added to the wells for 30 min at 37 °C. Then, cells were washed twice with PBS, lysed in cell lysates, and centrifuged at 15000*g* for 10 min at 4 °C. The DCF fluorescence intensity of the supernatant was measured via a fluorescence microplate reader at 485 nm excitation and 535 nm emission. Cellular ROS levels were expressed as relative DCF fluorescence per microgram of protein.[20]

AO–Ethidium Bromide (EB) and Hoechst 33258 Staining Assay. Cells were seeded into 35 mm polystyrene culture dishes at a seeding density of 1×10^4 cells/mL and cultured with 2 mL of cell culture medium overnight. After treatment, cells were washed with PBS twice, and then cells were incubated with 5 μL of 100 μg/mL AO–EB at room temperature in the dark, followed by observation under a fluorescence microscope. Cells were stained with 1 mg/mL Hoechst 33258 for 30 min at 37 °C and observed using a fluorescence microscope (Olympus Optical Co., Ltd., Tokyo, Japan).

Sodium Dodecyl Sulfate (SDS)–Polyacrylamide Gel Electrophoresis (PAGE) and Western Blot Analysis. After the cells were subjected to the indicated treatments, they were harvested and lysed with cell lysis buffer (Beyotime Institute of Biotechnology, Jiangsu, China) and nuclear extraction reagent (Xianfeng Biotechnology, Xian, China) as cytosolic extract (cytosol) and nuclear extract (nucleus), respectively. The total protein concentration was determined using the BCA protein kit (Thermo Fisher, Shanghai, China). The homogenates were treated with SDS sample buffer and then immediately heated at 95 °C for 10 min. The proteins were separated by SDS–PAGE and electrotransferred onto a polyvinylidene fluoride (PVDF) membrane (0.45 μm, Millipore) using a semi-dry transfer apparatus (Bio-Rad, Shanghai, China). Blocking was carried out for 2 h in 5% nonfat dry milk in TBST (20 mM Tris, 166 mM NaCl, and 0.05% Tween 20 at pH 7.5). Then, the membrane was washed with TBST for 15 min. The primary antibodies were added at the manufacturer-recommended dilutions in TBST buffer overnight at 4 °C. Secondary antibodies were added and incubated at 25 °C for 2 h. The blots were subjected to another three washes with TBST, developed with a chemiluminescent substrate (Thermo Fisher, China), and exposed using a Molecular Imager ChemiDoc XRS system (Bio-Rad, Shanghai, China).

Statistical Analysis. All experiments were performed 3 times, and the data are presented as the mean ± standard error (SE). Significant differences between measurements for the control and treated samples were analyzed using one-way factorial analysis of variance (ANOVA), followed by Duncan's post-hoc test (SPSS 16.0).

dx.doi.org/10.1021/jf500903g | J. Agric. Food Chem. 2014, 62, 5390–5400

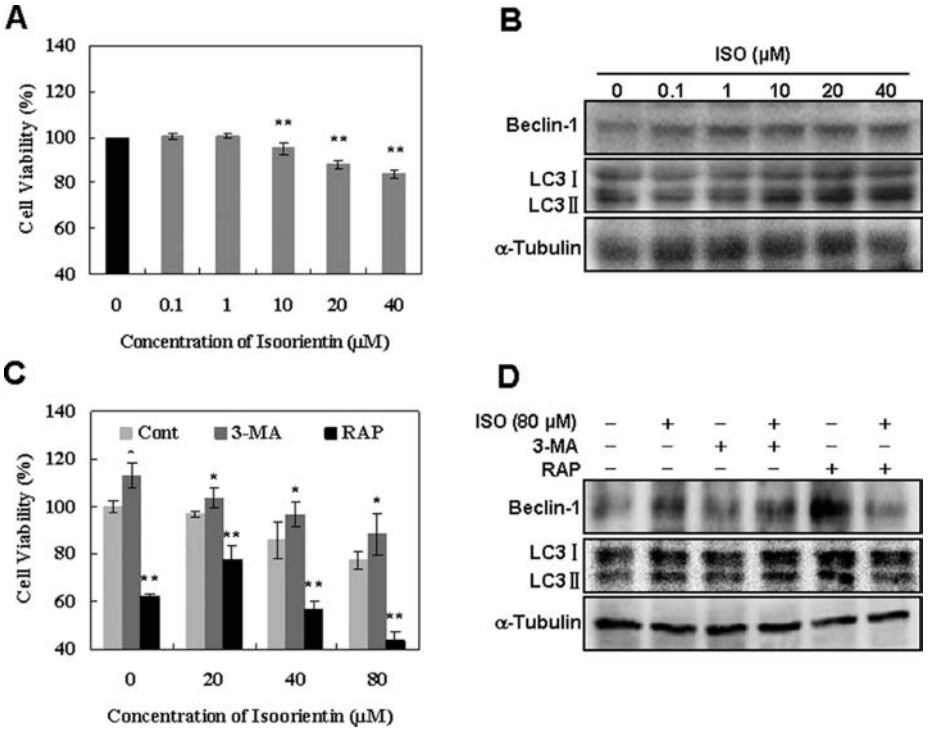

Figure 3. ISO induces autophagic cell death in HepG2 cells. (A) Cells were incubated with ISO at the indicated concentrations for 24 h and then processed for MTT assay. (B) Representative immunoblots for Beclin-1 and LC3 are shown. (C) Cells were incubated with variable concentrations of ISO for 24 h in the presence of 3-MA or RAP, respectively, and then processed for the MTT assay. The results are shown as the mean ± SD of nine separate experiments. (**) $p < 0.01$ and (*) $p < 0.05$ versus the corresponding control. (D) Cells were pretreated with 3-MA or RAP prior to exposure to ISO, respectively. Beclin-1 and LC3 were assessed by western blot analysis. α-Tubulin was used as an internal control.

RESULTS

Effect of ISO on Apoptosis in HepG2 Cells. Apoptosis includes two major pathways: the cell-death-receptor-mediated (extrinsic) apoptotic pathway and the mitochondrial-mediated (intrinsic) apoptotic pathway. We found that ISO induces apoptosis in HepG2 cells through the mitochondrial-mediated (intrinsic) apoptotic pathway. In the present study, we examined the effect of ISO on the cell-death-receptor-mediated (extrinsic) apoptotic pathway. As shown in Figure 1B, ISO increased the levels of TNF-α in HepG2 cells in a dose-dependent manner, but there was no significant difference in the TNF-α levels between the ISO-treated group and control group. ISO also notably increased the protein expression of Fas and FasL, decreased caspase-8 levels, and eventually caused the cleavage of Bid, increasing the protein levels of t-Bid (Figure 1C). In addition, we also found that ISO markedly increased p53 levels and the protein expression of NF-κB in the cytosol and decreased the phosphorylation of IκB and the level of NF-κB in the nucleus (Figure 1D). These results indicated that ISO induced apoptosis in HepG2 cells by activating the Fas receptor-mediated apoptotic pathway, increasing p53 levels and blocking the nuclear translocation of NF-κB.

Effect of ISO on Autophagy in HepG2 Cells. To investigate whether ISO induces autophagy in HepG2 cells, we examined the formation of autophagic vacuoles using the specific fluorescent dyes AO and MDC. Figure 2A shows predominantly green fluorescence in the control cells and considerable red fluorescence in a dose-dependent manner in the cells treated with ISO. ISO treatment also resulted in an increase in the accumulation of MDC, indicating an increased formation of the MDC-labeled vacuoles compared to the untreated cells. Furthermore, the fluorescence intensity of MDC was significantly ($p < 0.01$) enhanced by ISO in a dose- and time-dependent manner and reached its maximum intensity at an ISO dose of 80 μM for 24 h (Figure 2B). A TEM assay confirmed that numerous autophagic vacuoles and empty vacuoles were present in the HepG2 cells treated with 80 μM ISO (Figure 2C). Additionally, the expression level of Beclin-1 and the conversion of LC3-I to LC3-II, both of which indicate autophagy, were increased after ISO treatment in a dose- and time-dependent manner and reached their maximum levels at an ISO dose of 80 μM for 24 h (panels C and D of Figure 2). Taken together, the results suggest that ISO induces autophagy in HepG2 cells.

Effect of Autophagy on ISO-Induced Cell Death in HepG2 Cells. A significant inhibition in cell viability was observed in the ISO high-concentration groups (10, 20, and 40 μM), while no significant effects were observed in the lower concentration groups (0.1 and 1 μM) (Figure 3A), and the IC_{50} of ISO was 71.77 μM. There were also no significant changes in the protein expression of Beclin-1 and LC3-II in cells treated with ISO at 0.1 and 1 μM (Figure 3B). More importantly, the effects of the autophagy inhibitor 3-methyladenine (3-MA) and the autophagy activator rapamycin (RAP) on cell viability were also examined (Figure 3C); the results showed that 3-MA significantly ($p < 0.05$) increased cell viability and weakened the inhibitory effect of ISO on cell viability. However, RAP notably ($p < 0.01$) decreased cell viability and strengthened the inhibitory effect of ISO on cell viability. Additionally, 3-MA diminished the expression levels of Beclin-1 and LC3-II, and RAP increased their expression in HepG2 cells (Figure 3D). These results indicated that ISO induced autophagic cell death to decrease cell viability of HepG2 cells.

dx.doi.org/10.1021/jf500903g | J. Agric. Food Chem. 2014, 62, 5390−5400

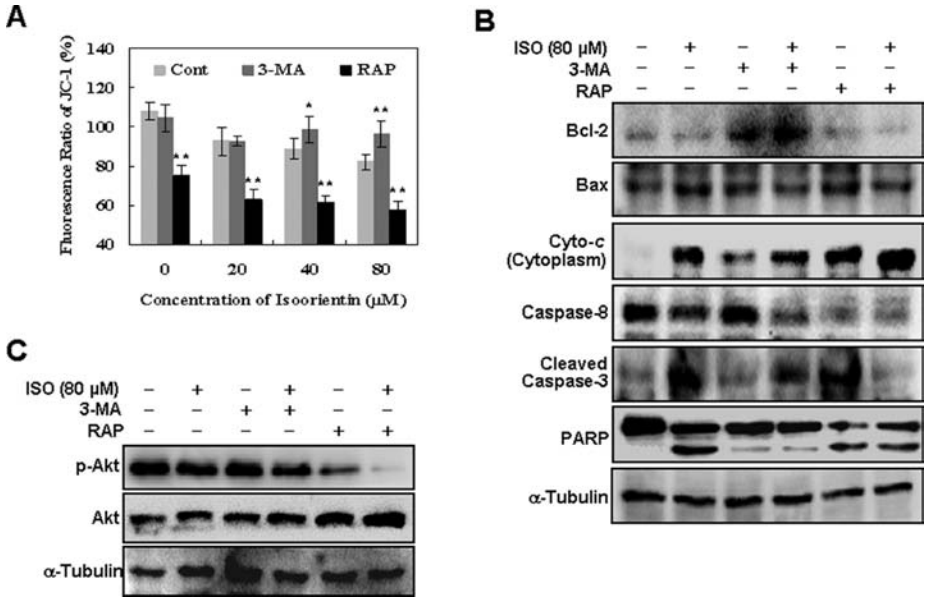

Figure 4. Effect of autophagy inhibitor and activator on ISO-induced apoptosis. (A) Cells were incubated with variable concentrations of ISO for 24 h in the presence of 3-MA or RAP, respectively. Then, cells were stained with JC-1 at 37 °C for 1 h. The fluorescence intensity of JC-1 was detected by a multifunctional microplate reader. The results are expressed as the mean ± SD of nine separate experiments. (**) $p < 0.01$ and (*) $p < 0.05$ versus the corresponding control. Representative image of immunoblots for (B) autophagic marker proteins and (C) Akt and p-Akt. α-Tubulin was used as an internal control.

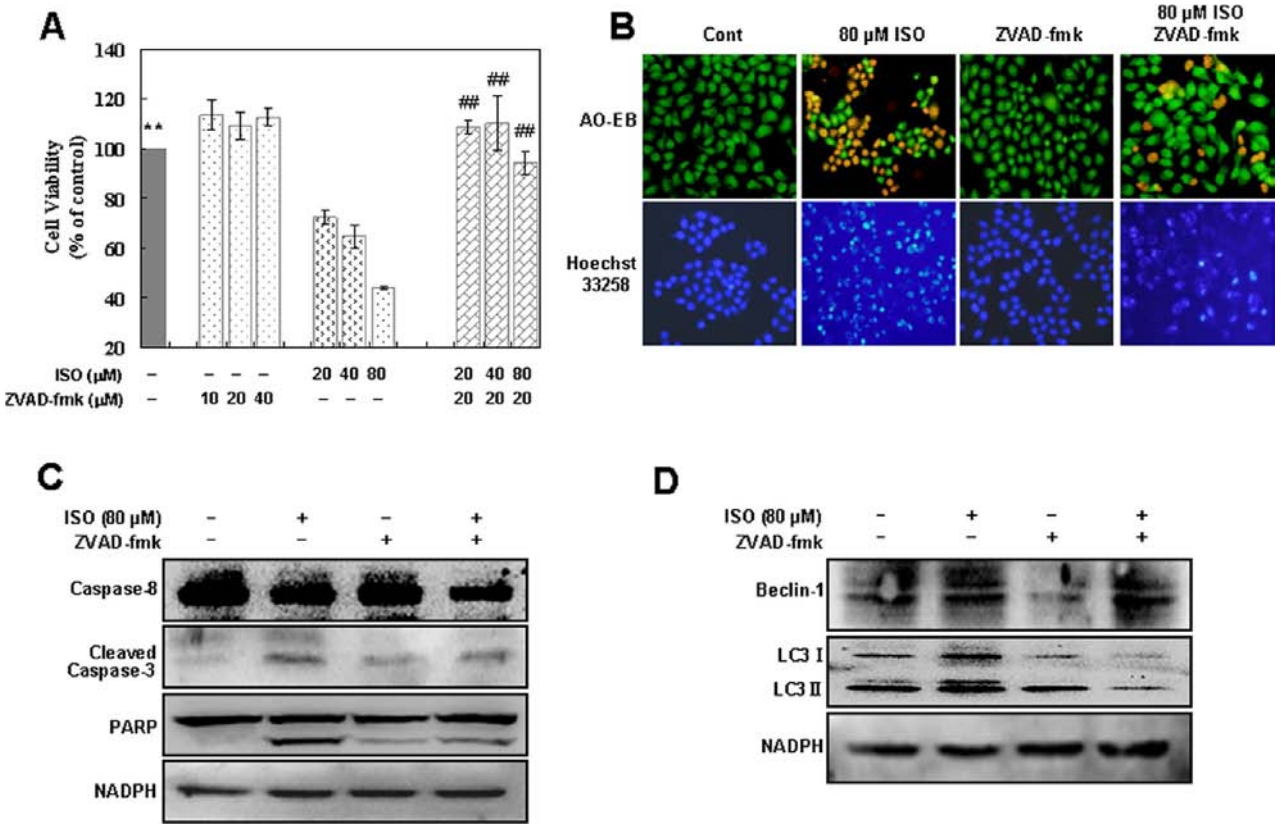

Figure 5. Effect of the apoptosis inhibitor on ISO-induced autophagy in HepG2 cells. (A) Cells were incubated with ISO for 48 h in the presence of ZVAD-fmk and then processed for the MTT assay. The results are shown as the mean ± SD of nine separate experiments. (**) $p < 0.01$ versus other treatments and (##) $p < 0.01$ versus the ISO treatment group. (B) Cells were incubated with ISO for 24 h in the presence of ZVAD-fmk, and then cells were exposed to AO−EB or Hoechst 33258. Green cells were counted as live cells; yellow cells were counted as early apoptotic cells; and orange cells were counted as late apoptotic cells. Chromatin condensation and nuclear fragmentation were considered to indicate apoptotic cells. Scale bar = 50 μm. (C) Caspase-8, cleaved caspase-3, and PARP and (D) Beclin-1 and LC3 were assessed by western blot analysis. NADPH was used as an internal control.

dx.doi.org/10.1021/jf500903g | J. Agric. Food Chem. 2014, 62, 5390−5400

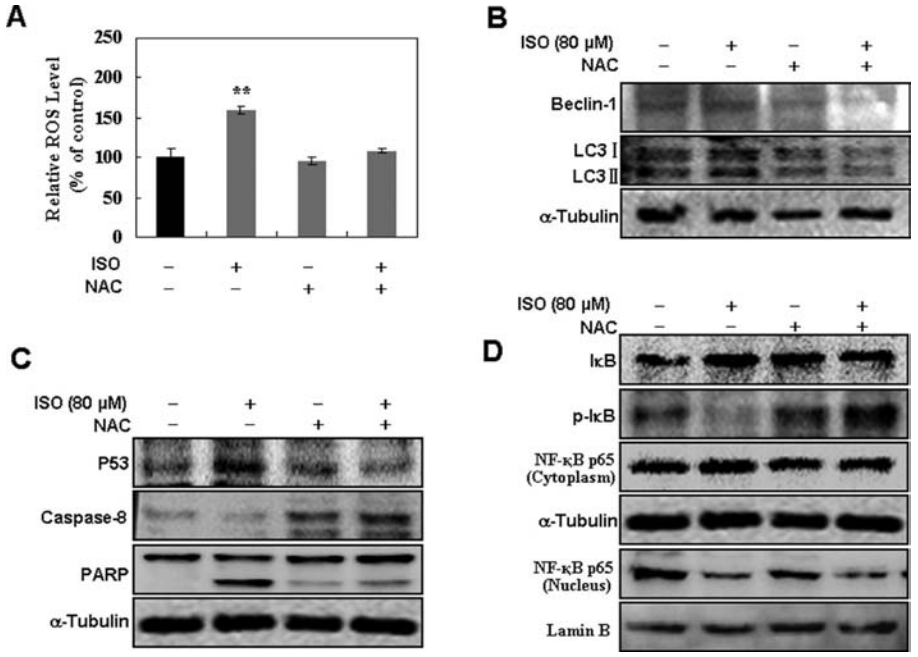

Figure 6. Effect of ROS on ISO-induced autophagy and NF-κB signaling pathway. (A) After treatment, cells were stained with H_2DCFDA for 30 min prior to detection using a fluorescence microplate reader. The results are expressed as the mean ± SD of nine separate experiments. (**) $p < 0.01$ versus the control group. (B) Beclin-1 and LC3 were assessed by western blot analysis. (C) Protein expressions of p53, caspase-8, and PARP were analyzed by western blotting. (D) Protein expressions of the NF-κB signaling pathway were analyzed by western blotting. α-Tubulin and lamin B were used as an internal control.

A complicated interplay exists between autophagy and apoptosis. To demonstrate whether ISO-triggered autophagy promotes or inhibits apoptosis, we examined apoptotic markers after treatment with the autophagy inhibitor 3-MA and the autophagy activator RAP. As shown in Figure 4A, 3-MA significantly ($p < 0.01$) attenuated the MMP collapse induced by ISO, while RAP increased MMP levels. In addition, in comparison to ISO alone, 3-MA markedly inhibited the expression of Bax, cytochrome *c* (in the cytoplasm), cleaved caspase-3, and PARP and increased the levels of Bcl-2 and caspase-8 in the presence of ISO (Figure 4B). In contrast, RAP notably enhanced the effects of ISO on the expression of these proteins. Furthermore, 3-MA significantly increased the phosphorylation of Akt. RAP strongly suppressed the phosphorylation of Akt, not only by itself but also in the presence of ISO (Figure 4C). These results suggest that the suppression of autophagy diminished the ISO-induced apoptosis in HepG2 cells.

To confirm these results, we further investigated the effect of the apoptosis inhibitor ZVAD-fmk on HepG2 cells. As shown in Figure 5A, the cell viability inhibition caused by ISO was strongly ($p < 0.01$) decreased in the presence of ZVAD-fmk and ZVAD-fmk alone did not have any cytotoxic effects. The fluorescence microscopy showed that the typical characteristics of apoptosis, such as cell shrinkage, chromatin condensation, and EB signals, were obviously attenuated in the cells treated with ZVAD-fmk and that ZVAD-fmk strongly reversed the apoptosis-inducing effect of ISO (Figure 5B). Other apoptotic hallmarks, including caspase-8, cleaved caspase-3, and PARP cleavage, were also suppressed by ZVAD-fmk in ISO-treated cells (Figure 5C). Additionally, ZVAD-fmk markedly decreased Beclin-1 and LC3-II levels, which had been increased by ISO, indicating that the inhibition of apoptosis blocks autophagy (Figure 5D). Taken together, these results suggest that ISO decreased cell viability simultaneously by inducing apoptosis and autophagy in HepG2 cells.

Effect of ISO-Stimulated ROS on Apoptosis and Autophagy. The molecular crosstalk between apoptosis and autophagy processes is complex, and they both may be triggered by common upstream signals; therefore, we next determined which interactions are demonstrated in the apoptosis and autophagy in HepG2 cells. Accumulating evidence indicates that intracellular ROS can trigger apoptosis and autophagy. We examined whether ROS stimulated by ISO induced apoptosis and autophagy in HepG2 cells. The ROS inhibitor NAC markedly ($p < 0.01$) decreased ROS generation, not only by itself but also in the presence of ISO (Figure 6A). NAC also significantly suppressed the protein expression of Beclin-1 and LC3-II and strongly reduced the effects of ISO on the expression of those proteins (Figure 6B). This suggests that a higher level of ROS may directly initiate autophagy. Similarly, a significant decrease in p53 and PARP cleavage and a increase in caspase-8, p-IκB, and NF-κB p65 (in the nucleus) were observed in NAC-treated cells (panels C and D of Figure 6). Taken together, these results showed that ROS is involved in the p53 signaling pathway, the phosphorylation of IκB, and the nuclear translocation of NF-κB as an upstream signal and that intracellular ROS controls apoptosis and autophagy induced by ISO.

Effect of the PI3K/Akt Signaling Pathway on Apoptosis and Autophagy. The PI3K/Akt signaling pathway is involved in the regulation of the cell cycle, growth, survival, metabolism, and tumorigenesis. In a previous study, we found that ISO induced apoptosis by inhibiting the PI3K/Akt pathway in HepG2 cells. To investigate the effect of the PI3K/Akt pathway on the crosstalk between the processes of apoptosis and autophagy, cells were pretreated with the PI3K/Akt inhibitor LY294002 prior to being exposed to ISO.

dx.doi.org/10.1021/jf500903g | J. Agric. Food Chem. 2014, 62, 5390−5400

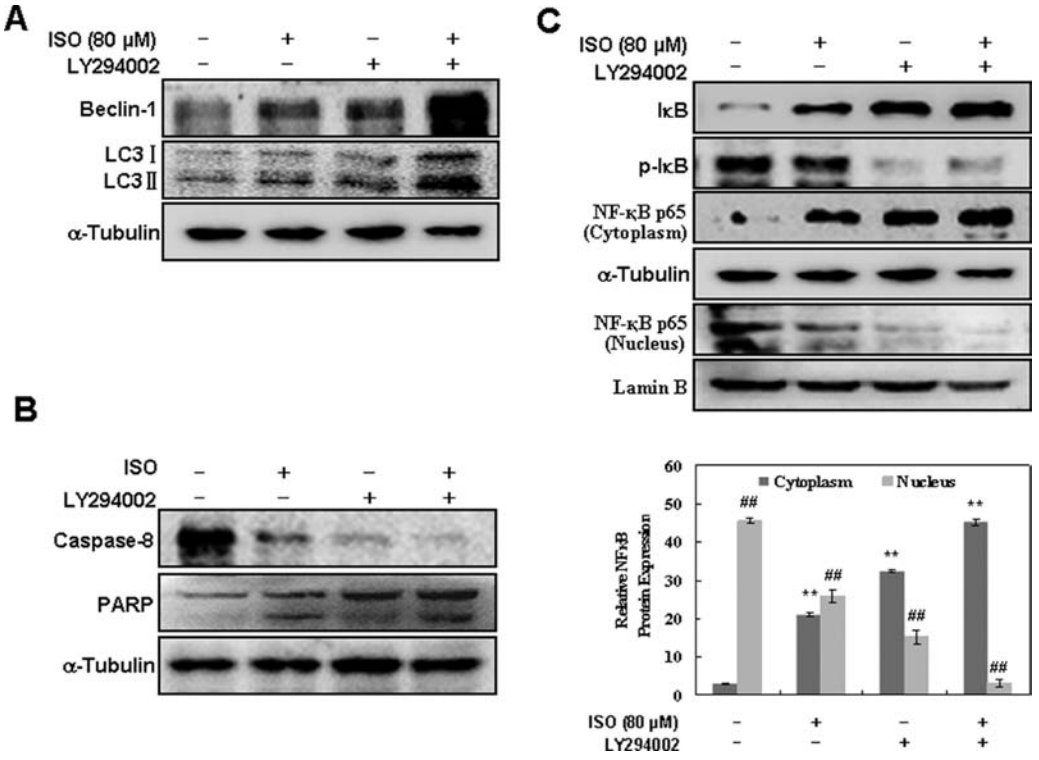

Figure 7. Effect of PI3K/Akt on ISO-induced autophagy and NF-κB. (A) Cells were incubated with 20 μM PI3K/Akt inhibitor LY294002 in the presence or absence of ISO. Beclin-1 and LC3 were assessed by western blot analysis. (B) Representative image of immunoblots for caspase-8 and PARP. (C) Protein expressions of NF-κB signaling pathway were analyzed by western blotting. α-Tubulin and lamin B were used as an internal control. The graph shows the levels of NF-κB in cytoplasm and nucleus. The densitometric analysis shows the mean ± SD of four independent experiments. (**) $p < 0.05$ and (##) $p < 0.05$ versus the control of cytoplasm and nucleus, repectively.

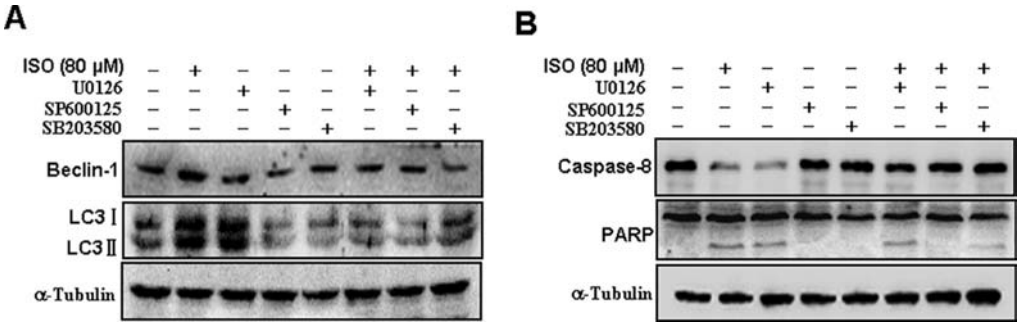

Figure 8. Effect of the MAPK signaling pathway on ISO-induced autophagy and apoptosis. Cells were treated with 5 μM U0126 (an ERK1/2 inhibitor), 10 μM SP600125 (a JNK inhibitor), or 10 μM SB203580 (a p38 inhibitor) for 30 min prior to exposure to ISO (80 μM) for 24 h. Representative images of immunoblots for (A) Beclin-1 and LC3 and (B) caspase-8 and PARP. α-Tubulin was used as an internal control.

In comparison to the control group, LY294004 markedly increased the protein expression of Beclin-1 and LC3-II, not only by itself but also in the presence of ISO (Figure 7A). Additionally, LY294004 significantly decreased caspase-8 levels and increased PARP cleavage levels in both the presence and absence of ISO (Figure 7B). Also, LY294004 obviously inhibited the phosphorylation of IκB and the nuclear translocation of NF-κB (Figure 7C). These data indicate that ISO induced apoptosis and autophagy simultaneously by inhibiting the PI3K/Akt signaling pathway.

Effect of the MAPK Signaling Pathway on ISO-Induced Apoptosis and Autophagy. To investigate the effect of the MAPK pathway on apoptosis and autophagy, cells were pretreated with U0126 (an ERK1/2 inhibitor), SP600125 (a JNK inhibitor), and SB203580 (a p38 inhibitor) prior to being exposed to ISO. As shown in Figure 8A, both SP600125 and SB203580 decreased the levels of Beclin-1 and LC3-II individually and in the presence of ISO and weakened the induced effect of ISO on the protein expression of Beclin-1 and LC3-II. It was interesting that the significant increase in Beclin-1 and LC3-II levels was observed in cells that were treated with U0126 alone, while U0126 inhibited the effect of ISO on Beclin-1 and LC3-II levels. In addition, U0126 markedly increased cleaved caspase-8 levels and PARP cleavage in the absence of ISO but did not change the activation effects of ISO on those protein levels. In contrast, SP600125 and SB203580 notably inhibited the levels of PARP cleavage, increased the protein expression of caspase-8, and reversed the activation effects of ISO on those protein levels (Figure 8B). Taken together, these results indicate that ISO induced apoptosis and autophagy by activating JNK and p38.

dx.doi.org/10.1021/jf500903g | J. Agric. Food Chem. 2014, 62, 5390−5400

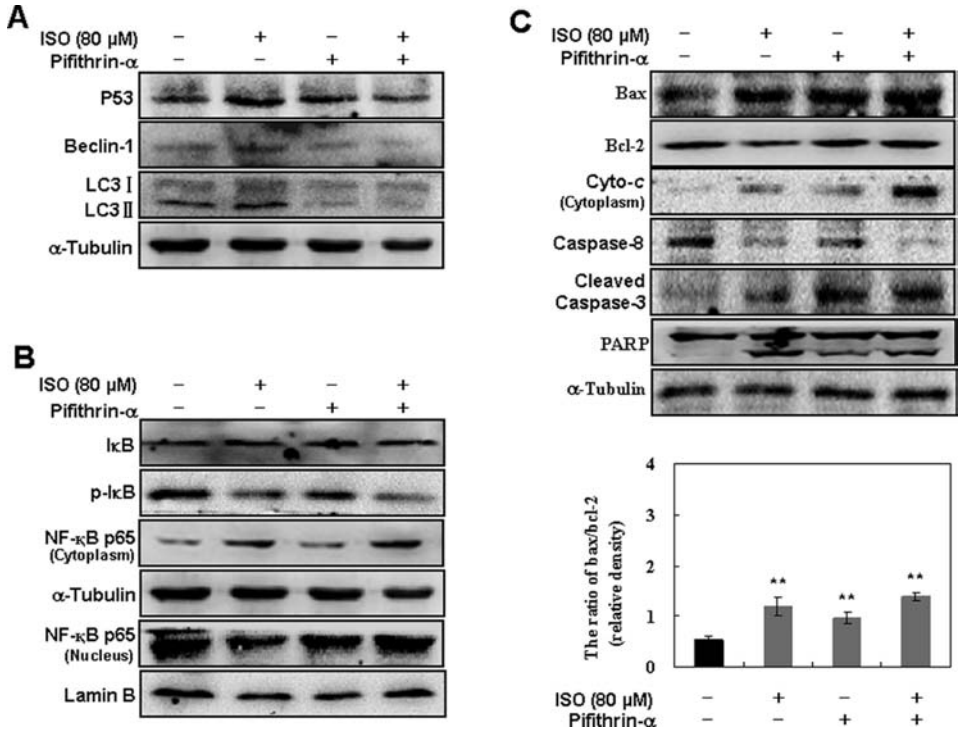

Figure 9. Effect of p53 on ISO-induced autophagy, apoptosis, and NF-κB. Cells were treated with 20 μM pifithrin-α (p53 inhibitor) for 30 min prior to exposure to ISO (80 μM) for 24 h. (A) Representative images of immunoblots for Beclin-1 and LC3 and (B) protein expressions of the NF-κB signaling pathway. (C) Apoptotic marker proteins were analyzed by western blotting. α-Tubulin was used as an internal control. The graph shows the ratio of Bax/Bcl-2 values. The densitometric analysis shows the mean ± SD of four independent experiments. (**) $p < 0.05$ versus the control.

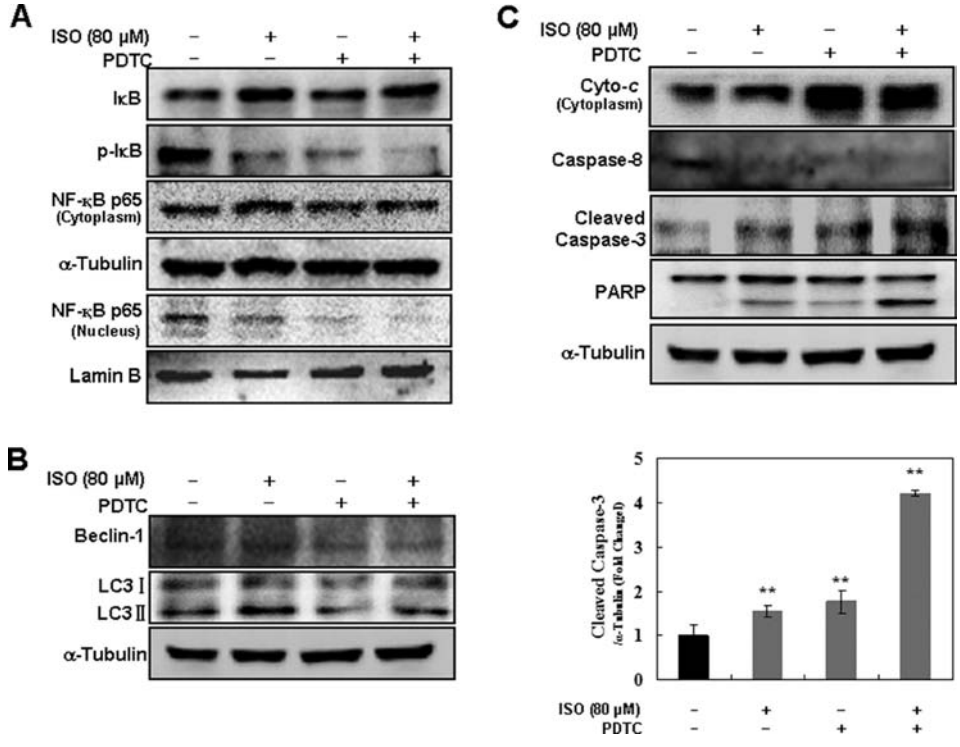

Figure 10. Effect of NF-κB on ISO-induced autophagy and apoptosis. Cells were treated with 50 μM PDTC (NF-κB inhibitor) for 30 min prior to exposure to ISO (80 μM) for 24 h. (A) Protein expressions of NF-κB signaling pathway were analyzed by Western blotting. (B) Representative images of immunoblots for Beclin-1 and LC3 and (C) apoptotic marker proteins. α-Tubulin was used as an internal control. The graph shows the relative expression of cleaved caspase-3. The densitometric analysis shows the mean ± SD of four independent experiments. (**) $p < 0.05$ versus the control.

dx.doi.org/10.1021/jf500903g | J. Agric. Food Chem. 2014, 62, 5390−5400

Effect of p53 on ISO-Induced Apoptosis and Autophagy. The effect of p53 on autophagy depends upon the cellular context. To determine the effects of p53 on autophagy and apoptosis, cells were exposed to the p53 inhibitor pifithrin-α prior to treatment with ISO. As shown in Figure 9A, pifithrin-α significantly inhibited the protein expression of p53, Beclin-1, and LC3-II and reversed the effects of ISO on p53, Beclin-1, and LC3-II (Figure 9A). This suggests that p53 promotes ISO-induced autophagy in HepG2 cells. In contrast, pifithrin-α upregulated the phosphorylation of IκB and the protein expression of NF-κB in the nuclear fraction of the cells (Figure 9B), indicating that p53 is involved in the activation of NF-κB as an upstream signaling molecule. Additionally, the upregulation of the Bax/Bcl-2 ratio, the release of cytochrome *c* into the cytosol, and an increase in the levels of cleaved caspase-3 and PARP cleavage were observed in pifithrin-α-treated cells in both the absence and presence of ISO (Figure 9C). Taken together, these data indicated that the activation of p53 induced apoptosis and autophagy in HepG2 cells.

Effect of NF-κB Activation on ISO-Induced Apoptosis and Autophagy. Accumulating evidence indicates that the activation of NF-κB inhibits apoptosis, activates autophagy, and regulates cell survival pathways. To confirm this evidence, cells were treated with the NF-κB inhibitor pyrrolidinedithiocarbamic acid (PDTC) prior to being exposed to ISO. PDTC notably decreased the phosphorylation of IκB and the protein levels of NF-κB in the nuclear fraction of the cells (Figure 10A). A significant decrease in the expression of Beclin-1 and LC3-II was also observed in cells treated with PDTC alone and in cells treated with PDTC and ISO (Figure 10B). In contrast, PDTC alone and with ISO caused a strong upregulation of cytochrome *c* (in the cytosolic fraction), cleaved caspase-3, and PARP cleavage levels, and PDTC enhanced the effects of ISO on these protein levels (Figure 10C). These results suggest that the inhibition of NF-κB suppresses autophagy and promotes apoptosis.

DISCUSSION

ISO is a naturally occurring *C*-glycosyl flavone and has been reported to reduce the proliferation of HepG2 cells, with no significant cytotoxicity on human liver cells (HL-7702) and buffalo rat liver cells (BRL-3A).[18] The present study showed that ISO induced cell death by activating both apoptosis and autophagy, which coexist and promote each other in HepG2 cells. ISO was able to induce apoptosis by activating the Fas receptor-mediated apoptotic pathway and suppressing the p53 and PI3K/Akt-dependent NF-κB signaling pathway. Also, we found that ROS-mediated p53, PI3K/Akt, JNK, and p38 were the common upstream signals that simultaneously triggered apoptosis and autophagy.

Apoptosis is a programmed cell death process, and a multitude of studies have suggested that the activation of apoptosis in tumor cells is an effective form of chemotherapy designed to hinder the development and progression of cancer.[3] Autophagy is another programmed cell death process, and it can have two effects on tumors. First, by removing damaged organelles, regenerating metabolic precursors, and reducing chromosomal instability, it aids the survival of cancer cells in a low-nutrient environment and increases the resistance of cancer cells to anticancer treatments preventing tumor suppression.[21] On the other hand, autophagy prevents tumor transformation and facilitates senescence, necrosis, and inflammation, processes that are induced by oncogenes; thus, autophagy eventually limits tumor growth.[22] A low level of constitutive autophagy has an important housekeeping role in cellular metabolism and is crucial for maintaining healthy cells. However, excessive autophagy or the activation of autophagy in a specific context has been implicated in autophagic cell death and may be harmful.[23] Numerous studies have revealed that autophagy is linked to cell death under certain circumstances. For example, the upregulation of autophagy contributes to the progress of cadmium-induced nephrotoxicity.[24] Also, our results showed that ISO decreased cell viability by inducing autophagic cell death in HepG2 cells (Figure 3).

Both apoptosis and autophagy are essential cellular degradation pathways that are often induced by similar stimuli and regulated by similar pathways. However, the relationship between apoptosis and autophagy is multifaceted, complex, and controversial. In some cellular settings, autophagy is necessary for apoptosis to occur. In other cellular settings, autophagy suppresses or delays apoptosis as a stress adaptation, and in some cell systems, the two processes occur independently.[8,25,26] In summary, autophagy and apoptosis can cooperate, antagonize, or assist each other to differentially influence the fate of the cell. It has been repotred that vitamin K2 induces autophagy and apoptosis simultaneously in leukemia cell,[4] and the survivin suppressant YM155 inhibits growth in both PC3 and LNCaP prostate cancer cells by inducing the autophagy-dependent apoptosis.[27] In the present study, the autophagy inhibitor 3-MA markedly inhibited ISO-induced apoptosis, and the apoptosis inhibitor ZVAD-fmk significantly decreased ISO-induced autophagy (Figures 4 and 5), suggesting that apoptosis and autophagy could exist simultaneously and work cooperatively in ISO-treated HepG2 cells.

ROS regulates a number of cellular pathways and, thus, plays critical roles in determining the fate of cells.[28] Accumulating evidence has revealed that autophagy can be stimulated in response to ROS injury in cancer cells, and ROS may have synergetic effects in apoptosis and autophagy.[29] Consistent with previous studies, we also found that both the autophagic markers (Beclin-1 and LC3-II) and apoptotic markers (caspase-8 and PARP) were suppressed by the ROS inhibitor NAC in ISO-treated cells (panels B and C of Figure 6). Our previous research showed that ROS is an upstream signal involved in the effects of ISO on the PI3K/Akt and MAPK signaling pathways, which impact apoptosis.[18,19] Numerous studies have demonstrated that autophagic cell death is triggered by the MAPK and PI3K/Akt pathways.[30−32] We further investigated the roles of the PI3K/Akt and MAPK pathways on the interactions of the apoptosis and autophagy processes. The results showed that the PI3K/Akt inhibitor LY294004 markedly increased autophagy; similarly, LY294004 notably promoted ISO-induced apoptosis (Figure 7), indicating that ISO simultaneously induced apoptosis and autophagy by inhibiting the PI3K/Akt signaling pathway. The mechanism behind this is the inhibition of the phosphorylation of mTOR by LY294002, resulting in the phosphorylation of autophagy protein-13 and the suppression of autophagy.[1] LY294002 also inhibits the phosphorylation of pro-apoptotic proteins, such as Bad, Bax, and caspase-9.[33,34] In addition, SP600125 (a JNK inhibitor) and SB203580 (a p38 inhibitor) obviously decreased autophagy that was induced by ISO (Figure 8A), and both SP600125 and SB203580 significantly inhibited ISO-induced apoptosis (Figure 8B). The effects of JNK and p38 on apoptosis and autophagy were consistent, because JNK and p38 kinases modulate the

expression and translocation of Bcl-2 and Bax in apoptotic cells.[35,36] JNK is able to trigger autophagy by targeting Bcl2/BclXL proteins and abrogating their binding to Beclin-1,[37] and p38 catalyzes the phosphorylation of mTOR.[38]

Furthermore, we found that the ROS inhibitor NAC also reversed the inhibitory effect of ISO on the protein expression of p53 and the nuclear translocation of NF-κB (panels C and D of Figure 6). The tumor suppressor p53 plays a major role in cell cycle arrest and/or apoptosis during the response of mammalian cells to stress, and p53 mutations and functional inactivation are linked to the pathology of more than half of all cancers.[39,40] Furthermore, p53 can both promote and inhibit autophagy, depending upon the cellular conditions.[8] In the current study, a p53 inhibitor promoted the induction of apoptosis by ISO and NF-κB nuclear translocation and inhibited autophagy (Figure 9). The transcription factor NF-κB is involved in the regulation of survival, death, differentiation, and migration.[41] The present study has shown that the NF-κB inhibitor PDTC efficiently suppressed ISO-induced autophagy and enhanced ISO-induced apoptosis (Figure 10). The results from several other studies also indicated that p53 and NF-κB promote apoptosis over autophagy.[42,43]

In summary, this study demonstrated that ISO simultaneously induced apoptosis and autophagy by inhibiting the ROS-related PI3K/Akt signaling pathway and activating the ROS-related JNK and p38 pathways. Moreover, ISO induced apoptosis by activating the Fas receptor-mediated apoptotic pathway and suppressing the p53 and PI3K/Akt-dependent NF-κB signaling pathway, with the subsequent increase in the release of cytochrome *c*, caspase-3 activation, and PARP cleavage. A schematic diagram of these observed effects of ISO is shown in Figure 11. These findings indicate that ISO inhibited cell viability by both apoptosis and autophagy and that autophagy induction by ISO may be a novel therapeutic method for the treatment of cancer.

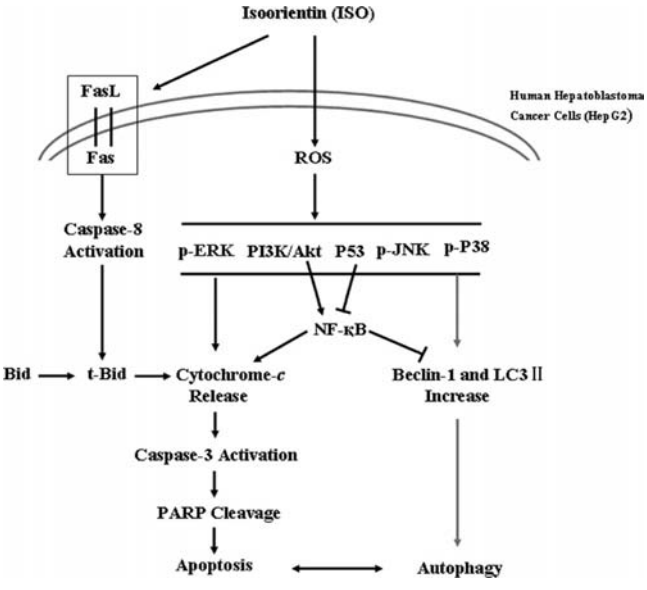

Figure 11. Possible molecular interplays between apoptosis and autophagy induced by ISO in HepG2 cells. → indicates activation or induction; ⊥ indicates inhibition or blockade; and ↔ indicates mutual promotion.

AUTHOR INFORMATION

Corresponding Author

*Telephone: 86-029-87092325. Fax: 86-029-87092817. E-mail: xueboliu@aliyun.com.

Funding

This work was financially supported by the National Natural Science Foundation of China (Grant 31271810) and the National "Twelfth Five-Year" Plan for Science and Technology Support (2012BAH30F03).

Notes

The authors declare no competing financial interest.

ABBREVIATIONS USED

HepG2 cells, human hepatoblastoma cancer cell line; ISO, isoorientin; PARP, poly(ADP-ribose) polymerase; ROS, reactive oxygen species; NAC, *N*-acetyl-L-cysteine; PDTC, pyrrolidinedithiocarbamic acid; 3-MA, 3-methyladenine; RAP, rapamycin

REFERENCES

(1) Maiuri, M. C.; Zalckvar, E.; Kimchi, A.; Kroemer, G. Self-eating and self-killing: Crosstalk between autophagy and apoptosis. *Mol. Cell. Biol.* **2007**, *8*, 741−745.

(2) Soldatenkov, V. A.; Smulson, M. Poly(ADP-ribose) polymerase in DNA damage-response pathway: implications for radiation oncology. *Int. J. Cancer* **2000**, *90*, 59−67.

(3) Ghobrial, I. M.; Witzig, T. E.; Adjei, A. A. Targeting apoptosis pathways in cancer therapy. *Ca-Cancer J. Clin.* **2005**, *55*, 178−194.

(4) Yokoyama, T.; Miyazawa, K.; Naito, M.; Toyotake, J.; Tauchi, T.; Itoh, M.; Yuo, A.; Hayashi, Y.; Georgescu, M. M.; Kondo, Y.; Kondo, S.; Ohyashiki, K. Vitamin K2 induces autophagy and apoptosis simultaneously in leukemia cells. *Autophagy* **2008**, *4*, 629−640.

(5) Bursch, W.; Ellinger, A.; Gerner, C.; Frohwein, U.; Schulte-Hermann, R. Programmed cell death (PCD). Apoptosis, autophagic PCD, or others? *Ann. N. Y. Acad. Sci.* **2000**, *926*, 1−12.

(6) Yang, C.; Kaushal, V.; Shah, S. V.; Kaushal, G. P. Autophagy is associated with apoptosis in cisplatin injury to renal tubular epithelial cells. *Am. J. Physiol.: Renal, Fluid Electrolyte Physiol.* **2008**, *294*, 777−787.

(7) Li, X.; Xu, H. L.; Liu, Y. X.; An, N.; Zhao, S.; Bao, J. K. Autophagy modulation as a target for anticancer drug discovery. *Acta Pharmacol. Sin.* **2013**, *34*, 612−624.

(8) Gump, J. M.; Thorburn, A. Autophagy and apoptosis: What is the interplay? *Trends Cell Biol.* **2011**, *21*, 387−392.

(9) Yong-Chun, J.; Lin, Y.; Yuan, K. A novel high- performance liquid chromatography fingerprint approach to discriminate *Phyllostachys pubescens* from China. *Pharmacogn. Mag.* **2012**, *8*, 42−48.

(10) Prinz, S.; Ring, A.; Huefner, A.; Pemp, E.; Kopp, B. 4″′-Acetylvitexin-2″-*O*-rhamnoside, isoorientin, orientin, and 8-methoxykaempferol-3-*O*-glucoside as markers for the differentiation of *Crataegus monogyna* and *Crataegus pentagyna* from *Crataegus laevigata*. *Chem. Biodiversity* **2007**, *4*, 2920−2931.

(11) Peng, J.; Fan, G.; Hong, Z.; Chai, Y.; Wu, Y. Preparative separation of isovitexin and isoorientin from *Patrinia villosa* Juss by high-speed counter-current chromatography. *J. Chromatogr. A* **2005**, *1074*, 111−115.

(12) Mitsuru, W.; Miyuki, I. Changes in antioxidative activity and flavonoid composition of the extracts from aerial parts of buckwheat during growth period. *Nippon Shokuhin Kagaku Kogaku Kaishi* **2002**, *49*, 119−125.

(13) Budzianowski, J.; Budzianowska, A.; Kromerb, K. Naphthalene glucoside and other phenolics from the shoot and callus cultures of *Drosophyllum lusitanicum*. *Phytochemistry* **2002**, *61*, 421−425.

(14) Afifi, F. U.; Khalil, E.; Abdalla, S. Effect of isoorientin isolated from *Arum palaestinum* on uterine smooth muscle of rats and guinea pigs. *J. Ethnopharmacol.* **1999**, *65*, 173−177.

(15) Ko, F. N.; Chu, C. C.; Lin, C. N.; Chang, C. C.; Teng, C. M. Isoorientin-6″-*O*-glucoside, a water-soluble antioxidant isolated from *Gentiana arisanensis*. *Biochim. Biophys. Acta* **1998**, *1389*, 81−90.
(16) Harborne, J. B. *The Flavonoids—Advances in Research since 1986*; Chapman and Hall: London, U.K., 1994.
(17) Pacifico, S.; Scognamiglio, M.; D'Abrosca, B.; Piccolella, S.; Tsafantakis, N.; Gallicchio, M.; Ricci, A.; Fiorentino, A. Spectroscopic characterization and antiproliferative activity on HepG2 human hepatoblastoma cells of flavonoid *C*-glycosides from *Petrorhagia velutina*. *J. Nat. Prod.* **2010**, *73*, 1973−1978.
(18) Yuan, L.; Wang, J.; Xiao, H. F.; Xiao, C. X.; Wang, Y. T.; Liu, X. B. Isoorientin induces apoptosis through mitochondrial dysfunction and inhibition of PI3K/Akt signalling pathway in HepG2 cancer cells. *Toxicol. Appl. Pharmacol.* **2012**, *265*, 83−92.
(19) Yuan, L.; Wang, J.; Xiao, H. F.; Xiao, C. X.; Wang, Y. T.; Liu, X. B. MAPK signalling pathways regulate mitochondrial-mediated apoptosis induced by isoorientin in human hepatoblastoma cancer cells. *Food. Chem. Toxicol.* **2013**, *53*, 62−68.
(20) Syama, S.; Reshma, S. C.; Sreekanth, P. J.; Varma, H. K.; Mohanan, P. V. Effect of zinc oxide nanoparticles on cellular oxidative stress and antioxidant defense mechanisms in mouse liver. *Toxicol. Environ. Chem.* **2013**, *95*, 495−503.
(21) Augustine, M. K.; Choi, M. D.; Stefan, W.; Ryter, P. D.; Levine, B. Autophagy in human health and disease. *New Engl. J. Med.* **2013**, *368*, 651−662.
(22) Lorin, S.; Hamaï, A.; Mehrpour, M.; Codogno, P. Autophagy regulation and its role in ancer. *Semin. Cancer Biol.* **2013**, *23*, 361−379.
(23) Nikoletopoulou, V.; Markaki, M.; Palikaras, K.; Tavernarakis, N. Crosstalk between apoptosis, necrosis and autophagy. *Biochim. Biophys. Acta* **2013**, *1833*, 3448−3459.
(24) Chargui, A.; Zekri, S.; Jacquillet, G.; Rubera, I.; Ilie, M.; Belaid, A.; Duranton, C.; Tauc, M.; Hofman, P.; Poujeol, P.; El May, M. V.; Mograbi, B. Cadmium-induced autophagy in rat kidney: An early biomarker of subtoxic exposure. *Toxicol. Sci.* **2011**, *121*, 31−42.
(25) Gozuacik, D.; Kimchi, A. Autophagy and cell death. *Curr. Top. Dev. Biol.* **2007**, *78*, 217−245.
(26) Baehrecke, E. H. Autophagy: Dual roles in life and death? *Nat. Rev. Mol. Cell Biol.* **2005**, *6*, 505−510.
(27) Wang, Q.; Chen, Z.; Diao, X.; Huang, S. Induction of autophagy-dependent apoptosis by the survivin suppressant YM155 in prostate cancer cells. *Cancer Lett.* **2011**, *302*, 29−36.
(28) Raza, H.; Annie, J.; Sheela, B. Acetylsalicylic acid-induced oxidative stress, cell cycle arrest, apoptosis and mitochondrial dysfunction in human hepatoma HepG2 cells. *Eur. J. Pharmacol.* **2011**, *668*, 15−24.
(29) Ling, L. U.; Tan, K. B.; Lin, H.; Chiu, G. N. The role of reactive oxygen species and autophagy in safingol-induced cell death. *Cell Death Dis.* **2011**, *2*, 129.
(30) Zhan, Y.; Gong, K.; Chen, C.; Wang, H.; Li, W. p38 MAP kinase functions as a switch in MS-275-induced reactive oxygen species-dependent autophagy and apoptosis in human colon cancer cells. *Free Radical Biol. Med.* **2012**, *53*, 532−543.
(31) Fimia, G. M.; Piacentini, M. Regulation of autophagy in mammals and its interplay with apoptosis. *Cell. Mol. Life Sci.* **2010**, *67*, 1581−1588.
(32) Takeuchi, H.; Kondo, Y.; Fujiwara, K.; Kanzawa, T.; Aoki, H.; Mills, G. B.; Kondo, S. Synergistic augmentation of rapamycin-induced autophagy in malignant glioma cells by phosphatidylinositol 3-kinase/protein kinase B inhibitors. *Cancer Res.* **2005**, *65*, 3336−3346.
(33) Liu, C. M.; Ma, J. Q.; Sun, Y. Z.; Liu, C. M. Puerarin protects rat kidney from lead-induced apoptosis by modulating the PI3K/Akt/eNOS pathway. *Toxicol. Appl. Pharmacol.* **2011**, *258*, 330−342.
(34) Franke, T. F.; Hornik, C. P.; Segev, L.; Shostak, G. A.; Sugimoto, C. PI3K/Akt and apoptosis: Size matters. *Oncogene* **2003**, *22*, 8983−8998.
(35) Chen, Y. J.; Liu, W. H.; Kao, P. H.; Wang, J. J.; Chang, L. S. Involvement of p38 MAPK- and JNK-modulated expression of Bcl-2 and Bax in *Naja nigricollis* CMS-9-induced apoptosis of human leukemia K562 cells. *Toxicon* **2010**, *55*, 1306−1316.
(36) Xie, N.; Wang, C.; Lin, Y.; Li, H.; Chen, L.; Zhang, T.; Sun, Y.; Zhang, Y.; Yin, D.; Chi, Z. The role of p38 MAPK in valproic acid induced microglia apoptosis. *Neurosci. Lett.* **2010**, *482*, 51−56.
(37) Wei, Y.; Sinha, S.; Levine, B. Dual role of JNK1-mediated phosphorylation of Bcl-2 in autophagy and apoptosis regulation. *Autophagy* **2008**, *4*, 949−951.
(38) Tang, G.; Yue, Z.; Talloczy, Z.; Hagemann, T.; Cho, W.; Messing, A.; Sulzer, D. L.; Goldman, J. E. Autophagy induced by Alexander disease-mutant GFAP accumulation is regulated by p38/MAPK and mTOR signaling pathways. *Hum. Mol. Genet.* **2008**, *17*, 1540−1555.
(39) Oren, M. Decision making by p53: Life, death and cancer. *Cell Death Differ.* **2003**, *10*, 431−442.
(40) Levine, A. J. p53, the cellular gatekeeper for growth and division. *Cell* **1997**, *88*, 323−331.
(41) Mayo, M. W.; Baldwin, A. S. The transcription factor NF-κB: Control of oncogenesis and cancer therapy resistance. *Biochim. Biophys. Acta* **2000**, *1470*, 55−62.
(42) Jiang, Y. Y.; Yang, R.; Wang, H. J.; Huang, H.; Wu, D.; Tashiro, S.; Onodera, S.; Ikejima, T. Mechanism of autophagy induction and role of autophagy in antagonizing mitomycin C-induced cell apoptosis in silibinin treated human melanoma A375-S2 cells. *Eur. J. Pharmacol.* **2011**, *659*, 7−14.
(43) Naugler, W. E.; Karin, M. NF-κB and cancer-identifying targets and mechanisms. *Curr. Opin. Genet. Dev.* **2008**, *18*, 19−26.

JOURNAL OF AGRICULTURAL AND FOOD CHEMISTRY

Letter

pubs.acs.org/JAFC

Detection of Melamine in Foods Using Terahertz Time-Domain Spectroscopy

ABSTRACT: The aim of this study was to investigate the feasibility of detecting melamine in foodstuffs using terahertz imaging. The terahertz (THz) spectra and images of melamine mixtures were obtained in the frequency range of 0.1−3 THz at room temperature using THz time-domain spectroscopy. Characteristic absorption peaks of melamine were found at 2, 2.26, and 2.6 THz, and these peaks showed the same frequencies in the different food matrices. At 2 THz, the THz images of melamine were dose-dependently distinguishable from those of food components with or without the packaging materials used. The calibration curve of melamine showed a regression coefficient (R^2) of >0.913 and a detection limit of <13%. These results suggest that terahertz imaging has the potential to be used for the qualitative detection of melamine in food as a nondestructive analytical tool.

KEYWORDS: *melamine, terahertz time-domain spectroscopy, terahertz imaging, food matrices*

INTRODUCTION

Melamine (1,3,5-triazine-2,4,6-triamine) is a nitrogen-rich molecule ($C_3H_6N_6$), with 40% nitrogen by number of atoms. Because of its high nitrogen content, this chemical has been illegally added to foods such as milk powder to increase the total nitrogen concentration, which is used as an indicator to estimate the protein content. Ingestion of melamine by pets, cattle, and infants is known to lead to serious health problems related to the reproductive system and kidneys, and it can cause death in some cases.[1] Currently, regulatory limits of 0.5−2.5 mg/kg in general food and feed and a tolerable daily intake of 0.2 mg/kg body weight/day for melamine are set by several countries and organizations.[1] Therefore, because it is of great concern for food safety, a rapid and accurate measurement method to detect this contaminant in foods is required, particularly for packaged foods.

Terahertz time-domain spectroscopy (THz-TDS) can be used as a detection method with the advantages of fast analysis and simplicity. The absorption features in the THz region are dominated by intermolecular vibrations corresponding to motion associated with coherent, delocalized movements of large numbers of atoms and molecules.[2,3] Because these properties are unique to a particular molecule, it is possible to obtain a "THz absorption peak", enabling the identification of a compound.[3,4] It was reported that THz-TDS was used for the identification of chemicals using the transmission method coupled with the standard pellet technique.[4,5] Although this method has the advantage in qualitative and quantitative analysis of a homogeneous sample, it has a limitation in heterogeneous materials such food. When the spectrum of a sample comprising a heterogeneous mixture is obtained, the differences between components cannot be distinguished clearly because the peaks appear as a sum of each component. To overcome this disadvantage, image mapping of THz spectroscopic data can be used.

The wavelength (100 μm−1 mm) of the THz region can be resolved spatially, which is sufficient for imaging applications; that is, specific absorption peaks can be used for both identification and mapping of chemicals with the spatial distribution of individual chemical components in a heterogeneous mixture. Moreover, the THz wave can determine the differences in density and dielectric constant. This is because the THz wave can penetrate a wide range of dielectric materials, such as clothing, paper, cardboard, wood, plastic, and ceramics.[6] These advantages can be successfully applied to the nondestructive inspection of chemicals.[7]

With this background, we explored the detection of melamine in three food matrices and examined the effect of packaging materials on the nondestructive detection of melamine.

MATERIALS AND METHODS

Sample Preparation. Melamine (Daejung Chemicals & Metals Co., Ltd., Siheung, Korea), HDPE (TeraView Ltd., Cambridge, UK; particle size < 10 μm), and food matrices (flour, milk powder, and chocolate powder) pellets were prepared in different concentrations of

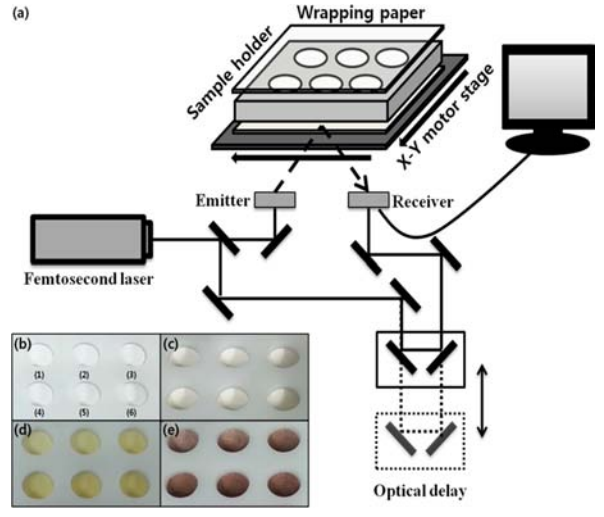

Figure 1. Schematic diagram of the terahertz imaging system and sample holder in reflection geometry (a). The THz image was scanned in the $X-Y$ plane using a motor stage. The sample holder was placed on the motor stage. Visible images of melamine and matrix mixtures in small box: HDPE (b), flour (c), milk powder (d), chocolate powder (e); 10% (1), 7.5% (2), 5% (3), 2.5% (4), 1% (5), and pure matrix (0%) (6).

Received: March 21, 2014
Revised: May 30, 2014
Accepted: June 2, 2014
Published: June 2, 2014

ACS Publications © 2014 American Chemical Society

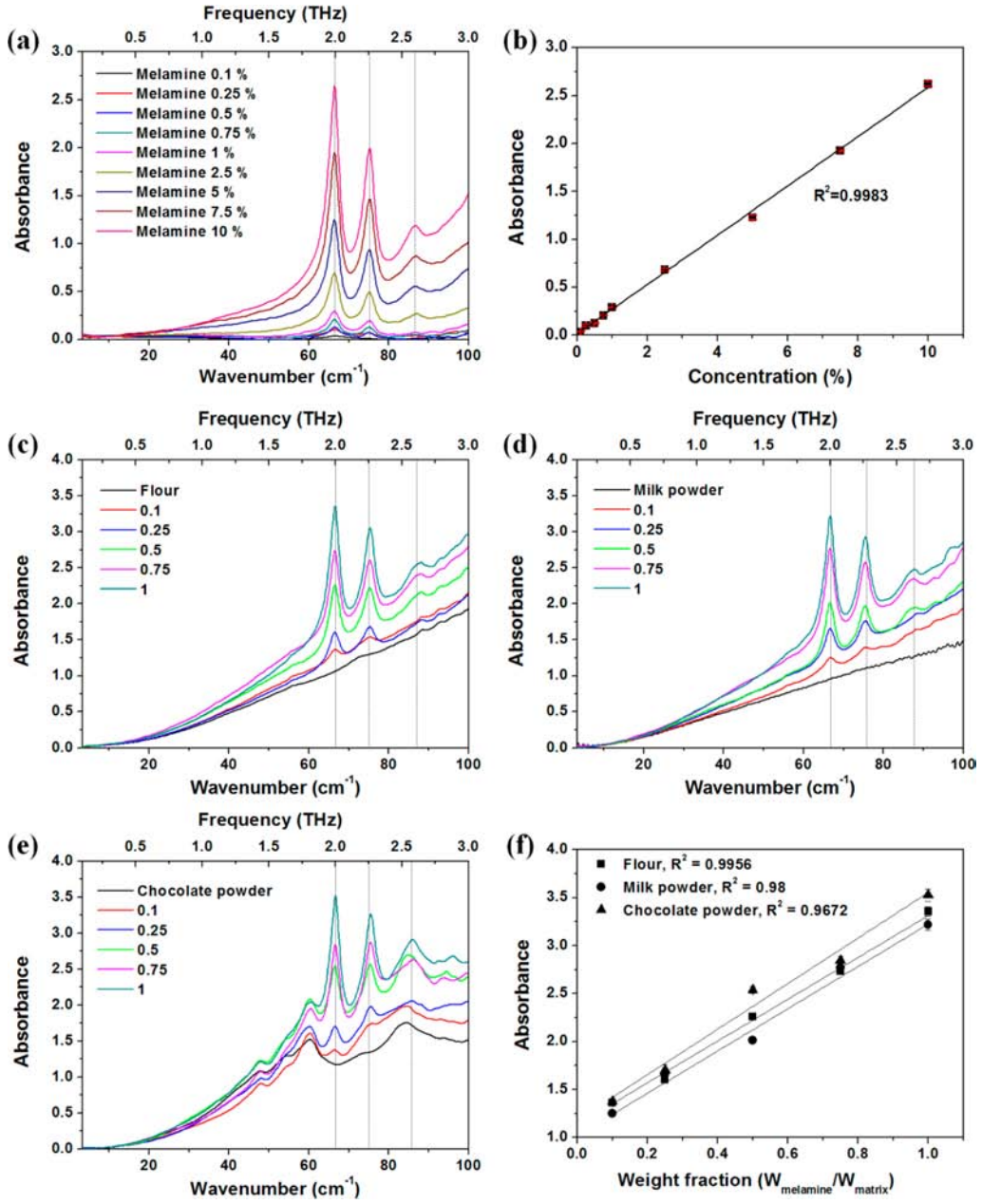

Figure 2. Absorption spectra of melamine mixtures in HDPE (a), flour (b), milk powder (c), and chocolate powder (d) and the calibration curve in HDPE (e) and the fitted curve in food matrices (f). Absorbance was measured using different ratios of melamine to matrices. The calibration curve and fitted curve were for absorbance at each ratio at 2 THz.

melamine, ranging from 0 to 10 wt %. Average particle sizes for flour, milk power, and chocolate powder were 50, 160, and 255 μm, respectively, and the water contents of three food matrices were <14%. The pellets were made of 360 mg of powder, using a hydraulic press (Specac Ltd., Orpington, UK; 13 mm diameter). To examine the effect of the packaging materials, oriented polypropylene/polyethylene (OPP/PE) film (vinyl film, thickness = 40 μm) and roll paper/polyethylene (roll paper/PE) film (paper film, thickness = 80 μm), which are widely used as food packaging materials, were selected. They were fixed at the top and bottom of the sample holder when the THz image was measured (Figure 1).

THz-TDS Spectra. The THz images and spectra of melamine mixtures were measured using a TPS spectra 3000 spectrometer (TeraView Ltd.).[8] This system acquired time-domain data using the time delay between the pulse generation and detection. The samples were measured in a stable and fast scan mode that allows 30 measurements in 1 s. Over a period of 1 min, 1800 scans were taken for each spectrum, and a Blackman−Harris three-term apodization was applied to the Fourier transformation. The signals that were transmitted by the pure HDPE pellets were used as the reference signal, and the signals that were transmitted by the center of the melamine mixture pellets were used as the sample signals.

Image Acquisition. THz spectral images were obtained by raster-scanning the reflected THz beam on the sample (Figure 1). For the analysis of melamine, a THz image was obtained at 2 THz. This was one of the frequencies for the absorption of melamine with a strong and clear peak. THz images were relatively expressed using false color for the THz signal amplitudes. The images indicate the highest THz signal in red and the lowest THz signal in blue.

Data Acquisition. The experiments and analyses were carried out at least in triplicate. Data were expressed as the mean ± standard deviation (n = 10). The calculation and statistical methods utilized were Excel and Origin 8.0 (Origin Lab, Northampton, MA, USA).

dx.doi.org/10.1021/jf501170z | J. Agric. Food Chem. 2014, 62, 5403−5407

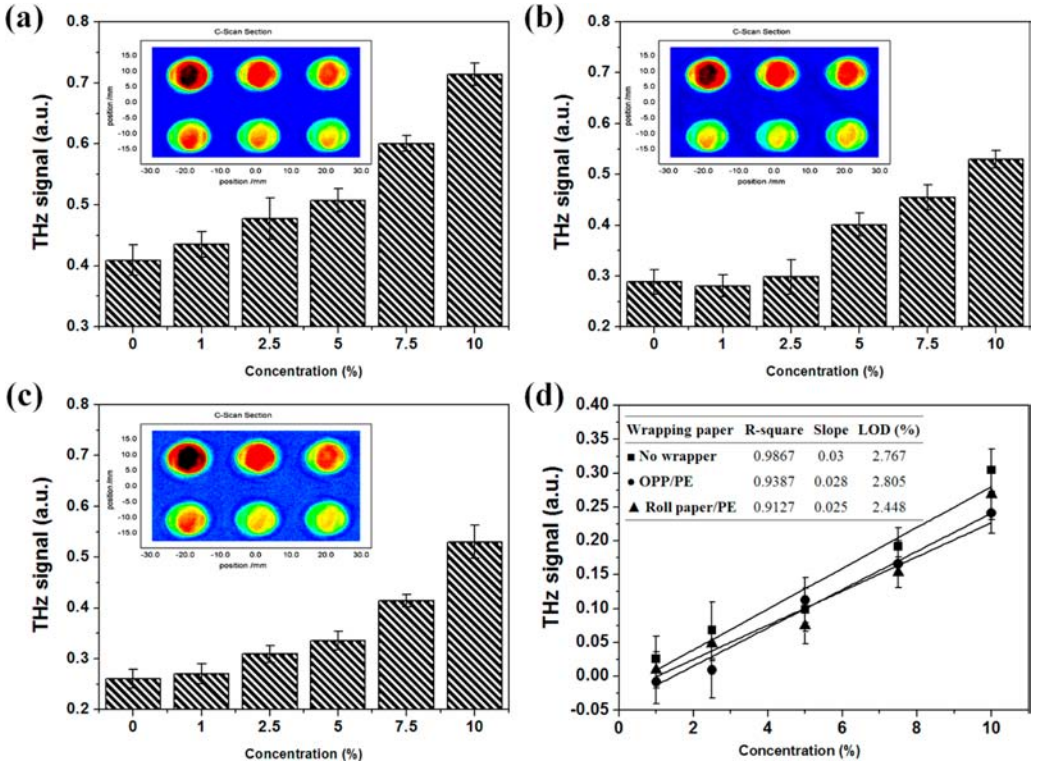

Figure 3. THz images and histograms of melamine in HDPE without wrapping materials (a), covered with OPP/PE (b) and covered with roll paper/PE (c), and their calibration curves (d). The fitted calibration curve of THz signals was extracted at 0% sample signal at 2 THz. The images indicate the highest THz signal in red and the lowest THz signal in blue.

RESULTS AND DISCUSSION

THz Spectra of Melamine in HDPE. The absorption spectra measured with different concentrations of melamine are shown in Figure 2a. The absorption peaks of melamine appeared at 2, 2.26, and 2.6 THz, which correspond to 66.6, 75.3, and 86.6 cm^{-1}, respectively. Harsha et al.[5] reported that melamine had specific absorbance peaks in the region of 0−3 THz. In their study, melamine exhibited absorption peaks at 2.01 and 2.26 THz, which correspond to 67 and 75.3 cm^{-1}, respectively.[5] On the basis of that study and our results, absorption peaks were identified at 2 and 2.26 THz. Because terahertz radiation is sensitive to the vibrational states of the entire molecule, these absorbance peaks were thought to correspond to the vibrational states of melamine.[4] However, further investigation in conjunction with solid-state theory is necessary to establish a relationship between the significant peaks and the molecular structure.[9] Figure 2b shows the calibration curves of absorbance at 2 THz. The calibration curve had a linear regression coefficient of >0.998 and a LOD of <0.2%. Because a linear relationship between the absorbance and the weight ratio was established, the qualitative and/or quantitative detection of melamine using our THz system can be feasible.

THz Spectra of Melamine in Food Matrices. The main absorption feature of melamine was identifiable when melamine was mixed with the three food matrices: flour, milk powder, and chocolate powder. Panels c−e of Figure 2 show the spectra of the melamine and food matrix mixtures measured at five different concentrations. Melamine absorption peaks were clearly identified in all of the measurements. The curves fitted by the absorbance of each pellet are shown in Figure 2f. The curves showed a linear relationship between the absorbance and the weight ratio with a linear regression coefficient (R^2) of >0.967. When the HDPE mixture was compared with the food matrices, a lower sensitivity was observed, possibly caused by scattering.[10]

THz Image of Melamine in HDPE. Figure 3 shows the THz image and THz signals of melamine in HDPE with different weight ratios (0, 1, 2.5, 5, 7.5, and 10%). The THz image and THz signal histogram obtained without wrapping materials are shown in Figure 3a. In the THz images, the false color of the pellets was changed from yellow to red as the concentration of melamine was increased from 0 to 10%. There was a clear contrast of absorption between melamine and the matrix; the false color of the 10% pellet was deep red, but the false color of the 0% pellet was light yellow. The THz images of the samples covered with the two wrapping materials (OPP/PE and roll paper/PE) are shown in Figure 3b,c. From Figure 3a−c we found that the wrapping materials had little effect on the THz image, suggesting that the wrapping materials have high transmittance in the THz region.[6] In Figure 3, the histogram shows the THz signals of each pellet, which increased as the concentration of melamine increased. The calibration curve obtained after the subtraction of 0% sample signal as a reference showed a linear regression coefficient (R^2) of >0.913. Thus, a linear relationship between the weight ratio of melamine and the amplitude of the THz signals is displayed. The LOD of melamine in HDPE was <2.45%, which suggested that the terahertz imaging method can be used to detect melamine in packaged foods.

THz Image of Melamine in Food Matrices. Figure 4 shows the THz images and histograms of melamine and mixtures of food matrices obtained from the amplitude of the THz signal. Those images and histograms were obtained from the samples containing the wrapping materials of OPP/PE wrapping material and roll paper/PE or not. As shown from all of the images, the false color of the pellets changed from yellow to red as the

dx.doi.org/10.1021/jf501170z | J. Agric. Food Chem. 2014, 62, 5403−5407

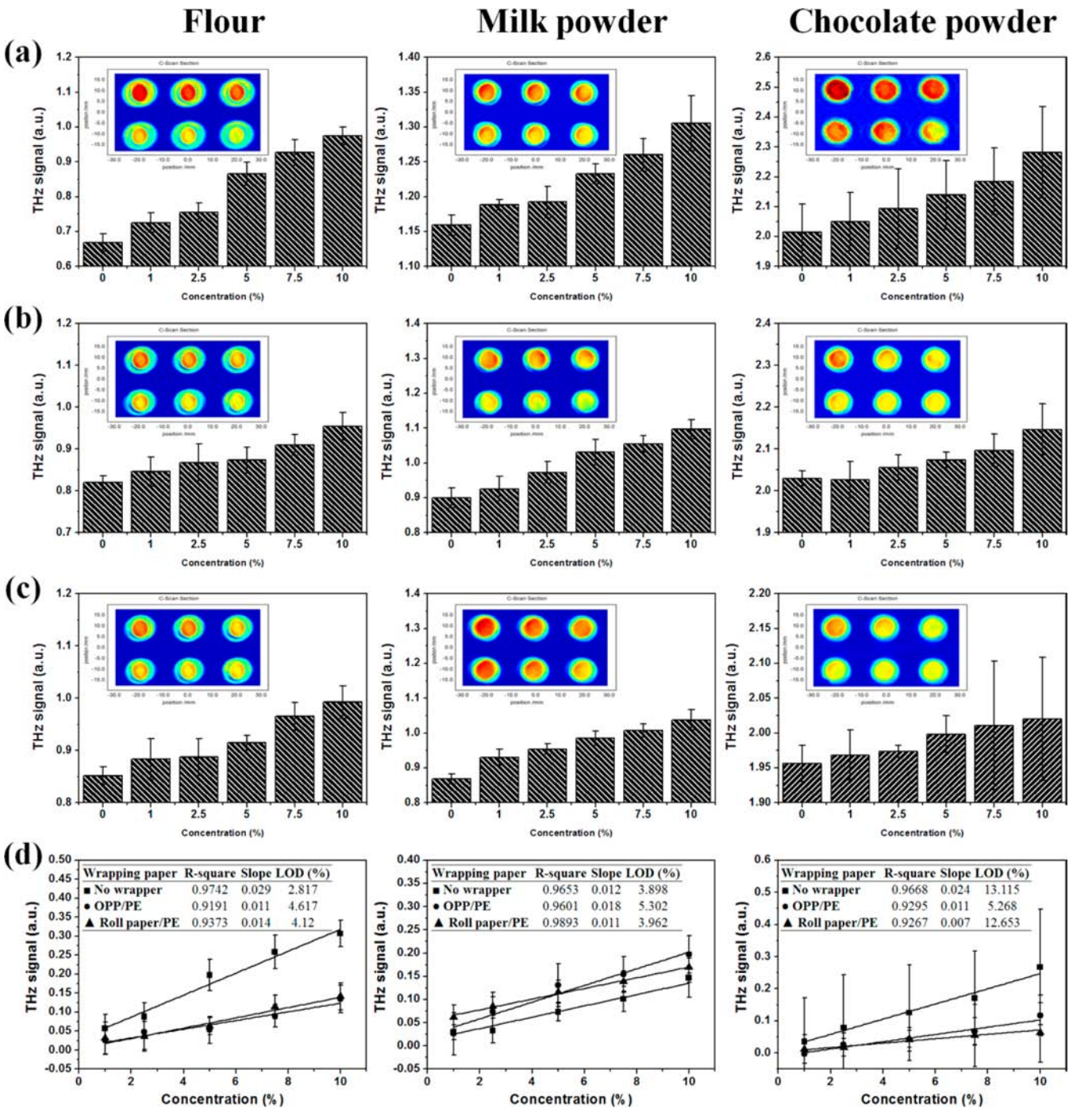

Figure 4. THz images and histograms of melamine in flour, milk powder, and chocolate powder without wrapping materials (a), covered with OPP/PE (b), and covered with roll paper/PE (c) and their fitted calibration curves (d). The fitted calibration curve of THz signals was extracted at 0% sample signal at 2 THz. The images indicate the highest THz signal fin red and the lowest THz signal in blue.

concentration of melamine increased from 0 to 10%. The images of the samples covered with wrapping materials showed a clear contrast of absorption between melamine and the matrix, like the images above. The histograms of the THz signals of each pellet are also shown in Figure 4. Similar to the images, the THz signals increased as the concentration of melamine increased. The calibration curves of THz signals are shown in panel d of Figure 4, for which the THz signal of a 0% sample was subtracted as a blank. The curve showed a linear regression coefficient (R^2) of >0.919, which indicated a good linear relationship between the weight ratio of melamine and the amplitude of the THz signals. The LOD of melamine in food was <13.12%. However, differences in the sensitivity among sample matrices with and without wrapping materials were found; the sensitivity was decreased in flour and chocolate powder covered with two wrapping materials. This decrease was assumed to be due to the combined effects of particle size and chemical composition of sample and wrapping material, and this assumption should be further investigated.

It was reported that terahertz imaging could be used not only for the identification of chemicals but also for the qualitative detection in a heterogeneous mixture.[8] Although the THz

dx.doi.org/10.1021/jf501170z | J. Agric. Food Chem. 2014, 62, 5403−5407

transmission method has a little higher sensitivity and lower LOD than the terahertz imaging method in this study, a terahertz imaging system can be a better choice for certain applications. For example, transmission spectral measurements require sample homogeneity, but the terahertz imaging system does not, because the terahertz imaging system scans the entire sample area, unlike the transmission method in which the THz ray is transmitted through the center of the sample. However, the terahertz imaging system had lower sensitivity and higher LOD than the other analytical methods. Considering that foods and agricultural products may contain contaminants in trace amounts, further research is required to improve the sensitivity and resolution.[11−13]

Overall, our results show the potential of THz-TDS for the qualitative analysis of melamine and for an identification and quantification technique in the food industry. Although THz-TDS cannot reach regulatory limits due to its low sensitivity, the ability of THz waves to pass through a wide variety of packaging materials can be used to characterize the molecular signature of many substances, which makes the terahertz imaging method attractive as a detection tool for enhanced food monitoring. For the routine application of THz spectroscopy, however, further research is required, including the development of a cost-effective THz spectrometer with high sensitivity and spectral databases for a wide variety of food chemicals.

Seung Hyun Baek[†,§]
Heung Bin Lim[§]
Hyang Sook Chun*[,†]

[†]School of Food Science and Technology, Chung-Ang University, Ansung, Gyounggi 456-756, Republic of Korea
[§]Department of Chemistry, Dankook University, Yongin, Gyounggi 448-701, Republic of Korea

AUTHOR INFORMATION

Corresponding Author

*(H.S.C.) Phone: +82-31-670-3290. Fax: +82-31-675-3108. E-mail: hschun@cau.ac.kr.

Funding

This research was supported by the Public Welfare & Safety research program through the National Research Foundation of Korea (NRF) funded by the Ministry of Education, Science and Technology (NRF-2010-0020819).

Notes

The authors declare no competing financial interest.

REFERENCES

(1) Sharma, K.; Paradakar, M. The melamine adulteration scandal. *Food Secur.* **2010**, *2*, 97−107.
(2) Walther, M.; Fischer, B. M.; Jepsen, P. U. Noncovalent intermolecular forces in polycrystalline and amorphous saccharides in the far infrared. *Chem. Phys.* **2003**, *288*, 261−268.
(3) Day, G. M.; Zeitler, J. A.; Jones, W.; Rades, T.; Taday, P. F. Understanding the influence of polymorphism on phonon spectra: lattice dynamics calculations and terahertz spectroscopy of carbamazepine. *J. Phys. Chem. B* **2006**, *110*, 447−456.
(4) Naftaly, M.; Miles, R. E. Terahertz time-domain spectroscopy for material characterization. *Proc. IEEE* **2007**, *95*, 1658−1665.
(5) Harsha, S. S.; Laman, N.; Grischkowsky, D. High resolution waveguide THz-TDS of melamine. *CLEO/QELS* **2008**, No. JWA40.
(6) Kodo, K.; Ogawa, Y.; Watanabe, Y.; Inoue, Y. Non-destructive terahertz imaging of illicit drugs using spectral fingerprints. *Opt. Express.* **2003**, *11*, 2549−2554.
(7) Watanabe, Y.; Kawase, K.; Ikari, T.; Ito, H.; Ishikawa, Y.; Minamide, H. Component spatial pattern analysis of chemicals using terahertz spectroscopic imaging. *Appl. Phys. Lett.* **2003**, *83*, 800−802.
(8) Shen, Y. C.; Taday, P. F.; Newnham, D. A.; Pepper, M. Chemical mapping using reflection terahertz pulsed imaging. *Semicond. Sci. Technol.* **2005**, *20*, S254−S257.
(9) Williams, M. R. C.; True, A. B.; Izmaylov, A. F.; French, T.; Schroeck, K.; Schmuttenmaer, C. A. Terahertz spectroscopy of enantiopure and racemic polycrystalline valine. *Phys. Chem. Chem. Phys.* **2011**, *13*, 11719−11730.
(10) Bandyopadhyay, A.; Sengupta, A.; Barat, R. B.; Gary, D. E.; Federici, J. F.; Chen, M.; Tanner, D. B. Effects of scattering on THz spectra of granular solids. *Int. J. Infrared Milli Waves* **2009**, *28*, 969−978.
(11) Shen, Y. C.; Taday, P. F.; Pepper, M. Elimination of scattering effects in spectral measurement of granulated materials using terahertz pulsed spectroscopy. *Appl. Phys. Lett.* **2008**, *92*, 051103-1−051103-3.
(12) Kaushik, M.; Ng, B. W.-H.; Fischer, B. M.; Abbott, D. Reduction of scattering effects in THz-TDS signals. *IEEE Photon. Technol. Lett.* **2012**, *24*, 155−157.
(13) Franz, M.; Fischer, B. M.; Walther, M. The Christiansen effect in terahertz time-domain spectra of coarse-grained powders. *Appl. Phys. Lett.* **2008**, *92*, 021107-1−021107-3.

JOURNAL OF AGRICULTURAL AND FOOD CHEMISTRY

Letter

pubs.acs.org/JAFC

Characteristics of an Organic Solvent-Tolerant β-Fructofuranosidase from *Arthrobacter arilaitensis* NJEM01 and Efficient Synthesis of Prebiotic Kestose

ABSTRACT: An organic solvent-tolerant β-fructofuranosidase (β-FFase) from *Arthrobacter arilaitensis* NJEM01 was purified, characterized, cloned, and overexpressed in *Escherichia coli*. The mature β-FFase contained 495 amino acid residues with an estimated molecular mass of 55 kDa. The purified β-FFase from strain NJEM01 was very stable in the buffer systems (pH 5.0−9.5) and showed high stability below 45 °C. Furthermore, the enzyme exhibited relatively high solvent stability in various aqueous organic mixtures and retained nearly 100% of its initial activity after incubation for 10 days in 20% (v/v) DMSO. In addition, the β-FFase exhibited high transfructosylation activity, synthesized prebiotic products of mainly 6-kestose (up to 476 g/L), and showed fructosyl receptor specificity to *C*-glucosyl flavone. A relatively high yield of FOS was achieved by the β-FFase from bacterium with a high concentration of sucrose. It made the β-FFase an exploitable biocatalyst for the production of glycosides of natural products and prebiotic kestose.

KEYWORDS: *β-fructofuranosidase, Arthrobacter arilaitensis NJEM01, high stability, overexpression, 6-kestose*

INTRODUCTION

Fructofuranosidases are powerful tools in industrial biotechnology, which catalyze the reactions of hydrolysis of sucrose and transfructosylation of fructose residue to suitable acceptors. The reaction is attractive owing to the feasibility and regio- and stereo-specificities controlling the synthesis of fructosyl-containing oligosaccharides and glycosides of aglycones.[1] Fructo-oligosaccharides (FOS) exhibit prebiotic properties, are a source of dietary fiber in food preparations, and exert a beneficial effect on human health because they are selectively fermented by colonic flora.[2,3]

We previously reported the glycosylation of puerarin/mangiferin to fructosyl puerarin/mangiferin derivatives with high concentration of substrate by the β-fructofuranosidase (β-FFase) from *Arthrobacter arilaitensis* NJEM01.[4,5] The greatesst advantage was that because of the highly efficient synthesis of fructosyl aglycones by the β-FFase in nonaqueous media using sucrose as donor, the β-FFase almost did not hydrolyze the newly formed glycoside products.[4,5] Thus, the great interest is the characteristics of the β-FFase to fully understand the enzyme's biological function.

In this paper, an organic solvent-tolerant β-FFase was purified, cloned, and heterologously expressed in *Escherichia coli*, and its biochemical properties were also investigated. In addition, the β-FFase was also applied to the efficient production of fructo-oligosaccharide, which suggested its potential use for prebiotic fructo-oligosaccharides.

MATERIALS AND METHODS

Strain and Culture Conditions for Producing β-FFase. The β-FFase producer, *A. arilaitensis* NJEM01 (deposited in China Center for Type Culture (CCTCC M2012155)),[5] culture media, and conditions were the same as in a previous study.[5] The β-FFase activity was analyzed by using 20% (w/v) sucrose as substrate (pH 6.5, 50 °C, for 15 min). One unit (U) of β-FFase activity was equivalent to 1.0 μmol of glucose liberated by the amount of the enzyme per minute.[6]

Purification and Biochemical Properties of Purified β-FFase. The purified β-FFase was obtained by employing $(NH_4)_2SO_4$ fractionation (50−90% saturation) and DEAE Sepharose FF chromatography. The purified β-FFase band on the SDS-PAGE gel was electrophoretically transferred to an Immobilon-PVDF membrane (Millipore, Bedford, MA, USA) and was used for N-terminal amino acid sequence analysis. The effects of pH on the activity and pH stability (40 °C, 2 h) of purified β-FFase were determined in various buffer systems (pH 3.0−11.0). The effects of temperature on the activity and thermostability (pH 6.5, 2 h) of purified β-FFase were determined at different temperatures (from 20 to 80 °C). The effects of metal ions (5 and 10 mM) on the activity of the β-FFase were investigated. For the analysis of organic solvent stability of the β-FFase, various solvents (DMF, methanol, ethanol, and DMSO (20%, v/v)) were added to the enzyme solution, respectively.

Cloning of β-FFase *aff* Gene and Expression of β-FFase in *Escherichia coli*. As the N-terminal sequence (containing 10 amino acid residues) of the β-FFase from strain NJEM01 showed 70% identity to the β-FFase from *Arthrobacter globiformis* IFO 3062,[6] the highly conserved region of the *aff* gene was amplified by using two primers (5′-GCTAGCGAACTCCCAAAACGT-3′ and 5′-GCTACTGCTTTGCCATTCTTCA-3′), designed on the basis of the nucleotide sequence alignment of the β-FFase from strain IFO 3062.[6] To determine the sequences upstream and downstream of the conserved region, an efficient PCR strategy called thermal asymmetric interlaced (TAIL) PCR was used. The basic procedure and thermal cycling conditions were described by Nakayama.[7] Each set of the nested specific primers was designed to accurately match a region of known sequence, and arbitrary degenerate primers were the same as Mishra described.[8]

The *aff* gene was amplified from the genomic DNA of strain NJEM01 by using the following primers: forward, 5′-GTTCATATG-GCCACCGAACCAGTGCCTG-3′ with an *Nco*I site (underlined), and reverse, 5′-CCCAAGCTTTTACTTTGCTACTGCTTTGC-3′) with a *Hin*d III site (underlined). The *Nco*I−*Hin*dIII-digested PCR-amplified fragment was cloned into the corresponding sites of pET-22b to produce recombinant plasmid pET-*aff*, which was then transformed into *E. coli* BL21 (DE3), and the expression of β-FFase was performed as described by Isono et al.[6] Then the cell-free supernatant after fermentation of the recombinant was used for enzyme activity assay and verified by SDS-PAGE.

Received: April 30, 2014
Revised: May 21, 2014
Accepted: May 22, 2014
Published: May 22, 2014

ACS Publications © 2014 American Chemical Society

dx.doi.org/10.1021/jf5020523 | J. Agric. Food Chem. 2014, 62, 5408−5411

Transfructosylation for FOS Production, Analysis, and Identification of the Product. After preliminary optimization, the fructo-oligosaccharide was synthesized (pH 7.5, 40 °C) in a reaction mixture containing 3.0 M sucrose and β-FFase (9.7 U/mL). The transfructosylation product was analyzed by HPLC and purified according to the method described by Mabel et al.[9] The purified product was further analyzed by MS (Voyager-DE MALDI-TOF MS, USA) and NMR spectrum (Bruker AV-500 spectrometer, Switzerland). All NMR spectra were obtained in D_2O using tetramethylsilane (TMS) as the internal standard.

RESULTS AND DISCUSSION

Purification and Characteristics of β-FFase from Strain NJEM01. The extracellular β-FFase was purified (Table S1). About 47.4% of total activity was covered with 22.8-fold purification to a specific activity of 348.43 U/mg protein. The purified β-FFase was homogeneous with an apparent molecular mass of 55 kDa by SDS-PAGE (Figure 1A). This molecular mass was similar to that of the β-FFase from strain IFO 3062 (54 kDa)[6] and from *Arthrobacter* sp. K-1 (60 kDa).[10]

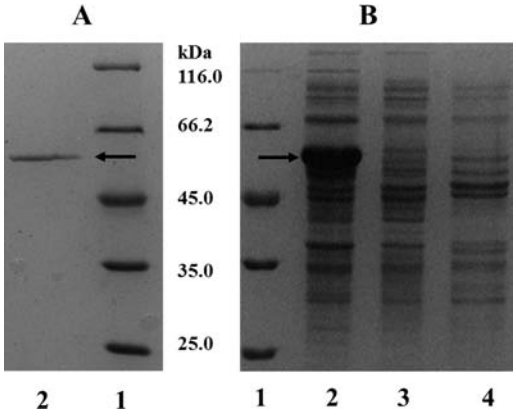

Figure 1. SDS-PAGE analysis of β-FFase purified from *A. arilaitensis* NJEM 01 (A) and β-FFase expressed in *E. coli* BL21 (DE3) (B). Lanes: 1 (A, B), marker; 2 (A), purified β-FFase; 2 (B), cell-free supernatant expressed in *E. coli*/pET-*aff* with IPTG; 3 (B), cell-free supernatant *E. coli*/ pET-*aff* without IPTG; 4 (B), cell-free supernatant *E. coli*/pET-22b with IPTG.

The purified β-FFase from strain NJEM01 showed a maximum activity at pH 6.5, and the enzyme was most active with broad range of pH from 5.0 to 7.0. Furthermore, the enzyme was very stable over the pH range of 5.0−9.5 for 2 h and retained >94% of its initial activity (Figure 2A). It has been reported that the action of hydrolysis and transfructosylation reactions of glycosidase preferentially occur at acidic and alkaline pH.[11] In addition, the hydrolyzing of product could be controlled by the alkaline pH.[11] Thus, the stability of β-FFase over the pH range of 5.0−9.5 would be beneficial for the regulation of transfructosylation.

The optimum temperature for the purified β-FFase was about 50 °C. The enzyme showed high stability below 45 °C (Figure 2B), which indicated its relatively good thermostability and was beneficial for the transfructosylation of functional and nutritional fructose-containing compounds.

There were no significant effects on the purified β-FFase activity with the supplementation of most of the metal ions and EDTA (Table S2). This finding was quite different from those reported enzymes from *Streptococcus salivarius* ATCC25975, *A. oxidans* J17-21, and *A. ureafacines* K2032,[12−14] which showed strong inhibition by several metal ions (Ni^{2+}, Mn^{2+}, Fe^{2+}, and Zn^{2+}). Interestingly, addition of 5 mM Fe^{3+} exhibited different effects on the hydrolysis and transfructosylation activities of the enzyme, whereas addition of Co^{2+} and EDTA could partially improve the transfructosylation activity of the purified β-FFase.

The purified β-FFase from strain NJEM01 exhibited relatively high stability in various hydrophilic solvent systems with concentration of 20% (v/v) (Figure 2C). It was noteworthy that activation of the β-FFase was obtained after 2 h of incubation in a medium containing 20% (v/v) DMSO. The β-FFase was very stable in the aqueous media with DMSO, retaining nearly 100% of its initial activity even after 10 days of incubation (data not shown). Enzymatic glycosylation in hydrophilic solvents could provide numerous industrially attractive advantages, such as reversal of the thermodynamic equilibrium of hydrolysis reactions and elimination of microbial contamination. In fact, in our previous studies, the β-FFase was successfully used in efficient and regioselective enzymatic fructosylation of puerarin[4] and mangiferin[5] in aqueous hydrophilic solvent system. Exceptionally high concentrations and high yields of mangiferin and puerarin fructosides were achieved by the solvent-stable β-FFase; the addition of hydrophilic solvents not only significantly promoted the solubility of flavone substrates (puerarin and mangiferin) but also produced a regulatory effect on the formation of the transfructosylation products,[5] the main products containing 111.3 g/L monofructosyl puerarin and 35.6 g/L difructosyl puerarin, with the total yield reaching 90%; 52.8 g/L

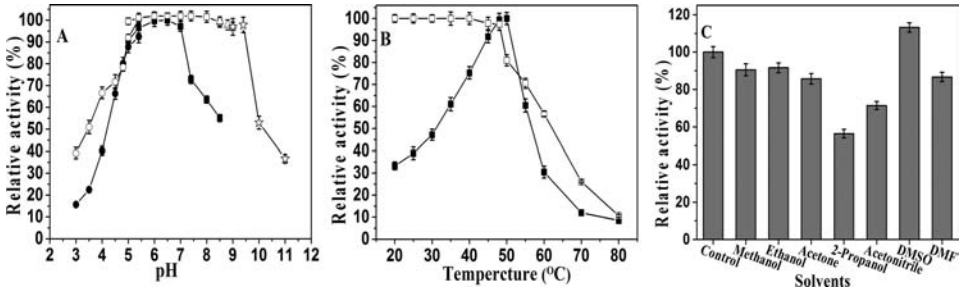

Figure 2. Characteristics of purified β-FFase: (A) effects of pH on the activity (solid symbols) of purified β-FFase and its pH stability for 2 h (hollow symbols); (B) effects of temperature on the activity (solid symbols) of purified fructofuranosidase and its thermostability for 2 h (hollow symbols); (C) solvent stability of purified β-FFase (the purified β-FFase was incubated in various solvent (20%, (v/v)) systems, at 40 °C for 2 h (under constant shaking at 200 rpm)). The β-FFase activities were measured in a buffer system (pH 6.5) at different temperatures and pH 3.0−5.4 (● and ○, citric acid buffer, 0.1 M), pH 5.0−8.6 (■ and □, KH_2PO_4−Na_2HPO_4, 0.05 M), pH 8.4−9.0 (△, Tris-HCl, 0.05 M), and pH 9.0−11.0 (☆, glycine−NaOH, 0.05 M).

dx.doi.org/10.1021/jf5020523 | J. Agric. Food Chem. 2014, 62, 5408−5411

monofructosyl mangiferin and 9.3 g/L difructosyl mangiferin were obtained, with the total yield reaching 91%.

Cloning and Expression of β-FFase. The N-terminal 10 amino acid residues of the purified β-FFase from strain NJEM01 were ATEPVPGFPQ and showed only 70% identity with the β-FFase from strain IFO 3062[6] and low similarity with the β-FFase from *Arthrobacter* sp. K-1[10] and strain K2032.[12] This suggested the differences of β-FFase from different strains.

The sequence of the *aff* gene had been elucidated in a patent.[15] The *aff* gene of the β-FFase from strain NJEM01 was cloned using degenerate PCR and TAIL PCR. The ORF of the *aff* gene (1647 bp) corresponded to the 548 residues (containing 53 residues of signal peptides) of the mature β-FFase of 495 residues. The amino acid sequence of the mature β-FFase from strain NJEM01 showed 91% identity with the β-FFase from strain IFO3062[6] and showed 80% identity to that from strain K-1.[10] This indicated the diversity of β-FFases from the *Arthrobacter* genus.

The recombinant plasmid pET-*aff* was constructed and the β-FFase was overexpressed in *E. coli* BL21 (DE3). The SDS-PAGE (Figure 1B) analysis indicated a thick band corresponding to a molecular mass of 55 kDa, which was the same as the purified native β-FFase. Furthermore, the recombinant β-FFase exhibited almost the same characteristics (data not shown) as the purified native β-FFase.

Efficient Production of FOS by the β-FFase. After preliminary optimization, the efficient transfructosylation was achieved in a reaction system (pH 7.5) containing a high concentration of the substrate (Figure 3). About 476 g/L 6-kestose was obtained from 3.0 M initial sucrose concentration, which corresponded to 45.7% (w/w) of the total carbohydrates in the reaction mixture. HPLC, MS, and NMR analyses suggested that the β-FFase from strain NJEM01 selectively synthesized almost only one kind of fructo-oligosaccharide. The amount of kestose obtained in the present work is much higher than that catalyzed by the β-FFase from *Schwanniomyces occidentalis* (including 4.2% (w/w) 1-kestose and 12.7% (w/w) 6-kestose).[16] The efficient production of FOS, including 1-kestose (234 g/L) and nystose (142 g/L), had also been produced by the β-fructofuranosidase from *Aspergillus* sp. 27H.[17] Moreover, the β-FFase from strain NJEM01 showed highly efficient transfructosylation of *C*-glucosyl flavone substrates, such as puerarin and mangiferin,[4,5] and also efficient transfructosylation for prebiotic fructo-oligosaccharide. A relatively high yield of prebiotic FOS was achieved by the β-FFase from bacterium NJEM01 with a high concentration of sucrose. All of these characteristics made it an exploitable biocatalyst for glycosides of natural products and prebiotic kestose.

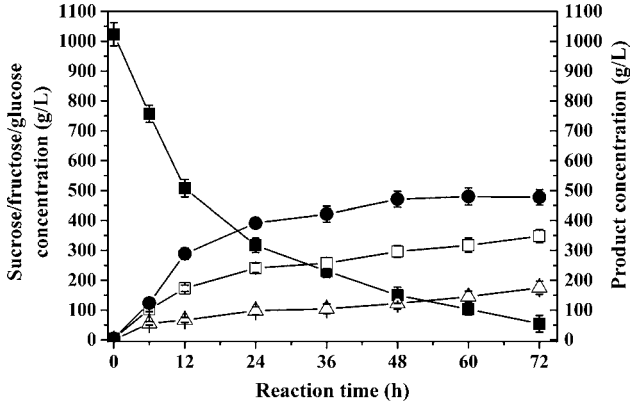

Figure 3. Time course of the transfructosylation for the production of microbial FOS by β-FFase from *A. arilaitensis* NJEM01: (■) sucrose; (●) FOS; (□) glucose; (△) fructose.

The fructo-oligosaccharide produced by the β-FFase was identified by combination of MS and NMR spectrum analyses. The purified product gave a main ion peak at m/z 527.16 $[M + Na]^+$ in a positive TOF-MS-ES spectrum. The NMR spectroscopic characterization (combination of HMBC, COSY, NOESY, and HSQC) revealed that the second fructose residue is β-(2 → 6)-linked to the fructose attached to the sucrose moiety. Thus, the fructo-oligosaccharide product was identical to that of an authentic 6-kestose.[9,16] The levan-type FOS (6-kestose, neokestose, and neonystose) exhibited increased prebiotic activity when compared to the usual inulin-type FOS (1-kestose, nystose, and ^{1}F-fructofuranosyl nystose).[18] The levan-type FOS could be selectively used by the beneficial intestinal bacteria, such as *Bifidobacterium adolescentis* and *B. longum*.[18]

The β-FFase could efficiently catalyze transfructosylation for the products of microbial FOS, with almost only one kind of kestose. In addition, exceptionally high concentrations and high yields of *C*-glucosyl flavone fructosides were also achieved.[4,5] Thus, this enzyme constitutes a profitable alternative for use in large-scale industrial prebiotic production while satisfying the growing needs of the population for healthy foods with bioactive compounds. Because of the important implications of the results obtained in the present work, further studies are currently underway to improve FOS production.

Jianlin Chu[†]
Xueming Wu[§]
Bin Wu[†]
Rui Wang[†]
Bingfang He*[,†]

[†]College of Biotechnology and Pharmaceutical Engineering, Nanjing University of Technology, 30 Puzhunan Road, Nanjing 211816, People's Republic of China

[§]College of Pharmaceutical Science, Nanjing University of Chinese Medicine, Nanjing 210046, Jiangsu, People's Republic of China

■ ASSOCIATED CONTENT

Ⓢ Supporting Information

Tables S1 and S2; ^{13}C NMR, ^{1}H NMR, and 2D-NMR spectroscopic data of the FOS product. This material is available free of charge via the Internet at http://pubs.acs.org.

■ AUTHOR INFORMATION

Corresponding Author

*(B.H.) E-mail: bingfanghe@njtech.edu.cn. Phone: 86-25-58139902. Fax: 86-25-58139902.

Funding

This work was supported by the National Natural Science Foundation of China (21376119), the Specialized Research Fund for the Doctoral Program of Higher Education (20123221130001), the National High Technology Program Research and Development Program of China (2012AA022200), and a Project Founded by PAPD.

Notes

The authors declare no competing financial interest.

REFERENCES

(1) Sangeetha, P. T.; Ramesh, M. N.; Prapulla, S. G. Recent trends in the microbial production, analysis and application of fructo-oligosaccharides. *Trends Food Sci. Technol.* **2005**, *16*, 442−457.

(2) Fukaya, M.; Takeuchi, S.; Tsukamoto, Y. Manufacture of 6-kestose containing oligosaccharides with *Acetobacter* or *Gluconobacter* and their uses. JP Patent 19970731, 1999.

(3) Silva-Santisteban, B. O. Y.; Maugeri, F. Agitation, aeration and shear stress as key factors in inulinase production by *Kluyveromyces marxianus*. *Enzyme Microb. Technol.* **2005**, *36* (5−6), 717−724.

(4) Wu, X. M.; Chu, J. L.; Wu, B.; Zhang, S.; He, B. F. An efficient novel glycosylation of flavonoid by β-fructosidase resistant to hydrophilic organic solvents. *Bioresour. Technol.* **2013**, *129*, 659−662.

(5) Wu, X. M.; Chu, J. L.; Liang, J. Y.; He, B. F. Efficient enzymatic synthesis of mangiferin glycosides in hydrophilic organic solvents. *RSC Adv.* **2013**, *3*, 19027−19032.

(6) Isono, N.; Tochihara, T.; Kusnadi, Y.; Win, T. T.; Watanabe, K.; Obae, K.; Ito, H.; Matsui, H. Cloning and heterologous expression of a β-fructofuranosidase gene from *Arthrobacter globiformis* IFO 3062, and site-directed mutagenesis of the essential aspartic acid and glutamic acid of the active Site. *J. Biosci. Bioeng.* **2004**, *97* (4), 4244−4249.

(7) Nakayama, T.; Soma, M.; Rahmutula, D.; Ozawa, Y.; Kanmatsuse, K. Isolation of the 5′-flanking region of genes by thermal asymmetric interlaced polymerase chain reaction. *Med. Sci. Monit* **2001**, *7* (3), 345−349.

(8) Mishra, R. N.; Singla-Pareek, S. L.; Nair, S.; Sopory, S. K.; Reddy, M. K. Directional genome walking using PCR. *Biotechniques* **2002**, *33* (4), 830−834.

(9) Mabel, M. J.; Sangeetha, P. T.; Srinivasan, K. P. K.; Prapull, S. G. Physicochemical characterization of fructooligosaccharides and evaluation of their suitability as a potential sweetener for diabetics. *Carbohydr. Res.* **2008**, *343* (1), 56−66.

(10) Ito, T.; Fujita, K.; Hara, K.; Tonozuka, T.; Sakano, Y. Cloning and expression of β-fructofuranosidase gene from *Arthrobacter* sp. K-1. *J. Appl. Glycosci.* **2002**, *49* (3), 291−296.

(11) Kurakake, M.; Onoue, T.; Komaki, T. Effect of pH on transfructosylation and hydrolysis by β-fructofuranosidase from *Aspergillus oryzae*. *Appl. Microbiol. Biotechnol.* **1996**, *45* (1−2), 236−239.

(12) Song, K. B.; Bae, K. S.; Lee, Y. B.; Lee, K. Y.; Rhee, S. K. Characteristics of levan fructotransferase from *Arthrobacter ureafaciens* K2032 and difructose anhydride IV formation from levan. *Enzyme Microb. Technol.* **2000**, *27*, 212−218.

(13) Song, D. D.; Jacques, N. A. Purification and enzymic properties of the fructosyl-transferase of *Streptococcus salivarius* ATCC25975. *Biochem. J.* **1999**, *341*, 285−291.

(14) Jang, K. H.; Ryu, E. A.; Park, B. S.; Song, K. B.; Kang, S. A.; Kim, C. H.; Uhm, T. B.; Park, Y. I.; Rhee, S. K. Levan fructotransferase from *Arthrobacter oxydans* J17-21 catalyzes the formation of the di-D-fructose dianhydride IV from levan. *J. Agric. Food Chem.* **2003**, *51*, 2632−2636.

(15) He, B. F.; Wang, R.; Wu, X. M.; Zhou, C.; Wu, B. An organic solvent tolerant glycosidase, its gene and application. CN Patent 201210185733.8, 2012.

(16) Álvaro-Benito, M.; de Abreu, M.; Fernandez-Arrojo, L.; Plou, F. J.; Jiménez-Barbero, J.; Ballesteros, A.; Polaina, J.; Fernández-Lobato, M. Characterization of a β-fructofuranosidase from *Schwanniomyces occidentalis* with transfructosylating activity yielding the prebiotic 6-kestose. *J. Biotechnol.* **2007**, *132* (1), 75−81.

(17) Fernández, R. C.; Maresma, B. G.; Juárez, A.; Martínez, J. Production of fructo-oligosaccharides by β-fructofuranosidase from *Aspergillus* sp. 27H. *J. Chem. Technol. Biot.* **2004**, *79* (3), 268−272.

(18) Fialho, M. B.; Simões, K.; de Almeida Barros, C.; Pessoni, R. A. B.; Braga, M. R.; Figueiredo-Ribeiro, R. C. L. Production of 6-kestose by the filamentous fungus *Gliocladium virens* as affected by sucrose concentration. *Mycoscience* **2013**, *54*, 198−205.

JOURNAL OF AGRICULTURAL AND FOOD CHEMISTRY

Article

pubs.acs.org/JAFC

Effect of Seed Roasting on Canolol, Tocopherol, and Phospholipid Contents, Maillard Type Reactions, and Oxidative Stability of Mustard and Rapeseed Oils

Kshitij Shrestha and Bruno De Meulenaer*

NutriFOODchem Unit, Department of Food Safety and Food Quality (Partner in Food2Know), Faculty of Bioscience Engineering, Ghent University, Coupure Links 653, B-9000 Ghent, Belgium

ABSTRACT: This work was carried out to study the effect of roasting on different compositional parameters and oil oxidative stability of three *Brassica* species (*Brassica juncea* (BJ), *B. juncea* var. *oriental* (BJO), and *Brassica napus* (rapeseed, RS)). After 10 min of roasting at 165 °C, canolol contents of BJ, BJO, and RS oil reached 297.8, 171.6, and 808.5 μg/g, and the phospholipid phosphorus contents reached 453.6, 342.6, and 224.2 μg/g oil, respectively. The BJ and BJO seeds showed more prominent browning reactions than RS, due to the presence of higher amounts of reducing sugars, lysine, arginine and the occurrence of Maillard type browning reactions of phospholipids. The UV−visible spectra, fluorescence, and pyrrole content showed the presence of browning reaction products in the roasted seed oils. Roasting increased the oxidative stability of all varieties. Canolol formation could only partially explain such observations. Other roasting effects such as phospholipid extraction and Maillard type browning reaction products were also responsible for the increased stability.

KEYWORDS: *2,6-dimethoxy-4-vinylphenol (canolol), mustard, rapeseed, lipid oxidation, seed roasting, phospholipid browning, Maillard type reactions*

INTRODUCTION

Seed roasting has been known to increase the oil oxidative stability of different seeds, such as mustard,[1] sesame,[2] *Pistacia terebinthus*,[3] pine nut,[4] cashew,[5] perilla,[6] apricot,[7] pumpkin,[8,9] walnut,[10] and rapeseed (RS).[11] However, there are considerable differences in the manner by which roasting improves the oil oxidative stability of these seeds. For instance, production of different radical scavengers, such as sesamol in sesame seed[2] and canolol in RS,[11−14] during seed roasting are considered to play an important role in the such phenomenon. In some cases, increased phospholipid extraction after seed roasting has also been suggested.[6,9] In most cases, Maillard browning reactions between amino acids and reducing sugars have been proposed as an important contributing factor for such observation.[1,3−5,8,10,11] These results suggest that roasting can have different effects in different types of seeds. Hence, it is important to understand the roasting effects and the manner by which it improves the oil oxidative stability of each type of seed, separately.

Mustard seeds are generally roasted before oil extraction, and the crude oil, extracted using a screw expeller, is consumed without refining in different south Asian countries such as India and Nepal.[1,15] The traditional mustard and RS varieties contain high amounts of erucic acid, whereas various low-erucic RS varieties have also been developed by breeding practices.[14] Although a number of seed roasting experiments have been reported for RS[11,12] and mustard varieties,[1,11] a clear insight to and an in-depth understanding of how roasting improves oxidative stability of these varieties are still lacking. For instance, all of these studies consider Maillard reactions to be partially responsible for increasing the oxidative stability of roasted seed oil; however, none of them clearly demonstrates the occurrence of such reactions by evaluating the loss of reducing sugars and amino acids and by analyzing the browning reaction markers in the roasted seed oil. Moreover, the formation of canolol and its contribution to the oxidative stability have been completely ignored in roasting experiments carried out on high-erucic mustard seed oil.[1] Recently, however, canolol formation during roasting has also been confirmed in those varieties.[14] Furthermore, most of the previous studies have ignored the possibility of Maillard type browning reactions involving the amino group containing phospholipid (e.g., phosphatidylethanolamine (PE)). Such browning reaction products have been demonstrated to be more lipophilic compared to Maillard reaction products between amino acids and reducing sugars.[16] Hence, they are more likely to be extracted with oil and can contribute to its antioxidative activity.[17,18] A correlation study considering the effect of all these different factors on the oxidative stability of roasted mustard seed oil has been published recently.[18] It has provided the novel insight that the presence of radical scavengers (such as canolol and tocopherol) could not solely explain the very high oxidative stability of roasted mustard seed oil. Such observation has been shown to be primarily linked with phospholipid content and the presence of lipophilic Maillard type browning reaction products, in addition to canolol that is formed during roasting.[18] However, that study was carried out on roasted mustard seed oils collected from the market and, hence, it does not clearly demonstrate how such antioxidative compounds are generated during seed roasting and if there exist

Received: January 31, 2014
Revised: May 27, 2014
Accepted: June 2, 2014
Published: June 2, 2014

ACS Publications © 2014 American Chemical Society

Table 1. Effect of Seed Roasting on Different Compositional Parameters and Browning Reaction Markers of Extracted Oil[a]

variety	roasting time (min)	canolol (μg/g oil)	α-tocopherol (μg/g oil)	γ-tocopherol (μg/g oil)	plastochromanol-8 (μg/g oil)	phospholipid phosphorus (μg/g)	absorbance (350 nm)	fluorescence[b] (ex 350 nm, em 440 nm)	pyrrole content (nmol/g)
BJ	unroasted	5.41 ± 0.01 a	89.56 ± 2.39 def	290.34 ± 2.36 hi	39.59 ± 1.43 hij	8.66 ± 1.81 a	0.03 ± 0.01 a	3.65 ± 0.19 a	6.97 ± 1.68 ab
BJ	10	297.76 ± 6.26 e	80.57 ± 0.99 cde	266.84 ± 2.16 efg	39.15 ± 0.81 hi	453.62 ± 51.65 k	0.56 ± 0.03 ghi	64.43 ± 1.34 efg	54.97 ± 4.64 c
BJ	20	301.19 ± 5.31 e	76.92 ± 2.02 cd	244.61 ± 17.93 d	38.16 ± 4.20 hi	319.23 ± 46.62 ijk	0.91 ± 0.13 k	56.71 ± 3.54 de	75.32 ± 6.87 efgh
BJ	30	255.31 ± 5.93 d	71.58 ± 1.89 bc	224.28 ± 3.79 c	36.63 ± 0.22 gh	175.54 ± 49.39 efgh	0.63 ± 0.02 hij	57.76 ± 3.19 de	86.45 ± 6.41 hi
BJ	45	234.56 ± 9.14 d	61.41 ± 5.57 b	221.74 ± 1.44 c	36.77 ± 0.69 hi	133.52 ± 35.91 def	0.63 ± 0.10 hij	64.57 ± 2.72 efg	65.04 ± 3.85 cde
BJ	60	181.82 ± 0.63 c	22.49 ± 1.81 a	200.09 ± 1.19 b	36.89 ± 0.60 hi	110.72 ± 30.13 de	0.70 ± 0.03 ij	71.34 ± 0.72 fghi	65.16 ± 4.43 cde
BJ	90	146.84 ± 12.39 b	12.96 ± 5.08 a	177.95 ± 11.47 a	32.99 ± 1.93 fg	117.74 ± 5.62 def	0.69 ± 0.01 ij	78.00 ± 2.73 ij	91.97 ± 5.66 ij
BJO	unroasted	5.06 ± 0.15 a	97.99 ± 0.82 f	358.49 ± 4.97 j	9.26 ± 0.25 b	15.66 ± 3.72 b	0.03 ± 0.01 a	3.51 ± 0.09 a	4.31 ± 1.50 a
BJO	10	171.64 ± 3.20 bc	89.72 ± 4.69 ef	295.40 ± 10.29 i	26.71 ± 0.88 c	342.57 ± 31.71 jk	0.26 ± 0.03 bc	42.72 ± 3.02 c	81.58 ± 2.44 fghi
BJO	20	174.32 ± 4.02 bc	87.30 ± 1.19 def	293.50 ± 1.57 i	27.61 ± 0.31 cd	271.75 ± 21.58 hijk	0.39 ± 0.02 cdef	43.62 ± 1.61 c	91.88 ± 2.05 ij
BJO	30	163.20 ± 1.25 bc	86.86 ± 0.58 def	291.26 ± 4.59 hi	29.50 ± 1.30 cdef	198.72 ± 21.46 fghi	0.52 ± 0.01 fgh	55.31 ± 1.87 d	89.02 ± 4.11 hi
BJO	45	154.23 ± 1.79 bc	85.65 ± 1.42 def	288.36 ± 4.23 hi	29.10 ± 1.13 cde	167.58 ± 46.28 efgh	0.65 ± 0.00 hij	67.41 ± 0.68 fgh	84.74 ± 2.36 ghi
BJO	60	157.98 ± 2.82 bc	85.42 ± 0.81 de	288.22 ± 2.06 hi	31.10 ± 0.14 def	128.29 ± 5.95 def	0.67 ± 0.00 ij	75.07 ± 2.51 hi	89.77 ± 0.89 hij
BJO	90	146.70 ± 0.49 b	76.61 ± 3.22 cd	283.36 ± 2.45 ghi	31.70 ± 0.80 ef	137.81 ± 41.53 defg	0.77 ± 0.09 jk	85.32 ± 1.73 j	172.31 ± 1.26 k
RS	unroasted	5.19 ± 0.09 a	214.89 ± 4.33 g	274.15 ± 3.81 fgh	1.80 ± 0.09 a	30.45 ± 9.38 c	0.04 ± 0.01 a	12.71 ± 0.28 b	1.92 ± 1.47 a
RS	10	808.48 ± 24.67 i	218.93 ± 14.31 gh	255.05 ± 14.61 de	40.29 ± 2.42 ij	224.15 ± 11.16 ghij	0.23 ± 0.09 b	68.90 ± 5.18 fgh	18.94 ± 9.64 b
RS	20	847.13 ± 22.30 j	222.79 ± 5.62 gh	258.10 ± 5.30 def	43.73 ± 0.77 jk	164.66 ± 19.28 efgh	0.27 ± 0.02 bcd	71.03 ± 1.17 fghi	60.12 ± 14.33 cd
RS	30	809.06 ± 4.22 i	224.49 ± 2.47 gh	260.62 ± 2.85 def	46.26 ± 0.98 kl	188.26 ± 47.47 fgh	0.45 ± 0.08 efg	68.96 ± 1.74 fgh	77.34 ± 1.56 efgh
RS	45	760.45 ± 31.19 h	229.81 ± 3.20 h	261.48 ± 2.61 def	48.01 ± 1.02 l	151.87 ± 12.68 efg	0.41 ± 0.02 defg	67.97 ± 0.71 fgh	71.36 ± 2.36 defg
RS	60	708.26 ± 15.97 g	225.77 ± 4.96 gh	257.19 ± 4.42 de	46.37 ± 0.58 kl	147.60 ± 39.54 defg	0.32 ± 0.11 bcde	63.54 ± 9.07 def	68.62 ± 5.30 cdef
RS	90	650.17 ± 13.83 f	227.06 ± 4.60 gh	257.06 ± 5.65 de	47.06 ± 1.14 kl	88.12 ± 4.96 d	0.36 ± 0.08 bcde	72.17 ± 3.00 ghi	102.20 ± 5.46 j

[a]Values with different letters in the same column are significantly different ($p < 0.05$). [b]Expressed as percent of fluorescence of quinine sulfate solution (1 μM in 0.1 M H_2SO_4).

dx.doi.org/10.1021/jf500549t | J. Agric. Food Chem. 2014, 62, 5412−5419

Table 2. Free Amino Acids Content (Milligrams per 100 g FFDM) of Seeds before and after 10 min of Roasting of Different Varieties[a]

amino acid	BJ (unroasted)	BJO (unroasted)	RS (unroasted)	BJ (roasted 10 min)	BJO (roasted 10 min)	RS (roasted 10 min)
aspartate	51.72 ± 1.12 d	92.18 ± 0.32 f	85.81 ± 1.74 e	10.23 ± 1.95 a	17.91 ± 0.93 b	25.96 ± 3.06 c
glutamate	269.00 ± 3.35 b	259.75 ± 4.49 b	304.92 ± 8.12 c	15.11 ± 2.81 a	13.93 ± 0.64 a	23.19 ± 3.82 a
asparagine	175.12 ± 1.93 e	100.69 ± 0.56 c	145.21 ± 4.04 d	17.76 ± 3.26 b	10.11 ± 0.68 a	21.64 ± 3.09 b
serine	19.75 ± 1.34 c	42.58 ± 3.55 d	15.34 ± 2.95 c	4.46 ± 0.88 ab	8.88 ± 0.09 b	2.96 ± 0.32 a
glutamine	6.99 ± 0.16 b	1.92 ± 3.75 a	7.54 ± 0.78 b	0.43 ± 0.07 a	0.36 ± 0.00 a	0.48 ± 0.15 a
histidine	8.20 ± 0.25 b	9.52 ± 0.64 c	12.13 ± 0.47 d	1.59 ± 0.39 a	1.56 ± 0.14 a	1.58 ± 0.07 a
glycine	6.35 ± 1.56 bc	12.23 ± 2.50 d	10.17 ± 2.56 cd	1.90 ± 0.37 a	2.99 ± 0.02 ab	3.04 ± 0.18 ab
threonine	5.68 ± 0.15 b	8.90 ± 0.46 d	6.80 ± 0.32 c	0.91 ± 0.16 a	1.25 ± 0.05 a	1.34 ± 0.19 a
arginine	28.11 ± 0.18 d	26.46 ± 0.16 c	22.34 ± 0.65 b	5.43 ± 1.03 a	4.14 ± 0.30 a	5.14 ± 0.65 a
alanine	7.08 ± 0.41 b	15.82 ± 1.10 c	25.16 ± 0.63 d	2.74 ± 0.50 a	4.28 ± 0.29 a	8.65 ± 0.79 b
tyrosine	4.33 ± 0.08 a	5.61 ± 0.32 b	5.84 ± 0.45 b	nd[b]	nd	nd
valine	7.82 ± 0.22 b	9.01 ± 0.54 c	11.73 ± 0.61 d	0.57 ± 0.11 a	0.84 ± 0.05 a	1.39 ± 0.30 a
methionine	1.62 ± 1.59 a	1.61 ± 1.57 a	0.64 ± 1.26 a	0.93 ± 0.11 a	1.17 ± 0.06 a	0.90 ± 0.00 a
tryptophan	8.38 ± 0.23 b	15.71 ± 0.39 c	7.73 ± 0.57 b	0.65 ± 0.16 a	1.08 ± 0.14 a	1.08 ± 0.14 a
phenylalanine	8.71 ± 0.06 c	15.46 ± 0.37 d	8.49 ± 0.43 c	1.83 ± 0.23 a	2.58 ± 0.14 b	2.26 ± 0.04 ab
isoleucine	3.08 ± 0.09 c	4.14 ± 0.23 d	4.84 ± 0.22 e	0.14 ± 0.14 a	0.24 ± 0.02 ab	0.58 ± 0.10 b
leucine	2.66 ± 0.19 b	5.00 ± 0.35 d	3.48 ± 0.53 c	0.08 ± 0.15 a	0.51 ± 0.04 a	0.45 ± 0.07 a
lysine	6.99 ± 0.32 c	8.96 ± 0.35 d	11.51 ± 1.10 e	1.38 ± 0.21 a	1.24 ± 0.09 a	3.42 ± 0.58 b
proline	3.47 ± 1.67 a	8.13 ± 0.21 b	8.46 ± 0.32 b	2.40 ± 0.27 a	2.83 ± 0.40 a	2.22 ± 0.36 a
total	625.07 ± 8.77 c	643.66 ± 10.26 c	698.14 ± 15.31 d	68.55 ± 12.03 a	75.90 ± 2.54 a	106.28 ± 13.13 b

[a]Values with different letters in the same row are significantly different ($p < 0.05$). [b]nd, not detected.

differences in the roasting effect among different mustard and RS varieties.

Therefore, the current study has been carried out to evaluate the seed roasting effect on different compositional parameters and oil oxidative stabilities of different *Brassica* species. The three species selected for the study were *Brassica juncea* (Indian mustard), *Brassica juncea* var. *oriental* (oriental mustard), and *Brassica napus* (European rapeseed).

MATERIALS AND METHODS

Materials and Reagents. The seeds of two high erucic acid mustard varieties (*B. juncea* (BJ) and *B. juncea* var. *oriental* (BJO)) and a low erucic acid rapeseed (RS) variety (*B. napus*) were collected from the local market of Ghent, Belgium. Tocopherol standard was obtained from DSM (New Jersey, USA). Syringaldehyde and 1,2-dioleoyl-*sn*-glycero-3-phosphoethanolamine were purchased from Sigma-Aldrich (Steinheim, Germany). Nonadecanoic acid was purchased from Fluka (Buchs, Switzerland). The HPLC grade hexane was bought from VWR International (Leuven, Belgium). Other reagents and solvents were of analytical grade and obtained from reliable commercial sources.

Synthesis of Canolol. Canolol was synthesized from syringaldehyde by condensation with malonic acid and then double decarboxylation under microwave condition as described previously.[14] Ultraviolet, fluorescence, liquid chromatography–mass spectrometry, and nuclear magnetic resonance spectra were used to confirm the identity and purity of the synthesized compound.[14] The synthesized canolol was used as a standard for quantification.

Analytical Methods. Fatty acid methyl esters were prepared using the boron trifluoride method (American Oil Chemists Society, 1990) and were analyzed on a gas chromatograph using the method described previously.[18] Nonadecanoic acid was used as an internal standard for the quantification.

Analysis of the total amino acid profile of seed sample was carried out using the previously described procedure[19] and included a full hydrolysis of the sample in acidic conditions and a liquid chromatographic analysis using fluorescence detection after derivatization. Thus, tryptophan and cysteine were lost and glutamine and asparagine were converted to glutamic and aspartic acid, respectively. Tryptophan was separately analyzed after basic hydrolysis followed by similar chromatographic conditions. Analysis of the free amino acids content was carried out after their extraction from the ground seeds with 15% trichloroacetic acid followed by similar chromatographic analysis, without acid hydrolysis. Sarcosine was used as an internal standard to quantify proline. Norvaline was used as an internal standard to quantify other amino acids.

Analysis of the sugar content in the seed sample was carried out gas chromatographically after aqueous extraction of the sugar and derivatization via oximation and silylation using the previously described procedure.[20] Phenyl-β-D-glucopyranoside was used as an internal standard for the quantification.

Tocopherol and canolol contents of the oils were analyzed in a high-pressure liquid chromatograph using a fluorescence detector, after separation in a silica column as described previously.[14]

The peroxide value (PV) of the oil was determined by using an iron-based spectrophotometric method.[21] A calibration curve was constructed using a standard iron(III) chloride solution as described in the same method. Calibration was done using six concentrations in duplicate in the range from 5 to 30 μg of iron(III). The multiple *R*-squared value was >0.99 for the calibration. Such a calibration curve was constructed just before the measurement of the peroxide value of the samples.

The phospholipid phosphorus content of the oil was analyzed spectrophotometrically after the formation of a phospholipid phosphorus–molybdate complex as described before.[18]

The pyrrolyzed phospholipid content of the oil samples was analyzed using a previously described procedure.[22] The absorbance of the Ehrlich adducts was measured at 512 nm, and the blank absorbance without Ehrlich reagent was subtracted during calculation. The reported value of the extinction coefficient of Ehrilich adducts (153000 M^{-1} cm^{-1}) with 1-[1-(2-hydroxyethyl)-1*H*-pyrrol-2-yl]-propan-1-ol was used in the calculation.[22]

UV–visible absorbance spectra of the oil solution in iso-octane (25 mg/mL) were measured using a Cary 50 UV–vis spectrophotometer (Varian) in a quartz cuvette. Fluorescence (excitation at 350 nm and emission at 440 nm) of the same oil solution was additionally measured using a Spectramax Gemini XS fluorescence spectrophotometer as described previously.[18] Fluorescence is expressed as the percentage fluorescence of 1 μM quinine sulfate solution in 0.1 M H_2SO_4.

Experimental Setup. Mustard seed and rapeseed were roasted in a beaker, which was dipped inside an oil bath maintained at 180 °C as reported earlier.[14] Briefly, 80 g of seed sample was added to a heated beaker placed in the oil bath (180 °C). The seed sample and heating oil were continuously agitated with two electric mechanical stirrers. The temperature of the seed sample and heating oil was continuously monitored using Testo thermostat probes. The oil temperature was maintained constant at 180 °C, and seed roasting was carried out for 10, 20, 30, 45, 60, and 90 min. The seed temperature profile with time followed the equation $T = 32.796 \ln(t) + 89.422$ ($R^2 = 0.99$) for the first 10 min of roasting, where T is the seed temperature (°C) and t is the roasting time (min). Afterward, seed temperature remained constant at 165 ± 3 °C.

The roasted and unroasted seeds were ground. The total amino acid profile was analyzed on unroasted seed powder. The reducing sugar content and free amino acid profile were analyzed on both unroasted and 10 min roasted seed powders.

The oil was extracted from unroasted and roasted seeds using petroleum ether.[14] Tocopherol, canolol, phospholipid, and browning reaction markers (absorbance, fluorescence, and pyrrolyzed phospholipid content) were analyzed on unroasted and roasted seed oils. The extracted oil (750 μL) was kept in a 1.5 mL loosely capped HPLC glass vial and stored at 104 °C to accelerate the oxidation process. Oil oxidation was monitored by analyzing PV at different time intervals. Both roasting and oxidation studies were carried out in independent triplicate experiments.

Statistical Analysis. All data are presented as mean values ± 95% confidence interval of the mean based on three independent experiments, unless otherwise stated. The logarithmic transformations of the different data were done, whenever necessary, to have homoscedasticity before the statistical analysis was carried out. ANOVA and post hoc Tukey test were performed using TIBCO Spotfire S+ 8.1 software. The significance level is $p < 0.05$, unless otherwise indicated.

RESULTS AND DISCUSSION

Effect of Roasting on Different Compositional Parameters. Mustard seed and rapeseed roasting is known to form canolol by decarboxylation of sinapic acid.[11,12,14,23,24] Roasting of seed before oil extraction increased the canolol content of oil in all varieties (Table 1). The maximum canolol content of oil was reached during 10−20 min of seed roasting. Oil from 20 min roasted RS contained the highest amount of canolol, which was 2.8 times higher compared to BJ seed oil and 4.9 times higher compared to BJO seed oil, roasted for the same time. Higher canolol formation in roasted RS compared to different mustard seed varieties was also reported previously.[14] Roasting for more than 20 min gradually reduced the canolol content in all varieties. The decrease in the canolol content during longer roasting time was also reported previously.[24] The canolol content of the roasted rapeseed oil was reported in a similar range previously.[23,24]

The tocopherol contents of the unroasted and roasted seed oils of different varieties are given in Table 1. The α-tocopherol content in the unroasted RS oil was more than double the amount present in both unroasted mustard seed oils. It remained stable during RS roasting, whereas a significant gradual degradation was observed for both BJ and BJO mustard varieties. The γ-tocopherol contents in all three varieties were quite comparable. Its degradation was observed in all varieties during 10 min of roasting. Afterward, it remained constant in RS, whereas a slight degradation was observed during BJO roasting. The BJ seed oil showed a gradual and the largest degradation in γ-tocopherol during longer roasting. The plastochromanol-8 content remained relatively stable in the BJ seed oil during roasting. On the other hand, a significant increment was observed in the BJO and RS oils during the first 10 min of roasting. The disruption of matrix during roasting could be responsible for the increased extractability. A longer roasting time had little effect on all varieties studied.

The phospholipid phosphorus content of the unroasted seed oils, extracted using petroleum ether, was in the range of 8−30 μg/g oil (Table 1). On the other hand, when the same unroasted seed powder was extracted with a chloroform/methanol solvent mixture (2:1, v/v), the phospholipid phosphorus content was 500−600 μg/g oil. Therefore, the lower phospholipid content of unroasted seed oil was due to the poor extractability with petroleum ether from the unroasted seed matrix. Roasting for 10 min significantly increased the oil phospholipid content for all varieties. This observation was similar to the increased extractability of plastochromanol-8 after seed roasting. The increased phospholipid content of the oil after seed roasting was also reported previously.[9] Roasting for more than 10 min showed a gradual decrease in the phospholipid phosphorus content in the oil of all varieties. The decrease in extractability could indicate its chemical modification; for instance, it could be covalently bound to matrix compounds.

The Maillard reaction is one of the most well-known nonenzymatic browning reactions in heat-treated food products. The possibility for such reactions during seed roasting was studied by evaluating the changes in the amino acid and reducing sugar contents. Among the free amino acids, RS contained a significantly higher quantity of glutamate, histidine, alanine, valine, isoleucine, and lysine compared to both BJ and BJO mustard varieties (Table 2). On the other hand, both BJ and BJO mustard varieties contained significantly higher quantities of free arginine compared to RS. After 10 min of roasting, >85% of free amino acids were lost, indicating the occurrence of Maillard reaction in all varieties. The losses of individual amino acids were quite comparable in all varieties. Therefore, the formation of low molecular weight antioxidative compounds from such reactions could also be comparable

Table 3. Total Amino Acids Content (Grams per 100 g FFDM) of Unroasted Seeds of Different Varieties[a]

amino acid	BJ	BJO	RS
aspartate	2.21 ± 0.04 c	2.07 ± 0.03 b	1.98 ± 0.03 a
glutamate	6.39 ± 0.10 c	5.96 ± 0.05 b	4.73 ± 0.06 a
serine	1.61 ± 0.05 c	1.51 ± 0.04 b	1.30 ± 0.02 a
histidine	1.19 ± 0.02 c	1.09 ± 0.02 b	0.86 ± 0.02 a
glycine	2.06 ± 0.04 c	1.94 ± 0.03 b	1.66 ± 0.03 a
threonine	1.68 ± 0.02 c	1.59 ± 0.02 b	1.45 ± 0.02 a
arginine	2.77 ± 0.04 c	2.59 ± 0.04 b	1.94 ± 0.03 a
alanine	1.67 ± 0.03 c	1.57 ± 0.01 b	1.38 ± 0.02 a
tyrosine	1.17 ± 0.03 c	1.08 ± 0.02 b	1.00 ± 0.02 a
valine	1.84 ± 0.03 b	1.86 ± 0.02 b	1.61 ± 0.03 a
methionine	0.55 ± 0.02 b	0.57 ± 0.05 b	0.46 ± 0.01 a
tryptophan	0.43 ± 0.03 ab	0.45 ± 0.03 b	0.37 ± 0.04 a
phenylalanine	1.68 ± 0.04 b	1.61 ± 0.04 b	1.32 ± 0.04 a
isoleucine	1.69 ± 0.03 c	1.60 ± 0.02 b	1.37 ± 0.03 a
leucine	2.71 ± 0.05 c	2.58 ± 0.05 b	2.18 ± 0.04 a
lysine	2.25 ± 0.08 b	2.21 ± 0.07 b	1.94 ± 0.06 a
proline	2.72 ± 0.03 c	2.57 ± 0.04 b	2.05 ± 0.03 a
total	34.62 ± 0.59 c	32.85 ± 0.49 b	27.60 ± 0.47 a

[a]Values with different letters in the same row are significantly different ($p < 0.05$).

Table 4. Changes in the Sugar Composition (Milligrams per Gram FFDM) in the Seed after 10 min of Roasting of Different Varieties[a]

variety	roasting time (min)	fructose	glucose	sucrose
BJ	unroasted	6.70 ± 0.29 d	46.60 ± 1.92 c	51.70 ± 1.62 b
BJO	unroasted	3.80 ± 0.18 b	48.56 ± 2.58 c	62.77 ± 1.37 c
RS	unroasted	3.94 ± 0.27 b	12.43 ± 0.94 b	70.42 ± 2.27 d
BJ	10	5.99 ± 0.22 cd	3.51 ± 0.12 a	33.37 ± 2.85 a
BJO	10	5.16 ± 0.84 c	4.49 ± 0.48 a	48.95 ± 3.04 b
RS	10	1.07 ± 0.03 a	1.44 ± 0.25 a	84.74 ± 5.15 e

[a]Values with different letters in thre same column are significantly different ($p < 0.05$).

Figure 1. Mustard (BJ and BJO) and rapeseed meals before and after 20 min of roasting.

among those varieties. On the other hand, the total amino acids content (on a fat-free dry matter (FFDM) basis) was higher in mustard varieties compared to that in RS (Table 3). Particularly notable was the presence of 30−40% higher arginine and 14−16% higher lysine in mustard varieties compared to that in RS. Because of the presence of a free amino group, these amino acids are particularly responsible for the Maillard reactions involving proteins. The formation of high molecular weight hydrophilic antioxidative compounds from such reactions could be much more pronounced in mustard varieties compared to that in RS.

The effect of seed roasting on the sugar content was additionally evaluated in all varieties (Table 4). Both mustard varieties contained significantly higher quantities of glucose and lower quantities of sucrose compared to RS before roasting. The fructose content of BJ mustard seed was also higher compared to both BJO seed and RS. After 10 min of roasting, the glucose content decreased significantly in all varieties compared to the amount present in the unroasted seed. The loss of glucose was around 4 times higher in both mustard varieties compared to that in rapeseed. Moreover, the sucrose content of both mustard varieties also decreased significantly, likely due to its hydrolysis into glucose and fructose. The increase in sucrose content in rapeseed after seed roasting could possibly due to its formation via the hydrolysis of stachyose and raffinose present in the matrix.[25]

The ground seed meals of different varieties before and after 20 min of roasting are shown in Figure 1. This picture illustrates that browning reactions during roasting were more pronounced in mustard varieties compared to RS. This could be linked with the presence of higher quantities of both reducing sugars and reactive amino acids (e.g., lysine, arginine) in mustard varieties compared to those in RS.

In addition to amino acids, the amino group containing phospholipid (e.g., PE) is also known to take part in the Maillard type browning reactions with reducing sugars.[17] Both types of browning reactions could be expected to happen simultaneously in the seed; however, their extraction in the oil could be affected by their polarity differences. In a previous study, it was shown that the amino group of PE was even more reactive with ribose than with lysine.[16] These authors reported that, when the aqueous reaction mixture of PE, ribose, and lysine was extracted with chloroform/methanol (2:1, v/v) to have phase separation, the brown compounds due to PE/ribose and lysine/ribose got separated into the organic and aqueous phases, respectively.[16] These observations showed that the

dx.doi.org/10.1021/jf500549t | J. Agric. Food Chem. 2014, 62, 5412−5419

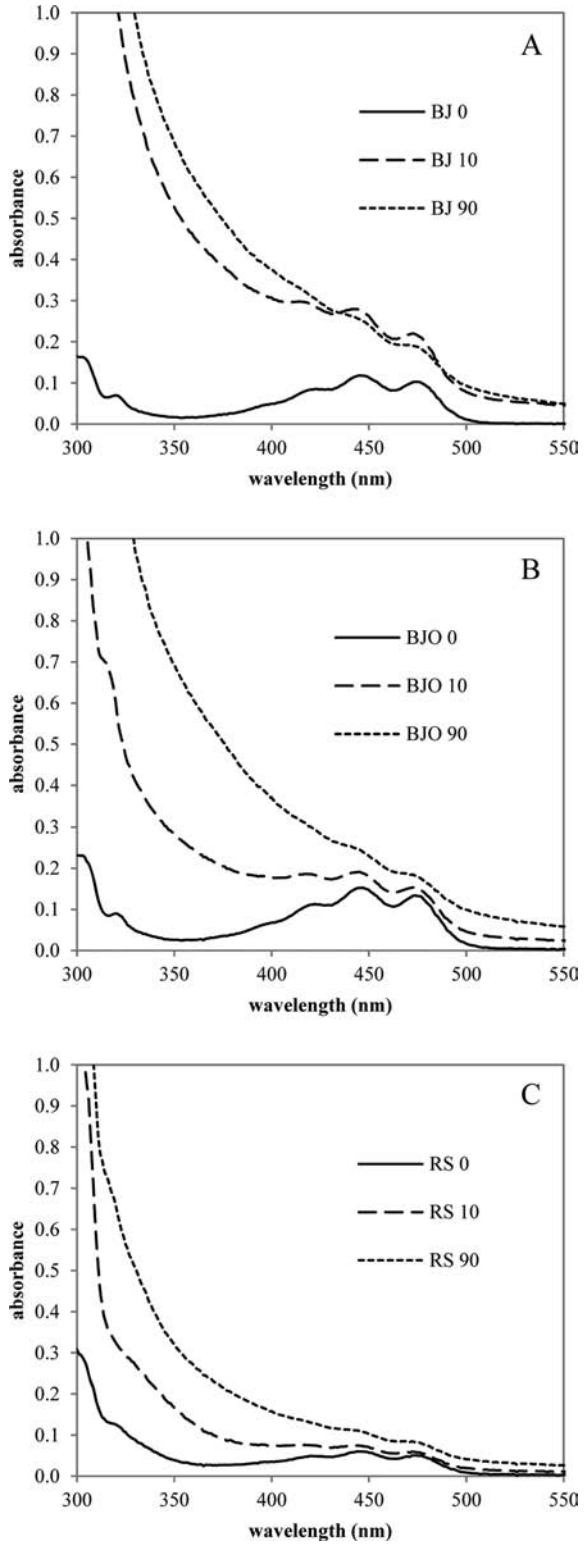

Figure 2. Changes in the visible spectrum of the oil after roasting of *B. juncea* (A), *B. juncea* var. *oriental* (B), and *B. napus* (rapeseed) (C).

lysine/ribose Maillard reaction products are more hydrophilic, whereas the PE/ribose reaction system could produce lipophilic Maillard type reaction products. The same extraction method was used to characterize the brown compounds in the roasted seed oil. It was observed that the major brown compounds of oil remained in the organic phase, indicating that these brown compounds could be mainly due to phospholipid browning compared to the reducing sugar amino acid Maillard reactions. The possibility of such phospholipid browning reaction products was also reported previously on the basis of the high correlation observed between the phospholipid content, absorbance, fluorescence, and pyrrolyzed phospholipid content in roasted mustard seed oil.[18]

Table 5. Fatty Acids Composition of Oil (Grams per 100 g Oil) from Different Mustard and Rapeseed Varieties

fatty acid	BJ	BJO	RS
16:0	2.6	2.5	4.4
16:1	0.1	0.1	0.2
18:0	1.1	1.3	1.1
18:1	17.8	18.8	53.9
18:2	18.1	19.0	19.8
20:0	1.1	1.2	1.1
20:1	8.4	8.2	0.3
18:3	15.4	13.9	9.7
20:2	1.0	0.9	nd[a]
22:0	0.2	0.3	nd
22:1	20.6	21.3	nd
24:1	1.2	1.2	nd

[a]nd, not detected.

Changes in the browning reaction markers in the oil after seed roasting of different varieties were further evaluated (Table 1). The absorbance of oil at 350 nm gradually increased during roasting in all varieties. The choice of this marker is based on the recent report that the oxidative stability of the roasted mustard seed oil is highly correlated at this wavelength.[18] The BJ seed oil showed the highest increment in the absorbance and reached a maximum after 20 min of roasting, which was >3 times compared to that of RS oil and >2 times compared to BJO seed oil roasted for the same time. After 45 min of roasting, the absorbance values of all varieties remained almost constant. The absorbance values after 45 min were comparable between BJ and BJO seed oil and were around double the amount compared to RS oil. To illustrate that more clearly, the changes in the UV−visible absorbance spectra of oil after roasting for 10 and 90 min for all varieties are shown in Figure 2. This figure shows that the increase in the UV−visible absorbance due to browning reactions within the 10 min of roasting was highest in BJ followed by BJO and rapeseed oil. After 90 min of roasting, BJ and BJO seed oil showed similar UV−visible absorbance spectra. On the other hand, the UV−visible absorbance spectrum of roasted rapeseed oil (even after 90 min of roasting) was lower than that of 10 min roasted BJ oil. This showed that browning reactions were more prominent in BJ and BJO mustard varieties compared to that in rapeseed variety. In addition, roasting increased the oil fluorescence (excitation 350 nm and emission 440 nm) in all varieties (Table 1). However, fluorescence development was comparable in all varieties and could not differentiate the extent of browning observed with the absorbance at 350 nm. Furthermore, the presence of the Maillard type browning reaction products in the roasted seed oil was supported by the increment in the pyrrolyzed phospholipid content after seed roasting in all varieties (Table 1).

Oxidative Stability of Roasted Seed Oil of Different Varieties. The fatty acid compositions of all the oils are given in Table 5. Both mustard varieties were rich in erucic acid, whereas RS was rich in oleic acid. However, total saturated,

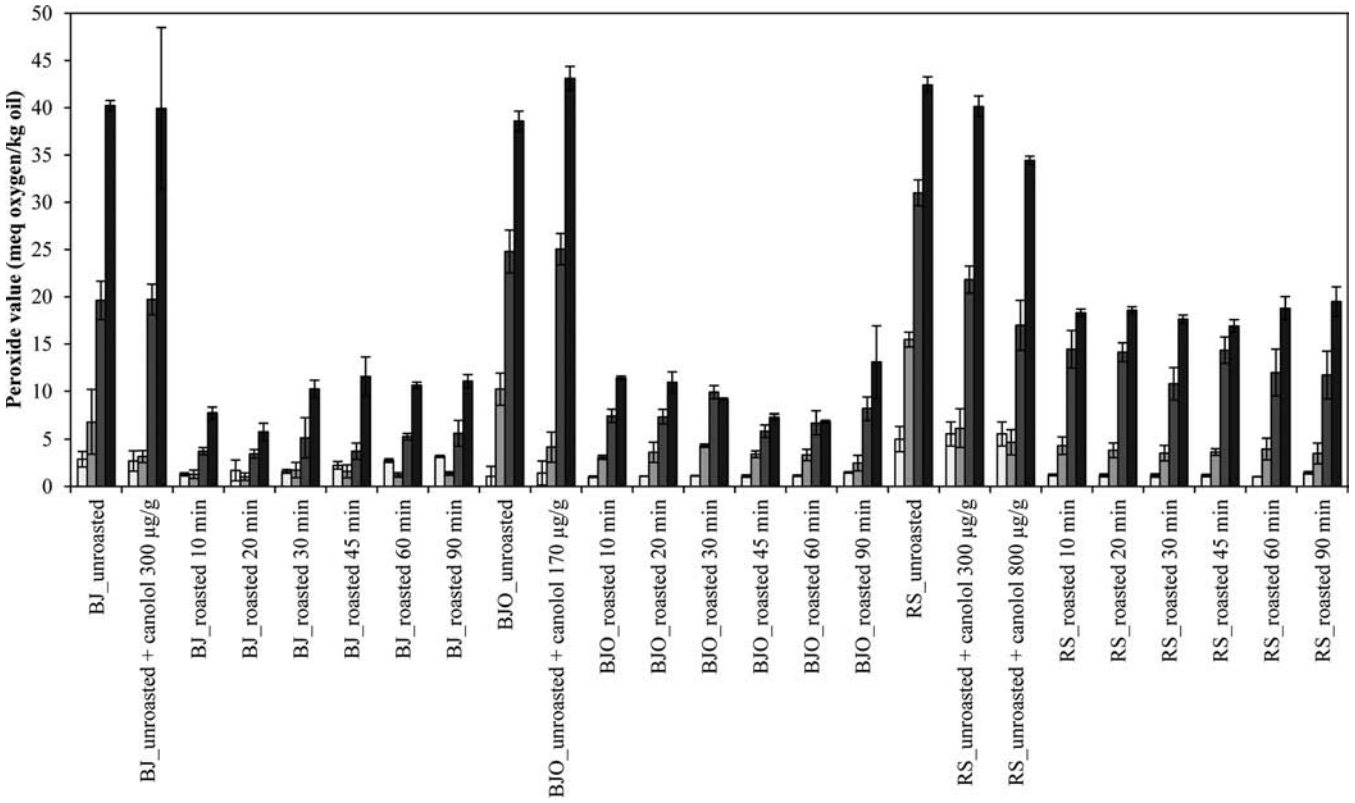

Figure 3. Changes in the PV of unroasted seed oil, roasted seed oil, and canolol added unroasted seed oil of different varieties stored at 104 °C (white bars, 0 h; light gray bars, 9 h; dark gray bars, 32 h; and black bars, 98 h).

monounsaturated, and polyunsaturated fatty acid contents were comparable in all varieties.

The oxidative stabilities of unroasted seed oil and roasted seed oil were evaluated by monitoring the changes in the PV during accelerated oxidation at 104 °C (Figure 3). A previous study showed that roasted mustard seed oil could have a very high oxidative stability with an induction period >60 days during storage at 50 °C.[18] Therefore, higher storage temperature (104 °C) was chosen to accelerate the oxidation. The vials were loosely capped so as to maintain a constant atmospheric oxygen concentration in the headspace. The experiment is similar to the active oxygen method used for the evaluation of oxidative stability of oil at 100 °C by saturating the oil with oxygen and monitoring the PV during storage. It is known that peroxides could degrade at this temperature and the oil oxidation could be different from the autoxidation; however, such effects could be similar in the oil samples with similar fatty acid compositions. Therefore, the results from this experiment should be taken as the relative oxidative stability among the samples with similar fatty acid compositions during accelerated oxidation.

Roasting for 10 min significantly improved the oxidative stability of all varieties compared to their respective unroasted seed oil (Figure 3). Such an increment in the oxidative stability due to roasting was more prominent in BJ and BJO varieties compared to the RS variety. Roasting for longer time had a smaller additional effect.

Canolol is a potent antioxidant and is known to play an important role in the oxidative stability of roasted rapeseed oil.[11,12] However, other factors in addition to canolol could also be responsible for the increased oxidative stability. To evaluate the role of canolol alone, oxidative stability was evaluated after the addition of canolol to the unroasted seed oil equivalent to the amounts formed after 10 min of roasting (Figure 2). In addition, the oxidative stability of unroasted rapeseed oil containing canolol equivalent to the amount in 10 min roasted BJ seed oil was also evaluated. Canolol addition to the unroasted mustard seed (BJ and BJO) could not increase their oxidative stability, whereas it showed a significant protective role in the rapeseed oil. In all varieties, 10 min roasted seed oil was more stable compared to the respective unroasted seed oil with an equivalent quantity of canolol added. These observations showed that canolol could play a significant role in increasing the oxidative stability of roasted RS oil; however, its formation alone could not be responsible for the increased oxidative stability after seed roasting. Furthermore, even though BJ and BJO varieties showed smaller increments in canolol during roasting compared to that in RS, the increment in oxidative stability after roasting was more prominent in BJ and BJO varieties compared to that in RS. This could be linked with other multiple effects of seed roasting such as increased extraction of phospholipid and formation of antioxidants via Maillard type reactions. Such roasting effects depend on the chemical composition of the seeds, which could be different in the different varieties. In the current example, BJ and BJO mustard seeds showed stronger Maillard type browning reactions compared to the RS variety. Maillard type browning reaction products are known to have strong antioxidative activity.[17,26] Such browning reaction products could be responsible for the increased oxidative stability of roasted mustard (BJ and BJO) seed oil in addition to the canolol formed during roasting. Further studies are required to isolate and identify the antioxidative compounds formed during such

reactions that can be used as a natural antioxidants in different food products.

AUTHOR INFORMATION

Corresponding Author

*(B.D.M.) E-mail: Bruno.DeMeulenaer@UGent.be. Phone: + 32 9 264 61 66. Fax: + 32 9 264 62 15.

Funding

The study was financially supported by the Special Research Fund − BOF, Ghent University, which is gratefully acknowledged.

Notes

The authors declare no competing financial interest.

ABBREVIATIONS USED

PV, peroxide value; BJ, *Brassica juncea*; BJO, *B. juncea* var. *oriental*; PE, phosphatidylethanolamine; RS, rapeseed; FFDM, fat-free dry matter

REFERENCES

(1) Vaidya, B.; Choe, E. Effects of seed roasting on tocopherols, carotenoids, and oxidation in mustard seed oil during heating. *J. Am. Oil Chem. Soc.* **2011**, *88* (1), 83−90.

(2) Lee, S. W.; Jeung, M. K.; Park, M. H.; Lee, S. Y.; Lee, J. Effects of roasting conditions of sesame seeds on the oxidative stability of pressed oil during thermal oxidation. *Food Chem.* **2010**, *118* (3), 681−685.

(3) Durmaz, G.; Gokmen, V. Changes in oxidative stability, antioxidant capacity and phytochemical composition of *Pistacia terebinthus* oil with roasting. *Food Chem.* **2011**, *128* (2), 410−414.

(4) Cai, L.; Cao, A.; Aisikaer, G.; Ying, T. Influence of kernel roasting on bioactive components and oxidative stability of pine nut oil. *Eur. J. Lipid Sci. Technol.* **2013**, *115* (5), 556−563.

(5) Chandrasekara, N.; Shahidi, F. Oxidative stability of cashew oils from raw and roasted nuts. *J. Am. Oil Chem. Soc.* **2011**, *88* (8), 1197−1202.

(6) Zhao, T.; Hong, S. I.; Lee, J.; Lee, J. S.; Kim, I. H. Impact of roasting on the chemical composition and oxidative stability of perilla oil. *J. Food Sci.* **2012**, *77* (12), C1273−C1278.

(7) Durmaz, G.; Karabulut, I.; Topcu, A.; Asilturk, M.; Kutlu, T. Roasting-related changes in oxidative stability and antioxidant capacity of apricot kernel oil. *J. Am. Oil Chem. Soc.* **2010**, *87* (4), 401−409.

(8) Nederal, S.; Skevin, D.; Kraljic, K.; Obranovic, M.; Papesa, S.; Bataljaku, A. Chemical composition and oxidative stability of roasted and cold pressed pumpkin seed oils. *J. Am. Oil Chem. Soc.* **2012**, *89* (9), 1763−1770.

(9) Vujasinovic, V.; Djilas, S.; Dimic, E.; Basic, Z.; Radocaj, O. The effect of roasting on the chemical composition and oxidative stability of pumpkin oil. *Eur. J. Lipid Sci. Technol.* **2012**, *114* (5), 568−574.

(10) Vaidya, B.; Eun, J. B. Effect of roasting on oxidative and tocopherol stability of walnut oil during storage in the dark. *Eur. J. Lipid Sci. Technol.* **2013**, *115* (3), 348−355.

(11) Wijesundera, C.; Ceccato, C.; Fagan, P.; Shen, Z. Seed roasting improves the oxidative stability of canola (*B. napus*) and mustard (*B. juncea*) seed oils. *Eur. J. Lipid Sci. Technol.* **2008**, *110* (4), 360−367.

(12) Koski, A.; Pekkarinen, S.; Hopia, A.; Wähälä, K.; Heinonen, M. Processing of rapeseed oil: effects on sinapic acid derivative content and oxidative stability. *Eur. Food Res. Technol.* **2003**, *217* (2), 110−114.

(13) Matthaus, B. Effect of canolol on oxidation of edible oils. In *Canola and Rapeseed: Production, Processing, Food Quality, and Nutrition*; Thiyam, U., Eskin, M., Mattaus, B., Eds.; CRC Press, Taylor & Francis Group: Boca Raton, FL, USA, 2012; pp 317−328.

(14) Shrestha, K.; Stevens, C. V.; De Meulenaer, B. Isolation and identification of a potent radical scavenger (canolol) from roasted high erucic mustard seed oil from Nepal and its formation during roasting. *J. Agric. Food Chem.* **2012**, *60* (30), 7506−7512.

(15) Vaidya, B.; Choe, E. Stability of tocopherols and lutein in oil extracted from roasted or unroasted mustard seeds during the oil oxidation in the dark. *Food Sci. Biotechnol.* **2011**, *20* (1), 193−199.

(16) Zamora, R.; Nogales, F.; Hidalgo, F. J. Phospholipid oxidation and nonenzymatic browning development in phosphatidylethanolamine/ribose/lysine model systems. *Eur. Food Res. Technol.* **2005**, *220* (5), 459−465.

(17) Zamora, R.; León, M. M.; Hidalgo, F. J. Free radical-scavenging activity of nonenzymatically-browned phospholipids produced in the reaction between phosphatidylethanolamine and ribose in hydrophobic media. *Food Chem.* **2011**, *124* (4), 1490−1495.

(18) Shrestha, K.; Gemechu, F. G.; De Meulenaer, B. A novel insight on the high oxidative stability of roasted mustard seed oil in relation to phospholipid, Maillard type reaction products, tocopherol and canolol content. *Food Res. Int.* **2013**, *54* (1), 587−594.

(19) Kerkaert, B.; Mestdagh, F.; Cucu, T.; Shrestha, K.; Camp, J.; Meulenaer, B. The impact of photo-induced molecular changes of dairy proteins on their ACE-inhibitory peptides and activity. *Amino Acids* **2012**, *43* (2), 951−962.

(20) De Wilde, T.; De Meulenaer, B.; Mestdagh, F.; Govaert, Y.; Vandeburie, S.; Ooghe, W.; Fraselle, S.; Demeulemeester, K.; Van Peteghem, C.; Calus, A.; Degroodt, J. M.; Verhe, R. Influence of storage practices on acrylamide formation during potato frying. *J. Agric. Food Chem.* **2005**, *53* (16), 6550−6557.

(21) Shantha, N. C.; Decker, E. A. Rapid, sensitive, iron-based spectrophotometric methods for determination of peroxide values of food lipids. *J. AOAC Int.* **1994**, *77* (2), 421−424.

(22) Zamora, R.; Olmo, C.; Navarro, J. L.; Hidalgo, F. J. Contribution of phospholipid pyrrolization to the color reversion produced during deodorization of poorly degummed vegetable oils. *J. Agric. Food Chem.* **2004**, *52* (13), 4166−4171.

(23) Wakamatsu, D.; Morimura, S.; Sawa, T.; Kida, K.; Nakai, C.; Maeda, H. Isolation, identification, and structure of potent alkylperoxyl radical scavenger in crude canola oil, canolol. *Biosci., Biotechnol., Biochem.* **2005**, *69* (8), 1568−1574.

(24) Spielmeyer, A.; Wagner, A.; Jahreis, G. Influence of thermal treatment of rapeseed on the canolol content. *Food Chem.* **2009**, *112* (4), 944−948.

(25) Shahidi, F. *Canola and Rapeseed: Production, Chemistry, Nutrition and Processing Technology*; Van Nostrand Reinhold: New York, 1990.

(26) Shrestha, K.; De Meulenaer, B. Antioxidant activity of Maillard type reaction products between phosphatidylethanolamine and glucose. *Food Chem.* **2014**, *161*, 8−15.

JOURNAL OF AGRICULTURAL AND FOOD CHEMISTRY

Article

pubs.acs.org/JAFC

Structural Characterization of Lignin from Grape Stalks (*Vitis vinifera* L.)

Sónia O. Prozil,[†] Dmitry V. Evtuguin,*[,†] Artur M. S. Silva,[†] and Luísa P. C. Lopes[‡]

[†]CICECO/QOPNA and Department of Chemistry, University of Aveiro, 3810-193 Aveiro, Portugal

[‡]CI&DETS and Department of Environment, Polytechnic Institute of Viseu, 3504-510 Viseu, Portugal

ABSTRACT: The chemical structure of lignin from grape stalks, an abundant waste of winemaking, has been studied. The dioxane lignin was isolated from extractive- and protein-free grape stalks (*Vitis vinifera* L.) by modified acidolytic procedure and submitted to a structural analysis by wet chemistry (nitrobenzene and permanganate oxidation (PO)) and spectroscopic techniques. The results obtained suggest that grape stalk lignin is an HGS type with molar proportions of *p*-hydroxyphenyl (H), guaiacyl (G) and syringyl (S) units of 3:71:26. Structural analysis by ^{1}H and ^{13}C NMR spectroscopy and PO indicates the predominance of *β*-*O*-4′ structures (39% mol) in grape stalk lignin together with moderate amounts of *β*-5′, *β*-*β*, *β*-1′, 5-5′, and 4-*O*-5′ structures. NMR studies also revealed that grape lignin should be structurally associated with tannins. The condensation degree of grape stalks lignin is higher than that of conventional wood lignins and lignins from other agricultural residues.

KEYWORDS: *grape stalks, dioxane lignin, nitrobenzene oxidation, permanganate oxidation, ^{1}H NMR, ^{13}C NMR, HSQC, FTIR, UV−vis*

INTRODUCTION

Winemaking is an important agricultural sector contributing substantially to national economies around the world. Total worldwide wine production is around 262 millions hL, 60% of which is produced by European Union countries.[1] The main wastes generated in the winemaking process (grape pomaces) are skins, pulp, stalks, and seeds, which account for 25−35 kg/hL of produced wine.[2] Grape stalks are one of the major byproducts of the wine industry. On average, 1 hL of wine generates up to 4 kg of grape stalks.[2] The utilization of wine byproducts is gaining increasing attention due to the environmental concerns and potential profitable applications.[3,4] Besides current uses of grape stalks as fertilizers,[5,6] the possibilities of using such materials for the production of biosorbents,[7] dietary fibers,[8] antioxidant supplements,[9] activated carbon,[10] and cellulosic pulp[11] have been demonstrated.

Grape stalks are a lignocellulosic fiber material composed essentially by cellulose, hemicelluloses, lignin, and tannins.[3,4] Similarly to jute, cotton stalks, dhaincha,[12] kenaf (*Hibiscus cannabinus*),[13] and reed (*Arundo donax*),[14] grape stalks may be considered an alternative to wood sources of fibers for papermaking and biocomposites.[4,15] Carbohydrates contribute to >50% of grape stalks,[4,16] the most abundant being cellulose (ca. 30−35%) and *O*-acetyl-4-*O*-methylglucurono-*β*-D-xylan (ca. 10−15%). One specific feature of grape stalks is the high content of tannins, their amount being comparable to the lignin content.[4] Grape stalks contain several classes of polyphenolic compounds, such as phenolic acids, flavonols, and flavanonols. The major part of tannins consist of polymeric proanthocyanidins composed of (−)-epicatechin units together with smaller amounts of (+)-catechin, (−)-epicatechin gallate, and (−)-epigallocatechin.[17] Among other polyphenolic compounds, quercetin 3-glucuronide, catechin, caffeoyltartaric acid, and dihydroquercetin 3-rhamnoside (astilbin) have been detected.[17]

Often, condensed tannins are determined together with lignin in the acid-insoluble residue called Klason lignin, thus overestimating its content by almost twice.[4] The accurate determination of Klason lignin is possible only after the preliminary removal of extractives, proteins, and condensed tannins from grape stalks. The Klason lignin content in grape stalks corrected for extractives, proteins, and tannins is around 17%.[4] Despite increased research activity on the chemical processing of grape stalks, practically no reliable information on the chemical structure of lignin is available. However, the undefined structure of lignin and/or its possible association with tannins was suggested to be a reason for the extremely difficult delignification of grape stalks by oxygen-alkali and organosolv,[11] soda,[18] and kraft[4] pulping.

The main goal of this work was the structural evaluation of lignin isolated from grape stalks by a soft acidolytic technique (dioxane lignin). Lignin was characterized by wet chemistry (nitrobenzene and permanganate oxidation) and spectroscopic techniques (1D and 2D NMR, FTIR, and UV spectroscopy). The molecular weight was assessed by size exclusion chromatography (SEC).

MATERIALS AND METHODS

Preparation of Plant Material. Grape stalks from red grape pomace (*Vitis vinifera*) were collected after destemming at the Quinta do Serrado in Penalva do Castelo, Region of Dão (Portugal). The material was dried at room temperature, milled on a cross-beater mill SKI (Retsch, Haan, Germany), and sieved to 0.5−1.0 mm sawdust. The grape stalks were submitted to Soxhlet extraction with acetone (6 h) to remove extractives, according to Tappi standard T 204 om-88. Proteins were removed by the treatment of the extractives-free grape

Received: February 7, 2014
Revised: May 22, 2014
Accepted: May 23, 2014
Published: May 23, 2014

ACS Publications © 2014 American Chemical Society

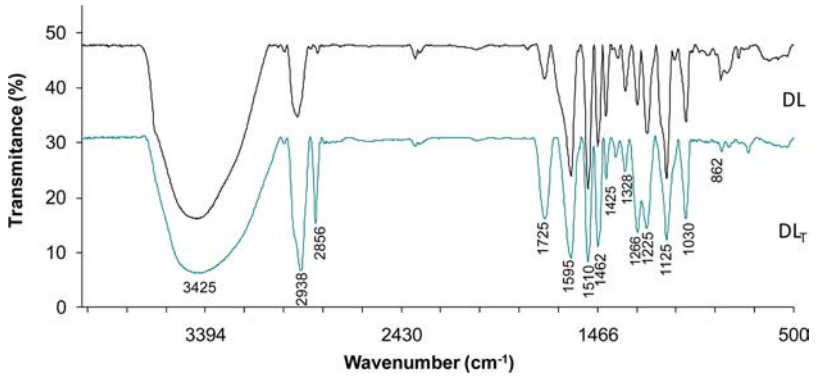

Figure 1. FTIR spectra of dioxane lignins isolated from grape stalks before (DL_T) and after (DL) removal of tannins.

Table 1. Results on Nitrobenzene Oxidation of Dioxane Lignins before (DL_T) and after Tannin Removal (DL) and Lignin of Grape Stalks

characteristic product	structural unit	% molar		
		DL	DL_T	grape stalks
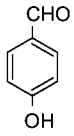 *p*-hydroxybenzaldehyde	**H**	1	2	3
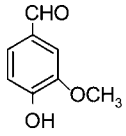 Vanillin	**G**	69	73	71
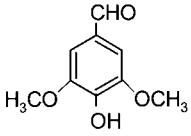 Syringaldehyde	**S**	30	25	26

stalks, with a 1% pepsin solution in 0.1 M HCl at 40 °C overnight, followed by hot water washing until neutral reaction of filtrate.[19] The tannins content was assessed in extractives- and proteins-free grape stalks by reflux with 0.3% NaOH solution (liquid-to-solid ratio of 100:1) under nitrogen atmosphere for 1 h. The lignin content was determined by the Klason method according to Tappi standard T 222 om-88, using grape stalks free of extractives, proteins, and tannins. The Klason lignin content in the grape stalks was 17.4%.

Isolation of Lignin. The lignin was isolated by acidolytic procedure from grape stalks free of extractives and proteins (DL_T) and from grape stalks free of extractives, proteins, and tannins (DL), according to the previously described method.[20] Typically, 10 g of dry extractives- and proteins-free grape stalks sawdust (0.5−1.0 mm) was submitted to three sequential extractions (each 60 min) with 500 mL of a dioxane/water solution (9:1, v/v) containing 0.1 M HCl, under a nitrogen atmosphere. The resulting extracts were further concentrated separately to a volume of ca. 150 mL. Finally, lignin was precipitated in distilled cold water (1.5 L), centrifuged, and washed with distilled cold water until filtrates were of neutral pH and vacuum-dried at room temperature (ca. 20 °C). Alternatively, another sample of dioxane lignin (DL) was isolated from extractives- and proteins-free grape stalks after additional treatment with 0.3% NaOH solution under nitrogen atmosphere, aiming to eliminate the concomitant condensed tannins.[4] The yields of DL_T and DL were about 70−75% of total lignin content in grape stalks (Klason lignin = 17.4%).

Chemical Analyses. The lignin in grape stalks sawdust and isolated dioxane lignins were characterized by oxidation with nitrobenzene under alkaline conditions, according to the previously described procedure.[21] The oxidation products were dissolved in 200 μL of pyridine and analyzed by GC-MS on a Trace Gas Chromatograph 2000 equipped with a Thermo Scientific DSQII mass spectrometer (Thermo Fisher Scientific, Austin, TX, USA). The conditions of GC analysis were as follows: column capillary, 30 m × 0.32 mm i.d. 0.25 μm, DB-1 (Agilent J&W, Santa Clara, CA, USA); initial temperature of the column, 100 °C; gradient of temperature, 4 °C/min; final temperature of the column, 270 °C; temperature of the injector, 240 °C; and temperature of the detector, 250 °C.

The permanganate oxidation of isolated lignin with tannins (DL_T) was performed as described previously.[22] The ethylated oxidation products were identified by GC-MS using the equipment as indicated above. The chromatographic conditions were as follows: initial temperature of the column, 180 °C; gradient of temperature, 4 °C/min; final temperature of the column, 290 °C; injector temperature, 250 °C.

Methoxy groups in lignins were analyzed according to the Zeisel−Vieböck−Schwappach method.[23]

dx.doi.org/10.1021/jf502267s | J. Agric. Food Chem. 2014, 62, 5420−5428

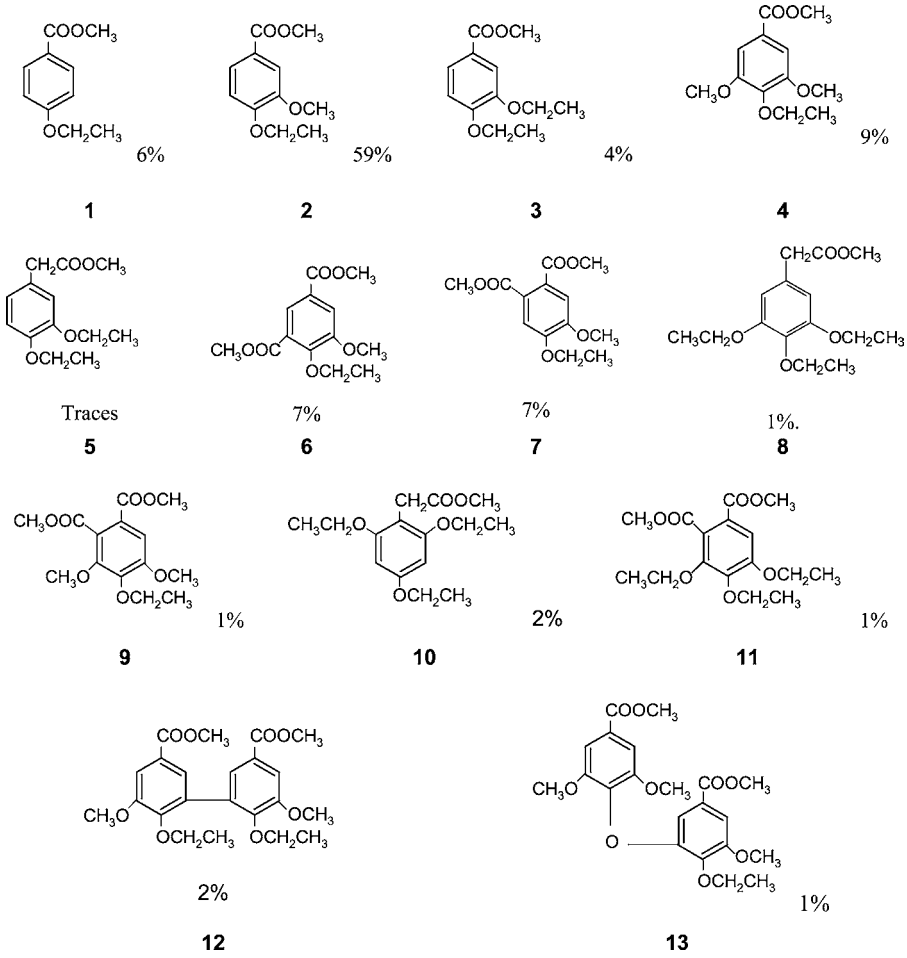

Figure 2. Frequency of occurrence (% mol) of carboxylic acid methyl esters obtained from oxidation of dioxane lignin (DL_T) with potassium permanganate.

Analysis by UV and FTIR Spectroscopy. Ultraviolet (UV) spectra of dioxane-lignin were recorded in 2-methoxyethanol on a JASCO V-560 UV−vis spectrophotometer (Jasco International, Tokyo, Japan), using 1 cm thick quartz cells. The FTIR spectrum of the dioxane-lignins was obtained on a Mattson 7000 spectrometer (Mattson Instruments, Madison, WI, USA), with a resolution of 4.0 cm^{-1} and 132 scans recorded in the medium-infrared area, which extends from 4000 to 400 cm^{-1}.

NMR Analyses. All NMR spectra were registered on an AVANCE 300 spectrometer (Bruker, Wissembourg, France). The ^1H NMR spectra of acetylated dioxane lignins dissolved in chloroform-d_1 (concentration ca. 3%), placed in a 5 mm diameter tube, have been carried out by operating at 300.1 MHz (298 K). The acquisition parameters were as follows: 12.2 μs pulse width (90°), 3 s relaxation delay, and 300 scans.

The quantitative ^{13}C NMR spectrum of dioxane lignin (DL) was recorded by operating at 75.47 MHz (318 K) with TMS as internal reference. DL was dissolved in DMSO-d_6 (ca. 25% concentration) and placed into 10 mm diameter tubes. The acquisition parameters were as follows: 4.1 ms pulse width (90° pulse angle), 12 s relaxation delay, 16K data points, and 20000 scans. The same lignin sample in DMSO-d_6 was placed into a 5 mm diameter tube, and 2D NMR spectra were recorded. The phase sensitive ^1H-detected heteronuclear single-quantum coherence (HSQC) spectrum was acquired over an F1 spectral weight of 12000 Hz and an F2 width of 2000 Hz with a 2048 × 1024 matrix and 128 transients per increment. The delay between scans was 2 s and the delay for polarization transfer was optimized for $^1J_{C-H}$ = 148 Hz. The heteronuclear multiple-bond correlation (HMBC) spectrum was recorded using a coupling evolution time of 110 ms ($^3J_{C-H}$ = 4.5 Hz).

Analysis by Size Exclusion Chromatography (SEC). Two dioxane lignins were analyzed by SEC using a PL-GPC 110 apparatus (Polymer Laboratories, Shropshire, UK), equipped with a precolumn, 10 μm, Plgel, and two 300 mm × 7.5 mm columns, 10 μm, Plgel MIXED D (Polymer Laboratories) and a refraction index detector. Columns and the injection system were maintained at a temperature of 70 °C. The eluent flow (0.1 M LiCl in DMF) was 0.9 mL/min. The lignin solutions (ca. 1%) were prepared just before the analysis by dissolution in eluent solution (0.1 M LiCl in DMF). The column calibration was carried out using lignin model compounds (monomers, dimers, and tetramers) and selected lignin samples (Mp = 950−3200 Da) previously characterized by ESI-MS.[24]

RESULTS AND DISCUSSION

Molecular Weight and Purity of Isolated of Dioxane Lignins. The molecular weights (M_w) of dioxane lignins free of extractives and proteins (DL_T) and free of extractives, proteins, and tannins (DL) were very close to each other (ca. 2600 Da). As could be expected, the removal of condensed tannins from grape stalks before the isolation of dioxane lignin led to much less contaminated lignin sample (DL). This fact was confirmed by FTIR spectroscopy and by analysis of methoxyl group content. Thus, the FTIR spectrum of DL_T showed typical strong signals for tannins and tannic acids at 2920/2860 cm^{-1} (sym/antisym C−H stretching in CH_2), 1718 cm^{-1} (C═O stretching in ketones), and 1610−1600 cm^{-1} (bending vibrations of aromatic ring),[25,26] which were drastically diminished in the spectrum of DL (Figure 1). The methoxyl

dx.doi.org/10.1021/jf502267s | J. Agric. Food Chem. 2014, 62, 5420−5428

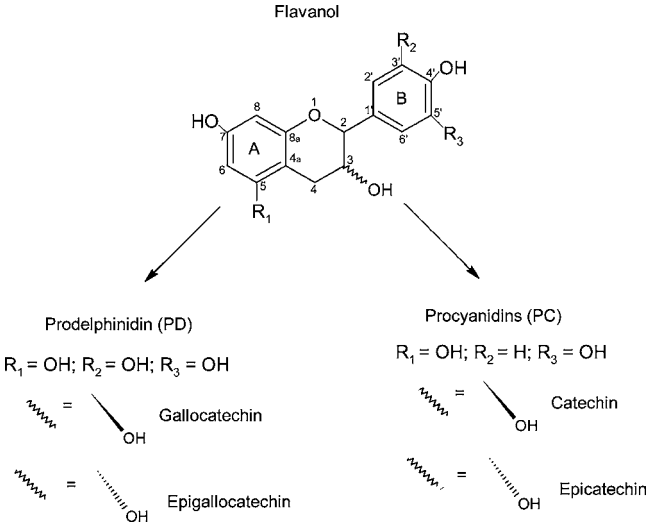

Figure 3. Monomeric units of representative flavanols constituting condensed tannins.

group content was 15.6% for DL_T and 17.3% for DL, which is consistent with the conclusion on the stronger contamination of the former with tannins. Because DL is purer than DL_T, the former is preferable for the qualitative and quantitative characterization by spectroscopic techniques. At the same time, the fact of preliminary alkaline extraction of grape stalks to remove tannins may cause the removal of the alkali-soluble lignin fraction. Hence, DL_T may provide some additional structural information when analyzed by degradation techniques.

FTIR and UV Spectroscopy. DL had FTIR spectrum patterns (Figure 1) typical for lignins constituted by guaiacyl (G) and syringyl (S) units.[27] Thus, besides characteristic aromatic ring bands at 1595, 1510, and 1425 cm^{-1} (aromatic skeletal vibrations in G and S rings), the bands at 1328 and 1266 cm^{-1} were detected and assigned to syringyl and guaiacyl rings breathing with Ar−OCH_3 stretching, respectively.[28] The shoulder at ca. 1636 cm^{-1} in the FTIR spectrum indicated the presence of lignin structures with C═C bonds in the propane chain conjugated to an aromatic ring.[29]

The UV spectrum of DL revealed the bands typically observed for dioxane lignins constituted by *p*-hydroxyphenyl (H), syringyl (S) and guaiacyl (G) units (HGS lignins) from kenaf[13] and banana plant.[30] The extinction coefficients (ε) at 212, 240, 284, and 320 nm were 54.8, 19.1, 9,8 and 5.7 L/g/cm, respectively. Attention is drawn to the bathochromic shifted band at 284 nm of relatively low intensity (ε = 9.7 L/g/cm) corresponding to the $\pi \rightarrow \pi^*$ electron transition in the aromatic ring, which usually appears in lignins at ca. 280 nm. Similar features were previously observed in dioxane lignin of kenaf bark contaminated by condensed tannins.[13] The relatively strong absorption at 320 nm could be assigned to the $n \rightarrow \pi^*$ transition in C═O groups conjugated to aromatic moieties and to $\pi \rightarrow \pi^*$ electronic transition in the aromatic ring conjugated with C═C moieties.[13,29]

Nitrobenzene Oxidation. Analysis of nitrobenzene oxidation (NO) products from DL, DL_T, and grape stalks was carried out to assess the molar ratio of structural units in lignin. It was evident that the grape stalk lignin is of HGS type with a relatively high proportion of G units and a small amount of H units (Table 1). H:G:S ratios were slightly different in terms of H unit abundance when NO was carried out on DL/DL_T or directly using grape stalk material (Table 1). This is especially notable for DL, which revealed a low content of H units. This can be tentatively explained by substantial alkaline hydrolysis of *p*-coumaric acid type structures during removal of condensed tannins prior to isolation of DL. The H:G:S ratio obtained by nitrobenzene oxidation of grape stalks was 3:71:26 and may be considered as the most credible because it was assessed on in situ lignin without modification during the isolation procedure.

By comparisin of the H:G:S ratios found in DL and DL_T, it may be proposed that during alkali pre-extraction of grape stalks, before the isolation of dioxane lignin, a small fraction of lignin rich in H and G structural units was removed from the starting material.

Permanganate Oxidation. The information about different "condensed" and "noncondensed" structures was assessed by analysis of products arising from permanganate oxidation (PO) of dioxane lignin isolated from extractives- and proteins-free grape stalks without preliminary alkaline extraction to remove condensed tannins (DL_T sample). DL_T was ethylated prior to oxidation, which allowed protection of the phenolic units against aromatic ring degradation and, at the same time, to distinguish PO products from lignin and structurally associated tannins, thus elucidating their eventual origin.

Detected and identified PO products and their frequencies of occurrence are summarized in Figure 2. Nearly 95% of PO products were identified, most of them belonging to lignin. Thus, products **1**, **2**, and **4** were assigned to noncondensed lignin structures derived from the *p*-hydroxyphenyl (**1**), guaiacyl (**2**), and syringyl (**4**) structural units, respectively. The isohemipinic acid methyl ester (**6**) originated from degraded phenylcoumaran (β-5′) structures, and the products **7** and **9** can be assigned to guaiacyl and syringyl units, respectively, linked by β-6′ and γ-*O*-α bonds (phenylisochroman type structures) or to some other type of still unknown condensed structures. The oxidation products **12** and **13** are derived from biphenyl-type structures (5-5′) and diaryl ether type (4-*O*-5′) structures, respectively. Attention is drawn to the high content of condensed guaiacyl units (products **6** and **7**), which are much more abundant than in lignins of such agricultural stuffs as kenaf,[13] reed, and [14] banana plant[30] or in hardwoods.[20,31] When the H:G:S ratio in DL_T (2:73:25) and the fact that only phenolic units are accessible for the PO analysis are taken into account, the relatively low abundance of syringyc acid methyl ester (**4**) among PO products (Figure 2) indicates that the lignin molecules constituted by syringic units should be much less ramified that those constituted of guaiacyl units. The ratio of uncondensed structural units (products **1**, **2**, and **4**) and the condensed units (products **6**, **7**, **9**, **12**, and **13**) was 64:21 (Figure 2), indicating a relatively higher degree of lignin condensation in grape stalks.

Rather abundant PO products **3**, **5**, **8**, and **10** belong to condensed tannins that are present in grape stalks. The same products were found previously in PO analysis of condensed tannins extracted from pine bark.[32] Thus, products **3** and **5** are derived from the B-ring of procyanidins and proanthocyanidins (Figure 3), which are the main types of condensed tannins in grape stalks.[4,11,17] The PO product **8** is derived from the B-ring of prodelphinidins and indicates the presence of this type of flavonoid in grape stalks. Accordingly, product **10** (Figure 2) is derived from the A-ring of the corresponding flavonoid units

dx.doi.org/10.1021/jf502267s | J. Agric. Food Chem. 2014, 62, 5420−5428

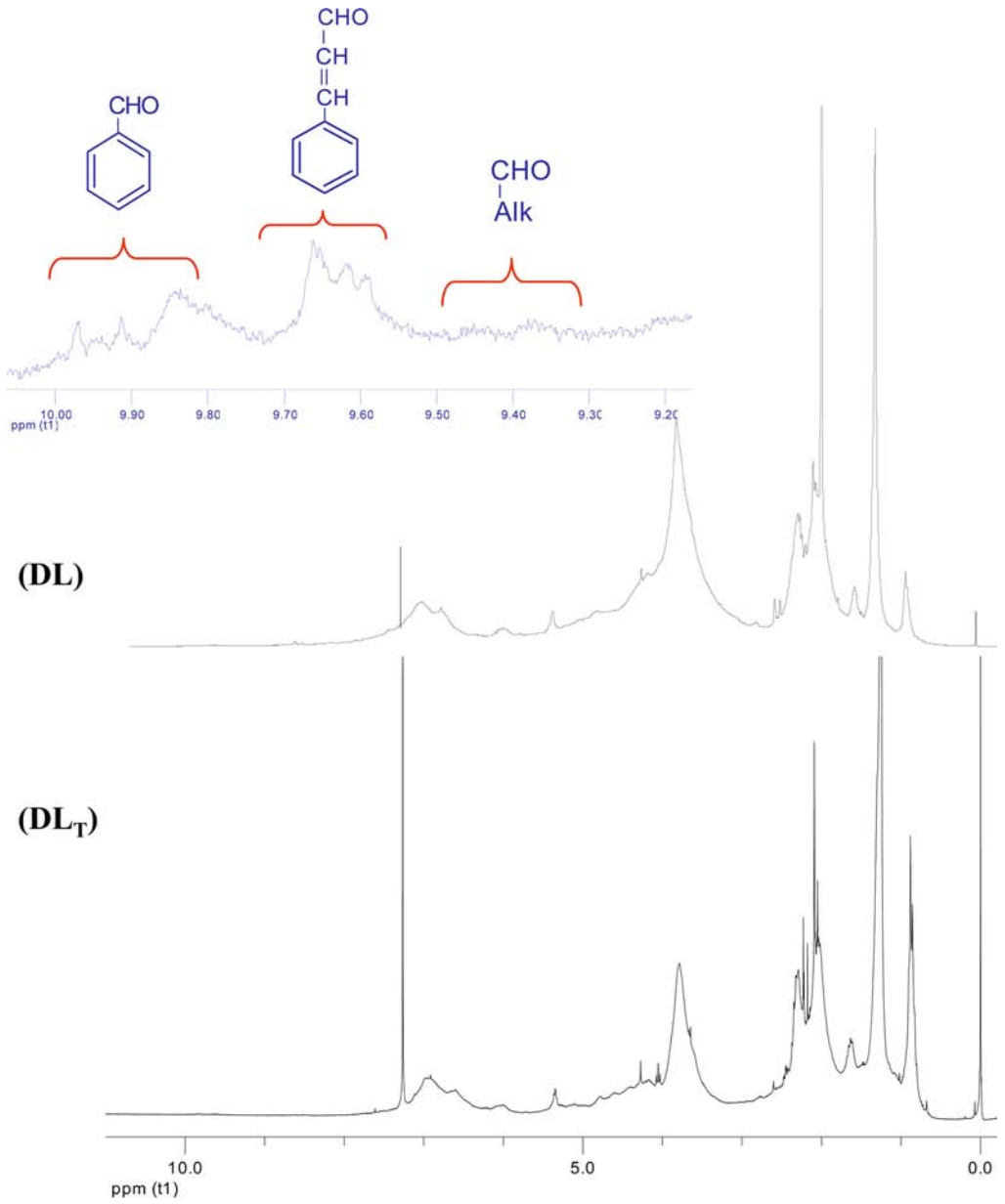

Figure 4. ^{1}H NMR spectrum (DMSO-d_6) of dioxane lignins (DL and DL$_T$) from grape stalks. Expanded range from 9 to 10 ppm shows resonances of formyl protons.

Table 2. Estimation of Frequency of Functional Groups and Major Interunit Linkages in Grape Stalk Dioxane Lignins DL$_T$ and DL As Determined by ^{1}H NMR Spectroscopy

	abundance/100 C_9	
structural element	DL$_T$	DL
OCH_3 (3.5−4.0 ppm)	123	129
aliphatic OH (CO−C$\underline{H}_3$ at 1.8−2.1 ppm)	80	85
phenolic OH (CO−C$\underline{H}_3$ at 2.1−2.5 ppm)	58	47
H_α in β-*O*-4 structures (5.8−6.3 ppm)	34	38
aromatc H (6.3−6.7 ppm; 6.7−7.3 ppm; 7.3−7.9 ppm)	205	212
CHO in benzaldehyde-type structures (9.8−10.0 ppm)	2	1
CHO in cinnamaldehyde-type structures (9.5−9.7 ppm)	2	2
CHO nonconjugated (9.3−9.5 ppm)	trace	trace

(Figure 3). Compound **11** was assigned to the PO product derived from ellagic acid originating from ellagitannins.

^{1}H NMR Spectroscopy. The amounts of hydroxyl and aldehyde groups and some interunit linkages were estimated from the ^{1}H NMR spectrum of acetylated DL. These data were compared with those obtained for DL$_T$ (Figure 4). The quantitation was carried out per phenyl propane unit (PPU) according to the previously defined methodology using the

dx.doi.org/10.1021/jf502267s | J. Agric. Food Chem. 2014, 62, 5420−5428

Table 3. Quantitative Estimation of Different Structural Elements in DL from Grape Stalks by ^{13}C NMR Spectroscopy (Figure 5)

structure element	calculation[a]	abundance/ C_6
β-O-4′	$I61.0-59.0 \times 6/(I_{156.0-102.0} - I_{139.5-138.5} - I_{125.7-124.0} - I_{128.0-127.4})$	0.39
β-5′	$I_{53.3-52.5} \times 6/(I_{156.0-102.0} - I_{139.5-138.5} - I_{125.7-124.0} - I_{128.0-127.4})$	0.03
β-β′	$I_{54.0-53.3} \times 6/(I_{156.0-102.0} - I_{139.5-138.5} - I_{125.7-124.0} - I_{128.0-127.4})$	0.06
β-1′ + *β-5′*	$I_{64.0-62.0} \times 6/(I_{156.0-102.0} - I_{139.5-138.5} - I_{125.7-124.0} - I_{128.0-127.4})$	006
Ar-O	$I_{156.0-140.0} \times 6/(I_{156.0-102.0} - I_{139.5-138.5} - I_{125.7-124.0} - I_{128.0-127.4})$	2.20
Ar-C	$I_{140.0-126.0} \times 6/(I_{156.0-102.0} - I_{139.5-138.5} - I_{125.7-124.0} - I_{128.0-127.4})$	1.50
Ar-H	$I_{124.0-102.0} \times 6/(I_{156.0-102.0} - I_{139.5-138.5} - I_{125.7-124.0} - I_{128.0-127.4})$	2.30
OCH_3	$I_{57.5-54.4} \times 6/(I_{156.0-102.0} - I_{139.5-138.5} - I_{125.7-124.0} - I_{128.0-127.4})$	1.27
S/G	$S/G = (I_{109.0-102.0} \times 3)/(I_{124.0-109.0} \times 2)$	0.56
H units	$I_{163.0-160.0} \times 6/(I_{156.0-102.0} - I_{139.5-138.5} - I_{125.7-124.0} - I_{128.0-127.4})$	0.02
S:G:H		34:64:2

[a] $(I_{139.5-138.5} + I_{125.7-124.0} + I_{128.0-127.4})$ − integral intensities from solvent contaminants.

resonance of methoxy groups at 3.6−4.0 ppm as an internal standard and integrating the proton intensities in the corresponding functionalities.[20] The average number of methoxy groups per PPU was calculated on the basis of the H:G:S ratio determined by NO in grape stalks and dioxane lignins (Table 1).

As was already highlighted by FTIR spectroscopy (Figure 1), the elimination of tannins from grape stalks by alkaline extraction before the lignin isolation by acidolytic technique allows much more pure lignin sample. This proposition was additionally confirmed by ^1H NMR showing the decrease of resonances at 0.7−1.8 ppm assigned to aliphatic moieties in extractives and the decrease of phenolic groups (OH_{ph}) in DL after tannin removal by alkaline extraction before the lignin isolation (Table 2). However, the amount of phenolic groups (OH_{ph}) in DL was still high (47/100 PPU) when compared to the amount of OH_{ph} usually reported in dioxane lignins (20−30/100 PPU).[20,31,33] This fact indicates that tannins still occur in this sample, which correlates with conclusions drawn by analysis of the UV−vis spectrum of DL suggesting the contamination of isolated lignin with condensed tannins.

The relatively low amount of *β-O-4′* structures detected in DL and DL_T (0.34−0.38/PPU), based on the H_α resonance in the corresponding structures at 5.8−6.3 ppm, may be explained by the significantly higher proportion of condensed structures (Table 3). The last proposition correlates with discussed data on PO analysis (Figure 2) and the relatively low content of aromatic protons per PPU detected in proton spectra of dioxane lignins (Table 3).

The amount of benzaldehyde- and cinnamaldehyde-type structures, calculated on the basis of the integral of formyl proton signals in the corresponding structures (Figure 4), was rather insignificant and similar in both studied lignins. Some lower amount of benzaldehyde type structures in DL than in DL_T may be explained by their partial removal during the alkaline extraction of grape stalks before lignin isolation.

^{13}C NMR Spectroscopy. The quantification of the main structures in grape stalk lignin was carried out by quantitative ^{13}C NMR spectroscopy of DL (Figure 5). The resonance assignments were done on the basis of the $^1H-^{13}C$ correlation

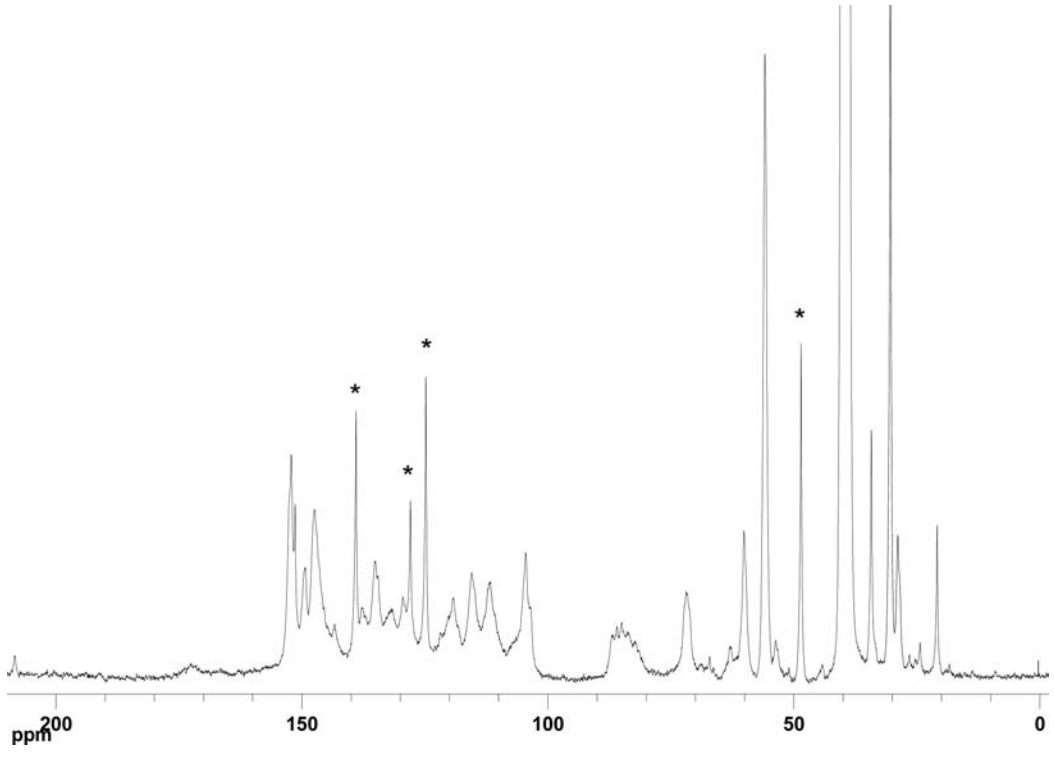

Figure 5. Quantitative ^{13}C NMR spectrum of dioxane lignin (DL) from grape stalks (DMSO-d_6). Solvent contaminants are marked by asterisks.

dx.doi.org/10.1021/jf502267s | J. Agric. Food Chem. 2014, 62, 5420−5428

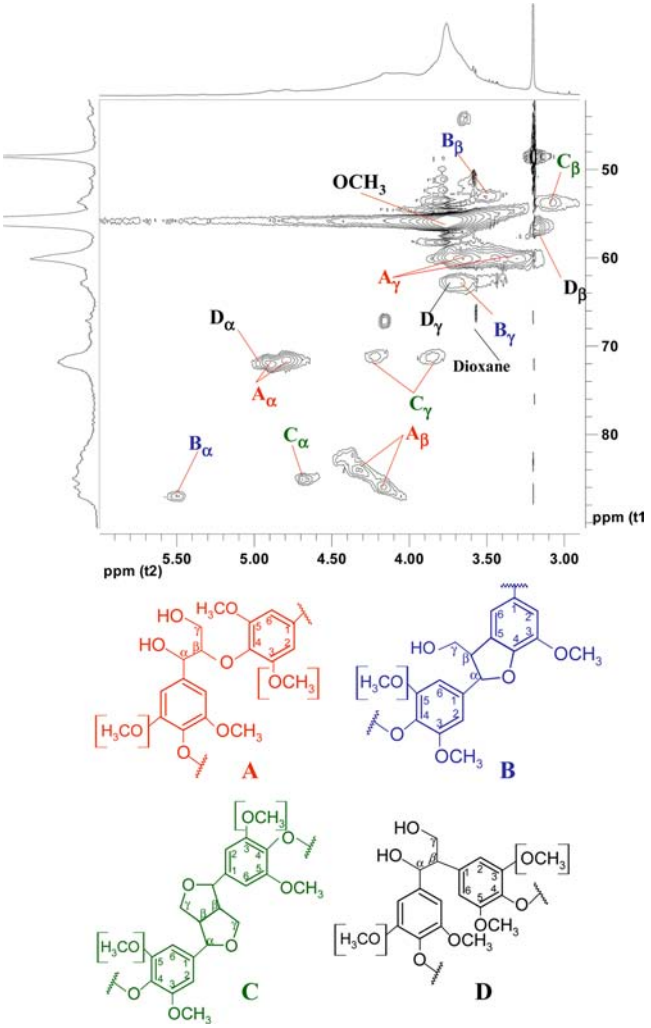

Figure 6. Oxygenated aliphatic region of HSCQ spectrum of DL from grape stalks. Major identified lignin structures, for which assignments are depicted in the spectrum, are presented below.

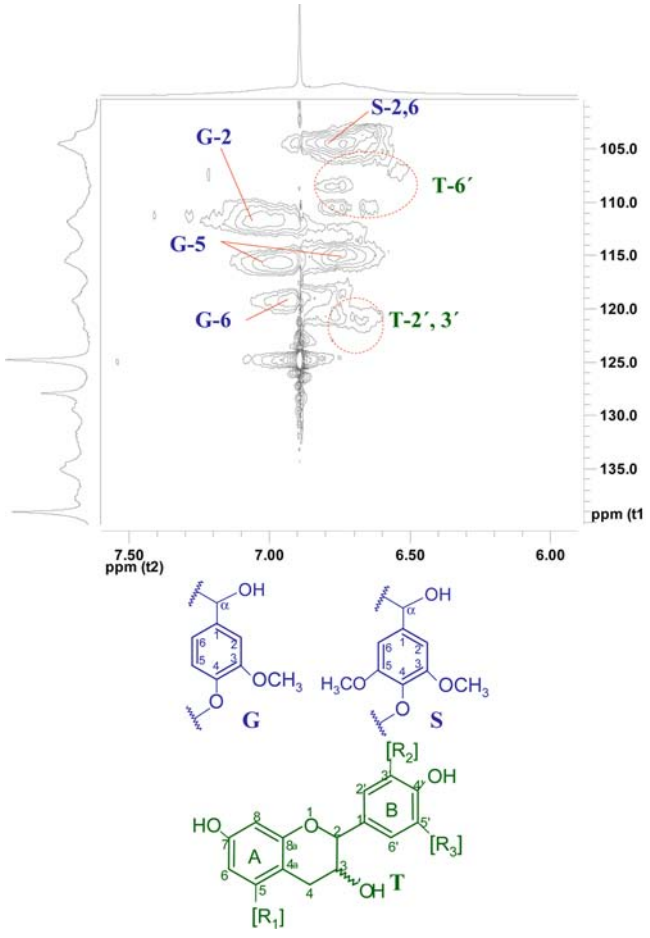

Figure 7. Aromatic region of HSCQ spectrum of DL from grape stalks. Identified guaiacyl (G), syringyl (S), and tannin (T) structures are depicted below.

(HSQC) spectra (Figures 6 and 7) using the well-known databases on lignin[34−36] and lignin model compounds.[37,38]

The primary analysis of the quantitative ^{13}C NMR spectrum of DL revealed unusual resonances for lignins in the range of 20−35 ppm assigned to aliphatic carbons (CH_3, CH_2, and CH) in extractives that were not eliminated during exhaustive extraction of grape stalks with acetone. The presence of condensed tannins was suspected on the basis of the unusually strong resonances for lignin at ca. 146 ppm (Figure 5) assigned to aromatic carbons in free phenolic moieties of proanthocyanidins.[39−41] In addition, the HSQC spectrum of DL (Figure 7) revealed $^{1}H-^{13}C$ correlation cross-peaks typical for the B-ring of procyanidins.[39−41] The cross-peaks typical for the A-ring of procyanidins were of a very low intensity, probably due to their lability under alkaline conditions[25,32,42] and the formation of a series of new structures difficult to assign. Due to the alkaline extraction of grape stalks at 100 °C before the isolation of DL, at least part of the procyanidins associated with DL might be in the form of catechinic acid arising as a result of intramolecular rearrangement reactions under alkaline conditions.[25,42] The notable resonance at ca. 208 ppm, assigned to ketone moieties in catechinic acid,[42] supports this proposition.

The fact of structural association of lignin with condensed tannins in grape stalk lignin supports earlier proposed chemical bonding between them.[4,11] The incorporation of tannins in a lignin network has been proposed in wood[43,44] and recently suggested in coconut coir[45] and in wheat straw[46] lignins. Hence, the formation of a lignin−tannin network could be realized also in the case of grape stalks. Besides this "natural" association, the new bonds could be formed between lignin and tannins during alkali pre-extraction of grape stalks and during acidolytic isolation of DL as depicted in Figure 8. The condensation of lignin with flavanols may explain the unusually high amounts of condensed structures detected in lignin by PO analysis (Figure 2). The cross peak at 44.3/3.62 ppm in the HSQC spectrum of DL (Figure 6) is very close to the corresponding carbon/proton chemical shifts reported for the C-2/H-2 condensed structures resulting from the reaction of procyanidins with phloroglucinol.[25] Unfortunately, the reliable identification of these lignin−tannin condensed structures using HMBC spectra was impossible due to their relatively low abundance in grape stalk lignin.

The quantification of major lignin structure has been done per aromatic ring (C_6) according to a previously described methodology.[20,30] The basic calculations involved are presented in Table 3, where the integral intensities of solvent contaminants were subtracted from intensities of carbons in the aromatic region at 102−156 ppm. Thus, the abundance of lignin structures linked by *β-O-4′* bonds was calculated on the

dx.doi.org/10.1021/jf502267s | J. Agric. Food Chem. 2014, 62, 5420−5428

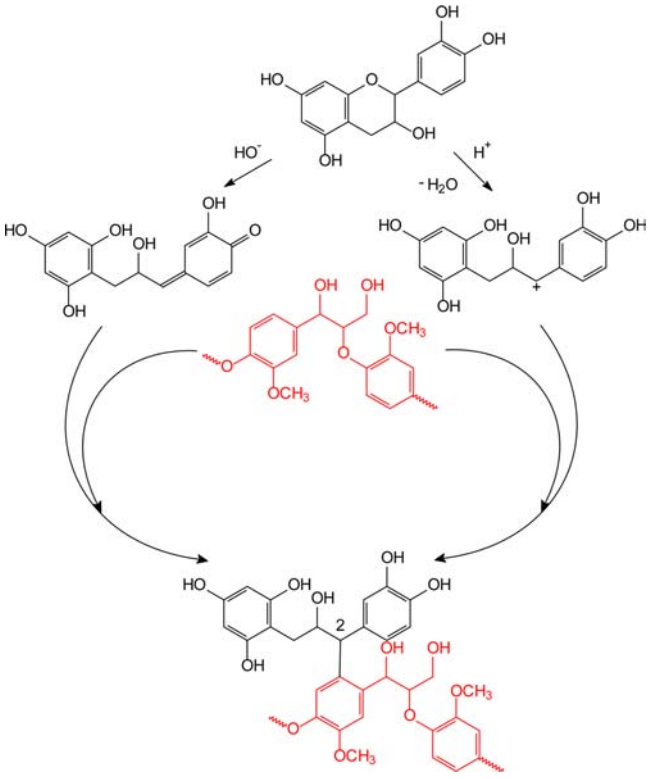

Figure 8. Schematic representation of lignin reaction with procyanidins under acidic and alkaline conditions.

basis of integral of signals at 59.0−61.0 ppm (C_γ resonance in *β*-*O*-4′ structures). The amounts of *β*-5′and *β*-*β*′ structures were assessed on the basis of C_β resonances in corresponding structures at 52.5−53.3 and 53.3−54.0 ppm, respectively, and the amount of *β*-1′ and *β*-5′ structures was calculated on the basis of the C_γ resonances in the spectrum region at 62.0−64.0 ppm (Table 3).

The data on abundance of *β*-*O*-4′ structures (Table 3) obtained by analysis of the ^{13}C NMR (0.39/C_6) in grape stalk dioxane lignin were consistent with those obtained by the ^{1}H NMR spectrum (0.38/C_9) (Table 3). A very similar abundance of *β*-*O*-4′ structures was reported previously for reed[14] and kenaf[13] dioxane lignins isolated from internode morphologic regions. ^{13}C NMR spectroscopy analysis (Table 3) also confirms a relatively high degree (Ar-C index of 1.50) of lignin condensation in grape stalks, which is comparable only to lignins isolated from nodes of reed.[14] According to the results of the PO analysis, most of the condensed lignin structures (ca. 17% mol) belongs to guaiacyl units substituted at C-5 and C-6 of the aromatic ring by aliphatic moieties (Figure 2). Meanwhile, the contribution of *β*-5′ structures (ca. 3% mol) (Table 3) to the total amounts of such condensed structures is not major. It may be proposed that a significant contribution to lignin condensation is due to its structural association with tannins. The condensation of tannins and lignin via ionic (e.g., quinone methide) mechanisms could occur under neutral/weakly acidic conditions due to tannin migration by diffusion from disintegrated cells to lignified cell tissues. Cell integrity may be violated both by natural reasons (e.g., down-regulated vacuole disrupts in parenchyma cells containing tannins) or by external factors during winemaking (e.g., during harvesting and destemming). In the last case the tannins from crushed grapes should also be taken into consideration. In addition, the contribution of the condensation reaction of lignin with tannins occurring under both alkaline (pre-extraction of grape stalks) and acidic (acidolysis) conditions during lignin isolation procedure cannot be excluded as well.

In conclusion, the results of the present study show that grape stalk lignin is of HGS type with a strong predominance of G units and a moderate amount of *β*-aryl ether structures, highly condensed, and, probably, structurally associated with tannins. This must be one of the reasons for difficult delignification of grape stalks by conventional pulping methods.

Unlike other lignins rich in G units, which possess a high abundance of biphenyl (5-5′), diaryl ether (4-*O*-5′), and *β*-5′structures, the high condensation degree of grape stalk lignin is due to unknown condensed structures of alkyl-aryl type. These structures, at least partially, must belong to lignin−tannin condensed structures. Among tannins involved in structural association with lignin, flavonols of gallocatechin and catechin types and ellagitannins were elucidated. The reasons for this lignin−tannin structural association are a challenge for future research.

AUTHOR INFORMATION

Corresponding Author

*(D.V.E.) Phone: +351 234 401 526. Fax: +351 34 37 00 84. E-mail: Dmitrye@ua.pt.

Funding

We thank the Portuguese Foundation for Science and Technology (FCT project PTDC/AGR-AAM/104911/2008) and the Operation Program of Competitive Factors (COMPETE, ref FCOMP-01-0124-FEDER-008734) for financial support of this work.

Notes

The authors declare no competing financial interest.

REFERENCES

(1) Meloni, G.; Swinnen, J. The political economy of European wine regulations. *J. Wine Econ.* **2013**, *8*, 244−284.

(2) Costa, J. M. Aproveitamento de subprodutos da vinificação. O bagaço como matéria-prima da indústria de óleos e grainha e de fabrico de rações para gado. In *First Congresso Nacional das Indústrias Agro-alimentares*; Junta Nacional dos Vinhos: Lisboa, Portugal, 1983.

(3) Spigno, G.; Pizzorno, T.; De Faveri, D. M. Cellulose and hemicelluloses recovery from grape stalks. *Bioresour. Technol.* **2008**, *99*, 4329−4337.

(4) Prozil, S. O.; Evtuguin, D. V.; Lopes, L. P. C. Chemical composition of grape stalks of *Vitis vinifera* L. from red grape pomaces. *Ind. Crops Prod.* **2012**, *35*, 178−184.

(5) Bertrán, E.; Sort, X.; Soliva, M.; Trillas, I. Composting winery waste: sludges and grape stalks. *Bioresour. Technol.* **2004**, *95* (2), 203−208.

(6) Bustamante, M. A.; Pérez-Murcia, M. D.; Paredes, C.; Moral, R.; Moreno-Caselles, J. Short-term carbon and nitrogen mineralisation in soil amended with winery and distillery organic wastes. *Bioresour. Technol.* **2007**, *98*, 3269−3277.

(7) Miralles, N.; Martınez, M.; Florido, A.; Casas, I.; Nuria Fiol, N.; Villaescusa, I. Grape stalks waste as low cost biosorbents: an alternative for metal removal from aqueous solutions. *Solv. Extr. Ion Exch.* **2008**, *26*, 261−270.

(8) Llobera, A.; Cañellas, J. Dietary fibre content and antioxidant activity of Manto Negro red grape (*Vitis vinifera*): pomace and stem. *Food Chem.* **2007**, *101*, 659−666.

(9) Cruz, J. M.; Dominguez, H.; Parajo, J. C. Assessment of the production of antioxidants from winemaking waste solids. *J. Agric. Food Chem.* **2004**, *52*, 5612−5620.

(10) Deiana, A. C.; Sardella, M. F.; Silva, H.; Amaya, A.; Tancredi, N. Use of grape stalk, a waste of the viticulture industry, to obtain activated carbon. *J. Hazard. Mater.* **2009**, *172*, 13−19.
(11) Ping, L.; Brosse, N.; Sannigrahi, P.; Ragauskas, A. Evaluation of grape stalks as a bioresource. *Ind. Crops Prod.* **2011**, *33*, 200−204.
(12) Jahan, M. S.; Chowdhury, D. A. N.; Islam, M. K.; Moeiz, S. M. I. Characterization of lignin isolated from some nonwood available in Bangladesh. *Bioresour. Technol.* **2007**, *98*, 465−469.
(13) Seca, A. M. L.; Cavaleiro, J. A. S.; Domingues, F. M. J.; Silvestre, A. J. D.; Evtuguin, D.; Pascoal Neto, C. Structural characterization of the bark and core lignins from kenaf (*Hibiscus cannabinus*). *J. Agric. Food Chem.* **1998**, *46*, 3100−3108.
(14) Seca, A. M. L.; Cavaleiro, J. A. S.; Domingues, F. M. J.; Silvestre, A. J. D.; Evtuguin, D.; Neto, C. P. Structural characterization of the lignin from the nodes and internodes of *Arundo donax* reed. *J. Agric. Food Chem.* **2000**, *48*, 817−824.
(15) Ping, L.; Brosse, N.; Chrusciel, L.; Navarrete, P.; Pizzi, A. Extraction of condensed tannins from grape pomace for use as wood adhesives. *Ind. Crops Prod.* **2011**, *33*, 253−257.
(16) Prozil, S. O.; Costa, E. V.; Evtuguin, D. V.; Lopes, L. P. C.; Domingues, M. R. M. Structural characterization of polysaccharides isolated from grape stalks of *Vitis vinifera* L. *Carbohydr. Res.* **2012**, *356*, 252−259.
(17) Souquet, J. M.; Labarbe, B.; Le Guernevé, C.; Cheynier, V.; Moutounet, M. Phenolic composition of grape stems. *J. Agric. Food Chem.* **2000**, *48*, 1076−1080.
(18) Ben-Ghedalia, D. Degradation of cell-wall monosaccharides of chemically treated grape branches by rumen microorganisms. *Eur. J. Appl. Microbiol. Biotechnol.* **1982**, *16*, 142−145.
(19) Neto, C. P.; Seca, A.; Fradinho, D.; Coimbra, M. A.; Domingues, F.; Evtuguin, D.; Silvestre, A.; Cavaleiro, J. A. S. Chemical composition and structural features of the macromolecular components of *Hibiscus cannabinus* grown in Portugal. *Ind. Crops Prod.* **1996**, *5*, 189−196.
(20) Evtuguin, D. V.; Neto, C. P.; Silva, A. M. S.; Domingues, P. M.; Amado, F. M. L.; Robert, D.; Faix, O. Comprehensive study on the chemical structure of dioxane lignin from plantation *Eucalyptus globulus* wood. *J. Agric. Food Chem.* **2001**, *49*, 4252−4261.
(21) Tanahashi, M.; Higuchi, T. Chemical degradation methods for characterization of lignins. In *Methods of Enzymology*; Abelson, J. N., Simon, M. I., Eds.; Academic Press: New York, 1988; pp 121−128.
(22) Gellerstedt, G. Chemical degradation methods: permanganate oxidation. In: *Methods in Lignin Chemistry*; Lin, S. Y., Dence, C. W., Eds.; Springer-Verlag: Berlin, Germany, 1992; pp 322−333.
(23) Zakis, G. F. *Functional Analysis of Lignins and Their Derivatives*; Tappi Press: Atlanta, GA, USA, 1994; pp 3−7.
(24) Evtuguin, D. V.; Domingues, P. N.; Amado, F. L.; Pascoal Neto, C.; Ferrer Correia, A. Electrospray ionization mass spectrometry as a tool for lignins molecular weight and structural characterization. *Holzforschung* **1999**, *53*, 525−528.
(25) Sears, K. D.; Casebier, R. L.; Hergert, H. L.; Stout, G. H.; McCandlish, L. E. The structure of catechinic acid. A base rearrangement product of catechin. *J. Org. Chem.* **1974**, *39*, 3244−3247.
(26) Pantoja-Castro, M. A.; González-Rodríguez, H. Study by infrared spectroscopy and thermogravimetric analysis of tannins and tannic acid. *Rev. Latinoam. Quim.* **2011**, *39*, 107−112.
(27) Faix, O. Fourier transform infrared spectroscopy. In *Methods in Lignin Chemistry*; Lin, S. Y., Dence, C. W., Eds.; Springer-Verlag: Berlin, Germany, 1992; pp 83−109.
(28) Herbert, H. L. Infrared spectra. In *Lignins. Occurrence, Formation, Structure and Reactions*; Sarkanen, K. V., Ludwig, C. H., Eds.; Wiley-Interscience: New York, 1971; pp 267−297.
(29) Oliveira, L.; Evtuguin, D. V.; Cordeiro, N.; Silvestre, A. J. D.; Silva, A. M. S.; Torres, I. C. Structural characterization of lignin from leaf sheaths of banana plant "Dwarf Cavendish". *J. Agric. Food Chem.* **2006**, *54*, 2598−2605.
(30) Oliveira, L.; Evtuguin, D.; Cordeiro, N.; Silvestre, A. J. D. Structural characterization of stalk lignin from banana plant. *Ind. Crops Prod.* **2009**, *29*, 86−95.
(31) Pinto, P. C.; Evtuguin, D. V.; Pascoal Neto, C. Chemical composition and structural features of the macromolecular components of plantation *Acacia mangium* wood. *J. Agric. Food Chem.* **2005**, *53*, 7856−7862.
(32) Fradinho, D. M.; Neto, C. P.; Evtuguin, D.; Jorge, F. C.; Irle, M. A.; Gil, M. H.; Pedrosa de Jesus, J. Chemical characterisation of bark and of alkaline bark extracts from maritime pine grown in Portugal. *Ind. Crops Prod.* **2002**, *16*, 23−32.
(33) Pinto, P. C.; Evtuguin, D. V.; Pascoal Neto, C. Effect of structural features of wood biopolymers on hardwood pulping and bleaching performance. *Ind. Eng. Chem. Res.* **2005**, *44*, 9777−9784.
(34) Robert, D. Carbon-13 Nuclear magnetic resonance spectrometry. In *Methods in Lignin Chemistry*; Lin, S. Y., Dence, C. W., Eds.; Springer Verlag: Berlin, Germany, 1992; pp 250−273.
(35) Kilpelaeinen, I.; Sipilae, J.; Brunow, G.; Lundquist, K.; Ede, R. M. Application of two-dimensional NMR spectroscopy to wood lignin structure determination and identification of some minor structural units of hard- and softwood lignins. *J. Agric. Food Chem.* **1994**, *42*, 2790−2794.
(36) Ralph, J.; Marita, J. M.; Ralph, S.; Hatfield, R. D.; Lu, F.; Ede, R. M.; Peng, J.; Quideau, S.; Helm, R. F.; Grabber, J. H.; Kim, H.; Jimenez-Monteon, G.; Zhang, Y.; Jung, H.-J. G.; Landucci, L. L.; MacKay, J. J.; Sederoff, R. R.; Chapple, C.; Boudet, A. Solution-state NMR of lignins. In *Advances in Lignocellulosics Characterization*; Argyropoulos, D. S., Ed.; Tappi Press: Atlanta, GA, USA, 1999; pp 55−108.
(37) Ralph, S. A.; Ralph, J.; Landucci, L. L. *NMR Database of Lignin and Cell Wall Model Compounds, 1996*; http://www.dfrc.wisc.edu/software.html (accessed March 22, 2006).
(38) Hise, R. G.; Chen, C. L.; Gratzl, J. S. Synthesis of β-aryl lignin model compounds. *J. Wood Chem. Technol.* **1985**, *5*, 379−390.
(39) Davis, A. L.; Cai, Y.; Davies, A. P.; Lewis, J. R. ^{1}H and ^{13}C NMR assignments of some green tea polyphenols. *Magn. Reson. Chem.* **1996**, *34*, 887−890.
(40) Porter, L. J.; Newman, R. H.; Foo, L. Y.; Wong, H.; Hemingway, R. W. Polymeric proanthocyanidins. ^{13}C N.M.R. studies of procyanidins. *J. Chem. Soc., Perkin Trans. 1* **1982**, *1*, 1217−1221.
(41) *Plant Polyphenols. Synthesis, Properties, Significance*; Hemingway, R. W., Laks, P. E., Eds.; Premium Press: New York, 1992; pp 295−338.
(42) Laks, P. E.; Hemingway, R. W.; Conner, A. H. Condensed tannins. Base-catalysed reactions of polymeric procyanidins with phloroglucinol: intramolecular rearrangements. *J. Chem. Soc., Perkin Trans. 1* **1987**, *6*, 1875−1881.
(43) Helm, R. F.; Ranatunga, T. D.; Chandra, M. Lignin-hydrolyzable tannin interactions in wood. *J. Agric. Food Chem.* **1997**, *45*, 3100−3106.
(44) Lange, W.; Faix, O. Lignin-polyphenol interaction in azobe (*Lophira alata*) heartwood. A study on milled wood lignin (MWL) and Klason residues. *Holzforschung* **1999**, *53*, 519−524.
(45) Rencoret, J.; Ralph, J.; Marques, G.; Gutiérrez, A.; Martínez, Á. T.; del Río, J. C. Structural characterization of lignin isolated from coconut (*Cocos nucifera*) coir fibers. *J. Agric. Food Chem.* **2013**, *61*, 2434−2445.
(46) del Río, J. C.; Rencoret, J.; Prinsen, P.; Martínez, Á. T.; Ralph, J.; Gutiérrez, A. Structural characterization of wheat straw lignin as revealed by analytical pyrolysis, 2D-NMR, and reductive cleavage methods. *J. Agric. Food Chem.* **2012**, *60*, 5922−5935.

JOURNAL OF AGRICULTURAL AND FOOD CHEMISTRY

Article

pubs.acs.org/JAFC

Design, Synthesis, Crystal Structure, Insecticidal Activity, Molecular Docking, and QSAR Studies of Novel N_3-Substituted Imidacloprid Derivatives

Mei-Juan Wang,[†,§] Xiao-Bo Zhao,[†,§] Dan Wu,[†] Ying-Qian Liu,[*,†] Yan Zhang,[†] Xiang Nan,[†] Huanxiang Liu,[*,†] Hai-Tao Yu,[‡] Guan-Fang Hu,[‡] and Li-Ting Yan[†]

[†]School of Pharmacy, Lanzhou University, Lanzhou 730000, P.R. China

[‡]Institute of Plant Protection, Gansu Academy of Agricultural Sciences, Lanzhou 730070, P.R. China

Supporting Information

ABSTRACT: Three novel series of N_3-substituted imidacloprid derivatives were designed and synthesized, and their structures were identified on the basis of satisfactory analytical and spectral (^{1}H NMR, ^{13}C NMR, MS, elemental analysis, and X-ray) data. Preliminary bioassays indicated that all of the derivatives exhibited significant insecticidal activities against *Aphis craccivora*, with LC_{50} values ranging from 0.00895 to 0.49947 mmol/L, and the insecticidal activities of some of them were comparable to those of the control imidacloprid. Some key structural features related to their insecticidal activities were identified, and the binding modes between target compounds and nAChR model were also further explored by molecular docking. By comparing the interaction features of imidacloprid and compound **26** with highest insecticidal activity, the origin of the high insecticidal activity of compound **26** was identified. On the basis of the conformations generated by molecular docking, a satisfactory 2D-QSAR model with six selected descriptors was built using genetic algorithm−multiple linear regression (GA-MLR) method. The analysis of the built model showed the molecular size, shape, and the ability to form hydrogen bond were important for insecticidal potency. The information obtained in the study will be very helpful for the design of new derivatives with high insecticidal activities.

KEYWORDS: *synthesis, insecticidal activity, X-ray diffraction, molecular docking, QSAR*

INTRODUCTION

Neonicotinoid insecticides (NNs), acting selectively on the insect nicotinic acetylcholine receptors (nAChRs), have attracted the widespread interest of scientists continuously due to their broad spectrum of biological activities and high selectivity for crop protection and public health.[1−3] Since imidacloprid (**1**) was introduced in the 1980s as an insecticide for crop protection, NNs have gained dramatic developments and many new generation NNs, such as thiacloprid (**2**), acetamiprid (**3**), nitenpyram (**4**), thiamethoxam (**5**), clothianidin (**6**), and dinotefuran (**7**), were commercialized successively with their own prominence (Figure 1) and they account for at least 26% of the global insecticide market.[4−8]

Despite the tremendous amount of effort invested in the development of neonicotinoids, it remains essential to continually explore novel neonicotinoid candidates because significant increases in resistance and cross-resistance have been observed in various insect species after frequent field applications.[9−13] Modification of the structures of existing neonicotinoids can be an effective tactic to combat resistance. Accordingly, strategies for designing and synthesizing neonicotinoids remain an ongoing, attractive research area. These modification strategies includes replacement of the pyridine ring with a thiazole or other bioisosteric heterocyclic rings, substitution of the nitroimino group with other electron-withdrawing groups, and transformation of the imidazolidine moiety to novel heterocyclic equivalents.[3,8,14−21] Through various modifications, some analogues were found to exhibit either enhanced or comparable activity to **1**. Intriguingly, an acyclic neonicotinoid, sulfoxaflor (**8**), emerged as an alternative to overcome the drawbacks of **1** and has widely been commercialized for agricultural use now.[22] Also, divalent neonicotinoids,[23] proinsecticides of imidacloprid,[24] nenicotinoids with extended *N*-substituted-imine,[25] bis-neonicotinoid,[26] and crown-capped imidacloprid[27] have appeared consecutively in the literature in recent years. Overall, the excellent activity profiles of some derivatives, including improved potency, broad insecticidal spectra, low mammalian toxicity, and good systemic properties, suggested this compound class could be optimized through rational structural modification.

Although many research papers that discussed the structure optimization of neonicotinoid insecticides (NNs) are based on cyclic NNs, such as imidacloprid, few studies have focused on the structural modification of NNs at 3-position.[28] As is well-known, bioactive functional fragments or skeletons play a crucial role in biologically active chemicals, and modifications in the functional groups could improve or change the biological activity of parent compounds.[29−32] Furthermore, amidines[33,34] and triazoles[35,36] are identified as important pharmacophores and are widely used in pesticide and drug molecular design; also, the introduction of a sulfonyl group into a wide range of

Received: March 5, 2014
Revised: May 17, 2014
Accepted: May 17, 2014
Published: May 17, 2014

ACS Publications © 2014 American Chemical Society

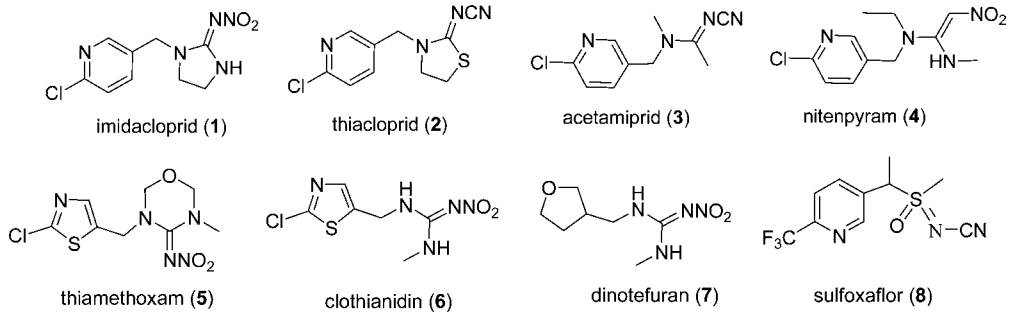

Figure 1. Structures of current commercially available neonicotinoid insecticides.

Scheme 1. Synthesis of Target Compounds 10−54

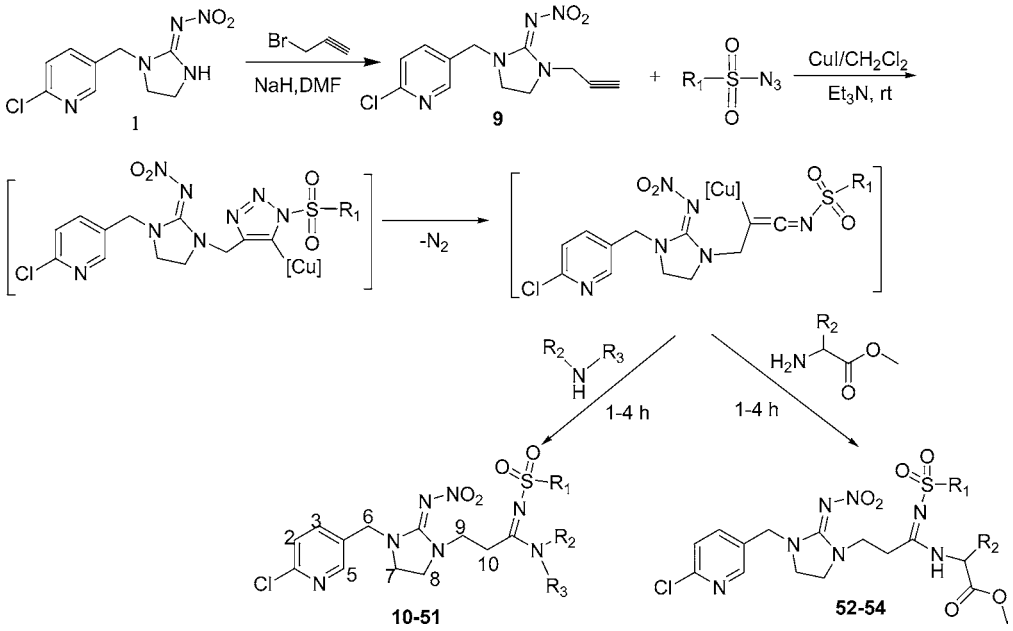

heterocyclic compounds results in significant changes in the bioactivity of the compounds,[37,38] thus it was indicated that sulfonylamidines and sulfonyltriazoles may be useful structural motifs for optimization in the scaffold of bioactive molecules. Given these considerations, we developed an idea that substitution of the hydrogen on the nitrogen atom of imidacloprid with sulfonylamidino or sulfonyltriazolo substituents could optimize physicochemical properties and improve the biological activity of imidacloprid. To verify our speculation, in the present study, we incorporated the functional fragment sulfonylamidino or sulfonyltriazolo into imidacloprid at the *N*-3 position and synthesized three novel series of imidacloprid derivatives according to Schemes 1-3. As compared to conventional synthetic methods, our studies noted that the one-pot synthesis of a *N*-sulfonylamidino group using Cu-catalyzed three component coupling of sulfonyl (or phosphoryl) azide, alkyne, and amine could be an efficient and convenient method to combine several active moieties into one molecule, and it could be convenient to implement structural modification via alternation of diverse starting materials. To further study the role of the sulfonyltriazolo substituents played in the biological activities, another series of sulfonyltriazole-derived imidacloprid analogues were also synthesized using modified click chemistry. The insecticidal activities of the target compounds were evaluated against *Aphis craccivora*, and the median lethal concentrations (LC_{50}) were calculated accordingly. Additionally, to identify some key structural features responsible for their potency, the quantitative structure−activity relationship model was developed. Furthermore, the binding modes between target compounds and nAChR model were also explored by molecular docking, which generated useful information for future design of new neonicotinoid pesticides.

MATERIALS AND METHODS

General. Reagents were purchased from commercial sources and were used as received. All reagents and solvents were of reagent grade or purified according to standard methods before use. Analytical thin-layer chromatography (TLC) and preparative thin-layer chromatography (PTLC) were performed with silica gel plates using silica gel 60 GF254 (Qingdao Haiyang Chemical Co., Ltd.). Melting points were determined in Kofler apparatus and were uncorrected. Mass spectra were recorded on a Bruker Daltonics APEXII49e spectrometer (Bruker Company, USA) with ESI source as ionization. NMR spectra were recorded on a Bruker AM-400 spectrometer (Bruker Company, USA) at 400 and 100 MHz using TMS as the reference. Elemental analyses were determined on a Vario El GmbH elemental analyzer.

Synthesis of Key Intermediate ***9.*** Sodium hydride (60% oil dispersion, 80 mg, 2 mmol) was added portionwise to a stirred solution of **1** (514 mg, 2 mmol) in dimethylformamide (DMF) (30 mL) with ice cooling. After the addition, the stirring was continued for a further 30 min at room temperature. The reaction mixture was cooled again with an ice bath and treated with propargyl bromide (297.5 mg, 2.5 mmol). The mixture was stirred overnight at room temperature and then 9 h at 50 °C. After quenching the reaction with a drop of acetic

dx.doi.org/10.1021/jf501108j | J. Agric. Food Chem. 2014, 62, 5429−5442

Scheme 2. Synthesis of Target Compounds 55−57

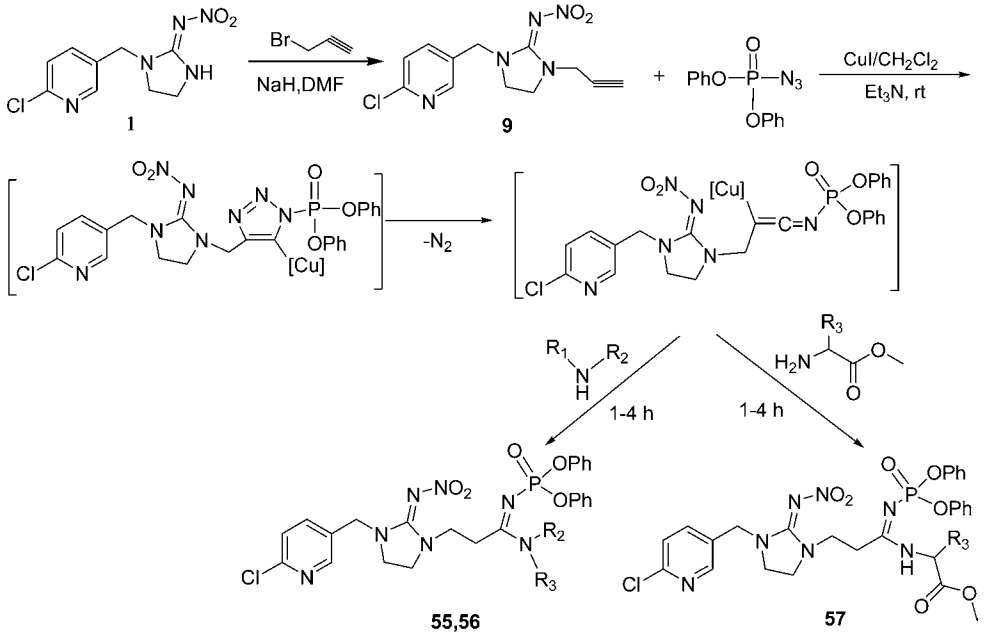

Scheme 3. Synthesis of Target Compounds 58−64

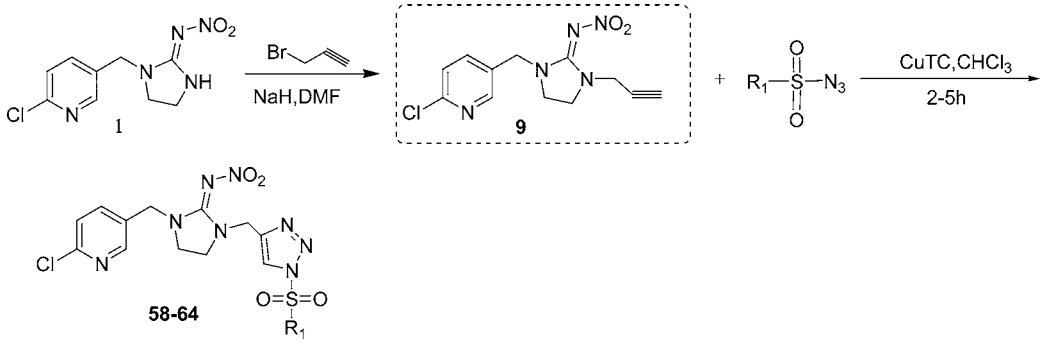

acid, the DMF was distilled off. The remaining solid was subjected to column chromatography on silica gel with ethyl acetate until no further **I** was detected in the fractions, then the elution was continued by replacing the eluting medium with ethyl acetate/methanol 5:1. The separated product was recrystallized from ethanol. Yield: 82%.

*General Synthetic Procedure for Target Compounds **10−54**.* Intermediate **9** (0.5 mmol) was added in CH_2Cl_2 (15 mL), and this mixture was stirred for 5 min when a clear solution was obtained. Under an N_2 atmosphere, sulfonyl azide (0.6 mmol), amines (0.5 mmol), and CuI (0.05 mmol) was added into this reaction mixture at room temperature. Triethylamine (0.6 mmol) was added. After the reaction was completed, as monitored by TLC, the reaction mixture was diluted by adding CH_2Cl_2 (4 mL) and aqueous NH_4Cl solution (6 mL). The mixture was stirred for an additional 30 min, and two layers were separated. The aqueous layer was extracted with CH_2Cl_2 (3 mL × 3). The combined organic layers were dried over $MgSO_4$, filtered, and concentrated in vacuo. The crude residue was purified by flash column chromatograph with an appropriate eluting solvent system.

*Data for Compound **10**.* Yield 52%; white solid; mp 120−123 °C. ^{1}H NMR (DMSO-d_6, 400 MHz) δ: 8.80 (s, 1H, NH), 8.37 (s, 1H, C5-H), 7.80 (d, 1H, J = 8.0 Hz, C3-H), 7.69 (d, 2H, J = 8.0 Hz, Ts-H), 7.52 (d, 1H, J = 8.4 Hz, C2-H), 7.33(d, 2H, J = 8.0 Hz, Ts-H), 4.42 (s, 2H, C6-H), 3.78 (t, 2H, J = 8.8 Hz, C7-H), 3.6 4(t, 2H, J = 9.6 Hz, C8-H), 3.58 (t, 2H, J = 6.8 Hz, C9-H), 3.07 (q, 2H, J = 6.4 Hz, $-\underline{CH_2}CH_2CH_3$), 2.91 (t, 2H, J = 6.8 Hz, C10-H), 2.50 (s, 3H, Ts-$\underline{CH_3}$), 1.45 (q, 2H, J = 7.6 Hz, $-CH_2\underline{CH_2}CH_3$), 0.82 (t, 3H, J = 7.6 Hz, $-CH_2CH_2\underline{CH_3}$). ^{13}C NMR (DMSO-$d_6$, 100 MHz) δ: 165.0, 160.5, 149.6, 149.5, 141.5, 141.4, 139.4, 130.3, 129.2, 125.6, 124.2, 46.6, 45.8, 45.2, 44.0, 43.1, 31.2, 20.9, 11.4. MS-ESI m/z: 544.1 $[M + Na]^+$. Anal. Calcd For $C_{22}H_{28}ClN_7O_4S$: C, 50.62; H, 5.41; N, 18.78. Found: C, 50.49; H, 5.48; N, 18.67.

*General Synthetic Procedure for Target Compounds **55−57**.* Amine nucleophile (0.75 mmol, 1.5 equiv) was added to the mixture of phosphoryl azide (0.5 mmol, 1.0 equiv), **9** (1 mmol, 2.0 equiv), and CuI (0.05 mmol, 10 mol %) in CH_2Cl_2 (1 mL) at room temperature under N_2 atmosphere. Triethylamine (0.75 mmol) was added after the addition of the amine if necessary. After the reaction was completed, the same procedure was followed as for N_3-sulfonyl amidines **10−54**.

*Data for Compound **55**.* Yield 56%; white solid; mp 80−82 °C. ^{1}H NMR ($CDCl_3$, 400 MHz) δ: 8.28 (s, 1H, C5-H), 7.65 (d, 1H, J = 6.4 Hz, C3-H), 7.22−7.64 (m, 9H, C2-H, $-(O\underline{Ph})_2$-H), 7.12 (t, 2H, J = 7.6 Hz, $-(O\underline{Ph})_2$-H), 4.45 (s, 2H, C6-H), 4.21 (m, 1H, $-N(\underline{CH}(CH_3)_2)_2$), 3.88 (t, 2H, J = 9.2 Hz, C7-H), 3.48 (m, 5H, C8-H, C9-H, $-N(\underline{CH}(CH_3)_2)_2$), 3.19 (t, 2H, J = 8.8 Hz, C10-H), 1.24 (d, 6H, J = 6.4 Hz, $-N(CH(\underline{CH_3})_2)_2$), 1.14 (d, 6H, J = 6.4 Hz, $-N(CH(\underline{CH_3})_2)_2$). ^{13}C NMR ($CDCl_3$, 100 MHz) δ: 163.9, 160.6, 151.6, 151.5, 149.2, 138.8, 129.3, 128.9, 124.7, 124.2, 120.4, 50.8, 47.9, 46.9, 46.3, 44.9, 44.8, 31.9, 20.7, 19.4. MS-ESI m/z: 749.3 $[M + H]^+$. Anal. Calcd For $C_{30}H_{37}ClN_7O_5P$: C, 56.12; H, 5.81; N, 15.27. Found: C, 56.03; H, 5.93; N, 15.34.

*General Synthetic Procedure for Target Compounds **58−64**.* Copper(I) thiophene-2-carboxylate (CuTC) (13.0 mg, 0.068 mmol) was added in 20 mL of $CHCl_3$. Then a solution of **9** (200 mg, 0.68 mmol) in 20 mL of $CHCl_3$ and a solution of sulfonyl azide

dx.doi.org/10.1021/jf501108j | J. Agric. Food Chem. 2014, 62, 5429−5442

(0.75 mmol) in 5 mL of $CHCl_3$ were added, and the reaction mixture was stirred for 6 h at room temperature. The resulting mixture was diluted with saturated NH_4Cl aq (50 mL) and extracted with $CHCl_3$ (3 × 50 mL). The combined organics were washed with brine, dried over $MgSO_4$, and concentrated under reduced pressure. The residue was purified by flash column chromatograph with an appropriate eluting solvent system.

Data for Compound ***58***. Yield 55%; white solid; mp 68−69 °C. ^{1}H NMR ($CDCl_3$, 400 MHz) δ: 8.28 (s, 2H, C5-H, triazole-H), 8.01 (d, 2H, J = 8.0 Hz, Ts-H), 7.66 (d, 1H, J = 8.0 Hz, C3-H), 7.42 (d, 1H, J = 8.0 Hz, C2-H), 7.35 (d, 2H, J = 8.0 Hz, Ts-H), 4.56 (s, 3H, C6-H), 4.47 (s, 3H, C9-H), 3.83 (t, 2H, J = 8.8 Hz, C7-H), 3.54 (t, 2H, J = 10.4 Hz, C8-H), 2.47 (s, 3H, Ts-$\underline{CH_3}$). ^{13}C NMR (DMSO-d_6, 100 MHz) δ: 160.5, 149.7, 149.5, 145.0, 140.3, 139.5, 138.1, 130.5, 128.3, 125.5, 124.3, 46.5, 45.7, 45.5, 41.0, 20.8. MS-ESI m/z: 513.1 [M + Na]$^+$. Anal. Calcd For $C_{19}H_{19}ClN_8O_4S$: C, 46.48; H, 3.90; N, 22.83. Found: C, 46.59; H, 4.06; N, 22.98.

X-ray Crystallography. X-ray quality crystal of **11** was obtained from a solution of acetone/methanol after 7 d. The crystal structure of compound **11** was determined, and X-ray intensity data were recorded on a Bruker APEX II diffractometer using graphite monochromated Mo Kα radiation (λ = 1.54180 Å). A total of 13962 reflections were measured, of which 4913 were unique (R_{int} = 0.1631) in the range of 3.802 < θ < 70.070° (h, −22 to 23; k, −17 to 18; l, −7 to 11), and 2576 observed reflections with $I > 2\sigma(I)$ were used in the refinement on F^2. The structure was solved by direct method with the SHELXTL-97 program. All of the non-H atoms were refined anisotropically by full-matrix least-squares to give the final R = 0.1319 and WR = 0.3098. All hydrogen atoms were computed and refined using a riding model. The atomic coordinates for **11** have been deposited at the Cambridge Crystallographic Data Centre. CCDC-970304 contains the supplementary crystallographic data for this paper. These data can be obtained free of charge from The Cambridge Crystallographic Data Centre via CCDC CIF Depository Request Form for data published from 1994.

Insecticidal Assay. All compounds were dissolved in acetone and diluted with water containing Triton X-100 (0.1 mg/L) to obtain series concentrations of 500, 250, 100, 50, and 10 mg L^{-1} and others for bioassays. For comparative purposes, imidacloprid was tested under the same conditions. Each concentration was tested three times in parallel. The insecticidal activities of title compounds against *Aphis craccivora* were tested by leaf-dip method according to a previously reported procedure.[23] Horsebean plant leaves with 30 apterous adults were dipped in diluted solutions of the chemicals containing Triton X-100 (0.1 mg L^{-1}) for 5 s, and the excess dilution was sucked out with filter paper; the burgeons were placed in the conditioned room (25 ± 1 °C, 50% relative humidity (RH)). Water containing Triton X-100 (0.1 mg L^{-1}) was used as control. Assessments were made after 24 h by the number of killed and size of live insects relative to that in the negative control, and evaluations were based on a percentage scale of 0−100, in which 0 = no activity and 100 = total kill. The deviation of values was ±5%. The mortality rates were subjected to probit analysis, and the median lethal concentrations (LC_{50}) were calculated accordingly. All bioassay results are summarized in Tables 1−4.

Molecular Docking Study. All molecular structures were sketched in SYBYL6.9[39] software package. Energy minimizations were performed using the Tripos force field with a distance dependent dielectric function and Powell method with a convergence criterion of 0.05 kcal/mol. Partial atomic charges were calculated using Geisteiger−Huckel method. The local minimum energy conformations of these minimized compounds were generated using the multisearch method. Schrödinger's LigPrep program[40] was used to process the generated conformations. The crystal structure of the acetylcholine binding protein (AChBP) from *Lymnaea stagnalis* (Ls-AChBP) in complex with imidacloprid (IMI) (PDB: 2ZJU) was used for the molecular docking studies because there is still no crystal structure of nAChR of insect *Aphis craccivora* and Ls-AChBP has high homology to the extracellular domain of nAChR. Actually, Ls-AChBP has been used to study the interaction between compounds with nAChR.[41−43] Chain A, chain B, and crystal waters were selected and prepared for subsequent grid generation using the Protein Preparation Wizard in the Schrodinger Suite. The structure was further treated by adding hydrogen atoms, assigning protonation states. Grids were then generated based on the ligand in the crystal structure using the Receptor Grid Generation module in Glide.[44] Lastly, the docking was performed using Glide.

Quantitative Structure−Activity Relationships Analysis. The docked conformations of these derivatives were imported into Dragon software[45] and molecular descriptors calculated. These descriptors are respectively 0D molecular descriptors (constitutional descriptors), 1D molecular descriptors (functional groups counts, atom-centered fragments), 2D molecular descriptors (topological descriptors, walk and path counts, connectivity indices, information indices, 2D auto-correlations, edge adjacency indices, Burden eigenvalues, topological charge index, eigenvalue-based index), 3D molecular descriptors (Randic molecular profiles, geometrical descriptors, RDF descriptors, 3D-MoRSE descriptors, WHIM descriptors, GETAWAY descriptors), and other molecular descriptors (charge descriptors and molecular properties). To reduce the nonuseful and redundant information, constant variables, near-constant variables, and one of any two descriptors with a correlation coefficient of 0.98 or higher were excluded, and thus 694 descriptors were used in next step.

To build and validate the QSAR model, 55 compounds were used as training set and test set, respectively. The insecticidal activities of these compounds against *A. craccivora* expressed as pLC_{50} values were defined as dependent variable for the following analysis.

To search the feature space and select descriptors related with the insecticidal activities, a combination of genetic algorithm and multiple linear regression (GA-MLR)[46] was used. GA-MLR method has been applied in many studies.[47,48] MobyDigs software[49] was used to build QSAR model of these derivatives. The leave-one-out (LOO) cross validation correlation coefficient (Q^2_{loo}) was used as the fitness function. The population size was set to 100, and maximum allowed variables in a model was 6. Other corresponding parameters were set as default.

To validate the built model, several statistic terms including correlation coefficient (R^2), leave-one-out (LOO) cross-validated correlation coefficient (Q^2_{loo}), and root-mean-square error (RMSE) were used. Moreover, the external validation correlation coefficient (Q^2_{ext}) of these compounds from the test set was used to evaluate the predictive ability of the QSAR model.

The hat value was used to evaluate the applicability domain (AD) of the model, defined as follows:

$$h_i = x_i(X^TX)^{-1}x_i^T \quad (i = 1, ..., m)$$

where x_i, m, and X are respectively row vector of the descriptors of the query compound i, the number of query compounds, and the $n \times k$ matrix of the descriptors of the training set (n and k are the number of descriptors of training set and the model, respectively). The plot of hat values and cross-validated standardized errors (the Williams plot) visually display the application domain of the built model. The horizontal and vertical dashed lines display the limits of normal values in the plot. For example, if the hat value of one compound id greater than h^*, this compound is considered as an X outlier. The cross-validated standardized error of a compound is more than 3.0 standard deviation units, and thus the compound is a Y outlier in a model. The warning hat (h^*) is defined by $3k'/n$. Here, n and k are the number of compounds in training set and the number of descriptors plus 1, respectively.

RESULTS AND DISCUSSION

Synthesis. The synthetic routes to target compounds are outlined in Schemes 1−3. As outlined in Schemes 1−2, briefly, starting from imidacloprid **1**, a propargyl group was first introduced in the N_3-position of **1** upon reaction with propargyl bromide in the presence of sodium hydride to give key precursor **9** in 82% yield. Subsequently, key precursor **9** was successfully employed as an efficient reacting partner in the Cu-catalyzed three-component reaction with sulfonyl azides and amines to produce the corresponding N_3-imidacloprid sulfonyl amidines **10**−**54** in moderate yields. Under the optimized

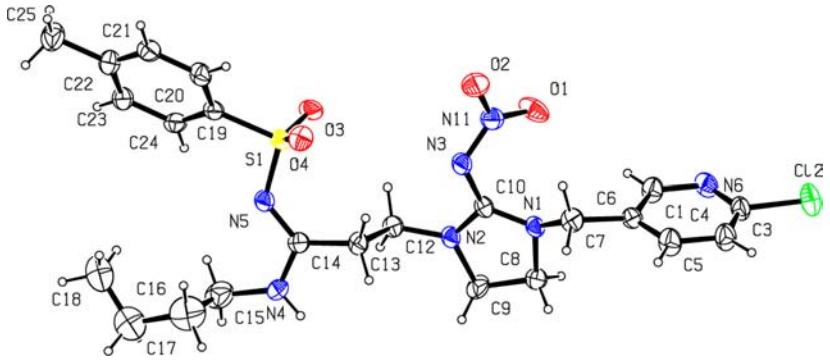

Figure 2. X -ray crystal structure of compound **11**.

conditions, a wide range of amines including primary, secondary, aliphatic, aryl, acyclic, and/or cyclic types were all efficiently coupled to furnish the corresponding amidines. Amino esters were likewise incorporated with almost the same efficiency. Moreover, the scope of the azide counterpart also turned out to be broad, and various types of such as sulfonyl azides and phosphoryl azides (**55**−**57**) were readily employed with high efficiency. The coupling reaction has a wide substrate scope, a high tolerance to various functional groups, and very mild reaction conditions. The reaction proceeds through a ketenimine intermediate, which is generated in situ from the triazole cycloadduct upon release of N_2 gas.[50]

As shown in Scheme 3, it has been reported that the introduction of a sulfonyl group into a wide range of heterocyclic compounds resulted in significant changes in the bioactivity of the compounds. Next, we initiate a new search for bioactive sulfonyl triazole molecules for structural modification using similar click chemistry. Interestingly, *N*-sulfonyl-1,2,3-triazoles **58**−**64** were expectedly obtained from **9** and sulfonyl azides in the absence of amines in good yields by the action of copper catalysts. In contrast to the traditional click methodology, the traditional click reaction using the $CuSO_4$/sodium ascorbate system resulted in both poorer conversions and selectivity. Addition of *tert*-butyl sulfide to the $CuSO_4$/sodium ascorbate system resulted in an improved ratio and maintained high conversion. During our attempts to achieve high conversion and selectivity by screening different copper(I) catalysts, copper(I) thiophene-2-carboxylate (CuTC) (Liebeskind's reagent) was found to be a convenient, effective catalyst for the synthesis of *N*-sulfonyl-1,2,3-triazoles at ambient temperature under anhydrous conditions. Furthermore, dichloromethane and chloroform were identified as optimal solvents for the CuTC-catalyzed 1-sulfonyl triazole synthesis, with both leading to complete reactions after 2−5 h.

All newly synthesized compounds were purified by column chromatography, and their structures were confirmed by ^{1}H NMR, ^{13}C NMR, ESI-MS, and elemental analysis. To obtain precise three-dimensional structural information and absolute configurations for **10**−**54**, compound **11** was recrystallized by slow evaporation from a solution of acetone/methanol and its single crystal structure was determined by X-ray crystallography as illustrated in Figure 2.

Insecticidal Activity against Aphis craccivora. On the basis of the methodology in Schemes 1−3, with 55 derivatives **10**−**64** in hand, we next examined their insecticidal activity against *Aphis craccivora*, imidacloprid was tested under the same conditions as a comparison compound. The results were summarized in Tables 1−4.

As shown in Tables1−4, all of the derivatives exhibited moderate to potent insecticidal activities against *Aphis craccivora*, with LC_{50} values ranging from 0.00895 to 0.49947 mmol/L. Among them, some of compounds were found to be equally potent or superior insecticidal activities to imidacloprid. For example, when *Aphis craccivora* were fed with the diet containing 500 mg L^{-1}, the corrected mortality rates of most of compounds had 100% inhibitory effect after 1 day. At reduced dosages, most of the target compounds still remaining had excellent inhibitory activity and had >80% mortality at 250 mg L^{-1}. Even at a 50 mg L^{-1} diet, compounds **18**, **26**, **41**, **47**, **48**, **49**, **62**, and **64** exhibited good insecticidal activity against *Aphis craccivora* and had >60% mortality. The LC_{50} values of those compounds were 0.05948, 0.00895, 0.07745, 0.07550, 0.06222, 0.07286, 0.06196, and 0.04470 mmol L^{-1}, respectively, whereas that of imidacloprid was 0.03602 mmol L^{-1}. Intriguingly, the insecticidal activity of compound **26** (LC_{50}: 0.00895 mmol L^{-1}) showed approximately 4-fold higher activities than that of imidacloprid based on the value of LC_{50}, which implied further possibilities for lead compound development.

As for the sulfonylamidine series **10**−**54**, the effects of different substituent groups in the sulfonylamidine side chains were investigated. As shown in Table 1, when the R_1 group was fixed as methylphenyl (**10**−**31**), changing the NR_2R_3 on in the sulfonylamidine side chains could lead to a remarkable change in activity. For example, linear alkyl groups, like *n*-propyl in **10**, lead to a much better efficacy than branched alkyl groups, like isopropyl in **14**. Substitution of the NR_2R_3 group with cycloalkyl (**15**), heterocycloalkyl (**16**−**19**), and amino esters (**52**−**54**) did not display a significant improvement in insecticidal activity as compared to **10**. Moreover, the potency of compounds with the aromatic or heterocycle rings (**20**−**31**) depended significantly upon the nature of the substitutes and their position at the aromatic ring, and compound **26** (*p*-Cl-C_6H_5) gave the best result compared with other synthetic derivatives. Interestingly, when the R_1 group was changed from methylphenyl to other substitutions (pyridinyl, dimethylamino, methyl, *p*-fluorophenyl, 2-naphthyl, etc.), the order of potency was somehow changed, and the substituents R_1 present in the functional group N═SO_2R_1 were also a crucial factor that governed activity. For example, the introduction of a pyridinyl group (**35**, 0.08106) into N═SO_2R_1 increased the insecticidal activities of the compounds (e.g., compounds **32**−**34**). While for compounds **37**−**39**, compound **39** bearing a fluorophenyl R_1 group displayed more potent activity than **38** with a pyridinyl R_1 group. Overall, considering the discussion above, these findings suggested that their insecticidal potency was dual-controlled by both the R_1 and NR_2R_3 groups in the sulfonylamidine side chain.

dx.doi.org/10.1021/jf501108j | J. Agric. Food Chem. 2014, 62, 5429−5442

Table 1. Insecticidal Activities of Compounds 1, 9, and 10−51 against *Aphis craccivora*

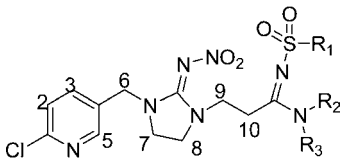

10-51

Compd	R_1	R_2R_3NH	*Aphis craccivora*			
			Mortality (%)			LC_{50} ($mmolL^{-1}$)
			500 mgL^{-1}	250mgL^{-1}	50 mg L^{-1}	
1			100	100	80.0	0.03602
9			100	100	83.3	0.01231
10	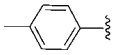	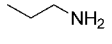	90.0	76.7	50.0	0.07857
11	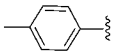	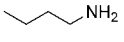	100	93.3	40.0	0.08856
12	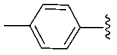		100	60.0	43.3	0.10636
13	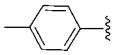	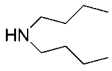	80.0	63.3	46.7	0.11618
14	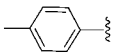		86.7	66.7	46.7	0.11719
15	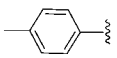	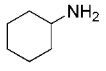	60.0	50.0	33.3	0.35768
16	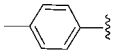		56.7	46.7	30.0	0.49947
17	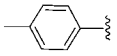		93.3	86.7	43.3	0.09324
18	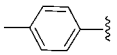		100	83.3	63.3	0.05948
19		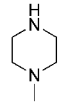	76.7	60.0	40.0	0.11882
20		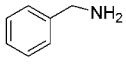	83.3	73.3	46.7	0.09959
21		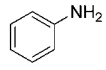	66.7	63.3	46.7	0.12530
22	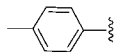	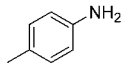	70.0	63.3	46.7	0.15676
23	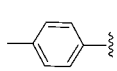	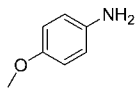	96.7	93.3	53.3	0.05606
24		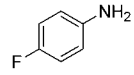	100	100	56.7	0.05062
25	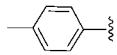	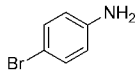	96.7	86.7	36.7	0.12407

dx.doi.org/10.1021/jf501108j | *J. Agric. Food Chem.* 2014, 62, 5429−5442

Table 1. continued

Compd	R_1	R_2R_3NH	*Aphis craccivora*			
			Mortality (%)			LC_{50} ($mmolL^{-1}$)
			500 mgL^{-1}	250mgL^{-1}	50 mg L^{-1}	
26	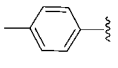	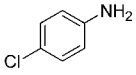	100	100	73.3	0.00895
27	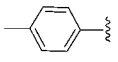	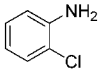	66.7	63.3	30.0	0.21021
28	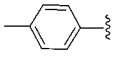	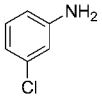	86.7	83.3	56.7	0.04983
29	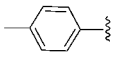	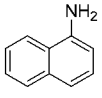	86.7	76.7	53.3	0.10938
30	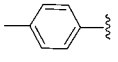	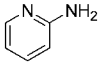	100	80.0	36.7	0.14435
31	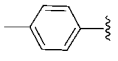	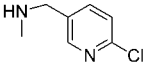	93.3	70.0	56.7	0.04158
32	CH_3	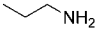	100	90.0	53.3	0.11050
33	CH_3CH_2	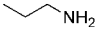	70.0	63.3	50.0	0.12537
34	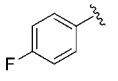	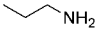	60.0	56.7	30.0	0.43204
35		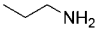	100	96.7	40.0	0.08106
36		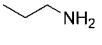	100	83.3	33.3	0.14723
37	CH_3	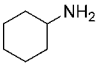	100	86.7	33.3	0.12918
38		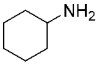	100	46.7	40.0	0.15976
39	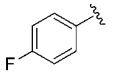	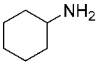	100	83.3	53.3	0.07086
40	CH_3	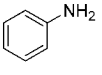	96.7	93.3	46.7	0.12849
41		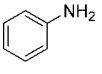	100	93.3	60.0	0.07745
42	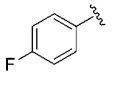	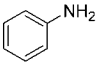	96.7	70.0	30.0	0.14967
43	CH_3	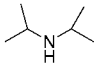	100	96.7	46.7	0.07592
44	$CH_3CH_2CH_2CH_2$	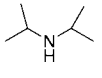	100	86.7	56.7	0.05374

dx.doi.org/10.1021/jf501108j | *J. Agric. Food Chem.* 2014, 62, 5429−5442

Table 1. continued

Compd	R_1	R_2R_3NH	*Aphis craccivora* Mortality (%) 500 mgL^{-1}	250mgL^{-1}	50 mg L^{-1}	LC_{50} (mmolL^{-1})
45	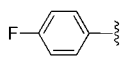	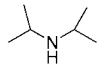	96.7	76.7	43.3	0.06884
46	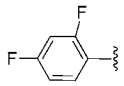	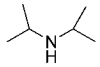	73.3	50.0	30.0	0.27860
47	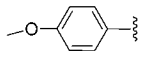	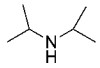	100	96.7	63.3	0.07550
48		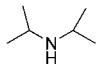	100	90.0	73.3	0.06222
49	CH_3		100	76.7	70.0	0.07286
50	CH_3	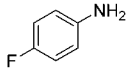	73.3	66.7	40.0	0.26891
51	CH_3	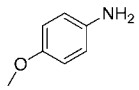	100	80.0	56.7	0.07500

Table 2. Insecticidal Activities of Compounds 52−54 against *Aphis craccivora*

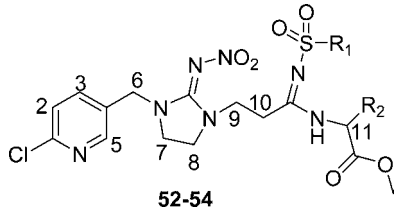

52-54

Compd	R_1	R_2	*A.craccivora* Mortality (%) 500 mgL^{-1}	250 mgL^{-1}	50 mgL^{-1}	LC_{50} (mmol L^{-1})
52	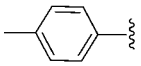	H	73.3	63.3	53.3	0.10362
53	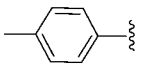	$CH_2CH(CH_3)_2$	100	93.3	30.0	0.08434
54	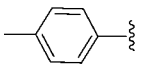	$PhCH_2$	100	76.7	36.7	0.08486

In addition to sulfonyl amidines, another two series of phosphoryl amidine derivatives (**55**−**57**) and sulfonyltriazolo-substituted 1-derivatives (**58**−**64**) were investigated as well. As indicated in Tables 3 and 4, all of the title compounds showed moderate to good insecticidal activities against *A. craccivora*, and some of them were either similar or better than that of imidacloprid. Significantly, compound **57** displayed the most potent activity among the tested compounds against *A. craccivora* and better than the positive control imidacloprid. In contrast, the activity of compounds with sulfonylamidino groups were predominantly higher than those of phosphoryl amidine or sulfonyltriazolo-substituted **1** derivatives, indicating that the electron distribution and substituents on N_3-position of **1** play an important role in the derivatives' activity. Taken together, these observations further underlined the insecticidal differences could be ascribed to a combination of factors, like the nature of the substituents (which may depend on the size of substituents, electronic characteristics of substituents, or other factors) or a different interaction at the site.

Meanwhile, it has been widely known that the physical properties of an insecticidal compound may be manipulated to obtain products with other selected types of activity by proper

dx.doi.org/10.1021/jf501108j | J. Agric. Food Chem. 2014, 62, 5429−5442

Table 3. Insecticidal Activities of Compounds 55−57 against *Aphis craccivora*

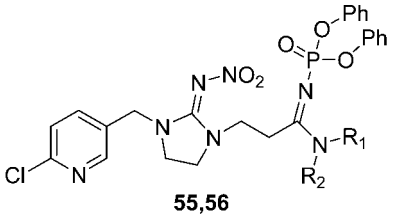

55,56

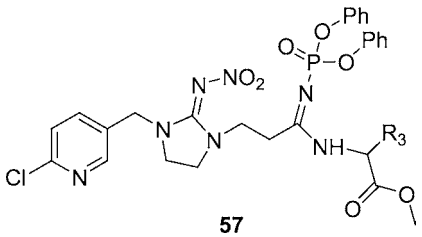

57

Compd	R_1R_2NH / R_3	*A.craccivora*			
		Mortality (%)			LC_{50} (mmol L^{-1})
		500 mgL^{-1}	250 mgL^{-1}	50 mgL^{-1}	
55	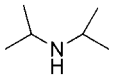	100	56.7	46.7	0.12393
56	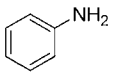	93.3	80.0	40.0	0.09175
57	$PhCH_2$	96.7	93.3	56.7	0.02464

Table 4. Insecticidal Activities of Compounds 58−64 against *Aphis craccivora*

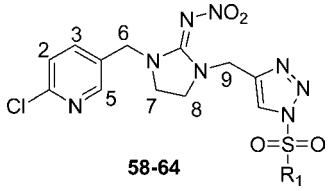

58-64

Compd	R_1	*A.craccivora*			
		Mortality (%)			LC_{50} (mmol L^{-1})
		500 mgL^{-1}	250 mgL^{-1}	50 mgL^{-1}	
58		90.0	63.3	43.3	0.13584
59	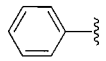	100	76.7	36.7	0.12591
60	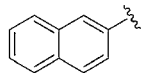	90.0	80.0	53.3	0.07506
61	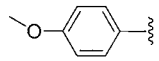	100	76.7	43.3	0.09127
62		100	96.7	63.3	0.06196
63	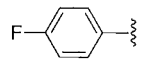	83.3	80.0	50.0	0.10122
64	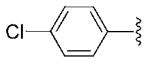	100	93.3	63.3	0.04470

selection of the derivative moiety. Encouraged by these investigations, some N_3-substituted imidacloprid derivatives, such as bis-imidacloprid,[26] crown-capped imidacloprid,[27] N_3-oxalyl imidacloprid derivatives,[51] have been prepared by different groups in recent years. It should be noted that these reported N_3-substituted compounds may act as pro-drug by hydrolyzing to IMI. Further biological data supported this conclusion that these N_3-substituted compounds as proinsecticides would likely be in vivo activated to release of the parent imidacloprid and such an assumption was supported by Kagabu et al.'s reported experimental method.[24] In the present study, the insecticidal effects of these derivatives may be similar to those seen in Kagabu's study. Therefore, one possibility is that these derivatives may be metabolized in vivo to regenerate imidacloprid, exerting insecticidal effects, although the exact mode is unknown.

Molecular Docking Analysis. It is noteworthy that the initially observed effects of these derivatives on *A. craccivora* were excitatory symptoms, such as tremors, followed by paralysis and mortality (personal observations). It could be postulated that the insecticidal activity of these synthetic derivatives could be due to potential effects on the insect nervous system, similar to the neuroactive imidacloprid.[52] To prove this hypothesis, imidacloprid and these derivatives were docked into the active site of AChBP. The most likely binding conformations were selected based on the score and the binding mode. In this way, the most possible conformations for all compounds were obtained. Imidacloprid was redocked to validate the docking reliability. The binding mode of redocked and co-crystallized imidacloprid is almost same in the active site of AChBP (Figures 3 and 4). For example, the nitrogen atom of the pyridine ring interacts with the carbonyl group of Leu102 and the amide group of Met114 by water-mediated hydrogen bonds. These H-bond interactions play important roles in the interaction of imidacloprid with the residues in the active site of AChBP.[41] The guanidine moiety of imidacloprid forms $\pi-\pi$ stacking interactions with the aromatic ring of Tyr185. The methylene (CH_2-CH_2) bridge of imidacloprid and Trp143 form $CH-\pi$ contacts.

After validating the docking reliability, all these derivatives were docked into the active site of AChBP. The 55 compounds show similar binding modes. To more clearly identify the origins of the high insecticidal activity of the compound **26**, the detailed interactions of compounds **26** and **11** with AChBP are shown in Figure 5. In the docked complex of compound **26** and AChBP, the imidacloprid skeleton of compound **26** is buried deep in the binding site and mainly interacts with loop D (Phe52-Trp58), loop B (Gly141-His145), and loop C (Tyr185-Glu193). Some studies have shown that these loops are essential to the high neonicotinoid sensitivity of insect nAChRs.[41] The nitro and sulfonyl group of compound **26** form hydrogen bonds with the side chain atoms of Tyr192 and Gln73, respectively. The pyridine ring forms $\pi-\pi$ stacking interactions with conserved Tyr185, which are crucial to the binding of imidacloprid derivatives with AChBP. The pyridine ring also contacts with the aromatic ring of Trp143 and side chain of Met114. The chlorine atom on the pyridine ring contacts the hydroxyl group of conserved Tyr185. The guanidine moiety of imidacloprid contacts the side chain of Tyr192. Arg104 and the nitro group have electrostatic interactions. The methylene (CH_2-CH_2) bridge of imidacloprid contacts the side chains of Cys187 and Cys188. The methylbenzene group of compound **26** has van der Waals

dx.doi.org/10.1021/jf501108j | J. Agric. Food Chem. 2014, 62, 5429−5442

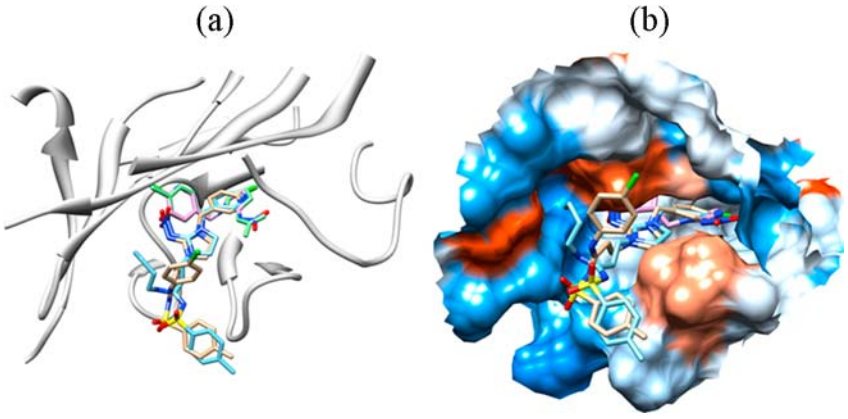

Figure 3. (a) The comparison of imidacloprid in the crystal structure and imidacloprid, compounds **26** and **11** in the docked complex by superimposing the coordinates of protein together. (b) A molecular surface of the active site of Ls-AChBP color-coded by amino acid hydrophobicity. The surface ranges from dodger blue for the most polar residues to orange−red for the most hydrophobic, with white in between. Imidacloprid in the crystal structure and imidacloprid, compounds **26** and **11** in the docked complex are shown in green, hot pink, orange, and cyan, respectively.

interactions with Cys188 and Pro189 of loop C. The main chain and side chain atoms of Arg104 form hydrogen bonds with main chain atom of Leu112 and side chain atom of Gln73, respectively (these H-bond interactions are not given in Figure 5). Under the influence of these hydrogen bonds, the side chain atoms of Leu112 contact with the aromatic ring of chloro-phenyl group.

The detailed interactions of compound **11** and residues of the active site of AChBP are shown in Figure 5b. The nitrogen atom (N4) of compound **11** and the side chain atom of Gln73 form one hydrogen bond. Like in compound **26**, the butyl group of compound **11** also contacts the side chain atoms of Leu112. The other interactions of compound **11** with AChBP are similar to the ones of compound **26**.

By comparing the binding mode and docking score of newly synthesized compounds and imidacloprid (shown in Figure 3.), the origin of the high insecticidal activity of the compound **26** can be identified. The docking scores of compound **26**, imidacloprid, and compound **11** are −7.078, −6.991, and −6.461, which are consistent with the insecticidal activity of these compounds. From the binding mode, in common, imidacloprid and the imidacloprid skeleton of compounds **26** and **11** are buried in the binding site and mainly interact with loop D (Phe52-Trp58), loop B (Gly141-His145), and loop C (Tyr185-Glu193). Several residues including Trp53, Met114, Trp143, Tyr185, and Tyr192 in the binding pocket form favorable hydrophobic and van der Waals interactions with imidacloprid and imidacloprid moieties of compound **26** and **11**. Differently, the methylbenzene groups of compound **26** and **11** form the additional van der Waals interactions with Cys188 and Pro189 compared with imidacloprid. The aromatic ring of chloro-phenyl group of compound **26** and the butyl group of compound **11** have favorable hydrophobic interactions with the side chain atoms of Leu112. Moreover, the hydrophobic contributions of aromatic ring of chloro-phenyl group of compound **26** are more favorable than ones of the butyl group of compound **11**. The nitrogen atom of the pyridine ring of imidacloprid forms hydrogen bonds with the carbonyl group of Leu102 and the amide group of Met114 by water. However, for compound **26**, there are two hydrogen bonds formed between the nitro group and the side chain atoms of Tyr192 and between the sulfonyl group and the side chain atoms of Gln73. For compound **11**, the nitrogen atom (N4) and the side chain atom of Gln73 form one hydrogen bond. Thus, the more favorable hydrophobic and van der Waals interactions and stronger hydrogen bonding interactions of compound **26** with the binding pocket contribute to its higher insecticidal activity.

QSAR Analysis. On the basis of the reasonable docked conformations, the following QSAR analysis was performed. GA method was used to select the most relevant descriptors to the insecticidal activities of these derivatives based on the training samples. The population size for the evolution was set to 100. Other parameters were set to the default value. The optimum number of variables (V_n) was selected when adding new descriptors did not improve the performance of the model significantly. Compared with the four-parameter model and five-parameter model, the six-parameter model with both higher internal and external predictive ability was adopted here.

The four-parameter and five-parameter models and corresponding statistical parameters were given as below:

$$\begin{aligned} pLC_{50} &= 0.01035T(O..Cl) - 0.66704EEig08d \\ &\quad + 0.04511RDF140u + 0.4984Mor12m \\ &\quad + 4.62595 \end{aligned}$$

$$N_{tr} = 46,\ N_{tst} = 10$$

$$R^2_{tr} = 0.7878,\ RMSE_{tr} = 0.1397$$

$$Q^2_{loo} = 0.7370,\ RMSE_{loo} = 0.1555$$

$$Q^2_{ext} = 0.7306,\ RMSE_{ext} = 0.1574$$

$$\begin{aligned} pLC_{50} &= 0.0097T(O..Cl) - 0.52152EEig08x \\ &\quad + 0.04153RDF140u + 0.56465Mor12m \\ &\quad + 0.40228Mor16m + 4.55723 \end{aligned}$$

$$N_{tr} = 46,\ N_{tst} = 10$$

$$R^2_{tr} = 0.9283,\ RMSE_{tr} = 0.0812$$

$$Q^2_{loo} = 0.9103,\ RMSE_{loo} = 0.0908$$

$$Q^2_{ext} = 0.8780,\ RMSE_{ext} = 0.1059$$

dx.doi.org/10.1021/jf501108j | J. Agric. Food Chem. 2014, 62, 5429−5442

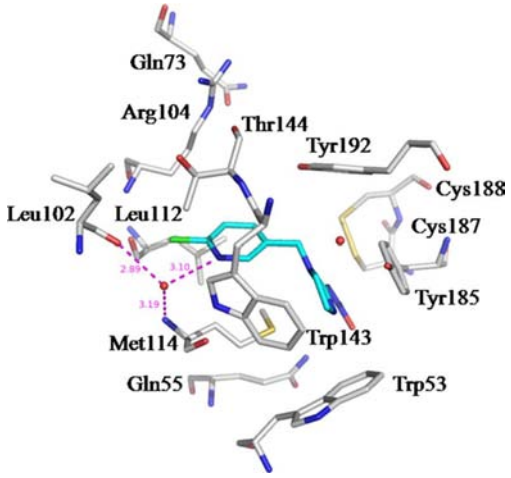

Figure 4. Interactions between imidacloprid and Ls-AChBP.

Compared with four-parameter model, the introduction of descriptor Mor16m into five-parameter model significantly improves the internal and external predictive abilities. The five-parameter model is statistically good with correlation coefficient R^2_{tr} of 0.9283, cross-validated correlation coefficient Q^2_{loo} of 0.9103, and the external validation coefficient Q^2_{ext} of 0.8780.

The best six-parameter model and corresponding statistical parameters were given as below:

$$\begin{aligned} pLC_{50} &= 0.00948T(O..Cl) - 0.65887EEig08x \\ &\quad + 0.52682BELm7 + 0.03658RDF140u \\ &\quad + 0.62012Mor12m + 0.40791Mor16m \\ &\quad + 4.31497 \end{aligned}$$

$$N_{tr} = 46,\ N_{tst} = 10$$

$$R^2_{tr} = 0.9479,\ RMSE_{tr} = 0.0692$$

$$Q^2_{loo} = 0.9287,\ RMSE_{loo} = 0.0810$$

$$Q^2_{ext} = 0.9270,\ RMSE_{ext} = 0.0819$$

Compared with five-parameter model, the external predictive ability of six-parameter model with Q^2_{ext} of 0.9270 was improved obviously by introducing the descriptor BELm7 (the lowest eigenvalue *n*, 7 of Burden matrix weighted by atomic masses).

The above results indicate that the built six-parameter model is stable, robust and predictive. The model exhibits a good external predictive ability with Q^2_{ext} of 0.9270 and $RMSE_{ext}$ of 0.0819. The experimental and predicted pLC_{50} are given in Table 5. The correlation plot of predicted and experimental values is shown in Figure 6. Figure 7 showed the Williams plot of the built model.

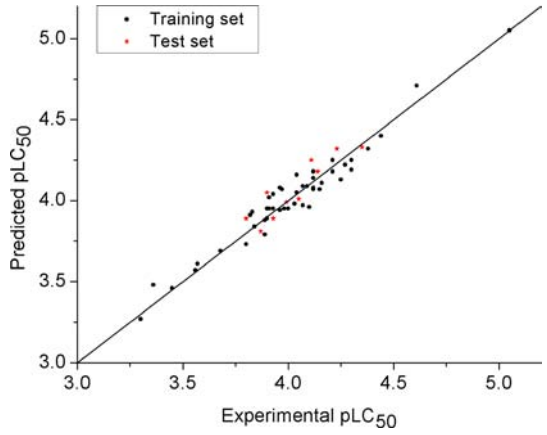

Figure 6. Experimental and predicted activities of target compounds in the training and test sets.

From Figure 7, it can be seen that the hat value (0.683) of imidacloprid is larger than the warning value (h^* = 0.457), and thus imidacloprid is considered as an *X* outlier. The molecular structure of imidacloprid differs greatly from other compounds. Moreover, the molecule docking also indicated the binding modes of this compound and other compounds with AChBP are different.

According to the regression model, the standardized regression coefficients (Std.Reg.Coeff) of the selected descriptors are 0.48696 (T(O..Cl)), −0.8566 (EEig08x), 0.25435 (BELm7), 0.47561 (RDF140u), 0.78685 (Mor12m), and 0.38254 (Mor16m),

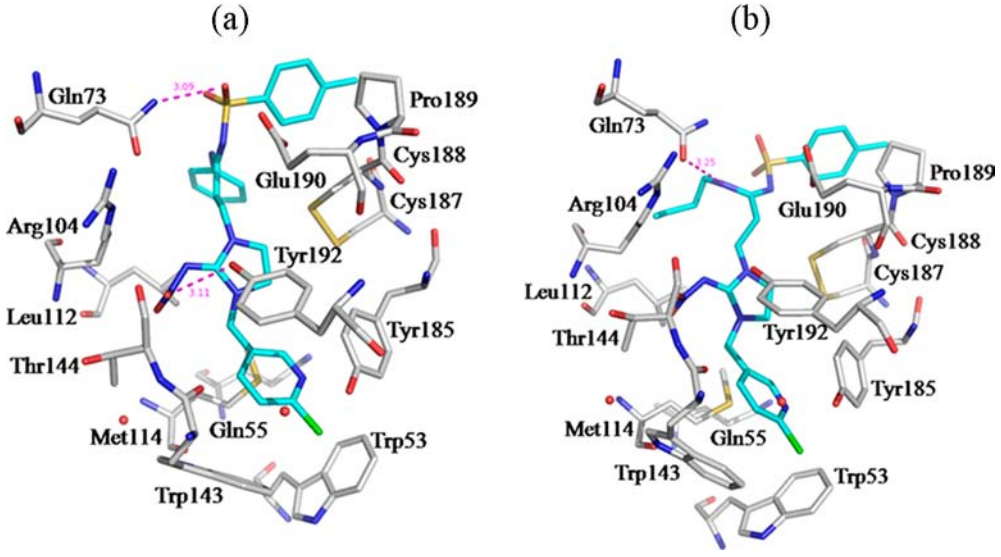

Figure 5. Binding mode of compounds **26** and **11** with Ls-AChBP. (a) Detailed interactions of compound **26** with the active site of Ls-AChBP. (b) Detailed interactions of compound **11** with the active site of Ls-AChBP.

dx.doi.org/10.1021/jf501108j | J. Agric. Food Chem. 2014, 62, 5429−5442

Table 5. Experimental and Predicted Activities against *A. craccivora* in the QSAR Model

no.	compd	exp pLC_{50}	pred pLC_{50}	absolute error
1	**1**	4.44	4.4	−0.04
2	**10**	4.1	3.96	−0.14
3	**11**[a]	4.05	4.01	−0.04
4	**12**	3.97	4.07	0.1
5	**13**[a]	3.93	3.89	−0.04
6	**14**	3.93	3.95	0.02
7	**15**	3.45	3.46	0.01
8	**16**	3.3	3.27	−0.03
9	**17**	4.03	3.98	−0.05
10	**18**[a]	4.23	4.32	0.09
11	**19**	3.93	4.04	0.11
12	**20**	4	3.95	−0.05
13	**21**[a]	3.9	4.05	0.15
14	**22**	3.8	3.73	−0.07
15	**23**	4.25	4.13	−0.12
16	**24**	4.3	4.19	−0.11
17	**25**	3.91	4.02	0.11
18	**26**	5.05	5.05	0
19	**27**	3.68	3.69	0.01
20	**28**	4.3	4.25	−0.05
21	**29**	3.96	3.94	−0.02
22	**30**	3.84	3.84	0
23	**31**	4.38	4.32	−0.06
24	**32**	3.96	4.08	0.12
25	**33**	3.9	3.95	0.05
26	**34**	3.36	3.48	0.12
27	**35**	4.09	4.09	0
28	**36**	3.83	3.93	0.1
29	**37**	3.89	3.79	−0.1
30	**38**[a]	3.8	3.89	0.09
31	**39**	4.15	4.07	−0.08
32	**40**	3.89	3.88	−0.01
33	**41**[a]	4.11	4.25	0.14
34	**42**	3.82	3.91	0.09
35	**43**	4.12	4.07	−0.05
36	**44**	4.27	4.22	−0.05
37	**45**	4.16	4.11	−0.05
38	**46**	3.56	3.57	0.01
39	**47**	4.12	4.18	0.06
40	**48**	4.21	4.25	0.04
41	**49**[a]	4.14	4.18	0.04
42	**50**	3.57	3.61	0.04
43	**51**	4.12	4.14	0.02
44	**52**	3.98	3.95	−0.03
45	**53**	4.07	4.09	0.02
46	**54**	4.07	3.97	−0.1
47	**55**	3.91	3.95	0.04
48	**56**	4.04	4.16	0.12
49	**57**	4.61	4.71	0.1
50	**58**[a]	3.87	3.81	−0.06
51	**59**	3.9	3.89	−0.01
52	**60**	4.12	4.08	−0.04
53	**61**	4.04	4.05	0.01
54	**62**	4.21	4.18	−0.03
55	**63**[a]	3.99	3.99	0
56	**64**[a]	4.35	4.33	−0.02

[a]Compounds in test set.

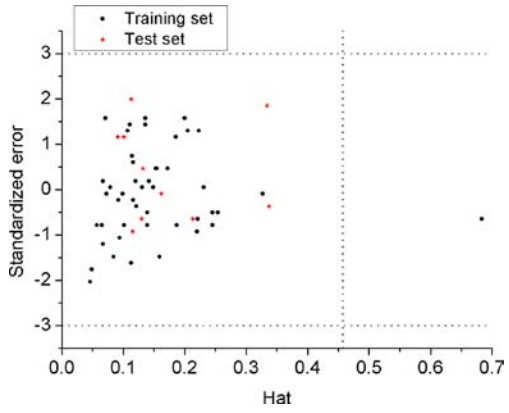

Figure 7. Williams plot of the training and test sets. The dashed lines are the warning value of hat (h^* = 0.457) and the 3σ limit, respectively.

respectively. The Std.Reg.Coeff determined the relative importance of these descriptors. The most important descriptor is an edge adjacency index EEig08x (eigenvalue 8 from edge adjacency matrix weighted by edge degrees).[53] This descriptor can reflect the molecular complexity and branching. The negative correlation coefficient of this descriptor indicates the larger the value of this descritpor is, the lower the biological activity of the compound is. The second important descriptor Mor12m is a 3D-molecule representation of structures based on electron diffraction (3D-MoRSE) descriptor. Mor12m is weighted by atomic masses.[54] It suggested that the molecular size has a close correlation with the activities of the studied compounds. The third important descriptor is T(O..Cl) descriptor (topological descriptors) representing the sum of topological distances between O and Cl.[55] From the above molecular docking analysis, the O and Cl atoms are involved in the formation of hydrogen bond between these derivatives and AChBP. The selection of the descriptor T(O..Cl) indicates the ability to form hydrogen bond of compounds has a high correlation with their activities. RDF140u (radial distribution function at 14.0 Å/unweighted) belongs to RDF descriptors which can be interpreted as the probability distribution of finding an atom in a spherical volume of radius R.[56] The RDF descriptors can provide information such as interatomic distances in the entire molecule, bond distances, ring types, planar, and nonplanar systems and atom types. Mor16m descriptor is another 3D-MoRSE descriptor. BELm7 is the lowest eigenvalue n 7 of Burden matrix weighted by atomic masses.[57] The Burden descriptors can reflect relevant aspects of molecular structure and are therefore useful for similarity searching. Except EEig08x, all other five descriptors have a positive correlation with the insecticidal activities of the studied compounds, indicating that the increase of the value of the descriptor will improve the biological activity of the compound in the application domain of the built model.

In summary, three novel series of N_3-substituted imidacloprid derivatives were designed and synthesized, and their structures were characterized by NMR spectroscopy, mass spectrometry, elemental analysis, and single-crystal X-ray diffraction analysis. The insecticidal activities against *Aphis craccivora* were evaluated. Preliminary bioassays indicated that some title compounds exhibited excellent insecticidal activities against *Aphis craccivora*, and their insecticidal activities against *Aphis craccivora* were comparable to those of the control imidacloprid. SAR analysis indicated that the size, electron density, and distribution of the substituents at the N_3 position are critical to the derivatives' activity. Furthermore, the

dx.doi.org/10.1021/jf501108j | J. Agric. Food Chem. 2014, 62, 5429−5442

molecular docking analysis indicated that imidacloprid and compounds **26** and **11** form the similar hydrophobic and van der Waals interactions with Trp53, Met114, Trp143, Tyr185, and Tyr192 in the binding pocket. Compared with imidacloprid, the more favorable van der Waals and hydrophobic interactions from the methylbenzene group and the aromatic ring of chloro-phenyl group of compound **26**, and stronger hydrogen bonding interactions from the nitro and sulfonyl group with the binding pocket contribute to higher insecticidal activity. From the QSAR analysis, the molecular size, shape, and the ability to form hydrogen bond are important for insecticidal potency. From the built QSAR model, the decrease of the value of selected descriptor EEig08x and the increase of the value of other descriptors will be favorable to improve the insecticidal activity of compound. These results can promote the understanding the interaction mechanism of these derivatives and nAChR and provide the useful information for further structural modification. Further structural optimization and mode of action studies are currently underway in our laboratories

■ ASSOCIATED CONTENT

Supporting Information

Melting point,^{1}H NMR, ^{13}C NMR, elemental analysis, and ESI-MS spectra for the target compounds. This material is available free of charge via the Internet at http://pubs.acs.org.

■ AUTHOR INFORMATION

Corresponding Authors

*For Y.-Q.L.: phone, +86(0)931-8618795; fax, +86(0)931-8915686; E-mail, yqliu@lzu.edu.cn.

*For H.-X.L.: phone, +86(0)931-8618795; fax, +86(0)931-8915686; E-mail, hxliu@lzu.edu.cn.

Author Contributions

§These authors contributed equally to this work.

Funding

This work was supported financially by the National Natural Science Foundation of China (30800720, 31371975, 31360451), the Fundamental Research Funds for the Central Universities (lzujbky-2013-69), and the Young Scholars Science Foundation of Lanzhou Jiaotong University (2011011).

Notes

The authors declare no competing financial interest.

■ REFERENCES

(1) Jeschke, P.; Nauen, R. Neonicotinoids—from zero to hero in insecticide chemistry. *Pest Manage. Sci.* **2008**, *64*, 1084−1098.

(2) Nauen, R.; Ebbinghaus, U.; Tietjen, K. Ligands of the nicotinic acetylcholine receptor as insecticides. *Pestic. Sci.* **1999**, *55*, 566−614.

(3) Tomizawa, M.; Kagabu, S.; Casida, J. E. Receptor Structure-Guided Neonicotinoid Design. *J. Agric. Food Chem.* **2011**, *59*, 2918−2922.

(4) Jeschke, P.; Nauen, R.; Schindler, M.; Elbert, A. Overview of the status and global strategy for neonicotinoids. *J. Agric. Food Chem.* **2011**, *59*, 2897−2908.

(5) Elbert, A.; Haas, M.; Springer, B.; Thielert, W.; Nauen, R. Applied aspects of neonicotinoid uses in crop protection. *Pest. Manage. Sci.* **2008**, *64*, 1099−1105.

(6) Uneme, H. Chemistry of clothianidin and related compounds. *J. Agric. Food Chem.* **2011**, *59*, 2932−2937.

(7) Maienfisch, P.; Angst, M.; Brandl, F.; Fischer, W.; Hofer, D.; Kayser, H.; Kobel, W.; Rindlisbacher, A.; Senn, R.; Steinemann, A.; Widmer, H. Chemistry and biology of thiamethoxam: a second generation neonicotinoid. *Pest. Manage. Sci.* **2001**, *57*, 906−913.

(8) Kovganko, N. V.; Kashkan, Z. N. Advances in the Synthesis of Neonicotinoids. *Russ. J. Org. Chem.* **2004**, *40*, 1709−1726.

(9) Nauen, R.; Denholm, I. Resistance of insect pests to neonicotinoid insecticides: current status and future prospects. *Arch. Insect Biochem. Physiol.* **2005**, *58*, 200−215.

(10) Ninsin, K. D. Acetamiprid resistance and cross-resistance in the diamondback moth *Plutella xylostella*. *Pest Manage. Sci.* **2004**, *60*, 839−841.

(11) Sanchez, D. M.; Hollingworth, R. M.; Grafius, E. J.; Moyer, D. D. Resistance and cross-resistance to neonicotinoid insecticides and spinosad in the Colorado potato beetle, *Leptinotarsa decemlineata* (Say) (Coleoptera: Chrysomelidae). *Pest. Manage. Sci.* **2006**, *62*, 30−37.

(12) Gorman, K. G.; Devine, G.; Bennison, J.; Coussons, P.; Punchard, N.; Denholm, I. Report of resistance to the neonicotinoid insecticide imidacloprid in *Trialeurodes vaporariorum* (Hemiptera: Aleyrodidae). *Pest. Manage. Sci.* **2007**, *63*, 555−558.

(13) Liu, Z. W.; Williamson, M. S.; Lansdell, S. J.; Denholm, I.; Han, Z. J.; Millar, N. S. A nicotinic acetylcholine receptor mutation conferring target-site resistance to imidacloprid in *Nilaparvata lugens* (brown planthopper). *Proc. Natl. Acad. Sci. U. S. A.* **2005**, *102*, 8420−8425.

(14) Jeschke, P.; Nauen, R.; Sparks, T. C.; Loso, M. R.; Watson, G. B.; Babcock, J. M.; Kramer, V. J.; Zhu, Y.; Nugent, B. M.; Thomas, J. D.; Crouse, G. D.; Dripps, J. E.; Waldron, C.; Salgado, V. L.; Schnatterer, S.; Holmes, K. A.; Pitterna, T. Nervous System. In *Modern Crop Protection Compounds*, 2nd ed.; Krämer, W., Schirmer, U., Jeschke, P., Witschel, M. Eds.; Wiley-VCH Verlag GmbH & Co. KGaA: Weinheim, Germany, 2012; Vol. *1*−*3*, Chapter 32.

(15) Su, W. C.; Zhou, Y. H.; Ma, Y. Q.; Wang, L.; Zhang, Z.; Rui, C. H.; Duan, H. X.; Qin, Z. H. *N*′-Nitro-2-hydrocarbylidenehydrazinecarboximidamides: design, synthesis, crystal structure, insecticidal activity, and structure−activity relationships. *J. Agric. Food Chem.* **2012**, *60*, 5028−5034.

(16) Tian, Z. Z.; Shao, X. S.; Li, Z.; Qian, X. H.; Huang, Q. C. Synthesis, insecticidal activity, and QSAR of novel nitromethylene neonicotinoids with tetrahydropyridine fixed cis configuration and exoring ether modification. *J. Agric. Food Chem.* **2007**, *55*, 2288−2292.

(17) Shao, X. S.; Li, Z.; Qian, X. H.; Xu, X. Y. Design, synthesis, and insecticidal activities of novel analogues of neonicotinoids: replacement of nitromethylene with nitroconjugated system. *J. Agric. Food Chem.* **2009**, *57*, 951−957.

(18) Tomizawa, M.; Durkin, K. A.; Ohno, I.; Nagura, K.; Manabe, M.; Kumazawa, S.; Kagabu, S. *N*-Haloacetylimino neonicotinoids: potency and molecular recognition at the insect nicotinic receptor. *Bioorg. Med. Chem. Lett.* **2011**, *21*, 3583−3586.

(19) Ye, Z. J.; Shi, L. N.; Shao, X. S.; Xu, X. Y.; Xu, Z. P.; Li, Z. Pyrrole- and Dihydropyrrole-Fused Neonicotinoids: Design, Synthesis, and Insecticidal Evaluation. *J. Agric. Food Chem.* **2013**, *61*, 312−319.

(20) Zhang, W. W.; Yang, X. B.; Chen, W. D.; Xu, X. Y.; Li, L.; Zhai, H. B.; Li, Z. Design, multicomponent synthesis, and bioactivities of novel neonicotinoid analogues with 1,4-dihydropyridine scaffold. *J. Agric. Food Chem.* **2010**, *58*, 2741−2745.

(21) Yu, H. B.; Qin, Z. F.; Dai, H.; Zhang, X.; Qin, X.; Wang, T. T.; Fang, J. X. Synthesis and insecticidal activity of *N*-substituted (1,3-thiazole)alkyl sulfoximine derivatives. *J. Agric. Food Chem.* **2008**, *56*, 11356−11360.

(22) Zhu, Y. M.; Loso, M. R.; Watson, G. B.; Sparks, T. C.; Rogers, R. B.; Huang, J. X.; Gerwick, B. C.; Babcock, J. M.; Kelley, D.; Hegde, V. B.; Nugent, B. M.; Renga, J. M.; Denholm, I.; Gorman, K.; DeBoer, G. J.; Hasler, J.; Meade, T.; Thomas, J. D. Discovery and characterization of sulfoxaflor, a novel insecticide targeting sap-feeding pests. *J. Agric. Food Chem.* **2011**, *59*, 2950−2957.

(23) Shao, X. S.; Fu, H.; Xu, X. Y.; Xu, X. L.; Liu, Z. W.; Li, Z.; Qian, X. H. Divalent and oxabridged neonicotinoids constructed by dialdehydes and nitromethylene analogues of imidacloprid: design, synthesis, crystal structure, and insecticidal activities. *J. Agric. Food Chem.* **2010**, *58*, 2696−2702.

(24) Ohno, I.; Hirata, K.; Ishida, C.; Ihara, M.; Matsuda, K.; Kagabu, S. Proinsecticide candidates *N*-(5-methyl-2-oxo-1, 3-dioxol-4-yl)-methyl derivatives of imidacloprid and 1-chlorothiazolylmethyl-2-nitroiminoimidaz olidine. *Bioorg. Med. Chem. Lett.* **2007**, *17*, 4500−4503.
(25) Zhang, W. W.; Chen, Y. B.; Chen, W. D.; Liu, Z. W.; Li, Z. Designing tetrahydroimidazo[1,2-*a*]pyridine derivatives via catalyst-free Aza-Diels−Alder reaction (ADAR) and their insecticidal evaluation. *J. Agric. Food Chem.* **2010**, *58*, 6296−6299.
(26) Ohno, I.; Tomizawa, M.; Durkin, K. A.; Casida, J. E.; Kagabu, S. Bis-neonicotinoid insecticides: observed and predicted binding interactions with the nicotinic receptor. *Bioorg. Med. Chem. Lett.* **2009**, *19*, 3449−3452.
(27) Kagabu, S.; Takagi, M.; Ohno, I.; Mikawa, T.; Miyamoto, T. Crown-capped imidacloprid: a novel design and insecticidal activity. *Bioorg. Med. Chem. Lett.* **2009**, *19*, 2947−2948.
(28) Nishiwaki, H.; Nakagawa, Y.; Ueno, T.; Kagabu, S.; Nishimura, K. Insecticidal and binding activities of N_3-substituted imidacloprid derivatives against the housefly *Musca domestica* and the α-bungarotoxin binding sites of nicotinic acetylcholine receptors. *Pest. Manage. Sci.* **2001**, *57*, 810−814.
(29) Wu, J.; Song, B. A.; Hu, D. Y.; Yue, M.; Yang, S. Design, synthesis and insecticidal activities of novel pyrazole amides containing hydrazone substructures. *Pest. Manage. Sci.* **2012**, *68*, 801−810.
(30) Zhang, J. F.; Xu, J. Y.; Wang, B. L.; Li, Y. X.; Xiong, L. X.; Li, Y. Q.; Ma, Y.; Li, Z. M. Synthesis and insecticidal activities of novel anthranilic diamides containing acylthiourea and acylurea. *J. Agric. Food Chem.* **2012**, *60*, 7565−7572.
(31) Wang, B. L.; Zhu, H. W.; Ma, Y.; Xiong, L. X.; Li, Y. Q.; Zhao, Y.; Zhang, J. F.; Chen, Y. W.; Zhou, S.; Li, Z. M. Synthesis, insecticidal activities, and SAR studies of novel pyridylpyrazole acid derivatives based on amide bridge modification of anthranilic diamide insecticides. *J. Agric. Food Chem.* **2013**, *61*, 5483−5493.
(32) Song, H. J.; Liu, Y. X.; Xiong, L. X.; Li, Y. Q.; Yang, N.; Wang, Q. M. Design, synthesis, and insecticidal evaluation of new pyrazole derivatives containing imine, oxime ether, oxime ester, and dihydroisoxazoline groups based on the inhibitor binding pocket of respiratory complex I. *J. Agric. Food Chem.* **2013**, *61*, 8730−8736.
(33) Greenhill, J. V.; Lue, P. Amidines and guanidines in medicinal chemistry. *Prog. Med. Chem.* **1993**, *30*, 203−326.
(34) Loso, M. R.; Nugent, B. M.; Zhu, Y.; Rogers, R. B.; Huang, J. X.; Renga, J. M.; Whiteker, G. T.; Breaux, N. T.; Daeuble, J. F. Heteroaryl (substituted) alkyl *N*-substituted sulfoximines as insecticides. World Patent WO 057131, 2008.
(35) Kolb, H. C.; Sharpless, K. B. The growing impact of click chemistry on drug discovery. *Drug Discovery Today* **2003**, *8*, 1128−1137.
(36) Yang, W.; Wu, H. X.; Xu, H. H.; Hu, A. L.; Lu, M. L. Synthesis of glucose−fipronil conjugate and its phloem mobility. *J. Agric. Food Chem.* **2011**, *59*, 12534−12542.
(37) Casini, A.; Scozzafava, A.; Mastrolorenzo, A.; Supuran, C. T. Sulfonamides and sulfonylated derivatives as anticancer agents. *Curr. Cancer Drug Targ.* **2002**, *2*, 55−75.
(38) Lamberth, C. Sulfur chemistry in crop protection. *J. Sulfur Chem.* **2004**, *25*, 39−69.
(39) Morris, G. *SYBYL software*, version 6.9; Tripos Associates: St Louis, MO, 2002.
(40) *Ligprep*, version 2.3; Schrodinger LLC: New York, , 2009.
(41) Ihara, M.; Okajima, T.; Yamashita, A.; Oda, T.; Hirata, K.; Nishiwaki, H.; Morimoto, T.; Akamatsu, M.; Ashikawa, Y.; Kuroda, S. i. Crystal structures of *Lymnaea stagnalis* AChBP in complex with neonicotinoid insecticides imidacloprid and clothianidin. *Invertebr. Neurosci.* **2008**, *8*, 71−81.
(42) Sun, C.; Yang, D.; Xing, J.; Wang, H.; Jin, J.; Zhu, J. Nitromethylene neonicotinoids analogues with tetrahydropyrimidine fixed cis-configuration: synthesis, insecticidal activities, and molecular docking studies. *J. Agric. Food Chem.* **2010**, *58*, 3415−3421.
(43) Sun, C.; Xu, X.; Xu, Y.; Yan, D.; Fang, T.; Liu, T. Synthesis, insecticidal activity, and molecular docking studies of nitenpyram analogues with a flexible ester arm anchored on tetrahydropyrimidine ring. *J. Agric. Food Chem.* **2011**, *59*, 4828−4835.
(44) *Glide*, version, 5.5; Schrödinger LLC: New York, 2009.
(45) Talete, S. *Dragon for Windows (Software for Molecular Descriptor Calculations)*, version 5.4; Talete, Srl: Milano, Italy, 2006; http://www.talete.mi.it.
(46) Papa, E.; Villa, F.; Gramatica, P. Statistically Validated QSARs, Based on Theoretical Descriptors, for Modeling Aquatic Toxicity of Organic Chemicals in *Pimephales promelas* (Fathead Minnow). *J. Chem. Inf. Model.* **2005**, *45*, 1256−1266.
(47) Gharagheizi, F. QSPR analysis for intrinsic viscosity of polymer solutions by means of GA-MLR and RBFNN. *Comput. Mater. Sci.* **2007**, *40*, 159−167.
(48) Saxena, A.; Prathipati, P. Comparison of MLR, PLS and GA-MLR in QSAR analysis. *SAR QSAR Environ. Res.* **2003**, *14*, 433−445.
(49) Todeschini, R.; Consonni, V.; Pavan, M. *MOBYDIGS Software (Version 1.2) for Windows*; Talete Srl: Milan, Italy, 2002.
(50) Yoo, E. J.; Ahlquist, M.; Bae, I.; Sharpless, K. B.; Fokin, V. V.; Chang, S. Mechanistic studies on the Cu-catalyzed three-component reactions of sulfonyl azides, 1-alkynes and amines, alcohols, or water: dichotomy via a common pathway. *J. Org. Chem.* **2008**, *73*, 5520−5528.
(51) Zhao, Y.; Li, Y. Q.; Wang, S. H.; Li, Z. M. Design, synthesis, and insecticidal activity of novel neonicotinoid derivatives containing *N*-oxalyl groups. *ARKIVOC* **2009**, *xi*, 152−164.
(52) Matsuda, K.; Buckingham, S. D.; Kleier, D.; Rauh, J. J.; Grauso, M.; Sattelle, D. B. Neonicotinoids: insecticides acting on insect nicotinic acetylcholine receptors. *Trends Pharmacol. Sci.* **2001**, *22*, 573−580.
(53) Estrada, E. Edge adjacency relationships in molecular graphs containing heteroatoms: a new topological index related to molar volume. *J. Chem. Inf. Comput. Sci.* **1995**, *35*, 701−707.
(54) Schuur, J. H.; Selzer, P.; Gasteiger, J. The coding of the three-dimensional structure of molecules by molecular transforms and its application to structure-spectra correlations and studies of biological activity. *J. Chem. Inf. Comput. Sci.* **1996**, *36*, 334−344.
(55) Todeschini, R.; Consonni, V. *Handbook of Molecular Descriptors*; Wiley: New York, 2008.
(56) Hemmer, M. C.; Steinhauer, V.; Gasteiger, J. Deriving the 3D structure of organic molecules from their infrared spectra. *Vib. Spectrosc.* **1999**, *19*, 151−164.
(57) Burden, F. R. Molecular identification number for substructure searches. *J. Chem. Inf. Comput. Sci.* **1989**, *29*, 225−227.

JOURNAL OF AGRICULTURAL AND FOOD CHEMISTRY

Article

pubs.acs.org/JAFC

High-Performance Liquid Chromatography Analysis of Phenolic Acid, Flavonoid, and Phenol Contents in Various Natural Yemeni Honeys Using Multi-walled Carbon Nanotubes as a Solid-Phase Extraction Adsorbent

A. Y. Badjah Hadj Ahmed,[†] Munir S. Obbed,[†] Saikh M. Wabaidur,*[,†] Zeid A. AlOthman, and Nora H. Al-Shaalan[‡]

[†]Advanced Materials Research Chair, Department of Chemistry, College of Science, King Saud University, Post Office Box 2455, Riyadh 11451, Kingdom of Saudi Arabia

[‡]Department of Chemistry, College of Science, Princess Nora Bint Abdul Rahman University, Riyadh, Saudi Arabia

ABSTRACT: A simple method has been described for simultaneous determination of phenolic acid, flavonoid, and other phenol contents in various natural honey samples collected from various regions of Yemen. Multi-walled carbon nanotubes were used as a solid-phase adsorbent for extraction of the polyphenols from honey samples. The total contents of phenolic acids, flavonoids, and phenolic components of the 12 different samples were found in the range of 363−2658, 261−1646, and 224−1355 μg/100 g of honey samples, respectively. The major phenolic acid, flavonoid, and phenolic compound in these samples were found to be 4-hydroxybenzoic acid (1410 μg/100 g), chrysin (850 μg/100 g), and cinnamic acid (1336 μg/100 g), respectively. A total of 25 compounds (10 phenolic acids, 9 flavonoids, and 6 phenols) were analyzed, and a total of 24 were detected, while only 23 compounds were determined quantitatively in the honey samples. The developed method showed potential usefulness for the analysis of honey and was used for the determination of polyphenols in honey extracts.

KEYWORDS: *liquid chromatography, honey, phenolic acids, flavonoids, phenols*

INTRODUCTION

Honey is a delicious viscous sweetener, which is made naturally by bees.[1] During the feast on flower, the bees collect the flower nectar and mix it with saliva inside their mouth to produce honey; they deposit it into the cells of the walls of the hive.[2] The honey can be made from a variety of different flowers, while its flavor and texture vary with the type of flower nectar from which it was collected.[2] Honey is a pure product and does not allow for the addition of any other substance.[3,4]

From the ancient times, honey has been used as both a confectionary food and a medicine. Many authors have reported that honey is a rich source of flavonoids and phenolic acids, which are mainly responsible for its significant antioxidant capacity.[5−9] It was reported that these phenolic constituents and flavonoids in honey could also be responsible for many pharmacologic effects, including wound healing,[10] contributing to the protection of cultured skin cells and tissues from oxidative damage,[11] and food preservation.[12,13] In addition, the quality of honey and its price is mainly evaluated on the basis of its floral origin and chemical composition.[14] Therefore, it is important to analyze honey and find out which flavonoids and phenolic compounds are present and in what amount.

Yemeni honey is a type of honey reputed for its flavor and medicinal qualities. It is a type of monofloral honey that has a characteristic taste because of the fact that the bees that produce it generally only gather nectar from one type of flower, the flowers of the "Sidr" tree (*Ziziphus spina-christi* L.). Numerous analytical methods have been reported in the literature for the analysis of honey contents and to make a correlation with floral source.[15−20] Many authors have reported the liquid chromatographic techniques for the analysis of organic acids in honey; these methods have proven to be very useful in determining the authenticity of the sample from the floral and geographical origin of honey.[15,18,21−23]

The aim of the present study was the separation and simultaneous quantitation of total phenolic acids, flavonoids, and phenols of various natural Yemeni honey using high-performance liquid chromatography (HPLC) and ultraviolet (UV) absorbance detection. Multi-walled carbon nanotubes (MWCNTs) were used as a solid-phase adsorbent for extraction of the polyphenols from honey samples, which show excellent recovery and regeneration properties. The developed HPLC−UV method was simple, sensitive, and easy to apply for routine analysis, and it would be a potential step forward in the analysis of various honey samples.

MATERIALS AND METHODS

Chemicals and Reagents. All solvents used were of HPLC grade. 4-Hydroxybenzoic acid, carvacrol, clorogenic acid, maleic acid, naringenin, and sinapic acid were purchased from Aldrich Chemicals Co. (Milwaukee, WI). Apigenin, caffeic acid, galangin, gallic acid, kaempferol, luteolin, *p*-coumaric acid, and quercetin were purchased from Sigma Chemicals Co. (St. Louis, MO). Acetic acid, acetonitrile, diethyl ether, ethanol, formic acid, hydrochloric acid, methanol, and

Received: March 12, 2014
Revised: May 28, 2014
Accepted: May 28, 2014
Published: May 28, 2014

ACS Publications © 2014 American Chemical Society

dx.doi.org/10.1021/jf5011758 | *J. Agric. Food Chem.* 2014, 62, 5443−5450

anhydrous sodium carbonate were purchased from BDH Chemicals Co. (U.K.). 4-Hydroxyphenyl acetic acid, chrysin, myricetin, naringin, syringic acid, thymol, and vanillic acid were purchased from Acros Organics (Morris Plains, NJ). Potassium acetate was purchased from Riedel de Haen Co. (Seelze, Germany). Benzoic acid was from Winlab. Cinnamic acid was from SAFC. Ferulic acid was from Fluka (St. Louis, MO). Phenol was from Merck (White House Station, NJ). Sodium sulfate was from Koch-Light Lab., Ltd. (Haverhill, Suffolk, U.K.). MWCNTs were from Timesnano (Chengdu Organic Chemicals Co., Ltd., China). Ultrapure water used for HPLC mobile phase and sample preparation was obtained using a Milli-Q water purification instrument from Millipore (Bedford, MA).

Sample Collection. All of the analyzed honey samples were collected from beehives fed with jujube flowers. Jujube (*Z. spina-christi* L.) is an evergreen tree native to southern and western Asia. It grows up to an elevation of 500 m. Mainly, 12 kinds of jujube honey from various Yemeni regions were collected in different harvesting seasons, to investigate the effect of geographical origin on the profile of polyphenols in honey composition. The samples were named as 1, 2, 3, 4, 5, 6, 7, 8, 9, 10, 11, and 12. All of these samples were preserved at a temperature below 0 °C. The production year and region of collection of these aforementioned honey samples are listed in Table 1.

Table 1. Jujube Honey Sample Collection Region and Year of Harvesting

sample	region (Yemen)	harvest (year)
1	Hadramout	2008
2	Hadramout	2011
3	Hadramout	2010
4	Hadramout	2009
5	Hadramout	2009
6	Hadramout	2009
7	Hadramout	2010
8	Hadramout	2010
9	Shabwa	2009
10	Hadja	2011
11	Dhamar	2010
12	Imran	2011

Extraction Procedure. In the present study, MWCNTs were used as a solid-phase adsorbent for extraction of the polyphenols from honey samples. The unique chemical, physical, mechanical, and thermal properties of MWCNTs provide exceptionally better sorption capacity and high stability to the extraction procedure.[24−26] Additionally, their unique properties in combination with their cave structure and ability to form a wide range of interactions with foreign molecules make their application highly useful for achieving efficient extraction methodologies.[27,28] The characteristics of the used MWCNTs in the extraction procedure are as follows: length, ∼30 μm; outer diameter, <8 nm; purity, >95 wt %; ash, <1.5 wt %; and specific surface area, >500 m^2/g. First, a 200 g sample of each honey was dissolved thoroughly in three parts of distilled water (200 mL each), and the solution was acidified with HCl at pH 2.0. To perform the solid-phase extraction of the phenolic compounds, 1 g of MWCNTs was added to this acidified aqueous solution of honey. The prepared mixture solution was then magnetically stirred for 20−30 min; the extreme large surface area and the unique tubular structure of MWCNTs[29,30] allow for the adsorption of honey phenolics onto that.[31] The MWCNTs were then being separated by vacuum filtration on a cellulose nitrate membrane filter (47 mm diameter and 0.45 μm porosity). After that, the separated MWCNTs were washed first with 100 mL of acidified water (at pH 2.0) and then with 300 mL of ultrapure water to remove sugars and other polar constituents.[32] Therefore, the phenolic compounds retained on the surface of MWCNTs were eluted with methanol (300 mL). This elute was then concentrated under reduced pressure in a rotary evaporator (Buchi, model V-850, Switzerland) at around 40 °C. The residue substance was then mixed with distilled water (6 mL), extracted with diethyl ether (5 mL × 3), and then reconcentrated by removing diethyl ether with nitrogen flushing. Finally, this concentrated residue was dissolved in 2 mL of methanol, filtered through a 0.45 μm membrane filter, and injected into the HPLC system. The washed MWCNTs can further be solvent-cleaned and then used for extraction of polyphenols from another honey sample.

Instrumentation. The HPLC analyses of phenolic acid, flavonoid, and phenol contents were performed using a Finnigan Surveyor Plus system from Thermo Scientific (Waltham, MA), equipped with a quaternary LC Pump Plus, a photodiode array (PDA) detector (PDA Plus), and an Autosampler Plus. The chromatographic separation of honey samples was performed using a reversed-phase column Betasil C_{18} column (Thermo Scientific, Waltham, MA), 150 mm length and 4.6 mm inner diameter, packed with a particle having a size of 3 μm. Several mobile phases of various compositions of water, acetonitrile, methanol, and mixtures of 1% formic acid aqueous solution with methanol or acetonitrile were tested at different flow rates (in the range of 0.2−1 mL/min) in both isocratic and gradient elution modes to achieve the best separations of the samples. The PDA detection wavelengths were investigated in the range between 200 and 600 nm.[28] The effect of the column oven temperature was also checked from 30 to 60 °C. The standards and honey extracts were injected to the system with an auto-injector, and the total flavonoids and phenolic compounds were detected using a PDA detector. A Welch Duo-Seal vacuum pump (model 1400, Niles, IL) was used for sample filtration. A shaker (Janke and Kunkel IKA Labortechnik Ks501D) was used for mixing the solutions, and a pH meter (Metrohm 6.0228.000) was used for mixing and pH measurements of the samples.

RESULTS AND DISCUSSION

Optimization of Chromatographic Conditions. The preliminary studies were carried out on a standard solution including 25 flavonoids and phenolic compounds. The optimization of chromatographic conditions was performed to obtain the best separation and a good peak resolution and to avoid peak tailing of the target compounds. To find the optimum HPLC conditions for all of these 25 compounds, the different chromatographic parameters, such as mobile-phase composition, flow rate, and detection wavelength, have been investigated. We have carried out several experiments using the mobile-phase flow rate between 0.1 and 0.5 mL/min and used different solvents (water, acetonitrile, and methanol) as the binary mixture with various compositions, in either isocratic or gradient elution mode. In gradient elution, different solvent programs were tested for each mixture.

The best separation in the shortest time was achieved using a linear gradient elution mode with a binary mobile phase mixture of aqueous 1% formic acid (A) and methanol (B) at a constant flow rate of 0.2 mL/min. The initial composition was 85% A, was decreased linearly to 20% in 70 min, and then remains constant up to the total run time of the system of 90 min. The temperature of the column oven was set at 40 °C. The samples were injected with an autosampler, and the constituents were detected using a PDA detector to obtain the UV spectrum of each of the various phenolic acids, flavonoids, and phenols. The chromatograms of all standard samples were monitored in the range of 200−600 nm, but 270 nm was chosen as the optimum, because the majority of the honey flavonoids and phenolic acids show their UV absorption maxima around this wavelength (Figure 1), which is in good agreement with the reported results obtained by Martos et al.[33] The injection volume was 10 μL for all samples. For convenience, the UV wavelength corresponding to the absorbance maximum of each individual component with its retention time is tabulated in Table 2. The table also lists the abbreviation of each analyte.

dx.doi.org/10.1021/jf5011758 | J. Agric. Food Chem. 2014, 62, 5443−5450

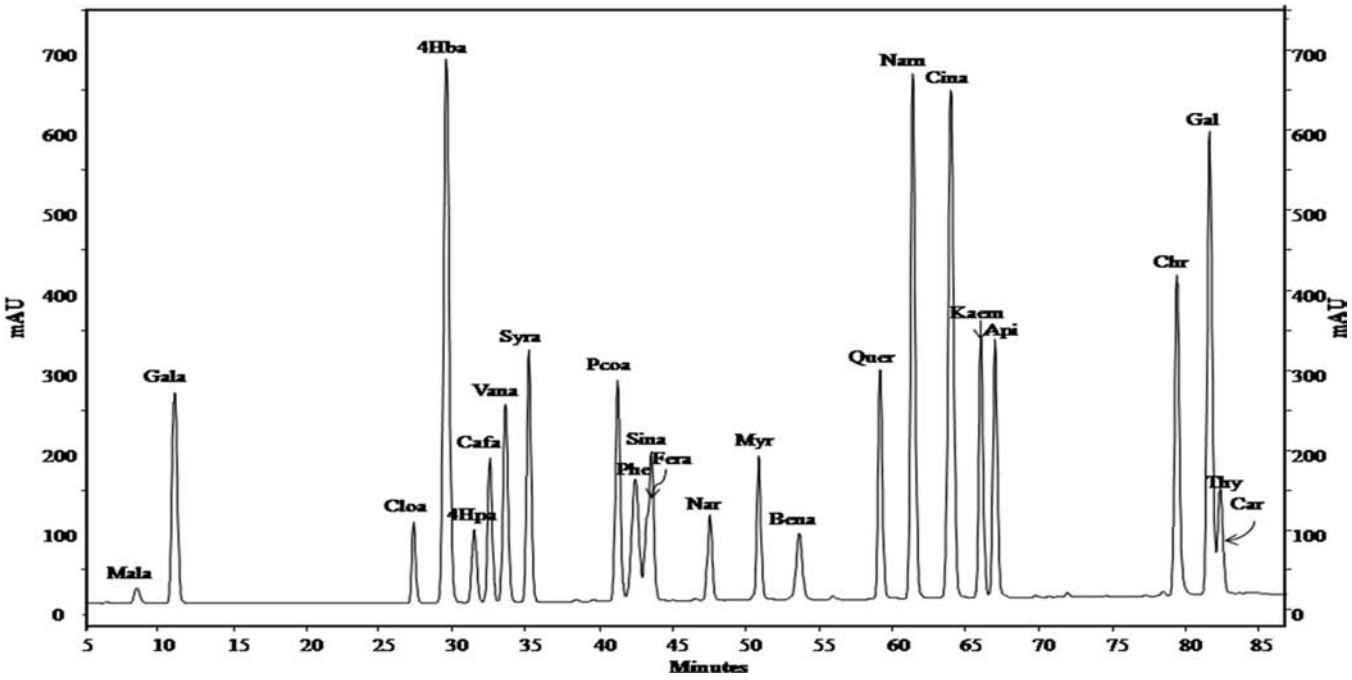

Figure 1. Chromatogram obtained by the HPLC−PDA system of a mixture of all 25 standards (λ_{max}, 270 nm): Mala, maleic acid; Gala, gallic acid; Cloa, clorogenic acid; 4Hba, 4-hydroxybenzoic acid; 4Hpa, 4-hydroxyphenyl acetic acid; Cafa, caffeic acid; Vana, vanillic acid, Syra, syringic acid; Pcoa, *p*-coumaric acid; Phe, phenol; Fera, ferulic acid; Sina, sinapic acid; Nar, naringin; Myr, myricetin; Bena, benzoic acid; Quer, quercetin; Narn, naringenin; Cina, cinnamic acid; Kaem, kaempferol; Api, apigenin; Ch, chrysin; Gal, galangin; Thy, thymol; and Car, carvacrol.

Table 2. UV Wavelength of Each Individual Component with Their Corresponding Abbreviations and Retention Times

analyte name	abbreviation used	retention time (min)	UV wavelength (nm)
maleic acid	Mala	8.8	248
gallic acid	Gala	12.3	273
clorogenic acid	Cloa	27.5	247−329
4-hydroxybenzoic acid	4Hba	29.5	255
4-hydroxyphenyl acetic acid	4Hpa	31.9	138−276
caffeic acid	Cafa	32.7	326
vanillic acid	Vana	33.8	261−293
syringic acid	Syra	35.5	274
p-coumaric acid	Pcoa	41.3	236−310
phenol	Phe	42.6	271
ferulic acid	Fera	43.6	323
sinapic acid	Sina	44.0	245−325
naringin	Nar	48.0	283−330
myricetin	Myr	51.0	255−375
benzoic acid	Bena	53.8	241−273
quercetin	Quer	59.2	255−372
luteolin	Lut		255−347
naringenin	Narn	61.3	290−330
cinnamic acid	Cina	63.8	274
kaempferol	Keam	66.2	266−366
apigenin	Api	67.1	268−337
chrysin	Ch	79.5	267−315
galangin	Gal	81.7	265−360
thymol	Thy	82.5	276
carvacrol	Car	83.0	272

Performance of the Proposed Method. Calibration standards at 0.05, 0.1, 0.5, 1, 5, 10, 50, and 200 μg/mL were prepared in methanol for each polyphenol. Under the optimal experimental conditions, a linear relationship of the suggested chromatographic quantitation method was established by investigating the detection signal as a function of the analyte concentration, with the aid of a linear regression equation by the method of least-squares. The calibration curve was plotted for each standard of phenolic acids, flavonoids, and phenols; it was linear over the range of 0.05−200 μg/mL. The correlation coefficient (r^2) obtained was >0.997 for each regression equation. The limit of detection (LOD) (corresponding to a signal-to-noise ratio of 3:1) and limit of quantification (LOQ) (signal-to-noise ratio of 10:1) values of the proposed method were calculated by analyzing three replicates of a blank sample (Milli-Q water) spiked with each standard at low concentration levels.[34] The LOD values were found between 0.015 and 0.041 μg/mL, while the LOQ values were between 0.051 and 1.35 μg/mL for each standard compound. The intra- and interday precisions of the proposed HPLC−PDA method were established by injecting five replicates of the standard mixture (100 μg/mL) on the same day and 15 replicates over 3 consecutive days (five replicates each day), respectively.[35] High intra- and interday precisions were achieved with relative standard deviation (RSD) values lower than 2.5% for all analyzed compounds. All obtained values of quality parameters are listed in Table 3. The low values of precision (<2.5% RSD) confirm that the proposed analytical method can be successfully used in the routine analysis of phenolic acids, flavonoids, and other phenols present in various natural samples, such as honey.

Real Sample Analysis. The recovery assay was performed to assess the applicability of the proposed extraction method for determination of phenolic acids, flavonoids, and phenol compounds. A total of 12 honey samples were analyzed in triplicate using the standard addition quantification method of two non-spiked and four spiked samples at different concentration levels (50, 100, 200, and 400%). The developed extraction

dx.doi.org/10.1021/jf5011758 | J. Agric. Food Chem. 2014, 62, 5443−5450

Table 3. Quality Parameters of the Proposed Method (HPLC−PDA)[a]

					precision (% RSD)[b]	
sample type	sample	LOD (μg/mL)	LOQ (μg/mL)	correlation coefficient (r^2)	interday	intraday
phenolic acids	4Hba	0.033	0.11	0.9976	1.9	2.3
	4Hpa	0.082	0.27	0.9992	1.7	2.1
	Cafa	0.026	0.086	0.9993	2.0	2.4
	Cloa	0.015	0.051	0.9996	1.9	2.5
	Fera	0.023	0.075	0.9999	1.8	2.2
	Gala	0.036	0.12	0.9989	2.1	2.3
	Pcoa	0.018	0.058	0.9999	2.0	2.5
	Sina	0.029	0.095	0.9999	1.8	2.1
	Syra	0.029	0.100	0.9997	1.9	2.2
	Vana	0.016	0.054	0.9997	2.1	2.4
flavonoids	Api	0.029	0.097	0.9998	1.7	2.0
	Ch	0.036	0.12	0.9998	1.9	2.2
	Gal	0.018	0.06	0.9997	2.1	2.4
	Keam	0.041	0.14	0.9987	1.5	2.0
	Lut	0.029	0.095	0.9992	1.8	1.9
	Myr	0.036	0.12	0.9999	1.8	2.4
	Nar	0.14	0.46	0.9999	2.0	2.2
	Narn	0.027	0.089	0.9997	1.9	2.4
	Quer	0.029	0.096	0.9994	1.8	2.0
other phenols	Bena	0.037	0.122	0.9996	1.8	1.9
	Car	0.018	0.06	0.9998	1.9	2.3
	Cina	0.034	0.11	0.9991	2.1	2.4
	Mala	0.400	1.35	0.9996	2.0	2.2
	Phe	0.037	0.12	0.9999	1.9	2.1
	Thy	0.038	0.13	0.9999	2.2	2.4

[a]4Hba, 4-hydroxybenzoic acid; 4Hpa, 4-hydroxyphenyl acetic acid; Cafa, caffeic acid; Cloa, clorogenic acid; Fera, ferulic acid; Gala, gallic acid; Pcoa, *p*-coumaric acid; Sina, sinapic acid; Syra, syringic acid; Vana, vanillic acid, Api, apigenin; Ch, chrysin; Gal, galangin; Kaem, kaempferol; Lut, luteolin; Myr, myricetin; Nar, naringin; Narn, naringenin; Quer, quercetin; Bena, benzoic acid; Car, carvacrol; Cina, cinnamic acid; Mala, maleic acid; Phe, phenol; and Thy, thymol. [b]Relative standard deviation (n = 5).

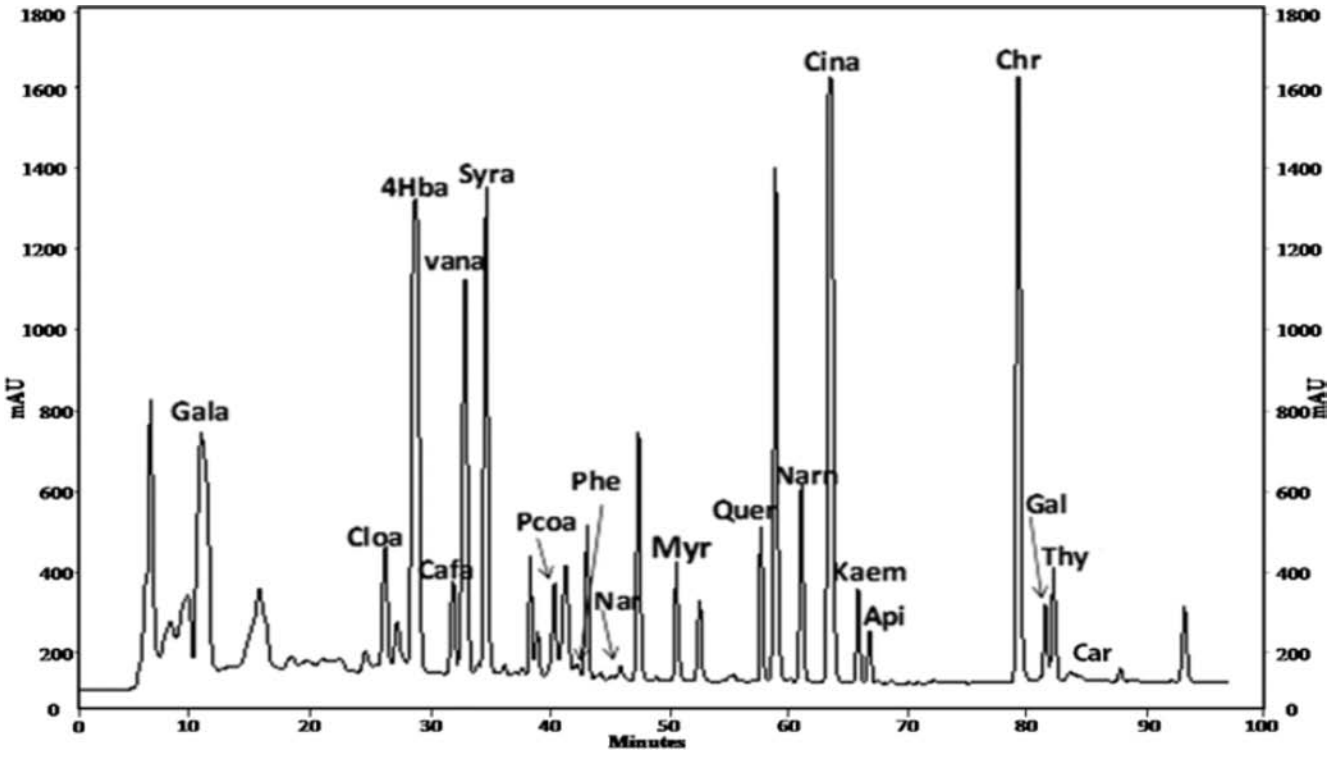

Figure 2. HPLC−PDA chromatogram of the analyzed phenolic acids, flavonoids, and phenol compounds in sample 8 (λ_{max}, 270 nm): Gala, gallic acid; Cloa, clorogenic acid; 4Hba, 4-hydroxybenzoic acid; Cafa, caffeic acid; Vana, vanillic acid; Syra, syringic acid; Pcoa, *p*-coumaric acid; Phe, phenol; Nar, naringin; Myr, myricetin; Quer, quercetin; Narn, naringenin; Cina, cinnamic acid; Kaem, kaempferol; Api, apigenin; Ch, chrysin; Gal, galangin; Thy, thymol; and Car, carvacrol.

dx.doi.org/10.1021/jf5011758 | J. Agric. Food Chem. 2014, 62, 5443−5450

Table 4. Quantitative Estimation of Phenolic Acids, Flavonoids, and Other Phenols in Honey Samples ± Standard Deviation (SD) (μg/100 g of Honey; $n = 3$)[a]

compound type	sample	Gala	Cloa	4Hba	4Hpa	Cafa	Vana	Syra	Pcoa	Fera	Sina	total
phenolic acids	1	nd[b]	nd	648 ± 1.1	84 ± 0.2	nd	344 ± 2.2	nd	nd	nd	26 ± 0.2	1102 ± 0.9
	2	188 ± 1.1	nd	1410 ± 2.9	nd	156 ± 1.1	nd	444 ± 2.6	60 ± 0.3	312 ± 2.5	87 ± 0.9	2657 ± 1.6
	3	33 ± 0.3	nd	1120 ± 1.9	nd	146 ± 1.2	258 ± 1.5	204 ± 1.3	26 ± 0.2	nd	nd	1791 ± 1.1
	4	171 ± 1.2	nd	nd	nd	149 ± 1.1	nd	175 ± 1.3	22 ± 0.1	nd	43 ± 0.5	560 ± 0.9
	5	240 ± 2.4	nd	1230 ± 2.5	nd	154 ± 1.6	422 ± 1.9	396 ± 1.9	nd	180 ± 1.1	nd	2618 ± 1.9
	6	79 ± 0.9	nd	332 ± 3.1	nd	nd	nd	nd	25 ± 0.2	nd	nd	436 ± 1.4
	7	127 ± 1.1	nd	794 ± 1.8	nd	72 ± 0.8	50 ± 0.5	53 ± 0.6	27 ± 0.3	nd	nd	1124 ± 0.9
	8	173 ± 1.7	106 ± 0.5	1040 ± 1.9	nd	37 ± 0.4	390 ± 1.4	636 ± 1.9	51 ± 0.5	nd	nd	2434 ± 1.2
	9	46 ± 0.2	nd	734 ± 1.8	nd	77 ± 0.6	nd	nd	nd	nd	nd	856 ± 0.9
	10	31 ± 0.3	22 ± 0.2	216 ± 1.4	nd	58 ± 0.5	nd	nd	nd	12 ± 0.2	25 ± 0.3	363 ± 0.5
	11	38 ± 0.5	31 ± 0.3	434 ± 1.8	198 ± 1.1	nd	nd	nd	89 ± 0.7	nd	79 ± 0.8	871 ± 0.9
	12	33 ± 0.1	nd	464 ± 1.6	nd	51 ± 0.8	nd	nd	36 ± 0.6	8 ± 0.1	28 ± 0.5	615 ± 0.6
	total	1159 ± 0.8	159 ± 0.3	8422 ± 1.8	282 ± 0.7	900 ± 0.9	1464 ± 1.5	1908 ± 1.6	336 ± 0.4	512 ± 1.0	288 ± 0.5	15428 ± 1.2
	average	106	53	766	141	100	293	318	42	128	48	1995[c]
	%[d]	7.52	1.03	54.59	1.84	5.84	9.49	12.37	2.16	3.31	1.85	

	sample	Nar	Myr	Lut	Quer	Narn	Kaem	Api	Ch	Gal	total
flavonoids	1	nd	nd	nd	93 ± 1.3	nd	10 ± 1.0	3 ± 0.2	51 ± 1.2	10 ± 0.2	167 ± 0.8
	2	117 ± 2.1	45 ± 1.9	nd	470 ± 2.6	83 ± 1.3	45 ± 2.5	13 ± 0.5	850 ± 2.9	23 ± 1.0	1646 ± 1.8
	3	25 ± 1.1	41 ± 1.6	nd	41 ± 1.5	21 ± 0.5	28 ± 2.2	3 ± 0.1	550 ± 2.9	21 ± 0.9	731 ± 1.3
	4	13 ± 0.8	nd	nd	27 ± 1.2	67 ± 1.2	37 ± 2.1	5 ± 1.0	113 ± 2.1	13 ± 0.5	275 ± 1.3
	5	29 ± 1.2	55 ± 2.1	nd	296 ± 2.5	67 ± 1.5	nd	13 ± 1.2	692 ± 2.5	21 ± 0.8	1173 ± 1.7
	6	nd	nd	nd	6 ± 0.4	nd	nd	nd	252 ± 2.5	2 ± 0.1	261 ± 1.0
	7	22 ± 1.1	24 ± 1.2	nd	39 ± 1.2	31 ± 1.2	21 ± 1.9	11 ± 1.1	404 ± 2.2	23 ± 0.9	573 ± 1.4
	8	4 ± 0.2	38 ± 1.9	nd	126 ± 2.1	95 ± 2.1	35 ± 1.2	9 ± 0.2	634 ± 2.8	15 ± 1.2	954 ± 1.4
	9	nd	3 ± 0.5	nd	nd	119 ± 2.5	nd	nd	712 ± 2.9	nd	834 ± 2.0
	10	13 ± 1.1	nd	nd	109 ± 2.2	nd	nd	nd	564 ± 2.2	nd	686 ± 1.8
	11	nd	nd	nd	186 ± 2.2	nd	37 ± 1.5	3 ± 0.2	626 ± 2.6	nd	852 ± 1.6
	12	9 ± 0.8	nd	nd	113 ± 2.0	134 ± 2.6	42 ± 1.5	3 ± 0.3	536 ± 2.9	nd	837 ± 1.7
	total	232 ± 1.1	206 ± 1.5	nd	1506 ± 1.6	617 ± 1.6	255 ± 1.7	63 ± 0.5	5984 ± 2.5	128 ± 0.7	8989 ± 1.5
	average	29	34	nd	137	78	32	7	498	16	831[e]
	%[f]	2.58	2.29		16.80	6.85	2.85	0.68	66.53	1.42	

	sample	Mala	Phe	Bena	Cina	Thy	Car	total
other phenols	1	nd	nd	3.2 ± 0.2	470.0 ± 2.6	3.2 ± 1.1	nd	476.8 ± 1.3
	2	nd	0.4 ± 0.1	5.6 ± 1.5	1336.0 ± 2.9	13.0 ± 1.8	nd	1355.0 ± 1.6
	3	nd	nd	nd	306.0 ± 2.1	12.0 ± 1.3	1.4 ± 0.5	319.4 ± 1.3
	4	nd	0.3 ± 0.1	nd	512.0 ± 2.6	6.6 ± 0.9	nd	518.8 ± 1.2
	5	nd	nd	nd	758.0 ± 2.7	20.6 ± 1.5	nd	778.6 ± 2.1
	6	nd	nd	nd	224.0 ± 0.9	nd	nd	224.0 ± 0.9
	7	nd	nd	nd	318.0 ± 1.2	nd	nd	318.0 ± 1.2
	8	nd	0.8 ± 0.1	nd	926.0 ± 2.8	68.8 ± 2.1	1.0 ± 0.4	996.6 ± 1.4
	9	nd	0.5 ± 0.1	nd	306.0 ± 1.3	8.6 ± 1.9	nd	315.0 ± 1.1
	10	nd	nd	nd	330.0 ± 1.5	nd	nd	330.0 ± 1.5

dx.doi.org/10.1021/jf5011758 | J. Agric. Food Chem. 2014, 62, 5443−5450

Table 4. continued

sample	Mala	Phe	Bena	Cina	Thy	Car	total
11	nd	nd	9.0 ± 1.2	410.0 ± 2.6	14.2 ± 1.1	nd	433.2 ± 1.6
12	nd	nd	6.4 ± 0.9	328.0 ± 1.2	46.4 ± 2.8	nd	380.8 ± 1.6
total		2.0 ± 0.1	24.2 ± 1.0	6220.0 ± 2.1	193.4 ± 1.6	2.4 ± 0.5	6446.0 ± 1.4
average		0.5	6.5	518.3	21.5	1.2	548.0[g]
%[h]	nd	0.03	0.35	96.49	3.00	0.04	

[a]Gala, gallic acid; Cloa, clorogenic acid; 4Hba, 4-hydroxybenzoic acid; 4Hpa, 4-hydroxyphenyl acetic acid; Cafa, caffeic acid; Vana, vanillic acid, Syra, syringic acid; Pcoa, *p*-coumaric acid; Fera, ferulic acid; Sina, sinapic acid; Nar, naringin; Myr, myricetin; Lut, Luteolin; Quer, quercetin; Narn, naringenin; Kaem, kaempferol; Api, apigenin; Ch, chrysin; Gal, galangin; Mala, maleic acid; Phe, phenol; Bena, benzoic acid; Cina, cinnamic acid; Thy, thymol; and Car, carvacrol. [b]nd = not detected. [c]Total phenolic acids averaged. [d]Percentage of each individual phenolic acid in the total phenolic acids. [e]Total flavonoids averaged. [f]Percentage of each individual flavonoid in the total flavonoids. [g]Total other phenols averaged. [h]Percentage of each individual other phenol in the total other phenols.

and HPLC−PDA method was applied for the simultaneous determination of all analyzed (total 25) phenolic acids, flavonoids, and phenol compounds in various natural honey samples. All of these target compounds were identified and quantitated with reference to their standard compounds mainly on the basis of the retention time and UV spectra.[18,23,33] The UV spectral data obtained by the developed HPLC−PDA method for the honey samples and their corresponding retention times were used as library data for the comparison and for identification for the phenolic acids, flavonoids, and phenol compounds. Figure 2 shows, as an example, the HPLC−PDA chromatogram and absorption spectra of all of the analyzed phenolic acids, flavonoids, and phenol compounds in sample 8. The chromatogram shows a good resolution, and no interferences from any other components were observed because no detectable matrix peaks were eluted in the retention time of the target compounds.[36]

The absorption spectra of the corresponding analyte were similar and found at the same wavelength as those obtained from analysis of the standard mixture solution (Figure 1). The compounds were quantitated by their absorbance in the HPLC chromatograms against the standards at their corresponding wavelength provided in Table 2. The percent recovery values were found between 89 and 96% depending upon the types of honey samples.

Phenolic Acids in Monofloral Jujube Yemeni Honeys. In the analyzed samples of Yemeni jujube (*Z. spina-christi* L.) honey, the total phenolic acid content was averaged to 1.921 mg/100 g of honey, while 4-hydroxybenzoic acid (54.59%) was the main component (0.766 mg/100 g of honey) (Table 4). On the other hand, syringic acid (12.37%) was the secondary compound (0.318 mg/100 g of honey) in all of the analyzed honey samples. The other phenolic acids present in the honey samples are relatively lower in proportion and were ranging from 1.84% (4-hydroxyphenyl acetic acid) to 9.49% (vanillic acid) of total phenolic acids (Table 4). However, the obtained results for all of the phenolic acids were different in each analyzed honey sample, and among them, sample 2 contains a much higher concentration of 4-hydroxybenzoic acid than other honey samples, while only in three samples, chlorogenic acid (1.03%) and 4-hydroxyphenyl acetic acid (1.84%) were found (Table 4).

Flavonoids in Monofloral Jujube Yemeni Honeys. The HPLC−PDA analysis of flavonoid compounds in Yemeni jujube honeys showed that chrysin was the main flavonoid present in most of the samples analyzed (Table 4). The experimental data show that, among the nine investigated flavonoids, eight were found in this type of honey and most of them occurred in small amounts, except chrysin. The total flavonoid content was found to be 8.989 mg/100 g of honey, with chrysin being 5.984 mg/100 g of honey (66.5%) (Table 4). In addition, quercetin (1.506 mg/100 g of honey) was found as the secondary main constituent representing 16.8% of the total flavonoids. The other flavonoids present in analyzed honey are in a lower proportion, ranging from 1.42 to 6.85% of the total flavonoids, while luteolin was not found in any honey sample. However, most of the analyzed honey samples showed a common flavonoid profile, comprising chrysin, quercetin, kaempferol, apigenin, and naringenin, suggesting that they could be used as characteristic floral markers for Yemeni jujube honeys.[32]

Other Phenols in Monofloral Jujube Yemeni Honeys. In the analyzed samples of Yemeni jujube honeys, the total other phenolic compounds were found to be 6.4460 mg/100 g

of honey, where the cinnamic acid (96.49%) was the main component (6.220 mg/100 g of honey) (Table 4). On the other hand, the other phenolic constituents present in the honey samples were relatively lower in proportion and were ranging from 0.0279% (phenol) to 3.001% (thymol) of total phenols.

However, the obtained results for all of the phenolic components were different in each analyzed honey sample, while sample 2 contains the highest concentration of cinnamic acid compared to other honey samples. In only four samples, carvacrol (0.0372%), benzoic acid (0.3754%), and phenol (0.0279%) were found in very low amounts, while maleic acid could not be detected in any honey sample (Table 4). According to the quantitative results showed in Table 4, there is no clear correlation between the geographical origin of the honey and its chemical composition because the concentration of each polyphenol varies in a wide range for samples collected from the same region.

In summary, a simple method has been described for the analysis of phenolic acid, flavonoid, and phenol contents in natural honey samples of Yemen. A total of 12 jujube honey samples were analyzed, and the total contents of phenolic acids, flavonoids, and phenolic components were found in the range of 363−2658, 261−1646, and 224−1355 μg/100 g (Table 4) of honey samples, respectively. Among phenolic acids, 4-hydroxybenzoic acid (1.41 mg/100 g) was found in a major quantity in all analyzed honeys, while chrysin (850 μg/100 g) was the main detected flavonoid and cinnamic acid was the main phenolic compound (1336 μg/100 g). Among the 25 investigated compounds, maleic acid and luteolin were not detected, while a common flavonoid profile corresponding to chrysin, quercetin, kaempferol, apigenin, and naringenin was established in all honey samples. In addition, the values of the quality parameters achieved with this proposed analysis method as well as the results obtained in the analysis of honey samples confirmed that they are sufficient to propose the extraction technique using MWCNTs coupled with HPLC−PDA as a new methodology for inexpensive and reliable analysis of polyphenols in natural honeys.

AUTHOR INFORMATION

Corresponding Author

*Telephone: +966545141396. Fax: +96614675992. E-mail: tarabai22@yahoo.com.sg.

Funding

The authors extend their appreciation to the Deanship of Scientific Research, College of Science Research Center, King Saud University, Riyadh, Saudi Arabia, for supporting this project.

Notes

The authors declare no competing financial interest.

REFERENCES

(1) Saif-ur, R.; Zia, F. K.; Tahir, M. Physical and spectroscopic characterization of Pakistani honey. *Cienc. Invest. Agrar.* **2008**, *35*, 199−204.

(2) Zander, E.; Koch, A. *Der Honig*; Eugen Ulmer Verlag: Stuttgart, Germany, 1994; p 201.

(3) Hall, C. W.; Farroll, A. W.; Rippen, A. L. *Encyclopedia of Food Engineering*; AVI Publishing: Westport, CT, 1986.

(4) Fox, B.; Cameron, A. *Food Science Nutrition and Health: Carbohydrates*, 6th ed.; Edward Arnold: London, U.K.; 1995; pp 95−105.

(5) Gheldof, N.; Wang, X. H.; Engeseth, N. J. Identification and quantification of antioxidant components of honeys from various floral sources. *J. Agric. Food Chem.* **2002**, *50*, 5870−5877.

(6) Nicholls, J.; Miraglio, A. M. Honey and healthy diets. *Cereal Foods World* **2003**, *48*, 116−119.

(7) Khalil, M. I.; Sulaiman, S. A.; Boukraa, L. Antioxidant properties of honey and its role in preventing health disorder. *Open Nutraceuticals J.* **2010**, *3*, 6−16.

(8) Lachman, J.; Hejtmánková, A.; Sýkora, J.; Karban, J.; Orsák, M.; Rygerová, B. Content of major phenolic and flavonoid antioxidants in selected Czech honey. *Czech J. Food Sci.* **2010**, *28*, 412−426.

(9) Lachman, J.; Orsák, M.; Hejtmánková, A.; Kováková, E. Evaluation of antioxidant activity and total phenolics of selected Czech honeys. *LWT—Food Sci. Technol.* **2010**, *43*, 52−58.

(10) Bergman, A.; Yanai, J.; Weiss, J.; Bell, D.; David, M. P. Acceleration of wound healing by topical application of honey: An animal model. *Am. J. Surg.* **1983**, *145*, 374−376.

(11) Phan, T. T.; Wang, L.; See, P.; Grayer, R. J.; Chan, S. Y.; Lee, S. T. Phenolic compounds of *Chromolaena odorata* protect cultured skin cells from oxidative damage: Implication for cutaneous wound healing. *Biol. Pharm. Bull.* **2001**, *24*, 1373−1379.

(12) Cherbuliez, T.; Domerego, R. *Medicine from the Bees*; Apimondia Standing Commission for Apitherapy, Apimondia: Rome, Italy, 2001.

(13) Cherbuliez, T.; Domerego, R. *L'apithérapie, Médecine des Abeilles*; Éditions Amyris: Brussels, Belgium, 2003.

(14) Cherchi, A.; Spanedda, L.; Tuberoso, C.; Cabras, P. Solid phase extraction and high-performance liquid chromatographic determination of organic acids in honey. *J. Chromatogr. A* **1994**, *669*, 59−64.

(15) Amiot, M. J.; Aubert, S.; Gonnet, M.; Tacchini, M. Les Composés Phénoliques des Miels: Étude Préliminaire sur L'identification et la Quantification par Familles. *Apidologie* **1989**, *20*, 115−125.

(16) Ferreres, F.; Tomas-Barberan, F. A.; Gil, M. I.; Tomas-Lorente, F. An HPLC technique for flavonoid analysis in honey. *J. Sci. Food Agric.* **1991**, *56*, 49−56.

(17) Gil, M. I.; Ferreres, F.; Ortiz, A.; Subra, E.; Tomas-Barberan, F. A. Plant phenolic metabolites and floral origin of rosemary honey. *J. Agric. Food Chem.* **1995**, *43*, 2833−2838.

(18) Martos, I.; Ferreres, F.; Tomas-Barberan, F. A. Identification of flavonoid markers for the botanical origin of Eucalyptus honey. *J. Agric. Food Chem.* **2000**, *48*, 1498−1502.

(19) Tomas-Barberan, F. A.; Martos, I.; Ferreres, F.; Radovic, B. S.; Anklam, E. HPLC flavonoid profiles as markers for the botanical origin of European unifloral honeys. *J. Agric. Food Chem.* **2001**, *81*, 485−496.

(20) Vit, P.; Soler, C.; Tomas-Barberan, F. A. Profiles of phenolic compounds of *Apismellifera* and *Melipona* spp. honeys from Venezuela. *Z. Lebensm.-Unters. -Forsch. A* **1997**, *204*, 43−47.

(21) Andrade, P.; Ferreres, F.; Amaral, M. T. Analysis of honey phenolic acids by HPLC, its application to honey botanical characterization. *J. Liq. Chromatogr. Relat. Technol.* **1997**, *20*, 2281−2288.

(22) Andrade, P.; Ferreres, F.; Gil, M. I.; Tomas-Barberan, F. A. Determination of phenolic compounds in honeys with different floral origin by capillary zone electrophoresis. *Food Chem.* **1997**, *60*, 79−84.

(23) Martos, I.; Ferreres, F.; Yao, L.; D_Arcy, B.; Caffin, N.; Tomas-Barberan, F. A. Flavonoids in monospecific Eucalyptus honeys from Australia. *J. Agric. Food Chem.* **2000**, *48*, 4744−4748.

(24) Valcarcel, M.; Cardenas, S.; Simonet, B. M.; Moliner-Martinez, Y.; Lucena, R. Carbon nanostructures as sorbent materials in analytical processes. *TrAC, Trends Anal. Chem.* **2008**, *27*, 34−43.

(25) Herrera-Herrera, A. V.; González-Curbelo, M. A.; Hernández-Borges, J.; Rodríguez-Delgado, M. A. Carbon nanotubes applications in separation science: A review. *Anal. Chim. Acta* **2012**, *734*, 1−30.

(26) Pérez-López, B.; Merkoci, A. Carbon nanotubes and graphene in analytical sciences. *Microchim. Acta* **2012**, *179*, 1−16.

(27) Ravelo-Pérez, L. M.; Herrera-Herrera, A. V.; Hernández-Borges, J.; Rodríguez-Delgado, M. A. Carbon nanotubes: Solid-phase extraction. *J. Chromatogr. A* **2010**, *1217*, 2618−2641.

(28) Herrero Latorre, C.; Álvarez Méndez, J.; Barciela García, J.; García Martín, S.; Peña Crecente, R. M. Carbon nanotubes as solid-

phase extraction sorbents prior to atomic spectrometric determination of metal species: A review. *Anal. Chim. Acta* **2012**, *749*, 16−35.
(29) Cai, Y. Q.; Jiang, G. B.; Liu, J. F.; Zhou, Q. X. Multi-walled carbon nanotubes packed cartridge for the solid-phase extraction of several phthalate esters from water samples and their determination by high performance liquid chromatography. *Anal. Chim. Acta* **2003**, *494*, 149−156.
(30) Cai, Y.; Jiang, G.; Liu, J.; Zhou, Q. Multiwalled carbon nanotubes as a solid-phase extraction adsorbent for the determination of bisphenol A, 4-*n*-nonylphenol, and 4-*tert*-octylphenol. *Anal. Chem.* **2003**, *75*, 2517−2521.
(31) Liang, P.; Liu, Y.; Guo, L.; Zeng, J.; Lu, H. Multiwalled carbon nanotubes as solid-phase extraction adsorbent for the preconcentration of trace metal ions and their determination by inductively coupled plasma atomic emission spectrometry. *J. Anal. At. Spectrom.* **2004**, *19*, 1489−1492.
(32) Yao, L.; Datta, N.; Tomas-Barberan, F. A.; Ferreres, F.; Martos, I.; Singanusong, R. Flavonoids, phenolic acids and abscisic acid in Australian and New Zealand *Leptospermum* honeys. *Food Chem.* **2003**, *81*, 159−168.
(33) Martos, I.; Cossentini, M.; Ferreres, F.; Tomas-Barberan, F. A. Flavonoid composition of Tunisian honeys and propolis. *J. Agric. Food Chem.* **1997**, *45*, 2824−2829.
(34) Khan, M. R.; Alothman, Z. A.; Ghafar, A. A.; Wabaidur, S. M. Analysis of aflatoxins in nonalcoholic beer using liquid−liquid extraction and ultra performance LC−MS/MS. *J. Sep. Sci.* **2013**, *36*, 572−577.
(35) Wabaidur, S. M.; Alothman, Z. A.; Khan, M. R. A rapid method for the simultaneous determination of L-ascorbic acid and acetylsalicylic acid in aspirin C effervescent tablet by ultra performance liquid chromatography−tandem mass spectrometry. *Spectrochim. Acta, Part A* **2013**, *108*, 20−25.
(36) Alothman, Z. A.; Wabaidur, S. M.; Khan, M. R.; Ghafar, A. A.; Habila, M. A.; Yacine, B. H. A. Determination of capsaicinoids in *Capsicum* species using ultra performance liquid chromatography−mass spectrometry. *J. Sep. Sci.* **2012**, *35*, 2892−2896.

JOURNAL OF AGRICULTURAL AND FOOD CHEMISTRY

Article

pubs.acs.org/JAFC

Study of the Surfactant Properties of Aqueous Stream from the Corn Milling Industry

X. Vecino,[†] L. Barbosa-Pereira,[†] R. Devesa-Rey,[†,‡] J. M. Cruz,[†] and A. B. Moldes*[,†]

[†]Chemical Engineering Department, School of Industrial Engineering (EEI), University of Vigo, Campus As Lagoas-Marcosende, 36310 Vigo-Pontevedra, Spain

[‡]Defense University Center, Naval Academy, University of Vigo, Plaza de España 2, 36920 Marín-Pontevedra, Spain

ABSTRACT: Corn steep liquor (CSL) is a liquid byproduct generated by the corn wet-milling industry. This agroindustrial residue is obtained when corn is digested with warm water and SO_2 in the presence of different spontaneously growing microorganisms. The microbial population of CSL includes lactic acid bacteria, which are widely known to produce biosurfactants. However, there is no information available about the possible existence of surface-active compounds in CSL. In this work the surface tension activity of CSL was evaluated and the biosurfactant contained in this residue was extracted with different organic solvents and characterized. The biosurfactant obtained from CSL was analyzed by Fourier transform infrared spectroscopy, and the composition in fatty acid was analyzed by gas chromatography−mass spectrometry. The hydrophobic chain of the biosurfactant contained in CSL comprised 50−55.2% linolelaidic acid, 15.7−22.2% oleic and/or elaidic acid, 5.9−14.6% stearic acid, and 14.9−19.6% palmitic acid.

KEYWORDS: *agroindustrial stream, corn steep liquor, biosurfactant, lipopeptide*

1. INTRODUCTION

Conventional corn wet-milling is designed to recover and purify starch and several other products, including germ, gluten, and steep liquor.[1] The process includes grain cleaning; steeping; germ, fiber, and gluten separation and recovery; and starch separation.[1] Corn steep liquor (CSL) is obtained when warm water is used to soften and swell the corn grain and the soluble material in the grain passes into the water. The corn is usually held in a series of silos through which the steep water passes.[2] The steeping process is carried out at approximately pH 4 and at 45−52 °C in the presence of SO_2 and active lactic acid fermentation. CSL contains soluble material collected at other stages of the milling or separation processes; as the processing water may be retained in the plant for approximately 2 weeks, additional fermentation often occurs at many times during the process.[3]

On the basis of the high nutritional content of CSL, various authors have proposed the use of this waste product as a nutrient supplement for microorganisms in diverse industrial fermentation processes.[4,5] Thus, CSL has been proposed as a nutritional supplement for producing transglutaminase,[6] lactic acid and biosurfactants,[7,8] succinic acid,[9] or ethanol.[10,11]

The annual global production of surfactants is about 13 million metric tons,[12,13] with approximately $23.9 billion of sales,[14] However, most of the surfactants produced worldwide are chemically synthesized using nonrenewable raw materials.

Several authors have recently proposed the use of biotechnological processes to produce microbial detergents, known as biosurfactants, as less toxic and more effective alternatives to chemical surfactants.[15] However, the major obstacle to the large scale industrial application of biosurfactants is the higher production cost and lower production rate in comparison with commercially available synthetic surfactants. Thus, in recent years several studies have focused on reducing the cost of producing biosurfactants by improving the yield and the use of either cost-free or low-cost feedstock or agricultural byproducts as carbon sources.[16]

Lactic acid bacteria (LAB) ferment water-soluble carbohydrates during the fermentation of many substrates. When LAB ferment food material, such as corn, they produce lactic acid, which inhibits microbiological growth by lowering the pH of the medium.[17] However, LAB produce many other substances in addition to lactic acid: bacteriocins, acetic acid, propionic acid, phenyl lactic acid, biosurfactants, and bioemulsifiers. However, the potential of CSL as a biosurfactant source has not yet been explored.

The aim of the present research was to explore the possible use of CSL as a source of biosurfactant and its stability. Biosurfactant from CSL was extracted using different organic solvents (chloroform, ethyl acetate, methyl *tert*-butyl ether, trichloroethylene, hexane, heptane, and dichloromethane) and characterized by Fourier transform infrared spectroscopy and gas chromatography−mass spectrometry.

2. MATERIAL AND METHODS

2.1. Chemicals. Chloroform stabilized with 50 ppm amylene (99.8%), ethyl acetate (99.5%), and methyl *tert*-butyl ether (99.8%) were purchased from Panreac (Barcelona, Spain). Trichloroethylene (≥99%) was supplied by Fluka Chemie AG (Buchs, Switzerland). Hexane (98%) and heptane (99%) were purchased from Analar Normapur (Fontenay-sois-Bois, France). Dichloromethane (99%) was supplied by Merk (Darmstadt, Germany).

Supelco37 Component FAME Mix: 10 mg mL^{-1} FAME reference standard mix in methylene chloride was purchased from Sigma-Aldrich (Steinheim, Germany).

Received: March 21, 2014
Revised: May 28, 2014
Accepted: May 30, 2014
Published: May 30, 2014

ACS Publications © 2014 American Chemical Society

Table 1. Description of the Corn Steep Liquors Used in This Study: Registry Number (CAS), Distributor, and Composition

product	CAS/lot	distributor	composition	observations
CSL-1	66071-94-1/MKBB5569	Sigma-Aldrich	concentrate of corn solubles, 50% solubles, pH = 4.2	store at room temp
CSL-2	66071-94-1/MKBH1451V	Sigma-Aldrich	concentrate of corn solubles, 45% solubles, pH = 4.5	store at 2−8 °C
CSL-3	66071-94-1/B1412	ChemCruz, Santa Cruz Biotechnology, Inc.	approx 50% solids (corn solubles, vitamins, amino acids, minerals, and other growth stimulants), glucose monohydrate, phytin, sulfur dioxide, water (>40%), pH = 4.5	store at 4 °C

2.2. Corn Steep Liquor. Three different batches of CSL were tested in this study: CSL-1 and CSL-2 were supplied by Sigma-Aldrich (St. Louis, MO, USA), and CSL-3 was provided by Santa Cruz Biotechnology (USA). Table 1 shows the properties of the three different CSLs as reported by the companies from which each batch was obtained. All are viscous concentrates of corn soluble substances such as vitamins, amino acids, minerals, and other growth stimulants.

2.3. Surface Activity Determination. Surface activity was evaluated using a KRUSS K6 tensiometer equipped with a 1.9 cm Du Noüy platinum ring, at room temperature. All the determinations were carried out in triplicate.

2.4. Determination of Critical Micelle Concentration of CSL. The critical micelle concentration (CMC) of CSL was determined from the intersection of the tangent to the curve at the inflection point with the horizontal tangent through the points at low concentration. The calibration curve was prepared using solutions containing different concentrations of CSL of known surface tension. When the concentration of CSL is lower than the CMC, the surface tension of water in the presence of CSL is linearly related to the concentration of surfactant, and thus it is possible to establish a relationship between the CSL concentration and the surface tension.[18] The CMC of CSL was expressed as g L^{-1}.

2.5. Study of the CSL Surfactant Stability. Three different batches of CSL at the CMC (CSL-1, CSL-2, and CSL-3) were exposed to different temperatures (4 °C, 25 °C, and 65 °C) and pH (4, 5, and 8). Experiments were carried out in 10 mL tubes for 1 h, and surface tension of samples was measured in triplicate, once samples reached room temperature. The pH of CSL was adjusted with HCl 1 M and NaOH 1 M using a pH-meter Basic 20 (Crison).

2.6. Extraction of Biosurfactant from CSL. Various organic solvents were tested: chloroform, ethyl acetate, methyl *tert*-butyl ether, trichloroethylene, hexane, heptane, and dichloromethane. The extraction was carried out with a CSL:solvent ratio of 1:10 (v/v), at 150 rpm, for 4 h at room temperature (25 °C), following the conditions used by Jamal et al.[19] to extract biosurfactants from fermentation media. The CSL was used at CMC by dilution from the commercial bottle. The percentage of biosurfactant extracted from CSL was calculated on the basis of the surface tension values obtained after the dissolution of biosurfactant extract in water. The amount of water added to the biosurfactant extract was fixed taking into account the volume of CSL used during the extraction.

2.7. Characterization of Biosurfactant Contained in CSL.

2.7.1. Biochemical Composition of Biosurfactant. Biochemical analysis of biosurfactant extracted from each CSL was carried out following standard methods. The carbohydrate content of the biosurfactants was determined by the phenol−sulfuric acid method, with D-glucose as a standard.[20] The protein content was determined by the Lowry method,[21] with bovine serum albumin as a standard. Lipid content of the extracted biosurfactant was assessed according to the procedure described by Folch et al.,[22] with cholesterol as a standard.

2.7.2. Fourier Transform Infrared Spectroscopy. Fourier transform infrared spectroscopy (FTIR) was used to determine the chemical nature of the biosurfactants via identification of the functional groups and chemical bonds present in the surface-active compounds. The biosurfactant extracted (1 mg) was ground with 10 mg of potassium bromide and pressed (7,500 kg for 30 s) to produce translucent pellets.

FTIR analyses were carried out in a Niocolet 6700 FTIR spectrometer (Thermo Scientific). The spectral measurements were made in the transmittance mode in a range of 400−4000 cm^{-1}, with a resolution of 4 cm^{-1} an average range of 32 data scanning, and a potassium bromide pellet for measuring background absorbance levels.

2.7.3. Fatty Acid Characterization of Biosurfactant by GC−MS. The fatty acid composition of the biosurfactants extracted from the different batches of CSL was determined by gas chromatography (Trace GC Ultra, Thermo Scientific) coupled to a mass spectrometer (Trace DSQ, Thermo Finnigan), after methylation and transesterification of fatty acids into fatty acid methyl esters (FAMEs), according to the method described in the European Standard, EN ISO 12966-2.[23] Nonadecanoic acid methyl ester (C19:0 ME) was added as an internal standard. A sample volume of 1 μL was injected using a split mode, at a split ratio of 1:50. FAMEs separation was performed on a ZB-WAX column (60 m × 0.25 mm i.d. × 0.25 μm film thickness) with an oven temperature gradient of 60 °C for 2 min, then 60−200 °C at 10 °C min^{-1}, held for 27 min, then increased to 240 °C at 5 °C min^{-1}, and finally held for 20 min. Helium was used as carrier gas at a flow rate of 1 mL min^{-1}, and the temperature of both injector inlet and the transfer line of detector was set at 250 °C.

The mass spectra were obtained using a mass selective detector under electron impact ionization at a voltage of 70 eV, and data were acquired over an m/z range of 40−400.

FAMEs were identified from a mass spectra library supplied with the GC−MS system and by comparison of retention times and mass spectra of a FAME standard mix, injected under the same conditions.

2.8. Statistical Analysis. Data were subjected to analysis of variance (ANOVA) performed using the SPSS 13.0 statistical software package. Significant differences were assessed by Duncan's test (at $p < 0.05$).

3. RESULTS AND DISCUSSION

3.1. Evaluation of the Biosurfactant Capacity of CSL. The effectiveness of CSL as a biosurfactant can be determined by its ability to lower the surface tension of water. It has been proposed that a good biosurfactant can lower the surface tension of water (air−water interface)[24] from 72 mN m^{-1} to 36.6 mN m^{-1}, although a substance can be considered biosurfactant when it is able to reduce the surface tension by 8 units.[25,26] Figure 1 shows the variation in surface tension of water in the presence of increasing concentrations (up to 40 g L^{-1}) of different commercially available varieties of CSL. Thus, when CSL was added to the water, the minimum surface tension values were 36.6, 46.7, and 43.1 mN m^{-1} for CSL-1, CSL-2, and CSL-3 respectively. The surface tension reduction of water achieved with CSL was higher than that obtained using for example biosurfactants produced by *Lactobacillus pentosus*,[27,28] *Bacillus subtilis* B30,[29] *Halobacteriaceae archaeon*,[30] or *Pseudomonas aeruginosa*.[31]

The CMC for CSL-1 was 15 g L^{-1}, whereas for CSL-2 and CSL-3 it was 10 g L^{-1}. CSL is an agroindustrial residue subject to spontaneous fermentation, which can occur at many points during corn wet-milling; the degree of fermentation can vary significantly from plant to plant, and considerably even in one plant from time to time.[32]

Although biosurfactants are environmentally friendly, biodegradable, and less toxic than chemical surfactants, knowing the stability of this surface-active compound at different pH and temperatures is of importance. Biosurfactants have surface-activity properties that make them excellent emulsifiers and foaming and dispersing agents. Biosurfactants are usually active at extreme temperature, pH, and salinity. However, when

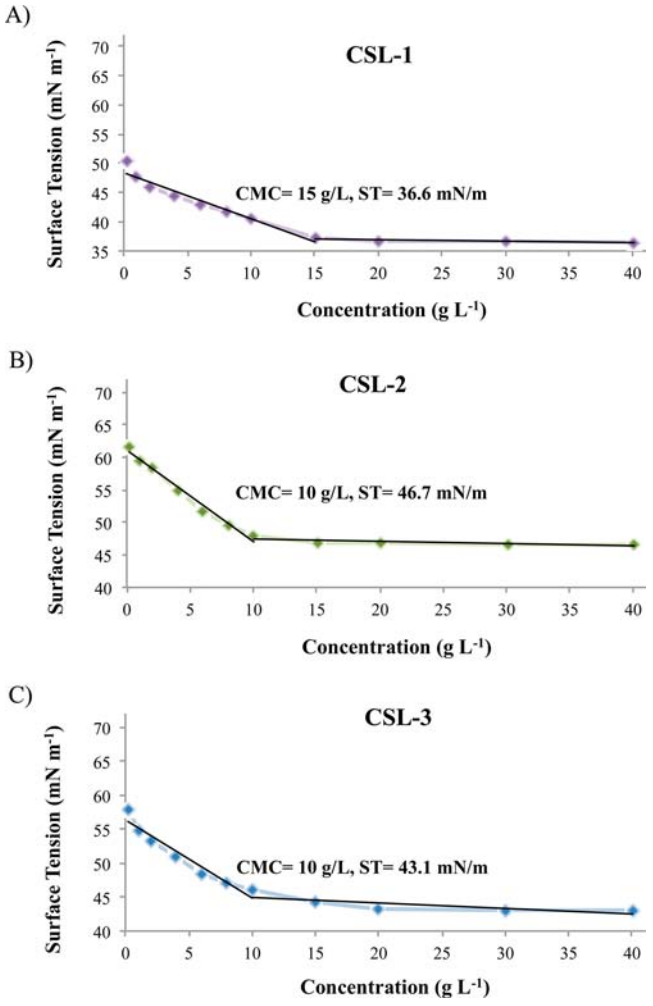

Figure 1. Variation in the surface tension of water at increasing concentrations of CSL-1 (A), CSL-2 (B), and CSL-3 (C).

Vecino-Bello et al.[33] studied the synergistic effects of pH, temperature, and salinity on the surface-active properties of biosurfactants produced by *L. pentosus*, they found that the emulsifying capacity of the biosurfactant was negatively affected at pH 3. Moreover, Bharali et al.[34] reported that the effectiveness of the biosurfactant produced by the thermophilic *Alcaligenes faecalis* was limited under both alkaline and neutral conditions. Figure 2 shows the variation in CSL surface tension with temperature and pH. Slight decreases in the surface tension were observed with increasing pH and temperature, although the differences were not significant in samples of CSL under different conditions. Figure 2A, Figure 2B, and Figure 2C show the surface-active reduction achieved in a water solution in the presence of CSL-1, CSL-2, and CSL-3 respectively at different pH (4, 5, and 8) and temperature (4 °C, 25 °C, and 65 °C).

From the data shown above, it can be speculated that CSL could be used in the bioremediation of hydrocarbon-contaminated soils. Thus, this waste material could be used to produce surface-active agents that would increase the solubilization of hydrophobic contaminants and also to supply important nutritients that would facilite the fermentation of hydrophobic substances in soil. Such an application would represent an important advance in environmental protection. Moreover, the biosurfactant isolated from CSL could find other aplications in the pharmacutical, biomedical, or comestics[35,36] as well as in food[37] and agriculture[38] industries to improve the solubilization of active principles.

The most powerful commercial biosurfactant known, surfactin, produced by *Bacillus subtilis*, is able to reduce the surface tension of water from 72 to 27 mN m^{-1} at a concentration of 10 mg L^{-1};[39] however, surfactin is of limited use for most applications involving consumer products because it is not water-soluble and it is very expensive (50 mg of surfactin costs about $820). Other authors have proposed the utilization of *Lactobacillus*,[40] *Candida*,[41] or *Pseudomona* strains[42] for producing biosurfactant, although the high cost of the nutritional components of the fermentation media and the biosurfactant purification could prevent their industrial commercialization. As CSL is a byproduct of the corn milling industry, and therefore cheap, the use of this waste material as a source of biosurfactant may represent an important advance in the production of inexpensive ecofriendly surfactants.

3.2. Extraction of Biosurfactant from CSL. In order to isolate the surface-active compounds contained in corn steep liquor, CSL-1 was submitted to liquid−liquid extraction with different organic solvents. The extraction study was carried out only with CSL-1 because CSL streams, evaluated in this work, have very similar characteristics, although, in order to corroborate the composition of the biosurfactant, the best extractant will be selected to isolate and characterize the biosurfactants contained in the other CSLs.

The minimum surface tension value achieved in the aqueous phase after the extraction and redissolution of biosurfactant obtained from CSL-1, at its CMC, was about 36 mN m^{-1}, when all the biosurfactant from CSL was extracted, and the maximum value obtained in the aqueous phase was about 72 mN m^{-1} when no biosurfactant was extracted. Of the solvents used, chloroform, methyl *tert*-butyl ether, and dichloromethane extracted almost 100% of the biosurfactant from CSL, as deduced by the surface tension value of water in the presence of the biosurfactant extracted from CSL-1 (36 mN m^{-1}).

3.3. Characterization of Biosurfactant Contained in CSL. Of the solvents used, chloroform was selected to extract the biosurfactant from CSL for chemical characterization. The biochemical analysis revealed that the biosurfactant, extracted from CSL, was composed of 21.9% proteins and 64.2% lipids. Moreover, FTIR spectroscopy was used to elucidate the molecular components of each biosurfactant extracted from the different batches of CSL. The FTIR spectra of the three biosurfactants are shown in Figure 3.

The spectral analysis of the biosurfactants indicated the presence of peptide groups resulting from N−H stretching and O−H stretching of carboxylic acids (wavenumbers between 3450 and 3300 cm^{-1}). Moreover, the FTIR spectrum of the biosurfactants indicated the presence of protein-related weak bands: C═O bond at 1750−1650 cm^{-1} (amide bonds) and N−H bonds at 1515 cm^{-1} (amides and amines bonds). The absorbance band between 3000 and 2850 cm^{-1} and bands at around 1465−1365 cm^{-1} denote the presence of C−H stretching corresponding to CH_2 and CH_3 groups of aliphatic chains. The bands at 1275 and 1750 cm^{-1} are stretching vibrations of C−O and C═O bonds in carboxyl esters. Furthermore, the bands at 1167 and 1240 cm^{-1} indicate the presence of fatty acid. The FTIR spectra of the biosurfactant extracted from CSL-1, CSL-2, and CSL-3 confirmed that this extract comprises lipids and proteins. The results obtained in this work are consistent with analytical data indicating that the biosurfactant is a

dx.doi.org/10.1021/jf501386h | J. Agric. Food Chem. 2014, 62, 5451−5457

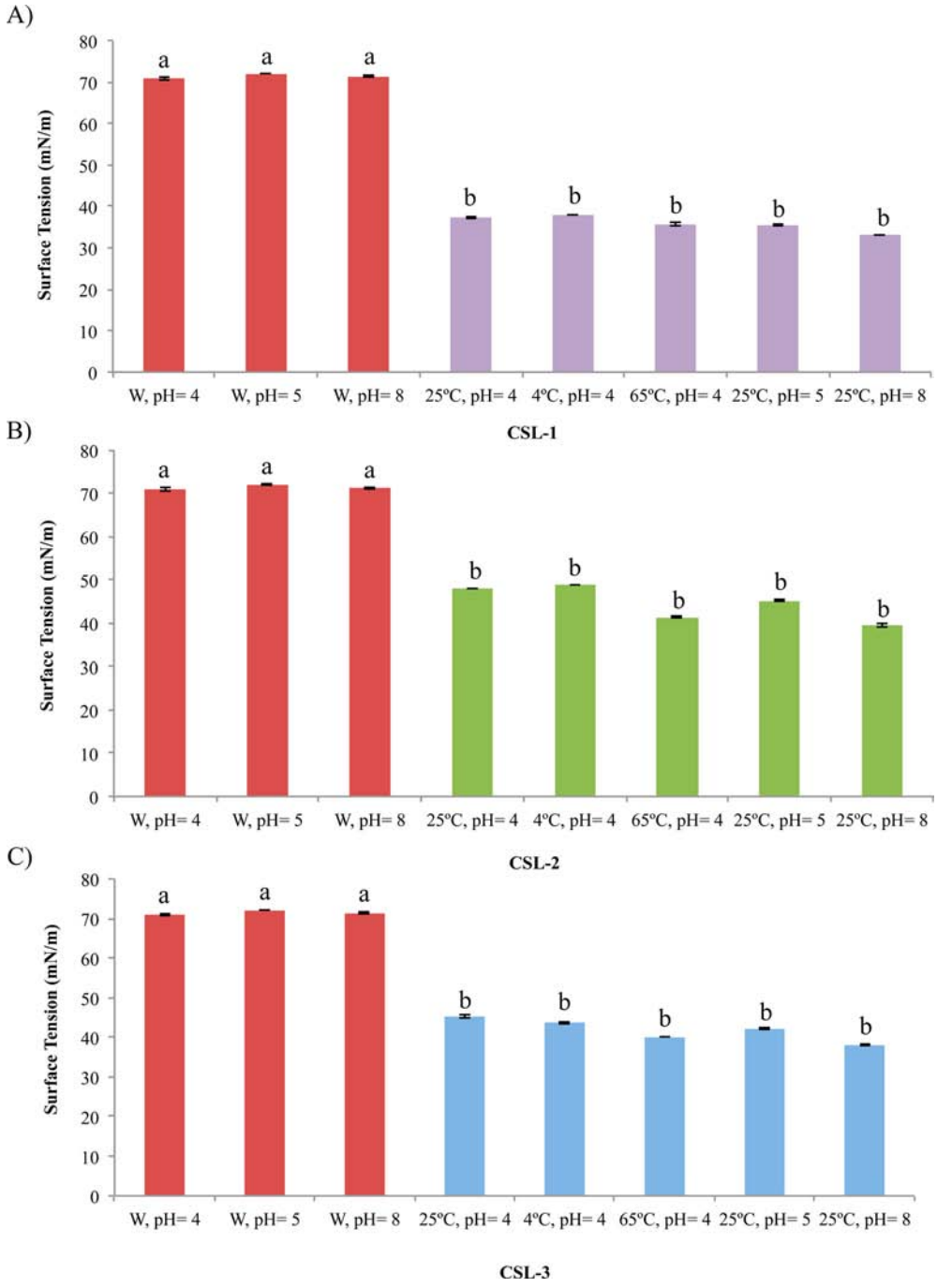

Figure 2. Influence of temperature and pH on the biosurfactant activity of CSL-1 (A), CSL-2 (B), and CSL-3 (C). Water (W) was included as control at different pH and 25 °C. Values are means of three determinations. Different letters indicate significant differences ($p < 0.05$).

lipopeptide. Thus, the hydrophobic chain of biosurfactant from CSL is composed of lipids, whereas the hydrophilic chain is mainly composed of proteins. The composition of the biosurfactant extracted from CSL is similar to the lipopeptide biosurfactant produced by *Selenomonas ruminantium*.[43]

Moreover, the fatty acid composition revealed that the biosurfactants obtained from CSL comprised linolelaidic acid, oleic and/or elaidic acids, stearic acid, and palmitic acid. The relative abundance of each fatty acid in the biosurfactants are shown in Table 2, indicating that the most abundant fatty acid was linolelaidic acid (50−55.2%). The fatty composition of the biosurfactant isolated from CSL is very similar to the fatty acid composition of the surfactin.[39]

Table 2. Fatty Acid Composition of the Biosurfactant Extracted with Chloroform from CSL-1, CSL-2, and CSL-3

retention time (min)	fatty acid	formula	rel abundance (%) CSL-1	CSL-2	CSL-3
24.3	palmitic acid	$C_{16}H_{32}O_2$ (C16)	16.7	14.9	19.6
32.1	stearic acid	$C_{18}H_{36}O_2$ (C18)	5.9	12.5	14.6
33.2	oleic or elaidic acid	$C_{18}H_{34}O_2$ (C18:1)	22.2	21.2	15.7
36.0	linolelaidic acid	$C_{18}H_{32}O_2$ (C18:2)	55.2	51.4	50.0

As a cheap and readily available byproduct of the corn wet-milling process, CSL could be used directly as a biosurfactant

dx.doi.org/10.1021/jf501386h | J. Agric. Food Chem. 2014, 62, 5451−5457

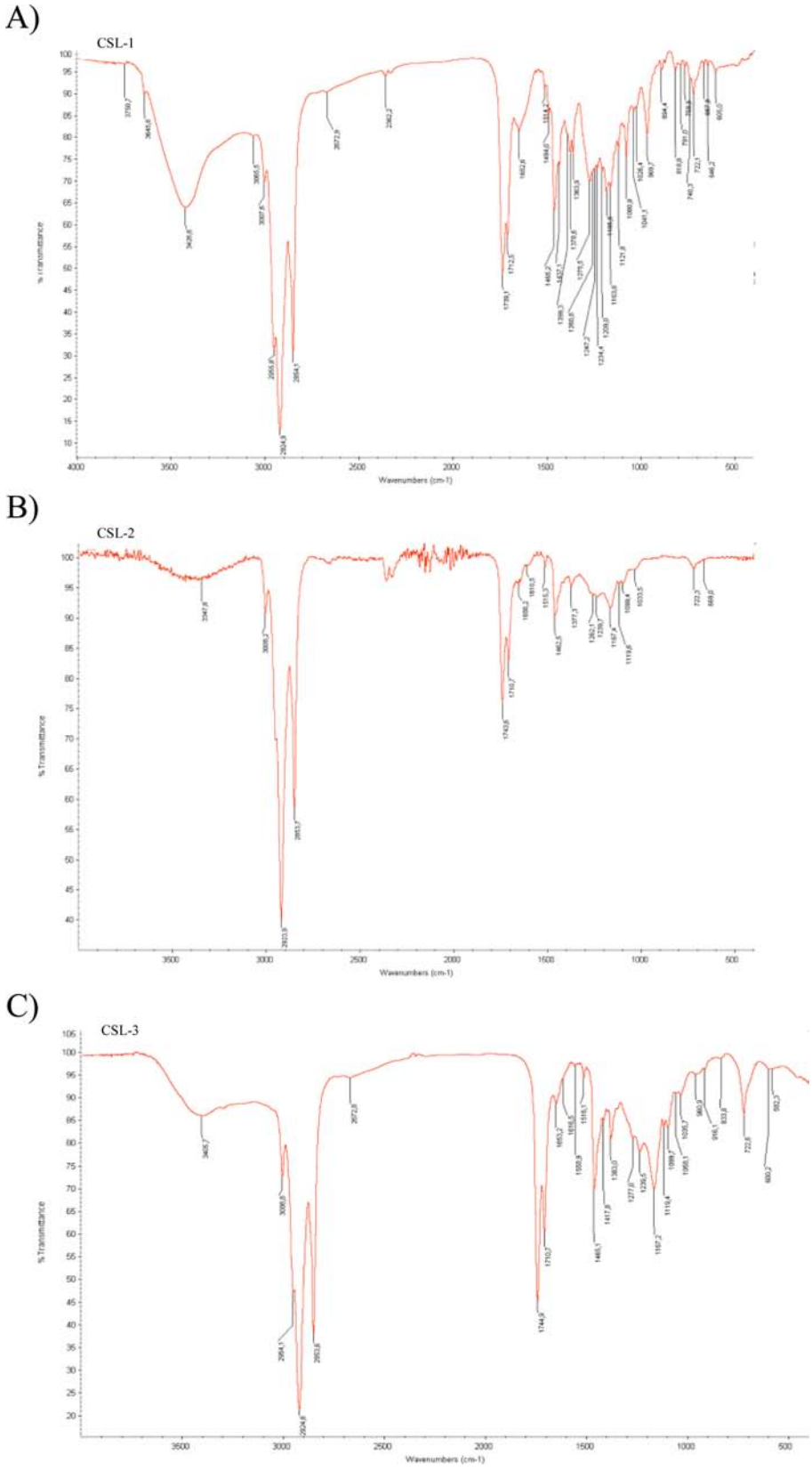

Figure 3. Fourier transform infrared spectrum of biosurfactant extracted from CSL-1 (A), CSL-2 (B), and CSL-3 (C).

agent, e.g., in the bioremediation of hydrophobic contaminated sites. The biosurfactant from CSL can be extracted using different organic solvents, and it is able to reduce the surface tension of water by more than 30 units. Moreover, the chemical characterization of this biosurfactant revealed that is a lipopeptide. Hence, the presence of biosurfactants in CSL may enable important advancements to be made in the industrial production of biosurfactants.

dx.doi.org/10.1021/jf501386h | J. Agric. Food Chem. 2014, 62, 5451−5457

AUTHOR INFORMATION

Corresponding Author

*Tel: +34 986812215. E-mail: amoldes@uvigo.es.

Funding

The authors wish to thank the Spanish Ministry of Economy and Competitiveness for funding this research (Project CTM2012-31873). X.V. gratefully acknowledges the University of Vigo for the award of a predoctoral contract.

Notes

The authors declare no competing financial interest.

REFERENCES

(1) Ramirez, E. C.; Johnston, D. B.; McAloon, A. J.; Yee, W.; Singh, V. Engineering process and cost model for a conventional corn wet milling facility. *Ind. Crops Prod.* **2008**, *27*, 91−97.

(2) Beuque, P.; Devos, F.; Huchette, M. Corn steeping process for products thus obtained and their use in the manufacture of penicillin. US Patent 4,359,528 (1982).

(3) Troostembergh J.; Winge, T.; Oudeene, F. Treatment of corn steep liquor. US Patent 4,980,282 (1990).

(4) Wang, Y.; Li, K.; Huang, F.; Wang, J.; Zhao, J.; Zhao, X.; Garza, E.; Manow, R.; Grayburn, S.; Zhou, S. Engineering and adaptive evolution of *Escherichia coli* W for L-lactic acid fermentation from molasses and corn steep liquor without additional nutrients. *Bioresour. Technol.* **2013**, *148*, 394−400.

(5) Sharma, N.; Prasad, G. S.; Choudhury, A. R. Utilization of corn steep liquor for biosynthesis of pullulan, an important exopolysaccharide. *Carbohydr. Polym.* **2013**, *93*, 95−101.

(6) Guerra-Rodríguez, E.; Vázquez, M. Technical and economical evaluation of microbial transglutaminase production on enzymatic hydrolysates of potato (*Solanum tuberosum*). *CyTA—J. Food* **2013**, *11*, 277−284.

(7) Téllez-Luis, S. J.; Moldes, A. B.; Alonso, J. L.; Vázquez, M. Optimization of Lactic acid production by *Lactobacillus delbrueckii* through response surface methodology. *J. Food Sci.* **2003**, *68*, 1454−1458.

(8) Bustos, G.; de la Torre, N.; Moldes, A. B.; Cruz, J. M.; Domínguez, J. M. Revalorization of hemicellulosic trimming vine shoots hydrolyzates trough continuous production of lactic acid and biosurfactants by *L. pentosus*. *J. Food Eng.* **2007**, *78*, 405−412.

(9) Xi, Y.-L.; Chen, K.-Q.; Dai, W.-Y.; Ma, J.-F.; Zhang, M.; Jiang, M.; Wei, P.; Ouyang, P.-K. Succinic acid production by *Actinobacillus succinogenes* NJ113 using corn steep liquor powder as nitrogen source. *Bioresour. Technol.* **2013**, *136*, 775−779.

(10) Maddipati, P.; Atiyeh, H. K.; Bellmer, D. D.; Huhnke, R. L. Ethanol production from syngas by Clostridium strain P11 using corn steep liquor as a nutrient replacement to yeast extract. *Bioresour. Technol.* **2011**, *102*, 6494−6501.

(11) Li, Y.; Gao, K.; Tian, S.; Zhang, S.; Yang, X. Evaluation of *Saccharomyces cerevisiae* Y5 for ethanol production from enzymatic hydrolysate of non-detoxified steam-exploded corn stover. *Bioresour. Technol.* **2011**, *102*, 10548−10552.

(12) Rust, D. *Surfactants: a market opportunity study update*; OmniTech International Ltd: Midland, MI, 2008.

(13) Levison, M. I. Surfactant production: present realities and future perspectives. In *Handbook of detergents part F: production*; Zoller, U., Eds.; CRC Press: Boca Raton, FL, 2009; pp 1−38.

(14) *Market Report, 2008. World Surfactant Market: markets, products, applications, innovations, chances & risks, competition, prospects to 2015*; Active Market Intelligence: Germany, 2008.

(15) Mulligan, C. N. Environmental applications for biosurfactants. *Environ. Pollut.* **2005**, *133*, 183−198.

(16) Moldes, A. B.; Torrado, A. M.; Barral, M. T.; Domínguez, J. M. Evaluation of biosurfactant production from various agricultural residues by *Lactobacillus pentosus*. *J. Agric. Food Chem.* **2007**, *55*, 4481−4486.

(17) Adams, M. R.; Moss, M. O. Fermented and Microbial Foods. In *Food Microbiology*, 3rd ed.; The Royal Society of Chemistry: Cambridge, U.K., 2008; pp 315−321.

(18) Kim, S. H.; Lim, E. J.; Lee, S. O.; Lee, J. D.; Lee, T. H. Purification and characterization of biosurfactants from *Nocardia* sp. L-417. *Biotechnol. Appl. Biochem.* **2000**, *31*, 249−253.

(19) Jamal, P.; Alam, M. Z.; Yusof, U. S. M.; Wan Nawawi, W. M. F. Optimization of process conditions for extraction of biosurfactant. *J. Appl. Sci. Res.* **2011**, *7*, 2156−2161.

(20) Dubois, M.; Gilles, K. A.; Hamilton, J. K.; Rebers, P. A.; Smith, F. Colorimetric method for determination of sugars and related substances. *Anal. Chem.* **1956**, *28*, 350−356.

(21) Lowry, O. H.; Rosebrough, N. J.; Farr, A. L.; Randall, R. J. Protein measurement with the Folin phenol reagent. *J. Biol. Chem.* **1951**, *193*, 265−275.

(22) Folch, J. M.; Lees, M.; Stanly, H. S. A simple method for the isolation and purification of total lipids from animal tissues. *J. Biol. Chem.* **1956**, *226*, 497−509.

(23) EN ISO 12966-2, 2011. Animal and Vegetable Fats and Oils-Gas Chromatography of Fatty Acid Methyl Esters: Part 2: Preparation of Methyl Esters of Fatty Acids, pp 1−23.

(24) Mulligan, C.; Gibbs, B. *Biosurfactants: Production. Properties. Applications*. Marcel Dekker: New York, 1993; pp 329−371.

(25) Velraeds, M.; Van der Mei, H.; Reid, G.; Busscher, H. Inhibition of initial adhesion of uropathogenic Enterococcus faecalis by biosurfactants from *Lactobacillus* isolates. *Appl. Environ. Microbiol.* **1996**, *62*, 1958−1963.

(26) Busscher, H.; Neu, T.; Van der Mei, H. C. Biosurfactant production by thermophilic dairy streptococci. *Appl. Microbiol. Biotechnol.* **1994**, *41*, 4−7.

(27) Moldes, A. B.; Torrado, A. M.; Barral, M. T.; Domínguez, J. M. Evaluation of biosurfactant production from various agricultural residues by *Lactobacillus pentosus*. *J. Agric. Food Chem.* **2007**, *55*, 4481−4486.

(28) Paradelo, R.; Moldes, A. B.; Dominguez, J. M.; Barral, M. T. Reduction of water repellence of hydrophobic plant substrates using biosurfactant produced from hydrolyzed grape marc. *J. Agric. Food Chem.* **2009**, *57*, 4895−4899.

(29) Al-Wahaibi, Y.; Joshi, S.; Al-Bahry, S.; Elshafie, A.; Al-Bemani, A.; Shibulal, B. Biosurfactant production by *Bacillus subtilis* B30 and its application in enhancing oil recovery. *Colloids Surf., B* **2014**, *114*, 324−333.

(30) Chooklin, C. S.; Maneerat, S.; Saimmai, A. Utilization of banana peel as a novel substrate for biosurfactant production by *Halobacteriaceae archaeon* AS65. *Appl. Biochem. Biotechnol.* **2014**, *173*, 624−645.

(31) Saikia, R. R.; Deka, S.; Deka, M.; Banat, I. M. Isolation of biosurfactant-producing *Pseudomonas aeruginosa* RS29 from oil-contaminated soil and evaluation of different nitrogen sources in biosurfactant production. *Ann. Microbiol.* **2012**, *62*, 753−763.

(32) Winston, R.; Koffler, H. Corn steep liquor in Microbiology. *Bacteriol. Rev.* **1948**, *12*, 297−311.

(33) Vecino-Bello, X.; Devesa-Rey, R.; Cruz, J. M.; Moldes, A. B. Study of the synergistic effects of salinity, pH, and temperature on the surface-active properties of biosurfactants produced by *Lactobacillus pentosus*. *J. Agric. Food Chem.* **2012**, *60*, 1258−1265.

(34) Bharali, P.; Das, S.; Konwar, B. K.; Thakur, A. J. Crude biosurfactant from thermophilic Alcaligenes faecalis: Feasibility in petro-spill bioremediation. *Int. Biodeterior. Biodegrad.* **2011**, *65*, 682−690.

(35) Gharaei-Fathabad, E. Biosurfactants in pharmaceutical industry: A mini-review. *Am. J. Drug Discovery Dev.* **2011**, *1*, 58−69.

(36) Gudiña, E. J.; Rangarajan, V.; Sen, R.; Rodrigues, L. R. Potential therapeutic applications of biosurfactants. *Trends Pharmacol. Sci.* **2013**, *34*, 667−675.

(37) Campos, J. M.; Montenegro Stamford, T. L.; Sarubbo, L. A.; de Luna, J. M.; Rufino, R. D.; Banat, I. M. Microbial biosurfactants as additives for food industries. *Biotechnol. Prog.* **2013**, *29*, 1097−1108.

(38) Sachdev, D. P.; Cameotra, S. S. Biosurfactants in agriculture. *Appl. Microbiol. Biotechnol.* **2013**, *97*, 1005−1016.

(39) Shaligram, N. S.; Singhal, R. S. Surfactin-a review on biosynthesis, fermentation, purification and applications. *Food Technol. Biotechnol.* **2010**, *48*, 119−134.
(40) Rodríguez-Pazo, N.; Salgado, J. M.; Cortés-Diéguez, S.; Domínguez, J. M. Biotechnological production of Phenyllactic Acid and biosurfactants from Trimming Vine Shoot Hydrolyzates by Microbial Coculture fermentation. *Appl. Biochem. Biotechnol.* **2013**, *169*, 2175−2188.
(41) Rufino, R. D.; Luna, J. M.; Sarubbo, L. A.; Rodrigues, L. R. M.; Teixeira, J. A. C.; Campos-Takaki, G. M. Antimicrobial and anti-adhesive potential of a biosurfactant Rufisan produced by *Candida* lipolytica UCP 0988. *Colloids Surf., B* **2011**, *84*, 1−5.
(42) Janek, T.; Łukaszewicz, M.; Krasowska, A. Identification and characterization of biosurfactants produced by the Arctic bacterium *Pseudomonas* putida BD2. *Colloids Surf., B* **2013**, *110*, 379−386.
(43) Saimmai, A.; Onlamool, T.; Sobhon, V.; Maneerat, S. An efficient biosurfactant-producing bacterium *Selenomonas ruminantium* CT2, isolated from mangrove sediment in south of Thailand. *World J. Microbiol. Biotechnol.* **2013**, *29*, 87−102.

JOURNAL OF AGRICULTURAL AND FOOD CHEMISTRY

Article

pubs.acs.org/JAFC

Identification of a Bioactive Bowman–Birk Inhibitor from an Insect-Resistant Early Maize Inbred

Eric T. Johnson,*[,†] Christopher Skory,[‡] and Patrick F. Dowd[†]

[†]Crop Bioprotection Research Unit and [‡]Renewable Product Technology Research Unit, National Center for Agricultural Utilization Research, Agricultural Research Service, U.S. Department of Agriculture , 1815 North University Street, Peoria, Illinois 61604, United States

Supporting Information

ABSTRACT: Breeding of maize, *Zea mays*, has improved insect resistance, but the genetic and biochemical basis of many of these improvements is unknown. Maize oligonucleotide microarrays were utilized to identify differentially expressed genes in leaves of three maize inbreds, parents Oh40B and W8 and progeny Oh43, developed in the 1940s. Oh43 had enhanced leaf resistance to corn earworm larvae, *Helicoverpa zea*, and fall armyworm larvae, *Spodoptera frugiperda*, compared to one or both parents. Among ca. 100 significantly differentially expressed genes, expression of a Bowman–Birk trypsin inhibitor (BBI) gene was at least ca. 8-fold higher in Oh43 than in either parent. The Oh43 BBI gene was expressed as a recombinant protein. Purified BBI inhibited trypsin and the growth of fall armyworm larvae when added to insect diet. These experiments indicate that comparative gene expression analysis combined with insect resistance measurements of early inbreds can identify previously unrecognized resistance genes.

KEYWORDS: *defense, metallothionein, trypsin inhibition, reactive oxygen species, ribosome-inactivating protein*

INTRODUCTION

Global management of crops due to insect damage costs billions of dollars annually.[1] Insect damage can also lead to the transmission of a variety of plant pathogens, including those that produce toxins that are harmful to people and animals in maize and other crops.[2] Past breeding efforts have shown some success in developing maize lines with significant insect resistance.[3] With the advent of successful transgene incorporation technology, new resistance gene sources have been identified and successfully deployed, such as the *Bacillus thuringiensis* crystal protein, which rely much less on source plant germplasm for trait improvement. However, recent and potential problems with pests developing resistance to these transgenic events[4] has provided additional incentive for looking at source plants for useful resistance alleles that can be incorporated by breeding or transgenic means.

Strategies for identifying new resistance genes are varied. Earlier work identified different bioactive chemicals in resistant plants, including DIMBOA-glucoside, maysin, and hemicellulose, which occurred at higher concentrations in resistant materials prior to insect damage.[5,6] More recent studies have identified proteins involved in maize resistance, such as proteases,[7] peroxidases,[8] or ribosome-inactivating proteins,[9,10] for which roles have been confirmed by diet incorporation or transgenic plant studies. With the advent of comparative expression analysis techniques, such as gene microarrays or RNA-Seq analysis, it has been possible to determine which genes that produce resistance molecules are up- or down-regulated, although the expression profiles often involve dozens of potential resistance candidates, making confirmation of a role in resistance onerous.[11] Additionally, the most effective resistance molecules are often expressed constitutively in some resistant material, whereas the same molecules are induced in other resistant material.[12]

Modern maize commercial varieties can be examined in the presence and absence of various pests, obtaining information on potential induced molecules, with the benefits and caveats mentioned above. Whereas yield increases have been relatively steady over the past several decades, over a dozen diseases have increased significantly in importance over the same period of time,[13] suggesting that resistance alleles have been lost during the process of breeding for yield. However, it is possible that useful resistance genes could be still expressed in "older" maize lines. Genome-wide examination of representatives of these older lines has yielded interesting examples of genes with utility.[14] Gene microarray comparisons can allow for parent/progeny comparisons where different pest resistance is present, as it is possible to examine the expression of many genes in the same tissue that also has been evaluated for insect resistance. Maize microarrays have been used to identify genetic differences among inbreds, especially in cases of hybrid vigor or heterosis,[15] but to our knowledge, no genomic profiling studies of closely related inbreds have integrated insect resistance results. We now report on an example of this type of comparison, using parent and progeny inbreds developed in the 1940s.[16] The inbreds were tested for leaf resistance to corn earworm and fall armyworm larvae. Maize microarrays were utilized to identify putative insect resistance genes differentially expressed in the leaves. A Bowman–Birk inhibitor, identified by

Received: March 21, 2014
Revised: May 28, 2014
Accepted: May 28, 2014
Published: May 28, 2014

ACS Publications This article not subject to U.S. Copyright. Published 2014 by the American Chemical Society

Table 1. PCR Primers Used for RT-qPCR of Maize Inbred or Control cDNA

oligonucleotide	top hit[a]	size (bp)	forward primer	reverse primer	PCR start	PCR end	PCR length (bp)
MZ00018241	NM_001 111495	983	CGTCTTCAGGTGGGCCGTCG	ACCACGTGGAAGCAGAGCAACA	760	969	210
MZ00055932	GRMZM2G007928_T01 utr3	596	TTCCGTTCGGAGCTCCATTT	CGAGTAAAAAGGCGACGAGC	42	137	96
luciferase	control RNA spike	1800	CCAGGGATTTCAGTCGATGT	AATCTGACGCAGGCAGTTCT	not known	not known	183

[a]From BLAST alignment to GenBank or the maize B73 genome.

this microarray analysis, was expressed in vitro and was bioactive against commercial trypsin and insect larvae.

MATERIALS AND METHODS

Insects. Corn earworms (CEW, *Helicoverpa zea* (Boddie)) and fall armyworms (FAW, *Spodoptera frugiperda* (J.E. Smith)) were reared on pinto bean based diet at 27 ± 1 °C, 50 ± 10% relative humidity, and a L14:D10 h photoperiod, as described previously.[17] First-instar larvae were used in bioassays.

Plants. Inbred maize parent lines W8 (Wisconsin Agricultural Experiment Station) and O40B (Ohio Agricultural Research and Development Center) and the inbred derived from the cross of these two parents, Oh43, were the subject of the study. Oh43, developed in 1949 by the Ohio Agricultural Experiment Station,[16] was produced with at least four generations of selfing following the initial Oh40B × W8 cross.[18] The W8 seed was obtained from Natalia de-Leon (Department of Agronomy, University of Wisconsin, Madison, WI, USA), and the Oh40B and Oh43 seeds were obtained from the USDA-ARS North Central Regional Plant Introduction Station. Prior studies indicated Oh40B had fair resistance to the corn leaf aphid *Rhopalosiphum maidis* (Fitch) and the European corn borer *Ostrinia nubilalis* (Hübner), whereas Oh43 had good resistance to these two insect species.[16] No reports of insect resistance of W8 were listed under its description,[16] although presumably it exhibits intermediate resistance against these insects. Seed was planted in soil mix 3.[19] Plants were grown in a climate-controlled room with light 14 h (24 ± 1 °C)/dark 10 h (18 ± 1 °C) and 50 ± 10% relative humidity. The third visible leaf from the top of a seven-leaf plant, which was fully expanded and mature, was used in bioassays.

Leaf Bioassays. Bioassays were performed as described previously.[19] Seven or eight plants of each inbred were used as a source of leaves. Approximately 20 cm of the anterior portion of the leaf was removed from each plant. Leaves were cut into approximately 1 × 2 cm sections with the posterior section used for corn earworms, and the adjacent anterior section was used for fall armyworms. The remaining leaf was frozen in liquid nitrogen for use in subsequent RNA extraction or protein assays. Individual leaf sections were placed on a piece of moistened filter paper in a 5 cm Petri dish with a tight-fitting lid, along with 10 newly hatched caterpillars. The total number of 1 mm^2 hole equivalents caused by feeding was determined after 2 days.[19] Survivors were weighed to the nearest 0.01 mg using an analytical balance.

Caterpillar Diet Disk Bioassays. Aliquots of recombinant protein (and corresponding quantities of background protein produced by wild-type yeast that eluted from a nickel column) were added to freeze-dried insect diet disks as previously described.[20] Briefly, for the 2 day bioassay, the protein solutions were absorbed into the diet disks at a rate of 30 μL per 15 mg disk and then added to a Petri dish with a tight-fitting lid containing 10 insect larvae. For the 5 day bioassay, 150 μL of the protein solutions was absorbed into 50 mg diet disks, and each disk was placed on top of a Teflon disk in a well of a 24-well plate containing 3% water agar. One insect larva was caged in each well, and the wells were covered with a sheet of parafilm. The assays were run for 5 days. Survivors were weighed to the nearest 0.01 mg using an analytical balance.

RNA Extraction and cDNA Labeling. RNA was extracted from the tissue, treated with DNase I (Qiagen, Valencia, CA, USA), and purified with the RNeasy kit (Qiagen) as previously described.[11] Ten micrograms of total RNA was converted into amino allyl modified cDNA by first adding 2 μg of oligo $d(T)_{12-18}$ primer and incubating at 70 °C for 5 min and then incubating on ice for 1 min. cDNA synthesis reactions were incubated at 46 °C for 3 h and included 1× Superscript III reaction buffer (Life Technologies, Carlsbad, CA, USA), 7.5 mM DTT, 1× dNTP mix with amino allyl dUTP (Stratagene, La Jolla, CA, USA), 20 units of RNase Block ribonuclease inhibitor (Stratagene), and 200 units of Superscript III reverse transcriptase enzyme (Life Technologies). Preliminary experimentation found that Superscript III enzyme resulted in better cDNA yield than the RT enzyme supplied in the FairPlay III Microarray Labeling Kit (Stratagene). After cDNA synthesis, 10 μL of 1 M NaOH was added and the sample was incubated at 70 °C for 10 min and then allowed to cool to room temperature before 10 μL of 1 M HCl was added to neutralize the pH. The cDNA was precipitated using 5 μL of 3 M sodium acetate, pH 4.5, 20 μg of glycogen, and 100 μL of ice-cold ethanol at −20 °C for 30 min. The cDNA was centrifuged at 14000*g* for 15 min, and the pellet was washed with 0.5 mL of ice-cold 70% ethanol followed by an additional spin at 14000*g* for 15 min. Ethanol was removed, and the pellet was allowed to dry before 5 μL of coupling buffer (Stratagene) was added to resuspend the cDNA. Samples were incubated at 37 °C for 15 min to aid in resuspension, then 5 μL of either Cy3 or Cy5 mono reactive dye (GE Healthcare Biosciences, Piscataway, NJ, USA) diluted in dimethyl sulfoxide (DMSO) was added, and samples were placed in the dark for 30 min at room temperature. Fifty microliters of water was added, and then labeled cDNA was purified from the unreacted dye using the illustra CyScribe GFX Purification Kit (GE Healthcare Biosciences).

Microarray Hybridization and Scanning. Maize microarray slides were purchased from the University of Arizona through the Maize Oligonucleotide Array Project funded by the NSF Plant Genome Research Program and contained ∼46000, 70mer oligonucleotides[21] (NCBI GEO Platform the GPL6438). Labeled cDNA was quantified with a Nanodrop 2000 spectrophotometer (Thermo Fisher Scientific, Wilmington, DE, USA) and subsequently evaporated to dryness in a Speedvac prior to resuspension. The probe solution (40 μL) included 40 pmol of Cy5-labeled cDNA, 40 pmol of Cy3-labeled cDNA, 25 μg of yeast tRNA, and 12 μg of salmon sperm DNA. Prehybridization of the microarray slide and hybridization of probes to the slide in a sealed hybridization chamber were carried out according to an established protocol[22] except for an additional high-stringency wash at room temperature. Each microarray slide was hybridized to two different maize inbred labeled cDNAs with the following arrangement: slide 1, W8-1 (Cy3) versus Oh40B-1 (Cy5); slide 2, Oh43-1 (Cy3) versus W8-2 (Cy5); slide 3, Oh40B-2 (Cy3) versus Oh43-2 (Cy5); slide 4, W8-3 (Cy3) versus Oh43-3 (Cy5); slide 5, Oh40B-3 (Cy3) versus W8-4 (Cy5); slide 6, Oh43-4 (Cy3) versus Oh40B-4 (Cy5). The slides were scanned at 10 μm resolution on an Axon GenePix 4100A microarray scanner using GenePix Pro software (both from MDS Analytical Technologies, Sunnyvale, CA, USA). Photomultiplier tube levels were adjusted using the Auto-PMT feature. Each slide was visually scanned for aberrant signals, and such signals were removed if necessary. Mean signal intensity, with the background subtracted, was utilized for expression calculations. Each set (four replicates) of signal intensities for one inbred was scaled to the one replicate with the highest mean intensity and then transformed to log2 values, using Microsoft Excel. Each inbred replicate set was imported

into the ArrayStar software program (version 4.1 DNASTAR, Madison, WI, USA). ANOVA analysis (*F* test procedure) with false discovery rate correction[23] was used to identify differentially expressed genes at 95% confidence. The normalized data are available at the NCBI Gene Expression Omnibus, accession no. GSE40107.

Reverse Transcriptase Quantitative PCR (RT-qPCR) Analysis. RNA was extracted as described above from maize leaves of three different biological replicates of each inbred that were different biological replicates from those used in the microarray experiments. Purified RNA (400 ng) was converted to cDNA using the AccuScript High Fidelity First Strand cDNA Synthesis Kit (Stratagene) with the provided oligo(dT) primer. Fifty picograms of luciferase RNA (Promega) was added to each cDNA reaction for normalization of target genes.[24] RNA was removed from cDNA using RNase H according to the manufacturer's instructions (New England Biolabs, Ipswich, MA, USA). Twenty-five microliter qPCR reactions were set up using 2× SYBR Green qPCR SuperMix Universal (Life Technologies), 10 μM of each forward and reverse primer, and 1 μL of cDNA reaction. Primers were designed with a melting temperature of 60 °C using Primer-BLAST (available at the NCBI Web site), OligoPerfect Designer (Life Technologies Web site), or Oligo Calc.[25] All primers used in this study are listed in Table 1. The cycling program consisted of the following: 50 °C for 2 min; 95 °C for 10 min; 40 cycles of 95 °C for 15 s, 60 °C for 60 s, plate read. After amplification, the following melting curve analysis was performed: 60−95 °C with a plate read every 1 °C; hold 1 s between reads. Cycling and fluorescence readings were performed on a Chromo 4 Detector (MJ Research, Waltham, MA, USA). Duplicate qPCR reactions for each primer combination and the luciferase control were completed for each biological replicate. A no-template control for each primer combination was also run for each plate to ensure the amplification did not include fluorescence due to primer dimers. Amplification of a single qPCR product close to the predicted size for each primer combination was confirmed using 3% agarose gel electrophoresis containing 1× SYBRsafe (Life Technologies) and visualized using a Molecular Imager ChemiDoc XRS+ (Bio-Rad, Hercules, CA, USA; at least one reaction was checked for each inbred). The crossover threshold (CT) value and efficiency for each reaction was calculated using the Real-time PCR Miner 4.0 algorithm[26] (software available through the Stanford University Office of Technology Licensing). The normalized initial fluorescence was calculated for each reaction for each target gene using the equation[27]

$$R_{0,T}/R_{0,R} = (1 + E_R)^{CT}{}_R/(1 + E_T)^{CT}{}_T$$

where R_0 is the SYBR Green initial fluorescence for the T, target gene, and R, reference (luciferase) gene, E is the efficiency, and CT is the crossover threshold value.

Trypsin Inhibitor Analysis. Trypsin inhibition (potentially due to a Bowman−Birk-type inhibitor) was determined using midgut homogenates of corn earworms and fall armyworms as the trypsin source and leaf homogenates of the three different maize inbreds as the source of trypsin inhibitor. N_α-Benzoyl-DL-arginine *p*-nitroanilide hydrochloride (BAPA) (Sigma-Aldrich, St. Louis, MO, USA) was used as the trypsin substrate[28] and is a suitable substrate for measuring trypsin activity in caterpillars.[29] BAPA was initially dissolved at the rate of 1 mg in 250 μL of dimethyl sulfoxide (DMSO). This stock of BAPA was diluted 1:50 in pH 8.0, 0.01 M sodium phosphate buffer, which was held at room temperature. Preliminary studies were used to determine an appropriate concentration of caterpillar midguts per volume of buffer to yield a linear reaction over 1 h at 30 °C. For the assays, three corn earworm and seven fall armyworm midguts were homogenized in 1400 μL of phosphate buffer.[30] The homogenates were centrifuged at 10000*g* for 10 min, and the supernatants were used in the assays. Maize leaf pieces approximately 1.5 × 0.5 cm from the same leaves used in bioassays and for array analysis were homogenized in 500 μL of phosphate buffer, centrifuged as described for midgut homogenates, and the supernatants were used as the inhibitor source, after adjustment for equivalent protein amounts in assays. The Bio-Rad protein assay dye reagent was used to quantitate protein, as described above. A typical assay consisted of 20 μL of enzyme source, 20 μL of inhibitor source, and 160 μL of substrate source; enzyme and inhibitor free controls were also used. Assays were performed in duplicate for each treatment using 96-well plates held at 30 °C for 1 h and read on a Spectramax 250 plate reader (Molecular Devices, Sunnyvale, CA, USA) at 410 nm. Maximum absorbance of uninhibited reactions ranged from approximately 0.1 to 0.2 absorbance units per h.

Recombinant Production of Maize BBI. The maize BBI gene that was expressed at higher levels in Oh43 leaves was amplified from Oh43 leaf cDNA (see above for cDNA preparation) on the basis of the B73 mRNA sequence (GRMZM2G007928_T01, which binds to maize oligonucleotide MZ00055932) using PCR Master mix (Roche Applied Science). The Oh43 BBI sequence was 100% identical to the B73 sequence (GRMZM2G007928_T01). The Oh43 BBI sequence (hereafter referred to as the Oh43 BBI), except for the 24 amino acid N-terminal signal peptide as predicted by SignalP,[31] was cloned by PCR into the *Eco*RI and *Xba*I sites of pPICZα A, a vector for secreted expression in *Pichia pastoris* X-33. The Oh43 BBI construct additionally contained a C-terminal hexahistidine tag for purification. The entire BBI sequence was checked for accuracy before transformation into *P. pastoris* by sequencing using a BigDye Terminator Cycle Sequencing Kit (Applied Biosystems, Foster City, CA, USA). Putative transformants were generated by electroporation and selection with 100 μg/mL zeocin on the following media: 1% yeast extract, 2% peptone, 2% dextrose, 1 M sorbitol, and 2% agar. Three different transformants were grown for 72 h, and Oh43 BBI clone 3 was chosen for further experimentation because of its high expression levels in the media as measured by Western blot analysis with a rabbit antihexahistidine antibody (Bethyl Laboratories, Montgomery, TX, USA).

Wild type *P. pastoris* and Oh43 BBI clone 3 were each grown in 25 mL of BMG media (100 mM potassium phosphate, pH 6.0, 1.34% yeast nitrogen base with ammonium sulfate (containing no amino acids), 4 × 10^{-5}% biotin, and 1% glycerol) overnight at 30 °C. The cells were resuspended in 120 mL of BMM media (same composition as BMG media, but with 0.5% methanol replacing the 1% glycerol) at OD 600 equal to 1.0 AU and then grown for 6 days at 30 °C with daily addition of methanol to 0.5%. The spent medium was recovered and adjusted to pH 6.5 with KOH. Three milliliters of nickel−nitrilotriacetic acid resin (Thermo Fisher Scientific) was washed with 10 mL of 20 mM $NaPO_4$, 300 mM sodium chloride, and 15 mM imidazole, pH 6.5. Approximately 50 mL of spent medium was mixed by rocking with the washed resin for 30 min at room temperature. The spent medium was removed and the resin added to a plastic 10 mL column (Bio-Rad) kept at 4 °C. The resin was washed with 2 column volumes of 20 mM $NaPO_4$, 300 mM sodium chloride, and 15 mM imidazole, pH 6.5. Histidine-tagged protein was eluted with 5 mL of 20 mM $NaPO_4$, 300 mM sodium chloride, and 250 mM imidazole, pH 6.5, and 1 mL fractions were collected. Fractions of wild type and BBI clone 3 were quantified by the Bio-Rad protein assay dye reagent. Aliquots of some of the fractions were separated by tricine SDS-PAGE using a 10% acrylamide gel[32] and transferred to polyvinylidene difluoride membrane in 10 mM 3-(cyclohexylamino)-1-propanesulfonic acid. Western blot analysis was performed as described previously[9] except for the following changes: the membrane was blocked for 1 h in 5% instant nonfat dry milk (Kroger, Cincinnati, OH, USA) in phosphate-buffered saline (with 0.01% Tween-20); the primary antibody was a rabbit antihexahistidine antibody from Bethyl Laboratories that was diluted 1:10000, and the secondary antibody was diluted 1:150000.

Reverse Zymography of Recombinant Maize BBI. Aliquots of eluted recombinant Oh43 BBI were subjected to reverse zymography as described previously[33] with some modifications. The 15% (w/v) acrylamide-SDS gels, which included 0.1% (w/v) gelatin, were made according to the method of Schägger.[32] Electrophoresis of the recombinant maize BBI, as well as soybean BBI (Sigma-Aldrich), was performed according to the method of Schägger[32] at 4 °C. Use of bovine pancreas type III trypsin (Sigma-Aldrich) at 450 μg per 100 mL in development buffer required incubation for only 2 h at 37 °C to digest the indicator background gelatin protein when inhibition did

Table 2. Biological Effects of Insect Larvae Feeding on Maize Leaves from Different Inbreds[a]

insect	W8	Oh40B	Oh43
CEW mean feeding	37.4 ± 1.2 (7) a	35.8 ± 1.5 (8) a	25.1 ± 0.9 (8) b
CEW mean weight (mg)	0.42 ± 0.02 (59) a	0.34 ± 0.02 (71) b	0.37 ± 0.02 (73) b
FAW mean feeding	49.9 ± 1.6 (7) a	43.5 ± 1.2 (8) b	31.8 ± 2.1 (8) c
FAW mean weight (mg)	0.53 ± 0.03 (68) a	0.62 ± 0.03 (79) a	0.40 ± 0.03 (73) b

[a]Feeding rate (1 mm^2 hole equivalents) and weight (±standard error) were determined after 2 days of leaf feeding. Values in rows followed by different letters are statistically different at $P < 0.05$ by ANOVA.

not occur. The gel was stained with Bio-Safe Coomassie stain (Bio-Rad) according to the manufacturer's instructions and visualized using a Molecular Imager ChemiDoc XRS+.

Statistical Analyses. Statistically significant ($P < 0.05$) differences in feeding rates, insect midgut trypsin inhibitor activity, initial reporter fluorescence values for RT-qPCR analysis, and insect survivor weights were determined by analysis of variance using Proc GLM of SAS for Windows version 8.0 or higher. Chi-square analysis was performed using Proc Freq of SAS, with significance at $P < 0.05$.

RESULTS AND DISCUSSION

Differential Insect Feeding on the Inbred Leaves. Results of bioassays indicate the Oh43 inbred was more resistant to CEW and FAW compared to one or both parents, as indicated by reduced amounts of feeding and lower weights of survivors (Table 2). For the CEW, those caged with Oh43 caused less damage and weighed less than those caged with W8 leaves. Although feeding rates were lower on day 2 for CEW caged with Oh43 versus Oh40B leaves, weights of survivors were not different. For the FAW, those caged with Oh43 leaves caused less damage to leaves and weighed less than both parents. Thus, there were differential effects of the three inbreds on these two species of caterpillars.

Differential Gene Expression of the Inbreds. Because the inbred lines displayed differential leaf resistance to the CEW and FAW, transcriptional profiling of the leaves was completed using maize oligonucleotide microarrays. These profiling experiments found 111 differentially expressed genes (with $P < 0.05$) among the three inbreds. Putative functions could be assigned to 90 of the differentially expressed genes. The majority of the differentially expressed genes (49/90) had a putative molecular function (Gene Ontology accession no. 0003674); this gene ontology describes the action of a gene product at the molecular level and could include catalysis or binding. The 20 genes with the lowest P values are listed in Table 3. A number of the genes in Table 3 could potentially contribute to differential insect resistance. Trypsin inhibitor (MZ00055932, described as a Bowman–Birk inhibitor by GenBank accession NP_001148299), which could inhibit trypsin proteases in insect digestive tracts, was more highly expressed in Oh43 than in W8 or Oh40B. The gene encoding ribosome-inactivating protein 2 (RIP2, MZ00018241), also known as rRNA *N*-glycosidase, was more highly expressed in Oh43 than in Oh40B or W8. Lastly, the *Bx1* gene (MZ00015105), which encodes the initial enzyme of DIMBOA biosynthesis, was more highly expressed in W8 than in the other inbreds. There were also a number of metallothionein-like genes and genes of unknown function differentially expressed among the three inbreds, which may be contributing to insect resistance.

RT-qPCR was used to analyze the differential expression of the putative insect resistance genes (Table 4). Both RIP and the BBI were more highly expressed in Oh43 leaves (at statistically significant levels) than in Oh40B or W8 leaves, respectively, but

Table 3. Differentially Expressed Genes in Maize Inbred Leaves Determined by Microarray Analysis

oligonucleotide	description[a]	Oh43/W8[b]	Oh43/Oh40B[b]	P
MZ00056633	Fe–S assembly protein	1.3	8.3	0.0051
MZ00041643	cupin3 domain	1.2	3.7	0.0072
MZ00020744	small nuclear RNA	9.1	17.8	0.0080
MZ00040089	histone	7.6	1.8	0.0080
MZ00039334	metallothionein-like	0.090	0.22	0.0084
MZ00055932	trypsin inhibitor (BBI)	8.4	7.8	0.0090
MZ00006035	nucleotide translocase	1.4	2.2	0.0090
MZ00018241	RIP2	3.1	9.4	0.010
MZ00021395	membrane protein	1.4	2.1	0.011
MZ00026722	expansin-like	1.1	2.8	0.012
MZ00028883	cytochrome P450	4.5	1.5	0.013
MZ00016005	peroxidase	0.81	2.7	0.013
MZ00014067	germin-like protein	0.27	1.0	0.013
MZ00017181	unknown protein	1.9	2.4	0.020
MZ00055047	run and tbc domains	1.0	27.0	0.020
MZ00037853	chloroplast 50S ribosomal protein	8.5	1.7	0.020
MZ00037704	isomerase	1.1	3.7	0.022
MZ00035390	Fe–S assembly protein	1.4	8.8	0.024
MZ00039519	unknown protein	1.3	3.0	0.030
MZ00015105	*Bx1*	0.13	1.9	0.030

[a]Annotation from the top hit of BLAST alignment of the maize B73 genome or NCBI GenBank. [b]Relative expression level.

at higher levels than measured using the microarrays. This might be due to the greater sensitivity of quantitative PCR methods.[34] A recent paper indicated that RIP2 mRNA and protein are rapidly induced (within 1 h) in maize Tx601 in response to fall armyworm feeding and RIP2 is active against FAW.[10] Our results suggest that some maize inbreds may have elevated levels of RIP2 prior to insect attack that would contribute to greater resistance.

Trypsin Inhibitor Experiments. Higher mRNA levels of a trypsin inhibitor (BBI) in Oh43 leaf extracts (Table 4) could contribute to reducing the trypsin activity of insect midguts compared to leaf extracts from the other inbreds. Some differences in levels of mean insect trypsin inhibition were significant for the crude inbred leaf extracts (Table 5). Oh40B trypsin inhibitory activity was significantly higher than that of W8 extract toward FAW trypsin and was more similar to levels for inhibition by Oh43 extract. For CEW trypsin activity, Oh40B and W8 inhibition levels were similar, but there were no statistically significant differences among the three inbred extracts. These results indicate that extracts from Oh43 leaves, as assayed, although sometimes more inhibitory than one or both parents, did not have significant trypsin inhibitory activity against CEW and FAW midgut trypsin that was higher than that of the parent inbred extracts. However, the crude mixture of plant and insect midgut extracts could contain components

Table 4. RT-qPCR Assay of Putative Insect Resistance Genes

oligonucleotide	description	inbred 1 $R_{0,T}/R_{0,luc}$[a]	inbred 2 $R_{0,T}/R_{0,luc}$[a]	RT-qPCR[b]	microarray[b]
MZ00055932	trypsin inhibitor	Oh43: 1.5 ± 0.38 c	W8: 0.012 ± 0.0082 d	125	8.4
MZ00018241	RIP2	Oh43: 0.78 ± 0.15 c	Oh40B: 0.0053 ± 0.0020 d	206	9.4

[a] $R_{0,T}/R_{0,luc}$ is the mean ± SE initial reporter fluorescence for the target (T) relative to the initial reporter fluorescence of luciferase; values in columns followed by different letters are statistically different at $P < 0.05$ by ANOVA analysis. [b] Relative expression level, Oh43/inbred.

Table 5. Inhibition of Insect Midgut Trypsin Activity by the Three Maize Inbreds[a]

inbred	% inhibition FAW	% inhibition CEW
W8	2.6 ± 3.6 a	18.4 ± 0.8 a
Oh40B	6.6 ± 1.5 b	19.4 ± 3.0 a
Oh43	6.7 ± 1.9 ab	25.0 ± 4.7 a

[a] Values in columns followed by different letters are significantly different at $P < 0.05$ by analysis of variance.

that mask the actual trypsin and antitrypsin activities of individual bioactive species. Hence, further experiments were undertaken with the BBI gene that was expressed at higher levels in Oh43 than in either parent.

Recombinant Oh43 BBI Added to Insect Diet Inhibits FAW Growth. To ascertain the insect inhibitory properties of the BBI gene elevated in Oh43, the gene was cloned for secreted recombinant protein production in *P. pastoris*. Western blot analysis of the nickel column elution fractions indicated wild-type *P. pastoris* did not secrete any detectable histidine-tagged proteins into the media, whereas the recombinant line secreted two small (<15 kDa) proteins and low levels of one ~50 kDa histidine-tagged protein (likely a multimer) into the media (Figure 1). The expected size of the recombinant maize

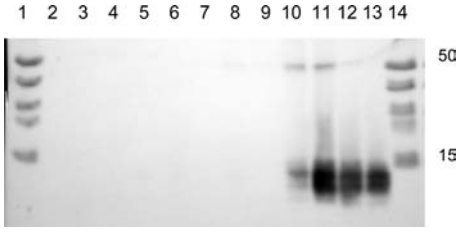

Figure 1. Western blot of elution fractions from *P. pastoris* spent media. Lanes: 1 and 14, molecular weight markers (numbers on the right side of the figure correspond to kilodalton standards); 2, flow-through of control media; 3–7, elution fractions 1–5 of the control media; 8, flow-through of Oh43 BBI media; 9–13, elution fractions 1–5 of Oh43 BBI media.

BBI was 10.3 kDa, which likely corresponds to one of the proteins below the 15 kDa protein marker. To test the activity of the recombinant Oh43 BBI, in-gel protease inhibitory activity experiments (zymography) were conducted. Protein from Oh43 BBI elution fractions 3 and 4 prevented trypsin activity below and above the 17 kDa marker (lanes 5–10), whereas there were no trypsin inhibitory proteins from control fraction 3 (lane 4) (Figure 2). The protein below the 17 kDa marker likely corresponds to one of the Oh43 BBI isoforms shown in Figure 1. In lanes 2 and 3 of Figure 2, a soybean BBI (8 kDa) was included as a control and was self-associating into higher molecular weight forms, which is likely the case for the higher molecular weight form seen in the recombinant BBI fractions examined (lanes 5–10 of Figure 2). Activity of the recombinant BBI was also noted in zymogram assays against

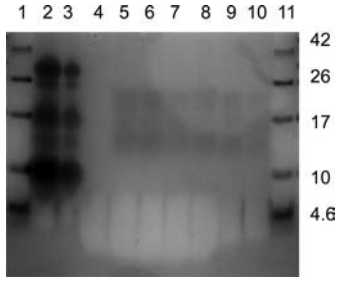

Figure 2. In-gel trypsin inhibitory activity of recombinant Oh43 BBI. Lanes: 1 and 11, molecular weight markers (numbers on the right side of the figure correspond to kilodaltons); 2 and 3, 3000 and 1000 ng, respectively, of soybean trypsin inhibitor; 4, control elution fraction 3; 5 and 6, 20 μL of Oh43 BBI elution fraction 3; 7 and 8, 20 μL of Oh43 BBI elution fraction 4; 9 and 10, 10 μL of Oh43 BBI elution fractions 3 and 4, respectively.

trypsin activity from midgut homogenates of fifth-instar FAW and whole body homogenates from newly hatched first-instar FAW (data not shown).

The recombinant form of BBI we produced did have some differing molecular forms. BBIs are known to self-associate into dimers in aqueous solutions.[35] Therefore, it is possible that the Oh43 BBI protein above the 17 kDa marker is a multimer that did not migrate at the expected molecular weight. A pea (*Pisum sativum*) BBI expressed in *P. pastoris* secreted two isoforms into the media, both of which inhibited trypsin and chymotrypsin activity; one of the isoforms was missing four amino acids at the C-terminus.[36] It is possible that the recombinant Oh43 BBI was altered as well, although probably not at the C-terminus, which ends with a hexahistidine sequence. In any case, it is clear that the recombinant Oh43 BBI had trypsin inhibitory activity.

The Oh43 BBI elution fractions with the highest protein concentration were added to insect diet that was fed to FAW larvae (control fraction 3, lane 5; Oh43 BBI fraction 3, lane 11) (Figure 1). The mean weight of FAW that fed on the 5.3 μg/g Oh43 BBI diet was much less than the mean weight of those that fed on the control diet after 2 days (Table 6), although the difference in the means was not statistically significant. However, a greater proportion of FAW larvae that weighed <0.40 mg were found among the larvae that fed on the Oh43 BBI diet compared to those that fed on the control diet. The length of the bioassay was extended to 5 days in an additional experiment. Again, the mean weight of FAW that fed on the 6.0 μg/g Oh43 BBI diet was less than the mean weight of those that fed on the control diet (Table 6), and the mean weights of the two treatments were very close to being statistically different at $P < 0.05$. A larger proportion of FAW larvae that weighed <17 mg were found among the larvae that fed on the Oh43 BBI diet compared to those that fed on the control diet. Inspection of the data indicated the 17 mg value was an appropriate value to select on the basis of the ranges of the values found for the different treatments. Identical experiments found that the recombinant Oh43 BBI did not inhibit the

Table 6. Recombinant Oh43 BBI Inhibits FAW Growth[a]

treatment	weight (mg) after 2 days	larvae <0.40 mg after 2 days	weight (mg) after 5 days	larvae <17 mg after 5 days
control	0.43 ± 0.045 (20)	25%	13.8 ± 2.6 (13)	69%
BBI	0.38 ± 0.021 (19)	58%	8.9 ± 0.9 (16)	100%
statistical measure	F = 3.04	P = 0.037	F = 3.9	P = 0.017
	P = 0.089		P = 0.059	

[a]Weights are mean ± standard error (N). Control contained 1.1 μg/g background *P. pastoris* protein for 2 day experiment. Control contained 1.2 μg/g background *P. pastoris* protein for 5 day experiment. BBI concentration was 5.3 μg/g for 2 day experiment and 6 μg/g for 5 day experiment. ANOVA was used for comparing mean weights in the same column. Chi-square analysis was used for comparing frequencies in the same column.

growth of CEW larvae (data not shown). It is possible that trypsins in the CEW larvae are not sensitive to the Oh43 BBI or degrade Oh43 BBI or that the CEW larvae synthesize novel insensitive trypsins after consuming the Oh43 BBI, as has been reported in studies in which insects have consumed other protease inhibitors.[29,37] Additional studies will be necessary to determine if there are trypsins in CEW that are insensitive to the Oh43 BBI. The adaptability of insects to protease inhibitors is justification for the development of transgenic crops expressing at least two protease inhibitors for effective resistance[38] or identifying protease inhibitors that do not induce resistant proteases.[39]

The maize genome contains at least 11 putative BBIs. To our knowledge, this is the first study demonstrating that a monocot BBI (the Oh43 BBI is gene GRMZM2G007928) has antitrypsin activity, can inhibit insect larva development, and could be a useful resistance gene for developing insect-resistant maize. The Oh43 BBI protein contains 12 cysteine residues, which are likely cross-linked in a pattern conserved in other monocotyledonous and dicotyledonous plants.[40] The Oh43 BBI has a single reactive site that contains conserved residues found in other monocotyledonous species.[40] Another maize BBI (gene GRMZM2G156632) in the Brio cultivar was induced by wounding and possibly protects the injured tissues from pathogens or insects.[41,42] Expression of one of the maize BBIs (gene GRMZM5G815098) potentially contributed to the increased insect resistance of maize plants that had been exposed to volatiles released after infestation with common armyworm, *Mythimna separata* Walker.[43] No other published studies describe a function for the other nine maize BBIs, including the BBI examined in the present study. Diet incorporation assays indicate BBIs from a number of dicot plant species are capable of inhibiting the growth of various insect larvae.[44,45]

Other Resistance Mechanisms Potentially Involved in Oh43 Insect Resistance. Expression of metallothionein genes was from 4- to 10-fold lower in Oh43 leaves than in the two parents. The potential involvement of metallothioneins in insect resistance is less obvious. A number of roles have been attributed to these proteins in plants, including complexing (and thus detoxifying) reactive oxygen species.[46] Reactive oxygen species are generated as part of a resistance response to insects or disease.[47] For example, as part of one resistance process, peroxidases interact with hydrogen peroxide and plant allelochemical substrates (such as ferulic acid in maize) to form reactive quinones and reactive oxygen species.[48] Both products can undergo additional reactions. Thus, the lowering of the level of reactive oxygen species, through the presence of metallothioneins, is likely to dampen any resistance response. Lower levels of metallothioneins would likely preserve reactive oxygen species for a longer period, resulting in a stronger resistance response. Transgenic overexpression of these proteins in rice has led to enhanced disease susceptibility.[49] Because the initial reactive components are compartmentalized in an intact cell, lower levels of metallothioneins are less likely to cause adverse effects on the intact cell. Reactive oxygen species are also important in signaling and stimulation of additional resistance responses.[47] Other genes, including some with uncharacterized roles, were expressed to a greater extent in Oh43 leaves compared to one or the other parent and may also be additively contributing to Oh43 insect resistance.

There was no clear-cut single gene responsible for greater resistance in Oh43 compared to either parent inbred. This is not surprising, considering multiple genes are known to confer insect resistance in maize.[50] However, from examination of relative expression levels, it is clear that Oh43 had expression trends higher or lower than one or both parents of most genes that could be considered as contributing to resistance (metallothionein-like, RIP2, BBI) and some genes of unknown function that may play a resistance role. We were able to identify where heterotic interactions were occurring (i.e., expression higher than either parent) and sources of resistance gene alleles in nonheterotic interactions (based on similar expression of genes in Oh43 and one or the other parent). In the future, performing quantitative trait loci (QTL) analysis on the parents W8 and Oh40B may clarify which insect resistance genes play a critical role in Oh43. It may be of interest to also identify resistance genes in leaves that are induced by insect feeding.

RIP2 and BBI genes have been demonstrated in this and other studies to produce proteins that can affect insects and/or pathogens. Studies involving transgenic over- or under-expression of these genes and genes of unknown function associated with expression differences in Oh43 will be required to more positively identify a role in insect resistance. However, the present study has demonstrated a bioactive Bowman−Birk inhibitor from maize leaves for the first time. Thus, comparative expression analyses of early inbred parent and progeny do have the potential to identify resistance genes present in earlier inbreds that have been lost due to yield-focused maize breeding.

■ ASSOCIATED CONTENT

Supporting Information

Entire list of differentially expressed genes, with their putative function. This material is available free of charge via the Internet at http://pubs.acs.org.

■ AUTHOR INFORMATION

Corresponding Author

*(E.T.J.) Phone: (309) 681-6177. Fax: (309) 681-6686. E-mail: eric.johnson2@ars.usda.gov.

Funding

The study was supported by CRIS Project 3620-42000-041-00D base funds. The mention of trade names or commercial products in this paper is solely for the purpose of providing specific information and does not imply recommendation or endorsement by the U.S. Department of Agriculture over other firms or similar products not mentioned.

Notes

The authors declare no competing financial interest.

■ ACKNOWLEDGMENTS

We thank D. Lee and M. Doehring for technical assistance. We are grateful to N. de-Leon and the North Central Regional Plant Introduction Station for providing seed. We appreciate F. Vega and C. Dunlap providing comments on prior versions of the manuscript.

■ ABBREVIATIONS USED

BBI, Bowman−Birk inhibitor; CEW, corn earworm; FAW, fall armyworm; MOD1, recombinant maize kernel ribosome-inactivating protein; RIP2, maize leaf ribosome-inactivating protein; RT-qPCR, reverse transcription-quantitative polymerase chain reaction analysis

■ REFERENCES

(1) Zalucki, M. P.; Shabbir, A.; Silva, R.; Adamson, D.; Liu, S.-S.; Furlong, M. J. Estimating the economic cost of one of the world's major insect pests, *Plutella xylostella* (Lepidoptera: Plutellidae): just how long is a piece of string? *J. Econ. Entomol.* **2012**, *105*, 1115−1129.

(2) Dowd, P. F; Johnson, E. T.; Williams, W. P. Strategies for insect management targeted toward mycotoxin management. In *Aflatoxin and Food Safety*; Abbas, H. K., Ed.; CRC Press: Boca Raton, FL, USA, 2005; pp 517−542.

(3) Painter, R. H. *Insect Resistance in Crop Plants.*; The University Press of Kansas: Lawrence, KS, USA, 1951; p 520.

(4) Benbrook, C. M. Impacts of genetically engineered crops on pesticide use in the U.S. − the first 16 years. *Environ. Sci. Eur.* **2012**, *24*, 24.

(5) Johnson, E. T.; Dowd, P. F.; Pinkerton, T. S. Altering plant secondary metabolism to achieve broad spectrum insect control and reduce mycotoxins. In *Genetically Modified Plants*; Wolf, T., Koch, J., Eds.; Nova Science Publishers: Happauge, NY, USA, 2008; pp 151−172.

(6) Williams, W. P.; Davis, F. M.; Buckley, P. M.; Hedin, P. A.; Baker, G. T.; Luthe, D. S. Factors associated with resistance to fall armyworm (Lepidoptera: Noctuidae) and southwestern corn borer (Lepidoptera: Crambidae) in corn at different vegetative stages. *J. Econ. Entomol.* **1998**, *91*, 1471−1480.

(7) Pechan, T.; Ye, L.; Chang, Y.; Mitra, A.; Lin, L.; Davis, F. M.; Williams, W. P.; Luthe, D. S. A unique 33-kDa cysteine proteinase accumulates in response to larval feeding in maize genotypes resistant to fall armyworm and other Lepidoptera. *Plant Cell* **2000**, *12*, 1031−1040.

(8) Dowd, P. F.; Johnson, E. T.; Pinkerton, T. S. Identification and properties of insect resistance-associated maize anionic peroxidases. *Phytochemistry* **2010**, *71*, 1289−1297.

(9) Dowd, P. F.; Johnson, E. T.; Price, N. P. Enhanced pest resistance in maize leaves expressing monocot crop plant derived ribosome inactivating protein and agglutinin. *J. Agric. Food Chem.* **2012**, *60*, 10768−10775.

(10) Chuang, W.-P.; Herde, M.; Ray, S.; Castano-Duque, L.; Howe, G. A.; Luthe, D. S. Caterpillar attack triggers accumulation of the toxic maize protein RIP2. *New Phytol.* **2014**, *201*, 928−939.

(11) Johnson, E. T.; Dowd, P. F.; Liu, Z. L.; Musser, R. O. Comparative transcription profiling analyses of maize reveals candidate defensive genes for seedling resistance against corn earworm. *Mol. Gen. Genom.* **2011**, *285*, 517−525.

(12) Glauser, G.; Marti, G.; Villard, N.; Doyen, G. A.; Wolfender, J. L.; Turlings, T. C.; Erb, M. Induction and detoxification of maize 1,4-benzoxazin-3-ones by insect herbivores. *Plant J.* **2011**, *68*, 901−911.

(13) Duvick, D. N. Genetic progress in yield of United States maize (*Zea mays* L.). *Maydica* **2005**, *50*, 195−202.

(14) Tian, F.; Bradbury, P.; Brown, P.; Sun, Q.; Flint-Garcia, S. A.; Rocheford, T. R.; McMullen, M. D.; Holland, J. B.; Buckler, E. S., IV. Genome-wide association study of maize identifies genes affecting leaf architecture. *Nat. Genet.* **2011**, *43*, 159−162.

(15) Thiemann, A.; Fu, J.; Schrag, T. A.; Melchinger, A. E.; Frisch, M.; Scholten, S. Correlation between parental transcriptome and field data for the characterization of heterosis in *Zea mays* L. *Theor. Appl. Genet.* **2010**, *120*, 401−413.

(16) Stringfield, G. H. *Maize Inbreds of Ohio*; Bulletin 831; Ohio Agricultural Experiment Station: Wooster, OH, USA, 1959; 67 pp.

(17) Dowd, P. F. Toxicological and biochemical interactions of the fungal metabolites fusaric acid and kojic acid with xenobiotics in *Heliothis zea* (F.) and *Spodoptera frugiperda* (J.E. Smith). *Pest. Biochem. Phys.* **1988**, *32*, 123−134.

(18) Guthrie, W. D.; Russell, W. A. Breeding methodologies and genetic basis of resistance in maize to the European corn borer. In *Toward Insect Resistant Maize for the Third World: Proceedings of the International Symposium on Methodologies for Developing Host Plant Resistance to Maize Insects*; CIMMYT: Mexico, D.F., Mexico, 1989; pp 192−202.

(19) Dowd, P. F.; Johnson, E. T.; Pinkerton, T. S. Oral toxicity of *β*-*N*-acetyl hexosaminidase to insects. *J. Agric. Food Chem.* **2007**, *55*, 3421−3428.

(20) Dowd, P. F.; Berhow, M. A.; Johnson, E. T. Differential activity of multiple saponins against omnivorous insects with varying feeding preferences. *J. Chem. Ecol.* **2011**, *37*, 443−449.

(21) Gardiner, J. M.; Buell, C. R.; Elumalai, R.; Galbraith, D. W.; Henderson, D. A.; Iniguez, A. L.; Kaeppler, S. M.; Kim, J. J.; Liu, J.; Smith, A.; Zheng, L.; Chandler, V. L. Design, production and utilization of long oligonucleotide microarrays for expression analysis in maize. *Maydica* **2005**, *50*, 425−435.

(22) Hedge, P.; Qi, R.; Abernathy, K.; Gay, C.; Dharap, S.; Gaspard, R.; Hughes, J. E.; Snesrud, E.; Lee, N.; Quackenbush, J. A concise guide to cDNA microarray analysis. *Biotechniques* **2000**, *29*, 548−562.

(23) Benjamini, Y.; Hochberg, Y. Controlling the false discovery rate: a practical and powerful approach to multiple testing. *J. R. Statist. Soc. Ser. B* **1995**, *57*, 289−300.

(24) Rehrig, E. M.; Appel, H. M.; Schultz, J. C. Measuring 'normalcy' in plant gene expression after herbivore attack. *Mol. Ecol. Res.* **2011**, *11*, 294−304.

(25) Kibbe, W. A. OligoCalc: an online oligonucleotide properties calculator. *Nucleic Acids Res.* **2007**, *35*, W43−W46.

(26) Zhao, S.; Fernald, R. D. Comprehensive algorithm for quantitative real-time polymerase chain reaction. *J. Computat. Biol.* **2005**, *12*, 1047−1064.

(27) Liu, W.; Saint, D. A. A new quantitative method of real time reverse transcription polymerase chain reaction assay based on simulation of polymerase chain reaction kinetics. *Anal. Biochem.* **2002**, *302*, 52−59.

(28) Erlanger, B. F.; Kokowsky, N.; Cohen, W. The preparation and properties of two new chromogenic substrates of trypsin. *Arch. Biochem. Biophys.* **1961**, *95*, 271−278.

(29) Paulillo, L. C.; Lopes, A. R.; Cristofoletti, P. T.; Parra, J. R.; Terra, W. R.; Silva-Filho, M. C. Changes in midgut endopeptidase activity of *Spodoptera frugiperda* (Lepidoptera: Noctuidae) are responsible for adaptation to soybean proteinase inhibitors. *J. Econ. Entomol.* **2000**, *93*, 892−896.

(30) Dowd, P. F. Responses of representative midgut detoxifying enzymes from *Heliothis zea* and *Spodoptera frugiperda* to trichothecenes. *Insect Biochem.* **1990**, *20*, 344−356.

(31) Nordahl Petersen, T.; Brunak, S.; von Heijne, G.; Nielsen, H. SignalP 4.0: discriminating signal peptides from transmembrane regions. *Nat. Methods* **2011**, *8*, 785−786.
(32) Schägger, H. Tricine-SDS-PAGE. *Nat. Protoc.* **2006**, *1*, 16−22.
(33) Le, Q. T.; Katunuma, N. Detection of protease inhibitors by a reverse zymography method, performed in a tris(hydroxymethyl)-aminomethane-tricine buffer system. *Anal. Biochem.* **2004**, *324*, 237−240.
(34) Czechowski, T.; Bari, R. P.; Stitt, M.; Scheible, W. R.; Udvardi, M. K. Real-time RT-PCR profiling of over 1400 *Arabidopsis* transcription factors: unprecedented sensitivity reveals novel root- and shoot-specific genes. *Plant J.* **2004**, *38*, 366−379.
(35) Birk, Y. The Bowman-Birk inhibitor. *Int. J. Pept. Protein Res.* **1985**, *25*, 113−131.
(36) Clemente, A.; Carmen Marín-Manzano, M.; Jiménez, E.; Carmen Arques, M.; Domoney. The anti-proliferative effect of TI1B, a major Bowman-Birk isoinhibitor from pea (*Pisum sativum* L.), on HT29 colon cancer cells is mediated through protease inhibition. *Br. J. Nutr.* **2012**, *108*, S135−S144.
(37) de Oliveira, C. F.; de Paula Souza, T.; Parra, J. R.; Marangoni, S.; de Castro Silva-Filho, C.; Macedo, M. L. Insensitive trypsins are differentially transcribed during *Spodoptera frugiperda* adaptation against plant protease inhibitors. *Comp. Biochem. Physiol. B* **2013**, *165*, 19−25.
(38) Dunse, K. M.; Stevens, J. A.; Lay, F. T.; Gaspar, Y. M.; Heath, R. L.; Anderson, M. A. Coexpression of potato type I and II proteinase inhibitors gives cotton plants protection against insect damage in the field. *Proc. Natl. Acad. Sci. U.S.A.* **2010**, *107*, 15011−15015.
(39) Srinivasan, A.; Chougule, N. P.; Giri, A. P.; Gatehouse, J. A.; Gupta, V. S. Podborer (*Helicoverpa armigera* Hübn.) does not show specific adaptations in gut proteinases to dietary *Cicer arietinum* Kunitz proteinase inhibitor. *J. Insect Physiol.* **2005**, *51*, 1268−1276.
(40) Mello, M. O.; Tanaka, A. S.; Silva-Filho, M. C. Molecular evolution of Bowman-Birk type proteinase inhibitors in flowering plants. *Mol. Phylogenet. Evol.* **2003**, *27*, 103−112.
(41) Eckelkamp, C.; Ehmann, B.; Schopfer, P. Wound-induced systemic accumulation of a transcript coding for a Bowman-Birk trypsin inhibitor-related protein in maize (*Zea mays* L.) seedlings. *FEBS Lett.* **1993**, *323*, 73−76.
(42) Rohrmeier, T.; Lehle, L. *WIP1*, a wound-inducible gene from maize with homology to Bowman-Birk proteinase inhibitors. *Plant Mol. Biol.* **1993**, *22*, 783−792.
(43) Ali, M.; Sugimoto, K.; Ramadan, A.; Arimura, G. Memory of plant communications for priming anti-herbivore responses. *Sci. Rep.* **2013**, *3*, 1872.
(44) Rahbé, Y.; Ferrasson, E.; Rabesona, H.; Quillien, L. Toxicity to the pea aphid *Acyrthosiphon pisum* of anti-chymotrypsin isoforms and fragments of Bowman-Birk protease inhibitors from pea seeds. *Insect Biochem. Mol. Biol.* **2003**, *33*, 299−306.
(45) Kaur, H.; Sohal, S. K.; Rup, P. J.; Kaur, A. Growth and development of melon fruit fly larvae under the influence of soybean trypsin inhibitors. *Int. J. Tropical Insect Sci.* **2010**, *30*, 200−206.
(46) Cobbett, C.; Goldsbrough, P. Phytochelatins and metal-lothioneins: roles in heavy metal find detoxification and homeostasis. *Annu. Rev. Plant Biol.* **2002**, *53*, 159−182.
(47) Fujita, M.; Fujita, Y.; Noutoshi, Y.; Takahashi, F.; Farusaka, Y.; Yamaguchi-Shinozaji, K.; Shinozaki, K. Cross talk between abiotic and biotic stress responses: a current view from the point of convergence in the stress signaling network. *Curr. Opin. Plant Biol.* **2006**, *9*, 436−442.
(48) Dowd, P. F; Lagrimini, L. M. The role of peroxidase in host insect defenses. In *Advances in Insect Control: The Role of Transgenic Plants*; Carozzi, N., Koziel, M., Eds.; Taylor & Francis: Bristol, PA, USA, 1997; pp 195−224.
(49) Wong, H. L.; Sakamoto, T.; Kawasaki, T.; Umemura, K.; Shimamoto, K. Down-regulation of metallothionein, a reactive oxygen scavenger, by the small GTPase *OsRac1* in rice. *Plant Physiol.* **2004**, *135*, 1447−1456.
(50) McMullen, M. D.; Simcox, K. D. Genomic organization of disease and insect resistance genes in maize. *Mol. Plant−Microb. Interact.* **1995**, *8*, 811−815.

JOURNAL OF AGRICULTURAL AND FOOD CHEMISTRY

Article

pubs.acs.org/JAFC

Stable Isotope Dilution Gas Chromatography−Mass Spectrometry for Quantification of Thymoquinone in Black Cumin Seed Oil

Okiemute Rosa Johnson-Ajinwo and Wen-Wu Li*

Guy Hilton Research Centre, Institute for Science and Technology in Medicine, Keele University, Thornburrow Drive, ST4 7QB Stoke-on-Trent, United Kingdom

Supporting Information

ABSTRACT: Black cumin seed (*Nigella sativa* L.) is a widely used spice and herb, where thymoquinone (2-isopropyl-5-methyl-1,4-benzoquinone) is the major bioactive compound. Here, a stable isotope dilution (SID) gas chromatography−mass spectrometry (GC−MS) technique was developed for the quantification of thymoquinone. A doubly deuterated thymoquinone ([$^2H_2$]-thymoquinone) was synthesized for the first time with more than 93% deuteration degree shown by mass spectrometry and proton nuclear magnetic resonance (^{1}H NMR). This compound was used as an internal standard for the quantification of thymoquinone using a SID GC−MS method. The validation experiment showed a recovery rate of 99.1 ± 1.1% relative standard deviation (RSD). Standard addition and external calibration methods have also been used to quantify thymoquinone, which cross-validated the developed stable isotope dilution assay (SIDA). In comparison to external calibration and standard addition methods, the SIDA method is robust and accurate. The concentration of thymoquinone in five marketed black cumin seed oils ranged between 3.34 and 10.8 mg/mL by use of SID GC−MS.

KEYWORDS: *Nigella sativa, thymoquinone, stable isotope dilution, GC−MS, quantification*

INTRODUCTION

Black cumin seed (*Nigella sativa* L.) is a widely used spice in Mediterranean countries, Pakistan, and India.[1,2] It is also used as a traditional medicine for the treatment of a range of diseases, such as diabetes, hypertension, fever, arthritis, inflammation, gastrointestinal disturbances, and cancer.[3] Studies into the biological activities of this plant have revealed that the volatile essential oil components, predominantly thymoquinone (**1**) (Figure 1),[4] possess antioxidant,[5] anti-inflammatory,[6] antidiabetic,[7] immunomodulatory,[8] and anti-tumor[9−11] activities.

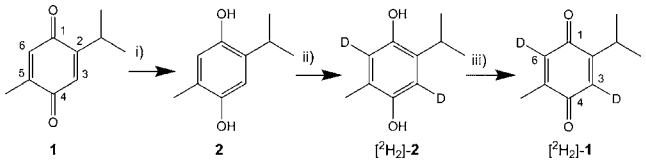

Figure 1. Scheme for synthesis of [$^2H_2$]-thymoquinone ([$^2H_2$]-**1**): (i) $Na_2S_2O_4$ in H_2O/MeOH at room temperature for 2 h, (ii) (a) 3.4 M D_2SO_4 in D_2O with reflux for 48 h and (b) cool to room temperature and workup with H_2O, and (iii) CrO_3 in 60% HOAc in H_2O at −4 °C for 2 h.

Thymoquinone was previously quantitated by means of high-performance liquid chromatography (HPLC),[12,13] high-performance thin-layer chromatography (HPTLC),[14] and a differential pulse polarographic method.[15] These methods could achieve high sensitivities and reproducibility, but they often need multi-steps of sample preparation and external calibrations; thus, the results could be influenced by complex matrices. Gas chromatography (GC) and/or gas chromatography−mass spectrometry (GC−MS) are preferred techniques for the analysis of volatile and semi-volatile compounds and have also been used for the quantification of thymoquinone[16] and identification of the composition of black cumin seed oil.[5,17] A stable isotope dilution assay/analysis (SIDA) should overcome the problem of the matrix effects, such as compound discrimination during extraction, chromatographic separation, and ultraviolet (UV)/mass spectrometry (MS)/electrochemical detection,[18,19] when a deuteriated thymoquinone is used as an internal standard. Stable isotope dilution coupled with GC−MS (SID GC−MS) has widely been used for determination of various compounds, e.g., methoxypyrazines in red wines,[19] dietary lignans in food,[20] natural estrogens in vegetables and fruits,[21,22] and alkypyrazines in coffee.[23] Here, we report synthesis of a stable deuterium (D or ^{2}H)-labeled thymoquinone (Figure 1) for the first time and its application as an internal standard for quantification of thymoquinone in black cumin seed oil by the means of SID GC−MS.

MATERIALS AND METHODS

Thymoquinone (99%), D_2-sulfuric acid (D_2SO_4, 99.5%), deuterated water [deuterium oxide (D_2O), 99.5%], sodium hydrosulfite ($Na_2S_2O_4$), and chromium trioxide (CrO_3) were purchased from Sigma-Aldrich. Hexane (analytical grade) was purchased from Fisher-Scientific, U.K. The following black cumin seed oils were purchased from Amazon: Manako black cumin oil, CEBRA *Nigella sativa* oil, Avena black cumin oil, Iman VERGIN black cumin oil, and This Health black seed oil.

Synthesis. The doubly deuteriated thymoquinone ([$^2H_2$]-**1**) (Figure 1) was prepared and purified according to a similar method

Received: January 21, 2014
Revised: May 22, 2014
Accepted: May 28, 2014
Published: May 28, 2014

ACS Publications © 2014 American Chemical Society

for preparation of deuterated 1,4-benzoquinones,[24,25] with modification.

2-Isopropyl-5-methyl-1,4-benenediol (2). A solution of sodium hydrosulfite (348 mg, 2.0 mmol) in 2.0 mL of water was added to a solution of thymoquinone (164 mg, 1.0 mmol) in 2.0 mL of methanol. The mixture was stirred for 2 h at room temperature. The methanol was evaporated, and the resultant solution was extracted with ethyl acetate (3 × 10 mL). The combined organic phase was washed with water (3 × 10 mL) and then dried over sodium sulfate. After evaporation of ethyl acetate, 2-isopropyl-5-methyl-1,4-benenediol (thymohydroquinone, **2**, 70 mg, yield of 42%) was obtained. MS [electron ionization (EI)] *m/z* (relative intensity, %): 166.1 (43) $[M]^{\bullet+}$, 151.1 (100) $[M - CH_3]^{\bullet+}$, 137 (4), 123.1 (11), 95.1 (10), 77.1 (10), 53.0 (3). Proton nuclear magnetic resonance (^{1}H NMR) (300 MHz, $CDCl_3$) δ: 6.56 (s, 1H), 6.47 (s, 1H), 3.06 (m, 1H), 2.10 (s, 3H), 1.14 (d, 6H, J = 7.2 Hz, $-CH(CH_3)_2$).

2-Isopropyl-5-methyl-1,4-dideuterobenenediol ($[^2H_2]$-2). 2-Isopropyl-5-methyl-1,4-benenediol (**2**, 68 mg, 0.40 mmol) was refluxed for 48 h in 3.4 M D_2-sulfuric acid (D_2SO_4, 0.9 mL) in deuterated water (D_2O, 4.2 mL). After cooling to room temperature, water (H_2O, 10 mL) was added and the mixture was extracted with ethyl acetate (3 × 10 mL). The ethyl acetate extract was washed with water (H_2O, 3 × 10 mL) and then dried over sodium sulfate. After evaporation of the solvent, 2-isopropyl-5-methyl-1,4-dideuterobenenediol ($[^2H_2]$-**2**, 45 mg) was obtained. MS (EI) *m/z* (relative intensity, %): 168.1 (44) $[M]^{\bullet+}$, 153.1 (100) $[M - CH_3]^{\bullet+}$, 139.1 (3), 125.1 (11), 97.0 (10), 79.1 (8), 55.0 (3).

2-Isopropyl-5-methyl-1,4-dideuterobenzoquinone ($[^2H_2]$-thymoquinone ($[^2H_2]$-1). 2-Isopropyl-5-methyl-1,4-dideuterobenenediol ($[^2H_2]$-**2**, 42 mg, 0.25 mmol) was dissolved in 60% acetic acid (2 mL) at −4 °C. Chromium trioxide (150 mg, 1.5 mmol) in 0.5 mL of 30% acetic acid was added, and the mixture was stirred at −4 °C for 2 h. Water (10 mL) was then added to the mixture, followed by extraction with ethyl acetate (2 × 10 mL). After drying over sodium sulfate, the solvent was removed under vacuum to give crude doubly deuteriated thymoquinone, which was sublimed to give pure 2-isopropyl-5-methyl-1,4-dideuterobenzoquinone ($[^2H_2]$-thymoquinone, $[^2H_2]$-**1**, 28.0 mg, 43% overall yield based on thymohydroquinone (**2**)). The purity of compound $[^2H_2]$-**1** was determined to be 97.7% by GC−MS using full-scan mode (see Figure S1 of the Supporting Information). The extent of double deuteration according to ^{1}H NMR (Figure 2) and MS (see Figure S2 of the Supporting Information) was greater than 93%. MS [electron ionization (EI)] *m/z* (relative intensity, %): 166.1 (100) $[M]^{\bullet+}$, 151 (54) $[M - CH_3]^{\bullet+}$, 138.1 (62) $[M - CO]^{\bullet+}$, 123.1 (73) $[M - CH_3CHCH_3]^{\bullet+}$, 110.1 (19), 95.1 (63), 79.1 (19), 69.1 (22), 54.1 (27) (see Figures S1 and S3 of the Supporting Information). ^{1}H NMR (300 MHz, $CDCl_3$) δ: 3.06 (m, 1H, $-CH(CH_3)_2$), 2.10 (s, 3H, CH_3), 1.10 (d, 6H, $-CH(CH_3)_2$) (Figure 2B).

^{1}H NMR Spectroscopy. ^{1}H NMR spectra were recorded on a Bruker DPX 300 MHz spectrometer using $CDCl_3$ as the solvent. Chemical shifts are quoted on the δ scale in parts per million (ppm) using $CDCl_3$ as the internal standard. NMR data were analyzed using an ACD/Laboratories 12 software. Multiplicities of signals are described as singlet (s), doublet (d), triplet (t), quadruplet (q), and multiplet (m).

GC−MS. The GC−MS system consisted of an Agilent 7890A GC system with split injection (250 °C; 1:10), coupled to an Agilent MS model 5975C mass selective detector (MSD) with a triple axis detector (Agilent Technologies, Santa Clara, CA).

A 30 m HP5-MS column [(5% phenyl)-methylpolysiloxane, 0.25 mm inner diameter, film thickness (df) = 0.25 μm, Agilent Technologies, Santa Clara, CA] was used for the quantification of thymoquinone. The GC heating program was as follows: initially at 80 °C, raised to 160 °C at 20 °C/min, then raised to 300 °C at 50 °C/min, and finally held at 300 °C for 3.2 min under a constant helium pressure (10 psi). MS was fitted with an EI source operating at an electron energy of 70 eV held at a temperature of 230 °C. Mass spectra and selected ion monitoring (SIM) were acquired using MSD ChemStation (Agilent Technologies, Santa Clara, CA). Full-scan mode was used to identify thymoquinone in the black cumin oil and characterize the synthetic compounds **2**, $[^2H]_2$−**2** and $[^2H]_2$−**1**. After observation of the major ions for thymoquinone (**1**) and doubly deuteriated thymoquinone ($[^2H]_2$-**1**), SIM mode (*m/z* 164.1 for compound **1** and *m/z* 166.1 for deuterium-labeled compound $[^2H]_2$-**1**) was performed for quantification of thymoquinone using SID GC−MS analysis. SIM mode (three selected ions at *m/z* 164.1, 149.1, and 136.1 for compound **1**) was applied for the quantification of thymoquinone using SIM GC−MS with standard addition and external calibration methods.

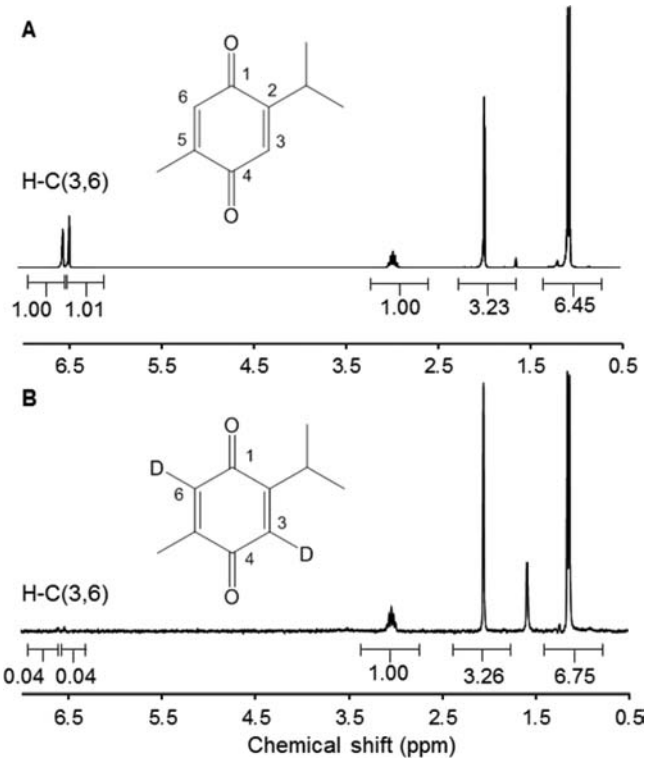

Figure 2. ^{1}H NMR spectra (300 MHz, $CDCl_3$) of (A) thymoquinone (**1**) and (B) $[^2H_2]$-thymoquinone ($[^2H_2]$-**1**). The disappearance of the signals at 6.52 and 6.45 ppm for H-3 and H-6 in the spectrum of compound $[^2H_2]$-**1** indicates >93% double substitution of deuterium for the two protiums of compound **1**.

Development of a SID GC−MS Method for Quantification of Thymoquinone. *Calibration.* The analyte thymoquinone (**1**) and the internal standard $[^2H_2]$-thymoquinone ($[^2H_2]$-**1**) were mixed in six ratios from 0.1 to 10 (5−500 μg/mL in hexane) and analyzed by means of GC−MS in triplicate. Calibration solutions were kept at 4 °C until analysis. The ratios of the area under the curve (AUC) of ion *m/z* 164.1 (AUC_{164}) for compound **1** to the AUC of ion *m/z* 166.1 (AUC_{166}) for compound $[^2H_2]$-**1** were plotted against the concentration ratio of compound **1** to compound $[^2H_2]$-**1** (see Figure S4 of the Supporting Information). The linearity of the calibration regression line was R^2 = 0.9952. The equation obtained was $y = 0.843x + 0.2297$ ($\mathbf{1}/[^2H_2]$-**1**). The limit of detection (LOD) was 0.16 μg/mL with a signal-to-noise ratio of 3:1, and the limit of quantification (LOQ) (10:1)[26] was 0.50 μg/mL, respectively. When using splitless injection mode, LOD and LOQ for thymoquinone were 0.04 and 0.16 μg/mL, respectively.

Quantitation of Thymoquinone in the Black Cumin Seed Oils by SID GC−MS. A sample of black cumin seed oil (50 μL) was added to a 10 mL volumetric flask, and hexane was added to the mark. Aliquots of the diluted oil (200-fold) in hexane (980 μL) was spiked and mixed with a solution of compound $[^2H_2]$-**1** in hexane (20 μL, 1.0 mg/mL). A total of 1 μL of sample was injected into the GC−MS instrument. Each black cumin seed oil sample was prepared 3 times and analyzed with three replicates.

dx.doi.org/10.1021/jf500357x | J. Agric. Food Chem. 2014, 62, 5466−5471

Method Validation. Recovery experiments were performed with a sample of Manako black cumin seed oil. An aliquot of the diluted Manako oil (200-fold) in hexane (920 μL) was spiked with an increasing amount (20, 40, and 60 μL) of compound **1** dissolved in hexane (1.0 mg/mL) and mixed with 20 μL of compound [$^2H_2$]-**1** in hexane (1.0 mg/mL). Finally, hexane was added to give 1.0 mL of black cumin seed oil solution. Aliquots (1 μL) of the diluted oils were analyzed using the SID GC−MS method described above. Three replicates were performed.

To study the intra- and interday imprecisions of the SID GC−MS method, diluted Manako oil in hexane (200-fold) was analyzed. Relative standard deviations (RSDs) were determined for intra- and interday variations based on a set of 9 (in 1 day) and 15 (on 5 different days) measurements.

SIM GC−MS Analysis of Thymoquinone Using Standard Addition and External Calibration. *Standard Addition.* An aliquot of the diluted (200-fold) Manako and Avena oil (800 μL) was added with an increasing amount of compound **1** in hexane to make oil solutions (1.0 mL) that contained an additional 40, 60, 80, 100, 120, 140, and 160 μg/mL of compound **1**. Linear calibration curves (R^2 > 0.99) were obtained by plotting the AUC for the three selected ions (m/z 164.1, 149.1, and 136.1) versus the concentration. Each measurement was repeated in triplicate.

External Calibration. Quantification of thymoquinone using external calibration was carried out by comparing the AUC for the three selected ions (m/z = 164.1, 149.1, and 136.1) of compound **1** in the diluted oil samples to those defined standard solutions of compound **1** dissolved in hexane. A sample of oil (50 μL) was diluted with hexane (10 mL) in a 10 mL volumetric flask, and an aliquot (1 μL) of the diluted samples were analyzed via SIM GC−MS. Each measurement was performed in triplicate. The quantity of thymoquinone was determined using a five-point response curve based on the analysis of standard solutions. Those solutions contained the defined amount of thymoquinone in different concentrations ranging from 5 to 80 μg/mL. The calibration curve (see Figure S5 of the Supporting Information) obtained was $y = 2.2852x - 6.5186$ (R^2 = 0.9956), where y is the AUC/10^3 and x is the concentration of thymoquinone (μg/mL). The LOD was 0.10 μg/mL with a signal-to-noise ratio of 3:1, and the LOQ (10:1) was 0.31 μg/mL. When using splitless injection mode, LOD and LOQ were 0.02 and 0.08 μg/mL, respectively.

RESULTS AND DISCUSSION

Synthesis of a Stable Isotope-Labeled Thymoquinone. The scheme of synthesis of the doubly deuterated thymoquinone ([$^2H_2$]-**1**) is shown in Figure 1. Thymoquinone (**1**) was first reduced to thymohydroquinone (**2**) by sodium hydrosulfite. The two protiums (H-3 and H-6) of compound **2** were then exchanged by deuterium in 3.4 M D_2SO_4 in D_2O under refluxing for 48 h. After cooling to room temperature, the deuterated thymohydroquinone ([$^2H_2$]-**2**) was obtained after workup with H_2O rather than expensive D_2O. Finally, compound [$^2H_2$]-**2** was oxidized with CrO_3 in 60% HOAc to yield compound [$^2H_2$]-**1** (17% overall yield).

GC−MS shows a single peak with high purity (97.7%) based on GC−MS (see Figure S1 of the Supporting Information) and ^{1}H NMR (Figure 2) for compound [$^2H_2$]-**1**. A comparison of the EI−MS spectrum of thymoquinone (**1**) to that of compound [$^2H_2$]-**1** (see Figures S1 and S2 of the Supporting Information) showed that a mass increase of the molecule ion m/z 164.1 by two deuterium atoms to m/z 166.1, which confirmed [$^2H_2$]-**1** was the predominant isotopologue. The electron impact fragmentation pathways for compounds **1** and [$^2H_2$]-**1** are very similar because of the substitution of H-3 and 6 of compound **1** by two deuteriums (see Figure S3 of the Supporting Information). The isotopic distribution of compound [$^2H_2$]-**1** detected by GC−MS was found to be 2.0% natural [^{2}H] abundant compound **1**, 5.0% compound [$^2H_1$]-**1**, and 93.0% compound [$^2H_2$]-**1**. Further comparison of the ^{1}H NMR of compound **1** (Figure 2A) to that of compound [$^2H_2$]-**1** (Figure 2B) shows the disappearance of peaks for H-3 and H-6 because of the protium/deuterium exchange, again confirming the presence and position of two deuterium atoms in 2-isopropyl-5-methyl-1,4-dideuterobenzoquinone ([$^2H_2$]-**1**). It shows only minor protium abundance of 4.0% at position C-3 and 4.0% at position C-6 of compound [$^2H_2$]-**1** (Figure 2B), which is consistent with a high degree of double deuteration of compound [$^2H_2$]-**1** found by GC−MS (see Figure S2 of the Supporting Information).

Because only 2.0% natural [^{2}H] abundant compound **1** was present in the synthetic compound [$^2H_2$]-**1** and less than 2.0% of the third isotopic peak of compound **1** (m/z 166.1) was detected, the ratios of the AUC for ion m/z 164.1 for compound **1** to the AUC for ion m/z 166.1 for compound [$^2H_2$]-**1** were used for the calibration and quantification of thymoquinone (**1**) using the SID GC−MS method. Compound [$^2H_2$]-**1** was found to be stable in hexane for more than 6 months in the dark and, therefore, is suitable to be used as an internal standard for the SIDA.

Establishment of a SID GC−MS Method. The conditions for gas chromatographic separation were optimized to quantify thymoquinone (**1**) in black cumin seed oil within only 10 min (Figure 3). Figure 3A shows a typical total ion current (TIC) gas chromatogram of the Manako oil sample spiked with compound [$^2H_2$]-**1** using full-scan mode. A number of compounds can be detected. SIM (m/z 164.1 and 166.1 for compounds **1** and [$^2H_2$]-**1**, respectively) mode was used to quantify compound **1** in the oil using SID GC−MS (chromatogram not shown). Panels B and C of Figure 3

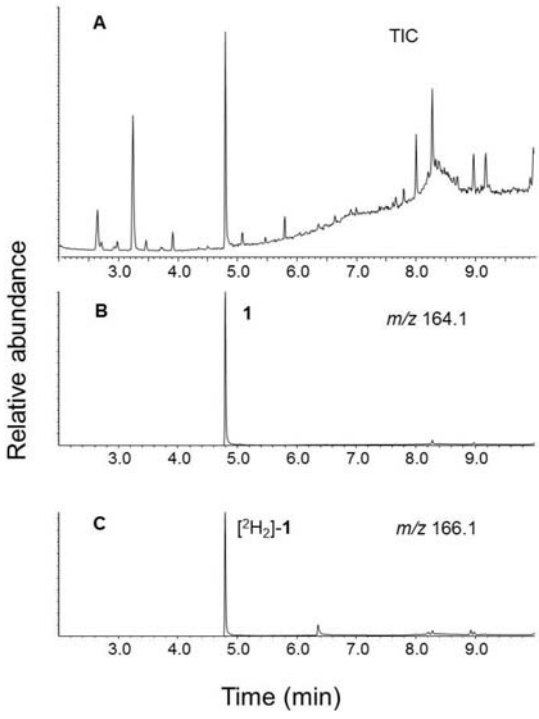

Figure 3. (A) Typical TIC chromatogram and reconstructed ion chromatograms of (B) thymoquinone (**1**) and (C) deuterium-labeled thymoquinone ([$^2H_2$]-**1**) in Manako black cumin seed oil spiked with compound [$^2H_2$]-**1**.

Table 1. Recovery Rates for the Quantification of Thymoquinone in the Diluted (1:200) Black Cumin Seed Oil (Manako) Determined by a SID GC−MS Method[a]

amount of compound **1** added (μg/mL)	concentration calculated (μg/mL)	concentration determined (μg/mL)	recovery (%)	average recovery (%)
		53.9 ± 0.01		
20.0	73.9 ± 0.01	73.3 ± 0.02	99.2 ± 0.02	
40.0	93.9 ± 0.01	94.0 ± 0.02	100.1 ± 0.02	99.1 ± 1.1
60.0	113.9 ± 0.01	111.5 ± 0.02	97.9 ± 0.02	

[a]Data are expressed as the mean ± RSD (n = 3).

show the reconstructed ion chromatograms of compounds **1** (m/z 164.1) and [$^2H_2$]-**1** (m/z 166.1) in the Manako black cumin seed oil. Compounds **1** and internal [$^2H_2$]-**1** were co-eluted at 4.81 min. A calibration graph (see Figure S4 of the Supporting Information) was plotted from a mixture of known mass ratios of compounds **1** and [$^2H_2$]-**1** and their corresponding peak area ratios in GC−MS by linear regression analysis. This calibration curve showing a linear response (R^2 = 0.9938) could enable the determination of the quantity of thymoquinone in the samples based on their measured ion intensities.

Recovery experiments were performed to check the trueness of the SIDA method. Specified quantities of thymoquinone (**1**) were added to the diluted Manako oil sample in three different concentrations before using SID GC−MS analysis. The quantity of compound **1** was measured and compared to those found in the blank diluted Manako oil sample as the control (Table 1). The mean recovery rate was determined to be 99.1 ± 1.1% RSD based on the amount of compound **1** added to the diluted oil sample. These results demonstrated that the developed SID GC−MS is a reliable, rapid, and accurate method for quantification of compound **1**. Thymoquinone in five marketed oil products was quantified, and their results are listed in Table 2. The concentration of thymoquinone ranged from 3.34 to 10.8 mg/mL. Manako oil has the highest content of thymoquinone, while CEBRA oil has the lowest content of thymoquinone.

Table 2. Quantification of Thymoquinone in Black Cumin Seed Oils via SID GC-MS, External Calibration, and Standard Addition Methods[a]

	concentration (mg/mL)		
black cumin seed oil	SID GC-MS	external calibration	standard addition
Manako	10.8 ± 0.01	8.95 ± 0.03	10.6 ± 0.13
Avena	7.27 ± 0.02	7.33 ± 0.08	7.17 ± 0.02
CEBRA	3.34 ± 0.03	2.96 ± 0.18	*b*
Iman	7.23 ± 0.02	6.02 ± 0.09	*b*
This Health	7.74 ± 0.04	7.03 ± 0.10	*b*

[a]Data are expressed as the mean ± RSD (n = 3). [b]Concentration not determined.

Cross-Validation of the SID GC−MS Method. The standard addition method can also overcome the matrix effects and is often used for the validation of the SIDA method.[18,27] To validate the SID GC−MS method developed above, the data obtained using SID GC−MS were compared to those found using standard addition and external calibration (Table 2). Three characteristic ions (m/z 164.1, 149.1, and 136.1) for compound **1** were selected for the quantification of thymoquinone using standard addition and external calibration. An external calibration curve with a linear response (R^2 = 0.9956) (see Figure S5 of the Supporting Information) was attained by linear regression analysis of the AUC versus the concentration.

Quantification based on the standard addition and external calibration showed 98.1 ± 1.2 and 82.9 ± 0.3% of compound **1** in Manako oil and 98.6 ± 0.4 and 100.8 ± 1.1% of compound **1** in Avena oil (calculated from data in Table 2) when compared to the results obtained by means of SID GC−MS, respectively. The standard addition and SID GC−MS results revealed very similar concentrations of compound **1** in Manako and Avena oils (differences are less than 2%), therefore validating the accuracy and advantage of the SIDA method. The concentrations of thymoquinone in all five oils determined by external calibration generally agreed with those determined from SIDA and/or standard addition methods (differences range between 1 and 17%). The slight discrepancies are probably due to matrix effects from the different preparations of these black cumin seed oils.[18]

The intraday precision of the SID GC−MS method for compound **1** showed a RSD of ±1.3% (n = 9) by analyzing diluted Manako oil in hexane in nine independent measurements in 1 day. Interday precision studies with diluted Manako oil revealed a RSD of ±5.9% (n = 15) in three independent measurements in each day for 5 days. These data again demonstrate that the SID GC−MS method is a reliable, rapid, and accurate analytic means for thymoquinone in black cumin seed oils.

In previous reports, thymoquinone was quantified by several other analytical techniques.[12−16] HPLC was used for quantification of thymoquinone in a commercial black cumin seed oil[12] and in different phytopharmaceuticals with a LOD of 0.006 μg/mL (10 μL of injection volume, ∼60 pg).[13] Quantification of thymoquinone in herbal extracts and oil was also achieved using HPTLC with LOD of 50 ng/spot.[14] A differential pulse polarographic method was developed for the determination of thymoquinone in black seed oil, where LOD was found to be 0.05 μg/mL (10 mL of volume, ∼500 ng).[15] The content of thymoquinone in black cumin seed oils was also found to be in the range of 0.13−0.17% (w/v) of the oil by GC.[16] In our GC−MS methods, where split injection mode (1:10) was used to avoid overloading samples, LODs of thymoquinone for SIM GC−MS and SID GC−MS were found to be 0.10 and 0.16 μg/mL (1 μL of injection volume, ∼100 and 160 pg), respectively. However, for trace analysis of thymoquinone, LODs can be further improved using splitless injection mode and range from 0.02 to 0.04 μg/mL (1 μL of injection volume, ∼20−40 pg). Therefore, the sensitivities of GC−MS methods are comparable to that of HPLC and are higher than those of HPTLC and differential pulse polarographic methods. Furthermore, GC−MS and/or SID GC−MS methods have advantages of identifying analytes and overcoming matrix effects over other analytical methods.[18,19]

dx.doi.org/10.1021/jf500357x | J. Agric. Food Chem. 2014, 62, 5466−5471

In summary, synthesis of a highly pure deuteriated thymoquinone has been achieved for the first time, which enables us to develop a SIDA of the biologically important thymoquinone in black cumin seed oil using GC−MS. Cross-validation using standard addition confirms the accuracy and reliability of the SIDA method, which can quantify a large number of black cumin seed oil products for their quality control in high-throughput means. Synthetic deuteriated thymoquinone and the SID GC-MS method should also be useful in the studies on the mechanism of binding thymoquinone to proteins,[24,28−30] *in vitro* and *in vivo* pharmacokinetics of thymoquinone, which are ongoing in our laboratory.[31]

■ ASSOCIATED CONTENT

Ⓢ Supporting Information

GC−MS chromatograms (Figure S1), mass spectra (Figure S2), possible electron impact fragmentation pathways of thymoquinone and doubly deuteriated thymoquinone (Figure S3), calibration curve for the SID GC−MS method (Figure S4), and external calibration curve for the SIM GC−MS method (Figure S5). This material is available free of charge via the Internet at http://pubs.acs.org.

■ AUTHOR INFORMATION

Corresponding Author

*Telephone: +44-0-1782-674382. Fax: +44-0-1782-747319. E-mail: w.li@keele.ac.uk.

Funding

This work was supported by Nigerian ETF (a Ph.D. studentship to Okiemute Rosa Johnson-Ajinwo) and Keele University.

Notes

The authors declare no competing financial interest.

■ ACKNOWLEDGMENTS

The authors thank John Clews for NMR measurements.

■ ABBREVIATIONS USED

AUC, area under the curve; EI, electron ionization; HPLC, high-performance liquid chromatography; HPTLC, high-performance thin-layer chromatography; GC, gas chromatography; GC−MS, gas chromatography−mass spectrometry; LOD, limit of detection; LOQ, limit of quantification; SIM, selected ion monitoring; MSD, mass selective detector; ^{1}H NMR, proton nuclear magnetic resonance; RSD, relative standard deviation; SID, stable isotope dilution; SIDA, stable isotope dilution assay/analysis; TIC, total ion current

■ REFERENCES

(1) Ramadan, M. F.; Morsel, J. T. Characterization of phospholipid composition of black cumin (*Nigella sativa* L.) seed oil. *Nahrung* **2002**, *46*, 240−244.

(2) Kiralan, M. Volatile compounds of black cumin seeds (*Nigella sativa* L.) from microwave-heating and conventional roasting. *J. Food Sci.* **2012**, *77*, C481−C484.

(3) Padhye, S.; Banerjee, S.; Ahmad, A.; Mohammad, R.; Sarkar, F. H. From here to eternity—The secret of Pharaohs: Therapeutic potential of black cumin seeds and beyond. *Cancer Ther.* **2008**, *6*, 495−510.

(4) El-Dakhakhny, M. Studies on the chemical constitution of Egyptian *N. sativa* L. seeds. *Planta Med.* **1963**, *11*, 465−470.

(5) Burits, M.; Bucar, F. Antioxidant activity of *Nigella sativa* essential oil. *Phytother. Res.* **2000**, *14*, 323−328.

(6) Hajhashemi, V.; Ghannadi, A.; Jafarabadi, H. Black cumin seed essential oil, as a potent analgesic and antiinflammatory drug. *Phytother. Res.* **2004**, *18*, 195−199.

(7) El-Mahmoudy, A.; Shimizu, Y.; Shiina, T.; Matsuyama, H.; El-Sayed, M.; Takewaki, T. Successful abrogation by thymoquinone against induction of diabetes mellitus with streptozotocin via nitric oxide inhibitory mechanism. *Int. Immunopharmacol.* **2005**, *5*, 195−207.

(8) Salem, M. L. Immunomodulatory and therapeutic properties of the *Nigella sativa* L. seed. *Int. Immunopharmacol.* **2005**, *5*, 1749−1770.

(9) Worthen, D. R.; Ghosheh, O. A.; Crooks, P. A. The in vitro anti-tumor activity of some crude and purified components of blackseed, *Nigella sativa* L. *Anticancer Res.* **1998**, *18*, 1527−1532.

(10) Sethi, G.; Ahn, K. S.; Aggarwal, B. B. Targeting nuclear factor-κB activation pathway by thymoquinone: Role in suppression of antiapoptotic gene products and enhancement of apoptosis. *Mol. Cancer Res.* **2008**, *6*, 1059−1070.

(11) Woo, C. C.; Kumar, A. P.; Sethi, G.; Tan, K. H. Thymoquinone: Potential cure for inflammatory disorders and cancer. *Biochem. Pharmacol.* **2012**, *83*, 443−451.

(12) Ghosheh, O. A.; Houdi, A. A.; Crooks, P. A. High performance liquid chromatographic analysis of the pharmacologically active quinones and related compounds in the oil of the black seed (*Nigella sativa* L.). *J. Pharm. Biomed. Anal.* **1999**, *19*, 757−762.

(13) Hadad, G. M.; Salam, R. A.; Soliman, R. M.; Mesbah, M. K. High-performance liquid chromatography quantification of principal antioxidants in black seed (*Nigella sativa* L.) phytopharmaceuticals. *J. AOAC Int.* **2012**, *95*, 1043−1047.

(14) Velho-Pereira, R. M.; Barhate, C. R.; Kulkarni, S. R.; Jagtap, A. G. Validated high-performance thin-layer chromatographic method for the quantification of thymoquinone in *Nigella sativa* extracts and formulations. *Phytochem. Anal.* **2011**, *22*, 367−373.

(15) Michelitsch, A.; Rittmannsberger, A. A simple differential pulse polarographic method for the determination of thymoquinone in black seed oil. *Phytochem. Anal.* **2003**, *14*, 224−227.

(16) Houghton, P. J.; Zarka, R.; de las Heras, B.; Hoult, J. R. Fixed oil of *Nigella sativa* and derived thymoquinone inhibit eicosanoid generation in leukocytes and membrane lipid peroxidation. *Planta Med.* **1995**, *61*, 33−36.

(17) Liu, X.; Abd El-Aty, A. M.; Cho, S. K.; Yang, A.; Park, J. H.; Shim, J. H. Characterization of secondary volatile profiles in *Nigella sativa* seeds from two different origins using accelerated solvent extraction and gas chromatography−mass spectrometry. *Biomed. Chromatogr.* **2012**, *26*, 1157−1162.

(18) Stanford, B. D.; Weinberg, H. S. Isotope dilution for quantitation of steroid estrogens and nonylphenols by gas chromatography with tandem mass spectrometry in septic, soil, and groundwater matrices. *J. Chromatogr. A* **2007**, *1176*, 26−36.

(19) Allen, M. S.; Lacey, M. J.; Boyd, S. Determination of methoxypyrazines in red wines by stable isotope dilution gas chromatography−mass spectrometry. *J. Agric. Food Chem.* **1994**, *42*, 1734−1738.

(20) Penalvo, J. L.; Haajanen, K. M.; Botting, N.; Adlercreutz, H. Quantification of lignans in food using isotope dilution gas chromatography/mass spectrometry. *J. Agric. Food Chem.* **2005**, *53*, 9342−9347.

(21) Lu, J.; Wu, J.; Stoffella, P. J.; Wilson, P. C. Analysis of bisphenol A, nonylphenol, and natural estrogens in vegetables and fruits using gas chromatography−tandem mass spectrometry. *J. Agric. Food Chem.* **2013**, *61*, 84−89.

(22) Lu, J.; Wu, J.; Stoffella, P. J.; Wilson, P. C. Isotope dilution−gas chromatography/mass spectrometry method for the analysis of alkylphenols, bisphenol A, and estrogens in food crops. *J. Chromatogr. A* **2012**, *1258*, 128−135.

(23) Pickard, S.; Becker, I.; Merz, K. H.; Richling, E. Determination of the alkylpyrazine composition of coffee using stable isotope dilution−gas chromatography−mass spectrometry (SIDA−GC−MS). *J. Agric. Food Chem.* **2013**, *61*, 6274−6281.

(24) Lu, S.; Li, W. W.; Rotem, D.; Mikhailova, E.; Bayley, H. A primary hydrogen−deuterium isotope effect observed at the single-molecule level. *Nat. Chem.* **2010**, *2*, 921−928.
(25) Charney, E.; Becker, E. D. Molecular vibrations of quinones. II. Infrared spectra (solution and vapor) of *p*-benzoquinone and *p*-benzoquinone-d_4. *J. Chem. Phys.* **1965**, *42*, 910−913.
(26) MacDougall, D.; Crummett, W. Guidelines for data acquisition and data quality evaluation in environmental chemistry. *Anal. Chem.* **1980**, *52*, 2242−2249.
(27) Stark, T.; Wollmann, N.; Losch, S.; Hofmann, T. Quantitation of resveratrol in red wines by means of stable isotope dilution analysis−ultra-performance liquid chromatography−Quan-time-of-flight mass spectrometry and cross validation. *Anal. Chem.* **2011**, *83*, 3398−3405.
(28) Li, W. W.; Heinze, J.; Haehnel, W. Site-specific binding of quinones to proteins through thiol addition and addition−elimination reactions. *J. Am. Chem. Soc.* **2005**, *127*, 6140−6141.
(29) Li, W. W.; Hellwig, P.; Ritter, M.; Haehnel, W. De novo design, synthesis, and characterization of quinoproteins. *Chemistry* **2006**, *12*, 7236−7245.
(30) El-Najjar, N.; Ketola, R. A.; Nissila, T.; Mauriala, T.; Antopolsky, M.; Janis, J.; Gali-Muhtasib, H.; Urtti, A.; Vuorela, H. Impact of protein binding on the analytical detectability and anticancer activity of thymoquinone. *J. Chem. Biol.* **2011**, *4*, 97−107.
(31) Li, W. W.; Johnson-Ajinwo, O. R.; Siddique, M. R.; Bajana, B.; J, S. S.; Richardson, A. Anti-cancer thymoquinone from *Nigella sativa*. *Planta Med.* **2013**, *79*, 1126.

JOURNAL OF AGRICULTURAL AND FOOD CHEMISTRY

Article

pubs.acs.org/JAFC

A Critical Point: The Problems Associated with the Variety of Criteria To Quantify the Antioxidant Capacity

M. A. Prieto,* J. A. Vázquez, and M. A. Murado

Group of Recycling and Valorization of Waste Materials (REVAL), Research Marine Institute (IIM-CSIC), Vigo 36208, Spain

ABSTRACT: The oxidant action implies interfering in an autocatalytic process, in which no less than five chemical species are present (oxygen, oxidizable substrate, radicals, antioxidants, and oxidation products); furthermore, reactions of first and second order can take place, and interactions can occur, at several levels of the process. The common and incorrect practice is to use the single-time dose−response of an established antioxidant as a calibration curve to compute the equivalent antioxidant capacity of a sample, which is only tested at one single time−dose, assuming too many false aspects as true. Its use is unreasonable, given the availability of computational applications and instrumental equipment that, combined, provide the adequate tools to work with different variables in nonlinear models. The evaluation of the dose−time dependency of the response of the β-carotene method as a case study, using the combination of strong quantification procedures and a high amount of results with lower experimental error (applying microplate readers), reveals the lack of meaning of single-time criteria. Also, it demonstrates that, in most of the reactions, the time-dependent response in the oxidation process is inherently nonlinear and should not be standardized at one single time, because it would lead to unreliable results, hiding the real aspects of the response. In food matrices, the application of single-time criteria causes deficiencies in the control of the antioxidant content. Therefore, it is logical that, in the past decade, researchers have claimed consensus to increase the determination and effectiveness of antioxidant responses.

KEYWORDS: *antioxidant capacity, β-carotene method, mathematical modeling, kinetic response*

INTRODUCTION

At present, there is no convenient assay that enables the evaluation of the antioxidant capacity (AC) in a food system, mainly because the factors affecting the oxidation reactions and ACs differ[1,2] greatly. The current methods to test the AC have still left many open questions.[3−7] The *in vitro* assays can only rank AC for its particular reaction system, and its relevance to *in vivo* health protective activities remains uncertain. Free radicals may be either oxygen-derived [reactive oxygen species (ROS)] or nitrogen-derived [reactive nitrogen species (RNS)]. In a normal cell, there is an appropriate balance, but this can be shifted in stress situations or when levels of antioxidants (A) are diminished. Therefore, an important factor that may counteract their effect is the alimentary intake of antioxidants. Hence, since two decades, the interest for evaluating the ACs present in all types of food and characterizing their specific mechanisms has increased noticeably.

The possibility to accumulate data rapidly has encouraged authors to use simple calculation formalisms to abbreviate the testing procedure, forcing the conditions of the assay to assume a linear kinetic response, in which samples are generally assessed using a single time and dose. Very often the same method is performed with different experimental protocols and formalisms for quantifying the activity. This has caused a loss of information and the risk of erroneous conclusions,[1] causing deficiencies in the control of the real AC of samples. The analysis of all of the particular problems associated with the diverse quantification criteria used for each method is unfeasible. However, because most of the methods share the main objectives and operative requirements, the β-carotene (βC) bleaching assay[8] has been chosen as a case study. This assay is a well-accepted model for testing the AC of samples, but the quantification approaches, considering or not the variation as a function of the time and dose, applied to analyze the response are diverse. This method, as many others, very often has a poor evaluation of the results,[1] despite the regularity of the oxidation and inhibition processes. Results are usually expressed at a fixed single time, which causes many difficulties to obtain a robust method. Although there are mathematical tools available to evaluate the lipid oxidation,[2,9−11] they are rarely applied to quantify the responses. The βC method is a highly reproducible procedure, currently performed in microplate readers,[12] providing an appropriate tool that ensures that samples, the reference antioxidant (usually commercial ones used to build the calibration curve), and the controls of the reaction can be simultaneously assessed as a function of the dose and time, producing abundant data with lower experimental error. It is, therefore, a robust and meaningful example that can be used as a case study for raising the discussion of the problems associated with the different quantification criteria applied when studying the responses generated for each method. When several common A are characterized, the problems of using single-time−dose quantification procedures, disregarding kinetic considerations, are discussed in detail. Furthermore, those criteria that take into account the kinetic of the process (dose−time-dependent behavior) are also evaluated and compared.

In consequence, the results prove that (1) the reduction to study the dose−response at one single time and dose, expecting

Received: February 11, 2014
Revised: May 7, 2014
Accepted: May 18, 2014
Published: May 18, 2014

ACS Publications © 2014 American Chemical Society

to find linear forms (as described by the non-kinetic approaches), leads frequently to unreliable results and (2) the preference for apparently simple assays, routinely applicable with minimal calculation requirements, is not very justifiable in our days, given the availability of computational applications and microplate readers, whose combination provides adequate tools to work with data sets that allow for the performance of accurate evaluations with nonlinear modeling. Such results can be easily extrapolated to the other *in vitro* and *in vivo* assays generally used to determine the capacity to counteract the oxidation products formed.

MATERIALS AND METHODS

βC Bleaching Method. *Assay Description.* The βC method is currently well-optimized and adapted to microplate readers.[12]

Equipment. Multiskan spectrum microplate photometers from Thermo Fisher Scientific and a Thermo Scientific Nunc 96-Well Polypropylene MicroWell plate with a flat bottom were used.

Main Reagents of the βC Bleaching Method. *cis,cis*-9,12-Octadecadienoic acid (linoleic acid), β-carotene, and polyoxyethylenesorbitan monopalmitate (Tween 40) were used.

Antioxidant Agents Used as an Example. Butyl-hydroxyanisole (BHA) is the main A used as a case study and/or calibration in the dose range 0.0−5.0 μM in intervals of 0.5. (2*R*)-2,5,7,8-Tetramethyl-2-[(4*R*,8*R*)-(4,8,12-trimethyltridecyl)]-6-chromanol or α-tocopherol (TOC) is A used as sample M1 in 0−40 nM in intervals of 4. Zinc chloride (Zn) is A used as sample M2 in 0−1070.5 μM in intervals of 107.5. Propyl-3,4,5-trihydroxybenzoate (PG) is A used as sample M3 in 0−80 μM in intervals of 8. Manganese sulfate (Mn^{2+}) is A used as sample M4 in 0−200 μM in intervals of 20. Butyl-hydroxytoluene (BHT) is A used as sample M5 in 0−20 μM in intervals of 2. 6-Ethoxy-2,2,4-trimethyl-1,2-dihydroquinoline or ethoxyquin (ETX) is A used as sample M6 in 0−3 nM in intervals of 0.3. All compounds were purchased from Sigma S.A. (St. Louis, MO).

Quantification Procedure. The most common criteria applied to quantify the responses, considering or not the variation as a function of the time and dose, are described in the following.

Original Quantification Approach. According to Marco,[8] when the absorbance at 470 nm is measured at increasing times and concentrations of an A, the response can be assessed through the percentage of the extended induction time (E_t) defined as

$$E_t\ (\%) = \frac{t_n - t_0}{t_{ref} - t_0} \times 100 \tag{1}$$

where t_0, t_n, and t_{ref} are the times at which the βC concentration reaches certain percentage values (p) in the absence of A, in the presence of a given concentration of the tested A, and in the presence of a reference A, respectively. The author uses the values of p = 50 and 70 and recommended to linearize (using logic paper) the sigmoid response obtained. He also noted that, for some common A, the relationship between the A concentration and its effect on βC-extended induction time was close to linearity.

Usual Non-kinetic Approaches To Quantify the Antioxidant Response of the βC Reaction. After the publication of the work by Marco,[8] several ways that abbreviate the procedure, avoiding the use of kinetic analysis with a probabilistic paper to quantify the response, were published. There is a high diversity of quantification criteria (Q) at a fixed time that has been used to analyze the responses. Next, the most common single time−dose typically applied in the βC reaction and the dose−response single-time methods are summarized. Several other methods have been excluded from the analysis, such as the method described by Mikami et al.,[13] because of the redundancy with one of the alternatives that would be described next.

Single-Time and Dose−Response Procedures. Q1: Percentage of Oxidation Inhibition (I) or Relative Activity. It is defined by Chatterjee et al.[14] as

$$I\ (\%) = \frac{C_0 - M_t}{C_0} \times 100 \tag{2}$$

where M_t is the final absorbance of the reagent in the presence of the sample and C_0 is the initial absorbance when the sample is replaced by water (control). The single time used to test their AC is usually 10, 20, or 30 min.

Q2: Antioxidant Activity Coefficient (AAC). One of the most common criteria[15−19] is defined as

$$\mathrm{AAC} = \frac{M_t - C_t}{C_0 - C_t} \times 1000 \tag{3}$$

where *C*, *M*, and t have the same meanings as in the previous criterion. Again, the time varies from 1 to 2 h, establishing *a priori*[20] or selecting an appropriate frame for interpolation, in view of the kinetic data.

Q3: Antioxidant Activity Coefficient Modified (AACm). An alternative way to the AACm is the normalized coefficient value of the antioxidant activity

$$\mathrm{AACm} = 100 - \frac{C_0 - C_t}{M_0 - M_t} \tag{4}$$

where the value meanings are the same as in previous cases.

Q4: Relative Rate of Degradation (RD). An example is used in refs 21−23

$$\mathrm{RD} = \frac{r_c - r_m}{r_c} \times 100 \tag{5}$$

where r_c and r_m are the specific rates of the control and sample βC bleaching, calculated assuming first-order kinetics

$$r_c = \frac{\ln C_0 - \ln C_t}{t - t_0} \quad \text{and} \quad r_m = \frac{\ln M_0 - \ln M_t}{t - t_0} \tag{6}$$

in which *C* and *M* are the control and sample, respectively, and *t* values are usual analytical times, usually 10, 20, and 30 min.

Q5: Ratio of Oxidation Rates (R_{OR}). This criterion[22−24] uses the relationship directly between specific rates previously defined

$$R_{OR} = \frac{r_c}{r_m} = \frac{\ln C_0 - \ln C_t}{\ln M_0 - \ln M_t} \tag{7}$$

Q6: Dose−Response at a Fixed Time. Other authors[9,25] used any of the above quantification criteria (Q1−Q5) or similar at a fixed time as a function of different doses of the sample and A as the reference. When the results behave linearly, the slope is used as the comparison term. When the response behaves in a nonlinear mode, typically, the dose at which the inhibition reaches 50% (IC_{50}) is used as the parameter for comparative analyses.

Methods Taking into Account the Kinetic Aspect of the Response To Quantify the AC. In this section, those quantification methods that take into account the kinetic part of the process are briefly described. Some may not have been applied directly in the βC bleaching method, but they were considered as valuable tools for describing the oxidation process and included for discussion.

Formal Mathematical Expressions. The range of mathematical expressions available is large and common to many fields of study. The preferable options are always models that have a lower number of parameters and models with parameters that provide direct meaning of the processes under analysis. In this sense, for the kinetic description of the A behavior, we have found three groups of alternatives in the references[2,9,10] covering a wide spectrum of profile responses, from potential to sigmoid responses, with and without intercepts.

Q7: Potential Functions without an Intercept. Power Equation. Recently, Terpinc et al.[9] adjusted the temporal progress of the oxidation to the following equation:

$$R = 1 - \frac{1}{(1 + at)^b} \tag{8}$$

where *R* is the oxidized substrate at each given time *t*, the response is standardized into a frame [0, 1], in which 0 is the initial response at *t* =

dx.doi.org/10.1021/jf5005995 | J. Agric. Food Chem. 2014, 62, 5472−5484

Table 1. Equations with or without an Intercept Used Are Summarized along with Several Other Properties[a]

potential function				
power function	$R = K - K[\tau/(\tau + (2^{1/b} - 1)t)]^b$	$\nu_m = \frac{ab}{(1 + at)^{b+1}}$	$\tau = \frac{2^{1/b} - 1}{a}$	
sigmoidal function with an intercept				
logistic	$R = \frac{K}{1 + e^{c(\tau - t)}}$	$\nu_m = \frac{Kc}{4}$	$\lambda = \tau - \frac{2}{c}$	$R = \frac{K}{1 + e^{c(\lambda - t) + 2}}$
sigmoidal function without an intercept				
Weibull	$R = K[1 - e^{-\ln 2(t/\tau)^\alpha}]$ $t = \tau[\ln(1 - R)/\ln 0.5]^{1/\alpha}$	$\nu_m = \frac{K\alpha \ln 2}{2\tau}$	$\lambda = \tau\left(1 - \frac{1}{\alpha \ln 2}\right)$	$R = K - Ke^{-\ln 2\left(t\left(1 - \frac{1}{\alpha \ln 2}\right)/\lambda\right)^\alpha}$

[a]The original or traditional forms of these equations were reformulated to facilitate comparisons; thus, all of them would have a positional parameter, such as the half-life (now on τ) and an asymptotic parameter (K), among the regression parameters of the functions. The third parameter (b, c, and α) would be related with steepness of the function.

0 and 1 is the response when the substrate is fully oxidized. The parameters a and b depend upon the concentration of A. The authors claim that this equation can fit different responses, such as the responses found in the DPPH and bleaching βC methods. Other interesting parameter values, such as the average rate and half-life (or time when 50% oxidation is achieved) can be obtained with further calculations using parameters a and b (Table 1).

Q8: Sigmoid Functions with an Intercept. Logistic Equation. Authors[2,10,26−29] have used the logistic equation, which can be written in its more functional form as follows:

$$R = \frac{K}{1 + \exp[\ln[(K/R_0) - 1] - \mu_m t]} \quad (9)$$

where R is the oxidized substrate (with R_0 and K as initial and asymptotic values, respectively) and μ_m is the specific-maximum rate. The equation can be reconfigured to explicitly highlight other valuable parameters, such as the oxidizable substrate half-life (τ), maximum speed (v_m), and lag phase (λ) (see Table 1 for more details).

Q9: Sigmoid Functions without an Intercept. Weibull Equation. Quantification was carried out using the accumulative Weibull distribution to describe satisfactorily the whole kinetic profile[2]

$$R = K\{1 - \exp[-\ln 2(t/\tau)^\alpha]\} \quad (10)$$

where K is the asymptote, τ is the substrate half-life or time when 50% oxidation is achieved, and α is a shape parameter associated with the maximum slope of the response. From this equation, other values of interest can be computed, such as the maximum speed (v_m) and lag phase (λ) (see Table 1 for more details).

Dose−Response of Single "Global Values" That Summarize the Kinetic Response. Q10: Lag Phase (λ) and Inhibition Time of Oxidation (t_{inh}). Those values are common criteria in the determination of the protective effect of A in a very diverse range of methods. We have not seen their application in the βC assay. Both values have nearly analogue meanings and very narrow differences.

The lag phase is typically used in those methods that the response shows clear sigmoid profiles, such as those that involve the oxidation of lipids.[10,29] The lag-phase value is commonly determined by univariate mathematical modeling with S-shaped equations as the ones described in Table 1. Pure geometric reparametrizations of those equations are used to directly perform the analysis and obtain the λ value as a parameter in the equation. Those rearrangements define λ as the intersection point obtained at the x axis (time units in this case) by a linear extrapolation tangent to the curve at the inflection point.

The t_{inh} value is the alternative solution to compute the λ parameter when certain assay conditions make it difficult to obtain the λ parameter.[30,31] For example, in the case of the low-density lipoprotein (LDL) oxidized by Cu^{2+}, the response is affected by two different actions. The LDL is oxidized spontaneously in the conditions of the assay and by the Cu^{2+} ions added, which is reflected in a biphasic curve. Because the spontaneous oxidizing rate is very low compared to the effect caused by Cu^{2+}, the spontaneous oxidation of LDL (baseline of the response) is subtracted graphically by drawing a line from the starting value at $t = 0$ parallel to the baseline of the response and the t_{inh} value is the intersection point with the line tangent to the main curve of the process.

Those values are computed in a dose−response format and expressed in min/μM. The higher this value, the stronger the A. Authors that support those approaches defended their simplicity and less experimental effort needed.

Q11: Area Units under the Curve. A simple approach to characterize the A action through a single value is achieved by calculating the area under the kinetic profile.[32−34] This has also been applied in more complex responses, as example, to simplify the variable time response to one value.[35] Even with the lack of a formal description of that profile, if R_i values are the responses along an arbitrary time series, it is possible to define a response in terms of area units (AU) that can be easily calculated by any numerical integration method, such as the trapezoidal rule as follows:

$$AU = \frac{R_1 \Delta t_1}{2} + \sum_{i=2}^{i=n-1} R_i \Delta t_i + \frac{R_n \Delta t_n}{2} \quad (11)$$

where i is the number of data measured along the time t, Δt is the interval of each measurement, and AU values are the area units under the curve. For the particular case analyzed here, the area values represent the accumulative amount of βC bleached during the total time (t) analyzed.

Numerical and Statistical Methods. Fitting the experimental results to the proposed equations was carried out in two phases. First, parametric estimates were obtained by minimization of the sum of quadratic differences between observed and model-predicted values, using the nonlinear least-squares (quasi-Newton) method provided by the macro Solver from a Microsoft Excel 2003 spreadsheet.[36] It allows for quick testing of hypotheses and display of its consequences. Subsequently, the determination of the parametric confidence intervals and model consistency (Student's t and Fisher's F tests, respectively, in both cases with $\alpha = 0.05$) were calculated using the "SolverAid" macro.[37,38] The "SolverStat" macro[39] was used to detect possible anomalies in the distribution of parametric estimates and residuals.

RESULTS

Non-kinetic Approaches (Q1−Q6). *Response at a Single Time and Single Dose (Q1−Q5).* Commonly, the mathematical determinations of the AC are based on a fixed end point without proper consideration of the kinetic behavior. The most typical practice is to use the single-time dose−response of one commercial A as a calibration curve (focusing on the concentration range that shows a linear pattern) and, afterward, to compute the equivalent AC of any type of sample by testing it only at one single-time dose, assuming too many false aspects as true. In Figure 1, we present a graphical representation of the problematic aspects when using single-time dose of a sample. On the left side of Figure 1, the kinetic results (32 time

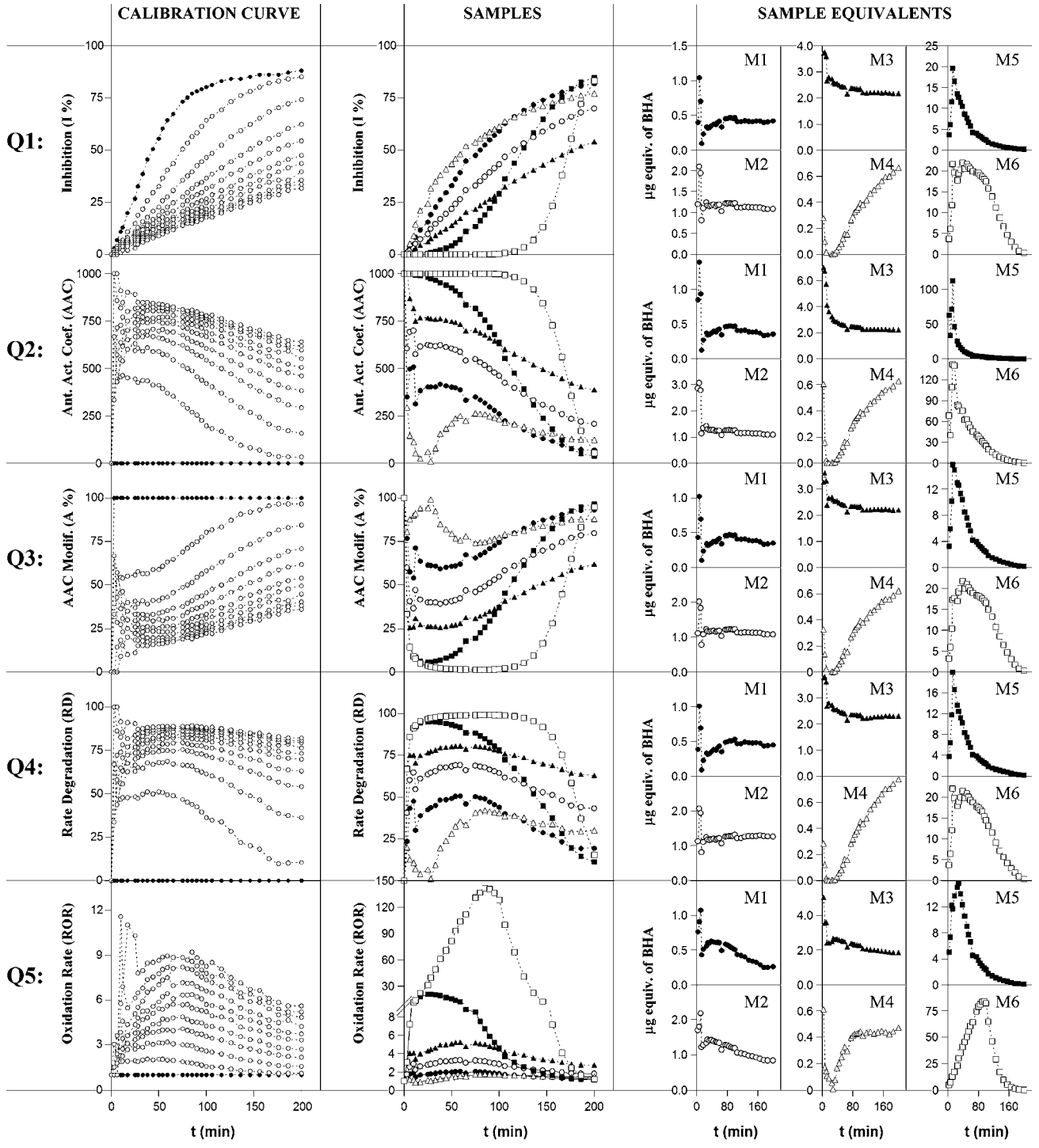

Figure 1. Analysis of the problems of single-dose quantification procedures at a fixed time (Q1−Q5). We use the dose−response of the antioxidant BHA in the range of 0.0−5.0 μM in intervals of 0.5 as the reference antioxidant and evaluate the results in the βC bleaching reaction from a kinetic point of view. Six samples (M1−M6) are used to test the robustness of the Q1−Q5 criteria. The doses used of the samples are 8 nM TOC for M1, 1007.5 μM Zn for M2, 80 μM PG for M3, 200 μM Mn for M4, 20 μM BHT for M5, and 4 nM ETX for M6.

measurements) of the βC reaction at increasing concentrations of BHA (as the calibration curve) are displayed in the format of each of the non-kinetic quantification criteria (Q1−Q5) described in the Materials and Methods. In the middle of Figure 1, six well-known A are presented as samples (M1−M6) and their kinetic activity is shown at one single dose for each of the non-kinetic criteria (Q1−Q5). Finally, on the right side, the equivalent activity computed by interpolation of each of the samples for each of the kinetic points analyzed is shown. It can be seen that the equivalent activity of BHA per each sample varies considerably as a function of the time of interpolation. The variations depend upon the level of similarity between the curves. The BHA dose−response is a specific case that we know[12] that behaves close to a first-order response in the βC bleaching reaction. For those sample responses in which their kinetic profile has a similar pattern, their equivalent kinetic

dx.doi.org/10.1021/jf5005995 | J. Agric. Food Chem. 2014, 62, 5472−5484

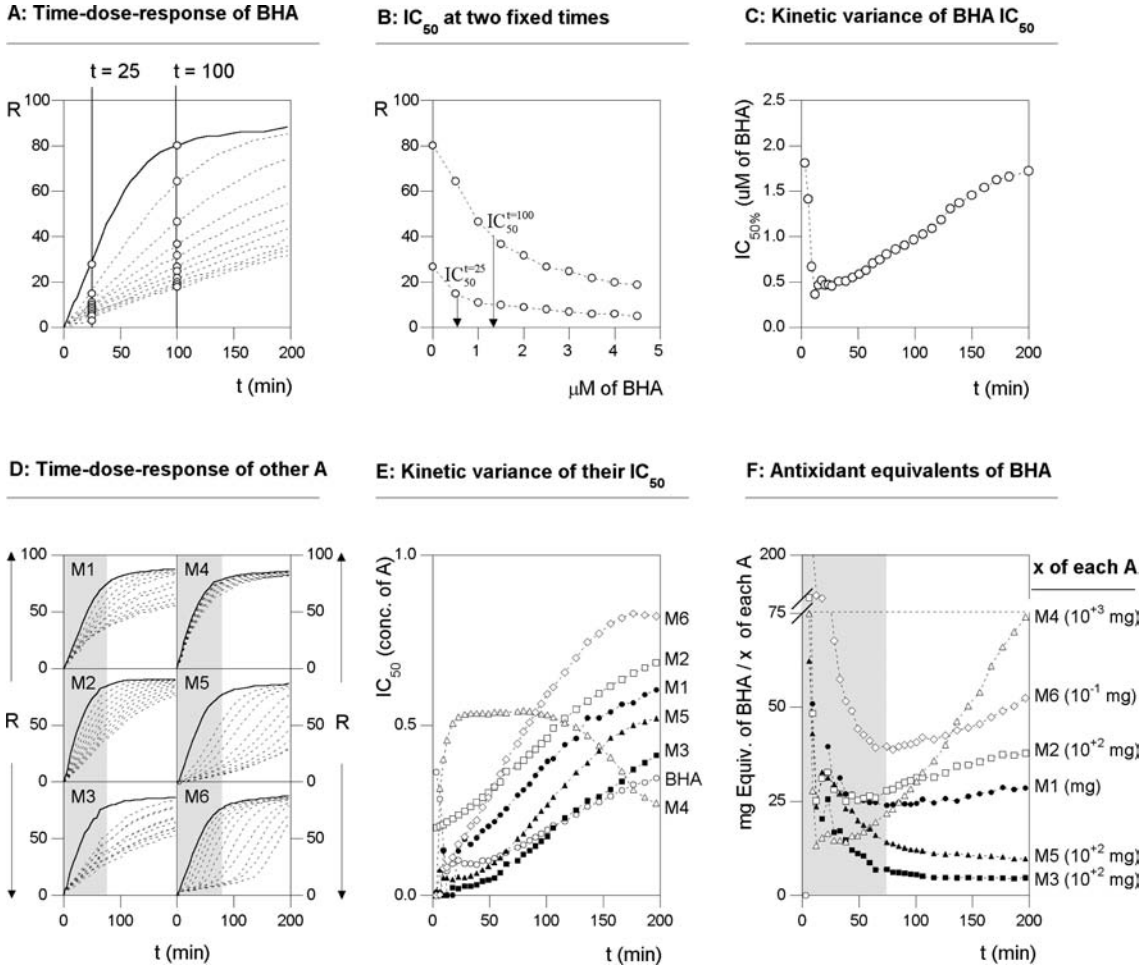

Figure 2. Analysis of the problems of dose−response quantification procedures at a fixed time (Q6). As an example, we use the dose−response of the antioxidant BHA in the range of 0.0−5.0 μM in intervals of 0.5 and evaluate the results in the βC bleaching reaction from a kinetic point of view. (A) Kinetic dose−response of BHA in the format of Q1 criterion. (B) Nonlinear dose−response of BHA at the fixed points selected in the previous graph. (C) Behavior of the computed value IC_{50} at all kinetic times measured. (D) Dose−response of samples M1−M6 (concentration ranges in the Materials and Methods). (E) Computed kinetic IC_{50} value for all samples. (F) Equivalent milligrams of BHA activity of all samples.

response is kept more or less constant, which is the case for M1, M2, and M3 samples. However, even in those responses with similar profiles, it can be seen that, performing the equivalent activity at initial kinetic points (<25 min), the response at which the major measurement errors are produced causes high equivalent activity inaccuracies. For all other cases, the type of response profile was different from that exhibited by the reference A, and this caused a considerably dependency upon the time at which the kinetic measure is performed. For example, cases M5 and M6 showed a different degree of sigmoid profiles; in consequence, their kinetic equivalent computation shows major differences at any time. The case of M4 shows a potential pattern as well as the previous cases, but in an opposite way, the kinetic equivalent activity estimation shows a clear dependency upon the fixed point selected.

Dose−Response at a Fixed Time (Q6). The problems explained above are not solved when the quantification involves computing the slope (linear responses) or the IC_{50} (nonlinear responses) of samples and reference A at a single or various fixed end points for any of the Q1−Q5 criteria or other similar approaches. Although testing samples and reference A in a dose−response way seems to be a more consistent approach, the calculated values (slope and IC_{50}) remain highly dependent upon the time and the similarities between the behaviors of the dose−response of the compounds.

On one hand, to illustrate the dependence upon the time, Figure 2A shows the kinetic dose−response of BHA in the format of criterion Q1. In this figure, we select "randomly" two possible fixed time points (25 and 100 min). Figure 2B shows the nonlinear dose−response of BHA at those fixed points, showing graphically the variance of the IC_{50} obtained. Figure 2C shows the behavior of the computed value IC_{50} at all kinetic times measured. Therefore, the fixed points initially chosen have a relevant impact on the final IC_{50} obtained. In the case of BHA, the dose−response tested was between 0 and 5 μM and the range of the computed IC_{50} was between 0.5 and 2 μM. Additionally, to extend our concerns regarding the applications of this type of quantification criteria, Figure 2D shows the dose−response of samples M1−M6 (concentration ranges in the legend of Figure 2). Figure 2E shows the computed kinetic IC_{50} value for all samples. The response was standardize into a [0, 1] format to distinguish the differences in a more graphical mode, in which 0 represents the absence of A and 1 represents the maximum tested dose of A. Thus, it can be examined that the kinetic variance of IC_{50} in some cases reaches values up to 70% of the dose−response tested.

dx.doi.org/10.1021/jf5005995 | J. Agric. Food Chem. 2014, 62, 5472−5484

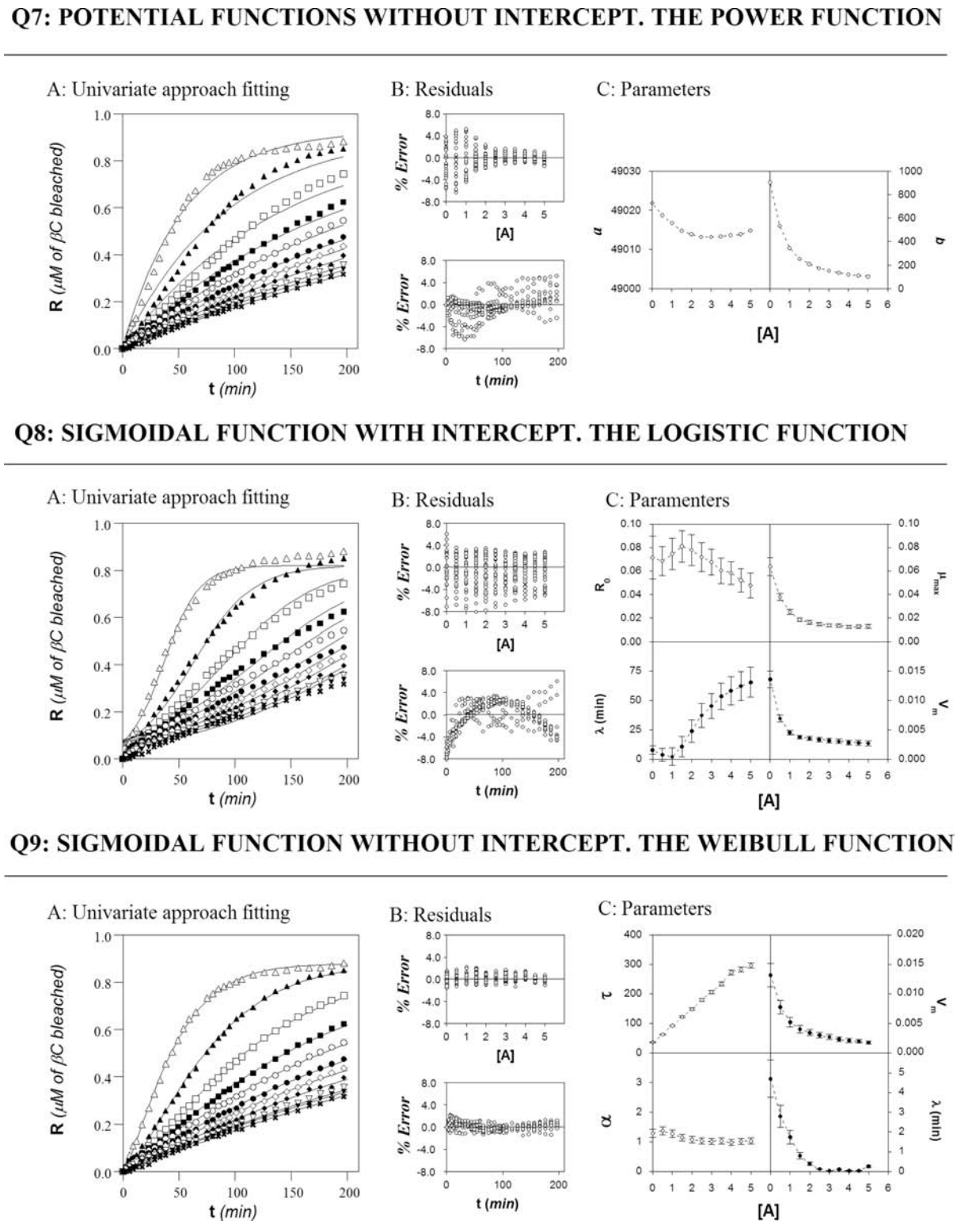

Figure 3. Kinetic description of βC bleaching, in the presence of the different concentrations of BHA in the range of 0.0−5.0 μM in intervals of 0.5 in the final solution with the available mathematical expressions as criteria *Q7*, *Q8*, and *Q9*. For each determination equation, three different subsections are graphically analyzed. (A) Univariate kinetic description of βC bleaching in the presence of the different concentrations of BHA in the range of 0.0−5.0 μM in intervals of 0.5 in the final solution (△, 0 μM; ▲, 0.5 μM; □, 1.0 μM; ■, 1.5 μM; ○, 2.0 μM; ●, 2.5 μM; ◇, 3.0 μM; ◆, 3.5 μM; ▽, 4.0 μM; ▼, 4.5 μM; and +, 5.0 μM). (B) Residual distribution of the fitting results for all of the doses assessed. (C) Main parameter pattern as a function of A doses.

On the other hand, to illustrate the dependency upon the type of dose−response profiles, we have computed the equivalent milligrams of BHA (Figure 2F) per *x* unit of concentration of each A (the corresponding *x* units of each A are clarified in the graph). It can be observed that those A that had similar kinetic IC_{50} profiles (M1, M2, M3, and M5 cases),

dx.doi.org/10.1021/jf5005995 | J. Agric. Food Chem. 2014, 62, 5472−5484

Table 2. Parametric Estimates and Confidence Intervals (α = 0.05) in Percentage of the βC Bleaching Kinetics

logistic function						
[A]	K	R_0	μ_{max}	v_m	λ	r^2
0.0	0.82 ± 0.01	0.071 ± 0.018	0.064 ± 0.007	0.0136	7.847	0.9913
0.5	0.82 ± 0.01	0.068 ± 0.012	0.038 ± 0.003	0.0070	3.918	0.9917
1.0	0.82 ± 0.01	0.075 ± 0.013	0.025 ± 0.002	0.0046	2.292	0.9833
1.5	0.82 ± 0.01	0.081 ± 0.013	0.019 ± 0.002	0.0038	11.02	0.9731
2.0	0.82 ± 0.01	0.078 ± 0.013	0.016 ± 0.002	0.0036	24.09	0.9638
2.5	0.82 ± 0.01	0.072 ± 0.012	0.015 ± 0.001	0.0034	37.45	0.9572
3.0	0.82 ± 0.01	0.068 ± 0.011	0.014 ± 0.001	0.0032	45.47	0.9588
3.5	0.82 ± 0.01	0.060 ± 0.011	0.013 ± 0.001	0.0031	53.65	0.9495
4.0	0.82 ± 0.01	0.058 ± 0.010	0.013 ± 0.001	0.0029	58.39	0.9498
4.5	0.82 ± 0.01	0.052 ± 0.010	0.013 ± 0.002	0.0028	62.45	0.9408
5.0	0.82 ± 0.01	0.048 ± 0.011	0.013 ± 0.002	0.0027	65.76	0.9284
potential function						
[A]	K	a	b	τ	r^2	
0.0	0.93 ± 0.05	2599.9 (NS)	47.85 (NS)	55.5	0.9920	
0.5	0.93 ± 0.05	2500.0 (NS)	27.32 (NS)	107.0	0.9918	
1.0	0.93 ± 0.05	2419.8 (NS)	17.21 (NS)	143.4	0.9915	
1.5	0.93 ± 0.05	2210.7 (NS)	11.64 (NS)	163.7	0.9934	
2.0	0.93 ± 0.05	2117.1 (NS)	9.19 (NS)	185.5	0.9958	
2.5	0.93 ± 0.05	2064.3 (NS)	7.43 (NS)	212.0	0.9968	
3.0	0.93 ± 0.05	2043.6 (NS)	6.49 (NS)	233.4	0.9961	
3.5	0.93 ± 0.05	2039.6 (NS)	5.66 (NS)	265.3	0.9967	
4.0	0.93 ± 0.05	2009.3 (NS)	4.99 (NS)	292.3	0.9972	
4.5	0.93 ± 0.05	2024.0 (NS)	4.68 (NS)	316.5	0.9982	
5.0	0.93 ± 0.05	2027.8 (NS)	4.37 (NS)	340.8	0.9985	
Weibull function						
univariate approach						
[A]	K	τ	α	v_m	λ	r^2
0.0	0.88 ± 0.01	36.83 ± 0.70	1.29 ± 0.04	0.0132	1.11	0.9993
0.5	0.88 ± 0.01	63.56 ± 0.71	1.37 ± 0.03	0.0078	3.02	0.9993
1.0	0.88 ± 0.01	92.89 ± 0.91	1.28 ± 0.03	0.0052	2.72	0.9991
1.5	0.88 ± 0.01	122.27 ± 1.67	1.15 ± 0.03	0.0041	1.01	0.9981
2.0	0.88 ± 0.01	148.31 ± 2.09	1.08 ± 0.03	0.0035	0.40	0.9982
2.5	0.88 ± 0.01	180.38 ± 3.03	1.04 ± 0.03	0.0030	0.13	0.9981
3.0	0.88 ± 0.01	206.49 ± 4.86	1.02 ± 0.03	0.0027	0.03	0.9973
3.5	0.88 ± 0.01	233.90 ± 5.13	1.04 ± 0.03	0.0024	0.11	0.9979
4.0	0.88 ± 0.01	273.46 ± 8.09	1.02 ± 0.03	0.0021	0.04	0.9979
4.5	0.88 ± 0.01	283.22 ± 5.77	1.02 ± 0.02	0.0020	0.04	0.9986
5.0	0.88 ± 0.01	296.95 ± 7.71	1.05 ± 0.03	0.0018	0.26	0.9981
bivariate approach						
control parameters		τ modifiers		α modifiers		
K	0.88 ± 0.02	m_τ	1.52 ± 0.2	m_α	0.14 ± 0.01	r^2 0.9983
τ	36.7 ± 1.1	n_τ		n_α	0.27 ± 0.02	
α	1.34 ± 0.19					
relative area units						
[A]	$\bar{P}$	parametric estimates to model eq 17				
0.0	0.000	P_m	0.511 ± 0.021		r^2	0.9987
0.5	0.120	r	0.614 ± 0.053			
1.0	0.239	F value	0.313 μM of βC protected/μM of A			
1.5	0.317					
2.0	0.361					
2.5	0.401					
3.0	0.425					
3.5	0.449					
4.0	0.467					
4.5	0.479					
5.0	0.490					

dx.doi.org/10.1021/jf5005995 | J. Agric. Food Chem. 2014, 62, 5472−5484

which only occurs after 75 min of the assay (probably when the protection of A has ended), showed "relative consistent" results. However, such an event seems to be more casual than a reliable measure. Any dose−response at a fixed point earlier than 75 min (dark area on plots D and F of Figure 2) resulted in serious inconsistencies.

When authors developed these evaluation criteria (*Q*1−*Q*5), in an effort to abbreviate the assay performance and obtain quick results, they related the rate of the process (decrease oxidizable substrate per unit time) of samples (in dose−response mode or not) and the dose−response of A as a reference. However, as nonlinear kinetic responses, this value varies with time; thus, the only useful rate value would be the maximum rate value, but the time at which the rate reaches its maximum cannot be established *a priori* and varies for each compound and concentration. In addition, the experimental effort necessary to calculate this value without much mistake allows, as we shall demonstrate, us to perform the analysis in more accurate and complete form than that derived from the non-kinetic approaches.

Kinetic Approaches with Formal Mathematical Expressions (*Q*7−*Q*9). Even if, in general, the criteria that applies mathematical expressions to analyze the kinetic part of the process produces much better results than those that abbreviate the response in a single-time value, there are specific problems with the type of expressions used. Next, we will discuss the problems and advantages of the mathematical expressions described in the references when applied to the oxidation process.

Univariate Approach. The detailed mechanistic description of lipid oxidation is complex and varies from one to another system, which has led to the search for empirical general models able to describe the most common profiles. As in many biological systems, such as microbiology, toxicology, pharmacology, immunology, population dynamics, etc., for wide diverse circumstances, it is usual to describe the effect of a response (independent variable) as a function of another variable (dependent) by a group of mathematical expressions (mechanistic or not) that translate the pattern of the response into parameters. Afterward, those parameters are used to deduce the meaning and/or quantify the effect of many possible dependent variables. Except for the particular case of responses linearly dependent, in almost all of the other cases, which are the most frequent cases in biology, nonlinear expressions must be used to properly describe the effects of variables.

The simple formal descriptions limiting the response in a two-dimensional (2D) framework, such as the power function alternative (*Q*7), are only acceptable in restricted situations. The power function (*Q*7) is a possible alternative[9] to adjust fractional-order kinetic profiles but fails in the description of first-order processes or sigmoid profiles. Figure 3 shows the fittings to the time−dose-dependent response of BHA, and it can be observed that the adjustments are reasonably acceptable. However, the parameters produced are not statistically significant (Table 2), even when the BHA is a particular case with profiles similar to those described for this type of function.

Other alternatives are those models that cover the maximum possible responses in a 2D frame and minimize the number of parameters, such as the sigmoid functions. In this regard, two mathematical expressions, the logistic (*Q*8) and Weibull (*Q*9) equations have been transferred from other fields to describe the oxidation action.[2,10] Both equations have been increasingly applied in different fields with diverse purposes (such as medicine, biology, pharmacology, microbiology, forestry, etc.) to describe the diversity profile from potential to sigmoid ones. They are appropriate for modeling processes, such as the lipid oxidation, to obtain key parameters to summarize the responses. In fact, both equations are able to describe the profile responses of the antioxidation kinetics of BHA accurately. However, as already underlined by other authors,[40] the equations with an intercept, such as the logistic, cause some problems, and in general, it is preferable to consider that the oxidative response is null at zero time. As seen in Figure 3 and Table 2, the results of the univariate fitting to the BHA case in the βC reaction are better performed by the criterion *Q*9 (Weibull equation) than by *Q*8. When the fitting is performed with a sigmoid function with an intercept, the residual distribution and the correlations between the observed and predicted data show higher deviations. The major issues arise when the criterion *Q*8 describes the initial states and the final part of the reaction. Such deviations disappear when the fitting is performed with approach *Q*9. In addition, criterion *Q*9 is an extremely versatile function (eq 10), whose shape is controlled by the parameter α: if $\alpha < 1$, it can describe the profiles generated by the model developed by Terpinc et al.;[9] if $\alpha = 1$, it describes a first-order kinetic; and if $\alpha > 1$, a large variety of sigmoid profiles are produced.

In general, the sigmoid function without an intercept (eq 10) is the best solution to fit individually the kinetic profiles corresponding to a series of increasing levels of an A agent. However, similar results are found, when instead of the Weibull equations, three other parameter sigmoid equations without interception are used, such as the Hill, Gompertz, or Richards−Chapman equations. Because the differences are narrow, we will use the Weibull equation as an example, but the results are easily extended to any other mentioned S-shaped curve without an intercept.

Unlike the *Q*1−*Q*6 alternatives, once a model is established, the variations of its parameter values, such as K, τ, and α, or others, such as ν_m and λ, can characterize the response and help to quantify the effect of the A agent. However, as stated by many authors before,[41,42] for living systems exposed to agents, any particular effect may be expected to be a function of both the dose in the external surroundings and the exposure time, in a bivariate form, as discussed in the following section.

Bivariate Approach. Simultaneous Analysis of Time and Dose To Evaluate the AC. Each component of a bivariate solution has a defined role in the evaluation of A. In general terms, the dose component would simply articulate the A availability, whereby the time component translates the affinity of A for the radicals generated. Adequate mathematical models are available for the analysis of such phenomena. Knowledge of the dose−time effect would be particularly important in the establishment of reference levels and to assess appropriately the effect of A. Additionally, optimal efficient data analysis should involve simultaneous description of all curves, rather than fitting each one individually because, if the necessary information to describe a parameter of the function is missing in one or various curves, this can be completed with the information from the other curves. Also, when the mathematical behaviors of the responses are unlocked, this information may provide the base for classification systems that could reveal A mechanistic patterns.

For the description of the time component of the function, we have discussed previously that the sigmoid equations (Weibull, Hill, Gompertz, or Richards−Chapman) are adequate

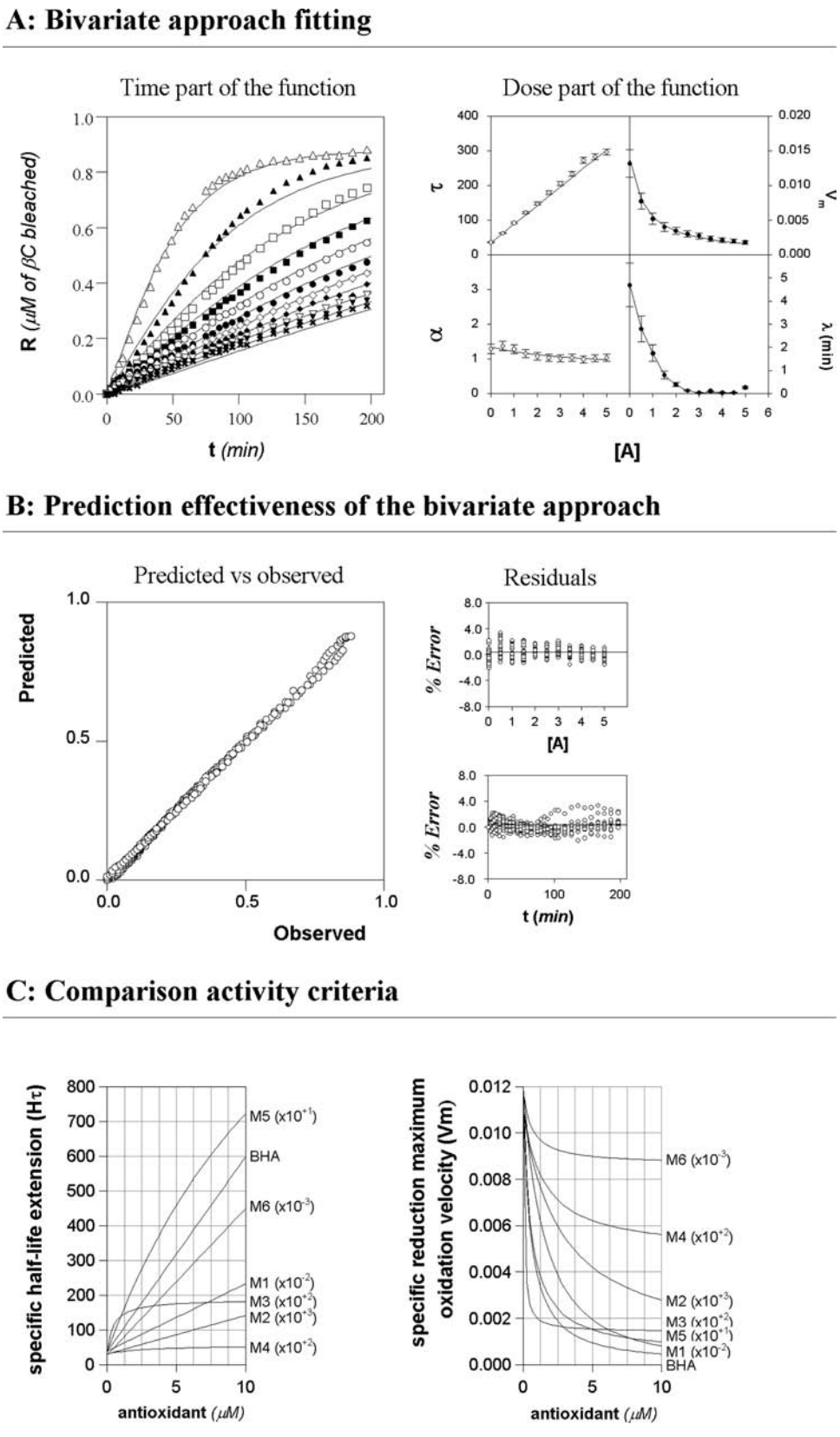

Figure 4. (A) Bivariate kinetic description of βC bleaching in the presence of the different concentrations of BHA in the range of 0.0−5.0 μM in intervals of 0.5 in the final solution. (B) Correlation between the predicted and observed data and residual distribution of the fitting results. (C) Specific behavior of the interesting parameters for all of the samples under study as a function of A doses.

approaches. For the description of the dose component of the function, those sigmoid equations could also be suitable. However, other authors[12,41,42] have made progress in the simultaneous analysis of dose−time response to evaluate the AC and found that the dose effect over any parameter (θ) of the function shows a saturable type effect.[43] Therefore, the

dx.doi.org/10.1021/jf5005995 | J. Agric. Food Chem. 2014, 62, 5472−5484

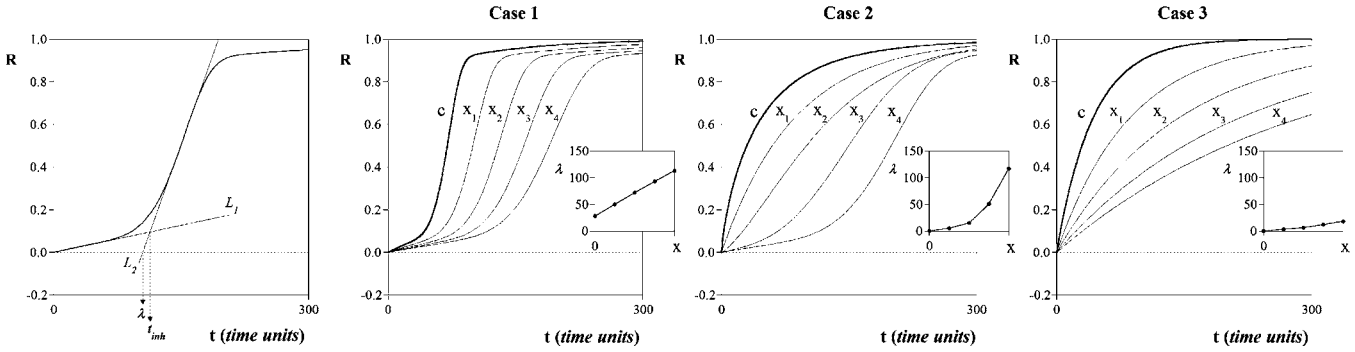

Figure 5. Illustration of the problems associated with the application of initial stage parameters, such as the lag phase (λ) or time of inhibition (t_{inh}).

equations that best fit these requirements are the following first-order, polynomial, or hyperbolic expressions:

$$\theta = \theta_0 H_\theta \begin{cases} H_\theta = 1 + m_\theta \exp(-n_\theta A) \\ H_\theta = 1 + m_\theta A + n_\theta A^2 \\ H_\theta = (1 + m_\theta A)/(1 + n_\theta A) \end{cases} \quad (12-14)$$

where θ represents the modified parameter (K, τ, or α), θ_0 is the parametric value when $A = 0$, and the pairs m_θ and n_θ are fitting coefficients. It should be noted that, in the absence of the effect, the first function requires $m_\theta = 0$ and $n_\theta \neq 0$, whereas the other two require $m_\theta = 0$ and $n_\theta = 0$. Moreover, in the third function, the condition $n_\theta A = -1$ produces a singularity; to avoid it, when A concentrations are coded in the interval $[0, 1]$, it is advisible to include the restriction $n_\theta > -0.999$ in the fitting algorithm. Thus, the model eq 10 turns into the following bivariate form:

$$R(t, A) = KH_K\left\{1 - \exp\left[-\ln 2\left(\frac{t}{\tau_0 H_\tau}\right)^{\alpha_0 H_\alpha}\right]\right\} \quad (15)$$

When any of the mentioned forms of H_θ (eqs 12−14) is inserted into eq 15, excellent simultaneous fittings were obtained in the case of BHA and all other sample cases (M1−M6), which confirms the specificity of the parametric variations found in the individual descriptions. However, when using eqs 12 and 13 to describe the dose effect, even if their parametric values are more informative, we have found, for some parameters, confident interval values with no statistically significant, which will lead to the rejection of the model, and therefore, it would be necessary to select a different approach. When solution eq 14 is used to insert the action of A in eq 15, the individual coefficients m_θ and n_θ lack proper meaning but jointly define a term as a function of the concentration of a given A. It allows for a useful way of quantification of the variations of the kinetic profiles, which characterize the different types of A, and provides even indications concerning modes of action. The advantage of eq 14 is that, if any of its parameters (m or n) is not statistically significant, by rejecting it, the analysis and fitting procedure could be continuous without altering the overall eq 15. Indeed, if $m = 0$ or $n = 0$, the equation would be a linear one (increasing or decreasing respectively), and if $m \neq n \neq 0$, the function would be a hyperbolic one. Figure 4A shows the results obtained with the hyperbolic function eq 14 in eq 15. Figure 4B shows the prediction effectiveness of the bivariate approach. These results were robust and consistent; the residuals were randomly distributed; and autocorrelations were not observed. The prediction was slightly worse than when the univariate approach with three parameter S-shaped equations with an intercept were used (Figure 3), but the joint solution provides a better understanding of the process. The parametric values of the bivariate analysis to the dose−time BHA data are presented in Table 2, showing low confidence intervals ($\alpha = 0.05$) and higher correlation coefficients.

Once the same expression is applied to samples (M1−M6), the profile defined by the specific action of the A, described by the parameters of eq 14, provides a meaningful way to compare their activities. As seen in Figure 4C, plotting the specific variations of the kinetic parameters as a function of A allows for the visualization of the agent-specific dynamics and their activities are compared straightforward.

Dose−Response of Single "Global Values" That Summarize the Kinetic Response (Q10 and Q11). *Lag Phase (λ) and Inhibition Time of Oxidation (t_{inh}).* The first part of Figure 5 shows an illustration of how narrow the meanings of λ and t_{inh} values are. They have analogue meanings, but as explained, the t_{inh} value must be understood as a solution when the common ways of describing λ have failed. Therefore, from now on, instead of discussing both values separately, we will only focus on λ.

In this sense, many authors emphasized the particular difficulties in estimating the lag-phase parameter.[44] Two reasons may explain those difficulties. The first problem has been studied in depth in other fields, notably in food microbiology, in which the estimations of λ has been found especially unreliable from different equations or graphical interpolations. Although different hypotheses provide similar estimates, the imprecision of the estimates is generally larger than the differences between the approaches used, which is highly dependent upon the quality of the data set. The second reason is related to the first reason and comes from the fact that the actual definition of parameter λ is purely geometric. To illustrate the problems, in the second part of Figure 5, we are presenting three different case scenarios (C1−C3) that can be found in the dose−time oxidation response of many methods. C1 shows dose−response curves with identical shape but with different starting points or lag phases. This particular case represents an ideal one, in which both values will be an excellent measure of the AC of compounds. However, C2 and C3 show other cases, in which such idyllic relations are not

dx.doi.org/10.1021/jf5005995 | J. Agric. Food Chem. 2014, 62, 5472−5484

fulfilled. C2 shows a case in which the shape of the curve varies with the concentration of A, which causes very short lag phases in the curves close to first-order profiles and more realistic values when the shape is more pronounced or sigmoid. C3 shows a dose−response case with static shape profiles as a function of A, which is very close to first-order ones. In this type of case, the resulting lag phases would always be low values. Overall, the three specific case responses have similar activity, but if we compare the resulting values found (graphically described in Figure 5), it becomes clear that those two global values λ and t_{inh} are very dependent upon the shape of the curve producing unreliable conclusions.

Area Units under the Curve (Q11). Once the area values are obtained (using for example approximation eq 11), there are many ways to transform these values into other useful ones. In the following, we will describe a simple process for the data under evaluation, which may possibly be valid for some type of A response. The area value response can be standardized in diverse types of formats. One that can be appropriate for our response is to rearrange them to the amount of molecules (micromolars) of βC protected ($\overline{P}$) during the time frame of the assay, in the presence of a dose−response of A, using the following relation:

$$\overline{P} = \frac{AU_C - AU_A}{t_T} \tag{16}$$

in which AU_C and AU_A are the area units corresponding to the kinetic profiles in the absence (C = control) and presence (A) of a concentration of A and t_T is the total time of the assay (minutes).

Typically, the dose−response of the value $\overline{P}$ is plotted against the concentration of A. On occasions, authors have shown a linear relation, but as discussed previously, such a behavior must only be true in a short range of concentrations or perhaps only for specific assays. For the case of BHA, the response found was nonlinear, suggesting that some radical-generating property of the system can be saturated.[43] This type of dose−response patterns can be adjusted to previous eqs 12−14 as the following asymptotic function:

$$\overline{P}(A) = P_m[1 - \exp(-rA)] \tag{17}$$

where A is the concentration of the A agent under study in micromolars, $\overline{P}(A)$ is the response behavior of the value $\overline{P}$ as a function of A, P_m is the asymptotic value of the parameter obtained (micromolars of the substrate protected), and r is the specific dose rate (per micromolars of A).

In addition, other interesting values can be computed, for example, by multiplying both parameters (P_m and r) estimated by eq 17 as follows:

$$F = P_m r \tag{18}$$

Therefore, the value F obtained corresponds to the average amount of molecules protected per unit of A (micromolars of the protected substrate per micromolars of A).

Figure 6A shows an illustration of how the relative values of area are obtained for one particular case of the dose−response of BHA. Figure 6B shows the dose−response curve profile fitted to eq 17 for the case of BHA. Figure 6C displays the F values that eq 18 produced for the BHA case and samples (M1−M6). Therefore, the AC of compounds could be summarized in one single value summarizing the dose−time response.

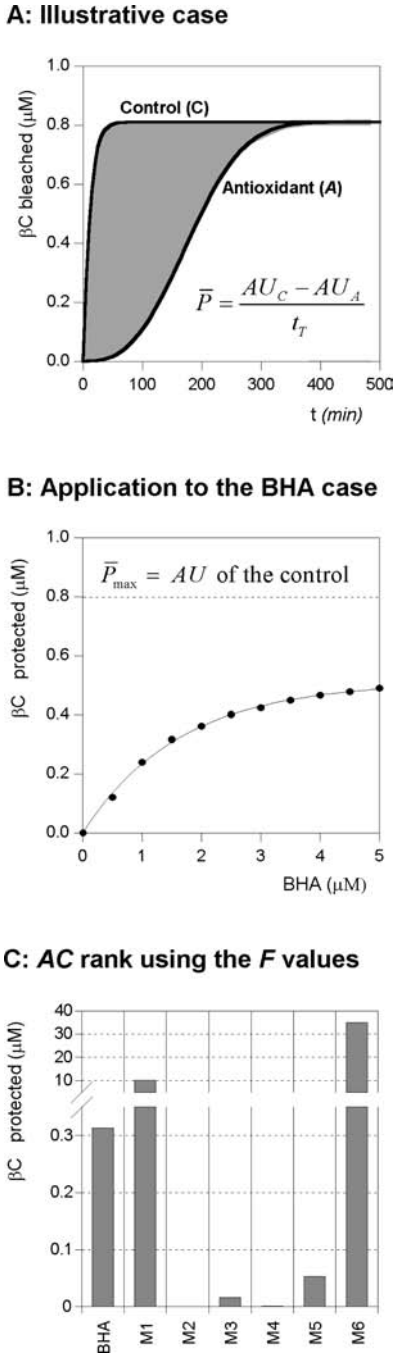

Figure 6. (A) Illustration of how the relative values of area are obtained for one particular case. (B) Dose−response curve profile fitted to eq 17 for the case of BHA. (C) AC rank obtained with the F values from eq 18 for the BHA case and the samples used (M1−M6).

The criterion Q11 represents a way of taking into account the kinetic profile but bypassing complex analytical expressions. The new microplate methods allow us to conduct large temporal data effortlessly with high accuracy. Its advantages are its simplicity[45] and synthetism. However, this second advantage is also its biggest drawback, because the lack of possible interrelations between their values and some possible mechanistic consequences that have a clear practical interest. However, in cases of complex responses, such as samples with more than one effector, either opposite effects (antioxidant versus pro-oxidant) or similar (antioxidant versus antioxidant),

dx.doi.org/10.1021/jf5005995 | J. Agric. Food Chem. 2014, 62, 5472−5484

the use of empirical models requires equations that integrate their interaction effects or, alternatively, their sum. In those types of complex matrices, the application of a globalizing parameter, such as the area under the curve, becomes very useful. It allows us to summarize the time part of the response in one global value and, therefore, to quantify the dose−time response with a simple equation. Thus, in our opinion, it is an useful, simple, and complete tool when complex responses need to be studied[35] and when the goal is to quantify.

DISCUSSION

The references are plentiful in experimental AC methods that are standardized in such a way that kinetic profiles are ignored, promoting the idea that rigorous protocols are needed to find the results in a proper format, normally as linear responses. The βC method presented here as a case study is just one example. In many other methods, as in the βC reaction to quantify the AC, authors have selected those conditions that hide the nonlinear character of the oxidation kinetics, selected commercial A that generates similar results to the linear specific response, and applied the traditional criteria to quantify the response (dose−response of one commercial A as a calibration curve to compute the equivalent AC of a sample, which is only tested at one single-time dose). In fact, when kinetic models are disregarded and measures are performed at a single-time dose, it is obvious that researchers tended to developed more complex protocols and impractical standardization. The results obtained when the activity is measured at one fixed time not only generates a serious reproducibility problem and prevents meaningful comparisons[4,5,26,27,34,46] but also makes it difficult to evaluate critical points that can be standardized.[3] Indeed, the reality is that the conclusions found may be limited and not reproduced anywhere else.

Antioxidants act by several mechanisms, e.g., by donating hydrogen to radicals, reducing power, free-radical-scavenging activity, metal-chelating ability, inhibition of βC bleaching, and quenching singlet oxygen. The method used to measure and calculate the AC has a major impact on the results because, in both *in vivo* and *in vitro*, the oxidation reactions are complex, in which the dominant mechanism depends upon many system conditions. Furthermore, we are using oxidizing substrates, initiators, and other components, and the activity is measured in different environments, such as bulk oils, emulsions, and multiphase, which may not represent the real systems. Avoiding the use of the kinetic part of the reaction to evaluate the capacity of antioxidants is incongruous. Today, the computer technology and development of microplate readers make it easier to obtain sufficient data in a time−dose format, and there are a diverse amount of tools that allows us to quantify properly the responses, such as criteria *Q*9 and *Q*11. Consequently, it does not seem reasonable to exclude these resources for routine assessments. In our opinion, any criterion avoiding kinetic focus is a misleading simplification. We are aware that criteria *Q*9 and *Q*11 are slightly elaborated than a single-time response, but it is also much less deceiving. It not only produces characterizing values of practical interest with high reproducibility but also enables the inclusion, if necessary, of environmental variables that modify the process as well as inference of mechanistic details that can be verified by other methods.

Perhaps using *Q*9 and *Q*11 as those solutions to describe the oxidation process, we are not helping to translate the results, because they may be related with the response itself, but at least we are able to (1) describe with precision the kinetics detected in many different reactions with antioxidants of very different nature, (2) obtain reproducible characterizing values of practical interest, (3) incorporate consistently, if necessary, environmental variables that modify the process, and (4) infer mechanistic details that can be verified by other methods.

The reduction to study the dose−response at one single time and expect to find linear forms (as described by the non-kinetic approaches) frequently leads to unreliable results and misinterpretations. The preference for apparently simple assays, routinely applied with minimal calculation requirements, is not very justifiable today, given the availability of computational applications and microplate readers, whose combination provides adequate tools to work with data sets that allow for accurate evaluations enabled by the nonlinear modeling. We believe that we have provided evidence that demonstrates the inadequate evaluation and quantification of the responses that focus on analyzing the results at a fixed time, avoiding the kinetic perspective. These results show the needs to apply a dose−time-dependent model to quantify the AC. Otherwise, the response will always be poorly described. We believe that those facts could be extended generally to almost all oxidative response methods.

AUTHOR INFORMATION

Corresponding Author

*E-mail: michaelumangelum@gmial.com.

Funding

The authors thank Ministerio de Ciencia e Innovación (Project CTM2010-18411, co-financed with FEDER funds by the European Union) for financial support. Miguel Ángel Prieto Lage was awarded one grant from the JAE predoctoral program co-financed by the CSIC and European Social Fund (ESF).

Notes

The authors declare no competing financial interest.

ACKNOWLEDGMENTS

Last but not least, the authors want to express their gratitude to Araceli Menduiña Santomé for her professional technical work.

REFERENCES

(1) Frankel, E. N.; Finley, J. W. *J. Agric. Food Chem.* **2008**, *56*, 4901−4908.
(2) Murado, M. A.; Vázquez, J. A. *J. Agric. Food Chem.* **2010**, *58*, 1622−1629.
(3) Dawidowicz, A. L.; Olszowy, M. *Eur. Food Res. Technol.* **2010**, *231*, 835−840.
(4) Frankel, E. N. *Trends Food Sci. Technol.* **1993**, *4*, 220−225.
(5) Frankel, E. N. *Trends Food Sci. Technol.* **1994**, *51*, 56−57.
(6) Ordoudi, S. A.; Tsimidou, M. Z. *J. Agric. Food Chem.* **2006**, *54*, 9347−9356.
(7) Prior, R. L.; Cao, G. *Free Radical Biol. Med.* **1999**, *27*, 1173−1181.
(8) Marco, G. J. *J. Am. Oil Chem. Soc.* **1968**, *45*, 594−598.
(9) Terpinc, P.; Bezjak, M.; Abramovič, H. *Food Chem.* **2009**, *115*, 740−744.
(10) Özilgen, S.; Özilgen, M. *J. Food Sci.* **1990**, *55*, 498−498.
(11) Ragnarsson, J.; Labuza, T. *Food Chem.* **1977**, *2*, 291−308.
(12) Prieto, M. A.; Rodríguez-Amado, I.; Vázquez, J. A.; Murado, M. A. *J. Agric. Food Chem.* **2012**, *60*, 8983−8993.
(13) Mikami, I.; Yamaguchi, M.; Shinmoto, H.; Tsushida, T. *Food Sci. Technol. Res.* **2009**, *15*, 171−178.
(14) Chatterjee, S.; Poduval, T. B.; Tilak, J. C.; Devasagayam, T. P. A. *Clin. Chim. Acta* **2005**, *352*, 155−163.
(15) Gonçalves, R.; Mateus, N.; de Freitas, V. *Food Chem.* **2011**, *125*, 665−672.

(16) Kato-Noguchi, H.; Macías, F. A.; Molinillo, J. M. G. *J. Plant Physiol.* **2010**, *167*, 1221−1225.
(17) Matthäus, B. *Society* **2002**, *50*, 11−14.
(18) Moure, A.; Franco, D.; Sineiro, J.; Domínguez, H.; Núñez, M. J.; Lema, J. M. *J. Agric. Food Chem.* **2000**, *48*, 3890−3897.
(19) Prasad, K. N.; Chew, L. Y.; Khoo, H. E.; Yang, B.; Azlan, A.; Ismail, A. *Food Chem.* **2011**, *124*, 1549−1555.
(20) Hsouna, A. B.; Trigui, M.; Culioli, G.; Blache, Y.; Jaoua, S. *Food Chem.* **2011**, *125*, 193−200.
(21) Othman, A.; Ismail, A.; Abdulghani, N.; Adenan, I. *Food Chem.* **2007**, *100*, 1523−1530.
(22) Suja, K. P.; Jayalekshmy, A.; Arumughan, C. *Food Chem.* **2005**, *91*, 213−219.
(23) Kubola, J.; Siriamornpun, S. *Food Chem.* **2008**, *110*, 881−890.
(24) Velioglu, Y. S.; Mazza, G.; Gao, L.; Oomah, B. D. *J. Agric. Food Chem.* **1998**, *46*, 4113−4117.
(25) Kulisic, T.; Radonic, A.; Katalinic, V.; Milos, M. *Food Chem.* **2004**, *85*, 633−640.
(26) Huang, D.; Ou, B.; Prior, R. L.; Ronald, L. *J. Agric. Food Chem.* **2005**, *53*, 1841−1856.
(27) Laguerre, M.; Lecomte, J.; Villeneuve, P. *Prog. Lipid Res.* **2007**, *46*, 244−282.
(28) Melton, S. *Food Technol.* **1983**, *37*, 105−111.
(29) Wardhani, D. H.; Fuciños, P.; Vázquez, J. A.; Pandiella, S. S. *Food Chem.* **2013**, *139*, 837−844.
(30) Esterbauer, H.; Gebicki, J.; Puhl, H.; Jürgens, G. *Free Radical Biol. Med.* **1992**, *13*, 341−390.
(31) Peyrat-Maillard, M. N.; Cuvelier, M. E.; Berset, C. *J. Am. Oil Chem. Soc.* **2003**, *80*, 1007−1012.
(32) Dávalos, A. *J. Agric. Food Chem.* **2004**, *52*, 48−54.
(33) Huang, D.; Ou, B.; Hampsch-Woodill, M.; Flanagan, J. A.; Deemer, E. K. *J. Agric. Food Chem.* **2002**, *50*, 1815−1821.
(34) Naguib, Y. M. *Anal. Biochem.* **2000**, *284*, 93−98.
(35) Prieto, M. A.; Murado, M. A.; Vázquez, J. A. *Food Res. Int.* **2014**, *60*, 218−229.
(36) Kemmer, G.; Keller, S. *Nat. Protoc.* **2010**, *5*, 267−281.
(37) Prikler, S. *Anal. Bioanal. Chem.* **2009**, *395*, 1945.
(38) Prieto, M. A.; Vázquez, J. A.; Murado, M. A. *Biotechnol. Prog.* **2012**, *28*, 372−381.
(39) Comuzzi, C.; Polese, P.; Melchior, A.; Portanova, R.; Tolazzi, M. *Talanta* **2003**, *59*, 67−80.
(40) Murado, M. A.; Prieto, M. A. *Sci. World J.* **2014**, DOI: 10.1155/2014/936202.
(41) De Lean, A.; Munson, P. J.; Rodbard, D. *Am. J. Physiol.* **1978**, *235*, E97−E102.
(42) Prieto, M. A.; Vázquez, J. A.; Murado, M. A. *Process Biochem.* **2011**, *46*, 1579−1588.
(43) Gieseg, S. P.; Esterbauer, H. *FEBS Lett.* **1994**, *343*, 188−194.
(44) Baty, F.; Delignette-Muller, M.-L. *Int. J. Food Microbiol.* **2004**, *91*, 261−277.
(45) Prior, R. L.; Wu, X.; Schaich, K. *J. Agric. Food Chem.* **2005**, *53*, 4290−4302.
(46) Koleva, I. I.; Van Beek, T. A.; Linssen, J. P. H.; De Groot, A.; Evstatieva, L. N. *Phytochem. Anal.* **2002**, *17*, 8−17.

JOURNAL OF AGRICULTURAL AND FOOD CHEMISTRY

Article

pubs.acs.org/JAFC

Determination of Grayanotoxins in Honey by Liquid Chromatography Tandem Mass Spectrometry Using Dilute-and-Shoot Sample Preparation Approach

Muammer Kaplan,* Elmas O. Olgun, and Oznur Karaoglu

Food Institute, TUBITAK Marmara Research Centre, P.O. Box 21, 41470 Gebze, Kocaeli, Turkey

ABSTRACT: A simple and rugged method of analysis for grayanotoxins I and III in honey using liquid chromatography triple quadrupole mass spectrometry with electrospray ionization was developed. This paper describes the first LC−MS/MS method for the quantitation and confirmation of the grayanotoxins in honey using "dilute-and-shoot" sample preparation approach. Honey sample was diluted 10-fold in methanol−water (1:4 v/v) prior to analysis. Chromatographic separation was achieved on a reversed phase HPLC column using a water−methanol gradient with 0.1% acetic acid. The method was fully validated for quantitative purposes. Overall recoveries, selectivity, overall intraday and interday repeatability, decision limit, and detection capability of the analytes was determined. The matrix effects, ruggedness, and analyte stability in standards and samples were studied. Ten real honey samples were successfully analyzed using the developed method. All the samples were found to contain residues of GTXs ranging from 0.1 to 39 mg/kg.

KEYWORDS: *grayanotoxin, mad honey, LC−MS/MS, dilute-and-shoot*

INTRODUCTION

Grayanotoxins (GTXs) are a group of chemical compounds found naturally in plants from the Ericaceous family which includes Rhododendrons. There are over 60 grayanotoxin-related compounds.[1] From these, grayanotoxins I and III are reported to be the most toxic.[2] Grayanotoxins cause intoxication by increasing the membrane permeability to sodium ions.[3] Grayanotoxin-containing Rhodendron species are grown naturally in different countries including United States, Brazil Spain, Portugal, Turkey, Nepal, and Japan.[4]

Toxic Rhododendron species, *Rhododendron ponticum*, native to the Black Sea region of Turkey, is commonly used as folk medicine to treat various health problems including colds, edema, and pains.[5] Honey produced from pollen and nectar of these flowers is known as "mad honey". Mad honey is also used as folk medicine to treat gastritis, ulcers, hyperglycemia, hypertension, arthritis, sexual impotence, and performance enhancement.[3,6] It is largely produced in the Black Sea region and marketed as folk medicine. The consumption of "mad honey" causes intoxications in humans, and the severity of symptoms may vary from mild to life-threatening depending on the amount consumed.[3] Grayanotoxin poisoning remains to be one of the most frequently encountered food toxicant in Turkey.[7] Cases of GTX poisoning have also been reported from Austria, Korea, Nepal, and a few other countries.[8] Moreover, recently, concerns about poisoning by mad honey were raised by the German Federal Institute for Risk Assessment (BfR- Bundesinstitut für Risikobewertung), calling for more systematic control of honey from specific regions.[9] Because of GTXs' unseen dangerous potential for public health, there is a great need for the development of rapid and reliable methods of analysis enabling the detection of GTXs in honey.

In the scientific literature, there are only very few analytical methods published for grayanotoxin determination in honey samples. Thin-layer chromatography[10] and direct spectrometric methods[11] were used for the analysis of grayanotoxins in plant materials and honey. Grayanotoxins in honey was carried out by gas chromatography (GC) with stainless steel capillary columns following trimethylsilyl derivatization.[12] A two-dimensional TLC was used for the qualitative analysis of GTXs in plant materials, gastrointestinal contents, and feces at a concentration of 0.2 μg/g.[13] Quantitative determination of GTXs in biological samples was performed using a liquid chromatography combined with an ion trap tandem mass spectrometry.[14] In a recent study, liquid chromatography coupled to high-resolution mass spectrometry was used to analyze plant toxins including GTX III at 50 μg/kg detection level in honey.[15] To the best of our knowledge, there is only one method published in the literature using liquid chromatography tandem mass spectrometry (LC−MS/MS) for determination of GTXs in honey.[16] In this method, honey samples were mixed with methanol and loaded onto a C18 SPE cartridge for cleanup, and the filtrate was diluted with water and analyzed. However, the method is relatively expensive and time-consuming due to SPE sample preparation step. SPE cleanup step is also prone to errors in sample preparation. Therefore, there is a great need for low cost, simple, and high-throughput analytical procedures for prompt detection and quantitative analysis of toxic GTXs that may coexist in honey. Recently, LC−MS/MS has become the most popular analytical tool for accurate and reliable determination of different residues and contaminants because of high specificity, selectivity, and sensitivity.[17−19]

In this study, we present the first triple quadrupole LC−MS/MS method developed and optimized for simultaneous

Received: April 2, 2014
Revised: May 31, 2014
Accepted: June 2, 2014
Published: June 2, 2014

ACS Publications © 2014 American Chemical Society

determination of grayanotoxins (GTX I and GTX III) in honey samples. The proposed method is rapid and very sensitive, using a methanol−water extraction for sample preparation. The avoidance of a cleanup step together with the optimized chromatography simplified the sample pretreatment and reduced the laboratory costs and the overall analysis time compared to prior methodology. The developed method was fully validated for grayanotoxin analysis in honey, and it is used routinely in our laboratory.

MATERIALS AND METHODS

Reagents and Chemicals. Glacial acetic acid (AA) (Emprove, 100%) and methanol (MeOH) (Lichrosolve purity ≥99.9) were obtained from Merck (Darmstadt, Germany). Grayanotoxin I was purchased from AnalytiCon Discovery GmbH, Potsdam, Germany, and grayanotoxin III was provided from Sigma-Aldrich. Pure water was obtained using a Milli-Q Plus system (Millipore, Billerica, MA).

Standard Solutions. Individual grayanotoxin stock solutions (1000 mg/kg) were prepared in methanol. A mixed intermediate standard solution (10 mg/kg) was obtained by dilution of GTX I and GTX III stock solutions in methanol. Working standard mixed solutions (0.01, 0.1, 0.5, 1, and 2 mg/kg) were prepared by diluting intermediate solution in MeOH−water (1:4 v/v). Stock and intermediate standard solutions were kept in amber flasks at 4 °C. They were stable more than 2 months under these conditions. Working standard solutions were prepared fresh daily.

Sample Preparation. Honey samples, upon arrival at our laboratory, were homogenized with a wooden spoon and were kept at room temperature (+22 ± 4 °C) until analysis. An aliquot of approximately 0.25 g of honey sample was weighed into a 15 mL glass tube. Then 2.5 mL of MeOH−water (1:4 v/v) with 0.1% AA was added, and the sample was vortexed vigorously for 1 min. The extract was filtered through a 0.45 μm filter prior to LC−MS/MS analysis. Honey samples obtained from local market were analyzed, and the ones containing no detectable amount of grayanotoxins were used as control blanks. Real mad honey samples were randomly acquired in local honey producers in different provinces from the Black Sea Region in Turkey between July and September 2013. Of the samples, five were from Duzce, two from Sinop, one from Rize, and two from Tokat province. The honey samples (about 500 g) were stored in their original packaging at room temperature until analysis.

LC−MS/MS Analysis. The HPLC system used for chromatographic analyses consisted of a binary pump (Shimadzu UFLC LC-20AD model), Shimadzu automatic injector (Auto Sampler SIL-20A HT model), and a column oven (CTO-20AC). Analytical columns, Kinetex 100 mm × 2.1 mm, 2.6 μm (Phenomenex, Torrance, USA), and Waters X Terra C18 150 mm × 2.1 mm, 5 μm (Waters, Milford, MA) were used. Chromatographic separation of grayanotoxins was performed using a Waters X Terra C18 column. The method used a binary gradient with mobile phases consisted of water (A) and methanol (B) containing 0.1% acetic acid. Optimized separation of all analytes was obtained using a gradient program as follows: 10−80% solution B in10 min, kept at 80% solution B for 10 min. The column was then returned back to its initial gradient conditions. Finally, the system was equilibrated to initial mobile phase conditions of 10% B and 90% A for 10 min before the next injection. A 10 μL sample was injected into the column maintained at 40 °C. The flow rate was 0.3 mL/min. The mass spectrometer used was an API 4000 Q-TRAP (Applied Biosystems, Foster City, CA) operating in the triple quadrupole mode. The MS/MS parameters were as follows: curtain gas 20 mL/min, exit potential 10 V, and drying and nebulizing gases (GS1 and GS2) were set to 50 mL/min. The ion spray voltage and turbo spray temperature were set to 5500 V and 550 °C, respectively. The mass spectra were acquired using positive ion ESI mode. Three transitions were monitored for each analyte. The selected molecular ion and optimized collision voltages of product ions used for quantification and confirmation are summarized in Table 1. For data acquisition and processing, Analyst version 1.6 (Applied Biosystems) was used. Quantification was made by comparison with a five-point calibration (0.01, 0.1, 0.5, 1, and 2 mg/kg).

Table 1. Optimized MS/MS Conditions Used for the Determination of Grayanotoxins

analyte	precursor ion (m/z)	fragment ions (m/z)[a]	declustering potential (V)	collision energy (eV)
grayanotoxin I	435	Q: 375	111	29
		C: 357	111	35
		C: 91	111	109
grayanotoxin III	335	Q: 299	81	15
		C: 91	81	75
		C: 316	81	9

[a]Q, transition used for quantification; C, transition used for confirmation.

Validation Study. The EU Decision 2002/657/EC[20] criteria were used for the validation of the analytical method developed for determination of GTX I and GTX III in honey. The parameters studied during validation of the method were selectivity, sensitivity, linearity, accuracy, and precision (intraday and interday reproducibility). Identification of grayanotoxins was achieved using retention time data and relative ion intensities of each compound. The Decision 2002/657/EC requires at least four identification points (IPs) for unequivocal confirmation of an analyte. Thus, 5.5 IPs were earned for each grayanotoxin by monitoring one precursor ion and the three most abundant fragment ions.

The Decision Limits (CCα) and Detection Capability (CCβ). The decision limit and detection capability that are the new parameters introduced by Commission Decision 2002/657/EC aimed at replacing the LOD and LOQ. In Decision 2002/657/EC, the CCα is described as "the limit at and above which it can be concluded with an error probability of α that a sample is non-compliant". CCβ is defined as "the smallest content of the substance that may be detected, identified and/or quantified in a sample with an error probability of β".[20] Ten blank honey samples were analyzed for the calculation of CCα and CCβ values. The CCα was calculated as three times the signal-to-noise ratio determined at the elution time of the analyte. The results obtained from the analyses of ten honey blanks spiked at CCα concentration level were used for the calculation of CCβ. The value obtained for CCα was added up to a value of 1.64 and multiplied by the corresponding standard error.

Stability. The stability of the grayanotoxins in both standard solution and honey sample was assessed. Stability in solution was evaluated for individual intermediate solutions prepared in methanol at 10 mg/L concentration level. The solutions were stored at room temperature under daylight and at −20 °C and +4 °C in darkness. Evaluation study was performed by comparing the original stored solution with a working solution prepared fresh daily. The stability of the GTXs in honey matrix was performed using mad honey sample containing residues of GTX I (1.5 mg/kg) and GTX III (0.25 mg/kg).

Matrix Effect. Matrix effects were evaluated using standard solvent and matrix matched calibration curves. The calibration curves were established using peak areas of the SRM transitions chosen for quantification. The slopes of the curves obtained with sample matrix and pure solvent were compared for the assessment of matrix-induced effects.

Ruggedness. Ruggedness of the method was extensively investigated. As the dilute and shoot approach involved injection of diluted honey samples directly to the LC−MS/MS system, it is possible to face column problems, accuracy, and precision loss and reduction in detection sensitivity. Therefore, the method ruggedness was studied using calibration standards and real mad honey sample and honey blanks prepared with honey purchased from a local market. Moreover, we have investigated the likelihood of sample carryover from one sample to the other.

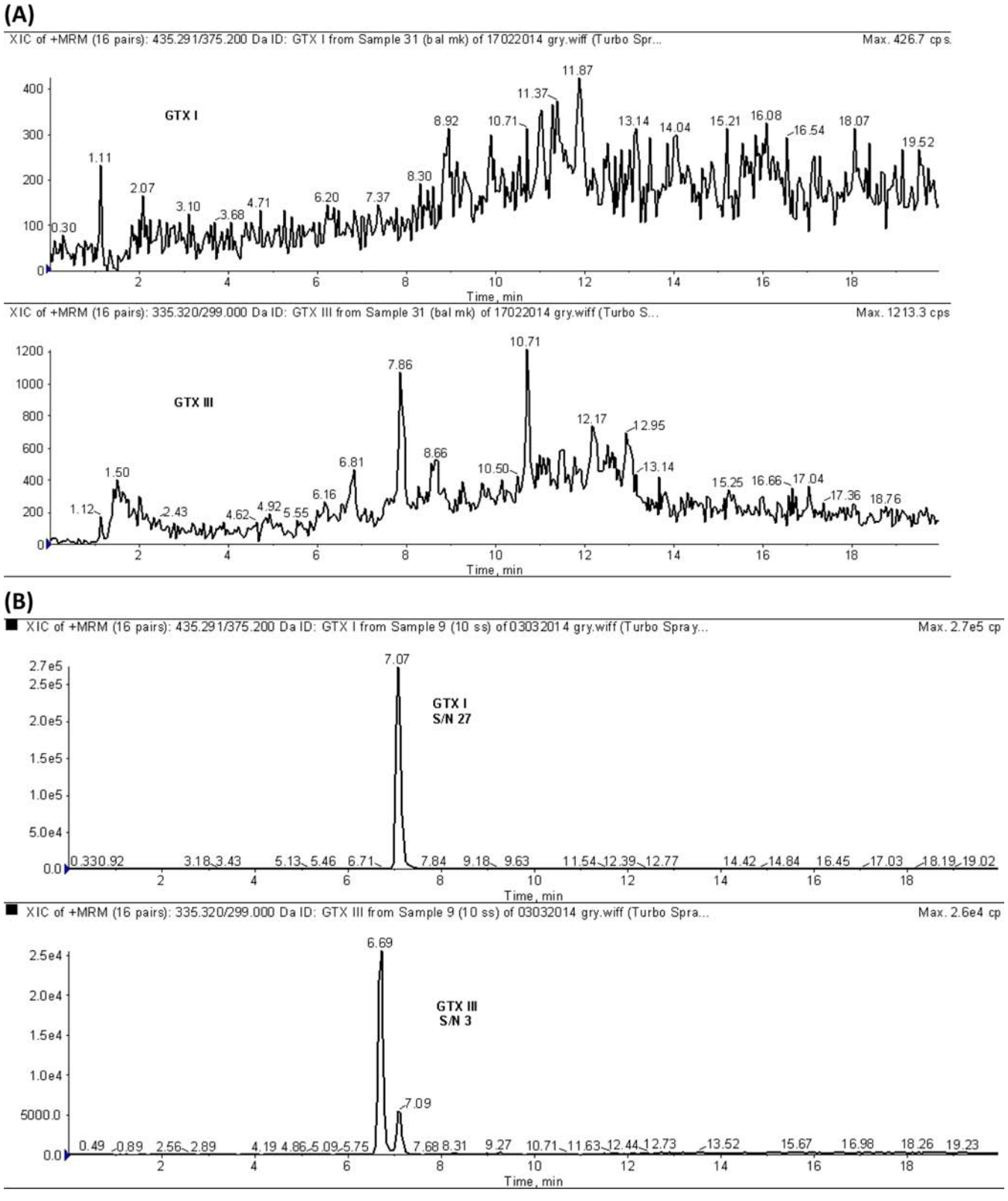

Figure 1. SRM chromatograms obtained from a honey blank (A) and honey spiked with 0.01 mg/kg of GTX I and GTX III (B) using dilute-and-shoot sample preparation.

RESULTS AND DISCUSSION

LC and MS Conditions. The initial stage of the method development was optimization of the mass spectrometer conditions for the detection of GTXs. MS/MS parameters were optimized by infusing GTX standard solutions individually. In the course of instrument tuning both positive (ESI+) and negative (ESI−) ionization modes were tested, and the mobile phase composition was compared. Satisfactory results were obtained only in the positive ionization mode. For each analyte, GTX I and GTX III, three most intensive transitions

dx.doi.org/10.1021/jf501560t | J. Agric. Food Chem. 2014, 62, 5485−5491

were chosen in this study. The most intensive fragment ion was selected for the quantitative determination and the remaining two ions were used for the confirmation of GTXs (Table 1).

Two LC columns with different particle sizes and lengths were assessed for the optimization of chromatographic separation and the signal intensity of grayanotoxins. Both Waters X Terra (150 mm × 2.1 mm, 5 μm) and Kinetex (100 mm × 2.1 mm, 2.6 μm) columns showed similar separation efficiency when MeOH−water solution containing 0.1% AA was used as the mobile phase. X Terra column produced slightly better peak intensities and therefore was chosen for the validation study. Under optimized gradient conditions good separation of GTXs in 7 min was achieved (Figure 1).

Development of Sample Pretreatment. Grayanotoxins are often extracted from the suspected products by classic extraction methods using methanol or dichloromethane.[13] These extraction solvents co-extract a range of other substances along with grayanotoxins. The ionization efficiency of the analytes is affected by the co-extracts especially when working with mass spectrometry in electrospray ionization mode. Therefore, to obtain a robust LC−MS/MS method, it is crucial to remove or minimize their presence. In this study, to overcome the matrix effects, the samples were prepared using dilute-and-shoot approach. For sample dilution, various solvents including water, MeOH, and MeOH−water solutions (1:2 and 1:4 v/v) were tested. The dilution solvents were acidified using acetic acid (0.1, 0.5 and 0.1%, v/v) in order to obtain the maximum signal response for the analytes of interest. Of these, MeOH−water solution (1:4 v/v) containing 0.1% AA gave the best results for both analytes and used for the dilution of honey samples. Furthermore, the efficacy of sample dilutions was examined. To maximize robustness of the procedure, the amount of honey injected per analysis was minimized. For this purpose, the signals obtained after sequential dilution of honey samples (1:4, 1:10, and 1:20) were compared with the signals obtained from the standard solutions prepared in pure solvent. Equally good peak responses were obtained for all dilutions, however, to reduce the instrument cleaning cycle and to meet the required method sensitivity, a 1:10 dilution with 10 μL injection volumes was selected and used for the method validation study. A typical SRM ion chromatogram obtained from a blank honey spiked with 0.01 mg/kg GTX I and GTX III is shown in Figure 1. The sample was prepared by diluting 0.25 g of honey in 2.5 mL of MeOH−water (1:4 v/v) with 0.1% AA. A 10 μL aliquot of this solution was injected.

Method Validation. *Selectivity.* The method selectivity was assessed by duplicate analysis of seven honey blanks from different floral sources (pine, chestnut, and flower honey). No peaks of interfering compounds were observed in the blank honey samples at the retention time of the target GTXs. Typical chromatograms obtained from the analysis of blank and spiked honey samples are given in Figure 1.

Linearity. Linearity was evaluated from the calibration curves by triplicate analyses of blank honey samples fortified with the analytes at five (0.01, 0.1, 0.5, 1, and 2 mg/kg) concentration levels. Linearity was expressed as the coefficient of linear correlation (r) and from the slope of the calibration curve. The correlation coefficients obtained over the concentration range studied was higher than 0.998 for both analytes, GTX I and GTX III.

Accuracy and Precision. The method accuracy and precision were assessed through recovery measurements analyzing honey blanks fortified at concentration levels of 0.01, 0.5, 1, and 2 mg/kg. The results obtained for the method accuracy and precision (Table 2) conform to the values given in Decision 2002/657/EC. Thus, the mean accuracy values obtained in the recovery tests were between 86 and 105%. The precision of the method was determined in two stages: intraday and interday repeatability. The repeatability of the results was expressed as RSDs calculated from six replicates analyzed using the same equipment with the same operator. The interday repeatability was expressed by the RSD of the results obtained from 18 measurements carried out on three different days, six analyses/day, using the same equipment by the same operator. The intraday and interday RSD values calculated for grayanotoxins analyzed using the developed method ranged between 3.7 and 8.3% and 7.2 and 15.9%, respectively (Table 2).

Table 2. Method Performance in Spiked Honey Samples at Concentration Levels Ranged between 0.01 and 2 mg/kg

analytes	spiked level (mg/kg)	average recovery (%) (n = 18)	intraday precision (RSD%, n = 6)	interday precision (RSD%, n = 18)
grayanotoxin I	0.01	86.0	8.3	13.8
	0.10	95.6	7.7	12.4
	0.50	98.0	5.9	12.1
	1.00	102.0	4.5	9.3
	2.00	105.0	3.9	7.2
grayanotoxin III	0.01	87.2	8.4	15.9
	0.10	98.0	7.0	14.7
	0.50	97.0	6.1	13.3
	1.00	103.7	5.8	10.1
	2.00	95.5	3.7	9.5

Decision Limits and Detection Capabilities. The decision limit (CCα) and detection capability (CCβ) values were calculated as 12 and 17 μg/kg for GTX I and 10 and 13 μg/kg for GTX III, respectively. Then, a preliminary experiment was conducted to check if all compounds were detected when spiked at their CCα level (Figure 1). As can be seen from Figure 1, very satisfactory S/N ratios were obtained for all analytes at CCα level.

Stability. The stability of GTX I and GTX III was assessed after storage in methanol solutions at room temperature under daylight and at −20 °C and +4 °C in darkness. Under these conditions, individual grayanotoxin solutions were stable following 8 weeks of storage. Real honey sample containing GTX I and GTX III at concentrations of 0.2 and 1.5 mg/kg, respectively, was stored at room temperature over 12 months period for stability study. GTXs were found to be very stable in honey matrix after 12 months of storage.

Matrix Effects. Evaluation of matrix effect is important during validation of analytical methods using the LC−MS/MS technique. Matrix interferences may affect the ionization efficiency of the analytes in ESI source. The degree of ion suppression or signal enhancement were evaluated using the calibration curves established with and without matrix. The slopes of these curves were used for the assessment of matrix-induced effects using the following formula: matrix effect (ME) = $1 - (a_{matrix}/a_{standard}) \times 100$, where a_{matrix} and $a_{standard}$ are the slopes for the calibration curves obtained in pure standard and matrix-matched honey, respectively. The matrix-matched curves were constructed using honey blanks (0.1 g/mL matrix

dx.doi.org/10.1021/jf501560t | J. Agric. Food Chem. 2014, 62, 5485−5491

equivalent) spiked with GTX I and GTX III (0.1, 0.5, 1, and 2 mg/kg) prepared in MeOH–water solution with 0.1% AA. Figure 2 shows the calibration curves for GTX I and GTXIII.

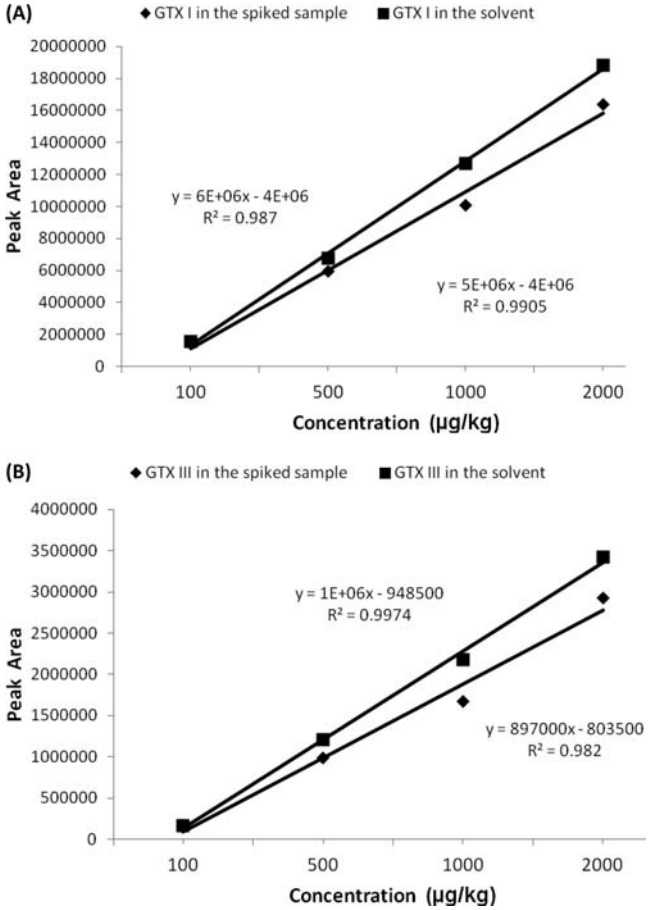

Figure 2. Calibration curves obtained for GTX I (A) and GTX III (B) prepared in pure solvent and fortified honey.

The upper curve represents the analyte signals in pure solvent, whereas the lower one shows the signals in a honey spiked with GTXs. The calibration curves prepared in the spiked samples have lower slope, indicating negligible ion suppression in GTX I (<16%) and GTX III (<11%). These results show that quantitation of GTXs in honey samples can effectively be performed with standard calibration, which is simpler and less time-consuming compared with matrix-matched calibration approach.

Ruggedness. The method ruggedness was demonstrated with sequential injections of 100 real honey sample containing GTX I (17 mg/kg) and GTX III (6 mg/kg) using the same analytical column. In the course of 100 injections, there was no significant increase in the column back pressure. Plots of GTX I and GTX III peak areas versus injection number are illustrated in Figure 3. The peak areas of the analytes stayed essentially constant over the entire run. Over 450 analyses were conducted with the same analytical column without any loss in chromatographic performance. The carryover from one sample to another was also tested by analyzing honey samples in the following order: a blank honey, a spiked honey (0.01 mg/kg), a honey blank, a spiked honey (1 mg/kg), and a honey blank. No peaks were observed in the nonspiked blanks, demonstrating

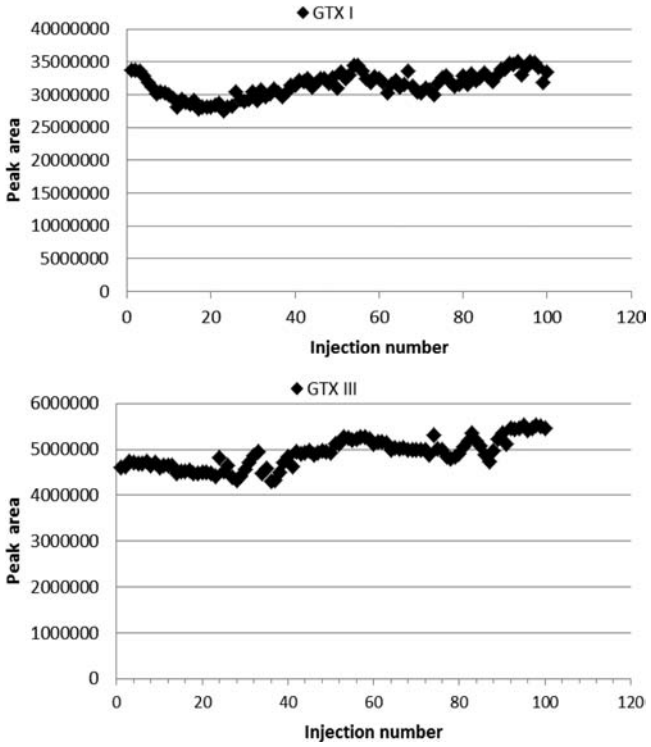

Figure 3. Plots of peak areas against injection number obtained from the sequential analysis of GTX I and GTX III in honey using dilute-and-shoot sample preparation methodology.

that there was no contamination or carryover from one sample to another.

Grayanotoxin Residues in Real Samples. The developed method was used for the analysis of 10 mad honey samples purchased from local honey producers in four different provinces of the Black Sea region. Table 3 shows the results

Table 3. Concentrations of GTX I and GTX III Detected in Honey Samples Collected from Different Provinces in the Black Sea Region, Turkey

sample	GTX I (mg/kg)	GTX III (mg/kg)
Duzce 1	18.4	7.4
Duzce 2	16.5	3.8
Duzce 3	20.2	3.3
Duzce 4	18.6	2.8
Duzce 5	17.1	6.3
Sinop 1	39.3	35.1
Sinop 2	1.5	0.3
Rize	ND[a]	0.1
Tokat 1	0.2	ND[a]
Tokat 2	1.8	0.4

[a]ND: not detected.

obtained for all ten samples. As seen in the table, eight of the honey samples contained residues of GTX I between 1.5 and 39.3 mg/kg and GTX III between 0.3 and 35.1 mg/kg. In one of the remaining two samples only GTX I and in the other one only GTX III was detected at lower concentrations of 0.2 and 0.1 mg/kg, respectively. Some of the SRM chromatograms obtained from real honey samples are shown in Figure 4. Positive identification of grayanotoxins in honey were confirmed when all the criteria for identification including

dx.doi.org/10.1021/jf501560t | J. Agric. Food Chem. 2014, 62, 5485–5491

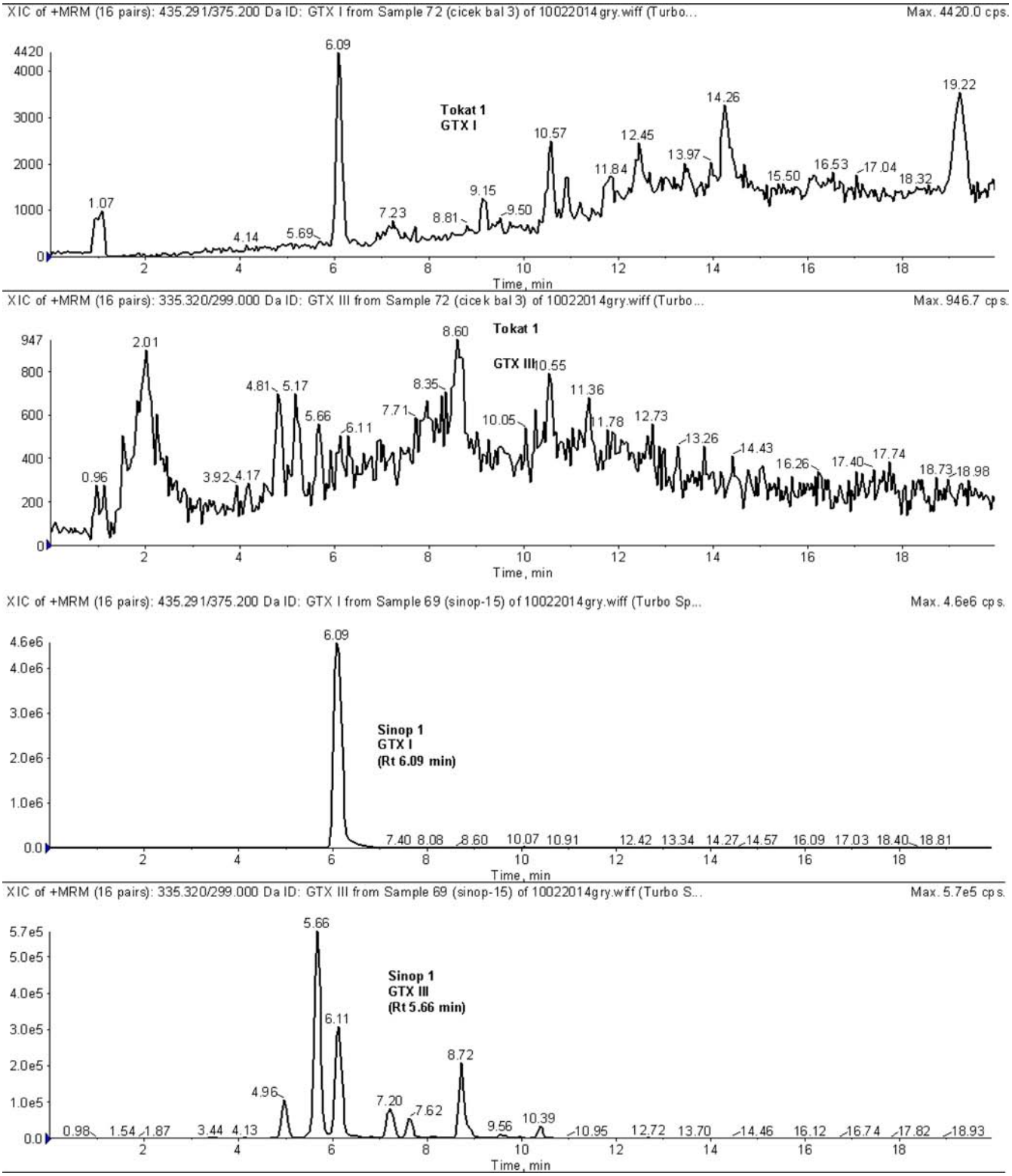

Figure 4. SRM chromatograms obtained for the selected samples of real honey. Amounts detected in each of the samples are given in Table 3

retention time data, molecular ion, fragment ions, and ion ratios (Table 4) were met. The utility of the proposed methodology is thus proved by real sample analyses.

In this study, it was shown that LC−MS/MS method using dilute-and-shoot sample preparation methodology enables a rapid and simple approach for quantitative determination of grayanotoxins in honey without compromising the method sensitivity. The developed method overcame a major disadvantage of current LC−MS/MS methods involving laborious extraction and SPE cleanup steps. It was demonstrated to be very selective and robust and enabling the determination of grayanotoxins after direct injection of diluted honey samples at very low concentrations. Consequently, the new method is a simple, sensitive, low-cost, and high-

dx.doi.org/10.1021/jf501560t | J. Agric. Food Chem. 2014, 62, 5485−5491

Table 4. Abundance Ratios of Three Transition Ion Pairs Obtained from Triplicate Analysis of GTX I and GTX III in Reference Standards and Spiked Samples

analyte	transition ion pairs (m/z)			concentration (mg/kg)	ion ratios reference standards
GTX III	335 > 299	335 > 91	335 > 316	0.01	100:16:89
				0.10	100:12:64
				0.50	100:14:62
				1.50	100:13:64
				2.00	100:12:64
GTX I	435 > 375	435 > 357	435 > 91	0.01	100:23:2
				0.10	100:32:2
				0.50	100:29:2
				1.50	100:23:2
				2.00	100:22:2

throughput methodology and well suited for use in the routine laboratory.

AUTHOR INFORMATION

Corresponding Author

*Phone: +90-262-6773241. Fax: +90-262-6432109. E-mail: muammer.kaplan@tubitak.gov.tr.

Notes

The authors declare no competing financial interest.

REFERENCES

(1) Terai, T.; Osakabe, K.; Katai, M.; Sakaguchi, K.; Narama, I.; Matsuura, T.; Katakawa, J.; Tetsumi, T. Preparation of 9-hydroxy grayanotoxin derivatives and their acute toxicity in mice. *Chem. Pharm. Bull.* **2003**, *51*, 351−353.

(2) Gunduz, A.; Tured, S.; Russell, R. M.; Ayaz, A. F. Clinical review of grayanotoxin/mad honey poisoning past and present. *Clin. Toxicol.* **2008**, *46*, 437−442.

(3) Koca, I.; Koca, A. F. Poisinig by mad honey: a brief review. *Food Chem. Toxicol.* **2007**, *45*, 1315−1318.

(4) Erturk, O.; Karakas, F. P.; Pehlivan, D.; Nas, N. The antibacterial and antifungal effects of rhododendron derived mad honey and extracts of four Rhododendron species. *Turk. J. Biol.* **2009**, *33*, 151−158.

(5) Tasdemir, D.; Demirci, B.; Demirci, F.; Donmez, A. A.; Baser, K. H. C.; Ruedi, P. Analysis of the volatile components of five Turkish Rhododendron species by headspace solid-phase microextraction and GC-MS (HS-SPME-GC-MS). *Z. Naturforsch.* **2003**, *58c*, 797−803.

(6) Lue, T. F. Erectile dysfunction. *N. Engl. J. Med.* **2000**, *342*, 1802−1813.

(7) Demir, H.; Denizbasi, A.; Onur, O. Clinical study mad honey intoxication: a case series of 21 patients. *ISRN Toxicol.* **2011**, *2011*, 1−3.

(8) Shrestha, P.; Vaidya, R.; Sherpa, K. Mad honey poisoning: a rare case report of seven cases. *Nepal Med. Coll. J.* **2009**, *11*, 212−213.

(9) *Vergiftungsfalle durch Grayanotoxine in Rhodendron-Honigen aus der Türkischen Schwarzmeerregion*; German Federal Institute for Risk Assessment (BfR), 2010; http://www.bfr.bund.de/cm/343/vergiftungsfaelle_durch_grayanotoxine_in_rhododendron_honigen_aus_der_tuerkischen_schwarzmeerregion.pdf, (Accessed March 20, 2014).

(10) Kerkvliet, J. D. Analysis of a toxic Rhododendron honey. *J. Apic. Res.* **1981**, *20*, 249−253.

(11) Terai, T.; Katai, M.; Meguri, H. Quantitative analysis of grayanotoxins. I. Spectrometric determination of grayanotoxin I, II, and III. *Yakugaku Zasshi* **1983**, *103*, 686−689.

(12) Terai, T.; Uda, T.; Katakawa, J.; Tetsumi, T. Assay of grayanotoxins by gas chromatography. *J. Jpn. Soc. Biosci. Biotechnol. Agrochem.* **1994**, *68*, 979−981.

(13) Holstege, D. M.; Francis, T.; Puschner, B.; Booth, M. C.; Galey, F. D. Multiresidue screen for cardiotoxins by two-dimensional thin-layer chromatography. *J. Agric. Food Chem.* **2000**, *48*, 60−64.

(14) Holstege, D. M.; Puschner, B.; Le, T. Determination of grayanotoxins in biological samples by LC−MS/MS. *J. Agric. Food Chem.* **2001**, *49*, 1648−1651.

(15) Mol, H. G. J.; Van Dam, R. C. J.; Zomer, P.; Mulder, P. P. J. Screening of plant toxins in food, feed and botanicals using full-scan high-resolution (Orbitrap) mass spectrometry. *Food Addit. Contam., Part A* **2011**, *28*, 1405−1423.

(16) Lee, S.; Choi, Y.; Lee, K.; Cho, T.; Kim, J.; Son, Y.; Park, J.; Im, S.; Choi, H.; Lee, D. Determination and monitoring of grayanotoxins in honey using LC−MS/MS. *Korean J. Food Sci. Technol.* **2008**, *40*, 8−14.

(17) Malik, A. K.; Blasco, C.; Picó, Y. Liquid chromatography−mass spectrometry in food safety. *J. Chromatogr., A* **2010**, *1217*, 4018−4040.

(18) Lohne, J. J.; Andersen, W. C.; Casey, C. R.; Turnipseed, S. B.; Madson, M. R. Analysis of stilbene residues in aquacultured finfish using LC−MS/MS. *J. Agric. Food Chem.* **2013**, *61*, 2364−2370.

(19) Kaplan, M.; Olgun, E. O.; Karaoglu, O. A rapid and simple method for simultaneous determination of triphenylmethane dye residues in rainbow trouts by liquid chromatography tandem mass spectrometry. *J. Chromatogr., A* **2014**, *1349*, 37−43.

(20) European Commission Decision 2002/657/EC. *Off. J. Eur. Communities* **2002**, *L221*, 8−36.

JOURNAL OF AGRICULTURAL AND FOOD CHEMISTRY

Article

pubs.acs.org/JAFC

6-Shogaol, a Major Compound in Ginger, Induces Aryl Hydrocarbon Receptor-Mediated Transcriptional Activity and Gene Expression

Kazutaka Yoshida,*[,†] Hideo Satsu,[‡] Ayano Mikubo,[‡] Haru Ogiwara,[‡] Takafumi Yakabe,[†] Takahiro Inakuma,[§] and Makoto Shimizu[‡]

[†]Research & Development Division, Kagome Co., Ltd., 17 Nishitomiyama, Nasushiobara 329-2762, Japan

[‡]Department of Applied Biological Chemistry, Graduate School of Agricultural and Life Science, The University of Tokyo, 1-1-1 Yayoi, Bunkyo-ku, Tokyo 113-8657, Japan

[§]Faculty of Contemporary Human Life Science, Department of Food and Nutrition, Tezukayama University, 3-1-3 Gakuenminami, Nara 631-8585, Japan

ABSTRACT: Xenobiotics are usually detoxified by drug-metabolizing enzymes and excreted from the body. The expression of many of drug-metabolizing enzymes is regulated by the aryl hydrocarbon receptor (AHR). Some substances in vegetables have the potential to be AHR ligands. To search for vegetable components that exhibit AHR-mediated transcriptional activity, we assessed the activity of vegetable extracts and identified the active compounds using the previously established stable AHR-responsive HepG2 cell line. Among the hot water extracts of vegetables, the highest activity was found in ginger. The ethyl acetate fraction of the ginger hot water extract remarkably induced AHR-mediated transcriptional activity, and the major active compound was found to be 6-shogaol. Subsequently, the mRNA levels of AHR-targeting drug-metabolizing enzymes (CYP1A1, UGT1A1, and ABCG 2) and the protein level of CYP1A1 in HepG2 cells were shown to be increased by 6-shogaol. This is the first report that 6-shogaol can regulate the expression of detoxification enzymes by AHR activation.

KEYWORDS: *aryl hydrocarbon receptor (AHR), luciferase assay, ginger, 6-shogaol, 6-gingerol*

INTRODUCTION

The human body is exposed to a wide variety of xenobiotics in one's lifetime, from food components to environmental toxins to pharmaceuticals; it has developed complex enzymatic mechanisms to detoxify these substances. Lipophilic xenobiotics are usually metabolized into more hydrophilic forms by drug-metabolizing enzymes, mainly in the liver, and excreted from the body. The metabolism of xenobiotics is commonly broken down into three systems: phase I, II, and III systems.[1,2] The phase I system is an oxidative process and is mainly mediated by the cytochrome P450 (CYP) supergene family. As a consequence of this step in the detoxification, reactive molecules, which may be more toxic than the parent molecule, are produced. In the phase II system, activated hydrophobic xenobiotics are converted into hydrophilic forms via conjugation reactions with glucuronide, sulfate, or glutathione. The phase II system is composed of conjugation enzymes such as glutathione-S-transferases (GSTs), sulfotransferases (SULTs), and uridine diphosphate glucuronosyltransferases (UGTs). The phase III system is composed of more than 40 different human ATP-binding cassette (ABC) transporter families and is involved in the exclusion of xenobiotics and their metabolites.

It has been shown that the gene expression of many of these drug-metabolizing enzymes and transporters is regulated by the aryl hydrocarbon receptor (AHR), which is a ligand-dependent transcription factor present in most cell and tissue types in the body.[3] AHR translocates into the nucleus and heterodimerizes with a protein known as the aryl hydrocarbon nuclear translocator (ARNT).[4] This AHR/ARNT complex binds to specific enhancer sequences adjacent to target promoters termed the xenobiotic-responsive element (XRE), which enhances the transcription of target genes encoding phase I metabolic enzymes such as CYP1A1 and CYP1A2, phase II metabolic enzymes such as UGT1A1 and UGT1A6, and phase III metabolic enzymes such as the ABC transporter subfamily G, member 2 (ABCG 2).[2,5−9] Therefore, AHR is regarded as a key regulator of xenobiotic metabolism.

The regulation of AHR by dietary factors is of considerable importance and interest because AHR regulates drug-metabolizing enzymes as described above, and so it is likely that metabolism of xenobiotics could be modulated by dietary factors via AHR. In previous studies, some substances contained in vegetables, such as flavonoids,[10−12] indole compounds,[13,14] and curcumin,[15] were shown to act as natural AHR ligands. However, it is possible that vegetables contain other AHR-activating compounds because there are so many plant-derived compounds in vegetables.

The aim of this study was to search for vegetable components that exhibited AHR-mediated transcriptional activity and modulation of xenobiotic metabolism. Previously, we established the stable AHR-responsive HepG2 cell line by cotransfection of an AHR expression vector (pcDNA-hAHR) and an AHR-responsive vector (pGL3-XRE) containing a luciferase gene and three tandemly arranged XRE elements into the human hepatoma cell line, HepG2.[16] Using this cell line, we

Received: November 14, 2013
Revised: May 13, 2014
Accepted: May 25, 2014
Published: May 26, 2014

ACS Publications © 2014 American Chemical Society

assessed the AHR-mediated transcriptional activity of vegetable extracts and identified new active compounds in vegetables. We also examined the regulation of mRNA and protein expressions of AHR-target xenobiotic-metabolizing genes by these active compounds.

MATERIALS AND METHODS

Cell Culture. The stable AHR-responsive HepG2 cells and HepG2/mock cells (empty vectors were transfected) were grown and maintained at 37 °C in Dulbecco's modified Eagle's medium (DMEM) High Glucose with L-glutamine and phenol red (Wako Pure Chemical Industries 044-29765 Osaka, Japan), containing 10% fetal bovine serum (Asahi Technoglass, Chiba, Japan), 40 U/mL penicillin, 40 μg/mL streptomycin, and 500 μg/mL G418 (Nacalai Tesque, Kyoto, Japan) in a 100% humidified atmosphere containing 5% CO_2. For culturing of HepG2 cells, G418 was removed from the same medium as that used for culturing the stable AHR-responsive HepG2 cells.

Preparation of Vegetables Extracts. Fresh vegetables were purchased from local markets in Nasushiobara, Japan (Table 1).

Table 1. List of the 23 Vegetables Used in This Study

Vegetable	Family name	Scientific name	Production area in Japan
Ashitaba	Apiaceae	*Angelica keiskei*	Ibaragi
Asparagus	Liliaceae	*Asparagus officinalis* L.	Tochigi
Beetroot	Chenopodiacea	*Beta vulgaris* L. ssp. vulgaris var. vulgaris	Nagano
Broccoli	Cruciferae	*Brassica oleracea* var. italica L.	Nagano
Broccoli sprout	Cruciferae	*Brassica oleracea* var. italica L.	Shizuoka
Burdock	Asteraceae	*Arctium lappa* L.	Tochigi
Cabbage	Cruciferae	*Brassica oleracea* var. capitata L.	Gunma
Carrot	Apiaceae	*Daucus carota* L.	Chiba
Celery	Apiaceae	*Apium graveolens* L.	Nagano
Chinese cabbage	Cruciferae	*Brassica rapa* L. ssp. Pekinensis	Ibaragi
Eggplant	Solanaceae	*Solanum melongena* L.	Kochi
Ginger	Zingiberaceae	*Zingiber officinale*	Miyazaki
Komatsuna	Cruciferae	*Brassica rapa* var. perviridis	Tochigi
Lettuce	Asteraceae	*Lactuca sativa* L.	Nagano
Molokhia	Tiliaceae	*Corchorus olitorius* L.	Tochigi
Onion	Liliaceae	*Allium cepa* L.	Saga
Paprika	Solanaceae	*Capsicum annuum* cv.	Chiba
Parsley	Apiaceae	*Petroselium crispum* Nym.	Nagano
Pumpkin	Cucurbitaceae	*Cucurbita maxima* L.	Tochigi
Spinach	Chenopodiacea	*Spinacia oleracea* L.	Tochigi
Tomato	Solanaceae	*Solanum lycopersicum* L.	Tochigi
Watercress	Cruciferae	*Nasturtium officinale* R. Br.	Tochigi
White radish	Cruciferae	*Raphanus sativus* L.	Hokkaido

Preparation of vegetable extracts was conducted as described in Figure 1. Each vegetable was chopped and boiled in four-times its weight of hot water for 1 h. The extraction liquid was then recovered and centrifuged at 8000*g* for 10 min at room temperature. A portion of the obtained supernatant (40 mL) was lyophilized, and the resultant powder was used as the "hot water extract (HWE)" sample. A portion of the supernatant (100 mL) was adjusted to pH 3.0 by adding 2 M hydrochloric acid, followed by addition of 200 mL of ethyl acetate. The mixture was then vigorously shaken in a separating funnel to separate it into the ethyl acetate layer and aqueous layer. This extraction was repeated four times. All the ethyl acetate layers were collected, and the ethyl acetate was evaporated. The obtained residue

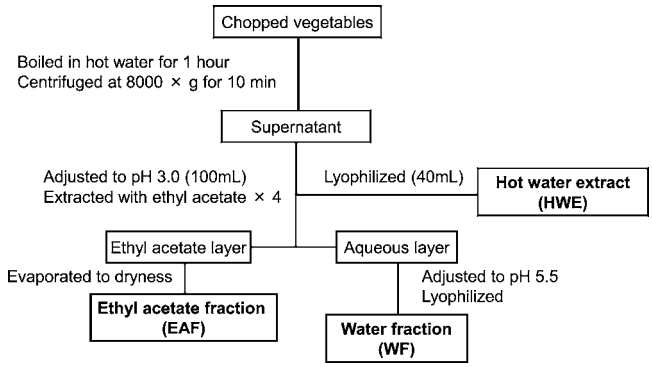

Figure 1. Preparation scheme of vegetable extracts.

was used as the "ethyl acetate fraction (EAF)" sample. The aqueous layer was adjusted to pH 5.5 by adding 2 M sodium hydroxide and lyophilized. The obtained lyophilized powder was used as the "water fraction (WF)" sample.

Chemicals. 3-Methylcholanthlene (3MC), 6-shogaol, 6-gingerol, 8-gingerol, and 10-gingerol were obtained from Wako Pure Chemical Industries. 8-Shogaol and 10-shogaol were obtained from ChromaDex (Irvine, CA, USA). Each phytochemical was dissolved in dimethyl sulfoxide (DMSO) at a concentration of 50 mM.

Luciferase Assay. The luciferase assay was carried out to assess AHR-mediated transcriptional activity as previously described.[17] The stable AHR-responsive HepG2 cells or HepG2/mock cells were seeded onto a 24-well plate (Corning-Coster Japan Product #3526, Tokyo, Japan) at a density of 1×10^5 cells/well. The 24-well plate was precoated with Type I-C collagen (Nitta Geratin, Osaka, Japan) for 30 min before the cells were seeded. After incubating overnight, the medium was replaced with a medium containing each test sample or 3MC (positive control). Each sample was diluted in the cell culture medium at the test concentration; the final concentration of DMSO was ≤0.1% (v/v) in the cell culture medium. After 24 h of culture, the cells were washed twice with 500 μL of PBS and then lysed with 100 μL of 1× passive lysis buffer (Promega). The lysate was centrifuged at 15000*g* for 5 min, and the supernatant was used for the luciferase assay. Luciferase activity was determined by a dual-luciferase reporter assay (Promega) with an LB9507 Lumet luminometer (Berthold Technologies, Bad Wildbad, Germany).

High-Performance Liquid Chromatography (HPLC) Analysis. The EAF from ginger and the standard phytochemicals were dissolved in methanol at concentrations of 10 mg/mL and 5 mM, respectively. HPLC analysis was performed using a photodiode array detector (L-2455, HITACH, Tokyo, Japan) and a PEGASIL-B ODS C18 column (250 mm × 4.6 mm, 4.6 μm; Senshu Scientific, Tokyo, Japan). The mobile phases were as follows: (a) acidified methanol (0.1% trifluoroacetic acid, TFA) and (b) acidified Milli-Q water (0.1% TFA). Pumps were programmed to perform the following gradient at a flow rate of 0.5 mL/min: from 20% solvent A to 80% solvent A over 50 min, to 100% solvent A at 55 min, and then to 0% solvent A at 60 min, with a column temperature of 35 °C. The separated compounds in the EAF were identified by comparison of the retention time and UV spectra to 6-shogaol or 6-gingerol standards.

Isolation of Total RNA and Real-Time PCR. The mRNA expression level of CYP1A1, UGT1A1, and ABCG 2, the target genes of AHR, was evaluated by real-time PCR. HepG2 cells were seeded onto a 24-well plate precoated with Type I-C collagen at a density of 1×10^5 cells/well. After overnight incubation, the medium was replaced with a medium containing 6-shogaol. After 24 h of culture, total RNA was extracted from the cells using Isogen. cDNA was prepared from 1 μg of the total RNA. Real-time PCR was performed with SYBR Premix Ex *Taq*II (TAKARA BIO INC., Otsu, Japan) and the 7900HT Fast Real-Time PCR System (Applied Biosystems, Tokyo, Japan). After denaturing at 95 °C for 30 s, PCR was performed for 40 cycles of denaturing at 95 °C for 5 s, annealing at 60 °C for 30 s, and dissociation at 95 °C for 15 s, followed by 60 °C for 60 s and 95 °C for

dx.doi.org/10.1021/jf405146j | J. Agric. Food Chem. 2014, 62, 5492−5499

Table 2. Primers Used for Real-Time PCR Analysis

Gene		Sequence (5′ → 3′)	T_m
ACTB (NM_001101)	Forward	TGGCACCCAGCACAATGAA	64.7
	Reverse	CTAAGTCATAGTCCGCCTAGAAGCA	62.3
CYP1A1 (NM_000499)	Forward	AGATGGTCAAGGAGCACTACA	69
	Reverse	CTGGACATTGGCGTTCTCAT	68
UGT1A1 (NM_000463)	Forward	TGGCTGTTCCCACTTACTGCAC	64.6
	Reverse	AGGGTCCGTCAGCATGACATC	64.7
ABCG2 (NM_001257386)	Forward	TGCCCAGGACTCAATGCAAC	64.5
	Reverse	TCGATGCCCTGCTTTACCAAATA	64.7

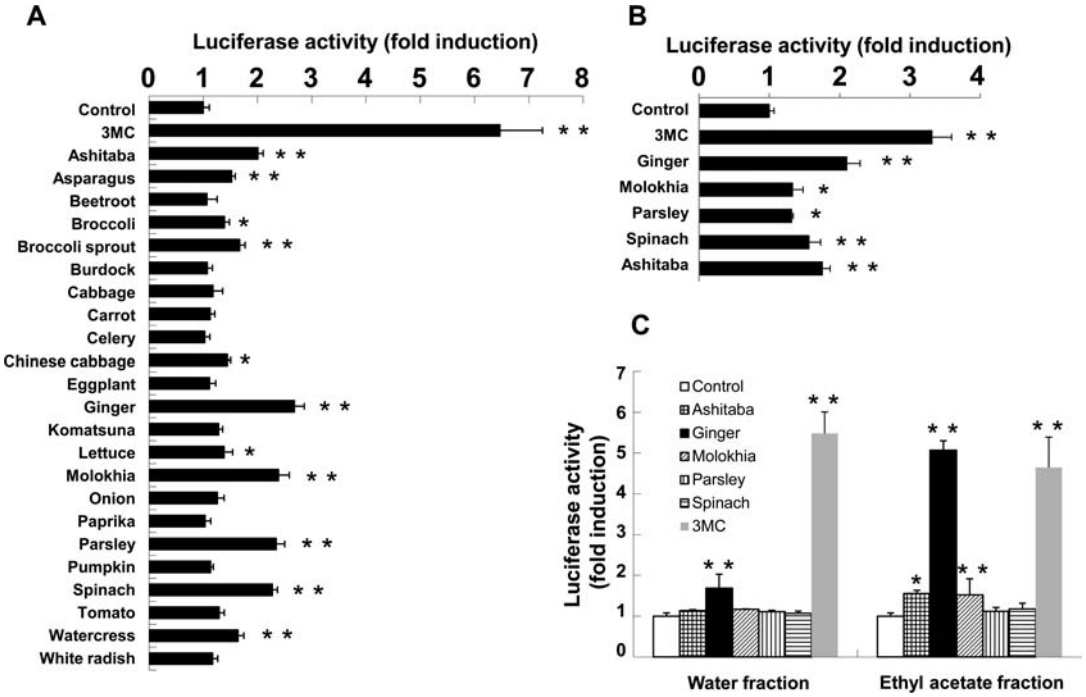

Figure 2. (A) Effects of the HWEs on AHR-mediated transcriptional activity. Stable AHR-responsive HepG2 cells were incubated with each HWE at 0.5 mg/mL for 24 h, and AHR-mediated transcriptional activity is shown as luciferase activity. Untreated cells were used as the control. (B) Effects of HWEs from ginger, molkhia, parsley, spinach, and ashitaba on AHR-mediated transcriptional activity corrected by AHR-nonspecific luciferase activity. Stable AHR-responsive HepG2 cells and HepG2/mock cells were incubated with each HWE at 0.25 mg/mL for 24 h, and AHR-mediated transcriptional activity is shown as luciferase activity. Luciferase activity in the stable AHR-responsive cells was divided by that in the HepG2/mock cells, and relative values were calculated. Untreated cells were used as the control. (C) Effects of EAFs and WFs from ginger, molkhia, parsley, spinach, and ashitaba on AHR-mediated transcriptional activity. Stable AHR-responsive HepG2 cells were incubated with each sample at 100 μg/mL for 24 h, and AHR-mediated transcriptional activity is shown as luciferase activity. The untreated and the 0.1% DMSO-treated cells were used as controls for WFs and EAFs, respectively. The relative luciferase activity measured for the control was taken as 1. 3MC was used as the positive control (5 μM). Each value is the mean ± SD (n = 3). Statistically significant differences from the value of the control were analyzed by the Dunnett's test; *p < 0.05; **p < 0.01.

15 s. The PCR primers used for CYP1A1 and UGT1A1 were synthesized at Invitrogen; the primers used for β-actin and ABCG 2 were synthesized at TAKARA BIO INC. The sequence of each primer is shown in Table 2.

Western Blot Analysis. HepG2 cells were seeded onto a 6-well plate precoated with Type I-C collagen at a density of 1×10^6 cells/well. After overnight incubation, the medium was replaced with a medium containing 6-shogaol. After 24 h of culture, cells were washed twice with PBS. Cells were scraped off and then suspended in 1 mL of PBS. The precipitate obtained by centrifugation at 1000g for 5 min at 4 °C was homogenized with 0.1 mL of RIPA lysis buffer (Santa Cruz Biotechnology, Santa Cruz, CA) with 0.1 mM phenylmethanesulfonyl fluoride, 0.1 mM sodium orthovanadate, and 0.1% protease inhibitor cocktail, and left on ice for 20 min. The homogenate was centrifuged at 18000g for 15 min at 4 °C. The resulting supernatant was dissolved in electrophoresis sample buffer (Santa Cruz Biotechnology) at 100 °C for 5 min.

Samples containing 30 μg of protein were loaded onto 12.5% polyacrylamide gel. Electrophoresis was conducted in an electrode buffer (25 mM Tris, 192 mM glycine, and 0.1% (w/v) SDS) with a fixed current (20 mA). An Immobilon polyvinylidene difloride (PVDF) membrane (Millipore, Bedford, MA) was treated with methanol and then blotting buffer (100 mM Tris, 192 mM glycine, and 20% methanol). The BioRad tank type of blotting apparatus was used for electrophoretic transfer of the gel to the PVDF membrane at 200 mM over 120 min.

After blotting, this PVDF membrane was blocked overnight at 4 °C by 0.1% Tween-20 and 5% skimmed milk dissolved in PBS. It was then incubated for 2 h with mouse monoclonal CYP1A1 antibody (1:100 dilution; sc-25304 Santa Cruz Biotechnology), or incubated for 1 h with mouse monoclonal β-Actin antibody (1:200 dilution; sc-47778 Santa Cruz Biotechnology) dissolved in a Can Get Signal immunoreaction enhancer solution (Toyobo, Japan). After the PVDF membrane had been washed three times with 0.1% Tween-20 dissolved in PBS for 5 min each, it was incubated for 1 h with

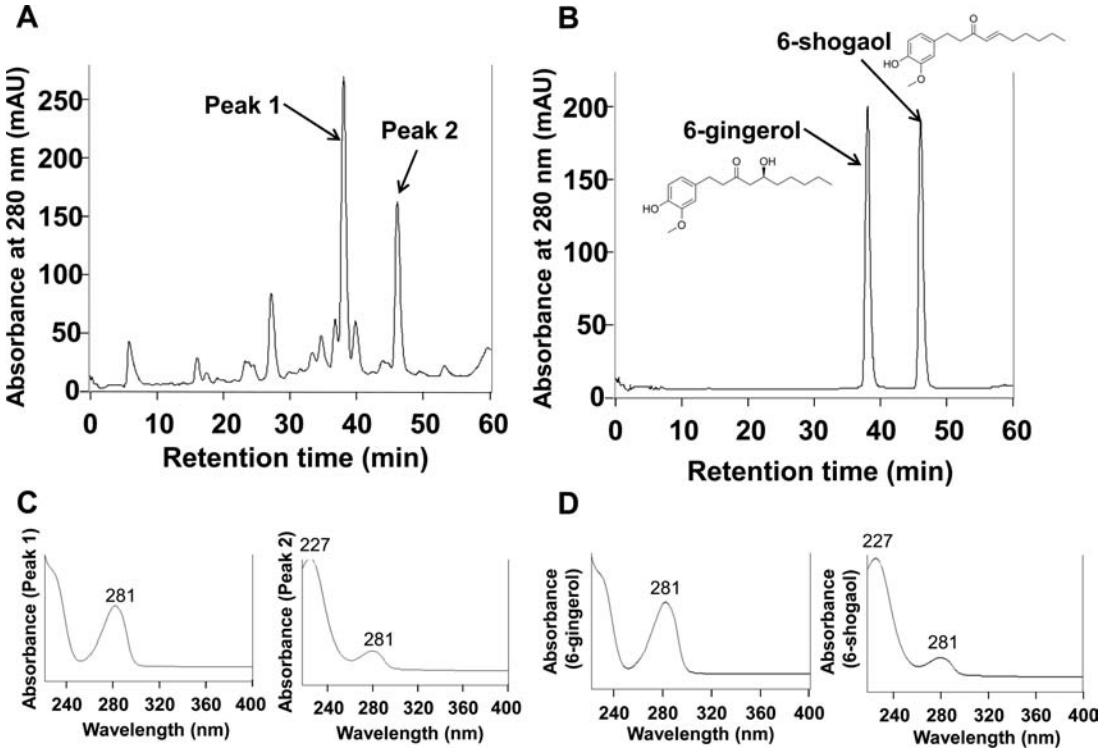

Figure 3. (A) HPLC profiles of the EAFs of ginger. (B) HPLC profiles and chemical structures of 6-gingerol and 6-shogaol. (C) UV spectra of peak 1 (left) and peak 2 (right). (D) UV spectra of 6-gingerol (left) and 6-shogaol (right).

antimouse immunoglobulin G-horseradish peroxidase (IgG-HRP; 1:2000 dilution; NA931, GE Healthcare, Buckinghamshire, U.K.) Proteins were detected by an ECL Prime Western Blotting Detection Reagent (GE Healthcare), followed by analysis with an LAS-1000 mini image analyzer and Multi Gauge Ver2.0 (Fuji Photo Film Co., Ltd., Tokyo, Japan).

Statistical Analysis. The data from the luciferase assay and real-time PCR were expressed as the mean ± SD. Statistical significance was analyzed using the Dunnett's test, and a p value of <0.05 was considered to indicate a statistically significant difference.

RESULTS

Effect of HWEs on AHR-Mediated Transcriptional Activity. HWEs from 11 vegetables significantly increased the relative luciferase activity as shown in Figure 2A. Among the 11 HWEs, five HWEs, namely ginger (2.68-fold induction), molokhia (2.3-fold induction), parsley (2.34-fold induction), spinach (2.27-fold induction), and ashitaba (2.01-fold induction), substantially increased the relative luciferase activity, showing more than a 2-fold induction compared with control. To confirm the results shown in Figure 2A, we further evaluated nonspecific induction of luciferase activity by the five HWEs using HepG2/mock cells. The stable AHR-responsive cells and HepG2/mock cells were treated with each HWE, and luciferase activity in the stable AHR-responsive cells was divided by that in the HepG2/mock cells. These data indicated that all five HWEs significantly induced luciferase activity (Figure 2B).

Effect of the EAFs and WFs from Ginger, Molokhia, Parsley, Spinach, and Ashitaba on AHR-Mediated Transcriptional Activity. As shown in Figure 2C, the EAF from ginger remarkably increased AHR-mediated transcriptional activity (5.07-fold induction). The EAFs from ashitaba and molokhia also significantly increased AHR-mediated transcriptional activity (1.56- and 1.52-fold induction, respectively). Only the WF from ginger significantly increased AHR-mediated transcriptional activity (1.69-fold induction).

HPLC Analysis of the EAF from Ginger. Since the EAF from ginger showed the highest AHR-mediated transcriptional activity (Figure 2C), it was further analyzed by HPLC. Two peaks (peak 1 and peak 2) appeared at retention times of 38 and 46 min (Figure 3A), which are the same retention times as those of 6-gingerol and 6-shogaol, respectively (Figure 3B). Figure 3C shows that the UV spectra of peaks 1 and 2 correspond to those of 6-gingerol and 6-shogaol (Figure 3D), respectively.

Effects of 6-Shogaol and 6-Gingerol on the Induction of AHR-Mediated Transcriptional Activity. Treatment of the stable AHR-responsive HepG2 cells with 6-shogaol for 24 h resulted in a significant increase in luciferase activity in a dose-dependent manner up to 50 μM (Figure 4A). On the other hand, treatment of the stable AHR-responsive HepG2 cells with 6-gingerol for 24 h had no effect on luciferase activity up to 50 μM (Figure 4B).

Effects of Gingerol and Shogaols on the Induction of AHR-Mediated Transcriptional Activity. Treatments of the stable AHR-responsive HepG2 cells with 6-, 8-, and 10-shogaol for 24 h resulted in significant increases of luciferase activity, and especially, 6- and 8-shogaol strongly increased luciferase activity (Figure 4C). On the other hand, treatments of the stable AHR-responsive HepG2 cells with 6-, 8-, and 10-gengerol for 24 h had no effects on luciferase activity.

mRNA Levels of AHR-Target Genes in HepG2 Cells after Treatment with Various Concentrations of 6-Shogaol. The expression levels of the AHR-target genes CYP1A1, UGT1A1, and ABCG 2 in HepG2 cells were measured by real-time PCR. Exposure of HepG2 cells to 6-shogaol significantly increased the expression level of CYP1A1 mRNA in a concentration-dependent manner up to 50 μM

dx.doi.org/10.1021/jf405146j | J. Agric. Food Chem. 2014, 62, 5492−5499

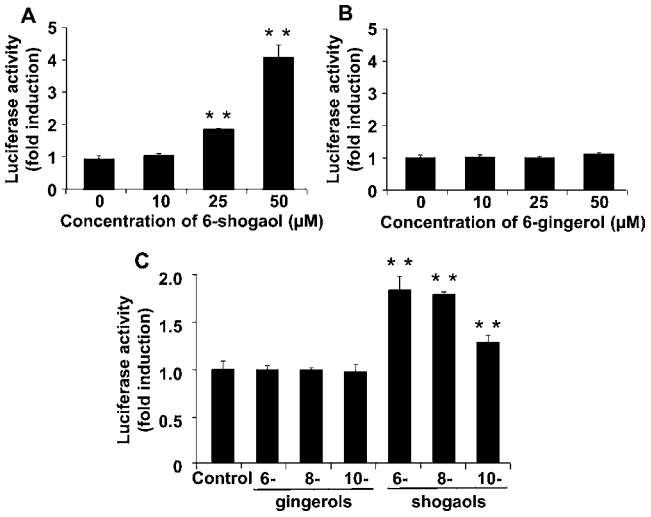

Figure 4. AHR-mediated transcriptional activity after treatment with various concentrations of 6-shogaol (A) and 6-gingerol (B). Stable AHR-responsive HepG2 cells were treated with 6-shogaol and 6-gingerol at the indicated concentrations for 24 h, and AHR-mediated transcriptional activity is shown as luciferase activity. The 0.1% DMSO-treated cells were used as the control. (C) Effects of gingerols and shogaols on the induction of AHR-mediated transcriptional activity in the stable AHR-responsive HepG2 cells. The stable AHR-responsive HepG2 cells were treated with each sample at 25 μM for 24 h, and AHR-mediated transcriptional activity is shown as luciferase activity. The 0.05% DMSO-treated cells were used as the control. The relative luciferase activity measured for the control was taken as 1. Each value is the mean ± SD (n = 3). Statistically significant differences from the value of the control were analyzed by the Dunnett's test; *p < 0.05; ** p < 0.01.

(Figure 5A). The expression levels of UGT1A1 and ABCG 2 indicated a significant increase after treatment of 6-shogaol only at 50 μM (Figure 5B, C).

Protein Level of CYP1A1 in HepG2 Cells after Treatment with Various Concentrations of 6-Shogaol. The protein expression levels of CYP1A1 in HepG2 cells were measured by Western blotting. Exposure of HepG2 cells to 6-shogaol increased the protein expression level of CYP1A1 to more than 2-fold of control by treatment with 25 and 50 μM 6-shogaol (Figure 5D).

DISCUSSION

Previous studies have reported that crude extracts of green tea, black tea, and propolis functioned as natural antagonists toward AHR.[18−20] Moreover, it was reported that extracts of vegetables, such as molokhia, suppressed AHR transformation in cell-free systems.[21] However, these reports focused on the suppressive effect of food extracts on AHR activation. De Waard et al. suggested that extracts of citrus pulp and grapefruit juice contained natural AHR agonists,[22] but detailed studies on AHR activation by vegetable extracts have not yet been reported. We examined the effect of HWEs from various vegetables on AHR-mediated transcriptional activity by the luciferase assay using the stable AHR-responsive HepG2 and HepG2/mock cell lines. The results showed that the HWEs from ginger, molokhia, parsley, spinach, and ashitaba increased AHR-mediated transcriptional activity (Figure 2A, B). These five HWEs increased the luciferase activity in a dose-dependent manner at concentrations of 0.5, 1.0, and 2.0 mg/mL (data not shown). In this study, the HWE from molokhia induced AHR-mediated transcriptional activity, even though the molokhia extract has previously been suggested to be an AHR

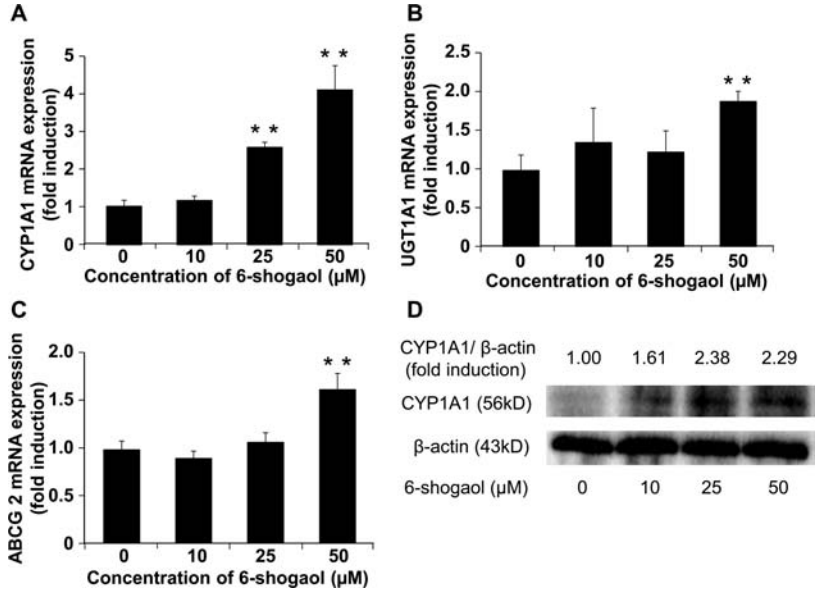

Figure 5. mRNA and protein expression levels of AHR-target genes in HepG2 cells after treatment with various concentrations of 6-shogaol. HepG2 cells were treated with 6-shogaol at the indicated concentrations for 24 h. Total RNA from the cells were extracted, and mRNA expression levels of CYP1A1 (A), UGT1A1 (B), and ABCG 2 (C) were evaluated by real-time PCR. The 0.1% DMSO-treated cells were used as the control. The mRNA levels of AHR-target genes were normalized to those of β-actin mRNA, and the relative mRNA expression measured for the control was taken as 1. Each value is the mean ± SD (n = 6). Statistically significant differences from the value of the control were analyzed by the Dunnett's test; **p < 0.01. (D) Protein level of CYP1A1 in HepG2 cells after treatment with various concentrations of 6-shogaol. HepG2 cells were treated with 6-shogaol at the indicated concentrations for 24 h, and the protein expression level of CYP1A1 was evaluated byWestern blotting. The 0.1% DMSO-treated cells were used as the control. The protein expression level of CYP1A1 was normalized to those of β-actin, and the relative protein expression measured for the control was taken as 1.

antagonist.[21] Molokhia contains quercetin in abundance,[23] which could function as an AHR antagonist[11] or an AHR agonist.[12,24] Therefore, compounds in molokhia such as quercetin could cause contradictory results. The results presented in this study are the first to indicate that some vegetable extracts can increase AHR-mediated transcriptional activity.

Our data indicated that the HWEs from five vegetables contained compounds that may activate AHR. We evaluated the AHR-mediated transcriptional activity of the WFs and EAFs of each vegetable to delineate the active compound in each HWE. Because HWEs were crude extracts, we used the HepG2/MOCK cell line to exclude nonspecific luciferase activity. Since nonspecific luciferase activity was not observed (Figure 2B), we did not use the HepG2/MOCK cell line in subsequent experiments. The luciferase assay using ethyl acetate and water fraction from all five vegetables showed that parsley and spinach had no activity in both fractions. In addition, the ethyl acetate fractions from molokhia and ashitaba had much less activity than that from ginger (Figure 2C), so we focused on the identification of active compounds in ginger. Therefore, to further identify the AHR-activating compounds, we analyzed this fraction by HPLC.

Shogaols and gingerols are the main compounds in ginger and ginger products, and 6-shogaol and 6-gingerol are the main components,[25−28] so we analyzed the EAF from ginger, 6-shogaol, and 6-gingerol. We showed that two major peaks appeared at retention times of 38 and 46 min (Figure 3A), and these peaks corresponded to the peaks of 6-gingerol and 6-shogaol, respectively (Figure 3B, C, D). This data suggested that 6-gingerol and 6-shogaol were the main compounds in EAF from ginger. Shogaols are compounds formed by dehydrating gingerols, and they are not thought to be present in fresh rhizome.[25,26] Gingerols are not stable during storage or thermal processing, and they generate shogaols.[25,26] It was suggested that the 6-shogaol detected in the EAF from ginger in this study resulted from the conversion of 6-gingerol to 6-shogaol during the extraction in hot water.

Treatment of the stable AHR-responsive HepG2 cells with 6-shogaol for 24 h resulted in significant increases in luciferase activity in a dose-dependent manner (Figure 4A). These data are the first to verify induction of AHR-mediated transcriptional activity by 6-shogaol. More interestingly, 6-gingerol had no effect on AHR-mediated transcriptional activity (Figure 4B). 6-Shogaol has been reported to have a much stronger inhibitory effect on the growth of various cancer cell lines than 6-gingerol.[29−31] Koliopanos et al. and Peng et al. reported that AHR agonists inhibited the growth of cancer cells.[32,33] Our finding that 6-shogaol, but not 6-gingerol, is a strong AHR activator may explain why 6-shogaol has a stronger inhibitory effect on the growth of cancer cells.

We think that only evaluation of the activities of the two most abundant components in ginger was insufficient to identify the active compounds in ginger. Therefore, 8-shogaol, 10-shogaol, 8-gingerol, and 10-gingerol, the major compounds in ginger other than 6-shogaol and 6-gingerol, were used for the luciferase assay. Figure 4C shows that 8-shogaol had the same activity as 6-shogaol, but 8-shogaol was not detected in the HPLC chromatogram of EAF from ginger shown in Figure 3A. These results show that 6-shogaol is the most major activator of AHR among shogaols and gingerols. Moreover, the concentration of 6-shogaol in the solution of EAF from ginger (100 μg/mL) was calculated to be about 27 μM by HPLC analysis (data not shown). In this study, the AHR-mediated transcriptional activity was 4−5 fold induction when 100 μg/mL of the EAF from ginger was used, whereas the transcriptional activity was about 2-fold induction when 25 μM of 6-shogaol was used. Based on these data, the activity of 6-shogaol accounted for about 50% of activity, so 6-shogaol is thought to be the most major activator of AHR in ginger.

6-Shogaol induced mRNA expression of the following AHR-target genes: phase I metabolic enzyme CYP1A1, phase II metabolic enzyme UGT1A1, and phase III metabolic enzyme ABCG 2 (Figure 5A, B, C) and protein expression of CYP1A1 (Figure 5D). These are the first data indicating that 6-shogaol induced expression of detoxification enzymes. Liska reported that a multifunctional inducer in detoxification systems was important.[1] Indeed, we have demonstrated the usefulness of 6-shogaol as a multifunctional inducer in this report.

The AHR has been found to favor hydrophobic molecular with a quasi-planar structure and to accommodate a ligand-binding pocket of approximately 14 × 12 × 5 Å.[34,35] Some flavonoids that induce AHR activity have molecular sizes and planar structures that could bind to a ligand-binding pocket of AHR.[10] Although there is no report about the detailed structure analysis of 6-shogaol, based on its structure, we guess that the molecular size of 6-shogaol is smaller than that of flavonoids and that 6-shogaol may bind to a ligand-binding pocket of AHR. Moreover, shogaols, but not gingerols, induced AHR activity in this study. Unlike gingerols, shogaols have the α,β-unsaturated ketone group. Compounds having this structure are good substrates for Michael addition reactions and are rendered electrophilic by conjugation with electron-withdrawing groups.[36] This difference of electrophilic nature based on the structures of shogaols and gingerols may cause the difference of AHR activities. Another possible mechanism of AHR activation by 6-shogaol is the effect of its metabolites. We evaluated the AHR-mediated transcriptional activity and mRNA expression of AHR-target genes by treatment of cells with 6-shogaol for 24 h. Most 6-shogaol has been shown to be metabolized to other reduced forms within 24 h in various cancer cell lines, and these metabolites retain their bioactivity.[37−39] Recently, the cysteine-conjugated metabolite of 6-shogaol, 5-cysteinyl-6-shogaol, exerts its bioactivity by acting as a carrier of 6-shogaol in cancer cells and showed strong growth inhibitory effects toward cancer cells.[39] These bioactive metabolites of 6-shogaol may contribute to induction of AHR activity. Further experiments are necessary to reveal whether or not the bioactive metabolites of 6-shogaol also exhibit induction of AHR-mediated transcriptional activity and mRNA expression of AHR-target genes.

We revealed for the first time that ginger more strongly induced AHR-mediated transcription compared to other vegetables such as molokhia, parsley, spinach, and ashitaba. We also found that 6-shogaol was the major active compound in ginger. The mRNA expression levels of AHR-targeting drug-metabolizing enzymes (CYP1A1, UGT1A1, ABCG 2) and the protein level of CYP1A1 in HepG2 cells were induced by 6-shogaol. These results are the first verification of AHR-mediated regulation of detoxification systems by 6-shogaol. This study suggests that AHR-mediated modulation of detoxification systems can be expected in the presence of 6-shogaol, although in vivo studies are needed to clarify whether AHR will be activated by the intake of 6-shogaol.

AUTHOR INFORMATION

Corresponding Author

*Tel: +81-287-36-2935. Fax +81-287-39-1038. E-mail: Kazutaka_Yoshida@kagome.co.jp.

Notes

The authors declare no competing financial interest.

REFERENCES

(1) Liska, D. J. The detoxification enzyme systems. *Altern. Med. Rev.* **1998**, *3*, 187−198.

(2) Nakata, K.; Tanaka, Y.; Nakano, T.; Adachi, T.; Tanaka, H.; Kaminuma, T.; Ishikawa, T. Nuclear receptor-mediated transcriptional regulation in Phase I, II, and III xenobiotic metabolizing systems. *Drug. Metab. Pharmacokinet.* **2006**, *21*, 437−457.

(3) Pohjanvirta, R.; Tuomisto, J. Short-term toxicity of 2,3,7,8-tetrachlorodibenzo-p-dioxinin laboratory animals: effects, mechanisms, and animal models. *Pharmacol. Rev.* **1994**, *46*, 483−549.

(4) Crews, S. T. Control of cell lineage-specific development and transcription by bHLH-PAS proteins. *Genes Dev.* **1998**, *12*, 607−620.

(5) Whitlock, J. P., Jr. Induction of cytochrome P4501A1. *Annu. Rev. Pharmacol. Toxicol.* **1999**, *39*, 103−125.

(6) Yueh, M. F.; Huang, Y. H.; Hiller, A.; Chen, S.; Nguyen, N.; Tukey, R. H. Involvement of the xenobiotic response element (XRE) in Ah receptor-mediated induction of human UDP-glucuronosyltransferase 1A1. *J. Biol. Chem.* **2003**, *278*, 15001−15006.

(7) Auyeung, D. J.; Kessler, F. K.; Ritter, J. K. Mechanism of rat UDP-glucuronosyltransferase 1A6 induction by oltipraz: evidence for a contribution of the aryl hydrocarbon receptor pathway. *Mol. Pharmacol.* **2003**, *63*, 119−127.

(8) Tan, K. P.; Wang, B.; Yang, M.; Boutros, P. C.; Macaulay, J.; Xu, H.; Chuang, A. I.; Kosuge, K.; Yamamoto, M.; Takahashi, S.; Wu, A. M.; Ross, D. D.; Harper, P. A.; Ito, S. Aryl hydrocarbon receptor is a transcriptional activator of the human breast cancer resistance protein (BCRP/ABCG2). *Mol. Pharmacol.* **2010**, *78*, 175−185.

(9) Ebert, B.; Seidel, A.; Lampen, A. Phytochemicals induce breast cancer resistance protein in Caco-2 cells and enhance the transport of benzo[a]pyrene-3-sulfate. *Toxicol. Sci.* **2007**, *96*, 227−236.

(10) Amakura, Y.; Tsutsumi, T.; Nakamura, M.; Kitagawa, H.; Fujino, J.; Sasaki, K.; Toyoda, M.; Yoshida, T.; Maitani, T. Activation of the aryl hydrocarbon receptor by some vegetable constituents determined using in vitro reporter gene assay. *Biol. Pharm. Bull.* **2003**, *26*, 532−539.

(11) Zhang, S.; Qin, C.; Safe, S. H. Flavonoids as aryl hydrocarbon receptor agonists/antagonists: effects of structure and cell context. *Environ. Health. Perspect.* **2003**, *111*, 1877−1882.

(12) Wang, H. K.; Yeh, C. H.; Iwamoto, T.; Satsu, H.; Shimizu, M.; Totsuka, M. Dietary flavonoid naringenin induces regulatory T cells via an aryl hydrocarbon receptor mediated pathway. *J. Agric. Food Chem.* **2012**, *60*, 2171−2178.

(13) Heath-Pagliuso, S.; Rogers, W. J.; Tullis, K.; Seidel, S. D.; Cenijn, P. H.; Brouwer, A.; Denison, M. S. Activation of the Ah receptor by tryptophan and tryptophan metabolites. *Biochemistry* **1998**, *37*, 11508−10515.

(14) Degner, S. C.; Papoutsis, A. J.; Selmin, O.; Romagnolo, D. F. Targeting of aryl hydrocarbon receptor-mediated activation of cyclooxygenase-2 expression by the indole-3-carbinol metabolite 3,3′-diindolylmethane in breast cancer cells. *J. Nutr.* **2009**, *139*, 26−32.

(15) Ciolino, H. P.; Daschner, P. J.; Wang, T. T.; Yeh, G. C. Effect of curcumin on the aryl hydrocarbon receptor and cytochrome P450 1A1 in MCF-7 human breast carcinoma cells. *Biochem. Pharmacol.* **1998**, *56*, 197−206.

(16) Satsu, H.; Yoshida, K.; Mikubo, A.; Ogiwara, H.; Inakuma, T.; Shimizu, M. Establishment of a stable aryl hydrocarbon receptor-responsive HepG2 cell line. *Cytotechnology* **2014**, *Mar 26*, Epub ahead of print.

(17) Hamada, M.; Satsu, H.; Natsume, Y.; Nishiumi, S.; Fukuda, I.; Ashida, H.; Shimizu, M. TCDD-induced CYP1A1 expression, an index of dioxin toxicity, is suppressed by flavonoids permeating the human intestinal Caco-2 cell monolayers. *J. Agric. Food Chem.* **2006**, *54*, 8891−8898.

(18) Williams, S. N.; Shih, H.; Guenette, D. K.; Brackney, W.; Denison, M. S.; Pickwell, G. V.; Quattrochi, L. C. Comparative studies on the effects of green tea extracts and individual tea catechins on human CYP1A gene expression. *Chem. Biol. Interact.* **2000**, *128*, 211−229.

(19) Fukuda, I.; Sakane, I.; Yabushita, Y.; Sawamura, S.; Kanazawa, K.; Ashida, H. Black tea extract suppresses transformation of aryl hydrocarbon receptor induced by dioxin. *Biofactors* **2004**, *21*, 367−369.

(20) Park, Y. K.; Fukuda, I.; Ashida, H.; Nishiumi, S.; Guzman, J. P.; Sato, H. H.; Pastore, G. M. Suppression of dioxin mediated aryl hydrocarbon receptor transformation by ethanolic extracts of propolis. *Biosci. Biotechnol. Biochem.* **2004**, *68*, 935−938.

(21) Nishiumi, S.; Yabushita, Y.; Fukuda, I.; Mukai, R.; Yoshida, K.; Ashida, H. Molokhia (Corchorus olitorius L.) extract suppresses transformation of the aryl hydrocarbon receptor induced by dioxins. *Food Chem. Toxicol.* **2006**, *44*, 250−260.

(22) De Waard, W. J.; Aarts, J. M.; Peijnenburg, A. A.; Baykus, H.; Talsma, E.; Punt, A.; de Kok, T. M.; van Schooten, F. J.; Hoogenboom, L. A. Gene expression profiling in Caco-2 human colon cells exposed to TCDD, benzo[a]pyrene, and natural Ah receptor agonists from cruciferous vegetables and citrus fruits. *Toxicol. In Vitro* **2008**, *22*, 396−410.

(23) Azuma, K.; Nakayama, M.; Koshioka, M.; Ippoushi, K.; Yamaguchi, Y.; Kohata, K.; Yamauchi, Y.; Ito, H.; Higashio, H. Phenolic antioxidants from the leaves of Corchorus olitorius L. *J. Agric. Food. Chem.* **1999**, *47*, 3963−3966.

(24) Ciolino, H. P.; Daschner, P. J.; Yeh, G. C. Dietary flavonols quercetin and kaempferol are ligands of the aryl hydrocarbon receptor that affect CYP1A1 transcription differentially. *Biochem. J.* **1999**, *340*, 715−722.

(25) Govindarajan, V. S. Ginger—chemistry, technology, and quality evaluation: part 1. *Crit. Rev. Food Sci. Nutr.* **1982**, *17*, 1−96.

(26) Ravindran, P. N. *Ginger. The Genus Zingiber*; CRC Press: Boca Raton, FL, 2005.

(27) Shao, X.; Lv, L.; Parks, T.; Wu, H.; Ho, C. T.; Sang, S. Quantitative analysis of ginger components in commercial products using liquid chromatography with electrochemical array detection. *J. Agric. Food Chem.* **2010**, *58*, 12608−12614.

(28) Ali, B. H.; Blunden, G.; Tanira, M. O.; Nemmar, A. Some phytochemical, pharmacological and toxicological properties of ginger (Zingiber officinale Roscoe): a review of recent research. *Food Chem. Toxicol.* **2008**, *46*, 409−420.

(29) Rhode, J.; Fogoros, S.; Zick, S.; Wahl, H.; Griffith, K. A.; Huang, J.; Liu, J. R. Ginger inhibits cell growth and modulates angiogenic factors in ovarian cancer cells. *BMC Complement Altern. Med.* **2007**, *7*, 44.

(30) Kim, J. S.; Lee, S. I.; Park, H. W.; Yang, J. H.; Shin, T. Y.; Kim, Y. C.; Baek, N. I.; Kim, S. H.; Choi, S. U.; Kwon, B. M.; Leem, K. H.; Jung, M. Y.; Kim, D. K. Cytotoxic components from the dried rhizomes of Zingiber officinale Roscoe. *Arch. Pharm. Res.* **2008**, *31*, 415−418.

(31) Sang, S.; Hong, J.; Wu, H.; Liu, J.; Yang, C. S.; Pan, M. H.; Badmaev, V.; Ho, C. T. Increased growth inhibitory effects on human cancer cells and anti-inflammatory potency of shogaols from Zingiber officinale relative to gingerols. *J. Agric. Food Chem.* **2009**, *57*, 10645−10650.

(32) Koliopanos, A.; Kleeff, J.; Xiao, Y.; Safe, S.; Zimmermann, A.; Büchler, M. W.; Friess, H. Increased arylhydrocarbon receptor expression offers a potential therapeutic target for pancreatic cancer. *Oncogene* **2002**, *21*, 6059−6070.

(33) Peng, T. L.; Chen, J.; Mao, W.; Liu, X.; Tao, Y.; Chen, L. Z.; Chen, M. H. Potential therapeutic significance of increased expression of aryl hydrocarbon receptor in human gastric cancer. *World J. Gastroenterol.* **2009**, *15*, 1719−1729.

(34) Gillner, M.; Bergman, J.; Cambillau, C.; Fernström, B.; Gustafsson, J. A. Interactions of indoles with specific binding sites

for 2,3,7,8-tetrachlorodibenzo-p-dioxin in rat liver. *Mol. Pharmacol.* **1985**, *28*, 357−363.
(35) Gasiewicz, T. A.; Kende, A. S.; Rucci, G.; Whitney, B.; Willey, J. J. Analysis of structural requirements for Ah receptor antagonist activity: ellipticines, flavones, and related compounds. *Biochem. Pharmacol.* **1996**, *52*, 1787−1803.
(36) Talalay, P. Mechanisms of induction of enzymes that protect against chemical carcinogenesis. *Adv. Enzyme Regul.* **1989**, *28*, 237−250.
(37) Chen, H.; Lv, L.; Soroka, D.; Warin, R. F.; Parks, T. A.; Hu, Y.; Zhu, Y.; Chen, X.; Sang, S. Metabolism of [6]-shogaol in mice and in cancer cells. *Drug Metab. Dispos.* **2012**, *40*, 742−753.
(38) Zhu, Y.; Warin, R. F.; Soroka, D. N.; Chen, H.; Sang, S. Metabolites of ginger component [6]-shogaol remain bioactive in cancer cells and have low toxicity in normal cells: chemical synthesis and biological evaluation. *PLoS One* **2013**, *8*, e54677.
(39) Chen, H.; Soroka, D. N.; Zhu, Y.; Hu, Y.; Chen, X.; Sang, S. Cysteine-conjugated metabolite of ginger component [6]-shogaol serves as a carrier of [6]-shogaol in cancer cells and in mice. *Chem. Res. Toxicol.* **2013**, *26*, 976−985.

JOURNAL OF AGRICULTURAL AND FOOD CHEMISTRY

Article

pubs.acs.org/JAFC

Naturally Occurring Angiotensin I-Converting Enzyme Inhibitory Peptide from a Fertilized Egg and Its Inhibitory Mechanism

Xiang Duan,[†,‡] Fengfeng Wu,[†,‡] Mei Li,[†,‡] Na Yang,[†,‡] Chunsen Wu,[†,‡] Yamei Jin,[†,‡] Jingjing Yang,[†] Zhengyu Jin,[†,‡] and Xueming Xu*[,†,‡]

[†]State Key Laboratory of Food Science and Technology, and [‡]School of Food Science and Technology, Jiangnan University, 1800 Lihu Road, Wuxi Jiangsu 214122, People's Republic of China

ABSTRACT: This study was performed to investigate the angiotensin I-converting enzyme (ACE) inhibitory activity of peptides derived from fertilized eggs and elucidate the inhibition mechanism of these peptides. During incubation, ACE inhibitory activity of the peptides remained stable before day 12 and then increased markedly on day 15. Two ACE inhibitory peptides, VGVIKAVDKKAGGAGKVT and HLFGPPGKKDPV, were purified from peptides on day 15 by consecutive chromatography. Because HLFGPPGKKDPV possessed a higher ACE inhibitory activity (IC_{50} = 125 μM), an antihypertensive effect of this peptide was further evaluated *in vivo*. The result showed that this peptide had an antihypertensive effect in spontaneously hypertensive rats (SHRs) at a dosage of 10 mg/kg. Furthermore, Lineweaver−Burk plots suggested that HLFGPPGKKDPV played as a non-competitive inhibitor against ACE, as supported by docking simulation. These data indicated that a fertilized egg has potential as antihypertensive components in functional foods and nutraceuticals.

KEYWORDS: *ACE inhibitory peptide, fertilized egg, inhibitory pattern, molecular docking, spontaneously hypertensive rat*

INTRODUCTION

Hypertension is one of the major risk factors for the development of cardiovascular diseases, stroke, and the end stage of renal disease.[1] Treatment of hypertension is an effective way to reduce the risk of these diseases.[2] The renin−angiotensin system (RAS) plays a key role in maintaining blood pressure homeostasis.[3] Angiotensin I-converting enzyme (ACE) is a key enzyme in RAS; it raises blood pressure by converting the inactive decapeptide angiotensin I to the potent vasoconstrictor octapeptide angiotensin II as well as inactivating the vasodilating nonapeptide bradykinin.[4] Therefore, inhibition of ACE is considered as an effective approach to controlling hypertension.[1] Since the discovery of ACE inhibitors in snake venom,[5] many chemical ACE inhibitors, such as captopril, enalapril, alacepril, and lisinopril, were designed.[6] However, these chemical ACE inhibitors are known to have various side effects, such as coughing, skin rashes, and angioedema.[7,8] Therefore, many studies have been initiated to develop novel, safe, and natural ACE inhibitors from natural sources.[9,10] In recent years, several ACE inhibitory peptides have been isolated from a wide range of food sources, such as gelatin,[11] casein,[12] tuna,[13] corn,[14] soy beans,[15] egg white,[16] and dried bonito.[17]

For a better understanding of inhibitory properties of peptides, the structure−activity relationship should be clarified. Terashima et al.[18] investigated a series of peptides derived from an ACE inhibitory peptide (VTVNPYKWLP) and concluded that the Pro residue in the C-terminal end strongly enhanced ACE inhibition activity. In addition, the length of peptides also played a key role in ACE inhibitory ability.[19] Recently, Wu et al.[20] have contructed a database consisting of 168 dipeptides and 140 tripeptides to study the quantitative structure−activity relationships of ACE inhibitory peptides. It showed that amino acid residues with bulky side chains as well as hydrophobic side chains were preferred for dipeptides, while for tripeptides, the most favorable residues for C terminus, middle position, and N terminus were aromatic amino acids, positively charged amino acids, and hydrophobic amino acids, respectively. However, these structure−activity correlation studies were mainly based on amino acid sequence analysis. In recent years, the crystal structures of ACE and its inhibitors have been analyzed to elucidate the relationship between the inhibition mechanism and the molecular structure of inhibitors.[21−23] These studies provided a new method to analyze the structure−activity relationship of ACE inhibitory peptides.

Traditionally, fertilized eggs are widely considered as natural dietary supplements in many Asian countries.[24] During chick embryonic development, RAS plays a principal role in regulation of blood pressure.[25] Savary et al.[25] reported that ACE was produced at a very early stage and its activity increased during incubation. Whether naturally occurring peptides derived from fertilized eggs have ACE inhibitory effect is still unknown. To our knowledge, this is the first research to investigate ACE inhibitory activity and the structure−activity relationship of the peptides from fertilized eggs. Because the fertilized eggs that are eaten by Asian consumers are commonly 12-day-old eggs,[26] the fertilized eggs before day 15 of incubation were chosen for investigation in this paper.

The objectives of the present study were to (1) determine ACE inhibitory activity of peptides derived from fertilized eggs and (2) investigate the inhibition mechanism of a purified ACE inhibitory peptide.

Received: November 20, 2013
Revised: May 19, 2014
Accepted: May 27, 2014
Published: May 27, 2014

ACS Publications © 2014 American Chemical Society

dx.doi.org/10.1021/jf501368a | *J. Agric. Food Chem.* 2014, 62, 5500−5506

MATERIALS AND METHODS

Materials. The fertilized eggs on days 3, 6, 9, 12, and 15 of the incubation period were prepared and lyophilized on the basis of our previous work.[27] The spontaneously hypertensive rats (SHRs, 10 weeks old, male, specific pathogen-free, 180−240 g of body weight) with tail systolic blood pressure (SBP) over 180 mmHg were obtained from Shanghai Slaccas Laboratory Animal Co., Ltd. (Shanghai, China). All animal protocols in this study adhered to the *Guide for the Care and Use of Laboratory Animals* (Ministry of Science and Technology of the People's Republic of China [(2006)398]) and were approved by the Ethics Committee of Jiangnan University, China (JN 28 2013). The testing chemicals including ACE (from rabbit lung) and substrate peptide hippuryl-L-histidyl-L-leucine (HHL) were purchased from Sigma Chemical Co. (St. Louis, MO). All other reagents were of analytical grade (Shanghai Chemical Reagents Co., Shanghai, China).

Preparation of Naturally Occurring Peptides. Peptides were prepared with the method described by Park et al.,[28] with some modification. The lyophilized egg samples (1.0 g) were prepared in 100 mL of Milli-Q water. After centrifugation at 10000*g* for 20 min at 4 °C, the supernatant was microfiltered through a 0.45 μm membrane and then ultrafiltrated through a 3 kDa cellulose membrane (Amicon, Beverly, MA). The filtrates were lyophilized and then stored at −20 °C until use.

Assay of ACE Inhibitory Activity. The ACE inhibitory activity assay was performed with the method described by Terashima et al.[29] Peptides (50 μL, 10 mg/mL in deionized water) with 50 μL of ACE solution (25 mU/mL) were preincubated at 37 °C for 10 min, and the mixture was then incubated with 50 μL of substrate (8.3 mM HHL in 50 mM sodium borate buffer containing 0.5 M NaCl at pH 8.3) for 60 min at the same temperature. The reaction was terminated by the addition of 1.0 M HCl (200 μL). The reaction mixture was filtered with Millex-LG (Nihon Millipore Co., Ltd., Tokyo, Japan), and 10 μL of the filtrates was injected into the high-performance liquid chromatography (HPLC) system (Shimadzu LC-10 AD, Shimadzu, Kyoto, Japan) equipped with a hydrophobic column (Cosmosil 5C18-MS-II, 4.6 × 150 mm). An isocratic mobile phase composed of 80% Milli-Q water containing 0.1% (v/v) trifluoroacetic acid and 20% acetonitrile containing 0.1% (v/v) trifluoroacetic acid was used at a flow rate of 1.0 mL/min. Peak areas for hippuric acid (HA) generated by the ACE reaction was monitored at 228 nm with a detector (Shimadzu SPD-20A). ACE inhibitory activity was obtained by the following equation:

ACE inhibitory activity (%) = $[(V_m - V_{in})/V_m] \times 100$, where V_m was the peak area without the sample solution and V_{in} was that with the sample solution.

Purification of ACE Inhibitory Peptides. The ACE inhibitory peptides were purified according to the method described in our previous work.[27] Briefly, on the basis of the ACE inhibition result, the peptides on day 15 showed the strongest inhibitory activity and, thus, were employed for purification of ACE inhibitory peptide. The lyophilized peptides on day 15 were loaded onto a Mono Q 5/50 GL ion-exchange column with the ÄKTA purifier system (Amersham Pharmacia Biotech, Uppsala, Sweden) equilibrated with 20 mM Tris−HCl (pH 8.0) and eluted with a linear gradient of NaCl (0−1.0 M) in the same buffer at a flow rate of 2 mL/min. Each fraction was monitored at 280 nm, collected, and lyophilized for ACE inhibitory activity assay at a concentration of 1 mg/mL. The lyophilized fraction having the highest activity was further dissolved in phosphate buffer (0.05 M sodium phosphate and 0.15 M NaCl at pH 7.2) and subjected to a Superdex Peptide 10/300GL column at a flow rate of 0.5 mL/min. Each peak was collected and lyophilized, and ACE inhibitory activity was also investigated at a concentration of 1 mg/mL. The most active fraction was lyophilized for further research.

Identification and Synthesis of the Purified Peptide. The fraction with the strongest inhibitory activity was dissolved in 0.1% formic acid in deionized water for liquid chromatography−tandem mass spectrometry (LC−MS/MS) analysis. LC−MS/MS analysis was performed using a LTQ mass spectrometer (Thermo Electron, Bremen, Germany) coupled with a a nanoelectrospray ionization source. Samples were loaded onto a reversed-phase C18 column with a diameter of 0.15 mm × 10 cm and particle size of 5 μm. Separation of the peptides was performed using a gradient going from 5 to 90% acetonitrile in 0.1% formic acid over 40 min. The MS/MS raw data were acquired using Thermo-Xcalibur data acquisition, and the acquired data were searched against the NCBI chicken-specific database using SEQUEST software (Bioworks 3.1 package, Thermo Electron). Peptides were searched using the following parameters: peptide tolerance, 2.0 amu; enzyme, trypsin (KR/P); enzyme limits, fully enzymatic (cleaves at both ends); and maximum missed cleavages, 2. The filtering criterion were set as $\Delta C_n \geq 0.1$, and $X_{corr} \geq 1.9$ with charge state 1+, $X_{corr} \geq 2.2$ with charge state 2+, and $X_{corr} \geq 3.75$ with charge state 3+ were used as a cutoff for peptide identification.

To investigate the antihypertensive activity and inhibition pattern of peptides, the solid-phase technique was used to synthesize the purified peptides on a peptide synthesizer (Symphony, Protein Technologies, Inc., Tucson, AZ). [(9-Fluorenylmethyl)oxy]carbonyl (FMOC) amino acids were successively coupled in the presence of 2-(1*H*-benzotriazol-1-yl)-1,1,3,3-tetramethyluronium hexafluorophosphate (HBTU). ACE inhibitory activity of the synthesized peptides were investigated according to the above-described method. The IC_{50} value was the concentration of the sample that inhibited 50% of the ACE activity.

Antihypertensive Action in Spontaneously Hypertensive Rats. Conscious SHRs were housed individually in steel cages in a room kept at 25 °C with a 12 h light−dark cycle and fed a standard laboratory diet. Tap water was freely available. The purified peptide was dissolved in saline at a dose of 10 mg/kg of body weight and injected orally using a metal gastric zoned in SHR. Antihypertensive activity of P2 was evaluated by measuring the change of systolic blood pressure (SBP) at 1, 2, 3, 6, 9, 22, and 24 h after oral administration of 10 mg/kg of body weight. The lowering efficacy of the peptide on SBP was compared to that of captopril (10 mg/kg). Control rats were administrated with the same volume of saline solution. Following oral administration, SBP was measured by tail-cuff method with a CODA monitor (Kent Scientific Corporation, Torrington, CT) after warming up SHR in a chamber maintained at 37 °C for 10 min.

Determination of the Inhibition Pattern on ACE. To determine the ACE inhibition pattern of the purified peptide, various substrate (HHL) concentrations (1, 2, and 5 mM) were incubated with the ACE solution in either the absence or presence of 100 or 200 μM purified peptide at 37 °C. ACE inhibitory activity was determined according to the above-described method. The ACE inhibition pattern was determined with Lineweaver−Burk plots.[30]

Molecular Docking. To verify the inhibition pattern of the purified peptide, a docking simulation was performed. The structure of the purified peptide was constructed and optimized with the polypeptide builder function of the public domain web server PEP-FOLD, which predicted and optimized the conformation of side chains by calculating energy values. The conformation with the lowest energy was considered to display a fully native structure.[30] In addition, the model for ACE used in this study was the crystal structure labeled 1O8A in the Protein Data Bank (PDB), which represented the human testis ACE (tACE). The conformation of the peptide−tACE complex was constructed and optimized with a protein-docking program, ZDOCK, which performed the three-dimensional (3D) search of the spatial degrees of freedom between the two molecules. The default parameters of ZDOCK were used, and the conformation with the highest ZDOCK score was identified as the best docking mode.[31]

Statistical Analysis. The experiments were run in triplicate. The results were expressed as the mean ± standard deviation and were analyzed using SPSS 16.0 software (SPSS, Inc., Chicago, IL). Differences between means were analyzed by an analysis of variance (ANOVA) test with the least significant difference (LSD) post-hoc analysis ($p < 0.05$).

RESULTS AND DISCUSSION

Change in ACE Inhibitory Activity of Peptides. During incubation, the inhibitory activity remained stable up to day 12

and then dramatically increased on day 15, reaching 78.25% at 10 mg/mL (Figure 1). During chick embryonic development,

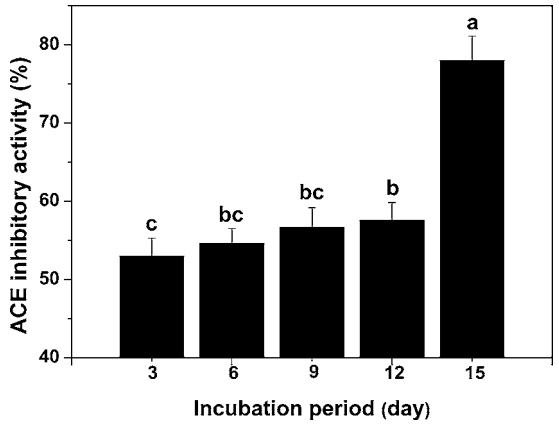

Figure 1. Change in ACE inhibitory activity of peptides derived from fertilized eggs at different developmental stages. The sample concentration was 10 mg/mL for measurement of ACE inhibitory activity. Different letters (a and b) above columns indicate significant differences ($p < 0.05$).

ACE was produced during early embryogenesis, at a stage when blood circulation is not yet established.[25] Girard has reported that the blood pressure increased rapidly and exponentially from 3 to 10 days of incubation; thereafter, the increase was slower.[32] This trend is in good agreement with the result that the inhibitory activity of peptides was low before day 12 and then increased markedly up to day 15. The results indicate that the peptides may play a potential role in regulating blood pressure by inhibiting ACE during incubation.

Purification and Identification of ACE Inhibitory Peptide. The peptides on day 15 exhibited the strongest ACE inhibitory activity and, thus, were employed for isolation of ACE inhibitory peptide. A Mono Q 5/50 GL column was used to fractionate the peptides, and the fractions were pooled to obtain fractions 1−6 (lower panel of Figure 2a). Although ACE inhibitory activity was observed in all of these fractions, fraction 2 exhibited the highest inhibitory activity (upper panel of Figure 2a). Thereafter, fraction 2 was eluted on a Superdex Peptide 10/300GL column, and six peaks were monitored (lower panel of Figure 2b). Among these peaks, fraction C expressed strong ACE inhibitory activity (upper panel of Figure 2b). Therefore, fraction C was subjected to linear trap quadrupole (LTQ) MS/MS analysis to identify its amino acid sequence. On the basis of mass spectrometric analysis, two peptides (named P1 and P2) were identified (Figure 3). Because the amino acid sequence of P2 has been reported in our previous work,[27] the mass spectrum of P2 was cited from ref 27. The two peptides were composed of 18 and 12 amino acid residues, and the amino acid sequences were VGVI-KAVDKKAGGAGKVT (molecular weight of 1698.03 Da) and HLFGPPGKKDPV (molecular weight of 1291.51 Da), respectively. To confirm ACE inhibitory activity of the two peptides, P1 and P2 were synthesized with a peptide synthesizer and their inhibitory activity was measured. The results showed that the half maximal inhibitory concentration (IC_{50}) of P2 was 125 μM, while P1 exhibited lower activity (IC_{50} > 250 μM). Therefore, P2 was selected for further research. Interestingly, our previous work indicated that HLFGPPGKKDPV also possessed antioxidant activity against the 1,1-diphenyl-2-picrylhydrazyl (DPPH) radical,[27] which is in accordance with the previous study reporting that peptides with high ACE inhibitory activity usually possessed a high level of DPPH radical scavenging activity at the same time.[33] Actually, since Hou et al.[34] suggested that some antioxidant peptides had effects on ACE, many multifunctional peptides have been

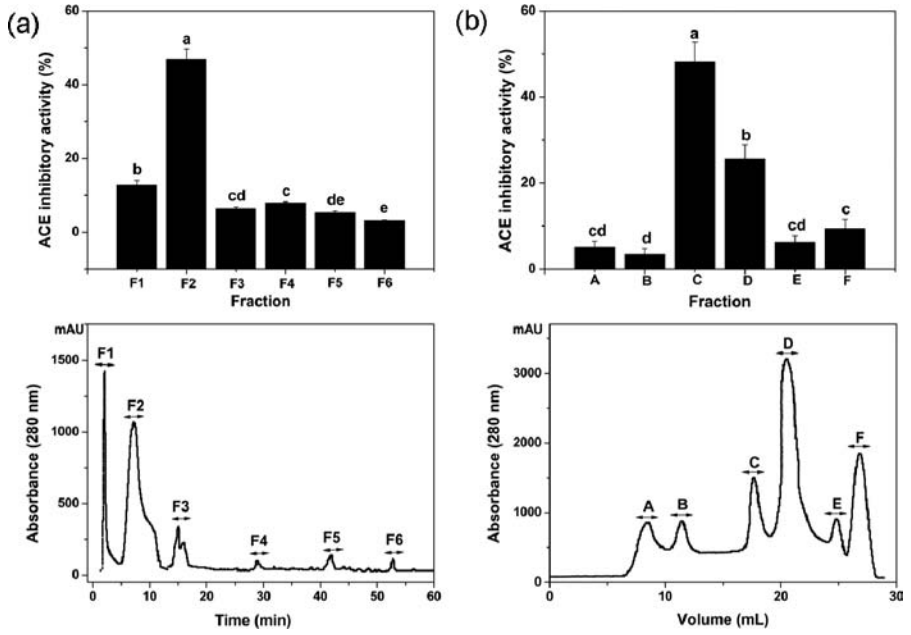

Figure 2. Purification profiles and ACE inhibitory activity of fractions derived from fertilized eggs on day 15. The sample concentration of each fraction was 1 mg/mL for measurement of ACE inhibitory activity. (a) Chromatography of peptides by a Mono Q 5/50 GL column (lower panel) and ACE inhibitory activity of each fraction (upper panel). (b) Chromatography of active fraction (fraction 2) by Superdex Peptide 10/300GL (lower panel) and ACE inhibitory activity of each fraction (upper panel). Different letters (a−e) above columns indicate significant differences ($p < 0.05$).

dx.doi.org/10.1021/jf501368a | J. Agric. Food Chem. 2014, 62, 5500−5506

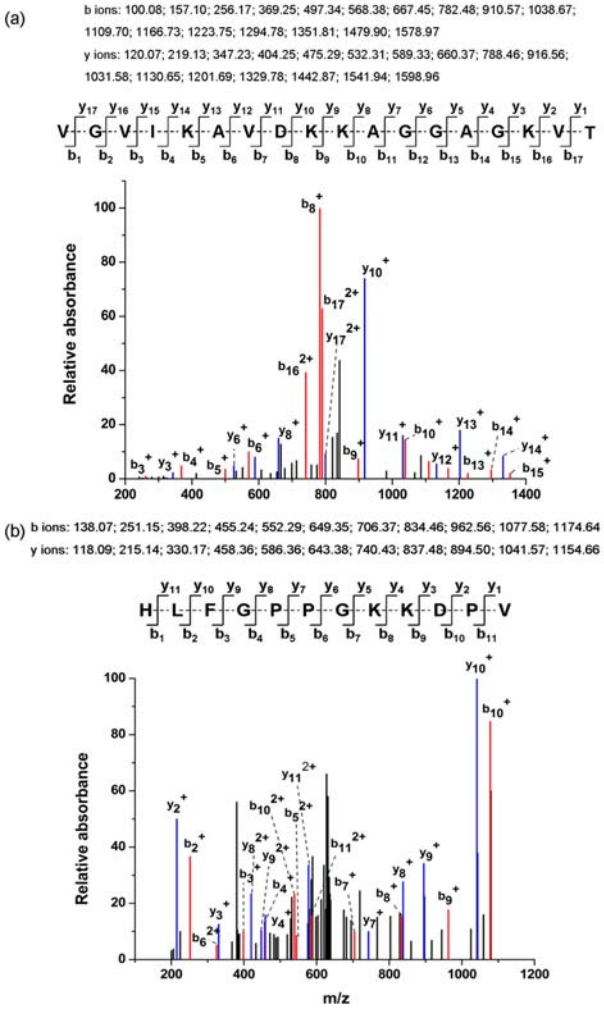

Figure 3. Identification of the amino acid sequence of the purified peptides (a) P1 and (b) P2. MS/MS experiments were performed on a LC system coupled to a linear ion trap mass spectrometer model LTQ (LC−ESI−LTQ). The mass spectrum of P2 was cited from ref 27.

purified from various food sources.[35,36] These active peptides have considerable potential for use as multifunctional ingredients in functional foods to control chronic diseases.

Basic Local Alignment Search Tool (BLAST) analysis revealed that HLFGPPGKKDPV corresponded to the fragment 302−313 of ovotransferrin.[27] Ovotransferrin is an iron-binding glycoprotein and appears to be a multifunctional protein.[37] Some ACE inhibitory peptides have been purified from ovotransferrin hydrolysates.[38−41] Lee et al.[41] have characterized an hexapeptide derived from ovotransferrin (KVREGT), possessing strong ACE inhibitory activity (IC_{50} = 9.1 μM). Lee et al.[38] also isolated an ovotransferrin octapeptide (KVREGTTY), which had an IC_{50} value of 102.8 μM against ACE. In recent research,[40] three novel tripeptides (IQW, IRW, and LKP) with high ACE inhibitory activity (IC_{50} lower than 3.0 μM) were purified from enzymatic hydrolysate of ovotransferrin. In this work, P2 had a relatively low activity compared to other reports. However, in contrast to those peptides obtained via enzymatic hydrolysis of proteins, P2 is the first naturally occurring ACE inhibitory peptide from a fertilized egg.

ACE inhibitory peptides usually contain 2−12 amino acid residues.[42] Thus, the molecular weight of P2 is in good agreement with the reported ACE inhibitory peptide size. Previous studies have demonstrated a good correlation between certain amino acid residues and ACE inhibitory activity of peptides.[21,43] Because the activity of ACE is to cleave the C-terminal dipeptide of oligopeptide substrates, the inhibitory activity of peptides is strongly influenced by their C-terminal tripeptide sequences.[30] Rohrbach et al.[44] demonstrated that the most potent ACE inhibitors contain hydrophobic amino acid residues at their three C-terminal positions. P2 contained six hydrophobic amino acid residues (L, F, P, and V), and two of them (P and V) were at the C-terminal tripeptide sequence. In addition, it was reported that most naturally occurring ACE inhibitory peptides contained P, K, or aromatic amino acid residues.[41] P2 contained the two amino acid residues (P and K) and one aromatic amino acid residue (F), which may play an important role in its inhibitory activity.

Antihypertensive Effect of the Purified Peptide on SHR. Antihypertensive activity of P2 was evaluated by measuring the change of SBP at 1, 2, 3, 6, 9, 22, and 24 h after oral administration. As shown in Figure 4, the SBP in the quiescent state of SHR was 188 ± 4.4 mmHg. After oral administration of P2 and captopril, SBP clearly decreased and the activities were maintained for 9 h. The maximal decrements in SBP of P2 and captopril treatment groups were 21.1 and 27.1 mmHg at 6 h, respectively. The blood pressure has been gradually recovered in 22 h for all groups. In addition, there was no significant change in the heart rate (HR) after administration, which suggested that the administration of P2 did not have a bad effect on the circulatory system of SHRs.

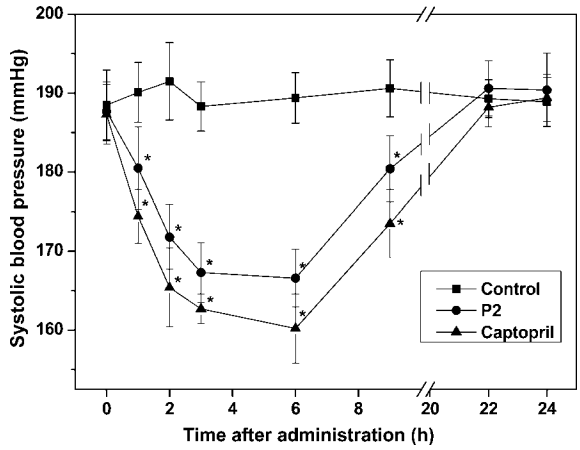

Figure 4. Changes in SBP of SHR after oral administration of P2. Captopril was used as a positive control. Single oral administration was performed with a dose of 10 mg/kg of body weight, and SBP was measured 0, 1, 2, 3, 6, and 9 h after administration. (*) Significant difference from the control at $p < 0.05$.

There have been many studies on ACE inhibitory peptides derived from egg proteins.[45−47] Some of these peptides have been shown to possess hypotensive activity in SHRs.[46,47] However, there is little information on the hypotensive activities of naturally occurring peptides from fertilized eggs. The depressor ability of P2 (21.1 mmHg) is higher than that of 20 mg/kg of ovokinin (13.5 mmHg), which was a heptapeptide derived from ovalbumin.[46] It is well-known that small peptides, such as di- or tripeptides are easily absorbed in their intact forms in the intestine.[3] Even though P2 has relatively high molecular weight compared to these small peptides, the result

dx.doi.org/10.1021/jf501368a | J. Agric. Food Chem. 2014, 62, 5500−5506

showed that P2 exerted a substantial effect on reduction of SBP in SHR. This meant that this peptide could be directly absorbed or undergo further hydrolysis in the digestive tract to release smaller size true inhibitors.

Inhibition Pattern on ACE. Various substrate (HHL) concentrations (1, 2, and 5 mM) were incubated with ACE solution in either the absence or presence of 100 or 200 μM P2. As shown in Figure 5, the three straight lines intersected at one

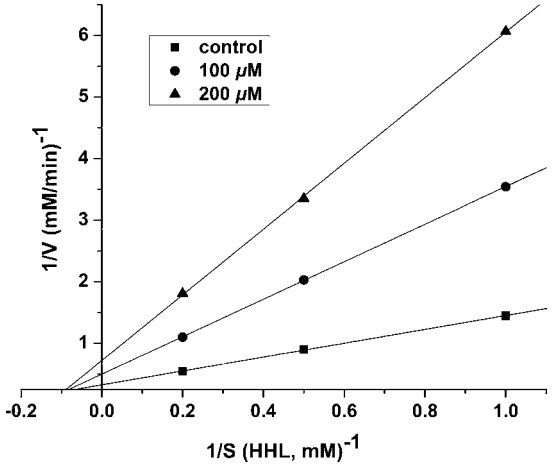

Figure 5. Lineweaver–Burk plot of ACE activity of P2: (■) control, (●) 100 μM the P2, and (▲) 200 μM P2.

point on the 1/*S* axis, which meant that this peptide was a non-competitive inhibitor.[30] Non-competitive inhibitors generally bind to non-catalytic sites of enzymes. They combine with enzyme molecules to produce a dead-end complex, regardless of whether a substrate molecule is bound or not.[3] In addition, a decrease in the V_{max} value was seen after incubating ACE with P2 (3.10, 2.01, and 1.39 mM/min for the absence and presence of 100 or 200 μM P2, respectively), whereas there was little effect on K_m (11.3, 12.5, and 13.9 μM for the absence and presence of 100 or 200 μM P2, respectively). This is in agreement with previous research reporting that non-competitive inhibition would lead to a decreased V_{max}, with minimal effects on K_m.[48] In recent years, several non-competitive inhibitory peptides have been purified from some food sources.[30,49] However, the relationship between the inhibition pattern and structure of these peptides has not been fully researched.[30]

Molecular Docking. The conformation with the highest ZDOCK score is shown in Figure 6a. It was observed that P2 (green) was located on the opposite side of the ACE (gray) active site, which included the zinc ion (red). Previous research reported that non-competitive ACE inhibitors cannot bind at the active site but at the other exclusive of the ACE active site.[3] Thus, P2 was further identified as a non-competitive inhibitor.

The interaction force between P2 and tACE is shown in Figure 6b. With Pymol software, the theoretical calculation indicated that the peptide formed hydrogen bonds with Asn-66, Lys-118, Arg-124, Tyr-394, Glu-403, and Arg-522 of tACE. His-1 donated its protons to Glu-403 and Tyr-394 to form hydrogen bonds, respectively. Gly-4 and Lys-9 in P2 accepted hydrogen bonds from Asn-66 and Arg-522, separately. Asp-10 and Pro-11 accepted protons from Arg-124 and Lys-118 to form hydrogen bonds, respectively. These interactions kept P2 away from the active site of tACE, and only Lys-9 formed a

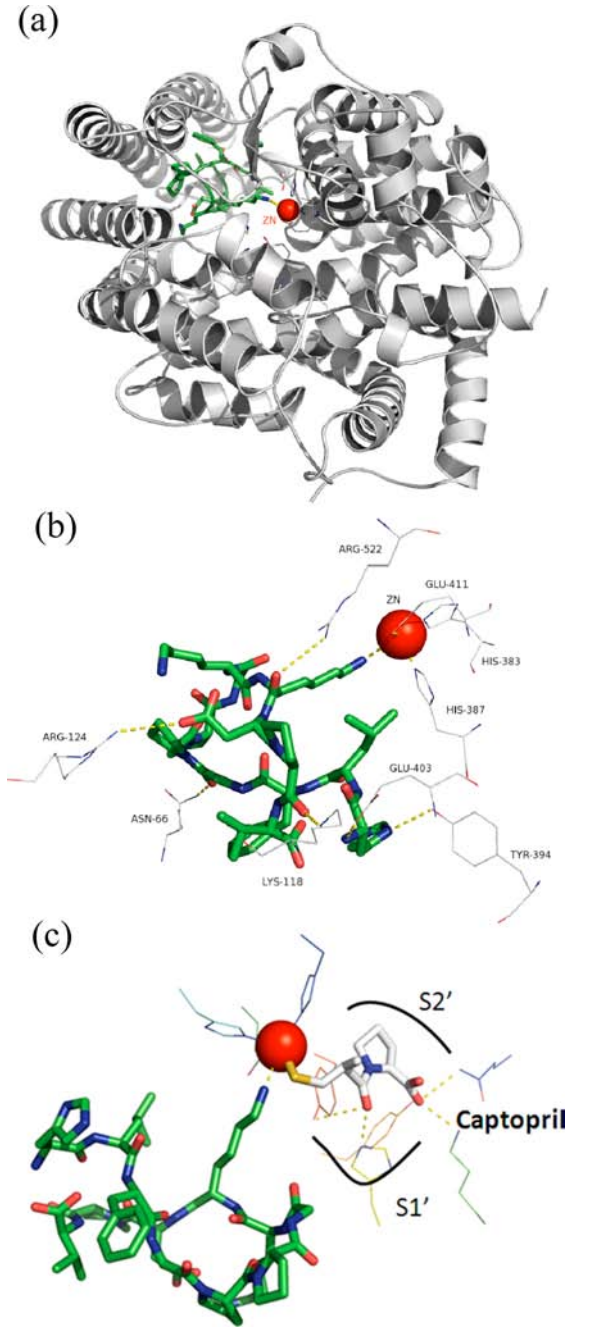

Figure 6. Docking simulation of P2 binding to tACE and captopril–tACE complex. The zinc ion (red ball) was present in the active site of tACE. (a) Docking simulation of P2 (green) binding to tACE (gray). (b) Interaction between P2 (shown as sticks) and the residues of tACE (shown as lines). (c) Overlap of captopril (white) in the crystal structure of the captopril–tACE complex with P2 (green).

coordination bond with the zinc ion that located in the active site. The zinc ion is the key ion in the active site of ACE; it plays a crucial role in opening up the catalytic site.[50] In the docking simulation, the zinc ion was attracted by Lys-9 of P2 through a coordination bond. Therefore, the zinc ion might be forced away from the active site, and thus, the substrate HHL bonded to ACE could not be catalyzed to produce HA.[30]

To further elucidate the inhibition pattern of P2, the docking simulation of P2 and the captopril–ACE complex (PDB code 1UZF) was performed (Figure 6c). Captopril is a specific

dx.doi.org/10.1021/jf501368a | J. Agric. Food Chem. 2014, 62, 5500–5506

competitive ACE inhibitor.[22] According to the crystal structure of the captopril−ACE complex, captopril (white) formed hydrogen bonds with key residues in ACE active site and occupied the key positions, which would be occupied by substrate HHL, such as the S1′ and S2′ subsites.[30] This is consistent with the competitive inhibition model. Contrarily, P2 (green) located away from the ACE active site (S1′ and S2′), and only Lys-9 interacted with the zinc ion (red). Therefore, we concluded that P2 could not compete with substrate for the active site, indicating that P2 is a non-competitive ACE inhibitor.

In summary, ACE inhibitory activity of peptides derived from fertilized eggs was investigated. During incubation, ACE inhibitory activity of peptides remained stable before day 12 and then markedly increased on day 15. The peptides on day 15 were then employed for isolation of ACE inhibitory peptide. An identified peptide (HLFGPPGKKDPV) exhibited potent ACE inhibitory activity with an IC_{50} value of 125 μM and acted as a non-competitive inhibitor against ACE. An antihypertensive effect in SHR revealed that oral administration of the peptide could decrease SBP significantly. These results showed that fertilized eggs could be seen as potential candidates to develop nutraceuticals against hypertension and its related disease.

AUTHOR INFORMATION

Corresponding Author

*Telephone/Fax: +86-510-85917100. E-mail: xmxu@jiangnan.edu.cn.

Funding

This work was supported by the National "Twelfth Five-Year" Plan for Science and Technology Support of China (2012BAD37B06), the Doctor Candidate Foundation of Jiangnan University (JUDCF13005), and the Graduate Student Innovation Project of Jiangsu Province (CXLX13_751).

Notes

The authors declare no competing financial interest.

ABBREVIATIONS USED

ACE, angiotensin I-converting enzyme; ANOVA, analysis of variance; BLAST, Basic Local Alignment Search Tool; DPPH, 1,1-diphenyl-2-picrylhydrazyl; FMOC, [(9-fluorenylmethyl)-oxy]carbonyl; HA, hippuric acid; HBTU, 2-(1*H*-benzotriazol-1-yl)-1,1,3,3-tetramethyluronium hexafluorophosphate; HHL, hippuryl-L-histidyl-L-leucine; HPLC, high-performance liquid chromatography; HR, heart rate; RAS, renin−angiotensin system; SBP, systolic blood pressure; SHR, spontaneously hypertensive rat; tACE, testis ACE

REFERENCES

(1) Du, L.; Fang, M.; Wu, H.; Xie, J.; Wu, Y.; Li, P.; Zhang, D.; Huang, Z.; Xia, Y.; Zhou, L.; Wei, D. A novel angiotensin I-converting enzyme inhibitory peptide from *Phascolosoma esculenta* water-soluble protein hydrolysate. *J. Funct. Foods* **2013**, *5*, 475−483.

(2) Chiang, W. D.; Tsou, M. J.; Tsai, Z. Y.; Tsai, T. C. Angiotensin I-converting enzyme inhibitor derived from soy protein hydrolysate and produced by using membrane reactor. *Food Chem.* **2006**, *98*, 725−732.

(3) Lee, S. H.; Qian, Z. J.; Kim, S. K. A novel angiotensin I converting enzyme inhibitory peptide from tuna frame protein hydrolysate and its antihypertensive effect in spontaneously hypertensive rats. *Food Chem.* **2010**, *118*, 96−102.

(4) Zhao, Y.; Li, B.; Dong, S.; Liu, Z.; Zhao, X.; Wang, J.; Zeng, M. A novel ACE inhibitory peptide isolated from *Acaudina molpadioidea* hydrolysate. *Peptides* **2009**, *30*, 1028−1033.

(5) Ferreira, S. H.; Bartelt, D. C.; Greene, L. J. Isolation of bradykinin-potentiating peptides from *Bothrops jararaca* venom. *Biochemistry* **1970**, *9*, 2583−2593.

(6) Vercruysse, L.; Van Camp, J.; Smagghe, G. ACE inhibitory peptides derived from enzymatic hydrolysates of animal muscle protein: A review. *J. Agric. Food Chem.* **2005**, *53*, 8106−8115.

(7) Antonios, T. F. T.; MacGregor, G. A. Angiotensin converting enzyme inhibitor in hypertension: Potential problems. *J. Hypertens.* **1995**, *13*, S11−S16.

(8) Vermeirssen, V.; Van Camp, J.; Verstraete, W. Optimisation and validation of an angiotensin-converting enzyme inhibition assay for screening of bioactive peptides. *J. Biochem. Biophys. Methods* **2002**, *51*, 75−87.

(9) Mine, Y.; Shahidi, F. *Nutraceutical Proteins and Peptides in Health and Disease*; CRC Press: Boca Raton, FL, 2005.

(10) Kovacs-Nolan, J.; Phillips, M.; Mine, Y. Advances in the value of eggs and egg components for human health. *J. Agric. Food Chem.* **2005**, *53*, 8421−8431.

(11) Oshima, G.; Shimabukuro, H.; Nagasawa, K. Peptide inhibitors of angiotensin I-converting enzyme in digest of gelatin by bacterial collagenase. *Biochim. Biophys. Acta* **1979**, *566*, 128−137.

(12) Maruyama, S.; Suzuki, H. A peptide inhibitor of angiotensin I-converting enzyme in the tryptic hydrolysate on casein. *Agric. Biol. Chem.* **1982**, *46*, 1393−1394.

(13) Kohama, Y.; Matsumoto, S.; Oka, H.; Teramoto, T.; Okabe, M.; Miura, T. Isolation of angiotensin-converting enzyme inhibitor from tuna muscle. *Biochem. Biophys. Res. Commun.* **1988**, *155*, 332−337.

(14) Miyoshi, S.; Ishikawa, H.; Kaneko, T.; Fukui, F.; Tanaka, H.; Maruyama, S. Structure and activity of angiotensin I-converting enzyme inhibitors in a α-zein hydrolysate. *Agric. Biol. Chem.* **1999**, *55*, 1313−1318.

(15) Kuba, M.; Tana, C.; Twata, S.; Yasuda, M. Production of angiotensin I-converting enzyme inhibitory peptides from soybean protein with *Monascus purpureus* acid proteinase. *Process Biochem.* **2005**, *40*, 2191−2196.

(16) Mine, Y.; Kovacs-Nolan, J. New insights in biologically active proteins and peptides derived from hen egg. *World Poultry Sci. J.* **2006**, *62*, 87−96.

(17) Yokoyama, K.; Chiba, H.; Yoshikawa, M. Peptide inhibitors for angiotensin I-converting enzyme from thermolysin digest of dried bonito. *Biosci., Biotechnol., Biochem.* **1992**, *56*, 1541−1545.

(18) Terashima, M.; Baba, T.; Ikemoto, N.; Katayama, M.; Morimoto, T.; Matsumura, S. Novel angiotensin-converting enzyme (ACE) inhibitory peptides derived from boneless chicken leg meat. *J. Agric. Food Chem.* **2010**, *58*, 7432−7436.

(19) Jimsheena, V. K.; Gowda, L. R. Angiotensin I-converting enzyme (ACE) inhibitory peptides derived from arachin by simulated gastric digestion. *Food Chem.* **2011**, *125*, 561−569.

(20) Wu, J.; Aluko, R. E.; Nakai, S. Structural requirements of angiotensin I-converting enzyme inhibitory peptides: quantitative structure−activity relationship study of di- and tripeptides. *J. Agric. Food Chem.* **2006**, *54*, 732−738.

(21) Natesh, R.; Schwager, S. L. U.; Evans, H. R.; Sturrock, E. D.; Acharya, K. R. Structural details on the binding of antihypertensive drugs captopril and enalaprilat to human testicular angiotensin I-converting enzyme. *Biochemistry* **2004**, *43*, 8718−8724.

(22) Natesh, R.; Schwager, S. L. U.; Sturrock, E. D.; Acharya, K. R. Crystal structure of the human angiotensin-converting enzyme−lisinopril complex. *Nature* **2003**, *421*, 551−554.

(23) Watermeyer, J. M.; Kroger, W. L.; O' Neill, H. G.; Sewell, B. T.; Sturrock, E. D. Probing the basis of domain-dependent inhibition using novel ketone inhibitors of angiotensin-converting enzyme? *Biochemistry* **2008**, *47*, 5942−5950.

(24) Duan, X.; Li, M.; Wu, F.; Yang, N.; Nikoo, M.; Jin, Z.; Xu, X. Post fertilization changes in nutritional composition and protein conformation of hen egg. *J. Agric. Food Chem.* **2013**, *61*, 12092−12100.

(25) Savary, K.; Michaud, A.; Favier, J.; Larger, E.; Corvol, P.; Gasc, J. M. Role of the renin−angiotensin system in primitive erythropoiesis in the chick embryo. *Blood* **2005**, *105*, 103−110.
(26) Li, X.; Su, Y.; Sun, J.; Yang, Y. Chicken embryo extracts enhance spleen lymphocyte and peritoneal macrophages function. *J. Ethnopharmacol.* **2012**, *144*, 255−260.
(27) Duan, X.; Ocen, D.; Wu, F.; Li, M.; Yang, N.; Xu, J.; Chen, H.; Huang, L.; Jin, Z.; Xu, X. Purification and characterization of a natural antioxidant peptide from fertilized eggs. *Food Res. Int.* **2014**, *56*, 18−24.
(28) Park, P. J.; Jung, W. K.; Nam, K. S.; Shahidi, F.; Kim, S. K. Purification and characterization of antioxidative peptides from protein hydrolysate of lecithin-free egg yolk. *J. Am. Oil Chem. Soc.* **2001**, *78*, 651−656.
(29) Terashima, M.; Oe, M.; Ogura, K.; Matsumura, S. Inhibition strength of short peptides derived from an ACE inhibitory peptide. *J. Agric. Food Chem.* **2011**, *59*, 11234−11237.
(30) Ni, H.; Li, L.; Liu, G.; Hu, S. Q. Inhibition mechanism and model of an angiotensin I-converting enzyme (ACE)-inhibitory hexapeptide from yeast (*Saccharomyces cerevisiae*). *PloS One* **2012**, *7*, No. e37077.
(31) Pierce, B. G.; Hourai, Y.; Weng, Z. Accelerating protein docking in ZDOCK using an advanced 3D convolution library. *PloS One* **2011**, *6*, No. e24657.
(32) Girard, H. Arterial pressure in the chick embryo. *Am. J. Physiol.* **1973**, *224*, 454−460.
(33) Lu, J.; Sawano, Y.; Miyakawa, T.; Xue, Y. L.; Cai, M. Y.; Egashira, Y.; Ren, D. F.; Tanokura, M. One-week antihypertensive effect of Ile−Gln−Pro in spontaneously hypertensive rats. *J. Agric. Food Chem.* **2010**, *59*, 559−563.
(34) Hou, W. C.; Chen, H. J.; Lin, Y. H. Antioxidant peptides with angiotensin converting enzyme inhibitory activities and applications for angiotensin converting enzyme purification. *J. Agric. Food Chem.* **2003**, *51*, 1706−1709.
(35) Hernández-Ledesma, B.; Miralles, B.; Amigo, L.; Ramos, M.; Recio, I. Identification of antioxidant and ACE-inhibitory peptides in fermented milk. *J. Sci. Food Agric.* **2005**, *85*, 1041−1048.
(36) Korhonen, H. Milk-derived bioactive peptides: From science to applications. *J. Funct. Foods* **2009**, *1*, 177−187.
(37) Mine, Y. Structure and chemical composition of eggs. *Egg Bioscience and Biotechnology*; Wiley: Hoboken, NJ, 2008.
(38) Lee, N.; Cheng, J.; Enomoto, T.; Nakamura, I. Antihypertensive effect of angiotensin-converting enzyme inhibitory peptide obtained from hen ovotransferrin. *J. Chin. Chem. Soc.* **2006**, *53*, 495−501.
(39) Liu, J.; Yu, Z.; Zhao, W.; Lin, S.; Wang, E.; Zhang, Y.; Hao, H.; Wang, Z.; Chen, F. Isolation and identification of angiotensin-converting enzyme inhibitory peptides from egg white protein hydrolysates. *Food Chem.* **2010**, *122*, 1159−1163.
(40) Majumder, K.; Wu, J. Purification and characterisation of angiotensin I converting enzyme (ACE) inhibitory peptides derived from enzymatic hydrolysate of ovotransferrin. *Food Chem.* **2011**, *126*, 1614−1619.
(41) Lee, N. Y.; Cheng, J. T.; Enomoto, T.; Nakano, Y. One peptide derived from hen ovotransferrin as pro-drug to inhibit angiotensin converting enzyme. *J. Food Drug Anal.* **2006**, *14*, 31−35.
(42) Yamamoto, N.; Akino, A.; Takano, T. Antihypertensive effect of the peptides derived from casein by an extracellular proteinase from *Lactobacillus helveticus* CP790. *J. Dairy Sci.* **1994**, *77*, 917−922.
(43) Pan, D.; Cao, J.; Guo, H.; Zhao, B. Studies on purification and the molecular mechanism of a novel ACE inhibitory peptide from whey protein hydrolysate. *Food Chem.* **2012**, *130*, 121−126.
(44) Rohrbach, M. S.; Williams, E. B.; Rolstad, R. A. Purification and substrate specificity of bovine angiotensin-converting enzyme. *J. Biol. Chem.* **1981**, *256*, 225−230.
(45) Fujita, H.; Usui, H.; Kurahashi, K.; Yoshikawa, M. Isolation and characterization of ovokinin, a bradykinin B1 agonist peptide derived from ovalbumin. *Peptides* **1995**, *16*, 785−790.
(46) Matoba, N.; Usui, H.; Fujita, H.; Yoshikawa, M. A novel antihypertensive peptide derived from ovalbumin induces nitric oxide-mediated vasorelaxation in an isolated SHR mesenteric artery. *FEBS Lett.* **1999**, *452*, 181−184.
(47) Fujita, H.; Sasaki, R.; Yoshikawa, M. Potentiation of the antihypertensive activity of orally administered ovokinin, a vaso-relaxing peptide derived from ovalbumin, by emulsification in egg phosphatidylcholine. *Biosci., Biotechnol., Biochem.* **1995**, *59*, 2344−2345.
(48) Cooper, C. E.; Brown, G. C. The inhibition of mitochondrial cytochrome oxidase by the gases carbon monoxide, nitric oxide, hydrogen cyanide and hydrogen sulfide: Chemical mechanism and physiological significance. *J. Bioenerg. Biomembr.* **2008**, *40*, 533−539.
(49) Ahn, C. B.; Jeon, Y. J.; Kim, Y. T.; Je, J. Y. Angiotensin I converting enzyme (ACE) inhibitory peptides from salmon byproduct protein hydrolysate by alcalase hydrolysis. *Process Biochem.* **2012**, *47*, 2240−2245.
(50) Watermeyer, J. M.; Sewell, B. T.; Schwager, S. L.; Natesh, R.; Corradi, H. R.; Acharya, K. R.; Sturrock, E. D. Structure of testis ACE glycosylation mutants and evidence for conserved domain movement. *Biochemistry* **2006**, *45*, 12654−12663.

JOURNAL OF AGRICULTURAL AND FOOD CHEMISTRY

Article

pubs.acs.org/JAFC

Activation of the Phase II Enzymes for Neuroprotection by Ginger Active Constituent 6-Dehydrogingerdione in PC12 Cells

Juan Yao, Chunpo Ge, Dongzhu Duan, Baoxin Zhang, Xuemei Cui, Shoujiao Peng, Yaping Liu, and Jianguo Fang*

State Key Laboratory of Applied Organic Chemistry and College of Chemistry and Chemical Engineering, Lanzhou University, Lanzhou, Gansu 730000, China

ABSTRACT: The cellular endogenous antioxidant system plays pivotal roles in counteracting or retarding the pathogenesis of many neurodegenerative diseases. Molecules with the ability to enhance the antioxidant defense thus are promising candidates for neuroprotective drugs. 6-Dehydrogingerdione (6-DG), one of the major components of dietary ginger, has received increasing attention due to its multiple pharmacological activities. However, how this pleiotropic molecule works on the neuronal system has not been studied. This paper reports that 6-DG efficiently scavenges various free radicals in vitro and displays remarkable cytoprotection against oxidative stress-induced neuronal cell damage in the neuron-like rat pheochromocytoma cell line, PC12 cells. Pretreatment of PC12 cells with 6-DG significantly up-regulates a panel of phase II genes as well as the corresponding gene products, such as glutathione, heme oxygenase, NAD(P)H:quinone oxidoreductase, and thioredoxin reductase. Mechanistic study indicates that activation of the Keap1-Nrf2-ARE pathway is the molecular basis for the cytoprotection of 6-DG. This is the first revelation of this novel mechanism of 6-DG as an Nrf2 activator against oxidative injury, providing the potential therapeutic use of 6-DG as neuroprotective agent.

KEYWORDS: *6-dehydrogingerdione, Nrf2, oxidative stress, neuroprotection, antioxidant*

INTRODUCTION

The cellular endogenous antioxidant system is crucial for counteracting reactive oxygen species (ROS)-mediated oxidative stress and preventing cell death. A well-elucidated universal pathway to induce intrinsic antioxidant defense involves transcriptional regulation through activation of the antioxidant-responsive element (ARE).[1,2] Under this circumstance, stimulants induce a set of genes encoding antioxidant and detoxifying enzymes ("phase II" enzymes), including heme oxygenase-1 (HO-1), NAD(P)H:quinone oxidoreductase 1 (NQO1), thioredoxin reductase 1 (TrxR1), thioredoxin (Trx), glutathione (GSH), γ-glutamylcysteine synthetase (γGCS), and γ-glutamyl cysteine ligase (γ-GCL), which provide efficient cytoprotection against oxidative stress and electrophilic assault.[3,4] The transcription factor NF-E2-related factor 2 (Nrf2) mediates transcription of phase II genes by binding to the ARE within nuclear DNA and subsequently initiates antioxidant genes transcription. Under basal conditions, the cytosolic regulatory protein Kelch-like ECH-associated protein 1 (Keap1) binds tightly to Nrf2, retaining it in the cytoplasm.[2] Molecules, such as electrophiles or oxidants, which could modify the critical cysteine residue(s) in the regulatory protein Keap1, would cause the release of Nrf2 and facilitate its translocattion into the nucleus and thus activate the transcription of phase II genes.[4−7]

In healthy cells, the level of ROS is tightly regulated by the antioxidant defense system. However, upon environmental stress or cellular damage, cells cannot readily detoxify the ROS generated and may thereby suffer from oxidative stress. As neuronal cells are particularly sensitive to oxidative stress, an increasing amount of experimental evidence has indicated that oxidative stress is a causal, or at least an ancillary, factor in the neuropathology of several adult neurodegenerative disorders such as Alzheimer's disease (AD) and Parkinson's disease (PD).[8,9] Besides the counteraction of various ROS by exogenous small molecule antioxidants, targeting the prevention of oxidative stress could be best achieved by stimulation of endogenous cytoprotective molecules known to serve this purpose because their actions are more sustained and are amplified by transcription-mediated signaling pathways. In this sense, activation of the Nrf2-ARE pathway is a promising therapeutic approach in neurodegenerative diseases.[3,10−12] Thus, the past years have witnessed expanding endeavors in identifying naturally occurring and synthetic neuroprotective small molecule activators of the Nrf2-ARE pathway,[13,14] including carnosic acid,[15] resveratrol,[16] curcumin,[17] sulforaphane,[18] quercetin,[19] epicatechin,[20] plumbagin,[21] luteolin,[22] and *tert*-butylhydroquinone.[18]

Ginger (rhizome of the dietary plant *Zingiber officinale*) has been commonly used as a popular spice or food supplement and has been equally reputed for its medicinal properties for centuries.[23,24] 6-Dehydrogingerdione (6-DG), one of the major components of dietary ginger, has received extensive attention due to its multiple pharmacological activities, such as inhibition of lipid peroxidation,[25] enhancement of skin cell proliferation,[26] and induction of cancer cell apoptosis.[27,28] However, how this pleiotropic molecule works on the neuronal system has not been elucidated. As part of our continuing effort in the discovery and development of novel redox active small

Received: December 11, 2013
Revised: May 26, 2014
Accepted: May 28, 2014
Published: May 28, 2014

ACS Publications © 2014 American Chemical Society

Scheme 1. Synthesis of 6-DG, M-6-DG, and DH-6-DG[a]

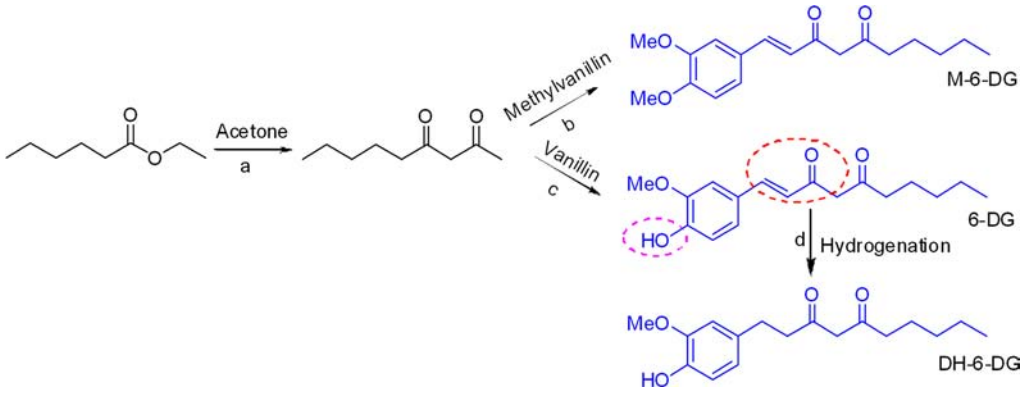

[a]The active motif of 6-DG is highlighted in circles. Reagents and conditions: (a) NaH, Et_2O, 64%; (b) boron trioxide, 78%; (c) boron trioxide, 71%; (d) 10% Pd–C, H_2, 70%.

molecules,[29−32] we determined herein the antioxidant activity of 6-DG in vitro and employed a neuron-like rat pheochromocytoma cell line, PC12, to assess the molecular mechanisms responsible for the neuroprotective effect of 6-DG. 6-DG, prepared from the readily available starting materials in two steps, efficiently scavenges free radicals and prevents erythrocytes from free radical-induced hemolysis. Importantly, 6-DG activates the Nrf2-ARE signaling pathway, leading to up-regulation of phase II enzyme expression and remarkable protection of PC12 cells from hydrogen peroxide (H_2O_2)- or 6-hydroxydopamine (6-OHDA)-induced neurotoxicity. We clarified that the hydroxyl group and the α,β-unsaturated ketone moiety are determinants of the biological function of 6-DG. Our results demonstrate that 6-DG is a novel small molecule activator of Nrf2-ARE pathway and suggest that 6-DG might be a potential candidate for the prevention of neurodegeneration. Targeting the Nrf2-ARE signaling pathway by 6-DG thus discloses a previously unrecognized mechanism underlying the biological action of 6-DG and provides a deep insight into understanding the neuroprotective effects of 6-DG.

MATERIALS AND METHODS

Chemicals and Enzymes. Dulbecco's modified Eagle's medium (DMEM), *N*-acetyl-Asp-Glu-Val-Asp-*p*-nitroanilide (Ac-DEVD-pNA), dimethyl sulfoxide (DMSO), yeast glutathione reductase (GR), Hoechst 33342, 2′,7′-dichlorfluorescein diacetate (DCFH-DA), 2,2′-azinobis(3-ethylbenzthiazoline-6-sulfonic acid) (ABTS), 2,2-diphenyl-1-picrylhydrazyl (DPPH), 5,5′-dithiobis(2-nitrobenzoic acid) (DTNB), 2,6-dichlorophenol-indophenol (DCPIP), NADH, 3-(4,5-dimethylthiazol-2-yl)-2,5-diphenyltetrazolium bromide (MTT), penicillin, and streptomycin were obtained from Sigma-Aldrich (St. Louis, MO, USA). NADPH was obtained from Roche (Mannheim, Germany). Fetal bovine serum (FBS) was obtained from HyClone. 6-Hydroxydopamine (6-OHDA) and antibodies against TrxR1, Trx1, actin, and Nrf2 were from Santa Cruz Biotechnology. Antibodies against HO-1 and NQO1 were from Sangon Biotech (Shanghai, China). The shRNA plasmids targeting coding regions of the rat Nrf2 gene (shNrf2) and the control nontargeting shRNA (shNT) were purchased from GenePharma Co, Ltd. (Shanghai, China). GeneTran III transfection reagent was obtained from Biomiga (San Diego, CA, USA). Bovine serum albumin (BSA), phenylmethanesulfonyl fluoride (PMSF), and sodium orthovanadate (Na_3VO_4) were from Beyotime (Nantong, China). All other reagents were of analytical grade.

Synthesis of 6-DG, Methylated 6-DG (M-6-DG), and Hydrogenated 6-DG (DH-6-DG). 6-DG, M-6-DG, and DH-6-DG described in this study were prepared using a straightforward chemistry (Scheme 1) by following the method described in the literature with minor modifications. Briefly, acetone reacts with ethyl hexanoate under basic condition (Claisen condensation) and gives 2,4-nonanedione in 64% yield. The dione reacting with vanillin and methylvanillin via Claisen–Schmidt condensation affords 6-DG and M-6-DG in 71 and 78% yields, respectively. Hydrogenation of 6-DG catalyzed by palladium on carbon furnished DH-6-DG in 70% yield. All compounds were fully characterized by NMR and MS.

2,4-Nonanedione.[33] To a stirred mixture of sodium hydride (1.2 g, 50 mmol) and ethyl hexanoate (7.2 g, 50 mmol) was added acetone (1.51 g, 26 mmol) in 7 mL of dry diethyl ether over a period of 30 min. The temperature of the reaction mixture was kept at 30–40 °C by occasional cooling with ice water. After the acetone was added, the reaction mixture was stirred at 40–50 °C for 1 h. Diethyl ether was continuously added to maintain a fluid reaction mixture. After continuous stirring at room temperature overnight, the reaction was quenched by sequential addition of 8 mL of ethanol and 80 mL of 0.75 M HCl. Extraction with diethyl ether (50 mL × 3) and removal of the solvent under vacuum gave a pale yellow oil, which was added to a hot solution of $CuSO_4·5H_2O$ (12.4 g, 40 mmol) in 60 mL of water. After cooling, crystals were collected and washed with 100 mL of hexane and further dissolved in 50 mL of 10% H_2SO_4. The resulting solution was extracted with diethyl ether and dried over Na_2SO_4. After removal of the solvent, the crude product purified by column chromatography on silica gel gave 2,4-nonanedione (64%). ^{1}H NMR (400 MHz, $CDCl_3$), δ 5.49 (s, 1H), 2.23–2.27 (t, 2H), 2.05 (s, 3H), 1.58–1.62 (m, 2H), 1.30–1.32 (m, 4H), 0.88–0.91 (t, 3H); ESI-MS $(M + 1)^+$, 157.2.

6-DG.[34] Vanillin (6.3 g, 42 mmol), 2,4-nonanedione (19.3 g, 124 mmol), and boron trioxide (11.5 g, 165 mmol) were mixed with 50 mL of *N*,*N*-dimethylformamide (DMF) and warmed to 90 °C. A solution of isobutylamine (40 mg, 0.4 mmol) in 40 mL of DMF was added dropwise for 2 h. After stirring at 85–90 °C for 1 h, ~60 mL of the solvent was evaporated in vacuo, and 250 mL of water was added. The resulting mixture was stirred at 60 °C for 1 h and at room temperature for 12 h. The reaction mixture was extracted with ethyl acetate (50 mL × 3), and the solvents were evaporated. The crude product was purified by column chromatography on silica gel to afford 6-DG (71%). mp, 84 °C; ^{1}H NMR (400 MHz, $CDCl_3$), δ 7.51–7.55 (d, J = 16 Hz, 1H), 7.09–7.11 (d, J = 8 Hz, 1H), 7.03 (s, 1H), 6.92–6.94 (d, J = 8 Hz, 1H), 6.33–6.37 (d, J = 16 Hz, 1H), 5.83 (s, 1H), 5.63 (s, 1H), 3.95 (s, 3H), 2.36–2.40 (t, 2H), 1.63–1.70 (m, 2H), 1.33–1.36 (m, 4H), 0.90–0.93 (t, 3H); ESI-MS $(M + 1)^+$, 291.2.

M-6-DG. The synthesis of M-6-HG exactly followed the procedure described for 6-DG except for the use of methylvanillin (6.9 g, 42 mmol) instead of vanillin. Yield, 78%; mp, 45 °C; ^{1}H NMR (400 MHz, $CDCl_3$), δ 7.53–7.57 (d, J = 16 Hz, 1H), 7.11–7.13 (m, 1H), 7.06 (s, 1H), 6.87–6.89 (d, J = 8 Hz, 1H), 6.35–6.39 (d, J = 16 Hz, 1H), 5.64 (s, 1H), 3.89 (s, 6H), 2.37–2.41(t, 2H), 1.26–1.34 (m, 6H), 0.9–0.93 (t, 3H); ESI-MS $(M + 1)^+$, 305.2.

dx.doi.org/10.1021/jf405553v | J. Agric. Food Chem. 2014, 62, 5507–5518

DH-6-DG.[31] To a mixture of 10 mg of Pd/C (10%) in 5 mL of ethyl acetate under a hydrogen atmosphere was added 10 mg of 6-DG. The reaction was kept at room temperature for 12 h. After the reaction, the Pd/C was removed by filtration, and the filtrate was concentrated and purified by silica gel column chromatography to afford DH-6-DG (70%). ^{1}H NMR (400 MHz, $CDCl_3$), δ 6.85−6.83 (d, J = 8 Hz, 1H), 6.70−6.68 (d, J = 8 Hz, 2H), 5.51 (s, 1H), 5.46 (s, 1H), 3.87 (s, 3H), 2.89−2.83 (m, 2H), 2.59−2.55 (t, 2H), 2.28−2.24 (t, 2H), 1.32−1.26 (m, 6H), 0.92−0.87 (m, 3H); ESI-MS $(M + Na)^+$, 315.3.

Free Radical-Scavenging Capacities. The various concentrations of antioxidants were mixed with the DPPH solution (50 μM), and the mixture was shaken vigorously and left to stand at room temperature for 30 min in the dark. The absorbance of the reaction solution was measured spectrophotometrically at 517 nm. The $ABTS^{\bullet+}$ scavenging ability was determined according to the published method.[35] The $ABTS^{\bullet+}$ solution, which was prepared from oxidation of ABTS (7 mM) by potassium persulfate (2.5 mM) for 12−16 h in the dark at room temperature, was diluted to an absorbance of 0.700 ± 0.020 at 734 nm. The $ABTS^{\bullet+}$ solution (2 mL) and the antioxidant solution (100 μL) were mixed, and the absorbance at 734 nm was recorded after 30 min.

Assay for Hemolysis of Red Blood Cells (RBCs) and Thiobarbituric Acid Reactive Substances (TBARS). Human RBCs were separated from heparinized blood that was drawn from a healthy donor. The 5% suspension of RBC in PBS (pH 7.4) was incubated under air at 37 °C for 5 min into which a PBS solution of AAPH was added to initiate hemolysis. The extent of hemolysis was determined spectrophotometrically as described previously.[36] Briefly, aliquots of the reaction mixture were taken out at appropriate time intervals, diluted with 0.15 M NaCl, and centrifuged at 3000 rpm for 5 min to separate the RBCs. The percentage hemolysis was determined by measuring the absorbance of the supernatant at 540 nm and compared with that of complete hemolysis by treating the same RBC suspension with distilled water. For measurements of TBARS, the erythrocyte ghost was incubated at 37 °C in 0.1 M PBS (pH 7.4) and diluted to a final protein concentration of 0.96 mg/mL. The peroxidation was initiated by the addition of AAPH. The reaction mixture was gently shaken at 37 °C, and aliquots of the reaction mixture were taken out at specific intervals to which a TCA−TBA−HCl stock solution (15% w/v trichloroacetic acid; 0.375% w/v TBA; 0.25 M HCl) was added, together with 0.02% w/v BHT. This amount of BHT completely prevents the formation of any nonspecific TBARS from the decomposition of AAPH during the subsequent boiling. The solution was heated in a boiling water bath for 15 min. After cooling, the precipitate was removed by centrifugation. TBARS in the supernatant were quantified at 532 nm using the extinction coefficient of 1.56×10^5 M^{-1} cm^{-1}.[37]

Cell Cultures. The rat adrenal pheochromocytoma cell line, PC12 cells, was obtained from Shanghai Institute of Biochemistry and Cell Biology, Chinese Academy of Sciences, and was cultured in DMEM supplemented with 10% FBS, 2 mM glutamine, and 100 units mL^{-1} penicillin/streptomycin and maintained in an atmosphere of 5% CO_2 at 37 °C.

MTT Assay and Lactate Dehydrogenase (LDH) Release Assay. To evaluate the cytotoxicity, PC12 cells (1×10^4 cells/well) were seeded in 96-well plates for 1 day followed by incubation with 6-DG or other agents for 24 h at 37 °C. For the H_2O_2 or 6-OHDA injury model, PC12 cells (1×10^4 cells/well) were plated in a 96-well plate and allowed to adhere for 24 h and then treated with the drugs for 24 h. After replacement with fresh medium containing 600 μM H_2O_2 for 12 h or 200 μM 6-OHDA for 24 h, cell viability was determined by MTT assay. At the end of the treatment, 10 μL of MTT (5 mg/mL) was added to each well and incubated for an additional 4 h at 37 °C. One hundred microliters of extraction buffer (10% SDS, 5% isobutanol, 0.1% HCl) was added, and the cells were incubated overnight at 37 °C. Cells treated with DMSO alone were used as controls. The absorbance was measured at 570 nm on a Multiskan GO (Thermo Scientific). For the LDH release assay, the cells (2×10^5 cells/well) were plated in 12-well plates. The following day, the cells were exposed to various concentrations of 6-DG for 24 h, followed by the addition of 600 μM H_2O_2 for an additional 12 h or 200 μM 6-OHDA for an additional 24 h. The leakage of LDH from cultured cells was quantified by measuring LDH activity in culture media. Briefly, 50 μL of culture medium was mixed with 110 μL of 100 mM Tris-HCl (pH 7.4) containing 20 μL of 2 mM NADH and 20 μL of 20 mM pyruvate, and the $A_{340\ nm}$ change was monitored every 20 s for 5 min. The content of LDH release was calculated by normalizing the LDH activity of samples to that measured in culture medium from the control cells.

Hoechst 33342 Staining and Assessment of the Intracellular ROS.[29,30] PC12 cells (2×10^5 cells/well) were seeded into 12-well plates. After 24 h, the cells were treated with 6-DG for another 24 h followed by replacement with fresh medium containing 600 μM H_2O_2 for 12 h or 200 μM 6-OHDA for 24 h. Hoechst 33342 was subsequently added to a final concentration of 5 μg/mL to stain the nuclei. The cells were visualized and photographed under a Leica inverted fluorescent microscope. For assaying the ROS, the medium was removed, and DCFH-DA in fresh FBS-free medium was added (10 μM); incubation was continued for 30 min at 37 °C in the dark. The cells were visualized and photographed under fluorescent microscopy.

Measurement of Caspase-3 Activity. PC12 cells (1×10^6 cells/well) were seeded in 60 mm dishes for 24 h and then treated with different concentrations of 6-DG for another 24 h. After replacement with fresh medium containing 600 μM H_2O_2 or 200 μM 6-OHDA for 24 h, the cells were lysed with RIPA buffer. The protein content was quantified using the Bradford procedure. The caspase-3 activity in the lystae was determined by following the published procedure.[38] Briefly, a cell extract containing 15 μg of total proteins was incubated with the assay mixture (50 mM Hepes, 2 mM EDTA, 5% glycerol, 10 mM DTT, 0.1% CHAPS, 0.2 mM Ac-DEVD-pNA, pH 7.5) for 4 h at 37 °C in a final volume of 100 μL. The absorbance at 405 nm was measured using a microplate reader. The same amounts of DMSO were added to the control experiments, and the activity was expressed as the percentage of the control.

Measurement of Total Glutathione, NQO1 Activity, Trx Activity, and TrxR Activity. PC12 cells (1×10^6 cells/well) were seeded in 60 mm dishes for 24 h and treated with different concentrations of 6-DG for another 24 h. After replacement with fresh medium containing H_2O_2 (600 μM) for 12 h or 6-OHDA (200 μM) for 24 h, cells were collected and resuspended in extraction buffer containing 0.1% Triton X-100 and 0.6% sulfosalicyclic acid in 0.1 M PBS with 5 mM EDTA, pH 7.5 (KPE buffer). The suspension was sonicated on ice for 2−3 min with vortexing every 30 s. The cells were centrifuged at 3000g for 4 min at 4 °C, and the supernatant was ready for the total GSH assay by enzymatic detection as described in the published protocols.[39] A 120 μL solution containing 0.33 mg/mL DTNB and 1.66 units/mL glutathione reductase was added to each sample (20 μL). β-NADPH (60 μL of 0.66 mg/mL) was then added quickly, and the absorbance at 412 nm was measured every 15 s for 2 min. The rate of chromophore production at 412 nm is proportional to the concentration of glutathione within the sample. The total glutathione content in the samples was determined by comparison with the predetermined glutathione standard curve. For measuring NQO1, Trx, and TrxR activity, the cells were lysed in RIPA buffer. The total protein content was quantified using the Bradford procedure. The NQO1 activity was determined spectrophotometrically by monitoring the reduction of the electron acceptor, DCPIP, at 600 nm.[40] The enzymatic reaction was initiated by the addition of cell lysate (5 μg of total protein) to the reaction mixture (20 mM Tris-HCl, pH 7.4, 200 μM NADH, and 40 μM DCPIP), and the decrease in absorbance at 600 nm was measured every 8 s for 2 min at room temperature in the presence or absence of 20 μM dicoumarol. The dicoumarol-inhibitable part of DCPIP's reduction was used to calculate the NQO1 activity. The same amounts of DMSO were added to the control experiments, and the activity was expressed as the percentage of the control. The Trx and TrxR activities in the lysate were determined by following the published protocols.[41] To determine the activity of TrxR, the cell extract containing 20 μg of total proteins was incubated in a final reaction volume of 50 μL containing 100 mM

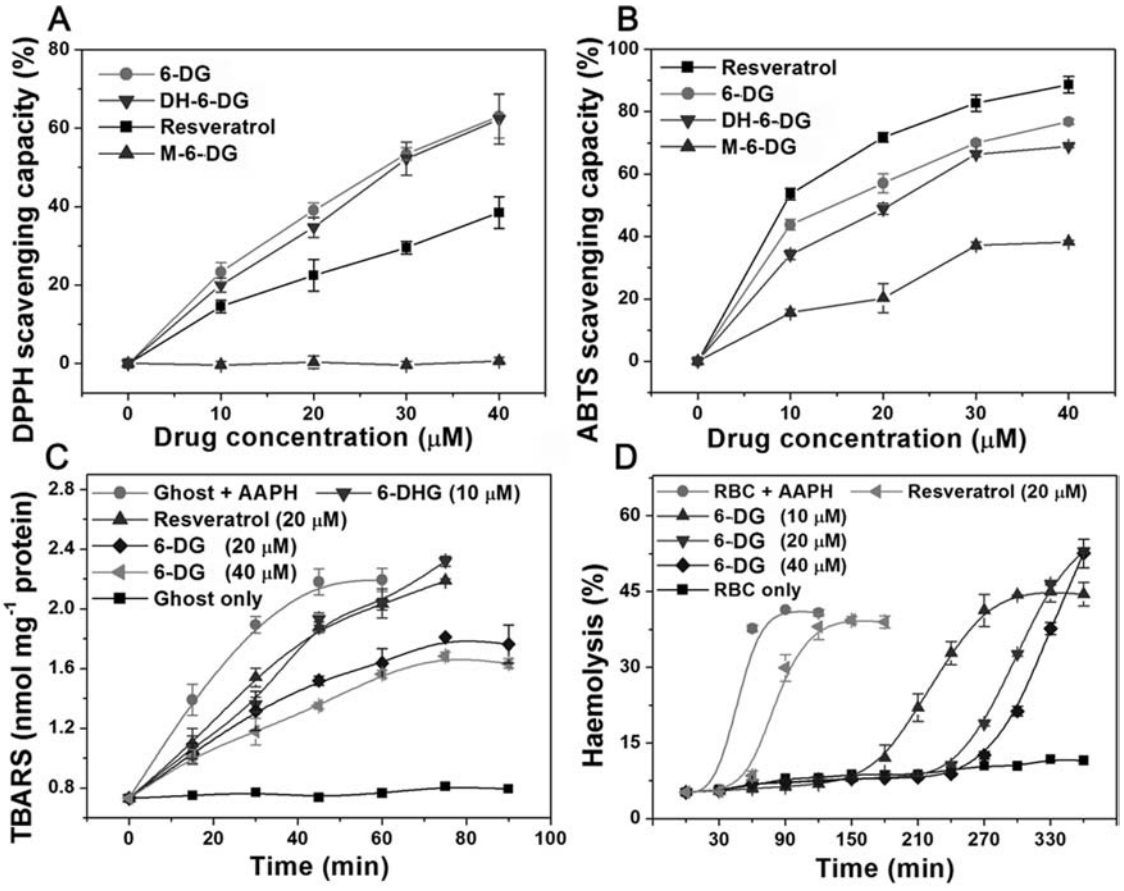

Figure 1. Antioxidant activity of 6-DG in vitro: (A) DPPH and (B) $ABTS^{\bullet+}$ scavenging abilities measured as described under Materials and Methods; (C) inhibition of TBARS formation during the AAPH-induced peroxidation of erythrocyte ghost by 6-DG; (D) protection of 6-DG against AAPH-induced hemolysis of RBC. Data represent the mean ± SD of three independent experiments.

Tris-HCl (pH 7.6), 0.3 mM insulin, 660 μM NADPH, 3 mM EDTA, and 15 μM *Escherichia coli* Trx for 30 min at 37 °C. To determine the activity of Trx, the cell extract containing 20 μg of total proteins was incubated in a final reaction volume of 50 μL containing 100 mM Tris-HCl (pH 7.6), 0.3 mM insulin, 660 μM NADPH, 3 mM EDTA, and 60 nM recombinant rat TrxR1 for 30 min at 37 °C. The reaction was terminated by adding 200 μL of 1 mM DTNB in 6 M guanidine hydrochloride, pH 8.0. A blank sample, containing everything except Trx (for TrxR assay) or TrxR (for Trx assay), was treated in the same manner. The absorbance at 412 nm was measured, and the blank value was subtracted from the corresponding absorbance value of the sample. The same amounts of DMSO were added to the control experiments, and the activity was expressed as the percentage of the control.

Real-Time Reverse Transcription-PCR (RT-PCR). PC12 cells (1×10^6 cells/well) were seeded in 60 mm dishes for 24 h and treated with 10 μM 6-DG for 0, 6, 12, and 24 h. Total RNA was isolated from cells using the RNAiso plus (TaKaRa, Dalian, China) according to the manufacturer's protocol and quantified through 260/280 absorbance. Reverse transcription was performed using Primescript RT reagent kit according to the manufacturer's protocol (TaKaRa). RT-PCR was performed on an Mx3005P RT-PCR System (Agilent Technologies) using SYBR Green PCR Master Mix (Takara) . The GAPDH was used as an internal control. Target gene expression was measured and was normalized to the GAPDH expression level. PCR primers specific to each gene are as follows: GAPDH, 5′-cagtgccagcctcgtctcat-3′ and 5′-aggggccatccacagtcttc-3′; HO-1, 5′-gccctggaagaggagatagag-3′ and 5′-tagtgctgtgtggctggtgt-3′; NQO1, 5′-tcaccactctactttgctccaa-3′ and 5′-ttttctgctcctcttgaacctc-3′; Trx1, 5′-ccttctttcattccctctgtgac-3′ and 5′-cccaacctttgaccctttttat-3′; TrxR1, 5′-actgctcaatccacaaacagc-3′ and 5′-ccacggtctctaagccaatagt-3′; GCLC, 5′-caaggacaagaacacaccatct-3′ and 5′-cagcactcaaagccataacaat-3′; GCLM, 5′-ggcacaggtaaaacccaatagt-3′ and 5′-ttcaatgtcagggatgctttct-3′. GAPDH was used as an internal control. Target gene expression was measured and was normalized to the GAPDH expression level.

Preparation of Different Protein Extracts for Western Blot Analysis.[42] For the whole cell protein extraction, PC12 cells were lysed with RIPA buffer. For the cytosolic and nuclear extracts, the cells were rinsed with ice-cold PBS and resolved in 100 μL of buffer A (10 mM Hepes, pH 7.9, 10 mM KCl, 0.1 mM EDTA, 0.1 mM EGTA, 1 μM DTT, and 1 μM protease inhibitor cocktail freshly added to buffer A). After 15 min of incubation, 10 μL of Nonidet-P40 (10%) was added, and the mixture was vortexed for 15 s. Thereafter, the lysate was repeatedly centrifuged for 10 min (1000*g*, 4 °C) to separate the nuclear from the cytosolic fraction. The pellet was resuspended in 100 μL of buffer B (20 mM Hepes, pH 7.9, 0.4 M NaCl, 1 mM EDTA, 1 mM EGTA, 1 μM DTT, and 1 μM protease inhibitor cocktail were freshly added to buffer B) and incubated on ice for 15 min, and the mixture was vortexed for 10−15 s every 2 min. After a final centrifugation step for 10 min (20000*g*, 4 °C), the supernatant was collected as the nuclear extract. The band intensity was analyzed and quantified by Image pro plus (IPP) software.

Knockdown of Nrf2 Expression Using Short Hairpin RNAs. Three shRNAs (shNrf2-842, shNrf2-184, and shNrf2-136) targeting rat Nrf2 gene and one shRNA with scrambled sequence (shNT) as control were used for Nrf2 knockdown experiments. Exponentially growing cells were transfected with different shRNAs using GeneTran III transfection reagent according to the manufacturer's instruction. After 48 h of transfection, the cells were maintained in DMEM, 10% FBS, 2 mM glutamine, 100 units/mL penicillin/streptomycin at 37 °C in a humidified atmosphere of 5% CO_2 and selected by

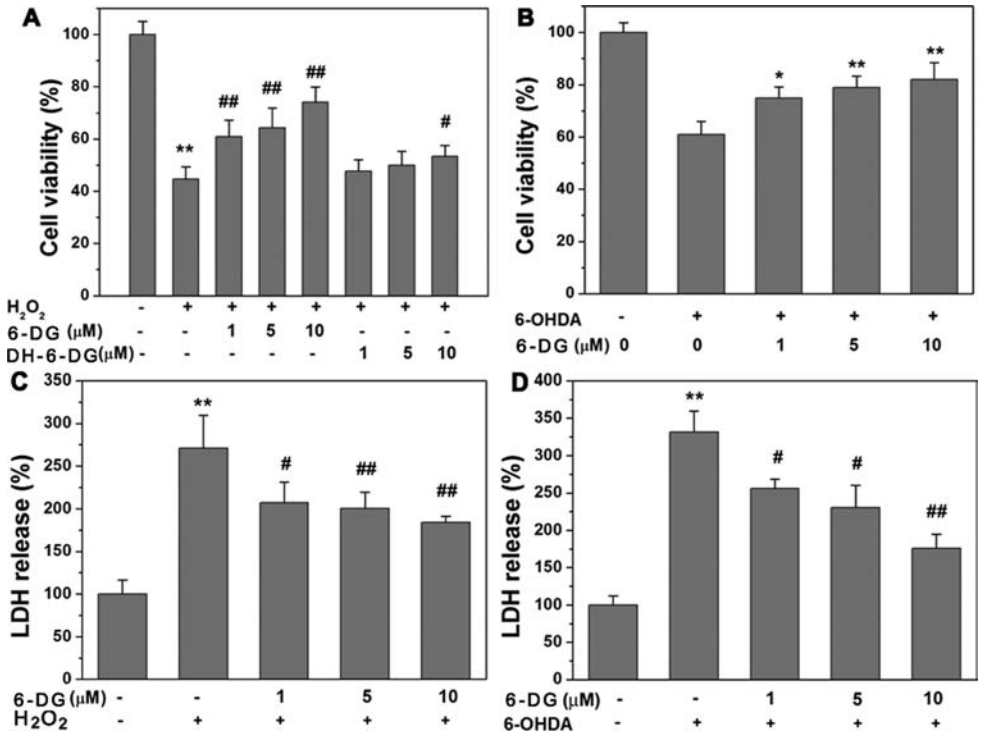

Figure 2. Protection of 6-DG against (A) H_2O_2- and (B) 6-OHDA-induced PC12 cell damage. PC12 cells (1×10^4 cells/well) were plated in a 96-well plate for 1 day and subsequently treated with 6-DG for another 24 h. After replacement of the medium containing H_2O_2 or 6-OHDA and continued incubation for indicated times, cell viability was measured by MTT assay. The content of LDH in the medium after H_2O_2 (C) or 6-OHDA (D) treatment was determined as described under Materials and Methods. All data represent the mean ± SD of three independent experiments. (*) $P < 0.05$ and (**) $P < 0.01$ versus the vehicle group; (#) $P < 0.05$ and (##) $P < 0.01$ versus the H_2O_2- or 6-OHDA-treated group.

supplementation with 0.5 mg/mL of G418. Knockdown of the Nrf2 expression in the cells was analyzed by Western blotting.

Statistics. Data are presented as the mean ± standard deviation (SD). Statistical differences between two groups were assessed by Student's *t* test. Comparisons among multiple groups were performed using one-way analysis of variance (ANOVA), followed by a post hoc Scheffe test. $P < 0.05$ was used as the criterion for statistical significance.

RESULTS

Scavenging of Free Radicals in Vitro. Previous studies have indicated that 6-DG is an effective antioxidant.[25] We further investigated herein the potency of 6-DG in scavenging free radicals in vitro. As shown in Figure 1A,B, 6-DG dose-dependently neutralizes DPPH and ABTS free radicals. To address the role of the hydroxyl group in scavenging radicals, we prepared M-6-DG, the methylated form of 6-DG. M-6-DG completely lost the ability to quench DPPH, whereas it retained partial capacity to scavenge ABTS. The remaining activity might be due to the 1,3-diketone structure in 6-DG as this moiety could also quench radicals.[25] Our results demonstrated the critical role of the hydroxyl group in scavenging free radicals. Thermal decomposition of AAPH in aqueous solution under aerobic condition constantly generates peroxyl radicals,[36] which attack membrane lipids to induce lipid peroxidation. We found 6-DG efficiently protects the erythrocyte ghost from AAPH-induced formation of TBARS, a biomarker of lipid peroxidation (Figure 1C). In the model of AAPH-induced hemolysis of intact human RBC, 6-DG remarkably retards the hemolysis with a clear concentration dependence (Figure 1D).

Protection of PC12 Cells from H_2O_2- and 6-OHDA-Induced Damage. As 6-DG demonstrates potent antioxidant activity in vitro, we next investigated if 6-DG has a protective effect against oxidative stress-induced neuronal cell death. 6-DG shows weak cytotoxicity toward PC12 cells, and significant cytotoxicity was observed only at high concentrations (>50 μM, data not shown). As shown in Figure 2A, compared with the control group, PC12 cells treated with H_2O_2 for 12 h showed about 60% cell death. However, pretreatment of cells with 6-DG at nontoxic concentrations (1−10 μM) for 24 h followed by H_2O_2 challenge significantly decreased the population of dead cells to about 30%. This protection was observed even at 1 μM 6-DG. However, hydrogenation of 6-DG to DH-6-DG almost completely blocked the protection, indicating the importance of the α,β-unsaturated ketone structure in 6-DG. The neurotoxin 6-OHDA has been widely used to generate an experimental model of PD. 6-OHDA-mediated neurotoxicity is engendered, at least in part, by generation of ROS.[43] 6-OHDA treatment reduced cell viability to about 60% of control (Figure 2B). Similarly, addition of 6-DG also markedly promoted cell viability to >80% of control. LDH is a soluble cytosolic enzyme that is released into the culture medium following loss of membrane integrity resulting from cell damage. To confirm the neuroprotection of 6-DG, we determined the content of LDH leakage after H_2O_2 or 6-OHDA insult (Figure 2C,D). Both H_2O_2 and 6-OHDA cause ∼3-fold increase of LDH release. Pretreatment of PC12 cells with 6-DG significantly reduces the leakage of LDH. Taken together, 6-DG at nontoxic concentration can significantly protect PC12 cells from H_2O_2- and 6-OHDA-induced cell damage.

Alleviation of H_2O_2- and 6-OHDA-Induced PC12 Cell Apoptosis by 6-DG. Apoptosis is a precisely regulated process of cell destruction with specific defining morphological and molecular features. Two known apoptotic signaling

dx.doi.org/10.1021/jf405553v | J. Agric. Food Chem. 2014, 62, 5507−5518

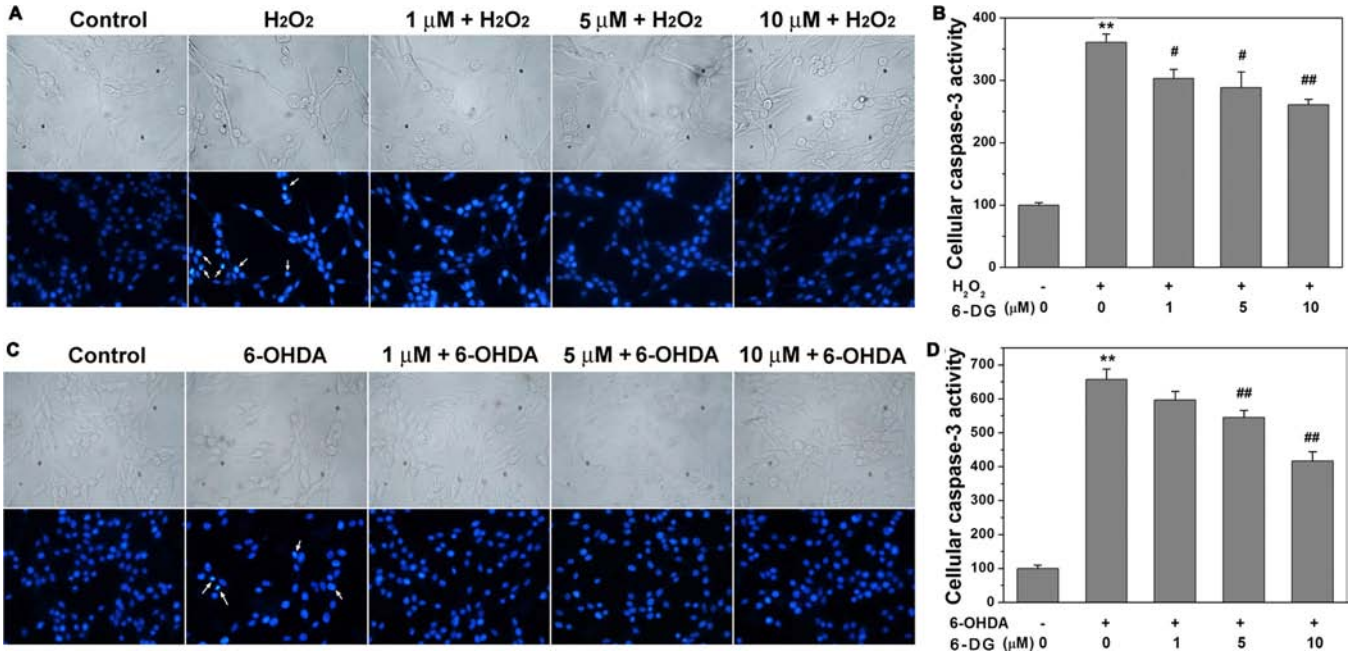

Figure 3. Inhibition of H_2O_2- or 6-OHDA-induced apoptosis in PC12 cells. PC12 cells were treated as described under Materials and Methods, and the morphological changes of nuclei were determined by Hoechst 33342 staining (A, C). Activation of the cellular caspase-3 was determined by a colorimetric assay as described under Materials and Methods. Data represent the mean ± SD of three independent experiments. (**) $P < 0.01$ versus the vehicle group; (#) $P < 0.05$ and (##) $P < 0.01$ versus the H_2O_2- or 6-OHDA-treated group.

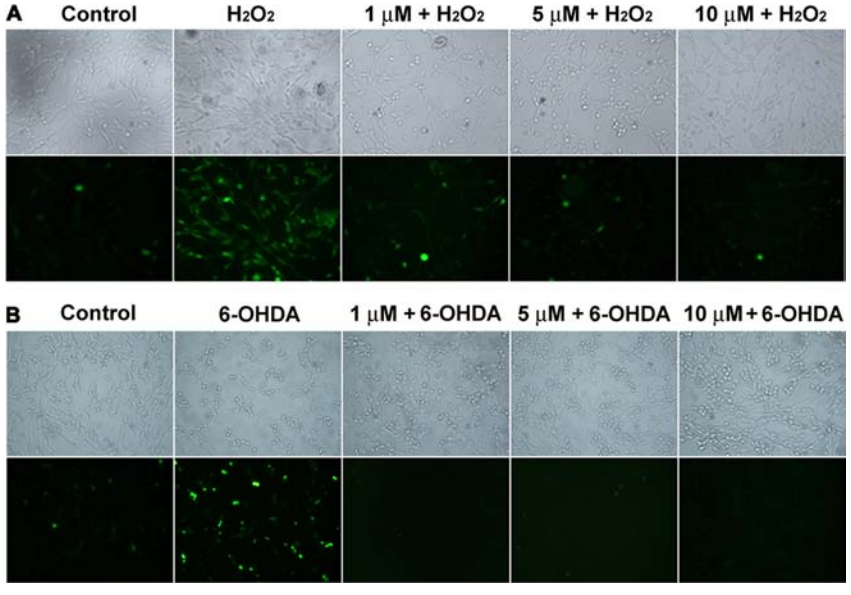

Figure 4. Prevention of ROS accumulation in PC12 cells by 6-DG. Pretreatment with 6-DG significantly alleviates ROS accumulation induced by H_2O_2 (A) or 6-OHDA (B) determined by DCFH-DA staining as described under Materials and Methods. The phase contrast (top panel) and fluorescence (bottom panel) images were acquired by inverted fluorescence microscopy.

pathways, the extrinsic cell surface receptor pathway[44] and the intrinsic mitochondrial pathway,[45] converge on the caspase activation.[46] As shown in Figure 3A,C, both H_2O_2 and 6-OHDA elicit apoptosis in PC12 cells evidenced by the appearance of apoptotic nuclei as highly fluorescent, condensed bodies (indicated by arrows), whereas no apoptotic nuclei were observed in control cells. Pretreatment of PC12 cells with 6-DG remarkably lowers the population of apoptotic nuclei. Activation of caspase-3 is a biochemical character in all apoptotic cells.[47] We thus further quantified the level of caspase-3 activation. Both H_2O_2 and 6-OHDA activate the cellular caspase-3, but with different potencies (Figure 3B,D). Again, 6-DG significantly alleviates the extent of caspase-3 activation in a concentration-dependent manner. Collectively, 6-DG, at nontoxic concentrations, can alleviate H_2O_2- and 6-OHDA-induced apoptosis in PC12 cells.

Inhibition of ROS Accumulation in PC12 Cells. DCFH-DA is a cell membrane permeable dye. After diffusing into cells, DCFH-DA is deacetylated by cellular esterases to non-fluorescent 2′,7′-dichlorodihydrofluorescin, which is rapidly converted to highly fluorescent 2′,7′-dichlorofluorescein upon reacting with ROS. Stimulation of the cells with H_2O_2 or 6-

OHDA leads to an intracellular burst of ROS, whereas the control cells display negligible ROS level (Figure 4). Pretreatment of the cells with 6-DG dose-dependently reduces the ROS accumulation. As oxidative stress, arising from the overproduction of ROS, has been implicated in a final common pathway for neurotoxicity in a wide variety of acute and chronic neurological disorders, the inhibition of ROS accumulation in neuronal cells might be the molecular basis of the neuroprotective action of 6-DG.

Induction of Phase II Gene Expression. Analysis of the chemical structure of 6-DG reveals that there is one Michael acceptor moiety (highlighted in a circle in Scheme 1), which is a core structure of many ARE inducers.[5,10,13] In analogy to known ARE activators, we thus hypothesized that 6-DG might activate the cellular ARE response. We measured the expression of Nrf2-driven antioxidant genes (HO-1, NQO1, Trx1, TrxR1, GCLC, and GCLM) after treatment with 6-DG (10 μM) in PC12 cells (Figure 5). The time course studies showed the highest induction of all genes at 6 h after stimulation with 6-DG. A >10-fold increase of the HO-1 mRNA was observed after 6 h of treatment, consistent with HO-1 being a sensitive marker for oxidative/electrophilic stress. The expression of the genes decreased after 6 h, but was still significantly higher at 12 h compared to the control. After treatment with 6-DG for 24 h, the mRNA levels of HO-1 and TrxR1 were back to the control level, whereas the others remained significantly elevated. Taken together, these results indicate that 6-DG is a potent activator of Nrf2-regulated antioxidant defenses.

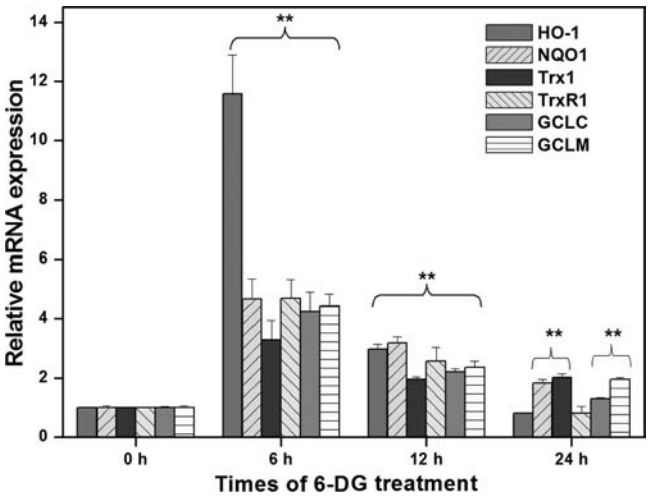

Figure 5. Induction of cytoprotective genes in PC12 cells by 6-DG. The cells were treated as described under Materials and Methods, and the mRNA levels of different genes were analyzed and normalized using GAPDH as an internal standard by qRT-PCR as described. Data represent the mean ± SD of three independent experiments. (**) $P < 0.01$ versus the control group (0 h).

Up-regulation of the Antioxidant Defense System in PC12 Cells. The induction of phase II detoxifying enzymes is an important defense mechanism against exogenous insult. As a series of phase II genes has been up-regulated at different levels, we then examined the corresponding gene products. 6-DG dose-dependently elevated HO-1, NQO1, Trx1, and TrxR1 protein expression and cellular GSH level in PC12 cells (Figure 6). By adopting the convenient assays, we further determined the cellular activity of NQO1, Trx1, and TrxR1. In line with the up-regulation of protein expression, all of the enzymes' activities were significantly increased (Figure 6E,H,K). After 6-DG (10 μM) treatment, the total GSH level (Figure 6L), NQO1 activity (Figure 6E), Trx activity (Figure 6H), and TrxR activity (Figure 6K) were increased by ∼1.6-, ∼2-, ∼1.7-, and ∼1.3-fold, respectively. H_2O_2 and 6-OHDA treatments caused serious GSH depletion (Figure 6M,N), whereas pretreatment with 6-DG gradually restored the total GSH level.

Promotion of Nrf2 Nuclear Localization by 6-DG. Induction of antioxidant gene expression via the Nrf2-dependent cytoprotective pathway requires translocation of Nrf2 from cytosol to nucleus. We therefore examined whether 6-DG could activate the Nrf2 signaling pathway in PC12 cells. Upon 6-DG treatment, immunoblotting results revealed that the Nrf2 expression slightly increased with peaking at 4 h and gradually decreased to the basal level (Figure 7A). Notably, the cytosolic Nrf2 decreased progressively, in coincidence with its continuous rise in the nucleus (Figure 7B,C), indicating the translocation of Nrf2 from cytosol to nucleus. The accumulation of Nrf2 in nuclei thus facilitates its binding to ARE and subsequently initiates the transcription process.

Involvement of Nrf2 in Neuroprotection of 6-DG. To further clarify whether 6-DG protects PC12 cells via the Nrf2 pathway, we conducted Nrf2 knockdown experiments in PC12 cells. The knockdown efficiency of different shRNAs (shNrf2-842, shNrf2-184, shNrf2-136, and shNT) was validated by Western blots (Figure 8A). The expression of Nrf2 protein in all cells transfected with shNrf2s was drastically decreased. Next, we evaluated the protective effect of 6-DG against oxidative insult toward the transfected cells. In line with the cytoprotective function of Nrf2, silence of Nrf2 expression slightly increased the cytotoxicity of H_2O_2 and 6-OHDA (Figure 8B,C). 6-DG displays a similarly protective pattern in PC12-shNT cells as observed in normal PC12 cells. However, this protection drops remarkably in PC12 cells transfected with different shNrf2 plasmids, and the most significant results were observed in PC12-shNrf2-842 cells, where the protection of 6-DG is almost completely abolished upon either H_2O_2- or 6-OHDA-induced cell death. In PC12-shNrf2-184 and PC12-shNrf2-136 cells, the protection of 6-DG is only partially lost. This could be due to the variation of the silence efficiency in cells. Although the protection of 6-DG declines to variable levels in different Nrf2 knockdown cells, the extents of all the decrease are significant. Taken together, these results indicate that the cytoprotection of 6-DG in PC12 cells was mediated through the action of Nrf2.

■ DISCUSSION

ROS are constantly produced under physiological metabolisms, and the intricate balance between their production and neutralization is controlled dynamically by the cellular antioxidant defense system. Oxidative stress, arising from excessive production of ROS, causes damage to proteins, lipids, and nucleic acids and eventually entails cell death. Neuronal cells in the brain are particularly vulnerable to oxidative stress as they possess high concentrations of oxidizable unsaturated fatty acids and high levels of pro-oxidants (e.g., iron) and show high oxygen consumption and low levels of antioxidant defense capacities.[48] Consistent with the above-described sense, there has been increasing evidence underpinning oxidative stress as a major cause in a number of neurodegenerative disorders such as AD and PD.[8,9] Treatment through replacing the dying or dead neurons in these diseases has been demonstrated with limited success.[49] Therefore, pharmacological interventions aiming at

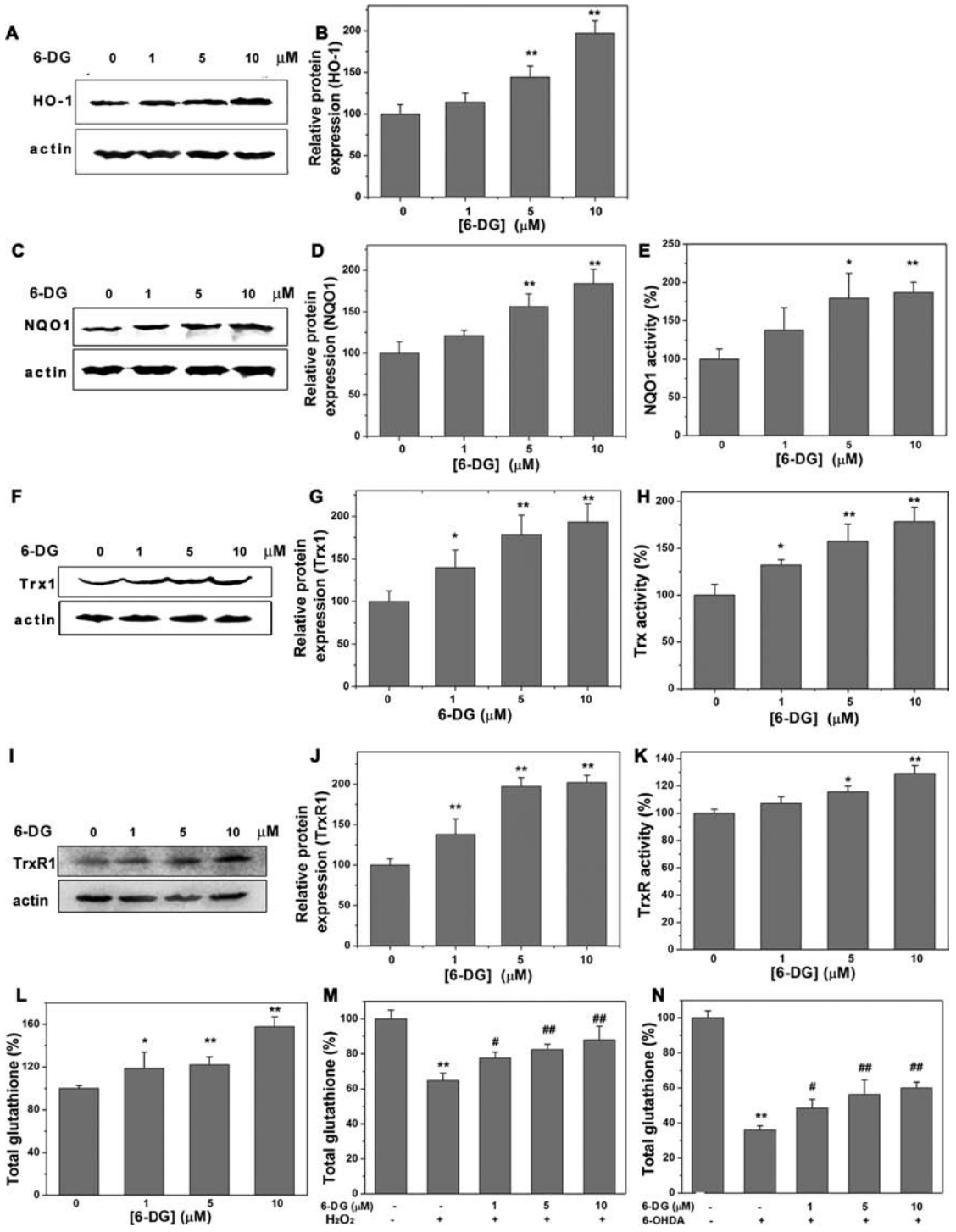

Figure 6. Up-regulation of antioxidant enzymes by 6-DG in PC12 cells. (A) Induction of HO-1 expression by 6-DG. (B) Quantification of the band intensity in panel A. (C) Induction of NQO1 expression and enzyme activity (E) by 6-DG. (D) Quantification of the band intensity in panel C. (F) Induction of Trx1 expression and total Trx enzyme activity (H) by 6-DG. (G) Quantification of the band intensity in panel F. (I) Induction of TrxR1 expression and total TrxR enzyme activity (K) by 6-DG. (J) Quantification of the band intensity in panel I. (L) 6-DG induces up-regulation of GSH in PC12 cells. (M, N) Prevention of H_2O_2- or 6-OHDA-induced GSH depletion by 6-DG. The total intracellular GSH was measured as described under Materials and Methods. Data are expressed as the mean ± SD of three experiments. (*) $P < 0.05$ and (**) $P < 0.01$ versus the vehicle group; (#) $P < 0.05$ and (##) $P < 0.01$ versus the H_2O_2- or 6-OHDA-treated group.

alleviating the oxidative stress are promising to confer protection to neuronal cells, eventually leading to retardation or blockage of the progression of these neurodegenerative diseases. Tactics against oxidative stress include direct antioxidant action by ROS neutralization, as well as indirect antioxidant defense by awakening the pathway(s) involved in the expression of endogenous cytoprotective molecules. In this regard, accumulating attention has been paid to discovering antioxidants or molecules that can induce endogenous

dx.doi.org/10.1021/jf405553v | J. Agric. Food Chem. 2014, 62, 5507−5518

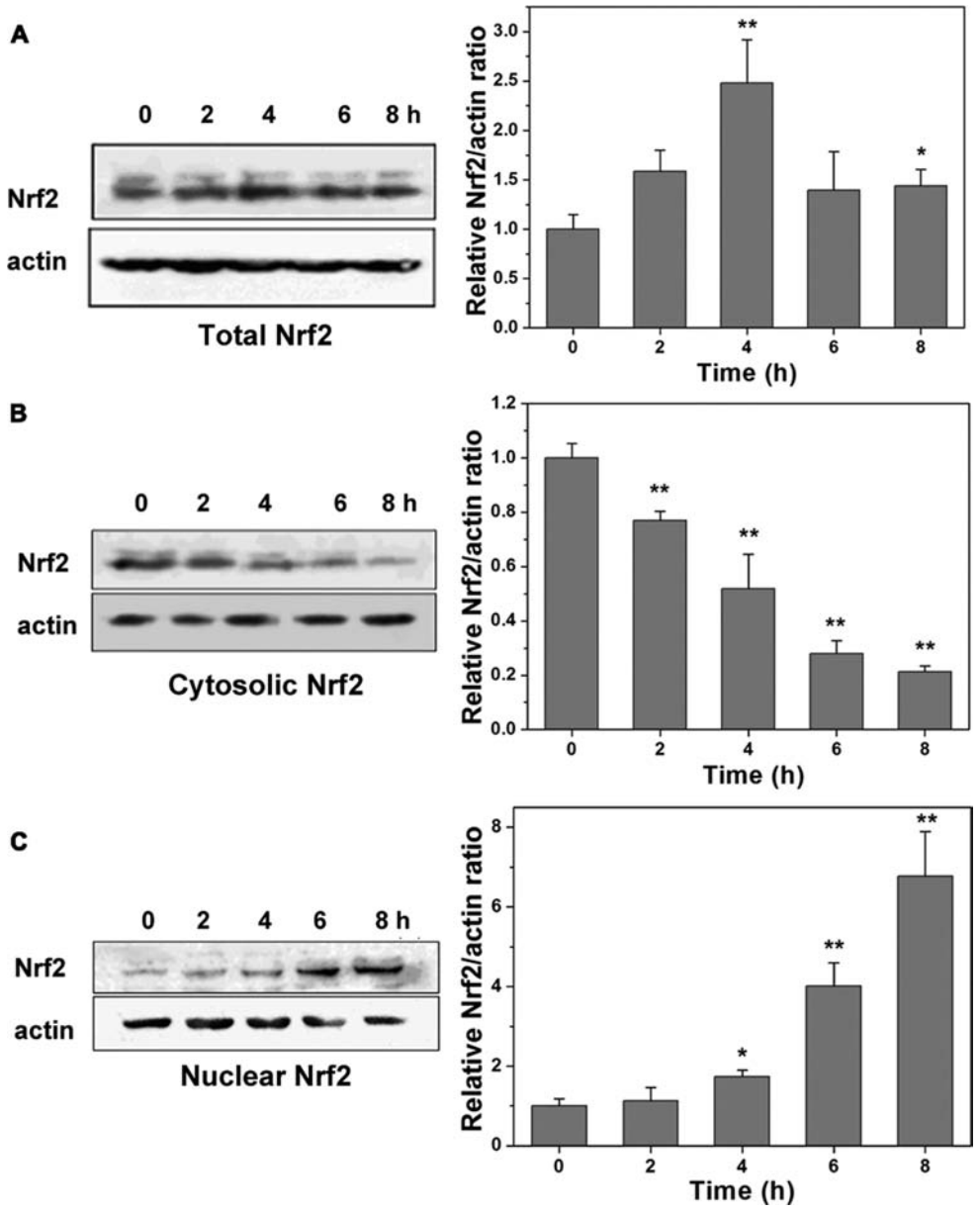

Figure 7. Promotion of Nrf2 nuclear accumulation by 6-DG. After the cells were treated with 6-DG (10 μM) for 0, 2, 4, 6, or 8 h, the cells were harvested and different cell extracts were prepared as described. Total Nrf2 (A), cytosolic Nrf2 (B), and nuclear Nrf2 (C) were analyzed by Western blotting with an antibody against Nrf2. Actin was used as a loading control. Quantification of the blots is presented in the right-hand panel. Data are expressed as the mean ± SD of three experiments. (*) $P < 0.05$ and (**) $P < 0.01$ versus the control group (0 h).

antioxidant defense as potential therapeutic agents for neurodegenerative diseases.[13,16,50,51]

This study demonstrated for the first time that 6-DG, an active constituent from dietary plant ginger, was a promising neuroprotective agent. Although 6-gingerol and 6-shogaol are two major components of ginger, the amount of 6-DG in ginger is also significantly high (up to 20 mg/100 g ginger).[52] Compared to 6-shogaol and 6-DG, 6-gingerol appears to have lower biological activity in different model systems.[53−57] 6-DG has a larger conjugated system than 6-shogaol and contains one additional active 1,3-diketone moiety, which could explain why 6-DG displays better antioxidant activity than 6-shogaol does.[53,54] Furthermore, 6-DG shows lower cytotoxicity than 6-shogaol.[55] The high antioxidant activity and low cytotoxicity make 6-DG an ideal molecule for further development as a therapeutic agent. In our present work, we found that 6-DG, as low as 1 μM, could significantly protect neuronal cells from oxidative insult. This concentration could be easily reached by daily intake of ginger or ginger products. The contribution of 6-DG to the observed activities of ginger and the physiological significance of the neuroprotective action of 6-DG require further investigation.

6-DG both acts as a direct antioxidant in scavenging free radicals in vitro and confers protective effects against oxidative stress-induced neuronal cell damage by activating the cellular antioxidant defense systems. As a phenolic compound, the direct antioxidant action depends primarily on the ability of 6-DG to donate its phenolic H atom to different radicals via a hydrogen abstraction reaction. Our result that M-6-DG almost completely lost free radical-scavenging activity (Figure 1A,B) supports that the hydroxyl group in 6-DG plays a key role in the direct antioxidant activity. More importantly, 6-DG, via

dx.doi.org/10.1021/jf405553v | J. Agric. Food Chem. 2014, 62, 5507−5518

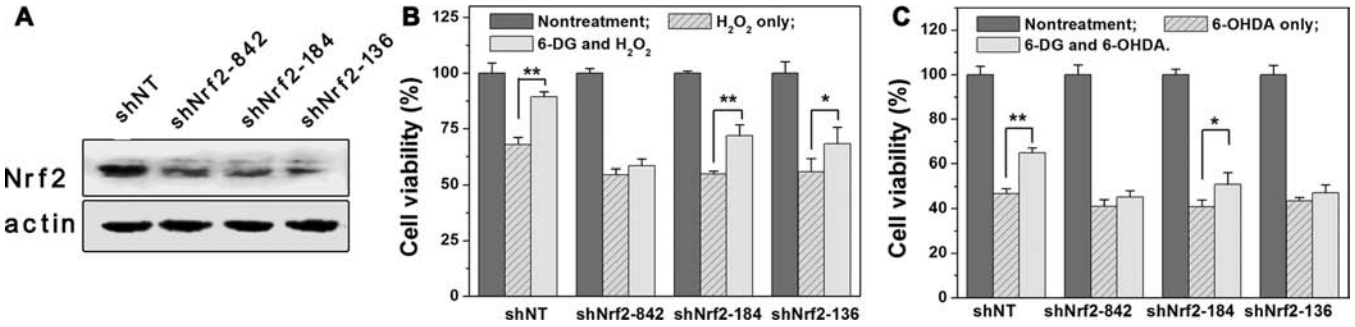

Figure 8. Involvement of Nrf2 in the cytoprotection of 6-DG in PC12 cells. (A) Evaluation of Nrf2 knockdown efficiency by different shRNAs. PC12 cells were transfected with shRNAs specifically targeting rat Nrf2 gene (shNrf2s) or nontargeting shRNA (shNT), and the efficiency of silencing Nrf2 was evaluated by Western blots. (B, C) Impairment of cytoprotection of 6-DG in Nrf2-knockdown cells. Different PC12 cells were treated with 6-DG for 24 h followed by treatment with 600 μM H_2O_2 for 12 h or 200 μM 6-OHDA for 24 h. Cell viability was determined by MTT assay. Results are represented as the mean ± SD (n = 6). (**) $P < 0.01$ and (*) $P < 0.05$.

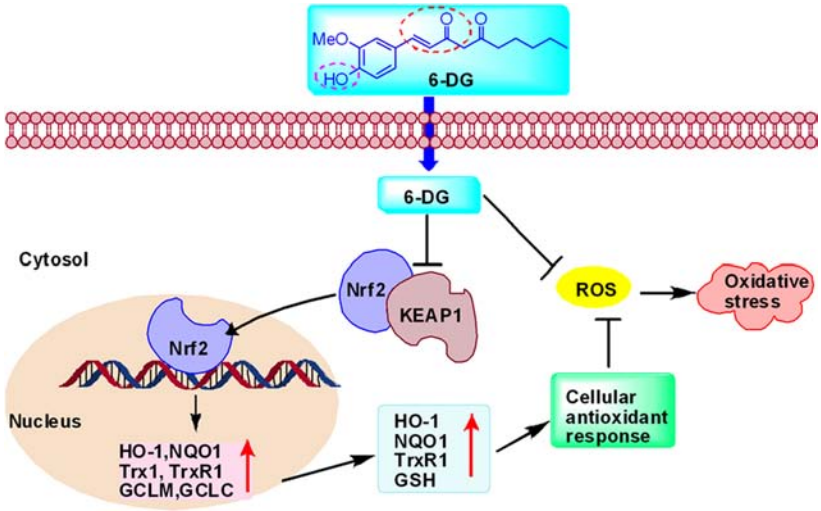

Figure 9. Dual neuroprotective mode of 6-DG in PC12 cells.

activation of the Keap1-Nrf2-ARE pathway, awakens the endogenous antioxidant defense system, including stimulation of GSH synthesis and up-regulation of diverse antioxidant enzyme expression and activity. The nuclear translocation of Nrf2 is a prerequisite for induction of the endogenous antioxidant defense. However, the mechanisms underlying such a process are not well understood but may involve oxidation/alkylation of key thiols in Keap1 and/or phosphorylation of Nrf2.[58] Upon exposure to electrophiles or oxidants, the Cys-rich protein Keap1 is modified by forming a covalent adduct or disulfide bonds within the protein, and it is this Cys-based modification of Keap1 that allows dissociation, accumulation, and subsequent nuclear translocation of Nrf2, where it initiates the transcription of cytoprotective genes (phase II genes).[58] Analysis of the chemical structure of 6-DG reveals that the molecule contains one α,β-unsaturated ketone moiety (highlighted in Scheme 1), a thiol-reactive electrophilic center that may covalently modify the Cys thiols. Many natural or synthetic molecules bearing such a structure are known to be effective inducers of phase II genes.[5,10,59] Thus, we speculated that alkylation of certain Cys residues might be the molecular basis for the activation of the Keap1-Nrf2-ARE pathway by 6-DG, which was supported by the observation that removal of the electrophilic center from 6-DG severely blocks the protection (Figure 2A). The observation that knocking down Nrf2 expression abolishes the effect of 6-DG suggests that the cytoprotection of 6-DG is mediated, at least in part, via Nrf2 activation.

Our findings suggest a dual neuroprotective mechanism of 6-DG shown schematically in Figure 9. The lipophilic character of 6-DG allows it to easily pass the plasma membrane and accumulate within cells. As a phenolic compound, 6-DG may directly counteract against various ROS. Furthermore, 6-DG, like many other electrophiles,[5,10,59] could selectively interact with the Cys residue(s) on the cytosolic protein Keap1, which is an adaptor protein for ubiquitinating Nrf2 and, thus, drives the continuous degradation of Nrf2. The binding of 6-DG to Keap1 perturbs the Keap1-Nrf2 complex and stabilizes Nrf2, causing the liberation of Nrf2 and enabling it to be translocated into nucleus, where it binds to ARE and stimulates the transcription of cytoprotective genes. Thus, 6-DG provides dual protection against oxidative stress-induced neuronal cell damage.

In conclusion, we have demonstrated that 6-DG was effective in preventing oxidative stress-induced neuronal cell damage. This neuroprotection may involve its capacity in directly neutralizing free radicals and activating endogenous cellular antioxidant defense. The hydroxyl group is critical for the direct antioxidant activity, whereas the α,β-unsaturated ketone structure is indispensable for activation of the Keap1-Nrf2-ARE pathway in cells. Our discovery will provide deep insights in understanding 6-DG effects in vivo, and this protective

dx.doi.org/10.1021/jf405553v | J. Agric. Food Chem. 2014, 62, 5507−5518

mechanism could lead to the development of novel small molecules as potential neuroprotective agents.

AUTHOR INFORMATION

Corresponding Author

*(J.F.) E-mail: fangjg@lzu.edu.cn. Fax: +86 931 8915557.

Funding

Financial support from Lanzhou University (Fundamental Research Funds for the Central Universities, lzujbky-2014-56), the National Natural Science Foundation of China for Fostering Talents in Basic Research of the (J1103307), and the 111 project is gratefully acknowledged.

Notes

The authors declare no competing financial interest.

REFERENCES

(1) Kobayashi, M.; Yamamoto, M. Nrf2-Keap1 regulation of cellular defense mechanisms against electrophiles and reactive oxygen species. *Adv. Enzyme Regul.* **2006**, *46*, 113−140.

(2) Itoh, K.; Wakabayashi, N.; Katoh, Y.; Ishii, T.; Igarashi, K.; Engel, J. D.; Yamamoto, M. Keap1 represses nuclear activation of antioxidant responsive elements by Nrf2 through binding to the amino-terminal Neh2 domain. *Genes Dev.* **1999**, *13*, 76−86.

(3) Suzuki, T.; Motohashi, H.; Yamamoto, M. Toward clinical application of the Keap1-Nrf2 pathway. *Trends Pharmacol. Sci.* **2013**, *34*, 340−346.

(4) Kensler, T. W.; Wakabayashi, N.; Biswal, S. Cell survival responses to environmental stresses via the Keap1-Nrf2-ARE pathway. *Annu. Rev. Pharmacol. Toxicol.* **2007**, *47*, 89−116.

(5) Satoh, T.; McKercher, S. R.; Lipton, S. A. Nrf2/ARE-mediated antioxidant actions of pro-electrophilic drugs. *Free Radical Biol. Med.* **2013**, *65C*, 645−657.

(6) Nguyen, T.; Nioi, P.; Pickett, C. B. The Nrf2-antioxidant response element signaling pathway and its activation by oxidative stress. *J. Biol. Chem.* **2009**, *284*, 13291−13295.

(7) Dinkova-Kostova, A. T.; Holtzclaw, W. D.; Kensler, T. W. The role of Keap1 in cellular protective responses. *Chem. Res. Toxicol.* **2005**, *18*, 1779−1791.

(8) Barnham, K. J.; Masters, C. L.; Bush, A. I. Neurodegenerative diseases and oxidative stress. *Nat. Rev. Drug Discov.* **2004**, *3*, 205−214.

(9) Klein, J. A.; Ackerman, S. L. Oxidative stress, cell cycle, and neurodegeneration. *J. Clin. Invest.* **2003**, *111*, 785−793.

(10) Wilson, A. J.; Kerns, J. K.; Callahan, J. F.; Moody, C. J. Keap calm, and carry on covalently. *J. Med. Chem.* **2013**, *56*, 7463−7476.

(11) Alfieri, A.; Srivastava, S.; Siow, R. C.; Modo, M.; Fraser, P. A.; Mann, G. E. Targeting the Nrf2-Keap1 antioxidant defence pathway for neurovascular protection in stroke. *J. Physiol.* **2011**, *589*, 4125−4136.

(12) de Vries, H. E.; Witte, M.; Hondius, D.; Rozemuller, A. J.; Drukarch, B.; Hoozemans, J.; van Horssen, J. Nrf2-induced antioxidant protection: a promising target to counteract ROS-mediated damage in neurodegenerative disease? *Free Radical Biol. Med.* **2008**, *45*, 1375−1383.

(13) Magesh, S.; Chen, Y.; Hu, L. Small molecule modulators of Keap1-Nrf2-ARE pathway as potential preventive and therapeutic agents. *Med. Res. Rev.* **2012**, *32*, 687−726.

(14) Surh, Y. J.; Kundu, J. K.; Na, H. K. Nrf2 as a master redox switch in turning on the cellular signaling involved in the induction of cytoprotective genes by some chemopreventive phytochemicals. *Planta Med.* **2008**, *74*, 1526−1539.

(15) Satoh, T.; Kosaka, K.; Itoh, K.; Kobayashi, A.; Yamamoto, M.; Shimojo, Y.; Kitajima, C.; Cui, J.; Kamins, J.; Okamoto, S.; Izumi, M.; Shirasawa, T.; Lipton, S. A. Carnosic acid, a catechol-type electrophilic compound, protects neurons both in vitro and in vivo through activation of the Keap1/Nrf2 pathway via S-alkylation of targeted cysteines on Keap1. *J. Neurochem.* **2008**, *104*, 1116−1131.

(16) Agrawal, M.; Kumar, V.; Singh, A. K.; Kashyap, M. P.; Khanna, V. K.; Siddiqui, M. A.; Pant, A. B. *trans*-Resveratrol protects ischemic PC12 Cells by inhibiting the hypoxia associated transcription factors and increasing the levels of antioxidant defense enzymes. *ACS Chem. Neurosci.* **2013**, *4*, 285−294.

(17) Wang, J.; Du, X. X.; Jiang, H.; Xie, J. X. Curcumin attenuates 6-hydroxydopamine-induced cytotoxicity by anti-oxidation and nuclear factor-kappa B modulation in MES23.5 cells. *Biochem. Pharmacol.* **2009**, *78*, 178−183.

(18) Kraft, A. D.; Johnson, D. A.; Johnson, J. A. Nuclear factor E2-related factor 2-dependent antioxidant response element activation by *tert*-butylhydroquinone and sulforaphane occurring preferentially in astrocytes conditions neurons against oxidative insult. *J. Neurosci.* **2004**, *24*, 1101−1112.

(19) Arredondo, F.; Echeverry, C.; Abin-Carriquiry, J. A.; Blasina, F.; Antunez, K.; Jones, D. P.; Go, Y. M.; Liang, Y. L.; Dajas, F. After cellular internalization, quercetin causes Nrf2 nuclear translocation, increases glutathione levels, and prevents neuronal death against an oxidative insult. *Free Radical Biol. Med.* **2010**, *49*, 738−477.

(20) Bahia, P. K.; Rattray, M.; Williams, R. J. Dietary flavonoid (−)epicatechin stimulates phosphatidylinositol 3-kinase-dependent anti-oxidant response element activity and up-regulates glutathione in cortical astrocytes. *J. Neurochem.* **2008**, *106*, 2194−2204.

(21) Son, T. G.; Camandola, S.; Arumugam, T. V.; Cutler, R. G.; Telljohann, R. S.; Mughal, M. R.; Moore, T. A.; Luo, W.; Yu, Q. S.; Johnson, D. A.; Johnson, J. A.; Greig, N. H.; Mattson, M. P. Plumbagin, a novel Nrf2/ARE activator, protects against cerebral ischemia. *J. Neurochem.* **2010**, *112*, 1316−1326.

(22) Wruck, C. J.; Claussen, M.; Fuhrmann, G.; Romer, L.; Schulz, A.; Pufe, T.; Waetzig, V.; Peipp, M.; Herdegen, T.; Gotz, M. E. Luteolin protects rat PC12 and C6 cells against MPP+ induced toxicity via an ERK dependent Keap1-Nrf2-ARE pathway. *J. Neural Transm. Suppl.* **2007**, *72*, 57−67.

(23) Shukla, Y.; Singh, M. Cancer preventive properties of ginger: a brief review. *Food Chem. Toxicol.* **2007**, *45*, 683−690.

(24) Grzanna, R.; Lindmark, L.; Frondoza, C. G. Ginger − an herbal medicinal product with broad anti-inflammatory actions. *J. Med. Food* **2005**, *8*, 125−132.

(25) Patro, B. S.; Rele, S.; Chintalwar, G. J.; Chattopadhyay, S.; Adhikari, S.; Mukherjee, T. Protective activities of some phenolic 1,3-diketones against lipid peroxidation: possible involvement of the 1,3-diketone moiety. *Chembiochem* **2002**, *3*, 364−370.

(26) Chen, C. Y.; Chiu, C. C.; Wu, C. P.; Chou, Y. T.; Wang, H. M. Enhancements of skin cell proliferations and migrations via 6-dehydrogingerdione. *J. Agric. Food Chem.* **2013**, *61*, 1349−1356.

(27) Hsu, Y. L.; Chen, C. Y.; Hou, M. F.; Tsai, E. M.; Jong, Y. J.; Hung, C. H.; Kuo, P. L. 6-Dehydrogingerdione, an active constituent of dietary ginger, induces cell cycle arrest and apoptosis through reactive oxygen species/c-Jun N-terminal kinase pathways in human breast cancer cells. *Mol. Nutr. Food Res.* **2010**, *54*, 1307−1317.

(28) Chen, C. Y.; Tai, C. J.; Cheng, J. T.; Zheng, J. J.; Chen, Y. Z.; Liu, T. Z.; Yiin, S. J.; Chern, C. L. 6-Dehydrogingerdione sensitizes human hepatoblastoma Hep G2 cells to TRAIL-induced apoptosis via reactive oxygen species-mediated increase of DR5. *J. Agric. Food Chem.* **2010**, *58*, 5604−5611.

(29) Duan, D.; Zhang, B.; Yao, J.; Liu, Y.; Sun, J.; Ge, C.; Peng, S.; Fang, J. Gambogic acid induces apoptosis in hepatocellular carcinoma SMMC-7721 cells by targeting cytosolic thioredoxin reductase. *Free Radical Biol. Med.* **2014**, *69*, 15−25.

(30) Duan, D.; Zhang, B.; Yao, J.; Liu, Y.; Fang, J. Shikonin targets cytosolic thioredoxin reductase to induce ROS-mediated apoptosis in human promyelocytic leukemia HL-60 cells. *Free Radical Biol. Med.* **2014**, *70C*, 182−193.

(31) Cai, W.; Zhang, B.; Duan, D.; Wu, J.; Fang, J. Curcumin targeting the thioredoxin system elevates oxidative stress in HeLa cells. *Toxicol. Appl. Pharmacol.* **2012**, *262*, 341−348.

(32) Zhang, L.; Duan, D.; Liu, Y.; Ge, C.; Cui, X.; Sun, J.; Fang, J. Highly selective off-on fluorescent probe for imaging thioredoxin reductase in living cells. *J. Am. Chem. Soc.* **2014**, *136*, 226−233.

(33) OHta, H.; Ozaki, K.; Tsuchihashi, G. Regio- and enantioselective reduction of α,γ-diketones by fermenting bakers' yeast. *Agric. Biol. Chem.* **1986**, *50*, 2499−2502.
(34) Ley, J. P.; Paetz, S.; Blings, M.; Hoffmann-Lucke, P.; Bertram, H. J.; Krammer, G. E. Structural analogues of homoeriodictyol as flavor modifiers. Part III: Short chain gingerdione derivatives. *J. Agric. Food Chem.* **2008**, *56*, 6656−6664.
(35) Re, R.; Pellegrini, N.; Proteggente, A.; Pannala, A.; Yang, M.; Rice-Evans, C. Antioxidant activity applying an improved ABTS radical cation decolorization assay. *Free Radical Biol. Med.* **1999**, *26*, 1231−1237.
(36) Fang, J. G.; Lu, M.; Ma, L. P.; Yang, L.; Wu, L. M.; Liu, Z. L. Protective effects of resveratrol and its analogues against free radical-induced oxidative hemolysis of red blood cells. *Chin. J. Chem.* **2002**, *20*, 1313−1318.
(37) Cai, Y. J.; Fang, J. G.; Ma, L. P.; Yang, L.; Liu, Z. L. Inhibition of free radical-induced peroxidation of rat liver microsomes by resveratrol and its analogues. *Biochim. Biophys. Acta* **2003**, *1637*, 31−38.
(38) Gurtu, V.; Kain, S. R.; Zhang, G. Fluorometric and colorimetric detection of caspase activity associated with apoptosis. *Anal. Biochem.* **1997**, *251*, 98−102.
(39) Rahman, I.; Kode, A.; Biswas, S. K. Assay for quantitative determination of glutathione and glutathione disulfide levels using enzymatic recycling method. *Nat. Protoc.* **2006**, *1*, 3159−3165.
(40) Benson, A. M.; Hunkeler, M. J.; Talalay, P. Increase of NAD(P)H:quinone reductase by dietary antioxidants: possible role in protection against carcinogenesis and toxicity. *Proc. Natl. Acad. Sci. U.S.A.* **1980**, *77*, 5216−5220.
(41) Fang, J.; Holmgren, A. Inhibition of thioredoxin and thioredoxin reductase by 4-hydroxy-2-nonenal in vitro and in vivo. *J. Am. Chem. Soc.* **2006**, *128*, 1879−1885.
(42) Jakubikova, J.; Sedlak, J.; Bod'o, J.; Bao, Y. Effect of isothiocyanates on nuclear accumulation of NF-kappaB, Nrf2, and thioredoxin in caco-2 cells. *J. Agric. Food Chem.* **2006**, *54*, 1656−1662.
(43) Przedborski, S.; Ischiropoulos, H. Reactive oxygen and nitrogen species: weapons of neuronal destruction in models of Parkinson's disease. *Antioxid. Redox Signal.* **2005**, *7*, 685−693.
(44) Locksley, R. M.; Killeen, N.; Lenardo, M. J. The TNF and TNF receptor superfamilies: integrating mammalian biology. *Cell* **2001**, *104*, 487−501.
(45) Desagher, S.; Martinou, J. C. Mitochondria as the central control point of apoptosis. *Trends Cell Biol.* **2000**, *10*, 369−377.
(46) Boatright, K. M.; Salvesen, G. S. Mechanisms of caspase activation. *Curr. Opin. Cell Biol.* **2003**, *15*, 725−731.
(47) Hengartner, M. O. The biochemistry of apoptosis. *Nature* **2000**, *407*, 770−776.
(48) Uttara, B.; Singh, A. V.; Zamboni, P.; Mahajan, R. T. Oxidative stress and neurodegenerative diseases: a review of upstream and downstream antioxidant therapeutic options. *Curr. Neuropharmacol.* **2009**, *7*, 65−74.
(49) Freed, C. R.; Greene, P. E.; Breeze, R. E.; Tsai, W. Y.; DuMouchel, W.; Kao, R.; Dillon, S.; Winfield, H.; Culver, S.; Trojanowski, J. Q.; Eidelberg, D.; Fahn, S. Transplantation of embryonic dopamine neurons for severe Parkinson's disease. *N. Engl. J. Med.* **2001**, *344*, 710−719.
(50) Leiros, M.; Alonso, E.; Sanchez, J. A.; Rateb, M. E.; Ebel, R.; Houssen, W. E.; Jaspars, M.; Alfonso, A.; Botana, L. M. Mitigation of ROS insults by *Streptomyces* secondary metabolites in primary cortical neurons. *ACS Chem. Neurosci.* **2014**, *5*, 71−80.
(51) Albarracin, S. L.; Stab, B.; Casas, Z.; Sutachan, J. J.; Samudio, I.; Gonzalez, J.; Gonzalo, L.; Capani, F.; Morales, L.; Barreto, G. E. Effects of natural antioxidants in neurodegenerative disease. *Nutr. Neurosci.* **2012**, *15*, 1−9.
(52) Shao, X.; Lv, L.; Parks, T.; Wu, H.; Ho, C. T.; Sang, S. Quantitative analysis of ginger components in commercial products using liquid chromatography with electrochemical array detection. *J. Agric. Food Chem.* **2010**, *58*, 12608−12614.
(53) Li, F.; Nitteranon, V.; Tang, X.; Liang, J.; Zhang, G.; Parkin, K. L.; Hu, Q. In vitro antioxidant and anti-inflammatory activities of 1-dehydro-[6]-gingerdione, 6-shogaol, 6-dehydroshogaol and hexahydrocurcumin. *Food Chem.* **2012**, *135*, 332−337.
(54) Wang, H. M.; Chen, C. Y.; Chen, H. A.; Huang, W. C.; Lin, W. R.; Chen, T. C.; Lin, C. Y.; Chien, H. J.; Lin, C. M.; Chen, Y. H. *Zingiber officinale* (ginger) compounds have tetracycline-resistance modifying effects against clinical extensively drug-resistant *Acinetobacter baumannii*. *Phytother. Res.* **2010**, *24*, 1825−1830.
(55) Sang, S.; Hong, J.; Wu, H.; Liu, J.; Yang, C. S.; Pan, M. H.; Badmaev, V.; Ho, C. T. Increased growth inhibitory effects on human cancer cells and anti-inflammatory potency of shogaols from *Zingiber officinale* relative to gingerols. *J. Agric. Food Chem.* **2009**, *57*, 10645−10650.
(56) Chen, B. H.; Wu, P. Y.; Chen, K. M.; Fu, T. F.; Wang, H. M.; Chen, C. Y. Antiallergic potential on RBL-2H3 cells of some phenolic constituents of *Zingiber officinale* (ginger). *J. Nat. Prod.* **2009**, *72*, 950−953.
(57) Kiuchi, F.; Iwakami, S.; Shibuya, M.; Hanaoka, F.; Sankawa, U. Inhibition of prostaglandin and leukotriene biosynthesis by gingerols and diarylheptanoids. *Chem. Pharm. Bull. (Tokyo)* **1992**, *40*, 387−391.
(58) Nguyen, T.; Yang, C. S.; Pickett, C. B. The pathways and molecular mechanisms regulating Nrf2 activation in response to chemical stress. *Free Radical Biol. Med.* **2004**, *37*, 433−441.
(59) Satoh, T.; Lipton, S. A. Redox regulation of neuronal survival mediated by electrophilic compounds. *Trends Neurosci.* **2007**, *30*, 37−45.

JOURNAL OF AGRICULTURAL AND FOOD CHEMISTRY

Article

pubs.acs.org/JAFC

Characterization of Antiproliferative Activity Constituents from *Artocarpus heterophyllus*

Zong-Ping Zheng,[†,∥] Yang Xu,[‡,∥] Chuan Qin,[†] Shuang Zhang,[†] Xiaohong Gu,[†] Yingying Lin,[‡] Guobin Xie,[‡] Mingfu Wang,[§] and Jie Chen*[,†,⊥]

[†]State Key Laboratory of Food Science and Technology, Jiangnan University, Wuxi, Jiangsu, People's Republic of China

[‡]School of Pharmaceutical Sciences, Xiamen University, Xiamen, Fujian, People's Republic of China

[§]School of Biological Sciences, The University of Hong Kong, Hong Kong, People's Reublic of China

[⊥]Synergetic Innovation Center of Food Safety and Nutrition, Jiangnan University, Wuxi, Jiangsu, People's Republic of China

Supporting Information

ABSTRACT: *Artocarpus heterophyllus* is an evergreen fruit tree cultivated in many tropical regions. Previous studies have shown that some of its compositions exhibited potential tyrosinase inhibition activities. This study indentified 8 new phenolic compounds, artoheterophyllins E−J (**1**−**6**), 4-geranyl-2′,3,4′,5-tetrahydroxy-*cis*-stilbene (**7**), and 5-methoxymorican M (**8**) and 2 new natural compounds (**9** and **10**), 2,3-dihydro-5,7-dihydroxy-2-(2-hydroxy-4-methoxyphenyl)-4*H*-benzopyran-4-one and 6-[(1*S*,2*S*)-1,2-dihydroxy-3-methylbutyl]-2-(2,4-dihydroxyphenyl)-5-hydroxy-7-methoxy-3-(3-methyl-2-buten-1-yl)-4*H*-1-benzopyran-4-one, together with 23 known compounds (**11**−**33**), from the ethanol extract of the wood of *A. heterophyllus*. The structures of the eight new compounds (**1**−**8**) and two new natural compounds were established by extensive 1D- and 2D-NMR experiments. The anticancer effects of the isolated compounds were examined in MCF-7, H460, and SMMC-7721 human cancer cell lines by MTT assay. Compounds **5**, **11**, **12**, and **30** significantly reduced the cell viabilities of these cell lines. Especially, compounds **11** and **30** resulted in more potent cytotoxicity than the positive control, 5-fluorouracil (5-Fu), in SMMC-7721 cell line, with IC_{50} values of 15.85 and 12.06 μM, whereas compound **30** exhibited more potent cytotoxicity than 5-Fu in NCI-H460 cell line, with an IC_{50} value of 5.19 μM. In addition, this study suggests that compounds **11** and **30** from the wood of *A. heterophyllus* have anticancer potential via MAPK pathways.

KEYWORDS: *Artocarpus heterophyllus, phenolic compounds, anticancer activity*

INTRODUCTION

Mitogen-activated protein kinases (MAPKs) are serine−threonine kinases, which include extracellular signal-regulated kinase (ERK), p38, and c-Jun NH_2-terminal kinase (JNK). MAPK pathways regulate intracellular signaling including cell apoptosis, proliferation, differentiation, survival, and death.[1] ERKs, JNKs, and p38 MAPKs play a complicated role in cancer development. These MAPK pathways could antagonize cell proliferation, survival, and invasion in some types of cells, whereas they could also promote morphological transformation and cell proliferation in cancer cells. The functions of MAPKs are accordingly dependent on the different cells' responses.[2−5] Especially, these MAPK pathways are expected to provide new strategies for anticancer therapeutic approaches.[1] Therefore, screening selective regulators to different types of cancer cell lines is likely to be a better route to cancer therapies targeted against MAPK pathways.

Artocarpus heterophyllus (jackfruit) is an evergreen fruit tree belonging to the *Artocarpus* genus of the family Moraceae, found in tropical and subtropical regions. *A. heterophyllus* is widely cultivated in tropical regions of India, Bangladesh, Nepal, Sri Lanka, Vietnam, Thailand, Malaysia, Indonesia, Philippines, Africa, and Brazil.[6] It is also an important tropical fruit in southern China, distributed and cultivated in Hainan, Guangdong, Guangxi, and Yunnan provinces.[7] Previous studies suggested that *A. heterophyllus* was rich in phenolic compounds, flavonoids, stilbenoids, and arylbenzofurans and possessed wide medicinal uses including antioxidant, anti-inflammatory, antibacterial, antifungal, antineoplastic, and hypoglycemic effects.[8−13] Furthermore, the extracts and chemicals prepared from *A. heterophyllus* were also found to exhibit cytotoxic effects on T47D, SMMC-7721, SGC-7901, hepatoma, choriocarcinoma, and melanoma cell lines in vitro.[14−18] However, little information is available on the systematic study of the phenolic compounds from *A. heterophyllus* with regard to cytotoxic effects on MCF-7, SMMC-7721, and NCI-H460 cells and pathways. Therefore, we used chromatography to isolate the active components and used NMR and MS to identify the compounds, combined with cytotoxic activity assay to confirm the in vitro anticancer effects of *A. heterophyllus*.

MATERIALS AND METHODS

General Experimental Procedures. Sephadex LH-20 was purchased from GE Healthcare Bio-Sciences AB (Uppsala, Sweden). Silica gel (200−300 mesh) for column chromatography and TLC plates (HSGF254) were purchased from Yantai Jiangyou Silicone Development Co., Ltd. (Yantai, China). Amberlite XAD16 was

Received: January 14, 2014
Revised: April 8, 2014
Accepted: May 22, 2014
Published: May 22, 2014

ACS Publications © 2014 American Chemical Society

purchased from Sigma Chemical Co (St. Louis, MO, USA). Semipreparative HPLC was carried out on a Waters 600 system equipped with a 2487 dual-wavelength detector, Masslynx V4.0 software, and a YMC C18 (2) column (250 × 20 mm, 5 μm). ^{1}H NMR, ^{13}C NMR, DEPT, HMQC, and HMBC spectra were obtained on a Bruker 400 NMR spectrometer. Molecular weights of compounds were analyzed on a Waters Maldi Syapt Q-Tof mass spectrometer. Cell morphologies were observed with Zeiss LSM 5 EXCITER and Zeiss AXIO IMAGER A1 microscopes. Antibodies, inhibitors, and other chemicals, except as otherwise noted, were purchased from Sigma-Aldrich Chemicals.

Plant Material. The wood of *A. heterophyllus* was collected in Wenchang county, Hainan province, China, in May 2012. Voucher specimens (accession no. 20120501) were deposited at the State Key Laboratory of Food Science and Technology, Jiangnan University.

Extraction and Isolation. The wood of *A. heterophyllus* (10 kg) was batched 20 times with 95% ethanol (3 × 2 L) under ultrasound condition. The extract was concentrated under vacuum at 45 °C with a rotor evaporator, and 272.2 g of crude extract was afforded. The crude extract was separated with an Amberlite XAD16 column (eluted with 20, 40, 60, 80, and 95% ethanol) to afford six fractions (1−6). Fraction 1 (5.5 g, 20% ethanol fraction) was subjected to Sephadex LH-20 and was eluted by MeOH/H_2O (1:1) to afford two fractions (1A and 1B). Fraction 1A (4.2 g) was purified by silica gel and was eluted by ethyl acetate/hexane (1:1) to afford **19** (3.8 g). Fraction 1B (86 mg) was further separated by preparative HPLC (eluted by 45% MeOH) to afford **27** (28 mg). Fraction 2 (2.0 g, 40% ethanol fraction) was subjected to silica gel and was eluted by ethyl acetate/hexane (3:1), and then it was separated by Sephadex LH-20 [eluted by MeOH/H_2O (1:1)] to afford **1** (8.8 mg) and another fraction (subfraction A). Subfraction A was further purified by HPLC to obtain **32** (1.9 mg) and **33** (3.4 mg). Fraction 3 (12.7 g, 60% ethanol fraction) was separated by silica gel [CH_2Cl_2/MeOH (20:1)] to give three fractions (3A−3C). Fraction 3A was further purified by Sephadex LH-20 [MeOH/H_2O (1:1)] to get **14** (752 mg). Fraction 3B was separated by Sephadex LH-20 [MeOH/H_2O (1:1)] to afford **16** (2596.4 mg), **22** (6.5 mg), **26** (8.4 mg), **21** (399.3 mg), and **8** (3.1 mg). Fraction 3C was separated by Sephadex LH-20 [MeOH/H_2O (1:1)] to afford two subfractions (B and C). Subfraction B was purified by silica gel [CH_2Cl_2/MeOH (25:1)] to give **28** (14.6 mg). Subfraction C was separated by silica gel [CH_2Cl_2/MeOH (30:1)] and HPLC (47% MeOH) to afford **3** (1.5 mg). Fraction 4 (15.8 g, 60% ethanol fraction) was separated by silica gel [hexane/ethyl acetate (3:1)] to give five fractions (4A−4E). Fraction 4A was purified by Sephadex LH-20 [MeOH/H_2O (1:1)] to afford **20** (2059.3 mg). Fraction 4B was separated by Sephadex LH-20 [MeOH/H_2O (1:1)] to get **23** (24.6 mg). Fraction 4C was purified by Sephadex LH-20 [MeOH/H_2O (1:1)] to obtain **24** (185 mg), **29** (18 mg), and another fraction (subfraction D). Subfraction D was purified by HPLC (60% MeOH) to obtain **7** (13.7 mg). Fraction 4E was separated by Sephadex LH-20 [MeOH/H_2O (1:1)] to afford **9** (88.8 mg). Fraction 5 (24.3 g, 80% ethanol fraction) was separated by silica gel and eluted by CH_2Cl_2, CH_2Cl_2/MeOH (50:1), and CH_2Cl_2/MeOH (25:1) to afford three fractions (5A−5C). Fraction 5A was further purified by silica gel (eluted by CH_2Cl_2) to get **25** (17.4 mg) and **31** (2.6 mg). Fraction 5B was separated by silica gel [eluted by CH_2Cl_2/MeOH (50:1)] to obtain **6** (4.3 mg). Fractioin 5C was separated by Sephadex LH-20 [MeOH/H_2O (3:2)] to offer three fractions (subfractions E−G). Subfraction E was purified by silica gel [CH_2Cl_2/MeOH (50:1)] and then further separated by HPLC (72% MeOH) to give **10** (0.4 mg), **4** (0.9 mg), and **5** (1.6 mg). Subfraction F was separated by silica gel [CH_2Cl_2/MeOH (50:1)] to get **30** (210.8 mg) and another fraction (subfraction H). Subfraction H was separated by Sephadex LH-20 [MeOH/H_2O (1:1)] to get **15** (56.8 mg) and **18** (48.6 mg). Subfraction G was purified by silica gel [CH_2Cl_2/MeOH (25:1)] to obtain **2** (6.4 mg). Fraction 6 (62 g, 95% ethanol fraction) was separated by silica gel and was eluted by CH_2Cl_2 to give **11** (28.9 g), **12** (16.9 g), **13** (1.2 g), and **17** (69 mg).

*Artoheterophyllin E (**1**):* brown amorphous powder; $C_{15}H_{12}O_5$; $[\alpha]^{20}_D$ +0.005 (*c* 0.002, acetone); UV (MeOH) 236, 277 nm; IR (KBr) ν_{max} 3379, 1612, 1463, 1111, 1007 cm^{-1}; ^{1}H NMR (acetone-d_6, 400 MHz) δ 9.28 (1H, s, OH-6′), 9.12 (1H, s, OH-4), 8.91 (1H, s, OH-4′), 7.08 (1H, d, *J* = 8.4 Hz, H-6), 6.31 (1H, dd, *J* = 8.4, 2.4 Hz, H-5), 6.18 (1H, d, *J* = 2.4 Hz, H-3), 5.94 (1H, d, *J* = 2.0 Hz, H-5′), 5.69 (1H, d, *J* = 2.0 Hz, H-3′), 5.20 (1H, m, H-1″), 5.15 (1H, m, H-3″), 2.12 (2H, m, H-2″); ^{13}C NMR (acetone-d_6, 100 MHz) δ 160.3 (C, C-4′), 160.2 (C, C-4), 158.2 (C, C-6′), 155.8 (C, C-2, 2′), 132.4 (CH, C-6), 114.0 (C, C-1), 108.9 (CH, C-5), 103.6 (CH, C-3), 102.4 (C, C-1′), 96.0 (CH, C-5′), 95.0 (CH, C-3′), 67.8 (CH, C-1″), 62.8 (CH, C-3″), 27.8 (CH_2, C-2″). HR-ESI-MS, *m*/*z* 273.0760 [M + H]$^+$ (calcd for $C_{15}H_{13}O_5$, 273.058).

*Artoheterophyllin F (**2**):* brown powder; $C_{24}H_{26}O_4$; $[\alpha]^{20}_D$ −0.008 (*c* 0.0001, $CHCl_3$); UV (MeOH) 246, 324 nm; IR (KBr) ν_{max} 3376, 2964, 1605, 1510, 1447, 1159 cm^{-1}; ^{1}H NMR (acetone-d_6, 400 MHz) δ 8.57 (1H, OH-2′), 8.42 (1H, s, OH-5), 8.39 (1H, s, OH-4′), 7.40 (1H, d, *J* = 8.4 Hz, H-6′), 7.35 (1H, d, *J* = 16.4 Hz, H-7′), 6.87 (1H, d, *J* = 16.4 Hz, H-8′), 6.71 (1H, d, *J* = 10.0 Hz, H-1″), 6.57 (1H, d, *J* = 1.2 Hz, H-2), 6.49 (1H, s, H-6), 6.44 (1H, d, *J* = 2.4 Hz, H-3′), 6.39 (1H, dd, *J* = 8.4, 2.4 Hz, H-5′), 5.58 (1H, d, *J* = 10.0 Hz, H-2″), 5.13 (1H, m, H-6″), 2.14 (2H, m, H-4″), 1.71 (2H, m, H-5″), 1.64 (3H, s, H-9″), 1.57 (3H, s, H-8″), 1.37 (3H, s, H-10″); ^{13}C NMR (acetone-d_6, 100 MHz) δ 159.3 (C, C-4′), 157.1 (C, C-2′), 155.3 (C, C-3), 154.1 (C, C-5), 140.7 (C, C-1), 132.0 (C, C-7″), 128.4 (CH, C-6′), 127.8 (CH, C-2″), 126.1 (CH, C-8′), 125.2 (CH, C-6″), 124.5 (CH, C-7′), 118.4 (CH, C-1″), 117.3 (C, C-1′), 109.4 (C, C-4), 108.6 (CH, C-5′), 106.4 (CH, C-2), 106.3 (CH, C-6), 103.7 (CH, C-3′), 78.7 (C, C-3″), 41.9 (CH_2, C-4″), 26.6 (CH_3, C-10″), 25.9 (CH_3, C-9″), 23.5 (CH_2, C-5″), 17.7 (CH_3, C-8″). HR-ESI-MS, *m*/*z* 379.1905 [M + H]$^+$ (calcd for $C_{24}H_{27}O_4$, 379.1904).

*Artoheterophyllin G (**3**):* yellow powder; $C_{20}H_{18}O_7$; UV (MeOH) 253 nm; ^{1}H NMR (CD_3OD, 400 MHz) δ 7.08 (1H, d, *J* = 8.8 Hz, H-6′), 6.41 (1H, s, H-3′), 6.40 (1H, dd, *J* = 8.8, 2.3 Hz, H-5′), 6.26 (1H, d, *J* = 2.0 Hz, H-8), 6.18 (1H, d, *J* = 2.0 Hz, H-6), 5.39 (1H, br t, *J* = 6.0 Hz, H-2″), 3.82 (2H, s, H-4″), 3.14 (2H, d, *J* = 7.2 Hz, H-1″), 1.46 (3H, s, H-5″); ^{13}C NMR (CD_3OD, 100 MHz) δ 184.3 (C═O, C-4), 166.3 (C, C-7), 164.4 (C, C-2), 164.0 (C, C-5), 162.7 (C, C-9), 160.4 (C, C-4′), 158.4 (C, C-2′), 137.0 (C, C-3″), 133.1 (CH, C-6′), 124.8 (CH, C-2″), 122.2 (C, C-3), 114.0 (C, C-1′), 108.8 (CH, C-5′), 104.6 (CH, C-3′), 106.1 (C, C-10), 100.3 (CH, C-6), 95.3 (CH, C-8), 69.6 (CH_2, C-4″), 25.3 (CH_2, C-1″), 14.3 (CH_3, C-5″). HR-ESI-MS, *m*/*z* 371.1126 [M + H]$^+$ (calcd for $C_{20}H_{19}O_7$, 371.1125).

*Artoheterophyllin H (**4**):* yellow powder; $C_{26}H_{26}O_8$; UV (MeOH) 277 nm; ^{1}H NMR (CD_3OD, 400 MHz) δ 7.08 (1H, d, *J* = 8.0 Hz, H-6′), 6.76 (1H, d, *J* = 16.4 Hz, H-1″), 6.68 (1H, d, *J* = 16.4 Hz, H-2″), 6.56 (1H, s, H-8), 6.41 (1H, overlapped, H-3′), 6.40 (1H, overlapped, H-5′), 5.10 (1H, t, *J* = 6.0 Hz, H-2‴), 3.93 (3H, s, OCH_3), 3.90 (3H, s, OCH_3), 3.11 (2H, d, *J* = 7.2 Hz, H-1‴), 1.59, 1.40 (each 3H, s, H-4‴,5‴), 1.37 (6H, s, H-4″,5″); ^{13}C NMR (CD_3OD, 100 MHz) δ 184.1 (C═O, C-4), 164.7 (C, C-7), 163.9 (C, C-2), 162.2 (C, C-2′), 160.5 (C, C-5), 158.7 (C, C-9), 158.0 (C, C-4′), 139.3 (CH, C-2″), 133.0 (C, C-3‴), 132.5 (CH, C-6′), 122.9 (CH, C-2‴), 122.5 (C, C-3), 119.9 (C, C-1′), 113.4 (CH, C-1″), 109.6 (C, C-6), 108.2 (CH, C-5′), 106.1 (C, C-10), 103.9 (CH, C-3′), 91.0 (CH, C-8), 77.6 (C, C-3″), 56.9 (OCH_3, OCH_3-7,4′), 27.9 (CH_3, CH_3-4″,5″), 26.5 (CH_3, CH_3-4‴), 25.1 (CH_2, CH_2-1‴), 17.8 (CH_3, CH_3-5‴). HR-ESI-MS, *m*/*z* 467.1703 [M + H]$^+$ (calcd for $C_{26}H_{27}O_8$, 467.1700).

*Artoheterophyllin I (**5**):* yellow powder; $C_{26}H_{30}O_7$; UV (MeOH) 266 nm; ^{1}H NMR (acetone-d_6, 400 MHz) δ 13.89 (1H, s, OH-5), 9.21 (2H, s, OH-2′,4′), 7.16 (1H, d, *J* = 8.4 Hz, H-6′), 6.67 (1H, dd, *J* = 16.4, 7.2 Hz, H-2″), 6.55 (1H, d, *J* = 16.4 Hz, H-1″), 6.52 (1H, s, H-8), 6.46 (1H, d, *J* = 2.4 Hz, H-3′), 6.44 (1H, dd, *J* = 8.4, 2.4 Hz, H-5′), 3.92 (3H, s, OCH_3), 2.45 (2H, m, H-1‴), 2.40 (1H, m, H-3″), 2.09, 1.05 (6H, s, H-4‴,5‴), 1.61 (2H, m, H-2‴), 1.07, 1.05 (6H, d, *J* = 6.0 Hz, H-4″,5″); ^{13}C NMR (acetone-d_6, 100 MHz) δ 184.2 (C═O, C-4), 164.5 (C, C-7), 163.1 (C, C-2), 162.1 (C, C-2′), 160.5 (C, C-5), 158.1 (C, C-9), 157.8 (C, C-4′), 142.8 (CH, C-2″), 132.7 (CH, C-6′), 123.7 (C, C-3), 117.6 (CH, C-1″), 113.5 (C, C-1′), 110.4 (C, C-6), 108.7 (CH, C-5′), 106.2 (C, C-10), 104.5 (CH, C-3′), 91.1 (CH, C-8), 70.8 (C, C-3‴), 57.2 (CH_3, OCH_3), 43.6 (CH_2, C-2‴), 34.5 (CH, C-3″), 31.2, 29.9 (CH_3, C-4‴,5‴), 23.7 (CH_3, CH_3-4″,5″), 21.8 (CH_2,

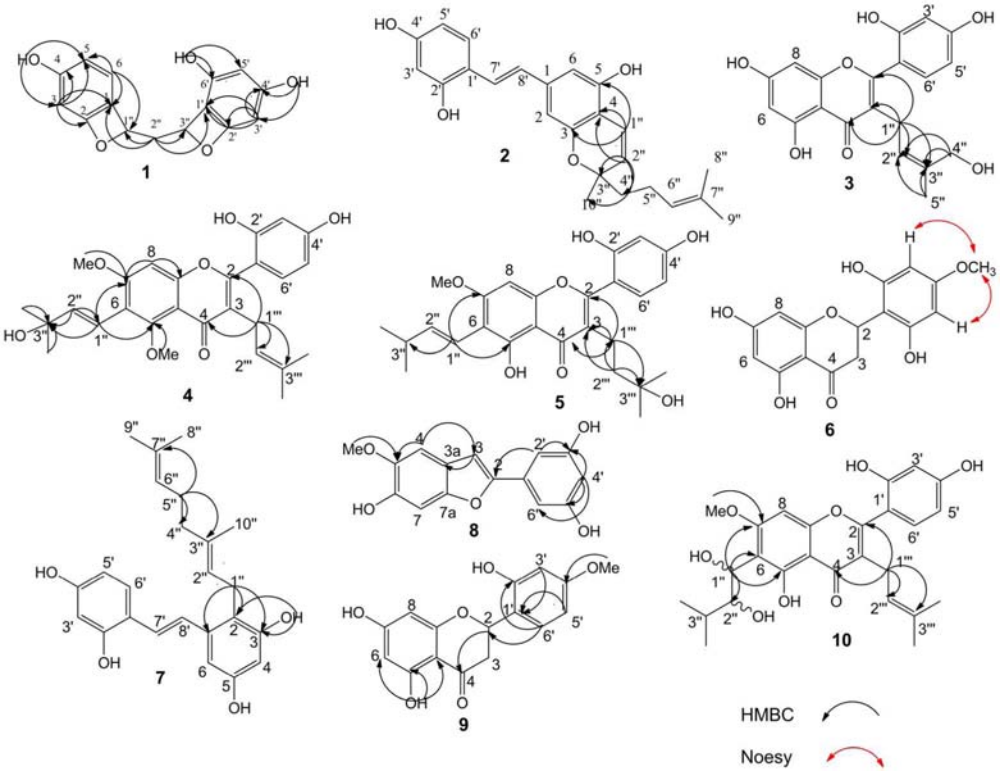

Figure 1. Key HMBC and NOESY of the compounds **1**−**10**.

C-1‴). HR-ESI-MS, *m*/*z* 455.2067 [M + H]$^+$ (calcd for $C_{26}H_{31}O_7$, 455.2064).

Artoheterophyllin J (***6***): pale yellow powder; $C_{16}H_{14}O_7$; $[\alpha]^{20}_D$ −200.0 (*c* 0.002, $CHCl_3$); UV (MeOH) 236, 288 nm; CD (MeOH, *c* 0.0009) $[\theta]_{276}$ +3566; IR (KBr) ν_{max} 3341, 1612, 1594, 1469, 1279, 1152 cm^{-1}; ^{1}H NMR (CD_3OD, 400 MHz) δ 5.97 (2H, s, H-3′,5′), 5.874 (1H, d, *J* = 2.8 Hz, H-8), 5.868 (1H, d, *J* = 2.8 Hz, H-6), 5.84 (1H, dd, *J* = 14.0, 2.8 Hz, H-2), 3.93 (1H, dd, *J* = 17.2, 14.0 Hz, H-3ax), 3.71 (3H, s, OCH_3), 2.41 (1H, dd, *J* = 17.2, 2.8 Hz, H-3eq); ^{13}C NMR (CD_3OD, 100 MHz) δ 199.9 (C═O, C-4), 168.1 (C, C-7), 166.1 (C, C-4′), 165.7 (C, C-9), 163.1 (C, C-5), 159.4 (C, C-2′, 6′), 117.9 (s, C-1′), 105.3 (CH, C-6), 103.4 (C, C-10), 96.9 (C, C-1′), 96.2 (CH, C-8), 94.6 (CH, C-3′,5′), 74.0 (CH, C-2), 55.7 (CH_3, OCH_3), 41.3 (CH_2, C-3). HR-ESI-MS, *m*/*z* 319.0814 [M + H]$^+$ (calcd for $C_{16}H_{15}O_7$, 319.0812).

2-Geranyl-2′,3,4′,5-tetrahydroxy-trans-stilbene (***7***): gray powder; $C_{24}H_{28}O_4$; UV (MeOH) 252, 271 nm; IR (KBr) ν_{max} 3357, 2910, 1609, 1454, 1270, 1137, 1004 cm^{-1}; ^{1}H NMR (acetone-d_6, 400 MHz) δ 8.60, 8.42, 7.38 (3H, OH-5,2′,4′), 8.15 (1H, OH-3), 7.38 (1H, d, *J* = 8.8 Hz, H-6′), 7.23 (2H, s, H-7′,8′), 6.66 (1H, d, *J* = 2.4 Hz, H-6), 6.44 (1H, d, *J* = 2.4 Hz, H-3′), 6.38 (1H, dd, *J* = 8.4, 2.4 Hz, H-5′), 6.33 (1H, d, *J* = 2.4 Hz, H-4), 5.22 (1H, m, H-6″), 5.19 (1H, m, H-2″), 3.45 (2H, d, *J* = 6.4 Hz, H-1″), 2.28 (1H, d, *J* = 7.2 Hz, H-5″), 2.25 (1H, d, *J* = 7.2 Hz, H-4″), 2.16 (1H, d, *J* = 7.2 Hz, H-4″), 2.12 (1H, d, *J* = 7.2 Hz, H-5″), 1.67 (3H, s, H-8″), 1.66 (3H, s, H-9″), 1.62 (3H, s, H-10″); ^{13}C NMR (acetone-d_6, 100 MHz) δ 159.1 (C, C-4′), 157.0 (C, C-2′), 156.9 (C, C-5), 156.8 (C, C-3), 140.1 (C, C-1), 134.6 (C, C-3″), 131.9 (C, C-7″), 128.3 (CH, C-6′), 126.1 (CH, C-2″), 125.6 (CH, C-7′), 125.5 (CH, C-6″), 124.5 (CH, C-8′), 118.4 (C, C-2), 117.7 (C, C-1′), 108.5 (CH, C-5′), 104.3 (CH, C-6), 103.8 (CH, C-3′), 102.5 (CH, C-4), 33.0 (CH_2, C-5″), 27.3 (CH_2, C-4″), 26.0 (CH_3, C-8″), 24.8 (CH_2, C-1″), 23.8 (CH_3, C-10″), 17.8 (CH_3, C-9″). HR-ESI-MS, *m*/*z* 381.2063 [M + H]$^+$ (calcd for $C_{24}H_{29}O_4$, 381.2060).

5-Methoxymorican M (***8***): gum; $C_{15}H_{12}O_5$; UV (MeOH) 244, 323 nm; ^{1}H NMR (acetone-d_6, 400 MHz) δ 8.57 (2H, s, OH-3′,5′), 7.82 (1H, s, OH-6), 7.12 (1H, s, H-4), 7.01 (1H, s, H-3), 7.00 (1H, s, H-7), 6.82 (2H, d, *J* = 2.4 Hz, H-2′,6′), 6.34 (1H, t, *J* = 2.4 Hz, H-4′), 3.89 (3H, s, OCH_3); ^{13}C NMR (acetone-d_6, 100 MHz) δ 160.0 (C, C-3′,5′), 155.7 (C, C-2), 150.7 (C, C-7a), 146.7 (C, C-6), 146.4 (C, C-5), 133.5 (C, C-1′), 121.6 (C, C-3a), 103.7 (CH, C-2′,6′), 103.5 (CH, C-4′), 103.4 (CH, C-4), 102.7 (CH, C-3), 98.5 (CH, C-7), 56.9 (CH_3, OCH_3). HR-ESI-MS, *m*/*z* 273.0959 [M + H]$^+$ (calcd for $C_{15}H_{13}O_5$, 273.0758).

2,3-Dihydro-5,7-dihydroxy-2-(2-hydroxy-4-methoxyphenyl)-4H-1-benzopyran-4-one (***9***): pale yellow powder; $C_{16}H_{14}O_6$; $[\alpha]^{20}_D$ −5.8 (*c* 0.0019, $CHCl_3$); UV (MeOH) 274, 299 nm; CD (MeOH, *c* 0.0009) $[\theta]_{276}$ +6512; IR (KBr) ν_{max} 3356, 2913, 1643, 1596, 1441, 1260, 1156 cm^{-1}; ^{1}H NMR (acetone-d_6, 400 MHz) δ 12.20 (1H, s, OH-5), 9.65 (1H, s, OH-7), 8.64 (1H, s, OH-2′), 7.41 (1H, d, *J* = 7.2 Hz, H-6′), 6.53 (1H, dd, *J* = 7.2, 2.4 Hz, H-5′), 6.52 (1H, d, *J* = 2.4 Hz, H-3′), 5.97 (1H, d, *J* = 2.0 Hz, H-8), 5.95 (1H, d, *J* = 2.0 Hz, H-6), 5.73 (1H, dd, *J* = 13.2, 2.8 Hz, H-2), 3.76 (3H, s, OCH_3), 3.17 (1H, dd, *J* = 17.2, 13.2 Hz, H-3ax), 2.74 (1H, dd, *J* = 17.2, 2.8 Hz, H-3eq); ^{13}C NMR (acetone-d_6, 100 MHz) δ 197.7 (C═O, C-4), 167.4 (C, C-7), 165.4 (C, C-5), 164.8 (C, C-9), 162.0 (C, C-4′), 156.3 (C, C-2′), 129.0 (CH, C-6′), 118.8 (C, C-1′), 106.1 (CH, C-5′), 103.3 (CH, C-10), 102.5 (CH, C-3′), 96.9 (CH, C-6), 95.9 (CH, C-8), 75.4 (CH, C-2), 55.6 (CH_3, OCH_3), 42.7 (CH_2, C-3). HR-ESI-MS, *m*/*z* 303.0865 [M + H]$^+$ (calcd for $C_{16}H_{15}O_6$, 303.0863).

6-[(1S,2S)-1,2-Dihydroxy-3-methylbutyl]-2-(2,4-dihydroxyphenyl)-5-hydroxy-7-methoxy-3-(3-methyl-2-buten-1-yl)-4H-1-benzopyran-4-one (***10***): yellow powder; $C_{26}H_{30}O_8$; UV (MeOH) 260 nm; ^{1}H NMR (CD_3OD, 400 MHz) δ 7.09 (1H, d, *J* = 8.4 Hz, H-6′), 6.58 (1H, s, H-8), 6.42 (1H, d, *J* = 2.0 Hz, H-3′), 6.41 (1H, dd, *J* = 8.4, 2.0 Hz, H-5′), 5.12 (1H, t, *J* = 7.6 Hz, H-2‴), 4.80 (1H, overlapped, H-1″), 4.33 (1H, dd, *J* = 8.8, 2.0 Hz, H-2″), 3.88 (3H, s, OCH_3), 3.11 (2H, d, *J* = 6.8 Hz, H-1‴), 2.66 (1H, s, H-3″), 1.59, 1.40 (each 3H, s, H-4‴,5‴), 0.95, 0.89 (each 3H, d, *J* = 6.8 Hz, H-4″,5″); ^{13}C NMR (CD_3OD, 100 MHz) δ 184.1 (C═O, C-4), 165.9 (C, C-7), 165.0 (C, C-2), 164.0 (C, C-2′), 162.2 (C, C-5), 159.8 (C, C-9), 158.0 (C, C-4′), 133.0 (C, C-3‴), 132.5 (CH, C-6′), 122.8 (CH, C-2‴), 122.8 (C, C-3), 113.3 (C, C-1′), 109.5 (C, C-6), 108.2 (CH, C-5′), 106.0 (C, C-10), 103.9 (CH, C-3′), 91.4 (CH, C-8), 79.8 (CH, C-1″), 77.4 (CH, C-2″), 56.8 (OCH_3, OCH_3-7), 31.1 (CH, C-3″), 26.0, 17.7 (CH_3,

dx.doi.org/10.1021/jf500159z | *J. Agric. Food Chem.* 2014, 62, 5519−5527

CH_3-4‴,5‴), 25.1 (CH_2, CH_2-1‴), 21.2, 15.5 (CH_3, CH_3-4‴,5‴). HR-ESI-MS, m/z 471.2013 $[M + H]^+$ (calcd for $C_{26}H_{31}O_8$, 471.2013).

Cell Culture and Drug Treatment. MCF-7, SMMC-7721, and NCI-H460 cells were cultured in Dulbecco's modified Eagle medium (high-glucose) and RPMI-1640, respectively, plus 10% fetal bovine serum under standard culture conditions. When the cells grew to about 80% confluence, they were subcultured or treated with drugs. The drugs' concentrations were based on the IC_{50} for a 48 h treatment of specific agents on the different cancer cell lines. To determine whether chemicals induced cancer cell apoptosis through caspase-dependent pathways, the spectrum caspase inhibitor 50 μM broad Z-VAD-fmk was applied for 1 h before compound **11** and **30** administrations. To determine whether chemicals induced cancer cell apoptosis via p38, JNK, and ERK pathways, their inhibitors were used to pretreat 1 h before chemical treatment, including 20 μM SB203580, 20 μM SP600125, and 20 μM PD98059.

Morphological Analysis of Apoptosis by DAPI Staining. Morphological changes of apoptosis were detected by fluorescence microscopy after staining with 1 μg/mL DAPI.[19] All experiments were repeated three times.

Growth Inhibition Study. The proliferation of cells was assessed by using the 3-(4,5-dimethylthiazol-2-yl)-2,5-diphenyltetrazolium bromide (MTT) assay, as reported previously.[20] Cells were plated on 96-well microplates in 200 μL (5×10^3/well). After 24 h, the cells were treated with complete medium containing compounds (10, 25, and 50 μM) for 48 h. At the end of experiments, 20 μL of 5 μg/mL MTT was directly added to each well. Cells were then incubated at 37 °C for 4 h. Formazan was solubilized by 100 μL of DMSO and measured at 570 nm. All experiments were repeated three times.

Western Blot Analysis. Total cell lysates were denatured with sample loading buffer and then subjected to SDS-PAGE for protein separation. After transfer onto membranes, the proteins were probed with corresponding antibodies and detected by ECL detection reagents (GE). The primary antibodies for PARP were from Cell Signaling (Beverly, MA, USA). Anti-β-actin was from Sigma. Secondary anti-mouse and -rabbit were from Thermo.

Statistical Analysis. Statistical analysis was done by using a two-tailed Student's t test, and $p < 0.05$ was considered significant. Data are expressed as the mean ± SD. All assays were performed in three independent experiments.

RESULTS AND DISCUSSION

Identification of Compounds 1−33. In total, 33 phenolic compounds, including 25 flavonoids (**3**−**6**, **9**−**27**, **30**, and **31**), 3 stilbene derivatives (**2**, **7**, and **29**), 2 simple resorcinols (**32** and **33**), 2 benzofuran derivatives (**8** and **28**), and one other type of compound (**1**) were isolated from the ethanol extract of woods of *A. heterophyllus*. Their structures were identified as artoheterophyllin E (**1**), artoheterophyllin F (**2**), artoheterophyllin G (**3**), artoheterophyllin H (**4**), artoheterophyllin I (**5**), artoheterophyllin J (**6**), 2-geranyl-2′,3,4′,5-tetrahydroxy-*cis*-stilbene (**7**), 5-methoxymorican M (**8**), 2,3-dihydro-5,7-dihydroxy-2-(2-hydroxy-4-methoxyphenyl)-4*H*-1-benzopyran-4-one (**9**),[21] 6-[(1*S*,2*S*)-1,2-dihydroxy-3-methylbutyl]-2-(2,4-dihydroxyphenyl)-5-hydroxy-7-methoxy-3-(3-methyl-2-buten-1-yl)-4*H*-1-benzopyran-4-one (**10**) (Figure 1),[22] artocarpin (**11**),[23] cycloartocarpin (**12**),[23] cycloartocarpesin (**13**),[23] steppogenin (**14**),[23] artocarpesin (**15**),[23] norartocarpetin (**16**),[23] brosimone I (**17**),[23] isoartocarpesin (**18**),[23] cyanomaclurin (**19**),[23] artocarpanone (**20**),[23] albanin A (**21**),[24] artocarmin A (**22**),[24] apigenin (**23**),[25] artocarpetin (**24**),[23] gemichalcone A (**25**),[24] artocarpfuranol (**26**),[23] morin (**27**),[26] moracin M (**28**),[18] artocarbene (**29**),[27] cudraflavone C (**30**),[28] hypargyflavones A (**31**),[29] 2,4-dihydroxybenzoic acid methyl ester (**32**),[30] and 2,4-dihydroxybenzaldehyde (**33**)[31] on the basis of spectral data and literature reports. Of these, excluding the 12 compounds (**11**−**20**, **24**, and **26**) that had been isolated and identified in our previous studies,[24] an additional 21 compounds, including 8 new compounds, artoheterophyllin E (**1**), artoheterophyllin F (**2**), artoheterophyllin G (**3**), artoheterophyllin H (**4**), artoheterophyllin I (**5**), artoheterophyllin J (**6**), 2-geranyl-2′,3,4′,5-tetrahydroxy-*cis*-stilbene (**7**), 5-methoxymorican M (**8**), and 2 new natural compounds, 2,3-dihydro-5,7-dihydroxy-2-(2-hydroxy-4-methoxyphenyl)-4*H*-1-benzopyran-4-one (**9**) and 6-[(1*S*,2*S*)-1,2-dihydroxy-3-methylbutyl]-2-(2,4-dihydroxy-phenyl)-5-hydroxy-7-methoxy-3-(3-methyl-2-buten-1-yl)-4*H*-1-benzopyran-4-one (**10**), were obtained and identified at this time.

The molecular formula of **1** was deduced to be $C_{15}H_{12}O_5$ by HR-ESI-MS. The ^{1}H NMR spectrum exhibited 12 proton signals, including 3 hydroxy signals at δ_H 9.28 (1H, s), 9.12 (1H, s), and 8.91 (1H, s), 3 proton signals of δ_H 7.08 (1H, d, J = 8.4 Hz), 6.31 (1H, dd, J = 8.4, 2.4 Hz), and 6.18 (1H, d, J = 2.4 Hz) forming one ABX system, 2 resonance signals at δ_H 5.94 (1H, d, J = 2.0 Hz) and 5.69 (1H, d, J = 2.0 Hz) making up a tetrasubstituted phenyl ring, and 3 other signals at δ_H 5.20 (1H, m), 5.15 (1H, m), and 2.12 (2H, m). In the ^{1}H−^{1}H COSY spectrum, the signal at 2.12 (2H, m) showed the correlations with signals at δ_H 5.20 (1H, m) and 5.15 (1H, m), which indicated the fragment of −CH−CH_2−CH−. Its ^{13}C NMR spectrum revealed the presence of 15 carbons, including 12 aromatic carbons, 2 oxygenated alkyl carbons, and 1 methylene. In the HMBC experiments, δ_H 9.12 had correlations with carbons δ_C 103.6, 108.9, and 160.2, followed by proton signals δ_H 7.08 with correlations with carbons δ_C 67.8, 108.9, 114.0, 155.8, and 160.2, δ_H 6.31 with correlations with carbons δ_C 103.6, 114.0, and 160.2, and δ_H 6.18 with correlations with carbons δ_C 108.9, 114.0, 155.8, and 160.2, indicating the presence of structural fragment A. On the other hand, the hydroxy signal of δ_H 9.28 had correlations with carbons δ_C 96.0, 102.4, and 158.2 and δ_H 8.91 with correlations with carbons δ_C 95.0 and 160.3. At the same time, proton signal δ_H 5.69 had correlations with carbons δ_C 96.0, 102.4, 155.8, 160.3, and proton signal δ_H 5.94 had correlations with carbons δ_C 95.0, 102.4, 160.3, supporting the presence of the structural fragment B. Furthermore, the proton signal at δ_H 2.12 exhibited correlations with carbons δ_C 62.8, 67.8, 102.4, and 114.0, suggesting the structural fragments A and B were joined by the methylene group. Thus, compound **1** was assigned as shown in Figure 1 and named artoheterophyllin E.

The molecular formula **2** was determined to be $C_{24}H_{26}O_4$ by its HR-ESI-MS data. Carefully analyzing the ^{1}H and ^{13}C NMR of **2**, we found that it had a structure similar to that of compound **29**, except for an additional 3,3-dimethylallyl group. Further examination of the remaining ^{1}H and ^{13}C NMR signals suggested that **2** contained a modified geranyl group that formed a 2-methyl-2-(4-methylpent-3-enyl) chromene structure on ring A [^{1}H δ 6.71 (1H, d, J = 10.0 Hz, H-1″), 5.58 (1H, d, J = 10.0 Hz, H-2″), 5.13 (1H, m, H-7″), 2.14 (2H, m, H-4″), 1.71 (2H, m, H-5″), 1.64 (3H, s, H-9″), 1.57 (3H, s, H-8″), 1.37 (3H, s, H-10″); ^{13}C δ 118.4 (C-1″), 127.8 (C- 2″), 78.57 (C-3″), 26.6 (C-10″), 41.9 (C-4″), 23.5 (C-5″), 125.2 (C-6″), 132.0 (C-7″), 17.7 (C-8″), 25.9 (C-9″)]. This unit should be situated at C-3 and C-4, and its placement was corroborated by the HMBC correlations from H-1″ to C-3 and C-5 and from H-2″ to C-4. The configuration of C-3″ in compounds can be defined by comparison of the optical rotation with those of reported compounds.[32] However, we can not get ideal data of optical rotation ($[\alpha]^{20}_D$ −0.008, c 0.0001, $CHCl_3$) for compound **2** due to the small amounts of material available.

Therefore, the absolute configuration for this compound was not further confirmed. On the basis of the above spectral evidence, the structure of **2** was established as shown in Figure 1, and the compound was given the trivial name artoheterophyllin F.

Compound **3** was a pale yellow powder, and its molecular formula was determined to be $C_{20}H_{18}O_7$ by its HR-ESI-MS data. The ^{1}H NMR and ^{13}C NMR spectra of **3** looked very similar to those of albanin A, which was also obtained from this plant, except for one of the prenyl methyl signals [δ_H 1.52 (3H, s), δ_C 25.9] changing to a hydroxy-substituted methylene [δ_H 3.82 (2H, s), δ_C 69.6]. In the HMBC experiment, proton δ_H 3.14 showed correlations with carbon δ_C 122.2 (C-3), 184.3 (C-4), 164.4 (C-2), 124.8 (C-2″), and 137.0 (C-3″), further confirming the hydroxy-substitutent prenyl group was attached at C-3 of the C ring. The key HMBC corrections are shown in Figure 1. Therefore, **3** was determined as (*Z*)-2-(2,4-dihydroxyphenyl)-5,7-dihydroxy-3-(4-hydroxy-3-methylbut-2-en-1-yl)-4*H*-chromen-4-one, named artoheterophyllin G.

The molecular formula of compound **4** was determined to be $C_{27}H_{26}O_8$ by its HR-ESI-MS data. The ^{1}H and ^{13}C NMR data for **4** were similar to those of artocarpin. However, the ^{1}H NMR spectrum exhibited a spin system that could be assigned to a 3-hydroxy-3-methyl-*trans*-but-l-enyl group [δ_H 6.76 (1H, d, J = 16.4 Hz), 6.68 (1H, d, J = 16.8 Hz), and 1.37 (6H, s)] and another methoxyl group (δ_H 3.90). This was supported by the ^{13}C NMR spectrum, displaying signals of two methyl groups (δ_C 27.9), one oxygenated carbon (δ_C 77.6), two olefinic carbons (δ_C 139.3 and 113.4) to form the 3-hydroxy-3-methyl-*trans*-but-l-enyl group, and another methoxyl group (δ_C 56.9).[33] The above information implied that the 3-methyl-1-butenyl group of artocarpin was replaced with a 3-hydroxy-3-methyl-*trans*-but-l-enyl group and that one hydroxy group was replaced with a methoxyl group in **4**. This was further confirmed by the HMBC correlations from the olefinic proton at δ_H 6.76 to C-5 (δ_C 160.5), C-7 (δ_C 164.7), and C-3″ (δ_C 77.6). Another methoxyl group was attached at C-5 by the HMBC corrlation of the methoxy proton at δ_H 3.90 with C-5 (δ_C 160.5). Thus, the structure of **4** was determined as 5,7-dimethoxy-3-(3-methylbut-2-enyl)-6-(3-hydroxy-3-methyl-*trans*-but-1-enyl)-flavone and named artoheterophyllin H.

The molecular formula of compound **5** was determined to be $C_{26}H_{30}O_7$ by its HR-ESI-MS data. The ^{1}H and ^{13}C NMR data for **5** were similar to those of artocarpin. However, the ^{1}H NMR spectrum exhibited a spin system that could be assigned to a 3-hydroxylated isoprenyl group [δ_H 2.45 (2H, m), 2.09, 1.05 (6H, s), 1.61 (2H, m)]. This was supported by the ^{13}C NMR spectrum, displaying signals of two methyl groups (δ_C 31.2 and 29.9), one oxygenated carbon (δ_C 70.8), and two methylene carbons (δ_C 43.6 and 21.8) to form the 3-hydroxylated isoprenyl group. In the HMBC spectrum, the correlations from δ_H 2.45 (H-1‴) to C-2 (δ_C 163.1), C-3 (δ_C 123.7), C-4 (δ_C 184.2), C-2‴ (δ_C 43.6), and C-3‴ (δ_C 70.8) and from H-2‴ to C-3 (δ_C 123.7), C-1‴ (δ_C 21.8), C-3‴ (δ_C 70.8), C-4‴ (δ_C 31.2), and C-5‴ (δ_C 29.9) indicated that the 3-hydroxylated isoprenyl group was attached to C-3. Thus, the structure of **5** was established as depicted and named artoheterophyllin I.

The molecular formula of compound **6** was determined to be $C_{20}H_{18}O_7$ by its HR-ESI-MS data. The ^{1}H NMR spectrum of **6** showed three one-proton double doublets at δ_H 5.84 (1H, dd, J = 14.0, 2.8 Hz), 3.93 (1H, dd, J = 17.2, 14.0 Hz), and 2.41 (1H, dd, J = 17.2, 2.8 Hz), attributed to the H-2, H-3ax, and H-3eq of a flavanone,[34] a two-proton singlet at δ_H 5.97 (2H, s) attributed to protons in the B ring nucleus, a pair of meta-coupled doublets at δ_H 5.874 (1H, d, J = 2.0 Hz) and 5.868 (1H, d, J = 2.0 Hz) assignable to H-6 and H-8, and one methoxyl signal at δ_H 3.71 (3H, s) assigned to the 5- or 7-position in the A ring or the 4′-position in the B ring. In the NOESY experiment, the methoxyl proton signal at δ_H 3.71 exhibited correlations with proton δ_H 5.97 (2H, s), suggesting that a methoxyl group was attached at the 4′-position in the B ring. According to the CD data at 270−290 nm ($[\theta]_{276}$ +3566), the C-2 configuration can be determined as *R* orientation of compound **6**.[35] Therefore, compound **6** was determined as 5,7,2′,6′-tretrahydroxy-4′-methoxyflavanone, named artoheterophyllin J.

The molecular formula of compound **7** was determined as $C_{24}H_{28}O_4$ by HR-ESI-MS. Its molecular mass was equal to that of chlorophorin.[36] Examination of the ^{1}H and ^{13}C NMR data of these two compounds further confirmed their structural similarities, with both as a tetrahydroxystilbene containing a geranyl substituent. However, in the ^{1}H NMR spectrum of compound **7**, the signal for H-2 was absent. Moreover, unlike chlorophorin, the observations of a pair of protons at δ_H 6.66 (H-6) and 6.33 (H-4) and a pair of nonsplitting protons δ_H 7.23 (2H, s, H-7′, 8′), due to the unsymmetrical substitution pattern of the A ring, implied that the geranyl unit should be attached at the 2- or 6-position in the A ring. These NMR spectroscopic properties indicated that **7** should have the geranyl unit attached at C-2. Conclusive evidence for the proposed structure of **7** came from the HMBC correlations that were found from δ_H 3.45 (H-1″) to C-1 (δ_C 140.1), C-2 (δ_C 118.4), C-3 (δ_C 156.9), C-2″ (δ_C 126.1), and C-3″ (δ_C 134.6) (Figure 1). Accordingly, compound **7** was identified as 2-geranyl-2′,3,4′,5-tetrahydroxy-*trans*-stilbene.

Compound **8** was obtained as a brown amorphous powder. Its molecular formula was determined as $C_{15}H_{12}O_5$ by HR-ESI-MS. Its ^{1}H and ^{13}C NMR spectra were similar to those of 2-(3,5-dihydroxyphenyl)-5,6-dihydroxybenzofuran,[37] except that another signal of a methoxy was present at δ_H 3.89. Analysis of HSQC and HMBC spectra of **8** suggested that the methoxy group was present at C-5. Therefore, compound **8** was determined as 2-(3,5-dihydroxyphenyl)-5-methoxy-6-hydroxybenzofuran. It was found that it was determined as wittifuran X by Tan et al.[38] However, in a further analysis of its ^{13}C NMR spectrum, we also found that several chemical shifts of carbons were greatly different from those reported by Tan et al. The chemical shifts of C-4, C-5, C-6, and C-7 were δ_C 103.4, 146.7, 146.4, and 98.5, respectively. However, it was found that they were δ_C 105.7, 147.5, 144.5, and 95.8 in the literature. On the other hand, we found that the chemical shifts of C-4 and C-7 were δ_C 106.0 and 98.4, respectively, when a hydroxy group was present at C-6 in another paper.[37] This is contradictory because if the structure of wittifuran X was determined as correct, the chemistry shifts of C-4 should not be δ_C 105.7 due to the effect of the methoxy group. It should move to the high field; that is, its chemical shift should be greatly different from the substituent of the hydroxy group, rather than similar. At the same time, the chemistry shifts of C-7 should not be δ_C 95.8 due to small effect of the methoxy group; its chemical shift should be similar to that of the substituent of the hydroxy group, rather than greatly difference. Therefore, wittifuran X determined by Tan et al. should actually be moracin J.[39] Therefore, compound **8** from our study was then named 5-methoxymorican M.

The molecular formula of compound **9** was determined as $C_{16}H_{14}O_6$ by HR-ESI-MS. By careful comparison of the ^1H and ^{13}C NMR spectra of **9** and artocarpanone, it was found that they were very similar, except for the different substitution position of the methoxy group. The methoxy group was present at the C-7 position of the artocarpanone, whereas it was present at C-2′ or C-4′ in the B ring of **9**. Analysis of the HMBC spectrum of **9** suggested that the methoxy group was present at C-4′. According to the CD data at 270−290 nm ($[\theta]_{276}$ +6512), the C-2 configuration can be determined as *R* orientation of compound **9**.[35] From the above analysis, the structure of **9** was determined as 2,3-dihydro-5,7-dihydroxy-2-(2-hydroxy-4-methoxyphenyl)-4*H*-1-benzopyran-4-one,[21] a new natural compound.

The molecular formula of compound **10** was determined to be $C_{26}H_{30}O_8$ by its HR-ESI-MS data. The ^1H and ^{13}C NMR data for **10** were similar to those of artocarpin. However, the ^1H NMR spectrum exhibited a spin system that could be assigned to a 1,2-dihydroxy-3-methylbutyl group [δ_H 4.80 (1H, overlapped), 4.33 (1H, dd, J = 8.8, 2.0 Hz), 0.95 (3H, d, J = 6.8 Hz), and 0.89 (3H, d, J = 6.8 Hz)]. This was supported by the ^{13}C NMR spectrum, displaying signals of two methyl groups (δ_C 26.0 and 17.7), two oxygenated carbon (δ_C 79.8 and 77.4), and one methine (δ_C 31.3). The HMBC correlations between the proton at δ_H 4.80 and carbons C-5 (δ_C 162.2), C-7 (δ_C 165.9), C-6 (δ_C 109.5), and C-2″ (δ_C 77.6) confirmed that the 1,2-dihydroxy-3-methylbutyl group was attached at C-6 in the A ring. Thus, the structure of **10** was determined as 2′,4′-dihydroxy-7-dimethoxy-3-(3-methylbut-2-enyl)-6-(1,2-dihydroxy-3-methylbutyl)flavone, 6-[(1*S*,2*S*)-1,2-dihydroxy-3-methylbutyl]-2-(2,4-dihydroxyphenyl)-5-hydroxy-7-methoxy-3-(3-methyl-2-buten-1-yl)-4*H*-1-benzopyran-4-one,[22] a new natural compound.

Effects of Compounds 1−33 on the Growth of MCF-7, SMMC-7721, and NCI-H460 Cells. To evaluate the effects of the compounds isolated from *A. heterophyllus*, cell viabilities were assessed via the MTT assay upon MCF-7, SMMC-7721 and NCI-H460 cancer cell lines. After 48 h of treatment, compounds **5**, **11**, **12**, and **30** reduced these three cell lines' viable cell percentages significantly, with IC_{50} values lower than 25 μM, whereas compounds **4**, **7**, **10**, **25**, **29**, and **31** showed moderate cytotoxic activity, with IC_{50} values ranging from 25 to 50 μM (Table 1). The other compounds exhibited weaker cytotoxic activity on these three cancer cell lines up to 50 μM (these compounds are not shown in Table 1). Furthermore, compound **30** showed the strongest inhibitory effect on the growth of MCF-7, SMMC-7721, and NCI-H460 cells (IC_{50} = 10.81, 12.06, and 5.19 μM) (Table 1). Especially, the inhibitory effects on the growth of SMMC-7721 and NCI-H460 cells were more potent than those of the positive control, 5-fluorouracil (5-FU) (IC_{50} = 17.53 and 7.31 μM) (Table 1).

Table 1. Inhibitory Effect of the Isolated Compounds against Different Cancer Cell Lines

	cancer cell line IC_{50} ± SD[a] (μM)		
compd	MCF-7	SMMC-7721	NCI-H460
4	>50	25−50	25−50
5	26.41 ± 0.95	25.28 ± 1.21	15.82 ± 0.61
7	25−50	25−50	16.66 ± 0.87
10	>50	≈50	25−50
11	11.3 ± 0.51	15.85 ± 0.79	11.01 ± 0.81
12	20.68 ± 1.01	23.7 ± 0.86	20.72 ± 0.63
25	25−50	25−50	25−50
29	25−50	25−50	25−50
30	10.81 ± 0.67	12.06 ± 0.75	5.19 ± 0.14
31	25−50	25−50	≈50
5-FU[b]	1.11 ± 0.13	17.53 ± 0.87	7.31 ± 0.33

[a]Values are means ± SD (n = 3). [b]Positive control.

As for flavonoids, one or two isoprenyl group substituents on the flavonoid skeleton seem to increase their cytotoxic activities, especially when the substituent is located at the 6-position of the A ring. Examples were compounds **15**, **16**, and **21**; compounds **15** and **21** have one isoprenyl group substituent at the 6-position and 3-position, respectively, whereas compound **16** lacks an isoprenyl group substituent in the skeleton. Cytotoxic activity test results showed that only compound **15** exhibited better cytotoxic activity, suggesting that the presence of an isoprenyl group at the 3-position in the skeleton cannot improve the cytotoxic activity relative to those with no isoprenyl group substituent. However, for those 6-isoprenyl flavonoids, the 3-isoprenyl substituent resulted in better cytotoxic activity. For example, compound **30** exhibited much stronger cytotoxic activity than compound **15** due to its additional 3-isoprenyl substituent. Moreover, cyclization of the isoprenyl groups, hydroxyl group substituent, and the position and saturation of double bonds of isoprenyl groups also affected cytotoxic activities. The case of compound **11** exhibited more potential cytotoxic activity than those of compounds **4**, **5**, and **10** because of its lack of a hydroxyl substituent at the 6-isoprenyl or 3-isoprenyl group, suggesting that the hydroxyl group substituent and saturation of the isoprenyl group reduced the cytotoxic activities. At the same time, compound **15** showed stronger cytotoxic activity than that of compound **13**. Meanwhile, compound **11** also exhibited better cytotoxic activity than that of compounds **12** and **31** due to the cyclization of the isoprenyl groups in the skeleton of the latter. In addition, compound **15** exhibited stronger cytotoxic activity than that of compound **18** because of the double bond at the 1,2-position of the latter, whereas it was at the 2,3-position of the former.

Effects of Compounds 11 and 30 on the Induction of Apoptosis. Apoptosis is an essential route of tissue development and homeostasis. It also works as a defense system avoiding the interruption of many toxic chemicals. It is well known that anticancer chemotherapies mainly exert their elimination of cancer cells via the apoptotic process, characterized by a number of cellular and biochemical hallmarks, including cell shrinkage, membrane blebbing, DNA chromatin fragmentation, nucleus condensation, and PARP cleavage.[40] To detect whether compounds **11** and **30** could induce apoptosis, DAPI staining was performed. Figure 2A shows that the indicated cell lines (including NCI-H460, MCF-7, and SMMC-7721) were administered by compounds **11** and **30** after 12, 24, and 48 h of incubation. The apoptotic bodies were observed clearly after 24 h of treatment and increased more at 48 h (Figure 2A). In addition, the apoptotic effect was validated through a significant increase of the cleaved-PARP proteins after chemical treatment in a time-dependent manner in these three cell lines (Figure 2B). All of these data demonstrate that compounds **11** and **30** obviously induced apoptosis in NCI-H460, MCF-7, and SMMC-7721 cell lines.

Effects of Compounds 11 and 30 on the Caspase Related-Apoptosis. When pretreated with 50 μM broad Z-VAD-fmk (spectrum caspase inhibitor) 1 h before compound

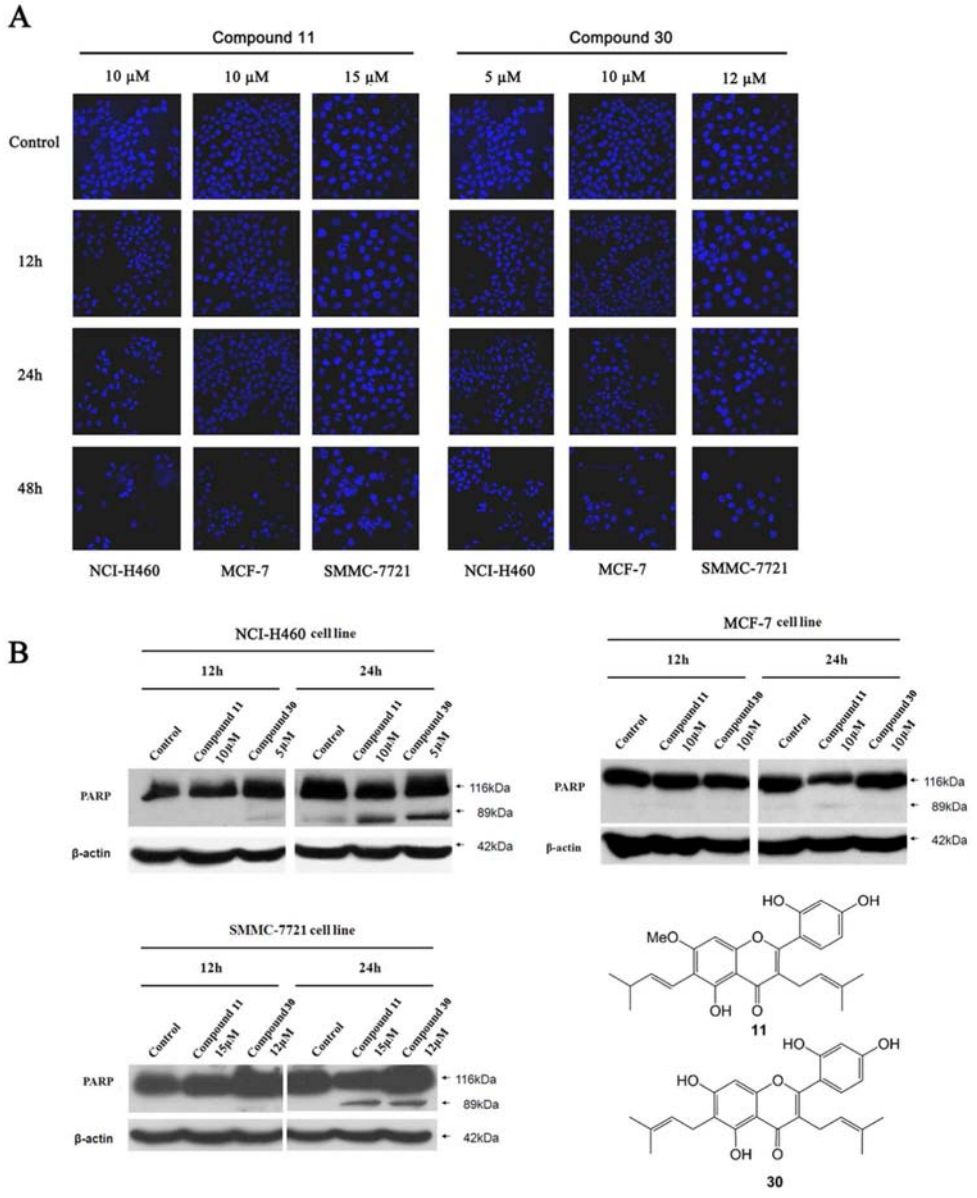

Figure 2. Compounds **11** and **30** induce apoptosis in NCI-H460, MCF-7, and SMMC-7721 cancer cell lines. (A) After drug administration at indicated concentrations, the cells were stained by DAPI and visualized by fluorescent microscope at 12, 24, and 48 h. (B) Western blot analysis was used to estimate PARP cleavage after drug administration for 48 h. Results are representative of three independent experiments (n = 3).

11 and **30** administration, with IC_{50} values for 48 h, we could observe the obvious increased cell number and improved cell morphology (Figure 3). These data indicated that compounds **11** and **30** induced apoptosis through caspase-dependent pathways.

Effects of Compounds 11 and 30 on MAPK Pathways Related Apoptosis. The MAPK signaling pathways, including ERK, p38, and JNK MAPK pathways, are all involved in affecting cell proliferation, differentiation, survival, and migration.[1] The MAPK pathway comprises several key signaling components and phosphorylation events that play a role in tumorigenesis. Especially, p38 and JNK MAPK pathways exhibit a complex function in cancer development. In HCC, higher JNK1 activation and lower p38 MAPK activity are correlated with an increased proliferation of tumor cells.[3] However, the increase of phosphorylated p38α has been detected in lung and breast cancer.[4,5] These investigations demonstrated that p38/JNK MAPK pathways have a selective function depending on the different types and stages of cancers. To determine whether compounds **11** and **30** induced cell apoptosis via the MAPK pathways, 20 μM JNK inhibitor (SP600125), 20 μM p38 MAPK inhibitor (SB203580), and 20 μM ERK inhibitor (PD98059) were pretreated to indicated cells 1 h before compound treatment. We observed the alteration of cancer cell morphology and number at 48 h after compound **11** and **30** administrations. In the SMMC-7721 cell line, pretreatment with SP600125 improved the cell morphology and increase the cell number (Figure 3). In MCF-7 cell line, pretreatment with SB203580, PD98059, and SP600125 improved the cell status noticeably (Figure 3). In the NCI-H460 cell line, pretreatment with SB203580 or PD98059 before treatment with compound **11** or **30** elevated the cell viability (Figure 3). These findings provide evidence demonstrating that the apoptosis-inducing effects of compounds **11** and **30** are mediated by down-regulation of different MAPK pathways in different cancer cell lines separately. All of the

dx.doi.org/10.1021/jf500159z | J. Agric. Food Chem. 2014, 62, 5519−5527

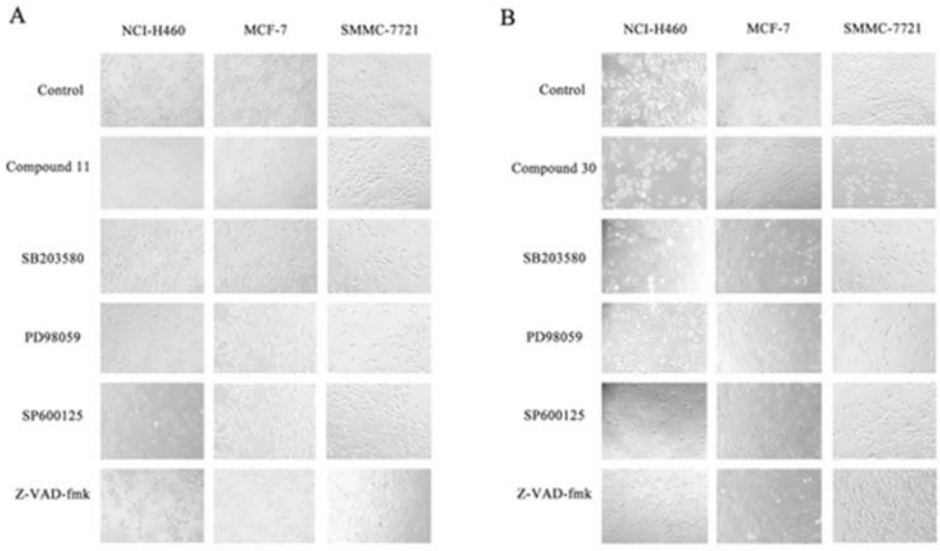

Figure 3. Effects of compounds **11** and **30** on the three MAPK pathway inhibitors: morphological and quantitative changes in NCI-H460, MCF-7, and SMMC-7721 cells in either control (untreated), treated with compounds **11** (10 μM for NCI-H460, 10 μM for MCF-7, and 15 μM for SMMC-7721) and **30** (5 μM for NCI-H460, 10 μM for MCF-7, and 12 μM for SMMC-7721) for 48 h, or pretreated with 20 μM SB203580, 20 μM PD98059, 20 μM SP600125, or 50 μM Z-VAD-fmk for 1 h before compound administration. Results are representative of three independent experiments (n = 3).

above results are consistent with previous findings[2−5] that MAPK pathways have a selective action on different cancer cell lines.

In this study, 8 new phenolic compounds, artoheterophyllin E−J (**1**−**6**), 4-geranyl-2′,3,4′,5-tetrahydroxy-*cis*-stilbene (**7**), and 5-methoxymorican M (**8**), and 2 new natural compounds (**9** and **10**), 2,3-dihydro-5,7-dihydroxy-2-(2-hydroxy-4-methoxyphenyl)-4*H*-1-benzopyran-4-one and 6-[(1*S*,2*S*)-1,2-dihydroxy-3-methylbutyl]-2-(2,4-dihydroxyphenyl)-5-hydroxy-7-methoxy-3-(3-methyl-2-buten-1-yl)-4*H*-1-benzopyran-4-one, together with 23 known compounds (**11**−**33**) were identified from the ethanol extract of the wood of *A. heterophyllus*. To our knowledge, this is the first systematic report of the phenolic compounds from the wood of *A. heterophyllus* with their cytotoxic effects on the three cell lines of MCF-7, SMMC-7721, and NCI-H460 at the same time. This study demonstrates that compounds **11** and **30** from the wood of *A. heterophyllus* inhibited the growth of the three cancer cell lines by inducing caspase-related apoptosis. Furthermore, the induction of apoptosis was accompanied by the activation of ERK, p38, and JNK MAPK pathways in a cell type-related manner. These data suggest that compounds **11** and **30** from the wood of *A. heterophyllus* have an anticancer potential and can be developed as anticancer drug leads.

■ ASSOCIATED CONTENT

Ⓢ Supporting Information

^{1}H NMR, ^{13}C NMR, HSQC, HMBC, and ^{1}H−^{1}H COSY spectra and HR-ESI-MS data of compounds **1**−**10** and ^{1}H and ^{13}C NMR data of compounds **1**−**10**. This material is available free of charge via the Internet at http://pubs.acs.org.

■ AUTHOR INFORMATION

Corresponding Author

*(J.C.) E-mail:chenjie@jiangnan.edu.cn. Phone: +86-510-85329032. Fax: +86-510-85919065.

Author Contributions

‖Z.-P.Z. and Y.X. contributed equally to this work.

Funding

We thank the National Basic Research Program of China (973 Program, 2012CB720801), the Fundamental Research Funds for the Central Universities (JUSRP11220), the Independent Research Program of State Key Laboratory of Food Science and Technology (5812060204120150), and the National Natural Science Foundation of China (81202956) for financial support.

Notes

The authors declare no competing financial interest.

■ REFERENCES

(1) Wagner, E. F.; Nebreda, A. R. Signal integration by JNK and p38 MAPK pathways in cancer development. *Nat. Rev. Cancer* **2009**, *9*, 537−549.

(2) Hui, L.; Zatloukal, K.; Scheuch, H.; Stepniak, E.; Wagner, E. F. Proliferation of human HCC cells and chemically induced mouse liver cancers requires JNK1-dependent p21 downregulation. *J. Clin. Invest.* **2008**, *118*, 3943−3953.

(3) Parekh, P.; Motiwale, L.; Naik, N.; Rao, K. V. Downregulation of cyclin D1 is associated with decreased levels of p38 MAP kinases, Akt/PKB and Pak1 during chemopreventive effects of resveratrol in liver cancer cells. *Exp. Toxicol. Pathol.* **2011**, *63*, 167−173.

(4) Greenberg, A. K.; Basu, S.; Hu, J.; Yie, T. A.; Tchou-Wong, K. M.; Rom, W. N.; Lee, T. C. Selective p38 activation in human non-small cell lung cancer. *Am. J. Respir. Cell Mol. Biol.* **2002**, *26*, 558−564.

(5) Esteva, F. J.; Sahin, A. A.; Smith, T. L.; Yang, Y.; Pusztai, L.; Nahta, R.; Buchholz, T. A.; Buzdar, A. U.; Hortobagyi, G. N.; Bacus, S. S. Prognostic significance of phosphorylated p38 mitogen-activated protein kinase and HER-2 expression in lymph node-positive breast carcinoma. *Cancer* **2004**, *100*, 499−506.

(6) Baliga, M. S.; Shivashankara, A. R.; Haniadka, R.; Dsouza, J.; Bhat, H. P. Phytochemistry, nutritional and pharmacological properties of *Artocarpus heterophyllus* Lam (jackfruit): a review. *Food Res. Int.* **2011**, *44*, 1800−1811.

(7) Li, Y.; Mao, Q.; Feng, F.; Ye, C. Genetic diversity within a jackfruit (*Artocarpus heterophyllus* Lam.) germplasm collection in China using AFLP markers. *Agric. Sci. China* **2010**, *9*, 1263−1270.

(8) Panthong, K.; Tohdee, K.; Hutadilok-Towatana, N.; Voravuthikunchai, S. P.; Chusri, S. Prenylated flavone from roots of a hybrid between *Artocarpus heterophyllus* and *Artocarpus integer* and its biological activities. *J. Braz. Chem. Soc.* **2013**, *24*, 1656−1661.
(9) Wei, B. L.; Weng, J. R.; Chiu, P. H.; Hung, C. F.; Wang, J. P.; Lin, C. N. Antiinflammatory flavonoids from *Artocarpus heterophyllus* and *Artocarpus communis*. *J. Agric. Food Chem.* **2005**, *53*, 3867−3871.
(10) Khan, M. R.; Omoloso, A. D.; Kihara, M. Antibacterial activity of *Artocarpus heterophyllus*. *Fitoterapia* **2003**, *74*, 501−505.
(11) Shanmugapriya, K.; Saravana, P. S.; Payal, H.; Mohammedaaa, S. P.; Bennai, W. A comparative study of antimicrobial potential and phytochemical analysis of *Artocarpus heterophyllus* and *Manilkara zapota* seed extracts. *J. Pharm. Res.* **2011**, *4*, 2587−2589.
(12) Arung, E. T.; Yoshikawa, K.; Shimizu, K.; Kondo, R. Isoprenoid-substituted flavonoids from wood of *Artocarpus heterophyllus* on B16 melanoma cells: cytotoxicity and structural criteria. *Fitoterapia* **2010**, *81*, 120−123.
(13) Fernando, M. R.; Thabrew, M. I.; Karunanayake, E. H. Hypoglycaemic activity of some medicinal plants in Sri-Lanka. *Gen. Pharmacol.* **1990**, *21*, 779−782.
(14) Kumar, R. N.; Jayapradha, R. Polyphenol analysis and antitumor activity of crude extracts from tegmen of *Artocarpus heterophyllus*. *Res. J. Biotechnol.* **2010**, *5*, 61−63.
(15) Arung, E. T.; Wicaksono, B. D.; Handoko, Y. A.; Kusuma, I. W.; Shimizu, K.; Yulia, D.; Sandra, F. Cytotoxic effect of artocarpin on T47D cells. *J. Nat. Med.* **2010**, *64*, 423−429.
(16) Zhu, G.; Yang, Y.; Hou, A.; Zhang, H.; Li, Q.; Zhang, C. Inhibitory effects of ACR-2 and ACR-3 on SMMC-7721 and SGC-7901 cell lines and enzyme activity of caspase-3. *Hunan Zhongyiyao Daxue Xuebao* **2007**, *27*, 24−27.
(17) Wang, H.; Ng, T. B.; Ooi, V. E. C.; Liu, W. K. Effects of lectins with different carbohydrate-binding specificities on hepatoma, choriocarcinoma, melanoma and osteosarcoma cell lines. *Int. J. Biochem. Cell Biol.* **2000**, *32*, 365−372.
(18) Fischer, E.; Khang, N. Q.; Brossmer, R. The α-galactosyl specific lectin from *Artocarpus integrifolia* distinguishes between two lymphoma lines with different metastatic potential. *Biochem. Cell Biol.* **1997**, *75*, 171−175.
(19) Xu, Y.; Chiu, J. F.; He, Q. Y.; Chen, F. Tubeimoside-1 exerts cytotoxicity in HeLa cells through mitochondrial dysfunction and endoplasmic reticulum stress pathways. *J. Proteome. Res.* **2009**, *8*, 1585−1593.
(20) Wu, S. B.; Su, J. J.; Sun, L. H.; Wang, W. X.; Zhao, Y.; Li, H.; Zhang, S. P.; Dai, G. H.; Wang, C. G.; Hu, J. F. Triterpenoids and steroids from the fruits of *Melia toosendan* and their cytotoxic effects on two human cancer cell lines. *J. Nat. Prod.* **2010**, *73*, 1898−1906.
(21) He, X.; Yang, F. Synthesis and characterization of homoeriodictyol and its analogs of B-ring. *Yiyao Gongye* **1987**, *18*, 534−537.
(22) Nagahata, T. Artocarpin derivative or artocarpin-like compound, and hair growth/restoration composition, skin-whitening cosmetic composition, pharmaceutical as anti-cancer, antiphlogistic/analgesic, antipyretic or antiallergic agent and pharmaceutical for treatment of pigmented skin lesion each comprising the same. *PCT Int. Appl.* WO 2008020490, 2008.
(23) Zheng, Z. P.; Cheng, K. W.; To, J. T. K.; Li, H.; Wang, M. Isolation of tyrosinase inhibitors from *Artocarpus heterophyllus* and use of its extract as anti-browning agent. *Mol. Nutr. Food Res.* **2008**, *52*, 1530−1538.
(24) Nguyen, N. T.; Nguyen, M. H. K.; Nguyen, H. X.; Bui, N. K. N.; Nguyen, M. T. T. Tyrosinase inhibitors from the wood of *Artocarpus heterophyllus*. *J. Nat. Prod.* **2012**, *75*, 1951−1955.
(25) Chari, V. M.; Ilyas, M.; Wagner, H.; Neszmelyi, A.; Chen, F. C.; Chen, L. K.; Lin, Y. C.; Lin, Y. M. Carbon-13 NMR spectroscopy of biflavanoids. *Phytochemistry* **1977**, *16*, 1273−1278.
(26) Mabry, T. J.; Kagan, J.; Roesler, H. Nuclear magnetic resonance spectra of trimethylsilyl ethers of flavonoid glycosides. *Phytochemistry* **1965**, *4*, 177−183.
(27) Shimizu, K.; Kondo, R.; Sakai, K. A stilbene derivative from *Artocarpus incisus*. *Phytochemistry* **1997**, *45*, 1297−1298.
(28) Hano, Y.; Matsumoto, Y.; Shinohara, K.; Sun, J.; Nomura, T. Constituents of the Moraceae plants. 10. Cudraflavones C and D, two new prenylflavones from the root bark of *Cudrania tricuspidata* (Carr.) Bur. *Heterocycles* **1990**, *31*, 1339−1344.
(29) Yu, M. H.; Zhao, T.; Yan, G. R.; Yang, H. X.; Wang, H. Y.; Hou, A. J. New isoprenylated flavones and stilbene derivative from *Artocarpus hypargyreus*. *Chem. Biodivers.* **2012**, *9*, 394−402.
(30) Tangdenpaisal, K.; Sualek, S.; Ruchirawat, S.; Ploypradith, P. Factors affecting orthogonality in the deprotection of 2,4-di-protected aromatic ethers employing solid-supported acids. *Tetrahedron* **2009**, *65*, 4316−4325.
(31) Achard, T. R. J.; Clegg, W.; Harrington, R. W.; North, M. Chiral salen ligands designed to form polymetallic complexes. *Tetrahedron* **2012**, *68*, 133−144.
(32) Starks, C. M.; Williams, R. B.; Norman, V. L.; Rice, S. M.; O'Neil-Johnson, M.; Lawrence, J. A.; Eldridge, G. R. Antibacterial chromene and chromane stilbenoids from *Hymenocardia acida*. *Phytochemistry* **2014**, *98*, 216−222.
(33) Na, M. K.; Jang, J. P.; Njamen, D.; Mbafor, J. T.; Fomum, Z. T.; Kim, B. Y.; Oh, W. K.; Ahn, J. S. Protein tyrosine phosphatase-1B inhibitory activity of isoprenylated flavonoids isolated from *Erythrina mildbraedii*. *J. Nat. Prod.* **2006**, *69*, 1572−1576.
(34) Lu, C. M.; Lin, C. N. The bioactive principles of formosan *Artocarpus* species. Part 5. Two 2′,4′,6′-trioxygenated flavanones from *Artocarpus heterophyllus*. *Phytochemistry* **1993**, *33*, 909−911.
(35) Chokchaisiri, R.; Suaisom, C.; Sriphot, S.; Chindaduang, A.; Chuprajob, T.; Suksamrarn, A. Bioactive flavonoids of the flowers of *Butea monosperma*. *Chem. Pharm. Bull.* **2009**, *57*, 428−432.
(36) Christensen, L. P.; Lam, J.; Sigsgaard, T. A novel stilbene from the wood of *Chlorophora excelsa*. *Phytochemistry* **1988**, *27*, 3014−3016.
(37) Tan, Y.; Liu, C.; Chen, R. 2-Arylbenzofuran derivatives from *Morus wittiorum*. *Yaoxue Xuebao* **2008**, *43*, 1119−1122.
(38) Tan, Y.; Yang, Y.; Zhang, T.; Chen, R. Y.; Yu, D. Q. Bioactive 2-arylbenzofuran derivatives from *Morus wittiorum*. *Fitoterapia* **2010**, *81*, 742−746.
(39) Takasugi, M.; Nagao, S.; Munoz, L.; Ishikawa, S.; Masamune, T.; Shirata, A.; Takahashi, K. The structure of phytoalexins produced in diseased mulberry. *Koen Yoshishu Tennen Yuki Kagobutsu Toronkai* **1979**, *22*, 275−282.
(40) Hacker, G. The morphology of apoptosis. *Cell Tissue Res.* **2000**, *301*, 5−17.

JOURNAL OF AGRICULTURAL AND FOOD CHEMISTRY

Article

pubs.acs.org/JAFC

Oleanolic Acid Induces Metabolic Adaptation in Cancer Cells by Activating the AMP-Activated Protein Kinase Pathway

Jia Liu,[†,§,∥] Lanhong Zheng,[‡,∥] Ning Wu,[†,∥] Leina Ma,[#] Jiateng Zhong,[⊥] Ge Liu,[†,§] and Xiukun Lin*[,†,△]

[†]Institute of Oceanology, Chinese Academy of Sciences, Qingdao 266071, China

[‡]Yellow Sea Fisheries Research Institute, Chinese Academy of Fishery Sciences, Qingdao 266071, China

[§]Graduate School, University of Chinese Academy of Sciences, Beijing 100049, China

[#]School of Medicine and Pharmacy, Ocean University of China, Qingdao 266003, China

[⊥]Department of Pathophysiology, Norman Bethune College of Medicine, Jilin University, Changchun 130021, China

[△]Department of Pharmacology, Capital Medical University, Beijing 100069, China

Supporting Information

ABSTRACT: Cancer cells are well-known to require a constant supply of protein, lipid, RNA, and DNA via altered metabolism for accelerated cell proliferation. Targeting metabolic pathways is, therefore, a promising therapeutic strategy for cancers. Oleanolic acid (OA) is widely distributed in dietary and medicinal plants and displays a selective cytotoxicity to cancer cells, primarily by inducing apoptosis and cell cycle arrest. This study investigated if OA inhibited growth of tumor cells by affecting their metabolism. OA was found to activate AMP-activated protein kinase (AMPK), the master regulator of metabolism, in prostate cancer cell line PC-3 and breast cancer cell line MCF-7. AMPK activation is required for the antitumor activity of OA on cancer cells. Lipogenesis, protein synthesis, and aerobic glycolysis were inhibited in cancer cells treated with OA, in an AMPK activation-dependent manner. The metabolic alteration was shown to mediate the tumor suppressor activity of OA on cancer cells. Collectively, this study provides evidence that OA, as a widely distributed nutritional component, is able to exert antitumor function by interfering in the metabolic pathway in cancer cells. This finding should encourage researchers to study if affecting cancer metabolism is a common mechanism by which nutritional compounds suppress cancers.

KEYWORDS: *aerobic glycolysis, AMPK, metabolism, oleanolic acid*

INTRODUCTION

Rapid and unlimited growth of cancer cells requires a constant supply of both energy and structural materials that is essential for cell division. Transformed cells usually adjust their metabolic machinery to these needs by modifying the activity and expression of key metabolic enzymes in a concerted fashion.[1] Metabolic switch is not only an adaptive response of preexisting malignant cells but also a driver of tumorigenicity.[2] The population that suffers from metabolic syndromes, such as diabetes, is more prone to cancers,[2] although the detailed mechanisms underlying increased tumor risk from altered metabolism are still unknown. Interfering with metabolism has been shown to retard the growth of tumor cells,[2] indicating it as a promising therapeutic target for cancer treatment.

Multiple kinases have been shown to participate in the regulation of metabolic activity. AMP-activated protein kinase (AMPK) is one of the most important kinases that trigger metabolic adaption in cells. As an energy sensor, AMPK is an enzyme consisting of three subunits (α, β, and γ). The α subunit is responsible for its catalytic activity, and the other two serve as regulatory parts. AMPK senses the increase in intracellular AMP/ATP ratio and responds to the changes by phosphorylating and activating/inactivating some key metabolic enzymes, thereby inducing metabolic switch from glycolysis and anabolism to oxidative phosphorylation and catabolism. This AMPK-mediated metabolic alteration compromises the generation of molecular intermediates that is essential for macromolecule synthesis and, hence, slows cell proliferation. AMPK, as evidenced by recent studies, is closely implicated in the correlation between metabolism and cancer. AMPK suppresses aerobic glycolysis in malignant cells and also hampers the growth of tumors in vivo.[3] In line with the tumor suppressor function of AMPK, the risk of cancer has been found to be lowered in type 2 diabetes patients who were administered metformin, an AMPK activator.[4] This observation raises the possibility that AMPK is likely to be a promising pharmacological target for cancer therapy.

Activated AMPK suppresses the activity of acetyl-CoA carboxylase (ACC) by phosphorylation at Ser218 and negatively regulated the expression of fatty acid synthase (FASN), finally inhibiting lipid synthesis in cancer cells. In parallel, the mammalian target of the rapamycin (mTOR) is a downstream effector of AMPK, which promotes protein synthesis by activating p70S6K and eIF-4E. Through phosphorylation-dependent activation of TSC1/TSC2, a major upstream negative regulator of mTOR activity, AMPK can abrogate the stimulatory effect of mTOR on mRNA translation in transformed cells. AMPK also promotes glycolysis by phosphorylating and activating 6-phosphofructo-2-kinase/fructose-2,6-biphosphatase 2 (PFKFB2),

Received: February 5, 2014
Revised: April 28, 2014
Accepted: May 23, 2014
Published: May 23, 2014

 © 2014 American Chemical Society

a key enzyme in the glycolytic pathway. Accumulated evidence has documented that enhanced glycolysis produces intermediates required for the synthesis of macromolecules. Above all, the activation status of AMPK determines the metabolism in cancer cells.[1] Biosynthesis of macromolecules, such as lipid, protein, and nucleic acids, may be slowed by reactivating the kinase function of AMPK in cancer cells that have no or low AMPK activity.

Oleanolic acid (OA) is a naturally occurring triterpenoid that is widely distributed in edible and medicinal plants. OA has been known, for a long time, to exert a variety of bioactivities, including a tumor-suppressing function.[5] However, the molecular mechanism by which OA was able to inhibit tumor growth has not been completely explored. In this study, we found that OA was able to induce AMPK activation in cancer cells. Sequentially, AMPK activation led to the metabolic alteration in OA-treated cancer cells. Finally, we demonstrated that AMPK-dependent alteration in the metabolic pattern is associated with the antitumor function of OA.

MATERIALS AND METHODS

Cell Culture. A human prostate carcinoma cell line, PC-3, and a human breast cancer cell line, MCF-7, were purchased from American Type Culture Collection (ATCC). A human normal liver cell, L-02, was obtained from Shanghai Cell Collection (Shanghai, China). PC-3 was cultured in RPMI-1640 supplemented with 10% fetal bovine serum (FBS; GIBCO-BRL) at 37 °C under a humidified 5% CO_2 condition. MCF-7 cells were cultured in DMEM.

Chemical Agents. OA was purchased from Sigma-Aldrich (O5504). An AMPK inhibitor, compound **C**, was purchased from Millipore (171260). The cells were incubated with compound **C** (20 μM) for 1 h prior to OA treatment. An mTOR activator, MHY1485, was purchased from Millipore (5.00554.0001). The cells were incubated with MHY1485 (2 μM) for 1 h prior to OA treatment. The above substances were all dissolved with DMSO for storing. PBS or culture medium was added to dilute the agents when needed.

Immunoblotting Assays. Total proteins were extracted from cells with M-PER Mammalian Protein Extraction Reagent (Thermo Scientific, USA), separated by electrophoresis with 10−12% SDS-PAGE gel and transferred onto 0.45 μm nitrocellulose membranes. Membranes were incubated in blocking solution (PBS, 0.1% Tween-20, and 5% nonfat dry milk powder) for 2 h at room temperature and then incubated with primary antibodies (1:1000, listed below). After overnight incubation, the membranes were washed with PBS containing 0.1% Tween-20 three times and then were incubated with horseradish peroxidase-conjugated secondary antibody for 1 h at room temperature. The involved antibodies were described as follows: phospho-AMPKα (Thr172), (Santa Cruz, sc-33524); AMPKα (CST, 2532); phospho-HMG-CoA reductase (Ser872) (Millipore, 09-356); HMG-CoA reductase (Millipore, ABS229); phospho-acetyl-CoA carboxylase (Ser79) (CST, 3661); acetyl-CoA carboxylase (CST, 3676); and fatty acid synthase (CST, 3180). The intensity of blots in some figures was determined with ImageJ software.

Immunofluorescence. PC-3 and MCF-7 cells were incubated with or without OA (100 μg/mL) for 6 h. The cells were fixed with 4% polyoxymethylene for 30 min and then incubated with phospho-AMPKα antibody (1:200) for 2 h at 4 °C. Subsequently, the cells were stained with FITC-conjugated secondary antibody and 4′,6′-diamidino-2-phenylindole (DAPI). A confocal microscope (CLS-2SS, Thorlabs) was used to observe the fluorescence.

Detection of Fatty Acid Synthesis Activity. A radioactive assay was employed to detect the effect of OA on lipid synthesis in PC-3 and MCF-7 cancer cells. The cells were incubated with [^{3}H]-acetyl-CoA (2 μCi) (PerkinElmer, NET290050UC) for 12 h as well as OA (50 or 100 μg/mL) for 6 or 12 h. Lipid was isolated with a mixture of water/methanol/chloroform (1:1:1) according to a procedure previously described.[6] The organic fraction that contains radioactive lipid was evaporated with N_2, followed by detection with a MicroBeta liquid scintillation counter (PerkinElmer).

Protein Synthesis Detection Assay. The effect of OA on nascent protein synthesis in cancer cells was detected using a Click-iT HPG Alexa Fluor Protein Synthesis Assay Kit (Life Technologies, C10428). Amounts of 5×10^3 PC-3 and MCF-7 cells were treated with 50 or 100 μg/mL OA for 6 or 12 h (Figure 3C). For the experiments in Figure 3E, 100 μg/mL OA was added to the culture of 5×10^3 PC-3 cells with or without 1 h of compound **C** (20 μM) pretreatment, and then the cells were incubated for another 12 h. The subsequent experiments were performed according to the procedures provided by the manufacturer. The fluorescence was detected and recorded with a confocal microscope (CLS-2SS, Thorlabs). The signal intensities were determined with ImageJ, and the relative values normalized by those in untreated control groups are presented in Figure 3C,E.

Glycolytic Activity Detection Assays. Glucose consumption of cancer cells treated with OA was assessed with a Glucose Uptake Colorimetric Assay Kit (BioVision, K676). Briefly, 5×10^3 PC-3 and MCF-7 cells were treated with 50 or 100 μg/mL OA for 6 or 12 h (Figure 4A). For the experiments shown in Figure 4D, 100 μg/mL OA was added to the culture of 5×10^3 PC-3 cells with or without compound **C** (20 μM) pretreatment for 1 h, and the cells were incubated for 12 h. Then, the cells were starved for glucose with 100 μL of Krebs−Ringer−phosphate−HEPES (KRPH) buffer containing 2% BSA for 30 min, followed by 20 min exposure with 100 nmol of 2-DG. Subsequent steps were done according to the manufacturer's instructions. The absorbance in each sample was measured with a microplate reader at 412 nm. Glucose consumption was determined on the basis of the established standard curves.

Lactate production was determined with a Lactate Colorimetric Assay Kit II (BioVision, K627) following the manufacturer's instructions. Briefly, 5 μL of culture medium was harvested from PC-3 and MCF-7 cells incubated with 50 or 100 μg/mL OA for 6 or 12 h (Figure 4B) and mixed with 45 μL of lactate assay buffer. Compound **C** (20 μM) was simultaneously added to PC-3 cells in some experiments (Figure 4E). A 10 kDa MW spin filter (BioVision, 1997-25) was used to remove the lactate dehydrogenase in serum. After 50 μL of reaction mix was added, the reaction was performed for 30 min at room temperature. The absorbance in each sample was measured with a microplate reader at 450 nm. The concentration of lactic acid in each sample was determined with the established standard curve. The values in each group relative to that untreated control group are shown in Figure 4B,E.

The oxygen consumption rate was determined with an Oxygen Consumption Rate Assay Kit (Cayman Chemical Co., 600800). PC-3 and MCF7 cells were treated with OA and/or compound **C** according to the procedures used to evaluate the glucose uptake and lactic acid production. After 12 h of OA stimulation, the cells were processed following the manufacturer's instruction. The signals in each sample were read at 650 nm with a VICTOR X3 multilabel plate reader (PerkinElmer). The oxygen consumption rate was presented as lifetime versus time (μs/h). The values were normalized by untreated control samples and are shown in Figure 4C,F.

Cell Cycle Analysis. Cell cycle analysis was performed by fluorescence-activated cell sorter (FACS)-based evaluation of DNA content with propidium iodide (PI) staining. PC-3 cells (2×10^5) were treated with OA for 12 h (indicated groups were pretreated with 20 μM compound **C** for 1 h prior to OA stimulation). The cells were fixed with cold 70% ethanol for 1 h. Subsequently, the cells were processed with RNase (20 μg/mL) at 37 °C for 1 h and then stained with PI (50 μg/mL), immediately followed by FACS-based cell cycle analysis (Aria II, BD Biosciences). A total of 5×10^4 cells were counted for each sample.

Colony Formation Assay. PC-3 cells (2×10^3) were plated in a 6-well plate and then cultured in medium with or without 100 μg/mL OA at 37 °C under a humidified 5% CO_2 condition for 10 days. Colonies consisting of more than 50 cells were counted after staining with crystal violet solution.

dx.doi.org/10.1021/jf500622p | J. Agric. Food Chem. 2014, 62, 5528−5537

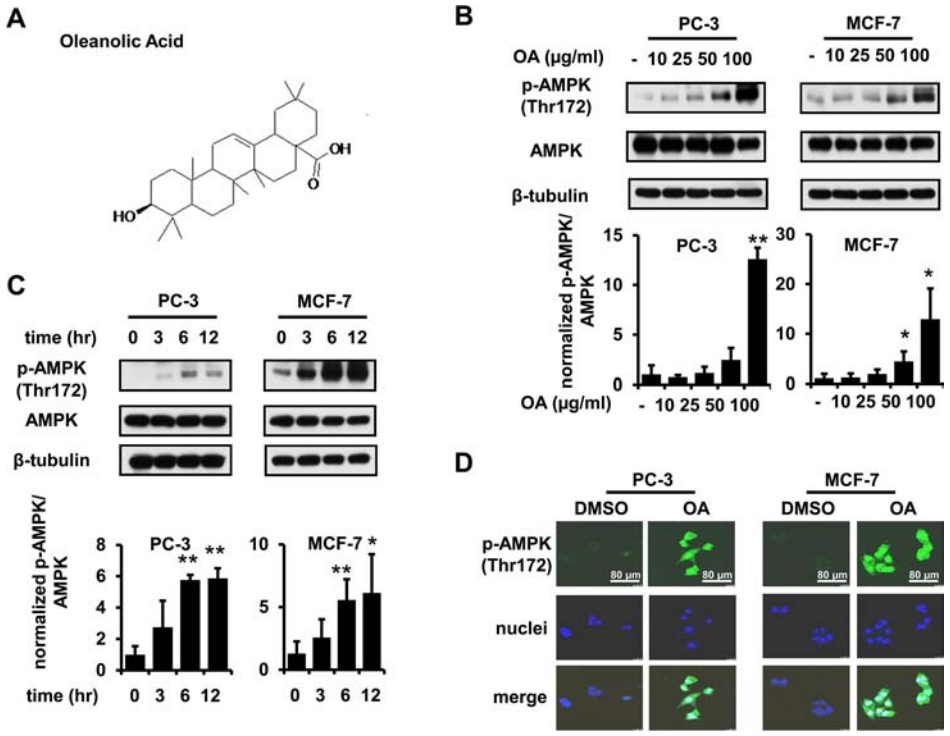

Figure 1. OA induces AMPK activation in cancer cells in a dose- and time-dependent fashion. (A) Chemical structure of oleanolic acid. (B) PC-3 and MCF7 cells were treated with OA for 3 h at 10, 25, 50, and 100 μg/mL. AMPK phosphorylation was detected by immunoblot assays (upper panel). The blot intensity quantified with ImageJ software is shown (bottom panel) as means ± SD of three independent experiments. (C) PC-3 and MCF7 cells were also treated with 100 μg/mL OA for 3, 6, and 12 h. AMPK phosphorylation was detected by immunoblot assays. Blots and their corresponding quantitative data are shown as means ± SD of three independent experiments. (D) PC-3 and MCF7 cells were stimulated with 100 μg/mL OA for 6 h. Phosphorylated AMPK was detected by immunofluorescent staining. Bars = 80 μm.

Animal Experiments. The animal experimental procedures were approved by the Committee on Animal Care in Jilin University (permission 2013032, Changchun, China). PC-3 cells (5×10^6) were injected into the flanks of 4–6-week-old male nude BALB/c mice (n = 18). OA (40 mg/kg, low dose; or 120 mg/kg, high dose) was orally administered every day for 4 weeks. The mice were divided into three groups: control (n = 6), low-dose OA (n = 6), and high-dose OA (n = 6). The diameters of tumors were periodically determined with calipers. The volumes were calculated using the following formula. Volume (mm^3) = length × $(width)^2/2$. The expression of indicated proteins was detected in the dissected tumors after the mice were sacrificed by immunoblot assay.

Statistical Analysis. The experiments except immunoblot assays were performed at least three times. All values are reported as means ± SD and compared at a given time point by unpaired, two-tailed t test. Data were considered to be statistically significant when $p < 0.05$ (*) and $p < 0.01$ (**).

RESULTS AND DISCUSSION

OA Induces AMPK Activation in Cancer Cells in a Dose- and Time-Dependent Fashion. The chemical structure of OA is shown in Figure 1A. First, AMPK activation was examined in OA-treated cancer cells by immunoblotting analysis of its phosphorylation at Thr172. AMPK phosphorylation was found to be increased in all tested cells (Figure 1B). The increase in phosphorylated AMPK expression was correlated with the dose of OA administered to cancer cells (Figure 1B). Also, the phosphorylation of AMPK was progressively elevated during the time when cancer cells were exposed with OA (Figure 1C). OA-induced phosphorylation of AMPK was also further confirmed in cancer cells by immunofluorescent staining (Figure 1D). These data showed that OA induced the phosphorylation and activation of AMPK in cancer cells in a concentration- and time-dependent manner.

OA has been demonstrated to exert multiple bioactivities, including anti-inflammation, anticancer, anticoagulation,[7] and hepatoprotection,[8] by affecting specific molecular pathways in cells. These signaling pathways are associated with apoptosis, cell cycle regulation, metastasis, angiogenesis, and inflammation. AMPK, the central modulator of metabolism, has been reported to be activated in mouse cardiomyocytes under OA treatment. In turn, AMPK activation protected cardiomyocytes from contractile dysfunction induced by hypoxia in a FOXO3-dependent manner.[9] This finding shed light on the mechanism of OA cardioprotective activity. However, it is still unclear whether OA is able to induce AMPK activation in cancer cells. In this study, we revealed that OA treatment resulted in the phosphorylation and activation of AMPK in cancer cells in both dose- and time-dependent fashions.

AMPK Activation Mediated the Antitumor Activity of OA on Cancer Cells. Subsequently, we aimed to establish the role of AMPK activation in tumor suppressor property of OA on cancer cells. Cell proliferation was determined by counting the cells at the different time points. An AMPK inhibitor, compound **C**, was used to block the AMPK activation in PC-3 cancer cells treated with OA (Figure 2A). OA was able to decelerate the proliferation of PC-3 cells, whereas compound **C**-mediated AMPK inactivation resulted in a partial recovery of the growth of PC-3 cells (Figure 2B). Cell cycle progression was also retarded by OA treatment. However, this effect was reversed by compound **C** (Figure 2C). Furthermore, compound **C** was also able to abolish the inhibitory activity of OA on the colony-forming ability of PC-3 cells (Figure 2D).

dx.doi.org/10.1021/jf500622p | J. Agric. Food Chem. 2014, 62, 5528–5537

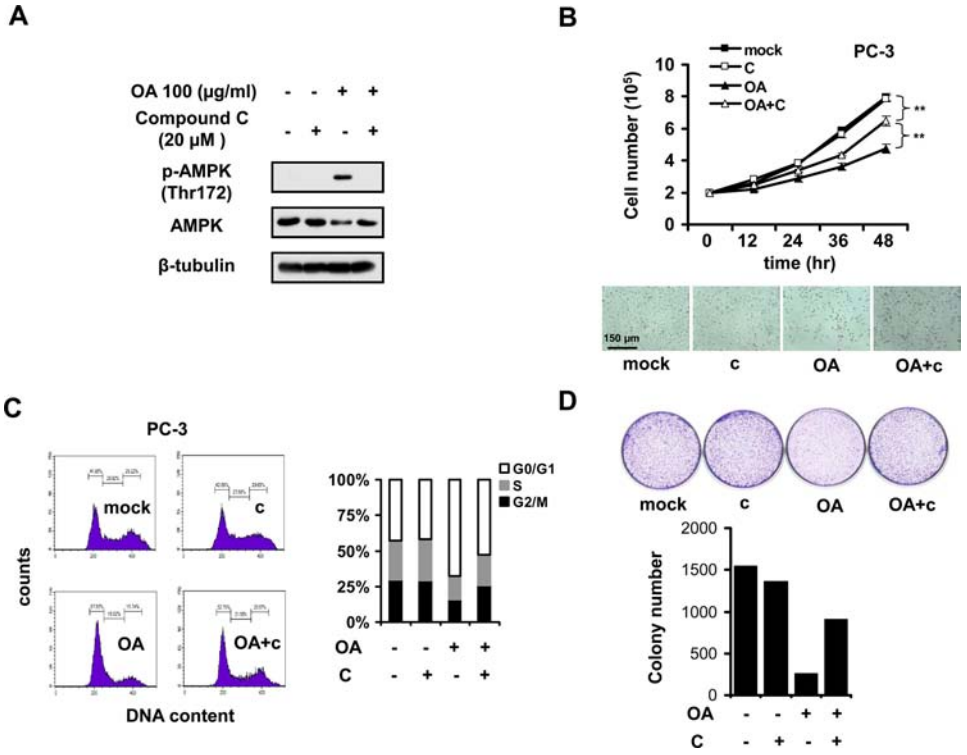

Figure 2. AMPK activation mediated the antitumor activity of OA on cancer cells. (A) PC-3 cells were pretreated with compound **C** (20 μM) for 1 h prior to OA (100 μg/mL) stimulation. Phosphorylated AMPK was detected by immunoblot assays. (B) PC-3 cells were analyzed for their proliferation at the indicated time points under the same treatment. Representative pictures are shown in the bottom panel. C, compound **C**. (C) Cell cycle analysis was performed on PC-3 cells under the same treatment. The percentages of G_0/G_1, S, and G_2/M population are presented as bars in the right panel. (D) Colony number of PC-3 cells treated with OA and/or compound **C** was counted and shown as both pictures (upper panel) and bars (bottom panel).

Subsequently, we aimed to establish the role of AMPK activation in the antitumor activity of OA. We found that the AMPK inhibitor, compound **C**, was able to rescue the effect of OA on PC-3 cells, suggesting that AMPK activation is required for OA to suppress tumor growth. AMPK activation has been also found to be essential for antitumor activity of other natural compounds. Curcumin induced apoptosis in CaOV3 ovarian cancer cells in an AMPK-dependent way. Blocking AMPK activation with compound **C** abolished curcumin induction of apoptotic event in cancer cells.[10] However, compound **C**-dependent AMPK inactivation in OA-treated cancer cells partially, not completely, abolished OA suppression of the proliferation, cell cycle progression, and colonigenecity of PC-3 cells, implying some molecular mechanisms other than AMPK activation are responsible for OA antitumor activity.

OA-Stimulated AMPK Activation Suppressed Lipid Biosynthesis in Cancer Cells. AMPK is a master kinase that regulates the cellular lipid metabolism. Its activation leads to a metabolic switch from anabolism to catabolism by phosphorylating several enzymes that play key roles in the biosynthesis of macromolecules, such as lipids.

As a rate-limiting enzyme for fatty acid synthesis, acetyl-CoA carboxylase 1 (ACC1) produces malonyl-CoA, an intermediate essential for fatty acid elongation, by catalyzing the carboxylation of acetyl-CoA. ACC1 is overexpressed in a variety of human cancers and highly contributes to the enhanced lipogenesis in cancer cells.[11] AMPK inhibits ACC1 activity by phosphorylating it at Ser79.[12] In OA-stimulated cancer cells, ACC1 phosphorylation was found to be augmented in both dose- and time-dependent manners (Figure 3A,B) and appeared to be closely correlated with OA-induced AMPK activation (Figure 1B,C). Compound **C** abolished ACC1 phosphorylation at Ser79 (Figure 3C), indicating the requirement of AMPK activation in OA-stimulated ACC1 phosphorylation.

Fatty acid synthase (FASN) is also a critical enzyme in the lipogenic pathway and is frequently found to be overexpressed in cancer cells.[13] Its transcription level is negatively regulated by AMPK-dependent SREBP1c phosphorylation.[14] As shown in Figure 3A,B, OA reduced the expression of FASN protein in cancer cells. This effect was associated with both OA concentration and the time of OA treatment (Figure 3A,B). After the treatment with OA, the protein levels of FASN were decreased. However, the protein levels of FASN were restored in the presence of compound **C** (Figure 3C).

In addition to the fatty acid, sterol is also required for the growth of cancer cells. 3-Hydroxy-3-methylglutaryl-CoA reductase (HMGR) is the enzyme responsible for generating mevalonic acid, an essential intermediate for the synthesis of cholesterol and isoprenoids. AMPK has been reported to phosphorylate and inactivate HMGR.[1] OA was found to increase the phosphorylation of HMGR in cancer cells, in both dose- and time-dependent fashions (Figure 3A,B). Compound **C** treatment was able to block the OA-induced phosphorylation of HMGR at Ser872 (Figure 3C).

Reactivation of AMPK has been documented to suppress the production of lipid in cancer cells. Radioactive assays revealed that OA was able to diminish the de novo lipid synthesis, shown as a reduced incorporation rate of [^{3}H] acetyl-CoA into lipid product of PC-3 cells (Figure 3D). OA suppression of lipid synthesis was rescued by compound **C** (Figure 3E), implying

dx.doi.org/10.1021/jf500622p | J. Agric. Food Chem. 2014, 62, 5528−5537

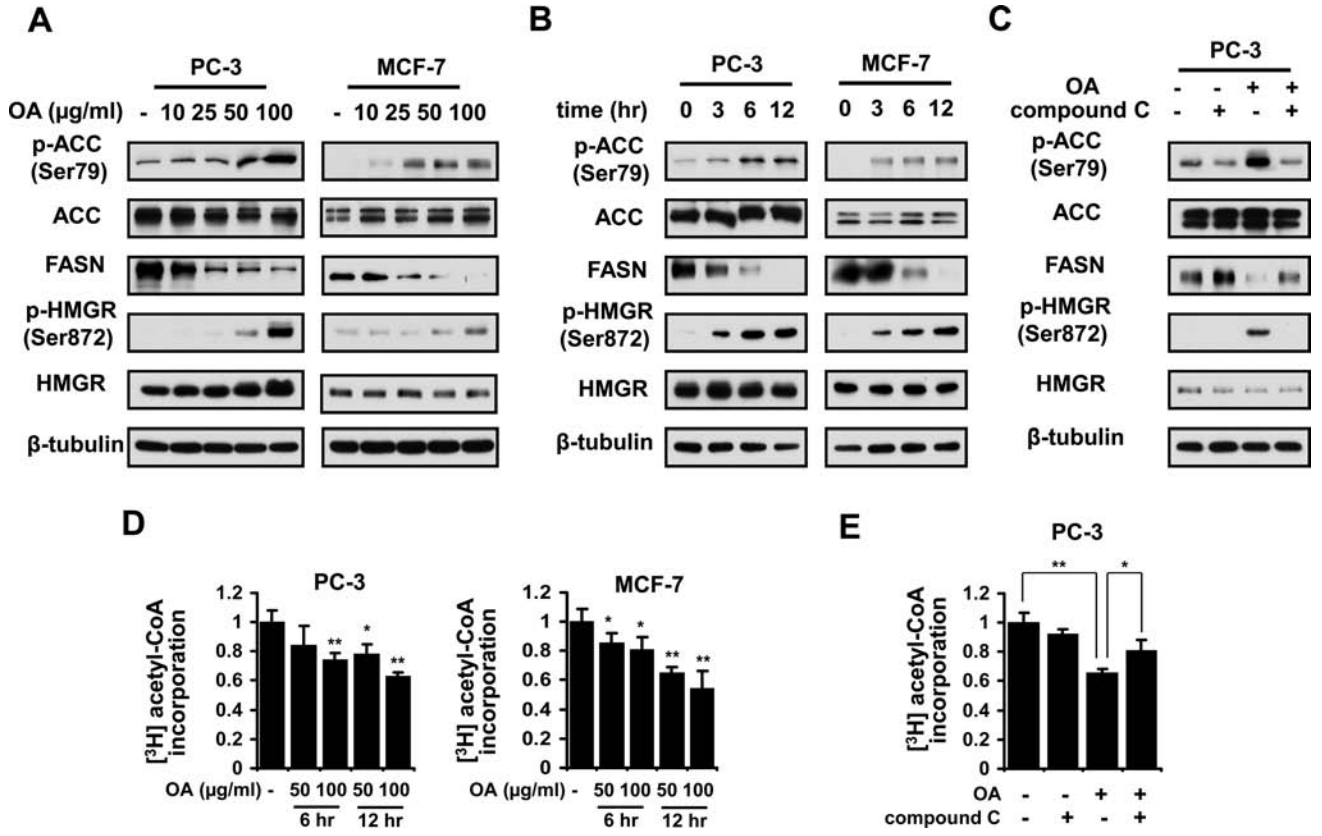

Figure 3. OA-stimulated AMPK activation suppressed lipid biosynthesis in cancer cells. PC-3 and MCF-7 cells were treated with OA of indicated concentrations for 3 h (A) or with 100 μg/mL OA for indicated times (B). PC-3 cells were also pretreated with compound **C** (20 μM) for 1 h prior to OA (100 μg/mL) stimulation (C). Then these cell lysates were used for immunoblot analysis of lipid metabolism-related gene expression. ACC, acetyl-CoA carboxylase; FASN, fatty acid synthase; HMGR, 3-hydroxy-3-methylglutaryl-CoA reductase. [^{3}H] acetyl-CoA incorporation was employed to evaluate the lipid synthesis of PC-3 and MCF-7 cells under the treatment of OA (50 and 100 μg/mL) for 6 or 12 h (D). Also, lipid synthesis of PC-3 cells treated with OA and/or compound **C** was also determined (E). The relative values are shown in panels D and E.

that AMPK activation is essential for its effect against fatty acid production.

Next, we investigated if OA was able to affect the lipogenesis of cancer cells by detecting the phosphorylation or expression of some lipid synthesis-associated genes, which have been confirmed as AMPK downstream effectors, and performing [^{3}H]acetyl-CoA incorporation assay. The results showed that OA was able to suppress the lipid synthesis in a dose- and time-dependent manner. Compound **C** abolished the inhibitory effect of OA on the lipogenic process in cancer cells, supporting the role of AMPK activation in OA suppression of lipid synthesis (Figure 3). Pomolic acid, a natural antitumor compound, was also found to suppress lipid synthesis in MCF-7 breast cancer cells in an AMPK-dependent manner.[15] There is a possibility that all of the compounds identified as AMPK activators may exert an inhibitory activity on lipogenic pathways.

Protein Synthesis Was Inhibited in Cancer Cells Treated with OA in an AMPK Activation-Dependent Way. AMPK reduces the activity of the mammalian target of rapamycin complex 1 (mTORC1) by phosphorylating its upstream inhibitory regulator, TSC2,[16] and its regulatory subunit, Raptor.[17] In OA-treated cancer cells, mTOR was shown to be less phosphorylated at Ser2448 (Figure 4A,B). The expression of phosphorylated p70S6K, a downstream effector of mTOR that hampers protein synthesis by inactivating S6 ribosomal protein, was consequently reduced in cancer cells under OA treatment (Figure 4A,B). This mTOR-dependent phosphorylation is required for the kinase activity of p70S6K.[18] The phosphorylation of another important mTOR downstream substrate, eukaryotic translation initiation factor 4E-binding protein 1 (4E-BP1), was also found to be decreased in OA-stimulated cancer cells (Figure 4A,B). The Thr37 and Thr46 phosphorylations prime 4E-BP1 for subsequent phosphorylations that abolish the inhibitory activity of 4E-BP1 on mRNA translation.[19] Therefore, OA-induced dephosphorylation of 4E-BP1 probably suppresses protein synthesis in cancer cells. Changes in the phosphorylation level of these protein synthesis-related factors were all abolished by compound **C** (Figure 4C), indicating that AMPK activation is required for OA inhibition of the mTOR signaling pathway.

A fluorescence-based protein synthesis assay kit was used to determine the effect of OA on protein synthesis in cancer cells. Microscopic observation revealed that the intensity of fluorescence was reduced in cells 3 and 12 h after the treatment of different dose of OA (Figure 4D), suggesting that OA compromised the nascent synthesis of protein. Compound **C** suppression of AMPK was able to partially prevent the reduction in protein synthesis in cancer cells treated with OA (Figure 4E).

We also studied the changes in protein synthesis in cancer cells treated with OA. The data showed that protein synthesis in PC-3 and MCF-7 cells was significantly compromised under OA stimulation. Consistently, the promoters of protein

dx.doi.org/10.1021/jf500622p | J. Agric. Food Chem. 2014, 62, 5528−5537

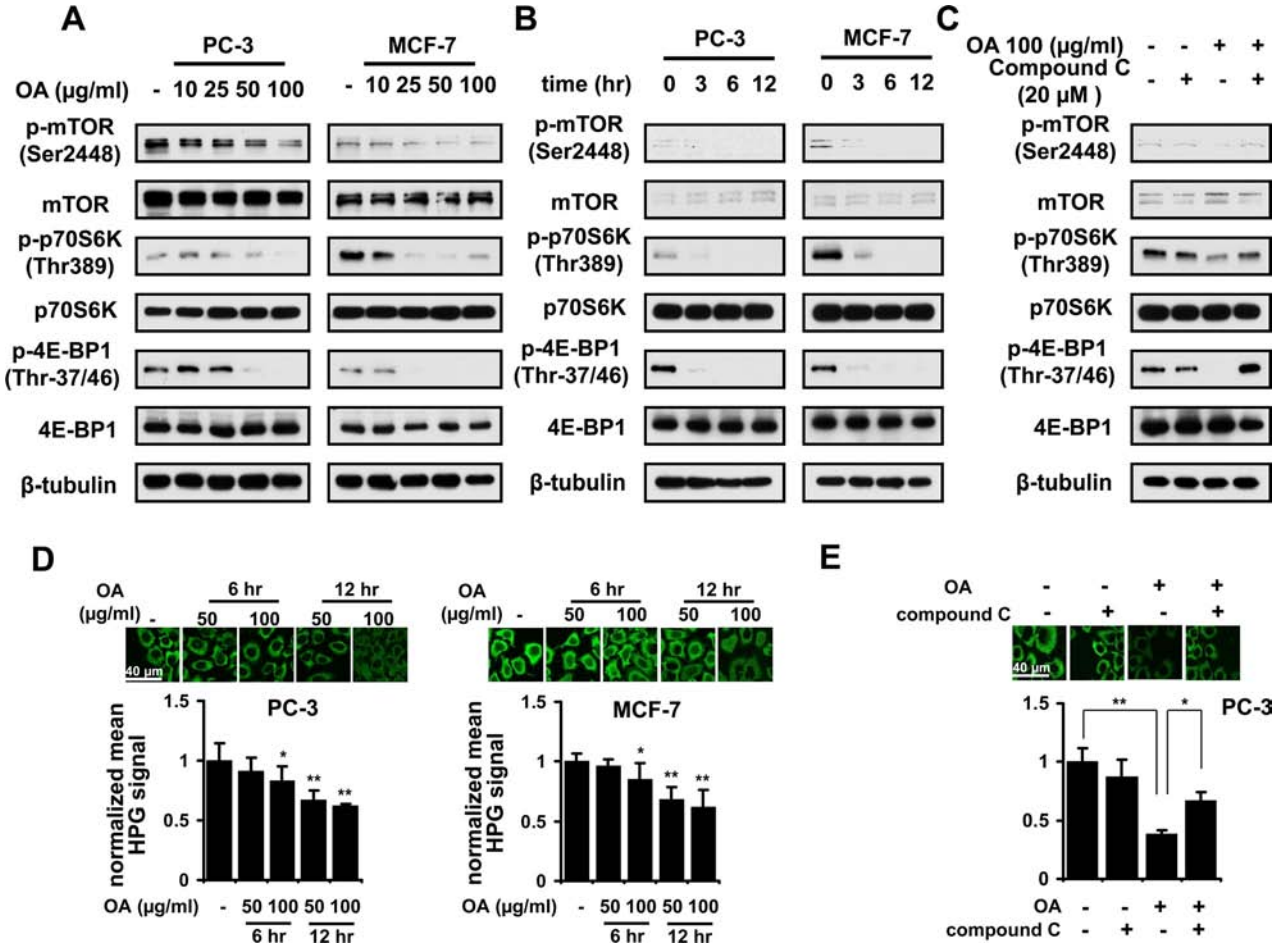

Figure 4. Protein synthesis was inhibited in cancer cells treated with OA in an AMPK activation-dependent way. PC-3 and MCF-7 cells were treated with OA of indicated concentrations for 3 h (A) or with 100 μg/mL OA for indicated times (B). PC-3 cells were also pretreated with compound **C** (20 μM) for 1 h prior to OA (100 μg/mL) stimulation (C). Then these cell lysates were used for immunoblot analysis of protein synthesis-related gene expression. mTOR, mammalian target of the rapamycin; 4EE-BP1, eukaryotic translation initiation factor 4E-binding protein 1. Nascent protein synthesis in PC-3 and MCF-7 cells under the treatment of OA (50 and 100 μg/mL) for 6 or 12 h was performed with a HPG-based Protein Synthesis Assay Kit (D). Also, PC-3 cells treated with OA and/or compound **C** were also detected for de novo protein synthesis (E). The relative values are shown in panels D and E. Representative pictures are shown in the upper panels.

synthesis were also inactivated under OA treatment, evidenced by decreased phosphorylation levels. Compound **C**-mediated AMPK inhibition revealed that AMPK activation is required for the inhibitory effect of OA on protein synthesis in cancer cells.

OA Suppressed Aerobic Glycolysis in Cancer Cells in an AMPK-Dependent Manner. AMPK has been recently demonstrated as a negative regulator of the Warburg effect in cancer cells.[3] The inhibitory effect of AMPK on glycolysis may be associated with its suppression of PKM2 activity via affecting mTOR activation.[20] Herein, we investigated if OA treatment affected the glycolytic metabolism in cancer cells. Glucose uptake was significantly reduced in cancer cells treated with OA (Figure 5A). Furthermore, cancer cells produced less lactic acid, which is the end product of glycolysis, under treatment with OA (Figure 5B). The changes in glucose consumption and lactate generation indicated that OA suppressed the glycolytic metabolism in cancer cells.

Cancer cells are also featured compromised mitochondrial oxidative phosphorylation, which contributes to the maintenance of malignant phenotypes. Oxygen consumption, an indicator for the efficiency of oxidative phosphorylation, was subsequently measured in OA-stimulated cancer cells. An increase in O_2 consumption was observed in cancer cells exposed to OA (Figure 5C).

Similar to the role of AMPK activation in lipid and protein synthesis, compound **C** was also able to partially inhibit OA-induced metabolic switch in cancer cells, evidenced by increases in glucose uptake, lactate production, and O_2 consumption in the cells treated with both OA and compound **C** (Figure 5D–F).

Increasing evidence indicated that the Warburg effect is critical for the unlimited growth of cancers, and targeting it seems to be an effective strategy for cancer treatment. We therefore examined if OA interferes with the metabolic pathways in cancer cells. The results on glucose uptake, lactate production, and oxygen consumption rates showed that OA switches metabolic patterns from aerobic glycolysis to mitochondrial oxidative phosphorylaion. Similarly, AMPK inhibition protected PC-3 cells from this metabolic change. However, it is unknown how OA-induced AMPK leads to the reversal of the Warburg effect.

AMPK-Dependent Metabolic Adaptation Contributes to the Tumor Suppressor Activity of OA on Cancer Cells. Finally, we aimed to study the contribution of metabolic alteration to the antitumor activity of OA on cancer cells. Therefore, we used a small molecule activator, MHY1485, to interfere with

dx.doi.org/10.1021/jf500622p | J. Agric. Food Chem. 2014, 62, 5528−5537

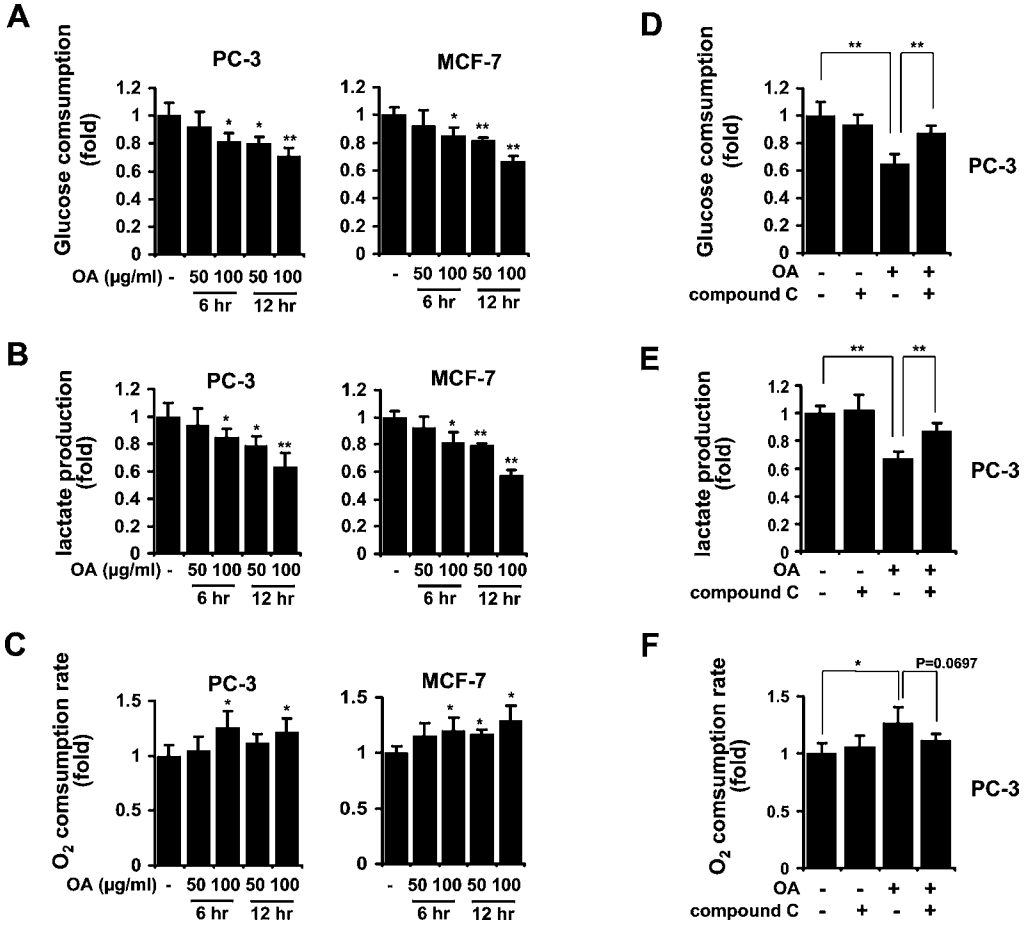

Figure 5. OA suppressed aerobic glycolysis in cancer cells in an AMPK-dependent manner. PC-3 and MCF-7 cells were treated with OA (50 and 100 μg/mL) for 6 or 12 h, followed by the assessment of glucose consumption (A), lactate production (B), and O_2 consumption rates (C). Furthermore, the above glycolysis-related parameters were estimated in PC-3 cells treated with OA and/or compound **C** (D−F). All data are shown as relative values. The methods were described under Materials and Methods.

the changes in the metabolic pathway without affecting AMPK activation.[21] mTOR inhibition was rescued by MHY1485 in OA-stimulated cancer cells, and AMPK activation was not affected under this treatment (Figure 6A). MHY1485 was able to counteract the inhibitory effect of OA on protein synthesis in cancer cells and to stop the metabolic switch from aerobic glycolysis to oxidative phosphorylation (data not known), through the mTOR pathway. The cell proliferation assay showed that MHY1485 could speed the growth of PC-3 cells under the treatment with OA (Figure 6B). The number of colonies in PC-3 cells was also increased by MHY1485 (Figure 6C).

We also determined the contribution of metabolic alteration to the antitumor activity of OA. Restoring protein synthesis and aerobic glycolysis in cancer cells partially abolished the AMPK effect on cancer cells (Figure 6), confirming the change in metabolic pattern is, at least partially, responsible for the antitumor activity of OA. The reason mTOR activators recovered proliferation and colony formation ability of PC-3 cells only in a partial manner may be that lipid synthesis was still not restored in OA-treated cells or that there are still some mechanisms underlying OA antitumor function, other than interfering with metabolism. For example, there is a possibility that OA may induce G_0/G_1 cell cycle arrest via the AMPK/p53/p21 pathway. Previous studies showed that AMPK phosphorylates p53 at Ser15, facilitates its accumulation, and enhances its transcription activity of p21CIP, a CDK inhibitor, in both normal and cancer cells.[22,23] p27KIP is also reported to be a substrate of AMPK kinase and phosphorylated at Thr-198. This phosphorylation event enhances the inhibitory function of p27KIP on cell cycle progression.[24] In addition, AMPK activation-induced FASN down-regulation may directly affect cell cycle progression in tumor cells.[25] Furthermore, p53-associated apoptosis is another possible mechanism by which OA may exert AMPK-dependent antitumor activity, based on a recent publication reporting AMPK overexpression led to increased p53 nuclear accumulation and apoptosis.[26]

Another question about OA induction of AMPK pathway is the mechanism by which OA initiates AMPK activation. Recently, H_2O_2 was found to induce AMPK activation in insulin-secreting cells.[27] AMPK signaling can be also activated in a p38 MAPK-dependent manner in cancer cells treated with antitumor compound.[10] Thus, further studies should be focused on these molecular pathways.

OA Reduced Tumor Growth and Activated AMPK Pathway in Mice. To further confirm the antitumor activity of OA and its stimulatory effect on the AMPK pathway, we established a tumor xenograft mouse model by injecting PC-3 cells into the flanks of mice. OA was orally administered every day at two different doses, followed by periodically measuring the diameters of tumors in mice. The results showed that tumor growth was significantly retarded by the administration of high-dose OA ($P < 0.01$), but not low-dose OA ($P = 0.145$)

dx.doi.org/10.1021/jf500622p | J. Agric. Food Chem. 2014, 62, 5528−5537

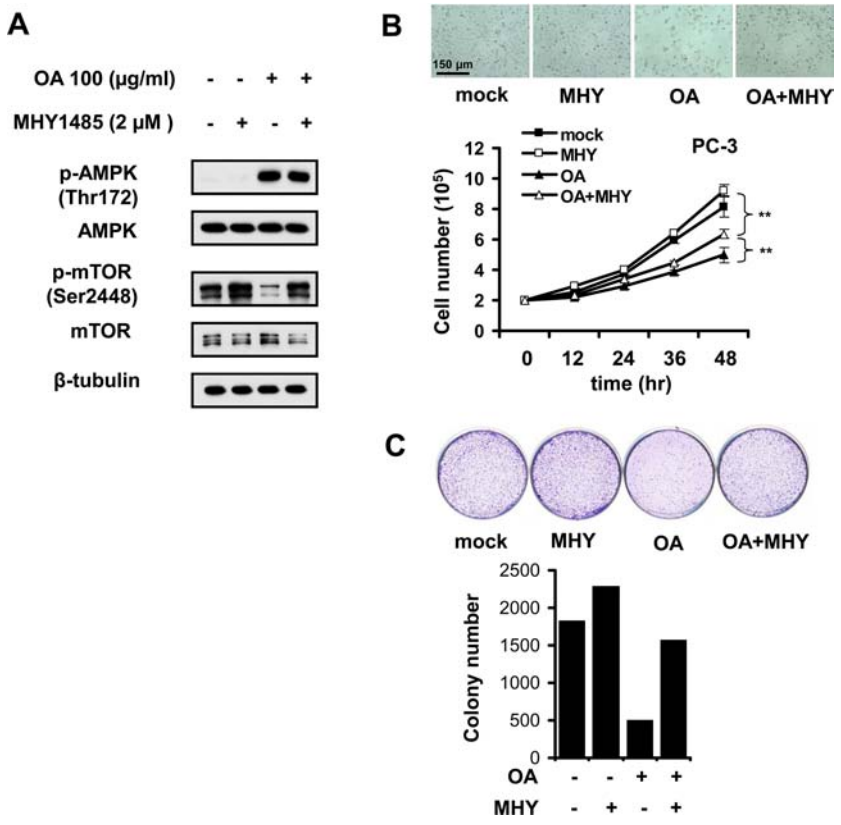

Figure 6. AMPK-dependent metabolic adaptation contributes to the tumor suppressor activity of OA on cancer cells. (A) PC-3 cells were pretreated with MHY1485 (2 μM) for 1 h prior to OA (100 μg/mL) stimulation. Phosphorylated AMPK and mTOR were detected by immunoblot assays. (B) PC-3 cells were analyzed for their proliferation at the indicated time points under the same treatment. Representative pictures are shown in the bottom panel. MHY, MHY1485. (C) Colony number of PC-3 cells treated with OA and/or MHY1485 was counted and shown as both pictures (upper panel) and bars (bottom panel).

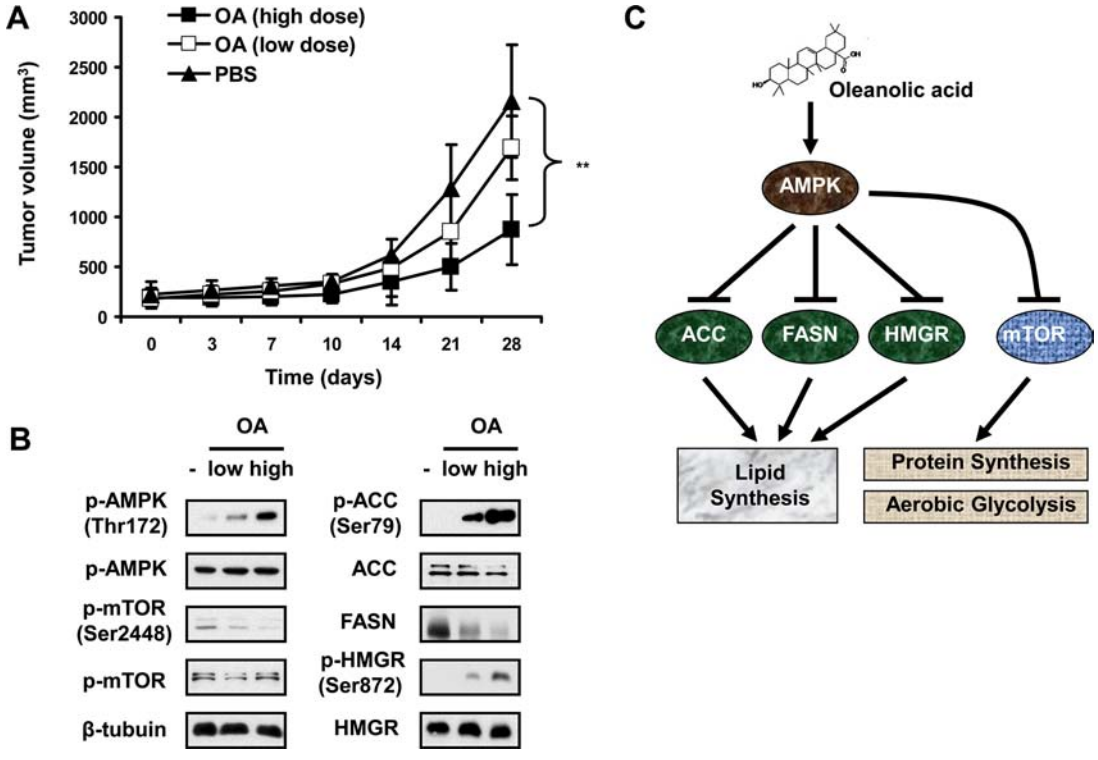

Figure 7. Action of OA on the activation of AMPK pathway in vivo. (A) OA (low dose, 40 mg/kg; high dose, 120 mg/kg) was orally administered every day for 4 weeks. Tumor volumes were periodically recorded as means ± SD. (B) The expression of phosphorylated AMPK, ACC, HMGR, and mOTR was detected in tumor xenografts. (C) Graphic illustration of molecular mechanisms by which OA alters the metabolic patterns via AMPK activation.

dx.doi.org/10.1021/jf500622p | J. Agric. Food Chem. 2014, 62, 5528−5537

(Figure 7A). Immunoblot analysis revealed that OA was able to induce the activation of AMPK in tumors (Figure 7B). Its downstream metabolism-related pathways were also affected by OA administration (Figure 7B). However, the low dose of OA indeed slightly suppressed the growth of tumor xenograft (Figure 7A), perhaps due to partial activation of AMPK and suppression of its downstream metabolic enzymes and key kinases (Figure 7B).

In addition, we detected the effect of OA on the metabolism of L-02 normal liver cells. Immunoblot assays revealed that the levels of phosphorylated AMPK are higher in normal cells than in cancer cells without OA treatment (Supporting Information panel A). OA was able to enhance AMPK phosphorylation in both cancerous and normal cells, but its effect on PC-3 cells appeared to be stronger than that in L-02 cells (Supporting Information panel A). Further metabolic assays showed that lipid and protein synthesis were higher in cancer cells than in normal cells, as well as aerobic glycolysis (Supporting Information panels B–E). OA was found to exert only a slight inhibitory effect on the above properties of normal cells (Supporting Information panels B–E).

In conclusion, we found that OA was able to induce AMPK activation and, consequently, change the metabolic patterns in cancer cells, which led to the decreased proliferation and colony formation of cancer cells (Figure 7C). We provided evidence that targeting metabolism is an effective anticancer strategy, and further preclinical and clinical studies based on metabolism as a therapeutic target should be performed.

■ ASSOCIATED CONTENT

Supporting Information

PC-3 cancer cell and L-02 normal cell were treated with or without OA (100 μg/mL). Twelve hours later, the cells were tested for total and phosphorylated AMPK levels (A), lipid synthesis (B), protein synthesis (C), glucose uptake (D), lactic acid production (E), and oxygen consumption (F). This material is available free of charge via the Internet at http://pubs.acs.org.

■ AUTHOR INFORMATION

Corresponding Author

*(X.L.) Phone: 86-10-83911837. Fax: 86-10-83911837. E-mail: linxiukun@yahoo.com.

Author Contributions

‖J.L., L.Z., and N.W. contributed equally to this work.

Funding

This work was supported by a national innovative drug development project (2014ZX-09102043-001) and an 863 High Technology Project (2014AA093503). The study was also supported in part by the National Foundation of Natural Science of China (81302906, 81273550, and 41306157) and Special Scientific Research Funds for Central Nonprofit Institutes, Chinese Academy of Fishery Sciences (2013B01YQ01).

Notes

The authors declare no competing financial interest.

■ REFERENCES

(1) Hardie, D. G.; Alessi, D. R. LKB1 and AMPK and the cancer-metabolism link – ten years after. *BMC Biol.* **2013**, *11*, 36.

(2) Khandekar, M. J.; Cohen, P.; Spiegelman, B. M. Molecular mechanisms of cancer development in obesity. *Nat. Rev. Cancer* **2011**, *11*, 886–895.

(3) Faubert, B.; Boily, G.; Izreig, S.; Griss, T.; Samborska, B.; Dong, Z.; Dupuy, F.; Chambers, C.; Fuerth, B. J.; Viollet, B.; Mamer, O. A.; Avizonis, D.; DeBerardinis, R. J.; Siegel, P. M.; Jones, R. G. AMPK is a negative regulator of the Warburg effect and suppresses tumor growth in vivo. *Cell Metab.* **2013**, *17*, 113–124.

(4) Chung, H. H.; Moon, J. S.; Yoon, J. S.; Lee, H. W.; Won, K. C. The relationship between metformin and cancer in patients with type 2 diabetes. *Diabetes Metab. J.* **2013**, *37*, 125–131.

(5) Wang, X.; Bai, H.; Zhang, X.; Liu, J.; Cao, P.; Liao, N.; Zhang, W.; Wang, Z.; Hai, C. Inhibitory effect of oleanolic acid on hepatocellular carcinoma via ERK-p53-mediated cell cycle arrest and mitochondrial-dependent apoptosis. *Carcinogenesis* **2013**, *34*, 1323–1330.

(6) Mullen, A. R.; Wheaton, W. W.; Jin, E. S.; Chen, P. H.; Sullivan, L. B.; Cheng, T.; Yang, Y.; Linehan, W. M.; Chandel, N. S.; DeBerardinis, R. J. Reductive carboxylation supports growth in tumour cells with defective mitochondria. *Nature* **2011**, *481*, 385–388.

(7) Lee, W.; Yang, E. J.; Ku, S. K.; Song, K. S.; Bae, J. S. Anticoagulant activities of oleanolic acid via inhibition of tissue factor expressions. *BMB Rep.* **2012**, *45*, 390–395.

(8) Reisman, S. A.; Aleksunes, L. M.; Klaassen, C. D. Oleanolic acid activates Nrf2 and protects from acetaminophen hepatotoxicity via Nrf2-dependent and Nrf2-independent processes. *Biochem. Pharmacol.* **2009**, *77*, 1273–1282.

(9) Wang, J.; Ma, H.; Zhang, X.; He, L.; Wu, J.; Gao, X.; Ren, J.; Li, J. A novel AMPK activator from Chinese herb medicine and ischemia phosphorylate the cardiac transcription factor FOXO3. *Int. J. Physiol. Pathophysiol. Pharmacol.* **2009**, *1*, 116–126.

(10) Pan, W.; Yang, H.; Cao, C.; Song, X.; Wallin, B.; Kivlin, R.; Lu, S.; Hu, G.; Di, W.; Wan, Y. AMPK mediates curcumin-induced cell death in CaOV3 ovarian cancer cells. *Oncol. Rep.* **2008**, *20*, 1553–1559.

(11) Zu, X.; Zhong, J.; Luo, D.; Tan, J.; Zhang, Q.; Wu, Y.; Liu, J.; Cao, R.; Wen, G.; Cao, D. Chemical genetics of acetyl-CoA carboxylases. *Molecules* **2013**, *18*, 1704–1719.

(12) Ha, J.; Daniel, S.; Broyles, S. S.; Kim, K. H. Critical phosphorylation sites for acetyl-CoA carboxylase activity. *J. Biol. Chem.* **1994**, *269*, 22162–22168.

(13) Menendez, J. A.; Lupu, R. Fatty acid synthase and the lipogenic phenotype in cancer pathogenesis. *Nat. Rev. Cancer* **2007**, *7*, 763–777.

(14) Li, Y.; Xu, S.; Mihaylova, M. M.; Zheng, B.; Hou, X.; Jiang, B.; Park, O.; Luo, Z.; Lefai, E.; Shyy, J. Y.; Gao, B.; Wierzbicki, M.; Verbeuren, T. J.; Shaw, R. J.; Cohen, R. A.; Zang, M. AMPK phosphorylates and inhibits SREBP activity to attenuate hepatic steatosis and atherosclerosis in diet-induced insulin-resistant mice. *Cell Metab.* **2011**, *13*, 376–388.

(15) Youn, S. H.; Lee, J. S.; Lee, M. S.; Cha, E. Y.; Thuong, P. T.; Kim, J. R.; Chang, E. S. Anticancer properties of pomolic acid-induced AMP-activated protein kinase activation in MCF7 human breast cancer cells. *Biol. Pharm. Bull.* **2012**, *35*, 105–110.

(16) Inoki, K.; Zhu, T.; Guan, K. L. TSC2 mediates cellular energy response to control cell growth and survival. *Cell* **2003**, *115*, 577–590.

(17) Gwinn, D. M.; Shackelford, D. B.; Egan, D. F.; Mihaylova, M. M.; Mery, A.; Vasquez, D. S.; Turk, B. E.; Shaw, R. J. AMPK phosphorylation of raptor mediates a metabolic checkpoint. *Mol. Cell* **2008**, *30*, 214–226.

(18) Weng, Q. P.; Kozlowski, M.; Belham, C.; Zhang, A.; Comb, M. J.; Avruch, J. Regulation of the p70 S6 kinase by phosphorylation in vivo. Analysis using site-specific anti-phosphopeptide antibodies. *J. Biol. Chem.* **1998**, *273*, 16621–16629.

(19) Gingras, A. C.; Gygi, S. P.; Raught, B.; Polakiewicz, R. D.; Abraham, R. T.; Hoekstra, M. F.; Aebersold, R.; Sonenberg, N. Regulation of 4E-BP1 phosphorylation: a novel two-step mechanism. *Genes Dev.* **1999**, *13*, 1422–1437.

(20) Sun, Q.; Chen, X.; Ma, J.; Peng, H.; Wang, F.; Zha, X.; Wang, Y.; Jing, Y.; Yang, H.; Chen, R.; Chang, L.; Zhang, Y.; Goto, J.; Onda, H.; Chen, T.; Wang, M. R.; Lu, Y.; You, H.; Kwiatkowski, D.; Zhang, H. Mammalian target of rapamycin up-regulation of pyruvate kinase

isoenzyme type M2 is critical for aerobic glycolysis and tumor growth. *Proc. Natl. Acad. Sci. U.S.A.* **2011**, *108*, 4129−4134.
(21) Choi, Y. J.; Park, Y. J.; Park, J. Y.; Jeong, H. O.; Kim, D. H.; Ha, Y. M.; Kim, J. M.; Song, Y. M.; Heo, H. S.; Yu, B. P.; Chun, P.; Moon, H. R.; Chung, H. Y. Inhibitory effect of mTOR activator MHY1485 on autophagy: suppression of lysosomal fusion. *PLoS One* **2012**, *7*, No. e43418.
(22) Jones, R. G.; Plas, D. R.; Kubek, S.; Buzzai, M.; Mu, J.; Xu, Y.; Birnbaum, M. J.; Thompson, C. B. AMP-activated protein kinase induces a p53-dependent metabolic checkpoint. *Mol. Cell* **2005**, *18*, 283−293.
(23) Imamura, K.; Ogura, T.; Kishimoto, A.; Kaminishi, M.; Esumi, H. Cell cycle regulation via p53 phosphorylation by a 5′-AMP activated protein kinase activator, 5-aminoimidazole-4-carboxamide-1-β-D-ribofuranoside, in a human hepatocellular carcinoma cell line. *Biochem. Biophys. Res. Commun.* **2001**, *287*, 562−567.
(24) Liang, J.; Shao, S. H.; Xu, Z. X.; Hennessy, B.; Ding, Z.; Larrea, M.; Kondo, S.; Dumont, D. J.; Gutterman, J. U.; Walker, C. L.; Slingerland, J. M.; Mills, G. B. The energy sensing LKB1-AMPK pathway regulates p27(kip1) phosphorylation mediating the decision to enter autophagy or apoptosis. *Nat. Cell Biol.* **2007**, *9*, 218−224.
(25) Li, N.; Lu, H.; Chen, C.; Bu, X.; Huang, P. Loss of fatty acid synthase inhibits the "HER2-PI3K/Akt axis" activity and malignant phenotype of Caco-2 cells. *Lipids Health Dis.* **2013**, *12*, 83.
(26) Fox, M. M.; Phoenix, K. N.; Kopsiaftis, S. G.; Claffey, K. P. AMP-activated protein kinase alpha 2 isoform suppression in primary breast cancer alters AMPK growth control and apoptotic signaling. *Genes Cancer* **2013**, *4*, 3−14.
(27) Sarre, A.; Gabrielli, J.; Vial, G.; Leverve, X. M.; Assimacopoulos-Jeannet, F. Reactive oxygen species are produced at low glucose and contribute to the activation of AMPK in insulin-secreting cells. *Free Radical Biol. Med.* **2012**, *52*, 142−150.

JOURNAL OF AGRICULTURAL AND FOOD CHEMISTRY

Article

pubs.acs.org/JAFC

Biological Activity and Molecular Docking Studies of Curcumin-Related α,β-Unsaturated Carbonyl-Based Synthetic Compounds as Anticancer Agents and Mushroom Tyrosinase Inhibitors

Syed Nasir Abbas Bukhari,*[,†] Ibrahim Jantan,*[,†] Oya Unsal Tan,[‡] Muhammad Sher,[§] M. Naeem-ul-Hassan,[§] and Hua-Li Qin[∥]

[†]Drug and Herbal Research Centre, Faculty of Pharmacy, Universiti Kebangsaan Malaysia, Jalan Raja Muda Abdul Aziz, 50300 Kuala Lumpur, Malaysia

[‡]Department of Pharmaceutical Chemistry, Faculty of Pharmacy, Hacettepe University, Ankara 06100, Turkey

[§]Department of Chemistry, University of Sargodha, Sargodha 40100, Pakistan

[∥]Department of Pharmaceutical Engineering, School of Chemical Engineering, Wuhan University of Technology, 205 Luoshi Road, Wuhan 430070, P.R. China

ABSTRACT: Hyperpigmentation in human skin and enzymatic browning in fruits, which are caused by tyrosinase enzyme, are not desirable. Investigations in the discovery of tyrosinase enzyme inhibitors and search for improved cytotoxic agents continue to be an important line in drug discovery and development. In present work, a new series of 30 compounds bearing α,β-unsaturated carbonyl moiety was designed and synthesized following curcumin as model. All compounds were evaluated for their effects on human cancer cell lines and mushroom tyrosinase enzyme. Moreover, the structure−activity relationships of these compounds are also explained. Molecular modeling studies of these new compounds were carried out to explore interactions with tyrosinase enzyme. Synthetic curcumin-like compounds (**2a−b**) were identified as potent anticancer agents with 81−82% cytotoxicity. Five of these newly synthesized compounds (**1a**, **8a−b**, **10a−b**) emerged to be the potent inhibitors of mushroom tyrosinase, providing further insight into designing compounds useful in fields of food, health, and agriculture.

KEYWORDS: *melanogenesis, Curcuma longa, cytotoxicity, antibrowning, synthesis*

INTRODUCTION

Throughout history, natural products have offered a rich source of compounds that have widespread applications in the fields of medicine, food and agriculture.[1] Structural modification of natural compounds or synthesis of new compounds, based upon designs following a natural compound scaffolding, have provided us a lot of important new commercialized drugs within the medicine, agriculture, and food spheres.[2,3] An important line in the discovery of modern anticancer drugs is exploration for enhanced cytotoxic agents principally with safety perspectives in view.[4] In line with the safety issues, plant-derived natural compounds have always fascinated scientists worldwide on grounds of being biocompatible, natural compounds that are deemed as potentially safe and effective skin lightening and anticancer agents.[5]

Curcumin, flavonoids, and numerous dietary chemopreventive compounds have shown potential in treating cancer or dermatological disorders.[6−8] Behind cardiovascular diseases, cancer is the second principal cause of death in the world. For treating a wide range and types of cancer, plentiful effort have been started for decades but it is only recently that chemoprevention has attracted due share of attention. Combinatorial chemistry along with high-throughput screening technique directed toward molecular targets and cancer cells are well-known methods for primary anticancer drug discovery.[9−11] Curcumin is a plant-derived polyphenol obtained from *curcuma longa;* Powdered rhizome of this plant, turmeric, has been widely used for color impartment and flavoring to foods and by tradition for the treatment of various inflammatory conditions and other diseases.[12−14] Curcumin (diferuloylmethane) possesses both anticancer and antityrosinase properties.[15−17]

Tyrosinase, a ubiquitous dinuclear copper enzyme, catalyzes the hydroxylation of phenols to catechols and the subsequent oxidation of catechols to quinones. This series of events take place by activation of dioxygen in the form of a side-on-bonded peroxide dicopper(II) species, crystallographically[18] and spectroscopically identified.[19,20] Melanin is a pigmented heteropolymer synthesized by differentiated melanocytes in specialized cellular organelles termed melanosomes. The entire process leading to the formation of melanin is called melanogenesis and is initiated with the first step of tyrosine oxidation to dopaquinone catalyzed by tyrosinase.

Melanin plays an important role in protecting human skin from the harmful effects of UV radiation from the sunlight. This is achieved by transfer of mature melanosomes to neighboring keratinocytes, which are arranged in a supranuclear cap, protecting the DNA against incident ultraviolet light (UV) irradiation.[21] By controlling skin tone, melanin also determines the human phenotypic appearance. Although photoprotection

Received: February 5, 2014
Revised: May 27, 2014
Accepted: June 5, 2014
Published: June 5, 2014

ACS Publications © 2014 American Chemical Society

dx.doi.org/10.1021/jf501145b | J. Agric. Food Chem. 2014, 62, 5538−5547

is melanin's main function in human skin, the accumulation of an abnormal amount of melanin in specific parts of the skin resulting in more pigmented patches might become an aesthetic problem. In addition, enzymatic browning caused by tyrosinase system in fruits and fungi is undesirable in, for example, fresh fruits, beverages, vegetables, and mushrooms. In commercial or domestic processing, handling and storage of foods, tyrosinase is contemplated to have a critical role. In bruised or cut fruits, vegetables and other plant foods, tyrosinase causes enzymatic browning which subsequently leads to a significant decrease in nutritional and market values.[22] The undesirable phenomenon of hyperpigmentation in human skin and enzymatic browning in fruits have ushered researchers to seek new, enhanced, and potent tyrosinase inhibitors for use in antibrowning of foods and skin whitening. Owing to the exclusively important roles in mammalian melanogenesis as well as enzymatic browning in fruits and fungi, tyrosinase inhibitors have been an important concern under the research radar for years.

Some tyrosinase inhibitors have been discovered and reviewed before.[23−26] Herein, a new series of 30 compounds bearing α,β-carbonyl moiety was designed and synthesized based on curcumin template (Figure 1) for potential use in

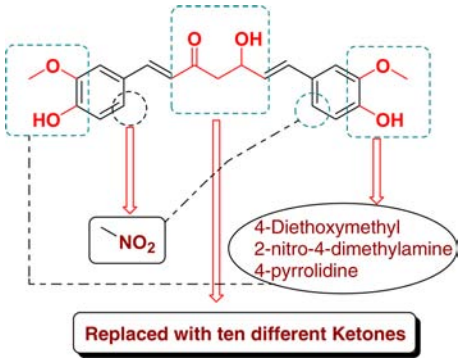

Figure 1. Chemical modifications in structure of curcumin.

cosmetics, clinical medicines, food industry, and agriculture. Effects of synthesized compounds on human cancer cell lines and mushroom tyrosinase enzyme were evaluated. Furthermore, structure−activity relationships of synthesized compounds were also discussed.

MATERIALS AND METHODS

Materials and General Procedures. All chemicals and reagents utilized in this research were purchased from Sigma-Aldrich (St. Louis, MO), Merck (Darmstadt, Germany) and Acros Organics (Geel, Belgium) of analytical grade, and were used as supplied, unless otherwise stated. A typical work-up included washing with brine and drying the organic layer with anhydrous magnesium sulfate before concentration in vacuo. ^{1}H and ^{13}C NMR spectra were recorded with a JEOL ECP spectrometer operating at 500 MHz, with Me4Si as internal standard and $CDCl_3$ or DMSO-d_6 as the solvent. High resolution mass spectra (HRMS) were determined by the Electrospray ionization mass spectrometry (ESI-MS) on MicroTOF-Q mass spectrometer (Bruker, Billerica, MA). Microanalyses data were obtained from the Fison EA 1108 elemental analyzer. Infrared spectra were recorded using KBr disc on a PerkinElmer 400 (FTIR) spectrometer. Flash column chromatography was performed with silica gel 60 (230−400mesh) (Merck) and thin layer chromatography (TLC) was carried out on precoated silica plates (kiesel gel 60 F_{254}, BDH). Melting points were determined on an electrothermal instrument and are uncorrected. Compounds were visualized by illumination under ultraviolet (UV) light (254 nm) or by the use of vanillin stain followed by charring on a hot plate.

Synthesis of Curcumin Related α,β-Unsaturated Carbonyl-Based Compounds. A direct coupling approach was employed in order to synthesize α,β-unsaturated carbonyl-based compounds. A general reaction proceeded by base catalyzed Claisen-Schmidt condensation, carried out by reacting a suitable aromatic aldehyde with different types of 10 ketones: at a molar ratio of 1:2 for synthesizing 21 compounds (**1a−7a**; **1b−7b**; **1c−7c**), and at a molar ratio of 1:1 for 9 compounds (**8a−10a**; **8b−10b**; **8c−10c**). A general synthesis method of α,β-unsaturated carbonyl-based compounds is illustrated in Figure 2. Briefly, in a single necked round-bottom flask, selected aromatic aldehyde (20 mmol, 2 equivalant) and ketone (10 mmol, 1 equiv) were mixed and dissolved in 15 mL of ethanol and stirred at 5 °C for a few minutes. A 40% NaOH solution (in ethanol) was then added into the above solution drop by drop over several minutes. The mixture obtained was stirred at room temperature (27 °C) for 1−24 h. Product formation was indicated by the appearance of precipitate and change in color of the reaction mixture. TLC was used to monitor the reaction and upon completion, acidified ice was added to the mixture for quenching the reaction. Column chromatography and/or recrystallization processes were used to isolate α,β-unsaturated carbonyl-based compounds.

*2,6-Bis[4-(diethoxymethyl)benzylidene]cyclohexanone (**1a**).* Yellow crystals (2.59 g, 54%). Mp: 112−114 °C; ^{1}H NMR (500 MHz, $CDCl_3$) δ: 7.89 (s, 2H), 7.29 (d, J = 8 Hz, 4H), 6.82 (d, J = 8 Hz, 4H), 5.89 (s, 2H), 3.42 (q, J = 7.5, 8H), 2.32 (t, J = 12.0 Hz, 4H), 1.82 (m, 2H), 1.24 (t, J = 7.5, 12H); ^{13}C NMR (500 MHz, $CDCl_3$) δ: 186.4, 152.9, 144.4, 136.5, 132.5, 127.3, 126.5, 101.1, 55.0, 28.3, 27.8, 16.2; HRMS (ESI) m/z: 479.68 $[M + H]^+$, Microanalysis calculated for $C_{30}H_{38}O_5$ (478.62), C: 75.28%, H: 8.00%. Found C: 75.42%, H: 8.12%.

*2,6-Bis(4-dimethylamino-2-nitro-benzylidene)-cyclohexanone (**1b**).* White powder (2.78 g, 62%). Mp: 139−140 °C; δ: 7.94 (s, 2H), 7.55 (d, J = 8 Hz, 2H), 7.41 (d, J = 8 Hz, 2H), 7.13 (s, 2H), 3.15 (s, 12H), 2.35 (t, J = 12.0 Hz, 4H), 1.87 (m, 2H); ^{13}C NMR (500 MHz, $CDCl_3$) δ: 190.7, 149.5, 145.7, 145.6, 140.1, 128.2, 118.6, 117.6, 106.5, 46.8, 29.1, 27.5; HRMS (ESI) m/z: 451.64 $[M + H]^+$, microanalysis calculated for $C_{24}H_{26}N_4O_5$ (450.49), C: 63.99%, H: 5.82%, N: 12.44%. Found C: 64.12%, H: 5.72%, N: 12.42%.

*3,5-Bis(4-diethoxymethyl-benzylidene)-tetrahydro-pyran-4-one (**2a**).* Pale-yellow crystals (3.06 g, 64%). Mp: 106−108 °C; ^{1}H NMR (500 MHz, $CDCl_3$) δ: 7.85 (s, 2H), 7.32 (d, J = 8 Hz, 4H), 6.95 (d, J = 8 Hz, 4H), 5.52 (s, 2H), 3.62 (q, J = 7.5, 8H), 2.69 (s, 4H), 1.18 (t, J = 8, 12H); ^{13}C NMR (500 MHz, $CDCl_3$) δ: 187.2, 152.7, 143.8, 136.7, 131.9, 126.2, 125.2, 101.5, 62.4, 55.2, 16.1; HRMS (ESI) m/z: 481.65 $[M + H]^+$, microanalysis calculated for $C_{29}H_{36}O_6$ (480.59), C: 72.48%, H: 7.55%. Found C: 72.62%, H: 7.72%.

*3,5-Bis[4-(dimethylamino)2-nitro-benzylidene]-1-methyl-piperidin-4-one (**4b**).* White powder (2.56 g, 55%). Mp: 181- 182 °C; ^{1}H NMR (500 MHz, $CDCl_3$) δ: 7.76 (s, 2H), 7.45 (d, J = 8 Hz, 2H), 7.23 (d, J = 8 Hz, 2H), 7.13 (s, 2H), 3.21 (s, 12H), 3.03 (s, 4H), 2.19 (s, 3H); ^{13}C NMR (500 MHz, $CDCl_3$) δ: 187.5, 148.9, 148.2, 143.2, 141.8, 126.7, 119.6, 118.9, 106.2, 44.5, 46.1, 38.8; HRMS (ESI) m/z: 466.72 $[M + H]^+$, microanalysis calculated for $C_{24}H_{27}N_5O_5$ (465.50), C: 61.92%, H: 5.85%, N: 15.04%. Found C: 61.99%, H: 5.91%, N: 15.19%.

*1,5-Bis(4-diethoxymethyl-phenyl)-penta-1,4-dien-3-one (**6a**).* Pale-brown solid (1.96 g, 45%). Mp: 98−100 °C; ^{1}H NMR (500 MHz, $CDCl_3$) δ: 7.82 (d, J = 6.5 Hz, 4H), 7.71 (d, J = 8 Hz, 2H), 7.49 (d, J = 6.5 Hz, 2H), 7.16 (d, J = 7 Hz, 4H), 5.25 (s, 2H), 3.52 (q, J = 7 Hz, 8H), 1.17 (t, J = 7.0, 12H); ^{13}C NMR (500 MHz, $CDCl_3$) δ: 190.5, 152.2, 148.6, 139.7, 136.4, 135.2, 132.8, 102.2, 55.5, 16.9; HRMS (ESI) m/z: 439.62 $[M + H]^+$, microanalysis calculated for $C_{27}H_{34}O_5$ (438.56), C: 73.94%, H: 7.81%. Found C: 74.12%, H: 7.89%.

*1,5-Bis(4-dimethylamino-2-nitro-phenyl)-penta-1,4-dien-3-one (**6b**).* Pale-yellow solid (2.97 g, 68%). Mp: 177−179 °C; ^{1}H NMR (500 MHz, $CDCl_3$) δ: 7.70 (d, J = 6 Hz, 2H), 7.68 (d, J = 8 Hz, 2H), 7.44 (d, J = 6 Hz, 2H), 7.25 (d, J = 8 Hz, 2H), 7.12 (s, 2H), 3.15 (s,

dx.doi.org/10.1021/jf501145b | J. Agric. Food Chem. 2014, 62, 5538−5547

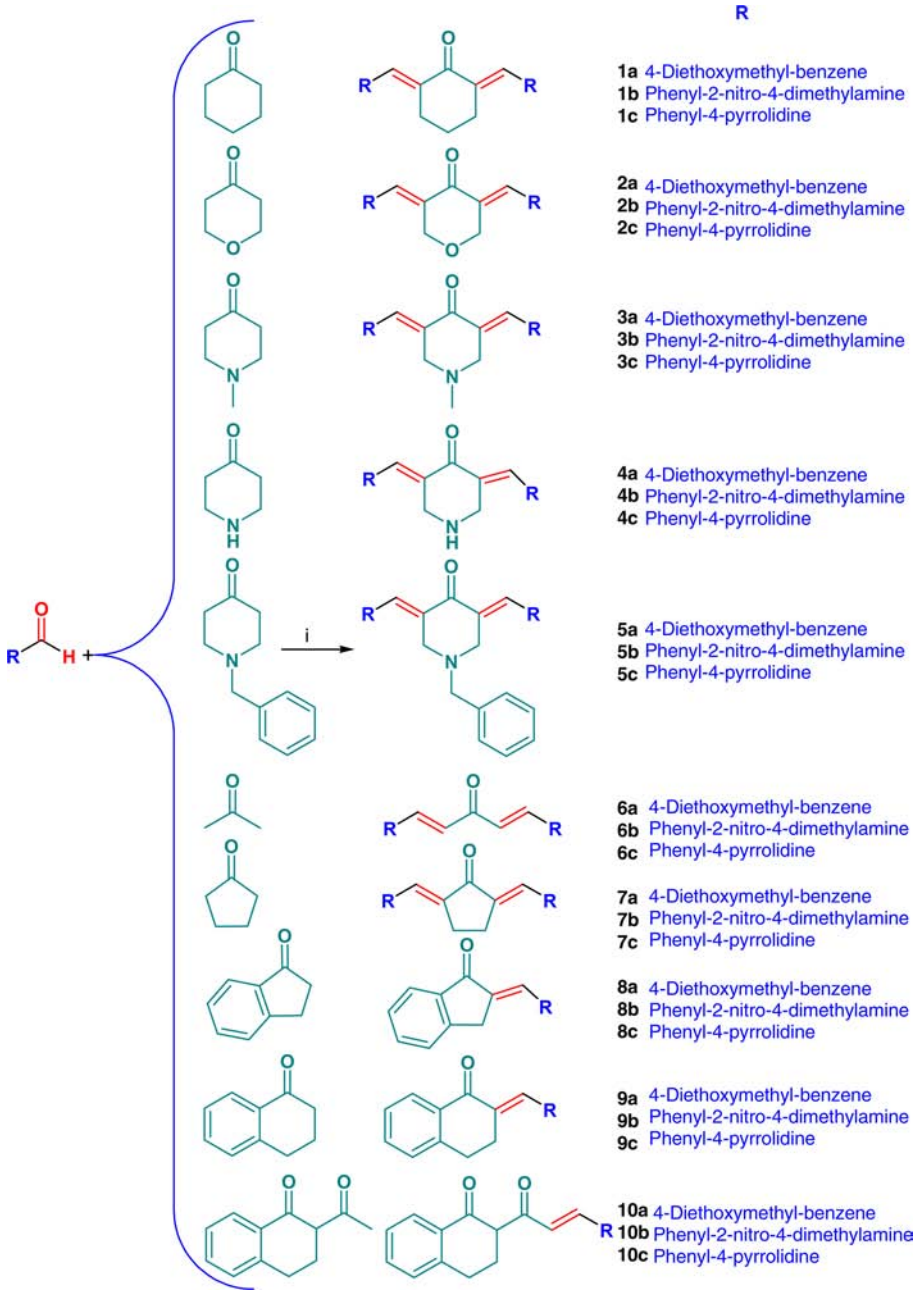

Figure 2. Synthesis of curcumin related *α,β*-unsaturated carbonyl-based compounds. Reagents and conditions: (i) NaOH, EtOH, Room temperature.

12H); ^{13}C NMR (500 MHz, $CDCl_3$) δ: 187.5, 150.9, 148.6, 144.4, 132.8, 128.1, 117.5, 113.8, 107.9, 46.7; HRMS (ESI) m/z: 409.45 $[M - H]^+$, microanalysis calculated for $C_{21}H_{22}N_4O_5$ (410.42), C: 61.45%, H: 5.40%, N: 13.65%. Found C: 61.48%, H: 5.62%, N: 13.77%.

*2,5-Bis(4-diethoxymethyl-benzylidene)-cyclopentanone (**7a**).* Light-yellow crystals (3.12 g, 67%). Mp: 88−89 °C; ^{1}H NMR (500 MHz, $CDCl_3$) δ: 7.69 (d, J = 6.5 Hz, 4H), 7.42 (s, 2H), 7.21 (d, J = 6.5 Hz, 4H), 5.45 (s, 2H), 3.62 (q, J = 7 Hz, 8H), 2.38 (t, J = 7 Hz, 4H), 1.22 (t, J = 7.0, 12H); ^{13}C NMR (500 MHz, $CDCl_3$) δ: 189.7, 149.4, 145.5, 138.7, 136.4, 133.9, 129.1, 100.9, 56.2, 32.5, 16.1; HRMS (ESI) m/z: 465.72 $[M + H]^+$, microanalysis calculated for $C_{29}H_{36}O_5$ (464.59), C: 74.97%, H: 7.81%. Found C: 75.18%, H: 7.87%.

*2,5-Bis(4-dimethylamino-2-nitro-benzylidene)-cyclopentanone (**7b**).* White powder (2.41 g, 55%). Mp: 156−157 °C; ^{1}H NMR (500 MHz, $CDCl_3$) δ: 7.92 (d, J = 6.5 Hz, 2H), 7.88 (d, J = 6 Hz, 2H), 7.75 (d, J = 6.5 Hz, 2H), 7.44 (s, 2H), 3.10 (s, 12H), 2.45 (t, J = 7 Hz, 4H); ^{13}C NMR (500 MHz, $CDCl_3$) δ: 188.9, 153.2, 149.9, 144.2, 143.8, 125.8, 118.1, 116.4, 108.3, 46.9, 32.6; HRMS (ESI) m/z: 437.72 $[M + H]^+$, microanalysis calculated for $C_{23}H_{24}N_4O_5$ (436.46), C: 63.29%, H: 5.54%, N: 12.84%. Found C: 63.42%, H: 5.48%, N: 12.72%.

*2-(4-Diethoxymethyl-benzylidene)-indan-1-one (**8a**).* White powder (2.52 g, 78%). Mp: 152−154 °C; ^{1}H NMR (500 MHz, $CDCl_3$) δ: 7.80 (d, J = 8 Hz, 2H), 7.69 (s, H), 7.48 (d, J = 8 Hz, 2H), 7.25 (d, J = 7.5 Hz, H), 7.20 (d, J = 7.5 Hz, H), 7.05 (t, J = 7.5 Hz, H), 6.94 (t, J = 7 Hz, H), 5.34 (s, H), 3.49 (q, J = 7 Hz, 4H), 2.75 (s, 2H), 1.29 (t, J = 6 Hz, 6H); ^{13}C NMR (500 MHz, $CDCl_3$) δ: 193.2, 144.5, 142.2, 140.1, 139.2, 138.8, 136.5, 130.4, 129.6, 128.1, 125.6, 125.1, 124.2, 102.2, 56.3, 29.9, 16.4; HRMS (ESI) m/z: 323.67 $[M + H]^+$, microanalysis calculated for $C_{21}H_{22}O_3$ (322.40), C: 78.23%, H: 6.88%. Found C: 78.44%, H: 6.92%.

*2-(4-Dimethylamino-2-nitro-benzylidene)-indan-1-one (**8b**).* Yellow semisolid (1.95 g, 63%). Mp: 169−171 °C; ^{1}H NMR (500 MHz, $CDCl_3$) δ: 7.56 (d, J = 8 Hz, H), 7.48 (s, H), 7.32 (d, J = 8 Hz, H), 7.12 (s, H), 6.98 (d, J = 7.5 Hz, H), 6.91 (d, J = 7.5 Hz, H), 6.74 (t, J =

dx.doi.org/10.1021/jf501145b | J. Agric. Food Chem. 2014, 62, 5538−5547

7.5 Hz, H), 6.65 (t, J = 7 Hz, H), 3.22 (s, 6H), 2.81 (s, 2H); ^{13}C NMR (500 MHz, $CDCl_3$) δ: 192.8, 145.6, 142.6, 141.3, 139.8, 138.2, 137.4, 130.9, 128.7, 128.0, 125.9, 123.8, 119.5, 117.6, 108.6, 46.8, 28.3; HRMS (ESI) m/z: 309.55 $[M + H]^+$, microanalysis calculated for $C_{18}H_{16}N_2O_3$ (308.33), C: 70.12%, H: 5.23%, N: 9.09%. Found C: 70.18%, H: 5.59%, N: 9.18%.

*2-(4-Diethoxymethyl-benzylidene)-3,4-dihydro-2H-naphthalen-1-one (**9a**).* Light-yellow solid (2.67g, 80%). Mp: 94−95 °C; ^{1}H NMR (500 MHz, $CDCl_3$) δ: 7.84 (d, J = 8 Hz, 2H), 7.59 (s, H), 7.47 (d, J = 8.5 Hz, 2H), 7.29 (d, J = 7.5 Hz, H), 7.22 (d, J = 7.5 Hz, H), 7.12 (t, J = 7.5 Hz, H), 7.02 (t, J = 7 Hz, H), 5.49 (s, H), 3.35 (q, J = 7 Hz, 4H), 2.29 (t, J = 7 Hz, 2H), 2.05 (t, J = 7 Hz, 2H), 1.17 (t, J = 6 Hz, 6H); ^{13}C NMR (500 MHz, $CDCl_3$) δ: 188.3, 152.2, 150.1, 148.5, 146.2, 143.9, 137.5, 134.4, 129.2, 127.2, 126.2, 124.8, 117.2, 101.7, 56.2, 29.5, 28.2, 16.0; HRMS (ESI) m/z: 337.51 $[M + H]^+$, microanalysis calculated for $C_{22}H_{24}O_3$ (336.42), C: 78.54%, H: 7.19%. Found C: 78.33%, H: 7.12%.

*2-(4-Dimethylamino-2-nitro-benzylidene)-3,4-dihydro-2H-naphthalen-1-one (**9b**).* White powder (2.50 g, 78%). Mp: 138−139 °C; ^{1}H NMR (500 MHz, $CDCl_3$) δ: 7.82 (d, J = 6.5 Hz, H), 7.57 (s, H), 7.42 (d, J = 6.5 Hz, H), 7.35 (s, H), 7.28 (d, J = 7 Hz, H), 7.20 (d, J = 7 Hz, H), 7.19 (t, J = 7.5 Hz, H), 6.92 (t, J = 8 Hz, H), 3.14 (s, 6H), 2.47 (t, J = 7 Hz, 2H), 2.14 (t, J = 7 Hz, 2H); ^{13}C NMR (500 MHz, $CDCl_3$) δ: 188.7, 152.8, 151.3, 148.9, 146.8, 144.2, 136.8, 134.6, 129.9, 127.6, 126.1, 125.3, 124.2, 107.8, 46.2, 29.9, 27.9; HRMS (ESI) m/z: 323.45 $[M + H]^+$, microanalysis calculated for $C_{19}H_{18}N_2O_3$ (322.36), C: 70.79%, H: 5.63%, N: 8.69%. Found C: 71.12%, H: 5.52%, N: 8.72%.

*2-[3-(4-Diethoxymethyl-phenyl)-acryloyl]-3,4-dihydro-2H-naphthalen-1-one (**10a**).* Yellow solid (3.16 g, 83%). Mp: 121−122 °C; ^{1}H NMR (500 MHz, $CDCl_3$) δ: 7.75 (d, J = 6 Hz, H), 7.52 (d, J = 6 Hz, H), 7.42 (d, J = 8 Hz, 2H), 7.39 (d, J = 8 Hz, 2H), 7.32 (d, J = 7 Hz, H), 7.29 (d, J = 7 Hz, H), 7.17 (t, J = 7 Hz, H), 6.89 (t, J = 7 Hz, H), 5.29 (s, H), 3.47 (q, J = 7 Hz, 4H), 3.29 (t, J = 8.5 Hz, H), 2.12 (t, J = 8 Hz, 2H), 1.95 (t, J = 7 Hz, 2H), 1.24 (t, J = 6.5 Hz, 6H); ^{13}C NMR (500 MHz, $CDCl_3$) δ: 194.6, 151.1, 148.9, 144.6, 142.3, 139.2, 138.4, 136.2, 135.5, 132.4, 130.6, 129.1, 125.2, 124.2, 103.1, 66.1, 55.7, 30.2, 28.6, 16.7; HRMS (ESI) m/z: 379.52 $[M + H]^+$, microanalysis calculated for $C_{24}H_{26}O_4$ (378.46), C: 76.17%, H: 6.92%. Found C: 76.21%, H: 6.91%.

*2-[3-(4-Dimethylamino-2-nitro-phenyl)-acryloyl]-3,4-dihydro-2H-naphthalen-1-one (**10b**).* Pale-yellow powder (2.93 g, 80%). Mp: 102−103 °C; ^{1}H NMR (500 MHz, $CDCl_3$) δ: 7.79 (d, J = 6.5 Hz, H), 7.62 (d, J = 6.5 Hz, H), 7.45 (d, J = 7.5 Hz, H), 7.32 (s, H), 7.29 (d, J = 7.5 Hz, H), 7.21 (d, J = 7.5 Hz, H), 7.14 (d, J = 7.5 Hz, H), 7.02 (t, J = 7.5 Hz, H), 6.94 (t, J = 7.5 Hz, H), 3.45 (t, J = 8.5 Hz, H), 3.10 (s, 6H), 2.22 (t, J = 8 Hz, 2H), 2.15 (t, J = 8 Hz, 2H); ^{13}C NMR (500 MHz, $CDCl_3$) δ: 193.8, 152.2, 148.7, 145.2, 142.8, 139.6, 137.1, 136.8, 135.6, 131.9, 130.5, 129.4, 124.8, 123.5, 116.5, 106.2, 65.8, 46.8, 31.3, 28.7; HRMS (ESI) m/z: 365.55 $[M + H]^+$, microanalysis calculated for $C_{21}H_{20}N_2O_4$ (364.39), C: 69.22%, H: 5.53%, N: 7.69%. Found C: 69.34%, H: 5.59%, N: 7.81%.4

MTT Assay. MTT assay was performed for determining the effect of synthetic compounds on normal (MCF-10A) mammary epithelial cells. MCF-10A cells were maintained in Dulbecco's modified Eagle's medium/Ham's F-12 medium (1:1) with 10% fetal calf serum, 2 mM glutamine, insulin (10 μg/mL), hydrocortisone (500 ng/mL), and epidermal growth factor (20 ng/mL). Cells were passaged every 2 to 3 days using trypsin EDTA (ethylenediaminetetraacetic acid). MCF-10A cells were plated at a density of 10^4 cells per milliliter in 96-well flat-bottomed plates. After 24 h, the medium was carefully aspirated and tested compounds (curcumin analogues) were added in quadruplicate in 200 μL of medium to give a final concentration of not more than 0.1% (v/v) dimethyl sulfoxide (DMSO). The cells were then permitted to grow for 96 h at 37 °C. The medium was removed and fresh medium with MTT (3-[4,5-dimethylthiazol-2-yl]-2,5-diphenyltetrazolium bromide) (0.4 mg/mL) was added to each well for 3 h. All medium was aspirated and the formazan product generated by viable cells was solubilized with 150 μL of DMSO. Plates were vortexed and the absorbance at 540 nm determined using a microplate reader. Results were expressed as the percentage inhibition of proliferation compared to controls containing 0.1% DMSO.

Anticancer Activity. For determining the anticancer activity a propidium iodide (PI) fluorescence assay was performed on MCF-7 (breast cancer cell line), PC-3 (prostate cancer cell line), HL-60 (promyelocytic leukemia cell line), H-460 (lung cancer cell line) and HT-29 (colon cancer cell line) cell lines.[27] Propidium iodide (PI), a dye which binds to DNA, provides a rapid and accurate means for quantitating total nuclear DNA. The principle of this assay is based on the fact that PI is not able to penetrate an intact cell membrane and the fluorescence signal intensity of the PI is directly proportional to the amount of DNA in each cell. So the cells which have damaged membranes or altered permemability profiles are scored as dead cells. For a typical PI cytotoxicity assay, cells, after trypsinization and counting, were seeded at 3000−7500 cells/well in 200 μL media in sterile tissue culture grade 96 well plates and allowed to recover for 24 h in humidified 5% CO_2 incubator at 37 °C. After this, compounds (in 0.1% DMSO) were added onto triplicate wells with 10 μM concentrations. 0.1% DMSO alone was used as control. Treatment with test compounds was continued for 48 h. After completion of designated treatment period, the medium was removed and cells were treated with 25 μL of propidium iodide (50 μg/mL in water/medium) per well. The above plates with samples were frozen at −80 °C for 24 h, then thawed and allowed to equilibrate to room temperature. Plates were read on a fluorometer (Polar-Star BMG Tech), using 530 nm excitation and 620 nm emission wavelength. Lastly, percent cytotoxicity of the compounds was calculated by using following formula:

$$\%\text{Cytotoxicity} = \frac{A_C - A_{TC}}{A_C} \times 100$$

where A_C = Absorbance reading of control and A_{TC} = Absorbance reading of treated cells. The results were compared with the standard drug inhibitors flavopiridol (0.5 μM).

Tyrosinase Assay. The spectrophotometric assay for tyrosinase was performed according to the reported method with slight modifications.[28] Briefly, L-DOPA was used as substrate to screen the synthesized compounds for the diphenolase inhibitory activity of tyrosinase. Positive controls in the assay were Kojic acid and 4-Butylresorcinol. 2% stock solutions of compounds were prepared in DMSO and diluted using phosphate buffer (pH = 6.8). These synthesized compounds were preincubated in 50 mM phosphate buffer (pH = 6.8) at 25 °C for 10 min with 30 units of mushroom tyrosinase (0.5 mg/mL). L-DOPA (0.5 mM) was then added to the reaction mixture. Reaction was monitored by following formation of L-DOPA chrome for 1 min measured by the change in absorbance at 475 nm. Triplicate measurements were taken for each concentration and average was used for further calculations. Dose−response curves were interpolated to obtain the IC_{50} values.

Molecular Modeling. Molecular modeling studies were performed with MOE (The Molecular Operating Environment) Version 2011.10, software available from Chemical Computing Group Inc., 1010 Sherbrooke Street West, Suite 910, Montreal, Canada H3A2R7, http://www.chemcomp.com. The ligands were built using the builder tool of the MOE program and subjected to energy minimization (MMFF94x, gradient: 0.05). The X-ray crystallographic structure of mushroom tyrosinase (PDB: 2Y9W)[29] was obtained from the Protein Data Bank. The errors of the protein were corrected by the Structure Preparation process in MOE. After correction, hydrogens were added and partial charges (Gasteiger methodology) were calculated. Site finder application was used to detect the possible binding pocket. The default Triangle Matcher placement method was applied for docking. GBVI/WSA dG scoring function which estimates the free energy of binding of the ligand from a given pose was used to rank the final poses. The ligand-enzyme complexes with lowest S score were selected for each ligand.

Statistical Analysis. Analysis was carried out using a complete randomized design and treatments were run in triplicates (n = 3). Statistical analysis was done using analysis of variance (ANOVA)

method of general linear model (GLM) procedure using SAS V8 (Cary, NC) for multiple comparisons. $P < 0.05$ was considered to be statistically significant.

RESULTS AND DISCUSSION

Chemistry. Claisen-Schmidt condensation was used for the synthesis of the desired α,β-unsaturated carbonyl-based compounds[30] by reacting different ketones and the appropriate aryl aldehyde. Twenty-one compounds (**1a**−**7a**; **1b**−**7b**; **1c**−**7c**) were synthesized in the presence of NaOH at a 1:2 molar ratio in ethanol while some compounds were synthesized in acetic acid by passing dry HCl gas through the mixture. Claisen-Schmidt condensation was also employed to synthesize nine compounds (**8a**−**10a**; **8b**−**10b**; **8c**−**10c**) similar to chalcone analogues however employing 1:1 molar ratio of ketone and aldehyde (Figure 2). Both types of catalytic systems, that is, NaOH and dry HCl gas mixture, were used to synthesize eight compounds (**7a**, **8a**, **10a**, **7b**, **8b**, **10b**, **7c**, **8c**). Catalytic system employing HCl gas mixture gave high percentage yields compared to NaOH. Using NaOH as a catalyst resulted in producing a mixture of several different unidentified products necessitating excessive purification using column chromatography.

Spectrophotometric techniques were used to characterize the synthesized compounds. An elemental analysis of C, H, and N, and melting points are represented. Representative carbon nuclear magnetic resonance spectra were also recorded. NH absorptions were not seen in the ^{1}H NMR spectra of the compounds **4a**, **4b** and **4c**, it has previously been shown by other researchers.[30,31]

Cytotoxicity toward MCF-10A Normal Mammary Epithelial Cells. The rule of three, relating to activity-exposure-toxicity, presents the single most difficult challenge in the design and advancement of drug candidates to the development stage. Absorption, distribution, metabolism and excretion (ADME) studies are widely used in drug discovery to optimize this balance of properties necessary to convert lead compounds into drugs that are both safe and effective for human patients.[32] Therefore, in vitro cell viability assay was performed by using the MCF-10A that is a normal cell line and was used as a comparison. MCF-10A cells were treated with synthetic compounds for 96 h and cell viability was measured using the MTT assay. Results are expressed in terms of percentage of toxicity (Table 1). The compounds were found to be nontoxic and majority of compounds showed more than 95% cell viability. Therefore, the compounds are biologically safe and can be used as the therapeutic agent for future drug discovery study.

Effects on Human Cancer Cell Lines. Anticancer activity of curcumin is one of the most widely explored activities among numerous others like anti-inflammatory activity. In vitro cytotoxicity assays performed in various cell lines originating from different organs show that curcumin have beneficial effects in, including but not limited to: prostate cancer cells,[33] ovarian cancer cells,[34] gastric carcinoma cells,[35] liver cancer cells, hepatocel- lular carcinoma cells,[36] cervical cancer cells,[37] breast cancer cells,[38] colon cancer cells,[39] lung carcinoma cell,[40] bladder cancer cells,[41] and pancreatic adenocarcinoma cell.[42] This provides strong preliminary data for the justification of clinical studies in humans.

Synthesized compounds were tested in present investigation for their capacity to inhibit the growth of five different cancer cell lines (PC-3, MCF-7, HL-60, H-460, and HT-29).

Table 1. Anticancer Activity and Inhibitory Effects of Synthetic Curcumin-Like Compounds against Mushroom Tyrosinase

	anticancer activity[a] (%)						
compounds	HT-29	PC-3	MCF-7	H-460	HL-60	MCF-10A	tyrosinase inhibitory activity (IC_{50} μM)
1a	55	56	59	52	60	0	10.11
1b	59	58	62	64	61	4	14.21
1c	42	40	41	48	45	0	45.66
2a	79	81	77	78	75	7	32.21
2b	81	82	79	80	80	12	36.23
2c	47	46	42	48	47	5	125.48
3a	69	64	61	61	59	2	51.82
3b	71	60	63	62	59	6	55.22
3c	59	51	52	55	53	5	>200
4a	72	71	70	71	69	9	66.32
4b	73	75	72	74	71	11	18.12
4c	31	32	45	31	30	0	>200
5a	41	41	40	43	44	0	102.44
5b	42	44	45	45	46	0	122.24
5c	21	22	22	20	21	0	ND
6a	42	43	41	42	40	0	11.04
6b	44	47	46	46	47	5	11.45
6c	12	11	13	15	15	0	77.83
7a	33	32	34	32	32	0	27.87
7b	35	36	35	38	39	0	23.22
7c	21	24	24	26	25	0	99.43
8a	12	14	13	13	15	0	06.83
8b	15	16	16	18	18	0	8.12
8c	09	11	15	12	16	0	45.84
9a	22	24	23	25	22	0	21.17
9b	25	26	26	27	25	0	26.22
9c	11	06	09	12	17	0	77.88
10a	47	45	46	44	43	4	5.34
10b	55	56	55	58	55	0	7.13
10c	23	26	28	21	20	2	56.76
flavopiridol[b]	77	70	72	79	74	–	–
4-butylresorcinol	–	–	–	–	–	–	33.16
Kojic acid	–	–	–	–	–	–	10.93

[a]HT-29 (colon cancer cell line), PC-3 (prostate cancer cell line), MCF-7 (breast cancer cell line), H-460 (lung cancer cell line), HL-60 (promyelocytic leukemia cell line), MCF-10A (normal mammary epithelial cell line). [b]0.5 μM concentration.

Compound **2b** was found to have highest anticancer activity inhibiting 82% of PC-3 cells; this was closely followed by compound **2a** showing 81% inhibition. These two compounds also show similarly comparative levels of anticancer activity (75−82%) on the other four cell lines used for experiments. Compound **2a** and **2b** were followed by six curcumin-like compounds (**2a**−**b**, **3a**−**b**, and **4a**−**b**) which had promising anti cancer activity (59−82%) (Figure 3). This was followed by 12 compounds (**1a**−**c**, **2c**, **3c**, **4c**, **5a**−**b**, **6a**−**b**, and **10a**−**b**) which show moderate effect (40−58%). Insignificant activity was shown by remaining compounds. For the anticancer activity experiments, positive control used was flavopiridol, which show 79% inhibition of H-460 cells at 0.5 μM concentration. Generally, curcumin like compounds show similar inhibitory anticancer activity on the tested cell lines and it was observed that the average difference in inhibitory activities was not more

dx.doi.org/10.1021/jf501145b | J. Agric. Food Chem. 2014, 62, 5538−5547

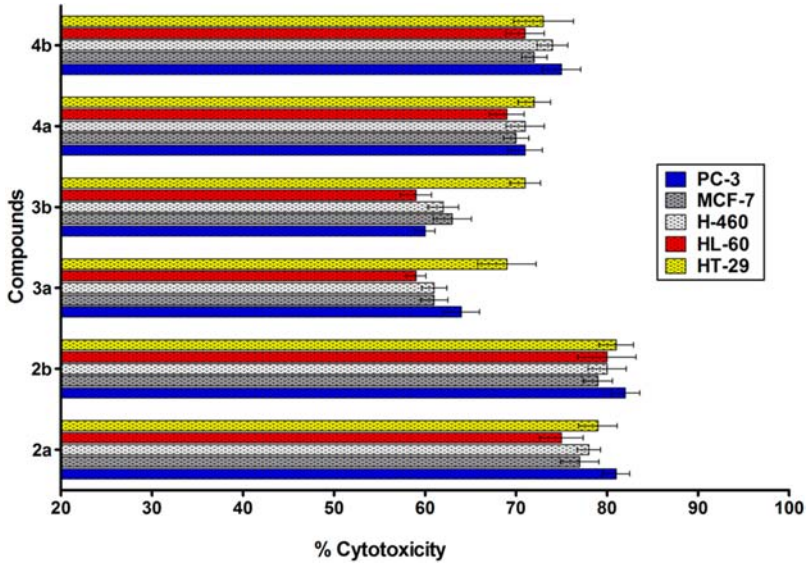

Figure 3. Percentage cytotoxicity of selected curcumin like synthetic compounds against various cancer cell lines.

Table 2. Physicochemical Properties and Cytotoxicity of Most Active Compounds 2a, 2b, 4a and 4b against Human Cancer Cell Lines

	anticancer activity IC_{50} (μM)					physicochemical properties[a]			
compound	HT-29	PC-3	MCF-7	H-460	HL-60	Clog$P$[b]	TPSA[c]	H-b(d)[d]	H-b(a)[e]
2a	2.39 ± 0.27	2.31 ± 0.62	2.42 ± 0.93	2.40 ± 0.22	2.45 ± 0.12	5.23	63.24	0	6
2b	1.06 ± 0.59	1.04 ± 0.42	1.08 ± 0.45	1.06 ± 0.41	1.05 ± 0.48	3.52	124.42	0	10
4a	2.79 ± 0.75	2.82 ± 0.11	2.81 ± 0.32	2.87 ± 0.59	2.85 ± 0.52	4.68	66.03	1	6
4b	2.72 ± 0.19	2.69 ± 0.64	2.63 ± 0.34	2.70 ± 0.74	2.77 ± 0.18	2.97	127.22	1	10

[a]Calculated with Molinspiration property engine v.2013.09 (http://www.molinspiration.com). [b]Calculated log P (molecular hydrophobicity). [c]Topological polar surface area of the molecules. [d]H-bond donors. [e]H-bond acceptors.

than 5% types of tested cancer cell lines. For most active compounds (**2a**, **2b**, **4a** and **4b**) the median inhibition concentration (IC_{50}) was calculated using GraphPad Prism software (GraphPad Software, San Diego, CA) and it was observed that compound **2b** was very potent anticancer agent among all other tested compounds with very low IC_{50} value in the range of 1.04 to 1.08 μM (Table 2).

Compounds **2a**, **2b**, **4a**, and **4b** were found to have high potency against different types of cancer cell lines. It can be depicted from their physicochemical properties (Table 2) that these compounds have potential to be new lead compounds in developing anticancer agents. Physicochemical properties of tested compounds were found within optimal range (Molecular weight <500; clog$P$ < 5 and TPSA <140).[43,44]

Effects on the Diphenolase Activity of Mushroom Tyrosinase. Tyrosinase inhibitory assay was performed for all synthesized curcumin-related compounds by measuring the oxidation of L-DOPA as previously reported.[28] A concentration-dependent enzyme activity inhibition by the compounds was observed. It was observed that the activity of remaining enzyme swiftly decreased when the concentration of compound (inhibitor) was increased. Table 1 summarizes the enzyme inhibition data expressed as IC_{50}. The majority of synthetic curcumin related compounds (**1a−c**, **2a−c**, **3a−b**, **6a−c**, **7a−c**, **8a−c**, **9a−c**, **10a−c**) exhibit <100 μM inhibitory activities against mushroom tyrosinase. With IC_{50} ranging from 5.34 to 10.11 μM, five compounds (**1a**, **8a−b** and **10a−b**) exhibited promising tyrosinase inhibitiory activity better than positive control Kojic acid (10.93 μM). Two of the synthesized compounds (**8a** and **10a**), with diethoxymethyl group at position 4, were found to be the strongest inhibitors among all tested compounds with IC_{50} values 6.83 and 5.34 μM respectively.

Structure−Activity Relationship Analysis. It was observed that the presence or absence of groups on the two aromatic rings and the linker between the two aromatic rings both played key roles in determining the anticancer inhibitory activity of the various analogues on the tested cancer cells. From their data for SAR of monocarbonyl analogues, the research group of G Liang, had shown previously that acetone and cyclohexanone spacers are much more favorable than the cyclopentanone one[45] for enhanced anticancer activity. Conclusion drawn by Liang's group is also afforded by present study as all synthetic compounds containing cyclopentanone ring system (**7a−7c**) have lesser anticancer activity when compared to compounds with acetone and cyclohexanone system. In fact, among these three group of compounds (**1**, **6**, **7**), compounds bearing cyclohexanone were found to be most active.

Different activity trends were observed among the different series of curcumin-related compounds when either linear or cyclic linkers were used between the two aromatic rings of curcumin related compounds. In general, tetrahydropyran-4-one (**2a−c**) linker containing compounds exhibited the strongest activities, moderate activity was exhibited by compounds with *N*-methyl-4-piperidone (**3a−c**), while three compounds (**4a−c**) with 4-piperidone showed good inhibition power however it was lesser compared to compounds bearing

dx.doi.org/10.1021/jf501145b | J. Agric. Food Chem. 2014, 62, 5538−5547

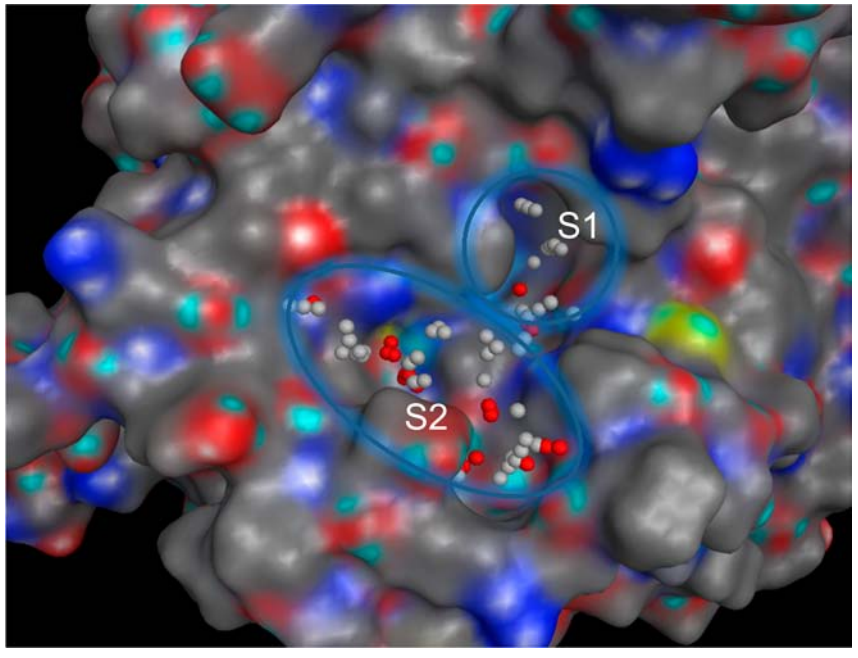

Figure 4. Binuclear copper binding site (S1) and its entrance (S2) region of mushroom tyrosinase enzyme.

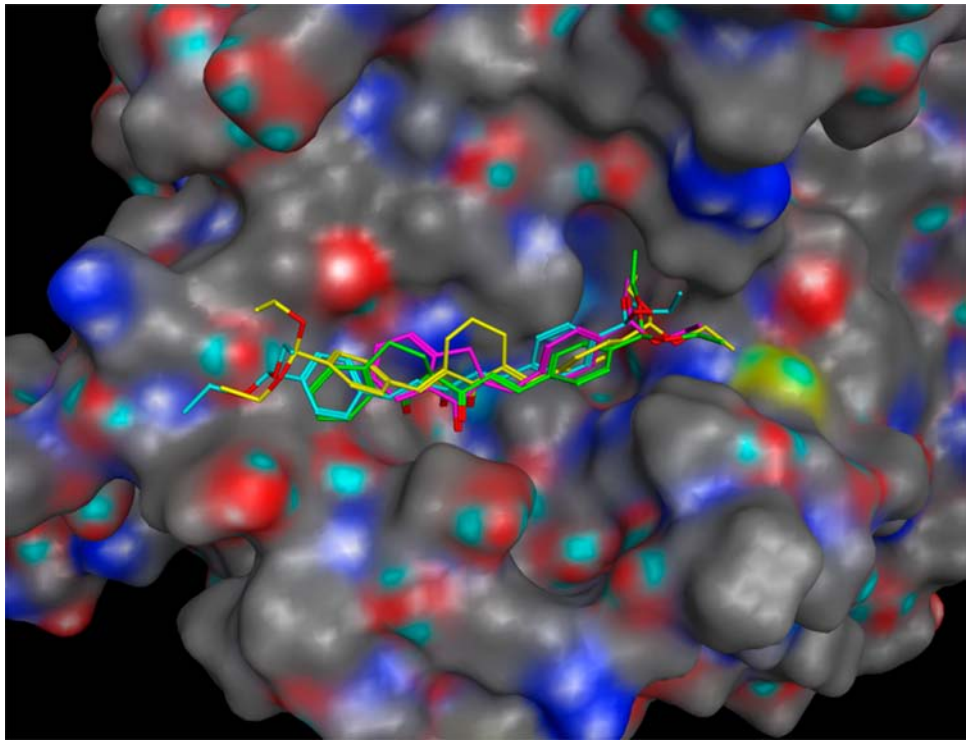

Figure 5. Superimposition of the best poses of compound **1a**, **6a**, **8a** and **10a** (**1a**, **6a**, **8a**, and **10a** are shown as yellow, blue, pink, and green, respectively).

N-methyl-4-piperidone. Bis-derivatives, bearing either 1-benzyl-4-piperidone (**5a**–**c**), acetone (**6a**–**c**) or cyclopentanone (**7a**–**c**) linker, were less active compared to the rest. Conversely, among the monoderivatives (**8**–**10**), merely compounds bearing dicarbonyl linker (**10a**–**b**) were shown to have moderate growth inhibitory anticancer activity in the tested cell lines.

Presence of a heteroatom linker in groups of compounds (**2**, **3**, **4**) resulted in enhanced anticancer activities compared to the compounds without a heteroatom linker (**1**, **6**, **7**). This finding suggests that flexibility of curcumin-like compounds could improve their anticancer activities which could be due to the ease of interactions with the DNA of cancer cells. Contrary to this, compounds with small and rigid linker would be less active due to the difficulty of interactions with DNA. Association of curcumin flexibility with curcumin-DNA interaction, which could be a possible explanation for antitumor activity, is a valuable and interesting finding.[46,47]

Effects of substitution of various groups curcumin related compound activity were compared. It was observed that introduction of 2-nitro-4-dimethylamine combination on the aromatic rings improved anticancer activity of curcumin related compounds. In all the three groups (based on substitution pattern **a**, **b**, **c**), compounds bearing combination of 2-nitro and 4-dimethylamine show exceptionally elevated anticancer activity whereas presence of diethoxymethyl group at position 4 of rings consequently produces markedly reduced anticancer activity. Further, presence of pyrrolidine at position 4 of compounds (**1**−**10c**) results in compounds which are not highly active.

Analysis of the effects of curcumin related compounds on tyrosinase activity produced structure−activity relationship with new and interesting findings. Based upon different substituted groups, with two exception (**4b** and **7b** more active than **4a** and **7a**), it was observed that compounds having diethoxymethyl group at position 4 of rings (group **a**) were most active against the mushroom tyrosinase activity. Like the anticancer activity, substitution of pyrrolidine at position 4 of compounds (**1**−**10c**) did not produce strongly active compounds for tyrosinase inhibition. An interesting finding was the presence of dicarbonyl group (**10a**−**b**) that resulted in maximum tyrosinase inhibition even better than the positive controls. In general, the monoderivatives (**8**−**10**) show better antityrosinase activity as compared to bis-derivatives (**2**−**7**). However, presence of a heteroatom linker (**2**, **3**, and **4**) did not result in compounds with a better antityrosinase activity when compared to those without a heteroatom linker (**1**, **6**, and **7**).

Molecular Docking Study. Tyrosinase enzyme has binuclear copper binding site and tropolone and kojic acid bind the entrance of this site.[29,48] In this study, Site Finder application in MOE was used to find the possible binding sites in the enzyme. The region consisting of S1 and S2 site was indicated as active pocket (Figure 4). S1 contains binuclear copper binding site where S2 locates near the entrance of this site.

To simplify, docking results were evaluated in groups. First of all, (a) the docking results of compound **1**−**7a** (bis-derivatives) which have different keton structures were considered. Compound **1a** and **6a** gave the same orientation (Figure 5) while the others oriented in a different way. It was seen that Val283 and His244 hold **1a** and **6a** at the entrance of copper binding site by H-arene interaction of the phenyl rings of both compounds (Figure 6). Furthermore, C═O moiety of compounds **1a** and **6a** might form a weak hydrogen bond with backbone NH of His85 (about 4 Å). Also, nonpolar part of cyclohexanone of compound **1a** made hydrophobic interactions with Val283 (less than 3 Å). Because of the hindrance of nonpolar part of Val283, synthetic compounds **2a**−**5a** and **7a** might be oriented in a different way. (b) The orientations of **8a**−**10a** (monoderivatives) occurred similar to that of bis-derivatives (except **9a**) by their interactions with Val283, His244 and His85 (Figure 6). (c) Compounds carrying pyrrolidine moiety (**1**−**10c**), were oriented so that C═O groups of the compounds located close to NH of Asn81 instead of His85. Substitution of pyrrolidine might decrease the flexibilities of these compounds at the entrance, which might cause a reduction in the activity.

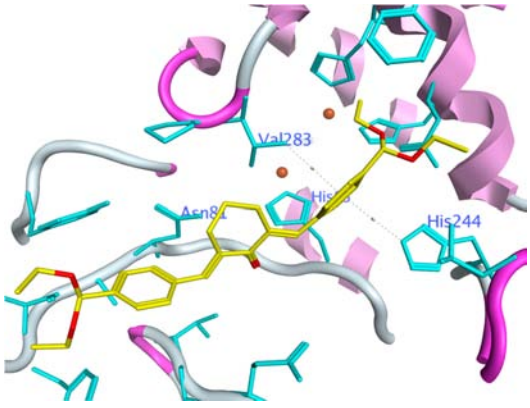

Figure 6. Orientations of compound **1a** in tyrosinase active site (**1a** and residues are shown as yellow and blue, respectively).

To conclude, 10 series containing 30 novel α,β-unsaturated carbonyl-based curcumin related compounds were successfully synthesized using the Claisen-Schmidt condensation reaction. All synthesized compounds were analyzed for anticancer and antityrosinase activity. Compounds **2a**−**b** were identified as potent anticancer agents with 81−82% inhibition of cancer cell lines. Five of these compounds (**1a**, **8a**−**b**, **10a**−**b**) emerged to be the potent inhibitors of Mushroom tyrosinase. Molecular modeling studies were also performed to see the interactions of synthetic compounds with X-ray crystallographic structure of mushroom tyrosinase. It also provided further insight into designing compounds with structural features that may translate into higher activity. Our studies have established that these curcumin-like compounds, with appropriate structural modifications, have the potential to be developed as anticancer agents for humans and can also be further studied for use in medicines, cosmetic products, food industry as well as agricultural purposes. Further studies are required for use and development of these synthetic compounds in food and agricultural field as antibrowning agents.

AUTHOR INFORMATION

Corresponding Authors

*E-mail: snab@pharmacy.ukm.my; snabphd@yahoo.com; snab_hussaini@yahoo.com.

*E-mail: ibj@pharmacy.ukm.my.

Funding

This research was supported by University Kebangsaan Malaysia (Grants no.: UKM-DLP-2013−013).

Notes

The authors declare no competing financial interest.

ACKNOWLEDGMENTS

Dr. Syed Nasir Abbas Bukhari thanks University Kebangsaan Malaysia for postdoctoral contract.

ABBREVIATIONS USED

PI, propidium iodide; DMSO, dimethyl sulfoxide; L-DOPA, L-3,4-dihydroxyphenylalanine; MOE, molecular operating environment; TPSA, topological polar surface area

REFERENCES

(1) Dias, D. A.; Urban, S.; Roessner, U. A historical overview of natural products in drug discovery. *Metabolites* **2012**, *2*, 303−336.

(2) Guo, Z. R. [Modification of natural products for drug discovery]. *Yao xue xue bao = Acta pharmaceutica Sinica* **2012**, *47*, 144−57.

(3) Valli, M.; Pivatto, M.; Danuello, A.; Castro-Gamboa, I.; Silva, D. H. S.; Cavalheiro, A. J.; Araújo, Â. R.; Furlan, M.; Lopes, M. N.; Bolzani, V. d. S. Tropical biodiversity: Has it been a potential source of

secondary metabolites useful for medicinal chemistry? *Química Nova* **2012**, *35*, 2278−2287.
(4) Bhatnagar, I.; Kim, S. K. Marine antitumor drugs: status, shortfalls and strategies. *Marine Drugs* **2010**, *8*, 2702−20.
(5) Prakash, O.; Kumar, A.; Kumar, P.; Ajeet, A. Anticancer potential of plants and natural products: A review. *Am. J. Pharmacol. Sci.* **2013**, *1*, 104−115.
(6) Brown, A.; Shi, Q.; Moore, T. W.; Yoon, Y.; Prussia, A.; Maddox, C.; Liotta, D. C.; Shim, H.; Snyder, J. P. Monocarbonyl curcumin analogues: Heterocyclic pleiotropic kinase inhibitors that mediate anticancer properties. *J. Med. Chem.* **2013**, *56*, 3456−3466.
(7) Gupta, A. K.; Gover, M. D.; Nouri, K.; Taylor, S. The treatment of melasma: A review of clinical trials. *J. Am. Acad. Dermatol.* **2006**, *55*, 1048−1065.
(8) Shakibaei, M.; Buhrmann, C.; Kraehe, P.; Shayan, P.; Lueders, C.; Goel, A. Curcumin chemosensitizes 5-fluorouracil resistant MMR-deficient human colon cancer cells in high density cultures. *PLoS One* **2014**, *9*, e85397.
(9) Lu, W.; Ogasawara, M. A.; Huang, P. Models of reactive oxygen species in cancer. *Drug Discovery Today: Disease Models* **2007**, *4*, 67−73.
(10) Rao, Y. K.; Fang, S.-H.; Tzeng, Y.-M. Differential effects of synthesized 2′-oxygenated chalcone derivatives: modulation of human cell cycle phase distribution. *Bioorg. Med. Chem.* **2004**, *12*, 2679−2686.
(11) Buolamwini, J. K. Novel anticancer drug discovery. *Curr. Opin. Chem. Biol.* **1999**, *3*, 500−509.
(12) Shoji, M.; Nakagawa, K.; Watanabe, A.; Tsuduki, T.; Yamada, T.; Kuwahara, S.; Kimura, F.; Miyazawa, T. Comparison of the effects of curcumin and curcumin glucuronide in human hepatocellular carcinoma HepG2 cells. *Food Chem.* **2014**, *151*, 126−132.
(13) Vaughan, R. A.; Garcia-Smith, R.; Dorsey, J.; Griffith, J. K.; Bisoffi, M.; Trujillo, K. A. Tumor necrosis factor alpha induces Warburg-like metabolism and is reversed by anti-inflammatory curcumin in breast epithelial cells. *Int. J. Cancer* **2013**, *133*, 2504−2510.
(14) Basnet, P.; Skalko-Basnet, N. Curcumin: An Anti-Inflammatory Molecule from a Curry Spice on the Path to Cancer Treatment. *Molecules* **2011**, *16*, 4567−4598.
(15) Hosoya, T.; Nakata, A.; Yamasaki, F.; Abas, F.; Shaari, K.; Lajis, N.; Morita, H. Curcumin-like diarylpentanoid analogues as melanogenesis inhibitors. *J. Nat. Med.* **2012**, *66*, 166−176.
(16) Lee, K.-H.; Ab. Aziz, F. H.; Syahida, A.; Abas, F.; Shaari, K.; Israf, D. A.; Lajis, N. H. Synthesis and biological evaluation of curcumin-like diarylpentanoid analogues for anti-inflammatory, antioxidant and anti-tyrosinase activities. *Eur. J. Med. Chem.* **2009**, *44*, 3195−3200.
(17) Youssef, D.; Nichols, C. E.; Cameron, T. S.; Balzarini, J.; De Clercq, E.; Jha, A. Design, synthesis, and cytostatic activity of novel cyclic curcumin analogues. *Bioorg. Med. Chem. Lett.* **2007**, *17*, 5624−5629.
(18) Matoba, Y.; Kumagai, T.; Yamamoto, A.; Yoshitsu, H.; Sugiyama, M. Crystallographic evidence that the dinuclear copper center of tyrosinase is flexible during catalysis. *J. Biol. Chem.* **2006**, *281*, 8981−8990.
(19) Solomon, E. I.; Sundaram, U. M.; Machonkin, T. E. Multicopper Oxidases and Oxygenases. *Chem. Rev.* **1996**, *96*, 2563−2606.
(20) Rolff, M.; Schottenheim, J.; Decker, H.; Tuczek, F. Copper-O2 reactivity of tyrosinase models towards external monophenolic substrates: molecular mechanism and comparison with the enzyme. *Chem. Soc. Rev.* **2011**, *40*, 4077−4098.
(21) Park, H. Y.; Kosmadaki, M.; Yaar, M.; Gilchrest, B. A. Cellular mechanisms regulating human melanogenesis. *Cell. Mol. Life Sci.* **2009**, *66*, 1493−1506.
(22) Artés, F.; Castañer, M.; Gil, M. I. Revisión: El pardeamiento enzimático en frutas y hortalizas mínimamente procesadas Review: Enzymatic browning in minimally processed fruit and vegetables. *Food Sci. Technol. Int.* **1998**, *4*, 377−389.
(23) Jiménez, M.; Chazarra, S.; Escribano, J.; Cabanes, J.; García-Carmona, F. Competitive inhibition of mushroom tyrosinase by 4-substituted benzaldehydes. *J. Agric. Food Chem.* **2001**, *49*, 4060−4063.
(24) Kubo, I.; Kinst-Hori, I. Flavonols from saffron flower: Tyrosinase inhibitory activity and inhibition mechanism. *J. Agric. Food Chem.* **1999**, *47*, 4121−4125.
(25) Okombi, S.; Rival, D.; Bonnet, S.; Mariotte, A.-M.; Perrier, E.; Boumendjel, A. Discovery of benzylidenebenzofuran-3(2H)-one (Aurones) as inhibitors of tyrosinase derived from human melanocytes. *J. Med. Chem.* **2005**, *49*, 329−333.
(26) Parvez, S.; Kang, M.; Chung, H.-S.; Bae, H. Naturally occurring tyrosinase inhibitors: mechanism and applications in skin health, cosmetics and agriculture industries. *Phytother. Res.* **2007**, *21*, 805−816.
(27) Dengler, W. A.; Schulte, J.; Berger, D. P.; Mertelsmann, R.; Fiebig, H. H. Development of a propidium iodide fluorescence assay for proliferation and cytotoxicity assays. *Anti-Cancer Drugs* **1995**, *6*, 522−532.
(28) Bao, K.; Dai, Y.; Zhu, Z.-B.; Tu, F.-J.; Zhang, W.-G.; Yao, X.-S. Design and synthesis of biphenyl derivatives as mushroom tyrosinase inhibitors. *Bioorg. Med. Chem.* **2010**, *18*, 6708−6714.
(29) Ismaya, W. T.; Rozeboom, H. t. J.; Weijn, A.; Mes, J. J.; Fusetti, F.; Wichers, H. J.; Dijkstra, B. W. Crystal structure of agaricus bisporus mushroom tyrosinase: Identity of the tetramer subunits and interaction with tropolone. *Biochemistry* **2011**, *50*, 5477−5486.
(30) Dimmock, J. R.; Padmanilayam, M. P.; Puthucode, R. N.; Nazarali, A. J.; Motaganahalli, N. L.; Zello, G. A.; Quail, J. W.; Oloo, E. O.; Kraatz, H.-B.; Prisciak, J. S.; Allen, T. M.; Santos, C. L.; Balzarini, J.; De Clercq, E.; Manavathu, E. K. A conformational and structure−activity relationship study of cytotoxic 3,5-bis(arylidene)-4-piperidones and related N-acryloyl analogues. *J. Med. Chem.* **2001**, *44*, 586−593.
(31) Das, U.; Alcorn, J.; Shrivastav, A.; Sharma, R. K.; De Clercq, E.; Balzarini, J.; Dimmock, J. R. Design, synthesis and cytotoxic properties of novel 1-[4-(2-alkylaminoethoxy)phenylcarbonyl]-3,5-bis-(arylidene)-4-piperidones and related compounds. *Eur. J. Med. Chem.* **2007**, *42*, 71−80.
(32) Nassar, A.-E. F.; Kamel, A. M.; Clarimont, C. Improvingthe decision-making process in structural modification of drug candidates: reducing toxicity. *Drug Discovery Today* **2004**, *9*, 1055−1064.
(33) Hour, T.-C.; Chen, J.; Huang, C.-Y.; Guan, J.-Y.; Lu, S.-H.; Pu, Y.-S. Curcumin enhances cytotoxicity of chemotherapeutic agents in prostate cancer cells by inducing p21WAF1/CIP1 and C/EBPβ expressions and suppressing NF-κB activation. *Prostate* **2002**, *51*, 211−218.
(34) Chan, M. M.; Fong, D.; Soprano, K. J.; Holmes, W. F.; Heverling, H. Inhibition of growth and sensitization to cisplatin-mediated killing of ovarian cancer cells by polyphenolic chemopreventive agents. *J. Cell. Physiol.* **2003**, *194*, 63−70.
(35) Koo, J. Y.; Kim, H. J.; Jung, K. O.; Park, K. Y. Curcumin inhibits the growth of AGS human gastric carcinoma cells in vitro and shows synergism with 5-fluorouracil. *J. Med. Food* **2004**, *7*, 117−121.
(36) Notarbartolo, M.; Poma, P.; Perri, D.; Dusonchet, L.; Cervello, M.; D'Alessandro, N. Antitumor effects of curcumin, alone or in combination with cisplatin or doxorubicin, on human hepatic cancer cells. Analysis of their possible relationship to changes in NF-kB activation levels and in IAP gene expression. *Cancer Lett.* **2005**, *224*, 53−65.
(37) Bava, S. V.; Puliappadamba, V. T.; Deepti, A.; Nair, A.; Karunagaran, D.; Anto, R. J. Sensitization of taxol-induced apoptosis by curcumin involves down-regulation of nuclear factor-kappaB and the serine/threonine kinase Akt and is independent of tubulin polymerization. *J. Biol. Chem.* **2005**, *280*, 6301−6308.
(38) Aggarwal, B. B.; Shishodia, S.; Takada, Y.; Banerjee, S.; Newman, R. A.; Bueso-Ramos, C. E.; Price, J. E. Curcumin suppresses the paclitaxel-induced nuclear factor-kappaB pathway in breast cancer cells and inhibits lung metastasis of human breast cancer in nude mice. *Clin. Cancer Res.* **2005**, *11*, 7490−7498.
(39) Lev-Ari, S.; Strier, L.; Kazanov, D.; Madar-Shapiro, L.; Dvory-Sobol, H.; Pinchuk, I.; Marian, B.; Lichtenberg, D.; Arber, N.

Celecoxib and curcumin synergistically inhibit the growth of colorectal cancer cells. *Clin. Cancer Res.* **2005**, *11*, 6738−6744.
(40) Sen, S.; Sharma, H.; Singh, N. Curcumin enhances Vinorelbine mediated apoptosis in NSCLC cells by the mitochondrial pathway. *Biochem. Biophys. Res. Commun.* **2005**, *331*, 1245−1252.
(41) Kamat, A. M.; Sethi, G.; Aggarwal, B. B. Curcumin potentiates the apoptotic effects of chemotherapeutic agents and cytokines through down-regulation of nuclear factor-kappaB and nuclear factor-kappaB-regulated gene products in IFN-alpha-sensitive and IFN-alpha-resistant human bladder cancer cells. *Mol. Cancer Ther.* **2007**, *6*, 1022−1030.
(42) Lev-Ari, S.; Vexler, A.; Starr, A.; Ashkenazy-Voghera, M.; Greif, J.; Aderka, D.; Ben-Yosef, R. Curcumin augments gemcitabine cytotoxic effect on pancreatic adenocarcinoma cell lines. *Cancer Invest.* **2007**, *25*, 411−418.
(43) Lipinski, C. A.; Lombardo, F.; Dominy, B. W.; Feeney, P. J. Experimental and computational approaches to estimate solubility and permeability in drug discovery and development settings. *Adv. Drug Delivery Rev.* **2001**, *46*, 3−26.
(44) Ertl, P.; Rohde, B.; Selzer, P. Fast calculation of molecular polar surface area as a sum of fragment-based contributions and its application to the prediction of drug transport properties. *J. Med. Chem.* **2000**, *43*, 3714−3717.
(45) Liang, G.; Shao, L.; Wang, Y.; Zhao, C.; Chu, Y.; Xiao, J.; Zhao, Y.; Li, X.; Yang, S. Exploration and synthesis of curcumin analogues with improved structural stability both in vitro and in vivo as cytotoxic agents. *Bioorg. Med. Chem.* **2009**, *17*, 2623−2631.
(46) Zsila, F.; Bikadi, Z.; Simonyi, M. Circular dichroism spectroscopic studies reveal pH dependent binding of curcumin in the minor groove of natural and synthetic nucleic acids. *Org. Biomol. Chem.* **2004**, *2*, 2902−2910.
(47) Caruso, F.; Rossi, M.; Benson, A.; Opazo, C.; Freedman, D.; Monti, E.; Gariboldi, M. B.; Shaulky, J.; Marchetti, F.; Pettinari, R.; Pettinari, C. Ruthenium−arene complexes of curcumin: X-ray and density functional theory structure, synthesis, and spectroscopic characterization, in vitro antitumor activity, and DNA docking studies of (p-cymene)Ru(curcuminato)chloro. *J. Med. Chem.* **2011**, *55*, 1072−1081.
(48) Sendovski, M.; Kanteev, M.; Ben-Yosef, V. S.; Adir, N.; Fishman, A. First structures of an active bacterial tyrosinase reveal copper plasticity. *J. Mol. Biol.* **2011**, *405*, 227−237.

JOURNAL OF AGRICULTURAL AND FOOD CHEMISTRY

Article

pubs.acs.org/JAFC

Xanthohumol, a Prenylated Chalcone from Beer Hops, Acts as an α-Glucosidase Inhibitor in Vitro

Ming Liu,[†,⊥] Hua Yin,[‡,⊥] Ge Liu,[§] Jianjun Dong,[‡] Zhonghua Qian,[‡] and Jinlai Miao*[,‡,∥]

[†]Key Laboratory of Marine Drugs, Ministry of Education, School of Medicine and Pharmacy, Ocean University of China, Qingdao 266003, China

[‡]State Key Laboratory of Biological Fermentation Engineering of Beer, Qingdao 266061, China

[§]Institute of Oceanology, Chinese Academy of Science, Qingdao 266071, China

[∥]Key Laboratory of Marine Bioactive Substance, The First Institute of Oceanography, State Oceanic Administration, Qingdao 266061, China

ABSTRACT: Xanthohumol (XN) is a unique prenylated flavonoid in hops (*Humulus lupulus L.*) and beer. XN alleviates hyperglycemia and has potential usage in the treatment of type 2 diabetes. In the present study, a series of in vitro experiments were performed to investigate whether XN was an effective inhibitor of α-glucosidase. The results showed that XN inhibited α-glucosidase in a reversible and noncompetitive manner, with an IC_{50} value of 8.8 μM and that XN inhibited the release of glucose from the maltose in the apical side of the Caco-2 cell monolayer. Fluorescence and circular dichroism spectra results indicated that XN directly bound to α-glucosidase and induced minor conformational changes of the enzyme. These results demonstrated that XN is a promising α-glucosidase inhibitor, which therefore could be used as functional food to alleviate postprandial hyperglycemia and as a potential candidate for the development of an antidiabetic agent.

KEYWORDS: *Humulus lupulus L., xanthohumol, α-glucosidase inhibitor*

INTRODUCTION

α-Glucosidase, a carbohydrate−hydrolase that releases glucose, is involved in diabetes and a variety of other diseases, such as viral infection and cancer, therefore, an attractive target for both pharmaceutical and functional food studies. Current clinically used antidiabetic agents, such as acarbose,[1] voglibose, and miglitol,[2] inhibit α-glucosidase and alleviate postprandial hyperglycemia. However, they are structurally confined to glycosidic derivatives, and continuous administration of these drugs can cause diarrhea and other intestinal disturbances,[3−5] as well as hepatotoxicity.[6] Therefore, novel drugs with fewer side effects will be needed to improve the treatment for type 2 diabetes mellitus (T2DM) patients.

Nutritional approaches that use phytonutrients for the prevention or treatment of T2DM are a rapidly emerging trend. Resveratrol has attracted much attention due to its therapeutic potential for T2DM and the related disorders;[7,8] Ginkgo biloba extract was shown to improve the cardiac function of diabetic rats;[9] and green tea extracts have a synergistic inhibitory effect on α-amylase and α-glucosidase when combined with acarbose.[10] Plant-based foods and dietary bioactives are more acceptable sources for the screening of α-glucosidase inhibitors due to their low cost and relative safety.[11−17] Dietary flavonoids and chalcones have already been proven good candidates to reduce postprandial hyperglycemia as α-glucosidase inhibitors.[18−24]

Xanthohumol (XN, Figure 1), the principal prenylated chalcone from the female inflorescences of the hop plant (hops, *Humulus lupulus L.*), is an ingredient of beer.[25,26] In vivo metabolism and pharmacokinetics of XN have been investigated previously.[27,28] XN has a good safety profile[29] and possesses beneficial health effects as an antioxidant,[30] anti-inflammatory,[31] antimicrobial,[32] anticancer agent,[33,34] and immune system modulator.[35] Recent studies demonstrated that XN lowered body weight and fasting plasma glucose in obese rats,[36,37] via mitochondrial uncoupling and stress response induction.[37] XN has also been found to ameliorate glucose metabolism and attenuates diabetes in KK-A^y mice.[38] These results implicate the benefits of using XN as treatment for obsesity and diabetes. Nevertheless, the mechanisms underlying the antidiabetes activity of XN are not fully clear.

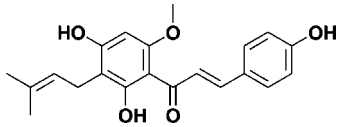

Figure 1. Structure of xanthohumol.

α-Glucosidase is an important enzyme that controls the postprandial blood glucose level and a drug target for the treatment of diabetes. In this study, the inhibitory effect of XN against α-glucosidase was investigated using both enzyme-based and cell-based assays; the inhibition mechanism was further explored using fluorescence spectra and circular dichroism (CD) spectra. This is the first study, to the best of our knowledge, which investigates the inhibition of α-glucosidase using XN.

Received: February 7, 2014
Revised: May 25, 2014
Accepted: May 26, 2014
Published: May 26, 2014

ACS Publications © 2014 American Chemical Society

dx.doi.org/10.1021/jf500426z | *J. Agric. Food Chem.* 2014, 62, 5548−5554

MATERIALS AND METHODS

Materials. XN (purity >98%) was purchased from Chengdu Biopurify Phytochemicals Ltd. (Chengdu, China). The baker's yeast α-glucosidase (EC 3.2.1.20), *p*-nitrophenyl glycosides, and bis-8-anilinonaphthalene-1-sulfonate (bis-ANS) were purchased from Sigma-Aldrich Chemical (St. Louis, MO, USA). Glucose detection kit was the product of Nanjing Jiancheng Bioengineering Institute (Nanjing, China). Other reagents were purchased from J&K Chemical Ltd. (Beijing, China).

Cell Culture. Caco-2 cells were obtained from the Cell Bank of the Chinese Academy of Sciences (Shanghai, China). Cells were grown at 37 °C and 5% CO_2 in minimal essential medium supplemented with 10% fetal calf serum, 1% nonessential amino acids, and 1% glutamine. The culture medium was renewed every 2 days, and subcultured using a 0.02% EDTA/0.05% trypsin solution when the cells reached 80−90% confluence.

Inhibitory Activity against α-Glucosidase. The α-glucosidase inhibitory activity of XN was evaluated using the method developed by Tsujii.[39] Briefly, α-glucosidase was dissolved using phosphate buffer (50 mM, pH 6.7) and treated with XN (0−100 μM) for 30 min. *p*-Nitrophenyl glycosides at 1 mM were used as a substrate and added to the reaction system to initiate the enzyme reaction. The enzyme reaction was carried out at 37 °C for 30 min. Na_2CO_3 (1 M) with 3-fold volume was added to terminate the reaction. The enzymatic activity of α-glucosidase was quantified by measuring the absorption at 405 nm and subtracting the background of XN. The inhibitory effect of XN was defined as inhibitory activity (%) = $(OD_{control} - OD_{XN\ treated})/OD_{control} \times 100$. Concentration−response assays were used to determine the potency (IC_{50}) of XN based on the logistic analysis of the concentration−response curve using Microsoft Excel.

Inhibitory Activity against α-Glucosidase on the Caco-2 Model System. α-Glucosidase inhibitory effect of XN on Caco-2 monolayers was performed based on the published protocol.[40,41] Caco-2 cells were cultured on polyethylene terephthalate membranes (Falcon, pore size, 0.4 μm; pore density, 1.6×10^6 pores/cm^2) in a 6 well plate for 20 days to form monolayers. The transepithelial electrical resistance (TEER) of the cell monolayer was measured using a Millicell-ERS electrical resistance measuring system, and the values that are more than 300 Ωcm^{-2} are considered as showing good integrity. Cell culture medium was then removed and washed with phosphate buffered saline (PBS). The apical chamber was replaced with XN solution (0−200 μM, 200 μL) or acarbose solution (0−200 μM, 200 μL), along with maltose solution in PBS (3 mM, 800 μL). In the basal chamber, after 1 mL of PBS was added, the plate was incubated at 37 °C in 5% CO_2 atmosphere for 2 h. The glucose concentration in both apical and basal chambers was measured by the glucose oxidase method.

Kinetics of Enzyme Inhibition. On the basis of the same assays detailed above, the kinetics of enzyme inhibition was performed with inhibitors at certain concentrations of XN (0−25 μM) and substrate (0.25, 0.5, 0.75, and 1.5 mM), respectively. The inhibitory kinetics of the investigated compounds on α-glucosidase was analyzed using the Lineweaver−Burk plot and the double-reciprocal plot of the substrate concentration and velocity (expressed as absorbance).

Dialysis Experiment. The dialysis experiment was conducted as previously reported by Lee with small modifications.[42] Briefly, using a ultrafiltration tube (4 K), α-glucosidase alone (0.25 mL, 100 U/mL, 2 groups) or α-glucosidase (0.25 mL, 100 U/mL) treated with XN (100 μM) were dialyzed in phosphate buffer (5 mM, pH 6.7) at 4 °C for 24 h. After dialysis, one of the α-glucosidase alone group was treated with XN (100 μM) for 20 min. The contents in the tubes were determined for residual enzyme activity as described above.

Intrinsic Fluorescence Measurements. α-Glucosidase (2 μM) was pretreated with certain concentrations of XN (0−100 μM) for 30 min at 37 °C. The intrinsic fluorescence spectra (300−400 nm) were measured using a Cary Eclipse fluorescence spectrophotometer (Varian Inc. USA) with the excitation wavelength at 295 nm.

Hydrophobic Analysis of α-Glucosidase Using Bis-ANS. α-Glucosidase (2 μM) was incubated at 37 °C for 30 min in the absence or presence of certain concentrations of XN (0−100 μM). Bis-ANS (15 μM) was then added, and fluorescence (395−545 nm) was measured after incubation at 37 °C for 15 min (λ_{ex} = 400 nm) using a FlexStation II microplate spectrofluorometer (Molecular Devices, USA).

Circular Dichroism Spectroscopy for Secondary Structure of α-Glucosidase. CD spectra (190−250 nm) of α-glucosidase (2 μM) treated with different concentrations of XN (0−100 μM) were measured with a JASCO 715 spectropolarimeter (JASCO, Tokyo, Japan). The spectra were collected and corrected by the reduction of noise and smoothing. The program JWSSE (JASCO) was used for estimation of the secondary structure percentage of α-glucosidase based on the method of Yang et al.[43]

Data Analysis. One-way ANOVA with Tukey's post-hoc test was used for the statistical analysis of the data. The results were expressed as the mean values ± SD. Differences of $p < 0.05$ were considered statistically significant.

RESULTS AND DISCUSSION

XN Inhibits α-Glucosidase in Vitro. We first tested XN's inhibition activity against the enzymatic activity of α-glucosidase. α-Glucosidase was pretreated with certain a concentration of XN (0−100 μM) for 30 min, and the enzymatic activity was measured using *p*-nitrophenyl glycoside as a substrate. As shown in Figure 2, XN significantly inhibited

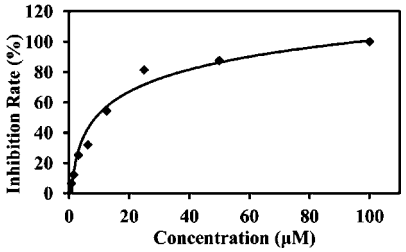

Figure 2. XN inhibits the activity of α-glucosidase in a concentration dependent manner. α-Glucosidase is pretreated with XN (0−100 μM) at room temperature for 30 min. *p*-Nitrophenyl glycosides at 1 mM was used as the substrate and added to the reaction system to initiate the enzyme reaction. Enzymatic activity was measured by the absorption at 405 nm, and the inhibition rate was calculated.

the activity of α-glucosidase in a concentration dependent manner, with an IC_{50} value of 8.8 μM. The determined inhibitory effect was stronger than that of other flavonoids and chalcones,[18,21−23] and the positive control acarbose (IC_{50} = 26.5 μM), indicating that XN is a powerful α-glucosidase inhibitor in vitro. Previous pharmacokinetics studies in both rats and humans have implied that XN could reach a high concentration in the intestinal tract when administrated orally[27,28,44] and that therefore XN could reach the concentration needed to inhibit the activity of α-glucosidase in vivo.

XN Inhibits Maltose Digestion in the Caco-2 Monolayer. To further confirm the inhibition effects of XN, the intestinal epithelial cell line Caco-2 was employed as a model of the intestinal brush border membrane. Caco-2 expresses α-glucosidases on the apical side and could hydrolyze maltose into glucose. As shown in Figure 3A, using a maltose solution as the substrate, the positive control acarbose inhibited the release of glucose from maltose on the apical side of the Caco-2 monolayer. Similarly, XN also inhibited the liberation of glucose from maltose, thus confirming its inhibitory activity against α-glucosidases in the cellular environment. On the basal side, there is no obvious difference in the glucose concentration

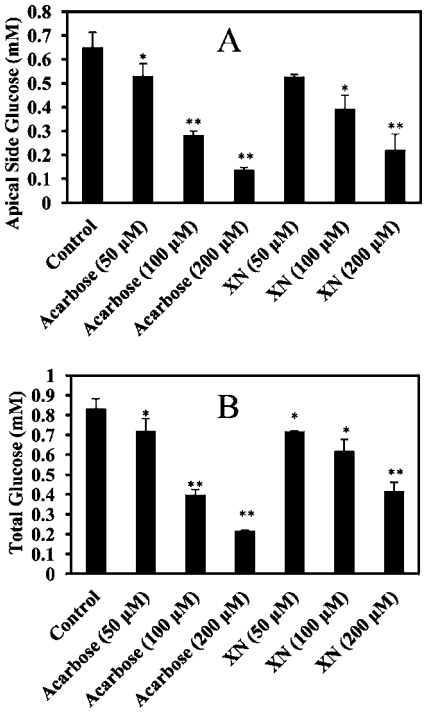

Figure 3. (A) XN inhibits the release of glucose from the maltose on the apical side of the Caco-2 monolayer. Caco-2 cells were cultured on polyethylene terephthalate membranes to form monolayers. The apical chamber was replaced with acarbose (0–200 μM), XN solution (0–200 μM), and maltose solution (3 mM, 800 μL), while the basal chamber was replaced with PBS. The plate was then incubated at 37 °C in 5% CO_2 atmosphere for 2 h, and then the glucose concentration in both the apical and basal chambers was measured by the glucose oxidase method. (B) XN inhibits the content of total glucose released from the maltose in the apical and basal sides of the Caco-2 monolayer. Values were expressed as the mean ± SD. Differences of $p < 0.05$ were considered statistically significant.

in the absence and presence of XN, indicating that XN does not inhibit the transport of glucose in the present experimental conditions (data not shown). The total glucose content included in both the basal and the apical side also decreased (Figure 3B). These results clearly demonstrated that XN can inhibit α-glucosidase enzymes in the Caco-2 monolayer.

In the Caco-2 monolayer model, to assay the inhibition against the α-glucosidases, higher concentrations of both acarbose and XN are needed. For example, a higher concentration (387 μM) of acarbose has been used as a positive control in other studies.[45] The possible reasons may include the higher concentration of substrate and nonspecific binding proteins in the system, which possibly compete against the α-glucosidase and XN interaction. Besides, a part of XN will be taken up and accumulated in the Caco-2 cells,[46] which will decrease the XN concentration in the apical side. The uptake and intracellular kinetics of XN may also explain why XN does not show a stronger inhibition than acarbose, which was observed in the enzyme assay.

XN Inhibits α-Glucosidase Noncompetitively. To explore the inhibitory mode of XN, double-reciprocal plots of α-glucosidase kinetics in the absence and presence of XN were analyzed. As shown in Figure 4, the value of 1/V increased with increasing concentrations of XN, but the intercept on the x-axis remains constant, and the K_m values remain at 0.65 mM. This result suggests a noncompetitive inhibition of XN. This

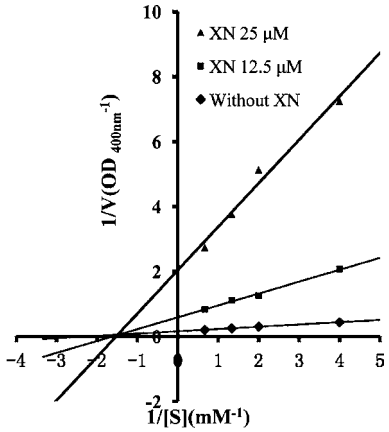

Figure 4. Double-reciprocal plots of the kinetics of α-glucosidase with and without XN. XN (0, 12.5, and 25 μM) was added in α-glucosidase buffer (50 μL and 10 U/mL) at room temperature for 30 min, and then, the substrate at different concentrations (0.25, 0.5, 0.75, and 1.5 mM) was added to initiate the enzyme reaction. Enzymatic activity was quantified by measuring the absorption at 405 nm.

inhibition mode is different from that of acarbose, which is a competitive inhibitor. Competitive inhibition is usually reversible, and an excessive amount of substrate will displace the inhibitor. In contrast, noncompetitive inhibition like that of XN is not influenced by the substrate concentration. The observed noncompetitive inhibition mode of XN indicates that XN may bind to a site different from the active site of α-glucosidase. Studies are in progress in our laboratory to identify those α-glucosidase residues that are critical for XN binding.

XN Inhibits α-Glucosidase Reversibly. We further investigated whether the inhibitory effect of XN is reversible using the dialysis experiment. The results are presented in Figure 5. After dialysis, the activity of α-glucosidase

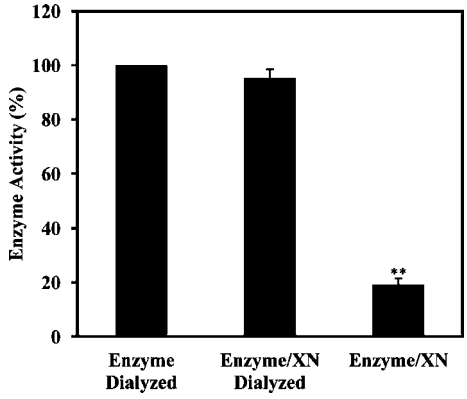

Figure 5. Recovery of α-glucosidase activity after dialysis. The inhibitor (100 μM) was added to α-glucosidase (100 U/mL) before dialysis. α-Glucosidase (0.25 mL and 100 U/mL) and XN (100 μM) treated α-glucosidase were dialyzed against phosphate buffer at 4 °C for 24 h, and the residual enzyme activities were measured.

preincubated with XN was similar to that of the untreated α-glucosidase, indicating that the enzymatic activity was recovered after dialysis. In contrast, α-glucosidase incubated with XN but without further dialysis showed relatively less activity. These results demonstrate that the inhibition of XN against α-glucosidase is reversible.

dx.doi.org/10.1021/jf500426z | J. Agric. Food Chem. 2014, 62, 5548–5554

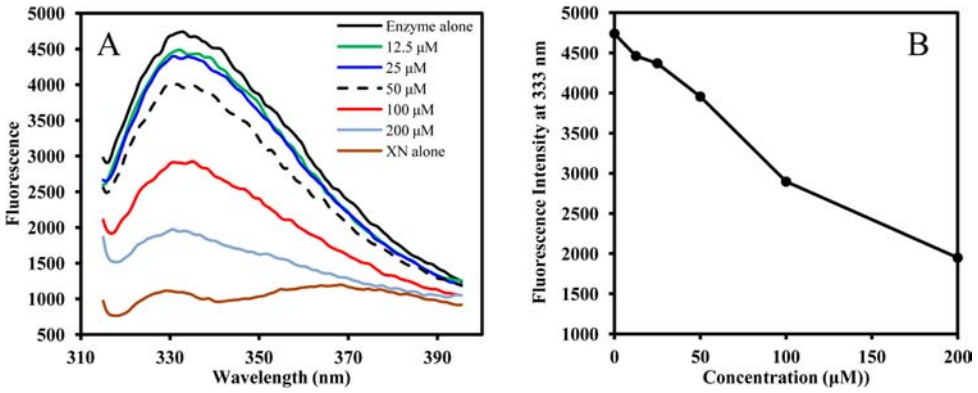

Figure 6. Variation of the intrinsic fluorescence spectra of α-glucosidase. The enzyme (2 μM) was incubated with specified concentrations of XN (0−200 μM) for 30 min at 37 °C. The excitation wavelength was 295 nm, and emission spectra were acquired by scanning from 300 to 400 nm. (B) XN quenches the intrinsic fluorescence of α-glucosidase in a concentration dependent manner.

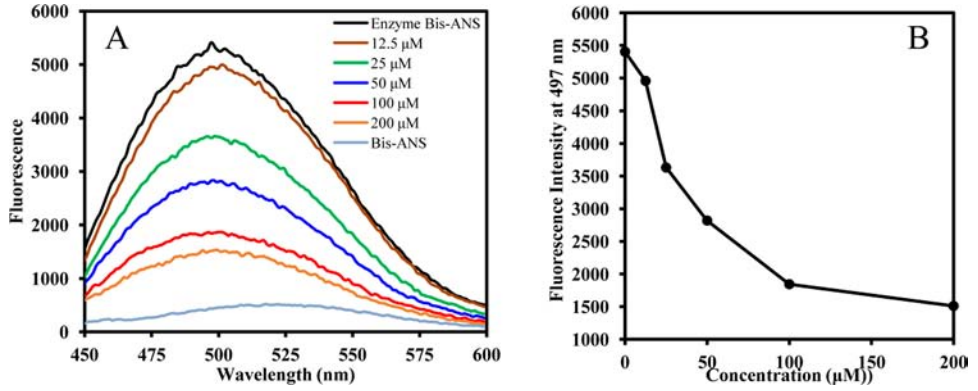

Figure 7. Changes of the α-glucosidase-bis-ANS complex's fluorescence by XN. (A) Fluorescence spectra of bis-ANS in the absence and presence of XN. α-Glucosidase (2 μM) was first incubated for 30 min at 37 °C in the absence or presence of specified concentrations of XN (0−200 μM). Bis-ANS (15 μM) was then added, and after 15 min of incubation at 37 °C, the fluorescence was measured (excitation at 400 nm) using a Cary Eclipse fluorescence spectrophotometer. (B) XN reduces the α-glucosidase-bis-ANS complex's fluorescence in a concentration dependent manner.

XN Quenches the Intrinsic Fluorescence of α-Glucosidase in Vitro. The in vitro inhibitory results of XN suggest that XN directly binds α-glucosidase. To test this hypothesis, we first investigated XN induced changes in intrinsic tryptophan fluorescence of the α-glucosidase enzymes. As shown in Figure 6A, when excited at 295 nm, XN had no obvious fluorescence emission from 300 to 400 nm. Therefore, the fluorescence interference contributed from XN was negligible. Excited at 295 nm, α-glucosidase alone has remarkable florescence at about 335 nm, which belongs to the tryptophan residues of α-glucosidase; the fluorescence intensity of XN-treated (12.5−200 μM) α-glucosidase was quenched gradually in a concentration dependent manner, and the fluorescence intensity almost vanished in the presence of the high concentration of XN (Figure 6B). These results confirmed that XN directly bound to α-glucosidase. Such XN binding might induce a conformational change of tryptophan residues in α-glucosidase, which subsequently hinders the active center formation and/or the substrate binding. The intrinsic fluorescence changes induced by XN are similar to those of other flavonoid compounds, which also quenched the intrinsic fluorescence of α-glucosidase.[18]

XN Reduces the Hydrophobicity of α-Glucosidase. The fluorescence probe bis-8-anilinonaphthalene-1-sulfonate (bis-ANS) is widely used in the measurement of protein surface hydrophobicity.[47] To further study the binding and interaction between XN and α-glucosidase, we measured the hydrophobicity of α-glucosidase using bis-ANS. The relative fluorescence intensities of bis-ANS in different statuses are shown in Figure 7A. Excited at 400 nm, there is barely a fluorescence signal for bis-ANS alone; however, significantly increased fluorescence intensity was observed when it was incubated with α-glucosidase. When treated with XN, the enzyme-bis-ANS fluorescence reduced remarkably in a concentration dependent manner (Figure 7B). These results suggested that XN might bind to a hydrophobic domain or/and reduce the hydrophobic surface of α-glucosidase. In our previous study, reduced enzyme hydrophobicity was also observed when α-glucosidase bound to other inhibitors, butyl-isobutyl-phthalate[16] and bis(2,3-dibromo-4,5-dihydroxybenzyl) ether.[48] Such inhibitor induced hydrophobicity decrease supports the notion that a poor hydrophobic surface usually hinders the formation of the active center of the enzyme molecules.

XN Influences the Secondary Structures of α-Glucosidase. To study the effect of XN on the secondary structure of α-glucosidase, we measured the CD spectra (190−250 nm) of α-glucosidase in the absence and presence of XN. As shown in Figure 8, minor changes in the CD spectrum of α-glucosidase were observed in the presence of XN (0−100 μM). The α-helix content increased slightly when treated with XN. The content of β-sheet decreased at a low concentration of XN (25 and 50 μM) but increased when treated with 100 μM XN. The content of β-turn decreased when treated with 25 and 100

dx.doi.org/10.1021/jf500426z | J. Agric. Food Chem. 2014, 62, 5548−5554

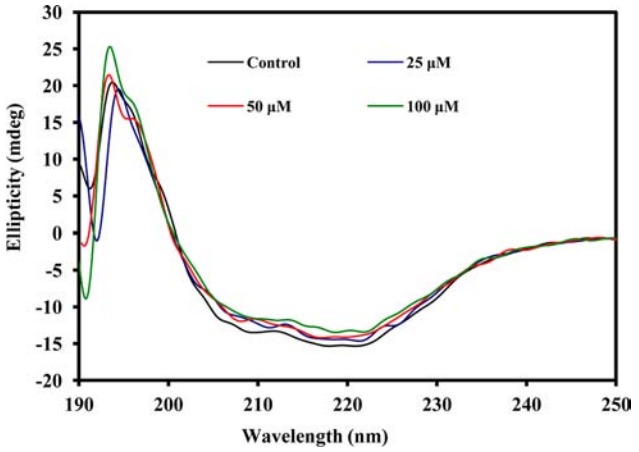

Figure 8. CD spectra of α-glucosidase in the absence or presence of XN. α-Glucosidase (2 μM, dissolved in 20 mM potassium phosphate buffer, pH 6.8) alone or incubated with XN (0−100 μM) at 37 °C for 30 min. CD spectra were acquired from 190 to 250 nm.

μM XN but increased a little in the presence of 50 μM XN. The predicted secondary structure content of α-glucosidase in the absence and presence of XN is shown in Table 1. The observed

Table 1. Secondary Structure Content of α-Glucosidase Influenced by XN[a]

XN (μM)	α-helix (%)	β-sheet (%)	β-turn (%)	random (%)
0	22	36.2	16.1	25.7
25	23.9	34	15.2	26.8
50	26.7	30	17	26.3
100	24.9	39.7	10.2	25.2

[a]The secondary structure content of α-glucosidase is predicted by the program JWSSE (JASCO).

XN-induced α-helix increase is similar to the effect of another α-glucosidase inhibitor, penicillamine,[49] but in contrast to the results of other α-glucosidase inhibitors, such as, curcuminoids analogues,[11] hydroxycoumarin derivatives,[50] and bicoumarin derivatives,[51] it decreased the α-helix content of the enzyme molecule. While CD spectra do not have the information needed to explain the different secondary structural changes induced by these inhibitors, it clearly further confirmed that XN directly bound to α-glucosidase and slightly changed its secondary structural conformations.

XN has a Michael acceptor moiety that can covalently interact with proteins. A number of studies have shown that the loss of protein function has been attributed to the Michael-type addition of cysteine residues with the α,β-unsaturated keto group of XN.[52,53] This reactivity possibly explains the interaction between XN and α-glucosidase. Since the Michael reactions are reversible, the release of XN recovers the enzyme function in the dialysis experiment and thus explains the reversible inhibitory mode. In addition, isoxanthohumol, a spontaneous cyclization product of XN with no electrophilic properties and Michael addition, does not possess an obvious inhibition against α-glucosidase. However, kuraridine, which has a structure similar to that of XN and contains the α,β-unsaturated keto group, possesses much stronger inhibitory activities against α-glucosidase.[54] Taken together, these investigations strongly indicate the Michael-type addition between XN and α-glucosidase could be the reason for the observed interaction and reversible inhibition mode. However, further experimental evidence is needed to prove this rationale.

In the present studies, we demonstrated, for the first time, XN inhibited α-glucosidase in a noncompetitive and reversible manner, and the inhibitory effect against α-glucosidase was confirmed in the Caco-2 cell monolayer assay. Our results indicated that XN directly bound to α-glucosidase and induced its conformational changes. The result that XN is a potent α-glucosidase inhibitor suggests that the α-glucosidase inhibition may contribute to the antidiabetic activity of XN. Nevertheless, α-glucosidase inhibition may not be the only mechanism underlying its antihyperglycemic effects. Other mechanisms, such as respiration uncoupling and induction of oxidant defense system,[37] acting as the ligand for farnesoid X receptor,[38] are likely also involved. Therefore, XN has the potential to be used in functional food and as a novel leading compound for the treatment of T2DM.

AUTHOR INFORMATION

Corresponding Author

*Tel: +86-532-88967430. Fax: +86-532-88967430. E-mail: miaojinlai@163.com.

Author Contributions

⊥These authors contributed equally to this work.

Funding

This study was supported by the Open Research Fund of State Key Laboratory of Biological Fermentation Engineering of Beer (in preparation) under grant number K2014002 and the National Natural Science Foundation of China (no. 31200097 and no. 31200272).

Notes

The authors declare no competing financial interest.

ACKNOWLEDGMENTS

We thank Dr. Wei Zhang, Southern Research Institute, MD for his revision of the manuscript.

REFERENCES

(1) Lefebvre, P. J.; Scheen, A. J. The use of acarbose in the prevention and treatment of hypoglycaemia. *Eur. J. Clin. Invest.* **1994**, *24* (Suppl 3), 40−44.

(2) Scott, L. J.; Spencer, C. M. Miglitol: a review of its therapeutic potential in type 2 diabetes mellitus. *Drugs* **2000**, *59*, 521−549.

(3) Campbell, L. K.; Baker, D. E.; Campbell, R. K. Miglitol: assessment of its role in the treatment of patients with diabetes mellitus. *Ann. Pharmacother.* **2000**, *34*, 1291−1301.

(4) Krentz, A. J.; Bailey, C. J. Oral antidiabetic agents: current role in type 2 diabetes mellitus. *Drugs* **2005**, *65*, 385−411.

(5) Nathan, D. M.; Buse, J. B.; Davidson, M. B.; Heine, R. J.; Holman, R. R.; Sherwin, R.; Zinman, B. Management of hyperglycaemia in type 2 diabetes: a consensus algorithm for the initiation and adjustment of therapy. A consensus statement from the American Diabetes Association and the European Association for the Study of Diabetes. *Diabetologia* **2006**, *49*, 1711−1721.

(6) Hsiao, S. H.; Liao, L. H.; Cheng, P. N.; Wu, T. J. Hepatotoxicity associated with acarbose therapy. *Ann. Pharmacother.* **2006**, *40*, 151−154.

(7) Timmers, S.; Hesselink, M. K.; Schrauwen, P. Therapeutic potential of resveratrol in obesity and type 2 diabetes: new avenues for health benefits? *Ann. N.Y. Acad. Sci.* **2013**, *1290*, 83−89.

(8) Lekli, I.; Szabo, G.; Juhasz, B.; Das, S.; Das, M.; Varga, E.; Szendrei, L.; Gesztelyi, R.; Varadi, J.; Bak, I.; Das, D. K.; Tosaki, A. Protective mechanisms of resveratrol against ischemia-reperfusion-induced damage in hearts obtained from Zucker obese rats: the role of

GLUT-4 and endothelin. *Am. J. Physiol. Heart Circ. Physiol.* **2008**, *294*, 7.
(9) Tosaki, A.; Pali, T.; Droy-Lefaix, M. T. Effects of Ginkgo biloba extract and preconditioning on the diabetic rat myocardium. *Diabetologia* **1996**, *39*, 1255−1262.
(10) Gao, J.; Xu, P.; Wang, Y.; Hochstetter, D. Combined effects of green tea extracts, green tea polyphenols or epigallocatechin gallate with acarbose on inhibition against alpha-amylase and alpha-glucosidase in vitro. *Molecules* **2013**, *18*, 11614−11623.
(11) Du, Z. Y.; Liu, R. R.; Shao, W. Y.; Mao, X. P.; Ma, L.; Gu, L. Q.; Huang, Z. S.; Chan, A. S. Alpha-glucosidase inhibition of natural curcuminoids and curcumin analogs. *Eur. J. Med. Chem.* **2006**, *41*, 213−218.
(12) Borges de Melo, E.; da Silveira Gomes, A.; Carvalho, I. alpha- and beta-glucosidase inhibitors: chemical structure and biological activity. *Tetrahedron* **2006**, *62*, 10277−10302.
(13) Kwon, Y. I.; Apostolidis, E.; Shetty, K. In vitro studies of eggplant (*Solanum melongena*) phenolics as inhibitors of key enzymes relevant for type 2 diabetes and hypertension. *Bioresour. Technol.* **2008**, *99*, 2981−2988.
(14) Tundis, R.; L, M.; Menichini, F. Natural products as alpha-amylase and alpha-glucosidase inhibitors and their hypoglycaemic potential in the treatment of diabetes: an update. *Mini-Rev. Med. Chem.* **2010**, *10*, 315−331.
(15) Ranilla, L. G.; Kwon, Y.-I.; Apostolidis, E.; Shetty, K. Phenolic compounds, antioxidant activity and in vitro inhibitory potential against key enzymes relevant for hyperglycemia and hypertension of commonly used medicinal plants, herbs and spices in Latin America. *Bioresour. Technol.* **2010**, *101*, 4676−4689.
(16) Liu, M.; Zhang, W.; Qiu, L.; Lin, X. Synthesis of butyl-isobutyl-phthalate and its interaction with alpha-glucosidase in vitro. *J. Biochem* **2011**, *149*, 27−33.
(17) Bu, T.; Liu, M.; Zheng, L.; Guo, Y.; Lin, X. alpha-Glucosidase inhibition and the in vivo hypoglycemic effect of butyl-isobutyl-phthalate derived from the *Laminaria japonica* rhizoid. *Phytother Res.* **2010**, *24*, 1588−1591.
(18) Li, Y. Q.; Zhou, F. C.; Gao, F.; Bian, J. S.; Shan, F. Comparative evaluation of quercetin, isoquercetin and rutin as inhibitors of α-glucosidase. *J. Agric. Food Chem.* **2009**, *57*, 11463−11468.
(19) Yilmazer-Musa, M.; Griffith, A. M.; Michels, A. J.; Schneider, E.; Frei, B. Grape seed and tea extracts and catechin 3-gallates are potent inhibitors of α-amylase and α-glucosidase activity. *J. Agric. Food Chem.* **2012**, *60*, 8924−8929.
(20) Choi, C. W.; Choi, Y. H.; Cha, M.-R.; Yoo, D. S.; Kim, Y. S.; Yon, G. H.; Hong, K. S.; Kim, Y. H.; Ryu, S. Y. Yeast α-glucosidase inhibition by isoflavones from plants of leguminosae as an in vitro alternative to acarbose. *J. Agric. Food Chem.* **2010**, *58*, 9988−9993.
(21) Ansari, F. L.; Umbreen, S.; Hussain, L.; Makhmoor, T.; Nawaz, S. A.; Lodhi, M. A.; Khan, S. N.; Shaheen, F.; Choudhary, M. I. Syntheses and biological activities of chalcone and 1,5-benzothiazepine derivatives: promising new free-radical scavengers, and esterase, urease, and alpha-glucosidase inhibitors. *Chem. Biodiversity* **2005**, *2*, 487−496.
(22) Seo, W. D.; Kim, J. H.; Kang, J. E.; Ryu, H. W.; Curtis-Long, M. J.; Lee, H. S.; Yang, M. S.; Park, K. H. Sulfonamide chalcone as a new class of α-glucosidase inhibitors. *Bioorg. Med. Chem. Lett.* **2005**, *15*, 5514−5516.
(23) Bak, E. J.; Park, H. G.; Lee, C.; Lee, T. I.; Woo, G. H.; Na, Y.; Yoo, Y. J.; Cha, J. H. Effects of novel chalcone derivatives on alpha-glucosidase, dipeptidyl peptidase-4, and adipocyte differentiation in vitro. *BMB Rep.* **2011**, *44*, 410−414.
(24) Kumar, S.; Narwal, S.; Kumar, V.; Prakash, O. Alpha-glucosidase inhibitors from plants: A natural approach to treat diabetes. *Pharmacogn. Rev.* **2011**, *5*, 19−29.
(25) Stevens, J. F.; Taylor, A. W.; Nickerson, G. B.; Ivancic, M.; Henning, J.; Haunold, A.; Deinzer, M. L. Prenylflavonoid variation in *Humulus lupulus*: distribution and taxonomic significance of xanthogalenol and 4′-O-methylxanthohumol. *Phytochemistry* **2000**, *53*, 759−775.
(26) Stevens, J. F.; Taylor, A. W.; Clawson, J. E.; Deinzer, M. L. Fate of xanthohumol and related prenylflavonoids from hops to beer. *J. Agric. Food Chem.* **1999**, *47*, 2421−2428.
(27) Legette, L.; Ma, L.; Reed, R. L.; Miranda, C. L.; Christensen, J. M.; Rodriguez-Proteau, R.; Stevens, J. F. Pharmacokinetics of xanthohumol and metabolites in rats after oral and intravenous administration. *Mol. Nutr. Food Res.* **2012**, *56*, 466−474.
(28) Nookandeh, A.; Frank, N.; Steiner, F.; Ellinger, R.; Schneider, B.; Gerhäuser, C.; Becker, H. Xanthohumol metabolites in faeces of rats. *Phytochemistry* **2004**, *65*, 561−570.
(29) Dorn, C.; Bataille, F.; Gaebele, E.; Heilmann, J.; Hellerbrand, C. Xanthohumol feeding does not impair organ function and homoeostasis in mice. *Food Chem. Toxicol.* **2010**, *48*, 1890−1897.
(30) Miranda, C. L.; Stevens, J. F.; Ivanov, V.; McCall, M.; Frei, B.; Deinzer, M. L.; Buhler, D. R. Antioxidant and prooxidant actions of prenylated and nonprenylated chalcones and flavanones in vitro. *J. Agric. Food Chem.* **2000**, *48*, 3876−3884.
(31) Peluso, M. R.; Miranda, C. L.; Hobbs, D. J.; Proteau, R. R.; Stevens, J. F. Xanthohumol and related prenylated flavonoids inhibit inflammatory cytokine production in LPS-activated THP-1 monocytes: structure-activity relationships and in silico binding to myeloid differentiation protein-2 (MD-2). *Planta Med.* **2010**, *76*, 1536−1543.
(32) Gerhäuser, C. Broad spectrum antiinfective potential of xanthohumol from hop (*Humulus lupulus* L.) in comparison with activities of other hop constituents and xanthohumol metabolites. *Mol. Nutr. Food Res.* **2005**, *49*, 827−831.
(33) Gerhauser, C.; Alt, A.; Heiss, E.; Gamal-Eldeen, A.; Klimo, K.; Knauft, J.; Neumann, I.; Scherf, H. R.; Frank, N.; Bartsch, H.; Becker, H. Cancer chemopreventive activity of xanthohumol, a natural product derived from hop. *Mol. Cancer Ther.* **2002**, *1*, 959−969.
(34) Colgate, E. C.; Miranda, C. L.; Stevens, J. F.; Bray, T. M.; Ho, E. Xanthohumol, a prenylflavonoid derived from hops induces apoptosis and inhibits NF-kappaB activation in prostate epithelial cells. *Cancer Lett.* **2007**, *246*, 201−209.
(35) Xuan, N. T.; Shumilina, E.; Gulbins, E.; Gu, S.; Gotz, F.; Lang, F. Triggering of dendritic cell apoptosis by xanthohumol. *Mol. Nutr. Food Res.* **2010**, *54* (Suppl 2), S214−S224.
(36) Legette, L. L.; Moreno Luna, A. Y.; Reed, R. L.; Miranda, C. L.; Bobe, G.; Proteau, R. R.; Stevens, J. F. Xanthohumol lowers body weight and fasting plasma glucose in obese male Zucker fa/fa rats. *Phytochemistry* **2013**, *91*, 236−241.
(37) Kirkwood, J. S.; Legette, L. L.; Miranda, C. L.; Jiang, Y.; Stevens, J. F. A metabolomics driven elucidation of the anti-obesity mechanisms of xanthohumol. *J. Biol. Chem.* **2013**, *288*, 19000−19013.
(38) Nozawa, H. Xanthohumol, the chalcone from beer hops (*Humulus lupulus* L.), is the ligand for farnesoid X receptor and ameliorates lipid and glucose metabolism in KK-Ay mice. *Biochem. Biophys. Res. Commun.* **2005**, *336*, 754−761.
(39) Tsujii, E.; Muroi, M.; Shiragami, N.; Takatsuki, A. Nectrisine is a potent inhibitor of α-glucosidases, demonstrating activities similarly at enzyme and cellular levels. *Biochem. Biophys. Res. Commun.* **1996**, *220*, 459−466.
(40) Toda, M.; Kawabata, J.; Kasai, T. Alpha-glucosidase inhibitors from clove (*Syzgium aromaticum*). *Biosci. Biotechnol. Biochem.* **2000**, *64*, 294−298.
(41) Hansawasdi, C.; Kawabata, J. Alpha-glucosidase inhibitory effect of mulberry (*Morus alba*) leaves on Caco-2. *Fitoterapia* **2006**, *77*, 568−573.
(42) Lee, D.-S.; Lee, S.-H. Genistein, a soy isoflavone, is a potent α-glucosidase inhibitor. *FEBS Lett.* **2001**, *501*, 84−86.
(43) Yang, J. T.; Wu, C. S.; Martinez, H. M. Calculation of protein conformation from circular dichroism. *Methods Enzymol.* **1986**, *130*, 208−269.
(44) Legette, L.; Karnpracha, C.; Reed, R. L.; Choi, J.; Bobe, G.; Christensen, J. M.; Rodriguez-Proteau, R.; Purnell, J. Q.; Stevens, J. F. Human pharmacokinetics of xanthohumol, an antihyperglycemic flavonoid from hops. *Mol. Nutr. Food Res.* **2014**, *58*, 248−255.

(45) Li, Z. Q.; Zuo, D. Y.; Qie, X. D.; Qi, H.; Zhao, M. Q.; Wu, Y. L. Berberine acutely inhibits the digestion of maltose in the intestine. *J. Ethnopharmacol.* **2012**, *142*, 474−480.
(46) Wolff, H.; Motyl, M.; Hellerbrand, C.; Heilmann, J.; Kraus, B. Xanthohumol uptake and intracellular kinetics in hepatocytes, hepatic stellate cells, and intestinal cells. *J. Agric. Food Chem.* **2011**, *59*, 12893−12901.
(47) Hawe, A.; Sutter, M.; Jiskoot, W. Extrinsic fluorescent dyes as tools for protein characterization. *Pharm. Res.* **2008**, *25*, 1487−1499.
(48) Liu, M.; Zhang, W.; Wei, J.; Lin, X. Synthesis and α-glucosidase inhibitory mechanisms of bis(2,3-dibromo-4,5-dihydroxybenzyl) ether, a potential marine bromophenol α-glucosidase inhibitor. *Marine Drugs* **2011**, *9*, 1554−1565.
(49) Kim, J. H.; Kim, H. J.; Park, H. W.; Youn, S. H.; Choi, D. Y.; Shin, C. S. Development of inhibitors against lipase and alpha-glucosidase from derivatives of monascus pigment. *FEMS Microbiol. Lett.* **2007**, *276*, 93−98.
(50) Shen, Q.; Shao, J.; Peng, Q.; Zhang, W.; Ma, L.; Chan, A. S.; Gu, L. Hydroxycoumarin derivatives: novel and potent alpha-glucosidase inhibitors. *J. Med. Chem.* **2010**, *53*, 8252−8259.
(51) Hu, X.-J.; Wang, X.-B.; Kong, L.-Y. α-Glucosidase inhibitors via green pathway: biotransformation for bicoumarins catalyzed by momordica charantia peroxidase. *J. Agric. Food Chem.* **2013**, *61*, 1501−1508.
(52) Liu, G.; Eggler, A. L.; Dietz, B. M.; Mesecar, A. D.; Bolton, J. L.; Pezzuto, J. M.; van Breemen, R. B. Screening method for the discovery of potential cancer chemoprevention agents based on mass spectrometric detection of alkylated Keap1. *Anal. Chem.* **2005**, *77*, 6407−6414.
(53) Harikumar, K. B.; Kunnumakkara, A. B.; Ahn, K. S.; Anand, P.; Krishnan, S.; Guha, S.; Aggarwal, B. B. Modification of the cysteine residues in IκBα kinase and NF-κB (p65) by xanthohumol leads to suppression of NF-κB−regulated gene products and potentiation of apoptosis in leukemia cells. *Blood* **2009**, *113*, 2003−2013.
(54) Kim, J. H.; Ryu, Y. B.; Kang, N. S.; Lee, B. W.; Heo, J. S.; Jeong, I. Y.; Park, K. H. Glycosidase inhibitory flavonoids from *Sophora flavescens*. *Biol. Pharm. Bull.* **2006**, *29*, 302−305.

JOURNAL OF AGRICULTURAL AND FOOD CHEMISTRY

Article

pubs.acs.org/JAFC

Genetic and Biochemical Evidence That Recombinant *Enterococcus* spp. Strains Expressing Gelatinase (GelE) Produce Bovine Milk-Derived Hydrolysates with High Angiotensin Converting Enzyme-Inhibitory Activity (ACE-IA)

Loreto Gútiez,[†] Juan Borrero,[†] Juan J. Jiménez,[†] Beatriz Gómez-Sala,[‡] Isidra Recio,[§] Luis M. Cintas,[†] Carmen Herranz,[†] and Pablo E. Hernández*[,†]

[†]Departamento de Nutrición, Bromatología y Tecnología de los Alimentos, Facultad de Veterinaria, Universidad Complutense de Madrid (UCM), 28040 Madrid, Spain

[‡]INNAVES S.A., 36475 Porriño, Pontevedra, Spain

[§]Instituto de Investigación en Ciencias de la Alimentación, CIAL (CSIC-UAM), C/. Nicolás Cabrera 8, 28049 Madrid, Spain

ABSTRACT: In this work, genes encoding gelatinase (*gelE*) and serine proteinase (*sprE*), two extracellular proteases produced by *Enterococcus faecalis* DBH18, were cloned in the protein expression vector pMG36c, containing the constitutive P_{32} promoter, generating the recombinant plasmids pCG, pCSP, and pCGSP encoding *gelE*, *sprE*, and *gelE*−*sprE*, respectively. Transformation of noncaseinolytic *E. faecalis* P36, *E. faecalis* JH2-2, *E. faecium* AR24, and *E. hirae* AR14 strains with these plasmids permitted detection of caseinolytic activity only in the strains transformed with pCG or pCGSP. Complementation of a deletion (knockout) mutant of *E. faecalis* V583 for production of gelatinase (GelE) with pCG unequivocally supported that *gelE* is responsible for the caseinolytic activity of the transformed strain grown in bovine skim milk (BSM). RP-HPLC-MS/MS analysis of hydrolysates of transformed *Enterococcus* spp. strains grown in BSM permitted the identification of 38 major peptide fragments including peptides with previously reported angiotensin converting enzyme-inhibitory activity (ACE-IA), antihypertensive activity, and antioxidant activity.

KEYWORDS: *lactic acid bacteria (LAB), Enterococcus faecalis, gelatinase (GelE), serine protease (SprE), ACE-inhibitory peptides, antihypertensive peptides*

INTRODUCTION

Many dietary proteins contain encrypted within their primary structure bioactive peptides with beneficial effects against cardiovascular diseases, inflammation, and cancer.[1,2] From the bioactive peptides, those with angiotensin converting enzyme-inhibitory activity (ACE-IA) and blood pressure-lowering effects have been extensively studied, due to the high prevalence of hypertension in the Western population.[3] Furthermore, peptides with ACE-IA known as ACE-inhibitory peptides (ACE-IP) are of interest due to their potential use in the treatment of elevated blood pressure and associated cardiovascular events.[4] Milk proteins are the main source of bioactive peptides, although other animal and plant proteins may also contain these peptides.[5−7] The release of ACE-IP from food proteins may be achieved by digestive enzymes, by hydrolysis with specific proteolytic enzymes, or by fermentation and ripening during food processing. Fermentation conditions and the proteolytic activity of specific lactic acid bacteria (LAB) seem to modulate the production of ACE-IP during their growth in milk.[8,9]

The enterococci are LAB that play a beneficial role in the development of the sensory characteristics of fermented foods being employed as starters in the food industry and as probiotics for humans and animals.[10] However, they are also gastrointestinal tract colonizers with lifestyles ranging from intestinal symbionts to multidrug-resistant pathogens responsible for nosocomial and, to a lesser extent, community-acquired infections.[11] Previous studies have shown that *Enterococcus faecalis* strains from food origin produce food-derived hydrolysates with ACE-IA[12−14] and that most, but not all, *E. faecalis* strains from food, environmental, and clinical origin produce milk-derived hydrolysates with high ACE-IA.[15] Accordingly, it would be convenient to identify those *E. faecalis* metabolic activities releasing milk-derived ACE-IP.

The zinc metalloprotease gelatinase (GelE) and the serine protease (SprE) are two secreted proteases produced by *E. faecalis*[16,17] that contribute to biofilm formation, stress response inside the host, host immune system evasion, and virulence.[18,19] On the other hand, the *fsr* (*E. faecalis* regulator) is a two-component quorum sensing-dependent regulatory system whose operon encodes the *fsrABCD* genes. The last gene encodes an autoinducing cyclic peptide, a gelatinase biosynthesis activating pheromone (GBAP) that is processed and exported out of the cells by the FsrB protein. Accumulation of GBAP outside the cells is sensed by the FsrC histidine kinase, leading to the activation of the response regulator FsrA. Activated FsrA induces expression of the *fsrBCD* genes. These *fsr* genes are involved in an autoregulatory circuit that results in a boost of GBAP signaling

Received: February 7, 2014
Revised: May 30, 2014
Accepted: May 30, 2014
Published: May 30, 2014

ACS Publications © 2014 American Chemical Society

and the induction of the Fsr regulon, among which the *gelE*−*sprE* operon is the most induced.[19,20] In the *gelE*−*sprE* operon, the gene encoding GelE is located immediately adjacent to the 3′ end of *fsrC* and is cotranscribed with *sprE*. However, despite their significance for *E. faecalis* virulence, both the *fsr* and the *gelE*−*sprE* loci are present in enterococcal isolates from different ecological environments, suggesting that both the Fsr system and the GelE and SprE proteins may play an additional role in the biology of *E. faecalis*,[18] not exclusively associated with virulence.

E. faecalis DBH18[21] is a bacteriocinogenic strain producer of bovine skim milk (BSM)-derived hydrolysates with high ACE-IA.[15] This strain may synthesize the GelE encoded by its *gelE*−*sprE* operon (GenBank no. JQ815406) as a 509 amino acid preproenzyme with a predicted N-terminal signal peptide of 29 amino acids, a prosequence of 480 amino acids, and the mature GelE of 318 amino acids, which is further subjected to C-terminal processing for full activation of protease activity, resulting in a molecular mass of 33 kDa.[22,23] Similarly, SprE may be synthesized as a 284 amino acid preproenzyme with a predicted N-terminal signal peptide of 32 amino acids, a prosequence of 252 amino acids, and the mature serine-type glutamyl endopeptidase (SprE) of 237 amino acids and a molecular mass of 25 kDa.[24] We describe in this work the cloning of the extracellular proteases GelE and SprE, produced by *E. faecalis* DBH18, in the protein expression vector pMG36c and the genetic and biochemical evidence that recombinant *Enterococcus* spp. strains expressing GelE produce BSM-derived hydrolysates with ACE-IA due to the production of ACE-IP.

MATERIALS AND METHODS

Bacterial Strains, Culture Conditions, Basic Genetic Techniques, and Enzymes. The bacterial strains and plasmids used in this study are listed in Table 1. *E. faecalis* DBH18[21] was used as the source of *gelE* and *sprE*. The nucleotide sequence of *gelE* from *E. faecalis* DBH18 (GenBank no. JQ815406) showed 99 and 98% homology with those of *E. faecalis* OG1RF (GenBank no. CP002621) and *E. faecalis* V583 (GenBank no. AE016830), respectively, whereas the nucleotide sequence of *sprE* showed a 98% homology with those of *E. faecalis* OG1RF and *E. faecalis* V583. The enterococcal strains were propagated at 37 °C in MRS broth (Oxoid Ltd., Basingstoke, UK). When needed, chloramphenicol (Cm) (Sigma Chemical Co., St. Louis, MO, USA) was added to the recombinant cultures at 10 μg/mL. Reconstituted 10% (w/v) bovine skim milk powder (BSM) (Oxoid), heated at 121 °C for 5 min, was seeded with a loop of frozen stocks of recombinant cultures and grown at 37 °C for 24 h. Three percent (v/v) grown cultures were added to freshly made reconstituted 10% (w/v) BSM, and the cultures were further grown at 37 °C for 24, 48, and 96 h. The fermentation process was discontinued by heating of the BSM-derived cultures at 75 °C for 1 min,[12] and the cultures were vigorously stirred and centrifuged at 8000*g* for 10 min. The resulting supernatants were filtered through 0.20 μm pore size filters (Whatman International Ltd., Maidstone, UK) and stored at −20 °C before use. Total genomic DNA from *E. faecalis* DBH18 was isolated using the Wizard DNA Purification Kit (Promega, Madison, WI, USA). Plasmid DNA isolation was carried out using the High Pure Plasmid Isolation Kit (Roche Diagnostics, East Sussex, UK), as suggested by the manufacturer, but with the cells suspended with lysozyme (40 mg/mL) and mutanolysin (500 U/mL) and incubated at 37 °C for 10 min before the kit instructions were followed. All DNA restriction enzymes were supplied by New England BioLabs (Beverly, MA, USA). Ligations were performed with the T4 DNA ligase (Roche Molecular Biochemicals, Mannheim, Germany). Electrocompetent *Enterococcus* spp. cells were obtained as previously described[25] and transformed with a Gene Pulser and Pulse Controller apparatus (Bio-Rad Laboratories, Hercules, CA, USA).

Determination of Gelatin and Bovine Skin Milk Hydrolysis by Different *E. faecalis* Strains. Well-characterized *E. faecalis* strains from food, environmental, and clinical origin including *E. faecalis* DBH18[21] and *E. faecalis* QA53[26] isolated from Mallard ducks (*Anas platyrhynchos*) and aged buffalo cheese, respectively, as well as *E. faecalis* P4 and *E. faecalis* P36, two medical isolates of clinical origin,[27] and *E. faecalis* H10 and *E. faecalis* 3Er1, two more human clinical isolates of the multilocus sequence typing (MLST)-derived clonal complex 2 (CC2) and CC9, respectively,[28] obtained from the Servicio de Microbiología, Instituto Ramón y Cajal de Investigación Sanitaria (IRYCIS), Hospital Universitario Ramón y Cajal, Madrid, (Spain), were evaluated for their ability to hydrolyze gelatin and bovine milk caseins. For detection of gelatinase activity, 5 μL of overnight cultures of *E. faecalis* strains, grown in MRS broth at 37 °C, were placed into Todd−Hewitt agar (Oxoid) containing 30 g of gelatin (Oxoid) per liter (TH-GEL), grown overnight at 37 °C, and placed at 4 °C for 5 h before examination of zones of turbidity around the cultures. The caseinolytic activity of *E. faecalis* strains was also evaluated by placing 5 μL of these cultures into Todd−Hewitt plates containing 1.5% (w/v) of BSM (TH-BSM) and grown overnight at 37 °C. A clear zone of hydrolysis within 24 h of growth was considered positive for caseinolytic activity.

PCR Amplification and Nucleotide Sequencing. Oligonucleotide primers were obtained from Sigma-Genosys Ltd. (Cambridge, UK). PCR amplifications were performed in 50 μL reaction mixtures containing 1 μL of purified DNA, 70 pmol of each primer, and 1 U of

Table 1. Bacterial Strains and Plasmids Used in This Study

strain or plasmid	description[a]	source and/or ref[b]
strains		
Enterococcus faecalis DBH18	*gel*E$^+$, *spr*E$^+$, GelE$^+$, used as the source of *gelE* and *sprE*	DNBTA, 21
Enterococcus faecalis QA53	GelE$^+$	DNBTA, 26
Enterococcus faecalis JH2-2	*gel*E$^+$, *spr*E$^+$, *fsrABC*$^-$, GelE$^-$	HRC, 50
Enterococcus faecalis V583	*gel*E$^+$, *sprE*$^+$, *fsrABCD*$^+$, GelE$^+$	LMG, 51
Enterococcus faecalis P4	*gelE*$^+$, *sprE*$^+$, GelE$^+$	IFR, 27
Enterococcus faecalis P36	*gelE*$^+$, *sprE*$^+$, GelE$^-$	IFR, 27
Enterococcus faecalis H10	GelE$^+$	HRC
Enterococcus faecalis 3Er1	GelE$^+$	HRC
Enterococcus faecium AR24	GelE$^-$	DAAUR
Enterococcus hirae AR14	GelE$^-$	DAAUR
plasmids		
pMG36c	Cm^r, pMG36e derivative	RUG-MG, 36
pCG	Cm^r, pMG36c derivative carrying the PCR product GEL[c]	this work
pCGSP	Cm^r, pMG36c derivative carrying the PCR product GEL/SPR[c]	this work
pCSP	Cm^r, pMG36c derivative carrying the PCR product SPR[c]	this work
pAS222	integrative vector, Amp^r	LMG,[30]
pAS222-KO-GelE	Amp^r, pAS222 derivative	this work

[a] Cm^r, choramphenicol resistant; Amp^r, ampicillin resistant. [b] DAAUR, Departamento de Agricultura y Alimentación, Universidad de la Rioja (Logroño, Spain); DNBTA, Departamento de Nutrición, Bromatología y Tecnología de los Alimentos, Facultad de Veterinaria, Universidad Complutense de Madrid (Madrid, Spain); HRC, Departamento de Microbiología, Hospital Universitario Ramón y Cajal (Madrid, Spain); IFR, Institute of Food Research (Norwich, UK); LMG, Laboratory of Microbial Gene Technology, Department of Chemistry, Biotechnology and Food Science, Norwegian University of Life Sciences (Ås, Norway); RUG-MG, Departament of Molecular Genetics, University of Groningen (Haren, The Netherlands). [c] See Table 2.

dx.doi.org/10.1021/jf5006269 | J. Agric. Food Chem. 2014, 62, 5555−5564

Table 2. Primers and PCR Products Used in This Study

primer or PCR product	nucleotide sequence (5′−3′) or description[a]	PCR product amplified
primers		
GERL-F	CATAGAGCTCTGTAA**GGAGG**ATTTTAGAAATGAAGGGAAATAAAATTTTATACAT	GEL, GEL/SPR
GERL-R	ATAAGTTAAGCTTGTATCATTCATTGACCAGAACAGATTCACTTG	GEL
SPL-F	CATAGAGCTCTGTAA**GGAGG**ATTTTAGAAATGAAAAAGTTCTCCATACGAAAAAT	SPR
SPL-R	ATAAGTTAAGCTTGTATTACGCTGCTGGCACAGCGGATAAAC	GEL/SPR, SPR
Pr1	TACTCGAGATTTCCCGTGATTCT	R1
Pr2	CTCTGCTGGAATCGGAGCT	R1
Pr3	AGCTCCGATTCCAGCAGAGGGTCACCAGTTGGCGAAGAAGT	R2a
Pr4	GGAAGGAGTTAATTGTTTCTAGAAGGGAAATAAAATTTTATAC	R2a
Pr5	GTATAAAATTTTATTTCCCTTCTAGAAACAATTAACTCCTTCC	R2b
Pr6	GCTATGGTATTGAGTTATGAGGGGC	R2b
PCR product		
GEL	1530 bp *Sac*I/*Hin*dIII fragment containing the P_{32} ribosome binding site and complete *gelE*	
SPR	903 bp *Sac*I/*Hin*dIII fragment containing the P_{32} ribosome binding site and complete *sprE*	
GEL/SPR	2400 bp *Sac*I/*Hin*dIII fragment containing the P_{32} ribosome binding site and complete *gelE*−*sprE*	

[a]Cleavage site for restriction enzymes is underlined; P_{32} ribosome binding site is shown in bold.

Platinum Pfx DNA Polymerase (Invitrogen S.A., Barcelona, Spain). Samples were subjected to an initial cycle of denaturation (97 °C for 2 min), followed by 35 cycles of denaturation (94 °C for 45 s), annealing (55−58 °C for 30 s), and elongation (68 °C for 40 s), ending with a final extension step at 68 °C for 7 min in a DNA thermal cycler Techgene (Techne, Cambridge, UK). The PCR-generated fragments were purified by a NucleoSpin Extract II Kit (Macherey-Nagel GmbH & Co. KG, Düren, Germany) before cloning into the expression vector and for nucleotide sequencing. Nucleotide sequencing of purified PCR products was done using the ABI PRISM BigDye Terminator cycle sequence reaction kit and the automatic DNA sequencer ABI PRISM model 377 (Applied Biosystems, Foster City, CA, USA) at the DNA Sequencing Service (Sistemas Genómicos, Valencia, Spain).

Recombinant Plasmids Derived from pMG36c. The primers and inserts used for construction of the recombinant plasmids are listed in Table 2. Restriction mapping analysis of the *gelE*−*sprE* operon of *E. faecalis* DBH18 indicated the absence of restriction sites for restriction enzymes *Sac*I and *Hin*dIII. Total genomic DNA of *E. faecalis* DBH18 was used as template for amplification with the GERL-F/GERL-R, SPL-F/SPL-R, and GERL-F/SPL-R primer pairs of a 1530 bp *Sac*I/*Hin*dIII fragment (GEL) containing *gelE*, a 903 bp *Sac*I/*Hin*dIII fragment (SPR) containing *sprE*, and a 2400 bp *Sac*I/*Hin*dIII fragment (GEL/SPR) containing *gelE* and *sprE*, respectively. Fragments GEL, SPR, and GEL/SPR were digested with the indicated restriction enzymes and inserted into plasmid pMG36c digested with the same enzymes. The ligation mixtures were used to transform *E. faecalis* P36 and the recombinant derivatives checked by their gelatinase and caseinolytic activities. The recombinant plasmids pCG, pCSP, and pCGSP were purified from *E. faecalis* P36 and analyzed by PCR and sequencing of the inserts. Subsequently, these recombinant plasmids were used to transform *E. faecalis* DBH18, *E. faecalis* JH2-2, *E. faecium* AR24, and *E. hirae* AR14. The caseinolytic activity of the recombinant enterococcal strains was determined by a stab-on-agar test (SOAT) during growth of the selected colonies in TH-BSM plates at 37 °C for 24 h and visualization of clear zones of hydrolysis.

Construction and Characterization of a Gelatinase (GelE) Deletion (Knockout) Mutant of *E. faecalis* V583. The deletion of *gelE* in *E. faecalis* V583 was achieved by double-crossover homologous recombination using pAS222 as the cloning vector.[29,30] The gene *sprE* located downstream of *gelE* and the initial sequence of *gelE* were the homologous sequences used in homologous recombination to remove *gelE*. The insert to be cloned into pAS222 was constructed by a three-step PCR. First, the entire *sprE* was amplified with primers Pr1 and Pr2 to obtain fragment R1. The fragment R2, with the initial sequence of *gelE*, was subjected to a two-step PCR to remove an internal Met codon that could cause residual expression of a truncated gene and further amplified using primer pairs Pr3−Pr4 and Pr5−Pr6 (Table 2). Fragments R1 and R2 were then fused using the primer pairs Pr1 and Pr6, and the construct was cloned into pAS222 resulting in plasmid pAS222-KO-GelE. To replace the genes on the chromosome with those in the construct, the latter plasmid was transformed into electrocompetent *E. faecalis* V583 cells,[25] and the selection for double-crossover events was performed as described by Biswas et al.[31] The replacement of *gelE* and the integrity of the flanking genes in *E. faecalis* V583 Δ*gelE* was confirmed by DNA sequencing.

Determination of the ACE-Inhibitory Activity. The ACE-IA of the supernatants of the recombinant *Enterococcus* spp. strains, grown in BSM, was determined by a fluorometric assay with modifications, as previously described.[15] The angiotensin converting enzyme (ACE, peptidyl-dipeptidase A, EC 3.4.15.1) was obtained from Sigma Chemical Co., and the ACE working solution was added to blank (B), control (C), or samples (S). The reaction was started by adding the fluorogenic substrate *o*-aminobenzoylglycyl-*p*-nitro-L-phenylalanyl-L-proline (Abz-Gly-p-Phe(NO_2)-Pro-OH) (0.45 mM, Bachem Feinchemikalien, Bubendorf, Switzerland), and the reaction mixture was incubated at 37 °C. The fluorescence of the samples was measured in a Multiscan Microplate Fluorimeter (FLUOstar optima, BMG Labtech, Offenburg, Germany) with the FLUOstar (version 1.32 R2, BMG Labtech) control system for processing of the data. The ACE-IA was expressed as the protein concentration required to inhibit 50% of the ACE activity (IC_{50}). The percentage of ACE-inhibitory activity was calculated as $100 \times (C - S)/(C - B)$. The protein concentration of the water-soluble extracts was determined by using the BCA protein assay (Pierce, Thermo Fisher Scientific Inc., Rockford, IL, USA).

Analysis of the Bovine Skim Milk-Derived Hydrolysates by Reversed-Phase High-Performance Liquid Chromatography−Tandem Mass Spectrometry (RP-HPLC-MS/MS). The RP-HPLC-MS/MS analysis of the supernatants obtained after growth of the recombinant *Enterococcus* spp. strains in BSM was performed on an Agilent 1100 HPLC System (Agilent Technologies, Waldbron, Germany) with column HiPore (RP318 C_{18} column 250 × 4.6 mm, 5 μm particle size; Bio-Rad, Richmond, CA, USA). The HPLC system was connected online to an Esquire 3000 quadrupole ion trap (Bruker Daltonik GmbH, Bremen, Germany) equipped with an electrospray ionization source, as previously described.[15] Solvent A was a mixture of water/trifluoroacetic acid (1000:0.37, v/v), and solvent B contained acetonitrile/trifluoroacetic acid (1000:0.27, v/v). Peptides were eluted with a linear gradient of solvent B in A from 0 to 45% in 60 min at a flow rate of 0.8 mL/min. Different spectra were recorded over the mass/charge (m/z) range of 100−1500. About five spectra were averaged in the MS and in the MS(n) analyses. The signal threshold to perform auto MS(n) analyses was 10000 (i.e., 5% of the total signal), and the precursor ions were isolated within a range of 4.0 m/z and fragmented with a voltage ramp from 0.35 to 1.4 V. The m/z spectral data were transformed to mass values by using the Data Analysis (version 3.0; Bruker Daltonik) control program. BioTools (version 2.1; Bruker

Daltonik) was used to process the MS(n) spectra for peptide identification and sequencing.

Statistical Analysis. A nonlinear adjustment of the data obtained was performed to calculate the IC_{50} values with the program PRISM version 4.02 for Windows (GraphPad Software, Inc., San Diego, CA, USA), as previously described.[32] The program gives the estimated value of the IC_{50} together with the standard error.

RESULTS

Hydrolysis of Gelatin and Bovine Milk Proteins by *E. faecalis* Strains from Different Origins. *E. faecalis* strains from food, environmental, and clinical origins were evaluated for production of gelatinase and their caseinolytic activity. With the exception of *E. faecalis* P36, previously recorded as *gelE*$^+$ and *sprE*$^+$ but GelE$^-$,[27] all strains produced a clear zone of turbidity or hydrolysis after growth on TH-GEL and TH-BSM plates (Figure 1). These results suggest that production of GelE and SprE and/

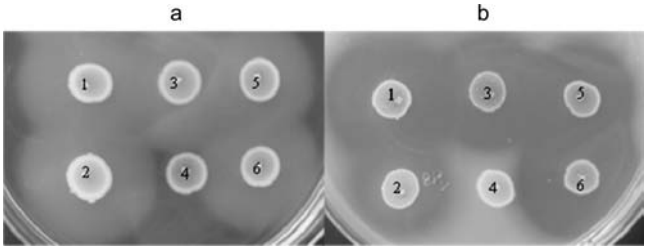

Figure 1. Gelatin (a) and bovine casein hydrolysis (b) by *E. faecalis* strains of food, environmental, and clinical origin grown in Todd Hewitt-gelatin (TH-GEL) and Todd Hewitt-bovine skim milk (TH-BSM) plates, respectively: (1) *E. faecalis* DBH18; (2) *E. faecalis* QA53; (3) *E. faecalis* P4; (4) *E. faecalis* P36; (5) *E. faecalis* 3Er1; (6) *E. faecalis* H10.

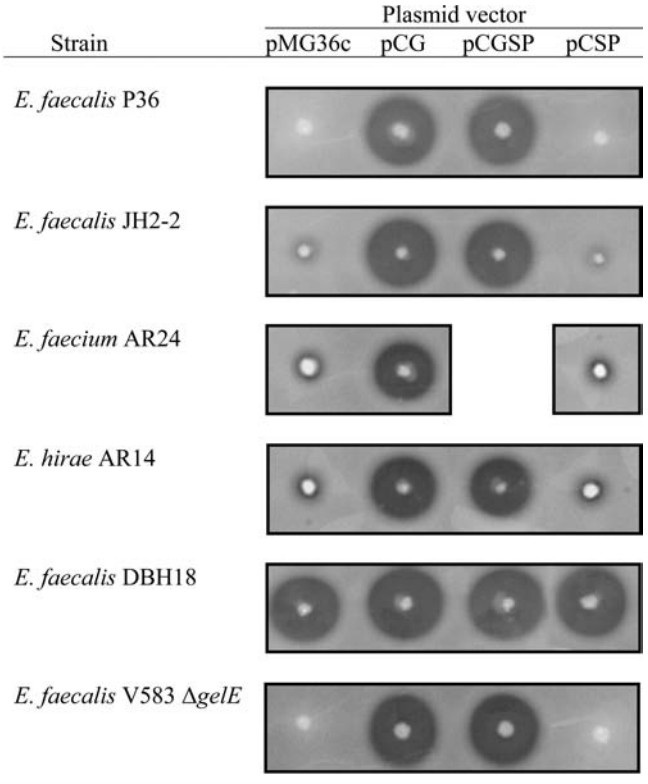

Figure 2. Caseinolytic activity of recombinant *E. faecalis* P36, *E. faecalis* JH2-2, *E. faecium* AR24, *E. hirae* AR14, *E. faecalis* DBH18, and *E. faecalis* V583 Δ*gelE* strains transformed with plasmids pMG36c, pCG, pCGSP, and pCSP.

or mutations in the regulatory *fsr* genes for induction of the production of both proteases could play a role in the hydrolysis of gelatin and bovine milk proteins.

Heterologous Production and Functional Expression of GelE and SprE by Recombinant *Enterococcus* spp. Strains. To determine the role of GelE and SprE in the caseinolytic activity of the *E. faecalis* strains during their growth in BSM, the genes encoding GelE (*gelE*) and SprE (*sprE*) in *E. faecalis* DBH18 were cloned in the protein expression vector pMG36c, containing the constitutive P_{32} promoter, to generate the plasmid-derived vectors pCG, pCSP, and pCGSP encoding *gelE*, *sprE*, and *gelE-sprE*, respectively. Transformation of the noncaseinolytic *E. faecalis* P36, *E. faecalis* JH2-2, *E. faecium* AR24, and *E. hirae* AR14 strains with the above cited plasmids showed halos of variable size, indicating casein hydrolysis, produced by *Enterococcus* spp. strains transformed with pCG or pCGSP but not with pMG36c or pCSP (Figure 2). The largest caseinolytic activity was observed in *E. faecalis* DBH18 transformed with pCG or pCGSP. A lower caseinolytic activity (<2 mm) was observed in *E. faecalis* JH2-2, *E. faecium* AR24, and *E. hirae* AR14 transformed with pMG36c. The caseinolytic activities of *E. faecium* AR24 transformed with pCG and *E. hirae* AR14 transformed with pCG or pCGSP were lower than those produced by the recombinant *E. faecalis* strains. Despite several attempts, the recombinant *E. faecium* AR24 (pCGSP) derivative was not obtained. On the other hand, no caseinolytic activity was observed in the *Enterococcus* spp. strains transformed with pCSP (Figure 2). *E. faecalis* V583, a Gel$^+$ and SprE$^+$ strain, was also evaluated to obtain a deletion (knockout) mutant of *gelE* unable to display GelE activity. Accordingly, using the plasmid pAS222-KO-GelE an *E. faecalis* V583 Δ*gelE* derivative lacking caseinolytic activity was obtained. Further transformation of *E. faecalis* V583 Δ*gelE* with plasmid pCG or pCGSP, but not with pMG36c or pCSP, resulted in a high caseinolytic activity of the recombinant strains after growth in TH-BSM plates (Figure 2).

Angiotensin Converting Enzyme-Inhibitory Activity of Recombinant *Enterococcus* spp. Strains Grown in Bovine Skim Milk. Supernatants of the recombinant *E. faecalis* P36, *E. faecalis* JH2-2, *E. faecium* AR24, *E. hirae* AR14, and *E. faecalis* DBH18 transformed with pMG36c, pCG, pCGSP, or pCSP were evaluated for their ACE-IA after growth in BSM (Table 3). Among the recombinant *Enterococcus* spp. only those transformed with pCG or pCGSP produced BSM-derived hydrolysates with high ACE-IA and IC_{50} values from 16.2 to 37.7 μg protein/mL. The lowest IC_{50} values correspond to the highest ACE-IA. Furthermore, the IC_{50} values of the BSM-derived hydrolysates showed that growth of the active recombinant strains at 37 °C during 48−96 h displayed a steady and high ACE-IA (Table 3). IC_{50} values for the BSM-derived hydrolysates produced by the strains transformed with pCG and pCGSP, respectively, were comparable. No ACE-IA was detected in the BSM hydrolysates of the enterococcal strains transformed with pMG36c or pCSP (Table 3).

Major Peptide Fragments and Identification of Angiotensin Converting Enzyme-Inhibitory Peptides (ACE-IP) in Supernatants of the Recombinant *Enterococcus* spp. Strains Grown in Bovine Skim Milk. BSM-derived hydrolysates of the recombinant *Enterococcus* spp. with high ACE-IA were subjected to RP-HPLC-MS/MS analysis. The peptide profiles by RP-HPLC of the supernatants of all

dx.doi.org/10.1021/jf5006269 | J. Agric. Food Chem. 2014, 62, 5555−5564

Table 3. Angiotensin Converting Enzyme-Inhibitory Activity (ACE-IA)[a] of Supernatants of Recombinant *Enterococcus* spp. Strains Grown in Bovine Skim Milk

strain	IC_{50} (μg protein/mL)			
	0 h	24 h	48 h	96 h
E. faecalis P36 (pMG36c)	NA[b]	NA	NA	NA
E. faecalis P36 (pCG)	NA	37.7 ± 4.6	24.1 ± 4.5	17.6 ± 1.6
E. faecalis P36 (pCGSP)	NA	33.5 ± 6.3	26.8 ± 5.0	20.0 ± 7.6
E. faecalis P36 (pCSP)	NA	NA	NA	NA
E. faecalis JH2-2 (pMG36c)	NA	NA	NA	NA
E. faecalis JH2-2 (pCG)	NA	23.3 ± 0.5	16.2 ± 5.4	21.5 ± 3.6
E. faecalis JH2-2 (pCGSP)	NA	25.0 ± 3.1	20.5 ± 3.7	19.7 ± 0.4
E. faecalis JH2-2 (pCSP)	NA	NA	NA	NA
E. faecium AR24 (pMG36c)	NA	NA	NA	NA
E. faecium AR24 (pCG)	NA	32.3 ± 1.2	31.0 ± 2.2	33.7 ± 2.6
E. faecium AR24 (pCSP)	NA	NA	NA	NA
E. hirae AR14 (pMG36c)	NA	NA	NA	NA
E. hirae AR14 (pCG)	NA	28.9 ± 3.3	26.8 ± 3.0	23.6 ± 2.5
E. hirae AR14 (pCGSP)	NA	26.4 ± 4.0	21.1 ± 7.9	23.7 ± 4.0
E. hirae AR14 (pCSP)	NA	NA	NA	NA
E. faecalis DBH18 (pMG36c)	NA	9.6 ± 0.7	14.0 ± 3.9	18.2 ± 0.6
E. faecalis DBH18 (pCG)	NA	27.0 ± 3.4	22.2 ± 5.6	19.9 ± 1.1
E. faecalis DBH18 (pCGSP)	NA	24.8 ± 5.1	17.8 ± 0.5	20.2 ± 1.6
E. faecalis DBH18 (pCSP)	NA	12.3 ± 2.1	16.5 ± 2.2	19.2 ± 1.8

[a]ACE-IA expressed as IC_{50} (μg protein/mL). Data are means from three independent determinations in triplicate. [b]NA, no ACE-IA detected.

recombinant strains were obtained after growth in BSM for 0, 24, 48, and 96 h, and those corresponding to *E. faecalis* P36 (pCG) and *E. faecalis* P36 (pCGSP) are shown in Figure 3. The main peptide profiles of each recombinant *Enterococcus* spp. were further analyzed by tandem MS, and peptide fragments from the total ion chromatogram with a signal >10000 units were considered as major fragments. Accordingly, the RP-HPLC-MS/MS analysis of the BSM-derived hydrolysates of the recombinant *E. faecalis* P36, *E. faecalis* JH2-2, *E. faecium* AR24, *E. hirae* AR14, and *E. faecalis* DBH18 strains with high ACE-IA allowed the identification of 38 major peptide fragments, 26 of which corresponded to bovine β-casein fragments and 12 to α_{s1}-casein fragments, including peptides with previously reported ACE-IA (Table 4).

DISCUSSION

LAB produce a broad range of bioactive peptides including those with ACE-IA due to the activity of bacterial extracellular proteases, cell-envelope associated proteases, and intracellular peptidases.[9,33] However, few studies have considered the role of LAB other than *Lactobacillus* spp., *Lactococcus* spp., and *Streptococcus* spp. in the production of peptides with ACE-IA due to the fermentation of milk and other proteinaceous food substrates.[9,34,35] In this study, the observation of halos surrounding colonies of the well-characterized *E. faecalis* DBH18, *E. faecalis* QA53, *E. faecalis* P4, *E. faecalis* 3Er1, and *E. faecalis* H10 strains from food, environmental, and clinical origins in both gelatin- and BSM-containing agar plates indicated their gelatinase and caseinolytic activities. However, the absence of these enzymatic activities in *E. faecalis* P36 and the recognition that this isolate is a well-characterized *gelE*$^+$ and *sprE*$^+$ but GelE$^-$ strain[27] suggest that GelE and SprE may play an important role in the ACE-IA and production of ACE-IP during growth of the *E. faecalis* strains in BSM.

To determine the role of GelE and SprE against BSM-derived proteins, the *gelE*, *sprE*, and *gelE*–*sprE* genes from *E. faecalis* DBH18 were cloned into pMG36c to generate the plasmid-derived vectors pCG (*gelE*), pCSP (*sprE*), and pCGSP (*gelE*–*sprE*). The expression vector pMG36c is a shuttle vector, able to replicate in *Escherichia coli*, *Bacillus subtilis*, and LAB that contain the low copy replication origin of pWV01 and the strong P_{32} promoter to drive the constitutive transcription of inserted genes into the multicloning site (MCS) of pUC18.[36] Transformation of the noncaseinolytic *E. faecalis* P36,[27] *E. faecalis* JH2-2,[37] *E. faecium* AR24, and *E. hirae* AR14 with plasmid pCG or pCGSP, but not with pCSP or pMG36c, resulted in caseinolytic activity of the transformed strains in plates with BSM, whereas transformants of the caseinolytic *E. faecalis* DBH18 strain with pCG or pCGSP originated larger BSM-derived halos of hydrolysis (Figure 1). Thus, recombinant *Enterococcus* spp. encoding *gelE* but not *sprE* are able to hydrolyze BSM-derived proteins during growth in BSM. Although previous studies reported that SprE is active on a variety of protein substrates[24] and that *sprE* contributes to virulence and infection in animal models,[17,38] the results of this work suggest that SprE by itself is not involved in the hydrolysis of BSM-derived proteins. Moreover, although the coexpression of *gelE* and *sprE* by *E. faecalis* may provide advantages, such as the effect of GelE on the maturation of SprE[24] and the role of SprE as an immunity protein against the killing action of GelE in the fratricide mechanism proposed for production of biofilms by *E. faecalis*,[18] the role of SprE in the hydrolysis of BSM-derived proteins is yet unknown.

The role of GelE in the hydrolysis of BSM-derived proteins was also evaluated in a deletion (knockout) mutant of the caseinolytic *E. faecalis* V583 lacking *gelE*. The deletion event was generated using the cloning shuttle vector pAS222, which contains the thermosensitive replicon of pG$^+$ host4.[29,30] Double-crossover events with pAS222-KO-GEL transformed into *E. faecalis* V583 permitted the selection of Δ*gelE* cells with loss of their caseinolytic activity. Restoration of the GelE$^+$ phenotype was achieved after transformation of *E. faecalis* V583 Δ*gelE* with pCG or pCGSP, but not with pMG36c or pCSP (Figure 2). The results of these complementation assays confirm that *gelE* from *E. faecalis* DBH18 confers caseinolytic activity.

Experiments were also performed to determine the ACE-IA of the recombinant *Enterococcus* spp. strains grown in BSM. A high ACE-IA was found in supernatants of *E. faecalis* P36, *E. faecalis* JH2-2, *E. faecium* AR24, and *E. hirae* AR14 transformed with plasmid pCG or pCGSP. However, no ACE-IA was observed in the *Enterococcus* spp. strains transformed with pCSP or pMG36c (Table 3). Most of the BSM-derived hydrolysates generated by the recombinant *Enterococcus* spp. showed a low IC_{50} and, consequently, a high ACE-IA. Considering that extended fermentation times involve higher energy and economical expenses and increase the chance of microbial contamination, the growth of the recombinant *Enterococcus* spp. in BSM at 37 °C

dx.doi.org/10.1021/jf5006269 | J. Agric. Food Chem. 2014, 62, 5555–5564

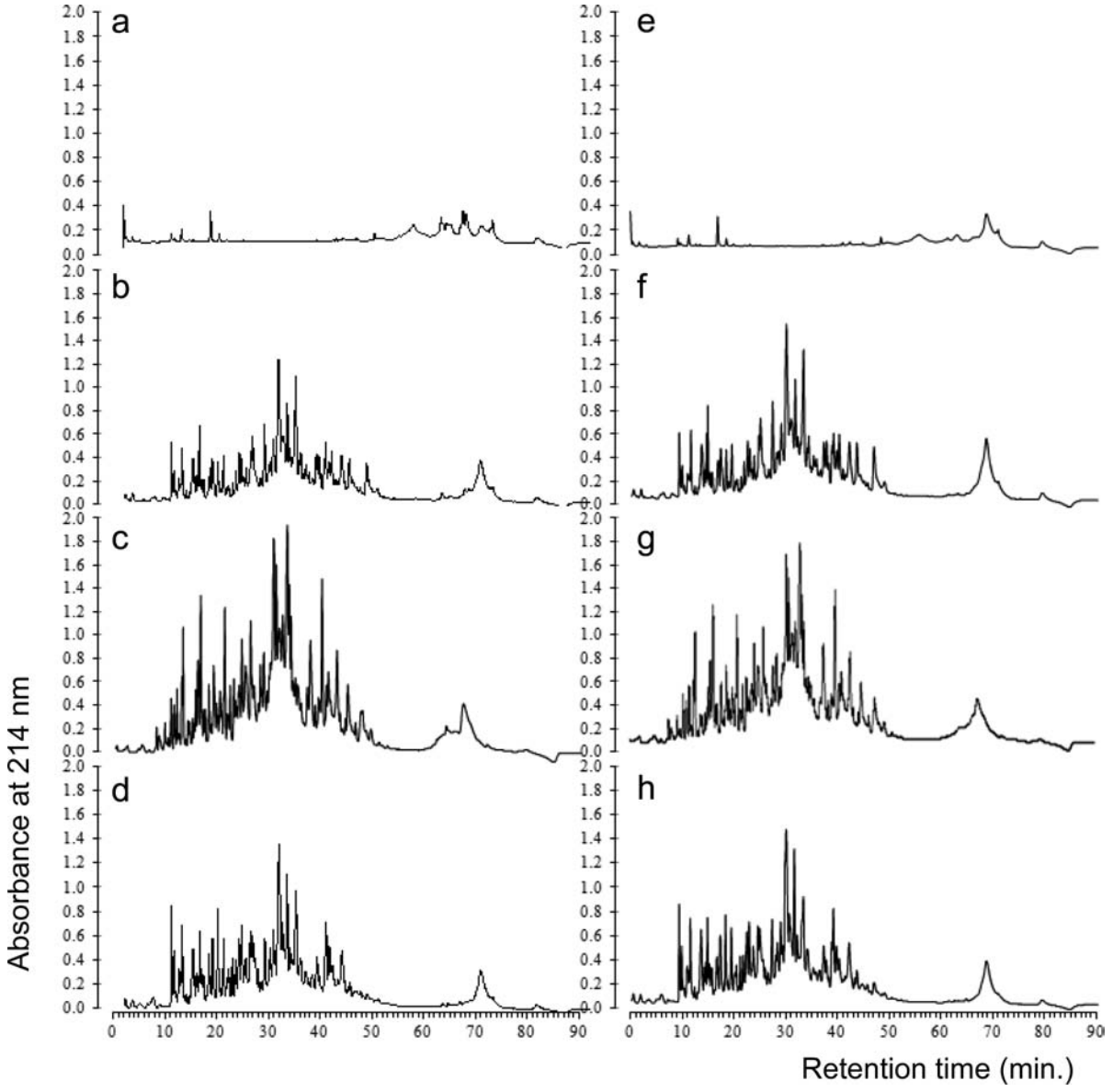

Figure 3. Peptide profiles by RP-HPLC of supernatants of *E. faecalis* P36 (pCG) (a–d) and *E. faecalis* P36 (pCGSP) (e–h) grown in bovine skim milk for 0 h (a, e), 24 h (b, f), 48 h (c, g), and 96 h (d, h).

for 48 h may be considered satisfactory for production of BSM-derived hydrolysates with high ACE-IA (Table 3). Because GelE may be produced by *E. faecalis* strains carrying antibiotic-resistance genes and/or genes coding other potential virulence factors, other enterococci as the recombinant *E. faecium* and/or *E. hirae* strains developed in this work could be used as safer and alternative bacterial hosts for production of GelE. Moreover, given that the N-terminal signal peptide of GelE (SP_{GelE}) drives the processing and transport of GelE out of the heterologous *Enterococcus* spp. producer cells, chimeras of the SP_{gelE} genetically fused to other enzymes, proteins, or biologically active peptides could permit their processing, heterologous production, and functional expression by other enterococci and, possibly, many other LAB.[39] *E. faecalis* DBH18 transformed with pCG or pCGSP originated larger halos of caseinolytic activity (Figure 2) but lower ACE-IA than the parent *E. faecalis* DBH18 (pMG36c) (Table 3). This lower ACE-IA of the transformed *E. faecalis* DBH18 derivatives with a higher production of GelE may be due to degradation of high molecular mass peptides with synergistic ACE-IA.[40,41]

Peptide profiles of BSM-derived hydrolysates of *E. faecalis* P36 (pCG) and *E. faecalis* P36 (pCGSP) grown in BSM are shown in Figure 3. No hydrolysis of BSM, evidenced by the absence of peptide fragments, was observed after growth of *E. faecalis* P36 (pCSP) and *E. faecalis* P36 (pMG36c) in BSM (results not shown). However, similar peptide profiles were generated by *E. faecalis* P36 (pCG) and *E. faecalis* P36 (pCGSP), suggesting that the hydrolysis of bovine caseins seems not to be affected by the coexpression of *gelE* and *sprE*. Similarly, few modifications were observed in the BSM-derived major peptide profiles during the fermentation process, suggesting that most of the release of ACE-IP takes place during the first 24 h of growth of the *E. faecalis* P36 strains transformed with pCG or pCGSP.

RP-HPLC-MS/MS analysis of BSM-derived hydrolysates from recombinant *Enterococcus* spp. with high ACE-IA permitted the identification of 38 major peptide fragments, including peptides with previously reported ACE-IA, antihypertensive

dx.doi.org/10.1021/jf5006269 | J. Agric. Food Chem. 2014, 62, 5555–5564

Table 4. Major Peptide Fragments in Supernatants of Recombinant *Enterococcus* spp. Strains Grown in Bovine Skim Milk

obsd mass	calcd mass[a]	protein fragment	peptide sequence	previously described ACE-inhibitory peptides[b]	*E. faecalis* strain[c]
477.2	477.266	β-CN *f*(187−190)	IQAF	RDMPIQAF	1
558.4	558.309	β-CN *f*(77−81)	LTQTP		14
561.2	561.320	β-CN *f*(165−169)	LSQSK		4, 6
656.5	656.397	β-CN *f*(82−87)	VVVPPF	VVVPPF	1, 2, 3, 4, 5, 6, 7, 8, 9, 10, 11, 12, 13, 14, 15
671.3	671.383	β-CN *f*(201−206)	VRGPFP	VRGPFP	1, 2, 3, 4, 5, 6, 7, 8, 10, 11, 12, 13, 14, 15
674.3	674.331	β-CN *f*(1−5)	RELEE		9
688.4	688.434	β-CN *f*(133−138)	LHLPLP	LHLPLP	1, 2, 3, 4, 5, 6, 7, 8, 9, 10, 11, 12, 13, 14, 15
697.2	697.299	β-CN *f*(119−124)	FTESQS		2, 5, 12, 13, 14, 15
740.6	740.393	β-CN *f*(62−68)	FPGPIPN	VYPFPGIPIPN	14
761.3	761.403	β-CN *f*(191−196)	LLYQEP		7, 8, 11, 12, 15
772.4	773.386	β-CN *f*(88−94)	LQPEVMG		9
779.4	779.498	β-CN *f*(170−176)	VLPVPQK		1, 2, 3, 4, 5, 6, 7, 8, 10, 11, 12, 13, 14, 15
788.6	788.425	β-CN *f*(148−154)	HQPLPPT		2, 3, 6, 13, 14
801.6	801.519	β-CN *f*(133−139)	LHLPLPL	LHLPLPL	1, 2, 3, 4, 5, 6, 7, 8, 9, 10, 11, 12, 13, 14, 15
804.5	804.391	β-CN *f*(155−161)	VMFPPQS		1, 2, 3, 4, 5, 6, 7, 8, 10, 11, 12, 13, 14, 15
849.7	849.478	β-CN *f*(45−51)	LQDKIHP	DKIHP	9
871.4	871.568	β-CN *f*(23−29)	ITRINKK		9
903.3	903.462	β-CN *f*(125−132)	LTLTDVEN		1, 2, 5, 9, 10, 11, 12, 15
939.5	939.473	β-CN *f*(127−134)	LTDVENLH		4, 7, 11
996.5	996.619	β-CN *f*(201−209)	VRGPFPIIV	VRGPFPIIV	1, 2, 4, 5, 6, 7, 8, 9, 10, 11, 12, 15
1037.4	1037.609	β-CN *f*(197−206)	VLGPVRGPFP	VLGPVRGPFP	9, 10
1112.8	1112.614	β-CN *f*(192−201)	LYQEPVLGPV		6, 13, 14
1172.5	1172.572	β-CN *f*(177−186)	AVPYPQRDMP		3, 4, 7, 8, 13, 14
1196.4	1196.688	β-CN *f*(77−87)	LTQTPVVVPPF	VVVPPF	1, 2, 4, 5, 10, 11, 12, 15
1281.8	1281.636	β-CN *f*(144−154)	HHQPHQPLPPT		7, 8, 12, 13, 14, 15
1323.0	1322.799	β-CN *f*(165−176)	LSQSKVLPVPQK		11
596.3	596.314	α_{s1}-CN *f*(150−153)	FRQF		8, 10, 11
633.2	633.356	α_{s1}-CN *f*(104−108)	YKVPQ		1, 2, 3, 4, 5, 6, 7, 8, 9, 10, 11, 12, 13, 14, 15
633.4	633.378	α_{s1}-CN *f*(1−5)	RPKHP		1, 2, 3, 4, 5, 6, 7, 8, 9, 10, 11, 12, 13, 14, 15
639.5	639.341	α_{s1}-CN *f*(76−80)	VEQKH		7, 8, 10, 11
656.5	656.477	α_{s1}-CN *f*(99−103)	LRLKK		1, 2, 3, 4, 5, 6, 7, 8, 9, 10, 11, 12, 13, 14, 15
706.6	706.409	α_{s1}-CN *f*(31−36)	VFGKEK		2, 7, 8, 9, 13, 14
825.6	825.431	α_{s1}-CN *f*(182−189)	IPNPIGSE		2
872.6	872.462	α_{s1}-CN *f*(149−154)	LFRQFY		2, 5, 8, 10, 11
949.4	949.505	α_{s1}-CN *f*(127−134)	IHAQQKEP		1, 2, 3, 5, 7, 11, 12, 13, 14, 15
1002.8	1002.630	α_{s1}-CN *f*(101−108)	LKKYKVPQ	KKYNVPQ	12
1141.4	1141.515	α_{s1}-CN *f*(158−168)	LDAYPSGAWY		1, 3, 4, 5, 7, 11, 12, 13, 14, 15
1218.8	1218.636	α_{s1}-CN *f*(25−35)	VAPFPEVFGKE		11

[a]Monoisotopic mass. [b]Previously described ACE-inhibitory peptides with ACE-IA or sharing, at least, three C-terminal residues with those found in this study. [c]Recombinant strains: 1, *E. faecalis* P36 (pCG), 24 h; 2, *E. faecalis* P36 (pCG), 48 h; 3, *E. faecalis* P36 (pCG), 96 h; 4, *E. faecalis* P36 (pCGSP), 24 h; 5, *E. faecalis* P36 (pCGSP), 48 h; 6, *E. faecalis* P36 (pCGSP), 96 h; 7, *E. faecalis* JH2-2 (pCG), 48 h; 8, *E. faecalis* JH2-2 (pCGSP), 48 h; 9, *E. faecium* AR24 (pCG), 48 h; 10, *E. hirae* AR14 (pCG), 48 h; 11, *E. hirae* AR14 (pCGSP), 48 h; 12, *E. faecalis* DBH18 (pMG36c), 48 h; 13, *E. faecalis* DBH18 (pCG), 48 h; 14, *E. faecalis* DBH18 (pCGSP), 48 h; 15, *E. faecalis* DBH18 (pCSP), 48 h.

activity, and antioxidant activity. Peptides such as LQDKIHP, FPGPIPN, VVVPPF, LHLPLP, LHLPLPL, IQAF, VLGPVRGPFP, VRGPFP, and VRGPFPPIIV were generated from bovine β-casein, whereas others, such as LKKYKVPQ, were derived from bovine α_{s1}-casein (Table 4). These peptide fragments are reported to be produced by *E. faecalis* strains from food, environmental, and clinical origins and show a high ACE-IA or share, at least, three C-terminal residues with those with known ACE-IA.[15] Moreover, the peptide LHLPLP resistant to gastrointestinal proteases is a true competitive inhibitor of ACE and shows a potent antihypertensive activity in spontaneously hypertensive rats (SHR).[42,43] On the other hand, the peptide VLPVPQK previously reported as antioxidant[44] has been also identified among the major peptides present in most *E. faecalis* hydrolysates (Table 4). The major peptides identified in the BSM-derived hydrolysates may be subject to variation due to complex interactions between growth of the enterococci and hydrolysis of their substrate. In this context, several β-casein-derived peptides such as VVVPPF, LHLPLP, and LHLPLPL or the α_{s1}-casein-derived peptides, such as RPKHP, LRLKK, and YKVPQ, were present in the hydrolysates of all the active *Enterococcus* spp., whereas other BSM-derived peptides were less frequent (Table 4). Interestingly, all of the BSM-derived hydrolysates produced by *E. faecalis* DBH18 and the active recombinant *E. faecalis*, *E. faecium*, and *E. hirae* derivatives contained, at least, the ACE-IP peptides LHLPLP, LHLPLPL, and VVVPPF, the antihypertensive peptide LHLPLP, and the antioxidant peptide VLPVPQK.

Most of the cleavage sites of the peptide fragments generated from β-casein and α_{s1}-casein were located before the hydrophobic amino acid residues leucine (L), isoleucine (I), or phenylalanine (F) (Figure 4), as previously described for the

dx.doi.org/10.1021/jf5006269 | J. Agric. Food Chem. 2014, 62, 5555−5564

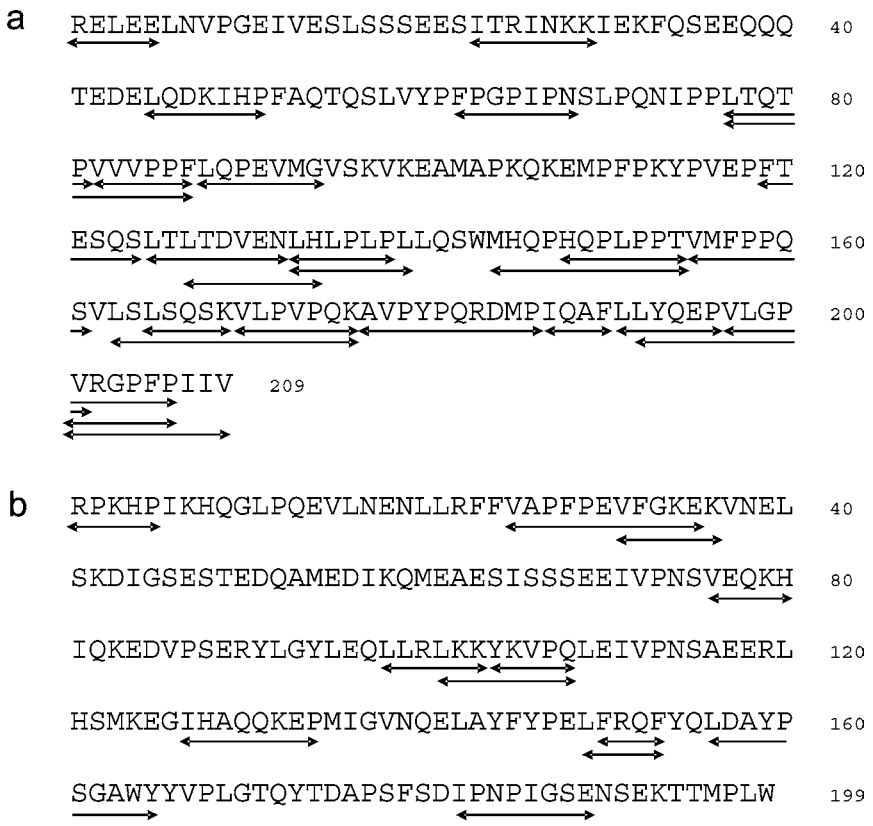

Figure 4. Location of the major peptides (doubled-ended arrows) identified in the primary sequences of β-casein (a) and α_{s1}-casein (b) present in bovine skim milk (BSM)-derived hydrolysates originated by the gelatinase (GelE) produced by recombinant *Enterococcus* spp. encoding *gelE* and *sprE* from *E. faecalis* DBH18.

purified GelE produced by *E. faecalis* OG1-10.[16] However, no glutamic acid (E)-Xaa cleavage fragments derived from a putative SprE proteolytic activity were detected.[24] Consequently, the pattern of β-casein and α_{s1}-casein breakdown and the release of bioactive peptides produced by the recombinant *E. faecalis* P36, *E. faecalis* JH2-2, *E. faecium* AR24, and *E. hirae* AR14, during growth in BSM, corresponds to the activity of the strongly hydrophobic metalloendopeptidase GelE from *E. faecalis* DBH18.

It has been reported that the GelE$^+$ phenotype of *E. faecalis* requires the concomitant presence of both the *fsr* and *gelE* genes and that loss of the GelE$^+$ phenotype is usually attributed to a 23.9 kb chromosomal deletion involving *fsrABC* that likely results from horizontal gene transfer and recombination.[19,45] However, in *E. faecalis* strains with apparently complete *fsr* and *gelE* loci, the Gel$^-$ phenotype also correlates with a specific nonsense codon in the FsrC protein, which prevents these isolates from sensing GBAP,[19] whereas in certain *E. faecalis* strains, even in the absence of a functional *fsr* system, a basal level of GelE and SprE is produced.[46] Furthermore, although the presence of a functional Fsr system and/or GelE production increases the severity of disease in animal, plant, and nematode models of *E. faecalis* infection, none of them are required for the organism to cause the disease.[45] Accordingly, it may be considered that *E. faecalis* strain producers of GelE may play an additional role, not associated with virulence, in the production of bioactive peptides with human health connotations and potential biotechnological applications.

To the best of our knowledge, the present study is the first to describe the genetic and biochemical implication of the GelE produced by *E. faecalis* in the production of BSM-derived bioactive peptides with ACE-IA, antihypertensive, and antioxidant activities. These results may strengthen the potential of GelE in the production of BSM-derived peptides with human health connotations and potential biotechnological applications. Furthermore, safer LAB and other microbial hosts could be engineered as heterologous producers of GelE to determine the biotechnological, medical, and veterinary applications of bioactive peptides derived from the GelE-mediated fermentation and/or hydrolysis of BSM and many other food substrates.[47−49]

AUTHOR INFORMATION

Corresponding Author

*(P.E.H.) Mail: Departamento de Nutrición, Bromatología y Tecnología de los Alimentos, Facultad de Veterinaria, Universidad Complutense de Madrid (UCM), Avenida Puerta de Hierro s/n, 28040 Madrid, Spain. Phone: +34-913943752. Fax: +34-913943743. E-mail: ehernan@vet.ucm.es.

Funding

This work was supported by Project AGL2012-34829 from the Ministerio de Economía y Competitividad (MINECO), by Projects AGL2009-08348 and AGL2011-24643 from the Ministerio de Ciencia e Innovación (MICINN), by a CENIT project (2006−2009) from the MITC-CDTI, by Grant GR35-10A from the BSCH-UCM, and by Grants S2009/AGR-1489 and P2013/ABI-2747 from the Comunidad de Madrid (CAM). L.G. holds a fellowship (FPU) from the Ministerio de Educación y Ciencia (MEC), J.B. held a research contract from the CAM, and J.J.J. was the recipient of a fellowship from the MICINN, Spain.

Notes

The authors declare no competing financial interest.

■ ACKNOWLEDGMENTS

We thank Dr. T. Eaton, Institute of Food Research, Norwich (UK), Dr. Rosa del Campo, Hospital Universitario Ramón y Cajal, Madrid (Spain), and Dr. Carmen Torres, Universidad de La Rioja, Logroño (Spain), for providing strains and Prof. I. F. Nes, Prof. D. B. Diep, and Z. Saleihan for help in obtaining *E. faecalis* V583 Δ*gelE*.

■ REFERENCES

(1) Hernández-Ledesma, B.; Contreras, M. M.; Recio, I. Antihypertensive peptides: production, bioavailability and incorporation into foods. *Adv. Colloid Interface. Sci.* **2011**, *165*, 23−35.

(2) Mills, S.; Ross, R. P.; Hill, C.; Fitzgerald, G. F.; Stanton, C. Milk intelligence: mining milk for bioactive substances associated with human health. *Int. Dairy J.* **2011**, *21*, 377−401.

(3) Martínez-Maqueda, D.; Miralles, B.; Recio, I.; Hernández-Ledesma, B. Antihypertensive peptides from proteins: a review. *Food Funct.* **2012**, *3*, 350−361.

(4) Phelan, M.; Kerins, D. The potential role of milk-derived peptides in cardiovascular disease. *Food Funct.* **2011**, *2*, 153−167.

(5) Contreras, M. M.; Carrón, R.; Montero, M. J.; Ramos, M.; Recio, I. Novel casein-derived peptides with antihypertensive activity. *Int. Dairy J.* **2009**, *19*, 566−573.

(6) Ryan, J. T.; Ross, R. P.; Bolton, D.; Fitzgerald, G. F.; Stanton, C. Bioactive peptides from muscle sources: meat and fish. *Nutrients* **2011**, *3*, 765−791.

(7) Yu, Z.; Yin, Y.; Zhao, W.; Chen, F.; Liu, J. Antihypertensive effect of angiotensin-converting enzyme inhibitory peptide RVPSL on spontaneously hypertensive rats by regulating gene expression of the renin−angiotensin system. *J. Agric. Food Chem.* **2014**, *62* (4), 912−917.

(8) Nielsen, M. S.; Martinussen, T.; Flambard, B.; Sørensen, K. I.; Otte, J. Peptide profiles and angiotensin-I-converting enzyme inhibitory activity of fermented milk products: effect of bacterial strain, fermentation pH, and storage time. *Int. Dairy J.* **2009**, *19*, 155−165.

(9) Otte, J.; Lenhard, T.; Flambard, B.; Sørensen, K. I. Influence of fermentation temperature and autolysis on ACE-inhibitory activity and peptide profiles of milk fermented by selected strains of *Lactobacillus helveticus* and *Lactococcus lactis*. *Int. Dairy J.* **2011**, *21*, 229−238.

(10) Franz, C. M. A. P.; Huch, M.; Abriouel, H.; Holzapfel, W.; Gálvez, A. Enterococci as probiotics and their implications in food safety. *Int. J. Food Microbiol.* **2011**, *151*, 125−140.

(11) Willems, R. J. L.; Hanage, W. P.; Bessen, D. E.; Feil, E. J. Population biology of Gram-positive pathogens: high-risk clones for dissemination of antibiotic resistance. *FEMS Microbiol. Rev.* **2011**, *35*, 872−900.

(12) Muguerza, B.; Ramos, M.; Sánchez, E.; Manso, M. A.; Miguel, M.; Aleixandre, A.; Delgado, M. A.; Recio, I. Antihypertensive activity of milk fermented by *Enterococcus faecalis* strains isolated from raw milk. *Int. Dairy J.* **2006**, *16*, 61−69.

(13) Chaves-López, C.; Serio, A.; Matruscelli, M.; Papparella, A.; Osorio-Cadavid, E.; Suzzi, G. Microbiological characteristics of kumis, a traditional fermented Colombian milk, with particular emphasis on enterococci population. *Food Microbiol.* **2010**, *28*, 1041−1047.

(14) Regazzo, D.; Da Dalt, L.; Lombardi, A.; Andrighetto, A.; Negro, A.; Gabai, G. Fermented milks from *Enterococcus faecalis* TH563 and *Lactobacillus delbrueckii* subsp. *bulgaricus* LA2 manifest different degrees of ACE-inhibitory and immunomodulatory activities. *Dairy Sci. Tecnol.* **2010**, *90*, 469−476.

(15) Gútiez, L.; Gómez-Sala, B.; Recio, I.; del Campo, R.; Cintas, L. M.; Herranz, C.; Hernández, P. E. *Enterococcus faecalis* strains from food, environmental, and clinical origin produce ACE-inhibitory peptides and other bioactive peptides during growth in bovine skim milk. *Int. J. Food Microbiol.* **2013**, *166*, 93−101.

(16) Mäkinen, P. L.; Clewell, D. B.; An, F.; Mäkinen, K. K. Purification and substrate specificity of a strongly hydrophobic extracellular metalloendopeptidase ("gelatinase") from *Streptococcus faecalis* (OG1-10). *J. Biol. Chem.* **1989**, *264*, 3325−3334.

(17) Qin, X.; Singh, K. V.; Weinstock, G. M.; Murray, B. E. Effects of *Enterococcus faecalis fsr* genes on production of gelatinase and a serine protease and virulence. *Infect. Immun.* **2000**, *68*, 2579−2586.

(18) Thomas, V. C.; Hiromasa, Y.; Harms, N.; Thurlow, L.; Tomich, J.; Hancock, L. E. A fratricidal mechanism is responsible for eDNA release and contributes to biofilm development in *Enterococcus faecalis*. *Mol. Microbiol.* **2009**, *72*, 1022−1036.

(19) Teixeira, N.; Santos, S.; Marujo, P.; Yokohata, R.; Iyer, V. S.; Nakayama, J.; Hancock, L. E.; Serror, P.; Silva Lopes, M. F. The incongruent gelatinase genotype and phenotype in *Enterococcus faecalis* are due to shutting off the ability to respond to the gelatinase biosynthesis-activating pheromone (GBAP) quorum-sensing signal. *Microbiology* **2012**, *158*, 519−528.

(20) Bourgogne, A.; Hilsenbeck, S. G.; Dunny, G. M.; Murray, B. E. Comparison of OG1RF and an isogenic *fsrB* deletion mutant by transcriptional analysis: the Fsr system of *Enterococcus faecalis* is more than activator of gelatinase and serine protease. *J. Bacteriol.* **2006**, *188*, 2875−2884.

(21) Sánchez, J.; Basanta, A.; Gómez-Sala, B.; Herranz, C.; Cintas, L. M.; Hernández, P. E. Antimicrobial and safety aspects, and biotechnological potential of bacteriocinogenic enterococci isolated from mallard ducks (*Anas platyrhynchos*). *Int. J. Food Microbiol.* **2007**, *117*, 295−305.

(22) Su, Y. A.; Sulavik, M. C.; He, P.; Mäkinen, K. K.; Mäkinen, P. L.; Fielder, S.; Wirth, R.; Clewell, D. B. Nucleotide sequence of the gelatinase gene (*gelE*) from *Enterococcus faecalis* subsp. *liquefaciens*. *Infect. Immun.* **1991**, *59*, 415−420.

(23) Del Papa, M. F.; Hancock, L. E.; Thomas, V. C.; Perego, M. Full activation of *Enterococcus faecalis* gelatinase by a C-terminal proteolytic cleavage. *J. Bacteriol.* **2007**, *189*, 8835−8843.

(24) Kawalec, M.; Potempa, J.; Moon, J. L.; Travis, J.; Murray, B. E. Molecular diversity of a putative virulence factor: purification and characterization of isoforms of an extracellular serine glutamyl endopeptidase of *Enterococcus faecalis* with different enzymatic activities. *J. Bacteriol.* **2005**, *187*, 266−275.

(25) Holo, H.; Nes, I. F. High frequency transformation by electroporation of *Lactococcus lactis* subsp. *cremoris* grown with glycine in osmotically stabilized media. *Appl. Environ. Microbiol.* **1989**, *55*, 3119−3123.

(26) Citti, R. *Aislamiento e identificación de bacterias lácticas bacteriocinogénicas de leches y quesos de búfala de Venezuela: actividad antimicrobiana y caracterización bioquímica y genética de sus bacteriocinas*. Ph.D. thesis, Universidad Complutense de Madrid, Madrid, Spain, 1989.

(27) Eaton, T. J.; Gasson, M. J. Molecular screening of *Enterococcus* virulence determinants and potential for genetic exchange between food and medical isolates. *Appl. Environ. Microbiol.* **2001**, *67*, 1628−1635.

(28) Ruiz-Garbajosa, P.; Bonten, M. J.; Robinson, D. A.; Top, J.; Nallapareddy, S. R.; Torres, C.; Coque, T. M.; Canton, R.; Baquero, F.; Murray, B. E.; del Campo, R.; Willems, R. J. L. Multilocus sequence typing scheme for *Enterococcus faecalis* reveals hospital-adapted genetic complexes in a background of high rates of recombination. *J. Clin. Microbiol.* **2006**, *44*, 2220−2228.

(29) Maguin, E.; Prévost, H.; Ehrlich, S. D.; Gruss, A. Efficient insertional mutagenesis in lactococci and other Gram-positive bacteria. *J. Bacteriol.* **1996**, *178*, 931−935.

(30) Jönsson, M.; Saleihan, Z.; Nes, I. F.; Holo, H. Construction and characterization of three lactate dehydrogenase-negative *Enterococcus faecalis* V583 mutants. *Appl. Environ. Microbiol.* **2009**, *75*, 4901−4903.

(31) Biswas, I.; Gruss, A.; Ehlrich, S. D.; Maguin, E. High-efficiency gene inactivation and replacement system for Gram-positive bacteria. *J. Bacteriol.* **1993**, *175*, 3628−3635.

(32) Quirós, A.; Ramos, M.; Muguerza, B.; Delgado, M. A.; Miguel, M.; Aleixandre, A.; Recio, I. Identification of novel antihypertensive peptides in milk fermented with *Enterococcus faecalis*. *Int. Dairy J.* **2007**, *17*, 33−41.

(33) Hebert, E. M.; Mamone, G.; Picariello, G.; Raya, R. R.; Savoy, G.; Ferranti, P.; Addeo, F. Characterization of the pattern of α_{S1}- and β-

casein breakdown and release of a bioactive peptide by a cell envelope protease from *Lactobacillus delbrueckii* subsp. *lactis* CRL 581. *Appl. Environ. Microbiol.* **2008**, *74*, 3682−3689.
(34) Gobbetti, M.; Di Cagno, R.; De Angelis, M. Functional microorganisms for functional food quality. *Crit. Rev. Food Sci. Nutr.* **2010**, *50*, 716−727.
(35) Miclo, L.; Roux, E.; Genay, M.; Brusseaux, E.; Poirson, C.; Jameh, N.; Perrin, C.; Dary, A. Variability of hydrolysis of β-, α_{s1}-, and α_{s2}-caseins by 10 strains of *Streptococcus thermophilus* and resulting bioactive peptides. *J. Agric. Food Chem.* **2012**, *60*, 554−565.
(36) van de Guchte, M.; van der Vossen, J. M.; Kok, J.; Venema, G. Construction of a lactococcal expression vector: expression of hen egg white lysozyme in *Lactococcus lactis* subsp. *lactis*. *Appl. Environ. Microbiol.* **1989**, *55*, 224−228.
(37) Mohamed, J. A.; Murray, B. E. Influence of the *fsr* locus on biofilm formation by *Enterococcus faecalis* lacking *gelE*. *J. Med. Microbiol.* **2006**, *55*, 1747−1750.
(38) Engelbert, M.; Mylonakis, E.; Ausubel, F. M.; Calderwood, S. B.; Gilmore, M. S. Contribution of gelatinase, serine protease, and *fsr* to the pathogenesis of *Enterococcus faecalis* endophtalmitis. *Infect. Immun.* **2004**, *72*, 3628−3633.
(39) Borrero, J.; Jiménez, J. J.; Gútiez, L.; Herranz, C.; Cintas, L. M.; Hernández, P. E. Protein expression vector and secretion signal peptide optimization to drive the production, secretion, and functional expression of the bacteriocin enterocin A in lactic acid bacteria. *J. Biotechnol.* **2011**, *156*, 76−86.
(40) Gobetti, M.; Ferranti, P.; Smacchi, E.; Goffredi, F.; Addeo, F. Production of angiotensin-I-converting-enzyme-inhibitory peptides in fermented milks started by *Lactobacillus delbrueckii* subsp. *bulgaricus* SS1 and *Lactococcus lactis* subsp. *cremoris* FT4. *Appl. Environ. Microbiol.* **2000**, *66*, 3898−3904.
(41) Raghavan, S.; Kristinsson, H. ACE-activity of tilapia protein hydrolysates. *Food Chem.* **2009**, *117*, 582−588.
(42) Miguel, M.; Recio, I.; Ramos, M.; Delgado, M. A.; Aleixandre, M. A. Antihypertensive effect of peptides obtained from *Enterococcus faecalis*-fermented milk in rats. *J. Dairy Sci.* **2006**, *89*, 3352−3359.
(43) Quirós, A.; Contreras, M. M.; Ramos, M.; Amigo, L.; Recio, I. Stability to gastrointestinal enzymes and structure-activity relationship of β-casein-peptides with antihypertensive properties. *Peptides* **2009**, *30*, 1848−1853.
(44) Rival, S. G.; Boeriu, C. G.; Wichers, H. J. Caseins and casein hydrolysates. 2. Antioxidative properties and relevance to lipoxygenase inhibition. *J. Agric. Food Chem.* **2001**, *49*, 295−302.
(45) Galloway-Peña, J. R.; Bourgogne, A.; Qin, X.; Murray, B. E. Diversity of the *fsr-gelE* region of the *Enterococcus faecalis* genome but conservation in strains with partial deletions of the fsr operon. *Appl. Environ. Microbiol.* **2011**, *77*, 442−451.
(46) Singh, K. V.; Nallaparedy, S. R.; Nannini, E. C.; Murray, B. E. Fsr-independent production of protease(s) may explain the lack of attenuation of an *Enterococcus faecalis fsr* mutant versus a *gelE-sprE* mutant in induction of endocarditis. *Infect. Immun.* **2005**, *73*, 4888−4894.
(47) Koyama, M.; Naramoto, K.; Nakajima, T.; Aoyama, T.; Watanabe, M.; Nakamura, K. Purification and identification of antihypertensive peptides from fermented buckwheat sprouts. *J. Agric. Food Chem.* **2013**, *61*, 3013−3021.
(48) Liu, L.; Liu, L.; Lu, B.; Chen, M.; Zhang, Y. Evaluation of bamboo shoot peptide preparation with angiotensin converting enzyme inhibitory and antioxidant abilities from byproducts of canned bamboo shoots. *J. Agric. Food Chem.* **2013**, *61*, 5526−5533.
(49) Estrada-Salas, P. A.; Montero-Morán, G. M.; Martínez-Cuevas, P. P.; González, C.; Barba de la Rosa, A. P. Characterization of antidiabetic and antihypertensive properties of canary seed (*Phalaris canariensis* L.) peptides. *J. Agric. Food Chem.* **2014**, *62*, 427−433.
(50) Jacob, A.; Hobbs, S. J. Conjugal transfer of plasmid-borne multiple antibiotic resistance in *Streptococcus faecalis* var. *zymogenes*. *J. Bacteriol.* **1974**, *117*, 360−372.
(51) Sahm, D. F.; Kissinger, J.; Gilmore, M. S.; Murray, P. R.; Mulder, R.; Solliday, J.; Clarke, B. *In vitro* susceptibility studies of vancomycin-resistant *Enterococcus faecalis*. *Antimicrob. Agents Chemother.* **1989**, *133*, 1588−1591.

JOURNAL OF AGRICULTURAL AND FOOD CHEMISTRY

Article

pubs.acs.org/JAFC

Non-cytotoxic Antifungal Agents: Isolation and Structures of Gageopeptides A−D from a *Bacillus* Strain 109GGC020

Fakir Shahidullah Tareq,[†,‡] Min Ah Lee,[‡] Hyi-Seung Lee,[‡] Yeon-Ju Lee,[‡] Jong Seok Lee,[‡] Choudhury M. Hasan,[§] Md. Tofazzal Islam,[∥] and Hee Jae Shin*[,†,‡]

[†]Department of Marine Biotechnology, Korea University of Science and Technology, Daejeon 350-360, Republic of Korea

[‡]Marine Natural Products Laboratory, Korea Institute of Ocean Science and Technology, Ansan 426-744, Republic of Korea

[§]Department of Pharmaceutical Chemistry, Faculty of Pharmacy, University of Dhaka, Dhaka 1000, Bangladesh

[∥]Department of Biotechnology, Bangabandhu Sheikh Muzibur Rahman Agricultural University, Dhaka 1706, Bangladesh

Supporting Information

ABSTRACT: Antifungal resistance and toxicity problems of conventional fungicides highlighted the requirement of search for new safe antifungal agents. To comply with the requirement, we discovered four new non-cytotoxic lipopeptides, gageopeptides A−D, **1**−**4**, from a marine-derived bacterium *Bacillus subtilis*. The structures and stereochemistry of gageopeptides were determined by NMR data analysis and chemical means. Gageopeptides exhibited significant antifungal activities against pathogenic fungi *Rhizoctonia solani*, *Botrytis cinerea*, and *Colletotrichum acutatum* with minimum inhibitory concentration (MIC) values of 0.02−0.06 μM. In addition, these lipopeptides showed significant motility inhibition and lytic activities against zoospores of the late blight pathogen *Phytophthora capsici*. These compounds also showed potent antimicrobial activity against Gram positive and Gram negative bacteria with MIC values of 0.04−0.08 μM. However, gageopeptides A−D did not exhibit any cytotoxicity (GI_{50} > 25 μM) against cancer cell lines in sulforhodamine B (SRB), 3-[4,5-dimethylthiazol-2-yl]-2,5-diphenyltetrazolium bromide (MTT), and WST-1 ((4-[3−4-iodophenyl]-2-(4-nitrophenyl)-2*H*-5-tetrazolio)-1,3-benzene disulfonate)) assays, demonstrating that these compounds could be promising candidates for the development of non-cytotoxic antifungal agents.

KEYWORDS: *Bacillus subtilis, gageopeptides, antifungal agents, non-cytotoxicity*

INTRODUCTION

Fungal diseases are very common crop-devastating diseases in agricultural practice. For example, *Rhizoctonia solani* (*R. solani*) is a plant pathogenic fungus with a wide host range and worldwide distribution. This pathogen is very destructive to many crops, including agronomic, ornamental, and forestry species.[1] This species has been reported to enormously reduce the growth and quality of crops such as cereals, potato, lettuce, and cotton in Spain.[2−5] *Phytophthora capsici* (*P. capsici*), another economically important pathogen, causes extensive damage in cucumber, pepper, tomato, and beans. It is well recognized to cause crown, leaf, and fruit blight, wilting of the whole plant, and dark purplish discoloration of the stem.[6] Similarly, a diverse group of fungi are recognized to cause severe plant diseases, resulting in a significant loss in agricultural practice.[7] Therefore, it is very important to control plant diseases to secure the level of yield both quantitatively and qualitatively.

Farmers often heavily rely on the application of commercial fungicides to secure the quality and production of crops. Most of the fungicides are not compatible with the environment or health; their excessive application and misuse can also cause acute and chronic toxicity.[8,9] According to a review by the International Labor Organization (ILO), about 14% of all occupational injuries were caused by exposure to synthetic pesticides and other agrochemicals.[10] Moreover, the World Health Organization (WHO) and the United Nations Environment Programme (UNEP) reported that three million farmers in the developing countries suffer from severe poisoning by commercial pesticides, resulting in the deaths of about 18,000 of them each year.[11] However, the environmental problems caused by synthetic fungicides have brought a significant change to people who work in the agricultural field toward the use of harmful pesticides. Therefore, it has now become an urgent issue to develop environmentally friendly alternative pesticides to synthetic chemicals to protect plants from diseases.

Lipopeptides produced nonribosomally by bacteria and fungi have been reported to be biodegradable and less toxic, and have various biomedical applications.[12] As illustrations, lipopeptides of surfactins, iturins, mycosubtilin, plipastatin, halobacillin, fengycin, and echinocandin families produced by bacterial origins have recently received much attention due to their potent biological activities, including antimicrobial, antitumor, antiviral, anti-inflammatory, and immunosuppressive activities.[13−18] In particular, echinocandins and pneumocandins are now approved antifungal drugs which inhibit the synthesis of glucan in the cell wall, via noncompetitive inhibition of the enzyme 1,3-β-D-glucan synthase in pathogenic fungi including

Received: February 13, 2014
Revised: May 25, 2014
Accepted: May 26, 2014
Published: May 26, 2014

ACS Publications © 2014 American Chemical Society

dx.doi.org/10.1021/jf502436r | J. Agric. Food Chem. 2014, 62, 5565−5572

Aspergillus and *Candida*.[19] In our previous studies,[20,21] we have discovered three novel lipotetrapeptides, gageotetrins A−C and surfactin like heptapeptides, gageostatins A−C with significant antimicrobial properties. Further investigations on the ethyl acetate (EtOAc) extract obtained from the same bacterium *Bacillus subtilis* (*B. subtillis*) afforded four new lipopeptides, gageopeptides A−D, **1**−**4** (Figure 1), which displayed

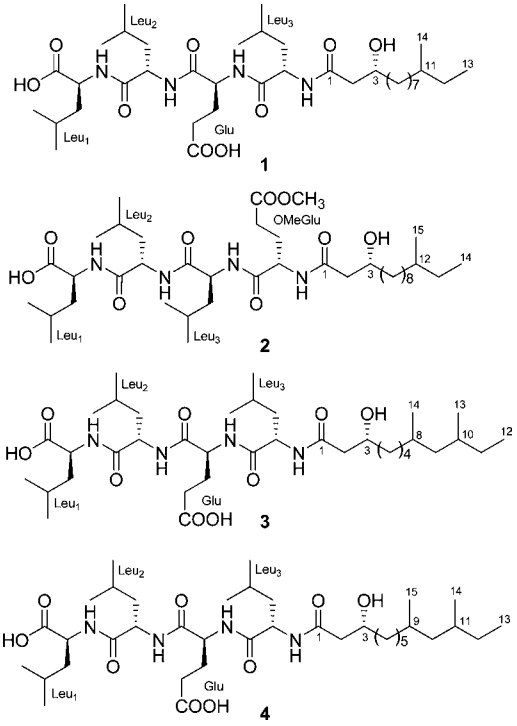

Figure 1. Structures of compounds **1**−**4**.

significant activity against pathogenic fungi and bacteria. The cytoxicity of gageopeptides against human cancer cell lines was also investigated during the study, and the results demonstrated that these new lipopeptides are potent non-cytotoxic antifungal agents.

MATERIALS AND METHODS

General Experimental Procedures. One- (1D) and two-dimensional (2D) NMR data were recorded on a Varian Unity 500 NMR spectrometer (Varian Inc., Palo Alto, CA, USA). IR spectra were measured on a JASCO FT/IR-4100 (JASCO, Easton, MD, USA). $[\alpha]_D$ values were obtained from a digital polarimeter (JASCO). Ultraviolet spectra were recorded on a Shimadzu UV-1650PC spectrometer (Shimadzu, Kyoto, Japan). HRESIMS data were obtained on a Shimadzu hybrid ion-trap time-of-flight mass spectrometer (Shimadzu). HPLC was performed with a column (250 mm × 4.6 mm i.d., 5 μm; YMC-Pack-ODS-A), with a PrimeLine Binary pump with RI-101 Shodex refractive index detector and M 525 variable UV detector (Shoko Scientific Co., Yokohama, Japan). Dextrose and agar were purchased from Junsei Chemical Co. Ltd. (Tokyo, Japan), and tryptone, yeast extract, and beef extracts were purchased from Becton, Dickinson and Co. (Sparks, MD, USA). All experimental chemicals were obtained from Duksan Pure Chemicals (Ansan, South Korea). For antimicrobial tests, type strains were collected from Korean Collection for Type Cultures (KCTC, Korea Research Institute of Bioscience and Biotechnology (KRIBB), Daejeon, South Korea).

Taxonomy of the Bacterial Strain. During an expedition in 2010, a sediment sample was collected from Gageocho reef, Republic of Korea, and the producing strain designated as 109GGC020 was isolated from the sample by serial dilution technique. The 16S rRNA sequence of the strain 109GGC020 was submitted to GenBank under accession number JQ927413. A BLAST search result showed the sequence of 109GGC020 to be 100% similar to *B. subtilis*.

Isolation of Compounds 1−4. Batch fermentation (60 L) of the strain *B. subtilis* 109GGC020 was carried out in 2 L flasks. For 1 L, the medium composition (w/v) was 1% dextrose, 0.1% yeast extract, 0.1% beef extract, 0.2% tryptone, 100% natural seawater, and pH 7.1. The culture broth was separated from the cells by centrifugation after 7 days of cultivation at 28 °C. The broth was extracted with EtOAc and the solvent was removed under reduced pressure at 40 °C to dryness. The EtOAc extract (11.8 g) was fractionated by an ODS open column chromatography using methanol:water (1:4, 2:3, 3:2, 4:1, and 100:0; v/v) as eluent. The 100% MeOH fraction was refractionated and purified by ODS semipreparative and analytical HPLCs with a solvent system of 95% MeOH in H_2O to yield **1**−**4**.

Gageopeptide A (**1**; 4.6 mg; 0.04%): amorphous solid; $[\alpha]^{27}_D$ −21 (*c* 0.1, MeOH). IR (MeOH; ν_{max}, cm^{-1}): 3285 (NH), 1620−1689 (CO), 2923 (aliphatic chain). ^1H and ^{13}C NMR data (CD_3OD): Table 1. HRESIMS (*m*/*z*): 735.4883 $[M + Na]^+$. Calcd for $C_{37}H_{68}N_4O_9$: 735.4884 $[M + Na]^+$;

Gageopeptide B (**2**; 1.8 mg; 0.02%): amorphous solid; $[\alpha]^{27}_D$ −40 (*c* 0.1, MeOH). IR (MeOH; ν_{max}, cm^{-1}): 3278 (NH), 1642 (CO), 2927 (aliphatic chain). ^1H and ^{13}C NMR data (CD_3OD): Table 1. HRESIMS (*m*/*z*): 763.5192 $[M + Na]^+$. Calcd for $C_{39}H_{72}N_4O_9$: 763.5197 $[M + Na]^+$.

Gageopeptide C (**3**; 5.9 mg; 0.05%): amorphous solid; $[\alpha]^{27}_D$ −20 (*c* 0.1, MeOH). IR (MeOH; ν_{max}, cm^{-1}) 3373 (NH), 1625 (CO), 2970 (aliphatic chain). ^1H and ^{13}C NMR data (CD_3OD): Table 1. HRESIMS (*m*/*z*): 735.4883 $[M + Na]^+$. Calcd. for $C_{37}H_{68}N_4O_9$: 735.4884 $[M + Na]^+$.

Gageopeptide D (**4**; 7.8 mg; 0.07%): amorphous solid; $[\alpha]^{27}_D$ −70 (*c* 0.05, MeOH). IR (MeOH; ν_{max}, cm^{-1}): 3287 (NH), 1629 (CO), 2959 (aliphatic chain). ^1H and ^{13}C NMR data (CD_3OD): Table 1. HRESIMS (*m*/*z*): 749.5044 $[M + Na]^+$. Calcd for $C_{38}H_{70}N_4O_9$: 749.5040 $[M + Na]^+$.

Determination of Absolute Stereochemistry of 1−4. The absolute stereochemistry of amino acid residues and at the stereocenter C-3 of 3-hydroxy fatty acids in **1**−**4** was determined by using the methods described previously.[20,21] In brief, compound **1** (1.9 mg) was hydrolyzed using 6 N HCl (500 μL) at 120 °C for 23 h. The hydrolysate was diluted with water and extracted with hexane. The hexane layer was evaporated by a stream of nitrogen, and the water layer was concentrated to dryness under reduced pressure. To determine the absolute configuration at the stereocenter C-3 of the fatty acid,[22] the hexane extract was derivatized with Mosher's reagent and the aqueous extract was used for the determination of absolute stereochemistry of amino acids by Marfey's method.[23] In an entirely analogous way, compounds **2**−**4** were hydrolyzed and their absolute stereochemistries were assigned.

Fatty acid in **1**: 1.5 mg; colorless oil. ^1H NMR data (CD_3OD): δ_H 2.34 (H-2a, dd, *J* = 15.0, 8.5 Hz), 2.43 (H-2b, dd, *J* = 15.5, 5.0 Hz), 3.96 (H-3, m), 1.33 (H-4a, m), 1.45 (H-4b, m), 1.47 (H_2-5, m), 1.29 (H_2-6−9, brs), 1.18 (H-10, m), 1.50 (H-11, m, overlapped), 1.29 (H-12, m, overlapped), 0.86 (H_3-13, t, *J* = 5.5 Hz), 0.87 (H_3-14, d, *J* = 6.5 Hz). LC-MS (*m*/*z*): 243.01 $[M - H]^-$. Optical rotation ($[\alpha]^{27}_D$): −26 (*c* o.1, MeOH).

Activity Study of 1−4 against *P. capsici*. *P. capsici* was received from Prof. W. Yuanchao of Nanjing Agricultural University, China. Mycelia of *P. capsici* were cultured on sterile clarified 10% V8 agar in Petri dishes and incubated at 25 °C in the dark for 4 days.[24] The agar culture from the Petri dishes incubated for 1−2 weeks was cut into six pieces, covered with sterile distilled water, and cultured in Petri dishes again at 25 °C in the dark to induce sporangium formation. Every 12 h, the water was replaced by fresh sterile distilled water. In this way, after changing the water 3 times, an abundance of sporangia were induced. The Petri dishes with large numbers of sporangia were incubated at 4 °C for 30 min, and kept at room temperature for another 30 min to induce zoospore release. The movement of sporangia and zoospores was checked on a regular basis under an Olympus light microscope. The zoospores remained motile for 10−12

dx.doi.org/10.1021/jf502436r | J. Agric. Food Chem. 2014, 62, 5565−5572

Table 1. ^{1}H and ^{13}C NMR Data of 1−4 in CD_3OD

		1		2		3		4	
units	no.	δ_H	δ_C	δ_H	δ_C	δ_H	δ_C	δ_H	δ_C
Leu_1	1		174.3		175.1		176.2		176.3
	2	4.44 m (α)	52.4	4.33 dd (8.5, 5.5, α)	54.0	4.45 m (α)	52.4	4.42 m (α)	52.4
	3	1.66 m (β)	41.4	1.66 m (β)	41.8	1.65 m (β)	41.4	1.63 m (β)	41.3
	4	1.66 m (γ)	26.1	1.66 m (γ)	26.1	1.65 m (γ)	26.0	1.63 m (γ)	26.0
	5	0.95 m (δ)	21.6	0.94 m (δ)	22.2	0.94 m (δ)	21.6	0.92 m (δ)	21.6
	6	0.95 m (δ)	23.6	0.94 m (δ)	23.8	0.94 m (δ)	23.5	0.92 m (δ)	23.5
	NH	8.00 d (6.5)[a]		7.89 d (8.0)[a]		7.97 d (6.5)		7.93 d (6.5)[a]	
Leu_2	1		174.8		174.7		174.8		174.8
	2	4.41 m (α)	53.3	4.40 m (α)	52.5	4.42 m (α)	53.2	4.39 m (α)	53.2
	3	1.66 m (β)	41.6	1.66 m (β)	41.6	1.65 m (β)	41.6	1.63 m (β)	41.6
	4	1.66 m (γ)	26.1	1.66 m (γ)	26.1	1.65 m (γ)	26.1	1.63 m (γ)	26.1
	5	0.95 m (δ)	22.0	0.94 m (δ)	22.0	0.94 m (δ)	22.0	0.92 m (δ)	22.0
	6	0.95 m (δ)	23.7	0.94 m (δ)	23.7	0.94 m (δ)	23.6	0.92 m (δ)	23.6
	NH	8.13 d (6.5)[a]		8.11 d (8.0)[a]		8.12 d (6.5)		8.09 d (6.5)[a]	
Glu	1		174.8		174.1		174.8		174.8
	2	4.33 dd (9.0, 6.0, α)	54.6	4.26 dd (9.0, 6.0, α)	54.4	4.33 dd (9.0, 6.0, α)	54.6	4.30 dd (9.0, 6.0, α)	54.6
	3	1.95 m (β)	28.2	1.95 m (β)	28.0	1.95 m (β)	28.1	1.92 m (β)	28.3
		2.09 m (β)		2.10 m (β)		2.09 m (β)		2.06 m (β)	
	4	2.41 m (γ)	31.5	2.45 m (γ)	31.3	2.41 m (γ)	31.5	2.39 t (4.5, γ)	31.4
	NH	8.23 d (6.5)[a]		8.23 d (7.0)[a]		8.23 d (6.5)[a]		8.20 d (6.5)[a]	
	COOH	176.7		175.1		176.7		176.8	
	OCH_3		3.66 s	52.4					
Leu_3	1		174.2		174.8		174.2		174.2
	2	4.27 dd (8.5, 6.0, α)	54.0	4.43 m (α)	53.2	4.27 dd (8.5, 6.0, α)	54.0	4.26 dd (8.5, 6.0, α)	54.0
	3	1.66 m (β)	41.4	1.66 m (β)	41.4	1.65 m (β)	41.7	1.63 m (β)	41.7
	4	1.66 m (γ)	26.1	1.66 m (γ)	26.0	1.65 m (γ)	26.1	1.63 m (γ)	26.1
	5	0.95 m (δ)	22.2	0.94 m (δ)	21.6	0.94 m (δ)	22.2	0.92 m (δ)	22.2
	6	0.95 m (δ)	23.8	0.94 m (δ)	23.6	0.94 m (δ)	23.8	0.92 m (δ)	23.8
	NH	8.27 d (6.5)[a]		8.19 d (7.0)[a]		8.27 d (6.5)[a]		8.23 d (6.5)[a]	
3-OH acid	1		175.0		174.9		174.9		174.9
	2	2.32 dd (8.5, 14.0)	44.7	2.32 dd (14.0, 8.5)	44.7	2.32 dd (14.0, 8.5)	44.7	2.43 dd (4.5, 14.5)	44.7
		2.46 dd (4.5, 14.5)		2.46 dd (10.0, 4.0)		2.46 dd (14.5, 4.5)		2.31 dd (8.5, 14.0)	
	3	3.98 m	70.0	3.97 m	70.0	3.98 m	70.0	3.96 m	70.0
	4	1.48 m	38.5	1.51 m	38.5	1.48 m	38.5	1.46 m	38.4
	5	1.44 m	26.9	1.48 m	26.9	1.47 m	26.9	1.45 m	26.9
		1.31 m		1.35 m		1.35 m		1.33 m	
	6	1.29 brs	30.6−30.9	1.29 brs	30.6−30.9	1.30 brs	30.6−31.3	1.28 brs	30.7−31.2
	7					1.17 m	40.4	1.28 brs	30.7−31.2
	8					1.52 m	29.3	1.15 m	40.4
	9					1.30 brs	30.8	1.49 m	29.3
	10					1.30 brs	35.8	1.28 brs	30.9
	11	1.29 brs	30.8	1.29 m	33.2	1.13 m	37.9	1.28 brs	35.8

dx.doi.org/10.1021/jf502436r | J. Agric. Food Chem. 2014, 62, 5565−5572

Table 1. continued

units	no.	1		2		3		4	
		δ_H	δ_C	δ_H	δ_C	δ_H	δ_C	δ_H	δ_C
	12	1.29 brs	33.2	1.29 m	30.6	1.30 brs 0.87 m	11.9	1.11 m 1.28 brs	37.9
	13	0.87 t	14.6	0.89, t (7.5)	14.6	0.87 m	19.8	0.87 m	11.9
	14	0.87 m	23.5	0.91, m	23.5	0.87 m	23.2	0.87 m	19.8
	15							0.87 m	174.9

[a]^{1}H NMR data recorded in CD_3OH.

h in sterile distilled water. The motility bioassay was carried out with the zoospores. A series of solutions for gegeopeptides were prepared in aqueous dimethyl sulfoxide (DMSO). The final concentration of DMSO in the zoospore suspension was less than 1% (v/v), a condition that does not affect the motility of zoospores. The bioassay for the motility inhibition and lysis of zoospores was investigated as described previously.[25,26] In brief, to a suspension (360 μL) of zoospores (ca.10^5/mL), 40 μL of sample solution was added and stirred with a glass rod. A 1% amount of aqueous DMSO was used as a control. Under a light microscope (×10 magnification), the time-course changes of motility and lysis of zoospores were evaluated as described previously.[27] The bioassay was repeated twice, and each treatment was replicated thrice. The mean value (%) was calculated (±SE, standard error) of the affected spores in each treatment. Minimum inhibitory concentration (MIC) values of individual compounds were converted to micromolar.[28]

Further Activity Study against Bacteria and Fungi. A standard "broth dilution assay"[29] was employed to evaluate the antimicrobial activity of gageopeptides against pathogenic fungi (*R. solani*, *Botrytis cinerea* (*B. cinerea*), and *Colletotrichum acutatum* (*C. acutatum*)), Gram positive bacteria (*B. subtilis* and *Staphylococcus aureus* (*S. aureus*)) and Gram negative bacteria (*Salmonella typhi* (*S. typhi*) and *Pseudomonas aeruginosa* (*P. aeruginosa*)). Briefly, a series of solutions for gegeopeptides were prepared over the range of 0.5−256 μg/mL in 96-well plates. Type strains were cultured overnight, and the final concentration (1.5×10^8 cfu/mL) of each strain in the culture broth was adjusted by comparing the culture turbidity with the 0.5 McFarland Standard. To each solution of gageopeptides **1**−**4**, 30 μL of culture broth was added and the final volume was adjusted to 200 μL using the respective fresh culture medium. The plates were incubated for 24 h at 37 °C for bacteria and 48 h at 30 °C for fungi.[28] The minimum inhibitory concentration (MIC, the lowest concentration of an antimicrobial compound that inhibits the visible growth of a microorganism) was recorded and expressed in micromolar in Result and Discussion.[28]

Cytotoxicity by SRB Assay. Cancer cell growth inhibitory activity of gageopeptides **1**−**4** was carried out according to a sulforhodamine B (SRB) assay.[30] The selected cancer cell lines (brest cancer, MDA-MB-231; colon cancer, HCT-15; prostate cancer, PC-3; lung cancer, NCI-H23; stomach cancer, NUGC-3; and renal cancer, ACHN) were added into 96-well plates. A series of solutions of gageopeptides with the concentrations of 6.25−50 μM were prepared and added to the plates. The plates were incubated for 48 h, and anchorage-dependent cells were fixed with 50% (w/v) trichloroacetic acid and stained for 60 min. The SRB solution (0.4% sulforhodamine B in 1% acetic acid) was used to wash out excess dye. The protein-bound dye was dissolved in 10 mM Tris base solution for optical density determination at 510 nm using a microplate reader. Using graphed prism software, the GI_{50} values of gageopeptides were calculated.

Cytotoxicity Test by WST-1 Assay. Inhibition of cancer cell growth for compounds **1**−**4** was determined by WST-1 (4-[3−4-iodophenyl]-2-(4-nitrophenyl)-2*H*-5-tetrazolio)-1,3-benzene disulfonate) assay.[31,32] In brief, the human myeloid leukemia K-562 cells were maintained in RPMI 1640 medium in 5% fetal bovine serum, supplemented with humidified air containing 5% CO_2 at 37 °C. Compounds **1**−**4** were added to the properly distributed cells (2×10^4 cells/mL) in 96-well plates. The plates were incubated for 5 days under the preceding condition. A 50 μL aliquot of WST-1 stock solution (1.0 mg/mL) was added to the suspensions, and the plates were further incubated for 4 h. After aspirating off the supernatant with a microplate washer, the formazen crystals were dissolved by adding 150 μL of DMSO in each well. Finally, the absorbance was measured using a microplate reader at 480 nm, and IC_{50} values were calculated.

Cytotoxicity Test by MTT Assay. The MTT assay was carried out to determine cancer cell viability.[33] In brief, the RAW 264.7 cells (mouse leukemic monocyte macrophage cell line, 5×10^4 cells/mL), were cultured in a 96-well plate at 37 °C, and treated with varying concentrations (6.25, 12.5, 25, and 50 μM) of gageopeptides **1**−**4** for 24 h. Cells treated only with medium were used as a negative control group. The supernatant of each well was removed, and 20 μL of MTT

solution (5 mg/mL in phosphate buffered saline) and 100 μL of medium were added into the plates. The plates were incubated for another 4 h, and the formazen crystals were dissolved in DMSO (100 μL). The absorbance at 540 nm was measured using a microplate reader. The relative cell viability (%) was measured as a percentage relative to the untreated control cells.

RESULTS AND DISCUSSION

The molecular formula of **1** was found to be $C_{37}H_{68}N_4O_9$ based on the HRESIMS data analysis. The ^{1}H NMR data (recorded in both CD_3OD and CD_3OH) analysis of pure compound **1** revealed its lipopeptidic nature (Table 1), showing amide proton signals at δ_H 7.99−8.28, α-methine groups at δ_H 4.26−4.44, a broad singlet at 1.29, and methyl signals at δ_H 0.88−0.97. This initial prediction of the lipopeptidic nature of **1** was further confirmed by the observation of carbonyl/carboxylic carbons at δ_C 174.2−176.7 and a group of CH_2 carbons at δ_C 30.6−30.9 in the ^{13}C NMR spectrum of **1**, which were attributable to amino acid residues and an aliphatic chain, respectively. Later, the detailed interpretation of NMR data revealed five partial structures **a**−**e**, corresponding to four amino acid residues and a lipid moiety that constitute **1** (Figure 2). The glutamic acid unit (substructure **c**) was elucidated from

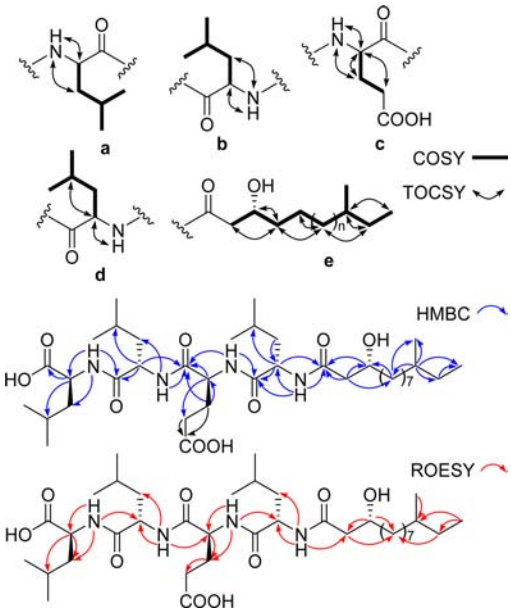

Figure 2. Assignment of partial structures by COSY and TOCSY correlations and complete structure with key HMBC and ROESY correlations of **1**.

the TOCSY correlations of the amide proton at δ_H 8.23 with an α-methine proton at δ_H 4.33 and the methylene signals at δ_H 1.95/2.09, and the α-methine proton also showed TOCSY correlations with the methylenes at δ_H 1.95/2.09 and 2.41. Furthermore, HMBC correlations were observed between the methylene signals at δ_H 1.95/2.09 and 2.41 and a carboxylic carbon resonating at δ_C 176.7, and between the protons at δ_H 1.95/2.09 and a carbonyl carbon at δ_C 174.8, confirming the glutamic acid residue in **1**. In a similar way, the substructures **a**−**e** were assigned by the analysis of 1D and 2D NMR data (Figure 2). The sequence of these amino acid residues was established as Leu_1-Leu_2-Glu-Leu_3 by the detailed interpretation of ROESY and HMBC correlations between α-methines, NH protons, and amide carbonyl carbons of respective amino acid residues. An additional oxygenated proton resonating at δ_H 3.98 displaying TOCSY and HMBC correlations with the carbonyl carbon at δ_C 175.0 and an aliphatic chain confirmed the presence of a fatty acid unit (**e**) in **1**. The ^{13}C NMR spectrum of **1** contained eight methyl carbons; six of them were found to constitute three Leu residues, and therefore, the remaining two methyls should be present in the fatty acid unit. The carbon resonating at δ_C 14.6 was assigned as a terminal methyl, and the methyl signal resonating at δ_C 23.5 was found to form a side chain with the fatty acid. By the detailed analysis of TOCSY and HMBC data, the position of the methyl group (δ_C 23.5) was determined to be at C-11 in the fatty acid chain. Judging from its molecular weight, the fatty acid was primarily assigned to be a C_{14} fatty acid connected to the N-terminal amine of the peptide. The LC-MS (m/z 243.01 $[M - H]^-$) analysis of the acid hydrolysate of **1** confirmed its chain length. Thus, the fatty acid was assigned as a 3-β-hydroxy-11-methyltridecanoic acid.[20,21] Finally, the structure of **1** was determined to be Leu_1-Leu_2-Glu-Leu_3-3-β-hydroxy-11-methyltridecanoic acid by HMBC and ROESY experiments (Figure 1).

The molecular formula of **2** was determined to be $C_{39}H_{72}N_4O_9$ according to the HRESIMS result. The ^{1}H and ^{13}C NMR data displayed a close similarity between **1** and **2** (Table 1), indicating the lipopeptidic nature of **2**. However, the presence of an additional oxygenated methyl peak at δ_H 3.66 and the molecular weight deference of **2** (C_2H_4 more) from **1** prompted us to conduct a detailed investigation of its structure. Therefore, a series of 1D and 2D NMR experiments were performed to clarify the structure of **2**. These NMR data analyses revealed the similar peptidic structure of **2**, consisting of Leu and Glu residues, but the methoxy proton at δ_H 3.66 did not show any correlations in both COSY and TOCSY spectra. However, HMBC correlations between this proton and a carboxylic carbon at δ_C 176.7 were found, indicating the presence of a OMeGlu unit in **2**. Based on the HMBC and ROESY spectra analysis, the sequence of these amino acid residues in the peptide moiety was assigned as Leu_1-Leu_2-Leu_3-OMeGlu. Similar to **1**, a 3-β-hydroxy fatty acid was also determined from the observation of correlations of the oxygenated methine proton at δ_H 3.97 with the methylene protons at δ_H 2.32/2.46 in the COSY and TOCSY spectra, as well as with a carbonyl carbon at δ_C 174.9 in the HMBC spectrum. Initially, the elemental composition and molecular formula of **2** suggested that the fatty acid had a molecular formula of $C_{15}H_{30}O_3$. Additional LC-MS results (m/z at 257.08 $[M - H]^-$) of the fatty acid obtained from the acid hydrolysis of **2** confirmed the molecular formula. Thus, the fatty acid was determined as a 3-β-hydroxy-12-methyltetradecanoic acid. Finally, the structure of lipotetrapeptide **2** was constructed as Leu_1-Leu_2-Leu_3-OMeGlu-3-β-hydroxy-12-methyltetradecanoic acid, based on the extensive 2D NMR data analysis (Figure 1).

The molecular formula of **3** was assigned to be $C_{37}H_{68}N_4O_9$ by means of the HRESIMS result, which was the same as that of **1**. Initially, the ^{1}H NMR data of **3** were found very similar to **1**. The difference between compounds **1** and **3** was the presence of several carbon resonances in the upfield region in the ^{13}C NMR data of **3**. The detailed analysis of a complete set of 1D and 2D NMR data of **3** indicated the presence of the same amino acid residues with the same sequence as **1**. Moreover, the primary investigation on the molecular weight of **3** and further LC-MS analysis of the hydrolysate of **3** revealed that the molecular formula of the fatty acid in **3** was the same as

dx.doi.org/10.1021/jf502436r | J. Agric. Food Chem. 2014, 62, 5565−5572

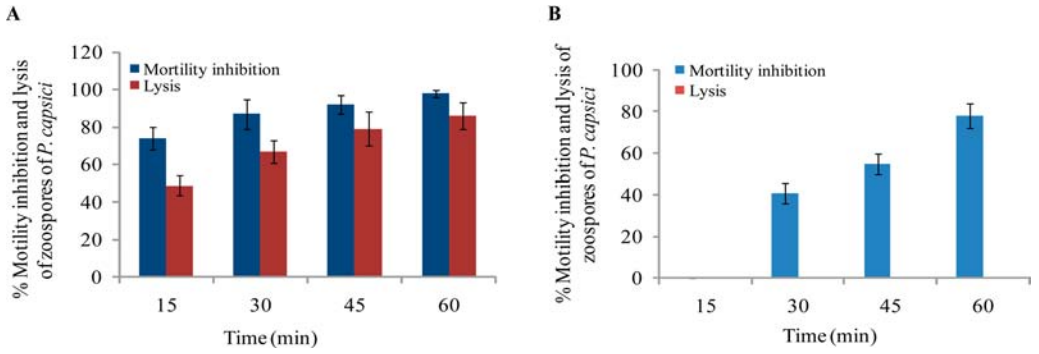

Figure 3. Time-course motility inhibitory and lytic activities of (A) compound **1** and (B) compound **2** against zoospores of the late blight pathogen *P. capsici* at 0.02 μM (investigations were performed in triplicate).

Table 2. Inhibitory and Lytic Activities of Compounds 1 and 2 against *P. capsici*

		motility inhibitory and zoosporicidal activity over control (% ± SE)[a]							
		15 min		30 min		45 min		60 min	
	dose (μM)	inhibited motility	lysed	inhibited motility	lysed	inhibited motility	lysed	inhibited motility	lysed
	0.02	74 ± whi6	49 ± 5	87 ± 8	67 ± 6	92 ± 5	79 ± 9	98 ± 2	86 ± 7
	0.04	89 ± 8	57 ± 4	100 ± 0	92 ± 5	100 ± 0	100 ± 0	nt	nt
1	0.07	100 ± 0	99 ± 1	100 ± 0	100 ± 0	nt	nt	nt	nt
	0.09	100 ± 0	100 ± 0	nt	nt	nt	nt	nt	nt
	0.02	0 ± 0	0 ± 0	41 ± 5	0 ± 0	55 ± 6	0 ± 0	78 ± 6	0 ± 0
	0.04	20 ± 3	0 ± 0	70 ± 8	0 ± 0	88 ± 8	10 ± 4	92 ± 10	21 ± 5
2	0.06	69 ± 6	0 ± 0	82 ± 9	14 ± 5	91 ± 9	21 ± 6	98 ± 3	26 ± 5
	0.09	84 ± 7	0 ± 0	98 ± 2	25 ± 9	98 ± 2	33 ± 7	100 ± 0	45 ± 7
	0.10	100 ± 0	0 ± 0	100 ± 0	34 ± 4	100 ± 0	49 ± 3	100 ± 0	65 ± 4

[a]Data presented here are the average value ± SE of at least three replications in each dose of compounds. nt, not tested. Compounds **3** and **4** did not show any activity against zoospores of *P. capsici* under the conditions tested.

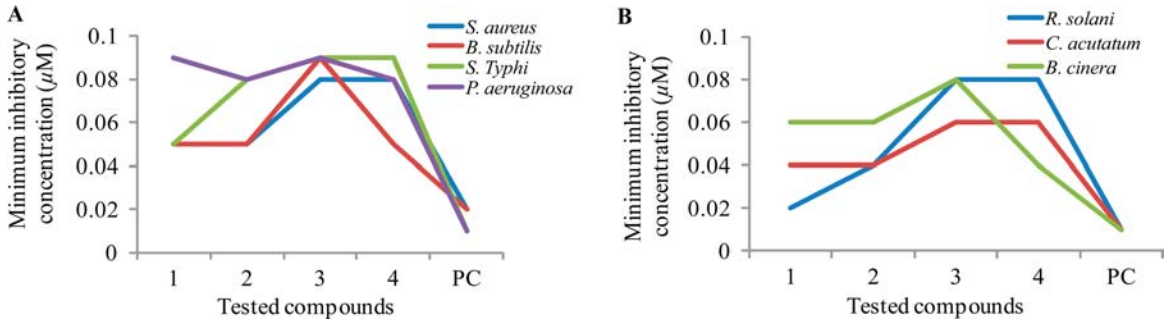

Figure 4. Minimum inhibitory concentrations (μM) of **1**−**4** against (A) Gram positive and Gram negative bacteria and (B) fungi.

that of **1**. However, the presence of additional methine carbons at δ_C 37.9 and 40.4 and methyl carbons at δ_C 11.9 and 19.8 in the ^{13}C NMR spectrum indicated that **3** had a different fatty acid from **1**. By the detailed interpretation of HMBC and TOCSY correlations, these additional methyl carbons were found to be located at C-9 and C-11 positions, and the fatty acid was assigned as a 3-β-hydroxy-9,11-dimethyltridecanoic acid.[20] Finally, the structure of **3** was determined as Leu_1-Leu_2-Glu-Leu_3-3-β-hydroxy-9,11-dimethyltridecanoic acid by the extensive interpretation of 2D NMR data (Figure 1).

The molecular formula of **4** was deduced to be $C_{38}H_{70}N_4O_9$ based on the HRESIMS data, and the ^1H and ^{13}C NMR data indicated that **4** was an additional analogue of **3**. But, it was found that compound **4** had a molecular weight 14 Da more than **3**, indicating the presence of an additional methylene group that could be present either in the fatty acid chain or in the peptide part. The careful interpretation of the NMR data revealed that compounds **3** and **4** had the same peptide moiety, suggesting the additional CH_2 group should be located in the fatty acid unit. This fact was further confirmed by the LC-MS analysis of the hexane phase of the acid hydrolysate of **4**. Thus, the molecular formula of the fatty acid in **4** was determined to be $C_{15}H_{30}O_3$. The fatty acid unit was found to possess same side chain as **3** with an additional methylene group and determined as a 3-β-hydroxy-9,11-dimethyltetradecanoic acid by 2D data analysis.[21] Thus, the final structure of **4** was assigned as Leu_1-Leu_2-Glu-Leu_3-3-β-hydroxy-9,11-dimethyltetradecanoic acid by HMBC and ROESY correlations (Figure 1).

The absolute stereochemistry of the amino acid residues in **1**−**4** was found to be L-form by Marfey's method. In addition, the absolute stereochemistry at C-3 of the fatty acid in **1** was assigned to be *R* by Mosher's MTPA method.[34] The absolute configuration of 3-hydroxy fatty acids in **2**−**4** (obtained from

dx.doi.org/10.1021/jf502436r | J. Agric. Food Chem. 2014, 62, 5565−5572

the hydrolysis of **2**−**4** followed by extraction with hexane) was also found to be *R* by the comparison of their optical rotation values {$[\alpha]^{27}_{D}$ −22 (*c* 0.1, MeOH), $[\alpha]^{27}_{D}$ −45 (*c* 0.1, MeOH), and $[\alpha]^{27}_{D}$ −24 (*c* 0.1, MeOH), respectively} with the optical rotation value $[\alpha]^{27}_{D}$ −26 (*c* 0.1, MeOH) of the 3-hydroxy fatty acid in **1**, as well as literature reviews, as the (*R*)-3-hydroxy fatty acid has the negative $[\alpha]_{D}$ value in MeOH.[20,21,35,36]

Compounds **1**−**4** were tested against both bacteria and fungi. These compounds were found to inhibit the growth of these microorganisms. In particular, compounds **1**−**4** displayed significant activity against *R. solani* and *P. capsici*. Compound **1** showed both inhibitory and lytic activity against *P. capsici* at a concentration of 0.02 μM, whereas compound **2** showed only inhibitory activity at the same concentration (Figure 3). However, compound **2** exhibited lytic activities against *P. capsici* when the concentration was increased (Table 2). It may be noteworthy that compound **2** had an OMeGlu amino acid residue in the peptide unit and an additional CH_2 group in the fatty acid chain compared to **1**. It was also revealed that compounds **1** and **2** exhibited stronger antifungal activity than **3** and **4** (Figure 4B). Compounds **1** and **2** were structurally different from compounds **3** and **4** in terms of having less side chains in the fatty acid units, suggesting that the side chain length and the additional methyl group in the aliphatic chain are important for antifungal activity. Usually, the fungal cell wall consists of three main components, chitin, glucans, and proteins. Antifungal agents display their activity by disrupting the integrity of this membrane or inhibiting sterol synthesis. Conversely, lipopeptides inhibit the synthesis of β-1,3-D-glucan in the cell wall. In fact, without β-1,3-D-glucan, the integrity of the fungal cell wall is compromised, leading to increased osmotic fragility and the eventual lysis of the fungal cell.[20,37] Since compounds **1**−**4** were found to exhibit potent antimicrobial activities, we became curious to know their possible cytotoxic effects. Accordingly, compounds **1**−**4** were tested against a panel of six human cancer cell lines according to a sulforhodamine B (SRB) assay. Interestingly, these compounds did not exhibit any activity (GI_{50} > 25 μM) against these cancer cell lines. The noncyotoxic character of these compounds was further checked against the leukemia cell line using WST-1 and MTT assays. From these detailed bioactivity results, it may be concluded that these lipotetrapeptides would be useful materials to develop environmentally friendly nontoxic antifungal agents.

■ ASSOCIATED CONTENT

Supporting Information

Figures showing ^{1}H, ^{13}C, and 2D NMR spectra of **1**−**4**, HPLC comparison of amino acid residues in **1** with Marfey's derivatives of standard L- and D-amino acids, LC-MS data for **3** and **4**. This material is available free of charge via the Internet at http://pubs.acs.org.

■ AUTHOR INFORMATION

Corresponding Author

*E-mail: shinhj@kiost.ac. Tel.: +82-31-400-6172. Fax: +82-31-400-6170.

Notes

The authors declare no competing financial interest.

■ ACKNOWLEDGMENTS

This research was supported in part by the Korea Institute of Ocean Science and Technology (Grant PE99273 to H.J.S.).

■ REFERENCES

(1) Anderson, N. A. The genetics and pathology of *Rhizoctonia solani*. *Ann. Rev. Phytopathol.* **1982**, *20*, 329−347.
(2) El Bakali, M. A.; Martin, M. P.; Garcia, F.; Moret, A.; Nadal, M.; Monton, C. First report of *Rhizoctonia solani* AG-3 in Catalonia (NE Spain). *Plant Dis.* **2000**, *84*, 806.
(3) El Bakali, M. A.; Martin, M. P.; Garcia, F.; Moret, A.; Nadal, M. Identification of Spanish isolates of *Rhizoctonia solani* from potato by anastomosis grouping, ITS-RFLP and RAMS-fingerprinting. *Phytopathol. Med.* **2003**, *42*, 167−176.
(4) Marin, J. P.; Segarra, J.; Almacellas, J. Enfermedades de los cereales en Cataluña en 1988−90. *Invest Agrar.: Prod. Prot. Veg.* **1992**, *7*, 261−275.
(5) Melero-Vara, J. M.; Jimenez-Diaz, R. M. Etiology, incidence and distribution of cotton seedling damping-off in southern Spain. *Plant Dis.* **1990**, *74*, 597−600.
(6) Akgül, D. S.; Mirik, M. Biocontrol of *Phytophthora capsici* on pepper plants by *Bacillus megaterium* strain. *J. Plant Pathol.* **2008**, *90*, 29−34.
(7) Strange, R. N.; Scott, P. R. Plant disease: A threat to global food security. *Ann. Rev. Phytopathol.* **2005**, *43*, 83−116.
(8) Suprapta, D. N. Potential of microbial antagonists as bio-control agents against plant pathogens. *J. ISSAAS* **2012**, *18*, 1−8.
(9) Nannipieri, P. The potential use of soil enzymes as indicators of productivity, sustainability and pollution. In *Soil biota-management in sustainable farming systems*; Pankhurst, C. E., Doube, B. M., Gupta, V. V. S. R., Grace, P. R., Eds.; CSIRO: Collingwood, Australia, 1994; pp 33−140.
(10) Wage workers in agriculture: condition of employment and work; sectoral activities program. *Report for discussion at the tripartite meeting on improving conditions of employment and work of agricultural wage workers in the context of economic restructuring*. International Labor Organization: Geneva, Switzerland, 1996.
(11) Miller, G. T. *Sustaining the Earth*, 6th ed.; Thompson Learning: Pacific Grove, CA, USA, 2004; Chapter 9, pp 211−216.
(12) Singh, P.; Cameotra, S. S. Potential applications of microbial surfactants in biomedical sciences. *Trends Biotechnol.* **2004**, *22*, 142−146.
(13) Cho, S. J.; Hong, S. Y.; Kim, J. Y.; Park, S. R.; Kim, M. K.; Lim, W. J. Endophytic *Bacillus* sp. CY22 from a balloon flower (*Platycodon grandiflorum*) produces surfactin isoforms. *J. Microbiol. Biotechnol.* **2003**, *13*, 859−865.
(14) Cao, X.; Wang, A. H.; Jiao, R. Z.; Wang, C. L.; Mao, D. Z.; Yan, L. Surfactin induces apoptosis and G2/M arrest in human breast cancer MCF-7 cells through cell cycle factor regulation. *Cell Biochem. Biophys.* **2009**, *55*, 163−171.
(15) Cao, X. H.; Wang, A. H.; Wang, C. I.; Mao, D. Z.; Lu, M. F.; Cui, Y. Q. Surfactin induces apoptosis in human breast cancer MCF-7 cells through a ROS/JNK-mediated mitochondrial/caspase pathway. *Chem.-Biol. Interact.* **2010**, *183*, 357−362.
(16) Vollenbroich, D.; Ozel, M.; Vater, J.; Kamp, R. M.; Pauli, G. Mechanism of inactivation of enveloped viruses by the biosurfactant surfactin from *Bacillus subtilis*. *Biologicals* **1997**, *25*, 289−297.
(17) Kim, S. D.; Cho, J. Y.; Park, H. J.; Lim, C. R.; Lim, J. H.; Yun, H. I. A comparison of the anti-inflammatory activity of surfactin A, B, C, and D from *Bacillus subtilis*. *J. Microbiol. Biotechnol.* **2006**, *16*, 1659.
(18) Park, S. Y.; Kim, Y. H. Surfactin inhibits immunostimulatory function of macrophages through blocking NK-jB, MAPK and Akt pathway. *Int. Immunopharmacol.* **2009**, *9*, 886−893.
(19) Kurtz, M. B.; Douglas, C. M. Lipopeptide inhibitors of fungal glucan synthase. *J. Med. Vet. Mycol.* **1997**, *35*, 79−86.
(20) Tareq, F. S.; Lee, M.; Lee, H. S.; Lee, Y. J.; Lee, J. S.; Hasan, C. M.; Islam, M. T.; Shin, H. J. Gageotetrins A−C, noncytotoxic

antimicrobial linear lipopeptides from a marine bacterium *Bacillus subtilis*. *Org. Lett.* **2014**, *16*, 928−93.
(21) Tareq, F. S.; Lee, M.; Lee, H. S.; Lee, Y. J.; Lee, J. S.; Shin, H. J. Gageostatins A−C, antimicrobial linear lipopeptides from a marine *Bacillus subtilis*. *Mar. Drugs* **2014**, *12*, 871−885.
(22) Ohtani, I.; Kusumi, T.; Kashman, Y.; Kakisawa, H. High-field FT NMR application of Mosher's method. The absolute configuration of marine terpenoids. *J. Am. Chem. Soc.* **1991**, *113*, 4092−4096.
(23) Marfey, P. Determination of D-amino acids. II. Use of a bifunctional reagent, 1,5-difluoro-2,4-dinitrobenzene. *Carlsberg Res. Commun.* **1984**, *49*, 591−596.
(24) Erwin, D. C.; Ribeiro, O. K. *Phytophthora Diseases Worldwide*; APS Press: St. Paul, MN, USA, 1996; 562 pp.
(25) Islam, M. T.; Hashidoko, Y.; Deora, A.; Ito, T.; Tahara, S. Suppression of damping-off disease in host plants by the rhizoplane bacterium *Lysobacter* sp. strain SB-K88 is linked to plant colonization and antibiosis against soilborne Peronosporomycetes. *Appl. Environ. Microbiol.* **2005**, *71*, 3786−3796.
(26) Islam, M. T.; Von, T. A.; Laatsch, H. Protein kinase C is likely to be involved in zoosporogenesis and maintenance of flagellar motility in the peronosporomycete zoospores. *Mol. Plant−Microbe Interact.* **2011**, *24*, 938−947.
(27) Islam, M. T.; Ito, T.; Sakasal, M.; Tahara, S. Zoosporicidal activity of polyflavonoid tannin identified in *Lannea coromandelica* stem bark against phytopathogenic oomycete *Aphanomyces cochlioides*. *J. Agric. Food Chem.* **2002**, *50*, 6697−6703.
(28) Tareq, F. S.; Kim, J. H.; Lee, M. A.; Lee, H. S.; Lee, J. S.; Lee, Y. J.; Shin, H. J. Antimicrobial gageomacrolactins characterized from the fermentation of the marine-derived bacterium *Bacillus subtilis* under optimum growth conditions. *J. Agric. Food Chem.* **2013**, *61*, 3428−3434.
(29) Appendino, G.; Gibbons, S.; Giana, A.; Pagani, A.; Grassi, G.; Stavri, M.; Smith, E.; Rahman, M. M. Antibacterial cannabinoids from *Cannabis sativa*: a structure-activity study. *J. Nat. Prod.* **2008**, *71*, 1427−1430.
(30) Skehan, P.; Storeng, R.; Scudiero, D.; Monks, A.; McMohan, J.; Vistica, D.; Warren, J. T.; Bokesch, H.; Kenney, S.; Boyed, M. R. New colorimetric cytotoxicity assay for anticancer-drug screening. *J. Natl. Cancer Inst.* **1990**, *82*, 1107−1112.
(31) Seo, Y.; Cho, K. W.; Lee, H. S.; Rho, J. R.; Shin, J. New acetylenic enol ethers of glycerol from the sponge *Petrosia* sp. *J. Nat. Prod.* **1999**, *62*, 122−126.
(32) Chucheep, K.; Kanlayanarat, S.; Maneerat, C.; Matsuo, T. Application of WST-1 to measurement of cell viability in low temperature-stressed explants of tropical vegetables. *J. Food Agric. Environ.* **2005**, *3*, 262−268.
(33) Mosmann, T. Rapid colorimetric assay for cellular growth and survival: Application to proliferation and cytotoxicity assays. *J. Immunol. Methods* **1983**, *65*, 55−63.
(34) Freire, F.; Seco, J. M.; Emilio, Q.; Riguera, R. Determining the absolute stereochemistry of secondary/secondary diols by ^{1}H NMR: basis and applications. *J. Org. Chem.* **2005**, *70*, 3778−3790.
(35) Jenske, R.; Vetter, W. Enantioselective analysis of 2- and 3-hydroxy fatty acids in food samples. *J. Agric. Food Chem.* **2008**, *56*, 11578−11583.
(36) Maider, P.; Francoise, P.; Jean, W. Solid-phase synthesis of surfactin, a powerful biosurfactant produced by *Bacillus subtilis,* and of four analogues. *Int. J. Pept. Res. Ther.* **2005**, *11*, 195−202.
(37) Kartsonis, N. A.; Nielsen, J.; Douglas, C. M. Caspofungin: the first in a new class of antifungal agents. *Drug Resist. Updates* **2003**, *6*, 197−218.

JOURNAL OF AGRICULTURAL AND FOOD CHEMISTRY

Article

pubs.acs.org/JAFC

Investigation of Anthocyanin Profile of Four Elderberry Species and Interspecific Hybrids

Maja Mikulic-Petkovsek,*[,†] Valentina Schmitzer,[†] Ana Slatnar,[†] Biljana Todorovic,[†] Robert Veberic,[†] Franci Stampar,[†] and Anton Ivancic[‡]

[†]Biotechnical Faculty, Department of Agronomy, Chair for Fruit, Wine and Vegetable Growing, University of Ljubljana, Jamnikarjeva 101, SI-1000 Ljubljana, Slovenia

[‡]Faculty of Agriculture and Life Sciences, Institute for Genetics, University of Maribor, SI-2000 Hoce, Slovenia

ABSTRACT: A total of 19 different anthocyanins have been detected in four elderberry species and eight hybrids and quantified with the use of HPLC−MS^n. The profile and content levels of anthocyanins varied considerably among the analyzed elderberry species and hybrids. Cyanidin-3-*O*-sambubioside and cyanidin-3-*O*-glucoside were the most abundant anthocyanins in *Sambucus nigra* fruits. On the other hand, the prevalent anthocyanin in *S. javanica* hybrids was identified as cyanidin-3-(*E*)-*p*-coumaroyl-sambubioside-5-glucoside. The highest content of total analyzed anthocyanins (TAA) was determined in berries of the interspecific hybrid *S. javanica* × *S. racemosa*, followed by *S. nigra*, (*S. javanica* × *S. nigra*) × cv. Black Beauty, and (*S. javanica* × *S. nigra*) × *S. cerulea*. Berries of *S. nigra* var. *viridis* contained significantly lower levels of TAA. Our results provide novel information for nutritional research in addition to breeding programs, which strive to create new hybrids or cultivars with enhanced levels of bioactive components.

KEYWORDS: *Sambucus cerulea, S. ebulus, S. javanica, S. nigra, S. racemosa, elderberry fruits, anthocyanins*

INTRODUCTION

The *Sambucus* L. genus was formerly grouped in the Caprifoliaceae family, but novel genetic research places it into the Adoxaceae family.[1,2] It includes between 5 and 30 species, depending on taxonomy, distributed in the temperate and subtropical regions of the Northern and Southern Hemisphere. The genus *Sambucus* mostly consists of perennial subshrubby herbs with creeping rhizomes, many-stemmed shrubs (sometimes rhizomatous), or small deciduous or semievergreen trees.[3]

The most important species are *S. cerulea* Raf. (blue elder), *S. javanica* Blume (Javanese elder, sin. Chinese elder), and *S. nigra* L. (common elderberry, syn. elderberry). The use of interspecific hybridization in the genetic breeding of the *Sambucus* species is a relatively novel approach. First systematic attempts to produce hybrid plants between *S. nigra* and *S. racemosa* were reported by Böcher[4] in Denmark, Winge[5] in North Zealand, and Nilsson[6] in southern Sweden. The resulting F_1 hybrids were usually sterile. Most of the phenotypical traits were intermediate between the parental species. According to Chia,[7] a higher fertility level was achieved in crosses between *S. canadensis* and *S. nigra*, and *S. cerulea* and *S. nigra*. On the other hand,[8] genetic sterility was reported in hybrids between *S. nigra* and *S. ebulus*.

Presently, one of the most important trends in food and pharmaceutical industries is the growing demand for valuable natural sources of antioxidant compounds. Among common fruits and vegetables, elderberry is one of the richest in anthocyanins, flavonols glycosides, and other polyphenolics, which contribute to the high antioxidant capacity of its berries.[9,10] Additionally, antioxidant properties of anthocyanins present in elderberries are associated with beneficial effects on human health due to their ability to protect against cancer or heart diseases,[11,12] asthma, arthritis,[13,14] cardiovascular diseases,[15] and different viral infections.[16,17]

High anthocyanin content makes elderberry fruits useful for processing to concentrates, jams, jellies, juices, and dried powders.[18,19] Because of their intense color, the concentrates are suitable for providing natural red/purple hues to different food products. Fruits of the cultivated elderberry are very dark purple, nearly black, but various species range from bright red to blue and dark purple shades.[20] In Europe, cultivars derived from *S. nigra* are mainly cultivated, whereas in the U.S. most of the cultivars belong to *S. Canadensis*.[21] The content and composition of anthocyanins vary between different species and cultivars[22−27] and are also environmentally triggered. Factors such as light, temperature, and stress during cultivation significantly modify their synthesis and accumulation.[28]

Recently, a great deal of renewed interest in anthocyanins has emerged due to their potential health benefits as antioxidants and antiinflammatory agents. As the market for healthy products requires new genotypes with different processing and quality characteristics, there is a strong need for the selection of genotypes optimal for increasing the quality of food products. Data on the chemical composition of elderberry fruits are scarce; only a few studies revealed anthocyanin levels of various *Sambucus* species or cultivars.[22−24] Although the content of fruit phenolics is affected by environmental conditions and the level of maturity at harvest, it is very important to know the chemical composition and the antioxidant capacity of different elderberry species to selectively

Received: March 12, 2014
Revised: May 15, 2014
Accepted: May 16, 2014
Published: May 16, 2014

ACS Publications © 2014 American Chemical Society

use them in pharmaceutical and alimentary industry. To our knowledge, there have been no comparative studies on the chemical composition of a large number of elderberry genotypes grown under the same ecological conditions.

Therefore, the purpose of the study was to determine a broad range of anthocyanins and their content in five genotypes belonging to four different elderberry species (*Sambucus cerulea*, *S. ebulus*, *S. nigra* − (var. *nigra* and var. *viridis*), and *S. racemosa* (var. *miquelli*)), and compare them to the anthocyanin profile of eight elderberry interspecific hybrids. The final aim is to select genotypes with favorable composition and content of anthocyanins. The biochemical evaluation of elderberry genetic resources and the identification of individual bioactive compounds and their properties as natural agents is of utmost significance to breeders. This is the first Article on anthocyanin composition of a large number of elderberry species and interspecific hybrids striving to select cultivars, which may prove interesting for different processing industries.

MATERIALS AND METHODS

Plant Material. The biochemical investigation included four species of the *Sambucus* genus (1, *Sambucus cerulea*; 2, *S. ebulus*; 3, *S. nigra*; 4, *S. racemosa* var. *miquelli*) and three groups of their interspecific hybrids (1, three hybrids of *S. cerulea*; 2, four hybrids of *S. nigra*; 3, one hybrid of *S. racemosa*) (Table 1). The self-incompatible genotype of *S. javanica* originating from tropical regions did not produce a sufficient quantity of berries and could not be included in chemical analyses; however, this species was crucial in the hybridization process. All interspecific hybrids were developed at the University of Maribor, Faculty of Agriculture and Life Sciences, by Anton Ivancic using *S. javanica* as a genetic bridge. The female components (*S. javanica* and some of the hybrids *S. javanica* × *S. nigra*) were highly self-incompatible, enabling pollination without emasculation. The hybrid origin of the majority of the interspecific hybrids was determined by molecular and morphological analyses.[29] The hybrid origin of *S. javanica* × *S. racemosa* hybrids, which were created later, was determined only by morphological markers: by comparing leaf, inflorescence, floret, infrutescence, and berry characteristics.

Hybrid plants are being maintained in the gene bank of the University of Maribor, Faculty of Agriculture and Life Sciences, near Hoce (Slovenia). For multiplication, a simple vegetative propagation by cuttings is used.

Table 1. *Sambucus* Species and Interspecific Hybrids Analyzed in the Study

species	abbreviation	origin
S. cerulea		Slovenia (local cultivated genotype)
S. ebulus		Slovenia (wild-growing genotype)
S. nigra var. *nigra* (common type)		Slovenia (local population)
S. nigra var. *viridis*		Slovenia (botanical garden Maribor)
S. racemosa var. *miquelli*		Slovenia (botanical garden Maribor)
interspecific hybrids	**abbreviation**	**origin**
S. cerulea Group		
S. javanica × *S. cerulea*	JA × CER	University of Maribor Gene Bank
(*S. javanica* × *S. nigra*) × *S. cerulea*	(JA × NI) × CER	University of Maribor Gene Bank
S. cerulea × *S. nigra*	CER × NI	University of Maribor Gene Bank
S. nigra Group		
S. javanica × *S. nigra*	JA × NI	University of Maribor Gene Bank
S. javanica × (*S. javanica* × *S. nigra*)	JA × (JA × NI)	University of Maribor Gene Bank
(*S. javanica* × *S. nigra*) × *S. nigra*	(JA × NI) × NI	University of Maribor Gene Bank
(*S. javanica* × *S. nigra*) × cv. Black Beauty		University of Maribor Gene Bank
S. racemosa Group		
S. javanica × *S. racemosa*	JA × RAC	University of Maribor Gene Bank

Chemicals. The following standards were used for the quantification of anthocyanins: cyanidin-3-*O*-glucoside, cyanidin-3,5-di-*O*-glucoside, and pelargonidin-3-*O*-glucoside from Sigma-Aldrich Chemie GmbH; and cyanidin-3-*O*-galactoside from Fluka Chemie GmBH. Methanol for the extraction of phenolics was acquired from Sigma-Aldrich Chemie. The chemicals for the mobile phases were HPLC−MS grade acetonitrile and formic acid from Fluka Chemie GmBH. Water for the mobile phase was double distilled and purified with the Milli-Q system (Millipore, Bedford, MA).

Extraction of Phenolic Compounds. For each genotype, six independent repetitions were done ($n = 6$). Until extraction, they were kept in deep freeze (−80 °C). The extraction of berries was performed as described by Mikulic-Petkovsek et al.,[30] with some modification. Elderberry fruits were ground to a fine paste with liquid nitrogen, and 3 g was extracted with 15 mL of methanol containing 3% (v/v) formic acid and 1% (w/v) 2,6-di-*tert*-butyl-4-methylphenol (BHT) in a cooled ultrasonic bath for 1 h. BHT was added to the samples to prevent oxidation.

After extraction, the fruit extracts were centrifuged for 10 min at 10.000 rpm. Each supernatant was filtered through a Chromafil AO-20/25 polyamide filter manufactured by Macherey-Nagel (Düren, Germany) and transferred to a vial prior to injection into the HPLC (high performance liquid chromatography) system.

Determination of Individual Phenolic Compounds Using HPLC-DAD-ESI-MS^n Analysis. Anthocyanins were analyzed on a Thermo Finnigan Surveyor HPLC system (Thermo Scientific, San Jose, CA) with a diode array detector at 530 nm. Spectra of the compounds were recorded between 200 and 600 nm. The column was a Gemini C_{18} (150 × 4.6 mm 3 μm; Phenomenex, Torrance, CA) operated at 25 °C. The elution solvents were aqueous 0.1% formic acid in double distilled water (A) and 0.1% formic acid in acetonitrile (B). Samples were eluted according to the linear gradient from 5% to 20% B in the first 15 min, followed by a linear gradient from 20% to 30% B for 5 min, then an isocratic mixture for 5 min, followed by a linear gradient from 30% to 90% B for 5 min, and then an isocratic mixture for 15 min before returning to the initial conditions.[31] The injection amount was 20 μL, and the flow rate was 0.6 mL min^{-1}.

All phenolic compounds presented in our results were identified by an HPLC-Finnigan MS detector and an LCQ Deca XP MAX (Thermo Finigan, San Jose, CA) instrument with electrospray interface (ESI) operating in positive ion mode. The analyses were carried out using full scan data-dependent MS^n scanning from m/z 110 to 1500. Column and chromatographic conditions were identical to those used for the HPLC-DAD analyses. The injection volume was 10 μL, and the flow rate was maintained at 0.6 mL min^{-1}. The capillary temperature was 250 °C, the sheath gas and auxiliary gas were 60 and 15 units, respectively, the source voltage was 4 kV, and normalized collision energy was between 20−35%. Spectral data were elaborated using the Excalibur software (Thermo Scientific). The identification of compounds was confirmed by comparing retention times and their spectra as well as by adding the standard solution to the sample and by fragmentation.

Concentrations of anthocyanins were calculated from peak areas of the sample and the corresponding standards and expressed in mg 100 g^{-1} fresh weight (FW) of elderberry fruits. For compounds lacking standards, quantification was carried out using compounds similar to the standards. Thus, pelargonidin-3-sambubioside was quantified in equivalents of pelargonidin-3-*O*-glucoside, and all cyanidin glycosides

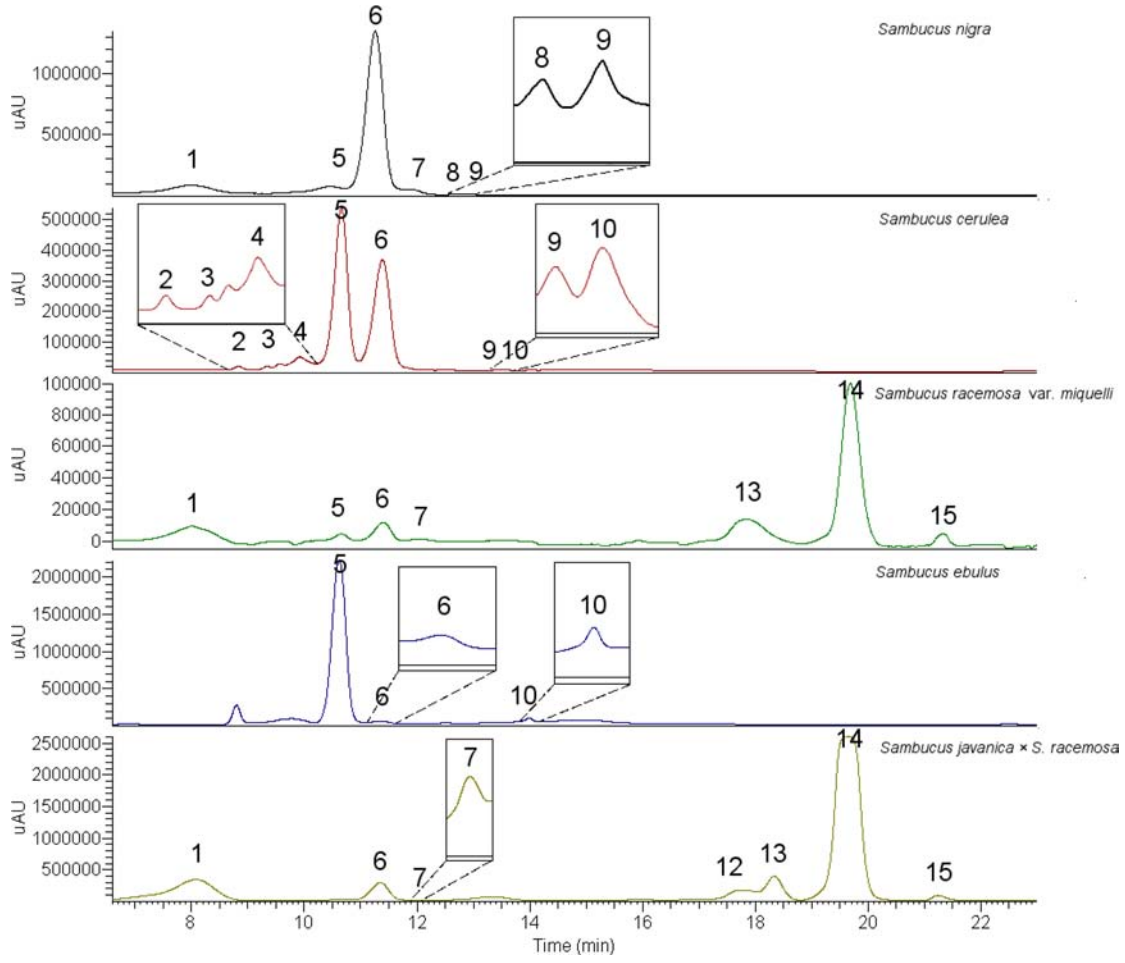

Figure 1. Anthocyanin profile of elderberry fruits of *Sambucus nigra*, *Sambucus cerulea*, *Sambucus racemosa* var. *miquelli*, *Sambucus ebulus*, and *Sambucus javanica* × *S. racemosa*. Peak numbers correspond to the compounds listed in Table 2.

(except for cyanidin-3-galactoside) were quantified in equivalents of cyanidin-3-*O*-glucoside.

Statistical Analysis. The data were analyzed with the Statgraphics Plus 4.0 program (Manugistics, Inc.) using one-way analysis of variance (ANOVA). The differences among the species and interspecific hybrids were tested using the Duncan test at the 0.05 significance level. The means and the standard errors of the means are reported (mean ± SE).

RESULTS AND DISCUSSION

All 13 elderberry genotypes were characterized by unique anthocyanin profiles. Because of limited space, only five representative chromatograms (species *S. nigra*, *S. cerulea*, *S. racemosa* var. *miquelli*, *S. ebulus*, and hybrid JA × RAC) are presented in Figure 1. A total of 19 different anthocyanins were detected in four elderberry species and eight hybrids. By comparing their MS data with recently published records,[20,24] 13 of them were identified. In all analyzed elderberries, cyanidin-based anthocyanins were the major anthocyanins, followed by glycosides of pelargonidin. Similar findings have previously been reported by Wu et al.[24] and Veberic et al.[32]

Peak 1 contained two compounds. The first had a $[M^+]$ at m/z 611, which on MS^2 produced a minor fragment at m/z 449 ($[M^+] - 162$, loss of glucosyl unit) and a major fragment at m/z 287 (cyanidin, $[M^+] - 162$ corresponding to a glucosyl moiety). This compound was, therefore, identified as cyanidin-3,5-diglucoside (also confirmed by the addition of an external standard). This cyanidin is one of the most common anthocyanins in plant tissue previously also confirmed in elderberry fruit.[24,33] Cyanidin-3,5-diglucoside was detected in *Sambucus nigra* fruit and its interspecific hybrids. On the other hand, *S. cerulea* (CER), *S. ebulus* (EB), and *S. racemosa* var. *miquelli* (MIQ) did not contain this anthocyanin. Cyanidin-3,5-diglucoside was also detected in two interspecific hybrids with *S. javanica*, JA × RAC and JA × CER. Although chemical analysis of *S. javanica* was not performed, it can be concluded that its fruits contain this anthocyanin as it is not present in RAC in CER fruit. Statistically the highest level of cyanidin-3,5-diglucoside was detected in fruit of JA × (JA × NI) hybrid, which contained 37.2 mg 100 g^{-1} FW. It seems that *S. javanica*, similar to *S. nigra*, accumulates high levels of this cyanidin. The content level of cyanidin-3,5-diglucoside in analyzed elderberry fruits is in accordance with the results of Kaack and Austed.[33] The second compound in peak 1 had an ion at $[M^+]$ m/z 743, which yielded MS^2 fragment at m/z 581 ($[M^+] - 162$, loss of a glucosyl unit) and MS^3 fragment at m/z 449/287 ($[M^+] - 132$, loss of a xylosyl and $[M^+] - 162$, a glucosyl unit). This corresponds to the fragmentation pattern of cyanidin-3-*O*-sambubioside-5-*O*-glucoside, a prior-identified elderberry anthocyanin.[34] The highest content of this cyanidin was quantified in JA × CER (146.9 mg 100 g^{-1}) hybrid, followed by (JA × NI) × cv. Black Beauty hybrid (136.8 mg 100 g^{-1}). In the former, *S. javanica* is probably responsible for the accumulation cyanidin-3-*O*-sambubioside-5-*O*-glucoside as the

dx.doi.org/10.1021/jf5011947 | J. Agric. Food Chem. 2014, 62, 5573−5580

Table 2. List of Anthocyanins Identified in Different Accessions of Elderberry Fruits and MS^n Specifications

peak no.[a]	t_R[b]	tentative identification	$[M]^{+c}$ (m/z)	MS^2	MS^3	identified in following species and interspecific hybrids[d,e]
1	7.99	cyanidin-3-*O*-sambubiosyl-5-*O*-glucoside	743	581	449/287	in all, except CER, EB
1	7.99	cyanidin-3,5-*O*-diglucoside	611	449/287		in all, except CER, EB
2	8.83	cyanidin-glycoside 1 (cyanidin-pentoside-hexoside 1)	581	449	287	CER
3	9.34	cyanidin-glycoside 2 (cyanidin-pentoside-hexoside 2)	581	449	287	CER
4	9.92	cyanidin-glycoside 3 (cyanidin-pentoside-hexoside 3)	581	449	287	CER
5	10.66	cyanidin-glycoside 4 (cyanidin-pentoside-hexoside 4)	581	449	287	in all, except JA × CER, JA × NI, VIR
5	10.66	cyanidin-3-*O*-galactoside	449	287		in all, except JA × NI, CER, EB, MIQ, VIR
6	11.40	cyanidin-3-*O*-sambubioside	581	449/287		in all
6	11.40	cyanidin-3-*O*-glucoside	449	287		in all
7	12.05	cyanidin-3-*O*-rutinoside	595	449	287	JA × CER, (JA × NI) × NI, (JA × NI) × cv. Black Beauty, NI
7	12.05	cyanidin-sambubioside-malonylglucoside	829	667	449/287	JA × CER, (JA × NI) × cv. Black Beauty, MIQ
8	12.54	cyanidin-dipentoside	551	419	287	CER, EB
9	12.66	pelargonidin-3-*O*-glucoside	433	271		NI, (JA × NI) × NI, (JA × NI) × CER, JA × (JA × NI), (JA × NI) × cv. Black Beauty
10	12.95	pelargonidin-3-*O*-sambubioside	565	433/271		NI, CER, (JA × NI) × NI, JA × (JA × NI), (JA × NI) × cv. Black Beauty
11	13.36	cyanidin-sambubioside-acetylglucoside	785	623	449/287	JA × RAC, JA × NI
12	17.73	cyanidin-xylosyl-dihexoside	905	743	449/287	JA × RAC, (JA × NI) × CER, JA × (JA × NI), JA × NI
13	18.33	cyanidin-3-(*Z*)-*p*-coumaroyl-sambubioside-5-glucoside	889	727	449/287	JA × RAC, (JA × NI) × CER, JA × (JA × NI), JA × NI, MIQ, CER × NI
14	19.65	cyanidin-3-(*E*)-*p*-coumaroyl-sambubioside-5-glucoside	889	727	449/287	JA × RAC, JA × CER, (JA × NI) × CER, JA × (JA × NI), JA × NI, (JA × NI) × cv. Black Beauty, MIQ, CER × NI
15	21.24	cyanidin-3-*p*-coumaroyl-sambubioside	727	433	287	JA × RAC, (JA × NI) × CER, JA × (JA × NI), JA × NI, MIQ, CER × NI

[a]Peak number. [b]Retention time. [c]Anthocyanins were obtained in the positive ion mode. [d]Abbreviations: CER, *Sambucus cerulean*; EB, *Sambucus ebulus*; JA, *Sambucus javanica*; NI, *Sambucus nigra* var. *nigra*; VIR, *Sambucus nigra* var. *viridis*; MIQ, *Sambucus racemosa* var. *miquelli*. [e]Abbreviations for interspecific hybrids are in Table 1.

fruit of *S. cerulea* does not contain it. However, research on *S. javanica* biochemistry is very limited, and no data comparison with literature could be made. Fruits of *S. ebulus* also lacked cyanidin-3-*O*-sambubioside-5-*O*-glucoside, but a high content of this anthocyanin was measured. Cyanidin-3-*O*-sambubioside-5-*O*-glucoside constituted from 3% to 44% total anthocyanins in elderberry fruit analyzed. Contrary to our results, Bridle and Garcia Viguera[35] reported cyanidin 3-*O*-sambubioside-5-*O*-glucoside as the major anthocyanin in the *S. nigra* sample, but Bronnumhansen and Hansen[36] reported cyanidin 3-glucoside as the prevalent pigment of *S. nigra*. The variations in results may be explained by differences of individual genotypes as well as specific growing conditions. It is often difficult to compare anthocyanin levels of elderberries in recent studies mainly because of the different methods and variable expression of the results (e.g., fresh weight vs dry weight).

MS data of peaks 2, 3, 4, and 5 shared the same mass spectral pattern: a molecular ion at 581 ($[M]^+$ m/z 581),a MS^2 fragment ion at m/z 449, and MS^3 fragment ion at m/z 287. The fragment loss of 132 (a pentose unit) and 162 (a hexose unit) suggests the anthocyanins to be cyanidin-pentoside-hexosides, and they were thus tentatively identified as cyanidin glycosides 1, 2, 3, and 4. Cyanidin glycosides 1−3 were only present in berries of *Sambucus cerulea*, but cyanidin glycoside 4 was identified in some others species and hybrids analyzed. An exceptionally high content of cyanidin glycoside 4 was detected in *S. ebulus* fruit (345.8 mg 100 g^{-1}, representing 97% TAA), followed by *S. cerulea* fruit (78.9 mg 100 g^{-1}, representing 53% TAA). Other analyzed species and hybrids contained less than 1 mg 100 g^{-1} of this anthocyanin. No cyanidin glycoside 4 could be detected in hybrids between *S. nigra* and *S. javanica* (JA × NI) (Table 3).

In addition to a $[M^+]$ ion at m/z 581, peak 5 yielded a $[M^+]$ ion at m/z 449. MS^2 fragmentation produced a cyanidin ion at m/z 287 ($[M^+]$ − 162, loss of a hexose moiety). This peak was thus identified as cyanidin-3-galactoside and further confirmed by cochromatography with a cyanidin-3-galactoside standard. A relatively high content of this anthocyanin was measured in fruit of JA × CER (32.2 mg 100 g^{-1}) hybrid, whereas other analyzed species and hybrids only contained traces of cyanidin-3-galactoside (less than 0.7 mg 100 g^{-1}).

Peak 6 contained an ion at m/z 581, which fragmented on MS^2 to produce a minor ion at m/z 449 ($[M]^+$ − 132, loss of a xylosyl unit) and a major fragment at m/z 287 ($[M]^+$ − 132 − 162, loss of xylosyl and glucosyl units). This compound was present in all studied elderberry species and hybrids and has been identified as cyanidin-3-*O*-sambubioside, previously confirmed in elderberry by Chandra et al.[37] and Lee and Finn.[20] Statistically the highest level of cyanidin-3-sambubioside was detected in *S. nigra* fruit (560 mg 100 g^{-1}), representing 61% TAA. Consequently, several interspecific *S. nigra* hybrids ((JA × NI) × CER and (JA × NI) × NI) also contained high levels of this anthocyanin. Similar content levels of cyanidin-3-sambubioside were reported by Veberic et al.[23] and Wu et al.[24] in various *Sambucus* species. *S. cerulea* fruit was also rich in this anthocyanin (representing 42% TAA); however, *S. racemosa*

dx.doi.org/10.1021/jf5011947 | J. Agric. Food Chem. 2014, 62, 5573−5580

Table 3. Individual Quantities (mean ± SE, mg 100 g^{-1} FW) of Each Anthocyanin Determined in Different Elderberry Species or Interspecific Hybrid

	C-3-sam-5-glu[a]			C-3,5-diglu			C-pent-hex 4			C-3-gal			C-3-glu			C-3-sam			C-3-rut		
	$\bar{x}$	SE		$\bar{x}$	SE		$\bar{x}$	SE		$\bar{x}$	SE		$\bar{x}$	SE		$\bar{x}$	SE		$\bar{x}$	SE	
JA × RAC	95.54	1.22	e[b]	32.49	0.42	f	0.51	0.02	a	0.64	0.03	a	32.37	1.06	b	10.68	0.35	ab			
JA × CER	146.91	2.70	g	33.64	0.62	f				32.27	0.62	b	31.91	0.61	b	13.78	0.26	ab	2.16	0.09	b
(JA × NI) × CER	13.97	0.83	b	17.86	1.06	d	0.47	0.12	a	0.13	0.03	a	59.05	5.89	c	111.64	11.14	d			
CER × NI	13.88	1.60	b	8.74	1.01	c	0.30	0.06	a	0.00	0.00	a	1.14	0.17	a	2.45	0.36	a			
JA × (JA × NI)	57.71	4.62	d	37.26	2.34	g	0.08	0.02	a	0.29	0.08	a	131.15	11.05	e	18.22	1.78	ab			
JA × NI	12.91	0.40	b	4.52	0.14	b							6.62	0.13	a	5.63	0.11	a			
(JA × NI) × NI	97.39	1.02	e	3.26	0.03	b	0.72	0.06	a	0.35	0.03	a	181.76	2.81	f	104.69	1.62	d	3.00	0.34	b
(JA × NI) × cv. Black Beauty	136.87	3.41	f	25.34	0.52	e	0.31	0.09	a	0.39	0.12	a	91.40	0.64	d	24.63	2.11	b	0.14	0.01	a
Sambucus cerulea							78.99	4.70	b				2.85	0.16	a	63.43	3.64	c			
Sambucus ebulus							345.82	5.44	c				0.49	0.01	a	6.56	0.18	a			
Sambucus racemosa var. *miquelli*	4.08	0.18	a				0.17	0.16	a				0.13	0.01	a	1.36	0.08	a			
Sambucus nigra	42.19	6.48	c	5.91	0.91	bc	1.08	0.32	a	0.32	0.09	a	190.63	15.98	f	344.48	20.65	e	9.36	1.11	c
Sambucus nigra var. *viridis*	0.09	0.06	a	0.02	0.01	a							0.55	0.34	a	1.03	0.64	a			

[a]Anthocyanin: C-3-sam-5-glu, cyanidin-3-*O*-sambubiosyl-5-*O*-glucoside; C-3,5-diglu, cyanidin-3,5-*O*-diglucoside; C-pent-hex 4, cyanidin-pentoside-hexoside 4; C-3-gal, cyanidin-3-*O*-galactoside; C-3-glu, cyanidin-3-*O*-glucoside; C-3-sam, cyanidin-3-*O*-sambubioside; C-3-rut, cyanidin-3-*O*-rutinoside. [b]Different letters (a−g) denote statistically significant differences in individual anthocyanins among elderberry species or interspecific hybrid by Duncan multiple range test at $P < 0.05$.

Table 4. Individual Quantities (mean ± SE, mg 100 g^{-1} FW) of Each Anthocyanin Determined in Different Elderberry Species or Interspecific Hybrid

	C-sam-malonylglu[a]			C-sam-acetylglu			C-xyl-dihex			C-3-(*Z*)-cou-sam-5-glu			C-3-(*E*)-cou-sam-5-glu			C-3-cou-sam			total anthocyanins		
	$\bar{x}$	SE		$\bar{x}$	SE		$\bar{x}$	SE		$\bar{x}$	SE		$\bar{x}$	SE		$\bar{x}$	SE		$\bar{x}$	SE	
JA × RAC				10.45	0.35	b	2.66	0.09	a	11.92	0.41	d	583.04	5.68	f	8.03	0.14	b	834.67	7.66	j
JA × CER	1.48	0.06	b[b]										0.83	0.32	a				331.88	4.16	e
(JA × NI) × CER							5.30	0.10	b	1.43	0.03	a	162.89	5.41	c	68.96	4.69	c	444.04	22.79	g
CER × NI										4.93	0.43	c	49.22	5.09	b	2.38	0.26	a	80.15	2.17	b
JA × (JA × NI)							12.05	0.48	c	1.92	0.13	ab	246.08	9.81	e	8.18	0.36	b	505.25	17.62	h
JA × NI				3.53	0.19	a	15.94	0.39	d	4.65	0.11	c	191.23	3.78	d	8.64	0.26	b	253.66	5.28	d
(JA × NI) × NI																			391.17	4.16	f
(JA × NI) × cv. Black Beauty	0.14	0.01	a										0.37	0.13	a				479.23	26.22	gh
Sambucus cerulea																			148.63	8.75	c
Sambucus ebulus																			353.37	5.38	ef
Sambucus racemosa var. *miquelli*	0.23	0.02	a							2.59	0.09	b	11.31	0.28	a	0.61	0.05	a	20.47	0.57	a
Sambucus nigra																			560.48	59.38	i
Sambucus nigra var. *viridis*																			1.69	1.05	a

[a]Anthocyanin: C-sam-malonylglu, cyanidin-sambubioside-malonylglucoside; C-sam-acetylglu, cyanidin-sambubioside-acetylglucoside; C-xyl-dihex, cyanidin-xylosyl-dihexoside; C-3-(*Z*)-cou-sam-5-glu, cyanidin-3-(*Z*)-*p*-coumaroyl-sambubioside-5-glucoside; C-3-(*E*)-cou-sam-5-glu, cyanidin-3-(*E*)-*p*-coumaroyl-sambubioside-5-glucoside; C-3-cou-sam, cyanidin-3-*p*-coumaroyl-sambubioside. [b]Different letters (a−j) denote statistically significant differences in individual anthocyanins among elderberry species or interspecific hybrid by Duncan multiple range test at $P < 0.05$.

dx.doi.org/10.1021/jf5011947 | J. Agric. Food Chem. 2014, 62, 5573−5580

var. *miquelli* (6% TAA) and *S. ebulus* only contained low amounts of cyanidin-3-sambubioside (less than 2% TAA). The second anthocyanin in peak 6 was identified as cyanidin-3-*O*-glucoside by its $[M]^+$ at m/z 449, which on MS^2 yielded a cyanidin fragment ion at m/z 287 formed by the cleavage of a 162 amu glucosyl unit. It was further confirmed by the addition of an external standard. *S. nigra* was characterized by highest levels of this anthocyanin (representing one-third of all anthocyanin analyzed in the fruit), followed by its hybrids: (JA × NI) × NI, JA × (JA × NI), and (JA × NI) × cv. Black Beauty. *S. ebulus* and *S. racemosa* var. *miquelli* contained only minor amounts of this anthocyanin. In accordance with our results, *S. nigra* samples analyzed by Watanabe et al.[38] contained more cyanidin-3-sambubioside than cyanidin-3-glucoside. On the other hand, Kaack and Austed[33] report higher levels of cyanidin-3-glucoside. In *S. nigra* berries analyzed in our study, cyanidin-3-sambubioside and cyanidin-3-glucoside combined represented approximately 95% TAA. These results are similar to those already reported in the literature by Seabra et al.[10] and Nakajima et al.[34]

Peak 7 showed a molecular ion at m/z 595, which fragmented to produce MS^2 ions at m/z 449 ($[M]^+ - 146$, loss of a rhamnosyl moiety) and m/z 287 ($[M]^+ - 308$, cleavage of rhamnosyl and glucosyl units), suggesting the presence of cyanidin-3-*O*-rutinoside. It was only present in specific hybrids; (JA × NI) × cv. Black Beauty was particularly rich in this anthocyanin (64.7 mg 100 g^{-1}) (Table 3). As one of the parents of the hybrid is *Sambucus nigra*, the results confirm the findings of Veberic et al.,[23] who reported 9.6 mg of cyanidin-3-rutinoside 100 g^{-1} in fruits of *S. nigra* 'Haschberg'. The second anthocyanin in peak 7 had an ion at m/z 829, which yielded a MS^2 fragment at m/z 667 ($[M]^+ - 162$, loss of a hexose unit) and MS^3 at m/z 449/287 ($[M]^+ - 132 - 162 - 86$, loss of xylosyl, glucosyl, and malonyl units). This compound is thus a cyanidin-pentosylhexoside-malonylhexoside, tentatively identified as cyanidin-sambubioside-malonyl-glucoside and present only in specific hybrids (JA × RAC, JA × CER, (JA × NI) × cv. Black Beauty, and MIQ). This is the first report of this compound in elderberry berries.

Peak 8 showed a molecular ion of m/z 551 and a neutral loss of 264 u, corresponding to two pentoses, so it was tentatively identified as a cyanidin dipentoside. It was detected in *S. cerulea* and *S. ebulus* fruit in levels below 0.5 mg 100 g^{-1}. This is the first report of cyanidin dipentoside ($[M]^+$ at m/z 551) in elderberry berries.

Peak 9 had $[M]^+$ at m/z 433 and on MS^2 yielded a fragment ion at m/z 271 (pelargonidin, $[M]^+ - 162$, loss of a hexosyl unit). On the basis of the mass spectra data, HPLC elution properties, and the addition of an external standard, peak 9 was identified as pelargonidin-3-*O*-glucoside. It was only detected in traces in berries of *S. nigra* and its hybrids (JA × NI) × NI, (JA × NI) × CER, JA × (JA × NI), and (JA × NI) × cv. Black Beauty (data not presented). Similarly, Lee and Finn[20] and Wu et al.[24] report low levels of pelargonidin-3-glucoside in *S. nigra* fruit.

The anthocyanin with a molecular ion of m/z 565 was identified as pelargonidin-3-*O*-sambubioside (peak 10). On MS^2 it produced a minor fragment at m/z 433 ($[M]^+ - 132$, loss of a xylosyl unit) and a major fragment at m/z 271 ($[M]^+ - 162$, loss of a glucosyl unit). It has been confirmed in the following species and hybrids: *S. nigra* and *S. cerulea*, (JA × NI) × NI, JA × (JA × NI), and (JA × NI) × cv. Black Beauty. Only low levels of this anthocyanin were quantified (data not presented), which is in accordance with Wu et al.[24] and their study on *S. nigra* fruit.

The compound in peak 11 showed a molecular ion at m/z 785 and MS^2 fragment at m/z 623 ($[M]^+ - 162$, loss of a hexose residue) and MS^3 fragment at m/z 449/287 ($[M]^+ - 42$ loss of acetyl; − 162 hexose and − 132 pentose moieties). This fragmentation pattern is similar to that observed for the compound in peak 6. Thus, peak 11 was identified as cyanidin 3-xylosylhexoside-acetyl-hexoside. Because sambubioside (i.e., 2-*O*-*β*-D-xylosyl-D-glucose) is the xylosylglucoside most frequently found as an anthocyanin substituent,[39] peak 11 could be tentatively identified as cyanidin-sambubioside-acetylglucoside. A similar fragmentation pattern of a cyanidin-based anthocyanin has previously been reported in *Sambucus* samples by Lee and Finn.[20] In our samples, it was merely present in two hybrids, JA × RAC (10.4 mg 100 g^{-1}) and JA × NI (3.5 mg 100 g^{-1}). Interestingly, hybrids of a similar origin (*S. javanica* as a mother plant) did not contain cyanidin-sambubioside-acetyl-glucoside.

Peak 12 presented a molecular ion $[M - H]^-$ at m/z 905, which yielded MS^2 fragment ion at m/z 743 ($[M]^+ - 162]^-$, loss of a hexoside moiety), and MS^3 fragment at m/z 449 ($[M]^+ - 132$, loss of a pentoside and − 162 a hexoside or caffeoyl moiety) and 287 (cyanidin, − 162 loss of a hexoside moiety). The fragmentation pattern is similar to that obtained for peak 1; the difference is one hexose or caffeoyl unit. The peak was tentatively identified as cyanidin-xylosyl-dihexoside or cyanidin-caffeoyl-sambubiosyl-glucoside. This anthocyanin was quantified in range of 2.6−15.9 mg 100 g^{-1} berries in the following hybrids: JA × RAC, (JA × NI) × CER, JA × (JA × NI), and JA × NI. As all hybrids share the same species, *S. javanica*, the latter potentially represents the genetic source for the accumulation of this specific anthocyanin.

Peaks 13 and 14 were characterized by the same mass spectral pattern. Both compounds had a molecular ion at m/z 889 that fragmented on MS^2 to produce ion at m/z 727 ($[M]^+ - 162$, loss of a glucosyl moiety) and on MS^3 produce the ions at m/z 449 ($[M]^+ - 132$ a pentosyl and − 146 a coumaroyl moiety) and 287 (cyanidin, − 162 a glucosyl moiety). According to the study of Lee and Finn[20] and Inami et al.,[40] this fragmentation pattern matches with cyanidin-3-(*Z*)-*p*-coumaroyl-sambubioside-5-glucoside and cyanidin-3-(*E*)-*p*-coumaroyl-sambubioside-5-glucoside. The results indicate that both anthocyanins are characteristic for *S. javanica* and *S. racemosa* fruit as they are only present in hybrids, where these species were used as parent plants. Statistically highest level of cyanidin-3-(*Z*)-*p*-coumaroyl-sambubioside-5-glucoside (11.9 mg 100 g^{-1}) and cyanidin-3-(*E*)-*p*-coumaroyl-sambubioside-5-glucoside (583 mg 100 g^{-1}) was determined in JA × RAC hybrid in which they combined to represent up to 71% total analyzed anthocyanins. On the other hand, *S. nigra*, *S. cerulea*, and *S. ebulus* fruit did not contain these two anthocyanins as reported also Jordheim et al.[41]

Peak 15 contained $[M]^+$ ion at m/z 727, which yielded MS^2 fragment at m/z 433 ($[M]^+ - 132$ and − 162, loss of xylosyl and glucosyl units) and MS^3 fragment at m/z 287 ($[M]^+ - 146$, loss of a coumaroyl unit). This corresponds to the fragmentation pattern of cyanidin-3-*p*-coumaroyl-sambubioside, which has previously been detected in elderberry fruit.[20,40] It was only detected in hybrids involving *S. javanica*, *S. cerulea*, or *S. racemosa* var. *miquelli* parent. The highest level of cyanidin-3-*p*-coumaroyl-sambubioside has been determined in (JA × NI) × CER (68.9 mg 100 g^{-1}) fruit. In accordance with our results,

Lee and Finn[20] reported that *S. nigra* fruit lacks cyanidin-3-*p*-coumaroyl-sambubioside.

Interestingly, berries of the CER × NI hybrid contained the last three mentioned anthocyanins (Table 4). The absence of the anthocyanins cyanidin-3-(*Z*)-*p*-coumaroyl-sambubioside-5-glucoside, cyanidin-3-(*E*)-*p*-coumaroyl-sambubioside-5-glucoside, and cyanidin-3-*p*-coumaroyl-sambubioside in *S. cerulea* and *S. nigra*, and their presence in their hybrid CER × NI, could be explained by homo- and heterozygosity in association with pollination system of elderberries, and genetic inheritance of these two anthocyanins (the interactions of two or more loci with dominant and recessive alleles and/or the involvement of inhibiting genes). Elderberries can be pollinated by wind and insects, and cross-pollination is probably more important than self-pollination.[3,42]

Elderberries are predominantly used as processed food or dietary supplements; therefore, it is useful to know their content of phenolic compounds, especially anthocyanins, which represent the highest share in elderberry fruit. The major anthocyanins detected in fruit of different species and interspecific hybrids were cyanidin-3-*O*-sambubioyl-5-*O*-glucoside, cyanidin-3,5-diglucoside, cyanidin-3-sambubioside, cyanidin-3-glucoside, and cyanidin-3-(*E*)-*p*-coumaroyl-sambubioside-5-glucoside. Conversely, in *S. javanica* and *S. racemosa*, hybrids cyanidin-3-(*Z*)-*p*-coumaroyl-sambubioside-5-glucoside and cyanidin-3-(*E*)-*p*-coumaroyl-sambubioside-5-glucoside prevailed. Total analyzed anthocyanins (TAA) varied greatly from hybrid to hybrid. Promising species or interspecific hybrids with TAA higher than 400 mg 100 g^{-1} were (JA × NI) × CER, (JA × NI) × cv. Black Beauty, *Sambucus nigra*, and, in particular, JA × RAC hybrid, which contained 834 mg 100 g^{-1} of anthocyanins. Berries of *S. nigra* var. *viridis* contained significantly lower levels of TAA, which is closely correlated with the pale color of their fruits; they are predominantly green with a slight hint of red color. Several minor anthocyanins have also been confirmed in different elderberries. Pelargonidin-3-glucoside, pelargonidin-3-sambubioside, cyanidin-3-galactoside, cyanidin-dipentoside ($[M]^+$ at m/z 551), and different cyanidin glycosides 1−3 ($[M]^+$ at m/z 581) were quantified in traces. Our results indicate that elderberry fruits are a superior source of anthocyanins to other fruit species, for example, apples, peaches, and strawberries.[43−45] However, a great variation in anthocyanin profile has been observed among elderberry species and hybrids. These differences may contain important implications and information, which may become evident in health effects studies. Some elderberry genotypes could be used to design new raw materials with high contents of anthocyanins, which can serve to produce elderberry products with health-promoting properties based on their positive health effects. Data from our research present new information for nutritional research in addition to breeding programs, which have turned their focus to fruit quality and strive to improve nutritional or health value to create new hybrids or cultivars with enhanced levels of bioactive components.

AUTHOR INFORMATION

Corresponding Author

*Tel.: +386 1 320 31 41. Fax: +386 1 423 10 88. E-mail: maja.mikulic-petkovsek@bf.uni-lj.si.

Notes

The authors declare no competing financial interest.

REFERENCES

(1) Jacobs, B.; Huysmans, S.; Smets, E. Evolution and systematic value of fruit and seed characters in Adoxaceae (Dipsacales). *Taxon* **2010**, *59*, 850−866.

(2) Eriksson, T.; Donoghue, M. J. Phylogenetic relationships of *Sambucus* and *Adoxa* (Adoxoideae, Adoxaceae) based on nuclear ribosomal ITS sequences and preliminary morphological data. *Syst. Bot.* **1997**, *22*, 555−573.

(3) Bolli, R. Revision of the genus Sambucus. *Diss. Bot.* **1994**, *223*, 1−227.

(4) Böcher, T. W. Højsommerekskursionen til Brædstrup, Bryrup og Vrads. *Bot. Tidsskr.* **1941**, *45*, 433−439.

(5) Winge, Ö. The Sambucus hybrid *S. nigra* × *S. racemosa*. Comptes-rendus des travaux du laboratoire Carlsberg. *Sér. Physiol.* **1944**, *24*, 73−78.

(6) Nilsson, A. Hybriden mellan fläder och druvfläder funnen i Skåne. *Sven. Bot. Tidskr.* **1987**, *81*, 174−175.

(7) Chia, C. L. A chromosome and thin-layer chromatographic study of the genus *Sambucus* L. Ph.D. Thesis, Cornell University, College of Agriculture and Life Sciences, Department of Plant Biology, New York, 1975; 50 pp.

(8) Koncalová, M. N.; Hrib, J.; Jicínská, D. The embryology of the *Sambucus* species and hybrids. In *Fertilization and Embryogenesis in Ovulated Plants. Proceedings of the VII International Cytoembryological Symposium*; Erdelská, O., Ed.; August, 1982, Bratislava, Czechoslovakia, 1983; pp 43−47.

(9) Thole, J. M.; Kraft, T. F. B.; Sueiro, L. A.; Kang, Y.-H.; Gills, J. J.; Cuendet, M.; Pezzuto, J. M.; Seigler, D. S.; Lila, M. A. A comparative evaluation of the anticancer properties of European and American elderberry fruits. *J. Med. Food* **2006**, *9*, 498−504.

(10) Seabra, I. J.; Braga, M. E. M.; Batista, M. T. P.; de Sousa, H. C. Fractioned high pressure extraction of anthocyanins from elderberry (*Sambucus nigra* L.) pomace. *Food Bioprocess Technol.* **2010**, *3*, 674−683.

(11) Jing, P.; Bomser, J. A.; Schwartzt, S. J.; He, J.; Magnuson, B. A.; Giusti, M. M. Structure-function relationships of anthocyanins from various anthocyanin-rich extracts on the inhibition of colon cancer cell growth. *J. Agric. Food Chem.* **2008**, *56*, 9391−9398.

(12) Schwarz, M.; Hillebrand, S.; Habben, S.; Degenhardt, A.; Winterhalter, P. Application of high-speed countercurrent chromatography to the large-scale isolation of anthocyanins. *Biochem. Eng. J.* **2003**, *14*, 179−189.

(13) Kilham, C. Health benefits boost elderberry. *HerbalGram* **2000**, *50*, 55−57.

(14) Kilham, C. Elderberries grow beyond folklore into mainstream functional foods. *Prepared Foods* **2001**, 39−41.

(15) Zafra-Stone, S.; Yasmin, T.; Bagchi, M.; Chatterjee, A.; Vinson, J. A.; Bagchi, D. Berry anthocyanins as novel antioxidants in human health and disease prevention. *Mol. Nutr. Food Res.* **2007**, *51*, 675−683.

(16) Zakay-Rones, Z.; Thom, E.; Wollan, T.; Wadstein, J. Randomized study of the efficacy and safety of oral elderberry extract in the treatment of influenza A and B virus infections. *J. Int. Med. Res.* **2004**, *32*, 132−140.

(17) Chen, C.; Zuckerman, D. M.; Brantley, S.; Sharpe, M.; Childress, K.; Hoiczyk, E.; Pendleton, A. R. Sambucus nigra extracts inhibit infectious bronchitis virus at an early point during replication. *BMC Vet. Res.* **2014**, *10*, 24.

(18) Steger-Mate, M.; Horvath, D.; Barta, J. Investigation of colourant content and stability in elderberry (*Sambucus nigra* L.). *Acta Aliment. Acad. Sci. Hung.* **2006**, *35*, 117−126.

(19) Kaack, K. 'Sampo' and 'Samdal', elderberry cultivars for juice concentrates. *Fruit Var. J.* **1997**, *51*, 28−31.

(20) Lee, J.; Finn, C. E. Anthocyanins and other polyphenolics in American elderberry (*Sambuclus canadensis*) and European elderberry (*S. nigra*) cultivars. *J. Sci. Food Agric.* **2007**, *87*, 2665−2675.

(21) Stang, E. Elderberry, highbush cranberry, and juneberry management. In *Small Fruit Crop Management*; Galletta, G. J., Himelrick, D. G., Eds.; Prentice-Hall: Englewood Cliffs, NJ, 1990; pp 363−374.

(22) Zadernowski, R.; Naczk, M.; Nesterowicz, J. Phenolic acid profiles in some small berries. *J. Agric. Food Chem.* **2005**, *53*, 2118−2124.
(23) Veberic, R.; Jakopic, J.; Stampar, F.; Schmitzer, V. European elderberry (*Sambucus nigra* L.) rich in sugars, organic acids, anthocyanins and selected polyphenols. *Food Chem.* **2009**, *114*, 511−515.
(24) Wu, X. L.; Gu, L. W.; Prior, R. L.; McKay, S. Characterization of anthocyanins and proanthocyanidins in some cultivars of *Ribes*, *Aronia*, and *Sambucus* and their antioxidant capacity. *J. Agric. Food Chem.* **2004**, *52*, 7846−7856.
(25) Wojdylo, A.; Jauregui, P. N. N.; Carbonell-Barrachina, A. A.; Oszmianski, J.; Golis, T. Variability of phytochemical properties and content of bioactive compounds in *Lonicera caerulea L.* var. *kamtschatica* berries. *J. Agric. Food Chem.* **2013**, *61*, 12072−12084.
(26) Ercisli, S.; Tosun, M.; Duralija, B.; Voca, S.; Sengu, M.; Turan, M. Phytochemical content of some black (*Morus nigra* L.) and purple (*Morus rubra* L.) mulberry genotypes. *Food Technol. Biotechnol.* **2010**, *48*, 102−106.
(27) Milivojevic, J.; Maksimovic, V.; Maksimovic, J. D.; Radivojevic, D.; Poledica, M.; Ercisli, S. A comparison of major taste- and health-related compounds of *Vaccinium* berries. *Turk. J. Biol.* **2012**, *36*, 738−745.
(28) Tomas-Barberan, F.; Espin, J. C. Phenolic compounds and related enzymes as determinants of quality in fruits and vegetables. *J. Sci. Food Agric.* **2001**, *81*, 853−876.
(29) Simonovik, B.; Ivancic, A.; Jakse, J.; Bohanec, B. Production and evaluation of interspecific hybrids within the genus *Sambucus*. *Plant Breed.* **2007**, *126*, 628−633.
(30) Mikulic-Petkovsek, M.; Slatnar, A.; Stampar, F.; Veberic, R. HPLC-MSn identification and quantification of flavonol glycosides in 28 wild and cultivated berry species. *Food Chem.* **2012**, *135*, 2138−2146.
(31) Wang, S. Y.; Zheng, W.; Galletta, G. J. Cultural system affects fruit quality and antioxidant capacity in strawberries. *J. Agric. Food Chem.* **2002**, *50*, 6534−6542.
(32) Veberic, R.; Jakopic, J.; Stampar, F. Flavonols and anthocyanins of elderberry fruits (*Sambucus nigra* L.). *Acta Hortic.* **2009**, *841*, 611−614.
(33) Kaack, K.; Austed, T. Interaction of vitamin C and flavonoids in elderberry (*Sambucus nigra* L.) during juice processing. *Plant Food Hum. Nutr.* **1998**, *52*, 187−198.
(34) Nakajima, J.; Tanaka, I.; Seo, S.; Yamazaki, M.; Saito, K. LC/PDA/ESI-MS profiling and radical scavenging activity of anthocyanins in various berries. *J. Biomed. Biotechnol.* **2004**, *5*, 241−247.
(35) Bridle, P.; GarciaViguera, C. Analysis of anthocyanins in strawberries and elderberries. A comparison of capillary zone electrophoresis and HPLC. *Food Chem.* **1997**, *59*, 299−304.
(36) Bronnumhansen, K.; Hansen, S. H. High-performance liquid-chromatographic separation of anthocyanins of *Sambucus nigra* L. *J. Chromatogr.* **1983**, *262*, 385−392.
(37) Chandra, A.; Rana, J.; Li, Y. Q. Separation, identification, quantification, and method validation of anthocyanins in botanical supplement raw materials by HPLC and HPLC-MS. *J. Agric. Food Chem.* **2001**, *49*, 3515−3521.
(38) Watanabe, T.; Yamanoto, A.; Nagai, S.; Terabe, S. Analysis of elderberry pigments in commercial food samples by micellar electrokinetic chromatography. *Anal. Sci.* **1998**, *14*, 839−844.
(39) Mazza, G.; Miniati, E. In *Anthocyanins in Fruits, Vegetables, and Grains*; Mazza, G., Miniati, E., Eds.; CRC Press: Boca Raton, FL, 1993; pp 1−362.
(40) Inami, O.; Tamura, I.; Kikuzaki, H.; Nakatani, N. Stability of anthocyanins of *Sambucus canadensis* and *Sambucus nigra*. *J. Agric. Food Chem.* **1996**, *44*, 3090−3096.
(41) Jordheim, M.; Giske, N. H.; Andersen, O. M. Anthocyanins in Caprifoliaceae. *Biochem. Syst. Ecol.* **2007**, *35*, 153−159.
(42) Charlebois, D.; Byers, P. L.; Finn, C. E.; Thomas, A. I. Elderberry: botany, horticulture, potential. In *Horticultural Reviews*; Janick, J., Ed.; Wiley-Blackwell: Oxford, 2010; Vol. *37*, pp 213−280.
(43) Mikulic-Petkovsek, M.; Slatnar, A.; Stampar, F.; Veberic, R. The influence of organic/integrated production on the content of phenolic compounds in apple leaves and fruits in four different varieties over a 2-year period. *J. Sci. Food Agric.* **2010**, *90*, 2366−2378.
(44) Mikulic-Petkovsek, M.; Schmitzer, V.; Slatnar, A.; Weber, N.; Veberic, R.; Stampar, F.; Munda, A.; Koron, D. Alteration of the content of primary and secondary metabolites in strawberry fruit by *Colletotrichum nymphaeae* infection. *J. Agric. Food Chem.* **2013**, *61*, 5987−5995.
(45) Orazem, P.; Mikulic-Petkovsek, M.; Stampar, F.; Hudina, M. Changes during the last ripening stage in pomological and biochemical parameters of the 'Redhaven' peach cultivar grafted on different rootstocks. *Sci. Hortic.* **2013**, *160*, 326−334. (This work is part of program Horticulture no. P4-0013-0481, funded by the Slovenian Research Agency (ARRS).)

JOURNAL OF AGRICULTURAL AND FOOD CHEMISTRY

Article

pubs.acs.org/JAFC

Stimulation of Osteogenic Activity in Human Osteoblast Cells by Edible *Uraria crinita*

Yi-Wen Mao,[†,‡] Rong-Dih Lin,[§] Hsiao-Chiao Hung,[‡] and Mei-Hsien Lee*[,‡,∥,⊥]

[†]School of Pharmacy, College of Pharmacy, Taipei Medical University, Taipei 110, Taiwan

[‡]Graduate Institute of Pharmacognosy, College of Pharmacy, Taipei Medical University, Taipei 110, Taiwan

[§]Department of Internal Medicine, Heping Branch, Taipei City Hospital, Taipei 110, Taiwan

[∥]Center for Reproductive Medicine & Sciences, Taipei Medical University Hospital, Taipei 110, Taiwan

[⊥]Ph.D. Program for the Clinical Drug Discovery from Botanical Herbs, Taipei 110, Taiwan

Supporting Information

ABSTRACT: *Uraria crinita* is an edible herb used as a natural food for childhood skeletal dysplasia. Ethyl acetate, *n*-butanol, and aqueous fractions of a 95% ethanol crude extract of *U. crinita* were obtained and the active ingredients isolated and purified using a bioguided method. In this manner, we isolated and identified a new active flavone glycoside, apigenin 6-*C*-*β*-D-apiofuranosyl(1→2)-*α*-D-xylopyranoside (**3**) and 10 known components with stimulatory activity on human osteoblast cells. The new compound **3** at 100 *μ*M significantly increased alkaline phosphatase activity (114.10 ± 4.41%), mineralization (150.10 ± 0.80%), as well as osteopontin (1.39 ± 0.01-fold), bone morphogenetic protein-2 (BMP-2, 1.30 ± 0.04-fold), and runt-related transcription factor 2 (Runx2, 1.43 ± 0.10-fold) mRNA expression through the activation of the BMP-2/Runx2 pathway. Two other components, dalbergioidin (**1**) and byzantionoside B (**9**), displayed similar effects. These results show that *U. crinita* and its active compounds may have the potential to stimulate bone formation and regeneration.

KEYWORDS: *Uraria crinita, human osteoblast cells, alkaline phosphatase, mineralization, apigenin 6-C-β-D-apiofuranosyl(1→2)-α-D-xylopyranoside, osteopontin, BMP-2/Runx2 pathway*

INTRODUCTION

Uraria crinita (L.) Desv. ex DC. (Fabaceae), an edible herb used in traditional medicine, is widely distributed throughout India, Thailand, Indonesia, southern China, and Taiwan. This herb has been reported to repress the formation of stress-induced ulcers[1] and to have antioxidant activity,[2] and its roots are used to treat chills, edema, and stomachache through effects that are possibly mediated by its anti-inflammatory activity.[3] In Taiwan, *U. crinita* is drunk as a tea that, similar to ginseng, is fragrant, sweet, and thirst-quenching, and it is therefore known as "Taiwanese ginseng." In traditional Chinese medicine, *U. crinita* roots are used as dietary supplements for treating childhood skeletal dysplasia as well as for sports injuries, stress fractures, sprains, and strains,[4] and its extracts are rich in *β*-sitosterol, flavonoids, butulin, stearic acid, and sucrose.[4,5]

Osteoblasts, the bone-forming cells that originate from mesenchymal stem cells, play a crucial role in creating and maintaining skeletal architecture. Bone formation involves a complex series of events that include the proliferation and differentiation of osteoblasts, and ultimately results in mineralization of the extracellular matrix (ECM).[6] Specific genes are sequentially expressed or repressed during each stage of osteoblast development; for example, histone 4 expression is a marker of proliferation, alkaline phosphatase (ALP) expression is a marker of differentiation,[7] and osteopontin (OPN) expression is a marker of mineralization.[8] Bone morphogenetic proteins (BMPs) are members of the transforming growth factor (TGF)-*β* family that activate SMAD proteins and other signaling pathways to stimulate the expression of a number of regulatory genes, including runt-related transcription factor 2 (Runx2). Both BMP growth factors and Runx2 transcription factors play essential roles in osteoblast differentiation and subsequent bone matrix mineralization.[9,10] Bone formation is necessary for the proper growth of bones in infants and children, prevention of bone mass loss in climacteric women, and healing and remodeling of bone fractures. Thus, there is a clinical need for nutritional and pharmacological agents that prevent bone loss and increase bone formation to support human health.

Primary osteoblast cell cultures are widely used as *in vitro* models to investigate the effects of new agents on osteoblast differentiation, matrix mineralization, and new bone formation. A number of factors influence the expression of the osteoblastic phenotype in cell culture.[11] For example, osteogenic supplements such as glucocorticoids, ascorbic acid, and *β*-glycerophosphate have been demonstrated to induce matrix mineralization in bone cell cultures and are extensively used to investigate agents that regulate bone formation *in vitro*.[6] Previous studies have revealed that many traditional Chinese herbal medicines affect bone formation, including *Puerariae radix*,[12] *Drynariae rhizome*,[13] and *Epimedium pubescens*.[14] However, there are no reports of the effects of *U. crinita* on osteoblasts. Therefore, this study was performed to determine whether *U. crinita* root extracts and their

Received: March 12, 2014
Revised: May 1, 2014
Accepted: May 2, 2014
Published: May 2, 2014

ACS Publications © 2014 American Chemical Society

Table 1. ^{1}H and ^{13}C NMR Data of Compound 3 (DMSO-d_6, 500 and 125 MHz)

position	δ_H (J in Hz)	δ_C	position	δ_H (J in Hz)	δ_C
2		163.5	1″	4.55, br s	72.1
3	6.75, s	102.8	2″	4.27, br s	72.6
4		181.8	3″	3.54, m	75.1
5		161.2	4″	3.74, m	69.4
6		108.8	5″	3.51, m	70.1
				3.77, m	
7		163.5	1‴	5.15, br s	109.1
8	6.51, s	94.0	2‴	3.58, m	75.9
9		156.4	3‴		79.0
10		103.2	4‴	2.52, m	73.6
				3.08, d (9.3)	
1′		121.1	5‴	2.99, d (11.0)	64.5
				3.18, d (11.0)	
2′, 6′	7.92, d (8.8)	128.5	5-OH	13.50, br s	
3′, 5′	6.91, d (8.8)	116.0			
4′		161.2			

active constituents have osteogenic effects on human osteoblast (HOb) cells.

MATERIALS AND METHODS

Plant Material. *Uraria crinita* roots were collected from the Mingjian Township Farmers' Association, Nantou, Taiwan and identified by Dr. Chao-Lin Kuo, School of Chinese Pharmaceutical Sciences and Chinese Medicine Resources, China Medical University, Taichung, Taiwan. A voucher specimen (M-343) was deposited at the Graduate Institute of Pharmacognosy, Taipei Medical University, Taipei, Taiwan.

Reagents and Chemicals. Dimethyl sulfoxide (DMSO), MTT, Triton X-100, *p*-nitrophenyl phosphate disodium, alizarin red-S, cetylpyridinium chloride monohydrate, ascorbic acid, and *β*-glycerophosphate disodium salt hydrate were purchased from Sigma-Aldrich (St. Louis, MO, USA). Phosphate-buffered saline (PBS) and trypsin were purchased from Gibco (Burlington, Canada). Osteoblast growth medium (OGM) and osteoblast differentiation medium (ODM) were purchased from Cell Applications (San Diego, CA, USA). A bicinchoninic acid (BCA) protein assay kit was purchased from Thermo Scientific (Rockford, IL, USA), 4-nitrophenyl phosphate disodium salt hexahydrate was obtained from Alfa Aesar (Ward Hill, MA, USA), High Pure RNA Isolation Kit and Universal Probe Library (UPL) probes were acquired from Roche (Mannheim, Germany), SuperScript II reverse transcriptase was obtained from Invitrogen (Burlington, Canada), and SafeView nucleic acid stain was purchased from NBS Biologicals (Huntingdon, UK). All chemicals and reagents were high-grade commercial products.

General Experimental Procedures. Optical rotations were measured on a Jasco P-1020 digital polarimeter (Tokyo, Japan). Ultraviolet spectra were recorded on a Hitachi U-2800 UV/vis spectrometer (Tokyo, Japan). 1D- and 2D-nuclear magnetic resonance (NMR) spectra were measured with a Bruker AM-500 spectrometer (Rheinstetten, Germany) using DMSO-d_6, methanol (MeOH)-d_4, and D_2O solutions. High-resolution eletrospray ionization mass spectroscopy (HRESI-MS) and ESI-MS analyses were performed using VG Platform Electrospray ESI/MS (Altrincham, Cheshire, UK).

Extraction and Isolation. Fresh roots (14.7 kg) of *U. crinita* were extracted three times with ethanol (EtOH, 95% v/v), and the filtrate was evaporated and dried under a vacuum. The dried extract (601.4 g) was suspended in H_2O and successively partitioned with ethyl acetate (EtOAc) and *n*-butanol (*n*-BuOH) to yield 32.0 and 133.9 g of extract, respectively. The EtOAc extract was subjected to Sephadex LH-20 column chromatography (Amersham Pharmacia Biotech, Uppsala, Sweden) and eluted with 95% EtOH to yield 9 fractions (UCE-1−9). Fraction UCE-3 was further separated by Sephadex LH-20 column chromatography and eluted with a MeOH/H_2O gradient (40−100%) to yield 17 fractions (UCE-3-1−17). Fraction UCE-3-7 was fractionated by MCI CHP-20 column chromatography (Supelco, Bellefonte, PA, USA) with an H_2O-MeOH gradient to yield 14 fractions (UCE-3-7-1−14). Compound **2** (98.1 mg) was obtained from the UCE-3-7-4 fraction after recrystallization from MeOH/H_2O. Fraction UCE-4 was further separated by Sephadex LH-20 column chromatography and eluted with a MeOH/H_2O gradient (50−100%) to yield 17 fractions (UCE-4-1−17). Fractions UCE-4-3 and UCE-4-10 were fractionated on an MCI CHP-20 column with a MeOH/H_2O gradient (30−100%) to yield 8 (UCE-4-3-1−8) and 11 (UCE-4-10-1−11) fractions, respectively. Compound **11** (12.0 mg) was obtained from the UCE-4-3-2 fraction after purification on a semipreparative C-18 reverse-phase HPLC column (Biotic Chemical Co., Taipei, Taiwan) with 10% MeOH as the eluent. Compound **4** (6.9 mg) was obtained from the UCE-4-10-2 fraction after purification on a semipreparative C-18 reversed-phase HPLC column with 25% acetonitrile as the eluent. Fraction UCE-5 was separated by MCI CHP-20 column chromatography with an H_2O−MeOH gradient to yield 24 fractions (UCE-5-1−24). Fractions UCE-5-15 and UCE-5-16 were subjected to Sephadex LH-20 column chromatography and eluted with 60% MeOH to yield 6 (UCE-5-15-1−6) and 10 (UCE-5-16-1−10) fractions, respectively. Compounds **3** (12.2 mg) and **1** (184.5 mg) were obtained from the UCE-5-15-1 and UCE-5-16-9 fractions, respectively, after purification on a semipreparative C-18 reversed-phase HPLC column with 55% MeOH as the eluent. The *n*-BuOH extract was subjected to Diaion HP-20 column chromatography (Mitsubishi Chemical Industries, Tokyo, Japan) and eluted with an H_2O−MeOH gradient to yield 6 fractions (UCB-1−6). Fractions UCB-3, UCB-4, and UCB-5 were further separated by Sephadex LH-20 column chromatography and eluted with 95% EtOH to yield 6 (UCB-3-1−6), 9 (UCB-4-1−9), and 6 (UCB-5-1−6) fractions, respectively. Fractions UCB-3-3 and UCB-5-2 were separated by MCI CHP-20 column chromatography with an H_2O−MeOH gradient to yield 6 (UCB-3-3-1−6) and 8 (UCB-5-2-1−8) fractions, respectively. Compounds **7** (38.3 mg) and **8** (15.3 mg) were obtained from the UCB-3-3-2 fraction. Compounds **5** (58.6 mg) and **6** (7.6 mg) were obtained from the UCB-3-3-3 and UCB-5-2-1 fractions, respectively, after purification on a semipreparative C-18 reversed-phase HPLC column with 20% MeOH as the eluent. Fractions UCB-4-3 and UCB-4-4 were separated on MCI CHP-20 columns and eluted with MeOH/H_2O gradients (60−100% and 20−100%, respectively) to yield 4 (UCB-4-3-1−4) and 9 (UCB-4-4-1−9) fractions, respectively. Compound **9** (38.5 mg) was obtained from the UCB-4-3-3 fraction after purification on a semipreparative C-18 reversed-phase HPLC column with 20% MeOH as the eluent. Compound **10** (13.5 mg) was obtained from the UCB-4-4-3 fraction after purification on a semipreparative C-18 reversed-phase HPLC column with 40% MeOH as the eluent.

Acid Hydrolysis of Compound 3. Compound **3** (1 mg) was dissolved in 6 N HCl and hydrolyzed at 80 °C for 6 h. The mixture was cooled, the acid was evaporated, and the remaining mixture was resuspended in double-distilled H_2O and filtered through a Millipore Millex-GX nylon membrane (EMD Millipore, Billerica, MA, USA).[15] Monosaccharides of **3** and polysaccharide hydrolysates were separated

Table 2. Primers and Probe Combinations Used for Q-RT-PCR

genes	forward primer	reverse primer	accession number	probe number
OPN	GGGCTTGGTTGTCAGCAG	TGCAATTCTCATGGTAGTGAGTTT	NM_001040058.1	63
BMP-2	CGGACTGCGGTCTCCTAA	GGAAGCAGCAACGCTAGAAG	NM_001200.2	49
Runx2	CAGTGACACCATGTCAGCAA	GCTCACGTCGCTCATTTTG	NM_001024630.3	41
GAPDH	AGCCACATCGCTCAGACAC	GCCCAATACGACCAAATCC	NM_002046.3	60

on a high-performance anion-exchange chromatographic (HPAEC) system (Dionex, Sunnyvale, CA, USA) using an anion-exchange column (Carbopac PA-10, 4.6 × 250 mm; Dionex, Sunnyvale, CA, USA). Monosaccharides were analyzed using isocratic elution with an 18 mM NaOH solution at ambient temperature.

*Apigenin 6-C-β-D-Apiofuranosyl(1→2)-α-D-xylopyranoside, **3**.* Yellow solid; $[\alpha]^{22}_{D}$ +21 (*c* 0.5, MeOH). UV (MeOH) λ_{max} (log ε): 272 (4.36), 329 (4.35) nm; ^{1}H NMR (DMSO-d_6, 500 MHz); and ^{13}C NMR (DMSO-d_6, 125 MHz); see Table 1. HRESI-MS *m*/*z* 535.1459 $[M + H]^+$ (calcd for $C_{25}H_{27}O_{13}$, 535.1452).

Cell Culture. HOb primary cells were derived from a normal femoral bone of a 63-year-old Caucasian female and obtained from Cell Applications (San Diego, CA, USA). HOb cells attach and spread on tissue culture surfaces, proliferate in OGM, and express differentiation and mineralization markers when cultured in ODM containing ascorbic acid and β-glycerophosphate at 37 °C in a 5% CO_2 humidified atmosphere. The growth medium was changed every other day. To maintain exponential growth, cells were subcultured every 7 days. HOb cells were used for all assays.

Cell Viability Assay. HOb cell viability was determined using the MTT assay as described elsewhere.[16] In brief, HOb cells were seeded in 96-well plates at a density of 4000 cells/well. After 24 h, the culture medium was replaced with fresh medium containing the test extracts or compounds. After 72 h, the incubation medium was removed, and the MTT reagent was added for 4 h. The MTT reagent was then replaced with 100 μL of DMSO, and the wells were thoroughly mixed to dissolve the dark-blue crystals. The absorbance at 600 nm was recorded using an enzyme-linked immunosorbent assay reader.

Alkaline Phosphatase (ALP) Assay. ALP activity in HOb cells was measured by a colorimetric assay using *p*-nitrophenyl phosphate as the substrate.[17] HOb cells were seeded in 96-well plates at a density of 4000 cells/well, and after 24 h, the culture medium was replaced with fresh ODM containing the test extracts or compounds. After 72 h, the incubation medium was discarded, and cells were rinsed twice with cold PBS and then lysed by adding lysis buffer (PBS containing 0.1% Triton X-100). The protein concentration in the supernatant was determined by a BCA assay. Supernatants were incubated with the BCA reagent for 1 h at 37 °C. The reaction was stopped by the addition of 1 M NaOH, and the absorbance was measured at 560 nm. ALP activity in the supernatants was assayed by incubation for 1 h at 37 °C in 0.1 M $NaHCO_3$−Na_2CO_3 buffer (pH 10) containing 0.1% Triton X-100, 2 mM $MgSO_4$, and 6 mM *p*-nitrophenyl phosphate. The reaction was stopped by the addition of 1 M NaOH, and the absorbance was measured at 405 nm. ALP activity was normalized to the protein concentration in each supernatant.

Mineralized Matrix Formation Assay. HOb cell mineralization was measured by alizarin red-S staining of calcium.[18] HOb cells were seeded in 24-well plates at a density of 7 × 10^4 cells/well, and after 3 days, the culture medium was replaced with mineralizing medium (ODM supplemented with 50 μg/mL ascorbic acid and 10 mM β-glycerophosphate) containing the test extracts or compounds. Cells were incubated for 12 days and then fixed in 75% EtOH. Calcium deposits were stained for 15 min at room temperature with an alizarin red-S solution (40 mM, pH 4.2). The bound stain was eluted with a solution of 10% (w/v) cetylpyridinium chloride in 10 mM sodium phosphate (pH 7.0), and the absorbance was measured at 550 nm.

RNA Extraction and Q-RT-PCR. HOb cells were seeded in 6 cm dishes at a density of 7 × 10^5 cells/dish, and after 24 h, the culture medium was replaced with fresh ODM containing the test extracts. After 24 h, total RNA was extracted with High Pure RNA Isolation Kit and reverse-transcribed with SuperScript II reverse transcriptase according to the manufacturer's instructions. Q-RT-PCR was used to measure OPN, Runx2, and BMP-2 mRNA expression. Specific primers were designed using the Universal Probe Library Assay Design Center (www.roche-applied-science.com) and the suggested Universal Probe Library (UPL) probes. The detailed sequences of primers and probes are given in Table 2. All reactions were performed in triplicate using a Roche LightCycler 480 detection system using the $2^{-\Delta\Delta Ct}$ method. Runx2, BMP-2, and OPN mRNA expression results were

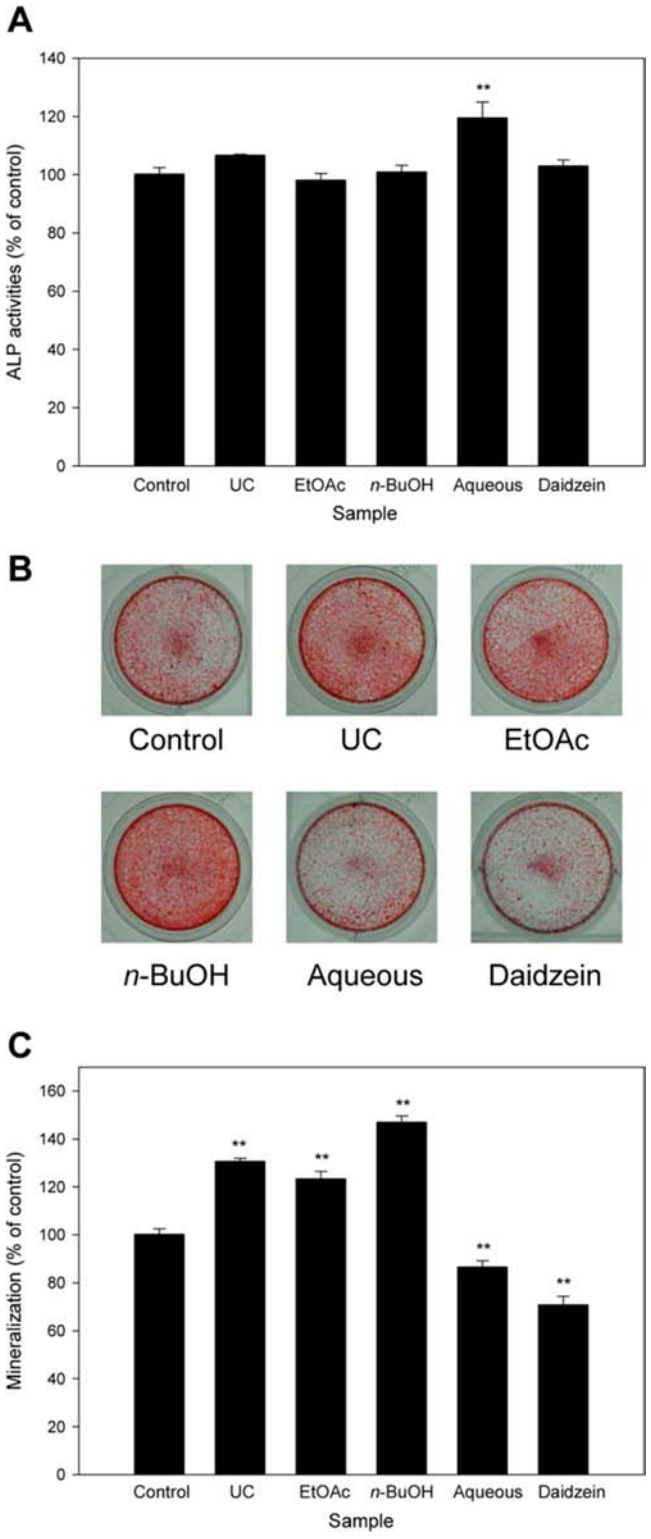

Figure 1. Effects of *U. crinita* extract (UC) and subfractions on ALP activity and mineralization in HOb cells. (A) HOb cells were seeded in 96-well plates and treated with 100 μg/mL of the indicated extracts for 72 h. ALP activity was measured using a colorimetric assay with *p*-nitrophenyl phosphate as the substrate. (B) HOb cells were plated in 24-well plates and treated with 100 μg/mL of the indicated extracts for 12 days. Mineralized nodule formation was assessed by alizarin red staining. (C) Quantitative analysis of the extent of mineralization. Daidzein (100 μM) was used as the positive control. Data are the presented as the mean ± SD (n = 3). * $p < 0.05$ and ** $p < 0.01$ compared to control cells.

dx.doi.org/10.1021/jf5012177 | J. Agric. Food Chem. 2014, 62, 5581−5588

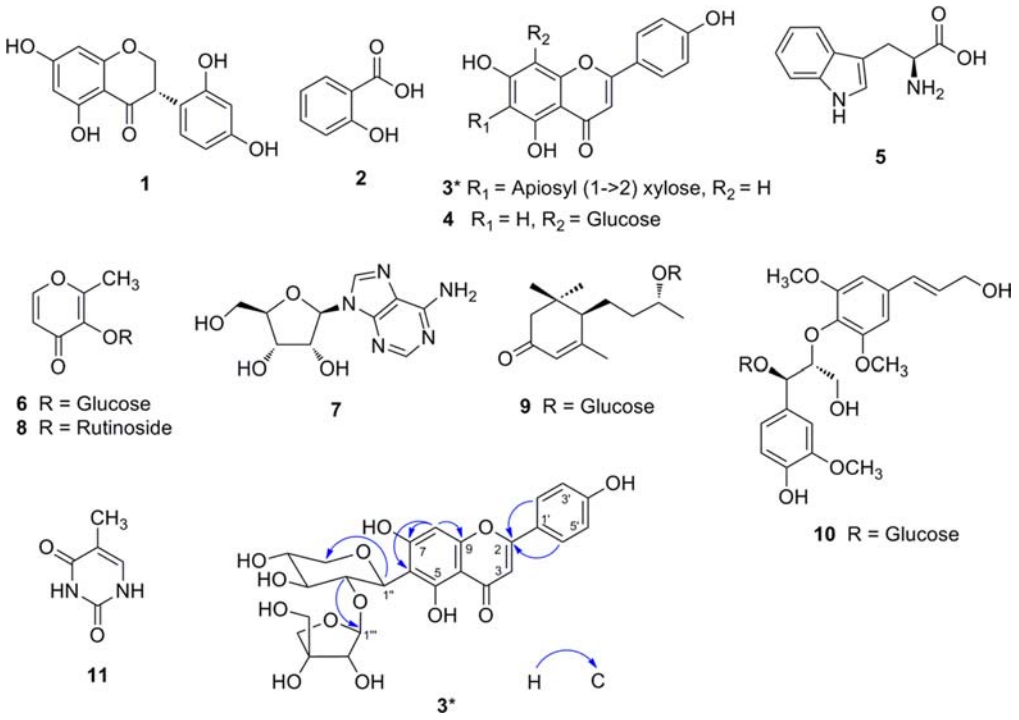

Figure 2. Schematic representation of the chemical structures of the isolated constituents from *U. crinita* and key HMBC correlations (H → C) for compound **3**.

normalized against GAPDH expression and expressed as relative expression compared with that of the controls.

Statistical Analysis. Data are expressed as the mean ± standard deviation (SD). Significant differences ($p < 0.05$ and $p < 0.01$) among the corresponding mean values were determined using one-way analysis of variance (ANOVA) followed by the Student−Newman−Keuls test. Probability values of $p < 0.05$ and $p < 0.01$ were considered statistically significant and extremely significant, respectively.

RESULTS AND DISCUSSION

Effect of *U. crinita* Extracts on Osteogenic Differentiation and Matrix Mineralization in HOb Cells. The fresh roots of *U. crinita* were extracted with 95% ethanol (EtOH) three times and the extract evaluated for osteogenic activity in HOb cells. This extract increased early bone differentiation marker alkaline phosphatase (ALP) activity and late mineralization activity by 106.51 ± 0.44 and 130.45 ± 1.51%, respectively (Figure 1A, B, and C). A bioguided method was then used to isolate and purify the active ingredients from the extract. Three fractions, EtOAc, *n*-BuOH, and aqueous fractions, were evaluated by the 3-(4,5-dimethylthiazol-2-yl)-2,5-diphenyltetrazolium bromide (MTT) assay. No significant toxic effects were observed in HOb cells when 100 μg/mL concentrations of these extracts were used. The effects of these fractions on ALP activity and the calcium contents of the mineralized matrix of the HOb cells were then evaluated. Treatment with the aqueous fraction caused a 119.36 ± 5.64% increase in ALP activity (Figure 1A). Treatment with either the EtOAc or *n*-BuOH fraction significantly increased the calcium content of the mineralized matrix by 123.11 ± 3.28 and 146.73 ± 2.85%, respectively (Figure 1B and C).

During bone formation, osteoblast maturation causes bone matrix synthesis, and the bone matrix becomes progressively mineralized in the terminal stages of synthesis. The EtOAc and *n*-BuOH fractions significantly increased the calcium content of the mineralized matrix in HOb cells; therefore, we purified their active compounds in subsequent studies.

Bioguided Isolation and Identification of Active Compounds from *U. crinita*. For purification of active compounds, the active EtOAc and *n*-BuOH fractions were subjected to column chromatography and high-performance lipid chromatography (HPLC). One new compound, **3**, and 10 known compounds were obtained. The structures of the 10 known compounds were clarified by spectroscopic analysis and comparisons with reported physical data, permitting the identification of dalbergioidin (**1**),[19,20] salicylic acid (**2**),[21] vitexin (**4**),[22] tryptophan (**5**),[23] maltol-3-*O*-β-D-glucopyranoside (**6**),[24] adenosine (**7**),[25] spatholosineside A (**8**),[26] byzantionoside B (**9**),[27] (7*R*,8*R*)-threo-guaiacylglycerol-8-*O*-4′-sinapyl ether 7-*O*-β-D-glucopyranoside (**10**),[28] and thymine (**11**)[29] (Figure 2).

The new compound **3** was obtained as a yellow solid. Its molecular formula was determined, from its positive HRESI-MS *m/z* 535.1459 $[M + H]^+$ (calculated for $C_{25}H_{27}O_{13}^+$, 535.1452), to be $C_{25}H_{26}O_{13}$, a result consistent with the NMR data (Table 1). The NMR spectrum showed δ_H 6.75 (1H, s, H-3) together with signals of δ_C 102.8 (C-3), 163.5 (C-2), and 181.8 (C-4), a spectrum that suggested the presence of flavone moieties. The presence of signals at δ_H 6.91 (2H, d, J = 8.8 Hz, H-3′, H-5′) and 7.92 (2H, d, J = 8.8 Hz, H-2′, H-6′) in an A_2X_2 coupling system, together with signals of δ_C 116.0 (C-3′, C-5′) and 128.5 (C-2′, C-6′) observed in the NMR spectra suggested a mono-substituted aromatic moiety (ring B) in **3**. In the hetero-nuclear multiple bond correlation (HMBC) spectrum (Figure 2), one aromatic signal, δ_H 6.51 (1H, s, H-8), was assigned at H-8 due to long-range coupling with C-6, C-7, and C-9. These data suggested that **3** had a 4′,5,7,-trihydroxyflavone (apigenin) skeleton. The NMR spectrum at δ_H 2.52 to 5.15 and δ_C 64.5 to 109.1 also showed two sugar signals in the structure. After acid hydrolysis of **3**, the aqueous layer was separated by HPLC and

dx.doi.org/10.1021/jf5012177 | J. Agric. Food Chem. 2014, 62, 5581−5588

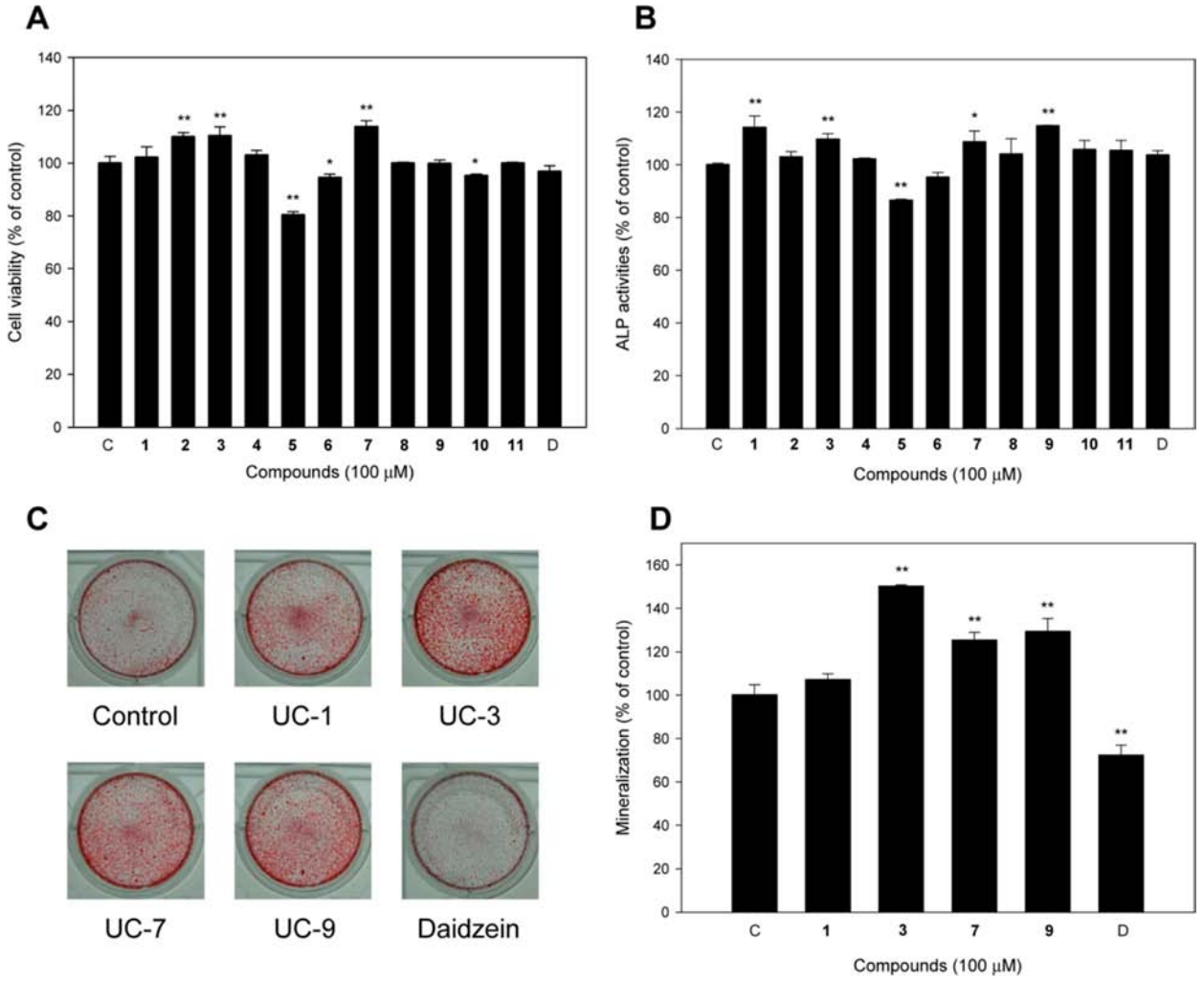

Figure 3. Effects of isolated compounds from *U. crinita* on cell viability, ALP activity, and mineralization in HOb cells. HOb cells were seeded in 96-well plates and treated with 100 μM of the indicated compounds for 72 h. (A) Cell viability was assessed using the MTT assay. (B) ALP activity was measured using a colorimetric assay with *p*-nitrophenyl phosphate disodium as the substrate. (C) HOb cells were plated in 24-well plates and treated with 100 μM of the indicated compounds for 12 days. Mineralized nodule formation was assessed by alizarin red-S staining. (D) Quantitative analysis of the extent of mineralization. Data are presented as the mean ± SD (n = 3). * $p < 0.05$ and ** $p < 0.01$ compared to control cells (C, control; D, daidzein).

compared to sugar standards to reveal one major sugar, apiose. The presence of *C*-D-xylopyranoside[30] and D-apiofuranoside[31] were determined from NMR, heteronuclear single quantum coherence (HSQC), ^{1}H−^{1}H correlation spectroscopy (COSY), HMBC spectra, and reported physical data.[32] Collectively, these data indicated that compound **3** was an apigenin linked with *C*-D-xylopyranoside and D-apiofuranoside moieties. The linkage of the sugar residues to the apigenin nucleus (C-1″ → C-6) was supported by the downfield NMR shifts of H-1″ (δ_H 4.55) of the *C*-D-xylopyranoside and the C-6 (δ_C 108.8) of the apigenin.[30,33,34] The position of the D-apiofuranoside and *C*-D-xylopyranoside linkage (C-1‴ → C-2″) was confirmed as C-1‴ at δ_C 109.1 and H-2″ at δ_H 4.27 (1H, brs) by HMBC correlations. The α-configuration of D-xylopyranoside and the β-configuration of D-apiofuranoside were deduced by the coupling constants of the anomeric protons H-1″ (δ_H 4.55, brs) and H-1‴ (δ_H 5.15, brs).[35] On the basis of these data, the structure of **3** was identified as apigenin 6-*C*-β-D-apiofuranosyl(1→2)-α-D-xylopyranoside.

Effects of the Isolated Compounds on Cell Viability, Osteogenic Differentiation, and Matrix Mineralization in HOb Cells. The effects of the isolated compounds on bone formation were assessed in HOb cells. Cell viability was measured using the MTT assay. Excluding compound **5**, none of the compounds at 100 μM reduced cell viability by more than 10% (Figure 3A). The effects of the nontoxic compounds on early osteoblast differentiation were investigated using an ALP activity assay, and their effects on late mineralization were assessed using alizarin red staining. The novel apigenin 6-*C*-β-D-apiofuranosyl(1→2)-α-D-xylopyranoside (**3**) and the known compounds dalbergioidin (**1**), adenosine (**7**), and byzantionoside B (**9**), significantly increased ALP activity in HOb cells by 109.68 ± 2.20, 114.10 ± 4.41, 108.70 ± 4.14, and 114.81 ± 0.18%, respectively (Figure 3B), when used at a concentration of 100 μM and also increased the calcium contents of the mineralized matrix by 150.10 ± 0.80, 107.09 ± 2.80, 125.21 ± 3.75, and 129.21 ± 6.13%, respectively (Figure 3C and D).

Effects of the Isolated Compounds on Osteogenesis-Related mRNA Expression in HOb Cells. We further investigated whether these four isolated compounds were able to promote osteogenesis-related mRNA expression by quantitative real-time PCR (Q-RT-PCR). At a concentration of 100 μM, dalbergioidin (**1**) upregulated the mRNA expression

dx.doi.org/10.1021/jf5012177 | J. Agric. Food Chem. 2014, 62, 5581−5588

of OPN, BMP-2, and Runx2 by 1.25 ± 0.05-, 1.21 ± 0.07-, and 1.71 ± 0.05-fold, respectively. Apigenin 6-*C*-*β*-D-apiofuranosyl-(1→2)-*α*-D-xylopyranoside (**3**) increased the expression of these substances by 1.39 ± 0.01-, 1.30 ± 0.04-, 1.43 ± 0.10-fold, respectively, adenosine (**7**) upregulated their expression by 1.14 ± 0.04-, 1.16 ± 0.09-, and 1.55 ± 0.05-fold, respectively, and byzantionoside B (**9**) increased their expression by 1.32 ± 0.07-, 1.21 ± 0.04-, and 1.28 ± 0.09-fold, respectively. The novel apigenin 6-*C*-*β*-D-apiofuranosyl(1→2)-*α*-D-xylopyranoside (**3**), dalbergioidin (**1**), adenosine (**7**), and byzantionoside B (**9**) increased OPN, BMP-2, and Runx2 mRNA expression in a concentration-dependent manner (Figure 4A, B, and C).

The BMP family plays an important role in the process of bone formation and remodeling.[36] In osteoblast cells, the action of BMP-2 is mediated by its binding to BMP-2 receptors and subsequent downstream regulation of the SMAD transcription factor SMAD1/5/8, which then forms a complex with SMAD4. Phosphorylated SMAD complexes translocate to the cell nucleus and bind to transcription factors including Runx2, Dlx5, and Osterix.[9,37] Extensive studies have demonstrated that BMPs stimulate osteoblast differentiation by upregulating Runx-2 expression and increasing the expression of ALP, type I collagen, OPN, and osteocalcin.[37] This is the first report demonstrating that apigenin 6-*C*-*β*-D-apiofuranosyl(1→2)-*α*-D-xylopyranoside (**3**), dalbergioidin (**1**), and byzantionoside B (**9**) significantly increase ALP activity in the early differentiation phase and OPN mRNA expression and bone nodule formation in the late mineralization phase in HOb cells. The osteogenic activity of the three compounds probably occurs through activation of the BMP-2/Smad/Runx2 signaling pathway, and these compounds had greater effects than daidzein (4′,7-dihydroxyisoflavone), the positive control, in HOb cells. Daidzein has been reported to induce the differentiation of rat or porcine osteoblast cells by upregulating BMP-2/Runx2 expression.[38,39] Adenosine (**7**) has been shown to increase osteoblast differentiation and bone formation in previous studies.[40,41] Natural isoflavonoids, such as daidzein, genistein (4′,5,7-trihydroxyisoflavone), and genistin (4′,5-dihydroxyisoflavone-7-*O*-glucoside), that enhance the expression of ALP, OCN, BMP-2, and osteoprotegerin have been reported to promote bone differentiation and mineralization both in vitro and in vivo.[39,42−44] Comparing dalbergioidin (**1**) (2′,4′,5,7-tetrahydroxyisoflavone) and the three isoflavones (genistein, genistin, and daidzein), we found that the OH groups at C-4′ and C-7 may be the important features of isoflavones needed for promoting bone formation. Additionally, compared with the flavonoid-6-*C*-glucosides of compound **3** and flavonoid 8-*C*-glucosides of compound **4**, we also observed that flavonoid-6-*C*-glycoside was an important unit for eliciting better osteogenic activity. The same pattern of flavonoid-6-*C*-glycoside was also found in the previous literature.[45] Our studies demonstrated that these four active compounds contained in *U. crinita* could stimulate osteogenic activity and enhance bone formation, possibly through the BMP-2/Smad/Runx2 pathway. Further studies are needed to understand the influence of different solvents and extraction methods on the osteogenic activity of *U. crinita*.

In conclusion, *U. crinita* extract contained the novel apigenin 6-*C*-*β*-D-apiofuranosyl(1→2)-*α*-D-xylopyranoside (**3**), which together with dalbergioidin (**1**), adenosine (**7**), and byzantionoside B (**9**) showed osteogenic activity by increasing ALP activity and calcium contents to regulate differentiation and mineralization in human osteoblast cells. Their mechanism of action may be through activation of the BMP-2 and Runx2 signal pathways. This is the first report that *U. crinita* and its active compounds exhibit osteogenic activity and suggests that in the future active constituents from this species may be applied for the prevention of bone loss and promotion of bone regeneration.

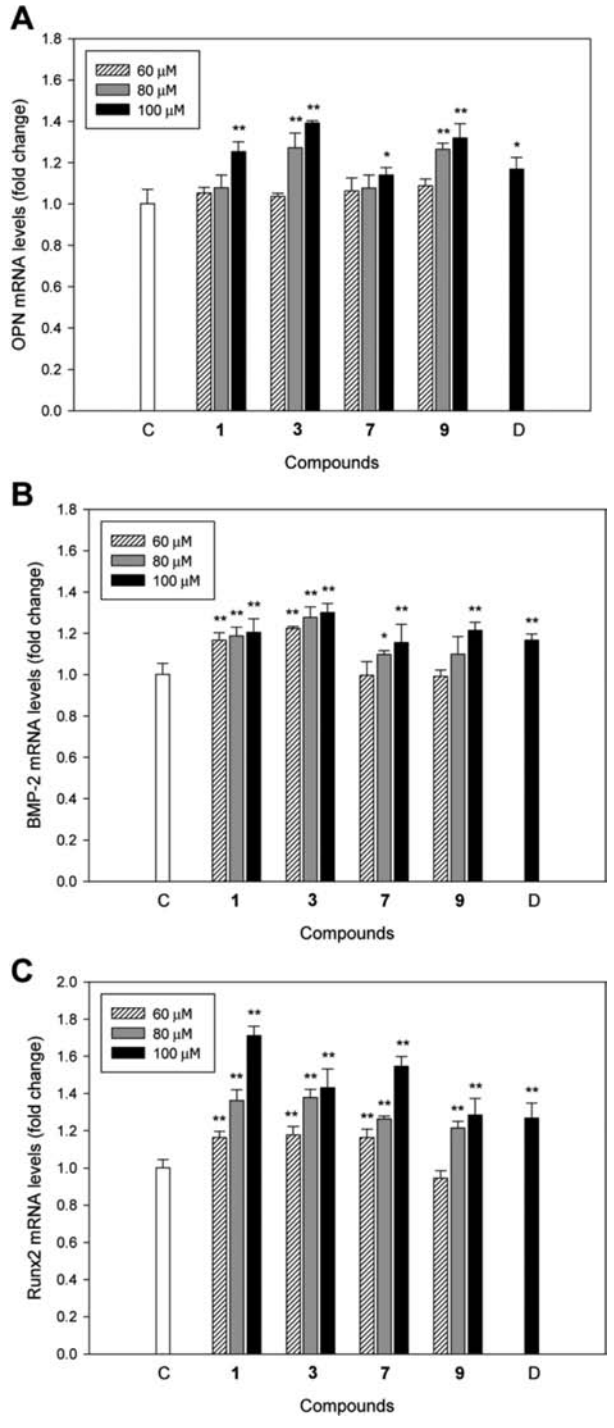

Figure 4. Effects of active compounds from *U. crinita* on osteogenesis-related mRNA expression in HOb cells. HOb cells were seeded in 6 cm dishes and treated with the indicated compounds for 24 h. Concentration-dependent effects of active compounds **1**, **3**, **7**, and **9** on (A) OPN, (B) BMP-2, and (C) Runx2 mRNA expression were determined by Q-RT-PCR analysis. Using the $2^{-\Delta\Delta Ct}$ method, Runx2, BMP-2, and OPN mRNA expression results were normalized against GAPDH expression. Data are presented as the mean ± SD (n = 3). * $p < 0.05$ and ** $p < 0.01$ compared to control cells (C, control; D, daidzein).

dx.doi.org/10.1021/jf5012177 | J. Agric. Food Chem. 2014, 62, 5581−5588

■ ASSOCIATED CONTENT

Supporting Information

NMR and HR-ESI-MASS spectra of compound **3**. This material is available free of charge via the Internet at http://pubs.acs.org.

■ AUTHOR INFORMATION

Corresponding Author

*Tel: +886-2-2736-1661 ext. 6151. Fax: +886-2-2735-7983. E-mail: lmh@tmu.edu.tw.

Funding

This study was supported by a grant from the National Science Council, Taiwan (NSC101-2320-B-038-014-MY3).

Notes

The authors declare no competing financial interest.

■ ACKNOWLEDGMENTS

We thank Shwu-Huey Wang (Instrumentation Center of Taipei Medical University) and Shou-Ling Huang (Nuclear Magnetic Resonance Lab, Instrumentation Center College of Science, National Taiwan University) for the NMR data acquisition and Dr. Mei-Kuang Lu (National Research Institute of Chinese Medicine, Taiwan) for acid hydrolysis and monosaccharide analysis.

■ ABBREVIATIONS USED

ALP, alkaline phosphatase; BCA, bicinchoninic acid; BMP, bone morphogenetic protein; BuOH, butanol; COSY, correlation spectroscopy; DMSO, dimethyl sulfoxide; ECM, extracellular matrix; EtOAc, ethyl acetate; EtOH, ethanol; HMBC, heteronuclear multiple bond correlation; HOb, human osteoblast; HPAEC, high-performance anion-exchange chromatography; HPLC, high-performance lipid chromatography; HRESI-MS, high-resolution eletrospray ionization mass spectroscopy; HSQC, heteronuclear single quantum coherence; MeOH, methanol; MTT, 3-(4,5-dimethylthiazol-2-yl)-2,5-diphenyltetrazolium bromide; ODM, osteoblast differentiation medium; OGM, osteoblast growth medium; OPN, osteopontin; NMR, nuclear magnetic resonance; PBS, phosphate-buffered saline; Runx2, runt-related transcription factor 2; TGF, transforming growth factor; UPL, Universal Probe Library

■ REFERENCES

(1) Hsu, S. Y.; Liu, K. C. *Studies on the Anti-ulcer Actions of Chinese Herbs and Folk Medicines (III)*; The Annual Reports of the National Research Institutes of Chinese Medicine; National Research Institutes of Chinese Medicine: Taipei, Taiwan, 1983; pp 31−41.

(2) Yen, G. C.; Lai, H. H.; Chou, H. Y. Nitric oxide-scavenging and antioxidant effects of *Uraria crinita* root. *Food Chem.* **2001**, *74*, 471−478.

(3) Liu, S. Y.; Liou, P. C.; Wang, J. Y.; Shyu, Y. T.; Hu, M. F.; Chang, Y. M.; Shieh, J. I. Production and Electrophoretic Analysis of Medical Plants in Taiwan. In *Proceeding of a Symposium on Development and Utilization of Resources of Medicinal Plants in Taiwan*; Tu, C. C., Lu, H. S., Liu, S. Y., Eds.; Taiwan Agricultural Research Institute: Taichung, Taiwan, 1995; pp 149−188.

(4) Wang, Y.; Zhang, X.; Gong, L.; Ruan, H.; Pi, H.; Zhang, Y. Studies on chemical constituents in roots of *Uraria crinita*. *Zhongguo Yaoxue Zazhi* **2009**, *44*, 1217−1220.

(5) Morita, N.; Arisawa, M.; Nagase, M.; Hsu, H. Y.; Chen, Y. P. Studies on the constituents of Formosan Leguminosae. II. The constituents in the leaves of *Uraria crinita* Desv. *Yakugaku zasshi* **1977**, *97*, 701−703.

(6) Muthusami, S.; Senthilkumar, K.; Vignesh, C.; Ilangovan, R.; Stanley, J.; Selvamurugan, N.; Srinivasan, N. Effects of *Cissus quadrangularis* on the proliferation, differentiation and matrix mineralization of human osteoblast like SaOS-2 cells. *J. Cell. Biochem.* **2011**, *112*, 1035−1045.

(7) Aubin, J. E.; Liu, F.; Malaval, L.; Gupta, A. K. Osteoblast and chondroblast differentiation. *Bone* **1995**, *17*, 77S−83S.

(8) Yang, H. M.; Shin, H. K.; Kang, Y. H.; Kim, J. K. *Cuscuta chinensis* extract promotes osteoblast differentiation and mineralization in human osteoblast-like MG-63 cells. *J. Med. Food* **2009**, *12*, 85−92.

(9) Chen, G.; Deng, C.; Li, Y. P. TGF-beta and BMP signaling in osteoblast differentiation and bone formation. *Int. J. Biol. Sci.* **2012**, *8*, 272−288.

(10) Phimphilai, M.; Zhao, Z.; Boules, H.; Roca, H.; Franceschi, R. T. BMP signaling is required for RUNX2-dependent induction of the osteoblast phenotype. *J. Bone Miner. Res.* **2006**, *21*, 637−646.

(11) Taira, M.; Nakao, H.; Takahashi, J.; Araki, Y. Effects of two vitamins, two growth factors and dexamethasone on the proliferation of rat bone marrow stromal cells and osteoblastic MC3T3-E1 cells. *J. Oral Rehabil.* **2003**, *30*, 697−701.

(12) Wang, X.; Wu, J.; Chiba, H.; Yamada, K.; Ishimi, Y. *Puerariae radix* prevents bone loss in castrated male mice. *Metabolism* **2005**, *54*, 1536−1541.

(13) Jeong, J. C.; Lee, J. W.; Yoon, C. H.; Lee, Y. C.; Chung, K. H.; Kim, M. G.; Kim, C. H. Stimulative effects of *Drynariae Rhizoma* extracts on the proliferation and differentiation of osteoblastic MC3T3-E1 cells. *J. Ethnopharmacol.* **2005**, *96*, 489−495.

(14) Hsieh, T. P.; Sheu, S. Y.; Sun, J. S.; Chen, M. H.; Liu, M. H. Icariin isolated from *Epimedium pubescens* regulates osteoblasts anabolism through BMP-2, SMAD4, and Cbfa1 expression. *Phytomedicine* **2010**, *17*, 414−423.

(15) Hsu, F. L.; Chou, C. J.; Chang, Y. C.; Chang, T. T.; Lu, M. K. Promotion of hyphal growth and underlying chemical changes in *Antrodia camphorata* by host factors from *Cinnamomum camphora*. *Int. J. Food Microbiol.* **2006**, *106*, 32−38.

(16) Scudiero, D. A.; Shoemaker, R. H.; Paull, K. D.; Monks, A.; Tierney, S.; Nofziger, T. H.; Currens, M. J.; Seniff, D.; Boyd, M. R. Evaluation of a soluble tetrazolium/formazan assay for cell growth and drug sensitivity in culture using human and other tumor cell lines. *Cancer Res.* **1988**, *48*, 4827−4833.

(17) Hsu, Y. L.; Chang, J. K.; Tsai, C. H.; Chien, T. T.; Kuo, P. L. Myricetin induces human osteoblast differentiation through bone morphogenetic protein-2/p38 mitogen-activated protein kinase pathway. *Biochem. Pharmacol.* **2007**, *73*, 504−514.

(18) Wang, Y. H.; Liu, Y.; Maye, P.; Rowe, D. W. Examination of mineralized nodule formation in living osteoblastic cultures using fluorescent dyes. *Biotechnol. Prog.* **2006**, *22*, 1697−1701.

(19) Benavides, A.; Bassarello, C.; Montoro, P.; Vilegas, W.; Piacente, S.; Pizza, C. Flavonoids and isoflavonoids from *Gynerium sagittatum*. *Phytochemistry* **2007**, *68*, 1277−1284.

(20) Durango, D.; Quinones, W.; Torres, F.; Rosero, Y.; Gil, J.; Echeverri, F. Phytoalexin accumulation in Colombian bean varieties and aminosugars as elicitors. *Molecules* **2002**, *7*, 817−832.

(21) Scott, K. N. Carbon-13 nuclear magnetic resonance of biologically important aromatic acids. I. Chemical shifts of benzoic acid and derivatives. *J. Am. Chem. Soc.* **1972**, *94*, 8564−8568.

(22) Krafczyk, N.; Glomb, M. A. Characterization of phenolic compounds in rooibos tea. *J. Agric. Food Chem.* **2008**, *56*, 3368−3376.

(23) Lee, M.; Phillips, R. S. Fluorine substituent effects for tryptophan in carbon-13 nuclear magnetic resonance. *Magn. Reson. Chem.* **1992**, *30*, 1035−1040.

(24) Ono, M.; Masuoka, C.; Tanaka, T.; Ito, Y.; Nohara, T. Antioxidative and antihyaluronidase activities of some constituents from the aerial part of *Daucus carota*. *Food Sci. Technol. Res.* **2001**, *7*, 307−310.

(25) Moyroud, E.; Strazewski, P. L-Ribonucleosides from L-xylose. *Tetrahedron* **1999**, *55*, 1277−1284.

(26) Yin, T.; Liu, H.; Wang, B.; Tu, G.; Liang, H.; Zhao, Y. Chemical constituents from *Spatholobus sinensis*. *Yaoxue Xuebao* **2008**, *43*, 67−70.

(27) Matsunami, K.; Otsuka, H.; Takeda, Y. Structural revisions of blumenol C glucoside and byzantionoside B. *Chem. Pharm. Bull.* **2010**, *58*, 438−441.
(28) Machida, K.; Sakamoto, S.; Kikuchi, M. Two new neolignan glycosides from leaves of *Osmanthus heterophyllus*. *J. Nat. Med.* **2009**, *63*, 227−231.
(29) Pouchert, C. J.; Behnke, J. *The Aldrich Library of ^{13}C and ^{1}H FT NMR Spectra*; Aldrich Chemical Company: Milwaukee, WI, 1993; pp 367.
(30) Fiorentino, A.; D'Abrosca, B.; Pacifico, S.; Izzo, A.; Letizia, M.; Esposito, A.; Monaco, P. Potential allelopathic effects of stilbenoids and flavonoids from leaves of *Carex distachya* Desf. *Biochem. Syst. Ecol.* **2008**, *36*, 691−698.
(31) Phan, V. K.; Nguyen, X. C.; Nguyen, X. N.; Vu, K. T.; Ninh, K. B.; Chau, V. M.; Bui, H. T.; Truong, N. H.; Lee, S. H.; Jang, H. D.; Kim, Y. H. Antioxidant activity of a new *C*-glycosylflavone from the leaves of *Ficus microcarpa*. *Bioorg. Med. Chem. Lett.* **2011**, *21*, 633−637.
(32) Dubois, M. A.; Zoll, A.; Bouillant, M. L.; Chopin, J. New *C*-glycosylflavones from *Cerastium arvense*. *Phytochemistry* **1982**, *21*, 1141−1143.
(33) Loizzo, M. R.; Said, A.; Tundis, R.; Rashed, K.; Statti, G. A.; Hufner, A.; Menichini, F. Inhibition of angiotensin converting enzyme (ACE) by flavonoids isolated from *Ailanthus excelsa* (Roxb) (Simaroubaceae). *Phytother. Res.* **2007**, *21*, 32−36.
(34) Aquino, R.; Morelli, S.; Lauro, M. R.; Abdo, S.; Saija, A.; Tomaino, A. Phenolic constituents and antioxidant activity of an extract of *Anthurium versicolor* leaves. *J. Nat. Prod.* **2001**, *64*, 1019−1023.
(35) Shie, J. J.; Chen, C. A.; Lin, C. C.; Ku, A. F.; Cheng, T. R.; Fang, J. M.; Wong, C. H. Regioselective synthesis of di-*C*-glycosyl-flavones possessing antiinflammation activities. *Org. Biomol. Chem.* **2010**, *8*, 4451−4462.
(36) Nishimura, R.; Hata, K.; Matsubara, T.; Wakabayashi, M.; Yoneda, T. Regulation of bone and cartilage development by network between BMP signalling and transcription factors. *J. Biochem.* **2012**, *151*, 247−254.
(37) Ryoo, H. M.; Lee, M. H.; Kim, Y. J. Critical molecular switches involved in BMP-2-induced osteogenic differentiation of mesenchymal cells. *Gene* **2006**, *366*, 51−57.
(38) De Wilde, A.; Lieberherr, M.; Colin, C.; Pointillart, A. A low dose of daidzein acts as an ERbeta-selective agonist in trabecular osteoblasts of young female piglets. *J. Cell. Physiol.* **2004**, *200*, 253−262.
(39) Jia, T. L.; Wang, H. Z.; Xie, L. P.; Wang, X. Y.; Zhang, R. Q. Daidzein enhances osteoblast growth that may be mediated by increased bone morphogenetic protein (BMP) production. *Biochem. Pharmacol.* **2003**, *65*, 709−715.
(40) Inoue, A.; Hiruma, Y.; Hirose, S.; Yamaguchi, A.; Hagiwara, H. Reciprocal regulation by cyclic nucleotides of the differentiation of rat osteoblast-like cells and mineralization of nodules. *Biochem. Biophys. Res. Commun.* **1995**, *215*, 1104−1110.
(41) Mediero, A.; Cronstein, B. N. Adenosine and bone metabolism. *Trends. Endocrinol. Metab.* **2013**, *24*, 290−300.
(42) Chang, H.; Jin, T. Y.; Jin, W. F.; Gu, S. Z.; Zhou, Y. F. Modulation of isoflavones on bone-nodule formation in rat calvaria osteoblasts *in vitro*. *Biomed. Environ. Sci.* **2003**, *16*, 83−89.
(43) Li, X. H.; Zhang, J. C.; Sui, S. F.; Yang, M. S. Effect of daidzin, genistin, and glycitin on osteogenic and adipogenic differentiation of bone marrow stromal cells and adipocytic transdifferentiation of osteoblasts. *Acta Pharmacol. Sin.* **2005**, *26*, 1081−1086.
(44) Morris, C.; Thorpe, J.; Ambrosio, L.; Santin, M. The soybean isoflavone genistein induces differentiation of MG63 human osteosarcoma osteoblasts. *J. Nutr.* **2006**, *136*, 1166−1170.
(45) Rawat, P.; Kumar, M.; Sharan, K.; Chattopadhyay, N.; Maurya, R. Ulmosides A and B: flavonoid 6-*C*-glycosides from *Ulmus wallichiana*, stimulating osteoblast differentiation assessed by alkaline phosphatase. *Bioorg. Med. Chem. Lett.* **2009**, *19*, 4684−4687.

JOURNAL OF AGRICULTURAL AND FOOD CHEMISTRY

Article

pubs.acs.org/JAFC

Cecal Succinate Elevated by Some Dietary Polyphenols May Inhibit Colon Cancer Cell Proliferation and Angiogenesis

Tomoaki Haraguchi,[†] Tomoko Kayashima,[*,‡] Yukako Okazaki,[§] Junji Inoue,[#] Shigeru Mineo,[⊥] Kiminori Matsubara,[⊗] Ei Sakaguchi,[△] Noriyuki Yanaka,[†] and Norihisa Kato[†]

[†]Graduate School of Biosphere Science, Hiroshima University, 1-4-4 Higashi, Hiroshima 739-8528, Japan

[‡]Faculty of Culture and Education, Saga University, 1 Honjou, Saga 840-8502, Japan

[§]Faculty of Human Life Sciences, Fuji Women's University, 4-5 Hanakawa Minami, Ishikari 061-3204, Japan

[#]Ahjikan Company Ltd., Hiroshima 733-0833, Japan

[⊥]Institutes of Health, BOURBON Corporation, Kashiwazaki 945-0114, Japan

[⊗]Graduate School of Education, Hiroshima University, 1-1-1 Higashi, Hiroshima 739-8524, Japan

[△]Graduate School of Natural Science and Technology, Okayama University, 1-1-1 Tsushimanaka, Kitaku, , Okayama 700-8530, Japan

ABSTRACT: This study demonstrated that 0.5% dietary rutin, ellagic acid, or curcumin markedly increased cecal succinate levels in rats fed a high-fat diet, whereas catechin, caffeic acid, and quercetin did not. Other organic acids were modestly or hardly affected by polyphenols. To clarify the effects of succinate levels increased by polyphenols, this study examined the effects of succinate on the growth and proliferation of colon cancer cells and angiogenesis. The growth and proliferation of HT29 human colon cancer cells and angiogenesis in an ex vivo model were significantly inhibited by succinate at a dose close to that in the cecum of rats fed polyphenols. Furthermore, succinate inhibited the migration of human umbilical vein endothelial cells. These findings suggest that the consumption of some polyphenols affects the health and diseases of the large intestine by elevating succinate.

KEYWORDS: *rats, polyphenols, succinate, colon cancer cells, angiogenesis*

INTRODUCTION

Polyphenols, which are abundant in plant foods, exhibit various beneficial activities such as antioxidative, antiatherogenic, antidiabetic, anticancer, antiviral, anti-inflammatory, and antiangiogenic activities.[1−3] We previously reported that the dietary addition of some polyphenols including curcumin, caffeic acid, catechin, rutin, and ellagic acid suppresses fecal levels of secondary bile acids, namely, deoxycholic acid and/or lithocholic acid (which are risk factors for colon diseases), in rats fed a high-fat diet.[4] A high-fat diet increases fecal secondary bile acids,[5,6] causing compensatory proliferation of colonic epithelium cells.[7,8] This suggests such polyphenols might have beneficial effects on colon health by reducing secondary bile acids in animals fed a high-fat diet.[4] High-fat diets not only increase fecal secondary bile acid levels but also lower cecal organic acid production.[6] Mounting evidence indicates the increased production of intestinal organic acids including butyrate and propionate is associated with a decreased risk of colon cancer and colitis.[9,10] Meanwhile, food constituents that are indigestible or digestible to only a limited extent, such as resistant starch[11] and inulin,[12] increase cecal organic acid levels in both rats and humans. However, there is limited information concerning the effects of dietary polyphenols on cecal organic acids. Therefore, this study examined the effects of dietary polyphenols on cecal levels of organic acids in rats fed a high-fat diet.

Succinate is an important metabolic molecule as an intermediate in the citric acid cycle. It is known as a "umami"-tasting substance and is found in shellfish, refined sake, and soy sauce. Recent studies suggest organic acids such as butyrate and propionate may contribute to intestinal immune and barrier function.[13−15] However, the role of succinate remains incompletely understood. In this study, we provide evidence that consumption of some polyphenols markedly elevated cecal succinate in rats fed a high-fat diet. Therefore, this study also examined the effect of succinate on the growth of colon carcinoma cells and angiogenesis.

MATERIALS AND METHODS

Materials. Rutin, curcumin, catechin, caffeic acid, quercetin, succinate disodium salt, and 3-(4,5-dimethylthiazol-2-yl)-2,5-diphenyl tetrazolium bromide (MTT) were purchased from Nacalai Tesque (Kyoto, Japan). Ellagic acid was obtained from Wako Pure Chemical Industry (Osaka, Japan). Human recombinant vascular endothelial growth factor (VEGF) was obtained from R&D Systems (Minneapolis, MN, USA). Other reagents were of special grade as commercially available.

Animals and Diets. Male Sprague−Dawley rats (Charles River Laboratories, Kanagawa, Japan) weighing 40−50 g (3 weeks old) were

Received: March 18, 2014
Revised: May 22, 2014
Accepted: May 23, 2014
Published: May 23, 2014

ACS Publications © 2014 American Chemical Society

Table 1. Effects of Dietary Addition of 0.5% Polyphenols on Cecal Organic Acids in Rats Fed a High-Fat Diet[s]

	control	rutin	ellagic acid	curcumin	catechin	caffeic acid	quercetin
wet weight of cecal digesta (g)	1.44 ± 0.12	1.83 ± 0.21	2.47 ± 0.16*	2.50 ± 0.18*	1.81 ± 0.16	1.75 ± 0.15	1.69 ± 0.11
organic acids (μmol/g wet digesta)							
succinate	7.0 ± 1.6	44.5 ± 9.8*	37.4 ± 6.4*	32.5 ± 9.0*	25.1 ± 4.8	23.8 ± 5.7	7.1 ± 3.0
formate	1.40 ± 0.20	1.48 ± 0.73	0.54 ± 0.26	0.82 ± 0.27	0.99 ± 0.30	1.27 ± 0.31	1.88 ± 0.43
acetate	24.1 ± 2.3	29.8 ± 2.8	26.6 ± 1.1	26.3 ± 2.1	29.0 ± 2.6	29.6 ± 4.4	35.4 ± 2.0*
propionate	6.34 ± 0.77	6.55 ± 0.83	6.66 ± 0.52	4.82 ± 0.60	5.18 ± 0.62	6.44 ± 0.74	7.63 ± 0.46
isobutyrate	1.24 ± 0.20	ND	ND	ND	0.80 ± 0.22	1.34 ± 0.41	0.67 ± 0.18
butyrate	4.50 ± 0.38	3.60 ± 0.48	2.96 ± 0.36	2.99 ± 0.48	5.99 ± 0.45	5.12 ± 0.98	7.78 ± 0.72*
isovalerate	1.58 ± 0.14	0.74 ± 0.31	0.78 ± 0.14	1.22 ± 0.34	1.24 ± 0.24	1.33 ± 0.28	0.58 ± 0.10*
valerate	1.12 ± 0.12	ND	0.32 ± 0.12	0.56 ± 0.24	0.88 ± 0.26	1.01 ± 0.32	ND
total	46.2 ± 5.0	86.9 ± 8.0*	75.6 ± 6.8*	69.8 ± 7.8	68.3 ± 3.2	70.2 ± 8.0	60.8 ± 5.8
pH	7.15 ± 0.12	6.40 ± 0.27*	6.97 ± 0.12	6.77 ± 0.19	6.71 ± 0.09	6.55 ± 0.20	6.81 ± 0.13

[s]Mean ± SE (n = 7). *, dignificantly different from the control group by Dunnett's multiple-range test ($p < 0.05$). ND, not detectable.

used. The rats were individually housed in metal separate cages in a temperature-controlled (24 °C) room with a 12 h light−dark cycle (lights on from 8:00 a.m. to 8:00 p.m.). The rats were allowed a 1 week acclimation period before the experiments. The rats were maintained according to the *Guide for the Care and Use of Laboratory Animals* established by Hiroshima University. The protocol was approved by the Committee on the Ethics of Animal Experiments of the Hiroshima University (permit D08-16). The control group received a high-fat diet that contained 30% fat, without polyphenols. The basal diet comprised 30% beef tallow, 20% casein, 20.3% corn starch, 20% sucrose, 5% cellulose, 3.5% salt mixture (AIN-93G),[16] 1% vitamin mixture (AIN-93),[16] and 0.2% L-cystine (made up to 100% with corn starch). Rats allocated to the 0.5% polyphenol groups received the high-fat diet supplemented with 0.5% polyphenols including rutin, ellagic acid, curcumin, catechin, caffeic acid, or quercetin. All rats were fed the same amount of experimental diet (9, 10, 12, 14, and 15 g for days 1, 2−4, 5−7, 8−13, and 14−21, respectively) to suppress any variation in food intake due to ad libitum feeding. All diets were provided daily at 7:00 p.m. in food cups in the cages, and all rats had completely consumed the diets by the next morning. All rats had ad libitum access to deionized water. After 3 weeks of diet feeding, the rats were euthanized between 1:00 and 3:00 p.m. The cecal contents were removed, weighed, and stored at −80 °C for later analysis.

Cecal Contents Analysis. The levels of organic acids in the cecum were measured by high-performance liquid chromatography (HPLC) as described previously.[17] Cecal contents (300 mg) were homogenized by ultrasonication in 2 mL of 10 mM sodium hydroxide aqueous solution containing 0.5 g/L crotonic acid and subsequently centrifuged at 10000*g* for 15 min. Fat-soluble substances in the supernatant were removed by extraction with chloroform. The aqueous phase was filtered through a membrane filter, and the samples were subjected to HPLC. Organic acids were separated with an ion exclusion column and detected using an H-type cation exchanger column with a column temperature of 45 °C, mobile phase of 5 mM *p*-toluene sulfonic acid aqueous solution, positive polarity electroconductivity detector at 45 °C, and detection reagent of 20 mM bis-Tris aqueous solution containing 5 mM *p*-toluenesulfonic acid and 100 μM EDTA.

Cell Lines and Culture Conditions. HT29 human colon cancer cells were cultured routinely in Dulbecco's modified Eagle medium (DMEM) supplemented with 10% fetal bovine serum, penicillin (100 units/mL), and streptomycin (100 units/mL). Subcultures of HT29 were obtained by treating cell cultures with 2% trypsin/EDTA buffer. Human umbilical vein endothelial cells (HUVECs) were purchased from Kurabo Industries (Osaka, Japan) and grown in HuMedia EG 2 medium (Kurabo), which is modified MCDB 131 medium containing 2% fetal bovine serum, 10 ng/mL recombinant human epidermal growth factor, 1 μg/mL hydrocortisone, 50 μg/mL gentamicin, 50 ng/mL amphotericin B, 5 ng/mL recombinant human basic fibroblast growth factor, and 10 μg/mL heparin. Subcultures of HUVECs were obtained by treating the HUVEC culture with Hanks'-based enzyme-free cell dissociation buffer (Gibco, Grand Island, NY, USA). HUVECs at passages 3−7 were used in the experiment. All cells were maintained at 37 °C in a humidified incubator with 5% CO_2.

MTT Assay. For the growth assay of HT29 cells, cells were suspended in DMEM and plated onto 96-well culture plates (3.0×10^3 cells/100 μL). For the growth assay of HUVECs, cells were suspended in HuMedia EG2Medium and plated onto 96-well culture plates (1.5×10^3 cells/100 μL). Cells were incubated for 24 h at 37 °C in a humidified incubator with 5% CO_2. The media were replaced with fresh media containing sodium succinate (1−30 mM) or vehicle [phosphate-buffered saline (PBS)]. After the cells had been exposed for 24 or 72 h, MTT solution (final concentration, 5 mg/mL MTT in PBS) was added to each well, and the cells were incubated for 3 h. The media were aspirated, and the cells were lysed in dimethyl sulfoxide. Absorbance was measured at 550 nm in an ELNX96 microplate reader (TFB Inc., Tokyo, Japan). Reported values represent the averages for six wells.

Bromo-deoxyuridine (BrdU) Incorporation Assay. Experiments were conducted in 6-well plates (1×10^6 cells/well) with two replicates. After the cells with or without the media containing sodium succinate (30 mM) had been exposed for 24 h, HT29 cells were incubated with 100 μM BrdU for 2 h at 37 °C in a humidified incubator with 5% CO_2. To detect BrdU immunoreactivity, cells were washed with PBS and fixed with 4% paraformaldehyde at room temperature for 10 min. After washing twice with PBS, cell samples were incubated with PBS with 1% Triton X-100 at room temperature for 10 min. Cells were again washed twice with PBS and incubated with 2 N HCl. After removal of the HCl, cells were washed three times with 0.1 mM borate buffer (pH 8.5). For blocking, 4% skim milk with PBS was added, and the cells were slowly shaken at room temperature. After 1 h of incubation, the blocking buffer was discarded, and BrdU antibody (1:1000; 1 mL/plate) and DAPI (40 mg/mL, 1:1000) were added. The cells were incubated at room temperature for 1.5 h and then washed three times with PBS. Cy3-labeled anti-mouse IgG was added as a secondary antibody (1:1000; 1 mL/plate), and the cells were incubated for 30 min at room temperature. The cells were then washed three times with PBS. The cells were visualized by fluorescence microscopy, and BrdU-positive cells were counted on 10 image fields. The average number of BrdU-positive cells in each sample was subsequently calculated.

Ex Vivo Angiogenesis Assay. Male Wistar rats (6 weeks old, Charles River Laboratories) were maintained according to the guide established by Hiroshima University Animal Research Committee as mentioned above. The ex vivo angiogenesis assay was carried out in the rat aortic model[18,19] with slight modifications.[20] Briefly, a rat aortic segment coved with the collagen gel was overlaid with 2 mL of culture medium (RPMI 1640 medium) containing sodium succinate (10 or 30 mM) or vehicle (PBS) and incubated for 10 days in a fully humidified system of 5% CO_2 at 37 °C. The culture medium with sample was changed on the seventh day. After 10 days of incubation, microscopic fields were photographed with a digital camera (DSE330-A system,

dx.doi.org/10.1021/jf501142k | J. Agric. Food Chem. 2014, 62, 5589−5594

Olympus, Tokyo, Japan), and the length of the capillary was measured using Adobe Photoshop software CS3. Each reported value represents the average of three or four culture samples.

Endothelial Cell Tube Formation and Chemotaxis Assays. The HUVEC tube formation assay was performed using BD Matrigel (BD Biosciences, Franklin Lakes, NJ, USA) as described previously.[20] Reported values represent the averages of three samples. The HUVEC chemotaxis assay was performed in a modified Boyden chamber.[20,21] Migrated cells were counted in three fields of each membrane at 200× magnification, and the average number of cells in each field was calculated. The experiment was performed in triplicate.

Statistical Analysis. Statistical analysis was conducted by one-way analysis of variation (ANOVA) and Dunnet's multiple-range test (Excel Statistics 2006 for Windows, Social Survey Research Information Co. Ltd., Tokyo, Japan). Statistical significance was estimated at $p < 0.05$.

RESULTS

Effect of Polyphenols on Cecal Organic Acids in Rats Fed a High-Fat Diet. Dietary addition of polyphenols did not affect the food intake, final body weight, or liver weight of the rats (data not shown). The wet weight of cecal contents was higher in the curcumin and ellagic acid groups than the control group ($p < 0.05$, Table 1). The cecal concentration (μmol/g wet digesta) of succinate was markedly higher in the rutin (6.4-fold), ellagic acid (5.3-fold), and curcumin (4.6-fold) groups than in the control group ($p < 0.05$). Meanwhile, dietary catechin and caffeic acid tended to increase cecal concentrations of succinate ($p < 0.1$). Acetate and butyrate concentrations were significantly higher and isovalerate concentration was significantly lower in the quercetin group compared to the control group ($p < 0.05$). The concentrations of other organic acids including formate, propionate, isobutyrate, and valerate were unaffected by dietary polyphenols. Dietary rutin and ellagic acid significantly increased the concentrations of total organic acids compared to the control (1.9- and 1.6-fold, respectively, $p < 0.05$). The pH of digesta was significantly lower in the rutin group than in the control group ($p < 0.05$).

Effects of Succinate on HT29 Cell Growth and Proliferation. Succinate significantly inhibited the growth of the HT29 cells at both 10 and 30 mM (Figure 1, $p < 0.05$). Analysis of cell proliferation by BrdU incorporation into the cells indicated 30 mM succinate significantly reduced (−30%) the proportion of proliferative cells (control vs succinate: 32.6 ± 2.0 and 22.8 ± 1.8%, respectively, $n = 6$, $p < 0.05$).

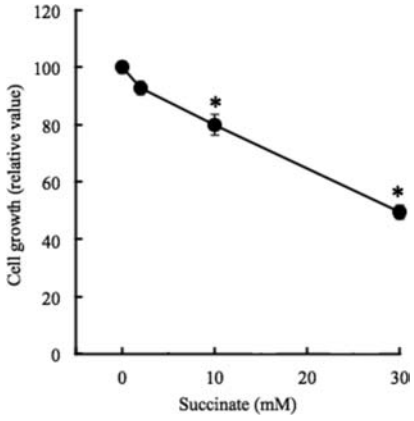

Figure 1. Effects of succinate on the growth of HT29 cells. Cultured cells (3.0×10^3 cells/well) were exposed to the medium for 24 h. Cell growth was determined by the MTT assay. Values are means ± SEM ($n = 6$). *, significantly different from the control by Dunnet's multiple-range test ($p < 0.05$).

Effects of Succinate on ex Vivo Angiogenesis and Endothelial Cell Functions. In the ex vivo angiogenesis model using a rat aortic ring, microvessels appeared from the ends of aortic rings and elongated in the absence of succinate (Figure 2A). Meanwhile, microvessel growth was significantly inhibited in the presence of 30 mM succinate (Figure 2C,D, $p < 0.01$).

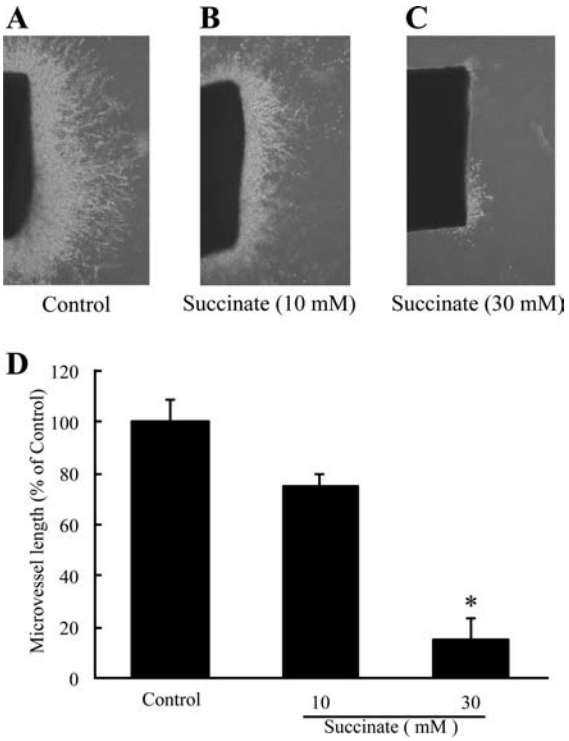

Figure 2. Effect of succinate on ex vivo angiogenesis with the use of a rat aortic ring: (A−C) representative result as to the inhibitory effects of succinate; (D) microvessel length measured on day 10 of culture. Values are means ± SEM ($n = 3, 4$). *, significantly different from the control by Dunnet's multiple-range test ($p < 0.01$).

The effects of succinate on HUVEC functions including tube formation on a reconstituted basement membrane, chemotaxis, and growth are shown in Figure 3. HUVECs inoculated onto a reconstituted basement membrane migrated, attached to each other, and finally formed tube structures in the tube formation assay model. In this assay, succinate did not significantly suppress HUVEC tube formation (Figure 3A). However, succinate at both 10 and 30 mM significantly inhibited HUVEC migration stimulated with VEGF in a gelatin-coated Boyden chamber (Figure 3B, $p < 0.01$). However, succinate did not significantly affect the growth of HUVECs (Figure 3C).

DISCUSSION

We previously reported that some dietary polyphenols suppress fecal levels of secondary bile acids, namely, deoxycholic acid and/or lithocholic acid, in rats fed a high-fat diet.[4] This study further provides novel evidence indicating dietary supplementation of rutin, ellagic acid, and curcumin to a high-fat diet markedly increase cecal succinate concentrations in rats. However, dietary catechin, caffeic acid, and quercetin hardly

dx.doi.org/10.1021/jf501142k | J. Agric. Food Chem. 2014, 62, 5589−5594

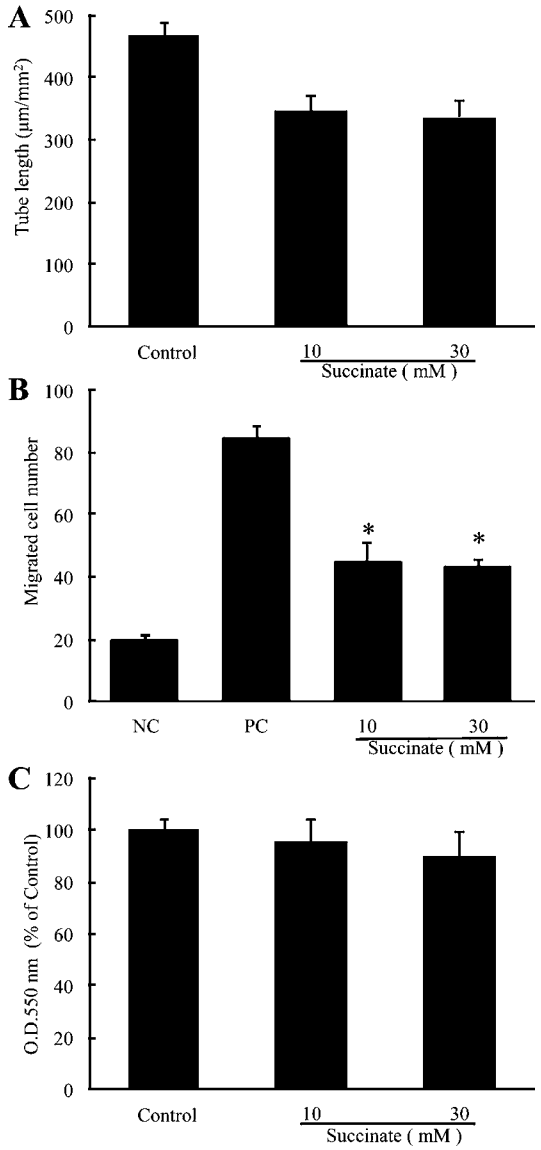

Figure 3. Effect of succinate on HUVEC functions. (A) Effect of succinate on HUVEC tube formation on reconstituted basement membrane. Capillary length was measured. Values are means ± SEM (n = 3). (B) Effect of succinate on HUVEC chemotaxis. HUVECs that migrated to the lower surfaces of the filters after 6 h of incubation were counted in three 200× fields of the filters. Means of a field of three filters ± SEM (n = 9) are shown. NC, negative control (medium without VEGF and sample); PC, positive control (VEGF containing medium without sample). (C) Effect of succinate on the growth of HUVEC. Cultured cells (1.5×10^3 cells/well) were exposed to the medium for 72 h. Cell growth was determined by the MTT assay. Values are means ± SEM (n = 6). *, significantly different from the positive control (PC) by Dunnet's multiple-range test ($p < 0.01$).

affected cecal succinate concentrations. Aprikian et al. report that adding a polyphenol-rich apple concentrate (~0.7 g polyphenol/kg diet) to a normal diet (with 5% corn oil) did not affect cecal succinate concentrations in rats.[22] Furthermore, in our preliminary study, dietary addition of 0.5% ellagic acid to a low fat-diet (5% beef tallow) failed to elevate cecal succinate levels in rats (Haraguchi et al., unpublished data), but the reason for the lack of an effect is unknown. Thus, the effect of polyphenols on cecal succinate levels might be dependent on dietary fat intake as well as the kinds and levels of polyphenols in the diet. Intriguingly, the dietary addition of rutin significantly increased cecal succinate levels, whereas quercetin did not. Quercetin and its glycosidic form, rutin, are common flavonoids in edible foods. However, the absorption processes of these polyphenols are quite different. Crespy et al. report quercetin can be partly absorbed in the stomach, whereas rutin cannot.[23] Dietary rutin likely escapes absorption in the stomach and small intestine to reach the large intestine, leading it to significantly affect cecal succinate production.

Because succinate is the major metabolite of *Bacteroides* in the large intestine,[24] we examined the effect of the polyphenols on the cecal profile of the microflora by 16S rDNA-based terminal restriction fragment length polymorphism analysis. The results indicate dietary 0.5% curcumin, ellagic acid, and rutin did not significantly affect the proportion of cecal microflora including *Bacteroides*, *Clostridium*, *Lactobacillales*, and *Bifidobacterium* (unpublished data). Thus, the increased production of cecal succinate by such polyphenols cannot be accounted for by the microfloral profile. In our previous study, besides 0.5% dietary curcumin, ellagic acid, and rutin, 0.5% dietary caffeic acid and catechin also markedly reduced fecal toxic secondary bile acids such as deoxycholic and lithocholic acid (which are risk factors for colon diseases) in rats fed a high-fat diet.[4] Therefore, the overall association between alterations in the cecal profile of organic acids and fecal secondary bile acids appears to be weak.

To gain further insight into the polyphenol-induced increase in cecal succinate levels, we examined the effects of succinate on colon cancer cells and angiogenesis. The results indicate 30 mM succinate, which corresponds to the cecal level in the rats fed various polyphenols, inhibits the growth and proliferation of HT29 colon cancer cells. An animal study by Inagaki et al. also demonstrates 100 mM succinate inhibits epithelial cell proliferation in the colon mucosa in rats.[25] Succinate accumulates in colon and stomach cancers,[26,27] although it remains unclear if succinate itself is related to colon cancer. Succinate is known to inhibit the function of HIF prolyl hydroxylases (PHDs); a line of data indicates PHDs have essential functions in cell growth and proliferation.[28] Therefore, it would be of interest to determine if the inhibitory effect of succinate on the growth and proliferation of colon cancer cells is mediated by the inactivation of PHDs.

Angiogenesis plays a key role in the development of malignant tumors and inflammatory bowel disease.[29] The inhibition of angiogenesis prevents tumor growth and metastases and, thus, inflammatory bowel disease. The results of the present ex vivo angiogenesis model indicate succinate has antiangiogenic effects at 30 mM, which is the dose corresponding to cecal levels in rats fed various polyphenols. Furthermore, the addition of succinate inhibited HUVEC migration but not HUVEC tube formation or growth. Thus, the antiangiogenic effect of succinate might be at least in part mediated by suppression in VEGF-induced HUVEC migration. Succinate at the micromolar order is reported to enhance retinal angiogenesis by mediating G-protein-coupled receptor 913.[30] However, in our study, the concentrations of succinate at 100−500 μM did not affect angiogenesis in an ex vivo model (unpublished data). This discrepancy might be due to differences in experimental models. Although succinate inhibits PHDs, some conflicting evidence indicates PHDs either suppress or activate angiogenesis.[28] Dietary rutin, ellagic acid, and curcumin are reported to suppress colon carcinogenesis in rodents.[31,32] This raises the question of whether the

suppression of colon cancer by polyphenols is related to the concentrations of intestinal succinate elevated by polyphenols.

Interestingly, this study indicated that dietary supplementation of quercetin increases cecal concentrations of butyrate and acetate in rats. Butyrate produced by intestinal microbial fermentation exerts potentially useful effects on prevention and inhibition of colonic carcinogenesis and other intestinal and extraintestinal disoders.[33] A recent study indicated moderate anti-inflammatory activity of acetate in LPS-stimulated RAW264.7 cells.[34] It was reported that fermentation of apple extracts containing quercetin compounds resulted in an increase of butyrate and acetate in vitro with human fecal flora.[35] To our knowledge, our study provides the first in vivo evidence for the elevations in these organic acids in the cecum of animals fed quercetin.

In summary, this study provides the first evidence that the consumption of some polyphenols remarkably increases cecal succinate levels in rats. Furthermore, succinate at levels close to those in the colonic ruminal environment suppressed the proliferation of colon cancer cells and angiogenesis. These findings provide novel insights into the roles of some polyphenols in the health and diseases of the large intestine.

AUTHOR INFORMATION

Corresponding Author

*(T.K.) Phone: +81-952-28-8380. Fax: +81-952-28-8380. E-mail: kaya@cc.saga-u.ac.jp.

Notes

The authors declare no competing financial interest.

ABBREVIATIONS USED

BrdU, bromo-deoxyuridine; DMEM, Dulbecco's modified Eagle medium; HPLC, high-performance liquid chromatography; MTT, 3-(4,5-dimethylthiazol-2-yl)-2,5-diphenyl tetrazolium bromide; PBS, phosphate-buffered saline; VEGF, vascular endothelial growth factor; HUVEC, human umbilical vein endothelial cell; PHDs, prolyl hydroxylases

REFERENCES

(1) Middleton, E., Jr.; Kandaswami, C.; Theoharides, T. C. The effects of plant flavonoids on mammalian cells: implications for inflammation, heart disease, and cancer. *Pharmacol. Rev.* **2000**, *52*, 673−751.

(2) Cao, Y.; Cao, R.; Brakenhielm, E. Antiangiogenic mechanisms of diet-derived polyphenols. *J. Nutr. Biochem.* **2002**, *13*, 380−390.

(3) Scalbert, A.; Manach, C.; Morand, C.; Remesy, C.; Jimenez, L. Dietary polyphenols and the prevention of diseases. *Crit. Rev. Food Sci. Nutr.* **2005**, *45*, 287−306.

(4) Han, Y.; Haraguchi, T.; Iwanaga, S.; Tomotake, H.; Okazaki, Y.; Mineo, S.; Moriyama, A.; Inoue, J.; Kato, N. Consumption of some polyphenols reduces fecal deoxycholic acid and lithocholic acid, the secondary bile acids of risk factors of colon cancer. *J. Agric. Food Chem.* **2009**, *57*, 8587−8590.

(5) Reddy, B. S. Dietary fat and its relationship to large bowel cancer. *Cancer Res.* **1981**, *41*, 3700−3705.

(6) Wu, W. T.; Chen, H. L. Effects of konjac glucomannan on putative risk factors for colon carcinogenesis in rats fed a high-fat diet. *J. Agric. Food Chem.* **2011**, *59*, 989−994.

(7) Bernstein, H.; Bernstein, C.; Payne, C. M.; Dvorakova, K.; Garewal, H. Bile acids as carcinogens in human gastrointestinal cancers. *Mutat. Res.* **2005**, *589*, 47−65.

(8) Hofmann, A. F. The continuing importance of bile acids in liver and intestinal disease. *Arch. Int. Med.* **1999**, *159*, 2647−2658.

(9) Scheppach, W. Effects of short chain fatty acids on gut morphology and function. *Gut* **1994**, *35*, S35−S38.

(10) Tang, Y.; Chen, Y.; Jiang, H.; Robbins, G. T.; Nie, D. G-protein-coupled receptor for short-chain fatty acids suppresses colon cancer. *Int. J. Cancer* **2011**, *128*, 847−856.

(11) Kleessen, B.; Stoof, G.; Proll, J.; Schmiedl, D.; Noack, J.; Blaut, M. Feeding resistant starch affects fecal and cecal microflora and short-chain fatty acids in rats. *J. Anim. Sci.* **1997**, *75*, 2453−2462.

(12) Kim, M.; Shin, H. K. The water-soluble extract of chicory influences serum and liver lipid concentrations, cecal short-chain fatty acid concentrations and fecal lipid excretion in rats. *J. Nutr.* **1998**, *128*, 1731−1736.

(13) Ishizuka, S.; Tanaka, S.; Xu, H.; Hara, H. Fermentable dietary fiber potentiates the localization of immune cells in the rat large intestinal crypts. *Exp. Biol. Med.* **2004**, *229*, 876−884.

(14) Shimotoyodome, A.; Meguro, S.; Hase, T.; Tokimitsu, I.; Sakata, T. Short chain fatty acids but not lactate or succinate stimulate mucus release in the rat colon. *Comp. Biochem. Physiol. A: Mol. Integr. Physiol.* **2000**, *125*, 525−531.

(15) Barcelo, A.; Claustre, J.; Moro, F.; Chayvialle, J. A.; Cuber, J. C.; Plaisancié, P. Mucin secretion is modulated by luminal factors in the isolated vascularly perfused rat colon. *Gut* **2000**, *46*, 218−224.

(16) Reeves, P. G.; Nielsen, F. H.; Fahey, G. C., Jr. AIN-93 purified diets for laboratory rodents: final report of the American Institute of Nutrition ad hoc writing committee on the reformulation of the AIN-76A rodent diet. *J. Nutr.* **1993**, *123*, 1939−1951.

(17) Okazaki, Y.; Utama, Z.; Suidasari, S.; Zhang, P.; Yanaka, N.; Tomotake, H.; Sakaguchi, E.; Kato, N. Consumption of vitamin B6 reduces fecal ratio of lithocholic acid to deoxycholic acid, a risk factor for colon cancer, in rats fed a high-fat diet. *J. Nutr. Sci. Vitaminol.* **2012**, *58*, 366−370.

(18) Kawasaki, S.; Mori, M.; Awai, M. Capillary growth of rat aortic segments cultured in collagen gel without serum. *Acta. Pathol. Jpn.* **1989**, *39*, 712−718.

(19) Mori, M.; Sadahira, Y.; Kawasaki, S.; Hayashi, T.; Notohara, K.; Awai, M. Capillary growth from reversed rat aortic segments cultured in collagen gel. *Acta. Pathol. Jpn.* **1988**, *38*, 1503−1512.

(20) Kayashima, T.; Matsubara, K. Antiangiogenic effect of carnosic acid and carnosol, neuroprotective compounds in rosemary leaves. *Biosci., Biotechnol., Biochem.* **2012**, *76*, 115−119.

(21) Kim, K. S.; Hong, Y. K.; Joe, Y. A.; Lee, Y.; Shin, J. Y.; Park, H. E.; Lee, I. H.; Lee, S. Y.; Kang, D. K.; Chang, S. I.; Chung, S. I. Anti-angiogenic activity of the recombinant kringle domain of urokinase and its specific entry into endothelial cells. *J. Biol. Chem.* **2003**, *278*, 11449−11456.

(22) Aprikian, O.; Duclos, V.; Guyot, S.; Besson, C.; Manach, C.; Bernalier, A.; Morand, C.; Rémésy, C.; Demigné, C. Apple pectin and a polyphenol-rich apple concentrate are more effective together than separately on cecal fermentations and plasma lipids in rats. *J. Nutr.* **2003**, *133*, 1860−1865.

(23) Crespy, V.; Morand, C.; Besson, C.; Manach, C.; Demigne, C.; Remesy, C. Quercetin, but not its glycosides, is absorbed from the rat stomach. *J. Agric. Food Chem.* **2002**, *50*, 618−621.

(24) Rotstein, O. D.; Pruett, T. L.; Fiegel, V. D.; Nelson, R. D.; Simmons, R. L. Succinic acid, a metabolic by-product of Bacteroides species, inhibits polymorphonuclear leukocyte function. *Infect. Immun.* **1985**, *48*, 402−408.

(25) Inagaki, A.; Ichikawa, H.; Sakata, T. Inhibitory effect of succinic acid on epithelial cell proliferation of colonic mucosa in rats. *J. Nutr. Sci. Vitaminol.* **2007**, *53*, 377−379.

(26) Kanazawa, K.; Konishi, F.; Mitsuoka, T.; Terada, A.; Itoh, K.; Narushima, S.; Kumemura, M.; Kimura, H. Factors influencing the development of sigmoid colon cancer. Bacteriologic and biochemical studies. *Cancer* **1996**, *77*, 1701−1706.

(27) Hirayama, A.; Kami, K.; Sugimoto, M.; Sugawara, M.; Toki, N.; Onozuka, H.; Kinoshita, T.; Saito, N.; Ochiai, A.; Tomita, M.; Esumi, H.; Soga, T. Quantitative metabolome profiling of colon and stomach cancer microenvironment by capillary electrophoresis time-of-flight mass spectrometry. *Cancer Res.* **2009**, *69*, 4918−4925.

(28) Jokilehto, T.; Jaakkola, P. M. The role of HIF prolyl hydroxylases in tumour growth. *J. Cell Mol. Med.* **2010**, *14*, 758−770.

(29) Folkman, J. Angiogenesis in cancer, vascular, rheumatoid and other disease. *Nat. Med.* **1995**, *1*, 27−31.
(30) Sapieha, P.; Sirinyan, M.; Hamel, D.; Zaniolo, K.; Joyal, J. S.; Cho, J. H.; Honoré, J. C.; Kermorvant-Duchemin, E.; Varma, D. R.; Tremblay, S.; Leduc, M.; Rihakova, L.; Hardy, P.; Klein, W. H.; Mu, X.; Mamer, O.; Lachapelle, P.; Di Polo, A.; Beauséjour, C.; Andelfinger, G.; Mitchell, G.; Sennlaub, F.; Chemtob, S. The succinate receptor GPR91 in neurons has a major role in retinal angiogenesis. *Nat. Med.* **2008**, *14*, 1067−1076.
(31) Volate, S. R.; Davenport, D. M.; Muga, S. J.; Wargovich, M. J. Modulation of aberrant crypt foci and apoptosis by dietary herbal supplements (quercetin, curcumin, silymarin, ginseng and rutin). *Carcinogenesis* **2005**, *26*, 1450−1456.
(32) Umesalma, S.; Sudhandiran, G. Ellagic acid prevents rat colon carcinogenesis induced by 1,2-dimethyl hydrazine through inhibition of AKT-phosphoinositide-3 kinase pathway. *Eur. J. Pharmacol.* **2011**, *660*, 249−258.
(33) Canani, R. B.; Costanzo, M. D.; Leone, L.; Pedata, M.; Meli, R.; Calignano, A. Potential beneficial effects of butyrate in intestinal and extraintestinal diseases. *World J. Gastroenterol.* **2011**, *17*, 1519−1528.
(34) Liu, T.; Li, J.; Liu, Y.; Xiao, N.; Suo, H.; Xie, K.; Yang, C.; Wu, C. Short-chain fatty acids suppress lipopolysaccharide-induced production of nitric oxide and proinflammatory cytokines through inhibition of NF-κB pathway in RAW264.7 cells. *Inflammation* **2012**, *35*, 1676−1684.
(35) Veeriah, S.; Hofmann, T.; Glei, M.; Dietrich, H.; Will, F.; Schreier, P.; Knaup, B.; Pool-Zobel, B. L. Apple polyphenols and products formed in the gut differently inhibit survival of human cell lines derived from colon adenoma (LT97) and carcinoma (HT29). *J. Agric. Food Chem.* **2007**, *55*, 2892−2900.

JOURNAL OF AGRICULTURAL AND FOOD CHEMISTRY

Article

pubs.acs.org/JAFC

High-Resolution Screening Combined with HPLC-HRMS-SPE-NMR for Identification of Fungal Plasma Membrane H^+-ATPase Inhibitors from Plants

Kenneth T. Kongstad,[†,§] Sileshi G. Wubshet,[†,§] Ane Johannesen,[†] Lasse Kjellerup,[‡] Anne-Marie Lund Winther,[‡] Anna Katharina Jäger,[†] and Dan Staerk*[,†]

[†]Department of Drug Design and Pharmacology, Faculty of Health and Medical Sciences, University of Copenhagen, Universitetsparken 2, DK-2100 Copenhagen, Denmark

[‡]PCOVERY, Ole Maaløes Vej 3, DK-2200 Copenhagen, Denmark

Supporting Information

ABSTRACT: Crude extracts of 33 plant species were assessed for fungal plasma membrane (PM) H^+-ATPase inhibition. This led to identification of 18 extracts showing more than 95% inhibition at a concentration of 7.5 mg/mL and/or a concentration-dependent activity profile. These extracts were selected for semi-high-resolution fungal PM H^+-ATPase inhibition screening, and, on the basis of these results, *Haplocoelum foliolosum* (Hiern) Bullock and *Sauvagesia erecta* L. were selected for investigation by high-resolution fungal PM H^+-ATPase inhibition screening. Structural analysis performed by high-performance liquid chromatography-high-resolution mass spectrometry-solid-phase extraction-nuclear magnetic resonance spectroscopy (HPLC-HRMS-SPE-NMR) led to identification of chebulagic acid (**1**) and tellimagrandin II (**2**) from *H. foliolosum*. Preparative-scale isolation of the two metabolites allowed determination of IC_{50} values for PM H^+-ATPase, and growth inhibition of *Saccharomyces cerevisiae* and *Candida albicans*. Chebulagic acid and tellimagrandin II are both potent inhibitors of the PM H^+-ATPase with inhibitory effect on the growth of *S. cerevisiae*.

KEYWORDS: *fungal plasma membrane H^+-ATPase, high-resolution screening, HPLC-HRMS-SPE-NMR, chebulagic acid, tellimagrandin II, antifungal, Haplocoelum foliolosum*

INTRODUCTION

Fungi are capable of colonizing a large variety of food and animal feed, and it has been estimated that 5−10% of the world's food production is lost due to fungal spoilage.[1] Fungal infections lead to substantial damage manifested as general spoilage such as discoloration and off-flavors as well as nutritional losses. The spoilage is often caused by excretion of exoenzymes during growth, and once inside the food the enzymes may continue their deteriorating activities despite the removal of the fungal mycelium. However, the most important aspect of fungal spoilage is the production of mycotoxins, which are often toxic to vertebrates and may lead to immune suppression and different types of cancers.[2] Thus, in addition to the financial consequences, fungal spoilage poses a serious threat to the health of immuno-compromised as well as healthy individuals. Fungi are also known to cause systemic infections in immunocompromised patients and are considered as a major healthcare problem. There are an increased number of infections that cannot be treated with the medicines available today, in part caused by infections with fungi that have become resistant to existing drugs,[3,4] but also due to infections with newly emerging fungal pathogens, which are not susceptible to the existing drugs.[5]

A large number of fungal proteins have been proposed as potential targets for novel antifungal agents.[3,6] However, current available antifungal agents are primarily targeting the intracellular membrane and cell wall biosynthesis,[3] and thus need to enter the fungus to act. In our search for novel and more efficient antifungal compounds, we are focusing on the plasma membrane (PM) H^+-ATPase enzyme as target. The PM H^+-ATPase enzyme consists of 10 trans-membrane helices and plays a pivotal role in eukaryotic cell physiology in maintaining the trans-membrane electrochemical proton gradient necessary for nutrient uptake.[7,8] Characterization of the PM H^+-ATPase from various fungi has shown it to comprise a single 100 kDa subunit, containing both a membrane-spanning transport domain as well as a catalytic ATP hydrolyzing domain located in the cytoplasm. The *PMA1* gene encoding for the enzyme has been shown to be highly conserved among fungi, but having only 32% sequence identity to its counterparts in plants[9,10] (sequence alignment of plant H^+-ATPase AHA2 (accession number P19456) and *Saccharomyces cerevisiae* H^+-ATPase PMA1 (accession number P05030) made with ClustalW2). Gene-disruption experiments with *S. cerevisiae* have confirmed the essential nature of the gene product of *PMA1*.[11] Thus, the low sequence identity with plant PM H^+-ATPases as well as its accessibility from the cell exterior, that is, circumventing potential problems with multidrug resistance pumps,[12,13] make the fungal PM H^+-ATPase a good target for new antifungal drugs.

Received: April 3, 2014
Revised: May 14, 2014
Accepted: May 16, 2014
Published: May 16, 2014

ACS Publications © 2014 American Chemical Society

Table 1. Percent Inhibition of Plasma Membrane H$^+$-ATPase at Crude Extract Concentrations of 7.5, 15, and 30 mg/mL[a]

				percent inhibition					
				7.5 mg/mL		15 mg/mL		30 mg/mL	
no.	species	family	plant part						
1	*Alafia barteri*	Apocynaceae	leaves + twigs	27	11	33	19	33	27
2	***Alchornea cordifolia***	**Euphorbiaceae**	**leaves + fruits**	**99**	**98**	**98**	**98**	**97**	**97**
3	*Avicennia marina*	Acanthaceae	root	−19	−12	−1	−7	8	−6
4	*Avicennia marina*	Acanthaceae	stembark	24	13	31	17	40	26
5	***Baissea leonensis***	**Apocynaceae**	**leaves + twigs**	**99**	**99**	**99**	**99**	**99**	**100**
6	***Baissea leonensis***	**Apocynaceae**	**fruit**	**98**	**98**	**98**	**98**	**97**	**97**
7	*Baissea leunensis*	Apocynaceae	root	−3	−6	−3	6	9	15
8	*Caloncoba echinata*	Achariaceae	leaves	50	39	54	46	57	46
9	*Caloncoba echinata*	Achariaceae	branches	10	−28	14	−18	29	−10
10	***Caloncoba gilgiana***	**Achariaceae**	**leaves**	**99**	**99**	**98**	**97**	**99**	**97**
11	*Croton longiracemosus*	Euphorbiaceae	branches	−8	−13	3	9	19	7
12	*Croton longiracemosus*	Euphorbiaceae	root bark	20	12	27	19	34	18
13	*Croton membranaceus*	Euphorbiaceae	leaves + twigs	40	18	40	28	53	41
14	*Dovyalis macrocalyx*	Salicaceae	stem	−4	−13	21	1	35	18
15	*Euadenia eminens*	Capparaceae	aerial parts	33	15	43	25	49	32
16	*Euadenia eminens*	Capparaceae	root	2	−47	4	−36	13	−7
17	*Gymnema sylvestre*	Apocynaceae	aerial parts	34	19	38	26	59	46
18	***Haplocoelum foliolosum***	**Sapindaceae**	**aerial parts**	**99**	**99**	**100**	**99**	**100**	**100**
19	***Hubertia ambavilla***	**Asteraceae**	**leaves + twigs**	**27**	**29**	**56**	**58**	**84**	**86**
20	***Hubertia tomentosum***	**Asteraceae**	**leaves**	**36**	**19**	**50**	**31**	**75**	**71**
21	***Hypericum scabrum***	**Hypericaceae**	**whole plant**	**59**	**51**	**96**	**75**	**97**	**96**
22	***Lophira alata***	**Achnaceae**	**leaves**	**41**	**38**	**60**	**56**	**96**	**90**
23	*Momordica charantia*	Curcurbitaceae	aerial parts	31	27	33	35	42	39
24	***Mussaenda tristigmatica***	**Rubiaceae**	**leaves + twigs**	**99**	**98**	**99**	**98**	**99**	**98**
25	*Nepeta glomerulosa*	Lamiaceae	whole plant	9	8	7	14	23	24
26	*Oncinotis glabrata*	Apocynaceae	leaves	0	−10	16	12	30	28
27	*Oncinotis glabrata*	Apocynaceae	branches	−12	−8	4	2	16	13
28	*Oncinotis glabrata*	Apocynaceae	stem	17	22	29	32	42	40
29	*Oncinotis gracilis*	Apocynaceae	leaves + twigs	−1	−20	3	−14	20	6
30	*Oncinotis pontyi*	Apocynaceae	leaves	17	7	22	12	29	29
31	*Oncinotis pontyi*	Apocynaceae	branches	8	−5	16	11	29	18
32	***Orthopichonia barteri***	**Apocynaceae**	**stem**	**22**	**30**	**45**	**51**	**97**	**95**
33	*Orthopichonia barteri*	Apocynaceae	leaves	21	22	25	25	35	37
34	***Pierreodendron kerstingii***	**Simaroubaceae**	**stem bark**	**3**	**9**	**18**	**29**	**55**	**49**
35	***Pierreodendron kerstingii***	**Simaroubaceae**	**leaves**	**99**	**98**	**99**	**99**	**99**	**98**
36	*Pierreodendron kerstingii*	Simaroubaceae	branches	35	21	38	25	47	36
37	***Pleiocarpa mutica***	**Apocynaceae**	**leaves**	**44**	**40**	**43**	**50**	**70**	**65**
38	*Protomegabaria stapfiana*	Euphorbiaceae	fruit	−4	−10	14	4	48	34
39	***Pycnocycla spinosa***	**Apiaceae**	**root**	**-1**	**-6**	**34**	**29**	**87**	**76**
40	*Pyrenacantha acuminata*[b]	Icacinaceae	branches	−16	−20	−16	−13	16	0
41	*Pyrenacantha acuminata*	Icacinaceae	leaves	48	38	52	39	51	37
42	*Pyrenacantha acuminata*[b]	Icacinaceae	branches	6	−4	7	−20	24	−2
43	***Salacia pyriformis***	**Celastraceae**	**leaves + twigs**	**99**	**98**	**99**	**99**	**98**	**97**
44	*Secamone afzelii*	Apocynaceae	stem	−2	−19	11	−4	25	10
45	***Sphenocentrum jollyanum***	**Menispermaceae**	**leaves + twigs**	**39**	**24**	**55**	**36**	**76**	**68**
46	***Sauvagesia erecta***	**Ochnaceae**	**whole plant**	**98**	**98**	**99**	**98**	**97**	**98**

[a]Extracts showing inhibition higher than 95% for all concentrations or extracts showing a concentration-dependent activity profile are marked with bold and were selected for semi-high-resolution screening. [b]Different collections.

Plants are exposed to a wide array of phytopathogenic fungi in their natural habitat, and have been forced to develop antifungal metabolites to survive.[14,15] Hence, as was previously suggested by Monk and co-workers,[16] it is reasonable to assume that the PM H$^+$-ATPase enzyme is a target for antifungal plant metabolites. However, plant extracts are very complex mixtures, and the traditional bioassay-guided fractionation used for identification of individual bioactive components is very time-consuming and suffers from inherently low resolution during the fractionation process.[17] To circumvent this, we have developed a bioanalytical platform that combines high-resolution microplate bioassays[18,19] with a hyphenated system consisting of high-performance liquid chromatography, solid-phase extraction, and nuclear magnetic resonance, that is, HPLC-SPE-NMR.[20,21] HPLC-SPE-NMR has proven successful for fast and efficient chemical analysis of crude plant extracts;[22−24] including the combination with circular dichroism to establish the absolute configuration of the separated analytes.[25] However, HPLC-SPE-NMR alone does not give any information about the pharmacological activity of the analytes,

dx.doi.org/10.1021/jf501605z | J. Agric. Food Chem. 2014, 62, 5595−5602

and therefore the extension with high-resolution assays, that is, HR-BIOASSAY/HPLC-SPE-NMR,[26−31] is probably the most important improvement to the basic HPLC-SPE-NMR setup in recent years.

Here, we report crude extract screening of 46 plant extracts (from 33 different plant species) for fungal PM H^+-ATPase inhibitors, followed by high-resolution bioassay and HPLC-HRMS-SPE-NMR analysis for identification of individual active constituents.

EXPERIMENTAL SECTION

Chemicals. Amphotericin B, RPMI 1640 medium, dimethyl sulfoxide, analytical grade HPLC solvents, and methanol-d_4 (99.8 atom % of deuterium) were purchased from Sigma-Aldrich (St. Louis, MO). Water used for HPLC was purified by deionization and 0.22 μm membrane filtration (Millipore, Billerica, MA).

Purification of the Yeast Plasma Membrane H^+-ATPase by Recombinant Expression. Heat competent *S. cerevisiae* RS72 yeast cells were prepared and transformed according to Gietz and Woods[32] with a yeast multicopy vector,[33] containing the full-length cDNA of the *S. cerevisiae* plasma membrane H^+-ATPase isoform *PMA1* under control of the *PMA1* promoter.[34,35] Transformed yeast cells were precultured in 100 mL of sterile SGAH medium (7.04 g/L yeast nitrogen base, 19.8 g/L galactose, 64 mg/L adenine, and 64 mg/L histidine) for 3 days at 25 °C and 150 rpm. The preculture was transferred to 500 mL of sterile SGAH medium and further incubated for 3−4 days. 100 mL from the cell culture was transferred to 1 L of YPAD medium (10 g/L yeast extract, 20 g/L bacto-peptone, 20 g/L glucose, 20 mg/L adenine) and incubated at 25 °C for 18−20 h. Recombinant yeast was harvested by 2−3 min of centrifugation at 3000*g* and 4 °C, followed by two times washing in milli-Q water. Harvested cells were incubated in 10% glucose for 10 min on a shaking table, and centrifuged at 3000*g* and 4 °C. Cells were resuspended in homogenization buffer (50 g/L glucose, 28.3% glycerol, 0.1 M Tris-HCl pH 7.25, 10 mM EDTA pH 8.0, 50 mM KCl, 1 mM DTT, 200 μM PMSF, 2 μg/mL Pepstatin A), and disrupted with 165 g of glassbeads (500 μm) by runs in a BeadBeater (Biospec Products, Bartlesville, OK). The disrupted cells were centrifuged at 4 °C for 5 and 15 min at 1400*g* and 12 000*g*, respectively. The supernatant was collected and centrifuged at 251 000*g* for 1 h with 112 μM phenylmethylsulfonyl fluoride (PMSF) and 1.1 μg/mL Pepstatin A. The resulting pellet was resuspended in $GTEK_{20}$ buffer (20% glycerol, 10 mM Tris-HCl pH 7.25, 25 mM KCl, 0.5 mM EDTA pH 8.0, 1 mM DTT, 0.2 mM PMSF, 2 μg/mL Pepstatin A) and centrifuged for 45 min at 251 000*g* and 4 °C. Pellet was then resuspended in $STKED_{20}$ buffer (200 g/L sucrose, 40 g/L glucose, 50 mM Tris-HCl pH 7.25, 50 mM KCl, 1 mM EDTA pH 8.0, 1 mM DTT, 0.2 mM PMSF, 2 μg/mL Pepstatin A), homogenized, and diluted with $STKED_{20}$ buffer. The plasma membranes were recovered at the interface of a 43%/53% (w/w) step sucrose gradient containing sucrose in 50 mM Tris-HCl pH 7.25, 50 mM KCl, 1 mM EDTA, and 1 mM DTT. Centrifugation was done for 16 h at 154 000*g* and 4 °C. The plasma membrane fraction was collected and diluted with $GTEK_{20}$ buffer and centrifuged for 1 h at 274 000*g*. Pellet was collected and homogenized in $GTEK_{20}$ buffer and stored at −80 °C.

Determination of Protein Activity. The protein activity was determined by measuring the amount of liberated phosphate (Pi) from the ATP hydrolysis reaction. Reactions, with or without 2 μL sample, were performed in an assay buffer consisting of 20 mM MOPS-NaOH pH 6.5, 8 mM $MgSO_4$, 50 mM KNO_3, 25 mM NaN_3, 250 μM Na_2MoO_4, and initiated by the addition of Na-ATP to a final concentration of 2.5 mM, followed by incubation for 30 min at 30 °C. The amount of Pi was measured after addition of STOP-solution (mixture of A, 170.3 μM $C_6H_8O_6$ in 0.5 M HCl; and B, 28.3 mM $(NH_4)_6Mo_7O_{24}\cdot 4H_2O$ in H_2O) with an incubation of 10 min at room temperature and thereafter addition of arsenite solution (154 mM $NaAsO_2$, 68 mM $Na_3C_6H_5O_7\cdot 2H_2O$, 0.35 M CH_3COOH). OD was measured at 860 nm after an additional incubation for 30 min at room temperature.

Protocol for Growth Assay. Minimum inhibitory concentrations (MICs) were determined on *S. cerevisiae* (FuSc041 − De Danske Gærfabrikker, Grenå, Denmark) and *Candida albicans* (SC5314 − LGC Standards, Borås, Sweden) as the lowest concentration that inhibited fungal growth with 50%. Fungal freeze stocks were transferred to YPD-agar plates (10 g/L yeast extract, 20 g/L bacto-peptone, 20 g/L glucose, 20 g/L agar) and incubated at 30 °C overnight (O/N). Cells were suspended in sterile H_2O, and the start OD_{600} was adjusted to *C. albicans* OD_{600} at 0.025, *S. cerevisiae* OD_{600} at 0.05. Three microliters of sample or DMSO, 100 μL of cell suspension, and 97 μL of 2 × RPMI-medium (20.8 g/L RPMI-1640 medium, 0.33 M MOPS, 36 g/L glucose) were pipetted into a microtiter plate and incubated for 24 h at 30 °C, followed by OD measurement at 490 nm.

Plant Material and Extractions. Ground plant material (0.3 g of dried material) of 46 plant samples from an in-house collection was extracted with 3.6 mL of ethanol (96%) by sonication for 2 h. Extracts were filtered (Q-Max RR 13 mm 0.45 μm Nylon, Frisenette, Denmark) and concentrated in vacuo before defatting by partitioning between 2 mL of 90% aqueous methanol and 1.5 mL of petroleum ether (bp 40−65 °C). Defatted extracts were dissolved in DMSO to a concentration of 30 mg/mL. Samples selected for HPLC-HRMS-SPE-NMR/bioassay analysis were extracted with 35 mL of ethanol (ca. 1.2 g of ground plant material) by sonication for 2 h. Extracts were concentrated in vacuo and defatted by partitioning between 20 mL of 90% aqueous methanol and 15 mL of petroleum ether (bp 40−65 °C). Defatted extracts were dissolved in methanol to a concentration of 10 mg/mL for semi-high-resolution bioassay analysis.

Crude Extract Screening. The defatted extracts of 46 plant samples (Table 1) were tested for PM H^+-ATPase inhibition at concentrations of 30, 15, and 7.5 mg/mL. The assay was performed in duplicate according to the protocol described above.

Semi-High-Resolution PM H^+-ATPase Inhibition Assay. Chromatographic separation of crude extracts was performed with an Agilent 1200 series instrument (Santa Clara, CA) consisting of a quaternary pump, a degasser, a thermostated column compartment, a photodiode-array detector, a high-performance auto sampler, and a fraction collector, all controlled by Agilent ChemStation ver. B.03.02 software and equipped with a reversed phase Luna $C_{18}(2)$ (Phenomenex, 150 × 4.6 mm, 5 μm, 100 Å) maintained at 40 °C. The aqueous eluent (A) consisted of water/acetonitrile (95:5, v/v), and the organic eluent (B) consisted of water/acetonitrile (5:95, v/v), both acidified with 0.1% formic acid. The eluent flow rate was maintained at 0.5 mL/min with the following elution profile: 0 min, 0% B; 5 min, 0% B; 35 min, 100% B; 43 min, 100% B; 45 min, 0% B, and 10 min equilibration with five successive injections of 10 μL. The column eluent was directed to an automated fraction collector, and eluent from 10 to 40 min was collected in 183 μL aliquots in 80 wells of a 96-well V-shaped microplate (Brand, Wertheim, Germany) (excluding outer columns), concentrated in vacuo, and redissolved in 25 μL of DMSO. Two microliters was transferred to a 96-well microplate, and the PM H^+-ATPase assay was conducted as described above.

High-Resolution PM H^+-ATPase Inhibition Assay. Chromatographic separation of the two selected plant extracts (*Haplocoelum foliolosum* and *Sauvagesia erecta* L.) was performed on the Agilent 1200 series instrument described above with similar conditions (column, solvent composition, temperature, and flow rate). The elution profiles were: 0 min, 5% B; 50 min, 40% B; 52 min, 100% B; 57 min, 100% B; 58 min, 5% B; and 10 min equilibration for *H. foliolosum*; and 0 min, 5% B; 50 min, 30% B; 52 min, 100% B; 57 min, 100% B; 58 min, 5% B; and 10 min equilibration for *S. erecta*. Single chromatographic separations after injection of 7 μL (from 170 mg/mL solution) and 30 μL (from 50 mg/mL solution) were used for microfractionation of *H. foliolosum* and *S. erecta*, respectively. The eluate from 10 to 40 min was collected in 94 μL aliquots in 160 wells of 2 × 96-well V-shaped microplates (excluding the outer columns). The chromatographic solvent was evaporated to dryness in vacuo, and the contents of each well were redissolved in 40 μL of DMSO. From each well, 3 × 2 μL and 3 × 3 μL were used for the PM H^+-ATPase and growth assays, respectively.

HPLC-HRMS-SPE-NMR. The HPLC-HRMS-SPE-NMR system consisted of an Agilent 1100 chromatograph comprising quaternary pump, degasser, thermostated column compartment, auto sampler, and photodiode array detector (Santa Clara, CA), a Bruker micrOTOF-Q II mass spectrometer (Bruker Daltonik, Bremen, Germany) equipped with an electrospray ionization source and operated via a 1:99 flow splitter, a Knauer Smartline 100 pump for postcolumn dilution (Knauer, Berlin, Germany), a Spark Holland Prospekt 2 SPE unit (Spark Holland, Emmen, The Netherlands), a Gilson 215 liquid handler equipped with a 1 mm needle for automated filling of 1.7 mm NMR tubes, and a Bruker Avance III 600 MHz NMR spectrometer (^{1}H operating frequency 600.13 MHz) equipped with a Bruker SampleJet sample changer and a cryogenically cooled gradient inverse triple-resonance 1.7 mm TCI probe-head (Bruker Biospin, Rheinstetten, Germany). Mass spectra were acquired in both positive and negative ion modes, using drying temperature of 200 °C, capillary voltages of −4100 and +4000 V for positive and negative ion modes, respectively, nebulizer pressure of 2.0 bar, and drying gas flow of 7 L/min. The negative ion mode HPLC-HRMS analysis was performed in a different experiment using identical chromatographic condition. A solution of sodium formate clusters was injected in the beginning of each run to enable internal mass calibration. Cumulative SPE trapping of *H. foliolosum* (peaks *3*−*6*) was performed after eight consecutive separations using the chromatographic conditions (column, solvent composition, temperature, flow rate, and elution profile) described above. The HPLC eluate was diluted with Milli-Q water at a flow rate of 1.5 mL/min prior to trapping on 10 × 2 mm i.d. resin GP (general purpose, 5−15 μm, spherical shape, polydivinyl-benzene phase) SPE cartridges from Spark Holland (Emmen, The Netherlands), and analytes were trapped using absorption thresholds (254 nm). Overlapped peaks (peaks *1* and *2* of *H. foliolosum*) were manually collected from repeated chromatographic separations, evaporated to dryness in vacuo, and reconstituted in methanol to afford 9 mg/mL. This solution was subjected to HPLC-HRMS-SPE-NMR analysis using the following isocratic elution profile: 0 min, 13% B; 24 min, 13% B; 25 min, 100% B; 30 min, 100% B; 31 min, 13% B; and 4 min equilibration. A total of eight cumulative trappings was performed using absorption thresholds (254 nm). SPE cartridges were conditioned with 1000 μL of methanol at 6 mL/min and equilibrated with 500 μL of Milli-Q water at 1 mL/min prior to trapping. Loaded cartridges were dried with pressurized nitrogen gas for 45 min each. Separations were controlled by Bruker Hystar version 3.2 software, automated filling of NMR tubes was controlled by PrepGilsonST version 1.2 software, and automated NMR acquisition was controlled by Bruker IconNMR version 4.2 software. NMR data processing was performed using Bruker Topspin version 3.2 software.

NMR Experiments. All NMR spectra were recorded in methanol-d_4 at 300 K. ^{1}H chemical shifts were referenced to the residual solvent signal (δ 3.31). One-dimensional ^{1}H NMR spectra were acquired in automation (temperature equilibration to 300 K, optimization of lock parameters, gradient shimming, and setting of receiver gain) with 30° pulses, 3.66 s interpulse intervals, 64k data points, and multiplied with an exponential function corresponding to line-broadening of 0.3 Hz prior to Fourier transform. Phase-sensitive DQF-COSY spectra were recorded using a gradient-based pulse sequence with a 20 ppm spectral width and 2k × 256 data points (processed with forward linear prediction to 1k data points). Multiplicity-edited HSQC spectra were acquired with the following parameters: spectral width 20 ppm for ^{1}H and 165 ppm for ^{13}C, 2k × 256 data points (processed with forward linear prediction to 1k data points), and 2.0 s relaxation delay. HMBC spectra (without a low-pass filter) were optimized for $^nJ_{C,H}$ = 10 Hz and acquired using the following parameters: spectral width 20 ppm for ^{1}H and 222 ppm for ^{13}C, 2k × 128 data points (processed with forward linear prediction to 1k data points), and 1.5 s relaxation delay.

Targeted Isolation and Determination of IC_{50} Values of 1 and 2. An injection solution of 0.17 g/mL (*H. foliolosum*) was subjected to a preparative chromatography using the Agilent 1100 system equipped with two preparative solvent delivery units, a multiple wavelength detector, an autosampler, and an optional fraction collector. Separation was performed using a 250 mm × 21.2 mm i.d. Phenomenex Luna C18 (5 μm) column operated at room temperature. Repeated injection (3 × 800 μL) of the above solution, followed by a gradient elution (similar to the one used for HR screening), afforded 9.5 mg of fraction A (collected in a retention time range 22−24 min). Fraction A was reconstituted in 800 μL of 50% MeOH and subjected to further preparation purification using an isocratic elution (12% B) for 30 min. Single injection of 400 μL was performed, and peaks *1* and *2* were manually collected. After concentration under reduced pressure and lyophilization, 0.82 mg of **1** and 0.49 mg of **2** were obtained. The two compounds were reconstituted in DMSO to a final concentration of 5 mM, and subsequently IC_{50} values in PM H^+-ATPase and fungal growth assays with *S. cerevisiae* and *C. albicans* were assessed.

RESULTS AND DISCUSSION

Crude Extract Screening. From our in-house plant collection, 33 different plant species were selected for this study. For some of the species, different parts were available, yielding a total of 46 samples of ground plant material (see Table 1). The material was extracted with ethanol, and the dried extracts were defatted by partitioning between 90% aqueous methanol and petroleum ether. The defatted extracts were tested for their ability to inhibit the PM H^+-ATPase enzyme at concentrations of 30, 15, and 7.5 mg/mL, and extracts showing inhibition higher than 95% for all concentrations or extracts showing a concentration-dependent activity profile (indicated with bold in Table 1) were selected for semi-high-resolution screening. Thus, *Alchornea cordifolia*, *Baissea leonensis* (fruits as well as leaves + twigs), *Caloncoba gilgiana*, *Haplocoelum foliolosum*, *Mussaenda tristigmatica*, *Pierreodendron kerstingii* (leaves), *Salacia pyriformis*, and *Sauvagesia erecta* were selected on the basis of the former criteria, whereas *Hubertia ambavilla*, *Hubertia tomentosum*, *Hypericum scabrum*, *Lophira alata*, *Orthopichonia barteri*, *Pierreodendron kerstingii* (stem bark), *Pleiocarpa mutica*, *Pycnocycla spinosa*, and *Sphenocentrum jollyanum* were selected on the basis of the latter criteria.

Semi-High-Resolution PM H^+-ATPase and Growth Inhibition Profiles. The 18 samples selected for semi-high-resolution screening were separated using a HPLC method starting at 5% acetonitrile (plus 0.1% formic acid) for 5 min, and using a linear gradient from 5% to 95% acetonitrile (plus 0.1% formic acid) from 5 to 35 min. The eluate from 10 to 40 min was collected in 80 wells of a 96-well microplate (omitting the first and last columns), yielding fractions of 183 μL. The eluate was evaporated, and the dried material in each well was redissolved in DMSO. These solutions were assayed for their ability to inhibit the PM H^+-ATPase as well as their ability to inhibit growth of *C. albicans* and *S. cerevisiae*. The results were plotted under the HPLC traces at 254 nm, and all semi-high-resolution biochromatograms are given in Supporting Information, Figures S1−S18. The results show that the tested extracts can be placed in three different groups as illustrated in Figure 1. The first group consists of *Hubertia ambavilla*, *Hubertia tomentosum*, *Hypericum scabrum*, *Lophira alata*, *Orthopichonia barteri*, *Pierreodendron kerstingii* (stem bark), *Pleiocarpa mutica*, *Pycnocycla spinosa*, *Salacia pyriformis*, and *Sphenocentrum jollyanum*, which show very low PM H^+-ATPase inhibition and/or no distinct peaks with PM H^+-ATPase inhibition. The second group consists of *Alchornea cordifolia*, *Baissea leonensis* (fruits as well as leaves + twigs), *Caloncoba gilgiana*, *Mussaenda tristigmatica*, and *Pierreodendron kerstingii* (leaves), where the observed PM H^+-ATPase inhibition is correlated with a broad hump at approximately 10−30 min. This hump is attributed to tannin-rich fractions, and the PM

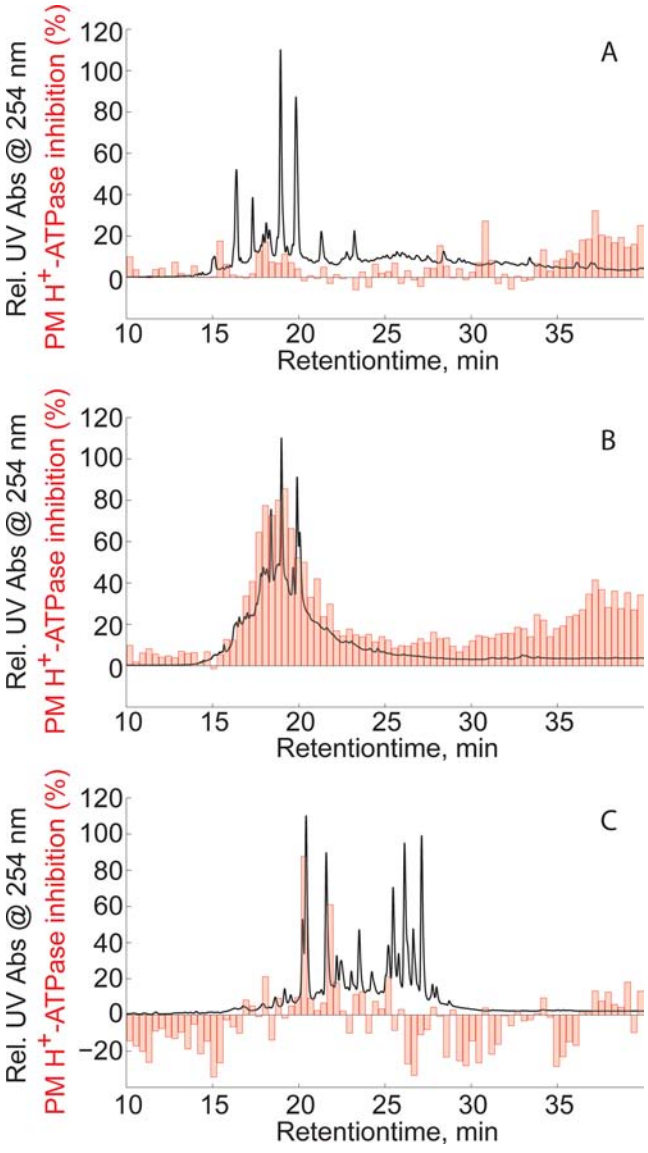

Figure 1. Three representative inhibition profiles obtained through semi-high-resolution antifungal screening: *Hypericum scabrum* (A, group 1), *Caloncoba gilgiana* (B, group 2), and *Haplocoelum foliolosum* (C, group 3).

H^+-ATPase inhibition is therefore likely to be caused by tannins, which are of little interest due to their inherent ability to precipitate proteins. The third group consists of two samples, *Haplocoelum foliolosum* and *Sauvagesia erecta*, showing direct correlation between individual peaks and inhibition of the PM H^+-ATPase. Therefore, the two plants from the last group were selected for a high-resolution PM H^+-ATPase assay to correlate the observed activities with individual metabolites.

High-Resolution PM H^+-ATPase Profiles. Extracts of *H. foliolosum* and *S. erecta* were reanalyzed using the high-resolution PM H^+-ATPase inhibition assay with optimized separation condition and a higher number of data points per retention time (5.33 points/min). Furthermore, higher chromatographic loading (1.2 and 1.5 mg for *H. foliolosum* and *S. erecta*, respectively) allowed triplicate assaying of the time-sliced fractions to assess statistical variations of the assay. The biochromatograms for the two plants were therefore plotted with standard deviation from the triplicate measurements (Figure 2 and Supporting Information Figure S19 for *H. foliolosum* and *S. erecta*, respectively). From *H. foliolosum* two

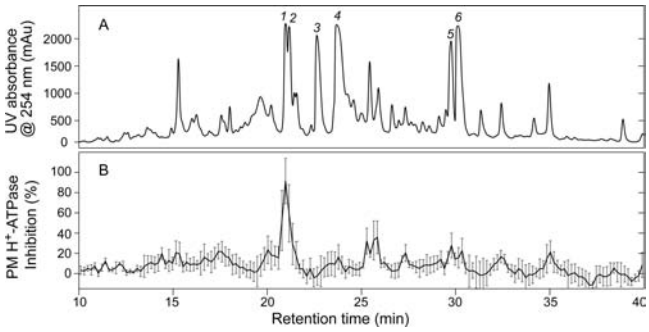

Figure 2. High-resolution antifungal screening of *Haplocoelum foliolosum* crude extract. (A) HPLC chromatogram at 254 nm. (B) High-resolution fungal plasma membrane H^+-ATPase inhibition profile (an average of triplicate measurements with standard deviations are plotted).

overlapping peaks at 23.6 min were correlated with >80% inhibition of the PM H^+-ATPase. *S. erecta*, however, did not show any peaks in the HPLC chromatogram correlating with a discrete peak in the inhibition profile of the optimized high-resolution assay (Supporting Information Figure S19). This is despite the noticeable inhibition in both the crude extract screening (Table 1) and the semi-high-resolution assay (Supporting Information Figure S18). This can be caused by loss of synergistic activities of multiple constituents that are separated in the high-resolution biochromatogram but assessed collectively in the semi-high-resolution biochromatogram as well as in the crude extract screening. Therefore, *S. erecta* was excluded from further investigation.

HPLC-HRMS-SPE-NMR. The two active peaks from *H. foliolosum* (peaks *1* and *2*) and four other major metabolites (peaks *3*–*6*) were subjected to HPLC-HRMS-SPE-NMR analysis. Detailed HRMS and NMR analysis resulted in identification of six compounds **1**–**6** (Figure 3) corresponding to peaks *1*–*6*, respectively. ^{1}H NMR, UV, and HRMS data of **1**–**6** obtained in the HPLC-HRMS-SPE-NMR mode are given in Table S1 in the Supporting Information.

HRMS data of compound **1** showed a base peak at *m*/*z* 785.0836, which was attributed to $C_{34}H_{25}O_{22}^+$. However, inverse-detected heteronuclear experiments revealed 41 carbon atoms. After a detailed analysis of 1D and 2D NMR experiments and comparison of the observed NMR data with literature data, the analyte was identified as chebulagic acid (**1**)[36] (molecular formula $C_{41}H_{30}O_{27}$). The observed base peak for **1** at *m*/*z* 785.0836 was assigned to a fragment ion [M + H − H_2O − galloyl]$^+$ ($C_{34}H_{25}O_{22}^+$, ΔM −0.5 ppm), similar to the fragment ion at *m*/*z* 769.0863 [M + H − H_2O − galloyl group]$^+$ ($C_{34}H_{25}O_{21}^+$, ΔM 2.5 ppm) observed as the base peak for compound **2**. Such fragmentation product has previously been reported for **1**.[37] The molecular ion peaks of compound **1** and **2** could not be detected in positive ion mode, even when studying extracted ions chromatograms from HPLC-HRMS. The molecular formulas are, however, supported by the presence of ammonium adducts in positive ion mode of *m*/*z* 972.1295 [M + NH_4]$^+$ ($C_{41}H_{34}NO_{27}^+$, ΔM 1.8 ppm) and *m*/*z* 956.1331 [M + NH_4]$^+$ ($C_{41}H_{34}NO_{26}^+$, ΔM 3.5 ppm) as well as molecular ion peaks in negative ion mode of *m*/*z* 953.0875 [M − H]$^-$ ($C_{41}H_{29}NO_{27}^-$, ΔM 2.8 ppm) and *m*/*z* 937.0924 [M −

dx.doi.org/10.1021/jf501605z | J. Agric. Food Chem. 2014, 62, 5595−5602

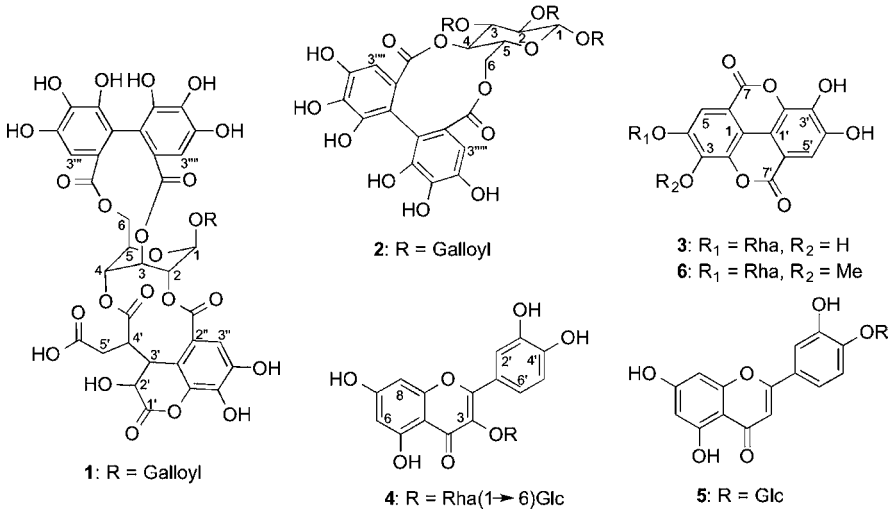

Figure 3. Structures of antifungal compounds chebulagic acid (**1**) and tellimagrandin II (**2**) as well as of compounds **3**–**6** showing no antifungal activity.

Table 2. IC_{50} Values for Fungal Growth Inhibition Assays and Fungal Plasma Membrane H^+-ATPase Inhibition

		growth inhibition[b]	
	plasma membrane H^+-ATPase inhibition[a]	*Saccharomyces cerevisiae* FuSc041[a]	*Candida albicans* SC5314[a]
chebulagic acid (**1**)	15.8 ± 7.9	1.8 ± 0.9	>75
tellimagrandin II (**2**)	10.6 ± 3.1	1.8 ± 0.9	>75
vanadate	2.3 ± 1.2		
amphotericin B		0.08 ± 0.05	0.08 ± 0.05
fluconazole		7.6 ± 4.9	0.9 ± 0.6

[a] n = 3, results reported in micromolar. [b] Determined as MIC for 50% inhibition.

$H]^-$ ($C_{41}H_{29}NO_{26}^-$, ΔM 2.9 ppm), compounds **1** and **2**, respectively.

The ^1H NMR spectrum of **2** shows five deshielded aromatic proton resonances, 7.05 (s, 2H, H-2′/H-6′), 6.95 (s, 2H, H-2″/H-6″), 6.92 (s, 2H, H-2‴/H-6‴), 6.62 (s, 1H, H-3⁗), and 6.49 (s, 1H, H-3⁗′). Three of these signals were integrated to two protons each, and thorough analysis of characteristic ^2J and ^3J HMBC correlations to the corresponding quaternary aromatic carbons and a carboxyl carbon revealed three galloyl groups. Seven relatively deshielded resonances with discrete COSY spin system were assigned to a glucose moiety with esterification of all hydroxyls. The esterification positions were established by ^3J HMBC correlations of the sugar proton resonances H-1 (δ 6.11, d, J = 8.2 Hz), H-2 (δ 5.55, dd, J = 9.1,8.4 Hz), and H-3 (δ 5.76, t, J = 9.6 Hz) with the galloyl carboxyl carbon resonances C-7′ (166.2 ppm), C-7″ (166.6 ppm), and C-7‴ (167.4 ppm), respectively. After identifying a hexahydroxydiphenoyl (HHDP) moiety bridging two oxygens of glucose at positions 4 and 6 through similar HMBC data analysis, the structure of peak 2 was confirmed as tellimagrandin II (**2**).[38]

In addition to the two active metabolites (**1** and **2**), four major metabolites (peaks 2–6) of *H. foliolosum* were investigated. HRMS analysis of peak 3 (HR-ESIMS(+) m/z 449.0698 $[M + H]^+$ [$C_{20}H_{17}O_{12}^+$, ΔM −3.7 ppm]) revealed the molecular formula of compound **3** to be $C_{20}H_{16}O_{12}$. After analysis of 1D and 2D NMR data and comparison of chemical shifts with literature values, compound **3** was identified as ellagic acid 4-*O*-α-L-rhamnopyranoside.[39] Peak 4 was identified as rutin (HR-ESIMS(+) m/z 611.1606 [$C_{27}H_{31}O_{16}^+$, ΔM −0.1 ppm]) by comparing HRMS and ^1H NMR data with an authentic reference compound. On the basis of HRMS analysis, peak 5 was assigned the molecular formula $C_{21}H_{20}O_{11}$ (HR-ESIMS(+) m/z 449.1075 [$C_{21}H_{22}O_{11}^+$, ΔM −0.8 ppm]). AMX and AX spin systems and a characteristic flavone H-3 resonance (6.63 ppm) observed in the downfield region of the ^1H NMR spectrum were in agreement with luteoline aglycone. A discrete spin system observed in COSY was attributed to a glucose moiety. After establishing the glycosidic linkage at C-4′ with ^3J HMBC correlations, compound **5** was identified as luteolin 4′-*O*-β-glucopyranoside.[40] The ^1H NMR spectrum of compound **6** (HR-ESIMS(+) m/z 463.0868 $[M + H]^+$ [$C_{21}H_{19}O_{12}^+$, ΔM 0.7 ppm]) displayed signals and multiplicity patterns similar to those of compound **3**, but with an additional methoxy resonance at 4.19 ppm. These observations and comparison of chemical shifts with literature revealed compound **6** as 3-*O*-methylellagic acid 4-*O*-α-L-rhamnopyranoside.[41]

After observation of their significant PM H^+-ATPase inhibitory effects in high-resolution screening, chebulagic acid (**1**) and tellimagrandin II (**2**) were isolated by preparative-scale HPLC, and the materials were used for assessing IC_{50} values in the PM H^+-ATPase inhibition assay and fungal growth inhibition assays (Table 2).

Chebulagic acid and tellimagrandin II had an inhibitory effect against PM H^+-ATPase with IC_{50} values of 15.8 and 10.6 μM, respectively. The two compounds also showed antifungal activity against *S. cerevisiae*, and were equally potent with MIC of 1.8 μM. This is better than Fluconazole that possess a MIC of 7.6 μM, but not as potent as Amphotericin B with a MIC of 0.08 μM for *S. cerevisiae*. Both compounds were also tested against *C. albicans*, but did not show any antifungal activity at concentrations lower than 75 μM, and this is despite conserved PM H^+-ATPase among the fungal species (83% sequence

dx.doi.org/10.1021/jf501605z | J. Agric. Food Chem. 2014, 62, 5595−5602

identity; sequence alignment of *C. albicans* PMA1 (accession number P28877) and *S. cerevisiae* H^+-ATPase PMA1 (accession number P05030) made with ClustalW2). Furthermore, the compounds have a higher IC_{50} value against the PM H^+-ATPase than MIC value against *S. cerevisiae*. Taken together, this could indicate that not only the inhibition of PM H^+-ATPase contributes to the antifungal effect of chebulagic acid and tellimagrandin II, but other factors may also play a role. Hydrolyzable tannins, including tellimagrandin II, have been shown to have membrane-damaging activity on liposomes prepared from egg-yolk phosphatidylcholin, but not affecting the viability of MKN-28 cells derived from human gastric epithelium.[42] It remains to be determined if chebulagic acid and tellimagrandin II, in addition to their PM H^+-ATPase inhibitory effect, have membrane-damaging activity on *S. cerevisiae*, which contributes to the observed antifungal activity.

In the literature, chebulagic acid has been identified as an active inhibitor of xanthione oxidase with an IC_{50} = 48.5 μM[43] and with both antibacterial and antifungal effect in doses of 100 μM.

In conclusion, chebulagic acid and tellimagrandin II are two potent inhibitors of the plasma membrane H^+-ATPase with inhibitory effect on the growth of *S. cerevisiae*. Further studies on isolated and/or semisynthetic analogues are planned to investigate the structure−activity relationship and specificity.

■ ASSOCIATED CONTENT

Supporting Information

Semi-high-resolution biochromatograms of selected plants, and UV, HRMS, and NMR data of **1**−**6**. This material is available free of charge via the Internet at http://pubs.acs.org.

■ AUTHOR INFORMATION

Corresponding Author

*Tel.: +45 3533 6177. Fax: +45 35336001. E-mail: ds@sund.ku.dk.

Author Contributions

[§]These authors contributed equally.

Funding

K.T.K. and S.G.W. supported by The Danish Research Council for Strategic Research − Food and Health. HPLC equipment used for high-resolution bioassay profiles was obtained via a grant from The Carlsberg Foundation. The 600 MHz HPLC-HRMS-SPE-NMR system used in this work was acquired through a grant from "Apotekerfonden af 1991", The Carlsberg Foundation, and the Danish Agency for Science, Technology and Innovation via the National Research Infrastructure funds.

Notes

The authors declare no competing financial interest.

■ REFERENCES

(1) Pitt, J. I.; Hocking, A. D. *Fungi and Food Spoilage*; Springer Science+Business Media LLC: Philadelphia, PA, 2009.

(2) Filtenborg, O.; Frisvad, J. C.; Thrane, U. Moulds in food spoilage. *Int. J. Food Microbiol.* **1996**, *33*, 85−102.

(3) Odds, F. C.; Brown, A. J. P.; Gow, N. A. R. Antifungal agents: mechanisms of action. *Trends Microbiol.* **2003**, *11*, 272−279.

(4) Sanglard, D.; Odds, F. C. Resistance of *Candida* species to antifungal agents: molecular mechanisms and clinical consequences. *Lancet Infect. Dis.* **2002**, *2*, 73−85.

(5) Garnica, M.; Nucci, M. Emerging fungal infections. In *Pulmonary Involvement in Patients with Hematological Malignancies*; Azoulay, E., Ed.; Springer-Verlag: Berlin Heidelberg, Germany, 2011; pp 337−348.

(6) De Backer, M. D.; Van Dijck, P.; Luyten, W. H. M. L. Functional genomics approaches for the identification and validation of antifungal drug targets. *Am. J. PharmacoGenomics* **2002**, *2*, 113−127.

(7) Scarborough, G. A. The plasma membrane proton-translocating ATPase. *Cell. Mol. Life Sci.* **2000**, *57*, 871−883.

(8) Serrano, R. Structure and function of plasma membrane ATPase. *Annu. Rev. Plant Physiol. Plant Mol. Biol.* **1989**, *40*, 61−94.

(9) Morsomme, P.; Slayman, C. W.; Goffeau, A. Mutagenic study of structure, function and biogenesis of the yeast plasma membrane H^+-ATPase. *Biochim. Biophys. Acta, Rev. Biomembr.* **2000**, *1469*, 133−157.

(10) Palmgren, M. G. Plant plasma membrane H^+-ATPase: Powerhouses for nutrient uptake. *Annu. Rev. Plant Physiol. Plant Mol. Biol.* **2001**, *52*, 817−845.

(11) Serrano, R.; Kielland-Brandt, M. C.; Fink, G. R. Yeast plasma membrane ATPase is essential for growth and has homology with (Na^+ + K^+), K^+- and Ca^{2+}-ATPases. *Nature* **1986**, *319*, 689−693.

(12) Seto-Young, D.; Monk, B.; Mason, A. B.; Perlin, D. S. Exploring an antifungal target in the plasma membrane H^+-ATPase of fungi. *Biochim. Biophys. Acta, Biomembr.* **1997**, *1326*, 249−256.

(13) Soteropoulos, P.; Vaz, T.; Santangelo, R.; Paderu, P.; Huang, D. Y.; Tamás, M. J.; Perlin, D. S. Molecular characterization of the plasma membrane H^+-ATPase, an antifungal target in *Cryptococcus neoformans*. *Antimicrob. Agents Chemother.* **2000**, *44*, 2349−2355.

(14) Bisson, J.; Waffo-Téguo, P.; Papastamoulis, Y.; Richard, T.; Corio-Costet, M.; Mérillon, J.; Cluzet, S. Phenolics and their antifungal role in grapevine wood decay: focus on the botryosphaeriaceae family. *J. Agric. Food Chem.* **2012**, *60*, 11859−11868.

(15) Maor, R.; Shirasu, K. The arms race continues: battle strategies between plants and fungal pathogens. *Curr. Opin. Microbiol.* **2005**, *8*, 399−404.

(16) Monk, B. C.; Perlin, D. S. Fungal plasma membrane proton pumps as promising new antifungal targets. *Crit. Rev. Microbiol.* **1994**, *20*, 209−223.

(17) Kool, J.; Giera, M.; Irth, H.; Niessen, W. M. A. Advances in mass spectrometry-based post-column bioaffinity profiling of mixtures. *Anal. Bioanal. Chem.* **2011**, *399*, 2655−2668.

(18) Shi, S.-Y.; Zhou, H.-H.; Zhang, Y.-P.; Jiang, X.-Y.; Chen, X.-Q.; Huang, K.-L. Coupling HPLC to on-line, post-column (bio)chemical assays for high-resolution screening of bioactive compounds from complex mixtures. *TrAC, Trends Anal. Chem.* **2009**, *28*, 865−877.

(19) Giera, M.; Heus, F.; Janssen, L.; Kool, J.; Lingeman, H.; Irth, H. Microfractionation revisited: a 1536 well high resolution screening assay. *Anal. Chem.* **2009**, *81*, 5460−5466.

(20) Kesting, J. R.; Johansen, K. T.; Jaroszewski, J. W. Hyphenated NMR techniques. In *Advances in Biomedical Spectroscopy*; Dingley, A. J., Pascal, S. M., Eds.; IOS Press: Amterdam, Netherlands, 2011; Vol. 3, pp 413−434.

(21) Seger, C.; Sturm, S. HPLC-SPE-NMR: A new hyphenation technique. *LC-GC Eur.* **2007**, *11*, 587−597.

(22) Sprogøe, K.; Stærk, D.; Jäger, A. K.; Adsersen, A.; Hansen, S. H.; Witt, M.; Landbo, A.-K. R.; Meyer, A. S.; Jaroszewski, J. W. Targeted natural product isolation guided by HPLC-SPE-NMR: Constituents of *Hubertia* species. *J. Nat. Prod.* **2007**, *70*, 1472−1477.

(23) Staerk, D.; Kesting, J. R.; Sairafianpour, M.; Witt, M.; Asili, J.; Emami, S. A.; Jaroszewski, J. W. Accelerated dereplication of crude extracts using HPLC-PDA-MS-SPE-NMR: Quinolone alkaloids of *Haplophyllum acutifolium*. *Phytochemistry* **2009**, *70*, 1055−1061.

(24) Johansen, K. T.; Wubshet, S. G.; Nyberg, N. T.; Jaroszewski, J. W. From retrospective assessment to prospective decisions in natural product isolation: HPLC-SPE-NMR analysis of *Carthamus oxyacantha*. *J. Nat. Prod.* **2011**, *74*, 2454−2461.

(25) Sprogøe, K.; Stærk, D.; Ziegler, H. L.; Jensen, T. H.; Holm-Møller, S. B.; Jaroszewski, J. W. Combining HPLC-PDA-MS-SPE-NMR with circular dichroism for complete natural product characterization in crude extracts: Levorotatory gossypol in *Thespesia danis*. *J. Nat. Prod.* **2008**, *71*, 516−519.

(26) Pukalskas, A.; van Beek, T. A.; de Waard, P. Development of a triple hyphenated HPLC-radical scavenging detection-DAD-SPE-

NMR system for the rapid identification of antioxidants in complex plant extracts. *J. Chromatogr., A* **2005**, *1074*, 81−88.
(27) Schmidt, J. S.; Lauridsen, M. B.; Dragsted, L. O.; Nielsen, J.; Staerk, D. Development of a bioassay-coupled HPLC-SPE-ttNMR platform for identification of α-glucosidase inhibitors in apple peel (*Malus* × *domestica* Borkh.). *Food Chem.* **2012**, *135*, 1692−1699.
(28) Grosso, C.; Jäger, A. K.; Staerk, D. Coupling of a high-resolution monoamine oxidase-A inhibitor assay and HPLC-SPE-NMR for advanced bioactivity profiling of plant extracts. *Phytochem. Anal.* **2013**, *24*, 141−147.
(29) Agnolet, S.; Wiese, S.; Verpoorte, R.; Staerk, D. Comprehensive analysis of commercial willow bark extracts by new technology platform: Combined use of metabolomics, high-performance liquid chromatography-solid-phase extraction-nuclear magnetic resonance spectroscopy and high-resolution radical scavenging assay. *J. Chromatogr., A* **2012**, *1262*, 130−137.
(30) Wubshet, S. G.; Schmidt, J. S.; Wiese, S.; Staerk, D. High-resolution screening combined with HPLC-HRMS-SPE-NMR for identification of potential health-promoting constituents in sea aster and searocket−New nordic food ingredients. *J. Agric. Food Chem.* **2013**, *61*, 8616−8623.
(31) Wiese, S.; Wubshet, S. G.; Nielsen, J.; Staerk, D. Coupling HPLC-SPE-NMR with a microplate-based high-resolution antioxidant assay for efficient analysis of antioxidants in food—Validation and proof-of-concept study with caper buds. *Food Chem.* **2013**, *141*, 4010−4018.
(32) Gietz, R. D.; Woods, R. A. Transformation of yeast by lithium acetate/single-stranded carrier DNA/polyethylene glycol method. *Methods Enzymol.* **2002**, *350*, 87−96.
(33) Hill, J. E.; Myers, A. M.; Koerner, T. J.; Tzagoloff, A. Yeast/E. coli shuttle vectors with multiple unique restriction sites. *Yeast* **1986**, *2*, 163−167.
(34) Villalba, J. M.; Palmgren, M. G.; Berberian, G. E.; Ferguson, C.; Serrano, R. Functional expression of plant plasma membrane H^+-ATPase in yeast endoplasmic reticulum. *J. Biol. Chem.* **1992**, *267*, 12341−12349.
(35) Buch-Pedersen, M. J.; Venema, K.; Serrano, R.; Palmgren, M. G. Abolishment of proton pumping and accumulation in the E_1P conformational state of a plant plasma membrane H^+-ATPase by substitution of a conserved aspartyl residue in transmembrane segment 6. *J. Biol. Chem.* **2000**, *275*, 39167−39173.
(36) Luo, W.; Wen, L.; Zhao, M.; Yang, B.; Ren, J.; Shen, G.; Rao, G. Structural identification of isomallotusinin and other phenolics in *Phyllanthus emblica* L. fruit hull. *Food Chem.* **2012**, *132*, 1527−1533.
(37) Wu, S.-B.; Dastmalchi, K.; Long, C.; Kennelly, E. J. Metabolite profiling of Jaboticaba (*Myrciaria cauliflora*) and other dark-colored fruit juices. *J. Agric. Food Chem.* **2012**, *60*, 7513−7525.
(38) Wilkins, C. K.; Bohm, B. A. Ellagitannins from *Tellima grandiflora*. *Phytochemistry* **1976**, *15*, 211−214.
(39) Yang, S.-W.; Zhou, B.-N.; Wisse, J. H.; Evans, R.; van der Werff, H.; Miller, J. S.; Kingston, D. G. I. Three new ellagic acid derivatives from the bark of *Eschweilera coriacea* from the Suriname rainforest. *J. Nat. Prod.* **1998**, *61*, 901−906.
(40) Kellam, S. J.; Mitchell, K. A.; Blunt, J. W.; Munro, M. H. G.; Walker, J. R. L. Luteoline and 6-hydroxyluteoline glycosides from *Hebe sericta*. *Phytochemistry* **1993**, *33*, 867−869.
(41) El-Toumy, S. A. A.; Rauwald, H. W. Two new ellagic acid rhamnosides from *Punica granatum* heartwood. *Planta Med.* **2003**, *69*, 682−684.
(42) Funatogawa, K.; Hayashi, S.; Shimomura, H.; Yoshida, T.; Hatano, T.; Ito, H.; Hirai, Y. Antibacterial activity of hydrolysable tannins derived from medicinal plants against *Helicobacter pylori*. *Microbiol. Immunol.* **2004**, *48*, 251−261.
(43) Fogliani, B.; Raharivelomanana, P.; Bianchini, J.-P.; Bouraïma-Madjèbi, S.; Hnawia, E. Bioactive ellagitannins from *Cunonia macrophylla*, an endemic Cunoniaceae from New Caledonia. *Phytochemistry* **2005**, *66*, 241−247.

JOURNAL OF AGRICULTURAL AND FOOD CHEMISTRY

Article

pubs.acs.org/JAFC

Protective Effect of Anthocyanidins against Sodium Dithionite-Induced Hypoxia Injury in C6 Glial Cells

Yu-Chun Lin, Pei-Feng Tsai, and James Swi-Bea Wu*

Graduate Institute of Food Science and Technology, National Taiwan University, P.O. Box 23-14, Taipei City 10672, Taiwan

ABSTRACT: The present study investigated the neuroprotective effect of anthocyanidins, including cyanidin, delphinidin, malvidin, pelargonidin, and peonidin, against hypoxia in C6 glial cells. The cells were first incubated with a medium containing anthocynidin in normoxia condition and then with a medium containing sodium dithionite ($Na_2S_2O_4$) in an anaerobic incubator for the hypoxia treatment. Methylthiazole tetrazolium test and evaluation of antioxidant enzyme activities and glutathione concentration were performed on the treated cells. At least 74% of the C6 cells preincubated with 25 mg/L of any of the five anthocyanidins in serum-free Dulbecco's modified Eagle's medium at 37 °C for 24 h survived the hypoxia treatment as compared with a survival rate between 47 and 59% for the control that was preincubated without an anthocyanidin. The cells preincubated with any of the five anthocyanidins showed higher catalase activity and glutathione concentration after the hypoxia treatment as compared with the corresponding samples without the preincubation with anthocyanidin. The cells preincubated with malvidin, pelargonidin, or peonidin also showed higher superoxide dismutase activities. The results of this study justify further research for the development of anthocyanidins into neuroprotective food ingredients against hypoxia injury.

KEYWORDS: *anthocyanin, anthocyanidin, antioxidant, hypoxia, glial cell*

INTRODUCTION

Mammalian cells rely on oxygen for survival. Hypoxia happens during various pathophysiologic conditions such as ischemia, respiratory disease, and tumorigenesis[1] and promotes the generation of reactive oxygen species (ROS), including superoxide anion ($O_2^{\bullet-}$), hydrogen peroxide (H_2O_2), and hydroxyl radicals, in the cell. The increase in ROS levels may lead to the occurrence of oxidative stress.[2] Oxidative stress has long been associated with the development of brain cell damage and neurodegenerative disorders.[3−5]

ROS are byproducts of both normal and irregular metabolic processes that utilize molecular oxygen. Antioxidant enzymes, such as catalase (CAT) and superoxide dismutases (SODs), are involved in the elimination of ROS.[6] Without the protection of antioxidant enzymes, various types of intracellular oxidative damages, such as DNA alteration[7] and lipid and protein peroxidations,[8] may occur and cause deterioration in health. Brain tissue is particularly vulnerable to oxidative damage, possibly due to its high consumption of oxygen and the consequent generation of high quantities of ROS during oxidative phosphorylation.[9]

Due to their abundance and ability to sustain the homeostatic environment of the central nervous system (CNS), glial cells play a critical role in maintaining neuronal function under both physiological and pathological conditions. Glial cells constitute the most common cell type in the brain and play critical roles in normal brain function and during infection and injury.[10,11] Astrocytes make up the largest subpopulation of glial cells and are a key factor in alleviating ischemic damage to neurons.[12] Impairment in the functions of these astrocytes during brain ischemia and other insults may be fatal to neurons.[13]

Astrocyte functions that are known to support the survival of neurons include glutamate uptake, glutamate release, free radical scavenging, water transport, and production of cytokines and nitric oxide.[14] The C6 glial cell line was originally derived from rat brain tumor induced by *N*-nitrosomethylurea. C6 cells are characterized with important functional analogy to normal rat brain astrocytes and therefore widely used to imitate astrocytes,[15] for example, in studies on oxidative stress with responsive effects to redox-active compounds.[16]

Anthocyanins occur widely in plants. They are well-known free radical scavengers against oxidative damage in the cell and are reported as a potential chempreventive agent.[17] A growing number of scientific papers show that anthocyanins and anthocyanin-rich berries or derived extracts exhibit a wide range of protective effects with potential benefits for human and animal health.[18] Ghosh et al.[19] proposed that the systemic antioxidative effects of absorbed anthocyanins or their metabolites may reduce oxidative stress and the risk of certain chronic and degenerative diseases. Anthocyanins are glycosides of polyhydroxyl and polymethoxyl derivatives of flavylium salts. Aglycons of anthocyanins, anthocyanidins, are widely present in pigmented fruits and vegetables such as pomegranate, berry, grape, sweet potato, red cabbage, and eggplant.[20,21]

There are quite a few cell studies investigating the effect of anthocyanidins to protect health.[22−24] Tarozzi et al.[25] studied the neuroprotective effect of cyanidin in SH-SY5Y cells under oxidative stress and proposed that it may play an important role in brain health promotion. However, little research has been done on the neuroprotective effect of anthocyanidins against hypoxia. The present study was to evaluate the effect of anthocyanidins in preventing hypoxia injury in the nervous

Received: April 11, 2014
Revised: May 17, 2014
Accepted: May 20, 2014
Published: May 20, 2014

ACS Publications © 2014 American Chemical Society

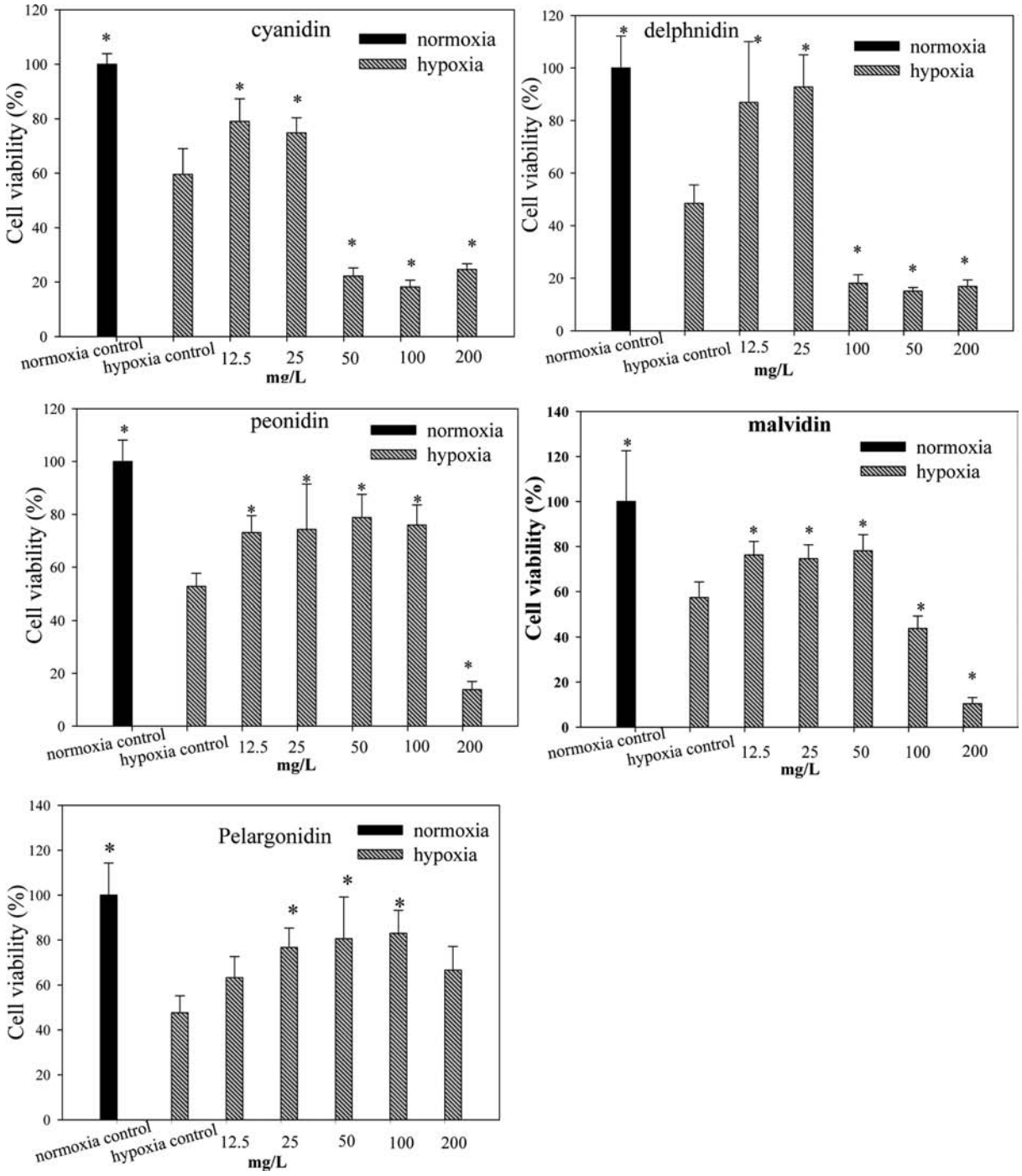

Figure 1. Neuroprotective effect of anthocyanidins on C6 cells against $Na_2S_2O_4$-induced hypoxia. The cells in the treatment groups were preincubated in DMEM containing an anthocyanidin in 12.5−200 mg/L at 37 °C for 24 h and then treated with 5 mM $Na_2S_2O_4$ for 30 min in anaerobic environment. Cell viability was evaluated by MTT test. Normoxia control: cells preincubated in DMEM containing no anthocyanidin and then treated with PBS in normoxia condition. Hypoxia control: cells preincubated in DMEM containing no anthocyanidin and then treated with PBS in hypoxia condition. Data are means ± SD from three independent experiments. Statistical analysis was performed using one-way ANOVA and Duncan's new multiple-range test. (∗) $p < 0.05$ versus the hypoxia control.

system. C6 glial cells were used to imitate brain astrocytes, whereas sodium dithionite ($Na_2S_2O_4$) was used to cause chemical hypoxia that mimics the hypoxic/ischemic condition.[26]

MATERIALS AND METHODS

Reagents. Anthocyanidins (cyanidin, delphinidin, malvidin, pelargonidin, and peonidin, all in chloride form) were obtained from Extrasynthese Corp. (Genay Cedex, France). 3-(4,5-Dimethylthiazol-2-yl)-2,5-diphenyl, bovine serum albumin (BSA), and trypsin/ethylenediaminetetraacetic acid (EDTA) were purchased from Sigma (St. Louis, MO, USA). Catalase (CAT), glutathione (GSH), and superoxide dismutase (SOD) activity kits were purchased from Cayman Chemical Co. (Ann Arbor, MI, USA). All the chemical reagents were of analytic grade.

Cultivation of Cells. C6 glial cells were obtained from Bioresource Collection and Research Center (Hsinchu, Taiwan). The cells were

dx.doi.org/10.1021/jf501564h | J. Agric. Food Chem. 2014, 62, 5603−5608

inoculated into Dulbecco's modified Eagle's medium (DMEM) (Gibco, Grand Island, NY, USA) supplemented with 10% fetal bovine serum (Gibco), containing 100 units/mL penicillin and 100 units/mL streptomycin, and then held in humidified 5% CO_2/95% air environment at 37 °C. Exponentially growing cells were detached from the culture flasks with the addition of 0.05% trypsin/EDTA and collected by centrifuging the suspension. For the methylthiazole tetrazolium (MTT) test, the harvested cells were suspended in serum-free DMEM at a density of 2×10^4 cells/well and then placed on 96-well plates. For CAT, SOD, and GSH assays, 6-well plates instead of 96-well plates were used. All of the plates were held at 37 °C for 24 h before the following treatments.

Preincubation. Preincubation of C6 cells with each of the five common anthocyanidins was practiced prior to the hypoxia treatment for revealing the protective effect of these anthocyanidins on neuronal cells from hypoxia injury. Anthocyanidins were dissolved in phosphate buffer saline (PBS, pH 7.2) in various concentrations from 12.5 to 200 mg/L and added into wells on the plate. After another 24 h of incubation, each well was rinsed with PBS. Samples containing no anthocyanidins were taken as controls.

Hypoxia Treatment. A 200 μL aliquot of 5 mM $Na_2S_2O_4$ was added to each well for the generation of hypoxia stress. The plates were then incubated at 37 °C for 30 min in an anaerobic incubator with 1% O_2, 5% CO_2, and 94% N_2 atmosphere.

MTT Test. The protective effects of anthocyanidins against hypoxia were determined by MTT test.[27] Samples of cultured cells were taken from the plates periodically. A filtered solution of 0.5 mg MTT/mL serum-free DMEM was added to each well. The plates were then incubated at 37 °C for 2 h. The supernatant, which contained unreacted dye, was removed. DMSO was added to dissolve the MTT formazan crystals left in each well. The 570 nm absorbance of each sample in the well was measured 15 min later. The viability of cells was calculated using the following equation:

$$\text{cell viability (\%)} = (\text{absorbance of sample}) / (\text{absorbance of normoxia control}) \times 100\%$$

CAT Assay. CAT activity was measured using a Catalase Assay Kit (Cayman). The cell samples were collected from the 6-well plate by a rubber policeman, mixed with 1 mL of cold buffer (pH 7.0, 50 mM potassium phosphate/1 mM EDTA), sonicated on ice, and then centrifuged at 10000*g* and 4 °C for 15 min. A 20 μL aliquot of the supernatant was placed in a well on a 96-well plate and mixed with 100 μL of assay buffer, 30 μL of methanol, and 20 μL of hydrogen peroxide. The plate was covered and incubated at room temperature for 20 min with shaking. To each well was then added 30 μL of potassium hydroxide to terminate the reaction, followed by 30 μL of Purpald for color development. The plate was covered again and incubated for an additional 10 min at room temperature with shaking. To each well was added 10 μL of potassium periodate, and then the plate was incubated at room temperature for 5 min with shaking. The protein content of the cell sample was evaluated using a protein assay dye (Bio-Rad, Hercules, CA, USA) following the above-described procedure. The absorbance at 540 nm was measured for evaluating the CAT activity in the cell sample, expressed as U/mg protein.

SOD Assay. SOD activity was measured using a Superoxide Dismutase Assay Kit (Cayman). The cell samples were collected from the 6-well plate by a rubber policeman, mixed with 1 mL of cold 20 mM HEPES buffer (pH 7.2, containing 1 mM EGTA, 210 mM mannitol, and 70 mM sucrose), sonicated on ice, and then centrifuged at 1500*g* and 4 °C for 5 min. A 10 μL aliquot of the supernatant was mixed with 200 μL of radical detector in a well on a 96-well plate. A 20 μL aliquot of xanthine oxidase was added followed by another mixing. The plate was covered and then incubated at room temperature for 20 min with shaking. The protein content of the cell sample was evaluated using a protein assay dye (Bio-Rad). The absorbance at 450 nm was measured for evaluating the SOD activity in the cell sample, expressed as U/mg protein.

GSH Assay. GSH was measured using a Glutathione Assay Kit (Cayman) following the protocol. Briefly, the cell samples were collected from the 6-well plate by a rubber policeman, mixed with 1 mL of cold buffer (50 mM phosphate at pH 6–7, containing 1 mM EDTA), sonicated on ice, and then centrifuged at 10000*g* and 4 °C for 15 min. A 50 μL aliquot of the supernatant was mixed with 150 μL of freshly prepared assay cocktail. The plate was covered and then incubated in the dark at room temperature for 25 min with shaking. The absorbance at 410 nm was measured for evaluating the GSH activity in the cell sample, expressed as μM.

Statistical Analysis. The data were analyzed by one-way ANOVA and Duncan's new multiple-range test. Differences with a p value <0.05 were considered significant.

RESULTS AND DISCUSSION

Protective Effects of Anthocyanidins against Hypoxia-Induced Cell Damage. In the present study, C6 glial cells, either preincubated with an anthocyanidin or not, were suspended in 5 mM $Na_2S_2O_4$ solution and incubated in an anaerobic environment at 37 °C for 30 min as the hypoxia treatment. The viability of cells preincubated without anthocyanidin was reduced in the hypoxia treatment to 47–59% of the original value (Figure 1). Preincubation of the cells with an anthocyanidin at proper concentration may effectively improve the viability in the hypoxia treatment. The concentration of an anthocyanidin up to 50–200 mg/L may cause cell toxicity. This might be because the anthocyanidins used in the present study are all in chloride form. The osmotic pressure or pH of solution may cause cell toxicity. Among the five anthocyanidins tested, delphinidin at 25 mg/L concentration showed the highest protective effect on C6 cells against the hypoxia treatment, by retaining >90% of the cell viability as compared with a survival rate between 47 and 59% for the hypoxia control that was preincubated without an anthocyanidin. The lowest protective effect came from peonidin, which retained 74% of the cell viability. The protective effect may be attributed to the antioxidant activity of anthocyanidins. Delphinidin and cyanidin are among those anthocyanidins that have a completely conjugated structure to allow ROS delocalizing their electrons and forming very stable radical products.[28] The antioxidant activities of these two anthocyanidins are therefore higher than the other three in the present study. The third hydroxyl group in the B ring also enhances the radical scavenging activity.[29] Delphinidin, which has hydroxyl groups in three positions, 3′-, 4′-, and 5′-, was more antioxidative than cyanidin, which has hydroxyl groups in only two positions, 3′- and 4′- (Figure 2). Higher stability, reactivity, and chemical antioxidant activity of an anthocyanidin may lead to higher cell antioxidant capacity at the cytosol level.[25]

No apparent dose dependency for the protective effect of anthocyanidins on C6 glial cells was observed. Generally, at least 74% of the C6 glial cells preincubated with an anthocyanidin at 25 mg/L survived the hypoxia treatment (Figure 1). The concentration of 25 mg/L was therefore chosen for the subsequent experiments.

Antioxidant Enzymes and Protein in Cells Subjected to Hypoxia Treatment. Hypoxia causes an increase of oxidative stress that is detrimental to cells. Extra activities of antioxidant enzymes, including CAT and SOD, and GSH may be induced in the cell to scavenge free radicals as a defensive response. The increments in antioxidant enzyme activities and GSH concentration can be indicators for the effectiveness of the antioxidant defense system in cells.[30] Intracellular superoxide anions could be converted to H_2O_2 by SOD and then to H_2O and O_2 by CAT.[31] GSH is the most abundant free cellular

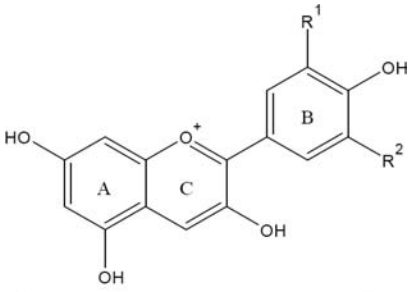

Anthocyanidin	R^1	R^2
Pelargonidin	H	H
Cyanidin	OH	H
Delphinidin	OH	OH
Peonidin	OCH_3	H
Malvidin	OCH_3	OCH_3

Figure 2. Structural formulas of five common anthocyanidins.

thiol in eukaryotes and a well-characterized ROS scavenger in the brain. The GSH content in cells is consumed to counteract the accumulation of ROS in hypoxia.[30]

In the present study, we treated C6 cells with five different anthocyanidins and assessed the activities of antioxidant enzymes CAT and SOD and the concentration of GSH in the cells for evaluating the effect of anthocyanidins on the antioxidant defense system.

CAT. CAT catalyzes the conversion of hydrogen peroxide into H_2O and O_2 in attenuating the oxidative stress. As shown in Figure 3, CAT activity in C6 glial cells preincubated with an anthocyanidin was increased in the hypoxia treatment ($p < 0.05$). The increments of CAT activity in cells in hypoxia were 49, 43, 33, 23, and 16%, in diminishing order, for delphinidin, peonidin, malvidin, pelargonidin, and cyanidin, respectively. C6 cells suffer from the increase of oxidative stress in hypoxia condition. Anthocyanidins may induce extra activities of CAT in the cell to scavenge more free radicals. The increase in CAT activity may be involved in the neuroprotective effect of anthocyanidins.

Propofol is a synthetic chemical that has been demonstrated to be neuroprotective in several in vivo and in vitro models of cerebral hypoxia reoxygenation injury.[32] Propofol contains a phenolic hydroxyl group, and thus its structure resembles that of α-tocopherol, a natural antioxidant. Moreover, propofol has been shown to induce and regulate intracellular signaling pathways, and the neuroprotective effects of propofol may also be mediated indirectly via the induction of cell-based antioxidant mechanisms. Its neuroprotective activity was attributed to the antioxidation activity from the phenolic chemical structure. Anthocyanidins are natural phenolic compounds and also have antioxidative activity. The anthocyanidins in the present study presumably protect the neuronal system in hypoxia on the basis of their phenolic structures as well.

Martin et al.[33] found that procyanidins may promote the activity of CAT in the cell. In the present study, we found similar promotion of cellular CAT activity in incubation with an anthocyanidin.

SOD. The presence of delphinidin in the culture medium resulted in a higher SOD activity in the aerobic preincubation as compared with the normoxia control and the presence of another anthocyanidin ($p < 0.01$) (Figure 4).

Cells preincubated with malvidin, pelargonidin, and peonidin were enabled to increase their SOD activity in the hypoxia treatment by 72, 11, and 49%, respectively, whereas those incubated with cyanidin and delphinidin showed decreased

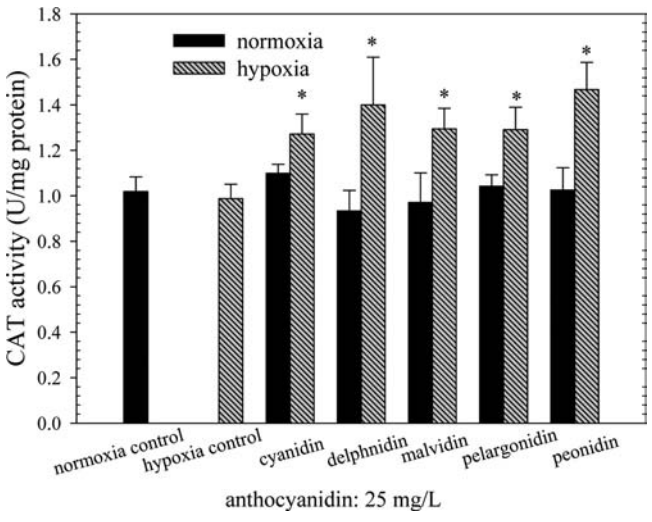

Figure 3. Effect of anthocyanidins on CAT activity in C6 cells in normoxia and hypoxia conditions. The C6 cells in the treatment groups were preincubated in DMEM containing an anthocyanidin at 37 °C for 24 h and then incubated for 30 min either in the hypoxia condition induced with 5 mM $Na_2S_2O_4$ under anaerobic environment or in the normoxia condition with PBS. CAT activity is expressed as U/mg protein. Normoxia control: cells preincubated in DMEM containing no anthocyanidin and then treated with PBS in normoxia condition. Hypoxia control: cells preincubated in DMEM containing no anthocyanidin and then treated with PBS in the hypoxia condition. (*) $p < 0.05$ versus the hypoxia control.

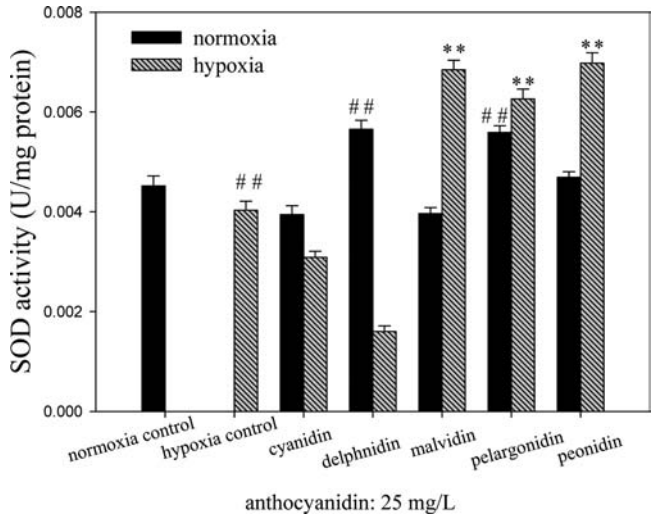

Figure 4. Effect of anthocyanidins on SOD activity in C6 cells in normoxia and hypoxia conditions. The cells in the treatment groups were preincubated in DMEM containing an anthocyanidin at 37 °C for 24 h and then incubated for 30 min either in the hypoxia condition induced with 5 mM $Na_2S_2O_4$ under anaerobic environment or in the normoxia condition with PBS. SOD activity is expressed as U/mg protein. Normoxia control: cells preincubated in DMEM containing no anthocyanidin and then treated with PBS in normoxia condition. Hypoxia control: cells preincubated in DMEM containing no anthocyanidin and then treated with PBS in the hypoxia condition. (##) $p < 0.01$ versus the normoxia control. (**) $p < 0.01$ versus the hypoxia control.

SOD activity. Wu et al.[34] reported that nerve growth factor (NGF) prevents hypoxic insults in cultured cerebral cortical neurons by increasing the activity of SOD. The increase in SOD activity may contribute to the neuroprotective effects of malvidin, pelargonidin, and peonidin in the present study. SOD activity readings in C6 cells preincubated with cyanidin and delphinidin were apparently decreased in the hypoxia treatment, by 21 and 72%, respectively (Figure 4), whereas the cell viability readings were maintained at 75 and 90%, respectively, which were better than the hypoxia control (Figure 1). Presumably, cyanidin and delphinidin do not provide protection on C6 cells against hypoxia by playing the role of promoters to SOD activity. The availability of the hydroxyl group on the B ring of an anthocyanidin, such as cyanidin and delphinidin, is fundamental to the antioxidant activity of these compounds because hydroxyl moieties can donate hydrogen to scavenge radicals.[35] Therefore, we postulate that playing antioxidants themselves may be an important mechanism for these two anthocyanidins to protect C6 cells against hypoxia.

GSH. The GSH concentrations in C6 cells were elevated in the aerobic preincubation with malvidin, pelargonidin, and peonidin ($p < 0.05$) (Figure 5). The increase in GSH continued

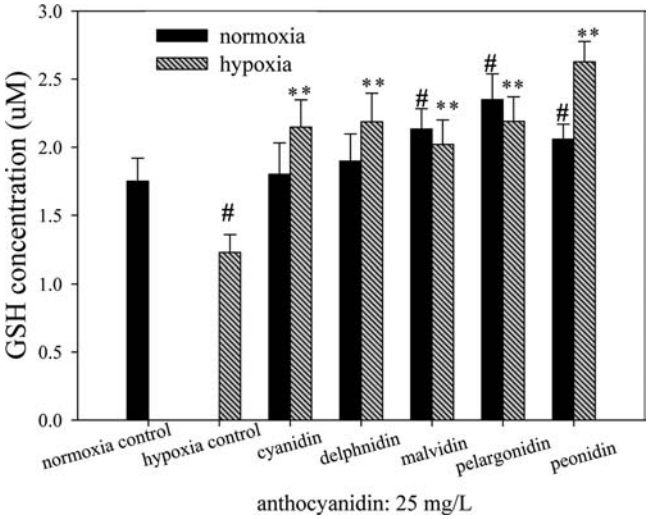

Figure 5. Effect of anthocyanidins on GSH concentration in C6 cells in normoxia and hypoxia conditions. The cells in the treatment groups were preincubated with an anthocyanidin at 37 °C for 24 h and then incubated for 30 min either in the hypoxia condition induced with 5 mM $Na_2S_2O_4$ under anaerobic environment or in the normoxia condition with PBS. GSH concentration is expressed as μM. Normoxia control: cells preincubated in DMEM containing no anthocyanidin and then treated with PBS in normoxia condition. Hypoxia control: cells preincubated in DMEM containing no anthocyanidin and then treated with PBS in the hypoxia condition. (#) $p < 0.05$ versus the normoxia control. (**) $p < 0.01$ versus the hypoxia control.

in the hypoxia treatment for cells preincubated with peonidin, by 27%. In response to the hypoxia-induced oxidative stress, a marked depletion in the concentration of GSH occurred in the brain.[36] In the present study, the preincubation with anthocyanidins enabled cells to increase their GSH concentrations in the subsequent hypoxia treatment. An explanation is that anthocyanidins initiate the promotion of GSH-related enzyme expressions in the preincubation.[37]

Several brain disorders are accompanied by a decrease in GSH and other indications of oxidative stress in cells.[38] The brain is particularly susceptible to oxidative insults, and its antioxidant defense is dependent on the GSH content.[39] The present study found that preincubations with malvidin, pelargonidin, and peonidin are able to increase GSH content in C6 cells, reconfirming the potential for these anthocyanidins to be used in the protection of the nervous system against hypoxia injury.

Limited information has been collected on the bioavailability, metabolism, and absorption of anthocyanins and anthocyanidins, although they generally appear in human plasma quickly after digestion.[40] Animal studies also confirm that these compounds rapidly cross the blood–brain barrier.[41,42] The present study provided supporting evidence in cell study for the development of anthocyanidins to be a health food ingredient for the prevention of neuronal injury in hypoxia condition.

Conclusion. In recent years, the inclusion of phytochemicals in the human diet has gained considerable attention. Anthocyanins occur widely in plant materials. Anthocyanidins are the aglycon part, which can be released from anthocyanins during digestion. The present study demonstrates the protective effect of five anthocyanidins, namely, cyanidin, delphinidin, malvidin, pelargonidin, and peonidin, on neuronal cells against hypoxia injury and supports the development of anthocyanidins as ingredients in health food. The results also indicate that the neuroprotective effect may be related to the increase in the activities of antioxidant enzymes CAT and SOD and the concentration of antioxidant protein GSH. Further studies to elucidate the mechanism for anthocyanidins to protect the nervous system shall be worthwhile.

AUTHOR INFORMATION

Corresponding Author

*(J.S.-B.W.) Phone: +886-2-3366-4117. Fax: +886-2-2362-0849. E-mail: jsbwu@ntu.edu.tw.

Notes

The authors declare no competing financial interest.

REFERENCES

(1) Xue, W. Hepatocyte growth factor protects against hypoxia/reoxygenation induced apoptosis in endothelial cells. *J. Biol. Chem.* **2004**, *279*, 5237–5243.

(2) Jayalakshmi, K.; Sairam, M.; Singh, S. B.; Sharma, S. K.; Ilavazhagan, G.; Banerjee, P. K. Neuroprotective effect of *N*-acetyl cysteine on hypoxia induced oxidative stress in primary hippocampal culture. *Brain Res.* **2005**, *1046*, 97–104.

(3) Medina, S.; Martinez, M.; Hernanz, A. Antioxidants inhibit the human cortical neuron apoptosis induced by hydrogen peroxide, tumor necrosis factor α, dopamine and β-amyloid peptide 1–42. *Free Radical Res.* **2002**, *36*, 1179–1184.

(4) Joseph, J. A.; Shukitt-Hale, B.; Casadesus, G. Reversing the deleterious effects of aging on neuronal communication and behavior: beneficial properties of fruit polyphenolic compounds. *Am. J. Clin. Nutr.* **2005**, *81*, 313S–316S.

(5) Halliwell, B. Oxidative stress and neurodegeneration: where are we now? *J. Neurochem.* **2006**, *97*, 1634–1658.

(6) Ahmad, S. *Oxidative Stress and Antioxidant Defenses in Biology*; Chapman and Hall: New York, 1995.

(7) Cozzi, R.; Ricordy, R.; Aglitti, T.; Gatta, V.; Perticone, P.; De Salvia, R. Ascorbic acid and β-carotene as modulators of oxidative damage. *Carcinogenesis* **1997**, *18*, 223–228.

(8) Berlett, B. S.; Stadtman, E. R. Protein oxidation in aging, disease, and oxidative stress. *J. Biol. Chem.* **1997**, *272*, 20313–20316.

(9) Castagne, V.; Gautschi, M.; Lefevre, K.; Posada, A.; Clarke, P. G. Relationships between neuronal death and the cellular redox status.

Focus on the developing nervous system. *Prog. Neurobiol.* **1999**, *59*, 397−423.
(10) Ransom, B. R.; Sontheimer, H. The neurophysiology of glial cells. *J. Clin. Neurophysiol.* **1992**, *9*, 224−251.
(11) Maeda, Y.; Matsumoto, M.; Hori, O.; Kuwabara, K.; Ogawa, S.; Yan, S. D.; Ohtsuki, T.; Kinoshita, T.; Stem, D. M. Hypoxia/reoxygenation-mediated induction of astrocyte interleukin 6: a paracrine mechanism potentially enhancing neuron survival. *J. Exp. Med.* **1994**, *180*, 2297−2308.
(12) Rossi, D. J.; Brady, J. D.; Mohr, C. Astrocyte metabolism and signaling during brain ischemia. *Nat. Neurosci.* **2007**, *10*, 1377−1386.
(13) Chen, Y.; Swanson, R. A. Astrocytes and brain injury. *J. Cereb. Blood Flow Metab.* **2003**, *23*, 137−149.
(14) Szydlowska, K.; Gozdz, A.; Dabrowski, M.; Zawadzka, M.; Kaminska, B. Prolonged activation of ERK triggers glutamate-induced apoptosis of astrocytes: neuroprotective effect of FK506. *J. Neurochem.* **2010**, *113*, 904−918.
(15) Ren, L. Q.; Garrett, D. K.; Syapin, M.; Syapin, P. J. Differential fibronectin expression in activated C6 glial cells treated with ethanol. *Mol. Pharmacol.* **2000**, *58*, 1303−1309.
(16) Slamon, N. D.; Pentreath, V. W. Antioxidant defense against antidepressants in C6 and 1321N1 cells. *Chem.−Biol. Interact.* **2000**, *127*, 181−199.
(17) Duthie, G. G.; Duthie, S. J.; Kyle, J. A. M. Plant polyphenols in cancer and heart disease: implications as nutritional. *Nutr. Res. Rev.* **2000**, *13*, 79−106.
(18) Zafra-Stone, S.; Yasmin, T.; Bagchi, M.; Chatterjee, A.; Vinson, J. A.; Bagchi, D. Berry anthocyanins as novel antioxidants in human health and disease prevention. *Mol. Nutr. Food Res.* **2007**, *51*, 675−683.
(19) Ghosh, D.; McGhie, T. K.; Zhang, J.; Adaim, A.; Skinner, M. Effects of anthocyanins and other phenolics of boysenberry and blackcurrant as inhibitors of oxidative stress and damage to cellular DNA in SH-SY5Y and HL-60 cells. *J. Sci. Food Agric.* **2006**, *86*, 678−686.
(20) Mazza, G. Anthocyanins in grapes and grape products. *Crit. Rev. Food Sci. Nutr.* **1995**, *35*, 341−371.
(21) Afaq, F.; Malik, A.; Syed, D.; Maes, D.; Matsui, M. S.; Mukhtar, H. Pomegranate fruit extract modulates UV-B-mediated phosphorylation of mitogen-activated protein kinases and activation of nuclear factor κB in normal human epidermal keratinocytes. *Photochem. Photobiol.* **2005**, *81*, 38−45.
(22) Noda, Y.; Packer, L.; Mori, A.; Kaneyuki, T. Antioxidant activities of pomegranate fruit extract and its anthocyanidins: delphinidin, cyanidin, and pelargonidin. *J. Agric. Food Chem.* **2002**, *50*, 166−171.
(23) Hou, D. X.; Yanagita, T.; Uto, T.; Masuzaki, S.; Fujii, M. Anthocyanidins inhibit cyclooxygenase-2 expression in LPS-evoked macrophages: structure−activity relationship and molecular mechanisms involved. *Biochem. Pharmacol.* **2005**, *70*, 417−425.
(24) Azevedo, L.; de Lima, P. A.; Gomes, J. C.; Stringheta, P. C.; Ribeiro, D. A.; Salvadori, D. M. F. Differential response related to genotoxicity between eggplant (*Solanum melanogena*) skin aqueous extract and its main purified anthocyanin (delphinidin) *in vivo*. *Food Chem. Toxicol.* **2007**, *45*, 852−858.
(25) Tarozzi, A.; Morroni, F.; Hrelia, S.; Angeloni, C.; Marchesi, A.; Cantelli-Forti, G.; Hrelia, P. Neuroprotective effects of anthocyanins and their in vivo metabolites in SH-SY5Y cells. *Neurosci. Lett.* **2007**, *424*, 36−40.
(26) Tang, J.; Yao, Y. J.; Zhong, L. NgR expression in oligodendrocyte precursor cells and its changes after oxygen & glucose deprivation in neonatal rats. *Zhongguo Dang Dai Er Ke Za Zhi* **2007**, *9*, 445−448.
(27) Chan, J. Y.; Siu, K. P.; Fung, K. P. Effect of arsenic trioxide on multidrug resistant hepatocellular carcinoma cells. *Cancer Lett.* **2006**, *236*, 250−258.
(28) van Acker, S. A.; van den Berg, D. J.; Tromp, M. N.; Griffioen, D. H.; van Bennekom, W. P.; van der Vijgh, W. J.; Bast, A. tructural aspects of antioxidant activity of flavonoids. *Free Radical Biol. Med.* **1996**, *20*, 331−342.
(29) Fukumoto, L. R.; Mazza, G. Assessing antioxidant and prooxidant activities of phenolic compounds. *J. Agric. Food Chem.* **2000**, *48*, 3597−3604.
(30) Kaminski, K. A.; Bonda, T. A.; Korecki, J.; Musial, W. J. Oxidative stress and neutrophil activation − the two keystones of ischemia/reperfusion injury. *Int. J. Cardiol.* **2002**, *86*, 41−59.
(31) Chen, Y.; Azad, M. B.; Gibson, S. B. Superoxide is the major reactive oxygen species regulating autophagy. *Cell Death Differ.* **2009**, *16*, 1040−1052.
(32) Huang, Y.; Zitta, K.; Bein, B.; Scholz, J.; Steinfath, M.; Albrecht, M. Effect of propofol on hypoxia re-oxygenation induced neuronal cell damage in vitro. *Anaesthesia* **2013**, *68*, 31−39.
(33) Martin, S.; Gonzalez-Burgos, E.; Carretero, M. E.; Gomez-Serranillos, M. P. Neuroprotective properties of Spanish red wine and its isolated polyphenols on astrocytes. *Food Chem.* **2011**, *128*, 40−48.
(34) Wu, J. F.; Zhang, J. T. Antagonistic effect of nerve growth factor on neuronal injury induced by hypoxia in cultured cerebral cortical neurons of rats. *Zhongguo Yao Li Xue Bao* **1999**, *20*, 47−51.
(35) Matsunaga, N.; Imai, S.; Inokuchi, Y.; Shimazawa, M.; Yokota, S.; Araki, Y.; Hara, H. Bilberry and its main constituents have neuroprotective effects against retinal neuronal damage *in vitro* and *in vivo*. *Mol. Nutr. Food Res.* **2009**, *53*, 869−877.
(36) Jiang, X.; Mu, D.; Manabat, C.; Koshy, A. A.; Christen, S.; Tauber, M. G.; Vexler, Z. S.; Ferriero, D. M. Differential vulnerability of immature murine neurons to oxygen-glucose deprivation. *Exp. Neurol.* **2004**, *190*, 224−232.
(37) Shih, P. H.; Yeh, C. T.; Yen, G. C. Anthocyanins induce the activation of phase II enzymes through the antioxidant response element pathway against oxidative stress-induced apoptosis. *J. Agric. Food Chem.* **2007**, *55*, 9427−9435.
(38) Schulz, J. B.; Lindenau, J.; Seyfried, J.; Dichgans, J. Glutathione, oxidative stress and neurodegeneration. *Eur. J. Biochem.* **2000**, *267*, 4904−4911.
(39) Feoli, A. M.; Siqueira, I.; Almeida, L. M.; Tramontina, A. C.; Battu, C.; Wofchuk, S. T.; Gottfried, C.; Perry, M. L.; Goncalves, C. A. Brain glutathione content and glutamate uptake are reduced in rats exposed to pre- and postnatal protein malnutrition. *J. Nutr.* **2006**, *136*, 2357−2361.
(40) McGhie, T. K.; Walton, M. C. The bioavailability and absorption of anthocyanins: towards a better understanding. *Mol. Nutr. Food Res.* **2007**, *51*, 702−713.
(41) Andrés-Lacueva, C.; Shukitt-Hale, B.; Galli, R. L.; Jauregui, O.; Lamuela-Raventos, R. M.; Joseph, J. A. Anthocyanins in aged blueberry-fed rats are found centrally and may enhance memory. *Nutr. Neurosci.* **2005**, *8*, 111−120.
(42) Talavéra, S.; Felgines, C.; Texier, O.; Besson, C.; Gil-Izquierdo, A.; Lamaison, J. L.; Remesy, C. Anthocyanin metabolism in rats and their distribution to digestive area, kidney, and brain. *J. Agric. Food Chem.* **2005**, *53*, 3902−3908.

JOURNAL OF AGRICULTURAL AND FOOD CHEMISTRY

Article

pubs.acs.org/JAFC

Structural Carbohydrates in a Plant Biomass: Correlations between the Detergent Fiber and Dietary Fiber Methods

Bruno Godin,*[,†,‡] Richard Agneessens,[†] Patrick Gerin,[‡] and Jérôme Delcarte[†]

[†]Walloon Agricultural Research Center, CRA-W. Valorisation of Agricultural Products Department, Biomass, Bioproducts and Energy Unit, Chaussée de Namur, 146, B-5030 Gembloux, Belgium

[‡]Université catholique de Louvain, Earth and Life Institute, Bioengineering group, Croix du Sud, 2 box L7.05.19, B-1348 Louvain-la-Neuve, Belgium

Supporting Information

ABSTRACT: We compared the detergent fiber and dietary fiber methods to analyze the cellulose and hemicellulose contents of commelinid and non-commelinid magnoliophyta biomass. A good linear correlation was found between both methods. Compared to the more accurate dietary fiber method, the detergent fiber method overestimates the content of cellulose, whereas the detergent fiber method, as compared to the dietary fiber method, overestimates and underestimates the hemicellulose content in commelinid and non-commelinid magnoliophyta biomass, respectively. Because of the good linear correlations, conversion factors were determined to predict the cellulose, hemicellulose, and xylan contents to be expected from the dietary fiber method, on the basis of analyses made by the faster, cheaper, and more commonly practiced detergent fiber method. Nevertheless, the dietary fiber method offers the advantage of providing the detailed composition of the hemicelluloses (xylan, arabinan, hemicellulosic glucan, galactan, and mannan), and that is of interest for biorefining purposes.

KEYWORDS: *cellulose, hemicelluloses, xylan, correlation, biofuels*

INTRODUCTION

The main chemical components of a plant biomass are generally cellulose (linear structural polysaccharide homogeneously composed of D-glucose units), hemicelluloses (ramified structural polysaccharides heterogeneously composed of D-xylose, L-arabinose, D-mannose, D-galactose, and D-glucose units) and lignin (phenyl propanoid polymer composed of syringyl, guaiacyl, and *p*-hydroxyphenyl units).[1,2] A plant biomass also contains other components such as pectins (ramified heterogeneous structural polysaccharides mainly composed of D-galacturonic acid units), starch (linear or ramified homogeneous nonstructural polysaccharide composed of D-glucose units), soluble sugars (D-glucose, D-fructose, sucrose, and fructans), proteins, and mineral compounds.[1,2]

The Van Soest sequential fiber solubilization method is widely used to assess the cellulose, hemicellulose, and lignin contents of plant feedstocks and to predict the nutritive value of these materials. This gravimetric method classifies the cell wall components of a plant biomass into three types of insoluble residues: neutral detergent fiber (NDF), acid detergent fiber (ADF), and acid detergent lignin (ADL) residues. The neutral detergent extraction is operated by refluxing a biomass sample in a boiling aqueous neutral detergent at pH 7 for 1 h.[3] The neutral detergent fiber residue represents the incompletely digestible portion of forages that is composed of cellulose, hemicelluloses, and lignin.[4] Acid detergent extraction is conducted by refluxing a biomass sample in a boiling aqueous detergent containing 0.5 mol/L sulfuric acid for 1 h.[5] Cellulose and lignin are the cell wall components recovered in the insoluble acid detergent fiber residue. The acid detergent extraction has been developed as a pretreatment prior to the measurement of lignin as acid detergent lignin. After the acid detergent procedure, the remaining structural carbohydrates of the acid detergent fiber residue are solubilized by 12.2 mol/L sulfuric acid at room temperature for 3 h.[5] The residual insoluble acid detergent lignin fraction represents an indigestible portion of forages.[4] The gravimetric difference between ADF and ADL insoluble residues is used to estimate the content of cellulose. The gravimetric difference between the NDF and ADF insoluble residues is used to estimate the content of hemicelluloses. The acid detergent lignin insoluble residue is used to estimate the content of lignin.[4,6] The detergent fiber method shows some deficiencies in accuracy. It overestimates the contents of cellulose and hemicelluloses and underestimates the content of lignin.[6−8] This can be explained by the fact that (1) the neutral detergent fiber residue contains some proteins,[6,7] (2) the acid detergent fiber residue contains some pectins when the analyzed biomass (such as a non-commelinid magnoliophyta biomass) has a high content of pectins,[4,6,9] (3) the acid detergent fiber residue contains some hemicelluloses,[10] and (4) the acid detergent lignin residue does not contain the acid soluble lignin.[6]

The dietary fiber method is based on the Uppsala method.[7,11] It is used to assess dietary fiber in animal and human food and in crop feedstocks that are of interest as a source of fibers, biofuels (such as bioethanol and biobutanol), and biobased chemicals.[11] The dietary fiber method is used to determine more accurately the contents of cellulose and hemicelluloses, compared to the accuracy of the detergent fiber method. This method quantitates the structural polysaccharides based on their monosaccharidic

Received: February 25, 2014
Revised: May 19, 2014
Accepted: May 19, 2014
Published: May 19, 2014

ACS Publications © 2014 American Chemical Society

components (D-glucose, D-xylose, L-arabinose, D-mannose, and D-galactose).[12−14] In the dietary fiber method, samples are first extracted one or several times by solvents (e.g., water, ethanol, neutral detergent, ether, and/or hexane) to remove all components that interfere with the subsequent sulfuric acid hydrolysis and chromatographic quantitation of the cellulosic and hemicellulosic monosaccharides. The total glucan, xylan, arabinan, galactan, and mannan contents are then determined by a two-stage sulfuric acid hydrolysis method (SAH). The first stage solubilizes the structural carbohydrates with 12.2 mol/L sulfuric acid at 30 °C for 1 h, and the second stage hydrolyzes these solubilized structural carbohydrates with 0.419 mol/L sulfuric acid at 121 °C for 1 or 2 h.[12−14] The released monosaccharides are separated and quantitated by liquid chromatography or gas chromatography. The content of hemicellulosic glucan is determined by the same dietary fiber method except that the cellulose solubilization step (incubation with 12.2 mol/L sulfuric acid at 30 °C for 1 h) is omitted. The content of cellulose (cellulosic glucan; i.e., D-glucose of cellulose in its polymeric form) is calculated as the difference between the total glucan and hemicellulosic glucan contents.[14] The monosaccharidic components (D-xylose, L-arabinose, D-glucose, D-mannose, and D-galactose) of hemicelluloses are expressed as their polymeric forms (xylan, arabinan, hemicellulosic glucan, mannan, and galactan, respectively).[14] In the dietary fiber method, the hemicellulose content is considered as the sum of the xylan, arabinan, hemicellulosic glucan, galactan, and mannan contents. To correct the results for any underestimation of the monosaccharide concentrations due to acidic degradation, a standard mixture of monosaccharides is treated with sulfuric acid in parallel with the samples.[12−14]

The relationship between the contents of cellulose and hemicelluloses determined by the detergent fiber and dietary fiber methods has been investigated on a data set that includes miscanthus (*Miscanthus sinensis* Anderss.), reed canarygrass (*Phalaris arundinacea* L.), smooth bromegrass (*Bromus inermis* L.), and alfalfa leaf and stem (*Medicago sativa* L.).[7] They showed that the detergent fiber method overestimates the content of cellulose and hemicelluloses, as compared to the dietary fiber method, except for alfalfa (a non-commelinid magnoliophyta biomass compared to other biomasses that are commelinids) where the detergent fiber method underestimates the content of hemicelluloses. The detergent fiber and dietary fiber methods have also been compared on alfalfa stems and on corn stover.[4,16] In spite of the bias mentioned above, there was a very good correlation between both methods. Cellulose results of one method can be consistently and confidently converted to the expected results of the other method because of this correlation. The reliability of this conversion has not been established for the other parameters, such as hemicellulose content.

The Van Soest detergent fiber method is faster, cheaper, and more commonly practiced than the dietary fiber method.[4,7,16] The advantage of the chromatographic dietary fiber method, as compared to the gravimetric detergent fiber method, is that the dietary fiber method also provides the monosaccharidic composition of the hemicelluloses (xylan, arabinan, hemicellulosic glucan, galactan, and mannan) and cellulose (cellulosic glucan).[14,15]

Predicting the cellulose, hemicellulose, and xylan contents directly from the results of the detergent fiber method would offer an interesting alternative to the time- and resource-consuming dietary fiber method. The purpose of this study is to check the feasibility and reliability of such a prediction on commelinid and non-commelinid magnoliophyta biomass. The correlation between the results of the dietary fiber and detergent fiber methods was therefore investigated for the contents of cellulose, hemicelluloses, the non-individualized sum of cellulose and hemicelluloses, and the hemicellulosic components (xylan, arabinan, hemicellulosic glucan, galactan, and mannan) of a wide diversity of plant biomasses. The sum of the cellulose and hemicellulose contents (cellulose+hemicelluloses) has also been taken into account in our assessment to compare more globally the dietary fiber and detergent fiber methods.

MATERIALS AND METHODS

Biomass Material. Miscanthus giganteus (*Miscanthus* × *giganteus* J. M. Greef and Deuter ex Hodk. and Renvoize), switchgrass (*Panicum virgatum* L.), fiber sorghum [*Sorghum bicolor* (L.) Moench], spelt straw [*Triticum aestivum* L. ssp. *spelta* (L.) Thell.], "cocksfoot-alfalfa" mixture (*Dactylis glomerata* L.-*M. sativa* L.), tall fescue (*Festuca arundinacea* Schreb.), immature rye (*Secale cereale* L.), fiber corn (*Zea mays* L.), hemp (*Cannabis sativa* L.), and Jerusalem artichoke leaves and stalks (*Helianthus tuberosus* L.) came from randomized block designed crop trials performed in 2007, 2008, 2009, and/or 2010 at Libramont, Belgium [498 m above sea level (asl), average annual temperature of 8.6 °C, average annual precipitation of 1260 mm, 49°55′N 05°24′E], and at Gembloux, Belgium (161 m asl, average annual temperature of 9.8 °C, average annual precipitation of 856 mm, 50°33′N 04°43′E). Depending on the crop, trials were performed with different nitrogen fertilization levels, different cultivars, and/or different harvest periods. For each biomass sample, a plot between 9 and 24 m^2 of the whole above ground biomass was harvested 10 cm from the ground and chopped.

Reed [*Phragmites australis* (Cav.) Trin. ex Steud], spelt grains [*T. aestivum* L. ssp. *spelta* (L.) Thell.], onion leaves and bulbs (*Allium cepa* L.), yucca leaves (*Yucca gloriosa* L.), tulip tree wood (*Liriodendron tulipifera* L.), Japanese knotweed [*Fallopia japonica* (Houtt.) Ronse Decr.], cabbage leaves (*Brassica oleracea* L.), rapeseed straw (*Brassica napus* L.), pumpkin leaves and stalks (*Cucurbita maxima* Duchesne), bean leaves and stalks (*Phaseolus vulgaris* L.), alfalfa leaves and stalks (*M. sativa* L.), lupine leaves and stalks (*Lupinus albus* L.), oak wood (*Quercus* sp.), beech wood (*Fagus sylvatica* L.), willow wood (*Salix* sp.), aspen wood (*Populus* sp.), flax straw (*Linum usitatissimum* L.), nettle (*Urtica dioica* L.), bramble leaves and stalks (*Rubus fruticosus* L.), comfrey leaves and stalks (*Symphytum officinale* L.), Jerusalem artichoke tubers (*H. tuberosus* L.), sunflower leaves and stalks (*Helianthus annuus* L.), tagetes (*Tagetes patula* L.), green (unforced) and white (forced) leaves of chicory (*Cichorium intybus* L.), unforced and forced roots of chicory (*C. intybus* L.), and leaves, stalks, and roots of carrot (*Daucus carota* L.) were harvested manually in 2010 and/or 2011 at Gembloux, Belgium, 10 cm from the ground and chopped.

Immediately after the harvest, two representative subsamples of 750 g of the whole of each biomass were dried at 60 °C for 72 h in a forced air oven. After being dried, the two subsamples were first milled with a 4 mm screen BOA hammer mill (Waterleau, Herent, Belgium) followed by a second milling step with a 1 mm screen Cyclotec cyclone mill (FOSS Benelux N.V., Brussels, Belgium). The samples were stored in airtight bags at room temperature and protected from light in a dark box.

Chemical Analysis. All chemicals were of analytical grade or equivalent. Duplicate aliquots were measured for each component quantitation on each of the 439 biomass samples.

Structural Polysaccharides Analyzed by the Van Soest Method. The neutral detergent fiber residue (NDF, weight of the neutral detergent fiber residue) of the Van Soest method was determined as described previously,[3] except that a 16.67 μkat/g of DM sample of an analytical thermostable α-amylase (Megazyme, Wicklow, Ireland) was added before the Van Soest neutral detergent step for biomass containing starch. The acid detergent fiber (ADF, weight of the acid detergent fiber residue corrected for its content of mineral compounds) residue, and acid detergent lignin (ADL, weight of the acid detergent lignin residue corrected for its content of mineral compounds) of the Van Soest method were determined as described previously,[5] except

Table 1. Data Set Statistics of the Structural Carbohydrate Contents in Commelinid (n = 333) and Non-Commelinid Magnoliophyta (n = 108) Biomass Determined by the Detergent Fiber and Dietary Fiber Methods

compound	mean (g/100 g of DM)	RSD (%)	minimum (g/100 g of DM)	maximum (g/100 g of DM)
commelinid biomass				
cellulose+hemicelluloses VS	59.5	22	25.1	79.3
cellulose+hemicelluloses SAH	53.1	23	21.8	76.9
cellulose VS	34.4	29	12.1	55.5
cellulose SAH	29.9	28	9.7	50.6
hemicelluloses VS	25.1	19	13.0	37.9
hemicelluloses SAH	23.3	19	10.3	34.3
xylan	17.1	24	5.8	27.8
arabinan	2.72	19	1.75	4.12
memicellulosic glucan	2.03	28	0.87	3.76
galactan	0.91	46	0.25	2.25
mannan	0.54	33	0.17	0.96
non-commelinid magnoliophyta biomass				
cellulose+hemicelluloses VS	41.1	48	7.6	80.1
cellulose+hemicelluloses SAH	36.2	52	5.0	71.2
cellulose VS	31.9	52	5.3	66.0
cellulose SAH	24.2	55	3.4	51.4
hemicelluloses VS	9.3	43	1.6	21.8
hemicelluloses SAH	12.0	49	1.2	25.8
xylan	7.3	61	0.3	20.4
arabinan	0.56	45	0.20	1.58
hemicellulosic glucan	1.20	51	0.15	3.05
galactan	1.73	40	0.34	3.43
mannan	1.20	58	0.18	2.74

that, prior to the acid detergent extraction, an extraction with the Van Soest neutral detergent without adding sodium sulfite was conducted as described for the Van Soest neutral detergent extraction. Cellulose +hemicelluloses of the Van Soest method was calculated as NDF − ADL. The cellulose VS content was calculated as ADF − ADL, and the hemicellulose VS content was calculated as NDF − ADF.[3,5] The term "detergent fiber method" will be used to refer to data generated by the Van Soest fiber data (NDF, ADF, ADL, and their combinations).

Structural Polysaccharides Analyzed by the Sulfuric Acid Hydrolysis Method. The samples were fractionated by the Van Soest neutral detergent extractions, with extraction 1 being 0.1 mmol/L phosphate buffer at pH 7 for 15 min at 90 °C where a 16.67 μkat/g of DM sample of an analytical thermostable α-amylase (Megazyme) was added when the sample contained starch and extraction 2 being Van Soest neutral detergent at 100 °C for 1 h.[14] The xylan, arabinan, galactan, mannan, and total glucan contents of the insoluble residue left after these extractions were determined by a two-stage sulfuric acid hydrolysis method (SAH), with stage 1 being solubilization by 12.2 mol/L sulfuric acid at 30 °C for 1 h and stage 2 being hydrolysis by 0.419 mol/L sulfuric acid at 121 °C for 2 h.[14] The released monosaccharides were separated and quantitated by a liquid chromatography system with an analytical liquid chromatography column [300 mm × 7.8 mm (inside diameter), 7 μm, Carbo Sep CHO-682 Pb (Interchrom, Montluçon, France)] at 80 °C using deionized water at a rate of 0.4 mL/min as the mobile phase, with a charged aerosol detector, as described previously.[14] The hemicellulosic glucan content was determined by the same sulfuric acid hydrolysis method except that the cellulose solubilization step (incubation with 12.2 mol/L sulfuric acid at 30 °C for 1 h) was omitted. The cellulose SAH (cellulosic glucan, i.e., D-glucose of cellulose in its polymeric form) content is calculated as the difference between the total glucan and hemicellulosic glucan contents. The hemicellulose SAH content is calculated as the sum of the xylan, arabinan, galactan, mannan, and hemicellulosic glucan contents. The content of cellulose+hemicelluloses SAH is calculated as the sum of the cellulose and hemicellulose contents. The term "dietary fiber method" will be used to refer to data generated by the dietary fiber data (total glucan, xylan, arabinan, galactan, mannan, hemicellulosic glucan, and their combinations). The monosaccharidic components (D-xylose, L-arabinose, D-glucose, D-mannose, and D-galactose) of hemicelluloses are expressed under their polymeric form (xylan, arabinan, hemicellulosic glucan, mannan, and galactan).

Hemicellulosic Components of the Acid Detergent Fiber and Weende Residues. The acid detergent fiber residue was prepared as described previously,[5] except that, prior to the acid detergent extraction, an extraction with the Van Soest neutral detergent (without adding sodium sulfite) was performed as mentioned above. The Weende residue was extracted as described previously.[17] Briefly, biomass samples were refluxed, in chronological order, with 0.13 mol/L boiling sulfuric acid for 30 min and with 0.13 mol/L boiling potassium hydroxide for 30 min. The xylan, arabinan, mannan, galactan, and hemicellulosic glucan contents of the acid detergent fiber and the Weende residues were determined by the same sulfuric acid hydrolysis method as described above.

Statistical Analysis. The linear least-squares regression analyses of structural carbohydrate contents between the detergent fiber and dietary fiber methods and the other statistical assessments were performed using JMP 11 (SAS Institute, Tervuren, Belgium). The prediction performance made by a linear regression line is considered excellent ($R^2p \geq 0.95$, and $RPDp \geq 4.0$), successful ($R^2p \geq 0.90$, and $RPDp \geq 3.0$), moderately successful ($R^2p \geq 0.80$, and $RPDp \geq 2.3$), or moderately useful (for the purpose of semiquantitative screening) ($R^2p \geq 0.70$, and $RPDp \geq 1.8$).[18]

The mean comparison tests (with $\alpha = 0.05$) were based on the Student's t test. The data were paired for the comparison between the detergent fiber and dietary fiber methods. The differences (with $\alpha = 0.05$) between two coefficients of correlation of prediction (Rp) were assessed using a Fisher z-transform. The differences (with $\alpha = 0.05$) between two root-mean standard errors of prediction (RMSEp) were assessed using an F-test of variances. These statistical analyses were performed using JMP 11 (SAS Institute).

RESULTS AND DISCUSSION

Main Structural Carbohydrates. The summary statistics of the mean structural carbohydrate contents among the 333 commelinid and the 108 non-commelinid magnoliophyta

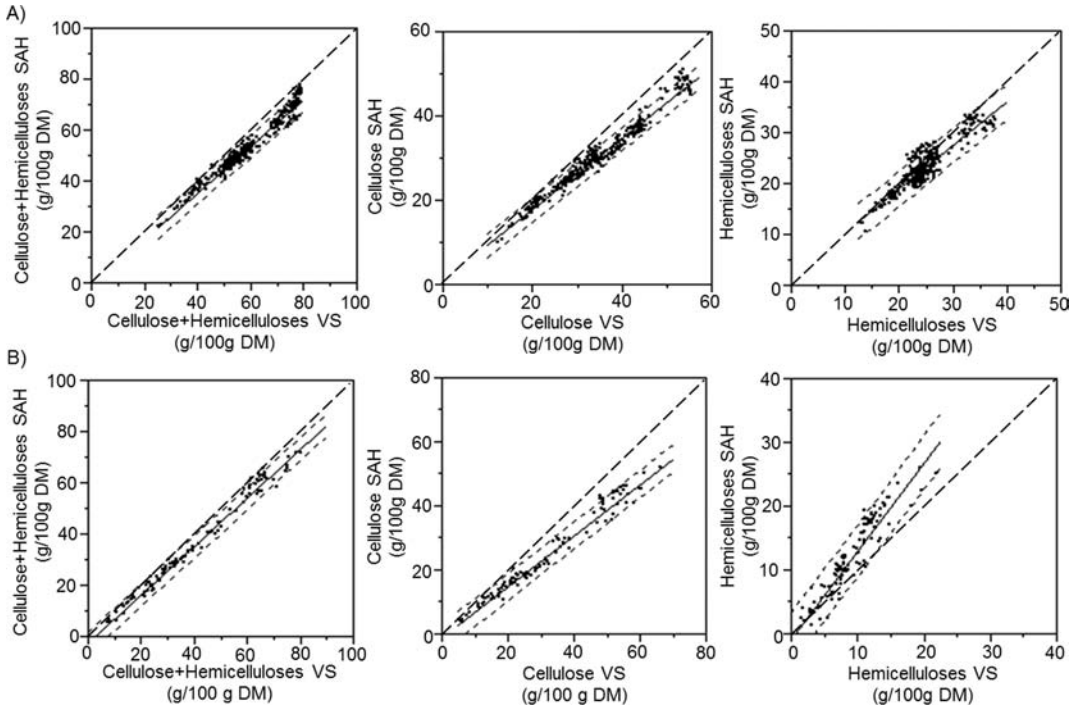

Figure 1. Relationship between the detergent fiber and dietary fiber methods for the contents of cellulose+hemicelluloses (left), cellulose (center), and hemicelluloses (right) in commelinid (n = 333) (A) and non-commelinid magnoliophyta (n = 108) (B) biomass. The black dashed line in each plot is the line of equality ($y = x$). The black plain line in each plot is the regression line. The black lines with smaller dashes in each plot are the 95% confidence lines of the regression.

Table 2. Linear Regression Lines and Their Prediction Performances for Structural Carbohydrate Contents in Commelinid (n = 333) and Non-Commelinid Magnoliophyta (n = 108) Biomass between the Detergent Fiber and Dietary Fiber Methods[a]

Figure	independent variable	dependent variable	slope	intercept	R^2p	RMSEp	RPDp
		Commelinid Biomass					
1A, left	cellulose+hemicelluloses VS	cellulose+hemicelluloses SAH	0.906 ± 0.010	−0.78 ± 0.58[b]	0.96	2.23	5.8
1A, center	cellulose VS	cellulose SAH	0.844 ± 0.008	0.81 ± 0.29	0.97	1.41	5.9
1A, right	hemicelluloses VS	hemicelluloses SAH	0.856 ± 0.020	1.82 ± 0.51	0.85	1.61	2.7
	NDF	cellulose+hemicelluloses SAH	0.758 ± 0.065	3.96 ± 0.44	0.98	1.84	6.6
	NDF	cellulose SAH	0.508 ± 0.010	−3.07 ± 0.66	0.89	2.64	3.2
	NDF	hemicelluloses SAH	0.250 ± 0.008	7.03 ± 0.52	0.76	1.94	2.3
	ADF	cellulose SAH	0.655 ± 0.006	3.81 ± 0.27	0.97	1.45	5.8
		Non-Commelinid Magnoliophyta Biomass					
1B, left	cellulose+hemicelluloses VS	cellulose+hemicelluloses SAH	0.945 ± 0.011	−2.64 ± 0.49	0.99	2.20	8.6
1B, center	cellulose VS	cellulose SAH	0.803 ± 0.012	−1.37 ± 0.44	0.98	2.11	6.3
1B, right	hemicelluloses VS	hemicelluloses SAH	1.381 ± 0.049	−0.79 ± 0.49[b]	0.88	2.04	2.9
	NDF	cellulose+hemicelluloses SAH	0.818 ± 0.013	−3.10 ± 0.70	0.97	3.05	6.2
	NDF	cellulose SAH	0.565 ± 0.014	−2.98 ± 0.76	0.94	3.26	4.1
	NDF	hemicelluloses SAH	0.252 ± 0.005	−0.12 ± 0.29[b]	0.95	1.24	4.7
	ADF	cellulose SAH	0.673 ± 0.015	−1.90 ± 0.65	0.95	2.91	4.6

[a]Uncertainties are expressed as ± the standard deviation. [b]The intercept of regression is not significantly different from zero ($p \geq 0.05$).

samples are listed in Table 1. These two types of biomass were separated because of the differences between their cell wall components. The statistical difference between these two types of biomass for each of the contents of the analyzed structural carbohydrate components is significant ($p < 0.001$, except cellulose VS that has a p value between 0.01 and 0.05) for each type of method. Commelinid magnoliophyta have higher cell wall contents of arabinoxylans, β-glucans, and lignin.[1,2] Non-commelinid magnoliophyta have higher cell wall contents of xyloglucans, mannans, and pectins.[1,2] The structural carbohydrates contained in these samples were determined by the detergent fiber and dietary fiber methods. Table 1 shows that cellulose and hemicelluloses are the main chemical components of the dry matter. The average content of cellulose+hemicelluloses represents more than the half of the dry matter of the analyzed commelinid biomass, while it is less than the half of the dry matter for the non-commelinid magnoliophyta biomass. The higher content of cellulose+hemicelluloses in commelinid magnoliophyta biomass can be explained by the higher content of hemicelluloses and lower content of pectins in their cell walls.[1,2]

Figure 1 illustrates the relationship among the contents of cellulose+hemicelluloses, cellulose, and hemicelluloses determined by the detergent fiber and dietary fiber methods. Table 2

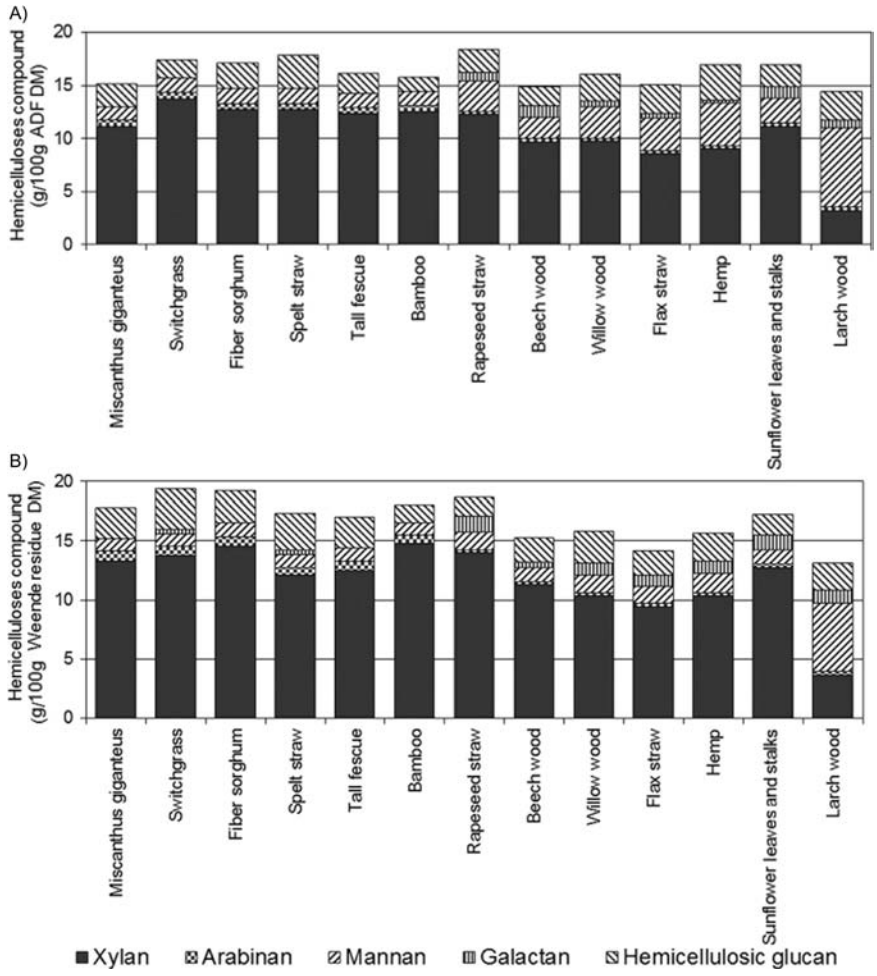

Figure 2. Hemicellulosic components detected in the acid detergent fiber residue (ADF) (A) and in the Weende residues (B).

presents the corresponding regression information. The contents of cellulose+hemicelluloses, cellulose, and hemicelluloses determined by the detergent fiber method are always higher than those determined by the dietary fiber method, except in the case of the content of hemicelluloses in non-commelinid magnoliophyta biomass (Tables 1 and 2 and Figure 1). The statistical difference between these two methods for the contents of cellulose+hemicelluloses, cellulose, and hemicelluloses is significant ($p < 0.001$) for each type of biomass. The overestimation of cellulose and hemicelluloses determined by the detergent fiber method can be explained by the fact that it is based on gravimetric differences between residues that are contaminated by undesired compounds, while the dietary fiber method measures specifically the monosaccharidic contents of cellulose and hemicelluloses.[6] The bias of the estimations of the contents of cellulose and hemicelluloses by the detergent fiber method depends mainly on the neutral detergent fiber residue, which also contains some proteins, and the acid detergent lignin residue, which does not contain the acid soluble lignin.[6] The acid soluble lignin fraction is higher in commelinid than in non-commelinid magnoliophyta biomass.[7] In commelinid magnoliophyta, lignin and hemicelluloses are bound through ferulate esters, which are indeed more sensitive to acid hydrolysis.[1,6] Non-commelinid magnoliophyta have cell walls with a content of pectins higher than that of cell walls of commelinids.[1] The presence of some pectins in their acid detergent fiber residue also explains an overestimation of cellulose and an underestimation of hemicelluloses by the detergent fiber method.[1,6,9] This information confirms that the relationship among the contents of cellulose+hemicelluloses, cellulose, and hemicelluloses determined by the detergent fiber and dietary fiber methods for commelinid and non-commelinid magnoliophyta biomass must be determined separately.

The slope of the regressions (Table 2) is an assessment of the bias between the detergent fiber and dietary fiber methods. The bias between these two methods affects, by order of increasing importance, the contents of cellulose+hemicelluloses, cellulose, and hemicelluloses. This could be explained by the fact that the acid detergent fiber residue of the detergent fiber method contains some residual hemicelluloses, as also suggested previously.[10] Indeed, an average of 16.3 g of hemicelluloses per 100 g was detected in the acid detergent fiber residue of the analyzed biomass (Figure 2A). An average of 16.8 g of hemicelluloses per 100 g was also detected in the Weende residue (Figure 2B). The Weende method aims to gravimetrically determine the cellulose content by means of an acid and alkaline extraction of all the other components, including hemicelluloses.

Hemicelluloses are made of four types of structural polysaccharides: arabinoxylan, xyloglucan (which also contains galactan), β-glucan, and mannan (which also contains galactan and hemicellulosic glucan).[19,20] In the acid detergent fiber and the Weende residues, the relative hemicellulosic components showed increased relative contents of hemicellulosic glucan and

dx.doi.org/10.1021/jf500924q | J. Agric. Food Chem. 2014, 62, 5609−5616

Table 3. Data Set Statistics of the Structural Carbohydrates Contents in Commelinid Biomass Determined by the Detergent Fiber and Dietary Fiber Methods, Expressed as the Relative Content of the Neutral Detergent Fiber (NDF) or Acid Detergent Fiber (ADF) Residues (n = 333)

compound	mean (g/100 g of DM)	RSD (%)	minimum (g/100 g of DM)	maximum (g/100 g of DM)
relative content in the NDF residue				
cellulose+hemicelluloses VS	92.2	3	85.0	96.6
cellulose+hemicelluloses SAH	82.3	4	74.4	94.1
cellulose VS	52.6	7	44.2	61.8
cellulose SAH	45.8	8	35.4	56.9
hemicelluloses VS	39.6	15	23.7	49.4
hemicelluloses SAH	36.5	11	26.9	47.2
xylan	26.5	9	19.1	32.0
arabinan	4.43	28	2.12	7.93
hemicellulosic glucan	3.33	35	0.97	6.87
galactan	1.48	48	0.28	3.64
mannan	0.87	28	0.19	1.39
relative content in the ADF residue				
cellulose VS	87.3	4	80.1	93.9
cellulose SAH	76.0	6	65.4	89.5

Table 4. Data Set Statistics of the Structural Carbohydrate Contents in Non-Commelinid Magnoliophyta Biomass Determined by the Detergent Fiber and Dietary Fiber Methods, Expressed as the Relative Content of the Neutral Detergent Fiber (NDF) or Acid Detergent Fiber (ADF) Residues (n = 108)

compound	mean (g/100 g of DM)	RSD (%)	minimum (g/100 g of DM)	maximum (g/100 g of DM)
relative content in the NDF residue				
cellulose+hemicelluloses VS	85.5	5	63.3	96.9
cellulose+hemicelluloses SAH	73.5	10	44.7	87.0
cellulose VS	65.3	9	43.3	76.4
cellulose SAH	48.9	14	29.7	62.0
hemicelluloses VS	20.3	23	9.2	38.8
hemicelluloses SAH	24.6	13	12.7	32.8
xylan	13.9	31	3.2	23.7
arabinan	1.60	86	0.28	8.94
hemicellulosic glucan	2.56	35	1.11	7.45
galactan	3.99	32	1.42	8.91
mannan	2.50	29	1.05	3.95
relative content in the ADF residue				
cellulose VS	81.8	7	54.2	95.0
cellulose SAH	61.3	12	38.2	75.5

mannan and decreased relative contents of xylan, arabinan, and galactan compared to the contents of the relative hemicellulosic components of native hemicelluloses of the analyzed samples, as described previously.[2] This suggests that interaction of cellulose is stronger with xyloglucan and mannan than with arabinoxylan. The high content of mannan in larch wood (Figure 2) is explained by its high content in the native hemicelluloses of the larch wood.[2] Larch wood is a part of pinophyta biomass, which is known to have a high content of mannan in their hemicelluloses.[1,2]

The higher relative bias for cellulose+hemicelluloses of commelinid biomass, as compared to non-commelinid magnoliophyta biomass, is mainly due to the acid soluble lignin fraction that is higher in commelinid biomass as explained above.[7] The higher relative bias for cellulose and hemicelluloses of non-commelinid magnoliophyta biomass, as compared to commelinid biomass, is mainly due to the presence of some pectins in the acid detergent fiber residue of non-commelinid magnoliophyta as explained above.[6,9]

Because of the large range of the contents of the various components and good prediction performances ($R^2p \geq 0.80$, and RPDp ≥ 2.3) (Table 2), the regression lines seem to be reliable enough to use the relatively simple detergent fiber method to predict quantitatively the values to be expected by the more expensive and time-consuming dietary fiber method.[4,7,16] This is especially the case for the prediction made by cellulose +hemicelluloses VS and cellulose VS.

The suitability of using directly the neutral detergent fiber content to predict the contents of cellulose+hemicelluloses SAH, cellulose SAH, and hemicelluloses SAH to be expected from the dietary fiber method was also tested (Table 2). The neutral detergent fiber residue-based predictions are generally less reliable for the commelinid magnoliophyta biomass, especially for the prediction of hemicelluloses SAH, which is not reliable. This last regression line for commelinid magnoliophyta biomass has prediction performances that are too low ($R^2p < 0.80$, and/or RPDp < 2.3) (Table 2). The generally lower prediction performances made by the neutral detergent fiber residue can be explained by the fact that it also contains cellulose and lignin. This lower prediction performance is only significant ($p < 0.05$) in terms of the coefficient of correlation of prediction (Rp) and the root-mean standard error of prediction (RMSEp) for the

Table 5. Best Linear Regression Lines and Their Prediction Performances for the Monosaccharidic Content of Hemicelluloses in Commelinid (n = 333) and Non-Commelinid Magnoliophyta (n = 108) Biomass between the Detergent Fiber and Dietary Fiber Methods[a]

independent variable	dependent variable	slope	intercept	R^2p	RMSEp	RPDp
Commelinid Magnoliophyta Biomass						
NDF	xylan	0.245 ± 0.005	1.21 ± 0.37	0.86	1.45	2.8
Non-Commelinid Magnoliophyta Biomass						
hemicelluloses VS	xylan	1.043 ± 0.038	−2.35 ± 0.38	0.88	1.48	3.0
NDF	xylan	0.185 ± 0.006	−1.57 ± 0.33	0.89	1.39	3.2

[a]Uncertainties are expressed as ± the standard deviation.

prediction of cellulose SAH of both types of biomass. In the case of the non-commelinid magnoliophyta biomass, the prediction performance of hemicelluloses SAH is more reliable on the basis of the neutral detergent fiber residue, as compared to that based on the hemicelluloses VS. This can be explained by the overestimation of hemicelluloses VS due to the presence of some pectins in the neutral detergent fiber residue.[6,9] This higher prediction performance is significant ($p < 0.05$) in terms of the coefficient of Rp and RMSEp.

The acid detergent fiber residue content can also be used to predict the cellulose SAH of the dietary fiber method because of the excellent prediction performances ($R^2p \geq 0.95$, and RPDp ≥ 4) (Table 2). This prediction is generally slightly less reliable than the cellulose VS-based prediction probably because of the presence of lignin in the acid detergent fiber residue. This difference of prediction is significant ($p < 0.05$) in terms of the coefficient of Rp for the non-commelinid magnoliophyta biomass and is not significant ($p \geq 0.05$) in terms of Rp for commelinid magnoliophyta biomass or in terms of RMSEp for both types of biomass. The acid detergent fiber residue always provides a slightly better prediction of the cellulose SAH compared to the same prediction given by the neutral detergent fiber residue, probably because of the higher cellulose content in the acid detergent fiber residue than in the neutral detergent fiber residue. This difference in prediction is significant ($p < 0.05$) in terms of the coefficient of Rp for the commelinid magnoliophyta biomass and not significant ($p \geq 0.05$) in terms of Rp for the non-commelinid magnoliophyta biomass or in terms of RMSEp for both types of biomass.

The relationship between the detergent fiber and dietary fiber methods is driven by the neutral detergent solubilized fraction (components such as nonstructural carbohydrates, pectins, proteins, organic acids, alcohols, pigments, lipids, and mineral compounds) for the contents of cellulose+hemicelluloses, cellulose, hemicelluloses, and xylan. Indeed, the neutral detergent fiber residue showed quite constant contents of these components for both commelinid and non-commelinid magnoliophyta biomass (Tables 3 and 4). When these contents are expressed without taking into account the solubilized fraction by the neutral detergent (i.e., as relative contents of the neutral detergent fiber residue, which is also called "extractives-free basis"), as compared to these contents expressed on the total dry matter, the relative standard deviation (RSD) and the range (maximum to minimum) of these contents decreased significantly (Tables 3 and 4). In addition, as compared to these contents expressed on the total dry matter, the neutral detergent fiber residue-based predictions of these contents expressed as relative contents of the neutral detergent fiber residue are no longer reliable for commelinid or non-commelinid magnoliophyta biomass (data not shown).

The relationship between the detergent fiber and dietary fiber methods is driven by the acid detergent solubilized fraction (components such as hemicelluloses, nonstructural carbohydrates, pectins, proteins, organic acids, alcohols, pigments, lipids, and mineral compounds) for the cellulose content. When it is expressed without taking into account the solubilized fraction by the acid detergent (i.e., as the relative content of the acid detergent fiber residue) (Tables 3 and 4), as compared to the cellulose content expressed on the total dry matter, the same observations are made as mentioned above for the neutral detergent fiber residue.

Monosaccharidic Components of Hemicelluloses. The mean composition of the hemicelluloses and the corresponding summary statistics are listed in Table 1 for the data set of the 333 commelinid and 108 non-commelinid magnoliophyta samples. The composition of the hemicelluloses can be determined by only the dietary fiber method. Xylan is the major hemicellulosic component of the analyzed samples, with contents more than 2 times higher in commelinid than in non-commelinid magnoliophyta biomass. The content of hemicelluloses is indeed known to be higher in commelinid cell walls, where hemicelluloses substitute for the pectins that are more present in non-commelinid magnoliophyta cell walls.[1,21−23] In addition, commelinid cell walls are known to have hemicelluloses with higher contents of arabinoxylan and β-glucan, whereas non-commelinid magnoliophyta cell walls have higher contents of xyloglucan and mannan.[1]

The average content of hemicellulosic components in commelinid biomass is, by order of decreasing importance, xylan, arabinan, hemicellulosic glucan, galactan, and mannan, while it is xylan, hemicellulosic glucan, galactan, mannan, and arabinan for non-commelinid magnoliophyta biomass (Table 1). This is consistent with the known hemicellulose compositions of these two types of biomass as mentioned above.[1,21−23]

Table 5 indicates that xylan is the only individual hemicellulosic component that is sufficiently correlated with the hemicelluloses VS and neutral detergent fiber residue to perform quantitative predictions ($R^2p \geq 0.80$, and RPDp ≥ 2.3), except for the hemicelluloses VS of commelinid magnoliophyta biomass. Further investigation showed that no useful linear regression lines with quantitative prediction performances ($R^2p < 0.80$, and/or RPDp < 2.3) can be detected between hemicelluloses VS or neutral detergent fiber residue and other individual SAH hemicellulosic components (data not shown). The fact that only xylan is highly correlated can be explained by its dominating contribution in the hemicellulosic component (73 mass percent in commelinids and 61 mass percent in non-commelinids magnoliophyta biomass) (Table 1) and its large range compared to those of the other hemicellulosic components.

Relevance of the Detergent Fiber and Dietary Fiber Methods in the Biomass Valorization Sector. Because of the reliable conversion factors determined in this study, the relatively simple detergent fiber method was used to predict the values to be expected by the more time- and resource-consuming dietary fiber method.[4,7,16] Nevertheless, the advantage of the chromatographic dietary fiber method is that it also provides the composition of the hemicelluloses (xylan, arabinan, hemicellulosic glucan, galactan, and mannan).[14,15] The detergent fiber method can then be very useful in the sector of biofuels (such as bioethanol and biobutanol) and biobased chemical production to rank plant feedstock samples with a good accuracy according to their contents of cellulose+hemicelluloses, cellulose, hemicelluloses, and xylan, while the dietary fiber method may be required for an optimal valorization of hemicellulosic components.

■ ASSOCIATED CONTENT

Ⓢ Supporting Information

Agronomic details about the mechanically and manually harvested biomass (Tables S1 and S2, respectively). This material is available free of charge via the Internet at http://pubs.acs.org.

■ AUTHOR INFORMATION

Corresponding Author

*Telephone: 00 32 81 62 71 49. Fax: 00 32 81 61 58 47. E-mail: b.godin@cra.wallonie.be.

Funding

This research was funded by the Walloon Agricultural Research Center (CRA-W) with the support of the Belgian Science Policy.

Notes

The authors declare no competing financial interest.

■ ACKNOWLEDGMENTS

We are grateful to Bridoux A for her technical support.

■ ABBREVIATIONS USED

ADF, acid detergent fiber; ADL, acid detergent lignin; asl, above sea level; DM, dry matter; NDF, neutral detergent fiber; RSD, relative standard deviation; RMSEp, root-mean-square error of prediction; Rp, coefficient of correlation of prediction; R^2p, coefficient of determination of prediction; RPDp, ratio of the standard deviation of the dependent variable to the RMSE of prediction; SAH, sulfuric acid hydrolysis; VS, Van Soest

■ REFERENCES

(1) Carpita, N.; McCann, M. The cell wall. In *Biochemistry and molecular biology of plants*; Buchanan, B., Gruissem, W., Jones, R., Eds.; American Society of Plant Physiologists: Rockville, MD, 2000; pp 52−108.

(2) Godin, B.; Lamaudière, S.; Agneessens, R.; Schmit, T.; Goffart, J.-P.; Stilmant, D.; Gerin, P.; Delcarte, J. Chemical composition and biofuel potentials of a wide diversity of plant biomasses. *Energy Fuels* **2013**, *27*, 2588−2598.

(3) Van Soest, P.; Wine, R. Use of detergents in the analysis of fibrous feeds. IV. Determination of plant cell wall constituents. *J. AOAC Int.* **1967**, *50*, 50−55.

(4) Jung, H.-J.; Lamb, J. Prediction of cell wall polysaccharide and lignin concentrations of alfalfa stems from detergent fiber analysis. *Biomass Bioenergy* **2004**, *27*, 365−373.

(5) Van Soest, P. Collaborative study of acid-detergent fiber and lignin. *J. AOAC Int.* **1973**, *56*, 781−784.

(6) Jung, H.-J. Analysis of forage fiber and cell walls in ruminant nutrition. *Nutr. J.* **1997**, *127*, 810S−813S.

(7) Theander, O.; Westerlund, E. Quantitative analysis of cell wall components. In *Forage cell wall structure and digestibility*; Jung, H., Buxton, D., Hatfield, R., Ralph, J., Eds.; American Society of Agronomy: Madison, WI, 1993; pp 83−104.

(8) Godin, B.; Agneessens, R.; Gofflot, S.; Lamaudière, S.; Sinnaeve, G.; Gerin, P.; Delcarte, J. Revue sur les méthodes de caractérisation des polysaccharides structuraux des biomasses lignocellulosiques. *Biotechnol., Agron., Soc. Environ.* **2011**, *15*, 165−182.

(9) Ampuero, S. *Détermination de la teneur en fibres dans les aliments pour animaux*; ALP Posieux: Posieux, France, 2008; pp 1−7.

(10) Morrison, I. Hemicellulosic contamination of acid detergent residues and their replacement by cellulose residues in cell wall analysis. *J. Sci. Food Agric.* **1980**, *31*, 639−645.

(11) Sluiter, J.; Ruiz, R.; Scarlata, C.; Sluiter, A.; Templeton, D. Compositional analysis of lignocellulosic feedstocks. 1. review and description of methods. *J. Agric. Food Chem.* **2010**, *58*, 9043−9053.

(12) Theander, O.; Aman, P.; Westerlund, E.; Andersson, R.; Pettersson, D. Total dietary fiber determined as neutral sugar residues uronic acid residues, and Klason lignin (the Uppsala method): Collaborative study. *J. AOAC Int.* **1995**, *78*, 1030−1044.

(13) Sluiter, A.; Hames, B.; Ruiz, R.; Scarlata, C.; Sluiter, J.; Templeton, D.; Crocker, D. *Determination of structural carbohydrates and lignin in biomass*; National Renewable Energy Laboratory: Golden, CO, 2008; pp 1−16.

(14) Godin, B.; Agneessens, R.; Gerin, P.; Delcarte, J. Composition of structural carbohydrates in biomass: Precision of a liquid chromatography method using a neutral detergent extraction and a charged aerosol detector. *Talanta* **2011**, *85*, 2014−2026.

(15) Englyst, H.; Quigley, M.; Hudson, G. Determination of dietary fibre as Non-starch polysaccharides with gas-liquid chromatographic, high-performance liquid chromatographic or spectrophotometric measurement of constituent sugars. *Analyst* **1994**, *119*, 1497−1509.

(16) Wolfrum, E.; Lorenz, A.; de Leon, N. Correlating detergent fiber analysis and dietary fiber analysis data for corn stover collected by NIRS. *Cellulose* **2009**, *16*, 577−585.

(17) European Union. Commission Regulation No 152/2009. *Off. J. Eur. Communities: Legis.* **2009**, *L54*, 1−130.

(18) Malley, D.; McClure, C.; Martin, P.; Buckley, K.; McCaughey, W. Compositional analysis of cattle manure during composting using a field-portable near-infrared spectrometer. *Commun. Soil Sci. Plant Anal.* **2005**, *36*, 455−475.

(19) Ishii, T. Structure and functions of feruloylated polysaccahrides. *Plant Sci.* **1997**, *127*, 111−127.

(20) Vogel, J. Unique aspects of the grass cell wall. *Cur. Opin. Plant Biol.* **2008**, *11*, 301−307.

(21) Godin, B.; Lamaudière, S.; Agneessens, R.; Schmit, T.; Goffart, J.-P.; Stilmant, D.; Gerin, P.; Delcarte, J. Chemical characteristics and biofuels potentials of various plant biomasses: Influence of the harvesting date. *J. Sci. Food Agric.* **2013**, *93*, 3216−3224.

(22) Godin, B.; Lamaudière, S.; Agneessens, R.; Schmit, T.; Goffart, J.-P.; Stilmant, D.; Gerin, P.; Delcarte, J. Chemical characteristics and biofuel potential of several vegetal biomasses grown under a wide range of environmental conditions. *Ind. Crops Prod.* **2013**, *46*, 1−12.

(23) Godin, B.; Ghysel, F.; Agneessens, R.; Schmit, T.; Gofflot, S.; Lamaudière, S.; Sinnaeve, G.; Goffart, J.-P.; Gerin, P.; Stilmant, D.; Delcarte, J. Détermination de la cellulose, des hémicelluloses, de la lignine et des cendres dans diverses cultures lignocellulosiques dédiées à la production de bioéthanol de deuxième génération. *Biotechnol., Agron., Soc. Environ.* **2010**, *14*, 549−560.

JOURNAL OF AGRICULTURAL AND FOOD CHEMISTRY

Article

pubs.acs.org/JAFC

Detection of Almond Allergen Coding Sequences in Processed Foods by Real Time PCR

Nuria Prieto,[†,‡] Elisa Iniesto,[†,‡] Carmen Burbano,[§] Beatriz Cabanillas,[∥] Mercedes M. Pedrosa,[§] Mercè Rovira,[⊥] Julia Rodríguez,[∥] Mercedes Muzquiz,[§] Jesus F. Crespo,[∥] Carmen Cuadrado,*[,§] and Rosario Linacero[†]

[†]Departamento de Genética, Facultad de Biología, Universidad Complutense de Madrid, 28040 Madrid, Spain

[§]Departamento de Tecnología de Alimentos, SGIT-INIA, Carretera La Coruña Km 7.5, 28040 Madrid, Spain

[∥]Servicio de Alergia, Instituto de Investigación Hospital 12 de Octubre (i+12), Avenida de Córdoba s/n, 28041 Madrid, Spain

[⊥]Institut de Recerca i Tecnologia Agroalimentàries IRTA-Mas de Bover, Carretera Reus-El Morell Km 3.8, 43120 Constantí, Spain

Supporting Information

ABSTRACT: The aim of this work was to develop and analytically validate a quantitative RT-PCR method, using novel primer sets designed on Pru du 1, Pru du 3, Pru du 4, and Pru du 6 allergen-coding sequences, and contrast the sensitivity and specificity of these probes. The temperature and/or pressure processing influence on the ability to detect these almond allergen targets was also analyzed. All primers allowed a specific and accurate amplification of these sequences. The specificity was assessed by amplifying DNA from almond, different *Prunus* species and other common plant food ingredients. The detection limit was 1 ppm in unprocessed almond kernels. The method's robustness and sensitivity were confirmed using spiked samples. Thermal treatment under pressure (autoclave) reduced yield and amplificability of almond DNA; however, high-hydrostatic pressure treatments did not produced such effects. Compared with ELISA assay outcomes, this RT-PCR showed higher sensitivity to detect almond traces in commercial foodstuffs.

KEYWORDS: *almond nut, allergen detection, real time-PCR, processed foods, thermal processing, pressure processing*

INTRODUCTION

In developed contries, food allergy is considered an important health problem. Its prevalence is about 3% in adults and 6 to 8% of the pediatric population.[1] Its clinical manifestations can be gastrointestinal, cutaneous, systemic, or respiratory symptoms, and even life-threatening anaphylaxis can be induced with some foods.[2,3] Tree nuts are one of the eight groups of potentially allergenic foods known to be responsible for almost 90% of human allergies caused by food ingestion. Almond (*Prunus dulcis* Miller) is currently the main tree nut crop in world production regarding plantings and value of its raw and processed kernels. Almond nut consumption could produce numerous immune reactions, including life-threatening anaphylaxis.[4,5] So far, eight allergenic proteins have been described in almond: Pru du 1 (PR-10 protein), Pru du 2 (thaumatin-like protein), Pru du 2S albumin, Pru du 3 (lipid transfer protein), Pru du 4 (profilin), Pru du 5 (60S ribosomal protein), Pru du 6 (11S-legumin), and Pru du γ-conglutin (7S vicilin).[6] Of these eight allergens, Pru du 3, Pru du 4, Pru du 5, and Pru du 6 are recognized as such and included in the WHO–IUIS allergen list.

Foods are subjected to several processing methods in order to improve their quality and safety. Thermal processing can degrade food constituents, modify them, or facilitate interactions with other food matrix components; therefore, this processing can modify allergenic properties of food proteins.[7] Thermal sterilization is still the most widely used method of food preservation.[8] Its basic function is to inactivate food spoilage by microorganisms in sealed containers of food using heat treatments at temperatures above the boiling point of water in pressurized steam retorts (autoclaves).[9] However, emerging technologies, such as high hydrostatic pressure (HHP), act by inactivation of microorganisms without the need for substantial heating.[10] HHP-treated foodstuffs are normally exposed for periods of a few seconds up to several minutes to hydrostatic pressures above 150 MPa.[11] These treatments have the potential to modify food proteins, which could alter food allergenicity, i.e., increasing or decreasing IgE reactivity.[12,13] From current information is not possible to identify which variables could be employed in the analysis of the effect of processing on protein allergenicity.[1,14,15] To date, the effects of HHP on food allergenicity have been studied in beef,[16,17] apple,[14,18] celery,[14] peanut,[18] and nuts such as almond.[19] HHP did not affect most food allergens, and even an increase of soybean antigenicity has been reported.[20] However, there is scarce information on the effects of such food processing techniques on almond allergenicity.

The European regulation (EU) 1169/2011/EC[21] requires labeling of food products regarding the contents of almond and other allergenic components. Similar requirements are in use in the USA[22] and in other countries. Several methodologies can be applied to detect potential allergens in foods.[3] According to these authors the limit of detection (LOD) for food allergens

Received: November 15, 2013
Revised: May 20, 2014
Accepted: May 23, 2014
Published: May 24, 2014

ACS Publications © 2014 American Chemical Society

should be less than 100 mg/kg. Data from a Spanish retrospective study indicated that 119 out of 530 food allergic reactions in adults were due to the exposure to "hidden" allergens which were not described in the label.[23] Since food contamination with hidden allergens might happen at any processing stage, some analytical approaches are necessary in order to ensure food safety for allergic consumers.

Enzyme-linked immunosorbent assay (ELISA) is the most common protein detection method used to detect the presence of food allergens in complex matrices. Currently, several almond specific ELISA assays are on the market.[6] However, as the food proteins could be affected by high temperature or high pressure and, hence, the integrity of the allergenic proteins too, consequently, the reliability of techniques based on protein for processed foods could be disminished.[7,18] A DNA-based method could be an advantegeous alternative for allergen detection, in which specific DNA sequences amplified by the polymerase chain reaction (PCR) are the target molecules. In spite of these techniques representing an indirect approach to detection of the allergenic components, DNA-based methods have higher stability vs seasonal and geographical variations than proteins and DNA is less affected and more efficiently extracted at severe conditions from food matrices.[3] Quantitative real-time PCR using fluorescence probes has been the most widely applied PCR strategy to detect food allergens. The target sequences of DNA could be a species-specific region of the allergenic food genome or gene coding for an allergenic protein.[24] Real-time PCR has been used to detect almond in food samples using different target sequences and dying methods.[25−31]

It is important to study the effects that food processing might exert on the detection of almond-allergen specific markers because consumers are commonly exposed to processed ingredients in complex food matrices.[32] The effects of high-temperature and/or high-pressure processing on the detectability of DNA targets in complex food matrices have been analyzed in peanut[24] and hazelnut.[33,34]

The aim of the present study was to set up and to analytically validate a quantitative SYBR Green real-time PCR method using specific primer sets designed de novo on Pru du 1, Pru du 3, Pru du 4 and Pru du 6 allergen-coding sequences in order to improve the sensitivity of RT-PCR techniques for detection of traces of almonds in commercial foods. In addition, how the detectability of almond DNA targets in complex food products is affected by high-temperature and/or high-pressure treatments was also analyzed.

MATERIALS AND METHODS

Samples. Almond cultivars (*Prunus dulcis* Miller) used in this work were provided by the almond collection of Institut de Recerca i Tecnología Agroalimentàries (IRTA-Mas de Bover, Tarragona, Spain). The four cultivars used were "Nonpareil", "Marcona", "Francolí", and "Vairo". "Nonpareil" and "Marcona" are both traditional cultivars of Californian and Spanish origins, respectively. "Nonpareil" is the main cultivar worldwide and used as reference. "Marcona" is a highly reputed cultivar used mainly in the Spanish almond industry.[35] "Francolí" and "Vairo" are both new releases from the IRTA's almond breeding program.[36−38] DNA from other *Prunus* species (peach *P. persica,* cherry *P. avium,* sand-cherry *P. besseyi,* bird-cherry *P. padus,* flowering almond *P. triloba*), other Rosaceae species as *Malus floribunda* and other common food plant species used as food ingredients (hazelnut, walnut, peanut, rice, wheat, barley, and rye) were employed in specificity analysis. To prepare the standards or spiked samples, binary mixtures containing 1; 10; 100; 1,000; 10,000; 100,000; and 500,000 mg/kg (0.0001% to 50% w/w) of defatted raw almond flour "Marcona" in defatted peanut flour matrices were prepared to a final weight of 200 g. The analytical validation of the method was carried out with several commercial foods (biscuits, chocolates, etc.) obtained in local food markets. All samples were grounded and homogenized using a kitchen robot (Thermomix 31-1, Vorwerk Elektrowerke, GmbH & Co. KG, Wüppertal, Germany).

Heat and High Hydrostatic Pressure (HHP) Treatments. Almond nuts were immersed in distilled water (1:5 w/v) and autoclaved using a Compact 40 Benchtop autoclave (Priorclave, London, U.K.) at 121 °C (120 kPa) and at 138 °C (260 kPa) for 15 and 30 min. Raw and autoclaved almond nuts were ground and defatted with *n*-hexane (34 mL/g of flour) for 4 h and air-dried after filtration of the *n*-hexane. High-pressure experiment conditions were carried out according to Omi et al.[39] and Kato et al.[40] Almond defatted flours were dissolved in distilled water (1:4 w/v) 20 h before HHP treatment, and the suspensions were subjected to HHP, using pressures of 300, 400, 500, and 600 MPa for 15 min in multivessel high-pressure equipment (HHP, ACB, France) at 15 °C.

Genomic DNA Isolation. DNA was extracted using the CTAB/phenol/chloroform-based method as previously described by Iniesto et al.[33] DNA was cleaned using a silica membrane in a spin column from Power Plant DNA isolation kit (MoBio, CA USA) and finally eluted in 50 μL of H_2O Milli-Q.

The CTAB-based extraction was selected to obtain DNA from raw and processed almond (200 mg), as well as from spiked samples and complex food matrices (400 mg). DNA quantity and quality was determined with NanoDrop ND-1000 spectrophotometer (Thermo-Fisher, Waltham, MA, USA) by measuring the absorbance at 230, 260, and 280 nm. DNA quality was also evaluated on 0.8% agarose gels.

Conventional PCR, Cloning, Sequencing, and RT-PCR Primer Design. Sets of primers were designed with Oligo Primer Analysis Software on the target coding sequences of the six Pru du genes (data not shown). The four most sensitive and specific to evaluate the almond content were used: Pru du 1 (GenBank accession no. EU424247.1, Pru du 1f AGTGTATTGTGATTGGCTCCC; Pru du 1r AGTCTTTGGCTTGCATTTGG), Pru du 3 (GenBank accession no. FJ652103, Pru du 3f GGCGGTGATGTGCTGC; Pru du 3r TGTAAGGGATGCCATTGACGG), Pru du 4 (GenBank accession no. AY081850.1 Pru du 4f AGTACGTCGATGACCACTTGA; Pru du 4r CTTAACAGTAATGCCACCAGA), and Pru du 6 (GenBank accession no. GU059261.1 Pru du 6 f GACAACCACATTCAGTCC; Pru du 6r CTTGTTGTTGCGGGTTA). These primers were used in conventional PCRs.

The PCR reactions were carried out using DNA from the cultivars Marcona, Vairo, and Francolí of almond, and the resulting amplicons were cloned in TOPO TA Cloning Kit (Invitrogen, Inc., U.K.), according to the manufacturer's instructions. Plasmid DNA was extracted using High Pure Plasmid Isolation Kit (Roche, Germany) and sequenced in an ABI PRISM 3700 sequencer (Applied Biosystems, Foster City, CA, USA) from "Unidad de Genómica, Parque Científico de Madrid". DNA sequences were edited using Chromas Pro 1.22 software (Technelysium Pty, Ltd., Australia). These sequences were compared with those present in the GenBank (NCBI) nonredundant nucleotide (nr/nt) databases through BLAST. Alignments between sequences of the same amplicon obtained from the three cultivars were performed using the ClustalW algorithm.[41]

Specific almond primer for real-time PCR was designed from the conserved sequences of Pru du 1, 3, 4, and 6 by Primer Express 2.0 (Applied Biosystems, Foster City, CA, USA) (data in Table 1 of Supporting Information). Primers met the following requirements: length between 20 and 24 bases and to produce an amplicon between 75 and 150 bp. A conventional PCR was performed using these pairs of primers in order to amplify the genomic DNA sequences of Pru du genes. The PCR products were electrophoresed on 2% agarose gels. The specificity of all primers was assessed by testing the amplification of non-almond DNA extracts from a wide variety of plant samples.

The conventional PCR reactions were carried out in 20 μL, containing 10 ng of DNA, 0.25 μM of each primer and 1× Taq PCR Master Mix (Qiagen, Germany). SensoQuest LabCycler (Progen

Scientific Ltd., Germany) was used and the following PCR program: an initial denaturation step at 95 °C, 4 min, followed by 35 cycles of denaturation at 94 °C for 45 s; annealing at 62−64 °C for 1 min; elongation at 72 °C for 1 min; last step at 72 °C for 6 min.

Real-Time PCR Conditions. Real-time PCR reactions were carried out in a volume of 20 μL, using 7900HT Fast Real-Time PCR System (Applied Biosystems, Foster City, CA, USA). Each reaction consisted of 10 μL of SYBR Premix Ex Taq (Takara, Japan), 2 μmol of primer, and a variable amount of template DNA. All samples were analyzed in duplicate. On each plate, at least two non template controls (NTC) were used to check the PCR performance. The following PCR program was used: initial denaturation at 95 °C for 10 min followed by 40 cycles of denaturation at 95 °C for 15 s and primer annealing and elongation at 60−65 °C for 1 min. Dissociation studies were performed on PCR products at a constant temperature increase (60−95 °C), recording fluorescence each 10 s.

Standard curves for real-time PCR were generated using the cycle threshold (Ct) value obtained from 10-fold serial dilutions of almond genomic DNA. The efficiency of each reaction was calculated from the slope of the standard curve (Ct vs log DNA concentration) as indicated in the Applied Biosystems manual. Standard curves for real-time PCR were generated using the cycle threshold (Ct) value obtained from 10-fold serial dilutions of almond genomic DNA. The efficiency of each reaction was calculated from the slope of the standard curve (Ct vs log DNA concentration) as indicated in the Applied Biosystems manual.

ELISA Assay. Almond protein detection by imunochemistry was performed using a commercial almond ELISA kit (RidaScreen Fast, R-Biopharm, Germany) according to the manufacturer's instructions. The kit includes microtiter strips coated with specific policlonal antibody against water-soluble almond proteins.

RESULTS AND DISCUSSION

Gene Target Selection, Primer Design, and Sequence Analyses. To specifically detect genes coding for different almond allergens (Pru du 1, Pru du 3, Pru du 4, and Pru du 6), sequences from these genes deposited in the GenBank database of NCBI were chosen to design the primers. These primers were checked for their specificity utilizing BLAST and employed for the amplifications of partial allergen-coding sequences of three almond cultivars. This procedure makes it possible to assess the intraspecific polymorphism which could produce false negatives.[42] All the amplicons showed the expected size, and their sequences were homologous to those employed for designing the specific primers (data in Table 1 of the Supporting Information). The sequences obtained for each primer pair from three cultivars (Marcona, Vairo, and Francolí) were aligned, showing a high similarity degree among them (Pru du 1 = 99.95%; Pru du 3 = 100%; Pru du 4 = 99.98%; Pru du 6 = 99%). The aligments were used to design the specific real-time PCR primers from each one of the target sequences.

The coding sequences of Pru du 1 (PR-10 protein), Pru du 3 (LTP), and Pru du 4 (profilin) proteins were chosen as target sequences since, until now, there has not been a specific RT-PCR method to detect them. So far, different RT-PCR protocols to detect almond have been developed by other authors,[6,28] and Pru du 6 (11S) and a nsLTP related to Pru du 3 genes have been previously used as targets.[27,28]

Optimization of Real-Time PCR Assays with SYBR Green. The first step to develop a reliable real-time PCR protocol is to optimize the DNA extraction regarding yield and quality values. Such parameters are important for the optimal detection of the target sequences besides other real-time PCR requirements such as efficiency, Ct, and R^2 values. As some nut components could inhibit polymerase reaction (polyphenols and fat),[43] they have to be eliminated from the DNA sample. To test DNA quality the 260/230 and 260/280 ratios were employed since these components absorb at 230 nm and the proteins at 280 nm.

By combining the CTAB−phenol−chloroform extraction with sample cleaning employing a silica membrane from Power Plant DNA Isolation Kit, the yield, concentration and quality of the extracted DNA were notably improved.[33] This procedure was employed for all the DNA extractions producing a high yield of good quality DNA from raw and processed almond foods and giving 260/280 = 2.11 ± 0.04 and 260/230 = 1.98 ± 0.06 ratios for raw samples.

Instead of a multiplex strategy, single RT-PCR reactions for each sequence were performed.[27] This procedure allows the analysis of the effect of each sequence on the most relevant parameters of RT-PCR (specificity, amplification efficiency, and sensitivity) and to compare them. The SYBR Green I methodology has been chosen because, giving equal sensitivity and performance as the TaqMan one, its cost is lower.[44]

Specificity. Through DNA amplification from almond by PCR, a 100−103 bp amplicon for each primer pair tested was obtained (Table 1 of the Supporting Information). To assess their specificity, DNA from different species of *Prunus* and other common food plant species used as food ingredients (hazelnut, walnut, peanut, rice, wheat, barley, and rye) were used as templates in conventional PCR, and the results of the amplification were electrophoresed on agarose. Primers for Pru du 1 and Pru du 4 genes were 100% specific for almond, while primers for Pru du 3 and Pru du 6 also amplify from peach DNA a product of the target size. As an example, Figure 1a shows the amplification of Pru du 6 and Figure 1b corresponds to Pru du 1.

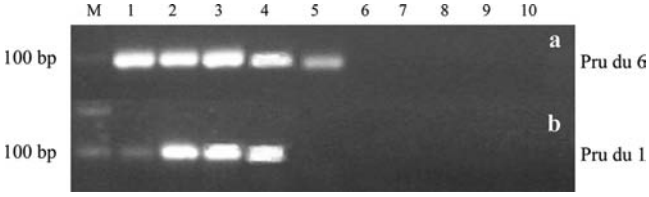

Figure 1. Real-time PCR primers specificity. Amplicons obtained with Pru du 6 (a) and Pru du 1 (b) primer pairs in different *Prunus*-related species. Lanes 1−4: *Prunus dulcis* cv Marcona, Vairo, Francoli, and Nonpareil. Lane 5: *P. persica*. Lane 6: *P. avium*. Lane 7: *P. besseyi*. Lane 8: *P. padus*. Lane 9: *P. triloba*. Lane 10: *Malus floribunda*. Electrophoresis in 2% (w/v) agarose gel. M: 100 pb ladder (Fermentas).

By the evaluation of the dissociation curves the primer specificity was confirmed (Figure 2). When DNA from almond cultivars was used as template, a single amplicon was observed and no amplification was detected from other plant samples. Similar results have been previously reported.[25,27,45]

Amplification Efficiency and R^2 Coefficient. To estimate the reaction amplification efficiency in a RT-PCR procedure, the slope of the standard curve is used. According to the supplier's instructions, a 100% efficient PCR reaction corresponds to a standard curve slope of −3.32. The R^2 describes the correlation between the Ct value and the logarithm of the amount of DNA in the standard curve. In order to produce the standard curves, three different DNA extractions of raw almond were carried out, the DNA was 10 times serially diluted, and 5 μL of each dilution was used in the reaction tube. The values obtained for all standard curves were optimal in agreement to ENGL

dx.doi.org/10.1021/jf405121f | J. Agric. Food Chem. 2014, 62, 5617−5624

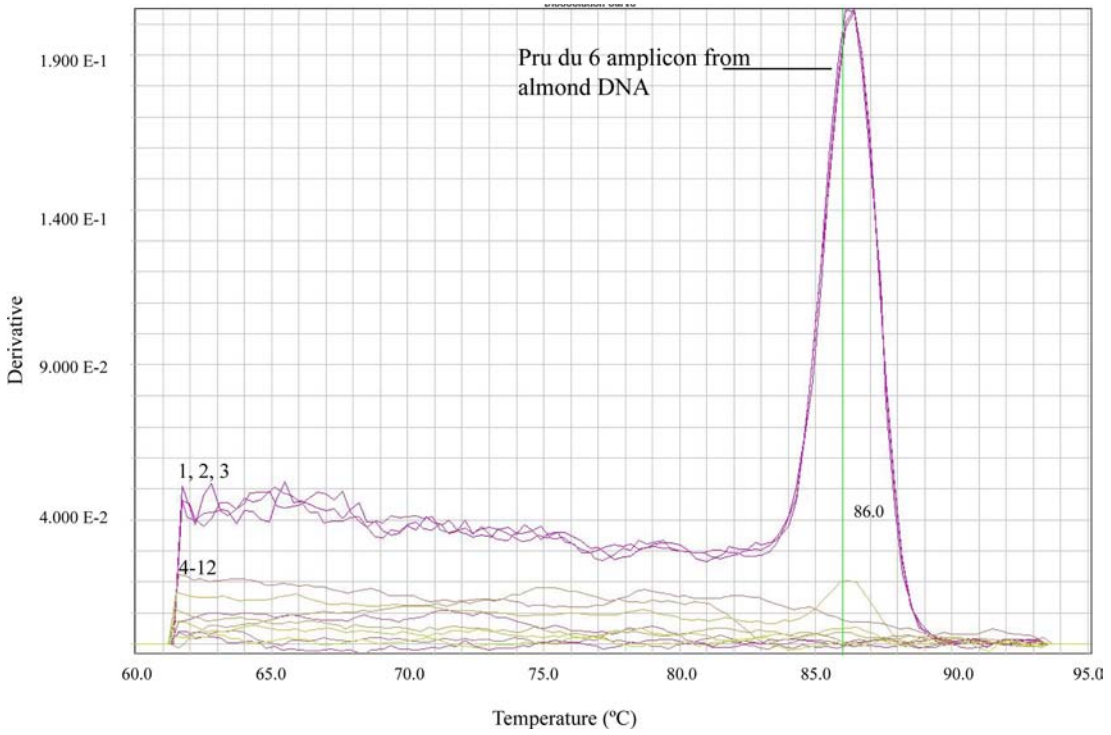

Figure 2. Melting curve obtained by real time-PCR. Amplification with SYBR Green dye target Pru du 6 gene of almond and applied to other food samples. 1, 2 and 3: almond cultivars. 4−12: other plants.

acceptance criteria (slope between −3.1 and −3.6 and correlation coefficient higher than 0.98).[46] The efficiency values were 102% for Pru du 1, 99.75% for Pru du 3, 99.75% for Pru du 4, and 97.5% for Pru du 6 (Figure 1 of the Supporting Information).

By overlapping the 3 standard curves obtained from separate samples in independent assays, the interassay reproducibility was studied. The Ct values were similar for all the varieties used, and the mean slope varied between −3.22 for Pru du 1 and −3.49 for Pru du 6; therefore, according to these results it can be concluded that this RT-PCR method is highly reproducible.

Sensitivity. At least three independent DNA extractions of almond have been used to assess the sensitivity of this RT-PCR protocol. Similarly to the efficiency experiments, the DNA was 10 times serially diluted, and 5 μL of each dilution was used in the reaction tube. The limit of detection (LOD) was 2.5 pg for Pru du 3 and 25 pg for Pru du 1, Pru du 4, and Pru du 6. This method allowed detection of a 1:10,000 dilution with the Pru du 3 primer pair. So far, the most sensitive RT-PCR method to detect almond had been described with the Pru du 5 probe, detecting up to 10 pg of almond DNA.[6,25]

In order to check the sensitivity of this procedure with food products, we carried out PCRs using defatted peanut flour mixed with known amounts of defatted almond flour (from 0.0001% to 1% w/w). The DNA of all spiking levels was extracted and analyzed by RT-PCR in duplicate. The LOD determined was 0.0001% w/w (1 mg/kg) of almond in peanut, that correspond to 1 ppm for the four allergen sequences. The literature on the specific detection of almond using real-time PCR reported a relative LOD of 50 mg/kg of almond in walnut,[25] 10 mg/kg of almond spiked in cookies,[26] and 5 mg/kg of almond in food products.[28] Taking this into account, the present procedure showed a higher sensitivity than those previously reported, this fact being its main advantage in comparison with others.

The sensitivity of this method could be related to the use of SYBR Green methodology for detection. Although SYBR Green is a non sequence-specific binding system, it showed a sensitivity and efficiency as high as other systems used to trace almond allergens, such as TaqMan probes[28] or high-resolution melting analysis.[25] The SYBR Green I methodology has been chosen because, according to other authors, it gives equal sensitivity and performance as the TaqMan one, but with lower cost.[44]

Effect of High-Pressure and Autoclave Treatments. To investigate the action of high-pressure and thermal treatments on the detection ability of this RT-PCR procedure, a calibration curve for each primer pair (Pru du 1, Pru du 3, Pru du 4, and Pru du 6) was performed using DNA extracted from the spiked samples made by mixing defatted peanut and known amounts of defatted almond flour (from 1% to 50% w/w). A linear regression was obtained in all cases, by plotting the Ct values against the logarithm of the almond quantity (Figure 2 of the Supporting Information). To quantify the amount of almond DNA in unprocessed and processed samples, these curves were used. From each treatment three DNA extracts were obtained and analyzed in duplicate. The mean values were normalized to the almond content measured in the unprocessed samples. Data are shown in Figure 3.

The autoclave treatment applied reduced significantly the ability to detect almond DNA. Similar results have been reported for hazelnut[33] and peanut,[24] all of which showed that thermal processing causes an important decrease in the DNA detectability when PCR methods are used. The samples treated only with high pressure did not show this reduction; on the contrary, the amount of almond detected in these samples was higher than in those untreated. These results could be related

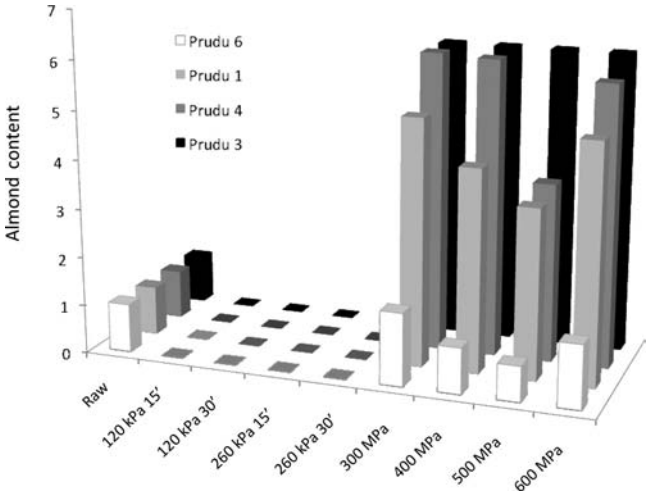

Figure 3. Estimation of almond content in different raw and treated samples. Raw; autoclaved 120 kPa, 15 min; autoclaved 120 kPa, 30 min; autoclaved 260 kPa, 15 min; autoclaved 260 kPa, 30 min; high-pressure 300 MPa; high-pressure 400 MPa; high-pressure 500 MPa; high-pressure 600 MPa.

to higher DNA extractability of HHP treated almond compared to the untreated samples. These findings are quite similar to the results obtained with protein in rice.[47] Therefore, while the autoclaving process strongly decreased the capability to detect almond DNA, high pressure at low temperature increased it. The effect of treatments on the detection of almond DNA may take place at two different levels: on the quality or on the amplificability of DNA.

In order to evaluate how processing can affect the amount and/or integrity of almond DNA, both were analyzed in the present work. DNA quantification of unprocessed and processed almond samples showed a progressive reduction in the extraction yield parallel to heat and time treatment increases (Table 1). The yield of DNA was disminished from

Table 1. DNA Extraction Yields Obtained from Raw and Processed Almond Samples[a]

almond samples	Yields ($nm \cdot mg^{-1}$)
raw	37.76 ± 6.64 a
autoclaved	
120 kPa, 15 min	23.66 ± 1.92
120 kPa, 30 min	3.23 ± 0.65
260 kPa, 15 min	1.53 ± 0.36
260 kPa, 30 min	0.56 ± 0.08
HHP	
300 MPa	52.19 ± 20.94 a,b
400 MPa	71.43 ± 14.53 b
500 MPa	59.53 ± 19.02 a,b
600 MPa	46.73 ± 15.81 a,b

[a]The mean values with the same letter are not significantly different when compared by Student's t test ($P < 0.05$).

37.76 ± 6.64 ng/mg in raw almond to 0.56 ± 0.08 ng/mg in autoclaved samples at 138 °C during 30 min. When DNA integrity was determined by agarose gel electrophoresis, the results were compatible with the DNA degradation in the heat processed samples (Figure 3 of the Supporting Information). High pressure (HHP) seems to increase the DNA extraction yield, but this treatment apparently breaks the DNA, since a smear at low molecular weight is observed when HHP treated samples are electrophoresed.

HHP treatment of foods can be used to create new products (new texture or taste) or to obtain analogue products with minimal effect on flavor, color, and nutritional value and without any thermal degradation. The effect of HHP on allergenicity is being currently investigated mainly through changes in protein structure.[48] Higher pressures can unfold the protein, and the usual pressure needed for the unfolding is about 500 MPa, but it can vary from protein to protein, ranging from 100 MPa to 1 GPa, or reaching even higher pressures in some cases.[48] The effects of HHP on food allergenicity have been studied in beef,[14,16−18] apple,[14,18] celery,[14] and nuts such as peanut.[18]

The DNA quality or integrity was also analyzed through amplificability studies in unprocessed and processed samples. For this objective the amount of DNA was standardized to 25 ng and the analysis was in duplicate. Unprocessed and high-pressure-treated almonds presented similar low Ct values, 24.96 ± 0.01 and 24.54 ± 0.03, respectively, but thermally treated almond (autoclaved) had higher Ct values, 33.74 ± 0.5 at 121 °C 30 min and 30.31 ± 0.08 at 138 °C 30 min. These data confirmed that degradation of DNA produced in the heat processed samples reduced the ability to amplify and detect almond by qRT-PCR. Although the high-pressure treatments at low temperature can break the DNA, they have no effect on their amplificability, because the expected size of the fragments is probably over the amplicon size (around 100 bp).

Scaravelli et al.[24] report a considerable peanut DNA extraction decrease as thermal treatment increases while DNA quality or integrity is not reduced. Our present data corroborated that the thermal treatment here applied decreased the DNA yield, aside from the almond DNA integrity or quality, is also affected, as previously described in hazelnut by Iniesto et al.[33] Such decrease was not detected in the almond samples treated only with high pressure at low temperature; on the contrary, the amount of almond detected in HHP treated samples was higher than in those untreated. This fact could be due to the smaller size of fragments, which makes their amplification easier. The effect of high-pressure treatments on the detection of allergenic tree nuts has been studied in hazelnut, where it did not affect the extraction yield, DNA quality, integrity, and amplicability.[33]

A similar conclusion has also been reported by other authors.[34] They concluded that food processing affects hazelnut detection using real-time PCR as well as ELISA. Moreover, they suggested that both methods lacked robustness in relation to food processing, without drawing any firm conclusion about the technique. This study hence illustrates that both food matrix and processing can lead to an erroneous quantification of the almond (DNA) content in food samples. This fact might pose a risk for the allergic consumer in cases where quantitative results are applied in risk assessment procedures.

Applicability on Commercial Foods. The applicability of this RT-PCR procedure for detecting almond allergens in food samples was evaluated by analyzing 10 commercial foodstuffs (chocolates, cookies, snacks, nougat, etc.). Two of these foods declared in the label the percentage of almond, six of them adverted that the product could have traces of tree nuts, and the other two did not declare any almond content. These commercial foodstuffs were also subjected to ELISA analysis, and the results are summarized in Table 2, in order to compare the outcomes of both techniques.

Table 2. Almond Detection in Commercial Food Products Analyzed through Real-Time PCR (Ct Value Average) and ELISA (+ = Detected; − = Nondetected)

commercial foods	almond declaration	Pru du 1	Pru du 3	Pru du 4	ELISA
cereal snack	contain	28.46 ± 0.33	26.69 ± 2.01	28.34 ± 0.20	+
chocolate with hazelnut	contain hazelnut	−	−	−	−
cereal snack I	might contain nuts	−	−	−	−
chocolate	might contain nuts	29.05 ± 0.33	−	−	−
chocolate with cereal	might contain nuts	25.62 ± 0.99	29.44 ± 2.12	28.08 ± 2.53	+
cookies with cereal and chocolate	might contain nuts	28.94 ± 0.62	−	−	+
cookies with fiber	not declared	−	−	−	−
nougat	might contain nuts	25.29 ± 0.19	26.72 ± 0.47	26.12 ± 0.12	+
chocolate snack with cookie	not declared	29.02 ± 0.79	−	−	−
Russian cake	contain	21.25 ± 0.21	22.36 ± 0.34	22.34 ± 0.48	+

The study was performed with the three primer pairs Pru du 1, Pru du 3, and Pru du 4, which were more sensitive to detect almond in the processed samples. The three primers detected the almond declared in the label, even at trace levels. This real-time PCR method based on three target sequences reduced the probability of false negatives or positives ensuring more reliable results.

The probe Pru du 1 was the most sensitive to detect almond traces in commercial food samples. There is correspondence between RT-PCR results and those obtained by ELISA for 8 of the 10 foods studied with Pru du 1, confirming the reliability of this method. In two samples (chocolate and chocolate snack with cookies), the signal obtained with the RidaScreen Fast ELISA assay was under its limit of detection (1.7 ppm), however, trace amounts of almond DNA were detected in these samples by the Pru du 1 primer. Röder et al.[28] described a similar relationship between the detectable signal and the amount of almond for both RT-PCR and ELISA.

According to Stephan and Vieths,[32] the detection of almond DNA by RT-PCR in a nondeclared sample whose results in the ELISA analysis were negative, such as chocolate snack with cookies, corroborates the higher sensitivity of such RT-PCR procedure. The method developed in this study seems to be more reliable than the ELISA assay tested.

In conclusion, a highly specific and sensitive RT-PCR procedure to detect almond DNA is described in this work. The primers designed de novo allow the amplification of DNA of the coding region of several almond allergens (Pru du 1, Pru du 3, Pru du 4, and Pru du 6). The present RT-PCR method seems to be the most sensitive of those previously reported for the detection of almond because of its very low LOD (1 ppm). In addition, when the outcome is compared with an ELISA assay, it offers a higher sensitivity to detect almond traces or even hidden almond allergens in food products where ELISA yields negative results. When processed samples or complex food products are analyzed, the effect of heat processing should be taken into account. In spite of the decrease in DNA quantitiy and quality elicited by the thermal treatment applied, the almond DNA detection has always been possible and accurate in the present study.

■ ASSOCIATED CONTENT

Supporting Information

Table 1 suppl (sequences, melting temperature, accession number for each locus, and amplicon size of specific primers used in real-time PCR studies), Figure 1 suppl (standard curve of DNA serial dilutions), Figure 2 suppl (calibration curve of Pru du primer pairs), and Figure 3 suppl (DNA degradation). This material is available free of charge via the Internet at http://pubs.acs.org.

■ AUTHOR INFORMATION

Corresponding Author

*E-mail: cuadrado@inia.es Departamento de Tecnología de Alimentos, SGIT-INIA, Ctra. Coruña Km 7.5, 28040 Madrid, Spain. Tel:+34913476925. Fax:+34913572293.

Author Contributions

‡Both first authors have collaborated on the work and the writing of the manuscript equally.

Funding

The AGL 2008-03453 and AGL 2012-39863 research projects supported this work.

Notes

The authors declare no competing financial interest.

■ ABREVIATIONS USED

Ct, cycle threshold; CTAB, hexadecyltrimethylammonium bromide; HHP, high hydrostatic pressure; NTC, nontemplate control; RT, real time

■ REFERENCES

(1) Sampson, H. A. Update on food allergy. *J. Allergy Clin. Immunol.* **2004**, *114*, 127−30.

(2) Ballmer-Weber, B. K. Allergic reactions to food proteins. *Int. J. Vitam. Nutr. Res.* **2011**, *81* (2−3), 173−80.

(3) Poms, R. E.; Klein, C. L.; Anklam, E. Methods for allergen analysis in food: a review. *Food Addit. Contam.* **2004**, *21* (1), 1−31.

(4) Chen, L.; Zhang, S. M.; Illa, E.; Song, L. J.; Wu, S. D.; Howad, W.; Arus, P.; van de Weg, E.; Chen, K. S.; Gao, Z. S. Genomic characterization of putative allergen genes in peach/almond and their synteny with apple. *BMC Genomics* **2008**, *9*, 15.

(5) Tawde, P.; Venkatesh, Y. P.; Wang, F.; Teuber, S. S.; Sathe, S. K.; Roux, K. H. Cloning and characterization of profilin (Pru du 4), a cross-reactive almond (Prunus dulcis) allergen. *J. Allergy Clin. Immunol.* **2006**, *118* (4), 915−22.

(6) Costa, J.; Mafra, I.; Carrapatoso, I.; Oliveira, M. B. Almond allergens: molecular characterization, detection, and clinical relevance. *J. Agric. Food Chem.* **2012**, *60* (6), 1337−49.

(7) Sathe, S. K.; Sharma, G. M. Effects of food processing on food allergens. *Mol. Nutr. Food Res.* **2009**, *53* (8), 970−8.

(8) Farid, M.; Ghani, A. G. A. A new computational technique for the estimation of sterilization time in canned food. *Chem. Eng. Process.* **2004**, *43* (4), 523−531.

(9) Simpson, R.; Almonacid, S.; Teixeira, A. Optimization criteria for batch retort battery design and operation in food canning-plants. *J. Food Process Eng.* **2003**, *25* (6), 515−38.

(10) Gould, G. W. Preservation: past, present and future. *Br. Med. Bull.* **2000**, *56* (1), 84−96.

(11) Guillard, V.; Mauricio-Iglesias, M.; Gontard, N. Effect of novel food processing methods on packaging: structure, composition, and migration properties. *Crit. Rev. Food Sci. Nutr.* **2010**, *50* (10), 969−88.
(12) Cabanillas, B.; Maleki, S. J.; Rodriguez, J.; Cheng, H.; Teuber, S. S.; Wallowitz, M. L.; Muzquiz, M.; Pedrosa, M. M.; Linacero, R.; Burbano, C.; Novak, N.; Cuadrado, C.; Crespo, J. F. Allergenic properties and differential response of walnut subjected to processing treatments. *Food Chem.* **2014**, *157*, 141−7.
(13) Cuadrado, C.; Cabanillas, B.; Pedrosa, M. M.; Varela, A.; Guillamon, E.; Muzquiz, M.; Crespo, J. F.; Rodriguez, J.; Burbano, C. Influence of thermal processing on IgE reactivity to lentil and chickpea proteins. *Mol. Nutr. Food Res.* **2009**, *53* (11), 1462−8.
(14) Husband, F. A.; Aldick, T.; Van der Plancken, I.; Grauwet, T.; Hendrickx, M.; Skypala, I.; Mackie, A. R. High-pressure treatment reduces the immunoreactivity of the major allergens in apple and celeriac. *Mol. Nutr. Food Res.* **2011**, *55* (7), 1087−95.
(15) van Boekel, M.; Fogliano, V.; Pellegrini, N.; Stanton, C.; Scholz, G.; Lalljie, S.; Somoza, V.; Knorr, D.; Jasti, P. R.; Eisenbrand, G. A review on the beneficial aspects of food processing. *Mol. Nutr. Food Res.* **2010**, *54* (9), 1215−47.
(16) Han, G. D.; Matsuno, M.; Ikeuchi, Y.; Suzuki, A. Effects of heat and high-pressure treatments on antigenicity of beef extract. *Biosci., Biotechnol., Biochem.* **2002**, *66* (1), 202−5.
(17) Yamamoto, S.; Mikami, N.; Matsuno, M.; Hara, T.; Odani, S.; Suzuki, A.; Nishiumi, T. Effects of a high-pressure treatment on bovine gamma globulin and its reduction in allergenicity. *Biosci., Biotechnol., Biochem.* **2010**, *74* (3), 525−30.
(18) Johnson, P. E.; Van der Plancken, I.; Balasa, A.; Husband, F. A.; Grauwet, T.; Hendrickx, M.; Knorr, D.; Mills, E. N.; Mackie, A. R. High pressure, thermal and pulsed electric-field-induced structural changes in selected food allergens. *Mol. Nutr. Food Res.* **2010**, *54* (12), 1701−10.
(19) Li, Y.; Yang, W.; Chung, S.-Y.; Chen, H.; Ye, M.; Teixeira, A.; Gregory, J.; Welt, B.; Shriver, S. Effect of Pulsed Ultraviolet Light and High Hydrostatic Pressure on the Antigenicity of Almond Protein Extracts. *Food Bioprocess Technol.* **2011**, *6* (2), 431−40.
(20) Peñas, E.; Gomez, R.; Frias, J.; Baeza, M. L.; Vidal-Valverde, C. High hydrostatic pressure effects on immunoreactivity and nutritional quality of soybean products. *Food Chem.* **2011**, *125* (2), 423−9.
(21) Official Journal of the European Union. (2011). Regulation (EU) 1169/2011EC of the European Parliament and of the Council of 25 October 2011on the provision of food information to consumers, amending Regulations (EC) No 1924/2006 and (EC) No 1925/2006 of the European Parliament and of the Council, and repealing Commission Directive 87/250/EEC, Council Directive 90/496/EEC, Commision Directive 1999/10/EC, Directive 2000/13/EC of the European Parliament and of the Council, Commision Directives 2002/67/EC and 2008/5/EC and Commission Regulation (EC) No 608/2004, L 304, pp 18−43.
(22) *Food Allergen Labeling and Consumer Protection Act of 2004. (Aug 2, 2004)*. Public law 108−282 (pp 905−11), 118 STAT.
(23) Añibarro, B.; Seoane, F. J.; Mugica, M. V. Involvement of hidden allergens in food allergic reactions. *J. Invest. Allergol. Clin. Immunol.* **2007**, *17* (3), 168−72.
(24) Scaravelli, E.; Brohee, M.; Marchelli, R.; van Hengel, A. J. The effect of heat treatment on the detection of peanut allergens as determined by ELISA and real-time PCR. *Anal. Bioanal. Chem.* **2009**, *395* (1), 127−37.
(25) Costa, J.; Mafra, I.; Oliveira, M. High resolution melting analysis as a new approach to detect almond DNA encoding for Pru du 5 allergen in foods. *Food Chem.* **2012**, *133* (3), 1062−9.
(26) Koppel, R.; van Velsen-Zimmerli, F.; Bucher, T. Two quantitative hexaplex real-time PCR systems for the detection and quantification of DNA from twelve allergens in food. *Eur. Food Res. Technol.* **2012**, *235* (5), 843−52.
(27) Pafundo, S.; Gulli, M.; Marmiroli, N. Multiplex real-time PCR using SYBR(R) GreenER for the detection of DNA allergens in food. *Anal. Bioanal. Chem.* **2010**, *396* (5), 1831−9.
(28) Röder, M.; Vieths, S.; Holzhauser, T. Sensitive and specific detection of potentially allergenic almond (Prunus dulcis) in complex food matrices by Taqman® real-time polymerase chain reaction in comparison to commercially available protein-based enzyme-linked immunosorbent assay. *Anal. Chim. Acta* **2011**, *685* (1), 74−83.
(29) Pafundo, S.; Gulli, M.; Marmiroli, N. SYBR GreenER Real-Time PCR to detect almond in traces in processed food. *Food Chem.* **2009**, *116* (3), 811−5.
(30) Costa, J.; Oliveira, M. B. P. P.; Mafra, I. Novel approach based on single-tube nested real-time PCR to detect almond allergens in foods. *Food Res. Int.* **2013**, *51* (1), 228−35.
(31) López-Calleja, I. M.; de la Cruz, S.; Pegels, N.; González, I.; Martín, R.; García, T. Sensitive and specific detection of almond (Prunus dulcis) in commercial food products by real-time PCR. *LWT—Food Sci. Technol.* **2014**, *56*, 31−9.
(32) Stephan, O.; Vieths, S. Development of a real-time PCR and a sandwich ELISA for detection of potentially allergenic trace amounts of peanut (Arachis hypogaea) in processed foods. *J. Agric. Food Chem.* **2004**, *52* (12), 3754−60.
(33) Iniesto, E.; Jiménez, A.; Prieto, N.; Cabanillas, B.; Burbano, C.; Pedrosa, M. M.; Rodríguez, J.; Muzquiz, M.; Crespo, J. F.; Cuadrado, C.; Linacero, R. Real Time PCR to detect hazelnut allergen coding sequences in processed foods. *Food Chem.* **2013**, *138*, 1976−81.
(34) Platteau, C.; De Loose, M.; De Meulenaer, B.; Taverniers, I. Quantitative detection of hazelnut (Corylus avellana) in cookies: ELISA versus real-time PCR. *J. Agric. Food Chem.* **2011**, *59* (21), 11395−402.
(35) Romero, A.; Vargas, F. J.; Tous Martí, J.; Ninot i Cort, A.; Miarnau, X. Parámetros de calidad del fruto interesantes en la mejora genética del almendro. *Rev. Frutic.* **2010**, *10*, 70−9.
(36) López, M.; Romero, M. A.; Vargas, F. J.; Batlle, I. 'Francolí', a late flowering almond cultivar re-classified as self-compatible. *Plant Breed.* **2005**, *124* (5), 502−6.
(37) Socias i Company, R.; Alonso, J. M.; Kodad, O.; Gradziel, T. M. Almond. In *Fruit Breeding, Handbook of Plant Breeding*; Badenes, M. L., Byrne, D. H., Eds.; Springer Science + Business Media: 2012; Vol. *8*, pp 697−728.
(38) Vargas, F. J.; Romero, M. A.; Clavé, J.; Vergés, J.; Santos, J.; Batlle, I. 'Vayro', 'Marinada', 'Constantí' and 'Tarraco' almonds. *HortScience* **2008**, *43* (2), 535−7.
(39) Omi, Y.; Kato, T.; Ishida, K.-I.; Kato, H.; Matsuda, T. Pressure-Induced Release of Basic 7S Globulin from Cotyledon Dermal Tissue of Soybean Seeds. *J. Agric. Food Chem.* **1996**, *44* (12), 3763−7.
(40) Kato, T.; Katayama, E.; Matsubara, S.; Omi, Y.; Matsuda, T. Release of allergenic proteins from rice grains induced by high hydrostatic pressure. *J. Agric. Food Chem.* **2000**, *48* (8), 3124−9.
(41) Thompson, J. D.; Higgins, D. G.; Gibson, T. J. CLUSTAL W: improving the sensitivity of progressive multiple sequence alignment through sequence weighting, position-specific gap penalties and weight matrix choice. *Nucleic Acids Res.* **1994**, *22* (22), 4673−80.
(42) D'Andrea, M.; Coisson, J. D.; Locatelli, M.; Garino, C.; Cereti, E.; Arlorio, M. Validating allergen coding genes (Cor a 1, Cor a 8, Cor a 14) as target sequences for hazelnut detection via Real-Time PCR. *Food Chem.* **2011**, *124* (3), 1164−71.
(43) Venkatachalam, M.; Sathe, S. K. Chemical composition of selected edible nut seeds. *J. Agric. Food Chem.* **2006**, *54* (13), 4705−14.
(44) Andersen, C.; Holst-Jensen, A.; Berdal, K.; Thorstensen, T.; Tengs, T. Equal performance of TaqMan, MGB, molecular beacon, and SYBR green-based detection assays in detection and quantification of roundup ready soybean. *J. Agric. Food Chem.* **2006**, *54* (26), 9658−63.
(45) Watanabe, S.; Taguchi, H.; Temmei, Y.; Hirao, T.; Akiyama, H.; Sakai, S.; Adachi, R.; Urisu, A.; Teshima, R. Specific detection of potentially allergenic peach and apple in foods using polymerase chain reaction. *J. Agric. Food Chem.* **2012**, *60* (9), 2108−15.
(46) European Network of GMO Laboratories (2005). *Definition of minimum performance requirements for analytical of GMO testing*. http://gmocrl.jrc.it/guidancedocs.htm. Accessed 25.11.07.

(47) Estrada-Giron, Y.; Swanson, B. G.; Barbosa-Canovas, G. V. Advances in the use of high hydrostatic pressure for processing cereal grains and legumes. *Trends Food Sci. Technol.* **2005**, *16* (5), 194−203.
(48) Somkuti, J.; Smeller, L. High pressure effects on allergen food proteins. *Biophys. Chem.* **2013**, *4622* (13), 98−7.

JOURNAL OF AGRICULTURAL AND FOOD CHEMISTRY

Article

pubs.acs.org/JAFC

Antroquinonol D, Isolated from *Antrodia camphorata*, with DNA Demethylation and Anticancer Potential

Sheng-Chao Wang,[†] Tzong-Huei Lee,[†,‡] Chun-Hua Hsu,[§] Yu-Jia Chang,[∥] Man-Shan Chang,[†] Yi-Ching Wang,[⊥] Yuan-Soon Ho,[#] Wu-Che Wen,[▽] and Ruo-Kai Lin*[,†,‡,¶]

[†]Graduate Institute of Pharmacognosy, Taipei Medical University, 250 Wu-Hsing Street Taipei, TW 110, Taiwan, R. O. C.

[‡]Ph.D. Program for the Clinical Drug Discovery from Botanical Herbs, Taipei Medical University, 250 Wu-Hsing Street Taipei, TW 110, Taiwan, R. O. C.

[§]Department of Agricultural Chemistry, National Taiwan University, No. 1, Sec. 4, Roosevelt Road Taipei, TW 10617, Taiwan, R. O. C.

[∥]Graduate Institute of Clinical Medicine, College of Medicine, Taipei Medical University, 250 Wu-Hsing Street Taipei, TW 110, Taiwan, R. O. C.

[⊥]Department of Pharmacology and Institute of Basic Medical Sciences, National Cheng Kung University, No.1, University Road, Tainan, TW 701, Taiwan, R.O.C.

[#]Graduate Institute of Biomedical Technology, Taipei Medical University, Taipei, TW 110, Taiwan, R. O. C.

[▽]Golden Biotechnology Corporation, 15F., No.27-6, Sec. 2, Zhongzheng E. Rd, Taipei, TW 110, Taiwan, R.O.C.

[¶]Master Program for Clinical Pharmacogenomics and Pharmacoproteomics, Taipei Medical University, 250 Wu-Hsing Street Taipei, TW 110, Taiwan, R. O. C.

S *Supporting Information*

ABSTRACT: DNA methyltransferase 1 (DNMT1) catalyzes DNA methylation and is overexpressed in various human diseases, including cancer. A rational approach to preventing tumorigenesis involves the use of pharmacologic inhibitors of DNA methylation; these inhibitors should reactivate tumor suppressor genes (TSGs) in tumor cells and restore tumor suppressor pathways. Antroquinonol D (3-demethoxyl antroquinonol), a new DNMT1 inhibitor, was isolated from *Antrodia camphorata* and identified using nuclear magnetic resonance. Antroquinonol D inhibited the growth of MCF7, T47D, and MDA-MB-231 breast cancer cells without harming normal MCF10A and IMR-90 cells. The SRB assay showed that the 50% growth inhibition (GI50) in MCF7, T47D, and MDA-MB-231 breast cancer cells following treatment with antroquinonol D was 8.01, 3.57, and 25.08 μM, respectively. D-Antroquinonol also inhibited the migratory ability of MDA-MB-231 breast cancer cells in wound healing and Transwell assays. In addition, antroquinonol D inhibited DNMT1 activity, as assessed by the DNMT1 methyltransferase activity assay. As the cofactor SAM level increased, the inhibitory effects of D-antroquinonol on DNMT1 gradually decreased. An enzyme activity assay and molecular modeling revealed that antroquinonol D is bound to the catalytic domain of DNMT1 and competes for the same binding pocket in the DNMT1 enzyme as the cofactor SAM, but does not compete for the binding pocket in the DNMT3B enzyme. An Illumina Methylation 450 K array-based assay and real-time PCR assay revealed that antroquinonol D decreased the methylation status and reactivated the expression of multiple TSGs in MDA-MB-231 breast cancer cells. In conclusion, we showed that antroquinonol D induces DNA demethylation and the recovery of multiple tumor suppressor genes, while inhibiting breast cancer growth and migration potential.

KEYWORDS: *breast cancer, DNA methyltransferase, DNA methylation, Antrodia camphorata, tumor suppressor genes, cell migration*

INTRODUCTION

The wild natural fruiting body of *Antrodia camphorata* has long been used by aboriginal peoples to treat hepatitis, cirrhosis and liver cancer and has been used in Taiwan to cure diarrhea, abdominal pain, hypertension, itching of the skin and liver cancer.[1] Due to its extremely slow growth rate and high host specificity for the endangered tree *Cinnamomum kanehira* Hay (Lauraceae), the fruiting body cannot be mass-produced for commercialization. Therefore, the mycelium of *A. camphorata* has recently been developed by industrial companies as a health food and has been reported to have antitumor effects.[2,3] The process of tumorigenesis is initiated and promoted by molecular abnormalities, including oncogene activation and tumor suppressor gene (TSG) inactivation.[4] Down-regulation of tumor suppressor genes (TSGs) by 5′CpG island hypermethylation is an important event in tumor development.[5] CpG island hypermethylation inactivates TSGs and is a major epigenetic modification of the mammalian genome that is not accompanied by changes in the DNA sequence.[6] Aberrant promoter hypermethylation of TSG-associated CpG islands can lead to transcriptional silencing and result in tumorigenesis.[7]

Received: December 23, 2013
Revised: March 18, 2014
Accepted: April 28, 2014
Published: May 1, 2014

ACS Publications © 2014 American Chemical Society

DNA methylation disorders give rise to several significant human diseases, including various cancers, neurological disorders, psychosis and cardiovascular diseases, many of which are mediated by altered DNA methyltransferase 1 (DNMT1) expression and activity.[8−12] Previous reports have indicated that DNMT1 is overexpressed in lung, hepatocellular, colorectal, gastric and breast tumors, as well as acute and chronic myelogenous leukemias.[13−18] Abnormal expression of DNMT1 in vivo induces cellular alterations such as transformation, whereas inhibition of DNMT1 expression or activity results in the reversal of fos transformation.[19] The inhibition of DNA methyltransferase (DNMT), the enzyme that methylates the cytosine residues of CpG islands, may inhibit or reverse the process of epigenetic silencing.[10] Therefore, the use of pharmacologic inhibitors of DNA methylation represents an attractive, rational approach to the reversal of epigenetic TSG silencing. These inhibitors will hopefully reactivate TSGs in tumors and restore activity in critical cellular pathways.

Several DNMT inhibitors have exhibited potent antitumor activities in human xenograft models, indicating their potential usefulness as new cancer therapeutic agents. The first extensively studied DNMT inhibitors were 5-azacytidine (Vidaza) and 5-aza-2′-deoxycytidine (decitabine), which have been approved by the US Food and Drug Administration (FDA) for the treatment of myelodysplastic syndrome. However, these inhibitors induced hematopoietic toxicity and neutropenia in clinical trials.[20−22] Some non-nucleoside drugs and natural compounds, such as epigallocatechin-3-gallate (EGCG), RG108, mithramycin A and procaine, have also been reported to inhibit DNMT activity.[23,24] However, 5-aza-2′-deoxycytidine and EGCG were found to be genotoxic,[25] and mithramycin A has been observed to cause marked hemorrhagic toxicity in patients.[26] Procaine and EGCG failed to induce significant genomic DNA demethylation in some of the tested cell lines.[25] Therefore, other effective, minimally toxic DNMT inhibitors could potentially be developed to provide additional DNMT inhibitors for clinical use.

In the present study, we discovered that a ubiquinone derivative, antroquinonol D, may act as a DNMT1 inhibitor. Antroquinonol D, isolated from the mycelium of *Antrodia camphorata* (*A. camphorata*), can inhibit DNMT1 enzyme activity, induce the re-expression of multiple tumor suppressor genes, increase cancer cell death without harming normal cells, and inhibit the migratory ability of MDA-MB-231 breast cancer cells.

MATERIALS AND METHODS

Isolation of Antroquinonol D. The culture conditions of *A. camphorata* and the extraction method of antroquinonol D were performed as previously reported.[2] From 500 g dried powder of cultured *A. camphorata* mycelium, 9.6 mg of antroquinonol D was obtained. ^{1}H- and ^{13}C NMR of antroquinonol D were acquired using a Bruker DMX-500 SB spectrometer (Ettlingen, Germany). Mass spectra were obtained using a Thermo Finnigan LCQ-Duo spectrometer (Waltham, MA). The following data were recorded for 3-demethoxyl antroquinonol (Figure 1): slight yellowish oil; $[\alpha]^{23}_{D}$: +52.2 (*c* 0.5, MeOH); ^{1}H NMR data (CD_3OD, 500 MHz): δ_H 5.91 (1H, d, *J* = 5.6 Hz, H-3), 5.21 (1H, t, *J* = 7.3 Hz, H-8), 5.10 (1H, t, *J* = 6.9 Hz, H-12), 5.09 (1H, t, *J* = 7.2 Hz, H-16), 4.48 (1H, dd, *J* = 5.6, 3.7 Hz, H-4), 3.59 (3H, s, H_3-23), 2.67 (1H, m, H-6), 2.26−1.95 (10H, H_2-7, -10, -11, -14 and -15), 1.78 (1H, m, H-5), 1.65 (3H, s, H_3-18), 1.62 (3H, s, H_3-21), 1.60 (3H, s, H_3-20), 1.57 (3H, s, H_3-19), 1.16 (3H, d, *J* = 6.9 Hz, H_3-22); ^{13}C NMR data (CD_3OD, 125 MHz): δ_C 198.7 (C-1), 152.0 (C-2), 138.1 (C-9), 136.0 (C-13), 132.1 (C-17), 125.5 (C-16), 125.3 (C-12), 123.3 (C-8), 116.6 (C-3), 65.0 (C-2), 55.3 (C-23), 47.5 (C-5), 43.4 (C-6), 41.0 (C-10), 40.9 (C-14), 28.2 (C-7), 27.8 (C-15), 27.4 (C-11), 25.9 (C-18), 17.8 (C-19), 16.3 (C-21), 16.2 (C-20), 13.1 (C-22); ESI-MS: *m*/*z* = 383 $[M + Na]^+$; HR-ESI-MS: *m*/*z* = 383.2560 $[M + Na]^+$; calculated for $C_{23}H_{36}O_3 + Na^+$: 383.2562.

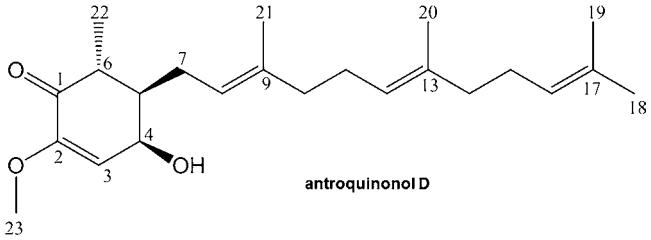

Figure 1. Structure of antroquinonol D. Antroquinonol D, a ubiquinone derivative, was isolated from the solid-state fermented mycelium of *Antrodia camphorata* (Polyporaceae, Aphyllophorales), a parasitic fungus that is indigenous to Taiwan. The structure of antroquinonol D is completely different from that of other non-nucleoside DNMT inhibitors, such as epigallocatechin-3-gallate (EGCG), RG108, mithramycin A and procaine.

Molecular Modeling and Docking. For the molecular docking experiments, the amino acid sequence of the DNMT1 catalytic domain was used as the query to perform a BLAST search against the RCSB Protein Data Bank. The crystal structure of DNMT1 in complex with sinefungin (PDB code 3SWR) was used to rebuild the model of the human DNMT1 catalytic domain. The DNMT3B catalytic domain was modeled using the crystal structure of DNMT3A (PDB code 2QRV) as a template. The structure was validated using Profile3D and PROCHECK. AutoDockTools 1.5.4 was used to prepare the pdbqt files for the ligands/protein and the control-parameter file for gridding and docking.[27] Autodock 4.2 was used to implement the docking process and calculate the binding energies.[28] The Autodock program software uses Monte Carlo-simulated annealing and a Lamarckian genetic algorithm to create a set of possible conformations. All of the ligand bonds were set to be rotatable. A grid box with a dimension of 50 × 80 × 50 points and default grid spacing of 0.375 Å was set around the active sites, covering the DNA-binding region and allowing ligands to move freely. Grid maps were generated using the Autogrid program. The best conformation was defined as the one with the lowest docked energy after the docking search had been completed. The interactions of the protein/ligand complex, including hydrogen bonds and bond lengths, were analyzed using Pymol.

DNMT1 and DNMT3B Methyltransferase Activity Assays. The drug screening was performed using a DNA Methyltransferase 1 Activity/Inhibitor Screening Assay Kit (Abnova). One hundred nanograms of the DNMT1 enzyme and the indicated concentrations of the potential DNMT inhibitors were added into a CpG-enriched DNA-coated 96-well plate and incubated for 2 h. The DNMT1 enzyme transfers a methyl group to cytosine from *S*-adenosyl methionine (SAM), thereby methylating the DNA substrate. The methylated DNA can be recognized using an anti-5-methylcytosine antibody. The ratio or amount of methylated DNA, which is proportional to the enzyme activity, can then be colorimetrically quantified using an ELISA-like reaction. Finally,

we detected the colorimetric reaction (OD450 nm) using an ELISA reader. The inhibitory effects of all of the drugs were calculated as follows: The relative DNMT1 activity (%) = (the OD450 of the sample-the OD450 of the blank)/(the OD450 of the DMSO control-the OD450 of the blank) × 100. To further confirm the specificity and underlying mechanism of the antroquinonol D-mediated DNMT inhibition, we measured the DNMT1 (Active Motif) and DNMT3B (BPS Bioscience, San Diego, CA) enzyme activity in the presence of 40, 80, or 160 μM of SAM following antroquinonol D, antroquinonol or EGCG (Sigma-Aldrich) treatment using an EpiQuik DNA Methyltransferase (DNMT) Activity/Inhibition Assay Kit (Epigentek, Farmingdale, NY). The key principles, methodology and protocols are similar to the DNA Methyltransferase 1 Activity/Inhibitor Screening Assay Kit. Antroquinonol D and antroquinonol were provided by Golden Biotechnology Corporation.

Cell Lines and Drug Treatments. The MCF7, T47D and MDA-MB-231 breast cancer cell lines were obtained from the Bioresource Collection and Research Center (BCRC, Hsinchu, Taiwan). MCF10A, a normal mammary gland cell line, was obtained from the American Tissue Cell Culture collection. IMR-90, a normal fibroblast-like cell line that was established from the lung tissue of a female fetus, was obtained from the BCRC. The MCF7, MDA-MB-231 and IMR-90 cell lines were cultured in DMEM (Invitrogen) supplemented with 10% fetal bovine serum and 1% penicillin/streptomycin. The T47D cell line was cultured in RPMI 1640 (Invitrogen) that had been supplemented with 10% fetal bovine serum and 1% penicillin/streptomycin. The cells were treated with DMSO, antroquinonol D, or the DNMT inhibitors 5-azacytidine (AZA) and decitabine (DAC) for the indicated durations. Antroquinonol D was dissolved in DMSO. AZA (Sigma-Aldrich) and DAC (Sigma-Aldrich) were dissolved in acetic acid/water (1:1).

Sulphorhodamine B (SRB) Assays. A sulphorhodamine B (SRB) assay was used to determine the cell growth rate. Based on the growth curves of the MCF7, T47D, MDA-MB-231, MCF10A and IMR-90 cell lines, the cells were seeded in 96-well plates at densities of 5000, 8000, 3000, 2000, and 6000 cells/well, respectively, and incubated with the indicated drugs for 3 days. Additionally, MCF7, T47D, MDA-MB-231, MCF10A and IMR-90 cells were seeded in 96-well plates at densities of 3000, 5000, 750, 500, and 4000 cells/well, respectively, and incubated with the indicated drugs for 6 days. The growth curves of the MCF7, T47D, MDA-MB-231, MCF10A and IMR-90 cell lines over 6 days are shown in Figure S1, Supporting Information. The cells were fixed with 10% trichloroacetic acid at the indicated times. Cell growth was assessed via OD determination at 515 nm using a microplate reader. The data for antroquinonol D were normalized to its solvent control (DMSO). The 5-azacytidine (AZA) and decitabine (DAC) data were also normalized to their solvent controls (50% acetic acid). The solvent controls were added in the same amounts as those used for the treatment drugs at the indicated concentrations. The growth inhibition rates were calculated using the following equation: Cell growth inhibition rate (%) = $100 - [(Ti - Tz)/(C - Tz)] \times 100$ ($Ti \geq Tz$). Cytotoxicity rate (%) = $[(Tz - Ti)/Tz] \times 100$ ($Tz \geq Ti$). Ti = the OD of the inhibitor sample. Tz = the OD of the basal cells. C = the OD of the control.

MTT Assays. The cells were seeded in 96-well microtiter plates (100 μL/well) at densities of 5000 cells/well and grown in culture medium. The next day, the culture medium was replaced with 100 μL of culture medium containing different concentrations of DMSO or a DNMT1 inhibitor, and cell viability was assayed using an MTT assay (3-(4,5-dimethylthiazol-2yl)-2,5-diphenyltetrazolium bromide) after 72 h of incubation. Cell viability was assessed using OD determinations at 570 nm using a microplate reader. MTT powder (Sigma-Aldrich) was dissolved in phosphate-buffered saline at 3.3 mg/mL and filtered.[29]

Wound Healing Assays for Migration Analyses. Treated and untreated cells were plated at densities of 2×10^5 cells in 10 cm culture dishes in quadruplicate and incubated at 37 °C. After the cells had been treated with 15 μM antroquinonol D for 6 days, wound healing assays were performed using Culture-Inserts (Ibidi). Cell-free gaps of 500 μm were created after removing the Culture-Inserts. After seeding the cells overnight, the Culture-Inserts were removed, and images of the wounded areas were acquired using an inverted microscope (Nikon) at the indicated time points. The percentage of closure of the wounded area was measured and analyzed using ImageJ software, and the migratory ability was calculated.

Transwell Assays for Migration Analyses. The Transwell consists of upper and lower chambers that are separated by a layer of membrane that has a pore size of 8 μm (Falcon). Approximately 2×10^4 treated and untreated MDA-MB-231 cells were seeded onto the upper chambers with 300 μL of serum-free medium containing drugs, and 800 μL of DMEM containing 10% FBS was added to the lower chambers as a chemoattractant. The seeded cells were incubated for 16 h. The cells that did not invade were removed using a scraper and washed twice with PBS, then fixed and stained using 1% crystal violet/ddH_2O for 60 min at room temperature. Five random views were photographed under a microscope (Nikon) and then counted and quantified using ImageJ.

Cell Migration Assays Using the xCELLigence Biosensor System. Migration assays were performed using the RTCA DP instrument (Roche Diagnostics GmbH, Germany), which was placed in a humidified incubator and maintained at 5% CO_2 and 37 °C, as previously described.[30] The cells were seeded into specifically designed 16-well plates (CIM-plate 16, Roche Diagnostics GmbH) that had 8 μm pores that were similar to conventional Transwells and contained microelectrodes on the undersides of the upper chamber's membranes. The cells (20 000 cells/well) were seeded into the upper chambers in serum-free medium, and media containing 10% FBS was added to the lower chambers. Each sample was treated under the same conditions in four independent wells. The CIM-plate 16 was monitored every 10 s for 40 min and once every hour thereafter. The greater the number of cells attached to the electrodes, the larger the increases in electrode impedance. The electrode impedance, which was displayed and recorded as the Cell Index (CI) value, reflected the biological statuses of the monitored cells, including the cell numbers, viabilities, morphologies and degrees of adhesion. The data analyses were performed using the RTCA software program v1.2, which was supplied with the instrument. The *t* test was to analyze the data differences.

DNA and RNA Extractions. Genomic DNA from the cell lines was prepared using the Blood and Tissue Genomic DNA Extraction Miniprep System (Viogene, Sunnyvale, CA). Total mRNA was extracted from the cells using the TRIzol reagent (Invitrogen). The DNA and RNA were quantified, and the

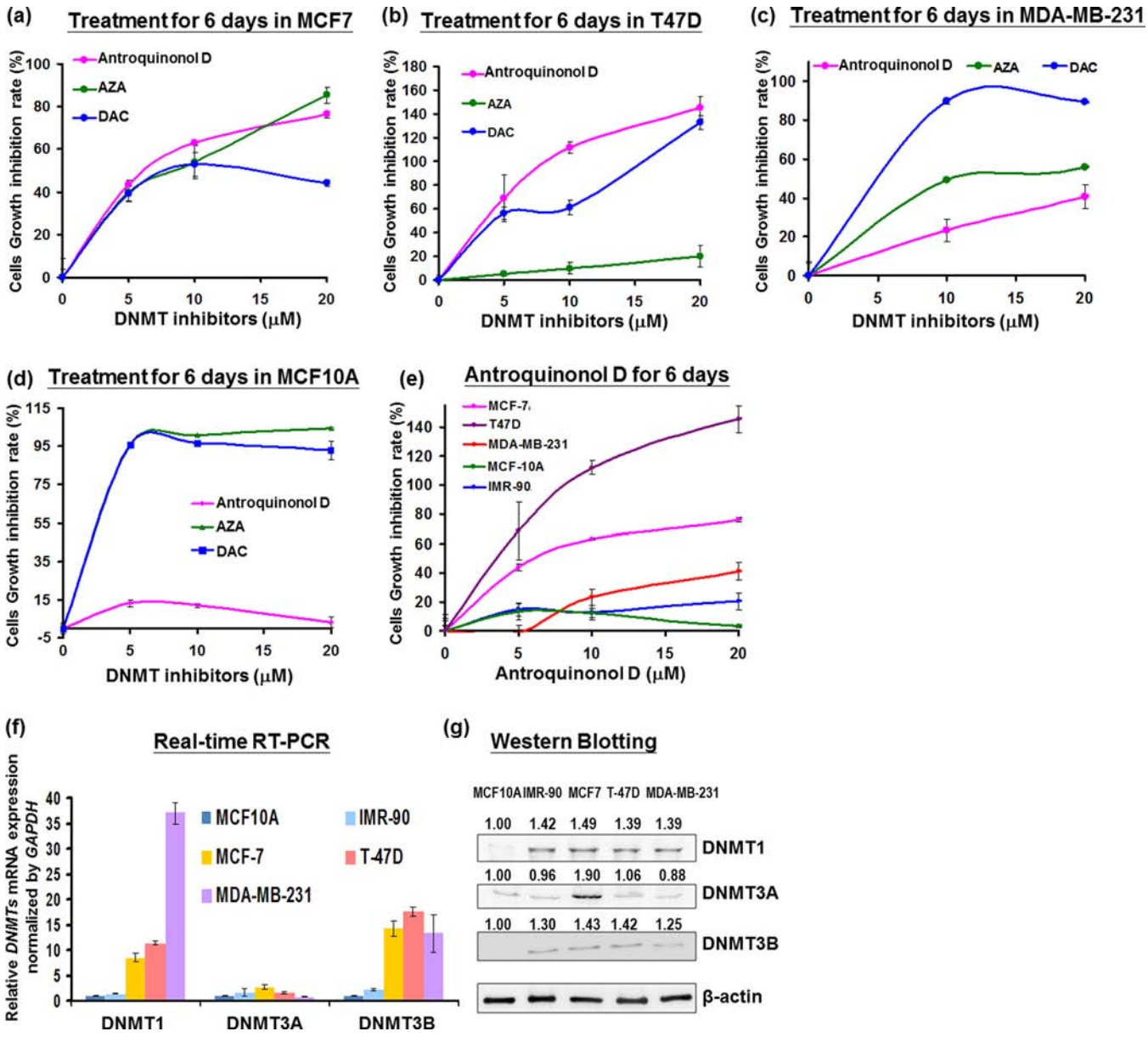

Figure 2. Growth of the breast cancer cell lines MCF7, T47D, MDA-MB-231 and the normal cell line MCF10A and IMR-90 following treatment with DNMT1 inhibitors. The growth of the MCF7 (a), T47D (b) and MDA-MB-231 (c) cancer cell lines, the MCF10A normal mammary gland cells, and the IMR-90 normal lung cell line (d and e), was determined using the SRB assay after the cells had been treated with antroquinonol D or the DNMT inhibitors azacitidine (AZA) and decitabine (DAC) at the indicated concentrations for 6 days. Cell growth inhibition rate (%) = 100 − [(Ti − Tz)/(C − Tz)] × 100 (Ti ≥ Tz). Ti = the OD of the inhibitor sample; Tz = the OD of the basal cells; C = the OD of the control. The cytotoxic effects of antroquinonol D in normal MCF10A and IMR-90 cells were lower than those of AZA and DAC after 6 days of treatment. (f) *DNMT1*, *DNMT3A* and *DNMT3B* mRNA expression levels were analyzed using real-time RT-PCR and were normalized to *GAPDH*. (g) DNMT1, DNMT3A and DNMT3B protein expression levels were analyzed using Western blotting. The data are presented as the means ± s.d. All experiments were performed with at least two biological duplicates and three technical replicates.

purities were verified by measuring the A_{260} and A_{260}/A_{280} ratios (which ranged from 1.8 to 2.0).

DNA Methylation Assays. The DNA methylation statuses of the MDA-MB-231 cells were determined following treatment with 15 μM antroquinonol D for 6 days. Five hundred nanograms of genomic DNA were bisulfite-converted using an EZ Methylation Gold kit (Zymo Research, Irvine, CA) according to the manufacturer's recommended protocol. The DNA methylation analyses were performed using Illumina Methylation 450 K array-based assays (Illumina, San Diego, CA). The array analyses were performed by Health GeneTech Corporation, Taiwan. Methylation scores for each CpG site were classified as "Beta" values that ranged from 0 (unmethylated) to 1 (fully methylated) by determining the ratios of the methylated signal intensities to the sums of the methylated and unmethylated signal outputs. Functional annotation clustering of differentially demethylated genes was performed using Functional DAVID Bioinformatics Resources 6.7.[31] Supporting Information Figure S9 was generated using XMind 3.2.1. The methylation patterns of the *FANCC* and *CACNA1A* genes were further confirmed and quantified using pyrosequencing. Because no primers were found that could be used for pyrosequencing that targeted the DNA regions of the *FANCC* and *CACNA1A* genes (which were detected using the

dx.doi.org/10.1021/jf4056924 | J. Agric. Food Chem. 2014, 62, 5625−5635

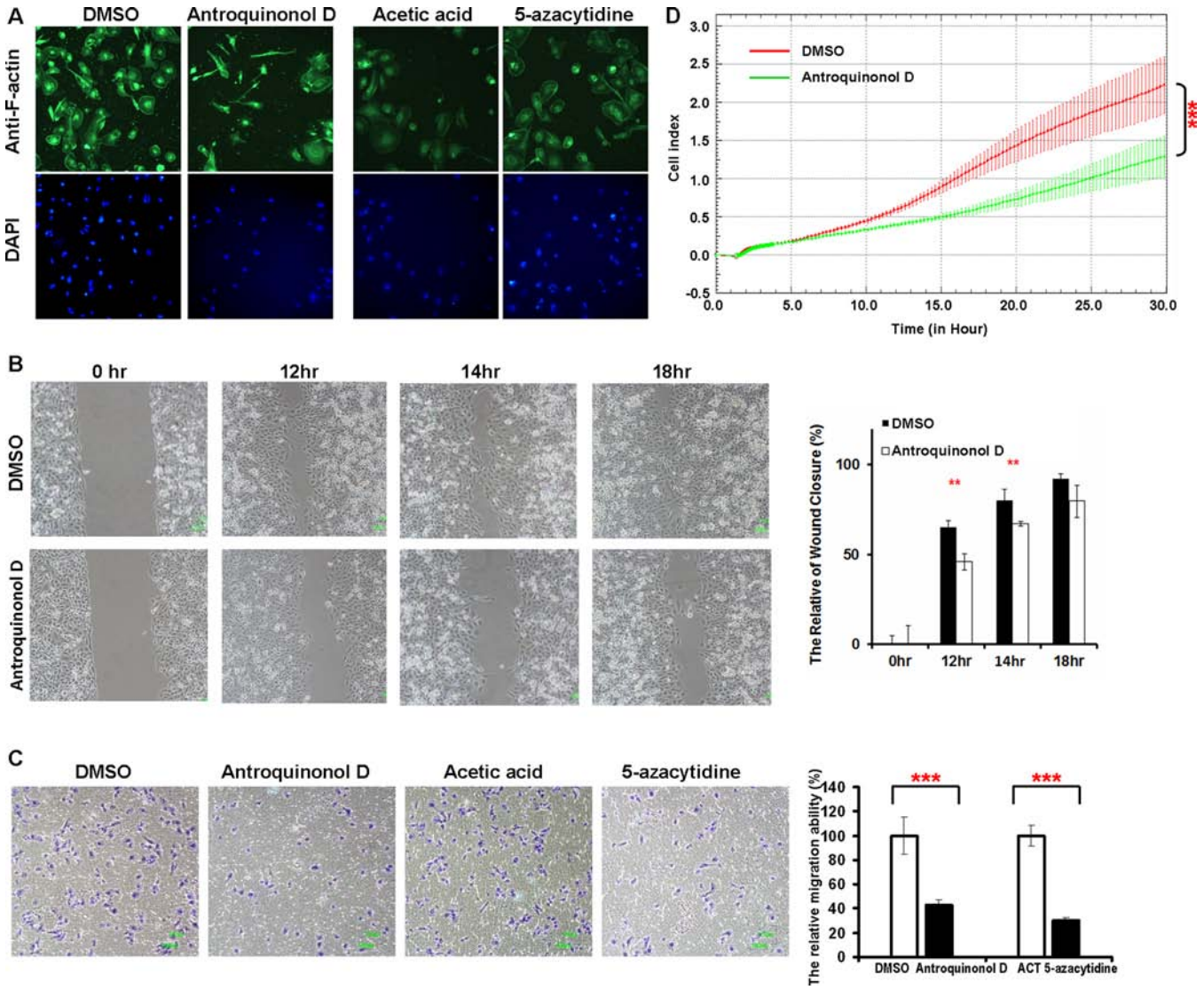

Figure 3. Antroquinonol D inhibits the migration of MDA-MB-231 breast cancer cells. (a) The distribution of F-actin (green) was detected by immunofluorescence staining and fluorescence microscopy using anti-F-actin antibody (original magnification 200X). DAPI was used to label cell nuclei (blue). (b) Wound healing was determined using a Culture-Insert assay to analyze the migratory abilities of the cells. The cells were photographed at 0, 12, 14, and 18 h. The images represent the untreated (upper panel) and treated (lower panel) cells (original magnification × 100). The data indicate that antroquinonol D decreased the migration of MDA-MB-231 cells compared to the DMSO control. The experiment was performed with at least two biological duplicates and three technical replicates. (c) A Transwell assay was used to further investigate the migratory abilities of the cells. The images represent treatment with DMSO, antroquinonol D, acetic acid (the solvent control for 5-azacytidine) or 5-azacytidine (original magnification ×100). The average number of migratory cells (those that passed through the membrane) was counted in five different fields. Antroquinonol D significantly decreased the migration of MDA-MB-231 cells. *** $p \leq 0.001$. The experiment was performed with three technical replicates. (d) Cell migration was also assessed using specifically designed 16-well plates (CIM-plate 16) that had 8 μm pores. The CIM-plate 16 was monitored every 10 s for 40 min and then once every hour. Data analyses were performed using the RTCA software v1.2 program that was supplied with the instrument. The Cell Index (CI) value reflects the biological status of the monitored cells, including the cell number, cell viability, morphology and degree of adhesion. The experiments were performed in technical quadruplicate. The data are presented as the means ± s.d. ** $p \leq 0.005$, *** $p \leq 0.001$. The t test was used to calculate group differences in all experiments.

Methylation 450 K array-based assay), we designed primers that were targeted to the promoter regions of the *FANCC* and *CACNA1A* genes for use in the pyrosequencing assay. The primers were designed using the MethPrimer[32] and Methyl Primer Express v1.0 (ABI) software programs. The PCR reactions were performed using biotinylated primers to convert the PCR products to single-stranded DNA templates. The pyrosequencing reactions and methylation quantification were performed using PyroMark Q24, which was provided by the Mission Biotech Corporation, Taiwan. The primers are described in Table S1, Supporting Information.

Real-time RT-PCR. The mRNA expression levels were measured by performing real-time RT-PCR using a LightCycler 480 (Roche Applied Science, Mannheim, Germany). Real-time PCR was performed using the LightCycler 480 Probe Master kit (Roche Applied Science) with the specific primers and the corresponding Universal Probe Library probe (Roche Applied Science) according to the manufacturer's instructions. Normalized gene expression values, which were calibrated to the control group, were obtained using the LightCycler Relative Quantification software program (ver. 2.0, Roche Applied

dx.doi.org/10.1021/jf4056924 | J. Agric. Food Chem. 2014, 62, 5625−5635

Science). *GAPDH* was used as a reference gene. The primers are described in Table S1, Supporting Information.

Cell Lyses and Immunoblotting Analyses. For Western blotting assays, the cells were lysed on ice in radioimmunoprecipitation buffer (0.05 M Tris-HCl [pH 7.4], 0.15 M NaCl, 0.25% deoxycholic acid, 1% Igepal CA-630, and 1 mM ethylenediaminetetraacetic acid). The lysates were then centrifuged at 13 000 r.p.m. at 4 °C for 10 min. The protein extracts were solubilized in sodium dodecyl sulfate (SDS) gel loading buffer (60 mmol/L Tris base, 2% SDS, 10% glycerol and 5% β-mercaptoethanol). Samples containing equal amounts of protein (40 μg) were separated on an 8% SDS-polyacrylamide gel using electrophoresis and electroblotted onto Immobilon-P membranes (Millipore, Bedford, MA) in transfer buffer. Immunoblotting was performed using antibodies that had been raised against DNMT1 (1:1000, GeneTex, TX), DNMT3A (1:1000, Cell Signaling, Danvers, MA), DNMT3B (1:250, Abcam, Cambridge, U.K.), FANCC (1:500, GeneTex, Hsin-Chu, Taiwan), and CACNA1A (1:250, Abcam, Cambridge, U.K.), total AKT (1:1000, Cell Signaling, Danvers, MA), phosphor-AKT Ser473 (1:500, Cell Signaling, Danvers, MA). β-Actin (1:5000, GeneTex, TX) was used as an internal control. For Immunofluorescence staining assays, cells were seeded in 4-well glass chamber slides (Nunc). After DNMT inhibitor treatment, cells were fixed in 4% formaldehyde and stained with anti-F-actin (1:200, Abcam, Cambridge, U.K.) cells. The image was detected by using the Olympus IX71 Inverted Microscope System.

RESULTS AND DISCUSSION

Identification of Antroquinonol D. Antroquinonol D was obtained as a slight yellowish oil. Its molecular formula, $C_{23}H_{36}O_3$, was deduced through analysis of the ^{13}C NMR and HRESIMS data. The ^1H NMR spectrum of antroquinonol D exhibited resonances compatible with those of antroquinonol except that a 3-methoxyl group at C-3 was substituted by an olefinic methine signal atδ_H 5.91 (d, J = 5.6 Hz, H-3) in antroquinonol D.[2] The difference was also reflected in the ^{13}C NMR of antroquinonol D, in which C-24 disappeared and a quaternary C-3 was replaced by a tertiary C-3 atδ_C 116.6. Thus, the gross structure of antroquinonol D was determined to be 3-demethoxyl antroquinonol. The relative configuration of cyclohexenone was consistent with that of antroquinonol. The configurations of Δ^8, Δ^{12} and Δ^{16} were *E* as corroborated by the chemical shifts of C-21, C-20 and C-19 at respectiveδ_C 16.3, 16.2, and 17.8. Accordingly, the structure of antroquinonol D is shown in Figure 1. We examined signals and noise in the 1H NMR spectrum of antroquinonol D, and the purity of antroquinonol D (LTH-0909−1) was determined to be greater than 95% (Supporting Information Figure S2).

Antroquinonol D Inhibits the Growth of Breast Cancer Cells, but not normal cells. Clinical toxicity is a major concern for the clinical application of anticancer agents. Therefore, we treated normal cell lines, MCF10A and IMR-90, and three breast cancer cell lines, MCF7, T47D and MDA-MB-231, with the DNMT inhibitor for 3 or 6 days. The drug treatment protocols are described in Supporting Information Figure S3. Antroquinonol D suppressed the growth of MCF7 and T47D cells as effectively as AZA and DAC treatment at 6 days (Figure 2a and Figure 2b). The SRB assay showed that the GI50 in MCF7, T47D and MDA-MB-231 breast cancer cells following antroquinonol D treatment is 8.01, 3.57, and 25.08 μM, respectively. Antroquinonol D could lead to cytotoxic effects in T47D and MCF7 cells (Figure S4a, Supporting Information). In addition, antroquinonol D treatment displayed lower cytotoxicity to normal mammary gland cells (MCF10A) and human fibroblast cells (IMR-90) than AZA and DAC treatment for 3 days (Figure S4b, Supporting Information) and 6 days (Figure 2d and Figure 2e), respectively. The antroquinonol D-mediated cell growth inhibition and cell death at 72 h, assessed by the MTT assay, was also stronger than that demonstrated by another DNMT inhibitor, EGCG, in MCF7 and NDA-MB-231 cells (Figure S4c, Supporting Information).

Antroquinonol D Inhibits the Migration of MDA-MB-231 Breast Cancer Cells. Metastasis is the primary cause of mortality for most cancer patients. The mobility of tumor cells is a key step in the metastatic process. The MDA-MB-231 cells exhibit invasive tumor features with rapid migration ability. The MDA-MB-231 cells are good cell models for analyzing whether antroquinonol D could also inhibit cell migration ability. We observed morphological changes in MDA-MB-231 cells, including cell shrinkage and fragmentation, after antroquinonol D treatment for 6 days (Supporting Information Figure S5 right panel) that were greater than those observed following DMSO treatment (Supporting Information Figure S5 left panel). Dynamic regulation of the filamentous actin (F-actin) cytoskeleton is critical to cell adhesion and migration.[33] Immunofluorescence imaging revealed that the network expansion of F-actin was not as extensive after antroquinonol D treatment as after DMSO control treatment (Figure 3a). Cell motility was further analyzed using wound healing and Transwell assays. The results of the wound healing assays indicated that the MDA-MB-231 cells migrated more slowly when treated with 15 μM antroquinonol D for 6 days compared to the DMSO control-treated cells (Figure 3b). The Transwell migration assays also revealed that antroquinonol D decreased the migration ability of MDA-MB-231 cells by 56.9% (Figure 3c). Antroquinonol D and a positive control DNMT inhibitor, AZA, displayed similar suppression effects on the migratory ability of MDA-MB-231 breast cancer cells. To further confirm that the DNMT inhibitor antroquinonol D influenced the migratory ability of breast cancer cells, a migration assay was performed using the xCELLigence biosensor system, and the numbers of cells that migrated were reflected by the cell index. As shown in Figure 3c, the cell indices in the DMSO-treated control cells and antroquinonol D-treated cells were 2.2 and 1.3, respectively, after 30 h. The migratory ability was reduced to approximately 41% in the antroquinonol D-treated cells compared to the DMSO-treated control cells (Figure 3d). These results indicate that this DNMT inhibitor can suppress the migratory ability of MDA-MB-231 breast cancer cells.

Antroquinonol D Can Inhibit DNMT1 Enzyme Activity. A previous study reported that antroquinonol induces anticancer activity in human pancreatic cancers through an inhibitory effect on PI3-kinase/Akt/mTOR pathways.[34] In our study, neither antroquinonol nor antroquinonol D can inhibit AKT phosphorylation in MDA-MB-231 cells (Supporting Information Figure S6), suggesting that the anticancer effect mediated by antroquinonol D is mediated through another pathway. Down-regulation of tumor suppressor genes (TSGs) by 5′CpG island hypermethylation is an important event in tumor growth and progression.[5] Blocking DNA methyltransferase (DNMT) could potentially inhibit or reverse the process of epigenetic silencing. To develop a new DNMT inhibitor and

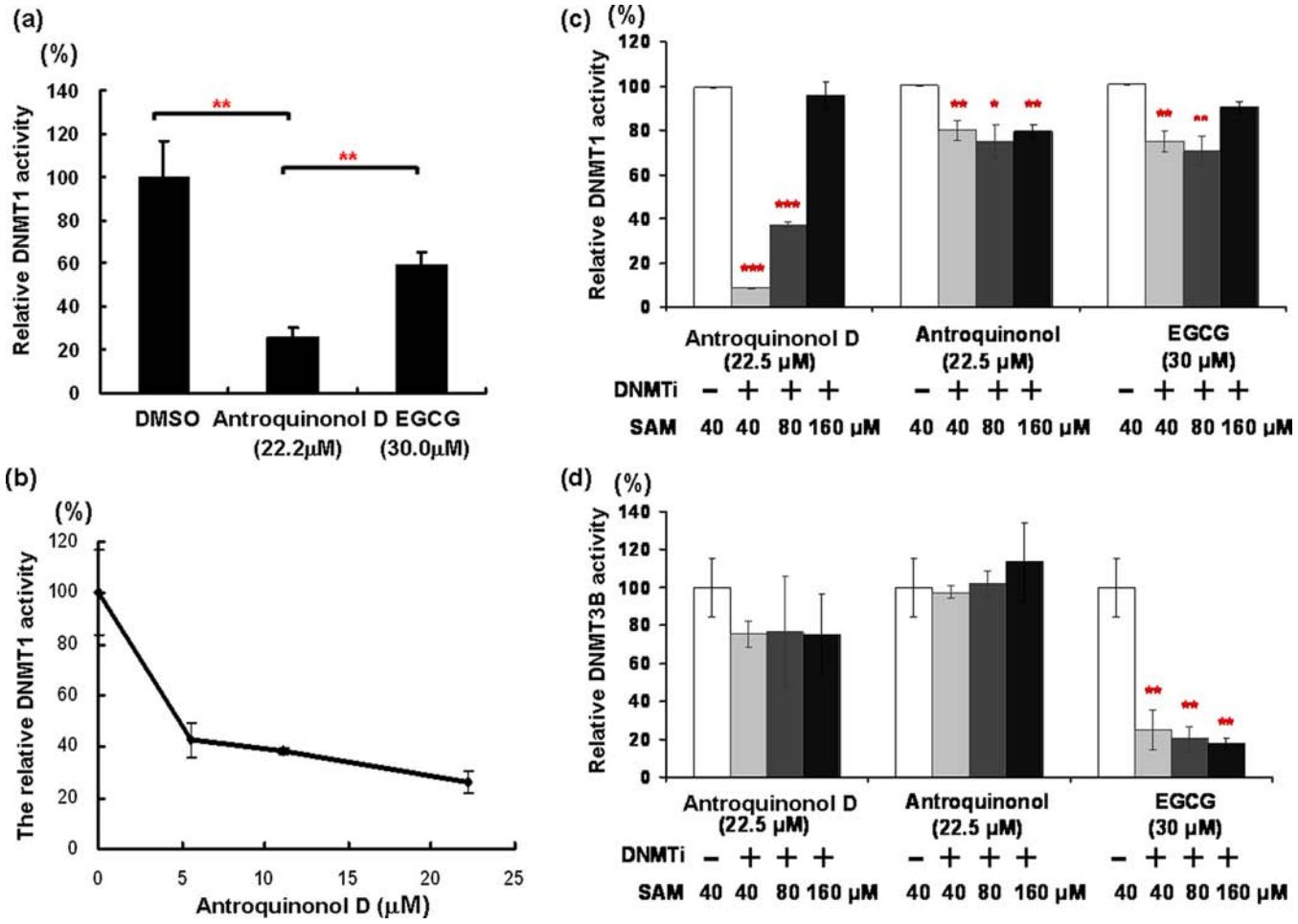

Figure 4. Antroquinonol D inhibits DNMT1 enzyme activity. (a) Antroquinonol D (22.5 μM) significantly suppressed DNMT1 activity. The experiments were performed with at least three biological and three technical replicates. (b) Antroquinonol D inhibited the methylation activity of DNMT1 followed by increasing of Antroquinonol D. The DNMT1 activity assays were analyzed based on the methylation levels catalyzed by DNMT1 in the presence of either an inhibitor or the control (DMSO). EGCG was used as a positive control DNMT inhibitor. The inhibitory effects of antroquinonol D, antroquinonol or EGCG on the DNMT1 (c) or (d) DNMT3B enzymes were analyzed in the presence of 40 to 80 and 160 μM of the cofactor SAM. * $p \leq 0.05$, ** $p \leq 0.005$, *** $p \leq 0.001$. The data are presented as the means ± s.d. All the experiments were performed with at least three technical replicates. The t test was used to calculate group differences in all experiments.

further determine whether the D-antroquinonol-mediated inhibition of cancer cell growth and migration resulted from the suppression of DNMT1 activity, we analyzed DNMT1 activity using the DNMT1 Activity/Inhibitor Screening Assay Kit. We collected natural compounds from the Graduate Institute of Pharmacognosy of Taipei Medical University, including phenolics, curcumin analogues, ubiquinone and sesquiterpene derivatives, and serially examined the DNMT1 activity. In addition to phenolics, curcumin analogues and sesquiterpene derivatives, we discovered that a ubiquinone derivative, antroquinonol D, may act as a DNMT1 inhibitor in vitro (Figures 1 and 4a, $P = 0.0036$). Its inhibitory effects were stronger than those of the positive control DNMT inhibitor, EGCG (Figure 4a, $P = 0.0027$). The IC50 of antroquinonol D on DNMT1 activity was much lower than 5 μM (Figure 4b). In addition, antroquinonol D inhibited DNMT1 activity in the presence of 40 μM SAM. After increasing the SAM concentration from 40 to 80 and 160 μM, the inhibitory effects of antroquinonol D on DNMT1 gradually decreased in a dose-dependent manner (Figure 4c). These results further indicate that antroquinonol D may be inserted into the putative cytosine pocket and compete with the cofactor SAM, resulting in decreased DNMT1 activity. One antroquinonol D analogue, antroquinonol, was isolated in 2007 and was reported to be toxic to cancer cells.[2] Antroquinonol does not inhibit DNMT1 enzyme activity as well as antroquinonol D does (Figure 4c). For DNMT3B enzyme activity assay, antroquinonol D only slightly reduced DNMT3B enzyme activity (Figure 4d). These results may also indicate that antroquinonol D competes for the same binding pocket in the DNMT1 enzyme as SAM, but does not compete for the binding pocked in the DNMT3B enzyme (Figure 4c and d). High levels of DNMT1 mRNA and protein expression were observed in three breast cancer cell lines (MCF7, T47D and MDA-MB-231) (Figure 2f and g) that were sensitive to antroquinonol D treatment compared to normal MCF10A cells (Figure 2d and e). However, real-time RT-PCR and Western blotting analyses found that DNMT1, DNMT3A and DNMT3B mRNA and protein levels were not significantly decreased after antroquinonol D treatment (Supporting Information Figure S7).

Molecular Modeling of the Interaction between antroquinonol D and DNMT1. To investigate the putative mechanisms involved in the antroquinonol D-mediated inhibition of DNMT1 activity, the crystal structure of

dx.doi.org/10.1021/jf4056924 | J. Agric. Food Chem. 2014, 62, 5625−5635

DNMT1 in complex with sinefungin (PDB code 3SWR) was used to build the model of the human DNMT1 catalytic domain (Figure 5a). Molecular docking of antroquinonol D

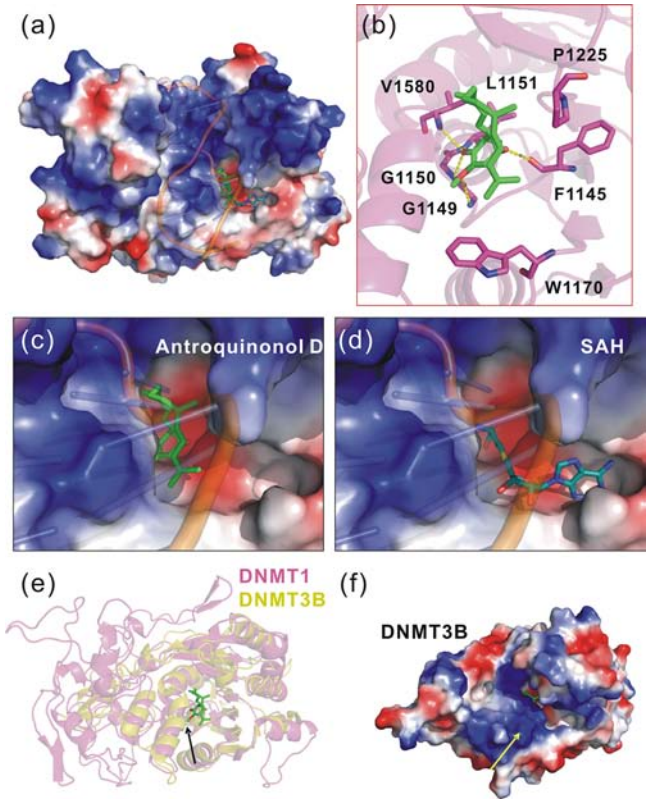

Figure 5. Molecular docking model of the DNMT1 catalytic domain binding to antroquinonol D or hemimethylated DNA. (a) Docking of antroquinonol D and hemimethylated DNA (brown line) in the catalytic pocket of DNMT1. (b) The binding mode of antroquinonol D upon docking to DNMT1. The hydrogen-bonding interactions of F1145, G1149, G1150, L1151 and V1580, and the van der Waals interactions with P1225 and W1170, are shown. Antroquinonol D (c) bound to the same pocket as SAH, which is the product of DNMT1 catalytic reactions (d). The ligands and site residues are shown in stick representation and colored by atom type, with the exception of the carbon atoms, which are indicated in green, cyan and purple for antroquinonol D, SAH, and the site residues, respectively. (e) Superimposition of DNMT1 (pink) and DNMT3B (yellow) structures revealed that antroquinonol D was not suitable to fit into the binding pocket of DNMT3B. (f) Bulky antroquinonol D had a crash (arrow) with the binding pocket of DNMT3B when overlapping antroquinonol D bound DNMT1 with DNMT3B.

onto the DNMT1 catalytic domain was performed. The hydrogen-bonding interactions of F1145, G1149, G1150, L1151 and V1580, and van der Waals interactions of P1225 and W1170 were observed on the residues of DNMT1 that were bound to antroquinonol D (Figure 5b). Antroquinonol D was found to bind to the same pocket as SAH, which is the SAM cofactor product of DNMT1 catalytic reactions (Figure 5c and d). DNMT3B catalytic domain was also modeled using the crystal structure of DNMT3A (PDB code 2QRV) as a template. Interestingly, when superimposing the structure of antroquinonol D bound DNMT1 with DNMT3B structure, antroquinonol D could fit into the binding pocket of DNMT3B (Figure 5e and f). The steric effect of DNMT3B on the bulky antroquinonol D entry may be the reason for the lower inhibition ability of antroquinonol D to DNMT3B compared to DNMT1 (Figure 5e and f). The enzyme activity assay and molecular modeling of the interaction between antroquinonol D and DNMTs support that antroquinonol D selectively inhibits the DNMT1 enzyme, but not DNMT3B. The structure–activity relationships between antroquinonol and antroquinonol D with the DNMT1 enzyme was also analyzed by molecular modeling. The data showed that antroquinonol, with an additional 3′-O–CH_3 group, may interfere with the binding of DNMT1 more than antroquinonol D does (Supporting Information Figure S8).

Antroquinonol D Induces Tumor Suppressor Gene Demethylation and Re-expression in Cancer Cells. Aberrant DNA hypermethylation of TSGs is an important mechanism underlying tumorigenesis.[21,35] Consequently, researchers are now searching for potential demethylating agents that can be used to reactivate TSGs in tumor cells, which may possibly lead to the suppression of cancer cell growth and invasion. To determine whether antroquinonol D can induce gene demethylation in cells, we analyzed changes in genomic methylation using the Illumina Methylation 450 K array-based assay. We discovered that treatment with 15 μM antroquinonol D for 6 days decreased the methylation status of 159 CpG sites and 113 specific genes in MDA-MB-231 breast cancer cells (Figure 6a and Supporting Information Table S2). Functional annotation clustering of differentially demethylated genes induced by following antroquinonol D treatment was performed using a Functional DAVID Bioinformatics Resources 6.7 analysis (Supporting Information Figure S9). The greatest decreases in methylation levels and increases in mRNA expression levels following antroquinonol D treatment were observed in five tumor suppressor genes: *FANCC*, *CACNA1A*, *CDH15*, *ASB9* and *COL4A2* (Figure 6a,b and Table 1). FANCC gene expression has been reported to be lower in stage III samples compared to stage I samples from ovarian cancer patients.[36] The CACNA1A gene encodes the α_{1A} pore-forming subunit of Ca^{2+} voltage-gated Cav2.1 channels. A recent report identified the *CACNA1A* gene as a novel tumor suppressor candidate that is methylated in lung cancer tumors.[37] Frequent promoter methylation of *CDH15* in hepatocellular carcinoma is associated with a poor prognosis.[38] Low expression of ASB9 in colorectal cancer is associated with a poor prognosis.[39] COL4A2 protein retards the growth of pancreatic cancer in a dose-dependent manner by inhibiting angiogenesis.[40] Pyrosequencing was used to further confirm the decreases in the methylation statuses of two of the tumor suppressor genes, *FANCC* and *CACNA1A*. The CpG island methylation levels in the *FANCC* and *CACNA1A* genes were decreased by approximately 9–51% and 20–51%, respectively, following antroquinonol D treatment (Figure 6c). We also used Western blotting to determine whether FANCC and CACNA1A protein expression was induced following antroquinonol D treatment. The data indicated that the FANCC and CACNA1A protein expression levels had also increased by 1.7- and 2.3-fold, respectively, following antroquinonol D treatment (Figure 6c). Note that DNA demethylation of the *ASB9* and *RPS6KA2* genes was detected using a Methylation 450 K array-based assay. However, RPS6KA2 mRNA expression cannot be detected using real-time RT-PCR. The ASB9 mRNA expression levels only increased 2-fold. A probable reason for these results may be that the DNA demethylation regions of RPS6KA2 and ASB9 were not close to the CpG islands (Table 1). Interestingly, the DNA demethylation regions of the

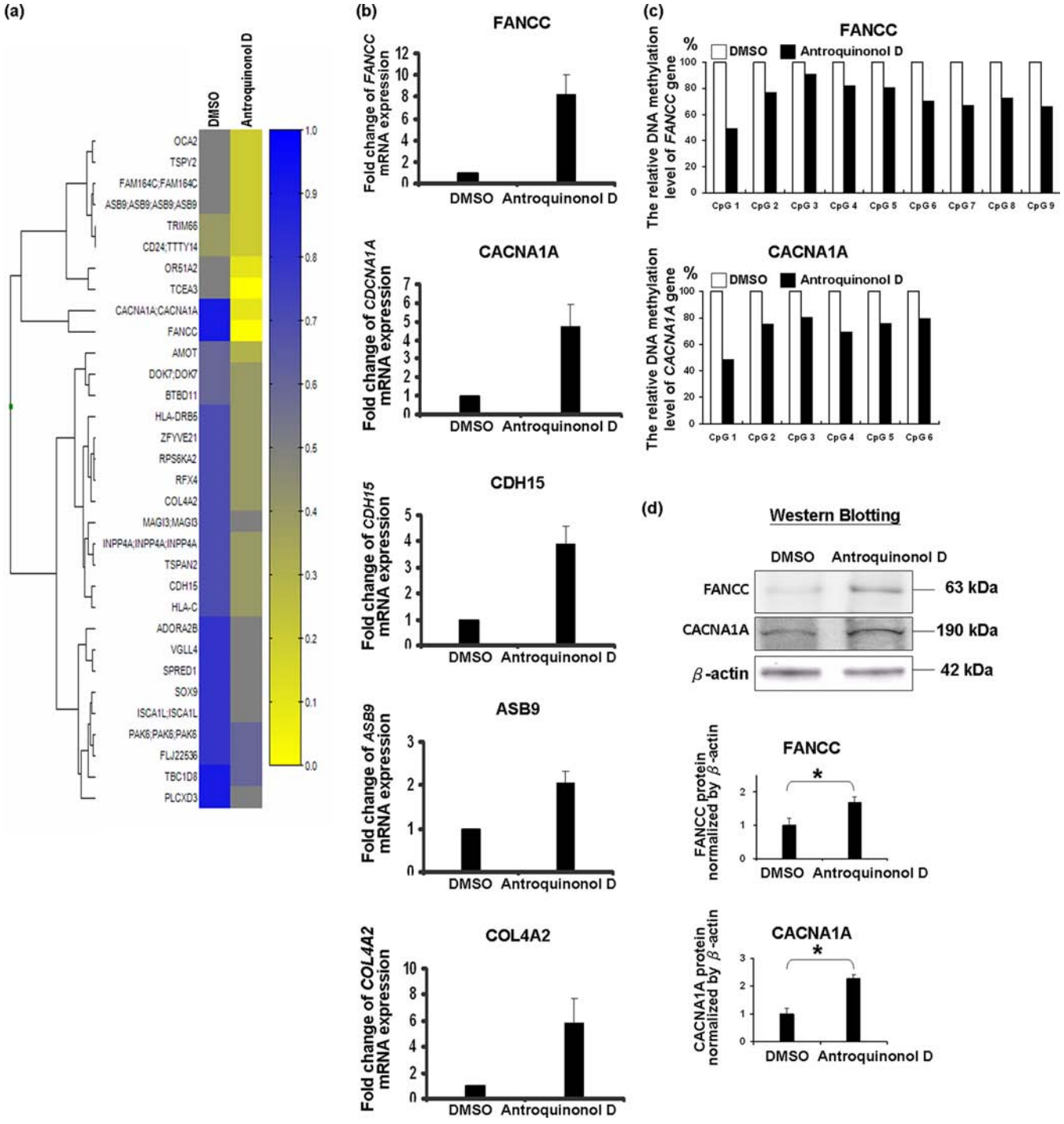

Figure 6. Antroquinonol D induces tumor suppressor gene demethylation and re-expression in cancer cells. (a) Methylation levels (ΔAvg_Beta >0.25) at the differentially methylated loci were identified using an Illumina Methylation 450 K array-based assay following treatment with DMSO or 15 μM antroquinonol D for 6 days in MDA-MB-231 cells and are represented on the heat map. The scale shows the relative methylation status (yellow indicates hypomethylation and blue indicates hypermethylation). (b) The mRNA levels of *FANCC*, *CACNA1A*, *CDH15*, *ASB9* and *COL4A2* were identified using real-time RT-PCR after the cells had been treated with 15 μM antroquinonol D for 6 days. The data are presented as the means ± s.d. Note that the DNA demethylation status of RPS6KA2 was detected using the Methylation 450 K array-based assay. However, RPS6KA2 mRNA expression cannot be detected using real-time RT-PCR. The experiments were performed with at least three technical replicates. (c) Pyrosequencing was used to confirm the DNA methylation status of the *FANCC* and *CACNA1A* genes following treatment with 15 μM antroquinonol D for 6 days in MDA-MB-231 cells. (d) The protein expression levels of FANCC and CACNA1A were analyzed via Western blotting following treatment with 15 μM antroquinonol D for 6 days. The data are presented as the means ± s.d. * $P \leq 0.001$. The experiments were performed with at least three technical replicates. The *t* test was used to calculate group differences in all experiments.

CACNA1A, *CDH15* and *COL4A2* genes were located within their gene bodies (Table 1). Whether those regions are important for gene expression requires further investigation. Fewer genes were demethylated following antroquinonol D treatment than were previously reported to be demethylated following DAC treatment.[41] We postulated that DAC

dx.doi.org/10.1021/jf4056924 | J. Agric. Food Chem. 2014, 62, 5625−5635

Table 1. Demethylation of Tumor Suppressor Genes

demethylation (Δ Avg_Beta)[a]	gene name	coverage of gene regions[b]	relation to CpG island[c]	function	reference
−0.881	FANCC	5′UTR	island shore	DNA repair	Low expression of FANCC is observed in late stage of ovarian cancer.[37]
−0.702	CACNA1A	gene body	island shore	calcium channels	High methylation of *CACNA1A* is determined in lung tumors.[38]
−0.323	CDH15	gene body	island shelf	cell−cell adhesion	Frequent promoter methylation of *CDH15* is associated with poor prognosis in liver cancer.[39]
−0.277	ASB9	TSS200	no	inhibition of cytokine signaling	Low expression of ASB9 in colorectal cancer is associated with poor prognosis.[40]
−0.274	RPS6KA2	gene body	no	inhibition of proliferation	RPS6KA2 reduces proliferation, causes G1 arrest, increases apoptosis.[43]
−0.253	COL4A2	gene body	within island	inhibition of angiogenesis	COL4A2 protein retards the growth of pancreatic cancer through inhibiting angiogenesis.[41,42]

[a]Demethylation (ΔAvg_Beta) indicates that the change level of DNA methylation in specific gene between DMSO control and antroquinonol D treatment. The data were calculated by antroquinonol D. Avg_Beta − DMSO.Avg_Beta. "Beta" scores are based on the ratio of methylated signal intensity to the sum of both methylated and unmethylated signal outputs. [b]The relative position between DNA demethylation region and the specific tumor suppressor gene. [c]The relative position between DNA demethylation region and the CpG island.

incorporates into replicating DNA, inducing the chelation and degradation of the DNMT1 protein, thereby preventing DNA methylation. Therefore, the mechanism underlying antroquinonol D-mediated DNMT1 inhibition differs from that of DAC and AZA, and therefore, antroquinonol D may be used as an alternative DNMT inhibitor. Antroquinonol D may induce far fewer cytotoxic effects than DAC because only certain genes are demethylated following antroquinonol D treatment. Therefore, antroquinonol D may still be worth optimizing to generate a more specific DNMT inhibitor.

In conclusion, we identified a new DNMT1 inhibitor, antroquinonol D, which induced DNA demethylation and reversed the silencing of multiple tumor suppressor genes, induced cancer cell death and inhibited cell migration. Further investigation of antroquinonol D using molecular biochemistry assays, animal studies, pharmacokinetics assays and clinical studies is required to determine whether antroquinonol D can be used clinically.

■ ASSOCIATED CONTENT

Supporting Information

The Supporting Information includes the DNMT1 inhibitor treatment protocols for the cells; the viability and cytotoxicity of breast cells after DNMT inhibitors treatment; images presenting morphological changes in MDA-MB-231 cells; Expression levels of DNMTs following antroquinonol D treatment; antroquinonol D effects on the AKT pathway; functional annotation clustering; the growth curves of cells over 6 days, assayed by Sulforhodamine B; a list of primer sequences and their reaction conditions used in the present study; the demethylation in genes. This material is available free of charge via the Internet at http://pubs.acs.org.

■ AUTHOR INFORMATION

Corresponding Author

*Tel.: +886 2 27361661, ext. 6162. Fax: +886 2 27361661, ext. 6162. E-mail: linruokai@tmu.edu.tw.

Funding

This work was supported in part by grant TMU99-AE1-B21 from the Taipei Medical University and grants NSC100−2320-B-038-002, NSC100−2320-B-038-014 and NSC99-2119-M-002-010 from the National Science Council (Republic of China).

Notes

The authors declare no competing financial interest.

■ ABBREVIATIONS USED

A. camphorata, *Antrodia camphorata*; ASB9, ankyrin repeat and SOCS box containing 9; Antroquinonol D, 3-demethoxyl antroquinonol; AZA, 5-azacytidine; DAC, 5-aza-2′-deoxycytidine (decitabine); BCRC, Bioresource Collection and Research Center; CACNA1A, calcium channel voltage-dependent P/Q type alpha 1A subunit; CDH15, cadherin 15 type 1 M-cadherin; CI, Cell Index; COL4A2, collagen type IV alpha 2; DNMT1, DNA methyltransferase 1; EGCG, epigallocatechin-3-gallate; TSG, tumor suppressor gene; FANCC, fanconi anemia complementation group C; F-actin, filamentous actin; GI50, 50% growth inhibition; NMR, Nuclear magnetic resonance; SAM, S-adenosyl methionine; FDA, US Food and Drug Administration; SDS, sodium dodecyl sulfate; SRB, Sulphorhodamine B

■ REFERENCES

(1) Geethangili, M.; Tzeng, Y. M. Review of pharmacological effects of Antrodia camphorata and its bioactive compounds. *Evid. Based Complement. Alternat. Med.* **2011**, *2011*, 212641.

(2) Lee, T. H.; Lee, C. K.; Tsou, W. L.; Liu, S. Y.; Kuo, M. T.; Wen, W. C. A new cytotoxic agent from solid-state fermented mycelium of Antrodia camphorata. *Planta Med.* **2007**, *73*, 1412−5.

(3) Nakamura, N.; Hirakawa, A.; Gao, J. J.; Kakuda, H.; Shiro, M.; Komatsu, Y.; Sheu, C. C.; Hattori, M. Five new maleic and succinic acid derivatives from the mycelium of Antrodia camphorata and their cytotoxic effects on LLC tumor cell line. *J. Nat. Prod.* **2004**, *67*, 46−8.

(4) Sekido, Y.; Fong, K. M.; Minna, J. D. Progress in understanding the molecular pathogenesis of human lung cancer. *Biochim. Biophys. Acta* **1998**, *1378*, F21−59.

(5) Jovanovic, J.; Ronneberg, J. A.; Tost, J.; Kristensen, V. The epigenetics of breast cancer. *Mol. Oncol.* **2010**, *4*, 242−54.

(6) Nephew, K. P.; Huang, T. H. Epigenetic gene silencing in cancer initiation and progression. *Cancer Lett.* **2003**, *190*, 125−33.

(7) Belinsky, S. A. Gene-promoter hypermethylation as a biomarker in lung cancer. *Nat. Rev. Cancer* **2004**, *4*, 707−17.

(8) Jamaluddin, M. S.; Yang, X.; Wang, H. Hyperhomocysteinemia, DNA methylation and vascular disease. *Clin. Chem. Lab. Med.* **2007**, *45*, 1660−6.

(9) Costa, E.; Dong, E.; Grayson, D. R.; Guidotti, A.; Ruzicka, W.; Veldic, M. Reviewing the role of DNA (cytosine-5) methyltransferase overexpression in the cortical GABAergic dysfunction associated with psychosis vulnerability. *Epigenetics* **2007**, *2*, 29−36.

(10) Egger, G.; Liang, G.; Aparicio, A.; Jones, P. A. Epigenetics in human disease and prospects for epigenetic therapy. *Nature* **2004**, *429*, 457−63.
(11) Rhee, I.; Bachman, K. E.; Park, B. H.; Jair, K. W.; Yen, R. W.; Schuebel, K. E.; Cui, H.; Feinberg, A. P.; Lengauer, C.; Kinzler, K. W.; Baylin, S. B.; Vogelstein, B. DNMT1 and DNMT3b cooperate to silence genes in human cancer cells. *Nature* **2002**, *416*, 552−6.
(12) Mastroeni, D.; Grover, A.; Delvaux, E.; Whiteside, C.; Coleman, P. D.; Rogers, J. Epigenetic changes in Alzheimer's disease: decrements in DNA methylation. *Neurobiol. Aging* **2010**, *31*, 2025−37.
(13) De Marzo, A. M.; Marchi, V. L.; Yang, E. S.; Veeraswamy, R.; Lin, X.; Nelson, W. G. Abnormal regulation of DNA methyltransferase expression during colorectal carcinogenesis. *Cancer Res.* **1999**, *59*, 3855−60.
(14) Lin, R. K.; Hsu, H. S.; Chang, J. W.; Chen, C. Y.; Chen, J. T.; Wang, Y. C. Alteration of DNA methyltransferases contributes to 5′CpG methylation and poor prognosis in lung cancer. *Lung Cancer* **2007**, *55*, 205−13.
(15) Girault, I.; Tozlu, S.; Lidereau, R.; Bieche, I. Expression analysis of DNA methyltransferases 1, 3A, and 3B in sporadic breast carcinomas. *Clin. Cancer Res.* **2003**, *9*, 4415−22.
(16) Saito, Y.; Kanai, Y.; Nakagawa, T.; Sakamoto, M.; Saito, H.; Ishii, H.; Hirohashi, S. Increased protein expression of DNA methyltransferase (DNMT) 1 is significantly correlated with the malignant potential and poor prognosis of human hepatocellular carcinomas. *Int. J. Cancer* **2003**, *105*, 527−32.
(17) Etoh, T.; Kanai, Y.; Ushijima, S.; Nakagawa, T.; Nakanishi, Y.; Sasako, M.; Kitano, S.; Hirohashi, S. Increased DNA methyltransferase 1 (DNMT1) protein expression correlates significantly with poorer tumor differentiation and frequent DNA hypermethylation of multiple CpG islands in gastric cancers. *Am. J. Pathol.* **2004**, *164*, 689−99.
(18) Mizuno, S.; Chijiwa, T.; Okamura, T.; Akashi, K.; Fukumaki, Y.; Niho, Y.; Sasaki, H. Expression of DNA methyltransferases DNMT1, 3A, and 3B in normal hematopoiesis and in acute and chronic myelogenous leukemia. *Blood* **2001**, *97*, 1172−9.
(19) Qiu, X.; Zhang, L.; Lu, S.; Song, Y.; Lao, Y.; Hu, J.; Fan, H. Upregulation of DNMT1 mediated by HBx suppresses RASSF1A expression independent of DNA methylation. *Oncol. Rep.* **2014**, *31*, 202−8.
(20) Issa, J. P.; Garcia-Manero, G.; Giles, F. J.; Mannari, R.; Thomas, D.; Faderl, S.; Bayar, E.; Lyons, J.; Rosenfeld, C. S.; Cortes, J.; Kantarjian, H. M. Phase 1 study of low-dose prolonged exposure schedules of the hypomethylating agent 5-aza-2′-deoxycytidine (decitabine) in hematopoietic malignancies. *Blood* **2004**, *103*, 1635−40.
(21) Esteller, M. Dormant hypermethylated tumour suppressor genes: questions and answers. *J. Pathol.* **2005**, *205*, 172−80.
(22) Lubbert, M.; Suciu, S.; Baila, L.; Ruter, B. H.; Platzbecker, U.; Giagounidis, A.; Selleslag, D.; Labar, B.; Germing, U.; Salih, H. R.; Beeldens, F.; Muus, P.; Pfluger, K. H.; Coens, C.; Hagemeijer, A.; Eckart Schaefer, H.; Ganser, A.; Aul, C.; de Witte, T.; Wijermans, P. W. Low-dose decitabine versus best supportive care in elderly patients with intermediate- or high-risk myelodysplastic syndrome (MDS) ineligible for intensive chemotherapy: final results of the randomized phase III study of the European Organisation for Research and Treatment of Cancer Leukemia Group and the German MDS Study Group. *J. Clin. Oncol.* **2011**, *29*, 1987−96.
(23) Medina-Franco, J. L.; Caulfield, T. Advances in the computational development of DNA methyltransferase inhibitors. *Drug Discovery Today* **2011**, *16*, 418−25.
(24) Lin, R. K.; Hsu, C. H.; Wang, Y. C. Mithramycin A inhibits DNA methyltransferase and metastasis potential of lung cancer cells. *Anticancer Drugs* **2007**, *18*, 1157−64.
(25) Stresemann, C.; Brueckner, B.; Musch, T.; Stopper, H.; Lyko, F. Functional diversity of DNA methyltransferase inhibitors in human cancer cell lines. *Cancer Res.* **2006**, *66*, 2794−800.
(26) Monto, R. W.; Talley, R. W.; Caldwell, M. J.; Levin, W. C.; Guest, M. M. Observations on the mechanism of hemorrhagic toxicity in mithramycin (NSC 24559) therapy. *Cancer Res.* **1969**, *29*, 697−704.
(27) Morris, G. M.; Huey, R.; Olson, A. J., Using AutoDock for ligand-receptor docking. *Curr. Protoc. Bioinform.* **2008**, Chapter 8, Unit 8 14.
(28) Huey, R.; Morris, G. M.; Olson, A. J.; Goodsell, D. S. A semiempirical free energy force field with charge-based desolvation. *J. Comput. Chem.* **2007**, *28*, 1145−52.
(29) Mosmann, T. Rapid colorimetric assay for cellular growth and survival: application to proliferation and cytotoxicity assays. *J. Immunol. Methods* **1983**, *65*, 55−63.
(30) Wei, P. L.; Kuo, L. J.; Wang, W.; Lin, F. Y.; Liu, H. H.; How, T.; Ho, Y. S.; Huang, M. T.; Wu, C. H.; Chang, Y. J. Silencing of glucose-regulated protein 78 (GRP78) enhances cell migration through the upregulation of vimentin in hepatocellular carcinoma cells. *Ann. Surg. Oncol.* **2012**, *19* (Suppl 3), 572−9.
(31) Huang da, W.; Sherman, B. T.; Lempicki, R. A. Systematic and integrative analysis of large gene lists using DAVID bioinformatics resources. *Nat. Protoc.* **2009**, *4*, 44−57.
(32) Li, L. C.; Dahiya, R. MethPrimer: designing primers for methylation PCRs. *Bioinformatics* **2002**, *18*, 1427−31.
(33) Stricker, J.; Falzone, T.; Gardel, M. L. Mechanics of the F-actin cytoskeleton. *J. Biomech.* **2010**, *43*, 9−14.
(34) Yu, C. C.; Chiang, P. C.; Lu, P. H.; Kuo, M. T.; Wen, W. C.; Chen, P.; Guh, J. H. Antroquinonol, a natural ubiquinone derivative, induces a cross talk between apoptosis, autophagy and senescence in human pancreatic carcinoma cells. *J. Nutr. Biochem.* **2012**, *23*, 900−7.
(35) Momparler, R. L. Cancer epigenetics. *Oncogene* **2003**, *22*, 6479−83.
(36) Ganzinelli, M.; Mariani, P.; Cattaneo, D.; Fossati, R.; Fruscio, R.; Corso, S.; Ricci, F.; Broggini, M.; Damia, G. Expression of DNA repair genes in ovarian cancer samples: biological and clinical considerations. *Eur. J. Cancer* **2011**, *47*, 1086−94.
(37) Castro, M.; Grau, L.; Puerta, P.; Gimenez, L.; Venditti, J.; Quadrelli, S.; Sanchez-Carbayo, M. Multiplexed methylation profiles of tumor suppressor genes and clinical outcome in lung cancer. *J. Transl. Med.* **2010**, *8*, 86.
(38) Yamada, S.; Nomoto, S.; Fujii, T.; Takeda, S.; Kanazumi, N.; Sugimoto, H.; Nakao, A. Frequent promoter methylation of M-cadherin in hepatocellular carcinoma is associated with poor prognosis. *Anticancer Res.* **2007**, *27*, 2269−74.
(39) Tokuoka, M.; Miyoshi, N.; Hitora, T.; Mimori, K.; Tanaka, F.; Shibata, K.; Ishii, H.; Sekimoto, M.; Doki, Y.; Mori, M. Clinical significance of ASB9 in human colorectal cancer. *Int. J. Oncol.* **2010**, *37*, 1105−11.
(40) He, X. P.; Li, Z. S.; Zhu, R. M.; Tu, Z. X.; Gao, J.; Pan, X.; Gong, Y. F.; Jin, J.; Man, X. H.; Wu, H. Y.; Xu, A. F. Effects of recombinant human canstatin protein in the treatment of pancreatic cancer. *World J. Gastroenterol.* **2006**, *12*, 6652−7.
(41) Tsai, H. C.; Li, H.; Van Neste, L.; Cai, Y.; Robert, C.; Rassool, F. V.; Shin, J. J.; Harbom, K. M.; Beaty, R.; Pappou, E.; Harris, J.; Yen, R. W.; Ahuja, N.; Brock, M. V.; Stearns, V.; Feller-Kopman, D.; Yarmus, L. B.; Lin, Y. C.; Welm, A. L.; Issa, J. P.; Minn, I.; Matsui, W.; Jang, Y. Y.; Sharkis, S. J.; Baylin, S. B.; Zahnow, C. A. Transient low doses of DNA-demethylating agents exert durable antitumor effects on hematological and epithelial tumor cells. *Cancer Cell* **2012**, *21*, 430−46.
(42) Bignone, P. A.; Lee, K. Y.; Liu, Y.; Emilion, G.; Finch, J.; Soosay, A. E.; Charnock, F. M.; Beck, S.; Dunham, I.; Mungall, A. J.; Ganesan, T. S. RPS6KA2, a putative tumour suppressor gene at 6q27 in sporadic epithelial ovarian cancer. *Oncogene* **2007**, *26*, 683−700.

JOURNAL OF AGRICULTURAL AND FOOD CHEMISTRY

Article

pubs.acs.org/JAFC

Coumestan Inhibits Radical-Induced Oxidation of DNA: Is Hydroxyl a Necessary Functional Group?

Gao-Lei Xi and Zai-Qun Liu*

Department of Organic Chemistry, College of Chemistry, Jilin University, Changchun 130021, China

Supporting Information

ABSTRACT: Coumestan is a natural tetracycle with a C═C bond shared by a coumarin moiety and a benzofuran moiety. In addition to the function of the hydroxyl group on the antioxidant activity of coumestan, it is worth exploring the influence of the oxygen-abundant scaffold on the antioxidant activity as well. In this work, seven coumestans containing electron-withdrawing and electron-donating groups were synthesized to evaluate the abilities to trap 2,2′-azinobis(3-ethylbenzothiazoline-6-sulfonate) cationic radical ($ABTS^{\bullet+}$), 2,2′-diphenyl-1-picrylhydrazyl radical (DPPH), and galvinoxyl radical, respectively, and to inhibit the oxidations of DNA mediated by $^{\bullet}OH$, Cu^{2+}/glutathione (GSH), and 2,2′-azobis(2-amidinopropane hydrochloride) (AAPH), respectively. It was found that all of the coumestans used herein can quench the aforementioned radicals and can inhibit $^{\bullet}OH$-, Cu^{2+}/GSH-, and AAPH-induced oxidations of DNA. In particular, substituent-free coumestan exhibits higher ability to quench DPPH and to inhibit AAPH-induced oxidation of DNA than Trolox. In addition, nonsubstituted coumestan shows a similar ability to inhibit $^{\bullet}OH$- and Cu^{2+}/GSH-induced oxidations of DNA relative to that of Trolox. The antioxidant effectiveness of the coumestan can be attributed to the lactone in the coumarin moiety and, therefore, a hydroxyl group may not be a necessary functional group for coumestan to be an antioxidant.

KEYWORDS: *coumestan, antioxidant, free radical, DNA oxidation*

INTRODUCTION

Coumestan is a naturally occurring skeleton with a coumarin moiety and a benzofuran moiety sharing a C═C bond (structure in Scheme 1). 2-Methoxy-3,8,9-trihydroxy coumestan, also called as wedelolactone, is the typically natural coumestan and exhibits various biological activities[1] such as antifibrotic,[2] antiadipogenesis,[3] and immunosuppressive effects.[4] However, the antioxidant effects of coumestans, especially substituent-free coumestans, are not usually reported.[5] In previously published studies, the pharmacological activities of coumestans are regarded as the contributions from hydroxyl groups.[6] In particular, the hydroxyl group attached to the benzofuran (ring D) mainly controls the redox state[7] and thus plays the major role in the biological activities for coumestans.[8] However, the influence of substituents at ring D on the antioxidant effectiveness remains unclear. In particular, it is worth clarifying the function of the coumestan scaffold itself (without any substituents attached) on the antioxidant effectiveness. These backgrounds encourage us to investigate the antioxidant effectiveness of coumestan with and without the substituent attached to ring D and to clarify whether the hydroxyl group is a necessary substituent for generating the antioxidant effectiveness.

The radical-induced oxidation of DNA is a suitable experimental system for estimating the antioxidant effectiveness of natural or synthetic compounds.[9] $^{\bullet}OH$, Cu^{2+}/glutathione (GSH), and 2,2′-azobis(2-amidinopropane hydrochloride) (AAPH) are usually used as radical initiators because they are able to mimic DNA undergoing oxidation caused by hydroxyl, glutathione, and peroxyl radicals. In addition, as the stable radicals at room temperature, 2,2′-azinobis(3-ethylbenzothiazoline-6-sulfonate) cationic radical ($ABTS^{\bullet+}$), 2,2′-diphenyl-1-picrylhydrazyl radical (DPPH), and galvinoxyl radical are applied to evaluate the ability of an antioxidant to donate its hydrogen atom to N- and O-centered radicals. Therefore,

Scheme 1. Coumestans Synthesized in This Work

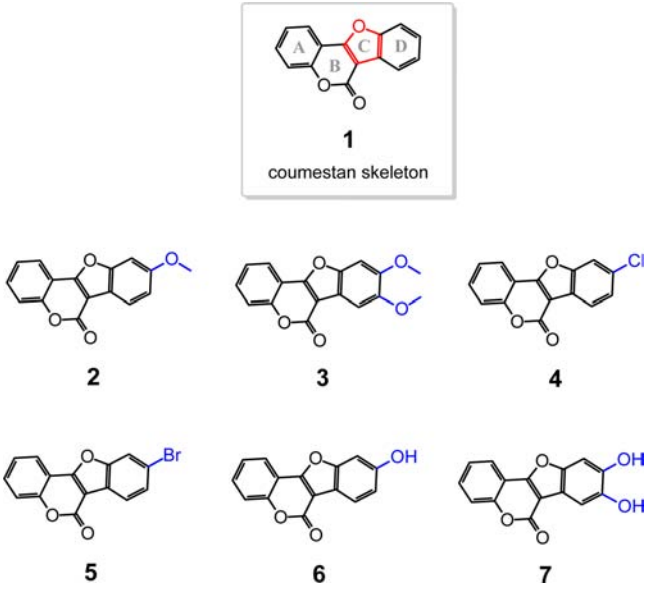

Received: January 2, 2014
Revised: June 1, 2014
Accepted: June 2, 2014
Published: June 9, 2014

ACS Publications © 2014 American Chemical Society

presented herein is a study on the antioxidant effects of seven coumestans with electron-withdrawing groups (−Cl, −Br) and electron-donating groups (−OCH_3 and −OH). The abilities to quench $ABTS^{\bullet+}$, DPPH, and galvinoxyl radical, respectively, and to inhibit the oxidations of DNA caused by $^{\bullet}OH$, Cu^{2+}/GSH, and AAPH, respectively, are estimated to reveal the role of the coumestan scaffold in the generation of antioxidant effectiveness.

MATERIALS AND METHODS

Materials and Instrumentation. ABTS, DPPH, and galvinoxyl radicals were purchased from Fluka Chemie GmbH, Switzerland, and AAPH and naked DNA sodium salt were purchased from Acros Organics, Belgium. Other agents were of analytical grade and used directly. The structures of products were identified by ^1H and ^{13}C NMR (Bruker Avance III 400 MHz sprctrometer), and the spectra are included in the Supporting Information.

Synthesis and Identification of Coumestan Structure. Esterification of Methyl Salicylate. To a mixture of methyl salicylate (1.52 g, 10 mmol) and the corresponding phenylacetic acid (11 mmol) in 10 mL of pyridine at 0−10 °C was added dropwise $POCl_3$ (1.1 mL, 12 mmol) within 0.5 h under stirring. After the above mixture was stirred for 3 h at 0−10 °C, the concentrated HCl was added to adjust pH 5−6 at the same temperature. The mixture was extracted by ethyl acetate at room temperature, and the organic phase was washed by brine and dried over Na_2SO_4. After the solvent was evaporated under vacuum, the obtained crude product was purified by silica chromatography with ethyl acetate and petroleum ether being eluents to afford a white product with a yield >70%.

Ester Condensation for the Formation of Coumarins. The phenylacetic ester of methyl salicylate (5 mmol) was mixed with anhydrous pyridine (5 mL), followed by the addition of KOH powder (0.7 g, 12.5 mmol) at room temperature. After the mixture was stirred for 6 h in a nitrogen atmosphere, pyridine was evaporated under vacuum, and 15 mL of NaOH (2.0 M) was added. The water phase was washed with ethyl acetate and then acidized by concentrated HCl to adjust the pH to 4−5. The aqueous solution was cooled to afford the crude product, a white solid with a yield >55%.

Oxidative Annulation for the Formation of Coumestans. To 30 mL of dried 1,2-dichloroethane solution of the ester condensation products (2.5 mmol) were added anhydrous $FeCl_3$ (1.625 g, 10 mmol) and silica powder (1.625 g), and the mixture was refluxed for 10 h. The solvent was then evaporated under vacuum, and the residue was purified by silica chromatography with ethyl acetate and petroleum ether being eluents to afford white coumestans with yields >60%.

To obtain hydroxyl-substituted coumestan, the methoxyl group should be converted into a hydroxyl group by demethylation. In brief, methoxyl-substituted coumestan (1.0 mmol, dissolved in 10 mL of anhydrous CH_2Cl_2) was added dropwise to 10 mL of CH_2Cl_2 solution of BBr_3 (1.0 M) within 30 min at 0 °C and stirred overnight at room temperature. The reaction mixture was hydrolyzed at 0 °C. The obtained precipitate was purified by silica chromatography with ethyl acetate and petroleum ether (1:2, v/v) being eluent to afford a white product with a yield >90%.

*6H-Benzofuro[3,2-c]chromen-6-one (**1**):* R_f = 0.40 (ethyl acetate/petroleum ether = 1:9, v/v), 0.38 g of white product, yield 64%; mp 177−179 °C; ^1H NMR (400 MHz, $CDCl_3$) δ 8.15 (d, J = 4.8 Hz, 1H), 8.04 (d, J = 7.2 Hz, 1H), 7.60−7.68 (m, 2H), 7.42−7.52 (m, 4H); ^{13}C NMR (100 MHz, $CDCl_3$) δ 159.9, 157.9, 155.4, 153.6, 131.9, 126.7, 125.2, 124.6, 123.4, 121.8, 121.8, 117.4, 112.5, 111.7, 105.8.

*9-Methoxy-6H-benzofuro[3,2-c]chromen-6-one (**2**):* R_f = 0.31 (ethyl acetate/petroleum ether = 1:9, v/v), 0.59 g of white product, yield 89%; mp 217−219 °C; ^1H NMR (400 MHz, $CDCl_3$) δ 7.98 (s, 2H), 7.57 (s, 1H), 7.50 (s, 1H), 7.40 (s, 1H), 7.19 (s, 1H), 7.07 (s, 1H), 3.91 (s, 3H); ^{13}C NMR (100 MHz, $CDCl_3$) δ 159.7, 159.3, 158.2, 156.8, 153.2, 131.3, 124.6, 122.0, 121.5, 117.4, 116.5, 113.6, 112.9, 106.1, 96.8, 55.9.

*8,9-Dimethoxy-6H-benzofuro[3,2-c]chromen-6-one (**3**):* R_f = 0.46 (ethyl acetate/petroleum ether = 3:7, v/v), 0.64 g of white product, yield 86%; mp 213−215 °C; ^1H NMR (400 MHz, $CDCl_3$) δ 7.97 (d, J = 7.6 Hz, 1H), 7.48−7.59 (m, 3H), 7.40 (t, J = 7.6 Hz, 1H), 7.21 (s, 1H), 4.01 (s, 3H), 4.00 (s, 3H); ^{13}C NMR (100 MHz, $CDCl_3$) δ 158.7, 158.3, 152.9, 150.2, 149.5, 148.1, 131.0, 124.5, 121.2, 117.3, 115.2, 112.8, 106.1, 102.1, 95.4, 56.4, 56.3.

*9-Chloro-6H-benzofuro[3,2-c]chromen-6-one (**4**):* R_f = 0.32 (ethyl acetate/petroleum ether = 1:19, v/v), 0.59 g of white product, yield 87%; mp 242−244 °C; ^1H NMR (400 MHz, $CDCl_3$) δ 8.01−8.06 (m, 2H), 7.69 (s, 1H), 7.63 (t, J = 8.0 Hz, 1H), 7.50−7.53 (m, 1H), 7.41−7.47 (m, 2H); ^{13}C NMR (100 MHz, $CDCl_3$) δ 160.5, 157.7, 155.5, 153.8, 132.7, 132.3, 130.7, 128.8, 126.1, 124.8, 122.4, 121.9, 117.6, 112.5, 112.4.

*9-Bromo-6H-benzofuro[3,2-c]chromen-6-one (**5**):* R_f = 0.39 (ethyl acetate/petroleum ether = 1:9, v/v), 0.42 g of white product, yield 53%; mp 213−215 °C; ^1H NMR (400 MHz, $CDCl_3$) δ 8.03 (t, J = 8.0 Hz, 2H), 7.87 (d, J = 1.2 Hz, 1H), 7.61−7.68 (m, 2H), 7.53−7.55 (m, 1H), 7.45 (t, J = 7.6 Hz, 1H); ^{13}C NMR (100 MHz, $CDCl_3$) δ 160.3, 157.7, 155.6, 153.8, 132.3, 128.8, 124.8, 122.7, 122.6, 121.9, 120.1, 117.6, 115.4, 112.3, 105.6.

*9-Hydroxy-6H-benzofuro[3,2-c]chromen-6-one (**6**):* R_f = 0.29 (ethyl acetate/petroleum ether = 1:2, v/v), 0.24 g of white product, yield 96%; mp 291−293 °C; ^1H NMR (400 MHz, DMSO-d_6) δ 10.16 (s, 1H), 8.03 (s, 1H), 7.78 (s, 1H), 7.69 (s, 1H), 7.60 (m, 1H), 7.49 (s, 1H), 7.22 (s, 1H), 7.00 (s, 1H); ^{13}C NMR (100 MHz, DMSO-d_6) δ 158.1, 157.7, 157.1, 156.4, 152.5, 131.5, 124.9, 121.2, 121.1, 117.0, 114.4, 114.3, 112.1, 105.3, 98.6.

*8,9-Dihydroxy-6H-benzofuro[3,2-c]chromen-6-one (**7**):* R_f = 0.18 (ethyl acetate/petroleum ether = 1:2, v/v), 0.24 g of white product, yield 91%; mp > 300 °C; ^1H NMR (400 MHz, DMSO-d_6) δ 9.65 (s, 1H), 9.53 (s, 1H), 8.00 (d, J = 8.0 Hz, 1H), 7.64−7.68 (m, 1H), 7.57−7.59 (m, 1H), 7.48 (t, J = 7.6 Hz, 1H), 7.30 (s, 1H), 7.24 (s, 1H); ^{13}C NMR (100 MHz, DMSO-d_6) δ 158.2, 157.9, 152.8, 149.9, 147.0, 145.2, 131.7, 125.4, 121.6, 117.5, 114.3, 112.9, 106.0, 105.4, 99.4.

Scavenging $ABTS^{\bullet+}$, DPPH, and Galvinoxyl Radicals. A 2.0 mL of aqueous solution containing 4.0 mM ABTS and 1.41 mM $K_2S_2O_8$ was kept for 20 h to form $ABTS^{\bullet+}$ and then diluted by 100 mL of ethanol. The absorbance of $ABTS^{\bullet+}$ was around 1.00 at 734 nm ($\varepsilon_{ABTS^{\bullet+}} = 1.6 \times 10^4\ M^{-1}\ cm^{-1}$). DPPH and galvinoxyl radicals were dissolved in ethanol directly. The absorbances of DPPH and galvinoxyl radicals were around 1.00 at 517 nm ($\varepsilon_{DPPH} = 4.09 \times 10^3\ M^{-1}\ cm^{-1}$) and 428 nm ($\varepsilon_{galvinoxyl} = 1.4 \times 10^5\ M^{-1}\ cm^{-1}$), respectively. A certain concentration of DMSO solution of a coumestan (0.1 mL) was added to 1.9 mL of $ABTS^{\bullet+}$, DPPH, and galvinoxyl radical solutions, respectively. The decreases of the absorbance of these radicals were recorded at 25 °C at a certain time interval.

Cu^{2+}/GSH- and $^{\bullet}OH$-Induced Oxidations of DNA. Cu^{2+}/GSH-induced oxidation of DNA was carried out according to the following description. Briefly, DNA, $CuSO_4$, and GSH were dissolved in phosphate-buffered solution (PBS_1: 6.1 mM Na_2HPO_4, 3.9 mM NaH_2PO_4), and coumestans were dissolved in dimethyl sulfoxide (DMSO) as the stock solution. Then, a solution of 2.0 mg/mL DNA, 5.0 mM Cu^{2+}, 3.0 mM GSH, and 0.2 mM coumestan was poured into test tubes with each containing 2.0 mL. The test tubes were incubated at 37 °C for initiating the oxidation of DNA. Three test tubes were taken out at 90 min and cooled immediately. PBS_1 solution of EDTA (1.0 mL, 30.0 mM) was added to chelate Cu^{2+}, followed by adding 1.0 mL of thiobarbituric acid (TBA) solution (1.00 g of TBA and 0.40 g of NaOH dissolved in 100 mL of PBS_1) and 1.0 mL of 3.0% trichloroacetic acid aqueous solution. The test tubes were heated in boiling water for 30 min and cooled to room temperature, and 1.5 mL of *n*-butanol was added and shaken vigorously to extract thiobarbituric acid reactive substance (TBARS) for measuring the absorbance at 535 nm.

$^{\bullet}OH$ can be generated in the mixture of H_2O_2 and tetrachlorohydroquinone (TCHQ, dissolved in DMSO as the stock solution). DNA and H_2O_2 were dissolved in phosphate-buffered solution (PBS_2: 8.1 mM Na_2HPO_4, 1.9 mM NaH_2PO_4, 10.0 μM EDTA). A solution of 2.0 mg/mL DNA, 4.0 mM TCHQ (dissolved in DMSO as the stock solution), 2.0 mM H_2O_2, and 0.2 mM coumestan (dissolved in DMSO as the stock solution) was poured into test tubes with each containing

dx.doi.org/10.1021/jf500013v | J. Agric. Food Chem. 2014, 62, 5636−5642

2.0 mL. The test tubes were incubated at 37 °C for initiating the oxidation of DNA. Three test tubes were taken out at 30 min and cooled immediately. Then, 1.0 mL of TBA solution (1.00 g of TBA and 0.40 g of NaOH dissolved in 100 mL of PBS_2) and 1.0 mL of 3.0% trichloroacetic acid aqueous solution were added and heated in boiling water for 30 min. After the test tubes were cooled to room temperature, 1.5 mL of *n*-butanol was added and shaken vigorously to extract TBARS for measuring the absorbance at 535 nm. In the aforementioned two tests, the absorbances in the control experiment and in the presence of coumestans were assigned as A_0 and A_{detect}, respectively. The effects of coumestans on the oxidation of DNA were expressed by $A_{detect}/A_0 \times 100$.

AAPH-Induced Oxidation of DNA Test. A solution of 2.0 mg/mL DNA (dissolved in PBS_2), 40 mM AAPH (dissolved in PBS_2), and a certain concentration of a coumestan (dissolved in DMSO as the stock solution) was poured into test tubes with each containing 2.0 mL. The test tubes were incubated at 37 °C for initiating the oxidation of DNA. Three of them were taken out every 2 h and cooled immediately. Then, 1.0 mL of TBA solution (1.00 g of TBA and 0.40 g of NaOH dissolved in 100 mL of PBS_2) and 1.0 mL of 3.0% trichloroacetic acid aqueous solution were added and heated in boiling water for 15 min. After the test tubes were cooled to room temperature, 1.5 mL of *n*-butanol was added and shaken vigorously to extract TBARS for measuring the absorbance at 535 nm. The absorbance of TBARS was plotted versus the reaction period.

Statistical Analysis. All of the data were the average value from at least three independent measurements with the experimental error within 10%. The equations were analyzed by one-way ANOVA in Origin 6.0 professional software, and $p < 0.001$ indicated a significance difference.

RESULTS AND DISCUSSION

Synthesis of Coumestans and Scavenging Radicals. As a naturally occurring oxygen-abundant tetracycle, the structure of coumestan contains a coumarin and a benzofuran with a C═C shared by the lactone of coumarin and the furan ring. In the past decade, efforts contributing to the synthesis of coumestan have mainly focuseed on constructing the lactone ring.[10,11] The applications of some reactions such as Sonogashira and Suzuki coupling conditions simplify the ring closure of lactone in coumarin,[12,13] but the difficulty in the preparation of catalysts still limits the widespread use of the aforementioned method in the synthesis of coumestans. As shown in Scheme 2, we herein follow another paper, in which furan ring closure acts as the key step catalyzed by $FeCl_3$.[14]

$FeCl_3$ drives the dehydrogenation from the aromatic ring (D) and hydroxyl group (attaching to ring B) to form a furan ring in the refluxing 1,2-dichloroethane. An intramolecular ester condensation in phenylacetate of methyl salicylate leads to the formation of lactone in coumarin before the final step. Therefore, it can be found that substituents in coumestan should be allocated at phenylacetic acid and methyl salicylate in advance. In this work, chloro-, bromo-, and single- or double-methoxyl-substituted phenylacetic acids are used as the reagents, and the substituents locate at the benzofuran ring of coumestans. We herein used the results from our previous studies (shown in Scheme 3) to emphasize the importance of the coumestan structure for enhancing the antioxidant effectiveness. Therefore, xanthotoxol is selected as the model for a multiheterocycle containing a single hydroxyl group, whereas compounds MPCP and **4a** are chosen to be the model for a catechol moiety linking with coumarin via a single C−C bond. The antioxidant effect of the hydroxyl group in xanthotoxol, a furan-substituted coumarin, is not high enough.[15] In comparison with the high antioxidant effectives of coumestan, it can be concluded that a hydroxyl group directly attaching to the coumarin scaffold cannot exhibit high antioxidant effectiveness, but the coumarin scaffold can increase the antioxidant effectiveness of the hydroxyl group attaching to coumestan. Moreover, our previous research indicates that the hydroxyl group at coumarin in compound **4a** (see Scheme 3, the stoichiometric factor, *n*, is 6.15, for the physical meaning, see below) cannot improve the antioxidant effectivess of catechol moiety. Contrarily, a hydroxyl-free coumarin moiety enhances the antioxidant effectiveness of compound MPCP (see Scheme 3, the stoichiometric factor, *n*, is 6.60).[16] By comparing the stoichiometric factors (n) of compound **4a** and MPCP, it can be concluded that coumarin cannot remarkably influence the antioxidant effectiveness of the catechol moiety linking coumarin with a single C−C bond. Therefore, the result presented herein reveals that the benzofuran in combination with the coumarin scaffold is able to generate high antioxidant effectiveness even without an attached hydroxyl group.

Scheme 2. Synthetic Routines of Coumestans

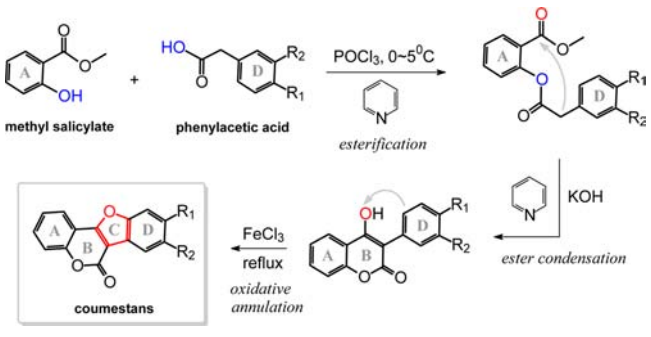

Scavenging radicals is regarded as the primary property of an antioxidant, and $ABTS^{\bullet+}$, DPPH, and galvinoxyl radicals are stable radicals at ambient temperature for evaluating the abilities of the antioxidant to reduce and to donate its hydrogen atom to N- and O-centered radicals, respectively.[17] Figure 1S in the Supporting Information outlines rapid decays of the concentrations of these radicals in the presence of coumestans. The coumestans are able to quench these radicals even in the absence of a hydroxyl group, indicating that the hydroxyl group is not a necessary functional group for coumestans to quench radicals. In addition to some thermodynamic methods for expressing the radical-scavenging ability of the antioxidant,[18] kinetic parameters such as the rate constant (k) can reveal the reaction rate between an antioxidant and a radical. We herein apply the rate constant to characterize the radical-scavenging abilities of coumestans. It has been proved that the reaction between an antioxidant and DPPH follows second-order kinetics as shown in eq 1.[19]

$$-\frac{\mathrm{d[DPPH]}}{\mathrm{d}t} = r = k[\mathrm{DPPH}][\mathrm{antioxidant}] \quad (1)$$

The above equation expresses the relationship among the concentrations of two reagents and the reaction rate (r) during the whole reaction period. Thus, eq 1 is also available when the reaction time is 0, and $[\mathrm{DPPH}]_{t=0}$ and $[\mathrm{antioxidant}]_{t=0}$ represent the concentrations of DPPH and the antioxidant at the beginning of the reaction. If the reaction rate at the beginning of the reaction (r_0) is measured according to the method in a previous paper[20] (data in Table 1S), the rate constant (k) can be calculated by using eq 2:

dx.doi.org/10.1021/jf500013v | J. Agric. Food Chem. 2014, 62, 5636−5642

Scheme 3. Contributions of Coumarin and Furan Moieties to the Antioxidant Effects

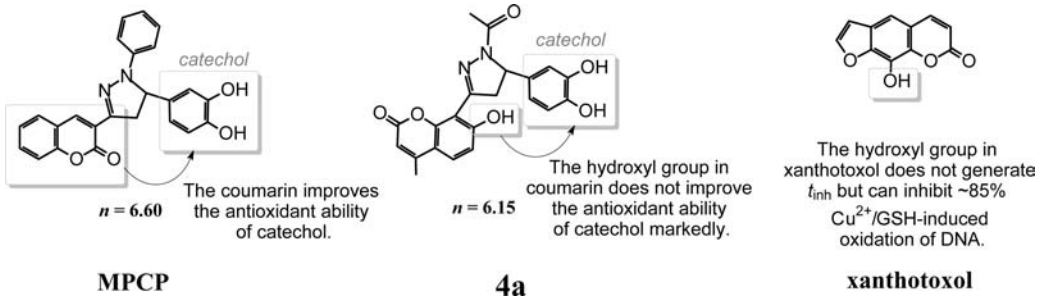

$$r_0 = k[\mathrm{DPPH}]_{t=0}[\mathrm{antioxidant}]_{t=0} \quad (2)$$

On the basis of the above method,[20] the rate constants (k) of coumestans in trapping $ABTS^{\bullet+}$, DPPH, and galvinoxyl radicals are obtained and listed in Table 1. It is worth noting that the reaction between an antioxidant and a radical behaves as first-order when the concentration of the antioxidant is in excess of the radical, but the concentration of the antioxidant should exceed that of the radical for ~100-fold to keep the concentration of the antioxidant almost constant during the reaction. As listed in the footnote of Table 1S, the antioxidant concentrations used herein are generally in excess of that of radicals by 5−10-fold, and thus, the reaction rate cannot be readily obtained following the first-order kinetics. As pointed out in eq 1, the reaction rate is simultaneously related to the concentrations of the antioxidant and the radical. Hence, a double-exponential function is selected to express the correlation of the reaction rate with the concentrations of two reagents to precisely estimate the reaction rate as shown in Table 1S, of which the important data are collected in Table 1. The data in the second column of Table 1 show that the k values of coumestans in trapping $ABTS^{\bullet+}$ are lower than that of Trolox. The reaction of an antioxidant with $ABTS^{\bullet+}$ shows the ability of the antioxidant to reduce the radical, and the coumestans possess low abilities to reduce the radical. This can be understood from a previous paper,[21] in which the oxidative potential of compound **7** (591.4 mV), a hydroxyl-substituted coumestan, is higher than that of general phenolic antioxidants. Therefore, the reductive ability of the coumestan is still dependent upon the phenolic hydroxyl group. On the other hand, the data in the third column of Table 1 show that the k values of coumestans in trapping DPPH are higher than that of Trolox (0.353 mM^{-1} s^{-1}). In particular, the k values of compounds **6** and **7** are as high as 7.20 and 14.81 mM^{-1} s^{-1}, respectively, and the k values of compounds **1**−**5** range from 0.6 to 1.0 mM^{-1} s^{-1}. The reaction between an antioxidant and DPPH shows the ability of the antioxidant to donate its hydrogen atom or electron to N-centered radicals, so the hydrogen atom of the hydroxyl group in coumestan still plays the major role in quenching N-centered radicals, and the coumestan scaffold (without the hydroxyl group attached) can also provide the electron for N-centered radicals. This is in agreement with a previous study on coumestan with electron-transferring efficiency higher than that of other phenols.[22] In this work,[22] coumestan was applied to modify an electrode for electro-oxidizing hydrazine with the anodic peak potential being 320 mV, whereas the oxidation cannot take place until 1100 mV on an unmodified electrode, demonstrating that coumestan plays the electron-transferring role in the oxidation at the electrode. This can be understood by eq 3 (see below), in which the cleavage of the C−O bond generates double single electrons for accepting electrons from other species. However, the electron-donating activity of coumestan also depends upon the electron receptor because, as can be seen from the data in the fourth column of Table 1, the coumestans used herein exhibit different properties in reacting with DPPH and galvinoxyl radicals. The hydroxyl-involved coumestans such as compounds **6** and **7** possess higher k values (2.40 and 6.99 mM^{-1} s^{-1}, respectively) than Trolox (1.70 mM^{-1} s^{-1}) in quenching the galvinoxyl radical, whereas the k values for compounds **1**−**5** (ranging from 0.1 to 0.5 mM^{-1} s^{-1}) are lower than that of Trolox. The galvinoxyl radical as an O-centered radical accepts the hydrogen atom from the hydroxyl group of coumestans readily but shows difficulty in accepting the electron from the coumestan scaffold. The hydroxyl group other than the coumestan scaffold plays the major role in quenching the O-centered radical. Thus, the coumestan scaffold can also be an electron donator for quenching radicals. This finding encourages us to test whether the radical-scavenging property of coumestans can also be applied to inhibit radical-mediated oxidation of biological species.

Table 1. Rate Constant (k) for Coumestans and Trolox in Scavenging $ABTS^{\bullet+}$, DPPH, and Galvinoxyl Radicals

	rate constant for coumestans and Trolox in scavenging radicals, k (mM^{-1} s^{-1})		
compd	$ABTS^{\bullet+}$	DPPH	galvinoxyl radical
1	0.14	0.73	0.17
2	0.19	0.65	0.34
3	0.14	1.02	0.14
4	0.23	0.79	0.34
5	0.25	0.79	0.44
6	3.06	7.20	2.40
7	8.95	14.81	6.99
Trolox	29.2	0.353	1.70

Inhibiting Cu^{2+}/GSH and $^{\bullet}OH$-Induced Oxidations of DNA. GSH can be oxidized by copper ions (Cu^{+} and Cu^{2+}) to form the glutathione radical ($GS^{\bullet}$) in vivo,[23] and $^{\bullet}OH$ is a well-known radical generated from the metabolism in the process of in vivo oxidative stress.[24] Both $GS^{\bullet}$ and $^{\bullet}OH$ are harmful radicals that can initiate oxidative damage of biological species, in which DNA is one of the susceptible biological species to the aforementioned radicals. The in vitro oxidations of DNA caused by $GS^{\bullet}$ and $^{\bullet}OH$ can be used as the experimental system for evaluating the antioxidant activity because the oxidative products from the oxidation of DNA can be readily detected after reaction with TBARS.[25] Thus, the activities of coumestans are characterized by inhibiting Cu^{2+}/GSH- and $^{\bullet}OH$-induced oxidations of DNA. The absorbances of TBARS

dx.doi.org/10.1021/jf500013v | J. Agric. Food Chem. 2014, 62, 5636−5642

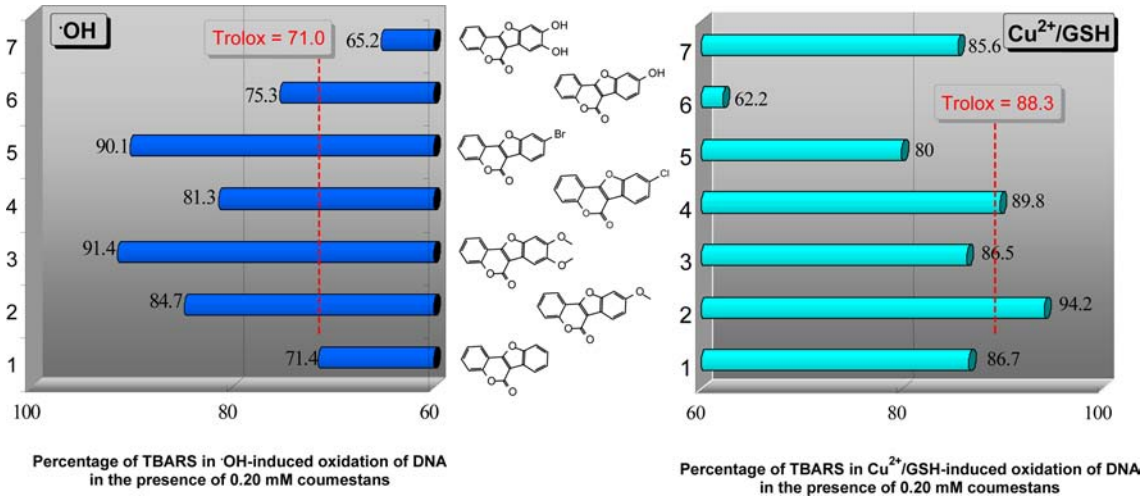

Figure 1. Percentage of TBARS in the presence of 0.20 mM coumestans when the oxidation of DNA (2.0 mg/mL) is caused by 5.0 mM Cu^{2+} and 3.0 mM GSH for 90 min (right panel) or 4.0 mM H_2O_2 and 2.0 mM tetrachlorohydroquinone (TCHQ) for 30 min (left panel).

when DNA undergoes Cu^{2+}/GSH-induced oxidation for 90 min and •OH-induced oxidation for 30 min are assigned to be 100% as the control. The absorbances of TBARS in the presence of 0.20 mM various coumestans and Trolox are compared with the control and shown in Figure 1, in which a low percentage of TBARS means a high antioxidant effectiveness.

The data in Figure 1 show that all of the coumestans used herein can inhibit both Cu^{2+}/GSH- and •OH-induced oxidations of DNA, and thus coumestans either containing a hydroxyl group or not behave as antioxidants to protect DNA against the aforementioned oxidative damage. Especially, the TBARS percentage of Trolox in inhibiting •OH-induced oxidation of DNA (71.0%) is similar to that of compound **1** (71.4%), revealing that the coumestan scaffold is able to protect DNA against •OH-induced oxidation. Compound **7** generates a low TBARS percentage (65.2%), because it contains double hydroxyl groups at adjacent positions, a classic structure for antioxidant. The TBARS percentages in the presence of other coumestans (compounds **2**–**6**) are higher than that of compound **1**, indicating that substituents are not beneficial for enhancing the antioxidant abilities of coumestans in this case. In the experimental system of Cu^{2+}/GSH-induced oxidation of DNA, the TBARS percentage in the presence of compound **1** (86.7%) also approaches that of Trolox (88.3%), indicating that the unsubstituted coumestan can also protect DNA against Cu^{2+}/GSH-induced oxidation. Moreover, as reported in our previous work, xanthotoxol (structure in Scheme 3) decreases the TBARS percentage only to 85%,[15] similar to that of the coumestan (86.7%). Therefore, one hydroxyl group attaching to the coumarin moiety (as xanthotoxol) results in the same antioxidative efficiency as the coumestan scaffold (without any substituents attached). Moreover, a hydroxyl group attaching to coumestan as in compound **6** decreases the TBARS percentage to 62.2%, indicating that one hydroxyl group attached to the benzofuran moiety leads to a high activity for coumestan to inhibit Cu^{2+}/GSH-induced oxidation of DNA. The TBARS percentages of other coumestans (compounds **2**–**5** and **7**) are around that of coumestan (86.7 ± 10%), implying that these substituents do not influence the inhibiting effects of coumestans on Cu^{2+}/GSH-induced oxidation of DNA markedly. The antioxidant mechanism of hydroxyl-substituted coumestan is undoubtedly attributed to the hydroxyl group providing a hydrogen atom to quench radicals. •OH is so reactive that it can attack any part of the molecule, including the aromatic rings. However, in a previous study the lactone of the coumarin moiety is hypothesized to be the receptor for the nucleophilic addition.[26] This may be a mechanism for coumestan to scavenge radicals. As shown in eq 3, the homolytic cleavage of the ester bond in the lactone (the only bond not participating in the aromatic system of coumestan) generates two single electrons, which can recombine with other radicals. Therefore, it is necessary to measure how many radicals can be trapped by one molecule of coumestan.

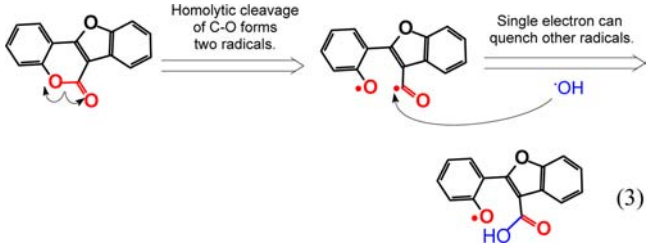

(3)

Inhibiting AAPH-Induced Oxidation of DNA. The AAPH-induced oxidation of DNA is selected to be the experimental system[27] because the number of radicals trapped by an antioxidant in this case can be calculated according to chemical kinetic deduction,[28] and the oxidative products from DNA can be followed by measuring TBARS as well. We have measured the numbers of radicals trapped by some antioxidants in this experimental system,[29] and here we also adopt the same experimental system for quantitatively comparing the antioxidant effectiveness of coumestans. Therefore, as shown in Figure 2S, an increase of the absorbance means that much TBARS is generated the longer the reaction time in the blank experiment. However, the addition of coumestan hinders the formation of the TBARS for a period, and then the TBARS are produced as in the blank experiment. The inhibition period (t_{inh}) can be measured from the beginning of the reaction to the cross point of tangents for the inhibition and the increasing period in the absorbance line. The relationships between t_{inh} and the concentrations of coumestans are outlined in Figure 3S

dx.doi.org/10.1021/jf500013v | J. Agric. Food Chem. 2014, 62, 5636−5642

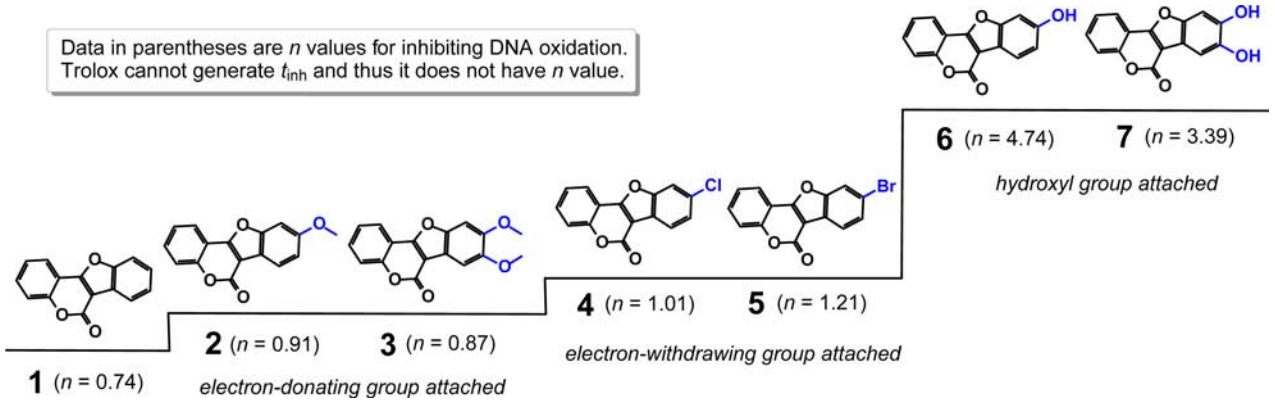

Figure 2. *n* values of coumestans in inhibiting 40 mM AAPH-induced oxidation of 2.0 mg/mL DNA at 37 °C.

and expressed by the equation of $t_{inh} \sim$ [coumestans] (listed in Table 2S). On the basis of the equation $t_{inh} \sim$ [coumestans], the number of radicals trapped by coumestans can be calculated following chemical kinetics.

In view of chemical kinetics, the t_{inh} correlates proportionally with the concentration of an antioxidant as shown as in eq 4:[30]

$$t_{inh} = (n/R_i)[\text{antioxidant}] \quad (4)$$

R_i refers to the initiation rate of the radical-induced reaction. Both AAPH and the sodium salt of DNA are water-soluble compounds, and radicals generated from AAPH can attack DNA at the same phase. R_i is thereby assumed to be equal to the radical generation rate (R_g, $R_g = (1.4 \pm 0.2) \times 10^{-6}$[AAPH] s^{-1}[30]). *n* stands for stoichiometric factor, which is the number of the radicals trapped by one molecule of the antioxidant. The coefficient in the equation of $t_{inh} \sim$ [coumestan] is equivalent to (n/R_i) in eq 4. Hence, when $R_i = R_g = 1.4 \times 10^{-6} \times 40$ mM s^{-1} = 3.36 μM min^{-1} in this experimental system, the *n* value is the product of the coefficient in the equation of $t_{inh} \sim$ [coumestan] and R_i. The obtained *n* values of coumestans (listed in Table 2S) are outlined at different steps in Figure 2, in which the structures of coumestans are involved for revealing the influence of coumestan structure on *n* values.

The data in Figure 2 show that compounds **1**−**3** can scavenge less than one radical and compounds **4** and **5** can trap about one radical. The coumestans even in the absence of hydroxyl groups or in the presence of electron-withdrawing groups such as −Cl and −Br are still able to inhibit AAPH-induced oxidation of DNA. Interestingly, compounds **6** and **7** can trap 4.74 and 3.39 radicals, respectively, revealing that the phenolic hydroxyl group remarkably improves the antioxidant abilities of coumestans. However, compound **6**, a single-hydroxyl-substituted coumestan, can trap more radicals (*n* = 4.74) than compound **7**, a double-hydroxyl-substituted coumestan (*n* = 3.39), revealing that compound **6** exhibits a higher antioxidant effect than compound **7**. This is in agreement with the observation on Cu^{2+}/GSH-induced oxidation of DNA, in which compound **6** is a stronger antioxidant than compound **7**. On the other hand, as shown in Scheme 3, MPCP and **4a** are coumarin-substituted dihydropyrazoles with 6.60 and 6.15 *n* values, respectively,[16] higher than that of coumestans used herein. Therefore, the coumarin moiety as a single substituent can improve the antioxidant effect of the catechol moiety within the same molecule. On the contrary, the coumarin moiety as a part of the tetracycle cannot markedly ameliorate the antioxidant effect of the catechol moiety. Figure 2 also shows that the *n* values of compounds **2** and **3** (0.91 and 0.87, respectively) are lower than those of compounds **4** and **5** (1.01 and 1.21, respectively), indicating that an electron-withdrawing group such as −Cl or −Br can improve the antioxidant effect more than the electron-donating group such as $-OCH_3$ and double $-OCH_3$. This fact can be understood from eq 3. The formation of a radical by the cleavage of lactone is the key step for coumestan to accommodate the single electron from other radicals. An electron-withdrawing group is beneficial for coumestan to dispense electrons around the benzofuran and phenolic rings. Furthermore, we have also detected the effects of Trolox and xanthotoxol on AAPH-induced oxidation of DNA.[15] It is found that Trolox and xanthotoxol just affect the increasing rate of TBARS and cannot generate t_{inh}, leading to the *n* values of Trolox, and xanthotoxol cannot be obtained. Thus, coumestan (compound **1** with a 0.74 *n* value) possesses a higher antioxidant effect than Trolox and xanthotoxol.

In conclusion, as a naturally occurring structure, coumestans exhibit wide antioxidant properties, which are attributed not only to the hydroxyl group but to the coumestan scaffold donating or accommodating a single electron. On the contrary, substituents are not beneficial for enhancing antioxidant effectiveness when coumestans are applied to inhibit Cu^{2+}/GSH- and $^{\bullet}OH$-induced oxidations of DNA. In addition, the coumestan scaffold is more active in inhibiting AAPH-induced oxidation than Trolox and xanthotoxol. Therefore, the hydroxyl group may not be a necessary factor in inhibiting radical-mediated oxidation of DNA, and the lactone shared with other heterocycles may be a novel structural feature in antioxidants.

■ ASSOCIATED CONTENT

Ⓢ Supporting Information

Additional experimental details. This material is available free of charge via the Internet at http://pubs.acs.org.

■ AUTHOR INFORMATION

Corresponding Author

*(Z.-Q. L.) Mail: Department of Organic Chemistry, College of Chemistry, Jilin University, No. 2519 Jiefang Road, Changchun 130021, China. E-mail: zaiqun-liu@jlu.edu.cn.

Funding

Financial support from the Jilin Provincial Science and Technology Department, China, is acknowledged gratefully (20130206075GX).

Notes

The authors declare no competing financial interest.

REFERENCES

(1) Kaushik-Basu, N.; Bopda-Waffo, A.; Talele, T. T.; Basu, A.; Costa, P. R.; da Silva, A. J.; Sarafianos, S. G.; Noël, F. Identification and characterization of coumestans as novel HCV NS5B polymerase inhibitors. *Nucleic Acids Res.* **2008**, *36*, 1482−1496.

(2) Xia, Y.; Chen, J.; Cao, Y.; Xu, C.; Li, R.; Pan, Y.; Chen, X. Wedelolactone exhibits anti-fibrotic effects on human hepatic stellate cell line LX-2. *Eur. J. Pharmacol.* **2013**, *714*, 105−111.

(3) Lim, S.; Jang, H.-J.; Park, E. H.; Kim, J. K.; Kim, J.-M.; Kim, E.-K.; Yea, K.; Kim, Y.-H.; Lee-Kwon, W.; Ryu, S. H.; Suh, P.-G. Wedelolactone inhibits adipogenesis through the ERK pathway in human adipose tissue-derived mesenchymal stem cells. *J. Cell. Biochem.* **2012**, *113*, 3436−3445.

(4) Li, L.; Deng, X.; Zhang, L.; Shu, P.; Qin, M. A new coumestan with immunosuppressive activities from *Flemingia philippinensis*. *Fitoterapia* **2011**, *82*, 615−619.

(5) Chen, Y.; Wei, X.; Xie, H.; Deng, H. Antioxidant 2-phenylbenzofurans and a coumestan from *Lespedeza virgata*. *J. Nat. Prod.* **2008**, *71*, 929−932.

(6) Pôças, E. S. C.; Touza, N. A.; da Silva, A. J. M.; Costa, P. R. R.; Noël, F. Synergistic interaction between ouabain and 8-methoxy-3,9-dihydroxy coumestan, a non-steroidal synthetic inhibitor of Na^+, K^+-ATPase. *Life Sci.* **2007**, *81*, 1199−1204.

(7) Zare, H. R.; Nasirizadeh, N.; Golabi, S.-M.; Namazian, M.; Mazloum-Ardakani, M.; Nematollahi, D. Electrochemical evaluation of coumestan modified carbon paste electrode: study on its application as a NADH biosensor in presence of uric acid. *Sensors Actuat. B* **2006**, *114*, 610−617.

(8) Benes, P.; Alexova, P.; Knopfova, L.; Spanova, A.; Smarda, J. Redox state alters anti-cancer effects of wedelolactone. *Environ. Mol. Mutagen.* **2012**, *53*, 515−524.

(9) Sakihama, Y.; Cohen, M. F.; Grace, S. C.; Yamasaki, H. Plant phenolic antioxidant and prooxidant activities: phenolics-induced oxidative damage mediated by metals in plants. *Toxicology* **2002**, *177*, 67−80.

(10) Chauder, B. A.; Kalinin, A. V.; Taylor, N. J.; Snieckus, V. Directed metalation linked to transition metal catalyzed cascade reactions: two total syntheses of plicadin, the alleged coumestan from *Psoralea plicata*. *Angew. Chem., Int. Ed.* **1999**, *38*, 1435−1438.

(11) Kraus, G. A.; Zhang, N. Hydrogen-atom abstraction/cyclization in synthesis. Direct syntheses of coumestan and coumestrol. *J. Org. Chem.* **2000**, *65*, 5644−5646.

(12) Li, C. C.; Xie, Z. X.; Zhang, Y. D.; Chen, J. H.; Yang, Z. Total synthesis of wedelolactone. *J. Org. Chem.* **2003**, *68*, 8500−8504.

(13) Liu, J.; Liu, Y.; Du, W.; Dong, Y.; Liu, J.; Wang, M. Pd-Catalyzed C-S activation for [3 + 3] annulation of 2-(methylthio)benzofuran-3-carboxylates and 2-hydroxyphenylboronic acids: synthesis of coumestan derivatives synthesis. *J. Org. Chem.* **2013**, *78*, 7293−7297.

(14) Tang, L.; Pang, Y.; Yan, Q.; Shi, L.; Huang, J.; Du, Y.; Zhao, K. Synthesis of coumestan derivatives via $FeCl_3$-mediated oxidative ring closure of 4-hydroxycoumarins. *J. Org. Chem.* **2011**, *76*, 2744−2752.

(15) Xiao, C.; Song, Z.-G.; Liu, Z.-Q. Synthesis of methyl-substituted xanthotoxol to clarify prooxidant effect of methyl on radical-induced oxidation of DNA. *Eur. J. Med. Chem.* **2010**, *45*, 2559−2566.

(16) Xi, G.-L.; Liu, Z.-Q. Antioxidant effectiveness generated by one or two phenolic hydroxyl groups in coumarin-substituted dihydropyrazoles. *Eur. J. Med. Chem.* **2013**, *68*, 385−393.

(17) Pinchuk, I.; Shoval, H.; Dotan, Y.; Lichtenberg, D. Evaluation of antioxidants: scope, limitations and relevance of assays. *Chem. Phys. Lipids* **2012**, *165*, 638−647.

(18) Munoz-Munoz, J. L.; Garcia-Molina, F.; Varon, R.; Tudela, J.; García-Cánovas, F.; Rodriguez-Lopez, J. N. Quantification of the antioxidant capacity of different molecules and their kinetic antioxidant efficiencies. *J. Agric. Food Chem.* **2010**, *58*, 2062−2070.

(19) Foti, M. C.; Daquino, C.; DiLabio, G. A.; Ingold, K. U. Kinetics of the oxidation of quercetin by 2,2-diphenyl-1-picrylhydrazyl (dpph$^\bullet$). *Org. Lett.* **2011**, *13*, 4826−4829.

(20) Wang, R.; Liu, Z.-Q. Solvent-free and catalyst-free Biginelli reaction to synthesize ferrocenoyl dihydropyrimidine and kinetic method to express radical-scavenging ability. *J. Org. Chem.* **2012**, *77*, 3952−3958.

(21) Namazian, M.; Zare, H. R. Computational electrode potential of a coumestan derivative: theoretical and experimental studies. *Biophys. Chem.* **2005**, *117*, 13−17.

(22) Zare, H. R.; Nasirizadeh, N. Electrocatalytic characteristics of hydrazine and hydroxylamine oxidation at coumestan modified carbon paste electrode. *Electroanalysis* **2006**, *18*, 507−512.

(23) Speisky, H.; Gómez, M.; Burgos-Bravo, F.; López-Alarcón, C.; Jullian, C.; Olea-Azar, C.; Aliaga, M. E. Generation of superoxide radicals by copper-glutathione complexes: redox-consequences associated with their interaction with reduced glutathione. *Bioorg. Med. Chem.* **2009**, *17*, 1803−1810.

(24) Jomova, K.; Vondrakova, D.; Lawson, M.; Valko, M. Metals, oxidative stress and neurodegenerative disorders. *Mol. Cell. Biochem.* **2010**, *345*, 91−104.

(25) Sugden, K. D.; Wetterhahn, K. E. Direct and hydrogen peroxide-induced chromium(V) oxidation of deoxyribose in single-stranded and double-stranded calf thymus DNA. *Chem. Res. Toxicol.* **1997**, *10*, 1397−1406.

(26) Pôças, E. S. C.; Touza, N. A.; Pimenta, P. H. C.; Leitão, F. B.; Neto, C. D.; da Silva, A. J. M.; Costa, P. R. R.; Noël, F. Insights into the mechanism of Na^+, K^+-ATPase inhibition by 2-methoxy- 3,8,9-trihydroxy coumestan. *Bioorg. Med. Chem.* **2008**, *16*, 8801−8805.

(27) Shao, J.; Geacintov, N. E.; Shafirovich, V. Oxidative modification of guanine bases initiated by oxyl radicals derived from photolysis of azo compounds. *J. Phys. Chem. B* **2010**, *114*, 6685−6692.

(28) McPherson, P. A. C.; Bole, A.; Cruz, K. A.; Young, I. S.; McEneny, J. A curvilinear approach to the kinetic analysis of linoleate peroxidation in aqueous liposomes by 2,2′-azobis(2-amidoino propane) dihydrochloride. *Chem. Phys. Lipids* **2012**, *165*, 682−688.

(29) Zhao, C.; Liu, Z.-Q. Diaryl-1,2,4-oxadiazole antioxidants: synthesis and properties of inhibiting the oxidation of DNA and scavenging radicals. *Biochimie* **2013**, *95*, 842−849.

(30) Bowry, V. W.; Stocker, R. Tocopherol-mediated peroxidation: the prooxidation effect of vitamin E on the radical-initiated oxidation of human low-density lipoprotein. *J. Am. Chem. Soc.* **1993**, *115*, 6029−6044.

JOURNAL OF AGRICULTURAL AND FOOD CHEMISTRY

Article

pubs.acs.org/JAFC

Characterizaiton of Barley Serpin Z7 That Plays Multiple Roles in Malt and Beer

Xiaomin Li,[†,‡,#] Zhao Jin,[†,‡,#] Fei Gao,[†,‡,#] Jian Lu,[†,*,‡,#,§] Guolin Cai,[†,‡,#] Jianjun Dong,[⊥] Junhong Yu,[⊥] and Mei Yang[⊥]

[†]The Key Laboratory of Industrial Biotechnology, Ministry of Education, Jiangnan University, 1800 Lihu Road, Wuxi 214122, People's Republic of China

[‡]National Engineering Laboratory for Cereal Fermentation Technology, Jiangnan University, 1800 Lihu Road, Wuxi 214122, People's Republic of China

[#]School of Biotechnology, Jiangnan University, 1800 Lihu Road, Wuxi 214122, People's Republic of China

[§]Industrial Technology Research Institute of Jiangnan University in Suqian, 888 Renmin Road, Suqian 223800, People's Republic of China

[⊥]State Key Laboratory of Biological Fermentation Engineering of Beer, Tsingtao Brewery Company, Ltd., Qingdao 266100, People's Republic of China

Supporting Information

ABSTRACT: Barley protein Z7 (BSZ7) is a well-known serine protease inhibitor that was regarded as a major effector of beer foam stability. Moreover, it has also been suggested to participate in haze formation and affect wort filterability. The present study purified BSZ7 from barley malt and characterized its secondary structure and modification, as well as its relationship with peroxidase, to elucidate the molecular base of BSZ7 that supports its multiple roles in malt and beer. It was found that after 30 min of heating, the secondary structure was not affected. BSZ7 has no inhibiting effect on nonspecific protease originated from malt, suggesting its negative role in wort filterability was accomplished by other means. Furthermore, the glycation of BSZ7 by the Maillard reaction may make some contribution to its survival during wort boiling. The interaction of BSZ7 with polysaccharides and polyphenols found by adding experiment may explain how it acts as a negative factor on wort filterability. Greater understanding of BSZ7 and other proteins of malts will lead to better improvements in brewing quality.

KEYWORDS: *BSZ7, secondary structure, glycation, melanoidins, wort filterability, peroxidase*

INTRODUCTION

Barley protein Z belongs to the serine protease inhibitor family (serpin). Due to the high lysine content, it acts as a storage protein in the endosperm. In addition, it is also responsible for defense against insect pathogens because of its protease-inhibiting activity.[1−3] Protein Z displays different isoforms, including protein Zx (BSZx), protein Z4 (BSZ4), and protein Z7 (BSZ7),[4] the latter two being major beer proteins with the capacity to survive during brewing.[5] The genes encoding BSZ4 and BSZ7 are present on chromosomes 4 and 7 of barley, respectively,[6] and BSZ4 comprises 80% of total protein Z in either barley or malt and thus is the predominant one.[7] Both of them are suggested to be positive effectors on foam stability.[8,9] BSZ7 was also found to be included in the silica eluent part during beer brewing, indicating it is a haze-forming protein in beer.[10] In our previous work, comparative proteomics was performed between Dan'er and Metcalfe malts showing different wort filterability, and multiple BSZ7 spots were found to be in more abundance in Dan'er malt, indicating its negative role in wort filterability.[11] Addition of BSZ7 to the mashing process significantly decreased the separation rate of wort, which further confirmed its effect on filterability.[11] Besides these, BSZ7 has been demonstrated to be an inhibitor of α-chymotrypsin.[12]

Although multiple roles of BSZ7 have been explored, the biochemical characterization of the protein was not fully studied. By Evans and Hejgaard,[7] the content of BSZ7 was observed to be 38−771 μg/g in barley seeds of 91 varieties and consisting of 397 amino acid residues with an apparent molecular mass of 39 kDa.[12,13] The primary structure of BSZ7 has been elucidated. BSZ7 shares 69, 72, and 71% identity with wheat chymotrypsin inhibitor WSZ1, barley BSZ4, and BSZx, respectively. Furthermore, BSZ7 shares 69−72 and 25−32% positional identity with plant and mammalian serpins. In the primary structure of BSZ7, four N-glycosylation sequences Asn-Xxx-Ser/Thr were found at positions 154, 171, 205, and 316, respectively.[13] The partial modification of lysine residues with sugars has been demonstrated by isoelectric focusing of protein Z.[14]

Dan'er and Metcalfe are typical malting malts in beer brewing. Dan'er is the most popular domestic barley in China. However, due to the deficiency in wort filterability of Dan'er malt, Metcalfe is imported from Canada every year and used for malting and brewing instead. In our previous study, proteomic

Received: December 19, 2013
Revised: May 8, 2014
Accepted: May 11, 2014
Published: May 12, 2014

ACS Publications © 2014 American Chemical Society

analysis and adding experiments confirmed the negative effect of BSZ7 on filterability.[11] Therefore, the two malts were selected for further purification and characterization of BSZ7 in the present study, to elucidate the structural and biochemical bases that support the multiple roles of BSZ7 during malting and brewing. More detailed analyses and better comprehension of BSZ7 may help improve brewing quality using the domestic barley Dan'er.

MATERIALS AND METHODS

Commercial Barley Malt. Samples of barley malts, the domestic Dan'er and the imprted Metcalfe, were collected from commercial maltsters in China and stored at 4 °C in our laboratory. Each maltster has its specialized malting conditions for these two barley cultivars. The Dan'er malt was produced with Dan'er barley that was harvested in 2011 in Jiangsu province of China. Barley of Metcalfe was harvested in 2011 in western Canada and imported to China for malting. Congress wort was obtained by the European Brewery Convention (EBC) Congress mash.

Total Protein Extraction from Malt and Wort of Dan'er and Metcalfe. Malt sample was ground into flour and then added into 5 times volume of 0.02 M PBS buffer (pH 5.5) supplemented with 0.1 M NaCl, to extract proteins at 4 °C overnight. The soluble proteins were obtained by centrifugation of crude extract at 4 °C (5000 *g*, 30 min) and precipitated with 100% saturation of ammonia sulfate. For wort sample, proteins were precipitated with 100% saturation of ammonia sulfate directly. All of the pellet was then resuspended in 0.02 M PBS buffer (pH 5.5) appending 0.1 M NaCl and then dialyzed against 2 L of the same buffer five times (4 h each time).

Purification of BSZ7 from Dan'er Malt. The soluble protein of Dan'er malt was fractionally precipitated with 20% and then 70% saturation of ammonia sulfate. The precipitant was collected and resuspended in 0.02 M PBS buffer (pH 5.5) containing 0.1 M NaCl and then dialyzed against 2 L of the same buffer five times (4 h each time). After that, the crude BSZ7 solution was incubated at 75 °C for 15 min to precipitate the hot unstable proteins, which were then removed by centrifugation at 10000 *g* for 15 min and filtered through a 0.22 μm membrane. The filtration was then loaded on a size exclusion column Hiload 26/60 Superdex 75 pg and then washed with 0.02 M PBS buffer (pH 5.5) containing 0.1 M NaCl at a flow rate of 2 mL/min. The eluted solutions were collected every 5 mL per tube. To discriminate the fraction containing BSZ7, 20 μL of sample in each tube was displayed on SDS-PAGE, and finally fractions containing the 39 kDa band corresponding to molecular weight of BSZ7 were pooled and concentrated by ultrafiltration for a second size exlusion column Hiload 26/60 Superdex 75 pg purification. After the two rounds of size exclusion purification, BSZ7 was collected and the protein concentration was analyzed using RC-DC quantity kit (GE Healthcare, Pittsburgh, PA, USA). To test the purity of collected BSZ7, 20 μL of sample was displayed on SDS-PAGE, and the corresponding band was then cut for MALDI-TOF/TOF identification. In detail, the 39 kDa band was manually excised from the SDS-PAGE gel and washed with the destaining buffer (25 mM ammonia sulfate, 50% (v/v) acetonitrile), followed by dehydration with 100% acetonitrile. The protein was in-gel digested by trypsin and then submitted to the Ultraflex MALDI-TOF/TOF mass spectrometer (Bruker-Daltonics Inc., Billerica, MA, USA) as described.[11]

Circular Dichroism (CD) Spectroscopy. BSZ7 was diluted with deionized water to a final concentration of 0.5 mg/mL and then submitted on the MOS-450 AF-CD (Biologic, France) for secondary structure determination. Far-ultraviolet (far-UV, 190−250 nm) and quartz cell with 0.2 mm path length were used. The secondary structure was analyzed with CONTIN software, and data were expressed as mean-residue ellipticity.

Hydrophobic Index Determination. A series of concentrations of BSZ7 (0.10, 0.15, 0.20, 0.25, 0.30, 0.35, and 0.40 mg/mL) was obtained by diluting the purified BSZ7 with 0.02 M PBS buffer (pH 7.0). Two hundred microliters of each sample was added to two separate wells of a 96-well plate, after which 2.5 μL of substrate solution (8 M 8-anilino-1-naphthalenesulfonate (ANS) dissolved in 0.02 M PBS buffer (pH 7.0)) was added to one well, whereas the other sample well without substrate buffer was used as blank control. The fluorescence intensity (FI) was determined using a SmartSpec microplate spectrophotometer (Bio-Rad, Hercules, CA, USA) with excitation and emission wavelengths at 390 and 470 nm, respectively. The protein hydrophobic index was calculated by plotting the FI on protein concentration. The hydrophobic index of total proteins in malt and wort of Dan'er and Metcalfe was detected with the same method.

Malt Nonspecific Protease Activity Assay. Protease was extracted with the following procedures. Three grams of finely ground malt was mixed with 30 mL of 0.1 M citric acid/Na_2PO_4 buffer (pH 5.2) and then incubated at 20 °C for 1 h in a water bath to extract the protease. The crude extracts were centrifuged at 8000*g* for 10 min and then filtered with Whatman no. 4 filter paper (Whatman PLC, Maidstone, UK). The supernatant was collected and stored for protease activity analysis at 680 nm by determining tyrosine produced. The reaction mixture for the hydrolysis reaction (2 mL) contained 1% (w/v) bovine hemoglobin in 0.1 M citric acid/Na_2PO_4 buffer (pH 5.2) and an appropriate amount of protease extract. Both the protease extract and bovine hemoglobin were preheated at 40 °C before being added into the assay mixture. Reactions were initiated by adding the protease extract and terminated by the addition of 0.4 M trichloroacetic acid (TCA) after incubation at 40 °C for 30 min. The mixture was then allowed to stand for 10 min to precipitate nonhydrolyzed proteins. For blank control, TCA was added together with the bovine hemoglobin before reaction initiation. All of the reactions were repeated in three parallels. After centrifugation, 1 mL of the supernatant was mixed with 5 mL of 0.4 M Na_2CO_3 and 1 mL of Folin's reagent and incubated at 40 °C for 20 min. Optical density was read at 680 nm, representing the tyrosine production. One unit of enzyme was defined as the amount of protease that produced 1 μg of tyrosine per minute at pH 5.2 and 40 °C.

Melanoidins Extraction and Detection. Malt melanoidins was extracted using an ethanol−water solution method.[15] Thirty grams of ground malt was added to 100 mL of 10% ethanol (v/v) and allowed to stand for 20 h to extract melanoidins. The crude extract was then centrifuged at 5000*g* for 10 min to remove insoluble material, after which the supernatant was added to ethanol to a final concentration of 65% and allowed to stand for 12 h to dissolve melanoidins. The ethanol was evaporated with a rotary evaporator RV10 (IKA, Staufen, Germany) before centrifugation. The corresponding supernatant was then mixed with isometric acetone to precipitate melanoidins and collected by centrifugation. As the acetone volatilized, melanoidins were resuspended with distilled water and dialyzed as soon as possible. The extracted melanoidins were separated by SDS-PAGE and detected with glycoprotein gel staining kit Protein Stains R (Sangon Biotech, Shanghai, China) following the manufacturer's instructions.

Adding Experiment of Purified BSZ7 to Mashing Process. A series of amounts of purified BSZ7 (0, 200, 400, and 600 μg/g malt) was added to the EBC Congress Mashing process with Dan'er malt. Macromolecular content and protease activity were measured as follows. The contents of arabinoxylan (AX), β-glucan, and polyphenaol were determined using the Douglas method,[16] Congo-Red method,[17] and Folin−Ciocalteu colorimetry,[18] respectively. High molecular weight protein (HWP) was precipitated with tannin[19] and then measured.

RESULTS AND DISCUSSION

Purification of BSZ7 from Dan'er Malt. BSZ7 is one of the thermally stable beer proteins that can survive during boiling. Therefore, the crude extracts were heated at 75 °C for 15 min prior to chromatographic separation, so that most of the hot unstable proteins were denatured and precipitated during the heating process. A few of the surviving proteins, including BSZ7, were then submitted to the Superdex G75 size exclusion column. All of the fractions collected were exhibited on SDS-PAGE gel (Figure 1a), and the one containing a single 39 kDa

band corresponding to BSZ7 was considered to be purified BSZ7, which was further confirmed by MALDI-TOF/TOF.

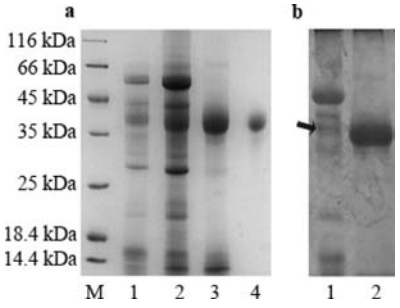

Figure 1. (a) SDS-PAGE of BSZ7 samples during the purification process: lane 1, crude extract; lane 2, salt fractionation; lane 3, heat treating; lane 4, size exclusion column. (b) SDS-PAGE of melanoidins and BSZ7 stained with the glycoprotein gel staining kit; the band corresponding to BSZ7 in melanoidins is indicated by the arrow.

Secondary Structure of BSZ7. CD was used to study the thermal and optical properties of BSZ7. There are two negative minima (280 and 222 nm) and a maximum (192−195 nm), representing a typical α-helix structure, in the far-UV spectra of purified BSZ7 (Figure 2). As shown in Table 1, a significant

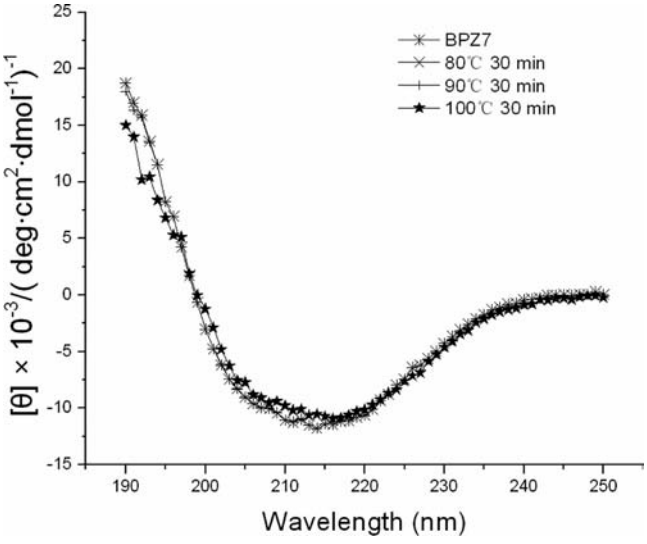

Figure 2. CD spectra of primary and heat-treated BSZ7.

Table 1. Secondary Structure Elements of Heat-Treated BSZ7

	secondary structure elements (%)			
heat treatment	α-helix	β-sheet	β-turn	random coil
untreated control	75.4	0.0	4.4	20.2
80 °C, 30 min	75.2	0.1	4.4	20.3
90 °C, 30 min	72.6	0.8	4.6	21.9
100 °C, 30 min	63.8	2.9	10.8	22.5

fraction of ordered secondary structural elements was found. There was a large amount of α-helix with a small proportion of random coil in the BSZ7 molecular, and no β-sheet or β-turn was found.

To observe the influence of wort boiling on BSZ7, SDS-PAGE and CD were performed following heat treatment of BSZ7 at different degrees for 30 min. There was no degraded band displayed in the SDS-PAGE gel (Supporting Information supplementary Figure 1), and there was only a decrease in band intensity of the heated BSZ7s spectra. No significant peak shifts were revealed (Figure 2). With increasing temperature the fraction of α-helix decreases, whereas the fraction of β-sheet and β-turn increases (Table 1). Despite these changes in secondary structure unit contents, the content of α-helix remains high, giving BSZ7 thermal stability.

Hydrophobicity of BSZ7. Compared with proteins in malt and wort, BSZ7 was the most hydrophobic one (Figure 3).

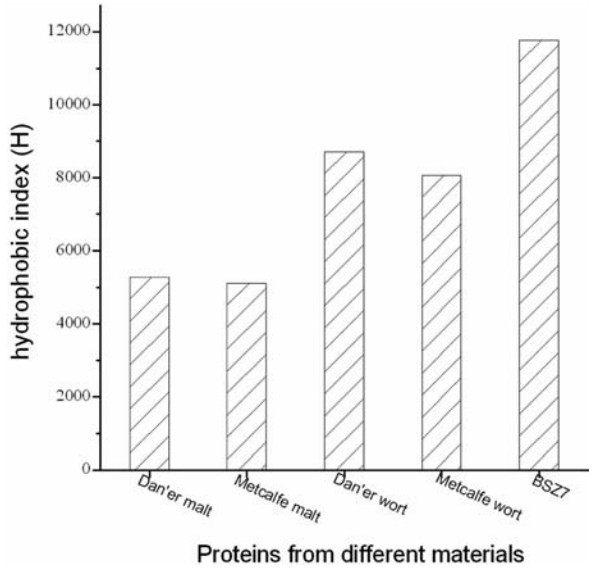

Figure 3. Surface hydrophobic index of BSZ7 and proteins from Dan'er malts and worts.

Previous studies have suggested that the hydrophobicity of a protein would increase its positive effect on beer foam.[20,21] Another well-known foam-promoting protein, LTP1, was found to decrease rapidly during boiling, thus reducing beer foam stability,[22] wheereas, after heating for 30 min, BSZ7 showed no degradation or secondary structure alteration (Supporting Information Supplementary Figures 1 and 2). This result suggested a greater contribution of BSZ7 than LTP1 in beer foam promotion. However, the high hydrophobicity of BSZ7 will also lead to its greater tendency to be left in the spent grain and precipitate to form beer haze, because it was suggested to be able to bind and precipitate with small fragments during wort boiling.[23]

No Inhibiting Effect of BSZ7 on Malt Nonspecific Protease. In the previous comparative proteomic research, it was found that the deficiency on filterability of Dan'er malt was partially caused by BSZ7.[11] The barley serpins were reported to be responsible for protecting the barley grain against insects and fungal infection by inhibiting the activity of pest proteases that digest the contents of grains.[24] However, none of these inhibitors has been shown to have inhibiting activity on the endogenous protease of barley or malt.[24] As a negative effecter on malt filterability, more BSZ7 in Dan'er malt was first thought to hinder the wort filtering through inhibiting protease activity and leaving more proteins in wort. Unexpectedly, the purified BSZ7 from malt showed no effect on nonspecific protease activity of malt (Suppporting Information supple-

dx.doi.org/10.1021/jf405699z | J. Agric. Food Chem. 2014, 62, 5643−5650

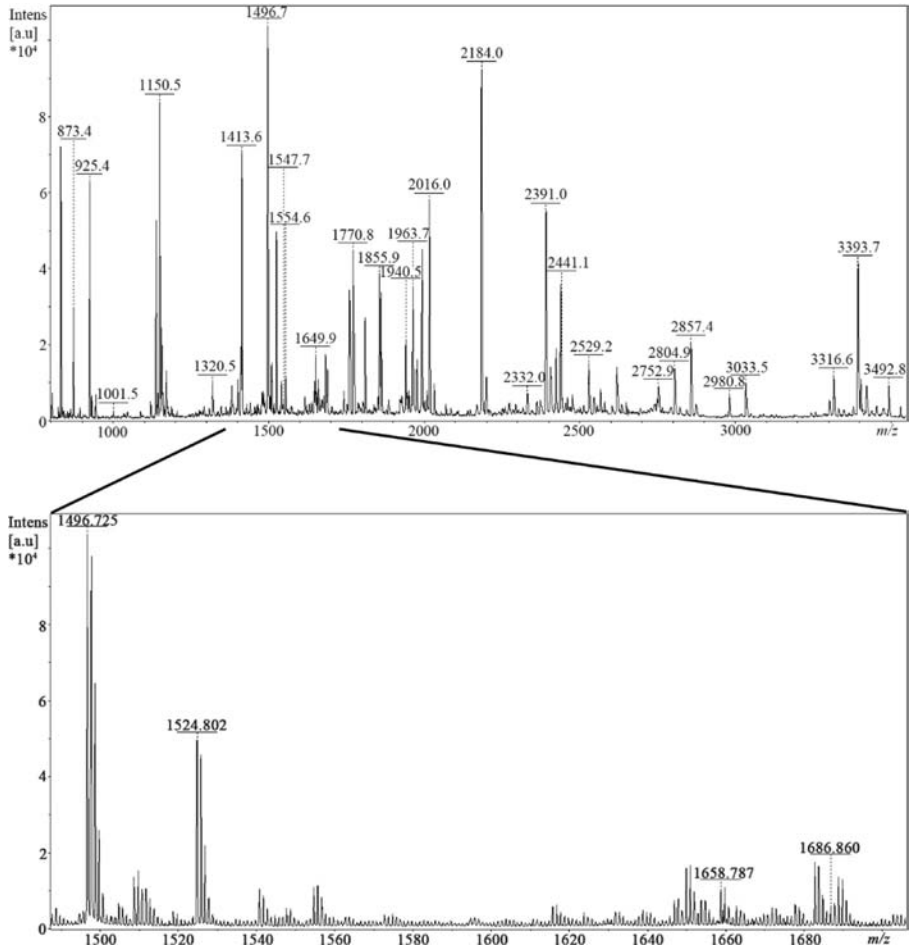

Figure 4. MALDI-TOF MS spectra of purified BSZ7. The marked signals correspond to the unmodified peptides and their glycated form with 162 Da increment of BSZ7.

mentary Figure 2), suggesting it plays its negative role in wort filterability through other actions.

BSZ7 Is a Component of Melanoidins. Melanoidins are complicated compound products of the Maillard reaction from sugars and proteins or amino acids during food processing and preservation.[25] BSZ7 was detected to display multiple spots in the 2DE maps (Supporting Information supplementary Figure 3).[26] Moreover, it has been suggested that protein Z was glycated during processing through the Maillard reaction in the previous study.[14,27] Therefore, BSZ7 was proposed to be one component of the melanoidin compounds. Stained with a glycoprotein gel staining kit, a band in the melanoidins lane showed a migration rate similar to that of the BSZ7 one (Figure 1b), indicating BSZ7 is a component of melanoidins, which was further identified by MALDI-TOF/TOF as described under Materials and Methods. In agreement with studies on the nonenzymatic glycated LTP1 and protein Z during malting and brewing processes,[27,28] several peaks in the MALDI-TOF MS spectra of BSZ7 were found to have 162 Da increments (Figure 4). Two peptides, m/z 1658.787 and 1686.860, were observed to have an increase of ~162 Da compared to the unmodified peptides m/z 1496.725 and 1524.802, both of which contained the glycation site lysine (K).[13] The glycation of protein Z has been proved to protect it from precipitation in the wort boiling process and improve foam stability.[29] In addition, the melanoidins participate in beer color formation and stabilize the oxidation−reduction processes,[25] which indicated another role of BSZ7 in malt and beer.

No peaks with increment of 162 Da were found in the MALDI-TOF MS spectra of the two BSZ7 spots in 2DE maps of Dan'er malt. As shown in Figure 5, panels a and b, the MS of one BSZ7 spot contained one cluster of peaks and the other showed two clusters, in which the major signals were m/z 1486.783 and 2421.329 and m/z 3052.489, respectively. Four peaks in the second cluster (m/z 3052.495, 3442.772, 3459.765, and 3456.799) were calculated to be glycopeptides analyzed by the oligosaccharide structure prediction tool GlycanMod (http://web.expasy.org/glycomod/). They were thought to be the glycation products of peptide NVTAGLIEEILPAGS-IDNTTR (154−174, m/z 2148.143), which contains two of the four N-glycosylation sequences Asn-Xxx-Ser/Thr (NXS or NXT) in BSZ7.[13] The N-oligosaccharide components were $HexHexNAc_1-NeuAc-PentPhos$ (m/z 550.13), $Hex_2HexNAc-Deoxyhexose_2NeuGc-Pent$ (m/z 1258.433), $Hex_2HexNAc_2-DeoxyhexosePent_3$ (m/z 1272.449), and $Hex_4HexNAc-Deoxyhexose_2Pent$ (m/z 1275.449), respectively. The latter three structures are paucimannose-type ($Man_nGlcNAc$-based structure), and the Pent is probably core xylosylation universally existing in plant glycoproteins.[30] BSZ7 purified from barley flour was shown to be non-glycosylated;[12] however, this does not mean that BSZ7 in malt was N-terminally blocked. As previously suggested, glycation can stabilize the protein conformation through hydrogen bonds

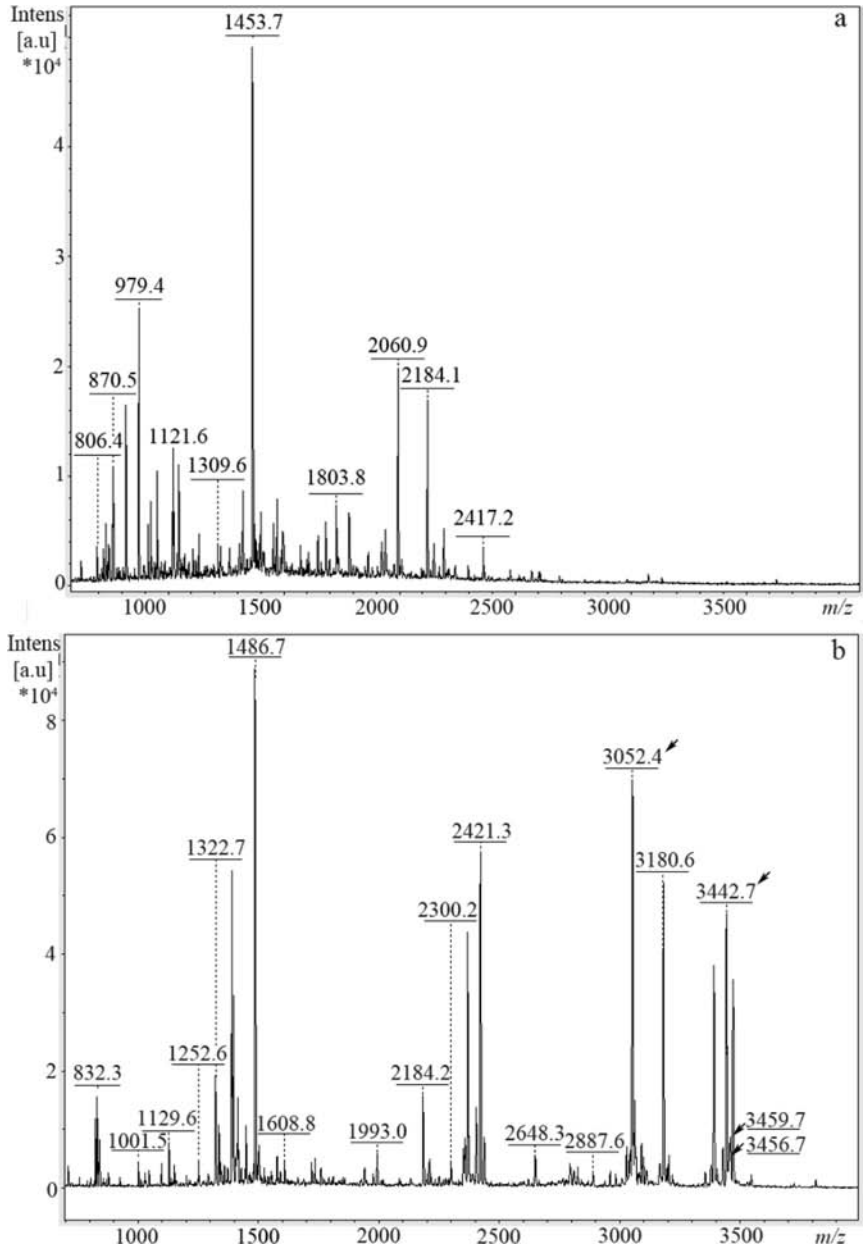

Figure 5. MALDI-TOF MS spectra of the two different spots corresponding to BSZ7 in the 2DE map of Dan'er barley malt. The putative glycopeptides are indicated by arrows.

or van der Waals contacts and thus endows the protein with resistance against wort boiling,[31] which further explains the superior thermal stability of BSZ7.

Effect of BSZ7 on Wort Filterability. According to BSZ7 content in various barley cultures, a series of amounts of purified BSZ7 was added as EBC Congress mashing with Dan'er malt to observe the effect of excess BSZ7 on wort filterability.

Our previous research has shown that extra BSZ7 will seriously decrease the wort separation rate and the turbidity, but have little effect on viscosity.[11] To explain this effect, macromolecular contents in the wort with distinct added BSZ7 were analyzed (Figure 6a–c). With increasing added BSZ7, the concentrations of polysaccharides including β-glucan and AX were decreased, and no difference in HWP among the wort was found. However, β-glucan and AX were degraded by their corresponding hydrolysis enzymes, which have not been reported to be affected by BSZ7. Therefore, we propose the hypothesis that the decreased contents of β-glucan and AX were due to their interaction with BSZ7 by the Maillard reaction, which well explained the unchanged viscosity of wort but decreased turbidity. Due to the high viscosity of polysaccharides, the strong hydrophobicity, and huge size of compounds, they cannot easily pass the filter membrane and therefore caused the decreased wort separation rate.

Besides these, the contents of polyphenols were also decreased significantly with increased extra BSZ7 (Figure 6d). It has been proved that the cross-link or oxidative polymerization between protein and polyphenols is an important negative factor in wort filterability.[32] However, there was no significant change of polyphenol concentrations in the wort using Metcalfe malt by adding a similar amount of BSZ7 (Supporting Information supplementary Figure 4), indicating there is an enzyme promoting the cross-link, and this enzyme

dx.doi.org/10.1021/jf405699z | J. Agric. Food Chem. 2014, 62, 5643–5650

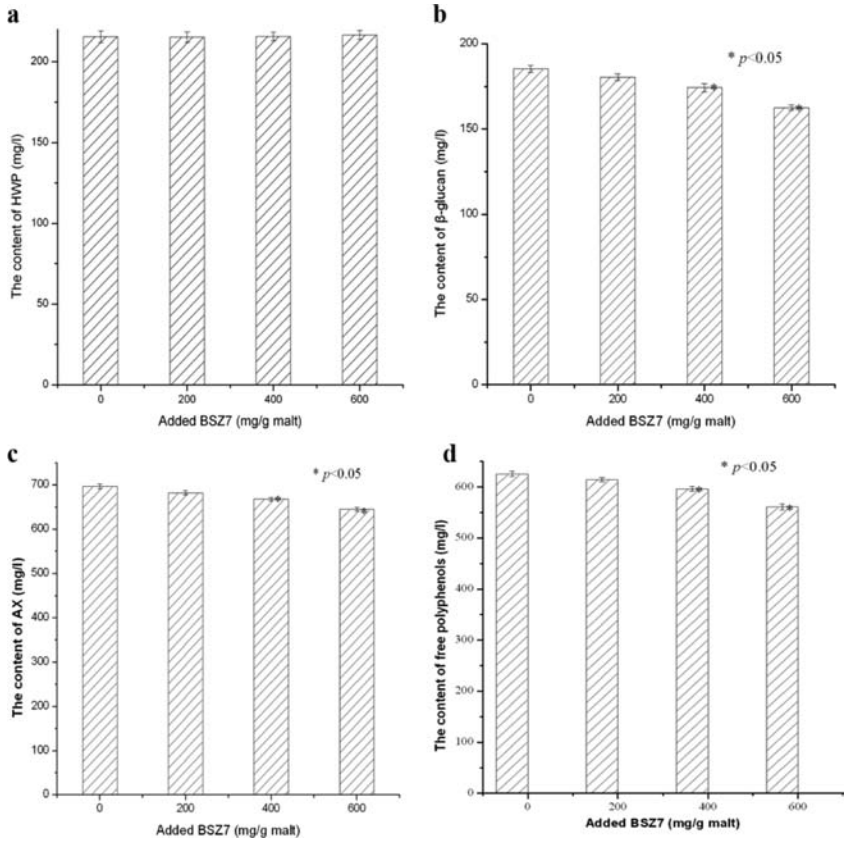

Figure 6. Effect of added BSZ7 during mashing on the contents of HWP (a), β-glucan (b), AX (c), and polyphenols (d) in wort.

was in a different redundancy or exhibited distinct activity between these two malts. Peroxidases (POD) from barley are heat-stable enzymes responsible for phenolic substrate oxidative polymerization, which caused the increased color and turbidity of wort.[33,34] They have been found to be in more abundance in Dan'er malt compared with Metcalfe malt.[11] Furthermore, the activity of POD was higher in Dan'er malt than in Metcalfe (Supporting Information supplementary Figure 5). Therefore, a series of amounts of horeadish peroxidase (0, 200, and 400 U/g malt, Sino-American Biotech., China) instead of malt POD was mixed with purified BSZ7 (600 μg/g malt) and then added simultaneously to test their synergetic effect on wort filterability. As peroxidase increased, the concentration of free polyphenols decreased significantly (Figure 7). At the same time, the wort separation rate was negatively hindered by them.

In conclusion, the present study has characterized BSZ7, a well-known serpin Z of barley playing multiple roles in barley, malt, and wort. The secondary structure and glycation facilitate its survival during wort boiling and improvement of foam stability in beer. Moreover, its existence in melanoidins indicated its potential role in the oxidation−reduction process. However, the high hydrophobicity of BSZ7 and its interaction with polysaccharides in the wort may hinder the compound's passing through the filter membrane, although it may decrease the viscosity to some degree. Finally, our data indicated that the cross-links induced by POD between polyphenols and BSZ7 may also create a negative effect on wort filterability. The glycation of BSZ7 and interaction between polysaccharides and BSZ7 still need more evidence. At the same time, the catalytic mechanism of POD is under study by another project.

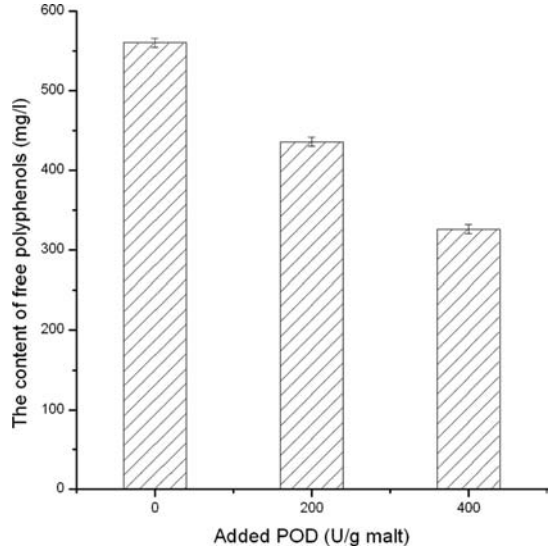

Figure 7. Effect of simultaneous addition of BSZ7 and POD on the content of polyphenols in wort.

■ ASSOCIATED CONTENT

Supporting Information

SDS-PAGE of heat-treated BSZ7; effect of distinct amount of added BSZ7 on the activity of protease from Dan'er malt; two BSZ7 spots in 2DE map of Dan'er malt; effect of distinct amount of added BSZ7 on the concentration of free polyphenols in Metcalfe malt; activity of POD in malts of different cultivars. This material is available free of charge via the Internet at http://pubs.acs.org.

AUTHOR INFORMATION

Corresponding Author

*(J.L.) E-mail: jlu@jiangnan.edu.cn. Phone: +86 510 8591 8191. Fax: +86 510 8591 8191.

Funding

This research was supported by the Major State Basic Research Development Program of China (973 Program, 2012CB720802 and 2013CB733602), the National High Technology Research and Development Program of China (863 Program, 2013AA102109), the National Natural Science Foundation of China (31171736), the Key Program of National Natural Science Foundation of China (31130043), the Key Project of Educational Commission of Jiangsu Province of China (JHB2012-26), the Fundamental Research Funds for the Central Universities (JUDCF10047, JUSRP1015, and JUSRP51302A), the Key Technologies R&D Program of Jiangsu Province of China (BE2012397), and the Program of Introducing Talents of Discipline to Universities (111 Project, 111-2-06).

Notes

The authors declare no competing financial interest.

REFERENCES

(1) Roberts, T. H.; Hejgaard, J. Serpins in plants and green algae. *Funct. Integr. Genomic* **2008**, *8*, 1−27.

(2) Ostergaard, H.; Rasmussen, S. K.; Roberts, T. H.; Hejgaard, J. Inhibitory serpins from wheat grain with reactive centers resembling glutamine-rich repeats of prolamin storage proteins − cloning and characterization of five major molecular forms. *J. Biol. Chem.* **2000**, *275*, 33272−33279.

(3) Thomas, J. C.; Adams, D. G.; Keppenne, V. D.; Wasmann, C. C.; Brown, J. K.; Kanost, M. R.; Bohnert, H. J. Protease inhibitors of *Manduca sexta* expressed in transgenic cotton. *Plant Cell Rep.* **1995**, *14*, 758−762.

(4) Yokoi, S.; Maeda, K.; Xiao, R.; Kamada, K.; Kamimura, M. Characeterization of beer proteins responsible for the foam of beer. *Proc. Eur. Brew. Conv. (Zurich)* **1989**, 593−600.

(5) Iimure, T.; Nankaku, N.; Hirota, N.; Zhou, T. S.; Hoki, T.; Kihara, M.; Hayashi, K.; Ito, K.; Sato, K. Construction of a novel beer proteome map and its use in beer quality control. *Food Chem.* **2010**, *118*, 566−574.

(6) Hejgaard, J. Gene products of barley chromosomes 4 and 7 are precursors of the major antigenic beer protein. *J. Inst. Brew.* **1984**, *90*, 85−87.

(7) Evans, D. E.; Hejgaard, J. The impact of malt derived proteins on beer foam quality. Part I. The effect of germination and kilning on the level of protein Z4, protein Z7 and LTP1. *J. Inst. Brew.* **1999**, *105*, 159−169.

(8) Iimure, T.; Takoi, K.; Kaneko, T.; Kihara, M.; Hayashi, K.; Ito, K.; Sato, K.; Takeda, K. Novel prediction method of beer foam stability using protein Z, barley dimeric α-amylase inhibitor-1 (BDAI-1) and yeast thioredoxin. *J. Agric. Food Chem.* **2008**, *56*, 8664−8671.

(9) Evans, D. E.; Sheehan, M. C. Don't be fobbed off: the substance of beer foam − a review. *J. Am. Soc. Brew. Chem.* **2002**, *60*, 47−57.

(10) Iimure, T.; Nankaku, N.; Watanabe-Sugimoto, M.; Hirota, N.; Zhou, T. S.; Kihara, M.; Hayashi, K.; Ito, K.; Sato, K. Identification of novel haze-active beer proteins by proteome analysis. *J. Cereal Sci.* **2009**, *49*, 141−147.

(11) Jin, Z.; Li, X. M.; Gao, F.; Sun, J. Y.; Mu, Y. W.; Lu, J. Proteomic analysis of differences in barley (*Hordeum vulgare*) malts with distinct filterability by DIGE. *J. Proteomics* **2013**, *93*, 93−106.

(12) Lundgard, R.; Svensson, B. A 39 kD barley seed protein of the serpin superfamily inhibits α-chymotrypsin. *Carlsberg Res. Commun.* **1989**, *54*, 173−80.

(13) Rasmussen, S. K.; Klausen, J.; Hejgaard, J.; Svensson, B.; Svendsen, I. Primary structure of the plant serpin BSZ7 having the capacity of chymotrypsin inhibition. *Biochim. Biophys. Acta−Protein Struct. Mol. Enzymol.* **1996**, *1297*, 127−130.

(14) Hejgaard, J.; Kaersgaard, P. purification and properties of the major antigenic beer protein of barley origin. *J. Inst. Brew.* **1983**, *89*, 402−410.

(15) Qin, L. K.; Ding, X. L. Extractions of melanoidins in the long-ripenned douchiba (DCB) and analyses of amino acid compositions in its peptide skeltons. *Food Sci.* **2006**, *27*, 125−129.

(16) Douglas, S. G. A rapid method for the determination of pentosans in wheat four. *Food Chem.* **1981**, *7*, 139−145.

(17) Naoyuki, I.; Masaru, O.; Masaharu, K.; Noriko, K. Improvement of the Congo Red method, a rapid β-glucan quantification method for the breeding of high quality malting barley. *Bull. Tochigi Prefectural Agric. Exp. Stn.* **1998**, *47*, 57−64.

(18) Zhao, H. F.; Fan, W.; Dong, J. J.; Lu, J.; Chen, J.; Shan, L. J.; Lin, Y.; Kong, W. B. Evaluation of antioxidant activities and total phenolic contents of typical malting barley varieties. *Food Chem.* **2008**, *107*, 296−304.

(19) Hough, J. S.; Briggs, D. E.; Stevens, R.; Young, T. W. *Malting and Brewing Science: Hopped Wort and Beer*; Chapman & Hall/Aspen Publishers: New York, 1999; p 460.

(20) Onishi, A.; Proudlove, M. O. Isolation of beer foam polypeptides by hydrophobic interaction chromatography and their partial characterization. *J. Sci. Food Agric.* **1994**, *65*, 233−240.

(21) Yokoi, S.; Yamashita, K.; Kunitake, N.; Koshino, S. Hydrophobic beer proteins and their function in beer foam. *J. Am. Soc. Brew. Chem.* **1994**, *52*, 123−126.

(22) Van Nierop, S. N. E.; Evans, D. E.; Axcell, B. C.; Cantrell, I. C.; Rautenbach, M. Impact of different wort boiling temperatures on the beer foam stabilizing properties of lipid transfer protein 1. *J. Agric. Food Chem.* **2004**, *52*, 3120−3129.

(23) Iimure, T.; Nankaku, N.; Kihara, M.; Yamada, S.; Sato, K. Proteome analysis of the wort boiling process. *Food Res. Int.* **2012**, *45*, 262−271.

(24) Jones, B. L. The endogenous endoprotease inhibitors of barley and malt and their roles in malting and brewing. *J. Cereal Sci.* **2005**, *42*, 271−280.

(25) Wang, H. Y.; Qian, H.; Yao, W. R. Melanoidins produced by the Maillard reaction: structure and biological activity. *Food Chem.* **2011**, *128*, 573−584.

(26) Jin, Z.; Mu, Y. W.; Sun, J. Y.; Li, X. M.; Gao, X. L.; Lu, J. Proteome analysis of metabolic proteins (pI 4−7) in barley (*Hordeum vulgare*) malts and initial application in malt quality discrimination. *J. Agric. Food Chem.* **2013**, *61*, 402−409.

(27) Bobalova, J.; Petry-Podgorska, I.; Lastovickova, M.; Chmelik, J. Monitoring of malting process by characterization of glycation of barley protein Z. *Eur. Food Res. Technol.* **2010**, *230*, 665−673.

(28) Jegou, S.; Douliez, J. P.; Molle, D.; Boivin, P.; Marion, D. Evidence of the glycation and denaturation of LTP1 during the malting and brewing process. *J. Agric. Food Chem.* **2001**, *49*, 4942−4949.

(29) Curioni, A.; Pressi, G.; Furegon, L.; Peruffo, A. D. B. Major proteins of beer and their precursors in barley − electrophoretic and immunological studies. *J. Agric. Food Chem.* **1995**, *43*, 2620−2626.

(30) Chow, L. P.; Chiu, L. L.; Khoo, K. H.; Peng, H. J.; Yang, S. Y.; Huang, S. W.; Su, S. N. Purification and structural analysis of the novel glycoprotein allergen Cyn d 24, a pathogenesis-related protein PR-1, from Bermuda grass pollen. *FEBS J.* **2005**, *272*, 6218−6227.

(31) Gowda, D. C.; Petrella, E. C.; Raj, T. T.; Bredehorst, R.; Vogel, C. W. Immunoreactivity and function of oligosaccharides in cobra venom factor. *J. Immunol.* **1994**, *152*, 2977−2986.

(32) Stephenson, W. H.; Biawa, J. P.; Miracle, R. E.; Bamforth, C. W. Laboratory-scale studies of the impact of oxygen on mashing. *J. Inst. Brew.* **2003**, *109*, 273−283.

(33) Billaud, C.; Louarme, L.; Nicolas, J. Comparison of peroxidases from barley kernel (*Hordeum vulgare* L.) and wheat germ (*Triticum aestivum* L.): isolation and preliminary characterization. *J. Food Biochem.* **1999**, *23*, 145−172.

(34) Billaud, C.; Kohler, B.; Boivin, P.; Nicolas, J. Polyphenolic substrates of cationic and neutral/anionic peroxidases from barley and malt using a chronometric method for the determination of pod activity. *J. Food Biochem.* **1999**, *23*, 519−545.

JOURNAL OF AGRICULTURAL AND FOOD CHEMISTRY

Article

pubs.acs.org/JAFC

Origin of the Pinking Phenomenon of White Wines

Jenny Andrea-Silva,[†,‡] Fernanda Cosme,[‡] Luís Filipe Ribeiro,[‡] Ana S. P. Moreira,[§] Aureliano C. Malheiro,[#] Manuel A. Coimbra,[§] M. Rosário M. Domingues,[§] and Fernando M. Nunes*[,†]

[†]CQ-VR, Chemistry Research Centre, Chemistry Department, Universidade de Trás-os-Montes e Alto Douro, 5001-801 Vila Real, Portugal

[‡]Institute for Biotechnology and Bioengineering, Centre of Genomics and Biotechnology, (IBB/CGB-UTAD), Edifício de Enologia, Universidade de Trás-os-Montes e Alto Douro, Apartado 1013, 5001-801 Vila Real, Portugal

[§]Mass Spectrometry Centre, QOPNA, Chemistry Department, Universidade de Aveiro, 3810-193 Aveiro, Portugal

[#]Centre for the Research and Technology of Agro-Environmental and Biological Sciences (CITAB), Universidade de Trás-os-Montes e Alto Douro, 5001-801 Vila Real, Portugal

Supporting Information

ABSTRACT: Pinking is the terminology used for the salmon-red blush color that may appear in white wines produced exclusively from white grape varieties. The isolation of pinking compounds and their analysis by RP-HPLC-DAD and ESI-MS^n showed that the origin of the pinking phenomenon in white wines from *Vitis vinifera* L. of Síria grape variety are the anthocyanins, mainly malvidin-3-*O*-glucoside. The analysis showed that the anthocyanins were located both in the pulp and in the skin. Wine pinking severity was negatively related with the increase of the average temperature of the first 10 days of October, the final period of grape maturation. The minimum amount of anthocyanins needed for the pink color visualization in wine was 0.3 mg/L. The appearance of pinking in white wines after bottling is due to the lowering of free sulfur dioxide, which leads to an increase of the relative amount of the anthocyanins red flavylium form and their polymerization, resulting in the formation of colored compounds resistant to pH changes and sulfur dioxide bleaching.

KEYWORDS: *Vitis vinifera, white grapes, Síria variety, white wines, pinking, anthocyanins*

INTRODUCTION

Pinking is a term that describes the appearance of a salmon-red blush in white bottled wines produced exclusively from white grape varieties. It is perceived as an undesirable phenomenon by both wine consumers and the industry.[1,2] Although with seasonal and regional variations, pinking has been observed worldwide, with predominance in white wines produced from *Vitis vinifera* L. grape varieties such as Chardonnay, Chenin blanc, Crouchen, Muscat Gordo blanco, Palomino, Riesling, Sauvignon blanc, Semillon, Sultana, and Thompson Seedless.[1,3]

Pinking is mainly observed when white wines are produced under reducing conditions.[1−4] The pinking phenomenon is usually observed after bottling and storage of white wines or after alcoholic fermentation, although sometimes it occurs as soon as the grape must is extracted.[5−7] Susceptibility of reductively produced wines to pinking may be effectively overcome by maintaining adequate levels of free sulfur dioxide, especially when ascorbic acid is used.[8,9] Pinking is thought to be due to oxidative changes in white wines when exposed to oxygen,[1,7] although the compounds responsible for the pinking phenomena are unknown.[10] In addition, inhibition of polyphenol oxidase activity has been linked to pinking potential in white wines,[11] and added hydrogen peroxide can induce it.[1] It has been proposed that white wine pinking can be a result of the rapid conversion of accumulated flavenes to the corresponding red flavylium salts formed from the hydrolysis of leucoanthocyanins.[12] However, this coloration may be caused by at least 10 different compounds and polymeric materials.[2] Also, it was reported that a 2-*S*-glutathionyl-caftaric acid derivative may be the pink chromophore.[4]

There are various preventive or curative enological treatments for the pinking problem, including adding polyvinylpolypyrrolidone (PVPP) or PVPP associated with bentonite or increasing the redox potential using ascorbic acid in the prebottling stage.[10] Nevertheless, the use of these treatments increases wine production costs and can change wine sensory properties.[13] Also, the use of high levels of ascorbic acid has been shown to increase the browning potential of white wines.[14] In white wine production, hyperoxidation of juice is not recommended, as it alters significantly the white wine flavor, decreasing the fruity aroma intensity and consequently the wine quality.[4,8]

The main purpose of this work was to get a deeper insight into the pinking phenomenon, its origin, and technological factors influencing its appearance in white wines. For this, Síria, a white grape variety, was used. Knowledge of the compounds responsible for this color alteration would increase the treatment efficiency of those wines by allowing the choice of the most correct treatment to optimize their removal.

Received: February 18, 2014
Revised: May 18, 2014
Accepted: May 24, 2014
Published: May 25, 2014

ACS Publications © 2014 American Chemical Society

MATERIAL AND METHODS

Chemicals. Oenin chloride, kuromanin chloride, and delphinidin 3-*O*-*β*-D-glucoside chloride were purchased from Sigma (USA).

Grape and Wine Samples. The white grapes and white wines from *V. vinifera* L., Síria variety, used in this study were from the vintages 2010−2012, harvested at the designation of origin Beira Interior, subregion Castelo Rodrigo, in Portugal, and provided by the Producers Union "Adega Cooperativa de Figueira de Castelo Rodrigo" (ACFCR). This region is characterized by an altitude ranging between 400 and 700 m. The soils are mostly granite or schist. In this subregion the principal white grape varieties are Síria and Malvasia Fina. The white wines from this region have medium acidity (4−5 g/L tartaric acid), pH 3.2−3.4, light color, medium sensitivity to oxidation, intense aroma, and balanced notes of unripe tropical and citrus fruits.

Winemaking was carried at the ACFCR, in Portugal. Grapes were manually harvested at optimum technological maturity (18−20 °Brix) and transported to the winery. They were immediately destemmed and crushed, and the grape juice was treated with sulfur dioxide (60 mg/L) to avoid must oxidation. Then, crushed grapes were pressed at a maximum pressure of 2 bar in a pneumatic press machine. Grape juice was clarified by decantation in a stainless steel tank during 24 h at 8 °C. The alcoholic fermentation was started using active dry yeasts, carried out at controlled temperature (14−15 °C), and finished when residual sugars were <2 g/L. After alcoholic fermentation, the wine was racked and the free sulfur dioxide was adjusted (~40 mg/L). All conventional analytical methods were performed according to OIV methods.[15]

Visible Absorption Spectra and Wine Chromatic Characteristics. The visible absorption spectra were acquired in a 4 cm path length glass cell from 380 to 780 nm. The spectra were converted into a 1 cm path length, and the chromatic characteristics of the wines according to CIELab were calculated by using the method MA-E-AS2-11-CARCHR of the OIV.[15] All analyses were performed in duplicate.

Isolation of the Pinking Compounds by PVPP Column Chromatography. To a white wine (1 L) presenting pinking, was added 0.8 g of PVPP (Polyclar V), and the suspension was filtered through a cheesecloth and washed with 100 mL of water followed by 100 mL of ethanol 95%. After this washing, the PVPP, presenting a pink color, was loaded on an empty SPE cartridge with frits and eluted sequentially with 3 mL of (1) acetonitrile, (2) acetone, (3) aqueous solution of 1% HCl, (4) ethanol, and (5) 0.1 M NH_3 in ethanol. Each eluent was separately collected, the solvent was removed by centrifugal evaporation, and the solution was reconstituted with 0.2 mL of a methanol/water (1:1 v/v) solution before analysis by HPLC. All analyses were performed in duplicate.

Isolation of Pinking Compounds by Reversed Phase Solid Phase Extraction. The pinking compounds present in the samples were purified and concentrated by reversed phase (C-18) solid phase extraction (Supelclean LC-18 SPE tube, 1 g of solid phase, and 6 mL volume). Briefly, 1 g of C-18 SPE column was conditioned by applying four times 5 mL of methanol and 4 times 5 mL of a 0.1 M HCl solution. Then, the samples were applied: (1) 35 mL of grape juice or must resulting from pressing Síria white grape varieties adjusted to pH 1 with 3 M HCl or (2) 100 mL of white wines from Síria grape variety or a blend from Síria and Malvasia Fina grape varieties adjusted to pH 1 with 3 M HCl. After application of the sample, the column was washed with four times with 5 mL of the 0.1 M HCl solution, and the compounds retained were eluted with four times 5 mL of methanol. The fractions were pooled, and the methanol was removed by rotary evaporation at 35 °C. The dried residue was dissolved in 2 mL of a methanol/water (1:1 v/v) solution and analyzed by HPLC. All analyses were performed in duplicate.

High-Performance Liquid Chromatography with Photodiode Array Detector. The chromatographic analysis of the phenolic compounds present in grape must and wine water/methanolic extract was performed by reversed phase (C-18) high-performance liquid chromatography using an Ultimate 300 solvent delivery system equipped with a PD-100 UV−vis diode array detector. Separation was performed by gradient elution on an ACE 5 C-18 column, 5 μm particle size (250 mm × 4.6 mm) (Advanced Chromatography Technologies, Scotland). Conditions of HPLC analysis were as follows: solvent A was a mixture of 95:5 water/formic acid (v/v), and solvent B was methanol. A linear gradient analysis for a total run time of 80 min was used as follows: starting from 5% solvent B during 2 min, increase to 80% solvent B over 68 min and then isocratic for 8 min, decrease to 5% solvent B over 2 min, and finally isocratic for 5 min. The sample volume injected was 100 μL, the flow rate was 1.0 mL/min, and the column temperature was maintained at 35 °C during the run. The eluent was continuously monitored from 250 to 600 nm with a photodiode array detector (PDA-100, Dionex). All analyses were performed in duplicate. Anthocyanin identifications were made by injection of pure standards in the case of cyanidin-3-*O*-glucoside, delphinidin-3-*O*-glucoside, and malvidin-3-*O*-glucoside and by comparison of their retention times and UV−vis spectra. Other anthocyanins were identified by comparison of the elution order and UV−vis spectra reported in the literature. Additionally, all anthocyanin-3-*O*-glucosides were confirmed by tandem mass spectrometry.

Determination of Total Monomeric Anthocyanins. Total monomeric anthocyanins were determined using the pH differential method AOAC Official Method 2005.02 with a minor modification.[16] Due to the low concentration of anthocyanins present in pinking white wines, for the anthocyanin determination by the pH differential method, the absorbance was measured at 520 and 700 nm using a 10 cm path length glass cell, and total monomeric anthocyanins were expressed as milligrams of malvidin-3-*O*-glucoside per liter (molar extinction coefficient of 28000 L/cm/mol and molecular weight of 493.4 g/mol). All analyses were performed in duplicate.

Electrospray Ionization Mass Spectrometry (ESI-MS). ESI-MS and tandem ESI-MS (ESI-MS^n) spectra of SPE-purified and concentrated must and wines were carried out on an LXQ linear ion trap mass spectrometer (Thermo Fisher Scientific Inc., Waltham, MA, USA). Typical operating conditions were as follows: electrospray voltage was 5 kV, capillary temperature was 275 °C, capillary voltage was 1 V, and tube lens voltage was 40 V. Samples were introduced at a flow rate of 8 μL/min into the ESI source. Nitrogen was used as nebulizing and drying gas. In the ESI-MS^n experiments, the collision energy used was set between 18 and 31 (arbitrary units). Data acquisitions were carried out on an Xcalibur data system. For all ESI-MS analyses, samples dissolved in water were diluted in methanol/formic acid (99:1, v/v), and the spectra were acquired in the positive mode, scanning the mass range from m/z 100 to 1500. All analyses were performed in duplicate.

Tissue Fractionation and Anthocyanin Content. For the analysis of anthocyanin distribution in Síria white grape variety, the skins were removed from the frozen grapes (hypodermal tissue samples) and the seeds were removed from the flesh (mesocarp tissue samples).[17] The hypodermal and mesocarp samples were homogenized in a mortar and pestle at 4 °C in the presence of 0.1% HC1 (v/v) in methanol containing 50 ppm of SO_2. The homogenate was centrifuged at 3400*g* for 6 min, and the supernatant was concentrated under vacuum. The residue was suspended in 2 mL of a water/methanol solution (1:1 v/v) and analyzed for anthocyanin by HPLC-DAD. All analyses were performed in duplicate.

Climate Data. The climate data corresponds to the period from 2005 to 2011 of the vineyards located at Figueira de Castelo Rodrigo (40° 52′ N, 6° 54′ W, 635 m). The climate is of the Mediterranean type (warm temperate climate with dry and warm summer) characterized by a sinusoidal pattern of precipitation with dry summers and wet winters. In the experimental area, long-term annual precipitation is about 590 mm, with roughly a third falling from April to September. Corresponding annual average minimum and maximum temperatures are 6.4 and 18.3 °C.[18]

Weather variables kindly supplied by the Portuguese state agricultural services (Direção Regional de Agricultura e Pescas do Centro) included daily records of maximum, minimum, and average temperatures and total precipitation, from which 10 day averages were computed. This set of data was recorded from a standard automatic weather station close to the experimental site. Additionally, thermal

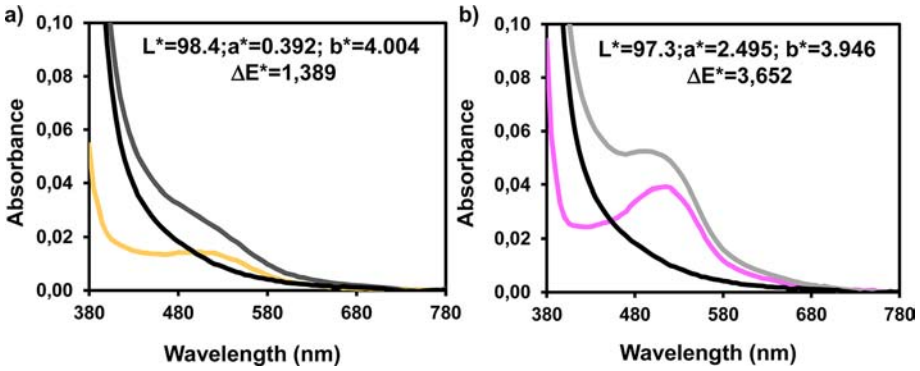

Figure 1. Visible absorption spectra and chromatic characteristics of (a) white wine (black curve), the same white wine exposed to oxygen in a glass for 24 h (gray curve), and difference spectrum (yellow curve) and (b) white wine (black curve), the same white wine with a pH 1 (gray curve), and difference spectrum (pink curve).

Table 1. Compounds Recovered from PVPP Used for Treatment of a White Wine with Pinking

no.	t_r (min)	spectra	λ_{max} (nm)	compound	identification[a]
1	21.58	A	523; 283	delphinidin-3-*O*-glucoside	R
2	24.27	B	516; 282	cyanidin-3-*O*-glucoside	R
3	26.77	C	526; 264	petunidin-3-*O*-glucoside	T
4	29.00	D	517; 280	peonidin-3-*O*-glucoside	T
5	30.68	E	527; 279	malvidin-3-*O*-glucoside	R
6	31.94			unknown	
7	33.03			unknown	
8	34.14			delphinidin-3-*O*-(6-*O*-acetyl)-glucoside	X
9	36.11			cyanidin-3-*O*-(6-*O*-acetyl)-glucoside	X
10	37.89			petunidin-3-*O*-(6-*O*-acetyl)-glucoside	X
11	41.29			unknown	
12	41.62			malvidin-3-*O*-(6-*O*-acetyl)-glucoside	X
13	42.05	F	530; 280	delphinidin-3-*O*-(6-*O*-coumaroyl)-glucoside	Z
14	43.13	G	527;281	cyanidin-3-*O*-(6-*O*-coumaroyl)-glucoside	Z
15	43.68	H	538; 281	petunidin-3-*O*-(6-*O*-coumaroyl)-glucoside	Z
16	46.52	I	529; 282	peonidin-3-*O*-(6-*O*-coumaroyl)-glucoside	Z
17	48.20	J	533; 283	malvidin-3-*O*-(6-*O*-coumaroyl)-glucoside	Z
18	52.64			unknown	

[a]Identification: R, identification based on retention time and UV−vis spectra match with reference compounds and tandem mass spectra; T, tentative identification by comparison of retention time and UV−vis spectra with those of the literature and tandem mass spectra; X, tentative identification by comparison of retention time with that of the literature; Z, tentative identification by comparison of retention time and UV−vis spectra with those of the literature.

amplitudes and growing degree days (with a 10 °C base temperature) were calculated.

The pinking severity over this period of time was indirectly calculated on the basis of the amount of PVPP used (grams) for white pinking treatment and the total volume of wine treated (liters).

To examine linear dependencies between climatic variables and pinking severity, Pearson correlation coefficients were computed. Statistical significance was considered at the 95% confidence level. As the synthesis of anthocyanins in berries occurs over the maturation period, the months used for the analysis included August (véraison), September, and October (harvest).

RESULTS AND DISCUSSION

Isolation of the Pinking Components and Characterization by HPLC-DAD. In Figueira de Castelo Rodrigo, designation of origin Beira Interior, subregion Castelo Rodrigo (Portugal), white wines are produced mainly from the Síria grape variety, although some white wines are produced by a blend of Síria and Malvasia Fina grape varieties. Producers at the ACFCR state that whatever wine they produce, monovarietal or blended, pinking has appeared in the past 12 years. In this period, the white wines have been produced under reducing conditions, although not with the same severity each year. Figure 1a presents the visible absorption spectra of a white wine (Síria 2010) and the same white wine where pinking was induced by standing in a glass during 24 h. After 24 h, the color of the wine changed from a clear pale yellow (L^* = 99.3; a^* = −0.471; b^* = 3.288) to a pale salmon (L^* = 98.4; a^* = 0.392; b^* = 4.004), with a clear increase in the absorbance in the visible region (ΔE^* = 1.39). After subtraction of the initial absorbance from the absorbance after 24 h, a peak in the visible region between 440 and 630 nm was clearly observed, with a maximum around 500−520 nm. This behavior is the pinking phenomenon described in the literature, where the appearance of the pink-salmon color is induced by oxidation of the white wines.[1]

In some years, pinking is observed before bottling, and the addition of PVPP is used to eliminate it. This strategy of using PVPP to remove the pinking from white wines was used in the present work as a first step for characterization of the pinking compounds present in white wines. After addition of PVPP to

dx.doi.org/10.1021/jf500825h | J. Agric. Food Chem. 2014, 62, 5651−5659

Table 2. Summary of the Ions Observed in the Product Ion Spectra of M^+ Ions of Anthocyanins Recovered from Pinking White Wines

	pelargonidin-3-*O*-glucoside	cyanidin-3-*O*-glucoside	peonidin-3-*O*-glucoside	delphinidin-3-*O*-glucoside	petunidin-3-*O*-glucoside	malvidin-3-*O*-glucoside
			MS^2			
M^+	433	449	463	465	479	493
$[M - H_2O]^+$	415	431	445	447	461	475
$[M - CH_3^\bullet - HO^\bullet]^+$	401	417	431	433	447	
$^{0,4}X_0$	373		403	405	419	433
$^{0,3}X_0$	343		473	375	389	403
$^{0,2}X_0$	313	329	343	345		
$M^+ - 132$ Da	301	317	331	333	347	361
$M^+ - 146$ Da	287	303	317	319		
Y_0	271	287	301	303	317	331
Z_0	253			285	299	
			MS^3			
Y_0	271	287	301	303	317	331
$[Y_0 - CH_3]^+$		272	286	288	302	316
$[Y_0 - CH_3^\bullet_H^\bullet]^+$						315
$[Y_0 - H_2O]^+$	253	269	283	285	299	
$[Y_0 - CO]^+$		259			289	
$[Y_0 - H_2CO]^+$		257		273		
$[Y_0 - OH^\bullet\text{-}CH_3^\bullet]^+$			269		285	299
$[Y_0 - HCO^\bullet - CH_3^\bullet]$	227	243		259		287
$[Y_0 - OH^\bullet - (H^\bullet + CO)]^+$		241		257		
$^{0,2}B^+$		137			167	
$^{0,2}A^{+\bullet}$						150
$^{0,2}A^{+\bullet}$		149		149		149
$^{0,2}B^+ - CO$						
$^{0,3}A^+$		121				

the wines, the PVPP becomes pink and the white wine recovered a pale yellow color. The PVPP-retained pink compounds, after extensive washing, were eluted with an ethanol solution containing 0.1 M NH_3, and a pink band was observed to migrate from the PVPP. When the compounds were eluted from the column, the pink color disappeared and, after neutralization of the solution with acetic acid, the pink color reappeared. The analysis of the compounds eluted from the PVPP by HPLC-DAD yielded a maximum of 18 peaks (Table 1), all with absorbance in the visible region, with maxima in the 500−540 nm range, which correspond to the wavelength of the pinking compounds.[1] Anthocyanins show a broad absorption band in the blue end of the visible spectra with maxima in the 500−535 nm region. Absorption bands in the UV region from about 277 to 284 nm are also observed due to the aromatic ring structure, and occasionally another weak UV band is observed in the region from about 328 to 346 nm. The UV−visible absorption spectra of the main compounds show that 10 of the 18 identified peaks recovered from the white wine with pinking, representing 86% of the total area, have a clear anthocyanin-like absorption spectra. Peaks at retention times of 21.58, 24.27, and 30.68 min were coincident with the retention times and UV spectra of pure standards of delphinidin-3-*O*-glucoside, cyanidin-3-*O*-glucoside, and malvidin-3-*O*-glucoside. Also, the retention times of all components match accordingly those of young red wines analyzed under the same conditions (data not shown). Although the analysis of the UV−vis spectra and retention times (Table 1) allows the assignment of the anthocyanins,[19,20] to confirm their presence in the white wines under study, the anthocyanins were recovered by reversed phase solid phase extraction. Also, other wines made from Síria and a blend made from Síria and Malvasia Fina grape varieties, from a different harvest, were also analyzed, allowing the clear identification of the presence of anthocyanins.

When the white wine was adjusted to pH 1 without previous exposure to air, it turned pink (L^* = 97.3; a^* = 2.495; b^* = 3.946). The change in the visible spectrum was much more intense than that observed for the wine in which pinking was induced by exposure to air (Figure 1b). These observations are also in accordance with the presence of anthocyanins, as will be further discussed below. When the difference absorption spectrum was calculated, the anthocyanin-like spectrum was observed, showing also that the pink color of the white wines in which the pinking phenomena are observed could arise from anthocyanins. The amount of total monomeric anthocyanins was determined by the differential pH method, and the higher amount of anthocyanins was observed for the Síria 2010 white wine, containing 0.33 mg of anthocyanins/L, followed by the blend 2012 white wine, containing 0.27 mg of anthocyanins/L, and the Síria 2012 white wine containing 0.20 mg of anthocyanins/L. When the white wines blend 2012 and Síria 2012 were left in a glass for 24 h, no pink color could be detected by eye, suggesting that the total amount of monomeric anthocyanins required to have the pink color is close to 0.3 mg/L.

These results show that the main compounds present in pinking Síria white wines, absorbing in the visible range of the light spectra, should be anthocyanins, as further confirmed by tandem mass spectrometry.

Tandem Mass Spectrometry Confirmation of the Chemical Nature of the Pinking Components. The

dx.doi.org/10.1021/jf500825h | J. Agric. Food Chem. 2014, 62, 5651−5659

identity of the different anthocyanins as the pinking-related compounds was confirmed by off-line mass spectral analysis, including MS^2 to MS^3 fragmentation. The ions at m/z 449, 463, 465, 479, and 493 were observed in the MS, attributed to the anthocyanidin-3-*O*-glucosides, which aglycones correspond to cyanidin, peonidin, delphinidin, petunidin, and malvidin, respectively (Table 2). It was also possible to observe an ion at m/z 433, attributed to pelargonidin-3-*O*-glucoside that could not be observed in the HPLC-DAD analysis as this anthocyanin is known to be present in grapes in insignificant amounts, preventing its detection by HPLC-DAD.[21]

To confirm the identities of selected ions, they were induced to fragment to obtain MS^2 and MS^3 spectra. Product ions formed in tandem mass spectrometry experiments of anthocyanidins bearing glycosyl residues are usually named according to the nomenclature proposed by Domon and Costello[22] and Ma et al.[23] (Scheme 1). Sugar fragment ions that retain the charge at the aglycone are designated X when originated by cross-ring cleavages, or Y and Z when originated by cleavage of the glycosidic linkage. Product ions that retain the charge at the sugar residue are designated A when originated by cross-ring cleavages or B and C when originated by cleavage of the glycosidic linkage. For free aglycones, the $^{i,j}\mathbf{A}^+$ and $^{i,j}\mathbf{B}^+$ labels are used to designate primary product ions containing intact A and B rings, respectively, in which the superscripts *i* and *j* indicate the C-ring bonds that have been broken (see Scheme 1). For conjugated aglycones, an additional subscript 0 to the right of the letter is used to avoid confusion with the A_i^+ and/or B_i^+ ($i \geq 1$) labels that have been used to designate carbohydrate fragments containing a terminal (nonreducing) sugar unit. The $^{i,j}\mathbf{A}^+$ and $^{i,j}\mathbf{B}^+$ ions can undergo further fragmentation by losing small neutral molecules, such as H_2O and CO, or combinations thereof. These product ions are denoted by the combined use of $^{i,j}\mathbf{A}^+$ (or $^{i,j}\mathbf{B}^+$) and the lost molecules. For simplicity, the ions formed by the direct loss of radicals or small neutral molecules such as a methyl group, water, carbon monoxide, and ketene from the M^+ ion are not indicated with special labels.

Scheme 1. Nomenclature of Fragment Ions from Anthocyanidin-3-*O*-glucosides according to Domon and Costello[29] and Ma et al.[30]

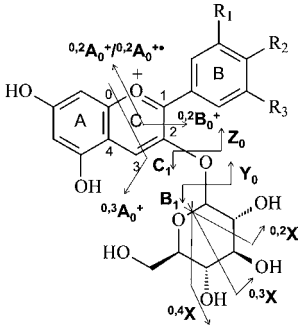

The ESI-MS^2 and MS^3 mass spectra of the anthocyanidin-3-*O*-glucosides corresponding to the ions at m/z 433, 449, 463, 465, 479, and 493 are shown in Figure 2, and the product ions observed are identified in Table 2. The fragmentation observed for the MS^2 spectra is consistent with the attributed structure (Figure 3) and in accordance with previous reports on anthocyanin fragmentation by tandem mass spectrometry.[24,25] For all ions a loss of a hexose residue (Hex_{res}; −162 Da) is observed, yielding the Y_0 ions corresponding to the respective aglycones (Table 2). Also observed in some MS^2 spectra are the Z_0 ions corresponding to the loss of a hexose (−180 Da). Observed in all spectra is one to all the possible cross-ring cleavage of the sugar residue, corresponding to the loss of 60, 90, and 120 Da, assigned as $^{0,4}X_0$, $^{0,3}X_0$, and $^{0,4}X_0$ ions. There are also small neutral losses including those corresponding to water (18 Da) and $CH_3^\bullet$ + $OH^\bullet$ (−32).

The MS^3 spectra were acquired and presented the typical fragmentation of anthocyanidins, corresponding to methyl loss,

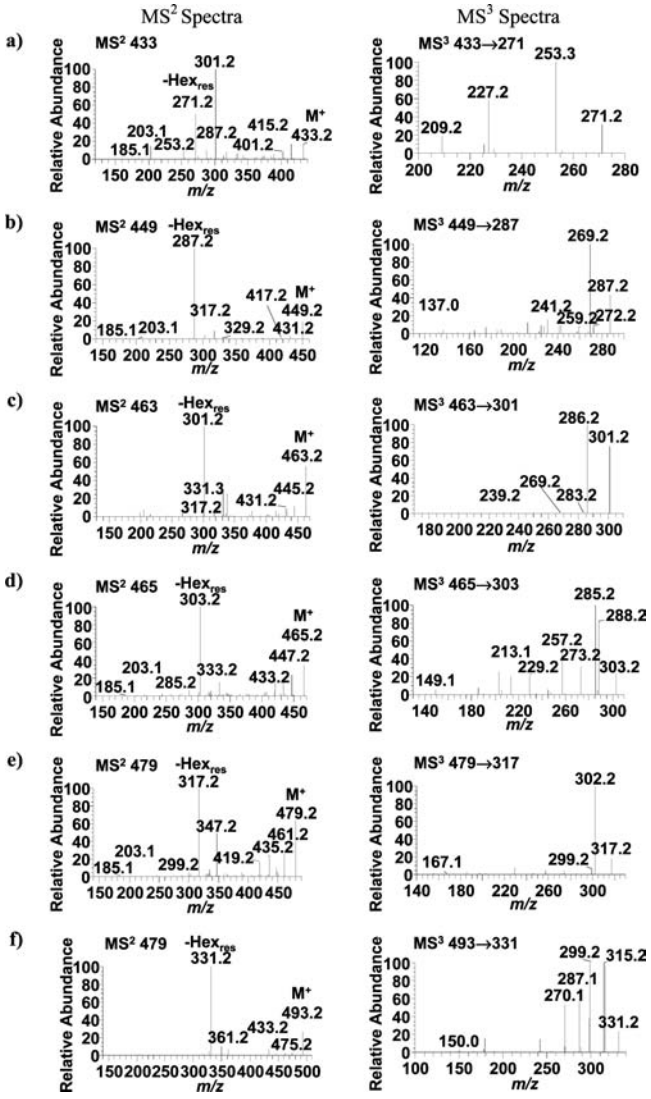

Figure 2. MS^2 and MS^3 spectra of (a) pelargonidin-3-*O*-glucoside, (b) cyanidin-3-*O*-glucoside, (c) peonidin-3-*O*-glucoside, (d) delphinidin-3-*O*-glucoside, (e) petunidin-3-*O*-glucoside, and (f) malvidin-3-*O*-glucoside.

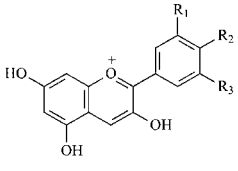

R_1	R_2	R_3	Anthocyanidins	MM	λmáx
H	OH	H	Pelargonidin	271	505
OH	OH	H	Cyanidin	287	515
OCH_3	OH	H	Peonidin	301	515
OH	OH	OH	Delphinidin	303	523
OH	OH	OCH_3	Petunidin	317	526
OCH_3	OH	OCH_3	Malvidin	331	530

Figure 3. Structure, monoisotopic mass, and maximum visible absorption wavelength of anthocyanidins in *Vitis vinifera*.

dx.doi.org/10.1021/jf500825h | J. Agric. Food Chem. 2014, 62, 5651−5659

water loss, CO loss, and H_2CO loss, among others. The diagnostic $^{0,2}B^+$, $^{0,3}A^+$, and $^{0,2}B^+$ ions could be detected in some but not all spectra. This is in accordance with previous reports that show that under low energy induced fragmentation, the neutral losses are more important than the formation of these fragment ions.[26]

The ions at *m/z* 521, 535, and 639 corresponding to petunidin-3-*O*-acetylmonoglucoside, malvidin-3-*O*-acetylmonoglucoside, and malvidin-3-*O*-(6-*O*-*p*-coumaroyl)monoglucoside were also observed in the MS spectra, and although the MS^2 spectra did not have enough quality due to the low abundance of these ions, a loss of 204 could be observed for the ions at *m/z* 521 and 535, consistent with the presence of an acetylated hexose residue. The loss of neutral molecules with 146 + 162 observed in the MS^2 of the ions at *m/z* 639 corresponds to the loss of a coumaroyl and hexose residue (data not shown).

Anthocyanin Distribution on Síria White Grapes and Effect of Pressing Method and Storage on the Pinking White Wine Anthocyanin Profile. As no pink color was observed in Síria white grape variety (Figure 4), it could be inferred that the anthocyanins were not concentrated in any particular grape berry tissue. Nevertheless, it was possible to detect anthocyanins in the skin and pulp of the Síria white grapes. Grapes may be either not-colored or colored, ranging from the lightest pink to the darkest purple tones according to the amount of anthocyanin accumulated in the berry skin, this being the primary factor characterizing the grapes and wines.[27] Síria grapes are undoubtedly accordingly classified as white grapes (Figure 4);[28] nevertheless, this variety has the capacity to synthesize small amounts of anthocyanins not concentrated in the skin as is common in red and pink grape varieties.[17,29] The synthesis of flavonoids in plants arises from the action of multiple enzymes of the phenylpropanoid pathway. Most of the genes coding for these enzymes have been identified in the *Vitis* genus.[30] White grapes contain the genes responsible for the synthesis of all enzymes in the anthocyanin pathway; some of them share in the formation of other polyphenols present in white grapes.[31] The absence of red color in the white varieties (i.e., the absence of anthocyanins) results from multiallelic mutations of the *VvMYBA1* and *VvMYBA2* genes,[29,32−34] which control the last biosynthetic step of anthocyanin synthesis, a glycosylation reaction mediated by the UDP-glucose flavonoid 3-*O*-glucosyltransferase enzyme. Also, the occurrence of light-red and rosy-skinned bud sports resulting from the color recovery in berries of grape of the white cultivar 'Italia' caused by a novel allele at the *VvmybA1* locus has been described.[35] Therefore, another possibility is that the clone of the Síria grape variety cultivated in Figueira de Castelo Rodrigo region is a bud sport of the original Síria white grape variety or that the Síria grape variety never completely lost the ability to produce anthocyanins. Furthermore, the Síria grape variety from this region presents the highest genetic diversity.[28] This point deserves further study.

Figure 4. Síria grape variety at technological maturity.

The 2012 vintage was followed in all steps of winemaking from Síria white grapes, from the reception of the grapes, their pressing to give the must, to the final product, the wine. The analysis of the must, just at the reception of the Síria white grapes, allowed the detection of anthocyanins, corroborating the presence of anthocyanins in Síria pulp. During grape pressing, the anthocyanin profile and amount of must sampled at different pressures show that higher amounts of anthocyanins were extracted at pressure stage 2. The must presented clearly a pink color, and the color changed with the change of pH, more intense at pH 1.39 and completely disappearing at pH 4.01. At pH 4.01 no pink color could be detected, showing that the anthocyanins were the only compounds with pink color present in the must. Lower amounts of anthocyanins were extracted at pressure stage 4, and the amount of anthocyanins extracted increased slightly again at pressure stage 6 due to the presence of anthocyanins also in the grape skin. White wine produced from these grapes also contained anthocyanins, even after PVPP treatment. In fact, when the white wine was exposed to oxygen, the appearance of pinking was observed from the top to the bottom of the bottle, attributed to the depletion of free sulfur dioxide due to the exposure to oxygen.

Anthocyanins are not stable during bottling. To follow their fate during storage in the pinking white wines, the Síria 2010 wine that turned pink after bottling was analyzed also after 12 months of storage. The chromatographic profile changed considerably, a lump and small amounts of malvidin-3-*O*-glucoside being observed. The observed lump is a feature characteristic of old red wines due to the polymerization of anthocyanins.[36] The amount of monomeric anthocyanins of the Síria 2010 white wine decreased to 0.035 mg/L after storage, showing that there was a decrease in the monomeric anthocyanin content during storage. This can explain the results previously reported by Jones, who described the pinking phenomena as being caused by at least 10 different compounds and polymeric material, suggesting that polymerization had occurred in the analyzed samples.[2]

The severity of pinking each year during the past 12 years in Figueira de Castelo Rodrigo wine was not the same, possibly due to the influence of weather conditions. Therefore, the pinking severity of each year was indirectly assessed by measuring the amount of PVPP used in winemaking in relation to the amount of white wine produced between 2005 and 2011, ranging from 0.111 g/L (2011) to 0.299 g/L (2008). This interannual variability was negatively related with the average temperatures of the first 10 days of October ($r = -0.92$, $p < 0.003$), suggesting that higher temperatures occurring during that period decreased the coloration of wines. No significant linear relationships were found for other periods of October (middle and last 10 days) and September. Nevertheless, they need to be cautiously interpreted as the data series is limited to seven vintages. On the other hand, August temperatures and thermal amplitudes displayed inconsistent outputs. The measures of heat accumulation, such as degree-days, did not show closer relationships. Furthermore, precipitation of the above periods presented no statistically significant correlations with pinking severity (data not shown). These results may be ascribed to the influence of temperature on anthocyanin

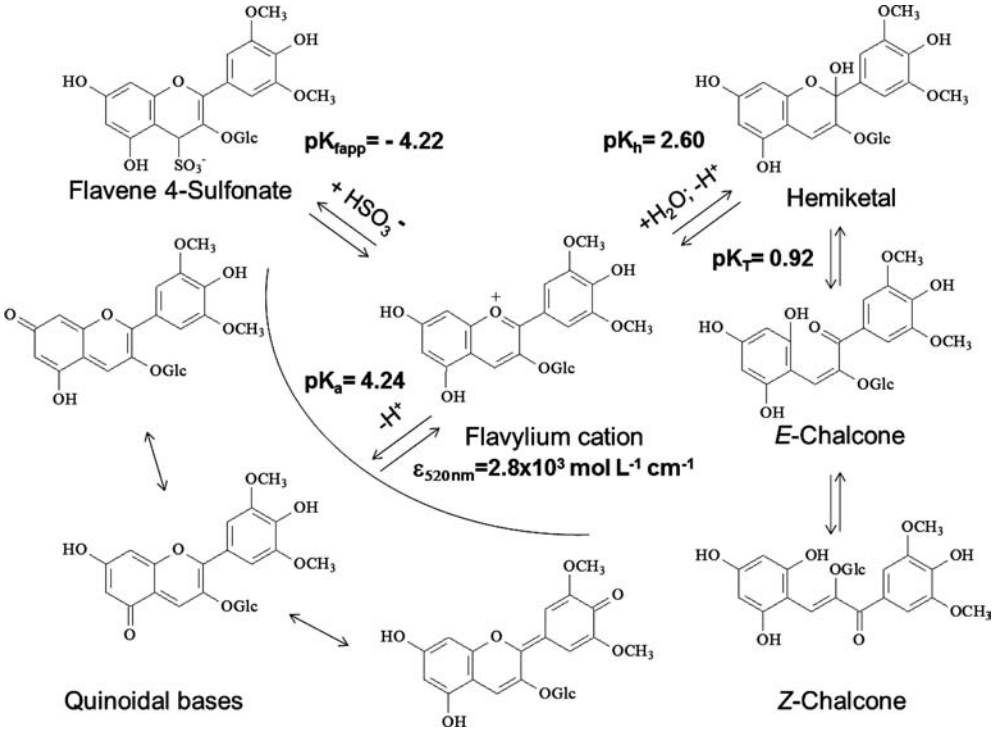

Figure 5. Effect of pH on anthocyanin equilibria in aqueous solution and in the presence of hydrogen bisulfite.

biosynthesis.[37,38] Therefore, it may be inferred that lower average temperatures in early October promote the synthesis of anthocyanins in Síria grape varieties and, consequently, white wine pinking.

Implications of Anthocyanins in White Wine Pinking. Although it cannot be excluded that the pinking of different grape varieties of white grapes can have a different origin from that observed for the Síria grape variety, all of the technical descriptions of the pinking process fit with the known chemical properties and reactivity of anthocyanins. It is described that the inhibition of wine PPO increases the pinking potential of white wines,[10] and hyperoxidation of grape must reduces pinking potency of white wines. In grape juice, PPO mainly catalyzes the oxidation of caftaric acid to the unstable *o*-quinones that bleach anthocyanins by two different mechanisms, depending on the anthocyanin structure.[39,40] The nonenzymatic generation of *o*-quinones from caftaric acid and other polyphenols containing an *o*-diphenol structure such as (+)-catechin/(−)-epicatechin, gallocatechin, gallic acid and its esters, and caffeic acid, which are the most readily oxidized wine compounds,[41,42] can occur under hyperoxidation of grape must. Anthocyanin bleaching can occur in the case of anthocyanins containing an *o*-diphenolic structure on the B-ring such as cyanidin, delphinidin, and petunidin by coupled oxidation to very unstable quinones, regenerating the initial caftaric acid or other quinones present in solution.[43] Condensation reactions of anthocyanin in its hemiketal form to the *o*-quinone produce a colorless adduct, which is then equilibrated to the corresponding flavylium form.[39,43] Pinking can be observed just after crushing of the grapes, and its decrease can be observed with the addition of sulfur dioxide to the grape must. The monomeric anthocyanins in solution, and in the presence of free sulfur dioxide, are involved in a series of dynamic equilibria among five major molecular forms (Figure 5), including the bisulfite addition flavene compound, the quinoidal base, the flavylium cation, the hemiketal or carbinol pseudobase, and the chalcone (*E*- and *Z*-forms). The relative proportions of each form are dependent on the pH, free sulfur dioxide concentration, and temperature.[44−48] At wine pH (3.0), using the available equilibrium constants[45−47] and the apparent formation constant for the bisulfite addition flavene compound[48] for malvidin-3-*O*-glucoside, the main anthocyanin present in the pinking white wines, and neglecting the effect of ionic strength and ethanol concentration, it is possible to calculate the relative proportion of all compounds in equilibrium with the flavylium cation (Figure 5). Without the presence of free sulfur dioxide, the flavylium cation represents 26% of all forms in equilibrium, with the most abundant being the hemiketal, which represents 65%. The presence of free sulfur dioxide changes considerably these proportions in a concentration-dependent manner. In the presence of 50 ppm of free sulfur dioxide, a normal level used in bottling of white wines, the flavylium cation abundance decreases significantly to 6%, the hemiketal form also decreases significantly to nearly 15%, and the bisulfite addition flavene compound becomes the most abundant form in equilibrium, representing 76% of all forms. The decrease in the free sulfur dioxide content to 20 ppm increases the relative abundance of the flavylium cation to 11%, increases the amount of the hemiketal form to 28%, and decreases the relative abundance of the bisulfite addition flavene compound to 56%. The appearance of pinking after bottling and after standing in the air can be explained by the decrease of the free sulfur dioxide in wine that increases the amount of the anthocyanins in the flavylium cation form to a level that can be perceived.

During storage, the polymerization of anthocyanins was also observed. As the color of the polymeric anthocyanins is resistant to sulfur dioxide bleaching,[49] the polymerization of anthocyanins can also contribute to the appearance of pinking during bottling. In fact, it is known that polymeric

dx.doi.org/10.1021/jf500825h | J. Agric. Food Chem. 2014, 62, 5651−5659

anthocyanins, besides being quite resistant to bleaching by sulfur dioxide, have a color much more insensitive to pH changes than the monomeric forms.[49] Probably, this is why often pinking is described as being insensitive to sulfur dioxide bleaching and pH change.[1]

The results obtained by the test developed by Simpson[1] to evaluate the pinking sensitivity of white wines can also be rationalized according to the equilibrium of anthocyanins and their polymerization under oxidative conditions. In this test, the addition of hydrogen peroxide (75 mg/L) is used presumably to accelerate the oxidation of the white wine pink color precursors. Nevertheless, the hydrogen peroxide consumes the available bisulfite (HSO_3^-)[50] present in wine (up to an equivalent amount of 141 mg sulfur dioxide/L when no other compounds able to consume the hydrogen peroxide are present), and in a normal white wine the amount of free sulfur dioxide is much lower than this value. This results in the increase of the relative proportion of the flavylium cation and the consequent appearance of pink color that can also be due to the polymerization of the anthocyanins under the oxidative conditions used in the test. In fact, the amount of free sulfur dioxide does not influence the outcome of the method as long the amount of free sulfur dioxide is below 40 mg/L.[1]

■ ASSOCIATED CONTENT

Supporting Information

Figures S1−S8. This material is available free of charge via the Internet at http://pubs.acs.org.

■ AUTHOR INFORMATION

Corresponding Author

*(F.M.N.) Phone: +351 259 350 273. Fax: + 351 259 350 480. E-mail: fnunes@utad.pt.

Funding

We appreciate the financial support provided to the Research Unit in Vila Real (PEst-OE/QUI/UI0616/2014), to the QOPNA Research Unit 62/94 (Project PEst-C/QUI/UI0062/2013; FCOMP-01-0124-FEDER-037296), and to IBB/CGB-UTAD by the Foundation for Science and Technology (FCT) and COMPETE.

Notes

The authors declare no competing financial interest.

■ ACKNOWLEDGMENTS

We gratefully acknowledge Direção Regional de Agricultura e Pescas (DRAP) Centro for providing the climate data and Adega Cooperativa de Figueira de Castelo Rodrigo for supplying the wine and grape samples used in this study. We also acknowledge the helpful discussion with José Miguel Ribeiro and António José Farias Madeira.

■ REFERENCES

(1) Simpson, R. Oxidative pinking in white wines. *Vitis* **1977**, *16*, 286−294.

(2) Jones, T. *Pinking of White Table Wines Further Studies*. Master of Science thesis, University of California, Davis, CA, USA, 1989; 125 pp.

(3) Du Toit, W.; Marais, J.; Pretorius, I.; Du Toit, M. Oxygen in must and wine: a review. *S. Afr. J. Enol. Vitic.* **2006**, *27*, 76−94.

(4) Van Wyk, C.; Louw, A.; Rabie, M. The effect of reductive wine making conditions on wine quality and composition. In *Proceedings of the 11 th International Oenological Symposium*, June 3−5, Sopron, Budapest, Hungary; International Association for Winery Technology and Management: Breisach, Germany, 1976; pp 180−200.

(5) Simpson, R.; Miller, G.; Orr, L. Oxidative pinking of whites wines: recent observations. *Food Technol. Aust.* **1982**, *34*, 46−47.

(6) Simpson, R.; Bennett, S.; Miller, G. Oxidative pinking of whites wines: a note on the influence of sulfur dioxide and ascorbic acid. *Food Technol. Aust.* **1983**, *35*, 34−36.

(7) Singleton, V.; Trousdale, E.; Zaya, J. Oxidation of wines. I. Young white wines periodically exposed to air. *Am. J. Enol. Vitic.* **1979**, *30*, 49−54.

(8) Singleton, V.; Zaya, J.; Trousdale, E. White table wine quality and polyphenol composition as affected by must SO_2 content and pomace contact time. *Am. J. Enol. Vitic.* **1980**, *31*, 14−20.

(9) Clark, A.; Pedretti, F.; Prenzler, P.; Scollary, G. The impact of ascorbic acid on the oxidative colouration and associated reactions of a model wine solution containing (+)-catechin, caffeic acid and iron. *Aust. J. Grape Wine Res.* **2008**, *14*, 238−249.

(10) Lamuela-Raventós, R.; Huix-Blanquera, M.; Waterhouse, A. Treatments for pinking alteration in white wines. *Am. J. Enol. Vitic.* **2001**, *52*, 156−158.

(11) Vaimakis, V.; Roussis, L. Must oxygenation and polyphenoloxidase inhibition and the oxidation of white wine. *Lebensm.Wiss. Technol.* **1993**, *26* (2), 133−137.

(12) Zoecklein, B.; Fugelsang, K.; Gump, B.; Nury, F. Phenolic compounds and wine color. In *Wine Analysis and Production*; Chapman and Hall: New York, 1995; pp 115−151.

(13) Sanborn, M.; Edwards, C.; Ross, C. Impact of fining on chemical and sensory properties of Washington State Chardonnay and Gewürztraminer wines. *Am. J. Enol. Vitic.* **2010**, *61* (1), 31−41.

(14) Bradshaw, M.; Cheynier, V.; Scollary, G.; Prenzler, P. Defining the ascorbic acid crossover from anti-oxidant to pro-oxidant in a model wine matrix containing (+)-catechin. *J. Agric. Food Chem.* **2003**, *51* (14), 4126−4132.

(15) OIV (Organisation International de la Vigne et du Vin). In *Recueil de Méthodes Internationales d'Analyse des Vins et des Moûts*; Edition Officielle: Paris, France, 2009; Vol. 1.

(16) Lee, J.; Durst, R.; Wrolstad, R. Determination of total monomeric anthocyanin pigment content of fruit juices, beverages, natural colorants, and wines by the pH differential method: collaborative study. *J. AOAC Int.* **2005**, *88*, 1269−1278.

(17) Ros Barceló, A.; Calderón, A.; Zapata, J.; Muñoz, R. The histochemical localization of anthocyanins in seeded and seedless grapes (*Vitis vinifera*). *Sci. Hortic.* **1994**, *57*, 265−268.

(18) I. N. M. G. O clima de Portugal. In *Fascículo XLIX*, 3rd Região, Normais climatológicas da região de "Trás-os-Montes e Alto Douro e Beira Interior", correspondentes a 1951−1980; Instituto Nacional de Meteorologia e Geofísica: Lisboa, Portugal, 1991; Vol. 3, 70 pp.

(19) Hong, V.; Wrolstad, R. Use of HPLC separation photodiode array detection for characterization of anthocyanins. *J. Agric. Food Chem.* **1990**, *38*, 708−715.

(20) Cho, M.; Howard, R.; Prior, R.; Clark, J. Flavonoid glycosides and antioxidant capacity of various blackberry, blueberry and red grape genotypes determined by high-performance liquid chromatography/mass spectrometry. *J. Sci. Food Agric.* **2004**, *84*, 1771−1782.

(21) He, F.; He, J.-J.; Pan, Q.-H.; Duan, C.-Q. Mass-spectrometry evidence confirming the presence of pelargonidin-3-*O*-glucoside in the berry skins of Cabernet Sauvignon and Pinot Noir (*Vitis vinifera* L.). *Aust. J. Grape Wine Res.* **2010**, *16*, 464−468.

(22) Domon, B.; Costello, C. A systematic nomenclature for carbohydrate fragmentations in FAB-MS/MS spectra of glycoconjugates. *Glycoconjugate J.* **1988**, *5*, 397−409.

(23) Ma, Y.; Vedernikova, I.; Van den Heuvel, H.; Claeys, M. Internal glucose residue loss in protonated *O*-diglycosyl flavonoids upon low-energy collision-induced dissociation. *J. Am. Soc. Mass Spectrom.* **2000**, *11*, 136−144.

(24) Oliveira, M.; Esperança, P.; Ferreira, M. Characterization of anthocyanidins by electrospray ionization and collision induced dissociation tandem mass spectrometry. *Rapid Commun. Mass Spectrom.* **2001**, *15*, 1525−1532.

(25) Giusti, M.; Rodríguez-Saona, L.; Griffin, D.; Wrolstad, R. Electrospray and tandem mass spectroscopy as tools for anthocyanin characterization. *J. Agric. Food Chem.* **1999**, *47*, 4657−4664.
(26) Montoro, P.; Tuberoso, C. I. G.; Perrone, A.; Piacente, S.; Cabras, P.; Pizza, C. Characterisation by liquid chromatography-electrospray tandem mass spectrometry of anthocyanins in extracts of *Myrtus communis* L. berries used for the preparation of myrtle liqueur. *J. Chromatogr., A* **2006**, *1112*, 232−240.
(27) Ramazotti, S.; Filippetti, I.; Intrieri, C. Expression of genes associated with anthocyanin synthesis in red-purplish, pink, pinkish-green and green grape berries from mutated 'Sangiovese' biotypes: a case study. *Vitis* **2008**, *47* (3), 147−151.
(28) Almadanim, M.; Baleiras-Couto, M.; Pereira, H.; Carneiro, L.; Fevereiro, P.; Eiras-Dias, J.; Morais-Cecílio, L.; Viegas, W.; Veloso, M. Genetic diversity of the grapevine (*Vitis vinifera* L.) cultivars most utilized for wine production in Portugal. *Vitis* **2007**, *46* (3), 116−119.
(29) Walker, A.; Lee, E.; Robinson, S. Two new grape cultivars, bud sports of Cabernet Sauvignon bearing pale-coloured berries, are the result of deletion of two regulatory genes of the berry colour locus. *Plant Mol. Biol.* **2006**, *62*, 623−635.
(30) Matus, J.; Poupin, M.; Canon, P.; Bordeu, E.; Alcalde, J.; Arce-Johnson, P. Isolation of WDR and bHLH genes related to flavonoid synthesis in grapevine (*Vitis vinifera* L.). *Plant Mol. Biol.* **2010**, *72*, 607−620.
(31) Holton, T. A.; Cornish, E. C. Genetics and biochemistry of anthocyanin biosynthesis. *Plant Cell* **1995**, *7*, 1071−1083.
(32) Kobayashi, S.; Goto-Yamamoto, N.; Hirochika, H. Retrotransposon-induced mutations in grape skin color. *Science* **2004**, *304*, 982.
(33) Walker, A.; Lee, E.; Bogs, J.; McDavid, D.; Thomas, M.; Robinson, S. White grapes arose through the mutation of two similar and adjacent regulatory genes. *Plant. J.* **2007**, *49*, 772−785.
(34) This, P.; Lacombe, T.; Cadle-Davidson, M.; Owens, L. Wine grape (*Vitis vinifera* L.) color associates with allelic variation in the domestication gene *VvmybA1*. *Theor. Appl. Genet.* **2007**, *114*, 723−730.
(35) Azuma, A.; Kobayashi, S.; Goto-Yamamoto, N.; Shiraishi, M.; Mitani, N.; Yakushiji, H.; Koshita, Y. Color recovery in berries of grape (*Vitis vinifera* L.) 'Benitaka', a bud sport of 'Italia', is caused by a novel allele at the *VvmybA1* locus. *Plant Sci.* **2009**, *176*, 470−478.
(36) Alcalde-Eon, C.; Escribano-Bailón, M. T.; Santos-Buelga, C.; Rivas-Gonzalo, J. C. Identification of dimeric anthocyanins and new oligomeric pigments in red wine by means of HPLC-DAD-ESI/MSn. *J. Mass Spectrom.* **2007**, *42*, 735−748.
(37) Kliewer, W. M.; Torres, R. E. Effect of Controlled day and night temperatures on grape coloration. *Am. J. Enol. Vitic.* **1972**, *23*, 71−77.
(38) Mori, K.; Sugaya, S.; Gemma, H. Decreased anthocyanin biosynthesis in grape berries grown under elevated night temperature condition. *Sci. Hortic.* **2005**, *105*, 319−330.
(39) Sarni-Manchado, P.; Cheynier, V.; Moutounet, M. Reaction of enzimatically generated quinones with malvidin-3-glucoside. *Phytochemistry* **1997**, *45*, 1365−1369.
(40) Yokotsuka, K.; Singleton, V. Disappearance of anthocyanins as grape juice is prepared and oxidized with PPO and PPO substrates. *Am. J. Enol. Vitic.* **1997**, *48* (1), 13−25.
(41) Sarni-Manchado, P.; Fulcrand, H.; Souillol, V.; Souquet, J.; Cheynier, V. Mechanisms of anthocyanin degradation in grape must-like model solutions. *J. Sci. Food Agric.* **1995**, *69*, 385−391.
(42) Li, H.; Guo, A.; Wang, H. Mechanisms of oxidative browning of wine. *Food Chem.* **2008**, *108*, 1−13.
(43) Wesche-Ebeling, P.; Montgomery, M. Strawberry polyphenoloxidase: its role in anthocyanin degradation. *J. Food Sci.* **1990**, *55*, 731−734, 745.
(44) Cheminat, A.; Brouillard, R. PMR investigation of 3-*O*-(β-D-glucosyl)malvidin structural transformations in aqueous solutions. *Tetrahedron Lett.* **1986**, *27*, 4457−4460.
(45) Brouillard, R.; Delaporte, B. Chemistry of anthocyanin pigments. 2. Kinetic and thermodynamic study of proton transfer, hydration, and tautomeric reactions of malvidin 3-glucoside. *J. Am. Chem. Soc.* **1977**, *99*, 8461−8468.
(46) Brouillard, R.; Dubois, J. E. Mechanism of the structural transformations of anthocyanins in acidic media. *J. Am. Chem. Soc.* **1977**, *99*, 1359−1364.
(47) Brouillard, R.; Delaporte, B.; Dubois, J. E. Chemistry of anthocyanin pigments. 3. Relaxation amplitudes in pH-jump experiments. *J. Am. Chem. Soc.* **1978**, *100*, 6202−6205.
(48) Berke, B.; Chèze, C.; Vercauteren, J.; Deffieux, G. Bisulfite addition to anthocyanins: revisited structures of colourless adducts. *Tetrahedron Lett.* **1998**, *39*, 5771−5774.
(49) Somers, T. The polymeric nature of wine pigments. *Phytochemistry* **1971**, *10*, 2175−2186.
(50) Hoffmann, M.; Edwards, J. Kinetics of the oxidation of sulfite by hydrogen peroxide in acidic solution. *J. Phys. Chem.* **1975**, *79* (20), 2096−2098.

JOURNAL OF AGRICULTURAL AND FOOD CHEMISTRY

Article

pubs.acs.org/JAFC

Characterization of a Grape Class IV Chitinase

Simone Vincenzi,*[,†] Jan Bierma,[‡] Samanthi I. Wickramasekara,[§] Andrea Curioni,[†] Diana Gazzola,[†] and Alan T. Bakalinsky[⊥]

[†]Department of Agronomy, Food, Natural Resources, Animals and the Environment, Padova University, 35020 Legnaro, Italy

[‡]Cellular and Molecular Bioscience, University of California at Irvine, Irvine, California 92697, United States

[§]Department of Chemistry, Environmental Health Sciences Center and [⊥]Department of Food Science and Technology, Oregon State University, Corvallis, Oregon 97331, United States

ABSTRACT: A chitinase was purified from *Vitis vinifera* Manzoni Bianco grape juice and characterized. On the basis of proteomic analysis of tryptic peptides, a significant match identified the enzyme as a type IV grape chitinase previously found in juices of other *V. vinifera* varieties. The optimal pH and temperature for activity toward colloidal chitin were found to be 6 and 30 °C, respectively. The enzyme was found to hydrolyze chitin and oligomers of *N*-acetylglucosamine, generating *N*,*N*′-diacetylchitobiose and *N*-acetylglucosamine as products, but was inactive toward *N*,*N*′-diacetylchitobiose. The enzyme exhibited both endo- and exochitinase activities. Because yeast contains a small amount of chitin in the cell wall, the possibility of growth inhibition was tested. At a concentration and pH expected in ripe grapes, no inhibition of wine yeast growth by the chitinase was observed.

KEYWORDS: *grape chitinase, chitinase activity, yeast inhibition*

INTRODUCTION

Chitinases (EC 3.2.1.14) are glycosyl hydrolases that catalyze the degradation of chitin, a β-1,4-linked polymer of *N*-acetylglucosamine (GlcNAc) found in fungal cell walls among other natural sources.[1] Although higher plants lack chitin, they harbor chitinase genes and express them in response to pathogens or developmental cues in susceptible tissues.[2,3] In *Vitis vinifera*, type IV chitinase activity has been reported to increase dramatically in berries during ripening, presumably to provide protection from potential fungal attack.[4] Type IV chitinases have been detected in the juice of a number of varieties of *V. vinifera* species[4−7] and in wines made thereof.[7−11] Chitinase concentration in bottled white wines has also been found to correlate with the formation of heat-induced turbidity, a recognized quality defect.[12] Chitinase activity was reported to decrease significantly from initial levels detected in Pinot noir berries through the various stages of sparkling wine production to undetectable levels in the final wine.[13]

Chitinases have been classified into two major categories: endochitinases and exochitinases.[14] However, the current nomenclature for chitinolytic enzymes is confusing, due in part to the fact that the former classification scheme has not been abandoned.[15,16] The former scheme distinguished the exochitinases (EC 3.2.1.29), which catalyze progressive release of dimeric chitobiose residues from the nonreducing end, from the *N*-acetyl-β-D-glucosaminidases (EC 3.2.1.30), which release monomeric GlcNAc residues from chitin oligomers.[14] Currently, the International Union of Biochemistry and Molecular Biology (IUBMB) recognizes a single β-*N*-acetylhexosaminidase class of enzyme, EC 3.2.1.52, that includes the former EC 3.2.1.29 and EC 3.2.1.30 enzyme classes. Furthermore, some authors have described the enzymes that release small oligomers (including dimers) from the reducing end as endochitinases (EC 3.2.1.14), differentiating them from even the strictly endotype enzymes.[17] In the present paper, we use the nomenclature proposed by Harman et al., in which the difference between endo- and exochitinases is substrate specificity: endochitinases require at least tetrameric GlcNAc, whereas the minimum substrate for an exochitinase is the GlcNAc trimer. In addition, we refer to the enzyme that catalyzes the release of dimers as chitobiosidase.[18]

Although a number of studies have characterized family 19 chitinases, which include the type IV enzyme,[19,20] to our knowledge, the grape type IV chitinase has been subjected to limited biochemical analysis.[21,22] Here, we determined enzyme activity and substrate specificity and asked whether chitinase activity likely to be present in ripe grapes has the potential to inhibit yeast growth during wine fermentation.

MATERIALS AND METHODS

Purification of Grape Chitinase. Initially, 6 L of grape juice from *V. vinifera* Manzoni Bianco was treated overnight at 4 °C with 4 g/L of polyvinylpolypyrrolidone (PVPP) (Fluka), 2 g/L activated charcoal (Sigma), and 3 g/L of pectolytic enzymes (Pectazina DC, Dal Cin). The juice was decanted, filtered through a GF/A filter (Whatman), adjusted to pH 3.0 with HCl, and then filtered through a 0.2 μm cellulose acetate filter (Sartorius). Chitinase was purified from the filtered juice essentially as described.[5] The only modification was the substitution of the MacroPrep High S resin with an S-Sepharose resin (220 mL). Fractions containing a single band at 31 kDa (corresponding to the molecular weight of grape chitinase) were pooled, dialyzed against water (3500 Da cutoff dialysis membrane), and freeze-dried. The purity of the protein was checked by HPLC as described.[6]

Received: March 17, 2014
Revised: May 20, 2014
Accepted: May 20, 2014
Published: May 20, 2014

 © 2014 American Chemical Society

Chitinase Identification by LC-MS/MS Analysis of Tryptic Peptides. The freeze-dried purified 31 kDa fraction was processed for in-solution trypsin (Promega Trypsin Gold) digestion in the presence of a protease enhancer (Promega ProteaseMAX Surfactant) according to the manufacturer's protocol. LC-MS/MS analysis was conducted on an LTQ-FT MS (Thermo Fisher Scientific, San Jose, CA, USA) instrument coupled to a nanoAcquity UPLC system (Waters Corp., Milford, MA, USA). A binary solvent system consisting of solvent A, water with 0.1% formic acid, and solvent B, acetonitrile with 0.1% formic acid, was used for the analyses. Tryptic peptides (2 μL) were loaded onto a peptide trapping column (Cap Trap, Michrom) and separated using a C18 column (Agilent Zorbax 300SB-C18, 250 × 0.3 mm, 5 μm). Peptides were trapped and washed with 3% solvent B for 3 min at a flow rate of 5 μL/min. Peptide separation was achieved using a linear gradient from 10 to 30% B at a flow rate of 4 μL/min over 102 min. The LTQ-FT mass spectrometer was operated using data-dependent MS/MS acquisition with an MS precursor ion scan, performed in the ICR cell, from m/z 350 to 2000 with the resolving power set to 100,000 at m/z 400, and MS/MS scans performed by the linear ion trap on the five most abundant doubly or triply charged precursor ions detected in the MS scan.

Thermo RAW data files were processed with Proteome Discoverer v1.4.0. Mascot software (v2.3) and were used to search against the *V. vinifera* database downloaded from UniprotKB on July 8, 2013 (http://www.uniprot.org/), which included common processing contaminants. The following parameters were used to search the database: the digestion enzyme was set to Trypsin/P, and two missed cleavage sites were allowed. The precursor ion mass tolerance was set to 10 ppm, whereas a fragment ion tolerance of 0.8 Da was used. Dynamic modifications that were considered included carbamidomethyl (+57.02 Da) for cysteine, oxidation (+15.99 Da) for methionine, and deamidination (+0.98 Da) of asparagine and glutamine. Scaffold_3.3.1 (Proteome Software, Portland, OR, USA) was used for search data compilation and data evaluation with an embedded X!Tandem database searching algorithm. Peptide identifications were accepted if they could be established at >90.0% probability. Peptide Probabilities from X! Tandem were assigned by the Peptide Prophet algorithm[23] with Scaffold delta-mass correction. Peptide Probabilities from Mascot were assigned by the Scaffold Local FDR algorithm. Protein identifications were accepted if they could be established at >90.0% probability and contained at least two identified peptides. Protein probabilities were assigned by the Protein Prophet algorithm.[24] Proteins that contained similar peptides and could not be differentiated on the basis of MS/MS analysis alone were grouped to satisfy the principles of parsimony. Identified MS/MS spectra were manually validated, and ion assignments were made according to the spectral output of the Scaffold program.

Purification of Chitin Oligomers. Two grams of crab shell chitin (Fluka 22780) were hydrolyzed by suspension in 32 mL of 12 M HCl initially for 10 min at room temperature followed by an additional 110 min at 40 °C. The solution was neutralized on ice by slow addition of 32 mL of 50% NaOH. Insoluble matter was removed by centrifugation, and the clear supernatant was adjusted to pH 7 and ultrafiltered on an apparatus equipped with a 500 Da cutoff membrane (Amicon) to remove excess salt and to concentrate the oligomers. When a volume of 3 mL was reached, 1.5 mL was loaded onto a Bio-Gel P2 (Bio-Rad Laboratories) column (100 × 1.5 cm) and eluted at a rate of 0.25 mL/min using distilled water. One milliliter fractions were collected, freeze-dried, and resuspended in 20 μL of water.

TLC Analysis. TLC analysis was performed using silica TLC plates and a butanol/acetic acid/water (2:1:1) solvent[25] to determine oligomer purity in the Biogel P2 fractions and subsequently to determine the mechanism of chitinase action. Two microliters of the Bio-Gel P2 fractions was analyzed, and fractions with the same profile were pooled and freeze-dried. *N*-Acetylglucosamine (GlcNAc) and $(GlcNAc)_{2-3}$ standards (Sigma-Aldrich, St. Louis, MO, USA) were used for reference. Higher oligomers, $(GlcNAc)_{4-6}$, that were not commercially available were identified on the basis of mobility relative to the monomer and $(GlcNAc)_{2-3}$ oligomers.

Amino sugars were detected by staining with a solution of aniline/diphenylamine (4 mL of aniline, 4 g of diphenylamine, 200 mL of acetone, 30 mL of 85% phosphoric acid), followed by incubation for 3 min at 180 °C.

Chitinase Activity. Colloidal chitin used as substrate was prepared essentially as described by Sheng et al. starting with crab shell chitin.[26] For the determination of pH and temperature optima, chitinase activity was measured using an assay that specifically detected GlcNAc by reaction with *p*-dimethylaminobenzaldehyde (DMAB).[27] One unit of activity was defined as the amount of enzyme that catalyzed the release of 1 nmol of GlcNAc per minute at 37 °C and pH 5.5. A different chitinase assay was used to quantify activity when the inhibition of yeast growth was assessed. Specifically, chitinase added to yeast cultures was assayed prior to the addition by determining a linear increase in soluble reducing sugar over 1 h[28] using a commercial kit (Thermo Scientific Pierce Micro BCA Protein Assay Kit 23235) and GlcNAc as standard. Although this Cu-based assay kit is designated for protein quantification, the same reaction measures reducing sugar as well.[29] For this assay, one unit of chitinase activity was defined as that which liberated 1 mg of GlcNAc equivalents per hour at 25 °C.

Activity versus pH Determination. Two buffers were prepared at 50 mM strength: a citric acid−phosphate McIlvaine buffer, covering the pH range from 2.5 to 8, and a glycine buffer, covering the pH range from 8.5 to 10.5. For each pH tested, 800 μL of colloidal chitin was washed three times with 2 volumes of the corresponding buffer and resuspended in a final volume of 1600 μL (0.5% w/v final chitin concentration). Half of the solution volume was kept as a control, whereas chitinase was added to the other 800 μL of substrate to a final concentration of 50 μg/mL. After 2 h at 37 °C, both the sample and the control were centrifuged (12000*g*, 5 min), and 250 μL of clear supernatant was used to quantify GlcNAc. The difference between the absorbance of the sample and that of the control was used to determine the enzyme activity.

Activity versus Temperature Determination. Chitinase activity was determined as a function of temperature in 50 mM sodium acetate buffer, pH 6. Colloidal chitin (800 μL) was washed three times with 2 volumes of buffer and resuspended in a final volume of 1600 μL (0.5% w/v final chitin concentration). After a 30 min equilibration of substrate at each chosen temperature, 50 μg/mL of enzyme was added to initiate reactions. After a 1 h incubation, samples were centrifuged (12000*g* for 5 min) and GlcNAc concentrations were determined in 250 μL of clear supernatant.

Determination of Substrate Specificity. Activity against *N,N′*-diacetylchitobiose and the oligomers $(GlcNAc)_{3-6}$ was assessed under the following conditions. Two microliters of individual substrates at 10 mg/mL in water was diluted into a final volume of 50 μL of 50 mM ammonium acetate, pH 5.5, to which 1 μL of enzyme (10 mg/mL) was added. Two control reactions were run per substrate: one with substrate but without enzyme and the other with substrate and heat-inactivated enzyme (100 °C for 5 min). After a 1 h incubation at 37 °C, samples were freeze-dried, during which the ammonium acetate was evaporated. The residues were then resuspended in 3 μL of water and loaded onto TLC plates.

Yeast Strains, Growth Media. Four strains of *Saccharomyces cerevisiae* were used; laboratory strain S288c (*MATα SUC2 gal2 mal mel flo1 flo8−1 hap1 ho bio1 bio6*); a brewing strain, 2007-Pilsen Lager (Wyeast Laboratories); and the wine strains EC1118 and RC212 (Lallemand). Strains were grown in yeast nitrogen base (YNB) without amino acids, pH 5.2 (Difco), containing 2% glucose (YNB + glu) or in YNB containing 2% glucose adjusted to pH 3.5 by the addition of 26.6 mM tartaric acid (YNB + glu + tartrate, pH 3.5).

Yeast Growth Assay. Growth inhibition was assessed as a reduction in cell yield (A_{600}) in treated versus control cells. Treated cells were grown in the presence of grape chitinase, whereas control cells were grown in the presence of the same amount of boiled grape chitinase. Cells were grown overnight in YNB + glu or YNB + glu + tartrate, pH 3.5, washed twice in sterile distilled water, and then diluted to an initial concentration of 10^3 cells/mL in 1 mL aliquots of YNB + glu or YNB + glu + tartrate, pH 3.5, respectively, containing 50 μg of chitinase or boiled chitinase (control). In 100 mM sodium

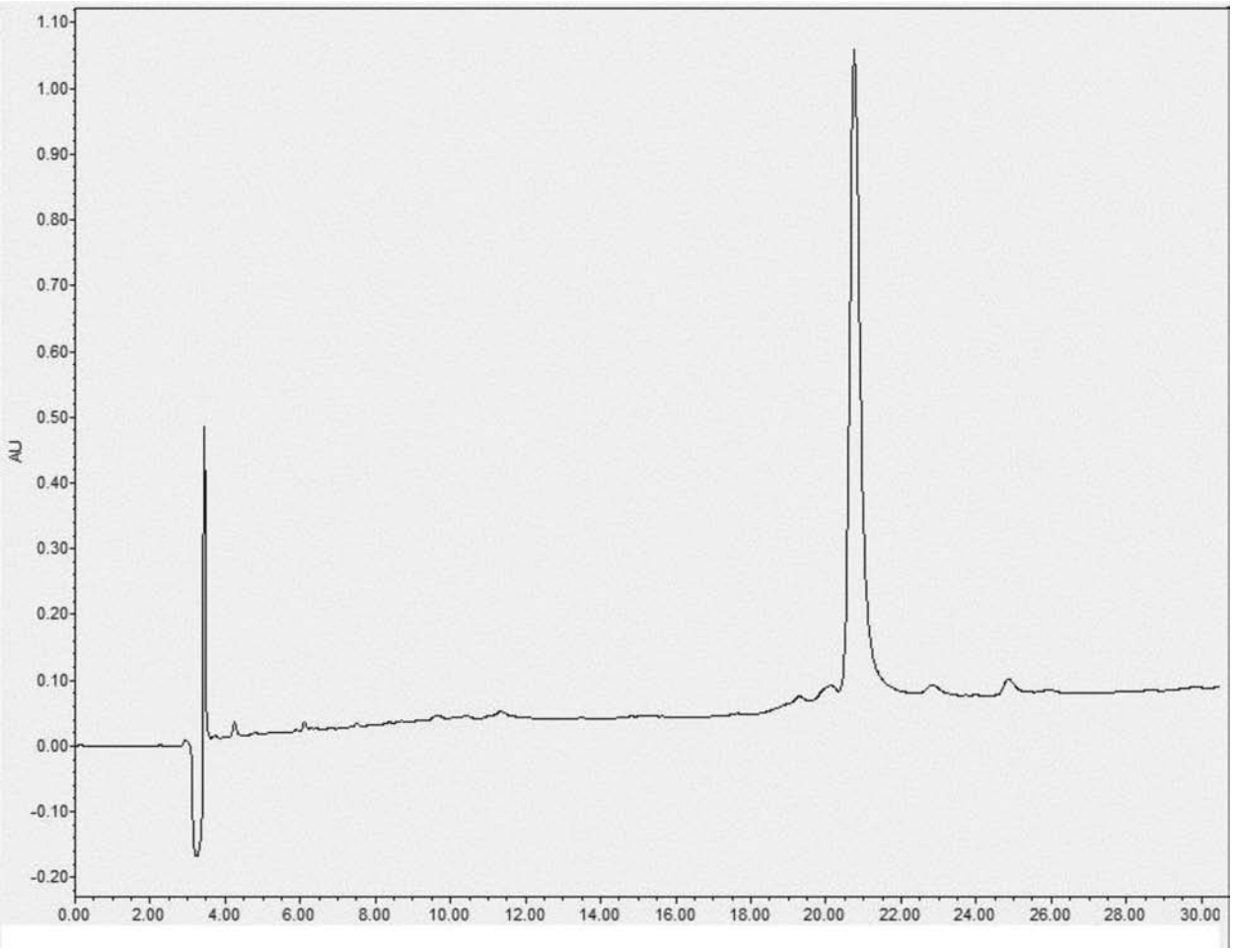

Figure 1. HPLC chromatogram of pooled fractions containing the purified 31 kDa protein (elution peak at 21 min).

Table 1. Identified Peptides with Matches in *V. vinifera* Chitinases Q7XAU6_VITVI and O24530

protein	sequence	Mascot ion score[a]	*m/z*
Q7XAU6_VITVI	AAFLSALNSYSGFGNDGSTDANKR	104.89	821.7239
	TALWFWMNNVHSVIGQGFGATIR	82.87	1303.17
O24530	AINGAVECNGGNTAAVNAR	105.66	929.9467

[a]Mascot ion score = $[-10 \log(P)]$, where P is the calculated probability that the observed MS/MS match between the experimental data and the database sequence is random.

phosphate at pH 6.0, 5.2, and 3.5, 50 μg of grape chitinase was found to contain $0.0237 \pm 9.7 \times 10^{-4}$, $0.0288 \pm 1.3 \times 10^{-3}$, and $0.0249 \pm 1.8 \times 10^{-3}$ units of activity ($n = 2$), respectively. Initial cell concentrations were determined by use of a hemacytometer. Cells were incubated in triplicate for 48 or 72 h at 30 °C and 200 rpm in 1.5 mL screw-capped polypropylene tubes, after which A_{600} values were measured. Growth inhibition was expressed as the ratio $[A_{600}$ (treated cells)$/A_{600}$ (control cells)$] \times 100$. The significance of differences was assessed using Student's two-sided, two-tailed t test ($p < 0.05$).

RESULTS AND DISCUSSION

Chitinase Purification and Identification. After the two purification steps, 130 mg of chitinase (97% purity by HPLC, calculated as peak area on the chromatogram) was obtained from 6 L of Manzoni Bianco grape juice (Figure 1), comparable to yields obtained by Van Sluyter et al., 45 and 10 mg/L for Semillon and Sauvignon blanc juices, respectively.[5]

The purified 31 kDa protein was identified as a type IV chitinase on the basis of significant matches with three different tryptic peptides (Table 1) shared by two enzymes designated Q7XAU6_VITVI (UniProtKB) based on the deduced amino acid sequence of cDNA VvChi4D (EMBL AAQ10093.1) and the *V. vinifera* chitinase designated O24530 (UniProtKB), the sequence of which was deduced from cDNA VvChi4A.[4] Q7XAU6_VITVI was previously detected in juice from Semillon and Sauvignon blanc grape varieties.[5,30,31] It is possible that the two proteins are allelic variants encoded by the same gene (Figure 2a). Tandem mass spectra of ion fragments derived from the three identified peptides are listed in Figure 2b–d. Although protein and peptide identification probabilities were set to >90%, the peptides listed in this figure have peptide identification probabilities of 100%.

Determination of Substrate Specificity. Because tetramers and larger oligomers of GlcNAc were unavailable commercially, these substrates were purified from a partial chitin hydrolysate by size exclusion chromatography. Figure 3 shows the purified oligomers $(GlcNAc)_{3-5}$ separated by TLC. The fractions were freeze-dried and resuspended in water at 10

a)

```
Q7XA-   1    MAAKLLTVLLVGALFGAAVAQNCGCASGLCCSKYGYCGTGSDYCGDGCQSGPCDSSSGSG  60
             MAAKLLTVLLVGALFGAAVAQNCGCASGLCCSKYGYCGTGSDYCGDGCQSGPCDSS   G
0245-   1    MAAKLLTVLLVGALFGAAVAQNCGCASGLCCSKYGYCGTGSDYCGDGCQSGPCDSS---G  57

Q7XA-   61   SSVSDIVTQSFFDGIINQAASSCAGKNFYTRAAFLSALNSYSGFGNDGSTDANKREIAAF  120
             SSVSDIVTQSFFDGII+QAASSCAGKNFYTRAAFLSALNSYSGFGNDGSTDANKREIAAF
0245-   58   SSVSDIVTQSFFDGIISQAASSCAGKNFYTRAAFLSALNSYSGFGNDGSTDANKREIAAF  117

Q7XA-   121  FAHVTHETGHFCYIEEINGASHNYCDSSNTQYPCVSGQNYYGRGPLQLTWNYNYGAAGNS  180
             FAHVTHETGHFCYIEEINGASHNYCDSSNTQYPCVSGQNYYGRGPLQLTWNYNYGAAGNS
0245-   118  FAHVTHETGHFCYIEEINGASHNYCDSSNTQYPCVSGQNYYGRGPLQLTWNYNYGAAGNS  177

Q7XA-   181  IGFNGLSNPGIVATDVVTSFKTALWFWMNNVHSVIGQGFGATIRAINGAVECNGGNTAAV  240
             IGFNGLSNPGIVATDVVTSFKTALWFWMNNVHSVIGQGFGATIRAINGAVECNGGNTAAV
0245-   178  IGFNGLSNPGIVATDVVTSFKTALWFWMNNVHSVIGQGFGATIRAINGAVECNGGNTAAV  237

Q7XA-   241  NARVQYYKDYCSQLGVSPGDNLTC  264
             NARVQYYKDYCSQLG SPGDNLTC
0245-   238  NARVQYYKDYCSQLGASPGDNLTC  261
```

Figure 2. continued

dx.doi.org/10.1021/jf501225g | J. Agric. Food Chem. 2014, 62, 5660−5668

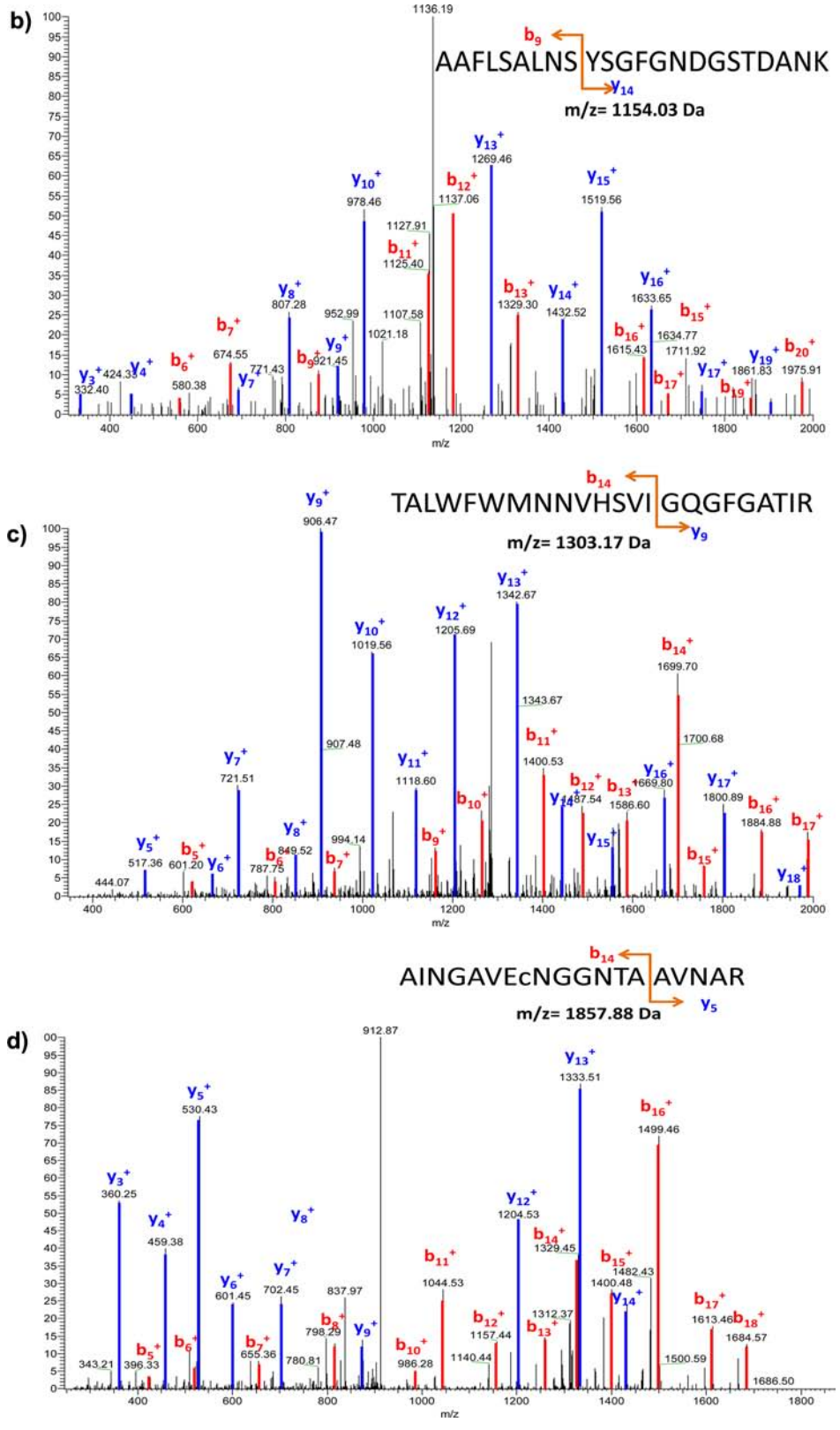

Figure 2. Sequence alignment of identified *V. vinifera* class IV chitinases and mass spectra for fragment ions derived from the three identified peptides. (a) Aligned sequences of UniProtKB Q7XAU6_VITVI (Q7XA-) and UniProtKB O24530 (0245-) with the identified peptides indicated in color and in bold font. Because the second and third peptides are contiguous, the third is in italicized bold font. Mass spectra for the major fragment ions (red, b ions; blue, y ions) matched the theoretically predicted fragmentation of (b) peptide AAFLSALNSYSGFGNDGSTDANK, (c) peptide TALWFWMNNVHSVIGQGFGATIR, and (d) peptide AINGAVECNGGNTAAVNAR.

mg/mL for subsequent analyses. The oligomers ($GlcNAc_1$–$GlcNAc_6$) were incubated with enzyme or heat-inactivated enzyme, and the reaction products were visualized by TLC (Figure 4). In Figure 4, spots are coded by letter and number.

dx.doi.org/10.1021/jf501225g | J. Agric. Food Chem. 2014, 62, 5660−5668

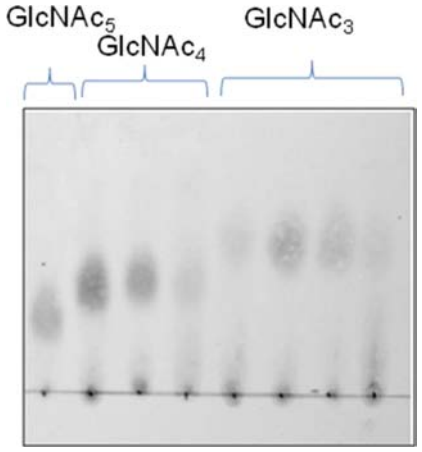

Figure 3. TLC analysis of a partial HCl hydrolysate of chitin fractionated by size exclusion chromatography. Lanes: 1, $(GlcNAc)_5$; 2−4, $(GlcNAc)_4$; 5−8, $(GlcNAc)_3$.

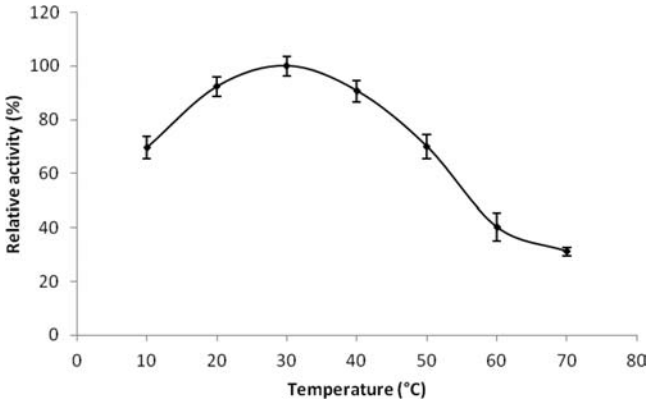

Figure 5. Chitinase activity as a function of temperature. Values are means of three replicates, and error bars are standard deviations.

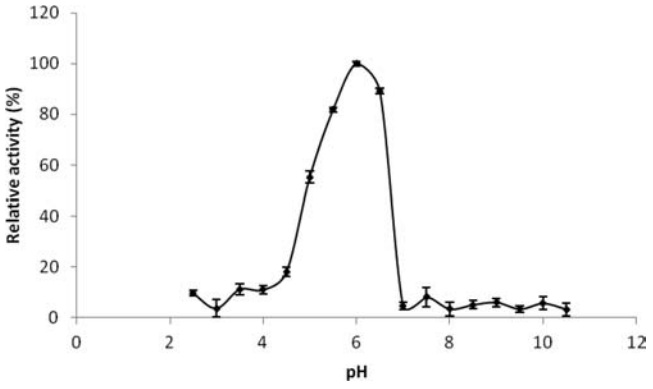

Figure 6. Chitinase activity as a function of pH. Values are means of three replicates, and error bars are standard deviations.

Letters A−F indicate substrates $GlcNAc_1$−$GlcNAc_6$, respectively. Numbers indicate treatment. Number 1 indicates incubation of substrate in the absence of enzyme. Numbers 2 and 3 indicate incubation with enzyme or heat-inactivated enzyme (100 °C for 5 min), respectively.

As expected, the monomer GlcNAc was not affected (Figure 4A1−A3), nor was *N,N′*-diacetylchitobiose degraded (Figure 4B1−B3), indicating an absence of 1,4-*β*-*N*-acetylglucosaminidase activity. On the other hand, chitotriose was split into the monomer GlcNAc and dimer *N,N′*-diacetylchitobiose (Figure 4C1−C3). Therefore, on the basis of the classification of Harman et al.,[18] this grape enzyme should be considered an exochitinase. However, as noted below, this designation is not consistent with the products generated from degradation of the tetramer $(GlcNAc)_4$. The degradation of $(GlcNAc)_4$ (Figure 4D1−D3) yielded both a dimer, as would be expected if chitobiosidase activity alone were present, and the monomer. On the basis of the absence of 1,4-*β*-*N*-acetylglucosaminidase activity (Figure 4B1−B3), we speculate that formation of the monomer was due to transient production of the trimer during cleavage, suggesting an endochitinase-based mechanism. Both monomer and dimer were also obtained from hydrolysis of the pentamer (Figure 4E1−E3) and hexamer (Figure 4F1−F3) as previously observed with other endochitinases.[25] The intermediate oligomers present in lanes E3 and F3 (Figure 4) are likely due to some chitinolitic activity present in the heat-denatured chitinase samples. This can be due to an incomplete denaturation of the catalytic domain or to its refolding upon cooling. Indeed, it was previously demonstrated that the grape chitinase is able to recover its activity after a 5 min treatment at

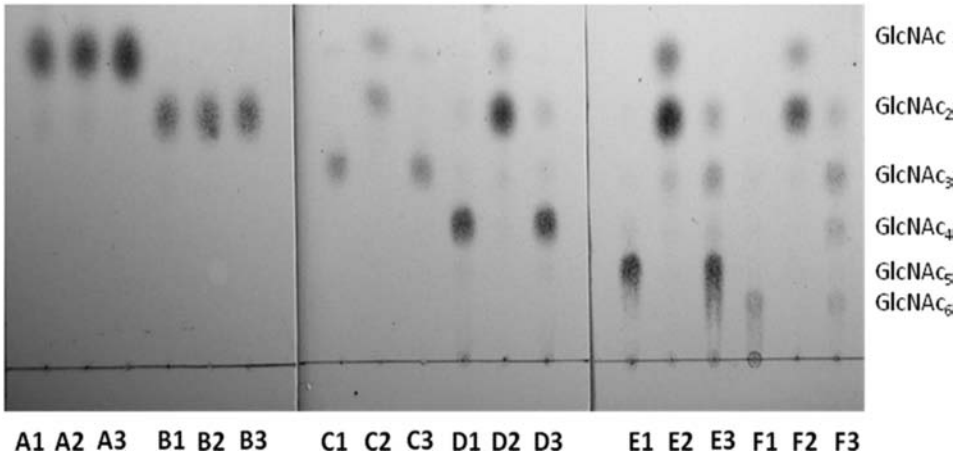

Figure 4. TLC analysis of reaction products generated by incubation of purified chitinase with purified oligomers of GlcNAc. Spots are coded by letter and number. Letters A−F indicate substrate $GlcNAc_1$ to $GlcNAc_6$, respectively. Number 1 indicates incubation of substrate in the absence of enzyme. Numbers 2 and 3 indicate incubation with enzyme or heat-inactivated enzyme (100 °C for 5 min), respectively.

dx.doi.org/10.1021/jf501225g | J. Agric. Food Chem. 2014, 62, 5660−5668

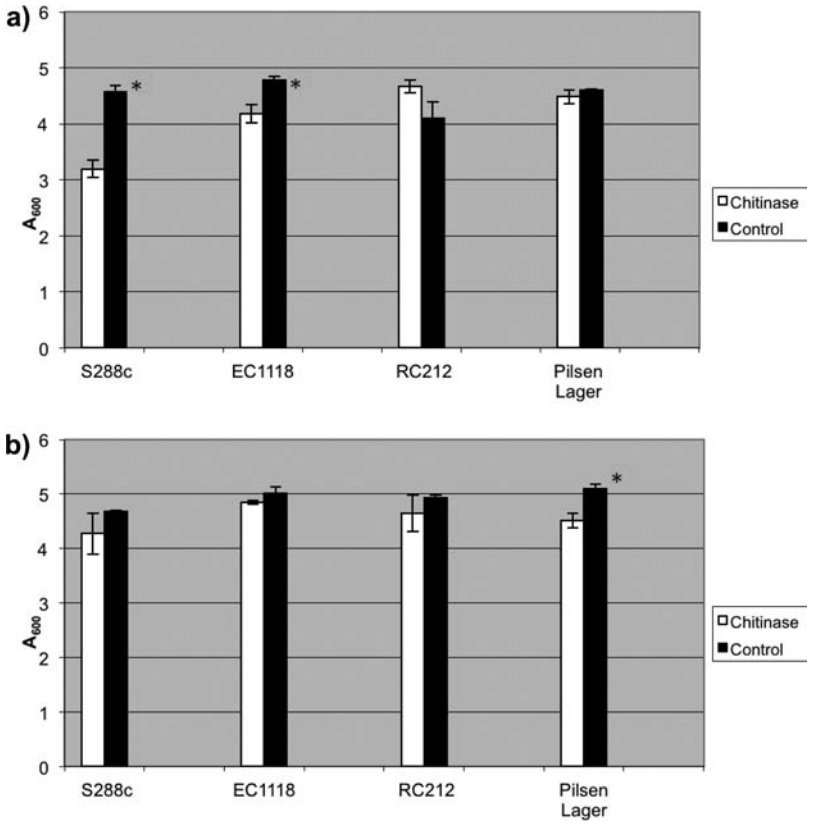

Figure 7. Inhibition of yeast growth: (A) inhibition after 48 h in YNB + glu assessed as a reduction in cell yield (A_{600}) in the presence of 50 μg of chitinase or boiled chitinase (control) starting with an initial inoculum of 10^3 cells/mL; (B) inhibition after 72 h in YNB + glu + tartrate, pH 3.5 assessed as a reduction in cell yield (A_{600}) in the presence of 50 μg of chitinase or boiled chitinase (control) starting with an initial inoculum of 10^3 cells/mL. Data are means of triplicate assays. An asterisk indicates a significant difference between treatment and control (Student's two-sided, two-tailed t test, $p < 0.05$).

100 °C followed by SDS-PAGE migration.[32] The presence of oligomers is consistent with endochitinase activity. These results are in agreement with a previous study that found the major grape chitinases to be class IV endochitinases on the basis of protein sequence.[4] However, a chitinase purified from *Bacillus brevis* characterized as an endosplitting enzyme produced mostly oligomers much larger than $(GlcNAc)_4$ from a substrate consisting of a hydrolysate of colloidal chitin.[26] In addition, it has been reported that to determine chitinase activity from a variety of sources (e.g., soybean seeds[33] or *Streptomyces*[34]), a specific chitobiase is needed to degrade the disaccharide to produce p-DMAB-reactive GlcNAc. In our case, it was possible to quantify enzymatic activity directly using p-DMAB without the addition of an exogenous chitobiase.

The pattern of degradation products observed here from various GlcNAc oligomers is very similar to that reported for an *Aspergillus fumigatus* chitinase, presumed to be a family 18 enzyme,[35] that exhibited exo- and endochitinase and transglycosylation activities.[36] On the other hand, a chitinase from *Pyrococcus kodakaraensis* classified as an endochitinase[25] produced $(GlcNAc)_2$ and GlcNAc from $(GlcNAc)_3$ and $(GlcNAc)_2$ along with small amounts of GlcNAc from $(GlcNAc)_{4-6}$.

In summary, both exochitinase activity and the previously described endochitinase activity are suggested for the enzyme purified from grape juice.

Determination of Temperature and pH Optima for Chitinase. Enzyme activity was assessed as a function of temperature and pH. The optimal temperature for chitinase activity was evaluated between 10 and 70 °C (Figure 5). Highest activity was observed between 30 and 40 °C, consistent with a 42 °C optimum found for grape chitinase isolated from *V. vinifera* Red Globe.[21] At temperatures above 50 °C, activity was found to decrease drastically, in agreement with a reported denaturation temperature of about 55 °C.[37] However, it must be noted that this latter result was obtained at pH 3 and that later it was reported that the melting temperature of the grape chitinase increased from 55 to 65 °C by raising pH from 3 to 4.[31] Therefore, the 30% residual activity found here after heating at 70 °C at pH 6 could be due to the effect of pH. More recently, Saito et al. described three chitinase isoforms in *V. vinifera* Semillon with temperature optima between 50 and 60 °C.[22]

The optimal pH for activity was found to be about 6, with relatively high activity observed in the range pH 5−6.5 (Figure 6). The same optimum was found by Gomes et al., although these researchers also detected a second peak of activity at about pH 3.[21] In our case, outside the pH 5−6.5 range, including the pH of grape juice, 3−3.5, activity was found to decrease sharply. On the other hand, chitinase isoforms purified from Semillon exhibited an optimal pH in the range of 4−4.5.[22]

Experiments performed at a pH and temperature close to those of winemaking conditions (25 °C and pH 3.2) demonstrated that the enzyme retained 12% of its maximal activity (data not shown), suggesting that residual activity could be present in grape must during fermentation.

Inhibition of Yeast Growth. Like other pathogenesis-related plant proteins, chitinases are synthesized in response to

biotic or abiotic stresses. However, in grapes, they are also generally expressed in a constitutive manner during ripening.[4] As a consequence, the concentration of chitinases can reach relatively high levels in grape juice.[38,39] The question of whether potential activity in grape juice could affect the major yeast species that mediates the wine fermentation is thus relevant because the cell wall of the wine yeast *S. cerevisiae* contains a small amount of chitin (1−2% dry wt), localized in bud scars.[40] Indeed, a class IV-like chitinase from *Streptomyces* was found to inhibit growth of *S. cerevisiae* at pH 5.8.[41] Because chitinase activity could potentially interfere with yeast growth under winemaking conditions, the effect of chitinase on cell yields of four different strains of *S. cerevisiae* was assessed using very low initial inoculum levels and an amount of chitinase expected in ripe grapes, 50 μg/mL. Although this concentration was found to reduce cell yield of the laboratory strain S288c by 30% and that of the wine strain EC1118 by 12% after 48 h in YNB + glu (Figure 7A), after 72 h, no reduction in cell yield was observed for any of the four strains tested (data not shown). In YNB + glu + tartrate, pH 3.5, a modest reduction in cell yield (12%) was observed only for the Pilsen Lager strain after 72 h (Figure 7B). No reduction was observed for either the laboratory or wine strains (data not shown). It is important to note that the chitinase activity tested here was about 10^4 less than that previously reported to inhibit growth of an unspecified strain of *S. cerevisiae*.[41]

These data suggest that yeast growth in a standard medium (YNB + glu) is slowed transiently if at all by the chitinase treatment and that cells recover if given sufficient time. After 72 h at pH 3.5, only growth of the brewing strain was reduced (modestly). Whether greater inhibition might be observed toward the wine strains during vinification in actual grape must (pH 3−4) when cells are exposed to greater osmotic stress at the higher initial sugar levels (∼20−25%) and higher ethanol levels is an open question.

In conclusion, we speculate that chitinase is unlikely to have an inhibitory effect on yeast growth during vinification, presuming the activity tested here is representative of that present in grape must and the fact that winemakers who use starter cultures typically inoculate with at least 10^6 cells/mL, which is about 10^3-fold higher than the level evaluated in the present study. Even if highly stressed cells might be more susceptible to chitinase-mediated growth inhibition, such cells in a wine fermentation have ceased growth for other reasons but continue to produce a significant amount of ethanol during stationary phase. Thus, growth inhibition per se would be unlikely to arrest fermentation, unless endogenous grape chitinase levels were high enough to inhibit initial growth of the starter culture or that of the naturally occurring yeasts present in uninoculated fermentations. On the other hand, we do not know if chitinase can interfere with fermentation in an indirect manner, unrelated to growth, by inhibiting other cellular processes.

AUTHOR INFORMATION

Corresponding Author

*(S.V.) E-mail: simone.vincenzi@unipd.it. Phone: (39) 0438 453052.

Notes

The authors declare no competing financial interest.

ACKNOWLEDGMENTS

The proteomic analysis was performed in the Oregon State University Environmental Health Sciences Center mass spectrometry facility, which is supported in part by a grant from the National Institute of Environmental Health Sciences (P30 ES000210).

REFERENCES

(1) Watanabe, T.; Kanai, R.; Kawase, T.; Tanabe, T.; Mitsutomi, M.; Sakuda, S.; Miyashita, K. Family 19 chitinases of *Streptomyces* species: characterization and distribution. *Microbiology* **1999**, *145*, 3353−3363.

(2) Samac, D. A.; Hironaka, C. M.; Yallaly, P. E.; Shah, D. M. Isolation and characterization of the genes encoding basic and acidic chitinase in *Arabidopsis thaliana*. *Plant Physiol.* **1990**, *93*, 907−914.

(3) Collinge, D. B.; Kragh, K. M.; Mikkelsen, J. D.; Nielsen, K. K.; Rasmussen, U.; Vad, K. Plant chitinases. *Plant J.* **1993**, *3*, 31−40.

(4) Robinson, S. P.; Jacobs, A. K.; Dry, I. B. A class IV chitinase is highly expressed in grape berries during ripening. *Plant Physiol.* **1997**, *114*, 771−778.

(5) van Sluyter, S. C.; Marangon, M.; Stranks, S. D.; Neilson, K. A.; Hayasaka, Y.; Haynes, P. A.; Menz, R. I.; Waters, E. J. Two-step purification of pathogenesis-related proteins from grape juice and crystallization of thaumatin-like proteins. *J. Agric. Food Chem.* **2009**, *57*, 11376−11382.

(6) Marangon, M.; van Sluyter, S. C.; Haynes, P. A.; Waters, E. J. Grape and wine proteins: their fractionation by hydrophobic interaction chromatography and identification by chromatographic and proteomic analysis. *J. Agric. Food Chem.* **2009**, *57*, 4415−4425.

(7) Le Bourse, D.; Conreux, A.; Villaume, S.; Lameiras, P.; Nuzillard, J.-M.; Jeandet, P. Quantification of chitinase and thaumatin-like proteins in grape juices and wines. *Anal. Bioanal. Chem.* **2011**, *401*, 1541−1549.

(8) Cilindre, C.; Jégou, S.; Hovasse, A.; Schaeffer, C.; Castro, A. J.; Clément, C.; Van Dorsselaer, A.; Jeandet, P.; Marchal, R. Proteomic approach to identify champagne wine proteins as modified by *Botrytis cinerea* infection. *J. Proteome Res.* **2008**, *7*, 1199−1208.

(9) Rowe, J. D. *Yeast Protein Release during Fermentation and Aging in a Model Wine*. M.S. thesis, Oregon State University, Corvallis, OR, 2008.

(10) Wigand, P.; Tenzer, S.; Schild, H.; Decker, H. Analysis of protein composition of red wine in comparison with rosé and white wines by electrophoresis and high-pressure liquid chromotagraphy-mass spectrometry (HPLC-MS). *J. Agric. Food Chem.* **2009**, *57*, 4328−4333.

(11) Tolin, S.; Pasini, G.; Curioni, A.; Arrigoni, G.; Masi, A.; Mainente, F.; Simonato, B. Mass spectrometry detection of egg proteins in red wines treated with egg white. *Food Control* **2012**, *23*, 87−94.

(12) Marangon, M.; Van Sluyter, S.; Neilson, K. A.; Chan, C.; Haynes, P. A.; Waters, E. J.; Falconer, R. J. Roles of grape thaumatin-like protein and chitinase in white wine haze formation. *J. Agric. Food Chem.* **2011**, *59*, 733−740.

(13) Manteau, S.; Lambert, B.; Jeandet, P.; Legendre, L. Changes in chitinase and thaumatin-like pathogenesis-related proteins of grape berries during the Champagne winemaking process. *Am. J. Enol. Vitic.* **2003**, *54*, 267−272.

(14) Cohen-Kupiec, R.; Chet, I. The molecular biology of chitin digestion. *Curr. Opin. Biotechnol.* **1998**, *9*, 270−277.

(15) Palanivelu, P.; Vaishna, L. Molecular cloning and characterization of a chitinase gene from the thermophilic fungus, *Thermomyces lanuginosus*. *J. Pharm. Biol. Sci.* **2013**, *5*, 99−107.

(16) Jacquoid, S.; Franqueville, L.; Cécillon, S.; Vogel, T. M.; Simonet, P. Soil bacterial community shifts after chitin enrichment: an integrative metagenomic approach. *PLoS One* **2013**, *8*, e79699.

(17) Ike, M.; Nagamatsu, K.; Shioya, A.; Nogawa, M.; Ogasawara, W.; Okada, H.; Morikawa, Y. Purification, characterization, and gene cloning of 46 kDa chitinase (Chi46) from *Trichoderma reesei* PC-3-7

and its expression in *Escherichia coli*. *Appl. Microbiol. Biotechnol.* **2006**, *61*, 294−303.
(18) Harman, G. E.; Hayes, C. K.; Lorito, M.; Broadway, R. M.; Di Pietro, A.; Peterbauer, C.; Tronsmo, A. Chitinolytic enzymes of *Trichoderma harzianum*: purification of chitobiosidase and endochitinase. *Phytopathology* **1993**, *83*, 313−318.
(19) Ohno, T.; Armand, S.; Hata, T.; Nikaidou, N.; Henrissat, B.; Mitsutomi, M.; Watanabe, T. A modular family 19 chitinase found in the prokaryotic organism *Streptomyces griseus* HUT 6037. *J. Bact.* **1996**, *178*, 5065−5070.
(20) Watanabe, T.; Kanai, R.; Kawase, T.; Tanabe, T.; Mitsutomi, M.; Sakuda, S.; Miyashita, K. Family 19 chitinases of *Streptomyces* species: characterization and distribution. *Microbiology* **1999**, *145*, 3353−3363.
(21) Gomes, L. P.; Ribeiro de Oliveira, C. I.; da Silva, M. C.; de Andrade, C. T.; Del Aguila, E. M.; Silva, J. T.; Paschoalin, V. M. F. Purification and characterization of grape (*Vitis vinifera* cv. Red Globe) chitinases for production of chitosan from shrimp chitin. *Quim. Nova* **2010**, *33*, 1882−1886.
(22) Saito, S.; Odagiri, M.; Furuya, S.; Suzuki, S.; Takayanagi, T. Inhibitory effect of chitinases isolated from Semillon grapes on growth of grapevine pathogens. *J. Plant Biochem. Biotechnol.* **2011**, *20*, 47−54.
(23) Keller, A.; Nesvizhskii, A. I.; Kolker, E.; Aebersold, R. Empirical statistical model to estimate the accuracy of peptide identifications made by MS/MS and database search. *Anal. Chem.* **2002**, *74*, 5383−5392.
(24) Nesvizhskii, A. I.; Keller, A.; Kolker, E.; Aebersold, R. A statistical model for identifying proteins by tandem mass spectrometry. *Anal. Chem.* **2003**, *75*, 4646−4658.
(25) Tanaka, T.; Fujiwara, S.; Nishikori, S.; Fukui, T.; Tajagi, M.; Imanaka, T. A unique chitinase with dual active sites and triple substrate binding sites from the hyperthermophilic archaeon *Pyrococcus kodakaraensis* KOD1. *Appl. Environ. Microbiol.* **1999**, *65*, 5338−5344.
(26) Sheng, L.; Zhi-An, Z.; Ming, L.; Zheng-Rong, G. C. Purification and characterization of a novel chitinase from *Bacillus brevis*. *Acta Biochim. Biophys. Sinica* **2002**, *34*, 690−696.
(27) Dinesh, K. P.; Santa Ram, A.; Shivanna, M. B. Studies on the chitinase activity in coffee (*Coffea arabica* L.). *Res. J. Agric. Biol. Sci.* **2010**, *6*, 449−452.
(28) Smith, P. K.; Krohn, R. I.; Hermanson, G. T.; Mallia, A. K.; Gartner, F. H.; Provenzano, M. D.; Fugimoto, E. K.; Goeke, N. M.; Olson, B. J.; Klenk, D. C. Measurement of protein using bicinchoninic acid. *Anal. Biochem.* **1985**, *150*, 76−85.
(29) Waffenschmidt, S.; Jaenicke, L. Assay of reducing sugars in the nanomole range with 2,2′-bicinchoninate. *Anal. Biochem.* **1987**, *165*, 337−340.
(30) Sauvage, F. X.; Bach, B.; Moutounet, M.; Vernhet, A. Proteins in white wines: thermo-sensitivity and differential adsorption by bentonite. *Food Chem.* **2010**, *118*, 26−34.
(31) Dufrechou, M.; Poncet-Legrand, C.; Sauvage, F. X.; Vernhet, A. Stability of white wine proteins: combined effect of pH, ionic strength, and temperature on their aggregation. *J. Agric. Food Chem.* **2012**, *60*, 1308−1319.
(32) Vincenzi, S.; Curioni, A. Anomalous electrophoretic behaviour of a chitinase isoform from grape berries and wine in glycol chitin-containing SDS-PAGE gels. *Electrophoresis* **2005**, *26*, 60−63.
(33) Wadsworth, S. A.; Zikakis, J. P. Chitinase from soybean seeds: purification and some properties of the enzyme system. *J. Agric. Food Chem.* **1984**, *32*, 1284−1288.
(34) Molano, J.; Duran, A.; Cabib, E. A rapid and sensitive assay for chitinase using tritiated chitin. *Anal. Biochem.* **1977**, *83*, 648−656.
(35) Hu, H.; Wang, G.; Yang, H.; Zhou, J.; Mo, L.; Yang, K.; Jin, C.; Jin, C.; Rao, Z. Crystallization and preliminary crystallographic analysis of a native chitinase from the fungal pathogen *Aspergillus fumigatus* YJ-407. *Acta Crystallgoraph. Sect. D* **2004**, *60*, 939−940.
(36) Xia, G.; Jin, C.; Zhou, J.; Yang, S.; Zhang, S.; Jin, C. A novel chitinase having a unique mode of action from *Aspergillus fumigatus* YJ-407. *Eur. J. Biochem.* **2001**, *268*, 4079−4085.
(37) Falconer, R. J.; Marangon, M.; Van Sluyter, S. C.; Neilson, K. A.; Chan, C.; Waters, E. J. Thermal stability of thaumatin-like protein, chitinase and invertase isolated from Sauvignon blanc and Semillon juice and their role in haze formation in wine. *J. Agric. Food Chem.* **2010**, *58*, 975−980.
(38) Tattersall, D. B.; Heeswijck, R.; Hoj, P. B. Identification and characterisation of a fruit-specific, thaumatin-like protein that accumulates at very high levels in conjunction with the onset of sugar accumulation and berry softening in grapes. *Plant Physiol.* **1997**, *114*, 759−769.
(39) Waters, E. J.; Hayasaka, Y.; Tattersall, D. B.; Adams, K. S.; Williams, P. J. Sequence analysis of grape (*Vitis vinifera*) berry chitinases that cause haze formation in wines. *J. Agric. Food Chem.* **1998**, *46*, 4950−4957.
(40) Klis, F. M.; Mol, P.; Hellingwerf, K.; Brul, S. Dynamics of cell wall structure in *Saccharomyces cerevisiae*. *FEMS Microbiol. Rev.* **2002**, *26*, 239−256.
(41) Yamashita, Y.; Okazaki, K. Antimicrobial activity of recombinant family 19 chitinase highly purified from *Escherichia coli* carrying *Streptomyces* chitinase gene. *Tech. Bull. Fac. Agric. Kagawa Univ.* **2007**, *59*, 71−77.

JOURNAL OF AGRICULTURAL AND FOOD CHEMISTRY

Article

pubs.acs.org/JAFC

Comparative Study of Phytosterol Derivatives in Monovarietal Olive Oils

Raquel B. Gómez-Coca,* Gabriel D. Fernandes, Chellah del Aguila-Sánchez, María del Carmen Pérez-Camino, and Wenceslao Moreda

Instituto de la Grasa-CSIC, Avenida Padre García Tejero 4, E-41012 Sevilla, Spain

ABSTRACT: Plant sterols and their derivatives are minor compounds that have been extensively studied in vegetable oils, mainly in olive oil, where they are closely related with its identity. The objective of this work is to determine the content of free and esterified steryl glucosides and their profiles in olive oil in relation to different geographical situation of olive orchards, cultivar, farming modality, and sampling time. The orchards under study were located in the outer ring of the submetropolitan area of Madrid (Spain), where olives from Cornicabra, Manzanilla Cacereña, Manzanilla Castellana, and Picual varieties were grown under traditional and organic modes, and harvested in four different samplings. Conclusions state that cultivar, farming mode, and light exposure do not have outstanding effects, whereas pedoclimate might affect the steryl glucoside presence in a substantial way. Further studies are being carried out presently in order to confirm such statement. Also glucoside derivative profiles are discussed, and reasons for differences with results in previous studies pointed out.

KEYWORDS: *olive oil, solid phase extraction (SPE), steryl glucoside (SG), esterified steryl glucoside (ESG), pedoclimate*

INTRODUCTION

Phytosterols, as well as their derivatives, are compounds of the unsaponifiable matter of vegetable oils, whose amount and profile are important parameters of oil identity. In the case of sterol derivatives, SG consist of a glucose moiety bound at the C3 position of the sterol residue via an acetyl bond. If additionally a fatty acid is esterified at the C6 position of the sugar, ESG are formed.

The presence of free and esterified steryl glucosides in edible matrices has been widely studied, although their synthesis pathway and influencing factors are not clear yet.[1] The health promoting effects of steryl glucosides have been unknown for a long time. Their use for the treatment of pathologies related to elevated cholesterol in blood was never compared to those of FS solutions[2] or functional foods,[3] and it was not until 2009 that studies in this field demonstrated the potential health benefits of glucosylated phytosterols in both free and esterified (acylated) forms.[4,5] Actually, SG could get reductions of around 37% in cholesterol absorption in the gut of human subjects, a value similar to the 30% obtained with SE.[4] As a consequence, research on possible steryl glucoside sources became more relevant and groups started publishing detailed data on the content and composition of glucosylated sterols in edible plant matrices to facilitate comparisons of the potential contribution of different foods as sources of steryl glucosides when included in the diet.[6] Those studies did not usually include olive oil, which justifies our studies on the presence of both SG and ESG in this matrix.

One would expect the SG and ESG composition to be closely related to the free sterol pool, and therefore the contribution of both SG and ESG to be bound to the oil identity. The procedure for isolating steryl glucosides from olive oil had been developed earlier. Initially the method was applied to a small number of oil samples of different categories and origins,[7] and then to a wider number also from different cultivars and treated with different refining processes,[8] reaching the conclusion that the only SG that might be present was BSSG, whose concentration in olive oil was never higher than 3 mg·kg^{-1}. Regarding ESG, mass spectrometry results confirmed that in the majority of the samples the only ESG present -at concentration sometimes above 8 mg·kg^{-1}- was EBSSG, possibly eluting just before small quantities of EAvSG.

In this case we have determined the composition and content of free and esterified steryl glucosides in a more systematic way, paying special attention to the contribution of each steryl glucoside to the total glucoside concentration. We have focused on monovarietal olive oils from different geographical situations, farming modalities, and sampling times. Our intention has been not only to start determining the factors affecting the steryl glucoside presence but also to contribute in a direct way to nutrient databases.

MATERIALS AND METHODS

Reagents. The internal standard ChSG, commercial mixtures of ESG and SG, and the analytical-grade chemical reagents used in the course of this research were the same as those utilized previously.[8]

Samples and Standard Solutions. Virgin olive oils were obtained from Cornicabra, Manzanilla Cacereña, Manzanilla Castellana, and Picual olive varieties. They were directly extracted in the laboratory of Doctor Pérez Jiménez group (IMIDRA) using an Abencor system identical to that described earlier.[8] Our blank sample (chemically refined olive-pomace oil) was obtained directly from the producers.

Stock solutions (100 μg·mL^{-1}) and samples were treated as described formerly,[7,8] in short: solutions of ESG standard were prepared by dissolving the standard mixture in chloroform. Stocks solutions of SG and of ChSG were made with a chloroform:methanol (2:1, by volume) blend. Samples consisted of 2 g of oil dissolved in 4 mL of chloroform, spiked with 100 μL of ChSG stock solution. The hydroxyl groups were

Received: March 18, 2014
Revised: May 26, 2014
Accepted: May 27, 2014
Published: May 27, 2014

ACS Publications © 2014 American Chemical Society

dx.doi.org/10.1021/jf501340q | J. Agric. Food Chem. 2014, 62, 5669−5674

derivatized (1 h at 60 °C) with 200 μL of a mixture of Py:HMDS:TMCS (9:3:1, by volume) before carrying out the GC analysis.

Olive Orchards and Olive Oil Extraction. The orchards were situated in Madrid, the center part of Spain, near the Manzanares River (Mediterranean climate), where they could be kept under optimal cultivation conditions. Specifically they were located in eight municipalities in the southern outer ring of the submetropolitan area (Table 1).

Table 1. Identification and Coding System of Studied Samples

variable	coding	assignment
cultivar	MCAC	Manzanilla Cacereña
	COR	Cornicabra
	MCLL	Manzanilla Castellana
	PIC	Picual
farming modality	T	Traditional
	O	Organic
municipality	AC	Anchuelo
	AG	Arganda
	AZ	Aranjuez
	CR	Campo Real
	CH	Chinchón
	TI	Tielmes
	VG	Valdelaguna
	VS	Villarejo de Salvanés
sampling time	1	Nov 14
	2	Nov 28
	3	Dec 12
	4	Dec 26

In these regions winters are cold due to the altitude (average of 667 m above sea level), January being the coldest month with temperatures between 3 and 10 °C, and 148 sunshine hours. These are dry climate areas; actually the common annual precipitations are between 400 and 500 mm per year in AC, AG, CR, CH, and VG, and below 400 mm per year in AZ, TI, and VS, which concentrate from October to May, October and December being the wettest months (56 mm).

Fruits from four different cultivars—Cornicabra, Manzanilla Cacereña, Manzanilla Castellana, and Picual cv.—were obtained from irrigated traditional orchards (drip irrigation). Additionally, olives from Manzanilla Castellana and Cornicabra cultivars were also obtained from organic orchards (Table 1).

The olive plantations were in a classical frame with around 300 trees per hectare. Fruits were handpicked according to the sampling time shown in Table 1.

To ensure maximum oil quality, olives were kept in darkness at 4 °C, and oil was extracted within 24 h after harvesting using an Abencor system and a small-quantity mill simulating commercial oil-extraction procedures (MC2 Ingeniería de Sistemas, Sevilla, Spain): the olives were crushed with an Abencor hammer mill equipped with a 4 mm sieve; 700 g of paste was processed using the system's malaxer and centrifuge during 1 min at 3500 rpm. Conditions: malaxation temperature, 27 °C; malaxation time, 20 min, plus 10 min after water addition; amount of distilled water added to the paste, 300 mL; amount of talc added, 20 g. The mixtures were left to decant during 24 h before proceeding to oil separation and filtration. To facilitate the work comprehension, the oil samples were coded according to Table 1.

Instrumentation. GC analyses of the sterol glucosides were carried out with an Agilent 6890N gas chromatograph (Agilent Technologies, Santa Clara, California) equipped with an Agilent 7683B automatic liquid sampler and FID. Acquisition of data was done with the Agilent ChemStation for GC System program. The conditions for the GC assays were as follows: TRB-5HT column (5% diphenyl−95% dimethylpoly-

Table 2. Total Steryl Glucoside Contents (mg·kg^{-1}) of Olive Oil from Different Cultivars, and Relative Composition Regarding Campesteryl Glucoside (CSG), Stigmasteryl Glucoside (SSG), β-Sitosteryl Glucoside (BSSG), and Δ5-Avenasteryl Glucoside (AvSG) (Part 1)[a]

	steryl glucosides														
	CSG			SSG			BSSG			AvSG			total		
samples	%	SD	*b*	%	SD	*b*	%	SD	*b*	%	SD	*b*	mg·kg^{-1}	SD	*b*
MCAC_T_CR_1	2.46	2.40	a,b	ND			86.89	3.14	c,d	10.65	0.73	c,d	2.08	0.05	d
MCAC_T_VS_2	ND			ND			90.30	1.00	d	9.70	1.00	c	1.83	0.14	c,d
MCAC_T_CR_3	5.25	0.37	b	ND			79.94	0.51	b	14.81	0.88	c,d	2.22	0.01	d
MCAC_T_VS_3	ND			11.91	1.45	b	81.21	1.13	b,c	6.88	0.33	b,c	2.33	0.05	d,e
MCAC_T_AZ_4	3.18	1.17	a,b	ND			90.72	1.84	d	6.10	0.66	b,c	2.15	0.24	d
MCAC_T_CR_4	13.38	0.03	c	3.30	0.82	a	70.52	1.18	a	12.81	0.39	c,d	2.28	0.02	d,e
COR_T_AZ_1	2.41	2.51	a,b	ND			91.38	0.13	d,e	6.21	2.63	b,c	1.74	0.07	c,d
COR_T_CH_1	ND	-		ND			96.59	3.50	e	3.41	3.50	a,b	1.53	0.04	b,c
COR_T_CH_2	2.06	2.04	a,b	ND			94.17	1.77	d,e	3.78	3.81	a,b	1.36	0.01	b,c
COR_T_AZ_2	4.67	0.70	b	ND			93.12	1.48	d,e	2.20	2.18	a,b	2.16	0.02	d
COR_T_CH_3	6.42	0.02	b	ND			90.41	3.17	d	3.17	3.15	a,b	1.68	0.01	b,c
COR_T_VS_3	5.29	0.83	b	ND			86.12	0.98	c	8.59	0.16	b,c	1.68	0.02	b,c
COR_T_AZ_3	4.59	0.57	b	ND			89.53	0.39	c,d	5.88	0.18	b,c	2.08	0.05	d
COR_T_CH_4	5.84	0.05	b	ND			91.92	2.16	d,e	2.24	2.21	a,b	2.38	0.03	d,e
COR_T_AZ_4	ND			ND			94.33	0.93	d,e	5.67	0.93	b,c	1.96	0.20	c,d
COR_T_VS_4	3.16	0.51	a,b	ND			89.29	0.81	c,d	7.55	0.30	b,c	2.14	0.11	d
COR_E_AZ_1	1.77	1.78	a,b	ND			92.29	1.23	d,e	5.94	0.55	b,c	1.63	0.01	b,c
COR_E_VG_1	3.69	3.53	a,b	ND			96.31	3.53	e	ND			1.61	0.07	b,c
COR_E_AZ_2	4.32	0.06	b	ND			90.45	0.11	d	5.22	0.05	b,c	1.93	0.12	c,d
COR_E_VS_2	1.77	1.78	a,b	ND			92.29	1.23	d,e	5.94	0.55	b,c	1.63	0.01	b,c
COR_E_CH_2	ND			ND			96.32	3.60	e	3.68	3.60	a,b	2.04	0.05	c,d
COR_E_AZ_3	4.21	0.18	a,b	ND			90.38	0.12	d	5.40	0.30	b,c	2.17	0.05	d

[a]A minimum of two independent measures was made in each case. The standard deviation is also given; ND (nondetected). [b]The use of the same letters (a−e) indicates the absence of statistical difference between samples (ANOVA/TUKEY test).

dx.doi.org/10.1021/jf501340q | J. Agric. Food Chem. 2014, 62, 5669−5674

Table 3. Total Steryl Glucoside Contents (mg·kg^{-1}) of Olive Oil from Different Cultivars, and Relative Composition Regarding Campesteryl Glucoside (CSG), Stigmasteryl Glucoside (SSG), β-Sitosteryl Glucoside (BSSG), and Δ5-Avenasteryl Glucoside (AvSG) (Part 2)[a]

	steryl glucosides													
	CSG			SSG		BSSG			AvSG			total		
samples	%	SD	*b*	%	SD	%	SD	*b*	%	SD	*b*	mg·kg^{-1}	SD	*b*
COR_E_VG_4	ND			ND		96.77	3.22	e	3.23	3.22	a,b	2.60	0.01	e
MCLL_T_TI_1	ND			ND		96.80	3.20	e	3.20	3.20	a,b	1.95	0.00	c,d
MCLL_T_AC_1	ND			ND		91.06	0.58	d,e	8.94	0.58	b,c	1.34	0.04	b,c
MCLL_T_AC_2	1.62	1.57	a,b	ND		88.89	1.92	c,d	9.49	0.34	b,c	1.54	0.04	b,c
MCLL_T_TI_2	ND			ND		95.13	0.02	d,e	4.87	0.02	a,b,c	2.00	0.02	c,d
MCLL_T_VS_2	7.61	1.72	b	ND		83.49	1.54	b,c	8.90	0.17	b,c	1.70	0.02	c
MCLL_T_VG_3	ND			ND		100.00			ND			0.59	0.01	a
MCLL_T_VS_3	ND			ND		100.00			ND			1.33	0.09	b
MCLL_T_VS_4	0.82	0.80	a	ND		89.53	0.60	c,d	9.66	1.40	b,c	1.57	0.03	b,c
MCLL_T_TI_4	ND			ND		94.98	0.20	d,e	5.02	0.20	a,b,c	2.02	0.01	c,d
MCLL_T_AC_4	3.77	3.60	a,b	ND		81.28	3.32	b,c	14.96	0.28	d	1.71	0.08	c
MCLL_E_VG_2	ND			ND		91.06	0.52	d,e	8.94	0.52	b,c	1.98	0.04	c,d
MCLL_E_VG_4	ND			ND		94.77	0.04	d,e	5.23	0.04	b,c	2.62	0.04	e
PIC_T_AZ_1	6.57	0.39	b	ND		85.69	0.27	c	7.73	0.66	b,c	1.90	0.04	c,d
PIC_T_AG_1	ND			ND		92.16	0.42	d,e	7.84	0.42	b,c	1.85	0.01	c,d
PIC_T_AG_2	ND			ND		94.26	0.42	d,e	5.74	0.42	b,c	1.89	0.02	c,d
PIC_T_CR_2	3.55	3.61	a,b	ND		87.85	0.25	c,d	8.59	3.36	b,c	2.41	0.04	d,e
PIC_T_AZ_3	5.25	0.93	b	ND		89.66	1.35	c,d	5.09	0.42	a,b,c	1.75	0.04	c,d
PIC_T_CR_3	ND			ND		94.56	0.00	d,e	5.44	0.00	b,c	2.61	0.14	e
PIC_T_CR_4	ND			ND		94.96	0.09	d,e	5.04	0.09	a,b,c	1.69	0.01	b,c
PIC_T_AG_4	ND			ND		94.49	0.79	d,e	5.51	0.79	b,c	1.99	0.03	c,d
PIC_T_AZ_4	ND			ND		94.25	0.69	d,e	5.75	0.69	b,c	2.13	0.06	d

[a]A minimum of two independent measures was made in each case. The standard deviation is also given; ND (nondetected). [b]The use of the same letters (a–e) indicates the absence of statistical difference between samples according to ANOVA and TUKEY test.

siloxane; 30 m × 0.32 mm i.d. × 0.10 μm film; Teknokroma, Sant Cugat del Vallés, Barcelona, Spain), 1.0 μL injection volume, hydrogen carrier gas at 3 mL·min^{-1}, and ECP cool on-column injection. The oven temperature program was as follows: 80 °C (1 min), 50 °C·min^{-1} to 320 °C (12 min), and 40 °C·min^{-1} to 360 °C (19 min). The detector temperature was 360 °C.

Steryl Glucoside Analysis. The SPE procedure developed previously[8] was utilized. The method consists of the conditioning of the cartridges (ExtraBond Si 1 g; Scharlab S.L., Barcelona, Spain) with 5 mL *tert*-butyl methyl ether, 5 mL hexane, 5 mL chloroform, and 10 mL of a newly prepared blend consisting of chloroform:methanol 4:1, by volume. Samples are then quantitatively transferred using 1 mL chloroform to wash the walls of the containers. The loaded cartridges are washed with 10 mL hexane, 10 mL of *tert*-butyl methyl ether, and 10 mL chloroform, applied one after the other. The steryl glucosides are eluted with 5 mL of the chloroform:methanol 4:1, by volume, solution. The procedure was carried out under negative pressure (1 mmHg) in a vacuum manifold. The eluted fractions are evaporated to dryness under nitrogen flux, derivatized and chromatographed using cool on-column injection.

The quantitative evaluation of the SG was carried out using ChSG as internal standard, whereas we quantified the ESG using three-point calibration curves (one specific curve for each ESG) built by spiking the in-house blank sample with the commercial standard mixture. This evaluation together with the purity, qualitative, and quantitative composition of the commercial standards is comprehensively described in our former work.[8]

All statistical analyses were run using the GraphPad Prism software, version 5.01 for Windows. The samples were compared by an ANOVA, with statistical significance of $p < 0.05$. After that they were differed by a TUKEY average comparison test.

RESULTS AND DISCUSSION

In the present study we have analyzed 44 oil samples, each of them at least in triplicate, in a relatively short time (six determinations/hour) and with fairly little solvent volumes, in comparison with former techniques, e.g., column chromatography.[9] This has proved the suitability of the system to be applied on a routine basis.

The quantitative results of the present study are shown in Tables 2–5. For the SG, the total amount is within the range 0.59 ± 0.01 to 2.62 ± 0.04 mg·kg^{-1}, the lowest and the highest amounts being those of Manzanilla Castellana samples from Valdelaguna, MCLL_T_VG_3 and MCLL_O_VG_4, respectively. If we compare them with those obtained previously,[8] it is clear that the SG concentration in virgin olive oils, devoid of defects, keeps constant within certain ranges. Consequently, we could assume that the SG concentration in virgin olive oils will be within the 0.6–2.7 mg·kg^{-1} range.

In the case of the SG profile, BSSG is always the main SG present, contributing at least with 70.52 ± 1.18% to the total. Actually, MCLL_T_VG_3 and MCLL_T_VS_3 only show BSSG. On the other hand, CSG and AvSG have great importance in almost all samples. MCAC_T_CR_4 has the highest CSG concentration (13.38 ± 0.03%) whereas MCLL_T_AC_4 exhibits the highest amounts of AvSG (14.96 ± 0.28%). SSG was present only in two Manzanilla Cacereña samples: MCAC_T_VS_3 (11.91 ± 1.45%) and MCAC_T_CR_4 (3.29 ± 0.82%). If we compare these results with the FS profile from olive oil, it is clear that there is no relationship between them beyond the fact that β-sitosterol derivatives are always present.

dx.doi.org/10.1021/jf501340q | J. Agric. Food Chem. 2014, 62, 5669–5674

Table 4. Total Esterified Steryl Glucoside Contents (mg·kg^{-1}) of Olive Oil from Different Cultivars, and Relative Composition Regarding Esterified Stigmasteryl Glucoside (ESSG), Esterified β-Sitosteryl Glucoside (EBSSG), and Esterified Δ5-Avenasteryl Glucoside (EAvSG) (Part 1)[a]

	esterified steryl glucosides													
	ESSG			EBSSG			EAvSG			total			SG:ESG	
samples	%	SD	*b*	%	SD	*b*	%	SD	*b*	mg·kg^{-1}	SD	*b*	%	*b*
MCAC_T_CR_1	ND			84.50	1.52	c,d	14.03	1.52	b,c	3.07	0.11	h	0.68	a
MCAC_T_VS_2	ND			84.14	3.88	c,d	15.86	3.88	c	2.01	0.08	e,f	0.92	a,b
MCAC_T_CR_3	ND			73.28	1.84	b,c	26.72	1.84	d	1.55	0.12	d,e	1.44	a,b
MCAC_T_VS_3	24.20	0.30	b	69.74	0.12	b	6.06	0.21	a,b	2.24	0.05	f,g	1.04	a,b
MCAC_T_AZ_4	ND			87.80	1.49	d	12.20	1.49	b,c	1.78	0.18	e,f	1.20	a,b
MCAC_T_CR_4	10.96	0.70	a	74.15	0.68	b,c	14.88	0.04	b,c	2.74	0.05	g,h	0.83	a,b
COR_T_AZ_1	ND			100.00			ND			0.64	0.06	b,c	2.75	b
COR_T_CH_1	ND			95.98	4.34	e	4.02	4.34	a,b	1.69	0.12	e	0.91	a,b
COR_T_CH_2	ND			89.93	0.69	d,e	10.07	0.69	b,c	0.85	0.06	c,d	1.60	a,b
COR_T_AZ_2	ND			100.00	-		ND	-		0.89	0.03	c,d	2.43	b
COR_T_CH_3	ND			89.05	0.78	d,e	10.95	0.78	b,c	1.82	0.02	e,f	0.92	a,b
COR_T_VS_3	ND			76.42	4.62	b,c	23.58	4.62	d	1.48	0.07	d,e	1.14	a,b
COR_T_AZ_3	ND			81.92	6.60	c,d	18.08	6.60	c,d	1.04	0.02	c,d	2.00	a,b
COR_T_CH_4	ND			79.27	1.00	c	20.73	1.00	c,d	0.39	0.03	b	6.20	c
COR_T_AZ_4	ND			96.77	3.45	e	3.23	3.45	a,b	1.10	0.07	c,d	1.77	a,b
COR_T_VS_4	ND			84.85	3.11	c,d	15.15	3.11	c	0.83	0.03	c	2.58	b
COR_E_AZ_1	ND			91.11	1.92	d,e	8.89	1.92	b,c	2.34	0.08	f,g	0.70	a
COR_E_VG_1	ND			100.00			ND			1.04	0.04	c,d	1.54	a,b
COR_E_AZ_2	ND			100.00			ND			0.96	0.06	c,d	2.01	a,b
COR_E_VS_2	ND			86.21	3.84	c,d	13.79	3.84	b,c	1.71	0.06	e,f	0.96	a,b
COR_E_CH_2	ND			100.00			ND			1.20	0.06	d	1.71	a,b
COR_E_AZ_3	ND			100.00			ND			0.46	0.01	b	4.73	c

[a]A minimum of two independent measures was made in each case. The standard deviation is also given; ND (nondetected). [b]The use of the same letters (a−e) indicates the absence of statistical difference between samples according to ANOVA and TUKEY test.

ESG contents are within a range from 0.18 ± 0.01 to 3.07 ± 0.07 mg·kg^{-1}. Previous studies[8] show varieties with very high ESG concentrations (e.g., Uovo di Pichone, 11.29 ± 2.75 mg·kg^{-1}, and Blanqueta, 9.63 ± 0.71 mg·kg^{-1}), which are not discussed here. If we compare the samples that were common to both studies (Cornicabra and Picual), ESG concentrations are nearly the same. Compiling global results from both studies, it is possible to establish a concentration interval from 0.2 to 14.0 mg·kg^{-1} for ESG presence in olive oil. As far as the profiles are concern, ECSG was never detected, while ESSG was seen only in two samples, which where those where SSG could be determined. EAvSG was detected in 70% of the samples (3.23−74.82% range). Except in the case of MCLL_T_VS_3, where EBSSG was 25.18 ± 2.34% of total ESG, in all the others samples, EBSSG was the main ESG, showing concentrations above 69%. Although it has already been demonstrated that there is no correspondence between the SG profile and that of their esterified counterparts,[6,8] this lack of any equivalence is still striking. Once again, it becomes clear that there is no connection between both SG and ESG concentrations, and that the SG:ESG rate does not have to be lower than 1 (Tables 4 and 5). Actually it is above 1 in more than 77% of the instances. Furthermore, there is not a correlation between global steryl glucoside quantities and their corresponding profiles. The fact of having high SG and/or elevated ESG concentration(s) does not imply richer profile(s), and vice versa. Actually, all four SG have been found in sample MCAC_T_CR_4 (Figure 1), together with three other ESG, and the respective concentrations of both kinds of sterol glucoside derivatives are not significantly higher than with "poorer" sets.

The cultivars tested in the present study cannot be considered different as far as the (E)SG content is concerned. However, we may observe that the Cornicabra variety shows the highest SG:ESG relationship, being in some cases surprisingly elevated (samples COR_O_VG_4, COR_T_CH_4, and COR_O_-AZ_3, with values of 8.6, 6.1, and 4.7, respectively). On the other hand the values are the lowest (around 1) in Manzanilla Cacereña cv. Finally, Picual cv. presents a more even distribution of the SG:ESG correlation.

Although correlation and cluster analysis, and other statistical analysis (PCA and HCA) did not let us get a clear distribution pattern to correlate sample characteristics with their (E)SG composition and content, calculation of three times the standard deviation allowed us to group results provisionally. Table 6 shows the SG and ESG results grouped according to the origin of the olive fruits. The fact of having somehow acceptable relative SD values (between 1 and 30%) when observing the SG concentration as a function of the location of the olive tree, and not on dependence of the cultivar, drives us to think that it might actually be the pedoclimate (soil water, nutrients, and aeration) that has any real influence on such values and not the fruit variety, as one might think a priori. Wider studies on this aspect are presently being carried out. On the other hand, the ESG behavior remains quite random, supporting our previous statement that both kinds of phytosterols (SG and ESG) behave independently of each other. The same trend is observed when classifying the results according to the sampling time (Table 7), whereas results on the two different farming modes (traditional and organic) cannot be conclusive, mainly due to the lack of enough sample material.

Table 5. Total Esterified Steryl Glucoside Contents (mg·kg^{-1}) of Olive Oil from Different Cultivars, and Relative Composition Regarding Esterified Stigmasteryl Glucoside (ESSG), Esterified β-Sitosteryl Glucoside (EBSSG), and Esterified Δ5-Avenasteryl Glucoside (EAvSG) (Part 2)[a]

	esterified steryl glucosides												
	ESSG		EBSSG			EAvSG			total			SG:ESG	
samples	%	SD	%	SD	*b*	%	SD	*b*	mg·kg^{-1}	SD	*b*	%	*b*
COR_E_VG_4	ND		100.00			ND			0.30	0.05	a,b	8.94	d
MCLL_T_TI_1	ND		88.31	1.52	d,e	11.69	1.52	b,c	1.30	0.07	d	1.51	a,b
MCLL_T_AC_1	ND		91.87	0.74	d,e	8.13	0.74	b,c	2.36	0.16	f,g	0.57	a
MCLL_T_AC_2	ND		80.73	1.53	c,d	19.27	1.53	c,d	2.33	0.07	f,g	0.66	a
MCLL_T_TI_2	ND		100.00			ND			1.36	0.10	d,e	1.47	a,b
MCLL_T_VS_2	ND		88.61	0.27	d,e	11.39	0.27	b,c	0.72	0.13	b,c	2.47	b
MCLL_T_VG_3	ND		100.00			ND			0.18	0.03	a,b	3.45	b,c
MCLL_T_VS_3	ND		25.18	2.34	a	74.82	2.34	e	0.45	0.05	b	3.01	b
MCLL_T_VS_4	ND		81.72	1.38	c,d	18.28	1.38	c,d	1.10	0.06	c,d	1.44	a,b
MCLL_T_TI_4	ND		89.53	4.28	d,e	10.47	4.28	b,c	1.01	0.06	c,d	2.00	a,b
MCLL_T_AC_4	ND		73.78	0.32	b,c	26.22	0.32	d	2.58	0.07	g	0.67	a
MCLL_E_VG_2	ND		83.61	4.05	c,d	16.39	4.05	c,d	1.36	0.01	d,e	1.46	a,b
MCLL_E_VG_4	ND		89.88	2.99	d,e	10.12	2.99	b,c	2.24	0.01	f,g	1.17	a,b
PIC_T_AZ_1	ND		90.72	2.04	d,e	9.28	2.04	b,c	2.05	0.18	f	0.93	a,b
PIC_T_AG_1	ND		100.00			ND			1.41	0.06	d,e	1.32	a,b
PIC_T_AG_2	ND		100.00			ND			0.86	0.04	c,d	2.21	b
PIC_T_CR_2	ND		94.58	1.38	d,e	5.42	1.38	a,b	2.04	0.30	e,f	1.21	a,b
PIC_T_AZ_3	ND		92.48	2.39	d,e	7.52	2.39	b	0.66	0.10	b,c	2.70	b
PIC_T_CR_3	ND		100.00			ND			0.90	0.01	c,d	2.89	b
PIC_T_CR_4	ND		100.00			ND			1.27	0.12	d	1.34	a,b
PIC_T_AG_4	ND		100.00			ND			1.17	0.06	c,d	1.70	a,b
PIC_T_AZ_4	ND		91.41	0.58	d,e	8.59	0.58	b,c	1.46	0.04	d,e	1.46	a,b

[a]A minimum of two independent measures was made in each case. The standard deviation is also given; ND (nondetected). [b]The use of the same letters (a−e) indicates the absence of statistical difference between samples according to ANOVA and TUKEY test.

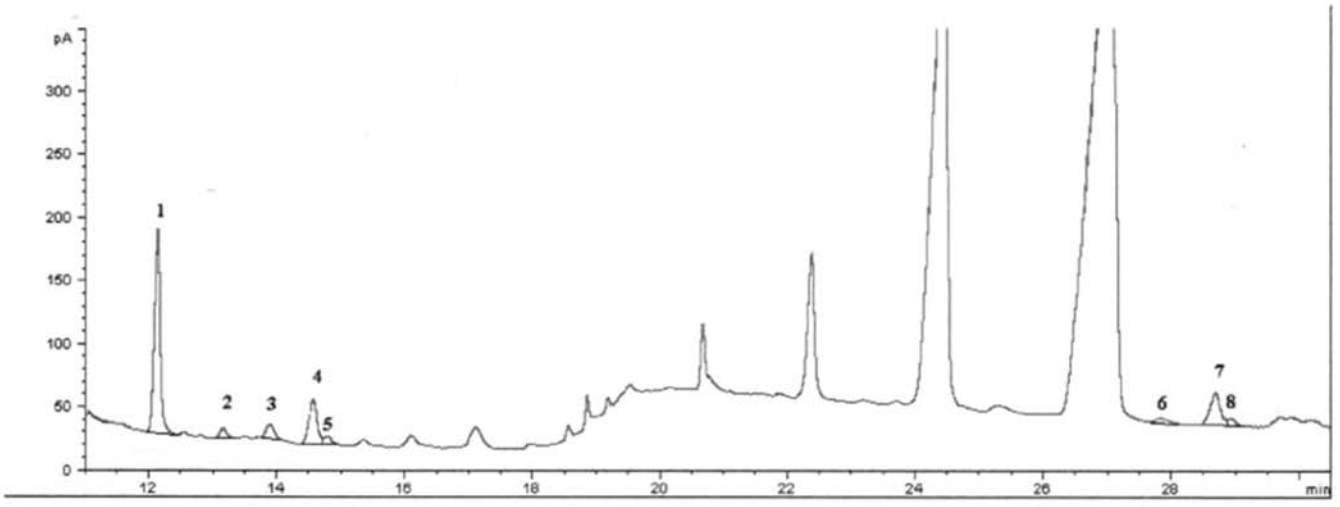

Figure 1. GC-FID chromatogram for steryl glucosides in virgin olive oil extracted from olive fruits of the Manzanilla Cacereña cultivar (sample MCAC_T_CR_4). This chromatogram has been obtained after analyzing the sample according to the proposed method and it shows the following: 1, the internal standard cholesterol glucoside; 2, campesteryl glucoside; 3, stigmasteryl glucoside; 4, β-sitosteryl glucoside; 5, (presumptive) Δ5-avenasteryl glucoside; 6, esterified stigmasteryl glucoside; 7, esterified β-sitosteryl glucoside; 8, (presumptive) esterified Δ5-avenasteryl glucoside.

To summarize we will conclude as follows: The performance of more than one hundred analyses in a relatively short time and with no waste of solvent has demonstrated the suitability of the procedure to be applied on a routine basis.

The presence of steryl glucosides in olive oil is not just limited to BSSG and EBSSG as thought previously, but also AvSG, EAvSG, and CSG have been found in an extensive number of samples. This might also be symptomatic either of different sample treatment or of differences during the oil extraction process. Actually it seems that industrial samples,[8] which have been obtained using a two or three phase decanter (higher water addition), have poorer (E)SG profiles than those samples

dx.doi.org/10.1021/jf501340q | J. Agric. Food Chem. 2014, 62, 5669−5674

Table 6. SG and ESG Contents of the Olive Oil Samples under Study Classified According to the Municipality of Origin[a]

municipality	SG ± 3SD	ESG ± 3SD
AC	1.52 ± 0.10	2.42 ± 0.05
AG	1.89 ± 0.01	1.15 ± 0.23
CR	2.19 ± 0.29	2.00 ± 2.58
CH	1.78 ± 0.50	1.19 ± 1.06
VG	2.28 ± 0.69	1.09 ± 1.77
AZ	1.88 ± 0.16	1.22 ± 0.98
TI	1.97 ± 0.01	1.22 ± 0.11
VS	1.80 ± 0.26	1.47 ± 1.41

[a]Three times the standard deviation is also given.

Table 7. SG and ESG Contents of the Olive Oil Samples under Study Classified According to Sampling[a]

sampling	SG ± 3SD	ESG ± 3SD
1	1.72 ± 0.13	1.63 ± 1.81
2	1.99 ± 0.34	1.44 ± 0.90
3	2.03 ± 0.58	1.40 ± 1.56
4	1.94 ± 0.35	1.38 ± 1.75

[a]Three times the standard deviation is also given.

obtained with the Abencor system, where water addition has been scarce. This reasoning seems to be supported by the fact of finding certain molecules (e.g., CSG) in Abencor samples, and not finding them in industrial oils. In any case a larger number of determinations under controlled circumstances must be carried out before drawing definite conclusions.

Olive cultivar, sampling time, and farming mode have no influence on the parameters under study. Pedoclimate (soil aeration, micronutrient presence, and water content) seems to have some influence on the glucoside presence. In this way further studies are being carried out to confirm such a relationship.

AUTHOR INFORMATION

Corresponding Author

*Tel: +34 954 611 550 (ext 251). Fax: +34 954 616 790. E-mail: raquel.coca@ig.csic.es.

Funding

The Spanish Ministry of Science and Innovation funded this work (ref AGL2009-07618).

Notes

The authors declare no competing financial interest.

ACKNOWLEDGMENTS

The authors would like to thank Ms. Diana Gómez Castillo for her assistance in the laboratory and Doctor María de los Ángeles Pérez Jiménez and Ms. Carmen Mena Uriarte from IMIDRA (Instituto Madrileño de Investigación y Desarrollo Rural, Agrario y Alimentario) for providing the varietal olive oil samples.

ABBREVIATIONS USED

ChSG, cholesterol β-D-glucoside; (E)AvSG, (esterified) Δ5-avenasteryl glucoside; (E)BSSG, (esterified) β-sitosteryl glucoside; (E)CSG, (esterified) campesteryl glucoside; ESG, esterified steryl glucosides; (E)SSG, (esterified) stigmasteryl glucoside; EVOO, extra virgin olive oil; FID, flame ionization detector; FS, free sterols; GC, gas chromatography; HMDS, hexamethyldisilazane; LOO, lampante olive oil; Py, pyridine; SD, standard deviation; SE, sterol esters; SG, free steryl glucosides; SPE, solid phase extraction; TMCS, trimethylchlorosilane; VOO, virgin olive oil.

REFERENCES

(1) Grille, S.; Zaslawski, A.; Thiele, S.; Plat, J.; Warnecke, D. The functions of steryl glucosides come to those who wait: recent advances in plants, fungi, bacteria and animals. *Prog. Lipid Res.* **2010**, *49*, 262−268.

(2) Pollak, O. J. Reduction of blood cholesterol in man. *Circulation* **1953**, *7*, 702−706.

(3) MacKay, D. S.; Jones, P. J. H. Phytosterols in human nutrition: type, formulation, delivery, and physiological function. *Eur. J. Lipid Sci. Technol.* **2011**, *113*, 1427−1432.

(4) Lin, X.; Ma, L.; Racette, S. B.; Anderson Spearie, C. L.; Ostlund, R. E. J. Phytosterol glycosides reduce cholesterol absorption in humans. *Am. J. Physiol.* **2009**, *296*, G931−G935.

(5) Lin, X.; Ma, L.; Moreau, R. A.; Ostlund, R. E., Jr. Glycosidic bond cleavage is not required for phytosteryl glycoside-induced reduction of cholesterol absorption in mice. *Lipids* **2011**, *46*, 701−708.

(6) Nyström, L.; Schär, A.; Lampi, A.-M. Steryl glycosides in plant foods reflect unique sterol patterns. *Eur. J. Lipid Sci. Technol.* **2012**, *114*, 656−669.

(7) Gómez-Coca, R. B.; Pérez-Camino, M. C.; Moreda, W. Specific procedure for analysing steryl glucosides in olive oil. *Eur. J. Lipid Sci. Technol.* **2012**, *114*, 1417−1426.

(8) Gómez-Coca, R. B.; Pérez-Camino, M. C.; Moreda, W. On the glucoside analysis: simultaneous determination of free and esterified steryl glucosides in olive oil. Detailed analysis of standards as compulsory first step. *Food Chem.* **2013**, *15*, 1273−1280.

(9) Lacoste, F.; Dejean, F.; Griffon, H.; Rouquette, C. Quantification of free and esterified steryl glucosides in vegetable oils and biodiesel. *Eur. J. Lipid Sci. Technol.* **2009**, *111*, 822−828.

JOURNAL OF AGRICULTURAL AND FOOD CHEMISTRY

Article

pubs.acs.org/JAFC

Thermodynamics of Dissolution of Calcium Hydroxycarboxylates in Water

Martina Vavrusova,[†] Ran Liang,[‡] and Leif H. Skibsted*[,†]

[†]Food Chemistry, Department of Food Science, University of Copenhagen, Rolighedsvej 30, DK-1958 Frederiksberg C, Denmark

[‡]Department of Chemistry, Renmin University of China, Beijing 100872, China

ABSTRACT: Aqueous solubility of calcium L-lactate, calcium D-gluconate, and calcium D-lactobionate increases with temperature (10−30 °C investigated), most significantly for the least soluble D-gluconate, while the calcium ion activity of the saturated solutions decreases with temperature, as measured electrochemically, most significantly for the most soluble D-lactobionate. This unusual behavior is discussed in relation to dairy processing and explained by endothermic binding of calcium to hydroxycarboxylate anions determined to have ΔH°_{ass} = (31 ± 3) kJ·mol^{-1} for L-lactate, (34 ± 2) kJ·mol^{-1} for D-gluconate, and (29 ± 3) kJ·mol^{-1} for D-lactobionate in 1:1 complexes with thermodynamic binding constants at 25 °C of K_{ass} = 49 (L-lactate), 88 (D-gluconate), and 140 (D-lactobionate). Quantum mechanical calculations within density functional theory (DFT) confirm the ordering of strength of binding. The complex formation is entropy driven with $\Delta S^{\circ}_{ass} > 0$, resulting in decreasing calcium ion activity in aqueous solutions for increasing temperature, even for the saturated solutions despite increasing solubility.

KEYWORDS: *calcium L-lactate, calcium D-gluconate, calcium D-lactobionate, calcium ion activity, endothermic calcium binding*

INTRODUCTION

Dairy products are an important source of dietary calcium, and calcium binding to the caseins and to proteins, peptides, and anions of the serum phase of milk prevents precipitation on calcium salts in the intestines during digestion ensuring high bioavailability of calcium.[1−4] Calcium is also important for structure development in fermented milk products and in cheeses as calcium binds electrostatically to caseins initiating protein network formation for conditions of decreasing pH and during enzymatic protein hydrolysis.[5−9]

An understanding of calcium binding to other milk components and to components added to dairy products or formed during milk processing accordingly is important both for improvement of dairy technology and for optimizing calcium bioavailability of dairy products.[10,11] Notably, it was recently shown that cooling of acidified skim milk for cheese production resulted in increased concentration of free calcium at the expense of complex bound calcium in the milk serum phase indicating that calcium binding is an endothermic process most likely involving carboxylate groups of peptides or of hydroxycarbolylates.[9]

Mixtures of hydroxycarboxylates of relevance for dairy products have further been shown to result in increased solubility of sparingly soluble calcium salts like calcium lactate otherwise known to precipitate in some cheeses during maturation.[11−14] Such synergistic effects on calcium hydroxycarboxylate solubility may for certain conditions of relevance for biomineralization even result in spontaneous formation of supersaturated solutions during isothermal dissolution.[15] Such phenomena, which at a first glance seem to violate thermodynamics, invite further investigations of the dissolution processes of calcium hydroxycarboxylates. It seems also of importance to make distinctions not only between bound and free calcium, but for the free calcium also between calcium ion concentration and calcium ion activity for the saturated and supersaturated calcium salt solutions.[6,16] Accordingly, we now report the results of investigations of calcium speciation in saturated solutions of calcium L-lactate, calcium D-gluconate, and calcium D-lactobionate combining electrochemical determination of calcium ion activity at varying temperature with quantum mechanical calculations of calcium binding to hydroxycarboxylate anions.

MATERIALS AND METHODS

Chemicals. Calcium L-lactate pentahydrate, calcium D-gluconate monohydrate, calcium D-lactobionate monohydrate, anhydrous calcium chloride, and ammonium purpurate 5,5-nitrilodibarbituric acid were all from Sigma-Aldrich (Steinheim, Germany). Ethylenediaminetetraacetic acid disodium salt dihydrate (EDTA), sodium chloride, and sodium hydroxide were all from Merck (Darmstadt, Germany). All aqueous solutions were made from purified water from Milli-Q Plus (Millipore Corporation, Bedford, MA).

Solubility Determination. Saturated aqueous solutions of calcium L-lactate pentahydrate and calcium D-gluconate monohydrate were prepared by combining 15.0 and 10.0 g with 100 mL of water, respectively, while 40.0 g of calcium D-lactobionate monohydrate was combined with 50 mL of water at 10 and 20 °C and with 35 mL at 30 °C. Equilibration time for each of the calcium salts to reach saturation was found to be less than 2 h under constant stirring at 10 °C, 20 °C, or 30 °C in a thermostated water bath. Samples were filtered (589/3, Whatman, Dassel, Germany) prior to each analysis. Total calcium concentration was determined by EDTA titration, and the calcium ion activity was determined by a calcium ion selective electrode for solutions of each of the three salts saturated at each of the three temperatures. pH was measured in the saturated solutions at the specified temperatures. All samples were prepared in duplicate.

Received: March 31, 2014
Revised: May 26, 2014
Accepted: May 28, 2014
Published: May 28, 2014

ACS Publications © 2014 American Chemical Society

EDTA Titration. Standardization of the EDTA solution for titration with the concentration of 0.0500 mol·L^{-1} was obtained against a 0.0200 mol·L^{-1} aqueous solution of $CaCl_2$. 1.000 mL of sample was transferred to a titration flask and diluted with 40 mL of water. 2.0 mL of 2.0 mol·L^{-1} solution of NaOH was added to each sample to maintain basic pH, and 0.30 mL of 0.50% murexid solution was used as an indicator. Samples were titrated until the initial pink color changed to dark purple, indicating the end point.

Electrochemical Measurement of Calcium Ion Activity. A calcium ion selective electrode ISE25Ca with a reference REF251 electrode from Radiometer (Copenhagen, Denmark) was calibrated using aqueous 1.00×10^{-4}, 1.00×10^{-3}, and 1.00×10^{-2} mol·L^{-1} $CaCl_2$ solutions prepared from a 1.000 mol·L^{-1} $CaCl_2$ stock solution at 10 °C, 20 °C, or 30 °C. Calcium ion activity, $a_{Ca}{}^{2+}$, in the standard solutions was calculated based on the relationship between activity and concentration according to

$$a_{Ca}{}^{2+} = c_{Ca}{}^{2+} \cdot \gamma^{2+} \quad (1)$$

where γ^{2+} is the activity coefficient calculated from the Davies equation:[17]

$$\log \gamma^{2+} = -A_{DH} z^2 \left(\frac{\sqrt{I}}{1 + \sqrt{I}} - 0.30I \right) \quad (2)$$

where A_{DH} is the Debye−Hückel constant with the numerical value of A_{DH} = 0.498, 0.506, or 0.515 at 10 °C, 20 °C, or 30 °C, respectively.[17] For aqueous solution, z (=2) is the charge of the calcium ion, and I is the ionic strength. The ionic strength was calculated as follows, taking all ions present in the solution into account including the calcium hydroxycarboxylate complexes:

$$I = \frac{1}{2} \sum cz^2 \quad (3)$$

The calcium ion activities of the standard solutions at 10 °C, 20 °C, or 30 °C may be found in Table 1. In the samples, the calcium ion activity, $a_{Ca}{}^{2+}$, was calculated from the linear relationship according to the Nernst equation between the electrode potential (in mV) measured for the calibration solutions and pCa (=−log $a_{Ca}{}^{2+}$) of the calibration solution, see Figure 1.

Table 1. Calcium Ion Activities in Standard Solutions at 10, 20, And 30 °C As Calculated According to Davies' Equation.[17]

	pCa = −log $a_{Ca}{}^{2+}$		
$c_{Ca}{}^{2+}$/mol·L^{-1}	10 °C	20 °C	30 °C
1.00×10^{-4}	4.034	4.034	4.035
1.00×10^{-3}	3.102	3.103	3.105
1.00×10^{-2}	2.276	2.281	2.286

DFT Calculation. Geometries of calcium hydroxycarboxylates in aqueous solutions were optimized using the Gaussian 09 package[18] on the basis of the B3LYP method combined with polarizable continuum model (PCM) at the 6-31G** level. Calcium binding enthalpies were calculated on the basis of stationary point energies of the calcium complexes and the hydroxycarboxylate anions at their optimized geometries, respectively, and relative association rate constants were calculated based on the approximation of

$$\Delta H_{binding} \approx \Delta G_{binding} = -RT \ln K_{rel} \quad (4)$$

RESULTS AND DISCUSSION

The aqueous solubility of the three calcium hydroxycarboxylates investigated for the temperature interval 10 to 30 °C in relation to calcium speciation and calcium salt precipitation in dairy products increased for increasing temperature and was in fair agreement with previous reports of calcium salt solubility.[11,12,19−21] The solubility of calcium L-lactate at 10, 20, and 30 °C, as determined by complexometric titration, is presented in Table 2, and the solubility of calcium D-gluconate and calcium D-lactobionate in Tables 3 and 4, respectively. The overall dissolution process for each of the three calcium hydroxycarboxylates is accordingly endothermic with $\Delta H^{\circ}_{dissol} > 0$, as for most food related calcium salts in water, except calcium sulfate, where a solid state phase transition around 40 °C makes the temperature dependence more complicated.[22] Calcium D-gluconate, the least soluble of the three hydroxycarboxylates investigated, showed a solubility ratio of 1.9 for the temperature interval of 20 °C investigated, the highest temperature sensitivity, while calcium D-lactobionate as the most soluble showed the lowest temperature sensitivity corresponding to a factor of 1.3. The solubility ratio for calcium D-gluconate and for calcium D-lactobionate was calculated by dividing the highest solubility by the lowest solubility to give an impression how much the solubilities of the investigated calcium hydroxycarboxylates will change with temperature.

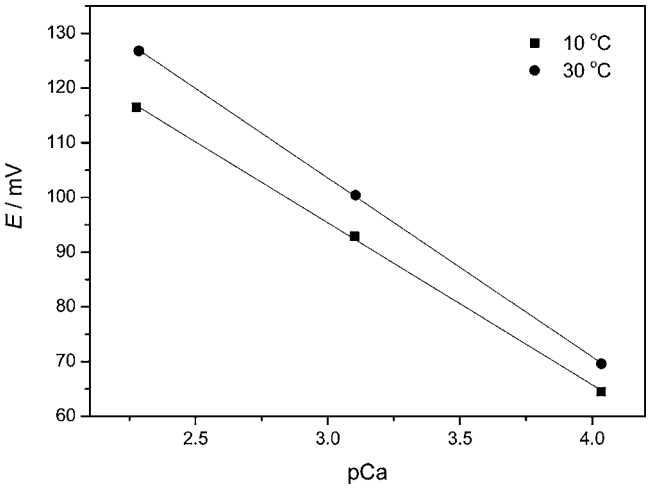

Figure 1. Calcium ion activity standardization of calcium selective electrode using the standard solutions of Table 1 based on the Davies equation. Slope of regression line at 10 °C is −29.6 mV^{-1} and at 30 °C −32.7 mV^{-1}.

The calcium ion activity of the saturated aqueous solutions of the three calcium hydroxycarboxylates showed opposite trends. The measured activities were based on activity standards correcting the calcium ion concentration according to the Debye−Hückel theory using the Davies equation for single ion activity.[17,23] Notably, activity standardization has to be performed at the actual temperature of measurement, and it is encouraging that the electrode response is in agreement with the Nernst equation and with an increasing slope for increasing temperature, see Figure 1. For each of the three calcium hydroxycarboxylates, the calcium activity in the saturated solution decreased with increasing temperature, which is remarkable, since the solubility increased. For the most soluble calcium D-lactobionate the effect was the largest, but still for calcium L-lactate and calcium D-gluconate, the effect is significant, compares Table 2, 3, and 4.

In order to understand this unusual effect of decreasing calcium ion activity for increasing calcium hydroxycarboxylate concentration, the calcium speciation needs to be considered. The dissolution of each of the three calcium hydroxycarboxylates occurs stepwise,[11,17,23]

dx.doi.org/10.1021/jf501453c | J. Agric. Food Chem. 2014, 62, 5675−5681

Table 2. Solubilities and the Thermodynamic Association Constants of Calcium L-Lactate in Aqueous Solutions at 10, 20, and 30 °C[a]

temp (°C)	pH	solubility (g/100 mL)	$c_{Ca^{2+}}$ (mol·L^{-1})	$a_{Ca^{2+}}$	I	$\gamma_{Ca^{2+}}$	[Ca^{2+}] (mol·L^{-1})	[$CaLact^{+}$] (mol·L^{-1})	[$Lact^{-}$] (mol·L^{-1})	K_{ass}
10	6.3	4.8 ± 0.1	0.219 ± 0.003	0.021 ± 0.002	0.36	0.294 ± 0.001	0.07 ± 0.01	0.149 ± 0.004	0.29 ± 0.01	25 ± 4
20	6.2	5.8 ± 0.1	0.266 ± 0.004	0.016 ± 0.001	0.38	0.28767 ± 0.00002	0.056 ± 0.002	0.21 ± 0.01	0.323 ± 0.001	40 ± 3
30	6.2	8.50 ± 0.02	0.390 ± 0.001	0.013 ± 0.001	0.48	0.2844 ± 0.0002	0.047 ± 0.002	0.342 ± 0.003	0.437 ± 0.002	59 ± 4

[a]Calcium ion activity, $a_{Ca^{2+}}$, was determined electrochemically. Free calcium ion concentration, [Ca^{2+}], activity coefficient, $\gamma_{Ca^{2+}}$, free lactate concentration, [$Lact^{-}$], the calcium complex concentration [$CaLact^{+}$], and the resulting ionic strength, I, were calculated by an iterative procedure.

$$CaL_2(s) \rightleftharpoons CaL^+ + L^- \quad (5)$$

$$CaL^+ \rightleftharpoons Ca^{2+} + L^- \quad (6)$$

with the reaction of eq 5 resulting in a complete dissociation into CaL^+ and L^-, where L^- is L-lactate, D-gluconate, or D-lactobionate, and CaL^+ the 1:1 complex of each of these anions with Ca^{2+}. The reaction of eq 6 corresponds to the dissociation of the complex, for which the association constant is defined as

$$K_{ass} = \frac{a_{CaL^+}}{a_{L^-}a_{Ca^{2+}}} = \frac{\gamma_{CaL^+}[CaL^+]}{\gamma_{L^-}[L^-]a_{Ca^{2+}}} \approx \frac{[CaL^+]}{[L^-]a_{Ca^{2+}}} \quad (7)$$

The approximation included in eq 7 is based on the assumption that the activity coefficient only depends on the charge of the ion as is also an assumption for the Davies equation.[17,23]

An iterative calculation procedure was used for each of the three salts for each of the three temperatures. From an initially estimated ionic strength neglecting complex formation ($I = 3c_{Ca^{2+}}$, where $c_{Ca^{2+}}$ is the concentration of calcium hydroxycarboxylate), $\gamma_{Ca^{2+}}$ was calculated according to eq 2 leading to a concentration of free ligand of

$$[L^-] = c_{Ca^{2+}} + [Ca^{2+}] = c_{Ca^{2+}} + \frac{a_{Ca^{2+}}}{\gamma_{Ca^{2+}}} \quad (8)$$

and a concentration of complex of

$$[CaL^+] = c_{Ca^{2+}} - [Ca^{2+}] = c_{Ca^{2+}} - \frac{a_{Ca^{2+}}}{\gamma_{Ca^{2+}}} \quad (9)$$

based on correction of $a_{Ca^{2+}}$ to free calcium concentration, [Ca^{2+}], using eqs 1 and 2. A new estimate of the ionic strength was made according to

$$I = \frac{1}{2}(4[Ca^{2+}] + [L^-] + [CaL^+]) \quad (10)$$

and the calculation procedure repeated until the ionic strength, I, was not influenced further, and the final values for the ion concentrations of the three calcium hydroxycarboxylates were calculated at each of the three temperatures.

The speciation for calcium L-lactate, calcium D-gluconate, and calcium D-lactobionate, resulting from measurement of total calcium, $c_{Ca^{2+}}$, and calcium ion activity, $a_{Ca^{2+}}$, and the iterative calculation procedure, is found in Tables 2, 3, and 4, respectively. Included in these tables are values for K_{ass} for the calcium complexes of L-lactate (Table 2), D-gluconate (Table 3), and D-lactobionate (Table 4), each at three temperatures as calculated from eq 7.

D-Lactobionate forms the strongest complex with calcium, L-lactate the weakest, with D-gluconate being intermediate according to the thermodynamic association constant for all of the three temperatures. The binding is, however, for each hydroxycarboxylate significant especially for the high concentrations of the saturated solutions, as evident from the speciation seen for the three calcium hydroxycarboxylates in Tables 2, 3, and 4. The temperature dependence of the three thermodynamic association constants further allows determination of ΔH°_{ass} and ΔS°_{ass} for the complex formation reaction using the van't Hoff equation.

$$\ln K_{ass} = -\frac{\Delta H^\circ_{ass}}{RT} + \frac{\Delta S^\circ_{ass}}{R} \quad (11)$$

The linearity of the plot of Figure 2 confirms the validity of the iterative calculation procedure and leads to the thermodynamic values of Table 5 including K_{ass} at 25 °C using standard regression methods. Since the complex formation is endothermic corresponding to $\Delta H^\circ_{ass} > 0$, the complex formation must be entropy driven with $\Delta S^\circ_{ass} > 0$. The increasing entropy resulting from binding seems related to release of water bound both to the calcium ion and to the carboxylic group of the hydroxycarboxylate. The association constants were determined for the natural pH around 6 of the saturated solutions, see Tables 2, 3, and 4. The pK_a values of the hydroxycarboxylic acids are around 3.6, and acid/base equilibria will accordingly not affect the calcium binding in the pH region of relevance for normal foods.[23]

The thermodynamic association constants for the three hydroxycarboxylate complexes of calcium and the derived thermodynamic parameters were determined in saturated aqueous solutions of each of the calcium hydroxycarboxylates. However, they should be of more universal use for aqueous solutions, since they are based on calcium ion activity rather than on calcium ion concentration as previously used.[11] Values available for K_{ass} are for other solution conditions, but for calcium L-lactate, a value of $K_{ass} = 35$ has been reported, which is comparable to the value of 49 of Table 2.[24] For D-gluconate a value $K_{ass} = 77$ was previously obtained by extrapolation of K_{ass} valid at varying ionic strength to infinite dilution.[23] Also this value for K_{ass} based on calcium ion activity compares well with the value of $K_{ass} = 88$ of Table 2. A more recent value based on ^{13}C NMR spectra is somewhat lower, with $K_{ass} = 63$.[25]

Binding of calcium to sugar derived ligands is of general interest for sugar metabolism, and structural assignment of the functional groups in the partly metabolized sugars binding calcium has been attempted.[25,26] Calcium seems to bind to a carboxylic group but also with involvement of hydroxylic groups apparently with equilibration between five- and six-membered rings.[25] In order to understand the structural effects on calcium binding for the three hydroxycarboxylates, quantum mechanical calculations within DFT were used to obtain optimized structures of the three calcium complexes in aqueous solution followed by calculation of $\Delta H_{binding}$ for the reaction correcting for solvent interaction:

$$Ca^{2+} + L^- \rightarrow CaL^+ \quad (12)$$

dx.doi.org/10.1021/jf501453c | J. Agric. Food Chem. 2014, 62, 5675−5681

Table 3. Solubilities and the Thermodynamic Association Constants of Calcium D-Gluconate in Aqueous Solutions at 10, 20, and 30 °C[a]

temp (°C)	pH	solubility (g/100 mL)	c_{Ca}^{2+} (mol·L^{-1})	a_{Ca}^{2+}	I	γ_{Ca}^{2+}	$[Ca^{2+}]$ (mol·L^{-1})	$[CaGl^+]$ (mol·L^{-1})	$[Gl^-]$ (mol·L^{-1})	K_{ass}
10	5.9	2.51 ± 0.01	0.0583 ± 0.002	0.0093 ± 0.003	0.11	0.373 ± 0.001	0.025 ± 0.001	0.033 ± 0.001	0.083 ± 0.001	43 ± 3
20	5.8	3.27 ± 0.04	0.076 ± 0.001	0.00813 ± 0.0004	0.12	0.355 ± 0.001	0.02291 ± 0.0004	0.053 ± 0.001	0.099 ± 0.001	66 ± 1
30	5.9	4.80 ± 0.04	0.112 ± 0.001	0.0064 ± 0.0001	0.15	0.3290 ± 0.0004	0.0194 ± 0.0002	0.092 ± 0.001	0.131 ± 0.001	110 ± 1

[a]Calcium ion activity, a_{Ca}^{2+}, was determined electrochemically. Free calcium ion concentration, $[Ca^{2+}]$, activity coefficient, γ_{Ca}^{2+}, free gluconate concentration, $[Gl^-]$, the calcium complex concentration $[CaGl^+]$, and the resulting ionic strength, I, were calculated by an iterative procedure.

The values of $\Delta H_{binding}$ are included in Table 5. The ordering of affinity of calcium ion to hydroxycarboxylates is D-lactobionate > D-gluconate > L-lactate, in agreement with the experimentally determined values for K_{ass}. Moreover, the relative strength of binding of calcium to D-gluconate and L-lactate is 1.6, as obtained from the theoretical calculations, which is surprisingly close to the ratio of 1.8 indicated by the experimentally determined values for K_{ass} at 25 °C, see Table 5.

The optimized structures of the calcium complexes are presented in Figures 3, 4, and 5. For L-lactate, calcium ion binds solely to the oxygen atoms of the carboxylate with equal bond lengths. For D-gluconate, calcium ion binds also to the two carboxylate oxygens but also to the hydroxyl group of C-3 of D-gluconate for the optimized (lowest energy) structure. However, separated by only 8.3 kJ·mol^{-1} is another conformation where calcium is bound to only one of the two carboxylic oxygens, but also to the hydroxyl groups both at C-2 and C-3, see Figure 4a. Calcium binding to D-lactobionate follows a similar pattern with the lowest energy conformation characterized by binding to the two carboxylic oxygens and to a hydroxyl group (C-5). As for D-gluconate, another conformation of the calcium complex of D-lactobionate is only 10.4 kJ·mol^{-1} above the optimized structure, with binding to only the two carboxylic oxygens as for L-lactate and not involving any hydroxyl groups, compare Figures 4 and 5. In the view of the small energy separation between the two local minima of calcium complexes of D-gluconate, it is suggested that they coexist in solution.

The strongest binding of calcium is characterized by three calcium-to-oxygen bonds as for D-gluconate and D-lactobionate, while the weaker binding of calcium for L-lactate only involves two oxygens. For D-lactobionate, an easy shift between binding to two carboxylic oxygens and binding including an additional hydroxyl group may explain the higher affinity for calcium by D-lactobionate than by D-gluconate.

The speciation of calcium in the saturated calcium hydroxycarboxylate solutions presented in Tables 2, 3, and 4 provides the information required to calculate the solubility product:

$$K_{sp} = a_{Ca^{2+}}a_{L^-}{}^2 \approx a_{Ca^{2+}}[L^-]^2\gamma_{L^-}{}^2 \quad (13)$$

The values for K_{sp} for each of the three calcium hydroxycarboxylates at three temperatures are presented in Table 6 applying the Davies equation for calculation of γ_{L^-} at the ionic strength of the saturated solutions. For the more soluble calcium L-lactate and calcium D-lactobionate, the uncertainty is rather large for these calculations, and since solubility products normally only are considered as a thermodynamic parameter for sparingly soluble salts, the temperature dependence on K_{sp} is only analyzed for the least soluble calcium D-gluconate as seen in Figure 6. Based on the van't Hoff equation as presented in eq 11, values of ΔH°_{sol} = (16 ± 1) kJ·mol^{-1} and $\Delta S^\circ_{sol} = -(26 \pm 5)$ J·mol^{-1}·K^{-1} were calculated, see Figure 6. The solubility product obtained for 20 °C, log K_{sp} = −4.26, is in good agreement with the value obtained by others, log K_{sp} = −4.19, also corrected for complex formation and based on activity standard.[21]

The dissolution of calcium hydroxycarboxylates in water involves the two reactions of eqs 5 and 6. While the thermodynamic parameters obtained for complex formation solely are associated with the process of eq 6, ΔH°_{sol} and ΔS°_{sol} obtained for calcium D-gluconate are valid for the hypothetical

Table 4. Solubilities and the Thermodynamic Association Constants of Calcium D-Lactobionate in Aqueous Solutions at 10, 20, and 30 °C[a]

temp (°C)	pH	solubility (g/100 mL)	$c_{Ca^{2+}}$ (mol·L^{-1})	$a_{Ca^{2+}}$	I	$\gamma_{Ca^{2+}}$	[Ca^{2+}] (mol·L^{-1})	[$CaLacto^+$] (mol·L^{-1})	[$Lacto^-$] (mol·L^{-1})	K_{ass}
10	5.7	42.8 ± 0.5	0.57 ± 0.01	0.012 ± 0.001	0.64	0.315 ± 0.002	0.038 ± 0.002	0.529 ± 0.005	0.61 ± 0.01	73 ± 5
20	5.7	45.2 ± 0.5	0.60 ± 0.01	0.0077 ± 0.0001	0.65	0.310 ± 0.001	0.0248 ± 0.002	0.57 ± 0.01	0.62 ± 0.01	120 ± 2
30	5.6	56.8 ± 0.3	0.752 ± 0.004	0.006 ± 0.001	0.79	0.330 ± 0.000	0.018 ± 0.002	0.73 ± 0.01	0.770 ± 0.002	162 ± 16

[a]Calcium ion activity, $a_{Ca^{2+}}$, was determined electrochemically. Free calcium ion concentration, [Ca^{2+}], activity coefficient, $\gamma_{Ca^{2+}}$, free lactobionate concentration, [$Lacto^-$], the calcium complex concentration [$CaLacto^+$], and the resulting ionic strength, I, were calculated by an iterative procedure.

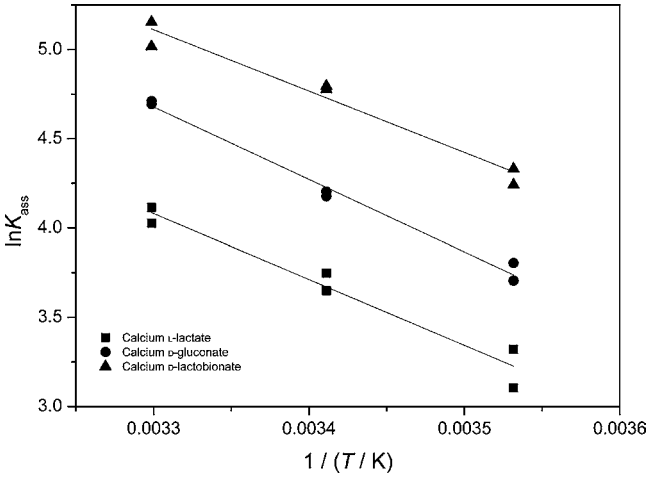

Figure 2. Effect of temperature on thermodynamic association constant of 1:1 complexes, K_{ass}, of calcium with (■) L-lactate, (●) D-gluconate, and (▲) D-lactobionate in water.

process of dissolving 1 mol of calcium D-gluconate in an already saturated solution of the specified temperature corresponding to the differential enthalpy and entropy of dissolution for a saturated solution as partial molar quantities. In order to assign the thermodynamic parameters directly to the dissolution process of eq 5, where a solid is dissolved in pure water to obtain integral enthalpy and entropy of dissolution, other types of experiments based on dissolution calorimetry are needed.

For a more practical use of the results in the food industry, the calcium ion activity in aqueous solutions was calculated for increasing concentration of each of the three calcium hydroxycarboxylates for 25 °C based on the association constants and correcting for the effect on the activity coefficient of calcium from the increasing ionic strength using iterative methods similar to those described for determination of the complex constants. The calculations were extended to concentrations above the saturation for each calcium hydroxycarboxylate as seen in Figure 7. The result is striking: up to saturation, the calcium ion activity continues to increasing steadily, but the continuing increase in activity is far less significant, when the concentration approaches the solubility limit especially for D-lactobionate and D-gluconate. For calcium

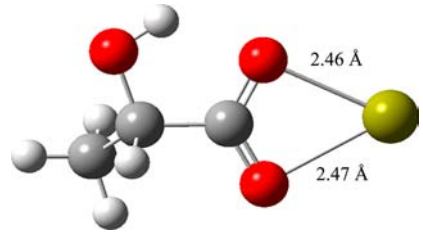

Figure 3. Calcium binding to L-lactate: DFT-optimized geometry with PCM solvent model (water).

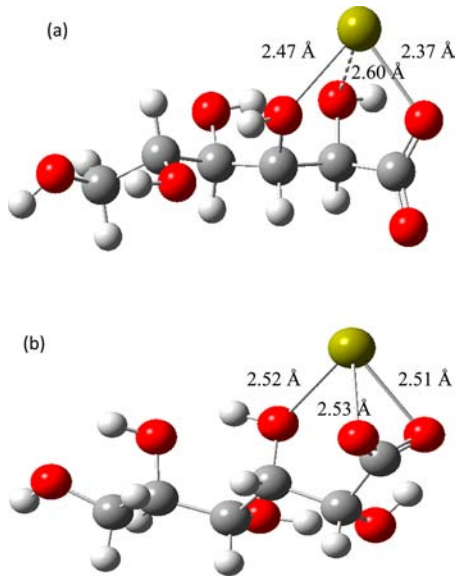

Figure 4. Calcium binding to D-gluconate: DFT-optimized local minima with PCM solvent model (water). Energy difference between two local minima: $E_a - E_b$ = 8.3 kJ·mol^{-1}.

D-gluconate, the calcium ion activity is rather constant for up to 10 times supersaturation and the driving force for precipitation becomes small. This seem to be part of the explanation for the well-known phenomenon that calcium D-gluconate forms a supersaturated solution which may stay supersaturated for years before precipitation starts.[15] D-Gluconate also protects against calcium L-lactate precipitation in cheeses during maturation, and similar effects of supersaturation may be involved.[14]

Table 5. Thermodynamic Association Constants of 1:1 Calcium Hydroxycarboxylate Complexes in Water at 25 °C and Thermodynamic Parameters ($\Delta G°_{ass}$, $\Delta H°_{ass}$, $\Delta S°_{ass}$) for Complex Formation from Electrochemical Measurement, Binding Enthalpy, $\Delta H_{binding}$, and Relative Stability Constant, K_{rel}, of Complexes Based on DFT Calculations

	K_{ass}	$\Delta G°_{ass}$ (kJ·mol^{-1})	$\Delta H°_{ass}$ (kJ·mol^{-1})	$\Delta S°_{ass}$ (J·mol^{-1}·K^{-1})	$\Delta H_{binding}$ (kJ·mol^{-1})	K_{rel}
calcium L-lactate	49	−9.7	31 ± 3	135 ± 11	−126.2	1
calcium D-gluconate	88	−11.1	34 ± 2	150 ± 6	−127.3	1.6
calcium D-lactobionate	140	−12.2	29 ± 3	137 ± 9	−133.6	20

dx.doi.org/10.1021/jf501453c | J. Agric. Food Chem. 2014, 62, 5675−5681

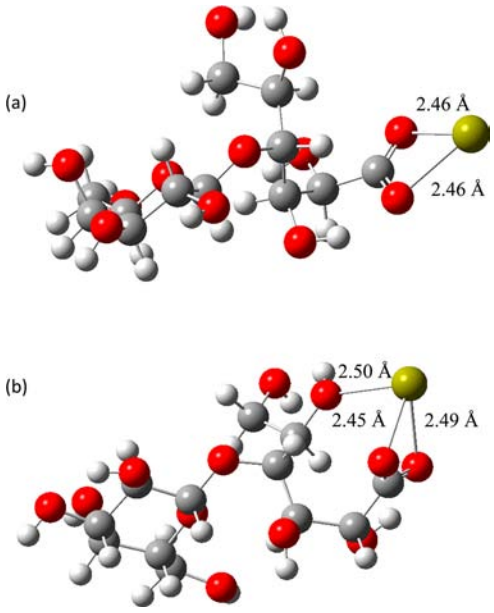

Figure 5. Calcium binding to D-lactobionate: DFT-optimized local minima with PCM solvent model (water). Energy difference between two local minima: $E_a - E_b = 10.4$ kJ·mol^{-1}.

Table 6. Thermodynamic Solubility Product, K_{sp}, of Calcium L-Lactate, Calcium D-Gluconate, and Calcium D-Lactobionate, Calculated from Experimental Data of Tables 2, 3, and 4

temp (°C)	K_{sp}
Calcium L-Lactate	
10	0.00090 ± 0.00010
20	0.00090 ± 0.00003
30	0.0014 ± 0.0001
Calcium D-Gluconate	
10	0.000039 ± 0.000002
20	0.000047 ± 0.000001
30	0.000063 ± 0.000001
Calcium D-Lactobionate	
10	0.0025 ± 0.0002
20	0.00166 ± 0.00001
30	0.0020 ± 0.0002

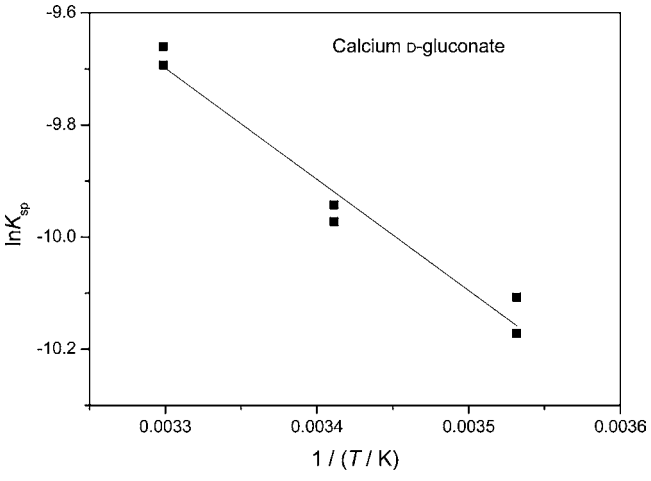

Figure 6. Effects of temperature on thermodynamic solubility product, K_{sp}, for calcium D-gluconate in water. Experimental data from Table 3.

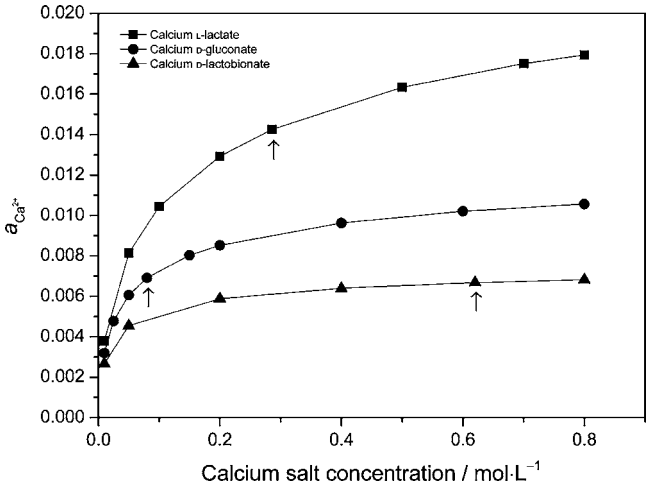

Figure 7. Calcium ion activity in calcium hydroxycarboxylate aqueous solutions of increasing concentration at 25 °C. Calcium concentration was corrected to calcium activity using the Davies equation based on an iterative calculation procedure correcting for complex formation. Solubilities (↑) of calcium L-lactate, calcium D-gluconate, and calcium D-lactobionate are 0.286 mol·L^{-1}, 0.080 mol·L^{-1}, and 0.620 mol·L^{-1}, respectively, in water at 25 °C.[11,19]

Calcium L-lactate, calcium D-gluconate, and calcium D-lactobionate also find use as calcium supplements because of their nonbitter taste in contrast to calcium chloride. Calcium bound in the hydroxycarboxylates is not bitter tasting, and in the mouth the increasing temperature will even mask any bitter taste after intake due to the entropy driven lowering of the calcium ion activity.

AUTHOR INFORMATION

Corresponding Author

*E-mail: ls@food.ku.dk. Tel: +45-35333221. Fax: +45-35283344.

Funding

Danish Dairy Research Foundation and Arla Food Ingredients are thanked for supporting the project "Calcium during whey processing".

Notes

The authors declare no competing financial interest.

ABBREVIATIONS USED

DFT, density functional theory; PCM, polarizable continuum model

REFERENCES

(1) Holt, C. An equilibrium thermodynamic model of the sequestration of calcium phosphate by casein micelles and its application to the calculation of the partition of salts in milk. *Eur. Biophys. J. Biophys. Lett.* **2004**, *33*, 421−434.

(2) Gaucheron, F. The minerals of milk. *Reprod. Nutr. Dev.* **2005**, *45*, 473−483.

(3) Parker, T. G.; Dalgleish, D. G. Binding of calcium-ions to bovine *β*-casein. *J. Dairy Res.* **1981**, *48*, 71−76.

(4) Hansen, C.; Werner, E.; Erbes, H. J.; Larrat, V.; Kaltwasser, J. P. Intestinal calcium absorption from different calcium preparations: Influence of anion and solubility. *Osteoporosis Int.* **1996**, *6*, 386−393.

(5) Ozcan, T.; Horne, D.; Lucey, J. A. Effect of increasing the colloidal calcium phosphate of milk on the texture and microstructure of yoghurt. *J. Dairy Sci.* **2011**, *94*, 5278−5288.

(6) Lewis, M. J. The measurement and significance of ionic calcium in milk—a review. *Int. J. Dairy Technol.* **2011**, *64*, 1−13.
(7) Mekmene, O.; Le Graet, Y.; Gaucheron, F. Theoretical model for calculating ionic equilibria in milk as a function of pH: comparison to experiment. *J. Agric. Food Chem.* **2010**, *58*, 4440−4447.
(8) Law, A. J. R.; Leaver, J. Effects of acidification and storage of milk on dissociation of bovine casein micelles. *J. Agric. Food Chem.* **1998**, *46*, 5008−5016.
(9) Koutina, G.; Knudsen, J. C.; Andersen, U.; Skibsted, L. H. Temperature effect on calcium and phosphorus equilibria in relation to gel formation during acidification of skim milk. *Int. Dairy J.* **2014**, *36*, 65−73.
(10) Vavrusova, M.; Skibsted, L. H. Calcium binding to dipeptides of aspartate and glutamate in comparison with orthophosphoserine. *J. Agric. Food Chem.* **2013**, *61*, 5380−5384.
(11) Vavrusova, M.; Munk, M. B.; Skibsted, L. H. Aqueous solubility of calcium L-lactate, calcium D-gluconate, and calcium D-lactobionate: Importance of complex formation for solubility increase by hydroxycarboxylate mixtures. *J. Agric. Food Chem.* **2013**, *61*, 8207−8214.
(12) Kubansteva, N.; Hartel, R. W.; Swearingen, P. A. Factors affecting solubility of calcium lactate in aqueous solutions. *J. Dairy Sci.* **2004**, *87*, 863−867.
(13) Pearce, K. N.; Creamer, L. K.; Gilles, J. Calcium lactate deposits on rindless Cheddar cheese. *N. Z. J. Dairy Sci. Technol.* **1973**, *8*, 3−7.
(14) Phadungath, C.; Metzger, L. E. Effect of sodium gluconate on the solubility of calcium lactate. *J. Dairy Sci.* **2011**, *94*, 4843−4849.
(15) Vavrusova, M.; Skibsted, L. H. Spontaneous supersaturation of calcium D-gluconate during isothermal dissolution on calcium L-lactate in aqueous sodium D-gluconate. *Food Funct.* **2014**, *5*, 85−91.
(16) Lucey, J. A.; Mishra, R.; Hassan, A.; Johnson, M. E. Rheological and calcium equilibrium changes during the ripening of Cheddar cheese. *Int. Dairy J.* **2005**, *15*, 645−653.
(17) Davies, C. W. *Ion association*: Butterworths: London, U.K., 1962.
(18) Frisch, M. J.; Trucks, G. W.; Schlegel, H. B.; Scuseria, G. E.; Robb, M. A.; Cheeseman, J. R.; Scalmani, G.; Barone, V.; Mennucci, B.; Petersson, G. A.; Nakatsuji, H.; Caricato, M.; Li, X.; Hratchian, H. P.; Izmaylov, A. F.; Bloino, J.; Zheng, G.; Sonnenberg, J. L.; Hada, M.; Ehara, M.; Toyota, K.; Fukuda, R.; Hasegawa, J.; Ishida, M.; Nakajima, T.; Honda, Y.; Kitao, O.; Nakai, H.; Vreven, T.; Montgomery, J. A., Jr.; Peralta, J. E.; Ogliaro, F.; Bearpark, M.; Heyd, J. J.; Brothers, E.; Kudin, K. N.; Staroverov, V. N.; Kobayashi, R.; Normand, J.; Raghavachari, K.; Rendell, A.; Burant, J. C.; Iyengar, S. S.; Tomasi, J.; Cossi, M.; Rega, N.; Millam, N. J.; Klene, M.; Knox, J. E.; Cross, J. B.; Bakken, V.; Adamo, C.; Jaramillo, J.; Gomperts, R.; Stratmann, R. E.; Yazyev, O.; Austin, A. J.; Cammi, R.; Pomelli, C.; Ochterski, J. W.; Martin, R. L.; Morokuma, K.; Zakrzewski, V. G.; Voth, G. A.; Salvador, P.; Dannenberg, J. J.; Dapprich, S.; Daniels, A. D.; Farkas, Ö.; Foresman, J. B.; Ortiz, J. V.; Cioslowski, J.; Fox, D. J. *Gaussian 09, Revision C.01*; Gaussian, Inc.: Wallingford, CT, 2009.
(19) Cao, X.; Lee, H. J.; Yun, H. S.; Koo, Y. M. Solubilities of calcium and zinc lactate in water and water-ethanol mixture. *Korean J. Chem. Eng.* **2001**, *18*, 133−135.
(20) Mishelevich, A.; Apelbalt, A. Solubilities of magnesium-L-ascorbate, calcium-L-ascorbate, magnesium-L-glutamate, magnesium-D-gluconate, calcium-D-gluconate, calcium-D-heptagluconate, L-aspartic acid and 3-nitrobenzoic acid in water. *J. Chem. Thermodyn.* **2008**, *40*, 897−900.
(21) Van Loon, L. R.; Glaus, M. A.; Vercammen, K. Solubility products of calcium isosaccharinate and calcium gluconate. *Acta Chem. Scand.* **1999**, *53*, 235−240.
(22) Azimi, G.; Papangelakis, V. G.; Dutrizac, J. E. Modelling of calcium sulphate solubility in concentrated multi-component sulphate solutions. *Fluid Phase Equilib.* **2007**, *260*, 300−315.
(23) Skibsted, L. H.; Kilde, G. Dissociation constant of calcium gluconate. Calculations from hydrogen ion and calcium ion activities. *Dan. Tidsskr. Farm.* **1972**, *46*, 41−46.
(24) Ghosh, R.; Mair, V. S. K. Studies of metal complexes in aqueous solution. 1. Calcium and copper lactates. *J. Inorg. Nucl. Chem.* **1970**, *32*, 3025−3032.
(25) Pallagi, A.; Sebok, P.; Forgo, P.; Jakusch, T.; Palinko, I.; Sipos, P. Multinuclear NMR and molecular modelling investigations on the structure and equilibria of complexes that form in aqueous solutions of Ca^{2+} and gluconate. *Carbohydr. Res.* **2010**, *345*, 1856−1864.
(26) Saladini, M.; Menabue, L.; Ferrari, E. Sugar complexes with metal (2+) ions: Thermodynamic parameters of associations of Ca^{2+}, Mg^{2+} and Zn^{2+} with galactaric acid. *Carbohydr. Res.* **2001**, *336*, 55−61.

JOURNAL OF AGRICULTURAL AND FOOD CHEMISTRY

Article

pubs.acs.org/JAFC

Physical and Molecular Changes during the Storage of Gluten-Free Rice and Oat Bread

Anna-Sophie Hager,* Geertrui M. Bosmans, and Jan A. Delcour

Laboratory of Food Chemistry and Biochemistry and Leuven Food Science and Nutrition Research Centre (LFoRCe), KU Leuven, Kasteelpark Arenberg 20, B-3001 Leuven, Belgium

ABSTRACT: Gluten-free bread crumb generally firms more rapidly than regular wheat bread crumb. We here combined differential scanning calorimetry (DSC), texture analysis, and time-domain proton nuclear magnetic resonance (TD ^{1}H NMR) to investigate the mechanisms underlying firming of gluten-free rice and oat bread. The molecular mobility of water and biopolymers in flour/water model systems and changes thereof after heating and subsequent cooling to room temperature were investigated as a basis for underpinning the interpretation of TD ^{1}H NMR profiles of fresh crumb. The proton distributions of wheat and rice flour/water model systems were comparable, while that of oat flour/water samples showed less resolved peaks and an additional population at higher T_2 relaxation times representing lipid protons. No significant crumb moisture loss during storage was observed for the gluten-free bread loaves. Crumb firming was mainly caused by amylopectin retrogradation and water redistribution within bread crumb. DSC, texture, and TD ^{1}H NMR data correlated well and showed that starch retrogradation and crumb firming are much more pronounced in rice flour bread than in oat flour bread.

KEYWORDS: *gluten-free, time-domain proton nuclear magnetic resonance, proton mobility, amylopectin retrogradation, crumb firming*

INTRODUCTION

Celiac disease is one of the most frequent genetically based food intolerances. It affects approximately 1% of the Western population.[1] The only available therapy is lifelong avoidance of storage proteins from wheat, rye, and barley, which, in the context of this disease, are termed gluten. While oat has been considered unsuitable for celiac patients, recent scientific evidence has allowed the conclusion that most gluten-intolerant people can consume oat without adverse health effects.[2] Today, a gluten-free diet is also followed by an increasing number of individuals who do not have celiac disease but appear to benefit from avoiding gluten. These include sufferers of non-celiac gluten sensitivity[3] and dermatitis herpetiformis.[4,5] In addition, the increasing number of individuals following a gluten-free diet as a life style choice creates an increasing demand for tasteful gluten-free bakery products with a texture comparable to that of their wheat counterparts. Because of the lack of a viscoelastic gluten network, production of leavened baked goods from non-wheat sources is challenging, and the resulting bread has low volume and a firm crumb.[6] Because of its wide availability, bland taste, and white color,[7] rice is the most commonly used gluten-free raw material.[8] However, rice flour contains levels of nutrients such as protein, fiber, and minerals lower than those of wheat flour.[9] Hence, rice-based gluten-free products are often nutritionally inferior to standard wheat products. Oat bread has not only better nutritional quality than rice bread but also improved volume, texture, and taste.[10]

Crumb firming of wheat bread is mainly related to changes in the starch fraction that result in a continuous, rigid, crystalline starch network.[11−15] On a molecular scale, amylose crystallizes during cooling after baking, while amylopectin does so over a longer time span in a process called retrogradation.[12,16−18] The amylose and amylopectin crystallites create network junction zones. These serve as nucleation sites for an intermolecular and maybe even intergranular mesoscale network[18] that includes unfreezable water. These changes can be monitored with differential scanning calorimetry (DSC) as an increase in melting enthalpy of retrograded amylopectin and a concomitant decrease in the amount of freezable water (FW).[15] The fast-forming amylose network and the thermoset gluten network are largely responsible for initial crumb firmness and resilience, while amylopectin retrogradation strengthens the network during bread storage.[18] In wheat bread crumb, part of the water included in the continuous starch network is withdrawn from the amorphous networks, which therefore lose plasticizing water. In addition, the thermodynamic incompatibility of starch and gluten causes water to diffuse from gluten to starch as shown for a model system.[19] The changes, which occur in the biopolymers during wheat bread baking as starch gelatinizes and gluten cross-links, and during storage as amylopectin retrogrades,[20] probably cause the water diffusion process to proceed until (new) equilibria are reached. Water not only is redistributed within bread crumb during storage but also migrates from crumb to crust, leading to a further local reduction in the moisture content of the biopolymer networks. As a result, the moisture content of the gluten network can drop below that needed for full plasticization during storage. The resulting increase in the stiffness of the gluten network then also contributes to crumb firming, mostly after storage for a couple of days.[15]

The molecular mobility of water and biopolymers in wheat model systems and wheat bread has already been studied with time-domain proton nuclear magnetic resonance (TD ^{1}H

Received: April 30, 2014
Revised: May 19, 2014
Accepted: May 26, 2014
Published: May 26, 2014

ACS Publications © 2014 American Chemical Society

NMR).[15,21−25] Six populations with different mobilities, depending on the local environment of the water and biopolymer protons, were categorized for fresh wheat bread crumb and interpreted by comparing the obtained NMR profiles to those of heated and cooled biopolymer model systems.[21] The least mobile and hence most rigid fraction contains nonexchanging CH protons of amylose crystals formed during cooling and of amorphous starch and gluten not in contact with water. Higher-mobility proton populations include CH protons of amorphous starch and gluten in little contact with water and exchanging protons of confined water, starch, and gluten. The largest population consists of mobile exchanging protons of water, starch, and gluten in the formed gel network. Finally, lipid protons represent a population with the highest T_2 relaxation time.[15,26−28] Molecular and physical changes that occur during the storage of starch-containing systems result in changes in proton distributions. Amylopectin retrogradation can be observed as an increase in the area of the population containing rigid CH protons and a decrease in areas of populations containing protons of amorphous starch due to a shift of protons to lower-mobility populations. In addition, the mobility of the exchanging protons is reduced, which can be attributed to strengthening of the starch network, loss of water from the gluten network, and migration of moisture from the crumb.[15] On the basis of this, TD ^{1}H NMR appears to be promising for also studying changes on a molecular scale during storage of gluten-free bread. So far and to the best of our knowledge, only one publication has reported on the use of ^{1}H NMR to investigate gluten-free bread. It stated that the mobility of the most mobile proton population, representing movable water, decreases during storage. However, no population assignment was conducted.[29]

Against this background, this study investigates the mechanisms underlying firming of the crumb of gluten-free rice and oat bread. Storage-related changes are studied on a macroscopic level (loaf volume and crumb texture) and on a molecular level (proton mobility, amylopectin retrogradation, and FW). Interpretation of complex NMR proton distributions in bread crumb is based on observations from simple oat and rice flour/water model systems.

MATERIALS AND METHODS

Materials and Analysis of Their Composition. Rice flour [11.8% moisture, 7.1% wet basis (wb) protein, 70.1% wb total starch, 0.9% wb lipids, and 0.46% wb ash] and commercial wheat flour (Crousti) (13.4% moisture, 11.4% wb protein, 65.5% wb total starch, 2.4% wb lipids, and 0.61% wb ash) were obtained from BENEO-Remy (Wijgmaal, Belgium) and Dossche Mills (Deinze, Belgium), respectively. Oat flour was purchased from E. Flahavan & Son (Kilmacthomas, Ireland) and sifted to obtain flour particle sizes of <400 μm. The sifted flour consisted of 10.7% moisture, 11.1% wb protein, 60.2% wb total starch, 6.6% wb lipids, and 1.39% wb ash. Dry yeast was obtained from Puratos (Groot-Bijgaarden, Belgium). Sugar and salt were purchased at a local supermarket. All reagents, solvents, and chemicals were purchased from Sigma-Aldrich (Bornem, Belgium) and were of analytical grade unless otherwise specified.

Flour and crumb moisture contents (MC) were determined according to AACC Approved Method 44-15.02.[30] The flour protein content was determined using an adaptation of the AOAC Official Method[31] with an automated Dumas protein analysis system (EAS VarioMax C/N, Elt, Gouda, The Netherlands). For the conversion of nitrogen content to protein content, the following factors were used: 5.7 for wheat, 5.8 for oat, and 6.0 for rice flour.[32] The starch content was calculated as 0.9 times the monosaccharide glucose content, determined by gas−liquid chromatography as described by Van Craeyveld et al.[33] The total lipid content was measured gravimetrically following extraction with water-saturated butanol (WSB). The ash content was determined according to AACC Approved Method 08-01.01.[34] All analyses were performed in triplicate.

Defatting of Oat Flour and Lipid Extraction. Oat flour was defatted with WSB. In practice, 1.0 g of oat flour was shaken in 10 mL of WSB for 60 min and the solvent was removed from the residue with a rotational vacuum concentrator (RVC, Q-Lab, Vilvoorde, Belgium) (60 °C, 1 mbar). This cycle was repeated twice before the resulting defatted flour was air-dried overnight, used to prepare flour/water model systems, and analyzed via TD ^{1}H NMR (see below).

The total lipid extract was obtained by WSB extraction of oat flour with an ASE200 (Dionex, Amsterdam, The Netherlands) as described previously by Gerits et al.[35] The obtained total lipid extract was then further purified to remove protein and other nonlipid material by discarding the upper phase obtained following addition of chloroform, methanol, and water [1:1:0.9 (v/v/v) ratio] to the total lipid extract and vigorous shaking as described by Bligh and Dyer.[36] Upon evaporation of the solvent with a RVC (40 °C, 1 mbar), the total lipid extract was transferred into NMR tubes and subjected to analysis (see below).

Flour/Water Model Systems. Flour/water model systems with an MC of 47% (representing a typical wheat dough MC) were prepared via the gentle stirring of flour and water to obtain homogeneous mixtures. After resting for 30−120 min, all model systems were analyzed with DSC and TD ^{1}H NMR before and after being heated and subsequently cooled to room temperature. Heating of the flour/water model systems was conducted in sealed NMR tubes placed in an oil bath (10 min at 110 °C).

Bread Making. Gluten-free formulations usually consist of complex mixtures of ingredients. To reduce the complexity and to allow comparison with wheat bread recipes, simple formulations based solely on flour, water, sugar, salt, and yeast described previously by Hager et al.[10] were used here. Batters were prepared by using 1.5% salt, 6.0% sugar, 3.0% yeast, and a water addition level of 95.0% for oat and rice (percentages based on flour weight). Optimal water addition levels were determined by preliminary baking tests. To control mold growth during storage, 0.1% calcium propionate and 1.6% potassium sorbate were added to oat and rice batter, respectively (percentages based on flour weight). Yeast was suspended in the water (30 °C) and rested for 10 min in a fermentation chamber (National Manufacturing, Lincoln, NE) at 30 °C and a relative humidity of 90%. The suspension was then added to the premixed dry ingredients. Mixing was conducted for 60 s at speed 1 with a KitchenAid KPM5 mixer (KitchenAid, St. Joseph, MI) equipped with a batter blade. The bowl content was scraped down and then further mixed for 90 s at speed 4. Greased baking tins [internal dimensions (width × length × height) of 8.0 cm × 14.5 cm × 5.5 cm] were filled with batter (350 g) and placed in the fermentation chamber for 30 min. Bread was then baked in a Condilux deck oven (Hein, Strasse, Luxemburg) for 45 min at 195 °C top and bottom heat. Prior to analyses, bread loaves were cooled for 2 h.

Bread Storage and Crumb Sampling. Cooled fresh bread loaves were wrapped in plastic foil and stored in sealed plastic bags for up to 120 h at 23 °C. Three bread loaves each were analyzed by crumb texture analysis and DSC 2, 48, and 120 h after removal from the oven. Additionally, center-crumb samples were withdrawn at these time points and transferred into NMR tubes, which were then sealed and analyzed (see below).

Loaf Volume and Crumb Texture Analysis. After the loaves had cooled for 2 h, loaf volume was determined using a VolScan Profiler (Stable Micro Systems, Surrey, U.K.). The firmness and springiness of crumbs were measured 2, 48, and 120 h after removal from the oven using an Instron 3342 instrument (Norwood, MA) equipped with a cylindrical probe (diameter of 25 mm). From the center of each of three fresh and stored bread loaves, three slices were cut (25 mm thickness), from which cylindrical samples were obtained with a cookie cutter (diameter of 35 mm). In a first test (test speed of 100 mm/min), one indentation was made. The force required to cause an indentation of 30% in the center of the samples is termed firmness. In

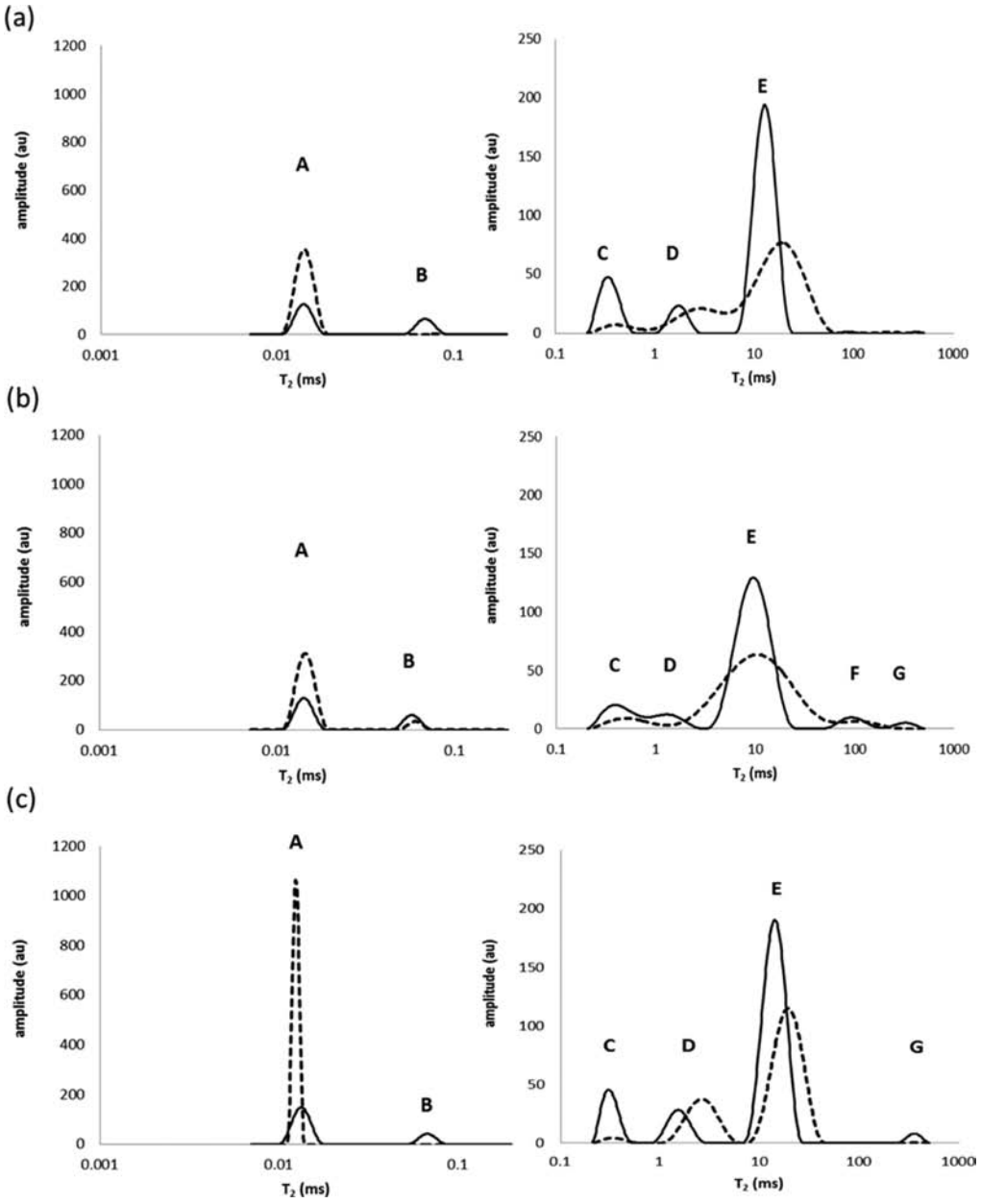

Figure 1. Proton distributions of unheated (---) and heated and cooled (—) flour/water model systems (water content of 47%) prepared from (a) wheat, (b) oat, and (c) rice flour obtained by the inverse Laplace transformation of the single-pulse free induction decay (left) and the decay obtained with the Carr−Purcell−Meiboom−Gill pulse sequence (right). Amplitudes are given in arbitrary units (au). The different proton populations are indicated with capital letters in order of their increasing mobility.

the second test (same test speed), two indentations of 30% in the center of the samples were made with a resting period of 60 s between them. The maximal force in the second indentation cycle divided by the maximal force in the first indentation cycle is the springiness, which is a measure of the reversibility of imposed bread crumb deformation.

Differential Scanning Calorimetry. DSC was conducted using a Q1000 DSC instrument (TA Instruments, New Castle, DE) previously calibrated with indium. To determine the temperatures and enthalpies corresponding to the melting of natively present amylopectin crystals or such crystals formed as a result of retrogradation, 2.5−4.0 mg of sample was accurately weighed in triplicate in aluminum pans (PerkinElmer, Waltham, MA). Deionized water was added in a sample dry matter:water ratio of 1:3 (w/w). Flour/water model systems were analyzed as such, while bread crumb was freeze-dried and ground prior to analysis. Pans were hermetically sealed and equilibrated at 0 °C together with an empty reference pan before being heated to 120 °C at a heating rate of 4 °C/min. Samples were measured after storage for 2, 48, and 120 h. The resulting endotherms were evaluated using TA Instruments Universal Analysis software. Enthalpies were expressed in joules per gram of sample dry base (db).

For the determination of the portion of FW, i.e., the water that transforms into ice during cooling to −40 °C, fresh bread crumb (10−15 mg) was accurately weighed in quadruplicate in aluminum pans. The samples were equilibrated at 15 °C and cooled to −40 °C at a rate of 4 °C/min. The portion of FW (eq 1) was calculated from the melting enthalpy of the sample ($\Delta H_{melting}$, in joules per gram of sample measured between −6 and 0 °C), the MC of the sample (grams of water per gram of sample), and the melting enthalpy of ice (ΔH_{ice} = 334 J/g of ice).

dx.doi.org/10.1021/jf502036x | J. Agric. Food Chem. 2014, 62, 5682−5689

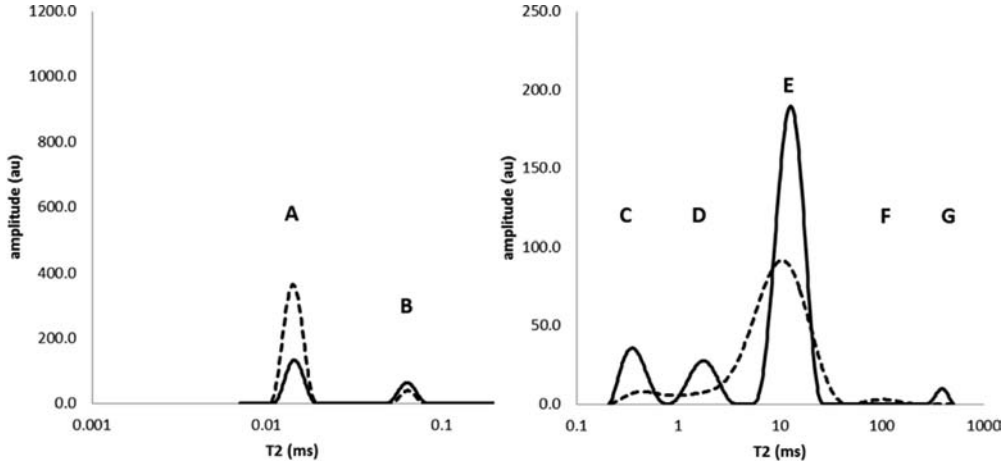

Figure 2. Proton distributions of unheated (---) and heated and cooled (—) flour/water model systems (water content of 47%) prepared from defatted oat flour (consecutive hexane and water-saturated butanol extraction) obtained by the inverse Laplace transformation of the single-pulse free induction decay (left) and the decay obtained with the Carr−Purcell−Meiboom−Gill pulse sequence (right). Amplitudes are given in arbitrary units (au). The different proton populations are indicated with capital letters in order of increasing mobility.

$$\%\mathrm{FW} = \frac{\Delta H_{\mathrm{melting}}}{\Delta H_{\mathrm{ice}} \times \mathrm{MC}} \times 100 \quad (1)$$

The FW content of fresh bread crumb was analyzed using samples withdrawn within 12 h of baking. Pans with fresh crumb withdrawn after baking and stored at 23 °C were also analyzed after storage for 48 and 120 h.

Time-Domain Proton Nuclear Magnetic Resonance. Measurements of proton distributions in model systems and bread were performed as described by Bosmans et al.[21] with a Minispec mq 20 TD NMR spectrometer (Bruker, Rheinstetten, Germany) at an operating resonance frequency of 20 MHz for ^{1}H (magnetic field strength of 0.47 T). An external water bath maintained the temperature of the probe head at 25 ± 1 °C. Relaxation curves were acquired using a single 90° pulse [free induction decay (FID)] and a Carr−Purcell−Meiboom−Gill (CPMG) pulse sequence with 90° and 180° pulse lengths of 2.86 and 5.42 μs, respectively. For the FID, an acquisition period of 0.5 ms was used and 500 data points were collected. For the CPMG sequence, the 90° and 180° pulses were separated by 0.1 ms and 2500 data points were acquired. For both measurements, a recycle delay of 3.0 s was used and 32 scans were accumulated to increase the signal-to-noise ratio. Three samples (approximately 0.3 g, accurately weighed) of a model system or bread crumb were placed in three different NMR tubes (10 mm external diameter). All samples were tightly compressed to a height of ∼8 mm to remove air bubbles. Each tube was analyzed in triplicate, and the exact sample weight in each tube was taken into account during the computations.

The CONTIN algorithm of Provencher[37] (software provided by Bruker) was applied to transform the transverse relaxation curves with an inverse Laplace transformation to a continuous distribution of transverse or spin−spin (T_2) relaxation times, which are related to proton mobility. The area under the curve of a population with a certain T_2 relaxation time is proportional to the number of protons in that population. The calculations were performed on 500 data points logarithmically spread between T_2 relaxation times of 0.007 and 0.5 ms and of 0.2 and 500 ms for the FID and CPMG measurements, respectively. Because the inhomogeneity of the static magnetic field affected the output for the most mobile FID population found around 0.5 ms,[38,39] this fraction was not taken into account in the following discussion.

Statistical Analysis. Statistical analysis was performed using R version 3.0.2 "Frisbee Sailing" (The R Foundation for Statistical Computing, Vienna, Austria) and the package "Agricolae". Analysis of variance was conducted, followed by the Shapiro Wilk normality test and Tukey's honest significant difference test.

RESULTS AND DISCUSSION

Flour/Water Model Systems. The molecular mobility of water and biopolymers in wheat, oat, and rice flour/water model systems and changes thereof after heating and subsequent cooling to room temperature were investigated first. The obtained proton distribution patterns of unheated and heated gluten-free flour/water models were comparable to those of wheat flour/water models,[21] and population assignment, therefore, was performed in a similar way. Figure 1 shows the FID and CPMG proton distributions of unheated and heated wheat, oat, and rice flour/water model systems. The unheated samples showed one predominant FID population (population A) (Figure 1, left panel). On the basis of previous studies, this population contains rigid CH protons of crystalline and amorphous starch[21,40] and proteins not in contact with water.[21,28]

With regard to the CPMG proton distributions, population E was most abundant in all samples (Figure 1, right panel). This population contains mobile OH protons of water in the extragranular space, which are in exchange with starch OH protons on the granule surface and with exchangeable protons of proteins.[21] Population C of the wheat flour/water model system contains CH protons of amorphous starch and gluten in contact with water.[21] Population D then contains OH protons of intragranular water and starch, but also some CH protons of gluten and exchanging protons of confined water and gluten.[21,41] It can reasonably be assumed that CH protons of rice or oat protein are also part of populations C and D.

For unheated rice and wheat samples, three distinct CPMG populations (C−E) were observed, even if these were not fully resolved for wheat. The difference from the oat samples is that in the latter population E was much broader and peaks C and D were not resolved. The total lipid extract from oat flour showed CPMG populations with T_2 relaxation times corresponding to populations C, E, and F of oat flour (results not shown). The lipid T_2 relaxation times apparently are too similar to those of the mobile and exchangeable protons of starch and protein to permit the clean separation of peaks. In the case of unheated oat flour, an additional proton population F was observed with a T_2 relaxation time of approximately 100 ms (Figure 1b, right panel). Prior removal of lipids from oat flour by WSB extraction

dx.doi.org/10.1021/jf502036x | J. Agric. Food Chem. 2014, 62, 5682−5689

Table 1. Melting Enthalpies of Retrograded Amylopectin (ΔH), Freezable Water (FW), Crumb Firmness, and Crumb Springiness of Oat and Rice Bread Loaves Stored for 2, 48, and 120 h at 23 °C[a]

	storage time (h)	ΔH (J/g of sample dry mass)	FW (%)	firmness (N)	springiness
oat bread	2	0	45.9 ± 6.1 a	2.2 ± 0.2 c	0.7 ± 0.0 a
	48	0.2 ± 0.1 b	44.0 ± 4.7 a	4.4 ± 1.0 b	0.6 ± 0.0 b
	120	0.5 ± 0.0 a	50.1 ± 4.8 a	8.3 ± 1.2 a	0.5 ± 0.0 c
rice bread	2	0.2 ± 0.1 C	59.3 ± 0.8 A	12.0 ± 1.4 C	0.6 ± 0.1 A
	48	3.4 ± 0.4 B	46.7 ± 2.8 B	47.5 ± 7.2 B	0.2 ± 0.1 B
	120	4.6 ± 0.1 A	51.7 ± 2.2 B	67.0 ± 5.3 A	0.1 ± 0.0 B

[a]Values in the same column followed by the same letter are not significantly different ($p < 0.05$).

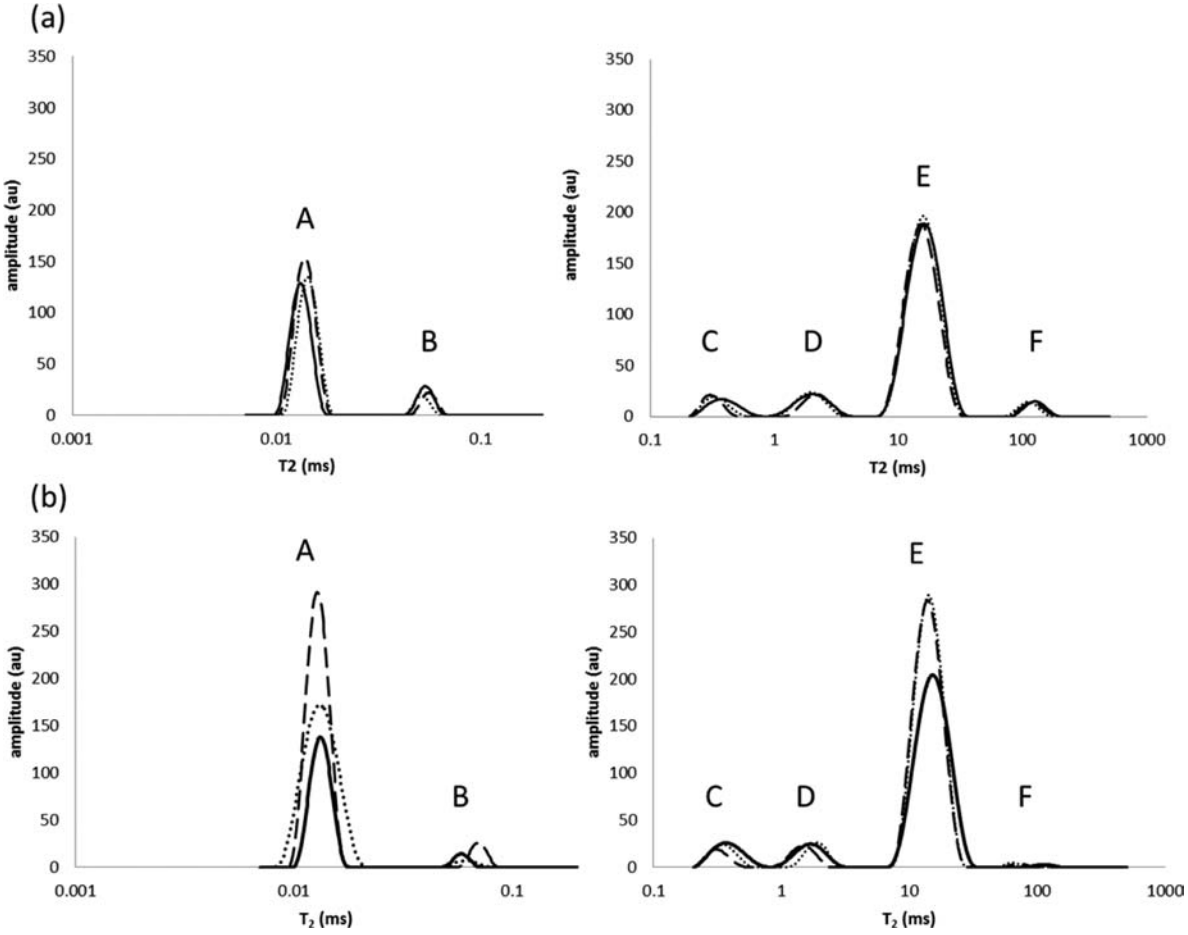

Figure 3. Proton distributions of oat (a) and rice (b) bread obtained by the inverse Laplace transformation of the single-pulse free induction decay (left) and the decay obtained with the Carr–Purcell–Meiboom–Gill pulse sequence (right) after storage for 2 h (—), 48 h (···), and 120 h (---). Amplitudes are given in arbitrary units (au). The different proton populations are indicated with capital letters in order of their increasing mobility.

reduced the area of population F (Figure 2, right panel). Thus, this peak probably represents protons of the lipid fraction. That such a peak was present in the oat flour/water model system is in line with the higher endogenous lipid content of oat than of either wheat or rice.

For heated flour/water model systems, DSC did not detect endothermic peaks (results not shown), confirming that heating model systems for 10 min at 110 °C fully gelatinized the starch in each flour model system.

Heat treatment and subsequent cooling of the flour/water model system resulted in similar changes in proton distributions. The area of population A decreased, while those of populations B and C increased (Figure 1). These changes were related to starch gelatinization, resulting in a decrease in the number of protons in a rigid environment due to melting of the starch crystals and swelling of the previously densely packed amorphous starch not in contact with water (present in population A), and an increase in the number of protons of amorphous starch in contact with water (present in populations B and C).[21] The area of population E, representing mobile protons in strong interaction with water, increased upon heating. The mobility of this population decreased during heat treatment. The reduced mobility was also observed for a starch/water model system and attributed to starch gelatinization and gelation.[21] After heating and subsequent cooling, this population consisted of mobile exchanging protons of water, starch, and proteins present in the formed gel network. The reduced mobility was possibly caused by more intense contact between the biopolymers and water.[21] The CPMG populations of heated wheat and rice flour/water model systems were well

dx.doi.org/10.1021/jf502036x | J. Agric. Food Chem. 2014, 62, 5682–5689

Table 2. T_2 Relaxation Times and Areas of the Free Induction Decay (FID) of Population A (rigid protons of starch crystals and amorphous starch and protein not in contact with water) and Carr−Purcell−Meiboom−Gill (CPMG) Population E (mobile exchanging protons of water, starch, and protein in the formed gel network) of Oat and Rice Bread Loaves Stored for 2, 48, and 120 h at 23 °C[a]

		FID population A		CPMG population E	
	storage time (h)	area (au)	T_2 (ms)	area (au)	T_2 (ms)
oat bread	2	4234 ± 83 b	0.013 ± 0.001 a	9576 ± 105 a	15.7 ± 0.4 a
	48	4627 ± 316 ab	0.013 ± 0.001 a	9500 ± 15 a	15.3 ± 0.2 a
	120	5636 ± 904 a	0.013 ± 0.002 a	9540 ± 110 a	14.3 ± 0.5 b
rice bread	2	4504 ± 26 C	0.012 ± 0.001 A	9745 ± 39 A	14.7 ± 0.4 A
	48	8451 ± 1059 B	0.013 ± 0.000 A	11578 ± 789 A	13.8 ± 0.1 B
	120	10229 ± 579 A	0.012 ± 0.000 A	11932 ± 168 A	13.1 ± 0.4 B

[a]Values in the same column followed by the same letter are not significantly different ($p < 0.05$).

resolved, while this was not the case for the heated oat flour/water model system. The broadness of the oat peaks can possibly be attributed to the presence of endogenous lipids, as clearly resolved peaks were observed after heating and subsequent cooling of the oat flour model system prepared with defatted flour (Figure 2). Heated model systems prepared with oat or rice flour contained an additional small population G with a T_2 relaxation time of 300 ms. The population was not influenced by defatting and, hence, does not contain protons of the lipid fraction, but possibly results from expulsion of water from the flour proteins during heating. This small proton population with a very high mobility was also observed for heated and cooled egg[28,42] and gluten.[21]

Oat and Rice Bread. The loaf specific volume was significantly higher ($p < 0.05$) for oat (1.9 ± 0.1 mL/g) than for rice (1.2 ± 0.0 mL/g) bread. During storage of wheat bread, the level of moisture gradually increases in the crust and decreases in the crumb.[15] Such water redistribution has also been reported for bread made from mainly cassava, maize, or rice starch[43] as well as for commercial gluten-free bread based on wheat starch and milk powder.[29] The crust moisture content could not be determined for oat and rice bread of this study because it was not possible to remove the fine crust from the crumb. Moisture contents of the crumb center of oat and rice bread were 51.4 ± 0.1 and 50.4 ± 0.4%, respectively, and did not change significantly ($p < 0.05$) over the examined storage period. Hence, crumb to crust moisture migration did not contribute to a significant degree to firming of these bread loaves.

The amylopectin melting enthalpy of crumb from fresh rice bread (0.22 ± 0.07 J/g) was comparable to that of wheat bread (0.25 ± 0.02 J/g) in the study of Bosmans et al.[15] Little if any melting enthalpy was detected for fresh oat crumb. As expected, the melting enthalpy of retrograded amylopectin significantly increased during storage of both bread types (Table 1). This increase was substantially more pronounced for rice bread. Concomitantly, the amount of FW significantly decreased from 59.3 to 50.1% during the storage of rice bread for 120 h, while no significant ($p < 0.05$) reduction in FW was observed for oat bread (Table 1). These differences between oat and rice bread can possibly be attributed to the high lipid content of oat.

Crumb firming, therefore, is mainly caused by formation of a rigid, partially crystalline starch network and the concomitant diffusion of water from the surrounding amorphous phase to the retrograding starch where it is rendered unfreezable, in line with observations of Bosmans et al.[15] for wheat bread crumb stored without crust.

The initial firmness was much lower for oat (2.3 ± 0.2 N) than for rice (12.0 ± 1.4 N) bread crumb (Table 1). Native oat starch lipids seem to reduce the level of leaching of amylose from the granule during baking, thereby reducing initial crumb firmness by lowering the extent of amylose network formation during cooling.[44] As a result of storage for 120 h, crumb firmness has increased and crumb springiness has decreased much more for rice than for oat bread (Table 1). This went hand in hand with less pronounced amylopectin retrogradation in oat bread than in rice bread such as observed with DSC (Table 1).

Proton distributions of gluten-free bread (Figure 3) were comparable to those of wheat bread[15,21] as well as those of the heated flour/water model systems investigated here (Figure 1). Therefore, population assignment was done in a similar way. Two FID populations (A and B) and four CPMG populations (C−F) were observed. Population F, related to protons of the lipid fraction, was not observed for the rice flour/water model system but could be detected in rice bread. These lipid protons probably originated from shortening used to grease the baking tins. For the oat bread, both endogenous oat lipids and shortening contribute to population F.

During the 120 h storage, no considerable changes were observed in the proton distributions of oat bread while those of rice bread changed significantly (Figure 3). The area of population A, containing rigid CH protons of amylose crystals formed during cooling and of amorphous starch and protein not in contact with water, increased during storage of rice bread. A positive relationship was observed between the area of population A and the melting enthalpy of retrograded amylopectin. The latter evidently is related to starch crystallinity, whereas population A of bread crumb contains protons not only from starch but also from other biopolymers such as protein. Nevertheless, the relation between both shows that the increase in the area of population A is associated with amylopectin retrogradation. This shift in protons to lower mobility can be explained by amorphous amylopectin CH protons from more mobile populations becoming incorporated into the forming crystalline structures, hence losing mobility and becoming part of population A.[15] The area of population D decreased for both gluten-free bread types, indicating that nonexchanging CH protons of protein and exchanging protons of confined water, protein, and starch became less mobile and shifted to populations with shorter T_2 relaxation times. The area of population E, containing exchanging protons of the formed gel network, did not significantly change for oat and rice bread (Table 2). This is in line with the observation that the overall crumb moisture content did not noticeably change

during storage. The T_2 relaxation time of population E decreased significantly during storage of oat and rice bread, showing that protons in this population had lost mobility. Because the overall moisture content of the bread loaves remained constant throughout the investigated storage period, this reduction in mobility must be attributed to changes in constituents within the bread crumb. Because amylopectin retrogradation results in a water-containing network,[15,45] the reduced mobility of population E was most probably caused by strengthening of the starch network and by the loss of water from proteins as observed for a gradually dried gluten/water model system.[15] A relation between the increase in firmness and the decrease in the T_2 relaxation time of population E was found. Hence, the extent of amylopectin retrogradation can be deduced from the NMR profiles as an increase in the area of population A, and the extent of crumb firmness can be deduced as a reduction in T_2 relaxation time of population E.

In conclusion, it can be said that the combination of DSC, texture analysis, and TD ^{1}H NMR allowed us to monitor molecular and textural changes during storage of oat and rice bread. The increase in melting enthalpy of retrograded amylopectin during storage was in line with the increase in the area of population A. The increase in firmness correlated well with the reduction of the T_2 relaxation time of population E. No loss of moisture from the crumb was observed, and hence, firming of oat and rice bread could mainly be related to changes in the starch fraction and redistribution of water within the crumb. Because of the increased extent of formation of amylopectin crystals, the crumb firmness of rice bread increased more rapidly than that of oat bread. The latter did not firm considerably during the observed storage period, possibly because of the higher endogenous lipid content of oat flour. This study hence showed that the use of oat flour for gluten-free bread making is beneficial in terms of shelf life.

AUTHOR INFORMATION

Corresponding Author

*E-mail: sophie.hager@biw.kuleuven.be. Phone: (+32)-16-379193. Fax: (+32)-16-321997.

Funding

J.A.D. is the W. K. Kellogg Chair of Cereal Science and Nutrition at KU Leuven. This work is part of Methusalem programme "Food for the future" (2007−2014).

Notes

The authors declare no competing financial interest.

ACKNOWLEDGMENTS

We acknowledge Raf Docx for technical support. Further, we thank Bram Pareyt and Lien Gerits for helpful discussions about lipids.

ABBREVIATIONS USED

au, arbitrary units; CPMG, Carr−Purcell−Meiboom−Gill; db, dry basis; DSC, differential scanning calorimetry; ΔH, melting enthalpy; FID, free induction decay; ^{1}H NMR, proton nuclear magnetic resonance; T, temperature; TD, time-domain; wb, wet basis; WSB, water-saturated butanol

REFERENCES

(1) Catassi, C.; Fasano, A. Celiac disease. *Curr. Opin. Gastroenterol.* **2008**, *24* (6), 687−691.

(2) Commission of the European Communities. Commission Regulation (EC) No. 41/2009 concerning the composition and labelling of foodstuffs suitable for people intolerant to gluten, 2009.

(3) Biesiekierski, J. R.; Newnham, E. D.; Irving, P. M.; Barrett, J. S.; Haines, M.; Doecke, J. D.; Shepherd, S. J.; Muir, J. G.; Gibson, P. R. Gluten as a cause of gastrointestinal symptoms in patients who do not have coeliac disease. *J. Gastroenterol. Hepatol.* **2009**, *24*, A229.

(4) Buckley, D. A.; McDermott, R.; O'Donoghue, D.; Rogers, S. Should all patients with dermatitis herpetiformis follow a gluten-free diet? *Journal of the European Academy of Dermatology and Venerology* **1997**, *9* (3), 222−225.

(5) Sapone, A.; Lammers, K. M.; Ciacci, C.; Dolinsek, J.; Green, P. H. R.; Hadjivassiliou, M.; Kaukinen, K.; Rostami, K.; Sanders, D. S.; Schumann, M.; Ullrich, R.; Villalta, D.; Volta, U.; Catassi, C.; Fasano, A. Spectrum of gluten-related disorders: Consensus on new nomenclature and classification. *BMC Med.* **2012**, *10*, 13.

(6) Gallagher, E.; Gormley, T. R.; Arendt, E. K. Crust and crumb characteristics of gluten free breads. *J. Food Eng.* **2003**, *56* (2−3), 153−161.

(7) Arendt, E. K.; Dal Bello, F. *Gluten-Free Cereal Products and Beverages*; Academic Press, Elsevier: London, 2008.

(8) Hager, A. S.; Axel, C.; Arendt, E. K. Status of Carbohydrates and Dietary Fiber in Gluten-free Diets. *Cereal Foods World* **2011**, *56* (3), 109−114.

(9) Hager, A. S.; Wolter, A.; Jacob, F.; Zannini, E.; Arendt, E. K. Nutritional properties and ultra-structure of commercial gluten free flours from different botanical sources compared to wheat flours. *J. Cereal Sci.* **2012**, *56* (2), 239−247.

(10) Hager, A. S.; Wolter, A.; Czerny, M.; Bez, J.; Zannini, E.; Arendt, E. K.; Czerny, M. Investigation of product quality, sensory profile and ultrastructure of breads made from a range of commercial gluten-free flours compared to their wheat counterparts. *Eur. Food Res. Technol.* **2012**, *235* (2), 333−344.

(11) Willhoft, E. M. Bread staling. 2. Theoretical study. *J. Sci. Food Agric.* **1971**, *22*, 180−183.

(12) Kim, S. K.; D'Appolonia, B. L. Bread staling studies. II. Effect of protein content and storage temperature on the role of starch. *Cereal Chem.* **1977**, *54*, 216−224.

(13) Ribotta, P. D.; Le Bail, A. Thermo-physical assessment of bread during staling. *LWT—Food Sci. Technol.* **2007**, *40*, 879−884.

(14) Lagrain, B.; Wilderjans, E.; Glorieux, C.; Delcour, J. A. Importance of gluten and starch for structural and textural properties of crumb from fresh and stored bread. *Food Biophys.* **2012**, *7*, 173−181.

(15) Bosmans, G. M.; Lagrain, B.; Ooms, N.; Fierens, E.; Delcour, J. A. Biopolymer Interactions, Water Dynamics, and Bread Crumb Firming. *J. Agric. Food Chem.* **2013**, *61* (19), 4646−4654.

(16) Gray, J. A.; Bemiller, J. N. Bread staling: Molecular basis and control. *Compr. Rev. Food Sci. Food Saf.* **2003**, *2*, 1−21.

(17) Hug-Iten, S.; Escher, F.; Conde-Petit, B. Staling of bread: Role of amylose and amylopectin and influence of starch-degrading enzymes. *Cereal Chem.* **2003**, *80*, 654−661.

(18) Goesaert, H.; Slade, L.; Levine, H.; Delcour, J. A. Amylases and bread firming: An integrated view. *J. Cereal Sci.* **2009**, *50*, 345−352.

(19) Grinberg, V. Y.; Tolstoguzov, V. B. Thermodynamic incompatibility of proteins and polysaccharides in solutions. *Food Hydrocolloids* **1997**, *11* (2), 145−158.

(20) Delcour, J. A.; Hoseney, R. C. *Principles of cereal science and technology*, 3rd ed.; AACC International: St. Paul, MN, 2010.

(21) Bosmans, G. M.; Lagrain, B.; Deleu, L. J.; Fierens, E.; Hills, B. P.; Delcour, J. A. Assignments of Proton Populations in Dough and Bread Using NMR Relaxometry of Starch, Gluten, and Flour Model Systems. *J. Agric. Food Chem.* **2012**, *60* (21), 5461−5470.

(22) Chen, P. L.; Long, Z.; Ruan, R.; Labuza, T. P. Nuclear magnetic resonance studies of water mobility in in bread during storage. *LWT—Food Sci. Technol.* **1997**, *30*, 178−183.

(23) Wynne-Jones, S.; Blanshard, J. M. V. Hydration studies of wheat starch amylopectin, amylose gels and bread by proton magnetic resonance. *Carbohydr. Polym.* **1986**, *6*, 289−306.

(24) Choi, S.-G.; Kerr, W. L. ^{1}H NMR studies of molecular mobility in wheat starch. *Food Res. Int.* **2003**, *36*, 341−348.
(25) Curti, E.; Carini, E.; Bubici, S.; Baroni, S.; Vittadini, E. Water molecular dynamics during bread staling by nuclear magnetic resonance. *LWT—Food Sci. Technol.* **2011**, *44*, 854−859.
(26) Assifaoui, A.; Champion, D.; Chiotelli, E.; Verel, A. Characterization of water mobility in biscuit dough using a low-field ^{1}H NMR technique. *Carbohydr. Polym.* **2006**, *64* (2), 197−204.
(27) Le Grand, F.; Cambert, M.; Mariette, F. NMR signal analysis to characterize solid, aqueous, and lipid phases in baked cakes. *J. Agric. Food Chem.* **2007**, *55* (26), 10947−10952.
(28) Luyts, A.; Wilderjans, E.; Waterschoot, J.; Van Haesendonck, I.; Brijs, K.; Courtin, C. M.; Hills, B.; Delcour, J. A. Low resolution ^{1}H NMR assignment of proton populations in pound cake and its polymeric ingredients. *Food Chem.* **2013**, *139* (1−4), 120−128.
(29) Purhagen, J. K.; Sjoo, M. E.; Eliasson, A. C. The anti-staling effect of pre-gelatinized flour and emulsifier in gluten-free bread. *Eur. Food Res. Technol.* **2012**, *235* (2), 265−276.
(30) Method 44-15.02. Moisture-Air-Oven Methods. *Approved methods of analysis*, 11th ed.; AACC International: St. Paul, MN, 1999.
(31) *Official methods of analysis*, 16th ed.; Association of Official Analytical Chemists: Washington, DC, 1995.
(32) Merrill, A.; Watt, B. *Energy value of foods: Basis and derivation—Agriculture Handbook no. 74*; Human Nutrition Research Branch, Agricultural Research Service, U.S. Department of Agriculture: Washinston, DC, 1955.
(33) Van Craeyveld, V.; Delcour, J. A.; Courtin, C. M. Extractability and chemical and enzymic degradation of psyllium (*Plantago ovata* Forsk) seed husk arabinoxylans. *Food Chem.* **2009**, *112* (4), 812−819.
(34) Method 08-01.01. Ash-Basic Method. *Approved methods of analysis*, 11th ed.; AACC International: St. Paul, MN, 1999.
(35) Gerits, L. R.; Pareyt, B.; Delcour, J. A. Single run HPLC separation coupled to evaporative light scattering detection unravels wheat flour endogenous lipid redistribution during bread dough making. *LWT—Food Sci. Technol.* **2013**, *53*, 426−433.
(36) Bligh, E. G.; Dyer, W. J. A rapid method of total lipid extraction and purification. *Can. J. Biochem. Physiol.* **1959**, *37*, 911−917.
(37) Provencher, S. W. Contin: A General-Purpose Constrained Regularization Program for Inverting Noisy Linear Algebraic and Integral-Equations. *Comput. Phys. Commun.* **1982**, *27* (3), 229−242.
(38) Farhat, I. A.; Ottenhof, M. A.; Marie, V.; de Bezenac, E. ^{1}H NMR relaxation study of amylopectin retrogradation. *Special Publication-Royal Society of Chemistry: Applications of magnetic Resonance in Food Science-Latest Developments*; Royal Society of Chemistry: London, 2003; Vol. *286*, pp 172−179.
(39) Tang, H. R.; Brun, A.; Hills, B. A proton NMR relaxation study of the gelatinisation and acid hydrolysis of native potato starch. *Carbohydr. Polym.* **2001**, *46* (1), 7−18.
(40) Tananuwong, K.; Reid, D. S. DSC and NMR relaxation studies of starch-water interactions during gelatinization. *Carbohydr. Polym.* **2004**, *58* (3), 345−358.
(41) Ritota, M.; Gianferri, R.; Bucci, R.; Brosio, E. Proton NMR relaxation study of swelling and gelatinisation process in rice starch-water samples. *Food Chem.* **2008**, *110* (1), 14−22.
(42) Juliano, P.; Toldra, M.; Koutchma, T.; Balasubramaniam, V. M.; Clark, S.; Mathews, J. W.; Dunne, C. P.; Sadler, G.; Barbosa-Canovas, G. V. Texture and water retention improvement in high-pressure thermally treated scrambled egg patties. *J. Food Sci.* **2006**, *71* (2), E52−E61.
(43) Osella, C. A.; Sanchez, H. D.; Carrara, C. R.; de la Torre, M. A.; Buera, M. P. Water redistribution and structural changes of starch during storage of a gluten-free bread. *Starch* **2005**, *57* (5), 208−216.
(44) Wang, L. Z.; White, P. J. Functional-Properties of Oat Starches and Relationships among Functional and Structural Characteristics. *Cereal Chem.* **1994**, *71* (5), 451−458.
(45) Eerlingen, R. C.; Deceuninck, M.; Declour, J. A. Enzyme-Resistant Starch. 2. Influence of Amylose Chain-Length on Resistant Starch Formation. *Cereal Chem.* **1993**, *70* (3), 345−350.

JOURNAL OF AGRICULTURAL AND FOOD CHEMISTRY

Article

pubs.acs.org/JAFC

Migration of Components from Cork Stoppers to Food: Challenges in Determining Inorganic Elements in Food Simulants

T. Corona, M. Iglesias, and E. Anticó*

Department of Chemistry, University of Girona, 17071 Girona, Spain

Supporting Information

ABSTRACT: The inorganic elements potentially migrating from cork to a food simulant [a hydroalcoholic solution containing 12 and 20% (v/v) ethanol] have been determined by means of inductively coupled plasma (ICP) with atomic emission and mass spectrometric detection. The experimental instrumental conditions were evaluated in depth, taking into account spectroscopic and nonspectroscopic interference caused by the presence of ethanol and other components in the sample. We report concentrations ranging from 4 $\mu g\ kg^{-1}$ for Cd to 28000 $\mu g\ kg^{-1}$ for Al in the food simulant (concentrations given in kilograms of cork). The values found for Ba, Mn, Fe, Cu, and Zn have been compared with the guideline values stated in EU Regulation 10/2011. In all cases, cork met the general safety criteria applicable to food contact material. Finally, we have proposed water as an alternative to the hydroalcoholic solution to simplify quantification of the tested elements using ICP techniques.

KEYWORDS: *elemental composition, cork, food simulant, migration, matrix interferences, spectroscopic interferences*

INTRODUCTION

Cork is a natural product obtained from the bark of *Quercus suber*, a common species in the Mediterranean region. Because of its unique physical properties, such as elasticity and low permeability, cork has long been used in the production of cork stoppers, frequently used in the wine industry to seal wine bottles.[1] The cork stopper fabrication process involves various steps: the stripping of the cork plank from the tree stem, a first rest or maturation in the field or factory, followed by boiling and resting in open air, a further boiling step and resting in the store room with a high relative humidity, and finally elimination of the outer corkback and the cork material cut and shaped according to use (stoppers for still wine and disks for sparkling wine). Surface modification is also performed using paraffins and other additives.[2]

The chemical characterization of cork has been investigated mainly with respect to organic compounds.[3,4] However, little attention has been paid to determining its elemental composition. The sources of the inorganic elements present in cork bark and cork stoppers may differ. On the one hand, plants and trees can accumulate trace elements, especially heavy metals, and act as passive receptors; the uptake of nutrients and trace elements through the roots has been extensively studied.[5] On the other hand, contamination from atmospheric particles, pesticides, and the cork stopper fabrication process itself may also contribute to the distribution of metals in cork material. Some studies have addressed the mineral composition of cork material and its relationship with mineral nutrition, the climate, or tree characteristics.[6] In these cases, it is mainly nutrients that are analyzed. In addition, some authors have used tree barks as bioindicators of heavy metal pollution in the atmosphere because of their ability to accumulate metals. The role of bark as a cation exchanger has been highlighted.[7]

Another very important issue to consider is the interaction of cork with wine when cork stoppers are used to seal wine bottles. European Regulation No. 1935/2004 (repealing Directives 80/590/EEC and 89/109/EEC) requires that food contact materials are safe and do not transfer their components into food in quantities that could endanger human health, change food composition in an unacceptable way, or deteriorate the taste and odor of the food.[8] Annex I of the regulation mentioned above lists the groups of materials that may be covered by specific measures, including cork. Specific regulations for cork are listed in Resolution ResAP(2004)2, adopted by the Committee of Ministers, in its composition restricted to Representatives of the States members of the Partial Agreement in the Social and Public Health Field.[9] Among other recommendations, the document states that Directives 82/711/EEC, 85/572/EEC, 93/8/EEC, 97/48/EEC, and 2002/72/EEC and their future amendments should be applied, and that there should be verification of compliance with the quantitative restriction according to the conditions laid out in "Technical document No.2-test conditions and methods of analysis for cork stoppers and other cork materials and articles intended to come in contact with foodstuffs". In this respect, a migration test should be performed under conditions simulating long-term storage (10 days at 40 °C) using a food simulant consisting of a 12% ethanol solution. The potential migrants from agglomerated cork stoppers associated with synthetic products (additives, surface treatments, and lubricants) have been previously studied in line with this approach.[10]

In general, elemental concentration in food simulant solutions obtained from corks is expected to be very low, and for this reason, extremely sensitive analytical techniques are needed. A common technique for determining elements in aqueous matrices is by means of inductively coupled plasma

Received: January 15, 2014
Revised: May 22, 2014
Accepted: May 26, 2014
Published: May 26, 2014

ACS Publications © 2014 American Chemical Society

dx.doi.org/10.1021/jf500170w | J. Agric. Food Chem. 2014, 62, 5690−5698

(ICP), which allows reliable results and high sample throughput. Depending on concentration level, different detection systems are available, such as ICP-AES (atomic emission spectroscopy) for elements present at concentrations higher than ~0.1 mg L^{-1} and ICP-MS (inductively coupled plasma with mass spectrometry detection) for those present at lower concentrations. The latter technique shows good analytical performance but suffers from interferences of different types, such as matrix and spectroscopic interferences.[11] In the particular case of a hydroalcoholic solution, the presence of a carbon source such as ethanol is of special concern. For example, some polyatomic interferences have been described for Cr ($^{12}C^{40}Ar$ and $^{13}C^{40}Ar$).[12] Additionally, the determination of elements with low ionization potential such as Zn, Se, and As is also challenging because of the increase in their degree of ionization in the plasma when an additional carbon source is simultaneously present.[13−15] To overcome these problems, several strategies were developed, including complex sample treatment procedures, the use of interference equations, collision cell devices, and high-resolution instruments.[15]

In this study, we have assessed the elemental composition of a food simulant originating from cork soaks with two objectives: (1) providing a reliable method for their determination, avoiding, if possible, the use of ethanol in calibration standards, and (2) ascertaining whether cork may be considered a safe material for use as a stopper for bottled wine according to the aforementioned EU directive.

MATERIALS AND METHODS

Reagents. The reagents used were analytical grade suprapur quality: nitric acid (Suprapur, Merck, Darmstadt, Germany) and hydrogen peroxide (Trace Select, Fluka, Gilligham, Dorset, U.K.). Water obtained from a Milli-Q purifier system (Millipore Corp., Bedford, MA) was used throughout the study. For matrix matching standards, ethanol absolute (UV-IR-HPLC) PAI was used, from Panreac.

Monoelemental ICP standard solutions (1000 or 5000 mg L^{-1} for Ba) for each element studied were purchased from Pure Chemistry, ROMIL, UKAS calibration.

Apparatus. An ETHOS PLUS Milestone microwave with an HPR-1000/10S high-pressure rotor (Sorisole, Bergamo, Italy) was employed for acid digestion of samples.

A sequential inductively coupled plasma atomic emission spectrometer (ICP-AES, Liberty RL, Varian) in radial configuration was used for major and minor element determination. For trace element determination, a quadrupole-based ICP-MS system (Agilent 7500c, Agilent Technologies, Tokyo, Japan) was used, equipped with an octapole collision reaction cell.

Sample Collection. Samples consisting of cork granules (samples C1 and C2) and cork slabs (C3) were obtained from local producers in Girona, Spain. In all cases, the cork material was obtained from the cork residues discarded in the final stages of the production process, i.e., shaping of the cork slab to obtain the cork stoppers or cork disks. Theses residues are ground in the manufacturing to obtain cork granules intended to be used in the fabrication of different synthetic cork and other cork types (samples C1 and C2). In the case of cork sample 3, we obtained from the producer cork slices that were ground in our laboratory using a conventional grinder (Moulinette D56, Moulinex España, Barcelona, Spain).

Sample Treatment. The migration tests were performed according to the European Directive using a hydroalcoholic (HA) solution [12% (v/v) ethanol] as a food simulant. Four grams of cork granules or previously ground cork slabs was immersed in 100 mL of a food simulant solution at 40 °C for a period of 10 days.[10] The solid parts were then separated by filtering the sample through glass wool. Prior to analysis, a precise weight of cork soak was taken, and the desired amount of the internal standard (IS) solution was added. A small volume of HNO_3 was also added to acidify the sample.

To determine the total content of elements in cork samples, the following procedure was followed.[16] Nine milliliters of concentrated HNO_3 and 1 mL of hydrogen peroxide were added to a 0.5 g cork sample placed in a Teflon reactor. Once the vessel was sealed, it was placed in the microwave oven and the following program was run: 5 min to reach 180 °C, 10 min at 180 °C, and finally a cooling period. After cooling to ambient temperature, the reactor was opened, and the resultant solution was quantitatively transferred to a vial, where the total weight was carefully measured.

To prepare the samples for analysis, the necessary amount of the IS solution was added to 5 g of the digested solution. The samples were measured using the prepared calibration set, as explained below.

To avoid the presence of ethanol in the samples and standards, we tried other migration treatments. In particular, we evaluated the possibility of performing the migration tests by using water instead of a hydroalcoholic solution at different temperatures.

Determination of Elements in the Food Simulant. *For Minor and Trace Element Determination (Ba, Mn, and Al).* Standard solutions were prepared in water or a hydroalcoholic solution. The calibration standards were prepared from individual standard solutions in 1% HNO_3, containing Y (1 mg L^{-1}) or Rh (3 mg L^{-1}) as an internal standard, as indicated. IS correction was conducted by taking into account the intensity of the line for the measured element and for the internal standard. Additionally, because of the different behavior traditionally observed for ionic and atomic lines, each ionic line was corrected using an ionic line from the internal standard and each atomic line was corrected using an atomic line[15] (see Table 1).

Table 1. Selected Atomic and Ionic Lines for ICP-AES Measurements

element	line type	wavelength (nm)	IS	line type	wavelength (nm)
Ba	II	455.403	Y	II	371.030
Zn	II	202.551	Y	II	371.030
Cu	I	324.754	Rh	I	343.489
Fe	II	259.940	Y	II	371.030
Mn	II	257.610	Y	II	371.030
Al	I	396.152	Rh	I	343.489

For Ultratrace Element Determination (Cr, Fe, Ni, Cu, Zn, Pb, Cd, As, and Se). From the commercial standard solutions, an intermediate solution in 1% (w/w) HNO_3 containing the measured elements over the appropriate range of concentrations was prepared and used to obtain the calibration set, either in water or in a hydroalcoholic solution.

The isotope ^{103}Rh was used for internal standard correction after checking that it was not present in the samples at the concentration range studied (results from a semiquantitative analysis). The concentration of IS in the standard solutions prepared for calibration and in the samples was around 3.7 ng g^{-1}.

The experimental conditions for determining this set of elements were optimized taking into account different criteria: abundance of the selected isotope, correction of isobaric and polyatomic interferences under the vented or pressurized collision cell, type and flow rate of the gas used in the pressurized collision cell, correction of matrix interferences by the IS used, and finally the presence of other matrix interferences that cannot be corrected with the IS.

Octopole and quadrupole potentials were varied according to cell conditions, being fixed at −12 and −11.1 V, respectively, when a pressurized cell was used and −6.4 and −4.5 V, respectively, under vented conditions.

Some other parameters, such as ion lens settings, were adjusted daily to obtain the maximal sensitivity and precision. The oxide level (CeO^+) and doubly charged ion level (Ce^{2+}) were kept under 1 and 3%, respectively.

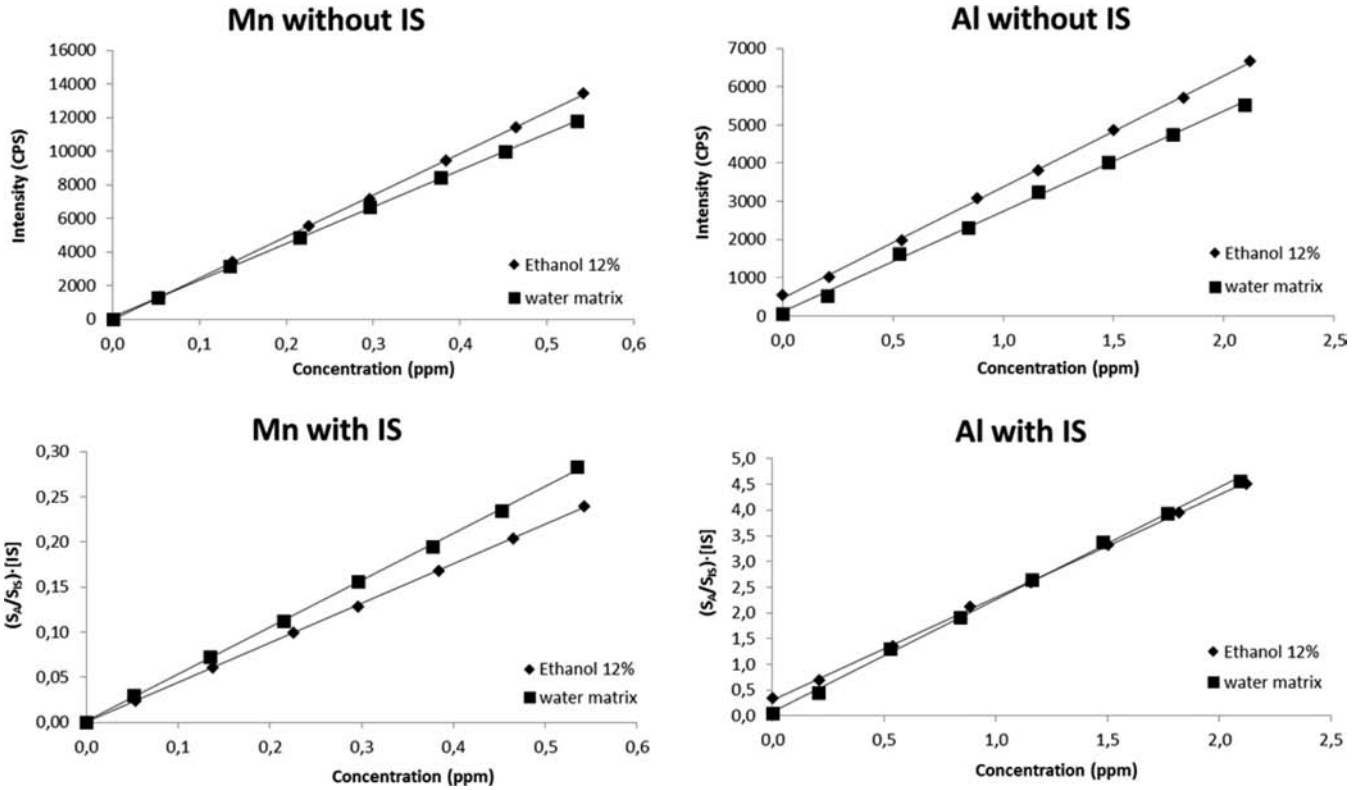

Figure 1. Calibration curves for Al and Mn with and without IS.

Statistical Analysis. The statistical package provided by Excel was used to perform analysis of variance to evaluate whether differences between treatments were significant ($p < 0.05$).

RESULTS AND DISCUSSION

Evaluation of Experimental Conditions for Determining Elements. The elements of interest were selected according to the results of preliminary semiquantitative studies conducted in our laboratory. To quantify these elements using ICP-AES and ICP-MS techniques, matrix interferences and spectral interferences are of great concern because of the presence of ethanol and other carbon sources in the matrix derived from the sample itself. In a previous work dealing with wine samples,[17] we evaluated the influence of the presence of ethanol and demonstrated that use of an adequate IS allows the calibration set to be prepared in water instead of a HA solution. For this reason, we devoted much effort here to studying whether choosing an adequate IS makes it possible to appropriately correct the different types of interferences. The elements determined by ICP-AES will be discussed separately from those measured by ICP-MS in the following sections.

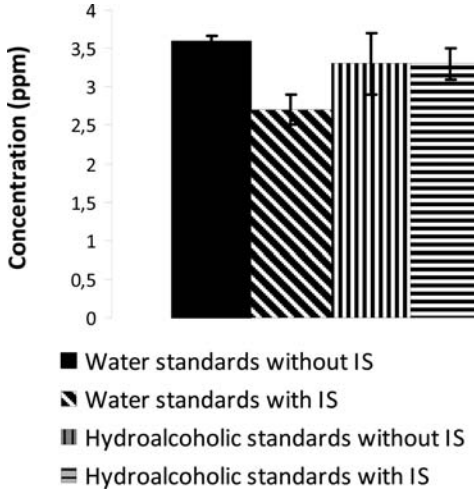

Figure 2. Results obtained for Mn determination in a cork soak under different calibration conditions.

Table 2. Main Isotopes and Possible Interferences

isotope	interferences
^{56}Fe	$^{40}Ar^{16}O$, $^{40}Ca^{16}O$, $^{40}Ar^{15}N^{1}H$, $^{38}Ar^{18}O$, $^{37}Cl^{18}O^{1}H$
^{57}Fe	$^{40}Ar^{16}O^{1}H$, $^{40}Ca^{16}O^{1}H$, $^{40}Ar^{17}O$, $^{38}Ar^{18}O^{1}H$, $^{38}Ar^{19}F$
^{60}Ni	$^{44}Ca^{16}O$, $^{23}Na^{37}Cl$, $^{43}Ca^{16}O^{1}H$
^{62}Ni	$^{46}Ti^{16}O$, $^{23}Na^{39}K$, $^{46}Ca^{16}O$
^{63}Cu	$^{31}P^{16}O_2$, $^{40}Ar^{23}Na$, $^{36}Ar^{12}C^{14}N^{1}H$
^{65}Cu	$^{49}Ti^{16}O$, $^{32}S^{16}O^{21}H$, $^{40}Ar^{25}Mg$, $^{40}Ca^{16}O^{1}H$, $^{36}Ar^{14}N_2{}^{1}H$, $^{32}S^{33}S$, $^{32}S^{16}O^{17}O$, $^{33}S^{16}O_2$, $^{12}C^{16}O^{37}Cl$, $^{12}C^{18}O^{35}Cl$, $^{31}P^{16}O^{18}O$
^{111}Cd	–
^{208}Pb	–
^{52}Cr	$^{40}Ar^{12}C$, $^{38}Ar^{14}N$, $^{35}Cl^{17}O$, $^{35}Cl^{16}O^{1}H$
^{53}Cr	$^{40}Ar^{13}C$, $^{37}Cl^{16}O$
^{75}As	$^{40}Ar^{35}Cl$
^{76}Se	$^{40}Ar^{36}Ar$
^{78}Se	$^{40}Ar^{38}Ar$
^{80}Se	$^{40}Ar^{40}Ar$
^{64}Zn	$^{40}Ar^{24}Mg$, $^{64}Ni^{36}Ar^{12}C^{16}O$, $^{38}Ar^{14}N_2$
^{66}Zn	$^{40}Ar^{26}Mg$, $^{38}Ar^{28}Si$, $^{38}Ar^{14}N_2$
^{68}Zn	$^{40}Ar^{14}N_2$, $^{36}Ar^{32}S$, $^{36}Ar^{16}O_2$, $^{38}Ar^{14}N^{16}O$

Metals Determined by ICP-AES (Ba, Mn, and Al). Table 1 shows the selected atomic and ionic lines taken for measure-

dx.doi.org/10.1021/jf500170w | J. Agric. Food Chem. 2014, 62, 5690−5698

Table 3. Isotope and Cell Conditions Selected for ICP-MS Measurements

isotope	conditions
^{111}Cd	vented cell
^{208}Pb	vented cell
^{56}Fe	He at 2 mL min^{-1}
^{60}Ni	He at 2 mL min^{-1}
^{63}Cu	He at 2 mL min^{-1}
^{53}Cr	He at 2 mL min^{-1}
^{66}Zn	He at 0.5 mL min^{-1} and H_2 at 3 mL min^{-1}
^{75}As	He at 0.5 mL min^{-1} and H_2 at 3 mL min^{-1}
^{78}Se	He at 0.5 mL min^{-1} and H_2 at 3 mL min^{-1}

ment. The main problem associated with determining the elements is sample composition due to the presence of the alcohol, which may cause differences in nebulization efficiency and aerosol transport compared to those of water samples. Figure 1 shows calibration curves for Al and Mn (see Table S1 of the Supporting Information for calibration parameters). As we can see, the addition of Rh and Y as internal standards allows for an appropriate correction of matrix interference due to the presence of ethanol for Al. Similar results were obtained for Ba. For Mn, calibration curves are statistically different [$p < 0.05$ (see Table S2 of the Supporting Information)] for both matrices even in the presence of the internal standard, which means that matrix effects other than nebulization efficiency and transport contribute to the response at the selected wavelength. To verify this fact, a sample was measured in triplicate and the manganese concentration was determined using the calibration plots shown in Figure 1, i.e., aqueous standards, aqueous standards with IS, standards in a hydroalcoholic solution, and standards in a hydroalcoholic solution with IS. The results obtained (Figure 2) demonstrate that the aqueous standards, even with IS, do not allow the correct determination of this element. On the other hand, when ethanol standards are used, the same result is obtained with and without IS, so the presence of ethanol is the main matrix effect in manganese determination.

Metals Determined by ICP-MS (Cr, Fe, Ni, Cu, Zn, Pb, Cd, As, and Se). For those elements present at lower concentrations, ICP-MS was used. In this case, spectroscopic and nonspectroscopic interferences are of particular concern and different situations can be envisaged: (1) when matrix interference due to the presence of ethanol in the samples is corrected by use of the appropriate IS, (2) when polyatomic interferences exist that are corrected by the use of a pressurized cell and the conditions in the cell need to be optimized, and (3) elements with a high ionization potential that also need special instrumental conditions.

We performed separate experiments depending on the characteristics of each element.

Cadmium, Lead, Iron, Nickel, and Copper. For lead and cadmium, no important polyatomic interferences have been described. Therefore, the most abundant isotope was selected for their measurement. Calibration curves were measured in water and hydroalcoholic solutions both with IS, and results showed that the use of the internal standard allows appropriate correction for the presence of ethanol in the solution. In both cases, without using the pressurized collision cell, calibration could be performed with standards prepared in water. Additionally, the values obtained for Cd and Pb, measured in a sample obtained from soaked cork, showed no significant differences when both calibration sets were used and with IS

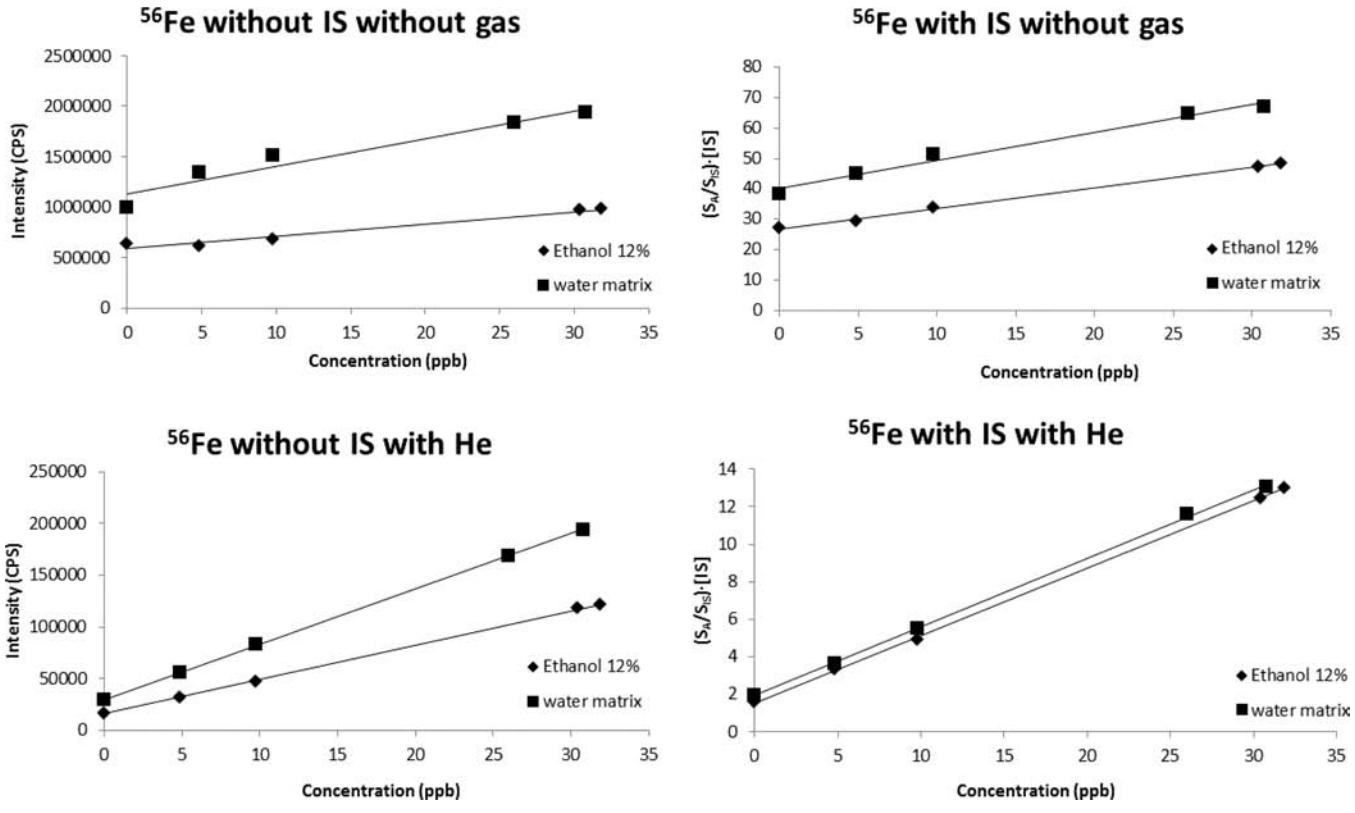

Figure 3. Calibration curves for ^{56}Fe under different conditions (pressurized cell with He at 2 mL min^{-1} and IS correction).

dx.doi.org/10.1021/jf500170w | J. Agric. Food Chem. 2014, 62, 5690−5698

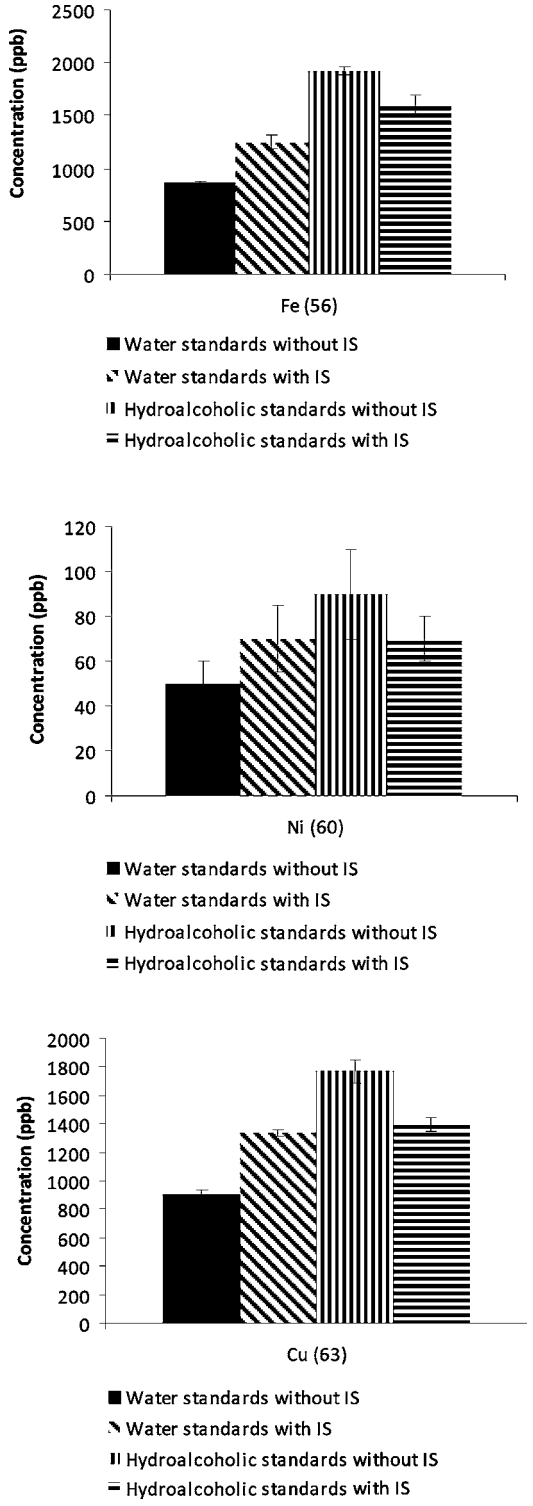

Figure 4. Results obtained for determination of ^{56}Fe, ^{60}Ni, and ^{63}Cu in a cork soak under different conditions.

correction. Some differences were encountered when the values obtained for calibration with ethanol were compared with the results obtained for calibration with ethanol and IS, probably due to matrix interferences other than ethanol.

For Ni, Fe, and Cu, common polyatomic interferences are known (see Table 2). Calibration data were compared for the most abundant isotopes under different conditions (internal standard and vented or pressurized cell). Similar behavior is observed in all six cases (two isotopes for each element): the use of the pressurized cell with He at 2 mL min^{-1}, as previously described,[18] allows for a good correction of polyatomic interferences, while matrix interferences deriving from the presence of ethanol can be mostly overcome by employing IS correction. The most abundant isotope providing better sensitivity was then chosen (Table 3). In Figure 3 and Table S3 of the Supporting Information, the case of ^{56}Fe is depicted by way of example.

The experimental conditions were verified by analyzing the three metal cations in a cork soak (Figure 4). When the results obtained from calibration with water standards were compared with those obtained with the hydroalcoholic solution, no significant differences were obtained for Ni and Cu if the IS is used for quantification. For Fe, the matrix interferences are not adequately corrected, and it is therefore compulsory to perform calibration using hydroalcoholic solutions. It should be taken into account that the cork soak solution has a complicated composition, so other matrix effects, different from those related to ethanol content, may be present.

Chromium. As explained in the Introduction, determination of chromium by means of ICP-MS is hampered by the presence of spectroscopic interferences due to the presence of carbon or chlorine in the sample matrix (see Table 2). Several strategies for overcoming these interferences have been proposed in the literature.[12] When the instrumentation available was taken into account, the use of pressurized cell conditions with He was chosen as the best alternative. As preliminary work, different He flow rates in the collision reaction cell were tested to obtain a high signal background ratio (SBR). A rate of 2 mL min^{-1} was finally chosen as a compromise between a low level of interferences and sufficient analyte signal. Calibration curves, with standards in water or a hydroalcoholic solution, were obtained under different conditions (vented and pressurized cell conditions and with and without IS) for the most abundant chromium isotopes, ^{52}Cr and ^{53}Cr. Additionally, the effect of the presence of chloride was also evaluated, because Cl has been determined to be an abundant element in cork.[19]

The addition of helium in chromium determination decreases spectroscopic interferences, which can be observed in Figure 5. However, the presence of a fairly important spectroscopic interference is still observed when ^{52}Cr is measured. In contrast, the use of He at a rate of 2 mL min^{-1} in the collision cell virtually eliminates the interference on ^{53}Cr. The use of IS does not result in much difference in this case.

Because chromium was present at a concentration level below the limit of detection in our particular samples, it could not be determined in the cork soak.

Arsenic, Zinc, and Selenium. These elements are also difficult to determine by means of ICP-MS because of their high ionization potential, which produces a low degree of ionization in the plasma. Additionally, they also suffer from spectroscopic interferences (see Table 2). It is already known that some of these elements show an important increase in sensitivity in ICP-MS when a quite large amount of C is present in the plasma source.[13] This effect has been explained as a charge transfer process from C ions to these elements and has been extensively studied for As and Se.[20] Some studies also include other elements with high ionization potentials, like Zn.[21]

The presence of important polyatomic interferences in As, Se, and Zn measurements makes it necessary to use pressurized cell conditions. Some studies found in the literature conclude

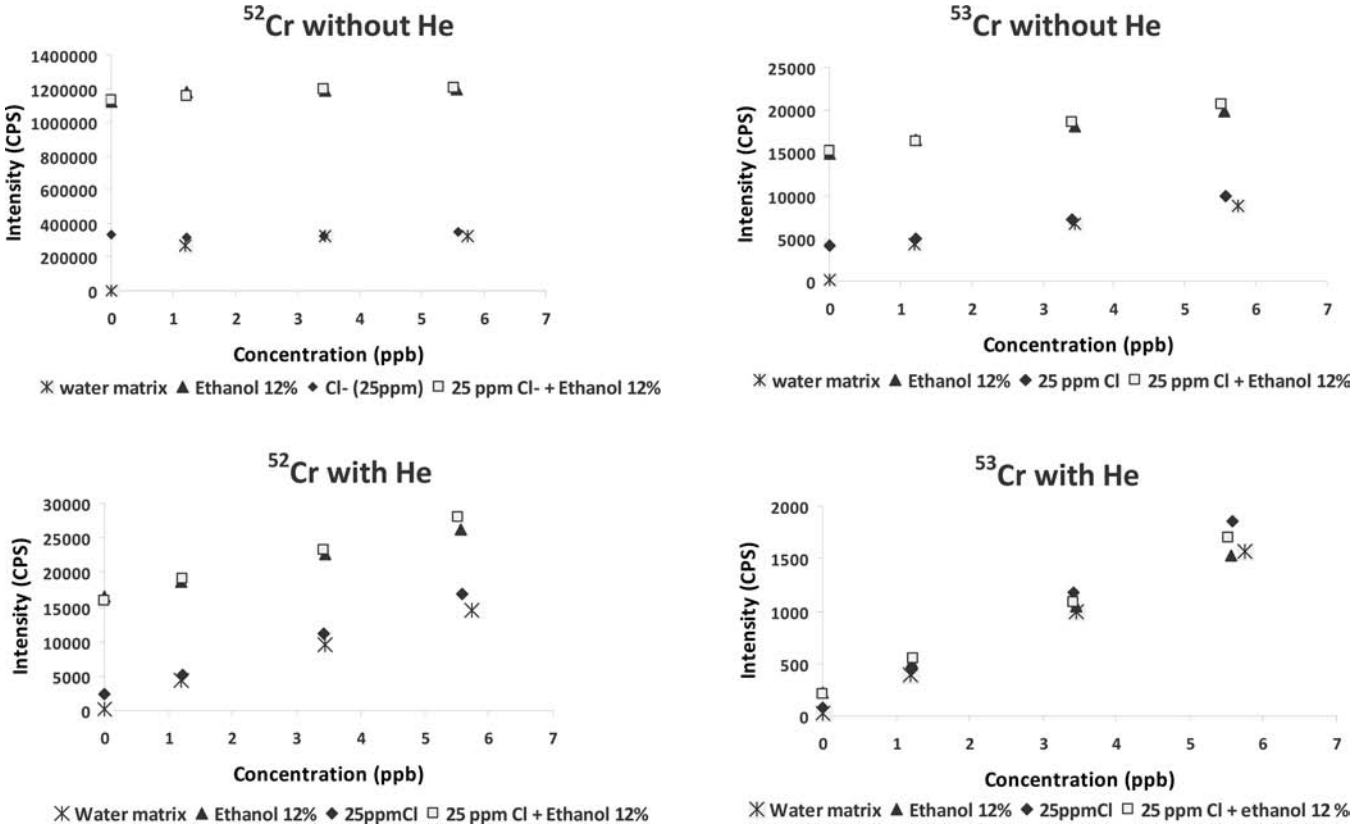

Figure 5. Intensity for ^{52}Cr and ^{53}Cr under different conditions in the collision cell. IS is used in all cases.

that the use of H_2 together with a small amount of He in the reaction cell (H_2 at 3 mL min^{-1} and He at 0.5 mL min^{-1}) gives good results for the determination of As and Se.[15] We therefore decided to use these conditions in our measurements. In the case of Zn, we compared the results obtained using He at 2 mL min^{-1} (same conditions used for Cr, Ni, Fe, and Cu) and H_2 at 3 mL min^{-1} and He at 0.5 mL min^{-1} (same conditions used for As and Se). Both gave similar results, so we decided to use the latter because of the greater sensitivity obtained in this case.

Upon comparison of the calibration curves obtained with and without ethanol and using IS, the internal standard does not correct properly for any of these elements, as expected. As already mentioned, the signal enhancement produced, due probably to a higher degree of ionization in the plasma, which in turn is related to the presence of C atoms from the matrix, is observed only for elements with high ionization potentials; this is not the case with Rh (our IS). The use of ethanol matrix standards to obtain the calibration curves is therefore once again compulsory. When a cork soak was measured (see Figure 6) and the results were compared, we again observed a difference between calibration in an aqueous matrix and calibration in a hydroalcoholic solution, both with IS. When standards in water are used, the concentration of these three elements is overestimated.

In Table 3, final collision cell conditions are summarized for the determination of arsenic, zinc, and selenium.

Method Validation. Because of the lack of certified cork soaked material, we validated the final conditions by performing recovery experiments. Three cork soaks were obtained, one for each sample type (C1−C3), and element concentrations were measured. The desired amount of stock solution was then added and a new measurement performed. Spiked levels and recoveries are listed in Table 4. Recovery values were obtained by using calibration curves with hydroalcoholic standards, with and without the IS correction. If we compare the data in the table for those elements measured with ICP-AES, the need to use the internal standard becomes clear because recoveries in the range of 130−176% were obtained without IS.

On the other hand, no statistical differences were obtained between the results for the other measured elements (recoveries obtained using calibration with IS compared with those without IS), except for As and Se. Taking into account the fact that the use of an IS is recommended in ICP-MS to account for variations in the plasma signal during one single run, we adopted this procedure to prepare the calibration set in the hydroalcoholic matrix.

Migration Tests. To calculate the percentage of an element that has migrated to the simulant, we previously determined the total concentration of each element in the three different cork samples (C1−C3). To do this, we used microwave-assisted acid digestion, establishing the condition described in the experimental part. Table 5 shows the concentrations found. We have also included some values obtained from the literature in the table. As shown in the table, few data are available for microelements. The results reported from PIXE analyses obtained from the bulk layer of a cork stopper[19] do not significantly differ from those obtained in our work in the case of Cu, while for Fe and Mn, PIXE concentrations are lower than ours. Additionally, when Pb is determined in a cork stopper used to seal a bottle of a French wine,[22] a relatively high concentration at the end in contact with the wine was found, compared with the concentration at the center of the cork. In this context, it has to be considered that lead content in wines is regulated,[23] and for that reason, its concentration in

dx.doi.org/10.1021/jf500170w | J. Agric. Food Chem. 2014, 62, 5690−5698

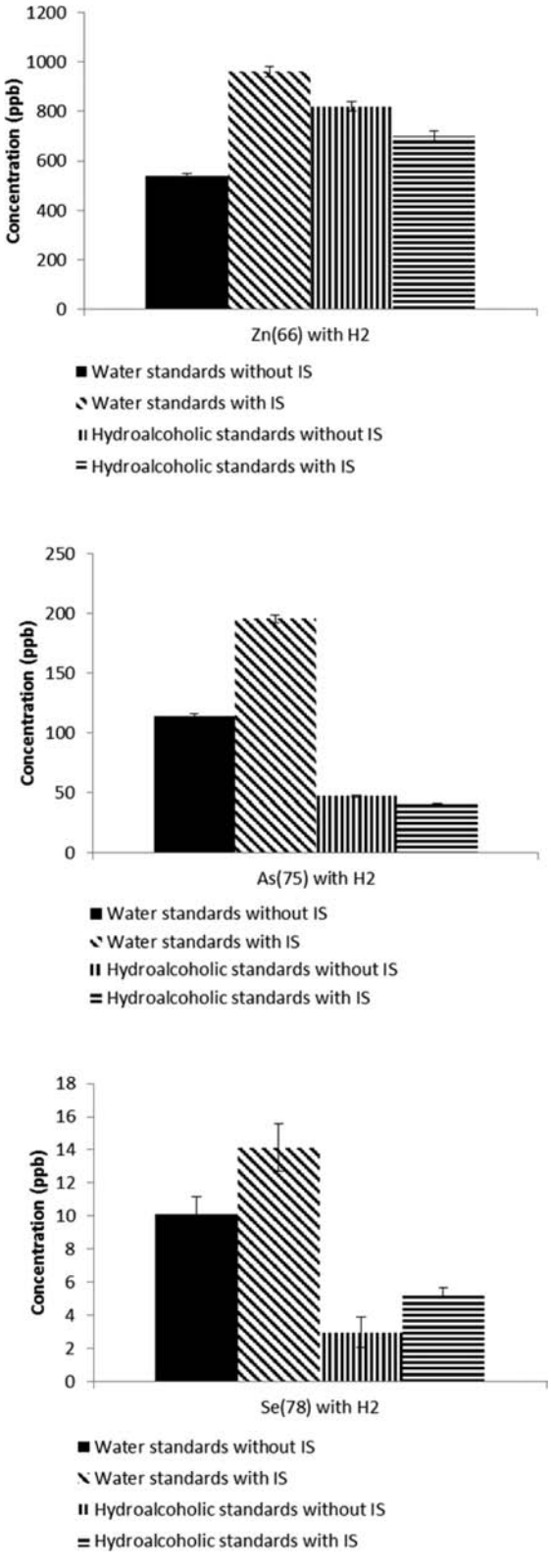

Figure 6. Results obtained for ^{66}Zn, ^{75}As, and ^{78}Se under different calibration conditions.

cork material and the migration to wine deserve special attention. With respect to the values we found for samples C1−C3, high variability was obtained between samples, presumably depending on the provenance of the cork. Catalonia is one of the most important regions producing cork stoppers, but the majority of producers obtain the cork material from forests in Andalusia, Extremadura, or Portugal. In this respect, it is hard to determine the precise origin of the material. It is also worth mentioning the differences between cork granules (corks 1 and 2) and cork slabs (cork 3), which may be attributed to the fabrication process applied to obtain cork granules, i.e., contamination due to the grinding process, when the cork material remains in close contact with the metallic parts of the machine for long periods of time.

Table 4. Recovery Results (R) Obtained for Spiked Samples

	added (μg/kg of food simulant)	R% without IS (SD)[a]	R% with IS (SD)[a]
Al	624	146	119
Ba	55	131 (5)	86 (4)
Mn	168	176 (24)	103 (9)
Cr	5.7	85 (6)	102 (6)
Fe	31−33.7	119 (7)	109 (2)
Ni	31−34.4	108 (6)	99 (2)
Cu	31−34.3	107 (7)	98 (4)
Zn	31−34.1	110 (6)	98 (4)
As	6−6.6	118 (4)	106 (2)
Se	5.6−6.1	116 (4)	104 (1)
Pb	6−6.5	92 (8)	83 (6)
Cd	6−6.5	96 (3)	106 (8)

[a]Three cork soaks (n = 3) were used, corresponding to each sample type (C1−C3), except for Ba and Mn (n = 2; C1 and C2) and Al (n = 1; C2).

The amount of each element transferred from the cork sample to the food simulant solution is presented in Table 6. The results are given as micrograms of the element measured in the solution divided by the total amount of cork used for the experiment. The percentage of the element migrated from the cork to the solution is also given. As we can see, the percentages vary from 0.6% for Ba to 67% for Se. Although this last migration percentage seems quite high, some studies in the literature reported Se migration values of up to 37% from yeast in hot water (50 °C) for 24 h.[24] It should be mentioned that selenoamino acids and inorganic Se (mainly selenite and selenate) are water-soluble.[25]

Prior to 2011, no reference values were established by the EU to determine whether these results might be considered safe. Recently, the EU has approved a new directive (EU directive 10/2011)[26] establishing maximal migration values for Ba, Cu, Fe, Mn, and Zn. Additionally, because cork stoppers are considered to be a material that comes into contact with wine, the new directive recommends the use of a food simulant consisting of 20% (v/v) ethanol in water. For this reason, we have measured the amount of the element that migrates not only in a 12% ethanol/water mixture but also in a hydroalcoholic solution with 20% ethanol. The values obtained for sample C2 are listed in Table 7. As we can see, the cork samples analyzed give migration results well below the maximum established, Ba and Mn being the most critical elements with respect to the maximal concentrations allowed. It is also worth mentioning that, in general, concentrations in a hydroalcoholic solution containing 20% ethanol are slightly higher than those in 12% ethanol, which may indicate that the solubility of metallic species increases at higher ethanol concentrations.

Migration Tests Using Water. Finally, we tested other conditions to perform the migration test using only water as a food simulant. In this way, we were able to avoid the presence

Table 5. Contents of Elements in Different Cork Samples [mean (SD)]

	Al[a]	Ba[a]	Mn[a]	Cu[a]	Fe[a]	Zn[a]	Cr[b]	Ni[b]	As[b]	Se[b]	Cd[b]	Pb[b]	ref
C1 (n = 4)	800 (100)	136 (4)	31 (4)	5 (2)	140 (10)	83 (6)	660 (50)	670 (60)	620 (10)	8 (0.3)	37.0 (0.8)	380 (20)	this work
C2 (n = 4)	68 (6)	142 (6)	35 (2)	6 (1)	26 (2)	92 (6)	330 (60)	520 (40)	23 (4)	8.86 (0.04)	42.3 (2)	350 (40)	this work
C3 (n = 4)	27 (8)	6.2 (0.2)	11.7 (0.4)	9 (4)	16.2 (0.3)	1.2 (0.4)	710 (20)	630 (40)	30 (4)	6.9 (0.8)	50 (10)	246 (8)	this work
	–	–	22–64	12–10	142–185	18–9.9	–	–	–	–	–	–	6
	–	–	–	–	–	–	–	–	–	–	–	60	22
	–	–	8.7 (2.3)	9.3 (1.5)	3.7 (1.9)	<3.6	–	–	–	–	–		19

[a]Milligrams per kilogram of cork. [b]Micrograms per kilogram of cork

Table 6. Results from the Migration Test with Sample C1 [mean (SD)]

element	concentration in the food simulant (μg/kg of cork) (n = 3)	% migration
Al	28000 (3000)	3.5
Ba	860 (70)	0.6
Mn	3300 (200)	10.6
Cr	not determined	not determined
Fe	1600 (100)	1.1
Ni	70 (30)	10.4
Cu	1400 (50)	28.0
Zn	700 (20)	0.8
As	41.1 (0.6)	6.6
Se	5.4 (0.3)	67.2
Cd	4 (2)	10.3
Pb	14 (3)	3.7

Table 7. Migration Results Compared with Data from EU Directive 10/2011 (C2; n = 3)[a]

element	HA 12% ethanol	HA 20% ethanol	EU Directive 10/2011
Ba	0.038 (0.009)	0.37 (0.01)	1
Cu	0.052 (0.003)	0.18 (0.01)	5
Fe	0.101 (0.005)	0.43 (0.02)	48
Mn	0.30 (0.02)	0.116 (0.004)	0.6
Zn	0.080 (0.003)	1.0 (0.2)	25

[a]Concentration in the food simulant given in milligrams per kilogram of food simulant [mean (SD)].

Table 8. Results from the Migration Test and Different Treatments (C1; n = 3) [mean (SD)]

element	W at 40 °C	W at 55 °C	W at 75 °C	HA at 40 °C
Al[a]	16.2 (0.9)	49 (6)	120 (20)	28 (3)
Ba[a]	0.2 (0.03)	0.9 (0.2)	3.5 (0.2)	0.86 (0.07)
Mn[a]	1.6 (0.2)	6.8 (0.5)	18.8 (0.5)	3.3 (0.2)
Fe[b]	930 (10)	2340 (60)	12800 (300)	1600 (100)
Ni[b]	37 (4)	100 (20)	195 (8)	70 (30)
Cu[b]	720 (30)	1960 (60)	3140 (50)	1400 (50)
Cd[b]	2.8 (0.2)	6.2 (0.3)	23 (0.6)	4 (2)
Pb[b]	4.83 (0.08)	9.3 (0.6)	28 (1)	14 (3)
Zn[b]	280 (30)	837.0 (0.1)	2720 (30)	700 (20)
As[b]	43 (2)	33 (2)	43 (0.9)	41.1 (0.6)
Se[b]	2.9 (0.3)	3.1 (0.3)	4.0 (0.3)	5.4 (0.3)

[a]Milligrams per kilogram of cork. [b]Micrograms per kilogram of cork.

of ethanol in the samples, resulting in fewer spectroscopic and nonspectroscopic interferences. Obviously, water is expected to have less extraction power than hydroalcoholic solutions. To address this difference, we increased the temperature (40–75 °C) while retaining the total contact time (10 days). Results are listed in Table 8, where those values that are similar to or slightly higher than those obtained for the food simulant [hydroalcoholic solution with 12% (v/v) ethanol] are underlined. As a general trend, we observe an increase in the amount of the element that migrated from the cork when the temperature is increased. With the exceptions of As and Se, the migration tests with water at 55 °C resulted in concentrations higher than those obtained with a HA solution. Taking into account the fact that most of the interferences in ICP-MS analysis of a food simulant are related to the presence of ethanol, we can propose the use of water at 55 °C as an alternative for making the analytical procedure easier.

■ ASSOCIATED CONTENT

Supporting Information

Tables S1−S3. This material is available free of charge via the Internet at http://pubs.acs.org.

■ AUTHOR INFORMATION

Corresponding Author

*E-mail: enriqueta.antico@udg.edu.

Funding

The Spanish National Research Program supported this work through Project CGL2010-22168-C03-03.

Notes

The authors declare no competing financial interest.

■ ACKNOWLEDGMENTS

We are grateful to Dr. E. Besalú for helping with the statistical analysis of the data.

■ ABBREVIATIONS USED

ICP-AES, inductively coupled plasma atomic emission spectroscopy; ICP-MS, inductively coupled plasma mass spectrometry; HA, hydroalcoholic; OIV, Organisation Internationale de la Vigne et du Vin; IS, internal standard; SD, standard deviation; PIXE, particle-induced X-ray emission

■ REFERENCES

(1) Fisher, C.; Fisher, U. Analysis of Cork Taint in Wine and Cork Material at Olfactory Subthreshold Levels by Solid Phase Microextraction. *J. Agric. Food Chem.* **1997**, *45*, 1995−1997.

(2) Ortega-Fernández, C.; González-Adrados, J. R.; García-Vallejo, M. C.; Calvo-Haro, R.; Cáceres-Esteban, M. J. Characterization of surface treatments of cork stoppers by FTIR-ATR. *J. Agric. Food Chem.* **2006**, *54*, 4932−4936.

(3) Conde, E.; Cadahía, E.; Garcia-Vallejo, M. C.; González-Adrados, J. R. Chemical characterization of reproduction Cork from Spanish Quercus Suber. *J. Wood Chem. Technol.* **1998**, *18*, 447−469.

(4) Juanola, R.; Subira, D.; Salvadó, V.; Garcia Regueiro, J. A.; Anticó, E. Evaluation of an extraction method in the determination of 2,4,6-trichloroanisole content in tainted cork. *J. Chromatogr., A* **2002**, *953*, 207−214.

(5) Kabata-Pendias, A. *Trace elements in soils and plants*, 3rd ed.; CRC Press: Boca Raton, FL, 2001.

(6) Robert, B.; Molinas, M.; Caritat, A.; Masson, P. The cork mineral composition, the cork characteristics and the cork-oak (*Quercus suber* L.) leaf mineral composition. In *Cork oak and cork*; Pereira, H., Ed.; European Conference on Cork Oak and Cork: Lisbon, 1997; pp 173−181.

(7) El-Hasan, T.; Al-Omari, H.; Jiries, A.; Al-Nasir, F. Cypress tree (*Cupressus semervirens* L.) bark as an indicator for heavy metal pollution in the atmosphere of Amman City, Jordan. *Environ. Int.* **2002**, *28*, 513−519.

(8) European Union, Regulation (EC) No. 1935/2004 of the European Parliament and of the Council of 27 October 2004 on materials and articles to come into contact with food and repealing Directives 80/590/EEC and 89/109/EEC. Official Journal of the European Union, L338/4 (November 13, 2004).

(9) Council of Europe. Public Health Committee. Appendix to Resolution ResAP(2004)2 on cork stoppers and other cork materials and articles intended to come into contact with foodstuffs (September 5, 2007).

(10) Six, T.; Feigenbaum, A. Mechanism of migration from agglomerated cork stoppers. Part 2: Safety assessment criteria of agglomerated cork stoppers for champagne wine cork producers, for users and for control laboratories. *Food Addit. Contam.* **2003**, *20*, 960−971.

(11) Beauchemin, D. Inductively Coupled Plasma Mass Spectrometry. *Anal. Chem.* **2010**, *82*, 4786−4810.

(12) Séby, F.; Gagean, M.; Garraud, H.; Castetbon, A.; Donard, O. F. X. Development of analytical procedures for determination of total chromium by quadrupole ICP-MS and high-resolution ICP-MS, and hexavalent chromium by HPLC-ICP-MS, in different materials used in the automotive industry. *Anal. Bioanal. Chem.* **2003**, *377*, 685−694.

(13) Allain, P.; Jaunault, L.; Mauras, Y.; Mermet, J. M.; Delaporte, T. Signal Enhancement of Elements Due to the Presence of Carbon-Containing Compounds in Inductively Coupled Plasma Mass Spectrometry. *Anal. Chem.* **1991**, *63*, 1497−1498.

(14) Hu, Z.; Hu, S.; Gao, S.; Liu, Y.; Lin, S. Volatile organic solvent-induced signal enhancements in inductively coupled plasma-mass spectrometry: A case study of methanol and acetone. *Spectrochim. Acta, Part B* **2004**, *59*, 1463−1470.

(15) Colon, M.; Hidalgo, M.; Iglesias, M. Arsenic determination by ICP-QMS with octopole collision/reaction cell. Overcome of matrix effects under vented and pressurized cell conditions. *Talanta* **2011**, *85*, 1941−1947.

(16) Marguí, E.; Queralt, I.; Carvalho, M. L.; Hidalgo, M. Comparison of EDXRF and ICP-OES after microwave digestion for element determination in plant specimens from an abandoned mining area. *Anal. Chim. Acta* **2005**, *549*, 197−204.

(17) Iglesias, M.; Besalú, E.; Anticó, E. Internal standardization-atomic spectrometry and geographical pattern recognition techniques for the multielement analysis and classification of Catalonia red wines. *J. Agric. Food Chem.* **2007**, *55*, 219−225.

(18) McCurdy, E.; Woods, G. The application of collision/reaction cell inductively coupled plasma mass spectrometry to multi-element analysis in variable sample matrices, using He as a non-reactive cell gas. *J. Anal. At. Spectrom.* **2004**, *19*, 607−615.

(19) Iochims dos Santos, C. E.; Dabastiani, R.; Przybylowicz, W.; Manfroi, V.; Amaral, L.; Yoneama, M. L.; Ferraz-Dias, J. Study of the elemental composition of wine stoppers using PIXE. *X-Ray Spectrom.* **2013**, *42*, 158−164.

(20) Floor, G. H.; Iglesias, M.; Roman-Ross, G. Selenium determination in volcanic soils by ICP-QMS: Influence of reaction cell pressurization and methanol addition on the occurrence of spectral interferences. *J. Anal. At. Spectrom.* **2009**, *24*, 944−948.

(21) Kralj, P.; Veber, M. Investigations into non spectroscopic effects of organic compounds in inductively coupled plasma mass spectrometry. *Acta Chim. Slov.* **2003**, *50*, 633−644.

(22) Rosman, K.; Chisholm, W.; Jimi, S.; Candelone, J. P.; Boutron, C. F.; Teissedre, P. L.; Adams, F. C. Lead concentrations and isotopic signatures in Vintages of France wine between 1950 and 1991. *Environ. Res.* **1998**, *78*, 161−167.

(23) OIV. Compendium of international methods of analysis. Maximum acceptable limits of various substances contained in wine. OIV-MA-C1-01:R; 2011.

(24) Huang, C.; Hu, B.; He, M.; Duan, J. Organic and inorganic selenium speciation in environmental and biological samples by nanometer-sized materials packed dual-column separation/preconcentration on-line coupled with ICP-MS. *J. Mass. Spectrom.* **2008**, *43*, 336−345.

(25) Polatajko, A.; Jakubowski, N.; Szpunar, J. State of the art report of selenium speciation in biological samples. *J. Anal. At. Spectrom.* **2006**, *21*, 639−654.

(26) European Union Commission Regulation (EU) No. 10/2011 of 14 January 2011 on plastic materials and articles intended to come into contact with food. Official Journal of the European Union, L12/1 (January 15, 2011).

JOURNAL OF AGRICULTURAL AND FOOD CHEMISTRY

Article

pubs.acs.org/JAFC

Identification of Atlantic Cod (*Gadus morhua*), Ling (*Molva molva*), and Alaska Pollock (*Gadus chalcogrammus*) by PCR–ELISA Using Duplex PCR

Ledicia Taboada,* Ana Sánchez, Amaya Velasco, Francisco J. Santaclara, Ricardo I. Pérez-Martín, and Carmen G. Sotelo

Instituto de Investigaciones Marinas (IIM-CSIC), Eduardo Cabello 6, E-36208 Vigo, Spain

ABSTRACT: Species-specific PCR–ELISA assays for the identification of Atlantic cod (*Gadus morhua*), Alaska pollock (*Gadus chalcogrammus*), and ling (*Molva molva*) in food products have been developed. The method, comprising a set of primers common to the first two species, a set of primers for *M. molva*, and a probe for each species, was designed using *ND4* and *cytochrome b* genes as molecular markers. The sensitivity and selectivity were then determined for each assay. These assays were afterward used to analyze DNA extracted from commercial fish products. The presence of the target species was successfully detected in all analyzed samples, demonstrating the applicability of this method to the analysis of food products.

KEYWORDS: *Gadus chalcogrammus, Gadus morhua, Molva molva, species identification, PCR–ELISA*

INTRODUCTION

The Gadidae family includes a large number of species, many of them of great economic value, such as *Gadus morhua*, which is marketed worldwide. However, due to several factors such as overfishing and climate change, some natural cod stocks are threatened, and the total world catch is currently <1 million tons, whereas in 1970 it was 3.5 million tons.[1]

Gadoid species can be identified in a relatively simple manner on the basis of their morphological characteristics in fresh and unprocessed fish; however, they are usually commercialized with some degree of processing, that being, frozen, gutted, filleted, smoked, canned, etc. Therefore, morphological characteristics that differentiate the species are, in many cases, absent. This situation favors some species eventually being replaced by other species, either accidentally or intentionally. This produces mislabeled fishery products, which affects directly or indirectly the consumer, the environment, and the industry. These consequences include human health risks[2−4] and overexploitation and depletion of some of the most consumed and valued species by consumers.[5−7] Other consequences are economic losses for the consumers[5] due to the addition of undeclared cheaper fish species or the sale of species that have a defined fishing quota and are captured over them, under the name of other species. For all this legislation is needed to control the correct labeling of fishery products.[8−13] European Union labeling regulations (EC No. 13/2000) specify that the commercial and scientific names should be included on the label of seafood products.

From this point of view, molecular DNA-based techniques are the most suitable option as an alternative to morphological analysis. Different genetic authentication techniques based on DNA have been proposed during the past decades for gadoid identification: polymerase chain reaction (PCR),[13,14] PCR–restriction fragment length polymorphism (RFLP),[16,17] real-time PCR,[15,18−21] forensically informative nucleotide sequencing (FINS),[22] single-stranded conformation polymorphism analysis (SSCP),[23] and single-nucleotide polymorphism (SNPs).[24]

One of the advantages of the PCR–ELISA methodology is that it can be applied to fresh, frozen, or processed products and that it requires only a conventional PCR system (thermocycler), because the results can be evaluated with the naked eye. This approach has been used in the detection of viruses,[25] bacteria,[26−28] and fish.[29,30]

The main objective of the present study was to develop a specific molecular technique to identify *G. morhua*, *Gadus chalcogrammus*, and *Molva molva* in seafood products.

MATERIALS AND METHODS

Fish Samples. Thirteen specimens of each of the Gadiformes target species were collected: *G. morhua*, *G. chalcogrammus*, and *M. molva*.

In addition, 20 representative specimens of other Gadiformes, Lophiiformes, Perciformes, and Cupleiformes orders were included in this study. Scientific and common names of these species are listed in Table 1.

During the validation step of the developed methodology, 19 commercial cod samples were used, purchased in different local markets (Table 2). All samples were analyzed in triplicate.

DNA Extraction. DNA was extracted from 0.3 g of thawed muscle and tissue of commercial samples, which were digested overnight in a thermoshaker at 56 °C with 860 μL of lysis buffer (1% SDS, 150 mM NaCl, 2 mM EDTA, and 10 mM Tris-HCl at pH8), 100 μL of 5 M guanidium thiocyanate (Sigma-Aldrich), and 40 μL of proteinase K (20 mg/mL) (Gibco Invitrogen, LifeTechnologies). After 3 h, extra proteinase K (40 μL) was added to the solution, and it was left overnight. After digestion, DNA was isolated employing the Wizard DNA Clean-Up System kit (Promega) following the manufacturer's instructions. DNA was quantified by using a NanoDrop 2000

Received: January 24, 2014
Revised: May 15, 2014
Accepted: May 25, 2014
Published: May 26, 2014

ACS Publications © 2014 American Chemical Society

Table 1. Reference Species Used for the Study

species	N	common name
order Gadiformes		
family Gadidae		
Gadus morhua	13	Atlantic cod
Gadus chalcogrammus	13	Alaska pollock
Gadus macrocephalus	1	Pacific cod
Gadus ogac	1	Greenland cod
Melanogrammus aeglefinus	1	haddock
Merlangius merlangius	1	whiting
Micromesistimus poutassous	1	blue whiting
Pollachius pollachius	1	pollack
Pollachius virens	1	saithe
Trisopterus luscus	1	pouting
family Merlucidae		
Macruronus magellanicus	1	Patagonian grenadier
Merluccius bilinearis	1	silver hake
Merluccius capensis	1	shallow-water Cape hake
Merluccius polli	1	Benguela hake
Merluccius hubbsi	1	Argentina hake
Merluccius merluccius	1	European hake
Merluccius paradoxus	1	deep-water Cape hake
Merluccius senegalensis	1	Senegalese hake
family Lotidae		
Brosme brosme	1	tusk
Molva dypterigia	1	blue ling
Molva molva	13	ling
order Lophiiformes		
family Lophiidae		
Lophius piscatorius	1	angler
order Cupleiformes		
family Engraulidae		
Engraulis encrasicolus	1	European anchovy
family Clupeidae		
Sardinella aurira	1	round sardinella
Sardina pilchardus	1	European pilchard
order Perciformes		
family Scombridae		
Thunnus alalunga	1	albacore
Thunnus obesus	1	bigeye tuna

spectrophotometer (Thermo Scientific) at 260 nm and the ratio 260/280, respectively. The 260/280 ratio was between 1.8 and 2.0. DNA concentration was adjusted to 50 ng/μL. The purified DNA was stored at −20 °C.

Design of PCR−ELISA Systems. An extensive number of partial DNA sequences (nuclear and mitochondrial) and a wide number of fish species were analyzed (data not shown) during the study.

Two PCR systems were designed to amplify two mitochondrial fragments: a small fragment of the *cytochrome b* gene and a fragment of the *ND4* gene. Specific sets of primers were designed for each system to include the previously identified polymorphisms among the target species and other gadoid using Oligo Analyzer v. 1.0.3 (Freeware, Teemu Kuulasmaa, Finland). The 5′ biotin-labeled probes Gmor_ND4-P, Gchal_ND4-P, and Mmol_Cytb-P were designed to hybridize with the specific polymorphism to *G. morhua*, *G. chalcogrammus*, and *M. molva* PCR amplification products, respectively (Figure 1). HPLC purification grade primers and probes were synthesized by Sigma Genosys. Primer and probe sequences designed and used are listed in Table 3.

PCR Amplification and Digoxigenin-11-dUTP (DIG) Labeling Conditions. Primers and magnesium chloride concentrations were optimized to perform PCR DIG-labeling reactions in a final volume of 25 μL containing molecular grade water, 1.5 mM final concentration magnesium chloride (Bioline), DIG dNTPs (Roche) final concentrations of 200 μM of each of dATP, dCTP, dGTP, 190 μM dTTP, 10 μM DIG-11dUTP, primers T/G_ND4-F and T/G_ND4-R (final concentration 0.24 μM), primers Mmol_Cytb-F and Mmol_Cytb-R (final concentration 0.36 μM), BIOTAQ DNA polymerase (final concentration 0.5 U), and 50 ng of DNA template. Thermal cycling parameters were as follows: 95 °C for 5 min; followed by 25 cycles of 95 °C for 20 s, 63 °C for 30 s, 72 °C for 30 s; and a terminal extension step of 72 °C for 5 min. Negative controls (molecular grade water) were included in each set of reactions. These PCR reactions were carried out in an Applied Biosystems 2720 thermocycler.

The amplification products were tested in a 2% agarose gel (Pronadisa), containing RedSafe 1× (iNtRON Biotechnology) in 0.5× TBE buffer (Sigma). DNA fragments were visualized using the Gel Documentation System Gel Doc XR System and the software Quantity One v 4.5.2 (Bio-Rad).

The PCR products were purified using the Nucleospin Extract II kit (Macharey-Nagel) according to the manufacturer's instructions. The concentration and purity were estimated by means of UV spectrometry at 260 nm using a NanoDrop 2000 spectrophotometer (Thermo Scientific).

To verify the correct assignation of the specimens used in the method setup, a new PCR product was amplified and sequenced on an ABI Prism 310 Genetic Analyzer (Applied Biosystems). This analysis was carried out using the primers L14735 and H15549D.[31] The resulting cytochrome *b* nucleotide sequences were also analyzed by FINS[32] and, to confirm, were compared with those present in the NCBI database using Megablast.

Once the correct performance of each PCR for the two designed systems was verified individually, a duplex PCR for the two systems was set up. Primer concentrations and thermal protocol were the same as the ones previously used in simplex PCR.

Detection of DIG-Labeled PCR Products by ELISA. The PCR−ELISA DIG detection kit (Roche) was used for the detection of labeled PCR products according to the manufacturer's instructions. A volume of 10 μL of each DIG-labeled PCR product (5 ng/ μL) was denatured in 20 μL of denaturation solution at 25 °C for 10 min; this solution and 170 μL of hybridization buffer, containing the biotinylated probe at a concentration of 5.3 nM, were then transferred to the wells of a streptavidin-coated microtiter plate strip, and the plate was incubated at 59 °C for 3 h. The microtiter plate wells then were washed, and anti-DIG-POD (anti-digoxigenin−peroxidase-conjugate) working solution (200 μL) was added to each well; the microtiter plate was incubated afterward at 37 °C for 30 min. After another washing step, peroxidase substrate, 2,2′-azinobis(3-ethylbenzthiazoline sulfonate) (ABTS), was added, and the plate was incubated at 37 °C for 30 min to allow color development. The absorbance of the contents of each well was read in a SynergyMx spectrophotometer (BioTek Instruments), at a wavelength of 405 nm.

To obtain the method's detection limit, mixtures of three species' DNA template were diluted in molecular biology grade water, obtaining 50 ng−50 pg per microliter. These dilutions were used in the PCR−ELISA reaction, and the labeled products were detected using the three probes.

Positive reactions were determined by a calculation of cutoff values as follows: cutoff = 4 × absorbance at 405 nm of the mean of 10 replicates of negative detection control.

Validation of the Methodology with Commercial Samples. Once the methods were optimized, they were applied to 19 commercial samples purchased in markets and shops from different places in Spain.

RESULTS AND DISCUSSION

The aim of the present study was the development and evaluation of a PCR−ELISA technique for the authentication of

Table 2. Commercial Products Used for the Study and Results of the PCR–ELISA Assay of Commercial Products

					PCR amplification		PCR–ELISA		
	commercial name	scientific name	remarks	FINS identification	Mmol_ Cytb	Gmor/Gchal_ ND4	*Gchal_ ND4-P*	*Gmor_ ND4-P*	*Mmol_ Cytb-P*
1	cod omelet	not available		mixed DNA	+	+	–	+	+
2	cod liver	not available	canned	*G. morhua*	–	+	–	+	–
3	Nordic cod	*G. morhua*	smoked	*G. morhua*	–	+	–	+	–
4	Iceland cod	*G. morhua*	salted	*G. morhua*	–	+	–	+	–
5	cod cheeks	*G. morhua*	desalted	*G. morhua*	–	+	–	+	–
6	cod	not available	croquettes	*G. morhua*	–	+	–	+	–
7	cod fritter	not available	frozen	*G. morhua*	–	+	–	+	–
8	cod filet	*G. morhua*	frozen	*G. morhua*	–	+	–	+	–
9	Iceland cod	*G. morhua*	frozen	*G. morhua*	–	+	–	+	–
10	cod	*Gadus* spp.	salted	*G. morhua*	–	+	–	+	–
11	ling loins	*M. molva*	frozen	*Molva dypterigia*	–	–			
12	cod liver	not available	canned	*G. morhua*	–	+	–	+	–
13	minced cod	*G. morhua*	salted	*M. molva*	+	–	–	–	+
14	Alaska pollock	*G. chalcogrammus*	salted	*G. chalcogrammus*	–	+	+	–	–
15	Alaska pollock loins	*G. chalcogrammus*	frozen	*G. chalcogrammus*	–	+	+	–	–
16	Alaska pollock	*G. chalcogrammus*	salted	*G. chalcogrammus*	–	+	+	–	–
17	Alaska pollock	*G. chalcogrammus*	frozen	*G. chalcogrammus*	–	+	+	–	–
18	ling roe	*M. molva*	dry-salted	*M. molva*	+	–	–	–	+
19	ling loins	*M. molva*	salted	*Molva dypterigia*	–	–			
20	*G. morhua*		reference sample		–	+	–	+	–
21	*G. chalcogrammus*		reference sample		–	+	+	–	–
22	*M. molva*		reference sample		+	–	–	–	+
23	*G. morhua* + *G. chalcogrammus* + *M. molva*		mix DNA		+	+	+	+	+

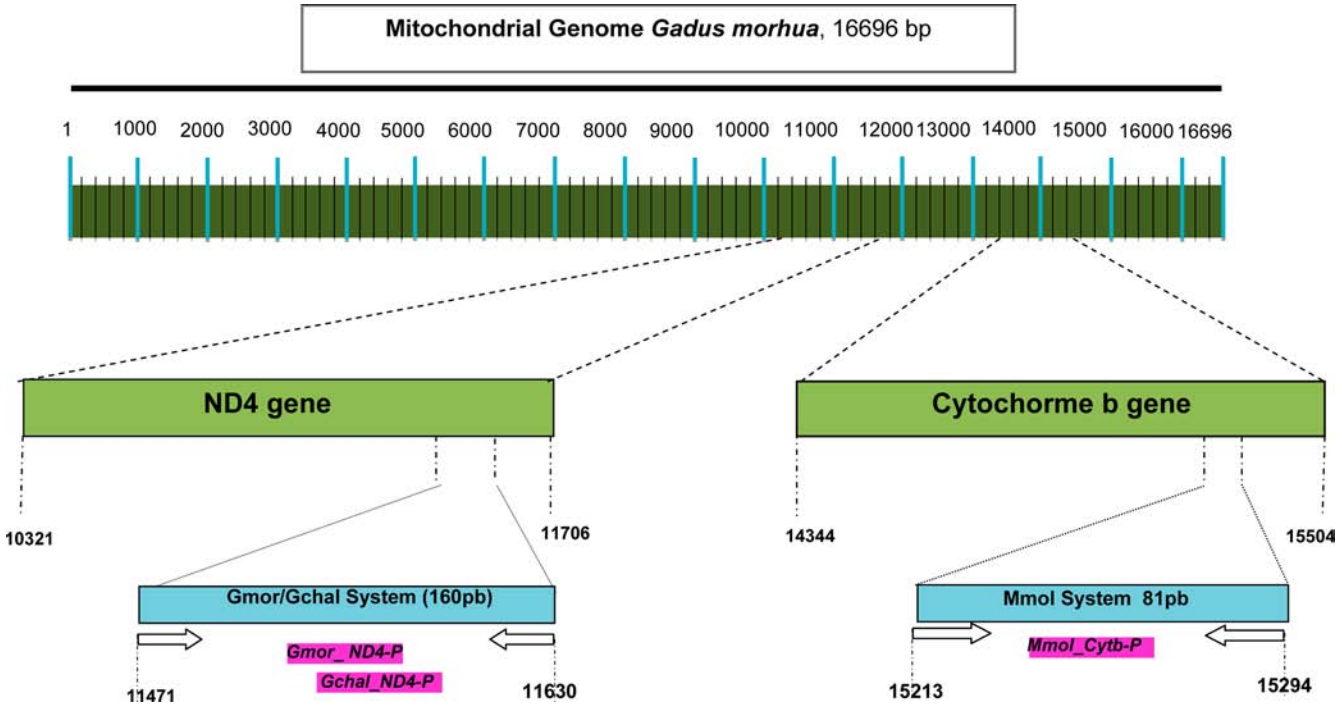

Figure 1. Location and position of primers and probes designed in this work.

G. morhua, *G. chalcogrammus*, and *M. molva* species in seafood products. Due to their low cost, when ling (*M. molva*) and Alaska pollock (*G. chalcogramma*) lose their morphological characteristics, they are highly susceptible to being used in fishery products for the replacement of more expensive fish species such as cod (*G. morhua*).[5]

PCR–ELISA System Design. For the correct design of the PCR–ELISA system, a large number of DNA sequences of nuclear and mitochondrial genes from a large number of fish

dx.doi.org/10.1021/jf500173j | J. Agric. Food Chem. 2014, 62, 5699–5706

Table 3. Primers and PCR−ELISA Probes Used in This Work

primer/probe name	PCR amplicon (pb)	molecular marker	sequence 5′−3′	size (bp)	T_a annealing/ hybridization
Gmor/Gchal_ND4-F	Gmor/Gchal (160)	*ND4*	5′-ACCTCCCTTTTTAACTGGTCT-3′	21	63
Gmor/Gchal_ND4-R			5′-TAACAAATGCTCTCGTGTGTAG-3′	22	
Gmor_ND4-P			5′-[biotin]GCCTACTCCCTGTATATATTCCT-3′	23	59
Gchal_ND4-P			5′-[biotin]TTCACTGTACATATTTCTGATGAG-3′	24	59
Mmol_Cytb-F	Mmol(81)	*Cyt b*	5′-GGGTTCTCGCACTTCTATTTTCA-3′	23	63
Mmol_Cytb-R			5′-ATGTTAGTCCTCGTTGTTTAGAGGTATG-3′	28	
Mmol_Cytb-P			5′-[biotin]TAGTTCTCATAGTAGTCCCCTTC-3′	23	59
L14735	Kocher (460)	*tRNAglu-cytb*	5′-GCICCTCARAATGAYATTTGTCCTCA-3′	26	59
H15149D			5′-AAAAACCACCGTTGTTATTCAACTA-3′	25	

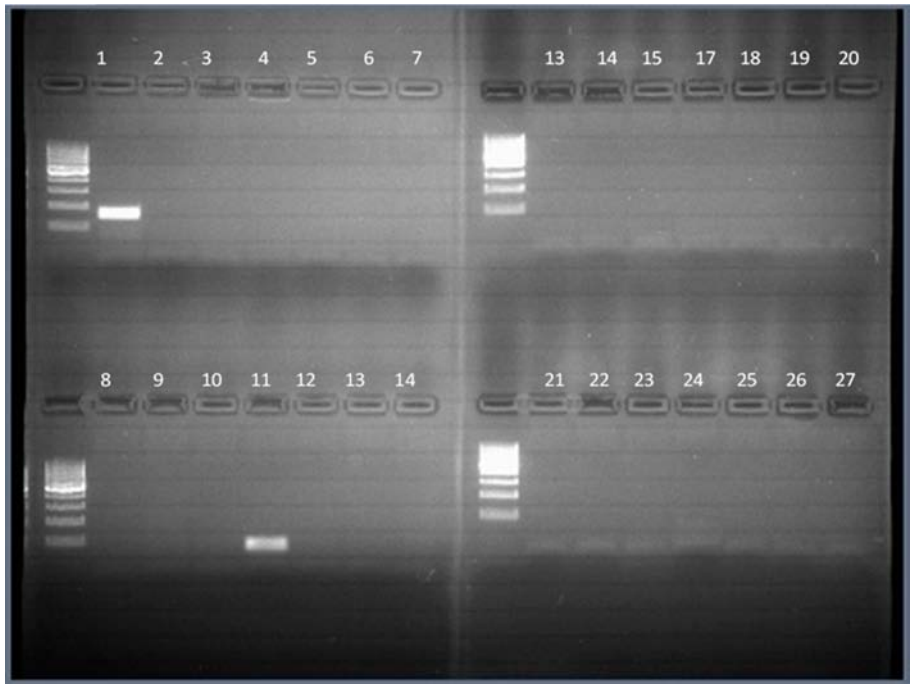

Figure 2. Agarose gel electrophoresis of amplification products obtained by a duplex PCR from DNA extracts of reference samples. Lanes: 1, *G. morhua*; 2, *G. macrocephalus*; 3, *G. ogac*; 4, *M. aeglefinus*; 5, *M. merlangius*; 6, *M. poutassous*; 7, *P. pollachius*; 8, *P. virens*; 9, *T. luscus*; 10, *B. brosme*; 11, *M. molva*; 12, *M. dypterigia*; 13, *M. magellanicus*; 14, *M. bilineariz*; 15, *M. capensis*; 16, *M. polli*; 17, *M. hubbsi*; 18, *M. merluccius*; 19, *M. paradoxus*; 20, *M. senegalensis*; 21, *L. piscatorius*; 22, *E. encrasicolus*; 23, *S. aurira*; 24, *S. pilchardus*; 25, *T. alalunga*; 26, *T. obesus*; 27, negative control.

species were analyzed previously. Mitochondrial DNA has been extensively studied and used as a marker for phylogenetic classification species of fish as well as for their detection in commercial products. This is because in the cells, mitochondrial DNA is more abundant than the nuclear, have a higher mutation rate, and contains more sequence diversity.[33,34]

To achieve sufficient sensitivity to accurately identify the species of Atlantic cod, ling, and Alaska pollock in processed samples, one of the objectives of this work was to find a system (comprising primers and probe) as short as possible.

This system must be designed in a region of DNA that contains sufficient interspecific variability and low or null intraspecific variability for the primers and biotin-labeled probe to be specifically bound and avoiding false negatives and false positives.[35]

The hybridization of the biotin-labeled probe with specific PCR products allows the detection of the target species, therefore increasing the number of interspecific differences the increasing the specificity. It is shown that this specificity is also dependent on the length, hybridization temperature,and GC content of the capture probe. Sails et al.[26] in their work onidentifying *Campylobacter jejuni* and *Campylobacter coli* observed that short capture probes (18−20 nucleotides) with nucleotide differences in the central region and high annealing temperatures (up to 55 °C) can identify a single nucleotide difference in the sequence target.

The designed systems consisted of a 160 bp fragment (Gmor/Gchal_ND4 system) and an 81bp fragment (Mmol_-cytb system) (Figure 1).

The sequences of the selected primers and probes are listed in Table 3.

Specificity of PCR−ELISA Assay. Detection of PCR products by simple electrophoresis in agarose gel may not be sufficiently specific, giving rise to false positives if a verification of the sequence is not performed by hybridization to specific probes;this may occur due to the difficulty in determining the exact size of the amplicons and the possible occurrence of artifacts with the same size as that of PCR products.[36] However,

the results of this assay showed that specific PCR products were always obtained and that non-false positives were produced in any case (Figure 2). The designed PCR systems allowed a certain degree of specificity to be obtained; for instance, if primer pair Gmor/Gchal_ND4 is used, a 160 bp DIG-labeled PCR product will be produced only when mitochondrial DNA used as template is from *G. chalcogrammus* and *G. morhua*.

Similarly, primer pair Mmol_Cytb generates an 81 bp DIG-labeled PCR product only when template DNA is from *M. molva*.

Both primer pairs were tested for their specificity using 50 ng/μL DNA of all species listed in Table 2.

Thanks to the joint use of specific sets of primers and probes, a highly specific hybridization is achieved, allowing the high specificity necessary to verify the DNA sequence of the PCR products, to avoid false positives, and to correctly identify the target species.

Detection of DIG-Labeled PCR Products. For the determination of the specificity of detection of the three labeled probes, these were tested for specific identification of labeled PCR products from the three problem species by measuring their absorbance at 405 nm (Table 4), considering positive those samples having an absorbance at 405 nm that was >0.604. This cutoff value was calculated as follows: cutoff = 4 × absorbance at 405 nm of the mean of 12 replicates of negative detection control (0.151 ± 0.009). Furthermore, the results showed a positive green coloration detectable to the naked eye.

Table 4. Comparative Specificity of the Different Probes for the Detection of *M. molva*, *G. chalcogrammus*, and *G.morhua*

sample	*N*	absorbance readings at 405 nm ± standard deviation
Molva molva	13	0.818 ± 0.07
Gadus chalcogrammus	13	1.904 ± 0.50
Gadus morhua	13	2.39 ± 0.8
negative	12	0.151 ± 0.00

With the purpose of evaluating the sensitivity and detection limit of the PCR–ELISA developed, a series of dilutions from 16 ng to 60 pg of the extracted sample of positive control DNA were amplified and subsequently used in an assay for PCR–ELISA and a conventional agarose gel electrophoresis assay to compare the signals obtained in both assays (Table 5; Figure 3). These assays showed that PCR–ELISA was at least 100-fold more sensitive than the detection method based on gel. The minimum amount of DNA template detectable in the PCR–ELISA assay with the Gmor_ND4-P probe was 123 pg, and with Gchal_ND4-P and Mmol_Cytb-P probes it was 416 pg, whereas with the conventional agarose gel electrophoresis method, the minimum amount of DNA template easily visually detected was 16.7 ng. The data here presented indicate that the PCR–ELISA technique based on the detection of cytochrome *b* and ND4 gene products is highly sensitive.

Table 5. PCR–ELISA Readings at 405 nm of Different Amounts of Purified PCR Products

DNA template	absorbance readings at 405 nm		
	G. morhua probe	*G. chalcogrammus* probe	*M. molva* probe
16.7 ng	2.59	1.74	1.72
1.7 ng	2.27	1.68	1.67
833 pg	2.6	1.92	2.04
416 pg	1.86	0.64	0.68
250 pg	1.31	0.29	0.31
123 pg	0.81	0.29	0.29
63 pg	0.47	0.21	0.20
0	0.11	0.12	0.13

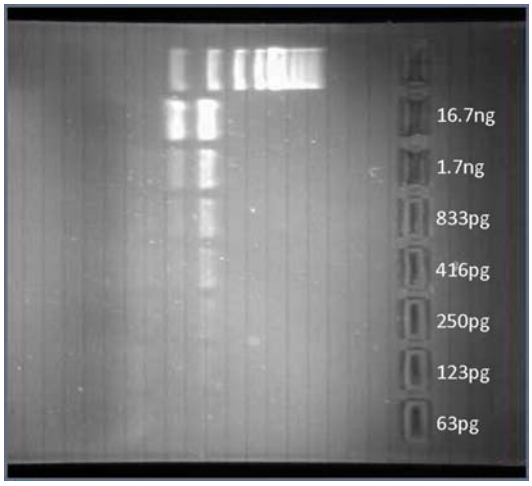

Figure 3. Agarose gel electrophoresis of amplification products obtained by a duplex PCR from mixtures of *G. morhua*, *G. chalcogrammus*, and *M. molva* DNA extracts, ranging from 16 ng to 60 pg of DNA of each DNA template.

Although there are other molecular detection techniques that require less time, such as TaqMan real-time PCR, PCR–ELISA can also be considered as a rapid technique, requiring less than a day's work to obtain the results.[27] The PCR–ELISA approach can be immediately adopted by most identification laboratories because the results can be visually read, eliminating the need for expensive equipment, and a large number of samples can be handled.

PCR Amplification and Sequencing. The success of the methodology used depends on the correct design of specific probes labeled with biotin that will be linked through an antigen–antibody reaction to a microplate with streptavidin and the incorporation, during the PCR process, of a triphosphate nucleotide labeled with DIG, allowing amplicon detection.

The annealing temperature was adjusted to allow the correct amplification of problem species while avoiding the amplification of other closely related species (Figure 2). Finally, this parameter was adjusted to 63 °C, because it allows the efficient amplification of *G. morhua*, *G. chalcogrammus* DNA with Gmor/Gchal_ND4 primers, and *M. molva* in Mmol_Cytb primers. Each primer set was independently tested and optimized first.

With the aim of reducing the number of steps of the identification methodology, PCR amplification of the two designed systems was grouped in a duplex PCR;[37] this also allows the identification of three species, even when mixed, in a single step.[38] The conditions were the same as used in simplex PCR. In these conditions, similar concentrations of PCR products were obtained in both duplex PCR.

The main advantage of multiplex PCR strategy is the reduction of the number of reactions required, decreasing labor time and total cost. It is particularly justified when a mix of

dx.doi.org/10.1021/jf500173j | J. Agric. Food Chem. 2014, 62, 5699–5706

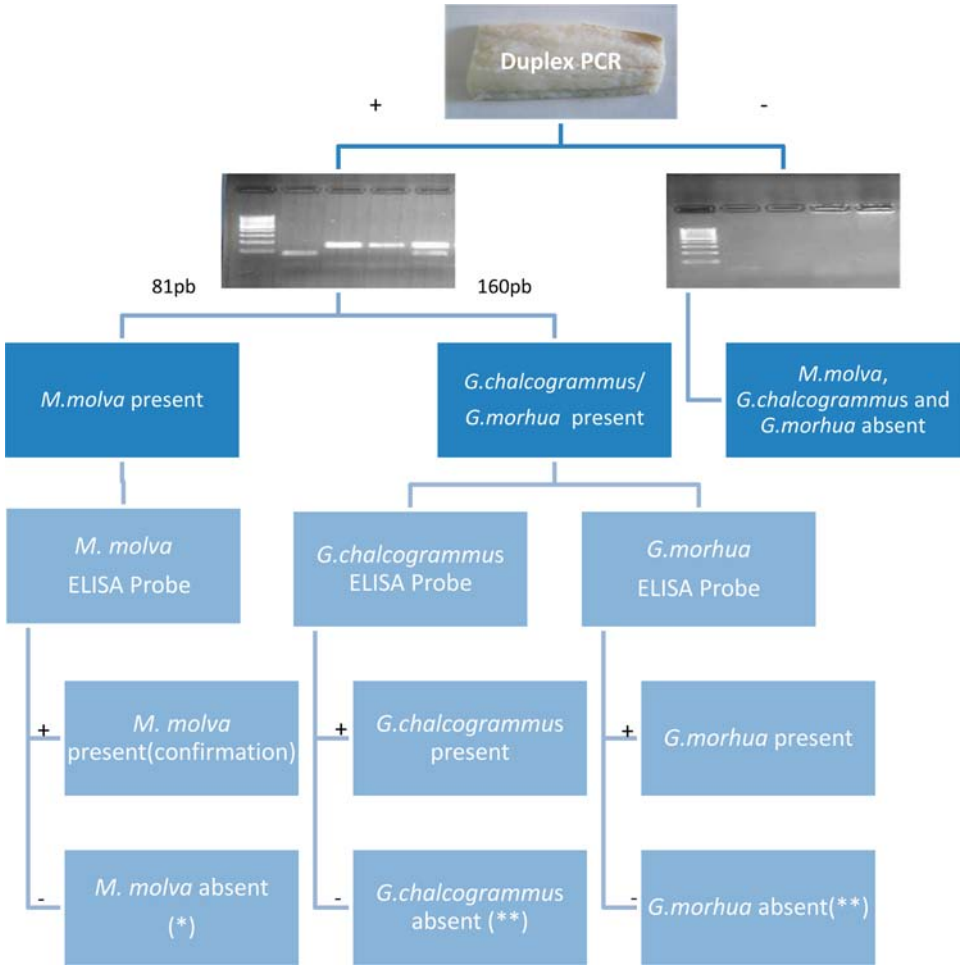

Figure 4. Flow diagram of the proposed method: *, unlikely to occur (if this occurs, it is recommended to check the ELISA test components including a positive control); **, 160 bp PCR product but double-negative hybridization of both *Gadus* probes is unlikely to occur (if this occurs it is recommended to check the ELISA test components including positive controls).

species is suspected in the sample or when the assurance of the presence/absence of the three target species is desired (Figure 4). The duplex PCR allows verification of the presence of *Gadus morhua/chalcogrammus* and/or *M. molva* DNA in a tissue or DNA mixture.

Alternatively, the individual use of each particular system is also possible, allowing determination of the presence of any of the three studied species.

The set of primers L14735 and H1549D was used as amplification control in PCR, to avoid the occurrence of false-negative amplifications due to problems associated with the samples, such as the presence of inhibitors and poor-quality or fragmented DNA associated with the transformation process.

To confirm the correct identification based on morphological characters, a 460 bp fragment from each of the specimens used in this study was amplified, sequenced, and analyzed by FINS. Moreover, to verify that these sequences were correctly assigned to particular species, they were compared with those present in the NCBI database using Megablast.

Validation of the Methodology with Commercial Samples. Once the method surpassed the validation step, it was applied to 19 commercial samples (Table 2) following the flowchart proposed (Figure 4), allowing us to evaluate and broadly determine the labeling situation of these products in the Spanish market. All samples analyzed were correctly identified. The positive and negative results were clearly visualized without the need of a spectrophotometer or ELISA plate reader (Figure 5). Four analyzed samples contained different species from those indicated on the label; one of them was identified as a mixture *G. morhua* and *M. molva*. This mislabeling would not have been possible to detect using DNA sequencing analysis (FINS) (Table 2).

In conclusion, the technique described in this paper represents a useful tool to unequivocally authenticate the species *G. morhua*, *M. molva*, and *G. chalcogrammus*.

In no cases were false negatives or false positives obtained. The purpose of this study was the development and evaluation of a PCR−ELISA technique for the detection of *G. morhua*, *M. molva*, and *G. chalcogrammus* in fish products, which has been successfully accomplished.

This methodology proves useful for enforcing labeling regulations in the authentication of fresh or elaborated fish products and could be used as a routine analysis in food control laboratories.

We indeed identified the species *M. molva* in these products, whereas, according to law, cod can only be manufactured with the species *G. morhua* and *G. macrocephalus*. *M. molva* is a less economically valued species and thus frequently used in transformed food products in which substitution is impossible to detect by simple visual inspection.

dx.doi.org/10.1021/jf500173j | J. Agric. Food Chem. 2014, 62, 5699−5706

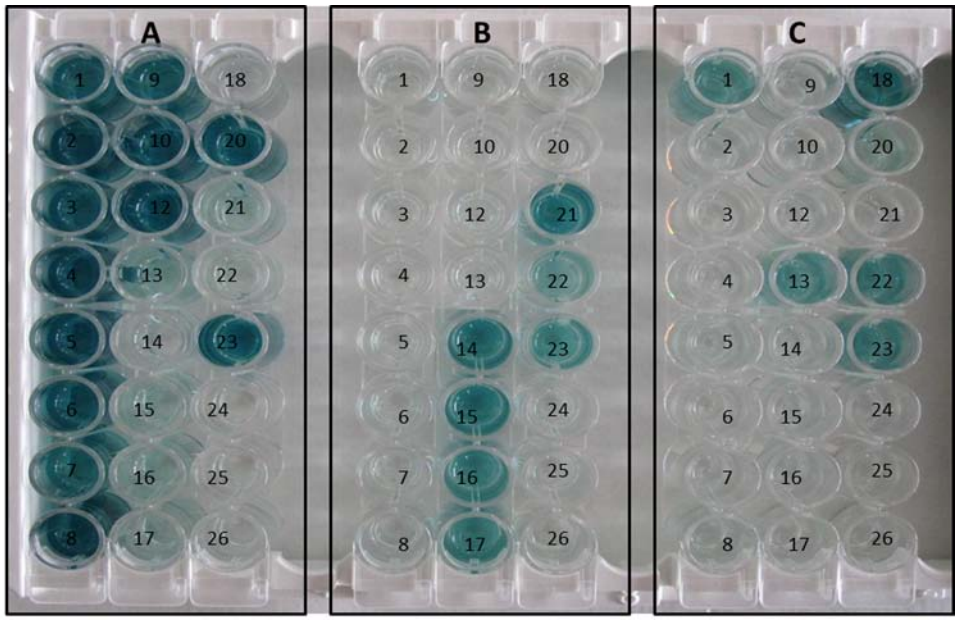

G. morhua Probe

A405nm	A405nm	A405nm
1 1,935	9 1,92	18 0,156
2 3,075	10 2,708	20 2,684
3 2,252	12 2,928	21 0,385
4 2,995	13 0,433	22 0,229
5 2,873	14 0,179	23 2,377
6 2,382	15 0,357	24 0,144
7 1,643	16 0,399	25 0,157
8 2,937	17 0,298	26 0,153

G. chalcogrammus Probe

A405nm	A405nm	A405nm
1 0,151	9 0,146	18 0,154
2 0,158	10 0,15	20 0,156
3 0,149	12 0,166	21 1,81
4 0,154	13 0,143	22 0,544
5 0,158	14 1,336	23 1,159
6 0,159	15 1,68	24 0,144
7 0,156	16 1,217	25 0,151
8 0,161	17 1,141	26 0,141

M. molva Probe

A405nm	A405nm	A405nm
1 0,989	9 0,145	18 1,534
2 0,193	10 0,177	20 0,37
3 0,142	12 0,186	21 0,167
4 0,152	13 0,918	22 1,236
5 0,196	14 0,17	23 1,165
6 0,144	15 0,195	24 0,152
7 0,151	16 0,192	25 0,15
8 0,196	17 0,164	26 0,145

Figure 5. PCR-ELISA results of commercial products. Wells 1−23 correspond to samples described in Table 2. Wells 24−26 correspond to negative samples. Positive and negative results could be clearly visualized without the need of a spectrophotometer or ELISA plate reader.

AUTHOR INFORMATION

Corresponding Author

*(L.T.) Phone: +34-986 231 930. Fax: +34-986 292 762. E-mail: lediciataboada@iim.csic.es.

Funding

The work was supported by the projects "GENTRASEA: Genetic traceability of fish products. Rapid methods with DNA hybridization probes" and "LABELFISH: Atlantic network on genetic control of fish and seafood labelling and traceability". The Spanish Ministry of Science and Innovation is gratefully acknowledged for the doctoral fellowship to L.T.

Notes

The authors declare no competing financial interest.

ACKNOWLEDGMENTS

We acknowledge Anxela Aldrey for her technical assistance. L.T. is a Ph.D. student at the University of Santiago de Compostela.

REFERENCES

(1) FAO. Fisheries and Aquaculture Department; http://www.fao.org/fishery/species/2218.

(2) Galland, A. V.; Dory, D. F.; Pons, L. F.; Chopin, C. F.; et al. Purification of a 41 kDa cod-allergenic protein. *J. Chromatogr.* **1998**, *706*, 63−71.

(3) Sakaguchi, M.; Toda, M.; Ebihara, T.; Irie, S.; et al. IgE antibody to fish gelatin (type I collagen) in patients with fish allergy. *J. Allergy Clin. Immunol.* **2000**, *106* (3), 579−584.

(4) Triantafyllidis, A.; Karaiskou, N.; Perez, J.; Martinez, J. L.; et al. Fish allergy risk derived from ambiguous vernacular fish names: forensic DNA-based detection in Greek markets. *Food Res. Int.* **2010**, *43* (8), 2214−2216.

(5) Miller, D. D.; Mariani, S. Smoke, mirrors, and mislabeled cod: poor transparency in the European seafood industry. *Front. Ecol. Environ.* **2010**, *8* (10), 517−521.

(6) Jacquet, J. L.; Pauly, D. Trade secrets: renaming and mislabeling of seafood. *Mar. Polym.* **2008**, *32* (3), 309−318.

(7) Marko, P. B.; Lee, S. C.; Rice, A. M.; Gramling, J. M.; et al. Fisheries: mislabelling of a depleted reef fish. *Nature* **2004**, *430* (6997), 309−310.

(8) Mackie, I. M.; Pryde, S. E.; Gonzales-Sotelo, C.; Medina, I.; et al. Challenges in the identification of species of canned fish. *Trends Food Sci. Technol.* **1999**, *10* (1), 9−14.
(9) Popping, B. The application of biotechnological methods in authenticity testing. *J. Biotechnol.* **2002**, *98*, 107−112.
(10) Dalmasso, A.; Fontanella, E.; Piatti, P.; Civera, T.; et al. Identification of four tuna species by means of real-time PCR and melting curve analysis. *Vet. Res. Commun.* **2007**, *31*, 355−357.
(11) Primrose, S.; Woolfe, M.; Rollinson, S. Food forensics: methods for determining the authenticity of foodstuffs. *Trends Food Sci. Technol.* **2010**, *21* (12), 582−590.
(12) Hubalkova, Z.; Kralik, P.; Kasalova, J.; Rencova, E. Identification of gadoid species in fish meat by polymerase chain reaction (PCR) on genomic DNA. *J. Agric. Food Chem.* **2008**, *56* (10), 3454−3459.
(13) Moran, P.; Garcia-Vazquez, E. Identification of highly prized commercial fish using a PCR-based methodology. *Biochem. Mol. Biol. Educ.* **2006**, *34* (2), 121−124.
(14) Bertoja, G. A rapid and high-throughput real-time PCR assay for species identification: application to stockfish sold in Italy. *Eur. Food Res. Technol.* **2009**, *229* (2), 191−195.
(15) Hird, H.; Chisholm, J.; Kaye, J.; Colyer, A. et al. Development of real-time PCR assays for the detection of Atlantic cod (*Gadus morhua*), Atlantic salmon (*Salmo salar*) and European plaice (*Pleuronectes platessa*) in complex food samples. *Eur. Food Res. Technol.* **2011**, *234* (1), 127−136.
(16) Akasaki, T.; Yanagimoto, T.; Yamakami, K.; Tomonaga, H.; Sato, S. Species identification and PCR-RFLP analysis of *Cytochrome b* gene in cod fish (order Gadiformes) products. *J. Food Sci.* **2006**, *71* (3), C190−C195.
(17) Di Finizio, A.; Guerriero, G.; Russo, G.; Ciarcia, G. Identification of gadoid species (Pisces, Gadidae) by sequencing and PCR-RFLP analysis of mitochondrial 12S and 16S rRNA gene fragments. *Eur. Food Res. Technol.* **2007**, *225* (3−4), 337−344.
(18) Herrero, B.; Madriñán, M.; Vieites, J. M.; Espiñeira, M. Authentication of Atlantic cod (*Gadus morhua*) using real time PCR. *J. Agric. Food Chem.* **2010**, *58* (8), 4794−4799.
(19) Hird, H.; Hold, G.; Chisholm, J.; Reece, P.; Russell, V. Development of a method for the quantification of haddock (*Melanogrammus aeglefinus*) in commercial products using real-time PCR. *Eur. Food Res. Technol.* **2005**, *220* (5−6), 633−637.
(20) Sánchez, A.; Quinteiro, J.; Rey-Mendez, M.; Perez-Martin, R.; Sotelo, G. C. Identification of European hake species (*Merluccius merluccius*) using real-time PCR. *J. Agric. Food Chem.* **2009**, *57* (9), 3397−3403.
(21) Taylor, M.; Fox, C.; Rico, I.; Rico, C. Species-specific TaqMan probes for simultaneous identification of cod (*Gadus morhua* L.), haddock (*Melanogrammus aeglefinus* L.) and whiting (*Merlangius merlangus* L.). *Mol. Ecol. Notes* **2002**, *2* (4), 599−601.
(22) Cutarelli, A.; Amoroso, M. G.; De Roma, A.; Girardi, S.; et al. Italian market fish species identification and commercial frauds revealing by DNA sequencing. *Food Control* **2014**, *37*, 46−50.
(23) Chapela, M.; Sánchez, A.; Suárez, M.; Perez-Martin, R.; Sotelo, G. C. A rapid methodology for screening hake species (*Merluccius* spp.) by single-stranded conformation polymorphism analysis. *J. Agric. Food Chem.* **2007**, *55* (17), 6903−6909.
(24) Maretto, F.; Reffo, E.; Dalvit, C.; Barcaccia, G.; Mantovani, R. Finding 16S rRNA gene-based SNPs for the genetic traceability of commercial species belonging to Gadiformes. *Ital. J. Anim. Sci.* **2007**, *6*, 161−163.
(25) Milne, S. A.; Gallacher, S.; Cash, P.; Porter, A. J. R. A reliable RT-PCR−ELISA method for the detection of infectious pancreatic necrosis virus (IPNV) in farmed rainbow trout. *J. Virol. Methods* **2006**, *132* (1−2), 92−96.
(26) Sails, A. D.; Fox, A. J.; Bolton, F. J.; Wareing, D. R. A.; et al. Development of a PCR ELISA assay for the identification of *Campylobacter jejuni* and *Campylobacter coli*. *Mol. Cell. Probes* **2001**, *15*, 291−300.
(27) Antolín, A.; González, I.; García, T.; Hernández, P. E.; Martín, R. Arcobacter spp. enumeration in poultry meat using a combined PCR-ELISA assay. *Meat Sci.* **2001**, *59* (2), 169−174.
(28) Kurupati, P.; Kumarasinghe, G.; Laa Poh, C. Direct identification of *Pseudomonas aeruginosa* from blood culture bottles by PCR-enzyme linked immunosorbent assay using oprI gene specific primers. *Mol. Cell. Probes* **2005**, *19* (6), 417−421.
(29) Asensio, L. PCR-ELISA for the semiquantitative detection of Nile perch (*Lates niloticus*) in sterilized fish muscle mixtures. *J. Agric. Food Chem.* **2004**, *52* (14), 4419−4422.
(30) Asensio, L.; Gonzalez, I.; Pavon, M.; Garcia, T.; Martin, R. An indirect ELISA and a PCR technique for the detection of grouper (*Epinephelus marginatus*) mislabeling. *Food Addit. Contam.* **2008**, *25* (6), 677−683.
(31) Kocher, T. D.; Thomas, W. K.; Meyer, A.; Edwards, S. V.; Pääbo, S.; Villablanca, F. X.; Wilson, A. C. Dynamics of mitochondrial DNA evolution in animals: amplification and sequencing with conserved primers. *Proc. Natl. Acad. Sci. U.S.A.* **1989**, *86* (16), 6196−6200.
(32) Bartlett, S. E.; Davidson, W. S. FINS (forensically informative nucleotide sequencing): a procedure for identifying the animal origin of biological specimens. *BioTechniques* **1992**, *12* (3), 408−411.
(33) Wilson, W. D.; Turner, T. F. Phylogenetic analysis of the Pacific cutthroat trout (*Oncorhynchus clarki* ssp.: Salmonidae) based on partial mtDNA ND4 sequences: a closer look at the highly fragmented inland species. *Mol. Phylogenet. Evol.* **2009**, *52*, 406−415.
(34) Rastogi, G.; Dharne, M. S.; Walujkar, S.; Kumar, A.; et al. Species identification and authentication of tissues of animal origin using mitochondrial and nuclear markers. *Meat Sci.* **2007**, *76*, 666−674.
(35) Ritzler, M.; Altwegg, M. Sensitivity and specificity of a commercially available enzyme-linked immunoassay for the detection of polymerase chain reaction amplified DNA. *J. Microbiol. Methods* **1996**, *27*, 233−238.
(36) Holzhauser, T.; Stephan, O.; Vieths, S. Detection of potentially allergenic hazelnut (*Corylus avellana*) residues in food: a comparative study with DNA PCR-ELISA and protein sandwich-ELISA. *J. Agric. Food Chem.* **2002**, *50*, 5808−5815.
(37) Edwards, M. C.; Gibbs, R. A. Multiplex PCR: advantages, development, and applications. *Genome Res.* **1994**, *3*, 65−75.
(38) Settanni, L.; Corsetti, A. The use of multiplex PCR to detect and differentiate food and beverage associated microorganisms. *J. Microbiol. Methods* **2007**, *69*, 1−22.

JOURNAL OF AGRICULTURAL AND FOOD CHEMISTRY

Article

pubs.acs.org/JAFC

Effect of Almond Processing on Levels and Distribution of Aflatoxins in Finished Products and Byproducts

Rosanna Zivoli, Lucia Gambacorta, Giancarlo Perrone, and Michele Solfrizzo*

Institute of Sciences of Food Production (ISPA), National Research Council of Italy (CNR), Via Amendola 122/O, 70126 Bari, Italy

ABSTRACT: The fate of aflatoxins during processing of contaminated almonds into nougat, pastries, and almond syrup was evaluated by testing the effect of each processing step (blanching, peeling, roasting, caramelization, cooking, and water infusion) on the distribution and levels of aflatoxins. Blanching and peeling did not reduce total aflatoxins that were distributed between peeled almonds (90−93%) and skins (7−10%). Roasting of peeled almonds reduced up to 50% of aflatoxins. Up to 70% reduction of aflatoxins was observed during preparation and cooking of almond nougat in caramelized sugar. Aflatoxins were substantially stable during preparation and cooking of almond pastries. The whole process of almond syrup preparation produced a marked increase of total aflatoxins (up to 270%) that were distributed between syrup (18−25%) and spent almonds (75−82%). The increase of total aflatoxins was probably due to the activation of almond enzymes during the infusion step that released free aflatoxins from masked aflatoxins.

KEYWORDS: *aflatoxin, almond, processing, pastries, nougat, syrup*

INTRODUCTION

Almonds are the edible seeds of the almond tree (*Prunus dulcis*) originating from regions of Central Asia and currently cultivated around the world in dry and temperate climates. The world production in 2012 was mainly distributed among the United States (mainly California, 37.2%), Spain (11.1%), Australia (7.4%), Iran (5.2%), Morocco (5.1%), Italy (4.6%), and the Syrian Arabic Republic (4.5%). The remaining production (24.9%) is distributed in other countries, each of them producing <4% of the total.[1] Almonds are used in the food industry to produce pastries (amaretti, cantucci biscuits, dragée, etc.), almond syrup, nougat, and marzipan. Among food commodities, almonds are considered to have an intermediate risk of aflatoxin contamination.[2] From 2010 the European maximum levels of total aflatoxins in almonds intended for further processing (15 μg/kg) and ready-to-eat (10 μg/kg) have been aligned with those of Codex Alimentarius after a positive opinion of the European Food Safety Authority (EFSA).[3−6] Among mycotoxins, aflatoxins are in the hazardous category, with the highest number of notifications in the European Union (EU) Rapid Alert System for Food and Feed (RASFF). The number of aflatoxin notifications for the category of nuts, nut products, and seeds decreased from 568 in 2007 (75 for almonds) to 214 in 2013 (8 for almonds).[7] The reduction of the number of lots rejected in 2013 could be probably due to the new EU limits for aflatoxins in tree nuts.

Freshly harvested almonds are dehulled, and in-shell almonds are dried until the water content is <6%.[8] Dried in-shell almonds can be stored for several months before being used by the food industry.[9] Factors affecting aflatoxin contamination in almonds are shell characteristics (soft or hard), insects, drought stress, and harvest techniques that can spread fungal contamination.[10−14]

Although aflatoxins are highly stable compounds, studies have indicated a reduction during thermal processing.[15] The efficacy of sorting, blanching, and electronic color sorting for reducing aflatoxins in pistachios, peanuts, and almonds has also been reported.[10,13,16] For almonds, the effect of some processing (e.g., peeling, roasting, cooking, and infusion) on aflatoxins has not been tested or limited. The objective of this study was to investigate the fate of aflatoxins during the different processing steps of almonds into pastries, nougat, and syrup (blanching, peeling, roasting, cooking, and water infusion), traditional Italian almond-based food products.[17] The mass balance approach was used to quantitatively determine the distribution of aflatoxins in final and waste fractions of almond processing.

MATERIALS AND METHODS

Safety. Aflatoxins are powerful human carcinogens and should be handled with care. All experiments were carried out in a fume hood using gloves and protective masks. All used laboratory glassware was treated with an aqueous solution of sodium hypochloride (5%) for 2 h and an equal volume of aqueous acetone for 30 min before discarding to minimize health and environmental risks due to aflatoxin contamination.

Production of Aflatoxin-Contaminated Almonds. Due to the unavailability of naturally contaminated almonds, shelled almonds were inoculated with a strain of *Aspergillus flavus* (ITEM 7828) that produces aflatoxins B_1 and B_2, taken from the Agri-Food Toxigenic Fungi Culture Collection of the Institute of Sciences of Food Production (ISPA), Bari, Italy.[18] In particular, 4 kg of shelled almonds (cv. Genco) was purchased in a local market in Conversano (Bari province, Italy) and subjected to a mild sterilization by immersion for 2 min in a solution of 1% sodium hypochlorite with manual agitation. Subsequently, almonds were washed with sterile water and then further surface-disinfected with 70% ethanol for 1 min as described above. Almonds were then transferred, under sterile conditions, in four 5 L sterile flasks, and each flask containing 1 kg of almonds was treated

Received: April 17, 2014
Revised: May 29, 2014
Accepted: May 29, 2014
Published: May 29, 2014

ACS Publications © 2014 American Chemical Society

dx.doi.org/10.1021/jf5018548 | J. Agric. Food Chem. 2014, 62, 5707−5715

with 300 mL of a conidial suspension containing 3.3×10^5 conidia/mL of *A. flavus*. The conidial suspension was obtained from *A. flavus* inoculated on plates of potato dextrose agar (PDA) and grown for 4 days in the dark. Fungal conidia were collected from the surface of plates by using a sterile spatula and sterile water. The concentration of conidial suspension was determined with a cell-counting Thoma chamber (HBG Henneberg-Sander GmbH, Gießen, Germany). Appropriate dilutions with sterile water were made to obtain a final concentration of 3.3×10^5 conidia/mL. After inoculation, flasks were manually stirred to uniformly distribute the conidial suspension on almonds' surface and closed with a stopper of raw cotton and a sheet of aluminum foil to avoid excessive water evaporation. The four flasks were incubated for 4 days at 28 °C in the dark. After incubation, almonds were dried at 50 °C for 24 h. Then three aliquots of almonds (20 g each) were randomly collected from each batch, content of flask, and analyzed for their aflatoxin content. The four batches of contaminated almonds were vacuum sealed and stored in the dark until used for processing experiments. In particular, batches 1−3 were used to evaluate the effect of steam blanching and peeling on levels and distribution of aflatoxins and to produce almond pastries and almond syrup. Almond nougat was prepared by using almonds of batches 1 and 3. Almonds of batch 4 were used to test the effect of peeling and roasting on levels and distribution of aflatoxins.

Blanching and Peeling of Almonds. Steam blanching was carried out in a model HD 9140 steamer (Philips Electroincs, Eindhoven, The Netherlands) for 40 min, whereas water blanching was carried out in boiling water for 5 min. Almonds of batches 1−3 and aliquots of batch 4 were submitted to steam blanching. For comparison, aliquots of almonds of batch 4 were submitted to water blanching. After water blanching, the almonds were separated from boiling water and peeled manually to separate peeled almond from skins. Wastewater was cooled, weighed, and stored at −20 °C until analysis. Steam-blanched almonds were also manually peeled. Peeled almonds and skins were separately cooled, freeze-dried, and weighed. Triplicate aliquots of peeled almonds, skins, and wastewater were sampled from each batch and analyzed for their aflatoxin content.

Roasting of Peeled Almonds. The effect of roasting on aflatoxin levels was evaluated at 120 and 150 °C for 30, 60, and 120 min on aliquots of peeled almonds of batch 4. Before roasting, peeled almonds were coarsely chopped with a knife and placed in two thin aluminum trays. For aflatoxin determination 3 × 10 g of chopped almonds was randomly sampled from each tray at 0, 30, 60, and 120 min. After each sampling, chopped almonds were mixed in the tray and put back in the oven. Samples of chopped almonds sampled before, during, and after roasting were analyzed for their aflatoxin content.

Aliquots (2 × 317 g) of peeled almonds from batches 1 and 3 were roasted without chopping at 150 °C for 30 min and used to prepare almond nougat.

Roasting experiments were also performed with blank peeled almonds that were spiked with the four aflatoxins at two levels and roasted for 30, 60, and 120 min at 150 °C. Aliquots of 10 g of peeled almonds (9−10 peeled kernels) were placed in aluminum trays, and each kernel was individually spiked on both sides with a standard solution containing the four aflatoxins. The two spiking levels of aflatoxins were 10 and 50 μg/kg for AFB_1 and AFG_1 and 2.5 and 12.5 μg/kg for AFB_2 and AFG_2. Quadruplicate experiments were performed for a total of 24 treatments.

Production of Almond Nougat, Almond-Based Pastries, and Almond Syrup. *Almond Nougat.* The two aliquots of roasted almonds of batches 1 and 3 were coarsely chopped and thoroughly mixed. From each batch, 40 g was sampled, ground, and analyzed in triplicate for their aflatoxin content. For each batch two types of nougat were produced (sugar nougat and sugar−honey nougat). In particular, 134 g of sugar was melted in a pot heated on a hot-plate to prepare the caramel. While the melted caramel was still hot, chopped roasted almonds (134 g) were added and mixed continuously for 7−10 min until the caramel adhered to the walls of the almonds. The mixture of almond and caramel was then manually shaped into small heaps by using a spoon and cooled at room temperature to reach their typical consistency. Sugar−honey nougat was prepared by melting 94 g of sugar and then adding 40 g of honey to obtain a homogeneous mixture. Then chopped roasted almonds (134 g) were hot mixed and portioned as described above. The four aliquots of nougats were singularly weighed, ground, and analyzed in triplicate for their aflatoxin content.

Almond Pastries. Aliquots of peeled almonds of batches 1−3 were separately ground with a blender and used to prepare almond pastries and almond syrup. The initial content of aflatoxins was determined in 3 × 10 g aliquots of each batch. Pastries were prepared by mixing ground peeled almonds (300 g) of each batch with sugar (180 g) and egg white meringue (from two eggs), and then each mixture was divided in three aliquots that were shaped in small spherical pastries and cooked at 140 °C for 30 min, at 160 °C for 20 min, or at 180 °C for 15 min, respectively. The inner temperatures of pastries (82, 95, and 98 °C, respectively) were measured with a thermometer at the end of each cooking period. After cooking, pastries were cooled, freeze-dried, and ground. Samples of initial ground peeled almonds and cooked pastries were analyzed in triplicate for their aflatoxin content.

Almond Syrup. Aliquots of peeled almonds of batches 1−3 were separately ground as described above and used to prepare almond syrup by using two procedures of water infusion. For the first procedure ground peeled almonds (100 g) were infused in tap water (300 mL) for 5 h at room temperature. After infusion, the soaked ground almonds were filtered under vacuum on a 9 cm diameter no. 4 filter paper (Whatman, Maidstone, UK) on a Büchner funnel fitted on a tailed vacuum flask. Spent ground almonds were collected from the filter paper, freeze-dried, and weighed. The infusion was sugared with 400 g of sugar and boiled until the solutions assumed the typical consistency of a syrup. For the second procedure ground peeled almonds (100 g) were infused in sugared water (300 mL of water + 400 g of sugar) for 5 h at room temperature. Almond syrups were cooled and stored at −20 °C until analysis. Samples of initial ground peeled almonds, syrup, and spent almonds were analyzed in triplicate for their aflatoxin content.

Chemicals and Reagents. Methanol (MeOH), acetonitrile (MeCN), and acetone were purchased from Carlo Erba (Rodano, Italy); 95% ethanol (EtOH) was purchased from Mallinckrodt Baker (Milan, Italy). Ultrapure water was produced with a Milli-Q system (Millipore, Bedford, MA, USA). AflaTest WB wide-bore affinity columns were purchased from Vicam L.P. (Watertown, MA, USA). The mixed aflatoxins standard solution (purity = 99 ± 1%), prepared in acetonitrile and containing 2.00 μg/mL AFB_1, 2.02 μg/mL AFG_1, 0.50 μg/mL AFB_2, and 0.50 μg/mL AFG_2, was purchased from Romer Laboratories Diagnostic (Tulln, Austria). This solution was used to prepare calibration solutions for HPLC-FLD determinations and to carry out recovery experiments.

Determination of AFB_1, AFB_2, AFG_1, and AFG_2. The method of Arranz et al.,[19] originally developed for determination of AFB_1 in medical herbs, was slightly modified and used herein for aflatoxin determination in almonds and derived products. In particular, the HPLC injection volume was 100 μL instead of 500 μL, the HPLC column was a pentafluorophenyl-propyl-bonded silica instead of C18-bonded silica, the HPLC mobile phase was MeCN/H_2O (30:70 v/v) instead of H_2O/MeCN/MeOH (60:20:30 v/v/v), and sample extracts with high aflatoxin content were directly analyzed by HPLC without immunoaffinity cleanup. Briefly, 10 g of dry ground sample was poured in a 250 mL Pyrex screw-capped glass flask, and 100 mL of extraction mixture of acetone/water (85:15 v/v) was added. The extraction was performed by sonication for 30 min. After filtration on fluted no. 4 filter paper (Whatman), 5 mL of filtered extract was diluted with 75 mL of ultrapure water and filtered with a GF/A glass microfiber filter (Whatman). Forty milliliters of filtered diluted extract (equivalent to 0.25 g of matrix) was passed through the immunoaffinity column (IAC) AflaTest (Vicam, Milford, MA) at the flow rate of 1−2 drops/s. Then the column was washed twice with 10 mL of ultrapure water, and aflatoxins were eluted with 1.5 mL (3 × 0.5 mL) of methanol. The three eluates were collected, diluted with ultrapure water up to 5 mL in a volumetric flask, and analyzed by HPLC-FLD. Immunoaffinity sample cleanup was not necessary for the determination of aflatoxins in samples of almonds and derived products obtained from almonds

inoculated with *A. flavus* due to the high levels of aflatoxins. In particular, after extraction with acetone/water (85:15 v/v), an aliquot of the filtered sample extract (0.5 mL) was diluted with 30 mL of MeCN/H_2O (30:70 v/v), stirred, filtered through a 0.45 μm PTFE filter (Sartorius Stedim Italy SpA, Bagno a Ripoli, Firenze, Italy), and injected into the HPLC system. Liquid samples (0.5 mL of almond syrup or wastewater from blanching) were diluted with 7.5 mL of MeCN/H_2O (30:70 v/v), stirred, filtered through a 0.45 μm PTFE filter, and injected into the HPLC system.

Calibration Curves. A mixed aflatoxins stock solution was prepared by diluting 500 μL of commercial standard solution to 10 mL with acetonitrile in a volumetric flask. The four HPLC calibration solutions of combined aflatoxins (AFB_1 + AFB_2 + AFG_1 + AFG_2) were prepared by diluting appropriate volumes of stock solution with MeOH/H_2O (40:60 v/v). The toxin concentration ranges of the four calibration solutions were 0.40−3.64 ng/mL for AFB_1 and AFG_1 and 0.10−0.90 ng/mL for AFB_2 and AFG_2.

HPLC-FLD Equipment and Conditions. The HPLC-FLD analyses were performed with an Agilent 1100 series (Agilent Technologies, Inc., Wilmington, DE, USA), consisting of a binary pump (G1312A), an autosampler (G1313A) with a 100 μL loop, a fluorescence detector (G1321A) fixed at 365 nm λ_{ex} and 435 nm λ_{em}, a thermostatic oven set at 30 °C, and software for Microsoft Windows 2000 (HP ChemStation). The column used was a 150 mm × 4.6 mm i.d., 3 μm, Luna PFP (2) (pentafluorophenyl-propyl) (Phenomenex, Torrance, CA, USA) with a 3 mm i.d., 0.45 μm pore size guard filter (Rheodyne, Cotati, CA, USA). The chromatographic separations were performed in the isocratic condition using a mixture of MeCN/H_2O (30:70 v/v) at flow rate of 0.8 mL/min. A photochemical postcolumn derivatization UVE system (LCTech, Dorfen, Germany) was used to enhance the fluorescence of AFB_1 and AFG_1.

Statistical Analysis. Mean and standard deviation (SD) of data were calculated with a SigmaPlot for Windows version 12.0 statistical software package (Sistat Software, Inc., Chicago, IL, USA). SigmaPlot was also used to perform one-way analysis of variance (ANOVA) followed by Tukey's pairwise multiple-comparison test and a least significant difference (LSD) test at 95% confidence levels ($p = 0.05$) to identify significant differences among groups.

Recovery Experiments. The performances of the analytical method that involves the use of the IAC column were checked on blank samples of shelled almonds, peeled almonds, skins, and almond-based pastries spiked in triplicate at 10.0 μg/kg AFB_1 and 24.9 μg/kg total aflatoxins. Each matrix was spiked in triplicate with 50 μL of commercial standard solution to check recovery and within laboratory repeatability of results. Spiked samples were left overnight in the dark at room temperature to allow solvent evaporation.

The performances of the "dilute and shoot" method were checked on blank samples of sugar nougat, sugar−honey nougat, almond syrup, and caramelized sugar spiked in triplicate at higher aflatoxin levels (394.7 μg/kg AFB_1 and 31.7 μg/kg AFB_2). The spiking solution for these recovery experiments was obtained from extracts of almonds inoculated with a strain of *A. flavus* producing AFB_1 and AFB_2. In particular, 10 g of aflatoxin contaminated almonds was extracted by sonication with 100 mL of acetone/water (85:15 v/v) and filtered with a fluted filter paper. The concentrations of AFB_1 and AFB_2 (AFG_1 and AFG_2 were not detected) in the filtered extract were measured by HPLC-FLD by using calibration curves of authentic standards of AFB_1 and AFB_2.

RESULTS AND DISCUSSION

Method Performance. Preliminary recovery experiments were carried out with the CEN/AOAC method[20] that uses a mixture of MeOH/H_2O (80:20 v/v) as extraction solvent mixture, IAC column cleanup, and HPLC-FLD end determination with post-column derivatization. Acceptable mean recoveries, between 69 and 90%, were obtained for shelled almonds, peeled almonds, and almond-based pastries, whereas low mean recoveries were obtained for almond skins, those being 33% for AFB_1 and 42% for total aflatoxins. It was therefore decided to test the method of Arranz et al.,[19] originally developed for medical herbs, that uses acetone/water (85:15 v/v) as extraction solvent mixture. As shown in Table 1, good mean recoveries, between 89 and 107%, and good within-laboratory repeatability of results, between 1 and 12%, were obtained for all of the matrices used in these studies including almond skins. Similar results were also obtained when the sample extracts in acetone/water (85:15 v/v) were diluted with HPLC mobile phase and directly analyzed by HPLC-FLD (Table 1). No interfering peaks at retention times of aflatoxins were visible in the chromatograms of tested sample extracts, and acceptable values of LOD and LOQ, ranging between 0.2 and 1.2 μg/kg and between 0.4 and 2.5 μg/kg, respectively, were obtained. The values of LOD and LOQ were calculated as signal-to-noise ratios of 3 and 6, respectively. Acetone/water (85:15 v/v) was therefore used as extraction solvent mixture for aflatoxin determination in all samples tested in this study.

Table 1. Results of Recoveries (Mean of Three Replicates) and Within-Laboratory Repeatability of Results (RSD_r) of Aflatoxins for Spiked Matrices

matrix	toxin	spiking level (μg/kg)	recovery (%)	RSD_r (%)
shelled almonds[a]	AFB_1	10.0	95	7
	AFtot	24.9	90	7
peeled almonds[a]	AFB_1	10.0	89	12
	AFtot	24.9	92	7
almond skins[a]	AFB_1	10.0	94	4
	AFtot	24.9	95	2
almond pastries[a]	AFB_1	10.0	91	9
	AFtot	24.9	92	3
sugar nougat[b]	AFB_1	394.7	109	4
	AFB_2	31.7	106	4
sugar−honey nougat[b]	AFB_1	394.7	101	2
	AFB_2	31.7	99	1
caramelized sugar[b]	AFB_1	394.7	101	3
	AFB_2	31.7	101	3
almond syrup[b]	AFB_1	394.7	103	2
	AFB_2	31.7	107	2

[a]Sample extracts were purified with immunoaffinity columns before HPLC analysis. [b]Sample extracts were appropriately diluted with MeCN/water (30:70 v/v) before HPLC analysis.

Aflatoxin Determination in Inoculated Almonds. The unavailability of naturally contaminated almonds prompted us to produce contaminated almonds by inoculating almonds with a toxigenic strain of *A. flavus*. Chromatographic analysis of diluted extracts of shelled almonds inoculated with *A. flavus* (ITEM 7828) showed the presence of AFB_1 and AFB_2 and the absence of AFG_1 and AFG_2, a typical toxigenic profile of *A. flavus* species as reported for this strain on the Web site of the ITEM culture collection.[18] Aflatoxin B_1 was identified and measured in batches 1, 2, 3, and 4 of inoculated almonds at mean levels of 8379, 49782, 2012, and 1383 μg/kg, respectively. The mean levels of AFB_2 were 2447, 11904, 993, and 135 μg/kg in batches 1, 2, 3, and 4, respectively. The four batches were kept separated and processed separately to determine the influence of different processing procedures on almonds containing different levels of aflatoxins. When possible, the contaminated almonds were thoroughly ground/blended before processing to homogenize aflatoxins within the sample

dx.doi.org/10.1021/jf5018548 | J. Agric. Food Chem. 2014, 62, 5707−5715

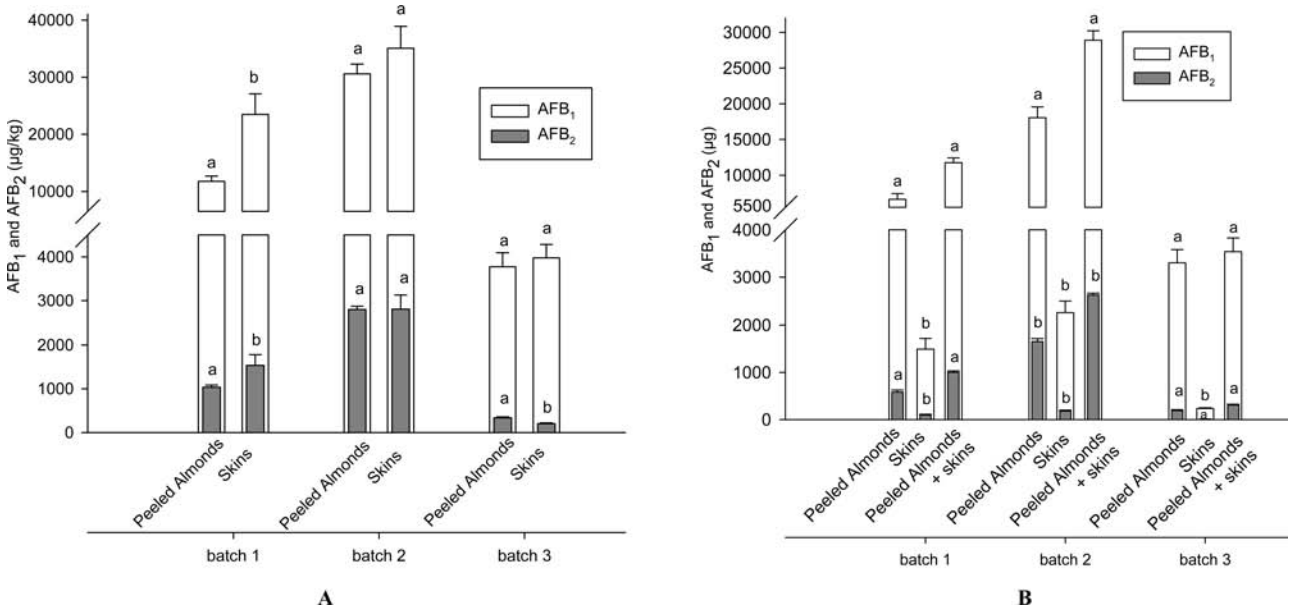

Figure 1. Steam blanching: (A) levels of aflatoxins in ground peeled almonds and ground almond skins; (B) relevant mass balance of aflatoxins.

Table 2. Effect of Roasting on AFB_1 and AFB_2 in Contaminated Almonds[a]

	AFB_1		AFB_2	
	level (μg/kg ± SD)	mean reduction (%)	level (μg/kg ± SD)	mean reduction (%)
initial level	5558.7 ± 4091.3 a		405.6 ± 378.0 a	
120 °C, 30 min	5258.6 ± 2708.9	5	543.7 ± 298.1	-
120 °C, 60 min	2295.4 ± 1376.6	58	283.3 ± 223.1	30
120 °C, 120 min	2571.4 ± 458.4	54	307.9 ± 53.0	24
150 °C, 30 min	2500.4 ± 974.8	55	322.8 ± 122.2	20
150 °C, 60 min	1465.8 ± 1006.1	74	207.2 ± 164.1	49
150 °C, 120 min	907.1 ± 611.9	84	124.9 ± 18.4	69

[a]SD, standard deviation of triplicate treatments. Statistical analysis of results within the column of each group showed no significant differences between treatments ($p > 0.05$).

and accurately measure the initial level of aflatoxins. It was not possible to grind/blend almonds when the effects of peeling, roasting, and nougat preparation were evaluated because these processes have to be performed with whole almonds (peeling) or at most with chopped almonds (roasted almonds and nougat).

Blanching and Peeling Procedures. The results of the effect of steam blanching on levels and distribution of aflatoxins between skins and peeled almonds are shown in Figure 1. In general, comparable levels of aflatoxins were measured in peeled almonds and skins (Figure 1A). However, from the mass balance of aflatoxins it was calculated that skins contained 10% AFB_1 and 7% AFB_2, whereas 90−93% of aflatoxins remained in peeled almonds. Similar results were obtained for water-blanched almonds with 7% AFB_1 and 6% AFB_2 measured in the skins, 92−93% measured in the peeled almonds, and only 0.9% in the water used for blanching. The very low transfer of aflatoxins from almonds into water during blanching could be explained by the low water solubility of aflatoxins and the high retention capacity of almonds for these mycotoxins. Considering that skin represents 6−7% of the total weight of shelled almond, these results suggest that aflatoxins do not accumulate in the skin and are homogeneously distributed between the kernel and the skin. The process of peeling, therefore, only partially reduces aflatoxins content in the almonds because 92−94% of the toxins remain in the peeled kernels. Although our results were obtained with almonds inoculated with *A. flavus* at laboratory scale, it is presumable that a similar aflatoxin distribution occurs in naturally contaminated almonds. To confirm this hypothesis, three samples of apricot kernels naturally contaminated with AFB_1 and AFB_2 and kindly provided by a local importer were submitted to steam blanching followed by peeling. The results of aflatoxin analyses showed that 94−96% of aflatoxins were found in peeled kernels, whereas 4.8−5.7% of aflatoxins were found in the skins (data not shown). No specific studies are available in the scientific literature on the distribution of aflatoxins among skins, peeled almonds, and water used for blanching.[10,13,14] Taken together, our results show that the passage of aflatoxins in boiling water is negligible and the separation of skins removed only 6−7% of total aflatoxins present in the shelled almonds as well as in naturally contaminated apricot kernels. In addition to the low water solubility of aflatoxins, the high capacity of almonds to retain the toxins may explain the negligible passage of aflatoxins from almonds to boiling water. The high levels of fat (54%) contained in almonds may explain the high capacity of almonds

dx.doi.org/10.1021/jf5018548 | J. Agric. Food Chem. 2014, 62, 5707−5715

Table 3. Effect of Roasting (150 °C) on AFB_1, AFG_1, AFB_2, and AFG_2 in Blank Spiked Almonds[a]

	AFB_1		AFG_1		AFB_2		AFG_2	
	level (μg/kg ± SD)	mean reduction (%)	level (μg/kg ± SD)	mean reduction (%)	level (μg/kg ± SD)	mean reduction (%)	level (μg/kg ± SD)	mean reduction (%)
spiking level	10		10		2.5		2.5	
30 min roasting	8.9 ± 0.54 a	11	9.5 ± 0.36 a	5	2.4 ± 0.12 a	6	2.1 ± 0.08 a	14
60 min roasting	7.2 ± 0.19 b	28	7.9 ± 0.22 b	21	2.1 ± 0.06 b	16	2.0 ± 0.08 b	22
120 min roasting	6.1 ± 0.35 c	39	6.8 ± 0.50 c	32	1.9 ± 0.09 c	25	1.8 ± 0.08 c	28
spiking level	50		50		12.5		12.5	
30 min roasting	38.7 ± 0.17 a	23	42.3 ± 0.92 a	16	10.7 ± 0.12 a	14	9.5 ± 0.37 a	24
60 min roasting	31.3 ± 1.52 b	38	34.5 ± 1.28 b	31	9.5 ± 0.25 b	24	8.5 ± 0.3 b	32
120 min roasting	25.9 ± 2.60 c	48	29.6 ± 2.79 c	41	8.6 ± 0.88 c	31	8.2 ± 0.34 c	34

[a]SD, standard deviation of quadruplicate treatments. Different letters within the column of each group indicate statistically significant differences among treatments ($p < 0.05$).

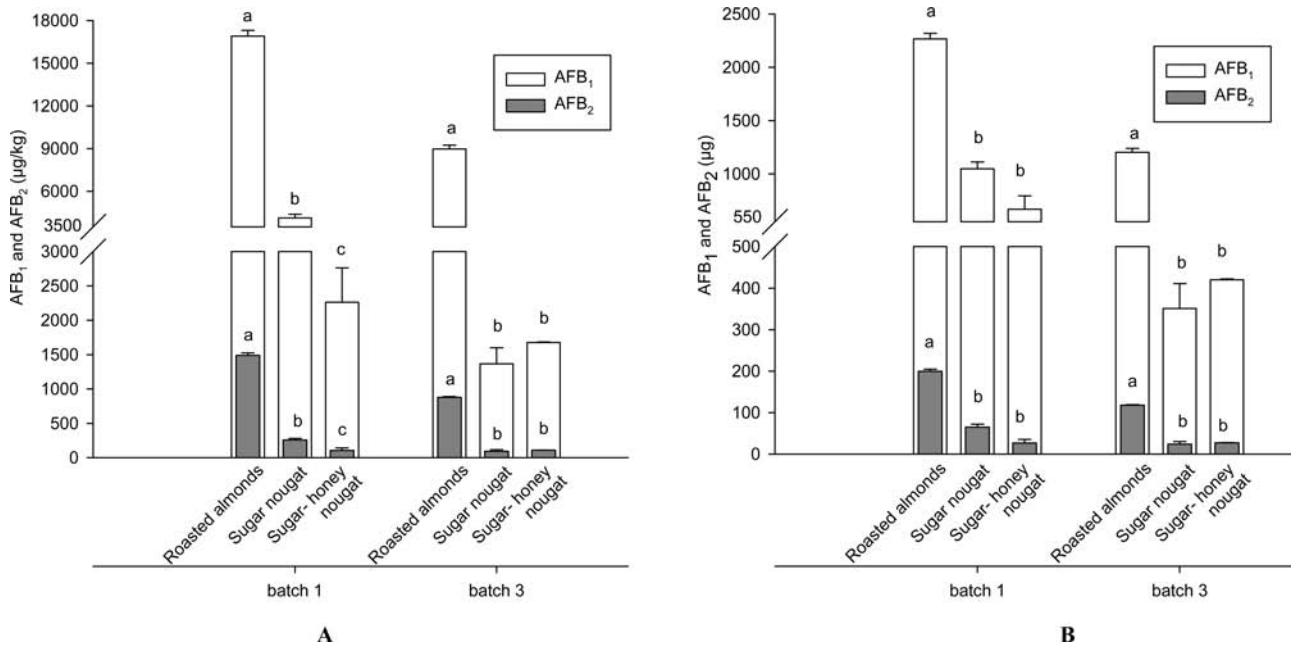

Figure 2. (A) Effect of nougat preparation and cooking on aflatoxin levels; (B) relevant mass balance of aflatoxins.

to retain aflatoxins, which belong to the less polar mycotoxins. In fact, when aflatoxin-contaminated ginger tea, a fat-free matrix, was steeped in boiling water for 5−10 min, 30−40% of aflatoxins passed in water.[21] On the other hand, a mean aflatoxin reduction of 27% was observed during blanching and peeling of roasted peanuts.[22] Sorting and sizing processes are used to separate aflatoxin-contaminated almonds from uncontaminated ones. In particular, up to 97% of total aflatoxins were found in almonds damaged by insects or mold or mechanically injured, whereas 3% of total aflatoxins were found in high-quality almonds that accounted for 84% of the total kernel mass.[13]

Roasting. The results of different roasting conditions on aflatoxin levels in peeled almonds are shown in Table 2. For almonds roasted at 150 °C, mean AFB_1 and AFB_2 reductions ranged between 55 and 84% and between 20 and 69%, respectively, after 30, 60, or 120 min. A lower reduction of aflatoxins was observed at 120 °C. However, these reductions were not statistically significant ($p > 0.05$) when compared to initial levels (Table 2). This was probably due to the inhomogeneous distribution of aflatoxins in chopped almonds that produced high values of standard deviation for replicate analyses that made problematic the statistical comparison of the mean levels measured before and after roasting. No aflatoxin reduction was observed for almonds roasted at 120 °C for 30 min, whereas mean reductions of 54−58% for AFB_1 and 24−30% for AFB_2 were observed after 60−120 min, although these reductions were not statistically significant. Similar mean reductions were observed at 120 °C for 120 min (54% for AFB_1, 24% for AFB_2) and at 150 °C for 30 min (55% for AFB_1, 20% for AFB_2) (Table 2). Taken together, these data suggest that AFB_2 may be more resistant to roasting because a lower reduction, compared to AFB_1, was observed at both 120 and 150 °C. However, the percent reduction may also be a function

dx.doi.org/10.1021/jf5018548 | J. Agric. Food Chem. 2014, 62, 5707−5715

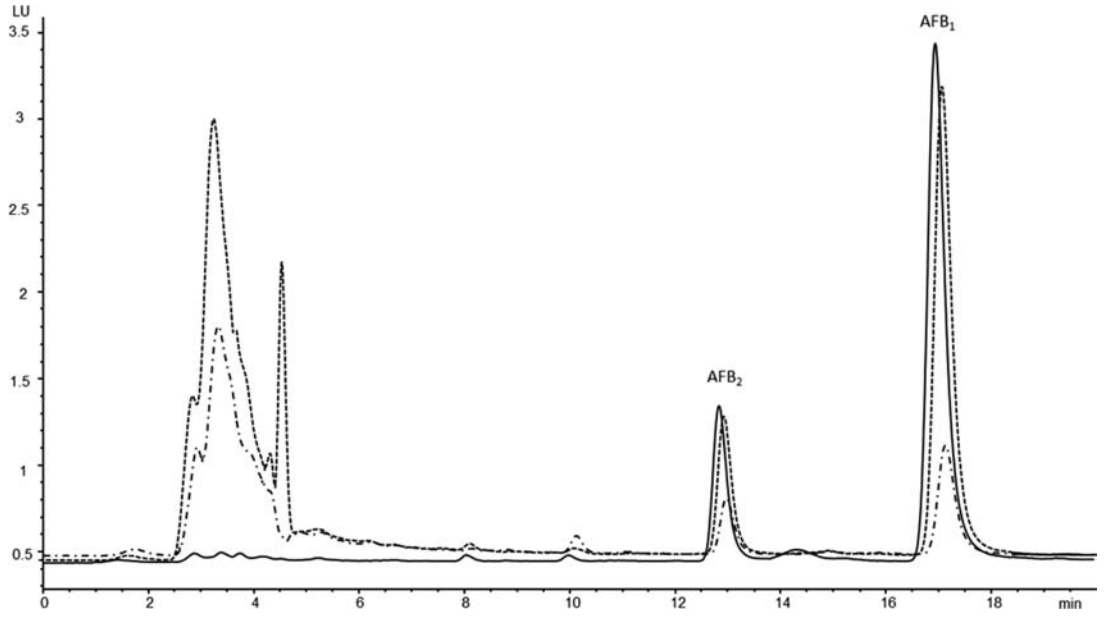

Figure 3. HPLC chromatograms of sugar spiked with AFB_1 (394.7 μg/kg) and AFB_2 (31.7 μg/kg) (- - -), sugar caramelized and then spiked with AFB_1 (394.7 μg/kg) and AFB_2 (31.7 μg/kg) (—), and sugar spiked with AFB_1 (394.7 μg/kg) and AFB_2 (31.7 μg/kg) and then caramelized (- · · -).

of aflatoxin concentration; that is, the higher the concentration, the higher the percent reduction, because the levels of AFB_2 tested in this study were always lower than those of AFB_1 (Tables 2 and 3). Although 150 °C for 120 min produced the highest reduction of aflatoxins, these conditions seem to be impracticable because roasted almonds appeared blackened/burned and most probably lost their organoleptic characteristics, making them inedible. The results of roasting experiments conducted at 150 °C with blank almonds spiked with the four aflatoxins at two levels are shown in Table 3. After 120 min, the AFB_1 reductions were 39 and 48% for the two spiking levels, whereas for AFB_2 the reductions were 25 and 31%, respectively. Lower reductions were observed after 30 min, those being 11 and 23% for AFB_1 and 6 and 14% for AFB_2 for the two spiking levels. As observed in the previous experiments, a higher reduction was observed for AFB_1 as compared to AFB_2, and roasting times >30 min (60−120 min) irreversibly altered the characteristics of almonds (color, smell etc.), making them unfit for consumption.

Although no data are available in the literature on the effect of roasting on aflatoxins in almonds, our results are comparable with those published for other nuts. Yazdanpanah et al.[23] reported that roasting pistachios at 90, 120, and 150 °C for 30, 60, and 120 min reduced the content of aflatoxins at levels ranging between 17 and 95%, and the maximum reduction was obtained at higher temperature and longer roasting time. Mean AFB_1 reductions of 78−80% were reported for spiked and naturally contaminated peanuts roasted at 150 °C for 120 min.[24] A similar reduction of AFB_1 (79%) was observed for peanuts inoculated with *A. flavus* and roasted at 150 °C for 30 min.[25] Roasting naturally contaminated and spiked peanuts at 150 °C for 30 min produced 48−61 and 30−44% AFB_1 reductions, respectively.[26]

No degradation products of aflatoxins have been isolated and chemically characterized from roasted nuts so far, and no attempts were performed in this study. Further studies are necessary to obtain these data that are necessary to establish the possible toxicity or harmlessness of degradation products and to define the roasting conditions that inactivate aflatoxins.[23−26]

Almond Nougat. The results of aflatoxin levels and aflatoxin mass balance in roasted almonds and nougat obtained from contaminated almonds of batches 1 and 3 and cooked with caramelized sugar or caramelized sugar−honey are reported in Figure 2. Clear reductions of AFB_1 and AFB_2 levels were observed in both types of nougat. The mass balance of toxins confirmed these reductions. For batch 1, the average reductions were 54 and 70% for AFB_1 and 83 and 93% for AFB_2 in sugar nougat and sugar−honey nougat, respectively. Similar reductions were observed for batch 3 (Figure 2B). The contact of almonds with hot caramel may have produced the reduction of aflatoxins. To verify this hypothesis, additional experiments were performed in the absence of almonds. In particular, aliquots of sugar were spiked with AFB_1 (394.7 μg/kg) and AFB_2 (31.7 μg/kg) and then caramelized in a pot and successively analyzed for aflatoxins. For comparison, aliquots of sugar were spiked with the same levels of AFB_1 and AFB_2 and successively analyzed for aflatoxins. The second control was constituted of aliquots of caramelized sugar that were spiked with AFB_1 and AFB_2 and successively analyzed for aflatoxins. As shown in Figure 3 the peaks of AFB_1 and AFB_2 in the chromatogram of spiked sugar submitted to caramelization are markedly lower than the corresponding peaks of spiked sugar and spiked caramelized sugar with an average reduction of 82% for both AFB_1 and AFB_2. This reduction is quantitatively equivalent to the reduction observed during nougat preparation; therefore, the caramelization of sugar may be responsible for aflatoxin reduction. However, mixing almonds with sugar during its caramelization should partially explain the big reduction of aflatoxin observed during nougat preparation because only the surface of almonds is affected by sugar caramelization. On the other hand, almonds contain high levels of sucrose (11−22%) followed by raffinose (0.7−2.1%), glucose (0.4−1.5%), and fructose (0.1−0.6%)[27] that should be caramelized during nougat preparation. Caramelization occurs when food surfaces are heated strongly.[28] Thermally induced

dx.doi.org/10.1021/jf5018548 | J. Agric. Food Chem. 2014, 62, 5707−5715

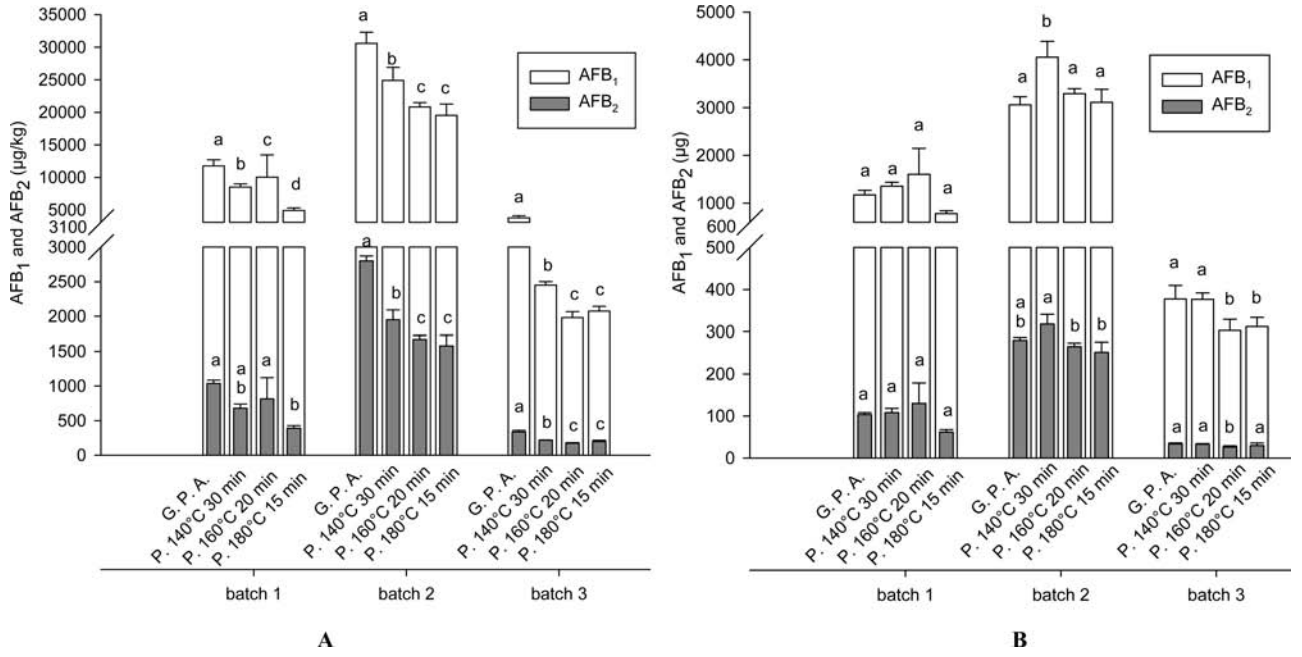

Figure 4. (A) Effect of almond pastry preparation and cooking conditions on aflatoxin levels; (B) relevant mass balance of aflatoxins. G.P.A., ground peeled almonds; P, pastries.

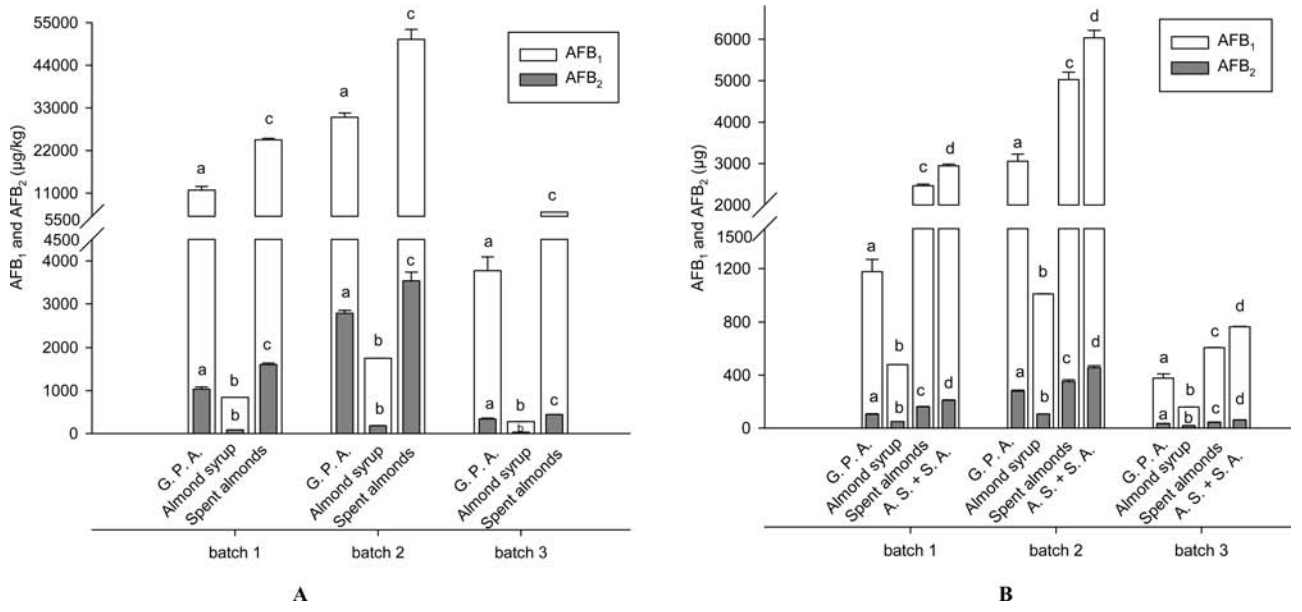

Figure 5. (A) Effect of almond syrup preparation on aflatoxin levels; (B) relevant mass balance of aflatoxins. G.P.A., ground peeled almonds; A.S., almond syrup; S.A., spent almonds.

caramelization of sugars contained in almonds may therefore contribute to the aflatoxin reduction occurring during nougat preparation. Caramelization of almond sugars may also occur during roasting of almonds and may explain the reduction of aflatoxins observed during almond roasting (Tables 2 and 3). Further investigations are necessary to understand if this reduction is a result of degradation or conjugation of aflatoxins with reactive sugar degradation products such as hydroxymethylfurfural, hydroxyacetylfuran, and hydroxydimethylfuranone that have been reported as degradation products formed during sugar caramelization.[28]

Almond Pastries. The results of aflatoxin levels and aflatoxin mass balance in ground peeled almonds and pastries obtained from contaminated almonds of batches 1−3 and cooked at three different temperatures and times are reported in Figure 4. The grinding of peeled almonds allowed a good aflatoxin homogenization as demonstrated by the low SD values for triplicate analyses performed for each batch. In general, mean levels of AFB_1 and AFB_2 in cooked pastries were lower than those measured in ground peeled almonds. However, these reductions were mainly due to the dilution effect of ingredients (sugar and egg white meringue) used for pastry preparation. The whole results of aflatoxin levels and relevant mass balance did not result in a clear trend related to cooking conditions. In particular, the increase of cooking temperature from 140 to 180 °C did not result in a clear

dx.doi.org/10.1021/jf5018548 | J. Agric. Food Chem. 2014, 62, 5707−5715

reduction of aflatoxins also because the increase of temperatures paralleled the reduction in cooking time. Altogether these results suggest that aflatoxins remained substantially stable during the cooking conditions tested in this study, probably because the maximum inner temperature measured in pastries was 98 °C and sugar caramelization should be excluded. The stability of aflatoxins during cooking and baking has been reported by various studies on different matrices. A substantial stability of aflatoxins during cooking of ground peanuts has been reported.[29] Experiments with microwave (700 W for 6 min) and home cooking (177 °C for 45 min) of spice sauces did not produce a significant decrease of aflatoxin levels in the sauce.[30] Baking of biscuits (10 min at 250 °C) produced only a 17% reduction of AFB_1, whereas a greater reduction (89%) was attributed to the mixing of contaminated wheat flour with leavening agents.[31] A significant reduction of AFB_1 was observed during the kneading in preparing bread, whereas no further reduction of AFB_1 was observed during baking.[32] On the other hand, a 34% reduction of AFB_1 was observed during cooking (20 min at 160 °C) of polished rice.[33] We did not use leavening agents for the preparation of almond pastries because they are not required by the recipe.

Almond Syrup. Almond syrup can be prepared by infusing ground peeled almonds with water or with sugared water. After infusion, spent almonds are separated from the infuse, which is boiled until reaching typical syrup consistency. For the infusion conducted only with water, the sugar is added to the infusion after separation of spent almonds. In Figure 5 are shown the results of aflatoxin levels and aflatoxin mass balances in ground peeled almonds, almond syrup, and spent ground peeled almonds obtained from contaminated almonds of batches 1−3. Surprisingly, the levels of AFB_1 and AFB_2 in spent almonds were significantly higher than those measured in ground peeled almonds. These results were confirmed with the mass balance of aflatoxins. On average, for the three batches, the sum of AFB_1 measured in the syrup and spent almonds was more than twice the amount the AFB_1 measured in the initial ground peeled almonds. Similar results were obtained for AFB_2 (Figure 5B). With regard to the passage of aflatoxins from almonds to the syrup, on average, for the three batches, the percentage of total AFB_1 that passed into the syrup was 18%, whereas for AFB_2 it was 25%. These percentages increased to 39 and 46% for AFB_1 and AFB_2, respectively, when they were calculated with respect to aflatoxin levels measured in the initial ground peeled almonds. These results were obtained by infusing ground peeled almonds with water that was successively sugared after separation from spent almonds. The same results were obtained when ground peeled almonds were infused in sugared water. A similar mean percentage of AFB_1 (14%) was transferred into the liquid phase during mashing of naturally contaminated maize grits and malted barley.[34] This is the first study that has monitored aflatoxins during water infusion of contaminated tree nuts. A possible explanation of this robust increment of aflatoxins during water infusion may be the presence of masked aflatoxins in almonds that were released by enzymatic activity because almonds are rich sources of various glycosidases.[35,36] Several masked mycotoxins have been reported to occur in plant-based foods and feeds, but no masked aflatoxins have been identified to date.[37] Further investigations are necessary to confirm the increase of aflatoxin levels during water infusion of naturally contaminated almonds and to isolate and chemically characterize the masked aflatoxins. In conclusion, the main outcomes of this study are the efficacy of processing such as caramelization in reducing aflatoxin levels in almonds and the increase of aflatoxin content in spent almonds after infusion.

AUTHOR INFORMATION

Corresponding Author

*(M.S.) E-mail: michele.solfrizzo@ispa.cnr.it. Phone: +39 080 5929367. Fax: +39 080 5929374.

Funding

This research was supported by EU-FPVII Project MYCORED (KBBE-2007-222690).

Notes

The authors declare no competing financial interest.

ACKNOWLEDGMENTS

We thank Filomena Epifani for her valuable technical assistance.

ABBREVIATIONS USED

AFB_1, aflatoxin B_1; AFB_2, aflatoxin B_2; AFG_1, aflatoxin G_1; AFG_2, aflatoxin G_2; AFtot, total aflatoxins; ISPA, Institute of Sciences of Food Production

REFERENCES

(1) FAOSTAT database, http://faostat3.fao.org/faostat-gateway/go/to/download/Q/QC/E (accessed April 15, 2014).

(2) Council for Agricultural Science and Technology (CAST). *Mycotoxins: Risks in Plant, Animal and Human Systems*, Task Force Report 139; CAST: Ames, IA, USA, 2003.

(3) European Commission. Commission Regulation (EC) no. 1881/2006 of 19 December 2006 setting maximum levels for certain contaminants in foodstuffs. *Off. J. Eur. Union* **2006**, *L364*, 5−24.

(4) European Commission. Commission Regulation (EC) no. 165/2010 of 26 February 2010 amending Regulation (EC) no. 1881/2006 setting maximum levels for certain contaminants in foodstuffs. *Off. J. Eur. Union* **2010**, *L50*, 8−11.

(5) Codex Standard 193−1995. Codex general standard for contaminants and toxins in food and feed, http://www.codexalimentarius.net/download/standards/17/CXS_193e.pdf (accessed April 15, 2014).

(6) EFSA (European Food Safety Authority). Opinion of the scientific panel on contaminants in the food chain on a request from the Commission related to the potential increase of consumer health risk by a possible increase of the existing maximum levels for aflatoxins in almonds, hazelnuts and pistachios derived products. *EFSA J.* **2007**, *446*, 1−127.

(7) RASFF (Rapid Alert System for Food and Feed). RASFF portal, https://webgate.ec.europa.eu/rasff-window/portal/index.cfm?event=searchForm&cleanSearch=1 (accessed April 15, 2014).

(8) Briamonte, L. Il comparto della frutta a guscio in Italia. In *I Quaderni dell'Ortofrutta*; INEA: Roma, Italy, 2007; pp 45−68.

(9) Garcia-Pascual, P.; Mateos, M.; Carbonell, V.; Salazar, D. M. Influence of storage conditions on the quality of shelled and roasted almonds. *Biosyst. Eng.* **2003**, *84*, 201−209.

(10) Campbell, B. C.; Molyneux, R. J.; Schatzki, T. F. Current research on reducing pre- and post-harvest aflatoxin contamination of U.S. almond, pistachio, and walnut. *J. Toxicol. Toxin Rev.* **2003**, *22*, 225−266.

(11) Schade, J. E.; McGreevy, K.; King, A. D.; Mackey, J. R. B.; Fuller, G. Incidence of aflatoxin in California almonds. *Appl. Microbiol.* **1975**, *29*, 48−53.

(12) Schatzki, T. F.; Ong, M. S. Dependence of aflatoxin in almonds on the type and amount of insect damage. *J. Agric. Food Chem.* **2001**, *49*, 4513−4519.

(13) Whitaker, T. B.; Slate, A.; Birmingham, T.; Adams, J.; Jacobs, M.; Grary, G. Correlation between aflatoxin contamination and various

USDA grade categories of shelled almonds. *Food Addit. Contam.* **2010**, *93*, 943−947.
(14) Rodrigues, P.; Venancio, A.; Lima, N. Mycobiota and mycotoxins of almonds and chestnuts with special reference to aflatoxins. *Food Res. Int.* **2012**, *48*, 76−90.
(15) Kabak, B. The fate of mycotoxins during thermal food processing. *J. Sci. Food Agric.* **2009**, *89*, 549−554.
(16) Whitaker, T. B.; Dorner, J. V.; Lamb, M.; Slate, A. B. The effect of sorting farmers' stock peanuts by size and color on partitioning aflatoxin into various shelled peanut grade sizes. *Peanut Sci.* **2005**, *32*, 103−118.
(17) Italian Ministry of Agriculture, Food and Forestry. Thirteenth revision of the national list of traditional food products in the art. 3 comma 3 of the Ministerial Decree of 8 September 1999 n. 350. Official Gazette of the Italian Republic 2013, no. 147, Ordinary Supplement 52.
(18) ITEM Culture Collection Homepage, available online http://www.ispa.cnr.it/Collection/ (accessed April 15, 2014).
(19) Arranz, I.; Sizoo, E.; van Egmond, H.; Kroeger, K.; Legarda, T. M.; Burdaspal, P.; Reif, K.; Stroka, J. Determination of aflatoxin B_1 in medical herbs: interlaboratory study. *J. AOAC Int.* **2006**, *89*, 595−605.
(20) AOAC Official Method 999.07. Aflatoxin B_1 and total aflatoxin in peanut butter, pistachio paste, fig paste and paprika powder. Immunoaffinity column liquid chromatography with post-column derivatization. First Action, 1999.
(21) Iha, M. H.; Trucksess, M. W. Aflatoxins and ochratoxin A in tea prepared from naturally contaminated powdered ginger. *Food Addit. Contam. A* **2010**, *27*, 1142−1147.
(22) Siwela, A. H.; Mukaro, K. J.; Nziramasanga, N. Aflatoxin carryover during large scale peanut butter production. *Food Nutr. Sci.* **2011**, *2*, 105−108.
(23) Yazdanpanah, H.; Mohammadi, T.; Abouhassain, G.; Cheraghali, A. M. Effect of roasting on degradation of aflatoxins in contaminated pistachio nuts. *Food Chem. Toxicol.* **2005**, 1135−1139.
(24) Arzandeh, S.; Jinap, S. Effect of initial aflatoxin concentration, heating time and roasting temperature on aflatoxin reduction in contaminated peanuts and process optimization using response surface modelling. *Int. J. Food Sci. Technol.* **2011**, *46*, 485−491.
(25) Ogunsanwo, B. M.; Faboya, O. O. P.; Idowu, O. R.; Lawal, O. S.; Bankole, S. A. Effect of roasting on the aflatoxin contents of Nigerian peanut seeds. *Afr. J. Biotechnol.* **2004**, *3*, 451−455.
(26) Pluyer, H. R.; Ahmed, E. M.; Wey, C. I. Destruction of aflatoxin on peanuts by oven and microwave roasting. *J. Food Prot.* **1987**, *50*, 504−508.
(27) Barreira, J. C. M.; Pereira, J. A.; Oliveira, M. B. P. P; Ferreira, I. C. F. R. Sugar profiles of different chestnut (*Castanea sativa* Mill.) and almonds (*Prunus dulcis*) cultivars by HPLC-RI. *Plant Foods Hum. Nutr.* **2010**, *65*, 38−43.
(28) Kroh, L. W. Caramelization in food and beverages. *Food Chem.* **1994**, *51*, 373−379.
(29) Njapau, H.; Muzungaile, E. M.; Changa, R. C. The effect of village processing techniques on the contest of aflatoxins in corn and peanuts in Zambia. *J. Sci. Food Agric.* **1998**, *76*, 540−456.
(30) MacDonald, S.; Castle, L. A UK retail survey of aflatoxins in herbs and spices and their fate during cooking. *Food Addit. Contam.* **1996**, *13*, 121−128.
(31) Amra, H. A.; Mahmoud, S. A. Z.; Taha, A. H.; El-Azab, M. A. Fate of afltoxins B_1 and G_1 residues during biscuit processing with or without leavening agents. *Mycotoxin Res.* **1996**, *12*, 99−104.
(32) Reiss, J. Mycotoxins in foodstuffs. XI. Fate of aflatoxin B_1 during preparation and baking of whole-meal bread. *Cereal Chem.* **1978**, *55*, 421−423.
(33) Park, J. W.; Lee, C.; Kim, Y.-B. Fate of aflatoxin B_1 during the cooking of Korean polished rice. *J. Food Prot.* **2005**, *7*, 1336−1534.
(34) Pietri, A.; Bertuzzi, T.; Agosti, B.; Donadini, G. Transfer of aflatoxin B_1 and fumonisin B_1 from naturally contaminated raw materials to beer during an industrial brewing process. *Food Addit. Contam.* **2010**, *27*, 1431−1439.
(35) Zeleny, R.; Leonard, R.; Dorfner, G.; Dalik, T.; Kolarich, D.; Altmann, F. Molecular cloning and characterization of a plant α1,3/4-fucosidase based on sequence tags from almond fucosidase I. *Phytochemistry* **2006**, *67*, 641−648.
(36) Schwartz, J.; Sloan, J.; Lee, Y. C. Mannosidase, glucosidase, and galactosidase in sweet almond emuIsin. *Arch. Biochem. Biophys.* **1970**, *137*, 122−127.
(37) Berthiller, F.; Crews, C.; Dall'Asta, C.; De Saeger, S.; Haesaert, G.; Karlovsky, P.; Oswald, I. P.; Seefelder, W.; Speijers, G.; Stroka, J. Masked mycotoxins: a review. *Mol. Nutr. Food Res.* **2013**, *57*, 165−186.

JOURNAL OF AGRICULTURAL AND FOOD CHEMISTRY

Symposium Introduction

pubs.acs.org/JAFC

Advances in the Understanding of Dairy and Cheese Flavors: Symposium Introduction

ABSTRACT: A symposium titled "Advances in the Understanding of Dairy and Cheese Flavors" was held in September 2013 at the American Chemical Society's 246th National Meeting in Indianapolis, IN, USA. The symposium, which was sponsored by the Division of Agricultural and Food Chemistry, was to discuss the state of the art in the detection and quantitation of flavor in dairy products. The authors of two of the presentations have been selected to expand on their talks by submitting full papers about their research.

The Division of Agricultural and Food Chemistry held the symposium "Chemistry and Flavors of Dairy Products" at the National Meeting of the American Chemical Society (ACS) in Philadelphia in August 2004. ACS Symposium Series Book 971, edited by co-organizers Keith R. Cadwallader, MaryAnne Drake, and Robert J. McGorrin, was published three years later and contained 14 chapters by the presenters. More progress has been made in this field since then, necessitating a new symposium held in September 2013 in Indianapolis.

Milk and the foods made from it are high in calcium, potassium, and protein, but these nutrients confer no advantage to a consumer who does not purchase the product. One study concluded that taste is a prime consideration in the selection of dairy foods, along with health, convenience, and process-related quality,[1] and a study of consumers revealed the top reason for choosing dairy beverages is sensory appeal, ahead of brand, price, health aspects, and other factors.[2] Therefore, much research has been performed around the world on identifying and improving flavors in dairy products. Reviews on flavor compounds in milk,[3] Cheddar cheese,[4] whey protein,[5] and yogurt[6] have been published since 2010, along with reviews of the relationship between sensory and instrumental analysis of dairy products,[7] aroma perception of dairy products,[8] and lactic acid bacteria in cheese flavor development.[9]

The two papers here deal with specific aspects of flavor in dairy products. Bitter peptides are the subject of the paper by Xiaowei Liu, Deshou Jiang, and Devin Peterson, which deals with whey protein hydrolysate. The authors have identified specific bitter peptide sequences and the proteins from which they originated. This research may result in the removal of bitter flavor from a dairy product.

The second paper, by Ming-Kai Cao, Tonya C. Schoenfuss, and Scott A. Rankin, describes the development of flavor in blue cheese, focusing on methyl ketones. The authors varied homogenization pressure and lipase treatment to determine the methyl ketone concentration and extent of lipolysis. Some two-way interactions were observed, indicating that flavor development of blue cheese flavor is complex.

We thank the Division of Agricultural and Food Chemistry for sponsoring the symposium, and we are grateful to the speakers/authors for their contributions. We also thank James Seiber and his editorial staff at the *Journal of Agricultural and Food Chemistry* for their invitation to publish these papers. We hope that they will provide a resource for furthering the progress in the area of dairy flavor analysis.

Michael H. Tunick*,[†]
Sanjay Gummalla[§]

[†]Dairy and Functional Foods Research Unit, Eastern Regional Research Center, Agricultural Research Service, U.S. Department of Agriculture, 600 East Mermaid Lane, Wyndmoor, Pennsylvania 19038, United States

[§]Givaudan Flavors Corp., 1199 Edison Drive, Cincinnati, Ohio 45216, United States

AUTHOR INFORMATION

Corresponding Author

*(M.H.T.) Phone: (215) 233-6454. Fax: (215) 233-6470. E-mail: Michael.Tunick@ars.usda.gov.

Notes

Mention of trade names or commercial products in this paper is solely for the purpose of providing specific information and does not imply recommendation or endorsement by the U.S. Department of Agriculture.

The authors declare no competing financial interest.

REFERENCES

(1) Grunert, K. G.; Bech-Larsen, T.; Bredahl, L. Three issues in consumer quality perception and acceptance of dairy products. *Int. Dairy J.* **2000**, *10*, 575−584.

(2) Krešić, G.; Herceg, Z.; Lelas, V.; Jambrak, A. R. Consumers' behaviour and motives for selection of dairy beverages in Kvarner region: a pilot study. *Mljekarstvo* **2010**, *60*, 50−58.

(3) Wolf, I. V.; Bergamini, C. V.; Perotti, M. C.; Hynes, E. R. Sensory and flavor characteristics of milk. In *Milk and Dairy Products in Human Nutrition: Production, Composition and Health*; Park, Y. W., Haenlein, G. F. W., Eds.; Wiley: Oxford, UK, 2013; pp 310−337.

(4) Murtaza, M.; Ur-Rehman, S.; Anjum, F. M.; Huma, N.; Hafiz, I. Cheddar cheese ripening and flavor characterization: a review. *Crit. Rev. Food Sci. Nutr.* **2014**, *54*, 1309−1321.

(5) Leksrisompong, P. P.; Miracle, R. E.; Drake, M. A. Characterization of flavor of whey protein hydrolysates. *J. Agric. Food Chem.* **2010**, *58*, 6318−6327.

(6) Cheng, H. Volatile flavor compounds in yogurt: a review. *Crit. Rev. Food Sci. Nutr.* **2010**, *50*, 938−950.

Special Issue: Advances in the Understanding of Dairy and Cheese Flavors

Received: August 29, 2013
Published: June 8, 2014

ACS Publications © 2014 American Chemical Society

(7) Croissant, A. E.; Watson, D. M.; Drake, M. A. Application of sensory and instrumental volatile analyses to dairy products. *Annu. Rev. Food Sci. Technol.* **2011**, *2*, 395−421.
(8) Gierczynski, I.; Guichard, E.; Laboure, H. Aroma perception in dairy products: the roles of texture, aroma release and consumer physiology. A review. *Flavour Fragrance J.* **2011**, *26*, 141−152.
(9) Steele, J.; Broadbent, J.; Kok, J. Perspectives on the contribution of lactic acid bacteria to cheese flavor development. *Curr. Opin. Biotechnol.* **2013**, *24*, 135−141.

JOURNAL OF AGRICULTURAL AND FOOD CHEMISTRY

Article

pubs.acs.org/JAFC

Identification of Bitter Peptides in Whey Protein Hydrolysate

Xiaowei Liu, Deshou Jiang, and Devin G. Peterson*

Department of Food Science and Nutrition, 145 FScN Building, University of Minnesota, 1334 Eckles Avenue, St. Paul, Minnesota 55108, United States

ABSTRACT: Bitterness of whey protein hydrolysates (WPH) can negatively affect product quality and limit utilization in food and pharmaceutical applications. Four main bitter peptides were identified in a commercial WPH by means of sensory-guided fractionation techniques that included ultrafiltration and offline two-dimensional reverse phase chromatography. LC-TOF-MS/MS analysis revealed the amino acid sequences of the bitter peptides were YGLF, IPAVF, LLF, and YPFPGPIPN that originated from α-lactalbumin, β-lactoglobulin, serum albumin, and β-casein, respectively. Quantitative LC-MS/MS analysis reported the concentrations of YGLF, IPAVF, LLF, and YPFPGPIPN to be 0.66, 0.58, 1.33, and 2.64 g/kg powder, respectively. Taste recombination analysis of an aqueous model consisting of all four peptides was reported to explain 88% of the bitterness intensity of the 10% WPH solution.

KEYWORDS: *whey protein hydrolysates, bitter, peptides sequence, antihypertensive*

INTRODUCTION

Whey protein is hydrolyzed to generate a product with unique functionality. Protein ingredients with smaller (versus larger) molecular weight peptides have been reported to be more rapidly digested and absorbed[1] to improve the heat stability and solubility in aqueous systems,[2] to be less allergenic than the nonhydrolyzed peptides,[3,4] and also to generate peptides possessing various biological and functional properties.[5−7] Common applications of whey protein hydrolysates (WPH) in the food and healthcare industry include the production of nutritional bars, sports drinks, and hypoallergenic infant formulas, among others.

Hydrolysis of protein can also introduce bitter-tasting attributes that limit the utilization of these ingredients because of their unfavorable influence on product acceptability.[8−11] The degree of hydrolysis on bitterness intensity has been previously investigated in WPH[9] as well as various other flavor defects.[12] In other dairy-based products, the breakdown of protein is well-known to generate bitterness such as cheese,[13−20] casein hydrolysates,[21,22] and other protein-rich ingredients such as soy protein hydrolysates.[23] Peptides have also been isolated to investigate, albeit with limited success, the structure−activity relationships related to bitterness perception.[16,23,24] To our knowledge, no studies have identified the peptides that impart bitterness in commercial WPH. The identification of the bitter peptides provides a more targeted basis to develop bitterness reduction strategies in related products.

The overall goal of this work was to identify the primary bitter peptides in a commercial WPH powder using sensory-directed taste fractionation techniques.

MATERIALS AND METHODS

Chemicals and Materials. A whey protein hydrolysate sample obtained from PGP International was stored at −20 °C. Trifluoroacetic acid, formic acid, and HPLC grade solvents were obtained from Sigma-Aldrich Co. Synthetic peptides YGLF, IPAVF, LLF, and YPFPGPIPN were obtained from EZBiolab Inc.

Ultrafiltration. WPH dissolved at 0.75% (w/v) in water was separated into a low molecular weight fraction (fraction 1) and a high molecular weight fraction (fraction 2) by means of an Amicon 8200 ultrafiltration cell (Millipore, Bedford, MA, USA) using a 3000 Da cutoff membrane (Millipore) at a nitrogen pressure of 30 psi; see Figure 1. Yields were 64 and 36% for fractions 1 and 2 after freeze-drying, respectively.

Preparative High-Performance Liquid Chromatography (Prep-HPLC). The prep-HPLC system consisted of a binary pumping system (Shimadzu, LC-8A), a manual injector (SIL-10vp), a water bath column heater, a variable-wavelength UV−vis detector (Shimadzu, SPD-10A), and a reverse phase C18 column (250 mm × 21.2 mm, pursuit 5, Varian, Palo Alto, CA, USA).

First-Dimensional HPLC Fractionation. Fraction 1 (<3000 Da) was dissolved in water (10%, w/v) and membrane filtered (cellulose acetate membrane syringe filter, 0.45 μm). Aliquots (10 mL) were separated by a preparative C18 column (250 mm × 21.2 mm, pursuit 5, Varian) maintained at 40 °C. Monitoring the effluent at 275 nm, the chromatography was performed using a binary solvent system of water (A) and methanol (B), both containing 0.1% trifluoroacetic acid. The mobile phase consisted of a linear gradient of B in A starting at 10% B in A (0−2 min), increasing to 100% B in A (2−30 min), and then held at 100% for 5 min (30−35 min). The flow rate was 15 mL/min. The effluent was collected into 26 fractions with a fraction collector (Figure 2). The corresponding fractions (termed 1-1−1-26) obtained from several runs were pooled and liberated from solvent (freeze-dried two times). The resulting residues obtained were then dissolved in water (10 mL) and evaluated for bitterness intensity by sensory analysis.

Second-Dimensional HPLC Fractionation. HPLC fractions 1-17, 1-18, and 1-19 were individually dissolved in 10 mL of water, and after membrane filtration (cellulose acetate membrane syringe filter, 0.45um), aliquots (5 mL) were further fractionated by preparative RP HPLC using a C18 column (250 mm × 21.2 mm, pursuit 5, Varian). The mobile phase consisted of a binary solvent system of 10 mM

Special Issue: Advances in the Understanding of Dairy and Cheese Flavors

Received: May 9, 2013
Revised: September 2, 2013
Accepted: September 3, 2013
Published: September 3, 2013

ACS Publications © 2013 American Chemical Society

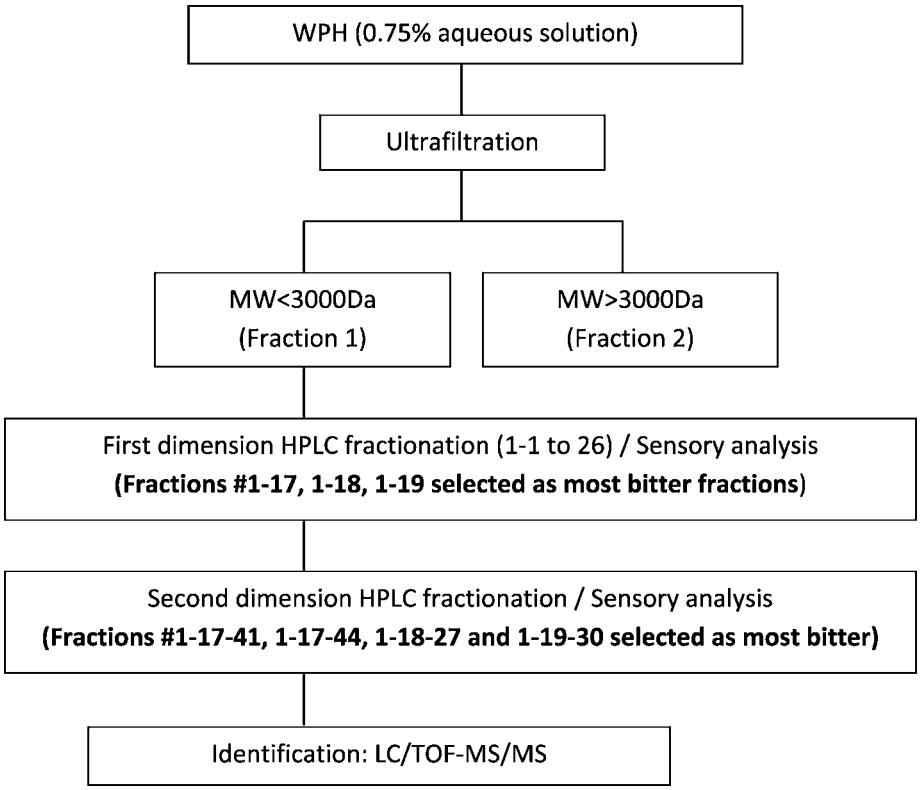

Figure 1. Separation scheme for identification of bitter peptides from WPH.

ammonium acetate, pH 5 (A), and acetonitrile (B). Chromatography was performed using a linear gradient at a flow rate of 15 mL/min monitored at 220 nm. The mobile phase conditions were as follows: for fraction 1-17, initially 15% B in A (0−25 min), increasing to 30% B in A (25−55 min), then held at 30% for 5 min (55−60 min); for fraction 1-18, initially 16% B in A (0−25 min), increasing to 35% B in A (25−60 min), then increasing to 100% B in A (60−61 min), held at 100% for 5 min (61−66 min); for fraction 1-19, initially at 17% B in A (0−25 min), increasing to 40% B in A (25−70 min), then increasing to 100% B in A (70−71 min), held at 100% for 5 min (71−76 min). Total numbers of subfractions collected were for fraction 1-17, 56 (1-17-1 to 1-17-56); for fraction 1-18, 58 (1-18-1 to 1-18-58); and for fraction 1-19, 58 (1-19-1 to 1-19-58). All subfractions were liberated from solvent (freeze-dried two times) and dissolved in water (5 mL) for subsequent sensory analysis.

LC-MS/MS-ESI. Analysis was performed with a Waters Ultra-Performance LC system (Waters ACQUITY UPLC) coupled with a Waters triple-quadrupole mass spectrometer (Waters Quattro Premier XE) equipped with an electrospray ionization (ESI) probe. The UPLC system included the ACQUITY UPLC sample organizer, column manager and heater/cooler, binary solvent manager, sample manager, and a reverse phase C18 column (XTerra RP18 column, 3.5 μm, 100 mm × 2.1 mm). Mass spectrometric ionization conditions were as follows: desolvation temperature, 250 °C; source temperature, 110 °C; capillary voltage, 3 kV. MRM methods setup, ion transitions, cone voltages, and collision energies were optimized via autotune.

LC-MS/Qtof-ESI. Analysis was conducted with an Acquity UPLC system coupled with a Waters Qtof G2 mass spectrometer equipped with an electrospray ionization (ESI) probe, run in positive mode. The UPLC system consisted of a degasser, a binary pumping system, an autosampler, a column heater, and a reverse phase C18 column (XBridge RP18 column, 2.5 μm, 50 mm × 2.1 mm). Mass spectrometric ionization conditions were as follows: desolvation temperature, 400 °C; source temperature, 120 °C; capillary voltage, 3 kV. For scan mode, the range of m/z was 100−2300; for daughter ion analysis, a collision energy ramp was used, ramping from 40 to 120 eV.

Purification of Synthetic Peptides. Purchased synthetic peptides were purified prior to use for sensory analysis. The individual peptides dissolved in water were purified by a preparative C18 column (250 mm × 21.2 mm, pursuit 5, Varian) using a water/methanol gradient at a flow rate of 15 mL/min. Purified peptides were freeze-dried twice prior to use.

Quantification of Bitter Peptides in WPH. Analysis was conducted using an Acquity UPLC system coupled with a Quattro Premier XE mass spectrometer (Waters Co., Milford, MA, USA). An Acquity UPLC 2.1 × 100 mm HSS C18 1.8 μm column with a VanGuard 2.1 × 5 mm HSS C18 1.8 μm precolumn was used for separation. The mass spectrometer was operated in positive ion mode, and the spectra were collected by multiple reaction monitoring (MRM). MRM methods were set up via autotune. For an internal standard, leucine enkephalin ion transition 556 → 136 was monitored. For peptides YGLF, YPFPGPIPN, IPAV,F and LLF, ion transitions 499 → 86, 1001 → 337, 546 → 169, and 392 → 199 were monitored, respectively. Individual synthetic peptides were dissolved in water, and five-point calibration curves were constructed using the peak areas obtained from corresponding ion transitions. Quantitative analysis was performed in triplicate.

Sensory Analysis. A trained sensory panel, ages 22 to 45 years, consisting of two males and five females evaluated the bitterness intensity of the peptide fractions, a commercial WPH sample, and recombination models. All evaluations were conducted with nose clips by a sip and spit method. Samples were evaluated on a 15-point intensity scale, anchored on the left with "none" and on the right with "extreme". Three reference levels were provided to panelists (0.03, 0.08, and 0.15% of caffeine w/w in water), corresponding to bitterness intensity ratings of 2, 5 and 10, respectively.[1] Judge's performance was evaluated by ANOVA. The reconstituted models and fraction samples were evaluated in duplicate. Panelists were instructed to wait 5 min between samples; water and unsalted crackers were used as palate cleansers. Sensory data were analyzed using ANOVA with mean separation to determine differences in bitterness between the commercial WPH sample and the recombinant model (Excel 2010, Microsoft).

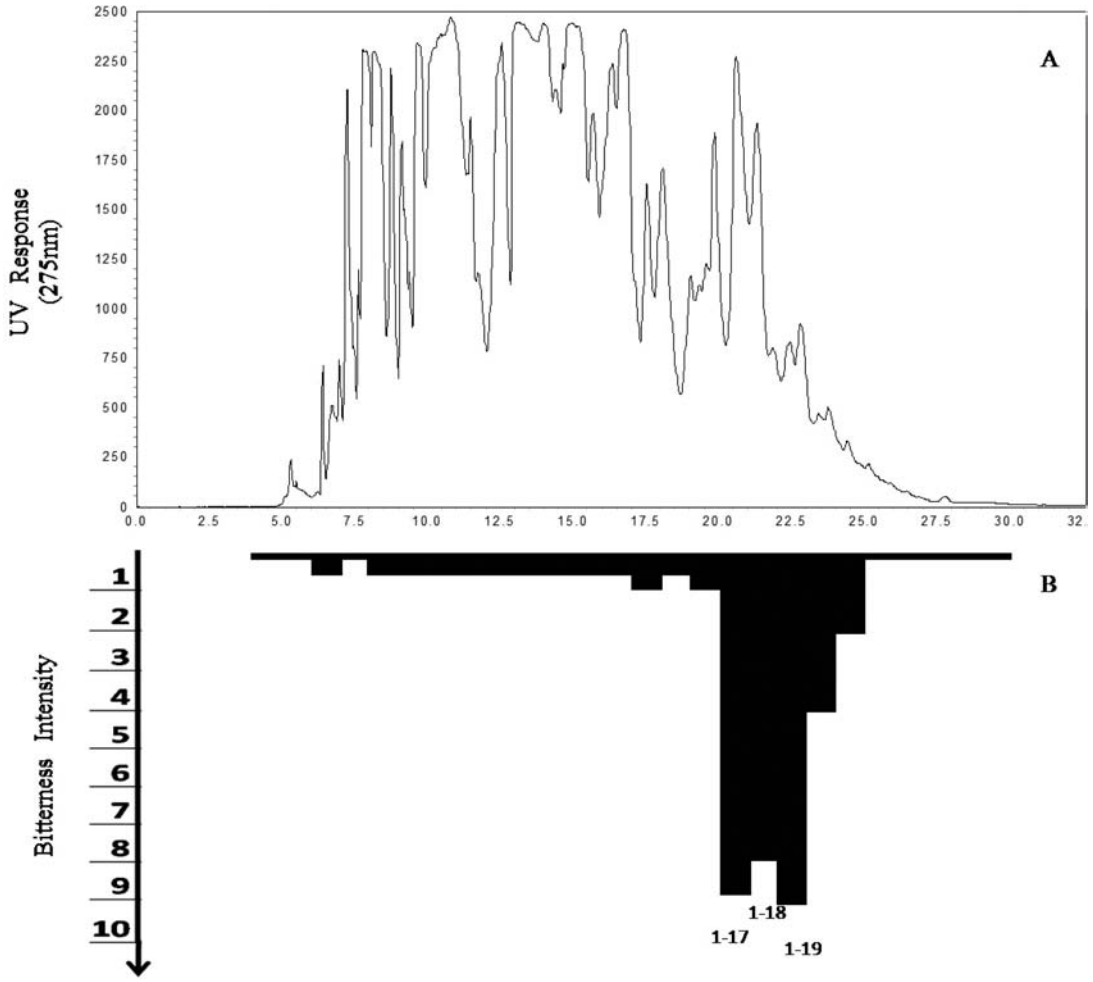

Figure 2. First-dimension HPLC-UV chromatogram (A) and taste intensity chromatogram (B) of low molecular weight fraction. Numbers listed indicate most bitter fractions perceived and selected for further investigation; bitterness scale levels of 2, 5, and 10 were equivalent to 0.05, 0.08, and 0.15% caffeine aqueous solution.

Recombination Sensory Analysis. A bitter taste 10% WPH model was prepared by dissolving four purified peptides, YGLF (0.66 mg), YPFPGPIPN (2.64 mg), IPAVF (0.58 mg), and LLF (1.33 mg), in 100 mL of water. A commercial WPH sample was also prepared for comparison by dissolving 10 g of WPH in 100 mL of water. The bitterness intensity of each individual peptide was also evaluated at the corresponding concentrations of a 10% WPH solution.

RESULTS AND DISCUSSION

The compounds responsible for the bitterness of a 10% w/v WPH solution (see Table 1) were characterized. On the basis of prior literature indicating that the bitter taste of WPH was correlated to lower molecular weight peptides,[12] ultrafiltration was selected as the initial preparative step. Using a 3 kDa cutoff membrane, the dissolved WPH sample was separated into a low molecular weight fraction and a high molecular weight fraction (Figure 1). These two fractions after freezing-drying were redissolved in water at the same concentrations as the original 10% (w/v) WPH solution. The 10% (w/v) WPH sample was also prepared for comparison. Sensory analysis of these three samples revealed that the bitter-taste peptides in WPH sample were located in the low molecular weight fraction, whereas the high molecular weight fraction was tasteless.

The low molecular weight fraction (1) was subsequently further separated by preparative RP-C18 column (mobile phase with TFA at pH 2) to give 26 fractions (Figure 2A), which were freed from solvents (freeze-dried twice), dissolved in 10 mL of bottled water for sensory analysis. Fractions 1-17, 1-18, and 1-19 were rated with the highest bitterness intensity, all of which were rated close to a score of 10, or similar to a 0.15% caffeine solution (Figure 2B).

Because the retention times of ionizable peptides on a RP column are sensitive to the mobile phase pH, second-dimensional HPLC was performed using the same RP column, but with different mobile phase pH. Separation of fractions 1-

Table 1. Mean Bitterness Intensity Ratings of a 10% WPH Aqueous Solution and Related Taste Recombination Models

sample	bitterness intensity[a]
10% WPH sample	8.5 ± 0.3
YGLF[b]	2.3 ± 0.2
YPFPGPIPN[b]	0.9 ± 0.1
IPAVF[b]	3.8 ± 0.3
LLF[b]	1.1 ± 0.2
taste recombination model − four peptides (YGLF, YPFPGPIPN, IPAVF, and LLF)[b]	7.5 ± 0.7

[a]Bitterness rankings 2, 5, and 10 are equivalent to 0.03, 0.08, and 0.15% caffeine aqueous solutions, respectively; 95% confidence interval shown. [b]Peptides at equivalent concentration as 10% WPH sample.

dx.doi.org/10.1021/jf4019728 | J. Agric. Food Chem. 2014, 62, 5719−5725

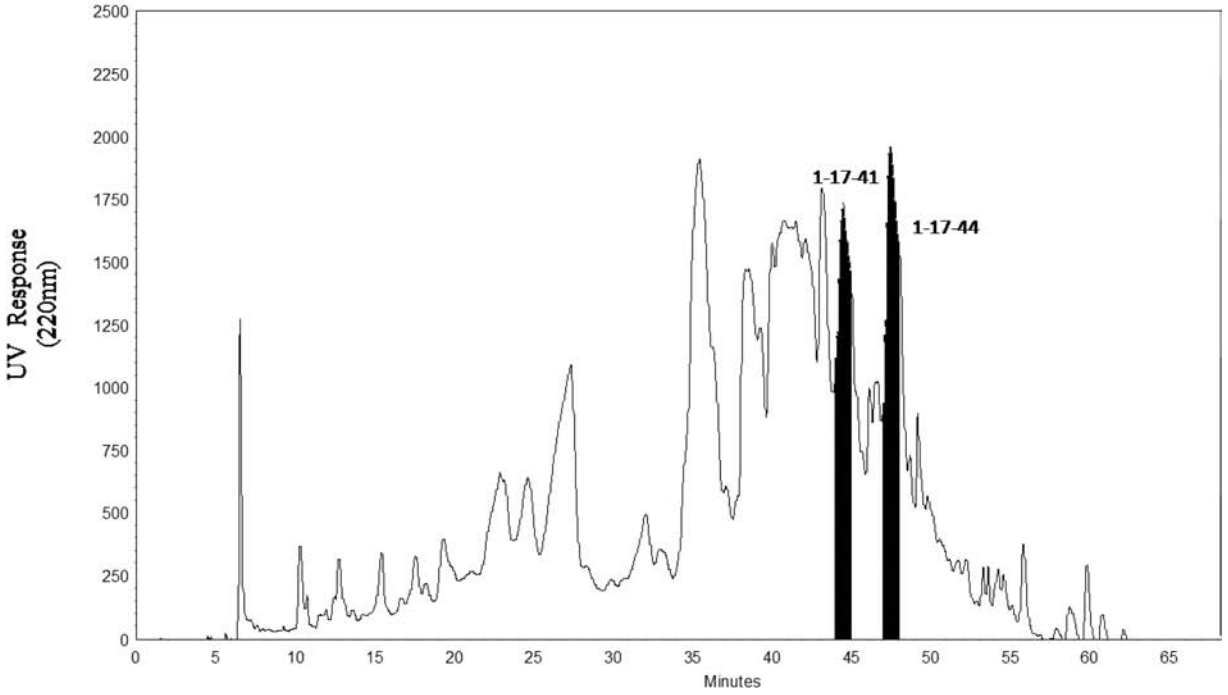

Figure 3. Second-dimension HPLC-UV chromatogram of fraction 1-17. Highlighted fractions are primary bitter fractions.

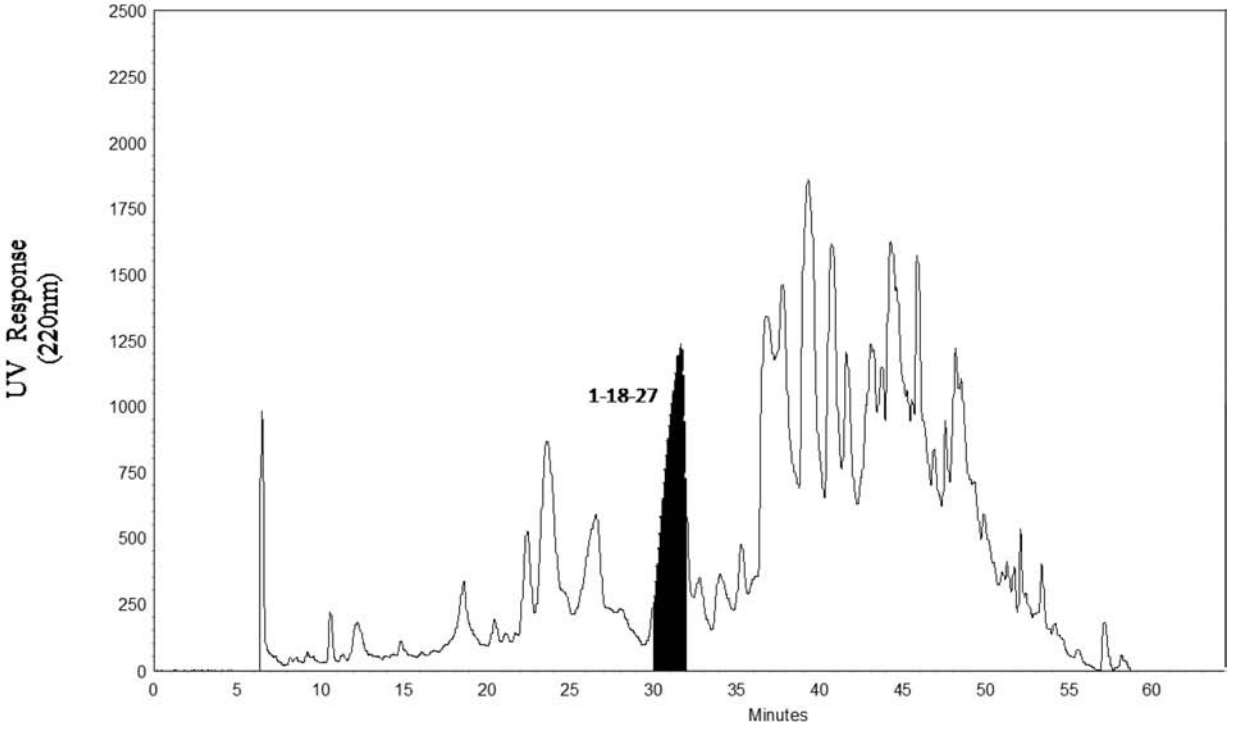

Figure 4. Second-dimension HPLC-UV chromatogram of fraction 1-18. Highlighted fraction is primary bitter fraction.

17, 1-18, and 1-19 by means of preparative RP C18 (mobile phase with ammonium acetate at pH 5) yielded 56 (1-17-1 to 1-17-56), 58 (1-18-1 to 1-18-58), and 58 (1-19-1 to 1-19-58) subfractions, respectively (Figures 3, 4, and 5). All of the subfractions were freed from solvents (freeze-dried twice) and dissolved in 4 mL of water for sensory analysis. Among these samples, four pronounced bitter subfractions were identified (1-17-41, 1-17-44, 1-18-27, and 1-19-30), the intensities of which were rated as 8, 10, 5, and 8, respectively, and were primarily responsible for the bitterness of the corresponding parent fractions. Each of these four subfractions was subsequently analyzed by LC-MS. One major peptide (based on m/z intensity) was reported in each respective fraction, and the sequence was identified by LC-TOF-MS/MS analysis with variable collision energy. The MS spectrum for one elucidated peptide (IPAVF) is shown in Figure 6; Y and B ions and possible internal ions are labeled. For subfraction 1-19-30, two peptide sequences were possible, ILF or LLF. The retention

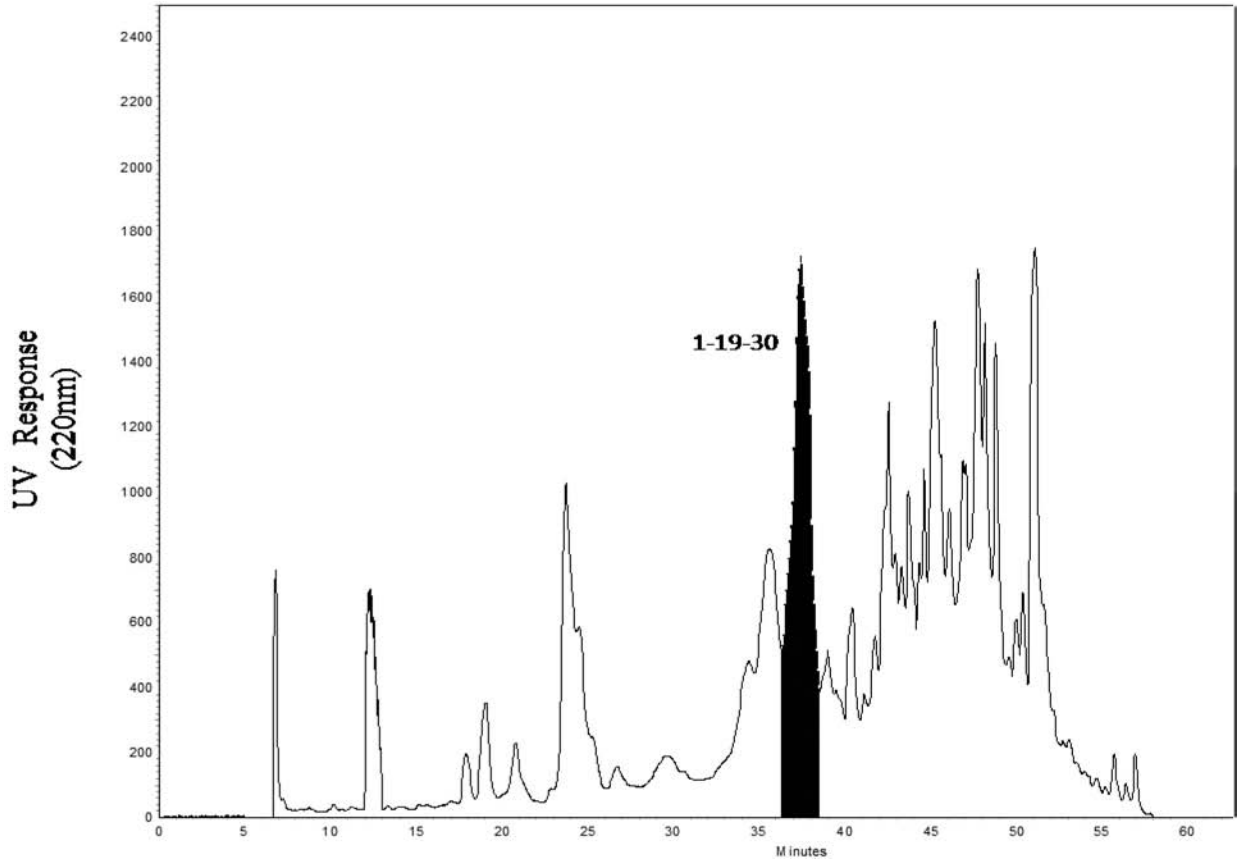

Figure 5. Second-dimension HPLC-UV chromatogram of fraction 1-19. Highlighted fraction is primary bitter fraction.

times of authentic peptides ILF and LLF were compared to the corresponding peptide in the sample, and the sequence LLF was correctly identified.

The concentrations of the bitter peptides YGLF, YPFPGPIPN, IPAVF, and LLF were subsequently determined to be 0.66, 2.64, 0.58, and 1.33 g/kg powder (Table 2). To determine the contribution of these peptides to the overall bitterness of the 10% WPH solution, the bitterness intensity of each peptide, as well as the resultant mixture, was evaluated by sensory analysis. Each peptide was reported to be bitter (Table 1) and, when added as a mixture, was reported to have a bitterness intensity rating of 7.5 compared to 8.5 for the reference (10% WPH solution); sample means were significantly different (p value = 0.02; LSD critical difference = 0.8). The four peptides explained on average 88% of the bitterness intensity reported in the reference WPH sample. Further evaluation of the bitterness potency of each peptide as measured by dividing the perceived bitterness intensity by the concentration of each peptide in the aqueous sample is shown in Table 2 (termed the taste intensity value (TIV)). The two peptides at the lowest concentrations were reported to be the most potent (YGLF and IPAVF) with the highest bitterness response per unit concentration.

On the basis of previously reported bitter peptides, researchers have attempted to elucidate structure−activity relationships. Ney[25] introduced the Q rule, pointing out a relationship existing between the degree of hydrophobicity and if a peptide was bitter (or not). The degree of hydrophobicity (the Q value) was calculated using the equation $(\sum\Delta f)/n$, where $\sum\Delta f$ is the sum of the hydrophobicity values of all the amino acid side chains of a peptide and n is the number of amino acid residues. Peptides (up to 6000 Da) with a Q value > 1400 cal/res were predicted to have a bitter taste. The Q values for the bitter peptides identified in the current study were also calculated on the basis of the free energy (Δf) values of amino acid side chains[26,27] and determined to be 1985, 2107, 2132, and 2497 cal/res for YGLF, YPFPGPIPN, IPAVF, and LLF, respectively. Although bitterness perception of a peptide cannot be solely predicted by the Q value,[16] our data supported the Q rule. The Q rule merely predicts peptides that may be bitter. The limitations of the Q calculation are that it does not account for the amino acid sequence (or geometry) on bitter taste, much less take into account if the compound is perceived (is above the sensory threshold). More recently, others[24] have correlated the bitterness of di- and tripeptides with a bulky hydrophobic amino acid at the C-terminus and a bulky amino acid at the N-terminus, whereas for larger peptides the bulky N-terminal amino acid was specific to basic amino acids. Our finding was in line with C-terminal postulation, but not in line with the N-terminal. Phenylalanine has been considered to be a functional residue of the bitter taste of peptides based on primary structures of three bitter peptides isolated from casein hydrolysates.[28] It has also been suggested that the bitterness of a peptide might be enhanced when its amino or carboxyl groups are blocked by forming peptide bonds.[10,28] This hypothesis was supported by our results. The four bitter peptides identified from the WPH sample all consist of a phenylalanine residue bonded with other amino acids via an amino group or both amino and carboxyl groups.

Whey proteins are typically considered a mixture of β-lactoglobulin, α-lactalbumin, and serum albumin. Sequence alignment of the four peptides identified in this study (see Figure 7) revealed the origin of YGLF in fraction 1-17-41 was

dx.doi.org/10.1021/jf4019728 | J. Agric. Food Chem. 2014, 62, 5719−5725

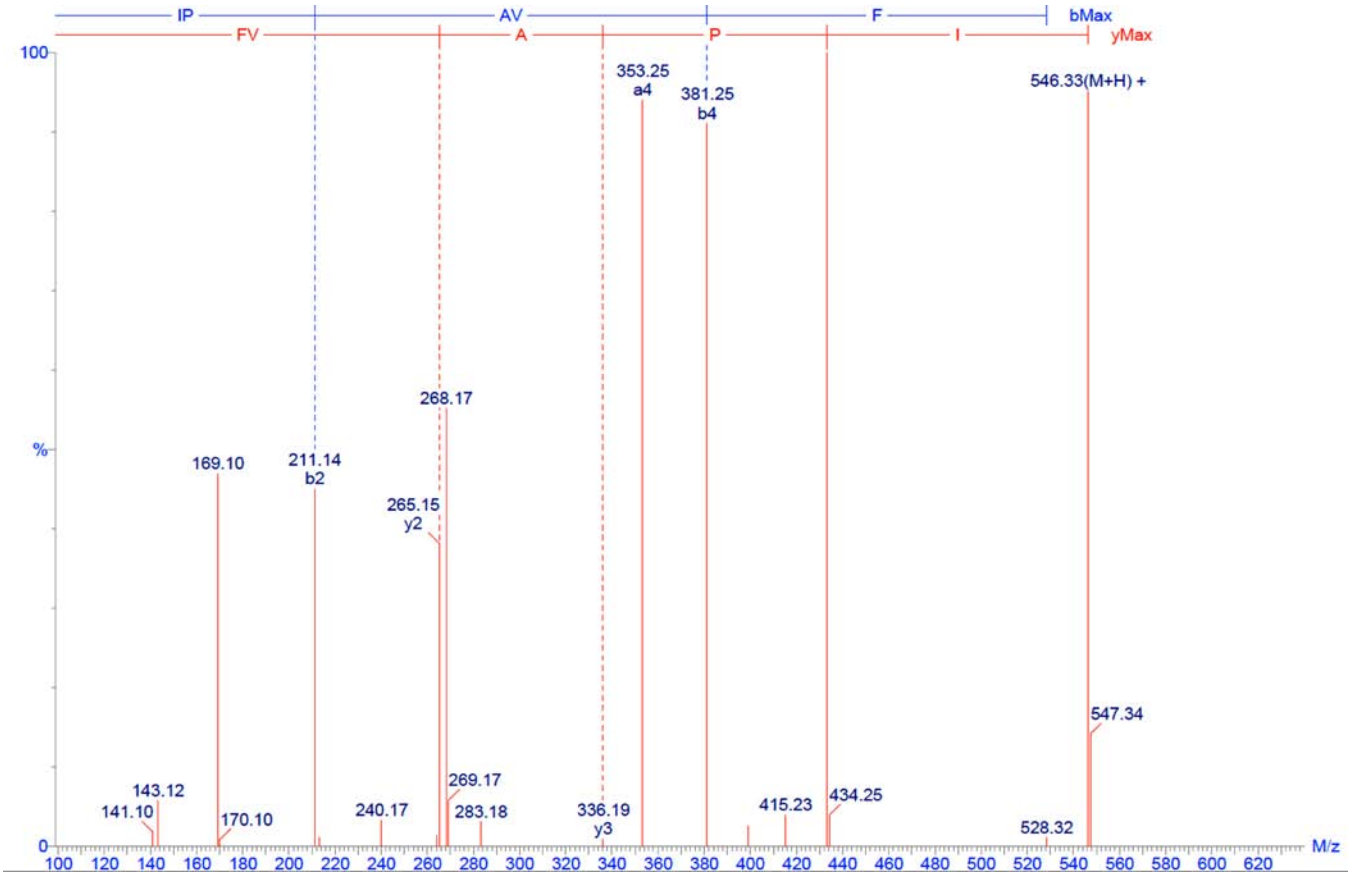

Figure 6. MS/MS spectrum (ESI^+) of the bitter peptide IPAVF in fraction 1-17-44.

Table 2. Concentration and Taste Intensity Value of Select Peptides in WPH

peptide	concentration, g/kg powder (% COV)[a]	taste intensity value (bitterness intensity/concentration)[b]
YGLF	0.66 (1.4)	3.6
YPFPGPIPN	2.64 (3.7)	0.3
IPAVF	0.58 (2.7)	6.5
LLF	1.33 (0.5)	1.1

[a]Average of triplicates (percent coefficient of variation). [b]At equivalent aqueous solution concentration as a 10% WPH solution.

from α-lactalbumin, IPAVF in fraction 1-18-27 was from β-lactoglobulin, and LLF in fraction 1-19-30 was from serum albumin, whereas YPFPGPIPN in fraction 1-17-44 originated from β-casein, which has also been identified as a bitter metabolite in cheese.[16] This indicated the bitterness of our WPH sample partly came from contamination of casein when whey was isolated from cheese.

Interestingly, the four bitter peptides identified in WPH in the current study have been previously reported to have positive health bioactivities. Peptides YGLF,[29,30] YPFPGPIPN,[30−32] and LLF[30,33] have been previously demonstrated to be antihypertensive peptides and lowered blood pressure in a spontaneously hypertensive rat (SHR) model. IPAVF could be

beta-lactoglobulin

61 elkptpegdl eillqkweng ecaqkkiiae ktkipavfki dalnenkvlv ldtdykkyll 120

alpha-lactalbumin

61 vqnndstevg lfqinnkiwc kddqnphssn icnisdkfl dddltddimc vkkildkvgi 120

serum albumin

1 mkwvtfisll llfssaysrg vfrrdthkse iahrfkdlge ehfkglvlia fsqylqqcpf 60

beta-casein

61 qdkihpfaqt qslvypfpgp ipnslpqnip pltqtpvvvp pflqpevmgv skvkeamapk 120

Figure 7. Select regions of primary structures of β-lactoglobulin, α-lactalbumin, serum albumin, and β-casein and related assignments of identified peptides.

dx.doi.org/10.1021/jf4019728 | J. Agric. Food Chem. 2014, 62, 5719−5725

transformed to IPA during digestion in the human intestinal tract, whereas IPA possessed antihypertensive activity in SHR.[34] This observation is another example of the correlation between bitter taste and potential bioactivity and suggests potential complications of removing bitterness for acceptability while maintaining potential positive health benefits.

AUTHOR INFORMATION

Corresponding Author

*(D.G.P.) E-mail: dgp@umn.edu. Phone: (612) 624-3201. Fax: (612) 625-5272.

Notes

The authors declare no competing financial interest.

REFERENCES

(1) Webb, K. E. Intestinal absorption of protein hydrolysis products: a review. *J. Anim. Sci.* **1990**, *68*, 3011−3022.

(2) Nathalie, C.; Gruppen, H. Hydrolysis of whey protein isolate with bacillus licheniformis protease: fractionation and identification of aggregating peptides. *J. Agric. Food Chem.* **2007**, *55*, 9241−9250.

(3) Isolauri, E.; Sutas, Y.; Turjanmaa, K. Efficacy and safety of hydrolyzed cow milk and amino acid-derived formulas in infants with cow milk allergy. *J. Pediatr.* **1995**, *127*, 550−557.

(4) Rango, V.; Giampietro, P. G.; Bruno, G.; Businco, L. Allergenicity of milk protein hydrolysate formulae in children with cow's milk allergy. *Eur. J. Pediatr.* **1993**, *152*, 760−762.

(5) Nnanna, I. A.; Wu, C. Diary protein hydrolysates. *Handbook of Food Products Manufacturing*; Hui, Y. H., Ed.; Wiley: Hoboken, NJ, 2007; Vol. 2, pp 537−556.

(6) Sinha, R.; Radha, C.; Prakash, J.; Kaul, P. Whey protein hydrolysate: functional properties, nutritional quality and utilization in beverage formulation. *Food Chem.* **2007**, *101*, 1484−1491.

(7) Gauthier, S. F.; Pouliot, Y. Functional and biological properties of peptides obtained by enzymatic hydrolysis of whey proteins. *J. Dairy Sci.* **2003**, *86*, 78−87.

(8) Lemieux, L.; Simard, R. E. Bitter flavor in dairy products. *Lait* **1992**, *72*, 335−382.

(9) Spellman, D.; Ocuinn, G.; FitzGerald, R. J. Bitterness in bacillus proteinase hydrolysates of whey proteins. *Food Chem.* **2009**, *114*, 440−446.

(10) Maehashi, K.; Huang, L. Bitter peptides and bitter taste receptors. *Cell. Mol. Life Sci.* **2009**, *66*, 1661−1671.

(11) Aubes-Dufau, I.; Seris, J. L.; Combes, D. Production of peptic hemoglobin hydrolysates: bitterness demonstration and characterization. *J. Agric. Food. Chem.* **1995**, *43*, 1982−1988.

(12) Leksrisompong, P. P.; Miracle, R. E.; Drake, M. Characterization of flavor of whey protein hydrolysates. *J. Agric. Food Chem.* **2010**, *58*, 6318−6327.

(13) Lee, K. P.; Warthesen, J. J. Preparative methods of isolating bitter peptides from cheddar cheese. *J. Agric. Food Chem.* **1996**, *44*, 1058−1063.

(14) Hamilton, J. S.; Hill, R. D.; Van Leeuwen, H. Bitter peptides from cheddar cheese. *Agric. Biol. Chem.* **1974**, *38*, 375−379.

(15) Champion, H. M.; Stanley, D. W. HPLC separation of bitter peptides from cheddar cheese. *Can. Inst. Food Sci. Technol. J.* **1982**, *15*, 283−288.

(16) Toelstede, S.; Hofmann, T. Sensomics mapping and identification of the key bitter metabolites in gouda cheese. *J. Agric. Food Chem.* **2008**, *56*, 2795−2804.

(17) Guigoz, Y.; Solms, J. Isolation of a bitter tasting peptide from alpkaese, a Swiss-mountain cheese. *Lebensm.-Wiss. Technol.* **1974**, *7*, 356−357.

(18) Huber, L.; Klostermeyer, H. Isolation and identification of a bitter peptide from butterkaese cheese. *Milchwissenschaft* **1974**, *29*, 449−455.

(19) Engel, E.; Nicklaus, S.; Septier, C.; Salles, C.; Le Quere, J. L. Evolution of the taste of a bitter camembert cheese during ripening: characterization of a matrix effect. *J. Agric. Food Chem.* **2001**, *49*, 2930−2939.

(20) Fallico, V.; McSweeney, P. L. H.; Horne, J.; Pediliggieri, C.; Hannon, J. A.; Carpino, S.; Licitra, G. Evaluation of bitterness in ragusano cheese. *J. Dairy Sci.* **2005**, *88*, 1288−1300.

(21) Nakatani, M.; Nakata, T.; Kouge, K.; Okai, H. Studies on bitter peptides from casein hydrolyzate. *Bull. Chem. Soc. Jpn.* **1994**, *67*, 438−444.

(22) Bumberger, E.; Belitz, H. D. Bitter taste of enzymatic hydrolysates of casein. *Z. Lebensm. Unters. Forsch.* **1993**, *197*, 14−19.

(23) Cho, M. J.; Unklesbay, N.; Hsieh, F. H.; Clarke, A. D. Hydrophobicity of bitter peptides from soy protein hydrolysates. *J. Agric. Food Chem.* **2004**, *52*, 5895−5901.

(24) Kim, H. O.; Li-Chan, E. C. Y. Quantitative structure-activity relationship study of bitter peptides. *J. Agric. Food Chem.* **2006**, *54*, 10102−10111.

(25) Ney, K. H. Prediction of bitterness of peptides from their amino acid composition. *Z. Lebensm. Unters. Forsch.* **1971**, *147*, 64−71.

(26) Tanford, C. Contribution of hydrophobic interactions to the stability of the globular conformation of proteins. *J. Am. Chem. Soc.* **1962**, *84*, 4240−4247.

(27) Ney, K. H. Bitterness of peptides: amino acid composition and chainlength. *ACS Symp. Ser.* **1979**, *No. 115*, 149−173.

(28) Matoba, T.; Hayashi, R.; Hata, T. Isolation of bitter peptides from tryptic hydrolysate of casein and their chemical structure. *Agric. Biol. Chem.* **1970**, *34*, 1235−1243.

(29) Nurminen, M. L.; Sipola, M.; Kaarto, H.; Piilola, K.; Korpela, R.; Tossavainen, O.; Korhonen, H.; Vapaatalo, H. α-Lactorphin lowers blood pressure measured by radiotelemetry in normotensive and spontaneously hypertensive rats. *Life Sci.* **2000**, *66*, 1535−1543.

(30) Hernandez-Ledesma, B.; Contreras, M. D. M.; Recio, I. Antihypertensive peptides: production, bioavailability and incorporation into foods. *Adv. Colloid Interface Sci.* **2011**, *165*, 23−35.

(31) Saito, T.; Nakamura, T.; Kitazawa, H.; Kawai, Y.; Itoh, T. Isolation and structural analysis of antihypertensive peptides that exit naturally in gouda cheese. *J. Dairy Sci.* **2000**, *83*, 1434−1440.

(32) Fitzgerald, R. J.; Murray, B. A. Bioactive peptides and lactic fermentations. *Int. J. Dairy Technol.* **2006**, *59*, 118−125.

(33) Hermandez-Ledesma, B.; Miquel, M.; Amigo, L.; Aleixandre, M. A.; Recio, I. Effect of simulated gastrointestinal digestion on the antihypertensive properties of synthetic β-lactoglobulin peptides sequences. *J. Dairy Res.* **2007**, *74*, 336−339.

(34) Janssen, J. G.; Schalk, J. (Unilever Intellectual Property Group, USA). Peptides having an ACE inhibiting effect. U.S. 20060216330A1, Sept 28, 2006.

JOURNAL OF AGRICULTURAL AND FOOD CHEMISTRY

Article

pubs.acs.org/JAFC

Homogenization and Lipase Treatment of Milk and Resulting Methyl Ketone Generation in Blue Cheese

Mingkai Cao,[†] Leorges M. Fonseca,[†,§] Tonya C. Schoenfuss,[#] and Scott A. Rankin*[,†]

[†]Department of Food Science, University of Wisconsin—Madison, 1605 Linden Drive, Madison, Wisconsin 53706, United States

[§]School of Veterinary Medicine, Universidade Federal de Minas Gerais, Av. Antonio Carlos 6627, Belo Horizonte, MG 31270-901, Brazil

[#]Department of Food Science and Nutrition, University of Minnesota, St. Paul, Minnesota 55108, United States

ABSTRACT: A specific range of methyl ketones contribute to the distinctive flavor of traditional blue cheeses. These ketones are metabolites of lipid metabolism by *Penicillium* mold added to cheese for this purpose. Two processes, namely, the homogenization of milk fat and the addition of exogenous lipase enzymes, are traditionally applied measures to control the formation of methyl ketones in blue cheese. There exists little scientific validation of the actual effects of these treatments on methyl ketone development. The present study evaluated the effects of milk fat homogenization and lipase treatments on methyl ketone and free fatty acid development using sensory methods and the comparison of selected volatile quantities using gas chromatography. Initial work was conducted using a blue cheese system model; subsequent work was conducted with manufactured blue cheese. In general, there were modest effects of homogenization and lipase treatments on free fatty acid (FFA) and methyl ketone concentrations in blue cheese. Blue cheese treatments involving *Penicillium roqueforti* lipase with homogenized milk yielded higher FFA and methyl ketone levels, for example, a ∼20-fold increase for hexanoic acid and a 3-fold increase in 2-pentanone.

KEYWORDS: *blue cheese, homogenization, lipase, ketone, GC-MS*

INTRODUCTION

Blue cheese is noted for its distinctive moldy flavor and blue-green veined appearance, both of which result from metabolic activities of the mold *Penicillium roqueforti*. Characteristic blue cheese flavor is caused by the presence of a collection of methyl ketones, especially 2-pentanone, 2-heptanone, and 2-nonanone, each derived from fatty acid metabolism[1] via β-oxidative pathways.[2] Current industry practices consider several practices for managing methyl ketone accumulation including the use of raw milk (as a source of native lipoprotein lipase), milk fat homogenization, and exogenous lipase addition. However, there is little scientific underpinning for the practices of homogenization and lipase addition.

Typical homogenization practices in the United States for dairy products involve the mechanical pumping of milk at high pressures through small openings, resulting in a partial disruption of the milk fat globule membrane, a reduction in the average particle size, and an increase in milk fat droplet surface area. As applied to blue cheese manufacture, these physical changes to the milk fat globule are thought to enable increased enzymatic and metabolic activities through improved access to the milk fat triglyceride substrate. Subsequently, lipase addition to homogenized milk, as an industry practice for blue cheese manufacture, is based on the hypothesis that increasing free fatty acid (FFA) concentration is a contributing factor for the conversion of milk fat into corresponding methyl ketone derivatives.

There are few data available to factually conclude that milk fat homogenization in conjunction with lipase addition is a functional control mechanism for the generation of methyl ketones and thus a means of controlling blue cheese flavor. Therefore, the present study examined the effects of milk fat homogenization and the addition of exogenous lipase on the generation of methyl ketones and blue cheese flavor. Lipase and homogenization variables were evaluated in a model system using instrumental measures of FFA and methyl ketone volatiles, followed by a subsequent study with pilot-scale manufactured blue cheeses evaluated for FFA and methyl ketone volatiles and by an evaluation of specific sensory attributes associated with blue cheese flavor and these treatment variables. The hypotheses of this work are that homogenization and lipase treatments of milk are means of controlling methyl ketone production in a blue cheese system through the modification of the milk fat globule and the liberation of FFA substrate, respectively.

MATERIALS AND METHODS

Materials and Reagents. Raw milk for the model system was obtained from Babcock Dairy Plant (Madison, WI, USA) and for the cheese manufacture from Land O'Lakes (Arden Hills, MN, USA). Fresh cheese for use as cheese matrix base was obtained from Roth Kase USA, Ltd. (Monroe, WI, USA). The following were obtained from Sigma-Aldrich (St. Louis, MO, USA): *p*-nitrophenyl butyrate, acetonitrile, porcine pancreatic lipase, butyric, pentanoic, hexanoic, octanoic, and *n*-decanoic acid, 4-methyl-2-pentanone, 2-pentanone, 2-

Special Issue: Advances in the Understanding of Dairy and Cheese Flavors

Received: October 31, 2013
Revised: January 23, 2014
Accepted: January 24, 2014
Published: January 24, 2014

ACS Publications © 2014 American Chemical Society

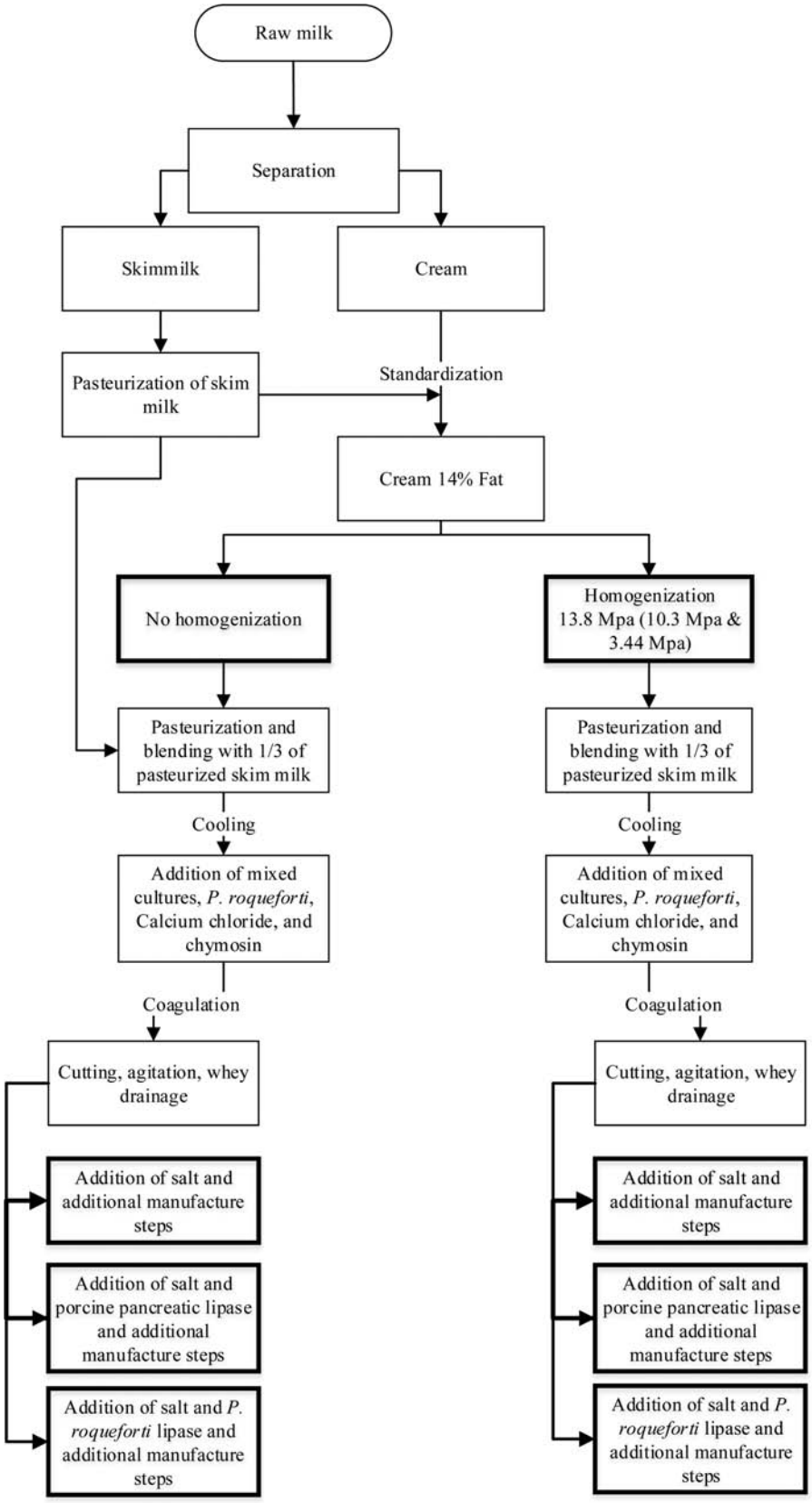

Figure 1. Flow diagram depicting the process of manufacture of blue cheeses for this study as well as the steps in which experimental treatments (homogenization, lipase treatment) were varied (bold boxes).

heptanone, 2-nonanone, 2-undecanone, 2-pentanol, 2-heptanol, 2-nonanol, and Triton X-100. Sodium phosphate monobasic, sodium phosphate, and sulfuric acid were from Fisher Scientific, Fair Lawn, NJ, USA. Sodium chloride was from Acros, Fair Lawn, NJ, USA. Lipase (EC 3.1.1.34) enzyme assay was obtained from Sigma-Aldrich. The following materials were obtained, as indicated: calf pregastric esterase

dx.doi.org/10.1021/jf4048786 | J. Agric. Food Chem. 2014, 62, 5726−5733

(Dairy Connection, Madison, WI, USA), *P. roqueforti* lipase (Biocatalysts, Wales, UK), porcine pancreatic lipase (Sigma, St. Louis, MO, USA), *P. roqueforti* spores for the model system (Danisco, Copenhagen, Denmark), *P. roqueforti* for the cheese manufacture (PR3, Chr. Hansen Inc., Milwaukee, WI, USA), and liquid chymosin (CHY-MAX 73863, Chr. Hansen Inc.). Direct vat set (DVS) mixed culture of *Lactobacillus helveticus* was obtained from Danisco (Madison, WI, USA) and FD-DVS Flora Danica (*Lactococcus lactis* subsp. *cremoris*, *Leuconostoc*, *Lactococcus lactis* subsp. *lactis*, *Lactococcus lactis* subsp. *lactis* biovar *diacetylactis*) from Chr. Hansen Inc. Antimycotic solution of natamycin (DelvoCid XT 1) was from DSM Food Specialties, Parsippany, NJ, USA.

Gas Chromatography (GC-MS). The gas chromatograph was an Agilent 6890N (Agilent Technologies, Inc., Palo Alto, CA, USA) with the following capillary column: 5% diphenyl−95% dimethyl polysiloxane fused silica capillary column (Rtx-5MS, 30 m, 0.25 mm i.d., 0.5 μm film thickness) (Restek Corp., Bellefonte, PA, USA). The carrier gas was helium, 99.999%. The mass selective detector used was an Agilent 5973 MS under the following conditions: mode, electron ionization, 70 eV; m/z scan range, 33−300 amu collected at 4.44 scans/s; ion source temperature, 230 °C. Chemstation software (rev, D.02.00 SP1, Agilent Technologies, Inc.) was used for signal analysis; compound identification was considered positive by matching unknown mass spectra to those in a published database (National Institute of Standards and Technology (NIST) version 1.7, Gaithersburg, MD, USA) and by common retention times of authentic standards.

Lipase Standardization. A solution of *p*-nitrophenyl butyrate in acetonitrile was used as the standardizing substrate. The three selected lipase enzyme treatments (calf pregastric esterase, *P. roqueforti* lipase, and porcine pancreatic lipase) were each separately dissolved in 100 mM sodium phosphate buffer with 150 mM sodium chloride and 0.5 mL/100 mL Triton X-100, and the pH was adjusted to 7.2 at 37 °C. Solution absorption was observed by a continuously temperature-controlled spectrophotometer (SpectraMax Plus384, Molecular Devices Corp, Sunnyvale, CA, USA) under the following conditions: 37 °C; light wavelength, 400 nm; 1 cm cuvette. One unit of activity produces 1.0 nmol (10^{-9} mol) of *p*-nitrophenol per minute at pH 7.2 and 37 °C.[3,4] Lipase activity was calculated according to EC 3.1.1.34 enzyme assay (Sigma-Aldrich) as follows:

$$\text{units/mL enzyme} = \frac{\left(\frac{\Delta A400}{\text{min}}\text{test} - \frac{\Delta A400}{\text{min}}\text{blank}\right)(1.01)(\text{df})}{(0.0148)(0.1)}$$

ΔA400/min is the maximum linear rate of absorption change per minute for both the test and blank; 1.01 is the volume (in milliliters) of the assay; df is the dilution factor; 0.0148 is the micromolar extinction coefficient of 4-nitrophenol at 400 nm; and 0.1 is the volume (in milliliters) of enzyme solution used.

Blue Cheese Model System Experimental Details. *Homogenization and Milk Fat Globule Size Measurement.* Homogenization was applied to pasteurized whole milk (3.5 g/100 g fat content) by a two-stage, high-pressure homogenizer (Gaulin K6-8TBS). As is typical in industry practices, the second stage of the homogenizer was fixed at 3.5 MPA, and the first stage was set at either 3.5 or 10.5 MPa. Unhomogenized milk was the third treatment; thus, there were three homogenization treatments: unhomogenized, 7 MPa total (3.5 MPa first stage, 3.5 MPa second stage), and 14 MPa total (10.5 MPa first stage, 3.5 MPa second stage). Milk samples were collected after pressure treatments, then pasteurized at 72 °C for 20 s, and stored at 4 °C. The fat globule size distributions in milk of different pressure treatments were measured by laser light scattering (Mastersizer 2000, Malvern, UK) with an absorption coefficient of 0.0001. Milk samples were preheated to 40 °C, and then 100 μL of each sample was diluted with 100 mL of distilled water to reach 12−13% laser obscuration (optimal conditions for particle size measurement). All analyses were performed in triplicate. Density was considered as 0.998 g/cm^3 (aqueous samples with dilute dispersed milk fat). Parameters reported by the system software included volume diameter ($D(4,3)$) and average surface area ($D(3,2)$). Refractive indices used were 1.456 for the milk fat globule and 1.33 for the aqueous dispersion medium with a ratio of 1.095.

FFA Profiles of Blue Cheese Model System Milks. Milk samples (100.0 g) were transferred into 150 mL flasks and heated to 40 °C. Each flask was treated with 2000 activity units of enzyme/100 g milk and then held for 3 h with continuous stirring.[5−7] FFA profiles were determined on the basis of previous methods as follows.[8,9] Samples of 10.00 g of lipolyzed milk with 1 mM pentanoic acid (internal standard) were placed into 20 mL septum-sealed headspace vials (Supelco, Bellefonte, PA, USA), and then the pH was adjusted to 1.5−1.6 with sulfuric acid (0.01 N). SPME analysis was conducted wherein the SPME fiber (85 μm carboxen/polydimethylsiloxane, Supelco) was exposed to the headspace for 30 min at 70 °C without agitation. Analysis of FFAs was carried out by GC-MS as described above with a flow rate of 1.5 mL/min and the following temperature program: from 40 to 250 °C, at 5 °C/min, initial holding 2 min, and equilibration time 0.50 min. MS parameters were as described above.

Blue Cheese Model System and Ketone Profiles. All glassware and tubing were heat sterilized in an autoclave (121 °C for 20 min). Sodium chloride (3.0 g) and 0.0010 g of *P. roqueforti* spores were added to yield a total of 100.00 g of lipolyzed milk sample while 50 mL/min of air was injected into the flask by a peristaltic pump. The milks were agitated by means of a magnetic stir bar. The reaction was conducted in an incubator at 20 °C for 24 h.

The method for volatile profiles was adapted from various references[10−12] and included the following parameters. A 1.00 g sample was placed into an 8 mL glass GC vial with 1.00 g of 4-methyl-2-pentanone water solution (50 μg/g final concentration) added as an internal standard. The SPME fiber (85 μm carboxen/polydimethylsiloxane, Supelco) was exposed to headspace for 30 min at 45 °C. Analysis of methyl ketones was carried out by GC-MS as described, with the following temperature program: injection temperature, 250 °C; 70 °C for 2 min; increased to 140 °C at 6 °C/min; 140 °C for 2 min; increased to 220 °C at 6 °C/min; and held at 220 °C for 5 min. MS parameters were as described above. The entire experiment was replicated three times.

Blue Cheese Experimental Details. *Cheese Manufacture (Figure 1).* Raw milk (544 kg) was centrifuged using a cream separator (Westfalia, Naperville, IL, USA); raw cream was standardized to 14 g/100 g fat using HTST pasteurized skim milk (73 °C for 15 s)[13] (APV, Goldsboro, NC, USA). Standardized cream was split into two parts, unhomogenized and two-stage homogenization (Gaulin, Delvan, WI, USA), at 13.8 MPa (10.3 MPa first stage, 3.44 MPa second stage). Each treatment was subsequently pasteurized and then blended with 1/3 pasteurized skim milk (final mik fat of 9.5 g/100 g) in an open cheese vat with mechanical stirring (Tetra Pak Cheese and Power System Inc., Fond du Lac, WI, USA). Direct vat set (DVS) mixed cultures of *Lactobacillus helveticus* (1.29 g/100 kg) and FD-DVS Flora Danica (*Lactococcus lactis* subsp. *cremoris*, *Leuconostoc*, *Lactococcus lactis* subsp. *lactis*, *Lactococcus lactis* subsp. *lactis* biovar *diacetylactis*) (2.02 g/100 g) were added to the standardized milks at 31 °C (DVS culture was incubated in pasteurized milk at 22.2 °C for 16 h before use). The following steps included the addition of *P. roqueforti* mold spores (1 g/100 kg milk) and calcium chloride (20 g/100 L milk) and mechanical stirring for 1 h. After renneting with liquid chymosin (10 mL/100 L), the curd was cut using 9.5 mm wire knives and agitated for 30 min at 31 °C, and the whey was drained at 20% of original volume, 50% after 30 min, and curd level after an additional hour of agitation. At a final pH of 6.05, 7.3 kg of cheese curds and 7.3 kg of whey were distributed into five tubs[14] followed by the addition of 392 g of salt blended with 0.61 g of each standardized lipase solutions. The whey−curd mixture was continuously stirred for 10 min and transferred into open-ended, perforated cheese hoops (diameter = 19.7 cm, height = 20.32 cm) on a stainless steel drain table and allowed to set and drain for 1 h before being inverted. Hoops were inverted every hour for the next 4 h and once again at 12 h post hooping. Wheels (still in hoops) drained overnight at room temperature on a drain table. Each cheese wheel was surface salted after removal from hoops on day 1 and subsequently on days 2 and 4 postmanufacture at 2, 1, and 0.5 g/100 g of initial cheese wheel weight,

respectively. During salting, cheese wheels were stored at 14 °C and 90% relative humidity. Cheese wheels were dipped into a 10 g/100 mL natamycin solution (DelvoCid) for mold control and pierced with 120 holes on each side using a single-wheel pneumatic punch with 40 needles. Cheeses were wrapped loosely in plastic bags and incubated at 14 °C and 90−95% relative humidity over 2 weeks for mold sporulation and then aged at 5 °C for 4 months.[15] Aged blue cheeses were vacuum-packed and stored at −20 °C for analysis.

Blue Cheese Volatile Analysis. Frozen blue cheese samples were thawed at 4 °C overnight. A composite sample of 10 g of cheese was placed in a 40 mL headspace vial with 10 mL of monosodium phosphate (25g/100 mL) containing 200 μg/g of 4-methyl-2-pentanone as internal standard and a magnetic stir bar.[10,16,17] Each vial was capped with a Teflon-lined septum. A manual SPME fiber holder unit with a carboxen polydimethylsiloxane fiber (Supelco) was exposed to the headspace at 65 °C for 30 min with continuous stirring at 600 rpm.[10,16] All analyses were performed in triplicate.

Gas Chromatography−Mass Spectrometry. Analysis of volatile compounds was carried out by GC-MS, as described above, with a 1.2 mL/min flow rate and the following temperature program: from 40 to 250 °C, at 5 °C/min, initial holding, 1.00 min; and equilibration time, 0.50 min.

Quantification of Compounds in Blue Cheese with Internal Standards by GC-MS-SPME. A multiple-point internal standard method was used to quantify selected volatile compounds in blue cheese samples.[18,19] Response factors of each analyte were tested using fresh cheese as cheese matrix base. Volatile profiles of fresh cheese were analyzed by GC-MS-SPME and showed no significant levels of FFAs or methyl ketones. Each analysis contained internal standard (4-methyl-2-pentanone) at 200 μg/g in 10 mL of monosodium phosphate (25 g/100 mL), 10.00 g fresh cheese, and each analyte of interest covering five-point concentration ranges as follows: butyric acid (5−8000 μg/g), hexanoic acid (20−2000 μg/g), octanoic acid (30−2000 μg/g), *n*-decanoic acid (100−700 μg/g), 2-pentanone (1−200 μg/g), 2-heptanone (2−400 μg/g), and 2-nonanone (1−400 μg/g). All analyses were performed in triplicate.

Descriptive Sensory Analysis (DSA) of Blue Cheese Samples. Fourteen panelists were trained through DSA for blue cheese. Flavor attributes included waxy, soapy, methyl ketone, chemical/medicinal, fruity, musty/cave, mushroom, salt, sweet, acid, and bitter (Table 1).[20−22] A linear scale from 0 (absent) to 15 (extreme) was used to measure flavor intensity. Blue cheese samples were stored at −20 °C to inhibit continued activity of *P. roqueforti* and, before analysis, defrosted overnight at 4 °C. Descriptive analysis of 0.5 cm size crumbles at 10 °C was done during eight separate days to prevent panel fatigue with three samples tested per day. Panelists were given 10 min to test each sample and 5 min between each sample. Panelists evaluated all cheeses within isolated, individual tasting booths with approximately 860 lx of white lighting.

Table 1. Terms and Definitions Used To Describe the Flavor of Blue Cheese Using Descriptive Analysis Method[a]

term	definition	standard (reference used neat or as noted in water)
rancid	aroma associated with milk fat lipolysis	butyric acid (500 mg/kg)
waxy	sweet aromatic associated with wax paper	capric acid
soapy	detergent-like taste and smell	lauric acid
methyl ketone	aroma associated with blue-vein cheeses	2-heptanone (40 mg/kg)
medicinal	aroma associated with unclean notes	*p*-cresol (100 mg/kg)
fruity	taste and aromatic blend of different fruits	ethyl hexanoate (10 mg/kg)
musty	aroma of a damp room, associated with closed air spaces	2,4,6-trimethoxy-benzaldehyde
mushroom	taste and aromatics associated with raw mushrooms	3-octan-3-ol (50 mg/kg)
basic tastes	salty, sweet, acid, bitter	salt, sugar, citric acid, caffeine (500 mg/kg)

[a]Adapted from Drake.[30]

Statistical Analyses. Statistical analysis was done using statistical software (JMP Pro 10, SAS Institute Inc., Cary, NC, USA). The main effects of exogenous lipase, homogenization pressure, and their interaction on each volatile compound's response in blue cheese samples were analyzed by least-squares model with an α of <0.05. The effects of lipase, pressure, and panelist on each flavor attribute were similarly evaluated with ANOVA at the same error rate.

RESULTS AND DISCUSSION

Homogenization Effects on Milk Fat Globule Size and Surface Area (Model System). The reported changes in milk fat globule size profiles are intended to demonstrate the relative degree of homogenization treatment variables achieved. Most noticeably, average diameters decreased and surface areas increased as homogenization pressures increased (Table 2), typical of commercial-scale homogenization processes.

Table 2. Mean (Standard Deviation) of Diameters and Surface Areas of Milk Fat Globules after Homogenization at Different Pressures[a]

first/second stage (MPa)	unhomogenized	3.5/3.5	10.5/3.5
diameter (μm)	3.62 (0.03)a	1.34 (0.04)b	0.37 (0.01)c
surface area (m^2/g)	1.78 (0.03)a	11.57 (1.20)b	25.10 (0.81)c

[a]Means within a row with different letters are significantly different at the α <0.05 level.

FFA Profiles of Homogenized, Lipase-Treated Milk (Model System). Overall triglyceride hydrolysis activities of calf pregastric, porcine pancreatic, and *P. roqueforti* were determined to be 2.12, 250, and 83.77 U/mg, respectively. Ten *n*-FFAs were positively identified in most treatments including butanoic (C4), hexanoic (C6), heptanoic (C7), octanoic (C8), nonanoic (C9), decanoic (C10), undecanoic (C11), dodecanoic (C12), tetradecanoic (C14), and hexadecanoic (C16) acids; C4, C6, C8, and C10 FFAs were selected for quantification on the basis of their potential to contribute to methyl ketones of significance to blue cheese aroma. The variation in FFA profiles and concentrations is expected to subsequently result in a difference in methyl ketone generation based on the conversion of FFA into methyl ketones. Overall, the main effects of homogenization treatment, lipase addition, and the two-way homogenization × lipase interactions significantly affected concentrations of the FFAs quantified (*n*-C4 to C10, even numbered). The mean concentrations and standard deviations of these FFAs in lipolyzed milk with different pressure treatments are shown in Table 3. The variation of the mean calculations was high for many treatments and probably results from a number of factors including slight differences in lipase activities and unexplained errors in the analytical steps. In general, significant increases in each [FFA] were observed by comparing the nonhomogenized milks to the 7 MPa homogenization treatment. However, that response was not further increased at the 14 MPa level and, in fact, the levels of some FFAs were decreased compared to the 7 MPa treatment.

Table 3. Average (Micrograms per Gram, Standard Deviations in Parentheses) FFA Concentrations as a Function of Homogenization and Lipase Treatments in Blue Cheese Model System[a]

lipase	pressure (total MPa)	butanoic	hexanoic	octanoic	decanoic
calf	0	530 (60)b	910 (97)b	630 (83)b	1700 (1100)d
calf	7	600 (87)b	1000 (74)b	660 (84)b	1100 (210)c
calf	14	600 (18)b	970 (67)b	590 (69)b	990 (370)c
P. roqueforti	0	42 (24)a	140 (59)a	160 (60)a	180 (95)a
P. roqueforti	7	540 (77)b	1300 (83)c	1100 (73)d	1800 (280)d
P. roqueforti	14	510 (62)b	1300 (76)c	1100 (70)d	2200 (26)d
porcine	0	440 (48)b	920 (75)b	590 (94)b	590 (180)b
porcine	7	700 (42)c	1300 (97)c	720 (69)c	630 (100)b
porcine	14	570 (46)b	1100 (99)bc	580 (58)b	530 (160)b

[a]Means within a column with different letters are significantly different at the α <0.05 level.

Table 4. Average (Micrograms per Gram, Standard Deviations in Parentheses) Methyl Ketone Concentrations as a Function of Homogenization and Lipase Treatments in Blue Cheese Model System[a]

lipase	pressure (total MPa)	2-pentanone	2-heptanone	2-nonanone
calf	0	22 (12)bc	180 (72)a	1100 (340)c
calf	7	24 (7.8)bc	280 (180)ab	1100 (360)c
calf	14	18 (1.1)b	270 (28)ab	840 (320)bc
P. roqueforti	0	6.6 (3.5)a	150 (30)a	240 (91)a
P. roqueforti	7	23 (3.7)bc	320 (51)b	930 (220)bc
P. roqueforti	14	37 (13)c	330 (100)b	200 (58)a
porcine	0	20 (5.4)b	250 (16)ab	810 (370)bc
porcine	7	36 (22)c	340 (170)ab	690 (200)b
porcine	14	25 (6.5)bc	280 (70)ab	440 (220)ab

[a]Means within a column with different letters are significantly different at the α <0.05 level.

Although statistically significant overall main and interaction effects were observed, the vast majority of treatment level combinations yielded only minor actual concentration changes with most treatment FFA concentrations falling in the 500−1300 μg/g range. The lowest levels of FFA were for the *P. roqueforti* × 0 MPa homogenization treatment at C4. Interestingly, the highest levels of lipolysis were for the *P. roqueforti* × 14 MPa treatments for C10, demonstrating that for this enzyme, homogenization strongly influences the hypothesized effect in aiding in the liberation of FFA. For octanoic acid (precursor for a key blue cheese flavor compound, 2-heptanone), neither calf nor porcine lipase demonstrated strong effects on changing the [FFA] as a function of homogenization. Alternatively, *P. roqueforti* lipase treated milk showed ≈10-fold increases in essentially all FFA concentrations when homogenization was applied at the 7 MPa level.

Calf pregastric esterase[23] and porcine pancreatic lipase[24] have shown preference for FFAs on sn-1 and sn-3 positions where most short-chain FFAs are located. *P. roqueforti* lipase has a preference similar to that of calf pregastric esterase and has been shown to display lower activity toward triglycerides of larger molecular weight.[24]

Ketone Generation in Blue Cheese Model System. There were eight ketones positively identified including 2-pentanone, 2-hexanone, 2-heptanone, 2-octanone, 8-nonen-2-one, 2-nonanone, 2-decanone, and 2-undecanone; 2-pentanone, 2-heptanone, and 2-nonanone were selected for quantitation on the basis of their known high impact on actual blue cheese flavor. The compound 8-nonen-2-one was found in every sample; this latter compound is thought to contribute to baked and mushroom-like aromas.[25] The formation of 8-nonen-2-one is associated with β-oxidation, but primarily results from the oxidation of specific unsaturated fatty acids, namely, linoleic or linolenic acid. Observations of ketone generation suggest loose patterns of correlation with the general patterns of FFA profiles, suggesting that the mechanism of ketone generation is only moderately influenced by FFA substrate availability rather than intact triglyceride. For example, hexanoic acid levels were not significantly different for the calf lipase, but increased for the *P. roqueforti* and porcine enzymes over the course of increasing homogenization. Subsequently, the hexanoic acid-derived methyl ketone, 2-pentanone, displayed a similar pattern of evolution across these enzyme/homogenization treatments. These results by no means denote stoichiometry or mass balance for such reactions, but do demonstrate that there is some correlation between the hypothesized substrate (FFA) and the generation of the corresponding methyl ketone. There is some evidence that *P. roqueforti* metabolism is thwarted by high FFA levels[26−28] and, as a result, the actual preferred conditions for metabolism may be more favorable under lower levels of lipolysis.[29]

The effects of homogenization and lipase treatment (and interactions) were significant but not for every methyl ketone. For instance, changes in homogenization pressure had little effect on 2-pentanone generation with the calf lipase treatment, but were positively correlated with increasing homogenization pressures (and increasing [FFA]) for *P. roqueforti* lipase treated samples (Table 4). In general, concentrations of methyl ketones were higher in samples made with homogenized milk compared to the unhomogenized samples. The 14 MPA homogenization treatment resulted in a numerical if not statistically significant reduction in methyl ketone concentration across most treatments, reflecting a similar trend in [FFA] values as noted above.

Identification of Volatile Compounds in Blue Cheese. Although entire volatile profiles were complex, efforts were

Table 5. Average and Total (Micrograms per Gram, Standard Deviations in Parentheses) FFA Concentrations as a Function of Homogenization and Lipase Treatments in Blue Cheese[a]

lipase	pressure (total MPa)	butanoic	hexanoic	octanoic	decanoic
none	0	210 (2.0)a	54 (0)a	100 (4.0)a	26 (0)a
none	13.8	4100 (400)b	360 (44)b	120 (4.0)a	920 (68)c
calf	0	12000 (710)c	770 (70)bc	160 (5.0)a	2400 (500)d
calf	13.8	9300 (1200)c	1000 (170)c	110 (6.0)a	4300 (980)e
P. roqueforti	0	530 (240)a	110 (21)a	120 (12)a	340 (130)b
P. roqueforti	13.8	29000 (5300)d	2100 (230)	274 (20)b	8400 (1600)e
porcine	0	3400 (860)b	340 (67)b	141 (3.4)a	1000 (200)c
porcine	13.8	7100 (1100)c	570 (76)b	150 (4.0)a	1600 (340)c

[a]Means within a column with different letters are significantly different at the α <0.05 level.

focused on specific volatile compounds wherein the following compounds were positively identified, including six *n*-FFA's (butanoic, hexanoic, octanoic, decanoic, dodecanoic, and tetradecanoic), acetic acid, five methyl ketones (acetone, 2-pentanone, 2-heptanone, 2-nonanone, and 2-undecanone), 8-nonen-2-one, and three secondary alcohols (2-pentanol, 2-heptanol, and 2-nonanol). These latter secondary alcohols are regarded as reduction products of the corresponding methyl ketones.

FFA Levels in Blue Cheese. In general, homogenization promoted lipolysis for each enzyme treatment across each fatty acid, but homogenization had little effect on the calf lipase treatment (Table 5). Interestingly, there was little effect on the concentrations of octanoic from either lipase or homogenization with the exception of the homogenized *P. roqueforti* lipase treated samples that had about a 2-fold increase over the other treatments. The treatment without added lipase (none) displayed a strong, positive effect of homogenization wherein [FFA] values increased by >10-fold (except octanoic). This lipolytic activity would most likely result from the innate lipolytic capabilities during *P. roqueforti* metabolism during ripening. Added *P. roqueforti* lipase also strongly responded to homogenization treatment of the milk, displaying >10-fold increases in [FFA]. Although not as dramatic, porcine lipase displayed modest activity in the cheese system toward FFA liberation, primarily for butyric acid. Compared to the model system work, there are some noted correlations, primarily relating to the *P. roqueforti* lipase treatment, wherein little lipolytic activity is displayed by this enzyme when homogenization is not employed.

Resulting Methyl Ketones in Blue Cheese. Although the premise is that an ability to increase the pool of FFA substrate (as affected by lipase and homogenization treatments) influences the resulting mass conversion into methyl ketone metabolites, no such cause and effect was readily noted (Table 6). Overall, the eventual ratio of FFA substrate and methyl ketone derivative was extremely low; for example, overall hexanoic acid concentrations ranged from 54 to 2100 μg/g, and the corresponding methyl ketone derivative, 2-pentanone, ranged from "not detected" to 49 μg/g. The *P. roqueforti* lipase treatment again showed the only response in harmony with the hypothesis wherein the presence of the enzyme and the application of homogenization generated significantly higher levels of methyl ketone as compared to the "none" treatment and the unhomogenized samples.

Descriptive Sensory Analysis. Means and standard deviations of sensory data are shown in Table 7. The sensory terms were primarily selected on the basis of the potential influence of the experimental variables on these terms. Only the terms *soapy* and *methyl ketone* displayed any form of significant treatment effects. Most notably, and consistent with the instrumental assays above, is the ability of the *P. roqueforti* lipase enzyme with homogenization treatment to increase the intensity of *soapy* and *methyl ketone*, wherein these terms were taught to the panel as resulting from the FFA lauric acid and 2-heptanone (Table 1), respectively. No changes in other sensory attributes were detected including *rancid* and *waxy*, despite changes in the concentrations of the compounds that contribute to these attributes. In general, the blue cheese samples presented an extremely high overall flavor intensity for sensory panelists. As such, fatigue and other panelist errors may have played a role in the outcomes we observed. However, to change the sensory response toward these somewhat related, lipid-derived compounds, the change in actual compound concentration must be quite large, especially in such a highly flavored cheese. For instance, a nearly 10-fold increase in concentration of butyric acid was found in milks classified as "distinctly rancid" compared to freshly pasteurized milks.

Table 6. Average and Total (Micrograms per Gram, Standard Deviations in Parentheses) Methyl Ketone Concentrations as a Function of Homogenization and Lipase Treatments in Blue Cheese[a]

lipase	pressure (total MPa)	2-pentanone	2-heptanone	2-nonanone
none	0	5.6 (2.1)a	2.9 (1.7)a	21 (7.8)a
none	13.8	5.2 (1.2)a	10 (2.7)b	63 (9.2)b
calf	0	22 (2.4)b	19 (1.8)c	130 (10)c
calf	13.8	ND	0.6 (0.3)a	42 (14)b
P. roqueforti	0	16 (6.3)b	19 (6.1)c	67 (16)b
P. roqueforti	13.8	49 (7.6)c	36 (4.1)d	390 (44)d
porcine	0	9.4 (1)a	10 (0.7)b	100 (7)c
porcine	13.8	7.7 (1.6)a	11 (1.3)b	122 (8.9)c

[a]Means within a column with different letters are significantly different at the α <0.05 level.

General Considerations. Blue cheese volatile chemistry results from a complex system of reactions involving milk quality, lipase activity, mold metabolism, aging parameters, oxygen availability/redox potential, and so forth. There is a dogma associated with the manufacture of blue cheese that suggests both homogenization and exogenous lipase addition influence characteristic blue cheese aroma through the mechanisms noted in the aforementioned hypothesis. Research designed to examine this hypothesis may range from the very basic to the very applied in scope; this work focused on the applied approach in design, but illustrates the need for a more basic understanding of the chemistry at hand. First, there is

dx.doi.org/10.1021/jf4048786 | J. Agric. Food Chem. 2014, 62, 5726−5733

Table 7. Sensory Analysis Results Averages and Standard Deviations (in Parentheses) for Each Flavor Attribute Assessed with a Scale from 0 (Absent) to 15 (Pronounced) from Blue Cheese Samples Treated with Homogenization and Lipase Enzymes[a]

lipase	pressure (total MPa)	salty	acid	bitter	sweet	rancid	waxy
none	0	6.90 (1.63)	5.35 (1.11)	1.68 (1.31)	0.50 (0.48)	0.60 (0.87)	1.02 (1.12)
none	13.8	6.37 (1.71)	4.84 (1.60)	1.33 (1.48)	0.22 (0.52)	0.39 (0.90)	1.35 (1.72)
calf	0	6.12 (1.48)	5.18 (1.50)	1.68 (1.73)	0.25 (0.59)	0.83 (1.27)	1.13 (1.24)
calf	13.8	6.20 (1.35)	4.55 (1.96)	1.24 (1.63)	0.35 (0.65)	0.68 (1.13)	1.38 (1.45)
P. roqueforti	0	6.55 (1.73)	5.22 (1.58)	1.50 (1.85)	0.65 (0.94)	0.48 (0.89)	0.92 (0.93)
P. roqueforti	13.8	5.48 (1.65)	4.58 (1.65)	1.45 (1.40)	0.25 (0.55)	0.56 (0.98)	1.52 (1.31)
porcine	0	6.84 (1.61)	5.62 (1.32)	1.16 (1.56)	0.47 (0.82)	0.73 (1.21)	0.83 (1.14)
porcine	13.8	6.08 (1.65)	5.08 (1.47)	1.33 (1.33)	0.35 (0.77)	0.63 (1.24)	1.13 (1.12)
lipase	pressure (total MPa)	soapy	methyl ketone	medicinal	fruity	musty	mushroom
none	0	2.72 (1.16)a	6.18 (2.13)a	2.26 (2.20)	0.66 (1.40)	1.68 (1.19)	3.42 (1.57)
none	13.8	3.22 (1.55)a	6.41 (2.23)a	3.20 (3.22)	0.50 (0.75)	2.15 (1.81)	3.57 (1.35)
calf	0	3.25 (1.49)a	7.56 (2.03)b	1.97 (2.05)	1.42 (3.09)	1.81 (1.63)	2.88 (1.15)
calf	13.8	3.28 (1.53)a	7.10 (2.72)ab	2.13 (2.02)	0.98 (1.34)	2.47 (1.55)	3.26 (1.77)
P. roqueforti	0	2.96 (1.34)a	6.75 (2.47)a	2.50 (2.15)	0.67 (1.23)	1.63 (1.53)	3.19 (1.65)
P. roqueforti	13.8	3.77 (1.25)b	8.10 (2.30)bc	3.33 (2.25)	0.46 (0.69)	2.08 (1.56)	3.15 (1.62)
porcine	0	3.08 (1.12)a	7.05 (1.63)ab	2.65 (2.21)	0.64 (1.20)	2.23 (1.42)	3.70 (1.70)
porcine	13.8	3.13 (1.24)a	7.90 (2.35)bc	2.09 (2.07)	0.63 (1.24)	2.13 (1.27)	3.15 (1.70)

[a]Means within a column with different letters are significantly different at the α <0.05 level.

some merit to the use of a model system as utilized in this work as a means of improved experimental control and expense. Such a system may be applied in future work to better understand the time course of methyl ketone generation and the relative roles of FFA versus triglyceride substrate for methyl ketone generation. Additionally, it is similarly critical to understand the conditions wherein methyl ketones are further reduced to their corresponding secondary alcohols (and resulting change of aroma), an element of this system not addressed by this work. Additionally, there is a further need to investigate the role of indogenous or native *P. roqueforti* lipase activity resulting from the metabolic activities of this mold during ripening or aging as well as the potential for native bovine lipoprotein lipase from raw milk to influence methyl ketone development.

However, albeit applied in nature, this work demonstrates the effectiveness of exogenous *P. roqueforti* lipase as an agent in ultimately increasing methyl ketones in cheese as well as the dependence of *P. roqueforti* lipase on homogenization of milk fat; other lipases were very much less effective toward this end, emphasizing the need for careful selection of lipase treatments.

AUTHOR INFORMATION

Corresponding Author

*(S.A.R.) Phone: (608) 263-2008. Fax: (608) 262-6872. E-mail: sarankin@wisc.edu.

Funding

We express our appreciation to Coordenação de Aperfeiçoamento de Pessoal de Nível Superior (CAPES)−Brazil Estagio Senior Process no. 18183/12-3 for financial support.

Notes

The authors declare no competing financial interest.

ABBREVIATIONS USED

FFA, free fatty acids; amu, atomic mass unity; *m*/*z*, mass to charge ratio; SPME, solid phase microextraction; DVS, direct vat set; DSA, descriptive sensory analysis; sn, stereospecific numbering

REFERENCES

(1) Jolly, R. C.; Kosikowski, F. V. A new blue cheese food material from ultrafiltrated skim milk and microbial enzyme-mold spore reacted fat. *J. Dairy Sci.* **1975**, *58*, 1272−1275.

(2) Kinsella, J. E.; Hwang, D. Biosynthesis of flavors by *Penicillium roqueforti*. *Biotechnol. Bioeng.* **1976**, *18*, 927−938.

(3) Kosikowski, F. V. Potential of enzymes in continous cheesemaking. *J. Dairy Sci.* **1975**, *58*, 994−1000.

(4) Shirai, K.; Jackson, R. L. Lipoprotein lipase-catalyzed hydrolysis of *p*-nitrophenyl butyrate. Interfacial activation by phospholipid vesicles. *J. Biol. Chem.* **1982**, *257*, 1253−1258.

(5) Iametti, S.; Versuraro, L.; Tragna, S.; Giangiacomo, R.; Bonomi, F. Surface properties of the fat globule in treated creams. *Int. Dairy J.* **1997**, *7*, 375−380.

(6) Kilcawley, K. N.; Wilkinson, M. G.; Fox, P. F. Determination of key enzyme activities in commercial peptidase and lipase preparations from microbial or animal sources. *Enzyme Microb. Technol.* **2002**, *31*, 310−320.

(7) Deegan, K. C.; McSweeney, P. L. H. Enhancement of lipolysis in cheese during ripening by low pressure homogenisation of cheese milk. *Aust. J. Dairy Technol.* **2006**, *61*, 212.

(8) Pinho, O.; Ferreira, I. M.; Ferreira, M. A. Solid-phase microextraction in combination with GC/MS for quantification of the major volatile free fatty acids in ewe cheese. *Anal. Chem.* **2002**, *74*, 5199−5204.

(9) Gonzalez-Cordova, A. F.; Vallejo-Cordoba, B. Detection and prediction of hydrolytic rancidity in milk by multiple regression analysis of short-chain free fatty acids determined by solid phase microextraction gas chromatography and quantitative flavor intensity assessment. *J. Agric. Food Chem.* **2003**, *51*, 7127−7131.

(10) Verzera, A.; Ziino, M.; Condurso, C.; Romeo, V.; Zappalà, M. Solid-phase microextraction and gas chromatography−mass spectrometry for rapid characterisation of semi-hard cheeses. *Anal. Bioanal. Chem.* **2004**, *380*, 930−936.

(11) Gkatzionis, K.; Linforth, R. S. T.; Dodd, C. E. R. Volatile profile of Stilton cheeses: differences between zones within a cheese and dairies. *Food Chem.* **2009**, *113*, 506−512.

(12) Wolf, I. V.; Perotti, M. C.; Zalazar, C. A. Composition and volatile profiles of commercial Argentinean blue cheeses. *J. Sci. Food Agric.* **2011**, *91*, 385−393.

(13) Jolly, R. C.; Kosikowski, F. V. Flavor development in pasteurized milk blue cheese by animal and microbial lipase preparations. *J. Dairy Sci.* **1975**, *58*, 846−852.

(14) Rabie, A. M. Acceleration of blue cheese ripening by cheese slurry and extracellular enzymes of *Penicillium roqueforti*. *Lait* **1989**, *69*, 305−314.
(15) Morris, H. A. *Blue-Veined Cheeses*; Pfizer: New York, 1981; Vol. VII.
(16) Delgado, F. J.; González-Crespo, J.; Cava, R.; García-Parra, J.; Ramírez, R. Characterisation by SPME−GC−MS of the volatile profile of a Spanish soft cheese P.D.O. Torta del Casar during ripening. *Food Chem.* **2010**, *118*, 182−189.
(17) Lee, J. H.; Diono, R.; Kim, G. Y.; Min, D. B. Optimization of solid phase microextraction analysis for the headspace volatile compounds of Parmesan cheese. *J. Agric. Food Chem.* **2003**, *51*, 1136−1140.
(18) Alonso, L.; Fontecha, J.; Juárez, M. Development of a headspace gas chromatographic-mass spectrometric method for determining methyl-ketones and secondary alcohols in blue cheese. *J. Chromatogr. Sci.* **1999**, *37*, 108−112.
(19) Tomaino, R. M.; Parker, J. D.; Larick, D. K. Analysis of free fatty acids in whey products by solid-phase microextraction. *J. Agric. Food. Chem.* **2001**, *49*, 3993−3998.
(20) Lawlor, J. B.; Delahunty, C. M.; Sheehan, J.; Wilkinson, M. G. Relationships between sensory attributes and the volatile compounds, non-volatile and gross compositional constituents of six blue-type cheeses. *Int. Dairy J.* **2003**, *13*, 481−494.
(21) Weimer, B. C. *Improving the Flavour of Cheese*; CRC Press: Boca Raton, FL, USA, 2007; p 580.
(22) Chambers, D. H.; Esteve, E.; Retiveau, A. Effect of milk pasteurization on flavor properties of seven commercially available French cheese types. *J. Sens. Stud.* **2010**, *25*, 494−511.
(23) Sweet, B. J.; Matthews, L. C.; Richardson, T. Purification and characterization of pregastric esterase from calf. *Arch. Biochem. Biophys.* **1984**, *234*, 144−150.
(24) Ha, J. K.; Lindsay, R. C. Release of volatile branched-chain and other fatty acids from ruminant milk fats by various lipases. *J. Dairy Sci.* **1993**, *76*, 677−690.
(25) Karahadian, C.; Josephson, D. B.; Lindsay, R. C. Contribution of *Penicillium* sp. to the flavors of Brie and Camembert cheese. *J. Dairy Sci.* **1985**, *68*, 1865−1877.
(26) Lawrence, R. C.; Hawke, J. C. The oxidation of fatty acids by mycelium of *Penicillium roqueforti*. *J. Gen. Microbiol.* **1968**, *51*, 289−302.
(27) Huang, Y.; Wilson, M.; Chapman, B.; Hocking, A. D. Evaluation of the efficacy of four weak acids as antifungal preservatives in low-acid intermediate moisture model food systems. *Food Microbiol.* **2010**, *27*, 33−36.
(28) Fan, T. Y.; Hwang, D. H.; Kinsella, J. E. Methyl ketone formation during germination of *Penicillium roqueforti*. *J. Agric. Food Chem.* **1976**, *24*, 443−448.
(29) King, R. D.; Clegg, G. H. The metabolism of fatty acids, methyl ketones and secondary alcohols by *Penicillium roqueforti* in blue cheese slurries. *J. Sci. Food Agric.* **1979**, *30*, 197−202.
(30) Drake, M. A. Defining cheese flavor. In *Improving the Flavor of Cheese*; Weimer, B., Ed.; CRC Press: Boca Raton, FL, USA, 2007; pp 370−395.

JOURNAL OF AGRICULTURAL AND FOOD CHEMISTRY

Review

pubs.acs.org/JAFC

Overview of Plant Chitinases Identified as Food Allergens

Mariateresa Volpicella,[†] Claudia Leoni,[†] Immacolata Fanizza,[†] Antonio Placido,[‡] Elide A. Pastorello,[§] and Luigi R. Ceci*[,‡]

[†]Department of Biosciences, Biotechnologies and Biopharmaceutics, University of Bari, Via Amendola 165/A, 70126 Bari, Italy

[‡]National Research Council, Institute of Biomembranes and Bioenergetics, Via Amendola 165/A, 70126 Bari, Italy

[§]Unit of Allergology and Immunology, Niguarda Ca' Granda Hospital, Piazza Dell'Ospedale Maggiore, 3, 20162 Milano, Italy

ABSTRACT: Food allergies are induced by proteins belonging to a limited number of families. Unfortunately, relationships between protein structure and capacity to induce the immune response have not been completely clarified yet, which precludes possible improvements in the diagnosis, prevention, and therapy of allergies. Plant chitinases constitute a good example of food allergenic proteins for which structural analysis of allergenicity has only been carried out partially. In plants, there are at least five structural classes of chitinases plus a number of chitinase-related polypeptides. Their allergenicity has been mostly investigated for chitinases of class I, due to both their higher prevalence among plant chitinases and by the high structural similarity between their substrate-binding domain and hevein, a well-known allergen present in the latex of rubber trees. Even if allergenic molecules have been identified for at least three other classes of plant chitinases, the involvement of the different structural motifs in the allergenicity of molecules has been disregarded so far. In this review, we provide a structurally based catalog of plant chitinases investigated for allergenicity, which could be a useful base for further studies aimed at better clarifying the structure−allergenicity relationships for this protein family.

KEYWORDS: *plant food, food allergy, chitinase, allergen*

INTRODUCTION

Food allergies are recognized as a major health concern, affecting about 4% of the total world population, and reaching peaks of 8% in infants.[1] In recent years, their occurrence in Westernized countries has shown a steady increasing trend, and currently no viable treatments are available for people with food allergies.[2] Food allergies are determined by a limited number of proteins, which, recognized as allergens by specific IgE, cause the release of histamine from mastocytes and basophils with resulting symptoms of variable severity, from mild pruritis to life-threatening anaphylaxis.

Among the more than 13,000 protein families listed in the Pfam database (http://pfam.sanger.ac.uk/),[3] food allergens fall within a relatively small group of about 30 families,[4−6] which are also described in Allfam (http://www.meduniwien.ac.at/allergens/allfam/), a database specific for allergen families.[4] Biological activity of these proteins is even more restricted being limited to few biochemical functions: hydrolysis of proteins, polysaccharides, and lipids; binding of metal ions and lipids; and storage of nutrients and cytoskeleton association.[4] These findings led to the assumption that allergens must meet specific, but not yet completely elucidated, structural features which are at the basis of their allergenic potency. Their disclosure could greatly accelerate research advances in the prevention, diagnosis, and therapy of allergies. Additionally, in the case of food allergens, uncovering the structural basis of allergenicity would provide insights for understanding the effects of food processing and contribute to a safer management of food proteins.[7] There are examples of food allergens which retain allergenic potency even after cooking or transformation processes as has been shown for Cor a 1 in roasted hazelnuts[8] and nonspecific lipid transfer proteins (nsLTP) in some plant derived foods (sterilized peach juice and polenta)[9] and fermented products (wine and beer).[10,11] While strong structural constraints (such as disulfide bridges) can be evoked to explain the maintaining of some conformational epitopes and allergenicity for cooked food proteins, the allergenic potency that unfolded proteins still maintain can be attributed to their linear epitopes, as in the case of "fermented" nsLTPs and caseins (Mills et al.[7] and references therein). In any case, at the moment there are no definitive, reliable ways to predict structural signatures for allergens in general and food allergens in particular.[4]

Food allergens can be distinguished as those that are directly involved in the sensitization process in the gastrointestinal tract, which generally show high stability toward heating and proteolysis, and those that cross-react with IgE related to pollen or other nonfood allergens, which are mostly easily degradable.[12] Cross-reactivity syndromes, i.e., the onset of food allergies in subjects already sensitized to nonfood allergens, are usually determined by similar structural features among allergens.[13]

Among food allergens, those of plant origin constitute an essential part, and numerous reviews are available reporting their classification and discussions about biological function, cross-reactivity syndromes, influence of protein structure on allergenic potency, and effects of cooking and other food processing as well.[1,6,7,13,14] Here, we report a comprehensive analysis on the involvement of plant chitinases in food-allergies.

Received: February 19, 2014
Revised: May 16, 2014
Accepted: May 19, 2014
Published: May 19, 2014

ACS Publications © 2014 American Chemical Society

dx.doi.org/10.1021/jf5007962 | J. Agric. Food Chem. 2014, 62, 5734−5742

Chitinases are enzymes that catalyze the hydrolysis of chitin, a linear homopolymer of β-1,4-*N*-acetyl-D-glucosamine units. They are ubiquitous in nature, having been detected in animals, plants, fungi, bacteria, and viruses. In plants, chitinases play a major role as pathogenesis related (PR) proteins, active in defense mechanisms against fungi and pathogens.[15,16] While a clear structural classification of plant chitinases has long been reported,[17−19] a precise classification of plant chitinases as allergens is still missing. The aim of this review is to update the knowledge on the relationships between the structures and properties of plant chitinases and their allergenicity. It will furnish the basis to establish in the future more detailed analyses of the structural determinants of allergenic chitinases.

CLASSIFICATION OF PLANT CHITINASES

Chitinases are classified into families 18 or 19 of glycoside hydrolases (GH), depending on the adoption of the so-called *retaining* or *inverting* hydrolysis mechanism, which results in the retention or inversion of the anomeric configuration of the hydrolysis product, respectively.[20] While chitinases of family 18 have heterogeneous origin, chitinases of family 19 mostly belong to plant and bacterial species.

From a structural point of view, plant chitinases of either families 18 or 19 can be further classified according to the presence of specific modules. Indeed, in addition to essential presequence (PM) and catalytic (CM) modules, the presence of additional chitin-binding (CtBM) and linker (LM) modules distinguishes particular classes. CMs can also exhibit different lengths, similarities, and architectures, according to the presence of structural loops on the protein surfaces. A schematic representation of the identified structural classes is reported in Figure 1. Only classes I and IV have the CtBM and

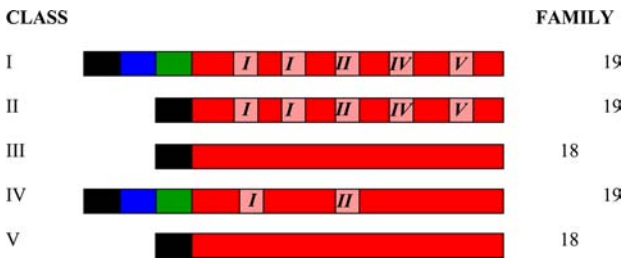

Figure 1. Schematic representation of different classes of chitinases of the 18 and 19 GH families. Color code: black = PM, blue = CtBM, green = LM, red = CM, and pink = surface loops. In order to adhere to previous literature, classes and surface loops have been both indicated with Roman figures, but italic font has been introduced for loops. Lengths of structural modules and positions of surface loops are only indicative. Adapted with permission from ref 24. Copyright 2009 Springer.

LM modules. CM modules can be distinguished on the basis of sequence similarities with reference enzymes (see Levorson and Chlan[21] and references therein). Class I and II chitinases, which share highly homologous CM modules, are at least 50% identical to tobacco Chia1 chitinases.[18] Chitinases of class III show no sequence similarities with class I or II chitinases and have higher than 50% sequence identities with a tobacco class III/lysozyme enzyme.[22] Class IV chitinases have CM modules which are at least 50% identical to the *Phaseolus vulgaris* PR-4 chitinase. CM modules in class IV chitinases are about 50 amino acids shorter than in class I and II chitinases. In chitinases of the classes I, II, and IV, up to five surface loops can be identified in the CM modules.[23,24] Chitinases of class V have CM modules which share consensus motifs with those of class III but are clearly distinguishable on the basis of an additional α/β domain (see the Class V section).

CLASSES OF PLANT CHITINASES AND ALLERGIES

The possibility that plant chitinases may act as food allergens[13] constitutes an important problem for human nutrition, also due to specific features of these proteins, which can be either overexpressed as PR-proteins[25−28] or can be unexpectedly present as transgenic chitinases, used for enhancing resistance to fungi and pathogens[29−31] (see the Class I section for a discussion about the induced expression of allergenic chitinases).

It has long been accepted that the allergenicity of plant chitinases derives from the presence of the CtBM, according to its high identity (65−70%) with hevein, a major allergen identified in the latex of rubber trees (*Hevea brasiliensis*).[32] Therefore, class I chitinases were the main object of the first studies on allergenic chitinases. It must be clarified that hevein, even if essentially constituted by a CtBM, is not a chitinase (its characteristics are further described in the Other Chitinase-Related Allergens section). Because of the presence of common or highly similar structural epitopes, hevein and class I chitinases have been indicated as largely responsible for the cross-reactive syndrome known as latex-fruit syndrome.[33,34] However, even at lower levels than hevein other latex allergens can be involved in latex-fruit cross-reactivity (see Radauer et al.[35] and references therein). Avocado, banana, chestnut, and kiwi fruits are considered as those with the highest degree of association to latex allergy.

Only more recently have chitinases from other classes been identified as allergens, resulting in a larger array of fruits and vegetables containing possible chitinase-type allergens. A summary of plant chitinases and structurally related proteins (hevein and other CtBM-like polypeptides), which have been indicated as allergens on the basis of their IgE-binding capacity, is reported in Table 1. With the exception of specific allergens detected in rubber tree latex, Japanese cedar pollen, and obeche dust, all the allergens can be regarded as food (or food-related) allergens. A literature-based list of allergenic chitinases is available in the Allergome database (http://www.allergome.org/). It must be emphasized that different approaches have been adopted to study the allergenicity of these chitinases (and of all allergens in general) and that not all are equivalent. For some of them, a rigorous analysis has been carried out, using both purified and recombinant proteins to study the alleged allergenicity. In a number of cases, the polypeptide has only been identified on the basis of partial sequence or mass-spectrometry analysis of molecules detected by either immunodetection assays using specific antibodies or immunoblot experiments carried out with sera of allergic patients. However, their isolation and complete characterization have not yet been accomplished. Up to now, chitinases acting as possible allergens have been identified in classes I−IV of plant chitinases. Details of studies carried out to investigate the allergenic activity of chitinases in each of the different structural classes, together with a short description of the main structural features, are given below.

Class I. This class contains most of the chitinases identified as allergens in plants. The first plant fruit chitinase with the capacity to bind IgE from allergic subjects was described in avocado (*Persea americana*) and is known by the name Pers a

dx.doi.org/10.1021/jf5007962 | J. Agric. Food Chem. 2014, 62, 5734−5742

Table 1. Classification of Plant Allergenic Chitinases[a]

plant	accession number	chitinase class	allergene (IUIS database)[b]	structure	ref
Actidinia chinensis (gold kiwi)	*c*	I			67, 68
Brassica rapa (turnip)	P81 729	I	Bra r 2		27
Carica papaya (papaya)	*d*				69
Castanea sativa (chestnut)	Q42 428	I	Cas s 5		38, 70
Hevea brasiliensis (rubber tree)	Q8GUD7	I	Hev b 11		39, 53
Lycopersicum esculentum (tomato)	Q05538	I			40
Musa sp. (banana)	B6UYK6, C3VD22, M0SI55, M0SI56, 022318, Q8VXF1	I	Mus a 2		37, 71, 72
Persea americana (avocado)	P93 680	I	Pers a 1		36, 38, 70, 73
Phaseolus vulgaris (green bean)	P36 361	I	*e*, *f*		26
Triplochiton scleroxylon (obeche)		I	Trip s 1 *e*(wood dust)		74
Triticum aestivum (wheat)	Q6T484	I	Tri a endochitinase[g,e,h]		28
Lycopersicum esculentum (tomato)	Q7Y0S1, Q05539	II	Sola I chitinase[g]		75, 76
Triticum aestivum (wheat)	Q4Z8L8	II	*e*		41
	Q8W429	II			
Coffea arabica (coffee) dust	D7REL9	III	Cof a 1		49
Hevea brasiliensis (rubber tree)		III			77, 78
Rubus ideaeu (raspberry)		III			48
Zizyphus mauritiana (Indian jujube)	Q2VST0	III	Ziz m 1		46
Cryptomeria japonica (red cedar)	Q5NTA4	IV	*e* (pollen)		39, 53
Vitis vinifera (grape)	AF532 966	IV	*e*		11, 39, 53, 79
Zea mays (maize)	ChiA/P29022	IV	*e*	4MCK	51, 52, 54
	ChiB/P29023		*e*		
Hevea brasiliensis (rubber tree)	Hevein/P02877	chitinase-related	Hev b 6	1HEV, 1Q9B	25, 32
Triticum aestivum (wheat)	agglutinin/isolectin P02876, P10 968	chitinase-related	Tri a 18	7WGA	80

[a]Chitinases identified as putative allergens are listed according to their classification into different classes. Chitinase-related polypeptides are listed separately. When available, protein names, accession numbers, IUIS allergen names, structure accession numbers in Protein Data Bank are reported. [b]IUIS is the acronym for International Union of Immunological Societies (http://www.allergen.org/). [c]Eight amino acids are available as the N-terminal sequence. This region shows homology with a class I chitinase (BAD02824) from *Taxodium distichum* (bald cypress). A 26 kDa allergen is recognized by a rabbit antichitinase antibody. Assignment to class I chitinase needs to be confirmed. [d]Data in the literature and databases are confusing. The Allergome site http://www.allergome.org/ reports the existence of a class I chitinase allergen, but contradictory cross-references are reported. The cited Uniprot sequence (P81241) leads to a class II sequence, and the literature citation[81] refers to a class IV chitinase. [e]Experimentally identified as an allergen but not yet added to the IUIS database. [f]Fourteen amino acids are available as the N-terminal sequence. This region shows 100% identity with Q6UZ78, a class I chitinase from kidney bean. [g]Allergen is present in the Allergome database and not in IUIS. [h]The gene is induced by the fungus *Fusarium graminearum*.[28]

1.[36] In this case, a 32 kDa protein from avocado fruit, identified by immune-reaction in the sera of 15 out of 20 avocado allergic patients, was purified and partially sequenced. The corresponding cDNA was also obtained. Analysis of polypeptides and cDNA sequences identified an open reading frame coding for a 326 amino acid protein with a leader peptide of 25 amino acids, a CtBM of 43 amino acids, and additional consensus motifs characteristic of a class I chitinase. The avocado mature chitinase, obtained as a recombinant molecule in *Pichia pastoris* cells, showed the expected endochitinase activity and was effective in inhibiting the binding of allergic patients' IgE to the 32 kDa protein in avocado extracts. Almost simultaneously, other plant chitinases were identified as allergens by procedures including purification of chitinases (with the aid of antihevein or specific antichitinase antibodies for their identification), N-terminal sequencing, immunoblot assays of plant protein extracts with sera of patients allergic to rubber latex, and immunoblot inhibition assays using purified chitinases (or hevein) as inhibitors. Two polypeptides of 32 and 33 kDa were identified as allergenic chitinases in banana (*Musa acuminata*). N-Terminal sequencing of the purified banana polypeptides revealed high identity (around 80%) with hevein.[37] A 32 kDa allergenic polypeptide was also identified as a class I chitinase in chestnut. The reported N-terminal sequence (27 amino acids) was 81% similar to hevein.[38] In this case also, the activity of the purified chitinase was assayed. Interestingly, in turnip (*Brassica rapa*), among polypeptides whose expression was enhanced in roots after chemical treatments for the activation of plant defense mechanisms, a class I allergenic chitinase was identified. The same polypeptide was not identifiable with antisera when proteins were extracted from untreated plants.[27] A strongly induced allergenic chitinase of class I was also identified in green bean subjected to ethylene treatment.[26]

Subsequently, a real class I chitinase from *Hevea brasiliensis* was described showing 58% identity between its CtBM and hevein and different IgE binding capacities.[39] Recently, a

putative class I allergenic chitinase has been identified in tomato fruits infected with *Pepino mosaic virus* by 2D comparative immunoblot assay with sera of tomato allergic subjects and mass spectrometry analysis.[40] Skin prick tests conducted with tomato allergic subjects did not, however, show any significant difference between infected and noninfected tomato fruits, indicating that the overall fruit allergenicity was, at least in this case, not appreciably changed by virus infection. More detailed studies have to be performed to clearly establish the allergenic risks due to inducible proteins like chitinases.

Other class I chitinases from plants which have been shown to react with IgE of allergic patients have been reported in kiwi, papaya, obeche, and wheat (Table 1).

Generally, relationships between chitinase three-dimensional structures and allergenicity have not so far received sufficient attention, perhaps due to the assumption that their allergenicity is mainly due to the CtBM. Evidence is emerging, however, indicating that other regions of chitinase molecules can act as allergen epitopes as well (see the Class II section) making a deeper structure−allergenicity analysis of their CM modules important. Knowledge about the structure of class I chitinases comes from a unique work carried out for the CM of the *Brassica juncea* chitinase (EBI accession number Q9SQF7). Even if there are no indications about its allergenicity, its structural analysis can be relevant for possible comparisons with known allergenic chitinases of other classes. The *B. juncea* chitinase is defined as a highly α-helical protein, with a single and irregular β-sheet.[23] The protein has a bilobate shape with a wide cleft in which the active site (Glu-212 and Glu-234) interacts with chitin. The overall structure is stabilized by three disulfide bridges and shows five flexible surface loops (*I*−*V* in Figure 1), some of which were located at the border of the active site cleft.

Class II. Chitinases of class II are highly similar to class I enzymes except for the absence of the CtBM module. They have not usually been considered as allergens, according to the assumption that allergenicity of chitinases mainly resides in the hevein-like CtBM. At least this is what emerged from a study on class II chitinases isolated from chestnuts and avocado fruits and assayed against the sera of allergic patients, for whom no IgE binding capacity was identified.[38] Data, however, are now emerging which indicate that the CM modules of class II chitinases can be the source of allergenicity. Recently, one class II chitinase has been identified as a possible allergen in wheat flour.[41] By immunoblotting analysis of wheat flour proteins with sera of 22 patients with a suspect history of wheat allergy and high levels of specific IgE, and successive mass-spectrometry analysis of reactive proteins, two chitinases were identified: a 26 kDa protein, which shows high similarity with a class I chitinase from *Hordeum vulgaris* (EBI accession number P11955), and an additional chitinase corresponding to a wheat class II chitinase (EBI accession number Q4Z8L8). The purified class II chitinase was reactive to at least 20 out of the 22 available patients' sera. No further details are available about the allergenicity of this molecule. Another wheat class II chitinase (EBI accession number Q8W429) is present in the Allergome database with the code 1274, for which additional information is not available.

Additionally, the Allergome database reports as allergen (code 1273) a class I chitinase from tomato fruits. It corresponds to two almost identical sequences (EBI accession numbers Q05539 and Q7Y0S1) which, however, do not contain the CtBM. The mature polypeptide has an acidic isoelectric point of 5.6, which further enables its classification among class II chitinases.[42] For these reasons, the allergen, named Sola 1 chitinase, has been listed in this review among class II chitinases (Table 1).

The structure of class II chitinases has been described for enzymes purified from barley,[43] papaya,[44] and rye,[45] for which there is currently no information about allergenicity. Also in these cases, as for class I enzymes, the structure is rich in α-helices and shows a substrate-binding groove located between two lobes, with three disulfide bridges contributing to protein folding.

Class III. Class III chitinases are structurally different from class I and class II enzymes and initially not considered as allergens. Recently, however, four plant chitinases belonging to this class have been identified as possible allergens.

The first plant fruit class III chitinase showing IgE binding capacity and IgE-cross reactivity with latex allergens has been identified in Indian jujube (*Zizyphus mauritiana*).[46] It is a protein of 330 amino acids, including a leader peptide of 25 residues. Both the purified and the recombinant proteins were immunoreactive with sera from latex and Indian jujube allergic patients (seven out of eight patients). This chitinase showed 45.2% identity with hevamine, a class III chitinase present in rubber tree latex, where it had been previously described as an unimportant allergen since only a reduced percentage of examined sera (about 3%) contained reactive IgE.[47]

Mass-spectrometry analysis of IgE-reactive proteins allowed the identification of a class III chitinase also among the allergens extracted from fresh raspberries (*Rubus ideaeus*).[48] As in the case of Indian jujube chitinase and different from hevamine, for raspberry fruits the protein was found to react with most (>80%) of the sera of patients allergic to raspberries. The involvement of plant chitinases of class III in allergic reactions has been recently confirmed by a study conducted on coffee (*Coffea arabica*) allergens.[49] By screening a phage display library of coffee cDNA with sera of two patients allergic to green coffee beans, a cDNA sequence corresponding to a class III chitinase was identified among those coding for IgE-reactive polypeptides. The recombinant polypeptide (rCofa 1) was subsequently produced and showed immunoreactivity with the sera of the two patients allergic to green coffee and 3 out of 17 sera from workers in coffee industries, all with allergenic symptoms to coffee dust. Immunoreactivity of rCof a 1 with IgE of sera from latex allergic patients was also found.

Currently, there are no studies about three-dimensional structures of class III chitinases among plant food proteins. Only for the nonfood plant chitinase hevamine has the structure been established.[50] It consists of an $(\alpha/\beta)_8$ barrel fold, different from that described for class I and II chitinases, leading to the assumption of a different structural base for allergenicity.

Class IV. As for class IV chitinases, IgE-binding capacity has been reported in maize kernels, grapes (*Vitis vinifera* and *V. lambrusca*), and wines by immunoblot analysis of plant protein extracts with sera of allergic patients, and subsequent mass spectrometry identification.[11,51,52] None of these allergens has been currently isolated, preventing further studies of their biological and structural characteristics. Only one chitinase of this class, identified as an allergen in Japanese cedar (*Cryptomeria japonica*) pollen, has been isolated and characterized for its enzymatic activity and allergenicity.[53] IgE binding was confirmed in all of the sera of the 31 tested allergic patients, with levels comparable with those observed for the Cry j 1 C.

A

```
                          10        20        30        40
                          .         .         .         .
Hevb6_P02877              -EQCGRQAGGKLCPNNLCCSQWGWCGSTDEYCSPDHNCQSNCKD--
CL_I_Brar2_P81729         ------QAGGQTCAGNXCCSQYGYCGTTADYCSPDNNCQ-------
Cl_I_Cass5_Q42428         -EQCGRQAGGAACANNLCCSQFGWCGNTAEYCGAG--CQSQCSSPT
Cl_I_Hevb11_Q8GUD7        -EQCGRQAGGALCPGGLCCSQYGWCANTPEYCGSG-CQSQCDGGV-
Cl_I_Le_Q05538            -EQCGSQAGGALCASGLCCSKFGWCGNTNEYCGPGNCQSQCPG--
Cl_I_Musa1_O22318         -EQCGRQAGGALCPGGLCCSQYGWCGNTDPYCGQG--CXSQCTGST
Cl_I_Prsa1_P93680         -EQCGRQAGGALCPGGLCCSQFGWCGSTSDYCGPT--CQSQCGGVT
Cl_IV_Cj_Q5NTA4           --------QNCGCN-GLCCSQYGYCGSGEAYCGAG--CKEGPCSSS
Cl_IV_Vv_Q7XAU6           --------QNCGCASGLCCSKYGYCGTGSDYCGDG--CQSGPCDS-
Cl_IV_Zm_P29022           --------QNCGCQPNFCCSKFGYCGTTDAYCGDG--CQSGPCRS-
Cl_IV_Zm_P29023           --------QNCGCQPNVCCSKFGYCGTTDEYCGDG--CQSGPCRS-
Tria18_P02876_1           -QRCGEQGSNMECPNNLCCSQYGYCGMGGDYCGKG--CQNGACWT-
Tria18_P02876_2           SKRCGSQAGGATCPNNHCCSQYGHCGFGAEYCGAG--CQGGPCRA-
Tria18_P02876_3           DIKCGSQSGGKLCPNNLCCSQWGFCGLGSEFCGGG--CQSGACST-
Tria18_P02876_4           DKPCGKDAGGRVCTNNYCCSKWGSCGIGPGYCGAG--CQSGGCDA-
Tria18_P10968_1           -QRCGEQGSNMECPNNLCCSQYGYCGMGGDYCGKG--CQNGACWT-
Tria18_P10968_2           SKRCGSQAGGATCTNNQCCSQYGYCGFGAEYCGAG--CQGGPCRA-
Tria18_P10968_3           DIKCGSQAGGKLCPNNLCCSQWGFCGLGSEFCGGG--CQSGACST-
Tria18_P10968_4           DKPCGKDAGGRVCTNNYCCSKWGSCGIGPGYCGAG--CQSGGCDG-
```

B

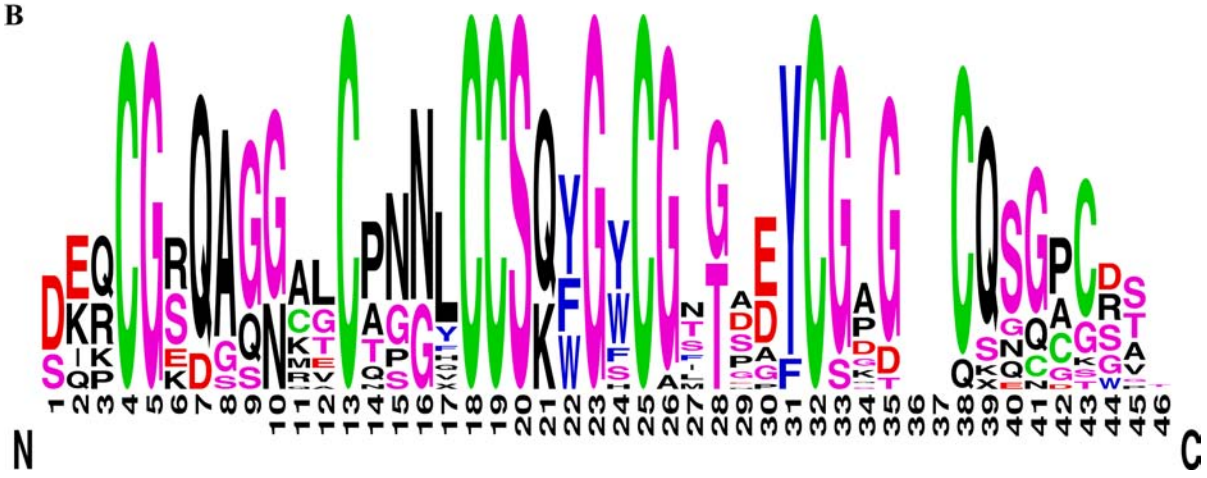

Figure 2. (A) Multialignment of hevein with CtBMs of class I and class IV chitinases and hevein-like regions of WGAs. With the exception of hevein, all the sequences are in the same order as that in Table 1. Class I (Cl_I) enzymes are reported before class IV (Cl_IV) enzymes. The last eight sequences refer to the chitinase-related polypeptides in Table 1. When possible, the sequence names report the name of the allergen; otherwise, the first letters of the plant's scientific name are indicated. All of the names of sequences contain the EBI accession number. Amino acids of the hevein linear epitopes have been underlined. Trp-21 and Trp-23, together with the other amino acids of the carbohydrate-binding site, are in bold. (B) Graphical representation of the hevein-CtBMs multiple sequence alignment obtained by the WebLogo program[66] with the following color code: green (C), purple (G, S, T), blue (Y, F, W), and red (D, E).

japonica major allergen. Interestingly, preincubation of the purified molecule with rubber tree latex completely inhibited IgE reaction in pooled sera of *C. japonica* allergic patients.

There are only two structures established for this class of chitinases. The first is that of the Norway spruce (*Picea abies*) chitinase.[24] The structure of the CM region shows a high content of α-helices and a small irregular β-sheet, assembled in a bilobate arrangement containing three disulfide bridges and forming a wide cleft exposed on the protein surface. The structure of the CtBM was obtained by homology modeling. It resembles those of class I enzymes and of hevein as well (see also the Other Chitinase-Related Allergens section). More recently, the 3D structure of the putative allergenic chitinase A from maize has also been determined.[54] In this case, a recombinant truncated form lacking the CtBM was investigated, which shows the same structural components of chitinases of the GH19 family and still retains activity levels comparable with those of the full-length enzyme.

Which module of class IV chitinases (CtBM or CM) is responsible for allergenicity has not been investigated yet. Even if the presence of a CtBM region, highly homologous to those of class I chitinases and hevein, can be considered as an obvious explanation of their allergenicity, the relatively close structural relationships between their CM modules with that of class II enzymes (among which allergens have been detected) open the possibility that other domains of these proteins could induce allergy. Obviously, this could be the case also for class I chitinases.

Class V. Allergens within this class have not yet been identified. Class V chitinases have been described only in *Arabidopsis thaliana*, *Nicotiana tabacum*, and *Cycas revoluta*, with structures established in the first two cases.[55,56] Putative chitinases have also been identified in *Medicago truncatula*, rice, and oil palm.[57,58] Class V chitinases share a similar $(\alpha/\beta)_8$ barrel fold with class III chitinases with which they also share the consensus DXDXE motif containing the catalytic glutamic acid. Other elements, however, clearly distinguish the two classes of chitinases. In particular, class V chitinases have an extra α/β region of about 65−70 amino acids and do not possess six cysteine residues involved in the formation of

dx.doi.org/10.1021/jf5007962 | J. Agric. Food Chem. 2014, 62, 5734−5742

disulfide bridges in class III chitinases. In addition, while the sequence identity of molecules within each class is relatively high (around 40% within class III and in the 40−60% range for class V), identity between members of classes III and V is less than 20%. If further confirmed, the absence of allergens within members of class V could provide valuable information to study structural determinants of allergenicity for class III chitinases.

Other Chitinase-Related Allergens. Hevein is the paradigm of chitinase-related allergens. It is a protein of 43 amino acids detected in the latex produced by specialized cells of the rubber tree (*Hevea brasiliensis*), with a possible role as a defense-related protein due to its capacity to bind chitin and inhibit the growth of chitin-containing fungi.[59] Additionally, thanks to its capacity to bind to glycosylated receptors, a role as a coagulation factor of rubber particles has also been assigned.[60] Hevein is known as a major allergen present in natural rubber latex which is the cause of allergies among people using latex-derived products, reaching percentages in the range of 3−17% for health-care workers.[32,61] The hevein gene encodes a polypeptide of 204 amino acids, constituted by a signal sequence of 17 amino acids, the hevein domain, and a 144 amino acid-long carboxy-terminal region showing high homology to wound-inducible potato polypeptides.[25] Hevein is rich in cysteine and glycine amino acids and shows high sequence similarities to the CtBM of class I chitinases (higher than 65%), the C-domain of wheat germ agglutinin (WGA) (around 60%), and the CtBM of class IV chitinases (in the 40−60% range). Similar domains have also been detected in other plant proteins (lectins, wound-induced proteins) and fungi (chitinases, toxins, and cell-wall enzymes).

The three-dimensional structure of hevein shows an ovoid shape containing an antiparallel β-sheet and a short four-amino-acid α-helix, assisted by four disulfide bonds.[62,63] More recent studies, carried out using chemically modified hevein molecules, highlighted the essential role of the surface exposed Trp-21 and Trp-23 amino acids for IgE recognition.[64] These amino acids are part of the carbohydrate binding site of the molecule and belong to a conformational epitope derived from the structural association of two previously identified linear epitopes.[65] Most of the aromatic and acid amino acids forming the hevein carbohydrate-binding site are present in other hevein-like molecules identified as allergens, such as WGA and class I and IV chitinases. All of these molecules share the consensus motif C(12)XXXXCCSXφXφCGXΩXAcYC(31) (where X = any amino acid; φ = an aromatic amino acid; Ω = Thr, Ser, or Gly; Ac = Glu or Asp).[64] Figure 2 reports the alignment of the hevein sequence with the corresponding region of class I and class IV chitinases, and with WGAs.

A recent study based on the cross-reactivity of recombinant hevein and specific plant class I chitinases from banana and avocado fruits, carried out by ELISA assays with sera of latex-allergic patients (for which the involvement in latex-associated plant food syndrome was not known), showed that only subfractions of patients' sera having hevein-specific IgE cross-reacted with banana and avocado chitinases. Also, cases of latex-allergic patients with IgE specific for the chitinases from the two fruits but without specificities for hevein could be observed. Structural analysis of hevein, CtBM-like domains of WGAs, and model structures of class I chitinases clearly indicated that surface variability of allergens is much higher than expected from the alignments of their amino acids sequences,[35] making the prediction of cross-reactivity even more challenging.

Conclusions and Perspectives. From the above-reported data, it appears that the general statement that plant chitinases can be allergenic molecules deserves more detailed clarifications. We can assume that plant food chitinases constitute a heterologous group of allergenic molecules, in which at least three different subgroups can be identified: the hevein-like (or CtBM-like) molecules (including both class I and class IV chitinases), the class II chitinases, and the class III chitinases. While a considerable amount of work has been carried out for the identification of class I chitinases as food allergens, chitinases of classes II, III and, IV have been little investigated so far for their potential allergenicity. It is notable that they have been identified as possible allergens in cultivated plants worldwide, widely used in human nutrition, in some cases even as raw food (e.g., salads and fresh fruits).

From a structural point of view, the identification of allergenic molecules belonging to class II chitinases, which do not contain the CtBM module, opens the possibility that the allergenicity of chitinases may not be exclusively due to the CtBM module. This aspect should be properly investigated among class I and class IV chitinases.

Plant chitinases are, therefore, a clear example of molecules for which further studies are required in the near future to better define their allergenic determinants and evaluate their relevance. Recombinant technologies, including techniques based on combinatorial approaches,[49] combined with advanced structural and physicochemical analysis[6] can provide useful tools to allergology investigations to firmly establish the structural determinants of allergenicity in chitinases.

AUTHOR INFORMATION

Corresponding Author

*Phone: +39 080 5443311. Fax: +39 080 5443403. E-mail: l.ceci@ibbe.cnr.it.

Funding

This work has been supported by a grant from Fondazione Cassa di Risparmio di Puglia (FCRP), Progetto "Studio di Proteine Allergeniche di mais mediante sistemi eterologhi e loro applicazioni in allergologia." C.L. was a recipient of a fellowship from FCRP.

Notes

The authors declare no competing financial interest.

ACKNOWLEDGMENTS

We are grateful to Stephan J. Reshkin (Department of Bioscience, Biotechnology and Biopharmaceutics, University of Bari) for critical reading of the manuscript.

ABBREVIATIONS USED

nsLTP, nonspecific lipid transfer proteins; PR, pathogenesis related; GH, glycoside hydrolases; PM, presequence module; CM, catalytic modules; CtBM, chitin-binding module; LM, linker module; WGA, wheat germ agglutinin

REFERENCES

(1) van Hengel, A. J. Food allergen detection methods and the challenge to protect food-allergic consumers. *Anal. Bioanal. Chem.* **2007**, *389*, 111−118.

(2) Otsu, K.; Fleischer, D. M. Therapeutics in food allergy: the current state of the art. *Curr. Allergy Asthma Rep.* **2011**, *12*, 48−54.

(3) Punta, M.; Coggill, P. C.; Eberhardt, R. Y.; Mistry, J.; Tate, J.; Boursnell, C.; Pang, N.; Forslund, K.; Ceric, G.; Clements, J.; Heger, A.; Holm, L.; Sonnhammer, E. L.; Eddy, S. R.; Bateman, A.; Finn, R.

D. The Pfam protein families database. *Nucleic Acids Res.* **2012**, *40*, D290−301.
(4) Radauer, C.; Bublin, M.; Wagner, S.; Mari, A.; Breiteneder, H. Allergens are distributed into few protein families and possess a restricted number of biochemical functions. *J. Allergy Clin. Immunol.* **2008**, *121*, 847−852 e847.
(5) Jenkins, J. A.; Breiteneder, H.; Mills, E. N. Evolutionary distance from human homologs reflects allergenicity of animal food proteins. *J. Allergy Clin. Immunol.* **2007**, *120*, 1399−1405.
(6) Harrer, A.; Egger, M.; Gadermaier, G.; Erler, A.; Hauser, M.; Ferreira, F.; Himly, M. Characterization of plant food allergens: an overview on physicochemical and immunological techniques. *Mol. Nutr. Food Res.* **2010**, *54*, 93−112.
(7) Mills, E. N.; Sancho, A. I.; Rigby, N. M.; Jenkins, J. A.; Mackie, A. R. Impact of food processing on the structural and allergenic properties of food allergens. *Mol. Nutr. Food Res.* **2009**, *53*, 963−969.
(8) Hansen, K. S.; Ballmer-Weber, B. K.; Luttkopf, D.; Skov, P. S.; Wuthrich, B.; Bindslev-Jensen, C.; Vieths, S.; Poulsen, L. K. Roasted hazelnuts–allergenic activity evaluated by double-blind, placebo-controlled food challenge. *Allergy* **2003**, *58*, 132−138.
(9) Pastorello, E. A.; Pompei, C.; Pravettoni, V.; Farioli, L.; Calamari, A. M.; Scibilia, J.; Robino, A. M.; Conti, A.; Iametti, S.; Fortunato, D.; Bonomi, S.; Ortolani, C. Lipid-transfer protein is the major maize allergen maintaining IgE-binding activity after cooking at 100 degrees C, as demonstrated in anaphylactic patients and patients with positive double-blind, placebo-controlled food challenge results. *J. Allergy Clin. Immunol.* **2003**, *112*, 775−783.
(10) Asero, R.; Mistrello, G.; Roncarolo, D.; Amato, S.; van Ree, R. A case of allergy to beer showing cross-reactivity between lipid transfer proteins. *Ann. Allergy Asthma Immunol.* **2001**, *87*, 65−67.
(11) Pastorello, E. A.; Farioli, L.; Pravettoni, V.; Ortolani, C.; Fortunato, D.; Giuffrida, M. G.; Perono Garoffo, L.; Calamari, A. M.; Brenna, O.; Conti, A. Identification of grape and wine allergens as an endochitinase 4, a lipid-transfer protein, and a thaumatin. *J. Allergy Clin. Immunol.* **2003**, *111*, 350−359.
(12) Steckelbroeck, S.; Ballmer-Weber, B. K.; Vieths, S. Potential, pitfalls, and prospects of food allergy diagnostics with recombinant allergens or synthetic sequential epitopes. *J. Allergy Clin. Immunol.* **2008**, *121*, 1323−1330.
(13) Hauser, M.; Egger, M.; Wallner, M.; Wopfner, N.; Schmidt, G.; Ferreira, F. Molecular properties of plant food allergens: a current classification into protein families. *Open Immunol. J.* **2008**, *1*, 1−12.
(14) Breiteneder, H.; Mills, E. N. Molecular properties of food allergens. *J. Allergy Clin. Immunol.* **2005**, *115*, 14−23.
(15) Bejosano, F. P.; Waniska, R. D.; Rooney, W. L. Antifungal proteins in commercial hybrids and elite sorghums. *J. Agric. Food Chem.* **2003**, *51*, 5911−5915.
(16) Ji, C.; Norton, R. A.; Wicklow, D. T.; Dowd, P. F. Isoform patterns of Chitinase and beta-1,3-glucanase in maturing corn kernels (*Zea mays* L.) associated with *Aspergillus flavus* milk stage infection. *J. Agric. Food Chem.* **2000**, *48*, 507−511.
(17) Beintema, J. J. Structural features of plant chitinases and chitin-binding proteins. *FEBS Lett.* **1994**, *350*, 159−163.
(18) Raikhel, N. V.; Lee, H. I.; Broekaert, W. F. Structure and Function of Chitin-Binding Proteins. *Ann. Rev. of Plant Physiol Plant Mol. Biol.* **1993**, *44*, 591−615.
(19) Neuhaus, J. M.; Fritig, B.; Linthorst, H. J. M.; Meins, F.; Mikkelsen, J. D.; Ryals, J. A revised nomenclature of Chitinase genes. *Plant Mol. Biol. Rep.* **1996**, *14*, 102−104.
(20) Davies, G.; Henrissat, B. Structures and mechanisms of glycosyl hydrolases. *Structure* **1995**, *3*, 853−859.
(21) Levorson, J.; Chalan, C. A. Plant Chitinase consensus sequences. *Plant Mol. Biol. Rep.* **1997**, *15*, 122−133.
(22) Collinge, D. B.; Kragh, K. M.; Mikkelsen, J. D.; Nielsen, K. K.; Rasmussen, U.; Vad, K. Plant chitinases. *Plant J.* **1993**, *3*, 31−40.
(23) Ubhayasekera, W.; Tang, C. M.; Ho, S. W.; Berglund, G.; Bergfors, T.; Chye, M. L.; Mowbray, S. L. Crystal structures of a family 19 Chitinase from *Brassica juncea* show flexibility of binding cleft loops. *FEBS J.* **2007**, *274*, 3695−3703.
(24) Ubhayasekera, W.; Rawat, R.; Ho, S. W.; Wiweger, M.; Von Arnold, S.; Chye, M. L.; Mowbray, S. L. The first crystal structures of a family 19 class IV Chitinase: the enzyme from Norway spruce. *Plant Mol. Biol.* **2009**, *71*, 277−289.
(25) Broekaert, I.; Lee, H. I.; Kush, A.; Chua, N. H.; Raikhel, N. Wound-induced accumulation of mRNA containing a hevein sequence in laticifers of rubber tree (*Hevea brasiliensis*). *Proc. Natl. Acad. Sci. U.S.A.* **1990**, *87*, 7633−7637.
(26) Sanchez-Monge, R.; Blanco, C.; Perales, A. D.; Collada, C.; Carrillo, T.; Aragoncillo, C.; Salcedo, G. Class I chitinases, the panallergens responsible for the latex-fruit syndrome, are induced by ethylene treatment and inactivated by heating. *J. Allergy Clin. Immunol.* **2000**, *106*, 190−195.
(27) Hanninen, A. R.; Mikkola, J. H.; Kalkkinen, N.; Turjanmaa, K.; Ylitalo, L.; Reunala, T.; Palosuo, T. Increased allergen production in turnip (*Brassica rapa*) by treatments activating defense mechanisms. *J. Allergy Clin. Immunol.* **1999**, *104*, 194−201.
(28) Kong, L.; Anderson, J. M.; Ohm, H. W. Induction of wheat defense and stress-related genes in response to *Fusarium graminearum*. *Genome* **2005**, *48*, 29−40.
(29) Iqbal, M. M.; Nazir, F.; Ali, S.; Asif, M. A.; Zafar, Y.; Iqbal, J.; Ali, G. M. Over expression of rice Chitinase gene in transgenic peanut (*Arachis hypogaea* L.) improves resistance against leaf spot. *Mol. Biotechnol.* **2012**, *50*, 129−136.
(30) Ceasar, S. A.; Ignacimuthu, S. Genetic engineering of crop plants for fungal resistance: role of antifungal genes. *Biotechnol. Lett.* **2012**, *34*, 995−1002.
(31) Waniska, R. D.; Venkatesha, R. T.; Chandrashekar, A.; Krishnaveni, S.; Bejosano, F. P.; Jeoung, J.; Jayaraj, J.; Muthukrishnan, S.; Liang, G. H. Antifungal proteins and other mechanisms in the control of sorghum stalk rot and grain mold. *J. Agric. Food Chem.* **2001**, *49*, 4732−4742.
(32) Alenius, H.; Kalkkinen, N.; Reunala, T.; Turjanmaa, K.; Palosuo, T. The main IgE-binding epitope of a major latex allergen, prohevein, is present in its N-terminal 43-amino acid fragment, hevein. *J. Immunol.* **1996**, *156*, 1618−1625.
(33) Blanco, C. Latex-fruit syndrome. *Curr. Allergy Asthma Rep.* **2003**, *3*, 47−53.
(34) Wagner, S.; Breiteneder, H. The latex-fruit syndrome. *Biochem. Soc. Trans.* **2002**, *30*, 935−940.
(35) Radauer, C.; Adhami, F.; Furtler, I.; Wagner, S.; Allwardt, D.; Scala, E.; Ebner, C.; Hafner, C.; Hemmer, W.; Mari, A.; Breiteneder, H. Latex-allergic patients sensitized to the major allergen hevein and hevein-like domains of class I chitinases show no increased frequency of latex-associated plant food allergy. *Mol. Immunol.* **2011**, *48*, 600−609.
(36) Sowka, S.; Hsieh, L. S.; Krebitz, M.; Akasawa, A.; Martin, B. M.; Starrett, D.; Peterbauer, C. K.; Scheiner, O.; Breiteneder, H. Identification and cloning of prs a 1, a 32-kDa endochitinase and major allergen of avocado, and its expression in the yeast *Pichia pastoris*. *J. Biol. Chem.* **1998**, *273*, 28091−28097.
(37) Mikkola, J. H.; Alenius, H.; Kalkkinen, N.; Turjanmaa, K.; Palosuo, T.; Reunala, T. Hevein-like protein domains as a possible cause for allergen cross-reactivity between latex and banana. *J. Allergy Clin. Immunol.* **1998**, *102*, 1005−1012.
(38) Diaz-Perales, A.; Collada, C.; Blanco, C.; Sanchez-Monge, R.; Carrillo, T.; Aragoncillo, C.; Salcedo, G. Class I chitinases with hevein-like domain, but not class II enzymes, are relevant chestnut and avocado allergens. *J. Allergy Clin. Immunol.* **1998**, *102*, 127−133.
(39) O'Riordain, G.; Radauer, C.; Hoffmann-Sommergruber, K.; Adhami, F.; Peterbauer, C. K.; Blanco, C.; Godnic-Cvar, J.; Scheiner, O.; Ebner, C.; Breiteneder, H. Cloning and molecular characterization of the *Hevea brasiliensis* allergen Hev b 11, a class I Chitinase. *Clin. Exp. Allergy* **2002**, *32*, 455−462.
(40) Welter, S.; Dolle, S.; Lehmann, K.; Schwarz, D.; Weckwerth, W.; Worm, M.; Franken, P. Pepino mosaic virus infection of tomato affects allergen expression, but not the allergenic potential of fruits. *PLoS One* **2013**, *8*, e65116.

(41) Sotkovsky, P.; Sklenar, J.; Halada, P.; Cinova, J.; Setinova, I.; Kainarova, A.; Golias, J.; Pavlaskova, K.; Honzova, S.; Tuckova, L. A new approach to the isolation and characterization of wheat flour allergens. *Clin. Exp. Allergy* **2011**, *41*, 1031−1043.
(42) Buchter, R.; Stromberg, A.; Schmelzer, E.; Kombrink, E. Primary structure and expression of acidic (class II) Chitinase in potato. *Plant Mol. Biol.* **1997**, *35*, 749−761.
(43) Hart, P. J.; Monzingo, A. F.; Ready, M. P.; Ernst, S. R.; Robertus, J. D. Crystal structure of an endochitinase from *Hordeum vulgare* L. seeds. *J. Mol. Biol.* **1993**, *229*, 189−193.
(44) Huet, J.; Rucktooa, P.; Clantin, B.; Azarkan, M.; Looze, Y.; Villeret, V.; Wintjens, R. X-ray structure of papaya Chitinase reveals the substrate binding mode of glycosyl hydrolase family 19 chitinases. *Biochemistry* **2008**, *47*, 8283−8291.
(45) Ohnuma, T.; Numata, T.; Osawa, T.; Inanaga, H.; Okazaki, Y.; Shinya, S.; Kondo, K.; Fukuda, T.; Fukamizo, T. Crystal structure and chitin oligosaccharide-binding mode of a 'loopful' family GH19 Chitinase from rye, *Secale cereale*, seeds. *FEBS J.* **2012**, *279*, 3639−3651.
(46) Lee, M. F.; Hwang, G. Y.; Chen, Y. H.; Lin, H. C.; Wu, C. H. Molecular cloning of Indian jujube (*Zizyphus mauritiana*) allergen Ziz m 1 with sequence similarity to plant class III chitinases. *Mol. Immunol* **2006**, *43*, 1144−1151.
(47) Alenius, H.; Kalkkinen, N.; Lukka, M.; Reunala, T.; Turjanmaa, K.; Makinen-Kiljunen, S.; Yip, E.; Palosuo, T. Prohevein from the rubber tree (*Hevea brasiliensis*) is a major latex allergen. *Clin. Exp. Allergy* **1995**, *25*, 659−665.
(48) Marzban, G.; Herndl, A.; Kolarich, D.; Maghuly, F.; Mansfeld, A.; Hemmer, W.; Katinger, H.; Laimer, M. Identification of four IgE-reactive proteins in raspberry (*Rubus ideaeus* L.). *Mol. Nutr. Food Res.* **2008**, *52*, 1497−1506.
(49) Manavski, N.; Peters, U.; Brettschneider, R.; Oldenburg, M.; Baur, X.; Bittner, C. Cof a 1: identification, expression and immunoreactivity of the first coffee allergen. *Int. Arch. Allergy Immunol.* **2012**, *159*, 235−242.
(50) Terwisscha van Scheltinga, A. C.; Hennig, M.; Dijkstra, B. W. The 1.8 A resolution structure of hevamine, a plant Chitinase/lysozyme, and analysis of the conserved sequence and structure motifs of glycosyl hydrolase family 18. *J. Mol. Biol.* **1996**, *262*, 243−257.
(51) Pastorello, E. A.; Farioli, L.; Pravettoni, V.; Scibilia, J.; Conti, A.; Fortunato, D.; Borgonovo, L.; Bonomi, S.; Primavesi, L.; Ballmer-Weber, B. Maize food allergy: lipid-transfer proteins, endochitinases, and alpha-zein precursor are relevant maize allergens in double-blind placebo-controlled maize-challenge-positive patients. *Anal. Bioanal. Chem.* **2009**, *395*, 93−102.
(52) Fasoli, E.; Pastorello, E. A.; Farioli, L.; Scibilia, J.; Aldini, G.; Carini, M.; Marocco, A.; Boschetti, E.; Righetti, P. G. Searching for allergens in maize kernels via proteomic tools. *J. Proteomics* **2009**, *72*, 501−510.
(53) Fujimura, T.; Shigeta, S.; Suwa, T.; Kawamoto, S.; Aki, T.; Masubuchi, M.; Hayashi, T.; Hide, M.; Ono, K. Molecular cloning of a class IV Chitinase allergen from Japanese cedar (*Cryptomeria japonica*) pollen and competitive inhibition of its immunoglobulin E-binding capacity by latex C-serum. *Clin. Exp. Allergy* **2005**, *35*, 234−243.
(54) Chaudet, M. M.; Naumann, T. A.; Price, N. P.; Rose, D. R. Crystallographic structure of ChitA, a glycoside hydrolase family 19, plant class IV Chitinase from *Zea mays*. *Protein Sci.* **2014**, *23*, 586−593.
(55) Taira, T.; Hayashi, H.; Tajiri, Y.; Onaga, S.; Uechi, G.; Iwasaki, H.; Ohnuma, T.; Fukamizo, T. A plant class V Chitinase from a cycad (*Cycas revoluta*): biochemical characterization, cDNA isolation, and posttranslational modification. *Glycobiology* **2009**, *19*, 1452−1461.
(56) Ohnuma, T.; Numata, T.; Osawa, T.; Mizuhara, M.; Lampela, O.; Juffer, A. H.; Skriver, K.; Fukamizo, T. A class V Chitinase from *Arabidopsis thaliana*: gene responses, enzymatic properties, and crystallographic analysis. *Planta* **2011**, *234*, 123−137.
(57) Salzer, P.; Feddermann, N.; Wiemken, A.; Boller, T.; Staehelin, C. Sinorhizobium meliloti-induced Chitinase gene expression in *Medicago truncatula* ecotype R108−1: a comparison between symbiosis-specific class V and defence-related class IV chitinases. *Planta* **2004**, *219*, 626−638.
(58) Yeoh, K. A.; Othman, A.; Meon, S.; Abdullah, F.; Ho, C. L. Sequence analysis and gene expression of putative oil palm Chitinase and Chitinase-like proteins in response to colonization of *Ganoderma boninense* and *Trichoderma harzianum*. *Mol. Biol. Rep.* **2013**, *40*, 147−158.
(59) Van Parijs, J.; Broekaert, W. F.; Goldstein, I. J.; Peumans, W. J. Hevein: an antifungal protein from rubber-tree (*Hevea brasiliensis*) latex. *Planta* **1991**, *183*, 258−264.
(60) Gidrol, X.; Chrestin, H.; Tan, H. L.; Kush, A. Hevein, a lectin-like protein from *Hevea brasiliensis* (rubber tree) is involved in the coagulation of latex. *J. Biol. Chem.* **1994**, *269*, 9278−9283.
(61) Chen, Z.; Posch, A.; Lohaus, C.; Raulf-Heimsoth, M.; Meyer, H. E.; Baur, X. Isolation and identification of hevein as a major IgE-binding polypeptide in Hevea latex. *J. Allergy Clin. Immunol.* **1997**, *99*, 402−409.
(62) Rodriguez-Romero, A.; Ravichandran, K. G.; Soriano-Garcia, M. Crystal structure of hevein at 2.8 A resolution. *FEBS Lett.* **1991**, *291*, 307−309.
(63) Andersen, N. H.; Cao, B.; Rodriguez-Romero, A.; Arreguin, B. Hevein: NMR assignment and assessment of solution-state folding for the agglutinin-toxin motif. *Biochemistry* **1993**, *32*, 1407−1422.
(64) Reyes-Lopez, C. A.; Hernandez-Santoyo, A.; Pedraza-Escalona, M.; Mendoza, G.; Hernandez-Arana, A.; Rodriguez-Romero, A. Insights into a conformational epitope of Hev b 6.02 (hevein). *Biochem. Biophys. Res. Commun.* **2004**, *314*, 123−130.
(65) Beezhold, D. H.; Kostyal, D. A.; Sussman, G. L. IgE epitope analysis of the hevein preprotein; a major latex allergen. *Clin. Exp. Immunol.* **1997**, *108*, 114−121.
(66) Crooks, G. E.; Hon, G.; Chandonia, J. M.; Brenner, S. E. WebLogo: a sequence logo generator. *Genome Res.* **2004**, *14*, 1188−1190.
(67) Bublin, M.; Mari, A.; Ebner, C.; Knulst, A.; Scheiner, O.; Hoffmann-Sommergruber, K.; Breiteneder, H.; Radauer, C. IgE sensitization profiles toward green and gold kiwifruits differ among patients allergic to kiwifruit from 3 European countries. *J. Allergy Clin. Immunol.* **2004**, *114*, 1169−1175.
(68) Gamboa, P. M.; Sanchez-Monge, R.; Diaz-Perales, A.; Salcedo, G.; Ansotegui, J.; Sanz, M. L. Latex-vegetable syndrome due to custard apple and aubergine: new variations of the hevein symphony. *J. Invest. Allergol. Clin. Immunol.* **2005**, *15*, 308−311.
(69) Diaz-Perales, A.; Collada, C.; Blanco, C.; Sanchez-Monge, R.; Carrillo, T.; Aragoncillo, C.; Salcedo, G. Cross-reactions in the latex-fruit syndrome: A relevant role of chitinases but not of complex asparagine-linked glycans. *J. Allergy Clin. Immunol.* **1999**, *104*, 681−687.
(70) Blanco, C.; Diaz-Perales, A.; Collada, C.; Sanchez-Monge, R.; Aragoncillo, C.; Castillo, R.; Ortega, N.; Alvarez, M.; Carrillo, T.; Salcedo, G. Class I chitinases as potential panallergens involved in the latex-fruit syndrome. *J. Allergy Clin. Immunol.* **1999**, *103*, 507−513.
(71) Karisola, P.; Kotovuori, A.; Poikonen, S.; Niskanen, E.; Kalkkinen, N.; Turjanmaa, K.; Palosuo, T.; Reunala, T.; Alenius, H.; Kulomaa, M. S. Isolated hevein-like domains, but not 31-kd endochitinases, are responsible for IgE-mediated in vitro and in vivo reactions in latex-fruit syndrome. *J. Allergy Clin. Immunol.* **2005**, *115*, 598−605.
(72) Sanchez-Monge, R.; Blanco, C.; Diaz-Perales, A.; Collada, C.; Carrillo, T.; Aragoncillo, C.; Salcedo, G. Isolation and characterization of major banana allergens: identification as fruit class I chitinases. *Clin. Exp. Allergy* **1999**, *29*, 673−680.
(73) Posch, A.; Wheeler, C. H.; Chen, Z.; Flagge, A.; Dunn, M. J.; Papenfuss, F.; Raulf-Heimsoth, M.; Baur, X. Class I endochitinase containing a hevein domain is the causative allergen in latex-associated avocado allergy. *Clin. Exp. Allergy* **1999**, *29*, 667−672.
(74) Kespohl, S.; Sander, I.; Merget, R.; Petersen, A.; Meyer, H. E.; Sickmann, A.; Bruening, T.; Raulf-Heimsoth, M. Identification of an obeche (*Triplochiton scleroxylon*) wood allergen as a class I Chitinase. *Allergy* **2005**, *60*, 808−814.

(75) Danhash, N.; Wagemakers, C. A.; van Kan, J. A.; de Wit, P. J. Molecular characterization of four Chitinase cDNAs obtained from *Cladosporium fulvum*-infected tomato. *Plant Mol. Biol.* **1993**, *22*, 1017−1029.
(76) Schwarz, D.; Welter, S.; George, E.; Franken, P.; Lehmann, K.; Weckwerth, W.; Dolle, S.; Worm, M. Impact of arbuscular mycorrhizal fungi on the allergenic potential of tomato. *Mycorrhiza* **2011**, *21*, 341−349.
(77) Bokma, E.; Spiering, M.; Chow, K. S.; Mulder, P.; Subroto, T.; Beintema, J. J. Determination of cDNA and genomic DNA sequences of hevamine, a Chitinase from the rubber tree *Hevea brasiliensis*. *Plant Physiol. Biochem.* **2001**, *39*, 367−376.
(78) D'Amato, A.; Bachi, A.; Fasoli, E.; Boschetti, E.; Peltre, G.; Senechal, H.; Sutra, J. P.; Citterio, A.; Righetti, P. G. In-depth exploration of *Hevea brasiliensis* latex proteome and "hidden allergens" via combinatorial peptide ligand libraries. *J. Proteomics* **2010**, *73*, 1368−1380.
(79) Falak, R.; Varasteh, A. R.; Ketabdar, H.; Sankian, M. Expression of grape class IV Chitinase in *Spodoptera frugiperda* (Sf9) insect cells. *Allergol. Immunopathol. (Madrid, Spain)* **2013**, DOI: doi: 10.1016/j.aller.2012.11.004.
(80) Sutton, R.; Skerritt, J. H.; Baldo, B. A.; Wrigley, C. W. The diversity of allergens involved in bakers' asthma. *Clin. Allergy* **1984**, *14*, 93−107.
(81) Chen, Y. T.; Hsu, L. H.; Huang, I. P.; Tsai, T. C.; Lee, G. C.; Shaw, J. F. Gene cloning and characterization of a novel recombinant antifungal Chitinase from papaya (*Carica papaya*). *J. Agric. Food Chem.* **2007**, *55*, 714−722.

JOURNAL OF AGRICULTURAL AND FOOD CHEMISTRY

Article

pubs.acs.org/JAFC

Radical Scavenging of White Tea and Its Flavonoid Constituents by Electron Paramagnetic Resonance (EPR) Spectroscopy

Nurul A. M. Azman,[†,‡] Sara Peiró,[†] Lluís Fajarí,[#] Luis Julià,*[,#] and Maria Pilar Almajano*[,†]

[†]Chemical Engineering Department, Technical University of Catalonia, Av. Diagonal 647, 08028 Barcelona, Spain

[‡]Chemical and Natural Resources Engineering Department, University of Malaysia, Pahang, 26000 Pahang, Malaysia

[#]Biological Chemistry and Molecular Modelling, Institute of Advanced Chemistry of Catalonia (CSIC), Jordi Girona 18-26, 08034 Barcelona, Spain

ABSTRACT: White tea (WT) presents high levels of catechins, which are known to reduce oxidative stress. WT is the least processed tea, unfermented and prepared only from very young tea leaves. The subject of this paper is the use of the spin trap method and electron paramagnetic resonance (EPR) spectroscopy as the analytical tool to measure, for the first time, the radical scavenging activity of WT and its major catechin components, epicatechin (EC), epicatechin-3-gallate (ECG), epigallocatechin (EGC), and epigallocatechin-3-gallate (EGCG), against the methoxy radical, using ferulic acid as antioxidant pattern. The antioxidant activity has been measured by the decrease of the intensity of the spectral bands of the adduct DMPO−OCH_3 in the EPR with the amount of antioxidant in the reactive mixture. Tea leaves and buds were extracted with waterless methanol. It has been proved that tea compounds with more antiradical activity against methoxy radical are those with the gallate group, EGCG and ECG.

KEYWORDS: *white tea, EPR, spin trap, antioxidant activity, radical scavenging*

INTRODUCTION

Tea (*Camellia sinensis* (L.)) is one of the world's most consumed beverages, and its medicinal properties have been widely explored. It can be classified in three types: unfermented (green and white teas), partially fermented (oolong tea), and completely fermented (black tea).[1] White tea (WT) is exclusively prepared from young tea leaves or buds, harvested before being fully opened. It is the least processed tea, because leaves are only air-dried and it does not suffer any fermentation process.[2−4] The strong antioxidant capacity of WT is linked to its high content in catechins. The main catechins of tea are epigallocatechin (EGC), catechin (C), epigallocatechin gallate (EGCG), epicatechin (EC), and epicatechin gallate (ECG).[2,5] Scavenging capacity of WT can be measured by different antioxidant tests such as ORAC, TEAC, FRAP, or DPPH, among others.[6] Nowadays, WT is used as a promising antioxidant additive medium, even better than green tea.[7] It is also suggested that the mechanism of protective actions of WT against oxidative stress in vitro is related to its antioxidant potential and the maintenance of the normal redox status of the cell when it is attacked by radicals or hydrogen peroxide (H_2O_2).[8]

In this context, radical scavenging measurements by traditional methods have their limitations. An essential antioxidant test, extensively used in the literature, deals with the scavenging activity of antioxidants against the hydroxyl radical ($HO^•$) or the superoxide ($O_2^{•−}$), which are the main harmful reactive oxygen species (ROS). The activity of the antioxidant is measured in a competitive reaction with 5,5-dimethyl-1-pyrroline-*N*-oxide (DMPO), an excellent $HO^•$ and $O_2^{•−}$ nitrone spin trap. Spin trapping is a technique in which a transient radical, very unstable under normal conditions, reacts with a spin trap to form a much more stable radical adduct, detected by electron paramagnetic resonance (EPR) spectroscopy. Nitrones have been the molecules chosen as spin trap species due to their specificity and ability to quantify transient ROS. It is well-known that the spin trapping technique can provide direct evidence of the presence of transient radicals in any reaction system and, therefore, it is very useful for discriminating trapped radical species. In fact, various short-lived radical intermediates have been identified by this technique.[9,10] Thus, EPR spectroscopy has been an indispensable tool for the detection of many harmful ROS ($O_2^{•−}$, $HO^•$, $HO_2^•$, $RO_2^•$, $RO^•$) via spin trapping.[10−13] Thereby, the antioxidant activity of a single polyphenol or a natural extract (mixture of polyphenols) is measured by the decrease of the intensity of the radical adduct spectra in the presence of the antioxidant relative to the decrease in the presence of an antioxidant pattern.[14−22]

Some studies about the radical scavenging activity of green and black teas against 2,2-diphenyl-1-picrylhydrazyl (DPPH) by using the EPR technique have been reported.[10,23−27] However, there are no publications about the use of EPR in the analysis of the antioxidant capacity of WT with a transient oxygen radical, much more unstable than DPPH.

Following our research work related to the antioxidant and antimicrobial properties of WT,[28−30] the aim of this paper is to measure the radical scavenging activity of WT and its major constituents, those being epicatechin (EC), epicatechin-3-gallate (ECG), epigallocatechin (EGC), and epigallocatechin-3-gallate (EGCG), against methoxy radical, generated in the Fenton reaction in methanol (MeOH) as solvent, using ferulic acid as antioxidant pattern. The alkoxy radicals are also considered

Received: December 5, 2013
Revised: May 28, 2014
Accepted: June 2, 2014
Published: June 2, 2014

ACS Publications © 2014 American Chemical Society

among ROS species in biological processes as critical mediators in several serious human diseases. The classical Fenton reaction in aqueous media is used in most cases to generate the harmful hydroxyl radical $HO^{\bullet}$. However, when the reduction of H_2O_2 with $FeSO_4$ is conducted in MeOH as solvent, the transient radical generated is the methoxy radical $CH_3O^{\bullet}$, as explained below.

MATERIALS AND METHODS

Materials. Commercially available WT was obtained from a local market. Ferulic acid, ECG, EGC, EGCG, and EC were bought from Sigma-Aldrich. Iron(II) sulfate ($FeSO_4$), DMPO, H_2O_2, and MeOH were of analytical grade and supplied by Panreac (Barcelona, Spain).

Extraction and Quantification of WT. The extraction was executed in two different ways: (a) Dried WT (10 g) was mixed with MeOH (100 mL) and extracted for 24 h at 4 ± 1 °C, stirred (103 rpm) and light protected. (b) Dried WT (10 g) was mixed with hot water (100 mL) and extracted for 4 min at 90 ± 1 °C, stirred (103 rpm) and light protected.

In both cases, the resulting infusions were filtered with qualitative filter papers (Watmann no. 1) in a vacuum system. To determine the soluble concentration of WT, the solvent was removed at low pressure (Buchi RE111, Flawil, Switzerland) and subsequently treated in a freeze-dryer (Unicryo MC2L ±60 °C, UniEquip, Martinsried/München, Germany). Finally, WT lyophilized pulps were weighed, and the concentration recovered from extract (g/L) was determined. The lyophilized extracts were kept in a desiccator, protected from light, until analysis.

An adequate dilution of each extract was prepared to be analyzed by HPLC method to determine the concentration of different flavonoids.

The results of the main catechins for the water extraction were (mg/100 g dry tea leaves) EC, 51.3 ± 3.7; EGC, 157 ± 9.5; EGCG, 1631 ± 97; and ECG, 280 ± 23.2.

In methanol, an average of 7.5 ± 0.2 g of soluble extract was collected from 100 g of dry WT. The major phenolic compounds found in methanolic WT extracts by HPLC analysis are listed in Table 1.

Table 1. Concentration of Polyphenols Found in MeOH WT Extracts by HPLC Analysis

compd	retention time (min)	concn (mg/100 g dry tea leaves)
EGC	1.913	260.9
EC	2.91	94.9
EGCG	4.715	2113.8
ECG	7.757	382.2

Determination of Methoxy Radical Scavenging Activity by EPR. The solutions of the different components were prepared in deoxygenated MeOH. A spin-trapping reaction mixture consisted of 100 μL of DMPO (35 mM); 50 μL of H_2O_2 (10 mM); 50 μL of pure polyphenols EC, ECG, EGC, and EGCG at different concentrations or WT extract (0−8.13 g/L) or 50 μL of ferulic acid used as reference (0−20 g/L) or 50 μL of pure MeOH used as a control; and, finally, 50 μL of $FeSO_4$ (2 mM), added in this order. The final solutions (250 μL) were passed to a narrow (inside diameter = 2 mm) quartz tube and introduced into the cavity of the EPR spectrometer. The spectrum was recorded 10 min after the addition of the $FeSO_4$ solution, when the radical adduct signal is greatest.

X-band EPR spectra were recorded with a Bruker EMX-Plus 10/12 spectrometer under the following conditions: microwave frequency, 9.8762 GHz; microwave power, 30.27 mW; center field, 3522.7 G; sweep width, 100 G; receiver gain, 5.02×10^4; modulation frequency, 100 kHz; modulation amplitude, 1.86 G; time constant, 40.96 ms; conversion time, 203.0 ms.

Each measurement was carried out three times. The first derivative of the absorption signal was twice integrated, resulting directly proportional to the concentration of the remaining radical adducts values, when the competitive reactions of the methoxy radical with DMPO and the antioxidant were completed. Then, these values were compared with those obtained with ferulic acid.

RESULTS AND DISCUSSION

Antioxidant Capacity Assay. In the present study, the free radical scavenging activity of WT extracts was evaluated against methoxy ($CH_3O^{\bullet}$) radical by a competitive method in the presence of DMPO as spin trap, using EPR spectroscopy. $CH_3O^{\bullet}$ radical was generated according to the Fenton procedure in MeOH instead of H_2O as solvent. Methoxy radical, with a relatively short half-life, was identified by EPR because of its ability to form a stable nitroxide adduct with DMPO, DMPO−OCH_3 (hyperfine splitting constants, a_N = 13.9 G and a_H = 8.3 G).[31]

Because iron has a variable valence, its oxidation by H_2O_2 may occur via one or two electron transfer reactions. Therefore, two different mechanisms of the Fenton reaction have been extensively discussed in the literature:[32−39] a radical mechanism with Fe(II) salt as one-electron donor and the generation of hydroxyl ($HO^{\bullet}$) radical (reaction 1)[40] and a nonradical mechanism, which involves a direct interaction between Fe(II) and H_2O_2. This interaction finally produces an iron oxide species of Fe(IV) (reaction 2).[41] In each case, the predominance of one mechanism over the other may depend on different variables, mainly the nature of the metal ligand, the solvent, and the pH of the medium.

$$Fe^{2+} + H_2O_2 \rightarrow Fe^{3+} + HO^- + HO^{\bullet} \quad (1)$$

$$Fe^{2+} + H_2O_2 \rightarrow [Fe^{2+}\cdot H_2O_2] \rightarrow [Fe^{IV}O]^{2+} + H_2O \quad (2)$$

As stated above, our experiments have been carried out in MeOH due to the low solubility of ferulic acid in water. Assuming a radical mechanism in the Fenton reaction in MeOH, the generated hydroxyl radical would abstract a hydrogen atom mainly from the α position of MeOH to yield a hydroxymethyl radical (reaction 3),[42]

$$HO^{\bullet} + CH_3OH \rightarrow H_2O + {}^{\bullet}CH_2OH \quad (3)$$

which, in turn, would react with DMPO to yield the radical adduct DMPO−CH_2OH[43] (reaction 4) (hyperfine splitting

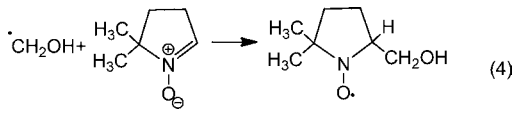

(4)

constants a_N = 14.7 G and a_H = 20.7 G).[44]However, in the reduction process of H_2O_2 with Fe(II) in MeOH as solvent in the presence of DMPO as spin trap, the unique bands of significant intensity shown in the EPR spectrum corresponded to those of the methoxy adduct, DMPO−OCH_3, and no relevant bands to the DMPO adducts with hydroxyl and α-hydroxymethyl radicals were detected. Therefore, we assume a nonradical process as the dominant mechanism in the Fenton reaction in these conditions (reaction 2), and we suggest that the oxidant action of Fe(IV) oxide in MeOH leads to the generation of methoxy radical in two consecutive one-electron paths (reactions eq 5 and eq 6) yielding

$$\left[Fe^{IV}O\cdot CH_3OH\right]^{2+} \downarrow \left[Fe^{III}(OH)^{2+}, {}^{\bullet}OCH3\right] \longrightarrow \left[Fe^{III}(OH)\right]^{2+} + {}^{\bullet}OCH3 \quad (5)$$

dx.doi.org/10.1021/jf501707p | J. Agric. Food Chem. 2014, 62, 5743−5748

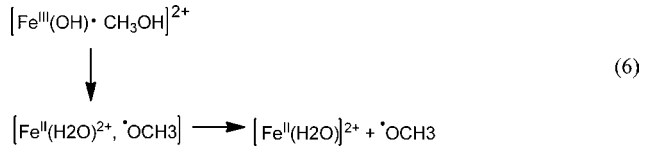

(6)

in the presence of the spin trap the radical adduct DMPO−OCH_3 (reaction 7). At this point, it should be emphasized that

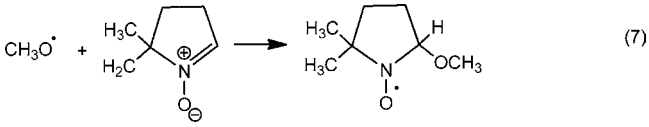

(7)

the involvement of an ionic mechanism in the formation of the radical adduct DMPO−$OCHH_3$ by nucleophilic addition of MeOH is discarded because the intensity of the EPR spectrum decreases with the addition of methoxy radical scavengers.Pure polyphenols or WT extracts added to methanolic solutions of H_2O_2 and small amounts of $FeSO_4$ in the presence of an excess of DMPO may compete with the spin trap in the scavenging of methoxy radicals. This effect reduces the amount of radical adducts and, accordingly, the intensity of the EPR signal decreases. The double-integration value of the signal of the spectrum for each experiment in the presence of an amount of antiradical relative to the value in the presence of the same amount of ferulic acid gives a measure of the antiradical activity of the test sample.

Figure 1 (left) shows the EPR spectra of the DMPO adduct of methoxy radical at different concentrations of ferulic acid. The

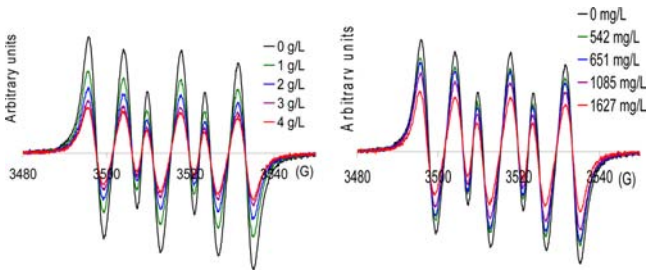

Figure 1. Electron paramagnetic resonance (EPR) spectra of the radical adduct DMPO−OCH_3 generated from a solution of H_2O_2 (2 mM) and $FeSO_4$ (0.04 mM) with DMPO (14 mM) as spin trap in MeOH as solvent: (left) decrease of the EPR signal with the increase of the concentration of ferulic acid as the reference sample; (right) decrease of the EPR signal with the increase of the concentration of the white tea extracts. EPR measurement conditions were as described under Materials and Methods.

spectra were recorded 10 min after the addition of $FeSO_4$ to the reaction mixture, when the radical adduct signal was the greatest. The signal intensity of the spectrum decreased with the increase of the amount of ferulic acid. Table 2 shows the values of the double integration at five different concentrations of ferulic acid. The best fitting with these data was an exponential function (Figure 2) that, if concentration values of ferulic acid are in grams per liter, corresponds to eq I:

$$y = 26.75\ e^{-0.21x};\ R^2 = 0.972 \quad (I)$$

The evolution of the signal intensity of the DMPO adduct in the presence of different amounts of WT extract is shown in Figure 1 (right). The radical scavenging activity values of WT extract against methoxy radical are presented in Table 3 as the

Table 2. Methoxy Radical Scavenging Activity of Ferulic Acid by the Spin Trap Technique with DMPO in EPR[a]

ferulic acid[b] (g/L)	ferulic acid[b] (mM)	DI EPR signal[c]
0	0	28.26
1	5.15	21.23
2	10.30	16.35
3	15.45	13.55
4	20.60	12.13

[a]Final concentration values of DMPO (14 mM), H_2O_2 (2 mM) and $Fe(SO_4)$ (0.4 mM) in 250 μL. [b]Final concentration values of ferulic acid in 250 μL. [c]Double integral of the EPR signal.

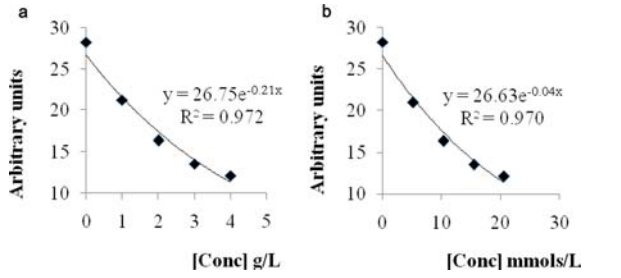

Figure 2. Decrease of the intensity of the spectrum of the spin adduct of methoxy radical with DMPO with increasing concentration of ferulic acid. The best-fitting function is an exponential curve with the equation given inside the graphic, (a) in g/L and (b) in mmol/L, and in the text.

Table 3. Methoxy Radical Scavenging Activity of White Tea (WT) Extracts by the Spin Trap Technique with DMPO in the EPR, Measured as Ferulic Acid (FA) Equivalents per Gram of the Active Sample[a]

WT concn[b] (mg/L)	DI EPR signal[c]	FA equiv[d] (mg/L)	FA equiv: WT[e]
0	28.26		
542	23.66	706.67	1.30
651	22.64	876.67	1.35
1085	20.70	1200.00	1.11
1627	14.94	2160.00	1.33

[a]Final concentration values of DMPO (14 mM), H_2O_2 (2 mM), and $Fe(SO_4)$ (0.4 mM) in 250 μL. [b]White tea extract final concentration in 250 μL. [c]Double integral of the EPR signal. [d]Ferulic acid equivalents in mg/L. [e]Ferulic acid equivalents in g/L per gram of white tea extract.

equivalents of ferulic acid in grams per liter per gram of WT. The scavenging activity of the WT extract is evaluated from four different concentrations of the extract. The last column in Table 3 shows that the activity of the extract is slightly higher than the activity of ferulic acid in grams per liter.

The radical scavenging activity of pure polyphenols toward methoxy radical was examined. Solutions of H_2O_2 (2 mM) and $Fe(SO_4)$ (0.4 mM) in the presence of DMPO (14 mM) and various amounts of polyphenol were introduced into the EPR cavity, and the double integration of the spectrum, obtained 10 min after the addition of the Fe(II) salt to the reaction mixture, was collected to calculate results. The overall chemical process can be defined as a system of two competing reactions between DMPO and the pure antioxidant over the methoxy radical. The action of the spin trap is to capture the methoxy radical to yield the radical adduct and, besides, the scavenging action of the antioxidant on the methoxy radical reduces the amount of radical adduct. In each experiment, the amount of spin trap was constant and the amount of antioxidant was varied. Then, the amount of

dx.doi.org/10.1021/jf501707p | J. Agric. Food Chem. 2014, 62, 5743−5748

radical adduct decreases exponentially as the amount of polyphenol increases, and the antioxidant efficiency is measured by the exponential coefficient α of eq II

$$y = y_0\, e^{-\alpha x} \quad \text{(II)}$$

where y is the value of the double integration of the spectrum of DMPO−OCH_3 at a given polyphenol concentration and y_0 represents the value of the double integration in the absence of polyphenol. The variable x represents the polyphenol concentration. Graphics for polyphenols EC, ECG, EGC, and EGCG are shown in Figures 3−6. In each case, experimental values are

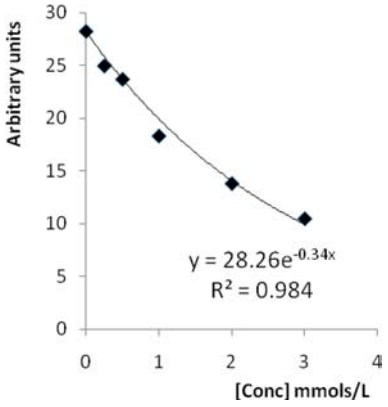

Figure 3. Decrease of the intensity of the spectrum of the spin adduct of the methoxy radical with DMPO with increasing concentration of EC. The best-fitting function is an exponential curve with the equation given inside the graphic and in the text.

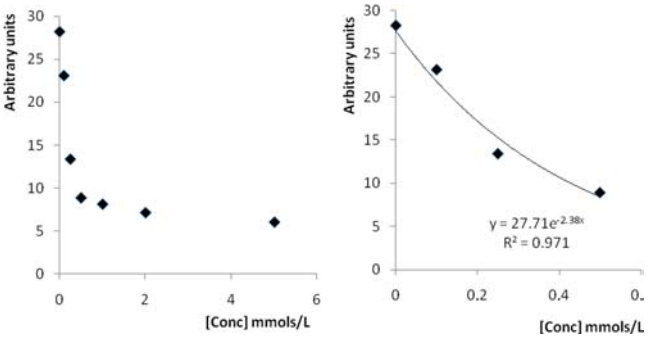

Figure 4. (Left) Decrease of the intensity of the spectrum of the spin adduct of the methoxy radical with DMPO with increasing concentration of ECG. (Right) Detail of the first values of the graph. The best-fitting function is an exponential curve with the equation given inside the graphic and in the text.

fitted to exponential functions inserted in the figures with good correlation coefficients (R), α being a measure of the antioxidant activity of polyphenols against the methoxy radical.

The graphics corresponding to ECG and EGCG (Figures 4 and 6) show some anomalies. For the exponential regression approach of the results, only low concentration values of polyphenol are well fitted to exponential functions. Both polyphenols show strong antioxidant properties at very low concentrations. High values of concentration give rise to values of integration well above the values that correspond to the exponential functions. This anomalous behavior may indicate the complex processes taking place to remove methoxy radicals within the reaction mixture. This is because the degradation byproducts of polyphenols may in turn act as radical scavengers.

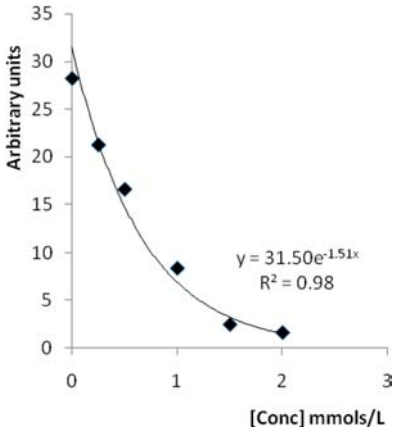

Figure 5. Decrease of the intensity of the spectrum of the spin adduct of the methoxy radical with DMPO with increasing concentration of EGC. The best-fitting function is an exponential curve with the equation given inside the graphic and in the text.

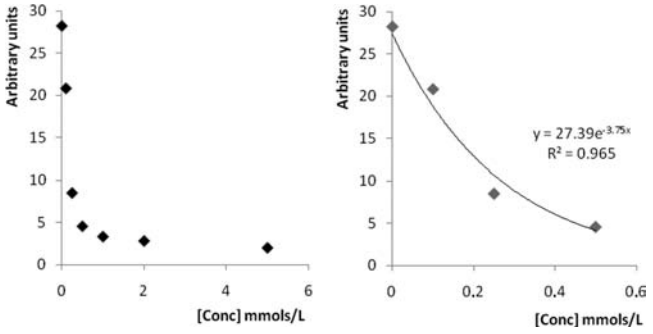

Figure 6. (Left) Decrease of the intensity of the spectrum of the spin adduct of the methoxy radical with DMPO with increasing concentration of EGCG. (Right) Detail of the first values of the graph. The best-fitting function is an exponential curve with the equation given inside the graphic and in the text.

The antioxidant efficiency coefficients of polyphenols relative to that of ferulic acid are displayed in Table 4. All polyphenols

Table 4. Values of the Antioxidant Activity Coefficients (α) of Pure Polyphenols EC, ECG, EGC, and EGCG toward the Methoxy Radical and Its Value Relative to Ferulic Acid (FA)

polyphenol	α (mmol/L)	α (FA relative)
FA	0.04	1
EC	0.34	8.5
ECG	2.43	60.75
EGC	1.51	37.75
EGCG	3.83	95.75

exhibit antioxidant efficiency well above that of the ferulic acid. The presence of the pyrogallol group and/or gallate group in the molecular structures of ECG, EGC, and EGCG greatly increases the methoxy radical scavenging relative to EC. EGCG is the most active polyphenol with both groups, gallate and pyrogallol.

These results with the spin trap method indicate that EGCG has the greatest radical scavenging activity, and it is consistent with those obtained by other more traditional methods, such as trolox equivalent antioxidant capacity (TEAC) with ABTS radical or oxygen radical antioxidant capacity (ORAC) with AAPH radical.[45,46] The values obtained with the spin trap method show a much greater difference in antioxidant activity

dx.doi.org/10.1021/jf501707p | J. Agric. Food Chem. 2014, 62, 5743−5748

Table 5. Antioxidant Activity of WT Tested by Different Methods with Ferulic Acid (FA) as Standard

	ORAC		TEAC		EPR		DPPH		FRAP	
WT[a]	FA equiv[b]	FA equiv/g sample[c]	FA equiv[b]	FA equiv/g sample[c]	FA equiv[b]	FA equiv/g sample[c]	FA equiv[b]	FA equiv/g sample[c]	FA equiv[b]	FA equiv/g sample[c]
542	68.06	1.67	17.46	0.54	2160.00	1.33	755.04	4.64	242.42	2.98
651	48.98	1.81	9.81	0.48	876.67	1.35	1057.11	4.55	154.02	2.84
1627	29.65	1.82	7.91	0.49	706.67	1.30	845.54	4.68	130.11	3.20

[a]Milligrams. [b]Ferulic acid equivalents in mg/L. [c]Ferulic acid equivalents in g/g of sample.

among the polyphenols than the other methods, although the order of activity is the same. An advantage of the spin method is that it works with ROS, the true mediators of human diseases, whereas TEAC and ORAC methods work with "atypical" and more stable radicals.

Table 5 shows the scavenging activity of WT methanolic extract with the different methods. The fact that the correlation is good in all of them is remarkable. The sensitivity of the EPR method is in the middle of the others (expressed in FA equiv/g sample (1.3 ± 0.3)) and near the value obtained for the ORAC (1.75 ± 0.6 FA equiv/g sample), the most sensitive radical scavenging method among traditional methods.

Moreover, the results obtained in this paper confirm that the presence of gallate in catechins leads to a higher radical scavenging activity. This also corroborates the results of ORAC or TEAC, which work similarly to the spin trap method. Furthermore, there is no correlation between the composition in catechins found in tea extract and the antioxidant activity values obtained by the spin trap method. That is, a greater proportion of ferulic acid equivalents in grams per liter than the value shown in Table 3 would be expected per gram per liter of tea extract. This anomaly may be because the competition established between catechins finally leads to non addition of the respective activities. It seems that the main catechin in the composition of WT, EGCG, is most responsible for the radical scavenging effect, measured by the spin trap method.

In conclusion, we have studied the antioxidant activity of WT extracts and the activity of the most abundant catechins of the WT versus methoxy radical, using ferulic acid as standard. An HPLC analysis of the extracts in MeOH shows the presence of EC, ECG, EGC, and EGCG in significant amounts. The source of methoxy radicals has been the reduction of H_2O_2 by $FeSO_4$ (Fenton reaction) in a ratio of 5:1, in MeOH as solvent. The experiments were conducted by EPR using the spin trap technique in the presence of DMPO, a good methoxy radical scavenger, and in the presence of various amounts of antioxidant. In these conditions, the oxidant mixture generates methoxy radical as the only radical species in significant amounts, being identified by EPR as the stable radical adduct DMPO−OCH_3. Therefore, we suggest that the dominant mechanism in the Fenton reaction in these specific conditions is a nonradical mechanism with a two-electron transfer process from Fe(II) to the formation of ferryl ion $[Fe^{IV}O]^{2+}$. This oxidizing species reacts with MeOH to give methoxy radical and regenerates Fe(II).

The antioxidant activity of the WT extracts and polyphenols has been measured by the decrease of the intensity of the spectral bands of the adduct DMPO−OCH_3 in the EPR with the increase of the amount of antioxidant. The activity of WT extracts is slightly higher than that of ferulic acid as shown in Table 4. In addition, the antioxidant efficiency of all catechins is much greater than that of the ferulic acid; being the activity of EGCG and ECG, which contain the gallate group, the highest and that of EC the lowest.

AUTHOR INFORMATION

Corresponding Authors

*(M.P.A.) E-mail: m.pilar.almajano@upc.edu. Phone: +34 934016686.

*(L.J.) E-mail: ljbmoh@cid.csic.es. Phone: +34 934006107.

Funding

Financial support for this research from the MCI (Spain) through Projects AGL2009-12374-C03-03/ALI, AGL2013-49079-C2-1-R and CTQ2012-36074 is gratefully acknowledged.

Notes

The authors declare no competing financial interest.

ACKNOWLEDGMENTS

We thank the EPR service of the Institute of Advanced Chemistry of Catalonia-CSIC (Spain) for recording the EPR spectra.

ABBREVIATIONS USED

WT, white tea; EC, epicatechin; ECG, epicatechin-3-gallate; EGC, epigallocatechin; EGCG, epigallocatechin-3-gallate; EPR, electron paramagnetic resonance; $HO^{\bullet}$, hydroxyl radical; $O_2^{\bullet-}$, superoxide radical; ROS, reactive oxygen species; DMPO, 5,5-dimethyl-1-pyrroline-*N*-oxide; $CH_3O^{\bullet}$, methoxy radical; MeOH, methanol; TEAC, trolox equivalent antioxidant capacity; ORAC, oxygen radical antioxidant capacity; FA, ferulic acid; DI, double integral; α, antioxidant activity coefficients

REFERENCES

(1) Moderno, P. M.; Carvalho, M.; Silva, B. M. Recent patents on *Camellia sinensis*: source of health promoting compounds. *Recent Pat. Food Nutr. Agric.* **2009**, *1*, 182−192.

(2) Venditti, E.; Bacchetti, T.; Tiano, L.; Carloni, P.; Greci, L.; Damiani, E. Hot vs. cold water steeping of different teas: do they affect antioxidant activity? *Food Chem.* **2010**, *119*, 1597−1604.

(3) Sharangi, A. B. Medicinal and therapeutic potentialities of tea (*Camellia sinensis* L.) − a review. *Food Res. Int.* **2009**, *42*, 529−535.

(4) Rusak, G.; Komes, D.; Likic, S.; Horzic, D.; Kovac, M. Phenolic content and antioxidative capacity of green and white tea extracts depending on extraction conditions and the solvent used. *Food Chem.* **2008**, *123*, 46−48.

(5) Peres, R. G.; Tonin, F. G.; Tavares, M. F. M.; Rodriguez-Amaya, D. B. Determination of catechins in green tea infusions by reduced flow micellar electrokinetic chromatography. *Food Chem.* **2011**, *127*, 651−655.

(6) Almajano, M. P.; Carbó, R.; Jiménez, J. A. L.; Gordon, M. H. Antioxidant and antimicrobial activities of tea infusions. *Food Chem.* **2008**, *108*, 55−63.

(7) Dias, T. R.; Alves, M. G.; Tomás, G. D.; Socorro, S.; Silva, B. M.; Oliveira, P. F. White tea as a promising antioxidant medium additive for sperm storage at room temperature: a comparative study with green tea. *J. Agric. Food Chem.* **2014**, *62*, 608−617.

(8) Yen, W. J.; Chyau, C. C.; Lee, C. P.; Chu, H. L.; Chang, L. W.; Duh, P. D. Cytoprotective effect of white tea against H2O2-induced oxidative stress in vitro. *Food Chem.* **2013**, *141*, 4107−4114.
(9) Janzen, E. G. Spin trapping. *Acc. Chem. Res.* **1971**, *4*, 31−40.
(10) Polovka, M. EPR spectroscopy: a tool to characterize stability and antioxidant properties of foods. *J. Food Nutr. Res.* **2006**, *45*, 1−11.
(11) Polovka, M.; Brezová, V.; Staško, A. Antioxidant properties of tea investigated by EPR spectroscopy. *Biophys. Chem.* **2003**, *106*, 39−56.
(12) Villamena, F. A.; Zweier, J. L. Detection of reactive oxygen and nitrogen species by EPR spin trapping. *Antioxid. Redox Signal.* **2004**, *6*, 619−629.
(13) Guo, Q.; Zhao, B.; Shen, S.; Hou, J.; Hu, J.; Xin, W. ESR study on the structure-antioxidant activity relationship of tea catechins and their epimers. *Biochim. Biophys. Acta* **1999**, *1427*, 13−23.
(14) Finkelstein, E.; Rosen, G. M.; Rauckman, E. J. Spin trapping. Kinetics of the reaction of superoxide and hydroxyl radicals with nitrones. *J. Am. Chem. Soc.* **1980**, *102*, 4994−4999.
(15) Thornalley, P. J.; Vasák, M. Possible role for metallothionein in protection against radiation-induced oxidative stress. Kinetics and mechanism of its reaction with superoxide and hydroxyl radicals. *Biochim. Biophys. Acta* **1985**, *827*, 36−44.
(16) Mitsuta, K.; Mizuta, Y.; Kohno, M.; Hiramatsu, M.; Mori, A. The application of ESR spin-trapping technique to the evaluation of SOD-like activity of biological substances. *Bull. Chem. Soc. Jpn.* **1990**, *63*, 187−191.
(17) Naito, Y.; Yoshikawa, T.; Tanigawa, T.; Sakurai, K.; Yamasaki, K.; Uchida, M.; Kondo, M. Reactions of captopril and epicaptopril with transition metal ions and hydroxyl radicals: an EPR spectroscopy study. *Free Radical Biol. Med.* **1995**, *18*, 117−123.
(18) Lauderback, C. M.; Breier, A. M.; Hackett, J.; Varadarajan, S.; Goodlett-Mercer, J.; Butterfield, D. A. The pyrrolopyrimidine U101033E is a potent free radical scavenger and prevents Fe(II)-induced lipid peroxidation in synaptosomal membranes. *Biochim. Biophys. Acta* **2000**, *1501*, 149−161.
(19) Polyakov, N. Carotenoids as antioxidants: spin trapping EPR and optical study. *Free Radical Biol. Med.* **2001**, *31*, 43−52.
(20) Sueishi, Y.; Yoshioka, C.; Olea-Azar, C.; Reinke, L. A.; Kotake, Y. Substituent effect on the rate of the hydroxyl and phenyl radical spin trapping with nitrones. *Bull. Chem. Soc. Jpn.* **2002**, *75*, 2043−2047.
(21) Kogure, K.; Tsuchiya, K.; Abe, K.; Akasu, M.; Tamaki, T.; Fukuzawa, K.; Terada, H. Direct radical scavenging by the bisbenzylisoquinoline alkaloid cepharanthhine. *Biochim. Biophys. Acta* **2003**, *1622*, 1−5.
(22) Mesa, J. A.; Chávez, S.; Fajarí, L.; Torres, J. L.; Juliá, L. A tri(potassium sulfonate) derivative of perchlorotriphenylmethyl radical (PTM) as a stable water soluble radical scavenger of the hydroxyl radical more powerful than 5,5-dimethyl-1-pyrroline-*N*-oxide. *RSC Adv.* **2013**, *3*, 9949−9956.
(23) Levêque, P. P.; Godechal, Q.; Gallez, B. EPR spectroscopy and imaging of free radicals in food. *Isr. J. Chem.* **2008**, *48*, 19−26.
(24) Morsy, M. A.; Khaled, M. M. Novel EPR characterization of the antioxidant activity of tea leaves. *Spectrochim. Acta A: Mol. Biomol. Spectrosc.* **2002**, *58*, 1271−1277.
(25) Biyik, R.; Tapramaz, R. An EPR study on tea: Identification of paramagnetic species, effect of heat and sweeteners. *Spectrochim. Acta A: Mol. Biomol. Spectrosc.* **2009**, *74*, 767−770.
(26) Morsy, M. A. Teas: direct test on quality and antioxidant activity using electron paramagnetic resonance spectroscopy. *Spectroscopy (Duluth, MN, U.S.)* **2002**, *16*, 371−378.
(27) Alvarez-Suarez, J. M.; Giampieri, F.; González-Paramás, A. M.; Damiani, E.; Astolfi, P.; Martinez-Sanchez, G.; Bompadre, S.; Quiles, J. L.; Santos-Buelga, C.; Battino, M. Phenolics from monofloral honeys protect human erythrocyte membranes against oxidative damage. *Food Chem. Toxicol.* **2012**, *50*, 1508−1516.
(28) Pérez-Llamas, F.; González, D.; Cabrera, L.; Espinosa, C.; López, J. A.; Larqué, E.; Almajano, M. P.; Zamora, S. White tea consumption slightly reduces iron absorption but not growth, food efficiency, protein utilization, or calcium, phosphorus, magnesium, and zinc absorption in rats. *J. Physiol. Biochem.* **2011**, *67*, 331−337.
(29) Almajano, M. P.; Vila, I.; Gines, S. Neuroprotective effects of white tea against oxidative stress-induced toxicity in striatal cells. *Neurotoxic. Res.* **2011**, *20*, 372−378.
(30) Espinosa, C.; López-Jiménez, J. Á.; Cabrera, L.; Larqué, E.; Almajano, M. P.; Arnao, M. B.; Zamora, S.; Pérez-Llamas, F. Protective effect of white tea extract against acute oxidative injury caused by adriamycin in different tissues. *Food Chem.* **2012**, *134*, 1780−1785.
(31) Janzen, E. G.; Liu, I. P. Radical addition reactions of 5,5-dimethyl-1-pyrroline-1-oxide. ESR spin trapping with a cyclic nitrone. *J. Magn. Reson.* **1973**, *9*, 510−512.
(32) Yamazaki, I.; Piette, L. H. ESR spin-trapping studies on the reaction of Fe^{2+} ions with H_2O_2-reactive species in oxygen toxicity in biology. *J. Biol. Chem.* **1990**, *265*, 13589−13594.
(33) Yamazaki, I.; Piette, L. H. EPR spin-trapping study on the oxidizing species formed in the reaction of the ferrous ion with hydrogen peroxide. *J. Am. Chem. Soc.* **1991**, *113*, 7588−7593.
(34) Gozzo, F. Radical and non-radical chemistry of the Fenton-like systems in the presence of the organic substrates. *J. Mol. Catal. A: Chem.* **2001**, *171*, 1−22.
(35) Deguillaume, L.; Leriche, M.; Chaumerliac, N. Impact of radical versus non-radical pathway in the Fenton chemistry on the iron redox cycle in clouds. *Chemosphere* **2005**, *60*, 718−724.
(36) Kremer, M. L. Promotion of the fenton reaction by Cu^{2+} ions: evidence for intermediates. *Int. J. Chem. Kinet.* **2006**, *38*, 725−736.
(37) Barbusinski, K. Fenton reaction − controversy concerning the chemistry. *Ecol. Chem. Eng.* **2009**, *16*, 347−358.
(38) Bataineh, H.; Pestovsky, O.; Bakac, A. pH-Induced mechanistic changeover from hydroxyl radicals to iron(IV) in the Fenton reaction. *Chem. Sci.* **2012**, *3*, 1594.
(39) Pestovsky, O.; Bakac, A. Reactivity of aqueous Fe(IV) in hydride atom transfer reactions. *J. Am. Chem. Soc.* **2004**, *126*, 13757−13764.
(40) Cannon, R. D. *Electron Transfer Reactions*, 1st ed.; Butterworth: London, UK, 1980; pp 315−351.
(41) Masarwa, M.; Cohen, H.; Meyerstein, D.; Hickman, D. L.; Bakac, A.; Espenson, J. H. Reactions of low valent transition metal complexes with hydrogen peroxide. Are they "Fenton-Like" or not? 1. The case of Cu^{+} aq and Cr^{2+}. *J. Am. Chem. Soc.* **1988**, *110*, 4293−4297.
(42) Asmus, K. D.; Moeckel, H.; Henglein, A. Pulse radiolytic study of the site of OH• radical attack on aliphatic alcohols in aqueous solution. *J. Phys. Chem.* **1973**, *77*, 1218−1221.
(43) Jurva, U.; Wikström, H. V.; Bruins, A. P. Electrochemically assisted Fenton reaction: reaction of hydroxyl radicals with xenobiotics followed by on-line analysis with high-performance liquid chromatography/tandem mass spectrometry. *Rapid Commun. Mass Spectrom.* **2002**, *16*, 1934−1940.
(44) Janzen, E. G.; Liu, J. I. P. Radical addition reactions of 5,5-dimethyl-1-pyrroline-1-oxide. ESR spin trapping with a cyclic nitrone. *J. Magn. Reson.* **1973**, *9*, 510−512.
(45) Zhang, Y.; Li, Q.; Xing, H.; Lu, X.; Zhao, L.; Qu, K.; Bi, K. Evaluation of antioxidant activity of ten compounds in different tea samples by means of an on-line HPLC−DPPH assay. *Food Res. Int.* **2013**, *53*, 847−856.
(46) Higdon, J. V.; Frei, B. Tea catechins and polyphenols: Health effects, metabolism, and antioxidant functions. *Crit. Rev. Food Sci. Nutr.* **2003**, *43*, 89−143.

JOURNAL OF AGRICULTURAL AND FOOD CHEMISTRY

Article

pubs.acs.org/JAFC

Nutritional and Nutraceutical Quality of Strawberries in Relation to Harvest Time and Crop Conditions

Ikram Akhatou and Ángeles Fernández-Recamales*

Department of Chemistry and Materials Science, Faculty of Experimental Sciences, and International Campus of Excellence CeiA3, University of Huelva, 21007 Huelva, Spain

ABSTRACT: Three strawberry varieties cultivated in soilless systems were studied for their content of primary and secondary metabolites in relation to harvest time and crop conditions. The three varieties were chosen based on their sensitivity level to environmental stress: Palomar (very sensitive), Festival (sensitive), and Camarosa (resistant). Throughout the campaign, three samplings were performed: December (extra-early production), January, and March (early production). Differences among cultivars and harvest times were observed based on the contents of sugars, organic acids, phenolic compounds, and antioxidant capacity. The higher levels for total anthocyanins and flavan-3-ols were found in Camarosa and Festival strawberries, both in the January harvest. The Palomar variety showed higher total sugar/total organic acids ratio in the March harvest. The influence of cultivation practices and environmental conditions was assessed by nested ANOVA and PLS-DA. Differences in the sugar and phenolic content were observed depending upon variety and coverage type. TEAC was most influenced by the substrate type.

KEYWORDS: *strawberry, quality, metabolites, cultivars, soilless system, crop conditions*

INTRODUCTION

Strawberries (*Fragaria* x *ananassa* Duch.) are one of the most popular berry fruits. They are widely used for industrial food processing but mainly consumed as fresh fruit. Its consumption has been increasing over the years due to the fact that epidemiological studies have revealed the relationship between diets which are rich in fruits and vegetables, and a lower incidence of some major human chronic diseases. Besides its proven health benefits,[1−3] strawberries have an attractive red color and flavor, and these attributes influence the choice of consumers and strawberries marketability.

The sugar content is very important from a nutritional point of view and, in combination with organic acids, contributes to strawberry taste and flavor. So, good taste is the result of a balance between sweetness provided by sugars and the sourness of organic acid. It depends not only on the total sugar and organic acid contents but also on the type and quantity of individual compounds. Different sugars differ from sweetness level percepted by human tongue. For this reason, the relative proportion of each sugar is important for sweetness perception and consumer acceptability.The strawberry color is related to the presence of pigments, among which, anthocyanins play an essential role. Moreover, anthocyanins and other phenolic compounds have attracted a great deal of attention due to their properties as antioxidants, which can protect the human body against cellular oxidation reactions through scavenging of free radicals. These antioxidants have been shown to reduce the risk of cardio- and cerebrovascular diseases, cancer and other age-related diseases[4,5] and also contribute to the high nutritional quality of the fruit. However, it should also be considered that antioxidants protective effect can be dose-dependent and some of them may be harmful at high doses.[6]

Recent studies postulated that the antioxidant potential of anthocyanins and other phenolic compounds, as a basic mechanism of biological activity, is compromised by their low level of bioavailability especially when compared to the concentrations of endogenous antioxidants. Consequently, further research in this area is required in order to target other mechanisms of action that could be involved in the health-promoting effects beyond antioxidant activity.[2,3]

Strawberry is widely cultivated in several areas under different cultivation conditions and every year new varieties come into trade and cultivation. In Spain, strawberry is one of the most important crops, especially in the south of Huelva (southwest of Spain) due to soil and climatic conditions and water quality. Strawberry production in this region is accounting for 35% of strawberry production in the EU and 90% of national production. The economic importance of this crop and its great competitivity in the strawberry market drive strawberry producers to develop new growing methods such as soilless culture,[7] and to use early varieties. These varieties come into market in winter with enhanced fruit quality, higher resistance to stresses (biotic and abiotic) as well as higher productivity.

The chemical composition of berry fruits is affected by a number of preharvest and postharvest factors. Among the preharvest factors, the variety is considered the main source of variation in composition. Their effects on the nutritional and sensorial quality are well-known[8−10] and several breeding and biotechnological programs are focused on them.[3] In addition, nutritional and nutraceutical quality is also influenced by crop conditions (environmental and cultivation techniques), sampling time and the degree of ripeness, among other factors.[11−17] Ripeness and maturity are the key factors that influence the taste of the fruit. In wild strawberry, climatic conditions, such as

Received: March 7, 2014
Revised: May 28, 2014
Accepted: May 29, 2014
Published: May 29, 2014

ACS Publications © 2014 American Chemical Society

dx.doi.org/10.1021/jf500769x | J. Agric. Food Chem. 2014, 62, 5749−5760

light, temperature, and rainfall are the main factors to be considered since fruit maturation is depending on these conditions. However, strawberry is currently cultured under controlled conditions, where light intensity is reduced by plastic covers; temperature is higher under plastic than in the outside mainly in coldest months and moisture is controlled by regular irrigation. Other factors such as soil composition and texture can affect phytochemical content and composition of fruits. The comparison between strawberries cultivated in soil and soilless systems revealed significantly differences in the mineral composition, content of sugars and related parameters.[18] Wang and Millner[13] studied the effect of matted row, black plastic mulch, and compost socks cultural systems on the phenolic and anthocyanin content of strawberry. They observed a higher phytochemical content in the compost sock system compared to the other two production systems.

Basic knowledge related to these aspects will allow the optimization of culture systems (environmental and agronomic conditions) and also may help to prevent some physiological disorders, such as the known as dry calyx.[19] This physiological disorder differs from salinity damage and its origin is unknown. For these reasons, the aim of the present work was to assess the influence of environmental, seasonal and genetic factors on nutritional and nutraceutical quality of strawberry fruits. Also, it will allow to correlate them with changes in concentration of primary (sugars and organic acids) and secondary (phenolic compounds) metabolites and their bioactivity (antioxidant activity).

MATERIAL AND METHODS

Experimental Design and Sampling. The study was conducted in experimental plantations managed by the University of Huelva, in southwestern Spain (latitude 37°14′N, longitude 6°53′W, and altitude 23 m) where strawberry plants (*Fragaria* x *ananassa* Duch.) were grown in soilless systems. The assay consisted of two macrotunnels whose dimensions were 60 × 6 m. One of them was covered with plastic Tricoat 800 gauges on the arched structure of galvanized iron, and the other one was uncovered. Each macrotunnel contained three breeding lines of plants grown under different conductivities. Each line of breeding plants was composed of three strawberry cultivars. Finally, each cultivar was grown in three different commercial substrates.

The experimental design (Table 1) was a strip-split-split-plot, where the main plot corresponds to crop covered (T) and culture exposed (D, without plastic cover). The subplot corresponds to the electrical conductivity of irrigation (EC = 1, 2, and 3 dS/m), the subsub-plot corresponds to the variety (Palomar, Festival and Camarosa) and the basic plot represents the substrate type (coconut fiber, perlite and rockwool). The three varieties were chosen basing on their sensitivity to environmental conditions: Palomar (very sensitive), Festival (sensitive), and Camarosa (resistant). Throughout the campaign, three samplings were performed: December (extra-early production), January (early production), and March (early production).

The strawberries were harvested at commercial ripeness, specifically when 75% of the surface showed a red color, which corresponds to stage 5 in terms of commercial criterion. For each treatment, several fruits were collected in our experimental plantations to generate a representative pooled fruit sample. Immediately after harvesting, fruits were sorted. Those showing damage, defects, or small size were removed. Then, sample lots were frozen in situ in a deep freezer and shipped to our laboratory in polystyrene punnents. Fruits were washed, sepals were dissected, and finally, fruits were gently homogenized by means of a kitchen mixer. The pastes obtained were subsequently stored for 2 months at −21 °C for further analysis.

Reagents, Materials, and Apparatus. Methanol, ethanol, and acetonitrile were of HPLC grade. Trolox (6-hydroxy-2, 5, 7, tetramethylchroman-2-carboxylic acid) and ABTS (2, 2′-azino-bis (3-

Table 1. Description of the Experimental Design[a]

	covered or uncovered macrotunnel																							
V1	EC1								EC2								EC3							
V2	Cam				Pal				Cam				Pal				Cam				Pal			
V3	Fes				Fes				Fes				Fes				Fes				Fes			
V4	C	P	R	C	P	R	C	P	R	C	P	R	C	P	R	C	P	R	C	P	R	C	P	R

[a] Abbreviations. V1= tunnel specifications. V2= Electrical conductivities. V3: Cultivars. V4: Substrate types. EC: electrical conductivity. Pal: Palomar. Cam: Camarosa. Fes: Festival. C: coconut fibers. P: perlite. R: rockwool. More details in the text.

dx.doi.org/10.1021/jf500769x | J. Agric. Food Chem. 2014, 62, 5749−5760

ethylbenzothiazoline-6 sulfonic acid)) were purchased from Sigma-Aldrich (Steinheim, Germany), and potassium persulfate was purchased from Panreac (Barcelona, Spain).

Standards (purity ≥99%) of fructose, glucose, malic acid, citric acid, oxalic acid, tartaric acid, and ascorbic acid were purchased from Merck (Darmstadt, Germany); sucrose was purchased from Panreac (Barcelona, Spain).

Polyphenol standards were supplied as follows: cyanidin-3-glucoside, pelargonidin-3-glucoside, peonidin-3-glucoside, malvidin-3-glucoside, petunidin chloride, procyanidin B1, luteolin, apigenin, quercetin-3-*O*-glucoside, kaempferol, and isorhamnetin were purchased from Extrasynthese (Genay, France); tyrosol, (+)-catechin, procyanidin B2, vanillic acid, *m*-coumaric acid, caffeic acid, and cinnamic acid were purchased from Fluka (Buchas, Switzerland); and epicatechin gallate, gallic acid, ellagic acid, *p*-coumaric acid, and quercetin were purchased from Sigma-Aldrich (Steinheim, Germany).

HPLC was used for separation, identification, and quantification of primary and secondary metabolites in strawberry. Chromatographic analyses were performed by means of an Agilent 1100 series HPLC system (Palo Alto, CA) equipped with a photodiode-array detector (PDA), which was set to scan from 200 to 770 nm, and RI detector.

Spectrophotometric determinations were carried out using a Helios Gamma UV−vis spectrophotometer (Thermo Fisher Scientific, USA) with 1 cm path length cuvettes.

Antioxidant Capacity Assay. To assess strawberries antioxidant power, 0.5 g of homogenized fruit were extracted with 10 mL of methanol−water (80% v/v) and the pH value was adjusted to 5.0 ± 0.2 with NaOH (0.5M) and then centrifuged (at 10.000 rpm for 10 min at 4 °C). The supernatant was filtered through 0.45 μm filter and diluted with ethanol in 1:15 ratio.

The free-radical scavenging activity was determined by ABTS radical cation decolorization assay according to the method of Pellegrini et al.[20] The assay was carried out using a Helios Gamma UV−vis Spectrophotometer. The ABTS was dissolved in water to a 7 mM concentration. The ABTS radical cation ($ABTS^{\bullet+}$) was produced by reacting ABTS stock solution with 2.45 mM potassium persulfate (final concentration), and the solutions were allowed to react at room temperature in the dark for 16 h. The ($ABTS^{\bullet+}$) solution was diluted with ethanol to obtain an absorbance of 0.70(±0.01) at 734 nm. An aliquot of 100 μL of the diluted extract was added to 2900 μL of diluted $ABTS^{\bullet+}$ solution and the absorbance was read exactly 6 min after initial mixing. The linear range of the calibration standard Trolox was 0.00−100 μM. Results from the assay were expressed in terms of micromoles of Trolox per gram of strawberry fresh weight (TEAC).

Extraction and Determination of Sugars and Organic Acids. Different extraction procedures were applied to strawberry samples for the determination of individual sugars (fructose, glucose and sucrose) and organic acids (citric, malic, oxalic, tartaric and ascorbic). Homogenized fruits (5.0 g) were dissolved with 25 mL of methanol, sonicated for 30 min and then centrifuged 10 min at 10 000 rpm 4 °C. Supernatants were concentrated by means of a rotary evaporator at 40 °C and the residues were redissolved in 3 mL of 50% methanol. The concentrated extracts were filtered through 0.45 μm filters (Hydrophilic PVDF, Millipore Millex-HV, Bedford, MA) prior to their injection in HPLC system for sugars analysis.

Separation of sugars was carried out using an Ultrabase NH_2 column (5 μm, 250 mm × 4.6 mm i.d.) with temperature maintained at 35 °C. Elution was performed at isocratic conditions with acetonitrile:water (70:30 v/v) as mobile phase, and at a constant flow rate of 0.5 mL/min. Refractive index (RI) detector was used for monitoring eluated sugars.

For extraction of organic acids, 1 g of strawberries was homogenized in 10 mL of phosphoric acid pH 2.20 (mobile phase) and then centrifuged at 10 000 rpm during 10 min. The supernatant was filtered through a 0.45 μm filter. The extract was diluted with phosphoric acid (pH 2.20) in 1:4 ratio (v/v).

Organic acids were analyzed by HPLC using an Ultrabase C18 column (2.5 μm, 100 mm × 4.6 mm i.d.) as stationary phase operating at a temperature of 50 °C. Organic acids were monitored at 210 nm and ascorbic acid at 254 nm. The mobile phase was phosphoric acid pH 2.20 prepared with Milli-Q water and the separation was carried out by isocratic elution, at a constant flow rate of 0.4 mL/min. The injection volume was set at 20 μL and the duration of analysis was 10 min.

Sugars in strawberry extracts were identified by comparison of their retention times to those of standards. The organic acids were identified by their retention times and UV spectra. For quantification, calibration curves were constructed using standards at 0.5−8 mg/L (ascorbic acid), at 1−60 mg/L (oxalic acid), at 20−100 mg/L (tartaric and malic acids), at 60−200 mg/L (citric acid), and at 1−50 g/L (sugars). Concentrations were expressed as g per kg fresh weight.

HPLC Analysis of Phenolic Compounds and Anthocyanins. Samples were prepared as described above for extraction of sugars. Extracts were injected (20 μL) into a reverse phase Ultrabase C18 column (2.5 μm, 100 mm × 4.6 mm i.d.) following the methodology previously described by our previous studies,[12] but adapted to the new column. The modified method was further validated and their performance characteristics were confirmed. As for anthocyanins, the HPLC analyses was carried out according to the methodology described by Kallithraka et al.[21]

For analysis of colorless flavonoids and phenolic acids, elution solvents were water:methanol:acetic acid (93:5:2) as eluent A, and methanol:acetic acid (98:2) as eluent B. Applied elution conditions were as follows: 0−29 min, 40% B isocratic; 29−34.8 min, linear gradient 40−60% B; 34.8−37.7 min, linear gradient 60−75% B; 37.7−40.6 min, linear gradient 75−100% B; 40.6−46.4 min 0% B. The flow was 0.8 mL/min, and the column temperature was set at 20 °C.

As for anthocyanins, the mobile phase consisted of 10% aqueous formic acid (A) and HPLC grade methanol (B). The gradient profile was as follows: 0−0.70 min, 5% B; 0.70−16.60 min, linear gradient 5-50% B; 16.60−18.60 min, linear gradient 50−95% B; 18.60−20.60 min 95% B isocratic. Flow rate was 0.8 mL/min and temperature of the column was set at 30 °C.

Identification of phenolic acids and flavonoids was achieved by comparison of their retention times and UV spectra at specific wavelenght with those of appropriate standards. For quantification, the external standard method was applied considering the following wavelengths: 260 nm for ellagic acid and derivatives, 280 nm for benzoic acids and flavan-3-ols, 320 nm for cinnamic acids, and 360 nm for flavonols. Each standard was dissolved in methanol at a concentration of 1 mg mL^{-1}, and five diluted solutions from these stock solutions were used to prepare calibration curves of each standard (for duplicate). Anthocyanins were monitored at 520 nm. Calibration curves were constructed using standards at 1−50 mg/L (cyanidin-3-glucoside) and at 10−200 mg/L (pelargonidin-3-glucoside). The obtained linear equation was used to calculate the concentration of anthocyanins in strawberries.

Statistical Analysis. ANOVA followed by the Newman-Keuls post hoc test was applied in order to make multiple comparisons of mean values to evaluate if there were significant differences between the studied strawberries cultivars at different times of harvesting. A significant difference was statistically considered at the level of $p < 0.05$. Nested ANOVA was carried out for assessing the influence of different cultural and environmental factors. Data processing was performed using Statistica software package for statistical analysis (Statsoft, USA).

Pattern recognition (PR) techniques, including principal component analysis (PCA) and partial least-squares discriminant analysis (PLS-DA), were also carried out using Statistica software (StatSoft, USA) and SIMCA-P v11.5 software (UMETRICS, Umeå, Sweden), respectively. PCA is one of the most powerful and common techniques used for reducing dimensionality of large sets of data without losses of information. New variables are obtained as a linear combination of the original ones. They are calculated in such a way to keep most of the original data set information, and mantain the least possible number of new variables or principal components (PCs). PLS-DA is a supervised pattern recognition method based on searching an optimal set of latent variables (or components) in order to discriminate between the previously defined categories. PLS-DA method consists of a classical PLS regression where the dependent

Table 2. Mean, Minimum, and Maximum Values of Antioxidant Activity and Primary and Secondary Metabolites in Three Strawberry Varieties

	Camarosa (n = 78)			Festival (n = 69)			Palomar (n = 60)		
compounds	mean	min	max	mean	min	max	mean	min	max
TEAC	11.55	9.77	12.85	11.71	10.39	12.97	11.74	9.77	13.10
cyanidin-3-O-glucoside	4.82	1.52	11.37	3.35	0.89	9.98	2.56	0.68	6.75
pelargonidin-3-O-glucoside	125.14	47.13	208.75	102.44	27.81	188.96	100.08	16.11	170.13
pelargonidin-3-rutinoside	56.69	18.72	103.32	35.25	10.55	66.78	31.13	7.75	57.02
pelargonidin derivative	7.10	1.35	18.85	3.41	0.50	9.56	3.83	0.57	7.41
procyanidin B1	52.98	8.07	108.11	60.17	5.89	116.54	39.20	8.49	109.77
tyrosol	8.08	0.03	65.02	7.96	1.51	34.86	9.07	1.72	52.58
(+)-catechin	38.02	9.27	64.49	39.92	4.64	72.84	34.45	4.04	195.28
procyanidin B2	31.02	2.06	106.15	33.19	1.98	142.70	35.11	2.39	101.54
vanillic acid	3.07	0.34	12.61	3.12	0.19	9.09	3.57	0.62	17.13
epicatechin gallate	2.75	0.13	5.60	1.77	0.13	4.11	2.91	0.13	28.63
m-coumaric acid	1.55	0.02	3.37	2.20	0.09	6.27	1.55	0.17	4.85
gallic acid	4.07	0.49	14.03	4.67	0.85	26.66	5.31	0.64	17.30
ellagic acid	9.33	3.72	24.86	10.07	4.67	24.92	8.69	3.98	21.32
ellagic acid derivative	9.67	0.23	63.75	8.43	0.76	16.88	7.44	0.23	15.36
caffeic acid	0.71	0.11	1.91	0.56	0.11	2.44	1.08	0.11	3.60
caffeic acid derivative	2.83	0.95	5.20	1.91	0.42	3.64	2.72	0.11	5.83
p-coumaric acid	1.60	0.08	7.58	1.53	0.08	4.39	2.20	0.08	8.92
luteolin	1.05	0.00	5.28	0.91	0.00	3.28	0.79	0.00	2.12
apigenin	1.72	0.85	3.38	2.39	1.33	10.74	2.47	1.07	5.02
quercetin-3-O-galactoside	2.80	0.14	33.68	3.98	0.15	41.11	2.59	0.07	30.65
quercetin	2.42	0.74	11.47	2.27	0.66	5.06	2.11	0.45	6.47
kaempferol	0.95	0.42	2.56	0.97	0.37	4.46	1.00	0.50	3.07
isorhamnetin	1.27	0.60	1.87	1.24	0.40	1.83	1.23	0.35	1.92
quercitrin	0.64	0.03	2.78	0.87	0.00	5.18	0.72	0.02	2.11
oxalic acid	1.41	0.44	2.92	0.88	0.15	1.47	1.16	0.25	2.52
tartaric acid	2.10	1.03	3.04	2.10	1.47	2.78	1.88	1.17	3.01
citric acid	6.36	4.62	8.41	5.70	4.16	7.54	5.48	3.28	7.24
malic acid	3.16	1.06	5.85	3.12	1.15	5.24	3.14	1.25	4.64
ascorbic acid	0.08	0.01	0.25	0.10	0.00	0.29	0.14	0.00	0.34
fructose	19.54	13.45	24.57	21.29	15.70	25.76	18.94	8.14	23.33
glucose	17.63	11.57	23.40	19.52	13.61	26.98	17.37	9.33	24.04
sucrose	3.22	0.90	6.60	4.09	1.15	9.80	2.71	0.61	7.33

variable Y is categorical and represents samples class membership. It can be conveniently used when the number of objects is fewer than the number of variables. The principle of PLS is to find the components in the matrix $\boldsymbol{X}$ (matrix of predictors) which describe, as much as possible, the relevant variations in the input variables and, at the same time, have maximal correlation with the target value in $\mathbf{Y}$ (matrix of responses). This gives less weight to the variations which are irrelevant or noisy.[22] That is, PLS searches for a set of components that performs simultaneous decomposition of X and Y with the constraint that these components explain, as much as possible, the covariance between X and Y. The optimal number of components is, in general, achieved by cross-validation techniques. The overall quality of PLS-DA models was described by $R_X{}^2$ and Q^2 values. $R_X{}^2$ is defined as the proportion of variance in data explained by models and indicates goodness of fit. Q^2 measures the predictive ability of the model.

The PCA and PLS-DA output consisted of scores plots and loading plots. They allow to visualize the contrast between different samples and to explain class separation, respectively. Prior to both, PCA and PLS-DA, data were mean-centered and scaled to "Unit Variance".

RESULTS AND DISCUSSION

Chemical Composition and Antioxidant Capacity. In this study, the chemical composition of three strawberry varieties cultivated in a soilless system was assessed. Table 2 shows the mean, minimum, and maximum values of data obtained from analysis of the different chemical parameters.

Table 3. Weather Parameters Recorded Outside the Macrotunnel During the Harvest Time

harvest time	min temp (°C)	max temp (°C)	rainfall (mm)	relative humidity (%)	global radiation (MJ/m^2)
December	8.2	16.1	156.9	86.4	197.78
January	6.6	15.9	55.2	88.9	246.45
March	7.5	18.8	124	82.4	504.37

Sugars, organic acids, and phenolic compounds were determined in strawberries and expressed on a fresh basis. Table 2 also shows antioxidant activity values.

The soluble sugars identified and quantified in strawberry fruits were fructose, glucose, and sucrose. Fructose was the major sugar (50% of total sugars) in all cultivars, glucose being the second one (45%). The relationship between the content of both sugars was about unity, regardless of the cultivar. In general, the analyzed fruits contained lower sucrose concentration compared to fructose and glucose, and its participation in total sugar content ranged from <LD (below the detection limit) to 20% of total sugar content. As regards the organic acids, citric acid was the major organic acid found in analyzed strawberries followed by malic acid (Table 2). Other organic acids such as oxalic, tartaric, and ascorbic acids were found in

dx.doi.org/10.1021/jf500769x | J. Agric. Food Chem. 2014, 62, 5749−5760

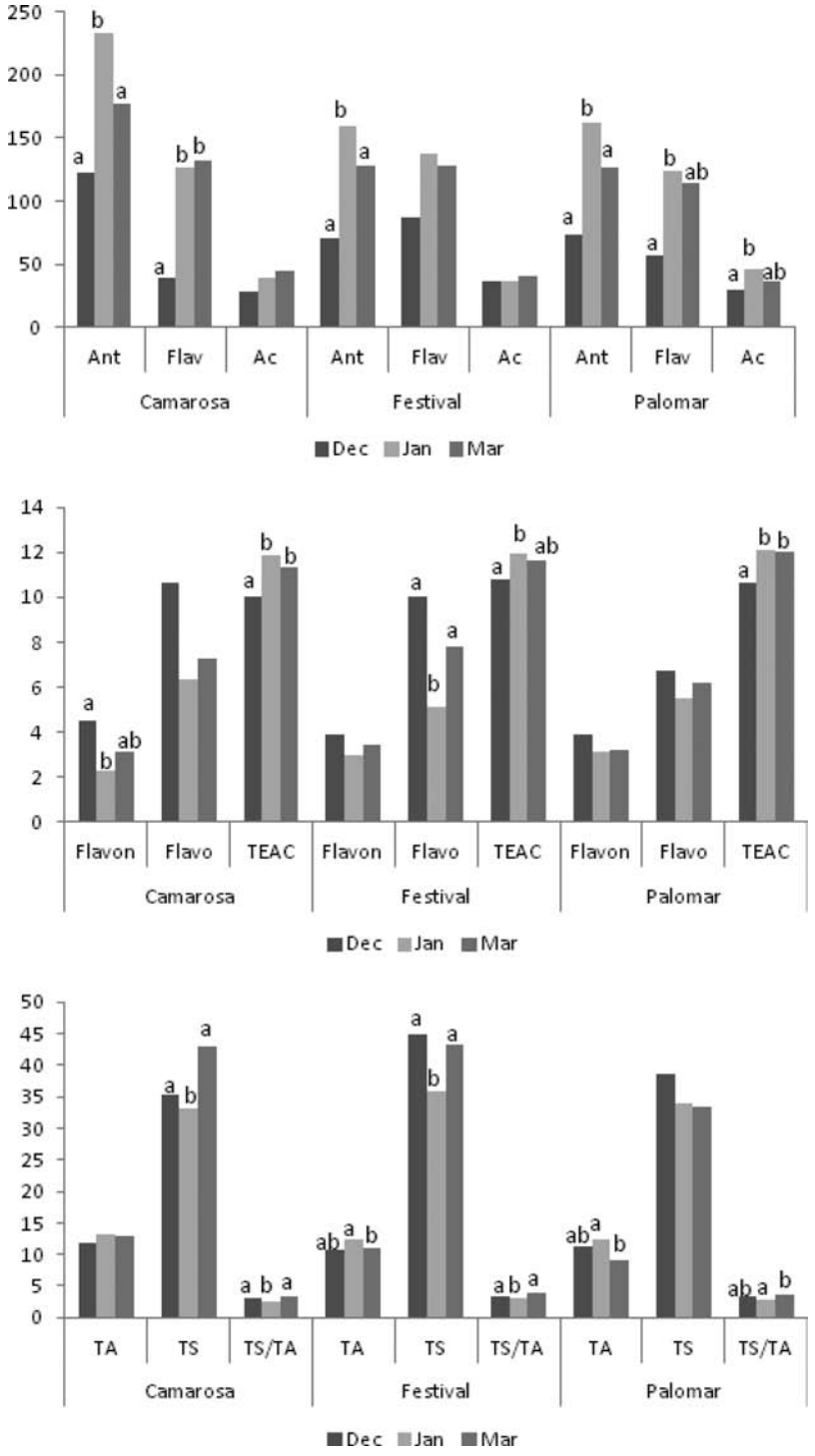

Figure 1. Content of phenolic compounds (sum of anthocyanins (Ant), flavan-3-ols (Flav), acids and derivatives (Ac), flavones (Flavon) and flavonols (Flavo)), sugars (TS), organic acids (TA), total sugars/total organic acids ratio (TS/TA), and antioxidant activity (TEAC) in three strawberry cultivars harvested in December (Dec; n = 14), January (Jan; n = 73), and March (Mar; n = 50). Columns belonging to the same set of data with different letters are significantly different (p < 0.05) by Kruskal–Wallis test.

lower concentrations. These results are in good agreement with those found in the literature.[13,15−17] The Festival variety presented the highest mean contents in the three sugar types (41.05 mg/g, as sum of sugars). The lowest level of total sugar was found in cv. Camarosa (38.92 mg/g), which had the highest contents of all acids (13.08 mg/g). In view of these results, Festival was the sweetest genotype and also had the highest total sugars/total acids ratio; therefore, this cultivar was seemingly more palatable and balanced. However, this should be confirmed by consumer panels.

Twenty five different phenolic compounds were identified and quantified. They were classified into five different groups: (a) phenolic acids and derivatives (gallic, vanillic, tyrosol, caffeic, *m*-coumaric, *p*-coumaric, caffeic derivative, ellagic and ellagic derivative acid); (b) flavonols (quercetin, kaempferol, hiperoside, isorhamnetin and quercetrin); (c) flavones (luteolin

dx.doi.org/10.1021/jf500769x | J. Agric. Food Chem. 2014, 62, 5749−5760

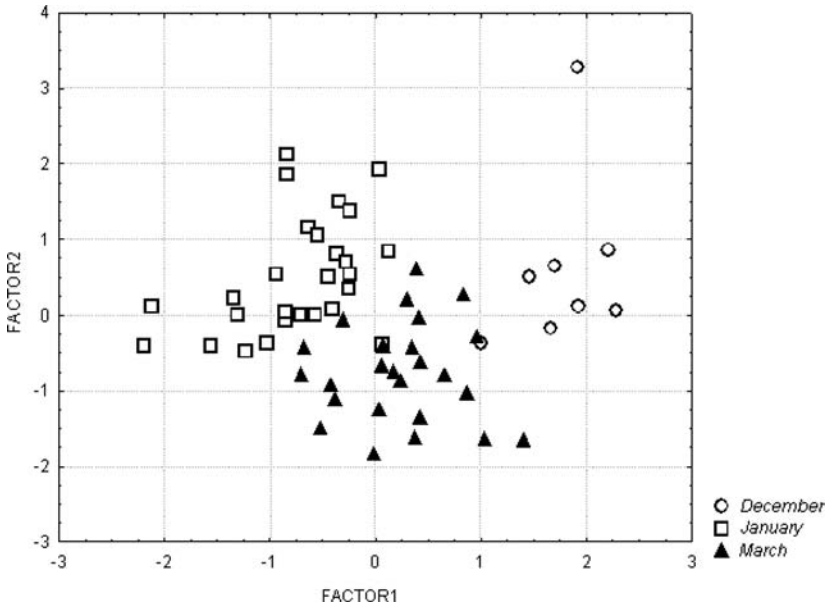

Figure 2. Scores plot of first two principal components obtained by PCA of quality attributes of strawberry samples.

Table 4. ANOVA Table for the Design Proposed and Calculation of Variance Component

source of variation	mean squares	F-ratio	variance component
coverage (A)	$MS_A^2 = \frac{rdcb\sum_{i=1}^{a}(\overline{x_i} - \overline{x})^2}{a-1}$	MS_A^2/MS_B^2	$(MS_A^2 - MS_B^2)/rdcb$
electrical conductivity (B(A))	$MS_B^2 = \frac{rdc\sum_{i=1}^{a}\sum_{j=1}^{b}(\overline{x_{ij}} - \overline{x_i})^2}{a(b-1)}$	MS_B^2/MS_C^2	$(MS_B^2 - MS_C^2)/rdc$
variety (C(B(A)))	$MS_C^2 = \frac{rd\sum_{i=1}^{a}\sum_{j=1}^{b}\sum_{k=1}^{c}(\overline{x_{ijk}} - \overline{x_{ij}})^2}{ab(c-1)}$	MS_C^2/MS_D^2	$(MS_C^2 - MS_D^2)/rd$
substrate (D(C(B(A))))	$MS_D^2 = \frac{r\sum_{i=1}^{a}\sum_{j=1}^{b}\sum_{k=1}^{c}\sum_{l=1}^{d}(\overline{x_{ijkl}} - \overline{x_{ijk}})^2}{abc(d-1)}$	MS_D^2/MS_R^2	$(MS_D^2 - MS_R^2)/r$
residual	$MS_R^2 = \frac{\sum_{i=1}^{a}\sum_{j=1}^{b}\sum_{k=1}^{c}\sum_{l=1}^{d}\sum_{n=1}^{r}(\overline{x_{ijkln}} - \overline{x_{ijkl}})^2}{abcd(r-1)}$		MS_R^2

and apigenin); (d) flavan-3-ols (catechin, epicatechin gallate and procyanidins B1 and B2); (e) anthocyanins (pelargonidin-3-glucoside, cyanidin-3-glucoside and pelargonidin-3-rutinoside).

Total phenolic content (considering the sum of all the individual phenolics) ranged from 307.43 μg/g of fresh fruit (cv. Palomar) to 373.82 μg/g of fresh fruit (cv. Camarosa). Anthocyanins were the predominant group, accounting for 48.0% of the total phenolic content. This is in agreement with results found in the literature.[3,23] As also previously reported,[10,24] the three major anthocyanins were pelargonidin-3-glucoside (mean value of 110.14 μg/g), pelargonidin-3-rutinoside (mean value of 41.95 μg/g) and cyanidine-3-glucoside (mean value of 3.66 μg/g). The levels of pelargonidin-3-glucoside and cyanidine-3-glucoside were in agreement with those reported by Crespo et al.[15] Other minor anthocyanins pelargonidin derivatives were observed but they could not be quantified. Camarosa cultivar was the richest in anthocyanins, which agreed well with our previous study findings[12] and with results reported by other authors.[25]

Flavan-3-ols was the second most important group in quantitative terms and accounted for 37.0% of the total phenolic content. In absolute terms, the highest levels were found in cv. Festival (143.01 μg/g of fresh fruit, as mean value) and the lowest in cv. Palomar (120.74 μg/g of fresh fruit, as mean value). Procyanidin B1 was the predominant flavanol in the three surveyed strawberry cultivars, with a mean value of 51.2 μg/g, following by catechin (37.6 μg/g) and procyanidin B2 (32.9 μg/g). Catechin has been reported to be the major flavan-3-ol in Spanish strawberries.[26] These authors found a global flavanols content of 4.9 mg/100 g, and the catechin content (1.57 mg/100 g) was lower than our results. However, Padula et al.[10] and Aaby et al.[27] reported higher contents of catechin in cv. Camarosa (5.86 mg/100g) and in Totem (6.2 mg/100 g) and Puget Reliance (9.0 mg/100 g) cultivars, respectively. With regard to the proanthocyanidins content, de Pascual et al.[26] reported the presence of four proanthocyanidins dimers (B1, B2, B3, and B4) in strawberry, being B3 the most abundant. Aaby et al.[23] quantified three procyanidin dimers, a trimer, and a pentamer in 27 strawberry cultivars using HPLC-DAD-MS^2. The total proanthocyanidin concentration ranged between 8.6 and 36.8 mg/100 g of fw. The results obtained by Buendía et al.[28] were higher (54−168 mg/100 g of fw), as expected, due to the fact that they used the phloroglucinolysis

dx.doi.org/10.1021/jf500769x | J. Agric. Food Chem. 2014, 62, 5749−5760

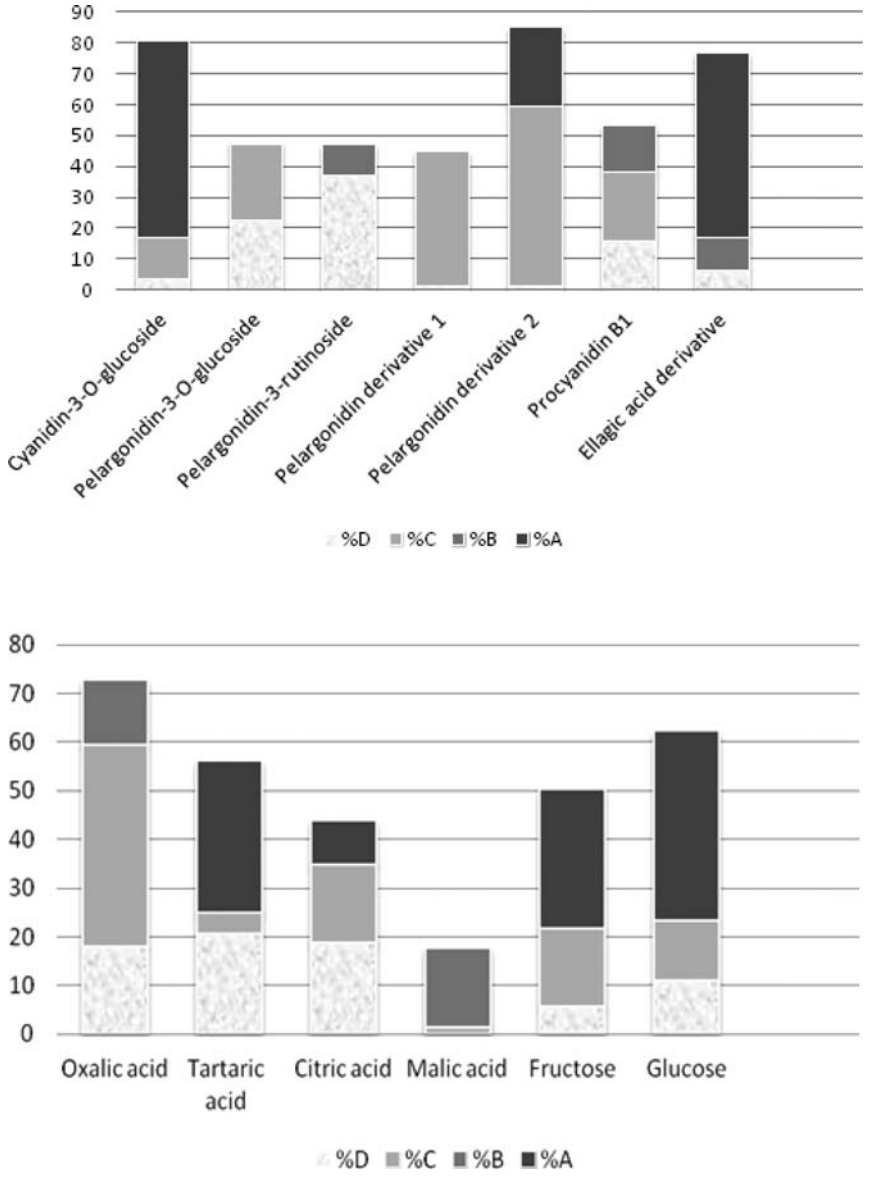

Figure 3. Variance component (%) corresponding to the different sources of variability coverage (A), electrical conductivity (B), variety (C), and substrate (D).

method. This approach generally leads to higher results compared with other methods. So, proanthocyanidins were the main strawberry phenolics found by these authors. In general, our results were lower than those previously found in the literature[27,28] and this could be explained by the analytical method used in addition to the differences between cultivars. Among the berries, the occurrence of galloyl esters was typical of strawberries.[29] Epicatechin gallate was found in the three surveyed strawberry cultivars (mean value 2.47 μg/g). Our results were lower than those reported by de Pascual et al.[26]

In general, the differences between results found in the literature and those shown here may be due to the variation in genotype, production area, soil and climatic conditions, and/or agricultural practices. Some of the differences may also stem from the variation in sample preparation and analysis procedures. Sample preservation and sample preparation parameters are critical for accurate estimation of phytochemicals present in foods. The freezing and thawing conditions can affect the content of strawberry phenolics. The extraction efficiency of phenolic compounds is influenced by the type of solvent, extraction procedure and conditions. Therefore, these factors must be taken into account when comparing data with literature.

The total content of phenolic acids of the three strawberry cultivars was similar among them, as can be seen in Table 2. This group of compounds comprised 12.0% of the total content of phenolics. Ellagic and ellagic derivative acids are the major phenolic acids in the samples studied and represent approximately 50% of the total phenolic acids). This was in consonance with other authors findings.[30] The highest level of *p*-coumaric acid was found in cv. Palomar (2.20 μg/g of fresh fruit, as mean value) and the lowest, in cv. Festival (1.55 μg/g of fresh fruit, as mean value). Other hydroxycinnamic acids such as *m*-coumaric acid, caffeic acid and caffeic acid derivative were also quantified. The last one was the most abundant (mean value 2.5 μg/g). Regarding hydroxybenzoic acids, vanillic (mean value 3.23 μg/g) and gallic (mean value 4.64 μg/g) acids were found in all samples analyzed. Previous

dx.doi.org/10.1021/jf500769x | J. Agric. Food Chem. 2014, 62, 5749−5760

Table 5. Results of the Nested ANOVA as p-Value[a]

	coverage	EC (coverage)	variety (coverage*EC)	substrate (coverage*EC*variety)
TEAC	**0.00024**	**0.00112**	**0.00199**	**0.00012**
cyanidin-3-O-glucoside	**0.00000**	**0.00071**	**0.00000**	**0.03459**
pelargonidin-3-O-glucoside	**0.00837**	**0.00025**	**0.00000**	**0.00049**
pelargonidin-3-rutinoside	**0.00263**	0.064 19	**0.00000**	0.086 43
pelargonidin derivative 1	0.326 28	0.058 72	**0.00000**	0.350 70
pelargonidin derivative 2	**0.00000**	0.158 53	**0.00000**	0.151 08
procyanidin B1	**0.00024**	**0.00000**	**0.00000**	**0.00262**
tyrosol	**0.03404**	0.959 24	0.075 52	0.129 37
(+)-catechin	0.411 43	0.072 56	0.353 37	0.386 87
procyanidin B2	0.857 75	0.441 90	0.188 71	**0.01656**
vanillic acid	**0.02789**	**0.02499**	0.861 20	0.231 98
epicatechin gallate	0.498 57	0.512 62	0.183 43	0.357 45
m-coumaric acid	**0.00049**	**0.00000**	**0.00010**	**0.00003**
gallic acid	0.843 41	0.067 58	**0.00053**	0.703 32
ellagic acid	0.128 05	**0.01965**	**0.01767**	0.275 33
ellagic acid derivative	**0.00000**	**0.00000**	0.151 49	**0.00709**
caffeic acid	**0.00001**	**0.00317**	**0.00000**	0.064 54
caffeic acid derivative	**0.00009**	**0.02595**	**0.00000**	0.106 99
p-coumaric acid	0.952 21	0.250 85	**0.02924**	0.074 07
luteolin	0.955 49	0.097 15	0.151 74	0.150 31
apigenin	**0.00309**	0.141 95	**0.00385**	0.125 73
quercetin-3-O-galactoside	**0.00410**	0.287 10	0.321 53	0.303 04
quercetin	**0.00000**	0.809 56	0.115 25	0.400 68
kaempferol	**0.00350**	0.508 23	**0.00002**	0.085 55
isorhamnetin	**0.00003**	**0.03369**	**0.00004**	**0.00495**
quercitrin	**0.00002**	**0.00018**	**0.00572**	**0.00010**
oxalic acid	**0.00042**	**0.00000**	**0.00000**	**0.00001**
tartaric acid	**0.00000**	**0.01491**	**0.00042**	**0.00026**
citric acid	**0.00025**	0.233 53	**0.00001**	**0.00335**
malic acid	0.271 15	**0.00011**	0.436 94	0.669 01
fructose	**0.00000**	0.284 61	**0.00002**	0.129 09
glucose	**0.00000**	0.286 17	**0.00000**	**0.00711**

[a]Figures in bold indicate significant F-tests at the level of significance showed in the table.

studies on strawberries have generally reported variable composition and contents of phenolic acids. Hydroxycinnamic acids occurred mainly as esters. Thus, *p*-coumaroyl-glucoside acid has been described as the major hydroxycinnamic acid in strawberries,[10,28,29,31,32] while *p*-coumaric acid has been described as the most abundant aglycon.[29,33] Padula et al.[10] reported relatively high contents of caffeic acid (from 0.7 to 11.40 mg/100 g fresh weight) and ferulic acid (from 0.76 to 13.99 mg/100 g fresh weight) in 20 strawberry cultivars grown in Italy. On the other hand, Mättila et al.[33] found caffeic, *p*-coumaric, *p*-hydroxybenzoic, cinnamic, and gallic acids in three strawberry cultivars grown in Finland (expressed as aglycones) but ferulic and vanillic acids were only detected in some of the strawberry cultivars. However, Määttä et al.[29] reported only the presence of p-coumarylester in cv. Jonsok.

The minor groups were flavonols and flavones, which accounted for 2.5 and 0.9%, of the total phenolic compounds, respectively. Regarding the family of flavonols, the mean content was 8.3 μg/g. The highest levels were found in cv. Festival (9.3 μg/g of fresh fruit, as mean value) and the lowest in cv. Palomar (7.6 μg/g of fresh fruit, as mean value). Hiperoside (quercetin-3-O-galactoside) was the most important flavonol in terms of quantity (3.15 μg/g) in the three cultivars. Other major flavonols were quercetin and isorhamnetin with mean values of 2.28 and 1.25 μg/g, respectively. Kaempferol and quercitrin were found in lower levels, whereas myricetin was not found at detectable levels in analyzed samples. Furthermore, two flavones, luteolin and apigenin, were detected in the three strawberry varieties. The mean content was 0.93 μg/g for luteolin and 2.16 μg/g for apigenin. As with the phenolic acids and other flavonoids, there are differences between results found in the literature. Glucosides and glucuronides of quercetin and kaempferol have been identified as the main flavonols in strawberry.[29,34] Our results for flavonol contents, averaging 8.4 μg/g, were low compared to those reported in the literature.[27−29]

The total antioxidant capacity was measured according to the ABTS method. Trolox (vitamin E analogue) was used as standard, and results, expressed as micromoles of Trolox equivalents per gram (TEAC), are displayed in Table 2. It can be observed that TEAC values were quite similar in the three surveyed strawberry cultivars, with a mean value of 11.66 μmoles TE/g. These results were of the same magnitude as those previously reported.[8,15] Jossuttis et al.[14] reported higher values of antioxidant capacity for two strawberry cultivars (Everest and Elsanta) grown in Germany. The cultivars were grown in three different conditions. Two of them were cultivated in a tunnel covered with two films which vary in their UV transparency, and another one was cultivated under open-field conditions.

Comparison of Harvest Time. The three varieties of strawberry were planted in September and harvested in

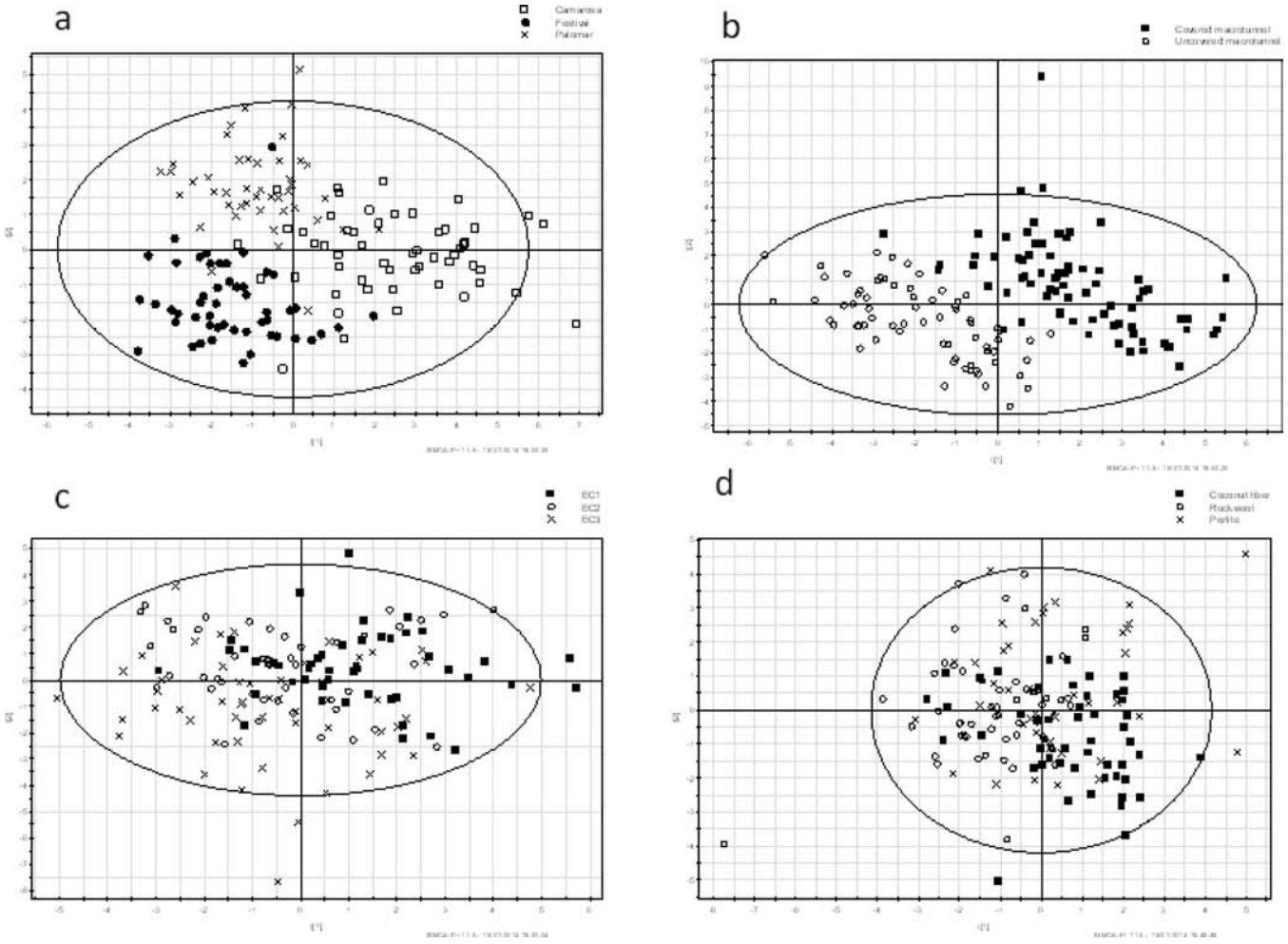

Figure 4. PLS-DA scores plots based on chemical composition of strawberry samples (n = 162) according to cultivars (a), covered or uncovered macrotunnel (b), electrical conductivity (c), and substrate (d).

December (extra-early production), January (early production), and March (early production) in order to assess differences in their profiles as a function of both variety and harvest time. Table 3 shows the monthly weather parameters (outside the macrotunnel) during the experimentation period. These values are considered normal according to the climatological data recorded in the area (period 1971−2000).

The contents of average total sugars, total organic acids and five groups of polyphenols and TEAC as a function of strawberry variety and harvest time are displayed in Figure 1. The comparison between three harvest times shows a similar trend in the three varieties. The amount of anthocyanins and flavan-3-ols (considering the sum of all individual phenolics) was higher in January (when rainfall, maximum and minimum temperatures were lower and relative humidity higher), whereas the total sugars content was more abundant in March (when maximum temperature and global radiation were higher). It has been previously observed that the content of many phenolic compounds and the antioxidant capacity increase in berry fruits as temperature increases.[32] On the other hand, low light intensity[35] and high temperatures[36] in day and night lead to decreased synthesis of sugar and ascorbic acid. Our results are apparently contradictory with these findings. However, Pereira et al.[37] observed it difficult to separate the effects of temperature from the photochemical effects. Moreover, the cultivation of strawberries under plastic tunnels decreases the dependency of quality on the climatic conditions.

The higher levels for total anthocyanins and flavan-3-ols were verified in cv. Camarosa and Festival strawberries, respectively, both in January harvest; while the fruits of Palomar variety showed higher total sugar/total organic acids ratio in March harvest.

In order to find out significant differences of analyzed compounds between the three considered harvested times, the multiple comparison test of Kruskal−Wallis was applied. Results are also shown in Figure 1. The harvests of December and January present statistical differences for anthocyanins and antioxidant activity in the three varieties. Additionally, Camarosa and Palomar cultivars also present differences for flavan-3-ols, and Festival cultivar for flavonols. Taste related parameters differentiate fruits harvested in January from March ones. The TS/TA ratio increased for the three varieties surveyed in March. Due to the importance of this parameter for strawberry flavor, seasonal changes in this ratio may influence consumer acceptance.

In order to confirm these results a principal component analysis (PCA) was carried out. PCA allows to visualize data trends and to provide a first evaluation for the discriminant power of the variables. PCA is applied to the data set to obtain linear combinations of variables, which are called principal components (PCs). It retains information about the variability

dx.doi.org/10.1021/jf500769x | J. Agric. Food Chem. 2014, 62, 5749−5760

of the data set, so that the first PC expresses the largest variability, and each successive PC represents as much of the residual variability as possible. In this case, five PCs, which account for 60% of the total variance, were extracted according to Kaiser Criterion (eigenvalues higher than 1.0). Figure 2 shows samples distribution in the plane defined by two first components. As can be observed, samples harvested in January and December appear separated along of PC1, while fruits harvested in March are located in the negative part of PC2. The variables that contribute most to the first component are pelargonidin-3-glucoside and the sum of anthocianyns and flavan-3-ols, all with negative loadings. In the case of PC2, the most contributing variables are glucose, sum of sugars and total sugar/total organic acids ratio, also with negative loadings. Regarding the meteorological variables, PC1 is positively correlated to minimum temperature and rainfall. PC2 is positively correlated to relative humidity and negatively to maximum temperature and global radiation.

Influence of Agronomical Practices. To meet the second overall objective of the study, that is, to examine changes in fruit quality depending on the cultivation practices and environmental conditions, a nested ANOVA was carried out. For this test, the expressions gathered in Table 4 were applied.

Nested ANOVA is used when the variation of the factor is subordinated to another variation factor. So, the survey had the following objectives: to explore whether chemical composition of strawberries varied in a purely random way across the two macrotunnels or whether it showed a variation due to different factors studied (electrical conductivity (B), variety (C), and substrate (D)). In the last case, the variance components associated with the levels of nested design is evaluated (Figure 3). The effect significance of factors is tested by Fisher F test.

Table 5 shows the F-test results (as p-value) from nested ANOVA for each variable. As can be observed, no statistically significant differences were found in the content of catechin, epicatechin gallate, and luteolin between two macrotunnels, electrical conductivity, variety or substrate. The type of coverage has a significant influence on the content of cyanidin-3-*O*-glucoside, pelargonidin-3-*O*-glucoside, pelargonidin-3-rutinoside, pelargonidin derivative 2, tyrosol, vanillic acid, *m*-coumaric acid, ellagic acid derivative, caffeic acid and caffeic acid derivative, apigenin, all flavonols, sugars and organic acids except for malic acid. So, the content of anthocyanins was higher in the cover macrotunnel, while the levels of flavan-3-ols, flavonols, ellagic acid and derivative, cinnamic acids and sugars were higher in the uncovered macrotunnel. These results were in agreement with those reported by Josuttis et al.[14] These authors found a higher content of flavonols and a lower total content of anthocyanins and pelargonidin related anthocyanins in open-field strawberry fruits compared to tunnel-grown fruits. The F-test also indicates significant differences between variety, mainly for the anthocyanins, sugars and organic acids. The electrical conductivity and type of substrate also influence the content of some studied compounds, mainly phenolic compounds. Keutgen and Pawelzik[38] observed that the NaCl stress significantly increased the concentration of most of organic acids in cv. Elsanta (sensitive), while remained fairly constant in cv. Korona (less sensitive). They also observed that in both cultivars the individual sugars decreased progressively due to NaCl. On the other hand, these authors found that moderate salt stress significantly increased the antioxidant capacity, total phenolic compounds and anthocyanins in cv Korona.[39]

Figure 3 shows, for a selection of variables, the estimated contribution of the various levels of the nested design to the total variance. For most variables, the variance of the residual errors was the largest variance component. For phenolic compounds the variance components associated with the coverage and variety contributed substantially to the total variance in addition to residual error. These findings are consistent with those found by other authors. They identify the genotype as the main source of variation for phenolic compounds[8,10,15] but they are also affected by crop conditions.[11,13,14] For sugars, the variance component due to coverage contributed noticeably to the total variance. Finally, the organic acids had different patterns of variation. The variance component associated with the substrate generally account for 1/5 of the total variance for citric, tartaric and oxalic acids. For oxalic and tartaric acids, the higher source of variability was due to variety and coverage, respectively.

The influence of agronomical practices was also investigated by multivariate chemometric method. Data were subjected to supervised chemometrics using partial least-squares discriminant analysis (PLS-DA). PLS-DA is a supervised method that explains the maximum variation in the data set (X) using a dummy matrix (Y), which can be used to sharpen the separation between groups or observations. Four models were constructed to assess the influence of strawberry cultivars and the growing conditions (macrotunnel type, electrical conductivity and substrate). In the first case, a two-component model was obtained with good quality of fit and validity (R^2 = 0.202) and prediction (Q^2 = 0.529). Figure 4a shows the scores plot obtained for the three strawberry cultivars, grouped accordingly to the first two components. As it can be observed, the separation between cultivars was satisfactory and they were clearly discriminated. PLS models also provided the possibility of obtaining a quantitative measure of the discriminating power of each variable by means of variable importance for the projection (VIP). This is a weighted sum of squares of the PLS loadings which takes into account the amount of explained Y-variance of each PLS component. X-variables, characterized by VIP values which are larger than 1, had major importance for modeling the responses, whereas variables with VIP values smaller than 0.5 had little or no influence on the model. The VIP scores indicated that anthocyanins were the most important parameters for cv. Camarosa, whereas glucose, fructose, total sugars and TS/TA ratio were more relevant for cv Festival and phenolics acids and flavonols for cv. Palomar.

A second model was obtained with data from strawberries grown in two macrotunnels, covered and uncovered. This three-component model explained 35.5% of the variance (R^2 = 0.355), and the t1 and t2 components allowed discrimination between two sets of samples (Figure 4b): strawberries grown in covered macrotunnel (positioned on the right side of the plot) and strawberries grown in uncovered macrotunnel (positioned on the left side of the plot). The variables which contribute the most to the discrimination between samples were anthocyanins, ellagic acid derivative, glucose and fructose contents and total sugars. All these variables had VIP values higher than 1.0. The loading plot showed how the first component (t1) was related to glucose, fructose, total sugars and ellagic acid derivative on the negative side where the uncovered grown samples were situated (data not shown), and with pelargonidin and their derivatives on the positive side where covered grown samples were situated, confirming the results discussed above.

The effect of the other two factors, electrical conductivity and substrate, was also evaluated. In this case, the PLS-DA scores plots showed a poor separation between samples (Figure 4c,d), resulting in low predictability of the models as indicated by a Q^2 of 0.0878 and 0.0188, for electrical conductivity and substrate, respectively.

In summary, we have shown that the content of several metabolites related to strawberry quality, including sugars, organic acids, phenolic compoundas and TEAC, depend on cultivar and growing conditions. Festival was the sweetest genotype and also had the highest total sugars/total acids ratio, whereas Camarosa was richest in anthocyanins. Considering the harvest time and after applying pattern recognition techniques such as PCA, it was concluded that strawberry harvested in January and March (early production) had higher quality. Fruits harvested in January were richer in phenolic compounds whereas fruits harvested in March were richer in taste-related compounds. The influence of agronomical conditions was investigated by nested ANOVA and PLS-DA. The type of coverage and the variety were the main source of variation for most of the variables studied mainly phenols and sugars. A good discrimination between three cultivars and macrotunnel type was also achieved by PLS-DA, confirming the results from Nested ANOVA. The VIP scores indicated that anthocyanins were the most important parameters for cv Camarosa, whereas glucose, fructose, total sugars and TS/TA ratio were more relevant for cv Festival and phenolics acids and flavonols for cv Palomar. Strawberries grown in covered macrotunnel were richer in pelargonidin and their derivatives. Uncovered grown samples were richer in glucose, fructose, total sugars, and ellagic acid derivative. Other growing conditions, such as electrical conductivity and substrate did not provide a clear discrimination between samples.

AUTHOR INFORMATION

Corresponding Author

*Tel: 34959 219958. Fax: 34959 219942. E-mail: recamale@uhu.es.

Notes

The authors declare no competing financial interest.

REFERENCES

(1) Giampieri, F.; Tulipani, S.; Alvarez-Suarez, J. M.; Quiles, J. L.; Mezzetti, B.; Battino, M. The strawberry: Composition, nutritional quality, and impact on human health. *Nutrition* **2012**, *28*, 9−19.

(2) Alvarez-Suarez, J. M.; Giamperi, F.; Tulipani, S.; Casoli, T.; Di Stefano, G.; González-Paramás, A. M.; et al. One-month strawberry-rich anthocyanin supplementation ameliorates cardiovascular risk, oxidative stress markers and platelet activation in humans. *J. Nutr. Biochem.* **2014**, *25*, 289−294.

(3) Giampieri, F.; Alvarez-Suarez, J. M.; Battino, M. Strawberry and Human Health: Effects beyond Antioxidant Activity. *J. Agric. Food Chem.* **2014**, DOI: 10.1021/jf405455n.

(4) Halliwell, B. Free radical, antioxidants and human disease: curiosity, cause or consequence. *Lancet* **1994**, *344*, 721−724.

(5) Battino, M.; Mezzetti, B. Update on fruit antioxidant capacity: a key tool for Mediterranean diet. *Public Health Nutr.* **2006**, *9*, 1099−1103.

(6) Niki, E. Do antioxidants impair signaling by reactive oxygen species and lipid oxidation products? *FEBS Lett.* **2012**, *586*, 3767−3770.

(7) Recamales, M. A.; Hernanz, D.; Toscano, G.; Peralbo, A.; Flores, F.; López-Medina, J. Strawberry Quality Cultivated in Soil-less Systems. *Sth International Strawberry Symposium*; The International Society for Horticultural Science and the Queensland Strawberry Growers Association; 2004.

(8) Capocasa, F.; Scalzo, J.; Mezzetti, B.; Battino, M. Combining quality and antioxidant attributes in the strawberry: The role of genotype. *Food Chem.* **2008**, *111*, 872−878.

(9) Tulipani, S.; Mezzetti, B.; Capocasa, F.; Bompadre, S.; Beekwilder, J.; De Vos, C. H. R.; et al. Antioxidants, phenolic compounds, and nutritional quality of different strawberry genotypes. *J. Agric. Food Chem.* **2008**, *56*, 696−704.

(10) Padula, M. C.; Lepore, L.; Milella, L.; Ovesna, J.; Malafronte, N.; Martelli, G.; et al. Cultivar based selection and genetic analysis of strawberry fruits with high levels of health promoting compounds. *Food Chem.* **2013**, *140*, 639−646.

(11) Anttonen, M. J.; Hoppula, K. I.; Nestby, R.; Verheul, M. J.; Karjalainen, R. O. Influence of Fertilization, Mulch Color, Early Forcing, Fruit Order, Planting Date, Shading, Growing Environment, and Genotype on the Contents of Selected Phenolics in Strawberry (Fragaria x ananassa Duch.) Fruits. *J. Agric. Food Chem.* **2006**, *54*, 2614−2620.

(12) Hernanz, D.; Recamales, A. F.; Melendez-Martinez, A. J.; Gonzalez-Miret, M. L.; Heredia, F. J. Assessment of the differences in the phenolic composition of five strawberry cultivars (Fragaria x ananassa Duch.) grown in two different soilles system. *J. Agric. Food Chem.* **2007**, *55*, 1846−1852.

(13) Wang, S. Y.; Millner, P. Effect of different cultural systems on antioxidant capacity, phenolic content, and fruit quality of strawberries (Fragaria × ananassa Duch.). *J. Agric. Food Chem.* **2009**, *57*, 9651−9657.

(14) Josuttis, M.; Dietrich, H.; Treutter, D.; Will, F.; Linnemannstöns, L.; Krüger, E. Solar UVB Response of Bioactives in Strawberry (*Fragaria x ananassa* Duch. L.): A Comparison of Protected and Open-Field Cultivation. *J. Agric. Food Chem.* **2010**, *58*, 12692−12702.

(15) Crespo, P.; Giné Bordonaba, J.; Terry, L. A.; Carlen, C. Characterisation of major taste and health-related compounds of four strawberry genotypes grown at different Swiss production sites. *Food Chem.* **2010**, *122*, 16−24.

(16) Ornelas-Paz, J. J.; Yahia, E. M.; Ramírez-Bustamante, N.; Pérez-Martínez, J. D.; Escalante-Minakata, M. P.; Ibarra-Junquera, V.; et al. Physical attributes and chemical composition of organic strawberry fruit (*Fragaria x ananassa* Duch., Cv. Albion) at six stages of ripening. *Food Chem.* **2013**, *138*, 372−381.

(17) Vandendriessche, T.; Vermeir, S.; Mayayo Martínez, C.; Hendrickx, Y.; Lammertyn, J.; Nicolaï, B. M.; Hertog, M. L. A. T. M. Effect of ripening and inter-cultivar differences on strawberry quality. *LWT-Food Sci. Technol.* **2013**, *52*, 62−70.

(18) Akhatou, I.; Fernández-Recamales, A. Influence of cultivar and culture system on nutritional and organoleptic quality of strawberry. *J. Sci. Food Chem.* **2014**, *94*, 866−875.

(19) Santos, M. B.; Chandler, C. K.; Whidden, A. J.; Sanchez, M. C. Assessing the possible causes for the "strawberry dried calyx disorder" in Florida and Spain. *VI International Strawberry Symposium*. ISHS Acta Horticulturae; 2008.

(20) Pellegrini, N.; Re, R.; Yang, M.; Rice-Evans, C. A. Screening of dietary carotenoids and carotenoid-rich fruit extracts for antioxidant activities applying the $ABTS^+$ radical cation decolorization assay. *Methods Enzymol.* **1999**, *299*, 379−389.

(21) Kallithraka, S.; Mohdaly, A. A-A.; Makris, D. P.; Kefalas, P. Determination of major anthocyanin pigments in Hellenic native grape varieties (*Vitis vinifera* sp.): association with antiradical activity. *J. Food Comp. Anal.* **2005**, *18*, 375−386.

(22) Berrueta, L. A.; Alonso-Salces, R. M.; Héberger, K. Supervised pattern recognition in food analysis. *J. Chromatogr. A* **2007**, *1158*, 196−214.

(23) Aaby, K.; Mazur, S.; Nes, A.; Skrede, G. Phenolic compounds in strawberry Fragaria x ananassa Duch.) fruits: composition in 27 cultivars and changes during ripening. *Food Chem.* **2012**, *132*, 86−97.

(24) Lopes da Silva, F.; Pascual, T.; Rivas-Gonzalo, J.; Santos-Buelga, C. Identification of anthocyanin pigments in strawberry (cv Camarosa)

by LC using DAD and ESI-MS detection. *Eur. Food Res. Technol.* **2002**, *214*, 248−253.
(25) Lopes da Silva, F.; Escribano-Bailón, M. T.; Pérez Alonso, J. J.; Rivas-Gonzalo, J. C.; Santos-Buelga, C. Anthocyanin pigments in strawberry. *Lebensm. Wiss.Technol.* **2007**, *40*, 374−382.
(26) De Pascual-Teresa, S.; Santos-Buelga, C.; Rivas-Gonzalo, J. C. Quantitative analysis of flavan-3-ols in Spanish foodstuffs and beverages. *J. Agric. Food Chem.* **2000**, *48*, 5331−5337.
(27) Aaby, K.; Skrede, G.; Wrolstad, R. E. Phenolic composition and antioxidant activities in flesh and achenes of strawberries (*Fragaria ananassa*). *J. Agric. Food Chem.* **2005**, *53*, 4032−4040.
(28) Buendía, B.; Gil, M. I.; Tudela, J. A.; Gady, A. L.; Medina, J. J.; Soria, C.; López, J. M.; Tomás-Barberán, F. A. HPLC-MS Analysis of Proanthocyanidin Oligomers and Other Phenolics in 15 Strawberry Cultivars. *J. Agric. Food Chem.* **2010**, *58*, 3916−3926.
(29) Määttä-Riihinen, K. R.; Kamal-Eldin, A.; Törrönen, A. R. Identification and quantification of phenolic compounds in berries of *Fragaria* and *Rubus* species (family Rosaceae). *J. Agric. Food Chem.* **2004**, *52*, 6178−6187.
(30) Häkkinen, S.; Heinonen, M.; Kärenlampi, S.; Mykkänen, H.; Ruuskanen, J.; Törrónen, A. Screening of selected flavonoids and phenolic acids in 19 berries. *Food Res. Int.* **1999**, *32*, 345−353.
(31) Schuster, B.; Herrmann, K. Hydroxybenzoic and hydroxycinnamic acid derivatives in soft fruits. *Phytochemistry* **1985**, *24*, 2761−2764.
(32) Wang, S. Y.; Zheng, W. Effect of plant growth temperature on antioxidant capacity in strawberry. *J. Agric. Food Chem.* **2001**, *49*, 4977−4982.
(33) Mattila, P.; Hellstrom, J.; Törrönen, R. Phenolic acids in berries, fruits, and beverages. *J. Agric. Food Chem.* **2006**, *54*, 7193−7199.
(34) Seeram, N. P.; Lee, R.; Scheuller, H. S.; Heber, D. Identification of phenolic compounds in strawberries by liquid chromatography electrospray ionization mass spectroscopy. *Food Chem.* **2006**, *97*, 1−11.
(35) Lee, S. K.; Kader, A. A. Preharvest and postharvest factors influencing vitamin C content of horticultural crops. *Postharvest Biol. Technol.* **2000**, *20*, 207−220.
(36) Wang, S. Y.; Camp, M. J. Temperatures after bloom affect plant growth and fruit quality of strawberry. *Sci. Hort.* **2000**, *85*, 183−199.
(37) Pereira, G. E.; Gaudillere, J.-P.; Pieri, P.; Hilbert, G.; Maucourt, M.; Deborde, C.; Moing, A.; Rolin, D. Microclimate Influence on Mineral and Metabolic Profiles of Grape Berries. *J. Agric. Food Chem.* **2006**, *54*, 6765−6775.
(38) Keutgen, A.; Pawelzik, E. Modifications of taste-relevant compounds in strawberry fruit under NaCl salinity. *Food Chem.* **2007**, *105*, 1487−1494.
(39) Keutgen, A.; Pawelzik, E. Modifications of strawberry fruit antioxidants pools and fruit quality under NaCl stress. *J. Agric. Food Chem.* **2007**, *55*, 4066−4072.

JOURNAL OF AGRICULTURAL AND FOOD CHEMISTRY

Article

pubs.acs.org/JAFC

Synthesis and Crystal Structure of New Temephos Analogues as Cholinesterase Inhibitor: Molecular Docking, QSAR Study, and Hydrogen Bonding Analysis of Solid State

Khodayar Gholivand,*[,†] Ali Asghar Ebrahimi Valmoozi,[†] and Mahyar Bonsaii[§]

[†]Department of Chemistry, Tarbiat Modares University, P.O. Box 14115-175, Tehran, Iran

[§]Department of Chemistry, Islamic Azad University, North Tehran Branch, Tehran, Iran

Supporting Information

ABSTRACT: A series of temephos (Tem) derivatives were synthesized and characterized by ^{31}P, ^{13}C, and ^{1}H NMR and FT-IR spectral techniques. Also, the crystal structure of compound **9** was investigated. The hydrogen bonding energies (E^2) were calculated by NBO analysis of the crystal cluster. The activities and the mixed-type mechanism of Tem derivatives were evaluated using the modified Ellman's and Lineweaver−Burk's methods on cholinesterase (ChE) enzymes. The inhibitory activities of Tem derivatives with a P═S moiety were higher than those with a P═O moiety. Docking analysis disclosed that the hydrogen bonds occurred between the OR (R = CH_3 and C_2H_5) oxygen and N−H nitrogen atoms of the selected compounds and the receptor site (GLN and GLU) of ChEs. PCA−QSAR indicated that the correlation coefficients of the electronic variables were dominant compared to the structural descriptors. MLR−QSAR models clarified that the net charges of nitrogen and phosphorus atoms contribute important electronic function in the inhibition of ChEs. The validity of the QSAR model was confirmed by a LOO cross-validation method with q^2 = 0.965 between the training and testing sets.

KEYWORDS: *bisphosphoramidothioate, crystal structure, cholinesterase inhibitor, QSAR, molecular docking*

INTRODUCTION

In recent years, organophosphorus compounds have been of great interest. A wide range of applications in the areas of medicinal, agricultural, and industrial chemistry have been found owing to their significant biological and physical properties.[1] Among many known phosphorus compounds, bisphosphoramidothioates (BPAT) with the general structure of $R_1R_2P(S)NH-X-NHP(S)R_1R_2$ comprise an important class of compounds that exhibit insecticide properties to inhibit cholinesterase (ChE) enzymes.[2] Little attention has been given to the interaction mechanism of the ChE enzymes and BPATs.[3,4] Temephos (Scheme 1) with the general formula is

Scheme 1. Synthesis Pathway and Chemical Structure of Compounds 1−24

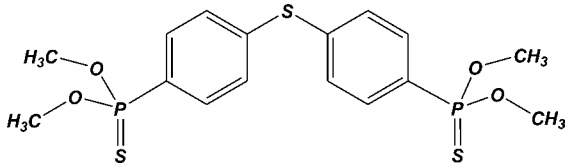

a useful insecticide to control the larvae of mosquitoes, midges, and moths;[5,6] however, it has side effects on humans as an anti-acetylcholinesterase (AChE) as well as carcinogenic potential.[7] Therefore, designing and producing the selective compounds of Tem category having high insecticide potential with fewer anti-AChE and carcinogenic effects are required. To extend and to evaluate this problem, two new methods have so far been introduced to overcome the inhibition mechanism.[8] Integrated molecular docking and QSAR approaches were employed to explore the binding interactions between the Tem analogues and the AChE and butyrylcholinesterase (BChE).[9] Molecular docking was performed to define a model for the comprehension of the binding interactions between ligands and receptor. QSAR models elucidated the effective parameters of molecular structure computed by the density function theory (DFT) in the inhibition process.[10]

In this study, 24 novel Tem analogues with the general formula of $(RO)_2P(X)YP(X)(OR)_2$, (X = O and S; Y = NH−$(CH_2)_2$−NH, NH−$CH(CH_3)$−CH_2−NH, N(CH_3)−$(CH_2)_2$−N(CH_3), NH−$(CH_2)_3$−NH, NH−CH_2−$C(CH_3)$−CH_2−NH, NH−$(CH_2)_4$−NH, N−$(CH_2)_4$−N, N−$(CH_2)_5$−N, and NH−(C_6H_{10})−NH; R = OCH_3 and OC_2H_5) (**1−24**) were synthesized and characterized by ^{31}P, ^{13}C, and ^{1}H NMR and IR spectroscopy. The solid state structure of $(CH_3O)_2P(S)$-$NH(C_6H_{10})NHP(S)(OCH_3)_2$ (**9**) was determined by X-ray crystallography and used as reference for quantum mechanical (QM) calculations at the B3LYP level. The electronic aspects of two different hydrogen bonds (P═S···H−N) in the crystal structure of compound **9** were studied by NBO and Atoms in Molecules (AIM) analyses. The activities of Tem derivatives on AChE and BChE were determined using a modified Ellman's method.[11] Also, the inhibition mechanisms of the prepared compounds were evaluated by Lineweaver−Burk plot.[12] Docking analysis was used to find the most efficient parameters to introduce a better mechanism of interaction between the

Received: March 11, 2014
Revised: June 3, 2014
Accepted: June 3, 2014
Published: June 3, 2014

ACS Publications © 2014 American Chemical Society

Scheme 2

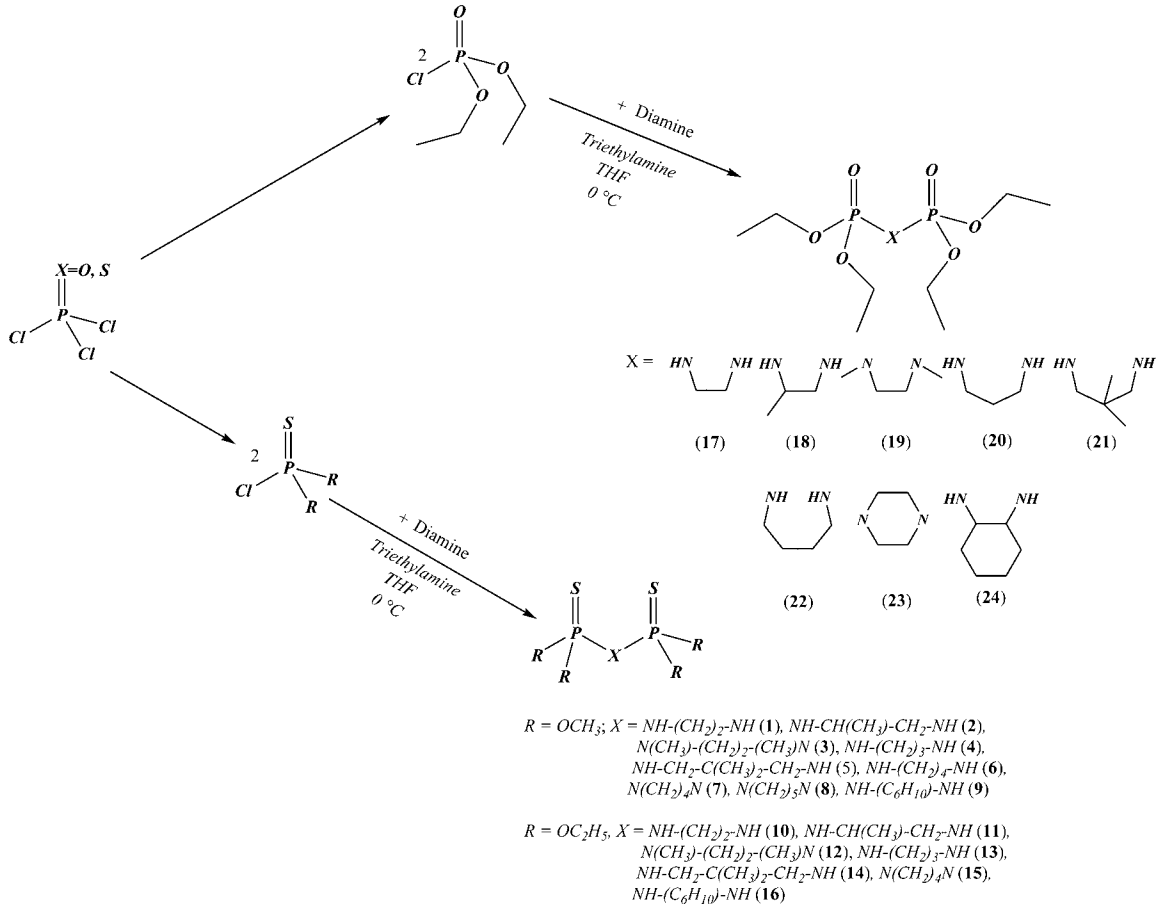

R = OCH_3; *X* = $NH\text{-}(CH_2)_2\text{-}NH$ (**1**), $NH\text{-}CH(CH_3)\text{-}CH_2\text{-}NH$ (**2**), $N(CH_3)\text{-}(CH_2)_2\text{-}(CH_3)N$ (**3**), $NH\text{-}(CH_2)_3\text{-}NH$ (**4**), $NH\text{-}CH_2\text{-}C(CH_3)_2\text{-}CH_2\text{-}NH$ (5), $NH\text{-}(CH_2)_4\text{-}NH$ (**6**), $N(CH_2)_4N$ (**7**), $N(CH_2)_5N$ (**8**), $NH\text{-}(C_6H_{10})\text{-}NH$ (**9**)

R = OC_2H_5, *X* = $NH\text{-}(CH_2)_2\text{-}NH$ (**10**), $NH\text{-}CH(CH_3)\text{-}CH_2\text{-}NH$ (**11**), $N(CH_3)\text{-}(CH_2)_2\text{-}(CH_3)N$ (**12**), $NH\text{-}(CH_2)_3\text{-}NH$ (**13**), $NH\text{-}CH_2\text{-}C(CH_3)_2\text{-}CH_2\text{-}NH$ (**14**), $N(CH_2)_4N$ (**15**), $NH\text{-}(C_6H_{10})\text{-}NH$ (**16**)

selected molecules and the receptor site of human AChE and BChE. The appropriate molecular structural parameters were computed by DFT method and adopted to construct QSAR equations.

MATERIALS AND METHODS

Instruments. The enzyme AChE (human erythrocyte; Sigma catalog no. C0663) and BChE (bovine erythrocyte, Sigma catalog no. B4186), acetylthiocholine iodide (ATCh, 99%, Fluka), 5,5′-dithiobis-(2-nitrobenzoic acid)) (DTNB, 98%, Merck), Na_2HPO_4, NaH_2PO_4 (99%), ethylenediamine, propylenediamine, 1,2-propylenediamine, 2,2-dimethylpropylenediamine, butylenediamine, and 1,2-cyclohexylanediamine (99%, Merck), *N*,*N*′-dimethylethylenediamine (95%, Alfa Aesar), piperazine (99%, Acros), homopiperazine (98%, Acros), triethylamine (99.5%, Merck), $CDCl_3$ (99%, Sigma-Aldrich), $(CH_3O)_2P(S)Cl$, $(CH_3CH_2O)_2P(S)Cl$, and $(CH_3CH_2O)_2P(O)Cl$ (97%, Sigma-Aldrich) were used as supplied. ^1H, ^{13}C, and ^{31}P spectra were recorded on a Bruker Avance DRX 500 spectrometer. ^1H and ^{13}C chemical shifts were determined relative to internal TMS and ^{31}P chemical shifts relative to 85% H_3PO_4 as external standard. Infrared (IR) spectra were recorded on a Shimadzu spectrometer (model IR-60) using KBr pellets. Melting points were obtained with an electrothermal instrument. A UV spectrophotometer was used using a Perkin-Elmer Lambda 25. The insecticide and anti-AChE activities of Tem derivatives were predicted by the Prediction of Activity Spectrum for Substances (PASS) software (version 1.193).[13] The three-dimensional X-ray structures of human AChE (PDB code 1B41) and BChE (PDB code 1POI) were chosen as the template for the modeling studies of selected compounds. The PDB files about the crystal structure of the ChE enzymes domain bound to P22303 (1B41.pdb) and P06276 (1POI.pdb) were obtained from the RCSB protein data bank (http://www.pdb.org). Molecular docking to both ChEs was carried out by using the AutoDock 4.2.3 package software.[14] The correlation analysis was performed by the Statistical Package for Social Scientists (SPSS), version 16.0 for Windows.[15] X-ray data of compound **9** were collected at 120 K on a Bruker SMART 1000 CCD area detector with graphite monochromated Mo Kα radiation (λ = 0.71073 Å) and refined by full-matrix least-squares methods against F^2 with SHELXL97.[16] CCDC 863609 contains the supplementary crystallographic data for compound **9**. These data can be obtained free of charge via http://www.ccdc.cam.ac.uk/conts/retrieving.html or from the Cambridge Crystallographic Data Centre, 12 Union Road, Cambridge CB2 1EZ, UK (fax (+44) 1223-336-033 or e-mail deposit@ccdc.cam.ac.uk).

Statistical Analysis. To identify the effect of descriptors on the activity of AChE and BChE, QSAR studies were undertaken using the model described by Hansch and Fujita.[17] The stepwise multiple linear regression (MLR) procedure was used for model selection, which is a common method used in QSAR studies for selection descriptors. MLR fits a linear model of the form (eq 1)

$$Y = b_0 + b_1X_1 + b_2X_2 + ... + b_nX_k + e \quad (1)$$

where Y is a dependent variable, X_1, X_2, ..., X_k are independent variables (descriptors), e is a random error, and b_0, b_1, b_2, ..., b_k are regression coefficients.[18] The MLR method performed by the software package SPSS 16.0 was used for selection of the descriptors. The electronic and structural descriptors (X) were obtained by both the quantum chemical calculations and theoretical studies.[19] The electronic descriptors include the highest occupied and the lowest unoccupied molecular orbital (E_{HOMO} and E_{LUMO}), electrophilicity (ω), polarizability (PL), and net atomic charges (Q). Dipole moment (μ) and molecular volume (Mv) are the structural descriptors. E_{HOMO}, E_{LUMO}, ω (expressed in terms of chemical potential and hardness), PL (the charge difference between the atoms in functional groups), Q, μ, and

dx.doi.org/10.1021/jf5011726 | J. Agric. Food Chem. 2014, 62, 5761−5771

Mv (the size and geometrical shape of the molecule, dependent on three-dimensional coordinate of atoms in a molecule) values were obtained from the DFT results by using the Gaussian 03 program package.[20] In this study, only the variables containing the information required for modeling were used. Principal component analysis (PCA) was utilized to find the relationship between the dependent and independent variables and reducing the set of independent variables (MINITAB software, version 14).[21] The linear combinations form a new set of variables, namely principal components (PCs), which are mutually orthogonal. The first PC contains the largest variance, the second new variable contains the second largest variance, and so on.[22] The validity of the QSAR model was evaluated by LOO cross-validation method, and an external data set was tested to evaluate the model. The high square value of the cross-validation coefficient (q^2) in the training set shows only a good internal validation; however, it does not automatically refer to its high validity for an external test set, because q^2 usually overestimates the validity of the model. Therefore, the QSAR model should be determined with a test set to confirm its validity. The performance of external validation was characterized by determination coefficient (R^2), standard error (S_{reg}), and q^2.[23]

Synthesis. The synthesis pathway of compounds **1**−**24** is represented in Scheme 2. For example, compound **1** was prepared by the reaction of a solution of diethylenamine (1 mmol), and triethylamine (2 mmol) in THF was added to a solution of $(OCH_3)_2P(S)Cl$ (2 mmol) in THF. After 4 h of stirring at 0 °C, the solvent was removed under vacuum, and the resulting white powder was washed with distilled solvent.

Crystal Structure Determination. A crystal suitable for X-ray crystallography was obtained from a mixture of THF at room temperature for compound **9** (Figure S1 in the Supporting Information). The solid state structure as starting point was fully optimized by using DFT calculations in the gas phase. Whereas X-ray crystallography cannot determine accurately the position of hydrogen atoms, optimization of hydrogen atom positions was performed to investigate the hydrogen bond characters in solid state structures. The H atoms of N−H groups were objectively localized in the difference Fourier synthesis and refined in isotropic approximation. To achieve this goal, the solid state structure of the crystal was modeled as a cluster, in which the target molecule is surrounded by two neighboring molecules (Figure 1). Other atoms were kept frozen during the optimization. Such computational justifications have also been used to describe well the geometry and electronic aspects of X-ray structure.[24,25] Taking into consideration the large number of atoms in the model cluster, all optimizations were performed at the B3LYP/6-311+G** level. NBO[26] analysis was performed to compare the electronic features of gas phase structures of compound **9** with those of the model clusters at the B3LYP/6-311+G** level. Natural population analysis (NPA) was performed at the same level by using the Reed and Weinhold scheme.[27] As part of this study deals with investigation of the hydrogen bonds between S···H atoms, AIM analysis at the B3LYP/6-311+G** level has much importance. Two hydrogen bonds with different lengths were observed in compound **9**. The hydrogen-bonding energies were calculated on the basis of energy difference between the hydrogen-bonded trimer and its fragments, as represented in the equation $E_{HB} = E_{trimer} - (E_{dimer} + E_{monomer})$, where dimer is composed of two monomers (central and neighboring molecules on the right, in Figure 1). Then the hydrogen-bonding energies were corrected for basis set superposition error (BSSE) using the counterpoise method.[24,28] All quantum chemical calculations were carried out by using the Gaussian 03 program package.[29]

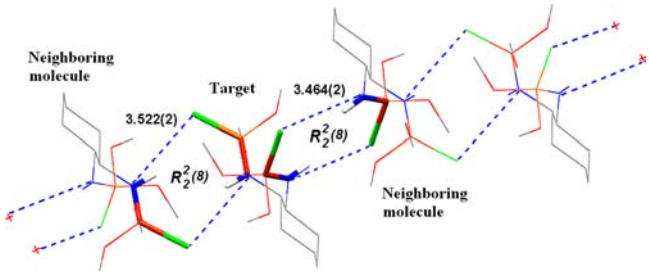

Figure 1. Illustration of $R_2^2(8)$ graph sets in $(CH_3O)_2P(S)NH(C_6H_{10})NHP(O)(OCH_3)_2$; a model to describe the hydrogen-bonded cluster for DFT calculations, in which the molecule is the target molecule in the center. A similar model was considered for another molecule, in which the molecule in the center is the target molecule.

Cholinesterase Assay. Human cholinesterase activity measurements were performed essentially according to the method of Ellman.[11] The reaction was carried out at 37 °C in millimolar phosphate buffer (Na_2HPO_4/NaH_2PO_4, pH 7.4) containing the AChE enzyme (10 μL volume, diluted 100 times in phosphate buffer, pH 7.4), DTNB (10^{-4} M concentration), and ATCh (1.35×10^{-4} M concentration). Each compound was dissolved in dimethyl sulfoxide (DMSO, 99%, Merck), which was then added to the buffer for in vitro cholinesterase assays. The highest concentration of DMSO used in the assays was 5%. In the independent experiments without the inhibitor, 5% DMSO had no effect on the inhibition activity of the enzyme. The absorbance change at 37 °C was monitored with the spectrophotometer at 412 nm for 3 min, and three replicates were run in each experiment (Supporting Information Figure S2). In the absence of inhibitor, the absorbance change was directly proportional to the enzyme level. The reaction mixtures for determination of IC_{50} values (the median inhibitory concentration) consisted of DTNB solution, 100 μL; inhibitor, x μL; acetylthiocholine iodide (ATCh) solution, 40 μL; phosphate buffer, $(850 - x)$ μL; and AChE (human erythrocyte; Sigma catalog no. C0663) solution, 10 μL (26.7 u). The activity of BChE (bovine erythrocyte, Sigma catalog no. B4186) was determined the same as the AChE activity by measuring the concentration of thiocholine, which reacted with DTNB after hydrolysis of BTCh. The lyophilized BChE was diluted with 100 mM phosphate buffer (pH 7.4) for use in the activity assay. The plot of V_I/V_0 (V_I and V_0 are the activity of the enzyme in the presence and absence of inhibitors, respectively) against log[I] (where [I] is the inhibitor's concentration) gave the IC_{50} values of 12 compounds **1**−**4**, **6**−**9**, **15**, **17** **18**, **20**, and **24** (as anti-AChE) and 11 compounds **1**, **2**, **4**, **6**−**11**, **13**, **15**, and **24** (as anti-BChE) (Table 1; Figure 2).

Inhibition Mechanism Study. One of the ways in which the inhibition of enzyme-catalyzed reactions can be discussed is in terms of the following general scheme (eq 2): It is assumed that the enzyme-

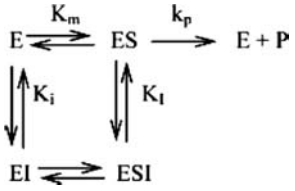

containing complexes are in equilibrium with each other, that is, the breakdown of ES to generate product does not significantly disturb the equilibrium. In the present work, all data obtained for a particular system were analyzed using the mixed model of enzyme inhibition as described in the equation

$$\frac{1}{V_0} = \frac{K_m\left(1 + \frac{[I_0]}{K_i}\right)}{V_{max}}\frac{1}{[S_0]} + \frac{\left(1 + \frac{[I_0]}{K_I}\right)}{V_{max}} \quad (2)$$

where V_0 is the initial reaction rate, V_{max} is the maximum reaction rate, K_m is the Michaelis constant for the substrate to the enzyme, and K_i and K_I are the inhibition constants for binding of the inhibitor to the enzyme or to the enzyme−substrate complex, respectively. In this model, a mixed inhibitor displays finite but unequal affinity for both the free enzyme (E) and the ES complex; hence, the dissociation constants from each of these enzyme forms inhibitors must be considered in their kinetic analysis.[12,30] K_i and K_I were determined using the secondary plots as described by the following equation:

dx.doi.org/10.1021/jf5011726 | J. Agric. Food Chem. 2014, 62, 5761−5771

Table 1. Experimental, Prediction, and External Validation Steps of the Biological Activity of the BPAT

	prediction (PASS)			experimental				external validation	
				IC_{50}		$\log(1/IC_{50})_{exptl}$		$\log(1/IC_{50})_{pred}$[a]	
no.	anti-AChE	carcinogenic	insecticide	AChE	BChE	AChE	BChE	AChE	res[b]
1	0.474	0.537	0.607	2546.83	273.53	−3.406	−2.437	−3.323	0.083
2	0.421	0.493	0.567	674.53	6338.70	−2.829	−3.802	−3.102	0.273
3	0.702	0.813	0.610	5.01		−0.700		−0.655	0.045
4	0.589	0.451	0.566	2805.43	7481.69	−3.448	−3.874	−2.357	1.091
5	0.420	0.477	0.582						
6	0.586	0.478	0.572	5636.37	175.39	−3.751	−2.244	−3.712	0.039
7	0.571	0.631	0.635	912.01	164.81	−2.960	−2.244	−0.616	2.344
8	0.466	0.514	0.561	1119.44	874.98	−3.049	−2.942	−0.645	2.404
9	0.527	0.547	0.580	602.56	891.25	−2.780	−2.950	−2.818	0.038
10	0.435	0.221	0.582		717.80		−2.855		
11	0.409	0.228	0.556		520.00		−2.716		
12	0.632	0.565	0.582						
13	0.553	0.000	0.546		346.73		−2.540		
14	0.409	0.206	0.571						
15	0.483	0.466	0.579	44.98	149.62	−1.653	−2.175	−1.715	0.062
16	0.491	0.249	0.558						
17	0.592	0.224	0.569	4055.08		−3.608		−3.701	0.093
18	0.540	0.000	0.524	11402.50		−4.057		−3.584	0.473
19	0.821	0.366	0.527						
20	0.680	0.000	0.532	3467.37		−3.540		−3.846	0.306
21	0.565	0.000	0.558						
22	0.677	0.000	0.539						
23	0.442	0.807	0.496						
24	0.569	0.232	0.507	363.08	851.14	−2.560	−2.930	−3.683	1.123

[a]Predictive activities were calculated using the QSAR model. [b]Residual for molecule is the difference between the experimental and predicted property.

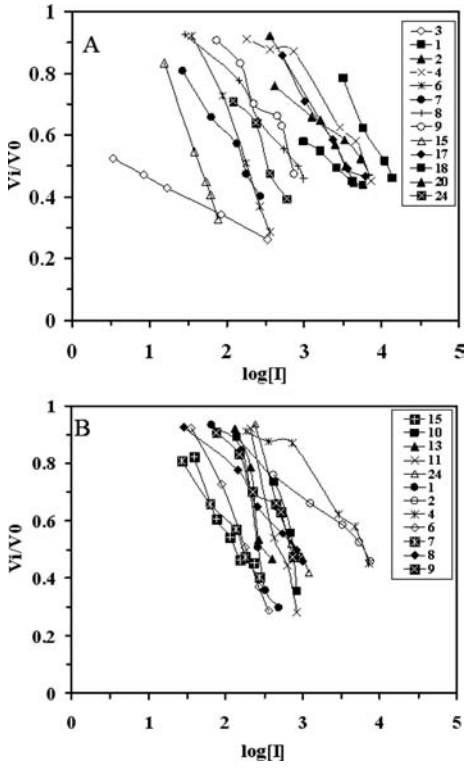

Figure 2. Plot of V_I/V_0 against log[I] for inhibitors. V_I and V_0 are the AChE (A) and BChE (B) enzyme's activities (OD min^{-1}), and [I] is the inhibitor concentration (μM).

$$\frac{1}{V'_{max}} = \frac{\left(1 + \frac{[I_0]}{K_I}\right)}{V_{max}} \quad (3)$$

slope for inhibited reaction

$$= \text{slope for uninhibited reaction} \times \left(1 + \frac{[I_0]}{K_i}\right)$$

Hence, a secondary plot of $1/V'_{max}$ against $[I_0]$ will be linear, and the intercept on $[I_0]$ axis gives $-K_I$; a graph of the slope of primary plot against $[I_0]$ will also be linear, and the intercept on $[I_0]$ axis gives $-K_i$. The Lineweaver−Burk plots related to the reversible inhibitory effects of compounds showed a typical pattern of mixed inhibition (Figure 3). The K_m and V_{max} values were calculated in the absence and presence of inhibitor from which the secondary plots were obtained, and the equilibrium dissociation constants, K_i and K_I, were calculated (Table 2). A mixed inhibitor displays affinity for both the free enzyme (K_i) and the enzyme−substrate complex (K_I). Thus, mixed-type inhibitors interfere with the substrate binding (increase K_m) and hamper the catalysis in the ES complex (decrease V_{max}). When $K_I > K_i$, the inhibitor preferentially binds to the free enzyme, and the plots cross to the left of the $1/V_0$ axis, but above the $1/[S_0]$ axis (Figure 3). In this situation, it is also termed competitive noncompetitive inhibition.

RESULTS AND DISCUSSION

Spectral Study. The ^{31}P NMR chemical shift at room temperature in $CDCl_3$ appears in the ranges of 68.31−78.82 ppm for P═S derivatives and 5.42−8.64 ppm for P═O derivatives. The ^{31}P NMR spectra of compounds **2**, **9**, **11**, and **18** appeared as two separate signals. The ^1H NMR spectrum of compound **3** revealed that two doublets at 2.76 ($^3J_{PNH}$ = 10.0 Hz) and 3.63 ($^3J_{POH}$ = 15.0 Hz) ppm are related to the methyl

dx.doi.org/10.1021/jf5011726 | J. Agric. Food Chem. 2014, 62, 5761−5771

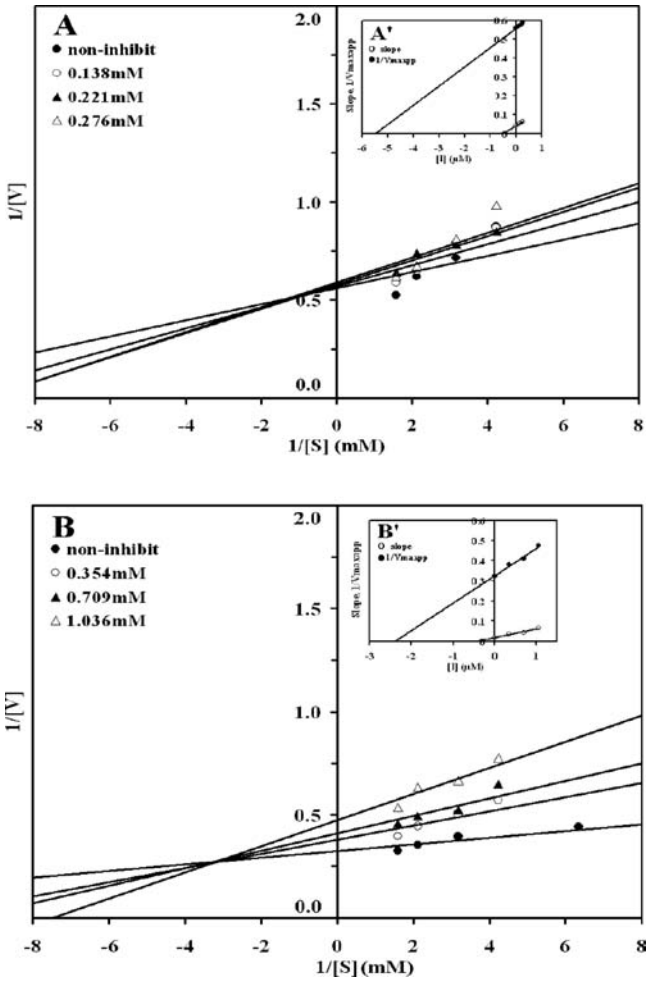

Figure 3. (A, B) Plot of 1/[V] against 1/[S] for the inhibitors **1** and **2** against BChE and AChE activation without inhibitor. [V] is the enzyme activity (OD min^{-1}), and [S] is the ATCh concentration (mM). (A′, B′) Steady state inhibition of AChE by compounds **1** and **2**. Secondary replots of the Lineweaver–Burk plot: $1/V_{max\ app}$ or slope versus various concentrations of the inhibitor.

Table 2. Experimental Parameters of the AChE and BChE Activities of Titled Compounds

enzyme	no.	K_m (mM)	K_i^c (mM)	K_I^b (mM)	V_m (mM/min)	inhibition mechanism
BChE	**1**	0.107	1.537	5.338	1.696	MT[c]
	2	0.133	0.362	2.286	2.108	MT
	3	0.084	1.925	1.137	2.716	MT
AChE	**4**	0.095	2.913	1.515	2.038	MT
	7	0.080	0.121	0.377	2.194	MT
	8	0.075	0.317	1.541	1.996	MT

[b]K_i = inhibitor affinity for the free enzyme; [c]K_I = inhibitor affinity for enzyme–substrate complex. [c]MT, mixed type.

proton in the NCH_3 and OCH_3 groups, respectively. The ^1H NMR spectra of compounds **9**, **16**, and **24** exhibited two signals for the methylene protons of the six-membered piperazinyl rings. Two protons of the NH group of all compounds exhibited as a multiple peak in the ranges of 3.48–5.37 ppm for P═S derivatives and 3.06–3.88 ppm for P═O derivatives. The ^{13}C NMR spectra of compounds **9**, **16**, and **24** indicated three separate peaks for the six carbon atoms that are due to different orientations of the aliphatic six-membered rings. The analysis of the IR spectra indicated that the fundamental ν(P═S) stretching modes for compounds **1**–**16** appeared in the range of 770.4–955.1 cm^{-1}. The P═O stretching frequencies for compounds **17**–**24** were exhibited over the range of 1223.8–1252.1 cm^{-1}. Moreover, the N–H stretching frequencies for all compounds were observed in the range of 3189.1–3580.0 cm^{-1}.

H-Bond Analysis. The crystal data and the details of the X-ray analysis of compound **9** are given in the Supporting Information (Table S1). The phosphorus centers are in typical tetrahedral environments. P═S bond lengths of 1.9288(9) and 1.9316(9) Å were observed for P(1)—S(1) and for P(2)—S(2), respectively, in $(CH_3O)_2P(S)NH(C_6H_{10})NHP(S)(OCH_3)_2$ (**9**). It seems that the difference in the bond lengths is correlated to the various orientations of cyclohexyldiamine rings and OCH_3 groups. These orientations lead to the creation of different hydrogen-bonding patterns between the P═S and N—H functional groups. The one-dimensional polymeric chains form in the crystal lattice with cyclic $R_2^2(8)$ motifs in which the monomers are connected to each other via two P═S···H—N hydrogen bond distances of 3.464(2) and 3.522(2) Å (Figure 1; Table 3). The $R_Y^X(Z)$ graph-set notation is descriptive of a Z-membered ring produced by the X hydrogen bonds between the Y donor–acceptor units.[31,32] Weak interactions, particularly P(2)–S(2)···H(3)–C(3) (2.970 Å) and P(2)–S(2)···H(2)–C(2) (2.902 Å), create different hydrogen-bonding lengths of the motifs. The large atomic radius and the low electronegativity of sulfur atoms decreased the strength of the hydrogen bonding between P═S and NH. The electronic parameters of the hydrogen-bonded clusters of compound **9** were calculated by AIM and NBO methods. The results of AIM and NBO analyses for the mentioned clusters are presented in Table 3 and Figure 1. As shown, the bond lengths in this cluster are equal to those obtained from the X-ray structures, except for the C–H and N–H bonds, because the optimizations have been performed only for the hydrogen atoms' positions. Also, the donor–acceptor distances for the hydrogen bonds in the model cluster are equal to the experimental values. The results of AIM analysis show that the electron density (ρ) value at the bond critical point (bcp) of S(1)···H(1) (0.104 $eÅ^{-3}$) bond path is larger in magnitude than the that calculated for the S(2)···H(2) (0.093 $eÅ^{-3}$) in the model cluster. The smaller ρ value at the bcp of the N–H bond confirms the presence of the stronger hydrogen bonds in P(1)–S(1)···(1)H–N(1) with the linear N–H···S contact angle in comparison with the values obtained for P(2)–S(2)···(2)H–N(2). The ρ value at the bcp of N–H bonds is 2.24 $eÅ^{-3}$ for the fully optimized structure in the gas phase, which decreases to 2.211 and 2.217 $eÅ^{-3}$, respectively, in N(1)–H(1) and N(2)–H(2). The mean N–H distance increases from the isolated molecules from 1.012 to 1.017 Å in their hydrogen bonded model cluster. The electronic delocalization of $Lp(S)_i \rightarrow \sigma^*(N–H)_j$ occurs when the hydrogen bonds are formed between the subunits i and j within a cluster. Such an electronic effect leads to weakening of the N–H bond. It has been previously explained that the stabilizing energy E^2 increases by a decrease in the donor–acceptor distance of hydrogen bond.[32] The stabilizing energies E^2 of $Lp(S)_i \rightarrow \sigma^*(N–H)_j$ electron density transfer in P═S···H–N hydrogen bonds in the model cluster have been calculated as 19.94 and 16.34 kJ mol^{-1}, respectively. This is in agreement with the values of distance for these hydrogen bonds in two P(1)—S(1)···(1)H—N(1)

dx.doi.org/10.1021/jf5011726 | J. Agric. Food Chem. 2014, 62, 5761–5771

Table 3. Hydrogen-Bond Data for the X-ray Structure (Values in Brackets), Model Cluster (at B3LYP/6-311+G), Charge Densities (from AIM Analysis), and Delocalization Energy (from NBO**

					ρ at the bcp (eÅ^{-3})			
D—H···A	d(N—H)	d(H···S)	d(N···S)	∠NHS	N—H	H···S	$E^{(2)a}$	$E_{HB}{}^{b}$
N(1)−H(1N)···S(1)[c]	[1.016] 0.850	[2.50] 2.70	[3.464(2)]	[157.1] 151.0	0.328	0.104	19.94	−33.3
N(2)−H(2N)···S(2)[d]	[1.017] 0.880	[2.55] 2.71	[3.522(2)]	[155.7] 154.0	0.329	0.093	16.34	−42.4

[a]Stabilizing energy E^2 refers to the effect of $Lp(X_P)_i \rightarrow \sigma^*(N-H)_j$ delocalization. [b]Binding energy in kJ mol^{-1} for N—H···S hydrogen bonds. [c]$-x+2, -y+1, -z$. [d]$-x+2, -y, -z+1$.

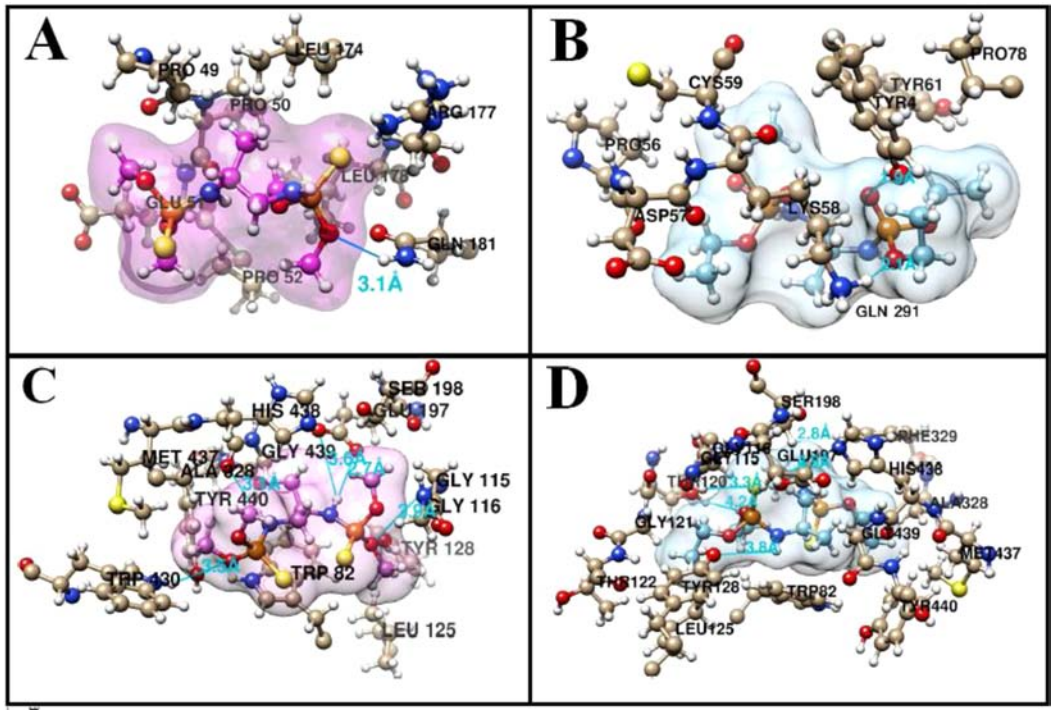

Figure 4. (A, B) 2D model of H-bond formation in the polar charged site, between the P—OCH_3 and P—OC_2H_5 oxygen **2** (A) and **18** (B) and the hydrogen of H−N of GLN181 (d = 3.131 Å) and GLN291 (d = 2.100 Å) of AChE enzyme. (C, D) 2D model of the hydrogen atoms of the N—H group of compounds **2** (C) and **11** (D) forming an H-bond with the C═O group containing GLU197 (d = 2.760 Å) and (d = 2.822 Å) of BChE enzyme.

(3.464(2) Å) and P(2)−S(2)···(2)H—N(2) (3.522(2) Å) models. The hydrogen-bonding energy in the P(1)—S(1)···(1)H—N(1) model (−33.3 kJ mol^{-1}) is smaller than the value calculated for P(2)—S(2)···(2)H—N(2) (−42.4 kJ mol^{-1}), although the stabilizing energies E^2 of P═S···H—N hydrogen bonds are larger in the former (Table 3).

It is noteworthy that the term E^2 refers to the stabilization energy of electronic delocalization between the donor−acceptor orbital and differs from the hydrogen-bonding energy. The molecule−molecule interaction energy is the sum of the total attractive and repulsive forces between two hydrogen-bonded fragments. The results of AIM analysis revealed some critical points with very small ρ values for the C—$H_{(methyl)}$···S(2)—P(2) and C—$H_{(cyclohexane)}$···S(2)—P(2) contacts. It can be said that the steric repulsion between the diaminocyclohexane, OCH_3 group, and P═S bond in the model crystal leads to a decrease in P(2)—S(2)···(2)H—N(2) hydrogen-bonding energy rather than the P(1)—S(1)···(1)H—N(1) model.

Prediction of Biological Potential. PASS software predicts 900 types of biological activities on the basis of the structural formula.[33] The default list of predictable biological activities (P_a) includes the main and side pharmacological effects, molecular mechanisms, and specific toxicities. The PASS prediction results for a compound are presented as a list of activity names and probability activity (Pa) values. The Pa values are interpreted as if Pa > 0.7, 0.5 < Pa < 0.7, and Pa < 0.5; then the chance of finding this activity in the experiments is high, low, and lower, respectively.[34,35] Insecticide potential, anti-AChE activity, and carcinogenic effect of 24 newly designed molecules were obtained by using PASS software (Table 1). Table 1 shows that anti-AChE and carcinogenic properties of compounds decrease owing to the change of $(CH_3O)_2P$═S to $(C_2H_5O)_2P$═S in compounds **1**−**16**. Furthermore, the replacement of P═S in **10**−**16** to P═O in **17**−**24** increased the anti-AChE property and decreased the carcinogenic activity. The insecticidal properties of all compounds are predicted in the range of 0.496−0.635. The comparison of experimental data and the prediction of anti-AChE activities are shown in Figure S2A in the Supporting Information. As shown in Figure S2B in the Supporting Information, a linear relationship gives the plot of probable insecticide potential against anti-AChE activity. To test the anti-ChE activity of the synthesized compounds, we evaluated the inhibitory potential of titled compounds against AChE and BChE enzymes.

dx.doi.org/10.1021/jf5011726 | J. Agric. Food Chem. 2014, 62, 5761−5771

Bioassay. The inhibition constant (IC_{50}) values of AChE against compounds **1**−**4**, **6**−**9**, **15**, **17**, **18**, and **20** were in the range of 5.01−11402.50 μM (Table 1). Compound **3** displayed the most potent inhibitory activity (IC_{50} = 5.01 μM). The inhibitory potential of compound **15** with OC_2H_5 was more greater than that of **7** with an OCH_3 substituent (Table 1). A review of the literature demonstrates that the inhibitory potential of monophosphoramides (P═O moiety) is higher than that of the monophosphoramidothiates (P═S moiety),[36] whereas comparison of bisphosphoramidothioate **2** (IC_{50} = 674.53 μM) and bisphosphoramide **18** (IC_{50} = 11402.50 μM) reveals the inhibitory activity of P═S to be greater than that of P═O in contrast with the AChE. In the present work, the synthesized compounds **1**, **2**, **4**, **6**−**11**, **13**, and **15** showed inhibition of BChE with IC_{50} values between 149.62 and 7481.69 μM. In general, the inhibitory activities of Tem derivatives with the P═S moiety were better than those of derivatives with the P═O moiety. The mixed-type and reversible mechanisms of these compounds were evaluated by Lineweaver−Burk plots (Table 2). To gain a better understanding of the inhibitory potential of the synthesized compounds and to study the reversible mechanism in more detail, it was necessary to examine the interaction of the Tem derivatives with the ChE structures by using the molecular docking method.

Molecular Docking Study. The interactions between Tem derivatives and AChE receptor were achieved by molecular docking, which can facilitate the selection of appropriate molecular parameters in the subsequent QSAR studies. The binding models of titled compounds against AChE and BChE are depicted in Figure 2. They are located in the active site gorge of both AChE and BChE so as to maximize the favorable contacts. The hydrogen bonds and van der Waals forces are the main features of the interactions of compounds **2** (Figure 4A) and **18** (Figure 4B) with the polar charged site of AChE, as well as the interactions of **2** (Figure 4C) and **11** (Figure 4D) with the esterastic site of BChE. H-bond formation in the polar charged site was found to occur between the P—OCH_3 and P—OC_2H_5 oxygen of compounds **2** (P═S) and **18** (P═O) with the hydrogen of H—N of GLN181 (d = 3.131 Å) and GLN291 (d = 2.100 Å), respectively. Panels C and D of Figure 4 show the 2D representation of the interaction mode of compounds **2** and **11** at the active site of BChE. It can be clearly seen from Figure 4C,D that the hydrogen atoms of the N—H group of compounds **2** and **11** form an H-bond with the C═O group containing GLU197 (d = 2.760 Å) and (d = 2.822 Å) moieties. The docking data including inhibition constant (K_i), electrostatic energy (E_{elect}) and the rest of the H-bonds distances are given for the ChEs in Table S3 in the Supporting Information. Panels A and A′ of Figure 3 indicate that the increase of the H-bond distances of RO···H—N enhances their inhibitory potential, whereas these correlations are reversed in the interaction between BChE and ligands (Figure 5B,B′). To continue work, the QSAR technique was used to find the effective electronic and structural parameters.

QSAR Analysis. QSAR studies were done to recognize the effect of descriptors on the activity of AChE and BChE enzymes. The stepwise MLR procedure, which is a common method used in QSAR studies, was used for model selection. The electronic and structural descriptors were obtained by quantum chemical calculations (Supporting Information Table S3). The number of independent variables is equal to the training set compounds, as shown in Tables 1 and S3

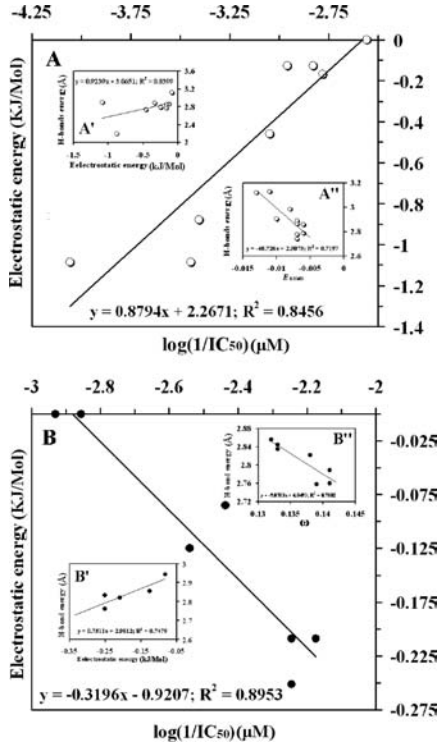

Figure 5. Linear plot of the electrostatic energy of docking analysis against $\log(1/IC_{50})$ for AChE (A) and for BChE (B); linear plot of the H-bond energy against the electrostatic energy of docking analysis for AChE (A′) and for BChE (B′); linear plot of the H-bond energy of docking analysis against ELUMO for AChE (A″) and against ω for BChE (B″).

(Supporting Information). Therefore, the PCA method was used to reduce the independent variables. The variable selection in PCA was performed by using the Fisher's weights approach,[37] and the results are summarized as eqs 4a and 4b:

$$PC_1 = +0.411Q_{P(1)} + 0.411Q_{P(2)} - 0.400Q_{X(S,O)} - 0.080Q_N + 0.410PL_{p=X} - 0.407E_{HOMO} - 0.052E_{LUMO} + 0.316\omega + 0.142\mu + 0.035Mv \quad (4a)$$

$$PC_2 = +0.064Q_{P(1)} + 0.053Q_{P(2)} - 0.042Q_{X(S,O)} + 0.547Q_N + 0.121PL_{p=X} - 0.028E_{HOMO} + 0.500E_{LUMO} - 0.334\omega + 0.343\mu + 0.035Mv \quad (4b)$$

The results showed the total variances of the first and second factor PC were 51.4 and 19.0%, respectively. Figure S3 in the Supporting Information shows the score and the loading plots of $PC_1 \times PC_2$. The score plot shows that separation of the compounds with P═O (right side) and P═S (left side) groups has been provided by PC_1, which contains the majority of the variance. From the above equations, it is deduced that the electronic parameters (Q_P, Q_X, Q_N, $PL_{P=X}$, E_{LUMO}, E_{HOMO}, and ω) are the largest compared to the structural parameters (μ and Mv). Consequently, these nine descriptors with higher correlation coefficients were selected to carry out the stepwise multiple linear regression (MLR) analysis, which led to an

dx.doi.org/10.1021/jf5011726 | J. Agric. Food Chem. 2014, 62, 5761−5771

optimal QSAR equation based on the anti-AChE potency (eq 5):

$$\log(1/IC_{50}) = +0.017\mu + 64.805Q_P + 1.690Q_{X(S,O)} - 8.967Q_N - 31.967PL_{P=X} - 25.193E_{HOMO} - 217.942E_{LUMO} - 243.834\omega + 0.016Mv - 33.690 \quad (5)$$

$$n = 13;\ R^2 = 0.721;\ S_{reg} = 0.966;\ F_{statistic} = 0.862$$

n is the number of compounds, R^2 is the determination coefficient of regression, S_{reg} is the standard deviation of regression, and $F_{statistic}$ is Fisher's statistic.[38] The variables with a high value of variance inflation factor (VIF > 10) are candidates for exclusion from the model.[39] The low determination coefficient value (R^2 = 0.721) and high residual value (S_{reg} = 0.966) with high VIF value (see Table 4) are associated with the multicollinearity problem. The improvement in eq 2 was carried out by omitting compounds **7**, **8**, and **24** from the training set compounds and replacing E_{LUMO} with ω and E_{HOMO}, as well as Q_P with $PL_{P=X}$ and Q_X. The linear regression was performed using the remaining five parameters that yielded the following model with increasing of R^2 = 0.922 and decreasing of S_{reg} = 0.438 (eq 6):

Table 4. VIF[a] Values for the QSAR Equations

	AChE		BChE	
independent variable	eq 2	eq 2	eq 3	eq 5
Q_P	5154.635	4.060	2416.392	2.122
$Q_{X(S,O)}$	82.623		70.221	
Q_N	46.154	12.411	31.865	3.105
$PL_{P=X}$	6368.558		3547.065	
E_{HOMO}	1677.977		313.179	
E_{LUMO}	1529.029	3.422	468.766	
ω	3249.905		688.616	2.629
μ	7.195	4.140	26.590	1.281
Mv	6.540	6.665	10.261	2.635

[a]VIF = $1/(1 - R_i^2)$, where R_i is the multiple correlation coefficient of the ith independent variable on all of the other independent variables.

$$\log(1/IC_{50}) = +0.175\mu + 0.845Q_P + 29.699Q_N - 129.903E_{LUMO} - 0.019Mv + 27.921 \quad (6)$$

$$n = 10;\ R^2 = 0.922;\ S_{reg} = 0.438;\ F_{statistic} = 9.473$$

The correlating parameters have VIF < 10; thus, there is no colinearity problem (Table 4). In this equation, the inhibitory potency of AChE is influenced mainly by the electronic parameters. E_{LUMO} with the coefficient value of −129.903 has the highest contribution to $\log(1/IC_{50})$ rather than the structural parameters. The negative sings of E_{LUMO} in $\log(1/IC_{50})$ disclose that the compound with lower E_{LUMO} is indicative of higher toxicity against the AChE enzyme. The net charge of the N−H nitrogen (Q_N) with the coefficient value of +29.699 reveals the highest effect of function on the inhibitory potential rather than the net charge of P═O phosphorus (+0.845). The correlation matrix was used to determine the interrelationship between the independent variables. A high interrelationship was observed between E_{LUMO} and Q_N (r = +0.456) (Table 5). Therefore, compound **3** with Q_N = −0.893 and compound **18** with Q_N = −1.031 showed the highest and the lowest inhibitory potentials, respectively. Consequently, the net charge of the nitrogen atom is able to control the influence of molecular orbital energy in the inhibition of human AChE. Also, the interaction of BChE as a secondary target was investigated against the tested compounds (**1**−**24**), and the same procedures were carried out. The QSAR modification model based on anti-BChE potency produced the following equation:

$$\log(1/IC_{50}) = -0.148\mu + 7.065Q_P + 1.720Q_{X(S,O)} + 0.430Q_N + 0.469PL_{P=X} + 100.702E_{HOMO} - 100.525E_{LUMO} - 104.965\omega - 0.002Mv + 22.751 \quad (7)$$

$$n = 12;\ R^2 = 0.566;\ S_{reg} = 0.862;\ F_{statistic} = 0.290$$

Table 4 shows that the regression equation is not favorable with VIF > 10. The improvement in eq 7 was performed by excluding compounds **1** and **24** from the selected compounds and replacing ω with E_{LUMO} and E_{HOMO}, as well as Q_P with $PL_{P=X}$ and Q_X. Consequently, a new multiple regression resulted without collinearity (eq 8):

$$\log(1/IC_{50}) = -0.116\mu + 3.768Q_P - 0.32Q_N - 106.212\omega + 0.004Mv + 3.397 \quad (8)$$

$$n = 10;\ R^2 = 0.848;\ S_{reg} = 0.352;\ F_{statistic} = 4.479$$

The model described by eq 8, similar to eq 6, depicts the share of molecular orbital energy in the inhibition of BChE. The most effective variable in the interaction of BChE and Tem derivatives was ω, with the coefficient value of −106.212. The interrelationships between the variables and the correlation matrix results are presented in Table 5. The high interrelationship between ω and Q_P (r = +0.680) shows that Q_P controls the affect of molecular orbital energy in the inhibition of human BChE. Compounds **5** (Q_P = +2.027) and **2** (Q_P = +1.997) are in order of the highest and the lowest inhibitory potentials.

Table 5. Correlation Matrix for the Anti-AChE and Anti-BChE Parameters and the Selected Variables in Equations 6 and 8

	AChE						BChE					
selected variable	μ	Q_P	Q_N	E_{LUMO}	Mv	selected variable	μ	Q_P	Q_N	ω	Mv	
μ	1.000					μ	1.000					
Q_P	+0.307	1.000				Q_P	+0.062	1.000				
Q_N	−0.520	−0.427	1.000			Q_N	+0.304	−0.204	1.000			
E_{LUMO}	+0.101	−0.209	+0.459	1.000		ω	−0.268	+0.680	−0.407	1.000		
Mv	+0.105	+0.417	+0.404	−0.033	1.000	Mv	+0.246	+0.077	+0.734	−0.049	1.000	

dx.doi.org/10.1021/jf5011726 | J. Agric. Food Chem. 2014, 62, 5761−5771

DFT-QSAR models of AChE and BChE revealed that changing in the net charge of nitrogen and phosphorus atoms contributes an important function in the inhibition mechanism of AChE and BChE, respectively. The above results are relatively good, but the validity of QSAR models and docking output must be examined by NBO and LOO cross-validation methods.

Validation of MLR-QSAR Model. The LOO cross-validation method was used for the training sets to select the optimum values of parameters. This procedure consists of three stages: (i) removing one sample from the training set, (ii) constructing the equation on the basis of only the remaining training data, and (iii) testing of the model on the removed and innovative samples.[40] A total of 10 samples was used as a training set, and the remaining compounds (**7**, **8**, and **24**) for AChE-QSAR (eq 6) were adopted as a test set for validating the models. A new equation is proposed to determine the outliers using LOO cross-validation coefficient q^2_{n-i}, which is equal to the q^2 of compound i computed by the new cross-validation procedure after leaving this datum from n compounds. The compound with an unduly high q^2_{n-i} value can be considered as an outlier, and the compound with a low value can be taken as an influential point. Compound **4** has too large a q^2_{n-i} value in the training set, so this compound can be confirmed to be an outlier from the AChE-QSAR model. After omission of compound **4**, two optimal models are obtained (eq 9):

$$\log(1/\mathrm{IC}_{50}) = +0.254\mu + 0.063Q_{\mathrm{P}} + 30.879Q_{\mathrm{N}} - 191.801E_{\mathrm{LUMO}} - 0.018\mathrm{Mv} + 29.838 \quad (9)$$

$$n = 9;\ R^2_{\mathrm{adj}} = 0.907;\ S_{\mathrm{reg}} = 0.335;\ r = 0.10$$

$$F_{\mathrm{statistic}} = 16.59;\ q^2 = 0.965;\ P < 0.0214$$

q^2 is the square of the LOO cross-validation coefficient. A good QSAR model has characters of large F, small r, and S_{reg}, low P value, and R^2 and q^2 values close to 1.[41] Therefore, the above-established eq 9 shows appropriate statistical quality. To check the validity of eq 9, we selected our previously omitted compound (**4**) as the test set; the dependent and independent variables with their residuals of test set compounds are shown in Table 1. Table 1 and particularly residuals data show that the inhibition results are the same in the empirical and prediction techniques. Figure 6 indicates that the predicted values of $\log(1/\mathrm{IC}_{50})$ are in good agreement with the experimental ones. The integrity was validated by the determination coefficient of $R^2 = 0.851$ with the residuals between the training and testing sets.

Natural Bond Orbital Analysis. The stabilization energy (E^2) data clarify that electron transfers lead to change in the net charge of phosphorus and nitrogen atoms and, accordingly, alter the inhibitory properties of compounds against enzymes. The NBO analysis reveals an electronic delocalization between the lone pair of X atom in the P = X(O, S) group, $\mathrm{Lp}(\mathrm{X_P})$, and the vacant σ^* ($\mathrm{P{-}O_2}$) orbital. Stabilization energies of 9.211 kJ/mol for compound **2** with the P═S moiety and 103.706 kJ/mol for compound **18** with the P═O moiety were obtained for the $\mathrm{Lp}(\mathrm{X_P}) \rightarrow \sigma^*$ ($\mathrm{P{-}O_2}$) interaction (Table 6). This interaction increases the electron density of OR (R = $\mathrm{CH_3}$ and $\mathrm{C_2H_5}$) oxygen atom and raises the hydrogen bond energy of $(\mathrm{R{-}O})_{\mathrm{ligand}}\cdots(\mathrm{H{-}N})_{\mathrm{enzyme}}$ type (Figure 4). Compared to **18**, compound **2** has a higher inhibitory potential in contrast to AChE. The H-bond energy of $\mathrm{CH_3{-}O\cdots H{-}N}$ (GLN181) for compound **2** is lower than the energy of $\mathrm{C_2H_5{-}O\cdots H{-}N}$ (GLN291) for compound **18**. Hence, there is not a direct correlation between the E^2 of $\mathrm{Lp}(\mathrm{X_P}) \rightarrow \sigma^*$ ($\mathrm{P{-}O_2}$) interaction and the hydrogen bond energy against the AChE activity. In other words, compound **2** with E^2 = 18.601 kJ/mol and compound **18** with E^2 = 16.218 kJ/mol for the $\mathrm{Lp}(\mathrm{X_P}) \rightarrow \sigma^*$ ($\mathrm{P{-}N_1}$) interaction (Table 6) prove that the negative charge of the nitrogen atom (Q_{N}) versus the hydrogen bond energy of $(\mathrm{R{-}O})_{\mathrm{ligand}}\cdots(\mathrm{H{-}N})_{\mathrm{protein}}$ affects the $\log(1/\mathrm{IC}_{50})$ factor. For instance, compound **3** with the highest E^2 and Q_{N} behaves as a strong inhibitor in the process of the inhibition of AChE. In addition, the high E^2 = 16.678 kJ/mol of $\mathrm{Lp}(\mathrm{N_1}) \rightarrow \sigma^*(\mathrm{P{-}O_2})$ interaction for compound **18** compared to compound **2** (E_2 = 12.582 kJ/mol) leads to the increase of the electron density of the oxygen atom on the alcohol substituent and consequently to the rise of the energy of the hydrogen bonding and to the decline of the inhibition potential. By investigating the interaction mechanism of ligand and BChE enzyme, it can be said that the $\mathrm{Lp}(\mathrm{O_2}) \rightarrow \sigma^*(\mathrm{P{-}N_1})$ interaction of selected compounds (**2** and **11**) increases the electron density of the N–H nitrogen and raises the hydrogen bond energy of $(\mathrm{N{-}H})_{\mathrm{ligand}}\cdots(\mathrm{O{=}C})_{\mathrm{enzyme}}$ type (Figure 4). The H-bond energy of $\mathrm{N{-}H\cdots O{=}C}$ (GLU197) for compound **2** is higher than that of **11**, whereas compound **2** has a lower inhibitory potential compared to compound **11** in contrast to BChE. Thiss means

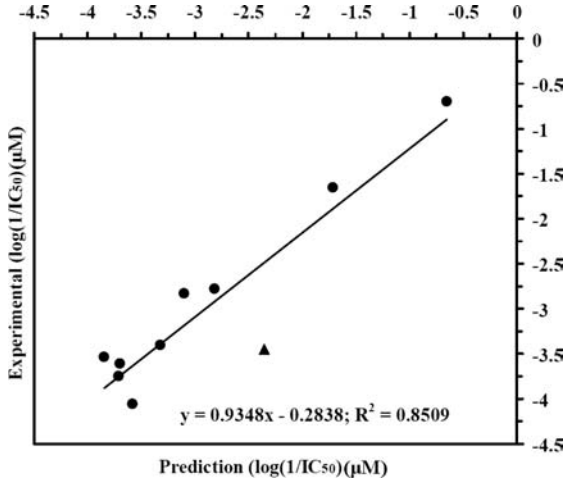

Figure 6. Plot of predicted activities versus experimental ones for the QSAR model, in which 10 compounds are the training set (●) and corresponding one compound is the test set (▲).

Table 6. Stabilization Energies (E^2) of the NBO Analysis of Some of the Compounds

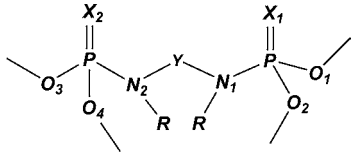

	E^2 (kJ/mol)			
electronic delocalization	**2**	**3**	**11**	**18**
$\mathrm{Lp}(X_1) \rightarrow \sigma^*$ (P − $\mathrm{N_1}$)	18.601	58.478		16.218
$\mathrm{Lp}(X_1) \rightarrow \sigma^*$ ($\mathrm{P{-}O_2}$)	79.211			103.706
$\mathrm{Lp}(\mathrm{N_1}) \rightarrow \sigma^*$ ($\mathrm{P{-}O_2}$)	12.582		14.254	16.678
$\mathrm{Lp}(\mathrm{O_2}) \rightarrow \sigma^*$ ($\mathrm{P{-}N_1}$)	39.124		38.999	
$\mathrm{Lp}(\mathrm{O_2}) \rightarrow \pi^*$ (P = X_1)	17.430		21.694	

dx.doi.org/10.1021/jf5011726 | J. Agric. Food Chem. 2014, 62, 5761−5771

that the net charge of the phosphorus atom's (Q_P) effect inverts the H-bond energy of $(N—H)_{ligand}\cdots(O=C)_{enzyme}$. Figures 5A″ and 5B″ demonstrate that the H-bond energy of the docking analysis of AChE and BChE is negative, proportional to the Q_N and Q_P parameters.

Concluding Remarks. Twenty-four bisphosphoramidothioates with the general formula of $(RO)_2P(S)XP(S)(OR)_2$ (**1**–**24**) were synthesized and characterized by spectroscopy methods. The cyclic motif of $(CH_3O)_2P(S)NH(C_6H_{10})NHP(S)(OCH_3)_2$ (**9**) was determined by X-ray crystallography. The results of NBO analysis showed that the H-bond energies in the P(1)–S(1)···(1)H–N(1) and P(2)–S(2)···(2)H–N(2) models were −33.3 and −42.4 kJ mol^{-1}, respectively. Docking analysis disclosed that reversible noncovalent interactions, especially hydrogen bonds, occurred between the OR (R = CH_3 and C_2H_5) oxygen and N—H nitrogen atoms of selected compounds, and the H—N atoms of GLN with O=C of GLU. The MLR-QSAR models (to R^2 = 0.922 and 3.422 < VIF < 12.411 for AChE and to R^2 = 0.845 and 1.281 < VIF < 3.105 for BChE) and correlation matrix clarified that the net charge of N–H nitrogen and R_2NP = X phosphorus atoms contributes an important electronic function in the inhibition of ChEs. The interrelationship shows that the net charge of nitrogen and phosphorus atoms controls the modification of the molecular orbital energy of Tem analogues. The predicted values of $\log(1/IC_{50})$ are in good agreement with the experimental ones; the validity of the QSAR model was confirmed by LOO cross-validation method with q^2 = 0.965 between the training and testing sets. Increasing E^2 for the $Lp(X_P) \rightarrow \sigma^*$ (P–N) and $Lp(N) \rightarrow \sigma^*$ (P–O) interactions and the electron density of the N–H nitrogen with the OR oxygen of Tem analogues verify the integrity of the QSAR equation and docking results in the inhibition process of ChE enzymes.

■ ASSOCIATED CONTENT

Supporting Information

Spectral data as indicated in the text relative to Tem analogues (**1**–**24**). This material is available free of charge via the Internet at http://pubs.acs.org.

■ AUTHOR INFORMATION

Corresponding Author

*(K.G.) Phone: +98 21 82883443. Fax: +98 21 8006544. E-mail: gholi_kh@modares.ac.ir.

Notes

The authors declare no competing financial interest.

■ ABBREVIATIONS USED

AChE, acetylcholinesterase; BPAT, bisphosphoramidothioate; ChE, cholinesterase; DFT, density function theory; IC_{50}, half-maximal inhibitory concentration; PASS, prediction of activity spectrum for substances; PCA, principal component analysis; PDB, Protein Data Bank; QSAR, quantitative structure–activity relationships; SPSS, Statistical Package for Social Scientists; Tem, temephos; VIF, variance inflation factor

■ REFERENCES

(1) Olszewski, T. K.; zowska, J. G.; Boduszek, B.; Kozłowski, H. New heterocyclic mono- and bis(α- hydroxymethyl)phosphinic acids: synthesis and cuii binding abilities. *Eur. J. Org. Chem.* **2007**, 3539–3546.

(2) Dos Santos, V. M. R.; Sant Anna, C. M. R.; Borja, G. E. M.; Chaaban, A.; Cortes, W. S.; Da Costa, J. B. N. New bisphosphorothioates and bisphosphoroamidates: synthesis, molecular modeling and determination of insecticide and toxicological profile. *Bioorg. Chem.* **2007**, *35*, 68–81.

(3) Kaboudin, B.; Emadi, S.; Hadizadeh, A. Synthesis of novel phosphorothioates and phosphorodithioates and their differential inhibition of cholinesterases. *Bioorg. Chem.* **2009**, *37*, 101–105.

(4) Fest, C.; Schmidt, K. J. *The Chemistry of Organophosphorus Pesticides*; Springer-Verlag: Berlin, Germany, 1982.

(5) Lores, E. M.; Moore, J. C.; Moody, P.; Clark, J.; Forester, J.; Knight, J. Temephose residues in stagnant pond after mosquito larvicide application by helicopter. *Bull. Environ. Contam. Toxicol.* **1985**, *35*, 308–313.

(6) Tikar, S. N.; Kumar, A.; Prasad, G. B. K. S.; Prakash, S. Temephos-induced resistance in *Aedes aegypti* and its cross-resistance studies to certain insecticides from India. *Parasitol. Res.* **2009**, *105*, 57–63.

(7) Hackenberger, B. K.; Perkusic, D. J.; Stepic, S. Effect of temephos on cholinesterase activity in the earthworm *Eisenia fetida* (Oligochaeta, Lumbricidae). *Ecotoxicol. Environ. Saf.* **2008**, *71*, 583–589.

(8) Ba-Omar, T. A.; Al-Jardani, S.; Victor, R. Effects of pesticide temephos on the gills of *Aphanius dispar* (Pisces: Cyprinodontidae). *Tissue Cell* **2011**, *43*, 29–38.

(9) Amadasi, A.; Mozzarelli, A.; Meda, C.; Maggi, A.; Cozzini, P. Identification of xenoestrogens in food additives by an integrated in silico and in vitro approach. *Chem. Res. Toxicol.* **2009**, *22*, 52–63.

(10) Modesto, C.; Luciana, S.; Antonio, C.; Cosimo, A.; Adele, N.; Saverio, C.; Angelo, C. Investigation of platelet aggregation inhibitory activity by phenyl amides and esters of piperidinecarboxylic acids. *Bioorg. Med. Chem.* **2003**, *11*, 439–1450.

(11) Ellman, G. L.; Coutney, K. D.; Andres, V. R.; Featherstone, M. A new and rapid colorimetric determination of acetylcholinesterase activity. *Biochem. Pharmacol.* **1961**, *7*, 91–95.

(12) Copeland, R. A. *Enzymes, A Practical Introduction to Structure, Mechanism, and Data Analysis*, 2nd ed.; Wiley-VCH: New York, 2000.

(13) Lagunin, A.; Stepanchikova, A.; Filimonov, D.; Poroikov, V. PASS: prediction of activity spectra for biologically active substances. *Bioinf. Appl. Note* **2000**, *16*, 747–748.

(14) Morris, G. M.; Goodsell, D. S.; Halliday, R. S.; Huey, R.; Hart, W. E.; Belew, R. K.; Olson, A. J. *J. Comput. Chem.* **1998**, *19*, 1639–1662.

(15) *SPSS for Windows*, version 10.05; SPSS Inc.: Bangalore, India, 1999.

(16) Sheldrick, G. M. A short history of *SHELX*. *Acta Crystallogr.* **2008**, *A64*, 112–122.

(17) Hansch, C.; Fujita, T. *p-σ-π* Analysis. A method for the correlation of biological activity and chemical structure. *J. Am. Chem. Soc.* **1964**, *86*, 1616–1626.

(18) Jung, M.; Tak, J.; Lee, Y.; Jung, Y. Quantitative structure–activity relationship (QSAR) of tacrine derivatives against acetylcholinesterase (AChE) activity using variable selections. *Bioorg. Med. Chem. Lett.* **2007**, *17*, 1082–1090.

(19) De melo, E. B. Multivariate SAR/QSAR of 3-aryl-4-hydroxyquinolin-2(1*H*)-one derivatives as type I fatty acid synthase (FAS) inhibitors. *Eur. J. Med. Chem.* **2010**, *45*, 5817–5826.

(20) Sharma, S. K.; Kumar, P.; Narasimhan, B.; Ramasamy, K.; Mani, V.; Mishra, R. K.; Majeed, A. A. Synthesis, antimicrobial, anticancer evaluation and QSAR studies of 6-methyl-4-[1-(2-substituted- phenylamino-acetyl)-1*H*-indol-3-yl]-2-oxo/thioxo-1,2,3,4-tetrahydropyrimidine-5-carboxylic acid ethyl esters. *Eur. J. Med. Chem.* **2012**, *48*, 16–25.

(21) Pinto, M. F. S.; Romero, O. A. S.; Pinheiro, J. C. Pattern recognition study of structure–activity relationship of halophenols and halonitrophenols against fungus *T. mentagrophytes*. *J. Mol. Struct. (THEOCHEM)* **2001**, *539*, 303–310.

(22) Malta, V. R. S.; Pinto, A. V.; Molfetta, F. A.; Honório, K. M.; de Simone, C. A.; Pereira, M. A.; Santos, R. H. A.; da Silva, A. B. F. The influence of electronic and steric effects in the structure–activity relationship (SAR) study of quinone compounds with biological activity against *Trypanosoma cruzi*. *J. Mol. Struct. (THEOCHEM)* **2003**, *634*, 271–280.

(23) Schuurmann, G.; Ebert, R. U.; Chen, J. W.; Wang, B.; Kuhne, R. External validation and prediction employing the predictive squared correlation coefficient — test set activity mean vs training set activity mean. *J. Chem. Inf. Model.* **2008**, *48*, 2140−2145.
(24) Mirzaei, M.; Elmi, F.; Hadipour, N. L. A systematic investigation of hydrogen-bonding effects on the ^{17}O, ^{14}N, and ^{2}H nuclear quadrupole resonance parameters of anhydrous and monohydrated cytosine crystalline structures: a density functional theory study. *J. Phys. Chem. B* **2006**, *110*, 10991−10996.
(25) Gholivand, K.; Ebrahimi Valmoozi, A. A.; Mahzouni, H. R. Structural and electronic aspects of hydrogen bonding in two polymorphs of butylene-*N*,*N*′-bis(*O*,*O*′-diarylphosphoramidate). *Acta Crystallogr.* **2013**, *B69*, 55−61.
(26) Reed, A. E.; Curtiss, L. A.; Weinhold, F. Intermolecular interactions from a natural bond orbital, donor−acceptor viewpoint. *Chem. Rev.* **1988**, *88*, 899−926.
(27) Carpenter, J. E.; Weinhold, F. Analysis of the geometry of the hydroxymethyl radical by the "different hybrids for different spins" natural bond orbital procedure. *J. Mol. Struct. (THEOCHEM)* **1988**, *169*, 41−46.
(28) Boys, S. F.; Bernardi, F. The calculation of small molecular interactions by the differences of separate total energies. Some procedures with reduced errors. *Mol. Phys.* **1970**, *19*, 553−566.
(29) Frisch, M. J.; Trucks, G. W.; Schlegel, H. B.; Scuseria, G. E.; Robb, M. A.; Cheeseman, J. R.; Montgomery, J. A.; Vreven, T.; Kudin, K. N.; Burant, J. C.; Millam, J. M.; Iyengar, S. S.; Tomasi, J.; Barone, V.; Mennucci, B.; Cossi, M.; Scalmani, G.; Rega, N.; Petersson, G. A.; Nakatsuji, H.; Hada, M.; Ehara, M.; Toyota, K.; Fukuda, R.; Hasegawa, J.; Ishida, M.; Nakajima, T.; Honda, Y.; Kitao, O.; Nakai, H.; Klene, M.; Li, X.; Knox, J. E.; Hratchian, H. P.; Cross, J. B.; Bakken, V.; Adamo, C.; Jaramillo, J.; Gomperts, R.; Stratmann, R. E.; Yazyev, O.; Austin, A. J.; Cammi, R.; Pomelli, C.; Ochterski, J. W.; Ayala, P. Y.; Morokuma, K.; Voth, G. A.; Salvador, P.; Dannenberg, J. J.; Zakrzewski, V. G.; Dapprich, S.; Daniels, A. D.; Strain, M. C.; Farkas, O.; Malick, D. K.; Rabuck, A. D.; Raghavachari, K.; Foresman, J. B.; Ortiz, J. V.; Cui, Q.; Baboul, A. G.; Clifford, S.; Cioslowski, J.; Stefanov, B. B.; Liu, G.; Liashenko, A.; Piskorz, P.; Komaromi, I.; Martin, R. L.; Fox, D. J.; Keith, T.; Al-Laham, M. A.; Peng, C. Y.; Nanayakkara, A.; Challacombe, M.; Gill, P. M. W.; Johnson, B.; Chen, W.; Wong, M. W.; Gonzalez, C.; Pople, J. A. *Gaussian 03*, revision D.01; Gaussian, Inc.: Wallingford, CT, USA, 2005.
(30) Dabirmanesh, B.; Khajeh, K.; Ranjbar, B.; Ghazi, F.; Heydari, A. Inhibition mediated stabilization effect of imidazolium based ionic liquids on alcohol dehydrogenase. *J. Mol. Liq.* **2012**, *170*, 66−71.
(31) Bernstein, J.; Davis, R. E.; Shimoni, L.; Chang, N. L. Patterns in hydrogen bonding: functionality and graph set analysis in crystals. *Angew. Chem., Int. Ed.* **1995**, *34*, 1555−1573.
(32) Gholivand, K.; Mahzouni, H. R. Solid-state and gas-phase structures of two conformers of *N*-(4- methylphenyl)-*N*′,*N*″-bis-(morpholinyl) phosphoric triamide; insights from X-ray crystallography and DFT calculations. *Acta Crystallogr.* **2011**, *B67*, 238−243.
(33) *PASS* software, version 1.917, July, 2005.
(34) Geronikaki, A. A.; Dearden, J. C.; Filimonov, D.; Galaeva, I.; Garibova, L.; Gloriozova, T.; Kranjneva, V.; Lagunin, A.; Macaev, F. Z.; Molodavkin, G.; Poroikov, V.; Pobrebnoi, S. I.; Shepeli, F.; Voronina, T.; Tsitlakido, M.; Vald, L. Design of new cognition enhancers: from computer prediction to synthesis and biological evaluation. *J. Med. Chem.* **2004**, *47*, 2870−2876.
(35) Lagunin, A.; Stepanchikova, A.; Filimonov, D.; Poroikov, V. PASS. *Bioinf. Appl. Note* **2000**, *16*, 747−748.
(36) Ghadimi, S.; Asad-Samani, K.; Ebrahimi-Valmoozi, A. A. Synthesis, spectroscopic characterization and structure-activity relationship of some phosphoramidothioate pesticides. *J. Iran. Chem. Soc.* **2011**, *8*, 717−726.
(37) Soltani, S.; Abolhasani, H.; Zarghi, A.; Jouyban, A. A. QSAR analysis of diaryl COX-2 inhibitors: comparison of feature selection and train-test data selection methods. *Eur. J. Med. Chem.* **2010**, *45*, 2753−2760.
(38) Roy, D. R.; Sarkar, U.; Chattaraj, P. K.; Mitra, A.; Padmanabhan, J.; Parthasarathi, R.; Subramanian, V.; Van Damme, S.; Bultinck, P. Analyzing toxicity through electrophilicity. *Mol. Divers.* **2006**, *10*, 119−131.
(39) Singh, J.; Shaik1, B.; Singh, S.; Agrawal, V. K.; Khadikar, P. V.; Deeb, O.; Supuran, C. T. Comparative QSAR study on para-substituted aromatic sulphonamides as CAII inhibitors: information versus topological (distance−based and connectivity) indices. *Chem. Biol. Drug. Des.* **2008**, *71*, 244−259.
(40) Hua, R.; Doucet, J. P.; Delamar, M.; Zhang, R. QSAR models for 2-amino-6-arylsulfonylbenzonitriles and congeners HIV-1 reverse transcriptase inhibitors based on linear and nonlinear regression methods. *Eur. J. Med. Chem.* **2009**, *44*, 2158−2171.
(41) Liao, S. Y.; Chen, J. C.; Qian, L.; Shen, Y.; Zheng, K. C. QSAR, action mechanism and molecular design of flavone and isoflavone derivatives with cytotoxicity against HeLa. *Eur. J. Med. Chem.* **2008**, *43*, 2159−2170.

JOURNAL OF AGRICULTURAL AND FOOD CHEMISTRY

Article

pubs.acs.org/JAFC

Cyclopent-4-ene-1,3-diones: A New Class of Herbicides Acting as Potent Photosynthesis Inhibitors

Jodieh O. S. Varejão,[†] Luiz C. A. Barbosa,*[,†,‡] Eduardo V. V. Varejão,[†] Célia R. A. Maltha,[†] Beatriz King-Díaz,[§] and Blas Lotina-Hennsen[§]

[†]Department of Chemistry, Federal University of Viçosa, Avenida Peter Henry Rolfs, s/n, 36570-000 Viçosa, Minas Gerais, Brazil

[‡]Department of Chemistry, Universidade Federal de Minas Gerais, Avenida Presidente Antônio Carlos, 6627, Campus Pampulha, 31270-901 Belo Horizonte, Minas Gerais, Brazil

[§]Department of Biochemistry, School of Chemistry, National Autonomous University of Mexico, Mexico City 04510, Mexico

Supporting Information

ABSTRACT: In a recent paper, we reported the synthesis and photosynthesis-inhibitory activity of a series of analogues of rubrolides. From quantitative structure−activity relationship (QSAR) studies, we found that the most efficient compounds are those having higher ability to accept electrons. On the basis of those findings, we directed our effort to synthesize new analogues bearing a strong electron-withdrawing group (nitro) in the benzylidene ring and evaluate their effects on photosynthesis. However, the employed synthetic approach led to novel cyclopent-4-ene-1,3-diones as major products. Here, we report the synthesis and mechanism of action of such cyclopent-4-ene-1,3-diones as a new class of photosynthesis inhibitors. These compounds block the electron transport at the Q_B level by interacting at the D1 protein at the reducing side of Photosystem II and act as Hill reaction inhibitors, with higher activity than the corresponding rubrolides. To the best of our knowledge, this is the first report on the photosynthesis inhibitory activity of cyclopentenediones.

KEYWORDS: *analogues of rubrolides, cyclopentenediones, chlorophyll a fluorescence, polarography, PSII inhibitors, Hill reaction inhibitors*

INTRODUCTION

Weed infestations constitute a major cause of crop losses worldwide, making agricultural yields highly dependent upon the management of such invasive plants.[1,2] Since the discovery of the herbicidal property of 2,4-dichlorophenoxyacetic acid (2,4-D) in the mid-1940s,[3] chemical control has been the most effective method for weed management. However, the continuous and repetitive use of herbicides has exerted selective pressure, leading to the replacement of sensitive by herbicide-resistant biotypes.[4−7] This problem has been worsened by the wide adoption of herbicide-resistant crops, which has contributed to an indiscriminate use of broad activity spectrum herbicides.[8−10] As a whole, this scenario has made the development of new herbicides a great concern and an important area of activity in industry and academy.

The use of phytotoxic natural products as models for the development of novel active molecules have been regarded as a promising strategy in the search for new herbicides.[11−14] Examples of the potential of such an approach are the commercial herbicides cinmethylin and mesotrione, derivatives from phytotoxic plant metabolites, and bialafos, synthesized from a phytotoxin isolated from species of the genera *Streptomyces*.[13,15] In line with such tendency, our research group have been using several natural compounds as models for the development of new bioactive molecules.[16−22]

In a recent paper, we reported the synthesis and photosynthesis-inhibitory activity of a series of analogues of rubrolides (Figure 1), a family of natural butenolides isolated from marine ascidians.[23] In that work, we found that derivatives bearing a nitro electron-withdrawing group at the *para* position in the benzylidene ring (Figures 1, compounds 2a and 2b) showed the higher activities, with IC_{50} 1 order of magnitude higher than that of commercial herbicides Diuron. In the same study, quantitative structure−activity relationship (QSAR) analyses indicated that the most efficient compounds are those having higher ability to accept electrons.

On the basis of these findings, we envisaged that rubrolide analogues bearing electron-withdrawing groups, such as nitro, for example, on the *meta* position of the benzylidene ring (Figure 1, compounds 3a and 3b), would be active as photosynthesis inhibitors. Because a nitro group acts as an electron-withdrawing group, its presence reduces the redox potential of the compound, making the molecule more able to accept an electron and interfere with the photosynthetic electron transport.[23] We then tried to prepare compounds **3a** and **3b**; however, this attempt led to unexpected and novel compounds, identified as 4-bromo-5-(2-methoxyphenyl)-2-(3-nitrophenyl)cyclopent-4-ene-1,3-dione (**4a**) and 4-bromo-5-(4-fluoro-2-methoxyphenyl)-2-(3-nitrophenyl) cyclopent-4-ene-1,3-dione (**4b**) (Figure 1), as major products. These compounds were assayed for their inhibitory activity on the photosynthetic electron transport chain and showed high

Received: March 31, 2014
Revised: June 3, 2014
Accepted: June 9, 2014
Published: June 9, 2014

ACS Publications © 2014 American Chemical Society

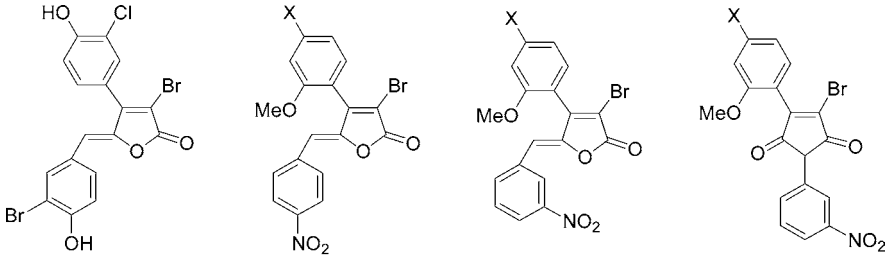

1: Rubrolide N

2a: X = H
2b: X = F

3a: X = H
3b: X = F

4a: X = H
4b: X = F

Figure 1. Rubrolide N, rubrolide analogues, and derived ciclopent-4-ene-1,3-diones.

activities. Their synthesis and photosynthesis-inhibitory activities are presented herein.

MATERIALS AND METHODS

General Experimental Procedures. All reagents and solvents were prepared following the procedure already reported in the literature[24] or were purchased from commercially available suppliers and used without any further purification. Compounds **5a** and **5b** were prepared employing a synthetic procedure previously reported.[23] Melting points are uncorrected and were obtained from a MQAPF-301 melting point apparatus (Microquimica, Brazil). Analytical thin-layer chromatography analysis was conducted on aluminum-packed pre-coated silica gel plates. Column chromatography was performed over silica gel 230−400 mesh. All compounds were fully characterized by infrared (IR), Electron ionization−mass spectrometry (EI−MS), ^{1}H and ^{13}C nuclear magnetic resonance (NMR), correlation spectroscopy (COSY), heteronuclear correlation (HETCOR), and nuclear Overhauser effect difference (NOEDIFF) NMR spectroscopy. IR spectra were recorded on a PerkinElmer Paragon 1000 fourier Transform infrared (FTIR) spectrophotometer using potassium bromide (1%, w/w) disks or as a thin liquid film on NaCl plates. Mass spectra were recorded on a Shimadzu GCMS-QP5050A instrument by direct insertion, using EI mode (70 eV). High-resolution mass spectra were recorded on a Bruker MicroToF [resolution = 10 000 full width at half maximum (fwhm)] under electrospray ionization (ESI) and are given to four decimal places. The ^{1}H and ^{13}C NMR spectra were recorded on a Varian Mercury 300 spectrometer at 300 and 75 MHz, respectively, using $CDCl_3$ as the solvent and tetramethylsilane (TMS) as the internal reference, unless otherwise stated. The energy gap between highest occupied molecular orbital (HOMO) and lowest unoccupied molecular orbital (LUMO) of the compounds was calculated with MOPAC[25] software using the AM1 method.[26,27]

Synthesis of Compounds 3a and 4a. In a two-necked round bottomed flask (25 mL) under a nitrogen atmosphere were added 3-bromo-4-(2-methoxyphenyl)furan-2(5*H*)-one (**5a**) (100 mg, 0.37 mmol), 3-nitrobenzaldehyde (67 mg, 0.44 mmol), dichloromethane (3 mL), *tert*-butyldimethylsilyl trifluoromethanesulfonate (TBDMSOTf) (101 μL, 0.44 mmol), and *N*,*N*-diisopropylethylamine (DIPEA) (130 μL, 0.74 mmol). The resulting mixture was stirred at room temperature for 1 h. After this period, 1,8-diazabicyclo[5.4.0]-undec-7-ene (DBU) (110 μL, 0.74 mmol) was added, and the resultant mixture was refluxed for 1 h before the addition of dichloromethane (70 mL). The organic phase was washed with 3 mol L^{-1} HCl (2 × 25 mL) and brine (2 × 25 mL). The combined organic layers were dried over magnesium sulfate, filtered, and concentrated under reduced pressure in a rotary evaporator. The residue obtained was purified by column chromatography on silica gel eluted with hexane/ethyl acetate (3:1, v/v), affording compound **4a** with a 42% yield. Compound **3a** was isolated in a 30% yield, but although observed as a unique peak in gas chromatography−mass spectrometry (GC−MS) analysis, it was unstable in $CDCl_3$.

(*Z*)-3-Bromo-4-(2-methoxyphenyl)-5-(3-nitrobenzylidene)-furan-2(5*H*)-one (3a). The compound was a yellow amorphous residue. FTIR (KBr) ν_{max}, cm^{-1}: 3068, 2923, 2847, 1771, 1606, 1531, 1491, 1281, 988, 750. ^{1}H NMR, δ_H (300 MHz, $CDCl_3$): 3.86 (s, 3H), 5.98 (s, 1H), 7.08−7.16 (m, 2H), 7.27 (dd, 1H, *J* = 8.0 and 1.5 Hz), 7.52−7.60 (m, 2H), 8.14−8.17 (m, 1H), 8.22 (brd, 1H, *J* = 8.1 Hz), 8.39−8.40 (m, 1H). ^{13}C NMR δ_C (75 MHz, $CDCl_3$): 55.6, 110.3, 111.7, 113.7, 117.1, 120.8, 123.4, 125.0, 129.9, 130.2, 132.3, 134.3, 135.7, 148.4, 149.4, 152.2, 156.5, 164.5. EM, *m*/*z* (%): 403 (98) $[M + 2]^{+\bullet}$, 401 (100) ($C_{18}H_{12}BrNO_5$) $[M^{+\bullet}]$, 322 (46), 294 (50), 281 (20), 279 (21), 277 (20), 219 (25), 205 (20), 189 (21), 176 (26), 163 (58), 131 (65), 119 (36), 115 (36), 103 (48), 102 (26), 95 (36), 91 (21), 89 (64), 88 (64), 77 (70), 63 (36), 51 (25), 39 (48).

4-Bromo-5-(2-methoxyphenyl)-2-(3-nitrophenyl)cyclopent-4-ene-1,3-dione (4a). The compound was a yellow amorphous residue. FTIR (NaCl, film) ν_{max}, cm^{-1}: 3080, 2955, 2923, 2852, 1750, 1709, 1604, 1529, 1486, 1463, 1347, 1265, 1144, 1021, 735, 732, 691. ^{1}H NMR, δ_H (300 MHz, $CDCl_3$): 3.89 (s, 3H), 4.38 (s, 1H), 7.05−7.14 (m, 2H), 7.37 (dd, 1H, *J* = 7.8 and 1.8 Hz), 7.50−7.58 (m, 1H), 7.60 (brd, 1H, *J* = 7.8 Hz), 7.67 (brd, 1H, *J* = 7.8 Hz), 8.16−8.17 (m, 1H), 8.22 (dt, 1H, *J* = 8.1 and 1.5 Hz). ^{13}C NMR, δ_C (75 MHz, $CDCl_3$): 55.8, 56.1, 111.6, 117.1, 120.7, 123.3, 123.4, 130.0, 132.8, 133.7, 135.3, 145.1, 148.5, 156.8, 156.9, 191.8, 194.1. EM, *m*/*z* (%): 403 (38) $[M + 2]^{+\bullet}$, 401 (38) ($C_{18}H_{12}BrNO_5$) $[M^{+\bullet}]$, 322 (28), 294 (28), 219 (22), 150 (41), 149 (20), 135 (21), 131 (84), 124 (31), 119 (36), 115 (34), 109 (23), 103 (39), 102 (19), 97 (23), 95 (27), 94 (24), 91 (21), 89 (61), 88 (79), 86 (58), 84 (87), 77 (100), 76 (26), 75 (31), 71 (20), 63 (49), 61 (28), 57 (34), 51 (81), 50 (24). High-resolution mass spectrometry (HRMS) (ESI) calculated for $[C_{18}H_{12}BrNNaO_5]^{+}$, 423.9791; found, 423.9787.

Synthesis of Compound 6. Compound **5b** (100 mg, 0.37 mmol), 3-nitrobenzaldehyde (67 mg, 0.44 mmol), dichloromethane (3 mL), TBDMSOTf (101 μL, 0.44 mmol), and DIPEA (130 μL, 0.74 mmol) were added to a two-necked round-bottom flask (25 mL), under a nitrogen atmosphere. The resulting mixture was stirred at room temperature for 1 h. The resulting organic phase was washed with 3 mol L^{-1} HCl (2 × 25 mL) and brine (2 × 25 mL). The combined organic layers were dried over magnesium sulfate, filtered, and concentrated under reduced pressure. The resulting residue was purified by column chromatography on silica gel eluted with hexane/dichlorometane (1:1, v/v). Compound **6** was obtained with 80% yield.

3-Bromo-5-((*tert*-butyldimethylsilyloxy)(3-nitrophenyl)-methyl)-4-(4-fluoro-2-methoxyphenyl)furan-2(5*H*)-one (6). The compound was a white solid. Melting point (mp): 161.2−162.8 °C. FTIR (KBr) ν_{max}, cm^{-1}: 2957, 2929, 2856, 2855, 1763, 1609, 1528, 1500, 1469, 1353, 1286, 1127, 1020, 837, 781. ^{1}H NMR, δ_H (300 MHz, $CDCl_3$): −0.38 (s, 3H), −0.28 (s, 3H), 0.78 (s, 9H), 3.92 (s, 3H), 4.84 (d, 1H, *J* = 2.4 Hz), 5.83 (d, 1H, *J* = 2.4 Hz), 6.72 (dd, 1H, *J* = 2.4 and 10.5 Hz), 6.80−6.86 (m, 1H), 7.50−7.54 (m, 1H), 7.66−7.74 (m, 2H), 8.03−8.05 (m, 1H), 8.13−8.16 (m, 1H). ^{13}C NMR, δ_C (75 MHz, $CDCl_3$): −5.7, −4.6, 17.8, 25.4, 55.9, 73.0, 86.1, 100.0 (d, *J* = 26.0 Hz), 108.0 (d, *J* = 21.7 Hz), 110.3, 114.7 (d, *J* = 3.3 Hz), 121.5, 123.3, 129.3, 132.3 (d, *J* = 10.4 Hz), 133.4, 141.9, 147.8, 156.1, 158.3 (d, *J* = 10.3 Hz), 165.2 (d, *J* = 251.9 Hz), 168.2. Electron microscopy (EM), *m*/*z* (%) (molecular ion does not appear): 496 (22), 494 (21), 415 (15), 345 (13), 343 (13), 342 (13), 267 (10), 266 (48), 264 (15), 150 (12), 115 (20), 75 (20), 73 (100), 59 (10), 45 (11).

dx.doi.org/10.1021/jf5014605 | J. Agric. Food Chem. 2014, 62, 5772−5780

Scheme 1. Synthesis of Compounds 3a and 4a

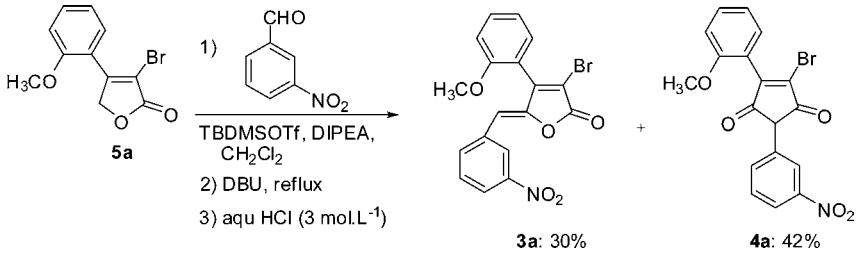

Synthesis of Compounds 3b and 4b. Compound **6** (100 mg, 0.18 mmol), dichloromethane (3 mL), and DBU (49 μL, 0.36 mmol) were added to a two-necked round-bottom flask (25 mL), under a nitrogen atmosphere. The resultant mixture was refluxed for 1 h. Dichloromethane (70 mL) was added, and the organic phase was washed with 3 mol L^{-1} HCl (2 × 25 mL) and brine (2 × 25 mL). The organic layer was dried over magnesium sulfate, filtered, and concentrated under reduced pressure. The residue obtained was purified by column chromatography on silica gel eluted with hexane/ethyl acetate (3:1, v/v) to afford compounds **3b** and **4b** in 35 and 49% yields, respectively.

(*Z*)-3-Bromo-4-(4-fluoro-2-methoxyphenyl)-5-(3-nitrobenzylidene)furan-2(5*H*)-one (3b). The compound was a yellow solid. mp: 156.1−158.6 °C. FTIR (KBr) ν_{max}, cm^{-1}: 3033, 2997, 2967, 2935, 1769, 1617, 1597, 1527, 1499, 1347, 1281, 987, 839. ^{1}H NMR, δ_H (300 MHz, $CDCl_3$): 3.86 (s, 3H), 5.96 (s, 1H), 6.80−6.89 (m, 2H), 7.23−7.28 (m, 1H), 7.58 (t, 1H, *J* = 8.1 Hz), 8.15−8.19 (m, 1H), 8.22 (d, 1H, *J* = 8.1 Hz), 8.39−8.40 (m, 1H). ^{13}C NMR, δ_C (75 MHz, $CDCl_3$): 56.0, 100.3 (d, *J* = 25.9 Hz), 107.8 (d, *J* = 22.0 Hz), 110.3, 112.6, 113.1 (d, *J* = 3.3 Hz), 123.6, 125.1, 129.9, 131.4 (d, *J* = 10.6 Hz), 134.2, 135.8, 148.4, 149.3, 151.2, 158.1 (d, *J* = 10.4 Hz), 164.3, 165.2 (d, *J* = 249.9 Hz). EM, *m*/*z* (%): 421 (99) $[M + 2]^{+\bullet}$, 419 (99) ($C_{18}H_{11}BrFNO_5$) $[M^{+\bullet}]$, 340 (30), 312 (30), 238 (25), 237 (36), 230 (23), 228 (23), 223 (23), 181 (65), 177 (27), 153 (27), 149 (100), 137 (28), 133 (37), 118 (20), 106 (43), 101 (93), 89 (56), 39 (38). HRMS (ESI) calculated for $[C_{18}H_{11}BrFNNaO_5]^+$, 441.9697; found, 441.9700.

4-Bromo-5-(4-fluoro-2-methoxyphenyl)-2-(3-nitrophenyl)-cyclopent-4-ene-1,3-dione (4b). The compound was a yellow solid. mp: 152.1−153.4 °C. FTIR (NaCl, film) ν_{max}, cm^{-1}: 3095, 2977, 2945, 2895, 1752, 1708, 1608, 1526, 1492, 1348, 1279, 1193, 1104, 1028, 952, 842, 808, 725, 670, 595, 488, 447. ^{1}H NMR, δ_H (300 MHz, $CDCl_3$): 3.88 (s, 3H), 4.37 (s, 1H), 6.77−6.86 (m, 2H), 7.36 (dd, 1H, *J* = 8.4 and 6.3 Hz), 7.57−7.62 (m, 1H), 7.64−7.68 (m, 1H), 8.14−8.15 (m, 1H), 8.22 (ddd, 1H, *J* = 8.1, 2.4, and 1.5 Hz). ^{13}C NMR, δ_C (75 MHz, $CDCl_3$): 56.0, 56.1, 100.2 (d, *J* = 26.2 Hz), 107.9 (d, *J* = 22.5 Hz), 113.1 (d, *J* = 3.1 Hz), 123.3, 130.0, 131.5 (d, *J* = 10.5 Hz), 133.6, 135.1, 145.0, 148.5, 158.0, 158.6 (d, *J* = 11.3 Hz), 165.7 (d, *J* = 251.0 Hz), 191.6, 194.0. EM, *m*/*z* (%): 421 (40) $[M^{+\bullet} + 2]$, 419 (40) ($C_{18}H_{11}BrFNO_5$) $[M^{+\bullet}]$, 181 (29), 153 (20), 149 (78), 133 (42), 118 (22), 101 (76), 89 (100), 75 (23), 74 (12), 63 (90), 62 (31), 51 (28), 50 (24), 39 (64), 30 (69). HRMS (ESI) calculated for $[C_{18}H_{11}BrFNNaO_5]^+$, 441.9697; found, 441.9692.

Study of the Conversion of Rubrolide Analogues to Cyclopentenediones. To verify the hypothesis that cyclopent-4-ene-1,3-dione was formed through rearrangement of the corresponding rubrolide analogues, we have tried to obtain compound **4b** by treating compound **3b** with DBU (2.0 equiv) in dichloromethane under reflux for 1 h. The resulting mixture was worked-up as described for the synthesis from compound **6**. Compound **4b** was obtained with 50% yield, and 50% of compound **3b** was recovered.

Chloroplast Isolation and Total Chlorophyll (Chl) Determination. Intact chloroplasts were obtained from market spinach leaves (*Spinacea oleraceae* L.) as published[28,29] by homogenization and differential centrifugation, and they were resuspended in a small volume of the following medium: 400 mM sucrose, 5 mM $MgCl_2$, 10 mM KCl, and 30 mM tricine−KOH (pH 8.0). The Chl concentration was determined as reported.[29,30]

Chl and Fluorescence Determinations. Chl *a* fluorescence transients of Photosystem II (PSII) were measured in thylakoids with a Handy plant efficient analyzer (PEA, Hansatech, King's Lynn, Norfolk, U.K.) as previously described.[31,32] The maximum fluorescence yield from the sample was generated by illumination for 2 s with continuous light (650 nm peak wavelength, intensity equivalent of 2830 μmol of photons m^{-2} s^{-1}, and gain of 0.7) provided by an array of three light-emitting diodes. The reaction medium set was that employed in basal non-cyclic electron transport measurements without methyl viologen (MV). To monitor Chl and fluorescence transients, aliquots of dark-adapted thylakoids for 5 min containing 60 μg of Chl were transferred to a filter paper by gravity with a dot-blot apparatus (Bio-Rad, Hercules, CA) to ensure a homogeneous and reproducible distribution of thylakoids. The filter paper was dipped immediately in 3 mL of the medium with different concentrations of the tested compounds, and the control contained medium plus the amount of dimethyl sulfoxide (DMSO) employed for dissolving each compound at the different used concentrations. Chloroplasts infiltrated with 50 μM 3-(3,4-dichlorophenyl)-1,1-dimethylurea (DCMU) were used as a positive control.

Measurement of Adenosine Triphosphate (ATP) Synthesis. To measure ATP synthesis, intact chloroplasts (20 μg/mL of Chl) were broken by osmotic rupture in non-buffered solution with 100 mM sorbitol, 10 mM KCl, 5 mM $MgCl_2$, 0.5 mM KCN, 50 μM MV (MV was used as an electron acceptor), 1 mM Na^+−tricine (pH 8.0), and 1 mM ADP (pH 6.7). The pH was adjusted to 8.0 with 50 mM KOH, and the mixture was illuminated for 1 min. The synthesized ATP was calculated as micromoles of ATP per milligram of Chl per hour.[29,33]

Measurement of the Rate of Non-cyclic Electron Transport. Electron flow (basal, phosphorylating, and uncoupled) from water to MV was monitored with a Yellow Springs Instrument (YSI) oxygraph using a Clark-type electrode.[29,34] Light-induced non-cyclic electron transport determinations were performed in the presence of 50 μM MV. Chloroplasts were efficiently lysed to yield free thylakoids prior to each experiment by incubating them in the following basal electron transport medium: 100 mM sorbitol, 10 mM KCl, 5 mM $MgCl_2$, 0.5 mM KCN, and 30 mM *N*-tris[hydroxymethyl]methylglicine (tricine) buffer (pH 8.0 with the addition of KOH). A total of 20 μg of Chl/mL of medium was illuminated for 1 min. Phosphorylating non-cyclic electron transport was measured as the basal non-cyclic electron transport medium in the addition of 1 mM ADP and 3 mM KH_2PO_4. Uncoupled electron transport was tested in the basal transport medium by adding 6 mM NH_4Cl as the uncoupler agent.

Uncoupled PSII and Photosystem I (PSI) Electron Flow Measurements. These experiments were performed in an uncoupled non-cyclic electron transport assay. The activities were monitored with a YSI oxygen monitor, model 5300A, using a Clark-type electrode. Uncoupled PSII from water to 2,5-dichloro-1,4-benzoquinone (DCBQ)[35] was monitored using the basal electron transport medium, and 1 μM 2,5-dibromo-6-isopropyl-3-methyl-1,4-benzoquinone (DBMIB), 100 μM DCBQ, and 6 mM NH_4Cl were added. MV was omitted. DCBQ accepts electrons at the D1 protein. Partial reaction of PSII electron transport from water to sodium silicomolybdate (SiMo) was determined as in PSII with the same basal electron transport medium without MV, and 50 μM SiMo and 10 μM DCMU were added.[35] These electron flow activities were monitored with a YSI oxygen monitor, model 5300, using a Clark-type electrode.

dx.doi.org/10.1021/jf5014605 | *J. Agric. Food Chem.* 2014, 62, 5772−5780

Scheme 2. Synthesis of Compounds 3b and 4b

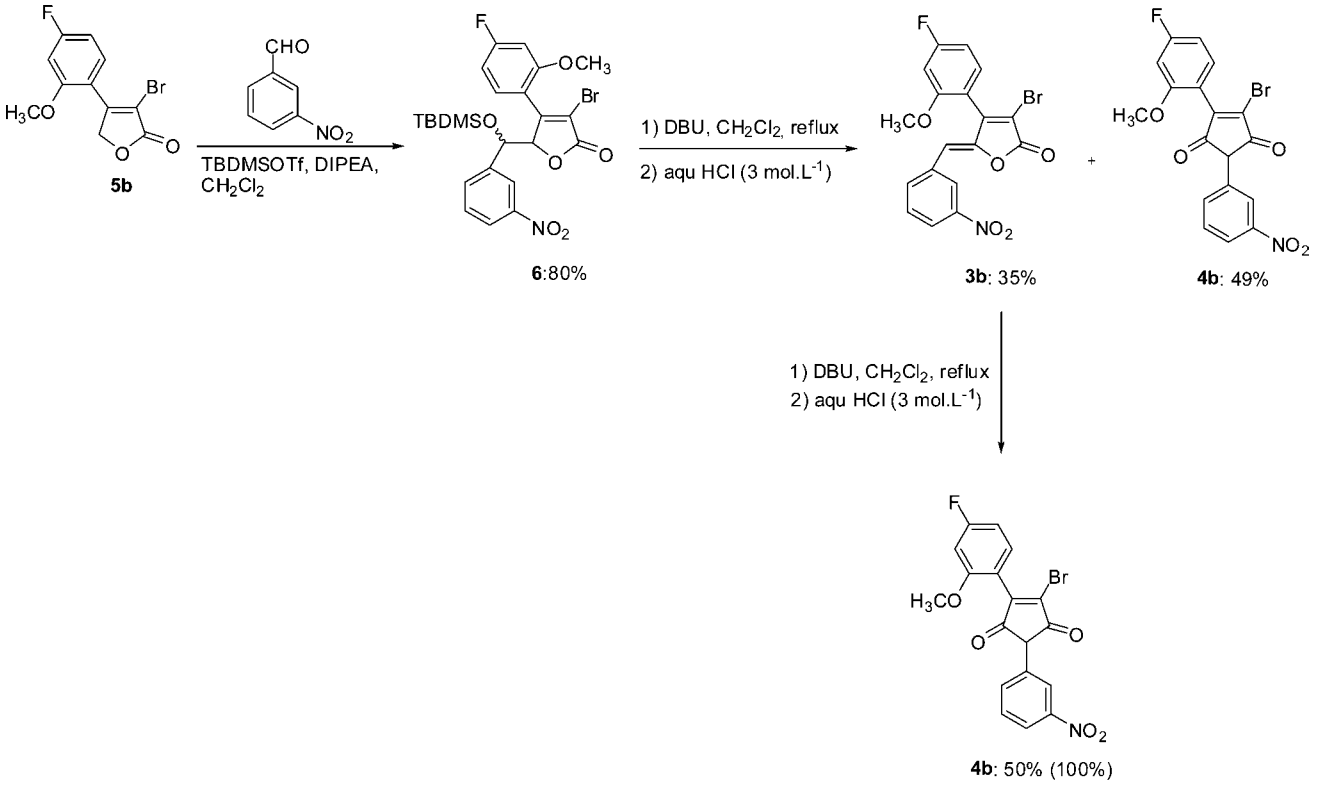

RESULTS AND DISCUSSION

Synthesis. In attempting to synthesize rubrolide analogues bearing a nitro group at the *meta* position (**3a** and **3b**), we employed the same approach used for the preparation of rubrolide analogues **2a** and **2b**.[23] Briefly, lactone **5a** (Scheme 1) was treated with *tert*-butyldimethylsilyl trifluoromethanesulfonate and *N*,*N*-diisopropylethylamine to yield the corresponding *tert*-butyldimethylsilyl intermediate, which was reacted *in situ* with 3-nitrobenzaldehyde. The silylated adducts were treated with DBU to afford the desired rubrolide analogue **3a** (30% yield). However, cyclopent-4-ene-1,3-dione **4a** was isolated as a major product (42% yield). This result was surprising and unexpected because this methodology has been previously applied for the preparation of other rubrolide analogues, and no rearranged products were reported.[23,36,37]

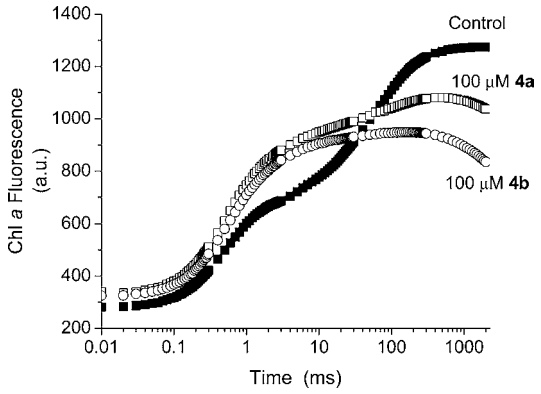

Figure 2. Fluorescence rise kinetics of freshly lysed broken chloroplasts infiltrated with (□) compound **4a** and (○) compound **4b** and compared to the (■) control chloroplasts. Chl *a* fluorescence induction curves were measured at room temperature. Details are in the Materials and Methods. Data are averages of three replicates.

Base-catalyzed rearrangement of alkylidenebutenolides to the isomeric cyclopentenediones has already been documented in the literature,[38−40] and this approach has been used for the synthesis of a range of natural cyclopent-4-ene-1,3-diones and derivatives.[40,41] Commonly, this procedure is carried out by treating butenolide with sodium methoxy in methanol. The suggested mechanism involves the electrophilic attack to carbon of the carbonyl group of benzylidene, which results in the opening of the ring, followed by a new cyclization to the cyclopentenedione ring.[40]

To verify if cyclopentenedione **4b** was in fact formed by means of a rearrangement of rubrolide **3b**, instead of being produced directly from the sililated intermediate, the former was reacted with DBU, in the same reaction conditions, affording compound **4b** with 50% yield (Scheme 2). Despite the strong Lewis basic property of DBU, it is not a good nucleophile and unlikely to be responsible for the opening of the butenolide ring.[42] A good example is the synthetic procedure reported by Tan and co-workers[41] for the synthesis of the natural cyclopentenedione known as methyl linderone. In this approach, the reaction of a precursor butenolide with sodium methoxy led to the desired cyclopent-4-ene-1,3-dione. However, treatment of the same precursor with DBU resulted in a basic catalyzed elimination reaction but not to the conversion of butenolide to cyclopentenedione. When the product of this elimination was reacted with NaOMe, cyclopentenedione was obtained with 71% yield.[41]

Thus, in view of the poor nucleophilic property of DBU, we supposed that the rearrangement of the rubrolide analogues to cyclopent-4-ene-1,3-diones could be caused by the presence of traces of water in DBU. In fact, Cota et al.[42] demonstrated that the DBU−water system acts as a basic catalyst for aldol

dx.doi.org/10.1021/jf5014605 | J. Agric. Food Chem. 2014, 62, 5772−5780

Table 1. Experimental Average Values Plus Standard Deviation of Parameters Obtained from Measurements of the Chl *a* Fluorescence Induction Curve in Control and Treated Chloroplasts with Different Concentrations of Compounds 4a and 4b[a]

compound	F_0	F_1	F_2	F_3	F_4	F_5	F_M	area
control	149 ± 4.0	159 ± 2.5	167 ± 5.7	208 ± 6.1	368 ± 14.5	385 ± 14.1	741 ± 15.3	29234 ± 503
[**4a**] (μM)								
25	153 ± 7.6	158 ± 7.8	168 ± 8.1	224 ± 13.2	423 ± 21.0	525 ± 18.2	694 ± 34.2	59,683 ± 12,230
50	132 ± 7.8	142 ± 8.9	154 ± 4.8	209 ± 5.5	403 ± 17.3	481 ± 16.4	584 ± 11.3	16,000 ± 529
[**4b**] (μM)								
12.5	149 ± 4.7	161 ± 4.7	170 ± 4.6	226 ± 6.6	418 ± 8.4	518 ± 12.2	694 ± 8.5	32,000 ± 16,116
25.0	167 ± 0	182 ± 1.4	193 ± 0	260 ± 1.4	478 ± 2.8	580 ± 4.2	709 ± 7.1	33100 ± 24,749
50.0	185 ± 4 0.2	199 ± 4.2	213 ± 11.3	277 ± 12.0	505 ± 24.0	592 ± 24.0	661 ± 15.6	7600 ± 848
50 μM								
DCMU	205 ± 5	224 ± 3.01	247 ± 6.1	346 ± 11.5	616 ± 18.0	716 ± 22.5	723 ± 22	1333 ± 115
control	269 ± 4.8	295 ± 5.7	317 ± 5.5	422 ± 5.9	665 ± 7.5	912 ± 27.0	1273 ± 23	140,960 ± 19,963
[**4a**] (μM)								
100	301 ± 9.9	335 ± 13.4	364 ± 16.3	500 ± 21.2	851 ± 14.1	1003 ± 0.7	1120 ± 44	14,600 ± 656
[**4b**] (μM)								
100	312 ± 13.8	341 ± 16.1	368 ± 19.4	485 ± 33.8	801 ± 55.7	964 ± 32.5	947 ± 71.1	2067 ± 808

[a]DCMU was used as a positive control.

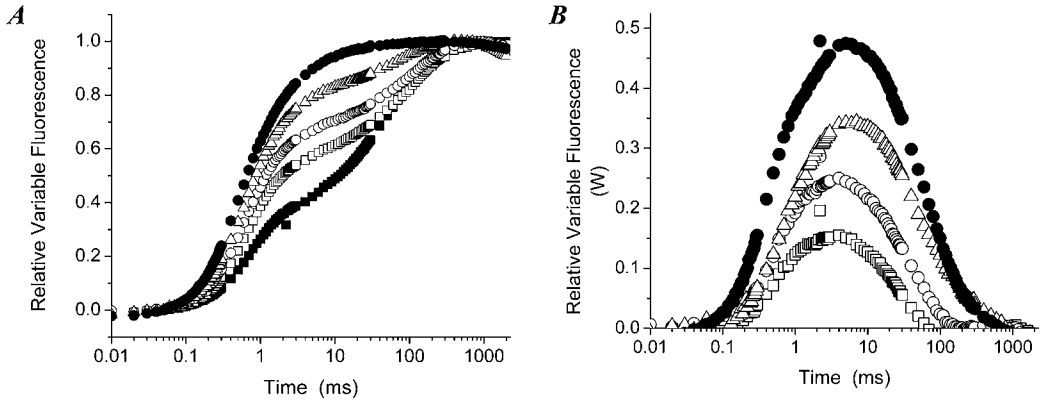

Figure 3. (A) OJIP curves normalized from F_1 to F_M at (○) 25 μM, (□) 50 μM, and (△) 100 μM compound **4a** in comparison to the (■) control and (●) 50 μM DCMU. (B) Calculated J band near 2 ms, as a result of the difference between the normalized treated and controls of the Chl *a* transients.

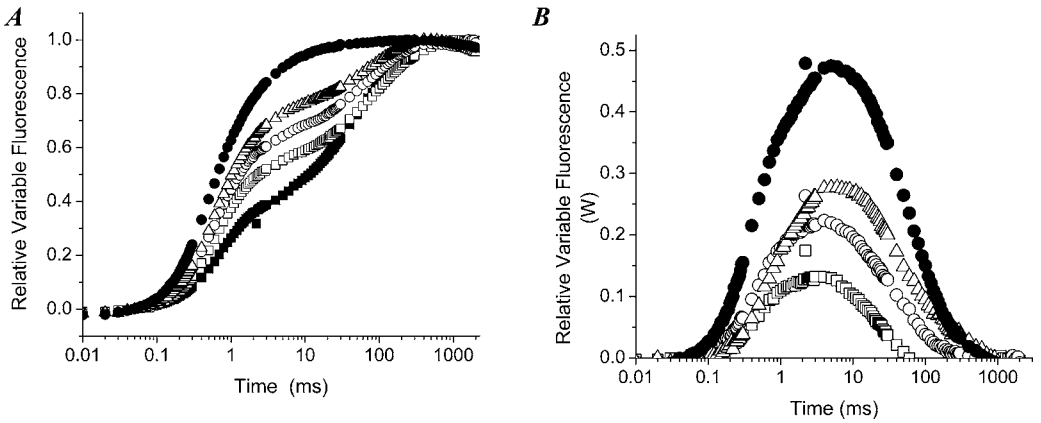

Figure 4. (A) OJIP curves normalized from F_1 to F_M at (○) 12.5 μM, (□) 25 μM, and (△) 50 μM of compound **4b** in comparison to the (■) control and (●) 50 μM DCMU. (B) J band near 2 ms, as a result of the difference between the normalized treated and controls of Chl *a* transients.

condensation reactions. By means of NMR studies, the authors showed that the reaction with water changes the DBU structure to a second resonance structure, which contains hydroxide ions responsible for the nucleophilic attack in the aldol condensation (see Scheme S1 of the Supporting Information).[42]

The presence of water in DBU used was confirmed by IR spectroscopy. Thus, we suppose that the water−DBU system is responsible for the rearrangement of rubrolide to cyclopentenedione. Also, this rearrangement can be facilitated by the presence of the electron-withdrawing NO_2 group in the benzylidene ring, which makes the lactone carbonyl more

dx.doi.org/10.1021/jf5014605 | J. Agric. Food Chem. 2014, 62, 5772−5780

Table 2. Derived Parameters, Their Description, and Their Formula Using Data Extracted from the Chl *a* Fluorescence (OJIP) Transient Presented in This Work

fluorescence parameters derived from the extracted data	
$M_0 = 4(F_{300\,\mu s} - F_0)/(F_M - F_0)$	approximated initial slope (in ms^{-1}) of the fluorescence transient $V = f(t)$
$Sm = (area)/(F_M - F_0)$	normalized total complementary area above the OJIP transient (reflecting multiple turnover Q_A reduction events)
yields or flux ratios	
$\varphi_{Po} = TR_0/ABS = [1 - F_0/F_M]$	maximum quantum yield of primary photochemistry at $t = 0$
$\varphi_{Eo} = ET_0/ABS = [1 - F_J/F_M)]$	quantum yield for electron transport at $t = 0$
$\psi_{Eo} = ET_0/TR_0 = (1 - V_J)$	probability (at $t = 0$) that a trapped exciton moves an electron into the electron transport chain beyond Q_A^-
$\varphi_{Do} = 1 - \varphi_{Po} = (F_0/F_M)$	quantum yield (at $t = 0$) of energy dissipation
$\delta R_0 = RE_0/ET_0 = (1 - V_I)/(1 - V_J)$	efficiency with which an electron can move from the reduced intersystem electron acceptors to the PSI end of electron acceptors of PSI
$\varphi R_0 = RE_0/ABS = \varphi_{Po}*\psi_{Eo}*\delta R_0 = 1 - (F_I/F_M)$	quantum yield for the reduction of end of acceptors of PSI per photon absorbed
$RE_0/TR_0 = \psi_{Eo}\delta R_0$	efficiency with which a trapped exciton moves an electron into the electron transport chain from Q_A^- to the PSI end of electron acceptors
specific energy fluxes or activities [per reaction Q_A^- reducing the PSII reaction center (RC)]	
$ABS/RC = M_0(1/V_J)(1/\varphi_{Po})$	absorption per RC
$TR_0/RC = M_0/V_J$	trapped energy flux per RC (at $t = 0$)
$ET_0/RC = M_0(1/V_J)(\psi_{Eo})$	electron transport flux per RC (at $t = 0$)
phenomenological energy fluxes [per excited cross-section (CS)]	
ABS/CS_0	absorption flux per CS
TR_0/CS_0	trapped energy flux per CS (at $t = 0$)
ET_0/CS_0	electron transport flux per CS (at $t = 0$)
de-excitation rate constants	
K_p	photochemical de-excitation rate constant
K_n	non-photochemical de-excitation rate constant
sum K	sum of photochemical and non-photochemical rate constants
performance index at $t = 0$	
	performance index on absorption basis

$$PI_{ABS} = \frac{RC}{ABS}\frac{\varphi_{Po}}{1-\varphi_{Po}}\frac{\psi_{Eo}}{1-\psi_{Eo}}$$

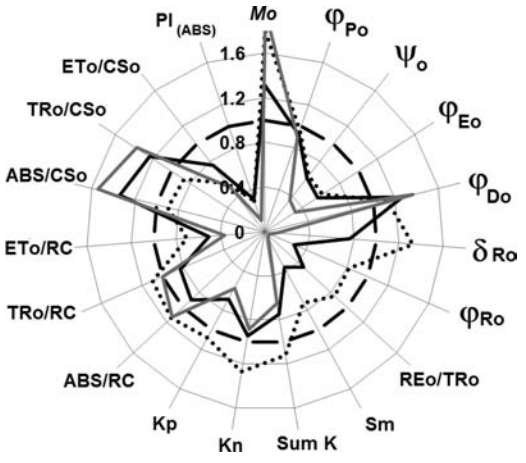

Figure 5. Radar graph showing the effects of compound **4a** (dotted line) and compound **4b** (black line) at 50 μM in comparison to 50 μM DCMU (gray line) on the derived parameters calculated from the OJIP transients of Chl *a* presented by dark-adapted freshly lysed chloroplasts. The control is represented by a dashed black line at the center of the radar and is equal to the unity.

electrophilic and susceptible to a nucleophilic attack. This supposition led us to speculate why cyclopentenedione was not isolated in our previous work[23] as a co-product of the reaction that afforded compounds **2a** and **2b**. Then, we decided to treat compound **2b** with the same DBU used in the present work, under the same reaction conditions. As the reaction was monitored by thin-layer chromatography (TLC), we observed a degradation of the starting material and no signs of the corresponding cyclopent-4-ene-1,3-dione. We suppose then that the reason for this degradation could be attributed to the higher electron-withdrawing effect of the nitro group in the *para* position, which, by means of the resonance effect, makes the lactone carbonyl even more susceptible to nucleophilic attack, resulting in different products. The formation of acyclic products from some other butenolides from the treatment with a strong base has already been reported.[40]

Chl and Fluorescence Transient Measurements in the Presence of Compounds 3b, 4a, and 4b. Chl *a* fluorescence measurements on photosynthetic organisms under different conditions, including stress, can be analyzed to provide detailed information about the structure, conformation, and function of the photosynthetic apparatus, especially of PSII and electron transport activity.[32] On this premise, different concentrations of compounds **3b**, **4a**, and **4b** were assayed on Chl *a* fluorescence of freshly lysed spinach chloroplasts. Compound **3a** was not tested because of degradation, as assessed by ^{1}H NMR experiments. Figure 2 shows the effects of compounds **4a** and **4b** at 100 μM on the induction curve of fluorescence of Chl *a*. Compound **3b** did not show any modification in the transients (data not shown).

OJIP transients were analyzed according to the JIP test, and the measured parameters are presented in Table 1: fluorescence intensity level (F_0) when plastoquinone electron acceptor pool, Q_A, is fully oxidized and fluorescence of the Chl *a* level when Q_A is transiently fully reduced (F_M). F_1 is the fluorescence Chl *a*

dx.doi.org/10.1021/jf5014605 | J. Agric. Food Chem. 2014, 62, 5772−5780

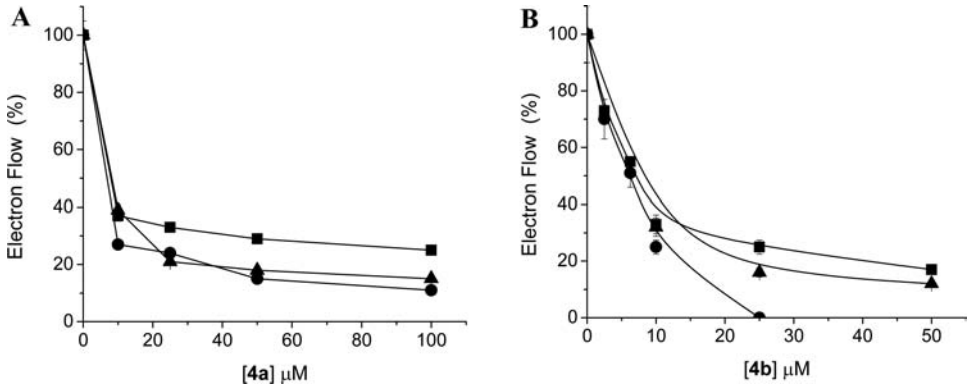

Figure 6. Effect of compound **4a** on electron transport flow: (■) basal, (●) phosphorylating, and (▲) uncoupled conditions. Control values in = 100% = 450, 880, and 1200 μequiv of e^- mg^{-1} of Chl h^{-1}, respectively. Each curve is the average of three replicates. Other conditions are indicated in the Materials and Methods.

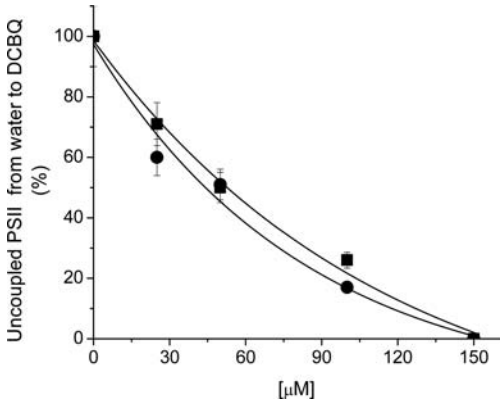

Figure 7. Effects of (■) compound **4a** and (●) compound **4b** on uncoupled electron transport flow of PSII measured from water to DCBQ. Control values = 100% = 300 μequiv of e^- mg^{-1} of Chl h^{-1}, respectively. Each curve is the average of three replicates.

intensity level at 0.05 ms; F_2 is the fluorescence Chl *a* intensity level at 0.1 ms; F_3 is the fluorescence Chl *a* intensity level at 0.3 ms; F_4 or F_J is the fluorescence Chl *a* intensity level at 2 ms; and F_5 is the fluorescence Chl *a* intensity level at 30 ms. The area is the area over the curve between F_0 and F_M and relates the pool size of PSII electron transport acceptors.[43,45]

The OJIP data were normalized using the equation $V_t = (F_t - F_0)/(F_M - F_0)$ and are presented as the kinetics of relative variable fluorescence between F_0 and F_M (Figures 3A and 4A). The difference between the normalized treated transients minus the control transients showed an increase in the 2−4 ms range, a J band (Figures 3B and 4B). The fluorescence rise to the J band provides information about single-turnover events of the primary reactions of the photochemistry, mainly Q_A reduction. This reflects light-driven accumulation of Q_A^- with Q_B, indicating that the electron transport beyond Q_A is blocked at the Q_B level, just like the commercial herbicide DCMU. These finds suggest that both compounds (**4a** and **4b**) interact at the D1 protein site and the unused energy is dissipated as heat.[32]

Using the program Biolyzer HP3 (from a laboratory at the University of Geneva; available at http://www.unige.ch/sciences/biologie/bioen), data from Table 1 were used to calculate other parameters related to the electron transport activity, such as the yield ratios φ_{Po}, ψ_{Eo}, φR_0, and RE_0/TR_0.[32] These derived parameters are depicted in Table 2, and the effects of compounds **4a** and **4b** and DCMU at 50 μM on these parameters are shown as a radar plot in Figure 5 (the effects at other concentrations are not shown for graph clarity). The normalized area (Sm), the electron transport per reaction center and per cross-section, and the performance index on an absorption basis were decreased by the compounds, while M_0 and φ_{Do} were increased by both compounds **4a** and **4b**. However, ABS/CS_0 and TR_0/CS_0 were increased only by compound **4b** and DCMU. These results suggest that compounds **4a** and **4b** inhibit the photosynthetic electron transport in the same site as herbicide DCMU, with compound **4b** being more potent than compound **4a**.

Effect of Cyclopent-4-ene-1,3-diones 4a and 4b on the Electron Transport Rate from Water to MV. To corroborate the site and mechanisms of action of cyclopentenediones on electron transport flow, different concentrations of compounds **4a** and **4b** were assayed by polarography on the electron transport under basal, phosphorylating, and uncoupled conditions. Because compound **3b** did not modify the Chl *a* fluorescence measurements, it was not subjected to this test. Panels A and B of Figure 6 show that all three conditions of the electron transport flow were inhibited by both compounds. The IC_{50} values (i.e., the concentration required to inhibit 50% of the activity) for the uncoupled electron flow were 9.5 and 8.4 μM for compounds **4a** and **4b**, respectively. These results indicate that both compounds act as Hill reaction inhibitors. DCMU inhibits both oxygen evolution and ATP synthesis at 5 μM;[44] therefore, compounds **4a** and **4b** have similar potency as an inhibitor to the PSII reducing side, just like DCMU.

To localize the target of compounds **4a** and **4b** on the thylakoid electron transport chain, effects on partial reactions of PSII and PSI electron transport were determined using appropriate artificial electron donors, electron acceptors, and electron transport inhibitors.[31,45] Figure 7 shows that compounds **4a** and **4b** inhibited PSII measured from water to DCBQ, with I_{50} values of 50 and 44 μM, respectively. Contrarily, these compounds showed no effects on PSI (data not shown). Furthermore, the activity of H_2O to SiMo was not affected by these compounds, indicating that the interaction and inhibition site of both compounds **4a** and **4b** are located in the PSII electron transport chain. These data corroborate the results obtained from measurements of the Chl *a* fluorescence transient.

The higher activity of compound **4b** when compared to compound **4a** may be related to the presence of the fluorine

dx.doi.org/10.1021/jf5014605 | J. Agric. Food Chem. 2014, 62, 5772−5780

substituent at the benzene ring of the first. Because of its high electronegativity, fluorine acts as an electron-withdrawing group and contributes to reduce the redox potential of compound **4b** relative to compound **4a**, thus enhancing the ability of compound **4b** to act as electron acceptors and inhibit the photosynthetic electron transport.

In a previous work, a QSAR study showed that the photosynthetic inhibition ability of rubrolide analogues was mainly correlated to the HOMO and LUMO energies.[23] However, using those data in attempting to explain the higher activity of cyclopentenediones is hindered by the difference in the structural skeleton between these two classes of compounds. On the other hand, a series of studies has concluded that biological activities (including herbicide properties) of various classes of organic compounds are related to the high-energy gap between HOMO and LUMO. For many of these studies, the higher the HOMO−LUMO energy gap of the compounds, the higher their biological activity.[46−50] Thus, we decided to calculate the HOMO−LUMO energy gap for compounds **3a**, **3b**, **4a**, and **4b**. Results obtained showed that cyclopentenediones **4a** and **4b**, which have higher biological activities, also have higher energy gaps (7.940 and 7.950 eV, respectively) than the corresponding rubrolides **3a** and **3b** (7.577 and 7.580 eV, respectively). This finding may suggest that the ability to accept electrons and interfere in the photosynthetic electron transport of these compounds may be related to higher energy gaps between HOMO and LUMO. Also, the energy gap between HOMO and LUMO for compound **4b** was found to be higher than that for compound **4a**, thus helping to explain the higher activity of the first in comparison to the former.

In this work, we have shown that rubrolide analogues bearing a nitro group at the benzylidene ring (*meta* position) can be converted into cyclopent-4-ene-1,3-diones using excess DBU with traces of water in the reaction medium. When assayed on Chl *a* fluorescence of freshly lysed spinach chloroplasts, these cyclopent-4-ene-1,3-diones were more active than the precursor rubrolides, displaying the same degree of potency as the commercial herbicide DCMU. Also, the presence of a fluorine atom at one of the benzene rings enhances the interference of cyclopent-4-ene-1,3-diones in the Chl *a* transients. By means of the polarography assay, we have further demonstrated that cyclopent-4-ene-1,3-diones act as Hill reaction inhibitors by binding the D1 protein at the reducing side of the PSII. These findings clearly show that cyclopent-4-ene-1,3-diones bearing electron-withdrawing groups at the aromatic rings can be regarded as promising candidates for the development of novel photosynthesis-inhibiting herbicides.

■ ASSOCIATED CONTENT

Supporting Information

^{1}H and ^{13}C NMR spectra of compounds **3b**, **4a**, and **4b** (Figures S1−S4, S7, and S8), COSY and HETCOR spectra of the compounds **4a** and **4b** (Figures S5, S6, S9, and S10), COLOQ spectrum of compound **4b** (Figure S11), and mechanistic proposal for the synthesis of compounds **4a** and **4b** (Scheme S1). This material is available free of charge via the Internet at http://pubs.acs.org.

■ AUTHOR INFORMATION

Corresponding Author

*Telephone: +55-31-34093396. E-mail: lcab@ufmg.br and/or lcab@outlook.com.

Funding

The authors are grateful to the following Brazilian agencies: Conselho Nacional de Desenvolvimento Científico e Tecnológico (CNPq) and Coordenação de Aperfeiçoamento de Pessoal de Nível Superior (CAPES) for research fellowships (to Célia R. A. Maltha, Eduardo V. V. Varejão, Jodieh O. S. Varejao, and Luiz C. A. Barbosa) and Fundação de Amparo à Pesquisa de Minas Gerais (FAPEMIG) for supporting our research in this area. The authors also gratefully acknowledge the financial support from Dirección General de Asuntos del Personal Académico (DGAPA)−National Autonomous University of Mexico (UNAM) Grants PAPIT IT102012-3 and PAIP 4290-03 from Faculty of Chemistry, UNAM.

Notes

The authors declare no competing financial interest.

■ REFERENCES

(1) Oerke, E. C. Crop losses to pests. *J. Agric. Sci.* **2006**, *144*, 31−43.
(2) Neve, P.; Vila-Aiub, M.; Roux, F. Evolutionary-thinking in agricultural weed management. *New Phytol.* **2009**, *184*, 783−793.
(3) Wood, H. E.; Olson, P. J. *A New Weed Killer, 2,4-D*; Manitoba Department of Agriculture and Immigration: Winnipeg, Manitoba, Canada, 1946; 201.
(4) Trezzi, M. M.; Felippi, C. L.; Mattei, D.; Silva, H. L.; Nunes, A. L.; Sebastiani, C.; Vidal, R. A.; Marques, A. Multiple resistance of acetolactate synthase and protoporphyrinogen oxidase inhibitors in *Euphorbia heterophylla* biotypes. *J. Environ. Sci. Health, Part B* **2005**, *40*, 101−109.
(5) Vila-Aiub, M. M.; Vidal, R. A.; Balbi, M. C.; Gundel, P. E.; Trucco, F.; Ghersa, C. M. Glyphosate-resistant weeds of South American cropping systems: An overview. *Pest Manage. Sci.* **2008**, *64*, 366−371.
(6) Powles, S. B. Evolved glyphosate-resistant weeds around the world: Lessons to be learnt. *Pest Manage. Sci.* **2008**, *64*, 360−365.
(7) Beckie, H. J. Herbicide-resistant weed management: Focus on glyphosate. *Pest Manage. Sci.* **2011**, *67*, 1037−1048.
(8) Duke, S. O.; Powles, S. B. Glyphosate: A once-in-a-century herbicide. *Pest Manage. Sci.* **2008**, *64*, 319−325.
(9) Duke, S. O.; Powles, S. B. Glyphosate-resistant crops and weeds: Now and in the future. *AgBioForum* **2009**, *12*, 346−357.
(10) Duke, S. O. Why have no new herbicide modes of action appeared in recent years? *Pest Manage. Sci.* **2012**, *68*, 502−512.
(11) Dayan, F. E.; Cantrell, C. L.; Duke, S. O. Natural products in crop protection. *Bioorg. Med. Chem.* **2009**, *17*, 4022−4034.
(12) Cantrell, C. L.; Dayan, F. E.; Duke, S. O. Natural products as sources for new pesticides. *J. Nat. Prod.* **2012**, *75*, 1231−1242.
(13) Hüter, O. F. Use of natural products in the crop protection industry. *Phytochem. Rev.* **2011**, *10*, 189−194.
(14) Barbosa, L. C. A.; Teixeira, R. R.; Montanari, R. M. In *Current Trends in Phytochemistry*; Epifano, F., Ed.; Research Singpost: Kerala, India, 2009; pp 21−59.
(15) Mitchell, G.; Bartlett, D. W.; Fraser, T. E. M.; Hawkes, T. R.; Holt, D. C.; Townson, J.; Wichert, R. A. Mesotrione: A new selective herbicide for use in maize. *Pest Manage. Sci.* **2001**, *57*, 120−128.
(16) Chaves, F. C.; Barbosa, L. C. A.; Demuner, A. J.; Silva, A. A. New helminthosporal analogues with plant-growth regulatory property synthesized via oxyallyl cation. *Z. Naturforsch.* **2006**, *61*, 1287−1294.
(17) Barbosa, L. C. A.; Ferreira, M. L.; Demuner, A. J.; Silva, A. A.; Pereira, R. C. Preparation and phytotoxicity of sorgoleone analogues. *Quim. Nova* **2001**, *24*, 751−755.
(18) Barbosa, L. C. A.; Costa, A. V.; Veloso, D. O.; Lopes, J. L. C.; Hernandez-Terrones, M. G.; King−Diaz, B.; Lotina-Hennsen, B. Phytogrowth-inhibitory lactones derivatives of glaucolide B. *Z. Naturforsch.* **2004**, *59c*, 803−810.
(19) Barbosa, L. C. A.; Demuner, A. J.; Alvarenga, E. S.; Oliveira, A.; King-Diaz, B.; Lotina-Hennsen, B. Phytogrowth- and photosynthesis-

inhibiting properties of nostoclide analogues. *Pest Manage. Sci.* **2006**, *62*, 214−222.
(20) Barbosa, L. C. A.; Teixeira, R. R.; Forlani, G.; Veloso, D. P.; Carneiro, J. W. M. Synthesis of photosynthesis-inhibiting nostoclide analogues. *J. Agric. Food Chem.* **2008**, *56*, 2321−2329.
(21) Barbosa, L. C. A.; Nogueira, L. B.; Maltha, C. R. A.; Teixeira, R. R.; Silva, A. A. Synthesis and phytogrowth properties of oxabicyclic analogues related to helminthosporin. *Molecules* **2009**, *14*, 160−173.
(22) Barbosa, L. C. A.; Varejão, J. O. S.; Petrollino, D.; Pinheiro, P. F.; Demuner, A. J.; Maltha, C. R.; Forlani, G. Tailoring nostoclide structure to target thechloroplastic electron transport chain. *ARKIVOC* **2012**, *iv*, 15−32.
(23) Barbosa, L. C. A.; Maltha, C. R.; Lage, M. R.; Barcelos, R. C.; Dona, A.; Carneiro, J. W. M.; Forlani, G. Synthesis of rubrolide analogues as new inhibitors of the photosynthetic electron transport chain. *J. Agric. Food Chem.* **2012**, *60*, 10555−10563.
(24) Perrin, D. D.; Armarego, W. L. F. *Purification of Laboratory Chemicals*, 5th ed.; Butterworth−Heinemann: Oxford, UK, 2003; p 609.
(25) Stewart, J. J. P. *MOPAC 2007, Version 7*; Stewart Computational Chemistry: Colorado Springs, CO, 2007.
(26) Dewar, M. J. S.; Thiel, W. Ground states of molecules. 38. The MNDO method. Approximations and parameters. *J. Am. Chem. Soc.* **1977**, *99*, 4899−4907.
(27) Dewar, M. J. S.; Zoebisch, E. G.; Healy, E. F. AM1: A new quantum chemical molecular model. *J. Am. Chem. Soc.* **1985**, *107*, 3902−3909.
(28) Mills, J. D.; Mitchell, P.; Schurmann, P. Modulation of coupling ATPase activity in intact chloroplasts. *FEBS Lett.* **1980**, *191*, 144−148.
(29) Morales-Flores, F.; Aguilar, M. I.; King-Díaz, B.; Lotina-Hennsen, B. Derivatives of diterpen labdane-8α,15-diol as photosynthetic inhibitorsin spinach chloroplasts and growth plant inhibitors. *J. Photochem. Photobiol., B* **2013**, *125*, 42−50.
(30) Strain, H. H.; Cope, T.; Svec, M. A. Analytical procedures for the isolation, identification, estimation and investigation of thechlorophylls. *Methods Enzymol.* **1971**, *23*, 452−466.
(31) Veiga, T. A. M.; King-Díaz, B.; Marques, A. S. F.; Sampaio, O. M.; Vieira, P. C.; da Silva, M. F. G. F.; Lotina-Hennsen, B. Furoquinoline alkaloids isolated from *Balfourodendron riedelianum* as photosynthetic inhibitors in spinach chloroplasts. *J. Photochem. Photobiol., B* **2013**, *120*, 36−43.
(32) Strasser, R. J.; Tsimilli-Michael, M.; Srivastava, A. In *Chlorophyll Fluorescence: A Signature of Photosynthesis*, Papageorgion, G. C., Govindjee, Eds.; Kluwer Academic Publishers: Dordrecht, Netherlands, 2004; pp 321−362.
(33) Dilley, R. A. Ion transport (H^+, K^+, Mg^{2+} exchange phenomena). *Methods Enzymol.* **1972**, *24*, 68−74.
(34) Izawa, S.; Hind, G. The kinetics of the pH rise in illuminated chloroplasts suspensions. *Biochim. Biophys. Acta* **1967**, *143*, 377−390.
(35) Yruela, I.; Montoya, G.; Alonso, P. J.; Picorel, R. Identification of the pheophytin-QA-Fe domain of the reducing side of the photosystem II as the Cu(II)-inhibitory binding site. *J. Biol. Chem.* **1991**, *266*, 22847−22850.
(36) Boukouvalas, J.; Lachance, N.; Oullet, M.; Trudeau, M. Facile access to 4-aryl-2(5*H*)-furanones by Suzuki cross coupling: Efficient synthesis of rubrolides C and E. *Tetrahedron Lett.* **1998**, *39*, 7665−7668.
(37) Boukouvalas, J.; McCann, L. C. Synthesis of the human aldose reductase inhibitor rubrolide L. *Tetrahedron Lett.* **2010**, *51*, 4636−4639.
(38) Tichotová, L.; Matoušová, E.; Spulák, M.; Kuneš, J.; Buchta, V.; Pour, I. M. Synthesis and biological activity of desmethoxy analogues of coruscanone A. *Bioorg. Med. Chem. Lett.* **2011**, *21*, 6062−6066.
(39) Krayushkin, M. M.; Pashchenko, D. V.; Lichitsky, B. V.; Irie, M.; Vorontsova, L. G.; Starikova, Z. A. Synthesis of photochromic dihetarylethenes with a cyclopentenedione bridge fragment. *Mendeleev Commun.* **2007**, *17*, 301−302.
(40) Gedge, D. R.; Pattenden, G. Rearrangement of 4-ylidenebutenolides to cyclopentene-1,3-diones: Synthesis of calythrone and related compounds. *J. Chem. Soc., Chem. Commun.* **1978**, *20*, 880−882.
(41) Tan, H.; Zheng, C.; Liu, Z.; Wang, D. Z. Biomimetic total syntheses of linderaspirone A and Bi-linderone and revisions of their biosynthetic pathways. *Org. Lett.* **2011**, *13*, 2192−2195.
(42) Cota, J.; Chimentao, R.; Sueiras, J.; Medina, F. The DBU−H_2O complex as a new catalyst for aldol condensation reactions. *Catal. Commun.* **2008**, *9*, 2090−2094.
(43) Jiang, H.-X.; Chen, L.-S.; Tang, N.; Smith, B. R. Aluminum-induced effects on photosystem II photochemistry in citrus leaves assessed by the chlorophyll *a* fluorescence transient. *Tree Physiol.* **2008**, *28*, 1863−1871.
(44) Giaquinta, R. T.; Dilley, R. A.; Crane, F. L.; Barr, R. Photophosphorylation not coupled to DCMU-insensitive photosystem II oxygen evolution. *Biochem. Biophys. Res. Commun.* **1974**, *59*, 985−991.
(45) Allen, J. F.; Holmes, N. G. In *Photosynthesis, Energy Transduction. A Practical Approach*; Hipkinns, M. F., Baker, N. R., Eds.; IRL Press: Oxford, U.K., 1986; pp 103−141.
(46) Refat, M. S.; El-Sayed, M. Y.; Adam, A. M. A.; Saad, H. A.; Eldaroti, H. H. Charge transfer complexes as a semiconductor models: Outline of spectroscopic studies on electron donor−acceptor complexes of hexane-1,6-diol with different π-acceptors. *Int. J. Electrochem. Sci.* **2013**, *8*, 4234−4259.
(47) Mahalakshmi, G.; Balachandran, V. FT-IR, FT-Raman and DFT study of 3,3′-bis(trifluoromethyl)benzophenone and its biological activity with other halogen (Cl, Br) atoms. *Spectrochim. Acta, Part A* **2014**, *124*, 328−340.
(48) Lamchouri, F.; Toufik, H.; Bouzzine, S. M.; Hamidi, M.; Bouachrine, M. Experimental and computational study of biological activities of alkaloids isolated from *Peganum harmala* seeds. *J. Mater. Environ. Sci.* **2010**, *S1*, 343−352.
(49) Wang, Z.; Song, J.; Han, Z.; Jiang, Z.; Zheng, W.; Chen, J.; Song, Z.; Shang, S. Quantitative structure−activity relationship of terpenoid aphid antifeedants. *J. Agric. Food Chem.* **2008**, *56*, 11361−11366.
(50) Balasubramanian, K. Molecular orbital basis for yellow curry spice curcumin's prevention of Alzheimer's disease. *J. Agric. Food Chem.* **2006**, *54*, 3512−3520.

JOURNAL OF AGRICULTURAL AND FOOD CHEMISTRY

Article

pubs.acs.org/JAFC

Continuous Stimulation of the Plant Immune System by the Peptide Elicitor PIP-1 Is Required for Phytoalexin Biosynthesis in Tobacco Cells

Yonghyun Kim, Eriko Komoda, Masahiro Miyashita,* and Hisashi Miyagawa

Division of Applied Life Sciences, Graduate School of Agriculture, Kyoto University, Kyoto 606-8502, Japan

Supporting Information

ABSTRACT: The peptide elicitor PIP-1 (YGIHTH-NH_2) induced various defense responses in tobacco cells. Types of defense responses induced by PIP-1 were different based on its concentration range: oxidative burst (an early response) was induced at low micromolar levels, but phytoalexin production (a late response) required about 10−50-fold higher concentrations than those required for oxidative burst. We assumed that rapid decreases in the PIP-1 concentration due to enzymatic hydrolysis in the culture media could cause this difference. To examine the potential impact of such degradation particularly on induction of phytoalexin biosynthesis, we designed a degradation-resistant analogue, MePIP-1, in which the amide bond between the fifth and sixth residues was N-methylated. MePIP-1 was considerably more stable than PIP-1 and induced significant phytoalexin production upon treatment at low micromolar levels. Further investigation of the mechanism of action of MePIP-1 showed a requirement of continuous elicitor stimulation for 3−6 h for the phytoalexin production, which is likely to be regulated by long-lasting MAP kinase activation.

KEYWORDS: *peptide elicitor, plant immunity, phytoalexin, MAP kinases*

INTRODUCTION

Plants face challenges from a variety of pathogens such as bacteria, fungi, and viruses. To maintain their growth and subsequent reproduction against pathogens, plants have evolved unique immune systems.[1,2] When plants sense pathogenic infections, they produce various defense responses, including oxidative burst, reinforcement of the cell wall, phytoalexin synthesis, and hypersensitive response (HR), to protect themselves.[3−5] Plants recognize various molecules derived from the pathogens, which are referred to as either elicitors or pathogen-associated molecular patterns, to initiate a series of defense responses.[6]

Elicitors with various chemical properties have been reported. Peptides are among the most well-studied elicitors, which include the following: flg22, a 22 amino acid peptide from bacterial flagellin; elf18, an 18 amino acid peptide from bacterial elongation factor Tu; and Pep13, a 13 amino acid peptide from transglutaminase of *Phytophthora sojae*.[7−9] In addition, several endogenous peptide elicitors released from host plants upon wounding and/or infection were identified. For example, a 23 amino acid peptide AtPep1 was isolated from *Arabidopsis* and its orthologue ZmPep1 from maize.[10,11] These elicitors are mainly perceived by distinct receptor-like kinases (RLKs). RLKs activate the downstream signaling networks controlled by mitogen-activated protein (MAP) kinase and/or calcium-dependent protein kinase cascades, which further regulate the production and the activity of transcription factors, enzymes, hormones, and phytoalexins.[12]

Recently, we discovered a peptide elicitor (YGIHTH-NH_2, PIP-1) by screening of a synthetic combinatorial random hexapeptide library.[13] PIP-1 induces typical defense responses, such as oxidative burst, phytoalexin biosynthesis, and defense-related gene expressions, in tobacco cells via a jasmonic acid signaling pathway. Intriguingly, the types of defense responses induced by PIP-1 were different based on its concentration range: oxidative burst, which is observed immediately after treatment of PIP-1, was induced at low micromolar concentrations, but for the induction of capsidiol biosynthesis (Figure 1), which is induced 6−24 h after treatment, 10−50-fold higher concentrations than those required for oxidative burst were necessary. Since PIP-1 is a linear short peptide, it readily undergoes enzymatic degradation in and/or on the surface of the plant cells. Although the exact fate of applied PIP-1 after treatment in the culture media of tobacco cells has not been examined yet, the decreases in PIP-1 concentrations due to degradation may affect the duration of the stimulation of immune systems, leading to failure to induce late-stage defense responses such as phytoalexin biosynthesis.

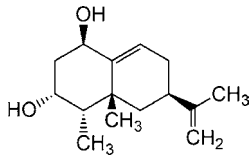

Figure 1. Structure of capsidiol.

In the present study, we hypothesized that inhibition of enzymatic degradation of PIP-1 can change the profile of

Received: April 9, 2014
Revised: May 30, 2014
Accepted: June 2, 2014
Published: June 2, 2014

ACS Publications © 2014 American Chemical Society

induced defense responses in tobacco, in which oxidative burst and phytoalexin production would be induced at the similar concentration range. Therefore, a degradation-resistant PIP-1 analogue was designed based on the degradation profile of PIP-1. Using this analogue, we examined the effect of elicitor stabilization on induction of defense responses including oxidative burst, phytoalexin biosynthesis, and HR-like cell death. To our knowledge, this is the first report demonstrating that enzymatic degradation of elicitors in the culture media considerably affects the induction of defense responses, particularly those in the late stage, such as phytoalexin biosynthesis in tobacco cells.

MATERIALS AND METHODS

Plant Cell Culture. Suspension-cultured tobacco cells (*Nicotiana tabacum* cv. Xanthi) were grown in a 100 mL Erlenmeyer flask with 25 mL of liquid Linsmaier and Skoog (LS) medium at pH 5.75 containing 1-napthalenacetic acid (10 μM), 5-benzyladenine (1 μM), and 3% sucrose. The cell suspensions were maintained at 25 °C under continuous illumination on a rotary shaker (100 rpm) with subculture every 2 weeks and used at 9 and 10 days after subculture for experiments.

Chemicals. *N*-(9-Fluorenylmethoxycarbonyl) (Fmoc)-protected amino acids, Fmoc-NH-SAL resin, and Cl-Trt(2-Cl) resin were purchased from Watanabe Chemical Industries (Hiroshima, Japan). (Carboxymethylaminocarbonyl)-4,4′-bis(dimethylamino)-diphenylamine sodium salt (DA-64) was obtained from Wako Pure Chemical Industries (Osaka, Japan). The peptides YGIHTH-NH_2, YGIHTH-OH and D-(YGIHTH)-NH_2 were previously synthesized in our laboratory.[13] K252a was obtained from LC laboratories (Woburn, MA).

Synthesis of Peptide Analogues. PIP-1 analogues (YGIHT-OH, YGIH-OH, and YGIHTmeA-NH_2) were manually synthesized by using the Fmoc-based solid-phase peptide synthesis technique. The C-terminal amino acids of YGIHT-OH and YGIH-OH were attached to Cl-Trt(2-Cl) resin, and that of YGIHTmeA-NH_2 was attached to Fmoc-NH-SAL resin. Fmoc was deprotected with 20% piperidine in *N*,*N*-dimethylformamide (DMF) three times for 3, 3, and 20 min. Each Fmoc-protected amino acid (3 equiv) was coupled in the presence of *O*-(benzotriazole-1-yl)-1,1,3,3-tetramethyluronium hexafluorophosphate (3 equiv), 1-hydroxybenzotriazole (3 equiv), and *N*,*N*-diisopropylethylamine (6 equiv) in DMF. The reaction was monitored by Kaiser test.[14] After completion of the coupling reaction, the resin was sequentially washed with DMF, diethyl ether, and methanol and dried in vacuo. Cleavage of peptides from the resin and removal of side-chain protecting groups were carried out using the solution A (trifluoroacetic acid (TFA)/triisopropylsilane (TIPS)/dimethoxybenzene (92.5:2.5:5, v/v/v)) for YGIHTmeA-NH_2 and solution B ((TFA/TIPS/distilled water (95:2.5:2.5, v/v/v)) for YGIHT-OH and YGIH-OH, which were reacted with each resin for 2 h at room temperature. After the resin was removed by filtration, cold diethyl ether was added to the filtrate to precipitate the peptides, followed by washing with cold diethyl ether twice and drying in vacuo. The desired peptides were purified by high-performance liquid chromatography (HPLC) using a 250 mm × 10 mm i.d., 5 μm, protein and peptide C18 semipreparative column (Grace, Columbia, MD), and lyophilized. Peptides were identified by electrospray ionization liquid chromatography/mass spectrometry (ESI-LC/MS) on a Shimadzu LCMS-2010 (Kyoto, Japan).

Evaluation of Degradation of PIP-1 and Its Analogues. Tobacco cells were collected using Miracloth (Calbiochem, San Diego, CA), and 0.2 g of cells was resuspended in a microtube containing 1 mL of LS medium. The cells were incubated for 1 h at 25 °C by a tube rotator, and the solution of PIP-1 or its analogues in distilled water (final concentration of 10 μM) was added to the cells. After incubation at 25 °C for a given time period (0−24 h), the media were collected and filtered through syringe filters (0.45 μm pore size). The filtrates were frozen in liquid nitrogen and stored at −80 °C to prevent further peptide degradation. Each sample was subjected to HPLC analysis using a 150 mm × 2.1 mm i.d., 3 μm, Discovery BIO wide pore C18 column (Supelco, St. Louis, MO) for quantitation. The following condition was used for HPLC analysis: flow rate, 0.2 mL/min; column temperature, 40 °C; mobile phase, 0.1% TFA in H_2O (solvent A) and 0.1% TFA in acetonitrile (solvent B); gradient, 10−30% solvent B for 20 min; UV detection, 215 nm. The amount of peptides in the medium was determined based on a calibration curve constructed using the synthesized standard peptides. Degradation products were identified by comparison of their m/z values and retention times on ESI-LC/MS analysis using an LCMS-2020 (Shimadzu) with those of the synthesized standard peptides.

Measurement of H_2O_2 Generation. H_2O_2 generation was measured as described previously.[15] Briefly, tobacco cells (0.2 g) resuspended in 1 mL of assay buffer (175 mM mannitol, 0.5 mM $CaCl_2$, 0.5 mM K_2SO_4, 2.0 mM MES, pH 5.75) were incubated for 1 h at 25 °C using a tube rotator. After incubation, the cells were treated with PIP-1 analogues (10 μL) and incubated for a given time period (0−12 h) including 2 min to allow cell sedimentation. The supernatants (60 μL) of cell suspension were mixed with the H_2O_2 indicator solution (140 μL; 100 mM DA-64, 1 U/mL horse radish peroxidase, 100 mM PIPES, pH 7.0) in a 96-well microplate, and incubated for 10 min at 37 °C. The absorbance at 727 nm was read with a Benchmark microplate reader (Bio-Rad, Hercules, CA). The amount of H_2O_2 was determined based on a calibration curve.

Quantitation of Capsidiol. Capsidiol was quantitated as described previously.[13] Tobacco cells (0.6 g) resuspended in 3 mL of LS medium were incubated for 1 h. The cells were treated with PIP-1 analogues and incubated for 24 h at 25 °C on a rotary shaker under continuous illumination. After incubation, the culture medium was extracted twice with 4 mL of ethyl acetate and dried in vacuo. The residue was dissolved in 1 mL of ethyl acetate and subjected to QP-2010 gas chromatography/MS (GC/MS) analysis (Shimadzu), equipped with a 30 m × 0.25 mm, 0.25 μm phase thickness, DB-5MS capillary column (J&W Scientific, Folsom, CA). For GC separation, helium was used as a carrier gas (100 kPa), and splitless injections were carried out at 220 °C. The column temperature was initially set at 100 °C for 2 min, then increased up to 270 °C at a rate of 4 °C/min for 42.5 min, and held at 270 °C for 2 min. The interface and ion source were set at 270 and 200 °C, respectively. Spectra were acquired in electron ionization mode with a scan range of m/z 45−500. Capsidiol was identified by comparison of spectra and retention times with authentic standards obtained from *Capsicum annuum* fruits.[16] The amount of capsidiol was quantitated from peak areas of the total ion chromatogram, based on a calibration curve constructed with authentic standards.

Cell Death Assay. Cell death assay was performed as described previously with slight modifications.[17] Tobacco cells (0.2 g) resuspended in 1 mL of LS medium were incubated for 1 h. The cells were treated with PIP-1 analogues and incubated for 24 h at 25 °C using a tube rotator. After incubation, the solution of Evans blue (Wako Pure Chemical Industries) was added into the cell suspension to a final concentration of 0.01%. The cells were reincubated for 15 min and then washed 3 times with distilled water to remove the unabsorbed dye. Washed cells were transferred into 50% methanol containing 1% SDS to extract the dye in the dead cells. After incubation for 1 h at 60 °C, the cells were centrifuged for 15 min at 1900*g*. Absorbance at 595 nm of the supernatant was read on a microplate reader (Bio-Rad).

Analysis of Gene Expressions. Tobacco cells (0.6 g) resuspended in 3 mL of LS medium were incubated for 1 h at 25 °C. The cells were treated with PIP-1 analogues for a given time period (0−6 h). After removal of the medium by filtration, cells were ground in liquid nitrogen using a mortar and pestle. Total RNA was extracted with Trizol reagent (Life Technologies, Carlsbad, CA) according to the manufacturer's instructions. The RNA (40 μg) was treated with 10 U of RQ1 RNase-free DNase (Promega, Madison, WI) for 30 min at 37 °C and then extracted by phenol and chloroform. Resultant RNA (1 μg) was reverse transcribed to cDNA in a final volume of 20 μL by using a PrimeScript RT reagent kit (Takara Bio, Otsu, Japan) according to the manufacturer's instructions. For

semiquantitative reverse transcription polymerase chain reaction (RT-PCR), 1 μL of the cDNA template was used for PCR in a solution (final volume of 20 μL) containing 0.5 U of TaKaRa Ex Taq (Takara Bio), 200 μM each of dNTP mixture, and 0.3 μM each of forward and reverse primers: *SIPK*, 5′-GATGTCTGATGCGGGGGCGG-3′ and 5′-GTGGCTCAACGTCGCCGGAA-3′; *WIPK*, 5′-CGGTGGAGGTCAATTCCCTG-3′ and 5′-CATTTACCAAAAGGTTGCTC-3′;[18] *Actin*, 5′-CCATTGGCTCAGAGAGGTTC-3′ and 5′-GTTGGAAGGTGCTGAGAG-3′.[19] PCR was performed on a T100 thermal cycler (Bio-Rad) at 95 °C for 3 min (first cycle), 95 °C for 30 s (denaturation), 54−56 °C for 30 s (annealing), 72 °C for 60 s (extension; 26−28 cycles), and 72 °C for 5 min (last cycle). PCR products were separated on a 2% or 3% agarose gel and stained by EtBr (0.5 μg/L) for visualization. For quantitative RT-PCR, 2 μL of the cDNA template was amplified on a Thermal Cycler Dice (Takara Bio) in the presence of amplification buffer (25 μL of final volume) containing SYBR Premix Ex *Taq*II (Takara Bio) and 0.4 μM each of following forward and reverse primers: *HMGR2*, 5′-GAGGGGAGAGGAAAGTCTGTAG-3′ and 5′-TCTCTATGTTCTGAGCTGGGTC-3′; *EAS*, 5′-GTAAGGACTCATGCTGACGA-3′ and 5′-TCCACCACCTTGATACTTCG-3′. The relative quantities were determined using *Actin* as a reference gene.

In-Gel Kinase Assay. Protein extraction and an in-gel kinase assay were performed as described previously with modifications.[20] Tobacco cells (0.6 g) resuspended in 3 mL of LS medium were incubated for 1 h at 25 °C. Cells were treated with PIP-1 analogues for a given time period (0−9 h). After removal of medium, tobacco cells were ground in liquid nitrogen using a mortar and pestle. Powdered tobacco cells were homogenized with 1.5 mL of extraction buffer (50 mM HEPES, pH 7.4, 5 mM EDTA, 5 mM EGTA, 5 mM DTT, 10 mM NaF, 10 mM Na_3VO_4, 50 mM β-glycerophosphate, 1 mM 4-(2-aminoethyl)-benzenesulfonyl fluoride, 2 μg/mL antipain, 2 μg/mL aprotinin, and 2 μg/mL leupeptin) and centrifuged at 16 000*g* for 30 min at 4 °C. Supernatants were quickly frozen in liquid nitrogen and stored at −80 °C. Extracts containing 10 μg of proteins were electrophoresed on 12% SDS-polyacrylamide gels embedded with 0.25 mg/mL myelin basic protein (MBP) (Sigma, St. Louis, MO) as a kinase substrate. After electrophoresis, the gel was washed with washing buffer (20% 2-propanol, 50 mM Tris, pH 8.0) three times for 20 min each at room temperature to remove SDS and incubated with buffer A (50 mM Tris, pH 8.0, 5 mM DTT) for 1 h. The proteins in the gel were denatured in denaturation buffer (50 mM Tris−HCl, pH 8.0, 6 M guanidine·HCl, 20 mM DTT, 2 mM EDTA) twice for 30 min each. The kinases were allowed to renature on incubation with buffer A containing 0.04% Tween 20 overnight at 4 °C with five changes of buffer. After equilibration with assay buffer (50 mM HEPES, pH 8.0, 2.0 mM DTT, 0.1 mM EGTA, and 20 mM $MgCl_2$) for 30 min at room temperature, the gel was incubated in 20 mL of assay buffer containing 30 μM ATP and 1.85 MBq of [γ-^{32}P]-ATP (111 TBq/mmol) (PerkinElmer, Waltham, MA) for 1 h at room temperature. The reaction was stopped by transferring the gel into the solution containing 10% trichloroacetic acid (w/v) and 1% sodium phosphate (w/v). The gel was washed five times with the same solution for 2 h each to remove unincorporated [γ-^{32}P]-ATP and dried on filter paper using a vacuum gel-dryer. The dried gel was exposed to BAS-MS2040 imaging plates (Fujifilm, Tokyo, Japan) and analyzed using BAS-2500 (Fujifilm). Prestained size markers (Nacalai Tesque, Kyoto, Japan) were used to estimate the size of the kinases.

RESULTS AND DISCUSSION

Phytoalexin Production Induced by PIP-1. Capsidiol is a major sesquiterpene phytoalexin accumulated in the extracellular medium of tobacco cells after elicitor treatment (Figure 1), which is synthesized through the mevalonate pathway in plants.[21,22] Treatment with PIP-1 at a 100 μM concentration induced a significant amount of capsidiol (4.24 ± 0.51 μg/g FW) in tobacco cells, whereas no capsidiol was detected after treatment with distilled water alone as reported previously.[13] On the other hand, only a marginal level of capsidiol production (0.04 ± 0.07 μg/g FW) was observed upon treatment with 10 μM of PIP-1, which is a 4.5-fold higher concentration than that required for a half-maximum response of oxidative burst. Oxidative burst is an early stage defense response initiated within 5 min, whereas phytoalexin production is a late-stage response observed 6−24 h after elicitor treatment.[23] Since linear peptides such as PIP-1 could be easily degraded in the presence of living cells, we assumed that a rapid decrease in PIP-1 concentrations due to the degradation was attributed to the requirement of high concentrations to induce phytoalexin biosynthesis. This also implies that early short stimulation by PIP-1 may not be enough for induction of phytoalexin biosynthesis. To explore this hypothesis, we first examined the effect of the duration of PIP-1 stimulation on capsidiol production by using various sample treatment procedures. When PIP-1 was removed from the culture media by washing the cells with fresh medium 1 h after treatment at 100 μM, no capsidiol production was detected. To further confirm that long-term stimulation by PIP-1 is required for capsidiol production, a small amount of PIP-1 was repeatedly added (1 μM, 10 times) to the medium over 3 h, which amounted to only 10 μM at most. This repeated treatment induced a significant level of capsidiol (2.17 ± 0.61 μg/g FW), indicating that continuous stimulation of the immune system by PIP-1 is required for capsidiol production in tobacco cells. These results motivated us to synthesize a degradation-resistance PIP-1 analogue, which should allow the induction of phytoalexin biosynthesis at low micromolar concentrations.

Design of Degradation-Resistant PIP-1. Prior to finding a way of preventing the degradation of PIP-1, we investigated its degradation process in the presence of tobacco cells by LC/MS analysis. While PIP-1 (m/z observed for $[M+2H]^{2+}$: 363.8) was detected in the extracellular medium at a retention time of 13.8 min immediately after its treatment at 10 μM, a new peak with m/z of 364.3 at a retention time of 14.9 min appeared as early as after 15 min (Figure 2). The observed molecular mass

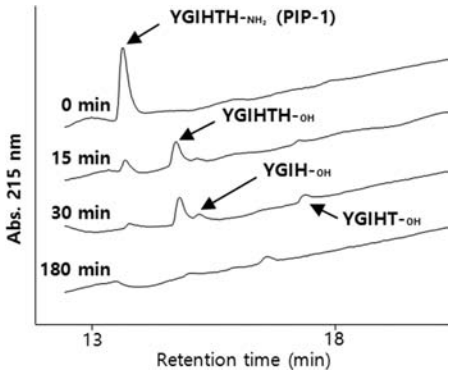

Figure 2. Degradation of PIP-1 (10 μM) in the culture medium of tobacco cells analyzed by LC/MS. Only LC/UV chromatograms were shown. Each peak was identified using synthesized standards.

was consistent with that of C-terminally deamidated PIP-1 (YGIHTH-OH, m/z calculated for $[M+2H]^{2+}$: 364.2).[13] After 30 min, two other peaks were detected at the retention times of 15.2 min (m/z 245.3) and 17.4 min (m/z 295.7), which were respectively identified to be YGIH-OH (m/z calculated for $[M+2H]^{2+}$: 245.1) and YGIHT-OH (m/z calculated for $[M+2H]^{2+}$: 295.7), based on the comparison with synthesized standards.

dx.doi.org/10.1021/jf501679p | J. Agric. Food Chem. 2014, 62, 5781−5788

Thereafter, PIP-1 and these degradation products underwent further degradation, and neither of them could be detected 3 h after the treatment. Thus, PIP-1 was found to be hydrolyzed rapidly from its C-terminal residue. This degradation could be catalyzed by proteases present in the extracellular space because PIP-1 cannot enter the cells due to its hydrophilic nature. In plants, several proteases have been identified from the extracellular space,[24] some of which are induced by pathogen infection.[25] Although further investigation is needed, proteases responsible for degradation of PIP-1 might be associated with defense responses in tobacco cells.

The bioassay data showed that, while YGIHTH-OH was significantly elicitor-active, YGIHT-OH and YGIH-OH were practically inactive, so it is noted that the activity was lost in the media within 3 h at the longest. This result supports the findings that the repeated additions of PIP-1 could induce the capsidiol production even at low concentrations.

On the basis of this degradation profile, we designed a degradation-resistant analogue of PIP-1 (Figure 3). Since

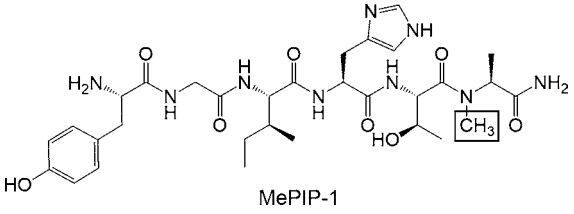

Figure 3. Structure of degradation-resistant PIP-1 analogue (MePIP-1).

methylation of amide nitrogen is known to improve stability against enzymatic degradation,[26,27] we introduced an N-methylated Ala residue into PIP-1 to substitute the C-terminal His residue, taking the observed hydrolysis of PIP-1 from the C-terminal end into consideration. As the previous study showed that the substitution of the C-terminal His residue with Ala had little effect on elicitor activity,[13] the PIP-1 analogue having N-methylated Ala at the C-terminus (MePIP-1) exhibited rather higher activity (about 3.5-fold) than PIP-1, in terms of oxidative burst induction. This is possibly due to a conformation change of the peptide as a consequence of N-methylation at the C-terminal residue, which may favorably interact with the receptor.[27,28] Since PIP-1 is likely to be recognized by the membranous receptors of plant cells,[13] the effect of a possible increase in intracellular uptake due to N-methylation can be ruled out.

We then monitored the degradation of MePIP-1 and compared it with that of PIP-1. When the tobacco cells were treated at 10 μM, MePIP-1 was present at 78% of the initial concentration after 3 h and was still detectable at 30% even after 24 h (Figure 4). This was in good contrast with the case of PIP-1, which was rapidly decreased to 3% of the initial concentration in 1 h upon the treatment with at 10 μM and completely disappeared after 3 h. The survival time of PIP-1 was extended to some extent when its initial concentration was raised to 100 μM, but it was decreased to an almost undetectable level as early as 6 h after the treatment. In this case, however, a significant level of elicitor-active YGIHTH-OH was present even after 6 h, which likely contributed to the induction of capsidiol production at least in part. Since no degradation products of MePIP-1 were detected 24 h after treatment, apparent reduction of MePIP-1 was likely due to its

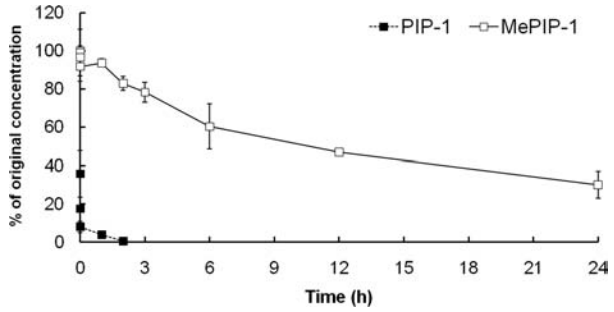

Figure 4. Comparison of degradation profiles of PIP-1 (10 μM) and MePIP-1 (10 μM) in the culture medium of tobacco cells. Vertical bars indicate ± SD of three independent replicates.

adsorption to tobacco cell surfaces rather than degradation. To confirm this, we evaluated the effect of adsorption using an elicitor-inactive but degradation-resistant PIP-1 analogue (D-PIP-1), which is composed of all D-forms of amino acid residues.[13] As expected, D-PIP-1 showed a decrease similar to MePIP-1 through 24 h incubation with tobacco cells. These results clearly indicate that MePIP-1 is highly resistant to enzymatic degradation in the presence of tobacco cells.

Defense Responses Induced by MePIP-1. We investigated the effect of degradation-resistance of MePIP-1 on defense responses induced in tobacco cells. In terms of the oxidative burst, both PIP-1 and MePIP-1 induced similar H_2O_2 production profiles over 12 h (Figure 5A). On the other hand, a significant difference was observed for capsidiol production between PIP-1 and MePIP-1. Treatment with 10 μM MePIP-1 induced significant capsidiol production (4.7 μg/g FW), whereas marginal levels of capsidiol were induced by 10 μM PIP-1 (Figure 5B). To confirm that this difference was due to its degradation-resistance, MePIP-1 was removed from the medium by washing the cells after treatment. As expected, no capsidiol production was observed when MePIP-1 was removed 1 or 3 h after treatment (Figure 5C). However, washing the cells 6 or 9 h after the treatment had no effect on the induction of capsidiol production, although the amount was relatively low. These results indicate that the degradation-resistance of MePIP-1 critically contributes to its higher potency in inducing capsidiol production by enabling the continuous stimulation of the immune system. Induction of HR-like cell death, which is also a late-stage defense response, was then examined (Figure 5D). As expected, a significant difference was observed between MePIP-1 and PIP-1: only MePIP-1 induced cell death when they were treated at 10 μM. This suggests that continuous stimulation by PIP-1 is also required for the HR induction, like in the case of capsidiol production.

Effects of MePIP-1 on MAP Kinase Activity. We then investigated the factors involved in triggering capsidiol biosynthesis in tobacco cells through continuous stimulation by MePIP-1. MAP kinase cascades play pivotal roles in signaling events associated with the recognition of pathogen and/or elicitors, which crucially affect downstream signaling events for induction of defense responses.[12] It is known that activation of salicylic acid induced protein kinase (SIPK) and/or wound-induced protein kinase (WIPK), representative MAP kinases in tobacco, is involved in defense responses induced by elicitors.[29,30] To investigate the possible involvement of MAP kinase activation in capsidiol production induced by MePIP-1, we first examined the effect of a kinase inhibitor on capsidiol production. When K252a, a general protein kinase inhibitor,

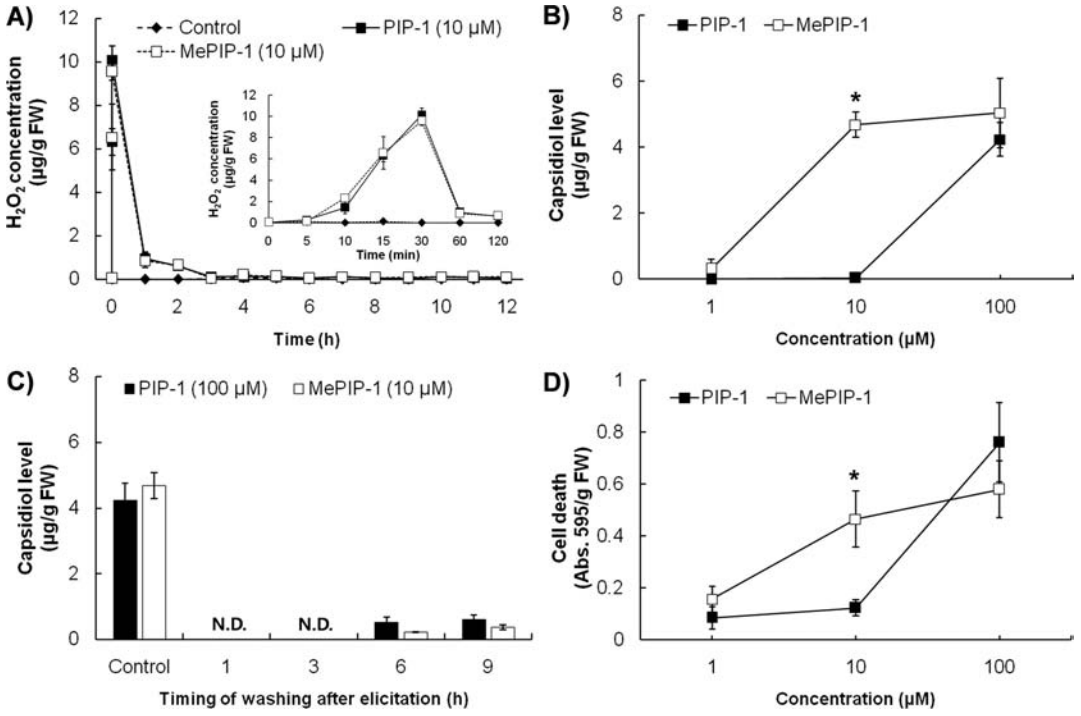

Figure 5. Comparisons of defense responses induced by PIP-1 and MePIP-1 in tobacco cells. (A) Time-course of H_2O_2 generation. Inset shows the enlarged view for 2 h after treatment. (B) Dose dependence of capsidiol production 24 h after treatment. (C) Effect of cell washing on capsidiol production. Amounts of capsidiol were quantitated 24 h after elicitation. (D) Dose dependence of HR-like cell death 24 h after treatment. Asterisks indicate significant differences at $P < 0.05$ according to the Student's paired t test. Vertical bars indicate ± SD of three independent replicates.

was added to the tobacco cells before addition of MePIP-1, production of capsidiol was inhibited in a dose-dependent manner (Figure 6). This suggested that activation of MAP

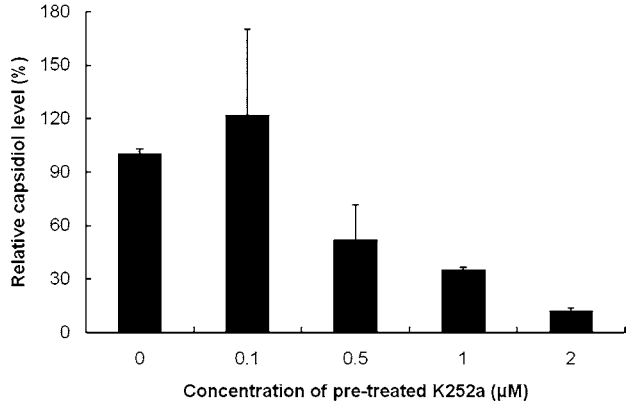

Figure 6. Inhibitory effect of K252a on capsidiol production induced by MePIP-1. Amounts of capsidiol were quantitated 24 h after treatment with MePIP-1. Capsidiol production without treatment with K252a was set at 100%. Vertical bars indicate ± SD of three independent replicates.

kinases, such as SIPK or WIPK, may be associated with capsidiol production. Thus, the effect of MePIP-1 on activation of SIPK and WIPK was investigated to examine its potential relevance to continuous elicitor stimulation prerequisite for capsidiol production. We first examined the expression of *SIPK* and *WIPK* transcripts. Consequently, no significant difference was observed between PIP-1 and MePIP-1 for induction of *SIPK* and *WIPK* transcripts (Figure 7A). Since it is known that the activity of these MAP kinases is regulated post-translation-

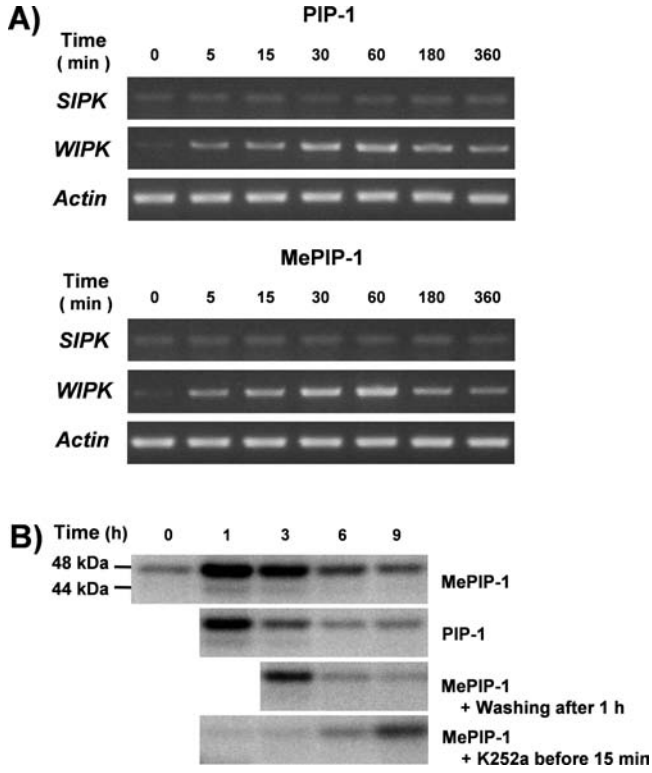

Figure 7. Effect of MePIP-1 on activation of MAP kinases. (A) Accumulation of transcripts of MAP kinases in response to PIP-1 and MePIP-1 at 10 μM. *Actin* was used as a control. (B) Activation of MAP kinases after treatment with PIP-1 or MePIP-1 at 10 μM. Activity was monitored by the in-gel kinase assay using MBP as a substrate.

dx.doi.org/10.1021/jf501679p | J. Agric. Food Chem. 2014, 62, 5781−5788

ally by phosphorylation, not by an increase in transcript or protein levels,[29,30] we then examined whether these MAP kinases are differently activated by PIP-1 and MePIP-1 by an in-gel kinase assay. Upon treatment of either PIP-1 or MePIP-1, a significant activation of a 48 kD kinase, which corresponds to SIPK, was observed. However, a considerable difference between PIP-1 and MePIP-1 was observed for their activation of SIPK in the late phase (Figure 7B). SIPK was activated 1 h after the treatment with PIP-1 but rapidly decreased to a base level after 6 h. In contrast, MePIP-1 induced a long-lasting activation of SIPK even up to 9 h after the treatment. When MePIP-1 was removed from the medium 1 h after the treatment by washing of the cells, SIPK activity was decreased 6 h after the treatment, which was similar to that of PIP-1 treatment. These results clearly indicate that a prolonged SIPK activation is induced by a continuous stimulation by MePIP-1. In addition, when K252a (1 μM) was pretreated, activity of SIPK was significantly suppressed. In this case, activation was observed 9 h after treatment, but it could have been caused by inactivation of the inhibitor, probably by its degradation.[31] These results strongly suggest that a prolonged SIPK activation is necessary for the activation of downstream signaling events that could be associated with capsidiol production.

It is known that the strength of a defense response can be influenced by the magnitude and duration of MAPK activation. For instance, cryptogein, a proteinaceous elicitor derived from *Phytophthora cryptogea*, caused a prolonged activation of both SIPK and WIPK, which is necessary for induction of late-stage defense responses, such as HR-like cell death and long-lasting production of reactive oxygen species, in tobacco cells.[32] When cryptogein was removed from the medium 0.5 h after treatment, no induction of HR-like cell death was observed, which coincided with rapid inactivation of both SIPK and WIPK. On the other hand, fungal cell wall elicitor, which induced only transient SIPK activation, failed to induce the late-stage responses such as HR-like cell death.[29] Although the reason why the fungal cell wall elicitor could not induce prolonged SIPK activation is unknown at present, it is possible that the enzymatic degradation of the elicitor by plant cells may be responsible for transient SIPK activation, which leads to failure to induce the late-stage responses, like in the case of PIP-1. Thus, the duration of SIPK activation may determine the induction of late-stage defense responses, which could be regulated transcriptionally and/or post-translationally.

Capsidiol Biosynthesis-Related Gene Expression Induced by MePIP-1. To examine the possible involvement of transcriptional regulation of capsidiol biosynthesis through prolonged SIPK activation, expression of capsidiol biosynthesis-related genes was investigated. Capsidiol is synthesized via the mevalonate pathway in plants.[21,22] In this pathway, 3-hydroxy-3-methylglutaryl CoA reductase (HMGR) is considered to be a key enzyme,[33] which catalyzes the rate-limiting step in the biosynthesis of all isoprenoid compounds, including capsidiol. The transcription level of this gene is known to be regulated by elicitor recognition.[34,35] Farnesyl pyrophosphate (FPP) is synthesized from mevalonate in several steps and is located at a final branch point for sesquiterpene and sterol synthesis. FPP is converted to capsidiol in several steps including the reaction catalyzed by 5-epi-aristolochene synthase (EAS), which is demonstrated to be induced in response to elicitor treatment.[21] To evaluate whether the degradation-resistance of MePIP-1 affects the transcription level of these capsidiol biosynthesis-related genes, we examined the expression of *HMGR2* and *EAS* genes after treatment either with PIP-1 or MePIP-1 using quantitative RT-PCR. Since continuous activation by MePIP-1 for 3−6 h was shown to be required for capsidiol biosynthesis in our result, we analyzed the gene expression 4 h after the treatment with PIP-1 or MePIP-1. Consequently, expression of these genes was induced by both PIP-1 and MePIP-1, and no statistically significant difference was observed between them (Figure 8). To further examine the effect of the degradation-

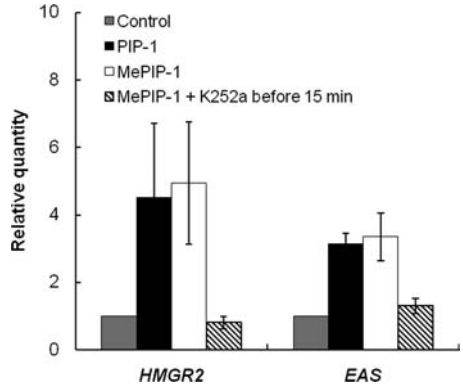

Figure 8. Relative transcription levels of capsidiol biosynthesis-related genes in response to PIP-1 and MePIP-1 at 10 μM. Values are the mean of three independent replicates. Vertical bars indicate ± SD.

resistance of MePIP-1 on the expression of *HMGR2* and *EAS* transcripts, time-course analysis for up to 18 h was conducted for both PIP-1 and MePIP-1. Again, no significant difference in these expression profiles was observed between them. These results indicate that the early short stimulation by PIP-1 is sufficient for expression of *HMGR2* and *EAS* genes but not enough for capsidiol biosynthesis. On the other hand, no induction of these genes was observed when K252a (1 μM) was pretreated (Figure 8), suggesting that the activation of SIPK in the early phase (<3 h) is necessary for induction of expression of these genes.

Isoprenoids play essential roles in plants as primary and secondary metabolites, which are synthesized in response to environmental and developmental cues or pathogen infection.[36] Biosynthesis of each isoprenoid is regulated at transcript and protein levels to control precursor availability via activation of biosynthesis-related enzymes or suppression of other branch-points.[37] In the present study, we found that the expression of *HMGR2* and *EAS* genes was induced by early short stimulation by PIP-1 but capsidiol production was initiated only after continuous stimulation by PIP-1. These facts suggest that capsidiol biosynthesis induced by PIP-1 is regulated translationally or post-translationally through long-lasting SIPK activation.

The early short-term activation of SIPK by PIP-1, which leads to increases in expression levels of capsidiol biosynthesis-related genes without production of capsidiol, could be comparable to the actions of chemicals referred to as "plant activators" that have so-called defense priming effects. These chemicals are known to stimulate the plant into a primed state, where the signal systems are ready for inducing the defense responses but still remain inactive.[38,39] Once activated into this primed state, the plant is able to display much faster and robust defense responses against subsequent biotic or abiotic stresses, compared to the nonprimed plant.[40−42] Conrath et al.[40] hypothesized that the primed plant accumulates the crucial

transcription factors to induce the relevant defense-related genes enabling their rapid expression in response to the subsequent stimulus. In *Arabidopsis*, priming is associated with the accumulation of the inactive forms of MPK3 and MPK6, orthologues of WIPK and SIPK, respectively.[39] Upon exposure to subsequent stress, these kinases are strongly activated to induce the enhanced defense responses. Thus, the state of the tobacco cells after the short-term stimulation by PIP-1 could be analogous to the primed state, where SIPK is transiently activated and mRNAs of WIPK and capsidiol biosynthesis-related enzymes are accumulated, and is ready for inducing the strong defense responses by the following continuous recognition of PIP-1. From an economic point of view, full activation of immune systems for the continuous production of phytoalexin or large-scale cell death is considered to require a substantial fitness cost and to be disadvantageous to the normal growth of the plant. Therefore, priming is believed to be more effective for the protection of plants from various stresses without major trade-off effects on growth and reproduction. The results of this study suggest that the plant may have a "suspending" system regarding the induction of defense reactions. The complete set of defense reactions are not induced until the plant judges the attack of a pathogen to be quite serious after continuously monitoring the elicitors for several hours, which should be beneficial for maintaining the balance of energy used for defense and growth.

In summary, we observed that PIP-1 was rapidly degraded in the media of suspension-cultured tobacco cells, probably by proteases from the cells. To prevent the degradation of PIP-1, we synthesized a degradation-resistant analogue, MePIP-1, in which the C-terminal His residues was substituted with Ala and the amide bond between fifth and sixth residues of PIP-1 was N-methylated. MePIP-1 induced H_2O_2 generation with a time-course similar to that by PIP-1, whereas significant differences were seen between PIP-1 and MePIP-1 in the late-stage defense responses such as phytoalexin production and HR-like cell death. Using the degradation-resistant PIP-1 analogue, we found that continuous stimulation of the immune system by PIP-1 is necessary for the induction of late-stage defense responses, and whether the late-stage responses are induced or not may depend on the duration of SIPK activation caused by the continuous elicitor stimulation.

■ ASSOCIATED CONTENT

Supporting Information

Extracted ion chromatograms of PIP-1 and its degradation products (Figure S1); degradation profile of PIP-1 at 100 μM (Figure S2); concentration changes of D-PIP-1 in the culture medium of tobacco cells (Figure S3); time-course analysis of *HMGR2* and *EAS* expression (Figure S4); and H_2O_2 generation activity of PIP-1 analogues (Table S1). This material is available free of charge via the Internet at http://pubs.acs.org.

■ AUTHOR INFORMATION

Corresponding Author

*Phone/fax: +81-75-753-6123; e-mail: miyamasa@kais.kyoto-u.ac.jp.

Funding

This study was partly supported by MEXT KAKENHI (grant nos. 21710226 and 23580148), Japan.

Notes

The authors declare no competing financial interest.

■ ACKNOWLEDGMENTS

We are grateful to Professor Ritsuo Nishida and Dr. Hajime Ono (Kyoto University) for quantitative RT-PCR analysis and to Professor Qing X. Li (University of Hawaii) for critical reading of the manuscript.

■ REFERENCES

(1) Nürnberger, T.; Brunner, F.; Kemmerling, B.; Piater, L. Innate immunity in plants and animals: Striking similarities and obvious differences. *Immunol. Rev.* **2004**, *198*, 249−266.

(2) Ausubel, F. M. Are innate immune signaling pathways in plants and animals conserved? *Nat. Immunol.* **2005**, *6*, 973−979.

(3) Hammond-Kosack, K. E.; Jones, J. D. Resistance gene-dependent plant defense responses. *Plant Cell* **1996**, *8*, 1773−1791.

(4) Glazebrook, J. Contrasting mechanisms of defense against biotrophic and necrotrophic pathogens. *Annu. Rev. Phytopathol.* **2005**, *43*, 205−227.

(5) Király, L.; Barna, B.; Király, Z. Plant resistance to pathogen infection: Forms and mechanisms of innate and acquired resistance. *J. Phytopathol.* **2007**, *155*, 385−396.

(6) Bent, A. F.; Mackey, D. Elicitors, effectors, and *R* genes: The new paradigm and a lifetime supply of questions. *Annu. Rev. Phytopathol.* **2007**, *45*, 399−436.

(7) Felix, G.; Duran, J. D.; Volko, S.; Boller, T. Plants have a sensitive perception system for the most conserved domain of bacterial flagellin. *Plant J.* **1999**, *18*, 265−276.

(8) Kunze, G.; Zipfel, C.; Robatzek, S.; Niehaus, K.; Boller, T.; Felix, G. The N terminus of bacterial elongation factor Tu elicits innate immunity in *Arabidopsis* plants. *Plant Cell* **2004**, *16*, 3496−3507.

(9) Brunner, F.; Rosahl, S.; Lee, J.; Rudd, J. J.; Geiler, C.; Kauppinen, S.; Rasmussen, G.; Scheel, D.; Nurnberger, T. Pep-13, a plant defense-inducing pathogen-associated pattern from *Phytophthora* transglutaminases. *EMBO J.* **2002**, *21*, 6681−6688.

(10) Huffaker, A.; Pearce, G.; Ryan, C. A. An endogenous peptide signal in *Arabidopsis* activates components of the innate immune response. *Proc. Natl. Acad. Sci. U.S.A.* **2006**, *103*, 10098−10103.

(11) Huffaker, A.; Dafoe, N. J.; Schmelz, E. A. ZmPep1, an ortholog of *Arabidopsis* elicitor peptide 1, regulates maize innate immunity and enhances disease resistance. *Plant Physiol.* **2011**, *155*, 1325−1338.

(12) Meng, X.; Zhang, S. MAPK cascades in plant disease resistance signaling. *Annu. Rev. Phytopathol.* **2013**, *51*, 245−266.

(13) Miyashita, M.; Oda, M.; Ono, Y.; Komoda, E.; Miyagawa, H. Discovery of a small peptide from combinatorial libraries that can activate the plant immune system by a jasmonic acid signaling pathway. *ChemBioChem* **2011**, *12*, 1323−1329.

(14) Kaiser, E.; Colescott, R. L.; Bossinger, C. D.; Cook, P. I. Color test for detection of free terminal amino groups in the solid-phase synthesis of peptides. *Anal. Biochem.* **1970**, *34*, 595−598.

(15) Miyata, K.; Miyashita, M.; Nose, R.; Otake, Y.; Miyagawa, H. Development of a colorimetric assay for determining the amount of H_2O_2 generated in tobacco cells in response to elicitors and its application to study of the structure-activity relationship of flagellin-derived peptides. *Biosci. Biotechnol. Biochem.* **2006**, *70*, 2138−2144.

(16) Whiteheah, I. M.; Threlfall, D. R.; Ewing, D. F. *Cis*-9,10-dihydrocapsenone: A possible catabolite of capsidiol from cell suspension cultures of *Capsicum annuum*. *Phytochemistry* **1987**, *26*, 1367−1369.

(17) Kadota, Y.; Watanabe, T.; Fujii, S.; Maeda, Y.; Ohno, R.; Higashi, K.; Sano, T.; Muto, S.; Hasezawa, S.; Kuchitsu, K. Cell cycle dependence of elicitor-induced signal transduction in tobacco BY-2 cells. *Plant Cell Physiol.* **2005**, *46*, 156−165.

(18) Seo, S.; Katou, S.; Seto, H.; Gomi, K.; Ohashi, Y. The mitogen-activated protein kinases WIPK and SIPK regulate the levels of jasmonic and salicylic acids in wounded tobacco plants. *Plant J.* **2007**, *49*, 899−909.

(19) Wang, J.; Ming, F.; Pittman, J.; Han, Y.; Hu, J.; Guo, B.; Shen, D. Characterization of a rice (*Oryza sativa* L.) gene encoding a

temperature-dependent chloroplast ω-3 fatty acid desaturase. *Biochem. Biophys. Res. Commun.* **2006**, *340*, 1209−1216.
(20) Romeis, T.; Piedras, P.; Zhang, S.; Klessig, D. F.; Hirt, H.; Jones, J. D. G. Rapid Avr9- and Cf-9-dependent activation of MAP kinases in tobacco cell cultures and leaves: Convergence of resistance gene, elicitor, wound, and salicylate responses. *Plant Cell* **1999**, *11*, 273−287.
(21) Vögeli, U.; Chappell, J. Induction of sesquiterpene cyclase and suppression of squalene synthetase activities in plant cell cultures treated with fungal elicitor. *Plant Physiol.* **1988**, *88*, 1291−1296.
(22) Kirby, J.; Keasling, J. D. Biosynthesis of plant isoprenoids: Perspectives for microbial engineering. *Annu. Rev. Plant Biol.* **2009**, *60*, 335−355.
(23) Zhao, J.; Davis, L. C.; Verpoorte, R. Elicitor signal transduction leading to production of plant secondary metabolites. *Biotechnol. Adv.* **2005**, *23*, 283−333.
(24) Delannoy, M.; Alves, G.; Vertommen, D.; Ma, J.; Boutry, M. Navarre, C. Identification of peptidases in *Nicotiana tabacum* leaf intercellular fluid. *Proteomics* **2008**, *8*, 2285−2298.
(25) Swaroopa Rani, T.; Podile, A. R. Extracellular matrix-associated proteome changes during non-host resistance in citrus−*Xanthomonas* interactions. *Physiol. Plant.* **2014**, *150*, 565−579.
(26) Cody, W. L.; He, J. X.; Reily, M. D.; Haleen, S. J.; Walker, D. M.; Reyner, E. L.; Stewart, B. H.; Doherty, A. M. Design of a potent combined pseudopeptide endothelin-A/endothelin-B receptor antagonist, Ac-DBhg^{16}-Leu-Asp-Ile-[NMe]Ile-Trp^{21} (PD 156252): Examination of its pharmacokinetic and spectral properties. *J. Med. Chem.* **1997**, *40*, 2228−2240.
(27) Biron, E.; Chatterjee, J.; Ovadia, O.; Langenegger, D.; Brueggen, J.; Hoyer, D.; Schmid, H. A.; Jelinek, R.; Gilon, C.; Hoffman, A.; Kessler, H. Improving oral bioavailability of peptides by multiple N-methylation: Somatostatin analogues. *Angew. Chem., Int. Ed.* **2008**, *47*, 2595−2599.
(28) Chatterjee, J.; Ovadia, O.; Zahn, G.; Marinelli, L.; Hoffman, A.; Gilon, C.; Kessler, H. Multiple N-methylation by a designed approach enhances receptor selectivity. *J. Med. Chem.* **2007**, *50*, 5878−5881.
(29) Zhang, S.; Du, H.; Klessig, D. F. Activation of the tobacco SIP kinase by both a cell wall−derived carbohydrate elicitor and purified proteinaceous elicitins from *Phytophthora* spp. *Plant Cell* **1998**, *10*, 435−449.
(30) Zhang, S.; Liu, Y.; Klessig, D. F. Multiple levels of tobacco WIPK activation during the induction of cell death by fungal elicitins. *Plant J.* **2000**, *23*, 339−347.
(31) Liu, Y.; Jin, H.; Yang, K.-Y.; Kim, C. Y.; Baker, B.; Zhang, S. Interaction between two mitogen-activated protein kinases during tobacco defense signaling. *Plant J.* **2003**, *34*, 149−160.
(32) Kadota, Y.; Fujii, S.; Ogasawara, Y.; Maeda, Y.; Higashi, K.; Kuchitsu, K. Continuous recognition of the elicitor signal for several hours is prerequisite for induction of cell death and prolonged activation of signaling events in tobacco BY-2 cells. *Plant Cell Physiol.* **2006**, *47*, 1337−1342.
(33) Chappell, J.; Nable, R. Induction of sesquiterpenoid biosynthesis in tobacco cell suspension cultures by fungal elicitor. *Plant Physiol.* **1987**, *85*, 469−473.
(34) Choi, D.; Ward, B. L.; Bostock, R. M. Differential induction and suppression of potato 3-hydroxy-3-methylglutaryl coenzyme A reductase genes in response to *Phytophthora infestans* and to its elicitor arachidonic acid. *Plant Cell* **1992**, *4*, 1333−1344.
(35) Takahashi, Y.; Uehara, Y.; Berberich, T.; Ito, A.; Saitoh, H.; Miyazaki, A.; Terauchi, R.; Kusano, T. A subset of hypersensitive response marker genes, including *HSR203J*, is the downstream target of a spermine signal transduction pathway in tobacco. *Plant J.* **2004**, *40*, 586−595.
(36) Chappell, J. Biochemistry and molecular biology of the isoprenoid biosynthetic pathway in plants. *Annu. Rev. Plant Physiol. Plant Mol. Biol.* **1995**, *46*, 521−547.
(37) Vranova, E.; Coman, D.; Gruissem, W. Network analysis of the MVA and MEP pathways for isoprenoid synthesis. *Annu. Rev. Plant. Biol.* **2013**, *64*, 665−700.
(38) Katz, V. A.; Thulke, O. U.; Conrath, U. A benzothiadiazole primes parsley cells for augmented elicitation of defense responses. *Plant Physiol.* **1998**, *117*, 1333−1339.
(39) Beckers, G. J.; Jaskiewicz, M.; Liu, Y.; Underwood, W. R.; He, S. Y.; Zhang, S.; Conrath, U. Mitogen-activated protein kinases 3 and 6 are required for full priming of stress responses in *Arabidopsis thaliana*. *Plant Cell* **2009**, *21*, 944−953.
(40) Conrath, U.; Beckers, G. J. M.; Flors, V.; García-Agustín, P.; Jakab, G.; Mauch, F.; Newman, M.-A.; Pieterse, C. M. J.; Poinssot, B.; Pozo, M. J.; Pugin, A.; Schaffrath, U.; Ton, J.; Wendehenne, D.; Zimmerli, L.; Mauch-Mani, B. Priming: Getting ready for battle. *Mol. Plant−Microbe Interact.* **2006**, *19*, 1062−1071.
(41) Heil, M.; Ton, J. Long-distance signalling in plant defence. *Trends Plant Sci.* **2008**, *13*, 264−272.
(42) Conrath, U. Molecular aspects of defence priming. *Trends Plant Sci.* **2011**, *16*, 524−531.

JOURNAL OF AGRICULTURAL AND FOOD CHEMISTRY

Article

pubs.acs.org/JAFC

Physical and Sensory Characterizations of Oral Coatings of Oil/Water Emulsions

S. Camacho,[†,‡] V. van Riel,[‡] C. de Graaf,[‡] F. van de Velde,[†,§] and M. Stieger*[,†,‡]

[†]TI Food and Nutrition, Post Office Box 557, 6700 AN Wageningen, The Netherlands

[‡]Agrotechnology and Food Sciences Group, Wageningen University, Post Office Box 8129, 6700 EV Wageningen, The Netherlands

[§]NIZO Food Research BV, Post Office Box 20, 6710 BA Ede, The Netherlands

ABSTRACT: The physical and sensory properties of oil coatings on the tongue formed by five oil/water emulsions varying in oil content were investigated. A total of 20 subjects processed orally each emulsion for 30 s in triplicate. *In vivo* fluorescence measurements at the front and back of the anterior tongue were made to quantify the oil fraction deposited at different time points. Calibration lines relating fluorescence intensity to oil fraction were determined using pig tongues at 37.5 °C to mimic oral conditions. The oil fraction on the tongue increased linearly with an increasing oil content of the emulsions. The oil fraction deposited at the back of the anterior tongue was 1.5−2.0× larger than at the front. The intensity of sensory attributes describing after-feel perception was related to the oil fraction by Weber−Fechner's law. This study uses *in vivo* fluorescence to study food behavior in the mouth and unravel new insights in after-feel perception of emulsions.

KEYWORDS: *oral coating, tongue, oral processing, fraction of oil, fluorescence, curcumin, emulsion, sensory perception, mouth-feel sensation, after-feel perception*

INTRODUCTION

Residues of foods and beverages that coat the oral mucosa after consumption are termed oral coatings. Only limited information is available on the chemical and physical properties of oral coatings. A method to quantify the lipid content of oral coatings has been proposed by rinsing the oral cavity after food ingestion and subsequently determining the turbidity of the spat out liquid.[1,2] de Jongh and Janssen used attenuated total reflection infrared (ATR IR) spectroscopy to analyze the chemical composition of oral coatings taken with swabs from distinct parts of the oral cavity.[3] This method allowed us to determine the relative content of fat, protein, and carbohydrate of oral coatings.[3] Pivk et al. developed an *in vivo* method to characterize the thickness of oral oil coatings on the tongue using fluorescence measurements.[4] Fluorescence was quantified with a fluorescence spectrometer coupled with a remote read fiber optic probe fitted with a tip for measurements on surfaces, such as the tongue.[4] Pivk et al. showed that thicker lipid coatings were formed at the back of the anterior tongue compared to the lateral tongue area.[5] The *in vivo* fluorescence method provides a direct measure of the thickness of oral coatings and allows us to study the spatial variation of coatings on the tongue and to link instrumental measurements to sensory perception.[5] Pivk et al. used thickness of the coating as the physical parameter to describe oil coatings.[4,5] Thickness suggests that a continuous, homogeneous film of oil is deposited on the tongue. That may be the case for orally processed oils, as studied by Pivk et al.[4,5] However, most beverages contain oil in water (o/w) emulsions and are stable under in-mouth conditions. When o/w emulsions form an oral deposit, it is likely that the coating consists of individual oil droplets adhering to the tongue surface rather than a continuous, homogeneous oil film. Therefore, the mass of oil deposited on the tongue is a more descriptive parameter to characterize oral coatings formed by o/w emulsions rather than thickness.

The calibration of fluorescence intensity versus coating deposition is a crucial step for the *in vivo* fluorescence method. Pivk et al. calibrated the fluorescence intensity with the thickness of the oil coating by spreading different volumes of medium-chain triglycerides (MCT) oil containing curcumin, a hydrophobic, food-grade fluorescent dye, in a Petri dish at room temperature to obtain oil coatings varying in thickness.[4,5] It is known that fluorescence intensity depends upon the temperature. Therefore, the calibration temperature should reflect the temperature of the coating in the oral cavity. The surface properties used for the calibration can also influence the fluorescence intensity. Thus, the surface should be as similar to the human tongue as possible. The surface of a Petri dish is different from the surface of a human tongue, which is rougher and covered with papillae. Pig tongues are considered to be good models for human tongues.[6,7] Pigs are omnivores, and the anterior part of their tongues is covered by fungiform papillae scattered between filiform papillae similar to human tongues.[8] Filiform papillae of the human and pig tongues have similar shapes.[8]

Oral coatings are one of the known factors that can influence after-feel, mouth-feel perception, and taste. de Wijk et al. demonstrated that fat containing oral coatings lubricate the movement of the food bolus, leading to decreased roughness and increased creaminess perception.[9,10] Lynch et al. showed that oral coatings formed by different oils reduce the subsequent perception of taste intensity of gels.[11] It was

Received: March 4, 2014
Revised: May 30, 2014
Accepted: May 31, 2014
Published: May 31, 2014

ACS Publications © 2014 American Chemical Society

dx.doi.org/10.1021/jf5010868 | J. Agric. Food Chem. 2014, 62, 5789−5795

suggested that oral fat coatings influence taste by modification of the partitioning of specific compounds between food, saliva, and taste receptors or forming a hydrophobic layer creating a physical barrier for hydrophilic tastants, limiting access to taste receptors.[11] Although it is well-known that oral coatings can linger in the mouth after swallowing, little is known about the influence of oral coatings on after-feel sensory perception (mouth-feel perception occurring after swallowing). We hypothesize that psychophysical relationships can describe the link between oil coatings lingering on the tongue after expectoration and after-feel perception.

This study is based on the method previously described by Pivk et al.[4,5] The aims of this study were to (i) develop an appropriate calibration method for *in vivo* fluorescence measurements, which represents closer the *in vivo* conditions occurring in the mouth, (ii) apply the method with the new calibration using o/w emulsions varying in oil content, and (iii) establish psychophysical relationships between oil coatings formed on the tongue and after-feel perception.

MATERIALS AND METHODS

Materials. Sunflower oil (Euroshopper, purchased from a local retailer), reverse osmosis water, sodium caseinate (Excellion sodium caseinate S, DMV International, Netherlands), and curcumin (7% curcumin solution in propylene glycol and polysorbate, L-WS, Sensient, Netherlands) were used. Pig tongues were provided by VION Food Group (Netherlands). All ingredients used were food-grade.

Emulsion Preparation. Five o/w emulsions were prepared with an oil content of 1, 5, 10, 15, and 20% (w/w). A total of 3.2% (w/w) sodium caseinate was added to the water phase of all emulsions independent of the oil content. The emulsions were pre-homogenized using an ultra turrax (IKA RW 20 Digital) and homogenized (Niro-Soavi S.p.A. NS1001L2K) with pressures between 300 and 400 bar. The droplet size distribution was determined by light scattering (Mastersizer 2000, Malvern Instruments, Goffin Meyvis). The average diameter of emulsion droplets ($d_{3,2}$) is presented in Table 1. Curcumin solution was added immediately before consumption to each o/w emulsion (Table 1) until saturation, which was verified through fluorescence intensity measurements (data not shown). All samples were prepared in a food-grade environment and stored at 4 °C for a maximum of 2 days.

Table 1. Composition of All o/w Emulsions Used in This Study and Average Diameter of Emulsion Oil Droplets ($d_{3,2}$)[a]

$[oil]_{emulsion}$ (%, w/w)	[curcumin] (‰, v/w)	oil droplet size $d_{3,2}$ ± standard error (μm)
1	0.027	1.16 ± 0.07
5	0.040	1.32 ± 0.12
10	0.070	1.37 ± 0.15
15	0.088	1.34 ± 0.16
20	0.105	1.17 ± 0.07

[a]All o/w emulsions contained 3.2% (w/w) Na caseinate.

Pig Tongue Preparation. Pig tongues were prepared and preserved as previously described.[6] The pig tongues were collected immediately after slaughter and stored in a physiological salt solution for transportation. The tongues had a length of about 18 cm. Only the middle part of about 6−8 cm was used because the back part of the tongue has larger papillae compared to the human tongue and the front part was damaged during processing in the slaughterhouse. The pig tongues were cut into three parts. The middle part was snap-frozen in liquid nitrogen and stored at −80 °C. The pig tongues were thawed shortly before use in tap water. The pig tongues were cut into pieces of 2 × 2 cm, resulting in a tongue surface area of 4 cm^2.

Confocal Laser Scanning Microscopy (CLSM): Microstructure of o/w Emulsions on Pig Tongues. The microstructure of the o/w emulsions on pig tongues was analyzed by CLSM (TCS SP5 confocal laser scanning microscope, Leica Microsystems, Heidelberg, Germany). The objective lens used was a dry HCPL apo 20×/0.70CS (zoom 2). A layer of human saliva was added to the pig tongues. Images were collected under three experimental conditions: (i) plain pig tongue with a layer of human saliva without o/w emulsion, (ii) pig tongue with a layer of human saliva and 10% (w/w) o/w emulsion, and (iii) pig tongue with a layer of human saliva and 10% (w/w) o/w emulsion after being rubbed with another piece of pig tongue to simulate the rubbing of the human tongue against the palate during drinking. The emulsions were stained with an aqueous solution of 0.5% (w/w) Nile Blue.

Fluorescence Measurements and Calibration. Calibrations were made to correlate fluorescence intensity of curcumin in the o/w emulsion to the oil content deposited on the tongue. For this purpose, a single-point fluorescence measurement (Fluorolog Instruments SA, Inc., Jobin Yvon Spex) was used with an excitation wavelength of 440 nm, an emission wavelength of 495 nm, a slit width of 0.95 mm, and a measurement time of 0.1 s. A fluorescence remote read fiber optic probe was used to measure on tongue surfaces. A plastic ring (diameter of 16.9 mm and height of 5 mm) was attached to the end of the probe to ensure that the distance between the probe and the surface remained constant. The probe was put gently on the tongue to avoid deformation of the tongue surface. For all measurements, the background (autofluorescence intensity of the surface without a sample) was measured first. The background measured immediately before the sample measurement was always subtracted afterward from the sample measurement.

The calibration correlates fluorescence intensity of curcumin of the o/w emulsions to the oil fraction per surface area of tongue. For this purpose, we used pig tongues at room temperature (21 ± 0.5 °C) and body temperature (37.5 ± 0.5 °C) as surfaces. For each measurement, a fresh piece of tongue was used. Five o/w emulsions at room temperature were spread on the pig tongue surface to achieve the target oil fraction (Table 2).

Table 2. Fraction of Oil (mg/cm^2) Used for the Calibrations at Room Temperature (21 °C) and Body Temperature (37.5 °C)[a]

oil fraction (mg/cm^2)	$V_{emulsion}$ (μL)	$[oil]_{emulsion}$ (%, w/w)
0.01	4	1
0.02	8	
0.15	12	5
0.20	16	
0.50	20	10
0.60	24	
1.05	28	15
1.20	32	
1.80	36	20

[a]Each fraction of oil was obtained by spreading the specified volume of o/w emulsion ($V_{emulsion}$) with the specified concentration ($[oil]_{emulsion}$) on pig tongues with a constant surface area of 4 cm^2.

The oil fraction was defined as

$$\text{oil fraction } (mg/cm^2) = \frac{m_{oil}}{A_{surface\ tongue}}$$

$$\text{with } m_{oil} = V_{emulsion}[oil]_{emulsion}$$

where m_{oil} is the mass of oil on the tongue, $V_{emulsion}$ is the volume of the emulsion spread on the tongue, $[oil]_{emulsion}$ is the concentration of oil in the emulsion, and $A_{surface\ tongue}$ is the surface area of the pig tongue where the sample is dispersed. The calibrations were made for

dx.doi.org/10.1021/jf5010868 | J. Agric. Food Chem. 2014, 62, 5789−5795

Table 3. List of Sensory Attributes with Attribute Definitions and Evaluation Protocol

sensory attribute	definition	evaluation protocol
roughness	roughness sensed on teeth, palate, and tongue	after spitting out the sample: analysis between tongue and palate by sliding, degree of roughness of the surface
fatty film	sensation of feeling a layer of oil covering the mouth	after spitting out the sample: slide the tongue on the palate and lips and the lips on one another
flavor intensity	overall flavor intensity of aroma and taste	after spitting out the sample: the flavor intensity perceived

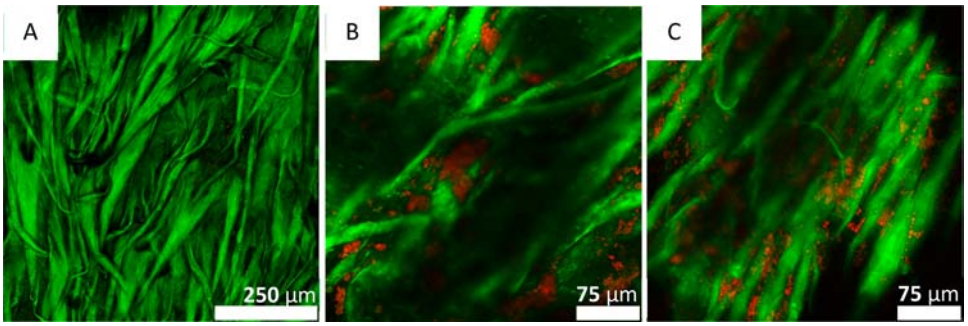

Figure 1. CLSM images: (A) pig tongue with a layer of human saliva, (B) pig tongue with a layer of human saliva and o/w emulsion (10%, w/w), and (C) pig tongue with a layer of human saliva and o/w emulsion (10%, w/w) after being rubbed with another piece of pig tongue. The same pig tongue was used to collect the three images. Papillae are represented in green, and oil droplets are represented in red.

targeted oil fractions between 0.01 and 1.8 mg/cm^2 (9 points) at room temperature (21 ± 0.5 °C) and body temperature (37.5 ± 0.5 °C). All measurements were performed in triplicate.

***In Vivo* Fluorescence Measurements.** A total of 20 untrained subjects (6 men and 14 women, with a mean age of 24 ± 1.7 years) tested the five o/w emulsions in triplicate. A randomized complete block design (randomization of five products per session) was used. Each sample was served in plastic cups in doses of 20 mL. The samples were coded with randomized three-digit numbers and served at room temperature. The test was performed in a controlled temperature and ventilated room. All subjects signed a written consent form and were given financial compensation. The materials and methods used did not require medical ethical approval under Dutch regulations.

Determination of the Oil Fraction on the Tongue. Each subject was instructed to ingest 20 mL of the o/w emulsion and process the sample in the mouth for 30 s while moving the sample around freely before spitting it out. This procedure was followed to create a maximum oil deposition on the tongue rather than to mimic natural drinking behavior. After expectoration, fluorescence measurements were made on the front and back of the anterior tongue at 0, 15, 30, 45, 60, 90, 120, and 180 s after expectoration. While waiting for the next measurements, subjects were free to swallow saliva and instructed to not speak or drink water. After 180 s, the subjects were given a recuperation time of approximately 5 min to cleanse their mouth with crackers, a tongue scraper, and warm (40 °C) and room temperature water to remove the residue of the oral coating. Before each sample was presented to the subject, a background fluorescence measurement (autofluorescence of the tongue) was made and subtracted from the subsequent sample measurement.

Sensory Perception of Oral Coatings. During the fluorescence measurement, the subjects were asked to rate the intensity of three sensory attributes: "roughness", "fatty film", and "flavor intensity". These attributes were chosen because they are descriptors that have been generated previously by quantitative descriptive analysis (QDA) panels to describe after-feel sensations of o/w emulsions.[12,13] In our study, the three attributes were evaluated by the untrained subjects after the stimuli were expectorated. The definition of descriptors and the evaluation protocol are shown in Table 3. The evaluation was performed using a continuous 100 mm visual analogue scale (VAS) line scale anchored with little and very at 5% from each end. The intensity of the attributes was rated 0, 30, 60, 90, 120, and 180 s after expectoration immediately after the fluorescence measurements.

Data Analysis. Descriptive statistics was used to obtain the mean and standard error (SE). A preliminary test for equal variances and normality was performed. Because these assumptions were not met for all of the fluorescence measurements, the data were normalized with a $\ln(x + 1)$ transformation. The effect of the position of the probe (within subject factor: front back), sample (within subject factor: 1, 5, 10, 15, and 20%, w/w), time (within subject factor: 0, 15, 30, 45, 60, 90, 120, and 180 s), and interactions on the oil fraction of the coating was tested by repeated-measures analysis of variance (ANOVA). For the sensory data, a repeated-measures ANOVA was used to investigate the effect of samples (within subject factor: 1, 5, 10, 15, and 20%, w/w) and time (within subject factor: 0, 30, 60, 90, 120, and 180 s) and the interactions on "roughness", "fatty film", and "flavor intensity"-scores. These analyses were performed in SPSS Statistics, version 19. A significance level of $p < 0.05$ was chosen.

RESULTS

Stability of o/w Emulsions under Mimicking In-Mouth Conditions. The stability of the 10% (w/w) o/w emulsion on a pig tongue was analyzed using CLSM (Figure 1). First, a layer of human saliva was added to the pig tongue in the absence of the 10% (w/w) o/w emulsion (Figure 1A). Second, the 10% (w/w) o/w emulsion was added to the pig tongue previously covered with human saliva (Figure 1B). Third, to mimic the oral processing behavior during drinking (i.e., rubbing of the tongue against the palate), the piece of pig tongue covered with a layer of human saliva and the 10% (w/w) o/w emulsion was rubbed against a second pig tongue (Figure 1C). The papillae are represented in green, and the oil droplets are represented in red. The microstructure of the 10% (w/w) o/w emulsion did not change considerably under the mimicked in-mouth conditions by mechanical stress through rubbing. A qualitative comparison between panels B and C of Figure 1 reveals no noticeable change in the microstructure of the emulsion. Panels B and C of Figure 1 both show individual oil droplets adhering to the tongue papillae. No coalescence of oil droplets after application of mechanical stress is observed.

Calibration Lines for *in Vivo* Fluorescence Measurements. Calibration lines were made using pig tongues as

dx.doi.org/10.1021/jf5010868 | J. Agric. Food Chem. 2014, 62, 5789−5795

surfaces at room temperature (21 ± 0.5 °C) and body temperature (37.5 ± 0.5 °C) to mimic in-mouth conditions (Figure 2). Five o/w emulsions were used to achieve the target

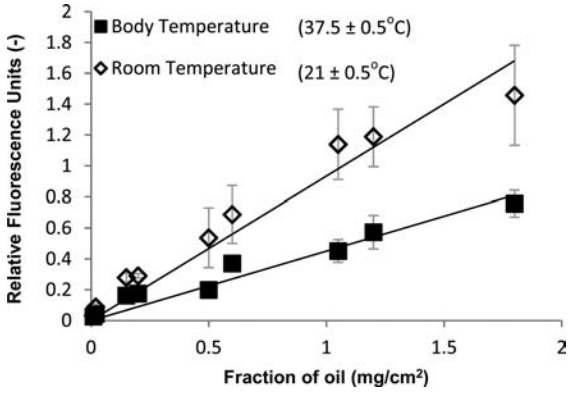

Figure 2. Calibration lines, relating the RFU to the fraction of oil on the tongue surface ($[oil]_{fraction}$). Error bars represent the standard deviation.

oil fractions for the calibration lines (Table 2). The five o/w emulsions were the same as the ones used for the *in vivo* fluorescence measurements. The data obtained from both calibrations were fitted with a linear regression to correlate the relative fluorescence units (RFU) with the oil fraction per surface area of tongue ($[oil]_{fraction}$). At room temperature (21 ± 0.5 °C), RFU = 0.94$[oil]_{fraction}$ (R^2 = 0.96) was obtained, and at body temperature (37.5 ± 0.5 °C), RFU = 0.45$[oil]_{fraction}$ (R^2 = 0.94). Both linear regressions passed through the origin. The increase of the temperature by 16.5 °C decreased the fluorescence intensity by 45%. In the following, the calibration line with the pig tongue at body temperature was used to calculate the oil fraction deposited on the tongue because the calibration resembles the in-mouth conditions closer.

Influence of the Oil Content of o/w Emulsions on Spatial Variation of Oral Coatings. Panels A and B of Figure 3 show the decay of the oil fraction deposited on the tongue after expectoration over time. The effects of probe position, sample, time, and their interactions on the oil fraction were statistically analyzed. Mauchly's test indicated that the assumption of sphericity had been violated for the main effect of the oil content of emulsions and the interactions. Therefore, the degrees of freedom were corrected using Greenhouse–Geisser estimates for sphericity. All effects are significant at $p < 0.001$. There was a significant main effect of probe position [$F(1, 59) = 166.5$], sample [$F(3.7, 215.9) = 52.5$], time [$F(7, 413) = 620.4$], and probe position × sample × time [$F(15.3, 903.6) = 2.07$; $p = 0.009$]. The oil fraction deposited on the front of the anterior tongue was significantly lower than on the back of the anterior tongue. The oil deposition on the front decreased on average by 42% after 15 s and by 67% after 45 s after expectoration. After 90 s, no significant difference of the oil fraction at the front of the anterior tongue was found between emulsions (Figure 3A). At the back of the anterior tongue, the oil fraction decreased in average by 34% after 15 s and by 60% after 45 s after expectoration (Figure 3B). After 120 s, there was no significant difference between emulsions. We conclude that the oil clearance was faster at the front of the anterior tongue compared to the back of the anterior tongue. The oil fraction on the front and back of the anterior tongue

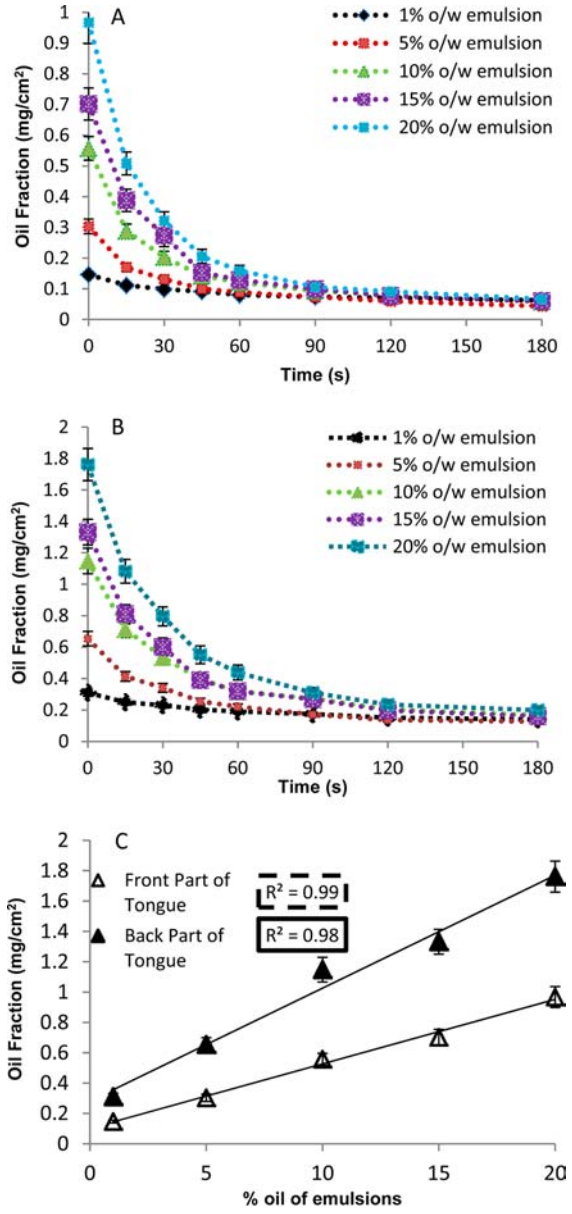

Figure 3. Oil fraction deposited on (A) front and (B) back of the anterior tongue over time for five o/w emulsions differing in oil concentration. Each point represents the average of n = 20 subjects and 3 replicates. Lines are drawn to guide the eye. Error bars represent the standard error. (C) Oil fraction deposited at the front and back of the anterior tongue immediately after expectoration (0 s) as a function of the emulsion oil concentration.

differed by a factor of 1.8 at 0 s, 2.2 at 30 s, and 2.4 at 180 s after expectoration.

The oil fraction deposited on the front and back of the anterior tongue surface immediately after expectoration of the stimulus (0 s) increased linearly with the oil content of the o/w emulsion (Figure 3C).

After-Feel Perception of Oral Coatings. Panels A and B of Figure 4 show the averaged intensities of the attributes "fatty film" and "flavor intensity" of the five o/w emulsions over time. The effect of sample, time, and sample × time on the attributes "fatty film", "flavor intensity", and "roughness" (data not shown) was tested. All effects were tested for sphericity with Mauchly's test. The effects that violated the sphericity assumption were corrected by Greenhouse–Geisser estimates.

dx.doi.org/10.1021/jf5010868 | J. Agric. Food Chem. 2014, 62, 5789–5795

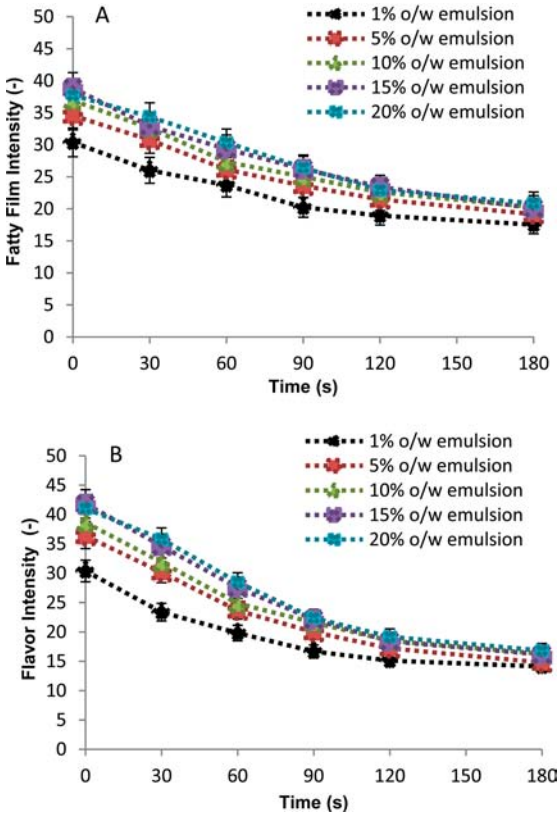

Figure 4. Intensity of the attributes (A) fatty film and (B) flavor intensity of five o/w emulsions over time. Each point represents the average of n = 20 subjects and 3 replicates. Lines are drawn to guide the eye. Error bars represent the standard error.

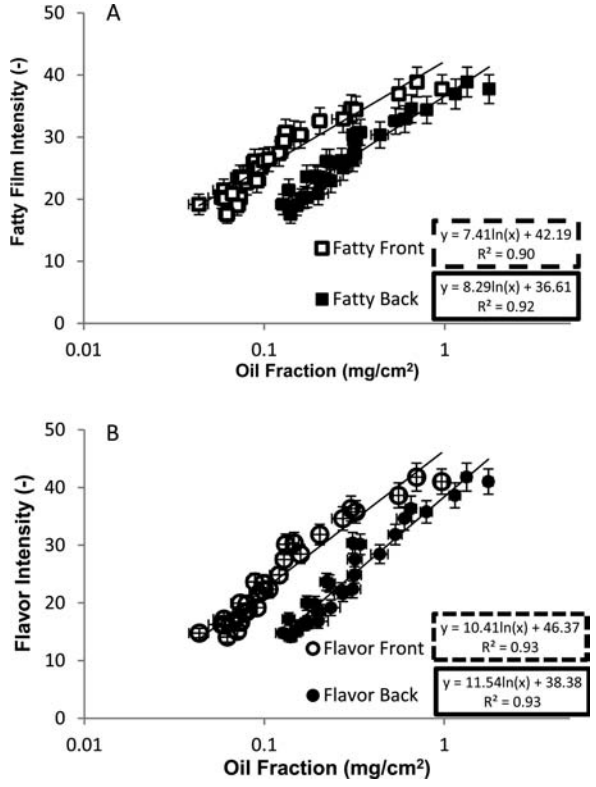

Figure 5. (A) Fatty film intensity and (B) flavor intensity as a function of oil deposition of different emulsions at the front and back of the anterior tongue at 0, 30, 60, and 90 s. Each point represents the average of n = 20 subjects and 3 replicates. Lines represent the linear regression of all points. Error bars represent the standard error.

For the attribute "roughness", all effects were not significant (sample, p = 0.11; time, p = 0.063; and sample × time, p = 0.175). For the attribute "flavor intensity", the effects of sample [F(3.2, 189.1) = 25.3], time [F(1.8, 108.6) = 94.0], and the interaction sample × time [F(9.5, 562.3) = 6.2] were significant at p < 0.001. The attribute "fatty film" was significantly influenced by the same effects: sample [F(4, 236) = 15.2; p < 0.001], time [F(1.6, 91.6) = 117.5; p < 0.001], and the interaction sample × time [F(9.3, 548.3) = 2.3]. At time 0 s, both attributes were perceived as more intense with an increasing oil content of o/w emulsions (panels A and B of Figure 4). For both attributes, the 1% (w/w) o/w emulsion was perceived as significantly different from all other samples up to 120 s (p < 0.001). At time point 180 s, all samples were perceived equally intense. The attributes "fatty film" and "flavor intensity" were linearly correlated for all samples (R^2 > 0.98; regression data not shown).

Psychophysical Relationships between Oil Coatings Formed on the Tongue and After-Feel Perception. Panels A and B of Figure 5 show the relationships between the after-feel perception of attributes "fatty film" and "flavor intensity" with the oil fraction deposited on the tongue. Each data point represents a different sample at a different time point after expectoration of the stimulus. The perceived intensity of a stimulus can be related to the physical intensity of the stimulus by a logarithmic relationship known as Weber–Fechner's law: $P = k \log I$, where P is the perceived intensity of the stimulus, I is the physical intensity of the stimulus, and k is a constant.[14] The psychophysical relationships between the attributes "flavor intensity" and "fatty film" and the oil fraction deposited on the tongue after expectoration of the stimulus were fitted using Weber–Fechner's law to determine the psychophysical functions for after-feel perception of the o/w emulsions (panels A and B of Figure 5). Weber–Fechner's law described the relationships between after-feel perception of the two attributes and the oil fraction ($R^2 \geq 0.90$).

DISCUSSION

Stability of o/w Emulsions under Mimicking In-Mouth Conditions. The stability of the 10% (w/w) o/w emulsion was qualitatively determined under mimicking in-mouth conditions using CSLM. The oil droplets remained stable and did not reveal coalescence after application of mechanical stress through rubbing the pig tongue covered with the emulsion against another pig tongue. Dresselhuis et al. reported that the occurrence of coalescence in the mouth depends upon the characteristics of the emulsion (droplet size, interfacial layer, type of emulsifier, and type of fat), the shear applied, and the characteristics of the oral mucosa. The coalescence in the mouth was shown to be more probable when the emulsions were less stable, i.e., stabilized by a low concentration of emulsifier.[15] The concentration of emulsifier used in the preparation of all of our emulsions [3.2% (w/w) Na caseinate] was in excess to cover the o/w interface. Therefore, as expected, the oral coating formed by the emulsion consists of individual oil droplets embedded in a mixture of water and saliva adhering to the tongue papillae and does not consist of a homogeneous layer of coalesced oil. Hence, thickness should not be used as the physical parameter to describe and quantify oral coatings formed by (stable) emulsions. The oil fraction is a more

dx.doi.org/10.1021/jf5010868 | J. Agric. Food Chem. 2014, 62, 5789–5795

suitable physical parameter to describe the mass of oil that adheres to the surface of the tongue.

Calibration Lines for *in Vivo* Fluorescence Measurements. The first aim of this study was to develop a new calibration method for *in vivo* fluorescence measurements that represents closer the *in vivo* conditions occurring in the mouth. Pig tongues were used as the contact surface for the calibration because they are known to be a good model for human tongues.[6,7] The calibration of the fluorescence method was made with o/w emulsions. To test the effect of the temperature on fluorescence, calibrations were performed with pig tongues at body temperature and room temperature. We observed a large effect of the temperature on the fluorescence intensity of curcumin in the emulsions on the tongue surface. This clearly demonstrates the importance of performing the calibration at temperatures close to those occurring during the *in vivo* measurements in the oral cavity. The experimental conditions of the calibration should resemble the in-mouth conditions during the *in vivo* measurements as much as possible.

Influence of the Oil Content of o/w Emulsions on Spatial Variation of Oral Coatings. The second aim of this study was to apply the *in vivo* fluorescence method with the new calibration using o/w emulsions varying in oil content. The *in vivo* fluorescence measurements showed more oil deposition on the back of the anterior tongue than on the front of the anterior tongue (panels A and B of Figure 3). This spatial variation of the oil fraction increased over time. An explanation for this finding may lay in the morphology of the tongue. Fungiform papillae, which are the smallest papillae, are present on the front of the anterior tongue. The papillae circumvallate are located on the back of the anterior tongue and secret cleaning liquid.[16] The most important papillae for the formation of the oral coating might be the filiform papillae, which are more predominant at the back of the tongue. These papillae contribute considerably to the roughness of the tongue surface. The differences between the papillae result in a smoother surface at the front of the anterior tongue compared to the back.[17] The difference in the surface morphology might partly explain the observed differences in spatial variation of oral oil deposits because oil droplets are likely to be entrapped between the papilla. The movement of the tongue might also influence the spatial variation of the oil deposit. The participants were allowed to swallow freely during the experiments. When swallowing, the front of the tongue moves against the teeth and palate.[18,19] This movement results in friction, which might degrade the oil coating more on the front of the anterior tongue compared to the back. This effect might also explain the increase in spatial variation over time. The oil fraction deposited on the tongue surface immediately after expectoration (0 s) increased linearly with an increasing oil content of the o/w emulsion (Figure 3C). Dresselhuis et al. studied the effect of stable and unstable emulsions on the oil retention in the mouth. It was concluded that increasing the oil content of the emulsions resulted in larger amounts of oil deposition on the tongue.[15] In contrast, results by Pivk et al. showed that deposition of MCT oils in the mouth followed a logarithmic increase with increasing volumes of oil.[5] A reason for the difference between these results may lay in the level of saturation of the oil coverage of the surface of the tongue. Complete coverage of the tongue surface by oil (saturation) is more likely to be reached by oils than by emulsions that contain considerably less oil, and the oil droplets can be stable against coalescence.

After-Feel Perception of Oral Coatings. The decrease of the oil fraction on the tongue with time lead to a decrease of "fatty film" and "flavor intensity" with time (panels A and B of Figure 4). The oral coating might lead to a prolonged release of odor compounds into the nasal cavity and to a higher lubrication in the mouth. Hence, more coating might result in a higher concentration of odors and, thus, increase flavor perception.[1] The increase of after-feel intensity at $t = 0$ s with an increasing emulsion oil content was not a linear probably because the flavor release also does not linearly depend upon the oil content.[15] It should be noted that no flavor substances were added to the emulsion to examine flavor release over time. The flavor of the o/w emulsions comes from the inherent flavor of the sunflower oil. The attribute "flavor intensity" was used as an indirect measurement of the presence of an oral coating. The attribute "roughness" showed no significant differences for any of the effects tested. This might have been due to a low consensus for the attribute "roughness" between the untrained subjects. The definition of "roughness" might have been unfamiliar or unclear to the untrained subjects, leading to misinterpretations or confusion. This effect would probably have been suppressed when a trained panel would have been used.

Psychophysical Relationships between Oil Coatings Formed on the Tongue and After-Feel Perception. The third aim of the study was to establish psychophysical relationships between oil coatings formed on the tongue and after-feel perception. For both attributes "fatty film" and "flavor intensity", a semi-logarithmic relation with the oil fraction of the coating was found (panels A and B of Figure 5). The relationship between after-feel perception of the attributes "fatty film" and "flavor intensity" and oil fraction deposited on the tongue can hence be described by Weber–Fechner's law. The k values of Weber–Fechner's law are an indication for the sensitivity of the sensory system toward a specific physical stimulus. In our study, we cannot determine a meaningful k value from our data because we used a direct intensity scaling method to quantify after-feel perception. To determine the k value of Weber–Fechner's law, usually indirect methods, such as two alternative forced choices (2AFCs) and/or the method of constant stimuli, and/or magnitude estimation methods are used.[20−24] The indirect methods are known to work well to quantify k values for taste and smell perception. Our study demonstrates that after-feel perception of o/w emulsion is dynamic and intensity of attributes strongly depends upon time after expectoration. Using indirect sensory methods to determine after-feel perception while accounting for perceptual changes of after-feel in time will be challenging to perform. Because we cannot determine a meaningful k value from our data, we cannot compare it to k values reported in the literature for other sensory systems, such as taste and smell.

In conclusion, we developed a new calibration method for *in vivo* fluorescence measurements and applied the methodology to investigate the psychophysical relationships between the oil fraction deposited on the tongue after expectoration of o/w emulsions and after-feel perception. We recommend a new calibration method using pig tongue surfaces at body temperature for the calibration procedure to resemble in-mouth conditions. We conclude that the after-feel perception of oral coatings follows Weber–Fechner's law. This study demonstrates the potential of *in vivo* fluorescence measurements for studying food behavior in the mouth. We suggest to continue the studies focusing on the effect of beverage

composition on the formation and clearance of oral coatings for improved design of low-fat products.

AUTHOR INFORMATION

Corresponding Author

*Telephone: +31-317-481694. E-mail: markus.stieger@wur.nl.

Notes

The authors declare no competing financial interest.

ACKNOWLEDGMENTS

The authors thank Jan Klok (NIZO Food Research) for the help with the CSLM measurements, Rob Koehorst (Laboratory of Biophysics, Wageningen University) for the help with the fluorescence measurements, and VION Foods for providing us with fresh pig tongues.

ABBREVIATIONS USED

2AFC, two alternative forced choice; ANOVA, analysis of variance; ATR IR, attenuated total reflection infrared; CLSM, confocal laser scanning microscopy; MCT, medium-chain triglycerides; o/w, oil in water; RFU, relative fluorescence units; VAS, visual analogue scale

REFERENCES

(1) Prinz, J. F.; Huntjens, L.; de Wijk, R. A. Instrumental and sensory quantification of oral coatings retained after swallowing semi-solid foods. *Arch. Oral Biol.* **2006**, *51*, 1071−1079.

(2) De Wijk, R. A.; Kapper, C.; Borsboom, P.; Prinz, J. F. Persistence of oral coatings of CMC and starch-based custard desserts. *Food Hydrocolloids* **2009**, *23*, 896−900.

(3) De Jongh, H. H. J.; Janssen, A. M. Differential clearance kinetics of adhered layer constituents from the oral cavity as modulator for afterfeel of dressings: ATR FT-IR measurements of localized oral coatings. *J. Texture Stud.* **2007**, *38*, 70−86.

(4) Pivk, U.; Ulrih, N. P.; Juillerat, M. A.; Raspor, P. Assessing lipid coating of the human oral cavity after ingestion of fatty foods. *J. Agric. Food Chem.* **2008**, *56*, 507−511.

(5) Pivk, U.; Godinot, N.; Keller, C.; Antille, N.; Juillerat, M. A.; Raspor, P. Lipid deposition on the tongue after oral processing of medium-chain triglycerides and impact on the perception of mouthfeel. *J. Agric. Food Chem.* **2008**, *56*, 1058−1064.

(6) Dresselhuis, D. M.; de Hoog, E. H. A.; Cohen Stuart, M. A.; van Aken, G. A. Application of oral tissue in tribological measurements in an emulsion perception context. *Food Hydrocolloids* **2008**, *22*, 323−335.

(7) Kullaa-Mikkonen, A.; Hynynen, M.; Hyvonen, P. Filiform papillae of human, rat and swine tongue. *Acta Anat.* **1987**, *130*, 280−284.

(8) Montavon, P.; Lindstrand, K. Immunohistochemical localization of neuron-specific enolase and calcitonin gene-related peptide in pig taste papillae. *Regul. Pept.* **1991**, *36*, 2235−2248.

(9) de Wijk, R. A.; Prinz, J. F.; Janssen, A. M. Explaing perceived oral texture of starch-based custard desserts from standard and novel instrumental tests. *Food Hydrocolloids* **2006**, *20*, 24−34.

(10) de Wijk, R. A.; van Gemert, L. J.; Terpstra, M. E. J.; Wilkinson, C. L. Texture of semi-solids: Sensory and instrumental measurements on vanilla custard desserts. *Food Qual. Prefer.* **2003**, *14*, 305−317.

(11) Lynch, J.; Liu, Y. H.; Mela, D. J.; MacFie, H. J. H. A time-intensity study of the effect of oil mouthcoatings on taste perception. *Chem. Senses* **1993**, 121−129.

(12) Dresselhuis, D. M.; de Hoog, E. H. A.; Cohen Stuart, M. A.; Vingerhoeds, M. H.; van Aken, G. A. The occurrence of in-mouth coalescence of emulsion droplets in relation to perception of fat. *Food Hydrocolloids* **2008**, *22*, 1170−1183.

(13) Vingerhoeds, M. H.; Silletti, E.; de Groot, J.; Schipper, R. G.; van Aken, G. A. Relating the effect of saliva-induced emulsion flocculation on rheological properties and retention on the tongue surface with sensory perception. *Food Hydrocolloids* **2009**, *23*, 773−785.

(14) Lawless, H. T.; Heymann, H. *Sensory Evaluation of Food*; Springer: New York, 2010.

(15) Dresselhuis, D. M.; Cohen Stuart, M. A.; van Aken, G. A.; Schipper, R. G.; de Hoog, E. H. A. Fat retention at the tongue and the role of saliva: Adhesion and spreading of protein-poor versus protein-rich emulsions. *J. Colloid Interface Sci.* **2008**, *321*, 21−29.

(16) Bear, M. F.; Connors, B. W.; Paradiso, M. A. *Neuroscience: Exploring the Brain*; Lippincott Williams & Wilkins (LLW): Philadelphia, PA, 2001.

(17) Kawasaki, K.; Porntaveetus, T.; Oommen, S.; Ghafoor, S.; Kawasaki, M.; Otsuka-Tanaka, Y.; Blackburn, J.; Kessler, J. A.; Sharpe, P. T.; Ohazama, A. Bmp signalling in filiform tongue papillae development. *Arch. Oral Biol.* **2012**, *57*, 805−813.

(18) ChiFishman, G.; Stone, M. A new application for electro-palatography: Swallowing. *Dysphagia* **1996**, *11*, 239−247.

(19) Pouderoux, P.; Kahrilas, P. J. Deglutitive tongue force modulation by volition, volume, and viscosity in humans. *Gastroenterology* **1995**, *108*, 1418−1426.

(20) Schutz, H. G.; Pilgrim, F. J. Differential sensitivity in gustation. *J. Exp. Psychol.* **1957**, *54*, 41−48.

(21) Withers, C.; Gosney, M. A.; Methven, L. Perception of thickness, mouth coating and mouth drying of dairy beverages by younger and older volunteers. *J. Sens. Stud.* **2013**, 1−8.

(22) Hoppert, K.; Zahn, S.; Puschmann, A.; Ullmann, I.; Rohm, H. Quantification of sensory difference thresholds for fat and sweetness in dairy-based emulsions. *Food Qual. Prefer.* **2012**, *26*, 52−57.

(23) Orellana-Escobedo, L.; Ornelas-Paz, J. J.; Olivas, G. I.; Guerrero-Beltran, J. A.; Jimenez-Castro, J.; Sepulveda, D. R. Determination of absolute threshold and just noticeable difference in the sensory perception of pungency. *J. Food Sci.* **2012**, *77*, S135−S139.

(24) van Aken, G. A.; Vingerhoeds, M. H.; de Hoog, E. H. A. Food colloids under oral conditions. *Curr. Opin. Colloid Interface Sci.* **2007**, *12*, 251−262.

JOURNAL OF AGRICULTURAL AND FOOD CHEMISTRY

Article

pubs.acs.org/JAFC

Characterization of the Key Odorants in Light Aroma Type Chinese Liquor by Gas Chromatography−Olfactometry, Quantitative Measurements, Aroma Recombination, and Omission Studies

Wenjun Gao, Wenlai Fan,* and Yan Xu

Key Laboratory of Industrial Biotechnology, Ministry of Education, Synergetic Innovation Center of Food Safety and Nutrition, Laboratory of Brewing Microbiology and Applied Enzymology, School of Biotechnology, Jiangnan University, Wuxi, Jiangsu 214122, China

ABSTRACT: The light aroma type liquor is widely welcomed by consumers due to its pleasant fruity and floral aroma, particularly in northern China. To answer the puzzling question of which key aroma compounds are responsible for the typical aroma, three typical liquors were studied in this paper. A total of 66 aroma compounds were identified in three liquors by means of gas chromatography−olfactometry (GC-O) coupled with mass spectrometry (MS), and 27 odorants were further screened out as the important odorants according to quantitative study and odor activity values (OAVs). For OAV calculation, odor thresholds of the odorants were determined in a hydroalcoholic solution at 46% ethanol by volume. The typical light type aroma dominated by fruity and floral notes was successfully simulated by dissolving these important odorants in the 46% vol hydroalcoholic solution in their natural concentrations. Omission experiments further confirmed β-damascenone and ethyl acetate as the key odorants and revealed the significance of the entire group of esters, particularly ethyl lactate, geosmin, acetic acid, and 2-methylpropanoic acid, for the overall aroma of the light aroma type Chinese liquor.

KEYWORDS: *Chinese light aroma type liquor, gas chromatography−olfactometry, gas chromatography−mass spectrometry, odor activity value, aroma recombination and omission, β-damascenone*

INTRODUCTION

Chinese liquor, also called *baijiu* or *shaojiu*, is a worldwide consumed distilled alcoholic beverage of great reputation, especially in China. It commonly has an ethanol content of 40−55% by volume.[1] Due to the great varieties of production processes, Chinese liquors from different manufacturers have significant differences in aroma profile. On the basis of the aroma characteristics, they are generally classified into the following categories: light aroma type, strong aroma type, soy sauce aroma type, sweet and honey aroma type, and miscellaneous aroma type liquors.[2] Among them, light aroma type liquor is widely welcomed by consumers due to its pleasant fruity and floral aroma, particularly in northern China.

As known to all, the quality of a beverage is influenced by many factors, such as raw materials and the fermentation process. In general, the main raw materials used for light aroma type liquor production are sorghum, barley, and pea: the former is used for making liquor, and the latter two are used for making *qu*.[3] In addition, rice husks are used as a fermentation accessory. *Qu*, which is made of pulverized barley and pea, is usually used as a fermentation starter to initiate the fermentation process. The various microorganisms and complex enzyme system in *qu* can generate abundant aroma compounds during the fermentation process.[4] The major producing steps of light aroma type liquor are as follows: mixing raw materials with *qu*, solid-state saccharification and fermentation in a pottery jar (350−400 L) under anaerobic conditions, and distillation.[2] Subsequently, the freshly distilled liquors are aged in sealed ceramic jars to develop balanced aroma and taste. Finally, the aged liquors are adjusted to a target ethanol concentration and blended for a constant quality of the final product.[5]

The aroma of Chinese liquor is an important factor in product quality, and it is mostly influenced by the complex aroma active compounds. Some studies have been made previously, and various techniques have been applied to investigate these aroma compounds. Fan and co-workers[5−7] have identified 126 odorants in *Wuliangye* and *Jiannanchun* liquor by gas chromatography−olfactometry (GC-O) and gas chromatography−mass spectrometry (GC-MS) techniques in 2006; afterward, they studied 27 pyrazines in Chinese liquors using GC-MS and headspace solid phase microextraction (HS-SPME) coupled with gas chromatograpy−flame thermionic detector (GC-FTD) in 2007, and later in 2011, they quantitated 76 volatile compounds in *Langjiu* through stir bar sorptive extraction (SBSE) coupled with GC-MS. Moreover, Zhu et al.[8] have shown the great complexity of the composition in *Maotai* liquor with 528 volatiles identified by means of comprehensive two-dimensional GC−time-of-flight MS. However, most of these studies were focused on the identification and quantitation of aroma compounds, and none comprehensively explored the contribution of key odorants from numerous constituents to the overall aroma.

Recently, techniques including not only GC-O and quantitation analysis but also odor activity value (OAV) analysis, descriptive profile test, aroma recombination, and

Received: March 16, 2014
Revised: June 6, 2014
Accepted: June 8, 2014
Published: June 8, 2014

ACS Publications © 2014 American Chemical Society

dx.doi.org/10.1021/jf501214c | J. Agric. Food Chem. 2014, 62, 5796−5804

omission experiments are being extensively and successfully used to investigate the key aroma compounds of alcoholic beverages, such as whiskey,[9,10] beer,[11] brandy,[12] and Chinese rice wine,[13] as well as other foods.[14−17]

Therefore, to answer the puzzling question of which key aroma compounds are responsible for the typical aroma of light aroma type Chinese liquor, our study investigated three representative liquors in the following ways: identify and quantitate their potent aroma compounds in common, rate these compounds on the basis of OAVs and find the important odorants, and, finally, confirm the aroma contribution of selected important odorants by means of aroma recombination and omission experiments performed in the *Fenjiu* liquor. These data can be used for the optimization of the aroma and flavor of Chinese liquors during their production.

MATERIALS AND METHODS

Liquors. Three premium Chinese light aroma type liquors from different origins were under investigation: *Fenjiu* liquor (FJ, 45% ethanol by volume, from Shanxi province in north-central China), *Baofeng* liquor (BFJ, 46% ethanol by volume, from Henan province in central China), and *Qingke* liquor (QKJ, 52% ethanol by volume, from Qinghai province in northwestern China). All liquors (500 mL for each) were supplied by corresponding cooperant distilleries and stored at 4 °C until analysis.

Chemicals. Authentic standards were obtained from commercial sources: 1-Propanol, 1-butanol, 1-pentanol, 1-hexanol, 1-heptanol, 1-octanol, 2-methylpropanol, 3-methylbutanol, 1-octen-3-ol, 2-butanol, 2-heptanol, ethyl acetate, ethyl propanoate, ethyl 2-methylpropanoate, 2-methylpropyl acetate, ethyl butanoate, ethyl 3-methylbutanoate, 3-methylbutyl acetate, ethyl pentanoate, ethyl hexanoate, hexyl acetate, ethyl lactate, ethyl heptanoate, ethyl octanoate, ethyl nonanoate, ethyl decanoate, diethylbutanedioate, 3-methylbutyl hexanoate, ethyl undecanoate, ethyl dodecanoate, ethyl 2-hydroxyhexanoate, propanoic acid, 3-methylbutanoic acid, pentanoic acid, hexanoic acid, decanoic acid, 3-methylbutanal, hexanal, nonanal, decanal, 2-nonanone, (*E*,*Z*)-2,6-nonadienal, benzaldehyde, phenylacetaldehyde, ethyl benzoate, ethyl 2-phenylacetate, 2-phenylethyl acetate, ethyl 3-phenylpropanoate, benzenemethanol, 2-phenylethanol, phenol, 4-methylphenol, 4-methylguaiacol, 4-ethylguaiacol, furfural, 2-acetyl-5-methylfuran, *β*-damascenone, *γ*-hexalactone, *γ*-nonalactone, 1,1-diethoxyethane, 1,1,3-triethoxypropane, and geosmin were purchased from Sigma-Aldrich (Shanghai, China). Acetic acid, 2-methylpropanoic acid, butanoic acid, and naphthalene were obtained from Alfa Aesar (Tianjin, China). Octyl propanoate (internal standard, IS), 2,2-dimethylpropanoic acid (IS), pentyl acetate (IS), and L-menthol (IS) (Sigma-Aldrich, Shanghai, China) were used as internal standards. A C_5−C_{30} *n*-alkane mixture (Sigma-Aldrich, Shanghai, China) was employed for determination of linear retention indices (RIs). All of the substances used above were of GC quality, with at least 97% purity.

Sodium chloride (NaCl), anhydrous sodium sulfate (Na_2SO_4), sodium bicarbonate ($NaHCO_3$), sulfuric acid (H_2SO_4), and absolute ethanol were from China National Pharmaceutical Group Corp. (Shanghai, China). Diethyl ether and pentane from ANPEL Scientific Instrument Co., Ltd. (Shanghai, China) were freshly distilled before use.

Aroma Extraction and Fractionation. Following ref 5, liquors (50 mL) were diluted to 10% ethanol by volume with boiled ultrapure water, saturated with NaCl, and then extracted with diethyl ether (3 × 20 mL). The combined extracts were further separated into acidic/water-soluble, neutral, and basic fractions, using a mixture of pentane/diethyl ether (1:1 by volume) as extraction solvent. Afterward, each fraction was dried with anhydrous Na_2SO_4 overnight and concentrated under a gentle stream of nitrogen to a final volume of 200 μL. These concentrated fractions were stored at −20 °C prior to the GC-O analysis.

Identification by GC-O and GC-MS Analysis. GC-O and GC-MS analysis were performed on an Agilent 6890N GC coupled to an Agilent 5975 mass selective detector (MSD) and an olfactometer.

GC-MS Analysis. The concentrated fraction (1 μL) was injected in splitless mode. Samples were analyzed on both a DB-Wax column (30 m × 0.32 mm i.d. × 0.25 μm, J&W Scientific) and a DB-5 column (30 m × 0.32 mm i.d. × 1 μm, J&W Scientific). Helium at a constant flow rate of 2 mL/min was used as carrier gas. The injector was held at 250 °C. The oven temperature was held at 50 °C for 2 min, then programmed to 230 °C at a rate of 6 °C/min, and finally kept at 230 °C for 20 min. The column flow was split at the end of the capillary; one was directed to a heated olfactometer (Olfactory Detector Port ODP 2, Gerstel Inc., Mülheim, Ruhr, Germany), whereas the other one was directed to the MSD. The temperature of the olfactory port was 280 °C. Mass spectra in the electron ionization mode (MS-EI) were recorded at 70 eV ionization energy, and the ion source temperature was set at 230 °C. Full-scan acquisition was used in the 30−350 amu range of masses.

GC-O Analysis. Six trained panelists (three males and three females, 26 years old on average) from the Laboratory of Brewing Microbiology and Applied Enzymology at Jiangnan University were recruited to perform GC-O analysis. The panelists were trained for 3 months in GC-O using at least 30 odor-active reference compounds in a concentration 10 times above their odor thresholds in air. During a GC run described above, a panelist placed his/her nose close to the sniffing port, responded to the aroma intensity of the stimulus, and recorded the aroma descriptor and intensity value as well as retention time. The sniffing time of each run was not more than 30 min. The aroma descriptors were determined by an evaluation of the odor quality of reference odorants previously. A six-point scale ranging from 0 to 5 was used for intensity judgment: 0 = none, 1 = very weak, 2 = weak, 3 = moderate, 4 = strong, and 5 = very strong. The Osme value for aroma intensity was an average result of the six panelists.[18]

Identification of Aroma Compounds. Peak identifications of the odorants were performed by comparison of mass spectra with those of the NIST 05 a.L database (Agilent Technologies Inc., Santa Clara, CA, USA). Positive identification was achieved by comparison of their odors, retention indices (RIs), and mass spectra with those of pure standards. RIs of the odorants were calculated from the retention times of *n*-alkanes (C_5−C_{30}), according to a modified Kovats method.[19]

Quantitation by HS-SPME-GC-MS. An automatic headspace sampling system (MultiPurposeSample MPS 2 with a SPME adapter, from Gerstel Inc., Mülheim, Ruhr, Germany) with a 50/30 μm divinylbenzene/carboxen/poly(dimethylsiloxane) (DVB/CAR/PDMS) fiber (2 cm, Supelco Inc., Bellefonte, PA, USA) was used for extraction of volatile aroma compounds. The liquors were diluted with boiled ultrapure water to a final concentration of 10% ethanol by volume. A total of 8 mL of this diluted sample was transferred into a screw-capped vial, saturated with NaCl, and spiked with 10 μL of a mixed internal standard (octyl propanoate and L-menthol, with a final concentration of 66.7 or 125.2 μg/L, respectively). Tightly capped with a Teflon-faced silicone septum, the sample was equilibrated at 50 °C for 5 min and extracted for 45 min at the same temperature under stirring at the rotation speed of 250*g*. After extraction, the fiber was inserted into the injection port of GC for a 5 min desorption. The injector and oven temperatures were identical to those used for GC-MS analysis described previously, and a DB-Wax column was used. All samples were performed in triplicate

Selective ion monitoring (SIM) mass spectrometry was used to quantitate the aroma compounds. The ions monitored of octyl propanoate and L-menthol in the SIM run were *m*/*z* 75 and 138, respectively. The standard curve for individual volatile aroma compound was built up by plotting the response ratio of target compounds and corresponding ISs against the concentration ratio as reported (Table 2).[20]

Liquid−Liquid Microextraction (LLME) for Quantitation of Fatty Acids. Due to the poor adsorption of the DVB/CAR/PDMS fiber to strong polar fatty acids, LLME was used as a separate extraction of these acids. According to the method described by Wang and co-workers,[21] each liquor sample was diluted with boiled ultrapure water

Table 1. Aroma Compounds Identified by GC-O in Three Light Aroma Type Chinese Liquors

			RI			Osme values[c]		
no.	aroma compound[a]	descriptor	DB-Wax	DB-5	fraction[b]	FJ	BFJ	QKJ
1	ethyl acetate	pineapple	895	589	N	3.83	4.00	2.67
2	1,1-diethoxyethane	fruity	897	721	N	2.17	2.33	3.33
3	3-methylbutanal	green, malty	923	624	N	1.67	1.67	1.83
4	ethyl propanoate	banana	950	697	N	2.67	2.33	2.33
5	ethyl 2-methylpropanoate	fruity	958	750	N	2.83	2.50	2.83
6	2-methylpropyl acetate	fruity	978	776	N	2.33	2.17	2.67
7	2-butanol	fruity	1008		A	1.83	0.33	1.50
8	1-propanol	alcoholic	1027		A	1.83	1.83	1.67
9	ethyl butanoate	pineapple	1028	817	N	2.17	2.83	3.50
10	ethyl 3-methylbutanoate	apple	1064	856	N	2.50	2.33	2.83
11	hexanal	grassy, green	1080	803	N	2.83	2.17	2.50
12	2-methylpropanol	malty	1092	620	A	4.17	3.67	4.00
13	3-methylbutyl acetate	fruity	1112	868	N	2.50	2.83	2.83
14	ethyl pentanoate	apple	1126	913	N	2.17	2.00	2.50
15	1-butanol	alcoholic, solvent	1142	669	N+A	3.00	2.33	2.17
16	3-methylbutanol	malty	1197	789	B+A	3.33	4.00	2.50
17	ethyl hexanoate	fruity	1239	1028	N	2.67	2.83	2.83
18	hexyl acetate	fruity	1248	1021	N	1.83	1.33	1.50
19	1-pentanol	balsamic	1259	763	A	1.83	0.82	0.67
20	1,1,3-triethoxypropane	vegetal	1288	1128	N	1.50	1.33	1.17
21	2-heptanol	fruity	1299	902	A	2.67	2.17	2.00
22	ethyl heptanoate	fruity	1304	1115	N	2.83	2.33	2.83
23	ethyl lactate	fruity	1328	823	N	2.83	2.33	2.17
24	1-hexanol	floral	1350	892	A	2.83	2.50	2.67
25	nonanal	soapy	1361	1121	N	2.17	2.17	2.33
26	2-nonanone	floral	1376		N		1.17	1.33
27	ethyl octanoate	fruity	1413	1203	N	4.17	4.00	4.33
28	3-methylbutyl hexanoate	fruity	1419	1269	N	1.83	1.50	1.33
29	acetic acid	acidic, vinegar	1420	601	A	3.17	2.33	2.33
30	1-heptanol	alcoholic	1448	978	A	1.67	1.17	1.17
31	decanal	oily	1453	1214	N	2.33	2.17	2.17
32	furfural	sweet, almond	1459	840	N+A	2.17	2.50	2.33
33	1-octen-3-ol	mushroom	1469	994	N	2.83	2.67	3.67
34	benzaldehyde	fruity, floral	1497	978	N	2.17	2.33	2.33
35	ethyl nonanoate	fruity	1512	1289	N	2.83	2.33	2.50
36	propanoic acid	vinegar	1520		A	1.67	1.33	1.50
37	ethyl 2-hydroxyhexanoate	floral	1529	1068	N	1.67	1.50	1.50
38	1-octanol	fruity	1530	1090	A	1.83	1.00	1.33
39	2-methylpropanoic acid	sweaty, acidic	1551	792	A	3.67	2.33	3.17
40	2-acetyl-5-methylfuran	nutty, sweet	1587		N	3.50	2.33	2.17
41	butanoic acid	sweaty, acidic	1594	802	A	2.83	2.67	3.33
42	ethyl decanoate	fruity	1602	1398	N	2.67	2.17	2.17
43	phenylacetaldehyde	floral	1617	1052	N	3.83	2.67	3.17
44	ethyl benzoate	fruity	1639	1165	N	3.33	2.67	2.17
45	diethyl butanedioate	fruity	1657	1170	N	2.17	2.17	2.17
46	3-methylbutanoic acid	sweaty, acidic	1660	837	A	3.67	2.50	2.17
47	γ-hexalactone	sweet, coconut	1688		N	1.50		1.67
48	(*E*,*Z*)-2,6-nonadienal	green, cucumber	1694	1228	N	1.67	1.33	1.17
49	naphthalene	mothball-like	1715		N	1.67		1.67
50	pentanoic acid	sweaty, rancid	1718		A	2.83	2.17	2.00
51	ethyl undecanoate	fruity	1730		N	1.33	1.33	1.17
52	ethyl phenylacetate	rosy, honey	1772	1254	N	4.50	3.00	2.17
53	2-phenylethyl acetate	floral	1810	1271	N	4.50	2.17	2.50
54	ethyl dodecanoate	fruity	1819	1589	N	1.17	1.33	1.33
55	geosmin	earthy	1820	1450	N	2.33	2.50	2.17
56	β-damascenone	floral, honey	1837	1379	N	4.33	4.67	4.17
57	hexanoic acid	sweaty	1840	971	A	2.50	2.17	2.00
58	benzenemethanol	floral	1864		A	1.83	1.67	1.83
59	ethyl 3-phenylpropanoate	floral	1868	1348	N	3.33	3.67	3.17

dx.doi.org/10.1021/jf501214c | J. Agric. Food Chem. 2014, 62, 5796−5804

Table 1. continued

no.	aroma compound[a]	descriptor	RI DB-Wax	RI DB-5	fraction[b]	Osme values[c] FJ	Osme values[c] BFJ	Osme values[c] QKJ
60	2-phenylethanol	rosy, honey	1902	1132	N+A	4.50	4.67	4.00
61	4-methylguaiacol	smoky	1962	1199	N	2.17	2.50	2.17
62	phenol	phenol, medicinal	2014	991	N+A	2.17	2.17	2.00
63	γ-nonalactone	coconut	2014	1359	N	3.33	3.67	2.67
64	4-ethylguaiacol	clove	2041	1297	A	2.50	2.17	2.17
65	4-methylphenol	animal, horse stable-like	2098		A	2.33	2.33	2.00
66	decanoic acid	sweaty	2274		A	1.67	1.17	1.33

[a]The odorants were identified by comparing their RIs, mass spectra, and aroma attributes with those of standards. [b]The odorants were detected in fraction A, acidic/water-soluble fraction; N, neutral fraction; or B, basic fraction. [c]FJ, *Fenjiu* liquor; BFJ, *Baofeng* liquor; QKJ, *Qingke* liquor.

to a final concentration of 10% ethanol by volume. Eighteen milliliters of diluted liquor sample with 6 μL of IS solution (3.40 mg/L final concentration of 2,2-dimethylpropanoic acid (IS)) was saturated with NaCl and then mixed for 3 min with 1 mL of redistilled diethyl ether. After extraction, 1 μL of extract was injected into the injection port of the GC (250 °C) for analysis. The SIM method was used to quantitate the fatty acids (Table 2). The ion monitored of 2,2-dimethylpropanoic acid was m/z 57. The standard curves for fatty acids were built up as mentioned above.

GC-FID for Quantitation of Some Compounds with High Concentrations. GC-FID was employed for quantitation of ethyl acetate and ethyl lactate, because these two compounds have a high concentration of >1 g/L (Table 2). It was carried out using an Agilent 6890 GC equipped with a FID, modified from the method of ref 22. The column carrier gas was nitrogen at a constant flow rate of 1 mL/min. The separations were performed using a DB-Wax column (30 m length, 0.25 mm i.d., 0.25 μm film thickness; J&W Scientific) with an oven temperature program of 60 °C (3 min), ramped at 5 °C/min to 150 °C (15 min), and then ramped at 10 °C/min to 230 °C (5 min). One microliter of diluted liquor sample (40% ethanol by volume) with 176 mg/L final concentration of pentyl acetate was injected into the GC. The split ratio was 37:1. Injector and detector temperatures were 250 °C. The identification of compounds and the correction factors calculated in 40% ethanol by volume were performed according to ref 22.

Determination of Odor Thresholds. On the basis of the method previously described,[23] the orthonasal thresholds of the odorants were determined by a forced-choice test at seven concentration steps. A certain amount of the odorant in ethanol was pipetted into a Teflon vessel containing 50 mL of hydroalcoholic solution at 46% ethanol by volume, stirred for 2 min, and stepwise diluted (1:3 by volume, with the hydroalcoholic solution). Triangular series including one glass of the dilution and two glasses of hydroalcoholic solution were prepared. All of the series were labeled with random four-digit numbers and presented in decreasing concentrations. A sensory panel consisting of 32 panelists was asked to sniff each triangular series and select the differing one. The minimum concentration that the assessors correctly selected and the maximum concentration incorrectly selected were recorded. The odor threshold of each odorant was calculated by using the formulas described in ref 23. Sensory tests were performed at 21 ± 1 °C in a sensory room, and all of the panelists were national liquor tasters and had prior sensory training in Chinese liquor evaluation.

Aroma Recombination of FJ. A hydroalcoholic solution at 46% ethanol by volume was used as the matrix for recombination. All 27 odorants with OAVs ≥ 1 simultaneously in three liquors were dissolved in the matrix in their natural concentrations (Table 2) and then equilibrated for 10 min at ambient temperature; thus, a complete recombinate was obtained. This recombinate of 20 mL was finally presented in a glass covered with aluminum foil. Besides, a glass of FJ liquor was also prepared for the following sensory evaluation.

Descriptive profile tests were performed by 10 assessors (5 males and 5 females, 32 years old on average), 6 of whom were from the GC-O analysis and the other 4 were laboratory staff members familiar with the sensory attributes of Chinese liquors. All of the assessors were previously trained in orthonasal odor perception and participated regularly in sensory evaluation. Eight attributes were chosen as the most relevant odor to describe the overall aroma: fruity, floral, acid, earthy, alcoholic, grassy, mushroom, and coconut. The assessors were asked to evaluate the odor intensity of these attributes on a six-point scale from 0 to 5 (same as that described for GC-O analysis). The results obtained from 10 assessors were averaged and finally plotted in a spider web diagram. All of the tests were conducted in a sensory panel room at 20 ± 1 °C.

Omission Experiments. Triangle tests were performed to determine the significance of certain compounds according to the method previously reported.[24] For this purpose, 15 aroma omission models were prepared in the same way as complete recombinate but omitting one or a group of selected components, shown in Table 4. Three samples, including one omission model and two complete recombinates, were presented simultaneously to the assessors. All of the samples (20 mL) were randomly coded, and the assessors were the same people from the descriptive profile tests. The assessors were asked to sniff the samples and determine the differing one. The significance of difference between omission model and complete recombinates was determined according to the method described.[24]

RESULTS AND DISCUSSION

Identification of Odor-Active Constituents. By extraction with diethyl ether, an organic phase was obtained, which exactly elicited the typical light type aroma when sniffed by the panelists on a fragrance blotter. Thus, the isolation method used in this study turned out to be appropriate and reliable. For the purpose of facilitating GC-O analysis and compound identification, the extract obtained was further separated into acidic/water-soluble, neutral, and basic fractions to reduce complexity as previously described by Fan and Qian.[5] To identify the constituents responsible for the odors, odor-active areas were first located by GC-O and their RIs on both DB-Wax and DB-5 columns were determined. Besides, mass spectra in EI mode were recorded in the meantime, which were then compared with those available in NIST05a.L (Agilent Technologies, Inc.). To confirm these compounds further, their RIs, mass spectra, and aroma attributes were finally compared to the data obtained from the respective reference compounds.

Following this procedure, a total of 66 aroma compounds were identified in three light aroma type liquors in this study (Table 1). Among them, the highest Osme value of 4.67 was determined for β-damascenone and 2-phenylethanol. 2-Phenylethanol exhibited rosy and honey odors and β-damascenone presented honey and floral aromas. Both of these two compounds were previously reported as important odorants in whiskey, rum, and brandy.[9,12,25] One further compound with an Osme value above 4.00 simultaneously in three liquors was identified as ethyl octanoate, which showed an intense fruity odor. In addition, odorants with somewhat lower Osme values

Table 2. Standard Curves and Concentrations of 47 Odorants in Three Light Aroma Type Chinese Liquors

			standard curve		FJ[a]		BFJ[b]		QKJ[c]	
no.	aroma compound	quantitate ion	slope	intercept	av (μg/L)[d]	RSD[e] (%)	av (μg/L)	RSD (%)	av (μg/L)	RSD (%)
23	ethyl lactate[f,g]				4910	2	1060	2	1020	2
1	ethyl acetate[f,g]				2120	2	2760	8	3230	3
16	3-methylbutanol[g]	70	137	−16.4	514	2	886	9	454	4
2	1,1-diethoxyethane[g]	103	173	−2.38	419	4	214	7	558	4
29	acetic acid[h,g]	60	166	5.13	397	1	415	6	770	3
12	2-methylpropanol[g]	43	1870	−21.1	194	2	392	10	291	5
45	diethyl butanedioate[g]	101	13.1	−2.12	48.7	6	10.4	5	11.8	3
60	2-phenylethanol[g]	91	13.1	−0.79	11.1	2	20.3	9	42.7	3
4	ethyl propanoate	57	46.3	−0.80	9070	5	3070	4	4580	2
39	2-methylpropanoic acid[h]	73	5.27	0.366	7840	6	2030	4	2120	6
42	ethyl decanoate	88	1.06	−0.29	6570	9	7340	7	6820	4
24	1-hexanol	56	28.8	0.192	6300	2	7290	8	6710	2
15	1-butanol	56	29.4	0.624	6160	2	5520	10	10100	2
13	3-methylbutyl acetate	70	56.1	2.58	5870	4	13700	10	14100	3
27	ethyl octanoate	88	15.3	24.9	5040	2	6390	9	19300	3
17	ethyl hexanoate	88	8.24	−0.352	3090	4	5390	9	7680	1
32	furfural	96	109	31.8	2890	7	4370	3	27900	9
57	hexanoic acid[h]	60	27.2	1.89	2610	7	1670	5	1410	4
6	2-methylpropyl acetate	56	34.3	−0.162	2140	4	3500	7	1010	2
9	ethyl butanoate	71	37.9	−0.619	1820	7	3810	2	42800	2
43	phenylacetaldehyde	91	12	2.49	1780	7	535	4	784	2
46	3-methylbutanoic acid[h]	60	29.9	−0.211	1250	4	899	8	496	3
41	butanoic acid[h]	60	46	1.88	969	5	483	5	3320	3
31	decanal	57	5.3	0.036	798	2	253	8	587	3
53	2-phenylethyl acetate	104	0.218	−0.012	793	8	883	4	641	2
5	ethyl 2-methylpropanoate	71	316	−1.40	642	4	2100	7	8580	6
11	hexanal	56	37.1	−0.269	484	2	208	9	813	2
50	pentanoic acid[h]	60	46.5	1.33	416	2	313	2	292	3
35	ethyl nonanoate	88	3.93	−0.16	408	10	267	10	635	2
34	benzaldehyde	106	121	−3.47	354	1	222	8	21600	2
63	γ-nonalactone	85	8.32	0.033	275	6	169	7	324	2
14	ethyl pentanoate	57	73.1	13.6	256	3	498	5	8620	1
52	ethyl phenylacetate	91	0.312	−0.039	222	5	189	4	394	3
61	4-methylguaiacol	123	87.3	0.81	195	9	294	8	nd[i]	
44	ethyl benzoate	105 + 122	8.18	−0.01	190	1	602	7	408	4
59	ethyl 3-phenylpropanoate	104	9.09	−0.198	145	4	201	3	2780	4
62	phenol	94	6.91	0.022	122	3	263	6	103	6
10	ethyl 3-methylbutanoate	88	26.6	7.87	119	9	49.8	9	2870	3
25	nonanal	57	1.33	−0.032	117	2	160	9	287	1
22	ethyl heptanoate	88	13.6	0.021	110	3	53.9	8	245	1
64	4-ethylguaiacol	137	1.03	0.299	104	5	101	2	nd	
33	1-octen-3-ol	57	95.8	−0.129	48.2	5	23.3	5	52.4	5
21	2-heptanol	45	3.29	1.77	42.9	3	5.66	4	56.2	4
65	4-methylphenol	107	3.19	0.052	33.5	4	138	2	nd	
56	β-damascenone	69 + 121	0.192	0.018	19.1	2	28.6	4	11.5	1
40	2-acetyl-5-methylfuran	109	2.79	0.01	16.1	2	39.0	3	nd	
55	geosmin	112	1.29	−0.08	1.10	7	1.22	4	1.17	4

[a]FJ, *Fenjiu* liquor. [b]BFJ, *Baofeng* liquor. [c]QKJ, *Qingke* liquor. [d]av, average concentration of triplicates. [e]RSD, relative standard deviation of the average concentration. [f]These compounds were quantitated by GC-FID method. Correction factors of ethyl acetate and ethyl lactate were 1.47 and 1.54, respectively. [g]The concentration was mg/L. [h]These compounds were quantitated by LLME coupled with GC-MS method. [i]nd, not detected.

were identified as ethyl acetate (pineapple), 2-methylpropanol (malty), 3-methylbutanol (malty), ethyl phenylacetate (rosy and honey), and 2-phenylethyl acetate (floral). With their high Osme values, which were above 4.00 in at least one of the three liquors, these compounds were likely to contribute a lot to the overall light type aroma. However, other odorants, such as 3-methylbutanal (green and malty), 2-butanol (fruity), hexyl acetate (fruity), propanoic acid (vinegar), γ-hexalactone (sweet and coconut), naphthalene (mothball-like), and benzenemethanol (floral), appeared with lower Osme values below 2.00 in all three liquors. Most of these compounds have been earlier identified as aroma compounds in FJ, as well as in other aroma types of Chinese liquor.[5,8,26] Among them, β-damascenone was detected for the first time in BFJ and QKJ.

Quantitation of Odor-Active Compounds and OAV Analysis. Although GC-O analysis is an effective means for

dx.doi.org/10.1021/jf501214c | J. Agric. Food Chem. 2014, 62, 5796−5804

odorant identification, it could not indicate a final importance of the odorant to the overall aroma. One main reason is the fact that compounds in GC-O analysis were significantly separated and concentrated before sniffing, but in authentic liquors only the odorant present at a concentration above its odor threshold contributes to the overall aroma. Besides, as Grosch[27] reported, the influence of ethanol concentration on the volatility of an odorant should not be ignored. Taking these cases into consideration, the odor activity value (OAV) concept,[28] which correlated quantitative data to odor thresholds in a matrix, was applied to get closer to the liquors themselves.

For this reason, a total of 47 odorants with Osme values of ≥2.00 simultaneously in three liquors were quantitated (Table 2). Among these odorants, ethyl acetate and ethyl lactate, which had been reported as the most abundant odorants in light aroma type liquor,[29] appeared with the highest concentrations as expected. Both of them were >1.00 g/L. Besides, odorants 1,1-diethoxyethane, 2-methylpropanol, 3-methylbutanol, and acetic acid had higher concentrations of 0.1−0.9 g/L. However, two notable odorants, namely, β-damascenone (12−29 μg/L) and geosmin (1.0−1.2 μg/L), were present only in trace amounts, far lower than any other compounds.

To get as close as possible to the authentic liquor, the thresholds of single compounds were determined in a hydroalcoholic solution at 46% ethanol by volume, the typical ethanol content in Chinese liquor. Except that of geosmin, all of these thresholds were determined for the first time. As shown in Table 3, odorants such as ethyl acetate had a fairly high threshold of 32.6 mg/L in 46% vol hydroalcoholic solution. However, thresholds of some compounds present at trace amounts in Chinese liquors were extremely low, such as β-damascenone and geosmin. In this study, β-damascenone was determined with a threshold value of 0.12 μg/L, 10 times higher than that in water.[23] The threshold value of geosmin in 46% vol hydroalcoholic solution was determined at 0.11 μg/L according to the previous study, also 10 times higher than that in water.[1] These data revealed that the higher ethanol concentration in Chinese liquor might lead to a higher threshold than that in water.

Subsequently, OAVs of the odorants in light aroma type liquors were calculated and are summarized in Table 3. The results indicated that altogether 27 odorants were calculated with OAVs > 1 simultaneously in three liquors. These odorants should be the important contributors to the characteristic aroma of light aroma type Chinese liquor. Among these odorants, ethyl octanoate had the highest OAV value, which exhibited an intense fruity aroma. Two odorants, β-damascenone (floral and honey) and 1,1-diethoxyethane (fruity), could also be significant according to their higher OAVs (>100). Other odorants with high OAVs (>10) were 3-methylbutyl acetate, ethyl acetate, ethyl hexanoate, ethyl butanoate, ethyl 2-methylpropanoate, and geosmin. They could also contribute to the overall aroma but to a lesser degree.

Aroma Recombination and Omission Experiments. To confirm that the odorants showing high OAVs were actually the important odorants of light aroma type liquor, aroma recombination and omission experiments based on FJ (the most representative light aroma type liquor in China) were undertaken. For this purpose, an aroma recombinate, consisting of 27 odorants with OAVs ≥ 1 simultaneously in the three liquors in their natural concentrations (Table 2), was prepared.

Table 3. Orthonasal Thresholds and OAVs of 47 Odorants in Three Light Aroma Type Chinese Liquors

			OAV[b]		
no.	aroma compound	odor threshold[a]	FJ	BFJ	QKJ
27	ethyl octanoate	12.9	391	495	1500
2	1,1-diethoxyethane	2090	200	102	267
56	β-damascenone	0.12	159	238	96
1	ethyl acetate	32600	65	85	99
13	3-methylbutyl acetate	93.9	63	146	150
17	ethyl hexanoate	55.3	56	97	139
23	ethyl lactate	128000	38	8	8
9	ethyl butanoate	81.5	22	47	525
11	hexanal	25.5	19	8	32
10	ethyl 3-methylbutanoate	6.89	17	7	417
31	decanal	70.8	11	4	8
5	ethyl 2-methylpropanoate	57.5	11	37	149
55	geosmin	0.11[c]	10	11	11
14	ethyl pentanoate	26.8	10	19	322
33	1-octen-3-ol	6.12	8	4	9
12	2-methylpropanol	28300	7	14	10
43	phenylacetaldehyde	262	7	2	3
42	ethyl decanoate	1120	6	7	6
39	2-methylpropanoic acid	1580	5	1	1
63	γ-nonalactone	90.7	3	2	4
16	3-methylbutanol	179000	3	5	3
29	acetic acid	160000	2	3	5
6	2-methylpropyl acetate	922	2	4	1
15	1-butanol	2730	2	2	4
59	ethyl 3-phenylpropanoate	125	1	2	22
25	nonanal	122	1	1	2
24	1-hexanol	5370	1	1	1
46	3-methylbutanoic acid	1050	1	<1	<1
57	hexanoic acid	2520	1	<1	<1
41	butanoic acid	964	1	<1	3
50	pentanoic acid	389	1	<1	<1
60	2-phenylethanol	28900	<1	<1	1
32	furfural	44000	<1	<1	<1
53	2-phenylethyl acetate	909	<1	<1	<1
64	4-ethylguaiacol	123	<1	<1	
61	4-methylguaiacol	315	<1	<1	
52	ethyl phenylacetate	407	<1	<1	<1
4	ethyl propanoate	19000	<1	<1	<1
65	4-methylphenol	167	<1	<1	
45	diethyl butanedioate	353000	<1	<1	<1
44	ethyl benzoate	1430	<1	<1	<1
35	ethyl nonanoate	3150	<1	<1	<1
34	benzaldehyde	4200	<1	<1	5
21	2-heptanol	1430	<1	<1	<1
22	ethyl heptanoate	13200	<1	<1	<1
62	phenol	18900	<1	<1	<1
40	2-acetyl-5-methylfuran	40900	<1	<1	

[a]Thresholds in 46% volume hydroalcoholic solution detected in this study, μg/L. [b]FJ, *Fenjiu* liquor; BFJ, *Baofeng* liquor; QKJ, *Qingke* liquor. [c]Odor thresholds were taken from ref 1.

Descriptive profile tests were then conducted by a sensory panel consisting of 10 trained assessors, and odor attributes of the recombinate and original liquor were compared. As shown in Figure 1, the aroma profile of the recombinate was in good similarity to that of the original liquor. Consequently, this result indicated the success in simulating the typical aroma of the

dx.doi.org/10.1021/jf501214c | J. Agric. Food Chem. 2014, 62, 5796−5804

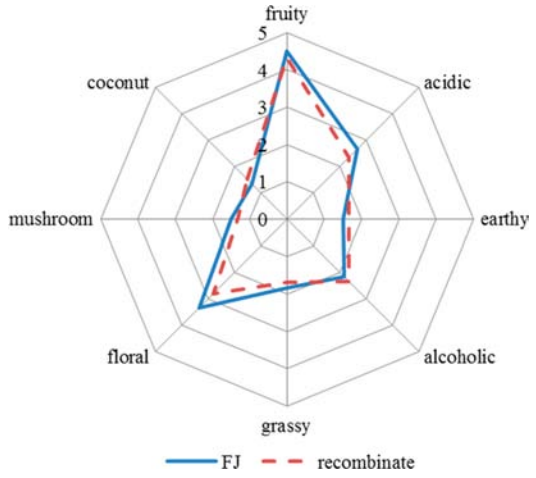

Figure 1. Aroma profile of FJ and the complete aroma recombinate.

investigated liquor by combining 27 odorants in their natural concentrations, using a 46% vol hydroalcoholic solution as the matrix.

To achieve a deeper investigation of the aroma contribution of certain compounds, 15 aroma omission models were prepared by omitting either a single odorant or a group of odorants from the complete recombinate (Table 4). Each of the omission models was presented to the assessors in comparison with the complete recombinate, using a triangle test. The results are shown in Table 4.

Table 4. Omission Experiments from the Complete Recombinate

no.	odorants omitted from the complete recombinate	n^a	significance[b]
1	all esters	10	***
1A	ethyl octanoate	4	
1B	ethyl acetate	8	**
1C	ethyl lactate	7	*
1D	ethyl acetate and ethyl lactate	8	**
1E	all esters except ethyl acetate and ethyl lactate	6	
2	1,1-diethoxyethane	5	
3	β-damascenone	9	***
4	aromatic compounds	5	
5	acetic acid and 2-methylpropanoic acid	8	**
6	all alcohols	6	
7	all aldehydes	3	
8	geosmin	8	**
9	γ-nonalactone	3	
10	1-octen-3-ol	2	

[a]Number of correct judgments from 10 assessors evaluating the aroma difference by means of a triangle test. [b]Significance: ***, very highly significant ($\alpha \leq 0.001$); **, highly significant ($\alpha \leq 0.01$); *, significant ($\alpha \leq 0.05$).

In the tests, all assessors were able to detect the omission model lacking the entire group of esters (model 1), thus leading to a very highly significant difference between the omission model and complete recombinate. This result revealed the fairly important role of these fruity note odorants to the overall aroma. Among them, ethyl octanoate was calculated for extremely high OAVs (Table 3), but as omission model 1A revealed, the absence of this compound was correctly detected by only 4 of 10 assessors in triangle tests. Therefore, no significant difference was determined for its omission compared with the complete recombinate. Thus, this compound was excluded as the most important aroma contributor. Ethyl acetate and ethyl lactate were traditionally regarded as the most potent aroma compounds because of their particularly high concentrations,[29,30] but in our study their OAVs were not so much high. Therefore, several omission models were set up for a deeper investigation. When ethyl acetate and ethyl lactate were omitted together (model 1D), a high significance was evaluated. However, no significant difference was observed when all esters except these two compounds (model 1E) were omitted. This indicated the important role of these two fruity note odorants. Furthermore, when solely lacking ethyl acetate (model 1B), the assessors could detect a highly significant difference, whereas the omission of single ethyl lactate (model 1C) was determined as only significantly different by the assessors. This revealed a slightly more important role of ethyl acetate compared with ethyl lactate. In conclusion, these data indicated that ethyl acetate and ethyl lactate together rather than ethyl octanoate were responsible for the typical fruity note of light aroma type liquor, probably due to their high concentrations, and this finding fitted well with the conclusion previously drawn.[30] As reported previously, esters were formed mainly through esterification of alcohols and fatty acids during the fermentation, distillation, and aging processes.[31,32]

However, another fruity-smelling odorant, 1,1-diethoxyethane, should be mentioned, just as the case of ethyl octanoate. Despite its relatively high OAV calculated in Table 3, omission of this compound was detected with no significant difference by the assessors (model 2). This might be due to the very intense fruity note of the esters, which made up for the absence of the single 1,1-diethoxyethane.

An omission model without β-damascenone was evaluated with a very highly significant difference compared to the complete recombinate (model 3), thereby pinpointing the crucial role of this floral- or honey-like-smelling compound for the typical aroma of light aroma type liquor. This result was in accordance with the high OAVs determined for β-damascenone (Table 3). However, no difference of the model lacking in aromatic compounds, which exhibited a floral odor as well, was detected by the assessors (model 4). Consequently, the floral note present in the profile of overall aroma could be greatly linked to β-damascenone rather than the aromatic compounds. β-Damascenone has already been detected in many alcoholic beverages, such as whiskey, wine, and beer.[9,33,34] Researchers have suggested that 3-hydroxy-7,8-dihydro-β-ionol was the key precursor for the formation of β-damascenone through an acid-catalyzed pathway.[35] On the basis of these findings, Poisson and Schieberle[10] assumed that cereals could contain similar precursors leading to the generation of β-damascenone during fermentation and/or distillation.

As shown in Table 4, the omission of acetic acid and 2-methylpropanoic acid (model 5) was rated with a highly significant difference. This elucidated the important role of these two acidic- or vinegar-smelling odorants to the overall aroma. In addition, the omission of the earthy-smelling odorant geosmin (model 8) also resulted in a highly significant difference from the complete recombinate. This compound was previously detected in Chinese liquors by Du and co-workers.[1] However, the model lacking in alcohols (model 6) was not determined as significantly different when compared with the complete recombinate; thus, the alcoholic note from the aroma profile could not be correlated to certain odorants in

dx.doi.org/10.1021/jf501214c | J. Agric. Food Chem. 2014, 62, 5796−5804

this study. Aldehydes mostly showed a grassy or green note; omission of this group of compounds was also determined with no significant difference by the assessors (model 7). The same results also occurred with γ-nonalactone (coconut smelling) and 1-octen-3-ol (mushroom smelling), as shown in models 9 and 10.

To sum up, with all of the findings above taken into account, conclusions can be drawn: (i) Aroma-active compounds in three representative Chinese light aroma type liquors have been successfully identified through GC-O analysis, and 27 odorants were further screened out as the important odorants according to quantitative study and OAV data. (ii) By means of aroma recombination and omission experiments, the typical light type aroma dominated by fruity and floral notes was successfully simulated using these 27 important odorants, and, additionally, ethyl acetate and β-damascenone were demonstrated as the key aroma contributors among them.

A careful literature inspection showed that this study is the first to investigate the key odorants of Chinese light aroma type liquor and to mimic its overall aroma through recombination and omission studies. Although limitations still exist, such as the simplified aroma model matrix that ignores the influence of nonvolatile compositions, our investigation could contribute to a better understanding of Chinese liquor.

AUTHOR INFORMATION

Corresponding Author

*(W.F.) Phone: 86-510-85197082. Fax: 86-510-85918201. E-mail: Wenlai.Fan@gmail.com.

Funding

Financial supports from National 863 Plan under No. 2013AA102108 and the Ministry of Science and Technology of China under No. 2012BAK17B11 are gratefully acknowledged.

Notes

The authors declare no competing financial interest.

REFERENCES

(1) Du, H.; Fan, W.; Xu, Y. Characterization of geosmin as source of earthy odor in different aroma type Chinese liquors. *J. Agric. Food Chem.* **2011**, *59*, 8331−8337.

(2) Xu, Y.; Wang, D.; Fan, W. L.; Mu, X. Q.; Chen, J. Traditional Chinese biotechnology. In *Biotechnology in China II*; Springer: Berlin, Germany, 2010; pp 189−233.

(3) Shen, Y. F. The main factors influencing the formation of liquor flavor. *Liquor Making Sci. Technol.* **2005**, *11*, 30−34.

(4) Fan, W. L.; Xu, Y. Research progress of enzyme in daqu. *Niangjiu* **2000**, *27*, 35−40.

(5) Fan, W.; Qian, M. C. Characterization of aroma compounds of Chinese "Wuliangye" and "Jiannanchun" liquors by aroma extract dilution analysis. *J. Agric. Food Chem.* **2006**, *54*, 2695−2704.

(6) Fan, W.; Xu, Y.; Zhang, Y. Characterization of pyrazines in some Chinese liquors and their approximate concentrations. *J. Sci. Food Agric.* **2007**, *55*, 9956−9962.

(7) Fan, W.; Shen, H.; Xu, Y. Quantification of volatile compounds in Chinese soy sauce aroma type liquor by stir bar sorptive extraction and gas chromatography−mass spectrometry. *J. Agric. Food Chem.* **2011**, *91*, 1187−1198.

(8) Zhu, S.; Lu, X.; Ji, K.; Guo, K.; Li, Y.; Wu, C.; Xu, G. Characterization of flavor compounds in Chinese liquor Moutai by comprehensive two-dimensional gas chromatography/time-of-flight mass spectrometry. *Anal. Chim. Acta* **2007**, *597*, 340−348.

(9) Poisson, L.; Schieberle, P. Characterization of the most odor-active compounds in an American Bourbon whisky by application of the aroma extract dilution analysis. *J. Agric. Food Chem.* **2008**, *56*, 5813−5819.

(10) Poisson, L.; Schieberle, P. Characterization of the key aroma compounds in an American Bourbon whisky by quantitative measurements, aroma recombination, and omission studies. *J. Agric. Food Chem.* **2008**, *56*, 5820−5826.

(11) Langos, D.; Granvogl, M.; Schieberle, P. Characterization of the key aroma compounds in two Bavarian wheat beers by means of the sensomics approach. *J. Agric. Food Chem.* **2013**, *61*, 11303−11311.

(12) Willner, B.; Granvogl, M.; Schieberle, P. Characterization of the key aroma compounds in Bartlett pear brandies by means of the sensomics concept. *J. Agric. Food Chem.* **2013**, *61*, 9583−9593.

(13) Chen, S.; Xu, Y.; Qian, M. C. Aroma characterization of Chinese rice wine by gas chromatography−olfactometry, chemical quantitative analysis, and aroma reconstitution. *J. Agric. Food Chem.* **2013**, *61*, 11295−11302.

(14) Pang, X.; Chen, D.; Hu, X.; Zhang, Y.; Wu, J. Verification of aroma profiles of Jiashi muskmelon juice characterized by odor activity value and gas chromatography−olfactometry/detection frequency analysis: aroma reconstitution experiments and omission tests. *J. Agric. Food Chem.* **2012**, *60*, 10426−10432.

(15) Chetschik, I.; Granvogl, M.; Schieberle, P. Quantitation of key peanut aroma compounds in raw peanuts and pan-roasted peanut meal. Aroma reconstitution and comparison with commercial peanut products. *J. Agric. Food Chem.* **2010**, *58*, 11018−11026.

(16) Christlbauer, M.; Schieberle, P. Evaluation of the key aroma compounds in beef and pork vegetable gravies a la chef by stable isotope dilution assays and aroma recombination experiments. *J. Agric. Food Chem.* **2011**, *59*, 13122−13130.

(17) Greger, V.; Schieberle, P. Characterization of the key aroma compounds in apricots (*Prunus armeniaca*) by application of the molecular sensory science concept. *J. Agric. Food Chem.* **2007**, *55*, 5221−5228.

(18) Fan, W.; Qian, M. C. Identification of aroma compounds in Chinese 'Yanghe Daqu' liquor by normal phase chromatography fractionation followed by gas chromatography−olfactometry. *Flavour Fragrance J.* **2006**, *21*, 333−342.

(19) Cates, V. E.; Meloan, C. E. Separation of sulfones by gas chromatography. *J. Chromatogr., A* **1963**, *11*, 472−478.

(20) Fan, W.; Xu, Y.; Jiang, W.; Li, J. Identification and quantification of impact aroma compounds in 4 nonfloral *Vitis vinifera* varieties grapes. *J. Food Sci.* **2010**, *75*, S81−S88.

(21) Wang, L.; Fan, W.; Xu, Y. Analysis of capillary chromatographic skeleton compounds in Chinese soy sauce aroma type liquor by liquid-liquid microextraction and aroma recombination. *Sci. Technol. Food Ind.* **2012**, 304−309.

(22) AQSIQ; SAC. Method of analysis for Chinese spirits. In *National Standard of the People's Republic of China*; Standardization Publishing House of China: Beijing, 2007; Vol. GB/T 10345-2007, pp 1−17.

(23) Czerny, M.; Christlbauer, M.; Christlbauer, M.; Fischer, A.; Granvogl, M.; Hammer, M.; Hartl, C.; Hernandez, N. M.; Schieberle, P. Re-investigation on odour thresholds of key food aroma compounds and development of an aroma language based on odour qualities of defined aqueous odorant solutions. *Eur. Food Res. Technol.* **2008**, *228*, 265−273.

(24) Jellinek, G. *Sensory Evaluation of Food. Theory and Practice*; Horwood: Chichester, UK, 1985.

(25) Pino, J. A.; Tolle, S.; Gök, R.; Winterhalter, P. Characterisation of odour-active compounds in aged rum. *Food Chem.* **2012**, *132*, 1436−1441.

(26) Ma, Y.; Qiao, H.; Wang, W.; Chen, T.; Du, X.; Zhai, X.; Zhang, S. Variations in physicochemical properties of Chinese Fenjiu during storage and high-gravity technology of liquor aging. *Int. J. Food Prop.* **2014**, *17*, 923−936.

(27) Grosch, W. Evaluation of the key odorants of foods by dilution experiments, aroma models and omission. *Chem. Senses* **2001**, *26*, 533−545.

(28) Schieberle, P. In *New Developments in Methods for Analysis of Volatile Flavor Compounds and Their Precursors*; Elsevier Science: Amsterdam, The Netherlands, 1995; pp 403−431.
(29) Wang, Y. T. Effects of the aain trace components and its quantity relative ratio relationship of Fen-flavor liquor on the sensory quality. *Liquor Making Sci. Technol.* **2004**, *3*, 3.
(30) Shen, Y. F. *Manual of Chinese Liquor Manufactures Technology*; Light Industry Publishing House of China: Beijing, China, 1996.
(31) Fan, W.; Qian, M. C. Headspace solid phase microextraction and gas chromatography-olfactometry dilution analysis of young and aged Chinese "Yanghe Daqu" liquors. *J. Agric. Food Chem.* **2005**, *53*, 7931−7938.
(32) Ledauphin, J.; Guichard, H.; Saint-Clair, J.-F.; Picoche, B.; Barillier, D. Chemical and sensorial aroma characterization of freshly distilled Calvados. 2. Identification of volatile compounds and key odorants. *J. Agric. Food Chem.* **2003**, *51*, 433−442.
(33) Guth, H. Identification of character impact odorants of different white wine varieties. *J. Agric. Food Chem.* **1997**, *45*, 3022−3026.
(34) Schieberle, P. Primary odorants of pale lager beer. *Z. Lebensm.-Unters. -Forsch.* **1991**, *193*, 558−565.
(35) Roberts, D. D.; Acree, T. E. Developments in the isolation and characterization of β-damascenone precursors from apples. In *Fruit Flavors, Biogenesis, Characterization and Authentication*; Rouseff, R. L., Leahy, M. M., Eds.; American Chemical Society: Washington, DC, USA, 1995; pp 190−199.

JOURNAL OF AGRICULTURAL AND FOOD CHEMISTRY

Article

pubs.acs.org/JAFC

Development of an Ultraperformance Liquid Chromatography–Tandem Mass Spectrometry Method for the Analysis of Perfluorinated Compounds in Fish and Fatty Food

Stephen W. C. Chung* and Chi Ho Lam

Food Research Laboratory, Food and Environmental Hygiene Department, 4/F Public Health Laboratory Centre, 382 Nam Cheong Street, Hong Kong SAR, China

Supporting Information

ABSTRACT: This paper reports the development of a method for the quantitative analysis of perfluorinated compounds (PFCs), including C_6–C_{14} perfluorinated carboxylic acids (PFCAs) and C_4–C_{12} perfluorinated sulfonates (PFSAs), in fish and fatty foods by ultraperformance liquid chromatography–electrospray ionization–tandem mass spectrometry (UPLC-ESI-MS/MS) in which the UPLC was equipped a PFC Analysis Kit to eliminate background contamination. Rapid baseline separation was achieved for 17 PFCs within 12 min, and PFCs were well-resolved from potential interferences from taurodeoxycholic acid and branched isomers of PFCs. The method was validated according to Commission Regulation 2002/657/EC of the European Commission with matrices including salmon, beef, egg, and butter. Average spiked recoveries, measured at concentration levels of 0.02 (method limit of quantification (MLOQ)), 0.2, and 2 μg/kg, were in the range of 68–117% with relative standard deviations below 20%. Matrix effects were evaluated and found to be correctable by internal standardization, especially for short- and long-chained PFCs. Trueness was verified against two certified reference materials. The method has also been successfully applied to the analysis of more than 200 food samples of a risk assessment study.

KEYWORDS: *perfluorinated compounds, PFCAs, PFSAs, fish, fatty food, UPLC-MS/MS*

INTRODUCTION

As perfluorooctanesulfonate (PFOS) and perfluoroctanoic acid (PFOA) are persistent and can bioaccumulate in animals, it is not surprising that various studies reported the general public is exposed to these two chemicals.[1,2] Food and water were found to be the main sources of exposure. Studies conducted by various authorities around the world, including Canada,[3] China,[4] the United States,[5] the United Kingdom,[6] Germany,[7] The Netherlands,[8] Spain,[9] Sweden,[10] and the European Union,[11] found that PFOS and PFOA can present in certain foods up to 20 μg/kg. Some of these reports stated that fish (marine and fresh water) contain higher levels of these two PFCs. Studies also found some fatty foods including beef, offal (e.g., liver and kidney), butter, etc., can have PFOS/PFOA.

Owing to the lack of native and labeled reference standards, early studies of PFCs in fish were concentrated in PFOS, PFOA, and PFCAs.[12−16] More standards are available recently, including perfluoropentanesulfonate, perfluorononanesulfonate, and perfluorododecanesulfonate. Ion-pair extraction[13,15,17] and solid–liquid extraction[12,14,18,19] were commonly used. Both approaches coextract other matrix constituents, including lipids, and affect the mass spectrometric analysis (signal suppression).[20] Alkaline digestion can reduce the interference from fatty matrix, but is time-consuming.[7,18] Besides, the former extraction method may have the problem of loss of analytes in the solvent exchange process,[13,17] whereas the latter would show low recoveries for long- and short-chain PFCs.[19] In 2010, Ballesteros-Gomez et al.[21] introduced the THF–water extraction method for the analysis of 14 PFCs in food and applied it to the dietary intake study of PFOS and PFOA in The Netherlands.[22] Although eight labeled standards were used, the correction of hydrophilic short-chained and hydrophobic long-chained PFCs for a range of complex and heterogeneous matrices was still found to inefficient. Besides, phase separation occurred for fatty fish samples.

According to the European Food Safety Authority (EFSA) report,[23] most occurrence data of PFOS were reported without information on the isomer types analyzed: linear, branched, or both types. Owing to differences in bioaccumulation potentials,[24] linear and branched isomers should be analyzed separately for better estimation of their dietary exposure. The developed ultraperformance liquid chromatography–mass spectrometry (UPLC-MS) method resolved linear PFOS from 10 different branched isomers and well-known interference taurodeoxycholic acid (TDCA). Besides, this method can quantify nine PFCAs and eight PFSAs within 12 min. Validation was performed with fish, meat, egg, and butter according to the requirement of the Commission Decision 2002/657/EC of the European Commission (EC), and the results fulfilled the recommendations in Commission Recommendation 2010/161/EU on monitoring of perfluoroalkylated substances in food. Furthermore, method accuracy and extraction efficiency were verified by two fish certified reference materials obtained from the National Institute of Standards and Technology.

Received: January 2, 2014
Accepted: June 5, 2014
Published: June 5, 2014

 © 2014 American Chemical Society

MATERIALS AND METHODS

Chemicals and Standards. LC-MS grade acetonitrile (MeCN) and methanol (MeOH) were purchased from Anaqua Chemicals Supply (Houston, TX, USA) and Fisher Scientific (Waltham, MA, USA), respectively. Water was purified through a Milli-Q synthesis system integral with LC-Pak polisher from Millipore (Billerica, MA, USA). Absolv. grade *n*-hexane was purchased from Tedia Co. (Fairfiled, OH, USA). Analytical reagent grade ammonia solution was purchased from VWR international (Poole, UK). HPLC grade tetrahydrofuran (THF), ammonium acetate, acetic acid, ammonium formate, and formic acid were purchased from Sigma-Aldrich (St. Louis, MO, USA).

Native perfluorinated compounds (PFCs), including perfluoro-*n*-hexanoic/heptanoic/octanoic/nonanoic/decanoic/undecanoic/dodecanoic/tridecanoic/tetradecanoic acid (PFHx/Hp/O/N/D/Ud/Do/TrD/TeDA) and sodium perfluoro-1-butane/pentane/hexane/heptane/octane/nonane/decane/dodecanesulfonate (PFB/Pe/Hx/Hp/O/N/D/DoS), were purchased from Wellington Laboratories (Ontario, Canada). Isotopically labeled standards perfluoro-*n*-[1,2,3,4,6-$^{13}C_5$]hexanoic acid ($^{13}C_5$PFHxA), perfluoro-*n*-[1,2,3,4-$^{13}C_4$]-heptanoic acid ($^{13}C_4$PFHpA), perfluoro-*n*-[$^{13}C_8$]octanoic acid ($^{13}C_8$PFOA), perfluoro-*n*-[$^{13}C_9$]nonanoic acid ($^{13}C_9$PFNA), perfluoro-*n*-[1,2,3,4,5,6-$^{13}C_6$]decanoic acid ($^{13}C_6$PFDA), perfluoro-*n*-[1,2,3,4,5,6,7-$^{13}C_7$]undecanoic acid ($^{13}C_7$PFUdA), perfluoro-*n*-[1,2-$^{13}C_2$]dodecanoic acid ($^{13}C_2$PFDoA), perfluoro-*n*-[1,2-$^{13}C_2$]-tetradecanoic acid ($^{13}C_2$PFTeDA), sodium perfluoro-1-[1,2,3-$^{13}C_3$]-hexanesulfonate (Na$^{13}C_3$PFHxS), and sodium perfluoro-1-[$^{13}C_8$]-octanesulfonate ($^{13}C_8$PFOS) were purchased from Wellington Laboratories (Ontario, Canada), and ammonium perfluoro-[$^{18}O_2$]-butanesulfonate ($^{18}O_2$PFBS) was obtained from RTI International (Research Triangle Park, NC, USA).

TDCA sodium salt was purchased from Steraloids Inc. (Newport, RI, USA), and perfluoro-1/-2/-3/-4/-5/-6-methylheptanesulfonate (P1/2/3/4/5/6MHpS), perfluoro-2/-3/-4/-5/-6-methylheptanoic acid (P2/3/4/5/6MHpA), perfluoro-4,4/-5,5/-3,5/-4,5-methylhexanesulfonate (P44/55/35/45DMHxS), and perfluoro-4,4/-5,5/-3,5/-4,5-methylhexanoic acid (P44/55/35/45DMHxA) in methanol were purchased from Wellington Laboratories.

Intermediate mixed standard solutions (10 mg/L) were prepared with methanol. Working standard solutions for calibration were freshly prepared with MeCN/water (5:5 v/v). All solutions were stored at −20 °C.

Sample Preparation. A portion of 10 g of homogenized sample was weighed and placed into a 50 mL polypropylene centrifuge (PP) tube (Sarstedt, Nümbrecht, Germany). Isotopically labeled internal standards each of 1 ng were spiked. The sample was then defatted by vortexing with 20 mL of *n*-hexane for 10 min with a multipulse vortexer (Glas-Col, LLC, Terre Haute, IN, USA). The mixture was centrifuged by a centrifuge (Kendro, Newtown, CT, USA), and the *n*-hexane layer was discarded. The defatted sample was then freeze-dried for 24 h to remove the sample moisture by a freeze-dryer (SP Industries, Warminster, PA, USA). Twenty milliliters of THF/water (75:25) solution was added for extraction. The mixture was vortexed for 10 min and was recentrifuged for 10 min at 8500 rpm (or 6770*g*) (Falcon 6/300, MSE, UK). Any residual oil layer was discarded. Ten milliliters of extract was pipetted into a 15 mL PP centrifuge tube (Sarstedt). The volume of extract was reduced to 6 mL under a slow stream of nitrogen at 50 °C and then made up to 15 mL with water before cleanup.

The 15 mL sample solution was loaded onto a preconditioned weak anion exchange cartridge, Strata X-AW (6 mL, 200 mg) obtained from Phenomenex, at a rate of 1 drop/s. After loading, the cartridge was washed with 4 mL of 25 mM acetate buffer at pH 4 and 6 mL of a 50:50 (v/v) THF/MeCN mixture at a rate of 2 drop/s. Then, the SPE WAX cartridge was coupled to the ENVI-carb cartridge (6 mL, 250 mg), which obtained from Sigma-Aldrich, via a suitable polyethylene (PE) adaptor cap. The target analytes were eluted out with 6 mL of 0.1% ammonia in MeOH. The eluate passed through the graphitized carbon cartridge, too. Cartridges were dried under vacuum to ensure maximal recovery of the eluate. The eluate was evaporated to dryness (50 °C, N_2) and reconstituted with 0.5 mL of MeCN/water 1:1 (v/v). Finally, the extract was filtered by syringe (Terumo, Leuven, Belgium) with a 0.2 μm regenerated cellulose syringe filter (Sartorius AG, Goettingen, Germany) into a PP LC vial with a PP screw cap (Waters) for UPLC-MS/MS analysis.

For fat/oil samples, no defatting and freeze-drying were done. The rest of the sample preparation was the same as described above.

Ultraperformance Liquid Chromatography−Mass Spectrometry. The chromatographic separation was carried out using a Waters Acquity UPLC system, which consisted of a sample manager, a column manager, and a binary solvent manager (Milford, MA, USA) equipped with a UPLC column with perfluoro-C8 stationary phase, Epic FO LB, 1.8 μm, 5 cm × 2.1 mm (ES Industries Chromega, West Berlin, NJ, USA). Column temperature was set at 35 °C. Gradient elution was made with MeCN and aqueous buffer with 1.3 mM ammonium formate and 0.7 mM formic acid at a constant flow rate of 0.45 mL/min. Initial mobile phase composition of 13% MeCN was held for 3 min. MeCN composition was linearly increased to 55% at 7.5 min and subsequently to 95% at 10 min. Washing with 95% MeCN was held from 2 min. MeCN composition was then reduced back to 13% and followed by a 3 min reconditioning of the column. The total run time was 15 min. Five microliters of extract was injected in this study. Besides, the UPLC system was installed with an Acquity PFCs analysis kit. Epic FO LB was used as an isolation column.

The UPLC system was coupled to a Qtrap 5500 triple-quadrupole mass spectrometer (AB Sciex, Framingham, MA, USA) equipped with a TurboV ion source for analysis. The data system was installed with Analyst software (version 1.5.2). The tandem mass spectrometer was operated in negative electrospray ionization mode (−ve ESI-MS/MS). Scheduled multiple reaction monitoring algorithm mode was used to maximize the instrument performance. Ion spray voltage was set at −4 kV. Nitrogen was used as collision gas and set at medium. Curtain gases, GS1 and GS2, were set at 20, 50, and 50, respectively. Source temperature was set at 600 °C. Both quadrupole 1 (Q1) and quadrupole 3 (Q3) resolution were set as unit. The entrance potential was set as −10 V. The optimized settings for collision energy (CE) and the declustering (DP), entrance (EP), and collision cell exit potentials (CXP) were tested for each target analyte and their ISs by flow injection analysis resulting from the most abundant precursor ion and are summarized in the Supporting Information (Table S1), as well as the indicative retention times on the column. All PFCAs were monitored as their deprotonated ions ($[M - H]^-$), whereas all PFSA anions were directly monitored ($[M]^-$). Softwares Acquity UPLC Console (Waters) and Analyst (AB Sciex) were used to operate the UPLC and MS/MS, respectively. Software MultiQuant (AB Sciex) was used for data processing.

Internal standardization was used for PFC quantification. Matching of native and labeled standards is summarized in Table S1 in the Supporting Information. Fifteen-point calibration curves with concentrations from 0.05 to 50 μg/L (which covered 3 orders of magnitude) using weighted linear regression were established for quantification. Two MRM transitions were monitored to fulfill the identification points and ion ratio requirement. The maximum permitted tolerances on the MRM ratio as well as relative retention time (RRT) deviation tolerances (2.5%) followed 2002/657/EC guidelines. The minimum signal-to-noise ratio for both quantification and confirmation MRM of a quantified signal was 3.

RESULTS AND DISCUSSION

Method Development. Despite more and more PFC standards becoming commercially available, PFCs being mainly present in fish and meat, linear and branched PFCs should be quantified separately, and improvement in high-throughput analytical procedure is requested. The key issue of this paper was to develop a new method with good resolution power of PFCs for rapid quantification in fatty foods. As PFPeS (C_5), PFNS (C_9), and PFDoS (C_{12}) are commercially available, the scope of analysis increased to nine PFCAs (C_6−C_{14}) and eight

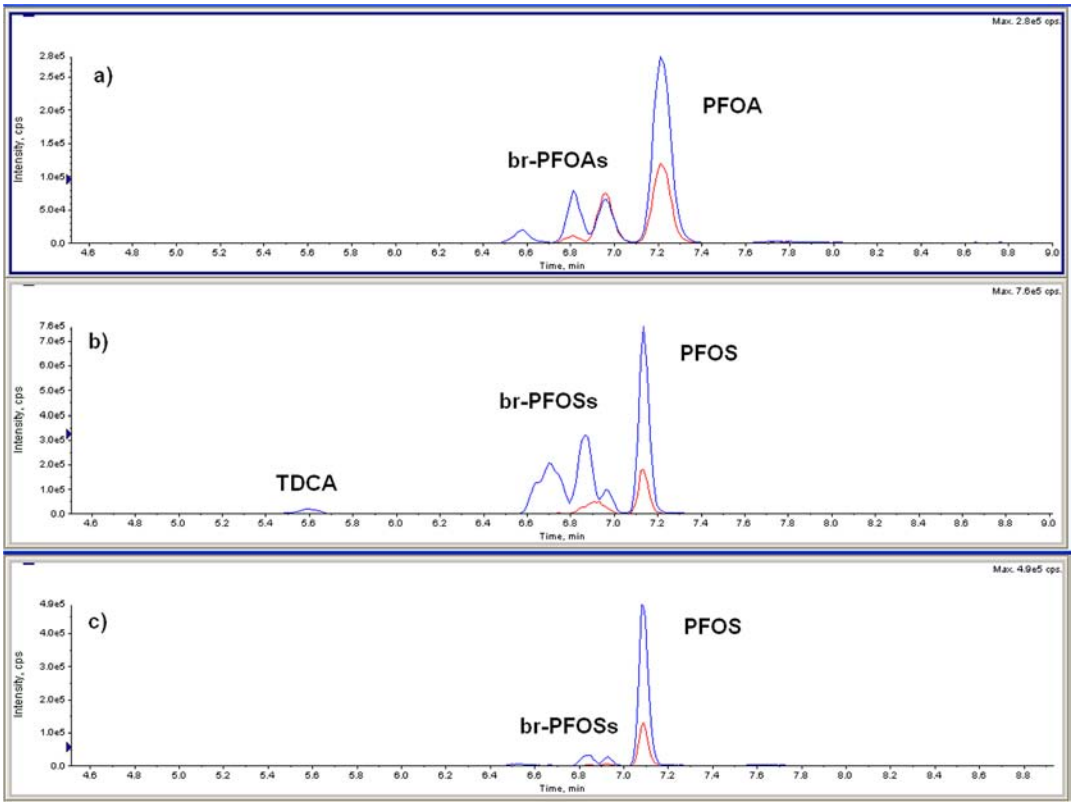

Figure 1. Chromatograms of the two MRM transitions of (a) PFOA and their branched isomers of a mixed standard solution, (b) PFOS, their branched isomers, and TDCA of a mixed standard solution, and (c) PFOS and their branched isomers of a fish sample. The blue trace refers to 413/369 and 499/80 for PFOA and PFOS, respectively, whereas the red trace refers to 413/169 and 499/99, respectively.

PFSAs (C_4−C_{12}). SPE WAX conditions were slightly modified for this wider scope of PFCs. We attempted to include perfluorohexadecanoic acid and perfluorooctadecanoic acid as well but did not succeed because their recoveries were comparatively low and none of the internal standards was found to be suitable for correction of recovery.

The run time was much shortened after the LC analysis migrated to a UPLC system. Seventeen PFCs were eluted within 12 min. It is worth mentioning that a small change in pH value of the buffering system affected PFC retentions. To ensure reproducibility, the mobile phase buffers were prepared by mixing of acid and salt solution instead of adjusting to the desired pH. Formic acid to ammonium formate ratios of 1:4, 1:2, and 1:1 in mobile phase were tested. PFBS was found to have no retention under buffer ratio 1:4, whereas PFTeDA had a strong retention, which led to undesirable peak boarding under buffer ratio 1:1. Although a systematic multivariate analysis of chromatographic conditions was not performed, the buffer system with an acid-to-salt ratio of 1:2 produced a suitable retention for both short- and long-chain PFCs.

Background PFCs Contamination. The UPLC-MS/MS offered excellent sensitivity to the PFCs, and analytes at the nanograms per liter level could be easily detected. As such, stringent control on background contamination from reagents, labware, and instrument was essential for reliable quantification of any trace amount of PFCs detected in samples. LC-MS grade MeOH (LabScan or Fisher) was used in the entire method as significant residual PFOA was noted in HPLC grade MeOH. Using PP centrifuge tubes, non-PTFE SPE vacuum manifold accessories, PP LC vials, and septumless polyethylene caps were necessary to reduce background. An Acquity PFC Analysis Kit was installed into the Waters UPLC system; those parts such as stainless steel tubings/screws/ferrules/filters of the LC system that contained PTFE parts were replaced by PEEK. An Epic FO LB was connected in-line between the solvent mixer and the injection of the LC system so that the PFCs leached out from the system were retained in it. The same type of column was used for both isolation and analytical separation such that the separation of the leached out PFCs could be ensured. High back pressure was generated by the isolator column of the PFC Analysis Kit and analytical separation column (i.e., two UPLC columns in series). The problem was resolved by replacing MeOH with MeCN as organic mobile phase and setting the analytical column temperature at 35 °C.

Trace amounts of PFHxA, PFHpA, and PFOA in method blank were controlled at ∼0.02 μg/L, which was less than the lowest calibration level at 0.05 μg/L in vial (i.e., 1/4 method limit of quantification (MLOQ)), whereas other PFC background contamination was much lower.

Method Performance. *Specificity.* The method specificity, which referred to the discrimination between analytes and closely related substances, was mainly focused on eliminating interference from branched PFCs isomers and TDCA as the method applied to fish and meat.

Branched (br-) PFOSs and PFOAs (dimethylhexane/methylheptane isomers) can also be monitored by the same principle transition from 499 to 80 and from 413 to 369 as PFOS and PFOA, respectively, but with different responses ranging from 7 to 340%. A similar observation was also noted for their secondary transitions from 499 to 99 and from 413 to 169. A systematic trend cannot be identified, and the MRM ratio varied among isomers. Thus, coelution of any branched

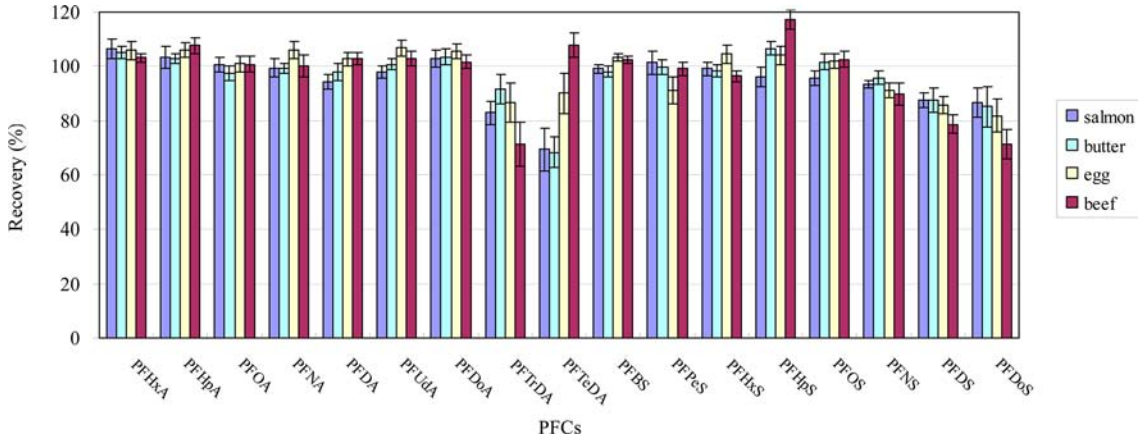

Figure 2. Average recovery and precision of sample spike of four matrices.

isomers could affect quantification as well as confirmation of PFOA/PFOS. Standard solutions of 10 br-PFOSs and 9 br-PFOAs at concentrations of 2 ng/mL were tested by the UPLC-MS/MS system and were baseline separated from their straight-chain isomer. Chromatograms of mixed standards of PFOAs and PFOSs are depicted in Figure 1, panels a and b, respectively, to show the separations achieved. From the real sample results, br-PFOS isomers were detected in almost all of the fish and seafood samples. Hence, good chromatographic separation was necessary for analyzing PFOS. An example is depicted in Figure 1c. In some cases, br-PFOS isomers could contribute to >30% of the signal, and overestimation occurred if br-PFOS isomer signals were not resolved. Further separation of branched isomers individually was not attempted.

TDCA in matrices of animal origin has been reported to interfere with the 499/80 MRM transition of PFOS, especially for fish. A standard solution of TDCA in 20 ng/mL was analyzed to evaluate the resolution of the UPLC program. It was found to elute much earlier than PFOS (Figure 1b). No interference from TDCA was expected as its retention time fell outside the MRM monitoring window in our finalized method.

Interference was noted for the MRM transition from 402 to 80 for $^{13}C_3$ PFHxS in fish samples. Thus, a matrix interference free of MRM transition of from 402 to 99 was used for correction.

Calibration. Linearity was checked through calibration curves, which were constructed by 15 concentration levels from 0.05 to 50 μg/L, equivalent to a working range from 0.005 to 5 μg/kg in sample, with coefficients of determination (R^2) values >0.995. Individual residual deviations were <15% for calibration levels greater than the MLOQ. Mandel's fitting test was performed to check the linearity. Calibration curves showed good linearity, with some exceptions. To achieve the linearity fulfilling Mandel's fitting, calibration ranges for PFPeS and PFHxA, PFNA and PFUdA, and PFTrDA and PFTeDA were narrowed to 0.05−40, 0.05−35, and 0.05−20 μg/L, respectively. Despite some working ranges being narrowed, we considered the calibrations were fit-for-purpose as high-level contaminations of these PFCs in real samples are rare.

Recovery, Precision, and Trueness. The accuracy and precision of the method were studied by means of spiked recovery experiments at three levels, MLOQ, 10× MLOQ, and 100× MLOQ (0.02/0.2/2 μg/kg), on four different days in four representative fatty matrices, namely, salmon, beef, egg, and butter. The overall performance of validation is summarized in Figure 2, with details given in Table S2 in the Supporting Information. The average recoveries in general fulfilled the recommended 70−120% in Commission Recommendation 2010/161/EU. Slightly lower recoveries (>65%) were observed for PFTeDA. Poor recoveries (>50%) and precision (>20%) of PFTrDA and PFTeDA in beef were improved when the recently available $^{13}C_2$PFTeA was used as internal standard for correction.

Method accuracy and trueness were also evaluated by four replicate analyses of certified reference materials (CRMs), fish tissues SRM 1946 and SRM 1947. Only reference values of PFOS were available in the two CRMs, and information values of PFNA, PFDA, PFUnDA, and PFTrDA were available in SRM 1947. Results obtained were compared to these values and are given in Table 1. Good method performance was observed for PFOS determination. The recoveries were about 103% with CV < 4%. Larger deviations were noted for the other PFCs with recoveries ranging from 84 to 119% and CV ranging from 2.0 to 6.2%.

Table 1. Recovery and Precision of CRM Analysis[a]

	reference value (μg/kg)	information value (μg/kg)	recovery (%)/ RSD (%)
SRM 1946 Lake Superior fish tissue			
PFOS	2.19 ± 0.08		103/3.9
SRM 1947 Lake Michigan fish tissue			
PFOS	5.90 ± 0.39		104/3.7
PFNA		0.20	110/4.6
PFDA		0.26	84/4.7
PFUnA		0.28	99/6.2
PFTrDA		0.20	119/2.0

[a]Number of replicates = 4.

CCα, CCβ, and Method Limit of Quantification. For the evaluation of decision limit (CCα) and detection capability (CCβ), matrix-matched calibration curves with four equidistant levels at concentrations close to MLOQ (which were 0.5×, 1×, 1.5×, and 2× MLOQ) were prepared in duplicate in the four fatty matrices. The calculation of CCα and CCβ was based on ISO 11843-2:2000 and referenced to Verdon et al.[25] The CCαs and CCβs calculated are summarized in Table S3 in the Supporting Information. Both CCα and CCβ obtained for each PFC were <0.01 μg/kg.

The lowest concentration of PFCs that was validated for all samples with satisfactory recovery and precision, 0.02 μg/kg,

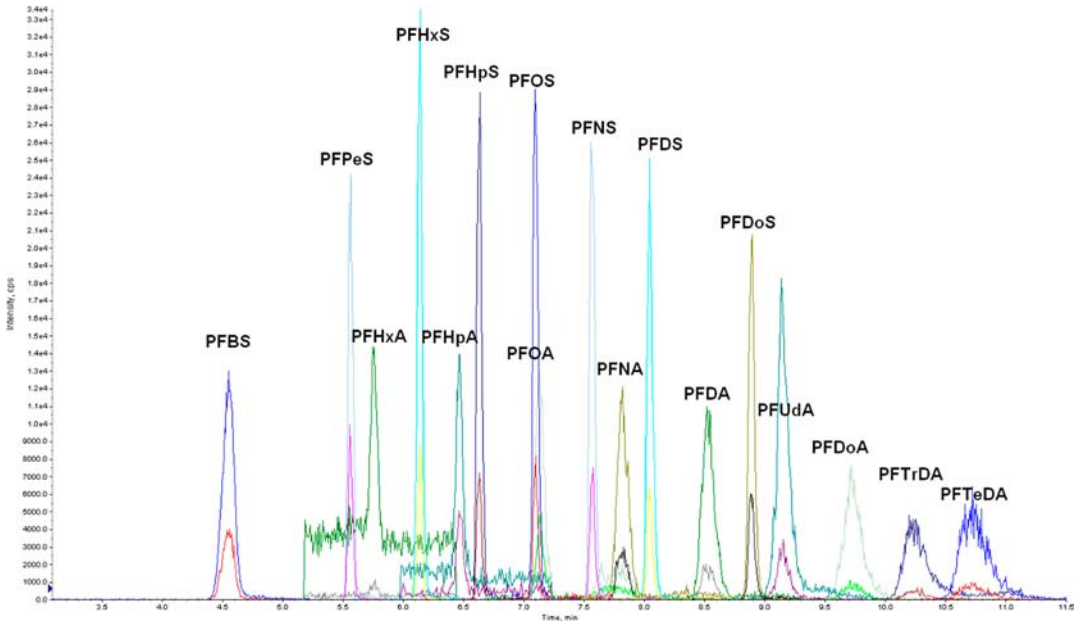

Figure 3. Chromatograms of PFCs at concentration MLOQ.

Table 2. Matrix Effects ($Slope_{matrix}/Slope_{solvent}$) in Four Fatty Matrices

	salmon		butter		egg		beef	
	w IS[a]	w/o IS[b]	w IS	w/o IS	w IS	w/o IS	w IS	w/o IS
PFHxA	1.05	2.05	1.05	0.92	1.05	1.72	1.05	1.38
PFHpA	1.07	1.80	1.00	1.04	1.03	1.99	0.87	1.26
PFOA	1.09	1.93	1.04	1.31	1.07	1.92	0.92	1.17
PFNA	0.92	1.42	1.08	0.96	0.95	1.32	1.01	0.90
PFDA	0.96	1.56	1.03	0.98	0.92	1.03	1.01	0.81
PFUdA	0.96	1.40	1.09	0.98	0.94	1.06	1.00	0.61
PFDoA	1.06	1.44	1.04	1.13	0.96	1.17	0.99	0.52
PFTrDA[c]	0.90	1.23	1.07	1.17	1.03	1.27	0.71	0.57
PFTeDA[c]	0.80	1.11	1.01	1.10	0.83	0.97	1.06	0.82
PFBS	1.05	1.26	1.07	1.07	1.08	1.04	1.00	1.00
PFPeS	1.05	1.34	1.10	1.13	1.01	1.10	0.86	1.01
PFHxS	1.08	1.38	1.04	1.07	1.05	1.14	0.82	0.96
PFHpS	0.91	1.11	1.04	1.10	1.05	1.18	1.06	1.01
PFOS	1.00	1.22	1.03	1.09	1.00	1.02	0.92	0.86
PFNS	1.00	1.22	0.99	1.05	0.99	1.04	0.88	0.84
PFDS	0.98	1.21	1.00	1.06	0.96	1.02	0.77	0.73
PFDoS	1.00	1.19	1.08	1.12	0.90	0.91	0.78	0.75

[a]Internal standardization values. [b]No internal standardization values. [c]PFTrDA and PFTeDA in beef were corrected by $^{13}C_2$PFTeDA.

was taken as the MLOQ, which was much lower than the 1 μg/kg recommended by Commission Recommendation 2010/161/EU. Figure 3 shows the UPLC-MS/MS chromatogram for 17 target analytes at the MLOQ level. It could be observed that a level below 0.01 μg/kg can be easily estimated.

Matrix Effect. It is well-known that the ionization of target analyte in LC-MS/MS analysis can be affected when competition between the analyte and coeluting component(s) for the available charge occurs. In most cases, signal suppression of the analyte is observed. The same set of CCα and CCβ study data was used for evaluation of the matrix effect. The matrix effect is obtained from the ratio of the slope of matrix-matched standards to that of solvent standards, and the matrix effects with and without internal standardization are summarized in Table 2.

Matrix effects were found to range from 0.52 to 2.05 when internal standard correction was not applied. Besides, PFCAs were noted to be subjected to greater matrix effect than PFSAs. Furthermore, the matrix effect could be different even on closely eluted PFCs, which indicated the matrix effect could be also analyte dependent. For example, the matrix effect was found to be ~1.9 for PFOA in salmon but only ~1.2 for PFOS, despite PFOA and PFOS being closely eluted.

When internal standard correction was applied, differences between slopes were found to be in general <10%. A larger difference was observed for PFTeDA when $^{13}C_2$PFDoA (quite different in retention time) was applied as internal standard for correction. In fact, slope ratios were closer to 1 for PFTeDA without the correction by $^{13}C_2$PFDoA. This further supports there were differences in matrix effects at different retention times.

dx.doi.org/10.1021/jf502326h | J. Agric. Food Chem. 2014, 62, 5805−5811

Strong ion suppression was noted in beef, especially for PFDoA and other late-eluting PFCs. The matrix effect for PFTeDA was found to be 1.56 when $^{13}C_2$PFDoA (eluted 1 min earlier) was used as internal standard for correction. Better correction was obtained when isotopically labeled $^{13}C_2$PFTeDA was made available recently. The supplementary validation with additional labeled $^{13}C_2$PFTeDA as internal standard was performed only in beef, but it was expected that the matrix effect should also be reduced for other matrices.

We performed quantitation with internal standardization instead of using matrix-matched calibration. This can avoid the trouble of finding a representative blank sample, especially for fish and seafood as they were commonly contaminated with PFOS.

Application of the Method to Real Samples. The method was applied for the analysis of 200 risk assessment study samples containing various types of food samples including fish and seafood, meat and meat products, eggs, fats, and oils. To ensure the quality of the results, method blank and duplicate samples spiked at 10× MLOQ were carried out with each batch of samples to avoid any false positives due to contamination and to assess the recovery, respectively. Average recoveries of the PFCs ranged from 65 to 120%.

Traces of PFCs, most of them were of <2 μg/kg, were detected in the samples. Only one freshwater fish sample was found to contain PFOS at >2 μg/kg. Besides, PFOS was the most frequently detected PFC in foods; it was detected in almost every fish or shellfish samples. For PFCAs, the most frequently detected were PFUdA and PFTrDA, then PFDoA, PFDA, PFNA, PFTeDA, and PFOA. Basically, such a sequence is similar to other reported findings in seafood.

In summary, the performance of the described methods for the determination of PFCs through different fatty matrices, especially with respect to the detection limit and its capability, was demonstrated. Moreover, the low detection limit (0.02 μg/kg) enabled us to quantify the content of PFCs at low parts per trillion level in various food products, which accounted for the major contributors of the dietary exposure of PFCs. This method gives quantitative results for C_6−C_{14} perfluorinated carboxylic acids (PFCAs) and C_4−C_{12} perfluorinated sulfonates (PFSAs), including PFPeS, PFNS, and PFDoS for comprehensive dietary exposure assessment. The analysis time has been shortened by using UPLC. Even so, 17 PFCs were eluted within 12 min with good separation of PFCs, especially on resolving branched PFOS and TDCA from PFOS. Comparability of the method was supported by satisfactory results for the analysis of CRMs.

■ ASSOCIATED CONTENT

Ⓢ Supporting Information

Tables S1−S3. This material is available free of charge via the Internet at http://pubs.acs.org.

■ AUTHOR INFORMATION

Corresponding Author

*(S.W.C.C.) E-mail: swcchung@fehd.gov.hk.

Notes

The authors declare no competing financial interest.

■ REFERENCES

(1) Hekster, F. M.; Laane, R. W.; de Voogt, P. Environmental and toxicity effects of perfluoroalkylated substances. *Rev. Environ. Contam Toxicol* **2003**, *179*, 99−121.

(2) Lehmler, H. J. Synthesis of environmentally relevant fluorinated surfactants − a review. *Chemosphere* **2005**, *58* (11), 1471−1496.

(3) Tittlemier, S. A.; Pepper, K.; Edwards, L. Concentrations of perfluorooctanesulfonamides in Canadian total diet study composite food samples collected between 1992 and 2004. *J. Agric. Food Chem.* **2006**, *54* (21), 8385−8389.

(4) Zhang, T.; Sun, H.; Lin, Y.; Wang, L.; Zhang, X.; Liu, Y.; Geng, X.; Zhao, L.; Li, F.; Kannan, K. Perfluorinated compounds in human blood, water, edible freshwater fish, and seafood in China: daily intake and regional differences in human exposures. *J. Agric. Food Chem.* **2011**, *59* (20), 11168−11176.

(5) Kato, K.; Wong, L. Y.; Jia, L. T.; Kuklenyik, Z.; Calafat, A. M. Trends in exposure to polyfluoroalkyl chemicals in the U.S. Population: 1999−2008. *Environ. Sci. Technol.* **2011**, *45* (19), 8037−8045.

(6) Food Standard Agency, United Kingdom. Fluorinated chemicals in food. Food Survey Information Sheet 05/09, 2009, http://www.food.gov.uk/science/surveillance/fsisbranch2009/fsis0509 (accessed May 9, 2014).

(7) Bundesinstitut für Risikobewertung (BfR). *Expert Panel Confirms: PFC Exposure of Consumers through Foodstuffs Is Very Low*; BfR Information Nr. 015/2010, March 30, 2010.

(8) Noorlander, C. W.; van Leeuwen, S. P.; Te Biesebeek, J. D.; Mengelers, M. J.; Zeilmaker, M. J. Levels of perfluorinated compounds in food and dietary intake of PFOS and PFOA in the Netherlands. *J. Agric. Food Chem.* **2011**, *59* (13), 7496−7505.

(9) Jogsten, I. E.; Perello, G.; Llebaria, X.; Bigas, E.; Marti-Cid, R.; Karrman, A.; Domingo, J. L. Exposure to perfluorinated compounds in Catalonia, Spain, through consumption of various raw and cooked foodstuffs, including packaged food. *Food Chem. Toxicol.* **2009**, *47* (7), 1577−1583.

(10) Vestergren, R.; Berger, U.; Glynn, A.; Cousins, I. T. Dietary exposure to perfluoroalkyl acids for the Swedish population in 1999, 2005 and 2010. *Environ. Int.* **2012**, *49C*, 120−127.

(11) European Food Safety Authority (EFSA). Perfluorooctane sulfonate (PFOS), perfluorooctanoic acid (PFOA) and their salts. Scientific Opinion of the Panel on Contaminants in the Food Chain. *EFSA J.* **2008**, *653*, 1−131.

(12) Tseng, C. L.; Liu, L. L.; Chen, C. M.; Ding, W. H. Analysis of perfluorooctanesulfonate and related fluorochemicals in water and biological tissue samples by liquid chromatography-ion trap mass spectrometry. *J. Chromatogr., A* **2006**, *1105* (1−2), 119−126.

(13) Nania, V.; Pellegrini, G. E.; Fabrizi, L.; Sesta, G.; De Sanctis, P.; Lucchetti, D.; Di Pasquale, M.; Coni, E. Monitoring of perfluorinated compounds in edible fish from the Mediterranean Sea. *Food Chem.* **2009**, *115* (3), 951−957.

(14) Malinsky, M. D.; Jacoby, C. B.; Reagen, W. K. Determination of perfluorinated compounds in fish fillet homogenates: method validation and application to fillet homogenates from the Mississippi River. *Anal. Chim. Acta* **2011**, *683* (2), 248−257.

(15) Llorca, M.; Farre, M.; Pico, Y.; Barcelo, D. Development and validation of a pressurized liquid extraction liquid chromatography-tandem mass spectrometry method for perfluorinated compounds determination in fish. *J. Chromatogr., A* **2009**, *1216* (43), 7195−7204.

(16) Llorca, M.; Farre, M.; Pico, Y.; Barcelo, D. Study of the performance of three LC-MS/MS platforms for analysis of perfluorinated compounds. *Anal. Bioanal. Chem.* **2010**, *398* (3), 1145−1159.

(17) van Leeuwen, S. P.; de Boer, J. Extraction and clean-up strategies for the analysis of poly- and perfluoroalkyl substances in environmental and human matrices. *J. Chromatogr., A* **2007**, *1153* (1−2), 172−185.

(18) Luque, N.; Ballesteros-Gomez, A.; van Leeuwen, S.; Rubio, S. Analysis of perfluorinated compounds in biota by microextraction with tetrahydrofuran and liquid chromatography/ion isolation-based ion-trap mass spectrometry. *J. Chromatogr., A* **2010**, *1217* (24), 3774−3782.

(19) Wang, L.; Sun, H.; Yang, L.; He, C.; Wu, W.; Sun, S. Liquid chromatography/mass spectrometry analysis of perfluoroalkyl carbox-

ylic acids and perfluorooctanesulfonate in bivalve shells: extraction method optimization. *J. Chromatogr., A* **2010**, *1217* (4), 436−442.
(20) van Leeuwen, S. P.; Swart, C. P.; van der Veen, I.; de Boer, J. Significant improvements in the analysis of perfluorinated compounds in water and fish: results from an interlaboratory method evaluation study. *J. Chromatogr., A* **2009**, *1216* (3), 401−409.
(21) Ballesteros-Gomez, A.; Rubio, S.; van Leeuwen, S. Tetrahydrofuran-water extraction, in-line clean-up and selective liquid chromatography/tandem mass spectrometry for the quantitation of perfluorinated compounds in food at the low picogram per gram level. *J. Chromatogr., A* **2010**, *1217* (38), 5913−5921.
(22) Esparza, X.; Moyano, E.; de Boer, J.; Galceran, M. T.; van Leeuwen, S. P. Analysis of perfluorinated phosponic acids and perfluorooctane sulfonic acid in water, sludge and sediment by LC-MS/MS. *Talanta* **2011**, *86*, 329−336.
(23) European Food Safety Authority (EFSA). Perfluoroalkylated substances in food: occurrence and dietary exposure. *EFSA J.* **2012**, *10* (6), 2743 (55 pp).
(24) O'Brien, J. M.; Austin, A. J.; Williams, A.; Yauk, C. L.; Crump, D.; Kennedy, S. W. Technical-grade perfluorooctane sulfonate alters the expression of more transcripts in cultured chicken embryonic hepatocytes than linear perfluorooctane sulfonate. *Environ. Toxicol. Chem.* **2011**, *30* (12), 2846−2859.
(25) Verdon, E.; Hurtaud-Pessel, D.; Sanders, P. Evaluation of the limit of performance of an analytical method based on a statistical calculation of its critical concentrations according to ISO standard 11843: application to routine control of banned veterinary drug residues in food according to European Decision 657/2002/EC. *Accredit. Qual. Assur.* **2006**, *11* (1−2), 58−62.

JOURNAL OF AGRICULTURAL AND FOOD CHEMISTRY

Article

pubs.acs.org/JAFC

Development of an Improved Reverse-Phase High-Performance Liquid Chromatography Method for the Simultaneous Analyses of *trans*-/*cis*-Resveratrol, Quercetin, and Emodin in Commercial Resveratrol Supplements

Jaclyn M. Omar,[†] Haifeng Yang,[†] Suzhen Li,[‡] Ronald R. Marquardt,[‡] and Peter J. H. Jones*[,†]

[†]Richardson Centre for Functional Foods and Nutraceuticals, University of Manitoba, 196 Innovation Drive, Winnipeg, Manitoba R3T 2N2, Canada

[‡]All Natural Nutritional Products, Incorporated, 196 Innovation Drive, University of Manitoba Smartpark, Winnipeg, Manitoba R3T 6C5, Canada

ABSTRACT: The objectives of the study were to develop a reverse-phase high-performance liquid chromatography method for the simultaneous analyses of *trans*-/*cis*-resveratrol, emodin, and quercetin and to determine the concentrations of these polyphenols in 28 resveratrol supplements. Samples were separated within 15 min in a C18 reversed-phase column using mobile phases containing 0.1% formic acid and methanol/0.1% formic acid. The calibration graphs for all four compounds were linear from 0.1 to 410 μg/mL ($r^2 = 0.99$). The concentration of resveratrol as stated on the labels was often different from the analytical results, with 21 and 11% of the total supplements having low or high values, respectively. Many of the supplements also contained variable but generally low levels of emodin, a compound known to cause diarrhea. The proposed method is a rapid, sensitive, accurate, and cost-effective procedure that can be used for the simultaneous quantification of four polyphenols in resveratrol supplements.

KEYWORDS: *reversed-phase HPLC method, trans-/cis-resveratrol, quercetin, emodin, extracts, Polygonum cuspidatum, supplements*

INTRODUCTION

Phenolic acids and flavonoids are bioactive compounds that are present in a wide variety of plants. They have been shown to possess beneficial biological properties through their strong antioxidative activity. Resveratrol is a polyphenolic phytoalexin (3,5,4′-trihydroxystilbene) that is found in the skin of red grapes and most notably in red wine. It has been acknowledged for its potent cardioprotective and other beneficial properties.[1−3] Resveratrol naturally occurs in two isoforms, *trans* and *cis* forms, of which *trans*-resveratrol is the isoform mainly present in red grapes, red wine, and other products and is largely responsible for its many health benefits.[4] Japanese knotweed (*Fallopia japonica* syn. *Polygonum cuspidatum*) is also found to have concentrated amounts of resveratrol and has become a common source of resveratrol for most dietary supplements.[5] Emodin and quercetin are additional phenolic compounds that are commonly found in varying amounts alongside resveratrol in dietary supplements depending upon the source of resveratrol. Quercetin is a flavanol that is found in the skins of grapes and, thus, is present in resveratrol supplements obtained from red grapes, including red wine extracts.[6,7] Emodin, in contrast, is generally absent in resveratrol supplements obtained from grapes but is naturally present in supplements obtained from *P. cuspidatum* in varying amounts.[8] Supplements made from lower purity *trans*-resveratrol may contain unacceptably high amounts of emodin and, as such, can act as a laxative, causing stomach cramping, gas production, bloating, and diarrhea.[8,9] However, moderate amounts of emodin has traditionally been used in Chinese and Japanese herbal medicine as a natural laxative and has more recently been shown to have antitumor properties.[8]

Currently, validated methods have been published for the detection of *trans*-resveratrol and, in some cases, *cis*-resveratrol, quercetin, and/or emodin. Most established analytical methods are based on gas chromatography−mass spectrometry (GC−MS),[10] reversed-phase liquid chromatography,[11−13] and high-performance liquid chromatography (HPLC) with tandem ultraviolet (UV) absorption and fluorimetric detection.[14] However, a single method that incorporates the simultaneous detection of all four polyphenolic compounds is lacking. Similarly, methods for the simultaneous detection of multiple polyphenols have been validated using capillary electrophoresis and have been found to be comparable qualitatively and quantitatively; however, sample preparation is laborious, and reproducibility and precision may be compromised because of the short capillary lifespan.[15−18] A previous evaluation of common analytical methods for the measurement of *cis*- and *trans*-resveratrol in commercial wines determined that reverse-phase (RP) HPLC with diode array detection was the most robust method for the simultaneous quantitation of multiple polyphenols of interest, which included *cis*- and *trans*-resveratrol, and may serve as an optimal method for routine quality control application, as compared to other methods (GC−MS and normal-phase HPLC).[19] Thus, the primary

Received: January 8, 2014
Revised: June 3, 2014
Accepted: June 3, 2014
Published: June 3, 2014

ACS Publications © 2014 American Chemical Society

dx.doi.org/10.1021/jf5001277 | J. Agric. Food Chem. 2014, 62, 5812−5817

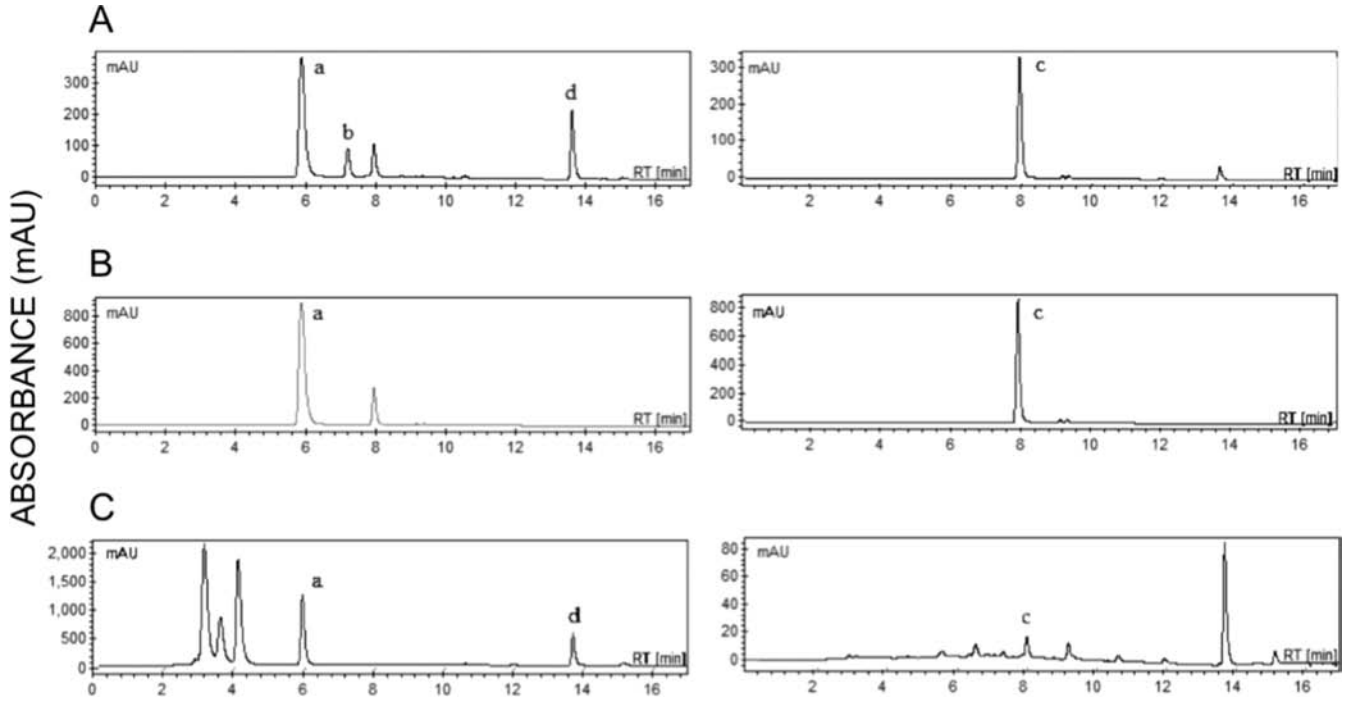

Figure 1. Representative HPLC chromatograms of resveratrol reference standards and resveratrol-containing products. Peaks detected at 290 nm are depicted on the left panel, and peaks detected at 369 nm are depicted on the right panel. (A) Reference standards: peak a, *trans*-resveratrol (20 μg/mL); peak b, *cis*-resveratrol (20 μg/mL); peak c, quercetin (10 μg/mL); and peak d, emodin (10 μg/mL); (B) commercial sample P2 (reference Table 3), consisting of resveratrol extract and quercetin; and (C) commercial sample P4 (reference Table 3), consisting of *P. cuspidatum* extract, green tea extract, and caffeine.

objective of this study was to develop and validate a rapid, simple, and cost-effective RP-HPLC analytical method for the simultaneous detection of *trans*-/*cis*-resveratrol, quercetin, and emodin in dietary supplements. The ability to determine the concentration of these polyphenols in resveratrol and other supplements using a sensitive and efficient method will aid in the quality assessment of commercially available dietary supplements because extract sources can originate from a variety of sources, each having a unique polyphenolic composition, as is the case in red wine extract and *P. cuspidatum* as sources of resveratrol. This will help to ensure that the consumer will obtain a product of known composition. A secondary objective was to measure *trans*-resveratrol in 28 commercially available resveratrol supplements using the validated method and compare these values to the labeled *trans*-resveratrol content as well as measure levels of detectable emodin and quercetin in each product.

MATERIALS AND METHODS

Samples. A total of 28 commercial resveratrol supplements were acquired via purchase from commercial Canadian and U.S. sources or generously donated as gifts. Samples were in the form of either tablets (n = 3), soft gel capsules (n = 3), or gelatin or vegetable capsules (n = 22).

Chemicals and Standards. *trans*-Resveratrol and *cis*-resveratrol standards were purchased from Cayman Chemical Company (Ann Arbor, MI). Emodin and quercetin standards were purchased from Santa Cruz Biotechnology, Inc. (Santa Cruz, CA). HPLC-grade methanol and formic acid were purchased from Fisher Scientific Canada. Ultrapure water (18.2 MΩ cm) was obtained using a Millipore Milli-Q 10 water system for the preparation of the buffer solution (Billerica, MA).

Standard Preparation. Stock solutions of each standard (*trans*-/*cis*-resveratrol, quercetin, and emodin) were prepared by dissolving each analyte (1 mg/mL) in pure methanol. The stock solution was aliquoted (1.5 mL) into LC vials and stored at −80 °C. The working solution was prepared by diluting the stock solution to obtain appropriate concentrations for calibration curves.

Sample Preparation. A total of 10 capsules/tablets/soft gels from each sample were weighed individually along with their respective empty capsules to determine the net weight of each sample. The content of the 10 capsules/tablets/soft gels were pooled and homogenized. A total of 100 milligrams of each sample was extracted with 20 mL of methanol for 10 min in a 25 mL aluminum-foil-covered volumetric flask using a bath sonicator, thermostatically set at 22 °C with a frequency of 33 kHz, and then brought to a final volume of 25 mL with methanol. The solution was then incubated for 10 min at room temperature, after which 100 μL of supernatant was diluted 20-fold. The diluted solution was filtered through a 0.2 μm syringe filter (Phenomenex, Torrance, CA), and an aliquot of 20 μL was injected onto a HPLC column for analysis in triplicate.

HPLC. Quantitative analysis was performed using a Varian 920LC HPLC coupled with an UV detector (Varian, Palo Alto, CA). The chromatographic separation was carried out on a Luna C18 (2) column (250 × 4.6 mm, 5 μm, Phenomenex, Torrance, CA) protected by a guard column (Security Guard Cartridge C18, 4 × 2.0 mm inner diameter, Phenomenex, Torrance, CA) and maintained at 35 °C. A linear elution gradient consisting of mobile phase A (0.1% formic acid) and B (methanol containing 0.1% formic acid) was programmed as follows: initially 50% A and 50% B, linearly changed to 100% B over 10 min, and then held for 5 min at 100% B. The system was then re-equilibrated for 7 min with the initial solvent (50% solvent A and 50% solvent B). The autosampler was operated at room temperature. The detection wavelength was set at 290 nm for *trans*-/*cis*-resveratrol and emodin and 369 nm for quercetin. System control and data acquisition were performed using Galaxie (Varian, Inc., Mississauga, Ontario, Canada).

Statistical Analysis. Statistical analysis was conducted using Statistical Analysis Software (SAS, version 9.4, Cary, NC), and values are expressed as the mean ± standard deviation (SD).

Table 1. Linearity Test[a]

compound	linear range (μg/mL)	slope (mean ± SD)	intercept (mean ± SD)	r^2	LOD (μg/mL)	LOQ	
						concentration (μg/mL)	precision (RSD %)
trans-resveratrol	0.1−400	0.72 ± 0.02	1.25 ± 2.47	0.99	0.03	0.1	10.11
cis-resveratrol	0.05−100	0.75 ± 0.04	−0.30 ± 0.50	0.99	0.01	0.05	0.79
emodin	0.095−380	1.09 ± 0.05	−0.81 ± 1.13	0.99	0.03	0.95	1.41
quercetin	0.095−380	1.10 ± 0.05	0.23 ± 0.32	0.99	0.03	0.05	5.09

[a]Regression equation, $y = ax + b$, where y is the peak area and x is the corresponding concentration. r^2 is the correlation coefficient. LOD, limit of detection; LOQ, limit of quantification; and RSD %, percent relative standard deviation.

Table 2. Intra- and Interday Precision of the Peak Area

compound	concentration (μg/mL)	intraday precision			interday precision		
		peak area[a]	SD	RSD (%)	peak area[b]	SD	RSD (%)
trans-resveratrol	2	3.9138	0.0243	0.62	3.8971	0.0149	0.38
	8	15.2925	0.0549	0.36	15.2793	0.0115	0.08
	20	36.8568	0.1762	0.48	36.9338	0.3415	0.92
	100	170.0153	0.3511	0.21	170.8047	3.1247	1.83
cis-resveratrol	1	0.6764	0.0102	1.50	0.6684	0.0075	1.12
	5	4.0318	0.0174	0.43	4.0205	0.0158	0.39
	20	15.2240	0.0452	0.30	15.2207	0.0495	0.33
	100	70.3522	0.4098	0.58	70.5788	0.2451	0.35
emodin	1	0.9010	0.0199	2.21	0.9210	0.0237	2.57
	20	5.3596	0.0422	0.79	5.3557	0.0165	0.31
	50	20.7074	0.0399	0.19	20.6449	0.0807	0.39
	100	100.5609	0.7761	0.77	100.7443	0.2845	0.28
quercetin	1	0.9376	0.0065	0.69	0.9306	0.0117	1.25
	20	5.5659	0.0413	0.74	5.5309	0.0594	1.07
	50	21.2631	0.0386	0.18	21.2032	0.1273	0.60
	100	103.0149	0.4939	0.48	103.0769	0.1099	0.11

[a]Mean value of triplicates analysis carried out within the same day. [b]Mean value of triplicates analysis per day over a period of 3 days.

RESULTS AND DISCUSSION

Optimization of the Chromatographic Condition. A RP-HPLC method was developed for the simultaneous analyses of four polyphenols: *trans*-resveratrol, *cis*-resveratrol, quercetin, and emodin. Several chromatographic conditions using different columns and elution systems were tested to determine optimum resolution, peak shape, efficiency, ease of operation, and cost-effectiveness of preparing the mobile phases. Conditions were established using a Luna C18 column (2) (250 × 4.6 mm, 5 μm) and a water/methanol mixture containing 0.1% (v/v) formic acid elution system for the detection of the different compounds. The UV detector was set at 290 nm for the monitoring of *trans*-/*cis*-resveratrol and emodin and 369 nm for the monitoring of quercetin. Previous methods have achieved individual maximum UV absorbance of emodin, *cis*-resveratrol, and *trans*-resveratrol at 254, 286, and 304 nm,[14,20,21] respectively; however, to achieve optimal UV absorbance for all three analytes, 290 nm was selected and demonstrated a high degree of sensitivity and precision. Interestingly, an emodin peak was detected at 369 nm but to a considerably lesser degree than at 290 nm. Maximum UV absorbance for quercetin has been reported at a variety of wavelengths, ranging from 280 to 370 nm, depending upon the sample and detector;[20−23] therefore, maximum UV absorbance was set at 369 nm for quercetin based on our objectives and equipment. Accordingly, quercetin was detected in Figure 1B at both 290 and 369 nm but at significantly greater absorbance at 369 nm. The use of methanol instead of acetonitrile significantly reduced solvent cost, reduced separation time (15 min/run), and demonstrated well-separated and defined peak shapes, consistent with previous reports.[14] Formic acid (0.1%) was selected as the mobile phase additive to provide improved pH control, simplified preparation, good methanol solubility, and high volatility, imparting a simpler and more efficient preparation, and was found to achieve good peak intensity and resolution when added to the aqueous solution. The peaks for each of the four reference compounds were well-resolved with retention times of 5.88, 7.20, 7.95, and 13.61 min, respectively (Figure 1).

HPLC Chromatograms. Chromatograms of standards and representative samples containing *trans*-/*cis*-resveratrol, quercetin, and emodin are shown in Figure 1. Figure 1A depicts reference standards of each analyte with their respective peak. Panels B and C of Figure 1 represent commercial resveratrol samples P2 and P4 (reference Table 3), respectively, as characteristic examples of resveratrol supplements containing *trans*-resveratrol and either quercetin or emodin, respectively. Of the polyphenols simultaneously analyzed, it was found that samples containing *trans*-resveratrol, quercetin, and emodin yielded distinct and large peaks, while the peak size for *cis*-resveratrol was low (Figure 1A) or undetected (panels B and C of Figure 1). *trans*-Resveratrol and quercetin but not emodin was detected in extracts prepared from grapes and grape extracts, whereas *trans*-resveratrol and emodin were detected in extracts from *P. cuspidatum*.

Method Validation: Linearity, Limits of Detection (LODs), and Limits of Quantification (LOQs). The linearity for each reference standard was investigated over the range of

dx.doi.org/10.1021/jf5001277 | J. Agric. Food Chem. 2014, 62, 5812−5817

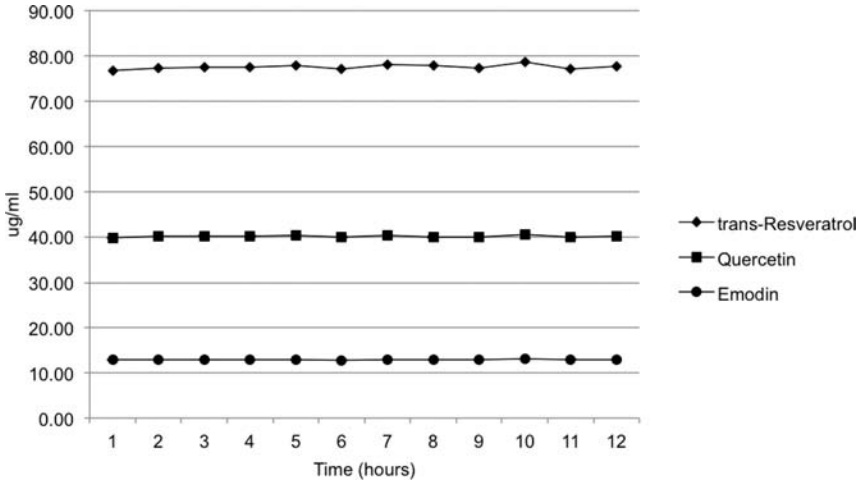

Figure 2. Stability of *trans*-resveratrol, quercetin, and emodin over 12 h stored in amber glass vials at room temperature using a standard solution containing 77.6 ± 0.6 μg/mL *trans*-resveratrol, 40.1 ± 0.1 μg/mL quercetin, and 12.9 ± 0.3 μg/mL emodin in duplicate.

Table 3. Amounts of *trans*-Resveratrol as Stated on the Product Label of Resveratrol Supplements Compared to Amounts of *trans*-Resveratrol, Emodin, and Quercetin as Determined by HPLC Analyses

	from the product label		HPLC-analyzed values				
sample[a]	net weight/capsule (mg)[b]	resveratrol/capsule (mg)	resveratrol/100 mg[c]	resveratrol/capsule (mg)	accuracy (%)[d]	emodin (%)[e]	quercetin (%)[f]
A5	279	245	98.2	274.1	112	ND	ND
G1	525	25	1.2	6.0	24	ND	ND
G2	258	245	87.3	225.3	92	ND	ND
P1	486	50	8.3	40.0	80	0.43	ND
P2	146	100	51.4	75.0	75	ND	26.7
P3	308	5	1.9	5.9	118	0.18	ND
P4	347	72.5	21.3	73.9	102	2.26	ND
P5	303	5	1.1	3.3	66	ND	ND
S1	406	100	23.7	96.3	96	0.66	ND
S2	245	3	1.3	3.2	107	0.13	ND
S3	398	50	11.9	47.4	95	0.68	ND
S4	1043	175	16.3	170.0	97	0.91	ND
S5	742	75	10.0	74.2	99	0.30	ND
S6	571	100	18.5	105.6	106	0.61	ND
S7	375	13	6.4	24.0	185	1.16	ND
S8	750	250	32.5	243.8	98	1.21	3.60
S9	628	50	7.9	49.6	99	0.39	ND
S10	403	125	36.2	145.9	117	0.14	ND
S12	215	20	8.3	17.8	89	0.13	ND
S13	417	75	18.6	77.6	103	1.16	ND
S14	428	50	12.1	51.8	104	0.47	ND
S15	827	250	30.9	255.5	102	1.29	12.1
S16	1044	250	23.2	242.2	97	1.09	ND
S17	487	100	20.3	98.9	99	1.74	ND
S18	583	100	15.9	92.7	93	0.64	ND
S19	177	5	2.5	4.4	88	0.34	ND
S20	150	5	8.7	13.1	262	0.12	ND
S21	447	37.5	7.7	34.4	92	0.81	ND

[a]S4, S5, and S16 were soft gels, and S7, S17, and S20 were tablets, while the remaining products were encapsulated in vegetable or gelatin capsules. [b]Weight of capsule minus empty weight of capsule. [c]Resveratrol per 100 mg of dry material. Values equal percentage of resveratrol in the product. [d]Accuracy = resveratrol/capsule as given on the label (mg) ÷ resveratrol/capsule as determined by HPLC (mg) × 100. [e]Emodin values as determined by HPLC analysis. Values are expressed as a percentage of net product weight. ND = not detected. [f]Quercetin values as determined by HPLC analysis. Values are expressed as a percentage of net product weight. ND = not detected.

concentrations: 0.1−400 μg/mL for *trans*-resveratrol, 0.095−380 μg/mL for quercetin and emodin, and 0.05−100 μg/mL for *cis*-resveratrol; all ranges were covered by 13 points (Table 1). *trans*-Resveratrol, quercetin, and emodin were prepared as a mixture, while *cis*-resveratrol was prepared separately because of the presence of *trans*-resveratrol as an impurity. The regression equation was plotted as the peak area versus the corresponding concentration of the analyte. The high linear correlation

dx.doi.org/10.1021/jf5001277 | J. Agric. Food Chem. 2014, 62, 5812−5817

coefficients (r^2 > 0.99) indicated good linearity between the peak area of the compound and its concentration. The LODs (signal/noise ratio > 3) for all analytes were below 0.03 μg/mL. The LOQs (signal/noise ratio > 10) for *trans*-resveratrol, *cis*-resveratrol, and quercetin were below 0.1 μg/mL and the LOQ for emodin was 0.95 μg/mL.

Precision and Reproducibility. The intra- and interday precision of the assay at four concentration levels for each compound are shown in Table 2. The method was found to be precise with the intraday relative standard deviation (RSD) values being between 0.21 and 0.62% for *trans*-resveratrol, between 0.30 and 1.50% for *cis*-resveratrol, between 0.19 and 2.21% for emodin, and between 0.18 and 0.74% for quercetin. Similarly, interday RSD values were within 0.08−1.83% for *trans*-resveratrol, 0.33−1.12% for *cis*-resveratrol, 0.28−2.57% for emodin, and 0.11−1.25% for quercetin. Intra- and interday RSDs below 2.6% for all compounds and concentrations indicate a high level of precision and reproducibility.

Stability. *trans*-Resveratrol, quercetin, and emodin were stable when stored at room temperature (24 °C) in amber glass vials over 12 h with no conversion of *trans*-resveratrol into its *cis* isomer (Figure 2). The RSDs of the peak area over this period were 0.58, 0.65, and 0.52% for *trans*-resveratrol, emodin, and quercetin, respectively. The stability of a cocktail of all standard compounds when stored over 21 days at 3 °C was also stable (data not shown). These results demonstrate that *trans*-resveratrol, quercetin, and emodin can be analyzed via HPLC without autosampler temperature control. *cis*-Resveratrol was found to be somewhat unstable at room temperature to isomerize to *trans*-resveratrol and requires preventative measures to maintain sample integrity, such as refrigeration, protection from light, and rapid processing times (data not shown).

Accuracy. The accuracy of the method was established by determining the recovery of *trans*-resveratrol, *cis*-resveratrol, emodin, and quercetin spiked to the sample in three known concentrations of the four mixed standards, corresponding to low, mid, and high (2, 10, and 20 μg/mL for *cis*-resveratrol and 10, 50, and 100 μg/mL for *trans*-resveratrol, quercetin, and emodin) LODs. The mean recovery of spiked samples for each concentration (low to high; n = 3) ranged from 96.7 to 103.0% for *trans*-resveratrol, from 97.3 to 99.8% for *cis*-resveratrol, from 97.5 to 101.8% for emodin, and from 98.0 to 104.7% for quercetin (data not shown). The proposed method had higher recovery rates for *trans*-resveratrol, quercetin, and emodin compared to previous HPLC methods using diode array detection[24] and HPLC−UV.[14]

HPLC Analysis of the Resveratrol Supplement. Resveratrol, emodin, and quercetin (Table 3) were simultaneously analyzed via the optimized HPLC−UV method in 28 resveratrol supplements using the conditions described above. Quantitative analyses were performed by means of the external standard methods. Product accuracy, as defined in the footnotes of Table 3, was determined by comparing the concentration of resveratrol as given on the product label with the HPLC-analyzed values. Six samples contained 11−76% less resveratrol than that stated on the label (21% of the total), while three samples had 18−162% higher contents of *trans*-resveratrol than that reported. The amounts of resveratrol in the remaining 18 samples were in fairly good agreement with those given on the product labels. Collectively, these data suggest only about 68% of the stated concentration of resveratrol in the supplements was reasonably accurate. In addition, there was a wide range in the concentrations of resveratrol per 100 mg of product among different commercial products, with some having relatively high concentrations (around 87.3−98.2 mg/100 mg; two products), some intermediate concentrations (20.3−51.4 mg/100 mg; nine products), and most relatively low concentrations (1.3−18.6 mg/100 mg) of resveratrol. Quercetin was only detected in three of the resveratrol supplements, of which quercetin was an added ingredient according to the product label, explaining the high concentrations in these few samples. Low concentrations of emodin were detected in many of the supplements derived from *P. cuspidatum* extracts, with values ranging from 0.12% to a maximum of 2.26%. The two supplements prepared from *P. cuspidatum* that had a high range of resveratrol (A5 and G2) did not contain detectable levels of emodin. The amount of emodin that will cause intestinal distress has not been reported in the literature, as far as the authors are aware, and therefore, the amount of emodin that can be consumed without an adverse effect is not known. However, it has been suggested that low-purity resveratrol (supplements from *P. cuspidatum* extracts with 50% or less resveratrol, having proportionately higher levels of emodin) should be avoided and only resveratrol supplements that are of high purity (i.e., >98% resveratrol) should be consumed.[24]

A simple, sensitive, accurate, and cost-effective RP-HPLC−UV method was developed and validated for the rapid and simultaneous analyses of *trans*-/*cis*-resveratrol, emodin, and quercetin in dietary resveratrol supplements. The proposed extraction and chromatographic method for the determination of resveratrol demonstrated good efficiency and stability with no shift in the *cis*/*trans* isomer ratio. The proposed method is superior to previously published isocratic RP-HPLC methods for the detection of *trans*-resveratrol in the recovery of product, repeatability, and speed of analysis, as previously published GC and HPLC methods can be time-consuming, costly and may cause instability of the *trans* isomer of resveratrol due to the extraction techniques, solvents used, and derivatization for enhanced volatility,[25,26] respectively. Overall, the proposed method demonstrates increased cost efficiency compared to other methods because of the substitution of acetonitrile for methanol and formic acid for phosphate buffers, which are commonly used solvents in most HPLC methods but are expensive and are becoming increasingly in short supply.[27−30] Most importantly, this novel method was optimized to simultaneously detect multiple polyphenols (*trans*-/*cis*-resveratrol, quercetin, and emodin) and may potentially serve as a basis for the simultaneous detection of other analytes.

Data from the current study demonstrate that the amount of resveratrol detected among different products tends to be highly variable and may not be as stated on product labels and that dietary resveratrol supplements derived from *P. cuspidatum* extract contain concentrations of emodin that are likely too low to induce a diarrheal effect. These results represent a need for this analysis for quality control systems by manufacturers and regulators to ensure efficacy and safety prior to production to prevent deleterious side effects or negligible and insignificant health benefits for the consumer public. The benefits of the applied RP-HPLC method demonstrate that this method is appropriate and feasible for the simultaneous quantification of multiple polyphenols of biological interest for routine application of quality control measures of commercial natural health products.

AUTHOR INFORMATION

Corresponding Author

*Telephone: +1-204-474-8883. Fax: +1-204-474-7552. E-mail: peter.jones@umanitoba.ca.

Funding

This research was support by the National Sciences and Engineering Research Council of Canada Engage Grant (EGP 428962-11).

Notes

The authors declare no competing financial interest.

REFERENCES

(1) Baur, J. A.; Sinclair, D. A. Therapeutic potential of resveratrol: The in vivo evidence. *Nat. Rev. Drug Discovery* **2006**, *5*, 493−506.

(2) Das, S.; Das, D. K. Resveratrol: A therapeutic promise for cardiovascular diseases. *Recent Pat. Cardiovasc. Drug Discovery* **2007**, *2*, 133−138.

(3) Olas, B.; Wachowicz, B. Resveratrol, a phenolic antioxidant with effects on blood platelet functions. *Platelets* **2005**, *16*, 251−260.

(4) Frankel, E. N.; Waterhouse, A. L.; Kinsella, J. E. Inhibition of human LDL oxidation by resveratrol. *Lancet* **1993**, *341*, 1103−1104.

(5) Jayatilake, G. S.; Jayasuriya, H.; Lee, E. S.; Koonchanok, N. M.; Geahlen, R. L.; Ashendel, C. L.; McLaughlin, J. L.; Chang, C. J. Kinase inhibitors from *Polygonum cuspidatum*. *J. Nat. Prod.* **1993**, *56*, 1805−1810.

(6) De Nisco, M.; Manfra, M.; Bolognese, A.; Sofo, A.; Scopa, A.; Tenore, G. C.; Pagano, F.; Milite, C.; Russo, M. T. Nutraceutical properties and polyphenolic profile of berry skin and wine of *Vitis vinifera* L. (cv. Aglianico). *Food Chem.* **2013**, *140*, 623−629.

(7) Zhu, L.; Zhang, Y.; Lu, J. Phenolic contents and compositions in skins of red wine grape cultivars among various genetic backgrounds and originations. *Int. J. Mol. Sci.* **2012**, *13*, 3492−3510.

(8) Srinivas, G.; Babykutty, S.; Sathiadevan, P. P.; Srinivas, P. Molecular mechanism of emodin action: Transition from laxative ingredient to an antitumor agent. *Med. Res. Rev.* **2007**, *27*, 591−608.

(9) Xu, J.-D.; Wang, W.; Li, L.-S.; Chen, X.; Zhu, J.-X. Involvement of endogenous prostaglandin in emodin-evoked rat colonic anion secretion. *Biol. Pharm. Bull.* **2007**, *30*, 2058−2062.

(10) Goldberg, D. M.; Yan, J.; Ng, E.; Diamands, E. P.; Karumanchiri, A.; Soleas, G.; Waterhouse, A. L. Direct injection gas chromatographic mass spectrometric assay for *trans*-resveratrol. *Anal. Chem.* **1994**, *66*, 3959−3963.

(11) Brizzi, A.; Brizzi, V.; Corradini, D. Identification and quantification of *trans*-resveratrol in dietary supplements by a rapid and straightforward RP-HPLC method. *J. Liq. Chromatogr. Relat. Technol.* **2008**, *31*, 2089−2100.

(12) Careri, M.; Corradini, C.; Elviri, L.; Nicoletti, I.; Zagnoni, I. Direct HPLC analysis of quercetin and *trans*-resveratrol in red wine, grape, and winemaking byproducts. *J. Agric. Food Chem.* **2003**, *51*, 5226−5231.

(13) Karacabey, E.; Mazza, G. Optimization of solid-liquid extraction of resveratrol and other phenolic compounds from milled grape canes (*Vitis vinifera*). *J. Agric. Food Chem.* **2008**, *56*, 6318−6325.

(14) Mandrioli, R.; Mercolini, L.; Ferranti, A.; Fanali, S.; Raggi, M. A. Determination of aloe emodin in *Aloe vera* extracts and commercial formulations by HPLC with tandem UV absorption and fluorescence detection. *Food Chem.* **2011**, *126*, 387−393.

(15) Gao, L.; Chu, Q.; Ye, J. Determination of *trans*-resveratrol in wines, herbs and health food by capillary electrophoresis with electrochemical detection. *Food Chem.* **2002**, *78*, 255−260.

(16) Mayer, B. X.; Muller, M.; Altria, K. Long-term analyses with capillary electrophoresis. *LC·GC Eur.* **2001**, *14*, 19−26.

(17) Prasongsidh, B. C.; Skurray, G. R. Capillary electrophoresis analysis of *trans*- and *cis*-resveratrol, quercetin, catechin and gallic acid in wine. *Food Chem.* **1998**, *62*, 355−358.

(18) Rodgriguez-Delgado, M. A.; Perez, M. L.; Corbella, R.; Gonzalez, G.; Garcia-Montelongo, F. J. Optimization of the separation of phenolic compounds by micellar electrokinetic capillary chromatography. *J. Chromatogr. A* **2000**, *871*, 427−438.

(19) Soleas, G. J.; Goldberg, D. M.; Ng, E.; Karumanchiri, A.; Tsang, E.; Diamandis, E. P. Comparative evaluation of four methods for assay of *cis*- and *trans*-resveratrol. *Am. J. Enol. Vitic.* **1997**, *48*, 169−176.

(20) Anastasiadi, M.; Pratsinis, H.; Kletsas, D.; Skaltsounis, A. L.; Haroutounian, S. A. Bioactive non-coloured polyphenols content of grapes, wine and vinification by-products: Evaluation of the antioxidant activities of their extracts. *Food Res. Int.* **2010**, *43*, 805−813.

(21) Bravo, M. N.; Silva, S.; Coelho, A. V.; Boas, L. V.; Bronze, M. R. Analysis of phenolic compounds in Muscatel wines produced in Portugal. *Anal. Chim. Acta* **2006**, *563*, 84−92.

(22) Rodríguez-Bernaldo de Quirós, A.; Lage-Yusty, M. A.; López-Hernández, J. HPLC analysis of polyphenolic compounds in Spanish white wines and determination of their antioxidant activity by radical scavenging assay. *Food Res. Int.* **2009**, *42*, 1018−1022.

(23) Tounsi, M. S.; Ouerghemmi, I.; Wannes, W. A.; Ksouri, R.; Zemni, H.; Marzouk, B.; Kchouk, M. E. Valorization of three varieties of grape. *Ind. Crops Prod.* **2009**, *30*, 292−296.

(24) Xu, J.-D.; Liu, S.; Wang, W.; Li, L.-S.; Li, Y.; Guo, H.; Ji, T.; Feng, X.-Y.; Hou, X.-L.; Zhang, Y.; Zhu, J.-X. Emodin induces chloride secretion in rat distal colon through activation of mast cells and enteric neurons. *Br. J. Pharmacol.* **2012**, *165*, 197−207.

(25) Goldberg, D. M.; Karumanchiri, A.; Ng, E.; Yan, J.; Diamands, E. P.; Soleas, G. Direct gas chromatographic-mass spectrometric method to assay *cis*-resveratrol in wines: Preliminary survey of its concentration in commercial wines. *J. Agric. Food Chem.* **1995**, *43*, 1245−1250.

(26) Trela, B. C.; Waterhouse, A. L. Resveratrol: Isomeric molar absorptivities and stability. *J. Agric. Food Chem.* **1996**, *44*, 1253−1257.

(27) Kolouchova-Hanzlikova, I.; Melzoch, K.; Filip, V.; Smidrkal, J. Rapid method for resveratrol determination by HPLC with electrochemical and UV detection in wines. *Food Chem.* **2004**, *87*, 151−158.

(28) Chen, X.; He, H.; Wang, G.; Yang, B.; Ren, W.; Ma, L.; Yu, Q. Stereospecific determination of *cis*- and *trans*-resveratrol in rat plasma by HPLC: Application to pharmacokinetic studies. *Biomed. Chromatogr.* **2007**, *21*, 257−265.

(29) Majors, R. E. The continuing acetonitrile shortage: How to combat it or live with it. *LCGC North Am.* **2009**, *27*, 458−471.

(30) Urpi-Sarda, M.; Zamora-Ros, R.; Lamuela-Raventos, R.; Cherubini, A.; Jauregui, O.; De la Torre, R.; Covas, M. I.; Estruch, R.; Jaeger, W.; Andres-Lacueva, C. HPLC−tandem mass spectrometric method to characterize resveratrol metabolism in humans. *Clin. Chem.* **2007**, *53*, 292−299.

JOURNAL OF AGRICULTURAL AND FOOD CHEMISTRY

Article

pubs.acs.org/JAFC

Dispersive Liquid-Phase Microextraction with Solidification of Floating Organic Droplet Coupled with High-Performance Liquid Chromatography for the Determination of Sudan Dyes in Foodstuffs and Water Samples

Bo Chen[†,‡] and Yuming Huang*[,†]

[†]State Key Laboratory Breeding Base of Eco-Environments and Bio-Resources of the Three Gorges Reservoir Region, College of Chemistry and Chemical Engineering, Southwest University, Chongqing 400715, People's Republic of China

[‡]Faculty of Environmental Science and Engineering, Kunming University of Science and Technology, Kunming 650500, People's Republic of China

Supporting Information

ABSTRACT: Dispersive liquid-phase microextraction with solidification of floating organic drop (SFO−DLPME) is one of the most interesting sample preparation techniques developed in recent years. In this paper, a new, rapid, and efficient SFO−DLPME coupled with high-performance liquid chromatography (HPLC) was established for the extraction and sensitive detection of banned Sudan dyes, namely, Sudan I, Sudan II, Sudan III, and Sudan IV, in foodstuff and water samples. Various factors, such as the type and volume of extractants and dispersants, pH and volume of sample solution, extraction time and temperature, ion strength, and humic acid concentration, were investigated and optimized to achieve optimal extraction of Sudan dyes in one single step. After optimization of extraction conditions using 1-dodecanol as an extractant and ethanol as a dispersant, the developed procedure was applied for extraction of the target Sudan dyes from 2 g of food samples and 10 mL of the spiked water samples. Under the optimized conditions, all Sudan dyes could be easily extracted by the proposed SFO−DLPME method. Limits of detection of the four Sudan dyes obtained were 0.10−0.20 ng g^{-1} and 0.03 $\mu g\ L^{-1}$ when 2 g of foodstuff samples and 10 mL of water samples were adopted, respectively. The inter- and intraday reproducibilities were below 4.8% for analysis of Sudan dyes in foodstuffs. The method was satisfactorily used for the detection of Sudan dyes, and the recoveries of the target for the spiked foodstuff and water samples ranged from 92.6 to 106.6% and from 91.1 to 108.6%, respectively. These results indicated that the proposed method is simple, rapid, sensitive, and suitable for the pre-concentration and detection of the target dyes in foodstuff samples.

KEYWORDS: *Sudan dyes, foodstuffs, dispersive liquid-phase microextraction, solidification of floating organic droplet, food analysis*

INTRODUCTION

Sudan dyes (Sudan I−IV; Scheme 1) are a class of artificially synthesized fat-soluble azo dyes.[1] The azo dyes have been widely used as organic colorants in all aspects of the chemical industry to improving the appearance of the products.[2] However, these lipophilic azo dyes are considered to be genotoxic carcinogens, imposing a threat to public health once entering the food chain.[3] For instance, Sudan dyes have been widely contacted by painters, hairdressers, etc., resulting in a high occurrence of bladder cancer.[4] In particular, Sudan I, a widely used additive in the food industry, has been reported to induce tumors in the liver of some animals, such as mice, and to show a carcinogenic potential for humans.[5] Because of this, the International Agency for Research Cancer (IARC) has listed the Sudan dyes as a category 3 carcinogenic to humans.[5] Many countries (including the European Union) have banned the use of Sudan dyes as an additive in the food industry.[6] However, Sudan dyes are still illegally used in some areas of Europe and Asia, where the contaminations of foodstuffs by Sudan dyes, in particular Sudan I, are reported.[7,8] Therefore, to monitor the illegal use of Sudan dyes in foodstuff samples, development of a

Scheme 1. Chemical Structures of Four Sudan Dyes (Sudan I, Sudan II, Sudan III, and Sudan IV)

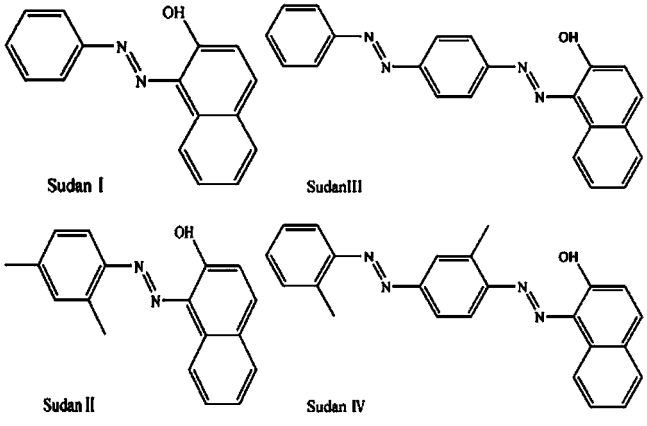

Received: February 6, 2014
Revised: June 3, 2014
Accepted: June 3, 2014
Published: June 3, 2014

ACS Publications © 2014 American Chemical Society

dx.doi.org/10.1021/jf5006403 | J. Agric. Food Chem. 2014, 62, 5818−5826

simple, rapid, and sensitive method for the detection of the target Sudan dyes in the contaminated food stuffs is desirable.

In the past few decades, various methods, including high-performance liquid chromatography (HPLC)−ultraviolet (UV),[1,7−11] HPLC−mass spectrometry (MS),[12] micellar electrokinetic chromatography,[13] and enzyme-linked immunoassay,[14] have been constructed for the analysis of Sudan dyes. Considering the complicated sample matrix as well as very low concentrations of Sudan dye residues in real samples, it is highly crucial to simultaneously isolate and enrich Sudan dyes using sample preparation methods before instrumental analysis. Various pretreatment procedures,[15−19] in particular, solid-phase extraction (SPE),[16−19] have been widely used for the separation and pre-concentration of Sudan dyes in foodstuffs.

Recently, a different mode of liquid-phase microextraction format using solidification of floating organic droplet (SFO−LPME), which incorporated sampling, extraction, and concentration into a single step, has attracted much attention.[20−24] In this technique, a drop of organic solvent is used for extraction. Thus, in comparison to liquid−liquid extraction (LLE), SFO−LPME is a miniaturized LLE technique.[23] When the extraction equilibrium is reached, the organic extract droplet is collected facilely via solidifying it in an ice bath because of the lower density than water and suitable melting point of the used organic extraction solvent. Thus, it has been used to the pre-concentration of organic and inorganic targets in various matrices.[24−30] However, the extraction time was somewhat long because of the long time required for equilibrium.

On the other hand, a dispersive liquid-phase microextraction (DLPME)-based pretreatment process has also gained much attention since the first one developed by Assadi and co-workers in 2006.[31] In DLPME, target extraction is realized by injection of a suitable mixture of extractant and dispersant into an aqueous sample, resulting in the formation of an emulsion solution. Because of the high dispersion of the extractant in the aqueous phase, the target extraction is completed within a few seconds because of the markedly enhanced contact area between phases. Thus, in comparison to classic liquid-phase microextraction (LPME), DLPME is a time-saving extraction technology and promises the advantages of simplicity and good extraction efficiency with a high pre-concentration factor.[32,33] Unfortunately, the commonly used extraction solvents, including $CHCl_3$, CCl_4, chlorobenzene, and CS_2, are difficult to be separated from the aqueous solution because the density of these solvents are higher than that of water. In addition, all of them are toxic and not environmentally friendly. Furthermore, the extract requires evaporation and reconstitution in an appropriate solvent for HPLC analysis. This leads to the increased analysis time and the risk of analyte losses.[23]

On the basis of the advantages of both DLPME and SFO−LPME, a new technique coupling dispersive liquid-phase microextraction and solidification of floating organic droplet (SFO−DLPME) has been proposed for extraction and pre-concentration of various organic targets, such as polycyclic aromatic hydrocarbons (PAHs),[34] phthalate esters,[35] chlorinated anilines,[36] and antidepressant drugs,[37] from aqueous matrices. It combines the best advantages of DLPME and SFO−LPME, eliminating or reducing their disadvantages. However, to the best of our knowledge, no investigation on the use of SFO−DLPME for extraction and enrichment of Sudan dyes from foodstuffs and water samples has been reported.

In present study, on the basis of solidification of the floating organic droplet, a new, rapid, and efficient dispersive liquid-phase microextraction method (SFO−DLPME) coupled with HPLC−UV is proposed for the extraction and sensitive detection of banned Sudan dyes (I, II, III, and IV) in foodstuffs and environmental water samples. Hence, the purposes of this work were (1) to confirm the suitability of the SFO−DLPME for the extraction of Sudan dyes, (2) to optimize the predominant factors affecting the enrichment efficiency of SFO−DLPME for Sudan dyes, and (3) to illustrate the feasibility of the developed method by analyzing the target Sudan dyes in foodstuffs and environmental water samples. The results demonstrate that this approach promises fastness, low consumption of organic solvent, and simplicity and is an interesting alternative for the concentration of organic targets in complex matrices.

EXPERIMENTAL PROCEDURES

Reagents and Chemicals. Sudan I and Sudan II were supplied by Shanghai Chemical Reagents Co. (Shanghai, China). Sudan III and Sudan IV were provided by Kasei Kogyo (Japan). An appropriate amount of four Sudan dyes was dissolved in methanol to obtain the standard stock solution, and the resulting solution was stored at 4 °C in the dark. The methanol was of HPLC grade and provided by Scharlau Chemie S.A. (Scharlau Chemie S.A., Spain). Humic acid (HA) was purchased from Sigma-Aldrich (Shanghai, China). Ultrapure water was supplied by a Milli-Q water purification system in our laboratory. 1-undecanol, 1-dodecanol, acetone, ethanol, HCl, acetonitrile, NaCl, and all other chemicals used were of analytical reagent grade, unless otherwise stated, and were provided by Chongqing Chemical Reagents Co. (Chongqing, China).

Instrumental Analysis. The HPLC system (JASCO Corporation, Japan) consisted of PU-2080i binary pumps, CO-2060 column thermostat, and UV-2075 detector. A Hypersil ODS chromatographic column (150 × 4.6 mm, 5 μm) was supplied by Waters Corporation (Milford, MA) and used for separation of four Sudan dyes. Methanol was used as the mobile phase. The flow rate of methanol was set to 1.0 mL min^{-1}. The column temperature was thermostated at 30 °C. The chromatographic peaks of Sudan I−IV were recorded at 506 nm. The injection volume was 20 μL.

SFO−DLPME Procedures. In all experiments, to optimize operational parameters of the SFO−DLPME procedure, 20 μg L^{-1} Sudan I, Sudan II, and Sudan III and 40 μg L^{-1} Sudan IV in a sample volume of 10 mL were used. The recovery of the target Sudan dyes was used as the criterion for optimizing the parameter for the proposed method. It was acquired on the basis of the ratio of the obtained content of Sudan dyes to the expected content of Sudan dyes, expressed as a percentage. The finally adopted SFO−DLPME procedure was as follows: after 1 g of NaCl (final concentration of 10% as w/v) and 10 mL of the fortified sample are introduced into a 15 mL centrifuge tube, 100 μL of 1-dodecanol and 400 μL of ethanol are rapidly injected by a microsyringe, leading to the formation of a homogeneous turbid solution. Then, the tube is immediately immersed in a water bath at 70 °C for 20 min, followed by centrifugation at 4500 rpm for 5 min, and finally placed in an ice bath for 5 min. The solid organic phase was transferred to a conical vial with the help of a spoon, and then it melts rapidly at room temperature. The melted organic solvent was mixed with 50 μL of methanol, and then 20 μL of the mixture was used for HPLC−UV analysis.

Sample Preparation. The foodstuffs, including tomato sauce, chili sauce, and chili oil samples used in this study, were obtained from the local market. For analysis of food samples, about 2 g of the selected food samples was put into a 10 mL glass centrifuge tube and mixed with 5 mL of ethanol. Then, the resulting mixture was shaken for 20 min at 30 °C and then centrifuged at 4000 rpm for 10 min. The transparent solution was transferred to a sample vial, dried under a nitrogen atmosphere, and then diluted to 10 mL with 10% NaCl (w/

dx.doi.org/10.1021/jf5006403 | J. Agric. Food Chem. 2014, 62, 5818−5826

v) solution (pH 7.0). Finally, the obtained sample solution was extracted with the optimized extraction protocols.

In this work, several aqueous samples, such as river water samples, tap water samples, and wastewater samples were pretreated by the proposed SFO–DLPME method for the analysis of four Sudan dyes. The river water samples were obtained from the Beibei section (Beibei, Chongqing) of the Jialingjiang River. The tap water samples and the sewage water samples were collected from our laboratory and a constructed wetland system for domestic sewage treatment situated in Southwest University (Beibei, Chongqing), respectively. Prior to analysis, all aqueous samples were passed through 0.45 μm micropore membranes and kept in glass bottles at 4 °C in a refrigerator. The extraction of target Sudan dyes from unspiked and spiked water samples was carried out according to the recommended SFO–DLPME procedures.

RESULTS AND DISCUSSION

Optimization of the SFO–DLPME Procedures. *Effect of the Kind and Volume of Extraction Solvent.* During the extraction process, selecting a suitable extraction solvent is a very important work using the SFO–DLPME method because the extraction efficiency was mainly determined by the extraction solvent in SFO–DLPME.[35] To improve extraction efficiency, three organic solvents, namely, 1-undecanol (melting point of 13–15 °C), 1-dodecanol (melting point of 22–24 °C), and *n*-hexadecane (melting point of 18 °C), were considered as

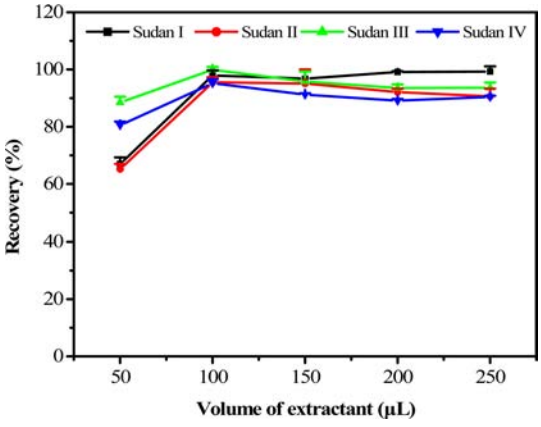

Figure 1. Effect of the volume of the extract solvent. Concentration of the sample solution, 20 μg L^{-1} Sudan I, 20 μg L^{-1} Sudan II, 20 μg L^{-1} Sudan III, and 40 μg L^{-1} Sudan IV; pH of the sample solution, 7.0; sample volume, 10 mL; extractant, 1-dodecanol; dispersion solvent, 400 μL of ethanol; extraction time, 20 min; extraction temperature, 70 °C; ion strength, 10% NaCl (w/v). Error bars stand for 1 standard deviation (n = 3).

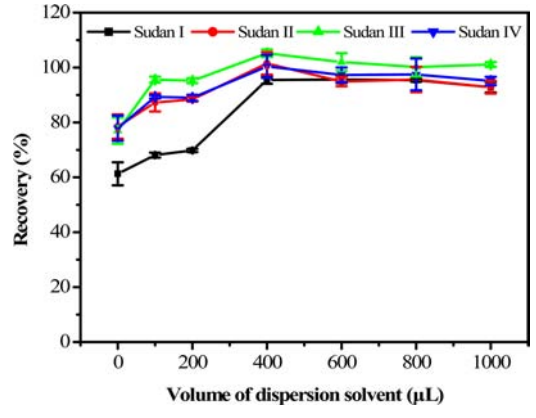

Figure 2. Effect of the volume of the dispersion solvent. Extract solvent, 100 μL of 1-dodecanol; dispersion solvent, ethanol; other conditions were the same as those in Figure 1. Error bars stand for 1 standard deviation (n = 3).

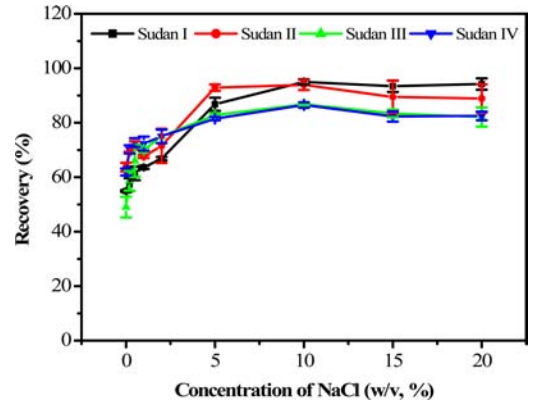

Figure 3. Effect of the concentration of NaCl. Extract solvent, 100 μL of 1-dodecanol; dispersion solvent, 200 μL of ethanol; extraction temperature, 50 °C; other conditions were the same as those in Figure 1. Error bars stand for 1 standard deviation (n = 3).

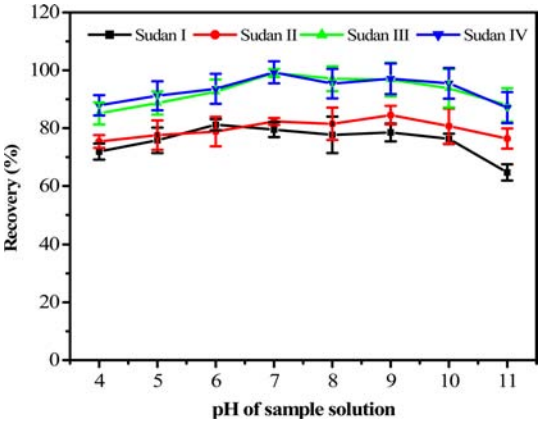

Figure 4. Effect of the sample solution pH. Extractant, 100 μL of 1-dodecanol; dispersion solvent, 200 μL of ethanol; extraction temperature, 50 °C; other conditions were the same as those in Figure 1. Error bars stand for 1 standard deviation (n = 3).

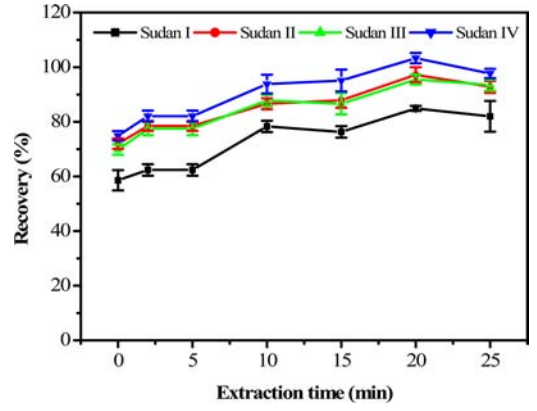

Figure 5. Effect of the extraction time. Extractant, 100 μL of 1-dodecanol; dispersion solvent, 400 μL of ethanol; other conditions were the same as those in Figure 1. Error bars stand for 1 standard deviation (n = 3).

dx.doi.org/10.1021/jf5006403 | J. Agric. Food Chem. 2014, 62, 5818–5826

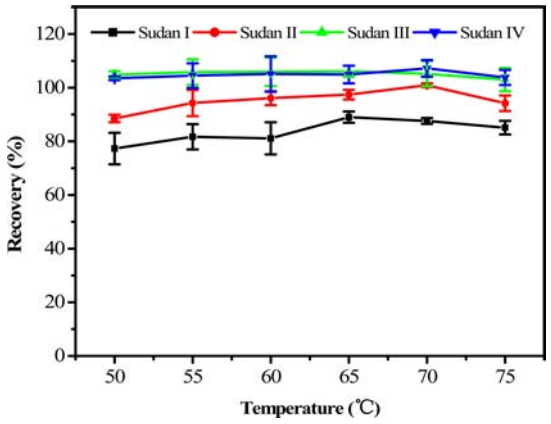

Figure 6. Effect of the solution temperature. Extractant, 100 μL of 1-dodecanol; dispersion solvent, 200 μL of ethanol; other conditions were the same as those in Figure 1. Error bars stand for 1 standard deviation (n = 3).

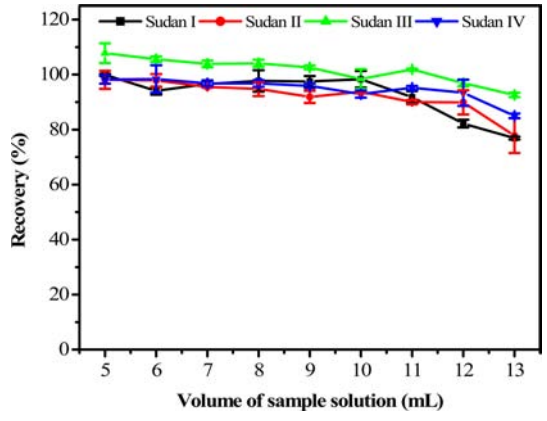

Figure 7. Effect of the sample volume. Extractant, 100 μL of 1-dodecanol; other conditions were the same as those in Figure 1. Error bars stand for 1 standard deviation (n = 3).

the extraction solvents in this work. Because of its high hydrophobicity, n-hexadecane is not miscible with a common dispersive solvent. Here, only 1-undecanol and 1-dodecanol were evaluated for extraction of Sudan dyes in this work. On the basis of the obtained result (see Figure S1 of the Supporting Information), the best extraction efficiency was obtained when 1-dodecanol was used as the extractant. Hence, 1-dodecanol was selected as the extraction solvent in the present work, and its volume was optimized in the range of 50−250 μL. From Figure 1, the recoveries of Sudan dyes rised rapidly when the volume of 1-dodecanol ranged from 50 to 100 μL and then remained stable ranging from 93.8 to 116.9%. Also, the effect of 1-dodecanol (as an extractant) volume on the pre-concentration factor (PF) was supplied in Table S1 of the Supporting Information. Here, PFs were obtained according to the following formula:

$$\mathrm{PFs} = C_p/C_i \quad (1)$$

where C_p and C_i are the concentrations of Sudan dyes in the floating phase after extraction and in the sample solution before extraction, respectively. As seen, the PFs decreased with an increase in the volume of 1-dodecanol. However, the quantitative recoveries of Sudan dyes were obtained with 100 μL of 1-dodecanol (Figure 1). Therefore, 100 μL of 1-

Table 1. Analytical Characteristics of the SFO−DLPME−HPLC Method for Sudan Dyes in Foodstuffs

	tomato sauce					chili oil					chili sauce				
			RSD (%)					RSD (%)				RSD (%)			
targets	linear range (ng g^{-1})	r^2	interday[a]	intraday[b]	LOD (ng g^{-1})	linear range (ng g^{-1})	r^2	interday[a]	intraday[b]	LOD (ng g^{-1})	linear range (ng g^{-1})	r^2	intraday[a]	intraday[b]	LOD (ng g^{-1})
Sudan I	1−1250	0.9964	4.0	2.8	0.15	1−1250	0.9990	2.0	2.3	0.15	1−1250	0.9948	4.0	2.8	0.15
Sudan II	1−1250	0.9948	1.6	1.6	0.15	1−1250	0.9974	2.2	2.6	0.15	1−1250	0.9923	1.6	1.6	0.15
Sudan III	1−1250	0.9921	3.5	2.4	0.10	1−1250	0.9934	3.8	4.8	0.10	1−1250	0.9921	3.5	2.4	0.10
Sudan IV	1−1250	0.9952	3.1	2.4	0.20	1−1250	0.9967	3.7	3.2	0.20	1−1250	0.9930	3.1	2.4	0.20

[a]Nine replicate determinations of 100 ng g^{-1} Sudan I, 100 ng g^{-1} Sudan II, 100 ng g^{-1} Sudan III, and 100 ng g^{-1} Sudan IV spiked foodstuff samples in 9 consecutive days. [b]Six replicate determinations of 100 ng g^{-1} Sudan I, 100 ng g^{-1} Sudan II, 100 ng g^{-1} Sudan III, and 100 ng g^{-1} Sudan IV spiked foodstuff samples in 1 day.

dx.doi.org/10.1021/jf5006403 | J. Agric. Food Chem. 2014, 62, 5818−5826

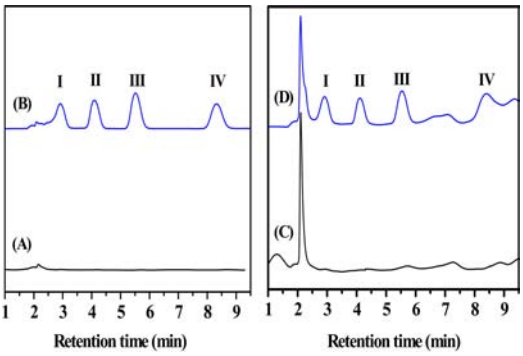

Figure 8. HPLC–UV chromatograms of food sample extraction with SFO–DLPME: (A) chili sauce and (C) chili oil without spiking and (B) chili sauce and (D) chili oil spiked with Sudan dyes standard at the 0.5 $\mu g\ g^{-1}$ level. I, Sudan I; II, Sudan II; III, Sudan III; and IV, Sudan IV.

Table 2. Recoveries of Four Sudan Dyes in Three Foodstuffs after SFO–DLPME

	spiked levels ($\mu g\ g^{-1}$)	tomato sauce recoveries[a] (%)	chili oil recoveries[a] (%)	chili sauce recoveries[a] (%)
Sudan I	0.05	99.3 ± 3.6	95.6 ± 4.1	95.6 ± 4.1
	0.1	93.9 ± 2.1	99.5 ± 2.3	96.4 ± 3.9
	0.5	92.8 ± 0.3	96.1 ± 0.3	99.0 ± 1.4
Sudan II	0.05	105.9 ± 3.1	95.6 ± 2.9	97.0 ± 1.8
	0.1	101.1 ± 3.3	97.3 ± 2.5	97.1 ± 1.5
	0.5	93.4 ± 4.8	103.4 ± 1.4	94.0 ± 4.2
Sudan III	0.05	106.6 ± 0.9	101.4 ± 5.8	97.0 ± 2.7
	0.1	95.3 ± 5.7	92.6 ± 4.5	97.1 ± 1.5
	0.5	98.8 ± 4.5	103.9 ± 0.9	102.8 ± 0.5
Sudan IV	0.05	96.3 ± 2.9	95.6 ± 6.9	98.1 ± 2.4
	0.1	99.3 ± 4.0	104.4 ± 3.3	101.9 ± 3.2
	0.5	97.9 ± 5.5	104.9 ± 5.6	102.4 ± 1.7

[a]Average of three determinations (mean ± SD; $n = 3$).

dodecanol was chosen as an appropriate extractant to obtain the quantitative results.

Effect of the Kind and Volume of Dispersion Solvent. Several organic solvents, namely, ethanol, acetonitrile, acetone, isopropanol, and methanol, were evaluated as the dispersion solvent for extraction of Sudan dyes. The experimental results indicated that acetone, ethanol, acetonitrile, and methanol gave better dispersion ability than that of isopropanol (see Figure S2 of the Supporting Information). In SFO–DLPME, the major consideration for choosing a dispersion solvent is mainly based on its miscibility with the extractant and aqueous phase. Generally, the good disperser solvent has good miscibility with the extraction solvent and sample solution.[30] In the selected dispersion solvents, ethanol, methanol, acetone, and acetonitrile are strong polar solvents, whereas isopropanol is a moderate polar solvent. The polarity of the five organic solvents follows the order of ethanol ≈ methanol > acetone > acetonitrile > isopropanol. Therefore, ethanol, methanol, acetone, and acetonitrile could be miscible with the water well, leading to the better dispersion ability than isopropanol. Because of low toxicity and low cost, finally, ethanol was selected as the dispersion solvent for further investigation. Also, the effect of the volume of ethanol ranging from 0 to 1000 μL was evaluated. From Figure 2, the recoveries of Sudan dyes increased when the volume of ethanol increased to 400 μL and then remained stable, ranging from 93.0 to 105.2%. A total of 400 μL of ethanol was selected to obtain high extraction efficiency in our work.

Effect of the Ion Strength and Sample pH. NaCl was used to study the effect of the ionic strength. The tested concentration of NaCl were in the range of 0–20% (w/v). As shown in Figure 3, the addition of NaCl into sample solution could efficiently improve the extraction efficiency of Sudan dyes when the concentration of NaCl was in the range of 0–10%. However, there is no obvious change of extraction efficiency of Sudan dyes if the concentration of sodium chloride exceeds 10%. This could be explained by the salting-out effect. The solubility of the hydrophobic organics in water samples was decreased when the salt was added. This could cause an increase in extraction efficiency.[38,39] On the basis of these results, 10% (w/v) NaCl solution was selected in the subsequent experiments.

The effect of solution pH, ranging from 4.0 to 11.0, on the extraction of Sudan dyes by SFO–DLPME was studied. From Figure 4, the extraction recoveries of four Sudan dyes remained a minor increase when solution pH ranged from 4.0 to 7.0 and then remained stable in the pH range from 7.0 to 9.0, above which it decreased. This is probably due to their instability in strong acid and alkali medium.[40] Hence, below pH 7.0 and above pH 9.0, the recoveries of Sudan dyes decreased. Considering that the best extraction of Sudan dyes was obtained at pH 7.0, the optimal pH 7.0 was adopted as solution pH in this work.

Effect of the Extraction Time and Solution Temperature. In SFO–DLPME, analytes are distributed between the sample solution phase and organic phase. Thus, the mass transfer of analyte between the aqueous phase and the organic solvent was greatly affected by the extraction time. To guarantee the equilibrium between phases as well as the maximal extraction of Sudan dyes, the extract time ranging from 0 to 25 min was investigated. According to Figure 5, the influence of the reaction time on recoveries of Sudan dyes was significant. This implies that the transfer of Sudan dyes from sample solution to extraction solvent is slow, which is probably due to the high fat-soluble property of Sudan dyes. A similar result was reported by Regueiro et al.,[26] working on extraction of fat-soluble contaminants by ultrasound-assisted emulsification–microextraction. It was found that extraction time presented a key role in the extraction of polycyclic musk fragrances, musk moskene, di-2-ethylhexyl phthalate (DEHP), and di-*n*-octyl phthalate (DOP). The recoveries of Sudan dyes increased with extraction time up to 20 min, above which no obvious change in extraction recovery was found. Finally, 20 min was selected for the subsequent experiments.

For liquid-phase microextraction, the efficient extraction can be achieved by increasing the temperature because an increasing temperature facilitates mass transfer of the targets from the aqueous phase to the organic phase, leading to shortening the analysis time.[41,42] Thus, the temperature effect was investigated from 50 to 75 °C by dispersing 1-dodecanol into the water samples containing Sudan dyes. According to Figure 6, the extraction recoveries of Sudan dyes were increased as the solution temperature increased from 50 to 70 °C. However, the higher temperature (>70 °C) resulted in a mild decrease in recovery. Thus, 70 °C was selected as the optimal temperature.

Effect of the Sample Volume. Increasing the volume of sample solution could increase the amount of targets migrated

dx.doi.org/10.1021/jf5006403 | J. Agric. Food Chem. 2014, 62, 5818–5826

Table 3. Comparison of Various Analytical Methods for the Detection of Sudan Dye in Foodstuffs

analytical method	real sample	preparation method	extraction time (min)	linear range (ng g^{-1})	recovery (%)	LOD (ng g^{-1})	RSD (%)	reference
HPLC−DAD	chili- and curry-based sauces and powdered spices	solvent extraction	>60	0−20000	51−100	200−2000	<15	1
HPLC−UV	tomato sauce and sausage	MIP SPE	25	4−1000	85.5	0.8−3.0	3.0	9
HPLC−UV	chili powder, dry red pepper, ketchup, and sausage	IL-modified microspheres	15	50−4000	92.5−106.1	4−14	≤5.7	10
UPLC−MS/MS	spices and chili foodstuffs	LLE	>60	10−50000	87−106	0.5−100	<20	12
HPLC−UV	red chili powder	cloud point extraction	30	not given	80.7−85.5	2−4	1.18−3.0	15
HPLC−UV	sausage	MIP SPE−DLLME	about 10	5−2000	86.3−107.5	1−5[a]	3.4−6.7	17
HPLC−UV	chili sauce	MIP SPE	>20	not given	87.5−103.4	3.3−5.0	1.94−5.33	18
HPLC−DAD	chili products	SPE	>20	50−2500[b]	93.2−103	4.1−5.8	0.3−4.9	43
HPLC−UV	chili powder	IL solvent extraction	about 40	20−20000[b]	76.8−109.5	7.0−8.2	2.0−3.5	47
HPLC−UV	egg yolk	MIP−MSPD−DLLME	>20	0.02−2	87.2−103.5	2.3−6.1	2.9−6.7	48
HPLC−DAD	tomato sauce, vinegar sauce, and meat sauce	supramolecular solvent ME	about 10	0.028−2	86−108	2.7−7.4	2−7	49
HPLC−UV	chili powder	magnetic MIP SPE	>20	25−5000	79.9−87.8	1.6−6.2	4.8−9.1	50
LC−MS/MS	chili products	solvent extraction	12	5−5500	72−103	3−24	1−15	51
LC−MS/MS	animal-derived foods and eggs of hen and duck	UAE	>10	0.1−10[b]	61.9−87.4	0.03−0.12	<19.1	52
LC−MS/MS	chili powder, pepper chili sauce, sausage, and chili meat	solvent extraction	10	1−500[b]	81.7−92.9	0.5−1.8	2.9−8.1	53
HPLC−UV	tomato sauce, chili oil, and chili sauce	SFO−DLPME	20	1−1250	92.6−106.6	0.1−0.2	1.6−4.8	this work

[a]Limit of quantification (LOQ). [b]In units of ng mL^{-1}.

into the extraction phase from aqueous phase, which improves the sensitivity of the proposed method. However, this also might lead to the decreased extraction recovery in a fixed extraction time.[28] The influence of the sample volume on the extraction of four Sudan targets was investigated by changing the sample volume from 5 to 13 mL. The results in Figure 7 indicated that the quantitative results (recovery of >95%) were obtained when the aqueous-phase volume varied from 5 to 11 mL. Finally, the volume of 10 mL was selected and used as the optimal sample volume in our work.

Application of the SFO−DLPME−HPLC Method to Real Foodstuff Samples. For the determination of Sudan dyes in foodstuffs, various solvents, including methanol,[10,16] acetonitrile,[1,6,17,43] and ethanol,[14,44,45] have been used alone for extraction of Sudan dyes in various foodstuffs. Considering that the recovery of Sudan IV could be improved using ethanol as an extraction solvent[44] and the ratio of the sample weight to the volume of the extractant has no obvious effect on extraction recovery,[46] in our work, about 2 g of the selected food samples was extracted with 5 mL of ethanol. To evaluate the potential application of the SFO−DLPME−HPLC method for the detection of Sudan dyes in real samples, the analytical characteristics were evaluated using the spiked food samples. The results are indicated in Table 1. As seen, the linear ranges, in terms of the peak area and sample concentration for four Sudan dyes, were in the range of 1−1250 ng g^{-1}. The correlation coefficients (r^2) were in the range of 0.9921−0.9990, demonstrating the good linearity of the proposed method. The limit of detection (LOD; S/N = 3) was in the range of 0.10−0.20 ng g^{-1}. Validation of the SFO−DLPME−HPLC method was evaluated by determining the recoveries of the spiked foodstuffs with Sudan I−IV at 0.05, 0.10, and 0.50 μg g^{-1}. The precision of the SFO−DLPME−HPLC method was evaluated by carrying out analysis of the spiked foodstuffs in 6 replicates in the same day and 9 successive days. The relative standard deviations (RSDs; precision) of inter- and intraday were ≤4.8% (Table 1), suggesting that the reproducibility was satisfactory. No target dyes were detected in the tomato sauce, chili oil, and chili sauce samples. Figure 8 shows the typical chromatograms of Sudan dyes from chili sauce and chili oil samples. The recoveries varied from 92.6 to 106.6% for the target Sudan dyes in tomato sauce, chili sauce, and chili oil (Table 2), showing that the proposed method was reliable for analysis of trace levels of Sudan dyes in complicated foodstuffs.

The proposed method was compared to other methods.[1,9,10,12,15,17,18,43,47−53] As seen from Table 3, the LODs of the proposed method in this work were lower than most methods reported. Meanwhile, a relatively short extraction time (20 min), good recoveries (92.6−106.6%), and low RSD were obtained with the reported pretreatment technique. This shows that the SFO−DLPME is an ideal microextraction technique in the pre-concentration of four Sudan dyes in real foodstuffs.

Application of the SFO−DLPME−HPLC Method to Environmental Water Samples. To assess the potential application of the SFO−DLPME−HPLC method for the detection of Sudan dyes in aqueous samples, first, the effect of the commonly co-existing ions (NO_3^-, CO_3^{2-}, PO_4^{3-}, Ca^{2+}, Mg^{2+}, K^+, NH_4^+, etc.) in natural waters was studied under the above-selected extraction conditions. The results demonstrated that quantitative recoveries of the target dyes were obtained in the presence of co-existing substances (see Table S2 of the Supporting Information), showing the good selectivity of the proposed SFO−DLPME method to Sudan dyes. Also, the effect of natural organic matter (NOM) on the extraction of Sudan dyes was evaluated because NOM is widely present in natural waters. To do this, sample solutions containing different concentrations of humic acid were treated by this SFO−

dx.doi.org/10.1021/jf5006403 | J. Agric. Food Chem. 2014, 62, 5818−5826

DLPME method. From Figure S3 of the Supporting Information, the quantitative recovery of Sudan dyes could be reached at less than the 5 mg L^{-1} level of humic acid. The humic acid contents in the natural waters are less than 4 mg L^{-1} for river water samples;[54] thus, it did not interfere with Sudan dye determination, indicating the good selectivity of the proposed SFO−DLPME method.

Second, under the selected extraction conditions indicated above, the analytical performance was tested. The analytical data, such as linear range, correlation coefficients, detection limits, and precision, are shown in Table S3 of the Supporting Information. As seen, good linear relationships could be obtained for four Sudan dyes between the peak area and the sample concentration from 0.2 to 500 $\mu g\ L^{-1}$. The LOD was 0.03 $\mu g\ L^{-1}$. The recoveries of Sudan dyes varied in the range of 91.1−108.6% when 10 mL of aqueous sample at three spiked concentration levels (5, 10, and 20 $\mu g\ L^{-1}$ Sudan dyes) were tested (see Table S4 of the Supporting Information), indicating the utility of the proposed method for the detection of Sudan dyes in environmental water samples.

In conclusion, for the first time, we demonstrated that the proposed SFO−DLPME−HPLC method can be used as a useful protocol for pre-concentration and detection of trace Sudan dyes. Our results indicate that SFO−DLPME is an efficient sample preparation technique for the extraction of banned Sudan dyes (I, II, III, and IV) in a complex matrix. The proposed method promises simplicity, less organic solvent consumption, and high sensitivity. Also, it allows for the determination of Sudan dyes in complex matrices with good accuracy and reproducibility.

■ ASSOCIATED CONTENT

Ⓢ Supporting Information

Pre-concentration factors of Sudan dyes by the SFO−DLPME method (Table S1), recoveries of Sudan dyes in the presence of foreign species (Sudan I−IV concentrations: 20, 20, 20, and 40 $\mu g\ L^{-1}$, respectively) (Table S2), analytical characteristics of the SFO−DLPME−HPLC method for Sudan dyes in aqueous solution (Table S3), determination results of Sudan dyes in environmental water samples (Table S4), effect of different extractants on the extraction efficiency of Sudan dyes (Figure S1), effect of different dispersion solvents on the extraction efficiency of Sudan dyes (Figure S2), and effect of humic acid on the extraction efficiency of Sudan dyes (Figure S3). This material is available free of charge via the Internet at http://pubs.acs.org.

■ AUTHOR INFORMATION

Corresponding Author

*Telephone/Fax: +86-23-68254843. E-mail: yuminghuang2000@yahoo.com.

Funding

Financial support by the National Natural Science Foundation of China (21277111) is gratefully acknowledged.

Notes

The authors declare no competing financial interest.

■ REFERENCES

(1) Cornet, V.; Govaert, Y.; Moens, G.; Van Loco, J.; Degroodt, J.-M. Development of a fast analytical method for the determination of Sudan dyes in chili- and curry-containing foodstuffs by high-performance liquid chromatography−photodiode array detection. *J. Agric. Food Chem.* **2006**, *54*, 639−644.

(2) Nohynek, G. J.; Fautz, R.; Benech-Kieffer, F.; Toutain, H. Toxicity and human health risk of hair dyes. *Food Chem. Toxicol.* **2004**, *42*, 517−543.

(3) Golka, K.; Kopps, S.; Myslak, Z. W. Carcinogenicity of azo colorants: Influence of solubility and bioavailability. *Toxicol. Lett.* **2004**, *151*, 203−210.

(4) Ahlstrom, L. H.; Eskilsson, C. S.; Bjorklund, E. Determination of banned azo dyes in consumer goods. *TrAC, Trends Anal. Chem.* **2005**, *24*, 49−56.

(5) Stiborová, M.; Martínek, V.; Rýdlová, H.; Hodek, P.; Frei, E. Sudan I is a potential carcinogen for humans: Evidence for its metabolic activation and detoxication by human recombinant cytochrome P450 1A1 and liver microsomes. *Cancer Res.* **2002**, *62*, 5678−5684.

(6) Anibal, C. V. Di; Odena, M.; Ruisánchez, I.; Callao, M. P. Determining the adulteration of spices with Sudan I-II-II-IV dyes by UV−visible spectroscopy and multivariate classification techniques. *Talanta* **2009**, *79*, 887−892.

(7) Zacharis, C. K.; Kika, F. S.; Tzanavaras, P. D.; Rigas, P.; Kyranas, E. R. Development and validation of a rapid HPLC method for the determination of five banned fat-soluble colorants in spices using a narrow-bore monolithic column. *Talanta* **2011**, *84*, 480−486.

(8) He, L.; Su, Y.; Fang, B.; Shen, X.; Zeng, Z.; Liu, Y. Determination of Sudan dye residues in eggs by liquid chromatography and gas chromatography−mass spectrometry. *Anal. Chim. Acta* **2007**, *594*, 139−146.

(9) Zhao, C.; Zhao, T.; Liu, X.; Zhang, H. A novel molecularly imprinted polymer for simultaneous extraction and determination of Sudan dyes by on-line solid phase extraction and high performance liquid chromatography. *J. Chromatogr. A* **2010**, *1217*, 6995−7002.

(10) Yan, H.; Gao, M.; Qiao, J. New ionic liquid modified polymeric microspheres for solid-phase extraction of four Sudan dyes in foodstuff samples. *J. Agric. Food Chem.* **2012**, *60*, 6907−6912.

(11) Ertaş, E.; Özer, H.; Alasalvar, C. A rapid HPLC method for determination of Sudan dyes and Para Red in red chilli pepper. *Food Chem.* **2007**, *105*, 756−760.

(12) Schummer, C.; Sassel, J.; Bonenberger, P.; Moris, G. Low-level detections of Sudan I, II, III and IV in spices and chili-containing foodstuffs using UPLC-ESI-MS/MS. *J. Agric. Food Chem.* **2013**, *61*, 2284−2289.

(13) Fukuji, T. S.; Castro-Puyana, M.; Tavares, M. F.; Cifuentes, A. Fast determination of Sudan dyes in chili tomato sauces using partial filling micellar electrokinetic chromatography. *J. Agric. Food Chem.* **2011**, *59*, 11903−11909.

(14) Wang, Y.; Yang, H.; Wang, B.; Deng, A. A sensitive and selective direct competitive enzyme-linked immunosorbent assay for fast detection of Sudan I in food samples. *J. Sci. Food Agric.* **2011**, *91*, 1836−1842.

(15) Liu, W.; Zhao, W. J.; Chen, J. B.; Yang, M. M. A cloud point extraction approach using Triton X-100 for the separation and preconcentration of Sudan dyes in chilli powder. *Anal. Chim. Acta* **2007**, *605*, 41−45.

(16) Long, C.; Mai, Z.; Yang, Y.; Zhu, B.; Xu, X.; Lu, L.; Zou, X. Synthesis and characterization of a novel molecularly imprinted polymer for simultaneous extraction and determination of water-soluble and fat-soluble synthetic colorants in chilli products by solid phase extraction and high performance liquid chromatography. *J. Chromatogr. A* **2009**, *1216*, 8379−8385.

(17) Yan, H.; Qiao, J.; Wang, H.; Yang, G.; Row, K. H. Molecularly imprinted solid-phase extraction combined with ultrasound-assisted dispersive liquid−liquid microextraction for the determination of four Sudan dyes in sausage samples. *Analyst* **2011**, *136*, 2629−2634.

(18) Zhang, Z.; Xu, S.; Li, J.; Xiong, H.; Peng, H.; Chen, L. Selective solid-phase extraction of Sudan I in chili sauce by single-hole hollow molecularly imprinted polymers. *J. Agric. Food Chem.* **2012**, *60*, 180−187.

(19) Puoci, F.; Garreffa, C.; Lemma, F.; Muzzalupo, R.; Splizzirri, U. G.; Picci, N. Molecularly imprinted solid phase extraction for detection of Sudan I in food matrices. *Food Chem.* **2005**, *93*, 349−353.

(20) Khalili-Zanjani, M. R.; Yamini, Y.; Shariati, S.; Jönsson, J. A. A new liquid-phase microextraction method based on solidification of floating organic drop. *Anal. Chim. Acta* **2007**, *585*, 286−293.
(21) Sobhi, H. R.; Yamini, Y.; Esrafili, A.; Abadi, R. H. H. B. Suitable conditions for liquid-phase microextraction using solidification of a floating drop for extraction of fat-soluble vitamins established using an orthogonal array experimental design. *J. Chromatogr. A* **2008**, *1196*−*1197*, 28−32.
(22) Khalili-Zanjani, M. R.; Yamini, Y.; Yazdanfar, N.; Shariati, S. Extraction and determination of organophosphorus pesticides in water samples by a new liquid phase microextraction−gas chromatography−flame photometric detection. *Anal. Chim. Acta* **2008**, *606*, 202−208.
(23) Vera-Avila, L. E.; Rojo-Portillo, T.; Covarrubias-Herrera, R.; Peña-Alvarez, A. Capabilities and limitations of dispersive liquid−liquid microextraction with solidification of floating organic drop for the extraction of organic pollutants from water samples. *Anal. Chim. Acta* **2013**, *805*, 60−69.
(24) Farahani, H.; Yamini, Y.; Shariati, S. M.; Khalili-Zanjani, R.; Mansour-Baghahi, S. Development of liquid phase microextraction method based on solidification of floated organic drop for extraction and preconcentration of organochlorine pesticides in water samples. *Anal. Chim. Acta* **2008**, *626*, 166−173.
(25) Faraji, H.; Tehrani, M. S.; Husain, S. W. Pre-concentration of phenolic compounds in water samples by novel liquid−liquid microextraction and determination by gas chromatography−mass spectrometry. *J. Chromatogr. A* **2009**, *1216*, 8569−8574.
(26) Regueiro, J.; Llompart, M.; Garcia-Jares, C.; Garcia-Monteagudo, J. C.; Cela, R. Ultrasound-assisted emulsification−microextraction of emergent contaminants and pesticides in environmental waters. *J. Chromatogr. A* **2008**, *1190*, 27−38.
(27) Dadfarnia, S.; Salmanzadeh, A. M.; Shabani, A. M. H. A novel separation/preconcentration system based on solidification of floating organic drop microextraction for determination of lead by graphite furnace atomic absorption spectrometry. *Anal. Chim. Acta* **2008**, *623*, 163−167.
(28) Bidabadi, M. S.; Dadfarnia, S.; Shabani, A. M. H. Solidified floating organic drop microextraction (SFODME) for simultaneous separation/preconcentration and determination of cobalt and nickel by graphite furnace atomic absorption spectrometry (GFAAS). *J. Hazard. Mater.* **2009**, *166*, 291−296.
(29) Rivas, R. E.; Lopez-Garcia, I.; Hernandez-Cordoba, M. Microextraction based on solidification of a floating organic drop followed by electrothermal atomic absorption spectrometry for the determination of ultratraces of lead and cadmium in waters. *Anal. Methods* **2010**, *2*, 225−230.
(30) Yamini, Y.; Rezaee, M.; Khanchi, A.; Faraji, M.; Saleh, A. Dispersive liquid−liquid microextraction based on the solidification of floating organic drop followed by inductively coupled plasma−optical emission spectrometry as a fast technique for the simultaneous determination of heavy metals. *J. Chromatogr. A* **2010**, *1217*, 2358−2364.
(31) Rezaee, M.; Assadi, Y.; Milani Hosseini, M. R.; Aghaee, E.; Ahmadi, F.; Berijani, S. Determination of organic compounds in water using dispersive liquid−liquid microextraction. *J. Chromatogr. A* **2006**, *1116*, 1−9.
(32) Birjandi, A. P.; Bidari, A.; Rezaei, F.; Hosseini, M. R. M.; Assadi, Y. Speciation of butyl and phenyltin compounds using dispersive liquid−liquid microextraction and gas chromatography−flame photometric detection. *J. Chromatogr. A* **2008**, *1193*, 19−25.
(33) Xiong, J.; Hu, B. Comparison of hollow fiber liquid phase microextraction and dispersive liquid−liquid microextraction for the determination of organosulfur pesticides in environmental and beverage samples by gas chromatography with flame photometric detection. *J. Chromatogr. A* **2008**, *1193*, 7−18.
(34) Xu, H.; Ding, Z.; Lv, L.; Song, D.; Feng, Y.-Q. A novel dispersive liquid−liquid microextraction based on solidification of floating organic droplet method for determination of polycyclic aromatic hydrocarbons in aqueous samples. *Anal. Chim. Acta* **2009**, *636*, 28−33.
(35) Kamarei, F.; Ebrahimzadeh, H.; Yamini, Y. Optimization of ultrasound-assisted emulsification microextraction with solidification of floating organic droplet followed by high performance liquid chromatography for the analysis of phthalate esters in cosmetic and environmental water samples. *Microchem. J.* **2011**, *99*, 26−33.
(36) Ramkumar, A.; Ponnusamy, V. K.; Jen, J.-F. Rapid analysis of chlorinated anilines in environmental water samples using ultrasound assisted emulsification microextraction with solidification of floating organic droplet followed by HPLC-UV detection. *Talanta* **2012**, *97*, 279−284.
(37) Ebrahimzadeh, H.; Saharkhiz, Z.; Tavassoli, M.; Kamarei, F.; Asgharinezhad, A. A. Ultrasound-assisted emulsification microextraction based on solidification of floating organic droplet combined with HPLC-UV for the analysis of antidepressant drugs in biological samples. *J. Sep. Sci.* **2011**, *34*, 1275−1282.
(38) Pan, L.; Adams, M.; Pawliszyn, J. Determination of fatty acids using solid-phase microextraction. *Anal. Chem.* **1995**, *67*, 4396−4403.
(39) Zhang, Z.; Duan, H.; Zhang, L.; Chen, X.; Liu, W.; Chen, G. Direct determination of anabolic steroids in pig urine by a new SPME−GC−MS method. *Talanta* **2009**, *78*, 1083−1089.
(40) Sun, S.; Wang, Y.; Yu, W.; Zhao, T.; Gao, S.; Kang, M.; Zhang, Y.; Zhang, H.; Yu, Y. Determination of Sudan dyes in red wine and fruit juice using ionic liquid-based liquid−liquid microextraction and high performance liquid chromatography. *J. Sep. Sci.* **2011**, *34*, 1730−1737.
(41) Bagheri, H.; Saber, A.; Mousavi, S. R. Immersed solvent microextraction of phenol and chlorophenols from water samples followed by gas chromatography−mass spectrometry. *J. Chromatogr. A* **2004**, *1046*, 27−33.
(42) López-Blanco, M. C.; Blanco-Cid, S.; Cancho-Grande, B.; Simal-Gándara, J. Application of single-drop microextraction and comparison with solid-phase microextraction and solid-phase extraction for the determination of α- and β-endosulfan in water samples by gas chromatography−electron-capture detection. *J. Chromatogr. A* **2003**, *984*, 245−252.
(43) Qi, P.; Zeng, T.; Wen, Z.; Liang, X.; Zhang, X. Interference-free simultaneous determination of Sudan dyes in chili foods using solid phase extraction coupled with HPLC−DAD. *Food Chem.* **2011**, *125*, 1462−1467.
(44) Zhang, Y.; Zhang, Z.; Sun, Y. Development and optimization of an analytical method for the determination of Sudan dyes in hot chilli pepper by high-performance liquid chromatography with on-line electrogenerated BrO^--luminol chemiluminescence detection. *J. Chromatogr. A* **2006**, *1129*, 34−40.
(45) Zhang, J.; Shao, J.; Guo, P.; Huang, Y. A simple and fast Fe_3O_4 magnetic nanoparticles-based dispersion solid phase extraction of Sudan dyes from food and water samples coupled with high-performance liquid chromatography. *Anal. Methods* **2013**, *5*, 2503−2510.
(46) Rebane, R.; Leito, I.; Yurchenko, S.; Herodes, K. A review of analytical techniques for determination of Sudan I−IV dyes in food matrixes. *J. Chromatogr. A* **2010**, *1217*, 2747−2757.
(47) Fan, Y.; Chen, M.; El-Sepai, F.; Wang, K.; Zhu, Y.; Ye, M. Ionic liquids extraction of Para Red and Sudan dyes from chilli powder, chilli oil and food additive combined with high performance liquid chromatography. *Anal. Chim. Acta* **2009**, *650*, 65−69.
(48) Yan, H.; Wang, H.; Qiao, J.; Yang, G. Molecularly imprinted matrix solid-phase dispersion combined with dispersive liquid−liquid microextraction for the determination of four Sudan dyes in egg yolk. *J. Chromatogr. A* **2011**, *1218*, 2182−2188.
(49) López-Jiménez, F. J.; Rubio, S.; Pérez-Bendito, D. Supramolecular solvent-based microextraction of Sudan dyes in chilli-containing foodstuffs prior to their liquid chromatography-photodiode array determination. *Food Chem.* **2010**, *121*, 763−769.
(50) Piao, C.; Chen, L. Separation of Sudan dyes from chilli powder by magnetic molecularly imprinted polymer. *J. Chromatogr. A* **2012**, *1268*, 185−190.
(51) Calbiani, F.; Careri, M.; Elviri, L.; Mangia, A.; Pistarà, L.; Zagnoni, I. Development and in-house validation of a liquid

chromatography−electrospray−tandem mass spectrometry method for the simultaneous determination of Sudan I, Sudan II, Sudan III and Sudan IV in hot chilli products. *J. Chromatogr. A* **2004**, *1042*, 123−130.

(52) Chen, D.; Li, X.; Tao, Y.; Pan, Y.; Wu, Q.; Liu, Z.; Peng, D.; Wang, X.; Huang, L.; Wang, Y.; Yuan, Z. Development of a liquid chromatography−tandem mass spectrometrywith ultrasound-assisted extraction method for the simultaneous determination of Sudan dyes and their metabolites in the edible tissues and eggs of food-producing animals. *J. Chromatogr. B: Anal. Technol. Biomed. Life Sci.* **2013**, *939*, 45−50.

(53) Sun, H.; Wang, F.; Ai, L. Determination of banned 10 azo-dyes in hot chili products by gel permeation chromatography−liquid chromatography−electrospray ionization-tandem mass spectrometry. *J. Chromatogr. A* **2007**, *1164*, 120−128.

(54) Li, L.; Huang, Y.; Wang, Y.; Wang, W. Hemimicelle capped functionalized carbon nanotubes-based nanosized solid-phase extraction of arsenic from environmental water samples. *Anal. Chim. Acta* **2009**, *631*, 182−188.

JOURNAL OF AGRICULTURAL AND FOOD CHEMISTRY

Article

pubs.acs.org/JAFC

Colorimetric Detection of Sulfite in Foods by a TMB−O_2−Co_3O_4 Nanoparticles Detection System

Wenjie Qin,[†,‡] Li Su,[§] Chen Yang,[†,‡] Yanhua Ma,[†,‡] Haijuan Zhang,[†,‡] and Xingguo Chen*[,†,‡]

[†]State Key Laboratory of Applied Organic Chemistry, Lanzhou University, Lanzhou 730000, China

[‡]Department of Chemistry, Lanzhou University, Lanzhou 730000, China

[§]School of Chemistry and Chemical Engineering, Henan Normal University, Xinxiang 453007, China

Supporting Information

ABSTRACT: In this paper, we first discovered that Co_3O_4 nanoparticles (NPs) possess intrinsic oxidase-like activity and can catalytically oxidize peroxidase substrates, such as 2,2′-azino-bis(3-ethylbenzothiazoline-6-sulfonic acid) diammonium salt (ABTS) and 3,3′,5,5′-tetramethylbenzidine (TMB), to form colored products, in the absence of exogenously added H_2O_2. The presence of sulfite inhibited the TMB−O_2−Co_3O_4 NPs reaction system and caused a change in color of the reaction system. On the basis of this phenomenon, a colormetric approach to detect sulfite was established with a good linear relationship ranging from 0.2×10^{-6} to 1.6×10^{-5} M and a detection limit of 5.3×10^{-8} M. The method was used to detect sulfite in foods. Good recoveries ranging from 93.8% to 100.5% were obtained. Furthermore, the mechanism was studied and results showed that the oxidase-like activity of the Co_3O_4 NPs was not from $^{\bullet}OH$ or $O_2^{\bullet-}$ radical generated. It may probably originate from their ability to transfer an electron between the peroxidase substrate and oxygen absorbed on the surface of the Co_3O_4 NPs.

KEYWORDS: *Co_3O_4 nanoparticles, oxidase mimic, colorimetry, sulfite, mechanism of oxidase-like activity*

INTRODUCTION

Sulfite is one of the oldest and most ubiquitous food additives, which has been widely used as blanching and preservative agents in a large variety of foodstuffs (dried fruit, vermicelli, preserves, etc.) to improve the appearance of food and prevent bacterial growth.[1,2] However, the ingestion of foods containing large amounts of sulfite can cause asthmatic attacks and allergic reactions in sensitive individuals.[3,4] Owing to the potential toxicity, the sulfite in foods is strictly limited in many countries.[5] Hence, sulfite determination in food products is essential for the purposes of public health, food assurance, and quality control. In recent years, numerous methods have been developed for determining sulfite in foods, including titrimetry, flow injection analysis, anodic stripping voltammetry, ion chromatography, chemiluminescence, gas chromatography, fluorometry, high-performance liquid chromatography, and colorimetry.[6−8]

Colorimetric biosensing has become more attractive because of its low cost, simplicity, and practicality. However, the key challenge for colorimetric sensors is transforming the detection events into color changes. Since color changes can be read by the naked eye, a colorimetric sensor does not require expensive or sophisticated instrumentation and can be applied to field analysis.[9−11] To this end, enzyme-like nanomaterials-based sensors have emerged as an important colorimetric tool. Since the first report of Fe_3O_4 magnetic nanoparticles (MNPs) possessing intrinsic peroxidase-like activity,[12] nanoparticles-based enzyme mimics have received great attention due to their merits relative to native enzymes (e.g., low cost, high stability, and tunability in catalytic activity). More and more nanoparticles have been found as enzymatic mimics, such as metal oxide nanomaterials,[13] sulfide nanomaterials,[14−17] selenide nanomaterials,[18,19] metal nanomaterials,[13,20] carbon nanomaterials,[13,20] nanocomposites,[21−28] and other nanomaterials.[29−31] These enzyme-like nanomaterials could be employed in colorimetry to detect nucleotides,[32] H_2O_2,[33−35] glucose,[33−35] melamine,[36] and so on. To the best of our knowledge, however, the colorimetric detection of sulfite in food using the enzyme-like property of nanoparticles has not been explored up to now, which might be attributed to the complication of food samples' matrices and the difficulties in constructing an effective nanoparticles-based enzyme mimic sensing platform to detect micro amounts of food additive.

Herein, we have developed a TMB−O_2−Co_3O_4 NPs colorimetric system for detection of sulfite in foods, based on the property of oxidase-like activity of Co_3O_4 NPs. In this method, the existence of sulfite can cause a change in color of the reaction system, and the color change can be visually observed directly. We also investigated the mechanism of oxidase-like activity of Co_3O_4 NPs by XPS, contrast experiments, and cyclic voltammetry.

EXPERIMENTAL PROCEDURES

Materials. $Co(CH_3COO)_2{\cdot}4H_2O$ were obtained from Tianjin Guangfu Chemical Reagent Factory (Tianjin, China). 3,3′,5,5′-Tetramethylbenzidine (TMB) and 2,2′-azinobis(3-ethylbenzothiazoline-6-sulfonic acid) diammonium salt (ABTS) were purchased from Sigma-Aldrich. Ammonium hydroxide (25−28 wt %) was purchased from Baiyin Liangyou Chemical Reagent Factory (Baiyin, China). Sodium acetate, glacial acetic acid, anhydrous sodium sulfite, sodium

Received: February 23, 2014
Revised: May 28, 2014
Accepted: June 2, 2014
Published: June 2, 2014

ACS Publications © 2014 American Chemical Society

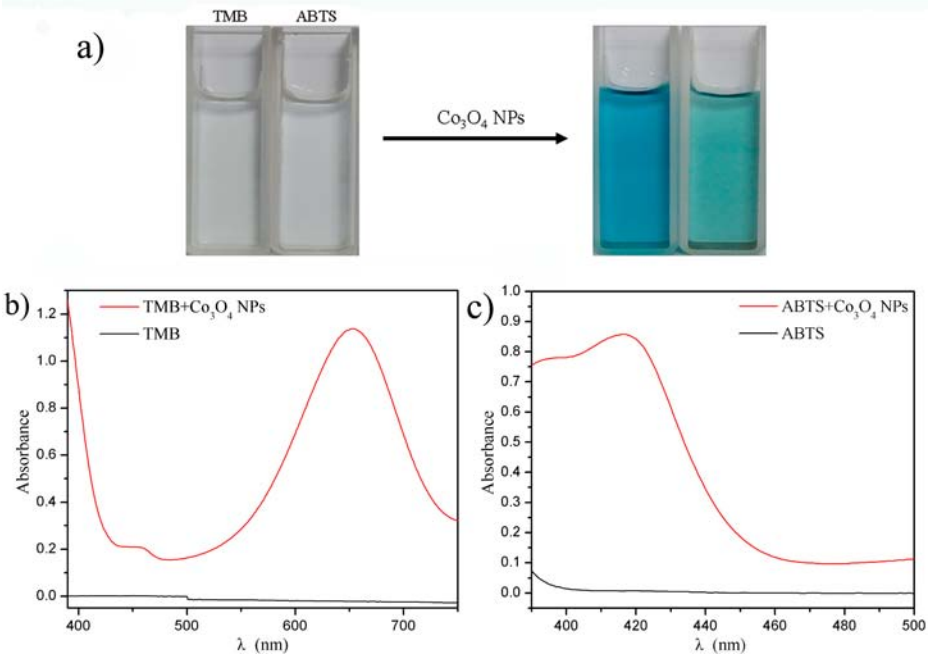

Figure 1. Images of the oxidation color reaction of TMB and ABTS by Co_3O_4 NPs (a). UV/vis spectra of TMB solution in 0.2 M acetic acid−acetate buffer (pH 4.0) at 40 °C for 10 min. The TMB and Co_3O_4 NPs concentrations were 0.25 mM and 40 μg mL^{-1}, respectively (b). UV/vis spectra of an ABTS solution in 0.2 M acetic acid−acetate buffer (pH 4.0) at 40 °C for 10 min. The ABTS and Co_3O_4 NPs concentrations were 0.25 mM and 40 μg mL^{-1}, respectively (c).

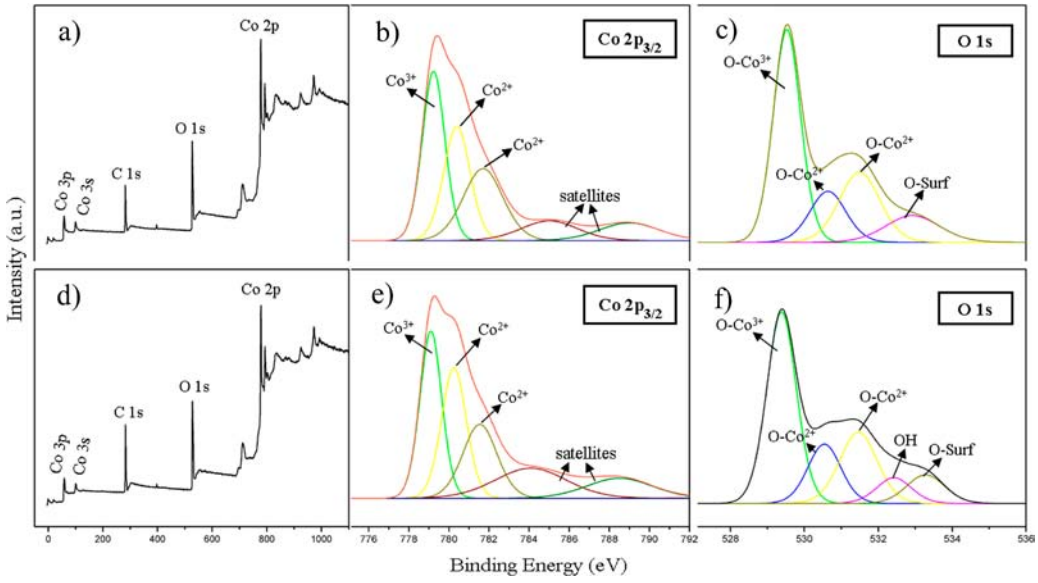

Figure 2. Survey XP spectra of Co_3O_4 NPs before and after reaction (a and d). Deconvoluted high-resolution Co $2p_{3/2}$ XP spectra of Co_3O_4 NPs before and after reaction (b and e). Deconvoluted high-resolution O 1s XP spectra of Co_3O_4 NPs before and after reaction (c and f).

dihydrogen phosphate, and other regents were obtained from Tianjin Guangfu Chemical Reagent Factory (Tianjin, China). A sulfite solution was prepared daily by dissolving anhydrous sodium sulfite in water and was standardized by iodimetric titration when needed. All other chemicals were of analytical reagent grade and used without further purification. Deionized water was used throughout the experiment.

Apparatus and Characterization. A TU-1901 double-beam UV−vis spectrophotometer (Beijing Purkine General Instrument Co. Ltd., China) was used to record absorption spectra and measure absorbance. A FEI Tecnai G^2 F30 microscope (TEM) was used for measuring the morphologies and size of Co_3O_4 NPs. The X-ray diffraction (XRD) pattern of Co_3O_4 NPs was determined on a Rigaku D/Max-2400 X-ray diffractometer with Cu Kα radiation (λ = 0.154056). The chemical state of the coating surface was analyzed using X-ray photoelectron spectroscopy (XPS, PerkinElmer PHI-5702 multifunctional photoelectron spectrometer). Element determination was measured by a 4300 DV inductively coupled plasma−atomic emission spectrometer (ICP-AES). Zeta potential measurements of Co_3O_4 NPs were performed with a Malvern Nano-ZS apparatus. ESR spectra were acquired using a JES-FA200 electron spin resonance spectrometer. Electrochemical experiments were performed on a CHI 832 electrochemical workstation (Shanghai Chenhua Instrument Co., China) and a conventional three-electrode system. The conventional three-electrode system contained a Pt wire counter electrode, a saturated calomel electrode as reference electrode, and an as-prepared

dx.doi.org/10.1021/jf500950p | J. Agric. Food Chem. 2014, 62, 5827−5834

working electrode. The specific surface area was measured using a multipoint Brunauer–Emmett–Teller technique (ASAP 2020, Micromeritics, USA).

Preparation of Co_3O_4 Nanoparticles. Co_3O_4 NPs were prepared using a hydrothermal method as described in the literature.[37] Briefly, 0.5 g of $Co(CH_3COO)_2{\cdot}4H_2O$ was dissolved in 25 mL of ethanol, and then 2.5 mL of ammonia solution was added under vigorous stirring. After stirring for 10 min, the obtained suspension was transferred into a 50 mL autoclave. Then the autoclave was sealed and kept at 150 °C for 3 h followed by cooling to room temperature naturally. Finally, the product was separated via centrifugation and alternately washed thoroughly several times with deionized water and ethanol until the pH of supernatant was about 7.0, then dried at 60 °C for 4 h.

Kinetic Assay of Oxidase-like Co_3O_4 NPs. Kinetic experiments were carried out at 40 °C using 120 μL of 1.0 mg mL^{-1} Co_3O_4 NPs in 2.8 mL of acetic acid–acetate buffer solution (0.2 M, pH 4.0) with 80 μL of TMB/ABTS as substrate, unless otherwise stated. Kinetic measurements were carried out in time course mode by monitoring the absorbance change at 652/417 nm for 4 min using a TU-1901 UV–vis spectrophotometer. The Michaelis–Menten constant was calculated using a Lineweaver–Burk plot:[12]

$$1/v = K_m/V_{max}(1/[S] + 1/K_m)$$

where v is the initial velocity, V_{max} represents the maximal reaction velocity, and [S] is the substrate concentration. K_m is the Michaelis–Menten constant, which is an indicator of enzyme affinity for its substrate.

Preparation of Samples. Dried lily bulbs, vermicelli, and haw roll were purchased randomly from a local market in Lanzhou, China. Samples were minced by a mixer. An accurately weighed minced sample was transferred to a beaker, and 40 mL of EDTA (1.0×10^{-4} M) was added.[5] After shaking and ultrasonication for 15 min, the mixture was filtered with a 0.45 μm syringe membrane filter. The filtrate was diluted to 100 mL with EDTA (1.0×10^{-4} M). All samples were stored in a refrigerator at 4 °C before analysis.

Detection of Sulfite. The amount of sulfite in samples was determined according to the following steps: (a) 80.0 μL of sample solution, 150.0 μL of 5 mM TMB, and 120.0 μL of Co_3O_4 NPs solution (1.0 mg mL^{-1}) were added into 2.65 mL of a 0.2 M acetic acid–acetate buffer solution (pH 4.0) and then thoroughly mixed to make it uniform; (b) the as-mixed solution was maintained in a 40 °C water bath for 10 min to hold the reaction and then kept in an ice–water bath for 10 min to terminate the reaction. The solution was then used to perform the adsorption spectroscopy measurement at 652 nm wavelength. For the control experiments, 80.0 μL of deionized water was used instead of sample solution.

RESULTS AND DISCUSSION

Oxidase-like Activity of Co_3O_4 NPs. The oxidase-like activity of Co_3O_4 NPs was evaluated in the catalysis of typical substrates TMB and ABTS in the absence of H_2O_2. As can be seen from Figure 1a, Co_3O_4 NPs catalyzed the oxidation of TMB and ABTS to produce the typical colored products.

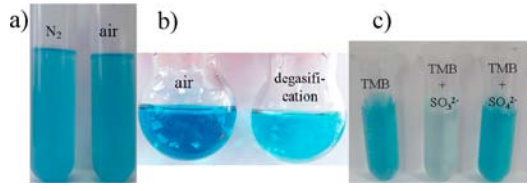

Figure 3. Photographs of TMB solutions in the absence and presence of an O_2 oxidation reaction catalyzed by Co_3O_4 NPs (a). Photographs of a TMB solution oxidation reaction catalyzed by Co_3O_4 NPs without degassing and Co_3O_4 NPs degassed by three freeze–pump–thaw cycles (b). Photographs of the oxidation color reaction of TMB, TMB-SO_3^{2-}, and TMB-SO_4^{2-} catalyzed by Co_3O_4 NPs, respectively (c).

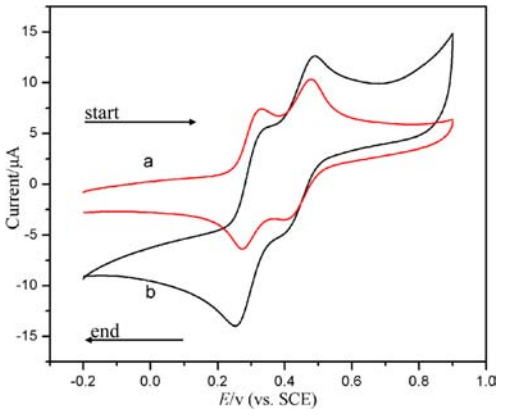

Figure 4. Cyclic voltammograms of bare GCE (a) and the Co_3O_4 NPs-modified GCE (b) in a 0.2 M acetic acid–acetate buffer (pH 4.0) + 0.25 mM TMB solution.

Similar to other peroxidase/oxidase mimic reactions, the maximum absorbance peaks of the oxidation products of TMB and ABTS were located at 652 and 417 nm, respectively.[12,33] Nevertheless, there was no absorbance at 652 or 417 nm in the absence of Co_3O_4 NPs in the system (Figure 1b and c). The results suggested that Co_3O_4 NPs exhibit intrinsic oxidase-like activity. The presence of mixed valence states of Co^{2+} and Co^{3+} ions in Co_3O_4 NPs is considered the key in their catalysis. As an oxidase mimic, the states of Co in the Co_3O_4 NPs did not change before or after the reaction.

In order to further confirm the property of oxidase mimic of the Co_3O_4 NPs, XPS was performed to find the oxidation state of Co in the Co_3O_4 NPs before and after the reaction. Figure 2e shows the deconvoluted XPS spectra of Co $2p_{3/2}$ of Co_3O_4 NPs after the reaction. The relative ratio of Co^{2+} and Co^{3+} was almost unchanged in Co_3O_4 NPs before and after the reaction. The high-resolution XPS spectra O 1s of unused and used Co_3O_4 NPs are presented in Figure 2c and f, respectively. The relative ratio of O–Co^{2+} and O–Co^{3+} peaks in O 1s XPS spectra was similar to Co $2p_{3/2}$ XPS results (Table S1). It is suggested that the states of Co in the Co_3O_4 NPs did not change before or after the reaction. These results confirmed that Co_3O_4 NPs exhibited intrinsic oxidase-like activity.

It is important to confirm the possibility that the observed activity was not caused by cobalt ions leaching from Co_3O_4 NPs in acidic solution. To test this, Co_3O_4 NPs were incubated in the reaction buffer (pH 4.0) for 2 h and then removed from the solution by centrifugation. As shown in Figure S5, comparing the activity of the leaching solution with that of Co_3O_4 NPs under the same conditions, the leaching solution had no activity, showing that the observed oxidase-like activity was due to intact Co_3O_4 NPs. Figure S6 shows the amount of cobalt ions leaked from Co_3O_4 NPs in the buffer solutions (pH 3.0–7.0) for 2 h, which was implemented by ICP-OES. The ICP results exhibited that there were few cobalt ions in the leaching solution. They probably came from residual Co_3O_4 NPs after centrifugation.

Possible Mechanism of Oxidase-like Activity of Co_3O_4 NPs. As an oxidase mimic, Co_3O_4 NPs catalyze an oxidation–reduction reaction involving oxygen (O_2) as the electron acceptor. However, in the reaction system of TMB–O_2–Co_3O_4 NPs, oxygen is present in the aqueous solution and also exists on the surface of Co_3O_4 NPs due to the high specific surface

dx.doi.org/10.1021/jf500950p | J. Agric. Food Chem. 2014, 62, 5827–5834

Scheme 1. Possible Mechanism for the TMB−O_2−Co_3O_4 NPs System

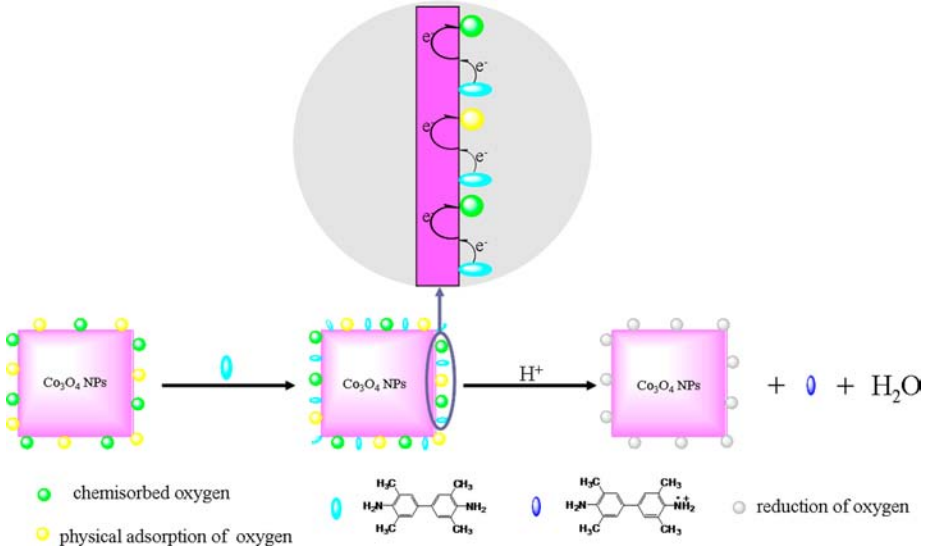

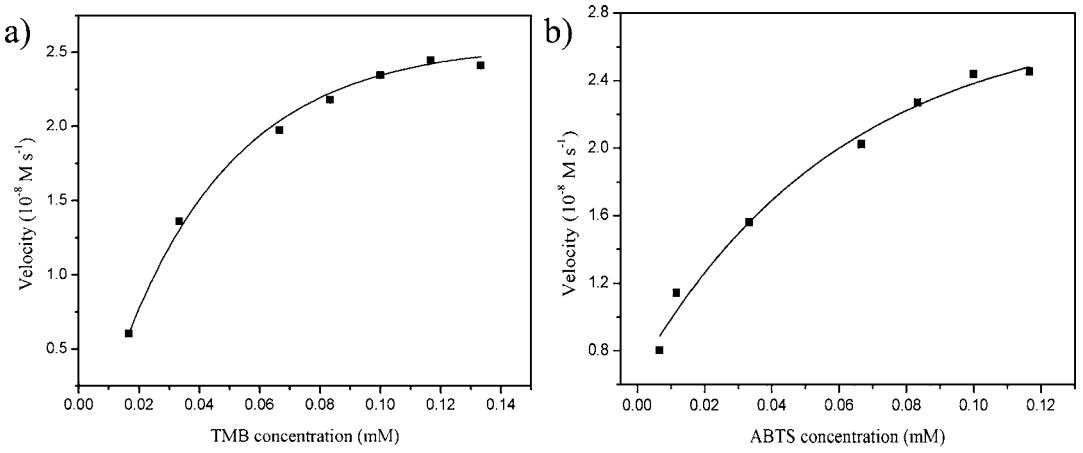

Figure 5. Michaelis−Menten curve of Co_3O_4 NPs with TMB (a). Michaelis−Menten curve of Co_3O_4 NPs with ABTS (b). Details are included in the Experimental Procedures.

area of nanomaterials. In order to determine whether the oxygen in the solution played a role in the TMB−O_2−Co_3O_4 NPs system, two sets of experiments were conducted: the first one was carried out in the presence of oxygen; the other was performed under high-purity nitrogen and the solution was degassed before the reaction, as in the photograph shown in Figure 3a. It was found that they exhibited the same color. The absorbance of the first one was 0.747; the other was 0.770 at 652 nm. The absorbance of the latter was higher than the former; one possible reason was that nitrogen played a role in mixing and speeded up the reaction. This indicated that the oxygen in the solution had no effect on the reaction, which was different from the behavior of some nanoparticles-based oxidase mimics reported.[8,38] For further study, the Co_3O_4 NPs without degassing and Co_3O_4 NPs degassed by three freeze−pump−thaw cycles that catalyze the oxidation of TMB were implemented in the degassed solutions. They produced different colors, as in the photograph shown in Figure 3b, and the degassed Co_3O_4 NPs also catalyzed the oxidation of TMB to produce the typical color reaction. It is suggested that the oxygen on the surface of Co_3O_4 NPs was due not only to physical adsorption. Chemisorbed oxygen probably existed on the surface of Co_3O_4 NPs because of the low oxygen Co−O bond strength of Co_3O_4 and the larger surface energy of nanomaterials caused by a large surface to volume ratio.[39] In addition, the O 1s peak at 533.0 eV in the XPS spectrum shown in Figure 2c indicated that there was chemisorbed oxygen on the surface of Co_3O_4 NPs.[40] It is indicated that both the physically absorbed and chemisorbed oxygen on the surface of Co_3O_4 NPs played a key role in the TMB−O_2−Co_3O_4 NPs system. In order to further confirm the above conclusion, oxidation experiments of TMB, TMB-SO_3^{2-}, and TMB-SO_4^{2-} catalyzed by Co_3O_4 NPs were carried out. The results are shown in Figure 3c. TMB-SO_3^{2-} system presented a lower absorbance than the other two systems. Since the volume of SO_3^{2-} is smaller than TMB, and Co_3O_4 NPs have a positive charge at pH 4.0 (Supporting Information), SO_3^{2-} is more easily adsorbed on the surface of Co_3O_4 NPs. Then SO_3^{2-} consumed oxygen absorbed on the surface of the Co_3O_4 NPs and interfered with the TMB−O_2−Co_3O_4 NPs system. This supported the above result that the oxygen absorbed on the surface of the Co_3O_4 NPs oxidized TMB in this system.

The oxidation of TMB is an electron transfer process.[41] The electrocatalytic behavior of a Co_3O_4 NP modified glassy carbon electrode (GCE) toward the electrochemical oxidation of TMB was studied using cyclic voltammetry (CV), in order to

dx.doi.org/10.1021/jf500950p | J. Agric. Food Chem. 2014, 62, 5827−5834

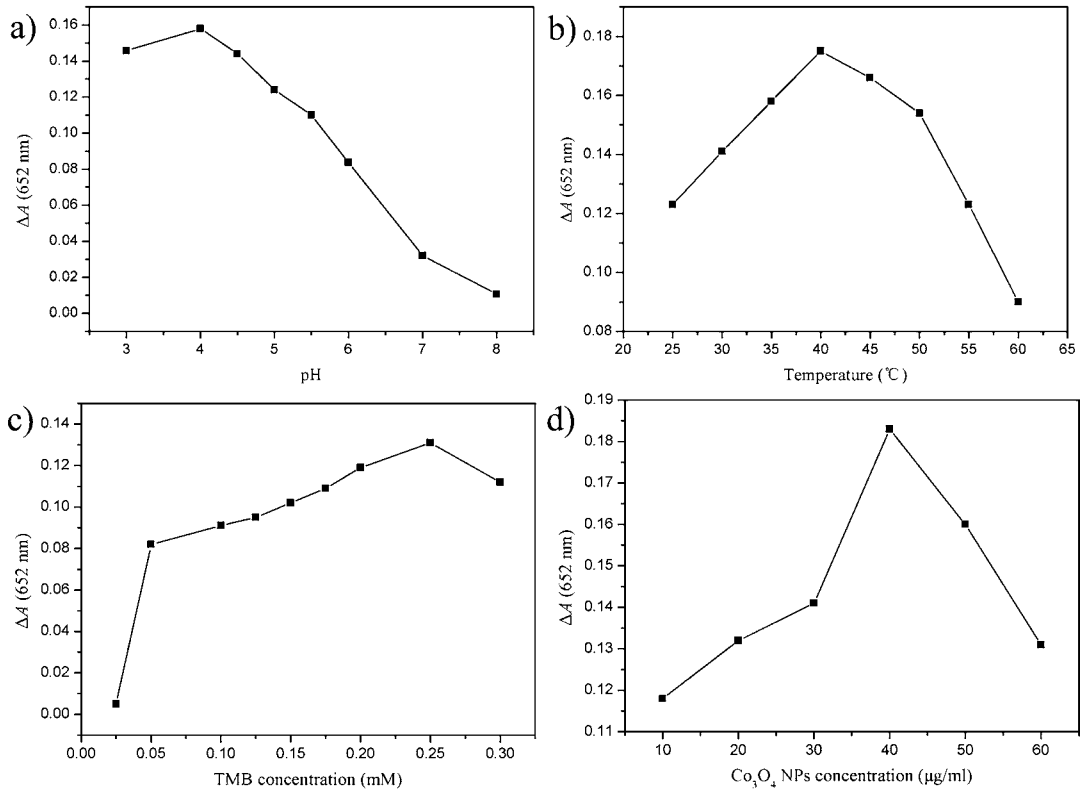

Figure 6. A pH−Δ*A* curve (a), a temperature−Δ*A* curve (b), a TMB concentration−Δ*A* curve (c), and a Co_3O_4 NPs concentration−Δ*A* curve (d) for 6 μM sulfite detection, where $\Delta A = A_{(blank,652nm)} - A_{(sulfite,652nm)}$, in 0.2 M acetic acid−acetate buffer solutions incubated for 10 min with the as-prepared Co_3O_4 NPs as oxidase mimics.

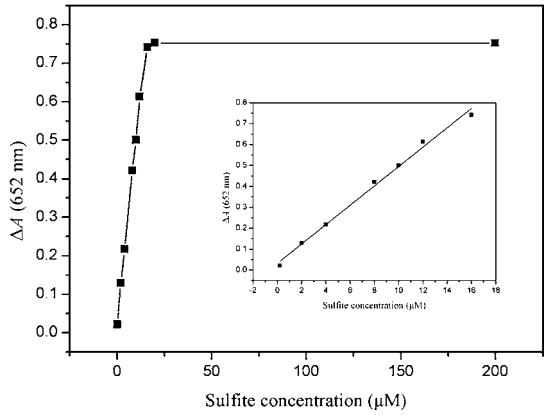

Figure 7. Dose−response curve for different concentrations of sulfite standard solutions under the optimum conditions. Inset: Linear calibration plot for sulfite detection.

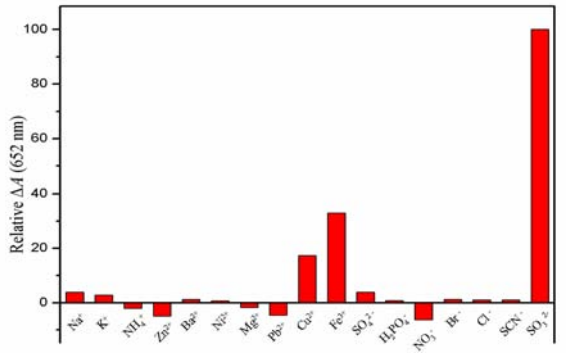

Figure 8. Δ*A* response of TMB solutions to blank and different common ions in the presence of sulfite (12 μM). The other ions added are 240 μM. Relative Δ*A*: $(\Delta A_{total} - \Delta A_{sulfite})/\Delta A_{sulfite}$.

investigate the mechanism of oxidase-like catalytic activity of Co_3O_4 NPs. The CVs of TMB at a bare GCE and the Co_3O_4 NPs-modified GCE are shown in Figure 4. Two pairs of redox peaks of TMB were found under the bare GCE, and increased current was obviously observed under the Co_3O_4 NPs-modified GCE. It is suggested that Co_3O_4 NPs exhibited an electrocatalytic activity to oxidate TMB, which indicated that the Co_3O_4 NPs had the ability to accelerate the electron transfer.[42]

In order to further demonstrate that the oxidase-like activity of the Co_3O_4 NPs was not from $O_2^{\bullet-}$ and $^{\bullet}OH$, an EPR spin trapping experiment was carried out under the optimized experimental conditions. The results revealed that no DMPO-$O_2^{\bullet-}$ or DMPO-$^{\bullet}OH$ spin adducts were detected (Figure S7).

Table 1. Results for the Determination of the Sulfite in Three Kinds of Foods

sample	initial amount (mg g^{-1})	added (μg mL^{-1})	recovery (%)	average recovery (%)	RSD (n = 3) (%)
dried lily bulbs	1.7	0.5	96.3−99.4	98.9	0.6
		1.0	94.4−99.5	96.5	2.8
		1.5	98.4−100.6	100.3	2.6
vermicelli	0.7	0.5	90.5−95.0	93.1	2.5
		1.0	91.6−96.2	93.8	2.5
		1.5	96.8−97.4	97.1	1.5
haw roll	2.9	0.5	95.2−99.4	96.3	1.1
		1.0	99.1−101.6	100.5	3.3
		1.5	97.8−99.9	98.9	1.1

dx.doi.org/10.1021/jf500950p | J. Agric. Food Chem. 2014, 62, 5827−5834

It is suggested that TMB was not oxidized by $O_2^{\bullet-}$ and $^{\bullet}OH$ radicals in the TMB−O_2−Co_3O_4 NPs system, which was different from the behavior of $CoFe_2O_4$ NPs.[8] Therefore, the nature of oxidase-like activity of the Co_3O_4 NPs does not originate from the $O_2^{\bullet-}$ and $^{\bullet}OH$ radicals generated.

Taken together, although the detailed mechanism remains unclear, these observations demonstrated that Co_3O_4 NPs accelerated the electron transfer from the peroxidase substrate to oxygen absorbed on the surface of the Co_3O_4 NPs. The possible mechanism of oxidase-like activity of Co_3O_4 NPs is presented in Scheme 1; that is, TMB was absorbed on the surface of the Co_3O_4 NPs and donated electrons to the Co_3O_4 NPs, resulting in an increase in electron density and mobility in the Co_3O_4 NPs, thus accelerating the electron transfer to oxygen absorbed on the surface of the Co_3O_4 NPs. After the completion of the electron transfer, the Co_3O_4 NPs reverted to their original state.

Steady-State Kinetic Assay of Co_3O_4 NPs. Since Co_3O_4 NPs exhibited oxidase-like activity, the kinetic parameters of only TMB/ABTS were determined by changing the concentration of TMB/ABTS. A typical Michaelis−Menten curve (Figure 5a,b) was obtained with TMB/ABTS by monitoring the absorbance change at 652/417 nm for 4 min (Figure S8a,b). The Michaelis−Menten constant (K_m) and maximum initial velocity (V_{max}) were obtained using a Lineweaver−Burk plot. The values of K_m and V_{max} for the Co_3O_4 NPs with TMB were 0.051 mM and 3.30×10^{-8} M s^{-1}. The values of K_m and V_{max} for the Co_3O_4 NPs with ABTS were 0.037 mM and 3.20×10^{-8} M s^{-1}. The K_m value of Co_3O_4 NPs with ABTS was smaller than that with TMB. It is suggested that Co_3O_4 NPs have higher affinity toward ABTS than TMB, because ABTS has a higher affinity toward a positively charged nanoparticle surface and TMB has a stronger affinity toward a negatively charged nanoparticle surface.[43]

Optimization of Experimental Conditions. The reaction conditions were optimized to establish the optimum analytical conditions. The pH value not only decides the charge of the surface of Co_3O_4 NPs (Supporting Information), which affects the interaction between Co_3O_4 NPs and sulfite, but also affects the catalytic activity of Co_3O_4 NPs. The catalytic activity of Co_3O_4 NPs is also dependent on the incubation temperature. In addition, the concentrations of TMB and Co_3O_4 NPs determine the color level of the reaction system. Therefore, they were investigated in this study as influencing factors. Figure 6a indicates that ΔA, where $\Delta A = A_{(blank,652nm)} - A_{(sulfite,652nm)}$, increased and then decreased with increasing pH and had a maximum at 4.0. The reaction temperature-dependent response curve is shown in Figure 6b. It showed that ΔA of the reaction system had a peak value at 40 °C. Therefore, 4.0 and 40 °C were taken as the optimal pH and temperature. The concentrations of TMB and Co_3O_4 NPs response curves are shown in Figure 6c and d; the optimal concentrations of TMB and Co_3O_4 NPs were 0.25 mM and 40 μg mL^{-1}, respectively.

Analytical Performance for Sulfite Determination. As an oxidase mimic, Co_3O_4 NPs can catalyze TMB to form colored product in the absence of H_2O_2. The sulfite inhibits the TMB−O_2−Co_3O_4 NPs system and causes a change in color of the reaction system, which suggested that sulfite can be indirectly detected. Since sulfite is easily adsorbed on the surface of Co_3O_4 NPs and consumes absorbed oxygen more easily than dissolved oxygen, the sulfite that is consumed by dissolved oxygen is neglected in the reaction. The calibration graphs for the determination of sulfite were constructed under the optimum conditions described above. The calibration data of ΔA versus sulfite concentration are shown in Figure 7. The results indicated that the concentration of detectible sulfite could be 0.2×10^{-6} M with a linear range from 0.2×10^{-6} to 1.6×10^{-5} M. The limit of detection (LOD) for sulfite was 5.3×10^{-8} M. (LOD = KS_0/S, where K is a numerical factor chosen according to the confidence level desired, S_0 is the standard deviation (SD) of the blank measurements ($n = 10$, $K = 3$), and S is the slope of the calibration curve.[44])

Effect of Foreign Substances. The effect of foreign substances was tested by analyzing the mixed solution and standard solution of sulfite (12 μM). The molar ratio of other ion and sulfite was 20 in the mixed solution. The relative ΔA values ($(\Delta A_{total} - \Delta A_{sulfite})/\Delta A_{sulfite}$) are presented in Figure 8. As can be seen, Fe and Cu were the main interferences for sulfite determination, since trace amounts of heavy metal ions in the water are believed to act as the catalyst in the oxidation of sulfite by oxygen.[45] EDTA was selected as a chelate reagent for the present study to eliminate the interferences derived from Fe, Cu, and other coexisting transient metals in the samples.

Detection of Sulfite in Real Samples. As an illustration of analytical application, the proposed method was used to determine sulfite in real samples under the optimal experimental conditions. The results are listed in Table 1. The recoveries of the three samples ranged from 93.8% to 100.5%. Hence, the proposed method can be considered a useful tool for the quantification of sulfites in real samples.

In summary, Co_3O_4 NPs were first found to possess oxidase-like activity and could catalyze the oxidation of TMB and ABTS to produce the typical color reaction in the absence of exogenously added H_2O_2. It was found that the oxygen absorbed on the surface of the Co_3O_4 NPs oxidizes the peroxidase substrate, rather than the oxygen dissolved in the solution. The oxidase-like activity of Co_3O_4 NPs was not from the generated $O_2^{\bullet-}$ or $^{\bullet}OH$ radical, probably originating from their ability to transfer an electron between the peroxidase substrate and oxygen absorbed on the surface of the Co_3O_4 NPs. Moreover, as the existence of sulfite inhibited TMB−O_2−Co_3O_4 NPs system and caused a change in color of the reaction system, a new colorimetric method for detecting sulfite was developed. The colorimetric method showed a good response toward sulfite detection with a linear range from 0.2×10^{-6} to 1.6×10^{-5} M and good recoveries ranging from 93.8% to 100.5% in three real samples using Co_3O_4 NPs as an oxidase mimic. The detection platform showed great potential applications in reducing substrates. In addition, Co_3O_4 NPs can be expected to provide potential applications for chemical sensing, biochemical analysis, electrochemical biosensing, and even clinical chemistry.

■ ASSOCIATED CONTENT

Ⓢ Supporting Information

This material is available free of charge via the Internet at http://pubs.acs.org.

■ AUTHOR INFORMATION

Corresponding Author

*E-mail: chenxg@lzu.edu.cn (X.-G. Chen). Tel: 86-931-8912763 Fax: 86-931-8912582.

Funding

The authors are grateful for financial support from the National Natural Science Foundation of China (No. 21375053) and the Specialized Research Fund for the Doctoral Program of Higher Education (No. 20130211110039).

Notes

The authors declare no competing financial interest.

REFERENCES

(1) Bush, R. K. Sulfites in foods: uses, analytical methods, residues, fate, exposure assessment, metabolism, toxicity, and hypersensitivity. *Adv. Food Res.* **1986**, *30*, 1−76.

(2) Sapers, G. Browning of foods: control by sulfites, antioxidants, and other means. *Food Technol. (Chicago, IL, U.S.)* **1993**, *47*, 75−84.

(3) Adams, J. Food additive-additive interactions involving sulphur dioxide and ascorbic and nitrous acids: a review. *Food Chem.* **1997**, *59*, 401−409.

(4) Vally, H.; Carr, A.; El-Saleh, J.; Thompson, P. Wine-induced asthma: a placebo-controlled assessment of its pathogenesis. *J. Allergy Clin. Immunol.* **1999**, *103*, 41−46.

(5) Filik, H.; Çetintaş, G. Determination of sulfite in water and dried fruit samples by dispersive liquid−liquid microextraction combined with UV−vis fiber optic linear array spectrophotometry. *Food Anal. Methods* **2012**, *5*, 1362−1367.

(6) Du, J.; Shao, Q.; Yin, S.; Jiang, L.; Ma, J.; Chen, X. Colorimetric chemodosimeter based on diazonium-gold-nanoparticle complexes for sulfite ion detection in solution. *Small* **2012**, *8*, 3412−3416.

(7) Pundir, C. S.; Rawal, R. Determination of sulfite with emphasis on biosensing methods: a review. *Anal. Bioanal. Chem.* **2013**, *405*, 3049−3062.

(8) Zhang, X.; He, S.; Chen, Z.; Huang, Y. $CoFe_2O_4$ nanoparticles as oxidase mimic-mediated chemiluminescence of aqueous luminol for sulfite in white wines. *J. Agric. Food Chem.* **2013**, *61*, 840−847.

(9) Stewart, M. E.; Anderton, C. R.; Thompson, L. B.; Maria, J.; Gray, S. K.; Rogers, J. A.; Nuzzo, R. G. Nanostructured plasmonic sensors. *Chem. Rev.* **2008**, *108*, 494−521.

(10) Liu, J.; Cao, Z.; Lu, Y. Functional nucleic acid sensors. *Chem. Rev.* **2009**, *109*, 1948−1998.

(11) Song, S.; Qin, Y.; He, Y.; Huang, Q.; Fan, C.; Chen, H.-Y. Functional nanoprobes for ultrasensitive detection of biomolecules. *Chem. Soc. Rev.* **2010**, *39*, 4234−4243.

(12) Gao, L.; Zhuang, J.; Nie, L.; Zhang, J.; Zhang, Y.; Gu, N.; Wang, T.; Feng, J.; Yang, D.; Perrett, S. Intrinsic peroxidase-like activity of ferromagnetic nanoparticles. *Nat. Nanotechnol.* **2007**, *2*, 577−583.

(13) Wei, H.; Wang, E. Nanomaterials with enzyme-like characteristics (nanozymes): next-generation artificial enzymes. *Chem. Soc. Rev.* **2013**, *42*, 6060−6093.

(14) Dai, Z.; Liu, S.; Bao, J.; Ju, H. Nanostructured FeS as a mimic peroxidase for biocatalysis and biosensing. *Chem.—Eur. J.* **2009**, *15*, 4321−4326.

(15) He, W.; Jia, H.; Li, X.; Lei, Y.; Li, J.; Zhao, H.; Mi, L.; Zhang, L.; Zheng, Z. Understanding the formation of CuS concave superstructures with peroxidase-like activity. *Nanoscale* **2012**, *4*, 3501−3506.

(16) Maji, S. K.; Dutta, A. K.; Dutta, S.; Srivastava, D. N.; Paul, P.; Mondal, A.; Adhikary, B. Single-source precursor approach for the preparation of CdS nanoparticles and their photocatalytic and intrinsic peroxidase like activity. *Appl. Catal. B: Environ.* **2012**, *126*, 265−274.

(17) Maji, S. K.; Dutta, A. K.; Srivastava, D. N.; Paul, P.; Mondal, A.; Adhikary, B. Peroxidase-like behavior, amperometric biosensing of hydrogen peroxide and photocatalytic activity by cadmium sulfide nanoparticles. *J. Mol. Catal. A: Chem.* **2012**, *358*, 1−9.

(18) Dutta, A. K.; Maji, S. K.; Mondal, A.; Karmakar, B.; Biswas, P.; Adhikary, B. Iron selenide thin film: peroxidase-like behavior, glucose detection and amperometric sensing of hydrogen peroxide. *Sens. Actuators, B* **2012**, *173*, 724−731.

(19) Dutta, A. K.; Maji, S. K.; Srivastava, D. N.; Mondal, A.; Biswas, P.; Paul, P.; Adhikary, B. Synthesis of FeS and FeSe nanoparticles from a single source precursor: a study of their photocatalytic activity, peroxidase-like behavior, and electrochemical sensing of H_2O_2. *ACS Appl. Mater. Interfaces* **2012**, *4*, 1919−1927.

(20) Xie, J.; Zhang, X.; Wang, H.; Zheng, H.; Huang, Y. Analytical and environmental applications of nanoparticles as enzyme mimetics. *TrAC Trends Anal. Chem.* **2012**, *39*, 114−129.

(21) Novoselov, K. S.; Geim, A. K.; Morozov, S.; Jiang, D.; Zhang, Y.; Dubonos, S.; Grigorieva, I.; Firsov, A. Electric field effect in atomically thin carbon films. *Science* **2004**, *306*, 666−669.

(22) Chen, H.; Li, Y.; Zhang, F.; Zhang, G.; Fan, X. Graphene supported Au-Pd bimetallic nanoparticles with core-shell structures and superior peroxidase-like activities. *J. Mater. Chem.* **2011**, *21*, 17658−17661.

(23) Kim, M. I.; Shim, J.; Li, T.; Lee, J.; Park, H. G. Fabrication of nanoporous nanocomposites entrapping Fe_3O_4 magnetic nanoparticles and oxidases for colorimetric biosensing. *Chem.—Eur. J.* **2011**, *17*, 10700−10707.

(24) Ye, Y.; Kong, T.; Yu, X.; Wu, Y.; Zhang, K.; Wang, X. Enhanced nonenzymatic hydrogen peroxide sensing with reduced graphene oxide/ferroferric oxide nanocomposites. *Talanta* **2012**, *89*, 417−421.

(25) Hao, J.; Zhang, Z.; Yang, W.; Lu, B.; Ke, X.; Zhang, B.; Tang, J. In situ controllable growth of $CoFe_2O_4$ ferrite nanocubes on graphene for colorimetric detection of hydrogen peroxide. *J. Mater. Chem. A* **2013**, *1*, 4352−4357.

(26) Jiang, Y.; Wang, W.; Li, X.; Wang, X.; Zhou, J.; Mu, X. Enzyme-mimetic catalyst-modified nanoporous SiO_2−cellulose hybrid composites with high specific surface area for rapid H_2O_2 detection. *ACS Appl. Mater. Interfaces* **2013**, *5*, 1913−1916.

(27) Lin, Y.; Li, Z.; Chen, Z.; Ren, J.; Qu, X. Mesoporous silica-encapsulated gold nanoparticles as artificial enzymes for self-activated cascade catalysis. *Biomaterials* **2013**, *34*, 2600−2610.

(28) Lin, Y.; Zhao, A.; Tao, Y.; Ren, J.; Qu, X. Ionic liquid as an efficient modulator on artificial enzyme system: toward the realization of high-temperature catalytic reactions. *J. Am. Chem. Soc.* **2013**, *135*, 4207−4210.

(29) Wang, J.; Han, D.; Wang, X.; Qi, B.; Zhao, M. Polyoxometalates as peroxidase mimetics and their applications in H_2O_2 and glucose detection. *Biosens. Bioelectron.* **2012**, *36*, 18−21.

(30) Wang, W.; Jiang, X.; Chen, K. $CePO_4$: Tb, Gd hollow nanospheres as peroxidase mimic and magnetic−fluorescent imaging agent. *Chem. Commun.* **2012**, *48*, 6839−6841.

(31) Wang, W.; Jiang, X.; Chen, K. Iron phosphate microflowers as peroxidase mimic and superoxide dismutase mimic for biocatalysis and biosensing. *Chem. Commun.* **2012**, *48*, 7289−7291.

(32) Song, Y.; Wang, X.; Zhao, C.; Qu, K.; Ren, J.; Qu, X. Label-free colorimetric detection of single nucleotide polymorphism by using single-walled carbon nanotube intrinsic peroxidase-like activity. *Chem.—Eur. J.* **2010**, *16*, 3617−3621.

(33) Wei, H.; Wang, E. Fe_3O_4 magnetic nanoparticles as peroxidase mimetics and their applications in H_2O_2 and glucose detection. *Anal. Chem.* **2008**, *80*, 2250−2254.

(34) Song, Y.; Qu, K.; Zhao, C.; Ren, J.; Qu, X. Graphene oxide: intrinsic peroxidase catalytic activity and its application to glucose detection. *Adv. Mater.* **2010**, *22*, 2206−2210.

(35) Su, L.; Feng, J.; Zhou, X.; Ren, C.; Li, H.; Chen, X. Colorimetric detection of urine glucose based $znfe_2o_4$ magnetic nanoparticles. *Anal. Chem.* **2012**, *84*, 5753−5758.

(36) Ding, N.; Yan, N.; Ren, C.; Chen, X. Colorimetric determination of melamine in dairy products by Fe_3O_4 magnetic nanoparticles−H_2O_2−ABTS detection system. *Anal. Chem.* **2010**, *82*, 5897−5899.

(37) Dong, Y.; He, K.; Yin, L.; Zhang, A. A facile route to controlled synthesis of Co_3O_4 nanoparticles and their environmental catalytic properties. *Nanotechnology* **2007**, *18*, 435602.

(38) Zhao, J.; Xie, Y.; Yuan, W.; Li, D.; Liu, S.; Zheng, B.; Hou, W. A hierarchical Co−Fe LDH rope-like nanostructure: facile preparation from hexagonal lyotropic liquid crystals and intrinsic oxidase-like catalytic activity. *J. Mater. Chem. B* **2013**, *1*, 1263−1269.

(39) Tang, X.; Li, J.; Hao, J. Synthesis and characterization of spinel Co_3O_4 octahedra enclosed by the {111} facets. *Mater. Res. Bull.* **2008**, *43*, 2912−2918.
(40) Yan, Q.; Li, X.; Zhao, Q.; Chen, G. Shape-controlled fabrication of the porous Co_3O_4 nanoflower clusters for efficient catalytic oxidation of gaseous toluene. *J. Hazard. Mater.* **2012**, *209*, 385−391.
(41) Josephy, P. D.; Mason, R. P.; Eling, T. Cooxidation of the clinical reagent 3,5,3′,5′-tetramethylbenzidine by prostaglandin synthase. *Cancer Res.* **1982**, *42*, 2567−2570.
(42) Mu, J.; Wang, Y.; Zhao, M.; Zhang, L. Intrinsic peroxidase-like activity and catalase-like activity of Co_3O_4 nanoparticles. *Chem. Commun.* **2012**, *48*, 2540−2542.
(43) Yu, F.; Huang, Y.; Cole, A. J.; Yang, V. C. The artificial peroxidase activity of magnetic iron oxide nanoparticles and its application to glucose detection. *Biomaterials* **2009**, *30*, 4716−4722.
(44) Chen, J.; Chen, H.; Zhou, C.; Xu, J.; Yuan, F.; Wang, L. An efficient upconversion luminescence energy transfer system for determination of trace amounts of nitrite based on $NaYF_4Yb^{3+}$ Er^{3+} as donor. *Anal. Chim. Acta* **2012**, *713*, 111−114.
(45) Humphrey, R. E.; Ward, M. H.; Hinze, W. Spectrophotometric determination of sulfite with 4, 4′-dithio-dipyridine and 5,5′-dithiobis (2-nitrobenzoic acid). *Anal. Chem.* **1970**, *42*, 698−702.

JOURNAL OF AGRICULTURAL AND FOOD CHEMISTRY

Article

pubs.acs.org/JAFC

Characterization of Grain-Specific Peptide Markers for the Detection of Gluten by Mass Spectrometry

Katherine L. Fiedler, Sara C. McGrath, John H. Callahan, and Mark M. Ross*

Center for Food Safety and Applied Nutrition, U.S. Food and Drug Administration, 5100 Paint Branch Parkway, College Park, Maryland 20740, United States

Supporting Information

ABSTRACT: Global and targeted mass spectrometry-based proteomic approaches were developed to discover, evaluate, and apply gluten peptide markers to detect low parts per million (ppm) wheat contamination of oats. Prolamins were extracted from wheat, barley, rye, and oat flours and then reduced, alkylated, and digested with chymotrypsin. The resulting peptides were subjected to LC-MS/MS analysis and database matching. No peptide markers common to wheat, barley, and rye were identified that could be used for global gluten detection. However, many grain-specific peptide markers were identified, and a set of these markers was selected for gluten detection and grain differentiation. Wheat flour was spiked into gluten-free oat flour at concentrations of 1−100,000 ppm and analyzed to determine the lowest concentration at which the wheat "contaminant" could be confidently detected in the mixture. The same 2D ion trap instrument that was used for the global proteomics approach was used for the targeted proteomics approach, providing a seamless transition from target discovery to application. A powerful, targeted MS/MS method enabled detection of two wheat peptide markers at the 10 ppm wheat flour-in-oat flour concentration. Because gluten comprises approximately 10% of wheat flour protein, the reported wheat gluten-specific peptides can enable detection of approximately 1 ppm of wheat gluten in oats.

KEYWORDS: *wheat, gliadin, proteomics, LC-MS/MS, celiac disease, gluten-free*

INTRODUCTION

Gluten is a complex network of proteins present in the endosperm of cereals that is responsible for giving dough its viscoelasticity.[1] Gluten is composed of two fractions: (1) monomeric, alcohol-soluble prolamins; and (2) polymeric, alcohol-insoluble glutelins.[2] Gluten proteins from wheat, barley, and rye can trigger an autoimmune disorder known as celiac disease (CD), and some wheat gluten and other wheat proteins can cause an IgE-mediated allergic response.[3,4] There are some celiac/allergy common immunoreactive proteins, and the only successful treatment for patients with a wheat allergy or CD is a wheat- or gluten-free (GF) diet devoid of these grains.[5] Although some oat cultivars have proven to be celiacogenic, pure oats can be an important source of nutrition in the GF diet because it is generally believed that the prolamins from oats (avenins) do not trigger an autoimmune response in most patients with CD, even though they are homologous to the prolamins from wheat (gliadins), barley (hordeins), and rye (secalins).[4,6,7] However, oats are frequently contaminated with one or more of the three celiacogenic grains during farming, transport, storage, and processing.[7,8]

Analytical techniques for the detection of gluten in food are important to ensure accurate food labeling and thereby protect consumers with CD from exposure to gluten. The U.S. FDA recently established that food labels bearing a "gluten-free" claim must contain <20 ppm of gluten from wheat, barley, rye, or their crossbred varieties.[9] Enzyme-linked immunosorbent assay (ELISA) is the only validated method available for the detection and quantitation of gluten; however, the different commercially available kits can respond differently to the gluten from wheat, barley, and rye. Recently, the accuracy of ELISA-based quantitation of gluten proteins has come into question due to the lack of a standardized reference material.[10] Concerns have also been raised with respect to the cross-specificity of the ELISA antibodies and the efficiency of the gluten protein extraction procedure, which can lead to over- or under-estimation of the total gluten content.[11] For example, most ELISA antibodies bind epitopes present in prolamins; however, the "cocktail" solution used to extract the gluten proteins can also extract glutelins. ELISA kits recommend multiplying the measured prolamin content by two to determine total gluten content; however, if the antibody cross-reacts with glutelins, then the total gluten content will be overestimated.[11]

Mass spectrometry (MS) offers a complementary method with unique capabilities that can provide molecularly specific information, including peptide identification, relative abundance determination, and protein inference. MS can be used to supplement or confirm ambiguous ELISA results, such as the differentiation of grains or the identification of specific protein sequences present in certain cultivars. MS-based proteomic strategies have been employed for the analysis of gluten for several years.[12] For example, MS has been used to identify the immunogenic gluten peptides responsible for causing CD and to determine how different gluten proteins affect flour quality.[13−16] The analysis of intact proteins by MS has been used to develop low-resolution fingerprints for gluten detection and grain source identification for the enforcement of gluten-

Received: February 26, 2014
Revised: May 15, 2014
Accepted: May 27, 2014
Published: May 27, 2014

ACS Publications This article not subject to U.S. Copyright. Published 2014 by the American Chemical Society

dx.doi.org/10.1021/jf500997j | J. Agric. Food Chem. 2014, 62, 5835−5844

free labeling regulations.[17,18] Bottom-up proteomics, which is based on enzymatic digestion of proteins and identification of the resulting peptides, was developed for mammalian proteomics, but has been less successful when applied to plants, for several reasons.[19] Incomplete genomes and poorly annotated protein databases for the three celiacogenic grains have made the identification of gluten proteins and peptides very challenging.[20] Nonetheless, bottom-up proteomic studies have been performed on wheat gluten, exclusively, and have yielded some candidate peptide markers that could be used to detect gluten from wheat in food.[21,22] The quantitation of gluten by mass spectrometry has been hindered by many challenges including, but not limited to, the lack of a standardized reference material, the large number of highly homologous proteins, cultivar heterogeneity, and variable growth conditions.

In this work, two proteomic strategies are used to develop a qualitative MS screening method to detect a gluten contamination of GF flour at concentrations below the maximum amount of gluten allowed in products labeled "gluten-free," which has been set at 20 ppm. In the first approach, a global proteomics analysis, which aims to characterize all of the proteins in a given sample, is used to identify grain-specific gluten peptide markers for wheat, barley, and rye that can be used for either total gluten detection or differentiation of the grains. In the second approach, a targeted proteomics assay is developed to detect low concentrations of wheat flour in GF oat flour. The complexity of the background matrix can greatly affect the sensitivity of mass spectrometric methods toward a particular analyte. Because wheat contamination of oats is common, oats are used here to provide a relevant matrix for the validation of the wheat candidate peptide markers.[7,8] The transition from a global proteomics method to a targeted method requires a thoughtful selection of the marker peptides according to a set of established guidelines[23] and rigorous verification of the gluten fragments that will serve as optimum markers of gluten in commercial foods. The selected wheat-specific peptide markers were targeted with a scheduled pseudo-selected reaction monitoring (pSRM) method.[24] This method involves acquiring full MS/MS spectra for each peptide of interest rather than following only a few selected parent-to-product ion transitions, as is done in traditional multiple reaction monitoring (MRM) methods.[25] pSRM is performed with the same instrument used for global proteomics analysis, a 2D linear ion trap, providing a seamless research pipeline from marker discovery to validation to application.[23]

MATERIALS AND METHODS

Gluten Sources. Gluten from wheat (Sigma), three single-grain flours, and seven commercial flours were obtained for this study: Duster wheat (hard red winter), King Arthur wheat (hard red), NIST standard reference material 1567a wheat (blend of hard red spring and hard red winter), Bob's Red Mill (BRM) wheat (hard red spring), Post90 barley, BRM barley, Wheeler rye, BRM dark rye, BRM oat, and BRM GF oat. The BRM GF oat flour was confirmed to be gluten-free via ELISA analysis with both R-Biopharm AG (R5 antibody) and Morinaga kits (data not shown). The three single-grain flours were prepared by grinding the whole grains with a Sorvall Omni-Mixer 17105 (DuPont) using a chamber assembly with cutting blades.

Wheat Flour-in-Oat Flour Sample Preparation. The 100,000 ppm wheat flour-in-oat flour mixture was prepared by mixing 0.5 g of BRM wheat flour and 4.5 g of BRM GF oat flour using a Spex SamplePrep Geno/Grinder 2010 at 1500 strokes/min for 5 min. Subsequent 10-fold dilutions of 0.5 g of wheat flour-in-oat flour mixtures with 4.5 g of BRM GF oat flour were made to produce 10000, 1000, 100, 10, and 1 ppm wheat flour-in-oat flour mixtures.

Gluten Extraction. The gluten extraction protocol used was an adaptation of the classic Osborne procedure.[26,27] For the neat wheat, barley, rye, and oat flours, 10 mg of each sample was washed twice with 1 mL of 0.5 M NaCl (1 h at 25 °C with vortexing) to remove albumins and globulins. After two washings with 1 mL of distilled water (1 h at 25 °C with vortexing), the prolamins were extracted twice with 1 mL of 70% ethanol (EtOH) or 50% EtOH for oats (1 h at 25 °C with vortexing), as recommended by Tatham et al.[26] The prolamin fraction was extracted from the Sigma wheat gluten sample with 70% EtOH without the NaCl and water washes. For the wheat flour-in-oat flour mixtures, 0.5 g of each sample was washed twice with 5 mL of 0.5 M NaCl and twice with 5 mL of distilled water and then extracted twice with 5 mL of 70% EtOH (each for 1 h at 25 °C on a Stuart SRT6 roller mixer at 33 rpm). A Qubit Protein Assay Kit (Invitrogen) was used to determine the amount of protein extracted from each sample by performing a spectroscopic measurement based on fluorescence according to the manufacturer's instructions. Experimental details for SDS-PAGE analysis of the prolamin extracts can be found in the Supporting Information.

Sample Digestion and Preparation. A 30 μg aliquot of each prolamin extract, as determined by Qubit analysis, was dried in a centrifugal evaporator (SpeedVac) without heating, resuspended with 20 μL of 50 mM ammonium bicarbonate and 5 μL 1% *Rapi*Gest SF (Waters) in 50 mM ammonium bicarbonate, and heated at 95 °C for 10 min. After the mixture had cooled to ambient temperature, 1.25 μL of 105 mM DTT was added to reduce the proteins with 5 mM DTT (final concentration) at 60 °C for 30 min. After the mixture had again cooled to ambient temperature, 1.25 μL of 330 mM iodoacetamide was added to alkylate the proteins with 15 mM iodoacetamide (final concentration) at 25 °C for 30 min. The proteins were then digested with either trypsin (1:100 enzyme-to-substrate ratio at 37 °C) or chymotrypsin (1:100 enzyme-to-substrate ratio at 25 °C) for approximately 18 h. To assess digestion efficiency, 60 pmol of intact bovine serum albumin (BSA, Sigma) was added to the samples prior to digestion. The resulting peptides were desalted using C18 spin columns (Pierce) according to the manufacturer's instructions. The samples were dried in a SpeedVac and reconstituted in an aqueous solution containing 0.1% formic acid (FA) and 3% acetonitrile (ACN) to obtain concentrations of 100 ng/μL prolamins and 200 fmol/μL BSA (based on the quantity of intact protein starting material) and subjected to mass spectrometric analysis. Angiotensin-II (A-II) was added to each sample at a concentration of 250 fmol/μL to serve as an injection internal standard to monitor run-to-run variations in instrument performance.

LC-MS/MS Analysis. A Thermo LTQ XL mass spectrometer equipped with a Waters nanoAcquity HPLC and Michrom CaptiveSpray source was used for global and targeted mass spectrometric analyses. For each sample, 1 μL was injected onto a Symmetry C18 (5 μm particle size, 180 μm i.d. × 20 mm length at 25 °C) trap column using an isocratic gradient at 0.5% B for 3 min at 5 μL/min (solvent A, 0.1% FA in water; solvent B, 0.1% FA in ACN). Peptide separation was accomplished with a BEH130 C18 column (1.7 μm particle size, 100 μm i.d. × 100 mm length at 35 °C) using a gradient of 3−40% B over 60 min at 500 nL/min. The LTQ was operated in either a Top9 data-dependent acquisition mode or a scheduled pSRM acquisition mode. For the Top9 method, a full MS scan was acquired first, and then the nine most abundant peaks were selected for MS/MS analysis. For the pSRM method, the global, non-data-dependent mass list and 5 min retention time (RT) windows were used for targeted MS/MS analysis of four wheat peptides, three BSA peptides, and the injection standard A-II. LTQ operation parameters include 35% collision energy, 2 Da precursor ion isolation width, 30 ms fragmentation time, 1.7 kV spray voltage, and 31 V capillary voltage. The automatic gain control (AGC) target values were 30000 and 10000 for full scans and MS^n or SIM scans, respectively. Maximum ion injection times were 10 and 100 ms for full scans and MS^n or SIM scans, respectively.

LC-MS/MS Data Analysis. The global proteomics data were searched with MASCOT (Matrix Science) to identify peptides and infer protein assignments from a database that consisted of the reviewed and unreviewed entries for the BEP clade (Bambusoideae, Ehrhartoideae, Pooideae) and PACMAD clade (Panicoideae, Arundinoideae, Chloridoideae, Micrairoideae, Aristidoideae, and Danthonioideae) of the Poaceae family listed in the Uniprot database (downloaded on November 1, 2012, filtered by taxonomy, ~380,000 entries). MASCOT search parameters included 2 maximum missed cleavages, +2 and +3 peptide charge states, ±1.8 Da peptide tolerance, ±0.8 Da MS/MS tolerance, carbamidomethyl (C) as a fixed modification, and oxidation (M) as a variable modification. Scaffold (Proteome Software) was used to organize and evaluate the confidence of peptide identifications and protein assignments. Scaffold filters applied to the search results included 99.0% protein threshold, two minimum peptides, and 95% peptide threshold. Scaffold results were exported to Excel as spectrum reports to enable spectral counting for individual peptides using pivot tables. All of the spectra assigned as "false" were removed (to avoid double counting of spectra), and the total number of spectra assigned to each peptide sequence was calculated. Skyline (University of Washington) was used to determine relative peptide abundances on the basis of the sum of the peak areas of the five most abundant fragment ions in the MS/MS spectra from each target peptide. Skyline allowed confirmation of the targeted peptides by visual inspection of peak shape to ensure coelution of the individual transition traces, as well as measurements of the RT and selected fragment ion abundance ratios. Xcalibur Qual Browser (Thermo) was used to interrogate the raw data by extracting ion chromatograms (XICs) and evaluating the full MS/MS spectra. Xcalibur was used to calculate the S/N ratio of the XIC peak areas for individual fragment ions via the ICIS peak detection model with default parameters.

RESULTS AND DISCUSSION

Digestion Optimization Using a Gluten Standard. Development of a global proteomics method usually begins with digestion optimization for the analyte of interest. Trypsin is traditionally used in bottom-up proteomics because it is reliable and specific, cleaving C-terminally to lysine and arginine residues. However, because prolamin proteins are low in lysine and arginine content, trypsin produces only a small number of very large peptides that are not of optimal size for ESI-MS/MS analysis. Chymotrypsin, which cleaves C-terminally to tyrosine, phenylalanine, tryptophan, and leucine (but not before proline), is less specific but is an acceptable alternative enzyme to trypsin.[28,29] A reduction and alkylation step is also traditionally included before digestion to cleave cysteine-cysteine disulfide bonds and derivatize the resulting free cysteines and thereby unfold the protein for improved digestion. The number of gluten peptides that could be identified in a 70% EtOH extract of the Sigma wheat gluten sample was evaluated using the four following digestion conditions: with or without reduction/alkylation and with either trypsin or chymotrypsin. The chymotryptic digestion with reduction and alkylation yielded the largest number of unique gluten peptide identifications; approximately 2 times more peptides were identified compared to the trypsin digestion with reduction and alkylation (125 vs 62 peptides, see Table 1).

A larger number of identified peptides demonstrates superior digestion efficiency and provides improved confidence in the protein assignments from database matching. In addition, a large pool of potential gluten peptide markers is preferred because not all peptides will be suitable markers after rigorous selection criteria are applied. For example, peptide markers should have 7−30 residues and average hydrophobicity and not contain potential modification sites, such as methionine residues, which can be oxidized.[23] A peptide marker should be reproducibly observed with high peak intensity, proper chromatographic peak shape, and a high-quality MS/MS spectrum with many abundant fragment ions with high S/N.[23]

Table 1. Number of Gluten Peptides Identified with the Indicated Digestion Conditions

digestion conditions			
trypsin	reduction/alkylation + trypsin	chymotrypsin	reduction/alkylation + chymotrypsin
33	62	96	125

The use of mulitple enzymes, separately or sequentially, has been reported.[13,20] However, multienzyme digestions require additional time and reagents, and because the chymotrypsin-alone digestion produced many candidate peptide markers, this strategy was used for the remainder of the experiments presented. The reduction/alkylation/chymotrypsin digestion protocol was further improved using the Sigma wheat gluten sample in a digestion time course study (2, 4, 8 and 18 h of digestion time) with various enzyme-to-substrate ratios (1:20, 1:50, 1:100, and 1:200). An enzyme-to-substrate ratio of 1:100 and a digestion time of 18 h were found to be optimal conditions for reproducible generation of gluten peptides (data not shown).

Characterization of Gluten Using a Global Proteomics Approach. A variety of flour samples were studied (Supporting Information Supplemental Table SI) to ensure that the technique developed will be applicable to a wide range of food products through the consistent production and detection of the selected markers. Gluten protein sequences may differ in these flours due to grain cultivar and plant growth conditions, as well as variable flour processing techniques such as bromation, bleaching, or refinement.[22] The wheat flours selected for the study are from hard red wheat and represent what is commonly used in the United States to make bread and hard-baked goods. The prolamin extracts were analyzed with SDS-PAGE to provide a coarse comparison of wheat gliadins, barley hordeins, rye secalins, and oat avenins; however, this technique offers a limited qualitative visualization. For instance, it would be difficult to determine a low-level gluten contamination via SDS-PAGE analysis. Supplemental Figure S1 in the Supporting Information is the SDS-PAGE image showing the most abundant prolamins extracted from wheat, barley, rye, and oat flours. Analysis of the second ethanol extract indicated an efficient first extraction because only 12.7 ± 1.4% more protein was extracted the second time.

Each prolamin extract was reduced, alkylated, and digested with chymotrypsin using the optimized digestion protocol and analyzed by LC-MS/MS. The reproducibility of the method was evaluated by extracting and digesting the BRM wheat, barley, rye, and GF oat flours three times. The LTQ mass spectrometer was operated in a Top9 data-dependent mode, and the data were analyzed in the same manner as described above (MASCOT search, Scaffold summary, Excel pivot table, and data compilation). The total numbers of unique peptides assigned to the top protein hits from each neat flour sample are summarized in Supplemental Table SII in the Supporting Information. For each type of flour tested, the protein matches derived from the MS/MS data cluster together by grain type (wheat, barley, rye, or oats). For example, peptides identified from each of the wheat flours matched the same top 10 wheat

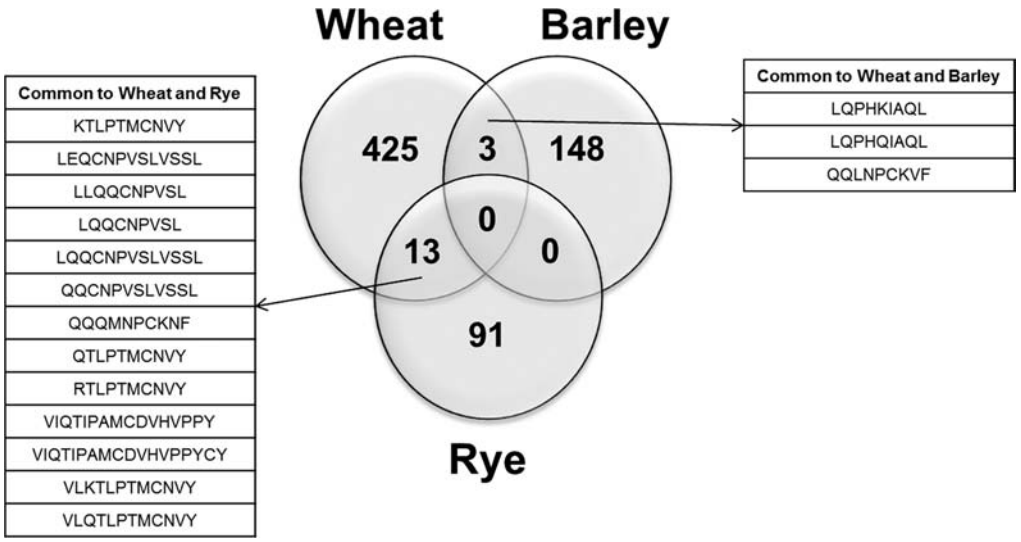

Figure 1. Venn diagram of the total number of unique gluten peptides identified in all wheat, barley, and rye flour samples.

Table 2. Candidate Wheat Markers Compiled from Wheat-Derived Peptides Detected in the Wheat Flour-in-Oat Flour Samples

peptide code	peptide sequence	Uniprot protein accession no.	gliadin class
W1	RPQQPYPQPQPQY[13,22]	J7HZV9_WHEAT	α/β
W2	QLVQGQGIIQPQQPAQY	B6UKP4_WHEAT	γ
W3	VQGQGIIQPQQL	H8Y0K0_PSAJU	γ
W4	LQLQPFPQPQLPY[16a]	Q9M4L9_WHEAT	α/β
W5	SQQQQVGQGSLVQGQGIIQPQQPAQL[30]	B6UKN7_WHEAT	γ
W6	VPPECSIIRAPF[30]	B6UKJ7_AEGTA	γ
W7	ASIVAGIGGQ	H8Y0I8_AEGUN	γ
W8	NIQVDPSGQVQW[30a]	Q9M6P7_WHEAT	γ
W9	SQEQPLPQQQPSVEEKQQL	I7KM78_WHEAT	γ
W10	QLIQGQGIIQPQQPAQL	J7I234_AEGUN	γ
W11	QQYPLGQGSF	Q3YFI1_9POAL	α/β
W12	RPQQPYPQSQPQY	Q9M4L6_WHEAT	α/β
W13	ASIVADIGGQ[30]	D0ES81_WHEAT	γ
W14	LQLQPFPQP**QLPYPQP**QPF[16]	J7HZV9_WHEAT	α/β
W15	GSSQPQQQTQLDQGW	D2KFG9_WHEAT	gliadin/avenin-like
W16	LQQCNPVSLVSSL[28a]	H8Y0I8_AEGUN	γ

[a]Peptide reported in the literature differs by a missed cleavage.

entries in the protein database and did not match confidently to proteins from any of the other grain types. Generally, the most abundant proteins from each grain source correlate to the specific prolamin type for that grain (wheat gliadins, rye secalins, barley hordeins, and oat avenins) except for one γ-gliadin, B6DQC4_LOPEL, which was observed in all of the wheat and rye flours.

To discover gluten peptide markers, the peptide identifications from each flour were grouped by grain source (wheat, barley, rye, or oats). The peptide lists were evaluated for peptides common to the grains (total gluten markers) and peptides unique to each grain (gluten grain source differentiation markers). Figure 1 displays the peptide identifications as a Venn diagram of the total number of unique peptides from gluten proteins that were identified in all of the flour samples from wheat, barley, and rye. No gluten peptide markers common to all three grains were identified; however, this does not imply that peptides common to all three grains do not exist. All MS-based proteomic strategies are limited by database quality because the identification of peptides and the assignment of proteins are restricted to the proteins present in the database. Unfortunately, the protein databases available for wheat, barley, rye, and oats are incomplete and not well curated. Because a unified gluten detection method is not possible using this strategy, a set of markers composed of representatives from each grain would be required to ensure the method is capable of gluten detection regardless of the grain source.

Many grain-specific peptides were identified for each grain, which could be used to differentiate wheat, barley, and rye. Wheat and rye were the most similar, with 13 peptides in common; wheat and barley had 3 peptides in common, and barley and rye did not have any peptides in common. Some of the peptides that were found in common between wheat and rye had similar sequence motifs and differ only by a single amino acid polymorphism (SAAP) or a missed cleavage site (e.g., five peptides contain the subsequence TLPTMCNVY and another five peptides contain QCNPVSL). Similarly, two of the three peptides common to wheat and barley have a SAAP (K → Q). None of the grain-specific peptide markers identified from wheat, barley, or rye were identified in oats.

Table 3. Peptides Targeted in the pSRM Method and the Transitions Monitored

peptide code	peptide sequence	protein	RT (min)	*m/z*	charge state	monitored fragment ions
W1	RPQQPYPQPQPQY	α/β-gliadin	20.7	814.4	+2	y_3 (*m/z* 407.2), b_{12}^{+2}(*m/z* 723.4), b_6 (*m/z* 770.4), b_8 (*m/z* 995.5), b_{10} (*m/z* 1220.6)
W2	QLVQGQGIIQPQQPAQY	γ-gliadin	30.1	949.1	+2	y_4 (*m/z* 478.2), y_7 (*m/z* 831.4), b_9 (*m/z* 937.5), b_{10} (*m/z* 1065.6), b_{13} (*m/z* 1418.8)
W3	VQGQGIIQPQQL	γ-gliadin	30.2	655.3	+2	y_4 (*m/z* 485.3), b_6 (*m/z* 583.3), y_5 (*m/z* 613.3), b_7 (*m/z* 696.4), b_8 (*m/z* 824.5)
W4	LQLQPFPQPQLPY	α/β-gliadin	42.8	785.4	+2	b_6 (*m/z* 727.4), y_7 (*m/z* 842.4), b_8 (*m/z* 952.5), y_9 (*m/z* 1086.6), b_{11} (*m/z* 1290.7)
B1	ICDNQDTISSKL	BSA	23.9	697.8	+2	y_4 (*m/z* 434.3), b_6 (*m/z* 746.3), b_8 (*m/z* 960.4), y_9 (*m/z* 1005.5), y_{10} (*m/z* 1120.5)
B2	SALTPDETYVPKAF	BSA	33.4	770.4	+2	y_4 (*m/z* 462.3), y_5 (*m/z* 561.3), b_{10} (*m/z* 1077.5), y_{10} (*m/z* 1166.6), y_{11} (*m/z* 1267.6)
B3	SQKFPKAEF	BSA	22.1	541.6	+2	b_2 (*m/z* 216.1), b_4 (*m/z* 491.3), y_5 (*m/z* 591.3), y_6 (*m/z* 738.4), y_7 (*m/z* 866.5)
A1	DRVYIHPF	A-II	27.7	524.1	+2	y_2 (*m/z* 263.1), b_7 (*m/z* 441.2), y_7 (*m/z* 466.3), b_5 (*m/z* 647.4), b_6 (*m/z* 784.4)

Global Proteomics Analysis of Wheat Flour Spiked into Gluten-free Oat Flour. To refine the group of wheat-specific peptides identified above into a set of useful peptide markers, a global proteomics analysis was performed on samples consisting of wheat flour spiked into GF oat flour at concentrations of 1−100,000 ppm. The different concentration levels were used to evaluate the peptide markers and determine those that would enable detection of the lowest concentration of the "contaminant" grain in the mixture.

The prolamin fraction was extracted from each flour mixture and digested using the optimized protocol. Using the global proteomics approach, 16 of the 425 wheat-specific peptides observed in the neat wheat flours were identified consistently in the wheat flour-in-oat flour samples with a linear signal intensity response from 1,000 to 100,000 ppm. Peptide sequences, protein accession numbers, and gliadin classes for the identified peptides are listed in Table 2. Almost half of the wheat-specific peptide makers that we identified have been reported in the literature.[13,16,22,28,30] The candidate peptide markers satisfy the selection criteria discussed previously and are of average length and hydrophobicity, do not contain methionine residues, and reproducibly provide high-quality LC-MS/MS data. Representative peptides from each prolamin class (α/β-, γ-, and ω-gliadins) are also preferred as well as peptides that contain ELISA epitopes. Because ELISA is the only validated method for gluten analysis, using peptide markers that contain ELISA epitopes will enable a direct comparison of a MS-based method with ELISA. Known gluten ELISA antibody epitopes include QLPYPQP for the A1 antibody from Romer Laboratories, QPQLPY for the G12 antibody from Romer Laboratories, and QQPFP for the R5 antibody from R-Biopharm AG.[31,32] Peptide W4 contains the G12 epitope (underlined), and peptide W14 contains the G12 epitope (underlined) and the A1 epitope (highlighted in bold).

Data from digests of the prolamin extracts from neat flours were searched to ensure that each of the 16 candidate peptide markers were reproducibly observed in the three replicate analyses of BRM wheat flour as well as in each different source of wheat flour. Most of the peptides were reproducibly detected in each replicate analysis except peptide W13, which was observed in only one BRM wheat flour replicate, and peptides W6, W7, and W15, which were observed in two of the three BRM wheat flour replicates. The majority of peptides (14 of 16) were observed in all of the wheat flour types except peptides W10 and W15, which were not observed in the Duster wheat flour. None of the candidate markers for wheat was observed in the barley, rye, or oat flours except peptide W16, which was observed in every rye flour. Although 15 of the 16 candidate makers matched specifically to wheat protein entries in the flours studied, no definite conclusion can be made on the absolute specificity of the wheat peptide makers because the databases for the other gluten-containing grains are incomplete. Because of the homology between these cereal grains, one should exercise caution when attempting to derive the grain source of gluten on the basis of the detection of a single peptide.

Targeted Proteomics Analysis of Wheat Flour Spiked into Gluten-free Oat Flour. Using the global proteomics approach, wheat flour could be confidently detected in the GF oat flour at concentrations of 1000 ppm or greater, which is significantly higher than the GF labeling threshold of 20 ppm. With a Top9 data-dependent acquisition mode, the wheat gluten peptides were not of sufficient abundance, with respect to the oats background, to trigger MS/MS analysis. Therefore, a targeted MS/MS method was developed so that the wheat-specific peptide markers could be observed at lower concentrations. Targeted methods can increase the selectivity and sensitivity of peptide detection by directing the mass spectrometer to analyze a small number of peptide ions with specified *m/z* and RT values. A scheduled pSRM method was used, in which the mass spectrometer collects full MS/MS spectra for selected precursor ions during designated RT windows.[24] The MS/MS scan events were time scheduled with small RT windows to minimize overlap between targets. Acquisition of MS/MS spectra for a small number of peptides at any given time increases the number of times the parent ion is sampled across the eluting LC peak (and therefore the number of data points per peptide), resulting in an improved measurement of peak area and relative abundance determination.

The pSRM approach is in contrast to a Top9 data-dependent method, which collects full MS scans and then MS/MS spectra for untargeted but highly abundant peptides, or an MRM method, which does not collect full MS/MS spectra and relies on specific parent-to-product ion transitions. A pSRM method maintains the selectivity advantage of MRM by monitoring product ion peaks in MS/MS spectra, which results in a peak that is more easily distinguished against the background. This is especially important for low-resolution instruments, such as the LTQ, where interferences from chemical noise result in low S/

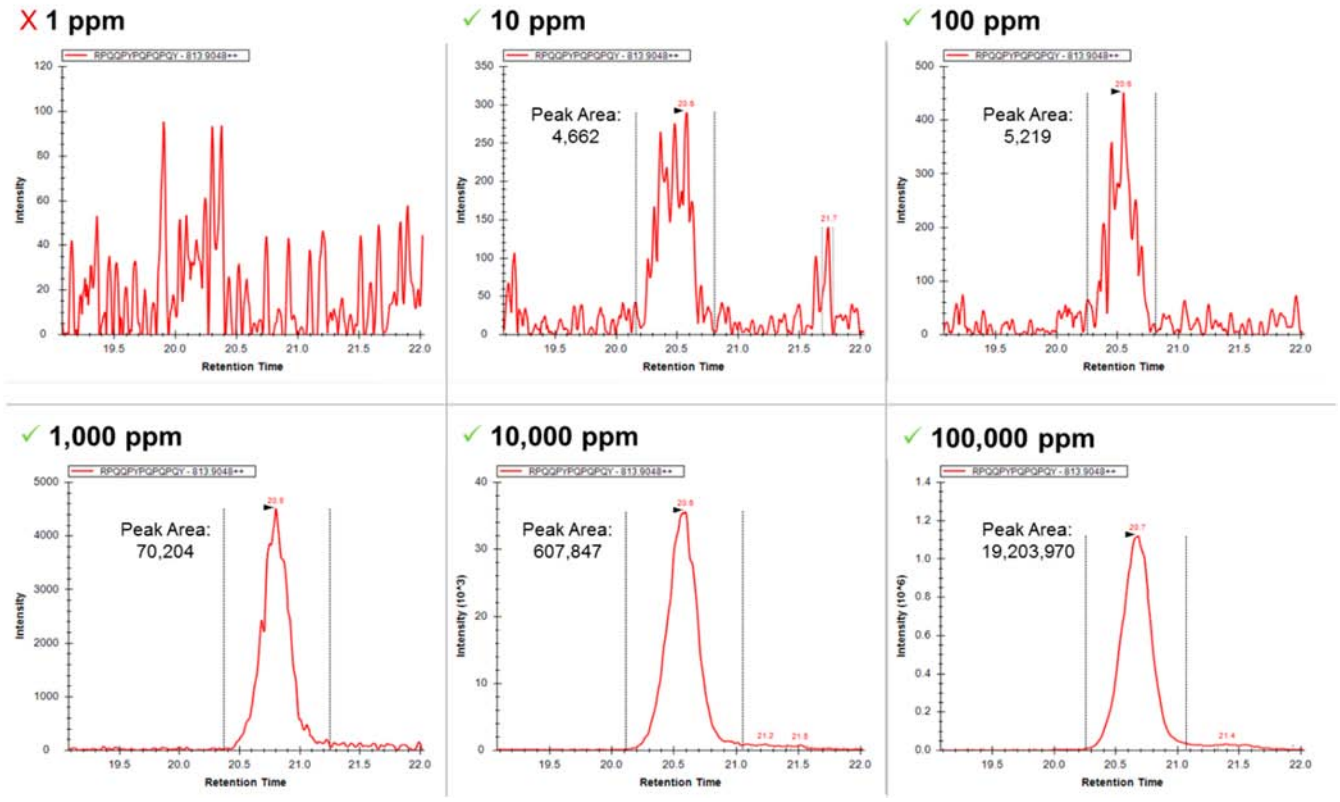

Figure 2. Chromatographic peaks representing the sum of the peak areas of the five most abundant fragment ions for peptide W1 as measured by pSRM analysis of the six wheat flour-in-oat flour samples.

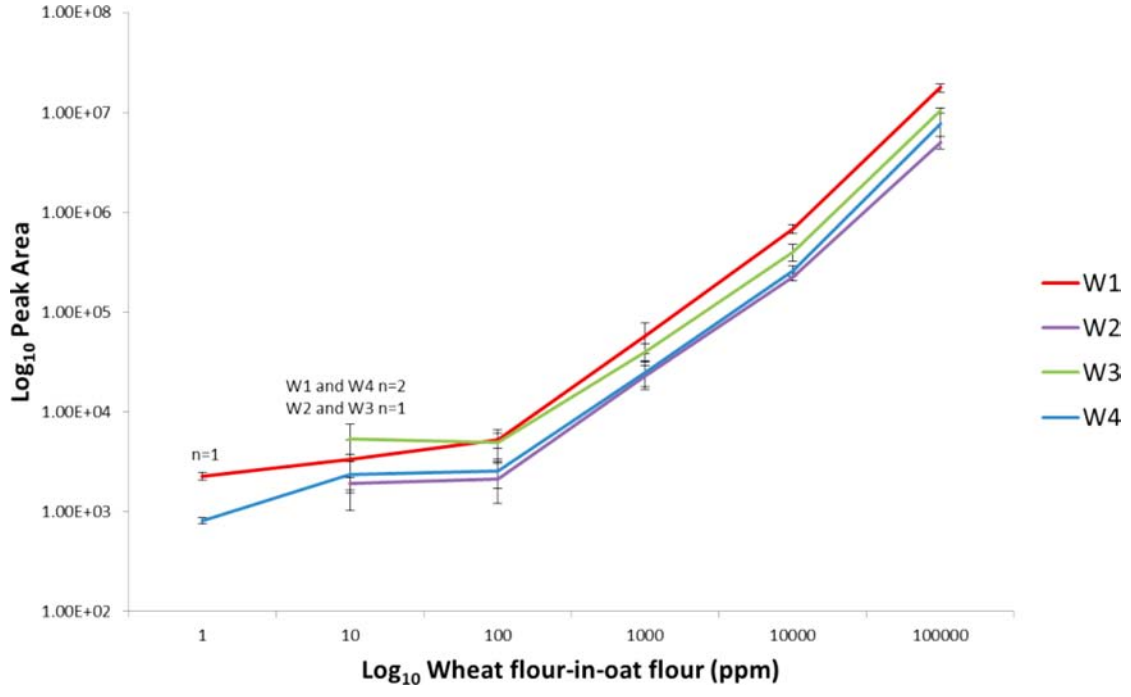

Figure 3. Log–log plot of the pSRM peak areas for the four targeted wheat-specific peptide markers versus the concentration of wheat flour in each wheat flour-in-oat flour sample. Data points correspond to the average of three replicate analyses. Lines connecting data points indicate a trend in decreasing peak area and do not represent a line of best fit.

N that can make distinction of precursor ion peaks (MS1) difficult. Because full MS/MS spectra are acquired with a pSRM method, false positives or negatives can be quickly verified by matching a large number of product ions in the acquired MS/MS spectrum with product ions in a reference spectrum. Data processing methods can be changed postacquisition to include as many product ions as is necessary to make a confident assignment, which is not possible with MRM.

dx.doi.org/10.1021/jf500997j | J. Agric. Food Chem. 2014, 62, 5835–5844

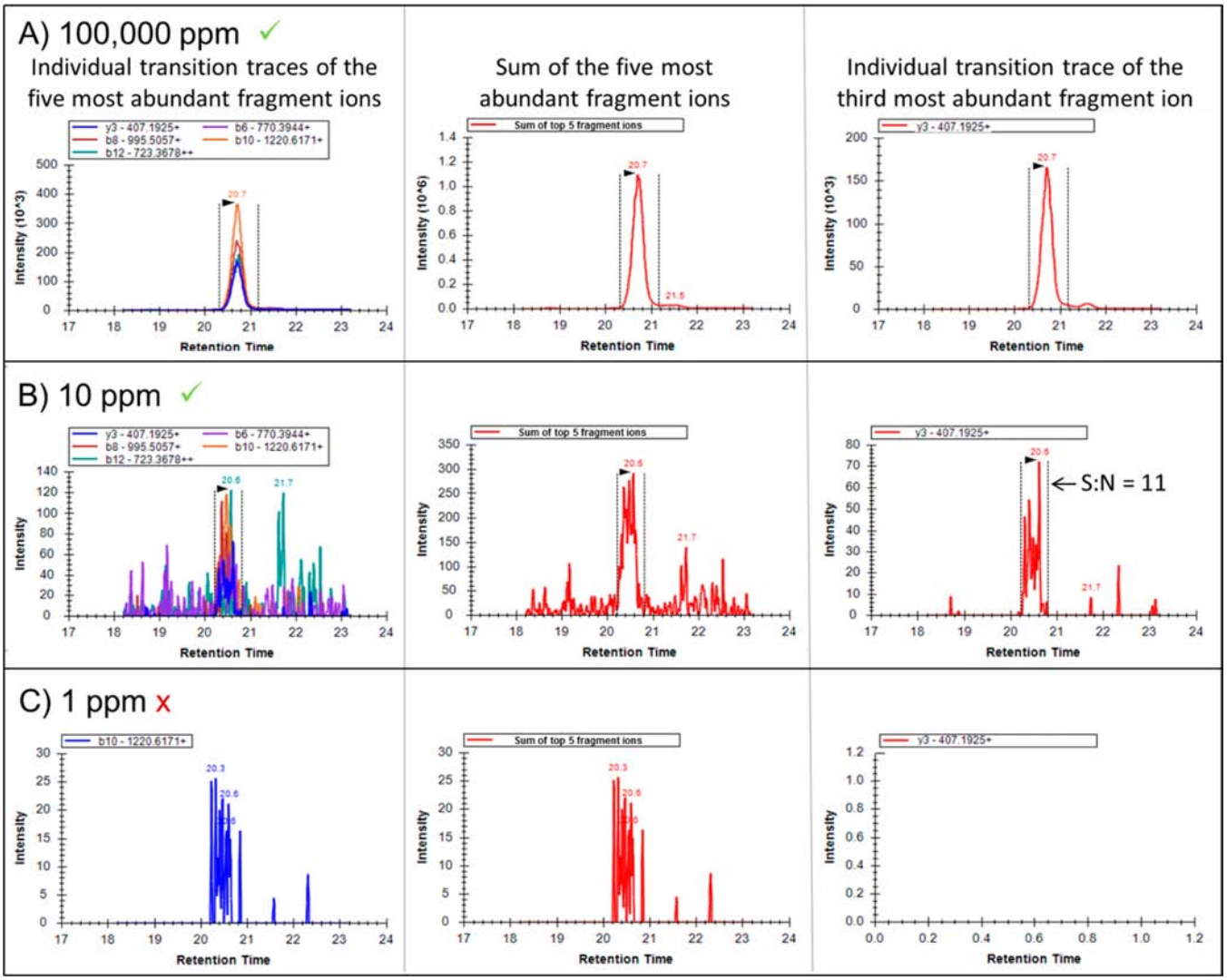

Figure 4. Chromatographic peaks for peptide W1 acquired by targeted analysis of the 100,000 ppm (A), 10 ppm (B), and 1 ppm (C) wheat flour-in-oat flour samples. Application of strict criteria ensured confident detection of peptide W1 at the 100,000 and 10 ppm concentrations, but not at the 1 ppm concentration. The leftmost column shows the individual transition traces for the five most abundant fragment ions. The middle column shows the sum XIC of the five most abundant fragment ions. The right column shows the individual transition trace for the third most abundant fragment ion.

With the global proteomics approach, 3 of the 16 wheat-specific candidate peptide markers, W1−W3, were observed at the 1000 ppm concentration ($R^2 \geq 0.991$). These peptides as well as an ELISA epitope-containing peptide (W4 contains the G12 ELISA epitope QPQLPY) were chosen for targeted analysis using pSRM. Three BSA peptides and A-II were also monitored to ensure proper digestion efficiency and instrument performance. Table 3 contains information on the pSRM targets including peptide sequence, protein source, m/z, and RT. The wheat flour-in-oat flour samples were mixed and digested three separate times at each concentration to ensure the reproducibility of the method.

Skyline was used to extract ion chromatograms and calculate the total peak area for each target peptide as the sum of the peak areas of the five most abundant fragment ions.[24,33] Figure 2 shows Skyline plots of pSRM data for peptide W1 at each concentration of the wheat flour-in-oat flour samples. The total peak area for each target peptide, determined using Skyline's default algorithm, was plotted versus wheat flour concentration to establish a dynamic range of the method. A log−log plot of the observed trend is shown in Figure 3. A linear response is observed from all four peptides for concentrations from 100 to 100,000 ppm. The peptides that were detected in samples below the 100 ppm concentration did not appear consistently in all replicates and did not continue the linear response, a phenomenon that has been observed by others.[24,34] Peptides W1 and W4 were detected at the 10 ppm concentration in two of the three sample replicates and observed at the 1 ppm concentration in one of the sample replicates. Peptides W2 and W3 were detected at the 10 ppm concentration in only one of the sample replicates.

To objectively and confidently confirm peptide detection at the lowest concentrations, the following six criteria were applied to pSRM data: (1) the transition traces from the five most abundant fragment ions from each peptide must coelute; (2) the retention time must agree with the authenticated retention time of the peptide ±15 s; (3) the individual XIC peak areas for the three most abundant fragment ions must have a S/N ≥ 3; (4) the m/z values for the more abundant b- and y-ions must be accurate and correctly represent the peptide

dx.doi.org/10.1021/jf500997j | J. Agric. Food Chem. 2014, 62, 5835−5844

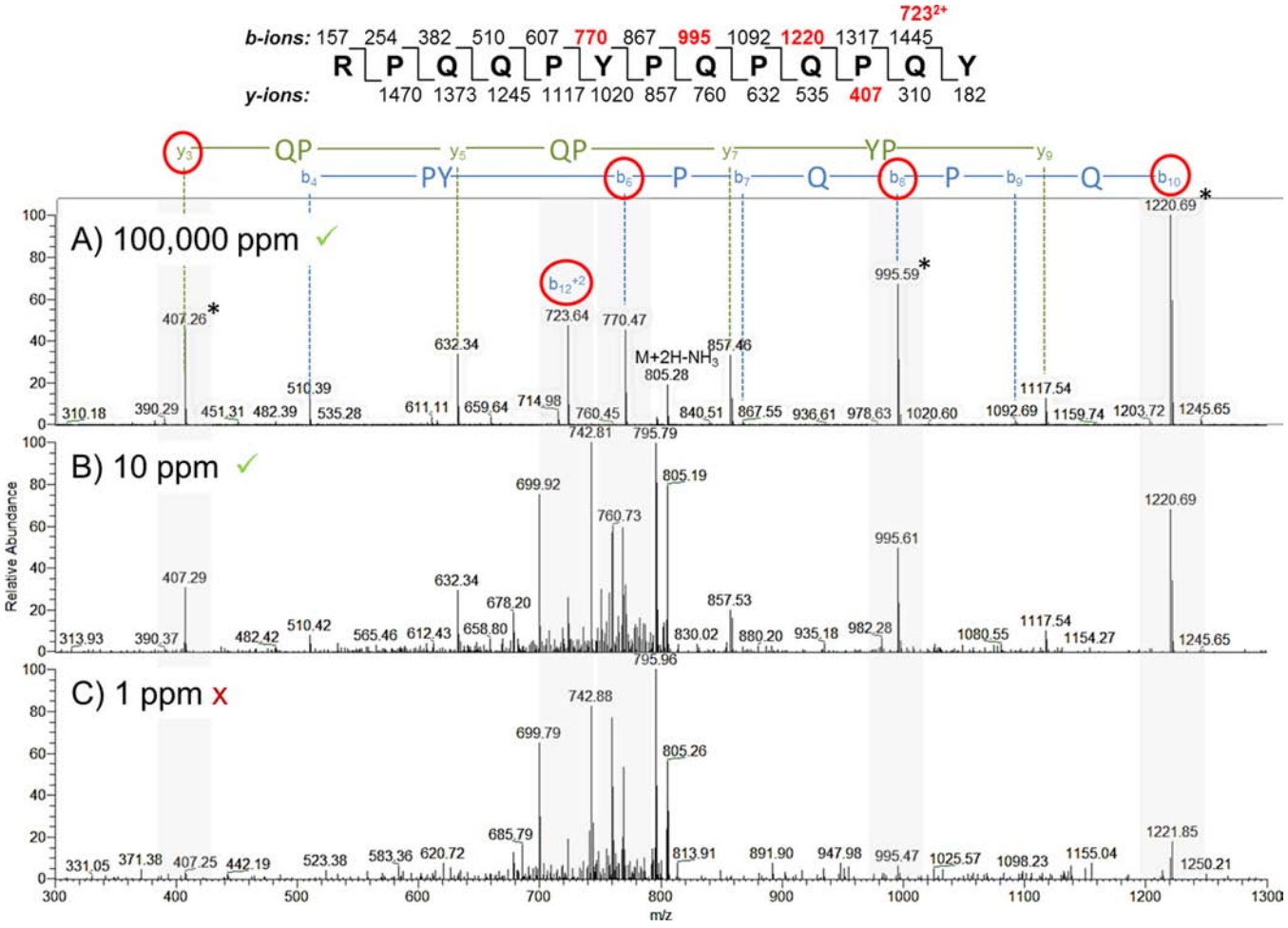

Figure 5. MS/MS spectra for peptide W1 at the 100,000 ppm (A), 10 ppm (B), and 1 ppm (C) concentrations obtained by averaging the MS/MS spectra across the XIC peaks in Figure 4. The b- and y-ion series were used to confirm the peptide sequence. The five most abundant fragment ions that were monitored in the pSRM data analysis are circled in red. The top three fragment ions (∗) were used to calculate the fragment ion abundance ratios.

sequence; (5) the abundance ratio of product ions must be within a prescribed range; (6) the peptide must be reproducibly observed in the replicate analyses. The criteria used are based on recommended guidelines established for the field of targeted peptide measurements.[35,36]

Figure 4 is representative XIC data for peptide W1, which was positively observed at the 100,000 ppm (A) and 10 ppm (B) wheat flour-in-oat flour concentrations, but not detected at 1 ppm (C). The left column shows the coelution of the individual transition traces for the five most abundant fragment ions for peptide W1. The middle column shows the sum of the five most abundant fragment ions for peptide W1, which was used to create the concentration−response relationship curve (Figure 3). The retention times of the peptides were consistent within 5.8 ± 1.4 s across the 6 orders of magnitude in concentration for the individual sample replicates, indicating the background matrix had minimal effect on chromatographic separation. The retention times of the peptides were consistent within 10.1 ± 1.7 s between the three sample replicates, which demonstrates the reproducibility of the method and instrument performance. The right column shows the individual transition trace for the third most abundant fragment ion for peptide W1, which must have a S/N ≥ 3 to ensure positive peptide observation. Peptide W2 fragments poorly and does not have many prominent peaks in its MS/MS spectrum; therefore, the second most abundant fragment ion was required to have a S/N ≥ 3.

Figure 5 is the model MS/MS spectrum for peptide W1 at 100,000 ppm (A), an acceptable spectrum at 10 ppm (B), and an unacceptable spectrum at 1 ppm (C) obtained by averaging the MS/MS spectra across each XIC peak in Figure 4 using the boundaries determined by Skyline. Even though only five fragment ions were used to calculate the peptide abundance, several additional fragment ions (b_4, y_5, y_7, and y_9) were detected with adequate S/N in samples with low concentrations of wheat flour-in-oat flour (Figure 5B). This ability of the pSRM method to capture full MS/MS spectra is important for reliable detection of low-concentration analytes in complex mixtures because it can provide increased confidence in peptide identifications. An acceptable fragment ion abundance ratio is determined by the ratio of the most abundant fragment ion with respect to the second and third most abundant fragment ions ±20−50% relative units depending on the relative intensity of the fragment ion with respect to the base peak.[37] Because the product ions could be assigned very reliably at high concentrations, the ion ratios from the 1000−100,000 ppm samples were used to establish the criteria for lower concentration samples. Overall, the fragment ion abundance

dx.doi.org/10.1021/jf500997j | J. Agric. Food Chem. 2014, 62, 5835−5844

ratios between the first and second most abundant fragment ions were within ±20%, except peptide W4 with a tolerance of ±40.9% at 1 ppm and a tolerance of ±21.1% at 10 ppm. The fragment ion abundance ratios between the first and third most abundant fragment ions were also within the accepted range. Although because full MS/MS spectra were acquired, the criterion for the fragment ion abundance ratios did not need to strictly apply for reliable peptide detection, if other criteria are sufficiently satisfied.[38]

The combination of these criteria allows a confident identification of wheat in oats at the 10 ppm concentration using peptides W1 and W4, which is below the 20 ppm "gluten-free" labeling threshold. Peptides W2 and W3 were not consistently observed at the 10 ppm concentration, which provides an example of why the largest initial pool of candidate markers is desired, as was previously discussed. It is very difficult to predict a priori which peptide markers will perform better in a complex sample due to factors such as suppression of ions of interest by coeluting peptides.

A unique aspect of this work is the use of the same mass spectrometer for the global and targeted proteomics methods, which has advantages over moving from a data-dependent method on an ion trap or QToF to a traditional MRM method on a triple-quadrupole instrument for targeted analysis. The optimal gluten peptide markers may change with different gluten sources because of the large number and variety of grain cultivars and processing techniques.[22] Gluten peptide marker discovery or confirmation by global proteomics may be necessary for different gluten-containing sample types prior to targeted analysis. Using the same instrument for both the discovery and validation phases streamlines the research and minimizes the time lost in transferring a method from one instrument platform to another. With the use of two different LC-MS systems, the peptide markers may differ with respect to chromatography, ionization, and fragmentation. In addition, the need for two mass spectrometers increases the cost per sample significantly.

Overall, we have demonstrated how a MS-based proteomics approach can be used for the qualitative detection of low concentrations of wheat in oats. After a global proteomics approach was used to identify a set of wheat-specific peptide markers (with respect to barley, rye, and oats), a targeted proteomics approach was used to enable detection of a 10 ppm wheat flour contamination of GF oat flour. The wheat flour used in this study consists of approximately 11.42% protein (micro-Kjeldahl analysis using a conversion factor of 5.7). Assuming 80% of wheat protein is gluten, the wheat flour contains approximately 9.1% gluten;[30] therefore, the concentration of gluten is approximately 1 ppm, which is well below the desired GF labeling threshold of 20 ppm. This combined global and targeted MS proteomics strategy is complementary to ELISA in that it can provide confirmatory, low-level, qualitative gluten detection with molecular specificity and enable grain differentiation. Because the detection of gluten has the potential to be complicated by variability in protein sequence due to differences in cultivar, growth conditions, and protein homology, a preliminary global proteomics analysis is important for each new application to confirm the validity of the gluten peptide markers or identify better peptide markers if necessary.

The strategy reported here could be improved by using an instrument with greater mass resolution and accuracy. Higher resolution will lead to fewer contaminants in the targeted m/z and RT window, and the increase in S/N could result in the observation of wheat gluten peptides at lower "contamination" concentrations.[39] Isotopically labeled peptide standards will be employed for an isotope dilution study to elucidate the extent of matrix suppression and background interference on the detection of the wheat-specific peptide markers. In addition, the method will be further developed toward the ultimate goal of a targeted quantitative method. Both MS and ELISA will be used to analyze gluten-incurred and suspected gluten-contaminated commercial foods to provide method performance comparison and determination of optimum gluten-in-food measurement strategies.

■ ASSOCIATED CONTENT

Ⓢ Supporting Information

Tables SI–SII and Figure S1. This material is available free of charge via the Internet at http://pubs.acs.org.

■ AUTHOR INFORMATION

Corresponding Author

*(M.M.R.) Phone: (240) 402-1987. Fax: (301) 436-2624. E-mail: markm.ross@fda.hhs.gov.

Notes

This paper is not an official U.S. Food and Drug Administration (FDA) guidance or policy statement. No official support or endorsement by the U.S. FDA is intended or should be inferred.

The authors declare no competing financial interest.

■ REFERENCES

(1) Shewry, P. R.; Halford, N. G.; Belton, P. S.; Tatham, A. S. The structure and properties of gluten: an elastic protein from wheat grain. *Philos. Trans. R Soc. London, B* **2002**, *357* (1418), 133–142.

(2) Wieser, H. Chemistry of gluten proteins. *Food Microbiol.* **2007**, *24* (2), 115–119.

(3) Catassi, C.; Fasano, A. Celiac disease. *Curr. Opin. Gastroenterol.* **2008**, *24* (6), 687–691.

(4) Mamone, G.; Picariello, G.; Addeo, F.; Ferranti, P. Proteomic analysis in allergy and intolerance to wheat products. *Expert Rev. Proteomics* **2011**, *8* (1), 95–115.

(5) Ciclitira, P. J.; Ellis, H. J.; Lundin, K. E. A. Gluten-free diet – what is toxic? *Best Practice Res. Clin. Gastroenterol.* **2005**, *19* (3), 359–371.

(6) Comino, I.; Real, A.; de Lorenzo, L.; Cornell, H.; López-Casado, M. Á.; Barro, F.; Lorite, P.; Torres, M. I.; Cebolla, Á.; Sousa, C. Diversity in oat potential immunogenicity: basis for the selection of oat varieties with no toxicity in coeliac disease. *Gut* **2011**, *60* (7), 915–922.

(7) Koerner, T.; Cléroux, C.; Poirier, C.; Cantin, I.; Alimkulov, A.; Elamparo, H. Gluten contamination in the Canadian commercial oat supply. *Food Addit. Contam.* **2011**, *28* (6), 705–710.

(8) Hernando, A.; Mujico, J. R.; Mena, M.; Lombardía, M.; Méndez, E. Measurement of wheat gluten and barley hordeins in contaminated oats from Europe, the United States and Canada by sandwich R5 ELISA. *Eur. J. Gastroenterol. Hepatol.* **2008**, *20* (6), 545–554.

(9) Food labeling; gluten-free labeling of foods. *Fed. Regist.* **2013**, *78* (150), 47154–47179.

(10) Diaz-Amigo, C.; Popping, B. Accuracy of ELISA detection methods for gluten and reference materials: a realistic assessment. *J. Agric. Food Chem.* **2013**, *61* (24), 5681–5688.

(11) Diaz-Amigo, C.; Popping, B. Gluten and gluten-free: issues and considerations of labeling regulations, detection methods, and assay validation. *J. AOAC Int.* **2012**, *95* (2), 337–348.

(12) Haraszi, R.; Chassaigne, H.; Maquet, A.; Ulberth, F. Analytical methods for detection of gluten in food – method developments in

support of food labeling legislation. *J. AOAC Int.* **2011**, *94* (4), 1006−1025.
(13) Sealey-Voyksner, J. A.; Khosla, C.; Voyksner, R. D.; Jorgenson, J. W. Novel aspects of quantitation of immunogenic wheat gluten peptides by liquid chromatography-mass spectrometry/mass spectrometry. *J. Chromatogr., A* **2010**, *1217* (25), 4167−4183.
(14) Shan, L.; Molberg, Ø.; Parrot, I.; Hausch, F.; Filiz, F.; Gray, G. M.; Sollid, L. M.; Khosla, C. Structural basis for gluten intolerance in celiac sprue. *Science* **2002**, *297* (5590), 2275−2279.
(15) Uvackova, L.; Skultety, L.; Bekesova, S.; McClain, S.; Hajduch, M. The MSE-proteomics analysis of gliadins and glutenins in wheat grain identifies and quantifies proteins associated with celiac disease and baker's asthma. *J. Proteomics* **2013**, *93*, 65−73.
(16) Altenbach, S. B.; Vensel, W. H.; DuPont, F. M. Integration of transcriptomic and proteomic data from a single wheat cultivar provides new tools for understanding the roles of individual alpha gliadin proteins in flour quality and celiac disease. *J. Cereal Sci.* **2010**, *52* (2), 143−151.
(17) Mamone, G.; Ferranti, P.; Chianese, L.; Scafuri, L.; Addeo, F. Qualitative and quantitative analysis of wheat gluten proteins by liquid chromatography and electrospray mass spectrometry. *Rapid Commun. Mass Spectrom.* **2000**, *14* (10), 897−904.
(18) Méndez, E.; Valdes, I.; Camafeita, E. Analysis of gluten in foods by MALDI-TOFMS. In *Mass Spectrometry of Proteins and Peptides*; Chapman, J. R., Ed.; Humana Press: Totowa, NJ, USA, 2000; Vol. 146, pp 355−367.
(19) Aebersold, R.; Mann, M. Mass spectrometry-based proteomics. *Nature* **2003**, *422* (6928), 198−207.
(20) Vensel, W. H.; Dupont, F. M.; Sloane, S.; Altenbach, S. B. Effect of cleavage enzyme, search algorithm and decoy database on mass spectrometric identification of wheat gluten proteins. *Phytochemistry* **2011**, *72* (10), 1154−1161.
(21) Simonato, B.; Mainente, F.; Tolin, S.; Pasini, G. Immunochemical and mass spectrometry detection of residual proteins in gluten fined red wine. *J. Agric. Food Chem.* **2011**, *59* (7), 3101−3110.
(22) Pompa, M.; Giuliani, M. M.; Palermo, C.; Agriesti, F.; Centonze, D.; Flagella, Z. Comparative analysis of gluten proteins in three durum wheat cultivars by a proteomic approach. *J. Agric. Food Chem.* **2013**, *61* (11), 2606−2617.
(23) Han, B.; Higgs, R. E. Proteomics: from hypothesis to quantitative assay on a single platform. Guidelines for developing MRM assays using ion trap mass spectrometers. *Brief. Funct. Genomics Proteomics* **2008**, *7* (5), 340−354.
(24) Sherrod, S. D.; Myers, M. V.; Li, M.; Myers, J. S.; Carpenter, K. L.; MacLean, B.; MacCoss, M. J.; Liebler, D. C.; Ham, A.-J. L. Label-free quantitation of protein modifications by pseudo selected reaction monitoring with internal reference peptides. *J. Proteome Res.* **2012**, *11* (6), 3467−3479.
(25) Keshishian, H.; Addona, T.; Burgess, M.; Kuhn, E.; Carr, S. A. Quantitative, multiplexed assays for low abundance proteins in plasma by targeted mass spectrometry and stable isotope dilution. *Mol. Cell. Proteomics* **2007**, *6* (12), 2212−2229.
(26) Tatham, A. S.; Gilbert, S. M.; Fido, R. J.; Shewry, P. R. Extraction, separation, and purification of wheat gluten proteins and related proteins of barley, rye, and oats. In *Celiac Disease*; Springer: Berlin, Germany, 2000; pp 55−73.
(27) Wieser, H.; Antes, S.; Seilmeier, W. Quantitative determination of gluten protein types in wheat flour by reversed-phase high-performance liquid chromatography. *Cereal Chem.* **1998**, *75* (5), 644−650.
(28) Rombouts, I.; Lagrain, B.; Brunnbauer, M.; Delcour, J. A.; Koehler, P. Improved identification of wheat gluten proteins through alkylation of cysteine residues and peptide-based mass spectrometry. *Sci. Rep.* **2013**, *3* (2279), 1−11.
(29) Šalplachta, J.; Marchetti, M.; Chmelík, J.; Allmaier, G. A new approach in proteomics of wheat gluten: combining chymotrypsin cleavage and matrix-assisted laser desorption/ionization quadrupole ion trap reflectron tandem mass spectrometry. *Rapid Commun. Mass Spectrom.* **2005**, *19* (18), 2725−2728.
(30) Altenbach, S.; Vensel, W.; DuPont, F. Analysis of expressed sequence tags from a single wheat cultivar facilitates interpretation of tandem mass spectrometry data and discrimination of gamma gliadin proteins that may play different functional roles in flour. *BMC Plant Biol.* **2010**, *10* (1), 7.
(31) Comino, I.; Real, A.; de Lourdes Moreno, M.; Montes, R.; Cebolla, Á.; Sousa, C. Immunological determination of gliadin 33-mer equivalent peptides in beers as a specific and practical analytical method to assess safety for celiac patients. *J. Sci. Food Agric.* **2013**, *93* (4), 933−943.
(32) Valdes, I.; Garcia, E.; Llorente, M.; Mendez, E. Innovative approach to low-level gluten determination in foods using a novel sandwich enzyme-linked immunosorbent assay protocol. *Eur. J. Gastroenterol. Hepatol.* **2003**, *15* (5), 465−474.
(33) MacLean, B.; Tomazela, D. M.; Shulman, N.; Chambers, M.; Finney, G. L.; Frewen, B.; Kern, R.; Tabb, D. L.; Liebler, D. C.; MacCoss, M. J. Skyline: an open source document editor for creating and analyzing targeted proteomics experiments. *Bioinformatics* **2010**, *26* (7), 966−968.
(34) Zhang, H.; Liu, Q.; Zimmerman, L. J.; Ham, A.-J. L.; Slebos, R. J. C.; Rahman, J.; Kikuchi, T.; Massion, P. P.; Carbone, D. P.; Billheimer, D.; Liebler, D. C. Methods for peptide and protein quantitation by liquid chromatography-multiple reaction monitoring mass spectrometry. *Mol. Cell. Proteomics* **2011**, DOI: 10.1074/mcp.M110.006593.
(35) Anderson, O. D.; Hsia, C. C.; Torres, V. The wheat γ-gliadin genes: characterization of ten new sequences and further understanding of γ-gliadin gene family structure. *TAG, Theor. Appl. Genetics* **2001**, *103* (2), 323−330.
(36) Carr, S. A.; et al. Targeted Peptide Measurements in Biology and Medicine: Best Practices for Mass Spectrometry-based Assay Development Using a Fit-for-Purpose Approach. *Mol. Cell. Proteomics* **2014**, *7*, mcp-M113.
(37) *Guidance for the Analysis and Documentation to Support Regulatory Action On Pesticide Residues*; U.S. Food and Drug Administration Office of Regulatory Affairs, Washington, DC, 2009; ORA-Lab.010, (1.4), 1−16.
(38) *Mass Spectrometry for Confirmation of the Identity of Animal Drug Residues*; U.S. Food and Drug Administration Center for Veterinary Medicine, Washington, DC, 2003; Final Guidance for Industry, (118).
(39) Peterson, A. C.; Russell, J. D.; Bailey, D. J.; Westphall, M. S.; Coon, J. J. Parallel reaction monitoring for high resolution and high mass accuracy quantitative, targeted proteomics. *Mol. Cell. Proteomics* **2012**, *11* (11), 1475−1488.

JOURNAL OF AGRICULTURAL AND FOOD CHEMISTRY

Article

pubs.acs.org/JAFC

Simultaneous Determination of Glutathione, Cysteine, Homocysteine, and Cysteinylglycine in Biological Fluids by Ion-Pairing High-Performance Liquid Chromatography Coupled with Precolumn Derivatization

Wenbing Zhang,† Pingliang Li,† Qianqian Geng, Yongheng Duan, Mingcheng Guo, and Yongsong Cao*

College of Agriculture and Biotechnology, China Agricultural University, Beijing, China, 100193

ABSTRACT: Biologically active low-molecular-mass thiols, mainly including glutathione (GSH), cysteine (Cys), homocysteine (Hcy), and cysteinylglycine (Cys-Gly), are important physiological components in biological fluids, and their analytical methods have gained continuous attention over recent years. We developed and validated a novel HPLC method for the quantification of GSH, Cys, Hcy, and Cys-Gly in human plasma, urine, and saliva using 4-chloro-3,5-dinitrobenzotrifluoride as the derivatization reagent. Analyses were linear from 0.15 to 500 μM with the coefficient regression range of 0.9987−0.9994. Detection limits ranged from 0.04 to 0.08 μM (S/N = 3). The developed method was applied to quantification of four thiols in human biological fluids collected from five donors with the concentration range of 2.50−124.25 μM, 0−72.81 μM, and 0−4.25 μM for plasma, urine, and saliva, respectively. The present method seemed to be an attractive choice for the determination of thiols in plasma, urine, and saliva.

KEYWORDS: *cysteine, glutathione, homocysteine, high performance liquid chromatography, precolumn derivatization, 4-chloro-3,5-dinitrobenzotrifluoride*

1. INTRODUCTION

Biologically active low-molecular-mass thiols, mainly including glutathione (GSH), cysteine (Cys), homocysteine (Hcy), and cysteinylglycine (Cys-Gly), are important physiological components in biological fluids and important biomarkers for a wide range of human diseases.[1,2] GSH is the most abundant nonprotein thiol, and its altered levels occur in plasma of patients with leukemia, diabetes, or AIDS.[3] Cys is involved in a variety of important cellular functions, and its levels in urine have been recognized as an important indicator for kidney stones and cystinuria.[4,5] The elevated level of Hcy in plasma is considered as a risk factor for cardiovascular disease.[1,6] Increased concentration of Cys-Gly in plasma or urine has been observed to be linked to rheumatoid arthritis.[1] Therefore, quantification of these thiols in biological fluids is important for monitoring some special pathological conditions of human.

There have been many analytical methods for these thiols, which mainly involved fluorescent assays,[7] electrochemical assays,[8] capillary electrophoresis,[9,10] gas chromatography,[11,12] high performance liquid chromatography (HPLC),[13−37] gas chromatography with mass spectrometry,[38,39] and liquid chromatography with mass spectrometry.[40,41] Recently, the derivatization followed by HPLC determination of the resulting derivatives attracted more attention because it is relatively simple and can simultaneously determine several thiols with good sensitivity.[33,42] The derivatization reagent is very important for the method sensitivity and recovery because it can provide chromophore or fluorophores and stabilize the thiol molecules. There have been a number of commonly used derivatization reagents, such as 2-chloro-1-methylquinolinium tetrafluoroborate (CMQT),[16−18] 5,5′-dithiobis(2-nitrobenzoic acid) (DTNB),[19] *o*-phthalaldheyde (OPA),[24,25] monobromobimane (mBrB),[26,27] ammonium-7-fluoro-2,1,3-benzoxadiazole-4-sulfonate (SBD-F),[28] and 4-(aminosulfonyl)-7-fluoro-2,1,3-benzoxadiazole (ABD-F).[29,30] Although these reagents have been well adapted in many fields, new labeling reagents are still needed to improve the detection properties.

Ion-pairing chromatography is a mature and valuable analytical and separation strategy in biological fluids. Its used has been reported in a very wide range of applications concerning organic and inorganic ions, neutrals, and zwitterionic compounds.[13−18] Therefore, the ion-pairing chromatography would be a better approach in separation and analysis of GSH, Cys, Hcy, and Cys-Gly in biological fluids.

In our previous studies, 4-chloro-3,5-dinitrobenzotrifluoride (CNBF) has been demonstrated to be a feasible and superior derivatization reagent for amino compounds.[43−45] CNBF has one activated halide leaving group which can be easily displaced by the thiol group (−SH), leading to formation of the stable thioether with well-defined absorbance at 230 nm. The aim of the present work is to develop and validate a novel HPLC method for the quantification of GSH, Cys, Hcy, and Cys-Gly in human plasma, urine, and saliva. Then the levels of thiols in three biological fluids collected from five healthy donors were determined with this novel method.

2. MATERIALS AND METHODS

2.1. Chemicals and Reagents. Glutathione, L-cysteine, DL-homocysteine, L-cysteinylglycine, trichloroacetic acid (TCA), 5,5′-

Received: March 22, 2014
Revised: June 9, 2014
Accepted: June 10, 2014
Published: June 10, 2014

ACS Publications © 2014 American Chemical Society

dx.doi.org/10.1021/jf5014007 | J. Agric. Food Chem. 2014, 62, 5845−5852

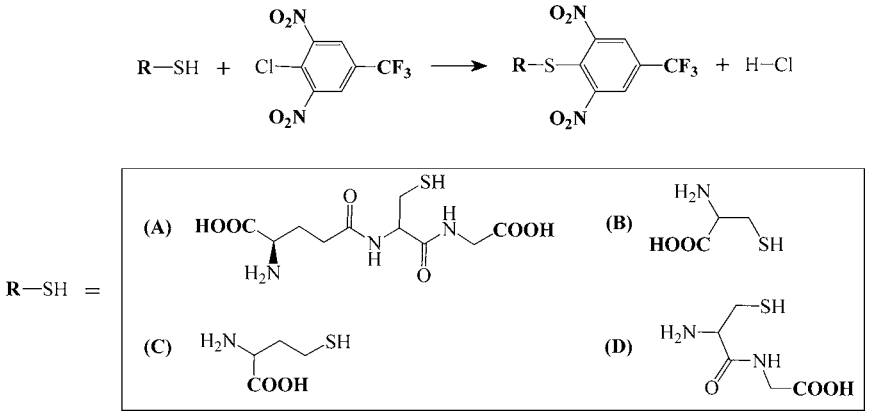

Figure 1. General reaction of thiols with 4-chloro-3,5-dinitrobenzotrifluoride.

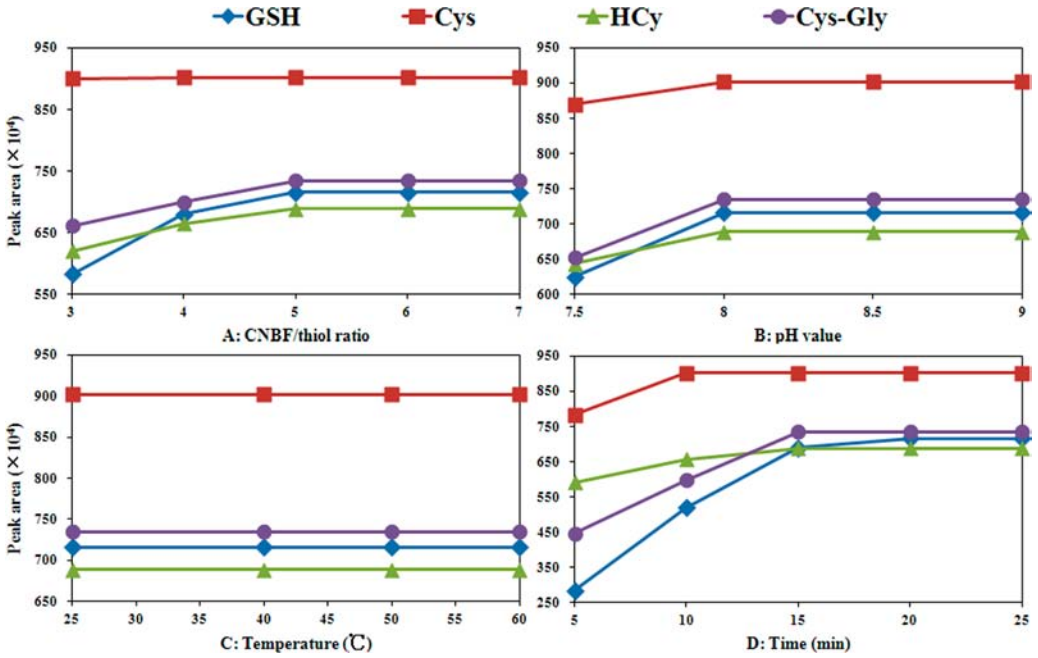

Figure 2. Effects of CNBF/thiol molar ratio (A), pH (B), reaction temperature (C), and reaction time (D) on the resulting peak areas of the thiol derivatives. (A) Constant conditions: thiol standard 100 μM, pH 8.0, 25 °C, 20 min. (B) Constant conditions: thiol standard 100 μM, CNBF 500 μM, 25 °C, 20 min. (C) Constant conditions: thiol standard 100 μM, CNBF 500 μM, pH 8.0, 20 min. (D) Constant conditions: thiol standard 100 μM, CNBF 500 μM, pH 8.0, 25 °C.

dithiobis(2-nitrobenzoic acid), and trifluoroacetic acid (TFA) were analytical grade reagent and purchased from Sinopharm Chemical Reagent Beijing Co., Ltd. (Beijing, China). CNBF was provided by Alfa Aesar (Ward Hill, MA, USA). Tris(2-carboxyethyl)phosphine (TCEP) was purchased from Fluka (Germany). Acetonitrile and methanol (HPLC grade) was purchased from J.T. Baker (Phillipsburg, NJ, USA). The ultrapure water was obtained by a Milli-Q water purification system (Millipore, Billerica, MA, USA). The standard solutions of 5.0 mM GSH, Cys, Hcy, and Cys-Gly were prepared in ultrapure water. The CNBF standard solution of 40.0 mM was prepared in methanol. The stock solutions were stored in the dark at 4 °C when not in use. H_3BO_3–$Na_2B_4O_7$ buffer was prepared by mixing 0.2 mol/L H_3BO_3 solution with 0.05 mol/L Na_2B_4O7 solution to the required pH value.

2.2. Instruments. A HPLC system, consisting of two LC-20ATvp pumps and an SPD-20Avp ultraviolet detector (Shimadzu, Japan), was applied for the separation and analysis. A reversed-phase Kromasil ODS C_{18} column (250 mm × 4.6 mm, 5 μm) and Chromatograph Solution Light Chemstation for LC system were employed to obtain and process chromatographic data.

2.3. Sample Preparation. In the present study, venous blood samples (about 2.0 mL), urine samples (about 5.0 mL), and saliva samples (about 1.0 mL) were collected from five healthy donors (male:female = 3:2, 23–30 years of age, Beijing, China) on April 27th, 2012. Blood samples were placed in precooled ethylenediaminetetraacetic acid (EDTA) Vacutainer tubes and immediately centrifuged at 2500*g* for 10 min at 4 °C. The supernatant liquid (plasma) was collected and stored at −80 °C for the analysis. The urine samples were collected and stored in a 5 mL tube at −80 °C until analysis. Five minutes after the gargling with distilled water, donors kept tongue in touch with palate and made the saliva naturally flow down into a 5 mL tube. Then the saliva samples were stored at −80 °C for analysis.

The pretreatment method was referenced to the report by Cevasco et al.[33] with some modifications. After thawing, 100 μL of sample (plasma, urine, or saliva) was mixed with 10 μL of a solution of TCEP (50 mM in borate buffer, pH 7.4) in a vial and incubated at 25 °C for 10 min. Then 90 μL of a solution containing 1% TCA and 1 mM EDTA was added and the total solution was centrifuged for 10 min at 10000*g*. The obtained supernatant was collected for the subsequent derivatization.

dx.doi.org/10.1021/jf5014007 | J. Agric. Food Chem. 2014, 62, 5845–5852

2.4. Derivatization Method. After the pretreatment step, 100 μL of the supernatant, 20 μL of 10 mM CNBF solution, 20 μL of methanol, and 50 μL of borate buffer (0.2 M, pH 8.0) were mixed and incubated at 25 °C for 20 min. Then the derivatization was terminated with 10 μL of 2 M HCl. The resulting solution was filtered through a 0.22 μm filter membrane (Millipore Corporation, Belfast, MA, USA) and injected into the chromatographic system.

2.5. Chromatographic Method. Before the analysis, the C_{18} column equipped with a C_{18} guard column (4 mm × 3 mm i.d.) was pre-equilibrated with the mobile phase for 20 min. HPLC separation of the thiol derivatives was carried out on a reversed-phase Kromasil ODS C_{18} column. The mobile phase was composed of acetonitrile (eluent A) and water with 0.1% (v/v) TFA (eluent B).

Optimum separation for plasma samples was achieved in gradient condition as follows (expressed as the proportion of eluent B): 0−9.0 min, a linear gradient starting from 70% to 20%; 9.0−10.0 min, 20%; 10.0−15.0 min, linear gradient from 20% to 70%. Optimum separation for urine and saliva samples (proportion of eluent B): 0−5.0 min, a linear gradient starting from 70% to 20%; 5.0−8.0 min, 20%; 8.0−11.0 min, linear gradient from 20% to 70%. The analysis was executed with injection volume of 20 μL, flow rate of 1.0 mL/min and UV detection wavelength at 230 nm. Each sample was injected in triplicate, and the analysis was carried out at 25 °C.

2.6. Comparison with a Reference Method. To validate this method, the thiols in the plasma samples from the five donors were also determined by a reference method[19] and the data from the two methods were compared by the Independent Sample t-Test using SPSS (version, 17.0). The plasma sample was derivatized with 10 mM DTNB at room temperature in pH 7.2 for 5 min, filtered, and injected into HPLC. The mobile phase was composed of methanol (A) and 100 mM KH_2PO_4 (B) with the ratio of 12:88 (A/B, v/v). The analysis was executed with injection volume of 20 μL, flow rate of 1.2 mL/min, and UV detection wavelength at 230 nm.

3. RESULTS AND DISCUSSION

3.1. Optimization of Derivatization Conditions. The general reaction of CNBF with thiols is shown in Figure 1. CNBF can react with thiols in low concentration to form stable thioether derivatives under alkaline conditions. The main factors affecting the derivatization yields were concentration ratio of CNBF to thiol, pH value, reaction temperature, and reaction time. To determine the optimum derivatization conditions, the effects of the four factors on the peak areas (yields) were investigated, and the results are shown in Figure 2.

The optimum concentration ratio of CNBF to thiol was of primary importance. Its effects on the peak areas are shown in Figure 2A. The thiol (100 μM) was reacted with various concentrations of CNBF (300, 400, 500, 600, and 700 μM, CNBF/thiol = 3−7:1). At concentration ratio ≥5:1, the peak areas of four thiols reached the most and kept constant. The levels of GSH, Cys, Hcy, and Cys-Gly in human fluids were reported to be in the range of 2.07−17.80, 72.0−312.70, 1.30−9.20, and 0.49−11.30 μM.[14,22,33] In the real analysis, 2.0 mM was the adequate concentration for CNBF to keep the concentration ratio ≥5:1. The optimum reaction pH value was determined by derivatizing thiols in H_3BO_3−$Na_2B_4O_7$ buffer with the pH values ranging from 7.5 to 9.0. Figure 2B shows that the peak areas of thiol-CNBF are the most at pH range of 8.0−9.0. Because high pH could lead to the hydrolysis of CNBF, pH 8.0 was selected for all experiments. A temperature range of 25−60 °C was used to study the optimum temperature. Figure 2C shows when other conditions are kept constant, temperature has no significant influence on the peak areas of four thiols. Therefore, 25 °C (room temperature) was selected for the derivatization temperature. The reaction time was also an essential factor, and its effects on derivatization were studied (Figure 2D). It can be seen that when the time ≥ 20 min, the peak areas of four thiol derivatives reached the most. Therefore, the derivatization time was 20 min.

CNBF has relatively poor water solubility, thus organic solvent should be added to the reaction medium to avoid the precipitation of the reagent and derivative. The tests showed the content of methanol in the total solutions should be more than 15%, especially for the derivatization of Cys.

3.2. Optimization of Separation Conditions. Test showed that, without ion-pairing reagents in the mobile phase, the thiol derivatives were too polar to be well retained on the reversed-phase column, which resulted in difficulty in the separation. In the present study, TFA was used as the ion-pairing agent to achieve fast and optimum separation of four thiol derivatives, CNBF, and matrix interferences. The effects of TFA concentration (range of 0.01−0.20%) on separation of the derivatives were also studied. It was found that high concentration may cause damage to the C18 column. Test also indicated 0.1% (v/v) TFA was the optimum adding concentration. To obtain better separation within shorter analysis time, the separation conditions for plasma, urine, and saliva were investigated respectively as previously mentioned in section 2.5. In the present work, a wavelength of 230 nm was selected in the HPLC-UV analysis to obtain good absorption and minimize the interferences.

Typical chromatograms of reaction of thiols with CNBF and plasma sample with spiking thiols are shown in Figure 3, in which the retention times of GSH, Hcy, Cys-Gly, and Cys were 4.05, 5.45, 7.50, and 11.80 min respectively and the separation can be completed within 15 min. Typical chromatograms of reaction of thiols with CNBF, urine sample with spiking thiols, and saliva sample with spiking thiols are shown in Figure 4, in which the retention times of GSH, Hcy, Cys-Gly, and Cys were 3.85, 4.95, 6.50, and 9.00 min respectively and the separation can be completed within 11 min.

3.3. Stability of the Derivative. The stability of thiol-CNBF in methanol−water (20:80, v/v) at 4 °C was investigated over 5 days without light irradiation. Results showed there was no significant change in the peak areas of GSH-CNBF, Cys-CNBF, Hcy-CNBF, and Cys-Gly-CNBF. When sample was illuminated by ordinary light of 100 W bulb for 24 h, there was also no significant change in the peak areas of the four thiol derivatives. Seven days later, the average degradation rates at room temperature were 4.20%, 5.05%, 5.40%, and 4.85% for GSH-CNBF, Cys-CNBF, Hcy-CNBF, and Cys-Gly-CNBF respectively. It appeared that the thiol derivatives were very stable.

3.4. Validation of the Method and Application to Sample Analysis. Text mixtures of different concentrations of thiols were prepared and analyzed by using the optimized derivatization procedure and separation conditions. Sensitivity of the method was determined by the limit of detection (LOD) at a signal-to-noise ratio of 3 and the limit of quantification (LOQ) at a signal-to-noise ratio of 10.[29,30] The usual numerical value used is the relative standard deviation (RSD) for reproducibility. The reproducibility of this analytical method was evaluated both intraday and interday with thiol concentration of 50 μM. The linear calibration range, regression equation, R^2, LOD, LOQ, and RSD of four thiols with this new method were calculated, and the results are listed in Table 1. Results showed that the correlation coefficients for

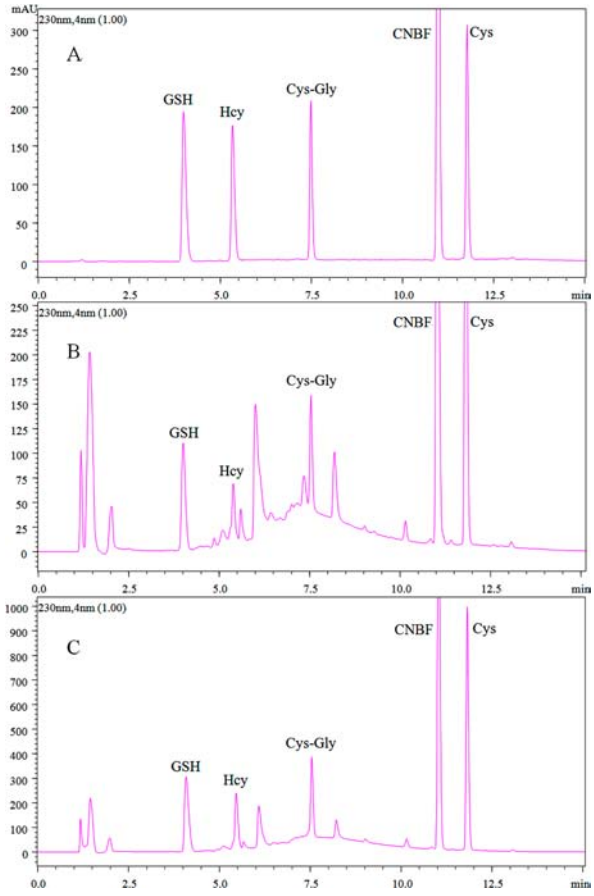

Figure 3. Chromatograms obtained from the reaction of CNBF with thiols (A, 40 μM of GSH, Cys, Hcy, and Cys-Gly; B, plasma samples; C, plasma samples with spiking 40 μM of GSH, Cys, Hcy, and Cys-Gly). Chromatographic conditions: column, reversed-phase Kromasil ODS C_{18} column (250 mm × 4.6 mm i.d., particle size 5 μm); UV detection, λ = 230 nm; mobile phase, acetonitrile (A) and water with 0.1% (v/v) TFA (B). Gradient conditions: B, 0−9.0 min, a linear gradient starting from 70% to 20%; B, 9.0−10.0 min, 20%; B, 10.0−15.0 min, linear gradient from 20% to 70%; flow rate, 1.0 mL/min; 25 °C.

these thiols were from 0.9987 to 0.9994. The RSDs for the thiol-CNBF are from 2.26% to 2.92% for within-day determination (n = 6) and from 2.65% to 3.55% for between-day determination (n = 6). The detection limits for four thiols ranged from 0.04 μM to 0.08 μM.

In the present work, the applicability of the proposed method was evaluated in plasma, urine, and saliva. Four thiol peaks were identified by spiking thiol standards to the fluid sample. Before adding the reducing reagent TCEP, the fluid sample was spiked with thiol standard 5 and 50 μM, respectively. Then the fluid samples with and without spiking were extracted and analyzed. Because the fluid contained thiols, the recovery should be calculated by the formula

$$\text{recovery} = (C - C_d)/C_s \times 100\%$$

where C represents the total found concentration of thiol after spiking, C_d represents the initially measured concentration before spiking, and C_s represents the spiked concentration. The recoveries of thiols from plasma, urine, and saliva were investigated. Table 2 shows the recoveries of thiols are in the range of 82.5% to 91.6% for plasma, 86.8% to 95.0% for urine, and 80.5% to 88.5% for saliva, depending on the sample

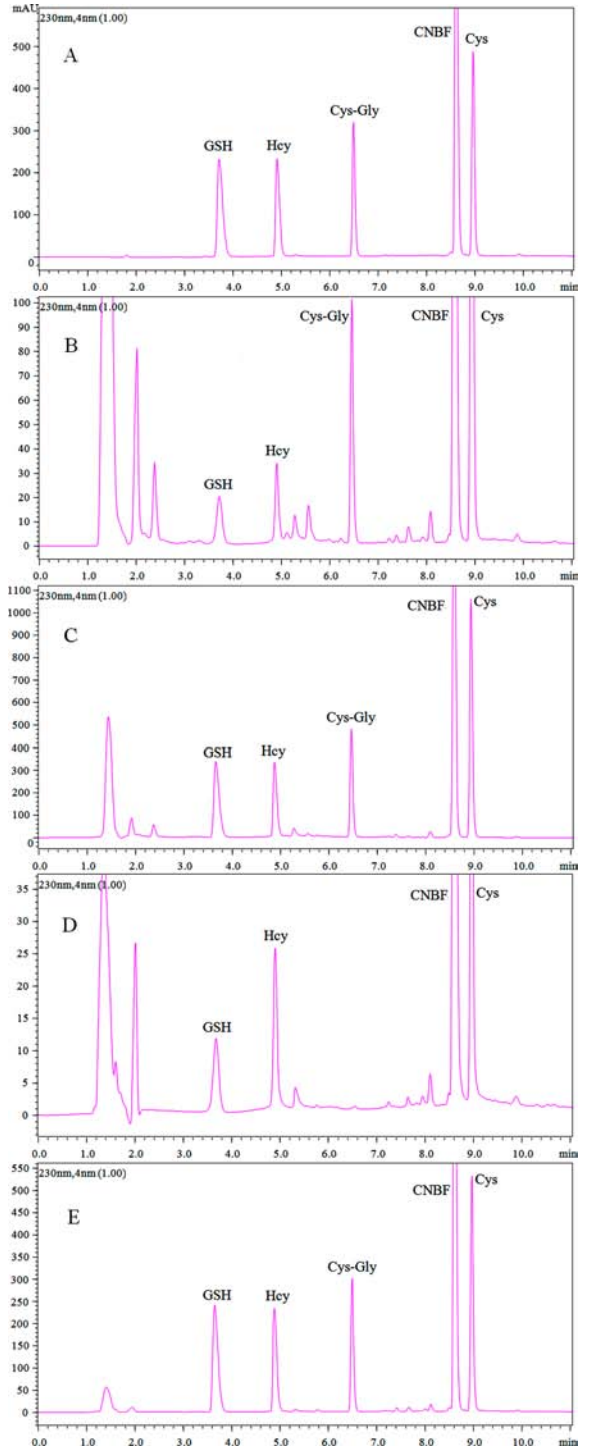

Figure 4. Chromatograms obtained from the reaction of CNBF with thiols (A, 50 μM of GSH, Cys, Hcy, and Cys-Gly; B, urine samples; C, urine samples with spiking 50 μM of GSH, Cys, Hcy, and Cys-Gly; D, saliva samples; E, saliva samples with spiking 50 μM of GSH, Cys, Hcy, and Cys-Gly). Chromatographic conditions: column, reversed-phase Kromasil ODS C_{18} column (250 mm × 4.6 mm i.d., particle size 5 μm); UV detection, λ = 230 nm; mobile phase, acetonitrile (A) and water with 0.1% (v/v) TFA (B). Gradient conditions: B, 0−5.0 min, a linear gradient starting from 70% to 20%; B, 5.0−8.0 min, 20%; B, 8.0−11.0 min, linear gradient from 20% to 70%; flow rate, 1.0 mL/min; 25 °C.

investigated. RSDs are from 1.75% to 3.62% for plasma, 1.85% to 3.84% for urine, and 2.00% to 4.08% for saliva.

dx.doi.org/10.1021/jf5014007 | J. Agric. Food Chem. 2014, 62, 5845−5852

Table 1. Linear Calibration Range, Regression Equation, R^2, LOD, LOQ, and RSD of Thiol-CNBF[a]

parameters	GSH-CNBF	Cys-CNBF	Hcy-CNBF	Cys-Gly-CNBF
calibration range (μM)	0.15−500.0	0.15−500.0	0.15−500.0	0.15−500.0
regression eq, y	71698x + 561.9	90251x − 1263	68920x + 865	73505x + 1106.5
coeff regression, R^2	0.9994	0.9987	0.9992	0.9994
RSD, n = 6				
within-day	2.46	2.85	2.92	2.26
between-day	2.90	2.70	3.55	2.65
LOD (μM)[b]	0.06	0.04	0.08	0.06
LOQ (μM)[c]	0.15	0.12	0.15	0.15

[a]x: concentration of thiol-CNBF (μM). y: peak area of thiol-CNBF. [b]S/N = 3, per 20 μL injection volume. [c]S/N = 10, per 20 μL injection volume.

Table 2. Average Recoveries of Thiols from Plasma, Urine, and Saliva Samples by Using Proposed Method

fluid	thiols	initial[a] (μM)	Spiked (μM)	total[b] (μM)	found[c] (μM)	recovery (%)	RSD[d] (%)
plasma	GSH	26.50	5.00	30.93	4.43	88.6	3.62
			50.00	72.30	45.80	91.6	2.05
	Cys	122.40	5.00	126.65	4.25	85.0	3.24
			50.00	165.50	43.10	86.2	2.05
	Hcy	5.70	5.00	9.83	4.13	82.5	2.58
			50.00	47.20	41.50	83.0	2.10
	Cys-Gly	19.25	5.00	23.70	4.45	89.0	2.90
			50.00	64.50	45.25	90.5	1.75
urine	GSH	5.40	5.00	10.02	4.62	92.3	3.02
			50.00	52.90	47.50	95.0	1.85
	Cys	72.81	5.00	77.24	4.43	88.5	3.84
			50.00	117.91	45.10	90.2	2.73
	Hcy	1.20	5.00	5.54	4.34	86.8	3.68
			50.00	45.20	44.00	88.0	3.50
	Cys-Gly	8.85	5.00	13.40	4.55	91.0	2.55
			50.00	55.75	46.90	93.8	2.32
saliva	GSH	2.80	5.00	6.95	4.15	83.0	3.62
			50.00	45.95	43.15	86.3	2.15
	Cys	3.54	5.00	7.57	4.03	80.5	4.08
			50.00	47.44	43.90	87.8	2.25
	Hcy	1.21	5.00	5.31	4.10	82.0	2.96
			50.00	43.71	42.50	85.0	2.05
	Cys-Gly	0	5.00	4.26	4.26	85.2	2.50
			50.00	44.25	44.25	88.5	2.00

[a]Mean value of six initial measured concentrations in biological fluid before spiking. [b]Mean value of six initial measured concentrations in biological fluid after spiking. [c]The total measured concentration minus the initial measured concentration. [d]Mean value of six determinations.

3.5. Comparison of CNBF with Other Derivatizing Reagents. The comparison of CNBF with these reported derivatizing reagents is given in Table 3. In comparison to the ultraviolet derivatizing reagents, CNBF was superior to CMQT and BCPB in the method sensitivity but inferior to them in the derivatization velocity. Although the methods with AuNPs (Au nanoparticles) and TCDI (1,1′-thiocarbonyldiimidazole) as the derivatizing reagent were more sensitive than the present method, the derivatization times with them were much longer (2 h). In comparison to several fluorescent reagents, the present method was more sensitive than the method with NDA or 5-BMF as the derivatizing reagent but showed no superiority to that with OPA, mBrB, SBD-F, SBD-BF, ABD-F, MIPBO, and TMPAB-o-M. However, derivatization with SBD-F, SBD-BF, ABD-F, MIPBO, and TMPAB-o-M required more time or higher temperature than that with CNBF. mBrB has the one drawback that the reagent itself, the hydrolysis products, and the impurities are fluorescent, which may interfere with analysis.[46] Apart from thiols, OPA can also very easily react with primary amino compounds in biological samples, resulting in an increase of interferences in the form of amino−OPA adducts.[42] CNBF can easily react with thiols (25 °C, pH 8.0), but its reaction with amines needed higher temperature (60 °C) and higher pH (9.0),[43−45] indicating that CNBF has good selectivity for the analysis of thiols. In conclusion, this CNBF-derivatization based method showed superiority in relative sensitivity and selectivity. Besides, HPLC with a UV detector, known for its stability, universality, and low demand in terms of maintenance, belongs to the standard instrumentation of an analytical laboratory for clinical samples.[2,23] Therefore, the proposed method is an attractive choice for the determination of thiols in human biological fluids.

3.6. Analysis of Fluid Samples and the Validation by the Reference Method. The developed method was applied to quantification of GSH, Cys, Hcy, and Cys-Gly in plasma, urine, and saliva collected from five donors. The detected concentrations of GSH, Cys, Hcy, and Cys-Gly are given in Table 4. In the plasma samples, the concentrations were in the range of 8.75 to 26.50 μM, 86.45 to 124.25 μM, 2.50 to 10.57 μM, and 11.20−27.00 μM for GSH, Cys, Hcy, and Cys-Gly

Table 3. Comparison of the Derivatization Conditions and Detection Limit of the Derivatizing Reagents Reported for Determination of Thiols in Different Matrix[a]

anal. meth	thiol analytes	derivatizing reagent	derivatization conditions	matrix	detection limit	ref
CE-LIF	GSH, Cys, Hcy, Cys-Gly	5-BMF	RT, 10 min	human plasma, urine	0.061−0.156 μM	9
CE-UV	GSH, Cys, Hcy, Cys-Gly	AuNPs	RT, 2 h	human plasma	10−65 nM	10
HPLC-UV	GSH, Cys, Hcy	CMQT	RT, 1 min	human plasma	0.1−0.3 μM	16
HPLC-UV	GSH, Cys, Hcy, Cys-Gly	CMQT	RT	human saliva	0.5 μM	17
HPLC-UV	GSH, Cys, Hcy, Cys-Gly	CMQT	RT	human plasma	0.5 μM	18
HPLC-UV	GSH, Cys, Hcy, Cys-Gly	DTNB	RT, 5 min	human plasma	ND	19
HPLC-UV	Cys, Hcy	CMPI	RT, 10 min	human plasma	4 pmol[b]	20
HPLC-UV	Cys	TCDI	RT, 2 h	ND	2 pmol[b]	21
HPLC-UV	Cys, Hcy, Cys-Gly	TCDI	RT, 2 h	human plasma, urine	ND	22
HPLC-UV	GSH, Cys, Hcy, Cys-Gly	BCPB	RT, 10 min	human plasma	0.2 μM	23
HPLC-FL	GSH	OPA	RT, 1 min	ND	25 fmol[c]	24
HPLC-FL	Hcy	OPA	Post column	human cell	100 fmol[c]	25
HPLC-FL	GSH, Cys, Hcy,	mBrB	RT, 5 min	human plasma	2 pmol[b]	26
HPLC-FL	GSH, Cys	mBrB	RT, 30 min	human muscle	30, 50 nM	27
HPLC-FL	GSH, Cys, Hcy, Cys-Gly	SBD-F	60 °C, 1 h	human plasma	ND	28
HPLC-FL	GSH, Cys	ABD-F	60 °C, 10 min	human plasma	20, 5 nM	29
HPLC-FL	GSH, Cys, Hcy, Cys-Gly	ABD-F	50 °C, 10 min	human plasma, urine, saliva	0.1−0.5 μM	30
HPLC-FL	GSH, Cys	MIPBO	40 °C, 35 min	human urine	3.5−15.0 fmol[c]	31
HPLC-FL	GSH, Cys, Hcy	MIAC	RT, 1 min	human plasma	1.2−2.0 pmol[b]	32
HPLC-FL	GSH, Cys, Hcy, Cys-Gly	SBD-BF	RT, 30 min	human plasma	0.01−0.1 μM	33
HPLC-FL	GSH	NDA	RT, 4 min	must and wine	0.1 μM	34
HPLC-FL	GSH, Cys,	TMPAB-o-M	37 °C, 6 min	pig liver	0.13−0.25nM	35
HPLC-UV	GSH, Cys, Hcy, Cys-Gly	CNBF	25 °C, 20 min	human plasma, urine, saliva	0.04−0.08 μM	this work

[a]CE-LIF, capillary electrophoresis with laser-induced fluorescent detection; CE-UV, capillary electrophoresis with ultraviolet detection; HPLC-UV, high performance liquid chromatography with ultraviolet detection; HPLC-FL, high performance liquid chromatography with fluorescent detection; 5-BMF, 5-(bromomethyl) fluorescein; CMQT, 2-chloro-1-methylquinolinium tetrafluoroborate; AuNPs, the synthesized triangular gold nanoparticles; CMPI, 2-chloro-1-methylpyridinium iodide; DTNB, 5,5-dithiobis (2-nitrobenzoic acid); TCDI, 1,1′-thiocarbonyldiimidazole; BCPB, 1-benzyl-2-chloropyridinium bromide; OPA, *o*-phthalaldheyde; mBrB, monobromobimane; SBD-F, ammonium-7-fluoro-2,1,3-benzoxadiazole-4-sulfonate; MIPBO, 5-methyl-(2-(*m*-iodoacetylaminophenyl) benzoxazole; MIAC, *N*-(2-acridonyl) maleimide; SBD-BF, 5-bromo-7-fluorobenzo-2-oxa-1,3-diazole-4-sulfonate; NDA, 2,3-naphthalenedialdehyde; TMPAB-o-M, 1,3,5,7-tetramethyl-8-phenyl-(2-maleimide) difluoroboradiaza-s-indacene; ABD-F, 4-(aminosulfonyl)-7-fluoro-2,1,3 -benzoxadiazole; RT, room temperature; ND, not described. [b]The full unit: pmol per injection (20 μL). [c]The full unit: fmol per injection (20 μL).

Table 4. Detected Concentrations of GSH, Cys, Hcy, and Cys-Gly in the Plasma, Urine, and Saliva Collected from Five Donors

sample[a]	donor	GSH (μM)		Cys (μM)		Hcy (μM)		Cys-Gly (μM)	
plasma	01	12.2 ± 0.85	12.0 ± 1.15[b]	124 ± 5.50	130 ± 8.20[b]	4.02 ± 0.12	4.35 ± 0.40[b]	11.2 ± 0.75	10.5 ± 0.95[b]
	02	8.75 ± 0.60	9.00 ± 0.64[b]	105 ± 7.25	105 ± 11.5[b]	10.6 ± 0.97	10.0 ± 0.46[b]	25.0 ± 1.68	25.0 ± 1.22[b]
	03	18.5 ± 1.40	17.9 ± 2.15[b]	86.5 ± 5.03	82.2 ± 2.55[b]	2.53 ± 0.22	2.12 ± 0.50[b]	27.0 ± 2.85	25.9 ± 0.70[b]
	04	26.2 ± 1.52	25.9 ± 1.93[b]	122 ± 10.20	120 ± 7.83[b]	5.70 ± 0.10	5.50 ± 0.50[b]	19.2 ± 1.02	20.0 ± 1.50[b]
	05	15.6 ± 0.95	15.5 ± 0.80[b]	90.8 ± 6.80	91.5 ± 6.40[b]	2.50 ± 0.20	2.24 ± 0.31[b]	23.0 ± 1.55	22.5 ± 2.40[b]
urine	01	5.40 ± 0.07		72.8 ± 1.25		1.20 ± 0.02		8.85 ± 0.24	
	02	12.1 ± 0.35		61.0 ± 0.87		2.45 ± 0.46		12.00 ± 1.22	
	03	1.43 ± 0.08		56.8 ± 1.04		0.82 ± 0.03		12.1 ± 0.53	
	04	6.57 ± 0.12		59.0 ± 3.25		1.10 ± 0.02		11.0 ± 0.88	
	05	9.35 ± 0.08		66.0 ± 1.95		ND[c]		3.24 ± 0.09	
saliva	01	1.43 ± 0.35		4.25 ± 0.60		0.84 ± 0.21		ND[c]	
	02	2.80 ± 0.50		3.54 ± 0.41		1.21 ± 0.06		ND[c]	
	03	3.20 ± 0.33		1.95 ± 0.05		0.75 ± 0.08		0.35 ± 0.04	
	04	1.25 ± 0.20		3.55 ± 0.70		0.98 ± 0.08		ND[c]	
	05	0.90 ± 0.11		1.24 ± 0.20		1.33 ± 0.12		0.55 ± 0.08	

[a]Each fluid sample was determined in triplicates. [b]The data was obtained with a reference method described in section 2.6. [c]Not detected.

respectively, with highest average concentration for Cys and lowest for Hcy. For urine samples, the concentration ranges were 1.43−12.11 μM, 56.75−72.81 μM, 0−2.45 μM, and 3.24−12.09 μM for GSH, Cys, Hcy, and Cys-Gly, respectively. As in saliva, the range values were 0.90−3.20 μM, 1.24−3.25 μM, 0.75−1.33 μM, and 0−0.55 μM for GSH, Cys, Hcy, and Cys-Gly, respectively. It can be concluded that the concentrations of total thiols in saliva were far lower than those in plasma or urine.

The data obtained with the reference method[19] is also given in Table 4. The data with two methods was compared, and significant differences were considered at the $P < 0.05$ level. The results showed that there were no significant differences

between the data ($P > 0.05$). Therefore, the data with the proposed method can be validated by the reference method.

Based on the reaction of CNBF with thiols, we developed a novel method for the determination of four physiologically important thiols, GSH, Cys, Hcy, and Cys-Gly, in plasma, urine, and saliva. The application of CNBF as a derivatization reagent seemed to be an attractive choice for the determination of thiols with TFA in mobile phase, which showed good separation of derivatized thiols from the interferences. The reaction of CNBF with thiols was rapid, required moderate reaction conditions, and led to stable products. In comparison to other derivatizing reagents for thiols, application of CNBF showed superiority in relative sensitivity, selectivity, and efficient derivatization procedure. The developed method was applied to quantification of four thiols in human biological fluids collected from five donors with the concentration range of 0−124.25 μM. This study provides a feasible HPLC method for the routine analysis of thiols required for clinical evaluation.

AUTHOR INFORMATION

Corresponding Author

*No. 2 Yuanmingyuan West Road, China Agricultural University, Beijing, P.R. China, 100193. Tel: 86-10-62734302. Fax: 86-10-62734302. E-mail: caoysong@126.com.

Author Contributions

†These authors contributed equally to this work.

Funding

This work was supported by National Department Public Benefit Research Foundation of China (201003065) and Research Fund for the Doctoral Program of Higher Education of China (20120008130006).

Notes

The authors declare no competing financial interest.

REFERENCES

(1) Kuśmierek, K.; Chwatko, G.; Głowacki, R.; Bald, E. Determination of endogenous thiols and thiol drugs in urine by HPLC with ultraviolet detection. *J. Chromatogr. B* **2009**, *877*, 3300−3308.

(2) Kuśmierek, K.; Chwatko, G.; Głowacki, R.; Kubalczyk, P.; Bald, E. Ultraviolet derivatization of low-molecular-mass thiols for high performance liquid chromatography and capillary electrophoresis analysis. *J. Chromatogr. B* **2011**, *879*, 1290−1307.

(3) Pastore, A.; Federici, G.; Bertini, E.; Piemonte, F. Analysis of glutathione: implication in redox and detoxification. *Clin. Chim. Acta* **2003**, *333*, 19−39.

(4) Goodman, M. T.; McDuffie, K.; Hernandez, B.; Wilkens, L. R.; Selhub, J. Case-control study of plasma folate, homocysteine, vitamin B12, and cysteine as markers of cervical dysplasia. *Cancer* **2000**, *89*, 376−382.

(5) Bald, E.; Glowacki, R.; Drzewoski, J. Determination by liquid chromatography of free and total cysteine in human urine in the form of its S-quinolinium derivative. *J. Chromatogr. A* **2001**, *913*, 319−329.

(6) Clarke, R. Homocysteine, B vitamins, and the risk of cardiovascular disease. *Clin. Chem.* **2011**, *57*, 1201−1202.

(7) Zuo, Q.-P.; Li, B.; Pei, Q.; Li, Z.; Liu, S.-K. A highly selective fluorescent probe for detection of biological samples thiol and its application in living cells. *J. Fluoresc.* **2010**, *20*, 1307−1313.

(8) Wang, W.; Li, L.; Liu, S.; Ma, C.; Zhang, S. Determination of physiological thiols by electrochemical detection with piazselenole and its application in rat breast cancer cells 4T-1. *J. Am. Chem. Soc.* **2008**, *130*, 10846−10847.

(9) Lochman, P.; Adam, T.; Friedecký, D.; Hlídková, E.; Škopková, Z. High-throughput capillary electrophoretic method for determination of total aminothiols in plasma and urine. *Electrophoresis* **2003**, *24*, 1200−1207.

(10) Chang, C. W.; Tseng, W. L. Gold nanoparticle extraction followed by capillary electrophoresis to determine the total, free, and protein-bound aminothiols in plasma. *Anal. Chem.* **2010**, *82*, 2696−2702.

(11) Kataoka, H.; Takagi, K.; Makita, M. Determination of total plasma homocysteine and related aminothiols by gas chromatography with flame photometric detection. *J. Chromatogr. B* **1995**, *664*, 421−425.

(12) Küster, A.; Tea, I.; Sweeten, S.; Rozé, J. C.; Robins, R. J.; Darmaun, D. Simultaneous determination of glutathione and cysteine concentrations and 2H enrichments in microvolumes of neonatal blood using gas chromatography−mass spectrometry. *Anal. Bioanal. Chem.* **2008**, *390*, 1403−1412.

(13) Khan, M. I.; Iqbal, Z. Simultaneous determination of ascorbic acid, aminothiols, and methionine in biological matrices using ion-pairing RP-HPLC coupled with electrochemical detector. *J. Chromatogr. B* **2011**, *879*, 2567−2575.

(14) Khan, A.; Khan, M. I.; Iqbal, Z.; Shah, Y.; Ahmad, L.; Nazir, S.; Watson, D. G.; Khan, J. A.; Nasir, F.; Khan, A.; Ismail. A new HPLC method for the simultaneous determination of ascorbic acid and aminothiols in human plasma and erythrocytes using electrochemical detection. *Talanta* **2011**, *84*, 789−801.

(15) Bronowicka-Adamska, P.; Zagajewski, J.; Czubak, J.; Wróbel, M. RP-HPLC method for quantitative determination of cystathionine, cysteine and glutathione: An application for the study of the metabolism of cysteine in human brain. *J. Chromatogr. B* **2011**, *879*, 2005−2009.

(16) Bald, E.; Chwatko, G.; Głowacki, R.; Kuśmierek, K. Analysis of plasma thiols by high-performance liquid chromatography with ultraviolet detection. *J. Chromatogr. A* **2004**, *1032*, 109−115.

(17) Bald, E.; Głowacki, R. Analysis of saliva for glutathione and metabolically related thiols by liquid chromatography with ultraviolet detection. *Amino Acids* **2005**, *28*, 431−433.

(18) Głowacki, R.; Bald, E. Fully automated method for simultaneous determination of total cysteine, cysteinylglycine, glutathione and homocysteine in plasma by HPLC with UV absorbance detection. *J. Chromatogr. B* **2009**, *877*, 3400−3404.

(19) Katrusiak, A. E.; Paterson, P. G.; Kamencic, H.; Shoker, A.; Lyon, A. W. Pre-column derivatization high-performance liquid chromatographic method for determination of cysteine, cysteinyl−glycine, homocysteine and glutathione in plasma and cell extracts. *J. Chromatogr. B* **2001**, *758*, 207−212.

(20) Kaniowska, E.; Chwatko, G.; Głowacki, R.; Kubalczyk, P.; Bald, E. Urinary excretion measurement of cysteine and homocysteine in the form of their S-pyridinium derivatives by high-performance liquid chromatography with ultraviolet detection. *J. Chromatogr. A* **1998**, *798*, 27−35.

(21) Amarnath, V.; Amarnath, K. Specific determination of cysteine and penicillamine through cyclization to 2-thioxothiazolidine-4-carboxylic acids. *Talanta* **2002**, *56*, 745−751.

(22) Amarnath, K.; Amarnath, V.; Amarnath, K.; Valentine, H. L.; Valentine, W. M. A specific HPLC-UV method for the determination of cysteine and related aminothiols in biological samples. *Talanta* **2003**, *60*, 1229−1238.

(23) Kuśmierek, K.; Bald, E. Reversed-phase liquid chromatography method for the determination of total plasma thiols after derivatization with 1-benzyl-2-chloropyridinium bromide. *Biomed. Chromatogr.* **2009**, *23*, 770−775.

(24) Mopper, K.; Delmas, D. Trace determination of biological thiols by liquid chromatography and precolumn fluorometric labeling with o-phthalaldehyde. *Anal. Chem.* **1984**, *56*, 2557−2560.

(25) Mukai, Y.; Togawa, T.; Suzuki, T.; Ohata, K.; Tanabe, S. Determination of homocysteine thiolactone and homocysteine in cell cultures using high-performance liquid chromatography with fluorescence detection. *J. Chromatogr. B* **2002**, *767*, 263−268.

(26) Ivanov, A. R.; Nazimov, I. V.; Baratova, L. Determination of biologically active low-molecular-mass thiols in human blood: I. Fast

qualitative and quantitative, gradient and isocratic reversed-phase high-performance liquid chromatography with photometric and fluorescence detection. *J. Chromatogr. A* **2000**, *895*, 157−166.
(27) Conlan, X. A.; Stupka, N.; McDermott, G. P.; Francis, P. S.; Barnett, N. W. Determination of intracellular glutathione and cysteine using HPLC with a monolithic column after derivatization with monobromobimane. *Biomed. Chromatogr.* **2010**, *24*, 455−457.
(28) Nolin, T. D.; McMenamin, M. E.; Himmelfarb, J. Simultaneous determination of total homocysteine, cysteine, cysteinylglycine, and glutathione in human plasma by high-performance liquid chromatography: application to studies of oxidative stress. *J. Chromatogr. B* **2007**, *852*, 554−561.
(29) Huang, K. J.; Han, C. H.; Li, J.; Wu, Z. W.; Liu, Y. M.; Wu, Y. Y. LC Determination of thiols derivatized with 4-(Aminosulfonyl)-7-fluoro-2,1, 3-benzoxadiazole after SPE. *Chromatographia* **2011**, *74*, 145−150.
(30) Persichilli, S.; Gervasoni, J.; Castagnola, M.; Zuppi, C.; Zappacosta, B. A reversed-phase HPLC fluorimetric method for simultaneous determination of homocysteine-related thiols in different body fluids. *Lab Med.* **2011**, *42*, 657−662.
(31) Liang, S. C.; Wang, H.; Zhang, Z. M.; Zhang, H. S. Determination of thiol by high-performance liquid chromatography and fluorescence detection with 5-methyl-(2-(m-iodoacetylamino-phenyl) benzoxazole. *Anal. Bioanal. Chem.* **2005**, *381*, 1095−1100.
(32) Benkova, B.; Lozanov, V.; Ivanov, I. P.; Todorova, A.; Milanov, I.; Mitev, V. Determination of plasma aminothiols by high performance liquid chromatography after precolumn derivatization with N-(2-acridonyl) maleimide. *J. Chromatogr. B* **2008**, *870*, 103−108.
(33) Cevasco, G.; Piątek, A. M.; Scapolla, C.; Thea, S. An improved method for simultaneous analysis of aminothiols in human plasma by high-performance liquid chromatography with fluorescence detection. *J. Chromatogr. A* **2010**, *1217*, 2158−2162.
(34) Marchand, S.; de Revel, G. A HPLC fluorescence-based method for glutathione derivatives quantification in must and wine. *Anal. Chim. Acta* **2010**, *660*, 158−163.
(35) Guo, X. F.; Zhao, P. X.; Wang, H.; Zhang, H. S. Simple and rapid determination of thiol compounds by HPLC and fluorescence detection with 1,3,5, 7-tetramethyl-8-phenyl-(2-maleimide)-difluoroboradiaza-s-indacene. *J. Chromatogr. B* **2011**, *879*, 3932−3936.
(36) Hoff, S.; Larsen, F. H.; Andersen, M. L.; Lund, M. N. Quantification of protein thiols using ThioGlo 1 fluorescent derivatives and HPLC separation. *Analyst* **2013**, *138*, 2096−2103.
(37) Zhang, X. Y.; Piao, Y. L.; Cui, S. Y.; Lee, Y. I. Determination of reduced glutathione, cystein and total thiols in pine pollen powder by in situ derivatization. *Microchem. J.* **2014**, *112*, 1−6.
(38) Herbst-Johnstone, M.; Piano, F.; Duhamel, N.; Barker, D.; Fedrizzi, B. Ethyl propiolate derivatisation for the analysis of varietal thiols in wine. *J. Chromatogr. A* **2013**, *1312*, 104−110.
(39) Warren, J. M.; Parkinson, D. R.; Pawliszyn, J. Assessment of thiol compounds from garlic by automated headspace derivatized in-needle-NTD-GC-MS and derivatized in-fiber-SPME-GC-MS. *J. Agric. Food Chem.* **2013**, *61*, 492−500.
(40) Guan, X.; Hoffman, B.; Dwivedi, C.; Matthees, D. P. A simultaneous liquid chromatography/mass spectrometric assay of glutathione, cysteine, homocysteine and their disulfides in biological samples. *J. Pharm. Biomed. Anal.* **2003**, *31*, 251−261.
(41) Huang, Y. Q.; Ruan, G. D.; Liu, J. Q.; Gao, Q.; Feng, Y. Q. Use of isotope differential derivatization for simultaneous determination of thiols and oxidized thiols by liquid chromatography tandem mass spectrometry. *Anal. Biochem.* **2011**, *416*, 159−166.
(42) Toyo'oka, T. Recent advances in separation and detection methods for thiol compounds in biological samples. *J. Chromatogr. B* **2009**, *877*, 3318−3330.
(43) Qian, K.; Tang, T.; Shi, T.; Wang, F.; Li, J.; Cao, Y. Residue determination of glyphosate in environmental water samples with high-performance liquid chromatography and UV detection after derivatization with 4-chloro-3,5-dinitrobenzotrifluoride. *Anal. Chim. Acta* **2009**, *635*, 222−226.
(44) Sun, Y.; Liu, P. F.; Wang, D.; Li, J. Q.; Cao, Y. S. Determination of amitrole in environmental water samples with precolumn derivatization by high-performance liquid chromatography. *J. Agric. Food Chem.* **2009**, *57*, 4540−4544.
(45) Tang, T.; Shi, T.; Qian, K.; Li, P.; Li, J.; Cao, Y. Determination of biogenic amines in beer with pre-column derivatization by high performance liquid chromatography. *J. Chromatogr. B* **2009**, *877*, 507−512.
(46) Camera, E.; Picardo, M. Analytical methods to investigate glutathione and related compounds in biological and pathological processes. *J. Chromatogr. B* **2002**, *781*, 181−206.

JOURNAL OF AGRICULTURAL AND FOOD CHEMISTRY

Article

pubs.acs.org/JAFC

Isoelectric Focusing and ELISA for Detecting Adulteration of Donkey Milk with Cow Milk

Rosa Pizzano*[,†] and Elisabetta Salimei[‡]

[†]Consiglio Nazionale delle Ricerche (CNR), Istituto di Scienze dell'Alimentazione, via Roma 64, I-83100 Avellino, Italy

[‡]Dipartimento Agricoltura Ambiente e Alimenti, Università degli Studi del Molise, via De Sanctis, I- 86100 Campobasso, Italy

Supporting Information

ABSTRACT: Donkey milk has been recently revalued intensely due to its nutritional properties. Moreover, donkey milk has been proposed as an effective alternative food for some infants with cow milk allergy. Two fast analytical methods were proposed to detect the fraudulent practice of blending cow milk to donkey milk. Detection of cow α_{s1}-casein bands along the profiles of experimental donkey−cow milk mixtures analyzed by isoelectric focusing was adequate to estimate cow milk used as adulterant of donkey milk starting from 5% (v/v). An ELISA-based method using the antipeptide antibodies raised against the 1−28 sequence stretch of cow β-casein was also developed for an accurate definition of composition of donkey−cow milk mixtures. The presence of cow milk at levels as low as 0.5% (v/v) was detected in donkey−cow milk mixtures prepared at laboratory scale and assayed by ELISA.

KEYWORDS: *donkey milk, adulteration, antipeptide antibodies, cow milk allergy, PAGIF, immunoblotting, ELISA*

INTRODUCTION

After a 5000 year partnership between human and donkey in agricultural work, mechanization led to a sharp decline of the donkey population in the world. Indeed, donkey has remained important only for rural economies in semiarid and mountainous regions of the world.[1] Over the past few decades the asinine species has been included in projects on equid diversity preservation and donkey milk has been intensively studied as a food source in the human diet. Current worldwide donkey distribution and milk production have been recently reported.[2] In Europe, some hundreds of dairy donkey farms (30−50 donkeys in average per farm) are experiencing an innovative multifunctional system where a wide variety of activities are carried out, from agritourism and agritainment to health and beauty activities, besides milk production. They are mainly located in marginal areas of Italy, France, Portugal, Spain, Greece, Belgium, and Cyprus. A special value has been ascribed to donkey milk since ancient times. Recently, preliminary experimental evidence based on in vitro tests has indicated that donkey milk possesses unique properties. Thus, bioactive compounds were found in donkey milk, displaying a variety of potentially health promoting activities.[3−8] In addition, donkey milk has been reported to be a potential food for the immune recovery of aged consumers[9] and may exert beneficial effects in the prevention of atherosclerosis.[10] Furthermore, donkey milk has been proposed as an alternative dietary ingredient in children with cow milk allergy.[11,12] Basics of donkey management and milking procedures have been established.[13] Like other expensive unconventional milks (buffalo, camel, horse, etc.), also donkey milk (10−15 €/L) is a potential target for adulteration through the fraudulent addition of the cheaper and more readily available cow milk (about 0.5 €/L). Ascertainment of milk genuineness is an important topic in the dairy sector, mainly for commercial reasons.[14] However, it becomes crucial for safety reasons when donkey milk is proposed in the diet therapy of cow milk allergic subjects. Indeed, intake of donkey milk adulterated by cow milk, even in trace, can be hazardous to the health of very sensitive patients. Two analytical methods for the detection of cow milk in donkey milk had been recently proposed. One of these had been developed according to stereospecific analysis of triacylglycerol fraction from milks of different animal species.[15] The other method had been based on monitoring of the two most abundant whey proteins (α-lactalbumin and β-lactoglobulin) from cow milk using matrix-assisted laser desorption/ionization time-of-flight mass spectrometry.[16] However, both these methods require expensive equipment and highly skilled operators, and the procedures for quantitative analysis are laborious and time-consuming. In addition, speciation analysis of donkey−cow milk mixtures based on the composition of the triacylglycerol fraction[15] can be impaired by adding defatted cow milk to donkey milk. On the other hand, the method based on the detection of cow α-lactalbumin and β-lactoglobulin[16] is fully reliable only if raw cow milk is used as adulterant, as whey proteins are susceptible to even mild heat treatments applied to milk, as previously reported.[17,18]

Immunoassay technology has been advantageously applied to dairy research since the early 1980s, leading to the development of a number of fast, sensitive, reliable, and user-friendly analytical methods.[19] Despite the overall complexity of the protein fraction in milk and dairy products, due to genetic variability, discrete phosphorylation, glycation, and limited hydrolysis by native milk proteinases, a single protein component could be selectively and sensitively recognized provided that the appropriate antibody preparation was used as

Received: March 25, 2014
Revised: May 30, 2014
Accepted: June 3, 2014
Published: June 3, 2014

ACS Publications © 2014 American Chemical Society

dx.doi.org/10.1021/jf5025533 | J. Agric. Food Chem. 2014, 62, 5853−5858

Table 1. Sequence Homology between the Main Proteins from Cow and Donkey Milk

	accession no.[a]		alignment between cow and donkey proteins[b]			
	cow	donkey	cow fragment	donkey fragment	no.[c]	% homology
α_{s1}-casein	P02662[d]	P86272	54−209	49−196	156	44.9
β-casein	P02666[d]	P86273	16−214	1−205	207	58.5
α_{s2}-casein	P02663[d]	B7VGF9[d]	1−221	1−235	235	60.0
κ-casein	P02668[d]	F0V6V5[d]	2−190	1−182	190	57.4
β-lactoglobulin	P02754[d]	P13613	19−178	3−162	160	56.9
α-lactalbumin	P00711[d]	P28546	20−142	1−123	123	71.5
serum albumin	P02769[d]	Q5XLE4[d]	1−607	1−607	607	74.1

[a]Primary accession number of the protein in UniProtKB/Swiss-Prot database. [b]Using the SIM alignment tool for protein sequences (ExPASy: Bioinformatics Resource Portal). [c]Amino acid residues overlapping. [d]Sequence including a signal peptide.

immunoreagent. Above all, definition of the composition of milk mixtures by immunochemical tools is a real challenge. As a rule, polyclonal antibodies raised against a specific milk protein also cross-react with the homologous counterparts included in milk from all of the other species. Consequently, cumbersome purification procedures, such as immunoabsorption and immunoaffinity chromatography, are required to avoid antibody cross-reactions. Alternatively, novel immunoreagents suited to milk speciation can be obtained by predetermining the antibody binding specificity, as allowed by the antipeptide antibody technology. Indeed, high levels of antibody species specificity can be attained using as immunogens peptides reproducing short sequence stretches within protein chains with species-specific features.

This work was directed to develop original, fast, and reliable analytical methods for the quantitative detection of cow milk in donkey milk. Two analytical approaches were planned. The first was based on the fact that cow α_{s1}-casein displays a p*I* different from that of donkey α_{s1}-casein, as described in a previous report.[20] The second aimed to develop an immunochemical assay using the antipeptide antibody preparation raised against the 1−28 peptide from cow β-casein, chosen as the immunoreagent according to its species-specific performances.[21]

MATERIALS AND METHODS

Protein Sequences and Determination of Homology Degrees. All of the milk protein amino acid sequences considered in the present work were drawn from the UniProtKB/Swiss-Prot database,[22] and their respective primary accession numbers were as specified in Table 1. In addition, the sequence marked as P11839 in UniProtKB/Swiss-Prot database was considered as sheep β-casein. Homology was calculated using the SIM alignment tool for protein sequences presently available in the ExPASy Web site,[23] according to the method used for comparative analysis of the protein sequences from milk of the animal species of dairy interest.[12]

Milk Sampling and Preparation of Milk Mixtures and Whole Casein. Raw cow milk was supplied by a local cattle farm (Savoia, Roccabascerana, Italy) and managed according to current sanitary regulations. Raw donkey milk from a private dairy donkey farm (Ciucolandia, Capestrano, Italy) was mechanically drawn according to the procedure previously described.[13] Standard mixtures of donkey milk containing 0.5, 1, 2, 5, 10, 20, 40, and 60% (v/v) of cow milk were prepared at laboratory scale. These milk mixtures as well as donkey milk and cow milk were subsequently centrifuged at 4500 rpm for 10 min at 4 °C using a Labofuge 400R equipped with a swinging bucket rotor 4 × 180 mL (Heraus, Germany), and the upper fat layer was manually removed. The skimmed milk mixtures and pure milk samples were diluted 1:5 in 50 mM NH_4HCO_3, pH 8.5, for competitive ELISA experiments whereas they were diluted with 9 M urea to a final concentration of 3.6 M urea for isoelectric focusing on polyacrylamide gel (PAGIF) analysis. Whole casein was recovered from defatted cow and donkey milk samples by adjusting pH to 4.6 with 1 M HCl under pHmeter control and centrifuging as described above for defatting. The humid pellet, after two washes with 10 mM of CH_3COONH_4 at pH 4.6, was dissolved at a final concentration of 70 mg/mL in 9 M urea containing 1% (v/v) β-mercaptoethanol and analyzed by immunoblotting.

Immunoreagents. The two antipeptide antibody preparations used to recognize cow β-casein and cow α_{s1}-casein were produced as described in previous works.[21,24,25] Apart from the peptide used as immunogen, reproducing a selected sequence stretch of either bovine β-casein or α_{s1}-casein, each antiserum was able to detect properly the parent protein. The antiserum developed against the 1−28 phosphopeptide of cow β-casein was kindly granted by Prof. F. Addeo (Department of Food Science, University of Naples, Portici, Italy).

Electrophoresis and Immunoblotting. PAGIF was performed essentially as previously described.[24] Aliquots of Pharmalyte (GE Healthcare, Uppsala, Sweden) 2.5−5.0, 4.5−5.4, and 4.0−6.5 were added to the polyacrylamide solution in the ratio 1.6:1.4:1 (v/v/v) to obtain a final pH gradient from 2.5 to 6.5 in the gel. The polyacrylamide solution was allowed to polymerize in the form of an ultrathin-layer gel (thickness, 0.25 mm). Gel prefocusing and protein separation were carried out on the PhastSystem apparatus (Pharmacia, Uppsala, Sweden). Coomassie Brilliant Blue G-250 staining was performed according to the procedure described by Blakesley and Boezi.[26] For immunoblotting analysis, the PAGIF profiles were transferred by capillary diffusion to a nitrocellulose paper previously rinsed in phosphate-buffered saline solution (PBS: 1.5 mM KH_2PO_4, 8.1 mM Na_2HPO_4, 136 mM NaCl, 2.7 mM KCl, pH 7.4). The paper was then held into blocking buffer (10% v/v heat-inactivated horse serum in PBS) for at least 1 h at room temperature. Immunodetection was carried out by incubating the paper with the appropriate rabbit antiserum at a 1:1000 dilution in blocking buffer for 1 h at room temperature and, after three washes with blocking buffer, with horseradish peroxidase-labeled goat anti-rabbit polyclonal antibodies (Bio-Rad, Hercules, CA) at a 1:2000 dilution in blocking buffer for 1 h at room temperature. For protein band detection, the nitrocellulose paper was placed in 10 mM Tris-HCl, pH 7.5, containing 0.5 mg/mL of 3,3-diaminobenzidine (Fluka, Buchs, Switzerland) and 0.06% (w/v) $NiCl_2$ hexahydrate (Fluka). To start the reaction between horseradish peroxidase-labeled goat anti-rabbit IgG antibodies and 3,3-diaminobenzidine, 100 μL of 30% (v/v) hydrogen peroxide was added to 20 mL of solution. Incubation of the nitrocellulose membrane was performed at room temperature with agitation and examined periodically until the protein bands became suitably dark (1 to 5 min). The reaction was stopped by rinsing the nitrocellulose membrane with distilled water.

Analysis of Donkey−Cow Milk Mixtures by Competitive ELISA. A 2 μg/mL solution of RP-HPLC purified bovine β-casein in 50 mM NH_4HCO_3, pH 8.5, was used to coat microtiter plates (cod. 3911, Falcon, Oxnard, CA). After overnight incubation at 4 °C and the saturation step, the wells were washed with PBS and then filled up with blocking buffer (10% v/v heat-inactivated horse serum in PBS) to

Table 2. Alignment of the C-Terminal Region of α_{s1}-Casein from Cow and Donkey Milk[a]

no.[b]	186	187	188	189	190	191	192	193	194	195	196		197	198	199
cow	Ile	**Gly**	Ser	Glu	Asn	Ser	Glu	Lys	Thr	**Thr**	**Met**		Pro	**Leu**	Trp
donkey	Ile	**Ala**	Ser	Glu	Asn	Ser	Glu	Lys	Thr	**Asp**	**Ile**	**Ile**	Pro	**Glu**	Trp
no.[c]	188	189	190	191	192	193	194	195	196	197	198	199	200	201	202

[a]Amino acid differences are reported in bold. [b]Amino acid numbering of mature cow α_{s1}-casein. [c]Amino acid numbering of donkey α_{s1}-casein.

saturate the remaining sites for protein binding. Microplates were placed at 37 °C for at least 1 h in a humid atmosphere. They were emptied and kept at −20 °C, ready for immediate use. Each milk sample was serially diluted ($1{:}4^n$, n = 1 to 4 except for defatted cow milk sample, where n = 1 to 8) in 50 mM NH_4HCO_3 pH 8.5, and each dilution was analyzed in duplicate. 50 μL aliquots of the serial dilutions were introduced in each well, and then 50 μL of a 1:2000 (v/v) dilution of the antiserum in the blocking buffer was added. Maximal binding of the antibodies to the plate was determined by adding to the wells 50 μL of 50 mM NH_4HCO_3 pH 8.5 instead of milk sample dilution. After 1 h at 37 °C in a humid atmosphere, the wells were emptied and washed five times with PBS. A 100 μL aliquot of a 1:2000 (v/v) dilution of horseradish peroxidase-labeled goat anti-rabbit IgG polyclonal antibodies (Bio-Rad, Hercules, CA) was then added to each well. Following incubation for 1 h at 37 °C in a humid atmosphere and five washings with PBS, 100 μL amounts of a solution of tetramethylbenzidine (Sigma, Saint Louis, MO) 0.1 mg/mL in 50 mM citrate−phosphate buffer, dimethyl sulfoxide 10% (v/v), pH 5.0, containing 0.01% (v/v) hydrogen peroxide were added to each microtiter well. After 10−15 min at room temperature the reaction was stopped by adding 100 μL of 1 M H_2SO_4. The ELISA signals were recorded at 450 nm with a Benchmark microplate reader (Bio-Rad, Hercules, CA). The net ELISA absorbance value of each dilution was used for calculations. It was the difference between each mean value of ELISA absorbance and the mean ELISA signal given by pure cow milk. Data were elaborated according to the log/logit curve fit method of Microplate Manager III Data Analysis software (Bio-Rad, Hercules, CA). Pure cow milk was used as internal standard, and its cow β-casein content was assumed as 100. Accordingly, the cow β-casein amounts detected in donkey−cow milk mixtures were obtained as percentages of the amount of cow β-casein included in pure cow milk.

RESULTS AND DISCUSSION

Donkey Milk Proteins in Comparison to Cow Milk Proteins. Similarity between the protein components included in milk from two different animal species reflects generally the phylogenetic relationship between the two mammals.[12] Both donkey and cow are members of the same class and superorder, that is Mammalia and Laurasiatheria, but are classified in a different order, Perissodactyla and Artiodactyla, respectively. Apart from the total protein content estimated in the two milks (3.2% w/w in cow milk versus 2.2% w/w in donkey milk), the ratio of casein to whey protein is clearly different, being 80:20 in cow milk whereas it is 58:42 in donkey milk. Based on current information about the primary structure of the main milk proteins, the percentage homology between the primary structures of the main proteins from cow and donkey milk is reported in Table 1. According to these data, homology between cow and donkey milk proteins was limited compared to that found between the proteins from cow and water buffalo milk (on average, about 96%) or from cow and sheep milk (on average, about 91%), especially as regards caseins.

PAGIF Detection of Cow Milk in Donkey Milk. Significant differences had been found by comparing the PAGIF electrophoretic profiles of caseins from cow and donkey milk.[20] Most importantly, cow α_{s1}-casein and its donkey counterpart were clearly separated by PAGIF due to their different pI values. Indeed, by immunostaining the PAGIF profiles with polyclonal antipeptide antibodies directed against the 186−199 sequence stretch of bovine α_{s1}-casein, the C-terminal region of the protein, the parent α_{s1}-casein was recognized as a group of bands migrating in the low pH zone of the electrophoretic profile of cow milk, as previously reported.[26] Donkey α_{s1}-casein was identified as a group of bands migrating in the pH zone diametrically opposite to that occupied by cow α_{s1}-casein.[20] Intriguingly, cross-reactivity of the antipeptide antibody preparation toward donkey α_{s1}-casein indicated that the substitution of four amino acids and the insertion of one amino acid, as found in the C-terminal region of donkey α_{s1}-casein (Table 2), did not prevent antibody recognition of the donkey counterpart of the C-terminal region of cow α_{s1}-casein. The different location of cow and donkey α_{s1}-casein in the PAGIF profiles was exploited to detect adulteration of donkey milk by cow milk. As shown in Figure 1, eight mixtures of donkey milk containing different amounts

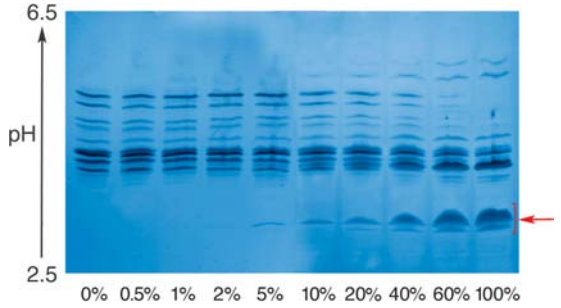

Figure 1. PAGIF analysis of donkey milk containing different percentages of cow milk (v/v) as reported. The gel area of cow α_{s1}-casein migration is indicated by the red arrow.

of cow milk were analyzed by PAGIF in addition to the two genuine milks. A group of protein bands focusing in the low pH gel zone was gradually detected in the profiles of the milk mixtures at increasing cow milk content from 5% v/v. These bands were selectively immunostained by the antipeptide antibodies directed against the 186−199 sequence stretch of bovine α_{s1}-casein (results shown in Figure S1, Supporting Information). Based on the results hitherto exposed, a direct PAGIF analysis of milk samples and Coomassie Brilliant Blue G-250 staining of the profiles proved to be effective in detecting more than 5% v/v of cow milk included in donkey milk using cow α_{s1}-casein as indicator of cow milk adulteration. Due to its rapidity, high-throughput, and cheapness, such a method can be usefully employed by competent authorities as a screening test of a large number of donkey milk samples. However, the method might not be sufficiently sensitive to detect trace amounts of cow milk, as required to guarantee safety of donkey milk designed for consumption by cow milk allergic patients. Immunostaining of the PAGIF profiles using antipeptide antibodies anti 186−199 bovine α_{s1}-casein could improve sensitivity of cow α_{s1}-casein detection with respect to Coomassie Brilliant Blue G-250 staining (results shown in

Table 3. 1-28 Sequence Stretch of β-Casein from Different Species[a]

no.[b]	1	2	3	4	5	6	7	8	9	10	11	12	13	14	15	16							17	18	19	20	21	22	23	24	25	26	27	28
cow	Arg	Glu	**Leu**	Glu	Glu	Leu	Asn	Val	**Pro**	Gly	Glu	**Ile**	Val	Glu	Ser	Leu	-	-	-	-	-	-	Ser	Ser	Ser	Glu	Glu	Ser	Ile	Thr	**Arg**	Ile	Asn	Lys
sheep	Arg	Glu	**Gln**	Glu	Glu	Leu	Asn	Val	**Val**	Gly	Glu	**Thr**	Val	Glu	Ser	Leu	-	-	-	-	-	-	Ser	Ser	Ser	Glu	Glu	Ser	Ile	Thr	**His**	Ile	Asn	Lys
donkey	Arg	Glu	**Lys**	Glu	Glu	Leu	Asn	Val	**Ser**	**Ser**	Glu	**Thr**	Val	Glu	Ser	Leu	**Ser**	Ser	Asn	Glu	Pro	Asp	Ser	Ser	Ser	Glu	Glu	Ser	Ile	Thr	**His**	Ile	Asn	Lys
no.[c]	1	2	3	4	5	6	7	8	9	10	11	12	13	14	15	16	17	18	19	20	21	22	23	24	25	26	27	28	29	30	31	32	33	34

[a]Amino acid differences are reported in bold. [b]Amino acid numbering of mature cow and sheep β-casein. [c]Amino acid numbering of donkey β-casein.

Figure S1, Supporting Information). Nevertheless, implementation of immunoblotting after PAGIF analysis, according to the method previously proposed for detecting cow casein in water buffalo milk,[24] would heavily affect quickness and simplicity of the analytical determinations. On the other hand, this antibody preparation was not suitable as an immunoreagent for developing an ELISA test to determine directly cow milk added to donkey milk because of its reactivity toward both cow and donkey α_{s1}-casein, simultaneously occurring in mixtures of cow and donkey milk.

ELISA Immunodetection of Cow Milk in Donkey Milk. In order to evaluate cow milk content in donkey milk samples by direct immunoassays, antibodies recognizing selectively any protein from cow milk were required. A broad library of antipeptide antibody preparations have been collected in our lab over about 20 years' work directed to the analysis of dairy products by immunochemical tools. In order to select immunoreagents suited for the specific detection of cow milk proteins in mixture with donkey milk proteins, the antipeptide antibody preparations directed against cow-specific sequence stretches of milk protein components were taken into consideration. According to previous results,[19,21] the antipeptide antibodies obtained by using the plasmin-released 1−28 phosphopeptide of cow β-casein as immunogen were able to recognize the parent β-casein from cow as well as water buffalo milk, but not from sheep and goat milk. Based on the 1−28 sequence stretch of β-casein from these four different animal species, the antibody binding specificity resulted to be strictly related to the amino acid residues located in positions 3, 9, and 12 of β-casein.[21] Similarly to sheep β-casein, donkey β-casein displayed three amino acid substitutions with respect to cow β-casein in the same positions 3, 9, and 12. Furthermore, the donkey N-terminal β-casein sequence included the insertion of six amino acid residues and two additional amino acid substitution. All of these differences are reported in Table 3, where the 1−28 sequence of cow β-casein was aligned with the homologous region of sheep and donkey β-casein to the best of juxtaposition.

Taken together, these findings suggested that the antipeptide antibodies raised against the 1−28 phosphopeptide of cow β-casein could be employed as a cow-specific reagent for the analysis of donkey−cow milk mixtures. To check this possibility, whole casein from cow milk was analyzed in comparison with whole casein from donkey milk by PAGIF and immunoblotting analysis using this antipeptide antibody preparation as immunoreagent. As shown in Figure 2, the two Coomassie Brilliant Blue G-250 stained profiles (panel A) reacted differently to the antibodies (panel B). A complex pattern of protein bands was recognized along the profile of whole casein from cow milk, as previously found.[21] By contrast, a very weak antibody cross-reaction was detected in the profile of whole casein from donkey milk. Occurrence of β-casein in donkey milk was verified by immunostaining the PAGIF

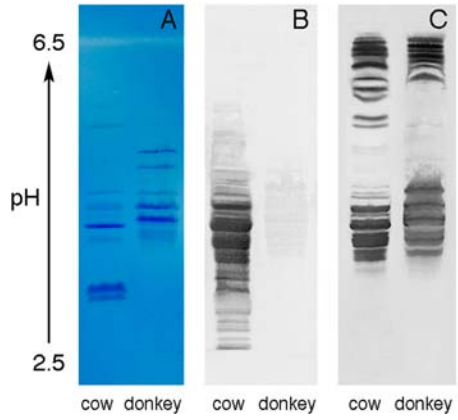

Figure 2. PAGIF analysis of whole casein from cow and donkey milks, as indicated. Panel A: aspecifical staining with Coomassie Brilliant Blue G-250. Panel B: immunostaining with the antipeptide antibodies raised against the 1−28 peptide of mature cow β-casein. Panel C: immunostaining with the antipeptide antibodies raised against the peptide 195−209 of cow β-casein.

profiles with another antipeptide antibody preparation, produced using the peptide reproducing the 195−209 sequence of cow β-casein as immunogen (panel C). Specific immunostaining of donkey β-casein using the antibodies raised against the 195−209 sequence of cow β-casein had been already obtained by proteomic tools.[20] Nevertheless, antibody cross-reactivity toward donkey β-casein was unusual. By comparing the amino acid sequences of the C-terminal region of β-casein from cow and donkey milk, a significant sequence homology could be found only in the last four amino acids of the two primary structures (Table 4). Therefore, antibody ability in detecting donkey β-casein in addition to cow β-casein seemed to indicate that the antipeptide antibodies were mainly directed against the last four amino acid residues of the peptide reproducing the 195−209 sequence of cow β-casein. It has been generally agreed that a peptide including at least six amino acid residues of a protein sequence has to be used as immunogen to obtain antipeptide antibodies able to detect the parent protein,[28] but even a peptide reproducing a sequence stretch of five amino acid residues had proved to be effective.[24] Furthermore, it is worth noting that the presence of a proline residue affects peptide conformation and that the protein sequences containing proline residues are generally more exposed on the surface of the native protein than the other sequences, as previously described.[27] Accordingly, the proline residue included in the last four amino acid residues of the peptide used as immunogen might have forced the immune response toward the terminal peptide sequence and/or might support the exposition of the sequence in the native protein for antibody attainment. Finally, additional homology between different regions along donkey β-casein and the 195−209

Table 4. C-Terminal Region of β-Casein from Cow and Donkey Milk[a]

no.[b]	195	196	197	198	199	200	201	202	203	204	205											206	207	208	209
cow	**Glu**	Pro	**Val**	Leu	Gly	**Pro**	**Val**	**Arg**	**Gly**	**Pro**	**Phe**	-	-	-	-	-	-	-	-	-	-	Pro	**Ile**	Ile	Val
donkey	**Asp**	Pro	**Gln**	Leu	Gly	**Leu**	**Thr**	**Gly**	**Glu**	**Phe**	**Asp**	**Pro**	**Ala**	**Thr**	**Gln**	**Pro**	**Ile**	**Val**	**Pro**	**Val**	**His**	**Asn**	Pro	**Val**	Ile	Val
no.[c]	201	202	203	204	205	206	207	208	209	210	211	212	213	214	215	216	217	218	219	220	221	222	223	224	225	226

[a]Amino acid differences are reported in bold. [b]Amino acid numbering of mature cow β-casein, without the signal peptide. [c]Amino acid numbering of donkey β-casein.

sequence of cow β-casein might be involved in antibody recognition of donkey β-casein, most likely the 63−77 sequence stretch of donkey β-casein displaying a 40% homology with the 195−209 sequence of cow β-casein. Once cow specifity of the antipeptide antibodies raised against the 1−28 phosphopeptide of cow β-casein was ascertained by immunoblotting, as recommended in the literature,[28] an ELISA-based assay of cow milk in donkey milk could be developed. A typical ELISA curve obtained in response to pure cow milk is shown in Figure S2, Supporting Information. A linear relationship was found between the experimental values of the cow β-casein concentration determined by ELISA and the actual volume percentages of cow milk included in the standard donkey−cow milk mixtures prepared at laboratory scale. By plotting the cow β-casein amount detected in donkey−cow milk mixtures, reported as the percentage of that detected in pure cow milk, versus the volume percentage of cow milk included in donkey−cow milk mixtures, a straight line with a slope very near to 1 was typically obtained (Figure 3). As shown in the inset of Figure 3, additions as low as 0.5% (v/v) of cow milk to donkey milk could be successfully detected. These results showed that cow β-casein, as detected by the antipeptide antibodies directed against its 1−28 phosphopeptide, could be regarded as a suitable marker of foreign cow milk in donkey milk. In addition to current advantages of ELISA-based determinations in terms of performance and convenience, this method was especially valuable as it did not require any pretreatment of the milk sample, except for a simple centrifugation to separate the aqueous phase including proteins from the lipid fraction. Furthermore, cow milk, largely available on commercial market, can be currently used as internal standard. Finally, this method, using thermostable cow β-casein to trace cow milk, was able to provide reliable evaluation of the cow milk amounts added to donkey milk up to 0.5% (v/v), regardless of either heat treatments or other technological expedients, such as defatting, applied to cow milk used as adulterant, overcoming some limits of available methods with similar sensitivity levels.[15,16]

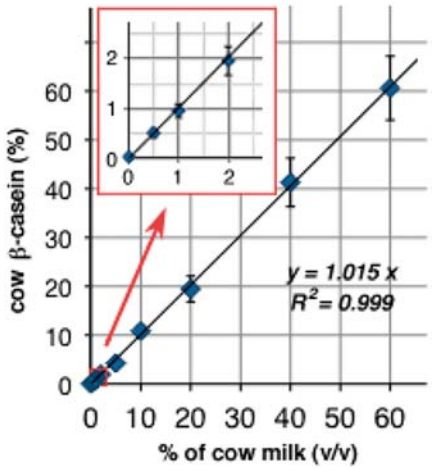

Figure 3. Analysis of donkey−cow milk mixtures by ELISA using the antipeptide antibodies raised against the 1−28 phosphopeptide of cow β-casein. The volume percentage of cow milk included in standard milk mixtures was placed in the *x*-axis. The cow β-casein amount detected in donkey−cow milk mixtures, reported as the percentage of that found in pure cow milk, was placed in the *y*-axis. The square of the diagram limited by red edges was magnified in the inset to emphasize the assay sensitivity. The estimated standard error of mean for concentration of each sample, calculated by using Microplate Manager III Data Analysis software (Bio-Rad), was graphically represented as *Y* error bar.

■ ASSOCIATED CONTENT

Supporting Information

Figure S1, PAGIF and immunoblotting analysis of donkey−cow milk mixtures; Figure S2, analysis of a cow milk sample by competitive ELISA. This material is available free of charge via the Internet at http://pubs.acs.org.

■ AUTHOR INFORMATION

Corresponding Author

*Tel: +39 825 299561. Fax: +39 825 781585. E-mail: rosa.pizzano@isa.cnr.it.

Notes

The authors declare no competing financial interest.

■ ABBREVIATIONS USED

ELISA, enzyme-linked immunosorbent assay; PAGIF, isoelectric focusing on polyacrylamide gel; PBS, phosphate-buffered saline solution (1.5 mM KH_2PO_4, 8.1 mM Na_2HPO_4, 136 mM NaCl, 2.7 mM KCl at pH 7.4); RP-HPLC, reversed-phase high-performance liquid chromatography

■ REFERENCES

(1) Faye, B.; Konuspayeva, G. The sustainability challenge to the dairy sector - The growing importance of non-cattle milk production worldwide. *Int. Dairy J.* **2012**, *24*, 50−56.

(2) Salimei, E.; Fantuz, F. Horse and donkey milk. In *Milk and Dairy Products in Human Nutrition: Production, Composition and Health*, 1st ed.; Park, Y. W., Haenlein, G. F. W., Eds.; John Wiley & Sons: Oxford, U.K., 2013; pp 594−613.

(3) Mao, X.; Gu, J.; Sun, Y.; Xu, S.; Zhang, X.; Yang, H.; Ren, F. Anti-proliferative and anti-tumour effect of active components in donkey milk on A549 human lung cancer cells. *Int. Dairy J.* **2009**, *19*, 703−708.

(4) Li, H.; Li, Q.; Zhong, J.; Lin, Q.; Shen, X.; Rao, P. Enzymatic Hydrolysis Mixture of Donkey Serum Albumin to Inhibit Tumor Cell Proliferation. *J. Food Biochem.* **2013**, *37*, 611−618.

(5) Li, H.; Zhong, J.; Huang, M.; Li, Z.; Rao, P. Antitumour effects of pentapeptide derived from donkey serum albumin both in vitro and in vivo. *Life Sci.* **2013**, *92*, 883−889.

(6) Sa, A.; Krishnaa, R. S.; Pavithrab, V.; Hemalathab, V.; Ingalea, P. Production and antibacterial activity of bacteriocin by Lactobacillus paracasei isolated from donkey milk. *Int. J. Curr. Sci.* **2011**, *1*, 109−115.
(7) Brumini, D.; Bø Furlun, C.; Comi, I.; Devold, T. G.; Marletta, D.; Vegarud, G. E.; Jonassen, C. M. Antiviral activity of donkey milk protein fractions on echovirus type 5. *Int. Dairy J.* **2012**, *28*, 109−111.
(8) Cotte, J. Le lait, une matière d'avenir pour la cosmétique. *Lait* **1991**, *71*, 213−224.
(9) Jirillo, E.; D'Alessandro, A. G.; Amati, L.; Tafaro, A.; Jirillo, F.; Pugliese, V.; Martemucci, G. Modulation of the human aged immune response by donkey milk intake. In *61st Annual Meeting of the European Association for Animal Production, Heraklion, Greece*, 23−27 August 2010; Wageningen Academic Publishers: Wageningen, The Netherlands, 2010; poster session 06, abstract no. 14, p 45.
(10) Tafaro, A.; Magrone, T.; Jirillo, F.; Martemucci, G.; DAlessandro, A. G.; Amati, L.; Jirillo, E. Immunological properties of donkey's milk: its potential use in the prevention of atherosclerosis. *Curr. Pharm. Des.* **2007**, *13*, 3711−3717.
(11) Salimei, E.; Fantuz, F. Equid milk for human consumption. *Int. Dairy J.* **2012**, *24*, 130−142.
(12) Restani, P.; Ballabio, C.; Di Lorenzo, C.; Tripodi, S.; Fiocchi, A. Molecular aspects of milk allergens and their role in clinical events. *Anal. Bioanal. Chem.* **2009**, *395*, 47−56.
(13) Salimei, E. Animals that produce dairy foods—Donkey. In *Encyclopedia of dairy sciences*, 2nd ed.; Fuquay, J. W., Fox, P. F., McSweeney, P. L. H., Eds.; Academic Press: San Diego, CA, 2011; Vol. *1*, pp 365−373.
(14) Scholl, P. F.; Farris, S. M.; Mossoba, M. M. Rapid turbidimetric detection of milk powder adulteration with plant proteins. *J. Agric. Food Chem.* **2014**, *62*, 1498−1505.
(15) Cossignani, L.; Blasi, F.; Bosi, A.; D'Arco, G.; Maurelli, S.; Simonetti, M. S.; Damiani, P. Detection of cow milk in donkey milk by chemometric procedures on triacylglycerol stereospecific analysis results. *J. Dairy Res.* **2011**, *78*, 335−342.
(16) Cunsolo, V.; Muccilli, V.; Saletti, R.; Foti, S. MALDI-TOF mass spectrometry for the monitoring of she-donkey's milk contamination or adulteration. *J. Mass Spectrom.* **2013**, *48*, 148−153.
(17) Manzo, C.; Pizzano, R.; Addeo, F. Detection of pH 4.6 insoluble β-lactoglobulin in heat-treated milk and Mozzarella cheese. *J. Agric. Food Chem.* **2008**, *56*, 7929−7933.
(18) Pizzano, R.; Manzo, C.; Nicolai, M. A.; Addeo, F. Occurrence of major whey proteins in the pH 4.6 insoluble protein fraction from UHT-treated milk. *J. Agric. Food Chem.* **2012**, *60*, 8044−8050.
(19) Pizzano, R.; Nicolai, M. A.; Manzo, C.; Addeo, F. Authentication of dairy products by immunochemical methods: a review. *Dairy Sci. Technol.* **2011**, *91*, 77−95.
(20) Chianese, L.; Calabrese, M. G.; Ferranti, P.; Mauriello, R.; Garro, G.; De Simone, C.; Quarto, M.; Addeo, F.; Cosenza, G.; Ramunno, L. Proteomic characterization of donkey milk "caseome". *J. Chromatogr. A* **2010**, *1217*, 4834−4840.
(21) Pizzano, R.; Nicolai, M. A.; Padovano, P.; Ferranti, P.; Barone, F.; Addeo, F. Immunochemical evaluation of bovine β-casein and its 1−28 phosphopeptide in cheese during ripening. *J. Agric. Food Chem.* **2000**, *48*, 4555−4560.
(22) UniProt. http://www.uniprot.org/.
(23) SIM Alignment Tool - Protein Sequences. In *ExPASy: Bioinformatics Resource Portal*. http://web.expasy.org/sim/.
(24) Addeo, F.; Pizzano, R.; Nicolai, M. A.; Caira, S.; Chianese, L. Fast isoelectric focusing and antipeptide antibodies for detecting bovine casein in adulterated water buffalo milk and derived mozzarella cheese. *J. Agric. Food Chem.* **2009**, *57*, 10063−10066.
(25) Pizzano, R.; Nicolai, M. A.; Addeo, F. Antipeptide antibodies as analytical tools to discriminate among bovine α_{s1}-casein components. *J. Agric. Food Chem.* **1998**, *46*, 766−771.
(26) Blakesley, R.; Boezi, J. A. A new staining technique for proteins in polyacrylamide gel using Coomassie Brilliant Blue G 250. *Anal. Biochem.* **1977**, *22*, 580−582.
(27) Harlow, E.; Lane, D. Immunizations. In *Antibodies. A Laboratory Manual*; Cold Spring Harbor Laboratory: Cold Spring Harbor, NY, 1988; pp 72−78.
(28) Pizzano, R.; Nicolai, M. A.; Addeo, F. Antigenicity of the 139−149 α_{s1}-casein region in different species revealed by ELISA and immunoblotting using antipeptide antibodies. *J. Agric. Food Chem.* **1997**, *45*, 2807−2813.

JOURNAL OF AGRICULTURAL AND FOOD CHEMISTRY

Article

pubs.acs.org/JAFC

Determination of Aristolochic Acids by High-Performance Liquid Chromatography with Fluorescence Detection

Yinan Wang and Wan Chan*

Department of Chemistry, The Hong Kong University of Science and Technology, Clear Water Bay, Kowloon, Hong Kong

ABSTRACT: Nephrotoxic and carcinogenic aristolochic acids (AAs) are naturally occurring nitrophenanthrene carboxylic acids in the herbal genus *Aristolochia*. The misuse of AA-containing herbs in preparing slimming drugs has caused hundred of cases of kidney disease in Belgium women in a slimming regime in the early 1990s. Accumulating evidence also suggested that prolong dietary intake of AA-contaminated food is one of the major causes to the Balkan endemic nephropathy that was first observed in the late 1950s. Therefore, analytical methods of high sensitivity are extremely important for safeguarding human exposure to AA-containing herbal medicines, herbal remedies, and food composites. In this paper, we describe the development of a new high-performance liquid chromatography coupled fluorescence detector (HPLC−FLD) method for the sensitive determination of AAs. The method makes use of a novel cysteine-induced denitration reaction that "turns on" the fluorescence of AAs for fluorometric detections. Our results showed that the combination of cysteine-induced denitration and HPLC−FLD analysis allows for sensitive quantification of AA-I and AA-II at detection limits of 27.1 and 25.4 ng/g, respectively. The method was validated and has been successfully applied in quantifying AAs in Chinese herbal medicines.

KEYWORDS: *aristolochic acids, high-performance liquid chromatography, fluorescence, cysteine, hydrogenolysis*

INTRODUCTION

Nephrotoxic aristolochic acids (AAs) are a mixture of nitrophenanthrene carboxylic acids derived from the herbal genus *Aristolochia* and are classified as members of the most potent carcinogens in the Carcinogenic Potency Database.[1,2] Major components of AAs include aristolochic acid I (AA-I) and aristolochic acid II (AA-II) that differ by a methoxy group, as shown in Figure 1. AA-containing herbs had been widely used as Chinese herbal medicines to treat tumors, rheumatism, snake bites, small pox, and pneumonia, until AAs were observed to be strong human carcinogens and nephrotoxins.[1−4] Currently, the use of AA-containing herbs is prohibited in regions including China, Hong Kong, Taiwan, Japan, U.S.A., U.K., and many European countries.[1,5]

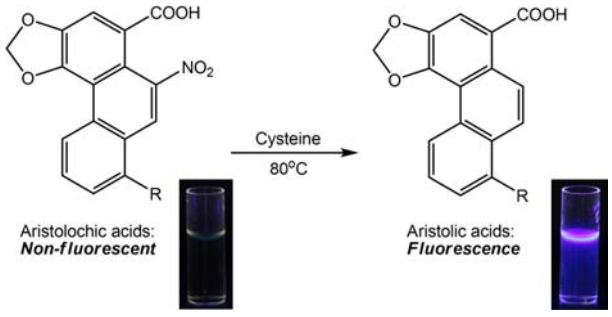

Figure 1. Cysteine-induced denitration of AA (AA-I, R = OCH_3; AA-II, R = H) forms of fluorescent aristolic acids for HPLC−FLD analysis.

Despite AA-containing herbs being banned from the markets worldwide, they are still available for sale on the Internet and misuse of AA-containing herbs exists.[6] For example, inadvertent substitution of *Stephania tetrandra* with AA-containing *Aristolochia fanghi* in the preparation of slimming drugs has caused about 100 cases of renal diseases in Belgium in the early 1990s.[1,4] The term Chinese herb nephropathy (CHN) has been used since then to describe this unique type of rapid progress renal fibrosis that is associated with prolonged exposure to AA-containing herbs or herbal products.[1,5] Cases of CHN were also reported in Australia, China, Hong Kong, Japan, Taiwan, U.K., and many other areas.[1]

Emerging evidence also suggested that chronic food poisoning through dietary intake of AA-contaminated flour, maize, and cucumber is responsible for the etiology of Balkan endomic nephropathy (BEN),[5−7] a peculiar renal disease that has been observed on thousands of farmers living alongside the Danube River for over the past 50 years. Because of the strong nephrotoxicity and potent human carcinogenicity of AAs and the reason that there is significant evidence showing that AAs are food/environmental contaminants,[7−10] analytical methods capable of detecting low concentrations of AAs in a complex matrix of herbal remedies, botanical products, and flour are highly necessary.

Current methods for AA determination include enzyme-linked immunosorbent assay (ELISA),[11] high-performance liquid chromatography with ultraviolet detection (HPLC−UV),[8−10] high-performance liquid chromatography with mass spectrometry (HPLC−MS),[11,12] capillary electrophoresis with ultraviolet detection (CE−UV),[13,14] capillary electrophoresis with electrochemical detection (CE−ECD),[15−19] and cyclic voltammetry.[20] As one of the most sensitive and selective analytical tools, the application of a fluorescence detector (FLD) on AA determination is only made possible recently by

Received: April 3, 2014
Revised: June 10, 2014
Accepted: June 11, 2014
Published: June 11, 2014

ACS Publications © 2014 American Chemical Society

converting the non-fluorescing AAs into their corresponding aristolactams that fluoresce.[2,10] However, these methods suffer from the drawbacks that individual samples have to be analyzed twice before the AA content can be determined. The reason underlying this is that the products from the derivatization reaction, i.e., the aristolactams, exist naturally in high abundance in the AA-containing herbs. The concentrations of endogenous aristolactams in the underivatized sample extracts must be determined and deducted from the total aristolactam levels in the derivatized sample extracts before the AA concentrations in the herbal samples can be elucidated. Consequently, although the developed high-performance liquid chromatography with fluorescence detection (HPLC−FLD) methods are sensitive, the necessities of duplicated analysis for a single sample rendered these methods inefficient for AA determination.

Herein, we report a novel HPLC−FLD method for the sensitive and efficient determination of AAs. The method makes use of cysteine-induced hydrogenolysis of AAs, in which the fluorescent-inhibiting nitro group is replaced by hydrogen and allows for sensitive and selective fluorometric determination of the otherwise non-fluorescing AAs by HPLC−FLD.[21] To the best of our knowledge, the application of the thiol-induced hydrogenolysis converting non-fluorescing nitroaromatics into fluorphores for their quantitative analysis by HPLC−FLD has not been reported before. Our proposed method offering superior sensitivity was validated and has been successfully applied in quantifying AAs in Chinese herbal medicines.

EXPERIMENTAL SECTION

Chemicals. All chemicals and reagents of the highest purity available were used without further purification, unless noted otherwise. AA (96% purity), a 1:1 mixture of AA-I and AA-II, was purchased from Acros (Morris Plains, NJ). Alanine, cysteamine, L-cysteine, cysteinylglycine, glutathione (GSH), and 2-mercaptoethanol were obtained from Sigma (St. Louis, MO). *Fructus Aristolochiae*, *Herba Aristolochiae*, *Aristolochiae mollissima*, *Radix Aristolochiae*, and *Aristolochiae cinnabarina* were purchased from the National Institute for the Control of Pharmaceutical and Biological Products (Beijing, China). *Herba Asari* and *Akebia Stem* were obtained from local Chinese drug stores in Hong Kong. HPLC-grade acetonitrile and methanol were purchased from Tedia (Fairfield, OH). Water was produced by a Milli-Q Ultrapure water purification system (18.2 MΩ, Millipore, Billerica, MA).

Sample Preparation. Herbal medicines and herbal preparations were powdered and sieved (size smaller than 100 μm) prior to analysis. Approximately 50 mg of the powdered samples were accurately weighted and extracted with 5.0 mL of methanol by sonication. After 30 min of sonication at 50 °C, 100 μL of the sample extracts were mixed with 900 μL of the denitrating reagent comprising 50 mM cysteine in potassium phosphate buffer (50 mM, pH 8.0). The reaction was conducted by heating the reaction mixture at 80 °C for 2 h. The cysteine-treated samples after being cooled to room temperature were centrifuged at 13 800 rpm for 5 min before the supernatant was transferred to a HPLC vial for HPLC analysis.

HPLC Analysis. HPLC analysis was conducted on an Agilent 1100 HPLC system coupled with a diode array detector (DAD) and a FLD connected in series (Palo Alto, CA). The DAD was set to monitor the UV absorption of the eluate at 254 nm, whereas the excitation and emission wavelengths for the FLD were set at 254 and 390 nm, respectively. A total of 10 μL of the cysteine-treated sample extract was injected into a Zorbax Eclipse XDB-C8 column (150 × 4.6 mm, 5 μm, Agilent). The HPLC mobile phases consisted of 20 mM, pH 7.0 ammonium acetate (A) and acetonitrile (B). A gradient elution program at a flow rate of 0.70 mL/min was applied to analyze the cysteine-treated samples. The solvent gradient was started from 10% B, programmed to 60% in 10 min, which was then ramped rapidly to 100% B in 0.1 min, and maintained 100% B for 5 min before reconditioning to 10% B for 8 min.

Calibration. A stock solution mixture of AA-I and AA-II each at 240 μg/mL was prepared in methanol and stored at −20 °C before use. Working standard solution mixtures of AA-I and AA-II of concentrations of 0.096, 0.24, 1.20, 2.40, and 4.80 μg/mL were prepared by diluting the stock solution with methanol. The calibration standard solutions were prepared by mixing 100 μL of the working standard solutions with 900 μL of the denitrating reagent, reacting, and HPLC analyzing as described above. Calibration curves were established by plotting the peak areas of the denitrated AAs against the AA concentrations in the calibration standard solutions.

Method Validation. The optimized method was also validated for analytical sensitivity, precision, and accuracy. The limit of detection (LOD) and limit of quantification (LOQ) were established as the amount of analyte in the blank sample extract that generated a signal 3 and 10 times the signal-to-noise ratio, respectively.[22,23] The method precision was evaluated by analyzing herbal extracts spiked with AAs at three different concentrations (0.096, 1.92, and 4.80 μg/mL), on the same day (n = 7) and over separate days in a month (n = 7). The method accuracy was determined by spiking AAs at the three stated concentrations to the blank herbal sample, processed, and analyzed as described above.

Method Comparison. The method accuracy was further gauged by direct liquid chromatography−mass spectrometry (LC−MS) analysis of AAs in the underivatized sample extracts on a Waters Acquity ultra-performance liquid chromatograph (UPLC) coupled with a Xevo G2 Q-TOF mass spectrometer with a standard electrospray ionization (ESI) interface (Milford, MA). AAs were resolved with a Waters BEH C18 column (50 × 2.1 mm, 1.8 μm) eluted with the following gradient of methanol in 20 mM ammonium acetate at a flow rate of 0.35 mL/min and 40 °C: 0−7 min, 1−40%; 7.1−9 min, 40−100%; 9−12 min, 100%; and 12.1−15 min, 1%. The LC eluate was analyzed by positive ESI−MS with the following parameters: capillary voltages, 3 kV; cone voltages, 25 V; desolvation temperature, 400 °C; and source temperature 120 °C. The peak areas of the pseudo-molecular ion ($[M + NH_4]^+$) of AAs (m/z 359 for AA-I and 329 for AA-II) were adopted quantifying AAs in the sample extracts. The results obtained from LC−MS analyses were compared to that obtained by HPLC−FLD analyses to evaluate the accuracy of the proposed method.

RESULTS AND DISCUSSION

Fluorometric Properties of AAs. Aromatic compounds generally fluoresce because of the presence of delocalized π electrons. However, the fluorescence of nitroaromatic hydrocarbons is not observed.[24] It is believed that the existence of a low-lying n → π* electronic transition in nitroaromatics that favors molecular relaxation by intersystem crossing the competing relaxation by fluorescence is therefore inhibited.[24]

AAs, although being rigid polycyclic aromatics, do not fluoresce.[2] The presence of an electron-withdrawing $-NO_2$ substituent inhibits their molecular fluorescence and, thus, hinders their fluorometric detections. Once the fluorescent inhibiting nitro group of AAs has been removed, the fluorescence of denitro AA products could be "turned on" to allow for sensitive and selective detection of AAs. To test this, we produced aristolic acids by reacting the mixed standard of AA-I and AA-II with cysteine and analyzed the reaction mixture by HPLC−FLD.

Characterization of the Cysteine-Induced Hydrogenolysis Product of AAs. Figure 2 depicts the chromatograms obtained from analyzing the underivatized (A and B) and cysteine-treated (C and D) AA-I and AA-II mixture. The HPLC analysis revealed the cysteine treatment of AAs indeed produced two fluorescing products at chromatographic

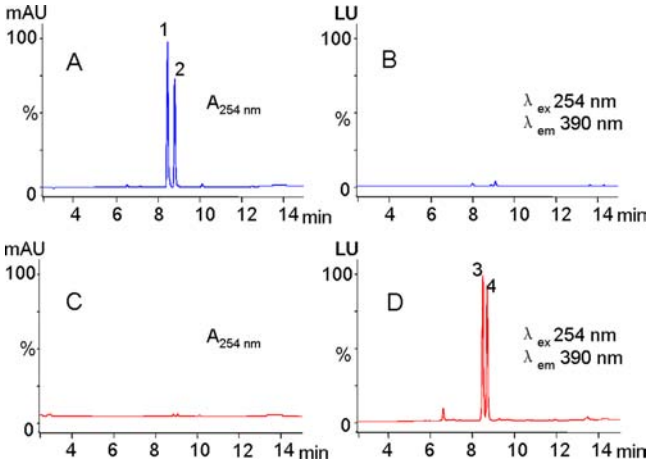

Figure 2. Typical chromatograms from HPLC analysis of underivatized (A, DAD trace; B, FLD trace) and cysteine-treated (C, DAD trace; D, FLD trace) AAs. Peaks 1, 2, 3, and 4 correspond to AA-II, AA-I, aristolic acid II, and aristolic acid I, respectively.

retention times of 8.71 and 8.91 min (Figure 2D), with their corresponding emission maxima at 385 and 390 nm, respectively (Figure 3A). UV absorbance measurements of

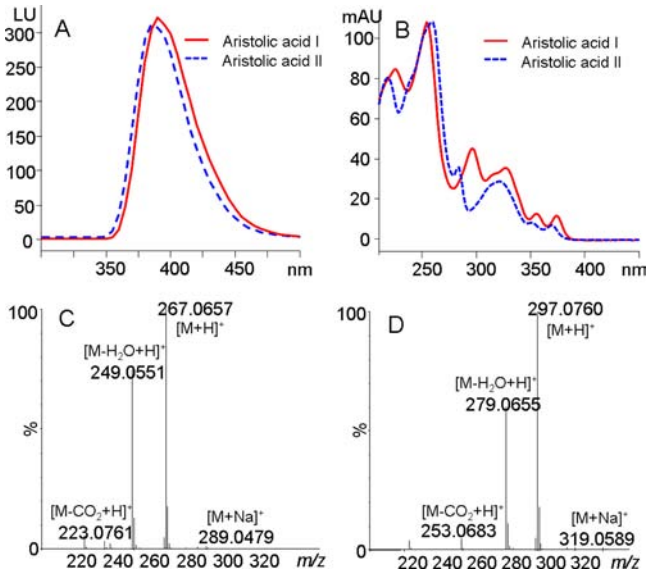

Figure 3. (A) Fluorescence emission and (B) UV absorption spectra of aristolic acids. (C and D) High-accuracy MS spectra of aristolic acid II and arstiolic acid I, respectively.

the chromatographic peak at 8.71 min revealed absorption maxima at 218, 258, 284, 320, 350, and 370 nm (Figure 3B). A similar UV absorption spectrum was also observed for the chromatographic peak at 8.91 min, with absorption maxima at 226, 254, 296, 326, 356, and 374 nm (Figure 3B).

High-accuracy MS analyses of the HPLC eluate collected at retention times of 8.71 and 8.91 min showed $[M + H]^+$ ions at m/z 267.0657 (Figure 3C) and m/z 297.0760 (Figure 3D), respectively. The close correlation between the measured (267.0657 and 297.0760) and theoretical (267.0657 and 297.0763) m/z values indicated that the fluorescing products were aristolic acid II ($C_{16}H_{11}O_4$) and aristolic acid I ($C_{17}H_{13}O_5$), respectively.

Selection of a Suitable Hydrogenolysis Reagent. As the basis for our method, Priestap and Barbieri recently reported that cysteine and GSH can induce hydrogenolysis of AAs at physiological relevant conditions, producing aristolic acids as the metabolites (Figure 1).[21] Aristolic acids, AAs with the fluorescent inhibiting nitro group replaced by hydrogen, exhibit fluorescence properties that allow for sensitive determination of AAs by spectrofluorometry (Figure 1).

With the hypothesis that other thiol-containing compounds may also be candidate denitrating reagents, cysteamine, cysteinylglycine, GSH, and 2-mercaptoethanol were investigated for their capabilites on producing the aristoloic acids from AAs. Our results showed that all of the tested thiol-containing reagents are capable of inducing AA hydrogenolysis, with cysteine being the most efficient reagent in removing the nitro group of AAs (Figure 4). Cysteine was therefore chosen as the hydrogenolysis reagent in this study.

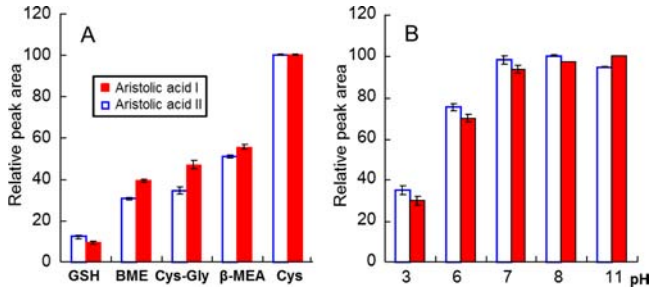

Figure 4. (A) Relative capability of some common thiol-containing compounds in inducing AA denitration and (B) effect of pH on the extent of cysteine-induced AA denitration. GSH, glutathione; BME, 2-mercaptoethanol; Cys-Gly, cysteinylglycine; *β*-MEA, cysteamine; and Cys, cysteine.

As an indirect approach to investigate the mechanism underlying the AA denitration reaction, we have also reacted AAs with alanine, an amino acid similar to cysteine but without the thiol functional group. Our results showed that no aristolic acids were produced in the alanine-catalyzed reaction, indicating that the thiol functional group is essential for the denitration process. Thus, we believed that the thiol functional group is participating in the electron transfer processes, which lead to the hydrogenolysis of AAs, producing the fluorophoric aristolic acids.

Optimization of the AA Hydrogenolysis Conditions. After the denitrating reagent was selected, the next step was to optimize the reaction conditions for AA denitration. Specifically, the formation of the aristoloic acids at different cysteine concentrations, pH values, temperatures, and reaction times were investigated. When the cysteine concentrations (from 10 to 150 mM) and pH (from 3.0 to 11.0) were changed in different reactions and the peak areas of aristolic acids in HPLC−FLD analyses were monitored, it was found that cysteine at 50 mM (Figure 5) and in pH 8.0 (Figure 4) is the most efficient for AA denitration. It is worth noting that the denitrating reaction is favored at alkaline conditions. This observation supports our proposed hydrogenolysis mechanism that the conjugated base of cysteine RS^- (pK_a = 8.36) initiated the AA denitration reaction and that the mechanism underlying the cysteine-induced denitration reaction appears to be

$$Ar{-}NO_2 + RS^- \rightarrow Ar{-}NO_2^{\bullet -} + RS^{\bullet}$$

dx.doi.org/10.1021/jf501609j | J. Agric. Food Chem. 2014, 62, 5859−5864

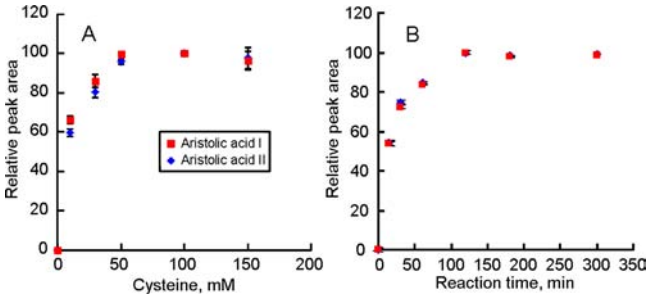

Figure 5. Influence of the (A) cysteine concentration and (B) reaction time on the denitration reaction of AAs. The data represent the mean ± standard deviation (SD) for three independent experiments with AAs at 4.80 μg/mL.

$$Ar{-}NO_2^{\bullet -} \rightarrow Ar^{\bullet} + NO_2^{-}$$

$$Ar^{\bullet} + H_2O \rightarrow - Ar{-}H + {}^{\bullet}OH$$

The influences of the reaction time and temperature on the extent of hydrogenolysis were studied over 1−5 h and from 25 to 80 °C, respectively. Our results showed that a 2 h reaction (Figure 5) at 80 °C (Figure 6) gave the best detector response.

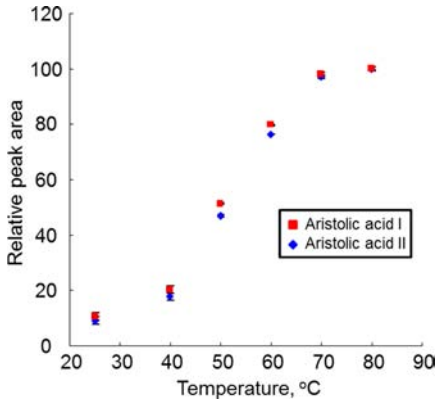

Figure 6. Influence of the reaction temperature on the cysteine-induced denitration reaction of AAs. The data represent the mean ± SD for three independent experiments with AAs at 4.80 μg/mL.

The optimized parameters above were selected and used in all studies. Under the developed hydrogenolysis conditions, the reaction yield of aristolic acid I and aristolic acid II from denitration of AA-I and AA-II were determined to be 95.2 and 96.4%, respectively.

Calibration and Method Validation. Calibration curves were constructed using standard solution mixture of AAs in triplicate reactions, with the concentrations of AA-I and AA-II ranging from 0.096 to 4.80 μg/mL. Depicted in Figure 7A is a typical chromatogram obtained from HPLC−FLD analysis of the reaction mixture containing AA-I and AA-II at 0.192 μg/mL. The peak areas of aristolic acids increased linearly over this concentration range, with r^2 values better than 0.9992. Table 1 summarizes the calibration slopes, intercepts, and coefficients of determination for the AAs determined in a calibration experiment.

The LODs defined as the concentrations of AA-I and AA-II that generated a signal 3 times the signal-to-noise ratio were 0.271 and 0.254 ng/mL,[22,25] respectively, corresponding to a method detection limit of 27.1 ng of AA-I and 25.4 ng of AA-II per gram of herbal medicines (Table 1). The LODs obtained

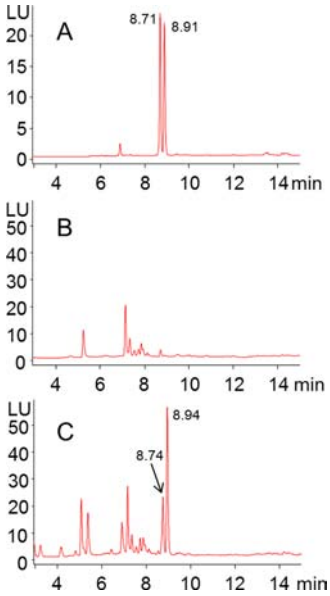

Figure 7. Typical chromatograms obtained from HPLC−FLD analyses of cysteine-treated AA-I (0.192 μg/mL) and AA-II (0.192 μg/mL), (A) standard mixture and (B) underivatized, and (C) cysteine-treated extracts of *Herba Aristolochiae* (*Tianxianteng*). The retention times of aristoic acid II and aristolic acid I were 8.7 and 8.9 min, respectively.

Table 1. Linear Regression Parameters of the Calibration Curves, Precision, Accuracy, and LOD of the Developed HPLC−FLD Method

	AA-I	AA-II
linear range (μg/mL)	0.096−4.80	0.096−4.80
slope	467.69	507.81
intercept	0.8259	0.3741
r^2	0.9992	0.9992
precision		
intraday (RSD, %)	0.45−1.48	0.57−1.31
interday (RSD, %)	0.64−2.95	0.71−2.82
accuracy (% mean deviation)	1.0−5.1	−3.3−8.5
LOD (ng/mL)	0.271	0.254
LOD (ng/g)[a]	27.1	25.4

[a]The LOD is the sample extract based on 50 mg of sample.

by the HPLC−FLD method are not differentiated from the existing LC−MS/MS (0.14−250 ng/mL)[15,16] and HPLC−FLD methods (0.39−26.0 ng/mL).[2,10]

The intra- and interday reproducibility of the developed method were determined by evaluating three individual reactions containing a mixture of AA-I and AA-II. The relative standard deviations for the intra- and interday reproducibility were less than 1.48 and 2.95%, respectively, at the tested concentrations (0.096, 1.92, and 4.80 μg/mL). The method accuracy as determined by spiking AAs at the three stated concentrations to blank herbal samples, cysteine treating, and HPLC analyzing was less than 8.5% deviated from the true values. The results of the reproducibility and accuracy of the HPLC−FLD method are summarized in Table 1. The robustness and high analytical precision of the data demonstrated a good performance of the HPLC−FLD method for AA determination.

HPLC−FLD Quantification of AAs in Herbal Medicine. The developed method combining cysteine-induced denitration

dx.doi.org/10.1021/jf501609j | J. Agric. Food Chem. 2014, 62, 5859−5864

Table 2. Determination of AAs (μg/g) in Selected Herbal Medical Samples by the Developed HPLC−FLD and LC−MS Methods[a]

	AA-I		AA-II	
	HPLC−FLD	LC−MS	HPLC−FLD	LC−MS
Fructus Aristolochiae (*Madouling*)[b]	617.2 ± 22.4	615.8 ± 16.8	55.7 ± 2.9	52.9 ± 3.4
Herba Aristolochiae (*Tianxianteng*)	53.7 ± 1.5	48.1 ± 2.2	25.2 ± 1.2	28.1 ± 8.5
Aristolochiae mollissima (*Xungufeng*)[b]	1086.7 ± 125.9	1004.4 ± 60.5	58.7 ± 0.4	55.7 ± 10.2
Radix Aristolochiae (*Qingmuxiang*)[b]	965.3 ± 38.4	927.3 ± 92.2	211.6 ± 27.2	201.4 ± 30.2
Aristolochiae cinnabarina (*Zhushalian*)[b]	911.3 ± 8.3	890.7 ± 54.7	658.7 ± 54.3	676.5 ± 17.3
Herba Asari (*Xixin*)[c]	<LOD	<LOD	<LOD	<LOD
Akebia Stem (*Mutong*)[c]	<LOD	<LOD	<LOD	<LOD

[a]The data represent the mean ± SD for three independent determinations. [b]Sample extracts were 10-fold diluted before the HPLC−FLD analysis. [c]Five samples of different origins from local drug stores in Hong Kong.

and HPLC−FLD analysis was applied for the determination of AAs in representative Chinese herbal medical samples. A total of 15 representative herbal samples were analyzed by the proposed HPLC method. Among the tested samples, five showed positive identification of AA-I and AA-II and *Aristolochiae mollissima* was found to contain the highest AA concentration (Table 2). Figure 7 shows the representative chromatograms obtained from HPLC analysis of underivatized (Figure 7B) and cysteine-treated (Figure 7C) sample extracts of *Herba Aristolochiae*. In agreement with previous studies, the concentration of AA-I is significantly higher than that of AA-II in all of the tested herbal medicine, which show a positive identification of AAs.

It is worth noting that the products from the cysteine-induced hydrogenolysis of AAs, the aristolic acids, were detected in only cysteine-treated sample extracts but none of the untreated samples. This observation implies that aristolic acids do not exist naturally in the tested herbal medicine and were only generated from hydrogenolysis of AAs. The absence of aristolic acids in herbal samples allows for AA quantification in a single HPLC analysis. In contrast to previous methods quantifying AAs by reducing AAs to aristolactams that require duplicated analyses of both the derivatized and underivatized sample extracts,[2,10] the current method has the advantage of being a more efficient and higher sample throughput for AA determination.

Method Comparison. The results from the HPLC−FLD analyses were also compared to that obtained from LC−MS analyses. Table 2 shows the result from LC−MS analysis of the sample extracts. No statistical difference was observed in the AA concentrations measured using the two methods. The mean deviation of the AA concentrations by the two methods was 4.89% for AA-I and 0.15% for AA-II, with no data pair difference exceeding 12%. With the strong correlation between the two methods, we believe that the newly developed HPLC−FLD method can accurately determine AA concentrations.

In conclusion, we have developed a new HPLC−FLD method for the sensitive and efficient detection of carcinogenic and nephrotoxic AAs. The method makes use of a novel cysteine-induced denitrating reaction converting the non-fluorescing AAs into aristolic acids that strongly fluoresce. This new derivatization methodology allows for fluorescence detection and quantification of AAs with high sensitivity. The method was validated for its accuracy, precision, and applied in quantifying AAs in herbal medical samples. It is believed that the developed HPLC−FLD method will find wide applications in detecting AAs in herbal preparations and food composites that are suspected to be AA-contaminated.

AUTHOR INFORMATION

Corresponding Author

*Telephone: +852-2358-7370. Fax: +852-2358-1594. E-mail: chanwan@ust.hk.

Funding

Wan Chan expresses his sincere thanks to The Hong Kong University of Science and Technology for supporting this research (Grant R9310).

Notes

The authors declare no competing financial interest.

ACKNOWLEDGMENTS

The authors thank Prof. Jianzhen Yu (Department of Chemistry, The Hong Kong University of Science and Technology) for providing the fluorescence detector for this research.

REFERENCES

(1) Arlt, V. M.; Stiborova, M.; Schmeiser, H. H. Aristolochic acid as a probable human cancer hazard in herbal remedies: A review. *Mutagenesis* **2002**, *17*, 265−277.

(2) Chan, W.; Lee, K. C.; Liu, N.; Cai, Z. A sensitivity enhanced high-performance liquid chromatography fluorescence method for the detection of nephrotoxic and carcinogenic aristolochic acid in herbal medicines. *J. Chromatogr. A* **2007**, *1164*, 113−119.

(3) Pfau, W.; Schmeiser, H. H.; Wiessler, M. N^6-adenyl arylation of DNA by aristolochic acid II and a synthetic model for the putative proximate carcinogen. *Chem. Res. Toxicol.* **1991**, *4*, 581−596.

(4) Vanherweghem, J. L.; Depierreux, M.; Tielemans, C.; Abramowicz, D.; Dratwa, M.; Jadoul, M.; Richard, C.; Vandervelde, D.; Verbeelen, D.; Vanhaelen-Fastre, R. Rapidly progressive interstitial renal fibrosis in young women: Association with slimming regimen including Chinese herbs. *Lancet* **1993**, *341*, 387−391.

(5) Martena, M. J.; A. van der Wielen, J. C.; J. van de Laak, L. F.; Konings, E. J. M.; de Groot, H. N.; Rietjens, I. M. C. M. Enforcement of the ban of aristolochic acids in Chinese traditional herb preparations on Dutch market. *Anal. Bioanal. Chem.* **2007**, *389*, 263−275.

(6) Gold, L. S.; Slone, T. H. Aristolochic acid, an herbal carcinogen, sold on the Web after FDA alert. *N. Engl. J. Med.* **2003**, *349*, 1576−1577.

(7) De Broe, M. E. Chinese herbs nephropathy and Balkan endemic nephropathy: Toward a single entity, aristolochic acid nephropathy. *Kidney Int.* **2012**, *81*, 513−515.

(8) Schmeiser, H. H.; Kucab, J. E.; Arlt, V. M.; Phillips, D. H.; Hollstein, M.; Gluhovschi, G.; Gluhovschi, C.; Modilca, M.; Daminescu, L.; Petrica, L.; Velciov, S. Evidence of exposure to aristolochic acid in patients with urothelial cancer from a Balkan endemic nephropathy region of Romania. *Environ. Mol. Mutagen.* **2012**, *53*, 636−641.

(9) Grollman, A. P.; Shibutani, S.; Moriya, M.; Miller, F.; Wu, L.; Moll, U.; Suzuki, N.; Fernandes, A.; Rosenquist, T.; Medverec, Z.; Jakovina, K.; Brdar, B.; Slade, N.; Turesky, R. J.; Goodenough, A. K.; Rieger, R.; Vukelic, M.; Jelakovic, B. Aristolochic acid and the etiology of endemic (Balkan) nephropathy. *Proc. Natl. Acad. Sci. U. S. A.* **2007**, *104*, 12129−12134.
(10) Pavlović, N. M.; Maksimović, V.; Maksimović, J. D.; Orem, W. H.; Tatu, C. A.; Lerch, H. E.; Bunnell, J. E.; Kostić, E. N.; Szilagyi, D. N.; Paunescu, V. Possible health impacts of naturally occurring uptake of aristolochic acids by maize and cucumber roots: links to the etiology of endemic (Balkan) nephropathy. *Environ. Geochem. Health* **2013**, *35*, 215−226.
(11) Yu, F. Y.; Lin, Y. H.; Su, C. C. A sensitive enzyme-linked immunosorbent assay for detecting carcinogenic aristolochic acid in herbal remedies. *J. Agric. Food Chem.* **2006**, *54*, 2496−2501.
(12) Chan, W.; Hu, K. M.; Poon, W. T.; Lee, K. C.; Cai, Z. Differentiation of herbs linked to "Chinese herb nephropathy" from the liquid chromatographic determination of aristolochic acids. *Anal. Chim. Acta* **2006**, *576*, 112−116.
(13) Yamasaki, K.; Tagami, T.; Kawaguchi, M.; Okihashi, M.; Takatori, S.; Sakagami, Y.; Sekita, S.; Satake, M. Simple and rapid analysis of aristolochic acid contained in crude drugs and Kampo formulations with solid-phase extraction and HPLC photodiode-array detection. *J. Nat. Med.* **2009**, *63*, 451−458.
(14) Yuan, J.; Liu, Q.; Zhu, W.; Ding, L.; Tang, F.; Yao, S. Simultaneous analysis of six aristolochic acids and five aristolactams in herbal plants and their preparations by high-performance liquid chromatography−diode array detection−fluorescence detection. *J. Chromatogr. A* **2008**, *1182*, 85−92.
(15) Kuo, C. H.; Lee, C. W.; Lin, S. C.; Tsai, I. L.; Lee, S. S.; Tseng, Y. J.; Kang, J. J.; Peng, F. C.; Wei-Chu, L. Rapid determination of aristolochic acids I and II in herbal products and biological samples by ultra-high-pressure liquid chromatography−tandem mass spectrometry. *Talanta* **2009**, *80*, 1672−1680.
(16) Kite, G. C.; Yule, M. A.; Leon, C.; Simmonds, M. S. Detecting aristolochic acids in herbal remedies by liquid chromatography/serial mass spectrometry. *Rapid Commun. Mass Spectrom.* **2002**, *16*, 585−590.
(17) Li, W.; Gong, S.; Wen, D.; Che, B.; Liao, Y.; Liu, H.; Feng, X.; Hu, S. Rapid determination of aristolochic acid I and II in *Aristolochia* plants from different regions by *β*-cyclodextrin-modified capillary zone electrophoresis. *J. Chromatogr. A* **2004**, *1049*, 211−217.
(18) Ong, E. S.; Woo, S. O. Determination of aristolochic acids in medicinal plants (Chinese) prepared medicine using capillary zone electrophoresis. *Electrophoresis* **2001**, *22*, 2236−2241.
(19) Zhou, X.; Zheng, C.; Sun, J.; You, T. Analysis of nephroloxic and carcinogenic aristolochic acids in *Aristolochia* plants by capillary electrophoresis with electrochemical detection at a carbon fiber microdisk electrode. *J. Chromatogr. A* **2006**, *1109*, 152−159.
(20) Sun, Z.; Liu, L.; Zheng, X.; Fan, C.; Wang, Q.; Li, G. An easy and rapid method to determine aristolochic acids I and II with high sensitivity. *Anal. Bioanal. Chem.* **2004**, *378*, 388−390.
(21) Priestap, H. A.; Barbieri, M. A. Conversion of aristolochic acid I into aristolic acid by reaction with cysteine and glutathione: Biological implications. *J. Nat. Prod.* **2013**, *76*, 965−968.
(22) Yu, Y.; Liu, H.; Horvatovich, P.; Chan, W. Liquid chromatography−electrospray ionization tandem mass spectrometric analysis of 2-alkylcyclobutanones in irradiated chicken by precolumn derivatization with hydroxylamine. *J. Agric. Food Chem.* **2013**, *61*, 5758−5763.
(23) Li, J.; Leung, E. M.; Choi, M. M.; Chan, W. Combination of pentafluorophenylhydrazine derivatization and isotope dilution LC−MS/MS techniques for the quantification of apurinic/apyrimidinic sites in cellular DNA. *Anal. Bioanal. Chem.* **2013**, *405*, 4059−4066.
(24) Valeur, B. *Molecular Fluorescence, Principles Applications*, 1st ed.; Wiley: New York, 2001; p 58.
(25) Leung, E. M.; Chan, W. A novel reversed-phase HPLC method for the determination of urinary creatinine by pre-column derivatization with ethyl chloroformate: Comparative studies with the standard *Jaffé* and isotope-dilution mass spectrometric assays. *Anal. Bioanal. Chem.* **2014**, *406*, 1807−1812.

JOURNAL OF AGRICULTURAL AND FOOD CHEMISTRY

Article

pubs.acs.org/JAFC

Effect of the Electric Field Frequency on Ascorbic Acid Degradation during Thermal Treatment by Ohmic Heating

Giovana Domeneghini Mercali,*[,†] Steven Schwartz,[‡] Ligia Damasceno Ferreira Marczak,[†] Isabel Cristina Tessaro,[†] and Sudhir Sastry[§]

[†]Chemical Engineering Department, Federal University of Rio Grande do Sul, Rua Engenheiro Luiz Englert s/n, Porto Alegre, Rio Grande do Sul 90040-040, Brazil

[‡]Department of Food Science and Technology, The Ohio State University, 235 Parker Food Science Building, 2015 Fyffe Court, Columbus, Ohio 43210, United States

[§]Department of Food, Agricultural and Biological Engineering, The Ohio State University, 590 Woody Hayes Drive, Columbus, Ohio 43210-1057, United States

ABSTRACT: In this work, the influence of the electric field frequency and solids content on the degradation kinetics of ascorbic acid during ohmic heating of acerola pulp and acerola serum was investigated. The degradation percentage of ascorbic acid in the pulp after 120 min of heating varied between 12 and 17%. For the serum, the degradation percentage was in the range of 13 and 18%. The results were fitted to the first-order model, and the kinetic rate constants ranged from 1.1 to 1.6 × 10^{-3} min^{-1} and from 1.1 to 1.5 × 10^{-3} min^{-1} for pulp and serum, respectively. *D* values ranged between 1480 and 2145 min for the pulp and between 1524 and 1951 min for the serum. A distinct behavior between the kinetic parameters of the pulp and serum in electric field frequencies ranging from 10 to 1000 Hz indicates that the presence of distinct amounts and types of solids might affect the rate of the electron transfer in electrochemical reactions. These variables may also affect the polarization process stimulated by the oscillating electric field. The non-achievement of the equilibrium of the polarization process may have an influence on oxidation reactions, affecting the predisposition to hydrogen donation from the ascorbic acid molecule.

KEYWORDS: *ohmic heating, ascorbic acid, electric field frequency, polarization, solids content*

INTRODUCTION

Increasing consumer interest for nutritive fresh-like food products is driving the development of emerging processing technologies to ensure food safety and high nutritional and sensory properties. Ohmic heating (OH) is one alternative heat treatment where an alternating current (AC) is passed through food materials, thereby leading to heat generation.[1,2] This technology is particularly suitable for viscous products and liquid−particulate food mixtures because the heat is generated inside the food product.[1] It allows for processing at the rate of high-temperature, short-time (HTST) processes, but without the limitation of conventional HTST methods relative to heat transfer to particulates.[2]

For some years, it was presumed that the effects of the OH during food pasteurization and sterilization were solely thermal and that the applied electric field had no effect on biological cells and bioactive compounds.[3] However, some studies have shown that non-thermal effects exist within the range of moderate electric field (MEF) strengths associated with OH.[4−9] From this standpoint, the interaction of electric fields with food at the molecular, cellular, and tissue levels is important and needs to be evaluated. The effects of MEF treatments on bioactive components of foods have not been always considered, and the precise mechanism of MEF-induced changes is still not deeply understood.

In OH devices, the signal is an alternating bipolar current. When an electric field is applied to a sample, the molecules of the sample attempt to align themselves with the oscillating electric field in a process known as polarization. The electronic polarization is the displacement of electrons of atoms with respect to the nucleus, and the atomic polarization is the displacement of the atomic nuclei within the molecules.[10] When a low-frequency alternating voltage is used, orientational movements of molecules that arise from the polarization process are slow and molecules have enough time to move and rotate in the field. However, when a high-frequency alternating voltage is applied, movements of molecules that arise from the polarization process become faster and may not be accomplished. The polarization depends upon the relaxation time of the molecular dipoles, which is, in turn, influenced by the molecular weight, mobility of the molecules, and temperature.[11]

This work aimed to study the impact of MEF processing conditions during OH on the stability of bioactive compounds in food systems. Regardless of specific motivations or process objectives, it is of fundamental scientific interest to understand the kinetics of inactivation under various processing conditions, so that future processes may be designed with a full understanding of these effects. In a previous study, the effects of the electric field frequency on ascorbic acid degradation and color changes in acerola pulp were evaluated.[12] The objective of this study was to compare the degradation kinetics of the

Received: October 4, 2013
Revised: March 31, 2014
Accepted: June 3, 2014
Published: June 3, 2014

ACS Publications © 2014 American Chemical Society

acerola pulp and the acerola serum to investigate the influence of the presence of solids when using different frequencies. Thus, our specific objectives were (1) to conduct experimental studies with acerola serum at different electric field frequencies (from 10 to 10^5 Hz) and (2) compare these results to those previously reported by Mercali et al.[12] to obtain a better understanding of the influence of solids content on the precise mechanism of MEF-induced changes.

MATERIALS AND METHODS

Chemicals. Standard L-ascorbic acid with a purity of 99.7% and *meta*-phosphoric acid with a purity of 33.5−36.5% were obtained from Fisher Scientific Co. (Fair Lawn, NJ) and Sigma-Aldrich (St. Louis, MO), respectively. Potassium phosphate monobasic was purchased from Sigma-Aldrich (St. Louis, MO). Deionized water was used throughout.

Acerola Pulp. Acerola pulp, supplied by EcoFruits Company (South Jordan, UT), was received frozen and was stored immediately at −18 °C. The product had an initial vitamin C content of 1657 ± 45 mg/100 g.

Samples were thawed before each experiment by immersion in cold water. For acerola pulp, the experiments were conducted immediately after thawing. For the serum, thawed samples were then centrifuged (3000*g* at 5 °C for 10 min) and the supernatant fraction was used immediately for conducting the experiments. The ratio between the serum and pulp was approximately 0.7 (w/w). The total solids contents of the pulp and serum were 12.8 and 9.9 g/100 g, respectively. The pulp was characterized as a high-acid product with a pH of 3.3 ± 0.3. The initial temperature of the samples before starting the heating experiments was approximately 10−13 °C.

OH Process. The OH apparatus used to conduct the experiments was comprised of a function generator (Tektronix, Inc., model AFG3252, Richardson, TX), a power amplifier (Industrial Test Equipment, model 500A, Port Washington, NY), an Agilent 34970A data acquisition unit and HP BenchLink Data Logger software (Agilent Technologies, Inc., Palo Alto, CA), a computer, and an ohmic cell. A more complete description of the OH setup can be found elsewhere.[12] The temperature was measured by two type-T thermocouples: one located close to the electrode and the other located away from the electrodes. The difference between the two measurements was lower than 2 °C. The ohmic cell (9.9 cm of height) consisted of a 500 mL glass vessel with a water jacket. It had a lid to prevent evaporation from the product. The electrodes were made of titanium and curved to conform to reactor dimensions. The maximum interelectrode gap was 7.5 cm, and the minimum gap was 5.7 cm. The electrode height was 5.0 cm. The product was stirred using a magnet inside the cell and a magnetic stirrer plate (Fisher Scientific, Model Isotemp, Fair Lawn, NJ). The velocity of the agitation is an important factor to be considered because it has influence on the amount of oxygen incorporated in the product. In this manner, the velocity of the agitation of both products was matched to eliminate this variable during the experiments (500 rpm for the pulp and 350 rpm for the serum). Five different electric field frequencies (FQs) were studied: 10, 10^2, 10^3, 10^4, and 10^5 Hz.

The kinetic experiments were conducted at 85 °C for up to 2 h. A critical consideration in such experiments (to ensure that an effect may be attributed to an electric field effect) is the need to maintain the same temperature history for both ohmic and conventional treatments. OH has its unique electrical heating mechanisms and temperature histories that are fundamentally different from the ones of the conventional process. To be able to match the time−temperature histories between electric field treatments and thermal controls, OH experiments were conducted using a controlled temperature cooling water in the jacket (in actual practice, it used 30 V and 75 °C water in the jacket simultaneously). In contrast, because conventional heat treatment lacked an internal energy source, the jacket was maintained at the test temperature (85 °C). This procedure allowed for the evaluation of the non-thermal effects of electricity because the temperature histories for conventional and ohmic treatments were the same. Sample plots of the thermal histories for OH and conventional heating (Figure 1) for acerola serum show that we were able to closely

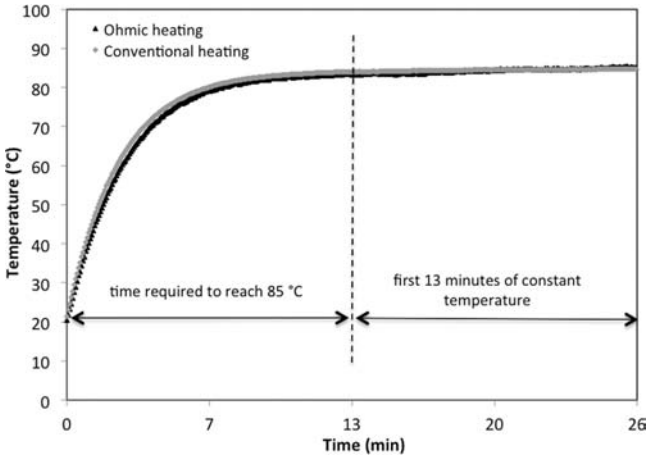

Figure 1. Time−temperature histories (the first 25 min of heating) of the ohmic and conventional treatments for acerola serum, showing closely matched thermal histories.

match temperature histories. Figure 1 represents the temperature measured close to the electrode. Time−temperature histories reported for acerola pulp showed a similar plot behavior.[12]

A model was developed to estimate the average electric field strength by solving Laplace's equation within the vessel domain. Figure 2 shows average electric field distribution within an ohmic cell when

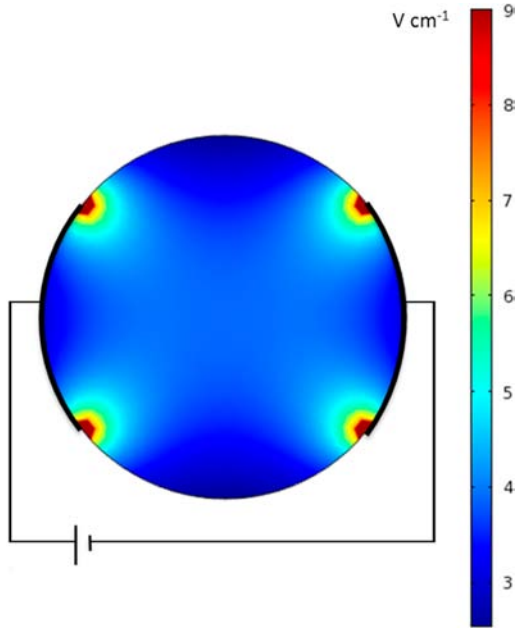

Figure 2. Average electric field distribution within the ohmic cell (cross-section) when 30 V is applied.

30 V is applied. The electric field within most of the cell is reasonably uniform, except for the electrode edges. The model did not account for the presence of the magnet and agitation. The agitation itself may not make a lot of difference unless the shape of the liquid surface is greatly changed by the agitation. The magnet will alter the local field, but the average field will likely be quite unaffected. In this manner, the assumed field strength was considered realistic.

The time zero was set when the sample reached the desired holding temperature. Samples were withdrawn at various heating times (0, 20,

40, 60, 80, 100, and 120 min). Determination of ascorbic acid levels was carried out immediately after the heating experiments.

Conventional Heating Process. The conventional heating process was conducted in the ohmic cell without an electric field. The samples were heated by passing hot water through the jacket using a thermostatic water bath (Brookfield Engineering Laboratories, model EX-100, Middleboro, MA). The kinetic experiments were conducted at the same temperature (85 °C), and samples were collected at the same heating times ranging from 0 to 120 min.

Determination of the Ascorbic Acid Content. The ascorbic acid content was quantified using high-performance liquid chromatography (HPLC, Hewlett-Packard, HP Agilent 1100 system, Norwalk, CT), reverse C_{18} Luna (5 μm, 250 × 4.6 mm, Phenomenex, Torrance, CA), and a diode-array detector (254 nm). The detailed methodology can be found elsewhere.[12]

Extraction of ascorbic acid was carried out adding *meta*-phosphoric acid solution to the samples. The mixture was homogenized for 30 s and centrifuged (1500*g* for 5 min). The supernatants were filtered through a 0.45 μm polytetrafluoroethylene (PTFE) membrane, diluted, and injected into the HPLC system. Samples were protected from light and kept on ice during all procedures.

Determination of the Kinetic Parameters. Traditionally, degradation of vitamin C in foods during thermal processing and storage has been described in terms of first-order kinetics and the Arrhenius equation.[13−16] Because the data seemed to follow a simple linear decrease, the zero-order kinetics was also considered. Then, a comparison between both models was carried out, and the model that better fit the experimental values was chosen to describe changes in ascorbic acid concentrations in acerola pulp during heating.

The zero- and first-order models are given by

$$C = C_0 - kt \quad (1)$$

$$C = C_0 \exp(kt) \quad (2)$$

where t is the time (min), k is the rate constant (min^{-1}), C_0 and C are the ascorbic acid contents at time zero and time t, respectively.

The decimal reduction time (D value), the time needed for a 10-fold reduction of the initial concentration at a given temperature, is related to k values according to eq 2.

$$D = \frac{\ln(10)}{k} \quad (3)$$

Statistical Analyses. Two independent experiments (replicates) were conducted for each frequency studied during OH and also for conventional heating. The results were fitted to the zero- and first-order models by linear and nonlinear estimation, respectively. The rate constants (k values) of all experiments were compared using the Tukey test (5% of the confidence level). Statistical analyses were performed using Statistica 7.0 (StatSoft, Tulsa, OK) and Microsoft Excel 2011 (MapInfo, Troy, NY).

The goodness of fit of the proposed models was evaluated by means of the χ^2 parameter, the determination coefficient (R^2), and the standard error of means (SEM). The average errors between the experimental values and the values predicted by the models (E) were also estimated.

RESULTS AND DISCUSSION

Degradation of ascorbic acid over time for acerola serum during conventional heating and OH (using different frequencies) is shown in Figure 3. Error bars have not been added because it would be impossible to distinguish between the different treatments. Standard deviations were lower than 3% for all experimental points. Figure 4 shows the results reported for acerola pulp.[12] The degradation percentage of ascorbic acid in acerola pulp after 120 min of heating varied between 12 and 17%. For the serum, the degradation percentage was in the range of 13 and 18%. These values were lower than expected on the basis of kinetic data reported in the literature.[16−20] It is likely that the oxygen dissolved in the medium is the limiting reactant because the vitamin C content in acerola is very high, approximately 40 times higher than that of orange juice (1657 mg/100 g compared to 40 mg/100 g). Therfore, there is not enough oxygen in the medium to react with this extremely high vitamin C content. Another possibility is the degradation of some other antioxidants (anthocyanins) that are competing for the available oxygen. According to de Rosso and Mercadante,[21] the high ascorbic acid content is the main cause of the low stability of anthocyanin extracts from acerola. A recently published study performed in our laboratory evaluated the degradation kinetics of monomeric anthocyanins in acerola pulp during thermal treatment by OH and conventional heating.[22] The anthocyanin degradation percentages after 90 min of OH at 75 and 90 °C were approximately 46 and 84%, respectively. This may be an indication that anthocyanin is degrading faster than ascorbic acid in acerola pulp. Another point that needs to be mentioned is that acerola has a very acidic pH (approximately 3.3), and at low pH, ascorbic acid is more stable.[23] When analyzing ascorbic acid degradation, it is important to consider that its stability is influenced by the intrinsic properties of the product and the process characteristics.[13,15,18,20,24−27] Vitamin C degradation can occur through aerobic and/or anaerobic pathways, depending upon a number

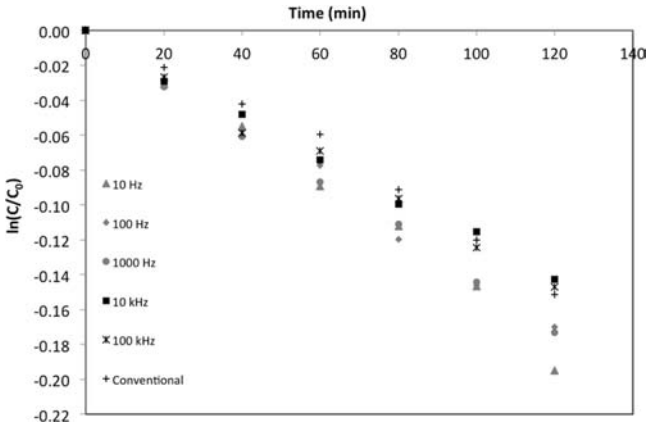

Figure 3. Degradation of ascorbic acid in acerola serum during OH and conventional heating processes. The standard deviations were lower than 3% for all experimental points.

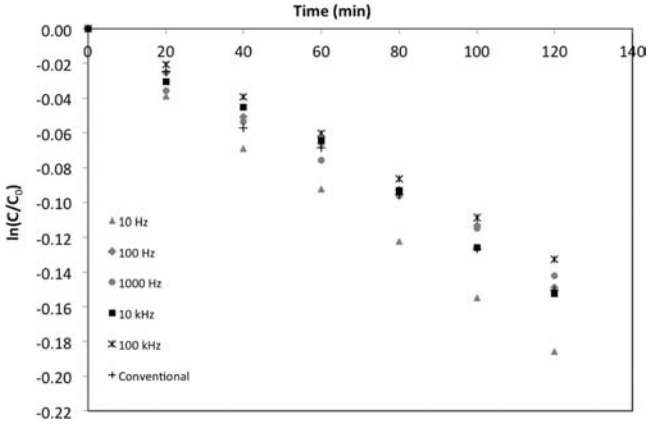

Figure 4. Degradation of ascorbic acid in acerola pulp during OH and conventional heating processes. The standard deviations were lower than 3% for all experimental points. Adapted with permission from ref 12 (Copyright 2013 Elsevier, License number 3305350538453).

Table 1. Statistical Parameters Evaluating the Zero- and First-Order Model Performance To Describe Ascorbic Acid Degradation during OH and Conventional Heating of Acerola Pulp

		zero-order model				first-order model			
process	FQ (Hz)	R^2	E (%)	χ^2	SEM	R^2	E (%)	χ^2	SEM
OH[a]	10	0.99	7.34	6.8×10^3	1.3×10^4	1.00	0.34	2.1×10^{-5}	3.9×10^{-5}
OH	10^2	0.99	5.66	2.7×10^3	5.0×10^3	0.99	0.40	1.9×10^{-5}	3.5×10^{-5}
OH	10^3	0.98	10.63	8.9×10^3	1.7×10^4	0.98	0.48	3.9×10^{-5}	7.3×10^{-5}
OH	10^4	0.99	7.85	4.8×10^3	9.1×10^3	0.99	0.55	3.4×10^{-5}	6.5×10^{-5}
OH	10^5	1.00	2.32	6.0×10^2	1.1×10^3	1.00	0.22	7.9×10^{-6}	1.5×10^{-5}
CH[b]	0	0.99	5.12	3.6×10^3	6.8×10^3	0.99	0.35	2.0×10^{-5}	3.7×10^{-5}

[a]OH = ohmic heating. [b]CH = conventional heating.

Table 2. Statistical Parameters Evaluating the Zero- and First-Order Model Performance To Describe Ascorbic Acid Degradation during OH and Conventional Heating of Acerola Serum

		zero-order model				first-order model			
process	FQ (Hz)	R^2	E (%)	χ^2	SEM	R^2	E (%)	χ^2	SEM
OH[a]	10	0.99	4.54	5.2×10^3	9.9×10^3	0.99	0.57	4.5×10^{-5}	8.6×10^{-5}
OH	10^2	1.00	4.04	3.6×10^3	6.8×10^3	1.00	0.33	1.9×10^{-5}	3.6×10^{-5}
OH	10^3	1.00	5.14	2.2×10^3	4.1×10^3	1.00	0.20	7.1×10^{-6}	1.3×10^{-5}
OH	10^4	0.99	5.82	2.7×10^3	5.2×10^3	1.00	0.23	8.1×10^{-6}	1.5×10^{-5}
OH	10^5	0.99	6.55	5.9×10^3	1.1×10^4	0.99	0.36	2.3×10^{-5}	4.3×10^{-5}
CH[b]	0	0.99	6.62	5.9×10^3	1.1×10^4	0.99	0.56	4.5×10^{-5}	8.5×10^{-5}

[a]OH = ohmic heating. [b]CH = conventional heating.

Table 3. Kinetic Parameters of the First-Order Model for Ascorbic Acid Degradation in Acerola Pulp and Acerola Serum during OH and Conventional Heating

		acerola pulp[a]		acerola serum	
process	FQ (Hz)	K $(min^{-1})^b$	D $(min)^b$	K $(min^{-1})^b$	D $(min)^b$
OH[c]	10	0.0016 ± 0.0001 a	1480 ± 72 a	0.00151 ± 0.00001 a	1524 ± 9 a
OH	10^2	0.0012 ± 0.0001 b	1948 ± 50 b	0.00143 ± 0.00008 a	1612 ± 86 a
OH	10^3	0.0012 ± 0.0001 b	1927 ± 183 b	0.00144 ± 0.00003 a	1599 ± 37 a
OH	10^4	0.0012 ± 0.0001 b	1889 ± 124 b	0.00112 ± 0.00007 b	1923 ± 110 b
OH	10^5	0.0011 ± 0.0001 b	2145 ± 179 b	0.00123 ± 0.00003 b	1867 ± 39 b
CH[d]	0	0.0012 ± 0.0001 b	1860 ± 151 b	0.00118 ± 0.00003 b	1951 ± 56 b

[a]Adapted with permission from ref 12 (Copyright 2013 Elsevier, License number 3305350538453). [b]Mean of two replicates ± standard error. Means in the same column with different letters (a and b) are significantly different ($p < 0.05$). [c]OH = ohmic heating. [d]CH = conventional heating.

of factors, such as pH, acidity, metal ions, light, humidity, water activity, temperature, presence of amino acids, carbohydrates, lipids, and enzymes, among others.[23]

From Figures 3 and 4, it can be observed that pulp and serum showed a distinct behavior when analyzing the degradation curves in the same range of frequencies. For a better comparison between treatments, the results of the ascorbic acid concentration against time were fitted to the zero- and first-order equations. The quality of the adjustment was evaluated through the statistical parameters presented in Tables 1 and 2. Both first- and zero-order equations proved to be suitable for modeling acid ascorbic degradation because the determination coefficients were above 0.98 for all treatments. When compared to the zero-order model, the first-order model yielded a better fit of the experimental data, with a smaller deviation between the values estimated by the model and experimental data and lower SEM and χ^2 values. The accuracy of the first-order model is confirmed by the small deviation between the values estimated by the model and the experimental data. Thus, the first-order model was chosen for predicting the ascorbic acid retention of acerola pulp and acerola serum during OH and conventional heating.

Table 3 presents the kinetic parameters of the first-order model obtained for each frequency evaluated during OH and also for the conventional process for both products. According to Mercali et al.,[12] the pulp showed kinetic rate constants ranging from 1.1 to 1.6×10^{-3} min^{-1} and D values ranging between 1480 and 2145 min. For the serum, the rate constants were between 1.1 and 1.5×10^{-3} min^{-1} and D values ranged from 1524 to 1951 min. Some points observed when comparing Figures 3 and 4 are confirmed by the statistical analysis. For acerola pulp, there was no difference ($p > 0.05$) between ascorbic acid degradation rates for experiments carried out with electric field frequencies ranging from 100 to 10^5 Hz. Also, the rate constants of these experiments did not differ from that found for the conventional heating treatment. The rate constant of the OH process at 10 Hz was higher than the rate constants of all other treatments. However, for the serum, a different behavior was observed. The rate constant of the OH process at 10 Hz was statistically similar to the rate constants of the treatments at 100 and 1000 Hz. These three conditions showed rate constants statistically different from the experiments conducted at 10^4 and 10^5 Hz. Also, the conventional process showed similar rate constants to the ones obtained for treatments using 10^4 and 10^5 Hz.

dx.doi.org/10.1021/jf500203u | J. Agric. Food Chem. 2014, 62, 5865−5870

Higher degradation rates at lower frequencies may be explained by the occurrence of electrochemical reactions (electrolysis of water and electrode corrosion). Electrolysis of water releases hydrogen and oxygen in the medium, which may cause additional oxidation of ascorbic acid.[28] Electrode corrosion releases metal ions that also catalyze the oxidation process.[28] Corrosion of electrodes and apparent (partial) electrolysis of the heating medium with most types of electrodes at low-frequency ACs were noticed in experiments carried out by Samaranayake and Sastry.[29] These authors verified that apparent electrolysis was seen at all pH values, even though titanium electrodes showed a relatively high corrosion resistance.

These electrochemical reactions occur within a narrow area between electrodes and the product, which acts as a capacitor. When an AC voltage starts flowing through the system, charges start to build up in this area close to the surface of the electrode. If a low-frequency alternating voltage is applied, there is enough time to reach the Faradaic threshold potential and the layer becomes saturated with charges. After the saturation point, any current that flows through it results in electrochemical reactions.[30] On the other hand, when a high-frequency alternating voltage is used, the potential raise and reverse before it reaches the Faradaic threshold potential point as a consequence the electrochemical reactions do not take place.

The distinct behavior shown between acerola pulp and acerola serum at frequencies ranging from 10 to 1000 Hz indicates that the presence of different amounts of solids may have an influence on this process. Moreover, the serum and pulp have a distinct composition of solids: in the serum, most of the solids are soluble solids, such as sugar, vitamins, and acids, while in the pulp, there are also insoluble solids, such as fibers, starch, pectin, and long-chain carbohydrates. The amount of solids and even the predominant type of solid (insoluble or soluble solids) may have affected the drag for ionic mobility and, consequently, the rate of electron transfer. The particle type, size, concentration, shape, and orientation in the electric field may affect the mass transport processes by diffusion and/or convection that occur in the narrow layer between the electrodes and the product, which, in turns, influences the rate of the electron transfer reactions.

In high frequencies (10^4 and 10^5 Hz), ascorbic acid degradation was similar to the degradation found in the conventional heating. This behavior was observed for both acerola pulp and serum. This means that the electrochemical reactions were probably minimized and the main mechanism of degradation was the oxidation. Some authors recommend the use of high-frequency ACs to effectively suppress electrochemical phenomena at electrode−solution interfaces.[2,28,31]

Another point that needs to be considered is the effect of the polarization stimulated by the oscillating electric field. The polarization process is critically dependent upon the relaxation time of the molecular dipoles. Relaxation time refers to the time taken by the dipoles to revert to random orientation when the field is removed and is influenced by their molecular weight, mobility, and temperature.[11,32] Because liquids and solids have different relaxation times, the polarization of the whole sample depends upon the relative contribution of the phases present in the sample. The acerola pulp had higher solids content and more insoluble solids (fibers, starch, pectin, and long-chain carbohydrates) than the serum, which makes them have different dielectric properties, and, consequently, different behaviors when subjected to electric fields.

The ascorbic acid is a small polar water-soluble molecule.[33] Even though its molecular weight is higher than water, some considerations can be performed comparing its behavior to the water molecule. When an electric field is applied at low frequencies to a polar liquid (such as water), the time interval taken for the field to reverse its polarity would presumably be longer than the relaxation times of the molecules. This means that there is enough time available for the molecules to respond and reorient in accordance to the direction of field changes. As the field frequency increases, the time interval between reverse movements in field polarity gradually becomes of a similar order to the relaxation times of the molecules. At this point, they still respond to the changing fields but with increasing lag time and energy absorption. At very high frequencies, the dipole motion can no longer keep up with the changing field. These molecules will cease to respond and remain in their random, steady-state orientations.[11,32]

However, in many materials, such as in acerola pulp, the water molecules are often chemically bound to other molecules in the material. The ascorbic acid is also chemically bound to water and other substances because of the presence of hydroxyl groups in its structure. According to Ryynänen,[34] hydrogen bonds restrict the free movement of the molecules, and therefore, bound molecules possess longer relaxation times. In the same way, the extensive intermolecular bonding interactions prevalent in solid materials restrict dipolar orientations.[11] In this manner, particle type, size, concentration, and polarity may affect bonding interactions and, consequently, influence the achievement of the equilibrium of the polarization process. These phenomena may have influenced the oxidation reactions during heating of acerola pulp and serum, affecting the predisposition to hydrogen donation from the ascorbic acid molecule.

This study highlights the importance of evaluating dielectric properties of food products to determine their behavior when subjected to an electric field. The increase in the use of electrical heating methods in recent years requires the knowledge of electrical properties and their effects on food processing. Further work is necessary to better understand the effects of the electric field frequency during OH.

AUTHOR INFORMATION

Corresponding Author

*Telephone: +55-51-3308-3638. Fax: +55-51-3308-3277. E-mail: gmercali@enq.ufrgs.br.

Funding

The authors acknowledge the financial support received from Conselho Nacional de Desenvolvimento Científico e Tecnológico (CNPq), Brazil, as a scholarship to the first author.

Notes

The authors declare no competing financial interest.

REFERENCES

(1) Goullieux, A.; Pain, J. P. Ohmic heating. In *Emerging Technologies for Food Processing*; Sun, D.-W., Ed.; Elsevier: Amsterdam, Netherlands, 2005; p 549.

(2) Ruan, R.; Ye, X.; Chen, P.; Doona, C. J. Ohmic heating. In *Thermal Technologies in Food Processing*; Richardson, P., Ed.; Woodhead Publishing Limited: Cambridge, U.K., 2001.

(3) Sastry, S. Ohmic heating and moderate electric field processing. *Food Sci. Technol. Int.* **2008**, *14*, 419−422.

(4) Loghavi, L.; Sastry, S. K.; Yousef, A. E. Effect of moderate electric field frequency on growth kinetics and metabolic activity of *Lactobacillus acidophilus*. *Biotechnol. Prog.* **2008**, *24*, 148−153.
(5) Loghavi, L.; Sastry, S. K.; Yousef, A. E. Effects of moderate electric field frequency and growth stage on the cell membrane permeability of *Lactobacillus acidophilus*. *Biotechnol. Prog.* **2009**, *25*, 85−94.
(6) Somavat, R.; Mohamed, H. M. H.; Chung, Y.-K.; Yousef, A. E.; Sastry, S. K. Accelerated inactivation of *Geobacillus stearothermophilus* spores by ohmic heating. *J. Food Eng.* **2012**, *108*, 69−76.
(7) Kulshrestha, S.; Sastry, S. K. Frequency and voltage effects on enhanced diffusion during moderate electric field (MEF) treatment. *Innovative Food Sci. Emerging Technol.* **2003**, *4*, 189−194.
(8) Wang, W.-C.; Sastry, S. K. Effects of moderate electrothermal treatments on juice yield from cellular tissue. *Innovative Food Sci. Emerging Technol.* **2002**, *3*, 371−377.
(9) Pereira, R. N.; Teixeira, J. A.; Vicente, A. A. Exploring the denaturation of whey proteins upon application of moderate electric fields: A kinetic and thermodynamic study. *J. Agric. Food Chem.* **2011**, *59*, 11589−11597.
(10) North, A. M. Dielectric relaxation in polymer solutions. *Chem. Soc. Rev.* **1972**, *1*, 49−72.
(11) Heng, P. W. S.; Loh, Z. H.; Liew, C. V.; Lee, C. C. Dielectric properties of pharmaceutical materials relevant to microwave processing: Effects of field frequency, material density, and moisture content. *J. Pharm. Sci.* **2010**, *99*, 941−957.
(12) Mercali, G. D.; Schwartz, S.; Marczak, L. D. F.; Tessaro, I. C.; Sastry, S. Ascorbic acid degradation and color changes in acerola pulp during ohmic heating: Effect of electric field frequency. *J. Food Eng.* **2014**, *123*, 1−7.
(13) Esteve, M. J.; Frígola, A.; Martorell, L.; Rodrigo, C. Kinetics of green asparagus ascorbic acid heated in a high-temperature thermoresistometer. *Z. Lebensm.-Unters. -Forsch. A* **1999**, *208*, 144−147.
(14) Polydera, A. C.; Stoforos, N. G.; Taoukis, P. S. Comparative shelf life study and vitamin C loss kinetics in pasteurised and high pressure processed reconstituted orange juice. *J. Food Eng.* **2003**, *60*, 21−29.
(15) Serpen, A.; Gökmen, V. Reversible degradation kinetics of ascorbic acid under reducing and oxidizing conditions. *Food Chem.* **2007**, *104*, 721−725.
(16) Lima, J. R.; Elizondo, N. J.; Bohuon, P. Kinetics of ascorbic acid degradation and colour change in ground cashew apples treated at high temperatures (100−180 °C). *Int. J. Food Sci. Technol.* **2010**, *45*, 1724−1731.
(17) Blasco, R.; Esteve, M. J.; Frígola, A.; Rodrigo, M. Ascorbic acid degradation kinetics in mushrooms in a high-temperature short-time process controlled by a thermoresistometer. *Lebensm.-Wiss. Technol.* **2004**, *37*, 171−175.
(18) Vikram, V. B.; Ramesh, M. N.; Prapulla, S. G. Thermal degradation kinetics of nutrients in orange juice heated by electromagnetic and conventional methods. *J. Food Eng.* **2005**, *69*, 31−40.
(19) Lima, M.; Heskitt, B. F.; Burianek, L. L.; Nokes, S. E.; Sastry, S. K. Ascorbic acid degradation kinetics during conventional and ohmic heating. *J. Food Process. Preserv.* **1999**, *23*, 421−443.
(20) Leizerson, S.; Shimoni, E. Effect of ultrahigh-temperature continuous ohmic heating treatment on fresh orange juice. *J. Agric. Food Chem.* **2005**, *53*, 3519−3524.
(21) de Rosso, V. V.; Mercadante, A. Z. The high ascorbic acid content is the main cause of the low stability of anthocyanin extracts from acerola. *Food Chem.* **2007**, *103*, 935−943.
(22) Mercali, G. D.; Jaeschke, D. P.; Tessaro, I. C.; Marczak, L. D. F. Degradation kinetics of anthocyanins in acerola pulp: Comparison between ohmic and conventional heat treatment. *Food Chem.* **2013**, *136*, 853−857.
(23) Gregory, J. Vitamins. In *Food Chemistry*, 4th ed.; Fennema, O. R., Srinivasan, D., Parkin, K. L., Eds.; CRC Press: Boca Raton, FL, 1996; p 1144.
(24) Mercali, G. D.; Jaeschke, D. P.; Tessaro, I. C.; Marczak, L. D. F. Study of vitamin C degradation in acerola pulp during ohmic and conventional heat treatment. *LWT—Food Sci. Technol.* **2012**, *47*, 91−95.
(25) Eison-Perchonok, M. H.; Downes, W. Kinetics of ascorbic acid autoxidation as a function of dissolved oxygen concentration and temperature. *J. Food Sci.* **1982**, *47*, 765−767.
(26) Odriozola-Serrano, I.; Soliva-Fortuny, R.; Gimeno-Añó, V.; Martín-Belloso, O. Kinetic study of anthocyanins, vitamin C, and antioxidant capacity in strawberry juices treated by high-intensity pulsed electric fields. *J. Agric. Food Chem.* **2008**, *56*, 8387−8393.
(27) Louarme, L.; Billaud, C. Evaluation of ascorbic acid and sugar degradation products during fruit dessert processing under conventional or ohmic heating treatment. *LWT—Food Sci. Technol.* **2012**, *49*, 184−187.
(28) Assiry, A.; Sastry, S. K.; Samaranayake, C. Degradation kinetics of ascorbic acid during ohmic heating with stainless steel electrodes. *J. Appl. Electrochem.* **2003**, *33*, 187−196.
(29) Samaranayake, C. P.; Sastry, S. K. Electrode and pH effects on electrochemical reactions during ohmic heating. *J. Electroanal. Chem.* **2005**, *577*, 125−135.
(30) Amatore, C.; Berthou, M.; Hébert, S. Fundamental principles of electrochemical ohmic heating of solutions. *J. Electroanal. Chem.* **1998**, *457*, 191−203.
(31) Bansal, B.; Chen, X. D. Effect of temperature and power frequency on milk fouling in an ohmic heater. *Food Bioprod. Process.* **2006**, *84*, 286−291.
(32) Içier, F.; Baysal, T. Dielectrical properties of food materials—1: Factors affecting and industrial uses. *Crit. Rev. Food Sci. Nutr.* **2004**, *44*, 465−471.
(33) Nováková, L.; Solich, P.; Solichová, D. HPLC methods for simultaneous determination of ascorbic and dehydroascorbic acids. *TrAC, Trends Anal. Chem.* **2008**, *27*, 942−958.
(34) Ryynänen, S. The electromagnetic properties of food materials: A review of the basic principles. *J. Food Eng.* **1995**, *26*, 409−429.

JOURNAL OF AGRICULTURAL AND FOOD CHEMISTRY

Article

pubs.acs.org/JAFC

Strawberry Ellagitannins Thwarted the Positive Effects of Dietary Fructooligosaccharides in Rat Cecum

Bartosz Fotschki,*[,†] Joanna Milala,[‡] Adam Jurgoński,[†] Elżbieta Karlińska,[‡] Zenon Zduńczyk,[†] and Jerzy Juśkiewicz[†]

[†]Division of Food Science, Institute of Animal Reproduction and Food Research, Polish Academy of Sciences, Olsztyn, Poland

[‡]Institute of Chemical Technology of Food, Technical University of Łódź, Łódź, Poland

Supporting Information

ABSTRACT: Forty-eight male Wistar rats were fed diets containing low (0.051% of diet) or high (0.153% of diet) levels of an ellagitannin-rich (ET) strawberry extract with dietary fructooligosaccharides (FOS) or cellulose (CEL) for 4 weeks. The in vivo study demonstrated that some positive changes in the cecal metabolism resulting from the ingestion of a diet enriched only with FOS were completely or slightly suppressed by the dietary ET. In particular, the pH value (7.21 vs 7.36), short-chain fatty acid production (41.2 vs 30.0 μmol/100g BW), and β-glucuronidase activity (20.2 vs 15.7 μmol/h/g) in the cecum of rats fed with FOS were affected upon the addition of the ET extract. Dietary FOS caused higher metabolism of the tested ET strawberry extract in the gastrointestinal tract of rats. Moreover, the systemic effect of the supplements when consumed together showed undesired serum HDL-cholesterol decrease (0.78 vs 1.02 mmol/L in the treatment with FOS only).

KEYWORDS: *strawberry extract, fructooligosaccharides, gastrointestinal tract, nasutin A, Wistar rats*

INTRODUCTION

"Fructan" is a general term used for naturally occurring plant oligo- and polysaccharides. As a type of fructan, FOS are plant-derived carbohydrates with well-established benefits for the modulation of gastrointestinal functions.[1] Currently, a number of studies have shown beneficial effects of the consumption of colorful fruits and vegetables that are rich in FOS and biologically active phytochemicals.[2,3] Dietary fiber including polyphenol-rich fiber complexes is resistant to endogenous enzymes of the upper part of the gut in humans as well as monogastric animals. Therefore, the compounds are transported in large quantities to the large intestine, where they undergo fermentation process.[1,4] In recent years, scientists have studied the impact of dietary fiber on the metabolism and absorption of phytochemicals.[5,6] However, there is little information regarding how phytochemicals may modulate the beneficial effects of FOS in the gastrointestinal tract.

An interesting source of phytochemicals, especially ellagic acid (EA) and anthocyanins, is the strawberry.[7] EA in this fruit occurs mainly in the form of macromolecular ET, whereas the free form of EA represents only a small proportion of the total content of its derivatives.[8] Numerous studies have demonstrated positive effects of ETs and EA on human health, primarily due to the antioxidant, anticarcinogenic, antineurodegenerative, and anti-inflammatory effects.[9,10] However, an increased content of polyphenols in the diet may inhibit the growth and reduce the abundance of gastrointestinal microflora.[11] ET polymers in the gastrointestinal tract can be absorbed after breaking the ester bonds, which leads to the formation of EA. EA absorption is very low, and the unabsorbed compounds released into the jejunum and colon are extensively metabolized to urolithins by specific microbiota.[12,13] The EA metabolism pathway is composed of many transitional forms. Some of the first forms are nasutin A and isonasutin derivatives, which are formed after removing the specific hydroxyls in the 3- and 3′-positions or in the 4- and 3′-positions of EA. Another form is urolithin, which is produced after opening the lactone rings in EA.[14,15] Urolithins easily pass into intestine−liver circulation, where they are glucuronidated and sulfated. Derivatives of urolithins that are transported in the blood may have a favorable effect on the levels and proportions of cholesterol fractions, the blood level of lipids, and vascular inflammation. In addition, some of the derivatives have proven biological activity, including as analogues of hormones.[9,14,16,17] Urolithins can remain in the body up to 4 days after the consumption of ET-containing foods, perhaps due to enterohepatic recirculation and slow microbial metabolism in the colon.[18]

The metabolism of ETs depends on the activity of individual colonic microflora.[18] Therefore, it can be assumed that high activity of the gastrointestinal microbiota will increase metabolism and absorption of the ETs derived from the diet. Well-known dietary ingredients that modulate microbiota are classified as nondigestible saccharides as part of dietary fiber, such as CEL and FOS. CEL has significantly lower susceptibility to fermentation processes in the hindgut than FOS, which has been shown to increase the production of short-chain fatty acids (SCFA) and to have a prebiotic effect.[5] In our earlier studies performed with a polyphenol concentrate, the addition of dietary FOS significantly enhanced the metabolic activity of quercetin.[6]

Received: December 23, 2013
Revised: May 5, 2014
Accepted: June 4, 2014
Published: June 4, 2014

ACS Publications © 2014 American Chemical Society

The environment of the large intestine is of paramount importance to host health. Our previous experiments showed beneficial action of dietary FOS[5] or strawberry polyphenols[17] in the rat's cecum. Therefore, in the reported experiment it was hypothesized that a dietary combination of both supplements, FOS and polyphenols, would increase the desired beneficial effect in the lower gut environment. Moreover, intensified metabolism of strawberry polyphenolic compounds when combined with dietary FOS was expected.

MATERIALS AND METHODS

Chemicals. Acetone (99.5%), pure p.a., was purchased from Basic POCH S.A. (Gliwice, Poland). Ethanol (96.2%), rectified, was purchased from "NORD CLAS" Sp. z o.o. (Łódz, Poland). Phloroglucinol for HPLC (≥99%), methanol for HPLC (99.9%), gradient grade, and sucrose, glucose, and fructose were purchased from Sigma-Aldrich (St. Louis, MO, USA). Acetic acid for HPLC (99−100%) and phosphoric acid (85−87%), ACS reagent grade, were purchased from J.T. Baker (Phillipsburg, NJ, USA). Ascorbic acid and hydrochloric acid (35−38%), pure p.a., were purchased from ChemPur (Piekary Śląskie, Poland). Acetonitrile (>99.9%), CHROMASOLV gradient grade for HPLC, was purchased from Sigma-Aldrich (Darmstadt, Germany).

FOS Preparation. A commercial FOS preparation (Raftilose P95) was kindly provided by Orafti (Oreye, Belgium). According to the producer's declaration, it contains 93.2−95.8% oligofructose, as 2−8 degree of polymerization (DP) of fructose polymers and no more than 7.0% of free fructose. The content of oligo-, di-, and monosaccharides in the preparation was characterized using an HPLC system (Knauer, Berlin, Germany) equipped with a EuroChrom 2000 data control system, RI K-2301 Knauer detector (Germany), and a Shodex NH2P (250 × 4 mm) column (Japan), using an acetonitrile−water mixture (67−33% v/v) as a mobile phase at a flow rate of 0.8 mL/min at 20 °C. FOS preparation (0.5 g) was weighed in a 50 mL volumetric flask and dissolved in water (concentration 10 mg/mL) and was injected to the chromatograph for separation and registration of signals by RI detector. The composition of the individual di- to heptamers was determined on the basis of registered areas of the signals. The results were as follows: fructose, 5.1%; DP 2, 2.7%; DP 3, 25.6%; DP 4, 31.2%; DP 5, 18.7%; DP 6, 12.3%; and DP 7, 4.4% (94.4% of oligofructose). Limit of detection for fructose as a standard was 0.06 mg/mL.

Strawberry Polyphenolic Extract. The strawberry press cake (750 kg) was taken from the concentrated juice production line of the Alpex Company (Łęczeszyce, Poland) and dried in an industrial vacuum dryer (Polfarmex Company, Kutno, Poland) at 70 ± 2 °C. After drying, the pomace (400 kg) was separated into a seed fraction (diameter 0.5−1 mm) and a seedless fraction (diameter 1−3 mm) using a vibration sieving machine with sieves of the sizes 0.5 mm, 1 mm, and 3 mm (each was designed by the company Polfarmex S.A. Kutno, Poland) equipped with a vibration device necessary to move the material on the sieve and to renew the surface of sieving. The material with particle sizes between 1 and 3 mm, constituting part of pomace devoid of seeds (achenes), was used for successive production of a strawberry polyphenolic extract applied in the present study. The water−acetone ET strawberry concentrate was prepared at laboratory scale using the seedless fraction and a 60% solution v/v of acetone (5 L per 1 kg of pomace). Extraction was conducted in two stages for a minimum of 12 h. After partial removal of the solvent by distillation, approximately 5% of the resulting solution was subjected to adsorption using 500 g of adsorbent Amberlite XAD 16 in a column with a diameter Φ of 40 mm and a height of 1000 mm. After washing away the saccharide dirt with water, the desorption of polyphenols was performed using 10%, 40%, and 60% solutions of ethanol successively in amounts of 0.5, 1, and 2 L per 1 kg of adsorbent, respectively. Solutions containing desorbed polyphenols from the Amberlite XAD were gathered and divided into fractions, of which only the eluates rich in ET were concentrated to approximately 15% of the dry weight and subjected to freeze-drying in a TG 5 Lyophilizer (VEB Hochvakuum Dresden, Germany). The yield of the dry weight of the preparation that was rich in polyphenols was 2.6% of the weight of the dried industrial, seedless strawberry pomace.

Chemical Analyses of the Polyphenolic Extract. The chemical composition of the preparations was determined by AOAC methods (2005)[19] using the following procedure: dry matter and ash content, 940.26; protein content, 920.152; crude fat, 930.09; total dietary fiber, 985.29. Sucrose, fructose, glucose, and other saccharides were measured after desalination of the strawberry extract solution in water (5 mg/mL) on an anion exchange column (two parts of Amberlite IRA 400 anion exchanger purchased from Sigma-Aldrich (Germany), one part of Amberlite IR 120 cation exchanger also purchased from Sigma-Aldrich (Germany)). The analysis was performed using an HPLC system (Knauer, Berlin, Germany) with an RI detector and a BIO-RAD Aminex HPX-87C column, 300 × 7.8 mm (Phenomenex, Torrance, CA, USA), with a flow rate of 0.5 mL/min at 85 °C. Sucrose (limit detection at 0.08 mg/mL), glucose (limit detection at 0.08 mg/mL), and fructose (limit detection at 0.04 mg/mL) were used as standards.

Determination of Polyphenols. The concentrations of EA and total ETs, such as agrimoniin, including agrimoniin alone and other polyphenols (anthocyanins and flavonols), were determined in 50% methanol solutions prepared by resolving 5−25 mg of the freeze-dried polyphenolic extract in 5 mL of methanol diluted in water to 10 mL according to Sójka et al. (2013).[20] The solution was then subjected to HPLC analysis. A Smartline (Knauer, Berlin, Germany) chromatograph equipped with degasser Smartline Manager 5000 unit, two pumps Smartline Pump 1000, mixing chamber, autosampler Smartline Autosampler 3950, column oven Jetstream 2 Plus, and detector Smartline PDA 2800 was used for the chromatographic analysis. The separation was conducted on a Phenomenex Gemini 5u C18 110A column (250 × 4.60 mm; 5 μm) (Phenomenex Torrance, CA, USA). The column was maintained at 35 °C. Eluent A contained 0.05% phosphoric acid in water, and eluent B contained 0.05% phosphoric acid in acetonitrile. The flow rate was 1.25 mL/min. The gradient program was as follows: 0−5 min, 4% eluent B; 5−12.5 min, 4−15% eluent B; 12.5−42.5 min, 15−40% eluent B; 42.5−51.8 min, 40−50% eluent B; 51.8−53.4 min, 50−55% eluent B; and 53.4−55 min, 4% eluent B. The volume of the injected sample was 20 μL. The detection conditions were as follows: 280 nm [*p*-coumaric acid, kaempferol-3-*O*-β-D-(6″-*E*-*p*-coumaroyl)-glucopyranoside, (+)-catechin agrimoniin], 360 nm (EA, quercetin, and kaempferol glycosides, quercetin, kaempferol), and 520 nm (anthocyanins). The data were registered by ClarityChrom (Knauer, Berlin, Germany) chromatography software. The following standards were used: EA, *p*-coumaric acid, and (+)-catechin (Sigma-Aldrich, St. Louis, USA) and quercetin-3-*O*-glucopyranoside, kaempferol-3-*O*-glucoside, quercetin, pelargonidin-3-*O*-glucoside, and kaempferol (Extrasynthese, Genay, France). The agrimoniin standard was obtained from strawberry press cake and was purified by preparative chromatography. The agrimoniin with limit detection at 0.55 mg/L was used as the basic standard for the ET content determination.

Analysis of Proanthocyanidins and Free Catechins. A proanthocyanidin degradation method in an acidic environment with an overdose of phloroglucinol was employed. The method was described by Kennedy and Jones (2001).[21] Approximately 20 mg of sample was weighed in a 2 mL Eppendorf tube, and 800 μL of a methanol solution containing phloroglucinol (75 g/L) and ascorbic acid (15 g/L) was added to the sample. Phloroglucinolysis was started by adding 400 μL of 0.2 mol/L hydrochloric acid to methanol. The incubation was conducted for 30 min at 50 °C. Next, the samples were instantly cooled in an ice bath, and the reaction was stopped by adding 600 μL of a 40 mmol/L sodium acetate solution. The samples were centrifuged for 5 min at 3600*g* and then diluted with a 40 mmol/L sodium acetate solution. The products of the acidic degradation of proanthocyanidins were separated with the Knauer Smartline chromatograph (Berlin, Germany) equipped with a UV−vis P2800 detector (Knauer, Berlin, Germany) and a fluorescent detector (FD) RF-10AXL (Schimadzu, Tokyo, Japan). The separation was conducted

on Gemini 5u C18 110A (250 mm × 4.6 mm; 5 μm) column (Phenomenex Torrance, CA, USA) using gradient elution with 2.5% water solution (v/v) of acetic acid (phase A) and 80% (v/v) acetonitrile in water (phase B). The following gradient was used: 0−10 min, 4−7% B; 10−27 min, 7−30% B; 27−29 min, 30−70% B; 29−34 min, 70% B; 34−35 min, 70−4% B; and 35−40 min, 4% B. The flow rate was 1 mL/min, the temperature was 25 °C, and the injection volume was 20 μL. The identification of components was conducted by comparing the retention times and the UV−vis spectra of standards of (−)-epicatechin, (+)-catechin, (−)-epicatechin-phloroglucinol, and (+)-catechin-phloroglucinol. Quantitative analyses of the released flavonols, i.e., (+)-catechin and (−)-epicatechin, were conducted based on chromatograms recorded with the FD detector set at an excitation wavelength of 278 nm and an emission wavelength of 360 nm. Quantities were calculated by standard curves of (−)-epicatechin (0.625−50 mg/L; detection limit at 0.03 mg/L) for terminal units, and (−)-epicatechin-phloroglucinol adduct for extender units (0.6−50 mg/L; detection limit at 0.3 mg/L). Phloroglucinol adducts were determined based on chromatograms registered with the PDA detector set at a 280 nm wavelength.

Extraction of Nasutin A (4,9-Dehydroxy-ellagic Acid) and Polyphenols. Polyphenol compounds, including nasutin A, were extracted with a 70% solution of acetone. A sample containing 0.5 g of the ground frozen digesta was placed in a 7 mL test tube; next, 5 mL of a solvent was added, mixed using a vortex (IKA Yellowline Test Tube Shaker TTS2, Wilmington, NC, USA) and sonicated (Inter Sonic IS-4, Inter Sonic s.c., Olsztyn, Poland) for 10 min. Following the sonication, the solution was left in the dark for 15 min for extraction. The solution was centrifuged for 5 min (4800*g*) and poured into a 20 mL tube with a cup. The above procedure was repeated three more times; the combined extracts were poured into a 20 mL tube with a cup. The obtained extracts were stored at 20 °C for a maximum of 3 days before further analysis. Next, the combined extracts were poured into a vacuum distillatory flask, and the solvent was removed. Next, the dry residue was dissolved in 2 mL of 70% methanol. The solution was centrifuged for 5 min (4800*g*) and was submitted to HPLC analysis. A Smartline (Knauer, Berlin, Germany) chromatograph equipped with the same elements as described above was applied for the chromatographic analysis. The separation was conducted on a Phenomenex Gemini 5u C18 110A (250 × 4.60 mm; 5 μm) column (Phenomenex, Torrance, CA, USA). The conditions of separation were the same as for the determination of polyphenols described above.

The urolithin A (3,8-dihydroxy-6*H*-dibenzo-[*β*-D]-pyran-6-one) was used as a standard for the determination of nasutin A. To date, commercial nasutin is not available. Urolithin A was prepared as described by Cerdá et al. (2004).[18] The raw material for the isolation of urolithin A was two liters of urine from three healthy volunteers (25−45 years old) who consumed 400 g of strawberry per day. The urine was acidified to pH 4.8 by acetic acid. Then, 1.2 mg of glucuronidase bovine liver (Sigma-Aldrich, St. Louis, MO, USA) was added, maintained at 37 °C for 60 min and passed through Amberlite XAd-7 (Sigma-Aldrich, St. Louis, MO, USA) resin for the absorption and purification of polyphenols. In the next step, the resin was washed, and the adsorbed polyphenols were desorbed by methanol. The methanol fractions rich in urolithin A were concentrated and subjected to purification on a Strata SPE 1 g column (Strata - x 33u Polymeric Reversed phase 1 g/20 mL, Giga Tubes Phenomenex, Torrance, CA, USA) and were separated on a preparative HPLC (Knauer, Berlin, Germany) chromatograph, composed of two pumps (Knauer K-501) forming gradient, Phenomenex Luna 10u C18 100A column (250 × 21, 20 mm; 10 μm) (Torrance, CA, USA), UV−vis detector, Foxy R1 Teledyne ISCO (Lincoln, USA) fraction collector, and Eurochrom chromatographic software. Two eluents were used for separation: eluent A, 0.1% water solution of formic acid; eluent B, 80% methanol. The flow rate was 15 mL/min. The following gradient was used: 0−15 min 30% eluent B; 15−50 min 30−75% eluent B; 50−60 min 75% eluent B; 60−63 min 75−30% eluent B; 63−66 min 30% eluent B; and 55−60 min 20% eluent B. The volume of injected sample was 500 μL. Selected fractions containing urolithin A were subjected to freeze-drying. The UV spectrum of the obtained substances had maxima at 246, 278, 305, and 356 nm, which was the same pattern as the main metabolite of ET detected in urine.[14,22]

Identification of Nasutin A. The UV spectra of polyphenols have often been used for their identification by HPLC DAD analysis. UV spectra are generally used for the identification of flavonoids and urolithins. In the present study, the spectra of ET metabolites were studied using HPLC UV-DAD to establish the structure of the microbial degradation of agrimoniin. The maximum UV wavelengths for the detected substance (with retention time 26 min) have been determined to be 250, 285, 373, and 389 nm. Next the solution of the substance, separated by HPLC, was directly injected into an ESI-MS/MS detector (LCQ DECA, Thermo-Finnigan). The analyses were conducted in the positive ion mode.[18] The source parameters were as follows: ion spray voltage 3.00 kV; capillary temperature 325 °C; sheath gas and auxiliary gas 30 and 10 units/min, respectively. To generate MS/MS data, the precursor ions were fragmented by helium gas collision in the ion trap by optimizing the collision energy in order to obtain an intensity of the precursor ion close to 10% of the relative scale of the spectrum. The MS $[M - H^+]$ 269 for the substance was determined. Data obtained for UV spectrum and value of $[M - H^+]$ indicate that nasutin A was the main metabolite in the experiment.[14]

In Vivo Experiment, Preparation of the Diets, and the Animal Protocol. The animal protocol used in this study was approved by the Local Institutional Animal Care and Use Committee, and the study was performed in accordance with EU Directive 2010/63/EU for animal experiments. The assessment was conducted on 48 male adult Wistar rats aged 130 d and weighing 440.3 g (pooled SEM 0.839). The rats were randomly divided into six groups of eight animals each. All animals were housed individually for 4 weeks in metabolic cages with free access to water and the experimental diets (Table 1). The selection of the animals and their maintenance over the 28 d experiment followed common regulations. The environment was controlled with a 12 h light−dark cycle, a temperature of 21 ± 1 °C, relative humidity of 50 ± 5%, and 20 air changes per h. Diets contained similar levels of protein (from casein supplemented with methionine), fat (soybean oil), and minerals and vitamins (from AIN-93 M mixtures)[23] and a similar content of fiber. However, the fiber was from different sources, i.e., insoluble *α*-cellulose (SIGMA, Poznań, Poland) or a prebiotic FOS that was fermentable in the lower gut (Orafti, Oreye, Belgium). In the standard-fiber diets, the content of CEL was 6%. In the prebiotic-supplemented diets, half of the dietary CEL was replaced with FOS. The strawberry polyphenolic preparation was added to each type of diet in an amount of 0.051% or 0.153% of the air-dried feed, which constituted 0.04% and 0.12% of total strawberry polyphenols in the diet, respectively (in regard to ETs, the main polyphenolic component of the extract, 0.03% and 0.09% of ETs, respectively). The individual BW and feed intake of the rats were recorded. At the termination of the experiment, the rats were anesthetized with sodium pentobarbital according to the recommendations for the euthanasia of experimental animals. After a laparotomy, blood samples were taken from the caudal vena cava, and then serum was prepared by solidification and low-speed centrifugation (350*g*, 10 min, 4 °C). The small intestine, cecum, and colon were removed and weighed. As soon as possible after euthanasia (ca. 10 min), the small intestinal, cecal, and colonic pH values were measured (pH meter model 301, Hanna Instruments, Vila do Conde, Portugal). The dry matter of the cecal digesta was determined at 105 °C for 4 h. In the fresh cecal digesta, ammonia (NH_3) was determined by microdiffusion analysis in Conway's dishes, and the SCFA were analyzed using GC as described previously.[24] For SCFA, the samples (0.2 g) were mixed with 0.2 mL of formic acid, diluted with deionized water, and centrifuged at 7211*g* for 10 min. The supernatant was loaded onto a capillary column (SGE BP21, 30 m × 0.53 mm) using an on-column injector. The initial oven temperature was 85 °C and was raised to 180 °C at a rate of 8 °C/min and held for 3 min. The temperatures of the flame ionization detector and the injection port were 180 and 85 °C, respectively. The sample volume for GC analysis was 1 μL. The cecal putrefactive SCFA (PSCFA) concentration was calculated as the sum of the isobutyrate, isovalerate, and valerate concentrations in the cecal

Table 1. Diet Composition (%)

	experimental diet					
	C_{CEL}	C_{FOS}	EL_{CEL}	EL_{FOS}	EH_{CEL}	EH_{FOS}
casein	14.8	14.8	14.8	14.8	14.8	14.8
DL-methionine	0.2	0.2	0.2	0.2	0.2	0.2
cellulose[a]	6	3	6	3	6	3
FOS	0	3	0	3	0	3
soya oil	8	8	8	8	8	8
cholesterol	0.5	0.5	0.5	0.5	0.5	0.5
mineral mix[b]	3.5	3.5	3.5	3.5	3.5	3.5
vitamin mix[c]	1	1	1	1	1	1
strawberry extract	0	0	0.051	0.051	0.153	0.153
corn starch	66	66	65.949	65.949	65.847	65.847
calcd dietary ellagitannins	0	0	0.030	0.030	0.090	0.090
calcd dietary polyphenols	0	0	0.040	0.040	0.120	0.120

[a]α-Cellulose preparation was obtained from Sigma-Aldrich (No. C8002). [b]AIN-93 M (Reeves 1997),[23] g per kg mix: 357 g of anhydrous calcium carbonate (40.04% Ca), 196 g of monobasic potassium phosphate (22.76% P, 28.73% K), 70.78 g of potassium citrate and tripotassium monohydrate (36.16% K), 74 g of sodium chloride (39.34% Na, 60.66% Cl), 46.6 g of potassium sulfate (44.87% K, 18.39% S), 24 g of magnesium oxide (60.32% Mg), 6.06 g of ferric citrate (16.5% Fe), 1.65 g of zinc carbonate (52.14% Zn), 1.45 g of sodium meta-silicate·$9H_2O$ (9.88% Si), 0.63 g of manganous carbonate (47.79% Mn), 0.3 g of cupric carbonate (57.47% Cu), 221.026 g of powdered sucrose, and 0.275 g of chromium potassium sulfate·$12H_2O$ (10.42% Cr). The following components were added in mg per kg mix quantities: 81.5 mg of boric acid (17.5% B), 63.5 mg of sodium fluoride (45.24% F), 31.8 mg of nickel carbonate (45% Ni), 17.4 mg of lithium chloride (16.38% Li), 10.25 mg of anhydrous sodium selenate (41.79% Se), 10 mg of potassium iodate (59.3% I), 7.95 mg of ammonium paramolybdate·$4H_2O$ (54.34% Mo), and 6.6 mg of ammonium vanadate (43.55% V). [c]AIN-93 M (Reeves 1997),[23] g per kg mix: 3.0 g of nicotinic acid, 1.6 g of Ca pantothenate, 0.7 g of pyridoxine−HCl, 0.6 g of thiamin-HCl, 974.655 g of powdered sucrose, 0.6 g of riboflavin, 0.2 g of folic acid, 0.02 g of biotin, 2.5 g of vitamin B_{12} (cyanocobalamin, 0.1% in mannitol). The following components were added in IU per g quantities: 15.0 IU of vitamin E (*all-rac*-α-tocopheryl acetate, 500), 0.8 IU of vitamin A (*all-trans*-retinyl palmitate, 500000), 0.25 IU of vitamin D_3 (cholecalciferol, 400000), and 0.075 IU of vitamin K-1 (phylloquinone).

digesta. The activity of selected bacterial enzymes (α- and β-glucosidase, α- and β-galactosidase, and β-glucuronidase) released into the cecal environment was measured by the rate of *p*- or *o*-nitrophenol release from their nitrophenyl glucosides, according to a method that has been described elsewhere.[24]

The serum concentration of glucose, triacylglycerol (TG), total cholesterol (TC), and its HDL fraction (HDL-C), as well as the activity of alanine aminotransferase (ALT) and aspartate aminotransferase (AST), were estimated with diagnostic sets from Alpha Diagnostics Limited (Warsaw, Poland).

Statistical Analyses. The data are expressed as the means and pooled standard error of the mean (SEM). The STATISTICA software, version 10.0 (StatSoft Corp., Krakow, Poland), was used to determine whether variables differed among the treatment groups. Two-way ANOVA was applied to assess the effects of the dietary addition of the strawberry extract (E), the type of diet (standard diet with 6% CEL and diet with 3% FOS added instead of 3% CEL; F), and the interaction between the investigated factors (E × F). When the ANOVA indicated significant treatment effects, the means were evaluated using Duncan's multiple range test. One-way ANOVA and Duncan's test were applied to analyze the concentration of nasutin A in the intestinal contents. The data were checked for normality before statistical analysis was performed. Differences with $P < 0.05$ were considered to be significant.

RESULTS

The preparation obtained from strawberry used in this study contained 78.7 g of polyphenols per 100 g of preparation (Table 2). The main phenolic compounds in the preparation were ETs (59.3%) and proanthocyanidins (16.9%). Other compounds, including flavonoids (quercetin and kaempferol, their glycosides, and anthocyanins), free EA, and *p*-coumaric acid and its derivatives were detected in relatively lower concentrations (1.0%, 1.3% and 0.2%, respectively). Chemical analysis showed that the tested preparation was also a source of cell wall saccharides (11.6%). In the examined extract, there was no dietary fiber.

Table 2. Basic Chemical and Polyphenolic Composition (%) of the Strawberry Extract

	composition	
	main components	polyphenols
chemical composition		
dry matter	93.2	
crude protein	2.5	
ether extract	0.0	
crude ash	0.4	
total dietary fiber	0.0	
carbohydrates[c], (including F+G < 1%)[a]	11.6	
polyphenols	78.7	
total polyphenolic compounds (HPLC-DAD):[b]		78.7
free ellagic acid		1.3
total ellagitannin[d] (containing 27% agrimoniin)		59.3
p-coumaric acid and derivatives		0.2
flavonoids[e]		1.0
proanthocyanidins		16.9

[a]F+G, content of fructose and glucose <1%. [b]HPLC-DAD, high-performance liquid chromatography with a diode array detector. [c]Calculated based on the balance of components. [d]The content of the substance calculated using agrimoniin as a standard. [e]The content of the substance calculated as the sum of quercetin and kaempferol, their glycosides, and anthocyanins.

The initial body weights of the rats did not differ among treatments (data not shown). The applied dietary treatments had no effect on the final body weight of the rats or the feed intake during the study (the latter not shown, Table 3). The pH value of the digesta in selected gut segments was significantly affected by the type of dietary fiber and the addition of the strawberry extract. The addition of FOS resulted in significantly higher stomach pH and significantly lower pH values in the small intestine and cecum. The dietary extract, irrespective of the dietary dosage, contributed to significantly higher pH value in the digesta of the stomach, small intestine, and cecum. In comparison with the rats receiving CEL in their diets, the addition of FOS significantly increased the relative weight of the cecal tissue. The relative mass of the cecal digesta was significantly increased by FOS addition, and the dietary extract (both dosages) had the opposite effect (Table 4). The concentration of DM in the cecal digesta was reduced ($P < 0.05$) in rats receiving diets with FOS; in the case of dietary strawberry extract, a statistical tendency toward an increased

dx.doi.org/10.1021/jf405612a | J. Agric. Food Chem. 2014, 62, 5871−5880

Table 3. Body Weight (BW), pH, and Mass of the Gastrointestinal Tissue in Rats[a]

			small intestine		cecum		colon	
	BW, g	stomach pH	tissue[b]	pH	tissue[b]	pH	tissue[b]	pH
group[c]								
C_{CEL}	478	2.84	1.49	7.23	0.158	7.32	0.347	7.33
C_{FOS}	492	3.82	1.56	7.05	0.183	7.10	0.351	7.24
EL_{CEL}	497	3.62	1.48	7.49	0.156	7.44	0.306	7.39
EL_{FOS}	490	4.06	1.52	7.17	0.189	7.26	0.359	7.16
EH_{CEL}	498	3.89	1.41	7.55	0.151	7.56	0.312	7.35
EH_{FOS}	496	3.99	1.42	7.31	0.179	7.19	0.333	7.27
SEM	7	0.11	0.03	0.04	0.003	0.03	0.009	0.03
extract (E)								
C	485	3.33 b	1.52	7.14 b	0.170	7.21 b	0.348	7.29
EL	493	3.84 a	1.50	7.33 a	0.173	7.35 a	0.332	7.28
EH	497	3.94 a	1.41	7.43 a	0.165	7.37 a	0.323	7.31
P value	0.818	0.045	0.267	0.002	0.643	0.042	0.522	0.912
fiber (F)								
CEL	491	3.45 b	1.46	7.42 a	0.155 b	7.44 a	0.322	7.36
FOS	493	3.96 a	1.50	7.18 b	0.184 a	7.18 b	0.347	7.24
P value	0.888	0.019	0.428	0.000	0.000	0.000	0.180	0.064
interaction E × F								
P value	0.860	0.229	0.903	0.695	0.863	0.331	0.560	0.630

[a]Mean values within a column with unlike letters a and b were shown to be significantly different ($P < 0.05$); differences among the groups C_{CEL}, C_{FOS}, EL_{CEL}, EL_{FOS}, EH_{CEL}, and EH_{FOS} were indicated only in the case of a statistically significant interaction E × F ($P < 0.05$). [b]g/100 g BW. [c]C_{CEL}, control diet with 6% cellulose (CEL) as the dietary fiber; C_{FOS}, control diet with 3% fructooligosaccharides (FOS) and 3% cellulose as the dietary fiber; EL_{CEL}, diet with a low level of the strawberry extract and CEL as the dietary fiber; EL_{FOS}, diet with a low level of the extract and FOS/CEL as the dietary fiber; EH_{CEL}, diet with a high level of the strawberry extract and CEL as the dietary fiber; EH_{FOS}, diet with a high level of the extract and FOS/CEL as the dietary fiber.

Table 4. Mass (g/100 g BW), Dry Matter (DM, %), and Ammonia Level (mg/g) of Cecal Digesta and the Activity of Selected Microbial Enzymes in the Cecum of Rats (μmol/h/g)[a]

	cecal digesta			activity of microbial enzymes[b]				
	mass	DM	NH_3	α-glu	β-glu	α-gal	β-gal	β-gluc
group[c]								
C_{CEL}	0.628	25.4	0.222	11.6	4.65	15.7	24.3	29.3 a
C_{FOS}	0.678	22.9	0.222	10.3	3.89	11.5	26.4	10.7 c
EL_{CEL}	0.532	26.1	0.215	8.62	2.94	12.8	22.4	14.7 bc
EL_{FOS}	0.587	24.5	0.243	12.3	3.76	12.2	32.8	14.1 bc
EH_{CEL}	0.485	26.1	0.209	9.54	2.67	11.5	25.9	14.6 bc
EH_{FOS}	0.607	24.6	0.221	10.7	3.61	13.7	31.0	19.2 b
SEM	0.018	0.3	0.005	0.43	0.21	0.6	1.2	1.2
extract (E)								
C	0.653 a	24.1	0.222	10.9	4.27 a	13.6	25.4	20.2 a
EL	0.559 b	25.3	0.229	10.5	3.35 b	12.5	27.6	14.4 b
EH	0.546 b	25.3	0.215	10.1	3.14 b	12.7	28.5	16.9 b
P value	0.026	0.061	0.634	0.739	0.049	0.684	0.500	0.036
fiber (F)								
CEL	0.548 b	25.8 a	0.216	9.91	3.42	13.3	24.2 b	19.5 a
FOS	0.624 a	24.0 b	0.229	11.1	3.75	12.4	30.1 a	14.7 b
P value	0.031	0.000	0.258	0.148	0.408	0.436	0.011	0.007
interaction E × F								
P value	0.625	0.631	0.618	0.066	0.151	0.088	0.322	0.000

[a]Mean values within a column with unlike letters a–c were shown to be significantly different ($P < 0.05$); differences among the groups C_{CEL}, C_{FOS}, EL_{CEL}, EL_{FOS}, EH_{CEL}, and EH_{FOS} were indicated only in the case of a statistically significant interaction E × F ($P < 0.05$). [b]α-Glu, α-glucosidase; β-glu, β-glucosidase; α-gal, α-galactosidase; β-gal, β-galactosidase; β-gluc, β-glucuronidase. [c]C_{CEL}, control diet with 6% cellulose (CEL) as the dietary fiber; C_{FOS}, control diet with 3% fructooligosaccharides (FOS) and 3% cellulose as the dietary fiber; EL_{CEL}, diet with a low level of the strawberry extract and CEL as the dietary fiber; EL_{FOS}, diet with a low level of the extract and FOS/CEL as the dietary fiber; EH_{CEL}, diet with a high level of the strawberry extract and CEL as the dietary fiber, EH_{FOS}, diet with a high level of the extract and FOS/CEL as the dietary fiber.

cecal DM percentage was observed ($P = 0.061$ vs treatment without extract). The applied dietary treatments had no significant effect on the concentration of ammonia in the cecal digesta. The feeding regimen with the strawberry extract diet caused a significant suppression in the activity of bacterial β-glucosidase released into the cecal environment, while the

dx.doi.org/10.1021/jf405612a | J. Agric. Food Chem. 2014, 62, 5871–5880

dietary FOS increased the activity of β-galactosidase. An interaction was observed between extract addition by dietary fiber type ($P < 0.05$) and cecal β-glucuronidase activity. Consumption of the FOS-diet without strawberry extract resulted in the lowest β-glucuronidase activity; the dietary application of the extract also significantly decreased β-glucuronidase activity compared to the C_{CEL} group, but to a lesser extent compared to FOS alone. Surprisingly, there was a significant difference in the activity of this bacterial enzyme in the cecal digesta between the C_{FOS} and EH_{FOS} groups ($C_{FOS} < EH_{FOS}$, $P < 0.05$).

The metabolism of ETs to nasutin A throughout the gastrointestinal tract is shown in Figure 1. The lowest

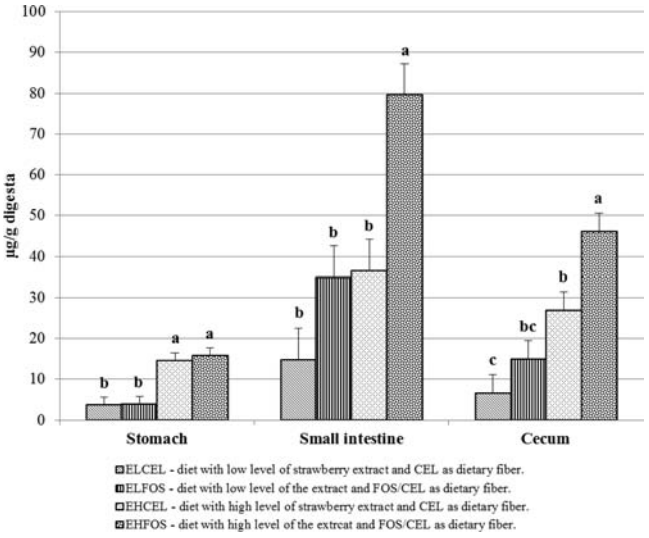

Figure 1. Concentration of nasutin A in the digesta of selected parts of the gastrointestinal tract. Mean values within a column with unlike letters a−c were shown to be significantly different ($P < 0.05$).

concentration of nasutin A was observed in the stomach (Figure 2, Supporting Information). Irrespective of the dietary fiber type, the groups with higher extract dosages had significantly increased concentrations of nasutin A in the stomach and cecal contents. As for the small intestine, the EH_{FOS} group was characterized by a significantly higher concentration of nasutin A (Figure 3, Supporting Information) compared to all other groups. A similar situation was observed in the cecum (Figure 4, Supporting Information) (EH_{FOS} > all other groups, $P < 0.05$). Additionally the EL_{CEL} rats had the lowest concentration of this metabolite, and it differed significantly in this respect from group EH_{CEL}.

Regardless of the diet type, the dietary application of both strawberry extract dosages significantly decreased the cecal concentration and pool of total SCFA, mainly due to the lower concentration of acetic acid (Table 5). The dietary supplementation with the higher dosage of strawberry extract significantly ($P < 0.05$) decreased the cecal concentration of putrefactive SCFA compared to the treatment without extract and with a lower extract dietary application. The dietary FOS significantly increased the cecal propionic and butyric acid concentrations and significantly decreased the concentration of total putrefactive SCFA. The cecal SCFA pool was also increased by dietary FOS application ($P < 0.05$). The analysis of the SCFA C2:C3:C4 profile indicates a lower ratio of acetic acid and an increased ratio of propionic and butyric acids after consumption of diets with added FOS (in all cases $P < 0.05$ vs treatment with 6% CEL).

Differences in the biochemical indicators in the blood serum from rats receiving the experimental dietary treatments are shown in Table 6. The results of a two-way ANOVA indicated that both main dietary treatments (both dosages of strawberry extract and FOS addition) significantly decreased the concentration of glucose in the serum. The lower serum TC concentration ($P = 0.068$) was observed in rats fed diets with added FOS. An interaction was observed between the extract addition by dietary fiber type ($P < 0.05$) and the serum HDL-C concentration and HDL-C profile. The C_{FOS} group was characterized by the highest HDL-C concentration ($P < 0.05$ vs other groups), that is, such a decrease was not observed when FOS was applied with the extract. The C_{FOS} group had the highest values of the HDL-C profile (percentage of the TC), and this group differed significantly not only from the C_{CEL} group but also from the EH_{CEL} and EH_{FOS} groups.

DISCUSSION

The results of the present study indicate that the ET strawberry extract obtained from strawberry press cake (including 2.4% proanthocyanidins; 1.5% free EA and its derivatives in the form of ETs; 0.11% flavonols and 0.09% anthocyanins) consisted of 785 g/kg of phenolic compounds, most of which were ETs (589 g/kg) and proanthocyanidins (169 g/kg). The range of the total content of phenolic compounds in fresh strawberry reported in other studies is very wide, ranging from 0.29 g/kg[25] to 1.44 g/kg.[26] Moreover, the contents of the key polyphenols present in this fruit (i.e., free and bound EA) are between 0.013 and 0.85 g/kg,[27,10] and for proanthocyanidins ranges have been reported from below 0.01 to greater than 0.16 g/kg.[28,29] The concentrations of these bioactive substances are strongly influenced by extrinsic factors, such as variations in plant type and growth, climate, season, temperature, and the degree of ripeness.[30] In this study, with the aid of the body surface area normalization method[31] and literature data for polyphenol content in the fruit, the higher dietary treatment was determined to correlate to a daily consumption of 0.38−1.8 kg fresh strawberries by an adult weighing 70 kg. Therefore, the diet used in this study could represent a realistic amount of fresh strawberries consumed by humans.

The addition of the extract to the diet did not reduce the diet intake or the body weight of the experimental rats, but it affected the activity of the intestinal microflora and its most important products. The administration of FOS leads to the enhancement of fermentative processes and SCFA production, which may decrease the pH of the digestive tract.[4−6] A number of authors have indicated that the acidification of the digesta promotes positive microbiota proliferation and decreases the growth of pathogenic bacteria species.[32] The present study showed that the addition of an ET strawberry extract and FOS together slightly diminished the beneficial effect of the latter on the acidification effect in the cecal digesta. The ET strawberry extract was a rich source of the ET, and it has been reported that this compound releases EA upon hydrolysis in vivo.[33] The higher pH value in the parts of the gastrointestinal tract can be explained by the poor solubility of EA in water and its ionization at physiological pH to form a complex with alkaline calcium and magnesium ions in the intestine.[34] Moreover, the poor solubility of EA most likely reduced the amount of bound water in the cecal digesta. This situation can also explain why dietary treatment with the ET strawberry extract significantly

Table 5. Short Chain Fatty Acid (SCFA) Concentration (μmol/g Digesta), Total Pool (μmol/100 g BW), and Profile (%)[a]

	SCFA concn									SCFA profile		
	C2[b]	C3	C4i	C4	C5i	C5	PSCFA	SCFA	SCFA pool	C2	C3	C4
group[c]												
C_{CEL}	42.0	8.36	0.73	6.57	0.61	1.06	2.40	61.7	36.9	68.0	13.6	10.5
C_{FOS}	45.0	10.7	0.60	9.23	0.64	1.13	2.36	69.7	45.5	65.0	15.3	13.0
EL_{CEL}	36.4	7.88	0.74	5.73	0.71	1.05	2.49	55.0	27.7	66.2	14.3	10.5
EL_{FOS}	35.7	9.36	0.50	6.21	0.52	0.93	1.95	55.2	31.5	65.1	16.8	11.0
EH_{CEL}	38.7	8.07	0.62	5.91	0.48	0.95	2.05	56.7	25.6	68.1	14.4	10.1
EH_{FOS}	37.6	9.68	0.43	8.27	0.43	0.93	1.80	59.2	35.2	63.4	16.4	14.1
SEM	0.95	0.27	0.02	0.36	0.03	0.03	0.07	1.5	1.4	0.5	0.3	0.4
extract (E)												
C	43.5 a	9.55	0.66 a	7.90	0.63 a	1.09	2.38 a	65.7 a	41.2 a	66.5	14.4	11.6
EL	36.1 b	8.62	0.62 a	5.97	0.61 a	0.99	2.22 a	55.1 b	29.6 b	65.7	15.5	10.7
EH	38.2 b	8.87	0.53 b	7.09	0.46 b	0.94	1.92 b	58.0 b	30.4 b	65.7	15.4	12.1
P value	0.004	0.283	0.015	0.061	0.035	0.185	0.026	0.008	0.000	0.709	0.053	0.307
fiber (F)												
CEL	39.0	8.10 b	0.70 a	6.07 b	0.60	1.02	2.32 a	57.8	30.1 b	67.4 a	14.1 b	10.4 b
FOS	39.5	9.92 a	0.51 b	7.90 a	0.53	1.00	2.04 b	61.4	37.4 a	64.5 b	16.2 a	12.7 a
P value	0.802	0.001	0.000	0.007	0.234	0.753	0.045	0.201	0.002	0.002	0.000	0.004
interaction E × F												
P value	0.583	0.720	0.570	0.342	0.291	0.555	0.320	0.494	0.520	0.281	0.715	0.189

[a]Mean values within a column with unlike letters a and b were shown to be significantly different ($P < 0.05$); differences among groups C_{CEL}, C_{FOS}, EL_{CEL}, EL_{FOS}, EH_{CEL}, and EH_{FOS} were indicated only in the case of a statistically significant interaction E × F ($P < 0.05$). [b]C2, acetate; C3, propionate; C4i, isobutyrate; C4, butyrate; C5i, isovalerate; C5, valerate; PSCFA, putrefaction short chain fatty acid (sum of C4i, C5i, and C5). [c]C_{CEL}, control diet with 6% cellulose (CEL) as the dietary fiber; C_{FOS}, control diet with 3% fructooligosaccharides (FOS) and 3% cellulose as the dietary fiber; EL_{CEL}, diet with a low level of the strawberry extract and CEL as the dietary fiber; EL_{FOS}, diet with a low level of the extract and FOS/CEL as the dietary fiber; EH_{CEL}, diet with a high level of the strawberry extract and CEL as the dietary fiber, EH_{FOS}, diet with a high level of the extract and FOS/CEL as the dietary fiber.

Table 6. Biochemical Indicators of the Blood Serum of Rats Fed Experimental Diets[a]

	U/L		mmol/L			mmol/L	
	ALT[b]	AST	TC	HDL	HDL profile, % of TC	TG	GL
group[c]							
C_{CEL}	33.0	93.9	2.08	0.75 b	36.5 b	0.97	8.81
C_{FOS}	34.3	93.6	2.10	1.02 a	48.7 a	1.03	7.59
EL_{CEL}	32.6	101	2.05	0.87 b	42.6 ab	0.99	6.53
EL_{FOS}	27.1	99.3	1.84	0.80 b	43.3 ab	0.87	6.47
EH_{CEL}	30.7	99.2	2.11	0.82 b	38.9 b	1.08	6.98
EH_{FOS}	32.3	99.8	1.91	0.75 b	39.5 b	0.90	6.16
SEM	1.1	2.6	0.03	0.02	1.0	0.04	0.20
extract (E)							
C	33.7	93.7	2.09	0.88	42.6	1.00	8.20 a
EL	29.8	99.9	1.95	0.83	42.9	0.93	6.50 b
EH	31.5	99.5	2.01	0.78	39.2	0.99	6.57 b
P value	0.378	0.593	0.268	0.074	0.172	0.770	0.000
fiber (F)							
CEL	32.1	97.9	2.08	0.81	39.3 b	1.01	7.44 a
FOS	31.2	97.6	1.95	0.85	43.9 a	0.93	6.74 b
P value	0.693	0.958	0.068	0.224	0.014	0.330	0.034
interaction E × F							
P value	0.356	0.990	0.313	0.000	0.014	0.447	0.326

[a]Mean values within a column with unlike letters a and b were shown to be significantly different ($P < 0.05$); differences among the groups C_{CEL}, C_{FOS}, EL_{CEL}, EL_{FOS}, EH_{CEL}, and EH_{FOS} were indicated only in the case of a statistically significant interaction E × F ($P < 0.05$). [b]ALT, alanine transaminase; AST, aspartate transaminase; TC, total cholesterol; TG, triglycerides; GL, glucose. [c]C_{CEL}, control diet with 6% cellulose (CEL) as the dietary fiber, C_{FOS}, control diet with 3% fructooligosaccharides (FOS) and 3% cellulose as the dietary fiber, EL_{CEL}, diet with a low level of the strawberry extract and CEL as the dietary fiber, EL_{FOS}, diet with a low level of the extract and FOS/CEL as the dietary fiber, EH_{CEL}, diet with a high level of the strawberry extract and CEL as the dietary fiber, EH_{FOS}, diet with a high level of the extract and FOS/CEL as the dietary fiber.

decreased the amount of cecal digesta and tended to increase the cecal dry matter concentration. It was also noted that the FOS and ET strawberry extract showed an opposite effect on the measured parameters.

dx.doi.org/10.1021/jf405612a | J. Agric. Food Chem. 2014, 62, 5871−5880

The activity of microbiota in the cecum depends on the supplied nutrients. Kosmala et al. (2014)[35] have shown that the inclusion of 5% FOS significantly decreased α-galactosidase, β-glucosidase, and β-glucuronidase activity, while the activity of α-glucosidase and β-galactosidase did not change statistically when compared to the CEL-enriched diet. In our experiment, the addition of 3% FOS to the diet significantly reduced the activity of β-glucuronidase and increased that of β-galactosidase in the cecal digesta compared to the CEL groups. The addition of ET strawberry extract improved the effect of ingested diet by significantly decreasing the activity of β-glucosidase in the cecal digesta. However, the addition of FOS and a high level of the ET strawberry extract (group EH) together reduced the beneficial effect of FOS by increasing the β-glucuronidase activity in the cecal digesta. These enzymes may exert toxic, carcinogenic, or mutagenic effects in the gastrointestinal tract.[36] It can be assumed that the addition of ETs to diet could selectively modulate the composition of the microbiota and thus increase potentially harmful species of bacteria which were responsible for the enhanced activity of β-glucuronidase in the cecum. FOS is known as a prebiotic, which selectively stimulates the growth of bifidobacteria, thus causing significant changes in the composition of the gut microflora by increasing the number of potentially health-promoting bacteria and reducing the number of potentially harmful species, including *Escherichia coli* and *Clostridium*.[37] Larrosa et al. (2010)[38] found that ETs and ET metabolites from pomegranate decreased enterobacteria and increased lactobacilli and bifidobacteria. The ET strawberry extract in addition to ETs is a source of proanthocyanidins, which may reduce the activity of digestive enzymes when present at elevated levels.[39] The ET strawberry extract used in this study was also a source of flavonoids; previously, a flavonoid extract applied as a dietary supplement was shown to decrease the activity of bacterial β-glucosidase and β- and α-galactosidases in the cecal digesta of rats.[11] Roberton et al. (1982)[40] suggested that the most important factor in the modulation of β-glucuronidase activity in the rat large bowel is bile flow. Indeed, dietary fiber is the main factor that intensifies peristalsis and thus the bile flow through the large intestine.[41]

In this study, the identification and determination of the ET metabolites in the gastrointestinal tract of the rats revealed the presence of nasutin A and EA. However, urolithins, which are considered to be typical reaction products of ET metabolism in the gastrointestinal tract of humans and experimental animals, were not detected.[12,13] One of the possible ways in which the intensification or modulation of the ET biodegradation processes may be occurring is through an increase in the population of the lactobacilli bacteria that are capable of producing tannase and changes in the pH of the environment.[42] Tannase causes hydrolysis of ester bonds, including the bonds between hexahydroxydiphenic acid (HHDP) and glucose; free HHDP can then undergo spontaneous lactonization to EA. Lactonization of the acid with the hydroxyl group of the benzene ring can be accompanied by decarboxylation of the second acid moiety and the subsequent loss of hydroxyl residues to form urolithins.[14,15] A small amount of experimental data[14] and the results of computer simulations of chemical reactions[12] indicated the formation of nasutin A and isonasutin as byproducts of lactonization with the removal of two hydroxyl residues from EA. Nevertheless, there is no clear explanation for the spontaneity or the conditions of the formation process of nasutin A. The data presented in Figure 1 show a significant increase in the concentration of nasutin A in the gastrointestinal tract after the consumption of the diet with FOS and variable doses of the ET strawberry extract. In this study, trace amounts of nasutin A were observed in the stomach; it can be speculated that hydroxyls can be removed from EA under the physiological conditions of the stomach. The acidic environment of the stomach leads to the production of EA.[7,14] The highest concentration of nasutin A was observed in the small intestines. Larrosa et al. (2006)[43] showed that ETs are mostly hydrolyzed to EA under the physiological conditions of the small intestine. In the cecum, a lower concentration of nasutin A was observed compared to the small intestine. When ETs or EA reach the distal part of the small intestine and the colon, they are largely metabolized by the gut microflora to urolithins;[42] we speculated that the main differences in the concentration of nasutin A were associated with specific microflora that are not the same in all parts of the gastrointestinal tract. Determining the causes of such a phenomenon requires further experiments.

Numerous studies have shown that the administration of FOS leads to an enhancement of SCFA production, mainly acetate, propionate, and butyrate.[3,6] After absorption, SCFAs play important roles in an organism. Propionate has a positive influence on lipid metabolism in liver, whereas butyrate is an energy substrate for colonocytes.[37] In this study, the addition of FOS into the diet improved the cecal production of propionate and butyrate acids. Thus, a higher concentration of butyric may explain the significantly higher mass of cecal tissue in the groups consuming FOS. Zduńczyk et al. (2006)[11] demonstrated that the presence of polyphenols in inulin-containing diets did not change the total SCFA production in the cecum of rats. In addition, Juśkiewicz et al. (2010)[6] reported that the polyphenol concentrate from apple pomace and FOS did not show any serious negative effects on the basic parameters of the cecum and SCFA production. However, the addition of the ET strawberry extract into the diet slightly reduced the beneficial effect of FOS on enhancing the production of SCFA, especially acetic acid in the cecum. The high content of ETs and their metabolites suppressed the activity of the microbiota and thereby decreased the production of SCFA. The results of other studies indicate that an increased content of polyphenols in the diet may inhibit the growth and reduce the abundance of gastrointestinal microflora.[11,38] In this study, the group with a high content of ET strawberry extract exhibited significantly reduced production of PSCFA, which may suggest less intensive anaerobic bacterial fermentation of polypeptides and amino acids.[24]

Based on the results obtained in this study, we assume that the above changes in the cecal concentrations of SCFA were consistent with blood markers of the lipid profile in the rats. Propionate is reported to be involved in the cholesterol-lowering effect of fiber by impairing acetate utilization, especially when cholesterol synthesis is activated to compensate for enhanced fecal losses of steroids.[44] In this study, rats that consumed the diet with FOS had a significantly higher value of HDL-C, a significantly lower concentration of glucose in the blood, and a statistical tendency ($P = 0.068$) toward a lower serum TC concentration compared to rats that consumed the diet with CEL. These results confirm earlier observations made by Giacco et al. (2004),[45] who reported that positive systemic effects of fructans could reduce plasma glucose as well as the total and LDL cholesterol concentrations. The combination of a high level of the ET strawberry extract with FOS in the diet caused a higher reduction of glucose in the blood, and the

HDL-C level in the serum was lower than in the group without the ET strawberry extract in the diet. Other authors have found that ET metabolites, urolithins, are responsible for serum and liver lipid reductions.[43,16] Moreover, some studies have shown that polyphenolic compounds may reduce the activity of endogenous enzymes in the small intestine and thereby may influence the regulation of blood glucose levels.[22,46]

In summary, the present experiment demonstrated that some of the positive changes in the cecal metabolism of rats that resulted from the ingestion of a diet enriched only with FOS were suppressed or slightly suppressed by the addition of an ET strawberry extract. The pH value, SCFA production, and β-glucuronidase activity in the cecum of rats fed with FOS were affected upon the addition of the ET strawberry extract. The addition of FOS to the diet resulted in higher metabolism of the tested ET strawberry extract in the gastrointestinal tract of rats. Moreover, the systemic effect of the supplements when consumed together showed undesired decrease in HDL-C.

■ ASSOCIATED CONTENT

Supporting Information

Figure 2: HPLC-DAD chromatogram (λ = 360 nm) of the rat gastric contents after the administration of high doses of ETs (EH) and FOS compared to the control group (C) without ETs and with FOS. Figure 3: HPLC-DAD chromatogram (λ = 360 nm) of the rat small intestine contents after the administration of high doses of ETs (EH) and FOS compared to the control group (C) without ETs and with FOS. Figure 4: HPLC-DAD chromatogram (λ = 360 nm) of the rat cecum contents after the administration of high doses of ETs (EH) and FOS compared to the control group (C) without ETs and with FOS. This material is available free of charge via the Internet at http://pubs.acs.org.

■ AUTHOR INFORMATION

Corresponding Author

*Phone: +48-89-523-4600. Fax: +48-89-524-0124. E-mail: b.fotschki@pan.olsztyn.pl.

Funding

This work was supported in part by the National Science Centre Poland (Grant DEC-2012/05/B/NZ9/03402) and by the Polish Ministry of Science and Higher Education as part of the resources allocated for science in 2010-2013 under research project No. NN312360139.

Notes

The authors declare no competing financial interest.

■ REFERENCES

(1) Sabater-Molina, M.; Larqué, E.; Torrella, F.; Zamora, S. Dietary fructooligosaccharides and potential benefits on health. *J. Physiol. Biochem.* **2009**, *65*, 315−328.

(2) Hannum, S. M. Potential impact of strawberries on human health: a review of the science. *Crit. Rev. Food Sci. Nutr.* **2004**, *44*, 1−17.

(3) Hyson, D. A. Comprehensive review of apples and apple components and their relationship to human health. *Adv. Nutr.* **2011**, *2*, 408−420.

(4) Nyman, M. Fermentation and bulking capacity of indigestible carbohydrates: the case of inulin and oligofructose. *Br. J. Nutr.* **2002**, *87*, 163−168.

(5) Jurgoński, A.; Juśkiewicz, J.; Zduńczyk, Z. Comparative effects of different dietary levels of cellulose and fructooligosaccharides on fermentative processes in the caecum of rats. *J. Anim. Feed Sci.* **2008**, *17*, 88−99.

(6) Juśkiewicz, J.; Milala, J.; Jurgoński, A.; Król, B.; Zduńczyk, Z. Consumption of polyphenol concentrate with dietary fructo-oligosaccharides enhances cecal metabolism of quercetin glycosides in rats. *Nutrition* **2010**, *27*, 351−357.

(7) Silva Pinto, M.; Lajolo, F. M.; Genovese, M. I. Bioactive compounds and quantification of total ellagic acid in strawberries (*Fragaria x ananassa Duch.*). *Food Chem.* **2008**, *107*, 1629−1635.

(8) Seeram, N. P.; Lee, R.; Scheuller, H. S.; Heber, D. Identification of phenolic compounds in strawberries by liquid chromatography electrospray ionization mass spectroscopy. *Food Chem.* **2006**, *97*, 1−11.

(9) Giménez-Bastida, J. A.; González-Sarrías, A.; Larrosa, M.; Tomás-Barberán, F.; Espín, J. C.; García-Conesa, M. T. Ellagitannin metabolites, urolithin A glucuronide and its aglycone urolithin A, ameliorate TNF-α-induced inflammation and associated molecular markers in human aortic endothelial cells. *Mol. Nutr. Food Res.* **2012**, *56*, 784−796.

(10) Landete, J. M. Ellagitannins, ellagic acid and their derived metabolites: a review about source, metabolism, functions and health. *Food Res. Int.* **2011**, *44*, 1150−1160.

(11) Zduńczyk, Z.; Juśkiewicz, J.; Estrella, I. Cecal parameters of rats fed diets containing grapefruit polyphenols and inulin as single supplements or in a combination. *Nutrition* **2006**, *22*, 898−904.

(12) Mertens-Talcott, S. U.; Jilma-Stohlawetz, P.; Rios, J.; Hingorani, L.; Derendorf, H. Absorption, metabolism, and antioxidant effects of pomegranate (*Punica granatum L.*) polyphenols after ingestion of a standardized extract in healthy human volunteers. *J. Agric. Food Chem.* **2006**, *54*, 8956−8961.

(13) Tomás-Barberan, F. A.; Garcia-Conesa, M. T.; Larrosa, M.; Cerdá, B.; Gonzalez-Barrio, R.; Bermudez-Soto, M. J.; Gonzalez-Sarrias, A.; Espín, J. C. Bioavailability, metabolism, and bioactivity of food ellagic acid and related polyphenols. *Recent Adv. Polyphenol Res.* **2008**, *1*, 263−277.

(14) González-Barrio, R.; Truchado, P.; Ito, H.; Espín, J. C.; Tomas-Barberán, F. A. UV and MS identification of urolithins and nasutins, the bioavailable metabolites of ellagitannins and ellagic acid in different mammals. *J. Agric. Food Chem.* **2011**, *59*, 1152−1162.

(15) Mazzone, G.; Toscano, M.; Russo, N. Density functional predictions of antioxidant activity and UV spectral features of nasutin A, isonasutin, ellagic acid, and one of its possible derivatives. *J. Agric. Food Chem.* **2013**, *61*, 9650−9657.

(16) Aviram, M.; Rosenblat, M.; Gaitini, D.; Nitecki, S.; Hoffman, A.; Dornfeld, L.; Volkova, N.; Presser, D.; Attias, J.; Liker, H.; Hayek, T. Pomegranate juice consumption for three years by patients with carotid arterial stenosis reduces common carotid-media thickness, blood pressure and LDL oxidation. *Clin. Nutr.* **2004**, *23*, 423−433.

(17) Jarosławska, J.; Juśkiewicz, J.; Wróblewska, M.; Jurgoński, A.; Król, B.; Zduńczyk, Z. Polyphenol-rich strawberry pomace reduces serum and liver lipids and alters gastrointestinal metabolite formation in fructose-fed rats. *J. Nutr.* **2011**, *141*, 1777−1783.

(18) Cerdá, B.; Espín, J. C.; Parra, S.; Martínez, P.; Tomás-Barberán, F. A. The potent in vitro antioxidant ellagitannins from pomegranate juice are metabolised into bioavailable but poor antioxidant hydroxy-6H-dibenzopyran-6-one derivatives by the colonic microflora of healthy humans. *Eur. J. Nutr.* **2004**, *43*, 205−220.

(19) AOAC. *Official methods of analysis of AOAC International*, 18th ed.; Horwitz, W., Latimer, G. W., Eds.; AOAC International: Gaithersburg, MD, 2005.

(20) Sójka, M.; Klimczak, E.; Macierzyński, J.; Kołodziejczyk, K. Nutrient and polyphenolic composition of industrial strawberry press cake. *Eur. Food. Res. Technol.* **2013**, *237*, 995−1007.

(21) Kennedy, J. A.; Jones, G. P. Analysis of proanthocyanidin cleavage products following acid-catalysis in the presence of excess phloroglucinol. *J. Agric. Food Chem.* **2001**, *49*, 1740−1746.

(22) Espín, J. C.; Gonzalez-Barrio, R.; Cerdá, B.; Lopez-Bote, C.; Rey, A. I.; Tomás-Barberan, F. A. Iberian pig as a model to clarify obscure points in the bioavailability and metabolism of ellagitannins in humans. *J. Agric. Food Chem.* **2007**, *55*, 10476−10485.

(23) Reeves, P. G. Components of the AIN-93 diets as improvements in the AIN-76A diet. *J. Nutr.* **1997**, *127*, 838S−841S.
(24) Juśkiewicz, J.; Zduńczyk, Z.; Żary-Sikorska, E.; Król, B.; Milala, J.; Jurgoński, A. Effect of the dietary polyphenolic fraction of chicory root, peel, seed and leaf extracts on caecal fermentation and blood parameters in rats fed diets containing prebiotic fructans. *Br. J. Nutr.* **2011**, *105*, 710−720.
(25) Oszmiański, J.; Wojdyło, A. Comparative study of phenolic content and antioxidant activity of strawberry puree, clear, and cloudy juices. *Eur. Food Res. Technol.* **2009**, *228*, 623−631.
(26) Panico, A. M.; Garufi, E.; Nitto, S.; Di Mauro, R.; Longhitano, R. C.; Magri, G.; Catalfo, A.; Serrentino, M. E.; De Guidi, G. Antioxidant activity and phenolic content of strawberry genotypes from Fragaria x ananasa. *Pharm. Biol.* **2009**, *47*, 203−208.
(27) Määttä-Riihinen, K. R.; Kamal-Eldin, A.; Törrönen, A. R. Identification and quantification of phenolic compounds in berries of Fragaria and Rubus species (family *Rosaceae*). *J. Agric. Food Chem.* **2004**, *52*, 6178−6187.
(28) Kähkönen, M. P.; Hopia, A. I.; Heinonen, M. Berry phenolics and their antioxidant activity. *J. Agric. Food Chem.* **2001**, *49*, 4076−4082.
(29) Buendía, B.; Gil, M. I.; Tudela, J. A.; Gady, A. L.; Medina, J. J.; Soria, C.; López, J. M.; Tomás-Barberán, F. A. HPLC-MS analysis of proanthocyanidin oligomers and other phenolics in 15 strawberry cultivars. *J. Agric. Food Chem.* **2010**, *58*, 3916−3926.
(30) Weisburger, J. H. Mechanisms of action of antioxidant as exemplified in vegetable, tomatoes, and tea. *Food Chem. Toxicol.* **1999**, *37*, 943−948.
(31) Reagan-Shaw, S.; Nihal, M.; Ahmad, N. Dose translation from animal to human studies revisited. *FASEB J.* **2008**, *22*, 659−661.
(32) Topping, D. L.; Clifton, P. M. Short-chain fatty acids and human colonic function: roles of resistant starch and nonstarch polysaccharides. *Physiol. Rev.* **2001**, *81*, 1031−1064.
(33) Daniel, E. M.; Ratnayake, S.; Kinstle, T.; Stoner, G. D. The effects of pH and rat intestinal contents on the liberation of ellagic acid from purified and crude ellagitannins. *J. Nat. Prod.* **1991**, *54*, 946−952.
(34) Seeram, N. P.; Lee, R.; Heber, D. Bioavailability of ellagic acid in human plasma after consumption of ellagotannins from pomegranate (*Punica granatum L.*) juice. *Clin. Chim. Acta* **2004**, *348*, 63−68.
(35) Kosmala, M.; Zduńczyk, Z.; Kołodziejczyk, K.; Klimczak, E.; Juśkiewicz, J.; Zduńczyk, P. Chemical composition of polyphenols extracted from strawberry pomace and their effect on physiological properties of diets supplemented with different types of dietary fibre in rats. *Eur. J. Nutr.* **2014**, *53*, 521−532.
(36) Gråsten, S. M.; Pajarib, A. M.; Liukkonenc, K. H.; Karppinenc, S.; Mykkänena, H. M. Fibers with different solubility characteristics alter similarly the metabolic activity of intestinal microbiota in rats fed cereal brans and inulin. *Nutr. Res. (N.Y.)* **2002**, *12*, 1435−1444.
(37) Roberfroid, M. B. Introducing inulin-type fructans. *Br. J. Nutr.* **2005**, *93*, 13−25.
(38) Larrosa, M.; Gonzalez-Sarrıas, A.; Yanez-Gascon, M. J.; Selma, M. V.; Azorın-Ortuno, M.; Toti, S.; Tomás-Barberan, F. A.; Dolara, P.; Espín, J. C. Anti-inflammatory properties of a pomegranate extract and its metabolite urolithin-A in a colitis rat model and the effect of colon inflammation on the phenolic metabolism. *J. Nutr. Biochem.* **2010**, *21*, 717−725.
(39) Beecher, G. R. Proanthocyanidins: biological activities associated with human health. *Pharm. Biol.* **2004**, *42*, 2−20.
(40) Roberton, A. M.; Lee, S. P.; Lindop, R.; Stanley, R. A.; Thomsen, L.; Tasman-Jones, C. Biliary control of beta-glucuronidase activity in the luminal contents of the rat ileum, cecum, and rectum. *Cancer Res.* **1982**, *42*, 5165−5166.
(41) Anderson, J. W.; Hanna, T. J. Impact of nondigestible carbohydrates on serum lipoproteins and risk for cardiovascular disease. *J. Nutr.* **1999**, *129*, 1457−1466.
(42) Cerdá, B.; Tomás-Barberán, F. A.; Espín, J. C. Metabolism of antioxidant and chemopreventive ellagitannins from strawberries, raspberries, walnuts and oak-aged wine in humans: identification of biomarkers and individual variability. *J. Agric. Food Chem.* **2005**, *53*, 227−235.
(43) Larrosa, M.; Tomás-Barberan, F. A.; Espín, J. C. The hydrolysable tannin punicalagin releases ellagic acid which induces apoptosis in human colon adenocarcinoma Caco-2 cells by using the mitochondrial pathway. *J. Nutr. Biochem.* **2006**, *17*, 611−625.
(44) Demigné, C.; Morand, C.; Levrat, M. A.; Besson, C.; Moundras, C.; Rémésy, C. Effect of propionate on fatty acid and cholesterol synthesis and on acetate metabolism in isolated rat hepatocytes. *Br. J. Nutr.* **1995**, *74*, 209−219.
(45) Giacco, R.; Clemente, G.; Luongo, D.; Lasorella, G.; Fiume, I.; Brouns, F.; Bornet, F.; Patti, L.; Cipriano, P.; Rivellese, A. A.; Riccardi, G. Effects of short-chain fructo-oligosaccharides on glucose and lipid metabolism in mild hypercholesterolaemic individuals. *Clin. Nutr.* **2004**, *23*, 331−340.
(46) Ramachandra, R.; Shetty, A. K.; Salimath, P. V. Quercetin alleviates activities of intestinal and renal disaccharidases in streptozotocin-induced diabetic rats. *Mol. Nutr. Food Res.* **2005**, *49*, 355−360.

JOURNAL OF AGRICULTURAL AND FOOD CHEMISTRY

Article

pubs.acs.org/JAFC

Modeling the Effect of Phase II Conjugations on Topoisomerase I Poisoning: Pilot Study with Luteolin and Quercetin

Luca Dellafiora,[†] Pedro Mena,[‡,§] Daniele Del Rio,*[,‡,§] and Pietro Cozzini*[,†]

[†]Molecular Modeling Laboratory, Department of Food Science, [‡]The Laboratory of Phytochemicals in Physiology, Human Nutrition Unit, Department of Food Science, and [§]LS9 Bioactives and Health, Interlaboratory Group, Department of Food Science, University of Parma, 43125 Parma, Italy

ABSTRACT: Topoisomerases are targeted by several drugs in cancer chemotherapy acting as key enzymes in cell viability. Some flavonoids and their glycosides may exert health protective effects through the poisoning of topoisomerases. However, previous studies did not consider the substantial modifications taking place after ingestion neglecting that only metabolites can interact with the internal compartments of the human body. Since the high number of possible metabolites hinders their systematic analysis, an in silico approach can be a valuable tool to prioritize compounds by identifying candidates for further characterization. Specifically focusing on luteolin and quercetin, among the most ubiquitous flavonoids in the human diet, this work reports a computational procedure to model the effect of hepatic phase II conjugative metabolism on poisoning of human Topoisomerase I. As a general effect, glucuronidation and sulphation might enhance and quench poisoning activity, respectively. Among all, quercetin-3-*O*-glucuronide represents a promising candidate to be analyzed more thoroughly.

KEYWORDS: *Topoisomerase I, poisoning, molecular modeling, flavones, metabolites, activity*

INTRODUCTION

Topoisomerases (Topos) are ubiquitous enzymes that control DNA supercoiling and intertwining. They allow DNA relaxing by introducing single- (Topo I) or double-strand breakage (Topo II) through respectively one or two transesterification reactions. When Topos activity is altered, abnormal DNA structures and delay of replication and transcription inevitably occur.[1] Both "canonical inhibition" and poisoning can disrupt Topos activity. The former requires the prevention/alteration of protein−DNA interaction, the latter turns the enzymes into a DNA damaging agent since poisoning compounds hinder DNA religation by stabilizing the so-called "cleavable complex".[2−4] Since Topos are involved in key steps of cell viability, topoisomerase inhibitors and poisons are widely used as antibacterial and anticancer agents.[5]

Flavonoids are low molecular weight secondary metabolites widely distributed in the plant kingdom. They are ubiquitous constituents of fruit- and vegetable-rich diets where they have potential protective effects against the onset of chronic conditions such as cancer and cardiovascular disease.[6] Among flavonoid subgroups, the most potent Topo I poisons are flavones and flavonols.[2] Quercetin, principally as glycoside conjugates, is an abundant flavonol in the human diet, occurring in products such as apples, red grapes, citrus, onions, garlic, and tea,[7] and its consumption has been linked to lower rates of certain cancers.[8] The flavone luteolin also occurs almost exclusively as glycoside conjugates and is found in carrots, peppers, celery, olive oil, peppermint, thyme, rosemary, and oregano.[7] Its consumption has been associated with a range of biological activities.[9]

Both quercetin and luteolin have been reported to poison DNA Topo I and II,[2,10,11] which supports their possible chemopreventive activity. However, results are conflicting and some works in the literature do not support flavonoids-mediated Topos poisoning.[12,13] A further factor to be taken into account is that, after consumption,[6] flavonoids are subjected to extensive phase II metabolism, and thus it would be their glucuronide and sulfate metabolites that might act as potential chemopreventive agents, rather than their parent compounds. The role of these circulating metabolites in poisoning Topo I has not been determined, yet. Therefore, considering that luteolin and quercetin are widely consumed through a normal balanced diet, it is relevant to investigate whether their phase II metabolites are able to act as Topo I poisons.

Nevertheless, the systematic characterization of metabolized forms of polyphenols based on in vitro assays may be a hard challenge due to the high number of hits and, sometimes, to the lack of commercially available standards at affordable costs. It becomes thus necessary a prioritizing system to drive experimental trials in a focused manner. The computational approach efficiently meet this need and because the Topos poisoning activity unequivocally involves protein/DNA complex-ligand recognitions, the use of 3D molecular modeling becomes paramount.[14] Hence, the present work presents a pilot study on luteolin and quercetin, with the aim of verifying the feasibility of modeling the effects of their phase II conjugation on Topo I poisoning by using already verified and effective technique.[15] In addition to plant-based glycosides (used for training procedure), several phase-II human metabolites, still untested to the best of our knowledge, were analyzed (luteolin-3′-*O*-glucuronide, luteolin-3′-*O*-sulfate, luteolin-4′-*O*-glucuronide, luteolin-7-*O*-glucuronide, luteolin-7-sulfate, quercetin-3-

Received: January 24, 2014
Revised: May 26, 2014
Accepted: May 29, 2014
Published: May 29, 2014

ACS Publications © 2014 American Chemical Society

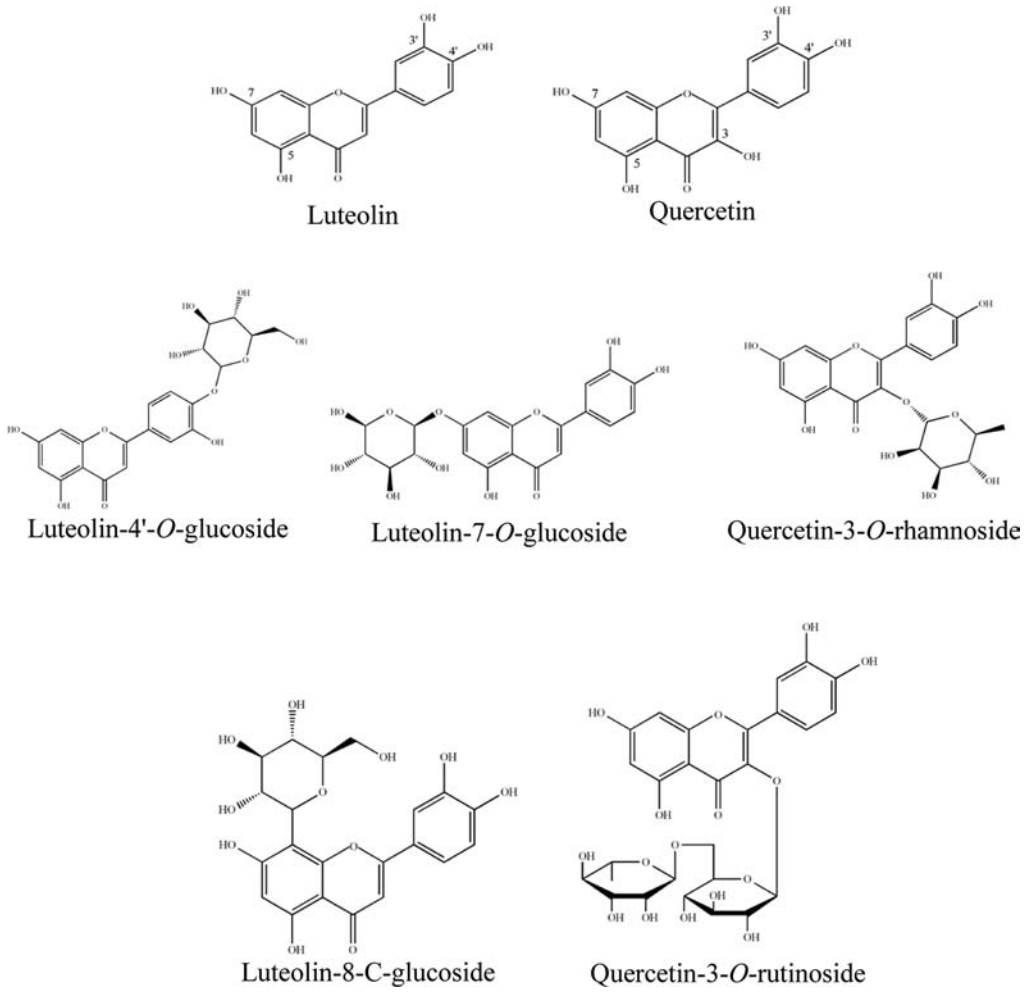

Figure 1. Molecules forming the training-set.

O-glucuronide, quercetin-3′-*O*-glucuronide, quercetin-3-sulfate, quercetin-4′-*O*-glucuronide, quercetin-7-*O*-glucuronide, and quercetin-7-sulfate)[16,17] and ranked according to physicochemical prioritization criteria.

MATERIAL AND METHODS

The procedure involved docking simulations followed by rescoring procedures using a proper scoring function. Our intention was to develop a procedure easy to perform, without excesses of software and hardware requirements and avoiding complex mathematical and statistical analysis.

All experimental data were retrieved from literature[2] and query set contained metabolites observed under in-vivo-like conditions whose might be the predominant occurring form in circulatory system.[16,17]

Molecular Modeling. The model used for docking simulation was derived from the high resolution structure of human Topo I retrieved from Protein Data Bank (http://www.rcsb.org; PDB code 1K4T).[18] Protein structure and small molecules were processed using the molecular modeling software Sybyl, version 8.1 (www.tripos.com). All atoms were checked for atom- and bond-type assignments. Amino- and carboxyl-terminal groups were set as protonated and deprotonated, respectively. Hydrogen atoms were computationally added to the protein and energy-minimized using the Powell algorithm whit a coverage gradient of ≤0.5 kcal (mol Å)$^{-1}$ and a maximum of 1500 cycles.

Docking Simulations. The docking simulations of all compounds were performed with the program GOLD version 5.1 (CCDC; Cambridge, U.K.; http://www.ccd.cam.ac.uk) on a double-quad cores machine equipped with 1.86 GHz processor. All crystallographic waters and ligands were removed and 30 poses for each compound were generated. No constraints were set up and the explorable space was defined in a radius of 10 Å from the centroid of the binding pocket. For each GOLD docking search, a maximum number of 100 000 operations were performed on a population of 100 individuals with a selection pressure of 1.1. Operator weights for crossover, mutation, and migration were set to 95, 95, and 10, respectively. The number of islands was set to 5 and the niche to 2. The hydrogen bond distance was set to 2.5 Å and the vdW linear cutoff to 4.0. Ligand flexibility options "flip pyramidal *N*", "flip amide bonds", and "flip ring corners" were allowed.

Rescoring Procedure and Hydropathic Analysis. The software HINT (Hydropatic INTeraction)[19] was used as postprocessing tool to rescore all poses generated by GOLD. The HINT scoring function calculates the favor of protein−ligand recognition trough a sum of hydrophobic atom constants which derived from experimental LogPo/w values (the partition coefficient of a molecule in 1-octanol/water). Thus, HINT appears as a "natural"[20] and intuitive force-field by providing empirical and quantitative evaluation of protein−ligand interaction as a sum of all single atom−atom contributions using the following equation:

$$\text{HINT score} = \sum_i \sum_j b_{ij} = \sum_i \sum_j (a_i S_i a_j S_j T_{ij} R_{ij} + r_{ij})$$

where *bij* is the interaction score between atoms *i* and *j*, *a* is the hydrophobic atomic constant, *S* represents the solvent accessible surface area, *Tij* is a logic function assuming +1 or −1 values, depending on the nature of the interatomic interaction, *Rij* and *rij* are functions of the distance between atoms *i* and *j*.

dx.doi.org/10.1021/jf501548g | J. Agric. Food Chem. 2014, 62, 5881−5886

Positive and high HINT score correlates with favorable binding free energy, allowing the evaluation of the thermodynamic benefit of predicted complexes.[21−24] Because different conformations of the same molecule may coexist contributing to the whole energy of binding, a Boltzman average calculation was applied. In this way the contributions of different conformations to the predicted interaction were taken into account.[25] Thus, from here, we referred to HINT score (HS) as Boltzman averaged score.

Replicas of Docking Simulation and Rescoring Procedure. Because GOLD uses a Lamarkian genetic algorithm, results may slightly change from run to run. This implies that computing twice the same molecule is impossible to record exactly the same score, because two identical poses (i.e., the exact *xyz* coordinates for each atom) are virtually impossible to obtain. This may be a nontrivial issue potentially disruptive in place of rescoring procedures. GOLD results are intrinsically ranked by its internal scoring functions. Because of this, it is not possible to separate GOLD's pose generation from its ranking, and we were forced to apply HINT only to rescore pregenerated poses. Thus, in order to avoid not-causative fluctuations due to random component of docking algorithm, each analysis was repeated 5-fold and the mean value was considered.

RESULTS

Training Procedure and Training-Set Results. When the validation of computational models may be not mandatory, as in this instance due to the lack of sufficient and inherent experimental data, training procedures are compulsory.[26] In the current study, the procedure exploited experimental data retrieved from the literature.[2] Specifically, a training-set has been formed by luteolin, luteolin-8-*C*-glucoside, luteolin-4′-*O*-glucoside, luteolin-7-O-glucoside, quercetin, quercetin-3-*O*-rhamnoside, and quercetin-3-*O*-rutinoside (Figure 1). Data and results concerning the training procedure are reported in Table 1. Taking into account the high variability and, in some cases, the proximity of experimental data, the absolute and quantitative rank of compounds was not easy to resolve. However, it was possible to perform a semiquantitative and relative comparison; instead of a global potency rank, we defined a binary categorization describing conjugation-dependent effects of enhancing and quenching on luteolin and quercetin, respectively. For instance, luteolin and luteolin-7-*O*-glucoside shared proximal values and the high variability of luteolin-7-*O*-glucoside made their relative potency indefinable, as ranges that totally overlap cannot be resolved. Conversely, luteolin-4′-*O*-glucoside (less active) and luteolin-8-*C*-glucoside (more active) were unequivocally separated from luteolin. Likewise quercetin-3-*O*-rhamnoside and quercetin-3-*O*-rutinoside clearly diverged down from quercetin.

Table 1. Results of the Training-Set[a]

compound	experimental activity	activity category	mean HS	predicted effect
luteolin	**55 ± 8.2**	/	**683 ± 28.0**	/
luteolin-8-*C*-glucoside	69 ± 5.6	↑	804 ± 107.0	↑
luteolin-4′-*O*-glucoside	19 ± 4.3	↓	562 ± 76.0	↓
luteolin-7-*O*-glucoside	51 ± 14.0	↑↓	747 ± 136.0	↑↓
quercetin	**57 ± 15.6**	/	**718 ± 42.0**	/
quercetin-3-*O*-rhamnoside	15 ± 12.0	↓	240 ± 140.0	↓
quercetin-3-*O*-rutinoside	5 ± 1.8	↓	383 ± 194.0	↓

[a]Enhancing and quenching effects with respect to the reference aglyconic compounds (in bold) are represented by up- or down-arrow, respectively "↑↓" indicates indefinable relative potency. Hint scores are expressed as mean value of 5 replicates. All experimental data were retrieved from the literature and express relative potency of compounds respect to the reference standard camptothecin.[2]

The training-set underwent docking simulations and rescoring procedure in order to assess the applicability of the procedure to this specific case study. Overall, good correlation between computed and experimental data was obtained (Figure 2). Specifically, computed results were in agreement with experimental data and the procedure was trained according to the fact that the augmentation and reduction of HSs correlated to conjugation-dependent enhancing and quenching of poisoning activity, respectively. However, it was not possible to compare the relative activity of luteolin and luteolin-7-*O*-glucoside due to the same reasons reported above (Table 1).

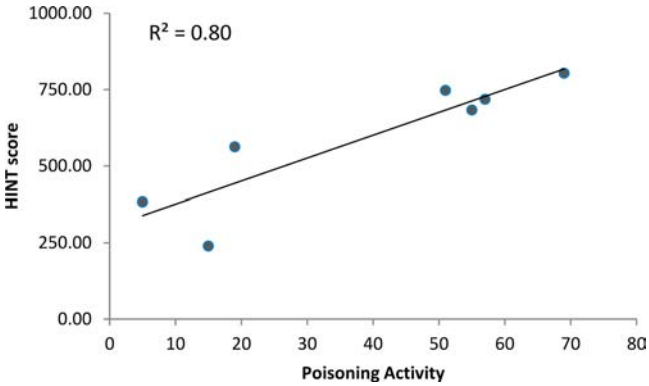

Figure 2. Correlation between computed results and experimental data. All experimental data were retrieved from the literature and express relative potency of compounds with respect to the reference standard camptothecin.[2]

Globally the procedure proved to be able to evaluate the relative effect of conjugations on poisoning activity of luteolin and quercetin.

Query-Set Results. The query-set underwent the same procedure of the training-set. Results were reported in Table 2.

Table 2. Results of the Query-Set[a]

compound	mean HS	predicted effect
luteolin	**683 ± 28**	/
luteolin-3′-*O*-glucuronide	756 ± 103	↑↓
luteolin-3′-sulfate	738 ± 24	↑
luteolin-4′-*O*-glucuronide	899 ± 163	↑
luteolin-7-*O*-glucuronide	891 ± 199	↑
luteolin-7-sulfate	354 ± 139	↓
quercetin	**718 ± 42**	/
quercetin-3-*O*-glucuronide	1766 ± 112	↑
quercetin-3′-*O*-glucuronide	782 ± 177	↑
quercetin-3′-sulfate	636 + 10	↓
quercetin-4′-*O*-glucuronide	756 ± 105	↑
quercetin-7-*O*-glucuronide	719 ± 41	–
quercetin-7-sulfate	618 ± 190	↓

[a]Enhancing and quenching effects with respect to aglyconic reference compounds (in bold) are represented by up- or down-arrow, respectively. "↑↓" indicates indefinable relative potency. "–" indicates comparable effect. HINT scores are expressed as mean value of 5 replicates.

dx.doi.org/10.1021/jf501548g | J. Agric. Food Chem. 2014, 62, 5881−5886

Overall, glucuronidation seemed to exert enhancing effects on both luteolin and quercetin, whereas sulphation, with the exception of luteolin-3′-sulfate, had the opposite effect. In addition, it is of interest to notice the out of range score of quercetin-3-*O*-glucuronide, indicating that this compound might be much more active than the others. Conversely, quercetin-7-*O*-glucuronide appeared virtually identical to quercetin and it could exert similar activity. Finally, once again, it was not possible to resolve the relative effect of luteolin-3′-*O*-glucuronide versus luteolin.

DISCUSSION

Topos I, as well as other topoisomerases, are key enzymes in cell viability which act on genome stability and accessibility during replication and transcription. Therefore, they are commonly targeted by antibacterial and anticancer chemicals. There are at least two mechanisms to disrupt Topo I activity: canonical inhibition by preventing protein−DNA recognition and poisoning by stabilizing DNA−protein complexes and hindering the DNA religation step. Enzyme poisoning rather than inhibition drives drug action. Several compounds act as Topo poisons, with many of them highly specific for Topo I, others for Topo II, and some promiscuous for both isoforms.[27] Currently camptothecin derivatives are the only anticancer drugs targeting Topo I approved by the FDA (Food and Drug Administration, http://www.fda.gov), although several promising compounds are under development.[5] Within this frame, flavonoids such as quercetin and luteolin might play critical roles. It is well-known that this class of compounds commonly occurs in edible parts of fruits and vegetables and exerts a broad spectrum of health-protective properties by interacting with several protein targets. Because advances in system biology suggest that multitarget compounds may prove higher efficacy rather than host-specific drugs,[28] these ubiquitous compounds might be of great relevance in cancer prevention, and TopoI poisoning may contribute to their health benefits. To better understand the underlying mechanisms of luteolin and quercetin putatively beneficial action, their metabolites, truly circulating in the bloodstream after their dietary intake, should be evaluated. Considering the wide array of possible metabolic phase II conjugation and the lack of commercially available standards, an in silico approach might be a useful prioritizing tool, acting by highlighting candidates for further characterization.

In silico techniques may be widely accessible and successfully applied also outside the boundaries of medicinal chemistry. The use of straightforward procedures (in terms of hardware and software requirements) may facilitate both the transition process and procedural automatizm in the field of the biological activity evaluation of phytocompounds. Several works in the literature show that computer driven analysis can contribute to decipher the mechanisms of action of a wide array of highly functional phytocomponents (e.g., refs 29−31). In addition, virtual screening has already proven to be a promising tool to make feasible the bioactivity evaluation of huge spectra of molecules of dietary origin,[32] including their metabolites,[33] or to discover novel enzymatic inhibitors.[34] However, to the best of our knowledge, relevant human metabolites of quercetin and luteolin have not been analyzed yet for their Topo I poisoning activity. For these reasons, we presented a virtual screening procedure performed on machines equipped with common hardware architecture similar to that of current portable devices (including laptops and smartphones). Concerning software, we chose GOLD, which is one of the most popular commercial docking software, and HINT, a natural and intuitive force-field to evaluate the favor of protein−ligand recognition. In addition, the use of such "linear" tools, avoiding complex mathematical and statistical models, contributes to reduce the risk of traps, such as overfitting phenomena and others erroneous or misleading results. The coupling of GOLD to perform docking simulations and HINT as rescoring function, has already proved to be a well working procedure to evaluate protein−ligand interaction,[33,35,36] thus no further validation was needed. Rather, as a proof of concept, we presented (i) the feasibility of a model able to evaluate the semiquantitative effect of conjugations on luteolin and quercetin by using the few inherent data available in literature and (ii) the application of such model to prioritize quercetin and luteolin metabolites for further experimental characterization. We focused on luteolin and quercetin due to their massive occurrence in plant-derived food and we took into account conjugated metabolites because glucuronidated and sulfated derivatives are the main circulating forms *in vivo*. Once assessed the capability to model the effect of conjugation on poisoning activity of luteolin and quercetin, glucuronidated and sulfated metabolites underwent the same procedure. In principle such approach can be applied to any other type of small molecule (and protein), but the procedural performance must be assessed case by case trough cross-check with experimental data.

Flavonoids able to effectively poison Topo I require hydroxyl group substitution at the C-3, C-7, C-3′, and C-4′ positions, a keto group at C-4, and a $\Delta^{2,3}$ double bond (3,3′,4′,7-tetrahydroxy-substituted flavones).[12] Quercetin and luteolin, as well as other flavonoids like apigenin, myricetin, fisetin, and morin, match these criteria and have been shown to poison Topo I.[2,11] However, the presence of sugar moieties has been pointed out to quench the poisoning effect of flavones and flavonols,[2] except for compounds glycosylated at the 8 position, as in the case of luteolin-8-*C*-glucoside (Table 1). In addition, the glucuronide form of SN-38, a potent topoisomerase I inhibitor derived from the pro-drug irinotecan (a derivative of camptothecin), has only 1% of the antitumor activity of its aglyconic active form.[37] Based on this observation, a limited poisoning effect of phase II metabolites containing a glucuronide conjugates should be expected. Nevertheless, most of the glucuronidated derivatives of the tested flavonoids showed enhanced Topo I poisoning effect with respect to their parent compounds (Table 2). On the contrary, sulfate derivatives, with the only exception of luteolin-3′-sulfate, showed a quenched effect when compared to aglycones.

In contrast to the marked role of the type of conjugation, its position in the flavonoid structure did not play a key role in the poisoning effect of these phenolic metabolites, with the exception of quercetin-3-*O*-glucuronide. The docking results revealed that the HINT score for quercetin-3-*O*-glucuronide was notably higher while the magnitude of the predicted effect was quite similar for most of the metabolites (Table 2). This might indicate that glucuronidation of flavonols at the C-3 position enhances their bioactivity as Topo I poisons. In this specific case, the substitution of the hydroxyl group by the glucuronide moiety occurs at the nonbenzene ring, the C ring. Thus, considering the essential role that the phenolic hydroxyl group plays in the activity of the chemotherapeutic SN-38,[37] this structural feature may at least partially explain the enhanced effect of quercetin-3-*O*-glucuronide. Overall, these results

indicate that quercetin-3-*O*-glucuronide is a promising candidate to be tested in further in vitro studies.

Sulfate and glucuronide conjugates are the major circulating metabolites of both quercetin and luteolin,[17,38−40] representing the physiological forms that may exert biological activities attributed to the consumption of their glycosidic precursors abundant in plant food. In the case of quercetin, quercetin-3′-*O*-sulfate and quercetin-3-*O*-glucuronide have been reported to be the predominant metabolites in plasma after the consumption of quercetin glycoside containing foods or supplements.[17,38−40] Therefore, in view of their putative quite opposite poisoning effect on Topo I, the study of their bioactivity on carcinogenic cell models could shed light on the real potential of dietary quercetin as Topo I poison. On the other hand, deconjugation processes consequent to cellular phenolic phase II conjugates uptake should also be taken into account, since this may condition their bioactivity, as already reported.[41]

In conclusion, the feasibility of an in silico model to evaluate conjugation-dependent effects of luteolin and quercetin on TopoI poisoning has been demonstrated by using literature experimental data. However, the applicability of the current model does not go beyond the prediction of potential effects and expanding the applicability of this model to other metabolic modifications and to other phenolic structures would be desirable. Further experimental results obtained on this specific biological feature will ultimately assess the validity of the applied model system. In addition, it is to be pointed out that in vivo effects cannot be inferred solely by using neither in silico models, nor cell-based or cell-free in vitro assays. However, such methods may suggest reasonable mechanisms of action that will then need to be deeply investigated.

This applied in silico model falls within the framework of "prospective" studies. The abuse of "retrospective" docking analysis, intended as aimed only at reproducing already published results, has been reported by several groups (e.g., ref 42). In this sense, our "pilot study" approach explored the feasibility of a good model that is neither definitive, nor a standalone analysis. Rather, it should be placed side by side to experimental works in order to help in prioritizing compounds by predicting putative activity.

Finally, the fact that different conjugations were linked, in this study, to opposite effects should be considered extremely relevant from a nutritional viewpoint, also beyond the results obtained within the specific applied model. The variability of hepatic phase II conjugation among subjects, as well as the interaction of dietary phytochemicals in this context, should be considered more complex than previously thought, and the putative beneficial nutritional effects of flavonoids, postulated by several epidemiological observations, should be evaluated taking carefully considering these observations.

AUTHOR INFORMATION

Corresponding Authors

*Tel: +39-0521-903830. Fax: +39-0521-903832. E-mail: daniele.delrio@unipr.it.

*Tel: +39-0521-905669. Fax: +39-0521-905556. E-mail: pietro.cozzini@unipr.it.

Notes

The authors declare no competing financial interest.

ABBREVIATIONS USED

FDA, Food and Drug Administration; HS, HINT score; PDB, Protein Data Bank; Topo, topoisomerase

REFERENCES

(1) Pommier, Y.; Leo, E.; Zhang, H.; Marchand, C. DNA topoisomerases and their poisoning by anticancer and antibacterial drugs. *Chem. Biol.* **2010**, *17*, 421−433.

(2) Webb, M. R.; Ebeler, S. E. Comparative analysis of topoisomerase IB inhibition and DNA intercalation by flavonoids and similar compounds: structural determinates of activity. *Biochem. J.* **2004**, *384*, 527−541.

(3) Vos, S. M.; Tretter, E. M.; Schmidt, B. H.; Berger, J. M. All tangled up: how cells direct, manage and exploit topoisomerase function. *Nat. Rev. Mol. Cell. Biol.* **2011**, *12*, 827−841.

(4) Burgos-Morón, E.; Calderón-Montaño, J.; Orta, M.; Pastor, N.; Pérez-Guerrero, C.; Austin, C.; Mateos, S.; López-Lázaro, M. The coffee constituent chlorogenic acid induces cellular DNA damage and formation of topoisomerase I- and II-DNA complexes in cells. *J. Agric. Food Chem.* **2012**, *60*, 7384−7391.

(5) Pommier, Y. Drugging topoisomerases: lessons and challenges. *ACS Chem. Biol.* **2013**, *8*, 82−95.

(6) Del Rio, D.; Rodriguez-Mateos, A.; Spencer, J. P.; Tognolini, M.; Borges, G.; Crozier, A. Dietary (poly)phenolics in human health: structures, bioavailability, and evidence of protective effects against chronic diseases. *Antioxid. Redox Signal.* **2013**, *18*, 1818−1892.

(7) Crozier, A.; Yokota, T.; Jaganath, I. B.; Marks, S.; Saltmarsh, M.; Clifford, M. N., Secondary metabolites as dietary components in plant-based foods and beverages. In *Plant Secondary Metabolites: Occurrence, Structure and Role in the Human Diet*; Crozier, A., Clifford, M. N., Ashihara, H., Eds.; Blackwell Publishing: Oxford, 2006; pp 208−302.

(8) Knekt, P.; Kumpulainen, J.; Järvinen, R.; Rissanen, H.; Heliövaara, M.; Reunanen, A.; Hakulinen, T.; Aromaa, A. Flavonoid intake and risk of chronic diseases. *Am. J. Clin. Nutr.* **2002**, *76*, 560−568.

(9) López-Lázaro, M. Distribution and biological activities of the flavonoid luteolin. *Mini Rev. Med. Chem.* **2009**, *9*, 31−59.

(10) Bandele, O. J.; Osheroff, N. Bioflavonoids as poisons of human topoisomerase IIα and IIβ. *Biochemistry* **2007**, *46*, 6097−6108.

(11) Boege, F.; Straub, T.; Kehr, A.; Boesenberg, C.; Christiansen, K.; Andersen, A.; Jakob, F.; Köhrle, J. Selected novel flavones inhibit the DNA binding or the DNA religation step of eukaryotic topoisomerase I. *J. Biol. Chem.* **1996**, *271*, 2262−2270.

(12) Constantinou, A.; Mehta, R.; Runyan, C.; Rao, K.; Vaughan, A.; Moon, R. Flavonoids as DNA topoisomerase antagonists and poisons: Structure-activity relationships. *J. Nat. Prod.* **1995**, *58*, 217−225.

(13) López-Lázaro, M.; Willmore, E.; Austin, C. A. The dietary flavonoids myricetin and fisetin act as dual inhibitors of DNA topoisomerases I and II in cells. *Mutat. Res., Genet. Toxicol. Environ. Mutagen.* **2010**, *696*, 41−47.

(14) Gleeson, M. P.; Modi, S.; Bender, A.; Robinson, R. L.; Kirchmair, J.; Promkatkaew, M.; Hannongbua, S.; Glen, R. C. The challenges involved in modeling toxicity data in silico: a review. *Curr. Pharm. Des.* **2012**, *18*, 1266−1299.

(15) Cozzini, P.; Dottorini, T. Is it possible docking and scoring new ligands with few experimental data? Preliminary results on estrogen receptor as a case study. *Eur. J. Med. Chem.* **2004**, *39*, 601−609.

(16) Boersma, M. G.; van der Woude, H.; Bogaards, J.; Boeren, S.; Vervoort, J.; Cnubben, N. H.; van Iersel, M. L.; van Bladeren, P. J.; Rietjens, I. M. Regioselectivity of phase II metabolism of luteolin and quercetin by UDP-glucuronosyl transferases. *Chem. Res. Toxicol.* **2002**, *15*, 662−670.

(17) Mullen, W.; Edwards, C. A.; Crozier, A. Absorption, excretion and metabolite profiling of methyl-, glucuronyl-, glucosyl- and sulpho-conjugates of quercetin in human plasma and urine after ingestion of onions. *Br. J. Nutr.* **2006**, *96*, 107−116.

(18) Staker, B. L.; Hjerrild, K.; Feese, M. D.; Behnke, C. A.; Burgin, A. B. J.; Stewart, L. The mechanism of topoisomerase I poisoning by a

camptothecin analog. *Proc. Natl. Acad. Sci. U.S.A.* **2002**, *99*, 15387−13592.
(19) Kellogg, E. G.; Abraham, D. J. Hydrophobicity: is LogP(o/w) more than the sum of its parts? *Eur. J. Med. Chem.* **2000**, *37*, 651−661.
(20) Amadasi, A.; Spyrakis, F.; Cozzini, P.; Abraham, D. J.; Kellogg, G. E.; Mozzarelli, A. Mapping the energetics of water-protein and water-ligand interactions with the "natural" HINT forcefield: predictive tools for characterizing the roles of water in biomolecules. *J. Mol. Biol.* **2006**, *358*, 289−309.
(21) Cozzini, P.; Fornabaio, M.; Marabotti, A.; Abraham, D. J.; Kellogg, G. E.; Mozzarelli, A. Simple, intuitive calculations of free energy of binding for protein-ligand complexes. 1. Models without explicit constrained water. *J. Med. Chem.* **2002**, *45*, 2469−2483.
(22) Fornabaio, M.; Cozzini, P.; Mozzarelli, A.; Abraham, D. J.; Kellogg, G. E. Simple, intuitive calculations of free energy of binding for protein-ligand complexes. 2. Computational titration and pH effects in molecular models of neuraminidase-inhibitor complexes. *J. Med. Chem.* **2003**, *46*, 4487−4500.
(23) Fornabaio, M.; Spirakis, F.; Mozzarelli, A.; Cozzini, P.; Abraham, D. J.; Kellogg, G. E. Simple, intuitive calculations of free energy of binding for protein-ligand complexes. 3. The free energy contribution of structural water molecules in HIV-1 protease complexes. *J. Med. Chem.* **2004**, *47*, 5507−4516.
(24) Marabotti, A.; Spyrakis, F.; Facchiano, A.; Cozzini, P.; Alberti, S.; Kellogg, G. E.; Mozzarelli, A. Energy-based prediction of amino acid-nucleotide base recognition. *J. Comput. Chem.* **2008**, *29*, 1955−1969.
(25) Salsi, E.; Bayden, A. S.; Spyrakis, F.; Amadasi, A.; Campanini, B.; Bettati, S.; Dodatko, T.; Cozzini, P.; Kellogg, G. E.; Cook, P. F.; Roderick, S. L.; Mozzarelli, A. Design of O-acetylserine sulfhydrylase inhibitors by mimicking nature. *J. Med. Chem.* **2010**, *53*, 345−356.
(26) Combes, R. D. In silico methods for toxicity prediction. *Adv. Exp. Med. Biol.* **2012**, *745*, 96−116.
(27) Khadka, D. B.; Cho, W. J. Topoisomerase inhibitors as anticancer agents: a patent update. *Expert Opin. Ther. Pat.* **2013**, *23*, 1033−1056.
(28) Russo, P.; Del Bufalo, A.; Cesario, A. Flavonoids acting on DNA topoisomerases: recent advances and future perspectives in cancer therapy. *Curr. Med. Chem.* **2012**, *19*, 5287−5293.
(29) Lambert, J.; Yennawar, N.; Gu, Y.; Elias, R. Inhibition of secreted phospholipase A2 by proanthocyanidins: a comparative enzymological and in silico modeling study. *J. Agric. Food Chem.* **2012**, *60*, 7417−7420.
(30) Puiggròs, F.; Sala, E.; Vaqué, M.; Ardévol, A.; Blay, M.; Fernández-Larrea, J.; Arola, L.; Bladé, C.; Pujadas, G.; Salvadó, M. In vivo, in vitro, and in silico studies of Cu/Zn-superoxide dismutase regulation by molecules in grape seed procyanidin extract. *J. Agric. Food Chem.* **2009**, *57*, 3934−3942.
(31) Shimmyo, Y.; Kihara, T.; Akaike, A.; Niidome, T.; Sugimoto, H. Flavonols and flavones as BACE-1 inhibitors: structure-activity relationship in cell-free, cell-based and in silico studies reveal novel pharmacophore features. *Biochim. Biophys. Acta* **2008**, *1780*, 819−825.
(32) Li, Y.; Frenz, C.; Li, Z.; Chen, M.; Wang, Y.; Li, F.; Luo, C.; Sun, J.; bohlin, L.; Li, Z.; Yang, H.; Wang, C. Virtual and in vitro bioassay screening of phytochemical inhibitors from flavonoids and isoflavones against xanthine oxidase and cyclooxygenase-2 for gout treatmen. *Chem. Biol. Drug. Des.* **2013**, *81*, 537−544.
(33) Dellafiora, L.; Mena, P.; Cozzini, P.; Brighenti, F.; Del Rio, D. Modelling the possible bioactivity of ellagitannin-derived metabolites. In silico tools to evaluate their potential xenoestrogenic behavior. *Food Funct.* **2013**, *4*, 1442−1451.
(34) Wang, J.; Tan, H.; Li, Y.; Ma, Y.; Li, Z.; Guddat, L. Chemical synthesis, in vitro acetohydroxyacid synthase (AHAS) inhibition, herbicidal activity, and computational studies of isatin derivatives. *J. Agric. Food Chem.* **2011**, *59*, 9892−9900.
(35) Amadasi, A.; Mozzarelli, A.; Meda, C.; Maggi, A.; Cozzini, P. Identification of xenoestrogens in food additives by an integrated in silico and in vitro approach. *Chem. Res. Toxicol.* **2009**, *22*, 52−63.
(36) Cozzini, P.; Dellafiora, L. In silico approach to evaluate molecular interaction between mycotoxins and the estrogen receptors ligand binding domain: a case study on zearalenone and its metabolites. *Toxicol. Lett.* **2012**, *214*, 81−85.
(37) Kaneda, N.; Nagata, H.; Furuta, T.; Yokokura, T. Metabolism and pharmacokinetics of the camptothecin analogue CPT-11 in the mouse. *Cancer Res.* **1990**, *50*, 1715−1720.
(38) Chen, T.; Li, L. P.; Lu, X. Y.; Jiang, H. D.; Su, Z. Absorption and Excretion of Luteolin and Apigenin in Rats after Oral Administration of Chrysanthemum morifolium Extract. *J. Agric. Food Chem.* **2007**, *55*, 273−277.
(39) Cialdella-Kam, L.; Nieman, D. C.; Sha, W.; Meaney, M. P.; Knab, A. M.; Shanely, R. A. Dose-response to 3 months of quercetin-containing supplements on metabolite and quercetin conjugate profile in adults. *Br. J. Nutr.* **2013**, *109*, 1923−1933.
(40) Jaganath, I. B.; Mullen, W.; Edwards, C. A.; Crozier, A. The relative contribution of the small and large intestine to the absorption and metabolism of rutin in man. *Free Radic. Res.* **2006**, *40*, 1035−1046.
(41) Menéndez, C.; Dueñas, M.; Galindo, P.; González-Manzano, S.; Jiménez, R.; Moreno, L.; Zarzuelo, M. J.; Rodríguez-Gómez, I.; Duarte, J.; Santos-Buelga, C.; Pérez-Vizcaíno, F. Vascular deconjugation of quercetin glucuronide: The flavonoid paradox revealed? *Mol. Nutr. Food Res.* **2011**, *55*, 1780−1790.
(42) Leach, A. R.; Shoichet, B. K.; Peishoff, C. E. Prediction of protein-ligand interactions. Docking and scoring: successes and gaps. *J. Med. Chem.* **2006**, *49*, 5851−5855.

JOURNAL OF AGRICULTURAL AND FOOD CHEMISTRY

Article

pubs.acs.org/JAFC

Toona sinensis Leaf Extract Inhibits Lipid Accumulation through Up-regulation of Genes Involved in Lipolysis and Fatty Acid Oxidation in Adipocytes

Hung-Wen Liu, Yue-Tseng Tsai, and Sue-Joan Chang*

Department of Life Sciences, National Cheng Kung University, Tainan, Taiwan

Supporting Information

ABSTRACT: *Toona sinensis* leaf (TSL) has been shown to lower plasma triacylglycerol levels and diminish the size of visceral fat cells in vivo. The molecular mechanism of TSL ethanol extract (TSL-E) on lipid metabolism in 3T3-L1 adipocytes was investigated in this study. Oil Red O staining as well as immunoblotting, real-time PCR, and dual-Luciferase reporter system were performed to investigate the effect of TSL-E on lipid accumulation and the regulation of lipid metabolism, respectively. In addition, active compounds in the TSL-E were analyzed by HPLC. TSL-E significantly decreased lipid accumulation, stimulated free fatty acid (FFA) release, and up-regulated peroxisome proliferator-activated receptor-α (PPARα) and genes involved in peroxisomal (acyl-CoA oxidase) and mitochondrial (uncouple protein 3) fatty acid oxidation. TSL-E also up-regulated cytoplasmic triacylglycerol hydrolysis gene (adipose triglyceride lipase) and genes related to fatty acid oxidation (AMP-activated protein kinase, acetyl-CoA carboxylase, carnitine palmitoyltransferase I, PPARγ, and adiponectin). The major constituents directly inducing PPARα transactivity in TSL-E are gallic acid, rutin, palmitic acid, linoleic acid, and α-linolenic acid. These results indicate that the inhibitory effect of TSL-E on lipid accumulation was through PPARα activation and further up-regulation of PPARα-mediated genes plus up-regulation of cytoplasmic genes involved in lipid catabolism.

KEYWORDS: *peroxisome proliferator-activated receptor alpha (PPARα), Toona sinensis Roem (T. sinensis), lipolysis*

INTRODUCTION

Dysregulation of lipid metabolism leading to lipid accumulation inside the body is a major risk factor for chronic diseases including diabetes, cardiovascular diseases, and hypertension.[1−4] To reduce the risk of these diseases, it is important to ameliorate the dysregulation of lipid metabolism to diminish deposition of extra fat.

Peroxisome proliferator-activated receptors (PPARs), PPARα, PPARδ, and PPARγ, a family of ligand-activated transcription factors, are involved in the regulation of glucose and lipid metabolism, inflammation, and cell differentiation.[5−8] Among these three nuclear receptors, PPARα predominantly expressed in metabolically active tissues including liver, heart, skeletal muscle, kidney, and brown adipose tissue[7,9] plays a central role in peroxisomal and mitochondrial fatty acid oxidation. The activation of PPARα up-regulates the transcription of target genes for fatty acid oxidation such as uncouple protein-1 (UCP1), carnitine palmitoyltransferase I (CPT-1), and acyl-CoA oxidase (ACO).[10,11] Most interestingly, recent studies indicate that the activation of PPARα enhances fatty acid oxidation in white adipose tissue and decreases the levels of circulating lipid profiles in obese diabetic patients.[12,13] Therefore, stimulating PPARα activity using PPARα agonist or herbal product-derived PPARα activator could modulate lipid catabolism in adipocytes.

TSL is extensively used as a vegetable in Asia and currently considered as a functional food. TSL improves health outcomes including antioxidant properties with effective protection for atherogenesis,[14] strong 2,2-diphenyl-1-picrylhydrazyl (DPPH) radical scavenging activities with inhibitory effects on lipid peroxidation,[15] against H_2O_2-induced oxidative stress, and DNA damage in epithelial Madin−Darby canine kidney (MDCK) cells,[16] anti-LDL glycative activity,[17] and improvement of learning and memory through the reduction of lipid peroxidation and β-amyloid plaques in the brains of senescence-accelerated mice.[18] In addition to a wide spectrum of health beneficial activities, TSL also significantly lowers plasma triacylglycerol levels and diminishes the size of visceral fat cells in high fat diet induced obese mice.[19] The precise mechanism underlying the lipid lowering effects of TSL through PPARα activation remains unclear. In the present study, differentiated 3T3-L1 adipocytes were used to investigate the molecular mechanism of the TSL ethanol extract (TSL-E) on PPARα mediated lipid metabolism. We hypothesized that TSL-E with lipid metabolism-modulating effects up-regulates genes associated with peroxisomal and mitochondrial fatty acid oxidation and cytoplasmic triglyceride hydrolysis. To test our hypothesis and elucidate the underlying mechanism of TSL-E on the regulation of lipid metabolism in 3T3-L1 adipocytes, we examined its effects on lipid accumulation, PPARα target gene expression, and PPARα transcriptional activation. Furthermore, high-performance liquid chromatography (HPLC) analysis was used to identify major constituents responsible for PPARα activation in TSL-E.

Received: February 12, 2014
Revised: May 28, 2014
Accepted: June 2, 2014
Published: June 2, 2014

ACS Publications © 2014 American Chemical Society

dx.doi.org/10.1021/jf500714c | J. Agric. Food Chem. 2014, 62, 5887−5896

MATERIALS AND METHODS

Preparation of TSL-E. The lyophilized extracts of TSL (1 g) purchased from the Taiwan Toona Biotech Corp. (Kaohsiung, Taiwan) were dissolved in 10 mL of ethanol (95%) and shaken at room temperature for 12 h. Crude extracts were collected from the supernatant and then concentrated by using a vacuum freeze-dryer. The TSL-E powder was collected and stored in the dark at room temperature for the following assays.

Cell Culture and Treatment. 3T3-L1 adipocytes (BCRC 60159) obtained from the Bioresource Collection and Research Center (Food Industry Research and Development Institute, Hsinchu, Taiwan) were grown in high-glucose DMEM (Gibco BRL, Rockville, MD, USA) supplemented with 10% bovine calf serum, 100 penicillin units/mL, and 100 μg/mL streptomycin (Hyclone, Logan, UT, USA) at 37 °C and 5% CO_2. When the cell density reached 100% confluence (day 0), adipocytes were grown in DMEM supplemented with 10% fetal bovine serum (FBS) (Biological Industries, Beit-Haemek, Israel), 10 μg/mL insulin (Humulin R, Lilly, Indianapolis, IN, USA), 1 μM dexamethasone (Sigma, St. Louis, MO, USA), and 0.5 mM isobutyl methyl xanthine (Sigma). After 4 days of differentiation (day 4), the medium was changed to DMEM with 10% FBS and 10 μg/mL insulin to induce lipid accumulation for a further 4 days (day 8). Unless noted otherwise, mature 3T3-L1 adipocytes with significant lipid accumulation were treated with dimethyl sulfoxide (DMSO) used as a control (Con) or other treatments dissolved in DMSO for an additional period of 4 days (days 8−12).

Oil Red O Staining. After an incubation period of 4 days (days 8−12), 3T3-L1 adipocytes were fixed with 10% formalin at room temperature for 10 min and then fixed with fresh 10% formalin for an additional 1 h. After fixation, cells were washed with 60% isopropanol and stained with Oil Red O (Sigma) at room temperature for 20 min. After staining, cells were washed four times with distilled water. Images were taken using a Nikon Eclipse TS100 inverted fluorescence microscope (Nikon Corp., Japan). After the image analysis, cells were lysed and dissolved in isopropanol (100%) and then harvested for lipid quantification.

Free Fatty acid (FFA) Quantification. Mature 3T3-L1 adipocytes with significant lipid accumulation (day 8) were treated with TSL-E (50 and 100 μg/mL) for 24 h (days 8 and 9). After 24 h of incubation, medium was collected. FFA concentrations were measured according to the manufacturer's instructions (BioVision, Milpitas, CA, USA).

Immunoblotting. After an incubation period of 4 days (days 8−12), 3T3-L1 adipocytes were sonicated for 10 s in ice-cold lysis buffer (20 mM Tris-HCl, 1 mM EDTA, 150 mM sodium chloride, 1 mM sodium orthovanadate, 1 mM sodium fluoride, 10 mM EDTA, 1% NP-40, 10 μg/mL aprotinin, 10 μg/mL leupeptin, and 2 mM PMSF), and the supernatant was obtained by centrifugation. Total protein in the supernatant was measured according to the BCA method (Bio-Rad, Hercules, CA, USA). An equal amount of protein (20−50 μg) for each preparation was added to an equal volume of 6× Laemmli sample buffer and separated using sodium dodecyl sulfate−polyacrylamide gel electrophoresis (SDS-PAGE). Protein was transferred on the PVDF membrane. The membrane was blocked with 5% nonfat dry milk in 0.1% Tween-Tris-buffered saline and then incubated in 5% dry milk Tween-Tris-buffered saline with PPARα, PPARγ (Santa Cruz Biotechnology, Dallas, TX, USA), adiponectin (Cell Signaling, Danvers, MA, USA), and β-actin (Novus Biologicals, Littleton, CO, USA) antibodies. β-Actin was used as loading control. Membranes were then washed and incubated with horseradish peroxidase-conjugated second antibody in Tween-Tris-buffered saline with 5% nonfat dry milk. Protein bands were visualized using a chemiluminescence kit (Millipore, Billerica, MA, USA), and densitometry analysis was performed using the LAS-4000 mini biomolecular imager (GE HealthCare Life Sciences, Pittsburgh, PA, USA).

RNA Extraction and Real-Time PCR. After an incubation period of 4 days (days 8−12), total RNA was isolated from all groups using a Trizol/chloroform procedure (Gibco BRL, Rockville, MD, USA). Total RNA concentration was quantified by the NanoDrop meter, and 1 μg of total RNA was reverse transcribed into cDNAs by using the kit (Invitrogen, Grand Island, NY, USA) according to the manufacturer's instructions. mRNA levels of PPARα, ACO, UCP3, CPT1, PPARγ, adiponectin, AMP-activated protein kinase (AMPK), acetyl-CoA carboxylase (ACC), and adipose triglyceride lipase (ATGL) in 3T3-L1 adipocytes were quantified using StepOnePlus real-time systems (Applied Biosystems, Foster City, CA, USA). Primer sequences are shown in the Supporting Information (Table 1). Real-time PCR was performed using a Fast Start SYBR Green master mix kit (Applied Biosystems). The PCR reaction included the following components: each primer at a concentration of 10 μM, diluted cDNA template, and Fast Start SYBR Green master mix and running 40 cycles. Each cDNA sample was run in triplicate, and GAPDH primers as an internal control were included in each run to correct sample-to-sample variation and to normalize mRNA levels. The relative mRNA level was calculated according to the comparative $\Delta\Delta$Ct method.

HPLC Analysis. Phytochemical compounds in TSL-E were analyzed by using an HPLC system consisting of a UV detector (Jasco UV157S, Jasco, Easton, MD, USA), an autosampler (Gilson 234, Gilson, Middleton, WI, USA), and a pump (Hitachi L-7100, Hitachi, Tokyo, Japan). Data were analyzed by chromatography EC2000 data system (Analab Corp., Taipei, Taiwan). The chromatography was performed on an Ascentis C18 column (250 mm × 4.6 mm i.d.). The mobile phase was a gradient prepared from (A) 100% methanol with 0.05% TFA and (B) 20% methanol with 0.05% TFA. A gradient was used as 0−9 min, 0−15% B; 9−12 min, 15% B; 12−17 min, 15−20% B; 17−35 min, 20−25% B; 35−55 min, 25−53% B; 55−65 min, 53% B. The flow rate was 1 mL/min at room temperature, and detection was performed at 280 nm.

To determine fatty acids in TSL-E, fatty acid was derivatized as described by Wood and Lee.[20] Fatty acid standards and TSL-E were converted to fatty acid *p*-bromophenacyl ester by reacting with α-bromoacetophenone and triethylamine. Bromophenacyl esters of fatty acids were used as standards for comparison of retention times to the derivatized TSL-E. Analytes were dissolved in a mixture of acetonitrile/acetone (1:1; v/v). The chromatographic elution was ACN + THF (99:1; v/v) at a flow rate of 1 mL/min. The injection volume was 20 μL, detection was at 258 nm, and all experiments were under room temperature. Calibration curves of fatty acids (palmitic acid, linoleic acid, α-linolenic acid; Sigma-Aldrich, St. Louis, MO, USA) and phytochemicals (gallic acid, catechin, methyl gallate, rutin, and quercetin; Sigma-Aldrich) were obtained by triplicate measurements on a single standard at increasing concentration.

Plasmids and Transfection Assay. The plasmids for PPARα-ligand binding domain (LBD) luciferase report assay, pBIND-PPARα-LBD and pG5luc-TK, were obtained from the Division of Biotechnology and Pharmaceutical Research, National Health Research Institutes, Taiwan.[21] HepG2 (human hepatocellular carcinoma cell line) cells were seeded (5×10^4 cells/well) in 12-well cell culture plates in DMEM supplemented with 10% FBS. After 24 h, transfections were performed using transfection reagent Lipofectamine 2000 (Life Technologies Corp., Carlsbad, CA, USA) according to the manufacturer's instruction. Cells were treated with bezafibrate, TSL-E, palmitic acid, linoleic acid, α-linolenic acid, gallic acid, methyl gallate, catechin, rutin, and quercetin for 24 h. Following treatment, cells were lysed, and firefly and renilla luciferase activities were measured using the Dual-Luciferase Reporter Assay System (Promega, Fitchburg, WI, USA). Bezafibrate was used as a positive control for PPARα activation. The results were expressed as fold difference compared to the Con group.

Statistical Analysis. Results are expressed as means ± standard error (SEM). When only the Con and TSL-E groups were involved, statistical analysis of the difference between the two groups was determined by using Student's *t* test (SigmaPlot 12.0). For multiple comparisons, one-way ANOVA was used to determine the statistical significance of the differences among the groups. ANOVA was followed by post hoc assessment by Student−Newman−Keuls method correction for multiple comparisons (SigmaPlot 12.0). A *P* value of <0.05 was considered to be statistically significant.

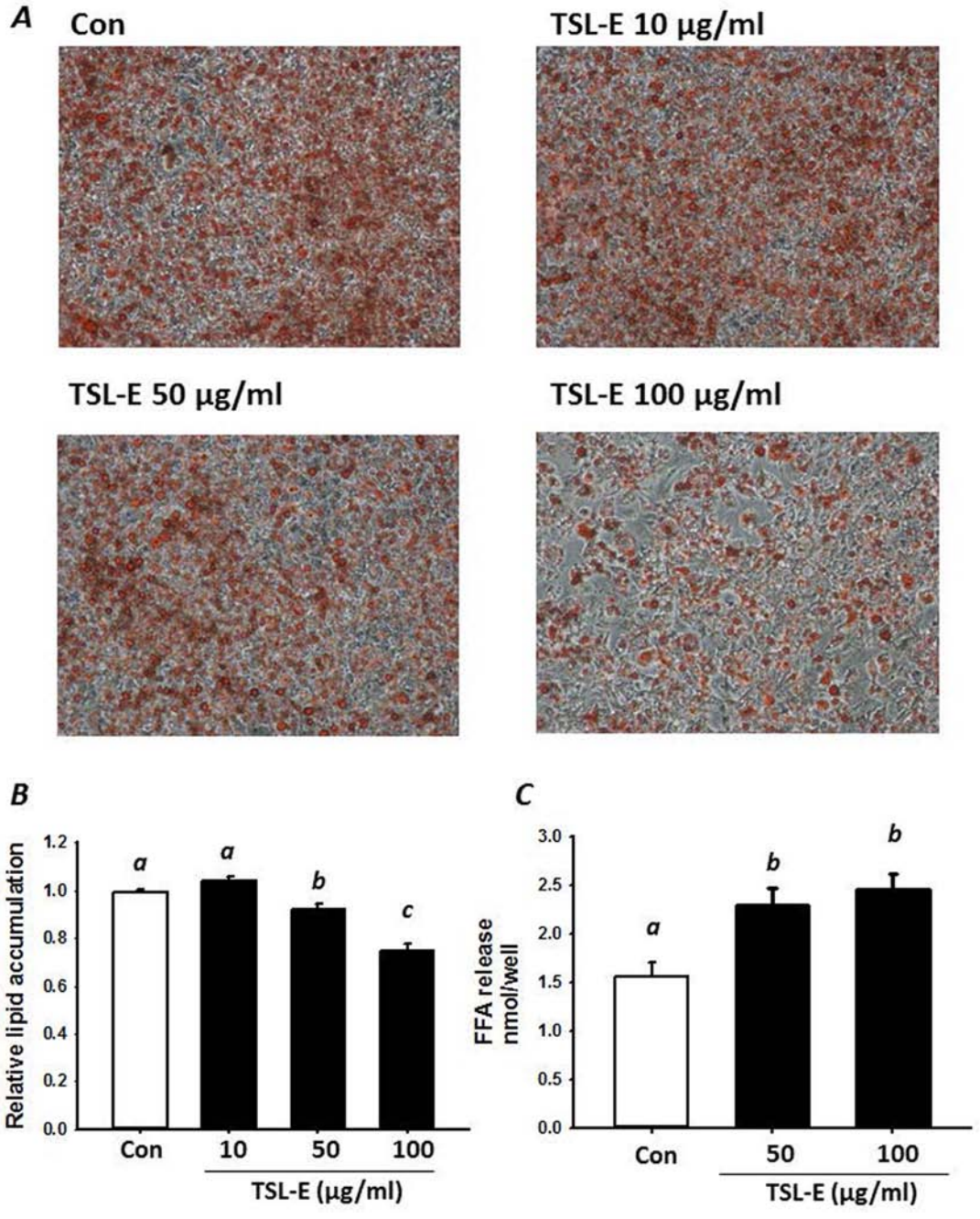

Figure 1. Lipid accumulation in mature 3T3-L1 adipocytes treated with TSL-E. Intracellular lipids were stained with Oil Red O (10× magnification) (A) and quantified (B) after treatment of TSL-E (10, 50, 100 μg/mL) or DMSO (Con) for 4 days (days 8−12). FFA were released in mature 3T3-L1 adipocytes treated with TSL-E (50, 100 μg/mL) or DMSO (Con) for 24 h (days 8−9) (C). Data represent the mean ± SE (n = 3, each in triplicate). Statistical analysis was performed using ANOVA followed by post hoc analysis using the Student−Newman−Keuls method. Significance ($P < 0.05$) among groups is denoted by different letters.

RESULTS

TSL-E Inhibits Lipid Accumulation and Stimulates FFA Release in 3T3-L1 Adipocytes. After 4 days of differentiation from preadipocytes into adipocytes (days 0−4) and 4 days of lipid accumulation (days 4−8), confluent cells were treated with TSL-E (0, 10, 50, and 100 μg/mL) for another 4 days (days 8−12). Oil Red O staining was performed to examine the content of lipid in mature 3T3-L1 adipocytes. As Figure 1B shows, there was no difference between a low concentration of TSL-E (10 μg/mL) and the Con group in lipid accumulation. Significantly lower lipid accumulation was observed at high concentrations of TSL-E extract (50 and 100 μg/mL) compared to the Con in mature 3T3-L1 adipocytes (Figure 1B). Release of FFA was significantly higher after 24 h of treatment of TSL-E (50 and 100 μg/mL) compared to the Con (Figure 1C).

TSL-E Up-regulates Protein and mRNA Expressions of Lipid Metabolism-Associated Genes in 3T3-L1 Adipocytes. To further understand the mechanisms underlying the inhibition of lipid accumulation by TSL-E, protein and mRNA from mature 3T3-L1 adipocytes were examined by Western blot and real-time PCR, respectively. A significant increase in

the protein expressions of PPARα and adiponectin was observed in mature 3T3-L1 adipocytes with TSL-E (100 μg/mL) compared to the Con group (Figure 2). Up-regulation of

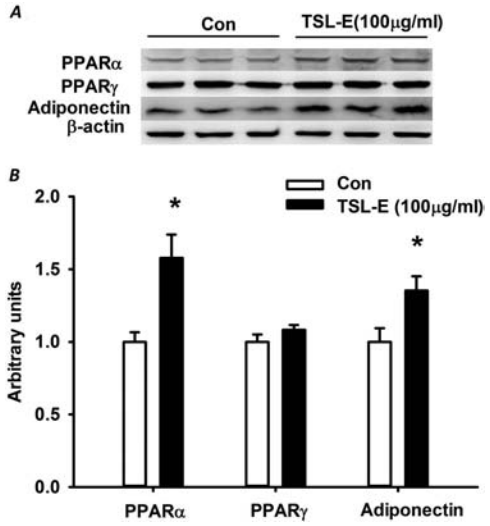

Figure 2. Protein expression in mature 3T3-L1 adipocytes treated with TSL-E for 4 days (days 8−12) and representative blots of three independent experiments (A). PPARα, PPARγ, and adiponectin relative levels were quantified by scanning densitometry of the bands (B). Results are expressed as means ± SE (n = 3/group). (*) $P < 0.05$.

PPARα gene expression was in parallel with protein expression after TSL-E treatment (Figure 3A). Other genes involved in peroxisomal (ACO) and mitochondrial (UCP3) fatty acid oxidation were significantly increased in mRNA levels after TSL-E treatment compared to the Con group in mature 3T3-L1 adipocytes. Moreover, the genes responsible for triacylglycerol hydrolysis (ATGL) and fatty acid oxidation related genes (CPT1, AMPK, and ACC) were significantly increased in mRNA levels after TSL-E treatment (Figure 3A,B). In addition to lipid catabolism, PPARγ and adiponectin involved in adipocyte differentiation and metabolism were also up-regulated by TSL-E (Figure 3C).

PPARα Antagonist GW6471 Attenuates the TSL-E-Induced Lipid Metabolism-Associated Gene Expression but Does Not Affect Lipid Accumulation in 3T3-L1 Adipocytes. To investigate whether the effect of TSL-E on inhibition of lipid accumulation is directly through the PPARα pathway, GW6471, a PPARα antagonist, was incubated with or without TSL-E in 3T3-L1 adipocytes (Figure 4). By using Oil Red O staining, a significant increase in lipid accumulation was observed in 3T3-L1 adipocytes incubated with GW6471 compared to the Con group. However, a marked decrease in lipid accumulation was observed in TSL-E and TSL-E + GW6471 compared to the Con, suggesting that TSL-E is not a specific agonist of PPARα.

With regard to lipid metabolism associated genes, as Figure 5 shows, no difference was observed between GW6471 and the Con group. GW6471 significantly attenuated TSL-E induced up-regulation of mRNA expression including PPARα (Figure 5A), CPT1, PPARγ, and adiponectin (Figure 5B). Furthermore, TSL-E mediated up-regulation of ACO, and UCP3 (downstream genes of PPARα) mRNA expression was completely inhibited by GW6471 (Figure 5A). Interestingly, TSL-E-mediated up-regulation of ATGL was not affected by GW6471 (Figure 5A).

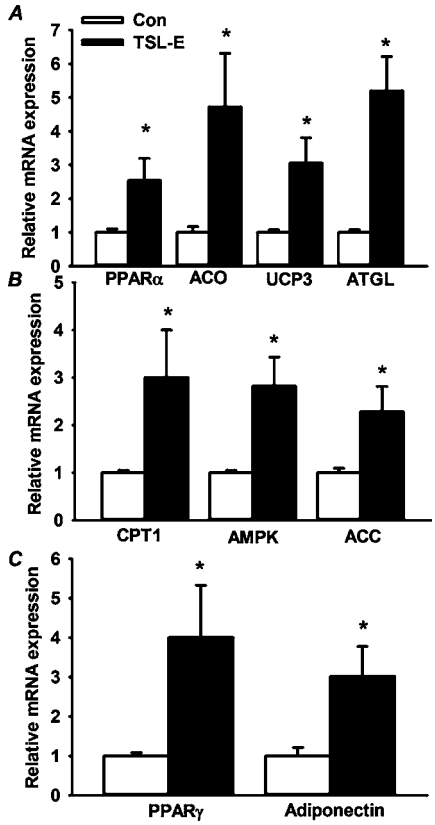

Figure 3. mRNA levels of lipid metabolism-associated genes in mature 3T3-L1 adipocytes treated with TSL-E for 4 days (days 8−12). mRNA levels of PPARα, ACO, UCP3, and ATGL (A), CPT1, AMPK, and ACC (B), and PPARγ and adiponectin (C) from the Con and TSL-E groups were determined by real-time PCR. mRNA levels are expressed as the mean ratio to control after normalization with GAPDH mRNA levels. Fold differences were calculated using the $\Delta\Delta$Ct method. Results are expressed as means ± SE (n = 3/group). (*) $P < 0.05$.

Phytochemicals and Fatty Acids in TSL-E Analyzed by HPLC. To identify active compounds in the TSL-E extract, major peaks (retention time) of TSL-E were observed at the same position as fatty acids and phytochemical standards (Figure 6). As compared to retention time and calibration at increasing concentrations of fatty acid standards, fatty acid compositions in TSL-E presented as a ratio of TSL-E were palmitic acid (2.1%), linoleic acid (2.1%), and α-linolenic acid (4.9%) identified in the present study (Figure 6A,B). In addition to various fatty acids, the identities of five phenolic compounds including gallic acid (4.1%), rutin (3.7%), catechin (0.6%), methyl gallate (0.5%), and quercetin (0.2%) were major phytochemicals in the TSL-E extract determined by comparison with standards (Figure 6C,D).

PPARα Luciferase Activity in TSL-E Extract, Polyphenols, and Fatty Acids. To investigate whether the induction of lipid metabolism associated genes in 3T3-L1 adipocytes by TSL-E resulted from a direct activation of PPARα, the PPARα ligand binding activity was examined by in vitro luciferase reporter assays. The results showed that TSL-E extract (50, 100, and 150 μg/mL) enhanced PPARα luciferase activity in a concentration-dependent manner (Figure 7A). To further examine whether fatty acids and phytochemicals in TSL-E act as bioactive ligands, PPARα luciferase activity in HepG2 cells transfected with PPARα reporter gene was also performed on palmitic acid, linoleic acid, α-linolenic acid, gallic

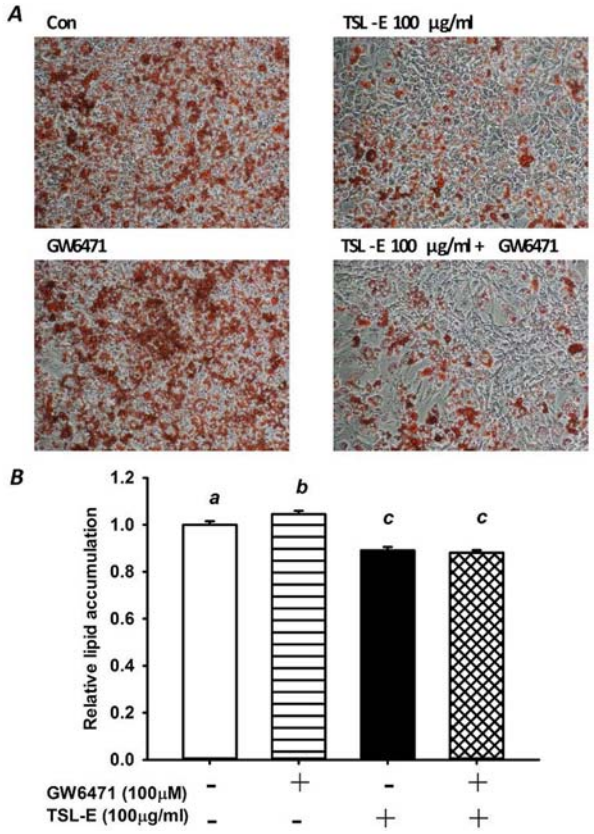

Figure 4. Lipid accumulation in mature 3T3-L1 adipocytes treated with or without PPARα antagonist GW6471 and TSL-E. Intracellular lipids were stained with Oil Red O (10× magnification) (A) and quantified (B) after treatment of DMSO-treated (Con), GW6471, TSL-E, and GW6471+TSL-E for 4 days (days 8−12). Data represent the mean ± SE (n = 3, each in triplicate). Statistical analysis was performed using ANOVA followed by post hoc analysis using the Student−Newman−Keuls method. Significance (P < 0.05) among groups is denoted by different letters.

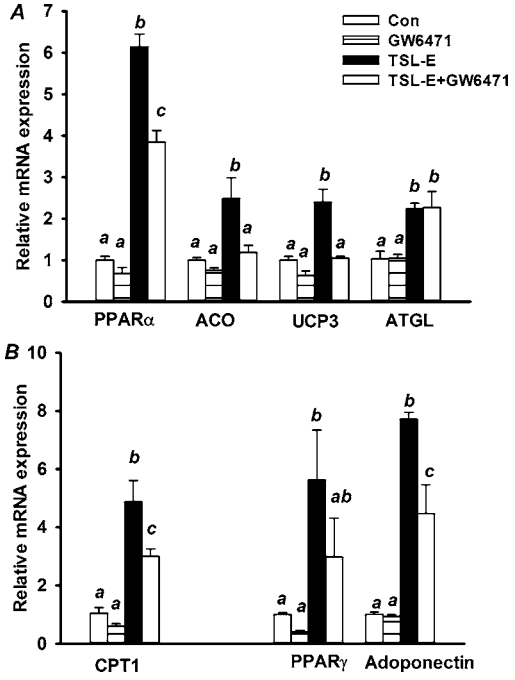

Figure 5. Lipid metabolism-associated genes in 3T3-L1 adipocytes treated with or without PPARα antagonist GW6471 and TSL-E for 4 days (days 8−12). mRNA levels of PPARα, ACO, UCP3, and ATGL (A) and CPT1, PPARγ, and adiponectin (B) from the Con, GW6471, TSL-E, and GW6471+TSL-E groups were determined by real-time PCR. mRNA levels are expressed as mean ratio to control after normalization with GAPDH mRNA levels. Fold differences were calculated using the ΔΔCt method. Results are expressed as means ± SE (n = 3, each in triplicate). Statistical analysis was performed using ANOVA followed by post hoc analysis using the Student−Newman−Keuls method. Significance (P < 0.05) among groups is denoted by different letters.

acid, methyl gallate, catechin, rutin, and quercetin in the present study. The concentration of each fatty acid as well as phytochemical used in PPARα luciferase activity was a ratio of TSL-E extract (150 μg/mL) based on HPLC analysis. Bezafibrate (an agonist for PPARα) was used as a positive control for PPARα activation. Transactivities of PPARα induced by palmitic acid, linoleic acid, α-linolenic acid, and bezafibrate (100 μM) were 1.7-, 1.9-, 2.5-, and 5.0-fold, respectively (Figure 7B). PPARα luciferase activity was significantly increased upon stimulation by palmitic acid, linoleic acid, and α-linolenic acid compared to the Con group. Among major phytochemicals in TSL-E, only gallic acid (1.4-fold) and rutin (1.14-fold) significantly enhanced PPARα luciferase activity compared to the Con group (Figure 7C).

DISCUSSION

The important finding of this study is that TSL-E is beneficial in suppressing lipid accumulation through activation of the PPARα pathway and up-regulation of genes involved in fatty acid oxidation in 3T3-L1 adipocytes. Fibrate drugs, the synthetic PPARα agonists commonly used to treat dyslipidemia,[22] have revealed potential adverse effects including elevated creatinine[23,24] and homocysteine levels,[25] which are biomarkers for renal disease and cardiovascular disease, respectively. Although the long-term effects of fibrates on these diseases require further examination, finding new PPAR modulators from natural products such as TSL-E with lower adverse effects is encouraged.

Results from a previous study indicate that PPARα is involved in the regulation of lipid metabolism through a ligand-dependent transcriptional activation of genes related to fatty acid oxidation.[26] PPARα agonists such as GW647 are known to up-regulate lipid regulatory genes including ACO (the rate-limiting enzyme for peroxisomal fatty acid oxidation) and CPT (the rate-limiting enzyme of mitochondrial fatty acid oxidation) in L6 myocytes.[27] A novel function of UCP2 is involved in mitochondrial fatty acid oxidation,[28] and hepatic UCP2 mRNA expression was up-regulated by using PPARα agonist, WY14643, in rodents.[12,29] In addition to liver and muscle, highly active metabolic tissues, recent studies demonstrated that PPARα was also expressed in white adipose tissue of humans and rodents.[12,26,30] Stimulating fatty acid oxidation through activation of PPARα in 3T3-L1 and human adipocytes[13,31] suggests that white adipose tissue is a potential pharmacological target for PPARα agonists to regulate lipid metabolism and whole body energy balance. TSL-E stimulated fatty acid oxidation through up-regulation of PPARα expression in protein and mRNA levels, leading to decreased lipid accumulation. ACO and UCP, PPARα downstream target genes, were up-regulated by TSL-E in mature 3T3-L1 adipocytes. The effect of TSL-E in augmented gene expression

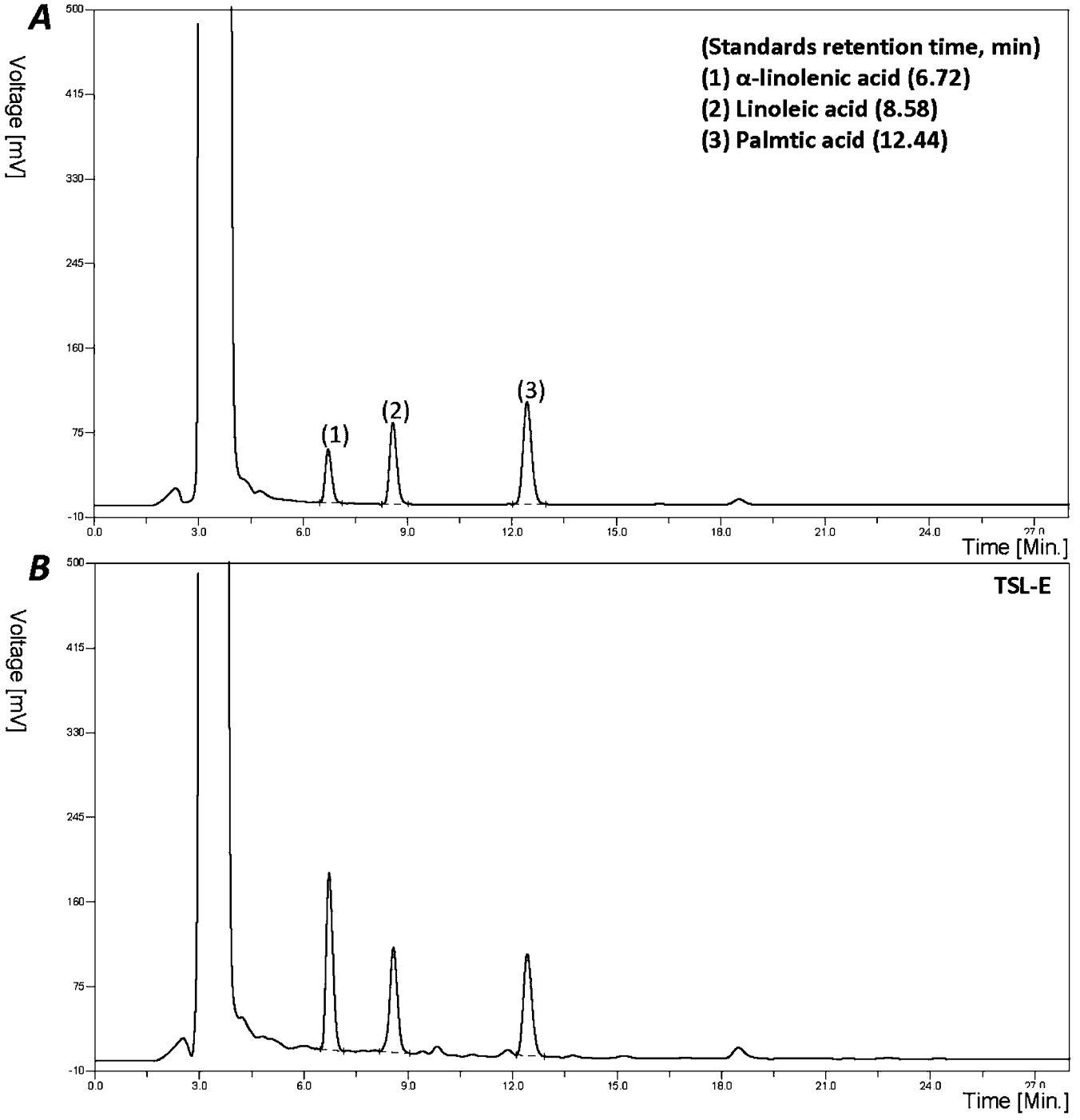

Figure 6. continued

dx.doi.org/10.1021/jf500714c | J. Agric. Food Chem. 2014, 62, 5887−5896

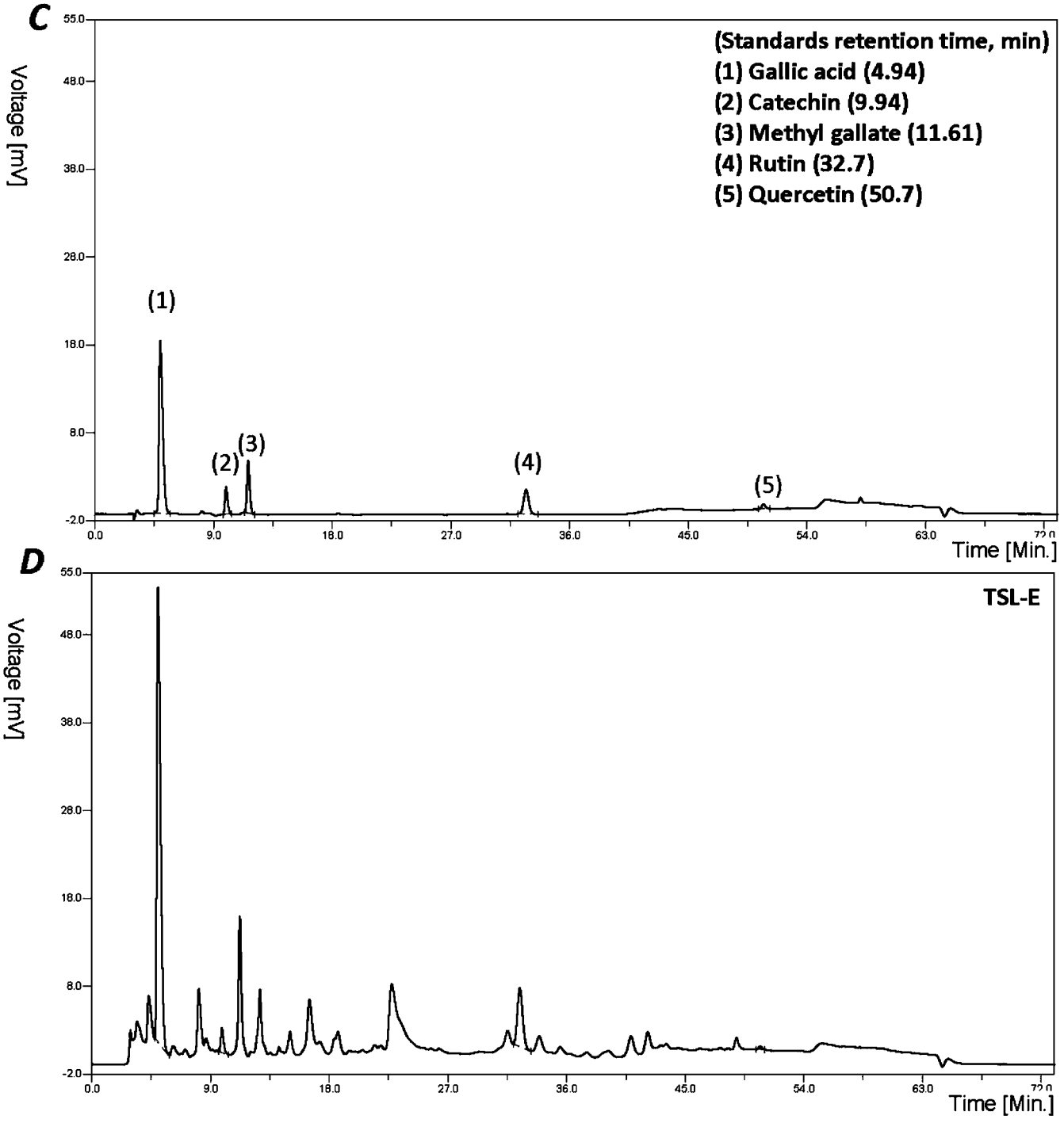

Figure 6. Diagram of the compounds in the TSL-E extracts analyzed using HPLC: chromatogram of TSL-E (B, D) as compared with a mixture of fatty acids standard (A) and phytochemical standards (C).

in adipocytes, particularly those involved in fatty acid β-oxidation such as ACO and CPT1, is similar to that of GW7647, a specific PPARα agonist.[13] The effect of TSL-E on lowering triacylglycerol content and increasing release of FFA via up-regulated ATGL mRNA expression (the key enzyme for the breakdown of triacylglycerol) was observed in the present study and an earlier report on 3T3-L1 cells.[32] Taken together, TSL-E promotes lipolysis through initiation of triacylglycerol hydrolysis into nonesterified fatty acid, followed by breakdown of fatty acids into acetyl-CoA by β-oxidation in adipocytes.

It is noteworthy that TSL-E not only up-regulates PPARα but also promotes PPARγ mRNA expression in this study. Unlike a small amount of PPARα expressed in fat cells, PPARγ is expressed predominantly in adipose tissue, with lower levels in liver and muscle. Activation of PPARγ is recognized to promote adipocyte differentiation.[33] Adipocyte differentiation induced by PPARγ activation increases the number of fat cells with a smaller average size, which are insulin-sensitive adipocytes.[33] As a result, an increase in adiponectin mRNA expression, a downstream target gene of PPARγ, was observed in 3T3-L1 cells treated with TSL-E, whereas a PPARγ agonist,

dx.doi.org/10.1021/jf500714c | J. Agric. Food Chem. 2014, 62, 5887−5896

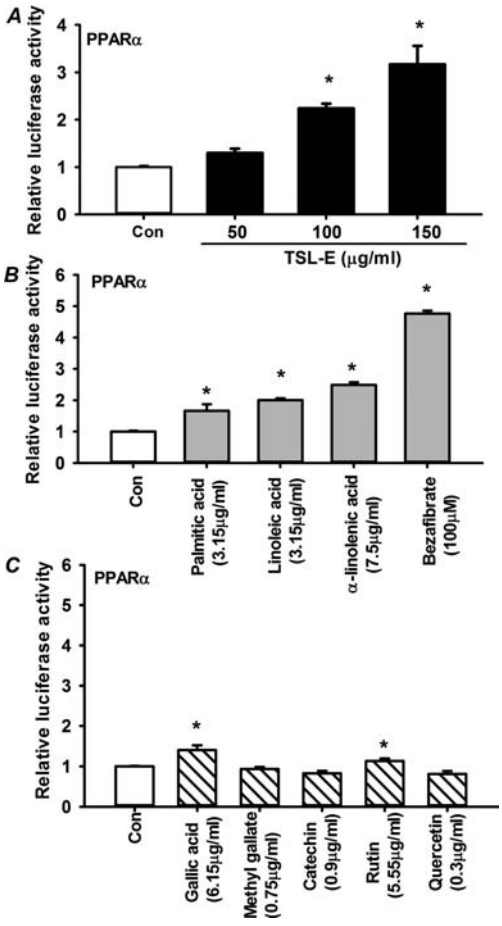

Figure 7. PPARα luciferase activity in HepG2 cells treated with TSL-E (A), various fatty acids (B), and phytochemicals (C) for 24 h. Results are expressed as means ± SE (n = 3, each in triplicate). Statistical analysis was performed using ANOVA followed by post hoc analysis using the Student−Newman−Keuls method. (*) $P < 0.05$ compared with Con.

thiazolidinedione, promotes small adipocyte differentiation, thereby preventing adipocyte hypertrophy.[34] It is generally accepted that there is an increased secretion of adiponectin from small adipocytes via the PPARγ pathway. Interestingly, synthetic PPARα agonists such as fenofibrate and bezafibrate have been reported to up-regulate adiponectin mRNA expression through PPARα activation in 3T3-L1 adipocytes.[26] Because adiponectin acts as an antidiabetic and antiatherosclerotic molecule,[35] such beneficial effects could be achieved by TSL-E-induced stimulation of adiponectin gene expression in adipocytes. In fact, antidiabetic property and normalized plasma adiponectin levels by TSL were observed in high fat diet induced obese mice.[19] Collectively, results from the present study suggest that PPARα as well as PPARγ is involved in the regulation of adipocyte differentiation by inducing PPARs pathways through TSL-E. Thus, the efficacy of TSL-E on adiponectin up-regulation mediated by PPARα/γ activation is a potential antidiabetic property.

Up-regulated gene expression of the AMPK/ACC pathway was also observed in 3T3-L1 cells treated with TSL-E in this study. The phosphorylation of AMPK on serine and threonine residues, a functional form of AMPK, was not determined in the present study. However, a previous study indicated that troglitazone, a PPARγ agonist, stimulated AMPK activation in the epididymal fat of rats.[36] In addition, direct AMPK activation by adiponectin was reported in 3T3-L1 adipocytes.[37] It is speculated that AMPK activation by TSL-E in 3T3-L1 adipocytes is through enhanced adiponectin expression and/or PPARs activation. Consequently, TSL-E plays an important role in the inhibition of anabolic pathways such as fatty acid, glycogen, and cholesterol synthesis and stimulation of catabolic pathways such as fatty acid oxidation and glycolysis in 3T3-L1 adipocytes.

To further elucidate whether TSL-E-mediated lipid catabolism is through the PPARα pathway or not, 3T3-L1 cells were treated with GW6471 (a PPARα antagonist), TSL-E, and the combination of GW6471 and TSL-E. Inhibition of lipid accumulation by TSL-E was not prevented by GW6471. In agreement with this result, GW6471 attenuated TSL-E-mediated lipid metabolism associated gene expression including PPARα, ACO, UCP, and CPT1. Interestingly, augmentation of ATGL mRNA expression mediated by TSL-E was not affected by GW6471, suggesting that TSL-E-mediated ATGL expression is not in a PPARα-dependent manner. As a result, the inhibitory effect of TSL-E on decreased lipid accumulation not only depends on activation of the PPARα pathway but also constantly promotes hydrolysis of triglycerides.

Because PPARα activation by TSL-E contributed to decreased lipid accumulation in adipocytes, active compounds responsible for PPARα activation were identified by HPLC analysis in TSL-E and indicated that palmitic acid, linoleic acid, α-linolenic acid, gallic acid, methyl gallate, catechin, rutin, and quercetin were the active fatty acids and phytochemicals in TSL-E extracts responsible for PPARα activation. It has been recognized that polyunsaturated fatty acids of 18−20 carbon groups consisting mainly of linoleic acid, α-linolenic acid, γ-linolenic acid, and arachidonic acid strongly induce PPARα transactivity.[38] Here we demonstrated that palmitic acid, linoleic acid, and α-linolenic acid in the TSL-E extract were the major active fatty acids to induce PPARα transactivity. Among the main five phytochemicals, only gallic acid and rutin act as PPARα agonists in vitro. It has been reported that rutin suppresses oleic acid induced lipid accumulation by up-regulating PPARα protein expression in hepatocarcinoma cells.[39] Similarly, gallic acid also effectively prevents lipid accumulation in the liver[40,41] and adipose tissue[40] from rodents fed a high-fat diet. Our results demonstrated that TSL-E-suppressed lipid accumulation was attributed to, at least in part, direct stimulation of PPARα activation by major constituents including long-chain fatty acids, gallic acid, and rutin. Taken together, an increase in adipose β-oxidation induced by TSL-E was the result of directly improved fatty acid oxidation enzymes at the PPARα-dependent transcriptional level.

In conclusion, activation of PPARα by TSL-E leading to the inhibition of lipid accumulation in mature 3T3-L1 adipocytes is due to attenuation of lipid accumulation by TSL-E on the regulation of systemic energy expenditure by the induction of molecules involved in fatty acid oxidation in adipocytes. Ultimately, results of this study are beneficial in the development of TSL-E as an antilipid accumulation agent for the prevention of obesity and obesity-related diseases.

■ ASSOCIATED CONTENT

Ⓢ Supporting Information

Table of primers for real-time PCR analysis. This material is available free of charge via the Internet at http://pubs.acs.org.

AUTHOR INFORMATION

Corresponding Author

*(S.-J.C.) Department of Life Sciences, National Cheng Kung University, No. 1 University Road, Tainan, Taiwan. E-mail: sjchang@mail.ncku.edu.tw. Fax: +886-6-2742583. Phone: +886-6-2757575, ext. 65542.

Funding

This work was supported by a grant from the National Science Council, Taiwan (NSC 97-2320-B006-028 and NSC 102-2120-S006-008).

Notes

The authors declare no competing financial interest.

ABBREVIATIONS USED

ACC, acetyl-CoA carboxylase; ACO, acyl-CoA oxidase; AMPK, AMP-activated protein kinase; ATGL, adipose triglyceride lipase; CTP-1, carnitine palmitoyltransferase I; FFA, free fatty acid; PPARs, peroxisome proliferator-activated receptors; TSL, *Toona sinensis* leaf; TSL-E, TSL ethanol extract; UCP1, uncouple protein-1

REFERENCES

(1) Reilly, M. P.; Rader, D. J. The metabolic syndrome: more than the sum of its parts? *Circulation* **2003**, *108*, 1546−1551.

(2) Miranda, P. J.; DeFronzo, R. A.; Califf, R. M.; Guyton, J. R. Metabolic syndrome: definition, pathophysiology, and mechanisms. *Am. Heart J.* **2005**, *149*, 33−45.

(3) Kahn, B. B.; Flier, J. S. Obesity and insulin resistance. *J. Clin. Invest.* **2000**, *106*, 473−481.

(4) Ginsberg, H. N. Insulin resistance and cardiovascular disease. *J. Clin. Invest.* **2000**, *106*, 453−458.

(5) Escher, P.; Wahli, W. Peroxisome proliferator-activated receptors: insight into multiple cellular functions. *Mutat. Res.* **2000**, *448*, 121−138.

(6) Desvergne, B.; Wahli, W. Peroxisome proliferator-activated receptors: nuclear control of metabolism. *Endocrine Rev.* **1999**, *20*, 649−688.

(7) Chinetti, G.; Fruchart, J. C.; Staels, B. Peroxisome proliferator-activated receptors (PPARs): nuclear receptors at the crossroads between lipid metabolism and inflammation. *Inflamm. Res.: Off. J. Eur. Histamine Res. Soc.* **2000**, *49*, 497−505.

(8) Duval, C.; Chinetti, G.; Trottein, F.; Fruchart, J. C.; Staels, B. The role of PPARs in atherosclerosis. *Trends Mol. Med.* **2002**, *8*, 422−430.

(9) Mandard, S.; Muller, M.; Kersten, S. Peroxisome proliferator-activated receptor alpha target genes. *Cell. Mol. Life Sci. (CMLS)* **2004**, *61*, 393−416.

(10) Tugwood, J. D.; Issemann, I.; Anderson, R. G.; Bundell, K. R.; McPheat, W. L.; Green, S. The mouse peroxisome proliferator activated receptor recognizes a response element in the 5′ flanking sequence of the rat acyl CoA oxidase gene. *EMBO J.* **1992**, *11*, 433−439.

(11) Roepstorff, C.; Halberg, N.; Hillig, T.; Saha, A. K.; Ruderman, N. B.; Wojtaszewski, J. F.; Richter, E. A.; Kiens, B. Malonyl-CoA and carnitine in regulation of fat oxidation in human skeletal muscle during exercise. *Am. J. Physiol.: Endocrinol. Metab.* **2005**, *288*, E133−E142.

(12) Tsuchida, A.; Yamauchi, T.; Takekawa, S.; Hada, Y.; Ito, Y.; Maki, T.; Kadowaki, T. Peroxisome proliferator-activated receptor (PPAR)alpha activation increases adiponectin receptors and reduces obesity-related inflammation in adipose tissue: comparison of activation of PPARalpha, PPARgamma, and their combination. *Diabetes* **2005**, *54*, 3358−3370.

(13) Goto, T.; Lee, J. Y.; Teraminami, A.; Kim, Y. I.; Hirai, S.; Uemura, T.; Inoue, H.; Takahashi, N.; Kawada, T. Activation of peroxisome proliferator-activated receptor-alpha stimulates both differentiation and fatty acid oxidation in adipocytes. *J. Lipid Res.* **2011**, *52*, 873−884.

(14) Hseu, Y. C.; Chang, W. H.; Chen, C. S.; Liao, J. W.; Huang, C. J.; Lu, F. J.; Chia, Y. C.; Hsu, H. K.; Wu, J. J.; Yang, H. L. Antioxidant activities of *Toona dinensis* leaves extracts using different antioxidant models. *Food Chem. Toxicol.* **2008**, *46*, 105−114.

(15) Cho, E. J.; Yokozawa, T.; Rhyu, D. Y.; Kim, H. Y.; Shibahara, N.; Park, J. C. The inhibitory effects of 12 medicinal plants and their component compounds on lipid peroxidation. *Am. J. Chinese Med.* **2003**, *31*, 907−917.

(16) Hsieh, T. J.; Liu, T. Z.; Chia, Y. C.; Chern, C. L.; Lu, F. J.; Chuang, M. C.; Mau, S. Y.; Chen, S. H.; Syu, Y. H.; Chen, C. H. Protective effect of methyl gallate from *Toona sinensis* (Meliaceae) against hydrogen peroxide-induced oxidative stress and DNA damage in MDCK cells. *Food Chem. Toxicol.* **2004**, *42*, 843−850.

(17) Hsieh, C. L.; Lin, Y. C.; Ko, W. S.; Peng, C. H.; Huang, C. N.; Peng, R. Y. Inhibitory effect of some selected nutraceutic herbs on LDL glycation induced by glucose and glyoxal. *J. Ethnopharmacol.* **2005**, *102*, 357−363.

(18) Liao, J. W.; Hsu, C. K.; Wang, M. F.; Hsu, W. M.; Chan, Y. C. Beneficial effect of *Toona sinensis* Roemor on improving cognitive performance and brain degeneration in senescence-accelerated mice. *Br. J. Nutr.* **2006**, *96*, 400−407.

(19) Hsieh, T. J.; Tsai, Y. H.; Liao, M. C.; Du, Y. C.; Lien, P. J.; Sun, C. C.; Chang, F. R.; Wu, Y. C. Anti-diabetic properties of non-polar *Toona sinensis* Roem extract prepared by supercritical-CO_2 fluid. *Food Chem. Toxicol.* **2012**, *50*, 779−789.

(20) Wood, R.; Lee, T. High-performance liquid chromatography of fatty acids: quantitative analysis of saturated, monoenoic, polyenoic and geometrical isomers. *J. Chromatogr., A* **1983**, *254*, 237−246.

(21) Chou, Y. C.; Prakash, E.; Huang, C. F.; Lien, T. W.; Chen, X.; Su, I. J.; Chao, Y. S.; Hsieh, H. P.; Hsu, J. T. Bioassay-guided purification and identification of PPARalpha/gamma agonists from *Chlorella sorokiniana*. *Phytother. Res.* **2008**, *22*, 605−613.

(22) Lefebvre, P.; Chinetti, G.; Fruchart, J. C.; Staels, B. Sorting out the roles of PPAR alpha in energy metabolism and vascular homeostasis. *J. Clin. Invest.* **2006**, *116*, 571−580.

(23) Hottelart, C.; el Esper, N.; Achard, J. M.; Pruna, A.; Fournier, A. [Fenofibrate increases blood creatinine, but does not change the glomerular filtration rate in patients with mild renal insufficiency]. *Nephrologie* **1999**, *20*, 41−44.

(24) Jun, M.; Zhu, B.; Tonelli, M.; Jardine, M. J.; Patel, A.; Neal, B.; Liyanage, T.; Keech, A.; Cass, A.; Perkovic, V. Effects of fibrates in kidney disease: a systematic review and meta-analysis. *J. Am. Coll. Cardiol.* **2012**, *60*, 2061−2071.

(25) Lever, M.; George, P. M.; Slow, S.; Elmslie, J. L.; Scott, R. S.; Richards, A. M.; Fink, J. N.; Chambers, S. T. Fibrates may cause an abnormal urinary betaine loss which is associated with elevations in plasma homocysteine. *Cardiovasc. Drugs Ther.* **2009**, *23*, 395−401.

(26) Hiuge, A.; Tenenbaum, A.; Maeda, N.; Benderly, M.; Kumada, M.; Fisman, E. Z.; Tanne, D.; Matas, Z.; Hibuse, T.; Fujita, K.; Nishizawa, H.; Adler, Y.; Motro, M.; Kihara, S.; Shimomura, I.; Behar, S.; Funahashi, T. Effects of peroxisome proliferator-activated receptor ligands, bezafibrate and fenofibrate, on adiponectin level. *Arterioscler. Thromb. Vasc. Biol.* **2007**, *27*, 635−641.

(27) Muoio, D. M.; MacLean, P. S.; Lang, D. B.; Li, S.; Houmard, J. A.; Way, J. M.; Winegar, D. A.; Corton, J. C.; Dohm, G. L.; Kraus, W. E. Fatty acid homeostasis and induction of lipid regulatory genes in skeletal muscles of peroxisome proliferator-activated receptor (PPAR) alpha knock-out mice. Evidence for compensatory regulation by PPAR delta. *J. Biol. Chem.* **2002**, *277*, 26089−26097.

(28) Pecqueur, C.; Bui, T.; Gelly, C.; Hauchard, J.; Barbot, C.; Bouillaud, F.; Ricquier, D.; Miroux, B.; Thompson, C. B. Uncoupling protein-2 controls proliferation by promoting fatty acid oxidation and limiting glycolysis-derived pyruvate utilization. *FASEB J.* **2008**, *22*, 9−18.

(29) Kelly, L. J.; Vicario, P. P.; Thompson, G. M.; Candelore, M. R.; Doebber, T. W.; Ventre, J.; Wu, M. S.; Meurer, R.; Forrest, M. J.; Conner, M. W.; Cascieri, M. A.; Möller, D. E. Peroxisome proliferator-activated receptors gamma and alpha mediate in vivo regulation of

uncoupling protein (UCP-1, UCP-2, UCP-3) gene expression. *Endocrinology* **1998**, *139*, 4920−4927.
(30) Loviscach, M.; Rehman, N.; Carter, L.; Mudaliar, S.; Mohadeen, P.; Ciaraldi, T. P.; Veerkamp, J. H.; Henry, R. R. Distribution of peroxisome proliferator-activated receptors (PPARs) in human skeletal muscle and adipose tissue: relation to insulin action. *Diabetologia* **2000**, *43*, 304−311.
(31) Lee, J. Y.; Hashizaki, H.; Goto, T.; Sakamoto, T.; Takahashi, N.; Kawada, T. Activation of peroxisome proliferator-activated receptor-alpha enhances fatty acid oxidation in human adipocytes. *Biochem. Biophys. Res. Commun.* **2011**, *407*, 818−822.
(32) Lasa, A.; Schweiger, M.; Kotzbeck, P.; Churruca, I.; Simon, E.; Zechner, R.; Portillo, M. P. Resveratrol regulates lipolysis via adipose triglyceride lipase. *J. Nutr. Biochem.* **2012**, *23*, 379−384.
(33) Spiegelman, B. M. PPAR-gamma: adipogenic regulator and thiazolidinedione receptor. *Diabetes* **1998**, *47*, 507−514.
(34) Yamauchi, T.; Kamon, J.; Waki, H.; Murakami, K.; Motojima, K.; Komeda, K.; Ide, T.; Kubota, N.; Terauchi, Y.; Tobe, K.; Miki, H.; Tsuchida, A.; Akanuma, Y.; Nagai, R.; Kimura, S.; Kadowaki, T. The mechanisms by which both heterozygous peroxisome proliferator-activated receptor gamma (PPARgamma) deficiency and PPARgamma agonist improve insulin resistance. *J. Biol. Chem.* **2001**, *276*, 41245−41254.
(35) Matsuzawa, Y. Therapy insight: adipocytokines in metabolic syndrome and related cardiovascular disease. *Nat. Clin. Pract. Cardiovasc. Med.* **2006**, *3*, 35−42.
(36) LeBrasseur, N. K.; Kelly, M.; Tsao, T. S.; Farmer, S. R.; Saha, A. K.; Ruderman, N. B.; Tomas, E. Thiazolidinediones can rapidly activate AMP-activated protein kinase in mammalian tissues. *Am. J. Physiol.: Endocrinol. Metab.* **2006**, *291*, E175−E181.
(37) Liu, Q.; Gauthier, M. S.; Sun, L.; Ruderman, N.; Lodish, H. Activation of AMP-activated protein kinase signaling pathway by adiponectin and insulin in mouse adipocytes: requirement of acyl-CoA synthetases FATP1 and Acsl1 and association with an elevation in AMP/ATP ratio. *FASEB J.* **2010**, *24*, 4229−4239.
(38) Mochizuki, K.; Suzuki, T.; Goda, T. PPAR alpha and PPAR delta transactivity and p300 binding activity induced by arachidonic acid in colorectal cancer cell line Caco-2. *J. Nutr. Sci. Vitaminol. (Tokyo)* **2008**, *54*, 298−302.
(39) Wu, C. H.; Lin, M. C.; Wang, H. C.; Yang, M. Y.; Jou, M. J.; Wang, C. J. Rutin inhibits oleic acid induced lipid accumulation via reducing lipogenesis and oxidative stress in hepatocarcinoma cells. *J. Food Sci.* **2011**, *76*, T65−T72.
(40) Jang, A.; Srinivasan, P.; Lee, N. Y.; Song, H. P.; Lee, J. W.; Lee, M.; Jo, C. Comparison of hypolipidemic activity of synthetic gallic acid-linoleic acid ester with mixture of gallic acid and linoleic acid, gallic acid, and linoleic acid on high-fat diet induced obesity in C57BL/6 Cr Slc mice. *Chem.−Biol. Interact.* **2008**, *174*, 109−117.
(41) Hsu, C. L.; Yen, G. C. Effect of gallic acid on high fat diet-induced dyslipidaemia, hepatosteatosis and oxidative stress in rats. *Br. J. Nutr.* **2007**, *98*, 727−735.

JOURNAL OF AGRICULTURAL AND FOOD CHEMISTRY

Article

pubs.acs.org/JAFC

Garlic Essential Oil Protects against Obesity-Triggered Nonalcoholic Fatty Liver Disease through Modulation of Lipid Metabolism and Oxidative Stress

Yi-Syuan Lai,[†] Wei-Cheng Chen,[†] Chi-Tang Ho,[†,§] Kuan-Hung Lu,[†] Shih-Hang Lin,[†] Hui-Chun Tseng,[†] Shuw-Yuan Lin,*[,∥] and Lee-Yan Sheen*[,†,‡,#]

[†]Institute of Food Science and Technology, National Taiwan University, Taipei 10617, Taiwan

[§]Department of Food Science, Rutgers University, New Brunswick, New Jersey 08901, United States

[‡]National Center for Food Safety Education and Research, National Taiwan University, Taipei 10617, Taiwan

[#]Center for Food and Biomolecules, National Taiwan University, Taipei 10617, Taiwan

[∥]Department of Nutrition, Hung-Kuang University, Taichung 43302, Taiwan

ABSTRACT: This study investigated the protective properties of garlic essential oil (GEO) and its major organosulfur component (diallyl disulfide, DADS) against the development of nonalcoholic fatty liver disease (NAFLD). C57BL/6J mice were fed a normal or high-fat diet (HFD) with/without GEO (25, 50, and 100 mg/kg) or DADS (10 and 20 mg/kg) for 12 weeks. GEO and DADS dose-dependently exerted antiobesity and antihyperlipidemic effects by reducing HFD-induced body weight gain, adipose tissue weight, and serum biochemical parameters. Administration of 50 and 100 mg/kg GEO and 20 mg/kg DADS significantly decreased the release of pro-inflammatory cytokines in liver, accompanied by elevated antioxidant capacity via inhibition of cytochrome P450 2E1 expression during NAFLD development. The anti-NAFLD effects of GEO and DADS were mediated through down-regulation of sterol regulatory element binding protein-1c, acetyl-CoA carboxylase, fatty acid synthase, and 3-hydroxy-3-methylglutaryl-coenzyme A reductase, as well as stimulation of peroxisome proliferator-activated receptor α and carnitine palmitoyltransferase-1. These results demonstrate that GEO and DADS dose-dependently protected obese mice with long-term HFD-induced NAFLD from lipid accumulation, inflammation, and oxidative damage by ameliorating lipid metabolic disorders and oxidative stress. The dose of 20 mg/kg DADS was equally as effective in preventing NAFLD as 50 mg/kg GEO containing the same amount of DADS, which demonstrates that DADS may be the main bioactive component in GEO.

KEYWORDS: *garlic essential oil, diallyl disulfide, nonalcoholic fatty liver disease, lipid metabolism, oxidative stress*

INTRODUCTION

Nonalcoholic fatty liver disease (NAFLD) is regarded as the hepatic manifestation of the metabolic syndrome and represents the major cause of liver-related morbidity and mortality with an increased prevalence of hyperlipidemia, obesity, insulin resistance, and diabetes mellitus.[1] Along with rising numbers of patients with metabolic syndrome, the increase in the prevalence of NAFLD directly correlates with the obesity epidemic. NAFLD is defined as fat accumulation in the liver exceeding 5% by weight in the absence of excessive alcohol consumption (<20 g per day).[2] It comprises a spectrum of liver diseases ranging from steatosis to nonalcoholic steatohepatitis (NASH), which can progress to fibrosis, cirrhosis, and hepatocellular carcinoma.[3]

The initiation and progression of NAFLD is primarily attributed to imbalanced lipid metabolism and insulin resistance that induce the accumulation of triglycerides (TG) in hepatocytes, leading to the development of NASH in combination with oxidative stress, inflammation, and hepatic injury.[4] However, no specific or conventional treatment for NAFLD is available; thus, current research focuses on the molecular mechanisms underlying the development of NAFLD.[5] Numerous studies have characterized the effects of sterol regulatory element-binding proteins (SREBPs) or peroxisome proliferator-activated receptor alpha (PPARα)-dependent pathways on lipogenesis and lipolysis in hepatic lipid metabolism.[6] SREBPs regulate the expression of lipogenic enzymes such as acetyl-CoA carboxylase (ACC), fatty acid synthase (FAS), and 3-hydroxy-3-methylglutaryl-coenzyme A reductase (HMGCR).[7] On the other hand, PPARα has been reported to be involved in fatty acid oxidation and to regulate the expression of carnitine palmitoyltransferase-1 (CPT-1), which catalyzes the rate-limiting step in fatty acid β-oxidation.[8] In addition, mounting evidence suggests that hepatic cytochrome P450 2E1 (CYP2E1) is a critical regulator of oxidative stress, inflammatory cytokines, and gut-derived endotoxins in the pathogenesis of NASH.[9] Therefore, it could act as a marker of oxidative stress associated with hepatic injury.

Garlic (*Allium sativum* L.) is a widely consumed traditional food and has various medicinal properties. Recent research has focused on the benefits of a variety of organosulfur compounds (OSCs) in garlic, which include water-soluble sulfur-containing compounds (*S*-allylcysteine (SAC), *S*-allylmercaptocysteine (SAMC), *S*-methylcysteine, and γ-glutamylcysteine derivatives) and oil-soluble sulfur-containing compounds (diallyl sulfide (DAS),

Received: February 15, 2014
Revised: April 21, 2014
Accepted: May 23, 2014
Published: May 23, 2014

ACS Publications © 2014 American Chemical Society

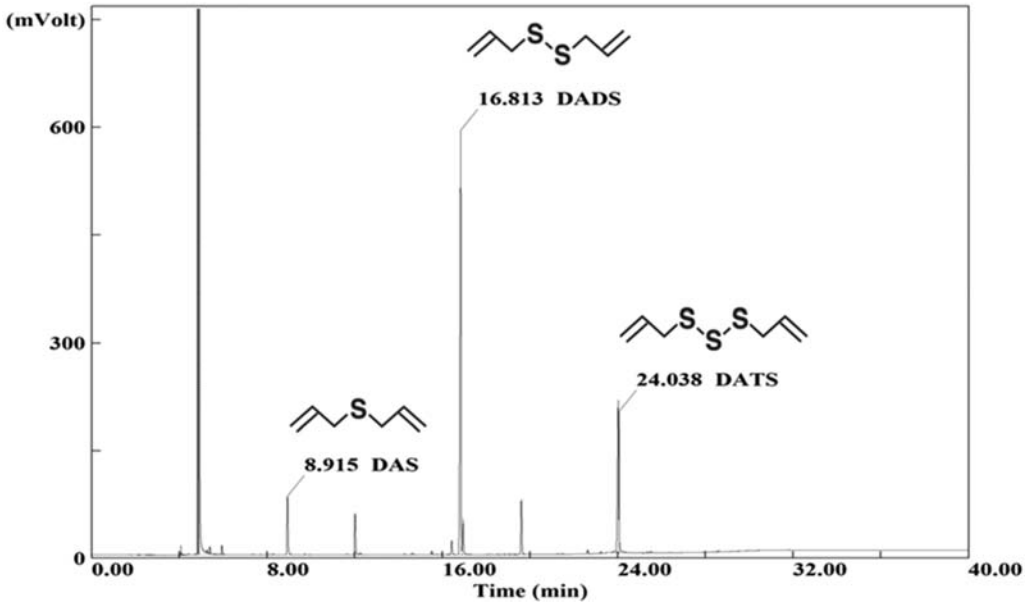

Figure 1. GC chromatogram of GEO. Retention times and chemical structures of the three major components present in GEO are shown. GC, gas chromatography; GEO, garlic essential oil; DAS, diallyl sulfide; DADS, diallyl disulfide; DATS, diallyl trisulfide.

diallyl disulfide (DADS), diallyl trisulfide (DATS), allyl methyl trisulfide, vinyldithiins, and ajoene).[10,11] The biological benefits of garlic include antioxidant,[12] antimicrobial,[13] antihyperlipidemic,[14] antiobesity,[15] hepatoprotective,[16] and anticancer effects.[17] Garlic essential oil (GEO) is a commercial garlic product obtained from crushed garlic by steam distillation or organic solvent extraction. GEO has been reported to contain more than 30 OSCs, and DAS, DADS, and DATS have been identified as the three major components.[11] Previous studies have indicated that GEO exhibits beneficial effects on acute ethanol-induced fatty liver and high-fat diet (HFD)-induced liver injury based on elevating the antioxidant and detoxification system.[18−20] However, the protective effects and underlying mechanisms of GEO on NAFLD have not been explored.

The present study evaluated the protective potential of GEO and its major organosulfur component (DADS) against lipid accumulation during the development of NAFLD in a mouse model of long-term HFD-induced obesity. We aimed to investigate the dose-dependent effects of GEO and DADS in a well-established animal model of NAFLD and to explore the possible role in preventing the development of NAFLD. We further identify the underlying molecular mechanisms involved in the hepatic lipid metabolism via SREBP-1c or PPARα-dependent pathways and oxidative liver injury through CYP2E1 expression. This study provides possibilities for new applications of GEO and DADS as functional food ingredients.

MATERIALS AND METHODS

Preparation and Chemical Analysis of GEO. Garlic (*A. sativum* L.) was obtained from the Yunlin County Farmers' Association (Yunlin, Taiwan). Extraction of GEO was performed according to the procedure of Sheen et al.[21] Briefly, garlic was stirred with 2 volumes of distilled water and extracted by steam distillation for 4 h. Volatile extracts were then dehydrated to obtain GEO and stored at −20 °C until use. The yield of the GEO from fresh garlic was 0.30 ± 0.05% (w/w), calculated according to the mean fresh weight of garlic used in each extraction procedure. The three major components in GEO, DAS, DADS, and DATS, were determined using a gas chromatograph (GC, Thermo Scientific Focus GC) equipped with an AI 3000 II autosampler, a flame ionization detector, and a Stabilwax (Crossbond Carbowax-PEG, Restek) capillary column (60 m × 0.32 mm, 1.0 μm thick film). The GC settings were as follows: initial column temperature, 50 °C, increased at 5 °C/min to 200 °C and held for 10 min; injector temperature, 200 °C; and detector temperature, 200 °C. Samples (1 μL, diluted 1:100 in acetone) were injected, with a split ratio of 80:1 and nitrogen as carrier gas (30 mL/min flow rate). Calibration curves were constructed with reference standards and used to determine the concentrations of DAS, DADS, and DATS in GEO. DAS (purity = 97%) and DADS (purity 80%) were purchased from Sigma-Aldrich Corp. (St. Louis, MO, USA). DATS (purity > 95%) was purchased from ChromaDex Inc. (Santa Ana, CA, USA). As shown in the GEO chromatogram (Figure 1), the three major components of GEO, DADS (40.7%), DATS (21.6%), and DAS (6.7%) accounted for 69.0% of the total oil. This result is similar to previous studies demonstrating that DADS is the major organosulfur compound in GEO.[18,22] Therefore, DADS was selected for comparison with GEO in the present study.

Animal Experiments. The protocol for the animal experiments was approved by the Institutional Animal Care and Use Committee (IACUC) of the National Taiwan University (IACUC approval no. NTU-101-EL-124). The protocol complied with guidelines described in the Animal Protection Law, amended on June 29, 2011, Hua-Zong-(1)-Yi-Tzi-10000136211, Council of Agriculture, Taiwan. Six-week-old male C57BL/6J mice were purchased from the Animal Center of the College of Medicine, National Taiwan University (Taipei, Taiwan). All mice were housed under controlled temperature (23 ± 2 °C), relative humidity (50−70%), and a 12 h light/12 h dark cycle in the animal house facility. The animals were allowed to acclimatize for 2 weeks prior to the experiments. Mice were randomly assigned to groups of 10 animals each. Animals in the control group were fed a normal diet (13.5% kcal from fat, Laboratory Rodent Diet 5001, Lab Diet/PMI Nutrition International, Purina Mills LLC, Gray Summit, MO, USA); those in the negative control group and treatment groups were fed an HFD (60% kcal from fat, D12492, Research Diets, Inc., New Brunswick, NJ, USA) for 12 weeks to develop NAFLD. Mice of the treatment groups were administered either GEO (25, 50, or 100 mg/kg) or DADS (10 or 20 mg/kg) by daily oral gavage. GEO or DADS was mixed with 0.1 mL of olive oil before administration to the mice. Animals of the control and HFD groups received the same amount of olive oil. All mice had free access to food and water at all times. Body weight and food intake for each mouse were recorded weekly throughout the study. At the end of the experiment, animals were fasted overnight and sacrificed by CO_2 asphyxiation.

Serum Biochemical Analysis. Blood was obtained by cardiac puncture and centrifuged at 1000*g* for 10 min at 4 °C to obtain serum samples. The levels of aspartate aminotransferase (AST), alanine aminotransferase (ALT), total cholesterol (TC), and TG were measured in serum using an automatic chemistry analyzer (SPOTCHEM EZ SP-4430, ARKRAY, Inc., Kyoto, Japan). Serum levels of free fatty acids (FFA; BioVision, San Francisco, CA, USA) and insulin (Mercodia AB, Uppsala, Sweden) were determined using commercial kits according to the manufacturers' instructions.

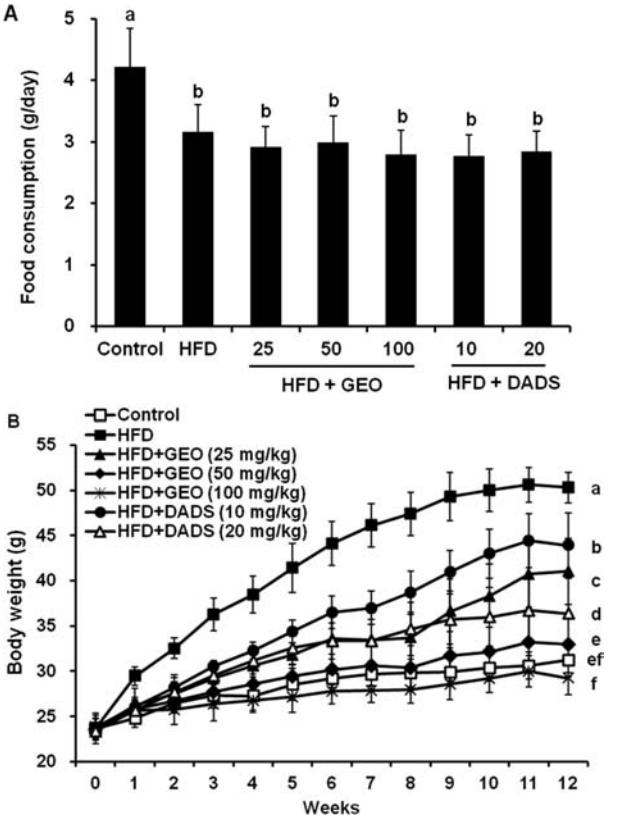

Figure 2. Effects of GEO and DADS on food consumption and body weight in C57BL/6J mice fed an HFD: (A) food intake and (B) body weight in mice fed a normal diet or HFD with/without GEO (25, 50, and 100 mg/kg) or DADS (10 and 20 mg/kg) administration by daily oral gavage for 12 weeks. Data are presented as the mean ± SD (n = 10 mice per group). Statistical analysis was performed using one-way ANOVA and Duncan's multiple-comparison test. Different letters indicate significant differences among groups at the level of $p < 0.05$ (letters are shown in panel B for the 12th week). HFD, high-fat diet; GEO, garlic essential oil; DADS, diallyl disulfide.

Histopathological Examination. Liver and fat pads (subcutaneous, epididymal, and perirenal fat) were collected, weighed, and photographed. A portion of the liver (the biggest lobe) was fixed overnight in 10% neutral-buffered formalin and then embedded in paraffin. Paraffin-embedded sections of liver tissue (5 μm) were stained with hematoxylin and eosin (H&E) to evaluate the morphological changes and assigned scores as an indicator of the degree of fatty liver by a pathologist. The extent of the lesions was graded from 1 to 5 according to severity: 1 = minimal (<1%); 2 = slight (1−25%); 3 = moderate (26−50%); 4 = moderate/severe (51−75%); 5 = severe/high (76−100%). Another portion of the liver was frozen-fixed in OCT mounting media (Sakura, Torrance, CA, USA), whereas the remaining part of the liver was immediately frozen at −80 °C for further investigations. Frozen sections of liver tissue (10 μm) were stained with Oil Red O (Muto Pure Chemicals Co., Ltd., Tokyo, Japan) to detect lipid droplets.

Liver Enzyme and Inflammatory Cytokines. Liver tissues (300 mg) were homogenized with 3 mL of cold homogenization buffer (8 mM KH_2PO_4, 12 mM K_2HPO_4, and 1.5% KCl, pH 7.4) and then centrifuged at 10000*g* for 30 min at 4 °C. The homogenate was stored at −80 °C for the following experiments. The total protein concentration of each sample was estimated with a Bio-Rad protein assay (Hercules, CA, USA) by using bovine serum albumin (BSA) as a standard and measuring the absorbance at 595 nm. The levels of hepatic TG, TC, and glutathione (GSH) and activities of glutathione peroxidase (GPx), glutathione reductase (GRd), glutathione *S*-transferase (GST), catalase (CAT), and superoxide dismutase (SOD) were assayed using commercial kits from Cayman Chemical Co. (Ann Arbor, MI, USA). Lipid peroxidation was evaluated by using a thiobarbituric acid-reactive substances (TBARS) assay kit obtained from Cayman Chemical Co. The levels of tumor necrosis factor-α (TNF-α), interleukin-1β (IL-1β), and interleukin-6 (IL-6) in liver were quantified by immunoassay kits from eBioscience Inc. (San Diego, CA, USA) according to the manufacturer's protocols.

Western Blot Analysis. Proteins from liver tissues (100 mg) were extracted with 1 mL of cold lysis buffer (7 M urea, 2 M thiourea, 2% CHAPS, 0.002% bromophenol blue, 60 mM DTT, and a protease and phosphatase inhibitor cocktail). All mixtures were then disrupted in an ice−water bath with an ultrasonic cell crusher for 5 min and then centrifuged at 17500*g* for 30 min at 4 °C. Total proteins of the supernatants (whole tissue extracts) were measured using the Bio-Rad protein assay. The protein samples were mixed with 5× sample buffer (62.5 mM Tris-HCl, 10% glycerol, 2% SDS, and 0.01% bromophenol blue) and boiled at 95 °C for 10 min.

Equal amounts of each protein sample were separated by SDS−polyacrylamide gel electrophoresis (SDS-PAGE) and electrotransferred to polyvinylidene difluoride (PVDF) membranes (Millipore Corp., Bedford, MA, USA). Membranes were blocked with a blocking solution containing 5% BSA or skim milk powder in TBST buffer (20 mM Tris-base, 150 mM NaCl, 0.05% Tween 20) for 2 h and rinsed three times with TBST buffer for 5 min each. Incubation with the primary antibody was performed overnight at 4 °C. After washing, the membranes were incubated with the horseradish peroxidase

Table 1. Effects of GEO and DADS Supplementation on Adipose Tissue Weight in Mice Fed an HFD[a]

group	total fat (g)	relative total fat (%)	subcutaneous fat (g)	epididymal fat (g)	perirenal fat (g)
control	0.78 ± 0.17 f	2.51 ± 0.57 d	0.25 ± 0.07 f	0.40 ± 0.08 d	0.13 ± 0.05 e
HFD	6.86 ± 0.85 a	13.63 ± 1.61 a	3.56 ± 0.65 a	2.01 ± 0.27 a	1.29 ± 0.25 a
HFD + GEO (25 mg/kg)	4.63 ± 0.86 c	11.22 ± 1.27 b	1.98 ± 0.49 c	1.84 ± 0.30 a	0.81 ± 0.12 b
HFD + GEO (50 mg/kg)	3.27 ± 0.95 d	9.92 ± 1.70 b	1.35 ± 0.49 de	1.36 ± 0.33 b	0.56 ± 0.15 c
HFD + GEO (100 mg/kg)	2.14 ± 0.55 e	7.27 ± 1.52 c	0.84 ± 0.22 e	0.94 ± 0.26 c	0.36 ± 0.10 d
HFD + DADS (10 mg/kg)	5.57 ± 0.98 b	12.66 ± 1.62 a	2.63 ± 0.73 b	2.04 ± 0.32 a	0.90 ± 0.12 b
HFD + DADS (20 mg/kg)	3.77 ± 0.97 d	10.23 ± 1.74 b	1.65 ± 0.48 cd	1.49 ± 0.37 b	0.63 ± 0.17 c

[a]C57BL/6 mice were fed a normal diet or HFD with/without GEO (25, 50, and 100 mg/kg) or DADS (10 and 20 mg/kg) administration by daily oral gavage for 12 weeks. The relative total fat is expressed as percentage of body weight (total fat/final body weight × 100). Data are presented as the mean ± SD (n = 10 mice per group). Statistical analysis was performed using one-way ANOVA and Duncan's multiple-comparison test. Different letters indicate significant differences among groups at the level of $p < 0.05$. HFD, high-fat diet; GEO, garlic essential oil; DADS, diallyl disulfide.

Table 2. Effects of GEO and DADS on Serum Biochemical Parameters in HFD-Fed Mice[a]

group	glucose (mg/dL)	insulin (ng/mL)	FFA (nmol/μL)	triglyceride (mg/dL)	total cholesterol (mg/dL)
control	210.58 ± 20.28 e	0.81 ± 0.29 b	0.78 ± 0.26 e	80.80 ± 7.35 c	86.00 ± 12.51 e
HFD	286.00 ± 17.62 a	2.07 ± 0.55 a	1.95 ± 0.33 a	113.25 ± 12.81 a	221.10 ± 18.12 a
HFD + GEO (25 mg/kg)	235.82 ± 20.74 bc	1.81 ± 0.43 a	1.45 ± 0.29 b	106.60 ± 13.51 ab	173.58 ± 15.69 c
HFD + GEO (50 mg/kg)	223.60 ± 31.21 cde	0.89 ± 0.27 b	1.07 ± 0.14 c	95.90 ± 11.05 b	139.33 ± 10.89 d
HFD + GEO (100 mg/kg)	213.00 ± 21.84 de	0.76 ± 0.48 b	0.89 ± 0.20 d	79.00 ± 14.94 c	130.00 ± 7.22 d
HFD + DADS (10 mg/kg)	252.45 ± 23.13 b	1.98 ± 0.33 a	1.63 ± 0.35 b	112.80 ± 11.16 a	206.33 ± 13.03 b
HFD + DADS (20 mg/kg)	232.50 ± 24.38 bcd	1.00 ± 0.25 b	1.19 ± 0.32 c	100.67 ± 12.26 b	154.42 ± 20.41 c

[a]C57BL/6J mice were fed a normal diet or HFD with/without GEO (25, 50, and 100 mg/kg) or DADS (10 and 20 mg/kg) administration by daily oral gavage for 12 weeks. Data are presented as the mean ± SD (n = 10 mice per group). Statistical analysis was performed using one-way ANOVA and Duncan's multiple-comparison test. Different letters indicate significant differences among groups at the level of $p < 0.05$. HFD, high-fat diet; GEO, garlic essential oil; DADS, diallyl disulfide; FFA, free fatty acid.

(HRP)-conjugated secondary antibody (GeneTex, San Antonio, TX, USA) at room temperature for 1 h and then washed again. Antibodies against SREBP-1c, FAS, ACC, HMGCR, PPARα, and CYP2E1 were purchased from GeneTex. The antibody against CPT-1 was obtained from Cell Signaling Technology Inc. (Beverly, MA, USA). The protein bands were finally visualized with enhanced chemiluminescence (ECL, PerkinElmer Life Sciences, Boston, MA, USA) and captured with a UVP BioSpectrum AC image system (UVP, Upland, CA, USA). Protein expression was quantified by densitometry using ImageJ software version 1.47 (NIH, Bethesda, MD, USA). The relative density of each individual protein band was normalized to that of the β-actin band and the results from three repeated and independent experiments.

Statistical Analysis. All data are expressed as the mean ± SD. Statistical comparisons among experimental groups were analyzed by one-way ANOVA and Duncan's multiple-comparison test using the SPSS software program (SPSS Inc., Chicago, IL, USA). p values <0.05 were considered statistically significant.

RESULTS

Body Weight, Food Consumption, and Adipose Tissue Weight. C57BL/6J mice were fed a normal diet or HFD (60% kcal from fat) for 12 weeks with treatment of GEO or DADS. Food intake and body weight were measured every week. As shown in Figure 2A, there was no significant difference among the diet groups with regard to food consumption; however, higher food intake during the study was noted in the control group. The average daily calorie intake of the HFD and treatment groups was 15.3 kcal, whereas that of mice fed the normal diet was 12.7 kcal. After 12 weeks, the average body weight of mice fed an HFD noticeably increased to 50.29 g from an initial weight of 23.67 g, whereas that of mice in the control group increased only to 31.23 g (Figure 2B). Daily oral administration of GEO or DADS significantly reduced the rate of body weight gain in mice, and the final average body weights of the groups treated with 25, 50, or 100 mg/kg GEO and 10 or 20 mg/kg DADS were 41.05, 32.95, 29.25, 43.92, and 36.38 g, respectively. The average body weight of mice treated with 100 mg/kg GEO was lower than that of mice in the control group, but the difference was not significant. Moreover, HFD-induced increase in the amount of subcutaneous, epididymal, and perirenal fat pads was significantly suppressed by GEO and DADS treatment in a dose-dependent manner (Table 1). Noticeably, treatment of 50 mg/kg GEO or 20 mg/kg DADS exerted a similar inhibitory effect on adipose tissue weight in mice fed an HFD for 12 weeks.

Serum Biochemical Analysis. As shown in Table 2, HFD significantly increased the serum levels of glucose, insulin, FFA, TG, and TC compared to the control group. Administration of GEO and DADS markedly suppressed the increase in the levels

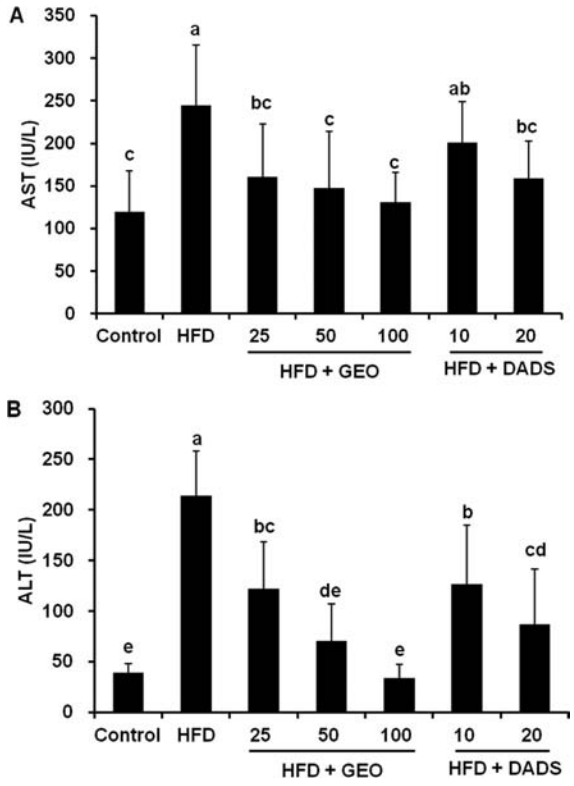

Figure 3. Effects of GEO and DADS supplement on serum AST and ALT levels in HFD-fed mice: serum levels of (A) AST and (B) ALT in C57BL/6J mice fed a normal diet or HFD with/without GEO (25, 50, and 100 mg/kg) or DADS (10 and 20 mg/kg) administration by daily oral gavage for 12 weeks. Data are presented as the mean ± SD (n = 10 mice per group). Statistical analysis was performed using one-way ANOVA and Duncan's multiple-comparison test. Different letters indicate significant differences among groups at the level of $p < 0.05$. HFD, high-fat diet; GEO, garlic essential oil; DADS, diallyl disulfide; AST, aspartate aminotransferase; ALT, alanine aminotransferase.

of serum biochemical markers in a dose-dependent manner. Treatment of 50 mg/kg GEO and 20 mg/kg DADS similarly reduced the elevated levels of glucose, insulin, FFA, and TG in HFD-fed mice. In addition, after 12 weeks of HFD, the serum levels of AST and ALT significantly increased by 2.0- and 5.5-fold, respectively (Figure 3). Supplementation of 25, 50, and 100 mg/kg of GEO resulted in the reduction of the serum AST levels by 34.1, 39.1, and 46.4%, respectively. Similarly, the serum ALT levels in mice treated with 25, 50, and 100 mg/kg GEO were decreased by 43.0, 67.1, and 84.2%, respectively.

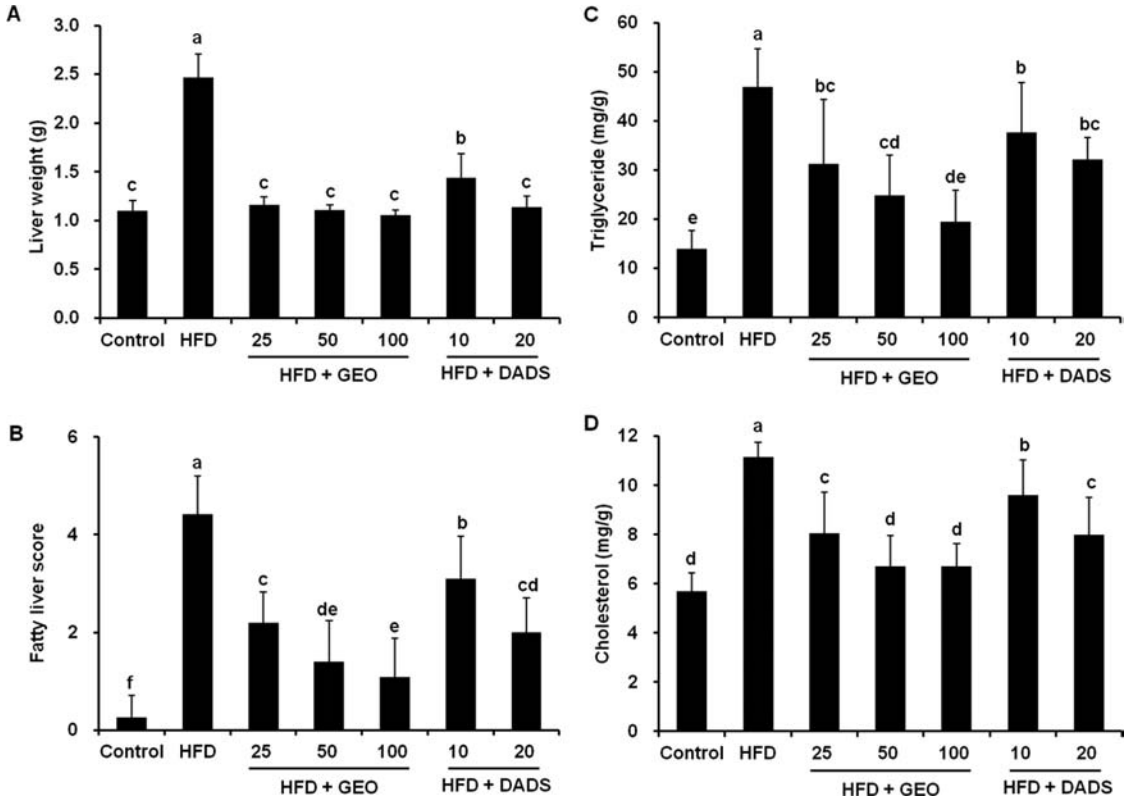

Figure 4. Effects of GEO and DADS on hepatic lipid content in HFD-fed mice: (A) liver weight, (B) fatty liver score, (C) hepatic triglyceride, and (D) total cholesterol in C57BL/6J mice fed a normal diet or HFD with/without GEO (25, 50, and 100 mg/kg) or DADS (10 and 20 mg/kg) administration by daily oral gavage for 12 weeks. Data are presented as the mean ± SD (n = 10 mice per group). Statistical analysis was performed using one-way ANOVA and Duncan's multiple-comparison test. Different letters indicate significant differences among groups at the level of $p < 0.05$. HFD, high-fat diet; GEO, garlic essential oil; DADS, diallyl disulfide.

The reduction of the serum AST and ALT levels by DADS treatment was similar to that observed for GEO treatment.

Hepatic Steatosis and Histopathological Analysis. Figure 4A shows that the average liver weight of HFD-fed mice was 2.2-fold higher than that of mice in the control group. Supplementation of GEO or DADS significantly suppressed the HFD-induced increase in liver weight. Hepatic lipid accumulation was further evaluated by H&E and Oil Red O staining. As shown in Figure 5, HFD-induced accumulation of lipid vacuoles and lipid droplets in mice liver was dramatically reduced by GEO and DADS treatments. Fatty liver scores were assessed in H&E-stained sections by morphometric analysis, which evidenced that the fatty infiltration with macrovesicles of hepatocytes was graded moderate/severe in the HFD-induced group (4.42), moderate in the 10 mg/kg DADS group (3.10), slight in the 20 mg/kg DADS group (2.00) and 25 mg/kg GEO group (2.20), and minimal in the 50 mg/kg GEO group (1.40) and 100 mg/kg GEO group (1.08) (Figure 4B). Similarly, the levels of hepatic TC and TG were significantly increased in HFD-fed mice and decreased dose-dependently by GEO or DADS treatment (Figure 4C,D).

Hepatic Oxidative Stress and Inflammation. Malondialdehyde (MDA) is a reactive aldehyde formed during lipid peroxidation. As shown in Table 3, the MDA levels in mice fed a normal diet and HFD were 3.15 and 4.60 nmol/mg protein, respectively. The MDA levels in mice fed HFD containing 25, 50, or 100 mg/kg GEO and 10 or 20 mg/kg DADS were 4.00, 3.36, 3.35, 4.37, and 3.63 nmol/mg protein, respectively, indicating that lipid peroxidation was attenuated by GEO treatment. The hepatic GSH level in HFD-treated mice was decreased by 29.0% compared to that of the control group, whereas treatment with 25, 50, or 100 mg/kg GEO and 10 or 20 mg/kg DADS resulted in increases in the hepatic GSH level by 17.7, 39.2, 47.7, 6.2, and 39.4%, respectively. In addition, 12 weeks of HFD feeding was accompanied by 16.7−49.5% inhibition of hepatic GPx, GRd, CAT, SOD, and GST activities compared to mice in the control group. The effect of HFD on the activities of these antioxidant enzymes was dose-dependently reversed by administration of GEO and DADS. Moreover, HFD induced a significant increase in the levels of TNF-α, IL-1β, and IL-6 in mouse livers, whereas the levels of these pro-inflammatory cytokines were also dose-dependently attenuated by GEO and DADS treatment. Furthermore, DADS at a dosage of 20 mg/kg, which is comparable to 50 mg/kg GEO, significantly reversed HFD-induced oxidative stress and inflammation after 12 weeks of treatment.

Hepatic Lipid Metabolism and Oxidative Stress. We further examined the effects of GEO or DADS administration on several representative hepatic proteins expression related to lipid metabolism and oxidative stress modulation by Western blotting. The expression of proteins involved in fatty acid synthesis in the liver are shown in Figure 6A−C; expression levels of SREPB-1c and its targets FAS and ACC in HFD-fed mice were 1.9-, 1.9-, and 2.4-fold higher than that in the control group, respectively. When compared to those of the mice in the HFD-fed group, the levels of SREPB-1c, FAS, and ACC were significantly down-regulated by GEO and DADS treatments in a dose-related manner. Figure 6D also shows that HFD-induced

dx.doi.org/10.1021/jf500803c | J. Agric. Food Chem. 2014, 62, 5897−5906

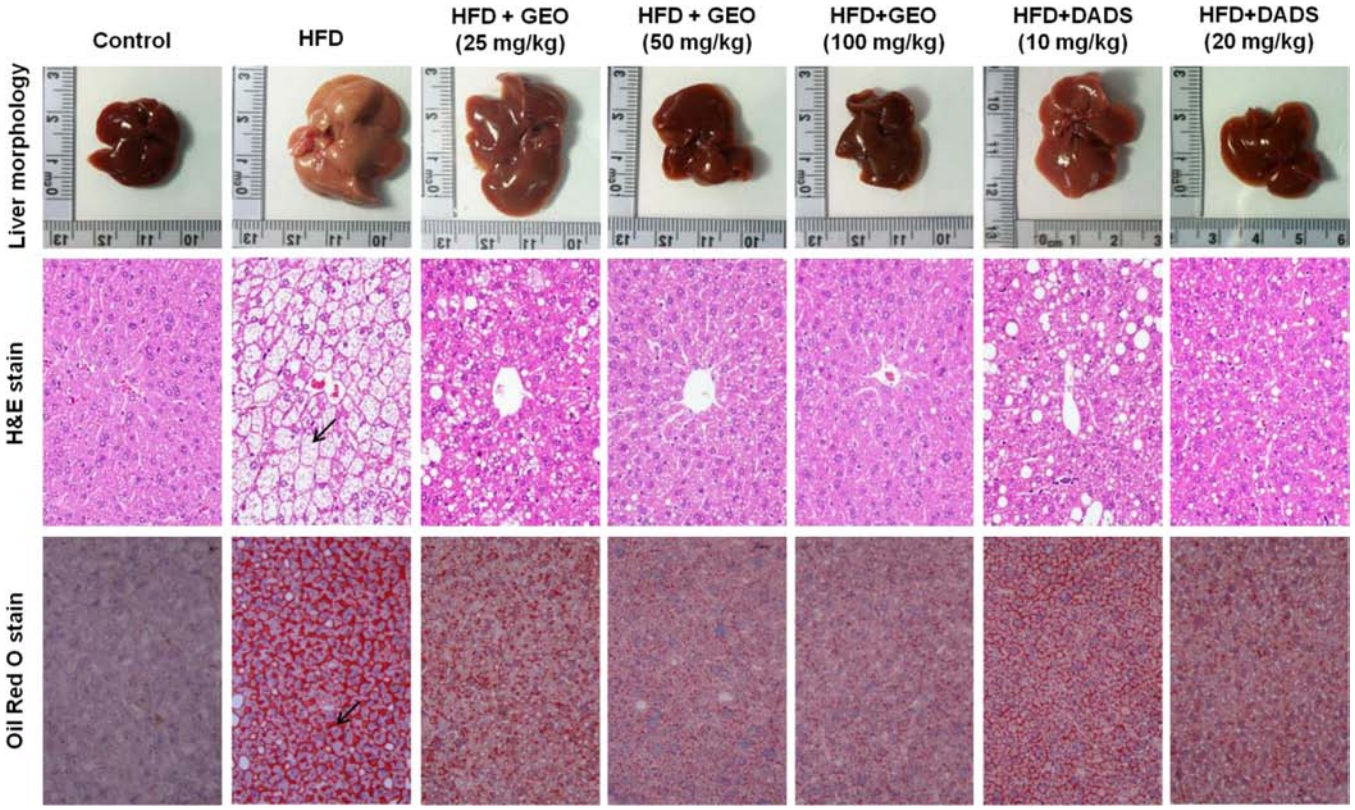

Figure 5. Effects of GEO and DADS supplement on liver histopathological alterations in HFD-fed mice. C57BL/6J mice were fed a normal diet or HFD with/without GEO (25, 50, and 100 mg/kg) or DADS (10 and 20 mg/kg) administration by daily oral gavage for 12 weeks. Liver morphology was assessed, and liver sections were stained with hematoxylin and eosin (H&E) and Oil Red O to visualize lipid droplets (in red). Representative images (magnification: 400×) of each group (n = 10 mice per group) are shown. Black arrows indicate regions of lipid vacuoles in H&E-stained sections and lipid droplets in Oil Red O-stained sections. HFD, high-fat diet; GEO, garlic essential oil; DADS, diallyl disulfide.

expression of the protein that regulates cholesterol synthesis, HMG-CoA reductase, was decreased by 10.7, 48.1, 52.4, 3.81, and 34.47% in the groups treated with 50, 100, or 200 mg/kg GEO and 10 or 20 mg/kg DADS, respectively. In contrast, the protein levels of lipid metabolism markers, PPARα and CPT-1, were significantly decreased by 44.0 and 49.3% in HFD-fed mice, respectively, compared to those in the control group (Figure 7A,B). Administration of 25, 50, or 100 mg/kg GEO and 20 mg/kg DADS to HFD-fed mice significantly up-regulated the hepatic PPARα and CPT-1 expression levels by 1.5−3.1-fold compared to those of HFD-fed mice. Moreover, CYP2E1 expression levels were significantly increased by 1.6-fold in livers of HFD-fed mice after 12 weeks. Administration of 50 or 100 mg/kg GEO and 20 mg/kg DADS markedly decreased the CYP2E1 expression levels by 20.4−42.7% compared to those in HFD-fed mice (Figure 7C). Similar results were observed that the HFD-induced increase in hepatic lipogenic protein expression and decrease of lipolytic protein expression were reversed by 12 weeks of treatment with DADS and GEO.

DISCUSSION

NAFLD is emerging as one of the most common causes of chronic liver disease, and obesity is intimately related to chronic metabolic disorders. Rodent animal models of NAFLD induced by HFD, which show the characteristics of metabolic disorders such as hyperlipidemia, obesity, and insulin resistance, have been widely used due to its similar pathogenesis in humans.[23] In the present study, we fed C57BL/6J mice an HFD (60% kcal from fat) for 12 weeks and found that glucose, TC, TG, AST, and ALT serum levels, hepatic TG and TC levels, and liver weight significantly increased; in addition, moderate levels of oxidative stress and inflammation were induced. However, earlier studies had failed to induce the development of NAFLD in combination with oxidative stress and inflammation.[24,25] These results suggest that long-term consumption of an HFD by mice causes typical NAFLD, with clinical characteristics similar to those observed in NAFLD patients. This model could help elucidate the alterations seen in target organs and the molecular mechanisms underlying the development of NAFLD.

The results of this study showed that administration of GEO and its major active component DADS imparted dose-dependent hepatoprotective effects in obese mice with long-term HFD-induced NAFLD. Administration of 50 or 100 mg/kg GEO and 20 mg/kg DADS lowered HFD-induced body weight and adipose tissue weight, accompanied by antihyperlipidemic effects by reducing serum TG and TC levels. Concurrently, supplementation of 50 or 100 mg/kg GEO and 20 mg/kg DADS resulted in a considerable reduction in FFA that were released by adipose tissue and improved insulin abnormalities by decreasing serum glucose and insulin levels. Imbalanced lipid metabolism and insulin resistance are regarded as key factors in the pathogenesis of NAFLD.[4] Serum AST and ALT, which are important clinical indicators of liver function, returned to levels similar to those observed in normal diet-fed mice through administration of GEO (50 or 100 mg/kg) and DADS (20 mg/kg). Histopathological analysis of liver sections revealed that GEO

dx.doi.org/10.1021/jf500803c | J. Agric. Food Chem. 2014, 62, 5897−5906

Table 3. Effects of GEO and DADS on Hepatic Antioxidant Capacity and Pro-inflammatory Cytokines in HFD-Fed Mice[a]

group	control	HFD	HFD + GEO (25 mg/kg)	HFD + GEO (50 mg/kg)	HFD + GEO (100 mg/kg)	HFD + DADS (10 mg/kg)	HFD + DADS (20 mg/kg)
MDA (nmol/mg protein)	3.15 ± 0.61 d	4.60 ± 0.61 a	4.00 ± 0.84 bc	3.36 ± 0.64 d	3.35 ± 0.69 d	4.37 ± 0.49 ab	3.63 ± 0.68 cd
GSH (nmol/mg protein)	56.70 ± 8.93 a	40.24 ± 4.95 c	47.36 ± 5.78 b	56.03 ± 7.03 a	59.42 ± 7.33 a	42.73 ± 6.39 bc	56.12 ± 8.61 a
SOD (U/mg protein)	74.80 ± 7.69 a	62.32 ± 9.95 c	70.17 ± 5.97 ab	73.23 ± 9.11 a	76.51 ± 6.71 a	63.70 ± 10.38 bc	71.39 ± 10.88 a
CAT (nmol/min/mg protein)	380.11 ± 40.60 a	222.41 ± 32.08 f	265.68 ± 36.97 de	309.72 ± 48.94 bc	339.39 ± 32.17 b	245.58 ± 65.65 ef	289.08 ± 29.45 cd
GPx (nmol/min/mg protein)	532.66 ± 38.64 a	435.05 ± 45.21 c	482.34 ± 61.68 bc	527.51 ± 51.09 ab	536.09 ± 40.79 a	451.43 ± 62.79 c	511.75 ± 56.38 ab
GRd (nmol/min/mg protein)	53.48 ± 7.86 a	26.97 ± 8.48 d	33.5 ± 13.19 cd	39.24 ± 8.37 bc	42.19 ± 6.12 b	28.89 ± 7.32 d	32.32 ± 4.90 cd
GST (nmol/min/mg protein)	426.55 ± 69.70 a	330.83 ± 43.47 c	354.49 ± 57.35 c	373.13 ± 35.24 bc	407.12 ± 28.67 ab	349.27 ± 18.88 c	364.00 ± 61.58 c
TNF-α (pg/mg protein)	120.44 ± 17.18 c	186.21 ± 33.50 a	175.31 ± 17.54 a	144.02 ± 20.01 b	143.60 ± 11.24 b	186.33 ± 37.61 a	167.24 ± 28.01 ab
IL-1β (pg/mg protein)	245.79 ± 55.81 d	373.04 ± 57.12 a	365.13 ± 26.03 ab	305.74 ± 47.20 c	308.50 ± 32.18 c	370.42 ± 88.24 a	321.14 ± 41.47 bc
IL-6 (pg/mg protein)	203.39 ± 26.71 b	238.81 ± 26.28 a	227.48 ± 11.04 ab	208.18 ± 22.70 b	205.88 ± 20.51 b	228.94 ± 47.55 ab	218.22 ± 46.40 ab

[a]C57BL/6J mice were fed a normal diet or HFD with/without GEO (25, 50, and 100 mg/kg) or DADS (10 and 20 mg/kg) administration by daily oral gavage for 12 weeks. Data are presented as the mean ± SD (n = 10 mice per group). Statistical analysis was performed using one-way ANOVA and Duncan's multiple-comparison test. Different letters indicate significant differences among groups at the level of $p < 0.05$. HFD, high-fat diet; GEO, garlic essential oil; DADS, diallyl disulfide; MDA, malondialdehyde; GSH, glutathione; SOD, superoxide dismutase; CAT, catalase; GPx, glutathione peroxidase; GRd, glutathione reductase; GST, glutathione *S*-transferase; TNF-α, tumor necrosis factor-α; IL-1β, interleukin-1β; IL-6, interleukin-6.

and DADS improved HFD-induced hepatic lipid deposition in mice. These data strongly suggest that GEO effectively prevents long-term HFD-induced obesity and NAFLD, which is positively correlated with the reduction in the serum levels of TG, TC, FFA, and insulin.

Oxidative stress and the inflammatory response have emerged as an important mechanism involved in the development and progression of NAFLD.[4] Excessive intake of dietary fats makes the liver vulnerable to toxins and oxidative stress, leading to hepatocyte inflammation by induction of oxidative stress, pro-inflammatory cytokines, and hepatocyte mitochondrial dysfunction. Sustained inflammatory infiltrate upon chronic hepatocellular damage further induces the development of NASH.[26] In this study, GEO and DADS supplementation dose-dependently decreased the levels of pro-inflammatory cytokines (TNF-α, IL-1β, and IL-6) in liver, accompanied by diminished oxidative stress through decreasing MDA levels, elevating GSH levels and antioxidant enzyme activities (CAT, SOD, GPx, GRd, and GST) in HFD-fed mice. Similar effects of garlic on HFD-induced metabolic disorders have been previously reported in the literature. The dietary intake of the ethanol extract of garlic stem at doses of 100, 250, and 500 mg/kg reversed the HFD-induced increase in body weight and adipose tissue weight gain and decreased the levels of antioxidant enzymes, as well as improved abnormal serum and liver lipid profiles in mice.[27] Garlic extract at concentrations of 250 and 500 mg/kg significantly decreased the plasma levels of insulin and TC, as well as oxidative stress markers in obese insulin-resistant rats.[28] Nevertheless, with regard to similar food or calorie intake, the improvements in long-term HFD-induced NAFLD and oxidative injury through administration of GEO and DADS might be attributed to changes in metabolic regulation.

Disorders of lipid metabolism play a central role in the initiation and progression of several metabolic disorders such as obesity, metabolic syndrome, and NAFLD. Experiments and clinical cases indicate that a reduction in FFA absorption in subjects results in elevated FFA concentrations in the peripheral system and entry into the liver, which stimulates the SREBP-1c or PPARα-dependent pathways.[6] This leads to an increase in hepatic SREBP-1c expression and the activation of downstream lipogenesis pathways,[29] including increased expression of lipogenesis markers involved in fatty acid synthesis (ACC and FAS), cholesterol synthesis (HMGCR and SREBP-2), and TG synthesis (glycerophosphate acyl transferase), as well as decreased expression of lipolysis markers (PPARα and CPT-1).[30] When the concentration of fatty acids exceeds the metabolic capacity for fatty acid β-oxidation, fatty acids are deposited in the liver in the form of TG, which results in NAFLD.[31] In the present study, administration of 50 or 100 mg/kg GEO and 20 mg/kg DADS reversed the enhanced synthesis of hepatic fatty acids and cholesterol and the reduced fatty acid degradation in HFD-fed mice as evidenced by decreased expression of SREBP-1c, FAS, ACC, and HMGCR, along with increased expression of PPARα and CPT-1. The results indicated that GEO and DADS dose-dependently prevented hepatic lipid accumulation by reducing serum FFA levels and regulating lipid metabolism in long-term HFD-fed mice.

CYP2E1 has been indicated as a marker of oxidative stress and inflammation associated with liver injury. In clinical and animal studies, up-regulation of CYP2E1 expression was found to be associated with decreased antioxidant enzyme activity in obesity-induced NAFLD or NASH.[32,33] The current study showed that treatment with 50 or 100 mg/kg GEO and

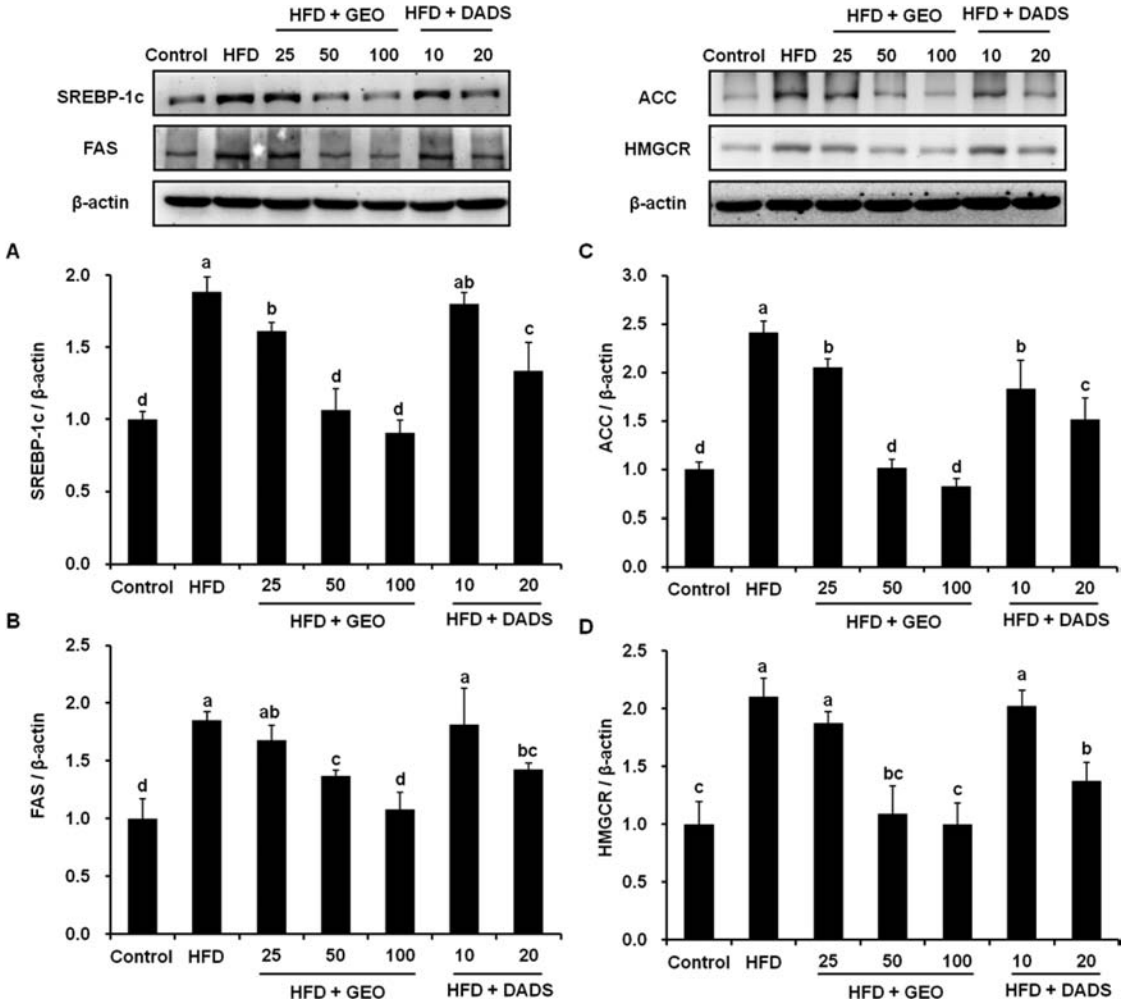

Figure 6. Effects of GEO and DADS supplementation on lipid synthesis-related hepatic protein expressions in HFD-fed mice. C57BL/6J mice were fed a normal diet or HFD with/without GEO (25, 50, and 100 mg/kg) or DADS (10 and 20 mg/kg) administration by daily oral gavage for 12 weeks. Protein expression of hepatic (A) SREBP-1c, (B) FAS, (C) ACC, and (D) HMGCR was analyzed by Western blot, and representative images are shown. Data are presented as the mean ± SD and analyzed with one-way ANOVA and Duncan's multiple-comparison test. Different letters indicate significant differences among groups at the level of $p < 0.05$.

20 mg/kg DADS significantly reversed the up-regulation in CYP2E1 protein expression induced by NAFLD. GEO and DADS restored the hepatic GSH level, enhanced the activities of the antioxidant enzymes, and prevented hepatocyte inflammation by reducing pro-inflammatory cytokine levels. Thus, the results indicated that treatment with GEO and DADS could protect against hepatic oxidative damage resulting from long-term HFD consumption. Moreover, the protection from liver damage may also be helpful for the regulation of fatty acid metabolism. GEO and DADS effectively regulated serum FFA concentrations and hepatic lipid metabolism; the regulation can help prevent SREBP-1c-mediated hepatic lipogenesis and the activation of PPARα-mediated hepatic lipolysis. This finding may explain the protective effects against HFD-induced oxidative injury and NAFLD that have been attributed to GEO and DADS. In addition, earlier studies have suggested that the sulfur compounds in garlic reduce HFD-induced hepatic steatosis and oxidative injury, possibly through modulation of SREBP-1c and CYP2E1.[34,35] The ability of garlic oil to prevent acute ethanol-induced fatty liver should be associated with its antioxidative activities.[20] Taken together, the results provided evidence that GEO and DADS not only prevented the occurrence of early-stage NAFLD but also protected the mice from developing NASH by regulating oxidative stress and suppressing inflammatory responses through CYP2E1 expression. Nonetheless, direct evidence for the mechanisms underlying the effects of GEO and DADS with respect to NASH still needs to be experimentally validated and further investigated.

In our study, the steam distillation of garlic produced GEO that was completely devoid of water-soluble compounds. The three major components of GEO are DADS (40.7%), DATS (21.6%), and DAS (6.7%), which account for 69.0% of the total oil. The various components in garlic work synergistically to provide various health benefits; however, because of garlic's chemical complexity, the efficacy of the preparation varies with the processing methods.[11] Previous studies on the sulfur-containing bioactive constituents of GEO, those being DAS, DADS, and DATS, have reported regulation of detoxification and the antioxidant system by these constituents.[18,36,37] However, the results of the present study suggest that administration of 50 or 100 mg/kg GEO and 20 mg/kg DADS significantly reduces the degree of HFD-induced NAFLD in mice by decreasing lipid accumulation and inflammation as well as by increasing hepatic antioxidant capacity. A single dose of 20 mg/kg DADS was more effective in controlling long-term HFD-induced adverse effects in

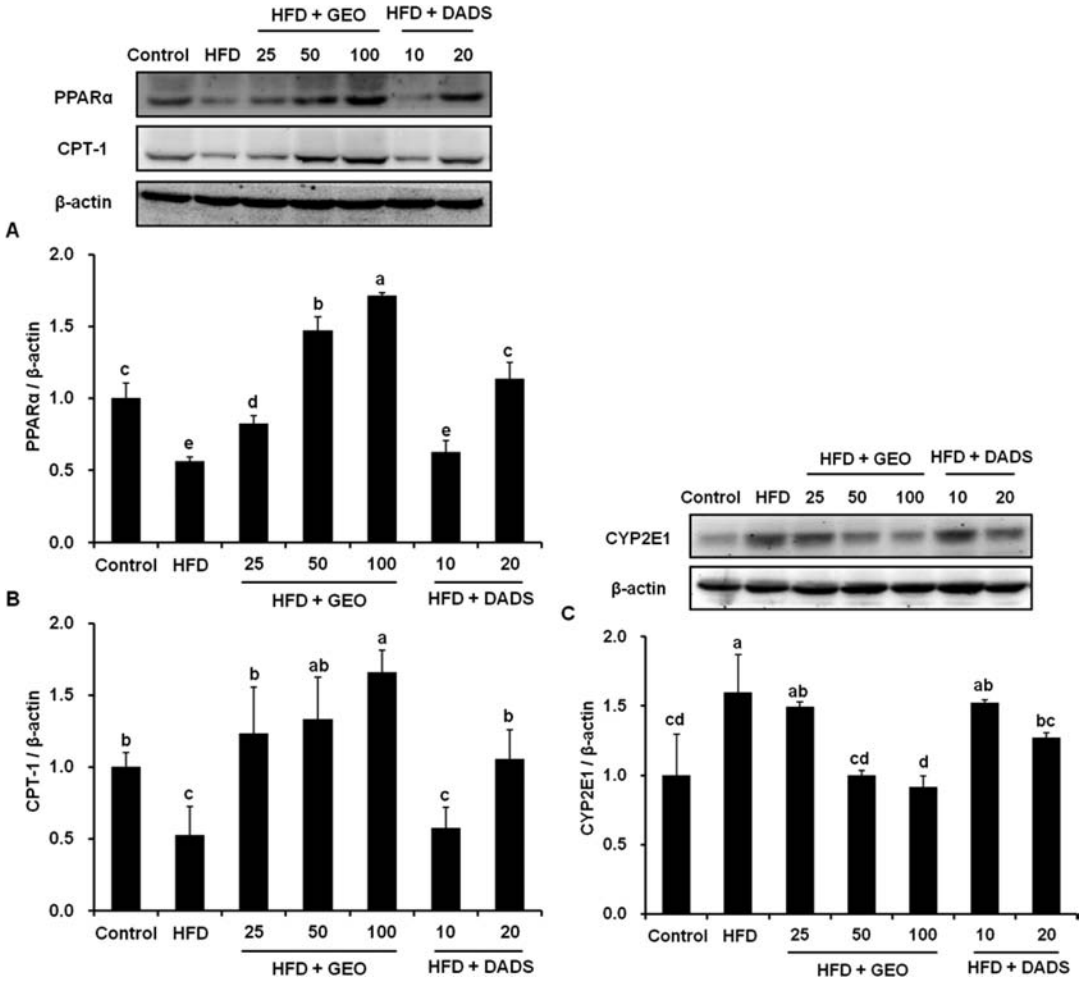

Figure 7. Effects of GEO and DADS supplementation on lipid oxidation-related hepatic protein expression and CYP2E1 expression in HFD-fed mice. C57BL/6J mice were fed a normal diet or HFD with/without GEO (25, 50, and 100 mg/kg) or DADS (10 and 20 mg/kg) administration by daily oral gavage for 12 weeks. Protein expression of hepatic (A) PPARα, (B) CPT-1, and (C) CYP2E1 was analyzed by Western blot, and representative images are shown. Data are presented as the mean ± SD and analyzed with one-way ANOVA and Duncan's multiple-comparison test. Different letters indicate significant differences among groups at the level of $p < 0.05$.

NAFLD mice than lower doses of DADS. This dose of DADS was equally effective in preventing obesity and NAFLD as 50 mg/kg GEO containing the same amount of DADS, which demonstrates that DADS may be the major active sulfur compound contributing to the protection by GEO.

This study is the first to demonstrate the potent protective effects of GEO and its major active component DADS administered to obese mice with long-term HFD-induced NAFLD. Moreover, the protective effects on regulation of hepatic lipid metabolism, antioxidant defense system, and inflammatory response are mainly mediated through SREBP-1c- and PPARα-dependent pathways and CYP2E1-dependent oxidative stress during NAFLD development. Furthermore, GEO and DADS could be considered as potent dietary supplements for preventing NAFLD-related metabolic diseases.

AUTHOR INFORMATION

Corresponding Author

*(S.-Y. L.) Postal address: No. 1018, Sec. 6, Taiwan Boulevard, Shalu District, Taichung City 43302, Taiwan. Phone: 886-4-26318652-5017. Fax: 886-4-22361569. E-mail: sylin@sunrise.hk.edu.tw.

*(L.-Y.S.) Postal address: No. 1, Section 4, Roosevelt Road, Taipei 106, Taiwan. Phone: 886-2-33664129. Fax: 886-2-23620849. E-mail: lysheen@ntu.edu.tw.

Funding

This research work was partially funded by the National Science Council (NSC-102-2628-B-002-010-MY2) and National Taiwan University (Aim For Top University Program 102R-7620), Taiwan.

Notes

The authors declare no competing financial interest.

ACKNOWLEDGMENTS

We thank Prof. Chih-Hsien Chiu for helpful discussions in animal experiments. We also thank Ying-Yu Chou, Ying-Chu Chen, Wan-Ching Lee, and Ya-Ling Huang for technical support.

REFERENCES

(1) Machado, M.; Cortez-Pinto, H. Non-alcoholic steatohepatitis and metabolic syndrome. *Curr. Opin. Clin. Nutr. Metab. Care* **2006**, *9*, 637–642.

(2) Ahmed, M. H.; Abu, E. O.; Byrne, C. D. Non-alcoholic fatty liver disease (NAFLD): new challenge for general practitioners and

important burden for health authorities? *Prim. Care Diabetes* **2010**, *4*, 129−137.
(3) Krawczyk, M.; Bonfrate, L.; Portincasa, P. Nonalcoholic fatty liver disease. *Best Pract. Res. Clin. Gastroenterol.* **2010**, *24*, 695−708.
(4) Malaguarnera, M.; Di Rosa, M.; Nicoletti, F.; Malaguarnera, L. Molecular mechanisms involved in NAFLD progression. *J. Mol. Med. (Berlin)* **2009**, *87*, 679−695.
(5) Rahimi, R. S.; Landaverde, C. Nonalcoholic fatty liver disease and the metabolic syndrome: clinical implications and treatment. *Nutr. Clin. Pract.* **2013**, *28*, 40−51.
(6) Serviddio, G.; Bellanti, F.; Vendemiale, G. Free radical biology for medicine: learning from nonalcoholic fatty liver disease. *Free Radical Biol. Med.* **2013**, *65*, 952−968.
(7) Shimano, H.; Yahagi, N.; Amemiya-Kudo, M.; Hasty, A. H.; Osuga, J.; Tamura, Y.; Shionoiri, F.; Iizuka, Y.; Ohashi, K.; Harada, K.; Gotoda, T.; Ishibashi, S.; Yamada, N. Sterol regulatory element-binding protein-1 as a key transcription factor for nutritional induction of lipogenic enzyme genes. *J. Biol. Chem.* **1999**, *274*, 35832−35839.
(8) Reddy, J. K.; Hashimoto, T. Peroxisomal β-oxidation and peroxisome proliferator-activated receptor α: an adaptive metabolic system. *Annu. Rev. Nutr.* **2001**, *21*, 193−230.
(9) Prompila, N.; Wittayalertpanya, S.; Komolmit, P. Hepatic cytochrome P450 2E1 activity in nonalcoholic fatty liver disease. *J. Med. Assoc. Thai.* **2008**, *91*, 733−738.
(10) Amagase, H.; Petesch, B. L.; Matsuura, H.; Kasuga, S.; Itakura, Y. Intake of garlic and its bioactive components. *J. Nutr.* **2001**, *131*, 955S−962S.
(11) Amagase, H. Clarifying the real bioactive constituents of garlic. *J. Nutr.* **2006**, *136*, 716S−725S.
(12) Banerjee, S. K.; Mukherjee, P. K.; Maulik, S. K. Garlic as an antioxidant: the good, the bad and the ugly. *Phytother. Res.* **2003**, *17*, 97−106.
(13) Fujisawa, H.; Watanabe, K.; Suma, K.; Origuchi, K.; Matsufuji, H.; Seki, T.; Ariga, T. Antibacterial potential of garlic-derived allicin and its cancellation by sulfhydryl compounds. *Biosci., Biotechnol., Biochem.* **2009**, *73*, 1948−1955.
(14) Jalal, R.; Bagheri, S. M.; Moghimi, A.; Rasuli, M. B. Hypoglycemic effect of aqueous shallot and garlic extracts in rats with fructose-induced insulin resistance. *J. Clin. Biochem. Nutr.* **2007**, *41*, 218−223.
(15) Lee, M. S.; Kim, I. H.; Kim, C. T.; Kim, Y. Reduction of body weight by dietary garlic is associated with an increase in uncoupling protein mRNA expression and activation of AMP-activated protein kinase in diet-induced obese mice. *J. Nutr.* **2011**, *141*, 1947−1953.
(16) Xiao, J.; Guo, R.; Fung, M. L.; Liong, E. C.; Chang, R. C.; Ching, Y. P.; Tipoe, G. L. Garlic-derived S-allylmercaptocysteine ameliorates nonalcoholic fatty liver disease in a rat model through inhibition of apoptosis and enhancing autophagy. *Evidence-Based Complement. Altern. Med.* **2013**, *2013*, 642920.
(17) Chu, Y. L.; Raghu, R.; Lu, K. H.; Liu, C. T.; Lin, S. H.; Lai, Y. S.; Cheng, W. C.; Lin, S. H.; Sheen, L. Y. Autophagy therapeutic potential of garlic in human cancer therapy. *J. Tradit. Complement. Med.* **2013**, *3*, 159−162.
(18) Sheen, L. Y.; Chen, H. W.; Kung, Y. L.; Liu, C. T.; Lii, C. K. Effects of garlic oil and its organosulfur compounds on the activities of hepatic drug-metabolizing and antioxidant enzymes in rats fed high- and low-fat diets. *Nutr. Cancer* **1999**, *35*, 160−166.
(19) Zeng, T.; Guo, F. F.; Zhang, C. L.; Zhao, S.; Dou, D. D.; Gao, X. C.; Xie, K. Q. The anti-fatty liver effects of garlic oil on acute ethanol-exposed mice. *Chem.−Biol. Interact.* **2008**, *176*, 234−242.
(20) Zeng, T.; Zhang, C. L.; Song, F. Y.; Zhao, X. L.; Xie, K. Q. Garlic oil alleviated ethanol-induced fat accumulation via modulation of SREBP-1, PPAR-α, and CYP2E1. *Food Chem. Toxicol.* **2012**, *50*, 485−491.
(21) Sheen, L. Y.; Lin, S. Y.; Tsi, S. J. Odor assessments for volatile compounds of garlic and ginger essential oils by sniffing method of gas chromatography. *J. Chin. Agric. Chem. Soc.* **1992**, *30*, 14−24.
(22) Banerjee, S. K.; Maulik, S. K. Effect of garlic on cardiovascular disorders: a review. *Nutr. J.* **2002**, *1*, 4.
(23) Takahashi, Y.; Soejima, Y.; Fukusato, T. Animal models of nonalcoholic fatty liver disease/nonalcoholic steatohepatitis. *World J. Gastroenterol.* **2012**, *18*, 2300−2308.
(24) Kang, J. S.; Lee, W. K.; Lee, C. W.; Yoon, W. K.; Kim, N.; Park, S. K.; Lee, H. S.; Park, H. K.; Han, S. B.; Yun, J.; Lee, K.; Lee, K. H.; Park, S. K.; Kim, H. M. Improvement of high-fat diet-induced obesity by a mixture of red grape extract, soy isoflavone and L-carnitine: implications in cardiovascular and non-alcoholic fatty liver diseases. *Food Chem. Toxicol.* **2011**, *49*, 2453−2458.
(25) Tzeng, T. F.; Lu, H. J.; Liou, S. S.; Chang, C. J.; Liu, I. M. *Cassia tora* (Leguminosae) seed extract alleviates high-fat diet-induced nonalcoholic fatty liver. *Food Chem. Toxicol.* **2013**, *51*, 194−201.
(26) Fromenty, B.; Robin, M. A.; Igoudjil, A.; Mansouri, A.; Pessayre, D. The ins and outs of mitochondrial dysfunction in NASH. *Diabetes Metab.* **2004**, *30*, 121−138.
(27) Kim, I.; Kim, H. R.; Kim, J. H.; Om, A. S. Beneficial effects of *Allium sativum* L. stem extract on lipid metabolism and antioxidant status in obese mice fed a high-fat diet. *J. Sci. Food Agric.* **2013**, *93*, 2749−2757.
(28) Supakul, L.; Pintana, H.; Apaijai, N.; Chattipakorn, S.; Shinlapawittayatorn, K.; Chattipakorn, N. Protective effects of garlic extract on cardiac function, heart rate variability, and cardiac mitochondria in obese insulin-resistant rats. *Eur. J. Nutr.* **2013**, DOI: 10.1001/s00394-013-0595-6.
(29) Kohjima, M.; Higuchi, N.; Kato, M.; Kotoh, K.; Yoshimoto, T.; Fujino, T.; Yada, M.; Yada, R.; Harada, N.; Enjoji, M.; Takayanagi, R.; Nakamuta, M. SREBP-1c, regulated by the insulin and AMPK signaling pathways, plays a role in nonalcoholic fatty liver disease. *Int. J. Mol. Med.* **2008**, *21*, 507−511.
(30) Pan, M. H.; Lai, C. S.; Tsai, M. L.; Ho, C. T. Chemoprevention of nonalcoholic fatty liver disease by dietary natural compounds. *Mol. Nutr. Food Res.* **2014**, *58*, 147−171.
(31) Browning, J. D.; Horton, J. D. Molecular mediators of hepatic steatosis and liver injury. *J. Clin. Invest.* **2004**, *114*, 147−152.
(32) Robertson, G.; Leclercq, I.; Farrell, G. C. Nonalcoholic steatosis and steatohepatitis. II. Cytochrome P-450 enzymes and oxidative stress. *Am. J. Physiol. Gastrointest. Liver Physiol.* **2001**, *281*, G1135−G1139.
(33) Lee, H. I.; Yun, K. W.; Seo, K. I.; Kim, M. J.; Lee, M. K. Scopoletin prevents alcohol-induced hepatic lipid accumulation by modulating the AMPK-SREBP pathway in diet-induced obese mice. *Metabolism* **2014**, *63*, 593−601.
(34) Xiao, J.; Ching, Y. P.; Liong, E. C.; Nanji, A. A.; Fung, M. L.; Tipoe, G. L. Garlic-derived S-allylmercaptocysteine is a hepato-protective agent in non-alcoholic fatty liver disease in vivo animal model. *Eur. J. Nutr.* **2013**, *52*, 179−191.
(35) Han, C. Y.; Ki, S. H.; Kim, Y. W.; Noh, K.; Lee da, Y.; Kang, B.; Ryu, J. H.; Jeon, R.; Kim, E. H.; Hwang, S. J.; Kim, S. G. Ajoene, a stable garlic by-product, inhibits high fat diet-induced hepatic steatosis and oxidative injury through LKB1-dependent AMPK activation. *Antioxid. Redox. Signal.* **2011**, *14*, 187−202.
(36) Shimada, M.; Liu, L.; Nussler, N.; Jonas, S.; Langrehr, J. M.; Ogawa, T.; Kaminishi, M.; Neuhaus, P.; Nussler, A. K. Human hepatocytes are protected from ethanol-induced cytotoxicity by DADS via CYP2E1 inhibition. *Toxicol. Lett.* **2006**, *163*, 242−249.
(37) Wu, C. C.; Sheen, L. Y.; Chen, H. W.; Kuo, W. W.; Tsai, S. J.; Lii, C. K. Differential effects of garlic oil and its three major organosulfur components on the hepatic detoxification system in rats. *J. Agric. Food Chem.* **2002**, *50*, 378−383.

JOURNAL OF AGRICULTURAL AND FOOD CHEMISTRY

Article

pubs.acs.org/JAFC

Quantitative Analysis of Alkaloidal Constituents in Imported Fire Ants by Gas Chromatography

Yu-Ting Yu,[†,‡] Hong-Yi Wei,[‡] Henry Y. Fadamiro,[§] and Li Chen*[,†,§]

[†]State Key Laboratory of Integrated Management of Pest Insects and Rodents, Institute of Zoology, Chinese Academy of Sciences, Beijing 100101, China

[‡]College of Agronomy, Jiangxi Agricultural University, Nanchang 330045, China

[§]Department of Entomology and Plant Pathology, Auburn University, Auburn, Alabama 36849, United States

ABSTRACT: A method based on silica gel chromatography and GC-MS/GC-FID analyses was developed for the quantitation of alkaloidal compounds in imported fire ants, *Solenopsis richteri*, *S. invicta*, and their hybrid found in the southern United States. The *cis* and *trans* alkaloids from fire ant body extracts were successfully separated by silica gel chromatography, identified by GC-MS, and quantitated by GC-FID. Piperideine compounds were eluted together with the *cis* and *trans* piperidines, but were well-resolved on a nonpolar GC column. Eight pairs of piperidine isomers and 12 piperideines were quantitated. The ratios of *trans* alkaloids to corresponding *cis* isomers ranged from 87 to 378:1 in *S. invicta* and were significantly higher than in *S. richteri* and hybrid ants. The results were discussed in relation to the evolution of fire ant venom alkaloids and their role as host location cues for parasitic *Pseudacteon* phorid flies.

KEYWORDS: *quantitation, venom, piperidine, Solenopsis richteri, Solenopsis invicta, hybrid*

INTRODUCTION

In the southern United States, the four main species of *Solenopsis* fire ants are *S. geminata*, *S. xyloni*, *S. richteri*, and *S. invicta*. The first two species are native to the southeastern coastal plain of Florida to Texas and south through Central America to northern South America.[1] However, the last two species were introduced into the United States from South America through the port of Mobile, AL, in the early 20th century. All four species produce venoms containing various 2-methyl-6-alkyl (or alkenyl) piperidines,[2−5] and, significantly, the venom of each species possesses a characteristic alkaloidal "fingerprint".[6−8] These alkaloids are species-specific as the venom of each species has groups of similar compounds either dominating or almost completely lacking. Chemical profiles of venom alkaloids have been widely used as a taxonomic tool to define fire ant populations.[8]

Hybrid fire ants, *S. richteri* × *S. invicta*, which were discovered many years after the introduction of their parent species, were indistinguishable from the parent species solely on the basis of the morphological characters. Vander Meer et al.[9] first presented chemical evidence of the natural occurrence of hybridization between the two imported fire ant species as hybrids exhibited intermediate gas chromatographic profiles of both piperidine alkaloids and cuticular hydrocarbons.[10−12]

In addition to *cis* and *trans* 2-methyl-6-alkyl (or alkenyl) piperidines, a series of $\Delta^{1,2}$- and $\Delta^{1,6}$-2-methyl-6-alkyl (or alkenyl) piperideines have been recently identified from imported fire ant workers and alate queens.[13−18] Furthermore, $\Delta^{1,6}$-piperideines in the imported fire ants, *S. richteri*, *S. invicta*, and hybrids, showed significant interspecific variations very similar to those of the *trans* 2,6-dialkylpiperidines.[14]

Previous studies have mainly focused on identification of alkaloidal components from *Solenopsis* fire ants by using a GC-MS technique. To the best of our knowledge, however, no proper analytical method has been developed that permits a detailed quantitative analysis of fire ant venom alkaloids. In the present study, GC-FID was used for quantitation of venom alkaloids because of low detection limits, wide linearity range, and general utility for various analytes. GC-MS was used for discrimination of alkaloidal components instead of quantitative analysis because the MS detector response that requires calibration for each individual compound is less uniform and less convenient for quantitation purposes compared to the FID. A primary goal of this work was to establish a routine analysis procedure to determine alkaloidal components of *Solenopsis* fire ants. A comparative study of the venom alkaloids in *S. richteri*, *S. invicta*, and hybrid fire ants was undertaken to further assess the distribution of these 2,6-disubstituted piperidines and piperideines. The results may contribute to an understanding of the evolution of fire ant venom alkaloids and mechanisms of host specificity and preference in *Pseudacteon* phorid flies, which are important biological control agents of imported fire ants.

MATERIALS AND METHODS

Reagents and Standard. HPLC grade *n*-hexane used for extraction and purification of the venom alkaloids was purchased from CNW Technologies GmbH (Düsseldorf, Germany). Anhydrous sodium sulfate, acetone, and triethylamine purchased from Beijing Chemical Reagent (Beijing, China) were of analytical reagent grade. Acetone and triethylamine were redistilled before use. Silica gel (300−400 mesh) for column chromatography was obtained from the Qingdao Marine Chemical Factory (Qingdao, China). 4-(2,6-

Received: March 24, 2014
Revised: May 27, 2014
Accepted: May 29, 2014
Published: May 29, 2014

ACS Publications © 2014 American Chemical Society

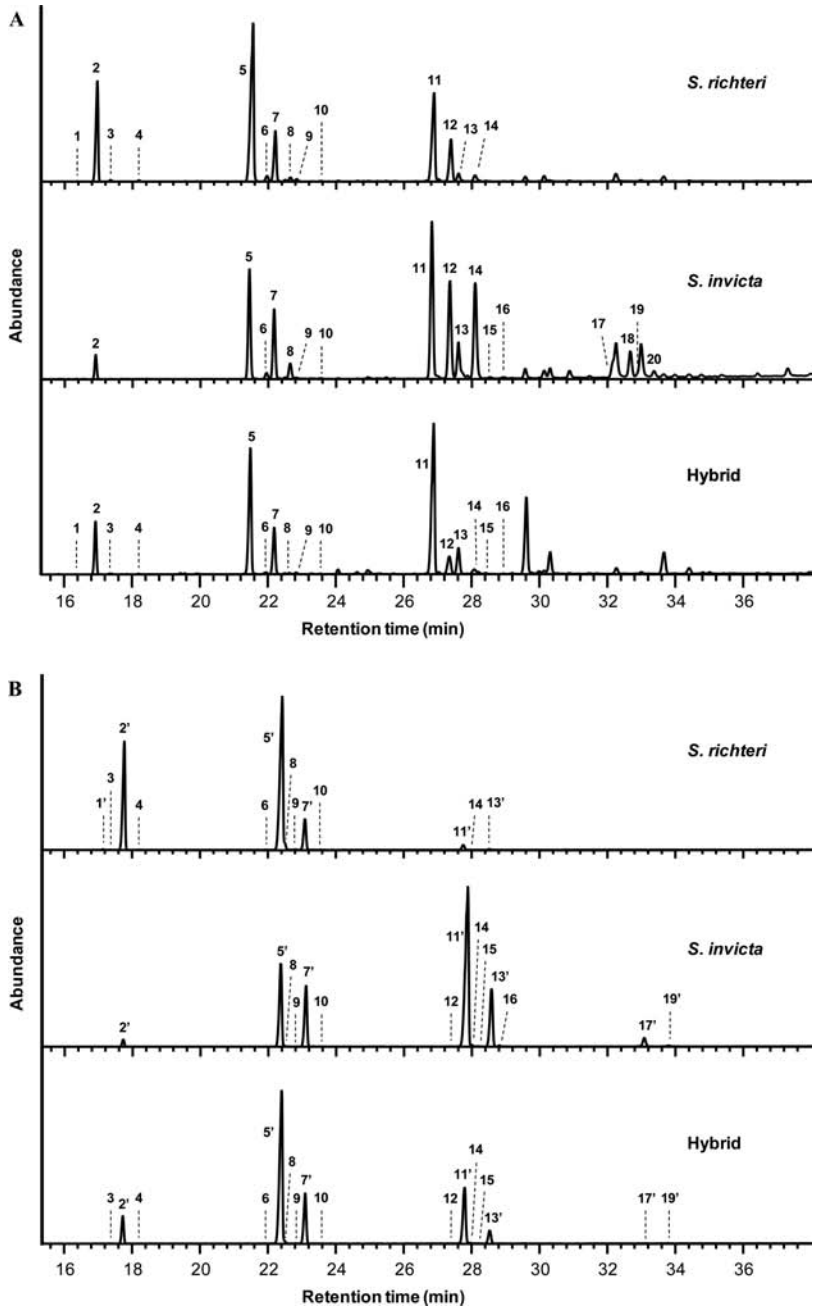

Figure 1. Typical GC-FID traces of the (A) *cis* and (B)*trans* alkaloid fractions.

Dimethyl-1-piperidinyl)-1-phenyl-1-butanone purchased from Sigma-Aldrich (St. Louis, MO, USA) was used as external standard for GC-FID analysis.

Collection and Identification of Fire Ant Colonies. Colonies of the black imported fire ant, *S. richteri* Forel, the red imported fire ant, *S. invicta* Buren, and their hybrid, *S. richteri* × *S. invicta*, were used in this test. We collected colonies of *S. richteri* in northern Mississippi and western Tennessee and colonies of *S. invicta* in Alabama (Auburn University campus) in mid-November 2011. At the same time, hybrid fire ant colonies were collected from northern Alabama and northeastern Mississippi, where hybrids are known to occur almost exclusively. Each colony containing workers, alates, broods, and queens was transferred in 1 gallon Rubbermaid plastic jars coated with Fluon to prevent escape. All colonies were reared in the laboratory and fed with 10% sugar water and crickets.

The identity of fire ant colonies was confirmed to be *S. richteri*, *S. invicta*, or hybrid fire ants by GC analysis using both alkaloid and hydrocarbon characters as previously reported.[17,19] Briefly, about 50 workers selected randomly from each colony were soaked in 1 mL of hexane for 2 h. A small aliquot (1 μL) of the hexane extract was injected into an Agilent 7890A GC equipped with a 30 m × 0.25 mm i.d., 0.25 μm, HP-5ms capillary column (Agilent Technologies) in splitless mode. Nitrogen was used as carrier gas at a flow rate of 2 mL/min. The injection port and detector temperatures were set at 270 and 280 °C, respectively. The GC oven was programmed at a rate of 15 °C/min from 90 to 270 °C, with a 2 min initial time and a 16 min final holding time.

Sample Preparation for Quantitative Analyses. A total of 32 colonies were analyzed in this study, including 8 colonies of *S. richteri*, 8 colonies of *S. invicta*, and 16 colonies of hybrids. Alkaloids were extracted and isolated from fire ant samples as previously reported.[15−17] For each colony, ant workers (1 g) were killed by freezing and extracted with hexane (enough hexane to cover ant bodies, ∼3.5 mL) for 24 h. The extract was dried over anhydrous

dx.doi.org/10.1021/jf501423y | J. Agric. Food Chem. 2014, 62, 5907−5915

Table 1. Quantitation of Alkaloids from *Solenopsis* Fire Ants

peak	structure	name	amount (μg/g ± SE)		
			S. richteri	*S. invicta*	hybrid
cis alkaloids					
1	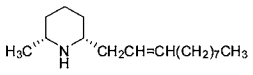	*cis*-C11:1[a]	+[b]		
2	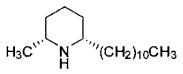	*cis*-C11	81.16 ± 12.28 a	1.48 ± 0.30 b	17.78 ± 2.76 b
5	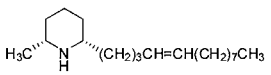	*cis*-C13:1	213.52 ± 33.97 a	16.25 ± 1.88 c	85.78 ± 7.73 b
7	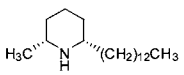	*cis*-C13	46.63 ± 7.59 a	8.99 ± 1.28 b	24.30 ± 3.76 b
11	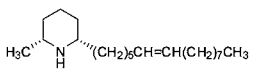	*cis*-C15:1	76.91 ± 11.71 ab	26.29 ± 3.26 b	151.84 ± 23.85 a
13	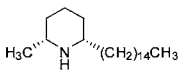	*cis*-C15	10.58 ± 1.72 b	6.26 ± 0.82 b	21.53 ± 3.02 a
17	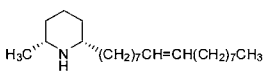	*cis*-C17:1		0.75 ± 0.15	
19	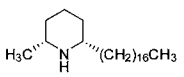	*cis*-C17		0.27 ± 0.05	
trans alkaloids					
1'	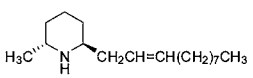	*trans*-C11:1	10.37 ± 1.73		
2'	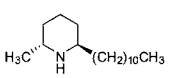	*trans*-C11	1851.85 ± 322.12 a	87.15 ± 11.76 b	510.58 ± 58.98 b
5'	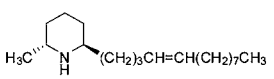	*trans*-C13:1	5618.02 ± 628.26 a	1997.26 ± 195.72 c	3844.62 ± 326.78 b
7'	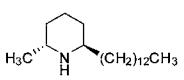	*trans*-C13	809.73 ± 96.40 b	1293.62 ± 141.51 a	966.70 ± 92.04 ab
11'	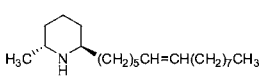	*trans*-C15:1	284.56 ± 48.61 c	4257.75 ± 315.05 a	1485.38 ± 162.63 b
13'	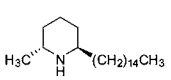	*trans*-C15	44.79 ± 12.77 c	1470.16 ± 152.36 a	332.38 ± 50.30 b
17'	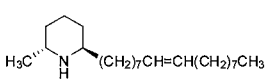	*trans*-C17:1		223.45 ± 34.64 a	17.36 ± 2.91 b
19'	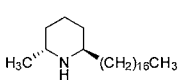	*trans*-C17		24.89 ± 3.40 a	7.04 ± 1.28 b

dx.doi.org/10.1021/jf501423y | J. Agric. Food Chem. 2014, 62, 5907−5915

Table 1. continued

peak	structure	name	amount (μg/g ± SE)		
			S. richteri	*S. invicta*	hybrid
piperideines					
3	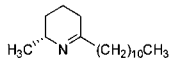	$\Delta^{1,6}$-C11	5.94 ± 0.74 a		0.42 ± 0.09 b
4	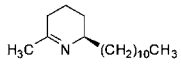	$\Delta^{1,2}$-C11	4.09 ± 0.63 a		0.25 ± 0.05 b
6	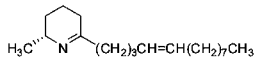	$\Delta^{1,6}$-C13:1	15.82 ± 1.34 a	2.75 ± 0.56 c	8.14 ± 1.05 b
8	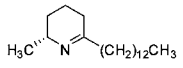	$\Delta^{1,6}$-C13	5.99 ± 0.81 a	4.73 ± 0.80 ab	3.39 ± 0.39 b
9	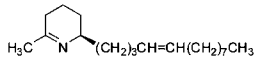	$\Delta^{1,2}$-C13:1	18.54 ± 2.16 a	2.30 ± 0.26 c	7.43 ± 0.93 b
10	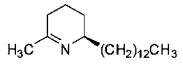	$\Delta^{1,2}$-C13	4.14 ± 0.42 a	2.50 ± 0.30 b	3.27 ± 0.38 ab
12	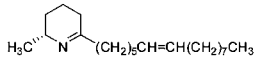	$\Delta^{1,6}$-C15:1	57.86 ± 7.67 b	26.73 ± 3.29 b	122.30 ± 15.64 a
14	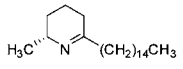	$\Delta^{1,6}$-C15	17.97 ± 2.96 b	21.81 ± 3.69 b	54.86 ± 4.44 a
15	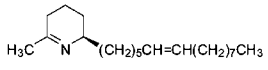	$\Delta^{1,2}$-C15:1		8.03 ± 0.82	5.87 ± 0.76
16	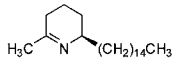	$\Delta^{1,2}$-C15		4.36 ± 0.31 a	0.88 ± 0.14 b
18	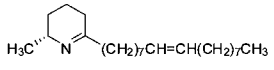	$\Delta^{1,6}$-C17:1		5.91 ± 1.11	
20	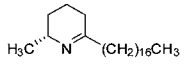	$\Delta^{1,6}$-C17		1.46 ± 0.24	

[a]Carbon numbers have been widely used to represent the trivial names of alkaloids found in *Solenopsis* fire ants, e.g., in *cis*-C11:1, with 11 referring to the chain length and 1 referring to the number of double bonds.[6] [b]Trace amount.

sodium sulfate, concentrated to 0.5 mL under a mild stream of N_2, and then loaded onto a 17 mm (o.d.) chromatography column (20 g of silica gel). The column was eluted with hexane containing 2% triethylamine and stepwise increasing amounts of acetone (hexane/acetone ratio ranging from 50:1 to 10:1) to obtain the alkaloids. The chemistry of each collection (ca. 2 mL) was analyzed by gas chromatography (GC) on an Agilent 7890A GC equipped with a flame ionization detector (FID) under the same GC conditions described above. The collections were pooled on the basis of changes observed in the GC chromatograms of each collection to obtain two major alkaloid fractions: *cis* and *trans* alkaloid fractions. The two alkaloid fractions of each colony were concentrated to a certain volume for GC-MS and GC-FID analyses. As imported *Solenopsis* fire ant workers contain large amounts of *trans* alkaloids compared to corresponding *cis* alkaloids, the final volume of the *trans* alkaloid fraction was 20 times more than that of the *cis* alkaloid fraction prior to GC injection to achieve proper concentrations of *trans* alkaloids for quantitation, that is, 2 mL for the *cis* alkaloid fraction and 40 mL for the *trans* alkaloid fraction.

A stock solution of standard compound, 4-(2,6-dimethyl-1-piperidinyl)-1-phenyl-1-butanone (2000 ng/μL), was prepared and then diluted to a series of concentrations ranging from 0.39 to 400 ng/μL. All dilutions were transferred to the GC autosampler, and 1 μL of each dilution was used for GC-FID analysis.

GC-MS and GC-FID Analysis. GC-MS analyses of alkaloid fractions were performed on an Agilent 7890A GC coupled to a 5975C mass selective detector, with an HP-5ms capillary column as described above. Helium was used as carrier gas at a flow rate of 1 mL/min. Injections (1 μL) were made in the splitless mode at an injector temperature of 230 °C. The GC oven temperature was programmed from 90 °C (isothermal for 1 min) to 160 °C at 10 °C/min, then to 250 °C at 3 °C/min, and held for 2 min. Total run time was 40 min. The transfer line temperature was set at 250 °C. Mass spectra were obtained using electron impact (EI, 70 eV). The chemical identities of alkaloids were determined by analysis of their mass spectra, as well as

by comparison of diagnostic ion fragments with published results on *Solenopsis* fire ants.[15−18]

Quantitative chromatographic analyses were carried out with the Agilent 7890A GC equipped with an FID. Nitrogen at a flow rate of 1 mL/min was used as the carrier gas. The GC conditions including the dimensions of capillary column, oven temperature program, and injection operation were the same as those for GC-MS. The detector temperature was set at 260 °C.

Statistical Analysis. A standard curve was calculated by linear regression analysis. The concentrations of the identified venom alkaloids were calculated against the standard curve. The absolute abundances of the alkaloids were analyzed using the PROC GLM procedure of one-way analysis of variance (ANOVA) followed by the Tukey−Kramer HSD comparison test ($P < 0.05$) to establish significant differences among the three fire ant species (we consider hybrid as a species in this study).[20] A PROC TTEST procedure ($P < 0.05$) was used to establish significant difference between, if applicable, any two of the three fire ant species.

RESULTS AND DISCUSSION

Fire ant venom alkaloids were readily extracted out of ant worker bodies by hexane. As previously reported,[15−17] the venom alkaloids of fire ant extract were separated into two alkaloid fractions (*cis* and *trans* alkaloid fractions) by silica gel chromatography, with the *cis* stereoisomers always being eluted before the corresponding *trans* stereoisomers. The two alkaloid fractions were then subjected to GC-MS analysis, and the chemical identities of alkaloidal components were determined by comparing mass spectrum and retention time with published data.[15−17] This routine procedure can be applied to the analysis of alkaloids from any *Solenopsis* or related alkaloid-containing ant species.

Typical GC-FID traces of the *cis* and *trans* alkaloid fractions of fire ant samples are shown in Figure 1. Both GC patterns of the two alkaloid fractions are species-specific. Almost all of the peaks show interspecific variations. Furthermore, both *cis* and *trans* alkaloids from hybrids show characteristics intermediate to those of the two parental species. A total of eight pairs of *cis* and *trans* alkaloids, those being **1**−**1′**, **2**−**2′**, **5**−**5′**, **7**−**7′**, **11**−**11′**, **13**−**13′**, **17**−**17′**, and **19**−**19′**, were identified by GC-MS on the basis of mass spectra with characteristic base peak m/z 98, molecular ion $[M^+]$, and $[M - 15]^+$,[2,3,5,6] meaning that there were eight pairs of diastereoisomers isolated from the three fire ant species (Table 1). Peaks 2, 5, 7, 11, 13 and their corresponding *trans* stereoisomers were found in all ant samples. However, peaks 1 and 1′ were not found in *S. invicta* samples, whereas peaks 17, 19, and their corresponding *trans* stereoisomers were not found in *S. richteri* samples. Peaks 17′ and 19′ were detected in trace amounts in the *trans* alkaloid fraction of hybrids, but their counterparts in the *cis* alkaloid fraction of hybrids were not detectable.

In both alkaloid fractions, two series of piperideines were found. $\Delta^{1,6}$-Piperideines, **3**, **6**, **8**, **12**, **14**, **18**, and **20**, were identified by characteristic mass ions m/z 96, 111, $[M^+]$, and $[M - 15]^+$, whereas $\Delta^{1,2}$-piperideines, **4**, **9**, **10**, **15**, and **16**, were identified by characteristic mass ions m/z 96, 97, 110, $[M^+]$, and $[M - 15]^+$.[6,13,15−17] As reduction of these piperideines to piperidine was proposed to be the final step of biosynthesis of piperidine alkaloids in *Solenopsis* fire ants, the absolute configuration of piperideines was established as (2*R*) or (6*R*).[15,21,22] GC trace of the *cis* alkaloid fraction had distinctive $\Delta^{1,6}$-piperideine peaks, mainly 12, 14, and 18 (for instance, in *S. invicta*), but fairly visible $\Delta^{1,2}$-piperideine peaks. GC traces of the *trans* alkaloid fraction also had $\Delta^{1,6}$-piperideine and $\Delta^{1,2}$-piperideine peaks in trace amounts. The intermolecular hydrogen bonding between nitrogen (−N═) of piperideine and hydrogen (H−*N*<) of piperidine might cause the inseparability of piperideines and piperidines and the slow elution of piperideines in the *trans* alkaloid fraction. The fact that we did not detect any alkaloidal components in the chromatographic collections between the *cis* and *trans* alkaloid fractions also supports this interpretation. The GC profile of piperideines in the *cis* alkaloid fraction of hybrids showed intermediate characteristics similar to those of the *cis* and *trans* alkaloids.

The external standard method was used to obtain the regression equation. We used log-transformed data to construct a calibration curve, $\log(A) = 0.9894 \log(C) + 1.2551$, where A is the peak area and C is the concentration of the standard compound (ng/μL). The selected piperidine standard showed good linearity ($r^2 = 0.9996$, $P < 0.001$) in relatively wide concentration ranges. Then the obtained calibration curve was used to determine alkaloidal components in all ant samples (Table 1).

Among the *cis* alkaloids, *cis*-C13:1 (peak 5) in *S. richteri* had the highest amount, 231.52 ± 33.97 μg/g, of ant workers. All three ant species had large amounts of shared *trans* alkaloids. *trans*-C13:1 (peak 5′) was quantitatively the most dominant component with 5618.02 ± 628.26 μg/g in *S. richteri*, whereas *trans*-C15:1 (peak 11′) was quantitatively the major component with 4257.75 ± 315.05 μg/g in *S. invicta*. These two components were both predominating in hybrids. The amounts of piperideines were all relatively low in the three ant species. In most cases, the amounts of these piperideines were under 10 μg/g of worker ants. The results of the statistical analysis showed that significant differences were detected for all peaks with only one exception, $\Delta^{1,2}$-C15:1 (peak 15), suggesting that there exists interspecific variation for all *cis* and *trans* alkaloids and piperideines. For any given alkaloidal component, the amount in hybrids was always intermediate to that of *S. richteri* and *S. invicta*. Although in some cases there was statistical nondifference between hybrids and the parental species, the amount of hybrids was always numerically either higher or lower than that of any parental species. Clearly, wide variation in alkaloid chemistry in hybrids resulted in the statistical indifference. This is why, in the current study, the number of hybrid colonies investigated was 2 times higher than that of the parental species. Peaks 11−14, however, were exceptions showing that these were higher in the hybrid than in both parental species. This inconsistency complicated the alkaloid chemistry of hybridization.

It has been previously hypothesized that the venom of ancestral *Solenopsis* species was simple (i.e., contained only a few components) and the evolution of venom alkaloids would have begun with a condition in which the venom contained abundant C11 and minute traces of C13, with the *cis* isomers dominating and the *trans* isomers at a much lower level.[23] The evolution of the alkaloidal compounds in *Solenopsis* could involve two steps: a switch from a probable normal production ratio of *cis*- and *trans*-C11 (**2** and **2′**), to a thermodynamically highly unfavorable decrease in *cis* and an increase in *trans* isomers and further evolution of abundant *trans*-C13 (**7′**) and *trans*-C13:1 (**5′**) and then the addition of *trans*-C15 (**13′**), *trans*-C15:1 (**11′**), *trans*-C17 (**19′**), and *trans*-C17:1 (**17′**), accompanied by a reduction in the production of *trans*-C11 (**2′**).[16,23,24] We first calculated the mean ratio of *trans* to *cis* alkaloids for *S. richteri*, *S. invicta*, and their hybrid (Table 2).

Table 2. Mean Ratio of *trans* Alkaloids to *cis* Alkaloids

no. of carbons	*S. richteri*	*S. invicta*	hybrid
unsaturated side chain			
C11	×[a]		
C13	32.33 ± 6.14 b	133.13 ± 16.92 a	47.76 ± 4.43 b
C15	4.00 ± 0.71 b	176.79 ± 21.22 a	13.31 ± 2.40 b
C17		377.65 ± 90.05	×
saturated side chain			
C11	28.31 ± 6.80 b	87.37 ± 24.23 a	38.21 ± 7.60 b
C13	20.37 ± 3.35 b	160.20 ± 22.06 a	50.25 ± 5.68 b
C15	4.17 ± 0.71 b	261.47 ± 38.62 a	17.65 ± 2.78 b
C17		110.61 ± 21.65	×
both unsaturated and saturated side chains			
C11	28.47 ± 6.84 b	87.37 ± 24.23 a	38.21 ± 7.60 b
C13	30.10 ± 5.44 b	142.70 ± 17.92 a	48.00 ± 4.49 b
C15	3.99 ± 0.68 b	192.47 ± 22.82 a	13.86 ± 2.46 b
C17		305.88 ± 73.42	×

[a]Only *trans* alkaloids were detected.

The ratios of *trans* to *cis* alkaloids in *S. invicta* were significantly greater than in *S. richteri*, and the ratios in hybrids were numerically but not significantly greater than in *S. richteri*, indicating that this character in hybrids was intermediate to both parental species. The ratios for combined alkaloids with the same length of unsaturated and saturated side chains in *S. invicta* ranged from 87.37 to 305.88, suggesting that *trans* alkaloids were extremely predominant in this ant species. Brand et al.[23] gave rough estimates of the ratio of *trans*-C11 (**2′**), to *cis*-C11 (**2**), collected from 10 individuals of *S. richteri* and of *S. invicta*, which were all 10:1. In this study, we present data calculated from 1 g of pooled ant samples. The ratios of *trans*-C11 (**2′**), to *cis*-C11 (**2**), for *S. richteri* and *S. invicta*, were 28.31 ± 6.80, and 87.37 ± 24.23, respectively, which were much greater than the reported data.[23] The venoms of several species native to the United States, *Solenopsis aurea*, *S. xyloni*, and *S. geminata*, consisted mainly of *cis*-C11 (**2**) and *trans*-C11 (**2′**). The ratio of *trans*-C11 (**2′**), to *cis*-C11 (**2**), in pooled samples of the first two species was about 1:4, whereas it was 1:1.2−1.5 in the latter species.[7,8,23,25] On this basis, *S. aurea*, *S. xyloni*, and *S. geminata* would appear to be the more primitive species, whereas *S. richteri* and *S. invicta* are relatively newer species. The venom of *Solenopsis eduardi* (a close relative of *S. geminata*) collected from Colombia consisted of > 98% *trans*-C11 (**2′**) and about 1% of the corresponding *cis* isomer (**2**),[8] which represented a major shift from *cis*-C11 (**2**) to *trans*-C11 (**2′**). Furthermore, the ratios of *trans* alkaloids to *cis* alkaloids for *S. invicta* were significantly higher than for *S. richteri*, suggesting that *S. invicta* is a much newer species than *S. richteri*.

Second, we calculated the total alkaloids with the same side-chain length at the 6-position of the piperidine and/or piperideine ring (Table 3). The *cis* alkaloids and piperideines were minor components, whereas the *trans* alkaloids were major components. Furthermore, the *cis* alkaloids and piperideines in *S. richteri* were relatively higher than in *S. invicta*. The *trans* alkaloids C11 (**2′**) and C13 (**5′** and **7′**) were predominant in *S. richteri*, whereas the *trans* alkaloids C13 (**5′** and **7′**) and C15 (**11′** and **13′**) were predominant in *S. invicta*. Hybrids showed intermediate characteristics between the two parental species. However, there were two exceptions, *cis*-C15 (including *cis*-C15 (**13**) and *cis*-C15:1 (**11**)) and piperideines C15 (including **12**, **14**, **15**, and **16**). Hybrids had significantly greater amounts of *cis*-C15 (**11** + **13**) and piperideines C15 (**12** + **14** + **15** + **16**) than *S. richteri* and *S. invicta*, which possibly resulted from wide variations in alkaloid chemistry among hybrid colonies. Data from Table 3 clearly demonstrated the dominance of *trans*-C13 (**5′** + **7′**) along with the addition of *trans*-C15 (**11′** + **13′**) and *trans*-C17 (**17′** + **19′**), accompanied by a reduction in the production of *trans*-C11 (**2′**).

Table 3. Total Amounts of Alkaloids with the Same Side Chain Length at the 6-Position of the Piperidine Ring

	amount (μg/g ± SE)		
no. of carbons	*S. richteri*	*S. invicta*	hybrid
cis alkaloids			
C11	81.16 ± 12.28 a	1.48 ± 0.30 b	17.78 ± 2.76 b
C13	260.15 ± 40.70 a	25.24 ± 3.01 c	110.08 ± 10.83 b
C15	87.49 ± 13.26 b	32.55 ± 4.04 b	173.36 ± 26.49 a
C17		1.01 ± 0.20	
trans alkaloids			
C11	1862.22 ± 323.69 a	87.15 ± 11.76 b	510.58 ± 58.98 b
C13	6427.74 ± 676.80 a	3290.88 ± 272.96 c	4811.32 ± 345.47 b
C15	329.35 ± 60.03 c	5727.91 ± 416.95 a	1817.76 ± 209.78 b
C17		248.34 ± 37.18 a	24.40 ± 3.86 b
piperideines			
C11	10.03 ± 1.21 a		0.68 ± 0.13 b
C13	44.49 ± 3.24 a	12.29 ± 1.28 c	22.24 ± 2.02 b
C15	75.83 ± 10.36 b	60.93 ± 7.10 b	183.92 ± 18.85 a
C17		7.37 ± 1.32	
total alkaloids[a]			
C11	1953.40 ± 320.55 a	88.63 ± 11.71 b	529.03 ± 60.89 b
C13	6732.39 ± 657.22 a	3328.41 ± 273.44 c	4943.64 ± 352.69 b
C15	492.67 ± 75.13 c	5821.38 ± 420.66 a	2175.04 ± 216.92 b
C17		256.72 ± 37.19 a	24.40 ± 3.86 b

[a]Total alkaloids mean sum of the *cis*, *trans* piperidines and piperideines with the same side chain length at the 6-position of the piperidine and piperideine rings.

Third, we calculated the total amounts of the *cis* and *trans* alkaloids and all alkaloids detected from all three ant species (Figure 2). *S. invicta* had a significantly lower amount of *cis*

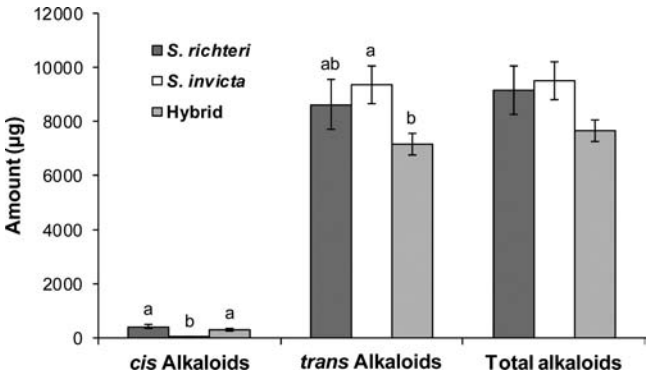

Figure 2. Amounts of alkaloids isolated from 1 g of ant workers. Total alkaloids are the sum of *cis* alkaloids, *trans* alkaloids, and piperideines. Means for same alkaloid type having no letter in common are significantly different ($P < 0.05$, Tukey–Kramer HSD test).

alkaloids than *S. richteri* and hybrids. In contrast, *S. invicta* had a significantly greater amount of *trans* alkaloids than hybrids and a relatively, but not significantly, greater amount than *S. richteri*. Hybrids produced a slightly lower amount of total alkaloids compared to the two parental species. The total amounts of alkaloids produced by 1 g of ant workers of the three species ranged from 8 to 10 mg, meaning that ant workers can produce up to 1% alkaloids of their body weight. The order of total amounts of alkaloids was *S. invicta* > *S. richteri* > hybrids even though the differences were not statistically significant (Figure 2). If the production of venom alkaloids represents competition ability of an ant species, a relatively lower production of total alkaloids in hybrids would decrease their fitness. It has been suggested that hybrid fire ants have reduced relative fitness compared to their parent species due to intrinsic selection.[26] Aggression toward heterospecifics has been used as a measure of fitness among sympatric congeneric species.[27] It was found that *S. invicta* had the lowest aggression threshold, whereas *S. richteri* was the least aggressive.[19] Moderate aggression threshold of hybrids might be related to intermediate chemistry in venom alkaloids shown in this study.

Piperideine alkaloid was first found in *S. xyloni* as $\Delta^{1,2}$-C11 (**4**).[6] Recently, several studies have reported the identification of a series of $\Delta^{1,2}$- and $\Delta^{1,6}$-piperideine alkaloids from the workers and alate queens of the imported fire ants.[13−18] The $\Delta^{1,2}$- and $\Delta^{1,6}$-piperideines have been proposed to function as precursors for biosynthesis of *cis* and *trans* alkaloids in fire ant venom.[15,22] Reduction of $\Delta^{1,6}$-piperideine or $\Delta^{2,3}$-piperideine gave a ratio of the *cis*-C11 to the *trans*-C11 of 4:1.[28,29] The composition of *cis*- and *trans*-C11 (**2** and **2′**), in *S. aurea* matched that of the equilibrium mixture formed during their chemical synthesis in the laboratory. This matchup supports the above hypothesis on the biosynthetic function of piperideines. As the imported *Solenopsis* fire ants have the biosynthetic capacity to synthesize mainly *trans* alkaloids, it is likely that enantioselective enzymes are present in these species which can reduce $\Delta^{1,2}$-piperideines exclusively into (2*R*,6*R*) dialkylpiperidines and $\Delta^{1,6}$-piperideines mainly into (2*R*,6*R*) and partially into (2*R*,6*S*) dialkylpiperidines. In most cases, the amount of $\Delta^{1,2}$-piperideine was similar to that of corresponding $\Delta^{1,6}$-piperideine (same side-chain length at the 6-position) (data shown in Table 1), suggesting that the two reduction routes are equally important in the biosynthesis of alkaloids in the imported fire ants.[15] In contrast, the detection of only $\Delta^{1,2}$-C11 (**4**) in *S. xyloni* together with a higher ratio of *cis*-C11 (**2**) to *trans*-C11 (**2′**) found in this species supported the hypothesis that the $\Delta^{1,2}$-C11 pathway could be more important than the $\Delta^{1,6}$-C11 pathway in more primitive *Solenopsis* species. Therefore, all *Solenopsis* fire ants may utilize similar biosynthetic pathways to produce both *cis* and *trans* alkaloids and even maintain favorable stereochemical composition diverging rather markedly from the thermodynamic equilibrium mixture.[15,16,22] Both $\Delta^{1,6}$-C17:1 (**18**) and $\Delta^{1,6}$-C17 (**20**) were found only in *S. invicta*, suggesting that this species possibly has evolved specific enzymes that could synthesize piperidines with longer and unsaturated side chains associated with greater toxicity and biological advantage.[8]

Pseudacteon phorid flies (Diptera: Phoridae) are parasitoids of ants, and many species are specific to *geminata* and/or *saevissima* species groups of the genus *Solenopsis*.[30] Nineteen of these parasitic flies are specifically associated with the *saevissima* group[31] and generally show an attack preference for imported fire ants over native fire ants.[32−40] Several phorid fly species, *Pseudacteon tricuspis*, *P. curvatus*, *P. litoralis*, *P. obtusus*, and *P. cultellatus*, have been introduced to the southern United States for biological control of the invasive imported fire ant complex in the past two decades.[41] Established populations of *P. tricuspis* have proved to be highly host specific to imported *Solenopsis* fire ants.[42] Previous studies have demonstrated that *P. tricuspis* utilizes fire ant venom alkaloids for host location.[43,44] In addition to five *cis* alkaloids (*cis*-C11 (**2**), *cis*-C13:1 (**5**), *cis*-C13 (**7**), *cis*-C15:1 (**11**), and *cis*-C15 (**13**)) and two *trans* alkaloids (*trans*-C11 (**2′**) and *trans*-C13:1 (**5′**)), two piperideine alkaloids, $\Delta^{1,6}$-C15:1 (**12**) and $\Delta^{1,6}$-C15 (**14**) from *S. invicta* were shown to elicit significant electrophysiological response in *P. tricuspis* by GC-EAD analysis. As shown in Figure 1 and Table 1, the quantities of these two $\Delta^{1,6}$-piperideines were relatively greater than those of the remaining piperideines. $\Delta^{1,6}$-C15:1 (**12**) and $\Delta^{1,6}$-C15 (**14**) from *S. richteri* and hybrids could also trigger a similar GC-EAD response in *P. tricuspis* (unpublished data). Dominance of the *cis* alkaloids suggests possible attraction of *P. tricuspis* to North America-native fire ants such as *S. xyloni* and *S. geminata*. *P. tricuspis* is frequently attracted to disturbed ant colonies, and venom release is part of the alarm response and probably a component of the complex alarm odor.[45] A recent study has proved that *P. tricuspis* was attracted to 2-ethyl-3,6 (or 5)-dimethylpyrazine, a commercially available mixture of fire ant alarm pheromone component (2-ethyl-3,6-dimethylpyrazine) and its isomer.[46] The alarm pheromone and venom alkaloids proved to act in concert to attract phorid flies to fire ant workers.[43] It is conceivable that the highly volatile pyrazine alarm pheromone serves as a general host location cue from long range, whereas the larger and less volatile venom alkaloids may play a major role in host preference and discrimination at close range.[43,46] As pyrazine alarm pheromone is a general odor in *Solenopsis* fire ants (R. K. Vander Meer, personal communication), it seems unlikely that phorid flies use ant alarm pheromone for host preference and discrimination.

Different *Pseudacteon* species display different levels of host specificity. Most fly species showed very low attack rate when tested in laboratory conditions against the native fire ant *S. geminata*. However, *P. curvatus* and *P. borgmeieri* freely attacked both *S. invicta* and *S. geminata*. Both fly species developed in *S.*

geminata but with apparent low success.[47] A recent study has demonstrated that *P. curvatus* preferred the alkaloid mixture (*cis* + *trans* alkaloids), whereas *P. tricuspis* showed relatively greater attraction to the *cis* alkaloids.[43] The alkaloid patterns, including the presence and quantity of individual alkaloid components, the ratios of the *trans* to *cis* alkaloids, and the presence of piperideines, are species-specific for *Solenopsis* fire ants. Attraction of *P. curvatus* and *P. borgmeieri* to *S. geminata* may be mediated by presence of the *cis* alkaloids, which generally predominate in native fire ants. A previous study showed that *P. tricuspis* is able to distinguish among *S. richteri*, *S. invicta*, and hybrid fire ants with greater preference for *S. invicta* and hybrids.[48] It is likely that the ratios of the *cis* and *trans* alkaloids, the presence of piperideines, and the quantitative difference in alkaloids detected in this study might be responsible for the reported host preference in phorid flies.

AUTHOR INFORMATION

Corresponding Author

*(L.C.) Phone: +86 10 64807780. Fax: +86 10 64807780. E-mail: chenli@ioz.ac.cn.

Funding

This work was supported by the National Basic Research Program of China (973 Program, Grant 2012CB114105), National Natural Science Foundation of China (Grant 30970402), and National Science and Technology Support Program (Grant 2012BAC11B06).

Notes

The authors declare no competing financial interest.

REFERENCES

(1) Trager, J. C. A revision of the fire ants, *Solenopsis geminata* group (Hymenoptera: Formicidae: Myrmicinae). *J. N. Y. Entomol. Soc.* **1991**, *99*, 141−198.

(2) MacConnell, J. G.; Blum, M. S.; Fales, H. M. Alkaloid from fire ant venom: identification and synthesis. *Science* **1970**, *168*, 840−841.

(3) MacConnell, J. G.; Blum, M. S.; Fales, H. M. Chemistry of fire ant venom. *Tetrahedron* **1971**, *27*, 1129−1139.

(4) MacConnell, J. G.; Williams, R. N.; Brand, J. M.; Blum, M. S. New alkaloids in the venoms of fire ants. *Ann. Entomol. Soc. Am.* **1974**, *67*, 134−135.

(5) Blum, M. S.; Fales, H. M.; Leadbetter, G.; Leonhardt, B. A.; Duffield, R. M. A new dialkylpiperidine in the venom of the fire ant *Solenopsis invicta*. *J. Nat. Toxins* **1992**, *1*, 57−63.

(6) Brand, J. M.; Blum, M. S.; Fales, H. M.; MacConnell, J. G. Fire ant venoms: comparative analyses of alkaloidal components. *Toxicon* **1972**, *10*, 259−271.

(7) Brand, J. M.; Blum, M. S.; Barlin, M. R. Fire ant venoms: intraspecific and interspecific variation among castes and individuals. *Toxicon* **1973**, *11*, 325−331.

(8) MacConnell, J. G.; Blum, M. S.; Buren, W. F.; Williams, R. N.; Fales, H. M. Fire ant venoms: chemotaxonomic correlations with alkaloidal compositions. *Toxicon* **1976**, *14*, 69−78.

(9) Vander Meer, R. K.; Lofgren, C. S.; Alvarez, F. M. Biochemical evidence for hybridization in fire ants. *Fla. Entomol.* **1985**, *68*, 501−506.

(10) Vander Meer, R. K.; Lofgren, C. S. Biochemical and behavioral evidence for hybridization between fire ants, *Solenopsis invicta* and *Solenopsis richteri* (Hymenoptera: Formicidae). *J. Chem. Ecol.* **1989**, *15*, 1757−1765.

(11) Ross, K. G.; Vander Meer, R. K.; Fletcher, D. J. C.; Vargo, E. L. Biochemical phenotypic and genetic studies of two introduced fire ants and their hybrid (Hymenoptera: Formicidae). *Evolution* **1987**, *41*, 280−293.

(12) Vander Meer, R. K.; Lofgren, C. S. Use of chemical characters in defining populations of fire ants, *Solenopsis saevissima* complex, (Hymenoptera: Formicidae). *Fla. Entomol.* **1988**, *71*, 323−332.

(13) Chen, J.; Cantrell, C. L.; Shang, H.-W.; Rojas, M. G. Piperideine alkaloids from the poison gland of the red imported fire ant (Hymenoptera: Formicidae). *J. Agric. Food Chem.* **2009**, *57*, 3128−3133.

(14) Chen, J.; Shang, H.; Jin, X. Interspecific variation of $\Delta^{1,6}$-piperideines in imported fire ants. *Toxicon* **2010**, *55*, 1181−1187.

(15) Chen, L.; Fadamiro, H. Y. Re-investigation of venom chemistry in *Solenopsis* fire ants. I. Identification of novel alkaloids in *S. richteri*. *Toxicon* **2009**, *53*, 463−478.

(16) Chen, L.; Fadamiro, H. Y. Re-investigation of venom chemistry in *Solenopsis* fire ants. II. Identification of novel alkaloids in *S. invicta*. *Toxicon* **2009**, *53*, 479−486.

(17) Chen, L.; Hu, Q.-B.; Fadamiro, H. Y. Reduction of venom alkaloids in *Solenopsis richteri* × *Solenopsis invicta* hybrid: an attempt to identify new alkaloidal components. *J. Agric. Food Chem.* **2010**, *58*, 11534−11542.

(18) Chen, L.; Lu, Y.-Y.; Hu, Q.-B.; Fadamiro, H. Y. Similarity in venom alkaloid chemistry of alate queens of imported fire ants: Implication for hybridization between *Solenopsis richteri* and *S. invicta* in the southern United States. *Chem. Biodivers.* **2012**, *9*, 702−713.

(19) Fadamiro, H. Y.; He, X.-F.; Chen, L. Aggression in imported fire ants: an explanation for shifts in their spatial distributions in southern United States? *Ecol. Entomol.* **2009**, *34*, 427−436.

(20) SAS Institute. *SAS User's Guide*; SAS Institute: Cary, NC, USA, 2004.

(21) Leclercq, S.; Thirionet, I.; Broeders, F.; Daloze, D.; Vander Meer, R. K.; Braekman, J. C. Absolute configuration of the solenopsins, venom alkaloids of the fire ants. *Tetrahedron* **1994**, *50*, 8465−8478.

(22) Leclercq, S.; Braekman, J. C.; Daloze, D.; Pasteels, J. M.; Vander Meer, R. K. Biosynthesis of the solenopsins, venom alkaloids of the fire ants. *Naturwissenschaften* **1996**, *83*, 222−225.

(23) Brand, J. M.; Blum, M. S.; Ross, H. H. Biochemical evolution in fire ant venoms. *Insect Biochem.* **1973**, *3*, 45−51.

(24) Brand, J. M. Fire ant venom alkaloids: their contribution to chemosystematics and biochemical evolution. *Biochem. Syst. Ecol.* **1978**, *6*, 337−340.

(25) Blum, M. S.; Brand, J. M.; Duffield, R. M.; Snelling, R. R. Chemistry of the venom of *Solenopsis aurea* (Hymenoptera: Formicidae). *Ann. Entomol. Soc. Am.* **1973**, *66*, 702.

(26) Shoemaker, D. D.; Ross, K. G.; Arnold, M. L. Genetic structure and evolution of a fire ant hybrid zone. *Evolution* **1996**, *50*, 1958−1976.

(27) Obin, M. S.; Vander Meer, R. K. Between- and within-species recognition among imported fire ants and their hybrids (Hymenoptera: Formicidae): application to hybrid zone dynamics. *Ann. Entomol. Soc. Am.* **1989**, *82*, 649−652.

(28) Hill, R. K.; Yuri, T. An approach to natural 2-alkyl-6-methylpiperidines via *N*-acyllactam rearrangement. *Tetrahedron* **1977**, *33*, 1569−1571.

(29) Jefford, C. W.; Jian, B. W. An enantiospecific synthesis of solenopsin A. *Tetrahedron Lett.* **1993**, *34*, 2911−2914.

(30) Porter, S. D. Biology and behavior of *Pseudacteon* decapitating flies (Diptera: Phoridae) that parasitize *Solenopsis* fire ants (Hymenoptera: Formicidae). *Fla. Entomol.* **1998**, *81*, 292−309.

(31) Porter, S. D.; Pesquero, M. A. Illustrated key to *Pseudacteon* decapitating flies (Diptera: Phoridae) that attack *Solenopsis saevissima* complex fire ants in South America. *Fla. Entomol.* **2001**, *84*, 691−699.

(32) Gilbert, L. E.; Morrison, L. W. Patterns of host specificity in *Pseudacteon* parasitoid flies (Diptera: Phoridae) that attack *Solenopsis* fire ants (Hymenoptera: Formicidae). *Environ. Entomol.* **1997**, *26*, 1149−1154.

(33) Folgarait, P. J.; Bruzzone, O. A.; Patrock, R. J. W.; Gilbert, L. E. Developmental rates and host specificity for *Pseudacteon* parasitoids (Diptera: Phoridae) of fire ants (Hymenoptera: Formicidae) in Argentina. *J. Econ. Entomol.* **2002**, *95*, 1151−1158.

(34) Porter, S. D.; Alonso, L. E. Host specificity of fire ant decapitating flies (Diptera: Phoridae) in laboratory oviposition tests. *J. Econ. Entomol.* **1999**, *92*, 110−114.
(35) Vazquez, R. J.; Porter, S. D.; Briano, J. A. Host specificity of a biotype of the fire ant decapitating fly *Pseudacteon curvatus* (Diptera: Phoridae) from northern Argentina. *Environ. Entomol.* **2004**, *33*, 1436−1441.
(36) Vazquez, R. J.; Porter, S. D. Re-confirming host specificity of the fire ant decapitating fly *Pseudacteon curvatus* (Diptera: Phoridae) after field release in Florida. *Fla. Entomol.* **2005**, *88*, 107−110.
(37) Porter, S. D.; Fowler, H. G.; Campiolo, S.; Pesquero, M. A. Host specificity of several *Pseudacteon* (Diptera: Phoridae) parasites of fire ants (Hymenoptera: Formicidae) in South America. *Fla. Entomol.* **1995**, *78*, 70−75.
(38) Porter, S. D. Host-specific attraction of *Pseudacteon* flies (Diptera: Phoridae) to fire ant colonies in Brazil. *Fla. Entomol.* **1998**, *81*, 423−429.
(39) Morrison, L. W.; Gilbert, L. E. Host specificity in two additional *Pseudacteon* spp. (Diptera: Phoridae), parasitoids of *Solenopsis* fire ants (Hymenoptera: Formicidae). *Fla. Entomol.* **1999**, *82*, 404−409.
(40) Estrada, C.; Patrock, R. W.; Folgarait, P. J.; Gilbert, L. E. Host specificity of four *Pseudacteon* spp. (Diptera: Phoridae), parasitoids of fire ants in Argentina (Hymenoptera: Formicidae). *Fla. Entomol.* **2006**, *89*, 462−468.
(41) Callcott, A.-M. A.; Porter, S. D.; Weeks, R. D., Jr.; Graham, L. C. F.; Johnson, S. J.; Gilbert, L. E. Fire ant decapitating fly cooperative release programs (1994−2008): two *Pseudacteon* species, *P. tricuspis* and *P. curvatus*, rapidly expand across imported fire ant populations in the southeastern United States. *J. Insect Sci.* **2011**, *11*, 1−25.
(42) Morrison, L. W.; Porter, S. D. Post-release host-specificity testing of *Pseudacteon tricuspis*, a phorid parasitoid of *Solenopsis invicta* fire ants. *BioControl* **2006**, *51*, 195−205.
(43) Sharma, K. R.; Fadamiro, H. Y. Fire ant alarm pheromone and venom alkaloids act in concert to attract parasitic phorid flies, *Pseudacteon* spp. *J. Insect Physiol.* **2013**, *59*, 1119−1124.
(44) Chen, L.; Sharma, K. R.; Fadamiro, H. Y. Fire ant venom alkaloids act as key attractants for the parasitic phorid fly, *Pseudacteon tricuspis* (Diptera: Phoridae). *Naturwissenschaften* **2009**, *96*, 1421−1429.
(45) Morrison, L. W.; King, J. R. Host location behavior in a parasitoid of imported fire ants. *J. Insect Behav.* **2004**, *17*, 367−383.
(46) Sharma, K.; Vander Meer, R. K.; Fadamiro, H. Y. Phorid fly, *Pseudacteon tricuspis*, response to alkylpyrazine analogs of a fire ant, *Solenopsis invicta*, alarm pheromone. *J. Insect Physiol.* **2011**, *57*, 939−944.
(47) Porter, S. D.; Gilbert, L. E. Assessing host specificity and field release potential of fire ant decapitating flies (Phoridae: Pseudacteon). In *Assessing Host Ranges for Parasitoids and Predators used for Classical Biological Control: A Guide to Best Practice*; van Driesche, R. G., Reardon, R., Eds.; Forest Health Technology Enterprise Team 2004-03; USDA Forest Service: Morgantown, WV, USA, 2004; pp 152−176.
(48) He, X. F.; Fadamiro, H. Y. Host preference in *Pseudacteon* phorid flies: response of *P. tricuspis* and *P. curvatus* to black, red and hybrid imported *Solenopsis* fire ants in multiple choice bioassays. *Biol. Control* **2009**, *51*, 116−121.

■ NOTE ADDED AFTER ASAP PUBLICATION

This article published June 11, 2014 with an error in Figure 1. The correct version published June 17, 2014.

JOURNAL OF AGRICULTURAL AND FOOD CHEMISTRY

Article

pubs.acs.org/JAFC

β-Lactoglobulin as a Vector for β-Carotene Food Fortification

Azza Mensi,[†,‡,§,∥] Patrick Borel,[‡,§,∥] Aurélie Goncalves,[‡,§,∥] Marion Nowicki,[‡,§,∥] Béatrice Gleize,[‡,§,∥] Stéphanie Roi,[‡,§,∥] Jean-Marc Chobert,[†] Thomas Haertlé,[†] and Emmanuelle Reboul*[,‡,§,∥]

[†]Biopolymères Interactions Assemblages, INRA, UR 1268, F-44316 Nantes, France

[‡]Nutrition, Obesity and Risk of Thrombosis, INRA, UMR 1260, F-13385 Marseille, France

[§]INSERM, UMR 1062, F-13385 Marseille, France

[∥]Aix Marseille Université, F-13385 Marseille, France

ABSTRACT: Food fortification is a strategy to overcome vitamin A deficiency in developing countries. Our aim was to investigate the involvement of the bovine milk protein β-lactoglobulin (β-Lg), a potential retinoid carrier, in vitamin A absorption. *In vivo* experiments were conducted by force-feeding mice with retinol or β-carotene associated with either β-Lg or oil-in-water emulsion, with subsequent determination of both vitamin A intestinal mucosa and plasma contents. Caco-2 cells were then used to investigate the mechanisms of vitamin A uptake when delivered by either β-Lg or mixed micelles. We showed that β-Lg was as efficient as emulsion to promote β-carotene, but not retinol, absorption in mice. Similar results were obtained *in vitro*. Interestingly, an inhibitor of the Scavenger Receptor Class B Type I significantly decreased the uptake of micellar β-carotene but not that of β-carotene bound to β-Lg. Overall, we showed that β-Lg would be a good vector for β-carotene food fortification.

KEYWORDS: *vitamin A, retinol, carotenoid, micelles, emulsion*

INTRODUCTION

Vitamin A insufficiency is still a public health issue in numerous countries. It affects more than 190 million children throughout the world, mostly in African and South East Asian developing countries.[1] Rising knowledge about the mechanisms of vitamin A absorption is therefore necessary to set up better approaches for ameliorating its bioavailability.[2]

Vitamin A refers to a group of polyunsaturated hydrocarbons playing important roles in different aspects of human development and health including gene transcription, vision, and dermatology.[3] It is found in the human diet either as preformed vitamin A in foods from animal origin, or as provitamin A carotenoids in foods from plant origin. The main molecules belonging to the preformed vitamin A are retinyl esters, and primarily retinyl palmitate, which is hydrolyzed to retinol during the digestion process.[4] The main provitamin A carotenoid is β-carotene, which is primarily converted to retinol in the intestine and somewhat in hepatic cells.[5]

β-lactoglobulin (β-Lg), the major whey protein of bovine milk, binds retinoids and carotenoids *in vitro* with apparent dissociation constants in the range of 10^{-8} M.[6] This protein belongs to the lipocalin family and shares similar structure with retinol binding protein (RBP).[7] Hattori et al. have shown that this protein protects retinoids from degradation and oxidation.[8] Due to its ability to bind various lipophilic molecules, β-Lg has been proposed as an oral drug carrier,[9] and its properties to transport retinol and some other lipophilic molecules through the intestinal cells have also been reported.[10−12] However, results concerning the intestinal transport of retinol bound to β-Lg by Caco-2 cells were not consistent with those found *ex vivo*. Indeed, Riihimaki and colleagues showed that retinol was transported in a more efficient manner across Caco-2 cells when it was free than when it was bound to β-Lg,[11] while other authors showed that the uptake of retinol by the intestinal tissues of suckling rat was higher when bound to β-Lg than when it was free.[13] Finally no data are available on the effect of β-Lg on β-carotene uptake by the enterocyte. Thus, the effect of β-Lg on vitamin A uptake by intestinal cells is barely known, and in spite of its interesting properties and its presumed carrier role, it is difficult to conclude its effect on vitamin A uptake as compared to vitamin A uptake in its physiological vehicle, i.e. mixed micelles.

The purpose of this study was thus to compare the uptake of vitamin A, either as retinol or as β-carotene, when it is associated with β-Lg or when it is incorporated into a lipid vector (micelles or emulsions). Retinol was chosen instead of retinyl palmitate in our experiments as in Caco-2 cells, the ester hydrolysis occurring during digestion cannot be mimicked.

MATERIAL AND METHODS

Chemicals. All-*trans*-retinol (≥99% pure), β-carotene (≥93% pure), 2-oleoyl-1-palmitoyl-*sn*-glycero-3-phosphocholine (phosphatidylcholine), 1-palmitoyl-*sn*-glycero-3-phosphocholine (lysophosphatidylcholine), monoolein, cholesterol, oleic acid, and sodium taurocholate, were purchased from Sigma-Aldrich (Saint-Quentin-Fallavier, France). Internal standards used were retinyl acetate (Sigma-Aldrich), echinenone (generously provided by DSM LTD formerly F. Hoffmann-La Roche, Basel, Switzerland) and tocopherol acetate (all-*rac*-α-TAC oil feed grade, purity: 95% generously provided by Adisseo, Anthony, France). Dulbecco's Modified Eagle Medium (DMEM) containing 4.5 g/L glucose, trypsin-EDTA (500 and 200 mg/L, respectively), nonessential amino

Received: April 11, 2014
Revised: May 23, 2014
Accepted: May 26, 2014
Published: May 26, 2014

ACS Publications © 2014 American Chemical Society

dx.doi.org/10.1021/jf501683s | J. Agric. Food Chem. 2014, 62, 5916−5924

acids and penicillin/streptomycin were purchased from Life Technology (Saint Aubin, France). FBS was from PAA (Velizy-Villacoublay, France). Blocks lipid transport 1 (BLT1), which is a specific inhibitor of Scavenger receptor class B type I (SR-BI) that does not interfere with receptor-mediated endocytosis or other forms of intracellular vesicular traffic,[14] was purchased from Chembridge (San Diego, CA, U.S.A). Ezetimibe-glucuronide (the active metabolite of ezetimibe, which is the specific inhibitor of Niemann-Pick C1 Like 1, NPC1L1[15]) was a generous gift from E. Levy (CHU Ste Justine, Montréal, Canada).

Preparation of Retinol and β-Carotene Enriched Vectors for Mouse and Cell Experiments. *Preparation of Retinol and β-Carotene Protein Complexes.* Cow β-Lg variant A (≥95%) was extracted as judged from high performance liquid chromatography as described before.[6] Human retinol binding protein (RBP, ≥85% pure) and bovine serum albumin (BSA, ≥95% pure) were from Sigma-Aldrich. Each protein was diluted in DMEM, and then mixed with either retinol in ethanol or β-carotene in tetrahydrofuran (THF) in appropriate concentrations. The final ethanol or THF concentrations in the medium were less than 0.1%. β-Lg was prepared at concentrations varying from 0.1 to 10 mg/mL, depending on the experiment. BSA and RBP were used at a concentration of 0.1 mg/mL. In all experiments, retinol and β-carotene concentrations were fixed between 3.8 and 5 μmol/L.

Preparation of Retinol and β-Carotene-Rich Emulsions. For the delivery of retinol or β-carotene to mice, oil-in-water vitamin A-rich emulsions were prepared as follows. An appropriate volume of retinol and β-carotene stock solution was transferred into Eppendorf tubes to obtain a final amount of 250 μg in each tube. Stock solution solvent was carefully evaporated under nitrogen. Dried residue was solubilized in 100 μL of peanut oil, and 200 μL of PBS solution was added. The mixture was vigorously sonicated in water (Branson 3510 sonication bath, Branson, MO, U.S.A.) for 15 min and used for force-feeding within 10 min.[16] The particle size of the emulsions was measured using a Malvern Mastersizer (Malvern Instruments, Orsay, France) and was around 30 μm in diameter.

Preparation of Retinol and β-Carotene-Rich Micelles. For the delivery of retinol and β-carotene to human intestinal Caco-2 clone TC7 cell monolayers, mixed micelles were prepared as published previously[17] to obtain the following final concentrations: 0.04 mmol/L phosphatidylcholine, 0.16 mmol/L lysophosphatidylcholine, 0.3 mmol/L monoolein, 0.1 mmol/L free cholesterol, 0.5 mmol/L oleic acid, 3.8−5 μmol/L retinol or β-carotene,[18] and 5 mmol/L taurocholate. Measurements of the size distribution of the micelles were carried out to control the stability of the micelle size (∼13 nm of diameter) with a Malvern Zetasizer Nano ZS.

Mouse Experiments. *Animals.* Six-week-old wild-type male C57BL/6 Rj mice were purchased from Janvier (Le-Genest-St-Isle, France). The mice were housed in a temperature-, humidity-, and light-controlled room. They were given a standard chow diet and water ad libitum. During acclimation period, mice were housed four per cage. Mice were fasted overnight before each experiment. Eight male mice weighing 21−24 g were used for retinol gavage and eight male mice weighing 24−28 g were used for β-carotene gavage. The protocol was approved by the ethics committee of Marseilles (Agreement #4-5032010).

Postprandial Blood Sample Collection. For absorption studies, mice were force-fed with either a retinol- or a β-carotene-rich emulsion (n = 4) or with retinol or β-carotene bound to β-Lg (n = 4). At t = 1.5 and 3 h, blood samples were taken by retro-orbital puncture under sevoflurane anesthesia. A last sample was taken at 4.5 h by intracardiac puncture before animal euthanasia. For zero baseline samples, four mice were killed upon fasting, and blood samples were collected. Blood samples were collected in tubes with heparin and immediately centrifuged to separate plasma, which was placed on ice and then stored at −80 °C.

Postprandial Intestinal Sample Collection. At 4.5 h after gavage, the mice were killed by cervical dislocation, and their intestines were collected, carefully washed with PBS, and cut into seven fragments corresponding to small intestine (5 fragments of 6 cm), cecum (1 fragment), and colon (1 fragment of 6 cm). All samples were immediately frozen in liquid nitrogen and stored at −80 °C until analysis. Samples suspended in 2 mL RIPA buffer were then homogenized with stainless-steel balls using MM301 ball mills (Retsch, Eragny sur Oise, France). Aliquots of samples were used to assess protein concentrations using a bicinchoninic acid kit (Pierce, Montluçon, France).

Cell Experiments. *Cell Culture.* The human intestinal Caco-2 clone TC-7 cells[19] were cultured in the presence of DMEM supplemented with 20% heat-inactivated FBS, 1% nonessential amino acids, and 1% antibiotics (complete medium) as previously described.[17] For each experiment, the cells were seeded and grown during 21 days on 1 μM filters to obtain confluent differentiated cell monolayers. Twelve hours before each experiment, the medium used in the apical and basolateral chambers was changed to a serum-free complete medium.

Vitamin A-Enriched Vectors Uptake by Caco-2 Cells. The vectors used for vitamin A uptake assessment by Caco-2 cells were either micelles or DMEM supplemented with β-Lg, RBP or BSA or a mixture of micelles and β-Lg at different concentrations.

The apical side received the retinol or β-carotene enriched vector whereas the basolateral side received serum-free complete medium. Cells were incubated for 30 to 240 min at 37 °C, depending on the experiment. At the end of each experiment, media were harvested. Cells were washed in 0.5 mL PBS to eliminate adsorbed vitamin A, then scraped and collected in 0.5 mL PBS. Absorbed vitamin A was estimated as vitamin A found in scraped cells plus vitamin A found at the basolateral side.[20] (No vitamin A was recovered in the basolateral chambers after β-carotene incubation). Aliquots of cell samples were used to assess protein concentrations using a bicinchoninic acid kit.

Effect of SR-BI and NPC1-L1 Chemical Inhibitors on Retinol and β-Carotene Uptake. Differentiated cell monolayers were pretreated with either DMSO (control), BLT1 at 10 μM,[17] or ezetimibe glucuronide at 100 μM[15] in serum-free complete medium for 1 h. The cells then received retinol-enriched micelles or retinol bound to β-Lg in serum-free complete media supplemented with either DMSO, 10 μM of BLT1, or 100 μM of ezetimibe glucuronide. Similar experiments were carried out with β-carotene, and vitamin A uptake was measured as described above.

Verification of Vector Protein Integrity during the Caco-2 Experiments. Due to the presence of enzymes on the Caco-2 cell brush border membrane, degradation state of β-Lg, RBP,

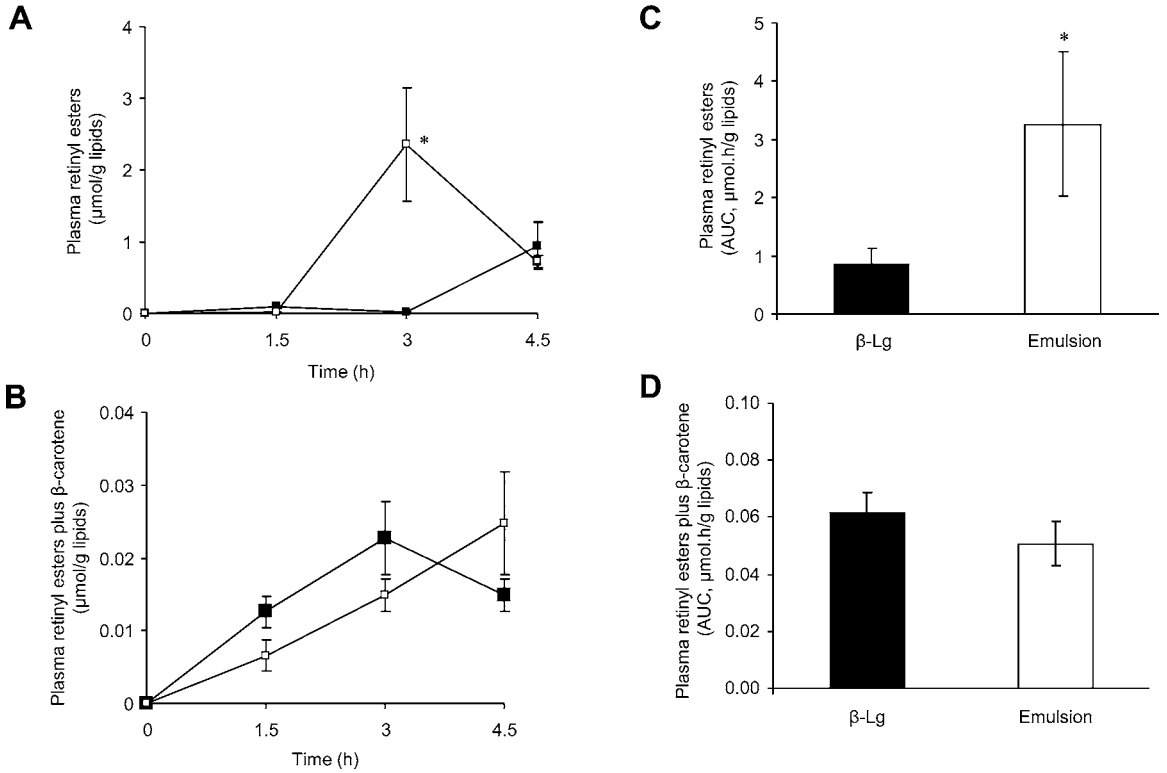

Figure 1. Postprandial changes in plasma total retinyl esters and β-carotene in wild type C57BL/6 Rj mice force fed with (A) retinol-enriched emulsion (□; $n = 4$) or retinol bound to β-Lg (■; $n = 4$) and (B) with β-carotene-enriched emulsion (□; $n = 4$) or β-carotene bound to β-Lg (■ ; $n = 4$). (C) Postprandial plasma retinyl ester responses (area under curves at 0−4.5 h) in mice force fed with retinol-enriched emulsion (□; $n = 4$) or retinol bound to β-Lg (■; $n = 4$). (D) Postprandial plasma retinyl ester plus β-carotene responses (area under curves at 0−4.5 h) after gavage with β-carotene-enriched emulsion (□; $n = 4$) or β-carotene bound to β-Lg (■; $n = 4$). Values are means ± SEM. Plasma samples were taken each 1.5 h after mice force-feeding and retinyl ester and β-carotene concentrations were analyzed. Asterisks indicate significant differences between β-Lg and emulsion ($p < 0.05$; Mann−Whitney U test).

and BSA after the incubation period was evaluated by SDS PAGE using 12% acrylamide gels under reducing conditions according to Laemelli:[21] samples from the apical side were compared to native protein at the same concentration.

Extraction and HPLC Analysis of Retinol, Retinyl Esters and β-Carotene. Retinol, retinyl esters, and β-carotene were extracted from 500 μL aqueous samples by using the following method. Distilled water was added to sample volumes <500 μL to reach a final volume of 500 μL. Retinyl acetate (internal standard for retinol experiments), echinenone (internal standard for *in vitro* β-carotene experiments), and tocopherol acetate (internal standard for *in vivo* β-carotene experiments) were added to the samples in 500 μL ethanol. The mixture was extracted once with 2 volumes of hexane for retinol and retinyl esters and twice with 2 volumes of hexane for β-carotene. All samples from intestinal explants were extracted twice. The hexane phases obtained after centrifugation (500 g, 10 min, 4 °C) were pooled if necessary and evaporated to dryness under nitrogen. The dried extracts were dissolved in either 200 μL acetonitrile/dichloromethane/methanol (70:20:10, vol:vol:vol) for retinol samples[20] or 200 μL acetonitrile/dichloromethane (65:35, vol:vol) for β-carotene.[22] A volume of 10−200 μL was used for HPLC analysis. Retinol experiment analyses were realized by using a 250 mm × 4.6 nm reversed-phase C18 5-μm Zorbax column (Interchim, Montluçon, France) maintained at a constant temperature (35 °C) and a guard column. β-Carotene analyses were performed on a 250 mm × 4.6 nm i.d. YMC C30 column maintained at 35 °C. Retinol was analyzed with a 70% acetonitrile, 20% dichloromethane and 10% methanol mobile phase (flow rate =1.8 mL/min), whereas β-carotene was analyzed with a gradient of methanol, methyl-*tert*-butyl ether, and water (flow rate =1 mL/min) according to Gleize et al.[22] The HPLC system comprised a Dionex separation module (P680 HPLC pump and ASI-100 Automated Sample Injector; Dionex, Aix-en-Provence, France), a Dionex UVD340U photodiode array detector (retinol, retinyl ester and β-carotene detection at 325 and 450 nm, respectively), and a fluorimetric detector (Jasco, Nantes, France). For the fluorimetric analysis, retinol and retinyl esters were detected at 450 nm after light excitation at 325 nm. Retinol, retinyl palmitate and β-carotene were identified by retention time compared with pure (>95%) standards. Quantification was performed by using Chromeleon software (version 6.50, SP4 Build 1000; Dionex Corporation) comparing peak area with standard reference curves. Retinyl linoleate, oleate, and stearate were identified by retention time and spectral analysis and quantified on the basis of their molecular extinction coefficiency ratio compared with retinyl palmitate.[20]

Statistical Analyses. Results are expressed as means ± SEM. Differences between the uptake efficiency in the different triplicates were analyzed by using the Kruskal−Wallis test. The Mann−Whitney U test was used as a post hoc test when the Kruskal−Wallis test showed significant differences ($p < 0.05$) between groups. $p < 0.05$ was considered significant. All

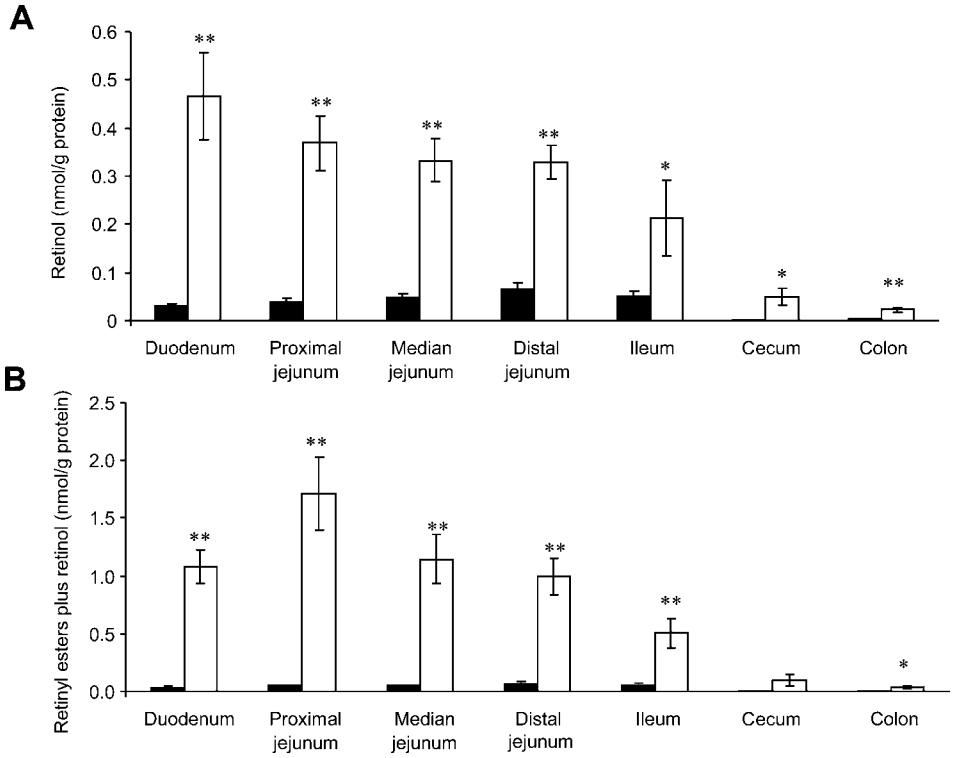

Figure 2. Retinol and retinyl ester contents of mouse intestinal fragments after force-feeding with retinol associated with either emulsion (□; $n = 4$) or β-Lg (■; $n = 4$); 250 μg of retinol were added to either 300 μL of oil-in-water emulsion or β-Lg at 50 mg/mL; 4.5 h after force feeding, mouse intestines were harvested and cut in seven fragments. Values are means ± SEMs. (A) Retinol recovered in the different segments of the intestine. (B) Retinol plus retinyl esters recovered in the different segments of the intestine. Values are means ± SEM. Asterisks indicate significant differences between emulsion and β-Lg (* $p < 0.05$, ** $p < 0.001$; Mann–Whitney U test).

statistical analyses were performed using the Statview software version 5.0 (SAS Institute, Cary, NC, U.S.A.).

RESULTS

Retinol and β-Carotene Absorption in Mice after Gavage. *Posprandial Plasma Vitamin A Concentration.* To understand the putative role of β-Lg in vitamin A intestinal absorption, we first compared retinol and β-carotene absorption in mice when delivered via either an emulsion or bound to β-Lg. During fasting, vitamin A circulates as nonesterified retinol (associated with RBP). Indeed, no retinyl esters were detected in fasting mouse plasma. The retinol absorbed by the enterocytes is massively esterified into retinyl esters (i.e., retinyl palmitate, retinyl oleate, retinyl stearate, and retinyl linoleate) by acylcoA-acyltransferase, ARAT, or lecithin retinol acyltransferase, LRAT.[2] These esters were thus measured in the postprandial samples. Postprandial plasma retinyl ester responses after gavage by either retinol-enriched emulsion or retinol bound to β-Lg were significantly different: lower ester concentrations were recovered in plasma when retinol was delivered by β-Lg (0.02 ± 0.00 μmol after 3 h) as compared to emulsion (2.36 ± 0.79 μmol after 3 h) (Figure 1A). The postprandial plasma retinyl ester responses expressed as area under the curve in the two conditions described above were also more than 3 times higher with emulsion than with β-Lg (3.27 ± 1.23 μM vs 0.87 ± 0.26 μM, respectively, $p < 0.05$, Figure 1B).

Conversely, postprandial plasma retinyl ester plus β-carotene responses expressed as area under the curve at 0–4.5 h after gavage with either β-carotene-enriched emulsion or with β-carotene associated with β-Lg were similar (0.06 ± 0.01 μM vs 0.05 ± 0.01 μM, respectively, Figure 1D).

Vitamin A Uptake by Mouse Intestine. Retinol was quantified in all segments of mouse intestine. Retinol was mainly recovered in the duodenum and proximal jejunum (Figure 2). Figure 2A shows that at 4.5 h post gavage, retinol was recovered at higher concentrations in the intestinal mucosa when delivered by the emulsion as compared to that when delivered bound to β-Lg (0.46 ± 0.09 nmol vs 0.03 ± 0.00; $p < 0.001$ in the duodenum, respectively). The formed esters were also measured in the different fragments of the intestine. Figure 2B shows the sum of retinyl esters plus retinol in the different fragments. In all fragments, more vitamin A was recovered when mice received the retinol-enriched emulsion than when they received retinol associated with β-Lg (for example in the duodenum: 1.07 ± 0.14 nmol vs 0.04 ± 0.01 nmol; $p < 0.001$, respectively).

Similar experiments were carried out with β-carotene-enriched emulsion and β-carotene bound to β-Lg. Figure 3A shows that β-carotene was mainly recovered in the distal jejunum, ileum, and cecum. Figure 3A also shows that β-carotene content was generally higher in all fragments with the emulsion condition compared to the β-Lg condition, but the differences were significant in the proximal jejunum and in the cecum only. Two pathways have been described for the metabolism of β-carotene in the enterocyte.[2] The major pathway is the central cleavage catalyzed by β-carotene 15,15′-monooxygenase 1 (βCMO1), which yields retinal and then retinol. The produced retinol is then esterified into retinyl esters. In Figure 3B, after considering β-carotene conversion into retinol and retinyl esters, these differences were abolished,

dx.doi.org/10.1021/jf501683s | J. Agric. Food Chem. 2014, 62, 5916–5924

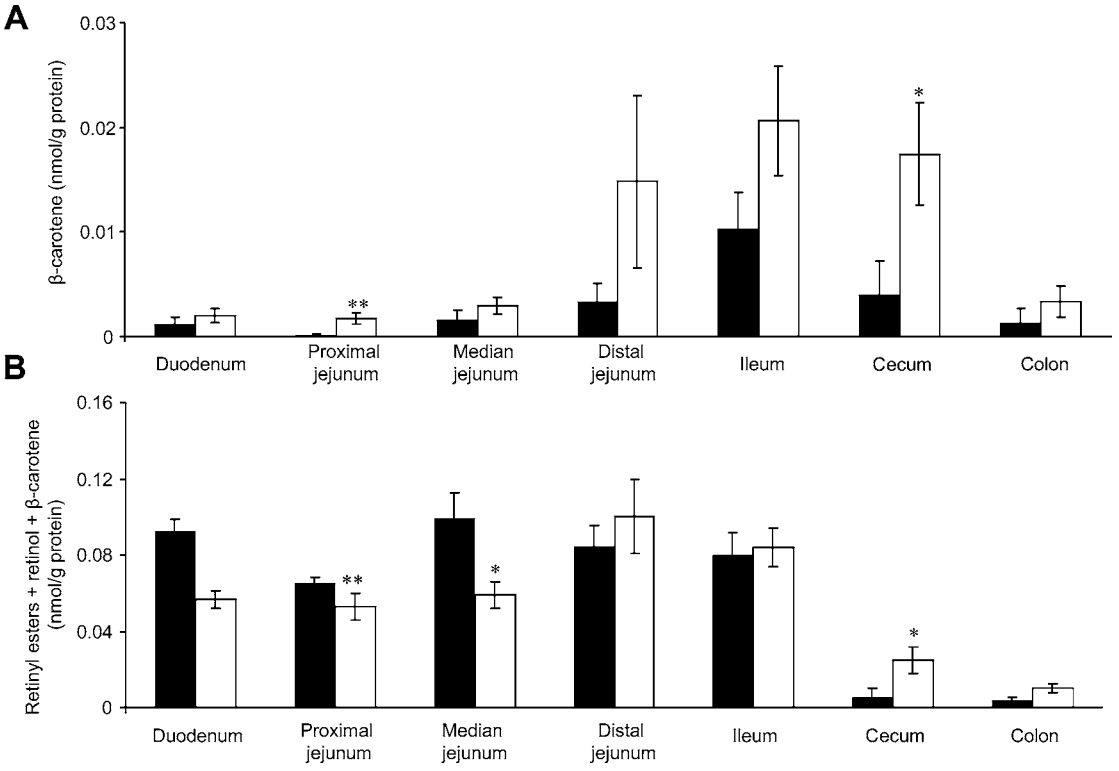

Figure 3. β-Carotene, retinol, and retinyl ester content of mouse intestinal fragments after force-feeding with β-carotene associated with either emulsion (□; $n = 4$) or β-Lg (■; $n = 4$); 250 μg of β-carotene was added to either 300 μL of oil-in-water emulsion or β-Lg at 50 mg/mL; 4.5 h after force-feeding, mouse intestines were harvested and cut in seven fragments. (A) β-Carotene recovered in the different segments of the intestine. (B) β-Carotene, retinol, and retinyl esters recovered in the different segments of the intestine. Values are means ± SEM. Asterisks indicate significant differences between emulsion and β-Lg (* $p < 0.05$, ** $p < 0.005$; Mann–Whitney U test).

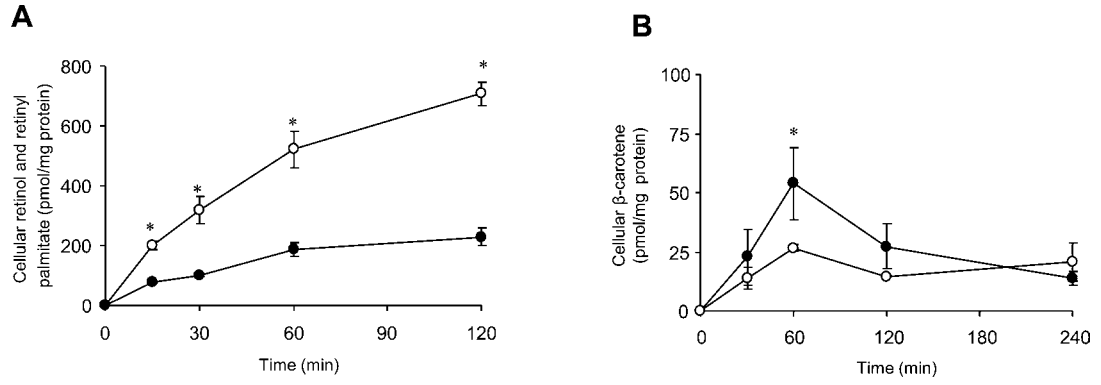

Figure 4. Uptake of retinol and β-carotene by Caco-2 TC-7 cells. The two vitamin A species were delivered either via mixed micelles (○; $n = 3$) or via β-Lg (●; $n = 3$). (A) Retinol uptake. The apical side received either retinol-enriched micelles at 3.8 μM, or retinol bound to β-Lg at 3.8 μM, and the basolateral side received FBS-free medium. Vitamin A absorbed = vitamin A recovered in the scraped cells + vitamin A recovered in the basolateral medium. (B) β-carotene uptake. The apical side received either β-carotene-enriched micelles at 5 μM, or β-carotene bound to β-Lg at 5 μM, and the basolateral side received FBS-free medium. Absorbed β-carotene was estimated as β-carotene found in scraped cells. Values are means ± SEM of three assays. Asterisks indicate significant differences between emulsion and β-Lg (* $p < 0.05$; Mann–Whitney U test).

and significantly higher vitamin A contents were recovered in the proximal and the median jejunum.

Retinol and β-Carotene Uptake by Caco-2 Cells. To focus on the mechanism involved in the uptake of retinol and β-carotene associated with the two different vectors, we then used Caco-2 cells. Figure 4 shows the kinetics of vitamin A uptake by Caco-2 cells when it was delivered via either micelles or β-Lg. After 2 h of incubation, retinol was more efficiently absorbed by Caco-2 cells when it was associated with micelles than when it was bound to β-Lg (Figure 4A). About 700 ± 40 pmol of retinol plus retinyl palmitate was recovered in cells incubated with retinol-rich micelles vs 228 ± 30 pmol in cells incubated with retinol associated with 2 mg/mL of β-Lg. Conversely, there was no significant difference between the amounts of micellar β-carotene and β-carotene bound to β-Lg after 4 h of incubation (Figure 4B).

Effect of β-Lg concentration on retinol and β-carotene uptake by Caco-2 cells. We investigated the effect of β-Lg concentration (varying from 0.1 to 10 mg/mL) on retinol and β-carotene uptake by differentiated Caco-2 cell

dx.doi.org/10.1021/jf501683s | J. Agric. Food Chem. 2014, 62, 5916–5924

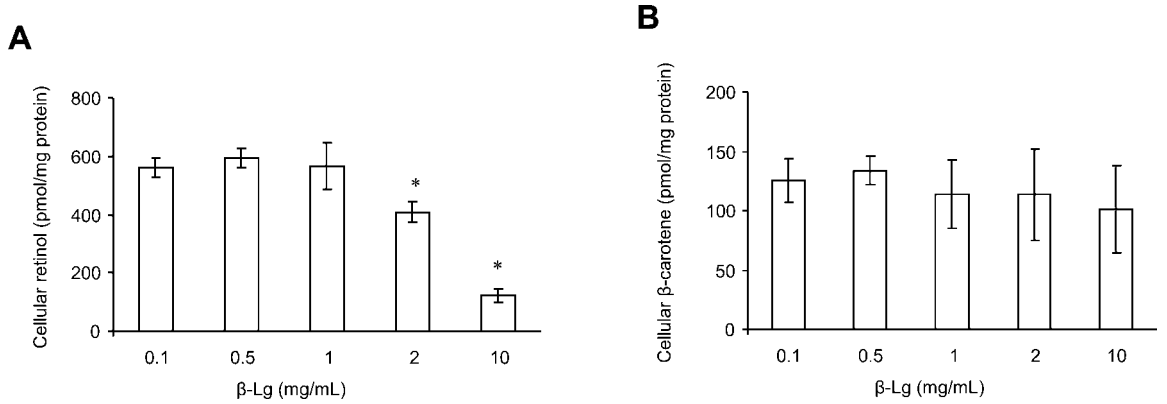

Figure 5. Effect of β-Lg concentration on retinol and β-carotene uptake by differentiated Caco-2 cell monolayers. (A) Retinol uptake by differentiated Caco-2 TC-7 monolayers during 120 min when delivered at 5 μM by different concentrations of β-Lg. The apical side received retinol bound to β-Lg, and the basolateral side received FBS-free medium. Vitamin A absorbed = vitamin A recovered in the scraped cells + vitamin A recovered in the basolateral medium. (B) β-Carotene uptake by differentiated Caco-2 TC-7 monolayers at 37 °C during 120 min when delivered at 5 μM by different concentrations of β-Lg. The apical side received 1 mL of β-carotene bound to β-Lg, and the basolateral side received 2 mL FBS-free medium. Absorbed β-carotene was estimated as β-carotene found in scraped cells. Values are means ± SEM of three assays. Asterisks indicate significant differences between different β-Lg concentrations (* $p < 0.05$; Mann–Whitney U test).

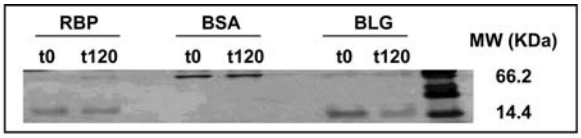

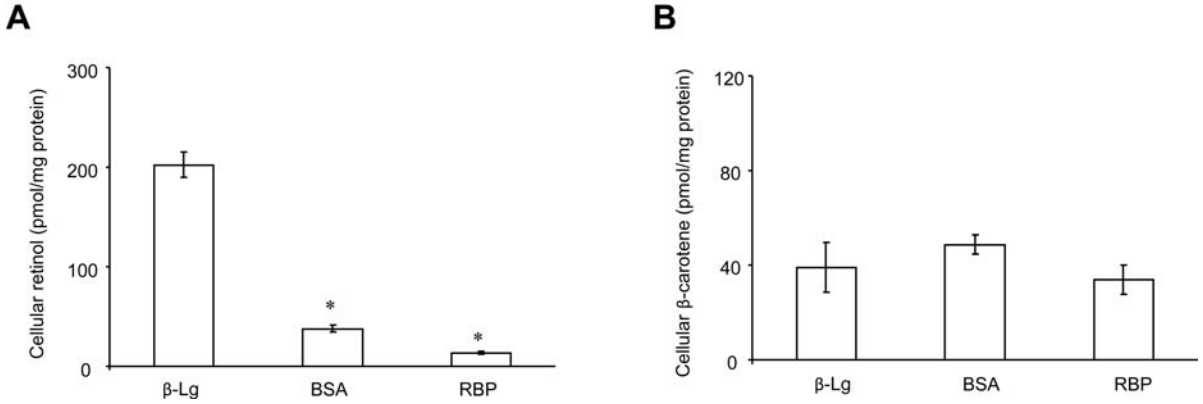

Figure 6. Uptake of retinol and β-carotene associated with lipocalins or BSA by differentiated Caco-2 cell monolayers. (A) The uptake of retinol associated with 0.1 mg/mL of either β-Lg, BSA, or RBP, was evaluated after 2 h of incubation. The apical side received each of the three proteins containing 5 μM of retinol. Vitamin A absorbed = vitamin A recovered in the scraped cells + vitamin A recovered in the basolateral medium. (B) The uptake of β-carotene associated with 0.1 mg/mL of either β-Lg, BSA, or RBP, was evaluated after 2 h of incubation. The apical side received each of the three proteins containing 5 μM of β-carotene and cellular β-carotene was quantified. Data are means ± SEM of 3 assays. Asterisks indicate significant differences between β-Lg, BSA, and RBP ($p < 0.05$; Kruskal–Wallis and Mann–Whitney U test). (Inset) SDS PAGE analysis of RBP, BSA, and β-Lg from the apical side of Caco-2 cells before ($t = 0$) and after incubation ($t = 120$ min).

monolayers during 2 h-incubations (Figure 5 A and B). Interestingly, high β-Lg concentrations significantly inhibited retinol but not β-carotene uptake.

Comparison of Two Lipocalins and BSA to Promote Retinol and β-Carotene Uptake by Differentiated Caco-2 Cell Monolayers. To understand whether the effect of β-Lg was specific to this protein, we compared its ability to deliver vitamin A to Caco-2 cells with 2 other proteins: RBP and BSA. We then compared vitamin A uptake after it was delivered by 0.1 mg/mL of β-Lg, by 0.1 mg/mL of BSA, or by 0.1 mg/mL of RBP. Figure 6A shows that retinol was more efficiently absorbed when bound to β-Lg (202.8 ± 7.4 pmol/mg protein) than when bound to BSA or RBP (37.9 ± 1.9; 13.3 ± 0.8 pmol/mg protein, respectively; $p < 0.05$). SDS PAGE analysis shows that, after 120 min of cells incubation, less β-Lg than BSA and RBP was recovered in the apical medium (Figure 6 inset).

Results obtained with β-carotene were completely different. The same amount of β-carotene was recovered into cells with the three proteins (Figure 6B).

Effect of SR-BI and NPC1L1 Chemical Inhibitors on the Uptake of Retinol and β-Carotene Delivered with Either β-Lg or Micelles to Differentiated Caco-2 Cell Monolayers. To evaluate whether the uptake pathways of vitamin A vectorized by either micelles or β-Lg were similar, we investigated the involvement of two membrane transporters

involved in micronutrient transport: SR-BI and NPC1L1, by using their respective inhibitors: BLT1 and ezetimibe glucuronide. The addition of BLT1 and ezetimibe glucuronide had no significant effect on retinol uptake when it was incorporated into either micelles or β-Lg (data not shown). Compared to the control condition (100%), the addition of BLT1 significantly decreased β-carotene uptake when incorporated into micelles (49.1 ± 3.9%) but not when fixed to β-Lg. Moreover, ezetimibe glucuronide significantly inhibited β-carotene uptake delivered by both micelles (31.9 ± 5.3%) and β-Lg (74.5 ± 2.1%).

DISCUSSION

In vivo studies were conducted at first to assess the effect of β-Lg on retinol and β-carotene absorption in mice. We compared (i) vitamin A postprandial plasma responses and (ii) vitamin A recovered in intestinal segments of mice force-fed with either retinol or β-carotene, which were delivered either in oil-in-water emulsions or associated with β-Lg. Plasma retinyl ester concentrations were higher when retinol was delivered by the emulsion as compared to β-Lg delivery. This difference may be explained by the fact that the presence of fatty acids likely increased retinyl ester synthesis and incorporation into chylomicrons,[23] which probably maintains the driving force for retinol uptake. To assess whether a similar mechanism occurred with carotenoids, we carried out the same experiment with β-carotene. Surprisingly, we found that plasma β-carotene and retinyl ester responses were similar when β-carotene was delivered by either emulsion or β-Lg. This is in agreement with a previous study that showed no effect of dietary fat (3 or 36 g) on the bioavailability of β-carotene from supplement.[24] The difference observed between retinol and β-carotene absorption may be explicated by the different stabilities of the two molecules into each vector. Retinol may be more degraded when bound to β-Lg than when included into an emulsion, which would induce a reduced absorption. On the contrary, the absence of difference between the two vectors with β-carotene suggests that β-carotene stability is similar in both vectors. This is consistent with previous results showing that retinyl palmitate, which is more stable toward oxidation than retinol,[25] was similarly absorbed by rats when incorporated into an oil carrier and when complexed to β-Lg.[26] Finally, it is interesting to note that, although less β-carotene was recovered in mouse intestinal mucosa with β-Lg compared to emulsion, β-Lg promoted β-carotene conversion in the enterocyte, leading to similar total vitamin A contents.

In order to clarify the mechanism involved in the intestinal absorption of retinol and β-carotene delivered by the two vectors, we studied their uptake in Caco-2 cell monolayers. First, retinol absorption efficiency was significantly higher than β-carotene absorption efficiency (30% for retinol vs 5% for β-carotene when delivered by micelles), similarly to what has been observed *in vivo* and according to our published data.[27] We observed that retinol uptake was more efficient when incorporated into micelles than when bound to β-Lg, which was also in accordance with our *in vivo* results. Moreover, this is in agreement with previous results in Caco-2 cells showing a low rate of retinol uptake when bound to β-Lg as compared to retinol delivered in ethanol.[11] Finally, results about β-carotene uptake were in agreement with our *in vivo* experiments as no significant difference was observed between uptake via β-Lg and via micelles.

Since it was demonstrated that both retinol and β-carotene have high affinity for β-Lg,[6] and that β-Lg may cross the intestinal cells,[10] we expected to observe a similar transport efficiency of retinol and β-carotene bound to β-Lg. This would support the hypothesis of the existence of a β-Lg ligand receptor at the brush border membrane.[13] However, retinol bound to β-Lg was more efficiently absorbed than β-carotene bound to β-Lg. Previous studies have similarly shown that retinol and palmitic acid transport efficiency across Caco-2 cells was different when bound to β-Lg[11] in spite of the high binding affinity of palmitic acid for the protein.[28] A possibility is that retinol and β-carotene dissociate from β-Lg before associating with cell membrane and/or with putative receptors. Indeed, it has been suggested that retinol dissociates from its binding protein before associating with liver cells[29] or with intestinal cells.[30] The putative dissociation of the complex β-carotene−protein is probably different than the complex retinol−protein as β-carotene and retinol were reported to have different binding sites on β-Lg.[6]

We then studied the effect of β-Lg concentration on retinol and β-carotene uptake. Retinol uptake by Caco-2 cells was significantly impaired by increasing amounts of β-Lg, according to previous data.[13] Conversely, β-carotene transport was not affected by high amounts of β-Lg. This finding can be attributed to their different uptake pathways.[31]

To further examine whether the effect of β-Lg was specific to this lipocalin, we compared its effect on vitamin A uptake with that of BSA and RBP, two other proteins that can bind vitamin A.[32,33] Results showed a lower absorption efficiency of retinol when it was bound to either BSA or RBP. This is in agreement with previous data showing that 26% of retinol associated with β-Lg was retained by Caco-2 cells vs 10% when bound to BSA after 24 h.[10] This may be explained by either a higher transport of β-Lg through cell monolayers or a higher hydrolysis of β-Lg by cell membrane enzymes compared to that of BSA,[10] as confirmed by the observed decrease of apical medium β-Lg content. Conversely, β-carotene was transported with the same efficiency with the three proteins used, which suggests unspecific uptake mechanisms.

Finally, we performed an uptake experiment in the presence of BLT1 and ezetimibe glucuronide, two specific chemical inhibitors of intestinal transporters that might be involved in uptake of vitamin A bound to β-Lg, i.e., SR-BI and NPC1L1, respectively. The uptake of retinol associated with either β-Lg or micelles was not inhibited by BLT1 and ezetimibe gluocuronide, according to the fact that neither BLT1[27] nor ezetimibe glucuronide[34] inhibited micellar retinol absorption in previous studies. Conversely, BLT1 significantly decreased the uptake of micellar β-carotene according to published data,[27] but not that of β-carotene bound to β-Lg. Ezetimibe glucuronide inhibited the uptake of micellar β-carotene, in agreement with previous results showing that β-carotene transport was decreased by 50% at 10 mg/mL of ezetimibe.[35] Interestingly, ezetimibe-glucuronide also inhibited the uptake of β-carotene bound to β-Lg. This finding suggests that SR-BI may be specifically implicated in the uptake of micronutrient included into a lipid vector, conversely to NPC1L1 that would not discriminate between the different vehicles. This may be due to the fact that NPC1L1 possibly acts like a cytosolic and not a membrane transporter,[36] and thus binds molecules after they dissociate from their vehicles in the cytosolic compartment.

In summary, our results show that β-Lg is at least as efficient as emulsion/micelles to promote the intestinal absorption of β-

carotene, but not that of retinol. β-Lg is thus a promising option for fortification with β-carotene. This should be taken into account in the formulation of vitamin A-fortified foods.

AUTHOR INFORMATION

Corresponding Author

*E-mail: Emmanuelle.Reboul@univ-amu.fr. Telephone number: +33 (0)4 91 29 41 03. Fax: +33 (0)4 91 78 21 01.

Notes

The authors declare no competing financial interest.

ACKNOWLEDGMENTS

This work was supported by a grant from the Ecole Doctorale VENAM (University of Nantes, France).

REFERENCES

(1) WHO. *Global Prevalence of Vitamin A Deficiency in Populations at Risk 1995−2005: WHO Global Database on Vitamin A Deficiency*. World Health Organization: Geneva, Switzerland, 2009.

(2) Harrison, E. H. Mechanisms involved in the intestinal absorption of dietary vitamin A and provitamin A carotenoids. *Biochim. Biophys. Acta* **2012**, *1821*, 70−77.

(3) Sklan, D. Vitamin A in human nutrition. *Prog. Food Nutr Sci.* **1987**, *11*, 39−55.

(4) Reboul, E.; Berton, A.; Moussa, M.; Kreuzer, C.; Crenon, I.; Borel, P. Pancreatic lipase and pancreatic lipase-related protein 2, but not pancreatic lipase-related protein 1, hydrolyze retinyl palmitate in physiological conditions. *Biochim. Biophys. Acta* **2006**, *1761*, 4−10.

(5) Lobo, G. P.; Amengual, J.; Palczewski, G.; Babino, D.; von Lintig, J. Mammalian carotenoid-oxygenases: Key players for carotenoid function and homeostasis. *Biochim. Biophys. Acta* **2012**, *1821*, 78−87.

(6) Mensi, A.; Choiset, Y.; Rabesona, H.; Haertlé, T.; Borel, P.; Chobert, J. M. Interactions of beta-lactoglobulin variants A and B with Vitamin A. Competitive binding of retinoids and carotenoids. *J. Agric. Food Chem.* **2013**, *61*, 4114−4119.

(7) Kontopidis, G.; Holt, C.; Sawyer, L. Invited review: beta-Lactoglobulin: binding properties, structure, and function. *J. Dairy Sci.* **2004**, *87*, 785−796.

(8) Hattori, M.; Watabe, A.; Takahashi, K. β-Lactoglobulin protects beta-ionone related compounds from degradation by heating, oxidation, and irradiation. *Biosci. Biotechnol. Biochem.* **1995**, *59*, 2295−2297.

(9) Eberini, I.; Fantucci, P.; Rocco, A. G.; Gianazza, E.; Galluccio, L.; Maggioni, D.; Ben, I. D.; Galliano, M.; Mazzitello, R.; Gaiji, N.; Beringhelli, T. Computational and experimental approaches for assessing the interactions between the model calycin beta-lactoglobulin and two antibacterial fluoroquinolones. *Proteins* **2006**, *65*, 555−567.

(10) Puyol, P.; Perez, M. D.; Sanchez, L.; Ena, J. M.; Calvo, M. Uptake and passage of beta-lactoglobulin, palmitic acid and retinol across the Caco-2 monolayer. *Biochim. Biophys. Acta* **1995**, *1236*, 149−154.

(11) Riihimaki, L.; Galkin, A.; Finel, M.; Heikura, J.; Valkonen, K.; Virtanen, V.; Laaksonen, R.; Slotte, J. P.; Vuorela, P. Transport properties of bovine and reindeer beta-lactoglobulin in the Caco-2 cell model. *Int. J. Pharm.* **2008**, *347*, 1−8.

(12) Diarrassouba, F.; Garrait, G.; Remondetto, G.; Alvarez, P.; Beyssac, E.; Subirade, M. Increased stability and protease resistance of the beta-lactoglobulin/vitamin D3 complex. *Food Chem.* **2014**, *145*, 646−652.

(13) Said, H. M.; Ong, D. E.; Shingleton, J. L. Intestinal uptake of retinol: enhancement by bovine milk beta-lactoglobulin. *Am. J. Clin. Nutr.* **1989**, *49*, 690−694.

(14) Nieland, T. J.; Penman, M.; Dori, L.; Krieger, M.; Kirchhausen, T. Discovery of chemical inhibitors of the selective transfer of lipids mediated by the HDL receptor SR-BI. *Proc. Natl. Acad. Sci. U.S.A.* **2002**, *99*, 15422−15427.

(15) Garcia-Calvo, M.; Lisnock, J.; Bull, H. G.; Hawes, B. E.; Burnett, D. A.; Braun, M. P.; Crona, J. H.; Davis, H. R., Jr.; Dean, D. C.; Detmers, P. A.; Graziano, M. P.; Hughes, M.; Macintyre, D. E.; Ogawa, A.; O'Neill K, A.; Iyer, S. P.; Shevell, D. E.; Smith, M. M.; Tang, Y. S.; Makarewicz, A. M.; Ujjainwalla, F.; Altmann, S. W.; Chapman, K. T.; Thornberry, N. A. The target of ezetimibe is Niemann-Pick C1-Like 1 (NPC1L1). *Proc. Natl. Acad. Sci. U.S.A.* **2005**, *102*, 8132−8137.

(16) Goncalves, A.; Gleize, B.; Bott, R.; Nowicki, M.; Amiot, M. J.; Lairon, D.; Borel, P.; Reboul, E. Phytosterols can impair vitamin D intestinal absorption in vitro and in mice. *Mol. Nutr. Food. Res.* **2011**, *55* (Suppl 2), S303−311.

(17) Reboul, E.; Abou, L.; Mikail, C.; Ghiringhelli, O.; Andre, M.; Portugal, H.; Jourdheuil-Rahmani, D.; Amiot, M. J.; Lairon, D.; Borel, P. Lutein transport by Caco-2 TC-7 cells occurs partly by a facilitated process involving the scavenger receptor class B type I (SR-BI). *Biochem. J.* **2005**, *387*, 455−461.

(18) Borel, P.; Pasquier, B.; Armand, M.; Tyssandier, V.; Grolier, P.; Alexandre-Gouabau, M. C.; Andre, M.; Senft, M.; Peyrot, J.; Jaussan, V.; Lairon, D.; Azais-Braesco, V. Processing of vitamin A and E in the human gastrointestinal tract. *Am. J. Physiol Gastrointest. Liver Physiol.* **2001**, *280*, G95−G103.

(19) Chantret, I.; Rodolosse, A.; Barbat, A.; Dussaulx, E.; Brot-Laroche, E.; Zweibaum, A.; Rousset, M. Differential expression of sucrase-isomaltase in clones isolated from early and late passages of the cell line Caco-2: Evidence for glucose-dependent negative regulation. *J. Cell Sci.* **1994**, *107*, 213−225.

(20) Reboul, E.; Trompier, D.; Moussa, M.; Klein, A.; Landrier, J. F.; Chimini, G.; Borel, P. ATP-binding cassette transporter A1 is significantly involved in the intestinal absorption of alpha- and gamma-tocopherol but not in that of retinyl palmitate in mice. *Am. J. Clin. Nutr.* **2009**, *89*, 177−184.

(21) Laemmli, U. K. Cleavage of structural proteins during the assembly of the head of bacteriophage T4. *Nature* **1970**, *227*, 680−685.

(22) Gleize, B.; Steib, M.; André, M.; Reboul, E. Simple and fast HPLC method for simultaneous determination of retinol, tocopherols, coenzyme Q(10) and carotenoids in complex samples. *Food Chem.* **2012**, *134*, 2560−2564.

(23) Sauvant, P.; Mekki, N.; Charbonnier, M.; Portugal, H.; Lairon, D.; Borel, P. Amounts and types of fatty acids in meals affect the pattern of retinoids secreted in human chylomicrons after a high-dose preformed vitamin A intake. *Metabolism* **2003**, *52*, 514−519.

(24) Roodenburg, A. J.; Leenen, R.; van het Hof, K. H.; Weststrate, J. A.; Tijburg, L. B. Amount of fat in the diet affects bioavailability of lutein esters but not of alpha-carotene, beta-carotene, and vitamin E in humans. *Am. J. Clin. Nutr.* **2000**, *71*, 1187−1193.

(25) Ball, G. F. M. *Vitamins in Foods: Analysis, Bioavailability, and Stability*; Taylor & Francis: Boca Raton, FL, 2006.

(26) Liu, Y.; Shaw, J.-J.; Swaisgood, H. E.; Allen, J. C. Bioavailability of oil-based and β-lactoglobulin-complexed vitamin A in a rat model. *ISRN Nutrition* **2013**, *2013*, 8.

(27) Borel, P.; Lietz, G.; Goncalves, A.; Szabo de Edelenyi, F.; Lecompte, S.; Curtis, P.; Goumidi, L.; Caslake, M. J.; Miles, E. A.; Packard, C.; Calder, P. C.; Mathers, J. C.; Minihane, A. M.; Tourniaire, F.; Kesse-Guyot, E.; Galan, P.; Hercberg, S.; Breidenassel, C.; Gonzalez Gross, M.; Moussa, M.; Meirhaeghe, A.; Reboul, E. CD36 and SR-BI are involved in cellular uptake of provitamin A carotenoids by Caco-2 and HEK Cells, and some of their genetic variants are associated with plasma concentrations of these micronutrients in humans. *J. Nutr.* **2013**, *143*, 448−456.

(28) Ragona, L.; Fogolari, F.; Zetta, L.; Perez, D. M.; Puyol, P.; De Kruif, K.; Lohr, F.; Ruterjans, H.; Molinari, H. Bovine beta-lactoglobulin: interaction studies with palmitic acid. *Protein Sci.* **2000**, *9*, 1347−1356.

(29) Van Bennekum, A. M.; Blaner, W. S.; Seifert-Bock, I.; Moukides, M.; Brouwer, A.; Hendriks, H. F. J. Retinol uptake from retinol-binding protein (RBP) by liver parenchymal cells in vitro does not specifically depend on its binding to RBP. *Biochemistry* **1993**, *32*, 1727−1733.

(30) Dew, S. E.; Ong, D. E. Absorption of retinol from the retinol:retinol-binding protein complex by small intestinal gut sheets from the rat. *Arch. Biochem. Biophys.* **1997**, *338*, 233−236.
(31) Reboul, E.; Borel, P. Proteins involved in uptake, intracellular transport and basolateral secretion of fat-soluble vitamins and carotenoids by mammalian enterocytes. *Prog. Lipid Res.* **2011**, *50*, 388−402.
(32) Belatik, A.; Hotchandani, S.; Bariyanga, J.; Tajmir-Riahi, H. A. Binding sites of retinol and retinoic acid with serum albumins. *Eur. J. Med. Chem.* **2012**, *48*, 114−123.
(33) Kanai, M.; Raz, A.; Goodman, D. S. Retinol-binding protein: the transport protein for vitamin A in human plasma. *J. Clin. Invest.* **1968**, *47*, 2025−2044.
(34) van Heek, M.; Farley, C.; Compton, D. S.; Hoos, L.; Davis, H. R. Ezetimibe selectively inhibits intestinal cholesterol absorption in rodents in the presence and absence of exocrine pancreatic function. *Br. J. Pharmacol.* **2001**, *134*, 409−417.
(35) During, A.; Dawson, H. D.; Harrison, E. H. Carotenoid transport is decreased and expression of the lipid transporters SR-BI, NPC1L1, and ABCA1 is downregulated in Caco-2 cells treated with ezetimibe. *J. Nutr.* **2005**, *135*, 2305−2312.
(36) Davies, J. P.; Levy, B.; Ioannou, Y. A. Evidence for a Niemann-pick C (NPC) gene family: Identification and characterization of NPC1L1. *Genomics* **2000**, *65*, 137−145.

JOURNAL OF AGRICULTURAL AND FOOD CHEMISTRY

Article

pubs.acs.org/JAFC

Gymnemic Acids Inhibit Sodium-Dependent Glucose Transporter 1

Yu Wang,[†,∥] Corinna Dawid,[†,∥] Gabor Kottra,[‡] Hannelore Daniel,[‡] and Thomas Hofmann*[,†]

[†]Chair of Food Chemistry and Molecular Sensory Science, Technische Universitaet Muenchen, Lise-Meitner-Straße 34, D-85354 Freising, Germany

[‡]Chair of Physiology of Human Nutrition, Research Center for Nutrition and Food Science, Molecular Nutrition Unit, Technische Universitaet Muenchen, Gregor-Mendel-Straße 2, D-85354 Freising, Germany

ABSTRACT: To evaluate the activity of botanicals used in Chinese Traditional Medicine as hypoglycemic agents for diabetes type II prevention and/or treatment, extracts prepared from 26 medicinal herbs were screened for their inhibitory activity on sodium-dependent glucose transporter 1 (SGLT1) by using two-electrode voltage-clamp recording of glucose uptake in *Xenopus laevis* oocytes microinjected with cRNA for SGLT1. Showing by far the strongest SGLT1 inhibitory effect, the phytochemicals extracted from *Gymnema sylvestre* (Retz.) Schult were located by means of activity-guided fractionation and identified as 3-*O*-*β*-D-glucuronopyranosyl-21-*O*-2-tigloyl-22-*O*-2-tigloyl gymnemagenin (**1**) and 3-*O*-*β*-D-glucuronopyranosyl-21-*O*-2-methylbutyryl-22-*O*-2-tigloyl gymnemagenin (**2**) by means of LC-MS/MS, UPLC-TOF/MS, and 1D/2D-NMR experiments. Both saponins exhibited low IC_{50} values of 5.97 (**1**) and 0.17 μM (**2**), the latter of which was in the same range as found for the high-affinity inhibitor phlorizin (0.21 μM). As SGLT1 is found in high levels in brush-border membranes of intestinal epithelial cells, these findings demonstrate for the first time the potential of these saponins for inhibiting electrogenic glucose uptake in the gastrointestinal tract.

KEYWORDS: *diabetes, SGLT1, inhibitor, Gymnema sylvestre, gymnemic acid V, gymnemic acid XV*

INTRODUCTION

Hyperglycemia is considered a major pathogenic factor in the development of acute and chronic diabetic complications such as diabetic ketoacidosis, retinopathy, nephropathy, and stroke.[1] Any practical and effective ways of maintaining long-time perfect glycemic control are lacking, thus leaving diabetics susceptible to developing acute and chronic complications such as cardiovascular diseases, blindness, amputation, and kidney failure.[2,3] Today, oral medication with euglycemic agents, such as sulfonylureas and thiazolidine derivatives,[4−6] combined with lifestyle intervention are applied to slow the progression of diabetic complications.[7−9] However, agents for glycemic control, targeting either insulin secretion or insulin action, can have significant adverse effects,[9] and thus additional treatment options are required. Lowering postprandial blood sugar excursions therefore becomes a focus in diabetes research and prevention programs.

Glucose is transported through biological membranes by the facilitative (GLUT) and sodium-dependent (SGLT) glucose transporters, which belong to the SLC2A and SLC5A gene families, respectively.[10] Facilitative glucose transport is mediated by 13 members of the GLUT protein family comprising GLUT1−12 and HMIT, which belong to a superfamily of transmembrane segment transporters identified in various tissue cells including liver, kidney, heart, brain, intestine, etc.[11] GLUT1, GLUT2, and GLUT4 have been reported to play a key role in glucose sensing in insulin secretion and for glucose uptake into insulin-sensitive organs.[12−14] The sodium/glucose cotransporters SGLT1 and SGLT2 are located primarily in epithelial cells of the intestine and kidney and transport glucose by the energy generated from the electrochemical gradient.[15] Exhibiting a high affinity to glucose and galactose, SGLT1 is predominantly located at the brush border membrane of the small intestine and carries these monosaccharides from the intestinal lumen into enterocytes.[15]

Both types of glucose transporters are currently targets in diabetes therapy. Among the GLUT protein family, for example, one strategy is to increase *m*RNA and protein expression of GLUT4 in the insulin-sensitive tissues or to increase the translocation of GLUT4.[16,17] For the sodium-dependent glucose transporters, the major strategy is to decrease glucose absorption by inhibiting or attenuating the transporter activity. SGLT1 in the kidney is responsible for only 2% of glucose reabsorption,[15] with the majority of glucose reabsorbed via SGLT2. Inhibitors of SGLT2 have been developed and are in clinical use and effectively increase glucose excretion via urine.[18] In contrast to kidney, the intestine only expresses SGLT1 that mediates glucose uptake through the apical membrane of intestinal epithelial cells. It could by its location be considered a promising target for diabetes prevention and/or therapy via specific inhibitors provided via the oral route.

To date, there are only a few studies published on natural SGLT1 inhibitors; for example, the dihydrochalcone phlorizin from apples was identified as a competitive inhibitor of glucose transporters including SGLT1 and was reported to normalize plasma glucose levels independent of insulin in diabetic animals.[19,20] To prevent its partial hydrolysis in the gastrointestinal (GI) tract, phlorizin was poly-*γ*-glutamylated and found to significantly decrease glucose-induced hyperglycemia.[21] Studies using two-electrode voltage clamp experiments

Received: April 14, 2014
Revised: May 22, 2014
Accepted: May 23, 2014
Published: May 23, 2014

ACS Publications © 2014 American Chemical Society

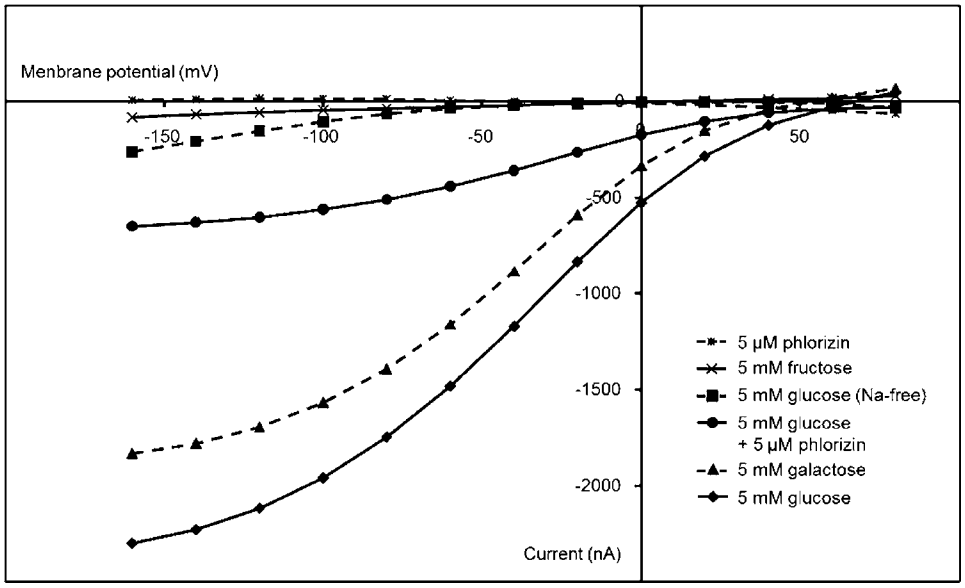

Figure 1. Comparative analysis of transporter currents induced by glucose, fructose, and galactose (5 mM each), and phlorizin (5 μM) and in a glucose/phlorezin mixture in *Xenopus* oocytes expressing hSGLT1. Data are mean values of 3−10 oocytes.

on *Xenopus* oocytes that express the human sodium-coupled glucose transporter hSGLT1 revealed that the inward current evoked by transport of α-methyl-D-glucopyranoside by SGLT1 is potently inhibited by the simultaneous application of flavonoid glycosides as well as by some aglycones.[22] Moreover, the green tea polyphenols epicatechin gallate and epigallocatechin gallate were found to have a modest SGLT1 inhibitory activity.[23]

Some medicinal herbs have been used in Asia for many centuries as hypoglycemic agents, for example, Huang Lian (*Rhizoma coptidis*), Mai Dong (*Radix ophiopogonis*), Fo-ti, Xuan Shen (*Radix scrophulariae*), Tian Men Dong (*Asparagi radix*), *Gymnema sylvestre* R. Schult, and Luo Han Guo (*Momordica grosvenori*).[24] However, their bioactive phytochemicals as well as their mechanisms of action remain elusive. The objective of the present study was to evaluate the SGLT1 inhibiting activity of a series of botanicals used in traditional Chinese medicine as hypoglycemic agents. Functional analysis was performed by two-electrode voltage-clamp recordings of glucose-associated transport currents in *Xenopus laevis* oocytes microinjected with the cRNA for hSGLT1 to identify the phytochemicals with SGLT1 inhibitory activity.

MATERIALS AND METHODS

Chemicals. The following compounds were obtained commercially: α-methyl-D-glucopyranoside (α-MDG), glucose, galactose, fructose, and phorizin as well as all chemicals used for preparation of the bath solution were obtained from Sigma-Aldrich (Taufkirchen, Germany). The bath solution (pH 7.5) contained 88 mM NaCl, 1 mM KCl, 0.8 mM $MgSO_4$, 0.4 mM $CaCl_2$, 0.3 mM $Ca(NO_3)_2$, 2.4 mM $NaHCO_3$, and 10 mM HEPES. Deuterated solvents were obtained from Euriso-Top (Gif-Sur-Yvette, France). All solvents were of HPLC grade (Merck, Darmstadt, Germany). Water for HPLC separation was purified by means of a Milli-Q Water Advantage A 10 water system (Millipore, Molsheim, France).

Medicinal Herbs. *Polygonatum sibiricum* Redouté (H1), *Polygonatum odoratum* (Mill.) Druce (H2), *Lycium chinense* Mill. (H3), *Arctium lappa* L. (H4), *Epimedium sagittatum* Maxim (H5), *Paeonia lactiflora* Pall. (H6), *Lycium barbarum* L. (H7), *Atractylodes macrocephala* Koidz. (H8), *Ligustrum lucidum* W. T. Aiton (H9), *Atractylodes macrocephala* Koidz. (H10), *Ophiopogon japonicus* (L.f.) Ker Gawl. (H11), *Rehmannia glutinosa* Steud. (H12), *Siraitia grosvenori* (H13), *Polygonatum odoratum* (Mill.) Druce (H14), *Angelica sinensis* (Oliv.) Diels (H15), *Eriobotrya japonica* (Thunb.) Lindl. (H16), *Cornus officinalis* Siebold & Zucc. (H17), *Panax ginseng* C. A. Mey. (H18), *Epimedium sagittatum* Maxim. (H19), *Coptis chinensis* Franch. (H20), *Cornus officinalis* Siebold & Zucc. (H21), *Paeonia lactiflora* Pall. (H22), *Panax ginseng* C. A. Mey. (H23), *Scrophularia ningpoensis* Hemsl. (H25), and *Paeonia lactiflora* Pall. (H26) were purchased from the Chinese Medicine Co. Tong Ren Tang (Beijing, China), *Gymnema sylvestre* (Retz.) R. Br. ex Schult (H24) was purchased from Magic Herbs (Ellerau, Germany).

Preparation of Oocytes. Maintenance of *Xenopus laevis* and the procedures of oocyte harvest were approved by the local authority for animal care in research (Regierung von Oberbayern, approval 211-2531.3-9/99). The surgical procedure and oocyte incubation were performed following the protocol reported earlier.[22] Oocytes were injected with 23 ng of hSGLT1-cRNA and incubated for 3−4 days at 17 °C. A solution of α-methyl-D-glucopyranoside (1 mM) was diluted with bath solution used as transport substrate for hSGLT1. In addition, oocytes that were not pretreated by cRNA injection and were lacking hSGLT1 were used as control.

Electrophysiology. Two-electrode voltage clamp experiments were performed as described previously in the literature[22] with oocytes placed in an open chamber and superfused (3 mL/min) with bath solution or with solutions containing the substrate. Oocytes were voltage-clamped, and transport current was measured at −60 mV using a TEC-05 amplifier and CellWorks software (npi electronic, Tamm, Germany). Current−voltage relationships were measured in a potential range from −160 to +80 mV, and the current generated by the transport at a given membrane potential was calculated as the difference of the currents measured in the presence and absence of substrate. The kinetic parameters of transport K_m and I_{max} (nA) were calculated from least-squares fits of at least three data points based on the Michaelis−Menten equation. The inhibition rate (IR) was calculated using the formula IR = [current(I) − current(0)]/(current(s) −current(0)), where current(0) is the transport current applied with bath solution and current(s) and current(I) are transport currents applied with α-MDG in the absence and presence of inhibitor, respectively. Dixon-type kinetic studies were performed at a membrane potential of −60 mV. To avoid errors due to the replenishment of the oocytes with α-MDG, the application time of the substrates was limited to 15 s at an increased (7 mL/min) perfusion speed. Activity of hSGLT1 in oocytes was measured for the monosaccharides glucose, fructose, and galactose (5 mM each) in bath solutions in the absence

or presence of phlorizin (5 μM) or as described above (Figure 1). In addition, 5 mM glucose in a sodium-free bath solution as well as a binary mixture of 5 mM glucose and 5 μM phlorizin in bath solution was analyzed.

Botanical extracts and subfractions as well as purified individual compounds were solubilized in DMSO at concentrations of 50−200 mM and were diluted with the α-MDG solution. The final concentration of DMSO in the test solutions was not higher than 1% (v/v).

Screening of Medicinal Herbs for SGLT1 Inhibitors. An aliquot of each ground botanical (10 g dry weight) was extracted with *n*-pentane (3 × 50 mL), followed by methanol/water (7:3, v/v; 3 × 50 mL) and methanol (3 × 50 mL). After removal of the solvents in a vacuum, aliquots (12 mg) of the pentane extractables (fraction I) and the methanol extractables (fraction II), respectively, were dissolved in small amounts of DMSO and made up with α-MDG solution to 50 mL to perform the hSGLT1 experiments (Figure 2). The final concentration of DMSO was not higher than 1% (v/v).

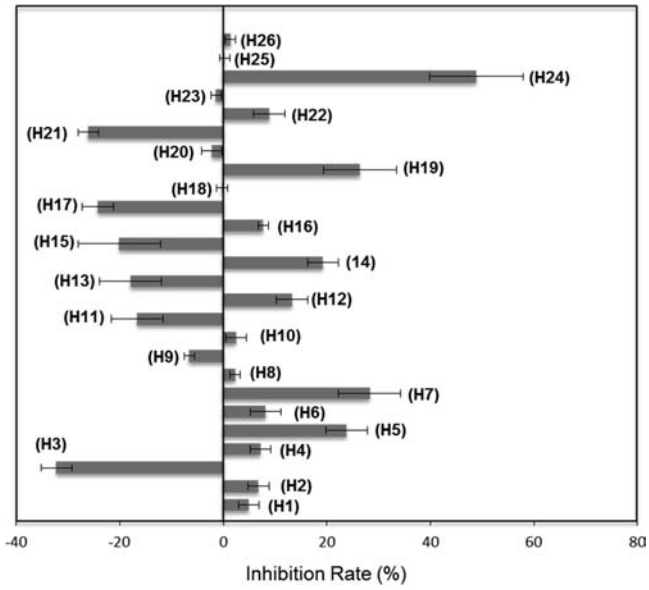

Figure 2. SGLT1 inhibitory activity of the methanol soluble fractions II of *Polygonatum sibiricum* Redouté (H1), *Polygonatum odoratum* (Mill.) Druce (H2), *Lycium chinense* Mill. (H3), *Arctium lappa* L. (H4), *Epimedium sagittatum* Maxim (H5), *Paeonia lactiflora* Pall. (H6), *Lycium barbarum* L. (H7), *Atractylodes macrocephala* Koidz. (H8), *Ligustrum lucidum* W. T. Aiton (H9), *Atractylodes macrocephala* Koidz. (H10), *Ophiopogon japonicus* (L.f.) Ker Gawl. (H11), *Rehmannia glutinosa* Steud. (H12), *Siraitia grosvenori* (H13), *Polygonatum odoratum* (Mill.) Druce (H14), *Angelica sinensis* (Oliv.) Diels (H15), *Eriobotrya japonica* (Thunb.) Lindl. (H16), *Cornus officinalis* Siebold & Zucc. (H17), *Panax ginseng* C. A. Mey. (H18), *Epimedium sagittatum* Maxim. (H19), *Coptis chinensis* Franch. (H20), *Cornus officinalis* Siebold & Zucc. (H21), *Paeonia lactiflora* Pall. (H22), *Panax ginseng* C. A. Mey. (H23), *Gymnema sylvestre* (Retz.) Schult (H24), *Scrophularia ningpoensis* Hemsl. (H25), and *Paeonia lactiflora* Pall. (H26).

Isolation and Identification of SGLT1 inhibitors from *Gymnemna sylvestre* (H24). Dried leaves of *Gymnemna sylvestre* (300 g) were ground, extracted with pentane (2 × 2L), and, finally, extracted with methanol/water (7:3, v/v; 2 × 2L), followed by methanol (2 × 2L). The latter two polar extracts were combined, solvents were separated by means of a Genevac Rocket evaporation system (Genevac Limited, Ipswich, UK), and the remaining residue was lyophilized to provide polar fraction II (104 g, 34.7% yield). Fraction II was dissolved in water (in sum 1 L), and 20 mL was applied each time onto a PP cartridge (i.d. = 40 mm, l = 150 mm) filled with RP18 material (LiChroprep RP18, 25−40 μm mesh material (Merck) and separated by MPLC by flushing the column with water (400 mL, fraction II-1), followed by methanol (400 mL, fraction II-2). After lyophilization, fractions II-1 and II-2 were both used for the SGLT1 bioassay. Fraction II-2 (51.7 g, 17.2%) showing SGLT1 inhibition was further separated by normal phase column chromatography using silica gel (400 × 30 mm, 5% water) as stationary phase and the following chloroform/methanol/water mixtures (v/v/v) as the mobile phase: fraction II-2/A (7:3:0.5), fraction II-2/B (6.9:3.1:0.57), fraction II-2/C (6.7:3.3:0.64), fraction II-2/D (6.6:3.4:0.71), fraction II-2/E (6.4:3.6:0.78), fraction II-2/F (6.3:3.7:0.86), fraction II-2/A (6.1:3.9:0.93), and fraction II-2/H (6:4:1) (Figure 3). An aliquot (1 g)

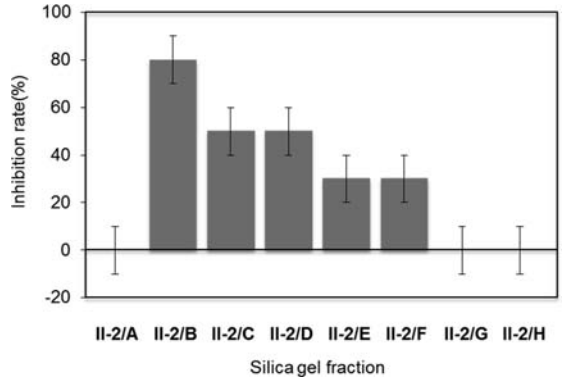

Figure 3. Inhibition of the hSGLT1 transport currents induced by α-methylglucose (1 mM) in the presence of fractions II-2/A−II-2/H isolated from *Gymnema sylvestre*. Data are mean values of 3−10 oocytes.

of fraction II-2/B was dissolved in acetonitrile/0.1% formic acid (30:70, v/v) and fractionated by means of preparative RP-HPLC. Twenty-eight fractions were collected individually in several runs, and the corresponding fractions were combined (Figure 4). HPLC fractions 22 and 24, showing the highest SGLT1 inhibitory activity, were separated from solvent using a Genevac Rocket evaporation system (Genevac Limited) and freeze-dried to yield gymnemic acids V (**1**) and XV (**2**), the structures of which were identified by means of LC-MS/MS, UPLC-TOF-MS, and 1D/2D-NMR experiments.

*Gymnemic acid V, **1**, Figure 5:* LC-MS (ESI$^-$), *m/z* 845 (100, [M − H]$^-$), 881 (12, [M + Cl]$^-$); MS/MS (DP = −64 V), *m/z* (%) 637 (89), 175 (74), 157 (100); LC-TOF-MS, *m/z* 845.4672 ([M − H]$^-$, measured), *m/z* 845.4687 ([M − H]$^-$, calcd for $C_{46}H_{69}O_{14}$); ^{1}H NMR (500 MHz, pyridine-d_5; COSY, *J*-RESOLVED, ROESY), δ 0.84−1.00 [m, 1H, H−C(1a)], 0.89 [s, 3H, H−C(25)], 0.92 [s, 3H, H−C(26)], 0.95 [s, 3H, H−C(24)], 1.02 [s, 3H, H−C(29)], 1.18−1.40 [m, 3H, H−C(6a,7a,19a)], 1.26 [s, 3H, H−C(30)], 1.30 [s, 3H, H−C(27)], 1.40−1.50 [m, 1H, H−C(1b)], 1.46 [d, 3H, *J* = 7.0 Hz, H−C(4‴)], 1.51−1.57 [m, 1H, H−C(15a)], 1.60 [d, 3H, *J* = 7.0 Hz, H−C(4″)], 1.62−1.73 [m, 4H, H−C(5,6b,7b,9)], 1.74−1.86 [m, 8H, H−C(11,5″,5‴)], 1.92−2.07 [m, 2H, H−C(2a,15b)], 2.14−2.27 [m, 1H, H−C(19b)], 2.27−2.35 [m, 1H, H−C(2b)], 3.11 [dd, 1H, *J* = 4.0 Hz, 14.0 Hz, H−C(18)], 3.74 [d, 1H, *J* = 10.8 Hz, H−C(23a)], 4.02 [d, 1H, *J* = 12 Hz, H−C(28a)], 4.10−4.19 [m, 1H, H−C(2′)], 4.19−4.28 [m, 1H, H−C(3′)], 4.23 [d, 1H, *J* = 12 Hz, H−C(28b)], 4.30−4.40 [m, 2H, H−C(3,23b)], 4.52−4.62 [m, 2H, H−C(4′,5′)], 4.99−5.08 [m, 1H, H−C(16)], 5.25 [d, 1H, *J* = 7.9 Hz, H−C(1′)], 5.33−5.39 [m, 1H, H−C(12)], 5.82 [d, 1H, *J* = 12.0 Hz, H−C(21)], 6.34 [d, 1H, *J* = 12.0 Hz, H−C(22)], 6.95−7.03 [m, 2H, H−C(3″,3‴)]; ^{13}C NMR (125 MHz, pyridine-d_5; HSQC, HMBC), δ 12.2 [C(5″)], 12.2 [C(5‴)], 13.6 [C(24)], 14.1 [C(4‴)], 14.2 [C(4″)], 16.2 [C(25)], 16.9 [C(26)], 18.1 [C(6)], 19.8 [C(30)], 23.9 [C(11)], 26.0 [C(2)], 27.4 [C(27)], 29.2 [C(29)], 32.5 [C(7)], 36.6* [C(10)], 36.8* [C(15)], 36.8 [C(20)], 38.8 [C(1)], 40.2 [C(8)], 42.6 [C(4)], 42.6 [C(18)], 43.5 [C(14)], 45.8 [C(19)], 47.1 [C(9)], 47.4 [C(5)], 48.0 [C(17)], 59.8 [C(28)], 64.4 [C(23)], 67.0 [C(16)], 73.5

dx.doi.org/10.1021/jf501766u | J. Agric. Food Chem. 2014, 62, 5925−5931

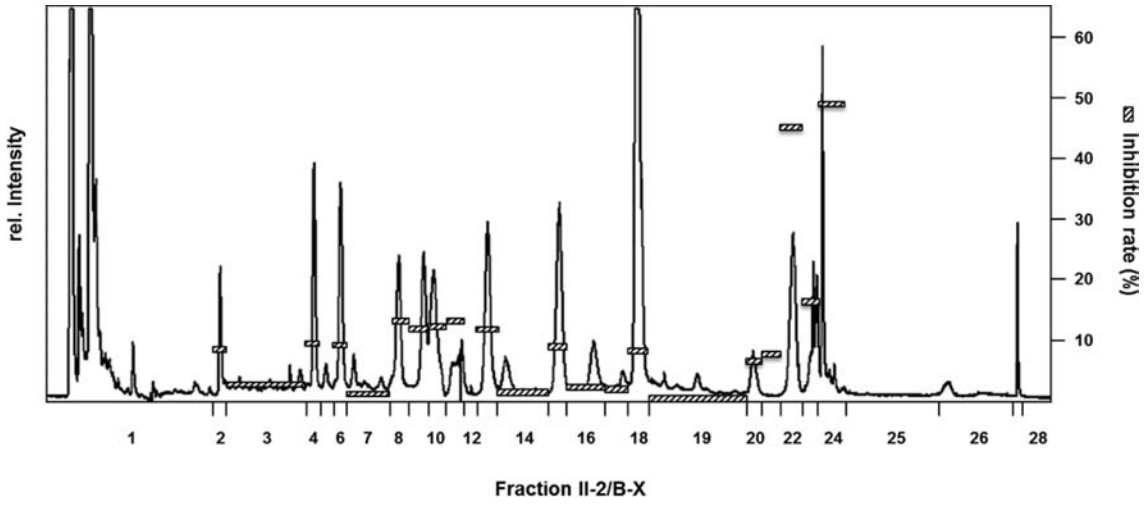

Figure 4. Inhibition of hSGLT1 transport currents induced by α-methylglucose (1 mM) in the presence of individual HPLC fractions in natural concentration ratios prepared from *Gymnema sylvestre* fraction II-2.

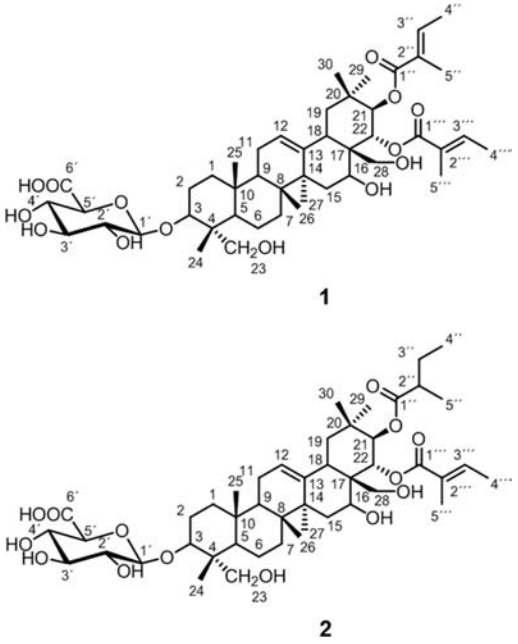

Figure 5. Chemical structures of hSGLT inhibitors gymnemic acid V (**1**) and gymnemic acid XV (**2**).

[C(4′)], 74.5 [C(22)], 75.4 [C(2′)], 76.6 [C(21)], 77.8 [C(5′)], 78.1 [C(3′)], 81.7 [C(3)], 106.2 [C(1′)], 123.8 [C(12)], 128.9 [C(2″)], 128.9 [C(2‴)], 137.7 [C(3″)], 137.9 [C(3‴)], 141.5 [C(13)], 167.5 [C(1‴)], 167.8 [C(1″)], 173.0 [C(6′)] (*, may be interchangeable).

*Gymnemic acid XV, **2**, Figure 5:* LC-MS (ESI$^-$), *m/z* 847 (100, [M − H]$^-$); MS/MS (DP = −54 V), *m/z* (%) 847 (100), 175 (4), 157 (4), 639 (2); LC-TOF-MS, *m/z* 847.4842 ([M − H]$^-$, measured), *m/z* 847.4844 ([M − H]$^-$, calcd for $C_{46}H_{71}O_{14}$); ^{1}H NMR (500 MHz, pyridine-d_5; COSY, *J*-RESOLVED, ROESY), δ 0.83−0.98 [m, 4H, H−C(1a,4″)], 0.89 [s, 3H, H−C(25)], 0.92 [s, 3H, H−C(26)], 0.95 [s, 3H, H−C(24)], 0.99 [s, 3H, H−C(29)], 1.11 [d, 1H, *J* = 7.1 Hz, H−C(5″)], 1.16−1.40 [m, 3H, H−C(6a,7a,19a)], 1.23 [s, 3H, H−C(30)], 1.30 [s, 3H, H−C(27)], 1.39−1.50 [m, 2H, H−C(1b,3″a)], 1.52 [d, 3H, *J* = 7.0 Hz, H−C(4‴)], 1.55−1.60 [m, 1H, H−C(15a)], 1.61−1.78 [m, 4H, H−C(5,6b,7b,9)], 1.73−1.90 [m, 6H, H−C(11,3″b,5‴)], 1.95−2.10 [m, 2H, H−C(2a,15b)], 2.13−2.28 [m, 1H, H−C(19b)], 2.27−2.35 [m, 1H, H−C(2b)], 2.41 [sex., 1H, *J* = 6.9 Hz, H−C(2″)], 3.06 [dd, 1H, *J* = 4.0 Hz, 14.2 Hz, H−C(18)], 3.70 [d, 1H, *J* = 10.8 Hz, H−C(23a)], 4.00 [d, 1H, *J* = 11.3 Hz, H−C(28a)], 4.10−4.18 [m, 1H, H−C(2′)], 4.18−4.27 [m, 1H, H−C(3′)], 4.20 [d, 1H, *J* = 11.3 Hz, H−C(28b)], 4.28−4.40 [m, 2H, H−C(3, 23b)], 4.51−4.62 [m, 2H, H−C(4′, 5′)], 4.96−5.06 [m, 1H, H−C(16)], 5.25 [d, 1H, *J* = 7.4 Hz, H−C(1′)], 5.32−5.43 [m, 1H, H−C(12)], 5.73 [d, 1H, *J* = 12.0 Hz, H−C(21)], 6.27 [d, 1H, *J* = 12.0 Hz, H−C(22)], 7.07−7.14 [m, 1H, H−C(3‴)]; ^{13}C NMR (125 MHz, pyridine-d_5; HSQC, HMBC), δ 11.8 [C(4″)], 12.3 [C(5‴)], 13.6 [C(24)], 14.2 [C(4‴)], 16.2 [C(25)], 16.7 [C(5″)], 16.9 [C(26)], 18.0 [C(6)], 19.8 [C(30)], 23.9 [C(11)], 26.0 [C(2)], 27.0 [C(3″)], 27.4 [C(27)], 29.2 [C(29)], 32.5 [C(7)], 36.7* [C(15)], 36.8 [C(20)], 36.9* [C(10)], 38.7 [C(1)], 40.2 [C(8)], 41.6 [C(2″)], 42.6 [C(18)], 43.5 [C(4)], 43.5 [C(14)], 45.8 [C(19)], 47.1 [C(9)], 47.4 [C(5)], 48.1 [C(17)], 60.0 [C(28)], 64.4 [C(23)], 66.9 [C(16)], 73.5 [C(4′)], 74.3 [C(22)], 75.4 [C(2′)], 76.1 [C(21)], 77.8 [C(5′)], 78.1 [C(3′)], 81.7 [C(3)], 106.1 [C(1′)], 123.8 [C(12)], 128.9 [C(2‴)], 138.4 [C(3‴)], 141.5 [C(13)], 167.4 [C(1‴)], 173.0 [C(6′)], 176.2 [C(1″)] (*, may be interchangeable).

Medium-Pressure Liquid Chromatography (MPLC). MPLC separation of the polar *Gymnemna sylvestre* extract was performed on a Sepacore chromatography system (Buchi, Flawil, Switzerland) consisting of two C-605 pumps with a C-615 pump manager, a manual Rheodyne injection port (20 mL loop), and a C-660 fraction collector. Data acquisition was performed by means of Sepacore Control 1.0 software (Buchi). Chromatographic separation was performed using PP cartridges (i.d. = 40 mm, l = 150 mm) and LiChroprep RP18, 25−40 μm, mesh material (Merck). Operated at a flow rate of 40 mL/min, the following gradient was used for chromatography: Starting with pure water (for 10 min) (water washing fraction), the methanol content was increased to 100% within 2 min and kept at 100% for 12 min (methanol/water fraction). Both fractions were individually collected; the solvent was removed using a Genevac Rocket evaporation system (Genevac Limited) and freeze-dried twice.

High-Performance Liquid Chromatography (HPLC). For analytical as well as for preparative analyses of fraction B, the HPLC apparatus (Jasco, Groß-Umstadt, Germany) was equipped with two PU-2087 Plus pumps, an AS-2055 Plus autosampler, a Sedex LT-ELSD detector model 85 (Sedere, Alfortville, France; split ratio was set to 1 mL/min for the ELSD; gain = 7), and a Rh 7725i type Rheodyne injection valve (Rheodyne, Bensheim, Germany). Data acquisition was performed by means of Chrompass 1.8.6.1 software (Jasco). Chromatographic separation was performed on a 250 × 21 mm i.d., 5 μm, NUCLEODUR C18 Pyramid column (Macherey-Nagel, Düren, Germany) operated with a flow rate of 20 mL/min. Using 0.1% formic acid in water (v/v) as solvent A and 0.1% formic acid in acetonitrile (v/v) as solvent B, chromatography was performed with the following gradient: 0 min, 30% B; 5 min, 30% B; 15 min, 40% B; 40 min, 40% B;

41 min, 45% B; 60 min, 45% B; 61 min, 65% B; 70 min, 65% B; 71 min, 100% B; 76 min, 100% B; 77 min, 30% B; 82 min, 30% B.

Liquid Mass Spectrometry (LC-MS). An API 4000 QTRAP mass spectrometer (AB Sciex, Darmstadt, Germany) with direct flow infusion was used to acquire electrospray ionization (ESI) mass spectra and product ion spectra. The MS system was operated in the full-scan mode detecting negative ions at an ion spray voltage at −4500 V. The MS/MS parameters were tuned for each compound to record fragmentation of the $[M - H]^-$ molecular ions into specific product ions. Data acquisition and instrumental control were performed with Analyst 1.4.2 software (AB Sciex).

UPLC/Time-of-Flight Mass Spectrometry (UPLC/TOF-MS). High-resolution mass spectra of the target substances were measured on a SYNAPT G2 HDMS (Waters UK Ltd., Manchester, UK) in the negative ESI and resolution modus with the following parameters: capillary voltage, 2.8 kV; sampling cone, 30; source temperature, 150 °C; desolvation temperature, 450 °C; cone gas, 5.0 L/h; and desolvation gas, 850 L/h. All saponins were dissolved in 1 mL water/methanol (90:10, v/v), and aliquots (1−5 μL) were injected into the UPLC/TOF-MS system. The samples were introduced into the instrument via an Acquity UPLC core system (Waters, Milford, MA, USA) consisting of a binary solvent manager, a sample manager, and a column oven. For chromatography, a 2 × 150 mm i.d., 1.7 μm, BEH C18 column (Waters) was operated with a flow rate of 0.4 mL/min at a temperature of 40 °C. The solvent system consisted of acetonitrile (A) and aqueous formic acid (0.1% in water, pH 2.5; B). The following gradient was used: 0 min, 50% B; 2 min, 100% B. The instrument was calibrated over a m/z range of 100−1200 using a solution of sodium formate (0.5 mM) in a 2-propanol/water mixture (90:10, v/v). All data were lock mass corrected using leucine enkephaline as the reference (m/z 556.2771, $[M + H]^+$). Data acquisition and interpretation were performed by using MassLynx software (version 4.1; Waters) and the tool "elemental composition".

Nuclear Magnetic Resonance Spectroscopy (NMR). 1D and 2D NMR spectra were acquired on a Bruker 500 MHz Avance III spectrometer (Bruker, Rheinstetten, Germany). 2D NMR experiments COSY, TOCSY, *J*-RESOLVE, HMQC/HSQC, DEPT, ROESY, and HMBC were carried out using the pulse sequences taken from the Bruker software library. Pyridine-d_5 was used as solvent, and chemical shifts are reported in parts per million relative to the pyridine-d_5 solvent signals (^{1}H NMR δ 7.19, 7.55, and 8.71; ^{13}C NMR δ 123.5, 135.5, and 149.5). Data processing was performed by using Topspin NMR software (version 3.1 and 2.1; Bruker) and Mestre-C (Mestrelab Research, A Coruña, Spain).

Statistical Analysis. Processing of raw data was done using Excel 2010 (Microsoft Corp.). Quantitative data are expressed as mean ± standard deviation unless otherwise noted. IC_{50} values were determined using Prism 6 software (GraphPad, La Jolla, CA, USA). A nonlinear regression was calculated using the log dose−response variable slope model.

RESULTS AND DISCUSSION

For identification of potent SGLT1 inhibitors from hypoglycemic botanicals used in traditional Chinese medication, a two-electrode voltage-clamp screening was used that records electronic glucose transport in *Xenopus laevis* oocytes microinjected with the cRNA for hSGLT1.

Functionality Testing. After the membrane voltage had been set to −60 mV, transport currents generated by SGLT1 were determined for glucose, fructose, and galactose (5 mM each) as well as the SGLT1 inhibitor phlorizin (Figure 1). As expected, neither application of fructose nor application of glucose in sodium-free solution caused any current, whereas a current was recorded when glucose or galactose was applied in the presence of sodium ions. These data confirmed the sodium dependency as well as the sugar specificity of SGLT1 as a selective glucose and galactose transporter. In the presence of only 5 μM phlorizin, glucose-mediated currents were significantly reduced, thus confirming the inhibitory activity of this polyphenol.[25]

Screening of Botanicals for SGLT1 Inhibition. A total of 26 Chinese medical herbs (H1−H26) were extracted with *n*-pentane, followed by methanol/water and, after removal of the solvents in a vacuum, the pentane extractables (fraction I) as well as the methanol extractables (fraction II) were used in the SGLT1-based screening. Whereas none of the pentane extracts showed any effect in the assay (data not shown), distinct SGLT1 inhibitory activities were found for some of the methanol-soluble fractions II (Figure 2). A total of nine botanical extracts increased SGLT1 activity and glucose transport, among which wolfberry (*Lycium chinense* Mill.; H3) and *Cornus officinalis* Siebold & Zucc. (H21) showed the highest activity by increasing the current by >30%. In comparison, 14 extracts induced a significant decrease in cellular sugar transport; the highest activity was found for *Gymnema sylvestre* (Retz.) Schult (H24), showing a 48% SGLT1 inhibition, followed by Digupi (*Lycium barbarum* L.; H7), Yin yang huo (*Epimedium sagittatum* Maxim; H5), and *Epimedium sagittatum* Maxim (H19) with somewhat lower SGLT1 inhibitory activities between 25 and 30%. As the leaves of *Gymnema sylvestre* R. Schult were found to show the highest SGLT1 inhibitory activity (Figure 2) and to exhibit hypoglycemic activities in diabetic subjects,[26−32] this botanical was selected for isolation of phytochemicals.

Activity-Guided Identification of SGLT1 Inhibitors in *Gymnemna sylvestre*. To identify the SGLT1 inhibitors, fraction II prepared from *Gymnema sylvestre* was separated by means of MPLC using water (fraction II-1) followed by methanol (fraction II-2) as the solvent. After lyophilization, fractions II-1 and II-2 were both used for the SGLT1 bioassay. Fraction II-1 did not exhibit any significant activity, but fraction II-2 showed SGLT1 inhibition similar to the activity found for the total fraction II (data not shown), thus suggesting the active target molecules to be present in fraction II-2. The latter fraction was, therefore, further separated by means of silica gel chromatography to afford eight fractions, namely II-2/A−II-2/H, which were again tested for their SGLT1 inhibitory activity (Figure 3).

Subfraction II-2/B showed the highest SGLT1 inhibition rate of 80% and was, therefore, further fractionated by means of preparative RP-HPLC using an evaporative light scattering detector. A total of 28 HPLC fractions were collected, separated from solvent in a vacuum and, finally, used for analysis of their SGLT1 inhibitory activity in their natural concentration ratios (Figure 4). By far the highest SGLT1 inhibition rates of 45 and 48%, respectively, were found for HPLC fractions 22 and 24, followed by fractions 2, 4, 6, 8−11, 13, 15, 18, 20, 21, and 23, all of which exhibited inhibition rates >5%. With the aim of determining the molecular structure of the molecules imparting the most intense SGLT1 inhibitory activity, LC-MS/MS, UPLC-TOF-MS, and 1D/2D-NMR experiments focused on the phytochemicals isolated from HPLC fractions 22 and 24 in semipreparative scale.

LC-MS(ESI$^-$) analysis of compound **1** isolated from HPLC fraction 22 revealed an intense pseudomolecular ion ($[M - H]^-$) with m/z 845, thus suggesting a molecular mass of 846 Da. This was confirmed by LC-TOF-MS indicating an empirical formula of $C_{46}H_{70}O_{14}$. Additional LC-MS/MS experiments led to the identification of the daughter ion m/z 669 $[M - 176 - H]^-$ and indicated the cleavage of one galacturonic acid moiety as expected for gymnema saponins.[33]

For further structure elucidation and NMR signal assignment, 1D/2D-NMR experiments including COSY, DEPT, TOCSY, *J*-RESOLVED, ROESY, HSQC, and HMBC were performed. The ^{13}C NMR spectrum showed a total of 46 signals for compound **1** resonating between 12.3 and 173.0 ppm, among which 30 signals were well in alignment with the aglycone structure of gymnemagenin.[33−35] After identification of the aglycone of **1**, the following spectroscopic experiments were focused on the structure determination of the intact saponin. As expected for tiglic acid ester moieties, the HMBC experiment revealed two long-range couplings between proton H−C(21) and H−C(22) resonating at 5.80 and 6.34 ppm and the carbon atoms C(1″) and C(1‴) observed at 167.8 and 167.5 ppm, which showed heteronuclear connectivity with the methyl protons H−C(5″) and H−C(5‴) at 1.76−1.86 ppm. In addition, 1D/2D-NMR spectroscopic experiments led to the identification of an anomeric proton resonating at 5.25 ppm. This proton signal showed a large coupling constant of 7.9 Hz, thus indicating a *β*-configuration of the galacturonic acid moiety. The full assignment of the carbohydrate moieties as well as their linkage alignment was achieved by means of COSY, TOCSY, and HMBC experiments; for example, the HMBC spectrum showed long-range correlations between H−C(1′) and C(3). With all of these findings taken into account, the phytochemical in fraction 22 was identified as 3-*O*-*β*-D-glucuronopyranosyl-21-*O*-2-tigloyl-22-*O*-2-tigloyl gymnemagenin, known as gymnemic acid V (**1**, Figure 5). Although the structure of **1** is known in the literature,[34−36] the SGLT1 inhibitory activity of this saponin has not yet been reported.

Separation of fraction 24 by means of semipreparative HPLC revealed the SGLT1 inhibiting key phytochemical **2** in a purity of >98%, which showed a pseudomolecular ion ($[M - H]^-$) with *m*/*z* 847 in the LC-MS spectrum recorded by means of electrospray ionization. This was confirmed by LC-TOF-MS experiments indicating an empirical formula of $C_{46}H_{72}O_{14}$. Comparison of the ^1H, ^{13}C, homonuclear (COSY, TOCSY), and heteronuclear (HMSC, HMBC) as well as ROESY data of **2** with those of **1** confirmed a methylbuturyl residue instead of a tiglinoyl moiety attached to aglycone carbon C(22). Comparison of all spectroscopic data with those reported in the literature[33−36] led to the unequivocal identification of compound **2** as 3-*O*-*β*-D-glucuronopyranosyl-21-*O*-2-methylbutyryl-22-*O*-2-tigloyl gymnemagenin, known as gymnemic acid XV (Figure 5). The SGLT1 inhibitory activity of **2** has not been previously reported.

SGLT1 Inhibitory Activity of Gymnemic Acids V and XV. Prior to cell experiments, the purity of the test compounds was confirmed by HPLC-MS as well as ^1H NMR spectroscopy to be >98%. Recording of dose/response functions, followed by the determination of IC_{50} data through Graphpad (Graphpad Prism 6), revealed $LogIC_{50}$ values of −5.224 for gymnemic acid V (**1**) and −4.781 for gymnemic acid XV (**2**), thus corresponding to IC_{50} values of 5.97 *μ*M for gymnemic acid V and 0.17 *μ*M for gymnemic acid XV, the structures of which are differing by just by the tigloyl and methylbutyryl moieties at position 21 of **1** and **2**, respectively. Interestingly, the IC_{50} value of gymnemic acid XV (**2**) matched the low value of 0.21 *μ*M measured for the high-affinity SGLT1 inhibitor phlorizin in our oocyte assay (Table 1). The latter value was in the same range as found for phlorizin in other studies by means of a radioactive (0.11 *μ*M)[37] as well as a nonradioactive assay (0.17 *μ*M)[38] using COS-7 cells transiently expressing human hSGLT1, but was lower when compared to an IC_{50} value of 42 *μ*M found for phlorizin when using a stably transfected Chinese hamster vvary (CHO) cell assay.[39]

Table 1. IC_{50} Values for SGLT1 Inhibitory Activity of Phytochemicals

compound	IC_{50} value[a] (*μ*M)
gymnemic acid V (**1**)[b]	5.97 ± 0.52
gymnemic acid XV (**2**)[b]	0.17 ± 0.05
phlorizin	0.21 ± 0.03

[a]IC_{50} values were calculated from dose−response recordings. [b]Structures of compounds are given in Figure 5.

Although gymnemic acids have been reported to decrease blood glucose level in rats after an oral glucose load,[40] the mechanism of action was not yet clear. Using the hSGLT1 bioassay, this is the first report on gymnemic acids as high-affinity SGLT1 inhibitors, among which gymnemic acids V and XV were found as the key molecules with the strongest SGLT1 inhibitory activity in *Gymnema sylvestre*. As SGLT1 is found in high levels in brush-border membranes of intestinal epithelial cells, our findings demonstrate for the first time the potential of these saponins for the inhibition of electrogenic glucose uptake in the GI tract.

AUTHOR INFORMATION

Corresponding Author

*(T.H.) Phone: +49-8161/71-2902. Fax: +49-8161/71-2949. E-mail: thomas.hofmann@tum.de.

Author Contributions

[‖]Y.W. and C.D. contributed equally to this work.

Funding

We thank the Alexander von Humboldt Foundation for a postdoctoral fellowship.

Notes

The authors declare no competing financial interest.

ACKNOWLEDGMENTS

We are grateful to Daniela Günzkofer for excellent technical assistance and Helene Prunkl for oocyte preparation. We acknowledge Kirsten Günther-Jordanland, Christian Schmid, and Dr. Oliver Frank for skillful acquisition of the NMR spectra.

REFERENCES

(1) World Health Organisation Department of Noncommunicable Disease Surveillance Definition. *Diagnosis and Classification of Diabetes Mellitus and Its Complications*; Geneva, Switzerland, 1999.

(2) Wild, S.; Roglic, G.; Green, A.; Sicree, R.; King, H. Global prevalence of diabetes: estimates for the year 2000 and projections for 2030. *Diabetes Care* **2004**, *27* (5), 1047−1053.

(3) Rother, K. I. Diabetes treatment — bridging the divide. *N. Engl. J. Med.* **2007**, *356* (15), 1499−1501.

(4) Rendell, M. The role of sulphonylureas in the management of type 2 diabetes mellitus. *Drugs* **2004**, *64*, 1339−1358.

(5) Norisada, N.; Masuzaki, H.; Fujimoto, M.; Inoue, G.; Hosoda, K.; Hayashi, T.; Watanabe, M.; Muraoka, S.; Yoneda, F.; Nakao, K. Antidiabetic and adipogenic properties in a newly synthesized thiazolidine derivatives, FPFS-410. *Metabolism* **2004**, *53*, 1532−1537.

(6) Gupta, D.; Ghosh, N. N.; Chandra, R. Synthesis and pharmacological evaluation of substituted 5-[4-[2-(6,7-dimethyl-1,2,3,4-tetrahydro-2-oxo-4 quinoxalinyl) ethoxy] phenyl] methylene] thiazolidine-2,4-dione derivatives as potent euglycemic and hypolipidemic agents. *Bioorg. Med. Chem. Lett.* **2005**, *15*, 1019−1022.

(7) Inzucchi, S. E. Oral antihyperglycemic therapy for type 2 diabetes. *JAMA, J. Am. Med. Assoc.* **2002**, *287*, 360−372.
(8) Buse, J. B.; Henry, R. R.; Han, J.; Kim, D. D.; Fineman, M. S.; Baron, A. D. Effects of exenatide (Exendin-4) on glycemic control over 30 weeks in sulfonylurea-treated patients with type 2 diabetes. *Diabetes Care* **2004**, *27*, 2628−2635.
(9) Chao, E. C.; Henry, R. R. SGLT2 inhibition − a novel strategy for diabetes treatment. *Nat. Rev./Drug Discovery* **2010**, *9*, 551−559.
(10) Wood, I. S.; Trayhurn, P. Glucose transporters (GLUT and SGLT): expanded families of sugar transport proteins. *Br. J. Nutr.* **2003**, *89*, 3−9.
(11) Joost, H. G.; Bell, G. I.; West, J. D.; Birnbaum, M. J.; Charron, M. J.; Chen, Y.; Doege, H.; James, D. E.; Lodish, H. F.; Moley, K. H.; Moley, J. F.; Mueckler, M.; Rogers, S.; Schurmann, A.; Seino, S.; Thorens, B. Nomenclature of the GLUT/SLC2A family of sugar/polyol transport facilitators. *Am. J. Physiol. Endocrinol. Metab.* **2002**, *282*, E974−E976.
(12) Marette, A.; Richardson, J. M.; Ramlal, T.; Balon, T. W.; Vranic, M.; Pessin, J. E.; Klip, A. Abundance, localization, and insulininduced translocation of glucose transporters in red and white muscle. *Am. J. Physiol.* **1992**, *263*, C443−C452.
(13) Guillam, M. T.; Hummler, E.; Schaerer, E.; Yeh, J. I.; Birnbaum, M. J.; Beermann, F.; Schmidt, A.; Deriaz, N.; Thorens, B.; Wu, J. Y. Early diabetes and abnormal postnatal pancreatic islet development in mice lacking Glut-2. *Nat. Genet.* **1997**, *17*, 327−330.
(14) Bady, I.; Marty, N.; Dallaporta, M.; Emery, M.; Gyger, J.; Tarussio, D.; Foretz, M.; Thorens, B. Evidence from glut2-null mice that glucose is a critical physiological regulator of feeding. *Diabetes* **2006**, *55*, 988−995.
(15) Wright, E. M.; Turk, E. M. The sodium/glucose cotransport family SLC5. *Pfluegers Arch.* **2004**, *447*, 510−518.
(16) Asano, T.; Ogihara, T.; Katagiri, H.; Sakoda, H.; Ono, H.; Midori, F.; Anai, M.; Kurihara, H.; Yasunobu, U. Glucose transporter and Na+/glucose cotransporter as molecular targets of anti-diabetic drugs. *Curr. Med. Chem.* **2004**, *11*, 2717−2724.
(17) Halaby, M. J.; Hibma, J. C.; He, J.; Yang, D. Q. ATM protein kinase mediates full activation of Akt and regulates glucose transporter 4 translocation by insulin in muscle cells. *Cell Signal.* **2008**, *20* (8), 1555−1563.
(18) Mckee, F. W.; Hawkins, W. B. Phlorhizin glucosuria. *Physiol. Rev.* **1945**, *25*, 255−280.
(19) Ehrenkranz, J. R. L.; Lewis, N. G.; Kahn, C. R.; Roth, J. Phlorizin: a review. *Diabetes Metab. Res. Rev.* **2005**, *21*, 31−38.
(20) Abdul-Ghani, M. A.; Norton, L.; deFronzo, R. A. Role of sodium-glucose cotransporter 2 (SGLT 2) inhibitors in the treatment of type 2 diabetes. *Endocrine Rev.* **2011**, *32* (4), 515−531.
(21) Ikumi, Y.; Kida, T.; Sakuma, S.; Yamashita, S.; Akashi, M. Polyphloridzin conjugates as an anti-diabetic drug that inhibits glucose absorption through the Na^+/glucose cotransporter (SGLT1) in the small intestine. *J. Controlled Release* **2008**, *125*, 42−49.
(22) Kottra, G.; Daniel, H. Flavonoid glycosides are not transported by the human Na^+/glucose transporter when expressed in xenopus laevis oocytes, but effectively inhibit electrogenic glucose uptake. *J. Pharmacol. Exp. Ther.* **2007**, *322*, 829−835.
(23) Kobayashi, Y.; Suzuki, M.; Satsu, H.; Arai, S.; Hara, Y.; Suzuki, K.; Miyamoto, Y.; Shimizu, M. Green tea polyphenols inhibit the sodium-dependent glucose transporter of intestinal epithelial cells by a competitive mechanism. *J. Agric. Food Chem.* **2000**, *48*, 5618−5623.
(24) Zhu, Y.-P. *Chinese Materia Medica. Chemistry, Pharmacology and Applications*; Harwood Academic Publisher: Amsterdam, The Netherlands, 1998; Vol. 29.
(25) Wright, E. M. The intestine Na+/glucose cotransporter. *Annu. Rev. Physiol.* **1993**, *55*, 575−589.
(26) Shanmugasundaram, K. R.; Panneerselvam, C.; Sumudram, P.; Shanmugasundaram, K. R. B. Enzym changes and glucose utilization in diabetic rabbits: the effect of *Gymnema sylvestre*, R.Br. *J. Ethnopharmacol.* **1983**, *7*, 205−234.
(27) Shanmugasundaram, E. R. B.; Leela Gopinath, K.; Rhada Shanmugasundaram, K.; Rajendran, V. M. Possible regeneration of the islets of Langerhans in streptozotocin-diabetic rats given *Gymnema sylvestre* leaf extract. *J. Ethnopharmacol.* **1990**, *30*, 265−279.
(28) Shanmugasundaram, E. R.; Rajeswari, G.; Baskaran, K.; Rajesh Kumar, B. R.; Radha Shanmugsundarama, K.; Kizar Ahmath, B. Use of *Gymnema sylvestre* leaf extract in the control of blood glucose in insulin-dependent diabetes mellitus. *J. Ethnopharmacol.* **1990**, *30*, 281−294.
(29) Shimizu, K.; Iino, A.; Nakajima, J.; Tanaka, K.; Nakajyo, S.; Urakawa, N.; Atsuchi, M.; Wada, T.; Yamashita, C. Supression of glucose absorption by some fractions extracted from *Gymnema sylvestre* leafs. *J. Vet. Med. Sci.* **1997**, *59* (4), 245−251.
(30) Persaud, S. J.; Al-Majed, H.; Raman, A.; Jones, P. M. *Gymnema sylvestre* stimulates insulin release in vitro by increased membrane permeability. *J. Endocrinol.* **1999**, *163*, 207−212.
(31) Sugihara, Y.; Nojima, H.; Matsuda, H.; Murakami, T.; Yoshikawa, M.; Kimura, I. Antihyperglycemic effects of gymnemic acid IV, a compound derived from *Gymnema sylvestre* leaves in streptocin-diabetic mice. *J. Asian Nat. Prod. Res.* **2000**, *2*, 321−327.
(32) Kenetkar, P.; Singhal, R.; Kamat, M. *Gymnema sylvestre*: a memoir. *J. Clin. Biochem. Nutr.* **2007**, *41*, 77−81.
(33) Yoshikawa, K.; Kondo, Y.; Arihara, S.; Matsuura, K. Antisweet natural products. IX [1] structure of gymnemic acids XV-XVIII from *Gymnema sylvestre* R. Br. V [2]. *Chem. Pharm. Bull.* **1993**, *41* (10), 1730−1732.
(34) Liu, H.; Kiuchi, F.; Tsuda, Y. Isolation and structure elucidation of gymnemic acids, antisweet principles of *Gymnema sylvestre*. *Chem. Pharm. Bull.* **1992**, *40* (6), 1366−1375.
(35) Mahato, S. B. Bioactive gymnemic acids and congeners from *Gymnema sylvestre*. In *Studies in Natural Product Chemistry*; Atta-ur-Rhaman, Ed.; Elsevier Science: Amsterdam, The Netherlands, 1996; Vol. 18, pp 649−676.
(36) Murakami, N.; Murakami, T.; Kadoya, M.; Matsuda, H.; Yamahara, J.; Yoshikawa, M. New hypoglycemic constituents in "gymnemic acid" from *Gymnema sylvestre*. *Chem. Pharm. Bull.* **1996**, *44* (2), 469−471.
(37) Pajor, A. M.; Randolph, K. M.; Kerner, S. A.; Smith, C. D. Inhibitor binding in the human renal low- and high-affinity Na/glucose cotransporters. *J. Pharmacol. Exp. Ther.* **2008**, *324*, 985−991.
(38) Chang, H.-C.; Yang, F.-F.; Huang, Ch.-Ch.; Lin, T.-S.; Liang, P.-H.; Lin, Ch.-J.; Lih-Ching Hsu, L.-Ch. Development of a novel non-radioactive cell-based method for the screening of SGLT1 and SGLT2 inhibitors using 1-NBDG. *Mol. BioSyst.* **2013**, *9*, 2010−2020.
(39) Castaneda, F.; Burse, A.; Boland, W.; Kinne, R. K.-H. Thioglycosides as inhibitors of hSGLT1 and hSGLT2: potential therapeutic agents for the control of hyperglycemia in diabetes. *Int. J. Med. Sci.* **2007**, *4*, 131−139.
(40) Yoshikawa, M.; Murakami, T.; Kadoya, M.; Li, Y.; Murakami, N.; Yamahara, J.; Matsuda, H. Medicinal foodstuffs. LX. [1] The inhibitors of glucose absorption from the leaves of *Gymnema sylvestre* R. Br. (Asclepiadaceae): structures of gymnemosides a and b. *Chem. Pharm. Bull.* **1997**, *45* (10), 1671−1676.

JOURNAL OF AGRICULTURAL AND FOOD CHEMISTRY

Article

pubs.acs.org/JAFC

Carnosine Ameliorates Lens Protein Turbidity Formations by Inhibiting Calpain Proteolysis and Ultraviolet C-Induced Degradation

Jiahn-Haur Liao,[†] I-Lin Lin,[§] Kai-Fa Huang,[†] Pei-Ting Kuo,[§] Shih-Hsiung Wu,[†] and Tzu-Hua Wu*[,§]

[†]Institute of Biological Chemistry, Academia Sinica, Taipei 115, Taiwan

[§]Department of Clinical Pharmacy, School of Pharmacy, College of Pharmacy, Taipei Medical University, Taipei 110, Taiwan

ABSTRACT: Carnosine (CAR) is an endogenous peptide and present in lens, but there is little evidence for its effectiveness in calpain-induced proteolysis inhibition and its differential effects toward different wavelengths of ultraviolet (UV) irradiation. This study aimed to develop three in vitro cataract models to compare the mechanisms underlying the protective activities of CAR. Crude crystallins extracted from porcine lenses were used for antiproteolysis assays, and purified γ-crystallins were used for anti-UV assays. The turbidity in those in vitro models mimics cataract formation and was assayed by measuring optical density (OD) at 405 nm. The effectiveness of CAR on calpain-induced proteolysis was studied at 37 and 58 °C. Patterns of proteins were then analyzed by SDS-PAGE. The turbidity was reduced significantly ($p < 0.05$) at 60 min measurements with the increased concentration of CAR (10−300 mM). SDS-PAGE showed that the decreased intensities at both ∼28 and ∼30 kDa protein bands in heat-enhanced assays were ameliorated by CAR at ≥10 mM concentrations. In UV-B studies, CAR (200, 300 mM) reduced the turbidity of γ-crystallin significantly ($p < 0.05$) at 6 h observations. The turbidity of samples containing γ-crystallins was ameliorated while incubated with CAR (100, 300 mM) significantly ($p < 0.05$) following 4 h of exposure to UV-C. SDS-PAGE showed that the presence of CAR reduced UV-B-induced aggregation of γ-crystallins at ∼44 kDa and resulted in less loss of γ-crystallin following UV-C exposure. The result of modeling also suggests that CAR acts as an inhibitor of calpain. In conclusion, CAR protects lens proteins more readily by inhibiting proteolysis and UV-C-induced degradation than aggregation induced by UV-B irradiation.

KEYWORDS: *carnosine, calpain proteolysis, UV insults, lens turbidity, molecular modeling*

INTRODUCTION

Carnosine (β-alanyl-L-histidine; CAR), discovered by Russian scientists in 1990, is a dipeptide present in meat,[1] lens,[2] and other tissues. The endogenous CAR acts as a natural antioxidant to scavenge free radicals[3] and lipid peroxides.[4] Its L-histidine, more specifically its imidazole moiety, appears to be the prime bioactive component and may react nonenzymically with protein carbonyl groups, a process termed "carnosinylation" to show its antiaging actions.[5] In eye lenses, crystallins are the proteins essential for their transparency. Among lens crystallin proteins, α-crystallin is able to prevent aggregation of the other destabilized proteins (especially of γ- and β-crystallins). The reported abilities of CAR in disaggregating crystallins, inhibiting fibril formations,[6,7] and protecting α-crystallins against glycation[8] provide an explanation for the anticataract activity exerted by CAR eye drops.

The aggregations or degradations of crystallins in cataractous eye lenses may result from intracellular or environmental insults. Recent studies have suggested that a major cause of the insolubilization of crystallins may be the unregulated proteolysis by calpains.[9] Calpain is one of the widely distributed calcium-dependent cysteine proteases. Among the subtypes of calpains, calpain II is the major type in human and rodent lenses[10,11] and is present in the superior cortical region.[12] Calpastatin is an endogenous inhibitor of calpain II in certain tissues. Inappropriate regulation of the calpain−calpastatin proteolytic system is associated with several important human pathological disorders including cataract formation.[13]

In addition, increased exposure to ultraviolet light results in increased photo-oxidative stress and will increase the risk of cataractogenesis.[14] The human lens can absorb visible light, UV-A and UV-B, but ocular protection from UV-B (290−320 nm) is recommended.[15] Moreover, accidental overexposure to UV-C (200−290 nm) during germicidal therapy can cause corneal burns and severe sunburn to the face and eyes. The consequences of overexposure to UV-C include increased production of free radicals, increased sensitivity of proteolysis, and decreased chaperone activity of α-crystallin[16,17] and further cause lens protein conformation destruction by cross-linking lens protein and further decreasing lens transparency.

Cataract is the leading cause of blindness, accounting for approximately 50% of blindness worldwide. Previously, we demonstrated that compounds that protect γ-crystallins from UV-C damage[18,19] or interact with calcium[20−22] may potentially be used as anticataract agents. In certain countries, CAR is available as a dietary supplement or eye drops in the health promotion market. Clinical eye drops containing its prodrug, *N*-acetylcarnosine, were also demonstrated to be absorbed intraocularly to prevent and reverse cataract.[23,24] However, claims that CAR possesses ophthalmological benefits are, as yet, insufficiently supported for the medical community to recommend CAR as a topical treatment for cataracts. For

Received: April 15, 2014
Revised: May 29, 2014
Accepted: June 5, 2014
Published: June 16, 2014

ACS Publications © 2014 American Chemical Society

example, the modulation role of CAR on the lens calpain−calpastatin system is still unclear. To date, only one study has investigated CAR's effect on aggregation of β-L-crystallins induced by UV,[25] but there are no details for CAR's effects on γ-crystallin exposure to UV-B or -C. This study aimed to clarify the effects of exogenous CAR on lens crystallin turbidity formation, especially resulting from calcium imbalance and UV-B/C photo-oxidation of lens crystallins using in vitro bioassay systems. Absorption spectroscopy and molecular modeling and docking were applied to propose the biochemical mechanisms of CAR underlying its multitarget activities in protecting lens proteins.

MATERIALS AND METHODS

General. Porcine lenses purchased from a slaughterhouse were decapsulated and homogenized in lens buffer containing 50 mM Tris-HCl, 0.1 M NaCl, 5 mM EDTA, 0.01% β-mercaptoethanol, and 0.02% sodium azide, at pH 8.0, as described previously.[18] After centrifugation at 16060*g* for 30 min (Hermle Z300 K, Hermle Labortechnik, Wehingen, Germany), the supernatant was collected, and the protein concentration was determined according to the Bradford method (Bio-Rad Laboratories, Irvine, CA, USA). γ-Crystallins were purified from crude porcine lens proteins by gel filtration as previous described.[19,26] CAR was purchased from Sigma (St. Louis, MO, USA). Samples for the turbidity assay were incubated at 37 °C using microtiter plates (Microtest 96; Falcon; Fisher Scientific, Franklin Lakes, NJ, USA) except those for heat-enhanced assays. Turbidity was measured as the optical density (OD) at 405 nm, using an enzyme-linked immunosorbent assay (ELISA) reader (TecanSunrise, Tecan Group, Männedorf, Switzerland).

m-Calpain-induced Proteolysis of Crystallins. To determine the in vitro exogenous calpain-induced lens protein turbidity, exogenous lens calpain (EC 3.4.22.17) was activated by adding 1.5 mM calcium[22] or further enhanced by heating according to the Shih et al. study.[27] Incubations of 200 μL were prepared by adding 5 mg of lens-soluble proteins/mL and 7.5 units of calpain II (from porcine kidney; Calbiochem, Torrey Pines, CA, USA) with various concentrations of CAR (0.1, 1, 10, 30, 100, 300 mM). Proteolysis was initiated by adding 1.5 mM Ca^{2+}, processed for 10 min at 37 °C (TKS OS1500, KANSAN Instruments Co. Ltd., Taipei, Taiwan) in nonheat assays or heating at 58 °C (Pantech Firefox 6100) in heat-enhanced assays. The proteolysis was terminated by the addition of EDTA to a final concentration of 3 mM. After the measurements, the mixture from each well was collected and centrifuged at 15000*g* and 4 °C for 15 min and subjected to a SDS-PAGE (12%) analysis followed by Coomassie brilliant blue R-250 staining. The intensity of each band was digitized by ImageJ, a Java-based image processing program developed at the National Institutes of Health, USA.

Photodamage of γ-Crystallins by UV-B or UV-C in Vitro. Chemical modifications of lens proteins by UV irradiation may also contribute to opacities and have been shown to cause the turbidity of γ-crystallin.[28] To develop a feasible anticataract activity assay against UV-B-[18,29] or UV-C-induced turbidity within 6 h, 20 or 0.4 mg/mL γ-crystallin exposure to UV-B (VilberLoumat biolink cross-linker; 312 nm; 4 J/h) or UV-C (UVP CL-1000; 254 nm; 14 J/h) for up to 6 or 4 h was used. In general, 200 μL of lens buffer mixtures containing γ-crystallins, with or without various concentrations of CAR for anti-UV-B or -UV-C assay, were exposed for 6 or 4 h, respectively. Anticataract activity of CAR at 1−300 mM was then determined. Protein patterns were then analyzed by SDS-PAGE and ImageJ. Ultraviolet−visible spectroscopy (UV−vis) was applied for CAR's UV-filtering property.

Molecular Modeling and Docking. The 3D-structural model of the *Sus scrofa* calpain II catalytic subunit (protein sequence entry NP_001093658) was generated with the program Discovery Studio (Accelrys Software Inc.) based on the structure of rat calpain II (PDB code 3BOW) as template. The model of CAR was docked into the active site of the resulting *S. scrofa* calpain II model based on the binding mode of calpastatin in rat calpain II (3BOW).[30] On the basis of the structures of rat calpain II bound to calpastatin, the model of CAR was manually docked into the active site of *S. scrofa* calpain II model with the program Coot to generate an initial binding pose of carnosine in *S. scrofa* calpain II. This model of the calpain II−CAR complex was optimized by energy minimization with the program Discovery Studio, and the resulting model with the lowest value of potential energy was selected. The stereochemical quality of the model was further checked with the programs 3D-profile and PROCHECK. The structure figures were generated with the program PyMOL (Schrödinger, New York, NY, USA).

Statistical Analysis. Average turbidity formation (in absolute OD 405 nm) changes from the baseline or percentage changes versus the controls were calculated. The changes of turbidity after various treatments are expressed as the mean ± standard error of the mean ($n \geq 3$). The data were analyzed using an unpaired *t* test between two groups or by Kruskal−Wallis one-way analysis of variance (ANOVA) on ranks with a post hoc Dunn's test, using SigmaStat 2.03 (Systat Software, San Jose, CA, USA). Differences were considered significant when the *p* value was <0.05. The intensity of each band for SDS-PAGE determined by ImageJ was further normalized against its normal controls or negative controls, which are the ones exposed to the insults without CAR treatments.

RESULTS

CAR Ameliorates m-Calpain-Induced Proteolysis of Crystallins. To test the effects of CAR on proteolysis, we compared the calcium/calpain II-induced turbidity of porcine lens crystallins to the normal controls. Figure 1 shows two

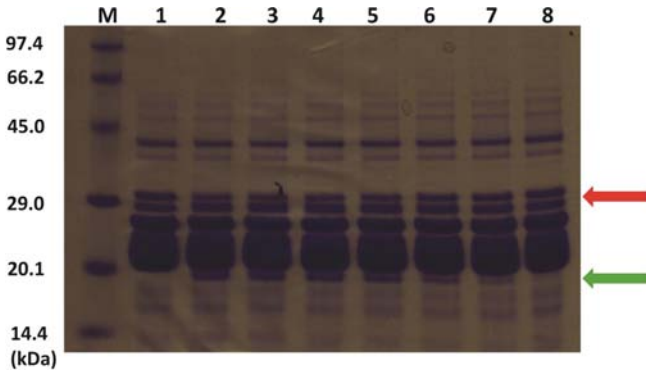

Figure 1. Effects of carnosine on exogenous m-calpain-induced cataract model. SDS-PAGE analysis of porcine eye lens crystallins subjected to exogenous calpain II induced proteolysis with or without carnosine. Lanes: M, markers; 1, normal crystallins; 2, crystallins with added calpain II; 3−8, crystallins with added calpain II solution containing 0.1, 1, 10, 30, 100, and 300 mM carnosine, respectively. Arrows indicate the noticeable crystallin band changes.

major differences: (1) The decreased β-crystallin band at ∼30 kDa was diminished in the presence of 30−300 mM CAR. The decreased β-crystallin band at ∼30 kDa was preserved in the presence of 30−300 mM CAR, but not at ∼28 kDa. (2) The appearance of degraded bands at ∼19 kDa increased by 42%, and the presence of CAR (0.1−100 mM) ameliorated the increased intensity of degraded protein bands by 1−27% when compared to the control or even prevented such proteolysis when incubated with 300 mM CAR.

To further confirm the effects of CAR, the heat-enhanced exogenous calpain II-induced proteolysis of crystallins was performed. The turbidity was measured at 0, 20, 40, and 60 min (Figure 2A). At 60 min, CAR at 0.1 and 1 mM did not inhibit turbidity formation, but CAR at higher concentrations (10, 100, 300 mM) decreased turbidity intensity values (0.14 ± 0.02,

dx.doi.org/10.1021/jf5017708 | J. Agric. Food Chem. 2014, 62, 5932−5938

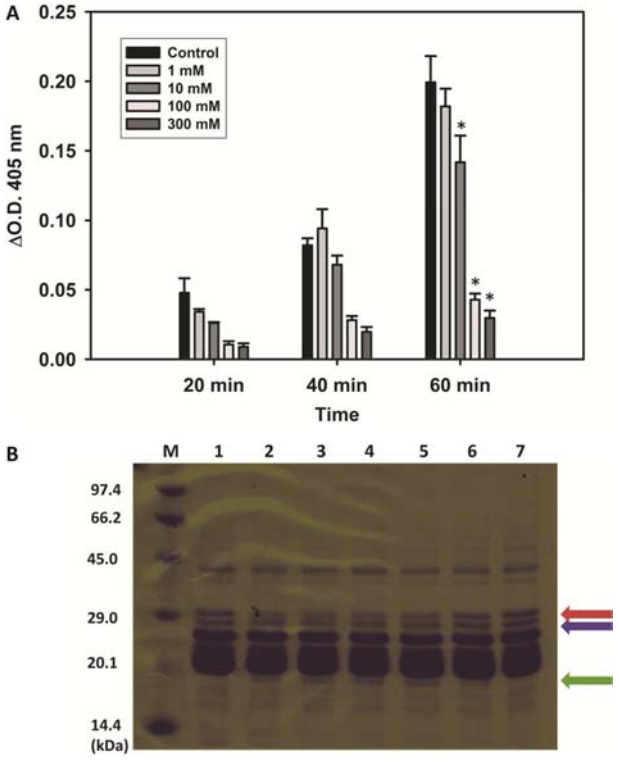

Figure 2. Effects of carnosine on heat-enhanced exogenous m-calpain-induced cataract model. (A) Turbidity changes of porcine eye lens crystallins subjected to heat-enhanced exogenous calpain II-induced proteolysis with various concentrations of carnosine. The control is the normal crystallins without carnosine incubations. The asterisk (∗) indicates statistically significant differences ($p < 0.05$). (B) SDS-PAGE analysis of porcine eye lens crystallins subjected to heat-enhanced exogenous calpain II-induced proteolysis. Lanes: M, markers; 1, normal crystallins; 2, crystallins with added calpain II after heating; 3−7, crystallins with added calpain II solution containing 0.1, 1, 10, 100, and 300 mM carnosine, respectively. Arrows indicate the noticeable changes of protein bands.

0.04 ± 0.01, 0.03 ± 0.01) in a dose-dependent manner compared with control (0.20 ± 0.02; $p < 0.05$). Digitalized image results of SDS-PAGE (Figure 2B) indicate that heat-enhanced exogenous calpain II induces proteolysis, which presented 11% decreases in proteins at ∼28 kDa compared to the ones without heating. CAR at concentrations ≥10 mM ameliorated the increased intensity of degraded protein bands at ∼28 kDa. The degraded proteins at ∼19 kDa increased by 22%, and the presence of CAR at a concentration of 100 mM ameliorated the increased intensity of degraded protein bands by 7% when compared to the negative control. According to the docking experiment of the 3D-structural model of the *S. scrofa* calpain II, CAR may bind to the calpain catalytic active site (Figure 3A) and possesses inhibitory activity similar to the activity of calpastatin. Multiple sequence alignments of calpain II showed high sequence identity among porcine, human, and rat (Figure 3B). The residues around the active site are conserved among these species.

Protective Effects of CAR from UV-B- and UV-C-Induced Photodamage of γ-Crystallins. Turbidity was determined at 405 nm for UV-B-induced photodamage of γ-crystallins after 0, 2, 4, and 6 h. CAR at 100 mM did not protect crystallins from UV insults; however, as shown in Figure 4A, after 6 h of UV-B exposure, the absolute turbidity of γ-crystallins without CAR (the controls) increased to 0.66 ± 0.02 and was significantly decreased to 0.30 ± 0.01 and 0.08 ± 0.01, respectively, in the presence of 200 or 300 mM CAR ($p < 0.05$). Results of SDS-PAGE revealed that there were no changes in the supernatants of γ-crystallin incubation samples (Figure 4B). With regard to the precipitate fractions of irradiated γ-crystallins, there are new protein bands at ∼44 kDa. A similar result was seen with 100 mM CAR. According to the digitalized image results of SDS-PAGE, precipitated fragments of irradiated γ-crystallins at ∼19 kDa decreased 22% when incubated with 200 or 300 mM CAR.

To evaluate CAR in protecting lens crystallins from UV-C damage, turbidity was determined after γ-crystallin solutions were exposed to UV-C for 0, 1, 2, 3, and 4 h. At 4 h, absolute turbidity of irradiated γ-crystallin incubated with 100 and 300 mM CAR increased to 0.36 ± 0.02 and 0.19 ± 0.01, whereas the ones without CAR increased to 0.51 ± 0.06 ($p < 0.05$) (Figure 5A). Compared to the intensity of normal controls, results of SDS-PAGE reveal that γ-crystallins degraded under UV-C irradiation, the intensity decreased 52%, and γ-crystallins were preserved 68% while 100−300 mM CAR was present (Figure 5B). The spectrum of CAR is shown in Figure 6.

DISCUSSION

In this study, we provided first evidence that CAR protects lens proteins by inhibiting calpain II activation regardless of incubations at 37 or 58 °C. Because the active sites of rat calpain II are conserved in porcine or human (Figure 3B), the calpain II inhibition activity of CAR may be common among these species. CAR's anti-UV activities are more precisely pronounced when UV-C is the source of insults rather than UV-B. Cataract is one of the main causes of blindness and low vision. Effective medications for preventing particular etiology of cataract formations remain important before cataract surgery is considered.

Activation of calpain II is related to cataract formation due to the cleavage of the N-terminal region of crystallins and resulting insolublization of these proteins.[31] The in vitro bioassay model of calcium-induced calpain II used in the current study mimicked this mechanism of senile cataract formation. The purpose of employing heating is to establish a fast turbidity formation assay system. The changes of porcine β-crystallins at ∼28 or ∼30 kDa and truncated α-crystallins at ∼19 kDa were similar to those proteolysis results previously reported by Shih et al.[27] When compared to the assays at 37 °C, less truncated α-crystallins at ∼19 kDa (22 vs 42%) were seen in heating condition. This may be because the truncated α-crystallins at ∼19 kDa were further broken down into smaller polypeptides due to thermal effects. Overall results reveal that CAR (10−300 mM) hampered proteolysis or degradation of β- and α-crystallins activated by calpain. Such results may[32] or may not[33] be related to complex formation by CAR with Ca^{2+}. Our modeling result shows that CAR may provide inhibitory effects on calpain and therefore subsequently inhibit calpain II-induced turbidity formation, which is similar to its antioxidation at levels of 5−15 mM in rabbit lenses.[34] CAR has shown good stability against intense heat treatments, even at temperatures as high as 120 °C for 20 min.[35] Therefore, the activity of this dipeptide in heat assays is assumed to be reserved. However, it cannot be ruled out that the presence of α-crystallins in the used crude lens proteins may also provide additional protective effects by their well-known chaperone activity, especially in assays of heat-enhanced calpain proteolysis.[28]

dx.doi.org/10.1021/jf5017708 | J. Agric. Food Chem. 2014, 62, 5932−5938

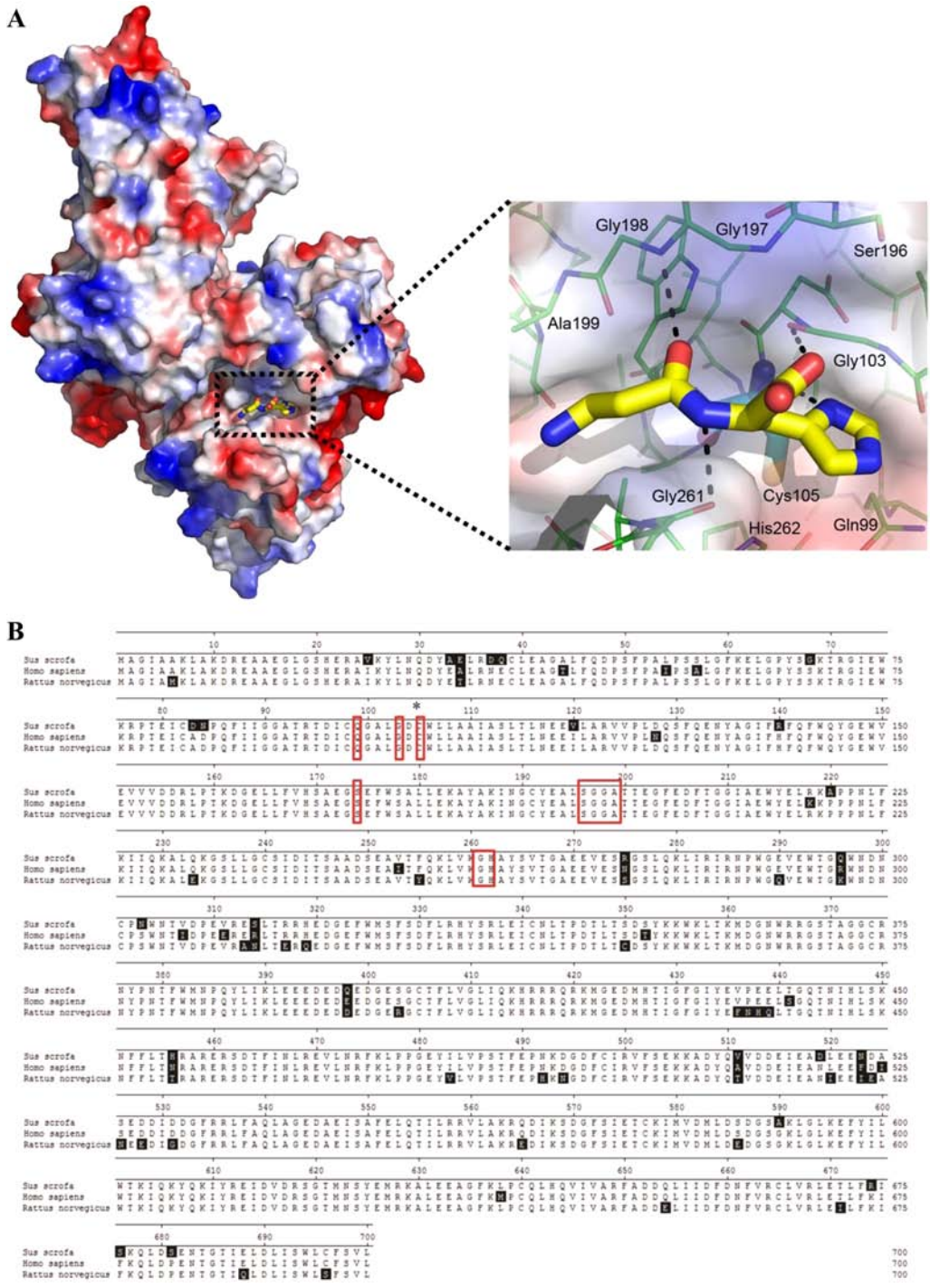

Figure 3. (A) 3D-structural model of *Sus scrofa* calpain II bound to carnosine. (Left) Surface representation of the *S. scrofa* calpain II catalytic subunit with yellow stick model depicting the bound carnosine molecule. The negative and positive charges of the surface are colored red to blue, respectively. (Right) Close-up view of the carnosine molecule bound in the active site of *S. scrofa* calpain II. The catalytic cysteine residue is drawn with a cyan stick model, and the possible hydrogen-bond interactions are indicated with dashed lines. (B) Multiple alignments of amino acid sequences of calpain II. Alignment was performed by using DNAstar MegAlign (Clustal W method). Human calpain II (*Homo sapiens*, NP_001739), porcine calpain II (*Sus scrofa*, NP_001093658), and rat calpain II (*Rattus norvegicus*, EDL94875) were used in this experiment. Nonidentical residues in all sequences are shaded in black, and the active site (Cys 105) is marked in asterisks (*). The conserved residues around the active site are shown in red boxes.

UV irradiation is a common risk factor of cataractogenesis in addition to calpain-induced proteolysis. α-Crystallin also provides additional protection against UV insults because it naturally presents with γ-crystallins in eye lenses. Even though the current results revealed that CAR required 100 or 200 mM or higher concentrations to protect γ-crystallins from UV-C or UV-B insults, doses of CAR needed for delaying lens opacity formation induced by daily light ultraviolet may be lower than the concentrations used in the current assays. Exposure of lens proteins to UV-C irradiation results in ROS production[36] and

dx.doi.org/10.1021/jf5017708 | J. Agric. Food Chem. 2014, 62, 5932−5938

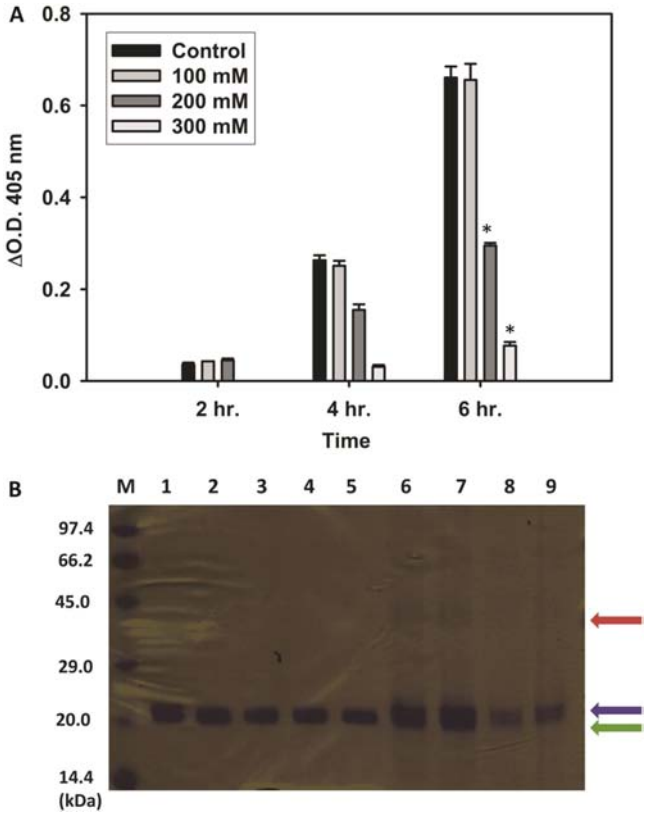

Figure 4. Anti-UV-B activity of carnosine. (A) Turbidity changes of crystallin solution with or without various concentrations of carnosine under UV-B irradiation for 2, 4, and 6 h. At 2 h, there is no turbidity change for the group with 300 mM CAR. The asterisk (∗) indicates statistically significant differences ($p < 0.05$). (B) Comparisons of supernatant and precipitate fractions by SDS-PAGE analysis: porcine γ-crystallins following UV-B irradiations. Lanes: M, markers; 1, normal γ-crystallin; 2−5, supernatant fractions of irradiated γ-crystallins incubated with carnosine (0, 100, 200, 300 mM); 6−9, precipitate fractions of irradiated γ-crystallin incubated with carnosine (0, 100, 200, 300 mM). Arrows indicate the noticeable crystallin bands changes.

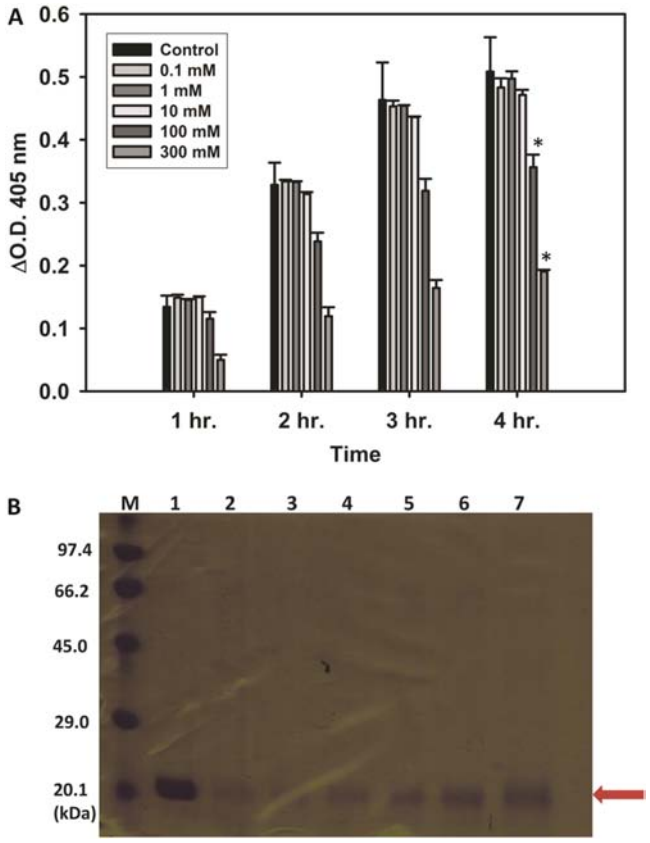

Figure 5. Anti-UV-C activity of carnosine. (A) Turbidity changes of crystallin solution with or without various concentrations of carnosine under UV-C irradiation. The asterisk (∗) indicates statistically significant differences ($p < 0.05$). (B) SDS-PAGE analysis of porcine γ-crystallin before and after UV-C irradiation. Lanes: M, markers; 1, normal γ-crystallin; 2−7, irradiated γ-crystallin incubated with carnosine (0, 0.1, 1, 10, 100, 300 mM). Arrows indicate the noticeable crystallin band changes.

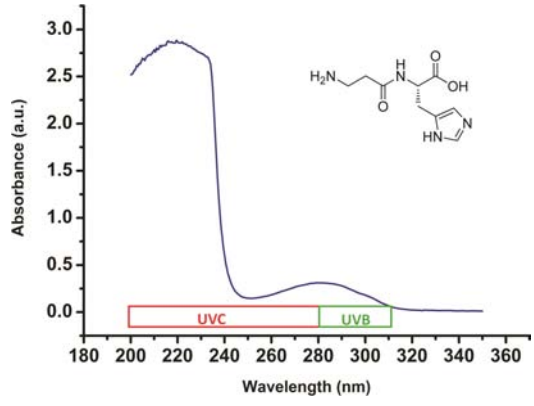

Figure 6. UV spectrum of carnosine in water (5 mg/mL). CAR absorbed in the UV-C domain, with a maximum absorption at 220 nm.

proteolytic degradation, whereas UV-B does not increase proteolytic susceptibility to the same extent but promotes the formation of cross-linked proteins[16,17] and increased content of carbonyl and disulfide bonding to form insoluble lens protein.[37]

Even though ultraviolet light is filtered by the dwindling ozone layer, increased exposure to UV-B is now considered to be a factor for increased cataract incidence. The observed UV-B-induced aggregation of γ-crystallins at ∼44 kDa (formation of dimers), similar to those of Andley et al.,[29] may be related to intermolecular disulfide bond formations induced by UV irradiation.[38] In addition, the protein bands at 15−18 kDa may have resulted from the degradation of γ-crystallins. The intensities of those new protein bands in precipitate fractions of irradiated γ-crystallins decreased when CAR increased to 100 mM. However, CAR at concentrations ranging from 1 to 100 mM provides little protective effect on γ-crystallins against UV-B. However, CAR provides better protection on porcine lens crystallins against UV-B irradiation and calpain proteolysis than pirenoxine[18] (an active ingredient of clinically used medication).

Moreover, our results suggest that CAR may possess better protective effects against UV-C than against UV-B insults because CAR at 100 mM significantly protects γ-crystallins from UV-C photodamage (accumulated intensity 56 J/4 h per 0.08 mg of γ-crystallins), but did not give adequate protection against UV-B, which was applied at lower intensity (accumulated intensity 24 J/6 h per 4 mg of γ-crystallins). The different anti-UV-B versus anti-UV-C activities exerted by CAR were also supported by its excellent UV filtering in the UV-C range between 200 and 240 nm, but not in the UV-B range (Figure

dx.doi.org/10.1021/jf5017708 | J. Agric. Food Chem. 2014, 62, 5932−5938

6). Therefore, the negative results of CAR reported by a Russian study[25] in inhibiting lens βL-crystallin aggregation are probably because UV-B was the choice of irradiation used in their assays. Moreover, the previously reported activity of CAR against free radicals, singlet oxygen, and superoxide[4] may provide support for its better anti-UV-C activity shown in the current study. However, CAR possesses slightly less protection in anti-UV-C activity when compared to pirenoxine.[18]

The physiological amount of CAR (16−30 μM) in lens[2] of healthy subjects may be enough to provide protection from ordinary UV light exposures, but predictably inadequate for intensive insults. Concentrations of 50−100 mM CAR show protective effects on in vitro crystalline fibrillation and decreased turbidity of lens organ cultures induced by quinidine.[6] A level of 50 mM CAR protects the chaperone activity of α-crystallin.[8] However, higher concentrations of CAR were also suggested to react with steroids after 1 week of incubation and to have a deleterious effect on the chaperone activity of α-crystallin.[39] The similar concentrations of CAR or higher used in this study are to counteract the applied thermally enhanced proteolysis and unusual irradiation insults; therefore, it may not suitable to directly apply our results for human trials. Therefore, further efforts to determine appropriate in vivo effective formulations and concentrations of eye drops containing prodrugs of CAR[24] to confirm the benefits of CAR instillation or supplementation in maintaining multifunctions of CAR in antiproteolysis or anti-irradiation from ordinary exposure to UV-B or UV-C are warranted.

In conclusion, the current study established convenient antiaggregation systems for assaying potential agents to prevent turbidity formation of lens proteins. The multifunctional effects of CAR in protecting lens proteins are more likely acting as an inhibitor on proteolysis and UV-C-induced degradation, rather than on aggregation induced by UV-B irradiation.

AUTHOR INFORMATION

Corresponding Author

*(T.-H.W.) Mail: Department of Clinical Pharmacy, School of Pharmacy, College of Pharmacy, Taipei Medical University, 250 Wu-Hsing Street, Taipei 110, Taiwan. Phone: 886-2-2736-1661, ext. 6172. Fax: 886-2-2735-8920. E-mail: thwu@tmu.edu.tw.

Funding

This work was supported by grants (NSC 100-2113-M-001-022-MY3, NSC 101-2313-B-038-003, NSC 102-2313-B-038-005) from the National Science Council, Taiwan.

Notes

The authors declare no competing financial interest.

ACKNOWLEDGMENTS

We thank Jhih Tian Yang for his assistance in sequence alignment.

REFERENCES

(1) Boldyrev, A. A.; Aldini, G.; Derave, W. Physiology and pathophysiology of carnosine. *Physiol. Rev.* **2013**, *93*, 1803−1845.

(2) Quinn, P. J.; Boldyrev, A. A.; Formazuyk, V. E. Carnosine: its properties, functions and potential therapeutic applications. *Mol. Aspects Med.* **1992**, *13*, 379−444.

(3) Babizhayev, M. A. Antioxidant activity of L-carnosine, a natural histidine-containing dipeptide in crystalline lens. *Biochim. Biophys. Acta* **1989**, *1004*, 363−371.

(4) Babizhayev, M. A.; Seguin, M. C.; Gueyne, J.; Evstigneeva, R. P.; Ageyeva, E. A.; Zheltukhina, G. A. L-Carnosine (β-alanyl-L-histidine) and carcinine (β-alanylhistamine) act as natural antioxidants with hydroxyl-radical-scavenging and lipid-peroxidase activities. *Biochem. J.* **1994**, *304* (Part 2), 509−516.

(5) Hipkiss, A. R.; Brownson, C.; Carrier, M. J. Carnosine, the anti-ageing, anti-oxidant dipeptide, may react with protein carbonyl groups. *Mech. Ageing Dev.* **2001**, *122*, 1431−1445.

(6) Attanasio, F.; Cataldo, S.; Fisichella, S.; Nicoletti, S.; Nicoletti, V. G.; Pignataro, B.; Savarino, A.; Rizzarelli, E. Protective effects of L- and D-carnosine on α-crystallin amyloid fibril formation: implications for cataract disease. *Biochemistry* **2009**, *48*, 6522−6531.

(7) Seidler, N. W.; Yeargans, G. S.; Morgan, T. G. Carnosine disaggregates glycated α-crystallin: an in vitro study. *Arch. Biochem. Biophys.* **2004**, *427*, 110−115.

(8) Yan, H.; Harding, J. J. Carnosine inhibits modifications and decreased molecular chaperone activity of lens α-crystallin induced by ribose and fructose 6-phosphate. *Mol. Vis.* **2006**, *12*, 205−214.

(9) Biswas, S.; Harris, F.; Dennison, S.; Singh, J.; Phoenix, D. A. Calpains: targets of cataract prevention? *Trends Mol. Med.* **2004**, *10*, 78−84.

(10) David, L. L.; Shearer, T. R. Purification of calpain II from rat lens and determination of endogenous substrates. *Exp. Eye Res.* **1986**, *42*, 227−238.

(11) Andersson, M.; Sjostrand, J.; Andersson, A. K.; Andersen, B.; Karlsson, J. O. Calpains in lens epithelium from patients with cataract. *Exp. Eye Res.* **1994**, *59*, 359−364.

(12) Sanderson, J.; Marcantonio, J. M.; Duncan, G. A human lens model of cortical cataract: Ca^{2+}-induced protein loss, vimentin cleavage and opacification. *Invest. Ophthalmol. Vis. Sci.* **2000**, *41*, 2255−2261.

(13) Carragher, N. O. Calpain inhibition: a therapeutic strategy targeting multiple disease states. *Curr. Pharm. Des.* **2006**, *12*, 615−638.

(14) Hollows, F.; Moran, D. Cataract − the ultraviolet risk factor. *Lancet* **1981**, *2*, 1249−1250.

(15) Taylor, H. R.; West, S. K.; Rosenthal, F. S.; Munoz, B.; Newland, H. S.; Abbey, H.; Emmett, E. A. Effect of ultraviolet radiation on cataract formation. *N. Engl. J. Med.* **1988**, *319*, 1429−1433.

(16) Sommerburg, O.; Ullrich, O.; Sitte, N.; von Zglinicki, D.; Siems, W.; Grune, T. Dose- and wavelength-dependent oxidation of crystallins by UV light − selective recognition and degradation by the 20S proteasome. *Free Radical Biol. Med.* **1998**, *24*, 1369−1374.

(17) Fujii, N.; Uchida, H.; Saito, T. The damaging effect of UV-C irradiation on lens α-crystallin. *Mol. Vis.* **2004**, *10*, 814−820.

(18) Hu, C.-C.; Liao, J.-H.; Hsu, K.-Y.; Lin, I. L.; Tsai, M.-H.; Wu, W.-H.; Wei, T.-T.; Huang, Y.-S.; Chiu, S.-J.; Chen, H.-Y.; Wu, S.-H.; Wu, T.-H. Role of pirenoxine in the effects of catalin on in vitro ultraviolet-induced lens protein turbidity and selenite-induced cataractogenesis in vivo. *Mol. Vis.* **2011**, *17*, 1862−1870.

(19) Liao, J.-H.; Wu, T.-H.; Hsu, F.-L.; Huang, Y.-S.; Chiang, P.-H.; Huang, Z.-Y.; Huang, C.-H.; Wu, S.-H.; Lin, M.-H. Anti-UVC irradiation and metal chelation properties of 6-benzoyl-5,7-dihydroxy-4-phenyl-chromen-2-one: an implications for anti-cataract agent. *Int. J. Mol. Sci.* **2011**, *12*, 7059−7076.

(20) Liao, J.-H.; Chen, C.-S.; Hu, C.-C.; Chen, W.-T.; Wang, S.-P.; Lin, I. L.; Huang, Y.-H.; Tsai, M.-H.; Wu, T.-H.; Huang, F.-Y.; Wu, S.-H. Ditopic complexation of selenite anions or calcium cations by pirenoxine: an implication for anti-cataractogenesis. *Inorg. Chem.* **2011**, *50*, 365−377.

(21) Chen, C.-S.; Wu, S.-H.; Wu, Y.-Y.; Fang, J.-M.; Wu, T.-H. Properties of astaxanthin/Ca^{2+} complex formation in the deceleration of cis/trans isomerization. *Org. Lett.* **2007**, *9*, 2985−2988.

(22) Wu, T.-H.; Liao, J.-H.; Hou, W.-C.; Huang, F.-Y.; Maher, T. J.; Hu, C.-C. Astaxanthin protects against oxidative stress and calcium-induced porcine lens protein degradation. *J. Agric. Food Chem.* **2006**, *54*, 2418−2423.

(23) Babizhayev, M. A.; Deyev, A. I.; Yermakova, V. N.; Semiletov, Y. A.; Davydova, N. G.; Kurysheva, N. I.; Zhukotskii, A. V.; Goldman, I.

M. *N*-Acetylcarnosine, a natural histidine-containing dipeptide, as a potent ophthalmic drug in treatment of human cataracts. *Peptides* **2001**, *22*, 979−994.
(24) Babizhayev, M. A.; Khoroshilova-Maslova, I. P.; Kasus-Jacobi, A. Novel intraocular and systemic absorption drug delivery and efficacy of *N*-acetylcarnosine lubricant eye drops or carcinine biologics in pharmaceutical usage and therapeutic vision care. *Fundam. Clin. Pharmacol.* **2012**, *26*, 644−678.
(25) Dizhevskaya, A. K.; Muranov, K. O.; Boldyrev, A. A.; Ostrovsky, M. A. Natural dipeptides as mini-chaperones: molecular mechanism of inhibition of lens β-L-crystallin aggregation. *Curr. Aging Sci.* **2012**, *5*, 236−241.
(26) Liao, J.-H.; Lee, J.-S.; Chiou, S.-H. C-terminal lysine truncation increases thermostability and enhances chaperone-like function of porcine αB-crystallin. *Biochem. Biophys. Res. Commun.* **2002**, *297*, 309−316.
(27) Shih, M.; David, L. L.; Lampi, K. J.; Ma, H.; Fukiage, C.; Azuma, M.; Shearer, T. R. Proteolysis by m-calpain enhances in vitro light scattering by crystallins from human and bovine lenses. *Curr. Eye Res.* **2001**, *22*, 458−469.
(28) Liao, J. H.; Lee, J. S.; Chiou, S. H. Distinct roles of αA- and αB-crystallins under thermal and UV stresses. *Biochem. Biophys. Res. Commun.* **2002**, *295*, 854−861.
(29) Andley, U. P.; Clark, B. A. Spectroscopic studies on the photooxidation of calf-lens γ-crystallin. *Curr. Eye Res.* **1988**, *7*, 571−579.
(30) Hanna, R. A.; Campbell, R. L.; Davies, P. L. Calcium-bound structure of calpain and its mechanism of inhibition by calpastatin. *Nature* **2008**, *456*, 409−412.
(31) David, L. L.; Shearer, T. R. β-Crystallins insolubilized by calpain II in vitro contain cleavage sites similar to β-crystallins insolubilized during cataract. *FEBS Lett.* **1993**, *324*, 265−270.
(32) Gaggelli, E.; Valensin, G. ^{1}H and ^{13}C NMR relaxation investigation of the calcium complex of β-alanyl-L-histidine (carnosine) in aqueous solution. *J. Chem. Soc., Perkin Trans. 2* **1990**, 401−406.
(33) Brow, C. E. Chelation chemistry of carnosine. Evidence that mixed complexes may occur in vivo. *J. Phys. Chem.* **1979**, *83*, 3314−3319.
(34) Babizhayev, M. A.; Yermakova, V. N.; Semiletov, Y. A.; Deyev, A. I. The natural histidine-containing dipeptide Nα-acetylcarnosine as an antioxidant for ophthalmic use. *Biochemistry (Moscow)* **2000**, *65*, 588−598.
(35) Aristoy, M.-C. n.; Soler, C.; Toldrá, F. A simple, fast and reliable methodology for the analysis of histidine dipeptides as markers of the presence of animal origin proteins in feeds for ruminants. *Food Chem.* **2004**, *84*, 485−491.
(36) Andley, U. P.; Clark, B. A. Generation of oxidants in the near-UV photooxidation of human lens α-crystallin. *Invest. Ophthalmol. Vis. Sci.* **1989**, *30*, 706−713.
(37) Wu, K.; Kojima, M.; Shui, Y. B.; Sasaki, K.; Hockwin, O. In vitro UV-B effect on lens protein solutions. *Ophthalmic Res.* **1997**, *29*, 75−82.
(38) Wang, S. S. S.; Wen, W.-S. Examining the influence of ultraviolet C irradiation on recombinant human γ-D-crystallin. *Mol. Vis.* **2010**, *16*, 2777−2790.
(39) Yan, H.; Guo, Y.; Zhang, J.; Ding, Z.; Ha, W.; Harding, J. J. Effect of carnosine, aminoguanidine, and aspirin drops on the prevention of cataracts in diabetic rats. *Mol. Vis.* **2008**, *14*, 2282−2291.

JOURNAL OF AGRICULTURAL AND FOOD CHEMISTRY

Article

pubs.acs.org/JAFC

Structural Features and Antioxidant Activities of Lignins from Steam-Exploded Bamboo (*Phyllostachys pubescens*)

Shao-Ni Sun,[†] Xue-Fei Cao,[‡] Feng Xu,[†] Run-Cang Sun,*[,†,‡] and Gwynn Lloyd Jones[§]

[†]Beijing Key Laboratory of Lignocellulosic Chemistry, Beijing Forestry University, Beijing 100083, China

[‡]State Key Laboratory of Pulp and Paper Engineering, South China University of Technology, Guangzhou 510640, China

[§]School of Natural Science, University of Wales, Bangor, LL57 2UW Gwynedd, Wales, United Kingdom

ABSTRACT: An environmentally friendly steam explosion process of bamboo, followed by alkali and alkaline ethanol delignification, was developed to fractionate lignins. Results showed that after steam explosion the lignins isolated showed relatively low carbohydrate contents (0.55−1.76%) and molecular weights (780−1050 g/mol). For each steam-exploded sample, alkali-extracted lignins presented higher phenolic OH values (1.41−1.82 mmol/g), *p*-coumaric acid to ferulic acid ratios (*p*CA/FA ratios 4.5−14.1), and syringyl to guaiacyl ratios (S/G ratios 5.0−8.5) than those from alkaline ethanol-extracted lignins (phenolic OH 0.85−1.35 mmol/g, *p*CA/FA ratios 1.6−5.2, and S/G ratios 3.5−4.8). The lignins obtained consisted mainly of β−O−4′ linkages combined with small amounts of β−β′, β−5′, and α−O−4/β−O−4 linkages. Antioxidant activities of the lignins obtained were tested by the 2,2-diphenyl-1-picrylhydrazyl, 2,2′-azobis(3-ethylbenzothiazoline-6-sulfonic acid), and ferric reducing activity power methods. It was found that alkali-extracted lignins obtained during the initial extraction process had higher antioxidant activities than alkaline ethanol-extracted lignins obtained during the second extraction process.

KEYWORDS: *Phyllostachys pubescens, steam explosion, alkaline delignification, lignin, antioxidant activity*

INTRODUCTION

Increasing concerns about global climate change and diminishing fossil resources have increased attention in the development of alternative forms of biofuels and materials from renewable resources. Lignocellulosic biomass, as the most abundant renewable resource, can serve as a source of carbon-neutral or carbon-negative feedback for the production of biofuels, chemicals, and polymers, generally referred to as the biorefinery. Nowadays, the most promising biorefinery is to integrate biofuel production into the process in which the major components (cellulose, hemicelluloses, and lignin) of the biomass can be converted into high value-added products.[1] Therefore, effective pretreatment technology is necessary to separate the three major components and enhance enzyme digestibility of cellulose.[2]

Generally, pretreatments include physical, chemical, and biological methods, such as steam explosion, dilute acid, organosolv, and aqueous lime or alkali pretreatments. Among these methods, steam explosion pretreatment offers several advantages as compared with other pretreatments, including opening up biomass structure effectively,[3] assisting in fractionation of biomass components,[4] and decreasing environmental impact and capital investment, as well as increasing energy efficiency. However, the pretreatment also has some limitations, such as only partial destruction of hemicelluloses and incomplete disruption of the lignin−carbohydrate matrix; therefore, lignin is removed only to a limited extent and redistributes on the cellulose surfaces.[5] To circumvent these drawbacks, a subsequent alkaline delignification process, namely, successive alkali and alkaline ethanol extractions, was developed to fractionate steam-exploded biomass. Alkaline treatment is effective to disrupt plant cell walls and cleave the hydrogen bonds and covalent bonds in the cell wall matrix.[6] In addition, alkaline ethanol treatment is also an effective method where ethanol swells the biomass structure and acts as a solvent for the lignin, therefore reducing surface tension of the refining liquor at high temperature and promoting penetration of alkali into the materials and diffusion of the breakdown products of lignin from the materials to the liquor.[7] This ensures that lignin can be extracted without extensive modification of its structure. The presence of sodium hydroxide prevents or reduces pentosan hydrolysis and improves the delignifying ability of ethanol.[7,8] Therefore, in the whole biorefinery process combining steam explosion with a two-step alkaline delignification (alkali and alkaline ethanol treatments), hemicelluloses and lignin can be effectively fractionated for the production of high value-added chemicals while cellulose can be used to produce biofuels. In this work, we focused on fractionating lignin from steam-exploded bamboo (*Phyllostachys pubescens*) by alkali and alkaline ethanol treatments.

Lignin is a heterogeneous polymer synthesized mainly from three *p*-hydroxycinnamyl alcohols differing in their degree of methoxylation: *p*-coumaryl, coniferyl, and sinapyl alcohols, each of which leads to a corresponding type of lignin unit named *p*-hydroxyphenyl (H), guaiacyl (G), and syringyl (S), respectively. The knowledge of lignin structure can not only provide valuable information to understand pretreatment mechanisms, and thus improve current approaches or develop new pretreatment methods, but also help to evaluate the potential utilization of lignin.[9] The present study focused on the application of steam explosion combined with alkali and

Received: December 7, 2013
Revised: June 3, 2014
Accepted: June 8, 2014
Published: June 8, 2014

ACS Publications © 2014 American Chemical Society

dx.doi.org/10.1021/jf5023093 | J. Agric. Food Chem. 2014, 62, 5939−5947

alkaline ethanol delignification in fractionating lignin from *Phyllostachys pubescens*, with the objective of determining the structure of the obtained lignin by sugar analysis, molecular weights, Fourier transform infrared (FT-IR), two-dimensional heteronuclear single-quantum coherence (2D HSQC), and ^{31}P NMR spectroscopies. Additionally, antioxidant activity of the lignins, which is closely related to lignin structure, was evaluated by 2,2-diphenyl-1-picrylhydrazyl (DPPH), 2,2′-azobis(3-ethylbenzothiazoline-6-sulfonic acid) (ABTS), and ferric reducing activity power (FRAP) methods.

MATERIALS AND METHODS

Materials. *Phyllostachys pubescens* was obtained from Jiangxi Province, China. The chemical composition (% w/w) was determined to be 39.8% glucan, 22.8% xylan, 25.1% acid-insoluble lignin, 1.4% arabinan, 0.3% galactan, 2.1% acid-soluble lignin, and 2.3% ash, according to National Renewable Energy Laboratory (NREL) standard analytical procedure.[10] The bamboo material was air-dried and cut into an average size of 100 mm × 15 mm × 15 mm. 2,2-Diphenyl-1-picrylhydrazyl (DPPH), deuterated chloroform, cyclohexanol, chromium(III) acetylacetonate, and 2-chloro-1,3,2-dioxaphospholane were purchased from Sigma−Aldrich (Shanghai, China). 2,4,6-Tripyridyl-*s*-triazine (TPTZ) was purchased from Xiya Reagents (Chengdu, Sichuan, China). 2,2′-Azobis(3-ethylbenzothiazoline-6-sulfonic acid) (ABTS) was obtained from Lanyi (Beijing, China), and Trolox was obtained from Aladdin (Shanghai, China). Methanol, potassium persulfate ($K_2S_2O_8$), and $FeCl_3{\cdot}6H_2O$ were purchased from Xilong Chemical Co., Ltd. (Shantou, Guangdong, China). Sodium hydroxide (NaOH), dimethyl sulfoxide (DMSO), anhydrous pyridine, hydrochloric acid, acetic acid, and sodium acetate were purchased from Beijing Chemical Works (Beijing, China), in which acetic acid and sodium acetate were used to make acetate buffer. Sodium hydrogen phosphate heptahydrate ($Na_2HPO_4{\cdot}7H_2O$) and $NaH_2PO_4{\cdot}H_2O$ were obtained from Guangdong Guanghua Chemical Factory Co., Ltd. (Guangzhou, Guangdong, China) and were used to make phosphate buffer.

Steam Explosion Pretreatment and Fractionation Process. Before steam explosion pretreatment, bamboo chips were separated into three batches (300 g for each batch). To evaluate the effect of water impregnation on subsequent steam explosion pretreatment, two batches were immersed in distilled water at 25 °C for 24 h and another batch was kept dry at room temperature (without water impregnation). The steam explosion pretreatment was carried out in a 7.5 L stainless steel vessel designed especially for the processing of biomass. The reactor was heated with saturated steam to reach the required pressure. At the end of the steaming, the pressure was instantaneously released to stop the reaction, and the exploded feedstock was collected. Specifically, the sample without water impregnation (sample 1) was treated at 2.0 MPa for 5 min, while the two water-immersed samples were treated at 1.8 MPa (sample 2) or 2.0 MPa (sample 3) for 5 min. Then the three steam-exploded samples were treated with 0.5% NaOH with a solid-to-liquor ratio of 1:20 (w/v) at 80 °C for 3 h to obtain lignin fractions L_{A1}, L_{A2}, and L_{A3}, respectively. Next the corresponding residuals were further treated with 60% ethanol containing 1.5% NaOH with a solid-to-liquor ratio of 1:20 (w/v) at 80 °C for 3 h to obtain other three lignin fractions, L_{AE1}, L_{AE2}, and L_{AE3}, respectively. The lignin fractions obtained with alkali and alkaline ethanol were categorized as lignin-A (L_{A1}, L_{A2}, and L_{A3}) and lignin-AE (L_{AE1}, L_{AE2}, and L_{AE3}), respectively. The purification procedure of all lignin fractions was performed according to a previous literature procedure.[11]

Characterization of Isolated Lignins. The associated carbohydrate composition of all lignin fractions was determined by high-performance anion-exchange chromatography (HPAEC). Lignin fractions (5 mg) were hydrolyzed with 1.475 mL of 6% sulfuric acid at 105 °C for 2.5 h. After hydrolysis, these fractions were diluted 50-fold and analyzed by HPAEC system (ISC 3000, Dionex, Beijing, China) with an amperometric detector and AS50 autosampler. The column used was a 250 mm × 4 mm, CarbopacTM PA-20, with a 30 mm × 3 mm i.d. guard column of the same material (Dionex, Beijing, China). The sugars were separated in 18 mmol/L of NaOH (carbonate-free and purged with nitrogen) with postcolumn addition of 0.3 M NaOH at a rate of 0.5 mL/min. Run time was 45 min, followed by 10 min elution with 0.2 M NaOH to wash the column and then a 15 min elution with 18 mmol/L of NaOH to re-equilibrate the column.

The average molecular weights and molecular weight distribution of lignin fractions were examined by gel-permeation chromatography (GPC, Agilent 1200) on a PL-gel 10 μm Mixed-B 7.5 mm i.d. column. The detector was a differential refractive index detector. A 4 mg sample was dissolved in 2 mL of tetrahydrofuran, and 20 μL aliquots of lignin solution were injected. The column was operated at ambient temperature and eluted with tetrahydrofuran at a flow rate of 1.0 mL/min.

FT-IR spectra of all lignin fractions were recorded on a spectrophotometer (Bruker Tensor 27 FT-IR) in the range 4000−400 cm^{-1} with a resolution of 4 cm^{-1}. A KBr disc containing 1% finely ground sample was used for measurement.

HSQC spectra of the lignin fractions were acquired on a Bruker AVIII 400 MHz spectrometer at 25 °C. About 90 mg of lignin was dissolved in 0.5 mL of DMSO-d_6. The spectral widths were 5000 and 20 000 Hz for the ^{1}H and ^{13}C dimensions, respectively. The number of collected complex points was 1024 for the ^{1}H dimension with a recycle delay of 1.5 s. The number of transients was 64 and 256 time increments recorded in the ^{13}C dimension. $^1J_{CH}$ was set to 146 Hz. Before Fourier transformation, the data matrices were zero-filled to 1024 points in the ^{13}C dimension. The central solvent (DMSO) peak was used as an internal chemical shift reference point (δC/δH 39.5/2.49). ^{31}P NMR spectra were acquired according to a previous method[12] with minor modifications. Twenty milligrams of dry lignin was dissolved in 500 μL of anhydrous pyridine and deuterated chloroform (1.6:1.0 v/v) under stirring, followed by addition of 100 μL of cyclohexanol (10.85 mg/mL) as an internal standard (IS) and 100 μL of chromium(III) acetylacetonate solution (5 mg/mL in anhydrous pyridine and deuterated chloroform, 1.6:1.0 v/v) as relaxation reagent. Finally, the mixture was reacted with 100 μL of phosphitylating reagent (2-chloro-1,3,2-dioxaphospholane) for 15 min and then used for subsequent NMR analysis.

Antioxidant Activity Analysis. The antiradical activity of different lignin fractions was estimated according to the procedure reported by Delgado-Andrade et al.[13] with some modifications. DPPH solution was prepared by dissolving 7.4 mg of DPPH with 100 mL of methanol to obtain an absorbance of 1.8 at 520 nm. A 200 μL aliquot of lignin fraction was allowed to react with 1 mL of 74 mg/L DPPH in methanol. The mixture was shaken for 1 h, and then absorption was measured at 520 nm. The temperature in the measurement chamber was set at 30 °C. The standard curve was linear between 10 and 400 μmol of Trolox. Results are expressed as micromole equivalents of Trolox per gram of sample.

The ABTS assay was performed according to the procedure reported by Delgado-Andrade et al.[13] with some modifications. Briefly, $ABTS^{+\bullet}$ was produced by reacting 7 mmol of ABTS stock solution with 2.45 mmol of potassium persulfate and keeping the mixture in the dark at room temperature for 12 h before use. The $ABTS^{+\bullet}$ solution was diluted with 5 mmol of phosphate-buffered saline (pH 7.4) to an absorbance of 0.70 at 730 nm. After addition of 10 μL aliquots of lignin fractions and Trolox standard to 4 mL of diluted $ABTS^{+\bullet}$ solution, an absorbance reading was taken at 20 min on an ultraviolet/visible spectrophotometer (Tec comp, UV 2300). Calibration was performed, as described previously, with Trolox solution. Results were expressed as micromole equivalents of Trolox per gram of lignins.

The FRAP assay was performed according to a previous study[14] with some modifications. Fresh FRAP reagent was prepared before use, which contained 25 mL of acetate buffer (300 mmol/L, pH 3.6), 2.5 mL of TPTZ (2,4,6-tripyridyl-*s*-triazine) solution (10 mmol/L in 40 mmol/L HCl), and 2.5 mL of $FeCl_3{\cdot}6H_2O$ solution (20 mmol/L) and then warmed at 37 °C before use. Lignin fractions and Trolox (150 mL) were allowed to react with 2850 mL of FRAP solution at 37

dx.doi.org/10.1021/jf5023093 | J. Agric. Food Chem. 2014, 62, 5939−5947

Table 1. Yields, Molecular Weights, Polydispersity, and Content of Lignin Fractions

	lignin fraction					
	L_{A1}	L_{A2}	L_{A3}	L_{AE1}	L_{AE2}	L_{AE3}
yield[a] (%)	62.8 ± 1.8	39.4 ± 1.1	59.7 ± 1.9	7.3 ± 0.4	24.1 ± 1.0	13.7 ± 0.6
M_w[b]	960	780	1040	1040	870	1050
M_n[c]	540	530	610	600	510	570
M_w/M_n[d]	1.78	1.47	1.70	1.73	1.71	1.84
Contents of Neutral Sugars and Uronic Acids (absolute %, w/w)						
arabinose	0.06	0.08	0.06	0.05	0.09	0.05
galactose	0.05	0.03	0.01	0.03	0.06	0.06
glucose	0.30	0.30	0.16	0.09	0.69	0.30
xylose	0.72	0.64	0.25	0.47	0.88	0.43
glucuronic acid	0.06	0.05	0.07	0.05	0.04	0.04
total[e]	1.19	1.10	0.55	0.69	1.76	0.88

[a]Yields of degraded acid-insoluble lignin fractions (% acid-insoluble lignin, w/w). [b]Weight-average molecular weight. [c]Number-average molecular weight. [d]Polydispersity. [e]Total associated carbohydrates in the lignin fractions (% dried lignin sample, w/w).

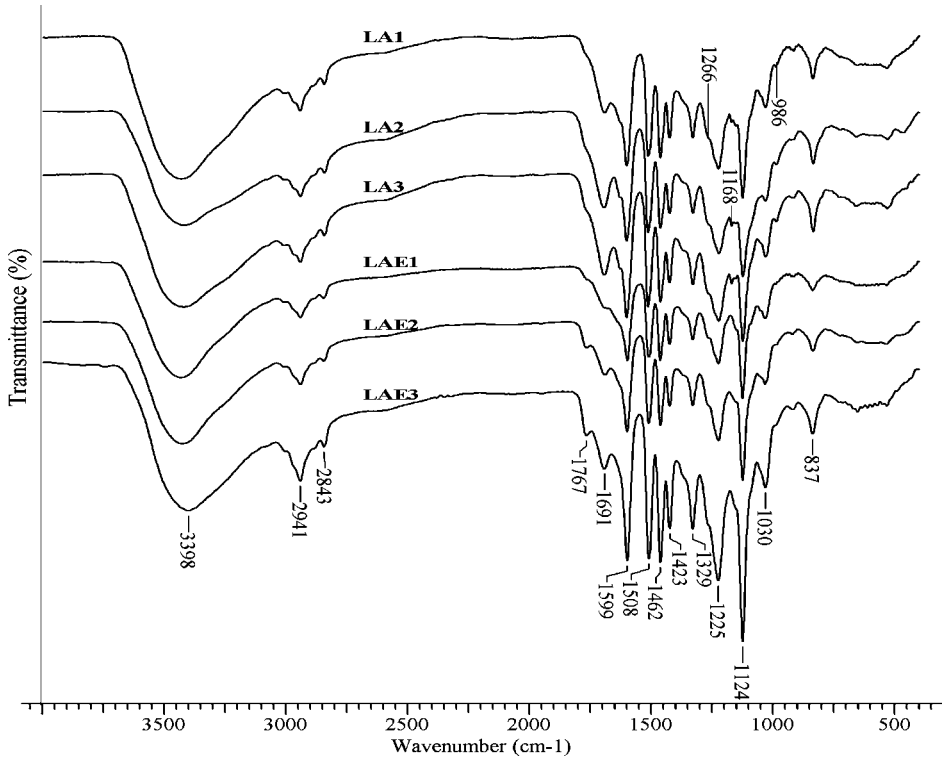

Figure 1. FT-IR spectra of lignin fractions.

°C for 30 min in the dark. Readings of the colored product were then taken at 593 nm. Trolox solution was used to perform the calibration curves. Results were also expressed as micromole equivalents of Trolox per gram of sample.

RESULTS AND DISCUSSION

Yields, Residual Carbohydrates, and Molecular Weight Distribution of Isolated Lignins. The yields of the lignin fractions (weight percent, oven-dried samples) and their residual carbohydrates are given in Table 1. In the present study, the yields of lignin fractions extracted with alkali and alkaline ethanol were 39.4−62.8% and 7.3−24.1% of the total acid-insoluble lignin, respectively. The total yields of lignins obtained from the two-step extraction procedure accounted for 70.1%, 63.5%, and 73.4% of total acid-insoluble lignin from steam-exploded samples 1, 2, and 3, respectively. Obviously, for water-immersed samples, the increase in steam pretreatment pressure from 1.8 MPa (sample 2) to 2.0 MPa (sample 3) resulted in a significant increment of total lignin yield in alkaline delignification. Besides, lignins extracted from sample 1 (without water impregnation) presented relatively lower yields as compared with those extracted from sample 3 (water impregnation), suggesting that water impregnation was an effective pretreatment method prior to steam explosion to increase the removal of lignin.

Obviously, the lignin fractions obtained by this process contained low levels of residual carbohydrates (0.55−1.76%), demonstrating that the two-stage process significantly cleaved ether bonds between lignin and carbohydrates in the plant cell walls of bamboo, in addition to partial saponification of hydroxycinnamic esters.[11] It is clear that xylose and glucose were the major sugars in the associated carbohydrates of lignins,

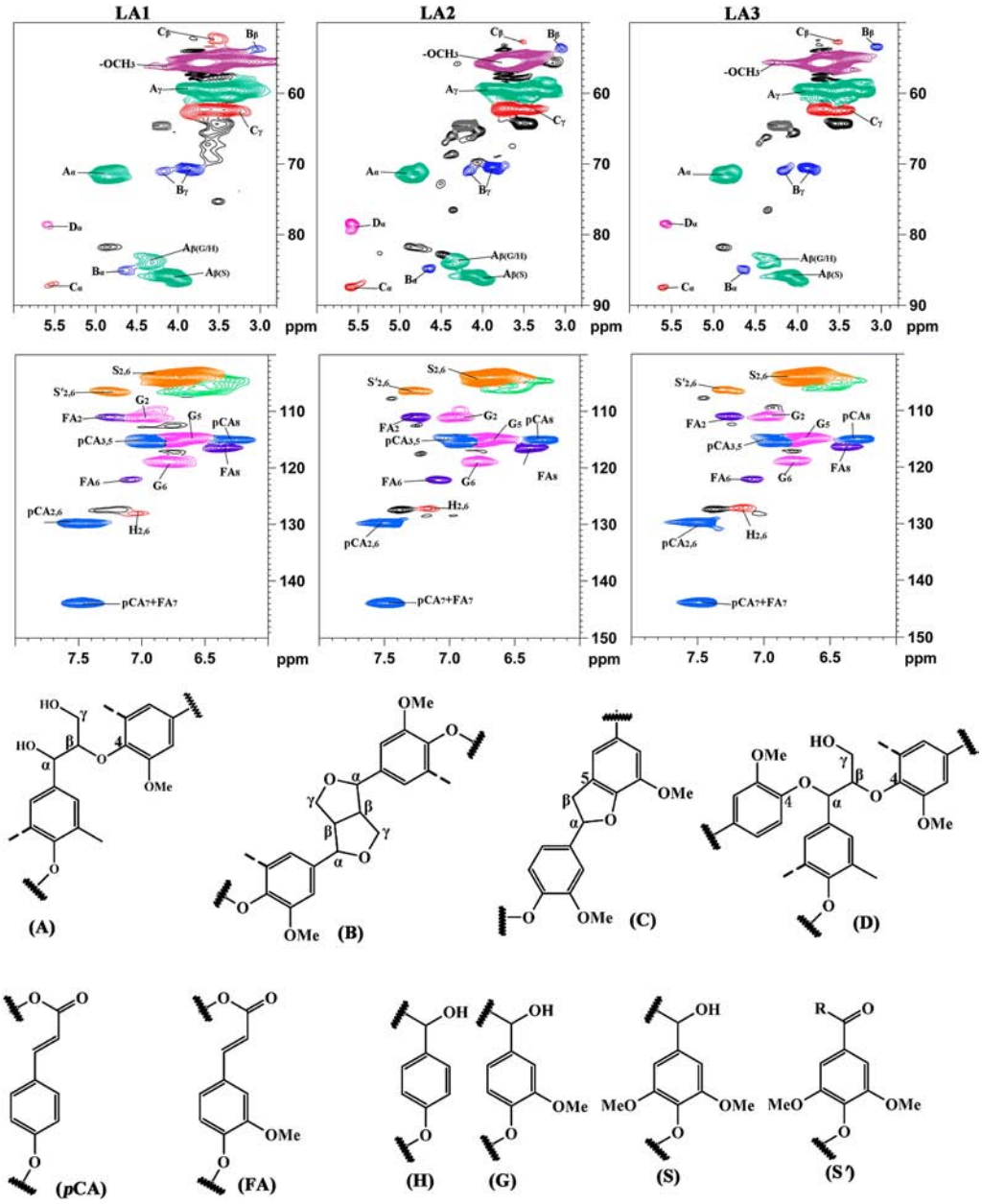

Figure 2. HSQC spectra of lignin-A fractions and their main substructures: **A**, β-aryl ether units (β−O−4′); **A′**, β−O−4′ alkyl aryl ethers with acylated γ-OH with *p*-coumaric acid; **B**, resinol substructures (β−β'); **C**, phenylcoumaran substructures (β−5′); and **D**, α,β-diaryl ethers (α−O−4/β−O−4). *p*CA, *p*-coumaric acid; FA, ferulic acid; H, *p*-hydroxyphenyl units; G, guaiacyl units; S, syringyl units; S′, oxidized syringyl units bearing a carbonyl at Cα.

whereas arabinose, galactose, and glucuronic acid were detected as minor quantities, as shown in Table 1. Therefore, low carbohydrate contents in the obtained lignins were beneficial for subsequent structure analysis of the lignins.

The weight-average (M_w) and number-average (M_n) molecular weights and the polydispersities (M_w/M_n) of all lignin fractions are also given in Table 1. The M_w and M_n values of the six lignin fractions were 780−1050 and 510−610 g/mol, which were lower than those of milled wood lignin (MWL, M_w = 6080 and M_n = 3230 g/mol), as reported by a previous study.[15] The results show that steam explosion, under the conditions given, significantly reduced M_w and M_n of the lignins, which were released during the steam explosion combined with alkali fractionation process. It should be noted that as the concentration of NaOH increased from 0.5% to 1.5%, M_w increased slightly from 780−1040 to 870−1050 g/mol. Apparently, in contrast to the M_w of L_{A1} and L_{AE1}, fractions L_{A3} and L_{AE3} present relatively higher M_w, implying that lignins obtained from dry sample had relatively lower M_w than those extracted from the water-immersed sample. This could be attributed to additional moisture adsorbing the heat applied during the steam explosion pretreatment, resulting in a decrease in the severity of treatment undergone by the chips at equivalent pretreatment condition,[16] thus presenting a low degradation degree of lignin in the water-immersed sample. Furthermore, for the water-immersed samples, an increase in steaming pressure from 1.8 to 2.0 MPa led to a slight increase in M_w from 780 to 870 g/mol for the alkali-extracted lignins and from 1040 to 1050 g/mol for the alkaline ethanol-extracted lignins. Additionally, all the lignin fractions showed narrow

dx.doi.org/10.1021/jf5023093 | J. Agric. Food Chem. 2014, 62, 5939−5947

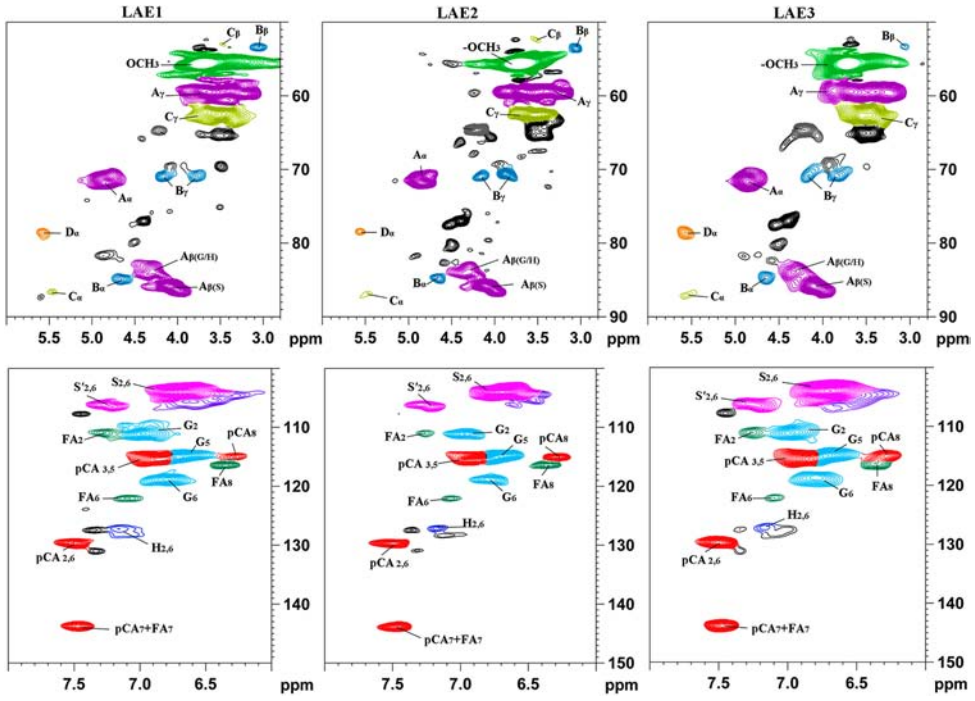

Figure 3. HSQC spectra of lignin-AE fractions.

molecular distributions (1.47−1.84), indicating homogeneous lignin fragment sizes.[17]

Fourier Transform Infrared Analysis. Figure 1 shows the FT-IR spectra of all lignin fractions; peaks were assigned according to the literature.[18,19] The band at 1691 cm^{-1} is related to carbonyl stretching in conjugated ketone and carboxylic acid groups, as indicated by the presence of *p*-coumaric acid (*p*CA). It can be observed that the weak intensity band at 1665 cm^{-1}, relating to carbonyl stretching of conjugated *p*-substituted aryl ketones, was present in lignin-A but almost disappeared in lignin-AE. This result implies that lignin-A had a relatively higher content of conjugated *p*-substituted aryl ketones as compared with lignin-AE. The bands at 1599, 1508, and 1423 cm^{-1} are assigned to aromatic skeletal vibrations and the band at 1462 cm^{-1} represents C−H deformation combined with aromatic ring vibration, indicating the primary structure of the obtained lignins. The bands at 1160 cm^{-1} (antisymmetric C−O stretching of ester groups) and 1125 cm^{-1} (aromatic C−H in-plane deformation) are typical for HGS lignin. It is worth mentioning that the band at 1160 cm^{-1} is less pronounced in lignin-A and almost disappeared in lignin-AE, suggesting that tiny ester bands in the initial fractionating lignins (lignin-A) were retained. However, this band disappeared in the subsequently isolated lignin-AE, indicating that the ester bonds of lignins were fundamentally cleaved during the alkaline ethanol extraction.

Two-Dimensional Heteronuclear Single-Quantum Correlation NMR. To further investigate the structural changes of lignins, 2D HSQC NMR was used. The HSQC spectra of lignin-A and lignin-AE are shown in Figures 2 and 3, respectively, and the main substructures are also depicted in Figure 2. The main assignments of lignin cross-signals in the HSQC spectra are listed in Table 2. From these well-resolved NMR spectra, $^{13}C-^{1}H$ correlations from all major units, representing the various linkages presenting in lignin units, were assigned according to previous literature.[20,21] In the side-

Table 2. Assignments of $^{13}C-^{1}H$ Cross-Signals in HSQC Spectra of Degraded Acid-Insoluble Lignin Fractions from Steam-Exploded Bamboo

label	$\delta C/\delta H$ (ppm)	assignment
C_β	52.4/3.51	$C_\beta-H_\beta$ in **C**[a]
B_β	53.6/3.04	$C_\beta-H_\beta$ in **B**
$-OCHH_3$	55.7/3.70	C−H in methoxyls
A_γ	59.6/3.66	$C_\gamma-H_\gamma$ in **A**
C_γ	62.4/3.71	$C_\gamma-H_\gamma$ in **C**
B_γ	71.0/3.88−4.17	$C_\gamma-H_\gamma$ in **B**
A_α	71.8/4.85	$C_\alpha-H_\alpha$ in **A**
D_α	78.4/5.58	$C_\alpha-H_\alpha$ in **D**
$A_{\beta(G/H)}$	84.1/4.33	$C_\beta-H_\beta$ in **A** linked to G/H unit
B_α	85.0/4.64	$C_\alpha-H_\alpha$ in **B**
$A_{\beta(S)}$	85.9/4.11	$C_\beta-H_\beta$ in **A** linked to S
C_α	87.2/5.57	$C_\alpha-H_\alpha$ in **C**
$S_{2,6}$	104.0/6.70	$C_{2,6}-H_{2,6}$ in S
$S'_{2,6}$	106.3/7.30	$C_{2,6}-H_{2,6}$ in S′
G_2	111.1/6.98	C_2-H_2 in G
G_5	114.7/6.71	C_5-H_5 in G
G_6	118.9/6.80	C_6-H_6 in G
$H_{2,6}$	127.4/7.21	$C_{2,6}-H_{2,6}$ in H
$pCA_{3,5}$	115.4/6.84	$C_{3,5}-H_{3,5}$ in *p*CA
$pCA_{2,6}$	129.8/7.50	$C_{2,6}-H_{2,6}$ in *p*CA
pCA_7	143.9/7.48	C_7-H_7 in *p*CA
pCA_8	115.1/6.29	C_8-H_8 in *p*CA
FA_2	111.0/7.27	C_2-H_2 in FA
FA_6	122.1/7.10	C_6-H_6 in FA
FA_7	143.9/7.48	C_7-H_7 in FA
FA_8	116.4/6.37	C_8-H_8 in FA

[a]Substructures are as follows: **A**, *β*-aryl ether units (*β*−O−4′); **B**, resinol substructures (*β*−*β*′); **C**, phenylcoumaran substructures (*β*−5′); **D**, *α*,*β*-diaryl ethers (*α*−O−4/*β*−O−4). *p*CA, *p*-coumaric acid; FA, ferulic acid; H, *p*-hydroxyphenyl unit; G, guaiacyl unit; S, syringyl unit; S′, oxidized syringyl unit bearing a carbonyl at C*α*.

dx.doi.org/10.1021/jf5023093 | J. Agric. Food Chem. 2014, 62, 5939−5947

chain region of the spectra, cross-signals from methoxyl groups (δC/δH 55.7/3.70) and side chains in β−O−4′ substructures **A** were most prominent. A signal located at δC/δH 71.8/4.85 is attributed to C_α−H_α in β−O−4′ substructure. Likewise, C_β−H_β correlations were identified at δC/δH 84.1/4.33 for β−O−4′ structure linked to G/H lignin units and at δC/δH 85.9/4.11 for β−O−4′ structure linked to S lignin units. The C_γ−H_γ correlations in β−O−4′ substructure were observed at δC/δH 59.6/3.66. Strong signals for resinol (β−β', **B**) substructures were observed, with the signals for their C_α−H_α and C_β−H_β correlations being observed at δC/δH 85.0/4.64 and 53.6/3.04, respectively, and those of C_γ−H_γ correlations showing the double signals at δC/δH 71.0/3.88 and 4.17. Interestingly, the signal for tetrahydrofuran (**B**′, formed by β−β' coupling of monolignols acylated at the γ-carbon)[22] substructures was observed in the spectra of MWL,[15] with characteristic C_α−H_α correlations at δC/δH 83.2/4.94, and the presence of substructures **B**′ is related to the high extent of γ-carbon acylation of S lignins.[23] However, this substructure was not detected in the lignins obtained, suggesting no or low extent of γ-carbon acylation of S lignins in the alkali and alkaline ethanol-extracted lignins obtained from steam-exploded bamboo. Signals for phenylcoumaran (β−5′, **C**) substructures were also observed in the spectra in noticeable amounts, with their C_α−H_α, C_β−H_β, and C_γ−H_γ correlations at δC/δH 87.2/5.57, 52.4/3.51, and 62.4/3.71, respectively. Finally, small signals corresponding to α,β-diaryl ethers (α−O−4/β−O−4, **D**) substructures could also be observed, with their C_α−H_α correlations being at δC/δH 78.4/4.58. Interestingly, although the substructures of spirodienones and γ-acylated cinnamyl alcohol end groups were found in MWL of *Phyllostachys pubescens*,[15] the two substructures were not observed in the alkali and alkaline ethanol-extracted lignins obtained from steam-exploded bamboo in this study. This difference was probably due to the different pretreatment and extraction methods. The lack of spirodienone units was potentially attributable to the steam explosion pretreatment because spirodienones are not stable under acidic conditions.[23] In addition, the γ-acylated cinnamyl alcohol end groups were cleaved as a result of subsequent alkaline treatment.

The main cross-signals in the aromatic regions of the HSQC spectra corresponded to different lignins and *p*-hydroxycinnamate units. Signals from H, G, and S units were observed. The S units show a prominent signal for $C_{2,6}$−$H_{2,6}$ correlations at δC/δH 104.0/6.70, whereas the signal for C_α-oxidized S units (S′) was observed at δC/δH 106.3/7.30. The G units show different correlations for C_2−H_2, C_5−H_5, and C_6−H_6 at δC/δH 111.1/6.98, 114.7/6.71, and 118.9/6.80, respectively. $C_{2,6}$−$H_{2,6}$ aromatic correlation signal from H units was observed at δC/δH 127.4/7.21. In addition, some condensed lignin structures likely occurred at $S_{2,6}$, but the detailed structures of the condensed lignin formed in S units remain unknown. One possible reason is that the condensed position in S units is located at C_α of the side chain and then can react with another lignin unit. In addition, signals corresponding to *p*CA were also observed in the HSQC spectra: $C_{2,6}$−$H_{2,6}$, $C_{3,5}$−$H_{3,5}$, C_7−H_7, and C_8−H_8 correlations at δC/δH 129.8/7.50, 115.4/6.84, 143.9/7.48, and 115.1/6.29, respectively. The correlations of ferulic acid (FA) were found at δC/δH 111.0/7.27 (C_2−H_2), 122.1/7.10 (C_6−H_6), 143.9/7.48 (C_7−H_7), and 116.4/6.37 (C_8−H_8).

According to semiquantitative methods, the relative amounts of interunit linkages present in lignins as well as *p*CA/FA and S/G molar ratios were calculated, and the results are shown in Table 3. These data indicate a similar composition in both alkali- and alkaline ethanol-extracted lignins. As seen in Table 3, the main lignin substructure was β−O−4′ aryl ether, which accounted for up to 73.9−79.0% of all interunit linkages, while low amounts of β−β', β−5′, and α−O−4/β−O−4 were also present. Furthermore, it was observed that alkali-extracted lignins had higher *p*CA/FA ratios than alkaline ethanol-extracted lignins. The ratios of S/G were estimated to be 5.0−8.5 for lignin-A and 3.5−4.8 for lignin-AE. This observation indicated that S-rich lignin was more easily released than G-rich lignin in the initial alkali process. Furthermore, the low S/G ratios of the alkaline ethanol-extracted lignins were probably due to the high content of condensed structure in these lignins because guaiacyl units were found to be reactive toward condensation.[24] All lignin fractions in this work had higher S/G ratios (3.5−8.5) than MWL (2.2). It has been reported that MWL mainly originates from middle lamella,[25] in which the lignin had fewer methoxyl groups per C9 than that in the secondary wall.[26] In other words, MWL with low yield (10%, acid insoluble lignin) had a low S/G ratio, while in this study the lignins with high yields (63.45−73.35% acid-insoluble lignin) had high S/G ratios, implying that the lignins from steam-exploded samples probably originated from whole plant cell walls.

Table 3. Characteristics of Degraded Acid-Insoluble Lignin Fractions from Quantitative 2D HSQC Spectroscopy

	lignin fraction					
	L_{A1}	L_{A2}	L_{A3}	L_{AE1}	L_{AE2}	L_{AE3}
A[a]	79.0	74.4	75.9	76.0	76.5	76.9
B	8.6	5.9	10.5	10.8	10.0	8.8
C	6.2	8.2	5.6	6.1	7.8	5.8
D	6.2	11.5	8.0	7.1	5.7	8.5
*p*CA/FA ratio[b]	14.1	4.5	5.3	1.6	3.2	5.2
S/G ratio[c]	8.5	7.4	5.0	4.3	3.5	4.8

[a]Relative quantitative method based on 2D HSQC spectra (without IS). Substructures are as follows: **A**, β-aryl ether units (β−O−4′); **B**, resinol substructures (β−β'); **C**, phenylcoumaran substructures (β−5′); **D**, α,β-diaryl ethers (α−O−4/β−O−4). [b]*p*CA, *p*-coumaric acid; FA, ferulic acid. *p*CA/FA ratio was obtained as $0.5I(pCA_{2,6})/I(FA_2)$. [c]G, guaiacyl unit; S, syringyl unit. S/G ratio was obtained as $0.5I(S_{2,6})/I(G_2)$.

^{31}P NMR and Antioxidant Activity Analyses. ^{31}P NMR spectroscopy is a facile and direct analytical tool for quantitating the major hydroxyl groups in lignin, and the concentrations of different hydroxyl groups were calculated on the basis of the internal standard (cyclohexanol) and the integrated peak areas. The results from ^{31}P NMR can particularly provide an insight into the absolute amounts of aliphatic OH (α-OH and primary OH), phenolic OH (S-OH, $G_{5,5}$-OH, G-OH, and *p*-coumarate OH), and carboxylic OH (COOH) in the six lignin fractions. Figure 4 provides typical ^{31}P NMR spectra of bamboo lignin, and Table 4 provides the contents of different hydroxyl groups. The data show that the hydroxyl content of lignin isolated from *Phyllostachys pubescens* decreased following the order aliphatic OH (1.93−2.88 mmol/g) > phenolic OH (0.85−1.82 mmol/g) > COOH (0.08−0.32 mmol/g). In the present work, for L_{A1} and L_{AE1}, no significant variations in the contents of aliphatic OH, phenolic OH, and COOH were observed. In comparison, L_{A2} and L_{A3} contained

dx.doi.org/10.1021/jf5023093 | J. Agric. Food Chem. 2014, 62, 5939−5947

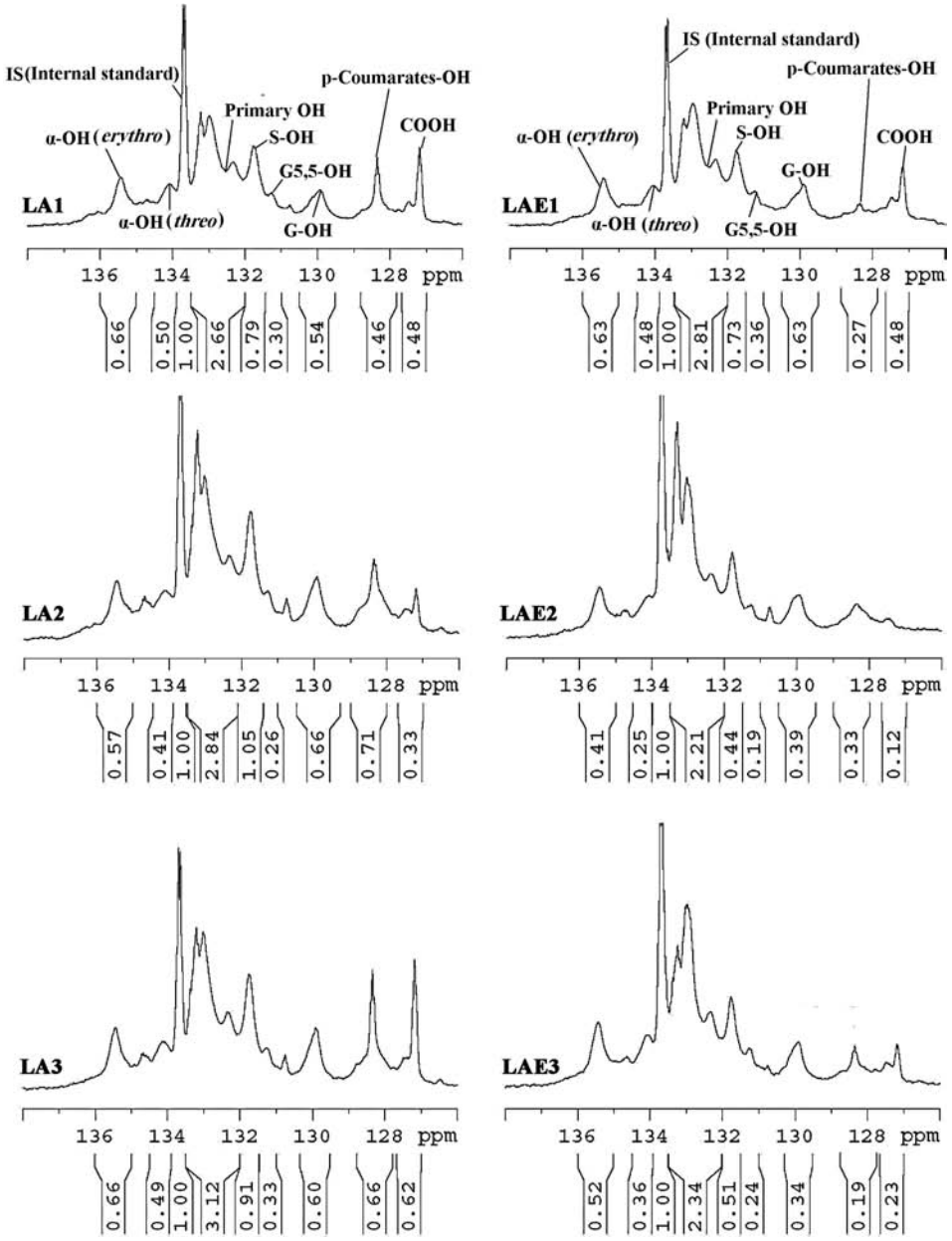

Figure 4. ^{31}P NMR spectra of lignin fractions.

Table 4. Hydroxyl Content (mmol/g) of Lignin Fractions as Determined by ^{31}P NMR

	lignin fraction					
	L_{A1}	L_{A2}	L_{A3}	L_{AE1}	L_{AE2}	L_{AE3}
α-OH (*erythro*)	0.44	0.38	0.45	0.43	0.27	0.35
α-OH (*threo*)	0.34	0.27	0.33	0.32	0.17	0.24
primary OH	1.79	1.92	2.10	1.90	1.49	1.58
S-OH	0.53	0.71	0.61	0.49	0.30	0.35
$G_{5,5}$-OH	0.20	0.18	0.22	0.24	0.13	0.16
G-OH	0.37	0.45	0.40	0.43	0.26	0.21
p-coumarates OH	0.31	0.48	0.44	0.19	0.22	0.13
COOH	0.32	0.22	0.42	0.32	0.08	0.15

relatively higher amounts of aliphatic OH, phenolic OH, and COOH than their corresponding samples L_{AE2} and L_{AE3}, respectively. The higher amounts of phenolic OH in the alkali-extracted lignins indicated the occurrence of cleavage of β−O−4′ linkages (HSQC NMR results). The decrease in β−O−4′ linkage further provided evidence for the cleavage of β-aryl ether structure in lignins. Moxley et al.[27] also revealed that cleavage of aryl ether lignin bonds resulted in lignin fragments with low M_w. From the above results, higher pressure in steam explosion pretreatment resulted in a higher content of phenolic OH, which also corresponded to the lower β−O−4′ content and M_w. As seen in Table 4, the increase in pressure (from 1.8 to 2.0 MPa) was accompanied by an increase of aliphatic OH and a decrease of phenolic OH. As compared with L_{A2}, the content of COOH in L_{A3} increased from 0.22 to 0.42 mmol/g, and the same correlation was also observed for L_{AE2} (0.08 mmol/g) and L_{AE3} (0.15 mmol/g). The increased COOH content suggested that the oxidation of aliphatic OH occurred during the high-pressure steam explosion pretreatment.

The antioxidant activities of the lignin fractions by the three selected methodologies are summarized in Table 5. Data are expressed as micromole equivalents of Trolox per gram of

dx.doi.org/10.1021/jf5023093 | J. Agric. Food Chem. 2014, 62, 5939−5947

Table 5. Antioxidant Activities of Lignin Fractions As Determined by DPPH, ABTS, and FRAP Assays[a]

lignin fraction	antioxidant activity (mmol of Trolox/g of lignins)		
	DPPH	ABTS	FRAP
L_{A1}	474 ± 12	2534 ± 19	848 ± 21
L_{A2}	371 ± 8	1926 ± 15	624 ± 17
L_{A3}	511 ± 17	2906 ± 28	953 ± 11
L_{AE1}	447 ± 10	2273 ± 25	767 ± 13
L_{AE2}	282 ± 10	1485 ± 17	579 ± 14
L_{AE3}	408 ± 9	2036 ± 18	657 ± 9

[a]DPPH, 2,2-diphenyl-1-picrylhydrazyl; ABTS, 2,2′-azobis(3-ethyl-benzothiazoline-6-sulfonic acid); FRAP, ferric reducing activity power.

lignins, a commonly used unit for antioxidant assays. It must be pointed out that DPPH and ABTS assays estimated the antiradical activity, developed in methanolic and aqueous media, respectively, whereas FRAP analyzed the ferric reducing ability of lignins. DPPH and ABTS assays presented a very different quantitative response for all the lignin fractions, although with the same trend in both. The low response by the DPPH method in methanolic medium was probably due to the fact that some components making an important contribution to the antioxidant activity of the aqueous dilutions were not soluble in methanol.[13] As seen from Table 5, the alkali-soluble lignins obtained during the initial extraction process had higher antioxidant activities than those of the alkaline ethanol-soluble lignins obtained during the second alkaline extraction process. The stronger antioxidant capacity of alkali-extracted lignin was probably due to the higher content of phenolic OH, which could act as a hydrogen donor antioxidant,[28,29] as revealed by ^{31}P NMR spectra. However, the effect of aliphatic OH on the radical scavenging activity of lignin is not very clear. Pan et al.[28] reported that aliphatic OH content had a negative effect on antioxidant activity of organosolv ethanol lignin, while Dizhbite et al.[30] reported that the aliphatic OH had a positive influence on the radical scavenging activity of lignin model compounds, which needs further investigation.

In summary, bamboo chips with or without water impregnation were pretreated by steam explosion, followed with alkali and alkaline ethanol delignification to fractionate lignins. The lignins obtained showed low levels of associated hemicelluloses (0.55−1.76%) and low molecular weights (780−1050 g/mol). However, the alkali-soluble lignins had higher *p*CA/FA and S/G ratios than the alkaline ethanol-soluble lignins. HSQC spectral analysis revealed that the main lignin substructure was β−O−4′ aryl ether (73.9−79.0%), while low amounts of β−β′, β−5′, and α−O−4/β−O−4 were also present. Additionally, the alkali-soluble lignins obtained during the initial extraction process had higher antioxidant activities than those of the alkaline ethanol-soluble lignins obtained during the second extraction process by alkaline ethanol. The results suggest that the combination of steam explosion and alkaline treatments is an effective method to separate lignin from bamboo. Comprehensive structure elucidation and its antioxidant activity will provide useful information for the application of lignins in industry. More importantly, the delignified bamboo will be more easily hydrolyzed and then fermented into bioethanol, and this biorefinery process allows all major components of biomass to be converted into high value-added products.

AUTHOR INFORMATION

Corresponding Author

*Telephone +86 10 62336903; fax +86 10 62336903; e-mail rcsun3@bjfu.edu.cn.

Notes

The authors declare no competing financial interest.

ACKNOWLEDGMENTS

We are extremely grateful for financial support from the Major State Basic Research Projects of China (973-2010CB732204) and the National Natural Science Foundation of China (31110103902).

REFERENCES

(1) Pan, X. J.; Arato, C.; Gilkes, N.; Gregg, D.; Mabee, W.; Pye, K.; Xiao, Z. Z.; Zhang, X.; Saddler, J. Biorefining of softwoods using ethanol organosolv pulping: Preliminary evaluation of process streams for manufacture of fuel-grade ethanol and co-products. *Biotechnol. Bioeng.* **2005**, *90*, 473−481.

(2) FitzPatrick, M.; Champagne, P.; Cunningham, M. F.; Whitney, R. A. A biorefinery processing perspective: Treatment of lignocellulosic materials for the production of value-added products. *Bioresour. Technol.* **2010**, *101*, 8915−8922.

(3) Zimbardi, F.; Ricci, E.; Braccio, G. Technoeconomic study on steam explosion application in biomass processing. *Appl. Biochem. Biotechnol.* **2002**, *98*, 89−99.

(4) Heitz, M.; Capek-Menard, E.; Koeberle, P.; Gagne, J.; Chornet, E.; Overend, R.; Taylor, J.; Yu, E. Fractionation of *Populus tremuloides* at the pilot plant scale: Optimization of steam pretreatment conditions using the STAKE II technology. *Bioresour. Technol.* **1991**, *35*, 23−32.

(5) Sun, Y.; Cheng, J. Hydrolysis of lignocellulosic materials for ethanol production: A review. *Bioresour. Technol.* **2002**, *83*, 1−11.

(6) Sun, S. L.; Wen, J. L.; Ma, M. G.; Sun, R. C. Successive alkali extraction and structural characterization of hemicelluloses from sweet sorghum stem. *Carbohydr. Polym.* **2012**, *92*, 2224−2231.

(7) Kleinert, T. N. Organosolv pulping with aqueous alcohol. *Tappi J.* **1974**, *57*, 99−102.

(8) McDonough, T. J. The chemistry of organosolv delignification. *Tappi J.* **1992**, *76*, 186−193.

(9) Sannigrahi, P.; Pu, Y.; Ragauskas, A. Cellulosic biorefineries-unleashing lignin opportunities. *Curr. Opin. Environ. Sustainability* **2010**, *2*, 383−393.

(10) Sluiter, A.; Hames, B.; Ruiz, R.; Scarlata, C.; Sluiter, J.; Templeton, D.; Crocker, D. Determination of structural carbohydrates and lignin in biomass. Technical Report NREL/TP-510-42618, 2008.

(11) Wang, K.; Jiang, J. X.; Xu, F.; Sun, R. C. Influence of steaming pressure on steam explosion pretreatment of *Lespedeza* stalks (*Lespedeza cyrtobotrya*). II. Characteristics of degraded lignin. *J. Appl. Polym. Sci.* **2010**, *116*, 1617−1625.

(12) Faix, O.; Argyropoulos, D. S.; Robert, D.; Neirinck, V. Determination of hydroxyl groups in lignins evaluation of ^{1}H-, ^{13}C-, ^{31}P-NMR, FTIR and wet chemical methods. *Holzforschung* **1994**, *48*, 387−394.

(13) Delgado-Andrade, C.; Rufián-Henares, J. A.; Morales, F. J. Assessing the antioxidant activity of melanoidins from coffee brews by different antioxidant methods. *J. Agric. Food. Chem.* **2005**, *53*, 7832−7836.

(14) Thaipong, K.; Boonprakob, U.; Crosby, K.; Cisneros-Zevallos, L.; Hawkins Byrne, D. Comparison of ABTS, DPPH, FRAP, and ORAC assays for estimating antioxidant activity from guava fruit extracts. *J. Food Compos. Anal.* **2006**, *19*, 669−675.

(15) Wen, J. L.; Sun, S. L.; Xue, B. L.; Sun, R. C. Quantitative structural characterization of the lignins from the stem and pith of bamboo (*Phyllostachys pubescens*). *Holzforschung* **2013**, 1−15.

(16) Chandra, R. P.; Bura, R.; Mabee, W.; Berlin, A.; Pan, X.; Saddler, J. Substrate pretreatment: The key to effective enzymatic hydrolysis of lignocellulosics? In *Biofuels*; Olsson, L., Ed.; Advances in Biochemical

Engineering/Biotechnology, Vol. *108*; Springer: Berlin and Heidelberg, Germany, 2007; pp 67−93.
(17) Wen, J. L.; Xue, B. L.; Xu, F.; Sun, R. C.; Pinkert, A. Unmasking the structural features and property of lignin from bamboo. *Ind. Crop. Prod.* **2013**, *42*, 332−343.
(18) Faix, O. Fourier transform infrared spectroscopy. In *Methods in Lignin Chemistry*; Lin, S. Y., Dence, C. W., Eds.; Springer Series in Wood Science; Springer: Berlin and Heidelberg, Germany, 1992; pp 83−109.
(19) Faix, O. Classification of lignins from different botanical origins by FT-IR spectroscopy. *Holzforschung* **1991**, *45*, 21−28.
(20) del Río, J. C.; Prinsen, P.; Rencoret, J.; Nieto, L.; Jiménez-Barbero, J.; Ralph, J.; Martínez, Á. T.; Gutiérrez, A. Structural characterization of the lignin in the cortex and pith of elephant grass (*Pennisetum purpureum*) stems. *J. Agric. Food Chem.* **2012**, *60*, 3619−3634.
(21) Villaverde, J. J.; Li, J.; Ek, M.; Ligero, P.; de Vega, A. Native lignin structure of *Miscanthus* × *giganteus* and its changes during acetic and formic acid fractionation. *J. Agric. Food Chem.* **2009**, *57*, 6262−6270.
(22) Lu, F. C.; Ralph, J. Novel tetrahydrofuran structures derived from $\beta-\beta$-coupling reactions involving sinapyl acetate in Kenaf lignins. *Org. Biomol. Chem.* **2008**, *6*, 3681−3694.
(23) Wen, J. L.; Xue, B. L.; Sun, S. L.; Sun, R. C. Quantitative structural characterization and thermal properties of birch lignins after auto-catalyzed organosolv pretreatment and enzymatic hydrolysis. *J. Chem. Technol. Biotechnol.* **2013**, *188*, 1663−1671.
(24) Hallac, B. B.; Pu, Y.; Ragauskas, A. J. Chemical transformations of *Buddleja davidii* lignin during ethanol organosolv pretreatment. *Energy Fuels* **2010**, *24*, 2723−2732.
(25) Hu, Z. J.; Yeh, T. F.; Chang, H. M.; Matsumoto, Y.; Kadla, J. F. Elucidation of the structure of cellulolytic enzyme lignin. *Holzforschung* **2006**, *60*, 389−397.
(26) Whiting, P.; Goring, D. Chemical characterization of tissue fractions from the middle lamella and secondary wall of black spruce tracheids. *Wood Sci. Technol.* **1982**, *16*, 261−267.
(27) Moxley, G.; Gaspar, A. R.; Higgins, D.; Xu, H. Structural changes of corn stover lignin during acid pretreatment. *J. Ind. Microbiol. Biotechnol.* **2012**, *39*, 1289−1299.
(28) Pan, X. J.; Kadla, J. F.; Ehara, K.; Gilkes, N.; Saddler, J. N. Organosolv ethanol lignin from hybrid poplar as a radical scavenger: Relationship between lignin structure, extraction conditions, and antioxidant activity. *J. Agric. Food Chem.* **2006**, *54*, 5806−5813.
(29) Lu, Q.; Liu, W.; Yang, L.; Zu, Y.; Zu, B.; Zhu, M.; Zhang, Y.; Zhang, X.; Zhang, R.; Sun, Z. Investigation of the effects of different organosolv pulping methods on antioxidant capacity and extraction efficiency of lignin. *Food Chem.* **2012**, *131*, 313−317.
(30) Dizhbite, T.; Telysheva, G.; Jurkjane, V.; Viesturs, U. Characterization of the radical scavenging activity of lignins-natural antioxidants. *Bioresour. Technol.* **2004**, *95*, 309−317.

JOURNAL OF AGRICULTURAL AND FOOD CHEMISTRY

Article

pubs.acs.org/JAFC

Selenium Speciation in Malt, Wort, and Beer Made from Selenium-Biofortified Two-Rowed Barley Grain

Sara Rodrigo,*[,†] Oscar Santamaria,[†] Yi Chen,[‡] Steve P. McGrath,[‡] and Maria J. Poblaciones[†]

[†]Department of Agronomy and Forest Environment Engineering, University of Extremadura, Avenida Adolfo Suárez s/n, 06007 Badajoz, Spain

[‡]Sustainable Soils and Grassland Systems, Rothamsted Research, Harpenden, Hertfordshire AL5 2JQ, United Kingdom

ABSTRACT: Selenium (Se) biofortification of barley is a suitable strategy to increase the Se concentration in grain. In the present paper, the suitability of this Se-biofortified grain for making Se-enriched beer is analyzed. The aim of the present study was to evaluate the effect of different Se fertilizer doses (0, 10, and 20 g of Se ha^{-1}) and forms (sodium selenate or sodium selenite) on the Se loss during the malting and brewing processes and Se speciation in grain, malt, wort, and beer. Samples were analyzed using inductively coupled plasma−mass spectrometry (ICP−MS) and high-performance liquid chromatography (HPLC)−ICP−MS for total Se and speciation. Mashing−lautering was the process with the greatest Se loss (83.8%). After malting and brewing, only 7.3% of the initial Se was retained in beer, mainly in selenite form. Even so, the fertilizer application of sodium selenate at 20 g ha^{-1} increased the total Se concentration almost 6-fold in the final beer in comparison to the use of grain derived from unfertilized barley. The present paper provides evidence that the use of Se-biofortified barley grain as a raw material to produce Se-enriched beer is possible, and the results are comparable to other methods in terms of efficiency.

KEYWORDS: *selenium, speciation, beer, brewing, HPLC−ICP−MS*

INTRODUCTION

Selenium (Se) is an essential trace element for humans and animals. An adequate Se intake has beneficial effects in humans, such as prevention of several cancers, benefits in immune system,[1] and some protection against the aging process and cardiovascular diseases.[2] According to Elmadfa,[3] the European recommended dietary allowance (RDA) of Se for humans is about 55 μg of Se day^{-1}, slightly lower than the current Se intake recommendation of 1 μg of Se kg^{-1} of body weight day^{-1} reported by the Committee on the Medical Aspects of Food Policy (COMA).[4] According to Roman Viñas et al.,[5] there is an inadequate intake of Se in more than 20% of the European population. In this context, the Se intake should be increased to reach the recommended values. Several strategies to remedy Se deficiency have been tried. Because yeast (*Saccharomyces cerevisiae* Meyen ex E. C. Hansen) has been shown to accumulate and transform inorganic Se to organo-Se compounds,[6] Se-enriched yeast supplements have been widely used.[7] Another strategy to remedy the Se-deficient intake is the use of Se-enriched common dietary foodstuff obtained by means of Se biofortification of crops.[8] Cereals constitute a major source of Se because they are consumed in large amounts in many human diets. Among cereals, two-rowed barley (*Hordeum vulgare* L. ssp. *distichum*) is one of the most ancient and widely distributed crops. Currently, about two-thirds of barley crops are used for animal feed, approximately one-third for malting and about 2% for human food directly. Spain produces annually more than 8 million tons of barley grain, and annual consumption is approximately 78 kg of beer per capita.[9]

Two-rowed barley has already demonstrated to be a suitable candidate to be included in Se biofortification programs under Mediterranean conditions.[10] However, that study was focused on the Se accumulation in the grain, but very scarce information is found regarding the effect of the biofortification in the final Se concentration in beer after the manufacturing process. At this regard, only a study carried out in Australia by Gibson et al.[11] has been found to deal with the use of Se-enriched barley grain by crop biofortification to obtain Se-enriched beer. However, in that study, the fertilizer application rates were much higher than those recommended in the literature for barley[10] and only total Se by inductively coupled plasma−mass spectrometry (ICP−MS) was analyzed, without analyzing the chemical forms of this Se. Other authors[12,13] proposed a different approach to increase the Se concentration in beer and other beverages, such as white wine. This procedure consisted of adding sodium selenite during the beer-making process directly to the fermentation medium to use the capacity of yeast to accumulate and biotransform Se. Finally, Gibson et al.[11] also proposed the Se biofortification of the grain during the malting process. In that case, the inorganic form of Se (especially sodium selenate) was added to the water used in the germination stage of the grain.

To obtain precise information about the Se benefit, it is important to know not only the amount of Se in beer but also the chemical forms in which Se is presented. According to Thiry et al.,[14] the organic Se forms, such as SeMet (selenomethionine), are the most efficient in the long term to prevent Se deficiency. Conversely, inorganic Se forms give a more rapid response to an acute shortage of Se, but they have a higher risk of becoming toxic in the long term. Several authors[15,16] have found differences in Se bioavailability in

Received: February 18, 2014
Revised: May 28, 2014
Accepted: May 28, 2014
Published: May 28, 2014

ACS Publications © 2014 American Chemical Society

Table 1. Percentage (Mean ± Standard Error) of Total ICP Selenium Loss, Related to the Total Se Remaining from the Previous Process, in Each Partial Process (Malting, Mashing−Lautering, and Fermentation−Maturation) and in the Whole Malting−Brewing Process, in Relation to the Dose and Form of Se in the Fertilizer[a]

treatment	malting	mashing−lautering	fermentation−maturation	whole brewing
0 g ha^{-1}	1.8 ± 2.5	76.8 ± 11.6	54.3 ± 18.0	88.6 ± 4.2
10 g of Se ha^{-1} selenate	11.9 ± 9.8	84.5 ± 0.6	58.0 ± 8.2	94.2 ± 1.5
20 g of Se ha^{-1} selenate	5.5 ± 7.7	84.6 ± 2.1	55.9 ± 2.4	93.6 ± 1.1
10 g of Se ha^{-1} selenite	3.3 ± 4.6	85.8 ± 2.4	45.4 ± 8.7	92.4 ± 0.6
20 g of Se ha^{-1} selenite	2.9 ± 3.2	87.2 ± 0.3	58.3 ± 5.0	94.8 ± 0.6
% average	5.1 ± 2.0 C	83.8 ± 8.8 A	54.4 ± 3.0 B	

[a]Letters indicate significant ($p < 0.05$) differences in the Se losses between the different brewing processes according to ANOVA and Fisher's LSD test. For each process, the one-way ANOVA on the effect of the treatment on the Se loss showed no significant effect ($p > 0.05$).

relation to different food sources, being higher in wheat (83%) than in garlic (78%), fish (56%), or mushrooms (5%). It is also important to distinguish between absorption, availability, and activity. While most dietary selenium is absorbed efficiently, the retention of organic forms for further bioactivity is higher than that of inorganic forms.[17] The U.S. Food and Nutrition Board Report[18] suggested that more than 90% of SeMet is absorbed; SeCys (selenocysteine) appears to be absorbed very well; although almost 100% of selenate is absorbed, a significant fraction is lost in the urine; and although 50% of selenite is absorbed, it shows better retention than selenate in the organism. It is already known that SeMet is the predominant form of selenium (56−83%) in the grain of many cereals, while other selenocompounds occur in smaller proportions (selenate, 12−19%; selenocysteine, 4−12%; Se-methyl-selenocysteine, 1−4%; and others, 4−26%).[19] However, to our knowledge, how Se fertilization affects such speciation in the barley grain and how the manufacturing process affects such speciation have not yet been studied.

Therefore, to advance the study of the two-rowed barley as a product able to increase the available Se levels in the organism and also to test beer as a "functional food", the aim of the present study was (1) to evaluate the effect of different Se doses and Se fertilizer forms on the total Se losses during the manufacturing processes (malting and brewing) and (2) to evaluate the influence of those Se doses and Se forms on the chemical speciation of Se accumulated in the different products derived from the manufacturing process (grain, malt, wort, and beer).

MATERIALS AND METHODS

Samples and Malting and Brewing Process. The barley grain used for malting and brewing in the present study was obtained from a previous Se biofortification field experiment.[10] The experiment had been conducted in the growing season 2011/2012, in Badajoz, southern Spain, on a Xerofluvents soil under rainfed Mediterranean conditions. The experiment was designed as a split plot arrangement with four repetitions, including two forms of Se [sodium selenate (Na_2SeO_4) and sodium selenite (Na_2SeO_3)], one per plot, and within the plot, three application doses (0, 10, and 20 g of Se ha^{-1} diluted in 3 L of water) were randomly distributed. The crop area for each treatment was 15 m^2 (3 × 5 m). Barley grain was harvested in early June. A more detailed description of the experiment is described by Rodrigo et al.[10]

Malting and brewing were carried out in our lab according to the guidelines by local brewers. Five barley grain samples (600 g), one per treatment obtained by mixing the four repetitions, were taken. Malt was obtained by germinating the barley seeds (20 °C, 100% humidity) in an incubator (GER-700, RADIBER, S.A., Barcelona) until the sprout reached $^2/_3$ of the seed size (after approximately 30 h), then air-dried for 24 h at room temperature, and kilning at 55 °C in an oven for a further 24 h. Roots were manually removed to obtain clean malt that was milled in a corundum mill (WolfgangMOC, Germany).

Brewing consisted of the following main processes: mashing, lautering, fermentation, and maturation. The mashing process was performed in 2 L of distilled water per sample for 1 h at 54 °C, followed by 1 h at 67 °C. For lautering, wort was separated from spent grains with a laboratory sieve and then boiled for 90 min. After boiling, wort was quickly cooled and filtered. For fermentation, 2 g of dried *S. cerevisae* yeast (SaftBrew T-58, Fermentis, Lesaffre Group, France) was added to wort. After a 9 day fermentation period, yeast was removed from the container bottom, and the resulting beer was left to mature for 20 days. Aliquots of grain, malt, wort, and beer were taken at the end of each process to evaluate the Se losses during malting, mashing−lautering, and fermentation−maturation.

Measurement of Total Se with ICP−MS and Se Speciation with High-Performance Liquid Chromatography (HPLC)−ICP−MS and Data Presentation. For each sample of each fraction (grain, malt, wort, and beer), total Se was determined by ICP−MS (Agilent 7500ce, Agilent Technologies, Palo Alto, CA) operating in the hydrogen gas mode. This analytical method was developed by the Elemental and Molecular Analysis Service of the University of Extremadura (Spain). Previously 1 g per sample was digested with ultrapure concentrated nitric acid (2 mL) and 30% (w/v) hydrogen peroxide (2 mL) using a closed-vessel microwave digestion protocol (Mars X, CEM Corp., Matthews, NC) and diluted to 25 mL with ultrapurified water.[20] Sample vessels were thoroughly washed with acid before use. For quality assurance, a blank and a standard (tomato leaf material, NIST 1573a) were included in each batch of samples. All of the results were reported on a dry weight basis.

Speciation was carried out by HPLC−ICP−MS following proteolytic digestion with protease and lipase[21] using an Agilent 1050 HPLC pump and a Hamilton PRPX100 250 × 4 mm column (Cole-Parmer, London, U.K.). It was performed following the methodology proposed by Li et al.[22] This method was slightly modified in the present study using 40 mM NH_4NO_3 instead of 50 mM NH_4NO_3 in the mobile phase, because it was found to be more effective. ICP−MS monitored m/z 78 and 80, with hydrogen flow into the octopole reaction cell of 4 mL min^{-1}. Peak areas for quoted species were measured, percentage value for a particular peak calculated relative to the total area under the chromatogram, and compared to the total Se content. Percentages of each fraction, selenomethionine (SeMet), selenite, selenate, oxidized selenomethionine (SeMetO), and others (unknown fraction), were calculated in each step of the brewing process. Three replicates from every fraction (grain, malt, wort, and beer) of the 10 g ha^{-1} sodium selenate treatment were analyzed to assess technical repeatability.

Statistical Analysis. In each manufacturing process (malting, mashing−lautering, and fermentation−maturation) as well as in the whole malting and brewing process, the effect of the fertilizer treatment (0, sodium selenate at a dose of 10 and 20 g ha^{-1}, and sodium selenite at a dose of 10 and 20 g ha^{-1}) and the manufacturing process (malting, mashing−lautering, and fermentation−maturation) on the percentage losses of total Se (determined by ICP−MS) was statistically analyzed by two-way analysis of variance (ANOVA) and multiple comparison tests [Fisher's least significant difference (LSD)

Table 2. Total ICP Se (μg kg^{-1}) and Total Se HPLC (μg kg^{-1}) in Barley Grain, Malt, Wort, and Beer as a Function of Se Form (Sodium Selenate and Sodium Selenite) and Se Dose Applied to the Crop[a]

				Se species (%)			
fraction	treatment	total ICP Se (μg kg^{-1})	total HPLC Se (μg kg^{-1})	SeMet	selenite	SeMetO	unknown
grain	0 g ha^{-1}	111.7 ± 16.3 e	91.2	59.0	41.0	0.0	0.0
	10 g of Se ha^{-1} selenate	880.0 ± 25.5 b	426.1 ± 26.6	90.2	9.8	0.0	0.0
	20 g of Se ha^{-1} selenate	1133.9 ± 6.4 a	466.5	90.4	9.6	0.0	0.0
	10 g of Se ha^{-1} selenite	270.0 ± 5.2 d	142.9	67.5	32.5	0.0	0.0
	20 g of Se ha^{-1} selenite	343.5 ± 12.9 c	146.1	74.2	25.8	0.0	0.0
malt	0 g ha^{-1}	128.8 ± 14.1 d	98.6	66.6	33.4	0.0	0.0
	10 g of Se ha^{-1} selenate	774.1 ± 63.8 b	357.7 ± 48.7	86.8	11.2	0.0	1.9
	20 g of Se ha^{-1} selenate	1076.2 ± 88.0 a	542.0	88.6	7.6	0.1	3.7
	10 g of Se ha^{-1} selenite	268.4 ± 27.7 c	125.4	66.8	32.5	0.6	0.0
	20 g of Se ha^{-1} selenite	333.8 ± 23.5 c	162.0	77.3	22.2	0.5	0.0
wort	0 g ha^{-1}	30.7 ± 18.2 b	3.9	0.0	100.0	0.0	0.0
	10 g of Se ha^{-1} selenate	120.2 ± 5.3 a	27.7 ± 1.2	61.5	38.5	0.0	0.0
	20 g of Se ha^{-1} selenate	166.3 ± 35.8 a	29.3	65.2	34.8	0.0	0.0
	10 g of Se ha^{-1} selenite	37.9 ± 2.4 b	8.9	0.0	100.0	0.0	0.0
	20 g of Se ha^{-1} selenite	42.7 ± 1.8 b	10.2	0.0	100.0	0.0	0.0
beer	0 g ha^{-1}	12.4 ± 2.8 c	6.6	0.0	100.0	0.0	0.0
	10 g of Se ha^{-1} selenate	50.7 ± 12.0 b	10.5 ± 0.9	0.0	100.0	0.0	0.0
	20 g of Se ha^{-1} selenate	73.0 ± 11.8 a	14.4	0.0	63.0	0.0	37.0
	10 g of Se ha^{-1} selenite	20.6 ± 2.0 c	6.9	0.0	100.0	0.0	0.0
	20 g of Se ha^{-1} selenite	17.9 ± 2.9 c	7.1	0.0	100.0	0.0	0.0

[a]Se species are presented as a percentage of total Se HPLC. In the total ICP Se column, mean ± standard error values are presented. Letters indicate significant ($p < 0.05$) differences among treatments for each product fraction according to ANOVA and Fisher's LSD test. Technical repeatability of the HPLC measurements was determined for the 10 g of Se ha^{-1} sodium selenate samples in each product fraction and expressed as the average ± standard error.

test]. The same effect of the fertilizer treatment was also analyzed by one-way ANOVA and LSD test on the total Se (determined by ICP–MS) accumulated in each product fraction (grain, malt, wort, and beer) obtained during the malting and brewing processes.

RESULTS

The two-way ANOVA performed to evaluate the effect of the fertilizer treatment and the manufacturing process on the losses of total Se resulting from the different malting and brewing processes showed a significant effect of the process [degrees of freedom (df) = 2; F statistic (F) = 284.42; $p < 0.001$] but not of the treatment (df = 4; F = 1.03; p = 0.426) nor the interaction (df = 8; F = 0.58; p = 0.781). For this reason, the multiple comparison test between the three different processes was carried out with the pooled data of the different treatments. The highest Se losses (obtained by ICP–MS) occurred significantly during the mashing–lautering processes, with a loss of 83.8% on average (Table 1). Although significantly lower, important Se losses were also observed during fermentation–maturation, with a loss percentage of 54.4%, in relation to the Se remaining after mashing–lautering. During the malting process, only 5.1% of Se was lost. On average, during the whole malting and brewing process, the loss of total ICP Se was 92.7%. As the ANOVA showed, similar Se loss patterns were observed in the different Se fertilization treatments used during barley cultivation (Table 1).

The fertilization treatment also significantly affected the total ICP–MS Se obtained in the different product fractions (grain, malt, wort, and beer) derived from the manufacturing process (Table 2). In the grain, the fertilization treatment significantly increased the Se concentration in comparison to controls. Sodium selenate was the most effective fertilizer form in boosting Se in the grain, and the higher fertilizer dose gave the highest Se accumulation in the grain (Table 2). With regard to malt, the pattern was similar, although no differences were found between the two doses of sodium selenite. In the wort, which had much lower Se concentrations than grain because of the already mentioned losses during the malting and mashing–lautering processes, fertilization with sodium selenate was the only treatment that significantly increased the Se concentration but no difference between doses. In the final beer, again the application of sodium selenate as a Se fertilizer was the only form able to increase the total Se in the manufactured product. A clear effect of the dose was observed, with the highest dose giving the highest Se concentration (Table 2).

On the basis of the Se speciation analysis (one example of a malt sample is given in Figure 1), the results obtained are shown in Table 2. The technical repeatability of the procedure, which can be observed in the total Se (HPLC) column in Table 2, can be considered adequate, because the relative standard error was less than 10% (n = 3) in almost all of the cases. Only

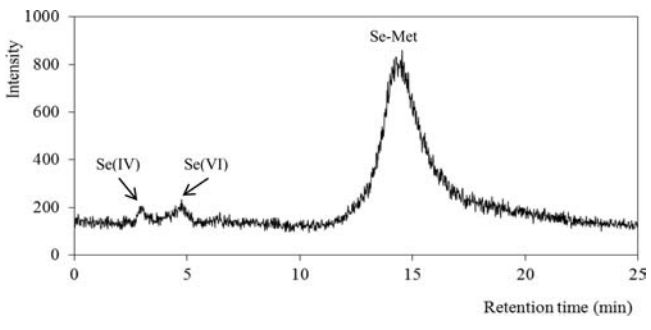

Figure 1. Se species of a malt sample separated by anion-exchange–HPLC–ICP–MS. The chromatogram was monitored at Se m/z 78.

dx.doi.org/10.1021/jf500793t | J. Agric. Food Chem. 2014, 62, 5948–5953

in the case of malt, it was a little bit higher (around 13%). In the grain, Se was mainly accumulated as SeMet, regardless of the chemical Se form used in the crop fertilization, although SeMet concentrations were higher when sodium selenate was used (on average 90.6%) in comparison to sodium selenite (on average 70.9%) and controls (on average 59.0%). The dose had a positive effect on the SeMet concentration in grain, only when Se was applied as sodium selenite but not when Se was applied as sodium selenate. In grain, selenite was also recorded, especially when Se was applied as sodium selenite (on average 29.2%). No other Se species were detected in the grain. In the control grain, the pattern was quite similar to that observed for the lower dose of selenite fertilizer, although the percentage of selenite was a little higher in detriment of the percentage SeMet. According to the results, the malting process did not have any substantial effect on the distribution pattern of the different Se species proportions (Table 2). In this case, a very small percentage of SeMetO (a SeMet oxidation product) was observed, and several unknown Se species occurred when the sodium selenate fertilizer was used, which slightly decreased the percentage of SeMet.

Important changes took place after the mashing–lautering process. In wort derived from non-Se-enriched barley and barley fertilized with sodium selenite, regardless of the dose, only the selenite form was detected. In wort from barley fertilized with sodium selenate, the proportion of SeMet was also substantially reduced but around 60% of SeMet was still recorded in these samples. This progressive removal of the SeMet fraction was completed after the fermentation–maturation processes. In almost all of the cases, Se measured in beer was in the selenite form. Only when barley was fertilized with the highest dose of sodium selenate, 37.0% of Se detected was unknown and the rest was in the selenite form.

DISCUSSION

The Se loss recorded in the present paper during the malting process (around 5% on average) was lower than the approximately 12–20% obtained by Gibson et al.[11] in their study dealing with the use of barley grain biofortified with Se during malting and brewing. Those authors determined that the amount of Se lost in this process was very similar to the amount of Se recorded in the rootlets. Therefore, the removal of rootlets from malt might explain in a high percentage the Se loss during this process. If the germination step had been stopped before in our study, then the rootlets should be smaller, and consequently, they might contain a lower amount of Se, which might explain the differences between both studies. However, not all of the Se loss during this process can be explained with the removal of rootlets. The rest of the Se loss observed during the malting process could be explained by Se phytovolatilization in the germination step. Grant et al.[23] found that plants transform the different Se forms during their metabolic activity. During germination and root development, part of Se contained in grain, mainly in the form of SeMet, may be transformed to selenomethylmethionine (SeMMet), which is the principal precursor of the volatile compound, dimethylselenide (DMSe). However, the slightly smaller proportion of SeMet that we found after malting might be explained in part by the transformation and volatilization hypothesis explained above but could also be a consequence of the transformation of SeMet to SeMetO, because easy oxidation of SeMet has already been demonstrated.[13] Even so, in our study carried out on barley, most Se recorded in grain and malt after biofortification has been found to be in the SeMet form, similar to findings in the grain of bread-making wheat,[24] hard wheat,[25] rice,[22] and chickpea.[26]

The highest loss of total Se was clearly produced during the mashing and lautering (a Se loss of around 85% on average). This Se loss was higher than that found in the same process in the already mentioned study by Gibson et al.[11] In that study, the Se loss was dependent upon the capacity of the pilot brew used. They used 20 and 500 L pilot breweries, which produced Se losses during mashing–lautering of about 71.5 and 64%, respectively. Therefore, taken into account that there appears to be a link between beer capacity (or brewing scale) and Se loss, the lab scale (in 2 L volumes) used in the present paper might explain the higher Se loss found in our study. With regard to the Se speciation analysis during this process, most SeMet was removed from the Se fraction. The cause could be thought to be the degradation of this compound because of the high temperatures during boiling. However, Poblaciones et al.[25] reported minimal SeMet losses after boiling in Se-enriched pasta. Thus, SeMet could be considered thermostable. Therefore, the most likely explanation for this loss would be that Se was strongly bound to the spent grain, and only a proportion of the most water-soluble compounds, such as selenite,[22] was able to pass to the wort. However, when the initial concentration of SeMet in the malt was high (more than 300 μg kg^{-1}), as occurred in the case of sodium selenate fertilization, not all SeMet was lost in the spent grain and approximately $^{1}/_{18}$ and $^{1}/_{25}$ of SeMet remained in the wort. Further experiments analyzing the Se concentration and the Se species contained in the spent grain should be performed to confirm this hypothesis.

Finally, during the fermentation–maturation process, a large proportion of total Se was also lost (around 54% on average). Yeast (*S. cerevisiae*) has been shown to accumulate Se in high concentrations.[27,28] This fact may explain the strong reduction in the total Se recorded in our study after this process removed the yeast from the fermented and matured wort. Thus, after malting and brewing, only around 7.3% (range of 5.2–11.4%) of the total Se contained in grain was maintained in the final beer. This proportion was only a little bit lower than 10.3 and 15.6% obtained by Gibson at al.[11] in the 20 and 500 L pilot breweries, respectively. Therefore, the quite similar results obtained in the two studies carried out in different conditions might reflect they are highly consistent, regardless of the conditions used. The Se concentration of the control beer was in line with that obtained for commercial beer, because in the Mediterranean area, it has been reported[13] to range between 9.2 and 17.2 μg kg^{-1}.

In the final beer obtained in the present study, no SeMet was found; instead, most Se was obtained in the selenite form. This lack of SeMet is a negative aspect of the use of Se-biofortified barley to obtain selenized beer because it is known that the bioavailability of Se organic forms is much higher than that of inorganic forms.[17] Nevertheless, it has been shown above that a large percentage of Se (around 37%) was in unknown forms in beer produced from barley fertilized with the largest dose of sodium selenate. In addition, when the total Se obtained by ICP–MS is compared to that obtained by HPLC–ICP–MS, it can be observed that there was a great amount of Se that was not considered in the speciation analysis because of accuracy limitations in the procedure. Further studies including more advanced techniques may allow for the identification of these fractions, the unknown fraction, and that not included in the

speciation analyses. At least, it would be very interesting to know if these fractions are in organic or inorganic forms to know accurately the bioavailability of the Se remaining in beer.

In addition to the approach to making Se-enriched beer through Se-biofortified barley indicated in the present study and that by Gibson et al.,[11] other authors[13] have proposed to add sodium selenite directly to wort during the brewing process, expecting biotransformation of selenite to organic selenium compounds by yeast. The same methodology was also used to obtain other Se-enriched beverages, such as white wine.[12] A variant of this method was also proposed by Gibson et al.[11] consisting of adding the inorganic form of Se in the water used for germination during malting. A comparison between these two approaches could be of great interest for farmers and beer manufacturers to establish their effectiveness, suitability, and convenience. Technically, both approaches reported a similar Se loss derived from the fermentation−maturation process (the only common in both methodologies), for example, 45−58% in our study and 40−57% in the study by Sánchez-Martinez et al.[13] In both approaches, the SeMet concentration reported in the final beer once removed yeast was either negligible or very low (1−2%). With regard to easiness and cost of the method, the brewer should choose one of the two following options, which correspond with each approach: to pay a little bit more money to farmers for Se-enriched barley (the method proposed in the present paper) or to introduce an additional step during the manufacturing process to include selenite/selenate in the wort or water for malting. The second option presents a high initial investment. It is true that it could be compensated in the long term if Se-enriched beer can be sold at higher prices than normal beer, but meanwhile, this investment is at risk to be lost. Conversely, the first option allows for examining the market trend year to year and, consequently, paying farmers for Se-enriched barley according to that trend. On the other hand, it is important to take into account that adding selenium during the beer-making process may be interpreted as the addition of an ingredient, and this may have a negative connotation to food health authorities and beer consumers.

For farmers, the application of Se would be very cheap because they can use the conventional fertilizer applications and incorporate Se at the same time. The cost of the product is also very cheap, around 4 € ha^{-1} (at a dose of 20 g ha^{-1}), easy to be compensated if beer manufacturers pay more for this Se-enriched product. The main weakness of the approach proposed in the present paper is the apparently low proportion of Se (ranging between 5.2 and 11.4% of the total Se contained in grain) remaining in the final beer after malting and brewing. Even so, Se biofortification provided barley grain able to produce beer with a much higher Se concentration than that obtained from non-Se-enriched barley. Beer produced with barley fertilized with sodium selenate at a dose of 20 g ha^{-1}, showed total ICP Se concentrations almost 6 times higher than beer produced with non-Se-fertilized barley. Gibson et al.[11] considered that 1 L of beer made from malt with a initial concentration of 2.2 mg of Se kg^{-1} would provide a male with over 100% of his recommended daily intake of Se. In our study, the maximum Se concentration in malt was 1076 μg kg^{-1}, obtained with a fertilizer application of sodium selenate at 20 g ha^{-1}. However, the biofortification of barley with sodium selenate in the same area at a dose of 40 g ha^{-1} has produced according to Rodrigo et al.[10] a Se concentration in grain of almost 2400 μg kg^{-1}, a concentration very close to that given by Gibson et al.[11] considering the Se loss during malting.

In following the methodology indicated in the present paper, it is also important to note that several Se-rich byproducts, generated during the brewing process, could be used as an important Se source. For example, spent grain, which includes approximately 25−30% of the malt weight, is an important byproduct from brewing that is commonly used for animal feed.[29] Therefore, considering that most Se, especially SeMet, might be bound in the spent grain, it could become a high-quality and an excellent feeding product for animals, able to remedy Se deficiencies and avoid their consequences for animal health and fertility.[30] Finally, it is also important to note that grain yield and quality parameters of grain were not affected by Se fertilization.[10] This is an important point, because it would be impossible to successfully implement a potential biofortification program if farmers obtained lower income gains as a consequence of Se application.

In conclusion, this paper provides an alternative approach to the already described methods to obtain Se-enriched beer, in our case through the use of Se-biofortified barley grain as raw material. Although after malting and brewing, only 7.3% of the initial total Se was retained in the beer, the use of grain from barley fertilized with sodium selenate at 20 g ha^{-1} increased the final Se concentration in grain almost 6-fold. Selenium was mainly lost during the mashing−lautering process because most Se seemed to be bound to the spent grain, which could be used consequently to prevent Se deficiency in the animal feeding. The present paper provides evidence that the use of Se-biofortified barley grain as a raw material to produce Se-enriched beer is possible, and the results are comparable to other methods in terms of efficiency. The final decision by farmers or brewers about the suitability of its use should be taken based on the importance of the positive or negative aspects of the different methods in each particular case and balancing investment risk and profitability according to the market preferences.

AUTHOR INFORMATION

Corresponding Author

*Telephone: +34-924-289-300. Fax: +34-924-286-201. E-mail: saramrodrigo@gmail.com.

Funding

Rothamsted Research receives strategic funding from the U.K. Biotechnology and Biological Sciences Research Council.

Notes

The authors declare no competing financial interest.

ACKNOWLEDGMENTS

The authors thank Teodoro García-White for his invaluable help with the laboratory work.

REFERENCES

(1) Thomson, C. D. Selenium. In *Encyclopedia of Human Nutrition*, 3rd ed.; Caballero, B., Allen, L., Prentice, A., Eds.; Academic Press: Oxford, U.K., 2013; Vol. *4*, pp 186−192.

(2) Flores-Mateo, G.; Navas-Acien, A.; Pastor-Barriuso, R.; Guallar, E. Selenium and coronary heart disease: A meta-analysis. *Am. J. Clin. Nutr.* **2006**, *84*, 762−773.

(3) Elmadfa, I. *The European Nutrition and Health Report*; Karger: Basel, Switzerland, 2006; Vol. *62*, p 412.

(4) Sneddon, A. *Selenium Nutrition and Its Impact on Health*; Food and Health Innovation Service (FHIS): Aberdeen, U.K., 2012, Aug, p 6.
(5) Roman Viñas, B.; Ribas Barba, L.; Ngo, J.; Gurinovic, M.; Novakovic, R.; Cavelaars, A.; de Groot, L. C. P. G. M.; van't Veer, P.; Matthys, C.; Serra Majem, L. Projected prevalence of inadequate nutrient intakes in Europe. *Ann. Nutr. Metab.* **2011**, *59*, 84−95.
(6) Alzate, A.; Fernández-Fernández, A.; Pérez-Conde, C.; Gutiérrez, A. M.; Cámara, C. Comparison of biotransformation of inorganic selenium by *Lactobacillus* and *Saccharomyces* in lactic fermentation process of yogurt and kefir. *J. Agric. Food Chem.* **2008**, *56*, 8728−8736.
(7) Suhajda, A.; Hegóczki, J.; Janzsó, B.; Pais, I.; Vereczkey, G. Preparation of selenium yeasts I. Preparation of selenium-enriched *Saccharomyces cerevisiae*. *J. Trace Elem. Med. Biol.* **2000**, *14*, 43−47.
(8) Broadley, M. R.; Alcock, J.; Alford, J.; Cartwright, P.; Foot, I.; Fairweather-Tait, S. J.; Hart, D. J.; Hurst, R.; Knott, P.; McGrath, S. P.; Meacham, M. C.; Norman, K.; Mowat, H.; Scott, P.; Stroud, J. L.; Trovey, M.; Tucker, M.; White, P. J.; Young, S. D.; Zhao, F.-J. Selenium biofortification of high-yielding winter wheat (*Triticum aestivum* L.) by liquid or granular Se fertilization. *Plant Soil* **2010**, *332*, 5−18.
(9) Food and Agriculture Organization (FAO). http://faostat.fao.org.
(10) Rodrigo, S.; Santamaría, O.; López-Bellido, F. J.; Poblaciones, M. J. Agronomic selenium biofortification of two-rowed barley under Mediterranean conditions. *Plant Soil Environ.* **2013**, *59* (3), 115−120.
(11) Gibson, C.; Park, Y. H.; Myoung, K. H.; Suh, M. K.; McArthur, T.; Lyons, G.; Stewart, D. The bio-fortication of barley with selenium. In *Proceedings of the Convention of the Institute of Brewing and Distilling, Asia Pacific Section*; Leishman Associates: Hobart, Australia, March 2006; pp 1−13.
(12) Pérez-Corona, M. T.; Sánchez-Martínez, M.; Valderrama, M. J.; Rodríguez, M. E.; Cámara, C.; Madrid, Y. Selenium biotransformation by *Saccharomyces cerevisiae* and *Saccharomyces bayanus* during white wine manufacture: Laboratory-scale experiments. *Food Chem.* **2011**, *124*, 1050−1055.
(13) Sánchez-Martínez, M.; da Silva, E. G. P.; Pérez-Corona, T.; Cámara, C.; Ferreira, S. L. C.; Madrid, Y. Selenite biotransformation during brewing. Evaluation by HPLC−ICP−MS. *Talanta* **2012**, *88*, 272−276.
(14) Thiry, C.; Ruttens, A.; De Temmerman, L.; Schneider, Y. J.; Pussemier, L. Current knowledge in species-related bioavailability of selenium in food. *Food Chem.* **2012**, *130*, 767−784.
(15) Thomson, C. D. Assessment of requirements for selenium and adequacy of selenium status: A review. *Eur. J. Clin. Nutr.* **2004**, *58*, 391−402.
(16) Fox, T. E.; Atherton, C.; Dainty, J. R.; Lewis, D. J.; Langford, N. J.; Baxter, M. J.; Crews, H. M.; Fairweather-Tait, S. J. Absorption of selenium from wheat, garlic, and cod intrinsically labelled with Se-77 and Se-82 stable isotopes. *Int. J. Vitam. Nutr. Res.* **2005**, *75*, 179−186.
(17) Fairweather-Tait, S. J.; Collings, R.; Hurst, R. Selenium bioavailability: Current knowledge and future research requirements. *Am. J. Clin. Nutr.* **2010**, *91*, 1484−1491.
(18) Food and Nutrition Board, Institute of Medicine. *Dietary Reference Intakes: Vitamin C, Vitamin E, Selenium, and Carotenoids*; National Academy Press: Washington, D.C., 2010.
(19) Whanger, P. Selenocompounds in plants and animals and their biological significance. *J. Am. Coll. Nutr.* **2002**, *21*, 223−232.
(20) Adams, M. L.; Lombi, E.; Zhao, F. J.; McGrath, S. P. Evidence of low selenium concentrations in UK bread-making wheat grain. *J. Sci. Food Agric.* **2002**, *82*, 1160−1165.
(21) Huerta, V. D.; Reyes, L. H.; Marchante-Gayón, J. M.; Sánchez, M. L. F.; Sanz-Medel, A. Total determination and quantitative speciation analysis of selenium in yeast and wheat flour by isotope dilution analysis ICP−MS. *J. Anal. At. Spectrom.* **2003**, *18*, 1243−1247.
(22) Li, H. F.; Lombi, E.; Stroud, J. L.; McGrath, S. P.; Zhao, F.-J. Selenium speciation in soil and rice: Influence of water management and Se fertilization. *J. Agric. Food Chem.* **2010**, *58*, 11837−11843.
(23) Grant, T. D.; Montes-Bayón, M.; LeDucb, D.; Fricke, M. W.; Terry, N.; Caruso, J. A. Identification and characterization of Se-methyl selenomethionine in *Brassica juncea* roots. *J. Chromatogr. A* **2004**, *1026*, 159−166.
(24) Hart, D. J.; Fairweather-Tait, S. J.; Broadley, M. R.; Dickinson, S. J.; Foot, I.; Knott, P.; McGrath, S. P.; Mowat, H.; Norman, K.; Scott, P. R.; Stroud, J. L.; Tucker, M.; White, P. J.; Zhao, F.-J.; Hurst, R. Selenium concentration and speciation in biofortified flour and bread: Retention of selenium during grain biofortification, processing and production of Se-enriched food. *Food Chem.* **2011**, *126*, 1771−1778.
(25) Poblaciones, M. J.; Rodrigo, S.; Santamaría, O.; Chen, Y.; McGrath, S. P. Agronomic selenium biofortification in *Triticum durum* under Mediterranean conditions: From grain to cooked pasta. *Food Chem.* **2014**, *146*, 378−384.
(26) Poblaciones, M. J.; Rodrigo, S.; Santamaria, O.; Chen, Y.; McGrath, S. P. Selenium accumulation and speciation in biofortified chickpea (*Cicer arietinum* L.) under Mediterranean conditions. *J. Sci. Food Agric.* **2014**, *94*, 1101−1106.
(27) Demirci, A.; Pometto, A. L. Production of organically bound selenium yeast by continuous fermentation. *J. Agric. Food Chem.* **1999**, *47*, 2491−2495.
(28) Ouerdane, L.; Mester, Z. Production and characterization of fully selenomethionine-labeled *Saccharomyces cerevisiae*. *J. Agric. Food Chem.* **2008**, *56*, 11792−11799.
(29) Fillaudeau, L.; Blanpain-Avet, P.; Daufin, G. Water, wastewater and waste management in brewing industries. *J. Clean Prod.* **2006**, *14*, 463−471.
(30) Underwood, E. J.; Suttle, N. F. *The Mineral Nutrition of Livestock*; CABI Publishing: Wallingford, U.K., 1999.

JOURNAL OF AGRICULTURAL AND FOOD CHEMISTRY

Article

pubs.acs.org/JAFC

Protein Matrix Involved in the Lipid Retention of *Foie Gras* during Cooking: A Multimodal Hyperspectral Imaging Study

Laëtitia Théron,[†,‡,§] Annie Vénien,[∥] Frédéric Jamme,[⊥,#] Xavier Fernandez,[†,‡,§] Frédéric Peyrin,[∥] Caroline Molette,[‡,†,§] Paul Dumas,[⊥] Matthieu Réfrégiers,[⊥] and Thierry Astruc*[,∥]

[†]INRA, UMR 1289 Tissus Animaux Nutrition Digestion Ecosystème Métabolisme, F-31326 Castanet-Tolosan, France

[‡]Université de Toulouse, INPT ENSAT, UMR 1289 Tissus Animaux Nutrition Digestion Ecosystème Métabolisme, ENSAT, F-31326 Castanet-Tolosan, France

[§]INPT ENVT, UMR 1289 Tissus Animaux Nutrition Digestion Ecosystème Métabolisme, F-31076 Toulouse, France

[∥]INRA Clermont-Ferrand Theix, UR370 QuaPA, F-63122 Saint-Genès-Champanelle, France

[⊥]Synchrotron SOLEIL, BP48, L'Orme des Merisiers, F-91120 Gif-sur-Yvette, France

[#]INRA, UAR1008 CEPIA, rue de la Géraudière, F-44316 Nantes, France

ABSTRACT: Denaturation of the protein matrix during heat treatment of duck *foie gras* was studied in relationship to the amount of fat loss during cooking. A low fat loss group was compared with a high fat loss group by histochemistry, FT-IR, and synchrotron UV microspectroscopy combination to characterize their protein matrix at different scales. After cooking, the high fat loss group showed higher densification of its matrix, higher ultraviolet tyrosine autofluorescence, and an infrared shift of the amide I band. These results revealed a higher level of protein denaturation and aggregation during cooking in high fat loss than in low fat loss *foie gras*. In addition, the fluorescence and infrared responses of the raw tissue revealed differences according to the level of fat losses after cooking. These findings highlight the importance of the supramolecular state of the protein matrix in determining the fat loss of *foie gras*.

KEYWORDS: *UV microspectroscopy, infrared microspectroscopy, histochemistry, foie gras, heating, fat loss, quality*

INTRODUCTION

In some birds such as palmipeds in which the liver is the main site of de novo lipogenesis, nonpathological steatosis can be triggered by dietary carbohydrates. This ability is used to produce *foie gras*, a coveted product highly appreciated for its flavor and sensorial qualities. Usually, ducks or geese are reared and overfed in standardized conditions. Immediately after slaughter, the *foie gras* is removed, trimmed, and seasoned before cooking. However, even under these standardized conditions, quality is uneven. Despite the controlled cooking conditions, fat loss ranges from 2% to 50%, with a marked impact on technological yield and organoleptic qualities. A study suggested that lipid and fatty acid characteristics are not closely related to fat loss during cooking.[1] However, a recent ultrastructural analysis showed that lipid staining intensity was linked to fat loss during cooking, thus suggesting a role of the composition of the lipid droplets in this effect.[2]

The protein component, though minor in amount, seems to play a major role in the molecular mechanisms underlying fat loss during cooking. Enzymes involved in redox processes are over-represented in livers with high fat loss during cooking;[3] this finding was interpreted as precocity in the steatosis stage. An extracellular matrix of hepatocytes forms the support tissue of cells. The integrity of this matrix is probably important for the structural support of lipid-filled hepatocytes. A proteomic study performed on duck livers showed that during postmortem storage, the proteolytic pattern was linked to fat loss during cooking.[4] A variation in the molecular composition of this matrix could affect its mechanical resistance during cooking and thereby modulate lipid retention. Cooking causes thermal denaturation of proteins[5] with consequent changes in the morphology of the protein components.[2] Using electron microscopy, these last authors found a coagulation of protein matrix that was difficult to quantify. New imaging tools allow a quantitative approach to the local chemical changes in composition and molecular structure, offering an opportunity to establish links between such changes and fat loss during cooking. This is the case of microspectroscopy tools consisting of an optical microscope coupled to a spectrometer. The microscope allows one to select an area of interest in the histological tissue section, and the spectrometer allows spectral acquisition in the same area. Results from different spectral acquisition modalities provide additional informations. From a series of spectral acquisition, it is possible to edit spectral maps of the region of interest. The image is multimodal when spectra come from different wavelength ranges such as infrared, visible, or UV.

Analysis of infrared spectra yields information on the molecular structure with a spatial resolution of 10 μm.[6] Synchrotron deep ultraviolet (DUV) fluorescence spectra provide knowledge of chemical composition with a spatial resolution that may reach 300 nm.[7,8] The simultaneous approaches of located microspectroscopy and histochemistry are therefore well-suited to characterize cellular morphology and molecular

Received: March 5, 2014
Revised: May 22, 2014
Accepted: May 25, 2014
Published: May 26, 2014

ACS Publications © 2014 American Chemical Society

dx.doi.org/10.1021/jf5009605 | J. Agric. Food Chem. 2014, 62, 5954−5962

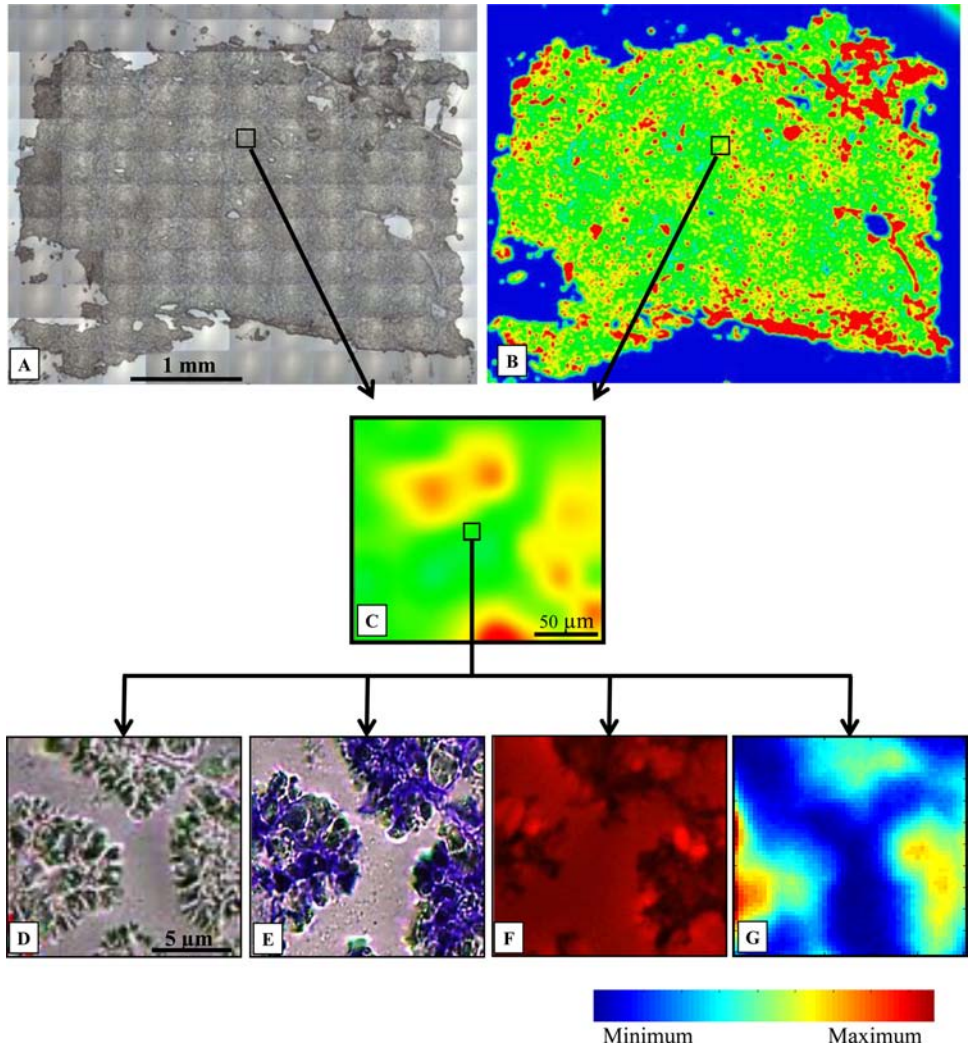

Figure 1. Multimodal and multiscale imaging (visible, IR, and UV) of the same raw *foie gras* tissue section. (A) Histological section of *foie gras* examined in bright field microscopy. (B) Infrared spectral distribution of the 1658 cm^{-1} band, assigned to the α-helix structure of proteins. (C) Magnification of the square delimited area of the infrared spectral image in B. (D,E,F,G) Magnification of the square delimited area depicted in C, characterized by different stains and UV spectroscopy imaging. (D) Bright field without stain. (E) Toluidine Blue staining highlighting the proteins in blue. (F) Histofluorescence of the Nile Red probe. Proteins in black; lipids in red. (G) Deep UV spectral image of the 290−375 nm emission band, assigned to the protein. The difference between the spatial resolution of FT-IR microspectroscopy (25 μm; B,C) and UV fluorescence microspectroscopy (1 μm; G) does not allow for a comparison of images at the same intensity. The UV spectrofluorescence imaging confirms protein histological identification without staining.

structures of targeted areas on the same tissue section. A recent study conducted by FT-IR microspectroscopy characterized the effect of heating on the secondary structure of muscle proteins previously identified by immunohistofluorescence.[9] The spatial resolution was reduced from about 25 to 6 μm by the use of a synchrotron source. In addition, the combination of FT-IR and UV fluorescence microspectroscopies allowed a fine in situ characterization of liver steatosis in human subjects.[10]

Considering the fat loss of *foie gras*, we suspected that slight differences in the molecular structure of the protein matrix could affect its mechanical resistance during cooking and thereby modulate lipid retention. So, our objectives were to characterize the in situ protein molecular structure changes of *foie gras* during cooking in order to find lipid loss markers and to acquire knowledge on the molecular mechanism involved in fat loss variability. Therefore, we conducted a multimodal imaging study combined with histological and spectroscopy analyses to characterize the thermal denaturation of *foie gras* proteins and to elucidate the molecular mechanisms underlying fat loss during cooking.

MATERIALS AND METHODS

Animals, *Foie Gras* Processing, and Sample Collection. Animals and samples were from an experiment that has been described in previous articles.[2,4] Briefly, 120 male mule ducks (*Cairina moschata* × *Anas platyrhynchos*) were reared with access to free range until age 13 weeks in a poultry house under natural conditions of light and temperature at the Agricultural College of Périgueux (EPLEFPA, 24, France). The ducks were then overfed in individual cages for 12 days by dispensing a soaked corn mixture (42% grain, 58% flour) twice a day. Ducks were slaughtered at the experimental slaughterhouse of the Agricultural College of Périgueux, 10 h after their last meal. The birds were electrically stunned head-only using scissor tongs and bled by ventral cutting of neck vessels within 10 s after the stun. After 5 min of bleeding, the carcasses were scalded and plucked.

The experiments described here fully comply with the legislation on research involving animal subjects in the European Communities Council Directive of November 24, 1986 (86/609/EEC). The investigators were

dx.doi.org/10.1021/jf5009605 | J. Agric. Food Chem. 2014, 62, 5954−5962

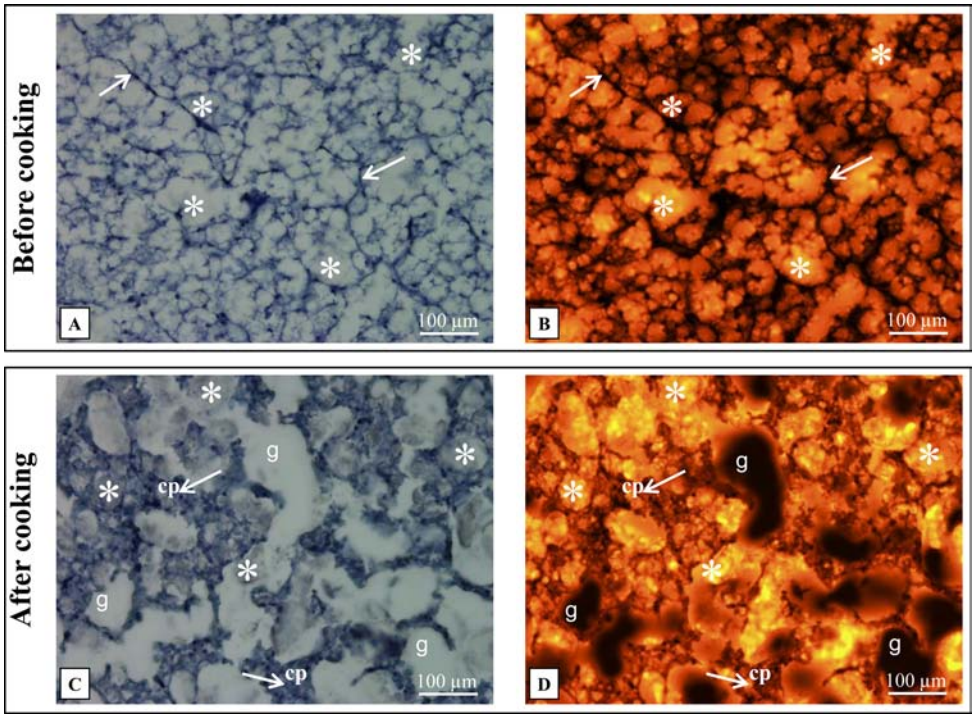

Figure 2. Cooking effect on *foie gras* tissue structure. Protein matrix (arrows) revealed by Toluidine Blue staining appeared thin before cooking (A) and thick after cooking (C) owing to coagulated proteins (cp). Lipids were stained with Nile Red fluorescent dye and were surrounded by the matrix, which appeared black before cooking (B) and fluorescent after cooking (D). Before cooking, the lipid droplets (stars) were small and spherical (B); after cooking, they were large and had lost their spherical shape (D). After cooking, gaps (g) are seen on the tissue sections (C and D).

certified by the French government authority to conduct these experiments (agreement no. 31-11.43.501).

At the end of the slaughter process, 20 min after bleeding, livers were removed from the carcasses and weighed. About 1 cm^3 was excised from each liver and frozen in cooled isopentane (−160 °C) chilled with liquid nitrogen (−196 °C). Samples were stored at −80 °C until use.

Livers were chilled on ice for 6 h and trimmed of their main blood vessels. Each *foie gras* was then transversally divided into three parts including its two lobes. In the middle part of each lobe, a slice of approximately 200 g was excised and placed in a closed glass jar. Salt (12 g/kg) and pepper (2 g/kg) were added, and the jars were left for 1 h in water in an autoclave ("Brouillon Process", Sainte-Bazeille, France) at 85 °C under a pressure of 0.8 bar. Temperature was controlled in the water and in two control jars equipped with temperature sensors. After 30 min of chilling (circulating cool water), the jars were stored at 4 °C for two months until opened for estimation of technological yield. The jars were opened, and the surface fat exuded during cooking was carefully removed from the liver. The technological yield was evaluated by the expression of fat loss during cooking as a percentage of initial liver weight: technological yield = (cooked liver weight trimmed of all visible fat/raw liver weight) × 100.

Among the 120 livers collected, 25 with similar lipid contents following Folch analysis[11] were selected for histological analysis, 13 with low cooking fat loss or high technological yield (89.9% ± 0.8%, mean ± SEM) and 12 with high cooking fat loss or low technological yield (68.3% ± 1.3%). Given the 96 h synchrotron beam time allocation, microspectroscopy analyses were performed on eight livers from the 25 selected, four livers with high technological yield (90.8% ± 1.6%) and four livers with low technological yield (67.0% ± 1.1%). About 1 cm^3 of cooked *foie gras* was cryofixed in cooled isopentane chilled with liquid nitrogen in the same way as that for raw *foie gras* and stored at −80 °C until use.

Tissue Section Preparation. Sections (10 µm thick) cut using a cryostat (Microm, HM 560) at −20 °C were collected on glass slides for histology and on infrared transparent BaF_2 windows for UV and IR microspectroscopy. Sections for both histology and microspectroscopy were dried and stored for several hours to several days at −20 °C until use.

Histochemistry. Slides were immersed in a 1% Toluidine Blue (EMS Company, Hatfield, PA 19440, USA) solution maintained at 4 °C for 10 min to contrast the nonlipidic matrix. Two washes of 1 min and one wash of 2 min were then performed in ultrapure water. After 1 h of drying, the same sections were stained with Nile Red fluorescent dye (Sigma-Aldrich corporation, St Louis, Missouri, USA) to reveal the lipids. Slides were incubated in a Nile Red solution (90 µg/mL in 75% glycerol) for 30 min in the dark at 4 °C. After three washes of 5 min in PBS buffer and one in ultrapure water, the slides were dried and stored at 4 °C in the dark until acquisition.

Image Acquisition and Image Analysis. Histological examination and image acquisitions were performed using an Olympus BX61 transmission bright field/fluorescence microscope coupled to a high-resolution digital acquisition kit (Olympus DP 71 digital camera and Olympus CellF software). Digital images were successively acquired on the same optical field in bright field and fluorescence mode (550 nm excitation and 570 nm emission). Proteins appeared in blue and lipids fluoresced in orange. Twenty-five images of each acquisition condition were acquired at 200× magnification on the same histological section.

For image analysis, the ×200-magnified Toluidine Blue stained section images were quantitatively analyzed with the open source ImageJ image processing software (http://rsbweb.nih.gov/ij) using exactly the same acquisition settings for all images. Each RGB-colored image was separated into its three monochromatic components (i.e., red, green, and blue) to keep only the green component of the image, which provided the best contrast between protein and lipid components. Protein matrix was extracted after thresholding segmentation of the gray levels, and its relative area was estimated by pixel counting of the region relative to the whole field-of-view area. The number of pixels stained was counted for each region of interest, in bright field acquisition mode, before and after cooking, and was expressed as a percentage of stained matrix per field. The protein matrix densification index, defined as the ratio of the percentage of stained matrix per field after to that before cooking, was calculated.

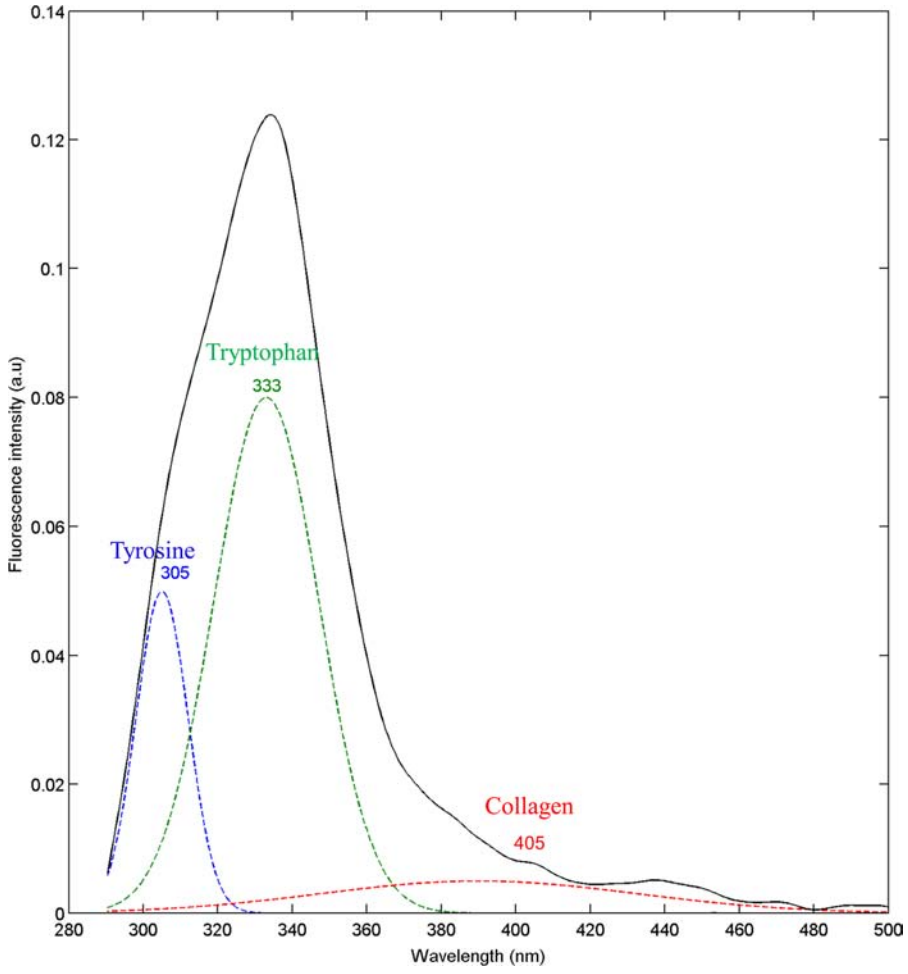

Figure 3. Representative UV fluorescence deconvoluted spectra of duck *foie gras*. Deconvolution of a UV spectrum of duck *foie gras* showing the autofluorescence bands assigned to Tyrosine (305 nm), tryptophan (333 nm), and to a lesser degree collagen (405 nm).

Lipid proportion was determined on the black and white images of Nile Red fluorescence. The same approach was used to extract lipid droplets. In each field of view, the total area of lipid droplets was estimated by its pixel count. A conversion factor was applied to express the measured surface areas in μm^2. The densification index was calculated as the ratio of percentage of matrix stained after/before cooking within each fat loss group.

Microspectroscopies Spectra Acquisitions. Synchrotron DUV microspectroscopy was performed on the DISCO beamline of the SOLEIL synchrotron radiation facility (Saint-Aubin, France).[7,8] DUV monochromatized light (typically between 270 and 330 nm) was used to excite tissue sections through a 40× ultrafluar immersion objective (Zeiss, Germany). The emission spectra were acquired from 290 to 539 nm and recorded with a 0.1 nm spectral resolution. The fluorescence spectrum from each excited pixel was recorded. Rastering of the sample allows the recording of a chosen map of interest. Mapping of 50 × 50 μm^2 was performed with 1 μm spatial resolution and a 3 s acquisition time per spectrum. Among all of the spectra acquired, 100 were selected for their high 335 nm peak intensity, characteristic of the protein target (tryptophan fluorescence).

FT-IR spectra acquisitions were performed on a Nicolet iN10 MX microscope (Thermo Scientific), using the internal (globar) infrared source, available at the SMIS beamline (Synchrotron SOLEIL, Saint-Aubin, France). Spectra were acquired on whole sections of each sample with a spectral resolution of 8 cm^{-1}. All spectra were recorded in transmission mode. The microscope comprises a motorized sample stage and a liquid nitrogen cooled array detector. A 15× Schwarzschild objective (NA = 0.5) was used, and all spectra were recorded in the mid-IR region from 4000 to 800 cm^{-1}. The spectra were saved in absorbance format using OMNIC software (Thermo Scientific).

Processing of Spectra. To study the chemical variations of interest, all of the spectra underwent data preprocessing before multivariate analysis. Autofluorescence spectra were spike- and noise-filtered using an in-house program written in MATLAB, version 7.3 (The MathWorks, Natick, MA), and images of each individual fluorescent component were produced. The Unscrambler software (v9.8, Camo Software AS, Norway) was used to perform a baseline adjustment to zero and to apply unit vector normalization.

Data processing of IR spectra was performed using the Unscrambler software (v9.8, Camo Software AS, Norway). An extended multiplicative signal correction (EMSC) was used as a flexible method for correcting artifacts in spectra by removing physical light scattering effects from chemical light absorbance effects.[12] The reference spectrum representative of the data set was calculated as the average of all spectra. The EMSC model was calculated over the 1700−1560 cm^{-1} range. On the basis of the 9-point Savitzky-Golay smoothing and using a third polynomial degree, the second derivative was first applied, and the calculated EMSC model was used to obtain the EMSC corrected spectra.

Statistical Analysis. Numerical variables of histology (protein matrix area) were expressed as the mean ± standard error of the mean (SEM). Variance analysis and mean comparisons were performed using one-way variance analysis and the Student−Newman−Keuls test under the general linear model procedure of the Statistical Analysis System software (Statistical Analysis Systems Institute Inc. SAS/STAT User's Guide, release 6.03, SAS Institute Inc., Cary, NC, 1988).

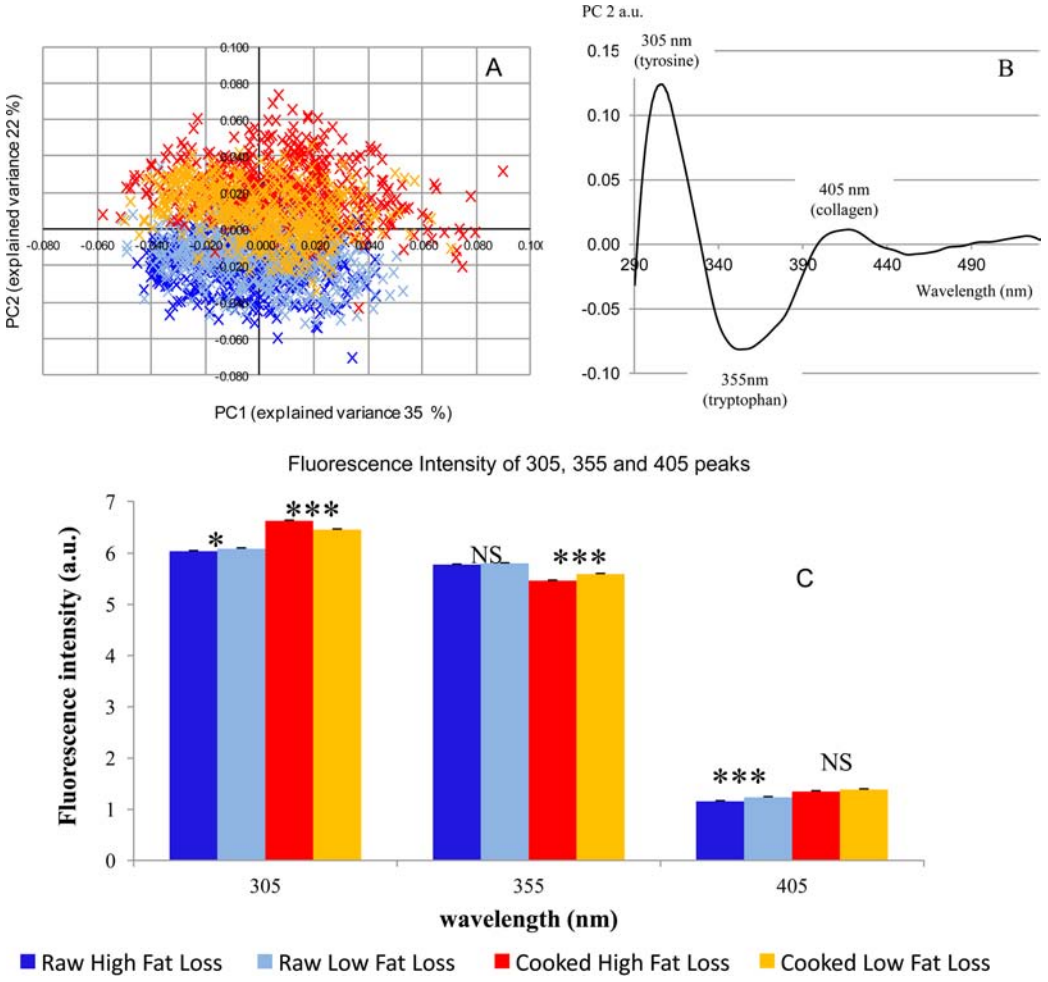

Figure 4. Synchrotron deep UV microspectroscopy comparison between raw and cooked *foie gras* within low and high fat loss groups. Dark blue, raw high fat loss; light blue, raw low fat loss; red, cooked high fat loss; and orange, cooked low fat loss. (A) Score plot of principal component analysis from the 290-510 nm fluorescence spectra. (B) PC2 loadings. (C) Autofluorescence intensity of 305, 355, and 405 nm bands. PCA score plots show that the groups separate along PC2. Compared to raw *foie gras*, cooked ones show higher fluorescence intensity at 305 and 405 nm wavelengths (assigned to tyrosine and collagen, respectively; $p < 0.001$) and lower fluorescence at 355 nm (assigned to the hydrophilic shift of tryptophan; $p < 0.001$). As shown in C, both the high and low fat loss groups are significantly different for raw *foie gras* at 305 and 405 nm and for cooked ones at 305 and 355 nm. NS: not significant; *, $p < 0.05$; **, $p < 0.01$; ***, $p < 0.001$. PC: principal component.

Processed spectra were analyzed by principal component analysis (PCA) using the Unscrambler software (v9.8, Camo Software AS, Norway). PCA was applied as an unsupervised approach to handle this new set of data and reveal variances or combinations of variables among this large multivariate data set. For this study, the infrared and fluorescence spectral domains were in the ranges 1700−1560 cm^{-1} and 290−530 nm, respectively. The number of possible components was always left sufficiently high (7). After analysis, the family label of each spectrum was revealed, and the first two components were plotted. The mean characteristic spectrum of each group was also plotted to relate the separation to spectral features. Score plots were used to show similarity maps allowing comparison of spectra regardless of sample categories. Loading plots derived from lists and second principal component X-loading plots were used to reveal and identify characteristic vibrational absorption bands.

RESULTS AND DISCUSSION

Complementarities of Imaging Modalities. The complementarity of the different imaging modalities used in this study is illustrated in Figure 1. The infrared maps of the spectral region 1600−1700 cm^{-1} allowed one to identify the protein matrix on the whole tissue section but with much lower spatial resolution than with fluorescence spectra imaging and histochemistry. A deep UV spectral image of the 290−375 nm emission band, which is assigned to proteins, evidences the protein matrix according to histology.

***Foie Gras* Ultrastructure.** The histological sample preparation performed in this study was used here on *foie gras* for the first time. Cryofixation followed by double staining with Toluidine Blue and the Nile Red fluorescent probe allowed the colocation of the lipid droplets and nonlipid matrix, composed mainly of protein. Previous histological studies of *foie gras* were carried out after fixation with formalin followed by organic solvent dehydration and inclusion in paraffin.[13,14] However, in this type of sample preparation, lipid esters are not fixed by formalin but are eluted by an organic solvent during dehydration.[15] In our study, cryo-fixation allowed lipid preservation in the tissue section, and the high contrast of the protein matrix facilitated its density measurement by image analysis. The *foie gras* ultrastructure study included characterizing the nonlipid structure (taken as protein) around the lipid droplets.

Before cooking, the protein matrix located around the lipid droplets (Figure 2A) was thin, and lipid droplets appeared

dx.doi.org/10.1021/jf5009605 | J. Agric. Food Chem. 2014, 62, 5954−5962

small (3.8 ± 0.7 μm^2) and spherical (Figure 2B) as already described for duck *foie gras* from a semithin section embedded in epoxy resin.[2] In fluorescence mode, the protein matrix was not visible, underlining the specificity of Nile Red fluorescent dye for lipids in raw *foie gras*.

After cooking, lipid droplets were larger (9.0 ± 3.6 μm^2) and had lost their spherical shape (Figure 2 D), probably because of the merging of droplets under heat treatment, as previously shown by Théron et al.[2]

The protein matrix appeared thicker than that before cooking (Figure 2C). These findings were consistent with results obtained on cooked meat.[16] Heating leads to protein aggregation through protein thermal denaturation[5,9,16] and protein oxidation[17] that can form disulfide and bityrosine bonds. Such protein aggregations probably explain the protein matrix structural changes. Also, in contrast to the raw *foie gras*, the protein matrix of cooked *foie gras* expressed fluorescence because of the affinity of Nile Red dye for protein aggregates.[17,18] These authors highlighted in situ protein aggregation on histological sections of cooked meat by detecting the Nile Red fluorescence dye fixed on protein aggregates formed during heating.

The protein matrix densification index, defined as the ratio of the percentage of stained matrix per field after to before cooking, was 1.55 ± 0.04 and 1.35 ± 0.02 ($p < 0.05$) in the high and low fat loss groups, respectively. These results evidence the link between the level of fat loss during cooking and the densification of the protein matrix, i.e., protein denaturation and aggregation.

Cooking Effects on the Protein Matrix Fluorescence Spectroscopy Response. The high brightness and high spatial resolution provided by the DISCO synchrotron beamline allowed the protein matrix to be characterized on an ultrastructural scale on raw and cooked *foie gras*. The UV spectra of duck *foie gras* (Figure 3) showed a marked peak at 333 nm assigned to the autofluorescence of tryptophan,[10,19] with a shoulder at 305 nm characteristic of tyrosine.[19] The band at 405 nm that could be assigned to collagen was not as well-defined as in human pathologic fibrosis studies.[10] This result is not surprising since *foie gras* is not the result of a disease, unlike human steatosis, which causes liver fibrosis. Figure 4A,B presents the score and loadings plots of the principal component analysis performed on UV spectra from the four groups: before and after cooking in low and high fat loss groups. The loadings show that cooking was characterized by peaks at 305, 355, and 405 nm. Cooking resulted in an increase in fluorescence intensity ($p < 0.001$) at 305 nm (tyrosine) and 405 nm (collagen), while fluorescence intensity decreased at 355 nm ($p < 0.001$); regardless of the fat loss during cooking.

The discriminatory effect of cooking at 355 nm could be due to a shift in the tryptophan peak as a consequence of changes in protein hydrophobicity[20] or to its partial degradation. Indeed, a decrease in tryptophan was still observed after meat cooking.[21] This amino acid can be oxidized in 5- and 7-hydroxytryptophan[22] or reacted with other molecules to form heterocyclic aromatic amines (HAAs).[23]

In Figure 4C, compared to raw *foie gras*, we observed an increase of fluorescence intensity of tyrosine in cooked *foie gras*. Thermal denaturation tends to move the hydrophobic amino acids to the external parts of proteins,[17,24] and tyrosine can be considered predominantly hydrophobic as its hydroxyl residue is not ionized at the pH of *foie gras* (about 6).[25] The hydrogen bond environment is known to affect the fluorescence intensity of a molecule.[26] In the present case, heating led to the cleavage of many hydrogen bonds, which probably helped to increase the fluorescence yield of tyrosine. The greater accessibility of the excitation radiation to well-exposed tyrosine residues, together with their lower molecular interactions, may explain this increase in tyrosine autofluorescence intensity.

In addition, heating causes melting and peroxidation of lipids, which are particularly abundant in *foie gras*. Aldehyde compounds from lipid peroxidation react with proteins and increase the fluorescence intensity of cooked meat.[27] This effect could be transposed to *foie gras*, where lipid movement during cooking could influence autofluorescence parameters of molecules in their vicinity. Before cooking, compared with high fat loss *foie gras*, we observed in low fat loss *foie gras*, a slight but significant increase in the fluorescence intensity at 305 nm assigned to tyrosine ($p < 0.05$) and at 405 nm that could be assigned to collagen ($p < 0.001$) (Figure 4 C). These results suggest that tyrosine and collagen autofluorescence of raw *foie gras* could be used to predict fat loss during cooking. Significant differences were observed after cooking on emission fluorescence between low and high fat loss groups. The low fat loss group showed a decrease in fluorescence at 305 nm ($p < 0.001$) and an increase at 355 nm ($p < 0.001$). This finding reflects different changes in the protein matrix structure and/or composition during cooking, related to fat loss level.

Cooking Effects on Protein Matrix Infrared Spectroscopy Response. FT-IR microspectroscopy was applied on the tissue sections to characterize the secondary structure of proteins in situ. The global profile obtained from FT-IR spectra (Figure 5) was similar to that observed on human nonalcoholic steatosis liver samples.[28] The spectrum shows major peaks at 3000−3060, 2800−3000, 1710−1780, and 1475−1710 cm^{-1} assigned to C = C, CH3-CH2, C = 0, and amide (I and II) bands of proteins, respectively.[28] The 1600−1700 cm^{-1} spectral range, was used to characterize the molecular structure of proteins.[29] A close-up of this part of the spectrum shows a peak at 1658 cm^{-1} reflecting α-helix structure.[29] Cooked samples

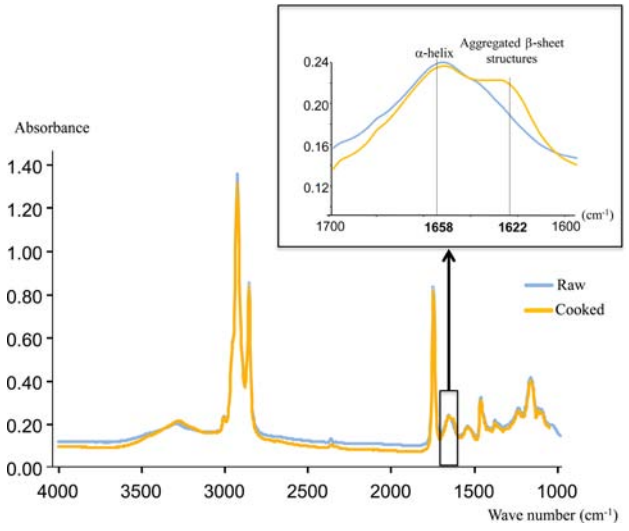

Figure 5. Mean infrared spectra of raw and cooked *foie gras*. The 1600-1700 cm^{-1} spectral range, which corresponds to the amide I band of protein, was used to characterize molecular structure. A close-up of this part of the spectrum shows that the cooked samples have a shoulder at 1622 cm^{-1}, assigned to aggregated β-sheet structures.

dx.doi.org/10.1021/jf5009605 | J. Agric. Food Chem. 2014, 62, 5954−5962

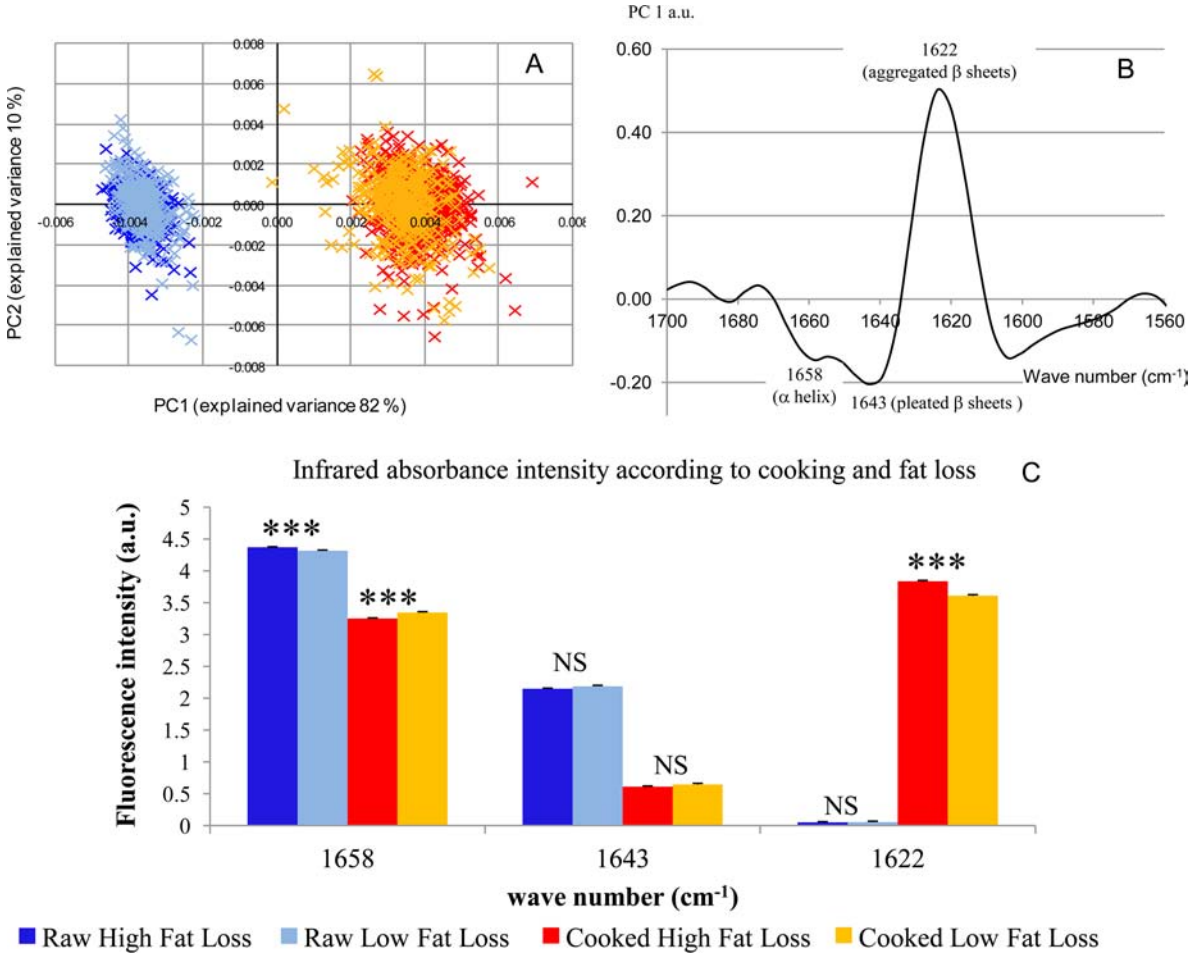

Figure 6. Infrared microspectroscopy comparison between raw and cooked *foie gras* within low and high fat loss groups. Dark blue, raw high fat loss; light blue, raw low fat loss; red, cooked high fat loss; orange, cooked low fat loss. (A) Score plot of principal component analysis from the 1558–1700 cm^{-1} band infrared spectra. (B) PC1 loadings. (C) Infrared response of 1658, 1643, and 1622 cm^{-1} bands. PCA score plots show that the groups separate along PC1. Compared to raw *foie gras*, cooked ones show lower infrared absorbance intensities at 1658 and 1643 cm^{-1} (attributed to α-helix and antiparallel β sheets structures, respectively; $p < 0.001$) and higher response at the 1622 cm^{-1} band assigned to aggregated β sheet structure ($p < 0.001$). From the ANOVA analysis, shown in C, the two fat loss groups (high and low) are significantly different for raw *foie gras* at 1658 cm^{-1} and for cooked ones at 1658 and 1622 cm^{-1}. NS, not significant; *, $p < 0.05$; **, $p < 0.01$; ***, $p < 0.001$. PC: principal component.

have a shoulder at 1622 cm^{-1}, assigned to aggregated β-sheet structures.[29]

Multivariate statistical analysis (Figure 6A,B) separated cooked samples from raw samples on the amide 1 band of proteins. This finding results in the changes in the secondary structure of proteins during heating characterized by changes in spectral bands at 1658, 1643, and 1622 cm^{-1}, as shown by PC1 loadings (Figure 6B) and the close-up of the amide 1 band (Figure 5). These bands are assigned to the α-helical structures, pleated (parallel/antiparallel) β-sheet structure, and aggregated β-sheet structure, respectively.[29−31] Compared with raw *foie gras*, after cooking, the peak heights at 1658 and 1643 cm^{-1} decreased by about 25% and 75%, respectively, while the peak height at 1622 cm^{-1} was increased by seven times (Figure 6).

These results agree with those of Kirschner et al.[32] and Astruc et al.[9] showing a decrease in α-helix and pleated β-sheet structures and an increase in aggregated β-sheet structures of skeletal muscle proteins subjected to heating. The decrease in native secondary structure of protein (α-helix and pleated β-sheet structures) associated with an increase of aggregated β-sheet structure is an illustration of the thermal denaturation of proteins.

The level of α-helix structure was slightly lower in the raw low fat loss group than in the raw high fat loss group, but the difference was highly significant ($p < 0.001$; Figure 6C). This finding could be linked to the lower content of heat shock proteins (HSP) in low fat loss *foie gras*,[3] which protects proteins against denaturation.

After cooking, the level of α-helix structures was higher, and the aggregated β-sheet structures were lower in the low fat loss group. Thus, the *foie gras* that was most sensitive to thermal denaturation of proteins also displayed lower lipid retention after cooking. It seems that the thermostability of proteins that maintain the structural integrity of hepatocytes is involved in the retention of lipid droplets during cooking.

The variability in protein thermal denaturation between high and low fat loss groups could also come from differences in the proportion of thermostable protein in the *foie gras* protein matrix. Indeed, FT-IR microspectroscopy does not allow for characterizing a specific single protein but does allow all proteins probed by the beam, i.e., a set of colocalized proteins. However, each protein has a specific thermal stability.[5] We have recently shown that myofibrillar proteins of muscle begin to denature at 40 °C, whereas elastin is thermostable up to at least

dx.doi.org/10.1021/jf5009605 | J. Agric. Food Chem. 2014, 62, 5954−5962

80 °C.[9] In the case of *foie gras*, the lower thermal denaturation of overall matrix proteins from low fat loss *foie gras* could be explained by a higher proportion of thermostable proteins.

Coupling morphological, multimodal imaging methods and spectroscopies enabled us to characterize the structure of *foie gras* at mesoscopic, ultrastructural, and supramolecular scales. The coagulation of heated proteins observed by histology is the result of their aggregation at the molecular scale after their thermal denaturation, which was characterized by microspectroscopy. Our results link the evolution of the protein matrix to the level of fat loss during cooking. Each of the three methods (histology, infrared microspectroscopy, and fluorescence microspectroscopy) showed that a reduced thermal change in *foie gras* proteins promotes better lipid retention and thereby enhances the technological quality of *foie gras*.

AUTHOR INFORMATION

Corresponding Author

*Tel: 33 4 73 62 41 56. Fax: 33 4 73 62 42 68. E-mail: Thierry.Astruc@clermont.inra.fr.

Funding

This work was supported by funding from INRA, CIFOG, and Région Midi-Pyrénées.

Notes

The authors declare no competing financial interest.

ACKNOWLEDGMENTS

Ducks were slaughtered and processed at the facilities of the Lycée Agricole de Périgueux (EPLEFPA, 24, France). We thank François Hérault (EPLEFPA) for technical supervision of the breeding and slaughter process. Microspectroscopy spectra acquisitions were performed at the SOLEIL synchrotron on the DISCO beamline in the framework of Project No. 20100044.

REFERENCES

(1) Hermier, D.; Salichon, M. R.; Guy, G.; Peresson, R. Differential channelling of liver lipids in relation to susceptibility to hepatic steatosis in the goose. *Poultry Sci.* **1999**, *78*, 1398−1406.

(2) Theron, L.; Astruc, T.; Bouillier-Oudot, M.; Molette, C.; Venien, A.; Peyrin, F.; Vitezica, Z. G.; Fernandez, X. The fusion of lipid droplets is involved in fat loss during cooking of duck "foie gras". *Meat Sci.* **2011**, *89*, 377−383.

(3) Theron, L.; Fernandez, X.; Marty-Gasset, N.; Pichereaux, C.; Rossignol, M.; Chambon, C.; Viala, D.; Astruc, T.; Molette, C. Identification by proteomic analysis of early post-mortem markers involved in the variability in fat loss during cooking of mule duck "foie gras". *J. Agric. Food Chem.* **2011**, *59*, 12617−12628.

(4) Theron, L.; Fernandez, X.; Marty-Gasset, N.; Chambon, C.; Viala, D.; Pichereaux, C.; Rossignol, M.; Astruc, T.; Molette, C. Proteomic analysis of duck fatty liver during post-mortem storage related to the variability of fat loss during cooking of "foie gras". *J. Agric. Food Chem.* **2013**, *61*, 920−930.

(5) Tornberg, E. Effects of heat on meat proteins - Implications on structure and quality of meat products. *Meat Sci.* **2005**, *70*, 493−508.

(6) Lasch, P.; Naumann, D. Spatial resolution in infrared micro spectroscopic imaging of tissues. *Biochim. Biophys. Acta, Biomembr.* **2006**, *1758*, 814−829.

(7) Giuliani, A.; Jamme, F.; Rouam, V.; Wien, F.; Giorgetta, J. L.; Lagarde, B.; Chubar, O.; Bac, S.; Yao, I.; Rey, S.; Herbeaux, C.; Marlats, J. L.; Zerbib, D.; Polack, F.; Refregiers, M. DISCO: a low-energy multipurpose beamline at synchrotron SOLEIL. *J. Synchrotron Radiat.* **2009**, *16*, 835−841.

(8) Jamme, F.; Villette, S.; Giuliani, A.; Rouam, V.; Wien, F.; Lagarde, B.; Refregiers, M. Synchrotron UV fluorescence microscopy uncovers new probes in cells and tissues. *Microsc. Microanal.* **2010**, *16*, 507−514.

(9) Astruc, T.; Peyrin, F.; Venien, A.; Labas, R.; Abrantes, M.; Dumas, P.; Jamme, F. In situ thermal denaturation of myofibre subtype proteins studied by immunohistofluorescence and synchrotron radiation FT-IR microspectroscopy. *Food Chem.* **2012**, *134*, 1044−1051.

(10) Petit, V. W.; Refregiers, M.; Guettier, C.; Jamme, F.; Sebanayakam, K.; Brunelle, A.; Laprevote, O.; Dumas, P.; Le Naour, F. Multimodal spectroscopy combining time-of-flight-secondary ion mass spectrometry, synchrotron-FT-IR, and synchrotron-UV microspectroscopies on the same tissue section. *Anal. Chem.* **2010**, *82*, 3963−3968.

(11) Folch, J.; Lees, M.; Sloane Stanley, G. H. A simple method for the isolation and purification of total lipides from animal tissues. *J. Biol. Chem.* **1957**, *226*, 497−509.

(12) Kohler, A.; Sule-Suso, J.; Sockalingum, G. D.; Tobin, M.; Bahrami, F.; Yang, Y.; Pijanka, J.; Dumas, P.; Cotte, M.; van Pittius, D. G.; Parkes, G.; Martens, H. Estimating and correcting Mie scattering in synchrotron-based microscopic Fourier transform infrared spectra by extended multiplicative signal correction. *Appl. Spectrosc.* **2008**, *62*, 259−266.

(13) Bénard, G.; Labie, C. In *Evolution histologique du foie des palmipèdes au cours du gavage*; 3èmeJournées de la Recherche sur les Palmipèdes à Foie Gras, Bordeaux, France, Oct 27−28, 1998; Bordeaux, ITAVI: Paris, France 1998; pp 31−35.

(14) Locsmandi, L.; Hegedus, G.; Andrassy-Baka, G.; Bogenfurst, F.; Romvari, R. Following the goose liver development by means of cross-sectional digital imaging, liver histology and blood biochemical parameters. *Acta Biol. Hung.* **2007**, *58*, 35−48.

(15) Fujimoto, T.; Ohsaki, Y.; Cheng, J.; Suzuki, M.; Shinohara, Y. Lipid droplets: a classic organelle with new outfits. *Histochem. Cell Biol.* **2008**, *130*, 263−279.

(16) Astruc, T.; Gatellier, P.; Labas, R.; Lhoutellier, V. S.; Marinova, P. Microstructural changes in m. rectus abdominis bovine muscle after heating. *Meat Sci.* **2010**, *85*, 743−751.

(17) Sante-Lhoutellier, V.; Astruc, T.; Marinova, P.; Greve, E.; Gatellier, P. Effect of meat cooking on physicochemical state and in vitro digestibility of myofibrillar proteins. *J. Agric. Food Chem.* **2008**, *56*, 1488−1494.

(18) Demeule, B.; Gurny, R.; Arvinte, T. Detection and characterization of protein aggregates by fluorescence microscopy. *Int. J. Pharm.* **2007**, *329*, 37−45.

(19) Pallu, S.; Rochefort, G. Y.; Jaffre, C.; Refregiers, M.; Maurel, D. B.; Benaitreau, D.; Lespessailles, E.; Jamme, F.; Chappard, C.; Benhamou, C. L. Synchrotron ultraviolet microspectroscopy on rat cortical bone: involvement of tyrosine and tryptophan in the osteocyte and its environment. *PLoS One* **2012**, *7*, 1−11.

(20) Lakowicz, J. *Principles of Fluorescence Spectroscopy*; Kluwer Academic and Plenum Publishers: New York, 1999.

(21) Gatellier, P.; Kondjoyan, A.; Portanguen, S.; Greve, E.; Yoon, K.; Sante-Lhoutellier, V. Determination of aromatic amino acid content in cooked meat by derivative spectrophotometry: Implications for nutritional quality of meat. *Food Chem.* **2009**, *114*, 1074−1078.

(22) Josimovic, L.; Jankovic, I.; Jovanovic, S. V. Radiation-induced decomposition of tryptophan in the presence of oxygen. *Radiat. Phys. Chem.* **1993**, *41*, 835−841.

(23) Skog, K. I.; Johansson, M. A. E.; Jagerstad, M. I. Carcinogenic heterocyclic amines in model systems and cooked foods: A review on formation, occurrence and intake. *Food Chem. Toxicol.* **1998**, *36*, 879−896.

(24) Morita, J. I.; Yasui, T. Involvement of hydrophobic residues in heat-induced gelation of myosin tail subfragments from rabbit skeletal-muscle. *Agric. Biol. Chem. Tokyo* **1991**, *55*, 597−599.

(25) Petsko, G. A.; Ringe, D. *Protein Structure and Function*; Lawrence, E., Robertson, M., Eds.; New Science Press Ltd.: London, U.K., 2004.

(26) Valeur, B. *Molecular Fluorescence: Principles and Applications*; Wiley-VCH: Weinheim, Germany, 2001.

(27) Gatellier, P.; Sante-Lhoutellier, V.; Portanguen, S.; Kondjoyan, A. Use of meat fluorescence emission as a marker of oxidation promoted by cooking. *Meat Sci.* **2009**, *83*, 651−656.
(28) Le Naour, F.; Bralet, M. P.; Debois, D.; Sandt, C.; Guettier, C.; Dumas, P.; Brunelle, A.; Laprevote, O. Chemical imaging on liver steatosis using synchrotron infrared and ToF-SIMS microspectroscopies. *PLoS One* **2009**, *4*, 1−10.
(29) Barth, A. Infrared spectroscopy of proteins. *Biochim. Biophys, Acta, Bioenerg.* **2007**, *1767*, 1073−1101.
(30) Jackson, M.; Mantsch, H. H. The use and misuse of ftir spectroscopy in the determination of protein-structure. *Crit. Rev. Biochem. Mol.* **1995**, *30*, 95−120.
(31) Bocker, U.; Ofstad, R.; Wu, Z. Y.; Bertram, H. C.; Sockalingum, G. D.; Manfait, M.; Egelandsdal, B.; Kohler, A. Revealing covariance structures in Fourier transform infrared and Raman microspectroscopy spectra: A study on pork muscle fiber tissue subjected to different processing parameters. *Appl. Spectrosc.* **2007**, *61*, 1032−1039.
(32) Kirschner, C.; Ofstad, R.; Skarpeid, H. J.; Host, V.; Kohler, A. Monitoring of denaturation processes in aged beef loin by Fourier transform infrared microspectroscopy. *J. Agric. Food Chem.* **2004**, *52*, 3920−3929.

JOURNAL OF AGRICULTURAL AND FOOD CHEMISTRY

Article

pubs.acs.org/JAFC

Raman Spectroscopic Study of Structural Changes upon Chilling Storage of Frankfurters Containing Olive Oil Bulking Agents As Fat Replacers

A. M. Herrero,*[,†] C. Ruiz-Capillas,[†] F. Jiménez-Colmenero,[†] and P. Carmona[‡]

[†]Institute of Food Science, Technology and Nutrition (ICTAN-CSIC), José Antonio Novais, 10, 28040 Madrid, Spain

[‡]Institute for the Structure of Matter, Serrano 121, 28006 Madrid, Spain

ABSTRACT: Technological properties and structural characteristics of proteins and lipids, using Raman spectroscopy, of frankfurters formulated with olive oil bulking agents as animal fat replacers were examined during chilling storage. Frankfurters reformulated with oil bulking agents showed lower ($P < 0.05$) processing loss and higher ($P < 0.05$) hardness and chewiness. Purge loss during chilling storage was relatively low, demonstrating a good water retention in the products. β-Sheet structures were enhanced by the use of olive oil bulking agents, and this effect was more pronounced in samples containing inulin. Reformulated frankfurters contained the least turns ($P < 0.05$). A significant decrease of β-sheets and an increase of turns were observed after 85 days of chilled storage. The lowest ($P < 0.05$) values of $I\nu_sCH_2/I\nu_{as}CH_2$ were recorded in frankfurters reformulated with oil bulking agents, which suggests more lipid acyl chain disorder. Structural characteristics were correlated to processing losses, hardness, and chewiness.

KEYWORDS: *lipid, protein, olive oil bulking agent, frankfurter, texture, processing loss, structure, Raman spectroscopy*

INTRODUCTION

Frankfurters are very popular, frequently consumed meat products. However, they are increasingly being associated with negative aspects relating to health. In order to minimize this negative aspect, frankfurters have been reformulated to improve their lipid composition by reducing fat content and/or replacing the animal fat present in the product with alternative fat whose characteristics are more in line with health recommendations.[1] In this context various strategies have been devised to incorporate these fats in meat products, for instance in liquid and solid forms, encapsulated, or as oil-in-water emulsions.[1] Our group has developed solid animal fat replacers such as oil bulking agents based on polysaccharide gels, which have been used in the formulation of meat batters.[2,3] The potential of a konjac matrix containing healthy oils to improve fat content in meat products has also been evaluated.[4−7] To properly develop this type of meat product, it is especially useful to look at reformulation processes that affect technological properties (water and fat binding properties, color, texture, etc.). It has been reported that food processing can potentially alter the structure of food proteins either as the result of intended unit operations or as a consequence of the physicochemical environment a protein encounters during processing.[8] In particular, the use of certain reformulation strategies based on replacement of animal fat in the development of healthier lipid meat products could alter both the structural properties of their main components (proteins, lipids, etc.) and technological properties of the final product. An understanding of the interactions that occur between meat proteins and other ingredients is vital for product quality and the development of new processed meat products.[9] The interactions of meat proteins with the other ingredients can significantly affect the properties of the end product, since many of these have a close bearing on the adequate formation of a protein network. Supplementary information relating to the structure/function relationship would clarify the mechanisms that act on them and help determine criteria for adjusting these. It would also aid to find conditions for certified aspects relating to processing and composition and their impact on technological properties of a complex meat system.

Raman spectroscopy can provide comprehensive structural information to highlight this structure/function relationship. Raman spectroscopy provides a means to approach the structure,[10−16] and particularly the interactions among the different components (protein, lipids, etc.) of these types of healthier-lipid meat products, modified by the addition of animal fat replacers as oil bulking agents. Studies have demonstrated that Raman spectroscopy is a useful tool for directly determining the changes occurring in lipids and proteins of meat batters due to the incorporation of various types of lipids.[2,17] These studies identify associations between the protein and lipid structure data obtained using Raman spectroscopy and the technological properties of the product such as texture and water binding.[2,17]

The primary objective of this work was to determine technological properties (processing loss, purge loss, and texture) and structural characteristics of protein and lipids, using Raman spectroscopy, of frankfurters formulated with olive oil bulking agents, as animal fat replacer. These bulking agents are based on the combination of olive oil, water, a cold set binding agent (alginate), and polysaccharides (inulin or

Received: March 14, 2014
Revised: June 4, 2014
Accepted: June 9, 2014
Published: June 9, 2014

ACS Publications © 2014 American Chemical Society

dextrin). Technological and structural properties were also evaluated as affected by chilling storage (85 days at 2 °C). The secondary objective was to examine the possible relationship between the technological properties and the protein and lipid structures of these frankfurters. A fuller understanding of this relationship could throw more light on the role of oil bulking agents in a meat matrix, which could be useful in optimizing the quality of frankfurters to which they are added.

MATERIALS AND METHODS

Materials. Ingredients used for preparation of oil bulking agents as fat replacers included the following: olive oil (13% SFA, 79% MUFA, and 8% PUFA) (Carbonell Virgen Extra, SOS Cuétara SA, Madrid, Spain); sodium alginate (90% carbohydrates) (Tradissimo, TRADES S.A., Barcelona Spain); calcium sulfate (Panreac Química, S.A. Madrid, Spain); tetra-sodium pyrophosphate anhydrous (STP) (Manuel Riesgo, S.A. Madrid, Spain); inulin consisting mainly of chicory inulin (>90% inulin) with a molecular weight of 1650 g/mol (TRADES S.A., Barcelona Spain); and white maize dextrin (molecular weight average approximate between 10 and 20 glucose molecule per polymer) (CARGILL S.L.U., CTS Rubi, Barcelona, Spain).

Fresh post-rigor pork (mixture of musculus *biceps femoris*, musculus *semimembranosus*, musculus *semitendinosus*, musculus *gracilis*, and musculus *adductor*) and pork backfat used for the preparation of frankfurters were obtained from a local meat market. The meat was trimmed of fat and connective tissue, and the pork fat was passed through a grinder with a 0.4 mm plate. Lots of approximately 1 kg were vacuum packed, frozen, and stored at −20 °C until use, which took place within 2 weeks.

Other ingredients and additives used were sodium chloride (Panreac Química S.A., Barcelona, Spain), sodium nitrite (Fulka Chemie GmbH, Buchs, Germany), and flavoring (Gewürzmüller, GmbH, Münchingen, Germany).

Preparation of Olive Oil Bulking Agents. Two different types of olive oil bulking agents were considered:[3] a combination of olive oil with sodium alginate, $CaSO_4$, STP, and dextrin, named A/D, or inulin, named A/I. These samples were prepared by mixing sodium alginate (1%), $CaSO_4$ (1%), STP (0.75%), and dextrin (2.25%) or inulin (2.25%) with water (40%) in a homogenizer (Thermomix TM 31, Vorwerk España M.S.L., S.C., Madrid) to prepare A/D or A/I respectively. The mixtures were prepared at 1500 rpm for 20 s. Olive oil (55%) was gradually added to this mixture with the homogenizer running (1500 rpm). Samples of each type were placed in metal molds under pressure to compact them and avoid air bubbles, and stored in a chilling room at 2 °C for 24 h until analysis. Each type of oil bulking agent was prepared in duplicate using two metal molds for each type of sample. These oil bulking agents were used as pork backfat replacers in the formulation of the frankfurters.

Preparation of Frankfurters. Frankfurters were prepared following the procedure previously reported.[7] Six different products were prepared as reported in Table 1: control normal fat (NFF-PF) and low fat (LFF-PF) frankfurter formulated with meat and pork backfat (PF); four reformulated samples in which the pork backfat was replaced by an equal amount of oil bulking agent A/D or A/I to formulate normal (NFF-A/D, NFF-A/I) and low (LFF-A/D, LFF-A/I) fat frankfurters. For frankfurter preparation a Stephan Universal Machine UM5 (Stephan u. Söhne GmbH and Co., Hameln, Germany) was used at 2 °C.

The meat batter was stuffed into 20 mm diameter Nojax cellulose casings (Viscase S.A., Bagnold Cedex, France), hand-linked, and heat processed in an Eller smokehouse (model Unimatic 1000, Micro 40, Eller, Merano, Italy). After that, the frankfurters were cooled (at room temperature), vacuum-packed in plastic bags (Cryovac BB3050), stored at 2 °C (±1 °C), and analyzed periodically (days 1, 45, and 85).

Proximate Analysis. Moisture and ash contents of the frankfurters were determined[18] in triplicate. Protein content was measured in triplicate with a LECO FP-2000 Nitrogen Determinator (Leco Corporation, St Joseph, MI, USA). Fat content was evaluated in triplicate.[19]

Table 1. Formulation (%) of Frankfurters[a]

			olive oil bulking agent[c]		
samples[b]	meat	pork backfat	A/D	A/I	water
NFF-PF	63.0	21.0			13.2
LFF-PF	63.0	9.0			25.2
NFF-A/D	63.0		32.5		1.7
LFF-A/D	63.0		14.0		20.2
NFF-A/I	63.0			32.5	1.7
LFF-A/I	63.0			14.0	20.2

[a]Additives added to all samples: 2.0 g/100 g NaCl; 0.30 g/100 g sodium tripolyphosphate; 0.012 g/100 g sodium nitrite; 0.5 g/100 g flavoring. [b]Frankfurter: normal fat (NF-) and low fat (LF-) frankfurter (F) formulated with pork backfat (NFF-PF and LFF-PF) or olive oil bulking agent containing dextrin (NFF-A/D and LFF-A/D) or inulin (NFF-A/I and LFF-A/I) as a fat replacer. [c]Olive oil bulking agent formulated with a combination of olive oil, water, sodium alginate, $CaSO_4$, sodium pyrophosphate, and dextrin (A/D) or inulin (A/I).

Energy values were estimated from both protein and carbohydrate content (×4.1 kcal/g) and fat content (×9.1 kcal/g).[6]

Processing Loss and Purge loss. Processing loss of frankfurters (expressed as % of initial sample weight) occurring after heat processing and chilling overnight at 2 °C was calculated in quadruplicate.

Three vacuum packs per formulation were used to determine purge loss during chilling storage for each storage time. After the frankfurters were removed from the package, the surface exudate (tiny drops) was wiped off with paper towels and the frankfurters were weighed again. The purge loss was calculated by weight difference and expressed as a percentage of the initial weight.

Texture Profile Analysis. Texture profile analysis (TPA) was performed in a TA.XTplus Texture Analyzer (Texture Technologies Corp., Scarsdale, NY, USA). Cylindrical cores (diameter = 20 mm, height = 20 mm) from each frankfurter formulation were axially compressed to 40% of their original height[20] with an aluminum cylinder probe P/25. Six replicates were performed for each frankfurter formulation. Force−time deformation curves were obtained with a 5 kg load cell, applied at a crosshead speed of 1 mm/s. Attributes were calculated as follows: hardness (Hd) = peak force (N) required for first compression; cohesiveness (Ch) = ratio of active work done under the second compression curve to that done under the first compression curve (dimensionless); springiness (Sp) = distance (mm) the sample recovers after the first compression; chewiness (Cw): Hd × Ch × Sp (N × mm). Measurement of samples was carried out at room temperature.

FT-Raman Spectroscopic Analysis. Various Raman spectra were measured and used as reference: spectra of heated homogenized raw meat, heated pork backfat, and heated olive oil bulking agent (A/I and A/D). Heating of these samples was performed in a water bath at 70 °C for 30 min (similar conditions to preparation of frankfurters). These Raman spectra were used to appropriately subtract their respective contribution in the spectra of frankfurters analyzed.

Spectra of frankfurters formulated according to Table 1 (NFF-PF, LFF-PF, NFF-A/D, LFF-A/D, NFF-A/I, and LFF-A/I) were also measured.

Portions (approximately 5 g) of the different samples were measured directly without previous treatment. These portions of samples were transferred to quartz cuvettes (ST-1/Q/10) (Teknokroma, Barcelona, Spain), which were filled to reach 1 cm sample length. For each sample 1500 scans were recorded. This procedure was carried out in triplicate. Measurements were performed on three samples from each formulation. Spectra were excited with the 1064 nm Nd:YAG laser line and recorded on a Bruker RFS 100/S FT-spectrometer. The scattered radiation was collected at 180° to the source, and frequency-dependent scattering of the Raman spectra was corrected by multiplying point by point with (ν_{laser}/ν).[4] The influence of the

dx.doi.org/10.1021/jf501231k | J. Agric. Food Chem. 2014, 62, 5963−5971

Table 2. Proximate Analysis (%) and Processing Loss (PL, %) of Frankfurters[a]

samples[b]	moisture	fat	protein	ash	PL (%)
NFF-PF	60.5 ± 0.2 b	20.4 ± 0.3 a	16.2 ± 0.5 a	2.90 ± 0.06 c	14.7 ± 0.7 d
LFF-PF	71.7 ± 0.1 a	9.9 ± 0.3 b	16.0 ± 0.5 a	2.79 ± 0.05 c	22.6 ± 0.9 a
NFF-A/D	60.6 ± 0.2 b	19.8 ± 0.3 a	15.0 ± 0.5 a	4.42 ± 0.02 a	13.8 ± 0.7 e
LFF-A/D	72.1 ± 0.3 a	9.6 ± 0.2 b	15.5 ± 0.6 a	3.49 ± 0.01 b	18.9 ± 0.9 b
NFF-A/I	60.9 ± 0.2 b	19.6 ± 0.4 a	15.2 ± 0.4 a	4.35 ± 0.02 a	12.9 ± 0.7 f
LFF-A/I	71.9 ± 0.2 a	9.8 ± 0.3 b	15.4 ± 0.5 a	3.57 ± 0.04 b	17.6 ± 0.9 c

[a]Means ± standard deviation. Different letters in the same column indicate significant differences ($P < 0.05$). [b]Frankfurter: normal fat (NF-) and low fat (LF-) frankfurter (F) formulated with pork backfat (NFF-PF and LFF-PF) or olive oil bulking agent containing dextrin (NFF-A/D and LFF-A/D) or inulin (NFF-A/I and LFF-A/I) as a fat replacer.

optics on the spectrometer was eliminated by means of Opus 2.2 software Raman correction command (Bruker, Karlsruhe, Germany). Raman spectra were resolved at 4 cm^{-1} resolution with a liquid nitrogen cooled Ge detector. The samples were illuminated by laser power at 300 mW, and the frequencies cited are accurate to ±0.1 cm^{-1}. Analysis of the ratios of the intensities of the Stokes and anti-Stokes Raman bands of the same frequency showed that there was no sample heating by using this laser power.

Spectroscopic Data Analysis To Determine Secondary Protein Structure. The secondary protein structure of meat proteins was determined as follows. First, the water spectrum was subtracted from the spectra following the same criteria as described previously.[21,22] In order to eliminate any spectral influence of lipids in the spectral region characteristic of proteins (800−1800 cm^{-1}), the corresponding spectrum of the heated oil bulking agent (A/D or A/I) was subtracted from the reformulated frankfurters (NFF-A/D, NFF-A/I, LFF-A/D, or LFF-A/I) by zeroing the bending =CH band located close to 1267 cm^{-1}, which is attributed to lipid molecules.[2,23] Similarly, the heated pork backfat spectrum was subtracted from the control (all pork backfat) frankfurters (NFF-PF or LFF-PF) following the same criteria.

The Phe ν-ring band located near 1003 cm^{-1} was used as an internal standard to normalize the spectra as it has been reported to be insensitive to the microenvironment.[13−15] The visible bands were assigned to vibrational modes of peptide backbone or amino acid side chains by comparing Raman spectra of model polypeptides or monographs of Raman spectra of proteins.[13−15] The intensity values of Raman bands from various atomic groups were determined after spectral normalization. Protein secondary structures were determined as percentages of α-helix, β-sheet, turns, and unordered conformations using a parametric method.[21] This method permits the determination of the quantitative secondary structure of proteins by using parameters of the Raman amide I band.[21]

Spectroscopic Data Analysis To Determine Lipid Structure. In order to eliminate any spectral influence of water in the samples in the spectral region 2800−3000 cm^{-1}, the spectral contribution of water was subtracted from the sample spectra.[2,21] The water-free spectra of the samples were then appropriately subtracted using the heated raw meat spectrum, based on elimination of the Phe ν-ring band by means of a subtraction factor so that the intensity of this Raman band near 1003 cm^{-1} is not visible. In this way, spectral influence of protein was eliminated.

Raman spectra were processed using Opus 2.2 (Bruker, Karlsruhe, Germany) and Grams/AI version 9.1 (Thermo Electron Corporation, USA) software. For intensity measurements, baselines were considered as straight lines drawn tangentially between the intensity minima occurring on either side of each band.

Statistical Analysis. One-way analyses of variance (ANOVA) to evaluate the statistical significance ($P < 0.05$) of the effect of formulation and two-way ANOVA as a function of formulation and storage time were performed using SPSS 13.0 (SPSS Inc., Chicago, IL, USA). Least squares differences were used for comparison of mean values among formulations and Tukey's HSD test to identify significant differences ($P < 0.05$) between formulations and storage times. In addition, Pearson product moment correlation (R) was performed to determine the relationships between technological properties (processing loss and texture parameters) and Raman spectroscopy data. These correlation coefficients range between −1 and +1 and measure the strength of the linear relationship between the variables. In this statistical analysis P-value tests the statistical significance of the estimated correlations. P-values below 0.05 indicate statistically significant nonzero correlations at the 95% confidence level. This statistical analysis was carried out using Statgraphics Plus version 5.0. Inc., Chicago, IL, USA).

RESULTS AND DISCUSSION

Proximate Analysis, Processing Loss, and Purge Loss. Proximate analysis of samples (Table 2) was in agreement with the target composition (Table 1). Protein content was similar ($P > 0.05$) in all frankfurters. Low fat frankfurters showed the highest moisture values according to formulation (Table 2). Ash contents varied between 2.79 and 4.42%. All animal fat samples (NFF-PF and LFF-PF) contained the lowest proportion of ash. These results are consistent with the composition of the components used in the preparation of oil bulking agents, which provide higher ($P < 0.05$) ash values in reformulated samples. Fat content ranged between 20.38% and 9.59% (Table 2), and the highest ($P < 0.05$) values were recorded in normal fat frankfurters (NFF-PF, NFF-A/D, and NFF-A/I).

The energy content of the oil bulking agent used to replace pork backfat was about 514 kcal/100 g, while the energy content of the pork backfat was around 810 kcal/100 g. This implies that if this oil bulking agent were used as animal fat replacer in the formulation of meat products, their energy content could be reduced by about 36.5%. In addition, frankfurters formulated with this oil bulking agent, which contain 55% olive oil, included around 13.5 g of olive oil per 100 g of product. These observations indicate that given the nature and composition of the lipid components of the olive oil included in the bulking agent, this approach could also be adopted to improve the fatty acid profiles of meat products.

Processing loss of frankfurters ranged from 12.9 to 22.6% (Table 2). The values of processing loss were highest ($P < 0.05$) in LFF-PF, which was also the sample with the most added water (Table 1). Reported values of processing loss in frankfurters normally oscillate between 10 and 20%.[7,24,25] Samples reformulated with oil bulking agents, both normal (NFF-A/D, NFF-A/I) and low (LFF-A/D and LFF-A/I) fat, showed significantly less processing loss than their respective counterparts (NFF-PF or LFF-PF) formulated with all pork backfat (Table 2). Processing losses were lowest ($P < 0.05$) in normal fat frankfurters prepared with A/D and A/I as pork backfat replacers (NFF-A/D and NFF-A/I), significantly more so in NFF-A/I. In these reformulated frankfurters with the added olive oil bulking agent, these agents encapsulated parts of the water and fat in the product, so that less was released during processing (Table 2). In previous assays cooking loss was found

Table 3. Textural Profile Analysis (TPA) Parameters (Hardness, Springiness, Cohesiveness, Chewiness) of Frankfurters[a] during Chilling Storage[b]

TPA params	samples[a]	days of storage		
		0	45	85
hardness (N)	NFF-PF	27.64 ± 0.40 b1	19.39 ± 0.64 b2	18.98 ± 0.71 a2
	LFF-PF	22.43 ± 0.52 d1	14.54 ± 0.71 d2	16.37 ± 0.80 c3
	NFF-A/D	28.46 ± 0.26 a1	18.85 ± 0.94 b2	19.91 ± 0.85 a2
	LFF-A/D	24.69 ± 0.52 c1	16.41 ± 0.47 c2	17.79 ± 1.05 b2
	NFF-A/I	29.83 ± 0.70 a1	21.42 ± 0.88 a2	19.47 ± 1.06 a2
	LFF-A/I	24.67 ± 0.19 c1	16.61 ± 1.05 c2	16.27 ± 0.85 c2
cohesiveness (dimensionless)	NFF-PF	0.66 ± 0.03 b3	0.73 ± 0.01 d2	0.73 ± 0.00 c1
	LFF-PF	0.69 ± 0.01 a3	0.75 ± 0.01 c2	0.77 ± 0.01 a1
	NFF-A/D	0.69 ± 0.00 a3	0.73 ± 0.01 d2	0.77 ± 0.01 a1
	LFF-A/D	0.70 ± 0.01 a2	0.75 ± 0.01 b1	0.75 ± 0.01 b1
	NFF-A/I	0.69 ± 0.00 a3	0.74 ± 0.01 d2	0.77 ± 0.02 a1
	LFF-A/I	0.69 ± 0.00 a2	0.76 ± 0.01 a1	0.77 ± 0.01 a1
springiness (mm)	NFF-PF	6.66 ± 0.06 b2	7.03 ± 0.04 b1	7.00 ± 0.12 b1
	LFF-PF	6.69 ± 0.02 b2	7.04 ± 0.06 b1	7.08 ± 0.11 b1
	NFF-A/D	6.95 ± 0.04 a2	7.24 ± 0.10 a1	7.18 ± 0.15 a1
	LFF-A/D	6.97 ± 0.05 a2	7.31 ± 0.16 a1	7.20 ± 0.11 a1
	NFF-A/I	6.93 ± 0.07 a3	7.23 ± 0.07 a3	7.30 ± 0.18 a1
	LFF-A/I	7.01 ± 0.05 a2	7.24 ± 0.17 a2	7.40 ± 0.15 a1
chewiness (N × mm)	NFF-PF	121.9 ± 1.3 c1	96.2 ± 1.8 2	97.8 ± 1.3 b2
	LFF-PF	98.9 ± 3.5 e1	75.6 ± 1.5 e3	80.1 ± 1.9 e2
	NFF-A/D	132.5 ± 1.2 a1	99.5 ± 1.4 b2	103.2 ± 1.8 a2
	LFF-A/D	117.3 ± 0.8 d1	90.6 ± 1.0 d3	95.5 ± 1.3 c2
	NFF-A/I	144.1 ± 1.2 a1	114.6 ± 2.4 a2	104.3 ± 2.0 a3
	LFF-A/I	121.3 ± 1.1 c1	88.5 ± 2.7 d2	88.4 ± 1.9 d2

[a]Frankfurter: normal fat (NF-) and low fat (LF-) frankfurter (F) formulated with pork backfat (NFF-PF and LFF-PF) or olive oil bulking agent containing dextrin (NFF-A/D and LFF-A/D) or inulin (NFF-A/I and LFF-A/I) as a fat replacer. [b]Means ± standard deviation. Different letters in the same column indicate significant differences ($P < 0.05$), and different numbers in the same row indicate significant differences ($P < 0.05$).

to be lower in meat batters where fat was replaced by polysaccharide matrices containing olive oil than in samples made with all pork backfat.[2] Similar behavior has been found in other products such as low fat pork batters formulated with animal fat replacers based on polysaccharides such as konjac gel.[26]

Purge loss is associated with unwanted purge accumulation in the packaged product during storage. This accumulation is undesirable for both commercial and microbiological reasons. Results showed that purge loss levels over storage were relatively low (ranging from 0.5 to 1.5%) and similar to those reported by other authors.[7,24,25] This fact was associated with appropriate stability during storage in terms of fat and water binding properties of the new meat derivate. The good stability found was independent of the formulation.

Texture Profile Analysis (TPA). Both types of formulation and chilling storage significantly influenced textural properties. Samples with normal fat content (NFF-PF, NFF-A/D, and NFF-A/I) presented the highest ($P < 0.05$) hardness and chewiness (Table 3). All frankfurters reformulated with oil bulking agents showed the highest ($P < 0.05$) springiness, while there was no significant difference in cohesiveness between samples. This difference in textural properties would appear to be due to two factors, the differences in fat and moisture content, and incorporation of an oil bulking agent as animal fat replacer. In normal fat frankfurters an increase in fat content and a decrease in water (Table 2) will raise the "effective" concentration of the protein that acts to form the gel/emulsion matrix. An increase in protein concentration generally entails the formation of a denser and more compact protein matrix,[27,28] a structure associated with harder products in normal fat samples (Table 3). The incorporation of fat replacers also seems to have affected the texture. Reformulated frankfurters containing a fat replacer, irrespective of fat content, produced stronger structures with higher ($P < 0.05$) hardness and chewiness values (Table 3). Given similar compositions (and the same fat level), the differences in hardness and chewiness were presumably attributable to the bulking agent, which should facilitate the formation of a gel/emulsion matrix in the samples, so that samples should be harder/firmer. Previous results indicated that meat products reformulated using fat replacers based on a mixed konjac/gellan gum gel,[29] oil in a konjac glucomannan matrix,[7] or pre-emulsified oils were more firm than those formulated with pork backfat.[17,24,25,30,31]

In general, the TPA parameters were affected ($P < 0.05$) by chilling storage (Table 3). However, no clear relationship was identified between these changes in texture during storage and the type of sample (Table 3). Results showed a significant decrease of hardness and chewiness and an increase ($P < 0.05$) of cohesiveness and springiness in all samples during chilling storage (Table 3). Previous studies have detected similar texture behavior in frankfurters formulated with emulsified oils as fat replacers.[25]

FT-Raman Spectroscopic Analysis. *Protein Structure.* Figure 1 shows representative Raman spectra in the 950−1800 cm^{-1} region from normal fat frankfurters (NFF-PF, NFF-A/D, and NFF-A/I), following elimination of the spectral influence of water and lipids (see Materials and Methods).

Amide III Band. This Raman band includes C−N stretching and N−H in-plane bending vibrations of the peptide bond.

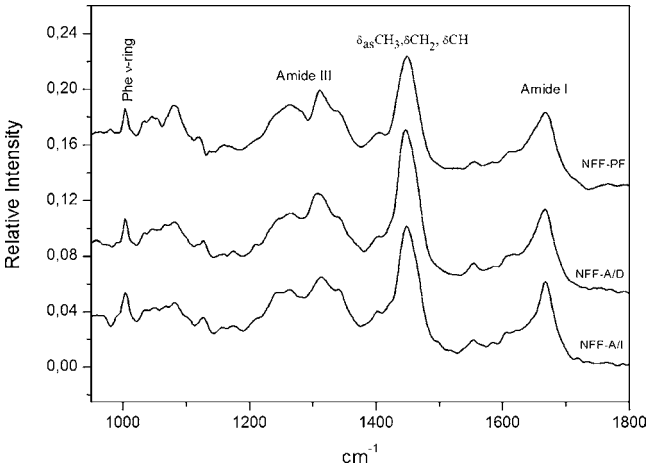

Figure 1. Raman spectra in the 950−1800 cm^1 region from the normal fat frankfurters with pork backfat (NFF-PF) or olive oil bulking agent containing alginate (A) and dextrin (NFF-A/D) or inulin (NFF-A/I) as a fat replacer.

Contributions from Cα−C stretching and C═O in-plane bending[13−15] were also detected (Figure 1). The amide III band provides information about the secondary structure of proteins. The amide III band in the spectra comprises a complex pattern of bands in the 1225−1350 cm^{-1} range (Figure 1) and for that reason is difficult to interpret.

Amide I Band. Figure 1 shows the amide I band, which offers valuable information about protein secondary structure.[13−15] The amide I band comprises mainly C═O stretching and, to a lesser extent, N−H in-plane bending of peptide groups.[13−15] In all spectra the amide I band was analyzed to elucidate the structural changes occurring in the meat protein due to the use of an olive oil bulking agent as pork backfat replacer. Figure 2 shows the amide I region (1620−1720 cm^{-1}) from the different frankfurters in detail. The alterations of frequency and intensity in this band revealed mainly changes in the secondary structure of meat proteins and variations in local environments. The highest frequency values were recorded in normal fat frankfurter when compared with the low fat one, both in control and in reformulated samples (NFF-PF, NFF-A/D, and NFF-A/I) (Figure 2). Some frequency upshifting from 1667.8 to 1668.3 cm^{-1} was detected, particularly in normal fat samples containing the oil bulking agent with inulin (Figure 2). This result may be related to increased β-sheet structure content in the meat protein in NFF-A/I. When the amide I bands of LFF-PF and reformulated frankfurters (LFF-A/D and LFF-AI) were compared, shifts of the frequency maximum from 1665.7 to 1666.1 cm^{-1} in LFF-A/D and from 1665.7 to 1667.2 cm^{-1} in LFF-A/I (Figure 2) were observed. These frequency upshifts are related to increased β-sheet structure content in the meat protein due to the use of a pork backfat replacer in the low fat frankfurters. As in the case of normal fat frankfurters, this effect was more pronounced in samples where the oil bulking agent contained inulin.

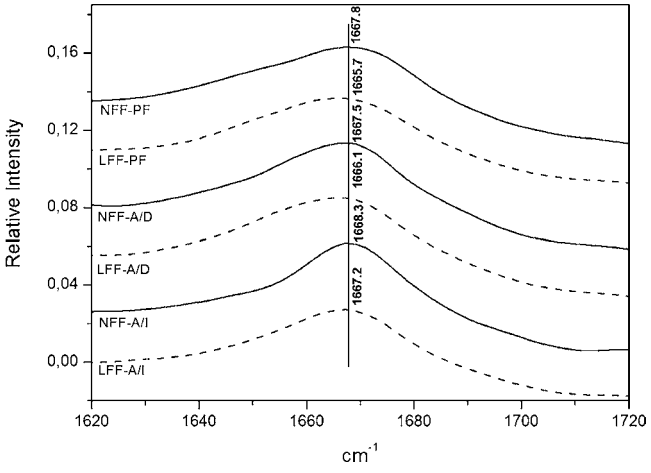

Figure 2. Raman spectra in the 1620−1720 cm^{-1} region from frankfurters formulated as normal fat (NFF-) and low fat (LFF-) formulated with pork backfat (NFF-PF and LFF-PF) or olive oil bulking agent containing alginate (A) and dextrin (NFF-A/D and LFF-A/D) or inulin (NFF-A/I and LFF-A/I) as a fat replacer.

Quantitative Percentages of Secondary Structure. In depth examination of amide I spectra profiles offered quantitative information about the percentages of secondary structure in the different frankfurters (Table 4). In general, values of α-helix content were lowest ($P < 0.05$) in normal fat frankfurters. Quantitative results of protein secondary structure confirm that β-sheet content was higher ($P < 0.05$) in normal than in low fat frankfurters, either control or reformulated. Among the normal fat frankfurters, β-sheet content was higher ($P < 0.05$) in samples reformulated with oil bulking agents as fat replacers (NFF-A/D and NFF-A/I) and highest ($P < 0.05$) of all in the sample with inulin in the oil bulking agent (NFF-A/I) (Table 4). Similar results were found when only low fat frankfurters were compared. β-Sheet content was significantly higher in LFF-A/D and LFF-A/I, with the highest values ($P < 0.05$) in the samples containing inulin in the oil bulking agent. These structural results were consistent with previous studies indicating that the use of animal fat replacers like olive oil bulking agents in meat batters, or oil-in-water emulsions in frankfurters, produces an increase in β-sheet structure.[2,32,33] The presence of aggregated intermolecular β-sheets in frankfurters has been associated with the formation of a compact network imparting more firmness.[2,17,32,33] These findings are consistent with our results (Tables 3 and 4). The formation of intermolecular β-sheets may result from the self-aggregation of the proteins. Studies of FT-Raman indicated the effect of modified celluloses, pectins, and NaCl on the secondary structure of gluten proteins. In general, a decrease in α-helix conformation and an increase in less ordered structures were observed with the addition of hydrocolloids.[34] It has been reported that certain systems based on mixes of milk proteins such as whey protein concentrate and sodium alginate were distinguished by a tendency to protein aggregation.[35] Interactions among muscle proteins and hydrocolloids, reflected in an enhancement of hydrogen bonding, have been suggested.[36]

The structural results show that, regardless of fat content, turn content was lowest ($P < 0.05$) in reformulated frankfurter, while differences among samples in term of unordered structure were nonsignificant.

Table 4 shows a decrease ($P < 0.05$) in β-sheet structure, in general accompanied by an increase in turn content at 85 days of chilled storage, while the rest of the protein secondary structure parameters (α-helix and unordered) remained constant throughout storage.

Relationship between Protein Structure and Technological Properties. Results showed that reformulation-induced changes in the secondary structure of meat protein were

dx.doi.org/10.1021/jf501231k | J. Agric. Food Chem. 2014, 62, 5963−5971

Table 4. Percentages of Protein Secondary Structure (α-Helix, β-Sheet, Turns, and Unordered) of Frankfurters during Chilling Storage[a]

protein secondary structure params (%)	samples[b]	days of storage		
		0	45	85
α-helix	NFF-PF	26.7 ± 0.6 d12	25.5 ± 0.8 c2	26.9 ± 0.79 b1
	LFF-PF	29.0 ± 0.5 b1	29.5 ± 0.7 a1	30.0 ± 0.8 a1
	NFF-A/D	26.5 ± 0.5 d1	27.4 ± 0.9 b1	27.2 ± 0.8 b1
	LFF-A/D	30.2 ± 0.6 a12	29.0 ± 0.7 a2	30.5 ± 0.5 a1
	NFF-A/I	27.9 ± 0.7 c1	27.6 ± 0.8 b1	27.4 ± 0.6 b1
	LFF-A/I	27.7 ± 0.9 c1	28.6 ± 0.5 ab1	27.9 ± 0.8 b1
β-sheet	NFF-PF	40.5 ± 0.8 d1	39.4 ± 0.6 12	38.6 ± 0.5 b2
	LFF-PF	36.7 ± 0.7 f1	37.0 ± 0.4 d1	35.3 ± 0.8 c2
	NFF-A/D	43.1 ± 0.6 b1	43.4 ± 0.7 a1	40.3 ± 0.6 a2
	LFF-A/D	38.5 ± 0.5 e1	39.1 ± 0.6 1	37.5 ± 0.4 b2
	NFF-A/I	45.6 ± 0.6 a1	43.4 ± 0.5 b2	41.2 ± 0.5 a3
	LFF-A/I	41.9 ± 0.7 c1	37.3 ± 0.7 d2	37.5 ± 0.7 b2
turn	NFF-PF	20.1 ± 1.6 b1	22.5 ± 1.2 b12	22.4 ± 1.4 b2
	LFF-PF	21.8 ± 1.2 b1	21.2 ± 1.6 b1	21.8 ± 1.1 b1
	NFF-A/D	18.3 ± 1.4 a1	19.3 ± 1.0 a1	19.9 ± 1.5 a12
	LFF-A/D	18.8 ± 1.5 a1	19.5 ± 1.2 a1	19.8 ± 1.1 a12
	NFF-A/I	16.2 ± 1.9 a1	16.9 ± 1.7 a1	18.6 ± 1.8 a2
	LFF-A/I	18.0 ± 1.5 a1	20.2 ± 1.2 a1	20.8 ± 1.5 a2
unordered	NFF-PF	12.7 ± 1.1 a1	12.6 ± 1.0 a1	12.1 ± 1.3 a1
	LFF-PF	12.5 ± 0.9 a1	12.3 ± 1.1 a1	12.9 ± 0.9 a1
	NFF-A/D	12.1 ± 1.2 a1	11.9 ± 1.4 a1	12.6 ± 0.8 a1
	LFF-A/D	12.5 ± 0.8 a1	12.1 ± 1.0 a1	12.5 ± 1.3 a1
	NFF-A/I	10.3 ± 2.2 a1	12.1 ± 0.9 a1	12.8 ± 1.0 a1
	LFF-A/I	12.4 ± 1.1 a1	13.9 ± 1.7 a1	13.8 ± 0.9 a1

[a]Means ± standard deviation. Different letters in the same column indicate significant differences ($P < 0.05$). [b]Frankfurter: normal fat (NF-) and low fat (LF-) frankfurter (F) formulated with pork backfat (NFF-PF and LFF-PF) or olive oil bulking agent containing dextrin (NFF-A/D and LFF-A/D) or inulin (NFF-A/I and LFF-A/I) as a fat replacer.

accompanied by changes in processing loss and texture. Thus, a correlation was found between processing loss and β-sheet ($R = -0.81$, $P < 0.0005$) and turn ($R = 0.74$, $P < 0.0005$) content. These correlations seem to indicate that in these types of meat products processing loss could be due to a specific meat protein structure in terms of β-sheet and turn content.

In addition, the results showed a positive correlation between β-sheet structure and hardness ($R = 0.77$, $P < 0.05$) and chewiness ($R = 0.92$, $P < 0.005$). There was also a negative correlation between turn and hardness ($R = -0.86$, $P < 0.005$) and chewiness ($R = -0.92$, $P < 0.005$). These findings indicate that reformulation-induced modifications in protein secondary structure could affect textural properties of the final meat product. Previous studies have reported a similar correlation between β-sheet content and hardness in frankfurters prepared with an olive oil-in-water emulsion.[32,33] Similarly, a positive correlation has been reported between β-sheet structures and textural behavior in meat products prepared with different lipids (pork fat, soybean oil, and dairy butter).[17] In particular, meat batters reformulated with soybean presented greater hardness, springiness, cohesiveness, chewiness, and resilience than meat batters made with pork fat or butter. These specific textural properties were accompanied by an increase of β-sheet structures.[17] This is consistent with the observation of increases of hardness associated with increases in β-sheet and turn structure in meat systems to which cold-set binding systems such as transglutaminase or fibrinogen/thrombin from porcine blood plasma have been added.[37,38]

Lipid Structure. In the Raman spectra obtained after removing the water and protein spectral contribution (see Materials and Methods), the 2800−3025 cm^{-1} region was studied to elucidate the lipid structure (Figure 3). This region contained bands that are characteristic of symmetric and asymmetric C−H stretching vibrations of methyl and methylene groups in aliphatic molecules.[23,39] There were prominent bands: a CH_2 asymmetric stretching band at 2897 cm^{-1}, a CH_3 symmetric stretching band at 2931 cm^{-1}, and a

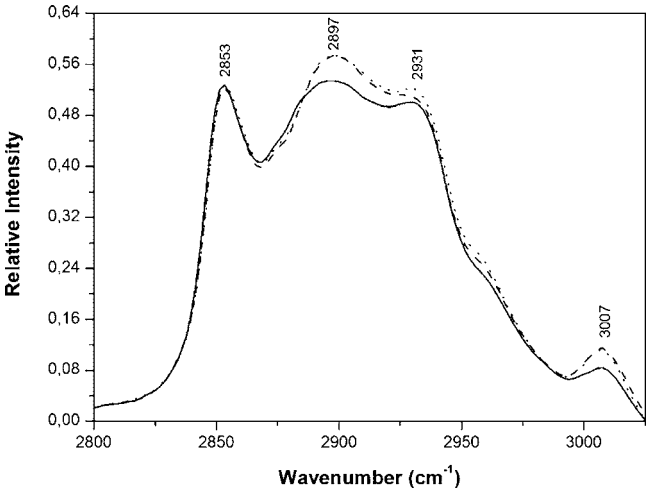

Figure 3. Raman spectra in the 2800−3025 cm^{-1} region from the low fat frankfurters with pork backfat (LFF-PF) (solid line) or olive oil bulking agent containing alginate (A) and dextrin (LFF-A/D) (dashed line) or inulin (LFF-A/I) (dotted line) as a fat replacer.

dx.doi.org/10.1021/jf501231k | J. Agric. Food Chem. 2014, 62, 5963−5971

Table 5. Relative Intensity of $I\nu_sCH_2/I\nu_{as}CH_2$ and $I\nu_sCH_3/I\nu_{as}CH_3$ of Frankfurters during Chilling Storage[a]

		days of storage		
	samples[b]	0	45	85
$I\nu_sCH_2/I\nu_{as}CH_2$	NFF-PF	0.94 ± 0.01 a1	0.93 ± 0.04 ab1	0.93 ± 0.01 b1
	LFF-PF	0.99 ± 0.05 b1	1.05 ± 0.01 a1	1.02 ± 0.03 a1
	NFF-A/D	0.91 ± 0.02 c1	0.90 ± 0.04 ab1	0.92 ± 0.01 bc1
	LFF-A/D	0.90 ± 0.03 c1	0.93 ± 0.05 ab1	0.89 ± 0.02 bc1
	NFF-A/I	0.89 ± 0.02 c1	0.85 ± 0.03 b2	0.88 ± 0.03 c2
	LFF-A/I	0.91 ± 0.01 c1	0.92 ± 0.02 ab1	0.83 ± 0.04 d1
$I\nu_{as}CH2/I\nu_sCH_3$	NFF-PF	1.12 ± 0.03 a1	1.13 ± 0.02 a1	1.15 ± 0.02 a1
	LFF-PF	1.08 ± 0.04 a1	1.11 ± 0.03 a1	1.14 ± 0.05 a1
	NFF-A/D	1.14 ± 0.02 a1	1.11 ± 0.01 a1	1.15 ± 0.03 a1
	LFF-A/D	1.13 ± 0.01 a12	1.15 ± 0.02 a1	1.13 ± 0.02 a1
	NFF-A/I	1.12 ± 0.03 a1	1.13 ± 0.02 a1	1.14 ± 0.03 a1
	LFF-A/I	1.11 ± 0.04 a1	1.12 ± 0.03 a1	1.11 ± 0.01 a1

[a]Means ± standard deviation. Different letters in the same column indicate significant differences ($P < 0.05$). [b]Frankfurter: normal fat (NF-) and low fat (LF-) frankfurter (F) formulated with pork backfat (NFF-PF and LFF-PF) or olive oil bulking agent containing dextrin (NFF-A/D and LFF-A/D) or inulin (NFF-A/I and LFF-A/I) as a fat replacer.

CH_2 symmetric stretching motion near 2853 cm^{-1} (Figure 3). Another Raman band at 3007 cm^{-1} attributable to *cis*-olefinic group =C−H stretching vibration is clearly visible.

Intensity Ratios $I\nu_sCH_2/I\nu_{as}CH_2$ and $I\nu_{as}CH_2/I\nu_sCH_3$. It has been reported that the peak height intensity ratios $I\nu_sCH_2/I\nu_{as}CH_2$ (I_{2850}/I_{2880}) and $I\nu_{as}CH_2/I\nu_sCH_3$ (I_{2880}/I_{2935}) are valuable references for gauging lipid packing effects and determining relative order/disorder of the intermolecular lipid chain.[40] In particular, the $I\nu_sCH_2/I\nu_{as}CH_2$ index reflects primarily interchain interactions whereas the $I\nu_{as}CH_2/I\nu_sCH_3$ intensity ratio evaluates effects resulting from modifications in intrachain trans/gauche isomerization superimposed on the chain−chain interactions. Intensity ratio $I\nu_{as}CH_2/I\nu_sCH_3$ was similar ($P < 0.05$) for all samples (Table 5). However, the intensity ratio values $I\nu_sCH_2/I\nu_{as}CH_2$ were lowest ($P < 0.05$) in frankfurter reformulated with olive oil bulking agent as pork backfat replacer (Table 4). These significant differences indicate that there was more lipid acyl chain disorder in frankfurters containing oil bulking agents than in samples made with animal fat, regardless of the fat content. There are a number of mechanisms that may explain fat stabilization in gel/emulsion meat products like frankfurters.[41] An "emulsion theory" has been proposed to the effect that a thin layer of myofibrillar proteins forms around the fat globules. The hypothesis assumes that this is accompanied by physical entrapment so that fat globules are stabilized within a gelled protein matrix.[41] On that assumption, the higher lipid chain disorder observed in frankfurters formulated with an oil bulking agent could be due to the fact that in reformulated samples more meat protein chains can be inserted between the acyl chains of the olive oil bulking agent than in control normal and low fat frankfurters containing pork backfat. This would imply more lipid−protein interactions in the reformulated products, which in turn implies more lipid acyl chain disorder (Table 4). Similar behavior has been found in meat batters in which oil bulking agents containing polysaccharide gels were used as fat replacers.[2] In general, $I\nu_sCH_2/I\nu_{as}CH_2$ and $I\nu_{as}CH_2/I\nu_sCH_3$ were not significantly affected by chilling storage (Table 4).

Relationship between Lipid Structure and Technological Properties. The possible relationship between lipid structure and processing loss and texture was also evaluated. Results showed that the observed changes in lipid structure due to the use of an olive oil bulking agent as pork backfat replacer were accompanied by changes in processing loss and textural properties of frankfurters. Thus, a positive significant correlation ($R = 0.80$; $P < 0.05$) was found between processing loss and intensity ratios $I\nu_sCH_2/I\nu_{as}CH_2$ related to lipid acyl chain order/disorder. This correlation suggests that disordering in oil acyl chains or lipid−protein interaction as a result of reformulation could affect the water and fat binding properties of the final meat product. In addition, order/disorder of lipid acyl chain correlated negatively or inversely with hardness ($R = -0.73$, $P < 0.005$) and chewiness ($R = -0.81$, $P < 0.05$).

The reformulation strategy employed could be used to reduce the energy content and improve the fat content of frankfurters. The implications of this study are that technological and structural characteristics of proteins and lipids were affected by the incorporation in frankfurters of olive oil bulking agent based on polysaccharides and cold-set binding agent like alginate as animal fat replacers. This reformulation process reduced processing loss while increasing hardness and chewiness of the frankfurters. The behavior of samples during chilling storage in terms of the technological properties considered was similar in all products regardless of the formulation.

Raman spectroscopy provided useful information on secondary protein structures in terms of enrichment of β-sheet structure, which was more pronounced in frankfurters containing inulin in the oil bulking agent. The high presence of aggregated intermolecular β-sheets in frankfurters suggests the formation of a denser network producing greater hardness. In addition a reduction in turn content was observed in response to reformulation.

In relation to how lipid structure was affected by this reformulation process, we should stress that it caused increased lipid acyl chain disorder, which involved more lipid−protein interactions when an oil bulking agent was used as a pork backfat replacer.

This study presented further advances in terms of how these reformulation processes influence the structures of the principal component proteins and lipids in these meat products, and how this affects the technological properties of the final meat product. This information can be helpful in improving these conditions and hence could be valuable for the development and formulation of healthier-lipid meat products. In addition, these correlations could be decisive for understand the

implications of both protein and lipid interactions in specific functional or technological properties such as texture or processing loss, which are very important for the acceptance of consumer.

AUTHOR INFORMATION

Corresponding Author

*Phone:+34 915616800. Fax: +34 91 5645557. E-mail: ana.herrero@ictan.csic.es.

Funding

This research was supported by projects AGL2010-19515 and AGL2011-29644-C02-01.

Notes

The authors declare no competing financial interest.

REFERENCES

(1) Jiménez-Colmenero, F. Healthier lipid formulation approaches in meat-based functional foods. Technological options for replacement of meat fats by non-meat fats. *Trends Food Sci. Technol.* **2007**, *18*, 567−578.

(2) Ruiz-Capillas, C.; Carmona, P.; Jiménez-Colmenero, F.; Herrero, A. M. Oil bulking agents based on polysaccharide gels in meat batters: A Raman spectroscopic study. *Food Chem.* **2013**, *141*, 3688−3694.

(3) Herrero, A. M.; Carmona, P.; Jiménez-Colmenero, F.; Ruiz-Capillas, C. Polysaccharide gels as oil bulking agents: Technological and structural properties. *Food Hydrocolloids* **2014**, *36*, 374−381.

(4) Triki, M.; Herrero, A. M.; Rodríguez-Salas, L.; Jiménez-Colmenero, F.; Ruiz-Capillas, C. Chilled storage characteristics of low-fat, n-3 PUFA-enriched dry fermented sausage reformulated with a healthy oil combination stabilized in a konjac matrix. *Food Control* **2013**, *31*, 158−165.

(5) Jiménez-Colmenero, F.; Triki, M.; Herrero, A. M.; Rodríguez-Salas, L.; Ruiz-Capillas, C. Healthy oil combination stabilized in a konjac matrix as pork fat replacement in low-fat, PUFA-enriched, dry fermented sausages. *LWT—Food Sci. Technol.* **2013**, *51*, 158−163.

(6) Triki, M.; Herrero, A. M.; Jiménez-Colmenero, F.; Ruiz-Capillas, C. Effect of preformed konjac gels, with and without olive oil, on the technological attributes and storage stability of merguez sausage. *Meat Sci.* **2013**, *93*, 351−360.

(7) Salcedo-Sandoval, L.; Cofrades, S.; Ruiz-Capillas, C.; Solas, M. T.; Jiménez-Colmenero, F. Healthier oils stabilized in konjac matrix as fat replacers in n − 3 PUFA enriched frankfurters. *Meat Sci.* **2013**, *93*, 757−766.

(8) Raynes, J. K.; Carver, J. A.; Gras, S. L.; Gerrard, J. A. Protein nanostructures in food—should we be worried?. *Trends Food Sci. Technol*. http://dx.doi.org/10.1016/j.tifs.2014.02.003.2014.

(9) Fernandez-Gines, J. M.; Fernandez-Lopez, J.; Sayas-Barbera, E.; Perez-Alvarez, J. A. Meat products as functional foods: a review. *J. Food Sci.* **2005**, *70*, R37−R43.

(10) Pedersen, D. K.; Morel, S.; Andersen, H. J.; Engelsen, S. B. Early prediction of water-holding capacity in meat by multivariate vibrational spectroscopy. *Meat Sci.* **2003**, *65*, 581−592.

(11) Böcker, U.; Ofstad, R.; Wu, Z.; Bertram, H. C.; Sockalingum, G.; Manfait, M.; Egelandsdal, B.; Kohler, A. Revealing covariance structures in FT-IR and Raman microspectroscopy spectra—A study on pork muscle fiber tissue subjected to different processing parameters. *Appl. Spectrosc.* **2007**, *61*, 1032−1039.

(12) Damez, J. L.; Clerjon, S. Meat quality assessment using biophysical methods related to meat structure. *Meat Sci.* **2008**, *80*, 132−149.

(13) Herrero, A. M. Raman spectroscopy a promising technique for quality assessment of meat and fish: A review. *Food Chem.* **2008**, *107*, 1642−1651.

(14) Herrero, A. M. Raman spectroscopy for monitoring protein structure in muscle food systems. *Crit. Rev. Food Sci.* **2008**, *48*, 512−523.

(15) Herrero, A. M.; Carmona, P.; Jiménez-Colmenero, F.; Ruiz-Capillas, C. Applications of vibrational spectroscopy to study protein structural changes in muscle and meat batter systems. In *Applications of vibrational spectroscopy to food science*; Chalmers, J., Griffiths, P., Li-Chan, E. Y. C., Eds.; John Wiley & Sons: West Sussex, U.K., 2010; pp 315−328.

(16) Yang, D. T.; Ying, Y. B. Applications of Raman spectroscopy in agricultural products and food analysis: a review. *Appl. Spectrosc. Rev.* **2011**, *46*, 539−560.

(17) Shao, J. H.; Zou, Y. F.; Xu, X. L.; Wu, J. Q.; Zhou, G. H. Evaluation of structural changes in raw and heated meat batters prepared with different lipids using Raman spectroscopy. *Food Res. Int.* **2011**, *44*, 2955−2961.

(18) AOAC. *Official Methods of Analysis of AOAC International*, 17th ed.; Association of Official Analytical Chemistry: Gaithersburg, MD, 2000.

(19) Bligh, E. G.; Dyer, W. J. A rapid method of total lipid extraction and purification. *Can. J. Biochem. Phys.* **1959**, *37*, 911−917.

(20) Bourne, M. C. Texture profile analysis. *Food Technol.* **1978**, *32*, 62−65.

(21) Alix, A. J. P.; Pedanou, G.; Berjot, M. Fast determination of the quantitative secondary structure of proteins by using some parameters of the Raman amide I band. *J. Mol. Struct.* **1988**, *174*, 159−164.

(22) Herrero, A. M.; Carmona, P.; López-López, I.; Jiménez-Colmenero, F. Raman spectroscopic evaluation of meat batter structural changes induced by thermal treatment and salt addition. *J. Agric. Food Chem.* **2008**, *56*, 7119−7124.

(23) Zou, M. Q.; Zhang, X. F.; Qi, X. H.; Ma, H. L.; Dong, Y.; Liu, C. W.; Guo, X.; Wang, H. Rapid authentication of olive oil adulteration by Raman spectrometry. *J. Agric. Food Chem.* **2009**, *57*, 6001−6006.

(24) Paneras, E. D.; Bloukas, J. G. Vegetable-oils replace pork backfat for low-fat frankfurters. *J. Food Sci.* **1994**, *59*, 725−728.

(25) Delgado-Pando, G.; Cofrades, S.; Ruiz-Capillas, C.; Jiménez-Colmenero, F. Healthier lipid combination as functional ingredient in sensory and technological properties of low-fat frankfurters. *Eur. J. Lipid Sci. Technol.* **2010**, *112*, 859−870.

(26) Fernández-Martín, F.; López-López, I.; Cofrades, S.; Jiménez Colmenero, F. Influence of adding Sea Spaghetti seaweed and replacing the animal fat with olive oil or a konjac gel on pork meat batter gelation. Potential protein/alginate association. *Meat Sci.* **2009**, *83*, 209−217.

(27) Carballo, J.; Fernández, P.; Barreto, G.; Solas, M. T.; Jiménez Colmenero, F. Morphology and texture of bologna sausage containing different levels of fat, starch and egg white. *J. Food Sci.* **1996**, *61*, 652−655.

(28) Jiménez Colmenero, F.; Carballo, J.; Solas, M. T. The effect of use of freeze-thawed pork on properties of bologna sausage with two fat levels. *Int. J. Food Sci. Technol.* **1995**, *30*, 335−346.

(29) Lin, K. W.; Huang, H. Y. Konjac/gellan gum mixed gels improve the quality of reduced-fat frankfurters. *Meat Sci.* **2003**, *65*, 749−755.

(30) Jiménez-Colmenero, F.; Herrero, A. M.; Pintado, T.; Solas, M. T.; Ruiz-Capillas, C. Influence of emulsified olive oil stabilizing system used for pork backfat replacement in frankfurters. *Food Res. Int.* **2010**, *43*, 2068−2076.

(31) Youssef, M. K.; Barbut, S. Fat reduction in comminuted meat products effects of beef fat, regular and pre-emulsified canola oil. *Meat Sci.* **2011**, *87*, 356−360.

(32) Carmona, P.; Ruiz-Capillas, C.; Jiménez-Colmenero, F.; Pintado, T.; Herrero, A. M. Infrared study of structural characteristics of frankfurter formulated with olive oil-in-water emulsion stabilized with casein as pork backfat replacer. *J. Agric. Food Chem.* **2011**, *59*, 12998−13003.

(33) Herrero, A. M.; Carmona, P.; Pintado, T.; Jiménez-Colmenero, F.; Ruíz-Capillas, C. Infrared spectroscopic analysis of structural features and interactions in olive oil-in-water emulsions stabilized with soy protein. *Food Res. Int.* **2011**, *44*, 360−366.

(34) Correa, M. J.; Ferrer, E.; Añón, M. C.; Ferrero, C. Interaction of modified celluloses and pectins with gluten proteins. Interaction of

modified celluloses and pectins with gluten proteins. *Food Hydrocolloids* **2014**, *35*, 91−99.
(35) Pereza, A. A.; Carrara, C. R.; Carrera Sánchez, C.; Rodríguez Patino, J. M.; Santiago, L. G. Interactions between milk whey protein and polysaccharide in solution. *Food Chem.* **2009**, *116*, 104−113.
(36) Yu, X.; Chen, C.; Cai, K.; Zhou, C.; Mao, D.; Sun, G. Combined effects of blood plasma powder, agar, and microbial transglutaminase on physicochemical and textural properties of pork muscle gels. *Food Sci. Biotechnol.* **2012**, *21*, 941−950.
(37) Herrero, A. M.; Cambero, M. I.; Ordóñez, J. A.; de la Hoz, L.; Carmona, P. Plasma powder as cold-set binding agent for meat system: Rheological and Raman spectroscopy study. *Food Chem.* **2009**, *113*, 493−499.
(38) Herrero, A. M.; Cambero, M. I.; Ordoñez, J. A.; de la Hoz, L.; Carmona, P. Raman spectroscopy study of the structural effect of microbial transglutaminase on meat systems and its relationship with textural characteristics. *Food Chem.* **2008**, *109*, 25−32.
(39) Muik, B.; Lendl, B.; Molina-Díaz, A.; Ayora-Cañada, M. J. Direct monitoring of lipid oxidation in edible oils by Fourier transform Raman spectroscopy. *Chem. Phys. Lipids* **2005**, *134*, 173−182.
(40) Levin, I. W.; Lewis, E. N. Fourier transform Raman spectroscopy of biological materials. *Anal. Chem.* **1990**, *62*, 1101A−1111A.
(41) Gordon, A.; Barbut, S. Mechanisms of meat batter stabilization:a review. *Crit. Rev. Food Sci.* **1992**, *32*, 299−332.

JOURNAL OF AGRICULTURAL AND FOOD CHEMISTRY

Article

pubs.acs.org/JAFC

Effect of Nitric Oxide on μ-Calpain Activation, Protein Proteolysis, and Protein Oxidation of Pork during Post-Mortem Aging

Yu-pin Li,[†] Rui Liu,[†] Wan-gang Zhang,*[,†] Qing-quan Fu,[‡] Nian Liu,[†] and Guang-hong Zhou[†]

[†]Lab of Meat Processing and Quality Control of EDU, College of Food Science and Technology, Synergetic Innovation Center of Food Safety and Nutrition, Nanjing Agriculture University, Nanjing, Jiangsu 210095, China

[‡]School of Biochemical and Environmental Engineering, Nanjing Xiaozhuang University, Nanjing, Jiangsu 211171, China

ABSTRACT: The aim of the current research was to examine the influence of nitric oxide (NO) on calpain activation, protein proteolysis, and oxidation in post-mortem pork. Five longissimus muscles were removed from carcass after slaughter, and samples were incubated with water, nitric oxide synthase (NOS) inhibitor, or NO donor for 24 h at 4 °C. The samples were taken out and then stored under 4 °C for 1, 4, and 7 d. Results showed that autolysis of μ-calpain increased by incubation with NOS inhibitor after storage for 1 d ($P < 0.05$). Degradation of titin and nebulin increased by treatment of NOS inhibitor among three treatments ($P < 0.05$). Higher levels of protein oxidation were observed after samples incubated with NO donor than treatment of NOS inhibitor ($P < 0.05$). These data indicated that NO could participate in regulating calpain activation and its proteolysis activity during post-mortem aging.

KEYWORDS: *nitric oxide, calpain, post-mortem proteolysis, protein oxidation*

INTRODUCTION

Protein *S*-nitrosylation, which is the thiol site of protein cysteine modified by a nitric oxide (NO) group, has many functions in diverse biological processes. However, whether NO and protein *S*-nitrosylation could affect meat quality during post-mortem aging remains to be unknown. Few studies have shown that fresh meat quality could be affected by the level of NO preslaughter[1] or postslaughter.[2,3] Changed meat quality might have a relationship with the modification of calpain by nitric oxide. However, no studies have focused on the influences of NO and protein *S*-nitrosylation on calpain activation and its proteolysis activity of pork during post-mortem aging.

It is well-known that early post-mortem biochemical and biophysical processes, especially protein degradation, could contribute to the variation of water-holding capacity and tenderness of pork. Many proteins that are involved in meat quality have been shown to be susceptible substrates of the cysteine protease calpain. Among the calpain system, μ-calpain is the main protease for the protein proteolysis during post-mortem aging.[4] The 80 kDa catalytic subunit of μ-calpain contains four domains in which the catalytic domain II contains an active cysteine residue at position 115.[5] Because μ-calpain has an active cysteine residue, it is very sensitive to oxidation and nitrosylation modification. The disulfide bond, which was formed between Cys108 and Cys115 within domain II of μ-calpain, was shown to inhibit its activity and autolysis upon exposure to an oxidating environment.[6] The activity of μ-calpain was changed slightly after treatment with nitric oxide enhancer under neutral pH. However, it turned out that 80% of its activity could be inhibited when the pH was shifted to 5.5.[7] This is particularly important, because pH declines from near neutral pH in living muscle to approximately 5.3−5.7 in normal pork.[8]

NO is generated when arginine is converted to citrulline with the catalysis of nitric oxide synthase (NOS). Brannan and Decker[9] investigated the NOS activity in post-mortem muscle and found that the pork diaphragm still showed NOS activity after 24 h aging. The activity of NOS was stable when the pH was in the range from 4.5 to 7.4, indicating that the generation of nitric oxide could not be influenced by post-mortem pH decline in skeletal muscle after slaughter. However, no study has been aimed to examine the influence of NO on protein modification in post-mortem pork by managing NOS activity. The objective of the current experiment was to examine the role of NO and NO-induced protein *S*-nitrosylation in regulating μ-calpain, its proteolytic activity, and protein oxidation during post-mortem storage.

MATERIALS AND METHODS

Samples and Treatment. Five 6-month-old crossbred pigs with live weight 100 ± 10 kg were slaughtered at Sushi Meat Co. in Huaian of Jiangsu Province. The longissimus muscle was removed from porcine carcasses after slaughter and then randomly dissected into small pieces (0.2 g/piece). The samples were randomly divided into one of three groups: control group containing deionized distilled water, NOS inhibitor group containing 0.1 M Nw-nito-L-arginine methyl ester hydrochloride (L-NAME, Sigma, MO), or NO donor group containing 1 mM diethylenetriamine/nitric oxide adduct (DETA/NO, Sigma, MO). DETA/NO is a NO generating agent. The ratio of meat and solution (w/v) was 1:1. The samples were kept for 24 h at 4 °C. After incubation, the samples were taken out from the solution and stored for 1, 4, or 7 d at 4 °C under vacuum package. The samples were kept at −80 °C for further analysis.

Sarcoplasmic Protein Extraction. Sarcoplasmic protein from the samples was prepared at 4 °C as in the description of Veiseth et al.[10] Ground muscle from the samples was homogenized with polytron (IKA T25 digital ultraturrox Made in IKA, German) twice at 15 000 rpm for 15 s. 0.5 g of the samples was homogenized with 6 volumes (w/v) of

Received: March 18, 2014
Revised: June 9, 2014
Accepted: June 9, 2014
Published: June 9, 2014

ACS Publications © 2014 American Chemical Society

solutions containing 10 mM EDTA, 100 mM Tris-HCl, and 0.1% β-mercaptoethanol (MCE) (v/v) (pH 8.3). After centrifugation under 4 °C at the speed of 15 000*g* for 30 min, the collected supernatant was utilized for concentration measurement using BCA Protein Assay Kit (Thermo, RD, U.S.). The concentration was adjusted to 6.4 mg/mL with ddH_2O. The samples were mixed with tracking dye buffer (30 mM Tris-HCl, 20% glycerol [v/v], 3% SDS [w/v], 3 mM EDTA, and 0.003% pyronin-Y [w/v], pH 8.0) with the ratio of 2:1 (v/v). Final protein concentration for gel sample was 4 mg/mL with 6.25% MCE. The samples of the sarcoplasmic protein were heated at 50 °C (20 min) and were kept in frozen storage.

Myofibrillar Protein Preparation. Myofibrillar proteins were extracted using the method of Etlinger et al.[11] One gram samples were homogenized with 7.5 mL of PRB solution that consisted of 2 mM $Na_4P_2O_7$, 1 mM NaN_3, 2 mM $MgCl_2$, 2 mM EGTA, 1 mM dithiothreitol (DTT), 100 mM KCl, and 10 mM Tris-maleate (pH 6.8). The homogenate of the samples was centrifuged at the speed of 1000*g* for 10 min. Precipitates then were collected for seven washes with 7.5 volumes of LSB buffer (same as PRB without pyrophosphate), and the condition was the same as above. After being suspended in EDTA (5 mM) and Tris-HCL (10 mM), myofibrils were vortex mixed, removed using eppendorf, and mixed with the treatment buffer (20% glycerol [v/v], 125 mM Tris-HCl, 4% SDS [w/v], pH 6.8). The myofibril was heated at 50 °C for 0.5 hour, and then the supernatant was obtained for protein concentration analysis using the BCA Protein Assay Kit (Thermo, RD, U.S.) after centrifugation for 30 min at the speed of 16 000*g*. The final concentration for SDS-PAGE was 3.5 mg/mL by mixing the samples with treatment buffer (same as above with 0.001% bromophenol blue and 10% MCE). Samples for SDS-PAGE were kept at 50 °C (20 min) and then at −80 °C.

Gel System. For determination of μ-calpain autolysis, a 10% polyacrylamide separating gel (0.05% ammonium peroxodisulfate (APS) [w/v], *N*,*N*-bis-methylene acrylamide:acrylamide = 1:100 [w/w], 0.1% SDS [w/v], 0.05% *N*,*N*,*N*,*N*′-tetramethylethyl-enediamine (TEMED) [v/v], 1.5 M Tris-HCl) was used. Stacking gel was 4% polyacrylamide gel that contained 0.075% APS [w/v], *N*,*N*-bis-methylene acrylamide:acrylamide = 1:100 [w/w], 0.1% SDS [w/v], 0.125% TEMED [v/v], and 0.5 M Tris-HCl. Degradation of titin and nebulin was detected by 5% polyacrylamide successive gel (pH 8.0, 2 mM EDTA, *N*,*N*-bis-methylene acrylamide:acrylamide = 1:100, 0.1% SDS, 0.067% TEMED, 0.1% APS, 1.5 M Tris-HCl).

SDS-PAGE and Western Blotting. Sixty micrograms of proteins was loaded per well for calpain autolysis. Sixteen micrograms of sarcoplasmic proteins was used for SDS-PAGE. A constant voltage of 120 V was set for all gels until the samples were at the bottom of the gels. Seventy micrograms of samples was loaded for titin and nebulin, and a constant current was set as 5 mA for each gel. Bio-Rad Mini-Protean II system (Bio-Rad, CA) was used to run gels for 18 h.[12] By following electrophoresis, the 10% gels for SDS-PAGE of sarcoplasmic proteins were stained using 7% glacial acetic acid [v/v], 40% ethanol [v/v] with 0.1% coomassie brilliant blue R-250 [w/v]. The proteins of calpain were then moved to polyvinylidene difluoride (PVDF) membranes at 4 °C (90 V, 1.5 h). The membranes were then blocked at room temperature with gentle agitation for 90 min in 5% nonfat dry milk, which was dissolved in PBST (100 mM sodium chloride, 20 mM sodium dihydrogen orthophosphate, 80 mM disodium hydrogen orthophosphate, and 0.1% (v/v) polyoxyethylene sorbitan monolaurate (Tween-20)). After blocking, the membranes with calpain proteins were put in PBST containing primary antibody (MA3-940, Aynity Bioreagents, CO) for 13 h at 4 °C. The dilution for the primary antibody was 1:10 000. The membranes were taken out from the cold room, washed 30 min (6 min per wash) using PBST, and then incubated with the second antibody (1:5000, goat antimouse) for 90 min followed by washing in PBST for another 30 min. After reacting with ECL reagent for 5 min, the blots were scanned with ImageQuant LAS4000[13] (GE, CT).

Semi Quantification of Targeted Proteins. Quantity One (Bio-Rad, U.S.) was the major software for analysis of the intensity of proteins. An approximately 2400 kDa band was a main indicator for the degradation of titin. Autolysis of μ-calpain was indicated by the intact calpain intensity of an approximately 80 kDa band and autolyzed 76 kDa band.

Carbonyl Content. The content of protein carbonyl was detected using the method of Lund et al.[14] with slight changes. Ground muscle from the sample was homogenized using a Ploytron (IKA T25 digital ultraturrox Made in IKA, German) at a speed of 18 000 rpm for 30 s (15 s × 2). One gram of muscle was homogenized in 10 volume of pyrophosphate buffer (w/v) containing 100 mM KCl, 2.0 mM $Na_4P_2O_7$, 10 mM tris-maleate, 2.0 mM EGTA, and 2.0 mM $MgCl_2$ (pH 7.4). Four milliliter solutions were removed from homogenate for two tubes equally. The samples were precipitated twice with 20% trichloroacetic acid (TCA, 2 mL) and followed by centrifugation at the speed of 12 000*g* (5 min). The 10 mM 2,4-dinitrophenylhydrazine (DNPH, 2 mL) in 2 M HCl or 2.0 M HCl (control) was reacted with pellets for 30 min at 25 °C. The samples were precipitated with the same solution, and the centrifugation condition was the same as described above. To eliminate the impact of the unreacted DNPH, the precipitates were washed with 10 mM HCl (5 mL) dissolved in ethanol-ethyl acetate (v/v = 1:1, three times). The absorbance was detected by a spectrophotometer (Shimadzu, Japan) at 370 nm after pellets reacted with guanidine hydrochloride (6.0 M, 2 mL), which was dissolved in 20 mM potassium hydrogen phosphate, pH 2.3) overnight under 4 °C. The amount of nanomolar DNPH in per milligram protein was the carbonyl content (nmol/mg).

Free Protein Thiol Groups. The amount of free thiol groups in protein was measured according to the method of Ellman.[15] The

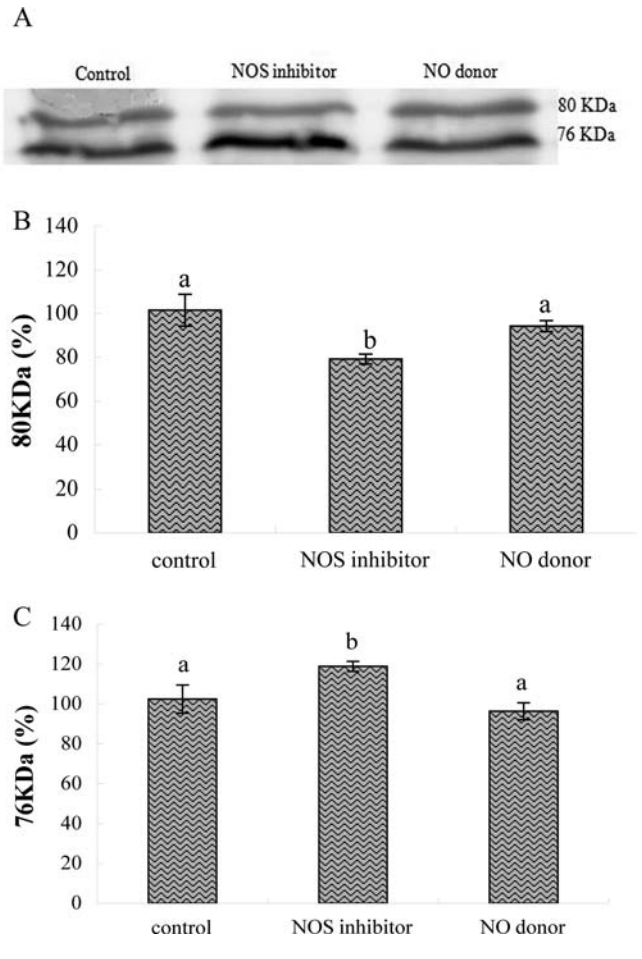

Figure 1. (A) Western blotting of μ-calpain. (B) Intensity of 80 kDa products of μ-calpain. (C) Intensity of 76 kDa products of μ-calpain. Ratios were calculated as the blot intensity of the μ-calpain fragment in each gel over the intensity of μ-calpain at 1 d control (100%). Vertical bars are mean ± SE (n = 5). Values with different letters show significant difference between treatments at $P < 0.05$.

dx.doi.org/10.1021/jf501332d | J. Agric. Food Chem. 2014, 62, 5972−5977

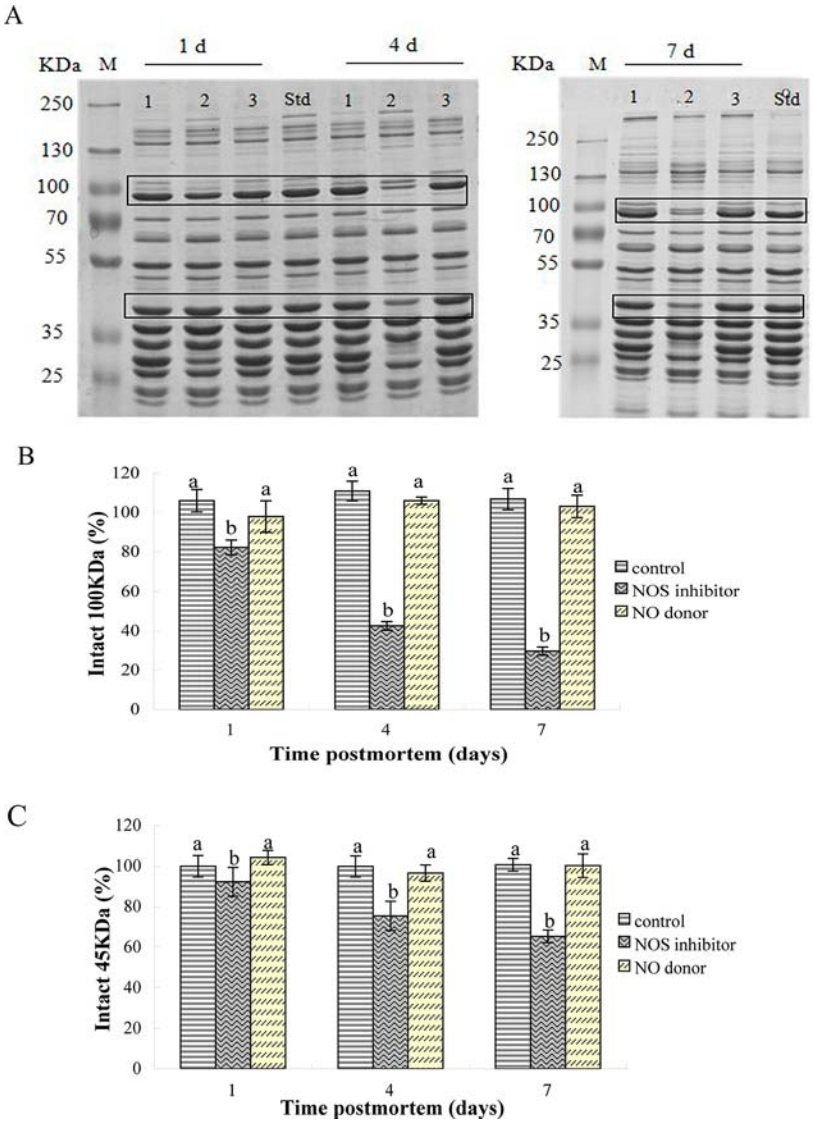

Figure 2. (A) 10% SDS-PAGE of sarcoplasmic proteins. 1, 2, and 3 represent control, NOS inhibitor group, and NO donor group, respectively. (B) The intensity of 100 kDa protein. (C) The intensity of 45 kDa protein. Ratios were calculated as intensity of the intact 100 and 45 kDa bands in each sample over intensity of 100 and 45 kDa bands at 1 d control (std). Values with different letters show significant difference between treatments at $P < 0.05$.

myofibril was dissolved in a solution containing 0.6 M NaCl, 50 mM Na_2HPO_4, and 50 mM NaH_2PO_4. Next, 0.5 mL of dissolved myofibril was added to 4 mL of Tris-Gly (86 mM Tris, 4 mM EDTA, 90 mM glycine, pH 8.0) and 0.4 mL of Ellman's reagent (Tris-Gly with 10 mM DTNB). The sample was vortex mixed, then incubated in 25 ± 1 °C for 1 h followed by centrifugation for 5 min at the speed of 12 000*g*. Free thiol groups were measured at 412 nm and calculated as nmol/mg protein.

Statistical Analysis. For statistical analysis, the version of SAS 9.2 was used. There were five replications in each group analyzed by ANOVA-one-way analysis of variance. The Bonferroni *t* test was used to analyze the difference among individual means, and the significant difference between treatments was considered at $P < 0.05$.

RESULTS AND DISCUSSION

***μ*-Calpain.** During the transformation of muscle to meat, *μ*-calpain plays a key role in proteolysis of some structural proteins.[16] The activation of *μ*-calpain has a close relationship with its autolysis. Because the autolysis from 80 to 76 kDa product had significance in early post-mortem muscle,[17] the intact 80 kDa band and the autolyzed 76 kDa band of calpain were investigated using Western blotting to examine the influence of L-NAME and DETA/NO treatment on calpain activation. The NOS inhibitor-treated group had less 80 kDa ($P < 0.05$, Figure 1B) and more 76 kDa products ($P < 0.05$, Figure 1C) as compared to control and NO donor group, suggesting that NO might inhibit the autolysis of *μ*-calpain. However, no significant differences were shown between control and NO donor group. Zhang, Lonergan, and Huff-lonergan[18] found that the rate of *μ*-calpain autolysis was slowed when it was first exposed to *S*-nitrosoglutathione before calcium at both pH 6.5 and pH 7.5, which was evidenced by more 80 and 78 kDa products and less 76 kDa products as compared to control group. Interestingly, endogenous purified *μ*-calpain was shown to be nitrosylated, and part of this nitrosylation could be reversed by DTT incubation. Koh and Tidball[19] used a NO enhancer, sodium nitroprussiate (SNP), to react with ionophore-treated cells. SNP pretreatment significantly reduced the degradation of talin and vinculin, indicating that NO might exert a negative influence on the activity of *μ*-calpain. Furthermore,

dx.doi.org/10.1021/jf501332d | J. Agric. Food Chem. 2014, 62, 5972−5977

calpain-mediated proteolysis could be reduced by modification with *S*-nitrosylation. Reduced *S*-nitrosylation of calpain during aging corresponded to the increased activity of calpain to cleave some proteins.[20]

Instead of μ-calpain, previous studies have shown that NO could inhibit other cysteine protease including papain, mammalian caspases, and cathepsins.[21] According to these studies, the activity of calpain was inhibited by NO through removal of the negative feedback by L-NAME at early stage post-mortem resulting in increased autolysis. However, the behind mechanism about the NO on the autolysis procedure of μ-calpain during post-mortem aging remains unknown and needs to be further studied.

Sarcoplasmic Protein. Sarcoplasmic proteins with molecular weights of about 100 and 45 kDa from NOS inhibitor group decreased during aging, and the differences were significant as compared to control and NO donor group ($P < 0.05$, Figure 2B and C). The sarcoplasmic protein of 100 kDa was tentatively considered as phosphorylase, while the protein of 45 kDa was believed as creatine kinase.[22,23] Creatine kinase is functionally coupled to enzymes and transport systems that participated in energy production and utilization,[24] and the enzyme of phosphorylase participates in glycogenolysis. Post-mortem degradation of creatine kinase has been observed in several studies.[25,26] Increased post-mortem glycolysis, evidenced by lower muscle glycogen and increased lactate concentration, was shown by inhibiting nitric oxide release preslaughter in ovine muscle.[1] *S*-Nitrosylation of kinase or phosphatase through a single Cys residue could have an inhibitory effect on its activity. In addition, *S*-nitrosylation could inhibit kinases directly through the suppression of kinase activity or by modulating the interaction of kinase and its substrate.[27] Further studies need to be conducted to investigate the mechanism of how NO and *S*-nitrosylation affects the enzymes during post-mortem storage.

Titin and Nebulin. Titin is the largest protein found in mammalian. One terminal end (C) of titin overlaps with M-line and the other terminal (N) overlaps with Z-line;[28] thus titin crosses one-half of a whole sarcomere. A major degradation product (T_2), which migrates at approximately 2400 kDa by using SDS-PAGE, could be observed when the intact titin is degraded. Nebulin, another mega-protein with MW 600−900 kDa, forms the fourth filament system in muscle.[29] The degradation of titin and nebulin could irreversibly cause myofibril fragmentation and also the integrity of muscle and result in improved tenderness.

The degradation product (T_2) of titin was not significantly different after 1 d of refrigerated storage ($P > 0.05$, Figure 3B), while significant difference was observed after 4 and 7 d by treatment with NOS inhibitor and water, and also by incubation with NOS inhibitor and NO donor ($P < 0.05$, Figure 3B). Lower levels of T_2 were observed by treatment of NOS inhibitor. Interestingly, another titin degradation product migrated below T_2 in NOS inhibitor group, which was reported in a previous study.[30] Although we could not analyze nebulin quantitatively, apparent differences could be observed from Figure 3A. The intact nebulin could not be detected from NOS inhibitor group after refrigerated storage of 1, 4, and 7 d. However, intact nebulin still could be observed by treatment of water and DETA/NO after storage of 4 and 7 d. Because titin and nebulin are susceptible substrates for μ-calpain, the increased activation of μ-calpain in NOS inhibitor group could result in a high degree of degradation.

The degradation of titin and nebulin is known to be associated with improved tenderness and increased water holding capacity.[31] Cottrell et al.[1] injected 30 mg/kg L-NAME into the ovine before slaughter and found the shear force of longissimus lumborum was significantly reduced. More importantly, the improved tenderness was independent of color parameters, pH decline, water holding capacity, or sarcomere length. Zhang et al.[2] incubated the broiler chicken meat with water, NO enhancer, and NOS inhibitor immediately after slaughter. The water holding capacity was lowered by treatment of incubation with *S*-nitrosoglutathione (a NO enhancer) after storage.

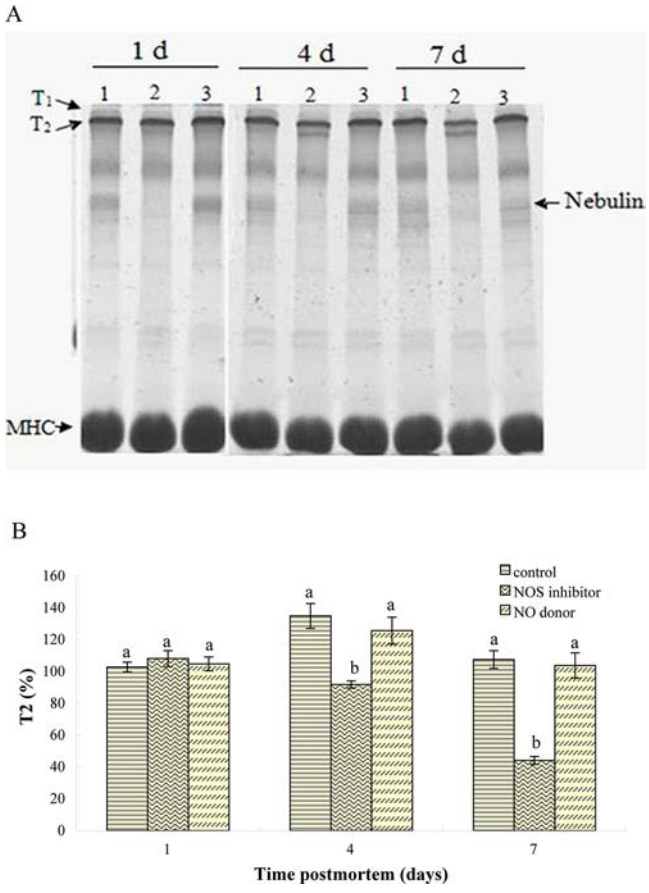

Figure 3. (A) SDS-PAGE (5%) showing degradation of titin and nebulin. 1, 2, and 3 represent control, NOS inhibitor group, and NO donor group, respectively. T_1 = intact titin, T_2 = large degradation of intact titin, MHC = myosin heavy chain. (B) The intensity of T_2. Ratios were calculated as intensity of 2400 kDa band in each sample over intensity of 2400 kDa band at 1 d control. Values with different letters show significant difference between treatments at $P < 0.05$.

Carbonyl Content. The carbonyl content by treatment with NO donor was higher than those in NOS inhibitor samples after storage of 1, 4, and 7 d ($P < 0.05$, Figure 4). No significant differences were observed by treatment with water and NOS inhibitor and by incubation with water and NO donor ($P > 0.05$, Figure 4). This indicated high content of nitric oxide might result in high levels of protein oxidation in post-mortem pork. Zhang et al.[2] injected the breast muscle with water, NOS inhibitor, or NO enhancer immediately after slaughter, and they reported similar results that the content of carbonyl by treatment of NO enhancer was improved. In that study, the higher content of carbonyl could not be the result of cross-reactions of protein oxidation products and lipid oxidation products because lipid oxidation just showed a significant difference after 7 d storage. The production of NO and superoxide ($O_2^{\bullet-}$) in muscle could contribute to the formation of peroxynitrite ($ONOO^-$). Protein thiols could be modified by peroxynitrite, whereas this modification cannot result in carbonyl

dx.doi.org/10.1021/jf501332d | J. Agric. Food Chem. 2014, 62, 5972−5977

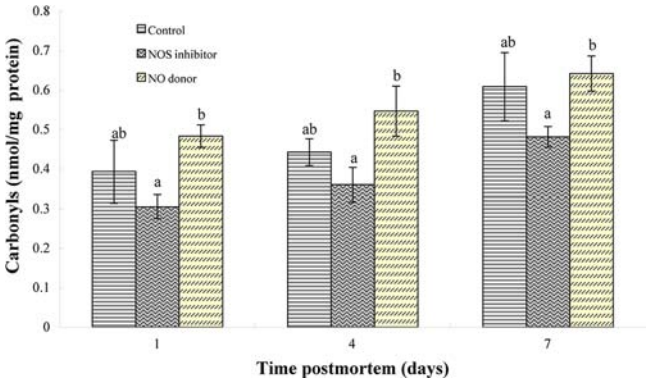

Figure 4. Carbonyl content. Vertical bars are mean ± SE (n = 5). Values with different letters show significant difference between treatments at $P < 0.05$.

formation.[32] A possible explanation could be that the NO donor group presented high levels of nitric oxide, and this might exert a high oxidative environment as compared to control and NOS inhibitor group. Antioxidant ability would decrease in pork samples during refrigerated storage and thus increased the content of the carbonyl group in the NO enhancer group.

Free Protein Thiol Group. The thiol content by incubation with NOS inhibitor was higher than the content in the other two groups after post-mortem storage of 1 and 4 d ($P < 0.05$, Figure 5). However, no significant difference was

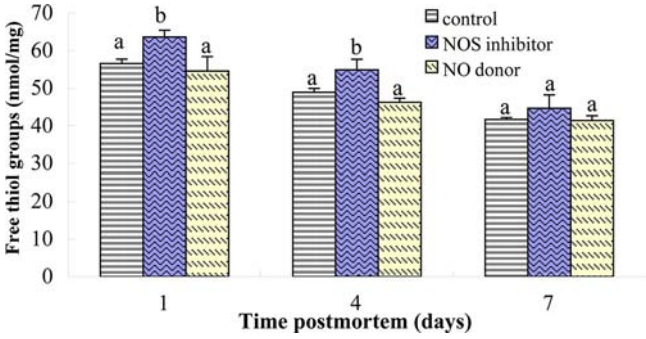

Figure 5. Free protein thiol group. Values with different letters show significant difference between treatments at $P < 0.05$ (n = 5).

shown by treatments with water and NO donor at 1 and 4 d. No significant difference was observed for free protein thiol content among three groups after refrigerated storage of 7 d ($P > 0.05$, Figure 5). Because of the decreased antioxidant system during refrigerated storage, NO could react with superoxide ($O_2^{\bullet-}$) in muscle, thus promoting the formation of peroxynitrite ($ONOO^-$). Peroxynitrite is a potent oxidant that mediates oxidation of both nonprotein and protein sulfhydryls. Besides, other reactive compounds derived from peroxynitrite ($ONOO^-$) could have a negative influence on the antioxidant capability during long-term storage.[9] Through inhibition of NOS activity at early stage post-mortem, less NO could be produced in the NOS inhibitor group than the other two groups, thus resulting in high levels of free thiol content after 1 and 4 d of storage.

AUTHOR INFORMATION

Corresponding Author

*Tel.: 86-25-84385341. Fax: 86-25- 84395341. E-mail: wangang.zhang@yahoo.com.

Funding

We thank the National Natural Science Foundation of China (31271899) for funding support.

Notes

The authors declare no competing financial interest.

ABBREVIATIONS USED

L-NAME, Nw-nito-L-arginine methyl ester hydrochloride; NOS, nitric oxide synthase; DETA/NO, diethylenetriamine/nitric oxide adduct; NO, nitric oxide; DTNB, 5,5-dithiobis (2-nitrobenzoic acid); TEMED, *N,N,N,N′*-tetramethylethyl-enediamine; APS, ammonium peroxodisulfate; DNPH, 2,4-dinitrophenylhydrazine

REFERENCES

(1) Cottrell, J. J.; McDonagh, M. B.; Dunshea, F. R.; Warner, R. D. Inhibition of nitric oxide release pre-slaughter increases post-mortem glycolysis and improves tenderness in ovine muscles. *Meat Sci.* **2008**, *80*, 511−521.

(2) Zhang, W. G.; Marean, A.; Samaraweera, H.; Lee, E. J.; Ahn, D. U. Breast meat quality of broiler chickens can be affected by managing the level of nitric oxide. *Poult. Sci.* **2013**, *92*, 3044−3049.

(3) Cook, C. J.; Scott, S. M.; Devine, C. E. Measurement of nitric oxide and the effect of enhancing or inhibiting it on tenderness changes of meat. *Meat Sci.* **1998**, *48*, 85−89.

(4) Huff-Lonergan, E.; Mitsuhashi, T.; Beekman, D. D.; Parrish, F. C.; Olson, D. G.; Robson, R. M. Proteolysis of specific muscle structural proteins by μ-calpain at low pH and temperature is similar to degradation in postmortem bovine muscle. *J. Anim. Sci.* **1996**, *74*, 993−1008.

(5) Goll, D. E.; Thompson, V. F.; Li, H.; Wei, W.; Cong, J. The calpain system. *Physiol. Rev.* **2003**, *83*, 731−801.

(6) Lametsch, R.; Lonergan, S.; Huff-Lonergan, E. Disulfide bond within μ-calpain active site inhibits activity and autolysis. *Biochim. Biophys. Acta* **2008**, *1784*, 1215−1221.

(7) Michetti, M.; Salamino, F.; Melloni, E.; Pontremoli, S. Reversible inactivation of calpain isoforms by nitric oxide. *Biochem. Biophys. Res. Commun.* **1995**, *207*, 1009−1014.

(8) Winger, R. J.; Pope, C. G. Osmotic properties of post-rigor beef muscle. *Meat Sci.* **1981**, *5*, 355−369.

(9) Brannan, R. G.; Decker, E. A. Nitric oxide synthase activity in muscle foods. *Meat Sci.* **2002**, *62*, 229−235.

(10) Veiseth, E.; Shackelford, S. D.; Wheeler, T. L.; Koohmaraie, M. Effect of postmortem storage on mu-calpain and m-calpain in ovine skeletal muscle. *J. Anim. Sci.* **2001**, *79*, 1502−1508.

(11) Etlinger, J. D.; Zak, R.; Fischman, D. A. Compositional studies of myofibrils from rabbit striated muscle. *J. Cell Biol.* **1976**, *68*, 123−141.

(12) Candiano, G. Blue silver: a very sensitive colloidal coomassie G-250 staining for proteome analysis. *Electrophoresis* **2004**, *25*, 1327−1333.

(13) Zhang, W. G.; Lonergan, S. M.; Gardner, M. A.; Huff-Lonergan, E. Contribution of postmortem changes of integrin, desmin and μ-calpain to variation in water holding capacity of pork. *Meat Sci.* **2006**, *74*, 578−585.

(14) Lund, M. N.; Hviid, M. S.; Magnussen, C. C.; Skibsted, L. H. Effects of dietary soybean oil on lipid and protein oxidation in pork patties during chill storage. *Meat Sci.* **2008**, *79*, 727−733.

(15) Ellman, G. L. Tissue sulfhydryl groups. *Arch. Biochem. Biophys.* **1959**, *82*, 70−77.

(16) Geesink, G. H.; Kuchay, S.; Chishti, A. H.; Koohmaraie, M. μ-Calpain is essential for postmortem proteolysis of muscle proteins. *J. Anim. Sci.* **2006**, *84*, 2834−2840.

(17) Melody, J. L.; Lonergan, S. M.; Rowe, L. J.; Huiatt, T. W.; Mayes, M. S.; Huff-Lonergan, E. Early postmortem biochemical factors influence tenderness and water-holding capacity of three porcine muscles. *J. Anim. Sci.* **2004**, *82*, 1195−1205.

(18) Zhang, W. G.; Lonergan, S. M.; Huff-Lonergan, E. S-nitrosogutathione affects the activity and autolysis of m- and μ-calpain. *Proceedings of 53rd International Congress of Meat Science and Technology*, Beijing, China; 2008; pp 201−202.
(19) Koh, T. J.; Tidball, J. G. Nitric oxide inhibits calpain-mediated proteolysis of talin in skeletal muscle cells. *Am. J. Physiol.* **2000**, *279*, 806−812.
(20) Samengo, G.; et al. Age-related loss of nitric oxide synthase in skeletal muscle causes reductions in calpain S-nitrosylation that increase myofibril degradation and sarcopenia. *Aging Cell* **2012**, *11*, 1036−1045.
(21) Ascenzi, P.; Salvati, L.; Bolognesi, M.; Colasanti, M.; Polticelli, F.; Venturini, G. Inhibition of cysteine protease activity by NO-donors. *Curr. Protein Pept. Sci.* **2001**, *2*, 137−153.
(22) Visessanguan, W.; Benjakul, S.; Riebroy, S.; Thepkasikul, P. Changes in composition and functional properties of proteins and their contributions to Nham characteristics. *Meat Sci.* **2004**, *66*, 579−588.
(23) Luca, D. A.; Mullen, A. M.; Elia, G.; Davey, G.; Hamill, R. M. Centrifugal drip is an accessible source for protein indicators of pork ageing and water-holding capacity. *Meat Sci.* **2011**, *88*, 261−270.
(24) Clapier, R. V.; Kuznetsov, A.; Veksler, V.; Boehm, E.; Anflous, K. Functional couping of creatine kinases in muscles: species and tissue specificity. *Dev. Mol. Cell. Biochem.* **1998**, *184*, 231−247.
(25) Lametsch, R.; Bendixen, E. Proteome analysis applied to meat science: Characterizing post mortem changes in porcine muscle. *J. Agric. Food Chem.* **2002**, *49*, 4531−4537.
(26) Purintrapiban, J.; Wang, M.; Forsberg, N. E. Identification of glycogenphosphorylase and creatine kinase as calpain substrates in skeletal muscle. *Int. J. Biochem. Cell Biol.* **2001**, *33*, 531−540.
(27) Hess, D. T.; Stamler, J. S. Regulation by S-nitrosylation of protein posttranslational modification. *J. Biol. Chem.* **2012**, *287*, 4411−4418.
(28) Huff-Lonergan, E.; Zhang, W. G.; Lonergan, S. M. Biochmistry of postmortem muscle-Lessons on mechanism of meat tenderization. *Meat Sci.* **2010**, *86*, 184−195.
(29) McElhinny, A. S.; Kazmierski, S. T.; Labeit, S.; Gregorio, C. C. Nebulin: The nebulous, multifunctional giant of striated muscle. *Trends Cardiovasc. Med.* **2003**, *13*, 195−201.
(30) Huff-Lonergan, E.; Parrish, F. C.; Robson, R. M. Effects of postmortem aging time, animal age, and sex on degradation of titin and nebulin in bovine longissimus muscle. *J. Anim. Sci.* **1995**, *73*, 1064−1073.
(31) Melody, J. L.; Lonergan, S. M.; Rowe, L. J.; Huiatt, T. W.; Mayes, M. S.; Huff-Lonergan, E. Early postmortem biochemical factors influence tenderness and water-holding capacity of three porcine muscles. *J. Anim. Sci.* **2004**, *82*, 1195−1205.
(32) Tien, M.; Berlett, B. S.; Levine, R. L.; Chock, P. B.; Stadtman, E. R. Peroxynitrite-mediated modification of proteins at physiological carbon dioxide concentration: pH dependence of carbonyl formation, tyrosine nitration, and methionine oxidation. *Proc. Natl. Acad. Sci. U.S.A.* **1999**, *96*, 7809−7814.

JOURNAL OF AGRICULTURAL AND FOOD CHEMISTRY

Article

pubs.acs.org/JAFC

Formation and Reduction of Furan in Maillard Reaction Model Systems Consisting of Various Sugars/Amino Acids/Furan Precursors

Heera Cho and Kwang-Geun Lee*

Department of Food Science and Biotechnology, Dongguk University—Seoul, 30, Pildong-ro-1-gil, Jung-gu, Seoul 100-715, Republic of Korea

ABSTRACT: To investigate the effect of the temperature on the formation of furan, various furan models were conducted at 90, 121, and 150 °C. A total 15 models, including alanine (ALA), serine (SER), ribose (RIB), RIB/ALA, RIB/SER, glucose (GLU), GLU/ALA, GLU/SER, sucrose (SUC), SUC/ALA, SUC/SER, furoic acid (FUR), GLU/FUR, acetaldehyde (ACET), and GLU/ACET, were prepared. The maximum level of furan was detected in the GLU/SER and GLU/ALA models at a molar ratio of 0.5:0.5. The formation of furan was proportional to the temperature in all models. The RIB/SER model generated the greatest amount of furan among the 11 models ranging from 2.1 to 4931.9 ng mL^{-1} under all temperature conditions. Among the precursor models, the FUR model formed the greatest amount of furan ranging from 1058.2 to 13 927.9 ng mL^{-1} at all temperatures.

KEYWORDS: *model system, furan, Maillard reaction HS-SPME, GC−MS*

INTRODUCTION

Furan (C_4H_4O) is a heterocyclic and highly volatile compound with a boiling point of 31.4 °C. Furan has received attention since 1995 because it was classified as "possibly carcinogenic to humans" by the International Agency for Research on Cancer.[1] Data have shown furan induces liver and kidney toxicity in rats and mice.[2,3] The Food and Drug Administration (FDA) announced that furan was present in a large number of thermally processed foods.[4] High amounts of furan have been detected in a variety of foods and beverages, including coffee, canned fish and vegetables, jarred source, fruit and vegetable juices, and bakery products.[5,6]

Furan is generated in food from multiple routes. Many researchers have reported that primary sources, such as sugars, amino acids, ascorbic acid, and polyunsaturated fatty acids, generate furan through thermal degradation, the Maillard reaction, and oxidation.[7,8] In particular, the Maillard reaction between the carbonyl groups of sugars and the amino groups of amino acids are regarded as major pathways of furan formation. Yaylayan proposed a pathway of furan formation with sugars and amino acids.[7] On the basis of this pathway, the degree of furan formation was evaluated using various heating sources. Ribose (RIB) as pentose, glucose (GLU) as hexose, and sucrose (SUC) as a disaccharide were chosen to determine the effect on the number of carbons. Serine (SER) and alanine (ALA) were used as amino group donors. In this study, single and binary primary source models were used. Single and binary models refer to one and two substrates, respectively. For example, a GLU or SER model is a single model and GLU/SER or GLU/ALA models are binary models. In this study, to determine the optimal molar ratio of a binary model, the concentration of furan of the GLU/SER and GLU/ALA models was compared at various molar ratios.

There are many precursors for furan formation, and they have occasionally been used as food additives. To confirm the effect of various precursors on furan formation, the heating process of the model including sugars, amino acids, and precursors was carried out in the same manner. Among furan precursors, we chose acetaldehyde (ACET) and 2-furoic acid, which are classified as edible synthetic flavoring substances.[9,10]

Several factors influence the formation of furan. Many studies have demonstrated that furan is formed in model systems during various heating processes.[7] Fan et al. reported that the heating time, temperature, and pH affect the formation of furan in food.[11−13] The aim of this study was to investigate the effect of the temperature and various ingredients in furan formation models. Each model was heated at 90, 121, and 150 °C. Eleven and four furan models were selected for clarification of the effect of the temperature and precursors on furan formation, respectively.

MATERIALS AND METHODS

Chemicals. L-ALA, D-SER, D-RIB, D-GLU, D-SUC, 2-furoic acid (FUR), and ACET were provided by Sigma-Aldrich Chemical (St. Louis, MO). Water and methanol were obtained from J.T. Baker (Phillipsburg, NJ).

Furan (+99%, purity) and d_4-furan (>99 atom % D) were purchased from Sigma-Aldrich. Stock solutions of furan and d_4-furan were prepared weekly by dissolving standard solutions in cold methanol at a concentration of 100 μg mL^{-1}. The stock solutions were further diluted in cold water to give a working solution with a concentration of 1 μg mL^{-1}. The stock and working solutions were stored in headspace vials closed with silicone−polytetrafluoroethylene (PTFE) septa and aluminum seals (Supelco, Bellefonte, PA) at 4 °C until analysis.

Method Validation for the Furan Analysis. The furan analytical method was validated using linearity, limit of detection (LOD), limit of quantification (LOQ), and repeatability. The calibration curve was drawn using the ratio of the area of furan versus the area of d_4-furan). A 10 μL aliquot of internal standard (1 μg mL^{-1}) was spiked in 10 mL

Received: April 4, 2014
Revised: June 3, 2014
Accepted: June 9, 2014
Published: June 9, 2014

ACS Publications © 2014 American Chemical Society

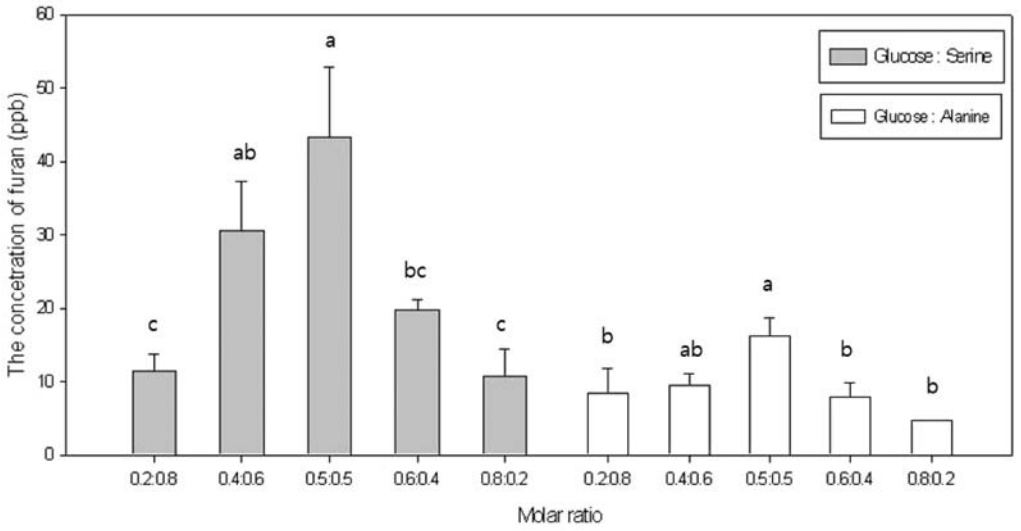

Figure 1. Effect of the molar ratio of amino acid to sugar on the furan formation. Within same figure, lower case alphabetical letters indicate spastically differences ($p < 0.05$, Duncan's multiple range test).

of water in a 20 mL headspace vial with a syringe to prepare the calibration curve. Seven different amounts (5, 10, 20, 50, 100, 500, and 1000 μL) of furan (1 μg mL^{-1}) were spiked into the vial. All experiments were performed at <4 °C to minimize furan loss.

Linearity was expressed as the correlation coefficient (r^2). LOD and LOQ were determined by the standard deviation (SD) of the response and the slope. LOD was calculated from the equation $3.3\sigma/S$, and LOQ was calculated from equation $10\sigma/S$, where σ is the SD of the response and S is the slope of the calibration curve. The SD, σ, is the SD of the blank in this study. The blank sample was analyzed 7 times.

Three concentrations (1, 5, and 10 ng mL^{-1}) of sample were analyzed to evaluate repeatability. Each concentration was investigated 5 times. Repeatability was presented as relative standard deviation (RSD, %).

Effect of the Molar Ratio of Amino Acid to Sugar on Furan Formation. GLU/SER and GLU/ALA models were selected to determine the effect of the sugar/amino acid molar ratio on furan formation. The two models (GLU/SER and GLU/ALA) were prepared by mixing both compounds at the following molar ratios in a headspace vial: 0.2:0.8, 0.4:0.6, 0.5:0.5, 0.6:0.4, and 0.8:0.2. Subsequently, 10 mL of water was added to the vial, and the solution was homogenized with a vortex machine (Scientific Industries, Bohemia, NY). The vial was heated at 121 °C for 25 min in a drying oven (OF-22, JEIO Tech., Daejeon, Korea). Immediately after heating, the sample was cooled in an ice box at <4 °C for a minimum of 30 min. Then, d_4-furan was spiked into a 20 mL vial with a syringe. After injection of 10 μL of d_4-furan (1 μg mL^{-1}), the fiber of a solid-phase microextraction (SPME) was injected into the headspace vial. All analyses were performed in triplicate.

Effect of the Heating Temperature on Furan Formation. Experiments were conducted at 90, 121, and 150 °C to identify the effect of the heating temperature on furan formation. The 11 models, including amino acid and sugar, were selected. The models were ALA, SER, RIB, RIB/ALA, RIB/SER, GLU, GLU/ALA, GLU/SER, SUC, SUC/ALA, and SUC/SER. A single compound (0.5 M) or a binary mixture (0.5:0.5 molar ratio) was transferred to a 20 mL headspace vial. After vortexing for 30 s, the samples were heated in a drying oven at 90, 121, and 150 °C for 25 min. Furan was then analyzed as described above.

Effect of Adding Various Precursors on Furan Formation. FUR, GLU/FUR, ACET, and GLU/ACET models were selected to investigate the effect of adding a direct precursor on furan formation. Each compound (0.5 M) was added to a 20 mL headspace vial and diluted with 10 mL of water. After vortexing for 30 s, the samples were heated in a drying oven at 90, 121, and 150 °C for 25 min. Furan was then analyzed as described above.

Analysis of Furan Using SPME–Gas Chromatography–Mass Spectrometry (GC–MS). A SPME fiber was pushed through a vial septum. The fiber was pushed out of the housing and exposed to the headspace (1.5 cm in depth) of the vial. Extraction was carried out at 50 °C for 20 min using a heating block. After extraction, the fiber was pulled into the housing and the SPME device was removed from the vial and inserted into the injection port of a gas chromatograph for thermal desorption analysis (4 cm in depth). The fiber was desorbed for 5 min at 230 °C to eliminate any residual volatile compounds.

The SPME fiber was a 75 μm Carboxen–polydimethylsiloxane (CAR–PDMS, Supleco, Bellefonte, PA) fiber. The extraction was carried out at 50 °C for 20 min on a heating block, and desorption was carried out at 230 °C for 5 min. GC–MS analyses were performed with an Agilent Technologies 6890 N GC system coupled with an Agilent Technologies 5975 mass selective detector (Palo Alto, CA) equipped with a HP-PLOT Q capillary column (HP-PLOT Q, 15 m × 0.32 mm inner diameter, 20 μm film thickness, J&W Scientific, Folsom, CA). Operational conditions were as follows: carrier gas, high-purity helium (99.999%); flow rate, 1 mL min^{-1}; and injector temperature, 230 °C. The oven temperature was programmed from 50 °C (held for 5 min) to 230 °C (held for 2 min). The mass spectrometer was operated in electron impact ionization mode (70 eV) and selected ion monitoring mode. The m/z (mass/charge) of 68 for furan and m/z of 72 for d_4-furan were used as quantification ions, and the m/z of 39 for furan and 42 for d_4-furan were used as confirmation ions.

Measurement of Ultraviolet (UV) Absorbance in Each Model System. A total of 1 mL of each sample was transferred to a cuvette. The absorbance of each sample was measured with a UV spectrometer (UV-1800, Shimadzu, Tokyo, Japan). The wavelength was set to 420 nm. Water was used as the control. All experiments were repeated 3 times.

Statistical Analysis. Results are presented as the mean ± SD. Data were analyzed by one-way analysis of variance (ANOVA), and multiple comparisons were performed with Duncan's test. The SAS 9.3 program was used for the statistical analysis (SAS Institute, Cary, NC). Statistical significance was set at $p < 0.05$.

RESULTS AND DISCUSSION

Method Validation for the Analysis of Furan and the Effect of the Sugar to Amino Acid Molar Ratio on Furan Formation. Satisfactory linearity was obtained with 0.997 correlation coefficient values. The LOD was 0.04 ng mL^{-1}, and the LOQ was 0.14 ng mL^{-1}. These LOD and LOQ values were

similar to those of a previous study.[5] RSD values for 1, 5, and 10 ng mL^{-1} were 9.33, 13.01, and 13.10%, respectively.

Figure 1 shows the effect of the molar ratio on furan formation in the GLU/SER and GLU/ALA models. Five molar ratios were selected for each model. The greatest amount of furan was formed at a molar ratio of 0.5:0.5 in both the GLU/SER and GLU/ALA models with 43.26 and 16.16 ng mL^{-1}, respectively. The molar ratio of 0.5:0.5 was selected as the optimal molar ratio for the sugar and amino acid binary models throughout this study.

Effect of the Heating Temperature on Furan Formation. All models were prepared by heating at 90, 121, and 150 °C to investigate the effect of the heating temperature on furan formation. The furan concentrations produced at 90, 121, and 150 °C are presented in Figures 2−4, respectively.

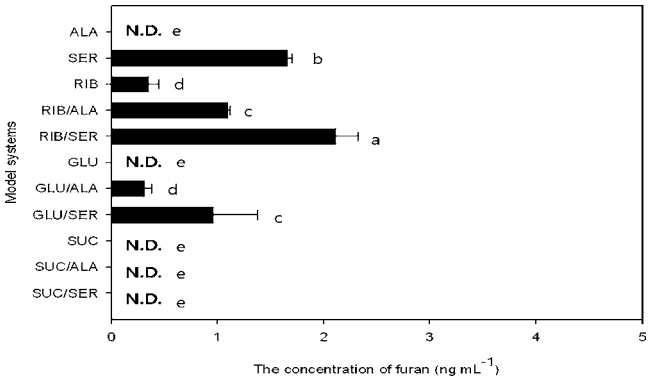

Figure 2. Concentration of furan in various model systems at 90 °C. Within same figure, lower case alphabetical letters indicate spastically differences (p < 0.05, Duncan's multiple range test). N.D.: Not detected.

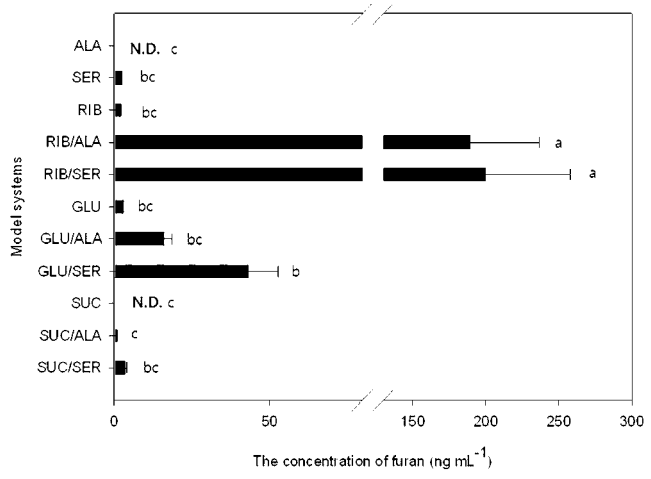

Figure 3. Concentration of furan in various model systems at 121 °C. Within same figure, lower case alphabetical letters indicate spastically differences (p < 0.05, Duncan's multiple range test). N.D.: Not detected.

The furan concentration was below the LOD in the ALA and SUC models at all temperatures. Furan formation ranged from not detectable to 8.5 ng mL^{-1} in the GLU model. Furan was not detected in any of the sugar single models at 90 °C, except for the RIB model. Although the RIB model generated furan (0.3 ng mL^{-1}) at 90 °C, no significant difference was observed in the GLU or SUC models. Furan was detected in the RIB model at concentrations of 1.9 and 44.9 ng mL^{-1} after heating at 121 and 150 °C, respectively. However, no significant difference with the GLU or SUC models was found.

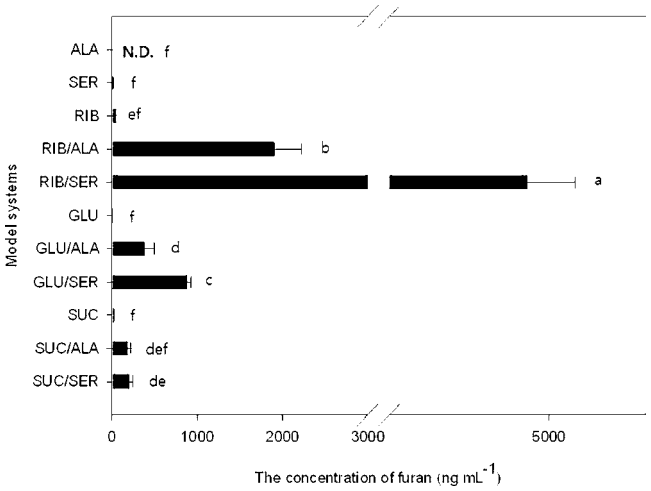

Figure 4. Concentration of furan in various model systems at 150 °C. Within same figure, lower case alphabetical letters indicate spastically differences (p < 0.05, Duncan's multiple range test). N.D.: Not detected.

SER formed furan at concentrations of 1.66−9.07 ng mL^{-1} at all temperatures; however, ALA produced no furan. Locas and Yaylayan explained the pathway of furan formation from sugars and amino acids.[14] Sugars and amino acids form ACET and glycolaldehyde by deamination and decarboxylation to produce furan. A previous study suggested the formation of furan from the aldol condensation reaction between ACET and glycolaldehyde.[14] Locas and Yaylayan reported that certain amino acids, such as SER, form ACET and glycoladehyde and eventually form furan. However, most amino acids, such as aspartic acid, ALA, and threonine, only generate ACET. These amino acids need a reducing sugar to generate glycoladehyde and eventually form furan.[14]

In contrast with the single model, the binary models, including an amino acid and sugar, produced more furan. For example, the RIB/SER model generated the greatest amount of furan ranging from 2.1 to 4931.9 ng mL^{-1} at all temperatures among the 11 models, followed by the RIB/ALA model (1.1−1901.3 ng mL^{-1}). Furan formation increased at higher temperatures for all model systems. For example, after heating at 150 °C, a significant increase in furan formation was observed in the RIB/SER model compared to heating at 90 °C (2347% increase). These results indicate that the temperature provides the main contribution to furan formation.

Effect of Various Precursors on Furan Formation. Four models were prepared to determine the effect of the precursor on furan formation. Figure 5 shows the furan concentration in these models. The FUR model formed the greatest amount ranging from 1058.2 to 13 927.9 ng mL^{-1} at all temperatures. The GLU/FUR model produced furan ranging from 628.1 to 9936.2 ng mL^{-1}. The formation of furan ranged from 647.9 to 834.2 ng mL^{-1} and from 600.1 to 742.9 ng mL^{-1} in the ACET and GLU/ACET models. However, no significant difference was observed between the ACET and GLU/ACET models.

The models including precursors generated more furan than the models including an amino acid and sugar. Amino acids and sugars undergo hydrolysis and elimination followed by decarboxylation, and they eventually form deoxyaldoltetrose.[15]

dx.doi.org/10.1021/jf501619e | J. Agric. Food Chem. 2014, 62, 5978−5982

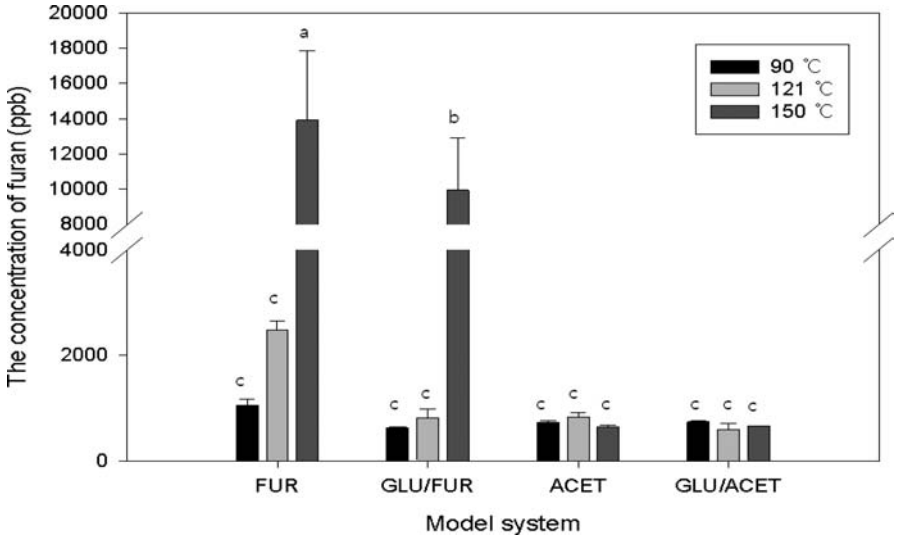

Figure 5. Concentration of furan in the model including precursors of furan. Within same figure, lower case alphabetical letters indicate spastically differences ($p < 0.05$, Duncan's multiple range test).

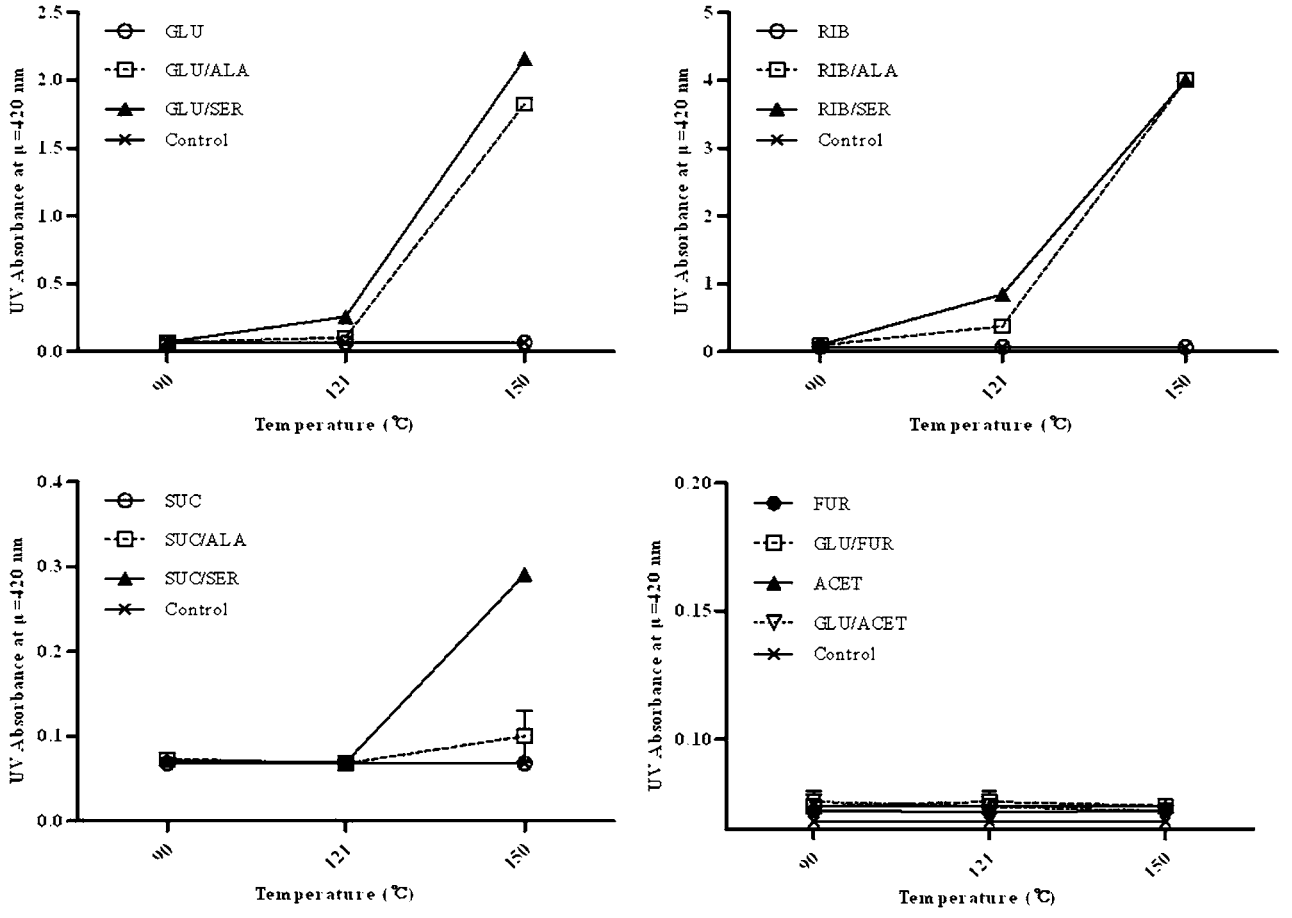

Figure 6. UV absorbance of the solution prepared in various models.

Deoxytaldoltetrose yields FUR and finally forms furan. However, FUR, which is a direct precursor of furan, can be produced only by decarboxylation and heating. These results explain why the FUR model formed furan at the greatest amount. FUR and ACET are used as food additives. However, FUR and ACET may potentially cause more furan formation during thermal processing.

Measurement of UV Absorbance in Each Model System. UV absorbance at 420 nm is often used to indicate the final products of the Maillard reaction, whereas UV absorbance at 294 nm is used to assess intermediate Maillard reaction products.[16] In the present study, changes in UV absorbance at 420 nm were investigated to identify the effects of the temperature on the Maillard reaction. Figure 6 shows the

dx.doi.org/10.1021/jf501619e | J. Agric. Food Chem. 2014, 62, 5978−5982

intensity of absorbance at 420 nm in the amino acid and sugar model systems. The intensity of absorbance in the RIB/SER model which had the greatest concentration of furan increased from 0.1 to 4.0 as the temperature increased. However, the intensity of the SUC model, which had the smallest concentration of furan, did not change. These results indicate that the Maillard reaction and formation of furan were promoted as the temperature increased. In contrast with the intensity of the Maillard reaction model, the intensity of models including furan precursors remained unchanged as the temperature increased. It was similar to the absorbance of the control. From these results, it was assumed that the models including precursors had different routes to produce furan during the Maillard reaction.

In summary, the effect of the sugar/amino acid molar ratio, heating temperature, and addition of precursor on furan formation was investigated. SPME−GC−MS was used to analyze furan production. The LOD and LOQ were 0.04 and 0.14 ng mL^{-1}, respectively. Repeatability by the RSD was 9.33−13.10%. Experiments were carried out at various molar ratios to investigate the effect of the molar ratio on furan formation, and the molar ratio of 0.5:0.5 was the optimal molar ratio for the binary model. Three heating temperatures and 11 binary models were selected to determine the effect of the heating temperature and type of sugar and amino acid. As the temperature increased, the formation of furan increased in all Maillard binary reaction models. Among the 11 models, the RIB/SER model generated the greatest amount of furan (2.10, 199.61, and 4931.97 ng mL^{-1} at 90, 121, and 150 °C, respectively). The FUR model formed the greatest amount of furan in an experiment to identify the effect of adding precursors on furan formation (1058.2−13 927.9 ng mL^{-1}) at all temperatures. In a future study, real food systems to form furan will be prepared and the furan level will be analyzed in the system.

AUTHOR INFORMATION

Corresponding Author

*Telephone: 82-2-2260-3370. Fax: 82-2-2285-3370. E-mail: kwglee@dongguk.edu.

Funding

This study was supported by the Research and Development Convergence Center Support Program, Ministry for Agriculture, Food and Rural Affairs, Republic of Korea.

Notes

The authors declare no competing financial interest.

ABBREVIATIONS USED

ALA, alanine; SER, serine; RIB, ribose; GLU, glucose; SUC, sucrose; FUR, furoic acid; ACET, acetaldehyde; LOD, limit of detection; LOQ, limit of quantification; SD, standard deviation; RSD, relative standard deviation; SPME, solid-phase microextraction; GC−MS, gas chromatography−mass spectrometry

REFERENCES

(1) International Agency for Research on Cancer (IARC). *Monographs on the Evaluation of Carcinogenic Risks to Humans: Dry Cleaning, Some Chlorinated Solvents and Other Industrial Chemicals*; IARC: Lyon, France, 1995; Vol. *63*, pp 3194−3407.

(2) Moser, G. J.; Foley, J.; Burnett, M.; Goldsworhy, T. L.; Maronpot, R. Furan-induced dose−response relationships for liver cytotoxicity, cell proliferation, and tumorigenicity (furan-induced liver tumorigenicity). *Exp. Toxicol. Pathol.* **2009**, *61*, 101−111.

(3) Selmanoglu, G.; Karacaoglu, E.; Kilic, A.; Akay, M. T. Toxicity of food contaminant furan on liver and kidney of growing male rats. *Environ. Toxicol.* **2010**, *27*, 613−622.

(4) Food and Drug Administration (FDA). *Exploratory Data on Furan in Food Data*; FDA: Silver Spring, MD, 2004; http://www.fda.gov/OHRMS/DOCKETS/AC/04/briefing/4045b2_09_furan%20data (accessed June 2013).

(5) Kim, T. K.; Kim, S. H.; Lee, K. G. Analysis of furan in heat-processed foods consumed in Korea using solid phase microextraction−gas chromatography/mass spectrometry (SPME−GC/MS). *Food Chem.* **2010**, *123*, 1328−1333.

(6) Wegener, J. W.; Lopez-Sanchez, P. Furan levels in fruit and vegetables juices, nutrition drinks and bakery products. *Anal. Chim. Acta* **2010**, *672*, 55−60.

(7) Yaylayan, V. A. Precursors, formation and determination of furan in food. *J. Consum. Prot. Food Saf.* **2006**, *72*, 5−9.

(8) Van Lancker, F.; Adams, A.; Owczarek-Fendor, A.; Meulenaer, B. D.; Kimpe, N. D. Mechanistic insights into furan formation in Maillard model systems. *J. Agric. Food Chem.* **2011**, *59*, 229−235.

(9) Korea Food and Drug Administration (KFDA). *Korean Food Code*; KFDA: Seoul, Korea, 2011.

(10) Adams, A.; Van Lancker, F.; De Meulenaer, B.; Owczarek-Fendor, A.; De Kimpe, N. On-fiber furan formation from volatile precursors: A critical example of artefact formation during solid-phase microextraction. *J. Chromatogr. B: Anal. Technol. Biomed. Life Sci.* **2012**, *897*, 37−41.

(11) Fan, X. Formation of furan from carbohydrates and ascorbic acid following exposure to ionizing radiation and thermal processing. *J. Agric. Food Chem.* **2005**, *53*, 7826−2831.

(12) Huang, X.; Duan, H.; Barringer, S. A. Effects of buffer and temperature on formation of furan, acetic acid and formic acid from carbohydrate model systems. *LWT—Food Sci. Technol.* **2011**, *44*, 1761−1765.

(13) Nie, S.; Huang, J.; Zhang, Y.; Wang, S.; Li, C.; Marcone, M.; Xie, M. Effect of pH, temperature and heating time on the formation of furan in sugar−glycine model systems. *Food Sci. Hum. Wellness* **2013**, *2*, 87−92.

(14) Locas, C. P.; Yaylayan, V. A. Origin and mechanistic pathways of formation of the parent furans—A food toxicant. *J. Agric. Food Chem.* **2004**, *52*, 6830−6836.

(15) Owczarek-Fendor, A.; Meulenaer, B.; Scholl, G.; Adams, A.; Lancker, F. V.; Yogendrarajah, P.; Eppe, G.; Scippo, M.-L.; Kimpe, N. Furan formation from vitamin C in a starch-based model system: Influence of the reaction conditions. *Food Chem.* **2010**, *121*, 1163−1170.

(16) Yu, X.; Zhao, M.; Hu, J.; Zeng, S.; Bai, X. Correspondence analysis of antioxidant activity and UV−vis absorbance of Maillard reaction products as related to reactants. *LWT—Food Sci. Technol.* **2012**, *46*, 1−9.

JOURNAL OF AGRICULTURAL AND FOOD CHEMISTRY

Article

pubs.acs.org/JAFC

Interactions of Casein Micelles with Calcium Phosphate Particles

Lucile Tercinier,[†,‡] Aiqian Ye,*[,†] Skelte G. Anema,[‡] Anne Singh,[‡] and Harjinder Singh[†]

[†]Riddet Institute, Massey University, Private Bag 11 222, Palmerston North 4442, New Zealand

[‡]Fonterra Research and Development Centre, Private Bag 11 029, Palmerston North 4442, New Zealand

ABSTRACT: Insoluble calcium phosphate particles, such as hydroxyapatite (HA), are often used in calcium-fortified milks as they are considered to be chemically unreactive. However, this study showed that there was an interaction between the casein micelles in milk and HA particles. The caseins in milk were shown to bind to the HA particles, with the relative proportions of bound β-casein, α_S-casein, and κ-casein different from the proportions of the individual caseins present in milk. Transmission electron microscopy showed no evidence of intact casein micelles on the surface of the HA particles, which suggested that the casein micelles dissociated either before or during binding. The HA particles behaved as ion chelators, with the ability to bind the ions contained in the milk serum phase. Consequently, the depletion of the serum minerals disrupted the milk mineral equilibrium, resulting in dissociation of the casein micelles in milk.

KEYWORDS: *milk, caseins, casein micelle, calcium phosphate, hydroxyapatite, adsorption*

INTRODUCTION

Calcium fortification is a growing trend in the food industry, especially for milk and dairy products. However, fortifying milk with calcium can be a challenge, especially if the product has to be heat treated. When soluble calcium salts are added to milk, the ionic calcium modifies the mineral equilibrium of the milk. Consequently, the physicochemical characteristics of the casein micelles are modified and their heat stability decreases.[1] Therefore, insoluble calcium phosphate particles such as hydroxyapatite (HA) or calcium carbonate, rather than soluble salts, are often used for the calcium fortification of milk. When HA particles were added to cow's milk or soy milk, they were reported not to modify the ionic calcium content or the pH of the milk and, therefore, did not affect the heat stability of the casein micelles when the milk was sterilized.[2−4] They are therefore considered to be unreactive when added to milk. However, it is known that proteins can interact with HA particles, for example, in chromatographic columns or nanoceramic materials.[5,6] HA particles are not homogeneously charged. Proteins can adsorb to both positive and negative adsorbing sites that are expressed at the surface of HA particles.

The negative sites are formed by oxygen atoms associated with phosphate and are called P-sites. Positively charged groups of proteins, such as amino groups, can adsorb to P-sites.[7] The positively charged sites, called C-sites, are formed by calcium ions in the crystal lattice. C-sites can complex specifically with negatively charged groups of proteins, such as carboxyl or phosphoserine groups.[7] As milk proteins are negatively charged at the natural pH of milk, they can adsorb to the C-sites of HA, as has been reported in several previous studies. For example, Reynolds and Wong[8] showed that, at pH 7, all of the main milk proteins (α_{S1}-casein, β-casein, κ-casein, β-lactoglobulin, and α-lactalbumin) adsorb onto HA disks and cause them to acquire an overall negative charge. In our previous work,[9] we showed that caseins from sodium caseinate (SC) adsorb onto HA particles, resulting in negatively charged particles and providing an electrosteric stabilization to the particles.

Whey proteins from whey protein isolate (WPI) are also able to bind to HA particles but to a lesser extent than the caseins.[9] They are believed to bind to HA particles through their carboxyl groups, whereas the caseins in SC are considered to bind more strongly onto HA particles through both their carboxyl groups and their phosphoserine groups. SC is a mixture of the natural caseins contained in milk, without the calcium and phosphate, which are removed from the micelles during processing and are replaced by sodium.[10] Therefore, in SC, the casein molecules reassociate randomly and their phosphoserine groups are available for binding to the calcium of HA particles. In milk, however, the phosphoserine groups of the caseins are involved in the casein micelle structure and are already bound to the colloidal calcium phosphate (CCP).[11] Therefore, if exogenous HA particles are added to milk, it is not certain whether the caseins in the micelles will be able to bind to the HA particles. Also, about 20% of the protein in milk is whey proteins, and these may also bind to HA particles.

The salt composition of milk is likely to affect the adsorption of proteins onto HA particles, as the binding of proteins has been shown to depend on the mineral composition of the suspending medium.[12,13] Potential-determining ions can change the surface charge of the HA particles, thereby affecting the amount of protein that can bind to them. For example, calcium ions have been shown to give a positive charge to the surface of HA, and this enhances protein adsorption by increasing the number of sites available for protein binding through their carboxyl and phosphoserine groups.[14] Preliminary experiments (unpublished data) showed that the adsorption of both caseins and whey proteins decreased in simulated milk ultrafiltrate (SMUF), and this was attributed to the binding of phosphate or citrate ions from the milk serum, which competed with the negatively charged groups of the

Received: April 16, 2014
Revised: June 3, 2014
Accepted: June 4, 2014
Published: June 4, 2014

ACS Publications © 2014 American Chemical Society

dx.doi.org/10.1021/jf5018143 | J. Agric. Food Chem. 2014, 62, 5983−5992

proteins for adsorption. As milk contains free calcium, phosphate, and citrate ions, it is likely that these ions will adsorb onto HA particles. If the ions in milk bind to the HA surface, the mineral equilibrium of the milk serum phase could be disrupted, potentially affecting the integrity of the casein micelles.[15]

As HA particles are often added to milk for calcium fortification, it is important to understand the interactions that could take place between the milk proteins, the milk minerals, and the HA particles and whether they are likely to cause any instability in the products. Therefore, the objective of this research was to investigate whether or not the casein micelles and whey proteins contained in skim milk (SM) adsorbed onto HA particles when HA was added. The binding of casein micelles onto HA particles was investigated using both SM and whey-protein-depleted skim milk (WPD-SM). Transmission electron microscopy (TEM) was used to check whether or not casein micelles could be observed at the surface of the HA particles. To check whether the milk mineral equilibrium was affected by the addition of HA particles, increasing levels of HA particles were added to SMUF and SM and the soluble minerals were quantified. SM was also dialyzed against SMUF or against SMUF containing HA particles to check whether the presence of HA particles caused disruption of the casein micelles when casein micelles and HA particles were separated.

EXPERIMENTAL PROCEDURES

Materials. Fresh SM was obtained from a local supermarket and was used to prepare the WPD-SM. Low-heat skim milk powder (SMP) was obtained from Fonterra Co-operative Group Ltd., New Zealand. The protein content of the SMP was 33% (w/w). Food grade HA powder was purchased from Budenheim (TCP 53-83, Budenheim, Germany). The median diameter $d_{(0.5)}$ was found to be 4.5 μm. The specific surface area of the powder was determined according to the Brunauer–Emmett–Teller (BET) method and was reported to be 65 m^2/g. SMUF was prepared according to the method of Jenness and Koops,[16] and the pH was adjusted to 6.67. All of the chemicals used were of analytical grade and were obtained from Sigma-Aldrich unless otherwise specified.

Preparation of WPD-SM. WPD-SM was prepared using a bench-scale microfiltration (MF) membrane unit (Amicon hollow fiber membrane, H1P30-43, pore size = 0.1 μm). This membrane unit allows the passage of the two main whey proteins (β-lactoglobulin and α-lactalbumin), the lactose, and the serum-phase minerals to the MF permeate, but retains the casein micelles. Fresh SM (1.3 L) was run through the membrane. The volume of the MF permeate was monitored and an equivalent volume of SMUF containing 5% (w/w) lactose was added back to the milk. Seven successive rinses with SMUF were necessary to obtain a final WPD-SM containing only ~5% of the initial whey proteins. The WPD-SM was then spray-dried using a Yamato Pulvis spray-dryer (model GB-22, Yamato Scientific Co., Tokyo, Japan), and the powder obtained was stored in an airtight container in a refrigerator until needed. The protein content of the WPD-SM powder was measured using the Kjeldahl method and was found to be 31% (w/w).

Adsorption Experiment. Stock solutions (10% (w/w) total solids (TS) on a powder basis, corresponding to 3.3% (w/w) total protein) of WPD-SM and SM, were reconstituted from WPD-SM powder and SMP in Milli-Q water. The solutions were stirred for at least 1 h and were left overnight at 4 °C to equilibrate.

The stock solutions were centrifuged at low speed (3000*g* for 2 min) prior to the adsorption experiment. A small pellet of casein micelles was centrifuged down at this speed (variable amount between 5 and 10% of the total casein micelles). The supernatants were carefully poured out and used for further experiments.

Ranges of WPD-SM and SM solutions at different concentrations (0.15–2.8% (w/w) total protein) were prepared by diluting appropriate volumes of the WPD-SM and SM stock solutions in SMUF. As protein adsorption varies with ionic strength, pH, and mineral composition, SMUF was used to prepare successive dilutions of the WPD-SM and SM solutions so that the casein micelles were suspended in a solution of similar pH, ionic strength, and mineral composition, for all samples. A constant weight of the WPD-SM or SM solutions (0.95 g) of various protein concentrations (0.15–2.8% (w/w)) was added to Eppendorf tubes containing the same amount of HA powder (50 mg).

The suspensions were stirred for 2 h at room temperature (approximately 20 °C), as preliminary experiments had shown that equilibrium was reached after 2 h of adsorption. The suspensions were then centrifuged (3000*g* for 2 min) to separate the HA particles from the WPD-SM and SM solutions. Preliminary work (unpublished data) had established that, under these conditions, <5% (w/w) of the HA particles remained in suspension after centrifugation; this did not affect the results. The supernatants (referred to in this paper as the adsorption supernatants) were kept aside for further analysis. The adsorption experiments were repeated at least twice.

Analysis of the Unabsorbed Protein Contained in the Adsorption Supernatant. *Determination of Surface Protein Concentration and Composition by SDS-PAGE.* The concentration of unadsorbed protein contained in the adsorption supernatants was determined as a percentage of that in the initial WPD-SM or SM sample, using microfluidic chip sodium dodecyl sulfate–polyacrylamide gel electrophoresis (SDS-PAGE), as described by Anema,[17] and conventional SDS-PAGE, as described by Tercinier et al.[9] The amount of adsorbed protein (in mg of protein/m^2 of HA surface available) was calculated by difference between the amount of protein in the initial WPD-SM or SM solution and that in the supernatant, as described by Tercinier et al.[9] No correction was applied for the small portion of casein micelles that were centrifuged down during the centrifugation of HA particles, as it could not be measured precisely and was different for all samples prepared at different initial concentrations. However, it was estimated to be always <5% of the total unadsorbed caseins and did not have a significant effect on the calculation of the amount of adsorbed protein.

Nonmicellar Casein Content. Nonmicellar caseins were defined as those that did not sediment from the adsorption supernatants during centrifugation at 21000*g* and 25 °C for 60 min using a bench centrifuge (centrifuge 5417R, Eppendorf AG, Hamburg, Germany). The serum containing the nonmicellar caseins was carefully removed from the pellet (containing the casein micelles), and the protein content was determined by microfluidic chip SDS-PAGE and was expressed as a percentage of the protein content in the adsorption supernatants.

Casein Micelle Diameter Measurement. Dynamic light scattering (DLS) was performed using a Malvern Zetasizer Nano ZS instrument (Malvern Instruments, Malvern, Worcestershire, UK) to determine the hydrodynamic diameter (D_h) of the casein micelles. The samples were diluted in SMUF (25 μL of sample in 5 mL of SMUF), and 1 mL was transferred to a plastic cuvette and placed in the instrument; the automatic attenuator setting was used, and the temperature of the cell was maintained at 20 °C for the duration of the experiments. Measurements of the dynamics of the scattered light were collected at a scattering angle of 173°. Average diffusion coefficients were determined according to the method of cumulants and were translated into average particle hydrodynamic diameters using the Stokes–Einstein relationship for spheres.

Transmission Electron Microscopy. Three selected samples were prepared for TEM observation: WPD-SM, HA particles suspended in water, and 50 mg of HA particles suspended in 0.9 mL of WPD-SM. The general TEM method was similar to the method used by McKenna et al.[18] The WPD-SM solution was pipetted into agarose tubes, and the ends of the tubes were sealed with agarose. The suspensions of HA particles in water and in WPD-SM were mixed with warm 3% low-temperature-gelling agarose at a ratio of 1:1. This solution was poured onto a microscope slide, was allowed to set, and was chopped into 1 mm^3 cubes. Agarose-embedded tubes and cubes were put into bijoux bottles containing 3% glutaraldehyde in 0.2 M

dx.doi.org/10.1021/jf5018143 | J. Agric. Food Chem. 2014, 62, 5983–5992

sodium cacodylate buffer and were left at 5 °C for 24 h. The glutaraldehyde was rinsed twice with 0.2 M sodium cacodylate buffer over 2 h. The agarose-embedded samples were then placed in 1% osmium tetroxide overnight at 5 °C. The samples were placed in 1% uranyl acetate for 30 min and then rinsed twice with distilled water before dehydration. The dehydration process consisted of successive rinses of the samples carried out at 5 °C in 25% acetone for 15 min and in 50, 70, and 90% acetone for 30 min each, followed by 100% acetone (three changes over 90 min). The acetone was then replaced by embedding resin (Procure 812), and the bottles were placed on a rotator for 36 h. The cubes (for samples containing HA particles) and the tubes (for samples containing only WPD-SM) were then placed into an embedding capsule containing resin and baked at 60 °C for 48 h. The embedded samples were then sectioned to a thickness of 90 nm using a Reichert Ultracut microtome (Reichert-Jung, Heidelburg, Germany). These sections were mounted on 3 mm copper grids and stained with lead citrate before examination in a Philips TEM 201C transmission electron microscope (Philips, Eindhoven, The Netherlands) at an accelerating voltage of 60 kV.

Dialysis Experiment. A dialysis experiment was carried out using 10% TS (w/w) SM. A 5% TS (w/w) SM solution was prepared by diluting the 10% TS SM in SMUF. These SM solutions are referred to as 10%-SM and 5%-SM in this paper. Samples of the 5%-SM and 10%-SM (10 mL) were placed in dialysis bags (MEMBRA-CEL MC25-16 × 100 CLR) and dialyzed overnight at room temperature against SMUF (control) or SMUF containing 10% HA particles. The SM samples were removed from the dialysis bags, their visual turbidity was assessed by taking photographs, and the samples were analyzed for hydrodynamic diameters of casein micelle and nonmicellar casein content.

Mineral Concentrations. Total calcium was measured by inductively coupled plasma−atomic emission spectrometry. The ionic calcium concentration was measured using a Radiometer (Copenhagen, Denmark) type F2112 Ca calcium-specific electrode paired with an Orion (Beverly, MA, USA) Sure-Flow model 90-02 Ag/AgCl double-junction electrode with 0.08 M KCl in the outer electrode chamber. The standards used were $CaCl_2$ solutions (1−5 mM) in 0.08 M KCl. Inorganic phosphate (PO_4^{3-}) was determined by automated colorimetric analysis using a Technicon Auto-Analyzer. The samples were pumped through a segmented flow injection system, and inorganic phosphate was determined by using a procedure involving measurement of the absorption at 420 nm of a complex formed by orthophosphate ions and a phosphate color reagent, containing ammonium molybdate and ammonium metavanadate. Citrate was measured by an enzymatic method, involving successive enzymatic reactions with citrate lyase, malate dehydrogenase, lactate dehydrogenase, and $NADH/H^+$. After the enzymatic reactions, the concentration of $NADH/H^+$, which was stoichiometric with the concentration of citric acid, was determined by measuring the absorbance at 365 nm.

Statistical Analysis. *t* tests and analysis of variance (ANOVA) tests were carried out using Minitab software (Minitab version 16, Minitab, Inc., State College, PA, USA) to determine the significance of the differences. Significance was established at $P < 0.05$.

RESULTS AND DISCUSSION

Adsorption of Caseins and Whey Proteins. The adsorption studies were carried out by adding a constant amount of HA to WPD-SM or SM solutions of different protein concentration (0.15−2.8% (w/w)). After 2 h of stirring, the HA was separated from the WPD-SM or SM solutions by centrifugation, and the supernatants (referred to as the adsorption supernatants) were analyzed for protein composition and concentration using SDS-PAGE. The adsorbed protein concentration was calculated as the difference between the total protein concentration and the unadsorbed protein concentration in each sample.

Figure 1 shows the unadsorbed protein concentration measured in the adsorption supernatants and the amount of

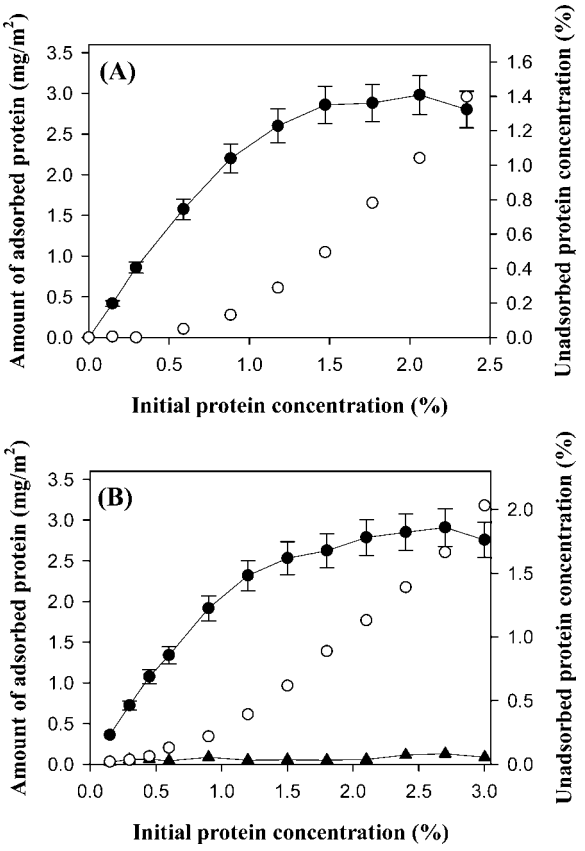

Figure 1. Amount of (●) caseins and (▲) whey proteins adsorbed onto HA particles (mg/m²) and (○) unadsorbed protein concentration (% (w/w)) as a function of initial protein concentration: (A) WPD-SM; (B) SM. Fifty milligrams of HA particles was added in 0.95 mL of WPD-SM and SM; the total surface area of HA was 3.25m². Results are means of duplicates or triplicates with error bars for the standard deviation.

adsorbed proteins on the surface of the HA particles as a function of the initial protein concentration for both WPD-SM (Figure 1A) and SM (Figure 1B). For both WPD-SM and SM, at low initial protein concentration (<0.5%), the amount of protein that remained in the supernatants (i.e., the unadsorbed protein) was very low. As the initial protein concentration increased, the amount of unadsorbed protein increased considerably. For both systems, the amount of adsorbed caseins increased gradually until it reached a plateau value, corresponding to a maximum protein coverage of the surface of the HA particles. For HA particles mixed with WPD-SM, the surface casein concentration increased gradually with the initial protein concentration up to about 1.5% (w/w, total protein) and reached a maximum value of ∼2.9 mg/m². For HA particles mixed with SM, the amount of adsorbed casein increased with the initial protein concentration up to about 2% (w/w, total protein) and reached a maximum value of ∼2.8 mg/m² (Figure 1B). These results clearly showed that the caseins from WPD-SM and SM adsorbed at the surface of HA particles, to similar maximum amounts of ∼2.9 mg/m². In contrast, the maximum amount of whey proteins from SM that bound to HA particles was ∼0.1 mg/m², which was negligible, as it represented only ∼3% of the total protein bound (Figure 1B).

Both caseins and whey proteins have been shown to bind to HA at pH ∼7, when adsorption studies are carried out in water or buffer.[8,9] As both caseins and whey proteins carry a net

dx.doi.org/10.1021/jf5018143 | J. Agric. Food Chem. 2014, 62, 5983−5992

negative charge at the milk pH, they mostly adsorb onto HA particles via an interaction between their negatively charged groups (carboxyl groups for the whey proteins, and both carboxyl and phosphoserine groups for the caseins) and the calcium sites (C-sites) on HA particles.[5−7] However, as the interactions between the C-sites and phosphoserine groups are stronger than those between the C-sites and carboxyl groups, caseins bind to HA to a greater extent than whey proteins.[9] As the phosphoserine groups of the caseins are grouped in clusters, the caseins probably also carry more anchor points to bind to the C-sites on HA particles than the whey proteins, which would partly explain the higher surface load for caseins compared with whey proteins.[19,20]

Also, in a milk environment, there is competition for binding between the milk ions and the milk proteins. Our previous work (unpublished data) on the binding of both caseins from SC and whey proteins from WPI in SMUF showed that the whey proteins from WPI could bind to HA particles only at a very low level (~0.5 mg/m^2), as they had to compete for binding with the divalent milk anions, mostly phosphate and citrate present in SMUF. However, as the interactions between caseins and HA are stronger, caseins could compete better with the milk ions for binding and more casein was bound (~2.4 mg/m^2). Negligible whey protein binding was therefore expected when HA particles were added to SM, and this is what was observed (Figure 1). Devold et al.[21] showed that, at the milk pH, only caseins were able to bind to the HA in tooth enamel and there was no whey protein binding.

The caseins in SC are in a nonmicellar form and can be present as individual molecules or small aggregates,[22] whereas the caseins in WDP-SM and SM are associated together to form casein micelles. The Langmuir model is often used in studies on the adsorption of protein onto HA, to compare the adsorption characteristics of different types of protein.[23−25] The Langmuir model was therefore fitted to the adsorption data obtained in this study for WPD-SM and SM and for SC in water and SMUF (unpublished data), to compare the adsorption characteristics of the caseins from SC, WPD-SM, and SM. The Langmuir model quantifies the amount of protein adsorbed onto HA as a function of the protein concentration once equilibrium has been reached (in this case, the unadsorbed protein concentration) at a given temperature. This model assumes that the proteins bind to a series of distinct empty sites on the HA surface. The surface is assumed to be energetically homogeneous, and the model allows only a monolayer coverage. The Langmuir model is given by eq 1

$$\frac{m_{abs}}{S} = q_m \times \frac{K[P]}{1 + K[P]} \quad (1)$$

where m_{abs}/S is the amount of protein bound to the surface expressed in mg/m^2, [P] is the concentration of protein at equilibrium (g/100 g), q_m is the maximum monolayer surface coverage (mg/m^2), and K is the Langmuir affinity constant and is dimensionless.

The Langmuir isotherm curves for casein adsorption onto HA for the adsorption experiments carried out with WPD-SM and SM are given in Figure 2. Table 1 gives the calculated Langmuir constants for each of the isotherms and for the adsorption data of SC onto HA in water and in SMUF. The maximum surface protein concentrations obtained for both WPD-SM and SM experiments (Figure 1) (3.0 and 2.7 mg/m^2, respectively) were not different from the maximum adsorption value obtained for SC in water (2.9 mg/m^2, $P < 0.05$) and were only slightly higher than the maximum adsorption value for SC in SMUF (2.4 mg/m^2).

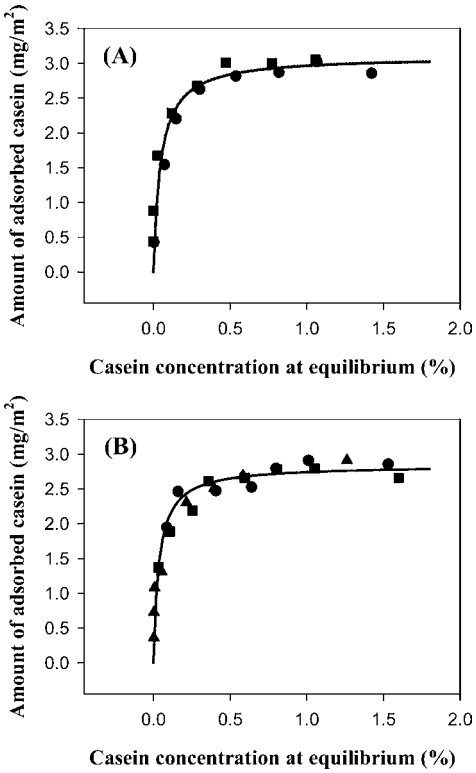

Figure 2. Adsorption isotherms of caseins onto HA particles: (A) WPD-SM; (B) SM; (●, ▲, ■) experimental data from different repeat experiments; (solid line) best-fit Langmuir curve.

Table 1. Parameters for the Adsorption of Caseins from WPD-SM, SM, and SC in Water and in SMUF, Calculated According to the Langmuir Model[a]

casein source	affinity constant, K	max surface coverage, q_m (mg/m^2)
WPD-SM	24.5ab ± 9	3.0a ± 0.02
SM	31.5a ± 7.1	2.7ab ± 0.15
SC in water	13.7b ± 4.8	2.9a ± 0.2
SC in SMUF	31.5a ± 3.6	2.4b ± 0.01

[a]Means with different letters differ significantly ($P < 0.05$; vertical comparison).

In food emulsion systems, casein micelles have been shown to bind as intact micelles onto oil droplets.[26,27] The surface protein concentration for casein-micelle-coated droplets has been reported to be much higher than that for SC-coated droplets,[27,28] with usually 2 or 3 times more adsorbed protein for casein micelles than for SC. As casein micelles are larger than SC aggregates, they form a thicker layer at the surface of the oil droplets so that the protein surface load is higher. The fact that the maximum amount of casein adsorbed onto HA was similar for WPD-SM, SM and SC in SMUF (Table 1) could indicate that casein micelles do not bind as intact micelles to HA particles. The affinity constant of the Langmuir model characterizes the initial slope of the adsorption isotherms and indicates a high affinity of protein for HA.[24] There was a variability of the affinity constants in this study (Table 1), as a small variation in the first points of the adsorption isotherms (Figure 2) can lead to a high variation of the slope and, therefore, of the affinity constant. However, it is interesting to

dx.doi.org/10.1021/jf5018143 | J. Agric. Food Chem. 2014, 62, 5983−5992

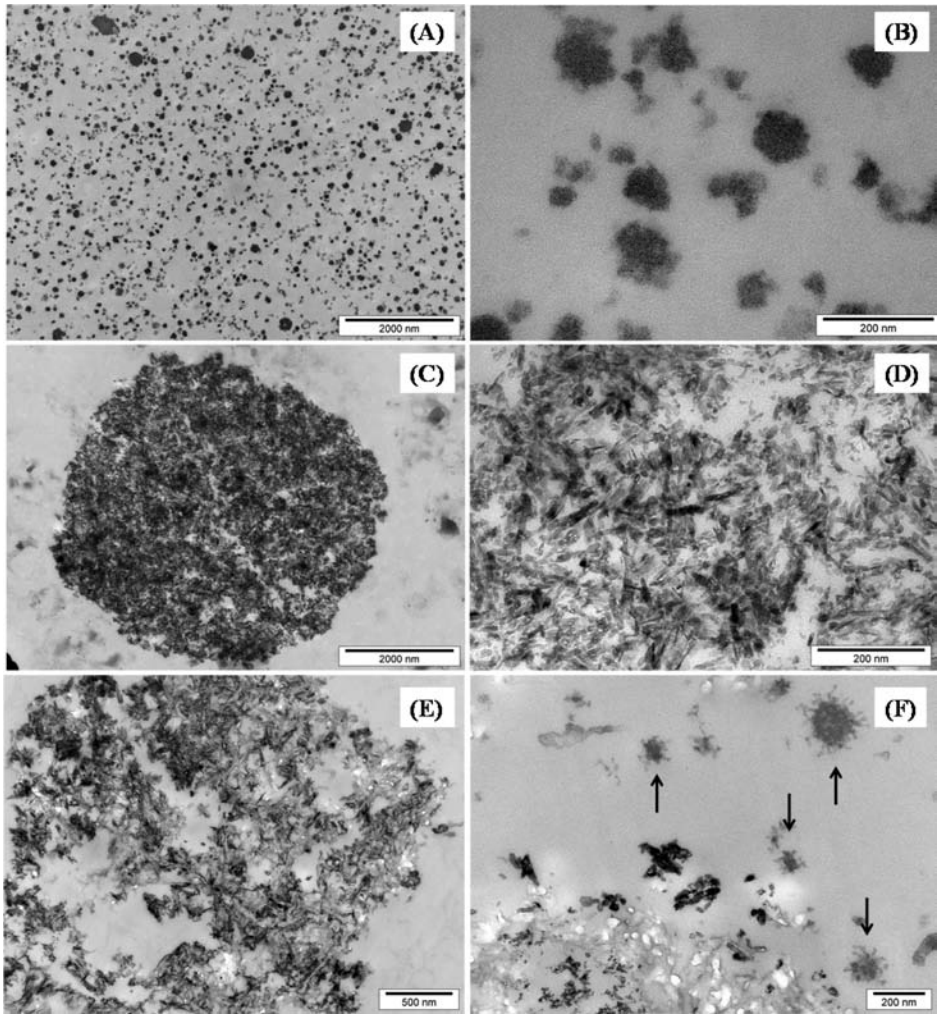

Figure 3. TEM micrographs obtained from (A, B) WPD-SM solution reconstituted from WPD-SMP in water (10% (w/w)); (C, D) suspension of HA particles in SMUF; (E, F) suspension of HA particles in WPD-SM solution, corresponding to a stage of adsorption at which the maximum amount of adsorbed protein was reached. The arrows show the remaining unbound casein micelles in the suspending phase.

note that the mean affinity constants were similar for the casein adsorption experiments carried out on SC in SMUF, WDP-SM, and SM binding to HA (Table 1). This suggests that the adsorption mechanisms and the affinity of HA for micellar and nonmicellar forms of caseins in a milk environment are somewhat similar.

Transmission Electron Microscopy. TEM was carried out to examine the structure of the adsorbed caseins at the surface of the HA particles. Panels A and B of Figure 3 show TEM images from a solution of WPD-SM. The casein micelles in WPD-SM appear to be dark spherical aggregates, to be well dispersed, and to have diameters ranging from ∼30 to 150 nm, consistent with the images of casein micelles observed in previous studies.[29−31] Panels C and D of Figure 3 show TEM images of the HA powder used in this study. It consists of particles of ∼4 μm average diameter. However, these particles are made of elementary nanometer-sized rod-like particles (Figure 3D) that aggregate together into micrometer-sized particles, as has been observed previously.[32,33]

Panels E and F of Figure 3 show images of the HA particles suspended in WPD-SM. As the particles had been stirred for 2 h in the WPD-SM before preparation for TEM, the caseins had adsorbed to the HA particles. The HA particles had an appearance similar to that of the HA particles in the control (Figure 3C). No casein micelles could be seen on the surfaces of the particles (Figure 3E,F). It was therefore hypothesized that the caseins did not adsorb as intact micelles, but as small aggregates and/or individual molecules, which would be too small to be observed with TEM. The unadsorbed casein micelles could still be seen in the suspending phase around the particles, as shown by the arrows in Figure 3F. These unadsorbed micelles had a hairy and disorganized appearance compared with the control (Figure 3A,B), which may have been because they were partly dissociated in the presence of HA particles.

Analysis of Unadsorbed Caseins. The initial adsorption measurements and TEM observations led to the hypothesis that casein micelles did not bind to HA particles as intact micelles, possibly because the micelles dissociated either before or shortly after binding. To verify this hypothesis, the supernatants containing the unadsorbed proteins were analyzed for casein content, particle size, and protein composition.

The supernatants were centrifuged at 21000*g* and 25 °C for 60 min; the pellet contained micellar caseins, whereas the nonmicellar caseins stayed in the serum phase. This serum phase was analyzed for protein content using microfluidic chip SDS-PAGE. Figure 4 shows the distribution of the unadsorbed caseins between micellar and nonmicellar forms (Figure 4A)

dx.doi.org/10.1021/jf5018143 | J. Agric. Food Chem. 2014, 62, 5983−5992

and their size (Figure 4B) as a function of the initial protein concentration.

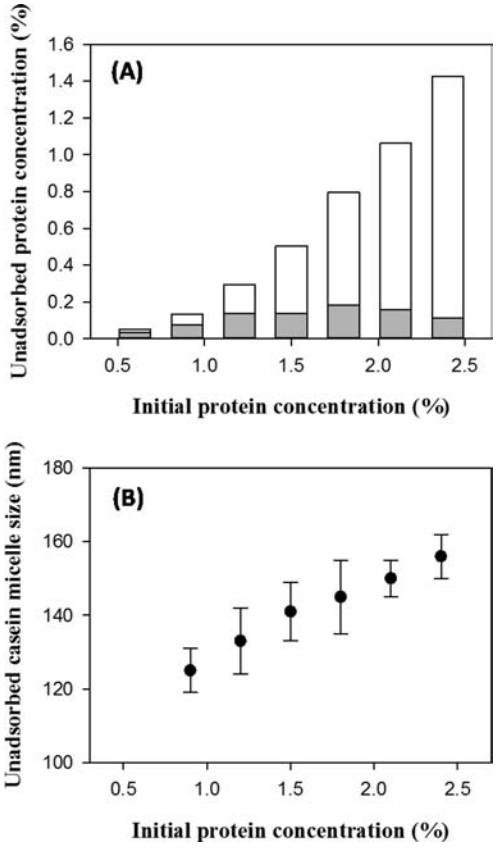

Figure 4. (A) Distribution of unadsorbed caseins between (white bar) micellar and (gray bar) nonmicellar forms and (B) diameters of unadsorbed caseins. Error bars represent standard deviation.

At low initial protein concentration, more than half of the unadsorbed caseins were in a nonmicellar form. For example, when the HA particles were prepared with WPD-SM containing 0.9% protein, 0.08% of the unadsorbed protein was nonmicellar (Figure 4A), which represented ∼57% of the unadsorbed proteins (total 0.14%). As the initial protein concentration increased, the proportion of nonmicellar casein in the unadsorbed protein decreased, reaching approximately 5% when HA particles were prepared with WPD-SM containing 2.4% protein (0.08% of 1.4% unadsorbed protein), which was close to the level of nonmicellar casein in the initial WPD-SM solutions (∼3% nonmicellar casein, data not shown).

At low initial protein concentration, the average diameter of the unadsorbed casein particles was about ∼122 nm (Figure 4B). As the initial protein concentration increased, the diameter increased, until it reached ∼155 nm, which was close to the size of the casein micelle in the initial WPD-SM solutions (160 nm).

Figure 5 shows the protein composition of the unadsorbed proteins as a function of the initial protein concentration. For the adsorption experiments carried out with WPD-SM containing <1% (w/w) protein, the ratio of unadsorbed κ-casein to unadsorbed α_S- and β-caseins was considerably greater than in the original WPD-SM (the composition of the original WPD-SM is indicated by the lines in Figure 5 and was α_S-casein 50%, β-casein 38%, and κ-casein 12%, based on the theoretical

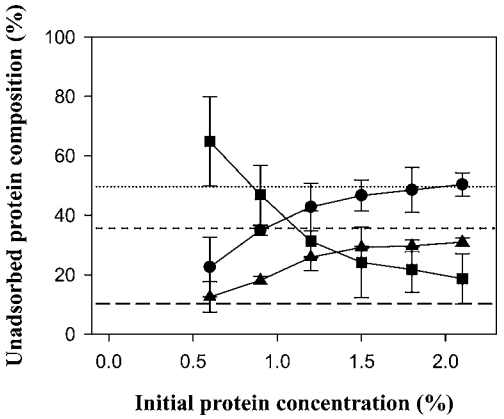

Figure 5. Composition of the supernatants containing the unadsorbed protein after adsorption of WPD-SM onto HA particles as a function of the initial protein concentration: (●) α_S-casein (α_{S1} + α_{S2}); (▲) β-casein; (■) κ-casein. The lines indicate the composition of the original WPD-SM in (dotted line) α_S-casein (α_{S1} + α_{S2}), (short dashed line) β-casein, and (long dashed line) κ-casein. Error bars represent standard deviation.

proportions of the individual proteins in SM[10]). For example, when HA particles were mixed with WPD-SM containing 0.6% protein, ∼60% of the unadsorbed protein was κ-casein, which is substantially higher than the proportion found in milk (12%). The ratio of unadsorbed α_S-casein to unadsorbed β-casein remained approximately constant. As the initial protein concentration in the SM increased, the relative proportions of the three unadsorbed individual caseins gradually approached the initial WPD-SM composition as more and more unadsorbed protein accumulated in the supernatant.

Analysis of the unadsorbed proteins showed that the proportions of micellar casein in the unadsorbed casein fraction (Figure 4A), the casein micelle size (Figure 4B), and the protein composition (Figure 5) were not constant across the range of initial protein concentrations studied. The unadsorbed caseins obtained at low initial protein concentrations contained a higher proportion of κ-casein, contained a higher proportion of nonmicellar casein, and were of a smaller size compared with the unadsorbed caseins obtained at high initial protein concentration. This confirmed that the caseins were not bound to the HA particles as intact micelles and that the casein micelle structure was disrupted by the addition of HA particles. However, it was not possible to determine whether the casein micelles dissociated first and then the liberated caseins bound to HA or casein micelles adsorbed as intact micelles and then dissociated, allowing only the strongly bound caseins to remain on the HA particle surface. However, as there was no change in the proportions of the different caseins adsorbed onto the HA particles as a function of time, from 1 min to 3 h (data not shown), it is believed that the caseins first dissociated from the micelles and then bound independently. However, further experiments would be needed to confirm this hypothesis.

The amounts of the individual proteins adsorbed onto HA were calculated from the composition of the unadsorbed protein and the original protein composition of the WPD-SM (Figure 6). When the initial protein concentration was varied from 0 to 2.5%, the amounts of adsorbed α_S-casein, β-casein, and κ-casein increased gradually until they reached maxima of ∼1.5, 1.3, and 0.15 mg/m^2, respectively. The maximum amount of bound κ-casein represented only ∼5% of the total bound

dx.doi.org/10.1021/jf5018143 | J. Agric. Food Chem. 2014, 62, 5983−5992

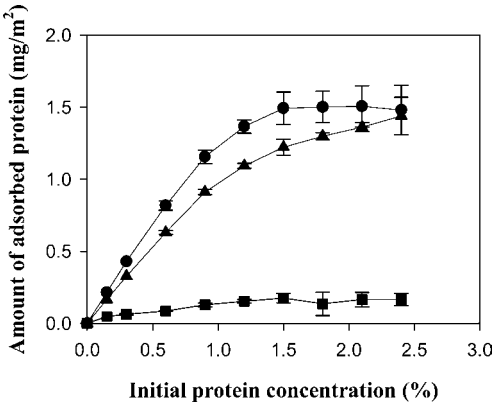

Figure 6. Estimated amount of adsorbed caseins (mg/m^2) on HA particles as a function of initial protein concentration of WPD-SM: (●) α_S-casein (α_{S1} + α_{S2}); (▲) β-casein; (■) κ-casein. Error bars represent standard deviation.

protein (0.15 mg/m^2 of 2.9 mg/m^2), even though the original WPD-SM contained ∼12% κ-casein. This confirms that α_S-casein and β-casein are preferentially adsorbed over κ-casein.

The preference for α_S- and β-caseins binding to HA has been shown previously and has been attributed to the high content of phosphoserine residues in both α_S- and β-caseins, compared with κ-casein.[9] Caseins adsorb mainly through their phosphoserine residues, which bind to calcium on the HA particles. α_{S1}-Casein, α_{S2}-casein, and β-casein contain 7−9, 10−13, and 5 phosphoserine residues, respectively, whereas κ-casein contains only 1 phosphoserine residue.[34] As α_S- and β-caseins carry more residues that can bind to the C-sites on HA particles, they can bind to a greater extent. As the casein micelles are probably disrupted by the addition of HA particles, the phosphoserine groups of α_S- and β-caseins must become available to bind to HA particles.

It has been shown previously that both α_S- and β-caseins contain specific phosphopeptides with a high ability to bind to calcium phosphate.[35−37] They contain similar calcium phosphate binding motifs, made of a sequence of amino acids containing three phosphoserine residues followed by two glutamic acid residues.[38] These casein-derived phosphopeptides (CPP) have been produced and purified by enzymatic digestion and have been bound to amorphous calcium phosphate (ACP) to form complexes (CPP−ACP).[39,40] It is probably the same motif of amino acids as involved in the CPP−ACP complexes that are involved in the binding of α_{S1}-casein, α_{S2}-casein, and β-casein to HA particles.

Mechanism of Casein Micelle Dissociation by HA Particles. This study has shown that the addition of HA particles to WPD-SM and SM causes dissociation of casein micelles into individual casein or casein aggregates that then bind to the HA particles. However, it is not known why the addition of HA particles causes the dissociation of the casein micelles. To further investigate the mechanism, a dialysis experiment and mineral quantification were carried out.

Dialysis Experiments. 10%-SM and 5%-SM were dialyzed overnight against SMUF (controls) or SMUF containing HA particles to ascertain whether the presence of HA particles caused the dissociation of the casein micelles when not in direct contact.

When removed from the dialysis bags, the 10%-SM and 5%-SM dialyzed against SMUF containing HA particles (cuvettes B and D, respectively, in Figure 7) were less turbid than their

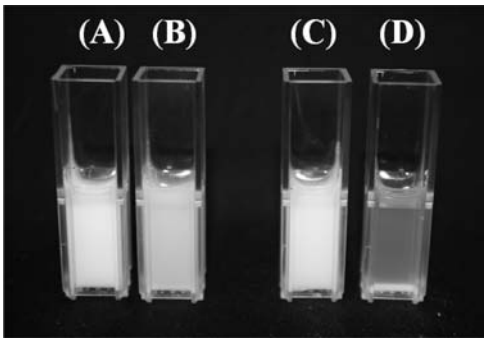

Figure 7. Visual turbidity of SM samples after dialysis against SMUF or against SMUF containing 10% (w/w) HA particles: (A) 10%-SM dialyzed against SMUF; (B) 10%-SM dialyzed against SMUF containing 10% (w/w) HA particles; (C) 5%-SM dialyzed against SMUF; (D) 5%-SM dialyzed against SMUF containing 10% (w/w) HA particles.

respective controls dialyzed against SMUF (cuvettes A and C, respectively, in Figure 7). For the lower concentration of SM (5%-SM), the sample dialyzed against SMUF containing HA particles was almost transparent, indicating that almost all of the casein micelles had dissociated. This shows that the casein micelles in the milks dialyzed against HA particles dissociated during the dialysis process, even though they were not in direct contact with the particles. This was confirmed by measurement of the nonmicellar casein content and the casein micelle diameter of the dialyzed milks (Table 2). The casein micelle diameter of the control SM was ∼230 nm for both 10%-SM and 5%-SM, and both milks contained <5% nonmicellar caseins, which was similar to the original nondialyzed SM. This shows that the milks dialyzed against SMUF were stable during dialysis. The 10%-SM and 5%-SM dialyzed against SMUF containing HA particles contained 73 and 94% nonmicellar caseins, respectively. The casein micelle diameter of 10%-SM dialyzed against SMUF containing HA particles was 165 nm; that of 5%-SM treated identically could not be measured by the Zetasizer because the sample did not show the required turbidity.

Table 2. Nonmicellar Casein Content and Casein Micelle Diameter of the Dialyzed Milks

sample	nonmicellar caseins (%)	casein micelle diameter (nm)
10%-SM		
dialyzed against SMUF	3	230
dialyzed against HA in SMUF	73	165
5%-SM		
dialyzed against SMUF	5	227
dialyzed against HA in SMUF	94	N/A[a]

[a]N/A, not applicable.

Mineral Quantification. The observations that HA caused the casein micelles to dissociate even when not in direct contact (Figure 7) led to the hypothesis that HA particles were able to draw out some of the minerals contained in SMUF, which would cause the casein micelles to dissociate. It has been shown previously that calcium, phosphate, and citrate ions can adsorb to HA.[12,41] The ions contained in SMUF must have adsorbed

dx.doi.org/10.1021/jf5018143 | J. Agric. Food Chem. 2014, 62, 5983−5992

onto HA particles, disrupting the salt balance in the SMUF. This hypothesis was tested by adding different amounts of HA particles (from 0 to 18% (w/w)) into SMUF and SM and then measuring ionic calcium, total calcium, and inorganic phosphate.

Figure 8 shows the variation in the ionic calcium concentration when HA particles at different concentrations

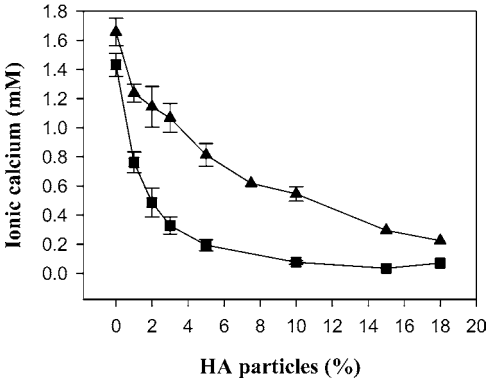

Figure 8. Effect of addition of HA particles in (■) SMUF and in (▲) SM on ionic calcium concentration. Error bars represent standard deviation.

(from 0 to 18% (w/w)) were added to SMUF or to SM. The SM and SMUF contained ∼1.7 and ∼1.45 mM ionic calcium, respectively, which was in accordance with the values reported in the literature.[42−44] As more HA particles were added to both SMUF and SM, the ionic calcium concentration decreased, with the decrease being more pronounced in SMUF. The addition of 10% (w/w) HA particles led to ionic calcium concentrations of ∼0.1 mM in SMUF and ∼0.55 mM in SM, which represented losses of 93 and 68% of the initial ionic calcium, respectively. The decrease in ionic calcium on the addition of HA particles indicates that ionic calcium binds to these particles. As ionic calcium binds to HA particles, CCP must be released from the casein micelles to compensate for the loss of ionic calcium in the serum, thereby explaining the smaller decrease in ionic calcium for SM than for SMUF. The binding of ionic calcium onto the HA particles was a relatively fast process; the ionic calcium concentration reached a stable level in <5 min (data not shown).

A mineral analysis was also carried out on SMUF and SM samples after the HA particles had been removed from the solution by centrifugation. As HA particles were added to SM at increasing concentration from 0 to 18% (w/w), the concentrations of total calcium, citrate, and inorganic phosphate decreased (Figure 9A). The initial SM contained ∼21.5 mmol/kg inorganic phosphate, ∼28.5 mmol/kg calcium, and ∼11 mmol/kg citrate, which are consistent with the values reported previously for SM.[15] On the addition of 18% HA particles to SM, the calcium concentration in the SM decreased by ∼93%, from 28.5 to 2.2 mmol/kg, the inorganic phosphate concentration decreased by ∼68%, from 21.6 to 6.8 mmol/kg, and the citrate concentration decreased by ∼74%, from 11 to 2.85 mmol/kg. Part of the decrease was probably because the calcium, phosphate, and citrate that were contained in the casein micelles before they dissociated and adsorbed on the HA particles sedimented out with the HA particles during centrifugation. However, CCP contains only ∼50% of the total inorganic phosphate, ∼70% of the total calcium, and ∼20% of the total citrate contained in milk. As the percentage decreases in calcium, phosphate, and citrate on the addition of 18% HA particles to SM were higher than the percentage of the corresponding mineral in CCP, calcium, phosphate, and citrate ions must have bound to HA particles, depleting the milk serum in these ions.

This was confirmed by the mineral analysis results when HA particles were added to SMUF (Figure 9B). On the addition of 15% HA particles to SMUF, the total calcium concentration decreased by ∼95%, from 8.7 to 0.5 mmol/kg, the inorganic phosphate concentration decreased by ∼53%, from 11.6 to 5.5 mmol/kg, and the citrate concentration decreased by ∼77%, from 9.8 to 2.3 mmol/kg. The decrease in calcium was faster and more pronounced than the decreases in phosphate and citrate, probably because phosphate and citrate have to compete for the same binding sites on the HA surface (positive sites, C-sites), whereas only calcium ions can bind to the negative sites (P-sites), and because more P-sites than C-sites are expressed on the surface of HA at pH ∼7, as shown by a negative zeta-potential of ∼ −9 mV (data not shown).

The disruption effect of HA on the integrity of the casein micelle and on the milk mineral equilibrium can also be explained by taking into account the thermodynamic aspects of calcium phosphate growth and sequestration. In milk, calcium and phosphate are sequestered in the form of calcium phosphate nanoclusters inside the casein micelle.[45] The phosphoserine groups of the caseins are bound to the calcium phosphate nanoclusters inside the micelles, keeping the calcium phosphate in a thermodynamically metastable state in which its precipitation and further growth are prevented.[46,47] However, when HA particles are added to milk, it is possible that the

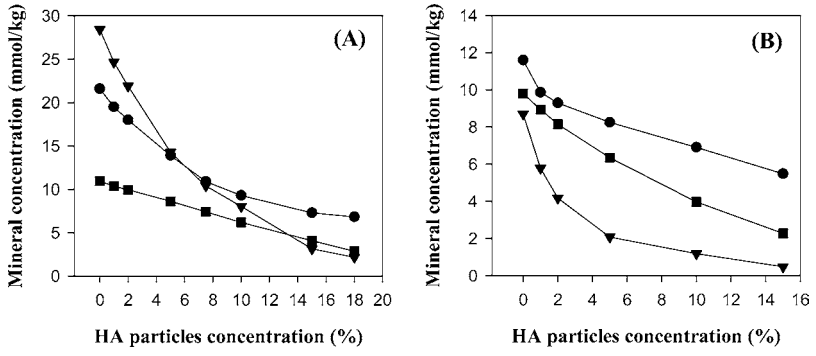

Figure 9. Effect of addition of HA particles in (A) SM and (B) SMUF on (▼) total calcium, (■) total citrate, and (●) inorganic phosphate concentrations. HA particles were removed from the solution by centrifugation before the measurements.

dx.doi.org/10.1021/jf5018143 | J. Agric. Food Chem. 2014, 62, 5983−5992

most stable form of calcium phosphate (HA) grows at the expense of the least stable form (calcium phosphate sequestered in the casein micelles). The calcium phosphate inside the casein micelles would therefore be released to contribute to the growth of the HA particles, leading to micelle dissociation. The process of calcium phosphate growth is generally very slow. However, the HA particles used in this study may have provided a very large surface of initially crystallized HA that would allow a fast crystallization of calcium phosphate from the minerals that were drawn out of the milk serum onto the HA particles.[48]

In conclusion, this study showed the existence of interactions between casein micelles and HA particles. The addition of HA particles to SM causes the dissociation of the casein micelles and the binding of the individual caseins to the particles. This dissociation of the casein micelles is a consequence of calcium, phosphate, and probably citrate ions contained in the milk serum binding to the surface of the HA particles. Consequently, CCP of casein micelle is drawn out of the micelles, and the structure of the casein micelles is disrupted. Therefore, the phosphoserine groups of α_S- and β-caseins become available to bind to HA particles. Both α_S- and β-caseins were preferentially bound compared with κ-casein, and this was attributed to the higher content of phosphoserine residues of both α_S- and β-caseins. The results of this study indicate that the addition of hydroxyapatite particles to milk may compromise the stability of the milk by disrupting the equilibrium of the milk minerals and dissociating the casein micelles.

AUTHOR INFORMATION

Corresponding Author

*(A.Y.) Phone: +64-6-350-5072. Fax: +64-6-350-5655. E-mail: a.m.ye@massey.ac.nz.

Funding

We gratefully acknowledge Fonterra Research and Development Centre for their financial support.

Notes

The authors declare no competing financial interest.

ACKNOWLEDGMENTS

We gratefully acknowledge Michael Loh for his help with TEM and Claire Woodhall for proofreading the manuscript.

ABBREVIATIONS USED

ACP, amorphous calcium phosphate; ANOVA, analysis of variance; CCP, colloidal calcium phosphate; CPP, casein-derived phosphopeptides; HA, hydroxyapatite; MF, microfiltration; SC, sodium caseinate; SDS-PAGE, sodium dodecyl sulfate−polyacrylamide gel electrophoresis; SM, skim milk; SMP, skim milk powder; SMUF, simulated milk ultrafiltrate; TEM, transmission electron microscopy; TS, total solids; WDP-SM, whey protein-depleted skim milk; WPI, whey protein isolate

REFERENCES

(1) Philippe, M.; Le Graët, Y.; Gaucheron, F. The effects of different cations on the physicochemical characteristics of casein micelles. *Food Chem.* **2005**, *90*, 673−683.

(2) Chaiwanon, P.; Puwastien, P.; Nitithamyong, A.; Sirichakwal, P. P. Calcium fortification in soybean milk and in vitro bioavailability. *J. Food Compos. Anal.* **2000**, *13*, 319−327.

(3) Omoarukhe, E. D.; On-Nom, N.; Grandison, A. S.; Lewis, M. J. Effects of different calcium salts on properties of milk related to heat stability. *Int. J. Dairy Technol.* **2010**, *63*, 504−511.

(4) Pathomrungsiyounggul, P.; Grandison, A. S.; Lewis, M. J. Effects of calcium-chelating agents and pasteurisation on certain properties of calcium-fortified soy milk. *Int. J. Food Sci. Technol.* **2010**, *45*, 2234−2240.

(5) Bernardi, G.; Kawasaki, T. Chromatography of polypeptides and proteins on hydroxyapatite columns. *Biochim. Biophys. Acta* **1968**, *160*, 301−310.

(6) Kawasaki, T. Hydroxyapatite as a liquid chromatographic packing. *J. Chromatogr., A* **1991**, *544*, 147−184.

(7) Gorbunoff, M. J.; Timasheff, S. N. The interaction of proteins with hydroxyapatite: III. Mechanism. *Anal. Biochem.* **1984**, *136*, 440−445.

(8) Reynolds, E. C.; Wong, A. Effect of adsorbed protein on hydroxyapatite zeta potential and *Streptococcus mutans* adherence. *Infect. Immun.* **1983**, *39*, 1285−1290.

(9) Tercinier, L.; Ye, A.; Anema, S.; Singh, A.; Singh, H. Adsorption of milk proteins on to calcium phosphate particles. *J. Colloid Interface Sci.* **2013**, *394*, 458−466.

(10) Wong, D. W. S.; Camirand, W. M.; Pavlath, A. E.; Parris, N.; Friedman, M. Structures and functionalities of milk proteins. *Crit. Rev. Food Sci. Nutr.* **1996**, *36*, 807−844.

(11) Dalgleish, D. G. On the structural models of bovine casein micelles − review and possible improvements. *Soft Matter* **2011**, *7*, 2265−2272.

(12) Yin, G.; Liu, Z.; Zhan, J.; Ding, F.; Yuan, N. Impacts of the surface charge property on protein adsorption on hydroxyapatite. *Chem. Eng. J.* **2002**, *87*, 181−186.

(13) Zhu, X. D.; Fan, H. S.; Li, D. X.; Xiao, Y. M.; Zhang, X. D. Protein adsorption and zeta potentials of a biphasic calcium phosphate ceramic under various conditions. *J. Biomed. Mater. Res., Part B* **2007**, *82*, 65−73.

(14) Wassell, D. T. H.; Hall, R. C.; Embery, G. Adsorption of bovine serum albumin onto hydroxyapatite. *Biomaterials* **1995**, *16*, 697−702.

(15) Holt, C. The milk salts: their secretion, concentrations and physical chemistry. In *Developments in Dairy Chemistry—3*; Fox, P. F., Ed.; Elsevier Applied Science Publishers: Amstersdam, The Netherlands, 1985; pp 143−181.

(16) Jenness, R.; Koops, J. Preparation and properties of a salt solution which simulates milk ultrafiltrate. *Neth. Milk Dairy J.* **1962**, *16*, 153−164.

(17) Anema, S. G. The use of "lab-on-a-chip" microfluidic SDS electrophoresis technology for the separation and quantification of milk proteins. *Int. Dairy J.* **2009**, *19*, 198−204.

(18) McKenna, A. B.; Lloyd, R. J.; Munro, P. A.; Singh, H. Microstructure of whole milk powder and of insolubles detected by powder functional testing. *Scanning* **1999**, *21*, 305−315.

(19) Johnsson, M.; Levine, M. J.; Nancollas, G. H. Hydroxyapatite binding domains in salivary proteins. *Crit. Rev. Oral Biol. Med.* **1993**, *4*, 371−378.

(20) Wang, K.; Zhou, C.; Hong, Y.; Zhang, X. A review of protein adsorption on bioceramics. *Interface Focus* **2012**, *2*, 259−277.

(21) Devold, T. G.; Rykke, M.; Isabey, D.; Sørensen, E. S.; Christensen, B.; Langsrud, T.; Svenning, C.; Borch-Iohnsen, B.; Karlsen, J.; Vegarud, G. E. In vitro studies of adsorption of milk proteins onto tooth enamel. *Int. Dairy J.* **2006**, *16*, 1013−1017.

(22) Pitkowski, A.; Durand, D.; Nicolai, T. Structure and dynamical mechanical properties of suspensions of sodium caseinate. *J. Colloid Interface Sci.* **2008**, *326*, 96−102.

(23) Iafisco, M.; Sabatino, P.; Lesci, I. G.; Prat, M.; Rimondini, L.; Roveri, N. Conformational modifications of serum albumins adsorbed on different kinds of biomimetic hydroxyapatite nanocrystals. *Colloids Surf., B* **2010**, *81*, 274−284.

(24) Iafisco, M.; Di Foggia, M.; Bonora, S.; Prat, M.; Roveri, N. Adsorption and spectroscopic characterization of lactoferrin on hydroxyapatite nanocrystals. *Dalton Trans.* **2011**, *40*, 820−827.

(25) Mohsen-Nia, M.; Massah Bidgoli, M.; Behrashi, M.; Mohsen Nia, A. Human serum protein adsorption onto synthesis nano-hydroxyapatite. *Protein J.* **2012**, *31*, 150−157.
(26) Euston, S. R.; Hirst, R. L. The emulsifying properties of commercial milk protein products in simple oil-in-water emulsions and in a model food system. *J. Food Sci.* **2000**, *65*, 934−940.
(27) Ye, A. Functional properties of milk protein concentrates: emulsifying properties, adsorption and stability of emulsions. *Int. Dairy J.* **2011**, *21*, 14−20.
(28) Singh, H.; Ye, A. Interactions and functionality of milk proteins in food emulsions. In *Milk Proteins. From Expression to Food*; Thompson, A., Boland, M., Singh, H., Eds.; Academic Press: San Diego, CA, USA, 2008; pp 321−345.
(29) Dalgleish, D. G. Food emulsions − their structures and structure-forming properties. *Food Hydrocolloids* **2006**, *20*, 415−422.
(30) Schmidt, D. G.; Buchheim, W. The application of electron microscopy in dairy research. *J. Microsc.* **1992**, *167*, 105−121.
(31) Titapiccolo, G. I.; Alexander, M.; Corredig, M. Rennet-induced aggregation of homogenized milk: impact of the presence of fat globules on the structure of casein gels. *Dairy Sci. Technol.* **2010**, *90*, 623−639.
(32) Sun, R.-x.; Lu, Y.-p. Fabrication and characterization of porous hydroxyapatite microspheres by spray-drying method. *Front. Mater. Sci. China* **2008**, *2*, 95−98.
(33) Xu, W.; Ganz, C.; Weber, U.; Adam, M.; Holzhüter, G.; Wolter, D.; Frerich, B.; Vollmar, B.; Gerber, T. Evaluation of injectable silica-embedded nanohydroxyapatite bone substitute in a rat tibia defect model. *Int. J. Nanomed.* **2011**, *6*, 1543−1552.
(34) Walstra, P.; Jenness, R. Proteins. In *Dairy Chemistry and Physics*; Wiley: New York, 1984; pp 98−122.
(35) Cross, K. J.; Huq, N. L.; Palamara, J. E.; Perich, J. W.; Reynolds, E. C. Physicochemical characterization of casein phosphopeptide-amorphous calcium phosphate nanocomplexes. *J. Biol. Chem.* **2005**, *280*, 15362−15369.
(36) Baum, F.; Ebner, J.; Pischetsrieder, M. Identification of multiphosphorylated peptides in milk. *J. Agric. Food Chem.* **2013**, *61*, 9110−9117.
(37) Reynolds, E. C.; Riley, P. F.; Adamson, N. J. A selective precipitation purification procedure for multiple phosphoseryl-containing peptides and methods for their identification. *Anal. Biochem.* **1994**, *217*, 277−284.
(38) FitzGerald, R. J. Potential uses of caseinophosphopeptides. *Int. Dairy J.* **1998**, *8*, 451−457.
(39) Cross, K. J.; Huq, N. L.; Reynolds, E. C. Casein phosphopeptides in oral health − chemistry and clinical applications. *Curr. Pharm. Des.* **2007**, *13*, 793−800.
(40) Reynolds, E. C. Anticariogenic complexes of amorphous calcium phosphate stabilized by casein phosphopeptides: a review. *Spec. Care Dentist.* **1998**, *18*, 8−16.
(41) López-Macipe, A.; Gómez-Morales, J.; Rodríguez-Clemente, R. The role of pH in the adsorption of citrate ions on hydroxyapatite. *J. Colloid Interface Sci.* **1998**, *200*, 114−120.
(42) Gao, R.; Temminghoff, E. J. M.; van Leeuwen, H. P.; van Valenberg, H. J. F.; Eisner, M. D.; van Boekel, M. A. J. S. Simultaneous determination of free calcium, magnesium, sodium and potassium ion concentrations in simulated milk ultrafiltrate and reconstituted skim milk using the Donnan Membrane Technique. *Int. Dairy J.* **2009**, *19*, 431−436.
(43) Lewis, M. J. The measurement and significance of ionic calcium in milk − a review. *Int. J. Dairy Technol.* **2011**, *64*, 1−13.
(44) Lin, M.-J.; Lewis, M. J.; Grandison, A. S. Measurement of ionic calcium in milk. *Int. J. Dairy Technol.* **2006**, *59*, 192−199.
(45) Little, E. M.; Holt, C. An equilibrium thermodynamic model of the sequestration of calcium phosphate by casein phosphopeptides. *Eur. Biophys. J.* **2004**, *33*, 435−447.
(46) Holt, C.; Wahlgren, N. M.; Drakenberg, T. Ability of a beta-casein phosphopeptide to modulate the precipitation of calcium phosphate by forming amorphous dicalcium phosphate nanoclusters. *Biochem. J.* **1996**, *314*, 1035−1039.
(47) Holt, C.; Timmins, P. A.; Errington, N.; Leaver, J. A core-shell model of calcium phosphate nanoclusters stabilized by β-casein phosphopeptides, derived from sedimentation equilibrium and small-angle X-ray and neutron-scattering measurements. J. *Eur. J. Biochem.* **1998**, *252*, 73−78.
(48) Nancollas, G. H.; Tomazic, B. Growth of calcium phosphate on hydroxyapatite crystals. Effect of supersaturation and ionic medium. *J. Phys. Chem.* **1974**, *78*, 2218−225.

JOURNAL OF AGRICULTURAL AND FOOD CHEMISTRY

Article

pubs.acs.org/JAFC

Structure Elucidation and Biological Activity of Two New Trichothecenes from an Endophyte, *Myrothecium roridum*

Ting Lin, Guanghui Wang, Yuqi Zhou, Dequan Zeng, Xiaoxuan Liu, Rong Ding, Xin Jiang, Dan Zhu, Wenjun Shan, and Haifeng Chen*

School of Pharmaceutical Sciences, Xiamen University, South Xiangan Road, Xiamen, Fujian 361102, China

Supporting Information

ABSTRACT: Worldwide, many different grains are infected by various fungi that may produce trichothecene mycotoxins. Fungi that produce trichothecenes, as well as the trichothecenes themselves, are potential problems for public health. On the other hand, trichothecenes possess multiple biological activities. Reduced toxicity may result in their applications in the pharmaceutical field. Two new trichothecenes along with seven known trichothecenes were isolated from an endophyte of the herb plant *Ajuga decumbens*. Their structures were deduced from 1D and 2D NMR data. The results of MTT assays revealed that new trichothecene 2′,3′-epoxymyrothecine A, **1**, and myrothecine A, **3**, exhibited much lower toxicity compared to other trichothecenes. New trichothecene 2′,3′-epoxymyrothecine A, **1**, could induce phosphorylation of JNK (c-Jun N-terminal protein kinase) protein and the PARP (poly ADP-ribose polymerase) cleavage, and eventually induce apoptosis in cancer cells. These results point out the possibility for application of trichothecenes as chemotherapeutic agent.

KEYWORDS: *trichothecenes, endophyte, mycotoxin, chemotherapeutic agent*

INTRODUCTION

Trichothecenes are a large family of chemically related mycotoxins produced by various species of *Fusarium*, *Myrothecium*, *Trichoderma*, *Trichothecium*, *Cephalosporium*, *Verticimonosporium*, and *Stachybotrys*.[1] These mycotoxins are produced in *Fusarium*-infested grains such as corn, wheat, and barley, and ingestion of contaminated grain can result in a variety of symptoms including diarrhea, hemorrhaging, and feed refusal.[2] Potentially hazardous concentrations of the trichothecene mycotoxins can occur naturally in moldy grains, cereals, and agricultural products.[3] They can be found worldwide in cereal grains and in animal feed and human food produced from contaminated grains, which creates a food safety risk.[1]

Trichothecenes can enter human and animal food chains through breakfast cereals, bakery products, snack foods, beer, and compound feeds made from small grains and maize.[4] These mycotoxins are characterized by a tricyclic 12,13-epoxytrichothec-9-ene (trichothecene) ring structure. They can be classified into two different types: simple or nonmacrocyclic trichothecenes, and macrocyclic trichothecenes. The simple or nonmacrocyclic trichothecenes can be divided further into two subgroups based on the presence or absence of a carbonyl function at C-8.[5] Type B trichothecenes have a keto function at C-8, while type A trichothecenes have a hydrogen, hydroxyl, or ester function at C-8.[2] Simple trichothecenes including type A and type B have variations at four sites (C-3, C-4, C-7, and C-15) and are subdivided into epoxy types and de-epoxy types, which are structural analogues bearing an ethylene group, which has not been epoxidized, and they may be biosynthetic intermediates on the pathway to corresponding epoxidized derivatives.[6] Type A trichothecenes are generally more toxic to animals. The naturally occurring macrocyclic trichothecenes are classified as verrucarins (mainly C27 compounds) and roridins (mainly C29 metabolites). They are characterized by a family of sesquiterpenols with a diacyl residue anchored at the 4β and 15 positions.

Among these trichothecenes, a number have been demonstrated to play a substantial role in malaria therapy,[7] immunomodulation,[8] and cancer prevention.[9] The inhibitory effect of trichothecene mycotoxins on rapidly dividing cells was the basis for their evaluation as antitumor chemotherapy drugs during the late 1970s and early 1980s.[10] They are cytotoxic to most eukaryotic cells and inhibit protein synthesis in a variety of eukaryotic cells.[11] Higher efficacy and lower toxicity trichothecenes might have significant potential for use as a chemotherapeutic agent in cancer treatment. Because of their multiple functions, the trichothecene mycotoxins have become a frequent research subject in the fields of medicine, agriculture, animal breeding, food safety, and toxicology.[12]

From an endophyte of the herb *Ajuga decumbens*, two new and seven known trichothecenes were isolated. Their structures were elucidated by spectroscopic methods, and cytotoxicity structure−activity relationships were investigated.

MATERIALS AND METHODS

General Experimental Procedures. NMR spectra were taken on a Avance III-600 NMR spectrometer (Bruker BioSpin International AG, Zurich, Switzerland) with TMS as an internal standard. HR-FT-MS data were acquired using an Apex Ultra 7.0 FT-MS (Bruker Corp., Billerica, MA, USA). Optical rotations were obtained on a PerkinElmer 341 automatic polarimeter (Waltham, MA, USA) with $CHCl_3$ as the solvent. IR spectra were recorded on a Nicolet Avatar 330 FT IR spectrometer (Thermo Electron Corp., Madison, WI, USA). Sephadex

Received: January 14, 2014
Revised: June 5, 2014
Accepted: June 8, 2014
Published: June 8, 2014

 © 2014 American Chemical Society

LH-20 (40−70 μm) (Amersham Pharmacia Biotech AB, Uppsala, Sweden), silica gel (200−300 mesh) (Qingdao Marine Chemical, Inc., Qingdao, China), and Lichroprep reversed-phase RP-18 silica gel (40−63 μm) (Merck, Darmstadt, Germany) were used for column chromatography. TLC was carried out using glass-precoated silica gel GF254 (Qingdao Marine Chemical, Inc., Qingdao, China) and visualized under UV light or by spraying with vanillin ethanol reagent, which contains H_2SO_4. The cell culture medium, Dulbecco's modified Eagle's medium (DMEM; high glucose, without sodium pyruvate, HyClone), and fetal bovine serum (FBS, HyClone) were purchased from HyClone Laboratories Inc. (Logan, UT, USA). Acrylamide/bis-acrylamide solution (30%; 29:1) was purchased from Bio-Rad Laboratories, Inc. (Hercules, CA, USA). Protein content was tested using a BCA kit (Thermo Fisher Scientific, Waltham, MA, USA). Anti-poly(ADP-ribose) polymerase-1 (PARP-1), anti-β-actin mouse antibody, horseradish peroxidase (HRP)-labeled anti-rabbit/mouse IgG (H + L), and dimethyl sulfoxide (DMSO) were obtained from Sigma-Aldrich Corp. (St. Louis, MO, USA). Cytochrome *c* was purchased from Beyotime Institute of Biotechnology (Jiangsu, China). DAPI (4′,6′-diamidino-2-phenylindole) was purchased from Pierce (Rockford, IL, USA).

Fungal Material. The fungus was isolated from current-year root of *Ajuga decumbens* collected from Fuzhou, Fujian, China. A BLAST search result showed that the internal transcribed spaces (ITS) sequence of this fungus was highly homologous (100% percent similarity) to that of *Myrothecium roridum* (E-1069), indicating that this fungus belongs to this genus.

Fermentation and Extraction. The strain was cultivated at 28 °C with 5 L of PDA (potato dextrose agar) media for 16 d. After fermentation, the culture medium was chopped and extracted with ethyl acetate/methanol (80:20) at room temperature overnight. The combined organic layer was concentrated under vacuum until 4.1 g of residue was obtained.

Isolation and Spectral Data. The crude extract (4.1 g) was separated into 18 fractions (fraction 1 to fraction 18) by column chromatography on RP-18 silica gel (100 g, 36 mm × 230 mm), eluted by methanol/H_2O (30:70, 50:50, 70:30, and 100:0, 1 L for each gradient, 100 mL per collection bottle). Fraction 1 (0.2315 g, fraction volume: 200 mL); fraction 2 (0.0380 g, fraction volume: 100 mL); fraction 3 (0.0611 g, fraction volume: 300 mL); fraction 4 (0.1080 g, fraction volume: 400 mL); fraction 5 (0.0431 g, fraction volume: 100 mL); fraction 6 (0.0836 g, fraction volume: 200 mL); fraction 7 (0.0386 g, fraction volume: 100 mL); fraction 8 (0.1195 g, fraction volume: 300 mL); fraction 9 (0.0674 g, fraction volume: 100 mL); fraction 10 (1.4100 g, fraction volume: 200 mL); fraction 11 (0.0745 g, fraction volume: 200 mL); fraction 12 (0.1649 g, fraction volume: 100 mL); fraction 13 (0.0476 g, fraction volume: 100 mL); fraction 14 (0.1802 g, fraction volume: 300 mL); fraction 15 (0.6822 g, fraction volume: 100 mL); fraction 16 (0.7478 g, fraction volume: 100 mL); fraction 17 (0.1352 g, fraction volume: 100 mL); and fraction 18 (0.0390 g, fraction volume: 400 mL).

Fraction 4 (108 mg) was separated using the Sephadex LH-20 (elution with 100% methanol, 25 mm × 1000 mm, 100 g, 400 mL) to give three subfractions (fraction 4-a to fraction 4-c). Fraction 4-a (0.0784 g, fraction volume: 15 mL) was separated by column chromatography on silica gel (2.35 g, 10 mm × 250 mm, elution with chloroform, 600 mL) to afford compound **1** (19.9 mg).

Fraction 6 (83.6 mg) was chromatographed on normal phase silica gel (2.51 g, 10 mm × 250 mm) and eluted with chloroform (120 mL) to yield compound **3** (9.0 mg, fraction volume: 30 mL).

Fraction 9 (67.4 mg) was purified using the Sephadex LH-20 (25 mm × 1000 mm, 100 g) column, eluted with methanol (300 mL), and two subfractions (fraction 9-a, 39.6 mg, and fraction 9-b, 20.4 mg) were obtained. Compound **9** (4.9 mg) was obtained from fraction 9-a eluted with petroleum ether−EtOAc [5:1(60 mL), 4:1 (100 mL), 3:1 (80 mL), 2:1 (60 mL), 1.5:1 (150 mL), 1:1 (100 mL), v/v] on column chromatography over normal phase silica gel (1.5 g, 10 mm × 250 mm).

Fraction 10 (1.41 g) was subjected to the Sephadex LH-20 (180 g) (25 mm × 1800 mm, elution with 100% methanol, 800 mL), and two fractions (fraction 10-a, 36.6 mg, and fraction 10-b, 841 mg) were collected. Fraction 10-b (841 mg) was fractionated on a silica gel column (8.4 g, 20 mm × 350 mm) eluted with petroleum ether−EtOAc of increasing polarity [4:1 (200 mL), 3:1 (240 mL), 2.5:1 (280 mL), 2:1 (90 mL), 1:1 (200 mL), v/v] to give compound **5** (4 mg, fraction volume: 10 mL), compound **6** (25.7 mg, fraction volume: 20 mL), and compound **2** (3.9 mg, fraction volume: 60 mL).

Fraction 11 (74.5 mg) was chromatographed on the Sephadex LH-20 (25 mm × 1000 mm, 100 g) and eluted with methanol (400 mL). Two fractions (fraction 11-a, 26 mg, and fraction 11-b, 43 mg) were made. Fraction 11-a (26 mg) was isolated with column chromatography over normal-phase silica gel [1.0 g, 8 mm × 250 mm, eluted with chloroform−methanol, v/v, 200:1 (100.5 mL)] to afford comopund **4** (6.8 mg).

Fraction 13 (47.6 mg) was purified by normal phase silica gel column chromatography (1.5 g, 10 mm × 250 mm), eluted with petroleum ether−chloroform [4:1 (100 mL), 3:1 (80 mL), 2:1 (90 mL), 1:1 (100 mL), 1:2 (80 mL), v/v], and compound **7** (4.1 mg, fraction volume: 35 mL) was obtained.

Fraction 14 (180.2 mg) was further subjected to the Sephadex LH20 (180 g, 25 mm × 1800 mm) column, eluted with methanol (600 mL). Subfraction 14-a (15.3 mg, fraction volume: 20 mL) was purified using a normal phase silica gel column [0.5 g, 8 mm × 250 mm, eluted with chloroform−methanol (100:1, v/v, 400 mL)] to yield compound **8** (3.0 mg, fraction volume: 10 mL).

2′,3′-Epoxymyrothecine A, 1: white powder; $[\alpha]_D^{20}$ +12.8 (*c* 0.525, chloroform); IR (KBr) ν_{max} 3428, 2920, 2850, 1745, 1711, 1461, 1383, 1181, 1098, 1058, 1023, 754 cm^{-1}; ^1H and ^{13}C NMR data shown in Table 1; HR-FT-MS, *m*/*z* 541.2045 $[M + Na]^+$ (calculated for $C_{27}H_{34}O_{10}Na$, 541.2146).

13′,14′-Hydroxymytoxin B, 2: white powder; $[\alpha]_D^{20}$ +60 (*c* 0.1, chloroform); IR (KBr) ν_{max} 3348, 2921, 2851, 1720, 1712, 1658, 1461, 1441, 1383, 1085, 1180 cm^{-1}; ^1H and ^{13}C NMR data shown in Table 1; HR-FT-MS, *m*/*z* 569.2361 $[M + Na]^+$ (calculated for $C_{29}H_{38}O_{10}Na$, 569.2465).

Cleaved-PARP and JNK Protein Phosphorylation Western Blotting. HepG2 (hepatocellular carcinoma, ATCC) cells were exposed to 5-Fu (5-fluorouracil) (20 and 50 μM) and compounds **1**−**9** at concentrations of **1** (50 μM), **2** (50 nM), **3** (50 μM), **4** (5 nM), **5** (50 nM), **6** (50 nM), 7 (50 nM), **8** (50 nM) and **9** (1 μM) for 8 h.

HepG2, A549 (human lung adenocarcinoma, ATCC) and MCF-7 (human breast adenocarcinoma, ATCC) cells were exposed to 2′,3′-epoxymyrothecine A, **1**, at concentrations of 0, 20, 50, and 100 μM for 8 h. HepG2 cells were treated with 20 μM **1** for different periods of time (0, 2, 4, and 8 h) respectively. After the treatment, cells were lysed with prepared lysis buffer with a WH-3 vortex machine (Shanghai Qingpu-Huxi Instruments Factory, Shanghai, China). For Western blot analysis, an amount of 25 μL of the protein sample containing 40 μg of protein was separated by 8% SDS−polyacrylamide gel electrophoresis and transferred to nitrocellulose membranes (Millipore, Bedford, MA, USA). The level of protein expression was determined using specific primary antibodies, PARP and β-actin, followed by rabbit/mouse HRP-conjugated secondary antibodies.

Cytotoxicity Assay. In vitro cytotoxicity of isolated compounds was evaluated by an MTT assay. Briefly, four different cancer cells [HepG2, MCF-7, A549, and SMMC-7721 (human hepatocellular carcinoma, Type Culture Collection of the Chinese Academy of Sciences, Shanghai, China)] were plated at 3000 cells/well in a 96-well plate and treated with the different concentrations of the isolated compounds for 48 h. Three independent experiments were performed and the results shown as the percentage of cell inhibition ratio.

Immunofluorescence Analysis of Cytochrome *c*. HepG2 cells were seeded onto glass coverslips and treated with compounds for 12 h. Cells were fixed with 4% paraformaldehyde in PBS for 20 min and permeabilized with 0.2% Triton X-100 in PBS for 10 min at room temperature. The cells were washed twice with PBS and blocked with 5% BSA in PBS for 30 min at room temperature. After washing, the cells were incubated with anti-cytochrome *c* (diluted 1:500 in PBS + 1% BSA) overnight at 4 °C. The cells were then washed twice in PBS

Table 1. ^{1}H NMR (600 MHz) and ^{13}C NMR (125 MHz) Data for Compounds 1 and 2 in $CDCl_3$

	1		2	
	δ_H, multi (J in Hz)	δ_C	δ_H, multi (J in Hz)	δ_C
1				
2	4.01, d (4.3)	80.8 d	3.86, m	79.1 d
3	1.83, m	28.4 t	2.49, dd (15.7, 8.1)	35.0 t
	1.56, m		2.11, m	
4	5.43, dd (7.9, 2.6)	77.9 d	5.80, dd (8.1, 3.5)	73.7 d
5		50.8 s		43.9 s
6		43.8 s	4.65	42.9 s
7	2.11, m	27.6 t	1.92, m	20.6 t
	1.47, dd (5.4, 14.0)			
8	1.40, m	30.4 t	2.05, m	27.6 t
	1.82, m		1.92, m	
9		72.6 s		140.4 s
10	2.16, m	43.9 d	5.45, d (4.6)	118.8 d
11	3.56, s	69.3 d	3.62, d (5.2)	67.9 d
12		76.6 s		65.6 s
13	2.23, m	39.9 t	3.14, d (4.0)	47.6 t
	1.88, m		2.82, m	
14	1.16, s	9.7 q	0.81, s	7.7 q
15	4.21, m	73.7 t	4.33, m	64.3 t
			4.03, m	
16	1.21, s	26.3 q	1.73, s	23.3 q
1′		167.6 s		166.4 s
2′	3.53, s	56.3 d	5.74, s	117.0 d
3′		65.3 s		155.1 s
4′	2.75, dt (5.6, 13.2)	22.9 t	3.71, d (13.2)	25.7 t
	1.71, dt (5.0, 14.4)		2.81, d (4.2)	
5′	4.24, m	66.9 t	4.10, m	63.9 t
	4.10, m		4.08, m	
6′		151.3 s		78.6 s
7′	4.61, dd (2.3, 10.6)	108.5 d	2.86, m	21.8 t
			1.96, m	
8′	4.16, dt (2.8, 11.6)	23.2 t	2.20, m	26.6 t
	2.51, ddd (2.3, 9.4, 14.4)			
9′	6.62, m	147.1 d	6.49, m	149.2 d
10′	5.96, dd (1.8, 11.4)	121.9 d	5.45, d (4.6)	118.8 d
11′		164.9 s		165.8 s
12′	3.57, s	74.0 d	3.85, s	77.6 d
13′			4.06, d (2.6)	75.8 d
14′			3.95, s	62.1 t

and detected by anti-mouse IgG conjugated with Cy3 (1:1000) at room temperature for 30 min. Cells were costained with DAPI to visualize nuclei. The images were taken using LSM-510 confocal laser scanning microscope system (Carl Zeiss, Oberkochen, Germany).

To investigate whether these compounds may induce the mitochondrial release of cytochrome *c*, we performed immunofluorescence analysis of cytochrome *c* in HepG2 cells treated with 5-Fu (50 μM), **1** (50 μM), **3** (50 μM), **5** (50 nM), **6** (50 nM), and **8** (50 nM) for 12 h, and observed that they can induce a diffuse cytosolic staining of cytochrome *c*.

Flow Cytometry for Cell Cycle Distribution. HepG2 cells (50% confluent) were synchronized by serum starvation for 24 h and treated with 5-Fu (50 μM), compound **1** (50 μM), **2** (50 nM), **3** (50 μM), **4** (5 nM), **5**−**8** (50 nM), and **9** (1 μM) in complete medium for 12 h. The cells were washed with cold PBS and centrifuged at 1000 rpm for 5 min. 70% ethanol was employed to fix the cells overnight at 4 °C. The cells were incubated using PBS with RNase (10 μg/mL) (Tiangen, Beijing, China) for 30 min, stained with propidium iodide (50 μg/mL) at room temperature for 30 min, and determined by FAC Plus flow cytometry (Beckman Coulter, Miami, FL, USA). The DNA histograms were further analyzed through the WinMDI 2.9 software program (Scripps Institute, La Jolla, CA, USA).

RESULTS AND DISCUSSION

Structure Elucidation. 2′,3′-Epoxymyrothecine A, **1**, was isolated as a white powder. The molecular formular was established as $C_{27}H_{34}O_{10}$. The ^{1}H and ^{13}C NMR spectra of **1** were similar to those of myrothecine A,[13] except for the presence of signals [δ_H 3.53 (1H, S, H-2′), δ_C 56.3 (C-2′), δ_C 65.3 (C-3′), δ_H 4.61 (1H, dd, J = 2.3, 10.6 Hz, H-7′), δ_C 108.5 (C-7′), δ_C 151.3 (C-6′)] and the absence of signals [δ_H 5.78 (1H, brs, H-2′), δ_C 117.3 (C-2′), δ_C 154.1 (C-3′), δ_H 1.96, 1.65 (2H, m, H-7′), δ_C 29.5 (C-7′), δ_C 87.3 (C-6′), δ_C 213.0 (C-13′), δ_H 2.30 (1H, s, H-14′), δ_C 28.7 (C-14′)] observed in the NMR spectra of myrothecine A due to the epoxidation between C-2′ and C-3′ in myrothecine A, **3**, the double bond of C-6′ and C-7′, and the absence of an acetyl group that was connected to C-6′ in myrothecine A. The HMBC correlations from proton δ_H 4.21 (2H, m, H-15) to C-1′ (δ_C 167.6), C-5 (δ_C 50.8), and C-7 (δ_C 27.6) revealed the linkage between C-15 and C-1′ via an oxygen bridge. The HMBC correlations from proton δ_H 4.01 (1H, d, J = 4.3 Hz, H-2) to C-13 (δ_C 39.9), C-5 (δ_C 50.8), and C-11 (δ_C 69.3) revealed the oxygen bridge between C-2 and C-11. The HMBC correlations from proton δ_H 5.43 (1H, dd, J = 2.6, 7.9 Hz, H-4) to C-12 (δ_C 76.6), C-2 (δ_C 80.8), and C-11′ (δ_C 164.9) revealed the ester linkage between C-4 and C-11′. The HMBC correlations from proton δ_H 4.24 (2H, m, H-5′) to C-3′ (δ_C 65.3) and C-6′ (δ_C 151.3) revealed the oxygen bridge linkage between C-5′ (δ_C 66.9) and C-6′. Other key HMBC correlations are shown in Figure 2. Therefore, the planar structure of compound **1** was determined. Moreover, the relative configuration of **1** was given by its nuclear Overhauser effect spectroscopy (NOESY) NMR spectrum which displayed the cross peaks of δ_H 4.01 (1H, d, J = 4.3 Hz, H-2) with δ_H 5.43 (1H, dd, J = 2.6, 7.9 Hz, H-4), δ_H 4.01 (1H, d, J = 4.3 Hz, H-2) with δ_H 2.21 (1H, m, H-10), δ_H 3.56 (1H, s, H-11) with δ_H 2.21 (1H, m, H-10), and δ_H 1.25 (3H, s, H-16) with δ_H 1.16 (3H, s, H-14).

13′,14′-Hydroxymytoxin B (**2**) was isolated as a white powder. The molecular weight and formula ($C_{29}H_{38}O_{10}$) were determined from the HR-FT mass spectrum ($C_{29}H_{38}O_{10}Na$) and the ^{13}C NMR data. The ^{1}H and ^{13}C NMR spectra of **2** were nearly identical to those of 14′-hydroxymytoxin B (**5**),[5] except for the presence of signals [δ_H 4.06 (1H, d, J = 2.6 Hz, H-13′), δ_C 75.8 (C-13′)] ascribable to a hydroxymethylene group and the absence of a signal at δ_C 214.1 (C-13′), observed in the NMR spectra of 14′-hydroxymytoxin B due to the 13′ carbonyl group. HMBC correlations from proton δ_H 4.33 (1H, m, H-15) to C-7 (δ_C 20.9), C-6 (δ_C 42.9), C-11′ (δ_C 68.7), and C-1′ (δ_C 166.4) revealed the ester linkage between C-15 and C-1′. The HMBC correlations from proton δ_H 3.16 (1H, m, H-2) to C-13 (δ_C 79.1) and C-11 (δ_C 67.9) revealed the oxygen bridge between C-2 and C-11. The HMBC correlations from proton δ_H 5.80 (1H, dd, J = 3.5, 8.1 Hz, H-4) to C-12 (δ_C 65.6), C-2 (δ_C 47.6), and C-11′ (δ_C 165.8) revealed the ester linkage between C-4 and C-11′. Other key HMBC correlations are shown in Figure 2. Therefore, the structure of 2 was deduced to be the 13′-hydroxy derivative of 14′-hydroxymytoxin B. The relative configurations of **2** were determined by the analysis of the NOESY spectrum which displayed the nuclear Overhauser effect (NOE) correlations of δ_H 5.45 (1H, d, J = 4.6 Hz, H-10) with δ_H 3.62 (1H, d, J = 5.2 Hz, H-11), δ_H 5.45 (1H, d, J = 4.6 Hz, H-10) with δ_H 1.73 (3H, s, H-16), δ_H 5.74 (1H, s,

dx.doi.org/10.1021/jf501724a | J. Agric. Food Chem. 2014, 62, 5993−6000

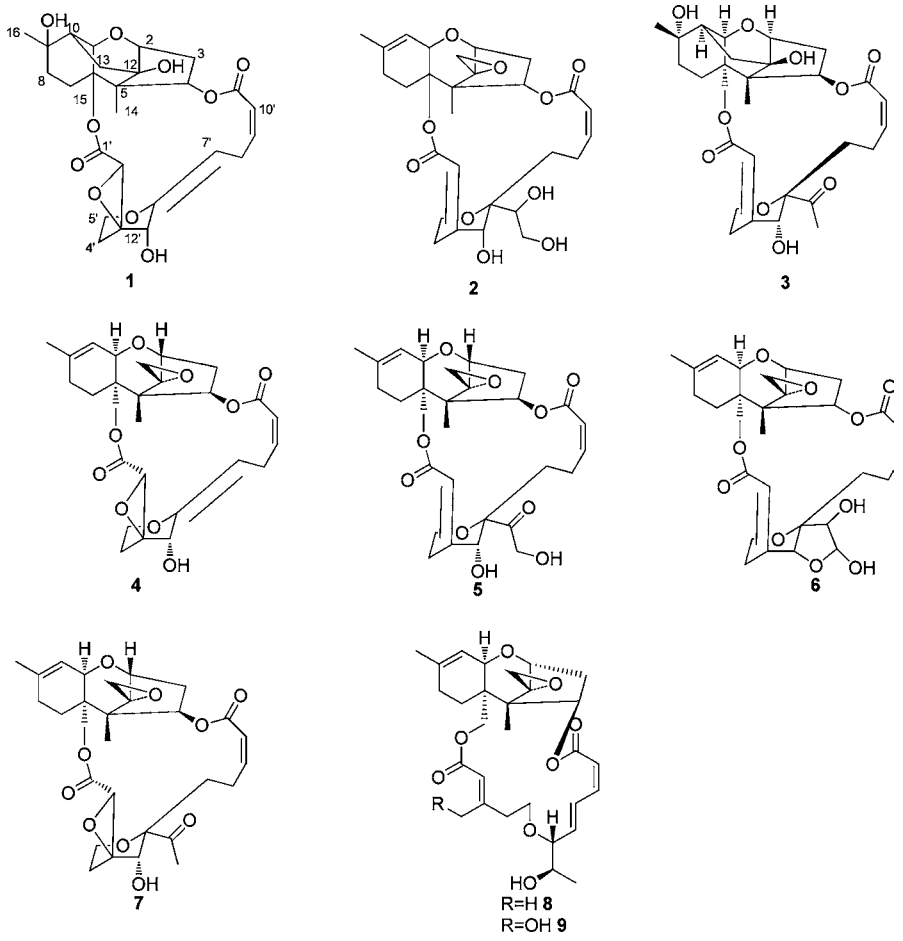

Figure 1. Compounds isolated from *M. roridum*: **1**, 2′,3′-epoxymyrothecine A; **2**, 13′,14′-hydroxymytoxin B; **3**, myrothecine A; **4**, myrotoxin A; **5**, 14′-hydroxymytoxin B; **6**, vertisporin; **7**, mytoxin C; **8**, roridin E; **9**, 12′-hydroxyroridin E.

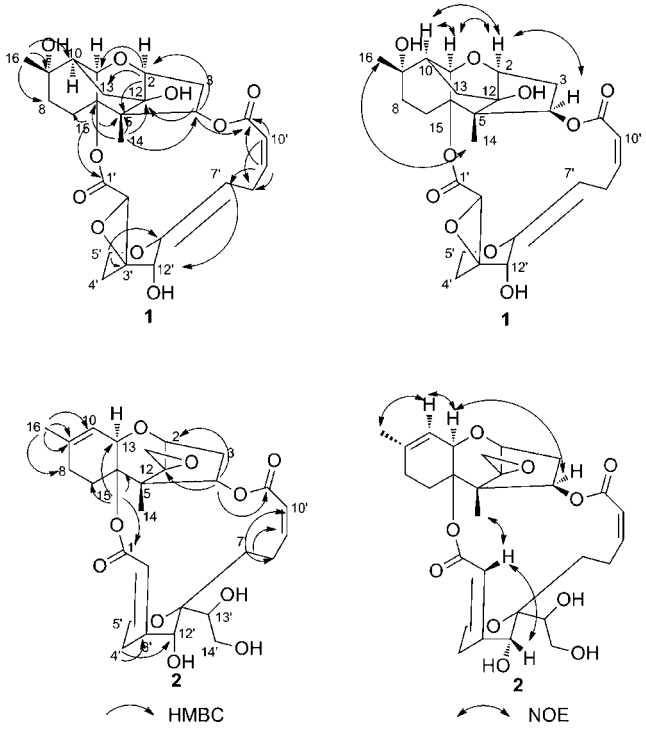

Figure 2. Key HMBC and NOE correlations of **1** and **2**.

H-2′) with δ_H 0.81 (3H, s, H-14), δ_H 5.74 (1H, s, H-2′) with δ_H 3.85 (1H, s, H-12′), and δ_H 0.81 (3H, s, H-14) with δ_H 3.62 (1H, d, J = 5.2 Hz, H-11).

Two new trichothecenes, 2′,3′-epoxymyrothecine A, **1**, and 13′,14′-hydroxymytoxin B, **2**, along with seven known trichothecenes, myrothecine A, **3**,[12] myrotoxin A, **4**,[13] 14′-hydroxymytoxin B, **5**,[5] vertisporin, **6**,[14] mytoxin C, **7**,[15] roridin E, **8**,[16] and 12′-hydroxyroridin E, **9**,[17] were isolated from an endophyte of the herb *Ajuga decumbens*; their structures are shown in Figure 1.

Since *Fusarium* and other related fungi that produce trichothecenes infect various agricultural products, especially important crops, they have been associated with intoxication of humans and animals all over the world. Trichothecenes are a well-known major class of mycotoxins. Many new macrocyclic trichothecenes have been isolated from different fungi possessing cytotoxic,[9] immunomodulation,[18] antimicrobial,[19] and phytotoxic[20] properties.

MTT assays were used to evaluate these trichothecenes' toxicity. 2′,3′-Epoxymyrothecine A, **1**, and myrothecine A, **3**, exhibited more than 1000-fold less toxicity than other trichothecenes (Table 2). The 12,13-epoxy ring is the most important structural feature leading to the remarkable differences in toxicity. A promising target for preharvest detoxification is the epoxide group located at C-12. 2′,3′-Epoxymyrothecine A, **1**, and myrothecine A, **3**, do not have an epoxy ring at C-12 and C-13. This variation can lead to

dx.doi.org/10.1021/jf501724a | J. Agric. Food Chem. 2014, 62, 5993−6000

Table 2. IC_{50} Values of Compounds (1−9) against Four Different Cancer Cell Lines (7721, A549, HepG2, MCF-7)

	A549	MCF-7	HepG2	7721
1	36.45 ± 2.79 μM	18.13 ± 3.89 μM	32.03 ± 2.94 μM	30.33 ± 9.71 μM
2	53 ± 3.36 nM	63 ± 2.38 nM	49 ± 3.35 nM	46 ± 2.88 nM
3	95 ± 3.51 μM	70 ± 2.50 μM	60 ± 3.54 μM	25 ± 2.13 μM
4	3.56 ± 1.23 nM	1.64 ± 0.23 nM	1.67 ± 0.19 nM	1.42 ± 0.25 nM
5	49 ± 1.26 nM	55 ± 1.46 nM	52 ± 3.36 nM	39 ± 2.29 nM
6	47 ± 3.30 nM	75 ± 2.80 nM	66 ± 5.65 nM	75 ± 2.80 nM
7	33 ± 1.86 nM	65 ± 2.20 nM	38 ± 1.22 nM	46 ± 1.79 nM
8	55 ± 3.33 nM	70 ± 1.9 nM	46 ± 1.66 nM	42 ± 3.23 nM
9	2.08 ± 0.71 μM	1.25 ± 0.11 μM	1.26 ± 0.08 μM	6.56 ± 4.15 μM

different trichothecene structures that result in differences in toxicity. 2′,3′-Epoxymyrothecine A, **1**, and myrothecine A, **3**, exhibited much lower toxicity compared to those trichothecenes which possess a 12,13-epoxy ring (Table 2). PARP-1 is a nuclear protein that has important roles in the maintenance of genomic integrity.[21] Cleavage of PARP-1 by caspases is considered to be a hallmark of apoptosis.[22,23] The PARP-cleavage activity of nine trichothecenes in HepG2 cells was tested (Figure 3). With the exception of trichothecenes **2**, **4**, **7**, and **9**, the other trichothecenes could induce PARP-cleavage in HepG2 cells (Figure 3). The results revealed that 2′,3′-epoxymyrothecine A, **1**, myrothecine A, **3**, 14′-hydroxymytoxin B, **5**, vertisporin, **6**, and roridin E, **8**, could induce apoptosis in HepG2 cells (Figure 3).

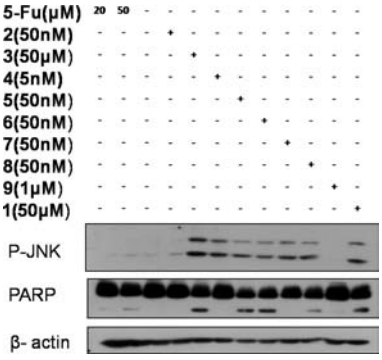

Figure 3. PARP-cleavage and phosphorylation of JNK protein in treated HepG2 cells. Cells were treated with 5-Fu (20 and 50 μM), **1** (50 μM), **2** (50 nM), **3** (50 μM), **4** (5 nM), **5**-**8** (50 nM), and **9** (1 μM) for 8 h.

Cytochrome *c* has been identified as an important mediator in apoptotic pathways.[24] The release of mitochondrial cytochrome *c* into the cytoplasm stimulates apoptosis and is commonly used as an indicator of the apoptotic process in the cell.[25] In order to confirm the apoptosis activity of these trichothecenes, cytochrome *c* releasing assays were carried out. The results confirmed that 2′,3′-epoxymyrothecine A, **1**, myrothecine A, **3**, 14′-hydroxymytoxin B, **5**, vertisporin, **6**, and roridin E, **8**, could promote the cytochrome *c* release from the mitochondria and subsequently cause apoptosis in HepG2 cells (Figure 4).

Cell cycle regulation in the G1 phase has attracted a great deal of attention as a promising target for the research and treatment of cancer. Many of the important genes associated with G1 regulation have been shown to play a key role in proliferation, differentiation and oncogenic transformation, and programmed cell death (apoptosis).[26] Cell cycle arrest experiments were carried out. Nine trichothecenes could induce the G1 cell cycle arrest in HepG2 cells (Figure 5). 2′,3′-Epoxymyrothecine A, **1**, and myrotoxin A, **4**, exhibited significant effects of G1 cell cycle arrest in HepG2, nearly 20% greater than the control (Figure 5). In structure comparions of these two trichothecenes to other trichothecenes, the most obvious difference was the substitution at C-6′. There was no substituent at C-6′ in these two trichothecenes (2′,3′-epoxymyrothecine A and myrotoxin A), whereas the other trichothecenes had a substitution group at C-6′. Therefore, this difference should be important for the G1 cell cycle arrest activity of trichothecenes.

Cells are continuously exposed to a variety of environmental stresses and have to decide "to live or die" depending on the types and strength of stress. Among the many signaling pathways that respond to stress, mitogen-activated protein kinase (MAPK) family members are crucial for the maintenance of cells.[27] Three subfamilies of MAPKs have been identified: c-Jun N-terminal kinases (JNKs), extracellular signal-regulated kinases (ERKs), and p38-MAPKs. It has been shown that ERKs are important for cell survival, whereas JNKs were deemed stress-responsive and thus involved in apoptosis.[27] JNK was discovered almost 20 years ago as the protein kinase responsible for phosphorylating c-Jun at Ser-63 and Ser-73.[28] JNKs belong to the family of mitogen-activated protein kinases (MAPK) that are responsive to a variety of environmental stimuli.[29,30] JNKs (also known as stress-activated protein kinases; SAPKs) are ubiquitously expressed, and the JNK stress pathways participate in many different intracellular signaling pathways that control a spectrum of cellular processes, including cell growth, differentiation, transformation, or apoptosis.[31−37]

Transient JNK activation promotes cell survival, while prolonged JNK activation induces cellular apoptosis.[38] In order to explain the structure−activity relationships of these trichothecenes, the PARP-cleavage and phosphorylation of JNK protein activities were carried out in HepG2 cells. With the exception of trichothecenes **2**, **4**, **7**, and **9**, all of the other trichothecenes could induce PARP-cleavage in HepG2 cells (Figure 3). Also, with the exception of trichothecenes **2** and **9**, all of the other trichothecenes could induce phosphorylation of JNK protein in HepG2 cells (Figure 3). Trichothecenes **1** and **3**, in which the epoxy ring typically located at C-12 and C-13 was absent and the olefinic bond, which is typically located at C-9 and C-10, was substituted with a hydroxy group, could induce PARP-cleavage and phosphorylation of JNK protein in HepG2 cells (Figure 3). These results indicated that the epoxy ring at C-12 and hydroxy substitution at C-9 were important for PARP-cleavage and phosphorylation of JNK protein in HepG2 cells. This conclusion can be further confirmed by the comparison of **1** and **4**. The epoxy ring at C-12 of **4** was open in **1**, and the olefinic bond at C-9 of **4** was substituted with a hydroxy group in **1**. For trichothecenes **1**, **4**, and **7**, the epoxy ring at C-12 and the hydroxy substitution at C-9 were absent in trichothecenes **4** and **7**. Among these three trichothecenes, the epoxy ring located at C-2′ and C-3′ did not play an important role in PARP-cleavage and phosphorylation of the JNK protein in HepG2 cells (Figure 3). For trichothecenes **2**, **5**, and **6**, the substituent group located at C-6′ was the major cause for the activities in HepG2 cells. In other two trichothecenes, **2** and **5**, no ring system existed at C-6′. In a comparison of these two trichothecenes, the only difference between them was that the

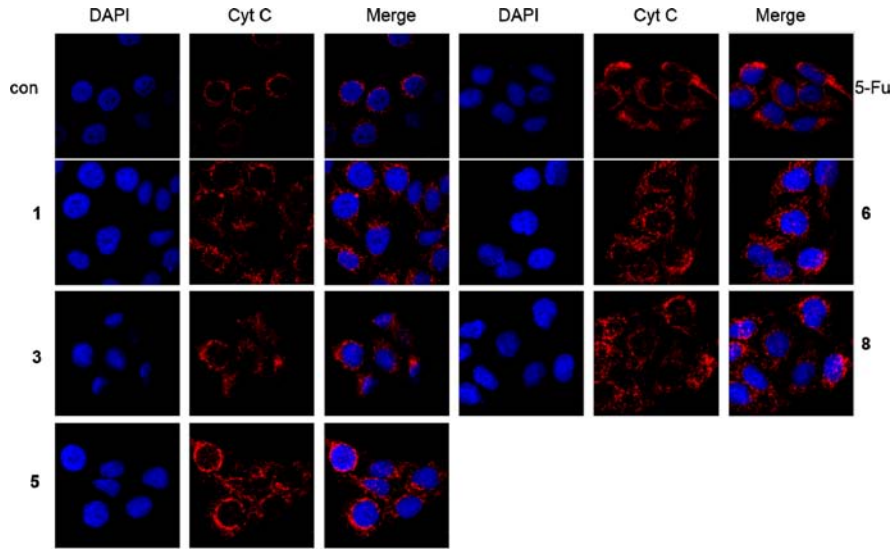

Figure 4. Trichothecene-induced release of cytochrome *c* in the HepG2 cell line. Cells were treated with 5-Fu (50 μM), **1** (50 μM), **3** (50 μM), **5** (50 nM), **6** (50 nM), and **8** (50 nM) for 12 h.

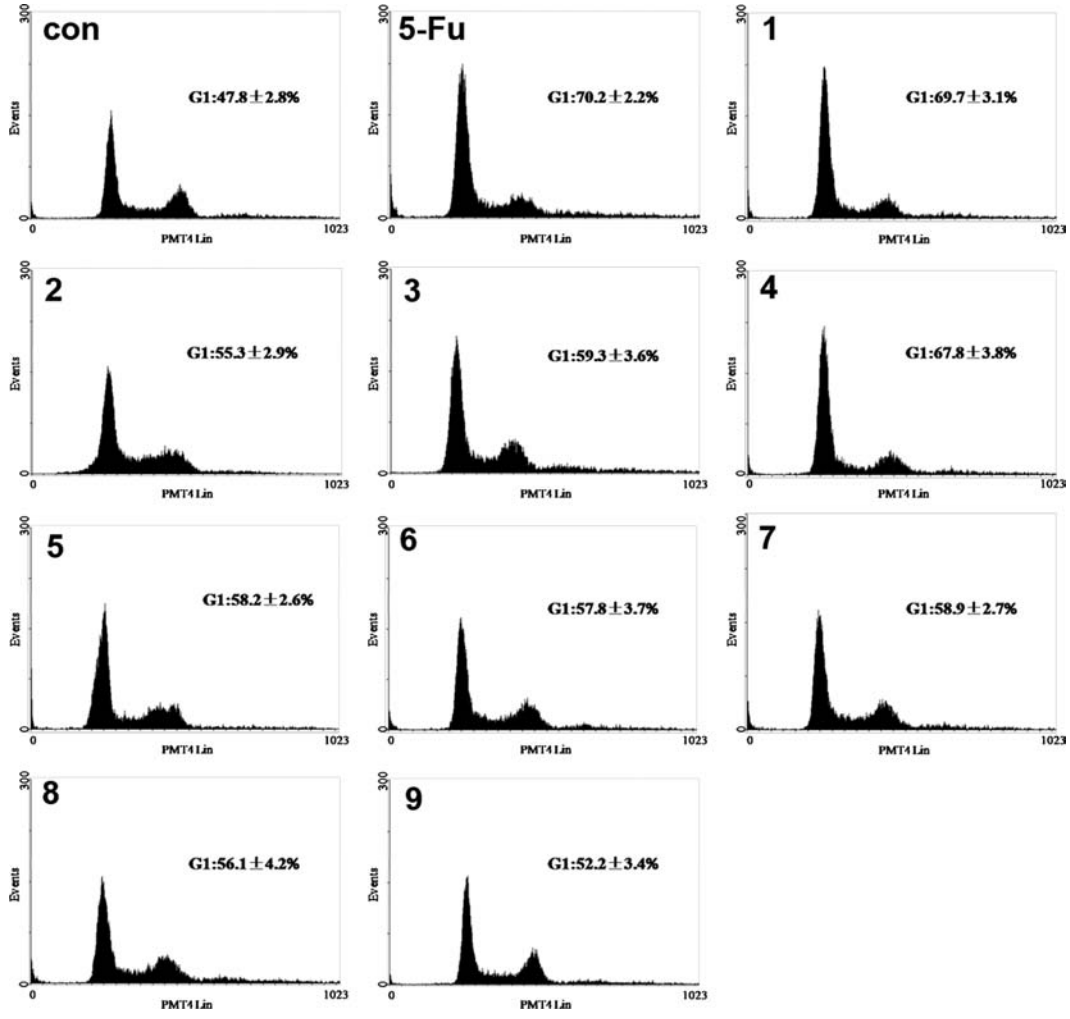

Figure 5. Trichothecene-induced G1 cell cycle arrest in the HepG2 cell line. Cells were treated with 5-Fu (50 μM), compounds **1** (50 μM), **2** (50 nM), **3** (50 μM), **4** (5 nM), **5**-**8** (50 nM), and **9** (1 μM) for 12 h).

hydroxy group located at C-13′ of **2** became a keto group in **5**. These results revealed that the keto group located at C-13′ was an important site for their activity in HepG2 cells (Figure 3).

For trichothecenes **8** and **9**, the only difference between them was the hydroxy group at C-12′. Roridin E, **8**, exhibited far stronger cytotoxicity than its derivative 12′-hydroxyroridin

dx.doi.org/10.1021/jf501724a | J. Agric. Food Chem. 2014, 62, 5993−6000

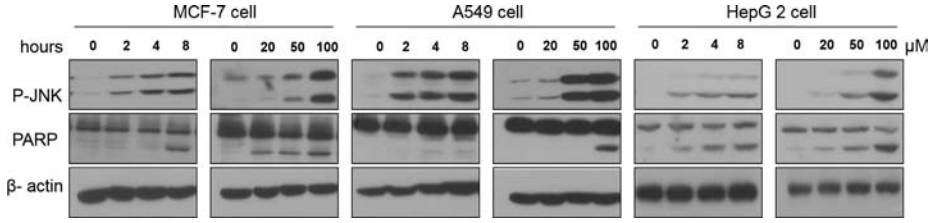

Figure 6. PARP-cleavage and protein JKN phosphorylation in treated MCF-7 cells, A549 cells, and HepG2 cells. Cells were incubated at concentration 50 μM of compound **1** for 0, 2, 4, and 8 h, respectively, or at concentrations 0, 20, 50, and 100 μM of compound **1** for 8 h.

E, **9**, and 12′-hydroxyroridin E, **9**, which exhibited no activity on PARP-cleavage and phosphorylation of JNK protein in HepG2 cells (Figure 3). These results indicated that hydroxy group substitution at C-12′ was vital for PARP-cleavage and phosphorylation of JNK protein in HepG2 cells.

2′,3′-Epoxymyrothecine A could induce the PARP-cleavage in a time- and dose-dependent manner in HepG2 and MCF-7 cells (Figure 6). Compared to HepG2 cells, 2′,3′-epoxymyrothecine A exhibited clear PARP-cleavage only after 8 h in MCF-7 cells, and the dose-dependency was much weaker (Figure 6). 2′,3′-Epoxymyrothecine A did not exhibit the same time-dependent effect on the PARP-cleavage in A549 cells. When A549 cells were treated with 2′,3′-epoxymyrothecine A (50 μM) for 8 h, the PARP-cleavage was unclear (Figure 6). For the dose-dependent experiment, 2′,3′-epoxymyrothecine A did not showed any PARP-cleavage activity until the concentration increased to 100 μM (Figure 6). All these results revealed that 2′,3′-epoxymyrothecine A showed much better apoptosis activity in HepG2 cells compared to A549 and MCF-7 cells.

2′,3′-Epoxymyrothecine A can induce phosphorylation of JNK protein in a time- and dose-dependent manner in HepG2 and MCF-7 cells (Figure 6). There were no significant differences of phosphorylation of JNK protein when A549 cells were treated with 50 μM 2′,3′-epoxymyrothecine A for 2, 4, and 8 h. In terms of dose-dependent manner, it seems that 50 μM 2′,3′-epoxymyrothecine A would achieve the plateau (Figure 6). From the perspective of JNK phosphorylation, 2′,3′-epoxymyrothecine A was more suitable for the treatment of HepG2 and MCF-7 cells. Based on these results, we can conclude that 2′,3′-epoxymyrothecine A can induce the G1 cell cycle arrest, phosphorylation of JNK protein, and the PARP-cleavage in a time- and dose-dependent manner, promote the cytochrome *c* release from the mitochondria, and eventually induce apoptosis in HepG2 liver cancer cells.

All these results indicated that a small change in trichothecenes could dramatically reduce the toxicity and still retain the apoptosis inducing activity in human cancer cells. These data provide a pilot study for future exploitation of the applicability of trichothecenes in cancer chemotherapy.

■ ASSOCIATED CONTENT

Ⓢ Supporting Information

1D and 2D NMR and HR-MS of compounds **1** and **2**. This material is available free of charge via the Internet at http://pubs.acs.org.

■ AUTHOR INFORMATION

Corresponding Author

*Phone: 86-592-2187225. Fax: 86-592-2181879. E-mail: haifeng@xmu.edu.cn.

Funding

This study were supported by the Natural Science Foundation of Fujian Province of China (No. 2011J01251) and National Natural Science Foundation of China (No. 81202439).

Notes

The authors declare no competing financial interest.

■ REFERENCES

(1) He, J. W.; Zhou, T.; Christopher, Y. J.; Boland, G. J.; Scottc, P. M. Chemical and biological transformations for detoxification of trichothecene mycotoxins in human and animal food chains: a review. *Trends Food. Sci. Technol.* **2010**, *21*, 67−76.

(2) McCormick, S. P; Alexander, N. J; Proctor, R. H. Trichothecene Triangle: Toxins, Genes, and Plant Disease. In *Phytochemicals, Plant Growth,and the Environment*; Gang, D. R., Bernards, M. A., Davin, L. B., Jetter, R., McCormick, S. P., Stevens, J. F., Eds.; Springer: New York, 2013; Vol. *42*, pp 1−2.

(3) Ueno, Y. Trichothecene mycotoxins: Mycology, chemistry, and toxicology. *Adv. Nutr. Res.* **1989**, *3*, 301−353.

(4) Lancova, K.; Hajslova, J.; Poustka, J.; Krplova, A.; Zachariasova, M.; Dostalek, P.; Sachambula, L. Transfer of *Fusarium* mycotoxins and 'masked' deoxynivalenol (deoxynivalenol-3-glucoside) from field barley through malt to beer. *Food Addit. Contam. A* **2008**, *25*, 732−744.

(5) Alvi, K. A.; Rabenstein, J.; Woodard, J.; Baker, D. D.; Bergthold, J. D.; Lynch, J.; Lieu, K. L.; Braude, I. A. 14′-Hydroxymytoxin B and 16-hydroxyroridin E, two new cytotoxic trichothecenes from *Myrothecium roridum*. *J. Nat. Prod.* **2002**, *65*, 742−744.

(6) Abbas, H. K.; Yoshizawa, T.; Shier, W. T. Cytotoxicity and phytotoxicity of trichothecene mycotoxins produced by *Fusarium* spp. *Toxicon* **2013**, *74*, 68−75.

(7) Isaka, M.; Punya, J.; Lertwerawat, Y.; Tanticharoen, M.; Thebtaranonth, Y. Antimalarial activity of macrocyclic trichothecenes isolated from the fungus *Myrothecium verrucaria*. *J. Nat. Prod.* **1999**, *62*, 329−331.

(8) Bondy, G. S.; Pestka, J. J. Immunomodulation by fungal toxins. *J. Toxicol. Environ. Health, Part B* **2000**, *3*, 109−143.

(9) Amagata, T.; Rath, C.; Rigot, J. F.; Tarlov, N.; Tenney, K.; Valeriote, F. A.; Crews, P. Structures and cytotoxic properties of trichoverroids and their macrolide analogues produced by saltwater culture of *Myrothecium verrucaria*. *J. Med. Chem.* **2003**, *46*, 4342−4350.

(10) Claridge, C. A.; Schmitz, H.; Bradner, W. T. Antitumor activity of some microbial and chemical transformation products of anguidine (4,15-diacetoxyscirpene-3-ol). *Cancer Chemother. Pharmacol.* **1979**, *2*, 181−182.

(11) Thompson, W. L.; Wannemacher, R. W., Jr. Detection and quantitation of T-2 mycotoxin with a simplified protein synthesis inhibition assay. *Appl. Environ. Microbiol.* **1984**, *48*, 1176−1180.

(12) Shen, L.; Jiao, R. H.; Ye, Y. H.; Wang, X. T.; Xu, C.; Song, Y. C.; Zhu, H. L.; Tan, R. X. Absolute configuration of new cytotoxic and other bioactive trichothecene macrolides. *Chemistry* **2006**, *12*, 5596−5602.

(13) Jarvis, B. B.; Comezoglu, F. T.; Wang, S.; Ammon, H. L. Myrotoxins from a plant pathogenic isolate of *Myrothecium roridum*. *Mycotoxin Res.* **1991**, *7*, 73−78.

(14) Hayakawa, S.; Kondo, E.; Wakisaka, Y.; Minato, H.; Katagiri, K. Vertisporin, a new antibiotic from *Verticimonosporium diffractum*. *J. Antibiot. (Tokyo)* **1975**, *28*, 550−551.
(15) Jarvis, B. B.; Taha Çömezoglu, F.; Lee, Y. W.; Flippen-Anderson, J. L.; Gilardi, R. D.; George, C. F. Novel Macrocyclic Trichothecenes from *Myrothecium Roridum*. *Bull. Soc. Chim. Belges.* **1986**, *95*, 681−697.
(16) Traxler, P.; Zurcher, W.; Tamm, C. Structure of the antibiotic roridin E. *Helv. Chim. Acta* **1970**, *53*, 2071−2085.
(17) Xu, J.; Takasaki, A.; Kobayashi, H.; Oda, T.; Yamada, J.; Mangindaan, R. E.; Ukai, K.; Nagai, H.; Namikoshi, M. Four new macrocyclic trichothecenes from two strains of marine-derived fungi of the genus *Myrothecium*. *J. Antibiot. (Tokyo)* **2006**, *59*, 451−455.
(18) Pestka, J. J.; Zhou, H. R.; Moon, Y.; Chung, Y. J. Cellular and molecular mechanisms for immune modulation by deoxynivalenol and other trichothecenes: unraveling a paradox. *Toxicol. Lett.* **2004**, *153*, 61−73.
(19) Kobayashi, M.; Kanasaki, R.; Ezaki, M.; Sakamoto, K.; Takase, S.; Fujie, A.; Hino, M.; Hori, Y. FR227244, a novel antifungal antibiotic from *Myrothecium cinctum* No. 002 Taxonomy, fermentation, isolation and physico-chemical properties. *J. Antibiot. (Tokyo)* **2004**, *57*, 780−787.
(20) Abbas, H. K.; Johnson, B. B.; Shier, W. T.; Tak, H.; Jarvis, B. B.; Boyette, C. D. Phytotoxicity and mammalian cytotoxicity of macrocyclic trichothecene mycotoxins from *Myrothecium verrucaria*. *Phytochemistry* **2002**, *59*, 309−313.
(21) Steffen, J. D.; Tholey, R. M.; Langelier, M. F.; Planck, J. L.; Schiewer, M. J.; Lal, S.; Bildzukewicz, N. A.; Yeo, C. J.; Knudsen, K. E.; Brody, J. R.; Pascal, J. M. Targeting PARP-1 allosteric regulation offers therapeutic potential against cancer. *Cancer Res.* **2013**, *74*, 31−37.
(22) Nguewa, P. A.; Fuertes, M. A.; Valladares, B.; Alonso, C.; Perez, J. M. Poly(ADP-ribose) polymerases: homology, structural domains and functions. Novel therapeutical applications. *Prog. Biophys. Mol. Biol.* **2005**, *88*, 143−172.
(23) Germain, M.; Affar, E. B.; D'Amours, D.; Dixit, V. M.; Salvesen, G. S.; Poirier, G. G. Cleavage of automodified poly(ADP-ribose) polymerase during apoptosis. Evidence for involvement of caspase-7. *J. Biol. Chem.* **1999**, *274*, 28379−28384.
(24) Bouchard, V. J.; Rouleau, M.; Poirier, G. G. PARP-1, a determinant of cell survival in response to DNA damage. *Exp. Hematol.* **2003**, *31*, 446−454.
(25) Liu, X.; Kim, C. N.; Yang, J.; Jemmerson, R.; Wang, X. Induction of apoptotic program in cell-free extracts: requirement for dATP and cytochrome c. *Cell* **1996**, *86*, 147−157.
(26) Delaval, B.; Birnbaum, D. A cell cycle hypothesis of cooperative oncogenesis (Review). *Int. J. Oncol.* **2007**, *30*, 1051−1058.
(27) Wada, T.; Penninger, J. M. Mitogen-activated protein kinases in apoptosis regulation. *Oncogene* **2004**, *23*, 2838−2849.
(28) Tournier, C. The 2 faces of JNK Signaling in cancer. *Genes Cancer* **2013**, *4*, 397−400.
(29) Dhanasekaran, D. N.; Johnson, G. L. MAPKs: function, regulation, role in cancer and therapeutic targeting. *Oncogene* **2007**, *26*, 3097−3099.
(30) Dhanasekaran, N.; Premkumar, R. E. Signaling by dual specificity kinases. *Oncogene* **1998**, *17*, 1447−1455.
(31) Seimiya, H.; Mashima, T.; Toho, M.; Tsuruo, T. c-Jun NH2-terminal kinase-mediated activation of interleukin-1beta converting enzyme/CED-3-like protease during anticancer drug-induced apoptosis. *J. Biol. Chem.* **1997**, *272*, 4631−4636.
(32) Waskiewicz, A. J.; Cooper, J. A. Mitogen and stress response pathways: MAP kinase cascades and phosphatase regulation in mammals and yeast. *Curr. Opin. Cell Biol.* **1995**, *7*, 798−805.
(33) Tibbles, L. A.; Woodgett, J. R. The stress-activated protein kinase pathways. *Cell. Mol. Life Sci.* **1999**, *55*, 1230−1254.
(34) Davis, R. J. Signal transduction by the JNK group of MAP kinases. *Cell* **2000**, *103*, 239−252.
(35) Chang, L.; Karin, M. Mammalian MAP kinase signalling cascades. *Nature* **2001**, *410*, 37−40.
(36) Johnson, G. L.; Lapadat, R. Mitogen-activated protein kinase pathways mediated by ERK, JNK, and p38 protein kinases. *Science* **2002**, *298*, 1911−1912.
(37) Werlen, G.; Hausmann, B.; Naeher, D.; Palmer, E. Signaling life and death in the thymus: timing is everything. *Science* **2003**, *299*, 1859−1863.
(38) Ventura, J. J.; Hubner, A.; Zhang, C.; Flavell, R. A.; Shokat, K. M.; Davis, R. J. Chemical genetic analysis of the time course of signal transduction by JNK. *Mol. Cell* **2006**, *21*, 701−710.

JOURNAL OF AGRICULTURAL AND FOOD CHEMISTRY

Article

pubs.acs.org/JAFC

An Advanced Glycation End Product (AGE)-Rich Diet Promotes Nε-Carboxymethyl-lysine Accumulation in the Cardiac Tissue and Tendons of Rats

Irene Roncero-Ramos,[†] Céline Niquet-Léridon,[‡] Christopher Strauch,[§] Vincent M. Monnier,[§] Frédéric J. Tessier,[‡] María Pilar Navarro,[†,∥] and Cristina Delgado-Andrade*[,†,∥]

[†]Instituto en Formación de Nutrición Animal, Estación Experimental del Zaidín, CSIC, 18100, Granada, Spain

[‡]Institut Polytechnique LaSalle Beauvais, 60026 Beauvais, France

[§]Departments of Pathology and Biochemistry, Case Western Research University, Cleveland, Ohio 44106, United States

ABSTRACT: The purpose of this study was to investigate the intake, excretion, and tissue accumulation of carboxymethyl-lysine (CML), after feeding rats a diet containing advanced glycation end products (AGEs) from a glucose−lysine (GL) model system. Rats were distributed into two groups and assigned to a control diet or a diet including 3% heated GL (GL diet) for three months. Feces and urine were collected over the last week. After sacrifice, serum was obtained and some organs were removed for CML analysis. The percentage of fecal CML was 2.5-fold higher in the animals fed the GL diet (33.2 vs 76.5% for control and GL group), whereby total recovery was 91.8% compared with a level of 54.6% in the animals fed the control chow, evidencing the importance of the chemical form and the net quantity of dietary CML on its elimination. We suggest that dietary dicarbonyl compounds from GL diet or dietary CML itself are responsible for CML accumulation in hearts and tendons. The most significant result of the present study is that the regular consumption of dietary AGEs in healthy individuals promotes CML accumulation in some organs.

KEYWORDS: *advanced glycation end products, carboxymethyl-lysine, bone, heart, tendon*

INTRODUCTION

Advanced glycation end products (AGEs) are compounds formed by the nonenzymatic reaction between reducing sugars and free amino groups in proteins, lipids, or nucleic acids, called the Maillard reaction. This reaction takes place during thermal processing of food by techniques such as frying, baking, or roasting and is responsible for the formation of characteristic flavors, colors, and tastes that are desirable to the consumer.[1] On the other hand, the formation of AGEs could lead to a decrease in the nutritional value of the food due to the destruction of vitamins,[2] loss of essential amino acids, or lower protein digestibility.[3,4]

AGEs may also be generated in biological systems by the reaction of α-dicarbonyl compounds with amino groups of endogenous proteins which accumulate in some tissues or are present in the systemic circulation and play a physiopathological role in cases of metabolic and degenerative disorders.[5] In addition to endogenous synthesis, food can provide a significant amount of AGEs, since glycation derivatives are widely consumed as part of the human diet.[6,7] AGEs are thought to be absorbed in the process of digestion, increasing the circulating level and being deposited in different tissues and organs.[8]

Carboxymethyl-lysine (CML) is one of the best characterized AGEs and is frequently used as a marker of glycation product formation in food and in vivo.[9] Several authors have correlated the CML accumulation in plasma and in different tissues with the progression of diabetes and with the acceleration of the aging process.[10,11] However, to date, its absorption, metabolism, and elimination have been only partially elucidated.[12] A direct correlation between the intake of CML and its elimination in feces and urine has been established in several studies. Thus, in the assay of Birlouez-Aragon et al.[13] carried out in humans, the urinary excretion of CML increased by 40% after the consumption of a diet rich in this compound compared with a low-AGE diet; moreover, its presence in plasma was 7% higher. Delgado-Andrade et al.[12] corroborated a higher CML elimination in feces when human volunteers consumed a diet containing large quantities of AGEs. However, the urinary excretion was weakly correlated, probably because renal excretion may be saturated or limited, exceeding the kidney's detoxification capacity. Renal clearance saturation has also been described in a rat study by Alamir et al.[14] after the intake of a diet based on crushed extruded biscuits rich in CML.

Derivatives from the glucose−lysine model system are frequently used to study diverse aspects of AGE effects. Their advantage is that they are easy to produce under laboratory conditions, and the results obtained after in vivo trials are often simpler and more easily interpreted. AGEs from lysine are commonly present in food, since this amino acid is very sensitive to thermal treatment and highly reactive in the Maillard reaction.[15]

The aim of the present study is to investigate CML intake and excretion after feeding rats a diet containing AGEs from a heated glucose−lysine model system. The main originality of

Received: March 3, 2014
Revised: May 12, 2014
Accepted: June 3, 2014
Published: June 3, 2014

ACS Publications © 2014 American Chemical Society

dx.doi.org/10.1021/jf501005n | J. Agric. Food Chem. 2014, 62, 6001−6006

Table 1. CML Daily Intake and Excretion during Last Week of the Assay. Percentage of Fecal, Urinary, and Total CML Excreted from the Intake[a]

	μg/day			CML excretion rate (%)		
groups	intake	feces	urine	feces	urine	total
control	30.2 ± 1.56 a	9.96 ± 0.63 a	6.41 ± 0.61 a	33.2 ± 1.88 a	21.4 ± 1.85 a	54.6 ± 2.21 a
GL	175 ± 14.7 b	135 ± 13.1 b	26.9 ± 3.25 b	76.5 ± 2.45 b	15.3 ± 1.20 b	91.8 ± 2.21 b

[a]Values are means ± SE (n = 6). Different letters within a column indicate significant differences between groups ($p < 0.05$).

this work is the seeking of possible target organs for the CML deposit in the organism of healthy subjects. For that reason, total CML in different tissues and the protein-bound fraction in serum were measured.

MATERIALS AND METHODS

Chemicals. All the chemical products and solvents for all the analyses were of the highest grade available and acquired from Sigma (Sigma-Aldrich, St. Louis, MO) and Merck (Darmstadt, Germany). CML and (D_2)-CML were provided by PolyPeptide Laboratories France SAS (Strasbourg, France).

Sample Preparation. Glucose (Merck, Darmstadt, Germany) and lysine (Sigma Chemical, St. Louis, MO., USA) were used to prepare the sample. Equimolar mixtures of glucose−lysine−HCl (GL) (40% moisture) were heated in open receptacles in an oven (Selecta 2000210; Barcelona, Spain) at 150 °C for 90 min to obtain the GL sample. This procedure tried to simulate usual home cooking. After heating, the reaction was stopped by cooling in an ice bath and the products were then removed, frozen, lyophilized, and stored at 4 °C as described by Delgado-Andrade et al.[16] until required for preparing the diets.

Preparation of Diets. The AIN-93G purified diet for laboratory rodents (Dyets Inc., Bethlehem, PA) was used as the control diet. The GL sample was added to the AIN-93G diet to reach a final concentration of 3%. This diet was termed GL. The individual analysis of the GL diet revealed no modification of the overall nutrient composition, compared with the control diet (AIN-93G). The mean ± SD nutrient content of the diets was as follows: moisture (%) 8.14 ± 0.08; protein (g/kg) 176.6 ± 3.1; fat (g/kg) 78.1 ± 0.9; and ashes (%) 2.55 ± 0.13.

The higher Maillard reaction product (MRP) content in the GL diet with respect to the control one was confirmed by analyzing the furosine and hydroxymethylfurfural (HMF) contents and total MRP associated fluorescence as described in previous publications.[17,18] The data obtained for furosine (mean ± SD) were as follows: 28.8 ± 0.5 and 1787.08 ± 7.31 mg/kg diet for control and GL diets, respectively. The results for HMF (mean ± SD) were as follows: 0.44 ± 0.06 and 5.15 ± 0.08 mg/kg diet for control and GL diets, respectively. In the case of total MRP associated fluorescence (mean ± SD), they were as follows: 1.1 ± 0.1 and 10.3 ± 0.1 × 10^5 fluorescence units/g diet for control and GL diets, respectively.

Biological Assays. Twenty-four weanling Wistar rats weighing 39.76 ± 0.85 g (mean ± SE) were used in the study. They were randomly distributed into two groups (12 animals per group), and each group was assigned to one of the dietary treatments. The animals were individually housed in metabolic cages in an environmentally controlled room under standard conditions (temperature: 20−22 °C with a 12 h light−dark cycle and 55−70% humidity). The rats had ad libitum access to their diets and demineralized water (Milli-Q Ultrapure Water System, Millipore Corps., Bedford, MA, USA).

The experiment involved a preliminary 81-day period during which solid food intake and body weight changes were monitored weekly, followed by a 7-day period in which feces and urine from each animal were collected daily and stored separately as a 1-week pool. The feces were weighed, lyophilized, powdered, and then homogenized. The urine was collected in 0.5% HCl (v/v), filtered (Whatman Filter Paper No. 40, ashless, Whatman, England), and diluted to an appropriate volume. On day 88, after an overnight fast, the animals were anesthetized with sodium pentobarbital (5 mg per 100 g of body weight) (Abbott Laboratories, Granada, Spain) and terminal exsanguination was performed by a cannulation of the carotid artery. Blood was drawn to obtain serum. Hearts, the right pelvic bones, and the tail tendons were removed, weighed, and frozen at −80 °C until CML analysis.

All management and experimental procedures carried out in this study were in strict accordance with the current European regulations (86/609 E.E.C.) regarding laboratory animals. The Bioethics Committee for Animal Experimentation at our institution (EEZ-CSIC) approved the study protocol.

Sample Preparation for CML Analysis. For CML determination, feces, urines, and hearts were lyophilized and powdered, while diets, serum, and tail tendons were directly processed. Bones were powdered and homogenized. In all samples, an equivalent to 10 mg of proteins was weighed to perform the CML determination. In the case of serum, a step prior to the acid hydrolysis was carried out for protein precipitation using trichloroacetic acid. Therefore, in this last case only protein-bound CML was quantified. The total content of CML (free and protein-bound) was measured in all other samples.

Analytical Techniques. The CML and lysine analysis in extracts of diets, feces, urine, serum, hearts, and bones were performed at the Institut Polytechnique LaSalle Beauvais. All the extractions were done in triplicate and analysis was done in duplicate, when possible, using the method recently developed by Niquet-Léridon and Tessier.[19] Each sample was treated with sodium borohydride to stabilize the Amadori products and to prevent their conversion into CML during the acid hydrolysis. A quantity of reduced sample, equivalent to 10 mg of protein, was dissolved in 5 mL of 6 M HCl and incubated at 110 °C for 20 h. Three hundred microliters of each acid hydrolysate was dried under vacuum and reconstituted in 300 μL of internal standard containing 0.15 μg of (D_2)-CML and 12.5 μg of ($^{15}N_2$)-lysine (dissolved in 20 mM nonafluoropentanoic acid (NFPA)) prior to analysis by LC−MS/MS. The use of internal standards which are isotopes of CML and lysine, respectively, increases the precision and the accuracy of the measurements compared with previous studies.[13] Liquid chromatography coupled to linear ion trap tandem mass spectrometry was used for the analysis of CML. The following instrumentation and criteria were used: Surveyor HPLC system coupled to an LTQ mass spectrometer working in its tandem operation mode (ThermoFisher Scientific, Courtaboeuf, France); thermostat, 10 °C; column Hypercarb, 100 mm × 2.1 mm, 5 μm with a guard column Hypercarb, 10 mm × 2.1 mm, 5 μm; injection volume, 10 μL; flow rate, 0.2 mL/min; mobile phase, 20 mM NFPA in a water−acetonitrile gradient (linear increase of acetonitrile from 0 to 50% over 20 min), electrospray ionization in positive mode; multiple reaction monitoring with the specific transitions m/z 205.0/130.0 and m/z 207.0/130.0 for CML and (D_2)-CML, respectively, with a normalized collision energy of 37% to achieve optimum fragmentations of the parent ions. Lysine and its isotope were detected with the specific transitions m/z 147.0/130.0 and m/z 149.0/131.0, respectively.

The CML and lysine analysis for tail tendons were carried out at Case Western Reserve University (Cleveland, OH). CML and lysine were determined in acid hydrolysates of processed collagen tendon samples and derivatized as its trifluoroacetyl methyl esters by selected ion monitoring gas chromatography GC/MS as previously described by Sell et al.[20]

Statistical Analysis. After checking the normal distribution of data, they were statistically tested with a Student's unpaired t test to compare means that showed a significant variation ($p < 0.05$). Analyses

were performed using Statgraphics Plus, version 5.1, 2001. Evaluation of the relationship between the different variables was carried out by computing the relevant correlation coefficient (Pearson's linear correlation) at the $P < 0.05$ confidence level.

RESULTS AND DISCUSSION

CML Intake and Excretion. The total CML content in the diets (mean ± SD) was 2.18 ± 0.03 and 12.5 ± 0.24 μg/g for the control and GL diets, respectively. As expected, the GL diet had a significantly higher CML content ($P < 0.05$). However, the control diet presented a basal CML content that was probably formed during storage of the diet or of its individual ingredients or even during their production.[21] However, due to the higher proportion of CML in the GL diet, the animals submitted to this diet had a much higher daily exposure to CML than the control group (Table 1). Previous assays conducted by our research group in designing AGE-rich diets for rats, using bread crust as a glycoprotein source, have also recorded significant amounts of CML in these animals and a subsequent higher CML intake, compared with the control diet.[22]

As a result of the high CML intake, fecal excretion was increased in the GL group, and CML intake and its elimination were highly correlated ($r = 0.981$, $p < 0.001$) (Figure 1), which is consistent with what other authors have described previously.[14,23,24] Despite the high proportion of CML eliminated in the feces after consumption of the GL diet (>75%) compared with the control diet (33%), its possible net absorption could be higher than in the control animals due to the great CML exposure of this diet (Table 1). The CML included in the GL diet and originated from a glucose−lysine model system is more likely present as a free adduct although other forms could exist (Table 1).

The animals in the GL group eliminated significantly more urinary CML than did those in the control group (Table 1). As before, this difference was related to the amount of CML consumed by each group; this is corroborated by the strong correlation between CML intake and its urinary elimination ($r = 0.943$, $p < 0.001$) (Figure 1). Previous studies have also reported CML intake to be significantly correlated with its urinary elimination, both in humans[13] and in rats.[14,23] However, the findings obtained by our research group working with AGEs derived from bread crust did not reflect any relationship between these parameters.[22] The lack of concordance between the two assays might be related to the form of CML preferentially ingested in each case. Whereas in the present assay free forms of CML were predominant in the GL diet, in our previous experiment bread crust was used as the source of glycoproteins, and in this latter case protein-bound CML forms would predominate. However, it is worthy to note that Alamir et al.[14] used a protein-bound CML source in their study and found a good correlation between dietary CML and its urinary excretion. Lastly, it must be also noticed that the excretion rate of urinary CML in the rats of the present assay was much higher than that recorded for humans in the ICARE study.[13] This fact points out strong differences between rats and human species with special relevance for CML metabolism.

The intake of free CML, a more absorbable form than the protein-bound compounds, could elevate the circulating CML and thus explain the high net renal clearance of CML in the GL diet (Table 1), which is corroborated by the existence of an important direct relationship between CML intake and its urinary elimination.

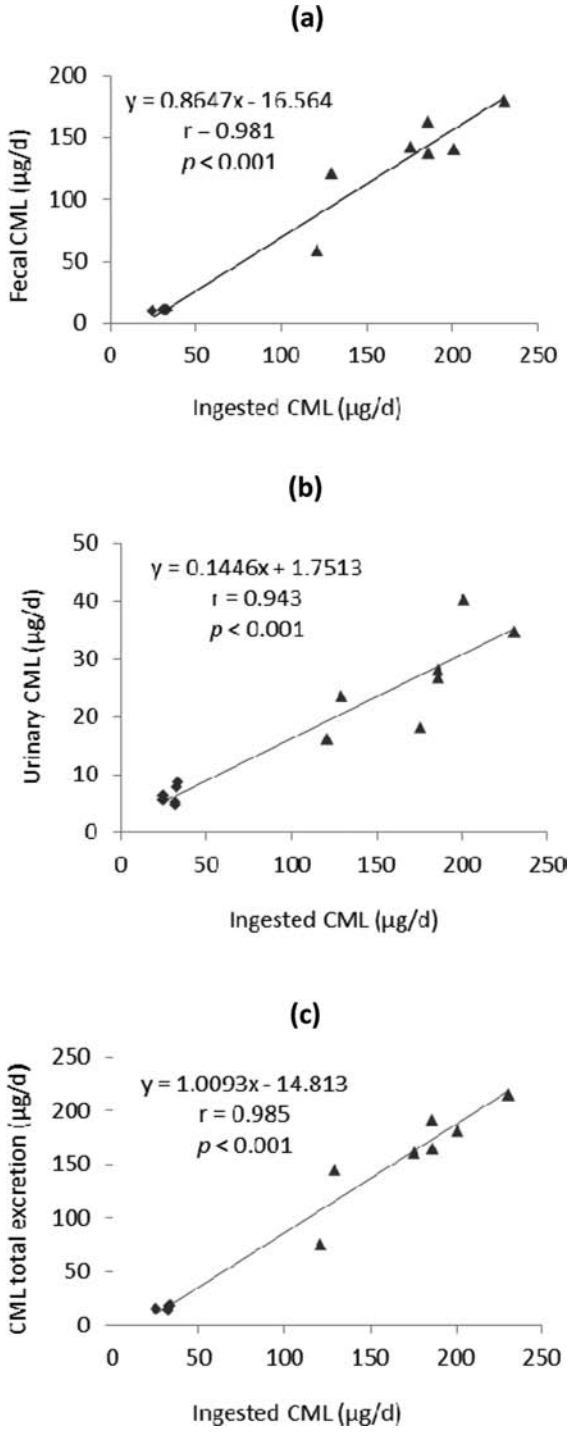

Figure 1. Relationship between CML intake (μg/day) and either fecal CML (a), urinary CML (b), or total excretion (c). $p < 0.05$ indicates the existence of a significant correlation (◆, control group; ▲, GL group).

With respect to the total percentage of CML excreted, the control group rats recovered approximately 50% while those in the GL group recovered 92% (Table 1). Results similar to those for our control group have been observed in other studies working with CML from food. Thus, Delgado-Andrade et al.[12] reported recovery rates of 45−50% in human volunteers, and Somoza et al.[25] found that 50% of the CML ingested was excreted in the feces and urine. Probably, the high difference between the recovery in the human studies and that from the

dx.doi.org/10.1021/jf501005n | J. Agric. Food Chem. 2014, 62, 6001−6006

GL group was mainly due to the great difference in the CML fecal elimination. Focused exclusively in the rate of total CML recovery, its high value in the GL group, once again, highlights the importance of the form of ingested CML (free or linked to a protein backbone) as well as the level of the oral dose of CML. Food-derived CML has a different chemical form and molecular weight to CML obtained from a model system. Available information regarding AGE absorption indicates that its absorption strongly depends on whether these compounds are present in protein-bound form or not. Low molecular weight AGEs may be relatively quickly absorbed, metabolized, and excreted; however, high molecular weight AGEs may remain relatively nonabsorbed due to insufficient degradation by gastrointestinal enzymes.[26]

The results obtained in the present paper for total CML recovery in the GL group (92%) are in line with the recovery described for pyrraline by Foerster and Henle.[27] However, unlike the CML, pyrraline was almost entirely absorbed from foods and, after its metabolic transit, was eliminated rapidly and almost completely in the urine, with only slight metabolism within the body.

CML in Plasma and Tissues. As has been observed previously, diets rich in AGEs can increase levels of circulating CML in serum.[25] Several authors have described a significant positive correlation between dietary intake of AGEs and CML concentrations in the blood.[28,29] In the present assay, the protein-bound CML in serum was measured and no differences were found between the GL group and the control group (Figure 2). Recent studies have described stability in protein-bound CML in serum after the consumption of diets rich in this AGE,[14,30] which is consistent with the results of the present work.[12] In the study by Alamir et al.,[14] in which rats were fed a diet based on crushed extruded biscuits, the protein-bound CML level in plasma did not vary, but the free fraction increased with consumption of this diet. In the light of these data it could be hypothesized that free CML is more affected by dietary exposure than protein-bound fraction, and this fact could be used to know the real index of the CML obtained from the diet. Unfortunately, this measurement could not be obtained in the present study.

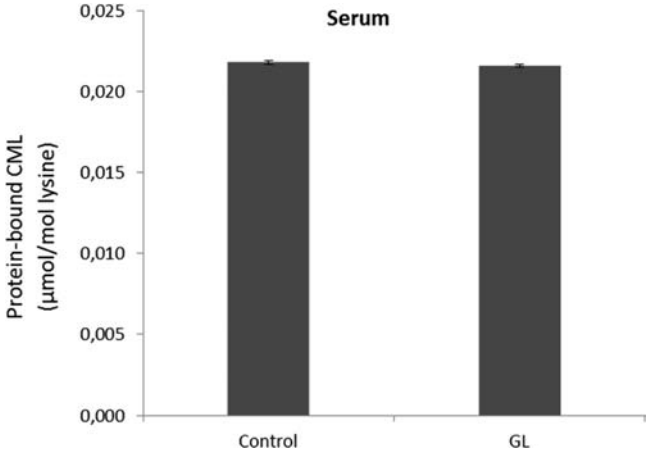

Figure 2. Protein-bound CML in serum expressed as μmol/mol lysine (mean ± SE, $n = 6$). No significant differences were found between the groups ($p > 0.05$).

A significant increase in tissue CML concentration has been observed under pathological conditions such as diabetes.[11] Although the accumulation of CML in the kidney, skin, and blood vessels in diabetic subjects is well established,[31] its accumulation in the heart has yet to be completely elucidated. Subsequent studies suggested that an increase in CML levels in cardiac tissue could play an important role in the pathogenesis of heart disease.[32,33] Moreover, our research group recently showed that after rats were fed an AGE-enriched diet elaborated from bread crust, the total CML level in cardiac tissue increased.[22] In the present assay, consumption of the GL diet significantly raised the total concentration of CML in the heart, in comparison with the animals given the control diet (Figure 3) ($p = 0.035$). In this respect, it should be noted that the remaining blood was not completely removed from the heart prior to the CML analysis, and so some contribution to the final CML content in the heart cannot be excluded. However, taking into account that no modifications were

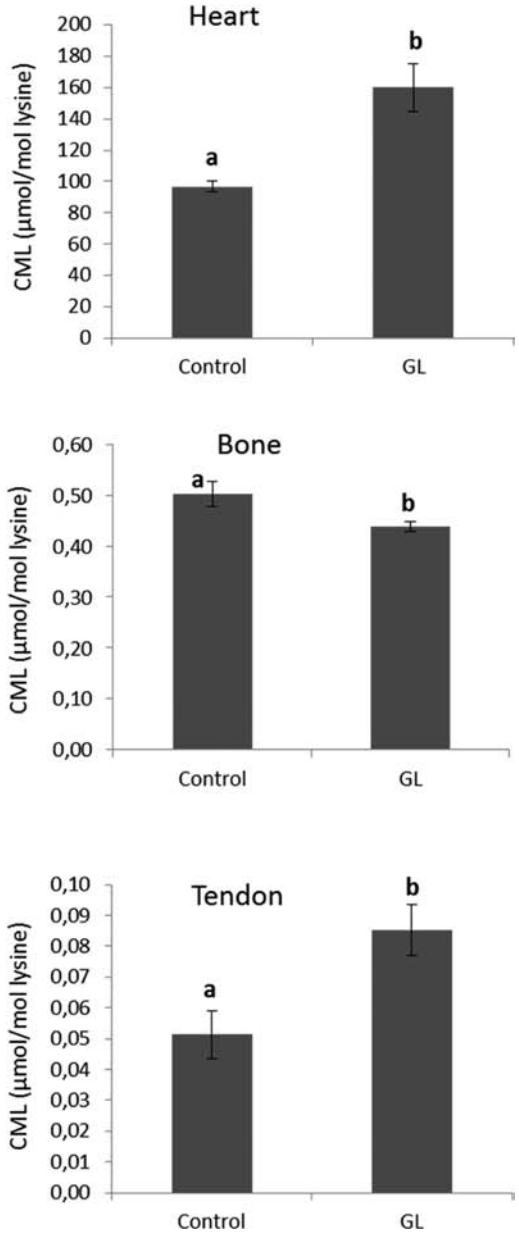

Figure 3. CML in heart, bone, and tail tendon (μmol/mol lysine) (mean ± SE, $n = 6$). Different letters indicate significant differences between the groups ($p < 0.05$).

dx.doi.org/10.1021/jf501005n | J. Agric. Food Chem. 2014, 62, 6001−6006

detected in the protein-bound CML of the plasma (which could be more representative of the endogenous CML), its accumulation in the heart could have a dietary origin. Supporting this hypothesis, a correlation between the daily intake of CML and its accumulation in the heart ($r = 0.785$; $p = 0.003$) was detected. But in any case, the in situ CML formation from dietary dicarbonyl compounds must be also considered due to the elevated recovery rate of the compound in urine and feces. The effect of a high dietary AGEs intake in increasing the heart AGEs content has been previously established.[34]

With respect to the concentration of CML in the bones, the GL group presented a significantly lower CML content than the control group. However, in the case of the tail tendons, total CML was significantly increased when the animals consumed the GL diet (Figure 3). This fact could be due to the tendon collagen being more susceptible to glycation than is bone collagen.[35] It has been reported that the mineral phase of bone provides some protection against glycation.[36] The high CML accumulation could also be explained by the lower turnover of collagen type I in the tendons and other connective tissues, such as cartilage or ligaments;[37] the turnover of this type of collagen in bones is faster, and this, too, could be significant in the lesser accumulation of AGEs. CML in the tendons might come from the direct deposition of ingested CML, and/or from absorbed dicarbonyl compounds, which could act as promoters for the in vivo formation of CML. Several authors have described the accumulation of AGEs in the bones[38] as well as in the tendons[39] under conditions of diabetes or aging,[40] but further studies are necessary to clarify the question of CML deposit or its formation by dietary exposure.

In summary, the results of the present study, together with those of previous work by our research group, underline the importance of the chemical form of dietary CML in its fecal and urinary excretion. The simpler forms of the compound in the diet increase its possible absorption, with a subsequent high renal clearance in comparison with the intake of the protein-bound CML. In view of the high rate of CML recovery observed in the GL group, we believe that, in addition to dietary CML, dietary dicarbonyl compounds could be partly responsible for CML accumulation in the heart. In parallel, those products could also be involved in the increased amount of CML in the tail tendons but not in the bones, due to the greater turnover of its collagen. Possibly the most significant result of the present study is the demonstration that the uninterrupted consumption of dietary AGEs promotes CML accumulations in the target tissues of healthy individuals, a fact which could have pathophysiological implications especially in the elderly population.

AUTHOR INFORMATION

Corresponding Author

*Instituto en Formación de Nutrición Animal, Estación Experimental del Zaidín, CSIC, Camino del Jueves s/n, 18100, Armilla, Granada, Spain. Tel: +34 958 572757. Fax: +34 958 572753. E-mail: cdelgado@eez.csic.es.

Author Contributions

‖These authors share the same authorship.

Funding

This work was supported by a project of the Spanish Ministry of Economy and Competitiveness.

Notes

The authors declare no competing financial interest.

ACKNOWLEDGMENTS

The authors thank Philippe Jacolot for his technical support.

REFERENCES

(1) Ames, J. M. Control of the Maillard reaction in food systems. *Trends Food. Sci. Technol.* **1990**, *1*, 150−154.

(2) Finot, P. A. BROWNING|Toxicology of nonenzymatic browning. In *Encyclopedia of Food Sciences and Nutrition (2nd)*, Caballero, B., Ed.; Academic Press: Oxford, 2003; pp 673−678.

(3) Seiquer, I.; Diaz-Alguacil, J.; Delgado-Andrade, C.; Lopez-Frias, M.; Munoz Hoyos, A.; Galdo, G.; Navarro, M. P. Diets rich in Maillard reaction products affect protein digestibility in adolescent males aged 11−14 y. *Am. J. Clin. Nutr.* **2006**, *83*, 1082−1088.

(4) Singh, S.; Wakeling, L.; Gamlath, S. Retention of essential amino acids during extrusion of protein and reducing sugars. *J. Agric. Food Chem.* **2007**, *55*, 8779−8786.

(5) Tessier, F.; Birlouez-Aragon, I. Health effects of dietary Maillard reaction products: the results of ICARE and other studies. *Amino Acids* **2012**, *42*, 1119−1131.

(6) Koschinsky, T.; He, C.-J.; Mitsuhashi, T.; Bucala, R.; Liu, C.; Buenting, C.; Heitmann, K.; Vlassara, H. Orally absorbed reactive glycation products (glycotoxins): An environmental risk factor in diabetic nephropathy. *Proc. Natl. Acad. Sci. U.S.A.* **1997**, *94*, 6474−6479.

(7) Vlassara, H. Advanced glycosylation in nephropathy of diabetes and aging. *Adv. Nephrol.* **1996**, *25*, 303−307.

(8) Luevano-Contreras, C.; Chapman-Novakofski, K. Dietary advanced glycation end products and aging. *Nutrients* **2010**, *2*, 1247−1265.

(9) Hull, G.; Woodside, J.; Ames, J.; Cuskelly, G. N-epsilon-(carboxymethyl)lysine content of foods commonly consumed in a Western style diet. *Food Chem.* **2012**, *131*, 170−174.

(10) Knecht, K. J.; Dunn, J. A.; McFarland, K. F.; McCance, D. R.; Lyons, T. J.; Thorpe, S. R.; Baynes, J. W. Effect of diabetes and aging on carboxymethyllysine levels in human urine. *Diabetes* **1991**, *40*, 190−196.

(11) Monnier, V. M.; Sell, D. R.; Nagaraj, R. H.; Miyata, S.; Grandhee, S.; Odetti, P.; Ibrahim, S. A. Maillard reaction-mediated molecular damage to extracellular matrix and other tissue proteins in diabetes, aging, and uremia. *Diabetes* **1992**, *2*, 36−41.

(12) Delgado-Andrade, C.; Tessier, F. J.; Niquet-Léridon, C.; Seiquer, I.; Navarro, M. P. Study of the urinary and faecal excretion of N^{ε}-carboxymethyllysine in young human volunteers. *Amino Acids* **2012**, *43*, 595−602.

(13) Birlouez-Aragon, I.; Saavedra, G.; Tessier, F. J.; Galinier, A.; Ait-Ameur, L.; Lacoste, F.; Niamba, C.-N.; Alt, N.; Somoza, V.; Lecerf, J.-M. A diet based on high-heat-treated foods promotes risk factors for diabetes mellitus and cardiovascular diseases. *Am. J. Clin. Nutr.* **2010**, *91*, 1220−1226.

(14) Alamir, I.; Niquet-Léridon, C.; Jacolot, P.; Rodriguez, C.; Orosco, M.; Anton, P. M.; Tessier, F. J. Digestibility of extruded proteins and metabolic transit of N(epsilon)-carboxymethyllysine in rats. *Amino Acids* **2012**, *16*, 16.

(15) Ashoor, S. H.; Zent, J. B. Maillard Browning of Common Amino Acids and Sugars. *J. Food Sci.* **1984**, *49*, 1206−1207.

(16) Delgado-Andrade, C.; Seiquer, I.; Nieto, R.; Navarro, M. P. Effects of heated glucose−lysine and glucose−methionine model-systems on mineral solubility. *Food Chem.* **2004**, *87*, 329−337.

(17) Roncero-Ramos, I.; Delgado-Andrade, C.; Rufián-Henares, J. A.; Carballo, J.; Navarro, M. P. Effects of model Maillard compounds on bone characteristics and functionality. *J. Sci. Food Agric.* **2013**, *93*, 2816−2821.

(18) Grasa, J.; Calvo, B.; Delgado-Andrade, C.; Navarro, M. P. Variations in tendon stiffness due to diets with different glycotoxins

affect mechanical properties in the muscle-tendon unit. *Ann. Biomed. Eng.* **2013**, *41*, 488−496.
(19) Niquet-Léridon, C.; Tessier, F. J. Quantification of N(epsilon)-carboxymethyl-lysine in selected chocolate-flavoured drink mixes using high-performance liquid chromatography-linear ion trap tandem mass spectrometry. *Food Chem.* **2011**, *126*, 655−663.
(20) Sell, D. R.; Strauch, C. M.; Shen, W.; Monnier, V. M. 2-Aminoadipic acid is a marker of protein carbonyl oxidation in the aging human skin: effects of diabetes, renal failure and sepsis. *Biochem. J.* **2007**, *404*, 269−277.
(21) Tan, A. L. Y.; Sourris, K. C.; Harcourt, B. E.; Thallas-Bonke, V.; Penfold, S.; Andrikopoulos, S.; Thomas, M. C.; O'Brien, R. C.; Bierhaus, A.; Cooper, M. E.; Forbes, J. M.; Coughlan, M. T. Disparate effects on renal and oxidative parameters following RAGE deletion, AGE accumulation inhibition, or dietary AGE control in experimental diabetic nephropathy. *Am. J. Physiol.* **2010**, *298*, F763−F770.
(22) Roncero-Ramos, I.; Delgado-Andrade, C.; Tessier, F. J.; Niquet-Leridon, C.; Strauch, C.; Monnier, V. M.; Navarro, M. P. Metabolic transit of N(epsilon)-carboxymethyl-lysine after consumption of AGEs from bread crust. *Food Funct.* **2013**, *4*, 1032−1039.
(23) Liardon, R.; De Weck-Gaudard, D.; Philippossian, G.; Finot, P. A. Identification of N.epsilon.-carboxymethyllysine: a new Maillard reaction product in rat urine. *J. Agric. Food Chem.* **1987**, *35*, 427−431.
(24) Tessier, F. J.; Niquet, C.; Rhaz, L.; Hedhili, K.; Seiquer, I.; Navarro, M. P.; Delgado-Andrade, C. N-Carboxymethyllysine: its origin in selected foods and its urinary and faecal excretions in healthy humans. In *Maillard Reaction Interface between Aging, Nutrition and Metabolism*; Thomas, M. C., Forbes, J. M., Eds.; RSC Publishing: Cambridge, 2010; Vol. *332*, pp 144−150.
(25) Somoza, V.; Wenzel, E.; Weiss, C.; Clawin-Radecker, I.; Grubel, N.; Erbersdobler, H. F. Dose-dependent utilisation of casein-linked lysinoalanine, N(epsilon)-fructoselysine and N(epsilon)-carboxymethyllysine in rats. *Mol. Nutr. Food Res.* **2006**, *50*, 833−841.
(26) Poulsen, M. W.; Hedegaard, R. V.; Andersen, J. M.; de Courten, B.; Bugel, S.; Nielsen, J.; Skibsted, L. H.; Dragsted, L. O. Advanced glycation endproducts in food and their effects on health. *Food Chem. Toxicol.* **2013**, *60*, 10−37.
(27) Foerster, A.; Henle, T. Glycation in food and metabolic transit of dietary AGEs (advanced glycation end-products): studies on the urinary excretion of pyrraline. *Biochem. Soc. Trans.* **2003**, *31*, 1383−1385.
(28) Uribarri, J.; Cai, W.; Peppa, M.; Goodman, S.; Ferrucci, L.; Striker, G.; Vlassara, H. Circulating glycotoxins and dietary advanced glyation endproducts: two links to inflammatory response, oxidative stress, and aging. *J. Gerontol., Ser. A* **2007**, *72*, 427−433.
(29) Uribarri, J.; Peppa, M.; Cai, W.; Goldberg, T.; Lu, M.; Baliga, S.; Vassalotti, J. A.; Vlassara, H. Dietary glycotoxins correlate with circulating advanced glycation end product levels in renal failure patients. *Am. J. Kidney Dis.* **2003**, *42*, 532−538.
(30) Šebeková, K.; Klenovics, K. S.; Boor, P.; Celec, P.; Behuliak, M.; Schieberle, P.; Heidland, A.; Palkovits, M.; Somoza, V. Behaviour and hormonal status in healthy rats on a diet rich in Maillard reaction products with or without solvent extractable aroma compounds. *Physiol. Behav.* **2012**, *105*, 693−701.
(31) Schleicher, E. D.; Wagner, E.; Nerlich, A. G. Increased accumulation of the glycoxidation product N(epsilon)-(carboxymethyl)lysine in human tissues in diabetes and aging. *J. Clin. Invest.* **1997**, *99*, 457−468.
(32) Hu, S.; He, W.; Liu, Z.; Xu, H.; Ma, G. The Accumulation of the Glycoxidation Product N(epsilon)-carboxymethyllysine in cardiac tissues with age, diabetes mellitus and coronary heart disease. *Tohoku J. Exp. Med.* **2013**, *230*, 25−32.
(33) Schalkwijk, C. G.; Baidoshvili, A.; Stehouwer, C. D. A.; van Hinsbergh, V. W. M.; Niessen, H. W. M. Increased accumulation of the glycoxidation product Nε-(carboxymethyl)lysine in hearts of diabetic patients: generation and characterisation of a monoclonal anti-CML antibody. *Biochim. Biophys. Acta, Mol. Cell Biol. Lipids* **2004**, *1636*, 82−89.
(34) Cai, W.; He, J. C.; Zhu, L.; Chen, X.; Zheng, F.; Striker, G. E.; Vlassara, H. Oral glycotoxins determine the effects of calorie restriction on oxidant stress, age-related diseases, and lifespan. *Am. J. Pathol.* **2008**, *173*, 327−336.
(35) Reddy, G. K. Glucose-mediated in vitro glycation modulates biomechanical integrity of the soft tissues but not hard tissues. *J. Orthop. Res.* **2003**, *21*, 738−743.
(36) Vashishth, D.; Gibson, G. J.; Khoury, J. I.; Schaffler, M. B.; Kimura, J.; Fyhrie, D. P. Influence of nonenzymatic glycation on biomechanical properties of cortical bone. *Bone* **2001**, *28*, 195−201.
(37) Eastell, R.; Colwell, A.; Hampton, L.; Reeve, J. Biochemical markers of bone resorption compared with estimates of bone resorption from radiotracer kinetic studies in osteoporosis. *J. Bone Miner. Res.* **1997**, *12*, 59−65.
(38) Silva, M. J.; Brodt, M. D.; Lynch, M. A.; McKenzie, J. A.; Tanouye, K. M.; Nyman, J. S.; Wang, X. Type 1 Diabetes in young rats leads to progressive trabecular bone loss, cessation of cortical bone growth, and diminished whole bone strength and fatigue life. *J. Bone Miner. Res.* **2009**, *24*, 1618−1627.
(39) Sell, D. R.; Monnier, V. M. Age-related association of tail tendon break time with tissue pentosidine in DBA/2 vs C57BL/6 mice: the effect of dietary restriction. *J. Gerontol., Ser. A* **1997**, *52*, B277−284.
(40) Verzijl, N.; DeGroot, J.; Oldehinkel, E.; Bank, R. A.; Thorpe, S. R.; Baynes, J. W.; Bayliss, M. T.; Bijlsma, J. W.; Lafeber, F. P.; Tekoppele, J. M. Age-related accumulation of Maillard reaction products in human articular cartilage collagen. *Biochem. J.* **2000**, *2*, 381−387.

JOURNAL OF AGRICULTURAL AND FOOD CHEMISTRY

Article

pubs.acs.org/JAFC

Partially Hydrolyzed Bamboo (*Phyllostachys heterocycla*) As a Porous Bioadsorbent for the Removal of Pb(II) from Aqueous Mixtures

Xiao-kun OuYang,* Ru-Na Jin, Le-Ping Yang, Zheng-Shun Wen, Li-Ye Yang, Yang-Guang Wang,* and Chong-Yu Wang

School of Food and Pharmacy, Zhejiang Ocean University, Zhoushan 316022, P. R. China

Supporting Information

ABSTRACT: A novel porous succinylated bioadsorbent was prepared by the partial enzymatic hydrolysis of bamboo (*Phyllostachys heterocycla*) and its subsequent modification with succinic anhydride. Pb(II) removal from solutions that also contained sodium chloride and an amino acid was investigated using the bioadsorbent. Enzymatic hydrolysis increased the number of accessible hydroxyl groups and surface area of the raw bamboo, and created many pores within the material. The porous succinylated bioadsorbent exhibited high efficiency for Pb(II) binding. The sodium chloride content significantly decreased the Pb(II) adsorption capacity, whereas a minor effect was observed in the presence of arginine. The experimental data could be accurately described by a pseudo-second-order kinetics model, and the adsorption proceeded via an ion exchange mechanism. Even in a solution containing sodium chloride and arginine, the maximum adsorption capacity of Pb(II) by the porous succinylated bioadsorbent was 99.5 mg/g at 303 K.

KEYWORDS: *partial enzymatic hydrolysis, porous biomass, Pb(II), arginine, sodium chloride, Phyllostachys heterocycla*

INTRODUCTION

Pb(II) is widely used in many industries despite its toxicity to humans.[1] Large volumes of contaminated wastewater are discharged into the oceans, where lead accumulates[2] and has the potential to move up the food chain through marine organisms.[3] Previous reports have revealed the contamination of some saltwater fish with Pb(II).[4,5] As a common practice, byproducts of the marine fish−processing industry are hydrolyzed to produce other products,[6,7] and China has set a hygienic limit on Pb(II) in aquatic protein hydrolysates.[8] A survey reported by Ip et al.[9] showed that the concentration of Pb(II) in edible fish muscle varied from 0.04 to 30.7 mg/kg. The Pb(II) concentrations in marine fish byproducts such as the liver and viscera are reportedly higher than that in muscles;[10] therefore, marine protein hydrolysates prepared from such byproducts may be contaminated with relatively high levels of Pb(II) residues. Thus, it is necessary and urgent to remove Pb(II) from marine protein hydrolysate solutions before the byproducts are used in the manufacture of other products.

Traditional methods[11] for the removal of heavy metal ions from aqueous solutions include coagulation, chemical precipitation, and chemical oxidation/reduction. However, these methods may introduce new pollutants or generate toxic products. Another method preferred for the removal of heavy metals from aqueous solutions is adsorption,[12] with activated carbon[13] being an effective adsorbent. However, the high cost of the adsorbent limits its application. Ion exchange resins[14] are also effective adsorbents; however, they may generate toxic pollutants during the adsorption process.[15] Therefore, from a food safety viewpoint, there is a demand for green adsorbents. Plant wastes[12] that can be used as bioadsorbents for the removal of Pb(II) residues from aqueous solutions are readily available, and many studies have reported their use.[12,16] However, raw plant waste is efficient only at high ion concentrations and in the absence of salts and amino acids. Marine protein hydrolysate solutions may contain high concentrations of amino acids[17] and salts.[7] Competition between heavy metal ions, sodium chloride,[18] and amino acids may dramatically affect the adsorption capacity of the adsorbent. Thus, there is demand for a bioadsorbent capable of high-efficiency Pb(II) adsorption in the presence of high concentrations of amino acids and salts.

The functional groups in a lignocellulosic biomass material are a key factor in its ability to adsorb heavy metal ions from solution,[12] and many efforts have been made to increase the number of these accessible functional groups.[19] Carboxylic acid functionalities are effective for binding metal ions[20] and can be introduced by the chemical modification of hydroxyl groups in the lignocellulosic biomass. The degree of biomass modification (e.g., by succinylation) is determined by the number of accessible hydroxyl groups. An adsorbent's structure has a significant influence on its metal ion adsorption abilities. For example, compactness reduces the accessibility and restricts the diffusion of metal ions into the interior of the biomass. If the compact lignocellulosic cell wall could be disrupted to some extent, the number of accessible functional groups would be increased and metal ion adsorption would take place in both the exterior and interior of the biomass. Zhong et al.[20] employed a new strategy to prepare a porous succinylated biopolymer by dissolving biomass in an ionic liquid. However, ionic liquid residues in the biomass have the potential to contaminate the solution, and previous reports[21] indicate that

Received: April 3, 2014
Revised: June 3, 2014
Accepted: June 3, 2014
Published: June 10, 2014

ACS Publications © 2014 American Chemical Society

ionic liquids also exhibit human toxicity. Thus, from a food safety viewpoint, a new strategy for the preparation of porous succinylated bioadsorbents with a high degree of efficiency and safety must be developed.

Enhancing the efficiency of enzymatic hydrolysis for the conversion of lignocellulosic biomass into sugars[22] to produce biofuel is quite difficult. However, natural biomass can be partially degraded by enzymatic hydrolysis: holes and cracks can be created within the material, thus increasing the accessible surface area and numbers of pores and hydroxyl groups in the biomass.

In this study, a porous succinylated bioadsorbent, prepared from lignocellulosic biomass by partial enzymatic hydrolysis coupled with a succinylation reaction, was used to remove lead ions from an aqueous solution in the presence of high concentrations of salts and amino acids. The adsorption behaviors of Pb(II) on the bioadsorbent were investigated under different experimental conditions. This study will help to ensure the safety of downstream products prepared from marine protein hydrolysates.

MATERIALS AND METHODS

Materials. Bamboo (*Phyllostachys heterocycla*) was collected in the summer of 2013 from a bamboo handicraft factory in AnJi City (Zhejiang province, China). A standard solution of Pb(II) (lead nitrate) was purchased from the National Analysis Center for Iron and Steel (Beijing, China). Cellulase was purchased from the Aladdin Reagent Co., Ltd. (Shanghai, China), with an enzyme activity of 10000 U/g. All other chemicals were of analytical grade. A stock solution of Pb(II) was prepared by diluting the standard solution with double-distilled water.

Preparation of Porous Succinylated Bioadsorbent. The collected bamboos were crushed into pieces, boiled in distilled water for 1 h to remove dust and soluble impurities, and thoroughly washed with distilled water until the supernatant was free of color and turbidity. The obtained materials were dried in an air oven for 24 h at 80 °C, and then ground and sieved to obtain <150 μm particles. The solids were subjected to successive ultrasonic treatments in 1 M hydrochloric acid and 1 M sodium hydroxide for 3 h. The solutions were filtered and the residues were washed with distilled water repeatedly until the washings were pH 7.0. The resulting powders were completely dried in an air oven at 80 °C for 48 h to obtain raw bamboo powder (RBP, mean size 99.6 μm). A portion of the RBP (10 g) was treated with cellulase (0.4 g, 4 g of enzyme/100 g of dry RBP) in acetic acid buffer solution (400 mL, pH 5.0) in a conical flask with a stopper, which was placed in a water bath shaker maintained at 50 °C and shaken at 150 rpm for 24 h. After this hydrolysis, the samples were placed in boiling water for 15 min to deactivate the enzyme. The mixture was centrifuged at 5000 rpm for 10 min. The solids were collected, washed three times with acetone until the washings were free of turbidity, and dried in air in an 80 °C oven for 48 h to obtain enzymatically hydrolyzed bamboo (EHP, mean size 110.9 μm). A portion of the EHP (5 g) was treated with succinic anhydride (10 g) in pyridine (120 mL) at reflux for 1 h. The resulting material was thoroughly washed with ethanol and dried in air in an 80 °C oven for 4 h. The material was then treated with saturated $NaHCO_3$ solution for 1 h and washed with double-distilled water and ethanol (95%). Finally, it was dried in an air oven at 80 °C to obtain the succinylated bamboo powder (SBP). A second succinylated bamboo powder was prepared by the reaction of RBP with succinic anhydride under similar succinylation conditions. This succinylated raw bamboo powder was called RSP. The prepared adsorbents were stored in a desiccator. Scanning electron microscopy (SEM) and Fourier transform infrared spectroscopy (FTIR) were used to characterize the bioadsorbents. FTIR analysis of RBP, EHP, and SBP was performed on a Thermo Nicolet 6700 spectrometer using KBr pellets. X-ray photoelectron spectroscopy (XPS) analysis was performed on AXIS ULTRA^{DLD} spectrometer (Kratos, England). SEM analysis of the materials was performed on a Philips XL30 ESEM (FEI Company, Germany) after coating of the samples with a thin layer of gold. The surface zeta potentials of the adsorbents were measured using Zetasizer 2000 (Malvern, United Kingdom). The particle size of the adsorbents was measured using a S3500 Microtrac Particle Size Analyzer (Microtrac Inc., USA).

Degree of Succinylation. The concentration of carboxylic acid functional groups per gram of bioadsorbent was determined by reverse-titration.[20] Briefly, the prepared bioadsorbent (100 mg) was mixed with NaOH solution (100 mL, 0.01 M) for 1 h while stirring. Thereafter, the materials were separated by filtration, and three aliquots of the obtained solution were titrated with aqueous HCl solution (0.01 M) by using phenolphthalein as an indicator. The concentration of the carboxylic acid functional groups was calculated using eq 1,

$$C_{COOH} = \frac{C_1V_1 - 5C_2V_2}{m} \quad (1)$$

where C_1 is the concentration (mol/L) and V_1 is the volume (L) of the NaOH solution; C_2 is the concentration (mol/L) and V_2 is the volume (L) of the HCl solution used in the titration of excess unreacted NaOH; and m is the mass of the bioadsorbent (g).

Preparation of Reagent Solutions. Aqueous solutions containing different concentrations of Pb(II) (5−100 mg/L), arginine (0−50 mg/mL), and sodium chloride (0−8 mg/mL) were prepared for use in the batch experiments.

Adsorption Experiments. Adsorption experiments were investigated in batch mode. Unless otherwise stated, these batch studies were conducted at pH 5.0 with an initial Pb(II) concentration of 50 mg/L and a contact time of 240 min, at 303 K. Except for the adsorbent dosage studies, all other experiments were performed by mixing aqueous Pb(II) solution (50 mL) with dry bioadsorbent (0.05 g). The initial pH of each Pb(II) solution was adjusted with 0.01 M HNO_3 or 0.01 M NaOH solution. The adsorbent/Pb(II) solution mixtures were shaken in a thermostatic shaker bath (GFL 1092 shaker) at 150 rpm at various temperatures for different contact times. At the end of the experiments, the solutions were centrifuged at 5000 rpm for 10 min to separate the bioadsorbents. Pb(II) concentrations before and after adsorption in the solutions were determined using an inductively coupled plasma (ICP) spectrometer (Prodigy XP, Teledyne Technologies Corp., USA). All experiments were performed in triplicate, and the average values were used in the data analysis. Data were analyzed using EXCEL 2003 (Microsoft).

The effect of pH on the adsorption capacity q_e of the adsorbents was investigated in the range 2.0−6.0. In these experiments, the Pb(II) concentration was 50 mg/L. The equilibrium absorption amount of Pb(II) absorbed on the adsorbent was calculated using eq 2,

$$q_e = \frac{(C_o - C_e)V}{m} \quad (2)$$

where q_e is the adsorption capacity of the adsorbent (mg/g), C_o is the initial concentration of Pb(II) (mg/L), C_e is the equilibrium Pb(II) concentration in solution (mg/L), m is the mass of adsorbent used (g), and V is the volume of Pb(II) solution (L).

To investigate the adsorption performance of EHP, SBP, and RSP, experiments were conducted by mixing aqueous Pb(II) solution (50 mL) with the dry bioadsorbent (0.05 g). This group of experiments was conducted under standard batch mode conditions.

Kinetics experiments were carried out with a series of different initial Pb(II) concentrations (5, 10, 20, 50, and 100 mg/L). The adsorption capacity of the adsorbents at any time was calculated using eq 3,

$$q_t = \frac{(C_o - C_t)V}{m} \quad (3)$$

where q_t (mg/g) is the adsorption capacity of Pb(II) on the adsorbent at any time t, and C_t (mg/L) is the Pb(II) concentration in solution at any time t.

To study the effect of temperature, isothermal experiments were conducted at 293, 298, 303, and 308 K. In this group of experiments, the initial Pb(II) concentration was varied from 5 to 100 mg/L. The effects of arginine (0−50 mg/mL) and sodium chloride (0−8 mg/mL) concentration, adsorbent dosage (0.05−0.25 g), and contact time (10−720 min) were also investigated.

Desorption Experiments. For the desorption study, batch experiments were conducted by mixing aqueous Pb(II) solution (50 mL, 50 mg/mL) with SBP (0.05 g) in the presence of sodium chloride (4 mg/mL) and arginine (20 mg/mL). The mixtures of the adsorbent and Pb(II) solutions were shaken in a thermostatic shaker bath at 150 rpm and 303 K for 240 min. After the attainment of equilibrium, the Pb(II)-loaded SBP was separated from the solution by centrifugation and washed three times with distilled water (50 mL) to remove unabsorbed Pb(II). Subsequently, the bioadsorbents were mixed with 0.1 M HCl (50 mL) and shaken for 240 min at 303 K. The solution was centrifuged at 5000 rpm for 10 min to collect the adsorbent and washed three times with distilled water. The obtained solids were dried in an air oven at 80 °C and reused for batch desorption studies. The adsorption and desorption experiments were performed over five cycles. The desorption efficiency was calculated using eq 4.

$$\text{desorption efficiency} = \frac{\text{amount of Pb (II) desorbed}}{\text{amount of Pb(II) adsorbed}} \times 100\% \quad (4)$$

RESULTS AND DISCUSSION

FTIR Analysis. The FTIR spectra of the adsorbents were obtained over the wavenumber range 400−4000 cm^{-1} with a resolution of 4 cm^{-1}. Figure 1 shows the FTIR spectra of (a) Pb(II)-loaded SBP, (b) as-prepared SBP, (c) EHP, (d) RSP, and (e) RBP. In the figure, the absorption at 3350 cm^{-1} may be attributed to hydroxyl group stretching vibrations.[23] In spectra b and d, the peak intensity at 3350 cm^{-1} decreases significantly, indicating that hydroxyl groups are involved in the succinylation reaction. The absorption at 2920 cm^{-1} is dominated by the stretching of the $-CH_2$ group.[24] As compared with spectrum e, the strong adsorptions at 1720 cm^{-1} in the spectra of SBP (spectrum b) and RSP (spectrum d)—attributable to carbonyl groups[24]—indicate the successful introduction of the succinyl groups. The peak intensity at 1720 cm^{-1} in SBP is stronger than that in RSP, suggesting that the enzymatically hydrolyzed biomass greatly favors the succinylation reaction. The peaks observed at 1590 cm^{-1} and between 1420 and 1360 cm^{-1} (spectra b and e) correspond to asymmetric and symmetric stretches of carboxylate ions.[20] The peaks at 1160 cm^{-1} belong to the C−O−C groups in the ester and carboxylic acid groups, and the band at 1030 cm^{-1} corresponds to C−O stretching.[20] As illustrated in Figure 1, the intensities of some peaks changes. In comparing spectra a and b, the peak intensities at 3350 cm^{-1} and 1720 cm^{-1} and between 1590 and 1160 dramatically decrease after Pb(II) loading, indicating that hydroxyl and carboxyl groups are involved in adsorption; these groups may be important in the adsorption of Pb(II) on SBP.

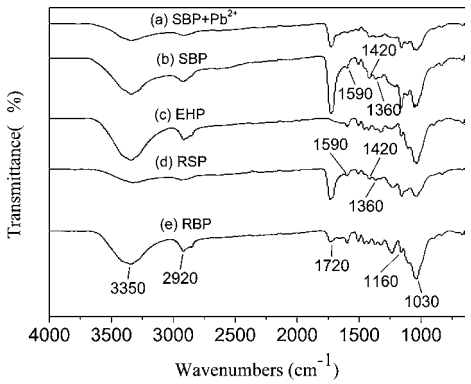

Figure 1. FTIR spectra of (a) Pb(II)-loaded porous succinylated bamboo, (b) porous succinylated bamboo, RBP; (c) partial enzymatically hydrolyzed bamboo, EHP; (d) succinylated bamboo prepared from raw bamboo material, RSP; and (e) raw bamboo material, RBP. The adsorption conditions were pH 5.0; contact time, 240 min; Pb(II) concentration, 50 mg/L; sodium chloride concentration, 4 mg/mL; arginine concentration, 20 mg/mL; adsorbent dosage, 0.05 g; and temperature, 303 K.

XPS analysis. XPS was used to characterize the changes in the main functional groups of SBP upon exposure to Pb(II) solution. From the XPS wide-scan spectra in Figure S1 (Supporting Information), distinct peaks for carbon and oxygen in both SBP and Pb(II)-loaded SBP were observed, as well as a peak due to sodium in SBP. After Pb(II) adsorption, the sodium peak disappeared and peaks for Pb(II) were observed in the Pb(II)-loaded SBP. It is evident that Pb(II) was bound to SBP through ion exchange. Figure 2 shows the C 1s region of the high-resolution XPS spectra of SBP before (a) and after (b) Pb(II) adsorption. The C 1s spectra can be deconvoluted into four peaks which can be assigned to C−C (aromatic), C−O (alcohol), O−C−O (ether), and O−C═O (carboxyl or ester) groups.[25] After Pb(II) adsorption, the binding energies of O−C and O−C═O shift from 286.3 and 289.0 eV to 286.2 and 288.8 eV, respectively. The changes in the C−O and O−C═O binding energies indicate that they are involved in the adsorption of Pb(II) onto the adsorbent.[26] In the XPS spectrum of Pb 4f (shown in Figure 2c), the peak observed at 139.0 eV, which corresponds to the characteristic binding energies of lead carbonate and lead oxalate compounds,[27,28] also indicates that Pb(II) is bound on SBP through hydroxyl and carboxyl groups. The results obtained above are consistent with the FTIR analysis.

Scanning Electron Microscopy (SEM) Analysis. Representative SEM micrographs of RBP, RSP, EHP, and SBP are given in Figure 3. Although RBP (Figure 3A) has a smooth and compact surface, after it is subjected to chemical modification with succinic anhydride, the resultant RSP (Figure 3B) has a rough surface morphology. The surface structure of EHP (Figure 3C) is significantly changed, with many observable pores and a rough surface, suggesting that enzymatic hydrolysis can create a porous structure in the RBP. By comparison with RBP, many cracks appeared on the surface of EHP, suggesting that surface area was increased after enzymatic hydrolysis. These changes should greatly favor subsequent chemical modification with succinic anhydride. Hence, the porous succinylated bioadsorbent, SBP (Figure 3D), with an enlarged surface area and considerable number of pores as well as COO^- groups was successfully prepared from enzymatically hydrolyzed bamboo. These structural changes in SBP will provide more binding sites for Pb(II) loading, as will the enhanced porosity, which will allow adsorption on both the exterior and interior of the bioadsorbent. As a result, the succinylated bioadsorbent will possess high adsorption efficiency.

Effect of Enzymatic Hydrolysis Modification on Pb(II) Uptake. Succinylated biomass has been used for the adsorption of heavy ion metals from solutions, and has exhibited excellent performance.[20] Carboxylic acid groups, which actively bind metal ions, can be introduced in the

dx.doi.org/10.1021/jf5015846 | J. Agric. Food Chem. 2014, 62, 6007−6015

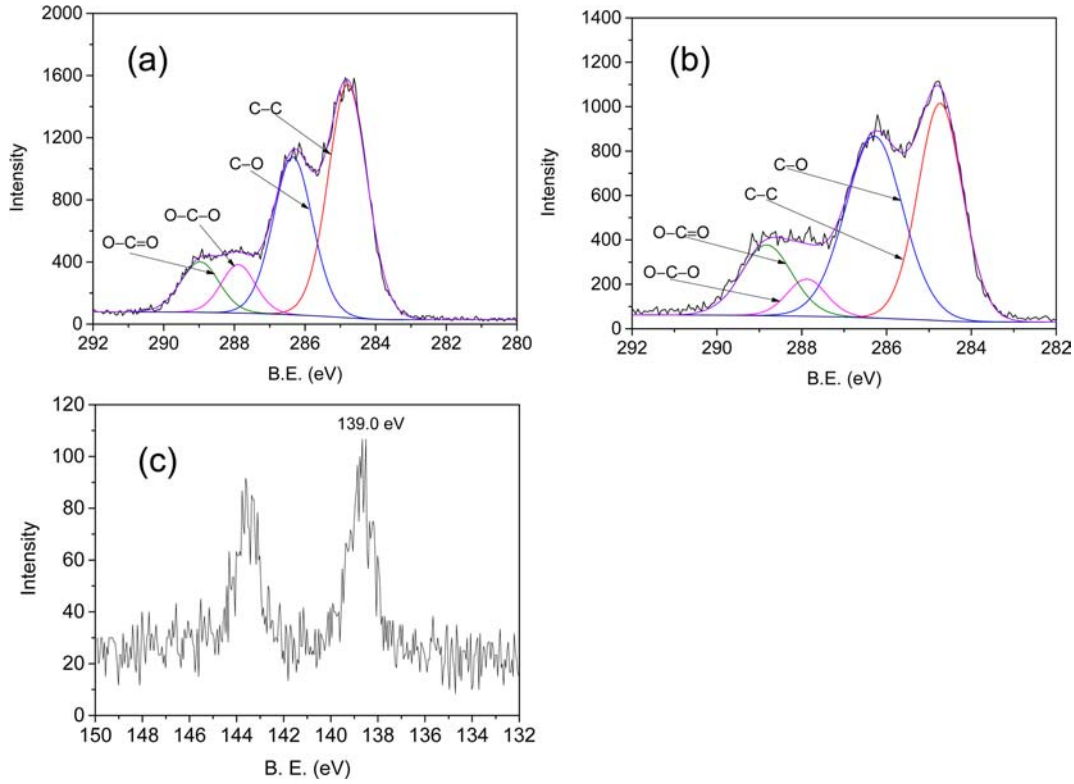

Figure 2. High-resolution of C 1s spectra of SBP (a), Pb(II)-loaded SBP (b), and Pb 4f spectrum on SBP (c). The adsorption conditions were pH 5.0; Pb(II) concentration, 50 mg/L; sodium chloride concentration, 4 mg/mL; arginine concentration, 20 mg/mL; adsorbent dosage, 0.05 g; and temperature, 303 K.

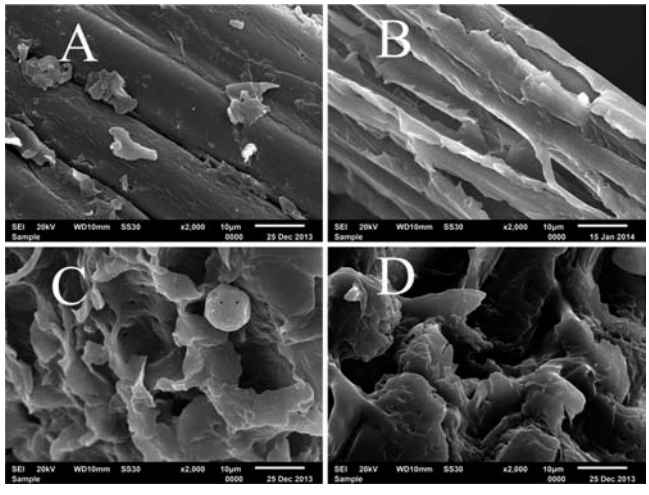

Figure 3. SEM images of adsorbents: (A) ground bamboo raw material, RBP; (B) RSP; (C) EHP (enzyme-to-bamboo ratio = 4:100 (g/g)); and (D) SBP.

biomass through the reaction of hydroxyl groups and succinic anhydride.[27,29] Hence, the degree of succinylation of the biomass largely depends on the number of accessible hydroxyl groups and the surface area. As mentioned above, enzymatic hydrolysis can create many pores within the bioadsorbent and roughen its surface. Enzyme treatment can dramatically affect the number of accessible hydroxyl groups and the biomass surface area, consequently influencing the carboxylic acid content introduced. Therefore, the effect of the enzyme-to-bamboo ratio on the introduction of carboxylic acid content to the bioadsorbent was investigated. The results are shown in Figure 4A. When the enzyme-to-bamboo ratio increased from 1:100 to 4:100 (g/g), the carboxylic acid content increased from 5.24 to 5.62 mmol/g, whereas the carboxylic acid content decreased gradually from 5.62 to 4.81 mmol/g when the enzyme-to-bamboo ratio increased from 4:100 to 24:100 (g/g). Hence, an enzyme-to-bamboo ratio of 4:100 (g/g) was selected to prepare the porous bamboo (EHP). This effect may be due to destruction of the RBP structure under higher enzymatic loads, resulting in a decreasing number of pores in the material. Consequently, the number of accessible hydroxyl groups would decrease, leading to a lower degree of succinylation. The carboxylic acid content of RSP is 5.06 mmol/g, suggesting that it may exhibit a higher q_e for Pb(II). A comparison of Pb(II) adsorption by RBP, EHP, SBP, and RSP (shown in Figure 4B) reveals a lower q_e toward Pb(II) for RSP (18.64 mg/g) than SBP (34.83 mg/g), and a higher q_e for EHP (24.44 mg/g) than RBP (12.97 mg/g). The higher q_e of SBP for Pb(II) over EHP suggests that the succinylated biomass adsorbs Pb(II) better than biomass without chemical modification. These results suggest that both the carboxylic acids and porous structure are important for higher q_e. In the other batch experiments, SBP was used as the bioadsorbent.

Effect of Pb(II) Solution pH on Uptake. Marine proteins are hydrolyzed in the pH range 3−11.[7,30] However, lead ions in solution will precipitate as lead hydroxides at pH values over 7.0.[31] To ensure the availability of Pb(II) in solution, therefore, in this group of experiments, the influence of the initial pH of the Pb(II) solution on the adsorption of lead ions by SBP was studied in the pH range 2−6. As illustrated in Figure 5A, the q_e increased slowly with pH, from 2.25 mg/g at pH 2.0 to 5.25 mg/g at pH 3.0, while a rapid increase in q_e occurred in the pH range from 3.5 (9.67 mg/g) to 6.0 (40.23 mg/g). As the pH

dx.doi.org/10.1021/jf5015846 | J. Agric. Food Chem. 2014, 62, 6007−6015

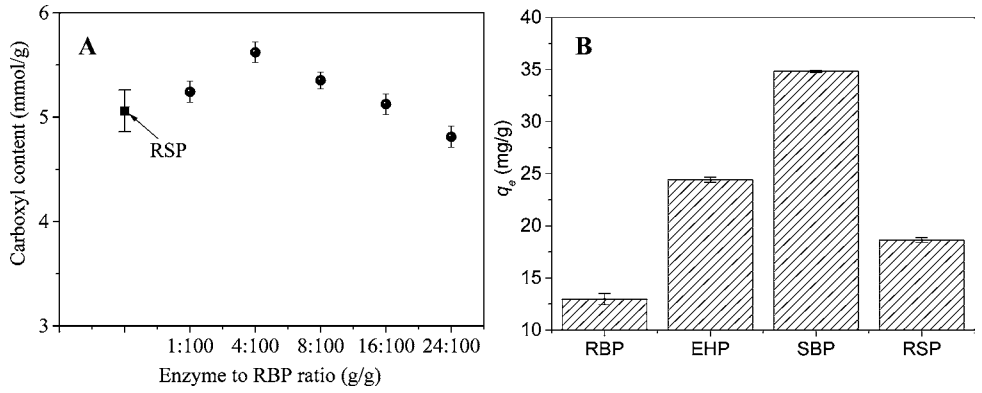

Figure 4. Effects of enzymatic hydrolysis modifications on Pb(II) uptake: (A) effect of enzyme-to-RBP ratio on carboxyl content in bioadsorbent; (B) effect of different adsorbents on the adsorption capacity q_e of Pb(II). The adsorption conditions were pH 5.0; contact time, 240 min; Pb(II) concentration, 50 mg/L; sodium chloride concentration, 4 mg/mL; arginine concentration, 20 mg/mL; adsorbent dosage, 0.05 g; and temperature, 303 K.

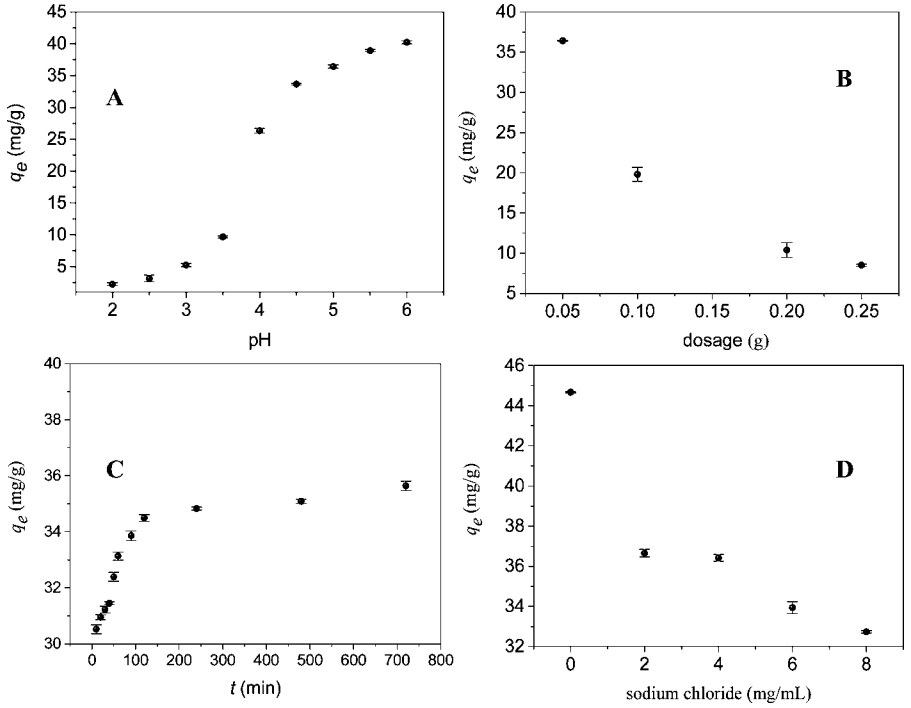

Figure 5. Effects of experimental conditions on Pb(II) adsorption by SBP: (A) pH, (B) adsorbent dose, (C) contact time, and (D) sodium chloride concentration. Studies were conducted at pH 5.0; initial Pb(II) concentration, 50 mg/L; contact time, 240 min; adsorbent dosage, 0.05 g; and temperature, 303 K, unless otherwise stated.

increases (3.5 to 6), the proton competition and electrostatic repulsion effects decrease, and the carboxylic acid groups become deprotonated (COO^-) and easily attract Pb(II); hence, the q_e significantly improves. Thus, it can be concluded that Pb(II) adsorption onto SBP mainly involves electrostatic interactions between Pb(II) and negatively charged carboxylate groups, and the adsorption process is an ion exchange mechanism.[20] Therefore, the rest of the batch experiments were conducted at pH 5.

Effect of Dosage and Contact Time on Pb(II) Uptake. The effect of SBP dosage on the equilibrium q_e of Pb(II) was investigated in the range 0.05−0.25 g, and the results are shown in Figure 5B. It can be found that q_e decreases from 36.42 to 8.51 mg/g as the dosage increases from 0.05 to 0.25 g. Similar results were observed in previous studies.[32] The reason for this phenomenon is likely to be adsorption sites remaining unsaturated during the adsorption process.[33] Another reason may be due to aggregation resulting from high adsorbent concentration.[34] This propensity can be assessed through the zeta potential, which is a measure of the electrokinetic potential in a colloidal system and of its stability.[35] The zeta potentials of SBP at concentrations of 1−5 mg/mL were measured to study the stability of the adsorbent. As can be seen from Figure S2 (Supporting Information), all the SBP zeta potentials are negative, but decrease from −29.55 to −10.1 mV as the adsorbent concentration increases from 1 to 5 mg/mL. The adsorbent surface becomes less negatively charged, thereby reducing the repulsive interactions between the particles and resulting in their aggregation.[35] Such aggregation would lead to a decrease in the total surface area of the adsorbent.

The effect of contact time (10−720 min) on the q_e of Pb(II) by SBP is shown in Figure 5C. Pb(II) adsorption on SBP is

dx.doi.org/10.1021/jf5015846 | J. Agric. Food Chem. 2014, 62, 6007−6015

rapid from 10 to 120 min, and the q_e increases continuously with increasing contact time within the first 120 min, increasing from 30.5 to 34.5 mg/g. Thereafter, the q_e increases slowly with contact time, increasing from 120 to 240 min. The rapid absorption behavior up to 120 min may be due to the abundance of vacant sites initially available for Pb(II) loading.[36] With increasing contact time, most of the SBP functional groups participate in the adsorption of Pb(II), reaching equilibrium. As illustrated in Figure 5C, there is no noticeable change in adsorption capacity after 240 min, thus ensuring that equilibrium is attained. Based on the data obtained in these batch experiments, 240 min was selected as the equilibrium time.

Effect of Sodium Chloride and Amino Acids on Pb(II) Uptake. Normally, marine protein hydrolysate contains high concentrations of sodium chloride.[7] The presence of sodium chloride leads to high ionic strength in the solution, which may significantly affect metal-ion adsorption on the bioadsorbent.[18] Hence, the effects of ionic strength on Pb(II) adsorption by SBP were examined by varying the concentration of sodium chloride from 0 to 8 mg/mL. The initial Pb(II) and arginine concentrations used in this study were 50 mg/L and 20 mg/mL, respectively. As can be seen from Figure 5D, increasing the sodium chloride concentration led to a decrease in Pb(II) adsorption on SBP; as the salt concentration increased from 0 to 8 mg/mL, the q_e decreased from 44.67 to 32 mg/g. The q_e sharply decreased at low sodium chloride concentrations (0−2 mg/mL). This can be explained by the formation of outer-sphere complexes, since Na^+ can compete with Pb(II) adsorbed on the outer-sphere sorption−active sites at a higher ionic strength.[18] Furthermore, the activity coefficients of Pb(II) would decrease with the increasing ionic strength induced by sodium chloride,[37] which limits Pb(II) ion transfer to the adsorbent surfaces. The surface charge of the adsorbent can also be changed by the increased ionic strength,[38] which should decrease the electrostatic force of attraction. A slight salt effect on Pb(II) adsorption by SBP was observed with sodium chloride concentrations from 2 to 4 mg/mL. According to the theory by Hayes,[39] Pb(II) adsorption by SBP at elevated NaCl concentrations (2−4 mg/mL) may take place by the formation of inner-sphere complexes, suggesting that Na^+ would not have competed for the inner-sphere sorption sites. A decreasing trend in the adsorption capacities can be found as sodium chloride concentrations increase from 4 to 8 mg/mL. Here, Na^+ may compete with Pb(II) adsorbed on both the inner- and outer-sphere sorption sites and thus reduce adsorption of the lead ions.

In addition to salts, marine protein hydrolysate contains abundant amino acids[17] that may affect Pb(II) adsorption. In this group of experiments, the effect of the amino acid arginine on the adsorption process was investigated at concentrations of 0−50 mg/mL. The initial Pb(II) and sodium chloride concentrations used in this study were 50 mg/L and 4 mg/mL, respectively. As illustrated in Figure 6, the equilibrium q_e of SBP decreased from 42.18 to 36.68 mg/g as the arginine concentration increased from 0 to 20 mg/mL. Thereafter, there was no obvious variation in q_e with the arginine concentration increasing from 20 to 50 mg/mL; a plateau value (approximately 35.5 mg/g) was observed after the concentration reached 20 mg/mL. These results indicate that amino acids affect the adsorption of Pb(II) on SBP to some extent. This adsorption behavior suggests that interactions do occur between the amino acids and adsorbents, indicating that

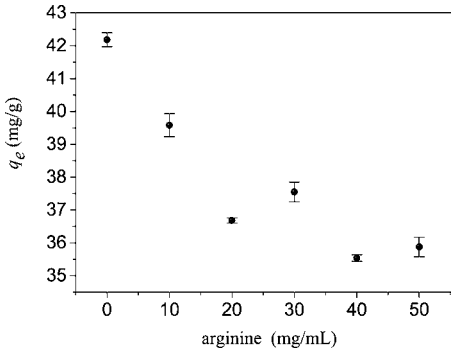

Figure 6. Effect of arginine concentration on Pb(II) adsorption by SBP. The adsorption conditions were pH 5.0; Pb(II) concentration, 50 mg/L; sodium chloride concentration, 4 mg/mL; contact time, 240 min; adsorbent dosage, 0.05 g; and temperature, 303 K.

amino acids could compete with lead ions for the adsorption sites of the bioadsorbents, and therefore, decrease the adsorption capacity.

Adsorption Kinetics Studies. Adsorption kinetics is very important for the design of adsorption systems. Therefore, the adsorption kinetics data for Pb(II) adsorption by SBP at different initial Pb(II) concentrations were fitted by applying pseudo-first-order and pseudo-second-order models, shown herein as eqs 5 and 6, respectively,[40]

$$\ln(q_e - q_t) = \ln q_e - k_1 t \tag{5}$$

$$\frac{t}{q_t} = \frac{1}{k_2 q_e^{\,2}} + \frac{t}{q_e} \tag{6}$$

where k_1 is the pseudo-first-order rate constant (min^{-1}), and k_2 is the pseudo-second-order rate constant of adsorption (g mg^{-1} min^{-1}). The values of $\ln(q_e - q_t)$ are calculated from the kinetics experimental data. The models are examined by linear plots of $\ln(q_e - q_t)$ versus t and (t/q) versus t, respectively. The models' characteristic parameters and regression coefficients are listed in Table 1. By comparing the two kinetics models, the

Table 1. Adsorption Kinetic Model Parameters for Pb(II) on SBP at Different Initial Pb(II) Concentrations

	C_0 (mg L^{-1})				
param	5	10	20	50	100
	Pseudo-First-Order Model				
$q_{e,exp.}$ [a]	3.81	7.609	14.407	35.94	58.65
$q_{e,cal}$ [b]	0.60	0.99	0.95	5.30	3.95
k_2	0.016	0.017	0.0080	0.0074	0.0061
R^2	0.980	0.997	0.954	0.940	0.867
	Pseudo-Second-Order Model				
$q_{e,cal}$ [b]	3.85	7.66	14.31	35.31	57.77
k_2	0.076	0.049	0.049	0.0081	0.014
R^2	0.999	0.999	0.999	0.999	0.999

[a]Experimental. [b]Calculated.

correlation coefficient values (R^2 > 0.999) calculated by the pseudo-second-order model at different initial Pb(II) concentrations are higher than those of the pseudo-first-order model, and the experimental $q_{e,exp}$ values agree with the calculated $q_{e,cal}$ values from the pseudo-second-order model. This suggests that the experimental data fits the pseudo-second-order model better than the pseudo-first-order model, and the rate is

dx.doi.org/10.1021/jf5015846 | J. Agric. Food Chem. 2014, 62, 6007−6015

proportional to the square of the number of unoccupied binding sites.[41] Hence, the adsorption of Pb(II) by SBP is dominated by chemisorption. The interactions may occur between the COO^- groups and the Pb(II) ions,[20] which means that the adsorption mechanism of SBP is ion exchange. This is consistent with the results of the analysis of the effects of sodium chloride.

Adsorption Isotherm Studies. Equilibrium adsorption isotherms are important to determine the mechanism of the adsorption systems. Hence, the Langmuir and Freundlich isotherm models were used to describe the adsorption process, and the corresponding adsorption isotherms were plotted. The Langmuir and Freundlich isotherms are expressed as eqs 7 and 8, respectively,

$$\frac{C_e}{q_e} = \frac{1}{bq_{max}} + \frac{C_e}{q_{max}} \quad (7)$$

$$\ln q_e = \ln K_f + \frac{1}{n} \ln C_e \quad (8)$$

where q_{max} is the maximum sorption capacity, and C_e and q_e have the same meanings as noted previously. In the Langmuir equation, b is the Langmuir constant, which can be determined from the intercept of the linear plot of experimental data of C_e/q_e versus C_e (shown in Figure S3, see the Supporting Information). In the Freundlich equation, K_f and $1/n$ are empirical constants that can be determined from the intercept and slope of the linear plot of ln q_e versus ln C_e (shown in Figure S4, see the Supporting Information).

Based on eqs 7 and 8, the values of the isotherm constants were obtained and are presented in Table 2. The Langmuir and Freundlich isotherms show no obvious difference in the adsorption of Pb(II) by SBP. Normally, the Langmuir isotherm assumes that the adsorption process only occurs at specific homogeneous sites within the adsorbent surface, with a uniform distribution of energy levels. It can be concluded that the adsorption process is monolayer in nature, based on the Langmuir isotherm.[42] However, the Freundlich isotherm supposes that the adsorption occurs at heterogeneous sites with a nonuniform distribution of energy levels. The Freundlich isotherm describes reversible adsorption and is not restricted to the formation of a monolayer.[43] These results suggests that the behavior of Pb(II) adsorption on SBP is complex due to the presence of sodium chloride and arginine.

Table 2. Isotherm Parameters for the Adsorption of Pb(II) on SBP at Different Temperatures

	T (K)			
param	293	298	303	308
	Langmuir Isotherm			
q_{max} (mg g^{-1})	99.11	101.83	99.50	100.40
b (L mg^{-1})	0.029	0.030	0.033	0.034
R_L	0.26	0.25	0.23	0.23
R^2	0.997	0.995	0.990	0.988
	Freundlich Isotherm			
K_f ($mg^{1-1/n}$ $L^{1/n}$ g^{-1})	3.25	3.40	3.64	3.91
n	1.29	1.28	1.30	1.32
R^2	0.995	0.995	0.994	0.996

R_L is a dimensionless constant referred to as a separation factor or equilibrium parameter, which can be used to describe the essential feature of the Langmuir isotherm. It is expressed as $R_L = 1/(1 + bC_o)$,[44] where C_o is the highest initial Pb(II) concentration. It is possible to predict whether an adsorption system is favorable by its R_L value.[44] As can be seen from Table 2, the R_L values are all between 0 and 1 at different temperatures, indicating that the adsorption of Pb(II) by SBP is favorable.

Effect of Temperature. The effect of temperature on Pb(II) adsorption by SBP was studied at four temperatures (293, 298, 303, and 308 K) and different initial Pb(II) concentrations (5−100 mg L^{-1}). The thermodynamic parameters can be calculated by eq 9,

$$\Delta G = -RT \ln \frac{q_e}{C_e} = -RT\left(-\frac{\Delta H}{RT} + \frac{\Delta S}{R}\right) \quad (9)$$

where R is the universal gas constant (8.314 J mol K^{-1}), and T is the absolute temperature (K). Changes in enthalpy (ΔH) and entropy (ΔS) can be calculated from the slope and intercept of the linear plot of $\ln(q_e/C_e)$ versus $1/T$. The changes in Gibbs free energy (ΔG), ΔH, and ΔS are given in Table 3. The negative ΔG values confirm the feasibility and spontaneous nature of the absorption of Pb(II) by SBP. Moreover, the decrease in the values of ΔG with increasing temperature suggests that adsorption is more favorable at higher temperatures.[45] The positive value of ΔH indicates the endothermic nature of the process. The positive values of ΔS indicate that there is an increase in the randomness at the solid/solution interface during Pb(II) adsorption by SBP. Normally, the values of ΔG for physisorption are between −20 and 0 kJ mol^{-1} and between −40 and −80 kJ mol^{-1} for chemisorption.[44] In this study, the ΔG values are not within either of these ranges, which indicates that Pb(II) adsorption by SBP is dominated by an ion exchange mechanism.

Desorption Studies. From an economic viewpoint, it is necessary to reuse adsorbents. As can be observed from Figure 7, no noticeable losses were observed in the adsorption capacity or desorption efficiency of SBP as the number of cycles increased. Even after five cycles of adsorption−desorption, the desorption efficiency of SBP was more than 91.2%. These results reveal that SBP can be reused without significant change in its adsorption performance.

Table 3. Thermodynamic Parameters for the Adsorption of Pb(II) Adsorption on SBP

	ΔG (kJ mol^{-1}) at temp (K)					
Pb(II) concn (mg L^{-1})	293	298	303	313.2	ΔH ($kJmol^{-1}$)	ΔS (J mol^{-1} K^{-1})
5	−19.26	−19.73	−20.31	−20.98	14.37	114.53
10	−19.35	−19.83	−20.31	−20.75	8.10	93.65
20	−18.91	−19.33	−19.70	−20.12	4.45	79.70
50	−18.40	−18.97	−19.51	−19.88	10.89	100.03
100	−17.39	−17.82	−18.17	−18.62	6.23	80.58

dx.doi.org/10.1021/jf5015846 | J. Agric. Food Chem. 2014, 62, 6007−6015

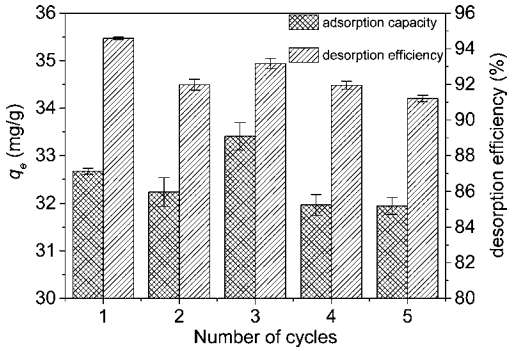

Figure 7. Adsorption−desorption studies of Pb(II) adsorption by SBP. The adsorption conditions were pH 5.0; contact time, 240 min; Pb(II) concentration, 50 mg/L; sodium chloride concentration, 4 mg/mL; arginine concentration, 20 mg/mL; adsorbent dosage, 0.05 g; and temperature 303 K.

In conclusion, enzymatic hydrolysis can be used as a new strategy for the preparation of porous bioadsorbents from biomass. Bamboo was subjected to enzymatic hydrolysis to increase its porosity, and then modified with succinic anhydride to obtain a porous succinylated bioadsorbent. Both the porous structure and the carboxylic acid content were found to significantly influence the adsorption capacity of the bioadsorbent. The carboxylate groups were found to be the main sites for Pb(II) binding. A pseudo-second-order kinetics model was a good fit for the SBP adsorption kinetics, and equilibrium data could be fitted well to the Langmuir isotherm. The adsorption isotherms and thermodynamic parameters suggested that the Pb(II) adsorption on SBP is favorable. SBP could be regenerated and high desorption efficiencies were obtained over five adsorption−desorption cycles. Sodium chloride content significantly affected Pb(II) adsorption by SBP. However, even in the presence of high concentrations of sodium chloride and arginine, the porous succinylated bioadsorbent showed high efficiency for Pb(II) binding, and the maximum adsorption capacity of Pb(II) was higher than 99 mg/g at different temperatures.

■ ASSOCIATED CONTENT

Supporting Information

XPS wide-scan spectra of the SBP and Pb(II)-loaded SBP. The adsorption conditions were pH 5.0; Pb(II) concentration, 50 mg/L; sodium chloride concentration, 4 mg/mL; arginine concentration, 20 mg/mL; adsorbent dosage, 0.05 g; and temperature, 303 K (Figure S1). Effect of adsorbent concentration on the zeta potential (Figure S2). Langmuir isotherms for Pb(II) adsorption by SBP at different temperatures (Figure S3). Freundlich isotherms for Pb(II) adsorption by SBP at different temperatures (Figure S4). This material is available free of charge via the Internet at http://pubs.acs.org.

■ AUTHOR INFORMATION

Corresponding Authors

*Tel: +86-580-2554781. Fax: +86-580-2554781. E-mail: xkouyang@zjou.edu.cn.

*Tel: +86-580-2554781. Fax: +86-580-2554781. E-mail: ygw0510@sohu.com.

Funding

The authors are grateful for the support of the Zhejiang Provincial Natural Science Foundation of China (Z3110487), China Spark Program (2012GA700212), Funds of Science and Technology Department of Zhejiang Province, China (2013C24028), and Funds of Zhoushan Municipal Bureau of China (2013C41006).

Notes

The authors declare no competing financial interest.

■ ACKNOWLEDGMENTS

Senior Engineer Guo-Zhou Cao and Senior Engineer Xiao-Yan Zhu (Ningbo Entry-Exit Inspection and Quarantine Bureau, NingBo, China) are acknowledged for their technical support.

■ ABBREVIATIONS USED

BE, binding energy; C_e, equilibrium Pb(II) concentration (mg/L); b, Langmuir constant; C_o, initial Pb(II) concentration (mg/L); C_t, Pb(II) concentration at time t (mg/L); C_x, concentration of species x (mol/L); ΔG, change in Gibbs free energy; ΔH, change in enthalpy; ΔS, change in entropy; EHP, enzymatically hydrolyzed bamboo; FTIR, Fourier transform infrared spectroscopy; k_1, pseudo-first-order rate constant of adsorption (min^{-1}); k_2, pseudo-second-order rate constant of adsorption (g mg^{-1} min^{-1}); K_b, empirical constant; m, mass of the bioadsorbent (g); $1/n$, empirical constant; q_e, adsorption capacity (mg/g); q_{max}, maximum adsorption capacity; q_t, adsorption capacity of the adsorbent at time t (mg/g); R, universal gas constant (8.314 J mol K^{-1}); R^2, correlation coefficient; RBP, raw bamboo powder; R_L, dimensionless separation factor (constant); RSP, succinylated raw bamboo powder; SEM, scanning electron microscopy; SBP, porous succinylated bamboo powder; T, absolute temperature (K); V_x, volume of species x (L); XPS, X-ray photoelectron spectroscopy

■ REFERENCES

(1) Cao, H.; Chen, J.; Zhang, J.; Zhang, H.; Qiao, L.; Men, Y. Heavy metals in rice and garden vegetables and their potential health risks to inhabitants in the vicinity of an industrial zone in Jiangsu, China. *J. Environ. Sci.* **2010**, *22*, 1792−1799.

(2) Manivannan, D.; Biju, V. M. Determination of toxic heavy metals in sea water by FAAS after preconcentration with a novel chelating resin. *Water Sci. Technol.* **2011**, *64*, 803−808.

(3) Bryan, G. W.; Langston, W. J. Bioavailability, accumulation and effects of heavy metals in sediments with special reference to United Kingdom estuaries: a review. *Environ. Pollut.* **1992**, *76*, 89−131.

(4) Hosseini, S. M.; Sobhanardakani, S.; Navaei, M. B.; Kariminasab, M.; Aghilinejad, S. M.; Regenstein, J. M. Metal content in caviar of wild Persian sturgeon from the southern Caspian Sea. *Environ. Sci. Pollut. Res.* **2013**, *20*, 5839−5843.

(5) Squadrone, S.; Prearo, M.; Gavinelli, S.; Pellegrino, M.; Tarasco, R.; Benedetto, A.; Abete, M. C. Heavy metals in Mugil cephalus (Mugilidae) from the Ligurian Sea (North−West Mediterranean, Italy). *Food Addit. Contam., Part B* **2013**, *6*, 134−138.

(6) Sathivel, S.; Bechtel, P. J.; Babbitt, J.; Smiley, S.; Crapo, C.; Reppond, K. D.; Prinyawiwatkul, W. Biochemical and functional properties of herring (Clupea harengus), byproduct hydrolysates. *J. Food Sci.* **2003**, *68*, 2196−2200.

(7) Kim, J. S.; Shahidi, F.; Heu, M. S. Characteristics of salt−fermented sauces from shrimp processing byproducts. *J. Agric. Food Chem.* **2003**, *51*, 784−792.

(8) Zeng, X. C.; Li, J.; Zheng, H. B.; Huang, Z. Y. Determination of Trace Lead in Fish Sauces by ID−ICP−MS After Mg(OH)(2) Coprecipitation. *J. Aquat. Food Prod. Technol.* **2013**, *22*, 584−594.

(9) Ip, C. C. M.; Li, X. D.; Zhang, G.; Wong, C. S. C.; Zhang, W. L. Heavy metal and Pb isotopic compositions of aquatic organisms in the Pearl River Estuary, South China. *Environ. Pollut.* **2005**, *138*, 494−504.

(10) Bellassoued, K.; Hamza, A.; van Pelt, J.; Elfeki, A. Seasonal variation of Sarpa salpa fish toxicity, as related to phytoplankton consumption, accumulation of heavy metals, lipids peroxidation level in fish tissues and toxicity upon mice. *Environ. Monit. Assess.* **2013**, *185*, 1137−1150.
(11) Namasivayam, C.; Ranganathan, K. Removal of Pb(Ii), Cd(Ii), Ni(Ii) and Mixture of Metal−Ions by Adsorption onto Waste Fe(Iii)/Cr(Iii) Hydroxide and Fixed−Bed Studies. *Environ. Technol.* **1995**, *16*, 851−860.
(12) Li, X. S.; Liu, S. L.; Na, Z. Y.; Lu, D. N.; Liu, Z. Adsorption, concentration, and recovery of aqueous heavy metal ions with the root powder of Eichhornia crassipes. *Ecol. Eng.* **2013**, *60*, 160−166.
(13) Lo, S. F.; Wang, S. Y.; Tsai, M. J.; Lin, L. D. Adsorption capacity and removal efficiency of heavy metal ions by Moso and Ma bamboo activated carbons. *Chem. Eng. Res. Des.* **2012**, *90*, 1397−1406.
(14) Ali, S. W.; Waqar, F.; Malik, M. A.; Yasin, T.; Muhammad, B. Study on the synthesis of a macroporous ethylacrylate−divinylbenzene copolymer, its conversion into a bi−functional cation exchange resin and applications for extraction of toxic heavy metals from wastewater. *Appl. Polym. Sci.* **2013**, *129*, 2234−2243.
(15) Wang, H. L.; Dong, W. J.; Liu, Y. L. Determination of resin residue in mulberry twig total alkaloids extract by head−space capillary GC. *Chin. J. Pharm.* **2010**, *41*, 216−218.
(16) Rajkumar, P.; Kumar, P. S.; Kirupha, S. D.; Vidhyadevi, T.; Nandagopal, J.; Sivanesan, S. Adsorption of Pb(II) ions onto surface modified Guazuma ulmifolia seeds and batch adsorber design. *Environ. Prog. Sustainable Energy* **2013**, *32*, 307−316.
(17) Shen, Q.; Guo, R.; Dai, Z.; Zhang, Y. Investigation of Enzymatic Hydrolysis Conditions on the Properties of Protein Hydrolysate from Fish Muscle (Collichthys niveatus) and Evaluation of Its Functional Properties. *J. Agric. Food. Chem.* **2012**, *60*, 5192−5198.
(18) Guo, X. Y.; Zhang, S. Z.; Shan, X. Q. Adsorption of metal ions on lignin. *J. Hazard. Mater.* **2008**, *151*, 134−142.
(19) Li, W. L.; Lu, Y. X. Adsorption study of Pb(II) by chemically modified cattail stem. *Desalin. Water Treat.* **2013**, *51*, 6824−6836.
(20) Zhong, L. X.; Peng, X. W.; Yang, D.; Sun, R. C. Adsorption of Heavy Metals by a Porous Bioadsorbent from Lignocellulosic Biomass Reconstructed in an Ionic Liquid. *J. Agric. Food Chem.* **2012**, *60*, 5621−5628.
(21) Cunha, E.; Pinto, P. C. A. G.; Carvalho, J. P. S.; Saraiva, M. L. M. F. S. Automated carboxylesterase assay for the evaluation of ionic liquids' human toxicity. *J. Hazard. Mater.* **2013**, *244*, 563−569.
(22) Hu, S.; Smith, T. J.; Lou, W.; Zong, M. Efficient Hydrolysis of Cellulose over a Novel Sucralose−Derived Solid Acid with Cellulose−Binding and Catalytic Sites. *J. Agric. Food Chem.* **2014**, *62*, 1905−1911.
(23) Li, Z.; Tang, X.; Chen, Y.; Wei, L.; Wang, Y. Activation of Firmiana Simplex leaf and the enhanced Pb(II) adsorption performance: Equilibrium and kinetic studies. *J. Hazard. Mater.* **2009**, *169*, 386−394.
(24) Hameed, B. H.; Krishni, R. R.; Sata, S. A. A novel agricultural waste adsorbent for the removal of cationic dye from aqueous solutions. *J. Hazard. Mater.* **2009**, *162*, 305−311.
(25) Puziy, A. M.; Poddubnaya, O. I.; Socha, R. P.; Gurgul, J.; Wisniewski, M. XPS and NMR studies of phosphoric acid activated carbons. *Carbon* **2008**, *46*, 2113−2123.
(26) Fukuda, R.; Yoshida, Y.; Nakayama, Y.; Okazaki, M.; Inoue, S.; Sano, H.; Suzuki, K.; Shintani, H.; Van Meerbeek, B. Bonding efficacy of polyalkenoic acids to hydroxyapatite, enamel and dentin. *Biomaterials* **2003**, *24*, 1861−1867.
(27) Tan, G.; Yuan, H.; Liu, Y.; Xiao, D. Removal of lead from aqueous solution with native and chemically modified corncobs. *J. Hazard. Mater.* **2010**, *174*, 740−745.
(28) Godelitsas, A.; Astilleros, J. M.; Hallam, K.; Harissopoulos, S.; Putnis, A. Interaction of calcium carbonates with lead in aqueous solutions. *Environ. Sci. Technol.* **2003**, *37*, 3351−3360.
(29) Gurgel, L. V. A.; Freitas, R. P. d.; Gil, L. F. Adsorption of Cu(II), Cd(II), and Pb(II) from aqueous single metal solutions by sugarcane bagasse and mercerized sugarcane bagasse chemically modified with succinic anhydride. *Carbohydr. Polym.* **2008**, *74*, 922−929.
(30) Wang, Q.; Li, W.; He, Y.; Ren, D.; Kow, F.; Song, L.; Yu, X. Novel antioxidative peptides from the protein hydrolysate of oysters (Crassostrea talienwhanensis). *Food Chem.* **2014**, *145*, 991−996.
(31) Ajmal, M.; Khan, A. H.; Ahmad, S.; Ahmad, A. Role of sawdust in the removal of copper(II) from industrial wastes. *Water Res.* **1998**, *32*, 3085−3091.
(32) Wang, F. Y.; Wang, H.; Ma, J. W. Adsorption of cadmium (II) ions from aqueous solution by a new low−cost adsorbent−Bamboo charcoal. *J. Hazard. Mater.* **2010**, *177*, 300−306.
(33) Yu, B.; Zhang, Y.; Shukla, A.; Shukla, S. S.; Dorris, K. L. The removal of heavy metal from aqueous solutions by sawdust adsorption—removal of copper. *J. Hazard. Mater.* **2000**, *80*, 33−42.
(34) Rao, M. M.; Rao, G. P. C.; Seshaiah, K.; Choudary, N. V.; Wang, M. C. Activated carbon from Ceiba pentandra hulls, an agricultural waste, as an adsorbent in the removal of lead and zinc from aqueous solutions. *Waste Manage.* **2008**, *28*, 849−858.
(35) Eastoe, J. Surfactant Aggregation and Adsorption at Interfaces. In *Colloid Science*; Blackwell Publishing Ltd.: 2009; pp 50−76.
(36) Acharya, J.; Sahu, J. N.; Mohanty, C. R.; Meikap, B. C. Removal of lead(II) from wastewater by activated carbon developed from Tamarind wood by zinc chloride activation. *Chem. Eng. J.* **2009**, *149*, 249−262.
(37) Guo, J. J.; Chen, W. B. Ionic Strength Effect on Copper(II) Biosorption by Folium camelliae Biomass: Equilibrium Study and Dynamic Modelling in Membrane Reactor. *Asian J. Chem.* **2013**, *25*, 3609−3612.
(38) Milojkovic, J. V.; Mihajlovic, M. L.; Stojanovic, M. D.; Lopicic, Z. R.; Petrovic, M. S.; Sostaric, T. D.; Ristic, M. D. Pb(II) removal from aqueous solution by Myriophyllum spicatum and its compost: equilibrium, kinetic and thermodynamic study. *J. Chem. Technol. Biotechnol.* **2014**, *89*, 662−670.
(39) Hayes, K. F.; Papelis, C.; Leckie, J. O. Modeling ionic strength effects on anion adsorption at hydrous oxide solution interfaces. *J. Colloid Interface Sci.* **1988**, *125*, 717−726.
(40) Chen, D. X.; OuYang, X. K.; Wang, Y. G.; Yang, L. Y.; Wu, K. J.; He, C. H. Adsorption of caprolactam from aqueous solution by novel polysulfone microcapsules containing [Bmim][PF_6]. *Colloids Surf., A* **2014**, *441*, 72−76.
(41) Ho, Y. S.; McKay, G. Pseudo−second order model for sorption processes. *Process Biochem.* **1999**, *34*, 451−465.
(42) Weber, T. W.; Chakravorti, R. K. Pore and solid diffusion models for fixed−bed adsorbers. *AIChE J.* **1974**, *20*, 228−238.
(43) Mohd Din, A. T.; Hameed, B. H.; Ahmad, A. L. Batch adsorption of phenol onto physiochemical-activated coconut shell. *J. Hazard. Mater.* **2009**, *161*, 1522−1529.
(44) Chen, H.; Dai, G.; Zhao, J.; Zhong, A.; Wu, J.; Yan, H. Removal of copper(II) ions by a biosorbent—Cinnamomum camphora leaves powder. *J. Hazard. Mater.* **2010**, *177*, 228−236.
(45) Ali, S. A.; Al Hamouz, O. C. S.; Hassan, N. M. Novel cross−linked polymers having pH-responsive amino acid residues for the removal of Cu^{2+} from aqueous solution at low concentrations. *J. Hazard. Mater.* **2013**, *248−249*, 47−58.

JOURNAL OF AGRICULTURAL AND FOOD CHEMISTRY

Article

pubs.acs.org/JAFC

Arsenic Speciation in Australian-Grown and Imported Rice on Sale in Australia: Implications for Human Health Risk

M. Azizur Rahman,*[,†] Mohammad Mahmudur Rahman,[‡,§] Suzie M. Reichman,[#] Richard P. Lim,[†] and Ravi Naidu*[,‡,§]

[†]Centre for Environmental Sustainability, School of the Environment, University of Technology Sydney, P.O. Box 123, Broadway, New South Wales 2007, Australia

[‡]Centre for Environmental Risk Assessment and Remediation (CERAR), University of South Australia, Mawson Lakes Campus, Mawson Lakes, South Australia 5095, Australia

[§]Cooperative Research Centre for Contamination Assessment and Remediation of the Environment (CRC-CARE), P.O. Box 486, Salisbury South, South Australia 5106, Australia

[#]School of Civil, Environmental and Chemical Engineering, RMIT University, G.P.O. Box 2476, Melbourne, Victoria 3001, Australia

ABSTRACT: Rice is an important route of arsenic (As) exposure to humans, especially populations with rice-based diets. Human health risk of As varies greatly with rice variety and country of origin. The purpose of the present study was to determine total and speciated As in Australian-grown and imported rice on sale in Australia to assess their health risk to consumers. The total As (tAs) concentrations in Australian-grown organic brown, medium grain brown, and organic white rice were 438 ± 23, 287 ± 03, and 283 ± 18 μg kg^{-1} dry weight (d wt), respectively. In Bangladeshi, Indian, Pakistani, and Thai rice imported and on sale in Australia, tAs concentrations were 56 ± 05, 92 ± 10, 82 ± 06 and 172 ± 24 μg kg^{-1}, respectively. Asian rice contained mainly inorganic As (iAs; 86−99%), whereas 18−26% of the tAs in Australian-grown rice was dimethylarsinic acid (DMA). Relatively higher concentrations of tAs in Australian-grown rice than that in imported rice of Asian origin suggest that Australian-grown rice may be a health risk for the consumers. It was estimated that Australian-grown organic brown rice can contribute up to 98% of the FAO/WHO recommended maximum tolerable daily intake limit of iAs (2.1 μg kg^{-1} body wt day^{-1}) for Asian immigrants. However, other Australian consumers including European immigrants are unlikely to be at risk to As from rice diets due to their lower rice consumption rates than that of Asian immigrants. The risk assessment showed that imported rice on sale in Australia was likely to pose a lower health risk to consumers than Australian-grown rice.

KEYWORDS: *arsenic speciation, rice, dietary intake, risk assessment, human health*

INTRODUCTION

Elevated concentrations of arsenic (As) in groundwater pose major health problems for the people of Bangladesh, West Bengal (India), and several other countries of Southeast (SE) Asia.[1−4] Arsenic-contaminated groundwater is used in South and SE Asian countries not only for drinking purposes but also for agricultural irrigation to grow crops such as rice and other food crops.[5,6] Increasing levels of As in agricultural soils are due to irrigation with contaminated groundwater, and its uptake in rice and other food crops has become a real health issue in this region.[5,7,8] Chronic effects of As toxicity to humans have been reported from many Asian countries through widespread water and crop contamination.[3] Around 200 million people in South and SE Asia are estimated to be exposed to As contamination from water and foods.[9] The recent incidence, where thousands of people are dying of arsenicosis and millions are potentially at risk, has led to renewed interest in As contamination worldwide.[10]

Arsenic pollution is also considered an important environmental issue in Australia;[11] however, the health risks of As to the Australian people from foods have not been fully determined. Whereas many of the emerging As problems in the Asian region are due to mobilization of As originating from natural processes, those recorded in Australia include contributions from both natural processes and anthropogenic activities associated with the use of arsenical pesticides, herbicides, sheep dip, atmospheric deposition, mining activities, waste disposal, and timber treatment processes.[12] Mining activities have contributed to the contamination of soil and water in Western Australia and Victoria; however, other anthropogenic activities such as agriculture, forestry, and a variety of industrial processes have also contaminated soil and water on a localized scale.[11]

The most significant concern related to human health risks from As toxicity is worldwide food-chain transfer with the expansion of the global food trade, as millions more people are potentially exposed to increased concentrations of As in imported food in situations where local As contamination does not occur. A study showed that rice imported into the United Kingdom (UK) from Bangladesh contained high concentrations of As.[13] These findings suggest that with supermarkets now sourcing their rice worldwide, As poisoning has potentially become a global problem exposing millions of

Received: March 3, 2014
Revised: June 2, 2014
Accepted: June 3, 2014
Published: June 3, 2014

ACS Publications © 2014 American Chemical Society

dx.doi.org/10.1021/jf501077w | J. Agric. Food Chem. 2014, 62, 6016−6024

consumers in countries not significantly affected by As-contaminated groundwater. Thus, As in rice and the associated possible risks to human health can no longer be considered just a regional issue, but an important global issue.

Australia is a multicultural country with significant numbers of immigrants from a range of countries including Asia and Europe. Rice is the staple food for a large number of Asian people living in Australia. Asian immigrants in Australia generally have strong preferences for rice imported from Asian countries, notably Bangladesh, West Bengal (India), Cambodia, and Vietnam. Because high concentrations of As in rice from As-endemic Asian countries have been reported,[8] rice on sale in Australia imported from these countries could be an important source of dietary As exposure for Australian consumers, particularly the Asian immigrants who are normally high consumers of rice. The objective of this study was to determine total and speciated As concentrations in Australian-grown and imported rice on sale in Australia from Asian countries with significant As contamination issues, particularly Bangladesh and India, to establish whether average Australians and Asian immigrants are likely to be at risk of As exposure via their rice diets. The forms of As present in rice were measured to predict the degree of As toxicity from this food source. The dietary contributions of Australian-grown and imported rice on sale in Australia to the maximum tolerable daily intake (MTDI) of total and inorganic As for Australian consumers (average Australian, and Asian and European immigrants) were also estimated on the basis of rice consumption rates and body weights.

MATERIALS AND METHODS

Chemicals and Reagents. All reagents were of analytical grade. Milli-Q (MQ) water (Milli-Q Plus system, Millipore, Bedford, MA, USA) was used throughout. Nitric acid (70%) and trifluoroacetic acid (TFA) were obtained from Mallinckrodt Chemicals, USA, and BDH Chemicals, UK, respectively. Sodium arsenite ($NaAsO_2$), monosodium arsenate ($Na_2HAsO_4{\cdot}7H_2O$), and monomethylarsonate ($CH_3AsNa_2O_3$) were obtained from Sigma Chemicals, and dimethylarsinate ($(CH_3)_2AsO(OH)$) was from Chem Service Inc. Phosphate buffer (30 mM, pH 5.6) was prepared from ammonium dihydrogen orthophosphate (Ajax Chemicals, Australia), and the pH was adjusted by adding ammonium hydroxide (Biolab, Australia). The buffer solution was filtered through a 0.22 μm nylon membrane before use.

Sample Collection and Preparation. Twenty-one samples representing 7 Australian-grown rice varieties and 51 samples of 17 different varieties of imported rice on sale in Australia were purchased from Australian and Asian shops in Sydney, Australia, during the month of January 2012. The samples were washed with tap water (three times) followed by deionized water (twice). The samples were then homogenized by grinding with a glass mortar and dried in an oven at 65 °C for 48 h before digestion for analysis.

Total As and As Speciation Analysis. Total As in the samples was determined following the method of Rahman et al.[4] Briefly, dried and ground samples (0.5 g) were each weighed into a digestion tube, and 5 mL of concentrated nitric acid (70%) was added and allowed to equilibrate overnight at room temperature. Then the tubes were placed on a digestion block (A. I. Scientific Block Digestion System AIM 500), and the temperature was increased from 75 to 140 °C over 8 h. Following digestion, tubes were removed, and after cooling, the samples were diluted to 20 mL with MQ water. Prior to analysis, all samples were filtered through 0.45 μm pore size filter paper (Whatman no. 41). The TFA extraction technique was used to determine As species in rice samples.[14]

An Agilent 7500c (Agilent Technologies, Tokyo, Japan) inductively coupled plasma mass spectrometer (ICP-MS) was used for the determination of total As (tAs) and As speciation. An Agilent 1100 liquid chromatography unit (Agilent, Tokyo, Japan) equipped with a guard column and a Hamilton PRP-1000 separation column (250 × 4.1 mm) was used for the determination of As species in the samples. The samples were injected using an 1100 autosampler (injection volume was 50 μL). The mobile phase contained 30 mM $NH_4H_2PO_4$ at pH 5.6, and the flow-rate was 1.0 mL min^{-1}. The details of the instrumental conditions for As speciation were described elsewhere.[15,16] All results in this paper are expressed on a dry weight (dw) basis.

Analysis of Standard Reference Materials (SRMs) and QC/QA. The analytical procedure was validated by analyzing certified standard reference material (SRM) of rice flour (SRM 1568a) from the National Institute of Standard and Technology (NIST), USA. The certified value of tAs in the SRM sample was 0.263 ± 0.012 μg g^{-1}, whereas the measured value was 0.290 ± 0.03 μg g^{-1}, indicating a recovery value of 110%. A reagent blank was also included in each batch of sample digestion and analysis to check the precision of the method. The detection limits for tAs and speciated As were evaluated by the analysis of solution matrix and determined to be 0.01 μg L^{-1} for tAs, 0.3 μg L^{-1} for As^V, 0.1 μg L^{-1} for As^{III} and dimethylarsinic acid (DMA), and 0.2 μg L^{-1} for methylarsonic acid (MMA). The precisions of five replicate determinations were 2.7, 1.5, 1.7, and 2.4% for As^V, As^{III}, DMA, and MMA, respectively.

There is no certified material currently available for As speciation in rice. In the present study, we used an established and published extraction method for As speciation in rice grain using 2 M TFA.[14] To validate the accuracy of our method and instrumental performance of As speciation analysis in rice grain sample, we analyzed As species in rice SRM (NIST 1568a) using the extraction procedures of 2 M TFA in a previous study, and the results were compared with those published by others.[17] Our results on As speciation in NIST SRM rice sample were consistent with those of other studies.

Dietary Exposure Estimates. According to the FAO/WHO,[18] three basic approaches can be used to determine the dietary intake of chemical contaminants from foods: (i) total diet study, (ii) duplicate diet method, and (iii) diary study. These approaches combine the concentration of specific contaminants in food with individual consumption rate. In the present study, the total diet study approach was used to determine the dietary intake of As from Australian-grown and imported rice on sale in Australia according to the equation

$$DI_{As} = C_{tAs\ or\ iAs} \times CR_{rice} \quad (1)$$

where DI_{As} is the dietary intake of As (μg $person^{-1}$ day^{-1}), C_{tAs} is the tAs concentration (μg kg^{-1}), C_{iAs} is the iAs concentration (μg kg^{-1}), and CR_{rice} is the rice consumption rate (kg $person^{-1}$ day^{-1}).

The health risk of total and inorganic As exposure from rice diet was estimated according to the equation

$$DE_{As} = DI_{tAs\ or\ As} \div BW_{av\ ind} \quad (2)$$

where DE_{As} is the dietary exposure (μg kg^{-1} body weight day^{-1}), DI_{tAs} is the dietary intake of tAs (μg $person^{-1}$ day^{-1}), DI_{iAs} is the dietary intake of iAs (μg $person^{-1}$ day^{-1}), and $BW_{av\ ind}$ is the average individual body weight of the consumers.

Total dietary intake and health risk of tAs and As species were estimated for three major consumer groups in Australia: (i) average Australian, (ii) Asian immigrants, and (iii) European immigrants. These consumer groups were selected because they represent the major populations in the country who consume rice on a regular basis. As the body weights and rice consumption rates of Asian and European immigrants living in Australia are not available, the dietary intake and health risk of As were estimated based on average body weights and rice consumption rates of Asian and European adults as reported by Walpole et al.[19] and Wailes and Chavez.[19]

RESULTS AND DISCUSSION

Total As Content in Australian-Grown and Imported Rice. The mean and range of tAs concentrations in Australian-grown rice were 270 and 188−438 μg kg^{-1}, respectively. The highest tAs was found in organic brown rice (438 ± 23 μg

Table 1. Concentrations of Total and Speciated Arsenic (Micrograms per Kilogram Dry Weight) in Australian-Grown and Imported Rice on Sale in Local Markets in Sydney, Australia[a]

				As species			% of total As		
origin	local name and type of rice	*n*	total	inorganic	MMA	DMA	inorganic	methylated	all species
Australia	brown rice (organic, medium grain)	3	438 ± 23	276 ± 25	<dl	115 ± 02	63	26	89
	brown rice (whole, medium grain)	3	287 ± 03	178 ± 22	<dl	68 ± 03	62	24	86
	brown rice (long grain)	3	198 ± 41	–	–	–	–	–	–
	white rice (organic, long grain)	3	283 ± 18	165 ± 08	<dl	52 ± 01	58	18	77
	Clever rice (long grain)	3	257 ± 05	–	–	–	–	–	–
	white rice (long grain)	3	241 ± 07	–	–	–	–	–	–
	sushi rice (sticky, Japanese style)	3	188 ± 06	177 ± 13	<dl	<dl	94	–	94
	all Australian rice (average)	21	270	–	–	–	–	–	–
Bangladesh	Chinigura (aromatic)	3	73 ± 03	68 ± 11	<dl	<dl	93	–	93
	Kalizira (aromatic)	3	38 ± 08	–	–	–	–	–	–
	all Bangladeshi rice (average)	6	56	–	–	–	–	–	–
Canada	wild rice (brown, long grain)	3	28 ± 03	19 ± 03	<dl	<dl	68	–	68
India	basmati (extra-long grain)	3	96 ± 13	94 ± 09	<dl	<dl	98	–	98
	basmati (long grain)	3	77 ± 09	–	–	–	–	–	–
	basmati (medium grain)	3	81 ± 08	–	–	–	–	–	–
	basmati (long grain, parboiled)	3	108 ± 07	–	–	–	–	–	–
	Sonamosori (small grain, aromatic)	3	99 ± 14	–	–	–	–	–	–
	all Indian rice (average)	15	92	–	–	–	–	–	–
Italy	Arborio (long grain)	3	547 ± 24	271 ± 25	<dl	107 ± 04	49	20	51
	Arborio (medium grain)	3	253 ± 10	–	–	–	–	–	–
	all Italian rice (average)	6	400	–	–	–	–	–	–
Pakistan	basmati (long grain)	3	86 ± 06	83 ± 13	<dl	<dl	96	–	96
	basmati (long grain, aromatic)	3	73 ± 08	–	–	–	–	–	–
	basmati (medium grain)	3	88 ± 05	–	–	–	–	–	–
	all Pakistani rice (average)	9	82	–	–	–	–	–	–
Thailand	white glutinous	3	159 ± 19	–	–	–	–	–	–
	jasmine (white, aromatic)	3	169 ± 08	168 ± 27	<dl	<dl	99	–	99
	Pin kiew glutinous	3	196 ± 35	168 ± 34	<dl	<dl	86	–	86
	Thai rice (long grain)	3	164 ± 36	–	–	–	–	–	–
	all Thai rice (average)	12	172	–	–	–	–	–	–

[a]Arsenic speciation was analyzed only in selected rice samples. –, As speciation data are not available for these rice varieties; dl, detection limit (0.01 $\mu g\ L^{-1}$ in solution matrix.

kg^{-1}) followed by medium-grain brown rice (287 ± 03 $\mu g\ kg^{-1}$) and organic white rice (283 ± 18 $\mu g\ kg^{-1}$). Total As concentrations in Australian-grown rice were higher than in imported rice on sale in Australia, except Italian Arborio rice (Table 1). In previous studies, Williams et al.[7] found tAs of 20–40 $\mu g\ kg^{-1}$ in Australian rice, with a mean of 30 $\mu g\ kg^{-1}$ ($n = 5$), whereas Juhasz et al.[20] reported 189 ± 18 $\mu g\ kg^{-1}$ in Australian long-grain white rice, which are both lower than the results of the present study for all rice varieties. It is notable that tAs concentration in Australian-grown organic brown rice exceeded the FAO/WHO recommended maximum permissible limit of 300 $\mu g\ kg^{-1}$.[21]

Although brown rice is generally considered healthier due to a higher fiber and nutrient content, the present study showed that it contains significantly higher concentrations of tAs than white rice (Table 1). Meharg et al.[22] also reported that brown rice contained more As than polished white rice. This is due to a higher As concentration in the outer layer (rice bran), which is removed in the polishing process to produce white rice, than in the inner layer of rice.[23] Why As concentration in the outer layer is higher than in inner layer is unclear. It is likely that the outer layer of rice bran acts as translocation barrier to As that prevents As movement into the inner layers.[23]

In a recent study, Jackson et al.[24] found tAs ranging from 2.2 to 12.6 $\mu g\ kg^{-1}$ in different infant formulas purchased from supermarkets in Hanover (Germany) and New Hampshire (USA). Another study by Vela and Heitkemper[25] reported 12–17 $\mu g\ kg^{-1}$ tAs in infant formulas and 63–320 $\mu g\ kg^{-1}$ tAs in rice-based cereals. Thus, not only the organic brown rice but also infant formulas and other foods manufactured from this rice can be sources of dietary As for both children and adults.[26−28] As brown rice and rice bran are the main ingredients in many of the previously tested baby and toddler food products (e.g., organic rice milk, organic rice syrup), high concentrations of tAs in Australian-grown organic brown rice, as found in the present study, could be of concern for babies eating significant quantities of such products in Australia.

Arsenic concentrations in long- and medium-grain Arborio rice of Italian origin were 547 ± 24 and 253 ± 10 μg kg^{-1}, respectively, which are comparable to tAs concentrations in some of the Australian-grown rice varieties (Table 1). The present study also showed that the tAs concentration in long-grain Arborio rice was about double that in medium-grain Arborio rice of Italian origin on sale in Australia (Table 1). Several market basket surveys have also reported tAs concentrations in different rice varieties of European origin.[7,20,29] Williams et al.[7] reported tAs concentrations as 220 ± 10 and 190 ± 30 μg kg^{-1} in medium-grain risotto and brown rice of Italian origin, respectively, and 170 ± 10 μg kg^{-1} in paella rice of Spanish origin. D'Amato et al.[30] reported 211 ± 7 μg kg^{-1} tAs in Italian origin Arborio rice. In a more recent study, Meharg et al.[29] reported tAs concentrations of 200 μg kg^{-1} (range = 50−820 μg kg^{-1}; n = 76) in Spanish rice, 280 μg kg^{-1} (range = 90−560 μg kg^{-1}; n = 33) in French rice, and 150 μg kg^{-1} (range = 70−330 μg kg^{-1}; n = 38) in Italian rice. The tAs concentration in medium-grain Arborio rice of Italian origin on sale in Australia (253 ± 10 μg kg^{-1}), as found in the present study, is similar to that in medium-grain risotto rice (220 ± 10 μg kg^{-1}) as reported by Williams et al.[7] The tAs concentration in medium-grain Arborio rice of Italian origin (547 ± 24 μg kg^{-1}), as found in the present study, is also comparable to the highest value in rice of French origin (560 μg kg^{-1}) as reported by Meharg et al.[29]

It is notable that in the present study, tAs concentrations in different rice varieties of Asian origin were lower than in Australian and Italian rice varieties on sale in Australia (Table 1). Among the Asian rices, tAs concentration in Thai rice was highest (mean = 172 μg kg^{-1}; range = 159−196 μg kg^{-1}) followed by Indian, Pakistani, and Bangladeshi rice (range = 38−108 μg kg^{-1}). Williams et al.[31] reported 110 ± 0.01 μg kg^{-1} of tAs in Thai rice, whereas in a later study, Williams et al.[7] found mean tAs to be 100 μg kg^{-1} with a range from 60 to 140 μg kg^{-1} in Thai rice. The tAs concentration in Thai rice, as found in the present study, was comparable to that reported by Meharg et al.[29] but higher than that reported by Williams et al.[7,31]

High concentrations of tAs in Indian (West Bengal) and Bangladeshi rice varieties cultivated in As-endemic areas (range = 150−1840 μg kg^{-1}) have been reported in many previous studies.[4,7,8,31] In the present study, the mean tAs concentrations in Indian and Pakistani rice on sale in Australia were 92 μg kg^{-1} (range = 77−108 μg kg^{-1}) and 82 μg kg^{-1} (range = 73−88 μg kg^{-1}), respectively (Table 1). Long- and medium-grain basmati rice is mainly imported into Australia from India and Pakistan. Williams et al.[31] reported tAs concentration in white basmati rice collected from Indian supermarkets as 50 μg kg^{-1} with a range of 30−80 μg kg^{-1}, which is comparable to that in Indian and Pakistani basmati rice used in the present study (Table 1). Indian basmati rice is mainly produced in the states of Haryana, Jammu, Kashmir, Himanchal Pradesh, Punjab, Delhi, Uttarakhand, and western Uttar Pradesh, where As contamination has not been reported to be extensive. Arsenic contamination is not wide spread in Pakistan either. Thus, it is consistent that tAs concentrations in Indian and Pakistani basmati rice on sale in Australia were found to be lower than those reported in rice of the As-contaminated Indian state of West Bengal (70−310 μg kg^{-1},[29] 110−440 μg kg^{-1},[32] and 30−480 μg kg^{-1}[33]).

As Speciation in Rice. Numerous studies have been conducted to determine As speciation in different varieties of Asian, European, and U.S. rice; however, little is known about As speciation in Australian-grown rice. In the present study, As speciation (inorganic and methylated As species) in 4 Australian-grown rice varieties (of 7) and 7 rice varieties (of 17) imported into Australia from Italy, Bangladesh, India, Pakistan, and Thailand was determined to estimate health risks of As exposure to Australian consumers from their rice diet. The results are presented in Table 1.

In the present study, the average iAs [As(III) + As(V)] and DMA in Australian-grown rice (except sushi rice) were found to be about 58−63 and 18−26% of the tAs, respectively (Table 1). In a previous study, Juhasz et al.[20] reported that the fractions of inorganic and organic As species were 86 and 14% of the tAs, respectively, in Australian Quest rice (a variety launched in 2003; it has a shorter growing cycle, making it more water efficient) grown in a greenhouse. Smith et al.[34] found As(III) and DMA as the major As species in Australian Quest rice grain. Notably, DMA was found to comprise 85−94% of the tAs concentration in the grain.

In the present study, iAs and DMA in Italian Arborio rice comprised 49 and 20% of the tAs, respectively (Table 1). Williams et al.[31] reported that 26−40% of the tAs in Italian rice was methylated species. D'Amato et al.[30] reported 31% of the tAs to be organic in Italian Arborio rice, which is slightly higher than that in the same rice of the present study. The iAs content in Asian rice on sale in Australia (86−99% of the tAs) is similar to that reported by Juhasz et al.[20] Australian-grown sushi rice contained only iAs representing 94% of the tAs and is comparable to As in Asian rice on sale in Australia (Table 1). With the exception for U.S. rice, iAs has been reported to be the main species (10−90% of the tAs) in most rice from other countries.[8] A small amount of the tAs has been found to be DMA, with a trace amount of MMA in some rice samples.[35] MMA was not detected in any rice samples used in the present study.

The present study reported As speciation (inorganic and methylated As) in field-grown Australian rice bought from the supermarket, for the first time. Although Juhasz et al.[20] determined As speciation in greenhouse-grown Australian rice, their As speciation data may not represent the rice that people consume regularly and, therefore, may not be true results of As speciation in Australian rice. A market basket survey of As speciation in U.S. rice showed that methylarsenic species (almost entirely as DMA) was the major species (36−65% of the tAs;[31]). Methylated As species have also been reported to be 10−15% in Chinese rice,[36] 12% in Indian rice,[31] and 11−43% in Bangladeshi rice.[36] In the present study, methylated As in Australian-grown rice was much higher than that in Asian rice on sale in Australia, but lower than that in U.S. rice, as reported in a previous study by Williams et al.[31]

Among the Australian-grown rice varieties, the highest concentration of DMA was found in organic brown rice (115 ± 02 μg kg^{-1}), which was ∼26% of the tAs. The concentration of iAs in this rice variety was 276 ± 25 μg kg^{-1}, which was ∼63% of the tAs (Table 1). Meharg et al.[22] reported mean concentrations of inorganic and organic As (mainly DMA with trace amounts of MMA) in U.S. brown rice as 170 and 140 μg kg^{-1}, which were about 45 and 28% of the tAs, respectively. The concentration of iAs in Australian-grown brown rice was higher than that in U.S. origin brown rice. As the speciation methodology for As remains technically challenging, the reason for the differences in iAs and DMA in Australian-grown and U.S. rice may lie in the high proportion of As where the species could not be determined. Additionally, rice types, varieties, and

Table 2. Estimated Dietary Intake of Total, Inorganic, and Methylated Arsenic Species (Micrograms per Person per Day) by Average Australian Consumers Including Asian and European Immigrants from Their Rice Diet Based on Rice Consumption Rates of 0.046, 0.016, and 0.44 kg Day^{-1} by Average Australian and European and Asian Adult Immigrants, Respectively[39] [a]

			average Australian			Asian immigrants			European immigrants		
country of origin	local name and variety of rice	*n*	total	inorganic	methylated	total	inorganic	methylated	total	inorganic	methylated
Australia	brown rice (organic, medium grain)	3	20.15	12.70	5.29	192.72	121.44	50.60	7.01	4.42	1.84
	brown rice (whole, medium grain)	3	13.20	8.19	3.13	126.28	78.32	29.92	4.59	2.85	1.09
	brown rice (long grain)	3	9.11	–	–	87.12	–	–	3.17	–	–
	white rice (organic, long grain)	3	13.02	7.59	2.39	124.52	72.60	22.88	4.53	2.64	0.83
	clever rice (long grain)	3	11.82	–	–	113.08	–	–	4.11	–	–
	white rice (long grain)	3	11.09	–	–	106.04	–	–	3.86	–	–
	sushi rice (sticky, Japanese style)	3	8.65	8.14	–	82.72	77.88	–	3.01	2.83	–
	all Australian rice (average)	21	12.42	9.15	3.60	118.80	87.56	–	4.32	3.18	–
Bangladesh	Chinigura (aromatic)	3	3.36	3.13	–	32.12	29.92	–	1.17	1.09	–
	Kalizira (aromatic)	3	1.75	–	–	16.72	–	–	0.61	–	–
	all Bangladeshi rice (average)	6	2.58	–	–	24.64	–	–	0.90	–	–
Canada	wild rice (brown, long grain)	3	1.29	0.87	–	12.32	8.36	–	0.45	0.30	–
India	basmati (extra-long grain)	3	4.42	4.32	–	42.24	41.36	–	1.54	1.50	–
	basmati (long grain)	3	3.54	–	–	33.88	–	–	1.23	–	–
	basmati (medium grain)	3	3.73	–	–	35.64	–	–	1.30	–	–
	basmati (long grain, parboiled)	3	4.97	–	–	47.52	–	–	1.73	–	–
	Sonamosori (small grain, aromatic)	3	4.55	–	–	43.56	–	–	1.58	–	–
	all Indian rice (average)	15	4.23	–	–	40.48	–	–	1.47	–	–
Italy	Arborio (long grain)	3	25.16	12.47	4.92	240.68	119.24	47.08	8.75	4.34	1.71
	Arborio (medium grain)	3	11.64	–	–	111.32	–	–	4.05	–	–
	all Italian rice (average)	6	18.40	–	–	176.00	–	–	6.40	–	–
Pakistan	basmati (long grain)	3	3.96	3.82	–	37.84	36.52	–	1.38	1.33	–
	basmati (long grain, aromatic)	3	3.36	–	–	32.12	–	–	1.17	–	–
	basmati (medium grain)	3	4.05	–	–	38.72	–	–	1.41	–	–
	all Pakistani rice (average)	9	3.77	–	–	36.08	–	–	1.31	–	–
Thailand	white glutinous	3	7.31	–	–	69.96	–	–	2.54	–	–
	jasmine (white, aromatic)	3	7.77	7.73	–	74.36	73.92	–	2.70	2.69	–
	Pin kiew glutinous	3	9.02	7.73	–	86.24	73.92	–	3.14	2.69	–
	Thai rice (long grain)	3	7.54	–	–	72.16	–	–	2.62	–	–
	all Thai rice (average)	12	7.91	–	–	75.68	–	–	2.75	–	–
average of all rice (irrespective of the origin)		72	8.13	7.15	1.75	77.72	68.42	12.54	2.83	2.49	0.46

[a] –, As speciation data are not available for these varieties.

sources of contamination may also be associated with the differences in iAs and methylated As ratios in rice as reported in several previous studies.[8] The variations in As speciation in rice have been suggested to reflect the source of As contamination, rice growing condition, the role of rhizosphere/soil microbial activity, and As uptake ability of the rice cultivars.[8,37] In Asian As-endemic countries, inorganic As-rich underground irrigation water is the main source of As contamination, and the agro-ecological condition of rice cultivation also favors iAs uptake by rice plants. On the other hand, arsenical pesticides consist of monosodium methanearsonate, disodium methanearsonate, calcium acid methanearsonate, and cacodylic acid, the main source of As for U.S. rice.[38] However, mining and arsenical pesticides, the sources of As in Australian paddy soils, have not been fully identified.

Dietary Intake of As from Rice Diet. Australians, who have been consuming locally grown rice and that imported from Bangladesh and other As-affected Asian countries, are likely to be unaware of the possible health risk of As from their rice diet. In the present study, dietary intake of As from Australian-grown and imported rice on sale in Australia was determined to establish whether Australian consumers, particularly the Asian immigrants who normally consume high amounts of rice (0.44 kg person^{-1} day^{-1} [39]), are likely to be at risk of As exposure from the rice in their diet. Australia is a multicultural country, and rice consumption rates in Australia differ substantially between the immigrants of different countries. In general, Asian people consume more rice than Australian and European people.[39] Per capita rice consumption data for different nationalities[39] have been used for the

dx.doi.org/10.1021/jf501077w | J. Agric. Food Chem. 2014, 62, 6016−6024

calculation of rice consumption rates by Bangladeshi, Cambodian, Laotian, and Vietnamese as the highest (between 0.59 and 80 kg person^{-1} day^{-1}), with an average of 0.44 kg person^{-1} day^{-1}. In contrast, average rice consumption rates by Australians and Europeans were 0.046 and 0.016 kg person^{-1} day^{-1}, respectively. On the basis of these data, we have estimated the daily dietary intake of total and speciated As from rice diet by the Australian consumers, particularly Asian and European immigrants (Table 2), for the assessment of health risk of As exposure from rice diet.

The results clearly show that the Asian immigrants in Australia are at higher risk of As exposure from their rice diet (77.72 and 68.42 μg of total and inorganic As person^{-1} day^{-1}, respectively) than the average Australian and European immigrants (2.83 and 2.49 μg of total and inorganic As person^{-1} day^{-1}, respectively) (Figure 1). This was due to the differences in rice consumption rates by Australian, Asian, and European people as reported by Wailes and Chavez.[39] It was estimated that an Asian immigrant in Australia may be exposed to 118.80, 40.48, 176.00, 36.08, and 75.68 μg of tAs day^{-1} from Australian, Indian, Italian, Pakistani, and Thai rice on sale in Australia, respectively. In contrast, the European immigrants may be exposed to 4.32, 1.47, 6.40, 1.31, and 2.75 μg of tAs day^{-1} from Australian, Indian, Italian, Pakistani, and Thai rice on sale in Australia, respectively (Table 2). Australian organic brown rice and Italian Arborio rice were the highest contributors of daily dietary total (192.72 and 240.68 μg person^{-1}, respectively) and inorganic (121.44 and 119.24 μg person^{-1}, respectively) As for Asian immigrants in Australia. In addition to inorganic As, Australian and Italian rices also contribute dietary intake of methylated As (mainly DMA) for Australian consumers. However, because organic As is far less toxic than iAs,[40] dietary intake of methylated As species from rice diet may not be a health issue for Australian consumers.

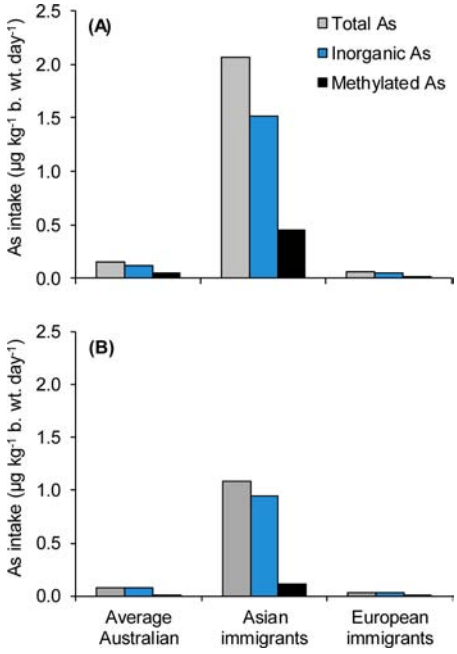

Figure 1. Estimated daily dietary intake of total, inorganic, and methylated As speciation by three consumer groups (average Australian and Asian and European immigrants) from Australian-grown (A) and imported (B) rice on sale in Australia.

The MTDI of tAs, as set by the FAO/WHO in 1967 and unrevised in 1989, is 50 μg kg^{-1} body weight (b wt).[41] For inorganic As, a provisional MTDI of 2.1 μg kg^{-1} b wt has also been set by the FAO/WHO for humans because of the higher toxicity of iAs than organic As species.[42,43] According to the Australian Bureau of Statistics,[44] on average, Australian adult men and women weigh 85.9 and 71.1 kg, respectively, with an average of 78.5 kg irrespective of gender. On the basis of these data, it was estimated that Australian-grown rice alone may contribute an average of 0.16 and 0.12 μg of total and inorganic As kg^{-1} b wt day^{-1} for Australian consumers, respectively (Figure 1A). Among all rice samples studied, Australian organic brown rice was found to be the highest contributor of tAs to MTDI (0.26 μg kg^{-1} b wt day^{-1}, which is about 0.51% of the MTDI) for Australian consumers, followed by Italian Arborio rice (0.23 μg kg^{-1} b wt day^{-1}; 0.64% of MTDI), Thai rice (0.10 μg kg^{-1} b wt day^{-1}; 0.20% of MTDI), and Indian and Pakistani basmati rice (0.05 μg kg^{-1} b wt day^{-1}; 0.10% of MTDI) (Table 3). These amounts are far less than the FAO/WHO recommended MTDI of total, suggesting that Australian consumers may not be at health risk of As exposure from their rice diet alone. On average, a European adult weighs 70.8 kg[19] and consumes 0.016 kg rice day^{-1}.[39] On the basis of these data, the estimated intakes of total and inorganic As were 2.83 and 2.49 μg day^{-1} for European immigrant in Australia (Table 2), which contribute 0.08 and 1.70% to the MTDI of total and inorganic As, respectively. Thus, the European immigrants are unlikely to have a health risk of As exposure from their rice diet alone.

The average body weight of an Asian adult is 57.7 kg,[19] and the rice consumption rate is 0.44 kg day^{-1}.[34,39] On the basis of these data, Australian-grown rice may contribute an average of 2.06 μg of tAs kg^{-1} b wt day^{-1} for an Asian immigrant (Figure 1A), which represents about 4% of the MTDI of tAs. Australian-grown organic brown rice alone may contribute 3.34 μg of tAs kg^{-1} b wt day^{-1} (about 7% of MTDI) for Asian immigrants, which is the highest among all rice varieties on sale in Australia, followed by Italian Arborio rice (3.05 μg kg^{-1} b wt day^{-1}; about 6% of MTDI), Thai rice (1.31 μg kg^{-1} b wt day^{-1}; about 2.6% of MTDI), and Indian and Pakistani basmati rice (0.63−0.70 μg kg^{-1} b wt day^{-1}; about 1.3−1.4% of MTDI) (Table 3). On average, the contribution of Australian-grown rice to daily dietary intake of total and inorganic As was higher than that of Asian rice for all Australian consumers (Figure 1). It is notable that Australian-grown organic brown rice and Italian Arborio rice were found to be the highest contributors of MTDI of iAs (2.07−2.10 μg kg^{-1} b wt day^{-1}, which is about 98−100% of MTDI) recommended by the FAO/WHO (2.1 μg kg^{-1} b wt day^{-1}[42,43]) for Asian immigrants in Australia (Table 3). Other Australian-grown rice varieties and Thai rice may also be significant sources of iAs (up to 65% of MTDI) for Asian immigrants.

The results indicate that Asian immigrants in Australia who regularly consume Australian-grown rice, particularly brown rice, and imported Italian Arborio rice may be at high health risk of iAs exposure. Several previous studies also reported high health risk of iAs to Asian populations from their rice-based diet.[31,45−47] However, the present study showed that Bangladeshi aromatic rice and Indian and Pakistani basmati rice on sale in Australia contribute very low amounts of total and inorganic As to the MTDI (Table 3), and hence, these imported rices may be safer than Australian-grown rice for the high rice-consuming Asian immigrants living in Australia. In a

Table 3. Dietary Intake of Total, Inorganic, and Methylated Arsenic Species (Micrograms per Kilogram Body Weight per Day) by Average Australian Consumers from Australian-Grown and Imported Rice on Sale in Australia Calculated Considering (i) Concentrations of Total and Speciated As in Rice of the Present Study, (ii) Body Weights of 78.5, 70.8, and 57.5 kg for Average Australian, and European and Asian Adult Immigrants, Respectively,[19] and (iii) Rice Consumption Rates of 0.046, 0.016, and 0.44 kg Day^{-1}for Average Australian, and European and Asian Adult Immigrants, Respectively[39]

			average Australian			Asian immigrants			European immigrants		
country of origin	local name and variety of rice	*n*	total	inorganic	methylated	total	inorganic	methylated	total	inorganic	methylated
Australia	brown rice (organic, medium grain)	3	0.26	0.16	0.07	3.34	2.10	0.88	0.10	0.06	0.03
	brown rice (whole, medium grain)	3	0.17	0.10	0.04	2.19	1.36	0.52	0.07	0.04	0.02
	white rice (organic, long grain)	3	0.17	0.10	0.03	2.16	1.26	0.40	0.06	0.04	0.01
	sushi rice (sticky, Japanese style)	3	0.11	0.10	–	1.43	1.35	–	0.04	0.04	–
Bangladesh	Chinigura (aromatic)	3	0.04	0.04	–	0.56	0.52	–	0.02	0.02	–
Canada	wild rice (brown, long grain)	3	0.02	0.01	–	0.21	0.14	–	0.01	0.00	–
India	basmati (extra-long grain)	3	0.06	0.06	–	0.73	0.72	–	0.02	0.02	–
Italy	Arborio (long grain)	3	0.32	0.16	0.06	4.17	2.07	0.82	0.12	0.06	0.02
Pakistan	basmati (long grain)	3	0.05	0.05	–	0.66	0.63	–	0.02	0.02	–
Thailand	jasmine (white, aromatic)	3	0.10	0.10	–	1.29	1.28	–	0.04	0.04	–
	Pin kiew glutinous	3	0.11	0.10	–	1.49	1.28	–	0.04	0.04	–

Table 4. Human Health Risk Assessment of Arsenic Exposure from Rice in the Diet[a]

			dietary intake of As species (μg kg^{-1} b wt day^{-1})						% contribution to MTDI of iAs for		
			average Australian		Asian immigrants		European immigrants				
country of origin	local name and variety of rice	*n*	inorganic	methylated	inorganic	methylated	inorganic	methylated	average Australian	Asian immigrants	European immigrants
Australia	brown rice (organic, medium grain)	3	0.16	0.02	2.08	0.29	0.06	0.01	7.59	98.82	2.96
	brown rice (whole, medium grain)	3	0.10	0.01	1.34	0.17	0.04	0.01	4.90	63.73	1.91
	white rice (organic, long grain)	3	0.10	0.01	1.24	0.13	0.04	0.00	4.54	59.08	1.77
	sushi rice (sticky, Japanese style)	3	0.10	–	1.33	–	0.04	–	4.87	63.37	1.90
Bangladesh	Chinigura (aromatic)	3	0.04	–	0.51	–	0.02	–	1.87	24.35	0.73
Canada	wild rice (brown, long grain)	3	0.01	–	0.14	–	0.00	–	0.52	6.80	0.20
India	basmati (extra-long grain)	3	0.05	–	0.71	–	0.02	–	2.59	33.66	1.01
Italy	Arborio (long grain)	3	0.16	0.02	2.04	0.27	0.06	0.01	7.46	97.03	2.91
Pakistan	basmati (long grain)	3	0.05	–	0.62	–	0.02	–	2.28	29.72	0.89
Thailand	jasmine (white, aromatic)	3	0.10	–	1.26	–	0.04	0.01	4.62	60.15	1.80
	Pin kiew glutinous	3	0.10	–	1.26	–	0.04	–	4.62	60.15	1.80

[a]Dietary intake of inorganic and methylated As species and percent contribution of rice diet to maximum tolerable daily intake (MTDI) of inorganic As were calculated considering (i) the concentrations of inorganic and methylated As species in rice grains, (ii) body weights of 78.5, 70.8, and 57.5 kg for average Australian, and European and Asian adult immigrants, respectively,[19] (iii) rice consumption rates of 0.046, 0.016, and 0.44 kg day^{-1} for average Australian, and European and Asian adult immigrants, respectively,[39] and (iv) bioavailability factors of 0.33 and 98.6 for organic and inorganic As species, respectively.[20].

recent evaluation conducted by the Joint FAO/WHO Expert Committee on Food Additives,[21] the provisional MTDI of iAs in rice has been withdrawn and is no longer valid as the iAs lower limit of the benchmark dose for a 0.5% increased the incidence of lung cancer. This was determined from epidemiological studies to be 3.0 μg kg^{-1} b wt day^{-1} (2−7 μg kg^{-1} based on the range of estimated total dietary exposure) using a range of assumptions to estimate total dietary exposure to iAs from drinking water and food.[48]

Bioaccessibility and bioavailability of As in rice are two important factors that have substantial influence on As toxicity to humans. The bioaccessibility and bioavailability of As in food mainly depend on the As speciation, and toxic iAs species are readily assimilated into the bloodstream.[5] Therefore, human health risk of iAs is greater than that of organic As species. Laparra et al.[49] investigated the bioavailability and bioaccessibility of iAs in cooked rice to assess the potential toxicological risk of this species to humans using the Caco-2 cell model. The results showed that iAs concentration in the bioaccessible fraction of cooked rice was 0.8−3.10 μg g^{-1} d wt, which suggests that a large proportion of iAs present in the cooked rice (63−100%) could be available for intestinal absorption. In another study, Juhasz et al.[20] investigated the bioavailability of As species in rice using the swine animal model to determine its significance for human health risk. The absolute bioavailability of iAs was found to be the highest [98.6% for iAs, which is the average of 103.9 and 92.5% for As(III) and As(V), respectively] followed by DMA (33.3%) and MMA (16.7%).[20]

On the basis of the As speciation data of the present study (Table 1) and bioavailability of As species as reported by Juhasz et al.,[20] dietary intake of inorganic and methylated As species and percent contribution to MTDI of iAs from Australian-grown and imported rice on sale in Australia were estimated (Table 4). Results showed that dietary intake of iAs from rice diet did not differ for total and bioavailable fractions of iAs in rice. However, dietary intake of methylated As differed substantially for total and bioavailable fractions of iAs in rice. The consumption of Australian-grown rice was estimated to contribute 4.5−7.6% (average = 5.5%) of the MTDI of iAs for Australian consumers, 59−98% (average = 71%) for Asian immigrants in Australia, and 1.8−3.0% (average = 2.1%) for European immigrants when the bioavailability of iAs (98.6%) was considered (Table 4). These values were slightly lower than those calculated without considering the bioavailability of the As species. Italian Arborio rice imported into Australia was estimated to contribute 7.5, 97, and 2.9% of the MTDI of iAs for average Australian, and Asian and European immigrants, respectively. In contrast, on average, the consumption of imported Asian rice on sale in Australia was estimated to contribute 0.5−4.6% (average = 2.8%) of the MTDI of iAs for average Australian consumers, 6.8−60.2% (average = 35.8%) for Asian immigrants, and 0.2−1.8% (average = 1.1%) for European immigrants when the bioavailability of iAs (98.6%) was considered (Table 4). The results showed that, if only the total concentration of iAs in rice is considered for assessing the human health risk of As from rice diet, the calculation may not reflect the real risk. Therefore, the bioavailability of As species should be taken into account to estimate dietary intake, MTDI, and human health risk of As.

Only small-grain aromatic rice is imported into Australia from Bangladesh in which tAs concentrations ranged between 38 and 73 μg kg^{-1}. This concentration is lower than the FAO/WHO recommended safe level (300 μg kg^{-1} [21]). Rice from other Asian countries such as India, Pakistan, and Thailand also contain tAs lower than the FAO/WHO recommended maximum level. However, the tAs concentration in Australian-grown organic brown rice exceeds the FAO/WHO recommended level, and because a significant fraction (about 63%) of tAs in this rice was inorganic As, Australian organic brown rice may be a matter of human health concern, especially for infants who eat cereals and formulas manufactured from organic brown rice and rice bran and for adults who regularly eat organic brown rice. Asian people consume much higher amounts of rice than those of other origins,[39] and therefore, regular consumption of high As-containing brown rice over an extended period may cause adverse health effects for Asian immigrants in Australia. The present study showed that compared to Australian-grown brown rice, Pakistani and Indian basmati rice and Thai rice may be safer for the Australian consumers, especially for high rice consuming Asian immigrants.

AUTHOR INFORMATION

Corresponding Authors

*(M.A.R.) E-mail: Mohammad.Rahman@uts.edu.au.

*(R.N.) E-mail: ravi.naidu@crccare.com. Phone: +61 8 8302 5041. Fax: +61 8 8302 3057.

Funding

We acknowledge the University of Technology, Sydney (UTS), for financial support to M.A.R. We further acknowledge the Centre for Environmental Risk Assessment and Remediation, University of South Australia (Supported Researcher Fund Scheme), for providing funds to M.M.R. to carry out this research. Finally, we gratefully acknowledge financial support from the Cooperative Research Centre for Contamination Assessment and Remediation of the Environment (CRC-CARE project 3.1.3.11/12), Australia.

Notes

The authors declare no competing financial interest.

ACKNOWLEDGMENTS

We extend our acknowledgement to the anonymous reviewers for their valuable comments and suggestions that helped to improve the quality of the paper.

REFERENCES

(1) Kohnhorst, A. Arsenic in groundwater in selected countries in south and southeast Asia: a review. *J. Trop. Med. Parasitol.* **2005**, *28*, 73−82.

(2) Mukherjee, A.; Sengupta, M. K.; Hossain, M. A.; Ahamed, S.; Das, B.; Nayak, B.; Lodh, D.; Rahman, M. M.; Chakraborti, D. Arsenic contamination in groundwater: a global perspective with emphasis on the Asian scenario. *J. Health Popul. Nutr.* **2006**, *24*, 142−163.

(3) Smedley, P. L. *Arsenic Occurrence in Groundwater in South and East Asia*; World Bank: Washington, DC, USA, 2005; pp 20−98.

(4) Rahman, M. M.; Owens, G.; Naidu, R. Arsenic levels in rice grain and assessment of daily dietary intake of arsenic from rice in arsenic-contaminated regions of Bangladesh − implications to groundwater irrigation. *Environ. Geochem. Health* **2009**, *31*, 179−187.

(5) Meharg, A. A.; Rahman, M. Arsenic contamination of Bangladesh paddy field soils: implications for rice contribution to arsenic consumption. *Environ. Sci. Technol.* **2003**, *37*, 229−234.

(6) del Ninno, C.; Dorosh, P. A. Averting a food crisis: private imports and public targeted distribution in Bangladesh after the 1998 flood. *Agric. Econ.* **2001**, *25*, 337−346.

(7) Williams, P. N.; Islam, M. R.; Adomako, E. E.; Raab, A.; Hossain, S. A.; Zhu, Y. G.; Feldmann, J.; Meharg, A. A. Increase in rice grain arsenic for regions of Bangladesh irrigating paddies with elevated arsenic in groundwaters. *Environ. Sci. Technol.* **2006**, *40*, 4903−4908.

(8) Rahman, M. A.; Hasegawa, H. High levels of inorganic arsenic in rice in areas where arsenic-contaminated water is used for irrigation and cooking. *Sci. Total Environ.* **2011**, *409*, 4645−4655.

(9) Sun, G.; Li, X.; Pi, J.; Sun, Y.; Li, B.; Jin, Y.; Xu, Y. Current research problems of chronic arsenicosis in China. *J. Health Popul. Nutr.* **2006**, *24*, 176−181.

(10) Perry, M. R.; Wyllie, S.; Prajapati, V. K.; Feldmann, J.; Sundar, S.; Boelaert, M.; Fairlamb, A. H. Visceral leishmaniasis and arsenic: an ancient poison contributing to antimonial treatment failure in the Indian subcontinent? *PLoS Negl. Trop. Dis.* **2011**, *5*, No. e1227.

(11) Smith, E.; Smith, J.; Smith, L.; Biswas, T.; Correll, R.; Naidu, R. Arsenic in Australian environment: an overview. *J. Environ. Sci. Health, Part A* **2003**, *38*, 223−239.

(12) Smith, E.; Naidu, R.; Alston, A. M. Arsenic in the soil environment: a review. In *Advances in Agronomy*; Donald, L. S., Ed.; Academic Press: San Diego, CA, USA, 1998; Vol. 64, pp 149−195.

(13) Al Rmalli, S. W.; Haris, P. I.; Harrington, C. F.; Ayub, M. A survey of arsenic in foodstuffs on sale in the United Kingdom and imported from Bangladesh. *Sci. Total Environ.* **2005**, *337*, 23−30.

(14) Abedin, M. J.; Cresser, M. S.; Meharg, A. A.; Feldmann, J.; Cotter-Howells, J. Arsenic accumulation and metabolism in rice (*Oryza sativa* L.). *Environ. Sci. Technol.* **2002**, *36*, 962−968.

(15) Chen, Z. L.; Akter, K. F.; Rahman, M. M.; Naidu, R. The separation of arsenic species in soils and plant tissues by anion-exchange chromatography with inductively coupled mass spectrometry using various mobile phases. *Microchem. J.* **2008**, *89*, 20−28.

(16) Farzana Akter, K.; Chen, Z.; Smith, L.; Davey, D.; Naidu, R. Speciation of arsenic in ground water samples: a comparative study of CE-UV, HG-AAS and LC-ICP-MS. *Talanta* **2005**, *68*, 406−415.

(17) Rahman, M. M.; Asaduzzaman, M.; Naidu, R. Arsenic exposure from rice and water sources in the Noakhali District of Bangladesh. *Water. Qual. Exp. Health* **2011**, *3*, 1−10.
(18) FAO/WHO. *Guidelines for the Study of Dietary Intakes of Chemical Contaminants*; World Health Organization: Geneva, Switzerland, 1985; p 104.
(19) Walpole, S.; Prieto-Merino, D.; Edwards, P.; Cleland, J.; Stevens, G.; Roberts, I. The weight of nations: an estimation of adult human biomass. *BMC Public Health* **2012**, *12*, 439.
(20) Juhasz, A. L.; Smith, E.; Weber, J.; Rees, M.; Rofe, A.; Kuchel, T.; Sansom, L.; Naidu, R. *In vivo* assessment of arsenic bioavailability in rice and its significance for human health risk assessment. *Environ. Health Perspect.* **2006**, *114*, 1826−1831.
(21) JECFA. *Report of the Sixth Session of the Codex Committee on Contaminants in Foods*; Joint FAO/WHO Food Standards Programme Codex Alimentarius Commission: Maastricht, The Netherlands, 2012; p 79.
(22) Meharg, A. A.; Lombi, E.; Williams, P. N.; Scheckel, K. G.; Feldmann, J.; Raab, A.; Zhu, Y.; Islam, R. Speciation and localization of arsenic in white and brown rice grains. *Environ. Sci. Technol.* **2008**, *42*, 1051−1057.
(23) Rahman, M. A.; Hasegawa, H.; Rahman, M. M.; Rahman, M. A.; Miah, M. A. M. Accumulation of arsenic in tissues of rice plant (*Oryza sativa* L.) and its distribution in fractions of rice grain. *Chemosphere* **2007**, *69*, 942−948.
(24) Jackson, B. P.; Taylor, V. F.; Punshon, T.; Cottingham, K. L. Arsenic concentration and speciation in infant formulas and first foods. *Pure Appl. Chem.* **2012**, *84*, 215−223.
(25) Vela, N. P.; Heitkemper, D. T. Total arsenic determination and speciation in infant food products by ion chromatography-inductively coupled plasma-mass spectrometry. *J. AOAC Int.* **2004**, *87*, 244−252.
(26) Blumberg, J. *Organic Food Sweetener May Be a Hidden Source of Dietary Arsenic*; Dartmouth: Hanover, NH, USA, 2012.
(27) Dangerously high levels of arsenic found in rice & rice products including infant cereals! http://thenutrifarm.com/dangerously-high-levels-of-arsenic-found-in-rice-rice-products-including-infant-cereals/; Accessed December 14, 2013.
(28) Allen, J. E.Organic brown rice syrup: hidden arsenic source. *ABC News Medical Unit*, Feb 16, 2012.
(29) Meharg, A. A.; Williams, P. N.; Adomako, E.; Lawgali, Y. Y.; Deacon, C.; Villada, A.; Cambell, R. C. J.; Sun, G.; Zhu, Y.-G.; Feldmann, J. Geographical variation in total and inorganic arsenic content of polished (white) rice. *Environ. Sci. Technol.* **2009**, *43*, 1612−1617.
(30) D'Amato, M.; Forte, G.; Caroli, S. Identification and quantification of major species of arsenic in rice. *J. AOAC Int.* **2004**, *87*, 238−243.
(31) Williams, P. N.; Price, A. H.; Raab, A.; Hossain, S. A.; Feldmann, J.; Meharg, A. A. Variation in arsenic speciation and concentration in paddy rice related to dietary exposure. *Environ. Sci. Technol.* **2005**, *39*, 5531−5540.
(32) Roychowdhury, T.; Uchino, T.; Tokunaga, H.; Ando, M. Survey of arsenic in food composites from an arsenic-affected area of West Bengal, India. *Food Chem. Toxicol.* **2002**, *40*, 1611−1621.
(33) Pal, A.; Chowdhury, U. K.; Mondal, D.; Das, B.; Nayak, B.; Ghosh, A.; Maity, S.; Chakraborti, D. Arsenic burden from cooked rice in the populations of arsenic affected and nonaffected areas and Kolkata city in West-Bengal, India. *Environ. Sci. Technol.* **2009**, *43*, 3349−3355.
(34) Smith, E.; Juhasz, A. L.; Weber, J.; Naidu, R. Arsenic uptake and speciation in rice plants grown under greenhouse conditions with arsenic contaminated irrigation water. *Sci. Total Environ.* **2008**, *392*, 277−283.
(35) Zhu, Y.-G.; Williams, P. N.; Meharg, A. A. Exposure to inorganic arsenic from rice: a global health issue? *Environ. Pollut.* **2008**, *154*, 169−171.
(36) Sun, G.-X.; Williams, P. N.; Carey, A.-M.; Zhu, Y.-G.; Deacon, C.; Raab, A.; Feldmann, J.; Islam, R. M.; Meharg, A. A. Inorganic arsenic in rice bran and its products are an order of magnitude higher than in bulk grain. *Environ. Sci. Technol.* **2008**, *42*, 7542−7546.
(37) Pillai, T. R.; Yan, W.; Agrama, H. A.; James, W. D.; Ibrahim, A. M. H.; McClung, A. M.; Gentry, T. J.; Loeppert, R. H. Total grain-arsenic and arsenic-species concentrations in diverse rice cultivars under flooded conditions. *Crop Sci.* **2010**, *50*, 2065−2075.
(38) Robinson, G. R.; Larkins, P.; Boughton, C. J.; Reed, B. W.; Sibrell, P. L. Assessment of contamination from arsenical pesticide use on orchards in the Great Valley region, Virginia and West Virginia, USA. *J. Environ. Qual.* **2007**, *36*, 654−663.
(39) Wailes, E. J.; Chavez, E. C. *World Rice Outlook: International Rice Baseline Projections, 2011−2020*; University of Arkansas, Department of Agricultural Economics and Agribusiness: Fayetteville, AR, USA, 2011; p 61.
(40) Jain, C. K.; Ali, I. Arsenic: occurrence, toxicity and speciation techniques. *Water Res.* **2000**, *34*, 4304−4312.
(41) FAO/WHO. *Evaluation of Certain Food Additives and Contaminants*; World Health Organization: Geneva, Switzerland, 1989; p 58.
(42) Dabeka, R. W.; McKenzie, A. D.; Lacroix, G. M. A. Dietary intakes of lead, cadmium, arsenic and fluoride by Canadian adults: a 24-h duplicate diet study. *Food Addit. Contam.* **1987**, *4*, 89−101.
(43) Llobet, J. M.; Falcó, G.; Casas, C.; Teixidó, A.; Domingo, J. L. Concentrations of arsenic, cadmium, mercury, and lead in common foods and estimated daily intake by children, adolescents, adults, and seniors of Catalonia, Spain. *J. Agric. Food Chem.* **2002**, *51*, 838−842.
(44) ABS. Profiles of health, Australia, 2011−12. In Statistics, A. B. o., Ed. Australian Bureau of Statistics; http://www.abs.gov.au/ausstats/abs@.nsf/Lookup/4338.0main+features212011-13, 2012.
(45) Ohno, K.; Yanase, T.; Matsuo, Y.; Kimura, T.; Hamidur Rahman, M.; Magara, Y.; Matsui, Y. Arsenic intake via water and food by a population living in an arsenic-affected area of Bangladesh. *Sci. Total Environ.* **2007**, *381*, 68−76.
(46) Schoof, R. A.; Yost, L. J.; Crecelius, E.; Irgolic, K.; Goessler, W.; Guo, H. R.; Greene, H. Dietary arsenic intake in Taiwanese districts with elevated arsenic in drinking water. *Hum. Ecol. Risk Assess.* **1998**, *4*, 117−135.
(47) Sun, G. X.; Williams, P. N.; Carey, A. M.; Zhu, Y. G.; Deacon, C.; Raab, A.; Feldmann, J.; Islam, R. M.; Meharg, A. A. Inorganic arsenic in rice bran and its products are an order of magnitude higher than in bulk grain. *Environ. Sci. Technol.* **2008**, *42*, 7542−7546.
(48) Rahman, M. M.; Asaduzzaman, M.; Naidu, R. Consumption of arsenic and other elements from vegetables and drinking water from an arsenic-contaminated area of Bangladesh. *J. Hazard. Mater.* **2013**, *262*, 1056−1063.
(49) Laparra, J. M.; Velez, D.; Barbera, R.; Farre, R.; Montoro, R. Bioavailability of inorganic arsenic in cooked rice: practical aspects for human health risk assessments. *J. Agric. Food Chem.* **2005**, *53*, 8829−8833.

JOURNAL OF AGRICULTURAL AND FOOD CHEMISTRY

Review

pubs.acs.org/JAFC

Antibacterial, Antiviral, and Antifungal Properties of Wines and Winery Byproducts in Relation to Their Flavonoid Content

Mendel Friedman*

Western Regional Research Center, Agricultural Research Service, U.S. Department of Agriculture, Albany, California 94710, United States

ABSTRACT: Grapes produce organic compounds that may be involved in the defense of the plants against invading phytopathogens. These metabolites include numerous phenolic compounds that are also active against human pathogens. Grapes are used to produce a variety of wines, grape juices, and raisins. Grape pomace, seeds, and skins, the remains of the grapes that are a byproduct of winemaking, also contain numerous bioactive compounds that differ from those found in grapes and wines. This overview surveys and interprets our present knowledge of the activities of wines and winery byproducts and some of their bioactive components against foodborne (*Bacillus cereus, Campylobacter jejuni, Escherichia coli, Listeria monocytogenes, Salmonella enterica, Staphylococcus aureus, Yersinia enterocolitica, Vibrio cholerae, Vibrio vulnificus*), medical (*Helicobacter pylori, Klebsiella pneumoniae*), and oral pathogenic bacteria, viruses (adeno, cytomegalo, hepatitis, noro, rota), fungi (*Candida albicans, Botrytis cinerea*), parasites (*Eimeria tenella, Trichomonas vaginalis*), and microbial toxins (ochratoxin A, Shiga toxin) in culture, in vivo, and in/on food (beef, chicken, frankfurters, hot dogs, lettuce, oysters, peppers, pork, sausages, soup, spinach) in relation to composition and sensory properties. Also covered are antimicrobial wine marinades, antioxidative and immunostimulating aspects, and adverse effects associated with wine consumption. The collated information and suggested research needs might facilitate and guide further studies needed to optimize the use of wines and byproducts to help improve microbial food safety and prevent or treat animal and human infections.

KEYWORDS: *adverse effects, antibacterial, antibiotic properties, antifungal, antiinflammatory effects, antioxidative effects, antiviral, flavonoids, food, grape pomace, grape seeds, grape skins, grapevine leaves and stems, human infections, immunostimulating effects, microbial food safety, microbial toxins, oral bacteria, parasites, pathogens, research needs, sensory properties, wine, wine byproducts, wine compostion, wine marinades*

INTRODUCTION

Grapes are the second largest fruit crop in the world after oranges. According to the Food and Agricultural Organization of the United Nations, >67 million tons of grapes is produced annually worldwide, with the United States contributing about 10% to the total.[1] Wines are classified into major groups, table wines with an alcohol content <14% and dessert wines produced from grapes high in sugar and low in acid content.[2] During the production of wines, up to 40% of the grapes ends up as byproducts.[3] Winery byproducts including grape pomace, seeds, skins, stems, and leaves are rich sources of inexpensive antioxidative phenolic compounds.[4−6] Numerous studies have demonstrated that these compounds exhibit health-promoting effects associated with cardioprotective, neuroprotective, and other health benefits.[7−13] The present paper seems to be the first review on the antimicrobial properties of wines and winery byproducts.

The literature indicates that the concentrations of the byproducts vary widely among the different grape cultivars from which they are derived. Because biological activities and health benefits may depend on both the total amounts and the specific amounts of highly bioactive phenolic compounds present in the byproducts, there is a need to relate the beneficial effects to the composition of the wines and byproducts.

Food safety researchers, regulatory agencies, microbiologists, virologists, epidemiologists, nutritionists, pharmacists, physicians, and the general public have been increasingly concerned about the growing number of foodborne illnesses caused by some pathogens. Antibiotic resistance of some pathogens associated with foodborne illness caused by the overconsumption of medicinal antibiotics seems to exacerbate these effects. There has been increasing interest in developing novel plant-derived safe antimicrobial compounds, including those present in grapes and grape products.

The main objective of this review is to unify and interpret widely scattered information on reported studies on the inhibitory effects of bioactive grape-derived polyphenolic compounds against pathogenic bacteria, viruses, and fungi in vitro and in/on food. The cited findings and suggested research outlined below may facilitate and guide further needed studies to optimize the use of wines and grape-derived products to improve microbial food safety and to protect animals and humans against infectious diseases.

POLYPHENOLIC COMPOUNDS IN GRAPES, WINES, AND WINERY BYPRODUCTS

In general, the phenolic composition of grapes may be influenced by variety, vineyard, micro- and macroclimate,

Received: March 13, 2014
Revised: June 2, 2014
Accepted: June 5, 2014
Published: June 19, 2014

ACS Publications

This article not subject to U.S. Copyright. Published 2014 by the American Chemical Society

viticultural practice, and winemaking techniques. To help provide a scientific rationale for the antibiotic properties, we will first provide brief summaries on the composition, sensory properties, and immunostimulating, antioxidative, and adverse aspects of wines.

Wines. The extraordinarily large number of structurally different wine flavonoids is illustrated in randomly selected recent studies.[14−16] Two review papers on structures of wine flavonoids by He et al.[17,18] list 25 free anthocyanin glycosides, 25 anthocyanin diglycosides, and 63 anthocyanin-derived pigments (pyranoanthocyanins), along with molecular and fragment ion mass spectral peaks and UV−vis absorption maxima for most of these compounds. Selected compositional aspects described below further demonstrate the presence of different classes and amounts of polyphenolic compounds in wines originally synthesized in grapes and numerous new ones formed during winemaking.

New Zealand Pinot noir and Pinot Meunier wines contain the following polyphenol compounds: (a) anthocyanins—cyanidin-3-glucoside, delphinidin-3-glcoside, malvidin-3-glucoside, peonidin-3-glucoside, petunidin-3-glucoside, and vitisin, with total depending on extraction solvent and ranging from 6.01 to 17.35 malvidin equivalents/g extracts; (b) flavanols—catechin, epicatechin, epicatechin gallate, procyanidin A, and procyanidin B; (c) flavonols—quercetin and quercetin methylglucoside; and (d) a nonflavonoid—gallic acid.[17] The procyanidin content of polymeric phenolic isolates from Pinot noir wine during fermentation varied from 27 to 54%.[18,19]

The analysis of wines by HPLC and LC-DAD/ESI-MS revealed the presence of the following classes of bioactive compounds in wines: (a) phenolic acids—caffeic, gallic, protocatechuic, 4-hydroxybenzoic, and syringic; (b) flavonoids—(+)-catechin, catechin dimer, (−)-epicatechin, epicatechin gallate trimer, procyanidin B1, procyanidin B2, quercetin-3-*O*-rhamnoside, *trans*-polydatin, and *trans*-resveratrol; and (c) total phenolic content of 327.6 gallic acid equivalents (GAE)/g extract.[20] A related study reported a TPC of 628 mg GAE/g in grape seed extracts originating from Turkish grapes.[21,22]

An Australian study found that the proximity of eucalyptus trees to grapevines can directly influence the concentration of the aroma compound 1,8-cineole present in the corresponding red wines, and a fermentation study showed that the amount of rotundone in red wine can be influenced by grapevine leaves and stems in the ferment.[23]

Statistical instruments based on artificial neural networks (ANN) can be used to predict relationships between the total phenolic, flavonoid, anthocyanin, and tannin levels and antioxidative activity and wine variety and authenticity.[24]

Using wine model solutions, Sousa et al.[25] demonstrated interactions between deoxyanthocyanidin (oaklins), catechin−pyrilium compounds formed in red wines aged in oak barrels, and copigment molecules that form new wine ingredients. Related studies reported that (a) postharvest treatment of grapes with ethylene before vinification affected wine composition[26] and (b) exposure of grapevine cv. Tempranillo fruit-bearing cuttings to UV-B radiation induced changes in the profiles of flavonoids and amino acids.[27]

Grape Pomaces. About 20% of the grape remains as pomace—peel (skins), seeds, and stems—after wine production.[28] Pomaces that are largely used as soil conditioners or as fertilizers contain significant quantities of phenolic compounds that are not extracted into the wines. A high-phenolic grape pomace residue that consists of skin and seeds after the winemaking fermentation process can be analyzed. Several chemical and biological methods have been used to determine antioxidant and antimicrobial properties of grape seed and skin extracts, including quantitative analysis of phytochemicals by HPLC and GC-MS, measuring antioxidant activities, determining total antioxidant capacity, and measuring antimicrobial activity using the agar well diffusion method.

The described approaches could serve as a model for the in vitro evaluation of grape products. The review by Fontana et al.[29] on grape pomace lists 25 reported solid−liquid extraction and 28 HPLC detection methods for the characterization of different classes of phenolic compounds in the extracts. The authors suggest that future studies should focus on simplified extraction methods and nontoxic solvents that meet generally accepted as safe (GRAS) requirements. The distribution of *p*-coumaric, ellagic, gallic, protocatechuic, syringic, and vanillic acids, (−)-epicatechin, myricetin, kaemferol, and quercetin of grape pomace extracts (GPE) from a mixture of Chilean grapes depended on the nature of the solvent used for the extraction.[30]

The pomace contains the following antioxidative polyphenolic categories: phenolic acids, flavonoids, lignans, and stilbenes.[31] The Brazilian investigators report that GPE also contains chlorogenic acid, *trans*-resveratrol, and rutin and that the total phenolic content (TPC) of seeds (213−1652 mg/of catechin equivalents (CE)/g is greater than that in the skins (66−184 CE/g).

Another detailed LC-MS study of 14 pomace samples originating from red wines showed (a) the presence of 13 anthocyanins, 12 phenolic acids, and 15 anthoxanthins and stilbenes; (b) the total anthocyanin content of peel separated from five grape pomaces from two vintages ranged from 2744 to 131,868 mg/kg DM, or a 48-fold variation from lowest to highest value, with malvidin-3-*O*-glucoside being the predominant anthocyanin followed by peonidin-3-*O*-glucoside; (c) the content of phenolic acids was much lower than that of anthocyanins and varied significantly among samples of different vintages, with caftaric acid being the predominant compound in all samples; (d) with the exception of the 3-flavan-3-ols in the seeds that ranged up to several grams per kilogram of dry matter, anthoxanthins and stilbenes were minor components; and (e) aside from lack of anthocyanins,there were no major differences in total, but there were differences among individual phenolic compounds among pomaces from red and white grapes.[28] The TPC of pomace extracts from five Turkish grape cultivars ranged from 6.63 to 20.1 mg/g.[32,33] Levels of 19 individual phenolic compounds in the extracts ranged from 0.0031 mg/g for *trans*- resveratrol to 50.83 mg/g for (+)-catechin.

An evaluation of Moroccan Cabernet Sauvignon, Merlot, and Syrah red wine fractions against four Gram-positive bacteria, nine Gram-negative bacteria, two yeasts, and four molds showed that the Cabernet Sauvignon wine, as well as fractions with the highest monomeric anthocyanin content, were the most active, suggesting that these compounds largely contribute to the antimicrobial effects associated with wine components.[34]

The high phenolic content of grape pomace is due to the fact that some of these bioactive compounds are poorly extracted into the wine during the vinification process. Environmental factors, such as climate and soil, and grape variety also influence the composition of the pomaces.[35]

These results indicate that studies on bioactivities of grape pomace, skins, and seeds need to take into account composi-

tional differences among the test substances. For example, juicemaking pomace from Cabernet Sauvignon wine is a better source of anthocyanins for use in functional foods than winemaking pomace.[36,37]

Grape Seeds. Grape seed extracts derived from whole grape seeds are a rich source of bioactive flavonoids such as resveratrol, oligomeric procyanidins, and linoleic acid. Microencapsulation has the potential to reduce the astringency and bitterness of grape seed extracts for use as a functional food.[38] An HPLC analysis of fatfree grape seeds extracted with acetone/water/acetic acid (90:9.5:0.5) showed the following contribution of nine procyanidins to the total (in %): monomers, 48; dimers, 16.5; trimers, 10.8; tetramers, 8.1; pentamers, 5.3; hexamers, 3.2; heptamers, 2.7; octamers, 3.0; and nonamers, 1.5.[39,40]

Analysis by HPLC and LC-DAD/ESI-MS revealed the presence of the following classes of bioactive compounds in the seeds from pomace: (a) phenolic acids—caffeic, gallic, protocatechuic, 4-hydroxybenzoic, and syringic; (b) flavonoids—(+)-catechin, catechin dimer, (−)-epicatechin, epicatechin gallate trimer, procyanidin B1, procyanidin B2, quercetin-3-*O*-rhamnoside, *trans*-polydatin, and *trans*-resveratrol; and (c) total phenolic content of 327.6 gallic acid equivalents (GAE)/g extract.[41] A related study reported a total phenolic content of 628 mg GAE/g in grape seed extracts originating from Turkey.[20]

Analysis of grape seeds and pomaces derived from six French grape varieties showed that the highest total phenolic content of 44.5 GAE/g dry wt was present in Alicante seeds compared with 31.6 GAE/g dry wt for pomace.[42] Additional studies showed pomaces also contained significant amounts of proanthocyanidins and anthocyanin glycosides and that seeds had the highest antioxidant capacity. Related studies found that (a) the percentage of prodelphinidins in the seed and skin extracts of two Croatian grape cultivars was negatively correlated with the bitterness (astringency) intensity of the skins[43] and (b) a grape seed proanthocyanidin extract improved the psychological and physical symptoms and reduced blood pressure in middle-aged menopausal women.[44]

Grapevine Stems and Leaves. The following selected results indicate that grape stems and leaves are additional sources of bioactive phenolic compounds. Püssa et al.[45] reported that grapevine *Vitis vinifera* stems contained *trans*-resveratrol and derivatives, flavan-3-ols, and phenolic acid glucosides. A factorial design and response surface method used to assess the extractability of phenolic compounds from the stems of three grape varieties followed by GC-MS analysis showed the presence of the following compounds: caffeic acid, flavanols, and derivatives, dehydroflavanols, and flavonols.[46] An evaluation of byproducts from 10 different grape varieties showed that stems from Callet, Syrah, Premsal Blanc, Parellada, and Mano Negro varieties contained the highest total phenolic and total proanthocyanidin content and showed the greatest antioxidant capacity; that Chardonnay and Merlot stems showed the lowest values; that no significant differences were apparent among stems from red or white varieties; and that the stems from the Callet variety are an especially rich source of polyphenols.[47] Results from a study on copigmentation effects of pomace, skins, seeds, and stem extracts suggest the possibility of reusing the byproducts to improve the biological value and color properties of red wines.[48] Grape stem extracts inhibited the growth of breast, colon, renal, and thyroid cancer cells,[49] suggesting that stem phenolics might also inhibit microbial cells.

Grapevine *V. vinifera* leaves contained flavonols, flavones, and stilbenes.[50] Flavonols slow the infection of grapevine leaves by *Plasmopara viticola* phytopathogens.[51] The total phenolic content of leaves from organically and conventionally grown *Vitis labrusca* plants was similar, but the organic leaves contained 10 times more resveratrol than did the conventional leaves.[52] Whether grapevine leaves can serve as an inexpensive source of bioactive phenolic compounds merits study.

SENSORY PROPERTIES OF WINES IN RELATION TO COMPOSITION

Because sensory properties of wines affect consumption and bioactivity, we present here summaries of selected studies on the relationship between composition and sensory properties such as astringency, bitterness, bouquet, color, flavor, and taste.[53−57]

An investigation of the sensory, olfactory, and hedonic properties of Italian wines showed that Italian students liked about equally wines prepared from grapes grown organically and conventionally and that 61% of respondents were willing to pay more for organically produced wines.[58] A study designed to define the relationship between phenolic composition and color of wines produced by 55 different grape samples found that the average ratios between wine and grape phenolics ranged from 0.25 and 7.9 for the different phenolic compounds, that individual wine phenolics correlated with several wine phenolics, and that there was a high correlation between predicted and measured total wine color ($r = 0.958$), suggesting that it is possible to predict the color and quality of fresh wines from grape measurements.[59] Ethyl phenylacetate, phenylacetic acid, and γ-decalactone were found to be key aroma compounds in sour rotten wines at levels above those found in controls, suggesting that rot infection affects sensory properties of Portuguese wines.[60,61] Measurements of the phenolic composition of grapes and wines from two maturity stages and two maturation times showed that (a) grape anthocyanin increased during ripening, (b) procyanidin content of wine decreased with extraction and maceration time, (c) wine made from riper grapes contained higher tannin levels, and (d) the color of the French wines was related to the content of anthocyanins and anthocyanin−tannin adducts, suggesting that sensory quality is linked to grape quality at harvest.[62,63] Storage of sweet red wines in the bottle for a year caused degradation of monomeric anthocyanins, with most of them being lost between 6 and 9 months, the appearance of stable oligomeric and polymeric pyranoanthocyanin and methylmethine-mediated condensation products, hydrolysis of glycosylated flavonols to aglycones, and retention of antioxidative and sensory properties.[55] By contrast, increasing storage temperature seems to reduce the antioxidative properties of California wines, especially Cabernet Sauvignon and other Chardonnay varieties.[64,65] Analysis of 67 red French wines showed that 3-methyl-2,4-nonadione is a good marker for defining quantitative changes in the oxidative potential.[66]

Related recent studies on the relationship between composition and sensory properties include (a) analytical characterization of red wines by aroma wheels;[67,68] (b) apparent relationships between starter cultures, sensory and chemical attributes, and consumer acceptance of South African wines;[67,68] (c) changes in composition and organoleptic properties of wines stored in wooden barrels;[43,69] (d) the

sensory quality of Cabernet wines related to grape quality at harvest and to anthocyanin, proanthocyanidins, and grape volatiles;[54,63,70,71] and (e) the greater impact of large-sized, water-soluble tannins on wine astringency and bitterness of Cabernet Sauvignon wines relative to smaller-sized hydrophobic, highly pigmented tannins.[72,73] Additional studies on sensory aspects include those by Vidal et al.,[74] Malherbe et al.,[75] Bindon et al.,[53] Schmidtke et al.,[76] Villamor and Ross,[77] and Ugliano.[78]

The cited studies suggest that grape composition, wine-making practices, and storage conditions significantly affect sensory and presumably health-promoting properties of wines. It is not known to what extent, if any, these complex relationships might also affect antimicrobial properties.

BIOMARKERS OF BIOACTIVITIES

Here, we will briefly highlight some of the biomarkers that have been reported to be related to the beneficial effects of wine compounds at the molecular and cellular levels that might be related to bioactivities of wines and wine compounds.

Immunomodulating and Anti-inflammatory Properties. Italian red wine induced the release of nitric oxide and both anti-inflammatory and pro-inflammatory cytokines in healthy human blood mononuclear cells, leading to the maintenance of the immune host; removal of the polyphenols from red wine abrogated these effects.[79] Exposure of macrophages stimulated by bacterial lipopolysaccharide to malvidin, the most abundant polyphenolic compound in red wine, induced a series of cellular and signaling events that protect cells against inflammation-mediated chronic diseases, suggesting that malvidin significantly contributes to the anti-inflammatory and antioxidant effects of red wine.[80,81] A human study with 67 high cardiovascular risk male volunteers found that the phenolic content of red wines may modulate leukocyte adhesion molecules and that ethanol polyphenols of red wine may modulate soluble inflammatory mediators in high-risk patients, suggesting that both ethanol and non-alcoholic compounds contribute to the anti-inflammatory effects.[82] On the basis of a review of the literature on the anti-inflammatory properties of flavonoids from different sources in humans, Peluso et al.[83] suggest the need for placebo-controlled trials to identify bioactive flavonoids in the anti-inflammatory effect of plant foods, including wines.

On the basis of the mechanism that seems to govern the anti-inflammatory action of a red wine extract, Nunes et al.[84] suggest that the wine extract may represent a simple and inexpensive therapeutic strategy against intestinal inflammation. This suggestion is supported by the observation that a grape seed extract enhances the chemotherapy of colon cancer in rats by the drug 5-fluorouracil by decreasing the severity of inflammation-related mucositis of the cancer cells.[85] Because macrophage cells associated with the immune system seem to have a strong affinity for pathogenic bacteria, and natural compounds protected mice against lethal effects of *Salmonella* via immunostimulation,[86−89] expectations are that wine flavonoids might exhibit similar in vivo antibiotic effects.

Antioxidative Properties. As illustrated by the following selected recent studies, the antioxidative properties of wine compounds seem to be paramount in neutralizing adverse effects of reactive oxygen species (ROS, free radicals) that induce oxidative stress in tissues that contributes to the cause of chronic diseases. Free radicals are highly reactive, short-lived molecules that can react with and damage essential structural proteins, enzymes, and DNA. Such damage has the potential to cause cancer, atherosclerosis, and cardiovascular and other diseases. Wine flavonoids have the potential to reduce such undesirable molecular events because the high-energy, highly reactive free electron on DNA is transformed to a less reactive and thus less damaging radical. Wine antioxidants inhibit the activation of the oxidative stress-related transcription nuclear factor κB (NF-κB) that participates in the regulation of inflammatory responses.[90]

A study of the effect of acute and chronic consumption by 19 obese men of red wine or dealcoholized red wine showed that consumption of moderate, but not high, amounts of red wine acutely increased plasma total antioxidant capacity (TEAC) and suppressed NF-κB activation, whereas chronic red wine, but not dealcoholized red wine, consumption increased oxidative lipid damage.[91] Romanian scientists found that mathematical modeling of red wines from different grape varieties showed that 57% of the observed variance in antioxidant capacity is linearly related to the age of the wines[92] and that neural networks can be used to predict antioxidant activities and classification of wines.[93] A Canadian study found that red wine intake by 12 healthy human volunteers induced a marked increase in salivary radical-scavenging activity within 30 min followed by a plateau up to 240 min, suggesting that the wine greatly improved the salivary antioxidant status.[94] An Australian study found that warmer climate wines had lower in vitro antioxidant capacity values but retained good ex vivo bioavailability compared to cool climate wines, suggesting the need for further studies of the effect of soil composition on the polyphenolic content.[95] A Slovakian in vitro interaction study of three red wine polyphenols and their mixtures found that the antioxidant activity of individual polyphenols is not a constant value in the presence of other polyphenols, suggesting that the antioxidant quality of individual polyphenols differs markedly when tested separately and in mixtures, presumably because interactions can cause additive, antagonistic, and synergistic effects.[96] The authors suggest the need for in vivo studies, where interactions among compounds always take place in a mixture. It is also worth noting that wine antioxidative properties seem to be influenced differently by each polyphenolic compound[97] and that the antioxidant potential of GSEs is 20- and 50-fold greater than those of vitamins C and E.[98] We do not know whether antioxidative properties of wine flavonoids correlate with antibiotic effects.

POSSIBLE ADVERSE EFFECTS OF WINES

To balance the largely beneficial properties of wines, here, we briefly mention some possible adverse effects of wine components.

Alcohol. Moderate consumption (one or two glasses per day) of red wines with an alcohol content of 12−13% has been associated with numerous health benefits mentioned earlier. Both alcohol and polyphenolic compounds of wine seem to contribute to these beneficial effects. To what extent, if any, excess consumption of wine might adversely affect human health merits study.

Biogenic Amines. Wine contains a class of compounds called biogenic amines naturally present in grapes and/or produced by amino acid transaminase induced transamination of aldehydes by decarboxylation of amino acids by microbial enzymes. Because the biogenic amines are reported to cause various symptoms in susceptible humans associated with allergic reaction,[99−101] there is an interest in their content in

different wine varieties. For example, the analysis of 67 Italian wines showed that red wines contained 19.3 mg/L total biogenic amines, rose wines, 9.2 mg/L, and white wines, 7.67 mg/L, with histamine, tyramine, and cadaverine as the most representative amines.[102]

Catecholamines. Bioactive compounds from wines and other foods can occasionally inhibit cytosolic sulfotransferases (SULTs) that catalyze the sulfonation (metabolism) of catecholamines (dopamine, epinephrine), resulting in increased plasma levels of these bioactive compounds that can trigger migraine headache, increased blood pressure, and atrial fibrillation.[103]

D-Amino Acids. Low levels of D-amino acids (D-Ala, D-Glu, and D-Lys) are produced by *Saccharomyces cerevisiae* and *Oenococcus oeni* during fermentation of wine.[104] Another study[105] found that the concentrations of D-amino amino acids relative to the corresponding L-enantiomers ranged for white wines from 0.4 to 3.9% D-Ala, from 0.9 to 8.3% D-Asx, and from 0.5 to 8.9% D-Glx; in red wines, from 2.9 to 10.6% D-Ala, from 2.2 to 10.9% D-Asx, and from 3.9 to 7.4% D-Glx. Storage times of bottled wines up to 24 years did not correlate with D-amino acid content. Studies on the nutrition and safety of D-amino acids reported that D-Lys is not bioavailable as a source of L-Lys and that certain D-amino amino acids inhibited the growth of mice.[106,107]

Homocysteine. Analysis of 32 different wines showed that the average homocysteine content, an amino acid that is linked to cardiovascular disease[106,108] and to macular edema and neuropathy in patients with type 2 diabetes,[109] was 10.31 and 6.11 μM and in red and white wines, respectively.[110]

Ochratoxin A. The possible human carcinogen ochratoxin A produced by *Aspergillus* and *Penicillium* fungal species[111] was found to be present in about 50% of all evaluated wines at levels that are generally lower than the European Union (EU) regulatory level of 2 μg/L.[112−117]

Sulfites. Sulfites added to wines as antimicrobial preservatives to extend shelf life may aggravate symptoms of allergic asthma.[8,118,119] Wine labels suggest that susceptible individuals need to be aware of the possible adverse effects of wines.

With the above brief overview of wine composition, sensory properties, bioactivities, and possible adverse effects as background, reported studies on the antimicrobial, antiviral, and antifungal potential of wines and wine byproducts, in culture, in vivo, and on/in food will now be described.

■ ANTIBACTERIAL PROPERTIES

Wines. This section presents brief overviews of reported studies on the growth inhibition of bacteria that can cause human illness. The individual pathogens are listed alphabetically followed by studies that cover multiple pathogens. General comments concerning pathogenicity are based on information listed in a book on foodborne pathogens[120] and in *The Merck Manual of Diagnosis and Therapy*.[121]

Bacillus cereus. This foodborne pathogen causes vomiting and diarrhea. A study on wine-induced inactivation of *B. cereus* found that (a) wine inactivated *B. cereus* cultures to undetectable levels in <10 s, (b) wine diluted with water was less effective, (c) *B. cereus* spores were highly resistant to inactivation, (d) wine organic acids strongly inhibited vegetative cells, (e) wine phenolic compounds were inactive, and (f) the addition of wine to a simulated intestine resulted in a reduction of the total number of vegetative cells and spores.[122] It can be suggested that these results show that drinking wine with a meal or consumption as a marinade might reduce the viable *B. cereus* organisms, thus lowering the toxic potential of this pathogen. A related study reported that tea catechins and theaflavins and whole teas exhibited exceptionally high activity against *B. cereus*.[123]

Campylobacter jejuni. This pathogen causes the gastrointestinal infection in humans called campylobacteriosis. A kinetic study on the inactivation of *C. jejuni* showed that (a) a Portuguese red wine rapidly inactivated the foodborne pathogen within 30 s, (b) ethanol and organic acid (malic, tartaric) wine fractions acted synergistically with an efficacy similar to that of wine itself, and (c) wine enhanced the anti-*Campylobacter* effect of a food- and gastric fluid-containing model stomach, suggesting that concurrent ingestion of wine with food might help prevent campylobacteriosis.[124] Related studies reported that *C. jejuni* was about 100 times more susceptible to inhibition by plant essential oils, oil compounds, and phenolic acids than three other foodborne pathogens.[125,126]

Listeria innocua. A study of the bactericidal effect of nonpathogenic *L. innocua* as a substitute for the pathogenic *L. monocytogenes* in a food matrix in a stomach model under simulated acid gastric conditions found that (a) red wine induced a 3−4 log CFU reduction of the initial pathogen count in <2 h, (b) the combination of ethanol and malic and tartaric acids was less effective than wine, and (c) the kinetics of the bactericidal effect of white wine differed from that of red wine, showing that the antimicrobial effects of wines depend on composition.[127] These results imply that ingestion of wine with food may reduce the *Listeria* level in the alimentary tract.

Pseudomonas savastanoi pv phaseolicola. This phytopathogen, the cause of halo bean blight, was inhibited by Hungarian red wines and, to a less extent, by white wines, with the inhibition directly related to the phenolic content of the wines.[128]

Wine Components. Wines are multicomponent solutions. Wine properties and components that have been reported to possess antimicrobial properties include acid pH (~3.00), alcohol (~12%), sulfur dioxide (sulfite), organic acids (caftaric, lactic), and numerous polyphenolic compounds. A factorial design study on the susceptibilities of *E. coli* O157:H7 and *S. aureus* to 20 min exposure to four of these factors[129] revealed the importance of pH, titratable acidity, and ethanol, but not total sulfur dioxide, in predicting inactivation, suggesting that lowering the pH would likely enhance the efficacy of the other parameters. The paramount role of phenolic compounds in inhibiting bacteria was not evaluated.

A study of the contribution of polyphenolic content, pH, ethanol content, and other components to the observed antimicrobial effects of Croatian wines against *E. coli* and *S. enterica* found the following order of activities: wine > phenol-stripped wine > dealcoholized wine > ethanol at low pH > low pH > ethanol, suggesting the antimicrobial efficacy of wine cannot be attributed to a specific component.[130] The average TPC of these wines (in mg GAE/L) was 3204; flavonoids, 2941; nonflavonoids, 262.6; catechins, 726.6. Anthocyanins were found at 239.7 mg M-3-G/L, and resveratrol was found at 2.00 mg/L.

A study of three Argentinean wine varieties found that (a) the TPC content of the Cabernet Sauvignon wine (2300 mg/L GAE) was lower than those of Malbec (2522 mg/L GAE) and Merlot (2704 mg/L GAE) varieties; (b) the relative antimicrobial activities against *E. coli* and *L. monocytogenes* in a meat model treated with 100 and 200 mg/L of isolated

phenolic compounds paralleled the phenolic content of the wines; and (c) the polyphenol effect was ethanol-independent, suggesting that phenolic content governs activity and the need to produce new wine varieties with high polyphenolic content.[131]

Wine Varieties. A study of the antimicrobial effects of three Argentinean wines with different phenolic contents against multiple organisms showed that *E. coli* was the most sensitive bacterium to Merlot wine and that clarified wines, prepared by exposure of red wines to charcoal to remove phenolic compounds, were inactive.[132]

A study of the composition and antioxidative and antimicrobial effect of six Serbian wines prepared from different grape varieties against nine different pathogenic bacteria showed that the contents of two wine flavonoids, quercetin and quercetin-3-glucoside, can be used as biochemical markers for antioxidative and antimicrobial bioactivities.[133]

An evaluation of Moroccan Cabernet Sauvignon, Merlot, and Syrah red wine fractions against four Gram-positive bacteria, nine Gram-negative bacteria, two yeasts, and four molds showed that the Cabernet Sauvignon wine, as well as fractions with the highest monomeric anthocyanin content, were the most active, suggesting that these compounds largely contribute to the antimicrobial effects associated with wine components.[34]

Winery Byproducts. An analytical and antimicrobial study of the polyphenolic profile of GSEs from seven red and seven white Croatian grape varieties showed that (a) the total phenols, flavonoids, catechins, flavanols, and individual polyphenols [(+)-catechin, (−)-epicatechin, epicatechin gallate, procyanidins B1 and B2, quercetin glucoside, resveratrol monomers, piceid, and astringin] was variety dependent; (b) the TPC (>70 mg/g DM) of red skins of red cultivars were much higher in phenolic content than the skins from white cultivars (>20 mg); (b) antioxidative properties were related to polyphenolic content; (c) the average content of highly bioactive *trans*-resveratrol of 0.29 mg/kg of fresh berry wt was lower than the corresponding value of 0.59 mg/kg of fresh berry wt in the extracts from the red varieties; (d) the corresponding values for *cis*-resveratrol were 0.30 and 0.80 mg/kg of fresh berry wt, respectively; (e) minimum inhibitory concentration (MIC) values against multiple organisms (Gram-positive *B. cereus* and *S. aureus* and Gram-negative *C. jejuni*, *E. coli*, and *Salmonella infantis*) ranged from 0.014 to 0.59 mg GAE/mL; and (f) MICs of white cultivars against *E. coli* and *Salmonella*, the most frequent causes of foodborne infections, were the lowest (highest activity).[134]

Resveratrol. Although present in small amounts in wine, resveratrol is probably the most widely studied flavonoid.[135−137] This phytoalexin phenolic compound is reported to inhibit the growth of microbial species (*S. aureus*, *Enterococcus faecalis*, and *Pseudomonas aeruginosa*) as well as several pathogenic fungal dermatophytes that cause skin infections,[138] to inhibit biofilm formation of *E. coli* O157:H7 and *P. aeruginosa*,[139,140] and *V. cholerae*,[141] to reduce the growth rates of numerous animal-associated bacteria in culture,[142] and to exhibit cytotoxicity against *T. vaginalis*, the cause of the sexually transmitted disease trichomoniasis.[143] It seems that resveratrol exhibits antimicrobial, antiparasitic, and anti-inflammatory properties that have the potential to benefit microbial food safety and human infections.

4-Hydroxytyrosol. We previously reported that this olive compound inhibited both the growth of foodborne pathogens and the biological activity of a bacterial toxin.[111,144,145] Because 30 Spanish red wines contained an average of 0.074 mg/L of 4-hydroxytyrosol,[146,147] the compound probably contributes to the antimicrobial properties of wines.

Gut Microbiota. A study of the effect of the consumption of Spanish Merlot red and dealcoholized red wines by 10 healthy volunteers for 4 weeks showed (a) a significantly increased number of native gut bacteria and (b) decreased blood pressure and cholesterol, triglyceride, and C-reactive plasma levels. The results of this in vivo study suggest that a moderate consumption of red wine can inhibit nonbeneficial bacteria from the human microbiota and stimulate the growth of probiotic bifidobacteria.[148] A related study found large interindividual differences in microbial metabolites in human feces following the consumption of red wine and dealcoholized red wine, suggesting differences in gut microbial composition among evaluated subjects.[149] These investigators also analyzed by HPLC the total and individual polyphenolic profile of the two wines. Dealcoholized red wine had the same composition of polyphenolic compounds as red wine, with respective TPC values of 733 and 798 GAE. Individual polyphenolic compounds consisted of six anthocyanins, three flavonols, four stilbenes, six flavan-3-ols, two hydroxybenzoic acids, four hydroxycinnamic acids, and tyrosol.

Wine Marinades. Here, we briefly describe the reported protection of wine marinades against adverse effects of foodborne pathogens and spoilage organisms on meat products.[150−156]

We developed a series of antimicrobial wine marinade recipes each consisting of red or white wine extracts of oregano leaves with added garlic juice and oregano oil, against *B. cereus*, *E. coli* O157:H7, *L. monocytogenes*, and *S. enterica*.[157] The results showed that (a) activities increased with incubation temperatures in the order 37 °C > 21 °C > 4 °C, (b) storage for up to 2 months did not affect activities against *Salmonella*, (c) combinations of antimicrobials in wine exhibited additive antimicrobial effects, and (d) polyphenolic compounds isolated by chromatography separation from red wine exhibited exceptional activity at nanogram levels against two strains of *B. cereus*. The cited beneficial effects seem to have stimulated interest in defining the efficacy of wine marinades against contaminated meat products outlined below.

The populations of *Carnobacterium maltaromaticum*, *L. monocytogenes*, *Brochothrix thermosphacta*, and *C. jejuni* bacteria were reduced by ∼1.5, 2, 3, and 6 log CFU, respectively, on contaminated pork meat submerged into Spanish red wine for 15 min followed by storage at 4 °C for 3 days.[151] Except for *C. maltaromaticum*, ultrasound treatment with red wine acted synergistically against the pathogens, suggesting that marinating can be used to enhance the taste, texture, and safety of pork meat counts (7 log CFU/mL) and low counts (3 logs CFU/mL) of *C. jejuni*. The bacteria were completely inactivated in both white and red wines. Immersion of poultry meat contaminated with this pathogen in both wine marinades was less effective in reducing the microbial levels.[152]

Immersion of contaminated beef fillets in Greek red wine or wine supplemented with 0.3% thyme oil for 12 h significantly reduced the levels of acid-adapted and -nonadapted *S. enterica* Typhimurium compared to nonmarinated control samples by 2.0 and 1.9 log CFU/g, respectively, during storage for 19 days at 5 °C.[155] The addition of thyme oil to the wine seems to increase the antimicrobial effect of marinades, suggesting the marinating can be used to extend the shelf life of meats.

Greek red wine with and without 0.5% oregano oil induced reduced levels of *S. enterica* and *L. monocytogenes* on contaminated beef pieces after storage at 5 °C for 18 h by 2.1 and 3.4 log CFU/cm^2.[156] Because the addition of oregano oil enhanced the antimicrobial activity and no changes in heat resistance were apparent during storage of the beef samples, wine marinating can enhance both safety and shelf life. Marinating with soy sauce or red wine marinades can control oxidation and microbial spoilage of raw beef, suggesting that marinating can extend the shelf life of meat.[158]

A wine-based marinade with added garlic powder or juice and a starter culture of *Lactobacillus sakei* induced loss of viability of *L. monocytogenes* and *Salmonella* spp. in a Portuguese dry sausage made from wine-marinated pork.[156] A related study optimized the drying conditions to protect the sausage against *Salmonella*, *Listeria*, and *S. aureus*.[159]

As described in detail elsewhere, there is a need to reduce both pathogens and heat-induced potentially carcinogenic heterocyclic amines in cooked meat products.[160,161] Wine marinades without and with added herbs used as meat flavoring (garlic, ginger, thyme, rosemary, and red chilli peppers) reduced the formation of heterocyclic amines in pan-fried beef.[162] Additional studies found no correlation between the marinade-induced antioxidant activities and individual or total heterocyclic amine formation.[162] Related studies on the reduction of amine formation by wine-fried chicken breast are described by Brusquest et al.[163] The concurrent reduction of both pathogens and heterocyclic amines by wine marinades with added herbs merits study.

Brannan found that 0.1% GSE inhibited the intensity of musty and rancid odor and rancid flavor, but caused color darkening, on ground chicken breast and thigh during refrigerated storage, suggesting that the seed extract may be an effective antioxidant in precooked chicken products.[164]

Grape Seed Extracts. This section presents brief overviews of reported studies on the inhibition of growth and/or destruction of pathogenic microorganisms by GSEs.

Brochothrix thermofacta. GSE incorporated into pea starch films with pork loins infected with the psychotrophic spoilage organism *B. thermofacta* reduced the bacterial growth on surface-inoculated pork loins by 1.3 log CFU/mL after 4 days of incubation at 4 °C.[20] Additional studies showed that GSE films also inhibited the growth of the following pathogens: *S. aureus*, *E. faecalis*, *E. faecium*, and *L. monocytogenes*. The authors suggest that biodegradable and edible GSE antimicrobial films have the potential to improve meat quality and extend shelf life.

Cronobacter sakazakii. *C. sakazakii* is a Gram-negative, anaerobic bacterium of the family Enterobacteriaceae reported to cause infection in adults and children, especially infants.[165] Freshly prepared red muscadine grape juices induced a 6 log reduction of *C. sakazakii* after a 2 h incubation at 37 °C, suggesting that red muscadine juice could inhibit the pathogen in baby food.[166]

Escherichia coli O157:H7. *E. coli* O157:H7 is a foodborne, toxin-producing enteropathogen responsible for hemorrhagic colitis, bloody diarrhea, and hemolytic uremic syndrome. Here, we will briefly review reported activities of grape-derived products against this organism.

A study on the effect of fresh and processed muscadine red grape juices against a 5 log cocktail of cells of *E. coli* O157:H7 incubated for 4 h at 37 °C showed that polar fractions containing malic, tartaric, and tannic acids showed strong antimicrobial activity and that synthetic tannic acid showed the highest activity.[167] These results indicate that muscadine juice can be used as an active antimicrobial ingredient against these pathogens in nonalcoholic beverages. A related study by the same investigators[168] found that water-soluble muscadine GSE prepared from the purple cultivar Ison and the bronze cultivar Carlos exhibited strong antimicrobial activity against a cocktail of three strains of *E. coli* O157:H7 and that heat treatment of both extracts increased antimicrobial activity, possibly because of increased acidity, tartaric acid, and individual and total phenolic content. These results suggest that water-soluble muscadine seed extracts could serve as natural preservatives in beverages.

Electrostatic spraying of GSE onto contaminated lettuce and spinach samples with GSE alone and in combination with lactic, malic, or tartaric acids reduced *E. coli* levels on spinach up to 4.0 log CFU/g and on spinach up 2.8 log CFU/g during the 14 day storage, suggesting that electrospraying technology could help lower risks due to pathogen contamination of fresh produce.[169]

Commercial grape seed and grape pomace extracts inhibited antitoxin properties of the Shiga toxins Stx1 and Stx2 produced by *E. coli* O157:H7 bacteria.[170] Because red and white wines and phenolic compounds isolated by chromatography from red wine exhibited strong antimicrobial activities against *E. coli* and other pathogens,[123] it would be of interest to find out whether the wine compounds can concurrently or consecutively inactivate the foodborne pathogens and the toxins produced by the pathogens. We previously reviewed the inactivation of food-related microbial, fungal, and plant toxins by natural compounds.[111,123,144]

Helicobacter pylori. *H. pylori*, a Gram-negative organism that has adapted to thrive in the acid conditions of the digestive tract, causes gastritis, peptic ulcers, and adenocarcinoma. To help overcome multidrug resistance, Brown et al.[171] evaluated the efficacy of muscadine grape skin and two polyphenolic constituents against *H. pylori*. They found that (a) grape skin and quercetin inhibited *H. pylori* infection in mice; (b) quercetin and resveratrol reduced the bacterial counts of the pathogen with MIC values of 256 and 128 μg/mL, respectively; (c) grape skin extracts were more effective than the two constituents; and (d) the inhibitions were dose dependent and pH independent.[172] The observed anti-*H. pylori* effects suggest that the extracts and components might be used in a diet-based approach for the prevention and/or treatment of *H. pylori* infection. A related study found that a comparison of the inhibition of *H. pylori* by grape seed, skin, and seed plus skin extracts of two grape varieties showed that the highest observed zone of inhibition was with the seed extracts, with MIC and minimum bactericidal concentration (BMC) values of 2048 μg/mL of the extracts of both varieties.[172,173]

Klebsiella pneumoniae. *K. pneumoniae* causes lung and urinary infections that occur mainly in hospital patients with diminished resistance. Because some isolates are resistant to medical antibiotics, there is a need for new antimicrobials to overcome infections associated with this pathogen. Ethanol extracts of grape seeds were found to be more effective in inhibiting *K. pneumoniae* than were grape skin extracts, suggesting a potential value for the seed extract against human infections.[174] These authors also found that the seed extract was also active against *E. faecalis* and *E. coli*.

Listeria monocytogenes. *L. monocytogenes* is a Gram-positive foodborne bacterial pathogen that causes human listeriosis, with symptoms ranging from headaches to

bacteremia, septicemia, encephalitis, and meningitis and a mortality rate of about 20−30%.[175] We now will record efforts to inactivate the pathogen with grape products.

Grape juice and skin extracts from black table grapes strongly inhibited multiple *L. monocytogenes* species but did not inhibit *B. cereus*, *Salmonella* Menston, *E. coli*, *S. aureus*, or *Y. enterocolitica* pathogens.[176] Fractionation of the extracts showed that the antilisterial activity was highest in the polymeric phenolic fractions, that activity of the red-pigmented fractions was pH dependent, and that the unpigmented polymeric phenolics from the seed showed pH-independent activity. The observed reduction was striking, from ∼log CFU7 to undetectable levels after 10 min. Evidently, both pigmented and unpigmented phenolic compounds from grapes were bioactive against *Listeria*, but apparently not against the other mentioned pathogens.

Chardonnay and black raspberry seed flour extracts at 165 and 160 μg seed flour equivalents/mL inhibited the growth of *L. monocytogenes* and *E. coli* with zero survival rates under the test conditions. These results and compositional and antioxidant activities suggest that the seed flours have the potential to serve as natural food preservatives for improving food stability, quality, and safety, and consumer acceptance.[177]

Dipping of surface-inoculated (log 6 CFU/g) turkey frankfurters into soy protein film-forming solutions without and with antimicrobials (1% GSE plus nisin, 10000 IU/mL) resulted in 2.8 log CFU reduction of *L. monocytogenes* after storage for 28 days at 4 or 10 °C, suggesting that the antilisterial activity of the combination was greater than that observed with the individual antimicrobials and that the use of antimicrobial films may enhance the microbial safety of meat products.[178] Because the combination of antimicrobials caused a much higher 9 log cycle reduction in culture, it seems that antimicrobial results in the absence of food do not predict the efficacy in a meat matrix.

Dipping contaminated turkey frankfurters with 1% GSE plus nisin (6400 IU/mL) reduced the *L. monocytogenes* population from ∼log 7 CFU/g to undetectable levels after storage at 4 or 10 °C for 21 days, suggesting that the combination can improve the antimicrobial efficacy against this pathogen in refrigerated ready-to-eat (RTE) meat and poultry storage.[179] A related study[180] found that soy protein edible films containing GSE, nisin, and EDTA were more effective in inhibiting the growth of *L. monocytogenes* (reduction of 2.9 log CFU/mL) than *E. coli* (1.8 log reduction) or *Salmonella* Typhimurium (0.6 log reduction), suggesting that the susceptibility of the pathogens to inhibition is not uniform.

Dipping turkey frankfurters contaminated with *L. monocytogenes*, *E. coli* O157:H7, or *Salmonella* Typhimurium (∼6 log CFU/g) into a whey protein isolate coating incorporated with GSE (0.5%) and nisin (6000 IU/g) followed by storage for 28 days at 4 °C reduced the bacterial population by 2.3, 4.6, and 1.0 log cycles, respectively, confirming that antimicrobial protein coatings can be used to inhibit foodborne pathogens in meat.[181]

Grape seed and stem extracts from the red Greek grape variety Mandilaria containing high concentrations of flavan-3-ols and derivatives represent a source of potent antilisterial compounds with low MIC values of 0.26−0.34. The extracts have the potential to serve as food additives to prevent the growth of *L. monocytogenes*.[182]

The addition of tartaric acid and grape seed and green tea extracts added to chicken marinades significantly reduced *L. monocytogenes* in vacuum-marinated irradiated chicken breast meat without affecting consumer acceptance of the product, suggesting that the combination of the plant formulations with levels of irradiation below the maximum allowed could contribute to the prevention of contamination by *Listeria*.[183]

Chitosan films impregnated with GSE inhibited *L. monocytogenes* as well as aerobic mesophiles and lactic acid bacteria on sausages during refrigerated storage, suggesting that the antimicrobial chitosan films could extend the shelf life of sausages.[184,185]

Maximum growth inhibition (∼2.0 log CFU/g) of *L. monocytogenes* was observed in chicken and turkey hot dogs treated with combinations of potassium lactate and sodium diacetate with green tea and grape seed extracts. The antilisterial effect was enhanced by heat treatment of the hot dogs, suggesting that the extracts can partially replace the chemical preservatives and enhance the antilisterial activities.[186]

Staphylococcus aureus. *S. aureus* is a Gram-positive, aerobic, toxin-producing foodborne pathogen that can also contaminate the skin, lung, heart, and other organs.

A total ethanol grape extract prepared by the percolation method of whole grapes inhibited *S. aureus*, suggesting that the extract represents a natural antibacterial for possible treatment of local skin infections.[187]

Pomace, seed, and skin extracts from New Zealand Pinot noir grapes were more effective against *S. aureus* bacteria than extracts from Pinot Meunier grapes, suggesting that extraction solvent, fraction, and grape variety significantly influence antimicrobial properties. A weak but significant relationship was observed between TPC and antimicrobial effects (r = 0.58).[17] A screening assay showed that bioactive polyphenols from pomace concentrated onto a protein-rich matrix inhibited the proliferation of *S. aureus* bacteria on the skin.[188]

Vibrio cholerae. *V. cholerae* produces a cholera toxin that causes watery diarrhea of cholera, an often fatal disease.[111] Two grape extracts sold as nutritional supplements inhibited the cholera toxin, as well as the heat-labile Shiga toxin produced by *E. coli* in cultured cells and intestinal loops by blocking toxin binding to the cell surface.[189,190] These results suggest that grape extracts could help ameliorate cholera in humans.

Vibrio vulnificus/Vibrio parahemolyticus. *V. vulnificus*, a Gram-negative foodborne bacterium present in estuarine environments where oysters are harvested, has a 40−50% fatality rate. Dipping of oysters contaminated with *V. vulnificus* in solutions of GSE (500 mg/mL), citric acid (300 mg/mL), or lactic acid (150 mg/mL) reduced the pathogens to levels lower than control samples during refrigerated storage for 20 days.[191]

The MIC value of *V. parahemolyticus* in artificially inoculated oysters dipped in GSE solutions was 10 mg/mL; a solution of 500 mg/mL of GSE reduced the population below detection level.[191]

Multiple Pathogens. An in vitro study showed that GSE was more effective in inhibiting Gram-positive bacteria (*S. aureus*, *L. innocua*, and *B. thermosphacta*) than Gram-negative ones (*E. coli*, *P. aeruginosa*, and *S. enterica*), suggesting that GSE can inhibit the most frequent causes of foodborne bacterial infections in developed countries.[174,192,193] A Turkish study found that GSEs completely inhibited Gram-positive (*B. cereus*, *B. coagulans*, *B. subtilis*, and *S. aureus*) and, less so, Gram-negative (*E. coli* and *P. aeruginosa*) bacteria.[194]

GSE with a high total phenolic content (628 mg GAE/g) inhibited the growth of the following spoilage and pathogenic bacteria: *Aeromonas hydrophila*, *Bacillus brevis*, *B. cereus*, *Bacillus*

megaterium, *Bacillus subtilis*, *Enterobacter aerogenes*, *E. faecalis*, *E. coli*, *K. pneumoniae*, *L. monocytogenes*, *Mycobacterium smegmatis*, *Proteus vulgaris*, *P. aeruginosa*, and *S. aureus*.[21,22] It seems that GSE with a high polyphenolic content can act as a broad-spectrum antibiotic in food contaminated with multiple pathogens.

Grape Pomace Extracts. Pomace extracts (5 and 10% concentration) from five Turkish grape varieties inhibited pathogenic (*S. aureus*, coliforms, Enterobacteriaceae, Enterococci, and *Salmonella*) as well as spoilage organisms (lactobacilli, lactococci, lipolytic bacteria, Micrococaceae, and proteolytic and psychotrophic bacteria) in beef patties, suggesting that the extracts could serve as antimicrobial agents that can prevent the deterioration of meat products.[32,195]

Pomaces from Pinot noir and Merlot Oregon grapes with TPC of 21.2−76.7 GAE/g DM, anthocyanin content of 0.35−0.76 mg Mal-3-glu/g DM, total flavonoid content (TFC) of 30.2−106.1 mg CE/g DM, and dietary fiber content of 57−63% of total dry matter (DM) showed higher activity against *L. innocua* than against *E. coli*.[196] The pomace extracts were more active against the bacteria than the skin extracts. All samples lost significant amounts of bioactive compounds during 16 weeks of storage, with freeze-dried samples retaining higher amounts of TPC than samples stored at ambient temperatures or 40 °C. The authors suggest that the two pomaces could be used as functional food ingredients that can promote human health.

An evaluation of the antimicrobial efficacy of grape pomace powder and pomace extracts from Turkish grape varieties showed that a 10% concentration of the powder completely inhibited *S. aureus* in vegetable soup at the end of 120 h and that this pathogen was more susceptible to inhibition than *E. coli*.[197] The same authors also analyzed the data by an adaptive neuro fuzzy inference system (ANFIS), an artificial neural network (ANN), and multiple linear regression (MLR) models to predict antibacterial effects of the two pathogens in the soup.

Supercritical fluid pomace extracts from Brazilian grapes were more effective against Gram-positive bacteria (*S. aureus* and *B. cereus*) than against Gram-negative ones (*P. aeruginosa* and *E. coli*).[41] Seed and skin extracts from grape winery byproducts of the Portuguese Arinto variety showed higher antimicrobial activity against five bacteria and yeast species (*E. coli*, *Salmonella* Poona, *B. cereus*, *S. cerevisiae*, and *C. albicans*) than did some of the individual components, suggesting that the extracts can both protect against the adverse effects of contaminated food and be used to prevent or treat animal and human infectious diseases.[198]

Pomace extract-based polysaccharide films induced ∼5 log reduction in bacterial activity against *E. coli* and up to a 3.0 log reduction against *L. innocua* on a Petri dish at the end of a 24 h test compared to the control, suggesting the need to evaluate the films for applicability to contaminated food.[20,199]

We evaluated the relative bactericidal activities of 10 presumed health-promoting food-based powders (neutraceuticals) and, for comparison, selected known components against the following foodborne pathogens: *E. coli* O157:H7, *S. enterica*, *L. monocytogenes*, and *S. aureus*.[144] The relative activities were evaluated using quantitative bactericidal activity (BA_{50} value, defined as the percentage of the sample in the assay mixture that resulted in a 50% decrease in colony-forming units). The BA_{50} values were determined by fitting the data to a sigmoidal curve by regression analysis using concentration−antimicrobial response data. Antimicrobial activity is indicated by a low BA_{50} value, meaning less material is needed to kill 50% of the bacteria. Olive pomace, olive juice powder, and oregano leaves were active against all four pathogens, suggesting that they behave as broad-spectrum antimicrobials. All powders exhibited strong antimicrobial activity against *S. aureus*. The following powders showed exceptionally high activity against *S. aureus* (as indicated by the low BA_{50} values shown in parentheses): apple skin extract (0.002%); olive pomace (0.008%); and GSE (0.016%). *Listeria* bacteria were also highly susceptible to apple skin extract (0.007%). The most active substances provide candidates for the evaluation of antimicrobial effectiveness in human foods and animal feeds.

■ ORAL PATHOGENIC BACTERIA

Several studies describe anticariogenic/cariostatic effects of grape products. These include the following observations. Phenolic extracts with highly variable anthocyanin and flavan-3-ol contents prepared from several red wine grape varieties and their fermented byproduct of winemaking (pomace) were highly effective against virulence traits of the dental pathogen *Streptococcus mutans*, suggesting their potential value against dental disease.[200−204] A study on bacterial adherence to enamel in the oral cavity of six human subjects revealed that rinses with red wine and teas induced up to a 66% reduction of adherent bacteria compared to controls, suggesting that these beverages might contribute to the prevention of biofilm-induced diseases in the oral cavity.[205]

A red wine GSE reduced plaque area on bovine teeth in an artificial mouth by 40% compared to the control. This value was, however, lower than corresponding reductions of 84.0 and 87.5%, respectively, observed with *Salvia officinalis* and *Rosmarinus officinalis* plant extracts.[206] An evaluation of the antibacterial activities of wine phenolic compounds and GSEs against potential respiratory pathogens present in the oral cavity that contribute to the formation of dental plaque showed that (a) gallic acid and ethyl gallate had the highest activity, (b) two commercial GSEs were more active than the phenolic compounds, and (c) Gram-positive bacteria (*E. faecalis*, *S. aureus*, and *Streptococcus pneumoniae*) were more susceptible to inactivation than Gram-negative bacteria (*Moraxella catarrhalis* and *P. aerations*).[207] Red wine alone and with added GSE inhibited oral microbiota in a five-species biofilm model of supragingival plaque.[208] These observations suggest the need to evaluate the germ-killing efficacy of wine compounds in oral rinses and chewing gums.

■ ANTIVIRAL ACTIVITIES

Viral contamination of food and infection of animals and humans is a major cause of numerous diseases. The mechanism of antiviral action of plant polyphenolic compounds is based on their abilities to act as antioxidants, to inhibit essential enzymes, to disrupt cell membranes, to prevent viral binding and penetration into cells, and to trigger the host cell self-defense mechanism.[209] Here, we present a brief overview of reported studies on the antiviral activities of grape products against pathogenic viruses.

Adenovirus. A polyphenol-based grape extract from Portuguese white-winemaking byproducts and resveratrol reduced adenovirus-5 production by 4.5 and 6.5 log ($TCID_{50}$/mL). In contrast to resveratrol, the extract irreversibly inhibited the replication of the adenovirus, suggesting its potential value as an antiviral agent.[210]

Cytomegalovirus. The wine polyphenolic compound resveratrol reduced human cytomegalovirus DNA replication to undetectable levels by blockage of epidermal growth factor receptor activation in human embryonic fibroblasts.[211]

Hepatitis Viruses and Virus Surrogates. A study of the effect of commercial GSE on human enteric virus surrogates and hepatitis A virus evaluated the infectivity of the virus exposed to GSE concentrations of 0.5, 1, and 2 mg/mL for 2 h at room temperature or 37 °C.[212,213] At high titer (~log 7 PFU/mL), the infectivity was reduced by up to 4.61 log PFU in a dose-dependent manner, suggesting that GSE has the potential to be used by the food industry as an inexpensive novel natural broad-spectrum antiviral alternative to reduce viral contamination and enhance food safety and quality.

Noroviruses. The foodborne norovirus causes gastroenteritis and diarrhea in humans. An examination of the effect of GSE against the human norovirus by a plaque and other bioassays for murine norovirus found that GSE at 0.2 and 2 mg/mL reduced the infectivity by >3 log PFU/mL of the murine virus and the binding of the human norovirus to salivary human histo-blood group antigen receptors.[213−215] The observed 1.5−2 log PFU/mL reduction in the murine virus titer following addition of 2 mg of GSE/mL to sanitized water in the washing bath of fresh-cut lettuce suggests the potential value of the treatment to reduce the viral burden of leafy greens. The mechanism of the antiviral effect seems to involve denaturation of the viral capsid protein.

GSE was also effective against these viruses on contaminated produce.[215] Thus, treatment of lettuce and jalapeno peppers (25−30 g) inoculated with human norovirus surrogates (feline calicivirus and murine norovirus) or hepatitis A virus with 0.25, 0.5, 1 mg/mL GSE or water for 30 s−5 min reduced the viral counts from ~7 log PFU/mL to 2.33, 2.58, and 2.71 log PFU on lettuce and to 2.20, 2.74, and 3.05 log PFU on peppers after 1 min at all three concentrations, respectively. The authors suggest that GSE should be considered for use as part of hurdle approaches that combine GSE with other antiviral treatments for foodborne virus reduction on produce.

Rotaviruses. Exposure of rotaviruses, the most common cause of severe diarrhea in children, to grape and cranberry juices and proanthocyanidins resulted in a loss of viral infectivity after 5 min via blockage of viral antigenic determinants caused by modification of viral integrity at physiological pH, suggesting that the fruit juices may help protect against viral-induced diarrheas.[216,217] A related study by Ko et al.[218] reported that an orally administered alcohol-free Cabernet Sauvignon red wine extract inhibited diarrhea in a neonatal mouse model of rotaviral infection, but did not prevent watery stools in the mice administered cholera toxin.[219,220]

Nair et al.[221] found that the flavonoid constituents of GSE seem to exert antiviral effects by inducing Th1-derived cytokine γ-interferon (IFN-γ) by peripheral mononuclear cells, suggesting that the beneficial immunostimulatory effect of GSE may be mediated through induction of IFN-γ.[222]

ANTIFUNGAL EFFECTS

***Botrytis cinerea* and Other Phytopathogens.** GPE fractions extracted with methanol or ethanol from a mixture of Chilean grape varieties exhibited in vitro antifungal activity against the phytopathogenic fungus *B. cinerea* that damages grapevines, resulting in extensive economic losses, suggesting that the pomace can provide a low-cost fungicide to help overcome this problem. Related studies reported that pomaces from other grape varieties inhibited the growth of *Zygosaccharomyces rouxii* and *Zygosaccharomyces bailii*[32,195] and that GPE from three Chilean grape varieties showed a large inhibitory effect on mycelia growth of *B. cinerea* with an IC_{50} value of 50 ppm.[30,35]

***Candida albicans* and Other Human Fungal Pathogens.** GPE from Brazilian Merlot grapes exhibited moderate activity against three fungal species (*C. albicans*, *Candida krusei*, and *Candida parapsilosis*), with MIC values ranging from 500 to 1000 μg/mL.[41] GSE acted synergistically with the medicinal antibiotic amphotericin B against *C. albicans*, the most common cause of fungal disease in humans, suggesting that the combination with 75% less antibiotic merits use in human fungal infections.[223−225] The authors suggest that synergism of natural compounds such as GSE with medicinal antibiotics has the potential to benefit the fight against human infectious diseases. Phenolic red and white wine extracts also inhibit *C. albicans*.[226]

MISCELLANEOUS ASPECTS

Anticoccidiosis Activity. GSE from grapes and other plant extracts significantly decreased adverse effects in broiler chickens infected with the parasitic organisms (*E. tenella*, *E. maxima*, and *E. acervulina*) that cause coccidiosis, a poultry disease that results in large economic losses.[227,228] The protection involved decreased mortality and improved feed conversion ratio (FCR), suggesting that antioxidant-containing plant extracts may be of benefit in the management of coccidiosis. A related study reported that a 0.1% GSE inhibited the intensity of musty and rancid odor and rancid flavor in chicken breast compared with control patties, suggesting that the extract may be an effective antioxidant in precooked chicken breast.[164,229]

Caenorhabditis elegans. Pomace flavanols and flavonols (122.75 and 23.11 mg/100 g dry pomace) from Zalema grapes seem to be responsible for the increased survival of *C. elegans* worms exposed to thermally induced oxidative stress.[230]

RESEARCH NEEDS AND OUTLOOK

In addition to the research needs mentioned earlier, future studies need to address the following food and medical aspects of the properties of wines and wine flavonoids. In this context the term "flavonoid" represents wines, grape pomace, seed, and skin extracts and their flavonoids.

- Determine whether the antibiotic activities of flavonoids and wines in vitro can be duplicated in vivo, especially in humans.
- Determine the relationship between wine consumption and lower risk of infection in humans. Will frequent consumption of red wine or flavonoids protect against infection and/or ameliorate the severity of infectious disease in humans?
- Determine how bioactivities of flavonoids vary, depending on whether they are tested or consumed in the free state or as part of a mixture or a food.
- Determine whether flavonoid metabolites formed after absorption into the circulation by animals and humans possess antimicrobial properties.
- Define additive or synergistic effects of mixtures of wine flavonoids with other plant antimicrobials, including plant essential oils, apple, and olive compounds, and

seashell-derived chitosans. Combinations of food ingredients that act synergistically will lessen amounts needed to design effective antimicrobial food formulations. They will be safer and affect flavor and taste less than individual compounds.

- Evaluate the effectiveness of wines and flavonoids against antibiotic resistant foodborne and medical pathogens, a largely unexplored area.[231−234]
- Determine whether flavonoids can additively or synergistically enhance antibiotic properties of medicinal antibiotics.
- Determine whether wine flavonoids can protect against bacterial infection through stimulation of the immune system.[88,89,235]
- Determine antibacterial, antiviral, antifungal, and antitoxin efficacies of wines and flavonoids in various contaminated foods including leafy greens, fruits and fruit juices, vegetables, dairy, meat, poultry, and seafood products.
- Develop methods to simultaneously reduce both pathogens and carcinogenic heterocyclic amine levels in processed meat products.
- Develop flavonoid-containing edible antimicrobial films and coatings to protect food against contamination by pathogens.
- Determine whether flavonoids can prevent biofilm formation by bacteria on contaminated food.
- Determine whether the flavonoid content of wines and byproducts can predict antibiotic activities.
- Determine whether molecular modeling of flavonoid structure−cell membrane interactions can be used to explain the antibiotic mechanisms of structurally different flavonoids.[236−238]
- Encourage growers to produce grapes with a high content of bioactive compounds.

In summary, because grape phenolic phytonutrients are considered to be generally accepted as safe, the cited and proposed studies will provide numerous benefits. The most active compounds could be used to protect liquid and solid foods against contamination by pathogenic and spoilage microorganisms and microbial toxins as well as therapeutically to treat animal and human infections. The grape pomace, seed, and skin extracts have the potential to provide inexpensive sources of compounds for use against a broad range of diseases. These byproducts will also provide a source of income to grape growers and wine producers. Growers will be encouraged to produce grapes with high levels of bioactive compounds.

AUTHOR INFORMATION

Corresponding Author

*E-mail: Mendel.Fridman@ars.usda.gov.

Notes

The authors declare no competing financial interest.

ACKNOWLEDGMENTS

I am most grateful to Carol E. Levin for assistance with the preparation of the manuscript, to colleagues for excellent scientific collaboration, and to journal reviewers for constructive comments.

ABBREVIATIONS USED

ANFIS, adaptive neuro fuzzy inference system; ANN, artificial neural network; BA_{50}, percent of sample that resulted in a 50% decrease in CFU; CE, catechin equivalents; CFU, colony-forming units; DAD, diode array detector; DM, dry matter; FCR, feed conversion ratio; IC_{50}, analogous to BA_{50}; GAE, gallic acid equivalent; GPE, grape pomace extract; GRAS, generally accepted as safe; GSE, grape seed extract; GSH, reduced glutathione; MIC, minimum inhibitory concentration; MLR, multiple linear regression; IFN-γ, γ-interferon; ROS, reactive oxygen species; SULTs, cytostolic sulfotransfrases; RTE, ready-to-eat; $TCID_{50}$, tissue concentration infectious dose 50%; TEAC, trolox equivalent antioxidant capacity; TFC, total flavonoid content; Th1, type 1 helper T cells; TPC, total phenolic content

REFERENCES

(1) FAO. FAOSTAT, http//faostat.fao (accessed March 10, 2014).
(2) Patil, V. K.; Chakrawar, V. R.; Narwadkar, P. R.; Shinde, G. S. Grape. In *Handbook of Fruit Science and Technology: Production, Composition, Storage, and Processing*; Salunkhe, D. K., Kadam, S. S., Eds.; Dekker: New York, 1996; pp 7−38.
(3) Moreno-Arribas, M. V.; Polo, M. C. Winemaking biochemistry and microbiology: current knowledge and future trends. *Crit. Rev. Food Sci. Nutr.* **2005**, *45*, 265−286.
(4) Cheynier, V. Flavonoids in wine. In *Flavonoids: Chemistry, Biochemistry, and Applications*; Andersen, Ø. M., Markham, K. R., Eds.; CRC Press: Boca Raton, FL, USA, 2006; pp 263−318.
(5) Cheynier, V. Phenolic compounds: from plants to foods. *Phytochem. Rev.* **2012**, *11*, 153−177.
(6) Cheynier, V.; Comte, G.; Davies, K. M.; Lattanzio, V.; Martens, S. Plant phenolics: recent advances on their biosynthesis, genetics, and ecophysiology. *Plant Physiol. Biochem.* **2013**, *72*, 1−20.
(7) Goldberg, D. M.; Soleas, G. J. Wine and health: a paradigm for alcohol and antioxidants. *J. Med. Biochem.* **2011**, *30*, 93−102.
(8) Pozo-Bayón, M. Á.; Monagas, M.; Bartolomé, B.; Moreno-Arribas, M. V. Wine features related to safety and consumer health: an integrated perspective. *Crit. Rev. Food Sci. Nutr.* **2012**, *52*, 31−54.
(9) Guilford, J. M.; Pezzuto, J. M. Wine and health: a review. *Am. J. Enol. Vitic.* **2011**, *62*, 471−486.
(10) Catalgol, B.; Batirel, S.; Taga, Y.; Ozer, N. K. Resveratrol: French paradox revisited. *Front. Pharmacol.* **2012**, *3*, 141.
(11) Zamora-Ros, R.; Knaze, V.; Luján-Barroso, L.; Romieu, I.; Scalbert, A.; Slimani, N.; Hjartåker, A.; Engeset, D.; Skeie, G.; Overvad, K.; Bredsdorff, L.; Tjonneland, A.; Halkjær, J.; Key, T. J.; Khaw, K.-T.; Mulligan, A. A.; Winkvist, A.; Johansson, I.; Bas Bueno-De-Mesquita, H.; Peeters, P. H. M.; Wallström, P.; Ericson, U.; Pala, V.; De Magistris, M. S.; Polidoro, S.; Tumino, R.; Trichopoulou, A.; Dilis, V.; Katsoulis, M.; María Huerta, J.; Martínez, V.; Sánchez, M.-J.; Ardanaz, E.; Amiano, P.; Teucher, B.; Grote, V.; Bendinelli, B.; Boeing, H.; Förster, J.; Touillaud, M.; Perquier, F.; Fagherazzi, G.; Gallo, V.; Riboli, E.; González, C. A. Differences in dietary intakes, food sources and determinants of total flavonoids between Mediterranean and non-Mediterranean countries participating in the European Prospective Investigation into Cancer and Nutrition (EPIC) study. *Br. J. Nutr.* **2013**, *109*, 1498−1507.
(12) Del Rio, D.; Rodriguez-Mateos, A.; Spencer, J. P. E.; Tognolini, M.; Borges, G.; Crozier, A. Dietary (poly)phenolics in human health: structures, bioavailability, and evidence of protective effects against chronic diseases. *Antioxid. Redox Signal.* **2013**, *18*, 1818−1892.
(13) Tognon, G.; Lissner, L.; Saebye, D.; Walker, K. Z.; Heitmann, B. L. The Mediterranean diet in relation to mortality and CVD: a Danish cohort study. *Br. J. Nutr.* **2014**, *111*, 151−159.
(14) Song, J.; Smart, R. E.; Dambergs, R. G.; Sparrow, A. M.; Wells, R. B.; Wang, H.; Qian, M. C. Pinot Noir wine composition from different vine vigour zones classified by remote imaging technology. *Food Chem.* **2014**, *153*, 52−59.

(15) Kilmister, R. L.; Mazza, M.; Baker, N. K.; Faulkner, P.; Downey, M. O. A role for anthocyanin in determining wine tannin concentration in Shiraz. *Food Chem.* **2014**, *152*, 475−482.
(16) Figueiredo-González, M.; Cancho-Grande, B.; Simal-Gándara, J.; Teixeira, N.; Mateus, N.; De Freitas, V. The phenolic chemistry and spectrochemistry of red sweet wine-making and oak-aging. *Food Chem.* **2014**, *152*, 522−530.
(17) Cheng, V. J.; Bekhit, A. E.-D. A.; McConnell, M.; Mros, S.; Zhao, J. Effect of extraction solvent, waste fraction and grape variety on the antimicrobial and antioxidant activities of extracts from wine residue from cool climate. *Food Chem.* **2012**, *134*, 474−482.
(18) Aron, P. M.; Kennedy, J. A. Flavan-3-ols: nature, occurrence and biological activity. *Mol. Nutr. Food Res.* **2008**, *52*, 79−104.
(19) Aron, P. M.; Kennedy, J. A. Compositional investigation of phenolic polymers isolated from *Vitis vinifera* L. cv. Pinot noir during fermentation. *J. Agric. Food Chem.* **2007**, *55*, 5670−5680.
(20) Corrales, M.; Han, J. H.; Tauscher, B. Antimicrobial properties of grape seed extracts and their effectiveness after incorporation into pea starch films. *Int. J. Food Sci. Technol.* **2009**, *44*, 425−433.
(21) Baydar, N. G.; Özkan, G.; Sagdiç, O. Total phenolic contents and antibacterial activities of grape (*Vitis vinifera* L.) extracts. *Food Control* **2004**, *15*, 335−339.
(22) Baydar, N. G.; Sagdiç, O.; Özkan, G.; Cetin, S. Determination of antibacterial effects and total phenolic contents of grape (*Vitis vinifera* L.) seed extracts. *Int. J. Food Sci. Technol.* **2006**, *41*, 799−804.
(23) Capone, D. L.; Jeffery, D. W.; Sefton, M. A. Vineyard and fermentation studies to elucidate the origin of 1,8-cineole in Australian red wine. *J. Agric. Food Chem.* **2012**, *60*, 2281−2287.
(24) Baykal, H.; Yildirim, H. K. Application of artificial neural networks (ANNs) in wine technology. *Crit. Rev. Food Sci. Nutr.* **2013**, *53*, 415−421.
(25) Sousa, A.; Petrov, V.; Araújo, P.; Mateus, N.; Pina, F.; De Freitas, V. Thermodynamics, kinetics, and photochromism of oaklins: a recent family of deoxyanthocyanidins. *J. Phys. Chem. B* **2013**, *117*, 1901−1910.
(26) Becatti, E.; Genova, G.; Ranieri, A.; Tonutti, P. Postharvest treatments with ethylene on *Vitis vinifera* (cv Sangiovese) grapes affect berry metabolism and wine composition. *Food Chem.* **2014**, *159*, 257−266.
(27) Martinez-Luscher, J.; Torres, N.; Hilbert, G.; Richard, T.; Sanchez-Diaz, M.; Delrot, S.; Aguirreolea, J.; Pascual, I.; Gomes, E. Ultraviolet-B radiation modifies the quantitative and qualitative profile of flavonoids and amino acids in grape berries. *Phytochemistry* **2014**, *102*, 106−114.
(28) Kammerer, D.; Claus, A.; Carle, R.; Schieber, A. Polyphenol screening of pomace from red and white grape varieties (*Vitis vinifera* L.) by HPLC-DAD-MS/MS. *J. Agric. Food Chem.* **2004**, *52*, 4360−4367.
(29) Fontana, A. R.; Antoniolli, A.; Bottini, R. Grape pomace as a sustainable source of bioactive compounds: extraction, characterization, and biotechnological applications of phenolics. *J. Agric. Food Chem.* **2013**, *61*, 8987−9003.
(30) Mendoza, L.; Cotoras, M.; Vivanco, M.; Matsuhiro, B.; Torres, S.; Aguirre, M. Evaluation of antifungal properties against the phytopathogenic fungus *Botrytis cinerea* of anthocyanin rich-extracts obtained from grape pomaces. *J. Chil. Chem. Soc.* **2013**, *58*, 1725−1727.
(31) Yu, J. M.; Ahmedna, M. Functional components of grape pomace: their composition, biological properties and potential applications. *Int. J. Food Sci. Technol.* **2013**, *48*, 221−237.
(32) Sagdic, O.; Ozturk, I.; Ozkan, G.; Yetim, H.; Ekici, L.; Yilmaz, M. T. RP-HPLC-DAD analysis of phenolic compounds in pomace extracts from five grape cultivars: Evaluation of their antioxidant, antiradical and antifungal activities in orange and apple juices. *Food Chem.* **2011**, *126*, 1749−1758.
(33) Sagdic, O.; Silici, S.; Yetim, H. Fate of *Escherichia coli* and *E. coli* O157:H7 in apple juice treated with propolis extract. *Ann. Microbiol.* **2007**, *57*, 345−348.
(34) Tenore, G. C.; Basile, A.; Novellino, E. Antioxidant and antimicrobial properties of polyphenolic fractions from selected Moroccan red wines. *J. Food Sci.* **2011**, *76*, C1342−C1348.
(35) Mendoza, L.; Yañez, K.; Vivanco, M.; Melo, R.; Cotoras, M. Characterization of extracts from winery by-products with antifungal activity against *Botrytis cinerea*. *Ind. Crops Prod.* **2013**, *43*, 360−364.
(36) Li, Y.; Ma, R.; Xu, Z.; Wang, J.; Chen, T.; Chen, F.; Wang, Z. Identification and quantification of anthocyanins in Kyoho grape juice-making pomace, Cabernet Sauvignon grape winemaking pomace and their fresh skin. *J. Sci. Food Agric.* **2013**, *93*, 1404−1411.
(37) Meral, R.; Dogan, I. S. Grape seed as a functional food ingredient in bread-making. *Int. J. Food Sci. Nutr.* **2013**, *64*, 372−379.
(38) Davidov-Pardo, G.; Arozarena, I.; Marín-Arroyo, M. R. Grape seed extract: additive and functional ingredient. *Agro Food Ind. Hi-Tech* **2013**, *24*, 41−43.
(39) Chen, L.; Yuan, P.; Chen, K.; Jia, Q.; Li, Y. Oxidative conversion of B- to A-type procyanidin trimer: evidence for quinone methide mechanism. *Food Chem.* **2014**, *154*, 315−322.
(40) Pechamat, L.; Zeng, L.; Jourdes, M.; Ghidossi, R.; Teissedre, P.-L. Occurrence and formation kinetics of pyranomalvidin-procyanidin dimer pigment in merlot red wine: Impact of acidity and oxygen concentrations. *J. Agric. Food Chem.* **2014**, *62*, 1701−1705.
(41) Oliveira, D. A.; Salvador, A. A.; Smânia, A.; Smânia, E. F. A.; Maraschin, M.; Ferreira, S. R. S. Antimicrobial activity and composition profile of grape (*Vitis vinifera*) pomace extracts obtained by supercritical fluids. *J. Biotechnol.* **2013**, *164*, 423−432.
(42) Ky, I.; Lorrain, B.; Kolbas, N.; Crozier, A.; Teissedre, P.-L. Wine by-products: phenolic characterization and antioxidant activity evaluation of grapes and grape pomaces from six different French grape varieties. *Molecules* **2014**, *19*, 482−506.
(43) Curko, N.; Kovacevic Ganic, K.; Gracin, L.; Dapic, M.; Jourdes, M.; Teissedre, P. L. Characterization of seed and skin polyphenolic extracts of two red grape cultivars grown in Croatia and their sensory perception in a wine model medium. *Food Chem.* **2014**, *145*, 15−22.
(44) Terauchi, M.; Horiguchi, N.; Kajiyama, A.; Akiyoshi, M.; Owa, Y.; Kato, K.; Kubota, T. Effects of grape seed proanthocyanidin extract on menopausal symptoms, body composition, and cardiovascular parameters in middle-aged women: a randomized, double-blind, placebo-controlled pilot study. *Menopause* **2014**, DOI: 10.1097/GME.0000000000000200.
(45) Püssa, T.; Floren, J.; Kuldkepp, P.; Raal, A. Survey of grapevine *Vitis vinifera* stem polyphenols by liquid chromatography-diode array detection-tandem mass spectrometry. *J. Agric. Food Chem.* **2006**, *54*, 7488−7494.
(46) Karvela, E.; Makris, D. P.; Kalogeropoulos, N.; Karathanos, V. T. Deployment of response surface methodology to optimize recovery of grape (*Vitis vinifera*) stem polyphenols. *Talanta* **2009**, *79*, 1311−1321.
(47) Gonzalez-Centeno, M. R.; Jourdes, M.; Femenia, A.; Simal, S.; Rossello, C.; Teissedre, P. L. Proanthocyanidin composition and antioxidant potential of the stem winemaking byproducts from 10 different grape varieties (*Vitis vinifera* L.). *J. Agric. Food Chem.* **2012**, *60*, 11850−11858.
(48) Jara-Palacios, M. J.; Gordillo, B.; Gonzalez-Miret, M. L.; Hernanz, D.; Escudero-Gilete, M. L.; Heredia, F. J. Comparative study of the enological potential of different winemaking byproducts: implications in the antioxidant activity and color expression of red wine anthocyanins in a model solution. *J. Agric. Food Chem.* **2014**, DOI: 10.1021/jf500978n.
(49) Sahpazidou, D.; Geromichalos, G. D.; Stagos, D.; Apostolou, A.; Haroutounian, S. A.; Tsatsakis, A. M.; Tzanakakis, G. N.; Hayes, A. W.; Kouretas, D. Anticarcinogenic activity of polyphenolic extracts from grape stems against breast, colon, renal and thyroid cancer cells. *Toxicol. Lett.* **2014**, DOI: 10.1016/j.toxlet.2014.1001.1042.
(50) Del-Castillo-Alonso, M. A.; Diago, M. P.; Monforte, L.; Tardaguila, J.; Martinez-Abaigar, J.; Núñez-Olivera, E. Effects of UV exclusion on the physiology and phenolic composition of leaves and berries of *Vitis vinifera* cv. Graciano. *J. Sci. Food Agric.* **2014**, DOI: 10.1002/jsfa.6738.

(51) Latouche, G.; Bellow, S.; Poutaraud, A.; Meyer, S.; Cerovic, Z. G. Influence of constitutive phenolic compounds on the response of grapevine (*Vitis vinifera* L.) leaves to infection by *Plasmopara viticola*. *Planta* **2013**, *237*, 351−361.
(52) Dani, C.; Oliboni, L. S.; Agostini, F.; Funchal, C.; Serafini, L.; Henriques, J. A.; Salvador, M. Phenolic content of grapevine leaves (*Vitis labrusca* var. Bordo) and its neuroprotective effect against peroxide damage. *Toxicol. In Vitro* **2010**, *24*, 148−153.
(53) Bindon, K.; Holt, H.; Williamson, P. O.; Varela, C.; Herderich, M.; Francis, I. L. Relationships between harvest time and wine composition in *Vitis vinifera* L. cv. Cabernet Sauvignon. 2. Wine sensory properties and consumer preference. *Food Chem.* **2014**, *154*, 90−101.
(54) Gonzalo-Diago, A.; Dizy, M.; Fernández-Zurbano, P. Contribution of low molecular weight phenols to bitter taste and mouthfeel properties in red wines. *Food Chem.* **2014**, *154*, 187−198.
(55) Marquez, A.; Serratosa, M. P.; Merida, J. Influence of bottle storage time on colour, phenolic composition and sensory properties of sweet red wines. *Food Chem.* **2014**, *146*, 507−514.
(56) Heymann, H.; Licalzi, M.; Conversano, M. R.; Bauer, A.; Skogerson, K.; Matthews, M. Effects of extended grape ripening with or without must and wine alcohol manipulations on Cabernet Sauvignon wine sensory characteristics. *S. Afr. J. Enol. Vitic.* **2013**, *34*, 86−99.
(57) Polásková, P.; Herszage, J.; Ebeler, S. E. Wine flavor: chemistry in a glass. *Chem. Soc. Rev.* **2008**, *37*, 2478−2489.
(58) Pagliarini, E.; Laureati, M.; Gaeta, D. Sensory descriptors, hedonic perception and consumer's attitudes to Sangiovese red wine deriving from organically and conventionally grown grapes. *Front. Psychol.* **2013**, *4*, 896.
(59) Jensen, J. S. Prediction of wine color attributes from the phenolic profiles of red grapes (*Vitis vinifera*). *J. Agric. Food Chem.* **2008**, *56*, 1105−1115.
(60) Barata, A.; Campo, E.; Malfeito-Ferreira, M.; Loureiro, V.; Cacho, J.; Ferreira, V. Analytical and sensorial characterization of the aroma of wines produced with sour rotten grapes using GC-O and GC-MS: identification of key aroma compounds. *J. Agric. Food Chem.* **2011**, *59*, 2543−2553.
(61) Barata, A.; Pais, A.; Malfeito-Ferreira, M.; Loureiro, V. Influence of sour rotten grapes on the chemical composition and quality of grape must and wine. *Eur. Food Res. Technol.* **2011**, *233*, 183−194.
(62) Cadot, Y.; Caillé, S.; Samson, A.; Barbeau, G.; Cheynier, V. Sensory dimension of wine typicality related to a terroir by quantitative descriptive analysis, just about right analysis and typicality assessment. *Anal. Chim. Acta* **2010**, *660*, 53−62.
(63) Cadot, Y.; Caillé, S.; Samson, A.; Barbeau, G.; Cheynier, V. Sensory representation of typicality of Cabernet franc wines related to phenolic composition: impact of ripening stage and maceration time. *Anal. Chim. Acta* **2012**, *732*, 91−99.
(64) Hopfer, H.; Buffon, P. A.; Ebeler, S. E.; Heymann, H. The combined effects of storage temperature and packaging on the sensory, chemical, and physical properties of a Cabernet Sauvignon wine. *J. Agric. Food Chem.* **2013**, *61*, 3320−3334.
(65) Hopfer, H.; Ebeler, S. E.; Heymann, H. The combined effects of storage temperature and packaging type on the sensory and chemical properties of Chardonnay. *J. Agric. Food Chem.* **2012**, *60*, 10743−10754.
(66) Pons, A.; Lavigne, V.; Darriet, P.; Dubourdieu, D. Role of 3-methyl-2,4-nonanedione in the flavor of aged red wines. *J. Agric. Food Chem.* **2013**, *61*, 7373−7380.
(67) Capone, S.; Tufariello, M.; Francioso, L.; Montagna, G.; Casino, F.; Leone, A.; Siciliano, P. Aroma analysis by GC/MS and electronic nose dedicated to Negroamaro and Primitivo typical Italian Apulian wines. *Sens. Actuators, B* **2013**, *179*, 259−269.
(68) Capone, S.; Tufariello, M.; Siciliano, P. Analytical characterisation of Negroamaro red wines by "aroma wheels". *Food Chem.* **2013**, *141*, 2906−2915.
(69) Michel, J.; Jourdes, M.; Le Floch, A.; Giordanengo, T.; Mourey, N.; Teissedre, P. L. Influence of wood barrels classified by NIRS on the ellagitannin content/composition and on the organoleptic properties of wine. *J. Agric. Food Chem.* **2013**, *61*, 11109−11118.
(70) Gonzalo-Diago, A.; Dizy, M.; Fernández-Zurbano, P. Taste and mouthfeel properties of red wines proanthocyanidins and their relation to the chemical composition. *J. Agric. Food Chem.* **2013**, *61*, 8861−8870.
(71) Forde, C. G.; Cox, A.; Williams, E. R.; Boss, P. K. Associations between the sensory attributes and volatile composition of Cabernet Sauvignon wines and the volatile composition of the grapes used for their production. *J. Agric. Food Chem.* **2011**, *59*, 2573−2583.
(72) Noble, A. C. Bitterness in wine. *Physiol. Behav.* **1994**, *56*, 1251−1255.
(73) McRae, J. M.; Schulkin, A.; Kassara, S.; Holt, H. E.; Smith, P. A. Sensory properties of wine tannin fractions: implications for in-mouth sensory properties. *J. Agric. Food Chem.* **2013**, *61*, 719−727.
(74) Kallithraka, S.; Kim, D.; Tsakiris, A.; Paraskevopoulos, I.; Soleas, G. Sensory assessment and chemical measurement of astringency of Greek wines: correlations with analytical polyphenolic composition. *Food Chem.* **2011**, *126*, 1953−1958.
(75) Malherbe, S.; Menichelli, E.; du Toit, M.; Tredoux, A.; Muller, N.; Naes, T.; Nieuwoudt, H. The relationships between consumer liking, sensory and chemical attributes of *Vitis vinifera* L. cv. Pinotage wines elaborated with different *Oenococcus oeni* starter cultures. *J. Sci. Food Agric.* **2013**, *93*, 2829−2840.
(76) Schmidtke, L. M.; Blackman, J. W.; Clark, A. C.; Grant-Preece, P. Wine metabolomics: objective measures of sensory properties of Semillon from GC-MS profiles. *J. Agric. Food Chem.* **2013**, *61*, 11957−11967.
(77) Villamor, R. R.; Ross, C. F. Wine matrix compounds affect perception of wine aromas. *Annu. Rev. Food Sci. Technol.* **2013**, *4*, 1−20.
(78) Ugliano, M. Oxygen contribution to wine aroma evolution during bottle aging. *J. Agric. Food Chem.* **2013**, *61*, 6125−6136.
(79) Magrone, T.; Jirillo, E. Polyphenols from red wine are potent modulators of innate and adaptive immune responsiveness. *Proc. Nutr. Soc.* **2010**, *69*, 279−285.
(80) Bognar, E.; Sarszegi, Z.; Szabo, A.; Debreceni, B.; Kalman, N.; Tucsek, Z.; Sumegi, B.; Gallyas, F., Jr. Antioxidant and anti-inflammatory effects in RAW264.7 macrophages of malvidin, a major red wine polyphenol. *PLoS One* **2013**, *8*, No. e65355.
(81) Quintieri, A. M.; Baldino, N.; Filice, E.; Seta, L.; Vitetti, A.; Tota, B.; De Cindio, B.; Cerra, M. C.; Angelone, T. Malvidin, a red wine polyphenol, modulates mammalian myocardial and coronary performance and protects the heart against ischemia/reperfusion injury. *J. Nutr. Biochem.* **2013**, *24*, 1221−1231.
(82) Chiva-Blanch, G.; Urpi-Sarda, M.; Llorach, R.; Rotches-Ribalta, M.; Guillen, M.; Casas, R.; Arranz, S.; Valderas-Martinez, P.; Portoles, O.; Corella, D.; Tinahones, F.; Lamuela-Raventos, R. M.; Andres-Lacueva, C.; Estruch, R. Differential effects of polyphenols and alcohol of red wine on the expression of adhesion molecules and inflammatory cytokines related to atherosclerosis: a randomized clinical trial. *Am. J. Clin. Nutr.* **2012**, *95*, 326−334.
(83) Peluso, I.; Raguzzini, A.; Serafini, M. Effect of flavonoids on circulating levels of TNF-α and IL-6 in humans: a systematic review and meta-analysis. *Mol. Nutr. Food Res.* **2013**, *57*, 784−801.
(84) Nunes, C.; Ferreira, E.; Freitas, V.; Almeida, L.; Barbosa, R. M.; Laranjinha, J. Intestinal anti-inflammatory activity of red wine extract: unveiling the mechanisms in colonic epithelial cells. *Food Funct.* **2013**, *4*, 373−383.
(85) Cheah, K. Y.; Howarth, G. S.; Bastian, S. E. Grape seed extract dose-responsively decreases disease severity in a rat model of mucositis; concomitantly enhancing chemotherapeutic effectiveness in colon cancer cells. *PLoS One* **2014**, *9*, No. e85184.
(86) Kim, S. P.; Moon, E.; Nam, S. H.; Friedman, M. Composition of herba pogostemonis water extract and protection of infected mice against *Salmonella* Typhimurium-induced liver damage and mortality by stimulation of innate immune cells. *J. Agric. Food Chem.* **2012**, *60*, 12122−12130.

(87) Kim, S. P.; Moon, E.; Nam, S. H.; Friedman, M. *Hericium erinaceus* mushroom extracts protect infected mice against *Salmonella* Typhimurium-induced liver damage and mortality by stimulation of innate immune cells. *J. Agric. Food Chem.* **2012**, *60*, 5590−5596.
(88) Kim, S. P.; Park, S. O.; Lee, S. J.; Nam, S. H.; Friedman, M. A polysaccharide isolated from the liquid culture of *Lentinus edodes* (shiitake) mushroom mycelia containing black rice bran protects mice against a *Salmonella* lipopolysaccharide-induced endotoxemia. *J. Agric. Food Chem.* **2013**, *61*, 10987−10994.
(89) Kim, S. P.; Park, S. O.; Lee, S. J.; Nam, S. H.; Friedman, M. A polysaccharide isolated from the liquid culture of *Lentinus edodes* (shiitake) mushroom mycelia containing black rice bran protects mice against salmonellosis through up-regulation of the Th1 immune reaction. *J. Agric. Food Chem.* **2014**, *62*, 2384−2391.
(90) Chiva-Blanch, G.; Arranz, S.; Lamuela-Raventos, R. M.; Estruch, R. Effects of wine, alcohol and polyphenols on cardiovascular disease risk factors: evidences from human studies. *Alcohol Alcohol.* **2013**, *48*, 270−277.
(91) Schrieks, I. C.; van den Berg, R.; Sierksma, A.; Beulens, J. W.; Vaes, W. H.; Hendriks, H. F. Effect of red wine consumption on biomarkers of oxidative stress. *Alcohol Alcohol.* **2013**, *48*, 153−159.
(92) Jäntschi, L.; Sestras, R. E.; Bolboaca, S. D. Modeling the antioxidant capacity of red wine from different production years and sources under censoring. *Comput. Math. Methods Med.* **2013**, *2013*, No. 267360.
(93) Hosu, A.; Cristea, V.-M.; Cimpoiu, C. Analysis of total phenolic, flavonoids, anthocyanins and tannins content in Romanian red wines: prediction of antioxidant activities and classification of wines using artificial neural networks. *Food Chem.* **2014**, *150*, 113−118.
(94) Varoni, E. M.; Vitalini, S.; Contino, D.; Lodi, G.; Simonetti, P.; Gardana, C.; Sardella, A.; Carrassi, A.; Iriti, M. Effects of red wine intake on human salivary antiradical capacity and total polyphenol content. *Food Chem. Toxicol.* **2013**, *58*, 289−294.
(95) Stockham, K.; Sheard, A.; Paimin, R.; Buddhadasa, S.; Duong, S.; Orbell, J. D.; Murdoch, T. Comparative studies on the antioxidant properties and polyphenolic content of wine from different growing regions and vintages, a pilot study to investigate chemical markers for climate change. *Food Chem.* **2013**, *140*, 500−506.
(96) Kurin, E.; Mucaji, P.; Nagy, M. In vitro antioxidant activities of three red wine polyphenols and their mixtures: an interaction study. *Molecules* **2012**, *17*, 14336−14348.
(97) Di Gioia, L.; Cuq, B.; Guilbert, S. Effect of hydrophilic plasticizers on thermomechanical properties of corn gluten meal. *Cereal Chem.* **1998**, *75*, 514−519.
(98) Shi, J.; Yu, J.; Pohorly, J. E.; Kakuda, Y. Polyphenolics in grape seeds − biochemistry and functionality. *J. Med. Food* **2003**, *6*, 291−299.
(99) Ancín-Azpilicueta, C.; González-Marco, A.; Jiménez-Moreno, N. Current knowledge about the presence of amines in wine. *Crit. Rev. Food Sci. Nutr.* **2008**, *48*, 257−275.
(100) Ancín-Azpilicueta, C.; González-Marco, A.; Jiménez-Moreno, N. Comparative study of the amine concentration in wines obtained from the traditional fermentation and from a more anaerobic fermentation method. *LWT−Food Sci. Technol.* **2010**, *43*, 771−776.
(101) Konakovsky, V.; Focke, M.; Hoffmann-Sommergruber, K.; Schmid, R.; Scheiner, O.; Moser, P.; Jarisch, R.; Hemmer, W. Levels of histamine and other biogenic amines in high-quality red wines. *Food Addit. Contam., Part A* **2011**, *28*, 408−416.
(102) Martuscelli, M.; Arfelli, G.; Manetta, A. C.; Suzzi, G. Biogenic amines content as a measure of the quality of wines of Abruzzo (Italy). *Food Chem.* **2013**, *140*, 590−597.
(103) Eagle, K. Toxicological effects of red wine, orange juice, and other dietary SULT1A inhibitors via excess catecholamines. *Food Chem. Toxicol.* **2012**, *50*, 2243−2249.
(104) Kato, S.; Ishihara, T.; Hemmi, H.; Kobayashi, H.; Yoshimura, T. Alterations in d-amino acid concentrations and microbial community structures during the fermentation of red and white wines. *J. Biosci. Bioeng.* **2011**, *111*, 104−108.
(105) Ali, H. S. M.; Pätzold, R.; Brückner, H. Gas chromatographic determination of amino acid enantiomers in bottled and aged wines. *Amino Acids* **2010**, *38*, 951−958.
(106) Friedman, M.; Levin, C. E. Nutritional value of D-amino acids, D-peptides, and amino acid derivatives in mice. In *Unnatural Amino Acids: Methods and Protocols*; Pollegioni, L., Servi, S., Eds.; Humana Press: New York, 2012; Vol. 794, pp 337−353.
(107) Friedman, M.; Levin, C. E. Nutritional and medicinal aspects of D-amino acids. *Amino Acids* **2012**, *42*, 1553−1582.
(108) Benkova, B.; Lozanov, V.; Ivanov, I. P.; Kalenderova, S.; Stoev, G.; Yordanova, N.; Milchova, M.; Mitev, V. Quantitation of the homocysteine content in wine. *Eur. Food Res. Technol.* **2009**, *230*, 361−365.
(109) Aydin, E.; Demir, H. D.; Ozyurt, H.; Etikan, I. Association of plasma homocysteine and macular edema in type 2 diabetes mellitus. *Eur. J. Ophthalmol.* **2008**, *18*, 226−232.
(110) Glowacki, R.; Borowczyk, K.; Bald, E. Fast analysis of wine for total homocysteine content by high-performance liquid chromatography. *Amino Acids* **2012**, *42*, 247−251.
(111) Friedman, M.; Rasooly, R. Review of the inhibition of biological activities of food-related selected toxins by natural compounds. *Toxins (Basel)* **2013**, *5*, 743−775.
(112) Tamura, M.; Takahashi, A.; Uyama, A.; Mochizuki, N. A method for multiple mycotoxin analysis in wines by solid phase extraction and multifunctional cartridge purification, and ultra-high-performance liquid chromatography coupled to tandem mass spectrometry. *Toxins (Basel)* **2012**, *4*, 476−486.
(113) Mao, J. F.; Lei, S. R.; Yang, X. F.; Xiao, D. Quantification of ochratoxin A in red wines by conventional HPLC-FLD using a column packed with core-shell particles. *Food Control* **2013**, *32*, 505−511.
(114) Novo, P.; Moulas, G.; Prazeres, D. M. F.; Chu, V.; Conde, J. P. Detection of ochratoxin A in wine and beer by chemiluminescence-based ELISA in microfluidics with integrated photodiodes. *Sens. Actuators, B* **2013**, *176*, 232−240.
(115) Quintela, S.; Villarán, M. C.; López de Armentia, I.; Elejalde, E. Ochratoxin A removal in wine: a review. *Food Control* **2013**, *30*, 439−445.
(116) Remiro, R.; Irigoyen, A.; González-Peñas, E.; Lizarraga, E.; López de Cerain, A. Levels of ochratoxins in Mediterranean red wines. *Food Control* **2013**, *32*, 63−68.
(117) Jiang, C. M.; Shi, J. L.; Cheng, Y. L.; Liu, Y. L. Effect of *Aspergillus carbonarius* amounts on winemaking and ochratoxin A contamination. *Food Control* **2014**, *40*, 85−92.
(118) Marenco Arellano, V.; Reaño Martos, M.; Rodriguez Cabreros, M.; Bueso Fernández, A.; Garcia Loria, J.; Rodríguez Mosquera, M. Sulfite sensitivity in a patient with allergic asthma. *Allergol. Immunopathol. (Madr.)* **2011**, *39*, 306−307.
(119) Costanigro, M.; Appleby, C.; Menke, S. D. The wine headache: consumer perceptions of sulfites and willingness to pay for non-sulfited wines. *Food Qual. Pref.* **2014**, *31*, 81−89.
(120) Fratamico, P. M.; Bhunia, A. K.; Smith, J. L. *Foodborne Pathogens − Microbiology and Molecular Biology*; Caister Academic Press: Norfolk, UK, 2005; p 454.
(121) Beer, M. H.; Porter, R. S.; Jones, T. V. *The Merck Manual of Diagnosis and Therapy*, 18th ed.; Wiley: Whitehouse Station, NJ, USA, 2006; p 3000.
(122) Vaz, M.; Hogg, T.; Couto, J. A. The antimicrobial effect of wine on *Bacillus cereus* in simulated gastro-intestinal conditions. *Food Control* **2012**, *28*, 230−236.
(123) Friedman, M. Overview of antibacterial, antitoxin, antiviral, and antifungal activities of tea flavonoids and teas. *Mol. Nutr. Food Res.* **2007**, *51*, 116−134.
(124) Carneiro, A.; Couto, J. A.; Mena, C.; Queiroz, J.; Hogg, T. Activity of wine against *Campylobacter jejuni*. *Food Control* **2008**, *19*, 800−805.
(125) Friedman, M.; Henika, P. R.; Mandrell, R. E. Bactericidal activities of plant essential oils and some of their isolated constituents against *Campylobacter jejuni*, *Escherichia coli*, *Listeria monocytogenes*, and *Salmonella enterica*. *J. Food Prot.* **2002**, *65*, 1545−1560.

(126) Friedman, M.; Henika, P. R.; Mandrell, R. E. Antibacterial activities of phenolic benzaldehydes and benzoic acids against *Campylobacter jejuni*, *Escherichia coli*, *Listeria monocytogenes*, and *Salmonella enterica*. *J. Food Prot.* **2003**, *66*, 1811−1821.
(127) Fernandes, J.; Gomes, F.; Couto, J. A.; Hogg, T. The antimicrobial effect of wine on *Listeria innocua* in a model stomach system. *Food Control* **2007**, *18*, 1477−1483.
(128) Király-Véghely, Z.; Móricz, Á. M.; Ott, P. G.; Kátay, G.; Bélai, I.; Tyihák, E. Comparison of components from red and white wines for antimicrobial activity by biodetection after OPLC separation. *J. Liq. Chromatogr. Relat. Technol.* **2009**, *32*, 1259−1272.
(129) Waite, J. G.; Daeschel, M. A. Contribution of wine components to inactivation of food-borne pathogens. *J. Food Sci.* **2007**, *72*, M286−291.
(130) Boban, N.; Tonkic, M.; Budimir, D.; Modun, D.; Sutlovic, D.; Punda-Polic, V.; Boban, M. Antimicrobial effects of wine: separating the role of polyphenols, pH, ethanol, and other wine components. *J. Food Sci.* **2010**, *75*, M322−M326.
(131) Rodríguez Vaquero, M. J.; Aredes Fernández, P. A.; Manca De Nadra, M. C.; Strasser De Saad, A. M. Effect of phenolic compounds from Argentinean red wines on pathogenic bacteria in a meat model system. *J. Food Biochem.* **2013**, *37*, 425−431.
(132) Vaquero, M. J. R.; Manca De Nadra, M. C. Growth parameter and viability modifications of *Escherichia coli* by phenolic compounds and Argentine wine extracts. *Appl. Biochem. Biotechnol.* **2008**, *151*, 342−352.
(133) Radovanovic, A. N.; Jovancicevic, B. S.; Radovanovic, B. C.; Mihajilov-Krstev, T.; Zvezdanovic, J. B. Antioxidant and antimicrobial potentials of Serbian red wines produced from international *Vitis vinifera* grape varieties. *J. Sci. Food Agric.* **2012**, *92*, 2154−2161.
(134) Katalinic, V.; Možina, S. S.; Skroza, D.; Generalic, I.; Abramovic, H.; Miloš, M.; Ljubenkov, I.; Piskernik, S.; Pezo, I.; Terpinc, P.; Boban, M. Polyphenolic profile, antioxidant properties and antimicrobial activity of grape skin extracts of 14 *Vitis vinifera* varieties grown in Dalmatia (Croatia). *Food Chem.* **2010**, *119*, 715−723.
(135) Aires, V.; Delmas, D. Resveratrol, a polyphenol with pleiotropic health benefits. In *Polyphenols: Chemistry, Dietary Sources and Health Benefits*; Sun, J., Prasad, K. N., Ismail, A., Yang, B., You, X., Li, L., Eds.; Nova Science Publishers: Hauppauge, NY, USA, 2012; pp 153−192.
(136) Latruffe, N.; Rifler, J.-P. Bioactive polyphenols from grapes and wine emphasized with resveratrol. *Curr. Pharm. Des.* **2013**, *19*, 6053−6063.
(137) Flamini, R.; Mattivi, F.; De Rosso, M.; Arapitsas, P.; Bavaresco, L. Advanced knowledge of three important classes of grape phenolics: anthocyanins, stilbenes and flavonols. *Int. J. Mol. Sci.* **2013**, *14*, 19651−19669.
(138) Chen, Y. M.; Chung, Y. C.; Wang, L. W.; Chen, K. T.; Li, S. Y. Antibacterial properties of chitosan in waterborne pathogen. *J. Environ. Sci. Health A: Toxic/Hazard. Subst. Environ. Eng.* **2002**, *37*, 1379−1390.
(139) Lee, J.-H.; Kim, Y.-G.; Ryu, S. Y.; Cho, M. H.; Lee, J. Resveratrol oligomers inhibit biofilm formation of *Escherichia coli* O157:H7 and *Pseudomonas aeruginosa*. *J. Nat. Prod.* **2014**, *77*, 168−172.
(140) Cho, H. S.; Lee, J.-H.; Ryu, S. Y.; Joo, S. W.; Cho, M. H.; Lee, J. Inhibition of *Pseudomonas aeruginosa* and *Escherichia coli* O157:H7 biofilm formation by plant metabolite ε-viniferin. *J. Agric. Food Chem.* **2013**, *61*, 7120−7126.
(141) Augustine, N.; Goel, A. K.; Sivakumar, K. C.; Kumar, R. A.; Thomas, S. Resveratrol − a potential inhibitor of biofilm formation in *Vibrio cholerae*. *Phytomedicine* **2014**, *21*, 286−289.
(142) Jung, D.-C.; Lee, S.-Y.; Yoon, J.-H.; Hong, K.-P.; Kang, Y.-S.; Park, S.-R.; Park, S. K.; Ha, S.-D.; Kim, G.-H.; Bae, D.-H. Inhibition of pork and fish oxidation by a novel plastic film coated with horseradish extract. *LWT−Food Sci. Technol.* **2009**, *42*, 856−861.
(143) Mallo, N.; Lamas, J.; Leiro, J. M. Hydrogenosome metabolism is the key target for antiparasitic activity of resveratrol against *Trichomonas vaginalis*. *Antimicrob. Agents Chemother.* **2013**, *57*, 2476−2484.
(144) Friedman, M.; Henika, P. R.; Levin, C. E. Bactericidal activities of health-promoting, food-derived powders against the foodborne pathogens *Escherichia coli*, *Listeria monocytogenes*, *Salmonella enterica*, and *Staphylococcus aureus*. *J. Food Sci.* **2013**, *78*, M270−M275.
(145) Brenes, M.; Medina, E.; García, A.; Romero, C.; De Castro, A. Olives and olive oil compounds active against pathogenic microorganisms. In *Olives and Olive Oil in Health and Disease Prevention*; Elsevier: Amsterdam, The Netherlands, 2010; pp 1013−1019.
(146) Piñeiro, Z.; Cantos-Villar, E.; Palma, M.; Puertas, B. Direct liquid chromatography method for the simultaneous quantification of hydroxytyrosol and tyrosol in red wines. *J. Agric. Food Chem.* **2011**, *59*, 11683−11689.
(147) Fernández-Mar, M. I.; Mateos, R.; García-Parrilla, M. C.; Puertas, B.; Cantos-Villar, E. Bioactive compounds in wine: resveratrol, hydroxytyrosol and melatonin: a review. *Food Chem.* **2012**, *130*, 797−813.
(148) Queipo-Ortuño, M. I.; Boto-Ordóñez, M.; Murri, M.; Gomez-Zumaquero, J. M.; Clemente-Postigo, M.; Estruch, R.; Cardona Diaz, F.; Andrés-Lacueva, C.; Tinahones, F. J. Influence of red wine polyphenols and ethanol on the gut microbiota ecology and biochemical biomarkers. *Am. J. Clin. Nutr.* **2012**, *95*, 1323−1334.
(149) Jiménez, A.; Sánchez-González, L.; Desobry, S.; Chiralt, A.; Tehrany, E. A. Influence of nanoliposomes incorporation on properties of film forming dispersions and films based on corn starch and sodium caseinate. *Food Hydrocolloids* **2014**, *35*, 159−169.
(150) Melo, A.; Viegas, O.; Petisca, C.; Pinho, O.; Ferreira, I. M. P. L. V. Effect of beer/red wine marinades on the formation of heterocyclic aromatic amines in pan-fried beef. *J. Agric. Food Chem.* **2008**, *56*, 10625−10632.
(151) Birk, T.; Knøchel, S. Fate of food-associated bacteria in pork as affected by marinade, temperature, and ultrasound. *J. Food Prot.* **2009**, *72*, 549−555.
(152) Isohanni, P.; Alter, T.; Saris, P.; Lyhs, U. Wines as possible meat marinade ingredients possess antimicrobial potential against *Campylobacter*. *Poult. Sci.* **2010**, *89*, 2704−2710.
(153) Istrati, D.; Ionescu, A.; Vizireanu, C.; Ciuciu, A. M. S.; Dinica, R. The tenderization of bovine Biceps femoris muscle using marinades on the basis of wine. *Rom. Biotechnol. Lett.* **2012**, *17*, 7787−7795.
(154) Linares, M. B.; Garrido, M. D.; Martins, C.; Patarata, L. Efficacies of garlic and *L. sakei* in wine-based marinades for controlling *Listeria monocytogenes* and *Salmonella* spp. in chouriço de vinho, a dry sausage made from wine-marinated pork. *J. Food Sci.* **2013**, *78*, M719−M724.
(155) Nisiotou, A.; Chorianopoulos, N. G.; Gounadaki, A.; Panagou, E. Z.; Nychas, G. J. Effect of wine-based marinades on the behavior of *Salmonella* Typhimurium and background flora in beef fillets. *Int. J. Food Microbiol.* **2013**, *164*, 119−127.
(156) Rhoades, J.; Kargiotou, C.; Katsanidis, E.; Koutsoumanis, K. P. Use of marination for controlling *Salmonella enterica* and *Listeria monocytogenes* in raw beef. *Food Microbiol.* **2013**, *36*, 248−253.
(157) Friedman, M.; Henika, P. R.; Levin, C. E.; Mandrell, R. E. Recipes for antimicrobial wine marinades against *Bacillus cereus*, *Escherichia coli* O157:H7, *Listeria monocytogenes*, and *Salmonella enterica*. *J. Food Sci.* **2007**, *72*, M207−M213.
(158) Kargiotou, C.; Katsanidis, E.; Rhoades, J.; Kontominas, M.; Koutsoumanis, K. Efficacies of soy sauce and wine base marinades for controlling spoilage of raw beef. *Food Microbiol.* **2011**, *28*, 158−163.
(159) Díez, J. G.; Patarata, L. Behavior of *Salmonella* spp., *Listeria monocytogenes*, and *Staphylococcus aureus* in Chouriço de Vinho, a dry fermented sausage made from wine-marinated meat. *J. Food Prot.* **2013**, *76*, 588−594.
(160) Friedman, M.; Zhu, L.; Feinstein, Y.; Ravishankar, S. Carvacrol facilitates heat-induced inactivation of *Escherichia coli* O157:H7 and inhibits formation of heterocyclic amines in grilled ground beef patties. *J. Agric. Food Chem.* **2009**, *57*, 1848−1853.
(161) Rounds, L.; Havens, C. M.; Feinstein, Y.; Friedman, M.; Ravishankar, S. Plant extracts, spices, and essential oils inactivate

Escherichia coli O157:H7 and reduce formation of potentially carcinogenic heterocyclic amines in cooked beef patties. *J. Agric. Food Chem.* **2012**, *60*, 3792−3799.
(162) Viegas, O.; Amaro, L. F.; Ferreira, I. M. P. L. V. O.; Pinho, O. Inhibitory effect of antioxidant-rich marinades on the formation of heterocyclic aromatic amines in pan-fried beef. *J. Agric. Food Chem.* **2012**, *60*, 6235−6240.
(163) Busquets, R.; Puignou, L.; Galceran, M. T.; Skog, K. Effect of red wine marinades on the formation of heterocyclic amines in fried chicken breast. *J. Agric. Food Chem.* **2006**, *54*, 8376−8384.
(164) Brannan, R. G. Effect of grape seed extract on descriptive sensory analysis of ground chicken during refrigerated storage. *Meat Sci.* **2009**, *81*, 589−595.
(165) Osaili, T. M.; Shaker, R. R.; Ayyash, M. M.; Al-Nabulsi, A. A.; Forsythe, S. J. Survival and growth of *Cronobacter* species (*Enterobacter sakazakii*) in wheat-based infant follow-on formulas. *Lett. Appl. Microbiol.* **2009**, *48*, 408−412.
(166) Kim, T. J.; Weng, W. L.; Silva, J. L.; Jung, Y. S.; Marshall, D. Identification of natural antimicrobial substances in red muscadine juice against *Cronobacter sakazakii*. *J. Food Sci.* **2010**, *75*, M150−M154.
(167) Kim, T. J.; Silva, J. L.; Jung, Y. S. Antibacterial activity of fresh and processed red muscadine juice and the role of their polar compounds on *Escherichia coli* O157:H7. *J. Appl. Microbiol.* **2009**, *107*, 533−539.
(168) Kim, T. J.; Weng, W. L.; Stojanovic, J.; Lu, Y.; Jung, Y. S.; Silva, J. L. Antimicrobial effect of water-soluble muscadine seed extracts on *Escherichia coli* O157:H7. *J. Food Prot.* **2008**, *71*, 1465−1468.
(169) Ganesh, V.; Hettiarachchy, N. S.; Griffis, C. L.; Martin, E. M.; Ricke, S. C. Electrostatic spraying of food-grade organic and inorganic acids and plant extracts to decontaminate *Escherichia coli* O157:H7 on spinach and iceberg lettuce. *J. Food Sci.* **2012**, *77*, M391−M396.
(170) Quiñones, B.; Massey, S.; Friedman, M.; Swimley, M. S.; Teter, K. Novel cell-based method to detect Shiga toxin 2 from *Escherichia coli* O157:H7 and inhibitors of toxin activity. *Appl. Environ. Microbiol.* **2009**, *75*, 1410−1416.
(171) Brown, J. C.; Huang, G.; Haley-Zitlin, V.; Jiang, X. Antibacterial effects of grape extracts on *Helicobacter pylori*. *Appl. Environ. Microbiol.* **2009**, *75*, 848−852.
(172) Brown, J. C.; Jiang, X. Activities of muscadine grape skin and polyphenolic constituents against *Helicobacter pylori*. *J. Appl. Microbiol.* **2013**, *114*, 982−991.
(173) Ghaedi, M.; Darvishi, S.; Rezaee, M. A.; Motaharinia, Y.; Ghavami, K.; Rahmani, M. R. Antibacterial activity of extracts of Halgho and Rashe grape cultivars against *Helicobacter pylori*. *J. Pure Appl. Microbiol.* **2013**, *7*, 1895−1901.
(174) Grace Nirmala, J.; Narendhirakannan, R. T. In vitro antioxidant and antimicrobial activities of grapes (*Vitis vinifera*. L) seed and skin extracts − Muscat variety. *Int. J. Pharm. Pharm. Sci.* **2011**, *3*, 242−249.
(175) Paoli, G. C.; Bhunia, A. K.; Bayles, D. O. *Listeria monocytogenes*. In *Foodborne Pathogens: Microbiology and Molecular Biology*; Fratamico, P. M.; Bhunia, A. K., Smith, J. L., Eds.; Caister Academic Press: Norfolk, UK, 2005; pp 295−325.
(176) Rhodes, P. L.; Mitchell, J. W.; Wilson, M. W.; Melton, L. D. Antilisterial activity of grape juice and grape extracts derived from *Vitis vinifera* variety Ribier. *Int. J. Food Microbiol.* **2006**, *107*, 281−286.
(177) Luther, M.; Parry, J.; Moore, J.; Meng, J.; Zhang, Y.; Cheng, Z.; Yu, L. L. Inhibitory effect of Chardonnay and black raspberry seed extracts on lipid oxidation in fish oil and their radical scavenging and antimicrobial properties. *Food Chem.* **2007**, *104*, 1065−1073.
(178) Theivendran, S.; Hettiarachchy, N. S.; Johnson, M. G. Inhibition of *Listeria monocytogens* by nisin combined with grape seed extract or green tea extract in soy protein film coated on turkey frankfurters. *J. Food Sci.* **2006**, *71*, M39−M44.
(179) Sivarooban, T.; Hettiarachchy, N. S.; Johnson, M. G. Inhibition of *Listeria monocytogenes* using nisin with grape seed extract on turkey frankfurters stored at 4 and 10°C. *J. Food Prot.* **2007**, *70*, 1017−1020.
(180) Sivarooban, T.; Hettiarachchy, N. S.; Johnson, M. G. Physical and antimicrobial properties of grape seed extract, nisin, and EDTA incorporated soy protein edible films. *Food Res. Int.* **2008**, *41*, 781−785.
(181) Gadang, V. P.; Hettiarachchy, N. S.; Johnson, M. G.; Owens, C. Evaluation of antibacterial activity of whey protein isolate coating incorporated with nisin, grape seed extract, malic acid, and EDTA on a turkey frankfurter system. *J. Food Sci.* **2008**, *73*, M389−M394.
(182) Anastasiadi, M.; Chorianopoulos, N. G.; Nychas, G.-J. E.; Karoutounian, S. A. Antilisterial activities of polyphenol-rich extracts of grapes and vinification byproducts. *J. Agric. Food Chem.* **2009**, *57*, 457−463.
(183) Over, K. F.; Hettiarachchy, N. S.; Perumalla, A. V. S.; Johnson, M. G.; Meullenet, J.-F.; Dickson, J. S.; Holtzbauer, M. J.; Niebuhr, S. E.; Davis, B. Antilisterial activity and consumer acceptance of irradiated chicken breast meat vacuum-infused with grape seed and green tea extracts and tartaric acid. *J. Food Sci.* **2010**, *75*, M455−M461.
(184) Moradi, M.; Tajik, H.; Razavi Rohani, S. M.; Oromiehie, A. R. Effectiveness of *Zataria multiflora* Boiss essential oil and grape seed extract impregnated chitosan film on ready-to-eat mortadella-type sausages during refrigerated storage. *J. Sci. Food Agric.* **2011**, *91*, 2850−2857.
(185) Friedman, M.; Juneja, V. K. Review of antimicrobial and antioxidative activities of chitosans in food. *J. Food Prot.* **2010**, *73*, 1737−1761.
(186) Perumalla, A. V. S.; Hettiarachchy, N. S.; Over, K.; Ricke, S. C.; Slavik, M. F.; Gbur, E.; Davis, B.; Acosta, S. Effect of partial replacement of potassium lactate and sodium diacetate by natural green tea and grape seed extracts and postpackaging thermal treatment on the growth of *Listeria monocytogenes* in hotdog model system. *Int. J. Food Sci. Technol.* **2013**, *48*, 918−926.
(187) Abtahi, H.; Ghazavi, A.; Karimi, M. Antimicrobial activities of ethanol extract of black grape. *Afr. J. Microbiol. Res.* **2011**, *5*, 4446−4448.
(188) Plundrich, N.; Grace, M. H.; Raskin, I.; Ann Lila, M. Bioactive polyphenols from muscadine grape and blackcurrant stably concentrated onto protein-rich matrices for topical applications. *Int. J. Cosmet. Sci.* **2013**, *35*, 394−401.
(189) Reddy, G. V. B.; Sen, A. R.; Nair, P. N.; Reddy, K. S.; Reddy, K. K.; Kondaiah, N. Effects of grape seed extract on the oxidative and microbial stability of restructured mutton slices. *Meat Sci.* **2013**, *95*, 288−294.
(190) Reddy, S.; Taylor, M.; Zhao, M.; Cherubin, P.; Geden, S.; Ray, S.; Francis, D.; Teter, K. Grape extracts inhibit multiple events in the cell biology of *Cholera* intoxication. *PLoS One* **2013**, *8*, No. e73390.
(191) Mahmoud, B. S. M. Controlling *Vibrio vulnificus* and spoilage bacteria in fresh shucked oysters using natural antimicrobials. *Lett. Appl. Microbiol.* **2014**, *58*, 1−7.
(192) Badet, C. Antibacterial activity of grape (*Vitis vinifera*, *Vitis rotundifolia*) seeds. In *Nuts and Seeds in Health and Disease Prevention*; Preedy, V. R., Watson, R. R., Patel, V. B., Eds.; Academic Press: London, UK, 2011; pp 545−552.
(193) Delgado Adámez, J.; Gamero Samino, E.; Valdés Sánchez, E.; González-Gómez, D. In vitro estimation of the antibacterial activity and antioxidant capacity of aqueous extracts from grape-seeds (*Vitis vinifera* L.). *Food Control* **2012**, *24*, 136−141.
(194) Jayaprakasha, G. K.; Selvi, T.; Sakariah, K. K. Antibacterial and antioxidant activities of grape (*Vitis vinifera*) seed extracts. *Food Res. Int.* **2003**, *36*, 117−122.
(195) Sagdic, O.; Ozturk, I.; Yilmaz, M. T.; Yetim, H. Effect of grape pomace extracts obtained from different grape varieties on microbial quality of beef patty. *J. Food Sci.* **2011**, *76*, M515−M521.
(196) Tseng, A.; Zhao, Y. Effect of different drying methods and storage time on the retention of bioactive compounds and antibacterial activity of wine grape pomace (Pinot noir and Merlot). *J. Food Sci.* **2012**, *77*, H192−H201.
(197) Sagdic, O.; Ozturk, I.; Kisi, O. Modeling antimicrobial effect of different grape pomace and extracts on *S. aureus* and *E. coli* in vegetable soup using artificial neural network and fuzzy logic system. *Expert Syst. Appl.* **2012**, *39*, 6792−6798.

(198) Serra, A. T.; Matias, A. A.; Nunes, A. V. M.; Leitão, M. C.; Brito, D.; Bronze, R.; Silva, S.; Pires, A.; Crespo, M. T.; San Romão, M. V.; Duarte, C. M. *In vitro* evaluation of olive- and grape-based natural extracts as potential preservatives for food. *Innovative Food Sci. Emerging Technol.* **2008**, *9*, 311−319.
(199) Deng, Q.; Zhao, Y. Physicochemical, nutritional, and antimicrobial properties of wine grape (cv. Merlot) pomace extract-based films. *J. Food Sci.* **2011**, *76*, 309−317.
(200) Daglia, M.; Papetti, A.; Grisoli, P.; Aceti, C.; Dacarro, C.; Gazzani, G. Antibacterial activity of red and white wine against oral *Streptococci*. *J. Agric. Food Chem.* **2007**, *55*, 5038−5042.
(201) Daglia, M.; Stauder, M.; Papetti, A.; Signoretto, C.; Giusto, G.; Canepari, P.; Pruzzo, C.; Gazzani, G. Isolation of red wine components with anti-adhesion and anti-biofilm activity against *Streptococcus mutans*. *Food Chem.* **2010**, *119*, 1182−1188.
(202) Thimothe, J.; Bonsi, I. A.; Padilla-Zakour, O. I.; Koo, H. Chemical characterization of red wine grape (*Vitis vinifera* and *Vitis* interspecific hybrids) and pomace phenolic extracts and their biological activity against *Streptococcus mutans*. *J. Agric. Food Chem.* **2007**, *55*, 10200−10207.
(203) Furiga, A.; Lonvaud-Funel, A.; Dorignac, G.; Badet, C. In vitro anti-bacterial and anti-adherence effects of natural polyphenolic compounds on oral bacteria. *J. Appl. Microbiol.* **2008**, *105*, 1470−1476.
(204) Gazzani, G.; Daglia, M.; Papetti, A. Food components with anticaries activity. *Curr. Opin. Biotechnol.* **2012**, *23*, 153−159.
(205) Hanning, I. B.; Nutt, J. D.; Ricke, S. C. Salmonellosis outbreaks in the United States due to fresh produce: sources and potential intervention measures. *Foodborne Pathog. Dis.* **2009**, *6*, 635−648.
(206) Smullen, J.; Finney, M.; Storey, D. M.; Foster, H. A. Prevention of artificial dental plaque formation in vitro by plant extracts. *J. Appl. Microbiol.* **2012**, *113*, 964−973.
(207) Cueva, C.; Mingo, S.; Muñoz-González, I.; Bustos, I.; Requena, T.; del Campo, R.; Martín-Álvarez, P. J.; Bartolomé, B.; Moreno-Arribas, M. V. Antibacterial activity of wine phenolic compounds and oenological extracts against potential respiratory pathogens. *Lett. Appl. Microbiol.* **2012**, *54*, 557−563.
(208) Muñoz-González, I.; Thurnheer, T.; Bartolomé, B.; Moreno-Arribas, M. V. Red wine and oenological extracts display antimicrobial effects in an oral bacteria biofilm model. *J. Agric. Food Chem.* **2014**, *62*, 4731−4737.
(209) Smulders, F. J. M.; Norrung, B.; Budka, H. *Foodborne Viruses and Prions and their Significance for Public Health*; Wageningen Academic Publishers: Wageningen, The Netherlands, 2013; p 373.
(210) Matias, A. A.; Serra, A. T.; Silva, A. C.; Perdigão, R.; Ferreira, T. B.; Marcelino, I.; Silva, S.; Coelho, A. V.; Alves, P. M.; Duarte, C. M. M. Portuguese winemaking residues as a potential source of natural anti-adenoviral agents. *Int. J. Food Sci. Nutr.* **2010**, *61*, 357−368.
(211) Campagna, M.; Rivas, C. Antiviral activity of resveratrol. *Biochem. Soc. Trans.* **2010**, *38*, 50−53.
(212) Sharaf, M.; El-Deeb, N. M.; El-Adawi, H. I. The potentiality of grape seed extract as a novel anti-hepatitis C virus agent. *J. Med. Sci.* **2012**, *12*, 107−113.
(213) Su, X.; D'Souza, D. H. Grape seed extract for control of human enteric viruses. *Appl. Environ. Microbiol.* **2011**, *77*, 3982−3987.
(214) Li, D.; Baert, L.; Zhang, D.; Xia, M.; Zhong, W.; Van Coillie, E.; Jiang, K.; Uyttendaele, M. Effect of grape seed extract on human norovirus GII.4 and murine norovirus 1 in viral suspensions, on stainless steel discs, and in lettuce wash water. *Appl. Environ. Microbiol.* **2012**, *78*, 7572−7578.
(215) Su, X.; D'Souza, D. H. Grape seed extract for foodborne virus reduction on produce. *Food Microbiol.* **2013**, *34*, 1−6.
(216) Lipson, S. M.; Gordon, R. E.; Ozen, F. S.; Karthikeyan, L.; Kirov, N.; Stotzky, G. Cranberry and grape juices affect tight junction function and structural integrity of rotavirus-infected monkey kidney epithelial cell monolayers. *Food Environ. Virol.* **2011**, *3*, 46−54.
(217) Lipson, S. M.; Ozen, F. S.; Karthikeyan, L.; Gordon, R. E. Effect of pH on anti-rotavirus activity by comestible juices and proanthocyanidins in a cell-free assay system. *Food Environ. Virol.* **2012**, *4*, 168−178.
(218) Ko, E.-A.; Jin, B.-J.; Namkung, W.; Ma, T.; Thiagarajah, J. R.; Verkman, A. S. Chloride channel inhibition by a red wine extract and a synthetic small molecule prevents rotaviral secretory diarrhoea in neonatal mice. *Gut* **2013**, *63*, 1120−1129.
(219) Roberts, P. R.; Zaloga, S. J.; Burney, J. D.; Zaloga, G. P. Wine components inhibit cholera toxin-induced intestinal secretion in rats. *J. Intensive Care Med.* **2000**, *15*, 48−52.
(220) Robots, P. R.; Zaloga, G. P. Wine inhibits enterotoxin-induced secretory diarrhea. *Crit. Care Med.* **1998**, *26*, A89.
(221) Nair, N.; Mahajan, S.; Chawda, R.; Kandaswami, C.; Shanahan, T. C.; Schwartz, S. A. Grape seed extract activates Th1 cells in vitro. *Clin. Diagn. Lab. Immunol.* **2002**, *9*, 470−476.
(222) Bak, M.-J.; Truong, V. L.; Kang, H.-S.; Jun, M.; Jeong, W.-S. Anti-inflammatory effect of procyanidins from wild grape (*Vitis amurensis*) seeds in LPS-induced RAW 264.7 cells. *Oxid. Med. Cell. Longev.* **2013**, *2013*, No. 409321.
(223) Han, Y. Synergic effect of grape seed extract with amphotericin B against disseminated candidiasis due to *Candida albicans*. *Phytomedicine* **2007**, *14*, 733−738.
(224) Jung, H. J.; Seu, Y. B.; Lee, D. G. Candicidal action of resveratrol isolated from grapes on human pathogenic yeast *C. albicans*. *J. Microbiol. Biotechnol.* **2007**, *17*, 1324−1329.
(225) Hyun, J. J.; In, A. H.; Woo, S. S.; Kang, H.; Beom, S. K.; Young, B. S.; Dong, G. L. Fungicidal effect of resveratrol on human infectious fungi. *Arch. Pharm. Res.* **2005**, *28*, 557−560.
(226) Papadopoulou, C.; Soulti, K.; Roussis, I. G. Potential antimicrobial activity of red and white wine phenolic extracts against strains of *Staphylococcus aureus*, *Escherichia coli* and *Candida albicans*. *Food Technol. Biotechnol.* **2005**, *43*, 41−46.
(227) Wang, M. L.; Suo, X.; Gu, J. H.; Zhang, W. W.; Fang, Q.; Wang, X. Influence of grape seed proanthocyanidin extract in broiler chickens: effect on chicken coccidiosis and antioxidant status. *Poult. Sci.* **2008**, *87*, 2273−2280.
(228) Naidoo, V.; McGaw, L. J.; Bisschop, S. P. R.; Duncan, N.; Eloff, J. N. The value of plant extracts with antioxidant activity in attenuating coccidiosis in broiler chickens. *Vet. Parasitol.* **2008**, *153*, 214−219.
(229) Kulkarni, S.; DeSantos, F. A.; Kattamuri, S.; Rossi, S. J.; Brewer, M. S. Effect of grape seed extract on oxidative, color and sensory stability of a pre-cooked, frozen, re-heated beef sausage model system. *Meat Sci.* **2011**, *88*, 139−144.
(230) Jara-Palacios, M. J.; Gonzalez-Manzano, S.; Escudero-Gilete, M. L.; Hernanz, D.; Duenas, M.; Gonzalez-Paramas, A. M.; Heredia, F. J.; Santos-Buelga, C. Study of Zalema grape pomace: phenolic composition and biological effects in *Caenorhabditis elegans*. *J. Agric. Food Chem.* **2013**, *61*, 5114−5121.
(231) Friedman, M. Antibiotic activities of plant compounds against non-resistant and antibiotic-resistant foodborne human pathogens. *ACS Symp. Ser.* **2006**, *No. 931*, 167−183.
(232) Moore-Neibel, K.; Gerber, C.; Patel, J.; Friedman, M.; Jaroni, D.; Ravishankar, S. Antimicrobial activity of oregano oil against antibiotic-resistant *Salmonella enterica* on organic leafy greens at varying exposure times and storage temperatures. *Food Microbiol.* **2013**, *34*, 123−129.
(233) Todd, J.; Friedman, M.; Patel, J.; Jaroni, D.; Ravishankar, S. The antimicrobial effects of cinnamon leaf oil against multi-drug resistant *Salmonella* Newport on organic leafy greens. *Int. J. Food Microbiol.* **2013**, *166*, 193−199.
(234) Mild, R. M.; Joens, L. A.; Friedman, M.; Olsen, C. W.; McHugh, T. H.; Law, B.; Ravishankar, S. Antimicrobial edible apple films inactivate antibiotic resistant and susceptible *Campylobacter jejuni* strains on chicken breast. *J. Food Sci.* **2011**, *76*, M163−M168.
(235) Kim, S. P.; Kang, M. Y.; Park, J. C.; Nam, S. H.; Friedman, M. Rice hull smoke extract inactivates *Salmonella* Typhimurium in laboratory media and protects infected mice against mortality. *J. Food Sci.* **2012**, *77*, M80−M85.
(236) Sirk, T. W.; Brown, E. F.; Sum, A. K.; Friedman, M. Molecular dynamics study on the biophysical interactions of seven green tea catechins with lipid bilayers of cell membranes. *J. Agric. Food Chem.* **2008**, *56*, 7750−7758.

(237) Sirk, T. W.; Brown, E. F.; Friedman, M.; Sum, A. K. Molecular binding of catechins to biomembranes: relationship to biological activity. *J. Agric. Food Chem.* **2009**, *57*, 6720−6728.
(238) Sirk, T. W.; Friedman, M.; Brown, E. F. Molecular binding of black tea theaflavins to biological membranes: relationship to bioactivities. *J. Agric. Food Chem.* **2011**, *59*, 3780−3787.

JOURNAL OF AGRICULTURAL AND FOOD CHEMISTRY

Article

pubs.acs.org/JAFC

Copper (Cu)−Silica Nanocomposite Containing Valence-Engineered Cu: A New Strategy for Improving the Antimicrobial Efficacy of Cu Biocides

Mikaeel Young[†,‡] and Swadeshmukul Santra[†,‡,#,*]

[†]Burnett School of Biomedical Sciences, [‡]NanoScience Technology Center, and [#]Department of Chemistry, University of Central Florida, Suite 400, 12424 Research Parkway, Orlando, Florida 32826, United States

Supporting Information

ABSTRACT: Copper (Cu) compounds are widely used as antibacterial/antifungal agents for protecting food crops. Prolonged use of Cu biocides would lead to undesirable Cu levels in agricultural soil. In the absence of a suitable alternative, prudent use of Cu biocides is required. This paper reports for the first time a composite material of sol−gel silica host matrix loaded with mixed-valence Cu as an alternative to conventional biocides. In this composite material, Cu is present in different oxidation states. The hydrophilic silica matrix serves as a water-dispersible delivery vehicle for antimicrobial Cu. It is hypothesized that a mixed-valence Cu system, specifically enriched with Cu(0) and Cu(I), will exhibit enhanced antimicrobial efficacy over traditional Cu(II) compounds. Materials were characterized by high-resolution transmission electron microscopy and X-ray photoelectron spectroscopy for the determination of particle size, morphology, crystallinity, and Cu oxidation states. Antimicrobial studies against *Xanthomonas alfalfae* and *Escherichia coli* (minimum inhibitory concentration) showed improved efficacy in MV-CuSiNG treatment compared to CuSiNG and other controls. Phytotoxicity studies performed (in *Vinca* sp. and Hamlin orange) under greenhouse conditions showed that the newly prepared nanocomposite is safe for plants, demonstrating potential usefulness of the material in agricultural biocides.

KEYWORDS: *copper, silica, antimicrobial, mixed-valence, agricultural biocide*

INTRODUCTION

In modern agriculture, copper (Cu)-based biocides are widely used for crop protection. Cu exhibits antimicrobial properties only at higher concentration (>50 μM),[1] as it is an essential micronutrient in many organisms including plants and animals.[2] Therefore, to achieve adequate protection, aggressive use of Cu is necessary, requiring multiple applications in one crop season.[3,4] For example, in the citrus industry, spraying Cu bactericides/fungicides is considered a standard measure for protection against a number of citrus diseases including citrus canker, scab, melanose, etc. In a season, running from March through October, Cu biocides are applied 5−15 times in citrus groves.[3] Extensive and continuous use of Cu-based biocides in agricultural field over years has caused undesirable accumulation of Cu in fertile soil, raising a huge environmental concern of Cu toxicity.[5−8] A serious concern for the citrus industry is the citrus canker disease caused by *Xanthomonas citri* subsp. *citri*. Studies conducted on *X. citri* subsp. *citri* and *Xanthomonas alfalfae* subsp. *citrumelonis* have revealed the development of Cu resistance.[9] Although there is no suitable alternative to Cu available to date, there is a strong need to improve the antimicrobial efficacy of the existing Cu-based biocides. Commercially available Cu compounds that are used in agriculture are primarily insoluble Cu(II) compounds such as basic copper(II) sulfate, copper(II) hydroxide, and copper(II) oxychloride.[4] Insoluble Cu(I) oxide and a mixed system containing both Cu(II) and Zn(II) are also available. All of these Cu-based products are traditional Cu compounds with known composition.[10]

Multiple mechanisms have been proposed to understand the biocidal activity of Cu, which has been correlated with its oxidation states, metallic (0), +1, and +2.[11] Cu(II) has been connected with a rapid decline in cell membrane integrity and specific binding for DNA, leading to cross-linking between strands and eventual denaturation.[2,12] Higher antimicrobial potency of Cu(I) over Cu(II) has been reported.[13−15] It has been suggested that Cu(I) is responsible for protein inactivation via its ability to strongly interact with thiol (−SH) groups of protein molecules.[16] It is also reported that Cu(I) is effective in producing reactive oxygen species via the Haber−Weiss reaction, leading to degradation of biomolecules.[17] Although the antimicrobial mechanism of Cu in its zero valence state (i.e., metallic Cu) is yet not fully understood, it has been suggested that metallic Cu surfaces such as Cu alloy based materials cause a rapid change in cell membrane potential, leading to damage in membrane integrity.[18,19] Release of ionic Cu from metallic Cu surfaces has been also suggested as a reason behind its antimicrobial effect.[19] Overall, Cu(I) and metallic Cu are shown to possess higher antimicrobial potency than the Cu(II) state.[1,13−15,18] To the best of our knowledge, there is no mixed-valence composite Cu system containing Cu(0), Cu(+1), and Cu(+2) reported to date.

Received: January 13, 2014
Accepted: June 9, 2014
Published: June 9, 2014

ACS Publications © 2014 American Chemical Society

In this paper, our objective is to design and synthesize a novel mixed-valence composite Cu system and study the role of mixed-valence Cu on overall antimicrobial efficacy. Amorphous silica is used as an inert environmentally friendly host matrix for embedding Cu in its mixed-valence states in this work. Our working hypothesis was that a mixed-valence copper system containing Cu(0), Cu(+1), and Cu(+2) will have an improved antimicrobial efficacy over a Cu(II)-only containing system. The goal is to improve overall Cu antimicrobial efficacy, which could potentially reduce the total amount of Cu biocide released into the environment.

EXPERIMENTAL PROCEDURES

Materials. All reagents used in synthesis and studies were purchased from commercial vendors and utilized without any further purification: tetraethylorthosilicate (TEOS, Gelest Inc.), copper(II) sulfate pentahydrate (CQ Concepts, Ringwood, IL, USA), concentrated hydrochloric acid (Fisher Scientific, USA), sodium borohydride (Sigma-Aldrich), neocuproine (Acros), ethylenediaminetetraacetic acid (EDTA) (Amresco, USA), Hyclone phosphate-buffered saline (PBS) (Fisher Scientific, USA), deionized (DI) water (Nanopure; Barnstead model D11911). Kocide 3000, a product of DuPont, was received as a gift from Dr. Jim Graham (Citrus Research and Education Center, Lake Alfred, FL, USA). Luria–Bertani (LB) broth and agar and nutrient broth and agar as well as Muller Hinton 2 (MH2) broth and agar were purchased from Fluka. Alamar blue dye was purchased from Life Technologies, Grand Island, NY, USA. *Escherichia coli* strain ATCC 35218 was obtained from the microbiology laboratory at the University of Central Florida, and *X. alfalfae* strain F1 ATCC 49120 was purchased from ATCC (U.S. Department of Agriculture permit P526P-12-04060). A cuprous ion efflux mutant of *E. coli*, *copA1(del)::kan* DW3110 CGSC#7968, was obtained from The Coli Genetic Stock Center (CGSC) at Yale University.

Synthesis of Composite Mixed-Valence Copper-Loaded Silica Nanogel (MV-CuSiNG). MV-CuSiNG was synthesized in two steps. In step 1, a water-soluble composite copper(II)-loaded silica nanogel (CuSiNG) was synthesized. The CuSiNG material was then converted to MV-CuSiNG material in step 2 using a reducing agent. Synthesis of CuSiNG material was done following a published protocol.[20] Briefly, 1.87 g of copper(II) sulfate pentahydrate was added to a mixture of 330 μL of 1% hydrochloric acid and 110 mL of deionized (DI) water. Then the solution was magnetically stirred for 30 min to ensure complete dissolution of copper sulfate crystals. Next, 778 μL of tetraethylorthosilicate (TEOS) was added a drop at time to the acidified copper sulfate solution, and stirring was continued for 24 h. The resulting composite CuSiNG solution was transparent, and the pH of the solution was measured to be 4. The CuSiNG nanocomposite loaded with Cu(II) was further converted to a mixed-valence Cu system by the treatment of sodium borohydride (a strong reducing agent). Briefly, about 183.3 mg of sodium borohydride was added directly to the CuSiNG solution, and the mixture was stirred for 1 h. The resulting mixture was then centrifuged at 10000 rpm for 10 min to remove residue. The supernatant containing the soluble form of MV-CuSiNG nanogel was used for further studies. The residue containing unreacted reagent was discarded. The pH of the MV-CuSiNG nanogel solution was 4 as measured by a pH-meter (Mettler, Toledo, OH, USA).

Nanogel Characterization. Nanogels, both CuSiNG and MV-CuSiNG, were characterized using high-resolution transmission electron microscopy (HRTEM, FEI Tecnai F30), X-ray photoelectron spectroscopy (XPS, Physical Electronics 5400 ESCA), UV–vis spectroscopy (Varian Cary 300), and atomic absorption spectroscopy (AAS, PerkinElmer AAnalyst 400 AA spectrometer).

HRTEM sample preparation was carried out by dipping carbon-filmed gold grids (400 square mesh) into the solution of nanogels followed by vacuum drying at room temperature overnight. Electron beam intensity of 100 kV was used for HRTEM. The HRTEM samples were analyzed at the Advanced Materials and Processing Center, Materials Characterization Facility (AMPAC-MCF) at the University of Central Florida. For XPS studies, 10 mL of each nanogel was lyophilized using a LabConco FreeZone 4.5 Liter Freeze-Dryer (model 7750020). AAS analysis was done by comparing nanogel samples with a series of copper standards. Samples for AAS were prepared by extracting Cu from lyophilized nanogel powder using saturated EDTA solution. EDTA strongly chelates with Cu and forms a water-soluble Cu–EDTA complex. The nanogel residue after EDTA treatment was also analyzed by AAS to confirm complete release of Cu from the nanogel material.

Copper(I) content within CuSiNG materials was observed using 2,9-dimethyl-1,10-phenanthroline (neocuproine, N_c assay) with UV–vis spectroscopy. Nc is a copper(I)-specific chelator, soluble in methanol and chloroform. The Cu(I)–Nc complex has a characteristic absorption band maxima at around 455 nm.[21,22] The Nc assay was done in a methanol–water mixed solvent. One milliliter of N_c solution (1 mg/mL) in methanol was combined with 1 mL of CuSiNG material solution (1 mg/mL). The resulting mixture was then stirred for 48 h using a stir plate. UV–vis absorption spectrum of the mixture was then recorded in the wavelength range between 350 and 550 nm.

Antimicrobial Studies. The antimicrobial properties of MV-CuSiNG and CuSiNG with control samples were investigated using a battery of standard microbiological techniques including minimum inhibitory concentration (MIC) and a bacterial growth inhibition assay using turbidity. Samples were tested against Gram-negative *Xanthomonas alfalfae* subsp. *citrumelonis* strain F1 (*X. alfalfae* F1, ATCC 49120, a nonpathogenic surrogate of citrus canker), Gram-negative *Escherichia coli* (ATCC 35218) and an *E. coli* efflux pump mutant *E. coli copA1(del)::kan*. The *E. coli* mutant was used to ascertain whether Cu(I) played a large role in Cu toxicity. The gene *copA* is known to be responsible for the development of Cu(I) efflux pumps. CopA translocates Cu(I) from the cytoplasm to periplasm when the Cu(I) concentration in cytoplasm reaches high levels.[23] *E. coli* and *E. coli copA1(del)::kan* were subcultured and maintained using LB agar and broth, whereas *X. alfalfae* was subcultured and maintained using nutrient agar and broth. Culturing and testing of *X. alfalfae* were done at 28 °C, whereas *E. coli* and *E. coli copA1(del)::kan* cultures and tests were conducted at 37 °C. All antimicrobial studies were conducted using LB and MH2 agar and broth with bacterial concentrations of 0.5 McFarland standard (10^8 CFU/mL). Kocide 3000 ("insoluble Cu" compound), copper sulfate ("soluble Cu" compound), and cuprous chloride ("insoluble Cu(I)" compound) were positive controls for growth inhibition, whereas silica nanogel (no Cu loaded) acted as the negative control. All test materials were standardized to a metallic Cu concentration of 3000 μg/mL before antimicrobial studies.

Determination of Minimum Inhibitory Concentration (MIC). The MIC values of MV-CuSiNG and CuSiNG with controls were determined along with those of Kocide 3000, copper sulfate, and cuprous chloride with equivalent Cu concentrations. MIC was carried out using broth microdilution in accordance with the guidelines of the Clinical and Laboratory Standards Institute (CLSI).[24] The accuracy of the MIC determination was improved by adding 5 μL of Alamar blue dye per 100 μL well volume and observing color changes (blue to pink for live organisms). This reduced an error produced from the cloudiness of the nanomaterial and control materials with broth.

Bacterial Alamar Blue Assay. The bacterial growth inhibition studies for the MV-CuSiNG and CuSiNG with controls were conducted using an Alamar blue assay with a microplate reader.[25] Briefly, different volumes of MV-CuSiNG and controls (5, 10, 15, 20, and 25 μL) were prepared in sterile MH2 or LB broth in separate wells within a 96-well flat-bottom, polystyrene microplate. Uniform growth potential was ensured by each well containing an equal amount of broth and equal final volumes (200 μL). Each well contained ~10^5 CFU/mL of bacteria. Appropriate "blank" wells were prepared containing no bacteria to compare with samples to determine bacterial growth. Microplates were incubated at the appropriate temperature for each bacterial species on a shaker at 200 rpm for 20–24 h. After incubation, 10 μL/well of Alamar blue dye was added to each well followed by further incubation. After 60 min of incubation, the absorbances of each well at both 570 and 600 nm were measured.

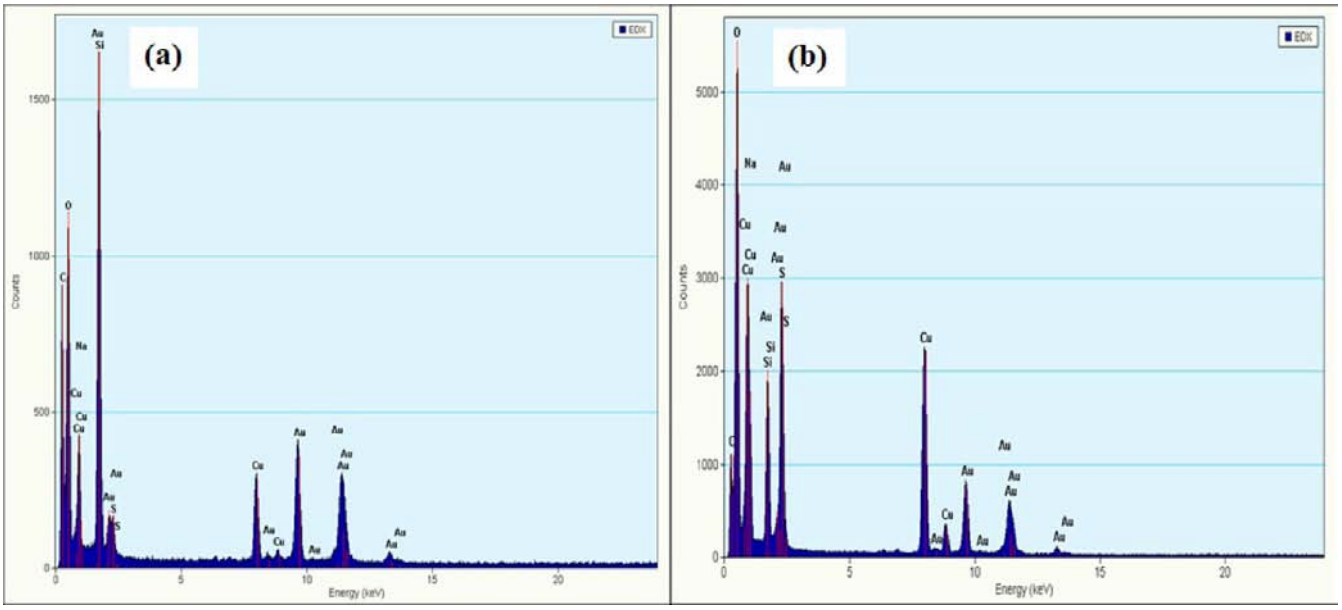

Figure 1. Energy-dispersive X-ray spectroscopy (EDX) for elemental analysis of (a) CuSiNG and (b) MV-CuSiNG during HRTEM.

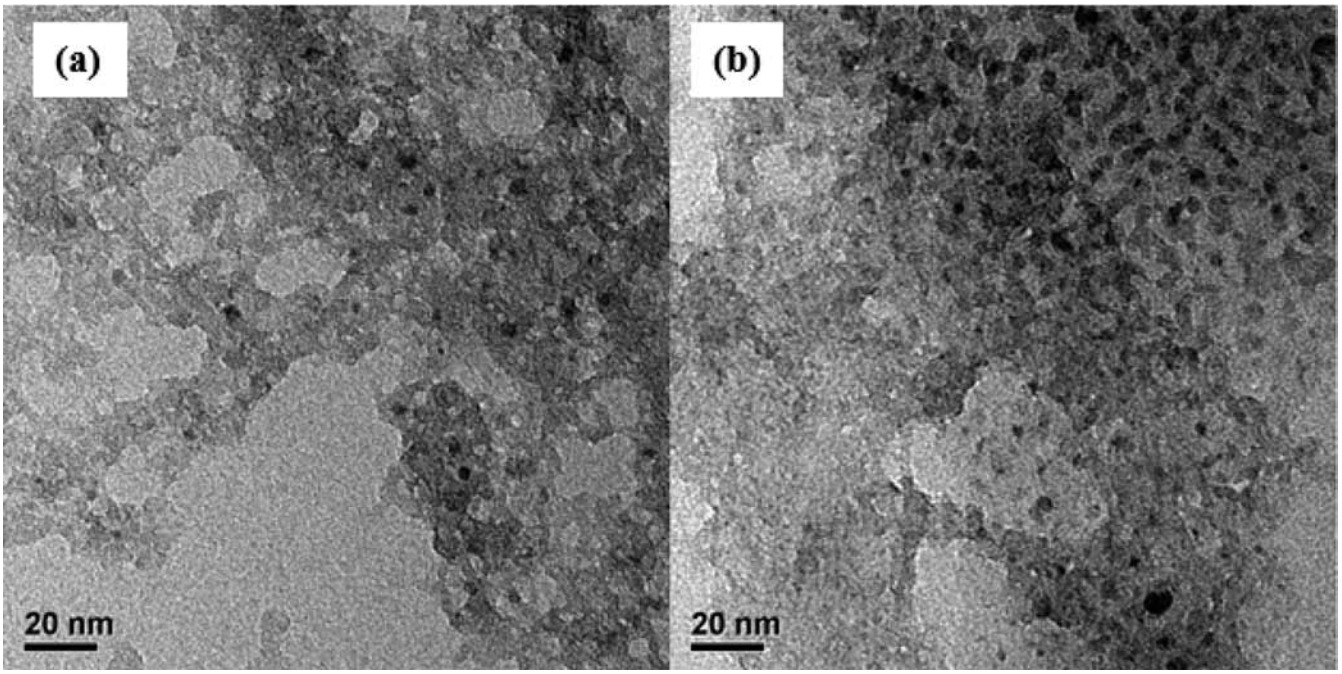

Figure 2. HRTEM image of (a) CuSiNG and (b) MV-CuSiNG at lower magnification with well-distributed material with light and dark contrast.

Wells containing sterile media with material controls and Alamar blue served as negative controls. Alamar blue assays for each bacterial strain were conducted at least three times to verify the results for reproducibility.

The percentage reduction of the dye was calculated by using the following formula as supplied by the manufacturer:

$$\frac{(\varepsilon_{ox})\lambda_2 A_{\lambda_1} - (\varepsilon_{ox})\lambda_1 A_{\lambda_2}}{(\varepsilon_{red})\lambda_1 A'\lambda_2 - (\varepsilon_{red})\lambda_2 A'_{\lambda_1}} \times 100$$

ε_{ox} is the molar extinction coefficient of Alamar blue oxidized form (blue), ε_{red} is the molar extinction coefficient of Alamar blue reduced form (pink), A is the absorbance of test wells, A' is the absorbance of negative control well, λ_1 = 570 nm, and λ_2= 600 nm.

Bacterial Viability Assay. The bactericidal activities of MV-CuSiNG and CuSiNG with controls were determined by colony-forming unit (CFU) assay. The copper concentration (225 μg/mL) that produced a significant decrease in viability over the lower concentration (150 μg/mL) as observed in the Alamar blue assay was used to perform the CFU assay. Treatment of bacteria with nanomaterial was carried out following the same procedure as described in the Alamar blue assay. After 24 h of nanomaterial treatment with the bacteria, each sample was serially diluted in 1× PBS and plated on LB or MH2 agar. After overnight incubation at species-appropriate temperatures, individual colonies were counted.

Phytotoxicity Studies. Phytotoxicity studies of MV-CuSiNG and CuSiNG with controls were carried out to observe potential plant tissue damage. Studies were conducted using *Vinca* sp., an annual ornamental plant purchased from a local Home Depot, and Hamlin orange, a citrus species purchased from Lukas Nursery in Oviedo, FL, USA. Ornamental species such as *Vinca* sp. and citrus were used to see if they exhibit differences in their levels of tolerance to oxidative stress,

dx.doi.org/10.1021/jf502350w | J. Agric. Food Chem. 2014, 62, 6043−6052

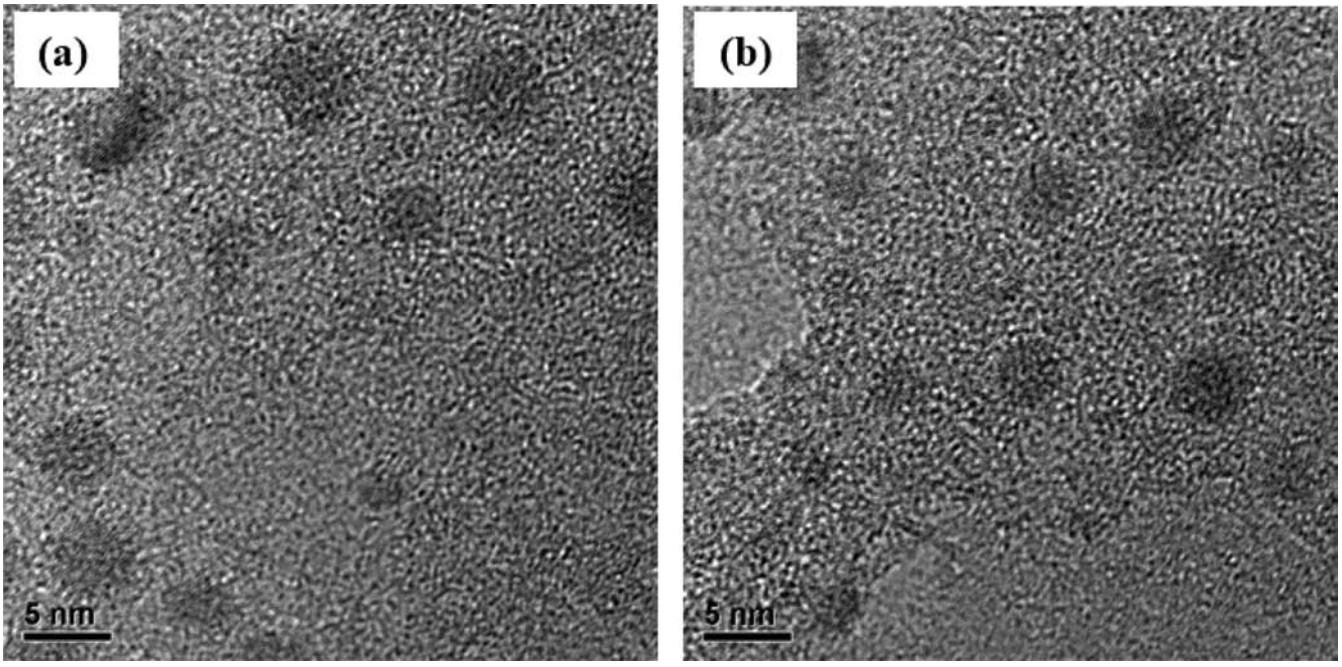

Figure 3. HRTEM image of (a) CuSiNG and (b) MV-CuSiNG at higher magnification with scattered dark contrast confirming presence of electron-rich material.

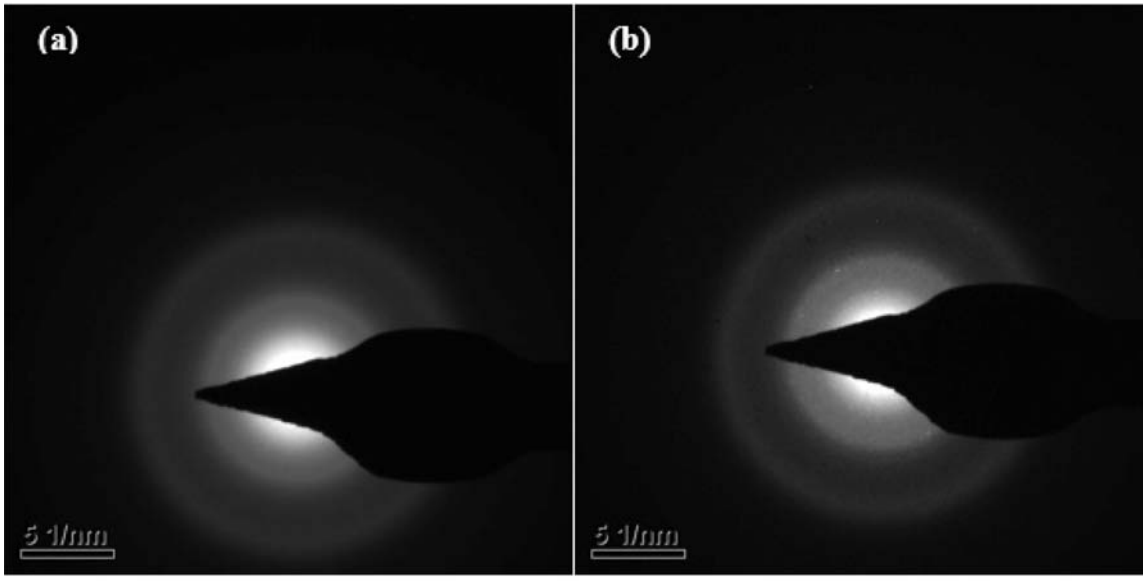

Figure 4. Selected area electron diffraction (SAED) image during HRTEM of (a) CuSiNG and (b) MV-CuSiNG.

thus giving a fair idea of how toxic or useful the agricultural material can be. Studies were carried out in a polyvinyl chloride (PVC) cold frame "mini greenhouse" covered in shade cloth and equipped with an Acurite temperature and humidity sensor purchased from Home Depot. Plants were purchased and placed in the greenhouse for at least 24 h prior to application of the formulation, allowing for acclimatization. Weather and conditions were monitored to ensure that plants were sprayed only on appropriate days for phytotoxicity (temperature > 80 °F, humidity 60−80%). CuSiNG and MV-CuSiNG were applied, along with Kocide 3000 ("insoluble Cu" compound), copper sulfate ("soluble Cu(II)" compound), cuprous chloride ("insoluble Cu(I)"), and SiNG (negative control containing no copper) used for comparisons. Formulations were sprayed at concentrations of 90, 450, and 900 ppm of metallic Cu at 8:00 a.m. before temperatures became too high, and observations were taken at 24, 48, and 72 h postspray application.

RESULTS AND DISCUSSION

Copper-loaded silica nanogel (CuSiNG) was successfully synthesized using an acid-catalyzed sol−gel method. CuSiNG was then converted to a mixed Cu valence state by using a reducing agent, sodium borohydride. Both the CuSiNG and MV-CuSiNG materials appeared as blue transparent solution and were stable for at least 12 months (Supporting Information Figure S1(a,b)). Copper loading within CuSiNG materials were confirmed from AAS measurements with Cu concentrations of ∼4300 μg/mL in both CuSiNG and MV-CuSiNG. AAS studies confirmed that the unreacted residue portion of the MV-CuSiNG material did not contain Cu.

HRTEM studies confirmed the state of dispersion and crystallinity of the nanogel materials. Energy-dispersive X-ray

dx.doi.org/10.1021/jf502350w | J. Agric. Food Chem. 2014, 62, 6043−6052

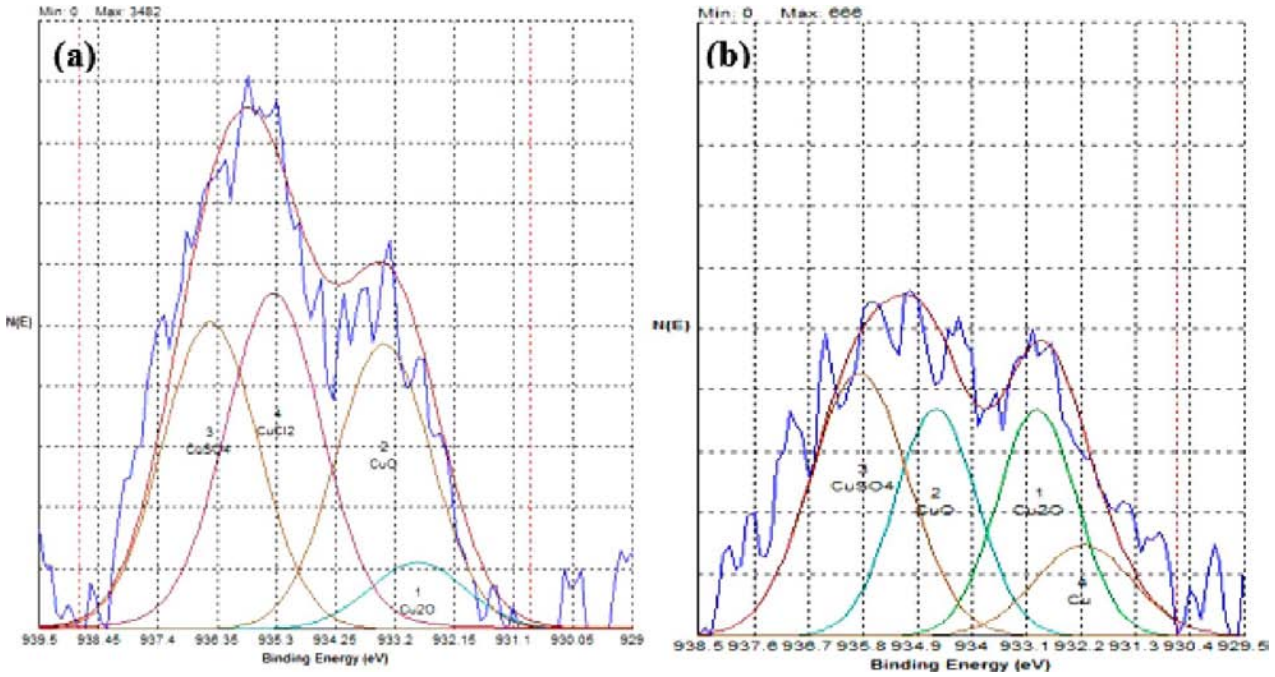

Figure 5. X-ray photoelectron spectroscopy high-resolution spectra of Cu in (a) CuSiNG and (b) MV-CuSiNG identifying $CuSO_4$, $CuCl_2$, CuO, Cu_2O, and metallic Cu.

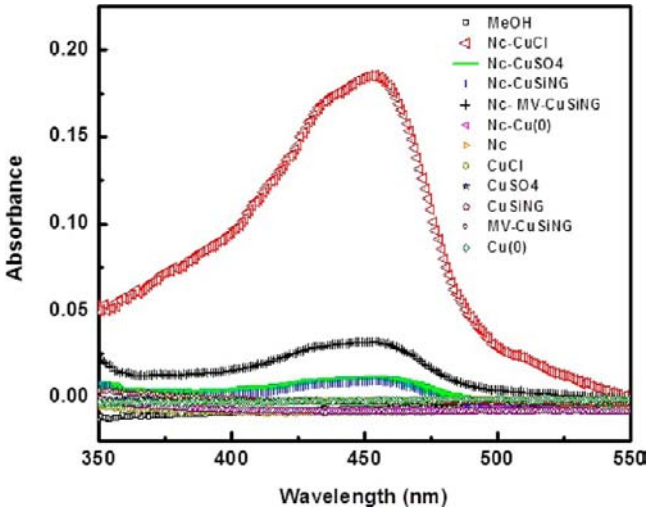

Figure 6. UV−vis spectra of CuSiNG materials chelated with neocuproine (Nc).

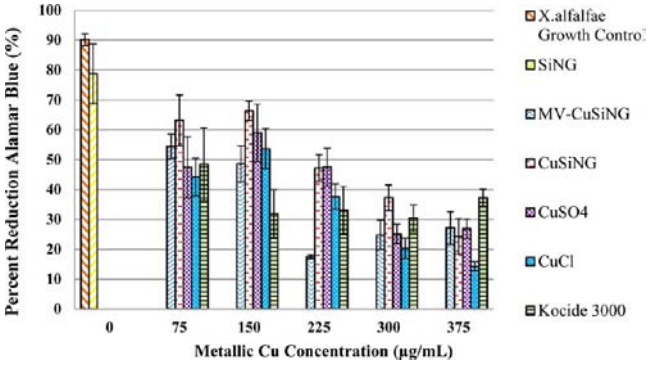

Figure 7. Histogram of Alamar blue reduction of *X. alfalfae* by MV-CuSiNG, CuSiNG, $CuSO_4$, CuCl, and Kocide 3000.

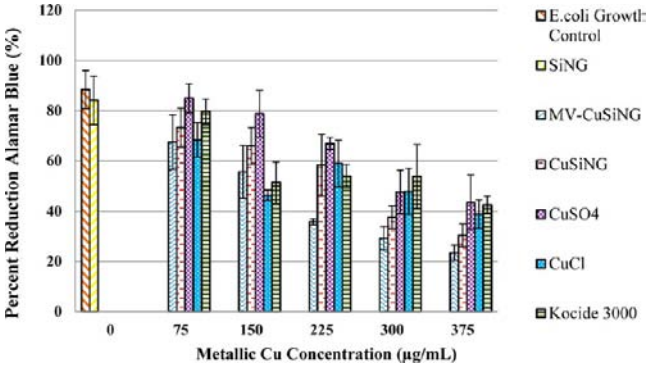

Figure 8. Histogram of Alamar blue reduction of *E. coli* by MV-CuSiNG, CuSiNG, $CuSO_4$, CuCl, and Kocide 3000.

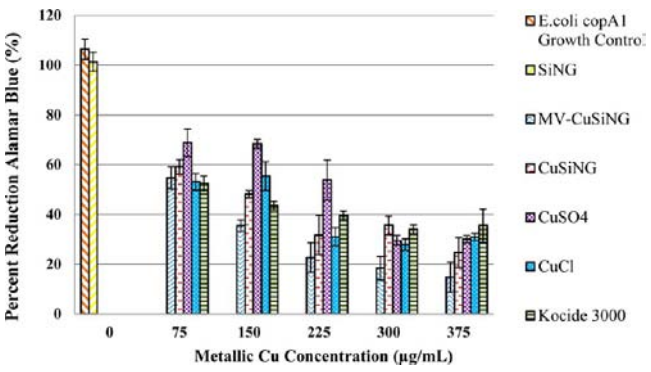

Figure 9. Histogram of Alamar blue reduction of *E. coli copA1 (del)::kan* by MV-CuSiNG, CuSiNG, $CuSO_4$, CuCl and Kocide 3000.

spectroscopy (EDX) elemental mapping confirmed the presence of elements Cu and Si in the nanogel materials. The appearance of Au peak was from the TEM grid (Figure 1). HRTEM studies revealed that ultrasmall size Cu crystallites were embedded in the amorphous silica matrix. The frequency

dx.doi.org/10.1021/jf502350w | J. Agric. Food Chem. 2014, 62, 6043−6052

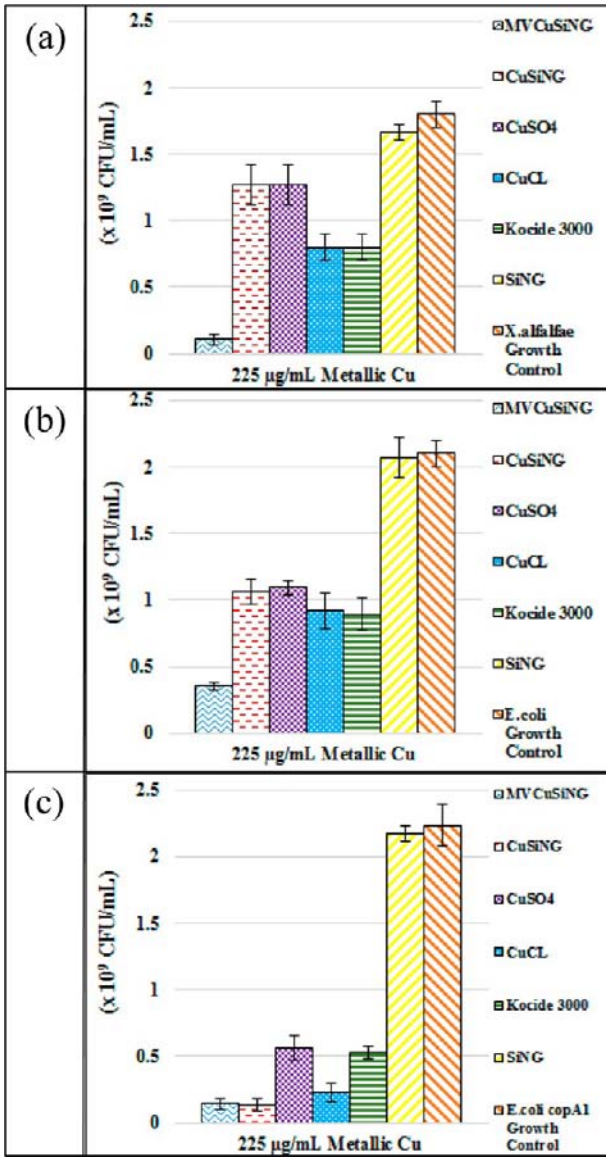

Figure 10. Bar graph of bacterial viability of (a) *X. alfalfae* (b) *E. coli*, and (c) *E. coli copA1 (del)::kan* by MV-CuSiNG, CuSiNG, $CuSO_4$, CuCl, and Kocide 3000 at 225 μg/mL metallic Cu.

Table 1. Minimum Inhibitory Concentration (MIC) of MV-CuSiNG and CuSiNG Compared with Controls against *X. alfalfae* and *E. coli*

	MIC (μg/mL Cu)		
	X. alfalfae	*E. coli*	*E. coli copA1(del)::kan*
MV-CuSiNG	187.5	187.5	93.75
CuSiNG	375	375	187.5
$CuSO_4$	375	375	375
CuCl	375	375	187.5
Kocide 3000	375	500	375

of cuprous oxide crystallites was higher in MV-CuSiNG as compared to CuSiNG, indicating a higher Cu(I) content. Lower magnification HRTEM images of CuSiNG and MV-CuSiNG showed well-distributed nanocomposite materials. Darker contrast indicated the presence of electron-dense material (Figure 2). High magnification HRTEM images of these darker contrast regions revealed the presence of ~4−8

Table 2. Data Collected from Phytotoxicity Studies of MV-CuSiNG and CuSiNG Materials with Controls on *Vinca* sp. at Various Cu Concentrations (90, 450, and 900 ppm) over a 3 Day Period[a]

		phytotoxicity rating		
tested material	metallic Cu content (μg/mL)	24 h	48 h	72 h
untreated	NA	−	−	−
SiNG	NA	−	−	−
MV-CuSiNG	90	−	−	−
	450	−	+	+
	900	+	+	+
CuSiNG	90	−	−	−
	450	−	+	+
	900	+	++	++
CuCl	90	−	−	−
	450	−	−	−
	900	−	+	+
$CuSO_4$	90	−	−	−
	450	+	+	+
	900	+	++	++
Kocide 3000	90	−	−	−
	450	−	−	−
	900	−	−	−

[a]Plant tissue damage rated on a scale of (−) nonphytotoxic, (+) slightly phytotoxic, and (++) moderately phytotoxic.

nm size crystalline material. Average lattice spacing between crystal planes was calculated. Values were determined as ~1.87, ~2.32, ~2.47, and ~3.02 Å to reveal Cu crystallites of cupric oxide[26] and cuprous oxide[26] in CuSiNG, whereas MV-CuSiNG possessed values of ~2.32, ~3.02, ~2.47, and ~2.09 Å, revealing cupric oxide,[26] cuprous oxide,[26] and metallic Cu[26] (Figure 3) . HRTEM selected area electron diffraction (SAED) measurements of CuSiNG and MV-CuSiNG showed a diffused diffraction pattern, suggesting the amorphous nature of the silica-rich matrix of the nanogel material (Figure 4).

Copper valence states were analyzed using XPS. Survey spectra were collected for CuSiNG and MV-CuSiNG materials. Characteristic XPS elemental signatures confirmed the presence of Cu, Si, S, O, C, and Cl (Supporting Information Figures S2 and S3). Detailed investigation of XPS spectra of Cu within CuSiNG and MV-CuSiNG was carried out to identify the Cu compounds and Cu valence states (Figure 5). Curve fitting and referencing through the National Institute for Science and Technology (NIST) XPS database indicated that $CuSO_4$,[27] $CuCl_2$,[28] CuO,[29] and Cu_2O[30] were found in CuSiNG, whereas $CuSO_4$,[27] CuO,[29] Cu_2O,[30] and metallic Cu[31] were found in MV-CuSiNG material. Nc assay was used to confirm the presence of Cu(I) in CuSiNG and MV-CuSiNG materials and its relative abundance. Nc is specific to Cu(I) only. The Cu(I)−Nc complex shows an absorption maximum around ~455 nm.[21,22] It was observed that Nc alone, methanol, Cu(II)SO_4, Cu(I)Cl, CuSiNG, and MV-CuSiNG do not absorb light at ~455 nm. Strongest 455 nm Nc−Cu(I) specific absorption for Nc−CuCl (positive control), moderate to high absorption for Nc−MV-CuSiNG, and low (insignificant) absorption for Nc−

dx.doi.org/10.1021/jf502350w | J. Agric. Food Chem. 2014, 62, 6043−6052

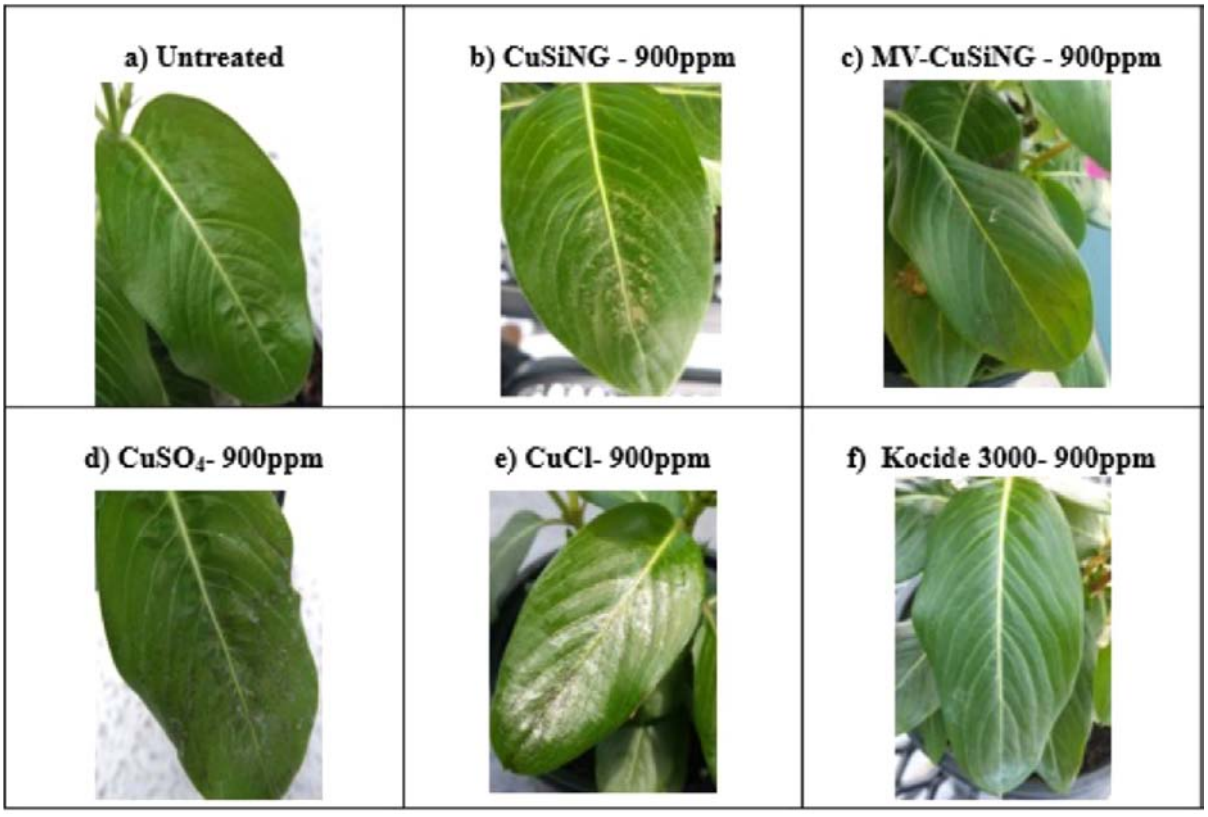

Figure 11. Images of *Vinca* sp. 72 h after application of CuSiNG materials and controls at a Cu concentration of 900 ppm.

Table 3. Data Collected from Phytotoxicity Studies of MV-CuSiNG and CuSiNG materials with controls on Hamlin Orange at Various Cu Concentrations (90, 450, and 900 ppm) over a 3 Day Period[a]

		phytotoxicity rating		
tested material	metallic Cu content (μg/mL)	24 h	48 h	72 h
untreated	NA	–	–	–
SiNG	NA	–	–	–
MV-CuSiNG	90	–	–	–
	450	–	–	–
	900	–	–	–
CuSiNG	90	–	–	–
	450	–	–	–
	900	–	–	–
CuCl	90	–	–	–
	450	–	–	–
	900	–	–	–
$CuSO_4$	90	–	–	–
	450	–	–	–
	900	–	–	–
Kocide 3000	90	–	–	–
	450	–	–	–
	900	–	–	–

[a]Plant tissue damage rated on a scale of (−) nonphytotoxic, (+) slightly phytotoxic, and (++) moderately phytotoxic.

CuSiNG were observed (Figure 6). Metallic Cu content was kept equal in each of these samples before exposure to Nc. XPS and HRTEM results support that Cu(0), Cu(I), and Cu(+2) are present in MV-CuSiNG material, whereas small amounts of Cu(I) and mostly Cu(+2) are present in CuSiNG material. The percentage of Cu_2O found within MV-CuSiNG was higher than that of CuSiNG, confirming higher Cu(I) content in MV-CuSiNG material. Cu(I) is increased in MV-CuSiNG, whereas CuSiNG primarily contains Cu(+2) as confirmed by the Nc assay. Therefore, the Nc assay clearly indicated that MV-CuSiNG had higher Cu(I) content in comparison to CuSiNG. This assay complements results from HRTEM and XPS studies and clearly supports the fact that Cu(I) content in MV-CuSiNG is increased after sodium borohydride reduction of CuSiNG material. HRTEM suggests that sodium borohydride further reduced some Cu(I) to Cu(0), indicated by the presence of metallic Cu crystallites.

Various antimicrobial assays were performed to measure the effectiveness of MV-CuSiNG and CuSiNG along with appropriate controls at inhibiting bacterial growth and/or causing bacterial cell death. Alamar blue assays were performed on *X. alfalfae* (Figure 7), *E. coli* (Figure 8), and *E. coli copA1(del)::kan* (Figure 9). Alamar blue dye is a colorimetric dye that is converted from an oxidized blue form to a reduced pink form by live cells. It is a semiquantitative assay that helps screen materials and can give an indication of antimicrobial effectiveness. The bacterial viability assay reported in CFU/mL was conducted to give a clear and quantitative measure of effectiveness of the MV-CuSiNG nanocomposite (Figure 10). MV-CuSiNG exhibited improved antimicrobial efficacy over CuSiNG material and controls, whereas CuSiNG composite material performed comparably to controls against all bacteria.

dx.doi.org/10.1021/jf502350w | J. Agric. Food Chem. 2014, 62, 6043−6052

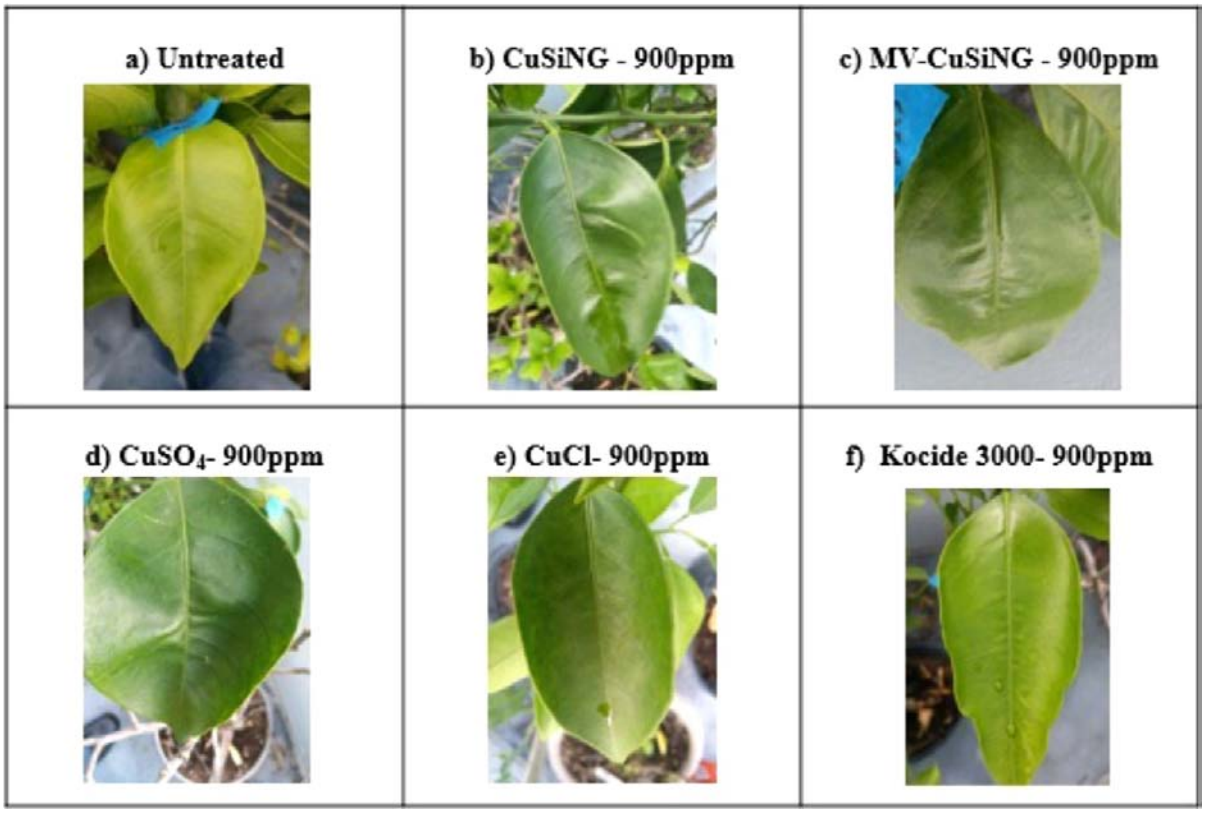

Figure 12. Images of Hamlin orange 72 h after application of CuSiNG materials and controls at a Cu concentration of 900 ppm.

The gene *copA* is responsible for limited Cu resistance within *E. coli*. It is responsible for Cu(I) efflux pumps, which transport Cu(I) ions from the cytoplasm to the periplasm to prevent Cu(I) accumulation.[23] *E. coli copA1(del)::kan* was far more susceptible to the MV-CuSiNG material than regular *E. coli*. Both MV-CuSiNG and CuSiNG along with CuCl materials performed better than the other controls against the *E. coli* mutant. This confirms the separate mechanism of Cu(I) toxicity. Improved efficacy of the mixed-valence Cu system has been correlated to the increased number of growth inhibition pathways in comparison to the Cu(II)-rich system. *E. coli copA1(del)::kan* was far more susceptible to the MV-CuSiNG material than regular *E. coli*, confirming the significant role of Cu(I) in growth inhibition. The high antimicrobial potency of Cu(I) was validated using the *E. coli copA1(del)::kan* model system (with no Cu(I) efflux pump) and MV-CuSiNG nanogel material enriched with Cu(I). MIC results reinforced and confirmed that the MV-CuSiNG formula was more efficient than Cu(II) only systems, exhibiting improved antimicrobial efficacy in *X. alfalfae*, *E. coli*, and *E. coli copA1(del)::kan* (Table 1).

Plant tissue damage potential (phytotoxicity) of MV-CuSiNG and CuSiNG with controls was tested on Hamlin orange and *Vinca* sp. *Vinca* sp. is highly susceptible to Cu phytotoxicity and therefore used as a model plant. *Vinca* sp. exhibited moderate to high levels of plant tissue damage when exposed to copper-containing agents including CuSiNG and MV-CuSiNG materials. Plant tissue damage was seen for all other copper formulations with the exception of Kocide 3000. All formulations showed no damage at 90 ppm but caused moderate to serious damage at 900 ppm (Table 2 and Figure 11). Hamlin orange was also tested as a model for citrus species. Hamlin orange exhibited strong tolerance to Cu-induced phytotoxicity even at the highest (900 ppm) metallic Cu concentrations for all formulations after 3 days (Table 3 and Figure 12). Phytotoxicty was absent in Hamlin orange, whereas it occurred in higher Cu concentrations in *Vinca* sp. for MV-CuSiNG material and controls. This could be attributed to residual copper ions present in the formulations. Copper hydroxide is the active Cu compound in Kocide 3000, and it is water-insoluble. Availability of Cu ions in Kocide 3000 is therefore very limited. As a result, Kocide 3000 exhibited no sign of phytotoxicity to *Vinca* sp. and Hamlin orange. These results indicate that MV-CuSiNG material requires further development before it can be used for protection of ornamental plant species, but in its current state it is very suitable for use in citrus crop protection.

We have successfully tested the hypothesis that a MV Cu system containing Cu in 0, +1, and +2 will exhibit improved antimicrobial potency relative to Cu(II) systems. Sodium borohydride (a model reducing agent) may not be a suitable reagent for large-scale production of MV-CuSiNG for agricultural applications; however, MV-CuSiNG material can be scaled up by using a mixture of Cu(I)- and Cu(II)-containing starting materials. We are currently characterizing such MV-CuSiNG materials and evaluating their antimicrobial efficacy. We will report our results in subsequent publications.

■ ASSOCIATED CONTENT

Supporting Information

Figures S1−S3 showing sample digital images and XPS survey spectra. This material is available free of charge via the Internet at http://pubs.acs.org.

AUTHOR INFORMATION

Corresponding Author

*(S.S.) Phone: (407) 882-2848. Fax: (407) 882-2819. E-mail: ssantra@mail.ucf.edu.

Author Contributions

The manuscript was written through contributions of all authors. All authors have given approval to the final version of the manuscript.

Funding

We ackowledge financial support from the Florida Department of Citrus (Grant 186) and the Citrus Research and Development Foundation, Inc. (Grants 328 and 544).

Notes

The authors declare no competing financial interest.

ACKNOWLEDGMENTS

We acknowledge Dr. Helge Heinrich (UCF Department of Physics) and Kirk Scammon (Materials Characterization Facility (MCF) at the UCF Advanced Materials and Processing Analysis Center (AMPAC) for their assistance with the HRTEM and XPS measurements. We thank Lisa Sorrentino and Veronica Maxwell at UCF Microbiology Preparatory Laboratory for providing the bacterial cultures. We recognize Ernie Gemeinhart at the UCF NanoScience Technology Center for his knowledge and assistance in constructing the "mini-greenhouse". We also acknowledge Dr. James Graham (Citrus Research and Education Center, University of Florida) for providing Kocide 3000 as a gift and for providing valuable information on citrus diseases, Cu bactericides/fungicides, and limitations of Cu products.

REFERENCES

(1) Outten, F. W.; Huffman, D. L.; Hale, J. A.; O'Halloran, T. V. The independent cue and cus systems confer copper tolerance during aerobic and anaerobic growth in *Escherichia coli*. *J. Biol. Chem.* **2001**, *276*, 30670−30677.

(2) Borkow, G.; Gabbay, J. Copper as a biocidal tool. *Curr. Med. Chem.* **2005**, *12*, 2163−2175.

(3) Behlau, F.; Belasque, J., Jr.; Graham, J. H.; Leite, R. P., Jr. Effect of frequency of copper applications on control of citrus canker and the yield of young bearing sweet orange trees. *Crop Prot.* **2010**, *29*, 300−305.

(4) Behlau, F.; Belasque, J., Jr.; Bergamin Filho, A.; Graham, J. H.; Leite, R. P., Jr.; Gottwald, T. R. Copper sprays and windbreaks for control of citrus canker on young orange trees in southern Brazil. *Crop Prot.* **2008**, *27*, 807−813.

(5) Pavlovic, M. A review of agribusiness copper use effects on environment. *Bulg. J. Agric. Sci.* **2011**, *17*, 491−500.

(6) Atha, D. H.; Wang, H.; Petersen, E. J.; Cleveland, D.; Holbrook, R. D.; Jaruga, P.; Dizdaroglu, M.; Xing, B.; Nelson, B. C. Copper oxide nanoparticle mediated DNA damage in terrestrial plant models. *Environ. Sci. Technol.* **2011**, *46*, 1819−1827.

(7) Cuypers, A.; Keunen, E.; Bohler, S.; Jozefczak, M.; Opdenakker, K.; Gielen, H.; Vercampt, H.; Bielen, A.; Schellingen, K.; Vangronsveld, J.; Remans, T. Cadmium and copper stress induce a cellular oxidative challenge leading to damage versus signalling. In *Metal Toxicity in Plants: Perception, Signaling and Remediation*; Gupta, D. K., Sandalio, L. M., Eds.; Springer: Berlin, Germany, 2012; pp 65−90.

(8) Sun, B.; Zhao, F. J.; Lombi, E.; McGrath, S. P. Leaching of heavy metals from contaminated soils using EDTA. *Environ. Pollut.* **2001**, *113*, 111−120.

(9) Behlau, F.; Canteros, B. I.; Minsavage, G. V.; Jones, J. B.; Graham, J. H. Molecular characterization of copper resistance genes from *Xanthomonas citri* subsp. *citri* and *Xanthomonas alfalfae* subsp. *citrumelonis*. *Appl. Environ. Microbiol.* **2011**, *77*, 4089−4096.

(10) Richardson, H. W. *Handbook of Copper Compounds and Applications*; CRC Press: Boca Raton, FL, USA, 1997.

(11) Konieczny, J.; Rdzawski, Z. Antibacterial properties of copper and its alloys. *Sci. Eng.* **2012**, *56*, 53−60.

(12) Aruoma, O. I.; Halliwell, B.; Gajewski, E.; Dizdaroglu, M. Copper-ion-dependent damage to the bases in DNA in the presence of hydrogen peroxide. *Biochem. J.* **1991**, *273*, 601−604.

(13) Finney, L. A.; O'Halloran, T. V. Transition metal speciation in the cell: insights from the chemistry of metal ion receptors. *Science* **2003**, *300*, 931−936.

(14) Huffman, D. L.; Huyett, J.; Outten, F. W.; Doan, P. E.; Finney, L. A.; Hoffman, B. M.; O'Halloran, T. V. Spectroscopy of Cu(II)-PcoC and the multicopper oxidase function of PcoA, two essential components of *Escherichia coli* pco copper resistance operon. *Biochemistry* **2002**, *41*, 10046−10055.

(15) Santo, C. E.; Lam, E. W.; Elowsky, C. G.; Quaranta, D.; Domaille, D. W.; Chang, C. J.; Grass, G. Bacterial killing by dry metallic copper surfaces. *Appl. Environ. Microbiol.* **2011**, *77*, 794−802.

(16) Macomber, L.; Imlay, J. A. The iron-sulfur clusters of dehydratases are primary intracellular targets of copper toxicity. *Proc. Natl. Acad. Sci. U.S.A.* **2009**, *106*, 8344−8349.

(17) Kehrer, J. P. The Haber−Weiss reaction and mechanisms of toxicity. *Toxicology* **2000**, *149*, 43−50.

(18) Santo, C. E.; Quaranta, D.; Grass, G. Antimicrobial metallic copper surfaces kill *Staphylococcus haemolyticus* via membrane damage. *Microbiol. Open* **2012**, *1*, 46−52.

(19) Grass, G.; Rensing, C.; Solioz, M. Metallic copper as an antimicrobial surface. *Appl. Environ. Microbiol.* **2011**, *77*, 1541−1547.

(20) Santra, S. *Silica-based antibacterial and antifungal nanoformulation*. In U.S. Patent 8221791, 2010.

(21) Brezova, V.; Valko, M.; Breza, M.; Morris, H.; Telser, J.; Dvoranova, D.; Kaiserova, K.; Varecka, L.; Mazur, M.; Leibfritz, D. Role of radicals and singlet oxygen in photoactivated DNA cleavage by the anticancer drug camptothecin: an electron paramagnetic resonance study. *J. Phys. Chem. B* **2003**, *107*, 2415−2425.

(22) Stephens, B.; Felkel, H., Jr.; Spinelli, W. Spectrophotometric determination of copper and iron subsequent to the simultaneous extraction of bis(2,9-dimethyl-1,10-phenanthroline) copper(I) and bis[2,4,6-tri(2-pyridyl)-1,3,5-triazine] iron(II) into propylene carbonate. *Anal. Chem.* **1974**, *46*, 692−696.

(23) Rensing, C.; Fan, B.; Sharma, R.; Mitra, B.; Rosen, B. P. CopA: an *Escherichia coli* Cu(I)-translocating P-type ATPase. *Proc. Natl. Acad. Sci. U.S.A.* **2000**, *97*, 652−656.

(24) CLSI. *Methods for Dilution Antimicrobial Susceptibility Tests for Bacteria That Grow Aerobically; Approved Standard*, 9th ed.; CLSI Document M07-A9; Clinical and Laboratory Standards Institute: Wayne, PA, USA, 2012.

(25) Pettit, R. K.; Weber, C. A.; Kean, M. J.; Hoffmann, H.; Pettit, G. R.; Tan, R.; Franks, K. S.; Horton, M. L. Microplate Alamar blue assay for *Staphylococcus epidermidis* biofilm susceptibility testing. *Antimicrob. Agents Chemother.* **2005**, *49*, 2612−2617.

(26) ICDD. *Powder Diffraction File Inorganic Phases Search Manual. Inorganic Phases*; Joint Committee on Powder Diffraction Standards: Newtown Square, PA, USA, 1984.

(27) Nefedov, V.; Zhumadilov, E.; Kopytova, T. Y. Comparison of the chemical shifts of X-ray electron and Auger lines. *J. Struct. Chem.* **1977**, *18*, 549−553.

(28) Yoshida, T.; Y, K.; Sawada, S. An X-ray photoelectron spectroscopic study of biuret metal complexes. *Bull. Chem. Soc. Jpn.* **1978**, *51*, 1561−1562.

(29) Strohmeier, B. R.; Levden, D. E.; Field, R. S.; Hercules, D. M. Surface spectroscopic characterization of $CuAl_2O_3$ catalysts. *J. Catal.* **1985**, *94*, 514−530.

(30) Ghijsen, J.; Tjeng, L.; Van Elp, J.; Eskes, H.; Westerink, J.; Sawatzky, G.; Czyzyk, M. Electronic structure of Cu_2O and CuO. *Phys. Rev. B* **1988**, *38*, 11322−11330.

(31) Schön, G. ESCA studies of Cu, Cu_2O and CuO. *Surf. Sci.* **1973**, 35, 96−108.

JOURNAL OF AGRICULTURAL AND FOOD CHEMISTRY

Article

pubs.acs.org/JAFC

Identification of Pheromone Synergists for *Rhynchophorus ferrugineus* Trapping Systems from *Phoenix canariensis* Palm Volatiles

Sandra Vacas,* María Abad-Payá, Jaime Primo, and Vicente Navarro-Llopis

Centro de Ecología Química Agrícola, Instituto Agroforestal del Mediterráneo, Universitat Politècnica de València, edificio 6C, 5ª planta, Cmno. de Vera s/n, 46022 Valencia, Spain

ABSTRACT: Trapping systems for the red palm weevil, *Rhynchophorus ferrugineus* Olivier, rely on the use of natural plant odor sources to boost the attractiveness of the aggregation pheromone. The identification of the key odorants involved in attraction is essential in the development of a synthetic pheromone synergist to replace the nonstandardized use of plant material in traps. Canary Islands date palms (*Phoenix canariensis*) have become preferred hosts for *R. ferrugineus* in Europe; thus, the volatile profile of different *P. canariensis* plant materials, including healthy and infested tissues, is investigated in the present work by means of solid phase microextraction (SPME-GC-MS), aimed to identify pheromone synergists. The electroantennography (EAG) response of the compounds identified was recorded, as well as the preliminary field response of several EAG-active compounds. The so-called "palm esters" (ethyl acetate, ethyl propionate, ethyl butyrate, and propyl butyrate) elicit the strongest EAG responses but performed poorly in the field. Mixtures of esters and alcohols give evidence of better performance, but release rates need further optimization.

KEYWORDS: *red palm weevil, Rhynchophorus ferrugineus (Coleoptera: Curculionidae), ferrugineol, kairomone, host attractants, Phoenix canariensis (Arecales: Arecaceae), Canary Islands date palm, SPME*

INTRODUCTION

Integrated pest management strategies play an important role in controlling the red palm weevil, *Rhynchophorus ferrugineus* (Olivier) (Coleoptera: Curculionidae), given this pest's concealed nature and its exceptional colonization capability. Larvae are the most destructive stage of this weevil as they penetrate deep into the stem, damage its internal tissues, disrupt nutrient transport, and even lead to tree collapse and death.[1] Red palm weevil was first described to attack coconut palms, but it has been reported to affect 30 palm species belonging to 17 different genera.[2−4] Since *R. ferrugineus* invaded the Mediterranean Basin and reached southern Europe in 1993,[5] it has become the most damaging pest for Canary Islands date palms [*Phoenix canariensis* (hort. ex Chabaud) (Arecales: Arecaceae)].[6−8] In the past 20 years in Europe, *R. ferrugineus* has demonstrated a strong preference for *P. canariensis* compared with other palm species such as *Phoenix dactylifera* L. or *Washingtonia* spp. In our region (the east coast of Spain), local government institutions have reported this preference on the basis of inspections made of thousands of palm trees. By way of example, 16% of a total of 2699 *P. canariensis* in the city of Valencia (eastern Spain) were infested during 2011−2012, whereas only 0.7% of a total 5925 *P. dactylifera* specimens were infested.[9] Moreover, the red palm weevil seems to prefer male to female Canary Islands palms. According to the Detection and Eradication Campaign developed by the regional Valencian government, 76.2% of the infested *P. canariensis* were male specimens, taking into account that the sex ratio in this area is ca. 60:40 (males/females) (data provided by Conselleria de Agricultura, Peixca i Alimentació, Generalitat Valenciana). The same was observed in the city of Valencia, where 74.7% of the attacked *P. canariensis* were males and 18.5% were females, with 6.8% undetermined.[9]

Generally, attack is detected only after the palm has been seriously damaged; thus, most efforts are made to develop methods that detect early stages of infestations, such as visual inspection, sniffing dogs,[10,11] and acoustic[12−14] and thermal detection.[15] Preventive and curative procedures have been investigated and proposed as control methods, which include chemical control[16−20] and biological control with entomopathogenic organisms, nematodes,[21−23] and fungi.[24,25] However, trapping systems through mass trapping play an important role for both detection and control purposes. This system does not create resistances, but allows population monitoring and helps enhance the efficacy of other control methods to reduce weevil populations and the number of insecticide applications. The introduction of pheromone-based trapping systems was possible thanks to the discovery of the red palm weevil aggregation pheromone component 4-methyl-5-nonanol (ferrugineol).[26] In general, male-produced aggregation pheromones for palm weevil consist of 8−10 carbon, methyl-branched secondary alcohols.[27] However, the attractant power of these pheromones tends to be weak in the traps deployed in the field, and the presence of synergistic plant tissues or other food attractants is required.[28−30] Unfortunately, this is a nonstandardized, costly, and cumbersome practice because the plant material needs to be replaced frequently to maintain the attractant level.

Received: February 26, 2014
Revised: June 11, 2014
Accepted: June 14, 2014
Published: June 14, 2014

ACS Publications © 2014 American Chemical Society

Table 1. Preliminary Field Tests

no.	date	location	no. of blocks	attractant[a]	reference[b]
1	May−Aug 2013	Godelleta (Valencia)	3	ph + acetoin ph + esters mix ph + esters mix + acetoin	ph
2	Sept−Oct 2013	Manises (Valencia)	3	ph + EtAc + EtOH ph + EtAc + alcohol mix	ph
3	Oct−Nov 2013	Valencia	3	ph + EtAc + phenyl-EtOH ph + EtAc + EtOH	ph
4	Sept−Nov 2013	Elche (Alicante)	5	ph + EtAc + alcohol mix ph + EtAc + phenyl-EtOH only ph	complete bait
5	Nov 2013−March 2014	Elche (Alicante)	5	ph + EtAc:EtOH (1:3) ph + EtAc:EtOH (3:1) ph + EtAc only ph	complete bait

[a]Attractant contained in Picusan traps: ph, aggregation pheromone dispenser (Ferosan RF); esters mix, (ethyl acetate + ethyl propionate + ethyl butyrate + propyl butyrate); EtAc, ethyl acetate; EtOH, ethanol; alcohol mix, (ethanol + 3-methyl-1-butanol); phenyl-EtOH, 2-phenylethanol. [b]Reference attractant employed for the main comparison: ph, aggregation pheromone; complete bait, molasses (10%) + water (2 L) + plant material (*P. canariensis* stem pieces).

Adult female weevils are attracted to and oviposit in healthy, stressed, or damaged palms[31] as they are attracted by a range of stimuli. However, attractiveness for weevils is generally boosted by the fermentation volatiles emanating from wounds or those resulting from infestation.[27,32] Ethyl esters are common volatile constituents in fermenting palm oils, sap, and plant tissues.[27,29,30] Many of these esters elicit significant electrophysiological responses in palm weevil species. Currently, however, they still prove less effective than the plant material used in traps when employed alone or combined.

This work investigates the volatile profile of different *P. canariensis* plant materials, including healthy and infested tissues, by means of solid phase microextraction (SPME), with a view to identifying pheromone synergists for red palm weevil. For this purpose, both the electroantennography (EAG) response of the identified volatiles and the preliminary field response of the most EAG-active compounds were recorded.

MATERIALS AND METHODS

Plant Material. Different *P. canariensis* palm materials were sampled for volatile collection and compound identification: (1) freshly cut petiole and rachis pieces of nonsprayed female and male *P. canariensis* palm leaves; (2) fresh healthy meristem stem tissues; (3) male inflorescence, including rachis and flowers; (4) infested stem tissues, upon which weevil larvae were feeding; (5) leaf pieces fermented in a 10% sugar water solution under field conditions; and (6) fermented stem pieces from the traps of the monitoring system deployed in Elche (Alicante, eastern Spain), which were also baited with a 10% molasses water solution. Fermented materials were collected when they still displayed attractant activity (1 or 2 weeks old).

Volatile Collection. The three replicates of each experimental case were simultaneously collected by SPME using Supelco SPME holders equipped with a polydimethylsiloxane/divinylbenzene fiber (PDMS/DVB), film thickness = 100 μm (Supelco Inc., Bellefonte, PA, USA). SPME fibers were conditioned before volatile sampling in a GC injector at 250 °C for 10 min under a 20 mL/min helium flow rate.

Each sample was placed inside a 1.3 L glass chamber with a screw-top polytetrafluoroethylene (PTFE)−silicone septum cap (Supelco Inc.) in the middle. Chambers were connected to the outlet of an air compressor (Jun-air Intl. A/S, Norresundby, Denmark) coupled with an AZ 2020 air purifier system (Claind Srl, Lenno, Italy) to provide ultrapure air (amount of total hydrocarbons <0.1 ppm). Before each chamber, an ELL-FLOW digital flowmeter (Bronkhorst High-Tech BV, Ruurlo, The Netherlands) was installed to run an air flow of 20 mL/min during sampling. Under these conditions, SPME needles were inserted through the septa, and fibers were exposed to each sample for the required period (3 h for the affected and fermented samples; 20 h for the green material) at 26 ± 1 °C. Then, fibers were removed and inserted into the GC injection port to desorb volatiles.

Detection and Identification of Volatiles. SPME fibers were thermally desorbed into the GC injection port, set at 250 °C for 1 min, and operated in the splitless mode. The extracted volatiles were analyzed by gas chromatography coupled with mass spectrometry (GC-MS) using a Clarus 600 GC-MS (PerkinElmer Inc., Wellesley, MA, USA). The column used was a 30 m × 0.25 mm i.d., 0.25 μm, ZB-5MS fused silica capillary column (Phenomenex Inc., Torrance, CA, USA). The oven was held at 40 °C for 3 min and then programmed at 3 °C/min to 60 °C, followed by 6 °C/min to 160 °C; when reached, temperature was raised to 260 °C at 12 °C/min and maintained at 260 °C for 5 min. Helium was used as the carrier gas with a flow rate of 1.2 mL/min. Detection was performed in the EI mode (ionization energy, 70 eV; source temperature, 180 °C), and spectra acquisition was done in the scanning mode (mass range m/z 35−400). Chromatograms and spectra were recorded with GC-MS Turbomass software version 5.4 (PerkinElmer Inc.).

Compounds were identified by comparing their retention times and mass spectra with those of pure standards (confirmed identification). They were all purchased from Sigma-Aldrich Química SA (Madrid, Spain), and their purity was ≥98−99% by GC-MS except for β-myrcene (≥90%); limonene, α-copaene, and aromadendrene (>90%, sum of enantiomers); ocimene and farnesene (90%, mixture of isomers); β-caryophyllene (≥80%); and 3-hydroxy-2-butanone (>96%). Unfortunately, it was not possible to obtain the commercial standards of some compounds, so their identification was tentative and based on high-probability matches (>80%) according to the NIST MS Search routine (NIST Mass Spectral Search Program for the NIST \EPA\NIH Mass Spectral Library, version 2.0, build 4/2005).

Electrophysiological Antennal Activity. Once identified, the electroantennographic response triggered by the compounds was

Table 2. Compounds Detected in the Different *P. canariensis* Samples

				percentage of the total chromatogram area[a] (mean ± SE)						
				palm leaves						
RT[b]	formula	name	ID[c]	female	male	healthy tissue	inflorescence	affected stem	fermented leaves	fermented stem
				Acids						
0.71	$C_2H_4O_2$	acetic acid	C					2.62 ± 0.94		
2.67	$C_3H_6O_2$	propanoic acid	C					2.07 ± 0.18		3.31 ± 0.92
5.57	$C_4H_8O_2$	butanoic acid	C					24.82 ± 1.34		6.09 ± 2.48
6.11	$C_4H_8O_2$	isobutanoic acid	C						0.31 ± 0.11	0.24 ± 0.15
7.85	$C_5H_{10}O_2$	isopentanoic acid	C					0.38 ± 0.14		
9.10	$C_5H_{10}O_2$	pentanoic acid	C					0.39 ± 0.04		
				Alcohols						
0.33	C_2H_6O	ethanol	C						3.76 ± 0.55	
0.51	$C_4H_{10}O$	1-butanol	C					0.66 ± 0.16		
1.02	$C_5H_{12}O$	2-methyl-1-butanol	C						0.07 ± 0.01	
2.53	$C_5H_{12}O$	3-methyl-1-butanol	C						0.61 ± 0.13	
2.61	$C_5H_{12}O$	1-pentanol	C					2.90 ± 0.45	0.65 ± 0.12	
16.30	$C_8H_{10}O$	2-phenylethanol	C					5.47 ± 0.56		
				Aldehydes						
4.47	$C_6H_{12}O$	hexanal	C				0.04 ± 0.02			
7.94	$C_7H_{14}O$	heptanal	C				0.16 ± 0.05			
12.73	$C_8H_{16}O$	octanal	C				0.02 ± 0.02			
14.28	C_8H_8O	2-phenylethanal	C				0.02 ± 0.02			
16.50	$C_9H_{18}O$	nonanal	C				0.24 ± 0.23			
19.65	$C_{10}H_{20}O$	decanal	C	1.52 ± 0.37	nd		0.04 ± 0.03			
				Alkanes						
19.58	$C_{12}H_{26}$	dodecane	C	0.43 ± 0.06	2.80 ± 0.60					
21.96	$C_{13}H_{28}$	tridecane	C			0.09 ± 0.03	0.03 ± 0.01		0.30 ± 0.05	
24.33	$C_{14}H_{30}$	tetradecane	C	0.76 ± 0.08	1.70 ± 0.40				0.18 ± 0.02	
26.56	$C_{15}H_{32}$	pentadecane	C				1.60 ± 0.28		2.74 ± 1.12	
28.40	$C_{16}H_{34}$	hexadecane	C			0.06 ± 0.01	0.03 ± 0.00			
30.25	$C_{17}H_{36}$	heptadecane	C				0.48 ± 0.20			
31.53	$C_{18}H_{38}$	octadecane	C				0.04 ± 0.00			
32.64	$C_{19}H_{40}$	nonadecane	C				0.24 ± 0.03			
				Alkenes						
26.33	$C_{15}H_{30}$	1-pentadecene	T						0.13 ± 0.07	
29.92	$C_{17}H_{34}$	3-heptadecene	T				0.51 ± 0.10			
32.37	$C_{19}H_{38}$	1-nonadecene	C				0.06 ± 0.02			
				Benzoates						
16.39	$C_8H_8O_2$	methyl benzoate	C			8.21 ± 0.50				
18.84	$C_9H_{10}O_2$	ethyl benzoate	C			85.42 ± 1.43		0.16 ± 0.04		0.58 ± 0.13
19.35	$C_8H_8O_3$	methyl salicylate	C			1.91 ± 0.98				
19.85	$C_{10}H_{12}O_2$	isopropyl benzoate	T			0.11 ± 0.08				
21.34	$C_9H_{10}O_3$	ethyl salicylate	C			1.24 ± 0.45				

dx.doi.org/10.1021/jf502663y | J. Agric. Food Chem. 2014, 62, 6053−6064

Table 2. continued

RT[b]	formula	name	ID[c]	percentage of the total chromatogram area[a] (mean ± SE)						
				palm leaves						
				female	male	healthy tissue	inflorescence	affected stem	fermented leaves	fermented stem
						Benzoates				
21.35	$C_{10}H_{12}O_2$	propyl benzoate	C			1.44 ± 0.27				
22.79	$C_{11}H_{14}O_2$	isobutyl benzoate	C			0.63 ± 0.08				
23.89	$C_{11}H_{14}O_2$	butyl benzoate	C			0.41 ± 0.22				
25.37	$C_{12}H_{16}O_2$	isopentyl benzoate	T			0.04 ± 0.01				
						Esters				
0.91	$C_4H_8O_2$	ethyl acetate	C			0.34 ± 0.16		4.41 ± 0.53	33.47 ± 0.74	
2.03	$C_5H_{10}O_2$	ethyl propionate	C					1.95 ± 0.30	0.05 ± 0.01	
3.18	$C_6H_{12}O_2$	*sec*-butyl acetate	C					0.54 ± 0.15		0.44 ± 0.17
3.49	$C_6H_{12}O_2$	isobutyl acetate	C					0.12 ± 0.02	0.27 ± 0.08	
3.95	$C_6H_{12}O_2$	ethyl butyrate	C					21.95 ± 2.97		
4.90	$C_6H_{12}O_2$	butyl acetate	C					0.56 ± 0.17	0.09 ± 0.01	
6.12	$C_7H_{14}O_2$	ethyl 2-methylbutyrate	C					0.76 ± 0.06		
6.39	$C_7H_{14}O_2$	ethyl 3-methylbutyrate	T					0.77 ± 0.12		
7.28	$C_7H_{14}O_2$	*sec*-butyl propionate	T							5.25 ± 1.79
7.51	$C_7H_{14}O_2$	isopentyl acetate	C					1.65 ± 0.36	20.46 ± 1.76	
8.10	$C_7H_{14}O_2$	propyl butyrate	C					0.46 ± 0.17		
8.33	$C_7H_{14}O_2$	ethyl pentanoate	C					1.50 ± 0.45		
8.75	$C_7H_{14}O_2$	pentyl acetate	C						0.14 ± 0.02	
8.92	$C_7H_{14}O_2$	butyl propionate	T					0.17 ± 0.06		
8.95	$C_7H_{14}O_2$	unknown (1)								0.67 ± 0.16
10.36	$C_8H_{16}O_2$	*sec*-butyl butyrate	T					1.29 ± 0.37		9.65 ± 4.82
10.80	$C_8H_{16}O_2$	isobutyl butyrate	C					0.37 ± 0.03		
11.51	$C_8H_{16}O_2$	isopentyl propionate	C					0.65 ± 0.06		
12.73	$C_8H_{16}O_2$	butyl butyrate	C					1.64 ± 0.09		
12.96	$C_8H_{16}O_2$	ethyl hexanoate	C					3.48 ± 0.26	0.08 ± 0.07	
14.24	$C_9H_{18}O_2$	isobutyl isopentanoate	T							0.58 ± 0.40
14.89	$C_9H_{18}O_2$	unknown (2)						2.40 ± 0.14		
15.14	$C_9H_{18}O_2$	isopentyl butyrate	C					5.45 ± 0.24		
16.58	$C_9H_{18}O_2$	ethyl heptanoate	C					1.06 ± 0.21		
17.64	$C_9H_{16}O_2$	ethyl cyclohexanecarboxylate	T					0.74 ± 0.10		
18.30	$C_{10}H_{20}O_2$	pentyl pentanoate	C					0.12 ± 0.02		
18.30	$C_9H_{10}O_2$	benzyl acetate	T						0.03 ± 0.01	
18.35	$C_{10}H_{20}O_2$	butyl hexanoate	T							0.16 ± 0.10
19.26	$C_{10}H_{20}O_2$	ethyl octanoate	C					3.95 ± 1.24	1.16 ± 0.37	
20.92	$C_{10}H_{12}O_2$	ethyl phenylacetate	C					0.36 ± 0.13	32.33 ± 1.17	
21.00	$C_{11}H_{22}O_2$	isopentyl hexanoate	T					0.05 ± 0.01		
21.10	$C_{10}H_{12}O_2$	*β*-phenylethyl acetate	C					0.38 ± 0.08		
21.83	$C_{11}H_{22}O_2$	ethyl nonanoate	C					0.38 ± 0.23	0.22 ± 0.03	
22.45	$C_{11}H_{14}O_2$	ethyl 3-phenylpropionate	T					0.09 ± 0.02		

dx.doi.org/10.1021/jf502663y | J. Agric. Food Chem. 2014, 62, 6053−6064

Table 2. continued

				percentage of the total chromatogram area[a] (mean ± SE)						
				palm leaves						
RT[b]	formula	name	ID[c]	female	male	healthy tissue	inflorescence	affected stem	fermented leaves	fermented stem
					Esters					
24.20	$C_{12}H_{24}O_2$	ethyl decanoate	C					1.13 ± 0.48	0.72 ± 0.12	
25.36	$C_{12}H_{16}O_2$	2-phenylethyl butyrate	T					0.11 ± 0.03		
28.20	$C_{14}H_{28}O_2$	ethyl laurate	C					0.17 ± 0.10	0.22 ± 0.06	
31.36	$C_{16}H_{32}O_2$	ethyl myristate	C				0.01 ± 0.00			
					Ketones					
0.93	C_4H_8O	2-butanone	C					2.14 ± 0.28		40.76 ± 12.11
2.11	$C_4H_8O_2$	3-hydroxy-2-butanone	C						0.10 ± 0.05	10.38 ± 2.23
4.68	$C_5H_{10}O_2$	2-hydroxy-3-pentanone	T							0.94 ± 0.19
8.10	$C_7H_{14}O$	2-heptanone	T							0.25 ± 0.10
16.14	$C_9H_{18}O$	2-nonanone	C					0.20 ± 0.13		1.70 ± 0.62
21.77	$C_{11}H_{22}O$	2-undecanone	T			0.09 ± 0.07				0.11 ± 0.06
					Phenols					
12.31	C_6H_6O	phenol	C							0.46 ± 0.09
15.68	C_7H_8O	*p*-cresol	C							0.64 ± 0.13
19.26	$C_8H_{10}O_2$	*p*-methylguaiacol	C					0.07 ± 0.05		
					Terpenes					
12.48	$C_{10}H_{16}$	*β*-myrcene	C	1.06 ± 0.30	1.30 ± 1.20					
13.81	$C_{10}H_{14}$	p-cymene	C	0.15 ± 0.15	0.80 ± 0.50					0.16 ± 0.03
13.97	$C_{10}H_{16}$	limonene	C	0.86 ± 0.32	0.60 ± 0.30					11.47 ± 3.97
14.33	$C_{10}H_{16}$	*Z*-*β*-ocimene	C	0.10 ± 0.07	0.60 ± 0.30					
14.72	$C_{10}H_{16}$	*E*-*β*-ocimene	C	1.39 ± 0.59	5.10 ± 0.90					
15.90	$C_{10}H_{16}$	*α*-terpinolene	C	0.26 ± 0.07	nd					
16.44	$C_{10}H_{18}O$	linalool	C							4.69 ± 1.22
22.72	$C_{15}H_{22}$	9,10-dehydroisolongifolene	T				0.10 ± 0.03			
23.29	$C_{15}H_{24}$	*α*-cubebene	C	1.11 ± 0.07	1.20 ± 0.30		2.22 ± 0.43		0.01 ± 0.01	
23.45	$C_{15}H_{24}$	unknown (3) (mw = 204)					0.11 ± 0.02			
23.57	$C_{15}H_{24}$	cyclosativene	T	12.30 ± 1.19	8.50 ± 1.60		0.70 ± 0.07			
23.81	$C_{15}H_{24}$	*α*-copaene	C	38.00 ± 2.24	33.20 ± 1.90		32.73 ± 2.54	0.05 ± 0.02	0.19 ± 0.10	0.03 ± 0.01
24.11	$C_{15}H_{24}$	*β*-cubebene	T	0.52 ± 0.28	0.50 ± 0.20		1.78 ± 0.49			
24.33	$C_{15}H_{24}$	unknown (4) (mw = 204)		0.44 ± 0.14	0.40 ± 0.10					
24.45	$C_{15}H_{22}$	unknown (5) (mw = 202)					45.10 ± 3.32			
24.52	$C_{15}H_{24}$	*α*-gurjunene	T	1.05 ± 0.04	1.00 ± 0.20		0.45 ± 0.01			
24.62	$C_{15}H_{22}$	unknown (6) (mw = 202)					0.59 ± 0.05			
24.85	$C_{15}H_{24}$	*β*-caryophyllene	C	2.72 ± 0.27	3.30 ± 0.50		0.68 ± 0.19		0.17 ± 0.18	
25.01	$C_{15}H_{24}$	unknown (7) (mw = 204)		0.40 ± 0.27	0.70 ± 0.05		0.07 ± 0.02			
25.24	$C_{15}H_{22}$	unknown (8) (mw = 202)					1.81 ± 0.21			
25.65	$C_{15}H_{24}$	*α*-caryophyllene	C				0.11 ± 0.02		0.02 ± 0.01	
25.67	$C_{15}H_{24}$	aromadendrene	C	2.03 ± 0.17	2.10 ± 0.30					
25.72	$C_{15}H_{24}$	alloaromadendrene	T				5.72 ± 0.40			

dx.doi.org/10.1021/jf502663y | J. Agric. Food Chem. 2014, 62, 6053−6064

Table 2. continued

RT[b]	formula	name	ID[c]	percentage of the total chromatogram area[a] (mean ± SE)						
				palm leaves						
				female	male	healthy tissue	inflorescence	affected stem	fermented leaves	fermented stem
				Terpenes						
26.02	$C_{15}H_{24}$	τ-muurolene	T	1.72 ± 0.18	1.00 ± 0.10		0.35 ± 0.16			
26.16	$C_{15}H_{24}$	germacrene D	T				1.12 ± 0.51			
26.47	$C_{15}H_{24}$	τ-elemene	T				0.40 ± 0.19			
26.54	$C_{15}H_{24}$	α-muurolene	T	1.42 ± 0.31	1.20 ± 0.30		0.30 ± 0.05			
26.67	$C_{15}H_{24}$	α-farnesene	C	5.07 ± 0.84	4.40 ± 0.70					
26.84	$C_{15}H_{24}$	τ-cadinene	T				0.09 ± 0.03			
26.95	$C_{15}H_{24}$	β-cadinene	T	25.69 ± 4.00	27.90 ± 4.70		1.82 ± 0.50	0.03 ± 0.01	0.43 ± 0.14	0.56 ± 0.30
27.06	$C_{15}H_{24}$	δ-cadinene	T				0.05 ± 0.02			
27.26	$C_{15}H_{24}$	unknown (9) (mw = 204)					0.23 ± 0.07			
				Other						
7.96	C_8H_8	styrene	C						0.02 ± 0.01	
13.01	$C_7H_{10}N_2$	2,3,5-trimethylpyrazine	T							0.29 ± 0.05
13.67	$C_8H_{10}O$	4-methylanisole	C						0.43 ± 0.06	
24.92	$C_{12}H_{12}$	2,6-dimethylnaphthalene	C	0.99 ± 0.41	2.10 ± 0.30				0.13 ± 0.04	
27.40	$C_{15}H_{20}$	calacorene	T					0.08 ± 0.04	0.92 ± 0.32	

[a]Means of three replicates. [b]RT, retention time (min) on ZB-5 column (30 m × 0.25 mm i.d. × 0.25 μm; Phenomenex Inc., Torrance, CA, USA). [c]Identification of the compound: C, confirmed with commercial standard; T, tentative with spectra and high probability matches (>80%) according to NIST mass spectral database.

dx.doi.org/10.1021/jf502663y | J. Agric. Food Chem. 2014, 62, 6053−6064

evaluated with a Syntech IDAC 2 acquisition controller and a Syntech CS-55 stimulus controller (Ockenfels Syntech GmbH, Kirchzarten, Germany), whereas GC-EAD 32 (v 4.3) software was employed for data acquisition. The EAG tests for each compound had seven replicates per sex, with each antenna belonging to seven different weevils. Individuals were collected from the field, maintained at 26 ± 2 °C under photoperiod conditions (10 h light and 14 h dark), and fed apples. Antennae were removed from living insects, cut off as close as possible to their base with fine-point stainless steel entomology scissors, whereas the club remained unaltered. After excision, the antenna was placed immediately on a fork holder, the flat tips of which had been previously covered with a small bead of Spectra 360 electrode gel (Parker Laboratories Inc., Fairfield, NJ, USA). The holder was then mounted in an EAG probe type PRG-2 (Syntech) to be connected directly to the IDAC-2 system. Test and control samples were prepared in hexane solution, and 1 μL aliquots were applied to filter paper strips. The solvent was allowed to evaporate for 30 s before the strip was placed into a disposable Pasteur pipet. The olfactory stimulus (1 s duration) was delivered into a continuous humidified charcoal-filtered air stream (400 mL/min) toward the antenna, after placing the pipet tip into the hole of the tube carrying the air stream. Each antenna was stimulated successively with the solvent, the positive reference (1 μg of ferrugineol), and no more than four different test compounds (1 μg). Stimuli were applied at 3 min intervals. To eliminate the variability of the response due to the different antennae conditions, the EAG test results are provided as the ratio: mV_C/mV_F, where C is the response for each compound and F is the response of the reference stimulus, which was 1 μg of ferrugineol in all cases.

Preliminary Field Tests. The compounds that triggered the most significant electrophysiological responses were included in the preliminary field tests to study the weevils' actual response under field conditions, using Picusan traps (Sansan Prodesing SL, Náquera, Valencia, Spain), the bases of which were filled with water.[33] All of the trials were designed as randomized block assays and were carried out in different locations in the Valencian community (on the Spanish eastern coast): Godelleta, Manises, Valencia, and Elche. The revision of catches and rotation of traps were performed on a weekly basis. In all of the trials, the traps within each block were separated by at least 30 m and the distance between blocks was at least 100 m.

The different attractants compared are detailed in Table 1, which also includes the number of blocks in each trial and the dates when the tests were conducted. The aggregation pheromone (ph) dispenser employed in all cases was Ferosan RF (Sansan Prodesing SL), loaded with 1 g of ferrugineol. Mixtures of compounds were formulated in low-density polyethylene vials to obtain controlled release rates. The gravimetric method was employed to assess the amount of active ingredients released in relation to the aging time. In parallel to the field trials, three corresponding dispensers of each type were aged under the same field conditions inside the same type of trap. These dispensers were weighed weekly in the laboratory on a precision balance. The weight differences over a period were referred to as the active mixture released from the dispenser. To obtain the mean emission level for each dispenser, recorded weights were fitted to linear regression models, $y = a + bx$, where y is the weight of the dispenser and x is the corresponding aging days. The resulting mean release rates refer to the mixtures released from the polyethylene vials. In addition, several samples of aged dispensers were also analyzed by gas chromatography (GC-FID) to check the proportions at which ethyl acetate and ethanol were emitted in the mixtures tested in trial 5.

The number of weevils captured with each experimental attractant was compared with that obtained in the traps baited only with ferrugineol (ph) or with the complete bait employed in the Valencian community red palm weevil monitoring network, which is composed of water, 10% molasses solution, and *P. canariensis* palm stem pieces.

The number of males, females, or total weevils recorded during each trapping period was divided by the number of days between dates to calculate the weevils per trap and day index (WTD). Log (WTD+1) transformation was applied to normalize the errors distribution prior to the analysis of variance (ANOVA), followed by LSD test (at $P < 0.05$). The Statgraphics Centurion XVI package was employed to perform the statistical analysis (Statpoint Technologies Inc., Warranton, VA, USA).

RESULTS AND DISCUSSION

Overview of Detected Compounds. Table 2 reports the 122 compounds detected in the different *P. canariensis* palm samples. Of these, 81 were confirmed with commercial standards and 32 were tentatively identified (most of them being sesquiterpenes with no available standards).

The main constituents of the palm leaf volatile samples were identified as cyclosativene, α-copaene, and δ-cadinene which, all together, assumed ∼70% of the total chromatogram area. Terpene hydrocarbons (mostly monoterpenes $C_{10}H_{16}$ and sesquiterpenes $C_{15}H_{24}$) are the largest group of airborne natural products emitted by vegetation and are responsible for both floral and fruity aromas and a mild, wood-like odor.[34] The remaining compounds detected in palm leaves were other terpenes, except for ∼5%, which comprised alkanes, aldehydes, and 2,6-dimethylnaphthalene (probably a contaminant from the aeration system). The volatile profiles of the female and male *P. canariensis* palm leaves were not significantly different if compared to the reported qualitative and relative composition (Table 2); only decanal and α-terpinolene were not detected in the male profile. Consequently, the volatile profile does not seem to explain the greater susceptibility of male palms observed in the field. Thus, other physical factors could affect the oviposition preferences of females or make larvae's feeding habits difficult.

Benzoates, such as ethyl and methyl benzoate, were the main constituents of the healthy tissue volatile profile (∼99% of the total chromatogram area), which are reported to confer floral and fruity odors.[35,36] As expected, male inflorescence presented traces of several aldehydes (0.5%), which are commonly found in essential oils and contribute to their favorable odors (citrusy, floral, and green aromas).[37] Several alkanes were also detected (2.4%), but sesquiterpenes were the main constituents. Unfortunately, it was not possible to identify the most abundant compound (45.1%), but the mass spectrum suggests a sesquiterpene structure [m/z 91 (50), 105 (45), 119 (100), 131 (40), 132 (50), 145 (38), 159 (25), 187 (21), 202 (12)] with a molecular weight of 202. Nonetheless, some GC-EAD coupled tests performed with SPME replicates of these samples did not evidence any electrophysiological activity for this unidentified compound (data not shown).

The volatile profile of the palm material dramatically changes when tissues are either affected by the pest or subjected to fermentation processes in traps; then esters, acids, alcohols, and ketones are the main constituents of the volatile profile of this plant material (Table 2). Short-chain fatty acids (acetic, propanoic, butanoic, etc.), associated with off-flavors, are the main products of the fermentative microorganisms responsible for anaerobic plant fiber degradation. A substantial part of many arthropods' diet consists of plant-derived polymers, such as lignin, hemicellulose, and cellulose,[38] which is the case for *R. ferrugineus* larvae. After egg hatching, larvae bore galleries into the palm and leave a frass, composed of excrements and plant debris with a high water content. The production of CO_2, 3-hydroxy-2-butanone (acetoin), ethanol, and ethyl lactate, among others, is associated with the bacterial community present in the frass.[39] In general, the relative distribution of the volatiles in degraded samples can be determined by several factors during fermentation, including microorganism species and/or strain, fermentation temperature, nutrient availability,

dx.doi.org/10.1021/jf502663y | J. Agric. Food Chem. 2014, 62, 6053−6064

Table 3. Relative[a] Electrophysiological Antennal Responses (Mean ± SE)[b] Triggered by Compounds Detected in the Different Palm Materials

compound	ratio males	ratio females	compound	ratio males	ratio females
Esters			**Ketones**		
propyl butyrate	1.24 ± 0.11	0.75 ± 0.06	3-hydroxy-2-butanone	1.10 ± 0.11	1.01 ± 0.03
ethyl propionate	1.20 ± 0.16	1.06 ± 0.09	6-methyl-5-hepten-2-one	0.83 ± 0.06	0.68 ± 0.06
ethyl butyrate	1.17 ± 0.07	0.93 ± 0.04	acetophenone	0.71 ± 0.05	0.70 ± 0.03
ethyl 2-methylbutyrate	1.11 ± 0.08	0.83 ± 0.04	2-pentanone	0.70 ± 0.04	0.73 ± 0.08
ethyl valerate	1.01 ± 0.05	0.74 ± 0.05	2-hexanone	0.67 ± 0.04	0.68 ± 0.04
ethyl acetate	0.77 ± 0.07	1.01 ± 0.16	2-nonanone	0.58 ± 0.05	0.67 ± 0.04
ethyl hexanoate	0.98 ± 0.11	0.78 ± 0.05	2-butanone	0.57 ± 0.06	0.58 ± 0.06
ethyl heptanoate	0.92 ± 0.09	0.68 ± 0.05	*p*-methylacetophenone	0.61 ± 0.04	0.51 ± 0.02
ethyl lactate	0.90 ± 0.05	0.77 ± 0.04	*p*-ethylacetophenone	0.59 ± 0.06	0.47 ± 0.05
isoamyl propionate	0.89 ± 0.08	0.79 ± 0.03			
propyl propionate	0.89 ± 0.04	0.88 ± 0.02	**Aldehydes**		
sec-butyl acetate	0.88 ± 0.08	0.71 ± 0.05	nonanal	0.82 ± 0.12	0.81 ± 0.06
butyl butyrate	0.85 ± 0.08	0.77 ± 0.10	hexanal	0.64 ± 0.05	0.69 ± 0.11
ethyl isobutyrate	0.84 ± 0.06	0.89 ± 0.06	decanal	0.59 ± 0.08	0.60 ± 0.06
methyl butyrate	0.84 ± 0.04	0.91 ± 0.06	heptanal	0.46 ± 0.03	0.44 ± 0.04
ethyl decanoate	0.81 ± 0.08	0.59 ± 0.11	octanal	0.40 ± 0.05	0.47 ± 0.06
isoamyl butyrate	0.78 ± 0.06	0.72 ± 0.10			
methyl isovalerate	0.74 ± 0.07	0.69 ± 0.05	**Benzoates**		
octyl acetate	0.72 ± 0.12	0.66 ± 0.07	methyl benzoate	0.79 ± 0.07	0.58 ± 0.06
isoamyl acetate	0.70 ± 0.04	0.66 ± 0.05	methyl salicylate	0.70 ± 0.05	0.61 ± 0.06
pentyl acetate	0.70 ± 0.06	0.57 ± 0.11	ethyl salicylate	0.68 ± 0.02	0.67 ± 0.05
ethyl octanoate	0.63 ± 0.02	0.85 ± 0.04	isobutyl benzoate	0.60 ± 0.05	0.61 ± 0.05
heptyl acetate	0.58 ± 0.08	0.54 ± 0.05	propyl benzoate	0.59 ± 0.04	0.55 ± 0.04
ethyl laurate	0.57 ± 0.07	0.53 ± 0.06	butyl benzoate	0.57 ± 0.02	0.51 ± 0.04
benzyl acetate	0.52 ± 0.04	0.56 ± 0.08	ethyl benzoate	0.52 ± 0.04	0.49 ± 0.04
ethyl myristate	0.49 ± 0.04	0.47 ± 0.02			
decyl acetate	0.49 ± 0.05	0.72 ± 0.12	**Phenols**		
butyl acetate	0.47 ± 0.03	0.61 ± 0.06	*p*-ethylguaiacol	0.60 ± 0.06	0.61 ± 0.07
			p-cresol	0.51 ± 0.05	0.44 ± 0.07
Alcohols			*p*-methylguaiacol	0.52 ± 0.06	0.51 ± 0.04
2-phenylethanol	0.85 ± 0.06	1.10 ± 0.12	phenol	0.50 ± 0.06	0.58 ± 0.05
2-methyl-1-butanol	0.87 ± 0.06	0.76 ± 0.05			
1-butanol	0.79 ± 0.11	0.89 ± 0.08	**Terpenes**		
3-methyl-1-butanol	0.79 ± 0.03	0.82 ± 0.04	limonene	0.69 ± 0.06	0.61 ± 0.05
1-pentanol	0.78 ± 0.07	0.86 ± 0.05	α-phellandrene	0.68 ± 0.05	0.46 ± 0.07
ethanol	0.63 ± 0.05	0.73 ± 0.04	α-pinene	0.67 ± 0.05	0.59 ± 0.03
2,3-butanediol	0.63 ± 0.03	0.64 ± 0.06	aromadendrene	0.65 ± 0.04	0.53 ± 0.05
1,3-butanediol	0.53 ± 0.06	0.43 ± 0.06	β-caryophyllene	0.53 ± 0.04	0.51 ± 0.08
			α-copaene	0.43 ± 0.06	0.53 ± 0.10
Acids			**Other**		
acetic acid	0.73 ± 0.12	0.74 ± 0.10	anisole	0.75 ± 0.03	0.80 ± 0.05
butyric acid	0.56 ± 0.08	0.78 ± 0.12	2-phenethyl acetate	0.76 ± 0.06	0.69 ± 0.06
isovaleric acid	0.45 ± 0.06	0.46 ± 0.08	dimethyl sulfide	0.61 ± 0.05	0.58 ± 0.04
			dimethyl disulfide	0.65 ± 0.06	0.50 ± 0.08

[a]Relative response: ratio = (mV compound)/(mV ferrugineol). [b]Means of seven replicates for each sex.

pH, unsaturated fatty acid levels, etc.[40−42] The formation of fatty acid ethyl esters and acetate esters confers floral and fruity sensory properties. Fatty acid esters (such as ethyl butyrate, ethyl hexanoate, and ethyl octanoate) result from the ethanolysis of acylCoA, which is produced during fatty acid synthesis or degradation. Acetate esters (such as butyl acetate, isoamyl acetate, hexyl acetate, and phenethyl acetate) are formed from the reaction of acetylCoA with the alcohols that result from the degradation of amino acids, carbohydrates, and lipids.[40,43] Biodegradation of lignin from plant tissues by rot fungi and bacteria can also generate the phenolic compounds detected (guaiacol, *p*-methylguaiacol, etc.),[44] which are associated with smoky or spicy trait.[45]

Electrophysiological Antennal Activity. Seventy-four compounds were tested for EAG responses (Table 3). The largest number of significant responses was elicited by the esters identified in the degraded samples for both male and female weevils, followed by alcohols and ketones. Propyl butyrate, ethyl propionate, ethyl butyrate, ethyl 2-methylbutyrate, ethyl valerate, and 3-hydroxy-2-butanone (acetoin) elicited the most significant responses, which were comparable to the reference ferrugineol (ratio ≥1) for males, whereas 2-phenylethanol, ethyl propionate, ethyl acetate, and acetoin

were the most active for females. The palm esters (ethyl propionate, ethyl acetate, ethyl butyrate, etc.) that elicited significant antennal responses have already been reported by Gries et al.[29] for *R. phoenicis* L., *R. palmarum* L., *R. cruentatus* (Fabricius), *R. ferrugineus*, *R. vulneratus* (Panz.), and *R. bilineatus* (Montrouzier). Later, while testing the antennal responses of several palm esters (ethyl acetate, ethyl butyrate, ethyl isobutyrate, and ethyl lactate), Guarino et al.[46] reported that ethyl propionate was the ester that elicited the strongest response for *R. ferrugineus* and for both females and males. Aldehydes and terpene hydrocarbons, these being characteristic compounds of inflorescence and palm leaves, elicited only intermediate responses in our tests.

Preliminary Field Activity. Nevertheless, the EAG tests do not provide conclusive ideas about the attractiveness and potential of each compound as semiochemical under field conditions. Indeed, the mechanisms responsible for EAG and field activity are different, and possible correlations between them should be considered with caution, as should the possible synergistic effects of blends for single compounds. For example, Giblin-Davis et al.[47] reported the attraction of *R. cruentatus* to some fermentation products. Yet, whereas isopropyl acetate elicited a major EAG response but not significant attractiveness in traps, ethanol elicited a minor relative EAG response, but proved attractive in the field when combined with the pheromone cruentol. This scenario coincides with the main findings of our preliminary field tests. In trial 1 (Figure 1A), when traps were baited with a mixture of the most EAG-active esters (ethyl acetate, ethyl propionate, ethyl butyrate, and propyl butyrate), the attractant power of the traps did not significantly differ from that of the traps baited only with pheromone for female, male, and total weevil catches (the significance of the factors is provided in Table 4 for the ANOVA performed using the data collected per sex and for total catches). Thus, the addition of these esters, in the proportion and at the emission level employed (Table 5), did not significantly improve weevil catches. The same was observed when ferrugineol was combined with acetoin or with esters and acetoin (Figure 1A and Table 4), these being the compounds that elicited the strongest EAG responses.

Whereas the combination of esters and ketones did not offer any advantage if compared to using the aggregation pheromone alone, the total weevil catches significantly increased when the ethyl acetate ester was combined with ethanol (Figure 1B), which was due mainly to the significant female captures obtained (trial 2) (Table 4). The total weevil catches almost doubled with this kairomonal mixture. When a second alcohol (3-methyl-1-butanol) was added to the mixture (alcohol mix in Figure 1B), catches did not significantly improve with regard to ethyl acetate + ethanol, suggesting that addition of this alcohol is irrelevant, at least under our particular test conditions (trial 2) (Table 5).

Although 2-phenylethanol elicited a strong antennal response for female *R. ferrugineus*, no synergistic effect was observed when it was added to traps in combination with ethyl acetate in trial 3 (Figure 1C and Table 4), whereas the combination (ethyl acetate + ethanol) still achieved significantly larger female, male, and total catches. The same was observed in Elche for trial 4 (Figure 1D and Table 4). Whereas the female catches obtained in traps baited with 2-phenylethanol combined with ethyl acetate did not significantly differ from those baited with only pheromone, the results obtained with ethyl acetate + ethanol + 3-methyl-1-butanol were significantly

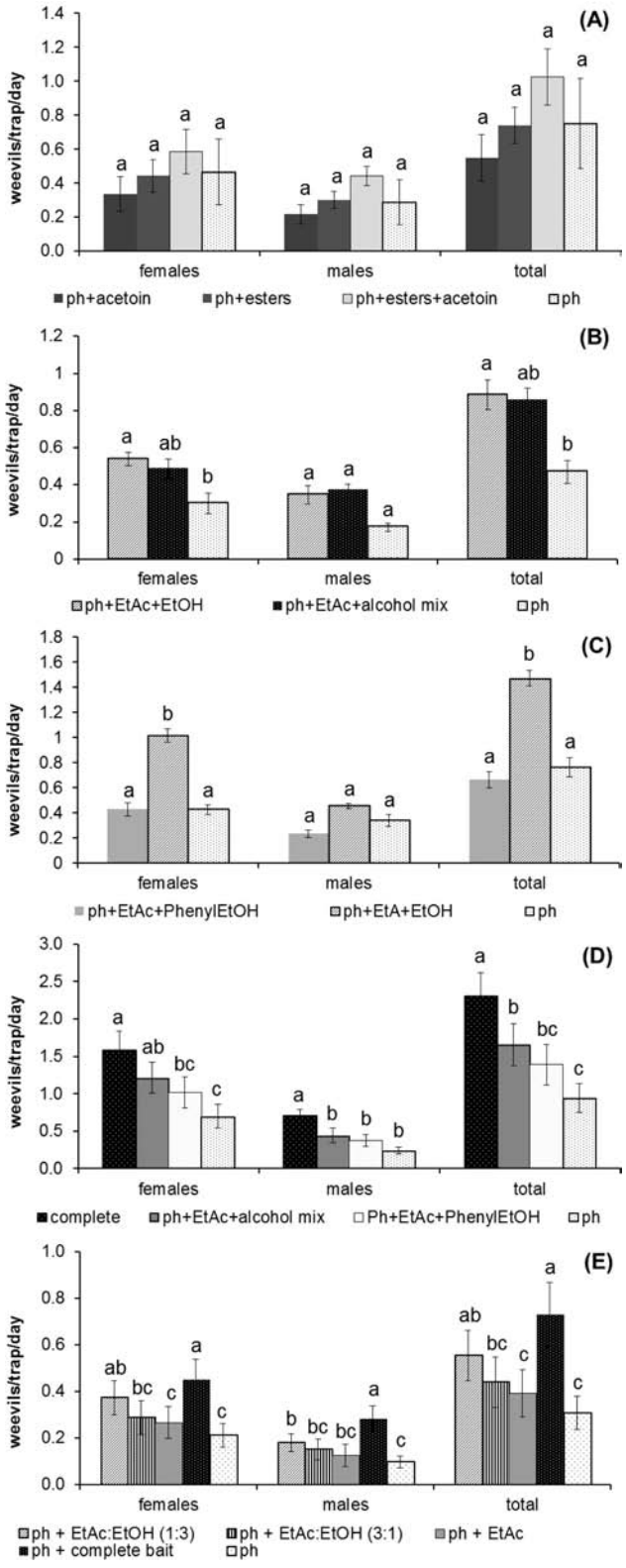

Figure 1. Number of weevils (females, males, and total) captured per trap and day in the different traps deployed in (A) trial 1, (B) trial 2, (C) trial 3, (D) trial 4, and (E) trial 5. All compounds combined with the aggregation pheromone (ph). Bars labeled with the same letter for each weevil case are not significantly different (ANOVA, LSD test at $P < 0.05$).

better than when using the pheromone alone. Moreover, the mean number of females trapped using this ester + alcohols

dx.doi.org/10.1021/jf502663y | J. Agric. Food Chem. 2014, 62, 6053−6064

Table 4. Statistical Parameters for the ANOVA Performed for Each Preliminary Field Trial

sex[a]	factor[b]	trial 1	trial 2	trial 3	trial 4	trial 5
females	attractant	$F_{3,39} = 0.50$; $P = 0.683$	$F_{2,39} = 7.00$; $P = 0.003$	$F_{2,28} = 9.60$; $P = 0.001$	$F_{3,52} = 6.98$; $P < 0.001$	$F_{4,143} = 6.41$; $P < 0.001$
	week	$F_{3,39} = 1.65$; $P = 0.193$	$F_{5,39} = 1.91$; $P = 0.115$	$F_{3,28} = 2.52$; $P = 0.078$	$F_{3,52} = 3.71$; $P = 0.017$	$F_{7,143} = 28.54$; $P < 0.001$
	block	$F_{2,39} = 7.51$; $P = 0.002$	$F_{2,39} = 7.59$; $P = 0.002$	$F_{2,28} = 3.00$; $P = 0.066$	$F_{3,52} = 3.08$; $P = 0.035$	$F_{3,143} = 5.63$; $P < 0.001$
males	attractant	$F_{3,39} = 0.64$; $P = 0.591$	$F_{2,39} = 3.89$; $P = 0.028$	$F_{2,28} = 1.28$; $P = 0.294$	$F_{3,52} = 9.43$; $P < 0.001$	$F_{4,143} = 6.27$; $P < 0.001$
	week	$F_{3,39} = 0.26$; $P = 0.851$	$F_{5,39} = 1.98$; $P = 0.104$	$F_{3,28} = 2.51$; $P = 0.080$	$F_{3,52} = 2.62$; $P = 0.061$	$F_{7,143} = 17.73$; $P < 0.001$
	block	$F_{2,39} = 2.63$; $P = 0.085$	$F_{2,39} = 3.83$; $P = 0.030$	$F_{2,28} = 3.53$; $P = 0.043$	$F_{3,52} = 1.78$; $P = 0.163$	$F_{3,143} = 10.86$; $P < 0.001$
total	attractant	$F_{3,39} = 1.14$; $P = 0.347$	$F_{3,39} = 8.37$; $P = 0.001$	$F_{2,28} = 7.82$; $P = 0.002$	$F_{3,52} = 9.15$; $P < 0.001$	$F_{4,143} = 7.49$; $P < 0.001$
	week	$F_{3,39} = 1.46$; $P = 0.240$	$F_{5,39} = 0.99$; $P = 0.438$	$F_{3,28} = 2.90$; $P = 0.052$	$F_{3,52} = 3.81$; $P = 0.015$	$F_{7,143} = 29.27$; $P < 0.001$
	block	$F_{2,39} = 8.40$; $P = 0.001$	$F_{2,39} = 9.03$; $P < 0.001$	$F_{2,28} = 3.87$; $P = 0.031$	$F_{3,52} = 3.15$; $P = 0.033$	$F_{3,143} = 8.13$; $P < 0.001$

[a]ANOVA was performed separately with the number of female, males, and total weevils captured. [b]Factors included in the multifactor ANOVA.

Table 5. Dispenser Types and Release Rates of the Semiochemicals Tested in Preliminary Field Trials

trial	semiochemical and dispenser type	initial load (g)	release rate[a] (mg/day)	R^2
all	LDPE Ferosan			
	ferrugineol (ph)	1	11.16	0.98
1	LDPE vial 50 mL			
	acetoin	1	10.4	0.99
	LDPE vial 25 mL			
	esters mix (1:1:1:1)	8.5	113	0.99
	acetoin + esters mix (0.5:2:2:2:2)	9	74	0.99
2	LDPE vial 100 mL			
	EtAc + EtOH (1:1)	18	118	0.98
	EtAc + alcohol mix (1:1:1)	28	125.8	0.99
3 and 4	LDPE vial 100 mL			
	EtAc + EtOH (1:1)	18	118	0.98
	EtAc + phenyl-EtOH (1:1)	18	107	0.97
5	LDPE vial 100 mL			
	EtAc + EtOH (1:3)	32	102	0.98
	EtAc + EtOH (3:1)	32	98	0.98
	EtAc	18	96	0.97

[a]Release profile studies by gravimetric method; linear model fittings (R^2) are also provided.

mixture did not substantially differ from that obtained with the complete bait (water + molasses + palm material + pheromone). Nevertheless, as found in trial 2, the activity of this synthetic mixture was due to ethyl acetate + ethanol, and the addition of 3-methyl-1-butanol did not improve efficacy.

Although ethyl acetate + alcohol mix in trial 4 performed significantly better than pheromone alone for the total weevil catches, the mixture did not reach the level of catches obtained with the complete bait, which was due mainly to the lack of differences in male catches (Figure 1D). Nevertheless, the data on the increased female catches offered promising results. Trial 5 was conducted in an attempt to adjust the proportion of the kairomonal active ingredients by testing 1:3 and 3:1 blends (v/v) of ethyl acetate/ethanol (Table 1). The results showed that the efficacy of Picusan traps baited with pheromone and the 1:3 ethyl acetate/ethanol blend did not significantly differ from those baited with the complete bait for the female, male, and total weevil catches (Figure 1E and Table 5). Although the mixture may still be incomplete, or need dose/proportion adjustments, the results suggest that it is possible to develop a synthetic kairomone to avoid the use of plant material to boost trap attractiveness.

The literature provides no conclusive results about currently employed synthetic kairomones having efficacy equal to or better than fermenting plant material for any *Rhynchophorus* sp. Ethyl acetate and several other esters were tested with cruentol to trap *R. cruentatus* in the field, but the efficacy was significantly poorer than that of fermenting sugar cane.[47] For *R. phoenicis*, ethyl propionate combined with phoenicol improved the efficacy of phoenicol + ethyl acetate, but it was still less effective than freshly cut oil palm tissues.[29] Rochat et al.[30] reported field trappings of *R. palmarum* with synthetic plant odors as compared to sugar cane. Despite not being significantly different, the complex synthetic blend ethyl acetate + ethanol + base fermentation odors + coconut volatiles (28 compounds) was 82% efficient if compared to sugar cane, but was better than the 1:1 ethyl acetate/ethanol blend, which can accomplish 50% efficacy compared to sugar cane. We found that this blend was synergistic for *R. ferrugineus*, as it increased weevil catches by 2 times as compared to aggregation pheromone alone (Figure 1B). Moreover, the 1:3 ethyl acetate/ethanol blend achieved 76% efficacy if compared to the total weevil catches obtained with the natural kairomone employed in Spain (palm stem + molasses), as found in trial 5. The GC-FID analysis of the aged dispenser samples demonstrated that the mixture was emitted in a 2:3 ratio (ethyl acetate/ethanol).

Many studies have shown that the addition of ethyl acetate to traps emitting aggregation pheromones (with or without food bait) increases attraction for *R. ferrugineus* adults.[48−50] Attraction of ethyl acetate + pheromone is sufficiently good if compared to pheromone + food bait (fermented date fruits) in

Oman.[50] Nevertheless, whether any of these combinations improves the efficacy of aggregation pheromone alone was not shown. Yet the results of our trial 5 (Figure 1E) reveal that the attraction of ethyl acetate + pheromone was significantly poorer than that of pheromone + food bait (palm stem pieces + molasses). This different result might be due to a greater efficacy of palm tissues + molasses if compared to date fruits as food baits, which highlights the importance of developing a synthetic kairomone to replace the use of nonstandardized food baits, which can provide diverse efficacy.

The results of the present study show the good field performance of ethyl acetate combined with ethanol, but further trials are required to optimize release rates. Designing dispensers that optimize the release rate of each compound can improve the results obtained in these trials. These findings can provide us with an inexpensive synthetic kairomone that is capable of avoiding trap servicing every 2 weeks, which would be a clear advantage for red palm weevil mass trapping and detection strategies.

AUTHOR INFORMATION

Corresponding Author

*(S.V.) Phone: +34 96 387 9058. Fax: + 34 96 387 9059. E-mail: sanvagon@ceqa.upv.es.

Funding

The research leading to these results has received funding from the 7th European Union Framework Programme under Grant Agreement FP7 KBBE 2011-5-289566 (PALM PROTECT).

Notes

The authors declare no competing financial interest.

ACKNOWLEDGMENTS

We thank Ecovisa (Godelleta) and Jose María Carrero from "Viveros Campo Arenal" (Manises) for providing us with their facilities to conduct the field trials. We are also grateful to the whole Tragsa team and especially to José Juan López Calatayud for field and technical assistance and for providing us with the insects for the laboratory trials. Finally, we thank Helen Warburton for English editing.

REFERENCES

(1) Murphy, S. T.; Briscoe, B. R. The red palm weevil as an alien invasive: biology and the prospects for biological control as a component of IPM. *Biocontrol News Inf.* **1999**, *20*, 35−46.

(2) European and Mediterranean Plant Protection Organization (EPPO). Data sheets on quarantine pests *Rhynchophorus ferrugineus*. *EPPO Bull.* **2008**, *38*, 55−59.

(3) El-Mergawy, R. A. A. M.; Al Ajlan, A. M.; Abdallah, N. A.; Nasr, M. I.; Silvain, J. F. Determination of different geographical populations of *Rhynchophorus ferrugineus* (Olivier) (Coleoptera: Curculionidae) using RAPD-PCR. *Int. J. Agric. Biol.* **2011**, *13*, 227−232.

(4) Fiaboe, K. K. M.; Peterson, A. T.; Kairo, M. T. K.; Roda, A. L. Predicting the potential worldwide distribution of the red palm weevil *Rhynchophorus ferrugineus* (Olivier) (Coleoptera: Curculionidae) using ecological niche modeling. *Fla. Entomol.* **2012**, *95*, 659−673.

(5) Barranco, P.; de la Peña, J. A.; Cabello, T. The red palm weevil, *Rhynchophorus ferrugineus* (Olivier) (Coleoptera, Curculionidae), a new pest in Europe. *Phytoma Espana* **1996**, *67*, 36−40.

(6) Ferry, M.; Gomez, S. The red palm weevil in the Mediterranean area. *Palms* **2002**, *46*, 172−178.

(7) Kontodimas, D. C.; Milonas, P.; Vassiliou, V.; Thymakis, N.; Economou, D. The occurrence of *Rhynchophorus ferrugineus* in Greece and Cyprus and the risk against the native greek palm tree *Phoenix theophrasti*. *Entomol. Hell.* **2006**, *16*, 11−15.

(8) Jacas, J. A.; Dembilio, Ó.; Llácer, E. Research activities focused on management of red palm weevil at the UJI-IVIA Associated Unit (region of Valencia, Spain). *EPPO Bull.* **2011**, *41*, 122−127.

(9) Uribarrena-Bollain, S. Protocole d'intervention local moyennant la coordination des activités de lutte contre le charançon rouge du palmier au sein de la municipalité de Valence, Espagne. In *Proceedings of AFPP−Palm Pest Mediterranean Conference*, Nice, France, Jan 16, 17 and 18, 2013; http://www.fredon-corse.com/standalone/3/DE9F2m0vhFaz8NCn9hf33W41.pdf (accessed May 29, 2014).

(10) Nakash, J.; Osem, Y.; Kehat, M. A suggestion to use dogs for detecting red palm weevil (*Rhynchophorus ferrugineus*) infestation in date palms in Israel. *Phytoparasitica* **2000**, *28*, 153−155.

(11) Suma, P.; La Pergola, A.; Longo, S.; Soroker, V. The use of sniffing dogs for the detection of *Rhynchophorus ferrugineus*. *Phytoparasitica* **2014**, DOI: 10.1007/s12600-013-0330-0.

(12) Pinhas, J.; Soroker, V.; Hetzroni, A.; Mizrach, A.; Teicher, M.; Goldberger, J. Automatic acoustic detection of the red palm weevil. *Comput. Electron. Agric.* **2008**, *63*, 131−139.

(13) Siriwardena, K. A. P.; Fernando, L. C. P.; Nanayakkara, N.; Perera, K. F. G.; Kumara, A. D. N. T.; Nanayakkara, T. Portable acoustic device for detection of coconut palms infested by *Rhynchophorus ferrugineus* (Coleoptera: Curculionidae). *Crop Prot.* **2010**, *29*, 25−29.

(14) Herrick, N. J.; Mankin, R. W. Acoustical detection of early instar *Rhynchophorus ferrugineus* (Coleoptera: Curculionidae) in Canary Island date palm, *Phoenix canariensis* (Arecales: Arecaceae). *Fla. Entomol.* **2012**, *95*, 983−990.

(15) Soroker, V.; Suma, P.; La Pergola, A.; Cohen, Y.; Cohen, V.; Alchanatis, V.; Golomb, O.; Goldshtein, E.; Hetzroni, A.; Galazan, L.; Kontodimas, D.; Pontikakos, C.; Zorovic, M.; Brandstetter, M. Early detection and monitoring of red palm weevil: approaches and challenges. In *Proceedings of AFPP−Palm Pest Mediterranean Conference*, Nice, France, Jan 16, 17, and 18, 2013; http://www.fredon-corse.com/standalone/3/D17FoIhi6a5DB6nF3478lK0W.pdf (accessed Feb 26, 2014).

(16) Abraham, V. A.; Koya, K. M. A.; Kurian, C. Evaluation of seven insecticides for control of red palm weevil *Rhynchophorus ferrugineus* Fabr. *J. Plant. Crops* **1975**, *3*, 71−72.

(17) Barranco, P.; De La Peña, J.; Martín, M. M.; Cabello, T. Eficacia del control químico de la nueva plaga de las palmeras *Rhynchophorus ferrugineus* (Oliver, 1790) (Col.: Cuculiondae). *Bol. San. Veg. Plagas* **1998**, *24*, 301−306.

(18) Llácer, E.; Dembilio, O.; Jacas, J. A. Evaluation of the efficacy of an insecticidal paint based on chlorpyrifos and pyriproxyfen in a microencapsulated formulation against *Rhynchophorus ferrugineus* (Coleoptera: Curculionidae). *J. Econ. Entomol.* **2010**, *103*, 402−408.

(19) Abo-El-Saad, M. M.; Al-Abdan, S. A.; Bou-Khowh, I. A. In vivo toxicity of beta-cyfluthrin insecticide against the red palm weevil, *Rhynchophorus ferrugineus* (Olivier). *J. Agric. Sci. Technol. A* **2012**, *2*, 1322−1331.

(20) Llácer, E.; Negre, M.; Jacas, J. A. Evaluation of an oil dispersion formulation of imidacloprid as a drench against *Rhynchophorus ferrugineus* (Coleoptera, Curculionidae) in young palm trees. *Pest Manage. Sci.* **2012**, *68*, 878−882.

(21) Abbas, M. S. T.; Saleh, M. M. E.; Akil, A. M. Laboratory and field evaluation of the pathogenicity of entomopathogenic nematodes to the red palm weevil, *Rhynchophorus ferrugineus* (Oliv.) (Col.: Curculionidae). *J. Pest Sci.* **2001**, *74*, 167−168.

(22) Llácer, E.; de Altube, M. M.; Jacas, J. A. Evaluation of the efficacy of *Steinernema carpocapsae* in a chitosan formulation against the red palm weevil *Rhynchophorus ferrugineus* in *Phoenix canariensis*. *BioControl* **2009**, *54*, 559−565.

(23) Dembilio, Ó.; Llácer, E.; Martínez de Altube, M. D. M.; Jacas, J. A. Field efficacy of imidacloprid and *Steinernema carpocapsae* in a chitosan formulation against the red palm weevil *Rhynchophorus ferrugineus* (Coleoptera: Curculionidae) in *Phoenix canariensis*. *Pest Manage. Sci.* **2010**, *66*, 365−370.

(24) Gindin, G.; Levski, S.; Glazer, I.; Soroker, V. Evaluation of the entomopathogenic fungi *Metarhizium anisopliae* and *Beauveria bassiana*

against the red palm weevil *Rhynchophorus ferrugineus*. *Phytoparasitica* **2006**, *34*, 370−379.
(25) Dembilio, Ó.; Quesada-Moraga, E.; Santiago-Álvarez, C.; Jacas, J. A. Potential of an indigenous strain of the entomopathogenic fungus *Beauveria bassiana* as a biological control agent against the red palm weevil, *Rhynchophorus ferrugineus*. *J. Invertebr. Pathol.* **2010**, *104*, 214−221.
(26) Hallett, R. H.; Gries, G.; Gries, R.; Borden, J. H.; Czyzewska, E.; Oehlschlager, A. C.; Pierce, H. D., Jr.; Angerilli, N. P. D.; Rauf, A. Aggregation pheromones of two Asian palm weevils, *Rhynchophorus ferrugineus* and *R. vulneratus*. *Naturwissenschaften* **1993**, *80*, 328−331.
(27) Giblin-Davis, R. M.; Oehlschlager, A. C.; Perez, A.; Gries, G.; Gries, R.; Weissling, T. J.; Chinchilla, C. M.; Peña, J. E.; Hallett, R. H.; Pierce, H. D., Jr.; González, L. M. Chemical and behavioral ecology of palm weevils (Curculionidae: Rhynchophorinae). *Fla. Entomol.* **1996**, *79*, 153−167.
(28) Oehlschlager, A. C.; Chinchilla, C. M.; González, L. M.; Jiron, L. F.; Mexzon, R.; Morgan, B. Development of a pheromone-based trapping system for *Rhynchophorus palmarum* (Coleoptera: Curculionidae). *J. Econ. Entomol.* **1993**, *86*, 1381−1392.
(29) Gries, G.; Gries, R.; Perez, A. L.; González, L. M.; Pierce, H. D., Jr.; Oehlschlager, A. C.; Rhainds, M.; Zebeyou, M.; Kouame, B. Ethyl propionate: synergistic kairomone for African palm weevil, *Rhynchophorus phoenicis* L. (Coleoptera: Curculionidae). *J. Chem. Ecol.* **1994**, *20*, 889−897.
(30) Rochat, D.; Nagnan-Le Meillour, P.; Esteban-Duran, J. R.; Malosse, C.; Perthuis, B.; Morin, J. P.; Descoins, C. Identification of pheromone synergists in American palm weevil, *Rhynchophorus palmarum*, and attraction of related *Dynamis borassi*. *J. Chem. Ecol.* **2000**, *26*, 155−187.
(31) Weissling, T. J.; Giblin-Davis, R. M. Fecundity and fertility of *Rhynchophorus cruentatus* (Coleoptera: Curculionidae). *Fla. Entomol.* **1994**, *77*, 373−376.
(32) Giblin-Davis, R. M.; Howard, F. W. Vulnerability of stressed palms to attack by *Rhynchophorus cruentatus* (Coleoptera: Curculionidae) and insecticidal control of the pest. *J. Econ. Entomol.* **1989**, *82*, 1185−1190.
(33) Vacas, S.; Primo, J.; Navarro-Llopis, V. Advances in the use of trapping systems for *Rhynchophorus ferrugineus* (Coleoptera: Curculionidae): traps and attractants. *J. Econ. Entomol.* **2013**, *106*, 1739−1746.
(34) El-Arem, A.; Saafi, E. B.; Flamini, G.; Issaoui, M.; Ferchichi, A.; Hammami, M.; Helall, A. N.; Achour, L. Volatile and nonvolatile chemical composition of some date fruits (*Phoenix dactylifera* L.) harvested at different stages of maturity. *Int. J. Food Sci. Technol.* **2012**, *47*, 549−555.
(35) Callejón, R. M.; Morales, M. L.; Ferreira, A. C. S.; Troncoso, A. M. Defining the typical aroma of sherry vinegar: sensory and chemical approach. *J. Agric. Food Chem.* **2008**, *56*, 8086−8095.
(36) Lasekan, O.; Khatib, A.; Juhari, H.; Patiram, P.; Lasekan, S. Headspace solid-phase microextraction gas chromatography-mass spectrometry determination of volatile compounds in different varieties of African star apple fruit (*Chrysophillum albidum*). *Food Chem.* **2013**, *141*, 2089−2097.
(37) Högnadóttir, Á.; Rouseff, R. L. Identification of aroma active compounds in orange essence oil using gas chromatography−olfactometry and gas chromatography−mass spectrometry. *J. Chromatogr., A* **2003**, *998*, 201−211.
(38) Cazemier, A. E. (Hemi)cellulose degradation by microorganisms from the intestinal tract of arthropods. Doctoral thesis, University of Nijmegen, Nijmegen, The Netherlands, 1999; http://repository.ubn.ru.nl/handle/2066/18826 (accessed Jan 14, 2014).
(39) Butera, G.; Ferraro, C.; Colazza, S.; Alonzo, G.; Quatrini, P. The culturable bacterial community of frass produced by larvae of *Rhynchophorus ferrugineus* Olivier (Coleoptera: Curculionidae) in the Canary Island date palm. *Lett. Appl. Microbiol.* **2012**, *54*, 530−536.
(40) Antonelli, A.; Castellari, L.; Zambonelli, C.; Carnacini, A. Yeast influence on volatile composition of wines. *J. Agric. Food Chem.* **1999**, *47*, 1139−1144.
(41) Plata, C.; Millan, C.; Mauricio, J. C.; Ortega, J. M. Formation of ethyl acetate and isoamyl acetate by various species of wine yeasts. *Food Microbiol.* **2003**, *20*, 217−224.
(42) Lee, S. J.; Rathbone, D.; Asimont, S.; Adden, R.; Ebeler, S. E. Dynamic changes in ester formation during chardonnay juice fermentations with different yeast inoculation and initial Brix conditions. *Am. J. Enol. Vitic.* **2004**, *55*, 346−354.
(43) Herraiz, T.; Ough, C. S. Formation of ethyl esters of amino acids by yeast during the alcoholic fermentation of grape juice. *Am. J. Enol. Vitic.* **1993**, *44*, 41−48.
(44) Bugg, T. D.; Ahmad, M.; Hardiman, E. M.; Singh, R. The emerging role for bacteria in lignin degradation and bio-product formation. *Curr. Opin. Biotechnol.* **2011**, *22*, 394−400.
(45) Qian, M. C.; Fang, Y.; Shellie, K. Volatile composition of Merlot wine from different vine water status. *J. Agric. Food Chem.* **2009**, *57*, 7459−7463.
(46) Guarino, S.; Lo Bue, P.; Peri, E.; Colazza, S. Responses of *Rhynchophorus ferrugineus* adults to selected synthetic palm esters: electroantennographic studies and trap catches in an urban environment. *Pest Manage. Sci.* **2011**, *67*, 77−81.
(47) Giblin-Davis, R. M.; Weissling, T. J.; Oehlschlager, A. C.; González, L. M. Field response of *Rhynchophorus cruentatus* (Coleoptera: Curculionidae) to its aggregation pheromone and fermenting plant volatiles. *Fla. Entomol.* **1994**, *77*, 164−177.
(48) Oehlschlager, A. C.; González, L. M. Advances in trapping and repellency of palm weevils. In *Proceedings of the 2nd International Conference on Date Palms*; United Arab Emirates University: Al-Ain, UAE, 2001; pp 358−365; http://www.pubhort.org/datepalm/datepalm2/datepalm2_40.pdf (accessed Dec 20, 2013).
(49) El-Sebay, Y. Ecological studies on the red palm weevil *Rhynchophorus ferrugineus* Oliv. (Coleoptera: Curculionidae) in Egypt. *Egypt. J. Agric. Res.* **2003**, *81*, 523−530.
(50) Abdallah, F. F.; Al-Khatri, S. A. The effect of pheromone, kairomone and food bait on attracting adults of red palm weevil, *Rhynchophorus ferrugineus*, in the Sultanate of Oman in date palm plantations. *Egypt. J. Agric. Res.* **2005**, *83*, 169−177.

JOURNAL OF AGRICULTURAL AND FOOD CHEMISTRY

Article

pubs.acs.org/JAFC

Glucose Positions Affect the Phloem Mobility of Glucose−Fipronil Conjugates

Zhiwei Lei,[†] Jie Wang,[†] Genlin Mao, Yingjie Wen, Yuxin Tian, Huawei Wu, Yufeng Li, and Hanhong Xu*

State Key Laboratory for Conservation and Utilization of Subtropical Agro-bioresources, and Key Laboratory of Natural Pesticide and Chemical Biology, Ministry of Education, South China Agricultural University, Guangzhou, Guangdong 510642, People's Republic of China

Supporting Information

ABSTRACT: In our previous work, a glucose−fipronil (GTF) conjugate at the C-1 position was synthesized via click chemistry and a glucose moiety converted a non-phloem-mobile insecticide fipronil into a moderately phloem-mobile insecticide. In the present paper, fipronil was introduced into the C-2, C-3, C-4, and C-6 positions of glucose via click chemistry to obtain four new conjugates and to evaluate the effects of the different glucose isomers on phloem mobility. The phloem mobility of the four new synthetic conjugates and GTF was tested using the *Ricinus* seedling system. The results confirmed that conjugation of glucose at different positions has a significant influence on the phloem mobility of GTF conjugates.

KEYWORDS: *phloem mobility, glucosyl conjugates, click chemistry, glycosyl azides, glucose positions*

INTRODUCTION

The phloem is one of the two long-distance transport pathways in plants.[1] The phloem mobility of pesticides is an essential requirement that contributes positively to its efficacy.[2] Pesticides with good phloem mobility can have an efficacious function in controlling hidden and soil-dwelling pests[3] because these pesticides can be distributed along with the nutrients via the phloem to pest-damaged sites.[4] In addition, the agricultural sector needs novel pesticides that have sufficient phloem mobility in plants because of their evolved resistance, environmental regulations, and economic considerations.[5] For modern synthetic insecticides, the most effective mode of transport in plants is via the xylem, and only a few phloem-mobile insecticides are available. An efficient and economical strategy to develop novel systemic pesticides has been mentioned, in which the structure of the parent compounds is modified by adding endogenous carboxylic acid, amino acid, and hexose derivatives.[2,3,6,7] For example, ε-(2,4-dichlorophenoxyacetyl)-L-Lys, a conjugate of an α-amino acid and an auxenic herbicide, exhibits high phloem mobility in broad bean (*Vicia faba*).[7] IPGN, a novel fluorescent conjugate containing glucose, could enter *Ricinus communis* phloem.[8]

Our research team focuses on exploring the possibility of glycosylation to develop new phloem-mobile pesticides. *N*-[3-Cyano-1-[2,6-dichloro-4-(trifluoromethyl)phenyl]-4-[(trifluoromethyl)-sulfinyl]-1*H*-pyrazol-5-yl]-1-(β-D-glucopyranosyl)-1*H*-1,2,3-triazole-4-methanamine (GTF) has been synthesized, and a systemicity test demonstrated that the glucose core confers phloem mobility to fipronil.[9] To fully understand the function of the sugar core in the phloem-mobile molecule, a series of monosaccharide−fipronil conjugates were synthesized in our further study. Phloem mobility tests in castor bean seedlings indicated that the hydroxyl of the monosaccharide has a significant effect on the phloem mobility of the conjugates.[10]

Glucosyl derivatives, which are conjugated at different carbons of glucose, have different properties. For example, the new glucosyl dopamine conjugates substituted at C-6 of the sugar were more potent inhibitors of glucose transport compared to C-1- and C-3-substituted derivatives.[11] (7-Nitrobenz-2-oxa-1,3-diazol-4-yl)-amine (NBD) replaced at C-6 of the sugar cannot be phosphorylated by hexokinase, but NBD substituted at C-2 can be metabolized to 2-NBDG-6-phosphate.[12] In addition, several different (C-2, C-3, C-4, and C-6) natural glucosides are found in nature.[13] Therefore, biological properties of the glucosides have a correlation with different positions of glucose.

All of the monosaccharide−fipronil conjugates were linked at C-1 of the monosaccharide,[8,9] which gives rise to consider if parent compounds linking different positions of the glucose may have different phloem mobilities. In the present work, four novel glucosyl conjugates were designed and synthesized by linking the fipronil to C-2, C-3, C-4, and C-6 of glucose via click chemistry to study the effects of the different positions of glucose on phloem mobility.

MATERIALS AND METHODS

General Information for Synthesis. Melting points were determined on a FP62 digital micro melting point apparatus. Nuclear magnetic resonance (NMR) spectra were obtained on a Bruker AV-600 instrument. Deuterated solvents were obtained from Cambridge Isotope Laboratories (Andover, MA). CD_3OD and $CDCl_3$ solvent peaks (3.31 and 7.26 ppm for ^1H and 49.0 and 77.0 ppm for ^{13}C, respectively) were used as internal chemical shift references. The mass spectra (MS) of new compounds were obtained by a Waters ZQ 4000 with electronspray ionization (ESI) or a Bruker maXis 4G ESI-Q-TOF mass spectrometer. Data were reported as m/z. Silica gel was used for column chromatography. Reagents and anhydrous solvents were used as purchased without further purification.

Plant Materials. Castor bean seeds (*R. communis*) No. 9, obtained from the Agricultural Science Academy of Zibo, Shandong, China, were sown and grown as previously described.[6] Six-day-old seedlings (the hypocotyl at about 20 mm in length) were relatively selected for further experiments.

Received: March 4, 2014
Revised: May 20, 2014
Accepted: June 11, 2014
Published: June 11, 2014

ACS Publications © 2014 American Chemical Society

dx.doi.org/10.1021/jf5010429 | J. Agric. Food Chem. 2014, 62, 6065−6071

Table 1. Properties of the Tested Compounds[a]

properties	GTF	2-GTF	3-GTF	4-GTF	5-GTF
MW	680.37	680.37	680.37	680.37	680.37
log K_{ow}	2.06	1.11	1.42	1.41	1.58
pK_a	12.8 ± 0.7	11.9 ± 0.7	12.0 ± 0.7	12.0 ± 0.7	12.1 ± 0.7
HBD	5	5	5	5	5
HBA	13	13	13	13	13

[a]The physicochemical properties of tested compounds were predicted by ACD Laboratories Percepta program, version 14.0. Log K_{ow} and pK_a values were classic values. 2-GTF, 3-GTF, 4-GTF, and 6-GTF mean that fipronil was conjugated at the C-2, C-3, C-4, and C-6 positions of glucose, respectively. All values (MW, HBD, and HBA) are the same for the different compounds.

Membrane Potential Measurements. Plasma membrane potential of the protoplasts of *R. communis* cotyledons was performed with flow cytometric analysis using a fluorescent membrane potential indicator dye bis(1,3-dibutylbarbituric acid)-trimethine oxonol [DiBAC4(3)]. The protoplasts were incubated with buffer solution without (control) or with the five glucosyl fipronil conjugates at 100 μM concentration for 5 h, and then the protoplast suspension was co-incubated with 3 μM DiBAC4(3) for 30 min at 28 °C prior to flow cytometric analysis.

Phloem Sap Collection and Analysis. The seedlings with 6 days of development were prepared for phloem sap collection. The phloem sap was collected from the upper part of the hypocotyl, which was similar to that recently described.[6,14] The cotyledons were removed from endosperm carefully without bending or crushing the cotyledons. The cotyledons were incubated in buffered solution supplemented with 100 μM glucosyl fipronil conjugtes. After 1 h of preincubation, the hypocotyl was severed in the hook region for phloem exudation. Phloem sap was collected from the upper part of the hypocotyl at a 1 h interval for 5 h and was stored at 4 °C until analysis.[15]

The collected phloem sap, diluted with pure water [1:4 (v/v) phloem sap/H_2O], was quantified by an Agilent 1100 HPLC system. Separations were made with a C8 reversed-phase column (5 μm, 250 × 4.6 mm inner diameter, Agilent Co.) at 30 °C. The injection was 10 μL, and the flow rate was 1 mL/min. The elution system consisted of acetonitrile and water (50:50, v/v). The conjugates detected in the phloem sap were further identified using ultra-performance liquid chromatography–mass spectrometry (UPLC–MS, Waters, Milford, MA). Samples were separated using an ACQUITY UPLC BEH C18 column (1.7 μm, 2.1 × 100 mm, Waters). The parameters were similar to our previously reported method.[16]

Physicochemical Properties. The physicochemical properties [molecular weight (MW), ionization constant in aqueous solution (pK_a), octanol/water partitioning coefficient (log K_{ow}), number of hydrogen bond donors (HBDs), and number of hydrogen bond acceptors (HBAs)] of different positions of glucose conjugates were predicted using ACD LogD suite version 14.0 software (Table 1).

*Synthesis of 1,3,4,6-Tetra-O-acetyl-2-azido-2-deoxy-β-D-glucoside (**2a**) (Scheme 1).* 2-Azido-2-deoxy-D-glucose (205 mg, 1 mmol) was dissolved in pyridine (5 mL), and then acetic anhydride (Ac_2O, 3 mL) was added with catalytic dimethylaminopyridine (DMAP, 6.1 mg, 0.05 mmol). After the solvents were stirred for 12 h at room temperature, they were removed under reduced pressure and the residue was diluted with CH_2Cl_2. The solution was washed with 1 M HCl and saturated $NaHCO_3$ solution, dried with $MgSO_4$, concentrated under reduced pressure, and purified by column chromatography (1:1 ethyl acetate/hexane) to obtain compound **2a**. White power; yield, 78%; melting point (mp), 80.4 °C; ^{1}H NMR (600 MHz, $CDCl_3$) δ, 5.54 (d, J = 8.6 Hz, 1H, H-1), 5.08 (t, J = 9.6 Hz, 1H, H-4), 5.03 (t, J = 9.6 Hz, 1H, H-3), 4.29 (dd, J = 12.5 and 4.5 Hz, 1H, H-6-a), 4.07 (dd, J = 12.5 and 2.1 Hz, 1H, H-6-b), 3.80 (ddd, J = 9.8, 4.5, and 2.2 Hz, 1H, H-5), 3.65 (dd, J = 9.9 and 8.6 Hz, 1H, H-2); ^{13}C NMR (150 MHz, $CDCl_3$) δ, 170.6, 69.8, 169.7, 168.6, 92.6, 72.8, 72.8, 67.9, 62.7, 61.5, 21.0, 20.8, 20.7, 20.6; MS–ESI [M + Na]$^+$, 396.1.

*Synthesis of 1,2,4,6-Tetra-O-acetyl-3-azido-3-deoxy-D-glucoside (Anomers α/β = 1:1) (**3a**).* A solution of 1,2:5,6-di-*O*-isopropylidene-3-azido-3-deoxy-α-D-glucofuranose (2 g, 7 mmol) in 80% CF_3COOH (10 mL) was stirred at room temperature for 3 h. Evaporation of the solvent afforded 3-azido-3-deoxy-D-glucose without further purification. The crude 3-azido-3-deoxy-D-glucose was per-acetylated according to the procedure of compound **2a** to obtain compound **3a**. α anomer: syrup; yield, 35%; ^{1}H NMR ($CDCl_3$, 600 MHz) δ, 6.25 (d, J = 3.6 Hz, 1H, H-1), 4.98 (t, J = 10.1 Hz, 1H, H-4), 4.90 (dd, J = 10.6 and 3.5 Hz, 1H, H-2), 4.17 (dd, J = 12.0 and 4.6 Hz, 1H, H-6-a), 4.05–3.99 (m, 1H, H-6-b), 3.93 (t, J = 10.3 Hz, 1H, H-3), 3.75 (m, H-5), 2.15–2.03 (4 s, 12H, $COCH_3$); ^{13}C NMR ($CDCl_3$, 150 MHz) δ, 171.0, 169.7, 168.6, 87.8, 73.2, 69.9, 69.8, 61.5, 60.5, 21.1, 20.9, 20.8, 20.8. β anomer: syrup; yield, 35%; ^{1}H ($CDCl_3$, 600 MHz) δ, 5.63 (d, J = 8.2 Hz, 1H, H-1), 4.99 (dd, J = 10.1 and 8.2 Hz, 1H, H-2), 4.18 (dd, J = 12.0 and 4.6 Hz, 1H, H-6-a), 4.04–3.96 (m, 3H), 3.66 (t, J = 10.1 Hz, 1H, H-3), 2.15–2.03 (4s, 12H, $COCH_3$); ^{13}C ($CDCl_3$, 150 MHz) δ, 171.0, 169.7, 168.6, 91.3, 69.6, 67.4, 66.0, 64.4, 61.5, 21.1, 21.0, 20.9, 20.8; MS–ESI [M + Na]$^+$, 396.1.

*Synthesis of 1,2,3,6-Tetra-O-acetyl-4-azido-4-deoxy-α-D-glucoside (**4a**).* To a solution of methyl 4-azido-4-deoxy-α-D-glucopyranoside (2 g, 9.13 mmol) in glacial acetic acid (10 mL) and acetic anhydride (10 mL) was added concentrated sulfuric acid (2 mL) dropwise with stirring. The solution was left at room temperature for 48 h. Then, 6.13 g of sodium acetate was added to neutralize the sulfuric acid, and chloroform (100 mL) was added. The mixture was pour into ice–water. The chloroform layer was washed with aqueous $NaHCO_3$ and aqueous NaCl, dried, and evaporated to dryness *in vacuo*. The brown oil was purified by column chromatography (1:1 ethyl acetate/hexane) to obtain compound **4a**. Syrup; yield, 68%; ^{1}H NMR (600 MHz, $CDCl_3$) δ, 6.12 (d, J = 3.6 Hz, 1H, H-1), 5.31 (t, J = 10.0 Hz, 1H, H-3), 4.88 (dd, J = 10.2 and 3.7 Hz, 1H, H-2), 4.18 (dd, J = 12.4 and 1.8 Hz, 1H, H-6-a), 4.12 (dd, J = 12.4 and 3.9 Hz, 1H, H-6-b), 3.80–3.72 (m, 1H, H-5), 3.58 (t, J = 10.2 Hz, 1H, H-4), 2.01 (s, 3H, $COCH_3$), 1.97 (s, 3H, $COCH_3$), 1.96 (s, 3H, $COCH_3$), 1.85 (s, 3H, $COCH_3$); ^{13}C (150 MHz, $CDCl_3$) δ, 170.1, 169.5, 169.4, 168.5, 88.8, 70.1, 69.9, 69.0, 62.1, 59.6, 20.5, 20.4, 20.3, 20.1; MS–ESI [M + Na]$^+$, 396.1.

*Synthesis of 1,2,3,4-Tetra-O-acetyl-6-azido-6-deoxy-D-glucopyranose (**6a**).* 1,2,3,4-Tetra-*O*-acetyl-6-*O*-*p*-tolylsulfonyl-D-glucopyranose[17] (7 g, 13.95 mmol) and sodium azide (5.0 g, 154 mmol) dissolved in dry *N*,*N*-dimethylformamide (DMF) (50 mL) were stirred at 50 °C for 4 h and then at room temperature for 16 h. The mixture was poured onto icy water and extracted with ether (4 × 50 mL). The organic extracts were washed twice with water and then dried over calcium chloride. After evaporation to dryness, 1,2,3,4-tetra-*O*-acetyl-6-azido-6-deoxy-α-D-glucopyranose (**6a**) was obtained (2.03 g). Needle solid; yield, 39%; mp, 146.2 °C; ^{1}H NMR (600 MHz, $CDCl_3$) δ, 6.33 (d, J = 3.7 Hz, 1H, H-1), 5.44 (t, J = 9.9 Hz, 1H, H-3), 5.09 (t-like, J = 9.6 Hz, 1H, H-4), 5.07 (dd, J = 10.3 and 3.7 Hz, H-2), 4.06 (m, 1H, H-5), 3.38 (dd, J = 13.5 and 2.7 Hz, 1H, H-6-a), 3.28 (dd, J = 13.5 and 5.5 Hz, 1H, H-6-b), 2.17 (s, 3H, $COCH_3$), 2.03 (s, 3H, $COCH_3$), 2.01 (s, 3H, $COCH_3$), 2.00 (s, 3H, $COCH_3$); ^{13}C NMR (150 MHz, $CDCl_3$) δ, 170.3, 169.7, 169.5, 168.8, 88.9, 70.8, 69.7, 69.3, 69.1, 50.8, 20.9, 20.7, 20.7, 20.5; MS–ESI [M + Na]$^+$, 396.1.

General Procedure for Synthesis of the Conjugates 2-GTF, 3-GTF, 4-GTF, and 6-GTF (Scheme 2). Fipronil–alkyne (474 mg, 1 mmol) was added to a vigorously stirred suspension of azide-containing glucoses (373 mg, 1 mmol) in 3 mL of *tert*-butyl alcohol. The reaction was initiated by the addition of a solution of $CuSO_4{\cdot}5H_2O$ (100 mg, 0.4 mmol) and sodium ascorbate (173 mg, 0.8 mmol) in distilled water (3 mL). The deep yellow suspension was stirred vigorously at 50 °C for 3 h. Distilled water (10 mL) was added, and the aqueous layer was

Scheme 1. Synthesis of Azido-Containing Acetylglucoses: (A) 1, $TMSN_3$, $SnCl_4$, CH_2Cl_2; (B) 1, TfN_3, $CuSO_4$, H_2O, MeOH, CH_2Cl_2; 2, Ac_2O, DMAP, Pyridine; (C) 1, Acetone, $ZnCl_2$, H_3PO_4; 2, Pyridinium Dichromate, Ac_2O, CH_2Cl_2; 3, $NaBH_4$, EtOH; 4, Tf_2O, CH_2Cl_2, Pyridine; 5, NaN_3, MeCN; 6, TFA, Ac_2O, DMAP, Pyridine; (D) 1, Benzoyl Chloride, Pyridine; 2, Tf_2O, CH_2Cl_2, Pyridine; 3, NaN_3, MeCN; 4, NaOMe, MeOH; 5, H_2SO_4, Ac_2O; and (E) 1, TsCl, Ac_2O, Pyridine; 2, NaN_3, DMF

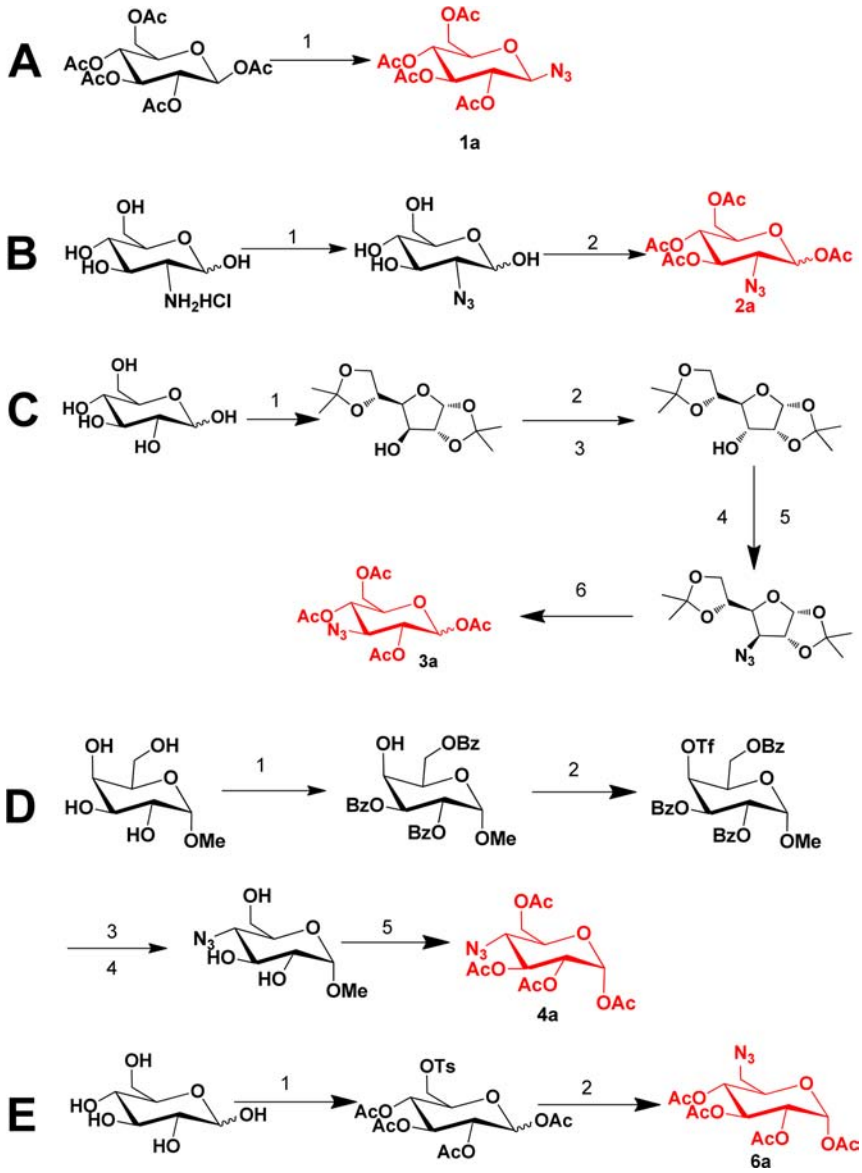

extracted with chloroform (10 mL × 3). The combined organic extracts were washed with aqueous sodium hydrogen carbonate and brine, dried with sodium sulfate, filtered, and evaporated *in vacuo*. The crude compound was added to a solution of sodium methoxide in dry methanol (0.05 M, 15 mL). The resultant solution was stirred for 30 min at room temperature. The mixture was neutralized with Amberlite IR 120 (H^+) resin and filtered, and the filtrate was then evaporated. The residues were purified by column chromatography (9:1 CH_2Cl_2/MeOH) to obtain the glucosyl fipronil conjugates.

D-Glucopyranose, 2-Deoxy-2-(4-(((1-(2,6-dichloro-4-(trifluoromethyl)phenyl)-4-((trifluoromethyl)sulfinyl)-3-cyano-1H-pyrazol-5-yl)amino)methyl)-1H-1,2,3-triazol-1-yl)- (2-GTF). White solid; yield, 88%, mp, 151.3 °C; ^{1}H NMR (CD_3OD, 600 MHz) δ, 8.08 (s, 2H), 8.00 (s, 1H), 7.89* (s, 1H), 5.28 (d, J = 3.2 Hz, 1H), 5.11* (d, J = 7.3 Hz, 1H), 4.09−4.21 (m, 2H), 3.93 (d, J = 11.3 Hz, 1H), 3.85 (d, J = 11.5 Hz, 1H), 3.74−3.81 (m, 1H), 3.44−3.55 (m, 2H), 3.32 (brs, 1H); ^{13}C NMR (CD_3OD, 150 MHz) δ, 151.7, 144.7, 144.4*, 137.9, 137.9, 137.8*, 136.0, 127.9, 127.9, 125.8, 125.7, 124.4, 123.5, 123.4*, 122.7, 112.2, 97.5, 96.1*, 78.1, 75.4, 73.2, 69.5, 66.7, 62.5, 62.4*, 41.1, 41.0*; HRMS (ESI) calcd for $C_{21}H_{17}Cl_2F_6N_7O_6SNa$ [M + Na]$^+$, 702.0140; found, 702.0135.

D-Glucopyranose, 3-Deoxy-3-(4-(((1-(2,6-dichloro-4-(trifluoromethyl)phenyl)-4-((trifluoromethyl)sulfinyl)-3-cyano-1H-pyrazol-5-yl)amino)methyl)-1H-1,2,3-triazol-1-yl)- (3-GTF). White solid; yield, 80%; mp, 156.8 °C; ^{1}H NMR (CD_3OD, 600 MHz) δ, 8.07 (s, 2H), 7.86 (s, 1H), 7.85* (s, 1H), 5.23 (d, J = 3.1 Hz, 1H), 4.50 (d, J = 3.0 Hz, 2H), 4.47* (d, J = 3.0 Hz, 2H), 4.29 (t, J = 10.1 Hz, 1H), 4.28* (t, J = 10.1 Hz, 1H), 4.04−4.08 (m, 1H), 4.02 (d, J = 10.0 Hz, 1H), 3.96* (d, J = 10.0 Hz, 1H), 3.93−3.96 (m, 1H), 3.89 (d, J = 11.9 Hz, 1H), 3.82* (d, J = 11.9 Hz, 1H), 3.72−3.80 (m, 2H); ^{13}C NMR (CD_3OD, 150 MHz) δ, 151.8, 144.7, 144.4*, 137.9, 136.3*, 136.0, 135.8, 127.9, 127.8, 125.9, 125.7, 124.5, 123.5, 122.5 112.1, 93.4, 79.2, 73.4, 71.7, 69.4, 67.8, 62.3, 41.0; HRMS (ESI) calcd for $C_{21}H_{17}Cl_2F_6N_7O_6SNa$ [M + Na]$^+$, 702.0140; found, 702.0135.

D-Glucopyranose, 4-Deoxy-4-(4-(((1-(2,6-dichloro-4-(trifluoromethyl)phenyl)-4-((trifluoromethyl)sulfinyl)-3-cyano-1H-pyrazol-5-yl)amino)methyl)-1H-1,2,3-triazol-1-yl)- (4-GTF). White solid; yield, 78%, mp, 177.9 °C; ^{1}H NMR (CD_3OD, 600 MHz) δ, 8.08 (s, 2H), 7.88 (d, J = 3.1 Hz, 1H), 7.86* (d, J = 3.1 Hz, 1H), 5.27 (d,

dx.doi.org/10.1021/jf5010429 | J. Agric. Food Chem. 2014, 62, 6065−6071

Scheme 2. Synthesis of Fipronil Conjugates for Replacement of C-1, C-2, C-3, C-4, and C-6 of D-Glucose: 1, *tert*-Butyl Alcohol, H_2O, $CuSO_4 \cdot 5H_2O$, Sodium Ascorbate, 50 °C, 3 h; 2, NaOMe, MeOH; Room Temperature, 30 min

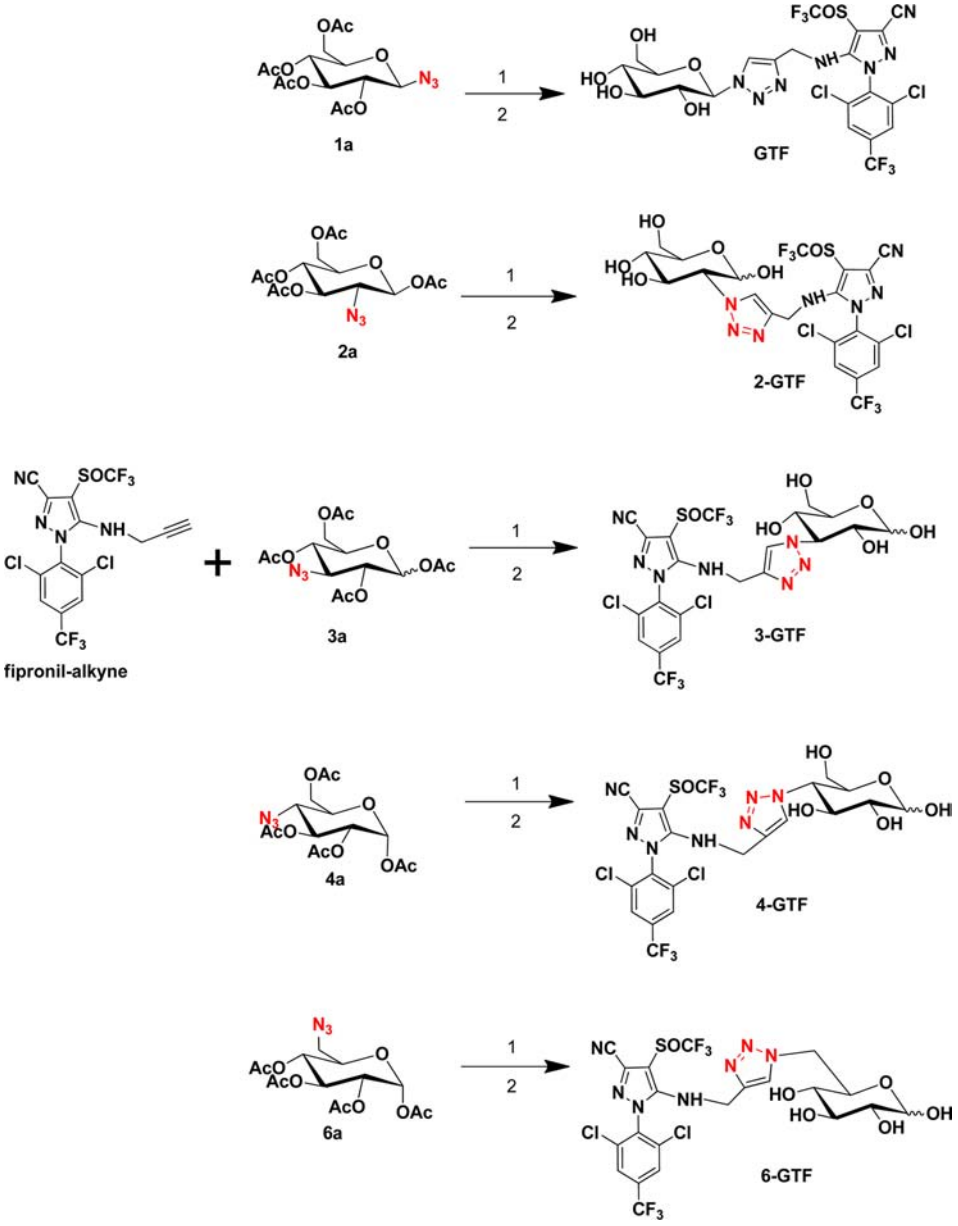

J = 3.1 Hz, 1H), 4.47−4.49 (m, 2H), 4.32−4.37* (m, 2H), 4.09 (dd, *J* = 9.1, 6.0 Hz, 1H), 4.02−4.05* (m, 1H), 3.53 (dd, *J* = 9.4, 3.6 Hz, 1H), 3.47−3.50 (m, 2H), 3.29 (t, *J* = 9.1 Hz, 1H), 3.29* (t, *J* = 9.1 Hz, 1H), 3.11−3.18 (m, 2H); ^{13}C NMR (CD_3OD, 150 MHz) *δ*, 151.8, 144.6, 137.9, 136.2, 136.0, 127.9, 127.8, 125.5, 125.3, 125.2, 124.5, 122.7, 112.1, 98.3, 94.2*, 76.9, 75.8, 75.3*, 74.4, 72.0, 71.1, 63.8, 63.6*, 61.6, 61.5*, 41.0, 40.9*; HRMS (ESI) calcd for $C_{21}H_{17}Cl_2F_6N_7O_6SNa$ $[M + Na]^+$, 702.0140; found, 702.0135.

D-Glucopyranose, 6-Deoxy-6-(4-(((1-(2,6-dichloro-4-(trifluoromethyl)phenyl)-4-((trifluoromethyl)sulfinyl)-3-cyano-1H-pyrazol-5-yl)amino)methyl)-1H-1,2,3-triazol-1-yl)- (6-GTF). White solid; yield, 88%, mp, 188.4 °C; ^{1}H NMR (CD_3OD, 600 MHz) *δ*, 8.08 (s, 2H), 7.89 (d, *J* = 3.1 Hz, 1H), 7.84* (d, *J* = 3.1 Hz, 1H), 5.06 (d, *J* = 3.2 Hz, 1H), 4.43−4.46 (m, 2H), 4.06−4.11 (m, 1H), 3.68 (d, *J* = 9.2 Hz, 1H), 3.68* (d, *J* = 9.2 Hz, 1H), 3.28−3.39 (m, 2H), 3.10 (t, *J* = 9.2 Hz, 1H), 3.04* (t, *J* = 9.2 Hz, 1H); ^{13}C NMR (CD_3OD, 150 MHz) *δ*, 151.7, 144.9, 137.8, 137.7, 135.9, 127.9, 127.8, 127.8, 125.4, 125.3, 124.4, 122.6, 112.1, 98.2, 94.0*, 77.6, 76.0, 75.6, 74.5, 73.5, 72.7, 72.6, 71.0, 52.3, 52.3*, 41.0, 40.9*. HRMS (ESI) calcd for $C_{21}H_{17}Cl_2F_6N_7O_6SNa$ $[M + Na]^+$, 702.0140; found, 702.0135.

RESULTS AND DISCUSSION

Various strategies for increasing the phloem mobility of pesticides have been considered. A feasible strategy is the use of endogenous transporter proteins to carry pesticides. In this work, D-glucose was chosen as a vector for several reasons. First, it is the most abundant and important monosaccharide in nature. Second, it could be transported by various monosaccharide transporters and their homologues through diverse plant species.[18] Third, D-glucose confers moderate phloem mobility to the non-phloem-mobile insecticide fipronil, as presented in our previous paper.[9,16] In the present work, to evaluate the effects of the different positions of glucose on phloem mobility, four novel GTF conjugates, namely, 2-GTF, 3-GTF, 4-GTF, and 6-GTF, were synthesized via click chemistry based on the synthetic method of GTF.[9] All of the novel structures were confirmed via ^{1}H and ^{13}C NMR spectroscopy and ESI mass spectrometry.

dx.doi.org/10.1021/jf5010429 | J. Agric. Food Chem. 2014, 62, 6065−6071

Synthesis of Azido-Containing Acetylglucoses (Scheme 1). 2,3,4,6-Tetra-*O*-acetyl-1-azido-1-deoxy-D-glucoside (**1a**) was prepared from glucose pentaacetate in the presence of azidotrimethylsilane and $SnCl_4$ (Scheme 1A).[19] Glucosamine hydrochloride was transformed into 2-azido-2-deoxy-D-glucose by diazo transfer from triflyl azide (TfN_3). 2-Azido-2-deoxy-D-glucose was subsequently acetylated using acetic anhydride with catalytic DMAP in pyridine to yield 1,3,4,6-tetra-*O*-acetyl-2-azido-2-deoxy-D-glucose (**2a**) (Scheme 1B).[20] The introduction of nitrogen at C-3 of glucose required a double inversion of the configuration. Thus, the usual oxidation/reduction sequence led to the fomation of diacetone allose, which was then converted to azide via a triflation/azide displacement sequence.[21] Treatment of furanose diacetonide with aqueous trifluoroacetic acid was followed by the complete acetylation of the crude products via treatment with acetic anhydride and pyridine, and pyranose acetates were produced as 1,2,4,6-tetra-*O*-acetyl-3-azido-3-deoxy-D-glucosise (**3a**)[22] (Scheme 1C). Methyl α-D-galactopyranoside (1 equiv) was benzoylated by benzoyl chloride (3.5 equiv) in pyridine to link selectively to methyl 2,3,6-tri-*O*-benzoyl-α-D-galactopyranoside because the axial C-4 hydroxyl in the favored conformation has a lower reactivity than C-2, C-3, and C-6.[23] Methyl 2,3,6-tri-*O*-benzoyl-α-D-galactopyranoside was then sulfonated by trifluoromethanesulfonic anhydride. The displacement of the trifluoromethanesulfonate by sodium azide in dimethylformamide gave a good yield of methyl 4-azido-2,3,6-tri-*O*-benzoyl-4-deoxy-α-D-glucopyranoside in syrup form.[24] The debenzoylation of methyl 2,3,6-tri-*O*-benzoyl-4-azido-4-deoxy-α-D-glucopy-ranoside with sodium methoxide resulted in crystalline methyl 4-azido-4-deoxy-α-D-glucopyranoside, which was subsequently peracetylated to obtain a syrupy 1,2,3,6-tetra-*O*-acetyl-4-azido-4-deoxy-α-D-glucose (**4a**). 1,2,3,4-Tetraacetyl-6-*O*-*p*-tolylsulfonyl-D-glucopyranose was prepared from D-glucose as previously described.[17] Conventional azidation in the presence of dimethylformamide resulted in the formation of 1,2,3,4-tetra-*O*-acetyl-6-azido-6-deoxy-D-glucopyranose (**6a**).[25]

Synthesis and Characterization of GTF Conjugates. The synthetic method of GTF conjugates was proposed by Yang et al.[9] To prepare these conjugates via click chemistry, tetraacetylglucosides containing the azide group were synthesized according to the same method mentioned above (Scheme 1). Propargyl was introduced into fipronil according to a previous method by Yang et al.[9] as a coupling partner. In Scheme 2, the $CuSO_4{\cdot}5H_2O$/ascorbate click reaction system was explored to prepare the acetyl glucose-containing fipronil conjugates, which were O-deacetylated via the Zemplén procedure to obtain the target products.

The ^{1}H NMR spectra of these compounds are complicated because fipronil has an asymmetrical sulfoxide and forms two enantiomers.[26,27] In addition, the α,β configuration of the glucosyl group also exists. Their configurations were confirmed on the basis of a chemical shift, coupling constants, and band shape of H-1. For example, the NMR signals of product 2-GTF were immediately measured after the dissolution of the glucosyl conjugates in denatured methanol. A one-proton doublet was observed at 5.28 and $J_{1,2}$ = 3.2 Hz. These results indicate that the substance was in the α-D-pyranose anomer form. The second doublet, observed at 5.11 and $J_{1,2}$ = 7.3 Hz, was assigned to H-1 of the β-D-pyranose anomer. The characteristic peaks at 8.00 in the ^{1}H NMR spectra and the peaks at 127.9 and 123.5 in the ^{13}C NMR spectra appeared after reaction. These results demonstrate that 1,2,3-triazole was produced and the target conjugate was obtained. The analysis via ESI−MS spectroscopy showed a specific peak at m/z 702.0135 $[M + Na]^+$, from which the MW was estimated at 702.0140 $[M + Na]^+$. From these results, the synthesized product was identified as 2-GTF.

Phloem Mobility. The castor bean seedling system is an ideal biological model to evaluate the phloem systemicity of xenobiotics because of its thin and highly permeable cuticle, which facilitates molecule diffusion to and within the cotyledon apoplast system.[28] The system was adopted to test the phloem mobility of GTF, 2-GTF, 3-GTF, 4-GTF, and 6-GTF. As presented in a previous study,[9] the plasma membrane potential of the conjugates was measured via flow cytometric analysis with DiBAC4(3) as the fluorescent dye indicator.[29] In comparison to the control sample, the relative fluorescence data did not have any remarkable changes during the treatment period (Figure 1).

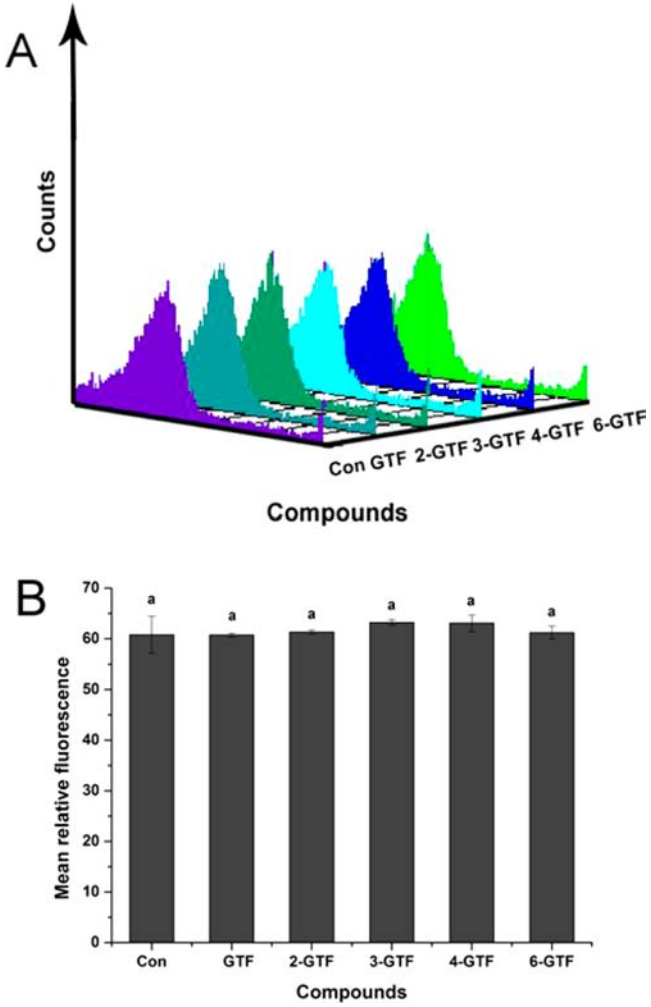

Figure 1. Plasma membrane potential in the protoplasts of *R. communis* cotyledons after 6 h of treatment. (A) Fluorescent intensity histogram marked DiBAC4(3) of the treatment of tested compounds and the control (Con). (B) Relative fluorescence of the treatment of tested compounds and the control (Con). The protoplasts were suspended in a buffered solution at pH 5.5 with or without (control) tested compounds (100 μM) for 5 h. The protoplasts were analyzed by flow cytometry for DiBAC4(3) fluorescence. The data [mean ± standard error (SE); n = 3] within a column are not significantly different, as shown by the Kruskal−Wallis test ($p > 0.05$).

The results indicate that the five conjugates have no depolarizing effects on the transmembrane potential. Therefore, the five

dx.doi.org/10.1021/jf5010429 | J. Agric. Food Chem. 2014, 62, 6065−6071

conjugates were not phytotoxic in the phloem mobility test during the 5 h experimental period.

After a 5 h incubation (including the 1 h pre-incubation period), the conjugates were clearly detected in the phloem sap. The phloem sap determination results indicate that the five conjugates (GTF, 2-GTF, 3-GTF, 4-GTF, and 6-GTF) all exhibited moderate phloem mobility in *Ricinus* seedlings (Figure 2). The GTF conjugates in the phloem sap were further

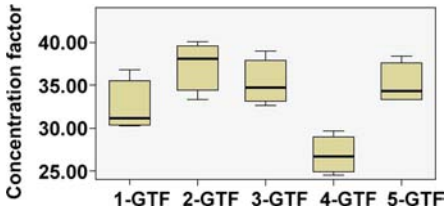

Figure 2. Phloem exudation collection of 4 sets of 12 castor bean seedlings for each conjugate at 5 h (mean ± SE). The Kruskal–Wallis tests at a 5% probability level were used to determine statistical differences among treatments ($p < 0.05$).

identified with UPLC–MS (see the figure in the Supporting Information). The UPLC–MS results indicated that the fipronil parent molecule was not detected in the phloem sap.

The "rule of five", which is widely adopted in the pharmaceutical industry, can also be used to predict the diffusion of endogenous molecules or xenobiotics through plant and animal membranes.[30] According to this rule, the passive absorption of small molecules is more likely to occur when their MW, log*P*, number of hydrogen bond donors, and number of hydrogen bond acceptors are less than 500 Da, 5, 5, and 10, respectively. Given the physical properties of the five conjugates (Table 1), their diffusion through the membranes should be very low. Models based on the physicochemical properties of pesticides are widely used to predict their phloem mobility. The Kleier model is widely used to predict the phloem systemicity of a compound based on the physicochemical properties (pK_a and log K_{ow}) of xenobiotics.[14,16,28] According to Kleier's prediction model, the physical properties of the five conjugates (Table 1) in terms of log K_{ow} and pK_a are found in non-mobile areas (Figure 3). In general, based on the "rule of five" and the Kleier prediction model, the five conjugates should have a low diffusion through the membrane and no phloem mobility should be observed. However, the experimental results of the phloem sap analysis violated the "rule of five" and the Kleier model. Specific carrier processes were probably involved in the phloem transport, as demonstrated in the phloem transport of GTF in *Ricinus* seedlings, which involves an active carrier-mediated mechanism that effectively contributes to GTF phloem loading.[16]

Among these conjugates, the analysis result showed that linking the fipronil to C-2, C-3, C-4, and C-6 of glucose affected phloem mobility of GTF conjugates. The concentrations of GTF, 2-GTF, 3-GTF, 4-GTF, and 6-GTF in phloem sap were 32.35 ± 1.51, 37.37 ± 1.44, 35.25 ± 1.32, 26.87 ± 1.07, and 35.10 ± 1.19 μM, respectively (Figure 2). In a previous work, sugar transporters have been shown to transport many glucose derivatives and glucose conjugates across the membrane. 2-NBDG is incorporated into mammalian cells through glucose transporters in a time-, concentration-, and temperature-dependent manner.[31] The uptake of IPNG into tobacco cells involves an active transport process.[32] Specifically, GTF can be mediated by sugar carrier systems during its phloem loading. The glucose conjugates (2-GTF, 3-GTF, 4-GTF, and 6-GTF) are isomers of GTF and

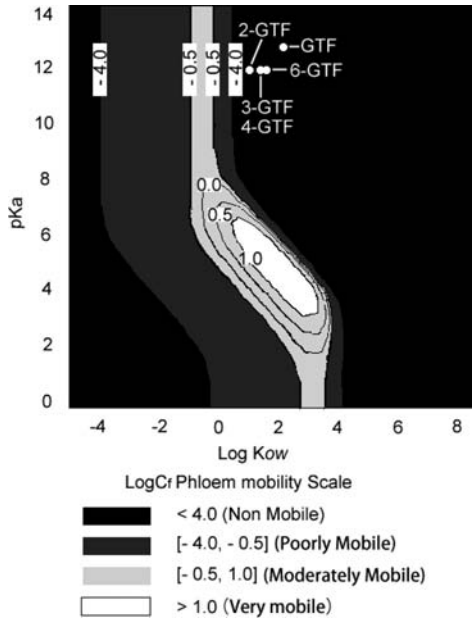

Figure 3. Prediction of phloem mobility of tested compounds (GTF, 2-GTF, 3-GTF, 4-GTF, and 6-GTF) using the Kleier map (log C_f as a function of log K_{ow} and pK_a) according to Kleier;[3,5] plant parameters are for a short plant.[3] Log K_{ow} and pK_a were calculated by the ACD Laboratories Percepta program, version 14.0, and log K_{ow} and pK_a values were classic values.

have very similar properties with each other (Table 1). Therefore, we speculate that sugar carrier systems are involved in the phloem loading of 2-GTF, 3-GTF, 4-GTF, and 6-GTF. Moreover, glucosyl derivatives, which are conjugated at different carbons of glucose, have a significant influence on affinities for sugar carriers. Among the O-methylsulfonyl derivatives of D-glucose, mesylation at C-4 and C-6 of glucose resulted in a slightly diminished affinity for the GLUT1, whereas mesylation at C-3 led to the complete loss of affinity.[33] Therefore, their phloem mobility difference of glucosyl conjugates might be caused by their different affinities for sugar carriers.

In conclusion, four new conjugates containing both fipronil and glucose moieties were synthesized via click chemistry. The phloem mobility tests in the 5 h experimental period demonstrated that the conjugates could enter into the phloem and exhibit moderate phloem mobility without being degraded. Results show that the phloem mobility was closely related to the position of the glucose. Crop protection and production technology have given increasing attention to the effective transport of pesticides through the phloem. Therefore, understanding the influence of the positions of glucose on phloem mobility provides a foundation for synthesis of excellent phloem-mobile sugar pesticides.

■ ASSOCIATED CONTENT

Supporting Information

UPLC–MS indicating that the GTF conjugates were not degraded in the phloem sap during the 5 h experiment. This material is available free of charge via the Internet at http://pubs.acs.org.

■ AUTHOR INFORMATION

Corresponding Author

*Telephone: +86-20-85285127. Fax: +86-20-38604926. E-mail: hhxu@scau.edu.cn.

Author Contributions

†Zhiwei Lei and Jie Wang contributed equally to this work.

Funding

This work was supported by the National Natural Science Foundation of China (Grant 31171886) and The Doctor Science Research Foundation of the Education Ministry of China (Grant 20114404110020)

Notes

The authors declare no competing financial interest.

REFERENCES

(1) Ruiz-Medrano, R.; Xoconostle-Cázares, B.; Lucas, W. J. Phloem long-distance transport of CmNACP mRNA: Implications for supracellular regulation in plants. *Development* **1999**, *126*, 4405−4419.

(2) Hsu, F. C.; Sun, K.; Kleier, D. A.; Fielding, M. J. Phloem mobility of xenobiotics VI. Preparation of a phloem-mobile pro-nematocide based on oxamyl, exhibiting root-specific activation in transgenic tobacco. *Pestici. Sci.* **1995**, *44*, 9−19.

(3) Kleier, D. A. Phloem mobility of xenobiotics. V. Structural requirements for phloem-systemic pesticides. *Pestic. Sci.* **1994**, *42*, 1−11.

(4) Lichtner, F. Phloem mobility of crop protection products. *Funct. Plant Biol.* **2000**, *27*, 609−614.

(5) Kleier, D. A.; Grayson, B. T.; Hsu, F. C. The phloem mobility of pesticides. *Pestic. Outlook* **1998**, *9*, 26−30.

(6) Chollet, J. F.; Rocher, F.; Jousse, C.; Delétage-Grandon, C.; Bashiardes, G.; Bonnemain, J. L. Synthesis and phloem mobility of acidic derivatives of the fungicide fenpiclonil. *Pest Manage. Sci.* **2004**, *60*, 1063−1072.

(7) Delétage-Grandon, C.; Chollet, J. F.; Faucher, M.; Rocher, F.; Komor, E.; Bonnemain, J. L. Carrier-mediated uptake and phloem systemy of a 350-Dalton chlorinated xenobiotic with an α-amino acid function. *Plant Physiol.* **2001**, *125*, 1620−1632.

(8) Lei, Z.; Wang, J.; Mao, G.; Wen, Y.; Xu, H. Phloem mobility and translocation of fluorescent conjugate containing glucose and NBD in castor bean (*Ricinus communis*). *J. Photochem. Photobiol., B* **2014**, *132*, 10−16.

(9) Yang, W.; Wu, H.; Xu, H.; Hu, A.; Lu, M. Synthesis of glucose−fipronil conjugate and its phloem mobility. *J. Agric. Food Chem.* **2011**, *59*, 12534−12542.

(10) Yuan, J.; Wu, H.; Lu, M.; Song, G.; Xu, H. Synthesis of a series of monosaccharide−fipronil conjugates and their phloem mobility. *J. Agric. Food Chem.* **2013**, *61*, 4236−4241.

(11) Fernández, C.; Nieto, O.; Fontenla, J. A.; Rivas, E.; Ceballos, M. L.; Fernández-Mayoralas, A. Synthesis of glycosyl derivatives as dopamine prodrugs: Interaction with glucose carrier GLUT-1. *Org. Biomol. Chem.* **2003**, *1* (5), 767−771.

(12) Barros, L. F.; Bittner, C. X.; Loaiza, A.; Ruminot, I.; Larenas, V.; Moldenhauer, H.; Oyarzun, C.; Alvarez, M. Kinetic validation of 6-NBDG as a probe for the glucose transporter GLUT1 in astrocytes. *J. Neurochem.* **2009**, *109*, 94−100.

(13) Grech, J. N.; Li, Q.; Roufogalis, B. D.; Duke, C. C. Novel Ca^{2+}-ATPase inhibitors from the dried root tubers of polygonum multiflorum. *J. Nat. Prod.* **1994**, *57*, 1682−1687.

(14) Rocher, F.; Chollet, J. F.; Jousse, C.; Bonnemain, J. L. Salicylic acid, an ambimobile molecule exhibiting a high ability to accumulate in the phloem. *Plant Physiol.* **2006**, *141*, 1684−1693.

(15) Kallarackal, J.; Orlich, G.; Schobert, C.; Komor, E. Sucrose transport into the phloem of *Ricinus communis* L. seedlings as measured by the analysis of sieve-tube sap. *Planta* **1989**, *177*, 327−335.

(16) Wu, H.; Yang, W.; Zhang, Z.; Huang, T.; Yao, G.; Xu, H. Uptake and phloem transport of glucose-fipronil conjugate in *Ricinus communis* involve a carrier-mediated mechanism. *J. Agric. Food Chem.* **2012**, *60*, 6088−6094.

(17) Jeong, L. S.; Schinazi, R. F.; Beach, J. W.; Kim, H. O.; Shanmuganathan, K.; Nampalli, S.; Chun, M. W.; Chung, W. K.; Choi, B. G.; Chu, C. K. Structure−activity relationships of β-D-(2*S*,5*R*)- and α-D-(2*S*,*S*)-1,3-oxathiolanyl nucleosides as potential anti-HIV agents. *J. Med. Chem.* **1993**, *36*, 2627−2638.

(18) Slewinski, T. L. Diverse functional roles of monosaccharide transporters and their homologs in vascular plants: A physiological perspective. *Mol. Plant* **2011**, *4*, 641−662.

(19) Cagnoni, A. J.; Varela, O.; Gouin, S. G.; Kovensky, J.; Uhrig, M. L. Synthesis of multivalent glycoclusters from 1-thio-β-D-galactose and their inhibitory activity against the β-galactosidase from *E. coli*. *J. Org. Chem.* **2011**, *76*, 3064−3077.

(20) Alper, P. B.; Hung, S.; Wong, C. Metal catalyzed diazo transfer for the synthesis of azides from amines. *Tetrahedron Lett.* **1996**, *37*, 6029−6032.

(21) Guo, J.; Frost, J. W. Kanosamine biosynthesis: A likely source of the aminoshikimate pathway's nitrogen atom. *J. Am. Chem. Soc.* **2002**, *124*, 10642−10643.

(22) Danac, R.; Ball, L.; Gurr, S. J.; Fairbanks, A. J. Synthesis of UDP-glucose derivatives modified at the 3-OH as potential chain terminators of β-glucan biosynthesis. *Carbohydr. Res.* **2008**, *343*, 1012−1022.

(23) Reist, E. J.; Spencer, R. R.; Calkins, D. F.; Baker, B. R.; Goodman, L. Derivatives of 4-amino-4-deoxy-D-glucose. *J. Org. Chem.* **1965**, *30*, 2312−2317.

(24) Sandbhor, M.; Bhasin, M.; Williams, D. T.; Hsieh, M.; Wu, S.; Zou, W. Synthesis of iminoalditol analogues of galactofuranosides and their activities against glycosidases. *Carbohydr. Res.* **2008**, *343*, 2878−2886.

(25) Saxon, E.; Luchansky, S. J.; Hang, H. C.; Yu, C.; Lee, S. C.; Bertozzi, C. R. Investigating cellular metabolism of synthetic azidosugars with the Staudinger ligation. *J. Am. Chem. Soc.* **2002**, *124*, 14893−14902.

(26) Teicher, H. B.; Kofoed Hansen, B.; Jacobsen, N. Insecticidal activity of the enantiomers of fipronil. *Pest Manage. Sci.* **2003**, *59*, 1273−1275.

(27) Zhao, Q.; Li, Y.; Xiong, L.; Wang, Q. Design, synthesis and insecticidal activity of novel phenylpyrazoles containing a 2,2,2-trichloro-1-alkoxyethyl moiety. *J. Agric. Food Chem.* **2010**, *58* (8), 4992−4998.

(28) Rocher, F.; Chollet, J. F.; Legros, S.; Jousse, C.; Lemoine, R.; Faucher, M.; Bush, D. R.; Bonnemain, J. L. Salicylic acid transport in *Ricinus communis* involves a pH-dependent carrier system in addition to diffusion. *Plant Physiol.* **2009**, *150*, 2081−2091.

(29) Konrad, K. R.; Hedrich, R. The use of voltage-sensitive dyes to monitor signal-induced changes in membrane potential−ABA triggered membrane depolarization in guard cells. *Plant J.* **2008**, *55*, 161−173.

(30) Bhal, S. K.; Kassam, K.; Peirson, I. G.; Pearl, G. M. The rule of five revisited: Applying log *D* in place of log *P* in drug-likeness filters. *Mol. Pharmaceutics* **2007**, *4*, 556−560.

(31) Yamamoto, T.; Nishiuchi, Y.; Teshima, T.; Matsuoka, H.; Yamada, K. Synthesis of 2-NBDLG, a fluorescent derivative of L-glucosamine; the antipode of D-glucose tracer 2-NBDG. *Tetrahedron Lett.* **2008**, *49*, 6876−6878.

(32) Hu, A.; Yang, W.; Xu, H. Novel fluorescent conjugate containing glucose and NBD and its carrier-mediated uptake by tobacco cells. *J. Photochem. Photobiol., B* **2010**, *101*, 215−223.

(33) Halmos, T.; Santarromana, M.; Antonakis, K.; Scherman, D. Synthesis of glucose-chlorambucil derivatives and their recognition by the human GLUT1 glucose transporter. *Eur. J. Pharmacol.* **1996**, *318* (2), 477−484.

JOURNAL OF AGRICULTURAL AND FOOD CHEMISTRY

Article

pubs.acs.org/JAFC

Design, Synthesis, and Biological Evaluation of Various α-Substituted Benzylpyrroles Based on the Structures of Insecticidal Chlorfenapyr and Natural Pyrrolomycins

Qiaoqiao Ma, Yuxiu Liu,* Pengxiang Zhang, Yongqiang Li, Lixia Xiong, and Qingmin Wang*

State Key Laboratory of Elemento-Organic Chemistry, Research Institute of Elemento-Organic Chemistry, Collaborative Innovation Center of Chemical Science and Engineering (Tianjin), Nankai University, Tianjin 300071, People's Republic of China

ABSTRACT: On the basis of the structures of chlorfenapyr and dioxapyrrolomycin, a series of 2-benzylpyrroles with a hydroxyl, an alkyloxy, an acyloxy, an alkylsulfanyl, or an oxime moiety at the α-position of benzyl were designed and synthesized. Their insecticidal, acaricidal, and fungicidal activities were extensively investigated. The structure−activity relationship showed that benzylpyrroles bearing shorter α-alkyloxy groups gave better activities against most of the insect species; the alkylation of pyrrole usually gave increased activity. Among all compounds, (4-bromo-2-(α-(2,2,2-trifluoroethoxy)-4-chlorobenzyl)-1-(ethoxymethyl)-5-(trifluoromethyl)-1*H*-pyrrole-3-carbonitrile) (**5′j**) exhibited the most outstanding insecticidal activities against oriental armyworm (IC_{50} = 10 mg L^{-1}), diamondback moth (0.07 mg L^{-1}), corn borer (50 mg L^{-1}), and mosquito (0.04 mg L^{-1}), which are very close to those of chlorfenapyr (**5**, 0.08, <25, and <0.025 mg L^{-1}, respectively). In addition, some compounds also exhibited a broad or selective fungicidal spectrum.

KEYWORDS: *chlorfenapyr, dioxapyrrolomycin, 2-benzylpyrrole, insecticidal activity, acaricidal activity, fungicidal activity*

INTRODUCTION

Using natural products as lead compounds to develop new pesticides with a novel structure and mechanism is one of the most effective drug design methods.[1,2] Dioxapyrrolomycin (Figure 1), isolated from the metabolites of the microorganism *Streptomyces* by the American Cyanamid Co. in 1987, is the first chiral pyrrole toxin found to have insecticidal, acaricidal, and fungicidal activities.[3] Chlorfenapyr is such a commercial arylpyrrole insecticide/acaricide optimized from dioxapyrrolomycin.[4−7] In fact, after chemical structure modification, chlorfenapyr has obvious changes in the skeleton compared with dioxapyrrolomycin. First, there is a carbon atom between the benzene ring and pyrrole ring in dioxapyrrolomycin, whereas in chlorfenapyr the benzene ring and pyrrole ring are directly connected. Second, the substituents on both the benzene ring and pyrrole ring of the two compounds are significantly different. Third, chlorfenapyr has an ethoxymethyl group on the pyrrole N, which is a necessary structural modification to solve the tough problem that the chlorfenapyr parent compound (**1**) has an intolerable phytotoxicity to the plants applied.[7]

Though dioxapyrrolomycin and chlorfenapyr have some differences in their skeletons, their insecticidal mechanisms are the same. Both dioxapyrrolomycin and the chlorfenapyr parent compound (**1**), acting as uncouplers of oxidative phosphorylation,[8] can uncouple respiratory electron transport in mitochondria and hinder ADP conversion to ATP.[9] Chlorfenapyr, as a precursor pesticide, shows same effect because it could be converted to **1** inside the insect body.[8] Thus, we speculated that when we retain all the substituents on the benzene and pyrrole rings of **1** but insert a methylene group between the two rings (compound **2**, Figure 1), such an alteration in the structure would not change the insecticidal mechanism and insecticidal/acaricidal activity, and the mentioned compound may also likely keep the fungicidal activity. To our delight, compound **2** and its N-alkylation product **3** were synthesized and found to have considerable insecticidal and/or acaricidal activity.[10]

Dioxapyrrolomycin contains a dioxane moiety in the structure; from another point of view, there is an oxygen-containing substituent on the methylene between the benzene ring and pyrrole ring. The presence of oxygen is thought to provide the possibility for the molecule to form a hydrogen bond with the target in the respiratory electron transport chain and therefore to give improved biological activity. Thus, in this paper, choosing compound **2** as the skeleton structure, we designed and synthesized a series of compounds with a hydroxyl group (**4**) and various alkyloxy groups (**5**) on the methylene and investigated the influence of different substituents on the insecticidal, acaricidal, and fungicidal activities; we also synthesized (α-(acyloxy)benzyl)pyrroles **6**, α-sulfanyl compounds **7**, and α-oxime ether compounds **8** to test their bioactivity. For (α-(alkyloxy)benzyl)pyrroles **5** with higher insecticidal activity, we further introduced an ethoxymethyl group onto the nitrogen atom of the pyrrole ring to get **5′** to compare the resulting changes in biological activity (Scheme 1). Herein, we present the synthesis and variety of bioactivities of the compounds mentioned above in detail. The structure−activity relationships are also discussed.

MATERIALS AND METHODS

Instruments. ^{1}H NMR and ^{13}C NMR spectra were obtained at 400 MHz using a Bruker AV400 spectrometer in $CDCl_3$ or DMSO-d_6

Received: March 22, 2014
Revised: June 3, 2014
Accepted: June 10, 2014
Published: June 10, 2014

ACS Publications © 2014 American Chemical Society

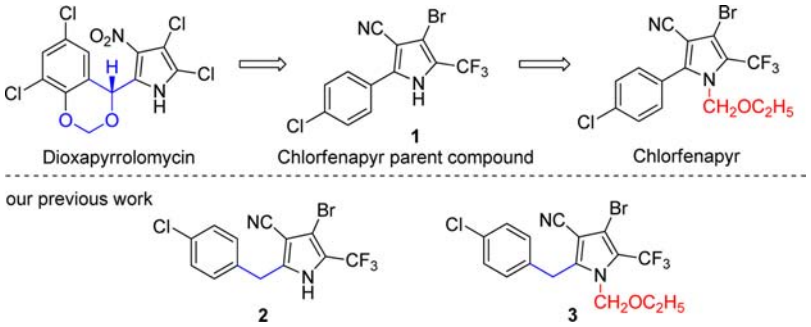

Figure 1. Structures of dioxapyrrolomycin, chlorfenapyr, and designed benzylpyrroles.

Scheme 1. Preparation of Target Compounds

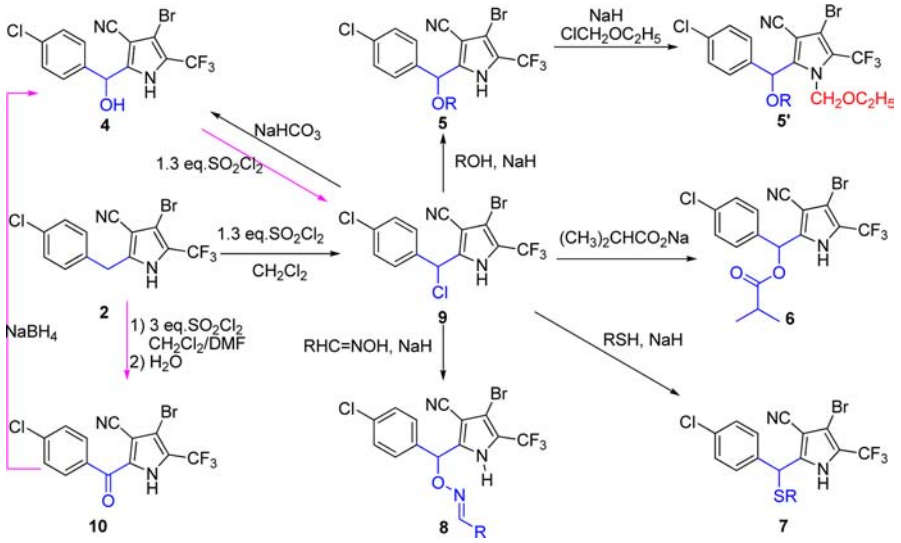

solution with tetramethylsilane as the internal standard. Chemical shift values (δ) are given in parts per million. In the ^{13}C NMR data, four peaks in one set of parentheses means that they are assigned to one carbon which is split by three adjacent F atoms. HRMS data were obtained on an FTICR-MS instrument (Ionspec 7.0 T). The melting points were determined on an X-4 binocular microscope melting point apparatus and are uncorrected. The yields were not optimized.

4-Bromo-2-(α-hydroxyl-4-chlorobenzyl)-5-(trifluoromethyl)-1*H*-pyrrole-3-carbonitrile (4). Method 1: A solution of **2** (0.50 g, 1.38 mmol) in dichloromethane (180 mL) was heated to reflux until all solid was dissolved. After this solution was cooled to room temperature, a solution of freshly distilled sulfonyl chloride (0.23 g, 1.70 mmol) in dichloromethane (10 mL) was added, and the reaction mixture was stirred at room temperature for 12 h. Saturated sodium bicarbonate aqueous solution (100 mL) was added, and the mixture was stirred for another 0.5 h. The organic layer was separated and washed with water and brine, dried over anhydrous magnesium sulfate, and concentrated to give **4** as a white solid (0.49 g, 90%): mp 158−159 °C; ^1H NMR (400 MHz, $CDCl_3$) δ 9.38 (s, 1H), 7.39 (d, J = 8.4 Hz, 2H), 7.35 (d, J = 8.4 Hz, 2H), 6.00 (s, 1H); ^{13}C NMR (100 MHz, $CDCl_3$) δ 142.8, 137.6, 135.6, 129.6, 128.0, (123.6, 120.9, 118.2, 115.6), (119.2, 118.8, 118.4, 118.0), 112.5, 101.7, 95.9, 69.0; HRMS (ESI) m/z calcd for $C_{13}H_6BrClF_3N_2O$ $(M - H)^-$ 376.9315, found 376.9310.

Method 2: To a solution of **2** (0.50 g, 1.38 mmol) in a mixed solvent of dichloromethane (50 mL) and DMF (5 mL) was added freshly distilled sulfonyl chloride (0.46 g, 3.40 mmol) in dichloromethane (10 mL), and the reaction mixture was stirred at room temperature for 12 h. Then water (100 mL) was added to the mixture, and the resulting mixture was stirred for another 0.5 h. The organic layer was separated and washed with water and brine, dried over anhydrous magnesium sulfate, and concentrated to give 4-bromo-2-(4-chlorobenzoyl)-5-(trifluoromethyl)-1*H*-pyrrole-3-carbonitrile (**10**) as a white solid (0.49 g, 94%): ^1H NMR (400 MHz, $CDCl_3$) δ 11.19 (s, 1H), 7.84 (d, J = 8.4 Hz, 2H), 7.55 (d, J = 8.4 Hz, 2H); HRMS (ESI) m/z calcd for $C_{13}H_3BrClF_3N_2O$ $(M - H)^-$ 374.9153, found 374.9153.

To a solution of **10** (1.0 g, 2.65 mmol) in THF (30 mL) was added $NaBH_4$ (0.15 g, 3.95 mmol), and the reaction mixture was stirred at room temperature for 12 h. The mixture was quenched with water, the solvent evaporated, and then the mixture extracted with dichloromethane. The organic layer was separated, washed with water and brine, dried over anhydrous magnesium sulfate, filtered, and then concentrated. The residue was purified by silica gel using petroleum ether/ethyl acetate as the eluent to give **4** as a white solid (0.50 g, 50%).

4-Bromo-2-(α-chloro-4-chlorobenzyl)-5-(trifluoromethyl)-1*H*-pyrrole-3-carbonitrile (9). Method 1: A solution of **2** (0.50 g, 1.38 mmol) in dichloromethane (180 mL) was heated to reflux until all solid was dissolved. After this solution was cooled to room temperature, a solution of freshly distilled sulfonyl chloride (0.23 g, 1.70 mmol) in dichloromethane (10 mL) was added, and the reaction mixture was stirred at room temperature for 12 h. Then the mixture was successively washed with water (3 × 100 mL) and brine, dried over anhydrous magnesium sulfate, an dconcentrated to give **9** as a white solid (0.51 g, 92%): mp 120−122 °C; ^1H NMR (400 MHz, $CDCl_3$) δ 9.23 (s, 1H), 7.42 (d, J = 8.4 Hz, 2H), 7.35 (d, J = 8.4 Hz, 2H), 6.20 (s, 1H).

Method 2: To a solution of **4** (0.50 g, 1.32 mmol) in dichloromethane (40 mL) was added freshly distilled sulfonyl chloride (0.46 g, 3.40 mmol) in dichloromethane (10 mL), and the reaction mixture was refluxed for 8 h. Then the mixture was successively

dx.doi.org/10.1021/jf501377t | J. Agric. Food Chem. 2014, 62, 6072−6081

washed with water (3 × 100 mL) and brine, dried over anhydrous magnesium sulfate, and concentrated to give **9** (0.47 g, 90%).

Synthesis of (α-Alkoxybenzyl)pyrrole (5). General Procedure. To a solution of the corresponding alcohol (4.5 mmol) in THF (40 mL) was added NaH (0.10 g, 4.1 mmol). After the mixture was refluxed for 1.5 h, crude **9** (0.60 g, 1.51 mmol) was added, and the mixture was refluxed for another 3 h. After the solvent was evaporated, the residue was dissolved in dichloromethane (50 mL), washed with water (3 × 25 mL) and brine, dried over anhydrous magnesium sulfate, and then concentrated. The crude was purified by silica gel using petroleum ether/ethyl acetate (10:1) as the eluent to give **5** as a white solid.

*Data for 4-bromo-2-(α-methoxy-4-chlorobenzyl)-5-(trifluoromethyl)-1H-pyrrole-3-carbonitrile (**5a**):* yield 63%; white solid; mp 51−53 °C; ^{1}H NMR (400 MHz, $CDCl_3$) δ 9.28 (s, 1H), 7.40 (d, J = 8.4 Hz, 2H), 7.31 (d, J = 8.4 Hz, 2H), 5.40 (s, 1H), 3.40 (s, 3H); ^{13}C NMR (100 MHz, $CDCl_3$) δ 141.1, 134.4, 130.1, 128.4, 127.5, (122.6, 119.9, 117.2, 114.5), (118.5, 118.1, 117.7, 117.3), 111.4, 100.3, 95.2, 76.3, 56.2; HRMS (ESI) m/z calcd for $C_{14}H_{13}BrClF_3N_3O$ $(M + NH_4)^+$ 409.9877, found 409.9867.

*Data for 4-bromo-2-(α-ethoxy-4-chlorobenzyl)-5-(trifluoromethyl)-1H-pyrrole-3-carbonitrile (**5b**):* yield 80%; white solid; mp 118−119 °C; ^{1}H NMR (400 MHz, $CDCl_3$) δ 9.15 (s, 1H), 7.40 (d, J = 8.0 Hz, 2H), 7.32 (d, J = 8.0 Hz, 2H), 5.52 (s, 1H), 3.60−3.48 (m, 2H), 1.28 (t, J = 6.8 Hz, 3H); ^{13}C NMR (100 MHz, $CDCl_3$) δ 141.5, 135.0, 134.1, 128.3, 127.4, 111.5, 100.3, 95.1, 74.4, 64.3, 14.0; HRMS (ESI) m/z calcd for $C_{15}H_{15}BrClF_3N_3O$ $(M + NH_4)^+$ 424.0034, found 424.0040.

*Data for 4-bromo-2-(α-propoxy-4-chlorobenzyl)-5-(trifluoromethyl)-1H-pyrrole-3-carbonitrile (**5c**):* yield 65%; yellow oil; ^{1}H NMR (400 MHz, $CDCl_3$) δ 9.23 (s, 1H), 7.39 (d, J = 8.4 Hz, 2H), 7.31 (d, J = 8.4 Hz, 2H), 5.50 (s, 1H), 3.45 (t, J = 6.4 Hz, 2H), 1.74−1.55 (m, 2H), 0.94 (t, J = 7.6 Hz, 3H); HRMS (ESI) m/z calcd for $C_{16}H_{17}BrClF_3N_3O$ $(M + NH_4)^+$ 438.0190, found 438.0193.

*Data for 4-bromo-2-(α-isopropoxy-4-chlorobenzyl)-5-(trifluoromethyl)-1H-pyrrole-3-carbonitrile (**5d**):* yield 86%; white solid; mp 62−64 °C; ^{1}H NMR (400 MHz, $CDCl_3$) δ 9.27 (s, 1H), 7.38 (d, J = 8.0 Hz, 2H), 7.33 (d, J = 8.0 Hz, 2H), 5.63 (s, 1H), 3.73−3.67 (m, 1H), 1.22 (dd, J = 12.4, 6.0 Hz, 6H); ^{13}C NMR (100 MHz, $CDCl_3$) δ 142.8, 136.5, 135.1, 129.4, 128.3, (120.9, 118.3), (119.0, 118.6, 118.2, 117.8), 112.5, 101.5, 96.2, 72.7, 70.9, 22.8, 21.4; HRMS (ESI) m/z calcd for $C_{16}H_{12}BrClF_3N_2O$ $(M - H)^-$ 418.9779, found 418.9786.

*Data for 4-bromo-2-(α-butoxy-4-chlorobenzyl)-5-(trifluoromethyl)-1H-pyrrole-3-carbonitrile (**5e**):* yield 74%; white solid; mp 72−74 °C; ^{1}H NMR (400 MHz, $CDCl_3$) δ 9.11 (s, 1H), 7.39 (d, J = 8.4 Hz, 1H), 7.31 (d, J = 8.4 Hz, 1H), 5.50 (s, 1H), 3.54−3.36 (m, 1H), 1.63 (dt, J = 13.6, 6.8 Hz, 1H), 1.49−1.27 (m, 1H), 0.91 (t, J = 7.6 Hz, 2H); ^{13}C NMR (100 MHz, $CDCl_3$) δ 141.6, 135.0, 134.1, 128.3, 127.3, (122.6, 119.9, 117.2, 114.6), (117.9, 117.5, 117.1, 118.3), 100.3, 95.1, 74.6, 68.6, 30.5, 18.2, 12.8; HRMS (ESI) m/z calcd for $C_{17}H_{19}BrClF_3N_3O$ $(M + NH_4)^+$ 452.0347, found 452.0339.

*Data for 4-bromo-2-(α-(hexyloxy)-4-chlorobenzyl)-5-(trifluoromethyl)-1H-pyrrole-3-carbonitrile (**5f**):* yield 80%; yellow oil; ^{1}H NMR (400 MHz, $CDCl_3$) δ 9.15 (s, 1H), 7.39 (d, J = 8.4 Hz, 2H), 7.31 (d, J = 8.4 Hz, 2H), 5.50 (s, 1H), 3.54−3.35 (m, 2H), 1.70−1.56 (m, 2H), 1.38−1.21 (m, 6H), 0.88 (t, J = 6.5 Hz, 3H); ^{13}C NMR (100 MHz, $CDCl_3$) δ 143.0, 136.6, 136.0, 130.1, 129.1, (121.6, 118.9), (119.5, 119.1), 113.1, 102.1, 97.2, 76.2, 70.7, 32.2, 30.1, 26.4, 23.3, 14.7; HRMS (ESI) m/z calcd for $C_{19}H_{18}BrClF_3N_2O$ $(M - H)^-$ 461.0249, found 461.0245.

*Data for 4-bromo-2-(α-(2-methoxyethoxy)-4-chlorobenzyl)-5-(trifluoromethyl)-1H-pyrrole-3-carbonitrile (**5g**):* yield 72%; yellow solid; mp 65−67 °C; ^{1}H NMR (400 MHz, $CDCl_3$) δ 11.26 (s, 1H), 7.37 (d, J = 8.4 Hz, 2H), 7.30 (d, J = 8.4 Hz, 2H), 5.61 (s, 1H), 4.01−3.89 (m, 1H), 3.80−3.71 (m, 1H), 3.70−3.62 (m, 1H), 3.60−3.54 (m, 1H), 3.50 (s, 3H); ^{13}C NMR (100 MHz, $CDCl_3$) δ 141.1, 135.0, 134.2, 128.2, 127.7, (122.8, 120.1, 117.4, 114.8), (118.2, 117.8, 117.4, 117.0), 111.6, (100.3, 100.2), 95.1, 75.6, 70.7, 68.3, 58.1; HRMS (ESI) m/z calcd for $C_{16}H_{17}BrClF_3N_3O_2$ $(M + NH_4)^+$ 454.0139, found 454.0131.

*Data for 4-bromo-2-(α-(cyclohexyloxy)-4-chlorobenzyl)-5-(trifluoromethyl)-1H-pyrrole-3-carbonitrile (**5h**):* yield 75%; white solid; mp 102−103 °C; ^{1}H NMR (400 MHz, $CDCl_3$) δ 9.38 (s, 1H), 7.40 (d, J = 8.4 Hz, 2H), 7.35 (d, J = 8.4 Hz, 2H), 5.71 (s, 1H), 1.97−1.95 (m, 1H), 1.85−1.83 (m, 1H), 1.78−1.75 (m, 2H), 1.60−1.51 (m, 1H), 1.47−1.33 (m, 2H), 1.31−1.18 (m, 3H); ^{13}C NMR (100 MHz, $CDCl_3$) δ 142.0, 135.6, 134.0, 128.3, 127.2, (122.6, 119.9, 117.2, 114.5), (118.0, 117.6, 117.2, 116.8), 111.6, 100.4, 95.1, 75.7, 71.3, 31.7, 30.6, 24.4, 23.0, 22.8; HRMS (ESI) m/z calcd for $C_{19}H_{16}BrClF_3N_3O_2$ $(M - H)^-$ 459.0092, found 454.0084.

*Data for 4-bromo-2-(α-(prop-2-ynyloxy)-4-chlorobenzyl)-5-(trifluoromethyl)-1H-pyrrole-3-carbonitrile (**5i**):* yield 67%; white solid; mp 127−129 °C; ^{1}H NMR (400 MHz, $CDCl_3$) δ 9.30 (s, 1H), 7.41 (d, J = 8.0 Hz, 2H), 7.33 (d, J = 8.0 Hz, 2H), 5.84 (s, 1H), 4.31 (d, J = 16.0 Hz, 1H), 4.06 (d, J = 16.0 Hz, 1H), 2.57 (s, 1H); ^{13}C NMR (100 MHz, $CDCl_3$) δ 141.3, 135.8, 134.3, 129.5, 129.0, (123.5, 120.9, 118.2, 115.5), (119.4, 119.0, 118.6, 112.2), (101.62, 101.59, 101.56, 101.54), 96.7, 77.6, 73.8, 56.1; HRMS (ESI) m/z calcd for $C_{16}H_7BrClF_3N_2O$ $(M - H)^-$ 414.9466, found 414.9462.

*Data for 4-bromo-2-(α-(2,2,2-trifluoroethoxy)-4-chlorobenzyl)-5-(trifluoromethyl)-1H-pyrrole-3-carbonitrile (**5j**):* yield 70%; yellow solid; mp 107−109 °C; ^{1}H NMR (400 MHz, $CDCl_3$) δ 9.20 (s, 1H), 7.45 (d, J = 8.3 Hz, 2H), 7.34 (d, J = 8.2 Hz, 2H), 5.72 (s, 1H), 3.95−3.79 (m, 2H); ^{13}C NMR (100 MHz, $CDCl_3$) δ 140.0, 136.4, 133.6, 129.9, 128.7, (127.5, 124.7, 122.0, 119.2), (123.4, 120.7, 118.1, 115.4), (120.0, 119.6, 119.2, 118.8), 112.0, 101.7, 97.2, 76.7, 66.5, 66.2, 65.8, 65.5; HRMS (ESI) m/z calcd for $C_{15}H_6BrClF_6N_2O$ $(M - H)^-$ 458.9340, found 458.9335.

*Data for 4-bromo-2-(α-(2,2,2-trichloroethoxy)-4-chlorobenzyl)-5-(trifluoromethyl)-1H-pyrrole-3-carbonitrile (**5k**):* yield 70%; white solid; mp 112−113 °C; ^{1}H NMR (400 MHz, $CDCl_3$) δ 9.37 (s, 1H), 7.45 (d, J = 8.4 Hz, 2H), 7.38 (d, J = 8.4 Hz, 2H), 5.90 (s, 1H), 4.15 (d, J = 11.2 Hz, 1H), 4.10 (d, J = 11.2 Hz, 1H); ^{13}C NMR (100 MHz, $CDCl_3$) δ 140.1, 136.3, 134.0, 129.8, 128.7, (120.8, 118.1), (119.6, 119.2), 112.0, 101.8, 97.3, 95.8, 80.4, 77.0; HRMS (ESI) m/z calcd for $C_{15}H_7BrCl_4F_3N_2O$ $(M - H)^-$ 506.8453, found 506.8450.

*Data for 4-bromo-2-(α-((1,1,1,3,3,3-hexafluoropropan-2-yl)oxy)-4-chlorobenzyl)-5-(trifluoromethyl)-1H-pyrrole-3-carbonitrile (**5l**):* yield 76%; white solid; mp 106−108 °C; ^{1}H NMR (400 MHz, $CDCl_3$) δ 9.16 (s, 1H), 7.48 (d, J = 8.4 Hz, 1H), 7.33 (d, J = 8.4 Hz, 1H), 5.96 (s, 1H), 4.19 (m, 1H); ^{13}C NMR (100 MHz, $CDCl_3$) δ 137.1, 136.2, 130.8, 129.0, 128.3, (124.5, 121.7, 118.9, 116.1), (123.8, 121.0, 118.2, 115.4), (122.2, 119.6, 116.9, 114.2), (119.7, 119.3, 118.9, 118.5), 110.4, (100.91, 100.88, 100.85, 100.82), 97.4, 77.1, (72.8, 72.6, 72.2, 71.9, 71.6, 71.2, 70.9); HRMS (ESI) m/z calcd for $C_{16}H_6BrClF_9N_2O$ $(M - H)^-$ 526.9214, found 526.9215.

*Data for 4-bromo-2-(α-(3-chloropropoxy)-4-chlorobenzyl)-5-(trifluoromethyl)-1H-pyrrole-3-carbonitrile (**5m**):* yield 40%; white solid; mp 71−73 °C; ^{1}H NMR (400 MHz, $CDCl_3$) δ 9.29 (s, 1H), 7.40 (d, J = 8.4 Hz, 2H), 7.31 (d, J = 8.4 Hz, 2H), 5.54 (s, 1H), 3.73−3.60 (m, 4H), 2.19−2.03 (m, 2H); HRMS (ESI) m/z calcd for $C_{16}H_{11}BrCl_2F_3N_2O$ $(M - H)^-$ 452.9389, found 452.9385.

*Data for 2-(α-(benzyloxy)-4-chlorobenzyl)-4-bromo-5-(trifluoromethyl)-1H-pyrrole-3-carbonitrile (**5n**):* yield 71%; white solid; mp 117−118 °C; ^{1}H NMR (400 MHz, $CDCl_3$) δ 9.20 (s, 1H), 7.43−7.37 (m, 5H), 7.34−7.28 (m, 4H), 5.58 (s, 1H), 4.62 (d, J = 11.2 Hz, 1H), 4.45 (d, J = 11.2 Hz, 1H); ^{13}C NMR (100 MHz, $CDCl_3$) δ 141.1, 135.0, 134.5, 134.3, 128.4, 127.8, 127.62, 127.58, 127.3, (122.5, 119.8, 117.2, 114.5), (118.4, 118.0, 117.6, 117.2), 111.4, (100.43, 100.40, 100.38, 100.35), 95.4, 73.4, 70.2; HRMS (ESI) m/z calcd for $C_{20}H_{11}BrClF_3N_2O$ $(M - H)^-$ 466.9779, found 466.9778.

*Data for 4-bromo-2-(α-((diethylamino)oxy)-4-chlorobenzyl)-5-(trifluoromethyl)-1H-pyrrole-3-carbonitrile (**5o**):* yield 60%; white solid; mp 104−106 °C; ^{1}H NMR (400 MHz, $CDCl_3$) δ 9.51 (s, 1H), 7.39 (d, J = 8.4 Hz, 2H), 7.30 (d, J = 8.4 Hz, 2H), 5.85 (s, 1H), 2.88−2.76 (m, 4H), 1.00 (t, J = 7.2 Hz, 6H); HRMS (ESI) m/z calcd for $C_{17}H_{18}BrClF_3N_3O$ $(M + H)^+$ 450.0190, found 450.0198.

Alternative Method for 5b. To a solution of **9** (0.55 g, 1.38 mmol) in ethanol (40 mL) was added sodium bicarbonate (0.35 g, 4.15 mmol), and the mixture was refluxed for 1 h. After the solvent was evaporated, the residue was dissolved in ethyl acetate (50 mL),

washed with water (3 × 25 mL) and brine, dried over anhydrous magnesium sulfate, and concentrated to give **5b** as a white solid (0.52 g, 93%).

4-Bromo-2-(α-ethoxy-4-chlorobenzyl)-1-(ethoxymethyl)-5-(trifluoromethyl)-1*H*-pyrrole-3-carbonitrile (5′b). To a stirred solution of **5b** (0.40 g, 1.24 mmol) in THF (20 mL) under an ice−salt bath was added sodium hydride (0.12 g, 6.19 mmol) in batches. After the mixture was stirred at room temperature for 10 min, chloromethyl ethyl ether (0.35 g, 3.71 mmol) was added, and the mixture was refluxed for 2.5 h. Then the solvent was removed by evaporation, and the residue was redissolved in ethyl acetate, successively washed with water and brine, dried over sodium sulfate, and concentrated give **5′b** as a white solid (0.50 g, 85%): mp 61−63 °C; ^{1}H NMR (400 MHz, $CDCl_3$) δ 7.36 (d, J = 8.4 Hz, 2H), 7.29 (d, J = 8.4 Hz, 2H), 5.77 (s, 1H), 5.27 (d, J = 10.4 Hz, 1H), 5.18 (d, J = 10.4 Hz, 1H), 3.63 (q, J = 6.8 Hz, 2H), 3.25 (hept, J = 6.8 Hz, 2H), 1.32 (t, J = 6.8 Hz, 3H), 1.06 (t, J = 6.8 Hz, 3H); ^{13}C NMR (100 MHz, $CDCl_3$) δ 142.7, 135.3, 133.5, 128.0, 126.6, (122.8, 120.7, 117.4, 114.7), (120.7, 120.4, 120.0, 119.6), 111.9, 101.9, 101.9, 99.0, 74.8, 73.9, 65.0, 63.4, 13.9, 13.5; HRMS (ESI) m/z calcd for $C_{18}H_{21}BrClF_3N_3O_2$ $(M + NH_4)^+$ 482.0452, found 482.0448.

4-Bromo-1-(ethoxymethyl)-2-(α-(2,2,2-trifluoroethoxy)-4-chlorobenzyl)-5-(trifluoromethyl)-1*H*-pyrrole-3-carbonitrile (5′j). The synthetic procedure was according to that of **5′b** using **5j** as the starting material: yield 90%; colorless oil; ^{1}H NMR (400 MHz, $CDCl_3$) δ 7.31 (d, J = 8.4 Hz, 2H), 7.24 (d, J = 8.4 Hz, 2H), 5.89 (s, 1H), 5.21 (d, J = 10.4 Hz, 1H), 5.10 (d, J = 10.4 Hz, 1H), 3.87 (q, J = 8.4 Hz, 2H), 3.25 (q, J = 6.8 Hz, 2H), 1.00 (t, J = 6.8 Hz, 3H); ^{13}C NMR (100 MHz, $CDCl_3$) δ 140.5, 134.5, 133.2, 128.4, 127.1, (126.7, 123.9, 121.1, 118.3), (122.7, 120.0, 117.4, 114.7), (121.2, 120.8, 120.5, 120.1), 111.4, 102.2, 99.4, 75.2, 74.9, (66.2, 65.9, 65.5, 65.2), 63.7, 13.4; HRMS (ESI) m/z calcd for $C_{18}H_{18}BrClF_6N_3O_2$ $(M + NH_4)^+$ 536.0170, found 536.0163.

(4-Bromo-3-cyano-5-(trifluoromethyl)-1*H*-pyrrol-2-yl)(4-chlorophenyl)methyl Isobutyrate (6). To a solution of sodium isobutyrate (0.28 g, 2.51 mmol) in dichloromethane (40 mL) was added the appropriate amount of molecular sieves, and the mixture was refluxed for 0.5 h. After compound **9** (0.50 g, 1.26 mmol) was added, the mixture was refluxed for another 1.5 h. Then the molecular sieves were filtrated, and the filtrate was washed with water (3 × 25 mL) and brine, dried over anhydrous magnesium sulfate, and then concentrated. The crude was purified by silica gel using petroleum ether/ethyl acetate (5:1) as the eluent to give **6** as a white solid: yield 71%; mp 101−102 °C; ^{1}H NMR (400 MHz, $CDCl_3$) δ 9.61 (s, 1H), 7.40 (d, J = 8.4 Hz, 1H), 7.35 (d, J = 8.4 Hz, 1H), 6.89 (s, 1H), 2.76 (hept, J = 7.0 Hz, 1H), 1.25 (d, J = 4.0 Hz, 3H), 1.23 (d, J = 4.0 Hz, 3H); ^{13}C NMR (100 MHz, $CDCl_3$) δ 176.5, 139.3, 135.7, 133.9, 129.6, 128.1, (123.4, 120.7, 118.0, 115.4), (120.2, 119.8, 119.4, 119.0), 112.1, 102.1, 97.7, 69.1, 34.1, 18.9, 18.6; HRMS (ESI) m/z calcd for $C_{17}H_{17}BrClF_3N_3O_2$ $(M + NH_4)^+$ 466.0139, found 466.0147.

Synthesis of (α-(Alkylsulfanyl)benzyl)pyrroles 7 and Benzylpyrrole α-Oxime Ethers 8. The synthetic procedures were according to that of **5** using compound **9** and 1.5−2 equiv of the corresponding alkanethiol or oxime as the starting material.

*Data for 4-bromo-2-(α-(ethylthio)-4-chlorobenzyl)-5-(trifluoromethyl)-1H-pyrrole-3-carbonitrile (**7a**):* yield 90%; pale yellow solid; mp 46−48 °C; ^{1}H NMR (400 MHz, $CDCl_3$) δ 9.50 (s, 1H), 7.34 (d, J = 8.4 Hz, 2H), 7.25 (d, J = 8.4 Hz, 2H), 5.32 (s, 1H), 2.64−2.28 (m, 2H), 1.28 (t, J = 7.6 Hz, 3H); ^{13}C NMR (100 MHz, $CDCl_3$) δ 140.4, 134.5, 133.6, 128.5, 127.9, (122.4, 119.8, 117.1, 114.4), (118.7, 118.3, 117.9, 117.5), 111.4, 100.3, 100.3, 97.1, 44.0, 25.9, 13.2; HRMS (ESI) m/z calcd for $C_{15}H_{10}BrClF_3N_2S$ $(M - H)^-$ 420.9394, found 420.9395.

*Data for 4-bromo-2-(α-(tert-butylthio)-4-chlorobenzyl)-5-(trifluoromethyl)-1H-pyrrole-3-carbonitrile (**7b**):* yield 62%; pale yellow solid; mp 147−149 °C; ^{1}H NMR (400 MHz, $CDCl_3$) δ 9.42 (s, 1H), 7.32 (d, J = 8.4 Hz, 2H), 7.16 (d, J = 8.4 Hz, 2H), 5.27 (s, 1H), 1.32 (s, 9H); ^{13}C NMR (100 MHz, $CDCl_3$) δ 141.5, 135.9, 133.3, 128.5, 127.8, (122.5, 119.8, 117.2, 114.5), (118.1, 117.7, 117.3, 116.9), 111.4, 100.6, 96.2, 45.1, 41.8, 29.9; HRMS (ESI) m/z calcd for $C_{17}H_{19}BrClF_3N_3S$ $(M + NH_4)^+$ 468.0118, found 468.0127.

*Data for (E)-4-bromo-2-(α-(((4-nitrobenzylidene)amino)oxy)-4-chlorobenzyl)-5-(trifluoromethyl)-1H-pyrrole-3-carbonitrile (**8a**):* yield 53%; yellow solid; mp 211−213 °C; ^{1}H NMR (400 MHz, DMSO-d_6) δ 13.94 (s, 1H), 8.67 (s, 1H), 8.28 (d, J = 8.8 Hz, 2H), 7.88 (d, J = 8.8 Hz, 2H), 7.53 (d, J = 8.4 Hz, 2H), 7.48 (d, J = 8.4 Hz, 2H), 6.54 (s, 1H); ^{13}C NMR (100 MHz, DMSO-d_6) δ 150.1, 148.3, 142.2, 137.3, 135.9, 133.6, 129.0, 128.9, 128.3, 124.1, (124.0, 121.3, 118.6, 115.9), (118.8, 118.4), 113.3, 100.7, 95.3, 79.0; HRMS (ESI) m/z calcd for $C_{20}H_{15}BrClF_3N_5O_3$ $(M + NH_4)^+$ 543.9993, found 543.9972.

*Data for (E)-4-bromo-2-(α-((((4-(dimethylamino)benzylidene)-amino)oxy)-4-chlorobenzyl)-5-(trifluoromethyl)-1H-pyrrole-3-carbonitrile (**8b**):* yield 50%; white solid; mp 86−88 °C; ^{1}H NMR (400 MHz, $CDCl_3$) δ 9.49 (s, 1H), 8.15 (s, 1H), 7.43 (d, J = 8.4 Hz, 2H), 7.39 (d, J = 8.4 Hz, 2H), 7.32 (d, J = 8.4 Hz, 2H), 6.76 (d, J = 8.4 Hz, 2H), 6.34 (s, 1H), 3.03 (s, 6H); ^{13}C NMR (100 MHz, $CDCl_3$) δ 152.3, 141.4, 140.5, 135.3, 135.1, 129.3, 128.9, 128.8, (120.9, 118.2), (119.8, 119.4, 119.0, 118.6), 112.4, 112.1, 101.4, 97.9, 40.3; HRMS (ESI) m/z calcd for $C_{22}H_{18}BrClF_3N_4O$ $(M + H)^+$ 525.0299, found 525.0299.

*Data for (E)-4-bromo-2-(α-(((3,3-dimethylbutan-2-ylidene)-amino)oxy)-4-chlorobenzyl)-5-(trifluoromethyl)-1H-pyrrole-3-carbonitrile (**8c**):* yield 68%; white solid; mp 97−99 °C; ^{1}H NMR (400 MHz, $CDCl_3$) δ 9.88 (s, 1H), 7.37 (d, J = 8.4 Hz, 2H), 7.22 (d, J = 8.4 Hz, 2H), 6.22 (s, 1H), 1.91 (s, 3H), 1.10 (s, 9H); ^{13}C NMR (100 MHz, $CDCl_3$) δ 167.1, 140.6, 134.4, 134.0, 128.1, 127.7, (125.6, 119.9, 117.2, 114.5), (118.8, 118.4, 118.0, 117.6), 111.3, (100.03, 100.00), 97.0, 75.8, 36.6, 26.4, 10.2; HRMS (ESI) m/z calcd for $C_{19}H_{19}BrClF_3N_3O$ $(M + H)^+$ 476.0347, found 476.0353.

4-Bromo-2-(α-(2,2,2-trifluoroethoxy)-4-chlorobenzyl))-5-(tris(2,2,2-trifluoroethoxy)methyl)-1*H*-pyrrole-3-carbonitrile (11). To a solution of **9** (0.05 g, 0.13 mmol) in trifluoroethanol (15 mL) was added sodium bicarbonate (0.10 g, 0.94 mmol), and the mixture was refluxed for 5 h. After the solvent was evaporated, the residue was dissolved in dichloromethane (25 mL), washed with water (3 × 25 mL) and brine, dried over anhydrous magnesium sulfate, and then concentrated to give **11** as a white solid (0.08 g, 90%): ^{1}H NMR (400 MHz, $CDCl_3$) δ 7.37 (d, J = 8.4 Hz,2H), 7.26 (d, J = 8.4 Hz, 2H), 5.60 (s, 1H), 3.93 (q, J = 8.0 Hz, 6H), 3.80 (q, J = 8.0 Hz, 2H).

Biological Assay. All bioassays were performed on representative test organisms reared in the laboratory. Each bioassay was replicated three times at 25 ± 1 °C for the statistical requirements. Mortalities were evaluated according to a percentage scale of 0−100%, in which 0% indicates no activity and 100% indicates total kill. When the mortality of the blank control was less than 5%, the test result was directly used. However, if the mortality of the blank control was less than 20%, the test result was corrected by means of $V = ((X - Y)/X) \times 100$ (V = value of the corrected mortality, X = livability of the blank control, and Y = livability of the treated organisms). To calculate IC_{50}, at least two mortalities at different concentrations had to be lower than 50%. The IC_{50} was taken from a graph plotting mortality (y-axis) against compound concentration (x-axis); the IC_{50} value is the concentration where the mortality crosses 50%.

Stock solutions of each test compound were prepared in dimethylformamide at a concentration of 600 or 200 mg L^{-1} and then diluted to the required concentration (100, 50, 25, 10, 5, 2, 1, 0.5, 0.25, 0.1, 0.05, 0.025, and 0.01 mg L^{-1}) with water containing 0.1% TW-20 (a type of emulsifier).

Insecticidal Activity. *Insecticidal Activities against Oriental Armyworm (Mythimna separata), Diamondback Moth (Plutella xylostella), Cotton Bollworm (Helicoverpa armigera), Corn Borer (Ostrinia nubilalis), Beet Armyworm (Spodoptera exigua), and Bean Aphid (Aphis craccivora).* The leaf-dip method was used. Leaf disks (5 cm × 3 cm) were cut from fresh cabbage leaves (or other leaves) and then dipped into the test solution for 3 s. After air-drying, the treated leaf disks were placed individually into vertical tubes (or Petri dishes), and the disks were infested with 10 larvae (for example, 2nd-instar diamondback moth larvae). The mortalities were evaluated 3 days after treatment.

dx.doi.org/10.1021/jf501377t | J. Agric. Food Chem. 2014, 62, 6072−6081

Scheme 2. Unexpected Reactions of 9 in Ethanol and Trifluoroethanol

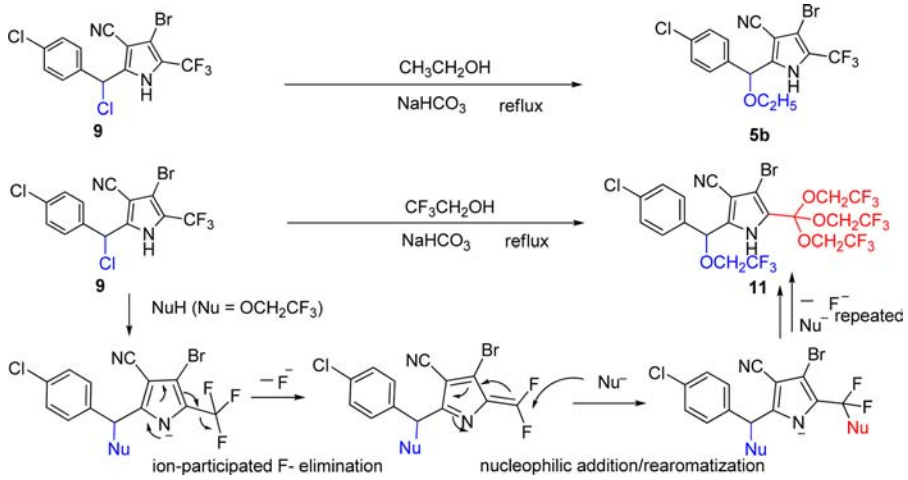

Table 1. Insecticidal Activity (Mortality Rates, %) against Different Insects' Larvae

Compd.	oriental armyworm	diamondback moth	cotton bollworm	corn borer	beet armyworm	bean aphid	mosquito larvae
	600[a]	600[a]	600[a]	600[a]	200[a]	200[a]	5[a]
2	100	100	45	45	-[b]	0	-
3	100	100	55	55	0	0	100
4	100	100	100	60	0	0	20
9	100	-	35	50	-	-	10
5a	100	100	100	100	40	0	100
5b	100	100	35	90	40	30	60
5'b	100	100	100	100	-	0	100
5c	100	100	100	100	0	0	100
5d	100	-	100	100	0	0	100
5e	50	100	65	85	0	0	100
5f	10	100	70	80	0	0	100
5g	100	100	-	-	0	0	100
5h	100	100	35	35	0	0	60
5i	100	100	45	85	60	-	40
5j	100	100	55	85	40	-	100
5'j	100	100	100	100	-	-	100
5k	100	100	80	70	-	0	100
5l	40	50	15	10	-	0	20
5m	100	100	100	100	-	-	100
5n	100	100	15	55	0	0	60
5o	100	100	100	40	0	0	35
6	40	100	30	25	0	0	30
7a	20	100	5	15	-	-	15
7b	100	100	70	60	0[c]	70[c]	100
8a	100	100	100	50	40[c]	30[c]	100
8b	100	100	100	50	0[c]	0[c]	100
8c	100	100	100	60	0[c]	0[c]	100
chlorfenapyr	100	100	100	100	100	0	100

[a]Concentration of the tested compounds. The units are milligrams per liter. [b]A dash means not tested. [c]The assay was conducted at a concentration of 600 mg L^{-1}.

Insecticidal Activities against Mosquito (Culex pipiens pallens). Twenty 4th-instar mosquito larvae were put into 10 mL of the test solution. The mortalities were evaluated 8 days after treatment.

Acaricidal Activity Assay. The detailed assay method against the eggs, larvae, and adults of the spider mite (*Tetranychus cinnabarinus*) was described in the literature.[10]

Fungicidal Activity Assay. In vitro assay: The compounds were evaluated in mycelial growth tests in artificial media against 10 phytopathogens, *Fusarium oxysporium*, *Cercospora arachidicola* Hori, *Physalospora piricola*, *Alternaria solani*, *Fusarium graminearum*, *Phytophthora infestans*, *Sclerotinia sclerotiorum*, *Botrytis cinerea*, *Rhizoctonia solani*, and *Phytophthora capsici*, at rate of 50 mg L^{-1}.

In vivo assay: The compounds were evaluated in leaf-piece assays at a rate of 200 mg L^{-1} for *Corynespora cassiicola* and *B. cinerea* on cucumber, *Blumeria graminis* f. sp. *tritici* on wheat, *S. sclerotiorum* on oilseed rape, *R. solani* on rice, and *Phytophthora* on pepper.

dx.doi.org/10.1021/jf501377t | J. Agric. Food Chem. 2014, 62, 6072−6081

Table 2. IC_{50} (mg L^{-1}) of Compounds against Insects' Larvae[a]

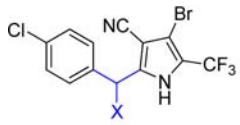

2, 4, 5, 6, 7, 8, 9

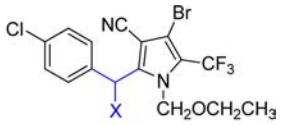

3, 5'

Compd.	X	oriental armyworm[b]	diamondback moth[c]	Cotton Bollworm[b]	Corn Borer[b]	Mosquito[d]
2	H	30	0.9	>600	>600	-
3	H	25	0.3	<600	<600	0.17
4	OH	75	2	180	60	>5.0
9	Cl	80	-	>600	600	>5.0
5a	OMe	13	<1	50	140	1.2
5b	OEt	10	<0.01	>600	<600	4.0
5'b	OEt	20	<10	130	<100	0.07
5c	OPr-*n*	8	<1	<100	<100	0.8
5d	OPr-*i*	13	-	140	120	1.6
5e	OBu-*n*	>600	90	<600	<600	2.5
5f	OHex-*n*	>600	110	<600	<600	1.6
5g	$OCH_2CH_2OCH_3$	10	4	-	-	1.6
5h	OHex-c	>200	125	>600	>600	4.0
5i	$OCH_2C{\equiv}CH$	13	0.05	>600	<600	>5.0
5j	OCH_2CF_3	6	0.04	<600	<600	0.15
5'j	OCH_2CF_3	10	0.07	60	50	0.04
5k	OCH_2CCl_3	8	0.07	<600	<600	0.15
5l	$OCH(CF_3)_2$	>600	600	>600	>600	>5.0
5m	$O(CH_2)_3Cl$	30	<10	200	<200	3.0
5n	OBn	80	0.2	>600	<600	4.0
5o	$ONEt_2$	115	2	350	>600	>5.0
6	OC(=O)Pr-*i*	>600	40	>600	>600	>5.0
7a	SEt	>600	35	>600	>600	>5.0
7b	SBu-*t*	13	4	<600	<600	1.2
8a	$4\text{-}NO_2C_6H_4CH{=}NO$	60	20	270	600	0.3
8b	$4\text{-}Me_2NC_6H_4CH{=}NO$	>200	180	180	600	1.2
8c	Me(t-Bu)C=NO	>200	180	200	<600	1.4
chlorfenapyr		5	0.08	<0.1	<25	0.025

[a]The data in blue mean good to excellent activity, and the data in pink mean moderate activity. [b]The concentrations were set as 600, 200, 100, 50, 25, 10, and 5 mg L^{-1} for calculation of IC_{50}. In the rectangular coordinate system, a line was drawn with concentration as the abscissa and mortality rate as the ordinate. The IC_{50} value was roughly read from the straight line that connected the two concentrations that gave mortality rates of just more and just less than 50%. Other IC_{50} values were calculated in the same way. [c]The concentrations were set as 600, 200, 100, 10, 1, 0.1, and 0.01 mg L^{-1} for calculation of IC_{50}. [d]The concentrations were set as 5, 2, 1, 0.5, 0.25, 0.1, 0.05, 0.025, and 0.01 mg L^{-1} for calculation of IC_{50}.

The detailed assay method was described in the literature.[10]

RESULTS AND DISCUSSION

Synthesis. Benzylpyrrole **2**, prepared according to our previous method,[10] was reacted with 1.3 equiv of sulfonyl dichloride to obtain *α*-monochlorinated benzylpyrrole **9**. As a key intermediate, **9** was treated with different nucleophiles such as sodium bicarbonate aqueous solution, sodium alkoxide, sodium carboxylate, thiol sodium salt, or oxime sodium salt to afford **4**, **5**, **6**, 7, or **8**, respectively (Scheme 1). **5** was further allowed to react with chloromethyl ethyl ether to obtain N-substituted compound **5′**. (*α*-(Aryloxy)benzyl)pyrroles or more (*α*-(acyloxy)benzyl)pyrroles were to be synthesized, but they were too unstable during the workup.

Note that, due to the poor solubility of **2** in dichloromethane, the preparation of intermediate **9** required a lot of solvent (0.50 g of **2** requires about 180 mL of warm dichloromethane), and adding dimethylformamide to increase the solubility was only to find an increased amount of *α*,*α*-dichlorinated benzylpyrrole. During the multiple repeated tests, it was also found that the amount of sulfonyl dichloride had to be changed depending on the degree of solvent dryness and even the humidity of the air because insufficient sulfonyl dichloride resulted in incomplete reaction, while excess sulfonyl dichloride produced more *α*,*α*-dichlorinated benzylpyrrole, and both circumstances made the reaction systems complicated. Therefore, preparing **9** directly from **2** was not always the quickest and the most convenient method. The preparation of **9** was then adopted as an alternative route (Scheme 1, route with purple arrows). **2** was first transformed to dichlorinated benzylpyrrole by using excess sulfonyl dichloride (3 equiv) in a mixed solvent of dichloromethane and dimethylformamide (0.5 g of **2** in 50 mL of dichloromethane and 5 mL of DMF) and after hydrolysis gave benzoylpyrrole **10**. Then **10** was reduced by $NaBH_4$ to (*α*-hydroxybenzyl)pyrrole **4**. Finally, **4** was treated with 1.3 equiv of sulfonyl dichloride to obtain *α*-monochlorinated benzylpyrrole **9**. This route needs three steps from compound **2**, **4** had much better solubility than **2**, and the chlorination step was not

dx.doi.org/10.1021/jf501377t | J. Agric. Food Chem. 2014, 62, 6072−6081

Table 3. Acarcidal Activity (Mortality Rates, %) against Spider Mite (*T. cinnabarinus* Boisduval)

Compd.	adults			larvae			eggs		
	600[a]	200[a]	100[a]	600[a]	200[a]	100[a]	600[a]	200[a]	100[a]
2	0	-[b]	-	0	-	-	0	-	-
3	100	90	70	97	85	70	100	100	70
4	0	-	-	85	-	-	90	-	-
9	85	0	0	95	90	60	95	70	0
5a	80	-	-	70	-	-	80	-	-
5b	100	90	60	90	80	0	100	95	70
5'b	70	0	-	0	-	-	0	-	-
5c	70	-	-	80	-	-	95	-	-
5e	0	-	-	0	-	-	30	-	-
5f	0	-	-	50	-	-	90	-	-
5g	0	-	-	0	-	-	0	-	-
5h	70	0	0	85	75	0	90	85	0
5i	95	50	0	90	90	50	90	80	50
5j	100	100	90	95	78	0	95	90	65
5'j	0	-	-	0	-	-	70	-	-
5k	0	-	-	0	-	-	50	-	-
5l	0	-	-	0	-	-	0	-	-
5m	85	0	-	65	-	-	70	-	-
5n	90	0	0	70	60	0	85	70	40
5o	0	-	-	75	-	-	70	-	-
6	40	-	-	0	-	-	0	-	-
7a	80	-	-	40	-	-	50	-	-
7b	40	-	-	70	-	-	70	-	-
8a	60	-	-	50	-	-	0	-	-
8b	60	-	-	88	-	-	85	-	-
8c	50	-	-	60	-	-	70	-	-
chlorfenapyr	100	100	100	100	100	100	100	100	100

[a]The data in blue mean good to excellent activity. Concentration of tested compounds. The units are milligrams per liter. [b]A dash means not tested.

so uncontrollable; thus, the purity of crude **9** prepared from **4** was better than that from **2**, which made the following nucleophilic substitution step clearer and the product easier to purify. Another thing to remember is that compound **9** is sensitive to alkaline aqueous solution, so whether it was prepared from **2** or **4**, during the workup the reaction mixture should be washed with sufficient water to remove excess sulfonyl dichloride but not with sodium bicarbonate aqueous solution.

Here we also mention some other experimental phenomena we encountered. (α-Alkoxybenzyl)pyrroles **5** were generally prepared from **9** and the corresponding sodium alkoxide, which were prepared in advance. Accidentally, we found (α-ethoxybenzyl)pyrrole **5b** also formed when **9** was refluxed in ethanol in the presence of sodium bicarbonate. The simpler procedure was then expected to be applied to other alcohols. However, when **9** was refluxed in trifluoroethanol, orthoester **11** was unexpectedly separated in high yield. In the structure of **11** not only the α-chloro atom but also the three fluorine atoms in the trifluoromethyl group on the pyrrole ring were replaced by trifluoroethoxyl (Scheme 2). The formation of the orthoester was thought to be via the repeated ion-participating F^- elimination and nucleophilic addition/rearomatization courses, which had been elucidated in detail in our previously published paper.[11] It seemed that an alcoholic solvent, a high reaction temperature (at least higher than the boiling point of dichloromethane), and a large excess amount of sodium bicarbonate jointly promoted the formation of the orthoester.

Bioactivity. The α-substituted benzylpyrroles were designed from insecticidal/acaricidal chlorfenapyr and dioxapyrrolomycin, so their insecticidal, acaricidal, and fungicidal activities were all assayed.

Insecticidal Activity. Table 1 shows the data of insecticidal activity against the larvae of oriental armyworm (*M. separata*), diamondback moth (*P. xylostella*), cotton bollworm (*H. armigera*), corn borer (*O. nubilalis*), beet armyworm (*Sp. exigua*), bean aphid (*A. craccivora*), and mosquito. Chlorfenapyr is included as a control.

As shown in Table 1, at 600 mg L^{-1}, most of the compounds exhibited 100% mortality against oriental armyworm, diamondback moth, and mosquito, and half of them gave 100% mortality against cotton bollworm and corn borer. However, for beet armyworm and bean aphid, no compounds gave the desired activity. Therefore, against those five species, the insecticidal activities at lower concentrations were determined, and the IC_{50} (the concentration of compounds resulting in 50% mortality) values of each species were roughly calculated (Table 2).

Table 2 shows clear structure−activity relationships for each insect species. For oriental armyworm, α-H-substituted (**2**), α-hydroxy-substituted (**4**), α-chloro-substituted (**9**), and most α-alkyloxy-substituted (**5a−n**) benzyl pyrroles gave moderate to

dx.doi.org/10.1021/jf501377t | J. Agric. Food Chem. 2014, 62, 6072−6081

Table 4. In Vitro Fungicidal Activity against Phytopathogens[a]

Compd.	inhibitory rate (%) at 50 mg L^{-1} in vitro									
	FO	CH	PP	AS	FG	PI	SS	BC	RS	PC
2	-[b]	-	-	50	35	15	55	60	35	30
3	20	15	30	25	25	10	40	35	35	40
4	-	-	-	81	65	65	87	87	50	92
9	45	65	75	60	55	45	81	70	80	85
5a	55	85	96	89	70	83	97	96	90	89
5b	70	88	97	88	50	75	85	83	88	75
5'b	25	60	65	40	20	20	80	80	40	60
5d	45	70	98	83	60	75	97	86	90	86
5e	45	0	95	80	65	75	87	75	80	70
5f	40	75	97	50	75	50	87	91	65	89
5g	45	75	97	70	55	70	94	70	60	83
5h	40	65	95	65	55	65	75	50	65	45
5i	65	70	98	70	55	60	85	65	85	75
5j	65	83	98	94	50	65	96	70	98	75
5'j	20	0	70	55	25	15	35	0	30	15
5k	65	92	96	89	55	83	92	65	84	75
5l	40	85	92	55	40	45	89	70	55	86
5m	55	75	96	83	40	83	94	65	80	83
5n	60	70	95	65	50	65	70	45	70	45
5o	25	85	96	60	45	65	83	70	55	70
6	45	70	65	55	25	35	83	65	60	89
7a	45	75	96	65	65	83	97	86	80	75
7b	40	75	92	65	55	70	83	65	70	80
8a	20	40	65	30	25	40	55	55	55	30
8b	30	60	50	30	35	20	70	65	50	65
8c	40	75	92	45	35	60	70	55	55	40

[a]The data in blue mean good to excellent activity. FO = *F. oxysporium*, CH = *C. arachidicola* Hori, PP = *Phys. piricola*, AS = *Al. solani*, FG = *F. graminearum*, PI = *Phyt. infestans*, SS = *S. sclerotiorum*, BC = *B. cinerea*, RS = *R. solani*, and PC = *Phyt. capsici*. [b]A dash means not tested.

excellent activity, except those bearing long or hindered alkyl groups such as **5e** (X = OBu-*n*), **5f** (X = OHex-*n*), **5h** (X = OHex-*c*), and **5l** (X = $OCH(CF_3)_2$). Compound **6** bearing an isobutyryloxy group at the α-position of benzylpyrrole also gave poor activity due to both steric and stereoelectronic effects. The α-alkylsulfanyl compounds **7a** and **7b** had structure−activity relationships different from those of α-alkyloxy compounds, as **7b** (X = SBu-*t*) had a more hindered substituent than **7a** (X = SEt) but exhibited much higher activity. Data for oxime ethers **8a−c** showed that an electron-withdrawing group played a significant role in the activity, as **8a** (4-$NO_2C_6H_4CH{=}NO$) gave much better activity than **8b** (X = 4-$Me_2NC_6H_4CH{=}$NO). In comparing *N*-ethoxymethyl compounds **3**, **5′b**, and **5′j** with corresponding NH compounds **2**, **5b**, and **5j**, the two types of structures did not show significant differences in the activity against oriental armyworm.

For diamondback moth, the compounds showed structure−activity relationships very similar to those for oriental armyworm. Benzylpyrroles with a shorter alkyloxy group at the α-position also gave better activity, with **5b** (X = OEt), **5i** (X = $OCH_2C{\equiv}CH$), **5j** (X = OCH_2CF_3), **5′j** (X = OCH_2CF_3), and **5k** (X = OCH_2CCl_3) having the lowest IC_{50} values (<0.1 mg L^{-1}), close to that of chlorfenapyr (0.08 mg L^{-1}).

The structure−activity relationships for cotton bollworm and corn borer were very similar to each other. However, neither of them had insecticidal ability comparable to that of chlorfenapyr.

For mosquito, most of the benzylpyrroles bearing shorter or longer α-alkyloxy groups (**5**) gave moderate to excellent activity, but the activity rule was not so distinct. The compounds with an oxime ether moiety (**8a−c**) also showed good activity. Notably, compounds **3**, **5′b**, and **5′j** with an ethoxymethyl group at the nitrogen of pyrrole all exhibited higher activity than their corresponding parent compounds **2**, **5b**, and **5j**, and the IC_{50} values for **5′b** and **5′j** (0.07 and 0.04 mg L^{-1}, respectively) were close to that of chlorfenapyr (0.025 mg L^{-1}).

Overall, benzylpyrroles bearing shorter α-alkyloxy groups gave better activities against most of the insect species. The alkylation of pyrrole usually gave increased activity. Among all the compounds, **5b** (X = OEt), **5i** (X = $OCH_2C{\equiv}CH$), **5j** (X = OCH_2CF_3), **5′j** (X = OCH_2CF_3), and **5k** (X = OCH_2CCl_3)

dx.doi.org/10.1021/jf501377t | J. Agric. Food Chem. 2014, 62, 6072−6081

Table 5. In Vivo Fungicidal Activity against Phytopathogens[a]

Compd.	inhibitory rate (%) at 200 mg L^{-1} in vivo					
	SS	RS	BG	CC	PH	BC
3	-[b]	-	85	-	-	-
4	-	-	60	50	83	30
5a	50	50	20	15	80	60
5b	-	-	50	-	-	-
5b'	40	25	-	40	25	45
5d	50	50	60	15	80	40
5e	40	50	0	55	25	35
5f	-	-	-	50	40	55
5g	65	40	80	40	80	40
5h	-	-	30	-	-	-
5i	-	-	30	-	-	-
5j	-	-	60	-	-	-
5j'	-	-	70	15	65	0
5k	45	45	70	15	80	15
5l	40	40	0	15	40	25
5m	35	40	40	15	87	20
5n	-	-	40	-	-	-
5o	30	30	75	50	60	30
6	45	65	70	40	55	40
7a	50	60	20	20	83	45
7b	30	45	60	20	80	40
8a	-	-	0	20	50	20
8b	30	45	0	55	55	35
8c	20	40	0	15	40	35
azoxystrobin	90	92	-	-	-	92
carbendazim	-	-	100	-	-	-
thiram	-	-	-	87	-	-
dimethomorph	-	-	-	-	92	-

[a]The data in blue mean good to excellent activity. SS = *S. sclerotiorum*, RS = *R. solani*, BG = *Bl. graminis*; CC: *Co. cassiicola*; PH: *Phytophthora*; BC = *B. cinerea*. [b]A dash means not tested.

exhibited excellent insecticidal activity against both oriental armyworm and diamondback moth; **5′j** also showed an eminent insecticidal effect against corn borer and mosquito.

Acaricidal Activity. Table 3 shows that few compounds exhibited satisfactory acarcidal activity; only compounds **3**, **9**, **5b**, **5i**, **5j**, and **5n** maintained certain mortality at a concentration of 100 mg L^{-1} against spider mite adults, larvae, and/or eggs, and none of them were comparable to chlorfenapyr. An interesting discovery is that though **5′b** and **5′j** had much lower activity than their parent products **5b** and **5j**, compound **3** gave much higher acarcidal activity than its parent product **2**.

Another thing to note is that no serious phytotoxicity was observed during the insecticidal and acaricidal assays; even those compounds without an ethoxymethyl group on the pyrrole N, such as compounds **2** and **5**, did not cause distinct harm to the leaves of the test plants at different concentrations.

Fungicidal Activity. The compounds were designed according to the structure of fungicidal dioxapyrrolomycin, so their fungicidal activities were also assayed to see if they could maintain fungicidal activity. The compounds were first evaluated in mycelial growth tests in artificial media against 10 species of phytopathogens at a rate of 50 mg L^{-1}. As shown in Table 4, most of the designed (α-(alkyloxy)benzyl)pyrroles **5** and α-alkylsulfanyl compounds **7** gave more than 80% inhibition against *Phys. piricola* (PP) and *S. sclerotiorum* (SS). **5a** (X = OMe) had the broadest fungicidal spectrum, with more than 80% inhibition against eight kinds of fungi. **5b** (X = OEt), **5d** (X = OPr-*i*), **5j** (X = OCH_2CF_3), **5k** (X = OCH_2CCl_3), and **5m** (X = $O(CH_2)_3Cl$) also gave broad fungicidal activity against at least five kinds of fungi.

Selected compounds were also tested for their fungicidal activity in vivo at 200 mg L^{-1}. Azoxystrobin, carbendazim, thiram, and dimethomorph were respectively used as contrast compounds for different fungi (Table 5). At the test concentration, most compounds exhibit certain fungicidal activity; especially **5a**, **5d**, **5g**, **6**, and **7a** gave better and broader fungicidal activity against at least three kinds of fungi. In contrast, **5m** showed some selectivity; it inhibited 87% of *Phytophthora*, which was very close to the value for dimethomorph. Thus, this kind of compound can be used as a lead compound for further fungicide research and development.

dx.doi.org/10.1021/jf501377t | J. Agric. Food Chem. 2014, 62, 6072−6081

In summary, on the basis of the structures of chlorfenapyr and dioxapyrrolomycin, a series of 2-benzylpyrroles with a hydroxyl, an alkyloxy, an acyloxy, an alkylsulfanyl, or an oxime moiety at the α-position of benzyl were designed and synthesized. The structure−activity relationships showed that benzylpyrroles bearing shorter α-alkyloxy groups gave better activities against most of the insect species; the alkylation of pyrrole usually gave increased activity. Several compounds were identified with excellent insecticidal and/or fungicidal activities, and the structure−activity relationship should be useful for future new active compound design and development.

AUTHOR INFORMATION

Corresponding Authors

*Phone: +86-(0)22-23503792. Fax: +86-(0)22-23503792. E-mail: liuyuxiu@nankai.edu.cn.

*Phone: +86-(0)22-23503952. Fax: +86-(0)22-23503952. E-mail: wangqm@nankai.edu.cn.

Funding

This work was supported by the National Key Project for Basic Research (Grant 2010CB126106), the National Natural Science Foundation of China (Grants 21121002, 21372131, and 21102077), and the Specialized Research Fund for the Doctoral Program of Higher Education (Grant 20130031110017).

Notes

The authors declare no competing financial interest.

REFERENCES

(1) Newman, D. J.; Cragg, G. M. Natural products as sources of new drugs over the 30 years from 1981 to 2010. *J. Nat. Prod.* **2012**, *75*, 311−335.

(2) Qian, X. H.; Lee, P. W.; Cao, S. China: Forward to the green pesticides via a basic research program. *J. Agric. Food. Chem.* **2010**, *58*, 2613−2623.

(3) Carter, G. T.; Nietsche, J. N.; Goodman, J. J.; Torrey, M. J.; Dunne, T. S.; Borders, D. B.; Testa, R. T. LL-F42248α, a novel chlorinated pyrrole antibiotic. *J. Antibiot.* **1987**, *40*, 233−236.

(4) Brown, D. G.; Diehl, R. E.; Siddens, J. K.; Wright, D. P., Jr. Arylpyrrole insecticidal, acaricidal and nematicidal agents and methods for the preparation thereof. US 5010098, 1988.

(5) Lovell, J. B.; Wright, D. P.; Gard, I. E.; Miller, T. P.; Treacy, M. F.; Addor, R. W.; Kamhi, V. M. AC 303,630—An insecticide/acaricide from a novel class of chemistry. *Brighton Crop Protection Conference. Pests and Diseases*; British Crop Protection Council: Alton, Hampshire, U.K., 1990; Vol. *1*, pp 37−40.

(6) Miller, T. P.; Treacy, M. F.; Gard, I. E.; Lovell, J. B.; Wright, D. P.; Addor, R. W.; Kamhi, V. M. AC 303,630—Summary of 1988−89 field trial results. *Brighton Crop Protection Conference. Pests and Diseases*; British Crop Protection Council: Alton, Hampshire, U.K., 1990; Vol. *1*, pp 41−45.

(7) Addor, R. W.; Babcock, T. J.; Black, B.; Brown, D. G.; Diehl, R. E.; Furch, J. A.; Kameswaran, V.; Kamhi, V. M.; Kremer, K. A.; Kuhn, D. G.; Lovell, J. B.; Lowen, G. T.; Miller, T. P.; Peevey, R. M.; Siddens, J. K.; Treacy, M. F.; Trotto, S. H.; Wright, D. P., Jr. Insecticidal pyrroles: discovery and overview. *Synthesis and Chemistry of Agrochemicals III*; ACS Symposium Series *504*; American Chemical Society: Washington, DC, 1992; Chapter 25, pp 283−297.

(8) Black, B. C.; Hollingworth, R. M.; Ahammadsahib, K. I.; Kukel, C. D.; Donovan, S. Insecticidal action and mitochondrial uncoupling activity of AC-303,630 and related halogenated pyrroles. *Pestic. Biochem. Physiol.* **1994**, *50* (2), 115−128.

(9) Weinbach, E. C.; Garbus, J. Mechanism of action of reagents that uncouple oxidative phosphorylation. *Nature* **1969**, *221*, 1016−1018.

(10) Liu, Y. X.; Zhang, P. X.; Li, Y. Q.; Song, H. B.; Wang, Q. M. Design, synthesis, and biological evaluation of 2-benzylpyrroles and 2-benzoylpyrroles based on structures of insecticidal chlorfenapyr and natural pyrrolomycins. *Mol. Diversity* **2014**, DOI: 10.1007/s11030-014-9515-9.

(11) Li, Y. Q.; Zhang, P. X.; Ma, Q. Q.; Song, H. B.; Liu, Y. X.; Wang, Q. M. The trifluoromethyl transformation synthesis, crystal structure and insecticidal activities of novel 2-pyrrolecarboxamide and 2-pyrrolecarboxlate. *Bioorg. Med. Chem. Lett.* **2012**, *22* (22), 6858−6861.

JOURNAL OF AGRICULTURAL AND FOOD CHEMISTRY

Article

pubs.acs.org/JAFC

Open Access on 06/16/2015

Quantitative Analysis of Neonicotinoid Insecticide Residues in Foods: Implication for Dietary Exposures

Mei Chen,[†] Lin Tao,[†] John McLean,[§] and Chensheng Lu*[,†]

[†]Department of Environmental Health, Harvard School of Public Health, 665 Huntington Avenue, Boston, Massachusetts 02115, United States

[§]Consultant Entomologist, Gisborne 4010, New Zealand

ABSTRACT: This study quantitatively measured neonicotinoids in various foods that are common to human consumption. All fruit and vegetable samples (except nectarine and tomato) and 90% of honey samples were detected positive for at least one neonicotinoid; 72% of fruits, 45% of vegetables, and 50% of honey samples contained at least two different neonicotinoids in one sample, with imidacloprid having the highest detection rate among all samples. All pollen samples from New Zealand contained multiple neonicotinoids, and five of seven pollens from Massachusetts detected positive for imidacloprid. These results show the prevalence of low-level neonicotinoid residues in fruits, vegetables, and honey that are readily available in the market for human consumption and in the environment where honeybees forage. In light of new reports of toxicological effects in mammals, the results strengthen the importance of assessing dietary neonicotinoid intakes and the potential human health effects.

KEYWORDS: *neonicotinoid insecticides, dietary exposure, pollen, honey*

INTRODUCTION

A growing body of research shows that fruits and vegetables are critical to promoting good health. Fruits and vegetables are major contributors of nutrients, such as folate, magnesium, dietary fiber, and vitamins A, C, and K, and essential for disease prevention. Diets rich in fruits and vegetables also help adults and children to achieve and maintain a healthy weight.[1] However, because of the wide usage of pesticides in agriculture, diet also becomes an important source of exposure to pesticides. Although relatively unknown to the public, neonicotinoids are the most commonly used insecticides in the world, which include acetamiprid, clothianidin, dinotefuran, imidacloprid, nitenpyram, thiacloprid, and thiamethoxam. Additionally, flonicamid has been categorized as a neonicotinoid insecticide,[2] although the mode of action is different from that of other neonicotinoids.[3] These insecticides act as nicotinic acetylcholine receptor (nAChR) agonists, which cause insect paralysis to death. Advantages of neonicotinoids in pest control, including a broad spectrum of insecticidal activity, high receptor specificity for insects relative to mammals, and versatility in application methods, have led to the replacement of organophosphates, carbamates, and synthetic pyrethroids.[4] They are now registered globally in more than 120 countries and extensively used in seed treatment (such as seed dressing or film coating) and soil treatment (by broadcast application, mechanical incorporation, soil drench, or soil injection) and are also directly applied to plant foliage for crop protection.[5,6] Additionally, neonicotinoids have been used as insect control on pets or companion animals, such as termite and flea control.[4,7]

Because of neonicotinoids' wide uses and their extreme toxicity to bees, neonicotinoids have been implicated in causing the steep decline of the global honeybee population and specifically colony collapse disorder (CCD).[8,9] Neonicotinoids are systemic insecticides and water-soluble, which means that they have superb plant-systemic activity.[4] When applied into the soil or as seed treatment, they are taken up by the roots and translocated through the entire plant.[10,11] Residue studies have detected low levels of neonicotinoids in the pollen of treated crops[10−12] and substantially high levels of resides in corn grown from imidacloprid-treated corn seeds.[13] When applied to the top surface of leaves and fruits, they penetrate into the plant tissues and afford long-term protection from piercing−sucking insects.[4] For example, substantial portions of thiacloprid and clothianidin residues and radiolabeled neonicotinoids were found to penetrate in and beyond the outer flesh regions of apples 24 h after topical application.[14,15] In another study, thiamethoxam and acetamiprid were detected in cherry leaves and the fruit's interior tissue 14 days after application.[16] Translocation of neonicotinoids into plant tissues (after either foliar application or seed/soil treatment) may potentially be subject to human consumption and subsequently dietary intake.

To estimate dietary exposure to neonicotinoids in humans, it is important to monitor neonicotinoid residues in and on foods that people consume. Although the U.S. Department of Agriculture (USDA) publishes Pesticide Data Program (PDP) reports annually, usually fewer than 15 fresh fruits and vegetables are included each year. Nevertheless, imidacloprid, the most commonly used insecticide in the world, had been detected in 81% of sweet bell peppers, 81% of broccoli, and 53% of grapes, as reported by the USDA PDP.[17] Imidacloprid is not only widely detectable in fruits and vegetables but also absorbed with high efficiency, as shown in a human intestinal cell model.[18] Imidacloprid and acetamiprid have also shown excitatory effects on cultured cerebellar neurons from neonatal

Received: March 31, 2014
Revised: June 11, 2014
Accepted: June 16, 2014
Published: June 16, 2014

 © 2014 American Chemical Society

rats, suggesting possible neurotoxicity in developing mammalian brains.[19] These results raise the concerns of potential health risks from chronic exposure to consumers by dietary intake of residues with food. Because half-lives for most neonicotinoids in aerobic soil can range from months to years,[20] neonicotinoids can become persistent in the environment for several years after repeated applications. Consequently, the persistence of neonicotinoids in soil would have created a reservoir of residues for plant to take up over a long period of time and, therefore, contaminate crops for human consumption. In addition, because of their systemic characteristics, neonicotinoids often occur as residues in the plant flesh and could not be washed off easily.

To the best of our knowledge, this is the first study aiming to demonstrate the presence of neonicotinoids in foods that people commonly consume. Only specific neonicotinoids (such as imidacloprid) in fruits and vegetables have been monitored and reported.[21,22] Most data on neonicotinoid residues in fruits and vegetables were from brief reports of the application of the newly developed analytical methods. In addition, in most of these brief reports, only up to six neonicotinoids were simultaneously monitored,[22−28] and eight neonicotinoids were monitored in only one study and in one commodity.[2] In recent years, the QuEChERS (quick, easy, cheap, effective, rugged, and safe) sample preparation procedure has been widely used for extraction of a wide variety of pesticides from various food matrices.[29−31] In this study, we used a sensitive and modified LC-MS/MS method along with the QuEChERS procedure to simultaneously measure eight neonicotinoid residues in various foods incluing fruits, vegetables, and honey and in pollen.[30] The results provided an initial assessment of the potential dietary exposure of neonicotinoids and will contribute to future epidemiological research linking neonicotinoid insecticide exposure to potential human health effects.

EXPERIMENTAL PROCEDURES

Materials. Acetamiprid, flonicamid, thiacloprid, thiamethoxam, and nitenpyram standard solutions were purchased from Accustandard (New Haven, CT, USA) with purity ≥99.7%. Imidacloprid and clothianidin were purchased from Sigma-Aldrich (St. Louis, MO, USA) with purity of 99.9%. Dinotefuran was purchased from Chem Service (West Chester, PA, USA) with purity of 99.2%. The isotope-labeled internal standards (IS) for imidacloprid-d_4 (99.2%), clothianidin-d_3 (98.9%), and thiamethoxam-d_3 (99.8%) were purchased from C/D/N Isotopes, Inc. (Quebec, Canada). LC-MS/MS grade formic acid and ammonium formate were purchased from Sigma-Aldrich. HPLC grade reagents, including acetonitrile and water, were purchased from J. T. Baker (Center Valley, PA, USA). Vial (1.5 mL with 0.2 μm nylon filter) were purchased from VWR international (Radnor, PA, USA). QuEChERS extraction salt packages, which include 4 g of $MgSO_4$, 1 g of NaCl, 1 g of sodium citrate, and 500 mg of of disodium citrate sesquihydrate in each salt pack, and 2 mL of QuEChERS dispersive SPE containing 50 mg of PSA + 50 mg of C18 + 150 mg of $MgSO_4$ or 50 mg of PSA + 50 mg of graphitized carbon black (GCB) + 150 mg of $MgSO_4$ or 25 mg of PSA + 7.5 mg of GCB + 150 mg of $MgSO_4$ ceramic homogenizer were purchased from Agilent Technologies (Santa Clara, CA, USA).

Liquid Chromatography−Mass Spectrometry (LC-MS/MS) Instrumentation. The HPLC system consists of a Shimadzu LC SCL-10AVP solvent delivery unit, an online solvent degasser, a gradient mixer, and a system controller (Shimadzu Scientific, Columbia, MD, USA), coupled with a CTC-PAL autosampler (LEAP Technologies, Carrboro, NC, USA) for injecting samples. The mass spectrometer is an API 4000 LC-MS/MS system (AB SCIEX, Framingham, MA, USA) equipped with a Turbo V IonSpray ionization source. The ShaQer 1500 from SPEX SamplePrep (Metuchen, NJ, USA) was used for mixing samples in the QuEChERS extraction procedure.

LC-MS/MS Conditions. Neonicotinoids in pollen and honey were analyzed by the LC-MS/MS method that was developed previously for pollen and high-fructose corn syrup (HFCS) samples.[30] Analysis of neonicotinoids in fruits and vegetables was conducted by using the modified method for pollen and HFCS. Briefly, the chromatographic separation was performed on a YMC ODS-AQ column (100 mm × 2.1 mm, 3 μm particle size, YMC, Allentown, PA, USA) with the mobile phase, consisting of water with 5 mM ammonium formate and 0.1% formic acid (mobile phase A) and acetonitrile/water (95:5 v/v) with 5 mm ammonium formate and 0.1% formic acid (mobile phase B), running gradient at 170 μL/min in 11 min for each analysis. The mobile phase gradient was as follows: 0% B for 1.3 min; linearly increased to 100% B from 1.3.0 to 2.3 min, and then maintained at 100% B from 2.3 to 7.5 min, back to 0% B from 7.5 to 8.0 min, and maintained at this proportion from 8.0 to 11.0 min. Injection volume into the LC-MS/MS is 10 μL. The mass spectrometer equipped with an electrospray was operated in the positive ionization mode with multiple reaction monitoring (MRM). The mass/charge (m/z) ratios monitored were 223/126, 250/169, 203/129, 230/203, 256/209, 271/225, 253/126, and 292/211 for acetamiprid, clothianidin, dinotefuran, flonicamid, imidacloprid, nitenpyram, thiacloprid, and thiamethoxam, respectively. A second transition was used for each analyte for identification purposes. The m/z of the internal standards (IS) of imidacloprid-d_4, clothianidine-d_3, and thiamethoxam-d_3 were 260/213, 253/172, and 294/214, respectively. The quantification of neonicotinoids was made from matrix-matched standard calibration curves using peak-area ratio of analyte versus IS. The calibration curves were constructed using weighted ($1/x$) linear least-squares regression. A calibration standard curve and two concentrations of QCs (QC low and QC high) in duplicate were incorporated into each analytical run. The QCs provide the basis for accepting or rejecting the run (within 20% of accuracy and precision).

Sample Collection. Twenty-nine fresh fruit and vegetable samples were purchased from several neighborhood grocery stores in Boston in 2012. Honey samples were collected directly from hives located in urban and suburban areas in Massachusetts (n = 3) or purchased from a local grocery store in Boston (n = 5) and from a store in Israel in 2012 (n = 2). Six pollen samples from New Zealand were collected by using pollen collectors set out under three hives located near a kiwifruit orchard during peak flowing for 2 days in 2011. The pollen samples were then separated into kiwifruit pollen and others (nonkiwifruit) pollen on the basis of the color of the pollen pellets. Another seven pollen samples were collected from hives located in seven different locations in the central Massachusetts area in July 2012.

Sample Preparation. *Calibration and QC Samples.* A prior analysis of neonicotinoid-free pollen, honey, and organic fruits and vegetable samples, which were used as blank matrix samples, was performed and confirmed to have no contamination of neonicotinoids. These blank samples were used for calibration, QCs, and blanks for the analysis. In addition, as a background check for any possible interference, blank matrix samples were also injected immediately after high-level standards to check the carry-over of the instrument. No carry-over was observed during the analysis. All calibration, QCs, and blanks were generated in 2 g blank matrix for pollen, 5 g for honey, and 10 g for fruits/vegetables. Calibration curves for eight neonicotinoids at seven levels ranging from 0.1 to 100 ng/g (except 0.1−50 ng/g for honey) were prepared by adding aliquots of intermediate standard solutions (preparation steps can be found in the previous study[30]) to blank sample matrix. The QC samples at two concentration levels, 5 (QCL) and 50 ng/g (QCH) (except 2 (QCL) and 40 ng/g (QCH) for honey), were prepared the same way as the blank sample matrix. The standards and QCs were stored at −20 °C.

Food Samples. The fruit and vegetable samples were washed under cold water for 15 s and allowed to drain for at least 2 min on paper toweling. Oranges were peeled, and the rinds of pumpkin and watermelon were removed. Anything that would not normally be consumed, such as apple core, pepper core, orange seeds, and the leafy tops of strawberries, were also removed. Then the samples were

No	Extraction Procedures	Pollen	Honey	Fruits and Vegetables		
				Olive	Spinach	Others
1	Weigh Xg of homogenized sample into a 50mL centrifuge tube	2g	5g	10g		
2	Add IS solution+ XmL of water	8mL	10mL	No water added		
3	Shake to dissolve	by hand	in water bath at 50 °C for 20 min	by hand		
3	Add 10mL of acetonitrile + XmL of n-hexane and shake for 30s	3mL	no hexane	5mL	no hexane	
4	Add one QuEChERS citrate salt package + one ceramic homogenizer, and shake for 40s and centrifuge					
5	Transfer 1mL of supernatant into a 2 mL d-SPE, and vortex 30s and then centrifuge	50mg PSA+50mg C18+150mg MgSO4			50mg PSA+50mg GCB+150mg MgSO4	25mg PSA+7.5mg GCB+150mg $MgSO_4$
7	Dispense 600μL of supernatant into a glass test tube, and dry under N_2 in water bath at 40 °C					
8	Reconstitute residues using 200μL of 15% Acetonitrile in water, transfer 150μL filtered solution into HPLC vials and analyze by LCMS/MS					

Figure 1. Sample extraction procedures in different matrices.

Table 1. Limit of Quantitation (LOQ) for Eight Neonicotinoid Insecticides in Various Sample Matrices

	LOQ (ng/g)							
	acetamiprid	clothianidin	dinotefuran	flonicamid	imidacloprid	nitenpyram	thiacloprid	thiamethoxam
matrix								
fruits/vegetables (n = 20)	0.1	0.1	0.1	0.2	0.1	0.1	0.1	0.1
honey (n = 5)	0.1	0.1	0.5	0.5	0.1	0.1	0.1	0.1
pollen (n = 5)	0.1	0.1	0.1	0.5	0.1	0.5	0.1	0.1
recovery (%)	110.4	97.5	96.1	95.6	101.6	97.4	99.6	101.5
RSD (%)	13	14	20	14	12	18	17	10

chopped into small pieces and blended in a Magic Bullet until a homogeneous paste was achieved. If the sample was homogenized in portions, all portions were mixed together in a clean container to ensure an evenly mixed sample.

The overall sample preparation procedure is shown in Figure 1. The sample extraction procedures for fruits and vegetables were modified from the method that we developed previously for pollen and HFCS samples, and the procedure for honey samples was the same as that for HFCS.[30] Ten grams of homogenized fruit and vegetable samples was weighed in a 50 mL centrifuge tube, and 10 mL of acetonitrile and 20 μL of IS solutions were added. For calibration standard and QCs, 10 g of homogenized organic samples was fortified with appropriate levels of working standard solutions. Double-blanks and blanks were also prepared in parallel with and without IS added, respectively. The tube was subsequently shaken for 30 s in a ShaQer at 1500 strokes per minute. Then one pack of QuEChERS salt and one ceramic homogenizer were added. An additional 5 mL of *n*-hexane was added to all olive samples. The tubes were shaken vigorously for 40 s in the shaker and centrifuged for 4 min at 4000*g*. One milliliter from the acetonitrile layer was transferred to a 2 mL QuEChERS dispersive SPE vial. Pollen, honey, and olive samples were added to d-SPE vials containing 50 mg of PSA, 50 mg of C18, and 150 mg of $MgSO_4$; spinach sample was added to d-SPE containing 50 mg of PSA, 50 mg of GCB, and 150 mg of $MgSO_4$; and all the rest of the fruits and vegetables were added to d-SPE containing 25 mg of PSA, 7.5 mg of GCB, and 150 mg of $MgSO_4$. The next d-SPE extraction, sample drying, and transfer steps were the same as presented before.[30]

RESULTS AND DISCUSSION

In this study, we analyzed various types of fruits, including oil fruits, stone fruits, pome fruits, citrus fruits, and berries, and vegetables, including leafy vegetables and root vegetables, as well as honey and pollen. Table 1 shows the performance of this method including the limit of quantification (LOQ) and the average recoveries (and the variations) of eight neonicotinoids in various sample matrices. LOQ was calculated as 10 times the signal-to-noise ratio of the quantitative ion transition in the matrix and was 0.1 ng/g for neonicotinoids in pollen, honey, fruits, and vegetables with the exceptions of 0.5 ng/g for flonicamid and 0.5 ng/g for nitenpyram in pollen and dinotefuran in honey. A sample was considered positive when residue levels were above the LOQ. As shown in Table 2, all fruit and vegetable samples in our study tested positive for one or more neonicotinoids, except nectarine and tomato. Five neonicotinoids, including clothianidin, dinotefuran, flonicamid, imidacloprid, and thiamethoxam, were detected in both fruits and vegetables; however, acetamiprid and thiacloprid were found only in fruits. Nitenpyram was the only neonicotinoid that is not detectable in any fruit or vegetable samples. Imidacloprid not only was detected with the highest concentration in a green pepper sample (7.2 ng/g), but also was the most frequently detected neonicotinoid in both fruits and vegetables with the overall detection rate of 70%. The results in Table 2 show that not only are neonicotinoids widely found in fruits and vegetables but also multiple neonicotinoids are often detected in a single sample, especially in apples. Seventy-two percent of fruits and 45% of vegetables were found to have multiple neonicotinoids. These percentages included 5 of 8 apples, which were detected with three different neonicotinoids, and 6 of 10 fruits and 5 of 11 vegetables were positive for two neonicotinoids. Because most commercially available products do not contain multiple neonicotinoids as the active ingredients, except for clothianidin, which could be the breakdown product of thiamethoxam, this result indicates that these fruit and vegetable plants were likely treated multiple times during their lifespan with different neonicotinoids or absorbed neonicotinoid residues accumulated in the soil. The persistence of neonicotinoids in aerobic soil is highly likely due

dx.doi.org/10.1021/jf501397m | J. Agric. Food Chem. 2014, 62, 6082−6090

Table 2. Concentrations of Neonicotinoids Measured in Conventional Fruits and Vegetables Purchased from a Local Grocery Store in Boston, MA, USA

		analyte concentrations[a] (ng/g)							
	types of foods	acetamiprid	clothianidin	dinotefuran	flonicamid	imidacloprid	nitenpyram	thiacloprid	thiamethoxam
fruits	apple (Cortland)	–	–	–	–	–	–	0.4	–
	apple (Granny Smith)	40.7	–	–	0.1	0.1	–	–	–
	apple (Fuji)	–	–	–	0.1	0.1	–	–	–
	apple (Red Delicious)	–	–	–	0.1	4.2	–	–	–
	apple (Golden Delicious)	0.3	0.2	–	–	0.6	–	–	–
	apple (Gala)	–	0.1	–	–	0.1	–	18.3	–
	apple (Honey Crisp)	100.7	–	–	0.2	0.1	–	–	–
	Apple (Macintosh)	–	1.9	–	–	0.1	–	4.7	–
	nectarine	–	–	–	–	–	–	–	–
	orange	–	–	–	0.2	0.9	–	–	–
		–	–	–	0.2	1.1	–	–	–
	strawberry	–	–	–	–	0.2	–	–	–
		19.5	–	–	–	–	–	–	–
	watermelon	–	–	–	–	0.1	–	–	0.2
		–	–	–	–	0.2	–	–	2.4
	cantaloupe	–	–	34.8	–	3.0	–	–	–
	honeydew	–	–	–	–	2.8	–	–	–
	olive	–	–	–	–	0.1	–	–	0.4
vegetables	spinach	–	–	–	0.4	6.5	–	–	–
	tomato	–	–	–	–	–	–	–	–
	yellow pepper	–	–	0.1	–	–	–	–	–
	green pepper	–	–	–	–	7.2	–	–	–
	potato	–	0.7	–	–	–	–	–	0.3
	eggplant	–	–	–	–	1.6	–	–	–
	cucumber	–	0.6	–	–	–	–	–	13.2
		–	–	–	–	2.76	–	–	–
	pumpkin	–	0.7	–	–	–	–	–	0.4
	zucchini	–	–	–	–	0.4	–	–	0.5
	summer squash	–	–	–	–	2.8	–	–	–

[a]–, below the limit of quantitation.

Table 3. Concentrations of Neonicotinoids Measured in Honey Samples

	concentration[a] (ng/g) of honey samples from different sources									
		suburban			foreign		raw honey		organic	
analyte	urban	1	2	rural	1	2	1	2	foreign	domestic
acetamiprid	–	–	–	–	–	0.2	–	–	–	–
clothianidin	–	0.1	–	–	–	–	–	–	0.5	–
dinotefuran	–	–	–	–	–	–	–	–	–	–
flonicamid	–	–	–	–	–	–	–	–	–	–
imidacloprid	0.1	0.3	0.2	–	0.7	0.8	0.2	0.1	0.2	1.3
nitenpyram	–	–	–	–	–	–	–	0.2	–	–
thiacloprid	–	–	–	–	–	–	–	–	–	–
thiamethoxam	–	–	–	–	–	–	–	–	–	0.4

[a]–, below the limit of quantitation.

to the accumulation of repeated applications of neonicotinoids, especially ones with long half-lives.[20]

In addition to fruits and vegetables, we analyzed 10 domestic and foreign honey samples collected from urban, suburban, and rural areas. Table 3 shows that five neonicotinoids, including acetamiprid, clothianidin, imidacloprid, nitenpyram, and thiamethoxam, were found in these honey samples. Similar to fruits and vegetables, imidacloprid was found in 9 of 10 honey samples, including 2 organic honey samples purchased from a local grocery store. The highest concentration of imidacloprid of 1.3 ng/g was found in a domestic organic honey sample. The USDA organic regulations allowed residues of prohibited pesticides up to 5% of the tolerance set by the U.S. Environmental Protection Agency (EPA) in organic products, but there are no defined tolerances for most neonicotinoids (including imidacloprid) in honey.[32] Five honey samples contained multiple neonicotinoids, including two organic honey samples. Only one honey sample collected from a hive located in the rural area was free from neonicotinoid contamination. The high frequency of detections of neon-

dx.doi.org/10.1021/jf501397m | J. Agric. Food Chem. 2014, 62, 6082−6090

Table 4. Concentrations[a] of Neonicotinoids Measured in Pollen Samples Collected from Central Massachusetts, USA, and New Zealand

pollen samples		acetamiprid	clothianidin	dinotefuran	flonicamid	imidacloprid	nitenpyram	thiacloprid	thiamethoxam
MA, USA[b]	1	–	–	–	–	2.3	–	–	–
	2	–	–	–	–	0.4	–	–	–
	3	–	–	–	–	2.2	–	–	–
	4	–	–	–	–	0.7	–	–	–
	5	–	–	–	–	–	–	–	–
	6	–	–	–	–	–	–	–	–
	7	–	–	–	–	0.6	–	–	–
New Zealand[c]	kiwi, A[d]	–	0.2	–	–	0.2	–	1.7	–
	others, A[e]	–	1.9	–	–	1.2	–	3.3	–
	kiwi, B[d]	–	0.5	–	–	–	–	1.3	–
	others, B[e]	–	2.6	–	–	0.5	–	0.1	–
	kiwi, C[d]	–	0.6	–	–	0.2	–	1.4	–
	others, C[e]	–	2.2	–	–	0.4	–	1.1	–

[a]–, below the limit of quantitation. [b]Pollen samples were collected from honeybees in hives from seven different locations of central Massachusetts. [c]Pollen samples were collected from 2 day collections from three hives in a kiwifruit orchard at the beginning of their pollination assignment in New Zealand in 2011. [d]Pollen samples were sorted by color; kiwifruit pollen was the dominant pollen. [e]Other pollens collected were a range of colors, according to their host plants, such as clovers and dandelions, in the proximity of the kiwi orchard.

Table 5. Summary of Neonicotinoids Concentrations in Foods

analyte	food type	total samples collected	no. of samples > LOQ	freq of detection (%)	concn range (ppb)	commodity with max concn
imidacloprid	fruits	17	15	82	0.1–4.2	apple
	vegetables	12	7	58	0.4–7.2	green pepper
	honey	10	9	90	0.1–1.3	organic, domestic
	pollen	13	10	77	0.2–2.3	MA
clothianidin	fruits	17	3	18	0.1–1.9	apple
	vegetables	12	3	25	0.6–0.7	potato, pumpkin
	honey	10	2	20	0.1–0.5	organic, foreign
	pollen	13	6	46	0.2–2.6	New Zealand, other
thiamethoxam	fruits	17	3	18	0.2–2.4	watermelon
	vegetables	12	4	33	0.3–13.2	cucumber
	honey	10	1	10	0.4	organic, domestic
acetamiprid	fruits	17	4	24	0.3–100.7	apple
	honey	10	1	10	0.2	foreign
dinotefuran	fruits	17	1	6	34.8	cantaloupe
	vegetables	12	1	8	0.1	yellow pepper
flonicamid	fruits	17	6	35	0.1–0.2	apple, orange
	vegetables	12	1	8	0.4	spinach
thiacloprid	fruits	17	3	18	0.4–18.3	apple
	pollen	13	6	46	0.1–3.3	New Zealand, other
nitenpyram	honey	10	1	10	0.2	raw

icotinoids, especially imidacloprid, in these samples indicates the wide usage of neonicotinoids in the environment where honeybees often foraged.

We also tested 13 pollen samples; 7 of them were from central Massachusetts and 6 from New Zealand. As shown in Table 4, imidacloprid continued to be the most commonly detected neonicotinoid with a detection frequency of 77% in all 13 pollen samples. Among the seven pollen samples from Massachusetts, the five that tested positive were collected from central Massachusetts within the so-called "quarantine area", where trees were injected with imidacloprid to combat the Asian Longhorn beetle problem in 2011–2012. The other two pollen samples containing no neonicotinoids were collected outside the "quarantine area", where neonicotinoid uses have not been observed or reported. The degree of neonicotinoid contamination in pollen samples collected in New Zealand is more extensive than that of samples collected from central Massachusetts areas, as shown in Table 4. All six samples contained multiple neonicotinoids, and five of those six samples contained three neonicotinoids. It is also noticeable that

dx.doi.org/10.1021/jf501397m | J. Agric. Food Chem. 2014, 62, 6082–6090

Table 6. Neonicotinoid Residues Measured in Fruits and Vegetables Reported by the USDA Pesticide Data Program (PDP) from 2004 to 2011

analyte	year	total samples collected	no. of samples with detection	freq of detection (%)	max concn (ppb)	commodity with highest freq of detection (freq of detection, %)[a]
imidacloprid	2004	5920	1510	26	780	sweet bell peppers (81%) (apple 30.2%)
	2005	6956	1567	23	470	cauliflower (85%) (apple 26.6%)
	2006	6930	1405	20	520	broccoli (81%) (applesauce 17.5%)
	2007	7107	1654	23	1000	broccoli (72%) (apple juice 0%)
	2008	8176	1389	17	1000	broccoli (67%) (apple juice 0%)
	2009	8981	1267	14	1100	grapes (53%) (apple 16.9%)
	2010	10322	1473	14	1100	grapes (48%) (apple 20.3%)
	2011	10480	1104	11	750	cauliflower/lettuce (36%) (no apple data)
	overall	64872	11369	18		
acetamiprid	2004	412	79	19		apples (100%)
	2005	1528	272	18		apples (70%)
	2006	3298	453	14		apple sauce (51.5%)
	2007	5284	350	7		summer squash (100%) (apple juice 34%)
	2008	8261	416	5		apple juice (33.3%)
	2009	9194	817	9		pears (41.1%) (apple 33%)
	2010	10323	552	5		apples (28.8%)
	2011	10096	295	3		baby food, pears (26.3%) (no apple data)
	overall	48396	3234	10		
clothianidin	2004					
	2005	123	0	0.0		watermelon (0%) (no apple data)
	2006	3482	29	1		summer squash (5.6%) (no apple data)
	2007	6381	28	0.4		summer squash (2.8%) (apple juice 0%)
	2008	7744	65	1		potatoes (5.3%) (apple juice 0%)
	2009	8447	104	1		grapes (4.8%) (apple 0%)
	2010	8739	172	2		hot peppers (11.3%) (no apple data)
	2011	9337	218	2		cherry tomatoes (14.1%) (no apple data)
	overall	44253	616	1		
flonicamid	2004					
	2005					
	2006	132	1	1		summer squash (0.8%)
	2007	2094	6	0		summer squash (1.1%) (apple 0%)
	2008	4661	73	2		spinach (13.9%) (apple 0%)
	2009	5990	58	1		cucumbers (6%) (apple 0.5%)
	2010	7910	114	1		cucumbers (6.9%) (apple 1.6%)
	2011	8162	139	2		lettuce (7.4%) (no apple data)
	overall	28949	391	1		
thiacloprid	2004					
	2005	480	4	1		apples (3%)
	2006	1853	96	5		apple sauce (12.8%)
	2007	1891	5	0		apple juice (4.7%)
	2008	3343	6	0		apple juice (4.6%)
	2009	7467	102	1		apples (9%)
	2010	7628	163	2		apples (12.6%)
	2011	6338	106	2		baby food, pears (no apple data)
	overall	29000	482	2		
dinotefuran	2009	7323	26	0		cucumbers (15%)
	2010	9580	150	2		cantaloupe (14.6%)
	2011	9678	153	2		cantaloupe (11.9%) (no apple data)
	overall	40085	472	1		
nitenpyram	overall	NA	NA	NA		
thiamethoxam	2009	10257	196	2		cucumbers (11.6%)
	2010	10602	422	4		sweet bell peppers (26.6)

dx.doi.org/10.1021/jf501397m | J. Agric. Food Chem. 2014, 62, 6082−6090

Table 6. continued

analyte	year	total samples collected	no. of samples with detection	freq of detection (%)	max concn (ppb)	commodity with highest freq of detection (freq of detection, %)[a]
	2011	10477	348	3		sweet bell peppers (17.1%) (no apple data)
	Overall	59778	1409	2		

[a]Frequency of detection (%) in apples or applesauce or apple juice as a comparison.

nonkiwifruit (others) pollen samples contained higher concentrations of imidacloprid and clothianidin than kiwifruit pollen. Those nonkiwifruit pollen samples were likely from nearby dandelion, clover, and other weed flowers, on the basis of the color of the pollen pellets. Because kiwifruit has little nectar, honeybees need to forage widely (as far as 2 km) to get their nectar feed for energy. In this search, bees could pick up other pollens containing higher levels of neonicotinoids around the kiwifruit orchard than the pollen of kiwifruit; therefore, higher levels of neonicotinoids showed up in these "others" pollen. This finding is consistent with the systemic property of neonicotinoids because upon application (such as spray), neonicotinoid residues can penetrate and translocate through the plant/weed, including nectar and pollen, located near the adjacent area. Because pollen is honeybees' main source of protein and neonicotinoids have been linked to CCD,[8,9] the widespread presence of neonicotinoids in these pollen samples could pose a potential threat to the survival of honeybees.

In addition, neonicotinoids, such as imidacloprid, clothianidin, and thiacloprid, have often been used as soil treatment for insect controls because of their long half-lives in aerobic soil (half-lives for imidacloprid and clothianidin are 26−229 and 148−1155 days, respectively) and water solubility.[6,20,33] A recent study has shown that clothianidin was found in both soil and dandelion flowers grown adjacent to a clothianidin-treated agriculture area.[34] Another study has shown that untreated sunflowers grown in fields previously treated with imidacloprid a year ago can still take up imidacloprid from the soil.[35] Therefore, some neonicotinoids can become persistent for several years and accumulated in the environment after repetitive applications and, therefore, cause concern for prolonged exposure.

This result from pollen samples is consistent with that from the fruit and vegetable samples in this study because most of these types of fruits and vegetables testing positive were pollinated by honeybees. Our study also raises the concern of pollen contaminated with neonicotinoids because not only is pollen the primary protein source for honeybees but also it could be readily available for human exposure via inhalation as well.

Table 5 shows the summary results of neonicotinoid residues detected in all samples that were analyzed in this study. Both imidacloprid and clothianidin were found in all four types of foods followed by thiamethoxam (three types of foods); acetamiprid, dinotefuran, flonicamid, and thiacloprid (two types of food); and nitenpyram (in only one honey sample). Results from this study were generally consistent with what have reported by the USDA PDP during 2004−2011 (Table 6). Consistent with having the highest frequency of detection among all neonicotinoids in samples that we analyzed, imidacloprid was found in seven of eight apple samples in this study, as well as in apples/applesauce/apple juice samples reported by PDP from 2004 to 2010 (Table 6). Along with imidacloprid, apples/applesauce/apple juice have the highest detection frequency of acetamiprid in almost every year from 2004 to 2010, although the frequency of detection for acetamiprid has gradually decreased from 100% in 2004 to approximately 30% in 2007. Similarly, apple, applesauce, or apple juice has consistently been the commodity with the highest frequency of detection for thiacloprid every year from 2004 to 2010 and has an increasing trend of use from 4.7% in 2007 to 9% in 2009 to 12.6% in 2010. Although clothianidin was not detectable in apples or apple juice in PDP from 2007 to 2009, clothianidin was found in three of eight apples in the current study conducted in 2012. Consistent with results from PDP, the current study has confirmed the wide use of imidacloprid, clothianidin, acetamiprid, flonicamid, and thiacloprid on apples, ranging from 38 to 88%. Unfortunately, we were not able to continue monitoring the trend of neonicotinoid residues in apples because they were not included in PDP after 2010. We found a higher frequency of detection of imidacloprid than USDA PDP reported primarily because we used a more sensitive analytical method with lower LOQs for all neonicotinoids in this study than those used by USDA PDP with a limit of detection ≥1 ng/g. Smaller sample sizes in our study could be another reason for higher frequency of detection; however, the commodities testing positive in our study matched the commodities reported by PDP. For instance, the highest concentration of thiamethoxam detected in our study was from a cucumber sample (13.2 ng/g), and cucumber was found with the highest detection rate of 12% in 2009 and an even higher rate of 16% in 2010 by PDP. The highest concentration of dinotefuran in our study was found in a cantaloupe sample, which was also reported by PDP in 2010 and 2011 with the highest detection rates of 15 and 12%, respectively.

This study has demonstrated the widespread presence of neonicotinoids in foods that people commonly consume and in pollen and honey that honeybees bring back to hives from the environment. Although those levels were low, studies have suggested a link to adverse health effects in honeybees as the results of sublethal exposure to neonicotinoids.[8,36,37] Neonicotinoid insecticides are known to selectively target insects' nicotinic acetylcholine receptors (nAChRs) and therefore were previously thought to pose less toxicity in mammals. However, a growing amount of evidence has shown that neonicotinoids are capable of directly activating and/or modulating the activation of mammalian nAChRs. Both in vitro and in vivo studies have shown that imidacloprid can change the membrane properties of mouse neurons,[38] significantly impair sensorimotor performance, and elevate glial fibrillary acidic protein expression in the motor cortex and hippocampus of neonatal rats after in utero exposure to a single sublethal dose.[39] Most mammalian adverse toxic effects of neonicotinoids are associated with their action on binding to the $\alpha4\beta2$ nAChR subtype.[40] In an in vitro study, imidacloprid and other neonicotinoids have been shown to directly activate and modulate human $\alpha4\beta2$ nAChR subtypes.[41] The $\alpha4\beta2$ nAChR subtype is the most prominent nAChR subtype in the mammalian brain, with the highest density of receptors in the

thalamus.[42] The $\alpha4\beta2$ nAChR is involved in various brain functions, such as cognition, memory, and behavior. There is strong evidence for a role of $\alpha4\beta2$ nAChR and alteration of the receptor density in CNS disorders, such as Alzheimer's disease, Parkinson's disease, schizophrenia, and depression.[43,44] In the developing brain (such as perinatal stage), $\alpha4\beta2$ nAChR subtypes have been implicated in neuronal proliferation, apoptosis, migration, differentiation, synapse formation, and neural-circuit formation.[45,46] It is likely that neonicotinoids could affect these processes when activating nAChRs. In addition, absorption studies using the human intestinal cell line have shown that neonicotinoids can be absorbed by active transportation.[18,47] Neonicotinoids and some of their metabolites are also shown to be able to pass through the blood–brain barrier in mice, and some metabolites having enhanced potency to nAChR are even more toxic than their parent compounds.[48] Therefore, there is an inevitable question if neonicotinoids could pose potential health risks to humans as well.

In conclusion, this is the first paper to document the widespread presence of neonicotinoid residues in fruits, vegetables, and honey that are readily available in the market for human consumption. We also reported neonicotinoid residues in pollen collected by honeybees in areas where neonicotinoids are known to be used, and the variation of neonicotinoid levels in pollen likely reflects the amount of neonicotinoids applied. It is important to note here that although all neonicotinoid residues reported in this study were below the maximum residue levels, or tolerances, established by the EPA, the determination of these tolerances is based on the best field practice and studies conducted in test animals exposed at acute and chronic toxic levels, and therefore does not take into sufficient account the protection of human health from long-term low-dose exposure. In light of the extensive use of neonicotinoids on fruit and vegetable crops and their widespread presence in foods along with new information on the toxicological effects of neonicotinoids in mammals, it is therefore warranted to conduct epidemiological studies to assess dietary neonicotinoid intakes in humans and the health effects.

AUTHOR INFORMATION

Corresponding Author

*(C.L.) Phone: (617) 998-8811. Fax: (617) 384-8728. E-mail: cslu@hsph.harvard.edu.

Funding

This project was supported by the Harvard–NIEHS Center for Environmental Health (P30ES000002) Pilot Project Program.

Notes

The authors declare no competing financial interest.

ACKNOWLEDGMENTS

We thank Dr. Christine Austin (University of Sydney, Sydney Australia), Erin Collin, Michaela Kapp (Harvard School of Public Health), and Barry Foster (New Zealand) for their assistance in sample collection, analytical method development, and sample preparation in the laboratory.

REFERENCES

(1) U.S. Department of Agriculture. Dietary guidelines for Americans, 2010; available online http://www.cnpp.usda.gov/DGAs2010-PolicyDocument.htm.

(2) Tanner, G.; Czerwenka, C. LC-MS/MS analysis of neonicotinoid insecticides in honey: and residue findings in Austrian honeys. *J. Agric. Food Chem.* **2011**, *59*, 12271–12277.

(3) U.S. Environmental Protection Agency. Flonicamid: report of the cancer assessment review committee, 2005; PC Code 128016.

(4) Tomizawa, M.; Casida, J. E. Neonicotinoid insecticide toxicology: mechanisms of selective action. *Annu. Rev. Pharmacol. Toxicol.* **2005**, *45*, 247–268.

(5) Agnes, R.; Gerard, A.; Marie-Pierre, H.; Frédérique, T. B. Modes of honeybees exposure to systemic insecticides: estimated amounts of contaminated pollen and nectar consumed by different categories of bees. *Apidologie* **2005**, *36*, 71–83.

(6) Elbert, A.; Haas, M.; Springer, B.; Thielert, W.; Nauen, R. Applied aspects of neonicotinoid uses in crop protection. *Pest Manage. Sci.* **2008**, *64*, 1099–1105.

(7) Vo, D. T.; Hsu, W. H.; Abu-Basha, E. A.; Martin, R. J. Insect nicotinic acetylcholine receptor agonists as flea adulticides in small animals. *J. Vet. Pharmacol. Ther.* **2010**, *33*, 315–322.

(8) Lu, C.; Warchol, K.; Callahan, R. In situ replication of honeybee colony collapse disorder. *Bull. Insectol.* **2012**, *65*, 99–106.

(9) Stokstad, E. How big a role should neonicotinoids play in food security? *Science* **2013**, *340*, 675.

(10) Stoner, K. A.; Eitzer, B. D. Movement of soil-applied imidacloprid and thiamethoxam into nectar and pollen of squash (*Cucurbita pepo*). *PLoS One* **2012**, *7*, No. e39114.

(11) Bonmatin, J. M.; Moineau, I.; Charvet, R.; Fleche, C.; Colin, M. E.; Bengsch, E. R. A LC/APCI-MS/MS method for analysis of imidacloprid in soils, in plants, and in pollens. *Anal. Chem.* **2003**, *75*, 2027–2033.

(12) Chauzat, M. P.; Faucon, J. P.; Martel, A. C.; Lachaize, J.; Cougoule, N.; Aubert, M. A survey of pesticide residues in pollen loads collected by honey bees in France. *J. Econ. Entomol.* **2006**, *99*, 253–262.

(13) Girolami, V.; Mazzon, L.; Squartini, A.; Mori, N.; Marzaro, M.; Di Bernardo, A.; Greatti, M.; Giorio, C.; Tapparo, A. Translocation of neonicotinoid insecticides from coated seeds to seedling guttation drops: a novel way of intoxication for bees. *J. Econ. Entomol.* **2009**, *102*, 1808–1815.

(14) Wise, J. C.; Vanderpoppen, R.; Vandervoort, C. Curative activity of insecticides on *Rhagoletis pomonella* (Diptera: Tephritidae) in apples. *J. Econ. Entomol.* **2009**, *102*, 1884–1890.

(15) Mota-Sanchez, D.; Cregg, B.; Hoffmann, E.; Flore, J.; Wise, J. C. Penetrative and dislodgeable residue characteristics of ^{14}C-insecticides in apple fruit. *J. Agric. Food Chem.* **2012**, *60*, 2958–2966.

(16) Hoffmann, E. J.; Vandervoort, C.; Wise, J. C. Plum curculio (Coleoptera: Curculionidae) adult mortality and associated fruit injury after exposure to field-aged insecticides on tart cherry branches. *J. Econ. Entomol.* **2010**, *103*, 1196–1205.

(17) U.S. Department of Agriculture (USDA). Pesticide Data Program: Annual Summary Calendar Year, 2004–2010.

(18) Brunet, J. L.; Maresca, M.; Fantini, J.; Belzunces, L. P. Human intestinal absorption of imidacloprid with Caco-2 cells as enterocyte model. *Toxicol. Appl. Pharmacol.* **2004**, *194*, 1–9.

(19) Kimura-Kuroda, J.; Komuta, Y.; Kuroda, Y.; Hayashi, M.; Kawano, H. Nicotine-like effects of the neonicotinoid insecticides acetamiprid and imidacloprid on cerebellar neurons from neonatal rats. *PLoS One* **2012**, *7*, No. e32432.

(20) U.S. Environment Protection Agency, Office of Pesticide Programs. Fact sheet clothianidin 2003, fact sheet Dinotefuran, 2004; 7501C.

(21) Kapoor, U.; Srivastava, M. K.; Srivastava, A. K.; Patel, D. K.; Garg, V.; Srivastava, L. P. Analysis of imidacloprid residues in fruits, vegetables, cereals, fruit juices, and baby foods, and daily intake estimation in and around Lucknow, India. *Environ. Toxicol. Chem.* **2013**, *32*, 723–727.

(22) Frenich, A. G.; Vidal, J. L.; López, T. L.; Aguado, S. C.; Salvador, I. M. Monitoring multi-class pesticide residues in fresh fruits and vegetables by liquid chromatography with tandem mass spectrometry. *J. Chromatogr., A* **2004**, *1048*, 199–206.

(23) Frenich, A. G.; Martínez Vidal, J. L.; Pastor-Montoro, E.; Romero-González, R. High-throughput determination of pesticide residues in food commodities by use of ultra-performance liquid chromatography-tandem mass spectrometry. *Anal. Bioanal. Chem.* **2008**, *390*, 947−959.
(24) Wiest, L.; Buleté, A.; Giroud, B.; Fratta, C.; Amic, S.; Lambert, O.; Pouliquen, H.; Arnaudguilhem, C. Multi-residue analysis of 80 environmental contaminants in honeys, honeybees and pollens by one extraction procedure followed by liquid and gas chromatography coupled with mass spectrometric detection. *J. Chromatogr., A* **2011**, *1218*, 5743−5756.
(25) Camino-Sánchez, F. J.; Zafra-Gómez, A.; Oliver-Rodríguez, B.; Ballesteros, O.; Navalón, A.; Crovetto, G.; Vílchez, J. L. UNE-EN ISO/IEC 17025:2005-accredited method for the determination of pesticide residues in fruit and vegetable samples by LC-MS/MS. *Food Addit. Contam. Part A: Chem. Anal. Control Exposure Risk Assess.* **2010**, *27*, 1532−1544.
(26) Botero-Coy, A. M.; Marín, J. M.; Ibáñez, M.; Sancho, J. V.; Hernández, F. Multi-residue determination of pesticides in tropical fruits using liquid chromatography/tandem mass spectrometry. *Anal. Bioanal. Chem.* **2012**, *402*, 2287−2300.
(27) Zhang, F.; Li, Y.; Yu, C.; Pan, C. Determination of six neonicotinoid insecticides residues in spinach, cucumber, apple and pomelo by QuEChERS method and LC-MS/MS. *Bull. Environ. Contam. Toxicol.* **2012**, *88*, 885−890.
(28) Ferrer, I.; García-Reyes, J. F.; Mezcua, M.; Thurman, E. M.; Fernánndez-Alba, A. R. Multi-residue pesticide analysis in fruits and vegetables by liquid chromatography-time-of-flight mass spectrometry. *J. Chromatogr., A* **2005**, *1082*, 81−90.
(29) Chung, S. W.; Lam, C. H. Development and validation of a method for determination of residues of 15 pyrethroids and two metabolites of dithiocarbamates in foods by ultra-performance liquid chromatography-tandem mass spectrometry. *Anal. Bioanal. Chem.* **2012**, *403*, 885−896.
(30) Chen, M.; Collins, E. M.; Tao, L.; Lu, C. Simultaneous determination of residues in pollen and high-fructose corn syrup from eight neonicotinoid insecticides by liquid chromatography-tandem mass spectrometry. *Anal. Bioanal. Chem.* **2013**, *405*, 9251−9264.
(31) Lozano, A.; Rajski, Ł.; Belmonte-Valles, N.; Uclés, A.; Uclés, S.; Mezcua, M.; Fernández-Alba, A. R. Pesticide analysis in teas and chamomile by liquid chromatography and gas chromatography tandem mass spectrometry using a modified QuEChERS method: validation and pilot survey in real samples. *J. Chromatogr., A* **2012**, *1268*, 109−122.
(32) 2010−2011 Pilot Study Pesticide Residue Testing of Organic Produce, USDA Agricultural Marketing Service, Nov 2012; available online http://www.ams.usda.gov/AMSv1.0/getfile?dDocName=STELPRDC5101234.
(33) California Department of Pesticide Regulation. Environmental fate, Imidacloprid, 2000; available online http://www.cdpr.ca.gov/docs/emon/pubs/fatememo/imid.pdf.
(34) Krupke, C. H.; Hunt, G. J.; Eitzer, B. D.; Andino, G.; Given, K. Multiple routes of pesticide exposure for honey bees living near agricultural fields. *PLoS One* **2012**, *7*, No. e29268.
(35) Bonmatin, J. M.; Marchand, P. A.; Charvet, R.; Moineau, I.; Bengsch, E. R.; Colin, M. E. Quantification of imidacloprid uptake in maize crops. *J. Agric. Food Chem.* **2005**, *53*, 5336−5341.
(36) Vidau, C.; Diogon, M.; Aufauvre, J.; Fontbonne, R.; Viguès, B.; Brunet, J. L.; Texier, C.; Biron, D. G.; Blot, N.; El Alaoui, H.; Belzunces, L. P.; Delbac, F. Exposure to sub-lethal doses of fipronil and thiacloprid highly increases mortality of honeybees previously infected by *Nosema ceranae*. *PLoS One* **2011**, *6*, No. e21550.
(37) Henry, M.; Rollin, O.; Aptel, J.; Tchamitchian, S.; Beguin, M.; Requier, F.; Decourtye, A. A common pesticide decreases foraging success and survival in honey bees. *Science* **2012**, *336*, 348−350.
(38) Bal, R.; Erdogan, S.; Theophilidis, G.; Baydas, G.; Naziroglu, M. Assessing the effects of the neonicotinoid insecticide imidacloprid in the cholinergic synapses of the stellate cells of the mouse cochlear nucleus using whole-cell patch-clamp recording. *Neurotoxicology* **2010**, *31*, 113−120.
(39) Abou-Donia, M. B.; Goldstein, L. B.; Bullman, S.; Tu, T.; Khan, W. A.; Dechkovskaia, A. M.; Abdel-Rahman, A. A. Imidacloprid induces neurobehavioral deficits and increases expression of glial fibrillary acidic protein in the motor cortex and hippocampus in offspring rats following in utero exposure. *J. Toxicol. Environ. Health A* **2008**, *71*, 119−130.
(40) Tomizawa, M.; Cowan, A.; Casida, J. E. Analgesic and toxic effects of neonicotinoid insecticides in mice. *Toxicol. Appl. Pharmacol.* **2001**, *177*, 77−83.
(41) Li, P.; Ann, J.; Akk, G. Activation and modulation of human $\alpha4\beta2$ nicotinic acetylcholine receptors by the neonicotinoids clothianidin and imidacloprid. *J. Neurosci. Res.* **2011**, *89*, 1295−1301.
(42) Lukas, R. J.; Changeux, J. P.; Le Novère, N.; Albuquerque, E. X.; Balfour, D. J.; Berg, D. K.; Bertrand, D.; Chiappinelli, V. A.; Clarke, P. B.; Collins, A. C.; Dani, J. A.; Grady, S. R.; Kellar, K. J.; Lindstrom, J. M.; Marks, M. J.; Quik, M.; Taylor, P. W.; Wonnacott, S. International Union of Pharmacology. XX. Current status of the nomenclature for nicotinic acetylcholine receptors and their subunits. *Pharmacol. Rev.* **1999**, *51*, 397−401.
(43) Toyohara, J.; Sakata, M.; Ishiwata, K. Chapter 6: Human brain imaging of acetylcholine receptors. *Imaging of the Human Brain in Health and Disease*; Book 1 in the Neuroscience-Net Reference Book Series; Philip, S., Bertha, M., Eds.; Elsevier: Oxford, UK, 2013; pp 113−143.
(44) Hogg, R. C.; Raggenbass, M.; Bertrand, D. Nicotinic acetylcholine receptors: from structure to brain function. *Rev. Physiol. Biochem. Pharmacol.* **2003**, *147*, 1−46.
(45) Role, L. W.; Berg, D. K. Nicotinic receptors in the development and modulation of CNS synapses. *Neuron* **1996**, *16*, 1077−1085.
(46) Dwyer, J. B.; McQuown, S. C.; Leslie, F. M. The dynamic effects of nicotine on the developing brain. *Pharmacol. Ther.* **2009**, *122*, 125−139.
(47) Brunet, J. L.; Maresca, M.; Fantini, J.; Belzunces, L. P. Intestinal absorption of the acetamiprid neonicotinoid by Caco-2 cells: transepithelial transport, cellular uptake and efflux. *J. Environ. Sci. Health B* **2008**, *43*, 261−270.
(48) Ford, K. A.; Casida, J. E. Chloropyridinyl neonicotinoid insecticides: diverse molecular substituents contribute to facile metabolism in mice. *Chem. Res. Toxicol.* **2006**, *19*, 944−951.

JOURNAL OF AGRICULTURAL AND FOOD CHEMISTRY

Article

pubs.acs.org/JAFC

Effect of Lignin Content and Subunit Composition on Digestibility in Clones of Timothy (*Phleum pratense* L.)

Anna Kärkönen,*[,†] Tarja Tapanila,[‡] Tapio Laakso,[‡] Mervi M. Seppänen,[†] Mika Isolahti,[§] Maarit Hyrkäs,[∥] Perttu Virkajärvi,[∥] and Pekka Saranpää[‡]

[†]Department of Agricultural Sciences, University of Helsinki, FI-00014 Helsinki, Finland

[‡]Finnish Forest Research Institute, METLA, FI-01301 Vantaa, Finland

[§]Boreal Plant Breeding Ltd., FI-31600 Jokioinen, Finland

[∥]MTT Agrifood Research Finland, FI-71750 Maaninka, Finland

ABSTRACT: Lignin amount and subunit composition were analyzed from stems and leaf sheaths of timothy (*Phleum pratense* L.) clones of different in vitro digestibility. Lignin concentration in stems and leaf sheaths was higher in clones of low digestibility than those of high digestibility. No change in lignin concentration occurred in stems as digestibility decreased. Intriguingly, the lignin concentration was lower and the syringyl/guaiacyl (S/G) ratio was higher in stems compared to leaf sheaths at all developmental stages studied. The developmental-associated decrease in digestibility correlated with the increase in S units in lignin in stems and leaf sheaths and in the amounts of *p*-coumaric acid and ferulic acid residues in the cell wall of stems. Yields of copper oxidation products increased in stems during maturation indicating qualitative changes in the lignin structure. This correlated strongly with the developmentally linked decrease in digestibility. The information obtained is valuable for breeding and for DNA marker development.

KEYWORDS: *cell wall, digestibility, ferulic acid, lignin amount, lignin subunit composition, lignin linkage structure, timothy*

INTRODUCTION

Grass silage is an important source of metabolizable energy for milk and beef production in many countries, particularly in the temperate and cool zones of Europe and North America.[1] The main goal in forage production is to obtain high herbage mass that is of high nutritive value and digestibility. Plant cell wall polysaccharides cellulose and hemicellulose are of great importance for the energy content of silage. In grasses, lignin, a phenolic component in the cell wall, increases with increasing maturity, as the need for structural strength increases during stem elongation. This is accompanied by a decrease in digestibility.[2] Lignin provides rigidity and structural support to the cell wall polysaccharides, and it also excludes water from the wall. In grasses and cereals, cell walls of several parenchymatous cell layers in the cortex thicken and lignify during stem development, i.e., a sclerenchyma ring develops.[3−5]

In grasses and cereals lignin is composed of guaiacyl (G), syringyl (S), and *p*-hydroxyphenyl (H) units originating from coniferyl alcohol, sinapyl alcohol, and *p*-coumaryl alcohol, respectively.[6] In addition, cell walls of grasses contain hydroxycinnamic acids (*p*-coumaric and ferulic acid).[7−10] The monolignol biosynthetic pathway leading to lignin precursors is well-known.[11,12] Each gene of the pathway has been individually down-regulated, and the effects on plant growth, lignin amount, and composition have been assayed. Down-regulation of certain genes in the pathway has led to reduced lignin content and/or change in lignin composition and improved digestibility, for example, in cultivars of maize (*Zea mays*) and alfalfa (*Medicago sativa*).[2,11]

Accumulation of lignin reduces digestibility of cell wall polysaccharides as lignin makes them inaccessible to rumenal enzymes that would normally digest them. Di- and oligoferulate cross-links between ferulic acid units ester-linked to arabinoxylans and linkages between ferulates/di- and oligoferulates and lignin further impede enzymatic degradation of cell wall polysaccharides.[2,6,7,13,14] Several studies have shown that there is a negative relationship between the amount of lignin and digestion.[4,15−17] The effect of lignin subunit composition on digestibility, however, remains unclear. In many forage crops both the lignin content and its S/G ratio increase during development.[4,16] In the case of alfalfa, no clear relationship was shown between in vitro digestibility and the S/G ratio.[16] In addition, in maize, artificially produced lignins had similar inhibitory effects on cell wall degradation independently of their monolignol composition.[18] In maize plants the lignin interunit linkage pattern (with uncondensed *β*-O-4 units correlating with low cell wall digestibility) and S units acylated with *p*-coumaric acid had a greater impact on cell wall degradability than lignin subunit composition.[19]

Whereas much is known about the relationship between lignification and digestibility in other major forage grass species,[4,15,17] in the case of timothy (*Phleum pratense* L.) there is relatively little information about this relationship. Timothy is the most important perennial forage grass grown for silage and hay production in Scandinavia[20] and is also widely grown in other cool and humid regions in Europe, Asia, and North America.[21] Earlier studies have shown that both total and

Received: April 11, 2014
Revised: June 11, 2014
Accepted: June 13, 2014
Published: June 13, 2014

ACS Publications © 2014 American Chemical Society

Table 1. Sampling Dates and Corresponding Weather Parameters in 2008−2012

	2008	2011	2012
	expt I	expt II	expt II
plant material	Tammisto II	clonal material, Tammisto II	clonal material
analysis	comparison of different quantitative methods	lignin analyses, microscopy, IVOMD; Tammisto II for Klason lignin determination and for AcBr assay as a standard	determination of leaf sheath−stem proportions and IVOMD of stems and leaf sheaths separately, microscopy
fertilizer application date	May 8th for the first cut	May 17th for the first cut; July 7th for the second cut	May 8th for the first cut
sampling date	June 30th	June 11th−13th	June 18th
days from onset of growth period	64	48−50	43
GDD,[a] °C	381.0	308.9−322.7	302.7

[a]GDD = growing degree days, °C (base temperature, 5 °C).

acid-insoluble lignin increase during the development of timothy tillers.[15] Increase in acid-insoluble lignin, expressed as a percentage of total lignin, was more closely related to decreasing in vitro digestibility than that in total lignin. The increased portion of acid-insoluble lignin in total lignin suggests that the quality of lignin changed during plant maturation.[15] In addition, by using histochemical stains and biochemical tests, Stafford observed that the lignin in xylem vessels of timothy is different from that in the subepidermal sclerenchyma which develops later.[3] It is known that S units become more abundant in lignin at later developmental stages,[4,18] a phenomenon also detected by Quicke and Bentley as an increase in methoxyl groups in total lignin.[15]

Because the digestibility of grass is crucial in ruminant production, the biological processes controlling the digestibility of harvested forage are therefore of great importance. Changes of digestibility in the stem fraction (true stem and leaf sheath) of cool-season grasses during plant development are much larger than in leaf blades.[22−24] Furthermore, the contribution of the stem fraction to yield formation of harvested grass is high.[24,25] Therefore, in this study we focused on lignification in the stem fraction.

The aims of the present study were to compare different analytical methods to quantitate lignin in timothy and to evaluate how the lignin amount and the subunit composition affect the organic matter (OM) digestibility in timothy clones selected for either high or low OM digestibility. It is well-known that the developmental stage of the tiller and the leaf to stem (which includes leaf sheath) ratio affect both the lignin component and the digestibility of timothy.[26,27] Therefore, these factors were taken into account in the sampling procedure. In addition we carried out the lignin analyses of leaf sheaths and stems separately, as the leaf sheaths are botanically part of the leaf though typically analyzed within the stem fraction.[22,24,26,27]

MATERIALS AND METHODS

Plant Material. For comparing several methods for quantitative lignin analyses cultivar (cv.) Tammisto II was used (expt I; collected in 2008). In order to explore the role of lignin in determining the in vitro organic matter digestibility (IVOMD) of different genotypes, timothy clones that were characterized as having either low or high digestibility were used (expt II; years 2011−2012). The clones originated from the breeding material of Boreal Plant Breeding Ltd. (Jokioinen, Finland). Based on the results of a previous experiment, six clones were selected for each of the low- and the high-digestibility groups. The selection was done by taking account of the stem proportion of each clone in order to avoid selection for leafiness only.[23] Three clones were selected from each of the two groups for this study. Clones 50, 51, and 85 represented the high-IVOMD group, whereas clones 41 and 84, together with cv. Grindstad, represented the low-IVOMD group. The cultivar Grindstad was chosen as a control because it is a high-yielding variety that has a relatively low IVOMD value when cut at the same date as the other cultivars based on the Finnish cultivar testing system.[28] The sampling dates and corresponding weather parameters are presented in Table 1.

The plant material was cultivated on a coarse loamy soil (Aquic Cryorthent) at the Maaninka Research Station of MTT Agrifood Research Finland, Maaninka, Finland (63°08′ N, 27°19′ E). The clones were propagated vegetatively, and cv. Grindstad and cv. Tammisto II were propagated from seeds. The clonal tillers and cv. Grindstad were grown individually in cardboard boxes (3 cm × 3 cm) in commercial garden peat (Kekkilä White 630 W; Kekkilä Ltd., Vantaa, Finland) in an unheated greenhouse and planted on Sept. 27 and 28, 2010 in 10 cm × 12.5 cm grids on the field in microplots of 50 cm × 100 cm. The plots were fertilized with N 100, P 15, and K 25 kg ha^{-1} for the first cut and N 100, P 0, and K 35 kg ha^{-1} for the second cut. Cultivar Tammisto II was sown on May 26, 2005 in plots of 12 m^2 in the field, and the plots were fertilized for the first cut in year 2008 with N 90, P 13.5, and K 22.5 kg ha^{-1}. In 2011 fertilization was at the same rates as applied to the clone microplots. The dates of fertilizer application are given in Table 1. Both 2008 and 2011 were the third grass year for cv. Tammisto II plots.

The experimental layout of the clonal plots was a randomized block design with four replicates. Due to the limited amount of plant material, the tillers collected from blocks 1 and 2 were used for lignin analyses, and the tillers from the blocks 3 and 4 were used for IVOMD analysis. There were no blocks for cv. Tammisto II samples.

The tillers were collected at three developmental stages according to Simon and Park[29] (stage 45, boot swollen; stage 56, three-fourths of the inflorescence emerged; stage 58, base of the inflorescence just visible). The sampling time corresponded to the time of spring harvesting, except in 2008 when fully mature generative plants were collected for lignin quantitative analyses. Tillers were harvested by cutting with a razor blade immediately above the soil, and the height to the uppermost ligule was measured after which the leaves, leaf sheaths, stems, and heads were separated. For chemical analyses, leaf sheaths and stems of six tillers collected from the same block were separately pooled and stored at −20 °C until dried. Two sets of pooled samples (i.e., biological replicates) were collected from blocks 1 and 2.

At the same time, 18−25 tillers of each clone at developmental stages 45 and 58 (see preceding descriptions) were collected for IVOMD analysis from blocks 3 and 4. These tillers were pooled due to a limited amount of plant material. Leaves and heads were removed, and stems and leaf sheaths were kept together and dried in a forced draft oven at 60 °C (approximately 40 h). Dry weights were determined and the proportions of the dry matter per tiller calculated. In order to determine the organ portions in each clone at the developmental stages studied, leaves, leaf sheaths, stems, and heads were separated from 10 (stages 45 and 56) or 30 tillers (stage 58) in year 2012. Fractions were dried at 60 °C (approximately 40 h) and

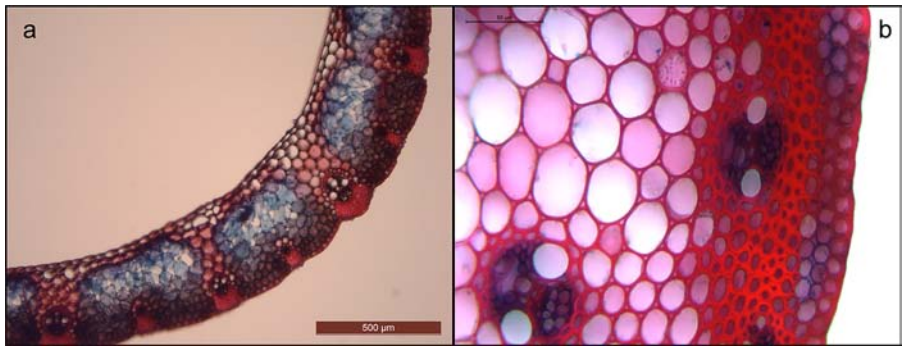

Figure 1. Cross-section of a timothy (a) leaf sheath and (b) stem stained with Alcian blue-Safranin O staining.

weighed. The proportions of leaf sheath and stem were determined by using dry weights.

Microscopy. The lignification stage of the tillers at each developmental stage was studied by microscopy. A sample (1 cm) was taken from the middle of the second lowest internode and fixed in a formalin (2%, v/v)−acetic acid (5%, v/v)−ethanol (63%, v/v) mixture (FAA). Hand-made or paraffin-embedded sections were made, and the developmental stage was observed after Alcian blue−Safranin O staining.[5]

Chemical Analyses. For lignin analyses plant material was dried in an oven at 60 °C and milled to a fine powder with a Retch ball mill (Retsch MM400, Haan, Germany; 50 mL grinding jars with one ball; stems, 4 × 30 s; leaf sheaths, (1−)2 × 30 s; frequency, 30 s^{-1}). To prevent warming of the samples during the milling, the grinding jars were cooled on carbon dioxide ice between samples. The extractive-free alcohol-insoluble residue (AIR) was obtained by extracting the powder for 8 times with 70% (v/v) ethanol in a water bath sonicator (25−30 °C; 30 min incubation in each extraction, with regular mixing) followed by 3 times with acetone. The tubes were centrifuged (4000 rpm, 10 min, at room temperature) before the solvent change. AIR was dried overnight at 60 °C and stored in firmly closed tubes in the dark at room temperature.

Since different quantitative methods for lignin determination are known to give different results,[30] we compared several methods by using AIR of cv. Tammisto II as a material (stems only, leaf sheaths removed). Permanganate lignin[31] was assayed in the MTT laboratory, and acid detergent lignin (ADL) by using the Foss Tecator Fibertec System M 1020 hot extractor and Fibertec System 1021 cold extractor, as described in Ordior Application Note AN 304, Ordior Application Sud Note ASN 3430 (AOAC-973.18) and USDA Forage Analyses Procedures, July 1993. Acid dioxane lignin was prepared as described.[32] Klason lignin was analyzed with a method commonly utilized by the Finnish Forest Research Institute.[33] For Klason lignin, the plant powder was sequentially extracted in a Soxhlet apparatus with acetone, ethanol, and water, 6 h each. The total nitrogen content of the Klason lignin was determined using a Leco CHN-1000 analyzer (St. Joseph, MI, USA), and the protein content calculated using the equation 6.25 × N%.[34]

Lignin content of timothy clones (stems and leaf sheaths separately; two pooled biological replicates) was analyzed with an acetyl bromide (AcBr) method[35] with modifications. Corresponding cv. Tammisto II samples of known Klason lignin content were used as standards. Briefly, 5 mg of AIR was transferred into a glass tube with a Teflon-coated lid. A 5 mL aliquot of AcBr reagent (20% AcBr (v/v) in glacial acetic acid without perchloric acid)[35] was added and the sample incubated at 50 °C for 3 h 15 min with regular mixing. The reaction was stopped in a −20 °C freezer for 15 min. An aliquot of 1.0 mL was transferred into a 10 mL volumetric flask containing 1 mL of 2 M NaOH and 2.4 mL of glacial acetic acid. After careful mixing, 0.1 mL of 7.5 M hydroxylamine−HCl was added. The volume was filled to 10 mL with acetic acid, and the absorbance at 280 nm was read with a Shimadzu UV-2401 spectrophotometer (Shimadzu Corp., Kyoto, Japan) against a blank that had been treated similarly to the samples.

Lignin subunit composition and *p*-hydroxycinnamic acid content in the cell wall of stems and leaf sheaths were studied by an alkaline cupric (II) oxidation method (CuO)[36] with modifications using AIR as a starting material. Oxidations were performed using a microwave digestion system MSD-2000 and a liquid phase hydrolysis accessory set (CEM Corp., Matthews, NC, USA). The gas chromatography−mass spectroscopy (GC-MS) detection of trimethylsilyl derivatives of CuO oxidation products was made using a HP 6890/HP 5972 (Hewlett-Packard, Palo Alto, CA, USA) equipped with a HP-5MS column (30 m; 0.25 mm i.d.; film thickness, 0.25 µm). The concentrations of individual compounds were calculated using response factors of commercially available standards. The internal standard, cinnamic acid, was added into the reaction vessel before microwave-assisted CuO treatment of samples. The method is time-consuming, and therefore the analysis was restricted to samples of one pooled biological replicate. Lignin subunit content was calculated as the percent of the corresponding total yield of CuO oxidation products, whereas *p*-coumaric acid and ferulic acid content was calculated as µmol g^{-1} AIR.

Digestibility Values. IVOMD (g kg^{-1} OM (cellulase))[37] with calculation of the results as described in Huhtanen et al.[38]), ash (g kg^{-1} dry matter (DM)), and neutral detergent fiber (NDF, g kg^{-1} DM) were assayed from the same clonal material (stems and leaf sheaths together) for the developmental stages 45 and 58 in the MTT laboratory. IVOMD was also determined separately for stems and leaf sheaths of clones at developmental stage 58 collected in 2012. Digestibility value (*D* value; g kg^{-1} DM) was calculated by (1000 − ash) × (IVOMD × 1000^{-1}).

Statistical Analyses. In order to study the relationship between measured IVOMD and the parameters obtained from lignin analyses, the lignin parameters were first calculated to correspond the same plant organs as the IVOMD analyses; i.e., we calculated weighted means for the whole stem (which includes leaf sheath; subsequently referred to as stem + leaf sheath) using original values of true stems and leaf sheaths separately, and their corresponding organic proportions that were determined in 2012 from the same plots. The generated weighted means for stem + leaf sheath were subjected to analysis of variance together with the original separate values for leaf sheath and stems.

Analysis of variance was performed using a mixed model with a residual maximum likelihood (REML) estimation method. In the model, the phenological stage, digestibility group, and their interaction were fixed effects, while clones were considered as a random effect. In the case of AcBr analyses with two biological replicates, the replicate was a random effect and the fixed effects were phenological stage and clone. Stage × clone interaction was not significant for any of the AcBr parameters, so it was not included in the model. The difference between digestibility groups was determined using contrast. The same model without a random effect was also used for the proportion of leaf sheaths and stems as there were no replicates. Pairwise comparisons between phenological stages were assessed by Tukey's test in all models. The MIXED procedure of SAS software (version 9.2; SAS Institute Inc., Cary, NC, USA).[39] The statistical dependences between IVOMD and other parameters were determined by Spearman's rank

correlation coefficient (r_s) using the CORR procedure of SAS software. Usage of r_s does not require the assumption of normality. Statistical significance was postulated at the 0.05 level of probability.

RESULTS AND DISCUSSION

Timothy clones of different in vitro digestibility were analyzed for lignin amount and subunit composition to evaluate their effects on digestibility. We separated leaf sheaths from stems before the analyses to assay the lignin in both organs separately. Timothy has a regular veining pattern in the leaf sheath that is an important support-giving structure for developing grass stems with intercalary meristems. Each vascular strand in the leaf sheath is accompanied by highly lignified sclerenchyma cells toward the adaxial epidermis (Figure 1a). The central area of the leaf sheath contains large, thin-walled cells that probably store water and are important for turgor-driven adjustment of the leaf sheath around the stem. In stems, xylem vessels in the vascular strands lignify first, followed by the sclerenchyma cells in and around the vascular strands (data not shown). The cell walls of the outer cortex cell layers also thicken and lignify during further development (Figure 1b).

Lignin Quantitative Analyses. Results obtained with various lignin quantitative methods differed (Figure 2), which is in accordance with a previous report.[30] Klason lignin and AcBr lignin (with acid dioxane standard) methods gave 3.5−6 times higher lignin concentrations than ADL, permanganate lignin, and acid dioxane lignin methods. Of the methods used, the ADL and Klason methods are gravimetric methods where cell wall carbohydrates are hydrolyzed with concentrated sulfuric acid, after which the residue that represents nonsoluble lignin is weighed. The acid-soluble part of the lignin is assayed from the solution and taken into account in the Klason estimate. The ADL procedure, which is based on the preparation of acid detergent fiber (ADF), however, underestimates the lignin content in grasses as a considerable amount of lignin (50% or more) is acid-soluble.[30] The S lignin, especially, is more soluble than other types of lignin during sulfuric acid hydrolysis.[32]

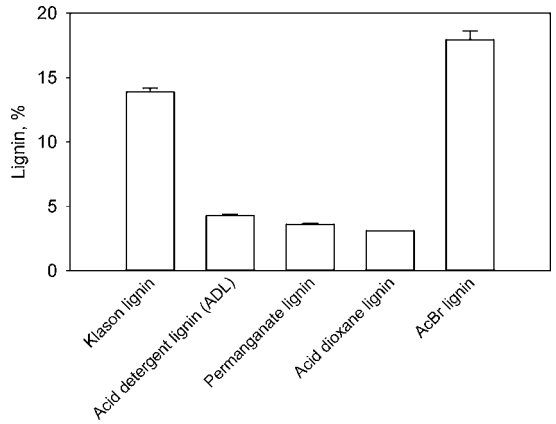

Figure 2. Lignin concentration (%) in stems of cv. Tammisto II as assayed by using several quantitative methods. AcBr = acetyl bromide. Error bars are standard errors of the means.

Timothy leaf sheaths were observed to contain more lignin than was present in stems. This occurred at all developmental stages studied, as calculated per mass unit of AIR, and was the case with AcBr lignin (Table 2) and Klason lignin (data not shown). The organ proportions (Table 2) were used to calculate the lignin concentration in stem + leaf sheath. Surprisingly, the phenological stage did not have any effect on the lignin concentration in AIR of stems, whereas that in AIR of leaf sheaths increased during development (Table 2). As the proportion of leaf sheaths decreased during development, however, the phenological stage had no effect on the calculated lignin concentration in AIR of stem + leaf sheath. The digestibility groups did not differ in the proportion of leaf sheaths but clones of low digestibility had higher lignin concentration both in AIR of stems and in AIR of leaf sheaths, and thus, also in the AIR of stem + leaf sheath (Table 2). This correlated negatively with IVOMD (Table 3). There were also some differences between individual clones in the lignin concentrations and also in the proportions of leaf sheaths (Table 2). The proportion of leaf sheaths did not, however, correlate with the IVOMD of the whole stem (stem that includes the leaf sheath; Table 3). The fact that the organ proportions were not determined in the same year as the samples for chemical analyses were collected may, however, weaken the relationship between plant organ proportions and chemical analyses.

Lignin Subunit Composition and Hydroxycinnamic Acids. Relatively mild oxidation with CuO induces cleavage of β-O-4 ether bonds in lignin;[36] thus, the subunit composition observed with this method originates from these noncondensed linkages. In timothy the abundance of S units in lignin increased during tiller development in both digestibility groups (Tables 4−6), correlating with the decrease in digestibility (Figure 3a; Table 3). In stems the S/G ratio was higher than in leaf sheaths at all developmental stages studied, suggesting that, in the case of timothy, the lignin subunit composition differs between stems and leaf sheaths (Tables 4 and 5). A similar difference in S/G ratio has been observed in leaf sheaths and stems of maize.[40] Interestingly, the relative increase in S units during development was higher in leaf sheaths than in stems of timothy. S units are able to form C−C bonds at the 8-position (β−β pinoresinol type structures), but they are unable to form C−C bonds in the 5-position due to methoxylation. Thus, an increase in S units observed during development suggests that the linkage structure in lignin changed. This conclusion is supported by the increased yields of CuO oxidation products obtained in stems at later developmental stages (Table 4) indicative of an increase in noncondensed β-O-4 bonds. There was, however, no developmental-related change in the yields of CuO oxidation products in leaf sheaths (Table 5) when both the lignin concentration (Table 2) and the proportion of S units increased. This indicates qualitative changes in lignin structure and possible cross-linking with carbohydrates.[40] The lower yields of CuO oxidation products obtained at earlier developmental stages from stems that contain higher relative proportions of S units than leaf sheaths, however, suggest that early in true-stem development the amount of β-O-4 linkages in stem lignin is less than in leaf-sheath lignin, but that during stem development S units are preferentially incorporated in these noncondensed linkages in stem lignin (Tables 4 and 5). Clones of low digestibility resulted in higher yields of CuO oxidation products in stem + leaf sheath than those of high digestibility (Table 6); furthermore, the increase in the yields CuO oxidation products strongly correlated with the decrease in digestibility during development (Figure 3b; Table 3).

Gramineous plants contain *p*-hydroxycinnamic acid residues esterified to arabinoxylan in the cell wall.[7,9,40] Ferulates can also be ether-linked to lignin. The ester-linked units can be released by saponification at room temperature whereas those residues

Table 2. Acetyl Bromide (AcBr) Lignin (Klason Standard) Concentration in Leaf Sheaths, Stems, and Stems + Leaf Sheaths (Calculated by Using the Proportions of These Organs in a Tiller As Determined from the Dry Weight) of Timothy Clones of High and Low Digestibility at Three Phenological Stages (Stage 45, Boot Swollen; Stage 56, Three-fourths of the Inflorescence Emerged; Stage 58, Base of the Inflorescence Just Visible)

digestibility group[a]	clone	lignin in leaf sheaths, g kg^{-1} AIR[b]	lignin in stems, g kg^{-1} AIR	lignin in stem + leaf sheath, g kg^{-1} AIR	proportion of leaf sheaths vs stems, %
high	clone 50	134	99	113	38
high	clone 51	124	95	108	44
high	clone 85	127	104	112	35
low	clone 41	140	111	123	42
low	clone 84	141	112	123	38
low	Grindstad	133	116	121	34
	SEM[c]	2.0	3.3	2.4	1.2
phenological stage					
45		130 a	104	114	40 b
56		132 a	110	119	39 ab
58		138 b	104	117	37 a
	SEM	1.4	2.4	1.9	0.9
high		128	100	111	39
low		138	113	122	38
P values	clone	<0.001	<0.001	<0.001	0.002
	phenological stage	<0.001	0.090	0.14	0.037
contrast	low−high	9.7	13.1	11.6	−0.7
P value		<0.001	<0.001	<0.001	0.47

[a]In relation to stem proportion. [b]Alcohol-insoluble residue. [c]Standard error of the mean. Values marked with the same letter do not differ (Tukey's test).

Table 3. Correlations between in Vitro Organic Matter Digestibility (IVOMD) and Other Parameters in Stems + Leaf Sheaths of Timothy Clones of Different Digestibility

	IVOMD, g kg^{-1} OM	
	r_s[a]	*P* value
proportion of leaf sheaths vs stems, %	0.48	0.11
stem height, cm	−0.90	<0.001
NDF, g kg^{-1} DM	−0.94	<0.001
AcBr lignin, g kg^{-1} AIR[b]	−0.59	0.042
total S units, %	−0.72	0.008
total G units, %	0.68	0.015
total P units, %	0.76	0.004
S/G	−0.58	0.048
p-coumaric acid, μmol g^{-1} AIR	−0.65	0.022
ferulic acid, μmol g^{-1} AIR	−0.77	0.003
total CuO oxidation products, mg g^{-1} AIR	−0.94	<0.001

[a]Spearman's rank correlation coefficient. [b]Alcohol-insoluble residue.

that are etherified to lignin can be released by high-temperature alkali treatment.[7] While being esterified to carbohydrates and etherified to lignin, ferulates make bridges between carbohydrates and lignin; these enhance the mechanical properties of the lignified cell walls and also contribute to digestibility decrease.[9,14] Ferulic and *p*-coumaric acid contents were higher in timothy stems than in leaf sheaths (Tables 4 and 5). The amount of ferulic acid in timothy cell walls increased during development in stems, and thus in stem + leaf sheath (Tables 4−6), correlating negatively with digestibility (Figure 3d; Table 3). This observation suggests that ferulates were continuously incorporated into the cell wall of stems leading to formation of di- and oligoferulate bridges as well as carbohydrate−lignin complexes.[14] Also, *p*-coumarate is associated with lignins, mainly esterified to S units.[14,41] In timothy, the level of cell wall-located *p*-coumaric acid rose slightly (ca. 1.1 times) in stems during development when S units increased (Table 4), suggesting that *p*-coumarates were at least partly coupled to S units. In leaf sheaths, however, no change in *p*-coumarate or ferulate concentration occurred during maturation (Table 5). This observation is interesting as ferulate cross-linking often correlates with reduced digestibility.[9,14] In maize, the concentrations of both ferulate esters and ferulate ethers increase between immature and mature (silage stage maturity) samples in both stems and leaf sheaths.[40] We do not know whether there are differences in the CuO procedure in the effectiveness of releasing of the hydroxycinnamic acids from the AIR of leaf sheaths and stems. However, none of the methods presently used in lignin analyses gives the absolute amounts of lignin subunits. The observation that the CuO method used in the present study gave repeatable results with different plant organs (leaf sheaths and stems, respectively) justifies making comparisons between these organs and the developmental stages. The results indicate that the ferulic acid content alone, and the cross-linking to arabinoxylans do not explain the differences observed in the digestibility of stems and leaf sheaths. A pronounced difference exists in cell wall-located *p*-coumarates in stems of timothy, a C3 plant, and maize, a C4 plant, because in maize stem the amount of *p*-coumarate esters increase by 2.6-fold during maturation,[40] whereas in maize leaf sheaths the situation is similar to that of timothy (1.2-fold increase in maize; no change in timothy). *p*-Coumarates in lignin are known to exist as terminal pendant groups; thus, the growth of the lignin polymer is restricted after incorporation of *p*-coumarylated S units.[6]

Table 4. Lignin Subunit Composition and the Concentration of Hydroxycinnamic Acids in Stems of Timothy Clones of High and Low Digestibility at Three Phenological Stages (Stage 45, Boot Swollen; Stage 56, Three-fourths of the Inflorescence Emerged; Stage 58, Base of the Inflorescence Just Visible) As Determined by the CuO Method

digestibility group[a]	phenological stage	total S units, %	total G units, %	total P units, %	S/G	*p*-coumaric acid, μmol g^{-1} AIR[b]	ferulic acid, μmol g^{-1} AIR	CuO oxidation products, mg g^{-1} AIR
	45	58 a	37	4.8 b	1.5	48 a	57 a	17 a
	56	60 ab	36	4.6 b	1.7	46 a	52 a	21 b
	58	62 b	35	3.2 a	1.8	54 a	89 b	26 c
SEM[c]		0.9	0.8	0.28	*d*	2.5	3.3	1.1
high		60	35	4.5	1.7	47	65	19
low		59	37	3.9	1.6	52	67	23
SEM		0.8	0.8	0.26	–	2.8	2.7	1.3
P values	phenological stage	0.040	0.108	0.005	0.086	0.049	<0.001	<0.001
	digestibility group	0.32	0.22	0.18	0.26	0.27	0.55	0.064
	stage × group	0.50	0.44	0.79	0.46	1.00	0.53	0.51

[a]In relation to stem proportion. [b]Alcohol-insoluble residue. [c]Standard error of the mean. [d]Logarithmic tranformation used; SEM not presented. Values marked with the same letter do not differ (Tukey's test).

Table 5. Lignin Subunit Composition and the Concentration of Hydroxycinnamic Acids in Leaf Sheaths of Timothy Clones of High and Low Digestibility at Three Phenological Stages (Stage 45, Boot Swollen; Stage 56, Three-fourths of the Inflorescence Emerged; Stage 58, Base of the Inflorescence Just Visible) As Determined by the CuO Method

digestibility group[a]	phenological stage	total S units, %	total G units, %	total P units, %	S/G	*p*-coumaric acid, μmol g^{-1} AIR[b]	ferulic acid, μmol g^{-1} AIR	CuO oxidation products, mg g^{-1} AIR
	45	43 a	52 b	4.5	0.8 a	35	43	23
	56	50 b	45 a	4.7	1.1 b	31	33	24
	58	54 b	42 a	3.8	1.3 b	34	43	25
SEM[c]		1.3	1.5	0.37	0.05	2.0	3.6	1.0
high		50	46	4.7	1.1	36	42	23
low		49	47	4.1	1.0	31	38	26
SEM		1.1	1.2	0.40	0.04	2.3	3.5	1.0
P values	phenological stage	<0.001	0.001	0.14	<0.001	0.22	0.099	0.21
	digestibility group	0.45	0.32	0.35	0.20	0.18	0.48	0.098
	stage × group	0.57	0.65	0.97	0.45	0.87	0.93	0.90

[a]In relation to stem proportion. [b]Alcohol-insoluble residue. [c]Standard error of the mean. Values marked with the same letter do not differ (Tukey's test).

Digestibility Values. The effect of the phenological stage was evident for tiller dry weight, stem height, NDF, IVOMD, and *D* value of the stem (including leaf sheath) in the clonal material (Table 7). The clones of the high-digestibility group had lower NDF and higher IVOMD and *D* values. The differences between digestibility groups in IVOMD and *D* value were more evident at the later development stage 58 than at the earlier stage 45. Surprisingly, similar interaction (stage × group) was not found in the lignin subunit composition analysis (Table 6). In general the measured NDF values of the stem fraction were similar to those of early and late maturing timothy cultivars[22] and logically higher than determined for the total DM yield of timothy.[27] Furthermore, the observed IVOMD in stems including leaf sheaths were markedly higher than in the results given by Nissinen and co-workers[24] even for stage 58 tillers of the low-digestibility group. The NDF concentration and stem height correlated strongly with the decrease in IVOMD (Table 3) referring to the role of fiber fraction (NDF) as mechanical support needed for higher stems.

There were clear differences in the lignin concentration and its subunit composition in stems and leaf sheaths of timothy clones. Unfortunately, in the IVOMD analyses these plant parts were not separated. When IVOMD was analyzed separately in stems and leaf sheaths for the clonal material collected in the following year (2012) from the same plots at stage 58, the leaf sheaths had lower digestibility (663 vs 650 g kg^{-1} DM, P = 0.020) and higher ADL lignin concentration (53 vs 62 g kg^{-1} DM, P = 0.020) than stems. Similarly, in cv. Tammisto II collected in 2011, the leaf sheaths had lower digestibility than stems (data not shown). This is probably due to higher lignin concentration in leaf sheaths than in stems. However, the yields of CuO oxidation products obtained from leaf sheaths at all developmental stages studied were approximately at the same level as in stems at stage 58, when digestibility had already decreased (Tables 4, 5, and 7). This finding suggests that lignin linkage structure in leaf sheaths is not optimal for digestion even at an early development stage.

Table 6. Lignin Subunit Composition and the Concentration of Hydroxycinnamic Acids in Stems + Leaf Sheaths of Timothy Clones of High and Low Digestibility at Three Phenological Stages (Stage 45, Boot Swollen; Stage 56, Three-fourths of the Inflorescence Emerged; Stage 58, Base of the Inflorescence Just Visible) As Determined by the CuO Method

digestibility group[a]	phenological stage	total S units, %	total G units, %	total P units, %	S/G	*p*-coumaric acid, μmol g^{-1} AIR[b]	ferulic acid, μmol g^{-1} AIR	CuO oxidation products, mg g^{-1} AIR
	45	52 a	44 b	4.6 b	1.3 a	43 ab	52 a	19 a
	56	56 b	39 a	4.6 b	1.5 b	41 a	45 a	22 b
	58	59 b	38 a	3.4 a	1.6 b	46 b	72 b	26 c
SEM[c]		0.8	0.8	0.22	0.05	1.6	2.3	0.8
high		56	39	4.5	1.5	43	56	20
low		55	41	3.9	1.4	44	57	24
SEM		0.7	0.7	0.23	0.04	1.7	2.1	0.8
P values	phenological stage	<0.001	<0.001	0.003	<0.001	0.042	<0.001	<0.001
	digestibility group	0.30	0.099	0.13	0.090	0.59	0.85	0.021
	stage × group	0.47	0.52	0.76	0.32	0.92	0.50	0.76

[a]In relation to stem proportion. [b]Alcohol-insoluble residue. [c]Standard error of the mean. Values marked with the same letter do not differ (Tukey's test).

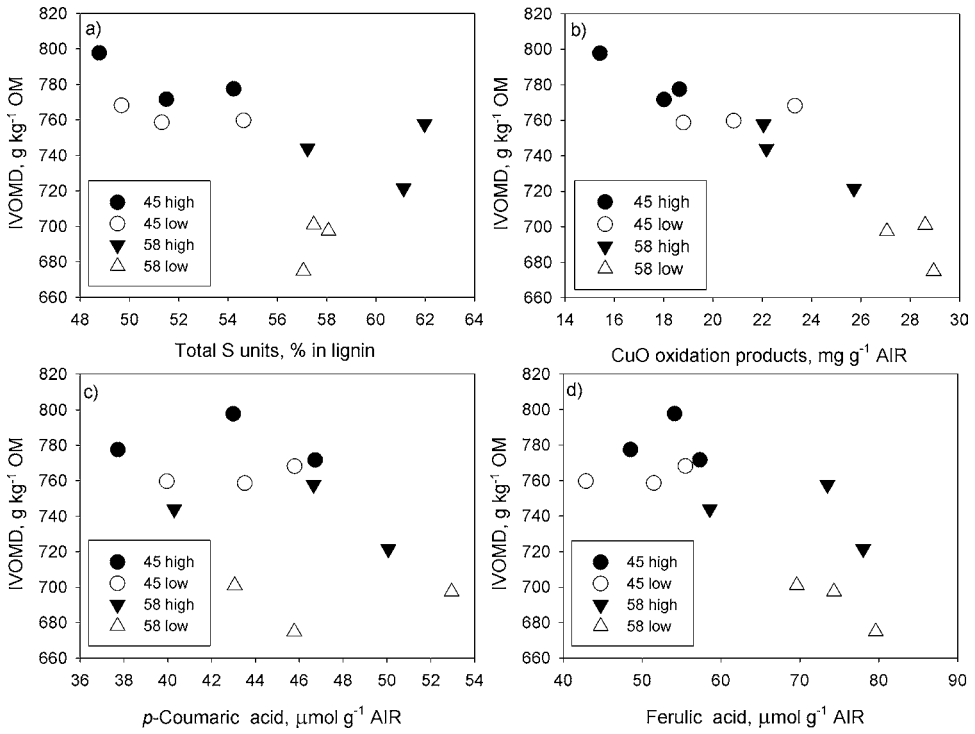

Figure 3. Relations between IVOMD (g kg^{-1} OM) and (a) amount of S units in lignin, (b) total yield of CuO oxidation products, (c) *p*-coumaric acid concentration, and (d) ferulic acid concentration in stems + leaf sheaths at different phenological stages (stage 45, boot swollen; stage 58, base of the inflorescence just visible) in high- and low-digestibility groups of timothy.

Summary. Lignin concentration in cell walls of timothy is the factor that explains the digestibility difference between clones of low and high digestibility. The developmental-associated decrease in digestibility correlates with the change in lignin subunit composition, and especially with the change in lignin linkage structure as shown by the increase in the yields of CuO oxidation products indicative of noncondensed β-O-4 linkages. In addition, the increase in the content of cell wall-located hydroxycinnamates contributes to the digestibility decrease during maturation. The difference in the lignin amount and the subunit composition between stems and leaf sheaths is interesting, as leaf sheaths have lower digestibility than stems. This is probably due to the fact that leaf sheaths contain more lignin than stems, but the lignin linkage structure may also contribute to this. Interestingly, there are less cell wall-bound hydroxycinnamic acids in leaf sheaths compared with stems. Considering that leaf sheaths, which consist of ca. one-third of the whole stem (stem including leaf sheath), are less digestible than stems, some goals in the future breeding efforts of timothy could include a reduction of the leaf-sheath proportion in the yield or a targeted lowering of the lignin concentration in leaf sheaths to the level of that in stems. It should be noted, however, that cell wall composition (lignin among other factors) in leaf sheaths is important in resistance

dx.doi.org/10.1021/jf5016494 | J. Agric. Food Chem. 2014, 62, 6091−6099

Table 7. Tiller Dry Weight, Stem Height and Contents of Neutral Detergent Fiber (NDF), in Vitro Organic Matter Digestibility (IVOMD), and Digestibility (*D*) Value of Timothy Clones (Stem Including Leaf Sheath) of High and Low Digestibility at Two Phenological Stages (Stage 45, Boot Swollen; Stage 58, Base of the Inflorescence Just Visible)

digestibility group[a]	phenological stage	tiller dry weight, mg tiller^{-1}	stem height, cm	NDF, g kg^{-1} DM	IVOMD, g kg^{-1} OM	*D* value, g kg^{-1} DM
high	45	382	35	641	782	724
low	45	296	36	660	762	703
high	58	606	47	670	741	686
low	58	652	52	695	691	640
SEM[b]		38.1	1.8	3.6	7.9	7.4
P values	phenological stage	<0.001	<0.001	<0.001	<0.001	<0.001
	digestibility group	0.67	0.22	<0.001	0.026	0.024
	stage × group	0.107	0.17	0.41	0.031	0.045

[a]In relation to stem proportion. [b]Standard error of the mean.

toward insects and diseases,[42] and against lodging, so the effects of the lignin decrease need to be evaluated in ways that also consider these aspects.

AUTHOR INFORMATION

Corresponding Author

*Tel.: +358 29 4157662. Fax: +358 29 4158727. E-mail: anna.karkonen@helsinki.fi.

Funding

This work was funded by the Ministry of Agriculture and Forestry (NurMI), MTT Agrifood Research Finland, Niemi Foundation, and Valio.

Notes

The authors declare no competing financial interest.

ACKNOWLEDGMENTS

We thank I. Luovula, L. Sarelainen, A. Leinonen, P. Korhonen, E. Oja, and V. Alonso Pablos for their skillful assistance in lignin analyses and microscopy. We also thank O. Haapala, T. Jalava, and P. Kiuru in MTT laboratories for lignin and digestibility analyses and J. Kanninen, M. Laasonen, and P. Issakainen for their assistance with field experiments.

ABBREVIATIONS USED

AcBr, acetyl bromide; ADL, acid detergent lignin; AIR, alcohol-insoluble residue; CuO, alkaline cupric (II) oxidation method; *D* value, digestibility value; DM, dry matter; G, guaiacyl unit; H, *p*-hydroxyphenyl unit; IVOMD, in vitro organic matter digestibility; NDF, neutral detergent fiber; OM, organic matter; S, syringyl unit; *S*/*G*, syringyl/guaiacyl ratio

REFERENCES

(1) Wilkinson, J. M.; Toivonen, M. I. *World silage: A survey of forage conservation around the world*; Chalcombe: Lincoln, U.K., 2003; pp 1−29.

(2) Jung, H.-J. G.; Samac, D.; Sarath, G. Modifying crops to increase cell wall digestibility. *Plant Sci.* **2012**, *185*−*186*, 65−77.

(3) Stafford, H. A. Histochemical & biochemical differences between lignin-like materials in *Phleum pretense* L. *Plant Physiol.* **1962**, *37*, 643−649.

(4) Chen, L.; Auh, C.; Chen, F.; Cheng, X.; Aljoe, H.; Dixon, R. A.; Wang, Z. Lignin deposition and associated changes in anatomy, enzyme activity, gene expression, and ruminal degradability in stems of tall fescue at differential developmental stages. *J. Agric. Food Chem.* **2002**, *50*, 5558−5565.

(5) Seppänen, M. M.; Pakarinen, K.; Jokela, V.; Andersen, J. R.; Fiil, A.; Santanen, A.; Virkajärvi, P. Vernalization response of *Phleum pratense* and its relationships to stem lignification and floral transition. *Ann. Bot.* **2010**, *106*, 697−707.

(6) Ralph, J. Hydroxycinnamates in lignification. *Phytochem. Rev.* **2010**, *9*, 65−83.

(7) Iiyama, K.; Lam, T. B. T.; Stone, B. A. Phenolic acid bridges between polysaccharides and lignin in wheat internodes. *Phytochemistry* **1990**, *29*, 733−737.

(8) Fry, S. C. Oxidative coupling of tyrosine and ferulic acid residues: Intra- and extra-protoplasmic occurrence, predominance of trimers and larger products, and possible role in inter-polymeric cross-linking. *Phytochem. Rev.* **2004**, *3*, 97−111.

(9) Buanafina, M. M. de O. Feruloylation in grasses: current and future perspectives. *Mol. Plant* **2009**, *2*, 861−872.

(10) Harris, P. J.; Trethewey, J. A. K. The distribution of ester-linked ferulic acid in the cell walls of angiosperms. *Phytochem. Rev.* **2010**, *9*, 19−33.

(11) Li, X.; Weng, J. K.; Chapple, C. Improvement of biomass through lignin modification. *Plant J.* **2008**, *54*, 569−581.

(12) Vanholme, R.; Demedts, B.; Morreel, K.; Ralph, J.; Boerjan, W. Lignin biosynthesis and structure. *Plant Physiol.* **2010**, *153*, 895−905.

(13) Grabber, J. H.; Hatfield, R. D.; Ralph, J. Diferulate cross-links impede the enzymatic degradation of non-lignified maize walls. *J. Sci. Food Agric.* **1998**, *77*, 193−200.

(14) Koshijima, T.; Watanabe, T. *Association between lignin and carbohydrates in wood and other plant tissues*; Springer Verlag: Berlin, Heidelberg, 2003; 329 pp.

(15) Quicke, G. V.; Bentley, O. G. Lignin and methoxyl groups as related to the decreased digestibility of mature forages. *J. Anim. Sci.* **1959**, *18*, 365−373.

(16) Reddy, M. S. S.; Chen, F.; Shadle, G.; Jackson, L.; Aljoe, H.; Dixon, R. A. Targeted down-regulation of cytochrome P450 enzymes for forage quality improvement in alfalfa (*Medicago sativa* L.). *Proc. Natl. Acad. Sci. U. S. A.* **2005**, *102*, 16573−16578.

(17) Casler, M. D.; Jung, H. G.; Coblenz, W. K. Clonal selection for lignin and etherified ferulates in three perennial grasses. *Crop Sci.* **2008**, *48*, 424−433.

(18) Grabber, J. H.; Ralph, J.; Hatfield, R. D.; Quideau, S. *p*-Hydroxyphenyl, guaiacyl, and syringyl lignins have similar inhibitory effects on wall degradability. *J. Sci. Food Agric.* **1997**, *45*, 2530−2532.

(19) Zhang, Y.; Culhaoglu, T.; Pollet, B.; Melin, C.; Denoue, D.; Barrière, Y.; Baumberger, S.; Méchin, V. Impact of lignin structure and cell wall reticulation on maize cell wall degradability. *J. Agric. Food Chem.* **2011**, *59*, 10129−10135.

(20) Höglind, M.; Hanslin, H. M.; Van Oijen, M. Timothy regrowth, tillering and leaf area dynamics following spring harvest at two growth stages. *Field Crops Res.* **2005**, *93*, 51−63.

(21) Bélanger, G.; Tremblay, G. F; Michaud, R. The nutritive value of timothy and its improvement through management and breeding. In *Timothy productivity and forage quality*, Nordiske Jordbrugsforskers Forening (Nordic Association of Agricultural Scientists) Seminar 384; Sveinsson, T., Ed.; Agricultural University of Iceland: Akureyri, Iceland, 2006; pp 15−25.

(22) Bélanger, G.; McQueen, R. E. Leaf and stem nutritive of timothy cultivars differing in maturity. *Can. J. Plant Sci.* **1997**, *77*, 237−245.
(23) Wilkins, P. W.; Humphreys, M. O. Progress in breeding perennial forage grasses for temperate agriculture. *J. Agric. Sci.* **2003**, *140*, 129−150.
(24) Nissinen, O.; Kalliainen, P.; Jauhiainen, L. Development of yield and nutritive value of timothy in primary growth and regrowth in northern growing conditions. *Agric. Food Sci.* **2010**, *19*, 252−268.
(25) Virkajärvi, P.; Pakarinen, K.; Hyrkäs, M.; Seppänen, M.; Bélanger, G. Tiller characteristics of timothy and tall fescue in relation to herbage mass accumulation. *Crop Sci.* **2012**, *52*, 970−980.
(26) Gustavsson, A. M.; Martinsson, K. Seasonal variation in biochemical composition of cell walls, digestibility, morphology, growth and phenology in timothy. *Eur. J. Agron.* **2004**, *20*, 293−312.
(27) Kuoppala, K.; Rinne, M.; Nousiainen, J.; Huhtanen, P. The effect of cutting time of grass silage in primary growth and regrowth and the interactions between silage quality and concentrate level on milk production of dairy cows. *Livest. Sci.* **2008**, *116*, 171−182.
(28) Laine, A.; Högnäsbacka, M.; Kujala, M.; Niskanen, M.; Jauhiainen, L.; Nikander, H. *Results of official variety trials 2006−2013*, MTT report 12; MTT Agrifood Research Finland: Jokioinen, Finland, 2014; 238 pp (in Finnish with tables in English).
(29) Simon, U.; Park, B. H. A descriptive scheme for stages of development in perennial forage grasses. In *Proceedings of the 14th international grassland congress*, Lexington, KY, USA; Smith, J. A., Hays, V. W., Eds.; Westview Press: Boulder, CO, USA, 1981; pp 416−418.
(30) Hatfield, R.; Fukushima, R. S. Can lignin be accurately measured? *Crop Sci.* **2005**, *45*, 832−839.
(31) Robertson, J. B.; Van Soest, P. J. The detergent system of analysis and its application to human foods. In *The analyses of dietary fibre in foods*; James, W. D. T., Theander, O., Eds.; Marcel Dekker: New York, NY, USA, 1981; pp 123−158.
(32) Fukushima, R. S.; Hatfield, R. D. Comparison of the acetyl bromide spectrophotometric method with other analytical methods for determining lignin concentration in forage samples. *J. Agric. Food Chem.* **2004**, *52*, 3713−3720.
(33) Raiskila, S.; Pulkkinen, M.; Laakso, T.; Fagerstedt, K.; Löija, M.; Mahlberg, R.; Paajanen, L.; Ritschkoff, A.-C.; Saranpää, P. FTIR spectroscopic prediction of Klason and acid soluble lignin variation in Norway spruce cutting clones. *Silva Fennica* **2007**, *41*, 351−371.
(34) Allen, S. E., Ed. *Chemical Analysis of Ecological Materials*, 2nd ed.; Blackwell: Oxford, England, 1989; p 179.
(35) Hatfield, R. D.; Grabber, J.; Ralph, J.; Brei, K. Using the acetyl bromide assay to determine lignin concentrations in herbaceous plants: Some cautionary notes. *J. Agric. Food Chem.* **1999**, *47*, 628−632.
(36) Goñi, M. A.; Montgomery, S. Alkaline CuO oxidation with microwave digestion system: Lignin analyses of geochemical samples. *Anal. Chem.* **2000**, *72*, 3116−3121.
(37) Nousiainen, J.; Rinne, M.; Hellämäki, M.; Huhtanen, P. Prediction of the digestibility of the primary growth of grass silages harvested at different stages of maturity from chemical composition and pepsin-cellulase solubility. *Anim. Feed Sci. Technol.* **2003**, *103*, 97−111.
(38) Huhtanen, P.; Nousiainen, J.; Rinne, M. Recent developments in forage evaluation with special reference to practical applications. *Agric. Food Sci.* **2006**, *15*, 293−323.
(39) Littell, R. C.; Milliken, G. A.; Stroup, W. W.; Wolfinger, R. D. *SAS system for mixed models.*; SAS Institute: Cary, NC, USA, 1996; 633 pp.
(40) Jung, H. G.; Phillips, R. L. Putative seedling ferulate ester (*sfe*) maize mutant: Morphology, biomass yield, and stover cell wall composition and rumen degradability. *Crop Sci.* **2010**, *50*, 403−418.
(41) Hatfield, R. D.; Marita, J. M. Enzymatic processes involved in the incorporation of hydroxycinnamates into grass cell walls. *Phytochem. Rev.* **2010**, *9*, 35−45.
(42) Santiago, R.; Barros-Rios, J.; Malvar, R. A. Impact of cell wall composition on maize resistance to pests and diseases. *Int. J. Mol. Sci.* **2013**, *14*, 6960−6980.

JOURNAL OF AGRICULTURAL AND FOOD CHEMISTRY

Article

pubs.acs.org/JAFC

Determination of Trace Acrylamide in Starchy Foodstuffs by HPLC Using a Novel Mixed-Mode Functionalized Calixarene Sorbent for Solid-Phase Extraction Cleanup

Wenfen Zhang,[†] Zhifen Deng,[†] Wenjie Zhao,*[,§] Ling Guo,[†] Wei Tang,[†] Huifang Du,[†] Lin Lin,[†] Qiong Jiang,[†] Ajuan Yu,[†] Lijun He,[§] and Shusheng Zhang*[,†]

[†]College of Chemistry and Molecular Engineering, Zhengzhou University, Zhengzhou 450001, People's Republic of China

[§]School of Chemistry and Chemical Engineering, Henan University of Technology, Zhengzhou 450001, People's Republic of China

ABSTRACT: In this paper, a rapid and effective HPLC method, using tetraazacalix[2]arene[2]triazine-modified silica gel (NCSi) as solid-phase extraction (SPE) sorbent, was developed for the purification and determination of trace acrylamide in starchy foodstuffs. The main influence factors of SPE including amount of NCSi sorbent, sample flow rate, and volume and composition of washing solution were investigated and evaluated in the sample pretreatment step. The optimized purification effect was achieved at the sample flow rate of 3 mL/min with 100 mg of NCSi and 2 mL of washing solution (water, 100%). The HPLC separation was carried out on a C18 column (250 × 4.6 mm i.d., 5 μm) with a mobile phase of methanol/water (10:90, v/v). The linear range of the calibration curve was 4−4000 ng/mL with s correlation coefficient of >0.9999. The intraday and interday RSDs (n = 5) of peak areas of acrylamide were 0.22 and 0.90% and the intraday and interday RSDs (n = 5) of retention times were 0.50 and 1.63%, respectively. In addition, overall recoveries through the extraction and NCSi-SPE purification ranged from 73.13 to 98%. Compared with the commercial SPE sorbents, NCSi featured excellent selectivity to retain polar and nonpolar interferences in the sample matrices. The improved method was simple, rapid, accurate, and promising for the determination of trace acrylamide in starchy foods with a complex matrix.

KEYWORDS: *tetraazacalix[2]arene[2]triazine-modified silica gel, SPE purification, HPLC, acrylamide, starchy foodstuffs*

INTRODUCTION

Acrylamide, a colorless and odorless crystalline powder, is known to be formed by the Maillard reaction during heating of starchy foodstuffs. In April 2002, the Swedish National Food Administration (NFA) and researchers from Stockholm University found high acrylamide levels in carbohydrate-rich foodstuffs fried/baked at high temperatures.[1] In recent years, research on acrylamide in different matrices has attracted extensive attention due to its demonstrated neurotoxicity, genotoxicity, and potential human carcinogenicity.[2]

In past years, a number of chromatographic methods have been developed to determine acrylamide such as gas chromatography (GC) with derivatization and high-performance liquid chromatography (HPLC) without derivatization.[3,4] Nowadays, most analytical methods are based on GC-MS and LC-MS/MS,[5−20] which appear to be acknowledged as the most useful and authoritative methods for the quantification of acrylamide in complex matrices. However, both GC-MS and LC-MS are high-cost and cannot be easily adopted by nonspecialized laboratories. On the contrary, HPLC with UV detection possesses the advantages of simplicity, lower cost, and strong maneuverability compared to MS techniques. Meanwhile, it is noteworthy that the matrix effect is a serious problem in the trace analysis of acrylamide in complex matrices such as chips and coffee,[7,12,13] which make quantification and identification difficult. Therefore, removal of the matrix effect and sample pretreatment are of great importance in trace analysis.

For the cleanup of acrylamide from complex samples, accelerated solvent extraction (ASE), liquid−liquid extraction (LLE), and solid-phase extraction (SPE), alone or in combination with other purification steps, were conducted by many laboratories. ASE and LLE with conventional organic solvent are time-consuming and labor-intensive. Furthermore, they can easily lead to loss of acrylamide in the scavenging process and require large amounts of toxic solvents. To overcome these shortcomings, SPE has been developed and applied in the cleanup of acrylamide in coffee and coffee products,[21,22] potato chips,[23] and so on. As acrylamide is a small, polar, and hydrophilic molecule, a large amount of matrix interferences tends to be extracted simultaneously with acrylamide, which makes it difficult for analysis using a single conventional SPE method employing reversed-phase (RP) or ion-exchange sorbents. With the aim of solving this problem, multiple retention mechanism cleanup procedures were developed. However, most of them consist of the combination of several SPE cartridges. Bortolomeazzi et al.[21] used a single SPE column consisting of 0.5 g of an in-house-prepared mixture of C18, strong cation (SCX), and anion exchange (SAX) sorbents in the ratio 2/1.5/1.5 (w/w/w) to extract and clean up roasted coffee samples.[24] Becalski et al. used a combination of three different cartridges including Oasis MAX (mixed mode

Received: April 2, 2014
Revised: June 9, 2014
Accepted: June 16, 2014
Published: June 16, 2014

ACS Publications © 2014 American Chemical Society

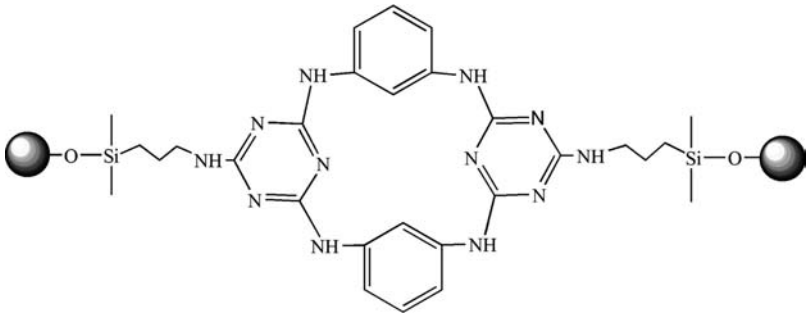

Figure 1. Chemical structure of the NCS stationary phase.[36]

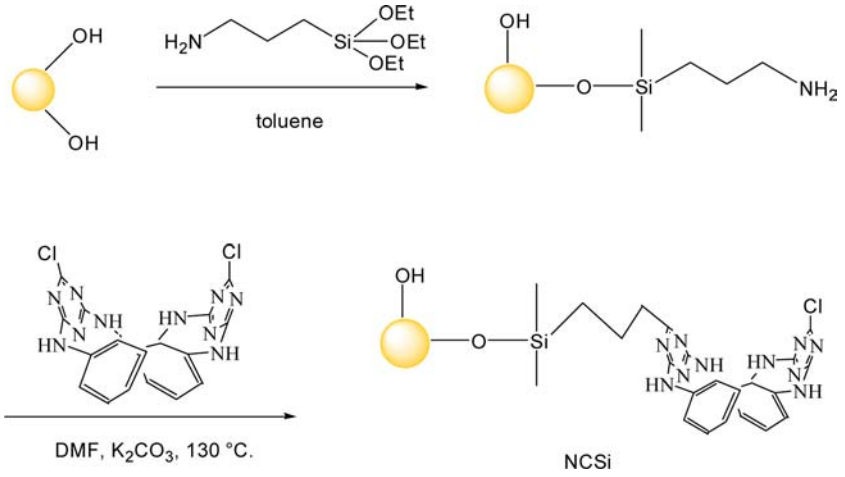

Figure 2. Synthesis of NCSi sorbent.

anion exchange), Oasis MCX (mixed-mode cation exchange), and ENVI-Carb (graphitized carbon) to treat various samples (potato fries, potato chips, crispbread, instant coffee, coffee beans, cocoa, chocolate, and peanut butter). A similar combination of SPE cartridges consisting of Bond Elut C18, Bond Elut Jr-PSA (anion exchange), and Bond Elut Accucat was chosen for cleanup samples.[24] However, these different SPE combination modes make the purification process cumbersome and expensive and even lead to loss of acrylamide in the cleanup process. Therefore, it is necessary to design a novel SPE sorbent with a multiple retention mechanism for the cleanup of acrylamide from complex sample matrices.

Calixarenes, following cyclodextrins and crown ethers, are considered to be a typical representative of the third generation of host supramolecules. They consist of phenol units linked via methylene bridges and can also form inclusion complexes like other host supramolecules. There are a number of selective factors in the configuration of calixarenes such as cavity size, conformation, and substituents. Since Glennon and his co-workers reported the application of calixarenes as the stationary phase, it has attracted extensive attention.[25−27] Our group has been comitted to the research of calixarene stationary phases for many years,[28−31] and a novel multi-interaction and mixed-mode stationary phase based on tetraazacalix[2]arene[2]-triazine modified silica gel (NCS, Figure 1) has been synthesized in our laboratory in 2012.[32] Being different from conventional calixarenes in which the aromatic rings are linked by methylene units, tetraazacalix[2]arene[2]triazine assembles aromatic rings by −NH− and adopts a 1,3-alternate conformation with two benzene rings nearly face-to-face parallel and two triazine rings tending to an edge-to-edge orientation in the solid phase. Our previous work indicated that the NCS exhibited high selectivity toward various compounds under different conditions with different mechanisms including hydrophobicity, $\pi-\pi$ stacking, hydrogen-bonding, inclusion, and anion-exchange interactions. A nNumber of compounds, including polycyclic aromatic hydrocarbons, nitrobenzene, organic bases, phenols, and inorganic anions, have been well separated on the NCS stationary phase.[33] Recently, a NCSi (tetraazacalix[2]arene[2]triazine functionalized silica) SPE sorbent (Figure 2)[34] was prepared utilizing preparation procedures similar to the NCS stationary phases in our laboratory. Because of the existence of multi-interaction, it is of great application value for purification or concentration trace analyte in a complex matrix. Furthermore, it has been successfully used for the extraction tobacco-specific *N*-nitrosamines, 4-(methylnitrosamino)-1-(3-pyridyl)-1-butanol, and a metabolite of 4-(methylnitrosamino)-1-(3-pyridyl)-1-butanone in rabbit plasma.[35]

In the present work, a novel multiple retention mechanism sorbent (NCSi) was used with the aim of developing a rapid and reliable sample preparation procedure for the determination of acrylamide in starchy foodstuffs. All of the main factors were optimized, and the results obtained by using the developed HPLC method based on NCSi SPE indicated that it is more suitable for the determination of acrylamide in the complex matrices.

MATERIALS AND METHODS

Chemicals, Materials, and Solutions. Tetraazacalix[2]arene[2]-triazine was synthesized in accordance with the previously published procedures.[32,36] 3-Aminopropyltriethoxysilane was purchased from

dx.doi.org/10.1021/jf501569q | J. Agric. Food Chem. 2014, 62, 6100−6107

Jingchun Chemical Reagent Co., Ltd. (Shanghai, China). Acrylamide (>99%) was purchased from Research Institute of Fine Chemical Industry (Tianjin, China). HPLC grade methanol (MeOH), *n*-hexane, ethyl alcohol, and acetonitrile were provided by Fisher (Fair Lawn, NJ, USA). Deionized water was purified by a Milli-Q system from Millipore (Bedford, MA, USA). The polypropylene column tube and 20 μm PTFE sieve plates used for SPE were bought from DIKMA (Beijing, China). Commercially available MCX, MAX, HLB, and C18 cartridges (100 mg/3 mL) were obtained from Waters (Milford, MA, USA).

Standard acrylamide was dissolved in water at a concentration of 40 μg/mL and stored at 4 °C as stock solutions. Five standard solutions at different concentration (4, 16, 40, 160, 400m and 4000 ng/mL) were prepared by diluting the standard stock solution with mobile phase.

Instruments and Measurement. The comparison of retention behaviors of acrylamide on NCS and octadecyl silane (ODS) stationary phases and all determinations were carried out on an Agilent 1260 (Agilent, USA) consisting of a G1311C quaternary pump with a vacuum degasser, a G13116A temperature-controlled column oven, a G1329B autosampler, and a G1314F VWD UV detector. A Flash EA 1112 elemental analyzer and a Bruker Vector 22 IR spectrograph were used for characterization of the NCSi SPE sorbent. A centrifuge (Zhongda Instrument Plant, Jiangsu, China) was used for centrifugal separation. A Vortex mixer (Shanghai jingke industrial LTD, Shanghai, China) was used for mixing solutions. A rotary evaporator was used for enrichment (Yarong, Shanghai, China). The HPLC separations were performed on an Ultimate XB-C18 column (250 × 4.6 mm i.d., 5 μm) with a solution of MeOH/water (10:90, v/v) at 0.5 mL/min. The wavelength was 200 nm, the injection volume was 20 μL, and the oven temperature was 30 °C. Under these chromatographic conditions, acrylamide and the food components in the tested samples were all baseline separated and eluted. Each separation and/or determination was performed in triplicate.

Synthesis of NCSi SPE Sorbent. As illustrated in Figure 2, NCSi sorbent was prepared by a two-step modification process as previously described.[32] First, aminopropyltriethoxyl-bonded silica gel (APS) was obtained. In the second step, APS was reacted with an excess of tetraazacalix[2]arene[2]triazine in anhydrous dimethylformamide (DMF) at 130 °C under nitrogen atmosphere. Different from the previous work, the spherical silica had a particle diameter of 40−60 μm instead of the previous 5 μm. The surface area is 500 m^2/g.

Retention Behaviors of Acrylamide on the NCS Stationary Phase. The retention behaviors were investigated on the previously studied NCS column (150 × 4.6 mm, 5 μm) and another four commercial columns (Agilent ZORBAX SB-C18, Waters XBridge Shield RP18, Ultimate XB-C18, and Hypersil ODS2) to evaluate the interactions between the NCS stationary phase and acrylamide. All tests were conducted at the same chromatographic conditions.

Sample Preparation. *Homogenization, Extraction, and Enrichment Process.* All samples (fried potato chips, rice crust, instant noodles, biscuit) were purchased from the local supermarket. Dry samples were ground, mesh size 1 mm. One gram of homogenized samples was weighed and put into 15 mL centrifuge tubes in triplicate. To each centrifuge tube was added 10 mL of acetonitrile followed by 30 s of vortexing to extract the target acrylamide. All of the centrifuge tubes were centrifuged for 5 min at 4000 rpm. Then the clear supernatant was transferred into a glass tube, this process was repeated, and the two clear supernatants were combined. About 20 mL of extraction solution was rotary evaporated to near 3 mL after the addition of 2 mL of water under vacuum at 30 °C.

SPE Cleanup. In this paper, a new purification procedure based on a novel homemade NCSi SPE sorbent is proposed for the analysis of acrylamide. The procedure consists of an acetonitrile extraction, centrifugation, and cleanup using homemade SPE cartridges. This method was compared with four different commercial SPE cartridges (C18, HLB, MAX, and MCX) with different interaction mechanisms to establish the best conditions for the determination of acrylamide in food products.

To investigate the availability of the NCSi SPE for the cleanup of acrylamide in complex matrix, 100 mg of NCSi sorbent was packed into a 3 mL SPE cartridge. The concentrated extracting solution (Sample Preparation) was passed through the five kinds of SPE cartridges, which had been preconditioned with 5 mL of MeOH and 5 mL of water, at the rate of 3 mL/min, and collected into a glass tube. The cartridges were then eluted with 2 mL of water and collected into the same glass tube, making the final volume approximately 5 mL. The 5 mL of collected aqueous solution was filtered through a 0.22 μm nylon filter (Agilent, USA) prior to HPLC analysis. All tests were performed in triplicate.

Recovery Test. The extraction and purification were validated by recovery investigation. We spiked test samples at three concentration levels of 40, 400, and 4000 ng/g by adding acrylamide to blank samples or real samples. Then, the recoveries were determined by HPLC method after the spiked test samples were treated by extraction and SPE cleanup procedures.

RESULTS AND DISCUSSION

Characterization of NCSi SPE Sorbent. In IR spectra of NCSi (Figure 3), the bands at 2937 and 2888 cm^{-1} are assigned

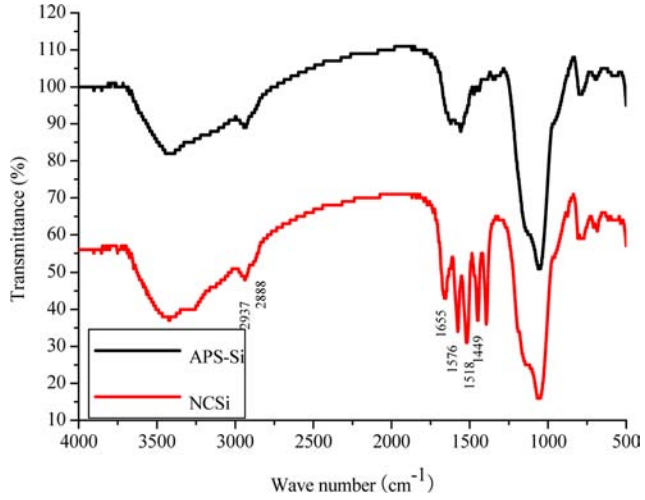

Figure 3. IR spectra of APS and NCSi sorbent.

to the stretching vibration of $-CH_2-$ groups. The characteristic absorption bands of the benzene rings appearing at 1449, 1518, and 1576 cm^{-1} confirmed that the macrocycle ligand was successfully immobilized on silica gel. Elemental analysis showed (Table 1) the bonding amount of tetraazacalix[2]-arene[2]triazine on NCSi sorbent was about 200 μmol/g.

SPE Optimization for Trace Acrylamide with the NCSi Sorbent. In this section, the main influence factors (amount of sorbent, flow rate of sample, composition and volume of washing solution) on the SPE recoveries (n = 3) of acrylamide

Table 1. NCS Stationary Phase and NCSi SPE Sorbent

	parameters of the silica gel		element analysis			
	particle size (μm)	specific surface area (m^2/g)	C (%)	H (%)	N (%)	bonded amount[a] (μmol/g)
NCS stationary phase	5	300	11.25	1.56	5.69	250
NCSi SPE sorbent	40−60	500	8.83	1.28	4.72	200

[a]Calculated from the carbon content.

dx.doi.org/10.1021/jf501569q | J. Agric. Food Chem. 2014, 62, 6100−6107

are evaluated in detail to obtain the optimal purification conditions.

The sorbent amount in the SPE cartridge is closely correlated with the purification effect. In this section, the influence of NCSi amount on the acrylamide's extraction was studied with the amount ranging from 50 to 250 mg. As shown in Figure 4,

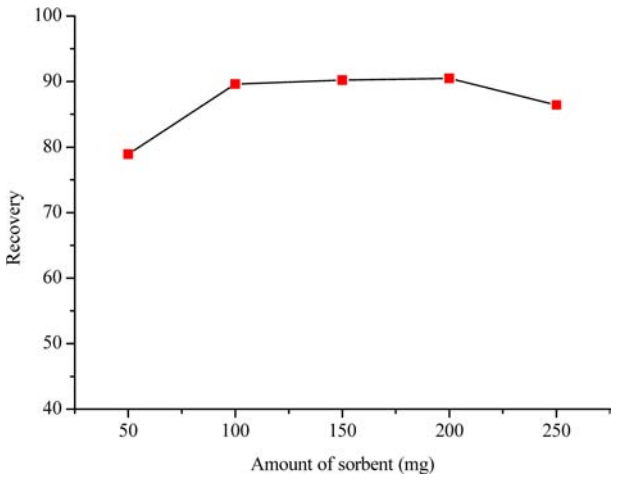

Figure 4. Recovery efficiency with different amounts of NCSi sorbent.

it is easily found that 100 mg of NCSi sorbent was enough to achieve satisfactory extraction and purification efficiency compared with 150 or 200 mg of NCSi sorbent. Thus, the optimal amount of sorbent was 100 mg.

As is known, the flow rate of the sample is another critical factor that not only affects the purification effect of analytes but also controls the sample pretreatment time. In this section, flow rates ranging from 1 to 5 mL/min were investigated, and it was found that 3 mL/min was the optimal flow rate to provide higher extraction recovery (Figure 5).

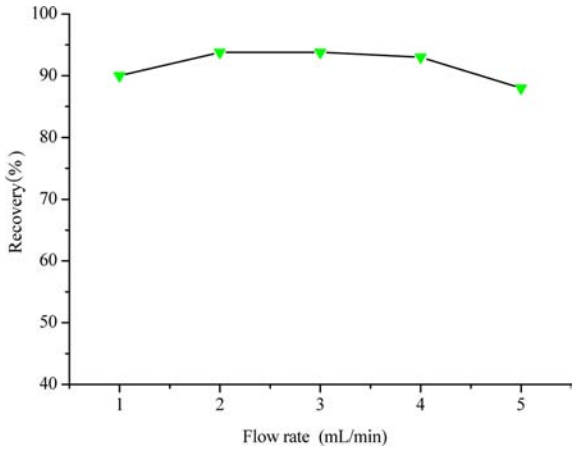

Figure 5. Recovery efficiency with different flow rates of sample.

A proper washing solvent is of great importance to reduce interfering substances and improve the recovery. Thus, the influence of the composition and volume of the washing solution on the purification of trace acrylamide (1 mL of working aqueous solution, 40 ng/mL) was studied. Different concentrations of MeOH solution (MeOH/water, v/v) at a constant volume (2 mL) were investigated. It was found that the recoveries showed no significant difference with the concentration of MeOH increasing from 0 to 20%; however, the interfering substances in the real samples increased along with the increasing proportion of MeOH. Meanwhile, a high concentration of MeOH may also result in loss of the target compounds. Therefore, a 100% water solution was selected as the optimal washing solution composition. For the selection of washing solution volume, various volumes (0.5−5 mL) of water solution were applied for the NCSi SPE process. The results display that the recoveries of acrylamide increased with the rise of the water solution volume from 0.5 to 2 mL. When the volume of water solution was >2 mL, the recoveries of acrylamide remained almost constant while the interference increased. As a result, 2 mL of water solution was chosen as the washing solution in this study.

Comparison of SPE Cleanup by NCSi Sorbent and Commercial Sorbents (MCX, MAX, HLB, and C18). *Comparison of SPE Cleanup by NCSi Sorbent and Commercial Sorbents.* Concentrated extracting solution of 1 g of blank cookies (Sample Preparation) was passed through NCSi and four kinds of commercial SPE cartridges (MCX, MAX, HLB, and C18) possessing the same specifications as the homemade NCSi SPE cartridge according to the SPE cleanup procedures as previous described, respectively. About 5 mL of purged aqueous solution was collected in the five glass tubes (Figure 6), respectively. As shown in Figure 6, it was found that

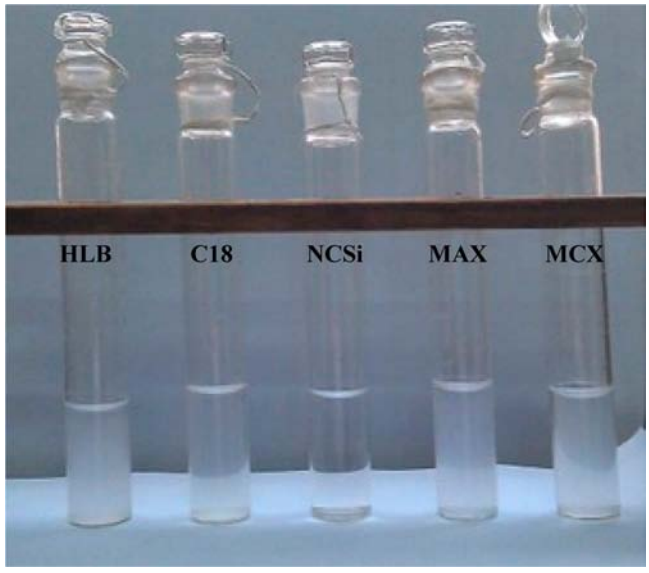

Figure 6. Turbidity comparison of the purged liquors from NCSi and four commercial SPE cartridges.

the type of sorbent used played an important role on the purification efficiency: the purged liquor from NCSi is obviously clearer than those from the other four kinds of commercial SPE cartridges. The purged liquor from NCSi was clear, but the purged liquors from C18 and HLB showed a little turbidity and the liquors from MAX and MCX were a milky white. These results imply that the fat and weak polar matrices could coelute out together with acrylamide during the purification of real samples through MCX, MAX, HLB, and C18 SPE cartridges. Therefore, NCSi SPE was selected as optimal for the extraction and purification of acrylamide in the actual samples.

To further evaluate the purification capacity of NCSi SPE sorbent, the above purged liquors from MCX and NCSi were

dx.doi.org/10.1021/jf501569q | J. Agric. Food Chem. 2014, 62, 6100−6107

defatted with hexane as described in the literature,[37,38] respectively. The defatting procedures are described as follows: add 15 mL of *n*-hexane to the 5 mL of purged liquor, then vortex for 30 s, allow to stand, and remove the upper hexane to get rid of lipid. The remaining liquids were clear, and 5 μL of liquid was injected for HPLC separation. As expected, it was found that the chromatograms of the defatted and non-defatted liquors from NCSi showed no difference, and they were similar to the chromatogram of the defatted liquor from the MCX SPE cartridge (Figure 7). These results prove that NCSi SPE could omit the defatting step and reduce acrylamide loss during the purification process.

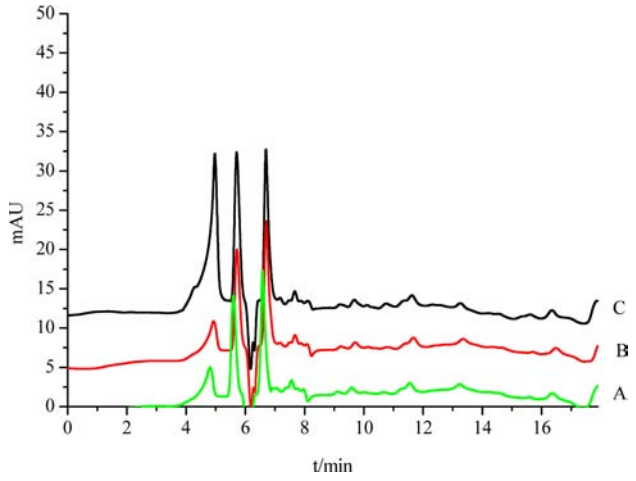

Figure 7. Chromatograms of purged liquors from MCX and NCSi with and without defatting steps in blank cookies. Conditions: column, Ultimate XB-C18 (250 × 4.6 mm i.d., 5 μm); mobile phase, MeOH/water (10:90, v/v); flow rate, 0.5 mL/min; detection wavelength, 200 nm; injection volume, 20 μL; column temperature, 30 °C. Chromatograms: (A) NCSi defatted; (B) NCSi without defatting; (C) MCX defatted.

Moreover, comparison of SPE purification efficiency between NCSi SPE and commercially available C18, HLB, MAX, and MCX SPE was carried out to further demonstrate the suitability of NCSi SPE for real samples. The sample cookies spiked at 40 ng/g acrylamide were performed under the extraction and SPE cleanup procedures. The 20 μL of purged liquor from NCSi and defatted liquor from the other four SPE sorbents was injected to perform HPLC separations. Their chromatograms are shown in Figure 8. The target peak of acrylamide by NCSi SPE cleanup showed more symmetry and higher UV response than those of the other commercially SPE cartridges, which makes the determination of trace acrylamide in complex matrix more accurate and sensitive. The NCSi sorbent exhibited high selectivity toward various interference and coprecipitation compounds with different mechanisms including hydrophobic, $\pi-\pi$ stacking, hydrogen-bonding, inclusion, and anion-exchange interactions. The proteins and carbohydrates were retained on NCSi depending on hydrogen-bonding and anion-exchange interactions, whereas fat and nonpolar matrices were held on the basis of hydrophobic interactions. For acrylamide, there is a weak hydrogen-bonding interaction with NCSi, which leads to its being weakly retained on NCSi.

Optimization of the Chromatographic Conditions. The chromatographic separation of acrylamide was performed by reverse-phase liquid chromatography using NCS and four

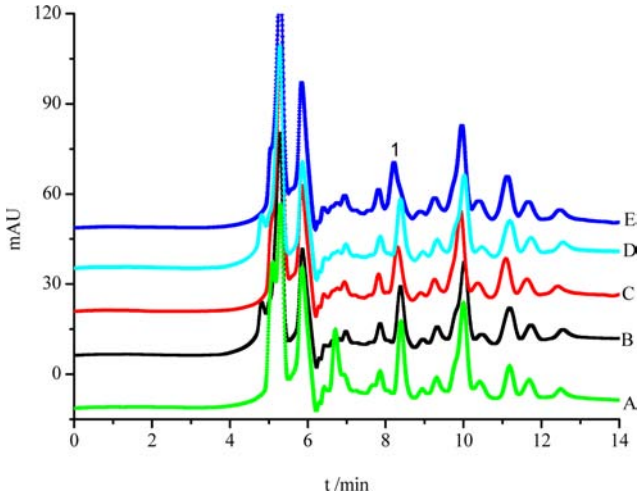

Figure 8. Chromatogram comparison of purged liquors from (A) NCSi without defatting step and from (B) C18, (C) HLB, (D) MAX, and (E) MCX with defatting steps. Conditions were as for Figure 7. Peak: 1, acrylamide.

different chromatographic columns. The retention properties of acrylamide are described in Table 2. From Table 2, NCS and

Table 2. Retention Properties of Acrylamide on Different Chromatographic Columns[a]

chromatographic column	retention time (min)	symmetrical factor	half-peak width
NCS (150 × 4.6 mm, 5 μm)	6.183	0.826	0.2542
Agilent ZORBAX SB-C18 (150 × 4.6 mm, 5 μm)	4.253	0.563	0.2442
Waters XBridge Shield RP18 (250 × 4.6 mm, 5 μm)	7.054	0.745	0.1239
Hypersil ODS2 (250 × 4.6 mm, 5 μm)	7.465	0.672	0.1653
Ultimate XB-C18 (250 × 4.6 mm, 5 μm)	8.487	0.929	0.1672

[a]Chromatographic conditions are given under Instruments and Measurement.

Ultimate XB-C18 provided better symmetry than the other columns, and Ultimate XB-C18 possessed higher theoretical plates than the others. Therefore, Ultimate XB-C18 (250 × 4.6 mm, 5 μm) was selected as the optimal column for the separation and determination of acrylamide in the real samples. However, it is noteworthy that the retention of acrylamide on the NCS column was a little bit stronger than those on the other ODS columns. Obviously, triazine rings and nitrogen bridges on the NCS stationary phase played an important role in acrylamide's retention. This result again displays that weak hydrogen bonding interaction exists between acrylamide and NCS.

We also carried out the HPLC separation of acrylamide with different mobile phases at different flow rates (detection wavelength at 200 nm). Chromatograms are shown in Figure 9. From Figure 9A,C,D, the retention time of acrylamide gradually reduced with the increase of MeOH content in the mobile phase from 5 to 15% at a flow rate of 0.5 mL/min. From Figure 9B,C,E, the retention time of acrylamide gradually decreases with the increase of flow rate from 0.4 to 0.6 mL/min with the mobile phase of 10% MeOH. Their retention times, peak areas, and theoretical plates were calculated and are presented in

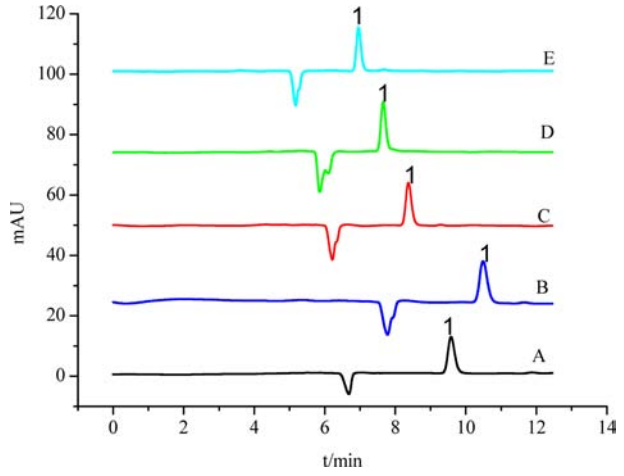

Figure 9. Chromatograms of acrylamide with different mobile phases and flow rates. Conditions: (A) methanol/water (5:95, v/v), 0.5 mL/min; (B) methanol/water (10:90, v/v), 0.4 mL/min; (C) methanol/water (10:90, v/v), 0.5 mL/min; (D) methanol/water (15:85, v/v), 0.5 mL/min; (E) methanol/water (10:90, v/v), 0.6 mL/min; others as for Figure 7. Peak: 1, acrylamide.

Table 3. As can be seen from Table 3, along with the increase of flow rate, both the retention time and peak area decrease. When

Table 3. Retention Time, Peak Areas, and Theoretical Plates of Acrylamide with Different Chromatographic Conditions[a]

chromatographic conditions	retention time (min)	peak area	theoretical plates (plates/m)
(A) methanol–water (5:95, v/v), 0.5 mL/min	9.58	166.6	32004.57
(B) methanol–water (10:90, v/v), 0.4 mL/min	10.492	207.2	31330.94
(C) methanol–water (10:90, v/v), 0.5 mL/min	8.373	166.1	34315.10
(D) methanol–water (15:85, v/v), 0.5 mL/min	7.659	178	34307.81
(E) methanol–water (10:90, v/v), 0.6 mL/min	6.959	136.7	35955.18

[a]Other chromatographic conditions are given underInstruments and Measurement.

5.0% methanol was invoked as the mobile phase at a flow rate of 0.6 mL/min, the peak area reduced 23.2% compared with 0.5 mL/min. The flow rate of 0.4 mL/min shows the largest response, but it also holds the disadvantage of longer retention time and solvent cost. With the retention time, peak area, and theoretical plate taken into consideration, a 10% v/v methanol mobile phase and 0.5 mL/min flow rate were chosen as optimal conditions for our HPLC-UV analysis of acrylamide in the samples.

Linear Regression Equation, LOD and LOQ of the Method. Method validation such as recovery, linearity, correlation coefficients, LODs, and LOQs were measured. The calibration curve was constructed by plotting peak area (y) versus the corresponding concentration of acrylamide (x, ng/mL) and its linear regression equation was obtained as follows:

$$y = 0.4357x + 0.2648 \ (n = 5, r^2 = 0.9999)$$

The results showed that good linearity was achieved in the range of 4–4000 ng/mL for acrylamide with a correlation coefficient of 0.9999. The limits of detection (LOD) and quantification (LOQ) of this method were determined with signal/noise ratios of 3 and 10, respectively. The LOD and LOQ were about 5 and 20 ng/g at a detection wavelength of 200 nm, respectively. This LOD or LOQ was low compared to those of published works by GC-MS[6] and LC-MS.[39,40] The intraday and interday RSDs (n = 5) of peak areas (400 ng/mL) were 0.22 and 0.90% and the intraday and interday RSDs (n = 5) of retention time were 0.50 and 1.63%, respectively.

Recovery and Application to Real Samples. The recovery investigations were carried out in accordance with the previous description. The standard acrylamide solutions at three levels (40, 400, and 4000 ng/mL) were added to real samples including potato chips, cookies, fried steamed buns, and rice crust. Then, the original samples and spiked samples were extracted, cleaned up by NCSi sorbent, and separated by HPLC. Typical chromatograms of potato chips are shown in Figure 10. The contents and recoveries of acrylamide were

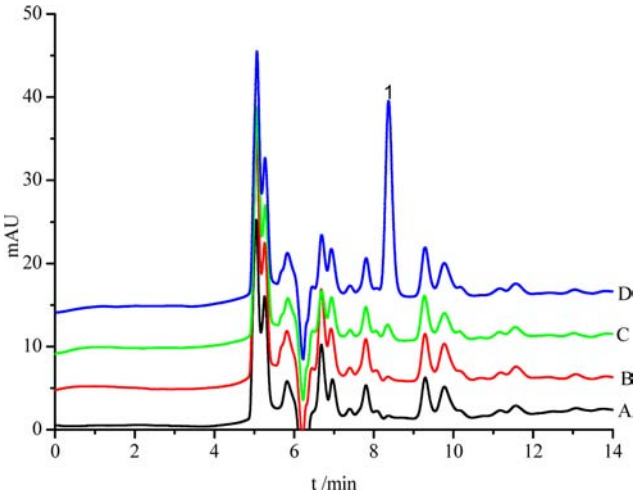

Figure 10. Chromatograms of potato chips and spiked potato chips. Chromatograms: (A) potato chips; (B) potato chips spiked at 40 ng/g; (C) potato chips spiked at 400 ng/g; (D) potato chips spiked at 4000 ng/g. Conditions were as for Figure 7. Peak: 1, acrylamide.

determined and are shown in Table 4. It can be seen from Table 4 that their recoveries ranged from 73.13 to 98%, indicating that the developed HPLC method based on NCSi SPE cleanup possessed high accuracy. The contents of acrylamide in these foods ranged from 13 to 28 ng/g; these values were much lower than the maximum residue limits (MRLs) recommended by the European Commission.[41] These foods can be safely consumed. From the results above, it is concluded that the present SPE method based on NCSi sorbent is more suitable for the determination of acrylamide in samples with a complex matrix.

In conclusion, an HPLC method based on NCSi-SPE cleanup has been successfully employed for the purification and determination of acrylamide in potato chip, cookie, fried steamed bun, and rice crust samples with complex matrices. The NCSi-SPE method enables a more efficient purification of acrylamide from a complex matrix due to its multi-interaction ability. The multi-interaction ability can selectively keep the main interferences (such as carbohydrates and proteins) from passing through NCSi while allowing acrylamide pass without any obstacle. The SPE procedure is simple and easy to operate; furthermore, NCSi-SPE offers higher accuracy for the determination of acrylamide in a complex matrix. The proposed

dx.doi.org/10.1021/jf501569q | J. Agric. Food Chem. 2014, 62, 6100–6107

Table 4. Analysis of Acrylamide in Various Foodstuffs

		spiking 40 ng/g		spiking 400 ng/g		spiking 4000 ng/g	
sample	concentration (ng/g)	recovery (%)	RSD (%, n = 3)	recovery (%)	RSD (%, n = 3)	recovery (%)	RSD (%, n = 3)
cookies	21	98	0.95	85.5	6.22	82.4	2.47
potato chips	28	77.5	2.63	76.9	4.53	81.3	3.09
fried steamed buns	13	80.6	4.30	82.9	1.57	73.13	4.42
rice crust	18	90.5	2.65	87.2	3.27	90.6	2.64

HPLC method based on NCSi-SPE is promising for use in the pretreatment and determination of acrylamide in starchy foodstuffs.

AUTHOR INFORMATION

Corresponding Authors

*(S. Zhang) Mail: Daxue Road 75, Zhengzhou 450052, P. R. China. Phone: 86 371 67763224. E-mail: zsszz@126.com.
*(W. Zhao) E-mail: wjiezh@126.com.

Funding

We acknowledge the support of NSF of China (21275133 and 21305030).

Notes

The authors declare no competing financial interest.

ACKNOWLEDGMENTS

We thank Dr. Julie Rimes and Dr. Simon Yang for assistance with editing the text.

REFERENCES

(1) Swedish National Food Administration (http://www.slv.se). *Information about Acrylamide in Food*, April 24, 2002.
(2) Scientific Committee on Toxicity Ecotoxicity and the Environment (CSTEE). Opinion on the results of the risk assessment of acrylamide. The 22nd CSTEE plenary meeting, Brussels, Belgium, March 6–7, 2001.
(3) Poole, C. F.; Sye, W. F.; Zlatkis, A.; Spencer, P. S. Determination of acrylamide in nerve tissue homogenates by electron-capture gas chromatography. *J. Chromatogr., A* **1981**, *217*, 239–245.
(4) Soares, C.; Cunha, S.; Fernandes, J. Determination of acrylamide in coffee and coffee products by GC-MS using an improved SPE clean-up. *Food Addit. Contam.* **2006**, *23*, 1276–1282.
(5) Lee, M. R.; Chang, L. Y.; Dou, J. P. Determination of acrylamide in food by solid-phase microextraction coupled to gas chromatography–positive chemical ionization tandem mass spectrometry. *Anal. Chim. Acta* **2007**, *582*, 19–23.
(6) Dunovská, L.; Čajka, T.; Hajšlová, J.; Holadová, K. Direct determination of acrylamide in food by gas chromatography–high resolution time-of-flight mass spectrometry. *Anal. Chim. Acta* **2006**, *578*, 234–240.
(7) Becalski, A.; Lau, B. P. Y.; Lewis, D.; Seaman, S. W. Acrylamide in foods: occurrence, sources and modeling. *J. Agric. Food Chem.* **2003**, *51*, 802–808.
(8) Inoue, K.; Yoshimura, Y.; Nakazawa, H. Development of high-performance liquid chromatography–electrospray mass spectrometry with size-exclusion chromatography for determination of acrylamide in fried foods. *J. Liq. Chromatogr. Relat. Technol.* **2003**, *26*, 1877–1884.
(9) Zhang, Y.; Ren, Y.; Zhao, H.; Zhang, Y. Determination of acrylamide in Chinese traditional carbohydrate-rich foods using gas chromatography with micro-electron capture detector and isotope dilution liquid chromatography combined with electrospray ionization tandem mass spectrometry. *Anal. Chim. Acta* **2007**, *584*, 322–332.
(10) Tareke, E.; Rydberg, P.; Karlsson, P.; Eriksson, S.; Törnqvist, M. Analysis of acrylamide, a carcinogen formed in heated foodstuffs. *J. Agric. Food Chem.* **2002**, *50*, 4998–5006.
(11) Leung, K. S.; Lin, A.; Tsang, C. K.; Yeung, S. T. K. Acrylamide in Asian foods in Hong Kong. *Food Addit. Contam.* **2003**, *20*, 1105–1113.
(12) Fernandes, J. O.; Soares, C. Application of matrix solid-phase dispersion in the determination of acrylamide in potato chips. *J. Chromatogr., A* **2007**, *1175*, 1–6.
(13) Arisseto, A. P.; Toledo, M. C. d. F.; Govaert, Y.; van Loco, J.; Fraselle, S.e; Degroodt, J.-M. A modified sample preparation for acrylamide determination in cocoa and coffee products. *Food Anal. Methods* **2008**, *1*, 49–55.
(14) DeArmond, P. D.; DiGoregorio, A. L. Characterization of liquid chromatography-tandem mass spectrometry method for the determination of acrylamide in complex environmental samples. *Anal. Bioanal. Chem.* **2013**, *405*, 4159–4166.
(15) Senyuya, H. Z.; Gökmen, V. Survey of acrylamide in Turkish foods by an in-house validated LC–MS method. *Food Addit. Contam.* **2005**, *22*, 204–209.
(16) Bermudo, E.; Moyano, E.; Puignou, L.; Galcera, M. T. Determination of acrylamide in foodstuffs by liquid chromatography ion-trap tandem mass-spectrometry using an improved clean-up procedure. *Anal. Chim. Acta* **2006**, *559*, 207–214.
(17) Karasek, L.; Wenzl, T.; Anklam, E. Determination of acrylamide in roasted chestnuts and chestnut-based foods by isotope dilution HPLC-MS/MS. *Food Chem.* **2009**, *114*, 1555–1558.
(18) Bortolomeazzi, R.; Munari, M.; Anesea, M.; Verardo, G.; Goeyens, L. Rapid mixed mode solid phase extraction method for the determination of acrylamide in roasted coffee by HPLC–MS/MS. *Food Chem.* **2012**, *135*, 2687–2693.
(19) Rosén, J.; Hellenäs, K. E. Analysis of acrylamide in cooked foods by liquid chromatography tandem mass spectrometry. *Analyst* **2002**, *127*, 880–882.
(20) Aguas, P. C.; Fitzhenry, M. J.; Giannikopoulos, G.; Varelis, P. Analysis of acrylamide in coffee and cocoa by isotope dilution. *Anal. Bioanal. Chem.* **2006**, *385*, 1526–1531.
(21) Bortolomeazzi, R.; Munari, M.; Anese, M.; Verardo, G. Rapid mixed mode solid phase extraction method for the determination of acrylamide in roasted coffee by HPLC–MS/MS. *Food Chem.* **2012**, *135*, 2687–2693.
(22) Soares, C.; Cunha, S.; Fernandes, J. Determination of acrylamide in coffee and coffee products by GC-MS using an improved SPE clean-up. *Food Addit. Contam.* **2006**, *23*, 1276–1282.
(23) Xu, L.; Zhang, L.; Qiao, X.; Xu, Z. J.; Song, J. Determination of trace acrylamide in potato chip and breadcrust based on SPE and HPLC. *Chromatographia* **2012**, *75*, 269–274.
(24) Zhang, Y.; Ren, Y. P.; Zhang, Y. New research developments on acrylamide: analytical chemistry, formation mechanism, and mitigation recipes. *Chem. Rev.* **2009**, *109*, 4375–4397.
(25) Glennon, J. D.; O'Connor, K.; Srijaranai, S.; Manley, K.; Harris, S. J.; McKervey, M. A. Enhanced chromatographic selectivity for Na^+ ions on a calixarene-bonded silica phase. *Anal. Lett.* **1993**, *26*, 153–158.
(26) Brindle, R.; Albert, K.; Harris, S. J.; Troltzsch, C.; Horne, E.; Glennon, J. D. Silica-bonded calixarenes in chromatography: I. Synthesis and characterization by solid-state NMR spectroscopy. *J. Chromatogr., A* **1996**, *731*, 41–47.
(27) Glennon, J. D.; Horne, E.; O'Connor, K.; Kearney, G.; Harris, S. J.; McKervey, M. A. Silica-bonded calixarenes in chromatography: II. Chromatographic retention of metal ions and amino acid ester hydrochlorides. *J. Chromatogr., A* **1996**, *731*, 47–56.

(28) Hu, K.; Qu, K.; Li, Y. B.; Ding, C. H.; Wang, X.; Zhang, J. X.; Ye, B. X.; Zhang, S. S. Investigation of the retention mechanism of naphthol and benzenediol on calix[4]arene stationary phase based on quantum chemistry calculations. *J. Sep. Sci.* **2008**, *31*, 2430−2433.
(29) Hu, K.; Liu, J. W.; Tang, C.; Wang, C. J.; Yu, A. J.; Wen, F. Y.; Zhao, W. J.; Ye, B. X.; Wu, Y. J.; Zhang, S. S. Preparation, characterization and application of a new 25,27-bis-[2-(5-methylthiadiazole)thioethoxyl]-26,28-dihydroxy-*para-tert*-butyl calix[4]arene stationary phase for HPLC. *J. Sep. Sci.* **2012**, *35*, 239−247.
(30) Zhao, W. J.; Hu, K.; Wang, C. J.; Liang, S.; Niu, B. L.; He, L. J.; Lu, K.; Ye, B. X.; Zhang, S. S. New oxo-bridged calix[2]arene[2]-triazine stationary phase for high performance liquid chromatography. *J. Chromatogr., A* **2012**, *1223*, 72−78.
(31) Hu, K.; Zhang, Y. H.; Liu, J. W.; Chen, K. K.; Zhao, W. J.; Zhu, W. X.; Song, Z. C.; Ye, B. X.; Zhang, S. S. Development of a new 25,27-bis(L-phenylalaninemethylester-*N*-carbonylmethoxy)-26,28-dihydroxy-*para-tert*-butylcalix[4]arene HPLC stationary phase and its application in food safety. *J. Sep. Sci.* **2013**, *36*, 445−453.
(32) Zhao, W. J.; Wang, W. J.; Chang, H.; Cui, S. W.; Hu, K.; He, L. J.; Lu, K.; Liu, J. X.; Wu, Y. J.; Qian, J.; Zhang, S. S. Tetraazacalix[2]arene[2]triazine modified silica gel: a novel multi-interaction and mixed-mode stationary phase for high performance liquid chromatography. *J. Chromatogr., A* **2012**, *1215*, 74−81.
(33) Zhang, S. S.; Zhao, W. J.; Liang, S.; Yu, A. J.; Hu, K.; Zhao, X. L.; Wu, Y. J. *Preparation and application of tetraazacalix[2]arene[2]triazine modified silica stationary phase*. Patent CN: 2011 1000 2890.6, 2011.
(34) Zhang, S. S.; Zhao, W. J.; Chang, H.; Jiang, Q.; Deng, Z. F.; Lu, J. *Preparation and application of tetraazacalix[2]arene[2]triazine modified silica sorbent for solid phase extraction*. Patent CN: 201210458997, 2012.
(35) Wang, L.; Yang, Ch. Q.; Zhang, Q. D.; Wang, S.; Lang, H. L.; Zhang, S. S.; Zhao, W. J.; Zhang, J. X. SPE-HPLC-MS/MS method for the trace analysis of tobacco-specific *N*-nitrosamines in plasma using tetraazacalix[2]arene[2]triazine modified silica sorbent. *J. Sep. Sci.* **2013**, *36*, 2664−2671.
(36) Wang, M.; Yang, H. A general and high yielding fragment coupling synthesis of heteroatom-bridged calixarenes and the unprecedented examples of calixarene cavity fine-tuned by bridging heteroatoms. *J. Am. Chem. Soc.* **2004**, *126*, 15412−15422.
(37) Gökmen, V.; Senyuva, H. Z.; Acar, J.; Sarıoğlu, K. Determination of acrylamide in potato chips and crips by high-performance liquid chromatography. *J. Chromatogr., A* **2005**, *108*, 193−199.
(38) Murkovic, M. Acrylamide in Austrian foods. *J. Biochem. Biophys. Methods* **2004**, *61*, 161−167.
(39) Govaert, Y.; Arisseto, A.; van Loco, J.; Scheers, E.; Fraselle, S.; Weverbergh, E.; Degroodt, J. M.; Goeyens, L. Optimisation of a liquid chromatography−tandem mass spectrometric method for the determination of acrylamide in foods. *Anal. Chim. Acta* **2006**, *556*, 275−280.
(40) Hoenicke, R.; Gatemann, W.; Harder, L. Analysis of acrylamide in different foodstuffs using liquid chromatography−tandem mass spectrometry and gas chromatography−tandem mass spectrometry. *Anal. Chim. Acta* **2004**, *520*, 207−215.
(41) European commission recommendation. 2013/647/EU, Nov 8, 2013.

JOURNAL OF AGRICULTURAL AND FOOD CHEMISTRY

Article

pubs.acs.org/JAFC

Plum and Soy Aglycon Extracts Superior at Increasing Bone Calcium Retention in Ovariectomized Sprague Dawley Rats

Jessica W. Pawlowski,[†,‡] Berdine R. Martin,[†] George P. McCabe,[§] Mario G. Ferruzzi,[†] and Connie M. Weaver*[,†]

[†]Department of Nutrition Science, College of Health and Human Sciences, Purdue University, 700 West State Street, West Lafayette, Indiana 47907, United States

[§]Department of Statistics, College of Science, Purdue University, 250 North University Street, West Lafayette, Indiana 47907, United States

ABSTRACT: Plant-derived polyphenols have been shown to influence bone turnover and bone properties in the estrogen-depleted state. We used a crossover design in ovariectomized rats (n = 16 rats for each diet) to investigate the effect of supplementation of two doses each of blueberry, plum, grape, grape seed extract, and resveratrol on bone. We tested the aglycon and glucoside forms of genistein to quantify differences in efficacy on bone calcium retention. Rats were given an intravenous dose of ^{45}Ca to prelabel bone, and bone calcium retention was assessed by urinary excretion of ^{45}Ca:Ca ratio during an intervention period compared with nonintervention. Genistein aglycon increased bone calcium retention significantly ($p < 0.05$) more than the glucoside (22% vs 13%, respectively). Plum extract (0.45% w/w total dietary polyphenols) and resveratrol (0.2% w/w total dietary polyphenols) were also effective, increasing bone calcium retention by 20% ($p = 0.0153$) and 14% ($p = 0.0012$), respectively. Several polyphenolic-rich diets improved bone calcium retention.

KEYWORDS: *genistein aglycon, genistein glucoside, bone calcium retention, bone resorption, plant-derived polyphenols*

INTRODUCTION

Various plant sources of polyphenolic compounds have been studied for their ability to prevent postmenopausal bone loss associated with estrogen deficiency. The link between soy consumption in the Asian diet and reduced fracture risk[1] has sparked many studies examining soy isoflavones and postmenopausal bone health. More recently, plum, blueberry, and grape products have also been implicated in preventing postmenopausal bone loss due to their polyphenolic components.[2−6]

In Western countries, soy is not consumed as often or in sufficient quantities to match the soy consumed in Asia, where beneficial effects to bone have been observed. In addition, soy in Western countries is typically consumed as an ingredient or in supplemental form that contains extracted isoflavones from soy rather than in whole soy foods.[7] The ability of soy isoflavones to attenuate bone resorption in an estrogen deficient state remains controversial.[8] Discrepancies have been attributed to a number of factors including an individual's ability to convert daidzein to equol, the effect of food matrix on bioavailability of isoflavones compared with extracted isoflavones, and specific isoflavone composition. In foods, isoflavones exist as glycosides and require cleavage of the sugar moiety in the gut to be absorbed in the intestine.[9] Although there have been contrary reports of bioavailability of glycoside compared with aglycon forms of genistein,[10,11] there is interest in comparing glycoside to aglycon forms for bone health as the aglycon form was used in various studies that have demonstrated a strong bone preserving effect in postmenopausal women.[12−15] The presence of the sugar moiety may have an influence on where the isoflavone is absorbed in the gut and how the isoflavone is subsequently conjugated inside the body.

Isoflavones and other phenolics have demonstrated estrogenic activity[16,17] and are being investigated for their biological effect on the estrogen-depleted state. Depletion of estrogen results in a marked increase in osteoclastogenesis, causing bone resorption. During this postmenopausal period, bone formation lags behind resorption, and net bone loss ensues.[18]

There is emerging evidence to suggest that certain fruits, vegetables, and other dietary compounds found in the Western diet may be protective to bone, especially from prune, grape products, and blueberries.[19−21] Grape seed extract has also shown promise in maintaining bone health as supplementation with grape seed extract was able to recover bone lost while on a calcium deficient diet in rats.[22] Dried plum is one of the most extensively studied botanicals for its role in bone health because of a potentially anabolic effect in bone. Dried plum was very effective in protecting bone in ovariectomized (OVX) rats when compared with the effect of intermittent teriparatide (parathyroid hormone 1−34) administration, which is the most effective anabolic drug therapy currently available for osteoporosis treatment.[3] Plum, as a daily supplement of 100 g/d dried plum for one year, was able to increase bone mineral density (BMD) in the spine and ulna of postmenopausal women compared with those who were supplemented with an equal amount of dried apple.[23] While these extracts appear to be diverse, they are rich sources of specific polyphenol forms

Received: August 8, 2013
Revised: May 9, 2014
Accepted: June 4, 2014
Published: June 4, 2014

ACS Publications © 2014 American Chemical Society

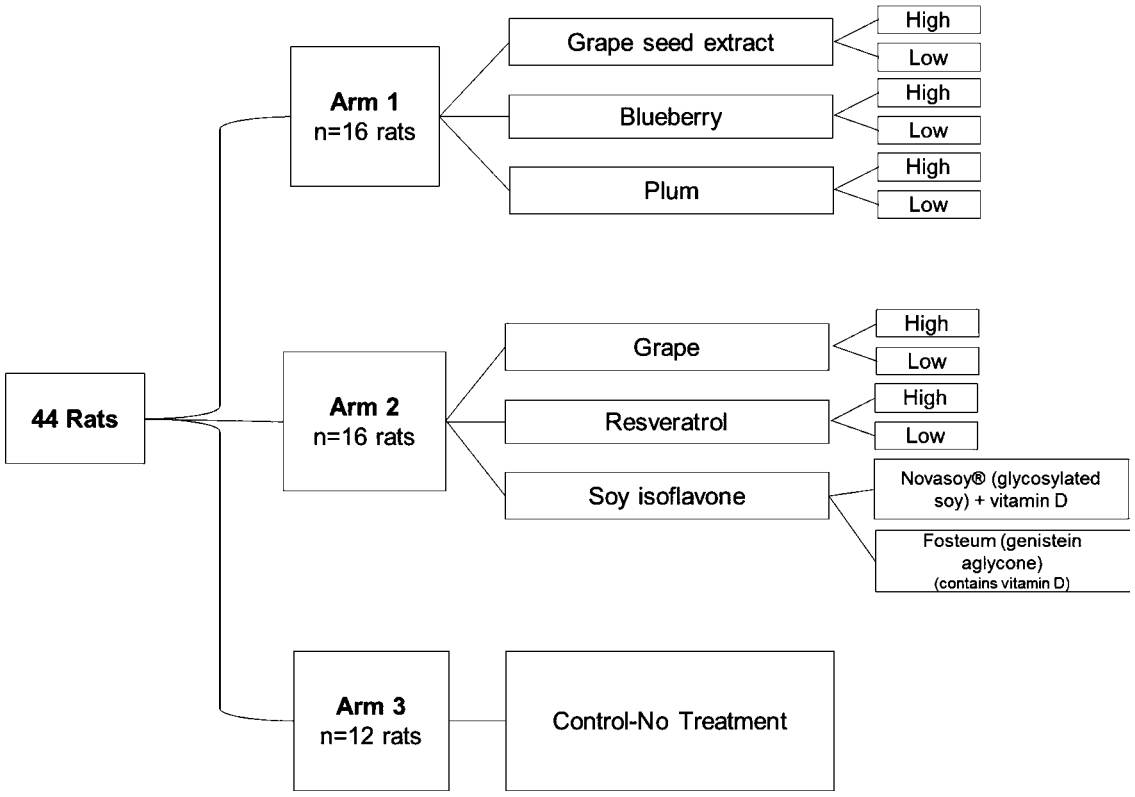

Figure 1. Study design. Forty-four rats were designated into one of three study arms. Rats in arm 1 (n = 16) received blueberry and plum fruit powder and grape seed extract to compare the effect of polyphenols in the whole fruit. Rats in arm 2 (n = 16) received whole fruit polyphenols from grape to compare against the isolated resveratrol polyphenols. Rats in arm 2 were also given genistein in the aglycon form and glycosylated soy to determine the effect of conjugation. Rats in arm 3 (n = 12) were not given a dietary botanical to establish an unperturbed excretion of ^{45}Ca excretion.

including quercetin, anthocyanins, proanthocyanidins, hydroxycinnamates, and resveratrol, which can be classified as possible bioactive agents responsible for observed bone health benefits associated with these foods. For example, resveratrol, found in grape products, extracts, and supplements, increased bone formation markers and decreased expression of receptor activator of nuclear factor kappa-B (RANK) in human primary monocytes,[21] showing potential to alter osteoclastogenesis.

Although the bioactive foods and ingredients described above have been shown to benefit bone by traditional measures of bone density and material properties, these approaches require chronic feeding and terminal measures. This has largely prevented comparisons among multiple diets and dose response effects. The aims of this study were to directly compare botanical sources and to study the effective dose of extracts to increase bone calcium retention in OVX rats using a novel technology that does not require sacrifice and evaluates responses quickly so that multiple comparisons can be efficiently tested. This involves prelabeling bones with ^{45}Ca as we have done previously with ^{41}Ca in human studies[24,25] as a means of screening botanical extracts for their ability to improve bone calcium retention. By injecting rats with ^{45}Ca, allowing the isotope to incorporate into bone, and quantifying the amount of ^{45}Ca in urine, a direct measure of net calcium tracer lost from bone is obtained. The long half-life of ^{45}Ca (163 days) allows multiple diets to be compared using a crossover design in the same rat, providing greater power to detect differences among diets. This method allows for screening of numerous diets on a relatively small number of rats during a short time period.

The method for determining bone calcium retention was derived from a well-established protocol using another bone seeking tracer, ^{3}H-tetracycline,[19,26−28] and adapted by us for calcium tracers in rats[29−31] and humans.[32] ^{3}H-tetracycline was the tracer of choice initially because it was assumed that it assessed only bone resorption from prelabeled bones in rats because it attaches tightly to hydroxyapatite and was slow to release.[33−35] However, we showed through kinetic modeling of both ^{3}H-tetracycline and calcium tracers that both isotopes leave bone during bone resorption and can re-enter bone during bone formation. Our findings suggest that these two tracers give comparable values and that net bone calcium retention is a more accurate description of what is being measured with bone seeking tracers.[30] Mühlbauer and Fleish[36] evolved the method to use daily measures of urinary ^{3}H-tetracycline from prelabeled bone of young rats given multiple injections of the tracer in order to continuously monitor bone resorption through 10-day diet periods and 10-day washout periods using a crossover design. We established that older OVX rats and a single isotope administration could be used in a study that evaluated effects of time of stabilization to OVX and time from dose on tracer behavior.[31] We further validated urinary tracer excretion against bone disappearance of the tracer[31] and adequacy of 10-day diet and washout periods.[29] Quantifying the urinary tracer appearance of a bone label enables rapid screening and multiple comparisons of efficacy of diets designed to improve bone calcium retention.

We hypothesized that both source and dose effects would be observed through testing high and low doses of various extracts from grape seed, grape, and blueberry, as well as plum powder,

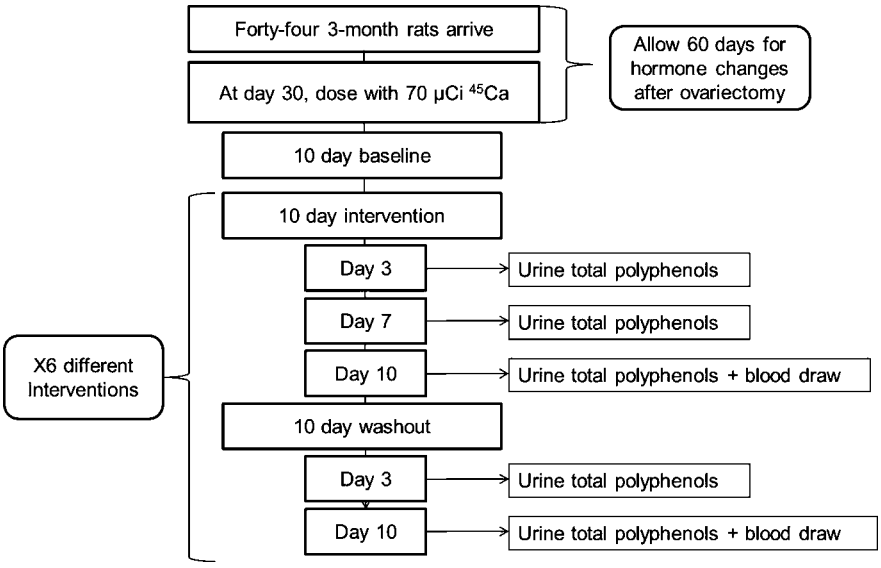

Figure 2. Study timeline for arrival of ovariectomized (OVX) rats, dosing with ^{45}Ca, and urine and blood collection pattern.

and resveratrol. We also used this screening method to determine whether genistein in an aglycon form is more effective at increasing bone calcium retention than its glucoside counterpart.

MATERIALS AND METHODS

Chemicals. A retrospective analysis of phenolic compounds from grape, blueberry, and plum extract was conducted after the conclusion of the study. Extracts were stored at −80 °C, reconstituted in 2% formic acid in ddH_2O at ∼1 mg/mL, and analyzed for key phenolic components by LC−MS as described by Song et al.[37]

Rats. Forty-four OVX Sprague Dawley rats (3 month old) were shipped from Harlan (Indianapolis, IN) and given approximately 30 days to acclimate to their environment, and to stabilize hormone changes post-OVX, while being fed AIN93-M polyphenol-free diet (soybean oil was replaced with corn oil) and distilled water ad libitum. The rats were housed individually in a humidity- and temperature-controlled room with a 12 h light and 12 h dark cycle. Food intake was monitored twice weekly, and body weight was recorded weekly. All procedures performed on rats were approved by and in compliance with the standards set by Purdue University's Animal Care and Use Committee.

Study Design. The study design (Figure 1) was a randomized, crossover intervention trial to evaluate 12 different polyphenolic-containing diets on bone turnover. The rats were randomized into one of three groups: (1) 16 rats received six diets of plum, blueberry, and grape seed extract at two doses, (2) 16 rats received six diets of grape extract and resveratrol at two doses each, and Novasoy (glycosylated soy) and Fosteum (genistein aglycon) at a single dose, and (3) 12 rats received no treatment to establish unperturbed ^{45}Ca excretion over time to verify that the regression lines computed from the nondiet periods were not confounded by diets for both calcium retention and the biomarker of bone turnover. Within each arm, the diets were randomized by polyphenolic source and then by dose.

The rats were injected with 70 μCi of ^{45}Ca in saline via a tail vein catheter approximately 30 days after arrival, moved to metabolic cages, and allowed 29 days for the isotope to be eliminated from soft tissues and fully incorporated into bone. Urine was collected for 24 h twice weekly during this equilibration period. The metabolic cages contained screens that prevented food debris and feces from contaminating the urine; the cages were cleaned once every 3 days throughout the duration of the experiment. Following the equilibration period, a baseline level of urinary tracer excretion was assessed during an initial 10 day baseline period (Figure 2), which was followed by a 10 day intervention and 10 day washout period. For each diet, there was n = 16 rats with 10 days of 24 h urine samples for each rat. The intervention and washout collections were repeated for 6 total intervention/washout cycles, and the total duration of the study was 189 days. Throughout the baseline, intervention, and washout, urine was collected for 24 h for 10 days during the intervention and 6 days during the washout. Urine was analyzed as a 24 h sample and was not pooled over multiple days. Food intake and body weight were monitored every 5 days. Blood was taken at the end of each diet and washout via the saphenous vein, and serum was stored at −80 °C to assay for bone-specific alkaline phosphatase. The urine collected at the end of each intervention and washout period was stabilized with 1% ascorbic acid at a 4:1 ratio immediately after the 24 h collection period, stored at −80 °C, and used to assay for total polyphenols and cross-linked N-telopeptides of type I collagen (NTx). Rats were killed using an excess of CO_2.

Diets. All diets were formulated to be isocaloric and to have approximately equal macronutrient, vitamin, and mineral content. The AIN93-M polyphenol-free diet[38] (Table 1) was used as a basal diet with the replacement of soybean oil with corn oil to prevent confounding from residual isoflavones. A higher amount of corn starch than in the original AIN93-M diet was used to facilitate the incorporation of up to 25% fruit powder, while maintaining the ability to pellet the diets. Research Diets, Inc. (New Brunswick, NJ),

Table 1. Modified AIN93-M Diet

ingredient	gm/kg
casein	140
L-cystine	1.8
corn starch[a]	495.692
maltodextrin[a]	125
sucrose	100
cellulose	50
corn oil[b]	40
tert-butylhydroquinone	0.008
mineral mix[c]	35
vitamin mix	10
choline bitartrate	2.5

[a]Modified from AIN93-M diet to enable pelleting while replacing up to 25% of corn starch with fruit powders. [b]Soybean oil in AIN93-M diet replaced with corn oil to avoid residual soy isoflavone interaction. [c]Mineral mix contains phosphorus at 3000 mg/kg diet and calcium at 5000 mg/kg diet.

dry blended the extracts and fruit powders into the basal diet prior to pelleting the diets. Each extract or fruit powder was added to the diet to create two doses of varying polyphenolic content and stored at −20 °C. The diets were formulated based on the goal of delivering 0.2% and 1% w/w total polyphenols for each extract where possible (Table 2). The total polyphenol content in the extracts was determined using the Folin−Ciocalteu method;[39] however, levels of resveratrol and soy isoflavones were added based on the manufacturers' specified levels of resveratrol and total isoflavones, respectively.

Table 2. Botanical and Total Polyphenol Composition in Modified AIN93-M Diet

botanical (% total polyphenols in extract)	exptl dose	% w/w diet	
		product	total polyphenols
grape seed extract (82.7)	high	1.2	1
	low	0.25	0.2
plum[a] (2.22)	high	20	0.45
	low	9	0.2
blueberry[b] (1.65)	high	25	0.4
	low	9	0.15
grape (32.8)	high	3	1
	low	0.6	0.2
resveratrol (99.9)	high	0.2	0.2
	low	0.1	0.1
genistein aglycon (6.67)	aglycon	0.6	0.04
glycosylated soy[c] (40.0)	glucoside	0.1	0.04

[a]Corn starch and cellulose in the AIN93-M diet were replaced by carbohydrates and fiber from plum powder. [b]Corn starch in the modified AIN93-M diet was replaced with maltodextrin from blueberry powder. [c]Additional 2960 IU of vitamin D/kg diet to match Fosteum (genistein aglycon).

We could achieve this goal with grape seed extract (Sensient, Indianapolis, IN) and grape skin extract (Sensient, Indianapolis, IN), which were both formulated to deliver 0.2% and 1% w/w total dietary polyphenols in the low and high doses, respectively. The blueberry and plum powder had lower phenolic content; therefore, these were added to the diet at levels that have been shown to be effective in bone.[3−6] The blueberry powder (Sensient, Indianapolis, IN) was added at levels of 9% and 25% w/w in the diet (delivering 0.15% and 0.40% w/w total dietary polyphenols, respectively) and plum powder (donated by the California Dried Plum Board, Los Altos, CA) was added at 9% and 20% w/w diet to deliver 0.20% and 0.45% w/w total dietary polyphenols, respectively. The added carbohydrates from the blueberry and plum powders were balanced by removing corn starch from the diet formula. Additionally, cellulose was removed to balance the added fiber in the plum powder. Resveratrol and isoflavones were added at lower levels than the fruit powders and extracts because they are isolated components rather than a complex botanical matrix. Resveratrol (Chromadex, Inc., Irvine, CA) was added at 0.1% and 0.2% w/w total dietary polyphenols. Novasoy (Archer Daniels Midland Company, Decatur, IL), which contains genistein glycoside plus other isoflavones, and Fosteum (Primus Pharmaceuticals, Inc., Scottsdale, AZ), which is genistein aglycon, were added to the diet to deliver an equivalent amount of total isoflavone content (0.04% w/w total dietary polyphenols) and to be consistent with the range of doses published in similar studies.[40,41] The diets delivered 5000 mg/kg diet calcium and 5000 mg/kg diet total phosphorus. Vitamin D was added to the Novasoy (glycosylated soy) diet at 2960 IU/kg diet to match the vitamin D present in the Fosteum supplement.

^{45}Ca and Total Calcium in Urine. Urine was centrifuged at 3500 rpm for 10 min at 4 °C, decanted, and diluted to the nearest 0.5 mL with ultrapure water; the total volume was recorded. Scintillation vials were prepared with 15 mL of Ecolite(+) (MP Biomedicals LLC., Solon, OH) and 1 mL of urine, and ^{45}Ca was measured on a Beckman LS 6500 scintillation counter (Beckman Instruments, Inc., Fullerton, CA). The ^{45}Ca values were corrected for decay and were reported as a percentage of original dose. Urinary total calcium was determined by vortexing, diluting, and analyzing urine samples on the atomic absorption spectrometer, AAnalyst 300 (PerkinElmer Instruments, Waltham, MA). For each 24 h urine sample of each rat, the ratio of percent dose ^{45}Ca to milligrams of total calcium was determined as the ^{45}Ca:Ca ratio. ^{45}Ca:Ca excretion during intervention was compared with ^{45}Ca:Ca excretion during nonintervention periods to determine percent bone calcium retention due to dietary polyphenols.

Biochemical Markers of Bone Turnover. Urine from day 10 of each intervention and washout period was stored at −80 °C for cross-linked N-telopeptides of type I collagen (NTx) analysis. Urine NTx was assayed in triplicate using an enzyme-linked immunosorbent assay (ELISA) from Wampole Laboratories R, Inc. (Princeton, NJ). The microtiter plate in the kit was precoated with an antibody specific to NTx. Samples and standards were added, followed by a series of reagents designed to produce a color change in the wells containing NTx. Bound NTx was analyzed spectrophotometrically at a wavelength of 450 nm, and concentration of NTx was determined by comparison to a standard curve.

Blood was taken at the end of each botanical diet period and washout period, and serum bone alkaline phosphatase was assayed using an ELISA from MyBioSource (San Diego, Ca). Serum samples were diluted 2-fold with saline and added to the wells of a microtiter plate that were precoated with an antibody specific to bone alkaline phosphatase. A series of reagents were added to produce a color change in the wells that contained bone alkaline phosphatase. Bone alkaline phosphatase was analyzed spectrophotometrically at 450 nm, and the concentration of bone alkaline phosphatase was determined by comparison to a standard curve.

Total Polyphenol Analysis. To confirm the dose dependent increase in polyphenol absorption from diets, urinary total polyphenols were quantified following solid phase extraction based on a modification of methods as described by Medina-Remón et al.[42] Briefly, urine samples were diluted to approximately 1 mL using a 50 mM sodium phosphate buffer (pH = 3.0). Strata-X polymeric reversed phase extraction tubes (Phenomenex Inc., Torrance, CA) were used for solid phase extraction. The tubes were initially washed with 3 mL of methanol, followed by 6 mL of phosphate buffer. The entire urine sample was applied to the column and washed with 6 mL of phosphate buffer, followed by 6 mL of 5% methanol. The samples were eluted with 6 mL of methanol, dried, and resolubilized with ethanol. Samples were then pipetted in triplicate onto a 96-well plate, along with gallic acid (Sigma-Aldrich, St. Louis, MO) in ethanol to create a standard curve, and an ethanol blank. The Folin−Ciocalteu reagent (2 N, Sigma-Aldrich, St. Louis, MO) was diluted to 0.2 N and added to the plate, and then samples were incubated for 7 min at room temperature. An equal amount of 7% sodium bicarbonate solution was added to the reaction, and the plate was incubated for 30 min prior to being analyzed by a spectrophotometer at 750 nm. Total polyphenols of the urine samples were calculated from the gallic acid standard curve and were reported as gallic acid equivalents.

Statistical Analysis. The ^{45}Ca:Ca ratio was transformed using the natural logarithm to correct for skewedness. For each rat, a simple linear regression model was fit through all of the nonintervention periods (baseline and washout data points) creating a regression line as illustrated in Figure 3A and Figure 3B. During the intervention period, a predicted value from the regression line for each observation of each rat was determined using the model described. The predicted value for each observation was subtracted from the experimental value measured during the botanical diet period, and the mean of differences was taken for that botanical diet of that rat. The means from each dietary intervention were averaged across all rats, and 95% confidence intervals were calculated. The values were exponentiated and reported in the original scale as percent improvement in calcium retention compared with baseline.

The data for food intake, weight change, feeding efficiency ratio, body weight, and total polyphenols were normal and were analyzed without transformation. Means and standard deviations were calculated for these variables, a repeated measures analysis of variance

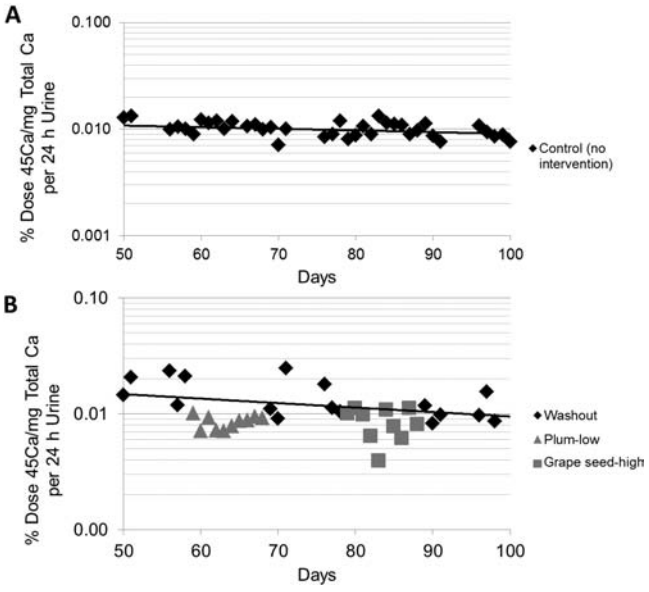

Figure 3. Plot of days vs ^{45}Ca:Ca ratio for (A) a control rat that did not receive a botanical diet and (B) two botanical diet periods and washout periods in one rat. Each data point represents a single 24 h urine collection. Different diets are indicated by different symbols. A regression line was fit through all of the nonintervention periods, which include baseline and washout data points. During the botanical diet periods, the residual was determined by finding the difference between the predicted value from the regression line and the experimental value.

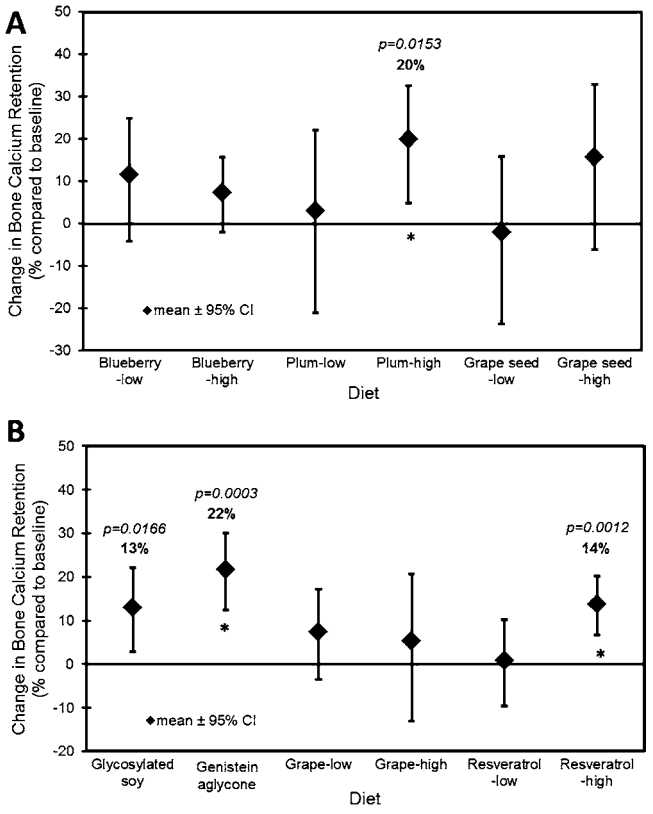

Figure 4. Effect of dietary botanicals on bone calcium retention in ovariectomized (OVX) rats (n = 16 rats per diet) was reported as mean ± 95% confidence intervals for (A) arm 1 and (B) arm 2. A value of "0" represents no change from the regression line computed from nonintervention periods. A confidence interval that excludes "0" indicates a significant change from the regression line at α = 0.05. The * indicates significant difference (p < 0.05) between high and corresponding low dose of the same dietary botanical as determined by a t test. For soy, the * indicates significant difference (p < 0.05) between genistein aglycon and glycosylated soy.

(ANOVA) was performed, and differences were determined by contrasts between high and low doses within each extract, and between genistein aglycon and glycosylated soy. t tests were performed for food intake, body weight, weight change, and feeding efficiency ratio to determine differences between control and botanical diets with a Bonferroni correction to adjust for multiple comparisons of means.

For each rat, NTx values were transformed to correct for skewedness using the natural logarithm. Subsequently, the difference in NTx between intervention and washout was determined for each botanical diet as change in NTx. The means and 95% confidence intervals of the differences were taken for each diet. A repeated measures ANOVA was performed followed by contrasts to determine differences between high and low doses of each diet, and between genistein aglycon and glycosylated soy. The means for each diet were transformed back to the original scale and reported as a ratio with 95% confidence interval. SAS software (version 9.3 SAS Institute, Cary, NC) was used for all analyses.

RESULTS

Bone Calcium Retention. Percent change in bone calcium retention was determined by finding the difference between the ^{45}Ca:Ca ratio excreted during the botanical diet compared with the residual line of all control diet periods. The urinary ^{45}Ca:Ca ratio of the control rats in arm 3 (Figure 1) verified that the regression line was not altered by diets in similarly aging rats (Figure 3A). The ratio of percent dose of ^{45}Ca to milligrams of Ca in the 24 h urine samples and residuals for two diets for one rat in arm 1 is shown in Figure 3B. Using this method, bone calcium retention was significantly improved due to dietary intervention with glycosylated soy (13%; p = 0.0166), genistein aglycon (22%; p = 0.0003), resveratrol-high (14%; p = 0.0012), and plum-high (20%; p = 0.0153) compared with baseline (Figures 4A and 4B). The genistein aglycon supplement, Fosteum, increased bone calcium retention 2-fold compared to glycosidic mixed isoflavone supplement, Novasoy (p < 0.05). The high dose of plum (0.45%) and resveratrol (0.2%) improved bone calcium retention compared with the lower doses (p < 0.05).

Food Intake and Body Weight. There was no significant difference in body weight between high and low doses of any botanical diet intervention despite some differences in the contributing factors (Table 3). In arm 1, plum-low increased the food intake, feeding efficiency ratio, and weight change compared with the plum-high diet (p < 0.0001). Blueberry-low increased the feeding efficiency ratio and weight change compared with the blueberry-high diet (p = 0.05). In arm 2, grape-low and resveratrol-high decreased the feeding efficiency ratio compared with control (p < 0.05), and glycosylated soy, grape-low, and resveratrol-high diets decreased the weight change of rats compared to those on the control diet (p < 0.05). There was a weak, but significant, positive correlation between change in body weight and net bone calcium retention (r = 0.21; p = 0.002); however, change in body weight was not correlated with NTx (p = 0.69).

Analysis of Extracts. Analysis of key phenolic compounds in grape, blueberry, and plum extracts highlighted some compositional differences between the different extracts (Table 4). The most prominent constituents in the plum

dx.doi.org/10.1021/jf403310q | J. Agric. Food Chem. 2014, 62, 6108−6117

Table 3. Food Intake, Body Weight, Weight Change, and Feeding Efficiency Ratio[a] for Ovariectomized Rats Expressed As Mean ± Standard Deviation

variable	feeding efficiency ratio	food intake, g/day	body wt, g	wt change, g/day
arm 1 rats				
blueberry-low	0.07 ± 0.05*	15.7 ± 1.3	354.2 ± 26.1	1.06 ± 0.70*
blueberry-high	0.03 ± 0.03	14.9 ± 1.44	351.4 ± 29.2	0.45 ± 0.56
plum-low	0.06 ± 0.05**	15.3 ± 2.2**	352.9 ± 22.1	0.92 ± 0.83**
plum-high	−0.02 ± 0.07	12.7 ± 2.3	346.1 ± 21.6	−0.20 ± 0.80
grape seed extract-low	0.03 ± 0.04	14.5 ± 1.0	351.1 ± 24.2	0.48 ± 0.64
grape seed extract-high	0.05 ± 0.03	15.1 ± 1.3	352.7 ± 25.0	0.78 ± 0.57
arm 2 rats				
glycosylated soy	0.03 ± 0.03	14.9 ± 1.1	377.0 ± 24.7	0.50 ± 0.40†
genstein aglycon	0.05 ± 0.04	15.0 ± 1.5	376.1 ± 28.2	0.74 ± 0.57
grape-low	0.06 ± 0.02†	16.0 ± 1.5	362.4 ± 22.5	1.01 ± 0.43†
grape-high	0.07 ± 0.03	17.0 ± 1.5	363.6 ± 20.3	1.14 ± 0.63
resveratrol-low	0.05 ± 0.03†	15.2 ± 1.5	360.1 ± 22.2	0.83 ± 0.60†
resveratrol-high	0.07 ± 0.03	15.2 ± 1.5	362.6 ± 22.0	1.05 ± 0.48
arm 3 control rats	0.16 ± 0.06	15.2 ± 1.2	370.2 ± 20.1	2.78 ± 1.24

[a]Feeding efficiency ratio as change in body weight/food intake. The * and ** denote significant differences with $p = 0.05$ and $p < 0.0001$, respectively, between low and corresponding high groups of the same extract diet as determined by contrasts after ANOVA. The † denotes significant difference from control with $p < 0.05$ as determined by t tests performed using a Bonferroni correction to adjust for multiple comparisons.

Table 4. Key Phenolic Compounds Identified in Extracts[a]

	mg/g extract[b]		
analytes	plum	grape	blueberry
phenolic acids			
gallic	0.15	11.85	0.45
ferulic		3.16	2.22
caffeic	2.82	0.37	0.45
stilbenoids			
resveratrol			
other stilbene derivatives		9.16	2.10
chlorogenic acids			
3-0-caffeoylquinic	11.62		4.19
caffeoylquinic (other forms)	21.75	3.28	1.85
flavonoids			
catechin		2.84	1.25
epicatechin		0.81	
quercetin- glucosides	0.09	0.14	0.23
genistein			
daidzein			
cyanidin-glycosides		0.94	1.85
acetylated cyanidins	0.27	0.71	0.19
peonidin-glycosides		3.21	1.21
acetylated peonidins		1.78	
delphinidin-glycosides		5.51	9.77
acetylated delphinidins	0.23	2.12	2.60
petunidin-glycosides		7.66	7.10
acetylated petunidins		2.61	
malvidin-glycosides		22.44	21.69
acetylated malvidins		7.72	
total polyphenols[c]	22.2	328	16.5

[a]Phenolic compounds were tested in duplicate using LC−MS[41] to assay for key compounds. [b]Resveratrol contained 295.12 mg resveratrol/g sample and grape seed extract contained 827 mg/g total polyphenols as determined using the Folin−Ciocalteu[38] method. Grape seed extract was unavailable for analysis using LC−MS. [c]Total polyphenols were determined through the Folin−Ciocalteu method.[38]

extract were chlorogenic acids (11.62 mg/g extract 3-0-caffeoylquinic and 21.75 mg/g extract other forms of caffeoylquinic), which were also notably higher than the content found in grape (3.28 mg/g extract chlorogenic acids) and blueberry (5.04 mg/g extract total chlorogenic acids). Grape and blueberry were both characterized as being higher in anthocyanins (54.7 mg/g extract and 44.41 mg/g extract total anthocyanins, respectively) compared with plum (0.5 mg/g extract total anthocyanins); however, grape had a greater amount of gallic acid compared with blueberry (11.85 mg/g extract compared with 0.45 mg/g extract, respectively), and blueberry contained a higher level of chlorogenic acids than grape (5.04 mg/g extract compared with 3.28 mg/g extract, respectively). Grape extract did not contain resveratrol, but did have other stilbene derivatives (9.16 mg/g extract).

Biochemical Markers of Bone Turnover. Grape seed extract-high ($p = 0.0056$) and grape-high ($p = 0.004$) dietary interventions reduced NTx compared with each corresponding baseline period (Figure 5A and Figure 5B). Resveratrol-low significantly increased NTx compared with the corresponding baseline period ($p = 0.0039$). Blueberry, plum, soy, grape seed extract, grape-low, and resveratrol-high diets did not produce a significant change in NTx.

The aglycon soy diet significantly increased serum bone alkaline phosphatase compared with baseline ($p = 0.03$, data not shown); however, none of the other diets impacted bone alkaline phosphatase.

Urine Total Polyphenols. There was a significant dose response of urinary total polyphenols in blueberry ($p = 0.005$) and grape seed extract ($p < 0.0001$) interventions of arm 1 and grape ($p = 0.0002$) dietary intervention of arm 2 rats (Figure 6A and Figure 6B). There was no difference in total polyphenols between glycosylated soy and genistein aglycon ($p = 0.27$).

DISCUSSION

In this crossover intervention trial in OVX rats, we identified that although both isoflavone-containing diets were effective at increasing bone calcium retention, the aglycon form of genistein was significantly more effective than the glucoside. In addition, we demonstrated that higher levels of resveratrol and plum (0.20% and 0.45% total polyphenols, respectively) increased bone calcium retention.

dx.doi.org/10.1021/jf403310q | J. Agric. Food Chem. 2014, 62, 6108−6117

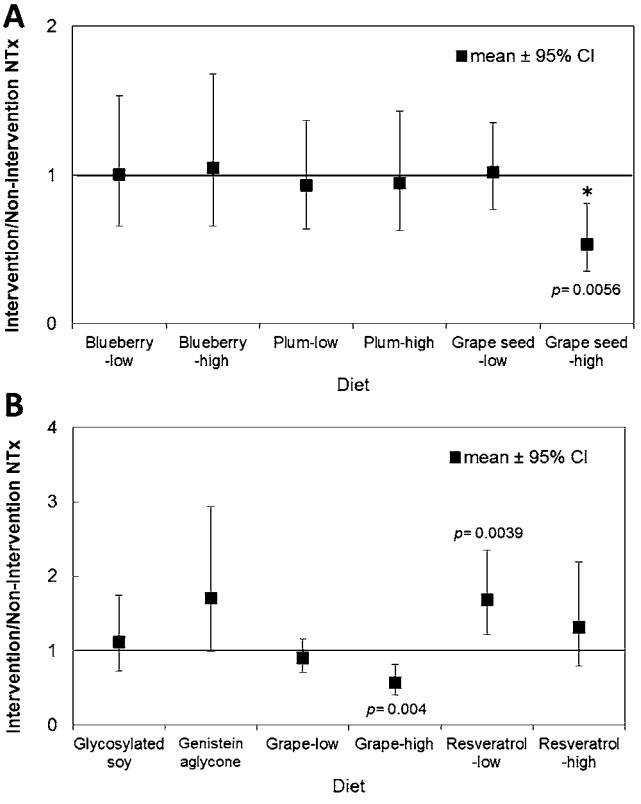

Figure 5. Effect of dietary botanicals on urinary NTx in ovariectomized (OVX) rats was reported as mean ± 95% confidence interval. A value of "1" represents no change from the regression line computed from nonintervention periods. A confidence interval that excludes "1" indicates a significant change from the regression line at α = 0.05. Contrasts were performed after ANOVA. For blueberry (n = 15 for low; n = 16 for high), plum (n = 15 for low; n = 14 for high), and grape seed extract (n = 14 for low; n = 15 for high) diets (A) * indicates a significant ($p < 0.05$) difference between NTx values during the low and corresponding high doses of the same diet. For soy (n = 14 for genistein aglycon; n = 15 for glycosylated soy), grape extract (n = 16 for low and high), and resveratrol (n = 16 for low and high) (B) there was a trend for NTx to be lower during the grape-high diet compared with the grape-low diet (p = 0.078). NTx, urinary collagen type 1 cross-linked N-telopeptide.

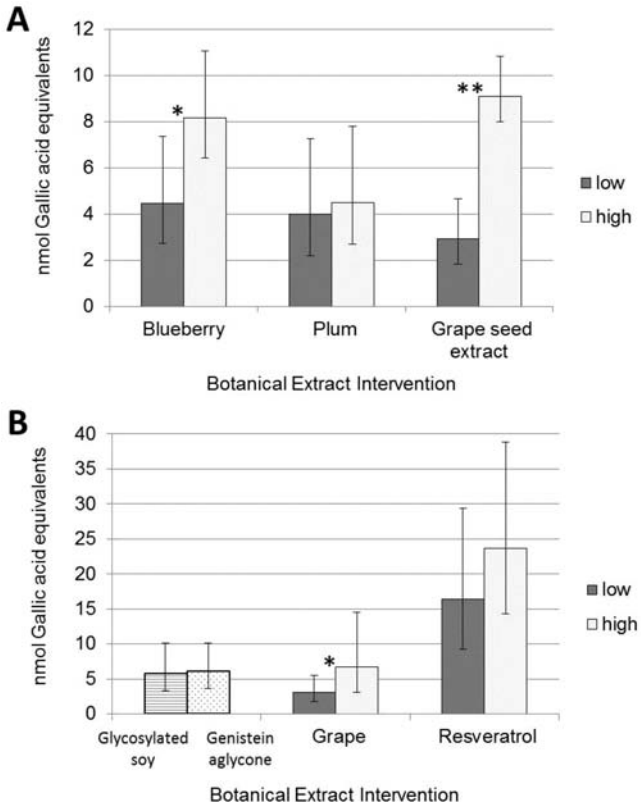

Figure 6. Effect of dietary botanicals on urinary total polyphenols in 24 h urine of ovariectomized (OVX) rats (n = 16 rats per diet). Values are reported as mean ± standard deviation with contrasts performed to detect differences between means. For blueberry, plum, and grape seed extract diets (A) * and ** indicate low is significantly different from high at p = 0.005 and $p < 0.0001$, respectively. All arm 1 diets were significantly different from baseline at p = 0.0015. For soy, grape, and resveratrol diets (B) * indicates that low is significantly different from high at p = 0.0002. There was a trend for total polyphenols during low to be different from high during the resveratrol-high diet with p = 0.06. All arm 2 diets were significantly different from baseline at $p < 0.0001$.

Dietary aglycon soy elicited an improvement to bone calcium retention that was approximately double the response from a diet with glycosylated soy (22% for aglycon soy compared with 13% for glycosylated soy), which supported our hypothesis that the aglycon form of genistein is more effective than the glucoside when tested on an equivalent mass basis of total polyphenols. We did not observe a difference in urinary total polyphenols between genistein aglycon and glycosylated soy, which supports that the glycosylated soy and genistein aglycon diets were formulated to have equivalent isoflavone content. We are first to directly compare soy aglycon to glucoside for effect on bone in an estrogen-depleted rodent model. Through this direct comparison, we were able to demonstrate that the aglycon form of genistein was more effective than glycosylated soy in increasing bone calcium retention.

Cleavage of the sugar moiety is believed to be required for genistin (glycosylated) to be effectively absorbed in the intestine,[9] but absorption of genistein (aglycon) occurs readily[11] and as early in the digestive process as in the stomach.[43] After the glucoside is hydrolyzed and absorbed in the gut, it is conjugated to mostly glucuronic acid by both intestinal and hepatic enzymes. Consumption of the aglycon form of genistein has the potential to lead to a higher presence of unconjugated genistein in the blood due to enhanced uptake in the gut and some absorption in the stomach. This is biologically important because unconjugated genistein has been shown to bind more strongly to estrogen receptor-β than its glucuronide metabolites,[16] demonstrating the potential for a more estrogenic effect on bone. We were able to demonstrate the enhanced efficacy of the aglycon form of genistein on bone in an estrogen-depleted rodent model. Future research should directly compare the metabolites produced from consumption of aglycon and glycoside soy to more closely link this mechanism to the increase in bone calcium retention from the aglycon form of soy.

Estrogen in bone works primarily by decreasing the production of inflammatory cytokines (interleukin (IL)-1, IL-6, and RANKL and M-CSF (macrophage colony stimulating factor)) in osteoblasts and precursor cells to regulate osteoclast activity.[44,45] A drop in estrogen leads to a prominent increase in osteoclast activity, which greatly increases bone resorption with a lag in subsequent bone formation.[18] Although the estrogenic activity of phytoestrogens such as isoflavones has been shown to elicit an antiresorptive response on bone,[24] we observed that

dx.doi.org/10.1021/jf403310q | J. Agric. Food Chem. 2014, 62, 6108−6117

genistein aglycon increased bone calcium retention, consistent with bone formation. This is evidenced by an increase in BAP, which is a marker of bone turnover and often an indicator of an anabolic effect to bone. Our finding suggests that the ability of isoflavones to reduce net bone loss works by stimulating the anabolic bone building effect to counter the increase in resorption caused by loss of estrogen, rather than by mitigating bone resorption only. Urinary calcium tracer excretion is specific to bone mineral balance and more precise than biochemical markers of bone turnover.

Our finding that short-term supplementation of dried plum at 20% w/w diet, delivering 0.45% w/w total dietary polyphenols (plum-high), to OVX rats resulted in a 20% increase in bone calcium retention was similar to the 15% increase in bone tracer retention observed by Mühlbauer et al. using a similar method in OVX rats with a lower percentage (8% w/w diet) of dried prune extract for 10 days.[19] The effects we observed on bone calcium retention from plum is also consistent with doses reported in the literature to be protective to bone in OVX rats, i.e., 15% and 25%.[3−5,46,47] In postmenopausal women, plum supplemented at 100 g/d prevented bone loss and increased BMD;[23,47] the control diet of 100 g/d dried apples also protected bone from loss, but to a lesser degree than dried plum supplementation.[23] This level of dried plum intake would be equivalent to the 25% w/w diet given to rodents and similar to the 20% w/w diet given in this study, assuming that food intake in women totals approximately 400 g/d on a dry weight basis.

We did not find a significant effect on bone with diets of blueberry, grape seed extract, or grape extract in OVX rats. Evaluation of the phenolic profiles of these extracts reveals that chlorogenic acids are more prominent in plum compared to the other extracts. Both chlorogenic acid[48] and dried plum powder[49] have been found to have an inhibitory effect on the RANKL pathway involved in osteoclastogenesis. However, we did not observe a decrease in NTx, a marker of bone resorption, with dietary supplementation with dried plum.

Previous work demonstrated that blueberry at 5% w/w diet prevented the loss of whole-body BMD in OVX rats.[50] Additionally, blueberry at 10% w/w diet fed to prepubertal[6,51] rats prevented bone loss later in life; the suggested mechanism was that phenolic acids found in blueberry promoted osteoblast differentiation. Although sera phenolic acid derivatives were described,[6] the phenolic profile of the blueberry extract was not reported. The lack of effect observed in our study could potentially be attributed to differences in blueberry phenolic profile and concentration of phenolic compounds in the extract. While abundant in anthocyanins, blueberry had lower levels of chlorogenic acids compared with the plum powder, which may have impacted the efficacy of the blueberry diet.

Grape seed extract when given with calcium was shown to have a protective effect on bone in adult and growing intact rats when given immediately following a low calcium diet.[2,22] We tested grape seed extract in an estrogen-depleted rodent model and did not find an effect on bone. Catechins, the most abundant polyphenols present in grape seed extract,[52] have been shown to have estrogenic activity,[53,54] and there is evidence to suggest that catechins from green tea have a role in preventing postmenopausal bone loss.[55,56] however, the binding affinity of different catechins to estrogen receptor-β should be investigated further as this receptor more directly impacts bone.

We did not see an effect of grape extract (0.2−1% w/w total polyphenols in diet) on bone calcium retention; however, we did find that resveratrol-high, which delivered 0.2% dry matter as total polyphenols in the diet, increased bone calcium retention by 14%. Mühlbauer et al.[19] fed rats 8% w/w diet red wine residue and observed a reduction in bone resorption; however, the measured total polyphenols and resveratrol content were not reported. Despite anthocyanins and gallic acid being more prominent in grape than the other extracts, our analysis of the phenolic profile of grape extract showed an absence of resveratrol, a compound which has been proven to have estrogenic activity[17] and was effective as an isolated compound in our study. Further analysis comparing grape extracts with varying levels of resveratrol should be tested to determine if efficacy is due primarily to resveratrol.

Total polyphenols were significantly higher during the botanical interventions than during baseline and washout periods, suggesting that polyphenols were absorbed and cleared into urine from test diets. Total polyphenols were not significantly different during the washout compared with baseline, which suggests clearance of prior diet in the system and no carryover effect.

Biochemical markers of bone turnover were not always consistent with bone calcium retention response to diets. Grape seed extract-high and grape-high supplementation decreased NTx without a change in bone calcium retention. Resveratrol-low induced an increase in NTx, but had no significant effect on bone calcium retention. The increase in bone calcium retention for glycosylated soy, aglycon soy, plum-high, and resveratrol-high failed to lower NTx or increase bone alkaline phosphatase.

In our crossover study with OVX rats, dietary plum, resveratrol, genistein glucoside, and genistein aglycon increased bone calcium retention by 13−22%. To our knowledge we are the first to directly compare and report the enhanced effect of genistein aglycon on bone. Additionally, we confirmed efficacy of dried plum on bone and highlighted chlorogenic acids as the group of phenolic compounds contributing to increased bone calcium retention. Although we did not observe a bone protective effect with a resveratrol-devoid grape extract, we did observe a strong bone protective effect with resveratrol, which suggests that resveratrol may be the active component in other grape products that have been shown to have bone protective effects. Future studies could extend this work by evaluating the effect of specific classes of botanical polyphenolics on bone strength measures.

AUTHOR INFORMATION

Corresponding Author

*Phone: (765) 494-8237. Fax: (765) 494-0674. E-mail: weavercm@purdue.edu.

Present Address

‡5450 Prairie Stone Parkway, Hoffman Estates, IL 60192.

Funding

This research was supported in part by the United States Department of Agriculture National Needs Fellowship for Foods for Health and by Grant P50-AT00477 from the National Institutes of Health.

Notes

The authors declare no competing financial interest.

■ ACKNOWLEDGMENTS

P. J. Lachcik is thanked for helping with handling and performing procedures on rats. J. R. Burgess is thanked for helping with designing and performing the plan for total polyphenol analysis.

■ ABBREVIATIONS USED

OVX, ovariectomized; BMD, bone mineral density; RANK, receptor activator of nuclear factor kappa-B; RANKL, receptor activator of nuclear factor kappa-B ligand; M-CSF, macrophage colony stimulating factor; IL, interleukin; NTx, cross-linked N-telopeptides of type I collagen; ANOVA, analysis of variance

■ REFERENCES

(1) Zhang, X.; Shu, X.; Li, H.; Yang, G.; Li, Q.; Gao, Y.; Zheng, W. Prospective cohort study of soy food consumption and risk of bone fracture among postmenopausal women. *Arch. Int. Med.* **2005**, *165*, 1890−1895.

(2) Kamitani, Y.; Maki, K.; Tofani, I.; Nishikawa, Y.; Tsukamoto, K.; Kimura, M. Effects of grape seed proanthocyanidins extract on mandibles in developing rats. *Oral Dis.* **2004**, *10*, 27−31.

(3) Bu, S. Y.; Lucas, E. A.; Franklin, M.; Marlow, D.; Brackett, D. J.; Boldrin, E. A.; Devareddy, L.; Arjmandi, B. H.; Smith, B. J. Comparison of dried plum supplementation and intermittent PTH in restoring bone in osteopenic orchidectomized rats. *Osteoporosis Int.* **2007**, *18*, 931−942.

(4) Halloran, B. P.; Wronski, T. J.; VonHerzen, D. C.; Chu, V.; Xia, X.; Pingel, J. E.; Williams, A. A.; Smith, B. J. Dietary dried plum increases bone mass in adult and aged male mice. *J. Nutr.* **2010**, *140*, 1781−1787.

(5) Franklin, M.; Bu, S. Y.; Lerner, M. R.; Lancaster, E. A.; Bellmer, D.; Marlow, D.; Lightfoot, S. A.; Arjmandi, B. J.; Brackett, D. J.; Lucas, E. A.; Smith, B. J. Dried plum prevents bone loss in a male osteoporosis model via IGF-1 and the RANK pathway. *Bone* **2006**, *39*, 1331−1342.

(6) Chen, J. R.; Lazarenko, O. P.; Wu, X.; Kang, J.; Blackburn, M. L.; Shankar, K.; Badger, T. M.; Ronis, M. J. J. Dietary-induced serum phenolic acids promote bone growth via p38 MAPK/β-catenin canonical Wnt signaling. *J. Bone Miner. Res.* **2010**, *25*, 2399−2411.

(7) Reinwald, S.; Weaver, C. M. Soy components vs. whole soy: are we betting our bones on a long shot? *J. Nutr.* **2010**, *140*, 2312S−2317S.

(8) North American Menopause Society. The role of soy isoflavones in menopausal health: report of The North American Menopause Society/Wulf H. Utian Translational Science Symposium in Chicago, IL (October 2010). *Menopause* **2011**, *7*, 732−753.

(9) Setchell, K. D. R.; Brown, N. M.; Zimmer-Nechemias, L.; Brashear, W. T.; Wolfe, B. E.; Kirschner, A. S.; Heubi, J. E. Evidence for lack of absorption of soy isoflavone glycosides in humans, supporting the crucial role of intestinal metabolism for bioavailability. *Am. J. Clin. Nutr.* **2002**, *76*, 447−453.

(10) Zubik, L.; Meydani, M. Bioavailability of soybean isoflavones from aglycone and glucoside forms in American women. *Am. J. Clin. Nutr.* **2003**, *77*, 1459−1465.

(11) Izumi, T.; Piskula, M. K.; Osawa, S.; Obata, A.; Tobe, K.; Saito, M.; Kataoka, S.; Kubota, Y.; Kikuchi, M. Soy isoflavone aglycones are absorbed faster and in higher amounts than their glucosides in humans. *J. Nutr.* **2000**, *130*, 1695−1699.

(12) Morabito, N.; Crisafulli, A.; Vergara, C.; Gaudio, V.; Lasco, A.; Frisina, N.; D'Anna, R.; Corrado, F.; Pizzoleo, M. A.; Cinotta, M.; Altavilla, D.; Ientile, R.; Squadrito, F. Effects of genistein and hormone-replacement therapy on bone loss in early postmenopausal women: a randomized double-blind placebo controlled study. *J. Bone Miner. Res.* **2002**, *17*, 1904−1912.

(13) Marini, H.; Minutoli, L.; Polito, F.; Bitto, A.; Altavilla, D.; Atteritano, M.; Gaudio, A.; Mazzaferro, S.; Frisina, A.; Frisina, N.; Lubrano, C.; Bonaiuto, M.; D'Anna, R.; Cannata, M.; Corrado, F.; Adamo, E.; Wilson, S.; Squadrito, F. Effects of the phytoestrogen genistein on bone metabolism in osteopenic postmenopausal women: a randomized trial. *Ann. Int. Med.* **2007**, *146*, 839−847.

(14) Bitto, A.; Burnett, B. P.; Polito, F.; Marini, H.; Levy, R. M.; Armbruster, M. A.; Minutoli, L.; Di Stefano, V.; Irrera, N.; Antoci, S.; Granese, S.; Squadrito, F.; Altavilla, D. Effects of genistein aglycone in osteoporotic, ovariectomized rats: a comparison with alendronate, raloxifene and oestradiol. *Br. J. Pharmacol.* **2008**, *155*, 896−905.

(15) Bitto, A.; Burnett, B. P.; Polito, F.; Levy, R. M.; Marini, H.; Di Stefano, V.; Irrera, N.; Armbruster, M. A.; Minutoli, L.; Altavilla, D.; Squadrito, F. Genistein aglycone reverses glucocorticoid- induced osteoporosis and increases bone breaking strength in rats: a comparative study with alendronate. *Br. J. Pharmacol.* **2009**, *156*, 1287−1295.

(16) Kinjo, J.; Tsuchihashi, R.; Morito, K.; Hirose, T.; Aomori, T.; Nagao, T.; Okabe, H.; Nohara, T.; Masamune, Y. Interactions of phytoestrogens with estrogen receptors α and β (III). Estrogenic activities of soy isoflavone aglycones and their metabolites isolated from human urine. *Biol. Pharm. Bull.* **2004**, *27*, 185−188.

(17) Bowers, J.; Tyulmenkov, V.; Jernigan, S.; Klinge, C. Resveratrol acts as a mixed agonist/antagonist for estrogen receptors alpha and beta. *Endocrinology* **2000**, *141*, 3657−3667.

(18) Reinwald, S.; Weaver, C. M. Soy isoflavones and bone health: A double-edged sword? *J. Nat. Prod.* **2006**, *69*, 450−459.

(19) Mühlbauer, R. C.; Lozano, A.; Reinli, A.; Wetli, H. Various selected vegetables, fruits, mushrooms and red wine residue inhibit bone resorption in rats. *J. Nutr.* **2003**, *133*, 3592−3597.

(20) Weaver, C. M.; Alekel, D. L.; Ward, W. E.; Ronis, M. J. Flavonoid intake and bone health. *J. Nutr. Gerontol. Geriatr.* **2012**, *31*, 239−253.

(21) Boissy, P.; Andersen, T. L.; Abdallah, B. M.; Kassem, M.; Plesner, T.; Delaissé, J. Resveratrol inhibits myeloma cell growth, prevents osteoclast formation, and promotes osteoblast differentiation. *Cancer Res.* **2005**, *65*, 9943−9952.

(22) Yahara, N.; Tofani, I.; Maki, K.; Kojima, K.; Kojima, Y.; Kimura, M. Mechanical assessment of effects of grape seed proanthocyanidins extract on tibial bone diaphysis in rats. *J. Musculoskeletal Neuronal Interact.* **2005**, *5*, 162−169.

(23) Hooshmand, S.; Chai, S. C.; Saadat, R. L.; Payton, M. E.; Brummel-Smith, K.; Arjmandi, B. H. Comparative effects of dried plum and dried apple on bone in postmenopausal women. *J. Chromatogr. A* **2011**, *913*, 397−413.

(24) Weaver, C. M.; Martin, B. R.; Jackson, G. S.; McCabe, G. P.; Nolan, J. R.; McCabe, L. D.; Barnes, S.; Reinwald, S.; Boris, M. E.; Peacock, M. Antiresorptive effects of phytoestrogen supplements compared with estradiol or risedronate in postmenopausal women using 41 Ca methodology. *J. Clin. Endocrinol. Metab.* **2009**, *94*, 3798−3805.

(25) Cheong, J. M. K.; Martin, B. R.; Jackson, G. S.; Elmore, D.; McCabe, G. P.; Nolan, J. R.; Barnes, S.; Peacock, M.; Weaver, C. M. Soy isoflavones do not affect bone resorption in postmenopausal women: a dose-response study using a novel approach with 41Ca. *J. Clin. Endocrinol. Metab.* **2007**, *92*, 577−582.

(26) Mühlbauer, R. C.; Lozano, A.; Reinli, A. Onion and a mixture of vegetables, salads, and herbs affect bone resorption in the rat by a mechanism independent of their base excess. *J. Bone Miner. Res.* **2002**, *17*, 1230−1236.

(27) Mühlbauer, R. C.; Li, F.; Lozano, A.; Reinli, A.; Tschudi, I. Some vegetables (commonly consumed by humans) efficiently modulate bone metabolism. *J. Musculoskeletal Neuronal Interact.* **2000**, *1*, 137−40.

(28) Mühlbauer, R. C.; Fleisch, H. The diurnal rhythm of bone resorption in the rat: effect of feeding habits and pharmacological inhibitors. *J. Clin. Invest.* **1995**, *95*, 1933−1940.

(29) Zhao, Y.; Cheong, J. M. K.; Lee, W. H.; Wastney, M.; Martin, B. R.; Weaver, C. M. Tetracycline and calcium kinetics are comparable in estimating bone resorption in rats. *J. Nutr.* **2010**, *140*, 1704−1709.

(30) Cheong, J. M. K.; Gunaratna, N. S.; McCabe, G. P.; Jackson, J. S.; Weaver, C. M. Bone seeking labels as markers for bone turnover:

effect of dosing schedule on labeling various bone sites in rats. *Calcif. Tissue Int.* **2009**, *85*, 444−450.
(31) Cheong, J.; Gunaratna, N.; McCabe, G.; Jackson, G.; Kempa-Steczko, A.; Weaver, C. M. Bone seeking labels as markers for bone turnover: Validation of urinary excretion in rats. *Osteoporosis Int.* **2011**, *22*, 153−157.
(32) Lee, W. H.; Wastney, M. E.; Jackson, G. S.; Martin, B. R.; Weaver, C. M. Interpretation of 41Ca data using compartmental modeling in post-menopausal women. *Anal. Bioanal. Chem.* **2011**, *399*, 1613−1622.
(33) Klein, L.; Van Jackman, K. Assay of bone resorption in vivo with 3H-Tetracycline. *Calcif. Tiss. Res.* **1976**, *20*, 275−290.
(34) DeMoss, D. L.; Wright, G. L. Analysis of whole skeleton 3H-tetracycline loss as a measure of bone resorption in maturing rats. *Calcif. Tiss. Int.* **1997**, *61*, 412−417.
(35) Klein, L. Direct measurement of bone resorption and calcium conservation during vitamin D deficiency or hypervitaminosis D. *Proc. Natl. Acad. Sci. U.S.A.* **1980**, *77*, 1818−1822.
(36) Mühlbauer, R. C.; Fleisch, H. A method of continual monitoring of bone resorption in rats: evidence for a diurnal rhythm. *Am. J. Physiol.* **1990**, *259*, R659−R689.
(37) Song, B. J.; Jouni, Z. E.; Ferruzzi, M. G. Assessment of phytochemical content in human milk during different stages of lactation. *Nutrition* **2013**, *29*, 195−202.
(38) Reeves, P. G.; Nielsen, F. H.; Fahey, G. C., Jr. AIN-93 purified diets for laboratory rodents: final report of the American Institute of Nutrition ad hoc writing committee on the reformulation of the AIN-76A rodent diet. *J. Nutr.* **1993**, *123*, 1939−1951.
(39) Saucier, C. T.; Waterhouse, A. L. Synergistic activity of catechin and other antioxidants. *J. Agric. Food Chem.* **1999**, *47*, 4491−4494.
(40) Reinwald, S.; Mayer, L. P.; Hoyer, P. B.; Turner, C. H.; Barnes, S.; Weaver, C. M. A longitudinal study of the effect of genistein on bone in two different murine models of diminished estrogen-producing capacity. *J. Osteoporosis* **2010**, *2010*, 1−14.
(41) Zhang, Y.; Li, Q.; Wan, H. Y.; Helferich, W. G.; Wong, M. S. Genistein and a soy extract differentially affect three-dimensional bone parameters and bone-specific gene expression in ovariectomized mice. *J. Nutr.* **2009**, *139*, 2230−2236.
(42) Medina-Remón, A.; Barrionuevo-González, A.; Zamora-Ros, R.; Andres-Lacueva, C.; Estruch, R.; Martínez- González, M.; Diez-Espino, J.; Lamuela-Raventos, R. M. Rapid Folin-Ciocalteu method using microtiter 96-well plate cartridges for solid phase extraction to assess urinary total phenolic compounds, as a biomarker of total polyphenols intake. *Anal. Chim. Acta* **2009**, *634*, 54−60.
(43) Piskula, M. K.; Yamakoshi, J.; Iwai, Y. Daidzein and genistein but not their glucosides are absorbed from the rat stomach. *FEBS Lett.* **1999**, *447*, 287−291.
(44) Rosen, C. J. Role of sex steroids in the pathogenesis of Osteoporosis. In *Primer on the metabolic bone diseases and disorders of mineral metabolism*, 7th ed.; American Society for Bone and Mineral Research: Washington, DC, 2008; pp 208−213.
(45) Jilka, R. L.; Hangoc, G.; Girasole, G.; Passeri, G.; Williams, D. C.; Abrams, J. S.; Boyce, B.; Broxmeyer, H.; Manolagas, S. C. Increased osteoclast development after estrogen loss: mediation by interleukin-6. *Science* **1992**, *257*, 88−91.
(46) Rendina, E.; Lim, Y. F.; Marlow, D.; Wang, Y.; Clarke, S. L.; Kuvibidila, S.; Lucas, E. A.; Smith, B. J. Dietary supplementation with dried plum prevents ovariectomy-induced bone loss while modulating the immune response in C57BL/6J mice. *J. Nutr. Biochem.* **2011**, *23*, 60−68.
(47) Arjmandi, B. H.; Khalil, D. A.; Lucas, E. A.; Georgis, A.; Stoecker, B. J.; Hardin, C.; Payton, M.; Wild, R. A. Dried plums improve indices of bone formation in postmenopausal women. *J. Women's Health Gender-Based Med.* **2002**, *11*, 61−68.
(48) Kwak, S. C.; Lee, C.; Kim, J. Y.; Oh, H. M.; So, H. S.; Lee, M. S.; Rho, M. C.; Oh, J. Chlorogenic acid inhibits osteoclast differentiation and bone resorption by down-regulation of receptor activator of nuclear factor kappa-B ligand-induced nuclear factor of activated T cells c1 expression. *Biol. Pharm. Bull.* **2013**, *36*, 1779−1786.
(49) Bu, S. Y.; Lerner, M.; Stoecker, B. J.; Boldrin, E.; Brackett, D. J.; Lucas, E. A.; Smith, B. J. Dried plum polyphenols inhibit osteoclastogenesis by downregulating NFATc1 and inflammatory mediators. *Calcif. Tissue Int.* **2008**, *82*, 475−488.
(50) Devareddy, L.; Hooshmand, S.; Collins, J.; Lucas, E.; Chai, S.; Arjmandi, B. J. Blueberry prevents bone loss in ovariectomized rat model of postmenopausal osteoporosis. *J. Nutr. Biochem.* **2008**, *19*, 694−699.
(51) Zhang, J.; Lazerenko, O. P.; Blackburn, M. L.; Shankar, K.; Badger, T. M.; Ronis, M. J. J.; Chen, J. R. Feeding blueberry diets in early life prevent senescence of osteoblasts and bone loss in ovariectomized adult female rats. *PLoS One* **2011**, *6*, 1−13.
(52) Shi, J.; Yu, J.; Pohorly, J. E.; Kakuda, Y. Polyphenolics in grape seed-biochemistry and functionality. *J. Med. Food.* **2003**, *6*, 291−299.
(53) Kuruto-Niwa, R.; Inoue, S.; Ogawa, S.; Muramatsu, M.; Nozawa, R. Effects of tea catechins on the ERE-regulated estrogenic activity. *J. Agric. Food Chem.* **2000**, *48*, 6255−6361.
(54) Goodin, M. G.; Fertuck, K. C.; Zacharewski, T. R.; Rosengren, R. J. Estrogen receptor-mediated actions of polyphenolic catechins in vivo and in vitro. *Toxicol. Sci.* **2002**, *69*, 354−361.
(55) Hegarty, V.; May, H.; Khaw, K. Tea drinking and bone mineral density in older women. *Am. J. Clin. Nutr.* **2000**, *71*, 1003−1007.
(56) Ko, C.; Lau, K.; Choy, W.; Leung, P. Effects of tea catechins, epigallocatechin, gallocatechin, and gallocatechin gallate, on bone metabolism. *J. Agric. Food Chem.* **2009**, *57*, 7293−7297.

JOURNAL OF AGRICULTURAL AND FOOD CHEMISTRY

Article

pubs.acs.org/JAFC

Profiling of Glucosinolates and Flavonoids in *Rorippa indica* (Linn.) Hiern. (Cruciferae) by UHPLC-PDA-ESI/HRMS^n

Long-Ze Lin,*[,†] Jianghao Sun,[†] Pei Chen,[†] Ren-Wei Zhang,[§] Xiao-E Fan,[§] Lai-Wei Li,[§] and James M. Harnly[†]

[†]Food Composition and Methods Development Laboratory, Beltsville Human Nutrition Research Center, Agricultural Research Service, U.S. Department of Agriculture, Building-161, BARC-East, 10300 Baltimore Avenue, Beltsville, Maryland 20705, United States

[§]Longjin Pharmaceutical Company, Ltd., Wujiadui News Road, Kunming, Yunnan 650228, China

ABSTRACT: An UHPLC-PDA-ESI/HRMS^n profiling method was used to identify the glucosinolates and flavonoids of *Rorippa indica* (Cruciferae), a wild vegetable and Chinese herb used to treat cough, diarrhea, and rheumatoid arthritis. Thirty-three glucosinolates, more than 40 flavonol glycosides, and 18 other phenolic and common organic compounds were identified. The glucosinolates and polyphenols were separated by UHPLC. High-resolution deprotonated molecules provided high accuracy mass values that were used to determine formulas and provide putative identification of the glucosinolates and flavonoids. The fragments from multistage mass spectrometry were used to elucidate the structures. The concentrations of the main components were based on UV peak areas and molar relative response factors with a single calibration standard. This study found this plant to be a rich source for glucosinolates, containing 24 new glucosinolates, including 14 glucosylated glucosinolates that were previously unidentified.

KEYWORDS: *glucosinolates, flavonol glycosides, Rorippa indica (Cruciferae), Chinese wild vegetable, Chinese herb, UHPLC-PDA-ESI/HRMS^n, compound identification, main compound quantification*

INTRODUCTION

Glucosinolates (GSs) are sulfur- and nitrogen-containing secondary metabolites found in cruciferous plants. A central carbon is connected to a thioglucose, to a sulfate via a nitrogen atom, and to a side chain (R) (Figure 1). The side chain determines whether the glucosinolate is defined as aliphatic (straight- or branched-chain alkyl, alkenyl, and oxo-, hydroxyl forms), aromatic, or indole. Many glucosinolates also contain one or two more sulfur atoms in the side chain to form another sulfur-containing unit, such as methyl-thio- (−S−), methyl-sulfinyl- (−SO−), methyl- or benzyl-sulfonyl- (−SO_2−), mercapto- (HS−), glucosyl-disulfanyl (−S−S−), and cysteinyl-thio- [HOOC−CH(NH_2)−CH_2−S−]. The glucosinolates and their enzyme-hydrolyzed products (thiocyanates, isothiocyanates, and nitriles) have shown important human health benefits, especially with respect to cancer prevention. Thus, many studies have been carried out on the isolation and structural elucidation of glucosinolates and their hydrolyzed products with respect to their biological activities and distribution in the plant kingdom.[1−7]

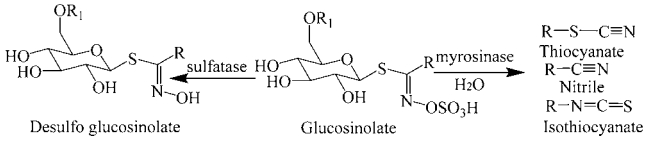

The identification code, name, and R and R_1 groups of the glucosinolates

GS-1 to GS-3 : R=9-(methylsulfonyl)nonyl (straight and branch chain, R_1=H
GS-4: R=7-methylsulfonylheptyl, R_1=H
GS-5: R=8-(methylsulfonyl)octyl, R_1=H
GS-6: R=10-methylsulfonyldecyl, R_1=H
GS-7: R=8-(methylsulfinyl)octyl, R_1=H
GS-8 and GS-9: R=9-(methylsulfinyl)nonyl(straight and branch chain), R_1=H
GS-10: R=10-(methylsulfinyl)decyl, R_1=H
GS-11: R=4-methoxyindol-3-ylmethyl, R_1=H
GS-12: R=hydroxyundecyl, R_1=H
GS-13 to GS-16: R=9-(methylsulfonyl)hydroxynonyl (straight and branch chain), R_1=H
GS-17 and GS-18: R=10-methylsulfonylhydroxydecyl (straight and branch chain), R_1=H
GS-19 to GS-22: R=9-(methylsulfonyl)nonyl (straight and branch chain), R_1=Glc
GS-23: R=9-(methylsulfinyl)nonyl, R_1=Glc
GS-24 to GS-26: R=10-methylsulfonyldecyl (straight and branch chain), R_1=Glc
GS-27 and GS-28 : R=9-(methylsulfinyl)nonyl, , R_1=Glc
GS-29: R=10-(methylsulfinyl)decyl, R_1=Glc
GS-30: R=methylthioethenylpentyl, R_1=Glc
GS-31: R=7-methylthio-3-oxoheptyl, R_1=Glc
GS-32: R=8-methylthiooctyl, R_1=Glc; R1=H: deoxyglucohirsutin in RS)
GS-33: R=7-(methylsulfinyl)heptyl, R_1=Glc

Figure 1. Structures of the glucosinolates of *Rorippa indica*.

To date, approximately 200 glucosinolates have been reported in plants. An electronic database of the structures, formulas, and accurate masses of 200 knownn and a further 180 predictedn GSs has been established.[8] Desulfoglucosinolates, glucosinolate-related nitriles, and isothiocyanates (Figure 1) formed by the loss of SO_3 or other functional groups through the action of sulfatase and myrosinase have been isolated from plants.[9,10] Glucosinolates, widely distributed in many plants of the Cruciferae family, have also been found in plants from other familiesn although at significantly reduced levels. The glucosinolate profiles of many foods derived from cruciferous plants have been studied qualitatively and quantitatively to

Received: December 12, 2013
Revised: May 28, 2014
Accepted: June 3, 2014
Published: June 3, 2014

ACS Publications © 2014 American Chemical Society

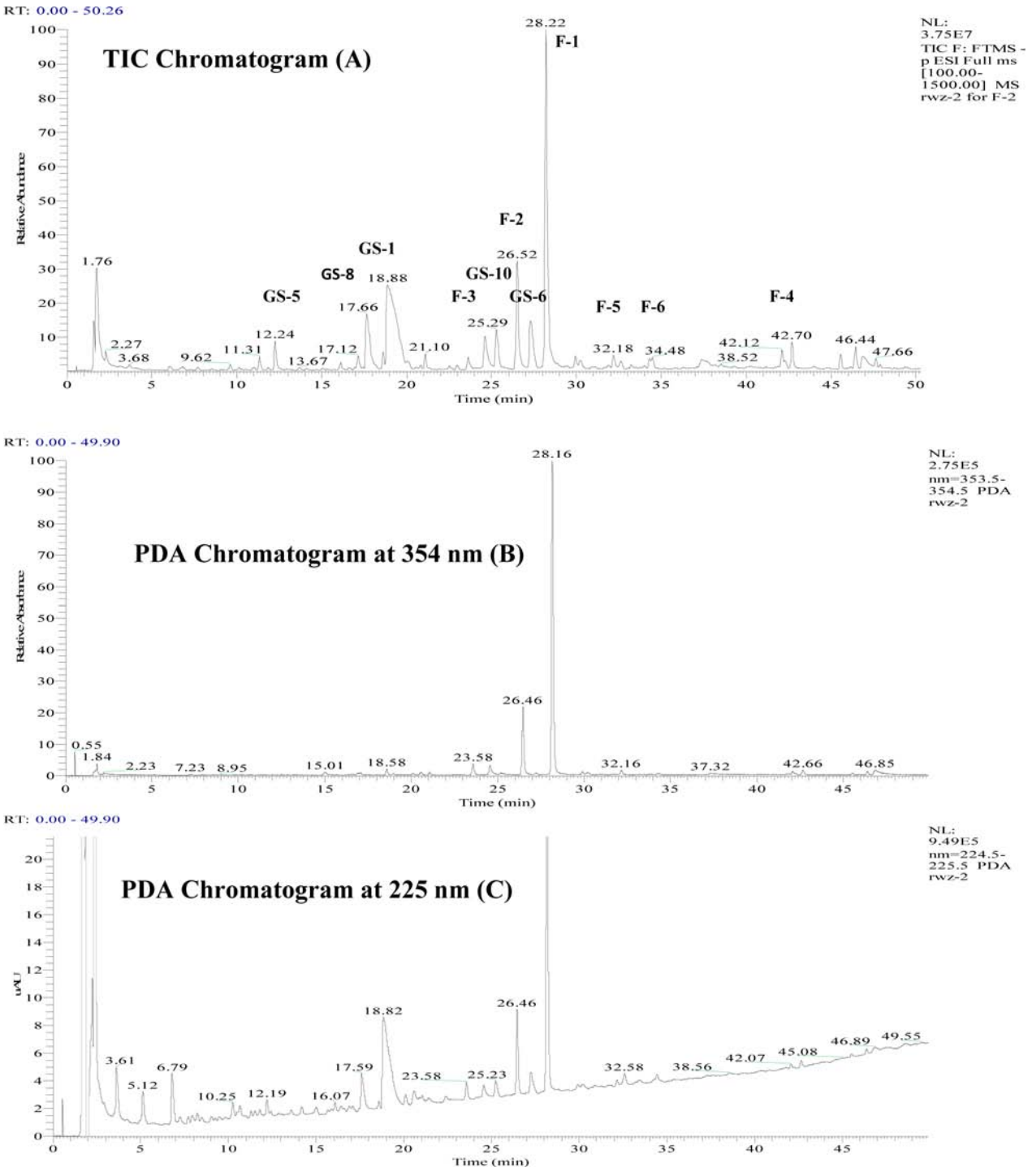

Figure 2. Chromatograms (A, TIC; B, PDA at 354 nm; and C, PDA at 225 nm) of *Rorippa indica* (only the main glucosinolates and flavonoids are labeled).

establish their dietary intake and relationship to health outcomes in biological, epidemiological, and clinical studies.[1−28]

The fragmentation patterns of glucosinolates have been studied using multistage mass spectrometry (MS^n), primarily in the negative ionization mode. High-performance liquid chromatography and MS^n with electrospray ionization (HPLC-ESI/MS^n) has been widely used to identify the intact glucosinolate components of plants.[8,11−18] Most glucosinolates have an ultraviolet (UV) absorbance maximum wavelength (λ_{max}) between 219 and 228 nm. They can be quantified directly from the UV absorbance at 225 nm when they are well separated.[8,14,19,20] However, in most cases, quantification has been based on absorbance of the desulfoglucosinolates following sulfatase hydrolysis. Quantification is based on calibration with a single compound and predetermined relative response factors (RRFs).[8,20−26]

Rorippa indica (Linn.) Hiern. is a perennial plant of the Cruciferae family that is widely distributed throughout the world. Its fresh spear-shaped leaves and tender seedlings are

dx.doi.org/10.1021/jf405538d | J. Agric. Food Chem. 2014, 62, 6118−6129

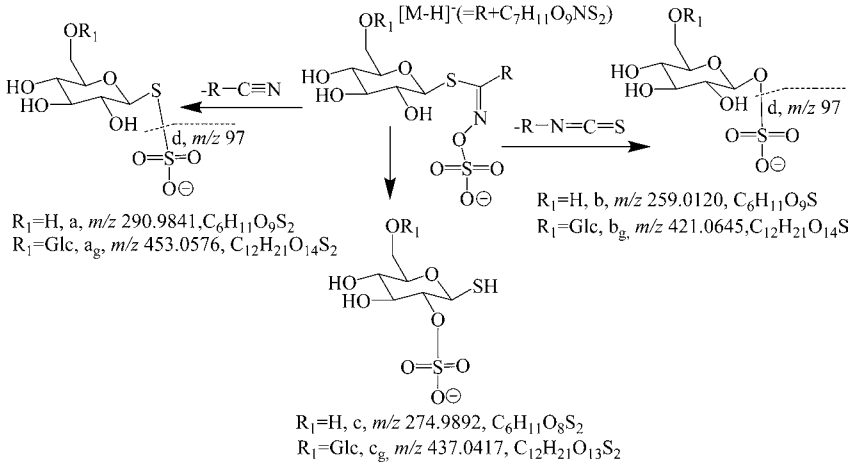

Figure 3. Molecular and typical fragments for the glucosinolates in *Rorippa indica*.

used as a healthy food, and the whole plant is used as an animal feed in China. The dried whole plant material is used as a Chinese traditional herb with purported diuretic, anti-inflammatory, antifever, and anticough properties and to help with blood circulation and rheumatoid arthritis.[27] Some glucosinolates have been reported in *R. indica* and several other *Rorippa* plants.[4,28] Ronifore (9-methylsulfonylnonyl nitrile) and its related amide (rorifamide) were isolated as the anticough components of *Rorippa montana*.[27,29] Fifteen isothiocyanates and desulfoglucosinolates were isolated from the roots of *Rorippa* plants, and several flavonol glycosides, phenolic acids, and derivatives, and other organic compounds have been reported.[9,28−30] This paper presents a comprehensive study of the glucosinolate and polyphenolic components of *R. indica*.

Phenolic compounds are widely distributed in plant-derived foods, whereas the glucosinolates are among the biologically active components of Cruciferous plants. Both types of compounds are known to have many potential benefits to human health. As a part of our project to systematically identify and quantify these compounds, both standardized HPLC-PDA-ESI/MS and UHPLC-PDA-ESI/HRMS^n methods were developed to identify and quantify the phenolics using their molar relative response factors (MRRFs) for UV absorbance.[31−33] In this study, the UHPLC-PDA-ESI/HRMS^n method was used to analyze the phenolic and glucosinolate profiles of *R. indica* and led to the identification of 33 glucosinolates, including 24 for the first time, and more than 40 flavonol glycosides. This study found that *R. indica* was a rich plant source for glucosinolates on the basis of its structural variety and total concentration of glucosinolates.[4,5,8]

MATERIALS AND METHODS

Standards and Other Chemicals. Glucocheirolin potassium salt [3-(methylsulfonyl)propyl glucosinolate-K, MW = 439 + 39 Da], rutin $3H_2O$ (MW = 610 + 54 Da), quercetin, kaempferol, and isorhamnetin were obtained from Chromadex, Inc. (Irvine, CA, USA). Formic acid, hydrochloric acid (~37%), HPLC grade methanol, and acetonitrile were purchased from VWR International, Inc. (Clarksburg, MD, USA). HPLC grade water was prepared from distilled water using a Milli-Q system (Millipore Lab., Bedford, MA, USA).

Standard Solutions. The stock standard solution consisted of dried rutin (1.27 mg) [34] and glucocheriolin-K (1.43 mg) in 10.0 mL of methanol/water (60:40, v/v). The stock solution was prepared at three concentrations (1, 1/2, and 1/4) to provide a range of signals suitable for the quantification of the main glucosinolates and phenolics of this sample. Each of the solutions (2 μL) was injected in triplicate, and the relative standard deviation (RSD) for each peak was <5.0%. The three standards provided a linear calibration curve for estimating the concentration of the main compounds of the extract.[31,32]

Plant Materials and Extracts. The dried *R. indica* plant materials were purchased by the Longjin Pharmaceutical Co., Ltd., from local herb stores in Chongqing, China. The plant materials were ground into powders and passed through 60 mesh sieves prior to extraction. The ground powder (200 mg) was extracted with 5.0 mL of methanol/water (60:40, v/v) using an FS30 ultrasonic sonicator (Fisher Scientific, Pittsburgh, PA, USA) for 60 min at room temperature. The slurry mixture was centrifuged at 2500 rpm for 15 min (IEC Clinical Centrifuge, Damon/IEC Division, Needham, MA, USA), and the supernatant (4.000 mL) was filtered through a 17 mm (0.45 μm) PVDF syringe filter (VWR Scientific, Seattle, WA, USA). Two microliters of the extract was injected in triplicate into the HPLC for analysis.[31−33]

Acidic Hydrolyzed Extracts. The filtered extracts (0.50 mL) were mixed with concentrated HCl (37%, 0.1 mL) and heated in a capped tube at 85 °C for 2 h. Then, 0.4 mL of methanol was added to the mixture, and the solution was sonicated for 10 min. The solution was refiltered prior to HPLC injection.[31]

UHPLC-PDA-ESI/HRMS^n Conditions. The UHPLC-DAD-ESI/HRMS-MS^n system used consisted of an LTQ Orbitrap XL mass spectrometer with an Accela 1250 binary Pump, a PAL HTC Accela TMO autosampler, a diode array detector (DAD) (ThermoScientific, San Jose, CA, USA), and a G1316A column compartment (Agilent, Palo Alto, CA, USA). The separation was carried out on an UHPLC column (200 mm × 2.1 mm i.d., Hypersil Gold AQ RP- C18, 1.9 μm) (ThermoScientific) with an HPLC/UHPLC precolumn filter (Ultra-Shield Analytical Scientific Instruments, Richmond, CA, USA) at a flow rate of 0.3 mL/min. The mobile phase consisted of a combination of A (0.1% formic acid in water, v/v) and B (0.1% formic acid in acetonitrile, v/v). The linear gradient was from 4 to 20% B (v/v) at 40 min, to 35% B at 60 min, to 100% B at 61 min, and held at 100% B to 65 min.[32] The PDA recorded spectra from 200 to 700 nm, and peak intensities at 225 and 354 nm were used for the quantification of the main glucosinolates and flavonoids, respectively.[33]

The MS was operated in the negative ionization mode using the following conditions: sheath gas at 70 (arbitrary units), auxiliary and sweep gas at 15 (arbitrary units), spray voltage at 4.8 kV, capillary temperature at 300 °C, capillary voltage at 15 V, and tube lens at 70 V. The scan range was from m/z 100 to 1500 with a resolution of 15000, FTMS AGC target at 2e5, FT-MS/MS AGC target at 1e5, isolation width of m/z 1.5, and maximum ion injection time of 500 ms. High-accuracy ion mass values were determined for all primary ions (i.e., the deprotonated molecular ions). The most intense ion was selected for the data-dependent scan to provide MS^2−MS^5 product ions with a normalized collision energy at 35% (CID).[33] The product ions were

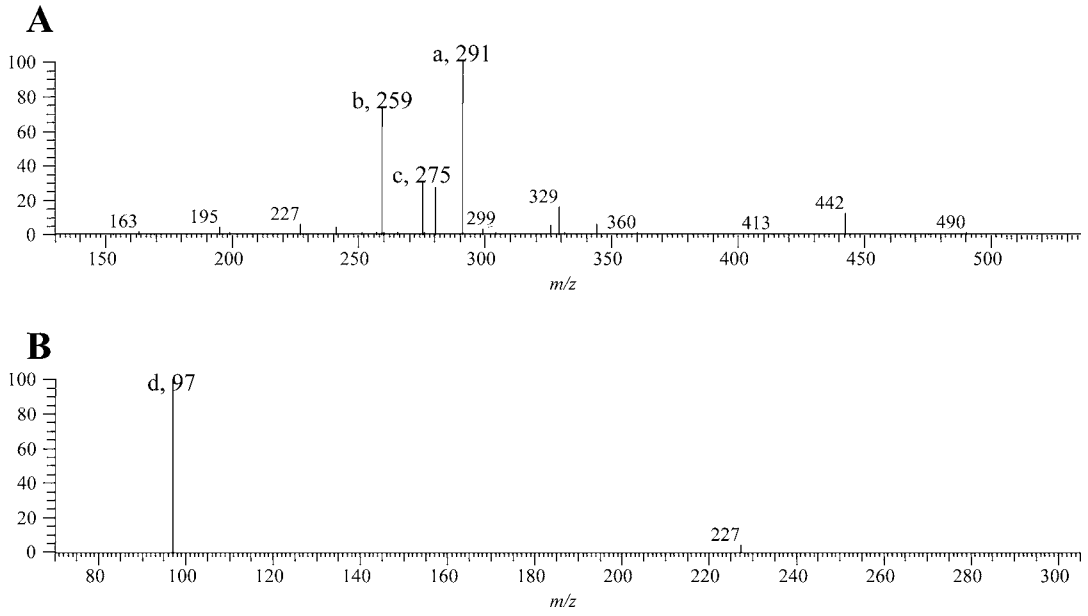

Figure 4. MS^2 (A) and MS^3 (B) spectra of 9-(methylsulfonyl)nonylglucosinolate (GS-1).

determined with nominal mass accuracy. An additional separate data-dependent scan with high-energy collisional dissociation (HCD) at 75% was also carried out for high-accuracy measurement of some of the MS^n ions with the resolution of 7500.

RESULTS AND DISCUSSION

Identification of Glucosinolates. Thirty-three glucosinolates were detected in the plant extract. Figure 1 lists the identification codes, putative identification, retention times (recorded on the TIC chromatogram), deprotonated molecule high-resolution mass, formula, error between the experimental and calculated values, and main and important fragments from MS^2, MS^3, and MS^4 fragmentations for each peak. The listing is in order of molecular weight. The TIC and PDA (at 225 nm) chromatograms are shown in Figure 2. Thirty-three of the compounds were putatively identified, and nine compounds could not be identified.

The main glucosinolates of this plant consisted of methylsulfonyl straight alkyl chain compounds ($CH_3S(O)_2(CH_2)_n$) (Figure 1). The most concentrated glucosinolate (GS-1) had TIC and UV peaks with retention times (t_R) at 18.88 and 18.83 min (Figure 2), UV λ_{max} at 225 nm, and a $[M - H]^-$ of 522.1134 Da for $C_{17}H_{32}O_{11}NS_3$ (calcd 522.1129 Da, with the error of −1.72 ppm) for 9-(methylsulfonyl)-nonylglucosinolate (GS-1). The assignment of this compound as 9-(methylsulfonyl)nonyl glucosinolate (GS-1) was based on the fact that the hydrolyzed products, desulfoglucosinolate, isothiocynate, and nitrile (rofifone), had been previously isolated from this plant.[9,27,28] Furthermore, the authors in China isolated the related nitrile from the same plant material and confirmed the structure by nuclear magnetic resonance.

GS-1 had major MS^2 fragments at m/z 291 (100%, $[C_6H_{11}O_9S_2]^-$), 275 (28%, $[C_6H_{11}O_8S_2]^-$), and 259 (73%, $[C_6H_{11}O_9S]^-$), ions a, c, and b in Figures 3 and 4A. MS^3 had a major fragment at m/z 97 (100%, $[HSO_4]^-$), ion d in Figure 4B. The compositions for ions a, c, and b were confirmed by the experimentally determined masses of 290.9842 (error −2.7 ppm), 274.9890 (error −3.9 ppm), and 259.0117 (error −4.8 ppm, Figure 3), respectively, from the additional data-dependent scan with activation in HCD.

Figure 3 illustrates the fragmentation pathway leading to the four product ions through the loss of RCN and RNCS groups. Some glucosinolates, such as 4-methoxyglucobrassin, glucobrassicin, 3′-hydroxyglucoisatisin, glucoisatinsin, and sinalbin, were reported to present an MS^2 fragment (b, 291 Da) with a relative intensity of 6−61%.[13,14,22] These diagnostic ions fully supported the identification of this compound as a glucosinolate.

Two minor peaks (GS-2 and GS-3, t_R = 10.39 and 21.00 min) had the same high-resolution deprotonated molecular ion masses as GS-1 and similar MS^2 and MS^3 fragments. Thus, they were determined to be isomers of GS-1. Most likely, the R groups are isomeric.

Three glucosinolates, GS4, GS-5, and GS-6, are analogues of GS-1 and identified as 7-methylsulfonylheptyl- (t_R = 6.67 min, $[M - H]^-$ = 494.0823 Da), 8-(methylsulfonyl)octyl- (t_R = 12.24 min, $[M - H]^-$ = 508.0978 Da), and 10-methylsulfonyldecylglucosinolates (t_R = 27.25 min, $[M - H]^-$ = 536.1301 Da), respectively. Their mass differences arise from the numbers of CH_2 units. Their retention times correlate with increasing mass, suggesting that the R groups are straight chains and the increasing number results in increased retention times as the polarity decreases. These data also confirmed the identification of these compounds as glucosinolates.

Four other glucosinolates (GS-7−GS-10) containing methylsulfinyl ($CH_3SO(CH_2)_n$) were detected. They were putatively identified as 8-(methylsulfinyl)octyl- (t_R = 11.39 time, $[M - H]^-$ = 492.1031 Da), 9-(methylsulfinyl)nonyl- (t_R = 17.66 and 18.71 min, $[M - H]^-$ close to 506.1189 Da, two isomers, GS-8 and GS-9), and 10-(methylsulfinyl)decyl glucosinolates (t_R = 25.28 min, $[M - H]^-$ = 520.1347 Da), respectively. All of them showed the same diagnostic fragments, confirming them as glucosinolates, and their elution time increased with increasing numbers of CH_2 units.

GS-11 (t_R = 11.85 min) contained an indole function and was putatively identified as 4-methoxyindol-3-ylmethylglucosinolate on the basis of its high-resolution mass value of 477.0635 Da. This compound showed the same fragmentation behavior observed above. Eight of the above glucosinolates (GS-1, GS-4,

dx.doi.org/10.1021/jf405538d | J. Agric. Food Chem. 2014, 62, 6118−6129

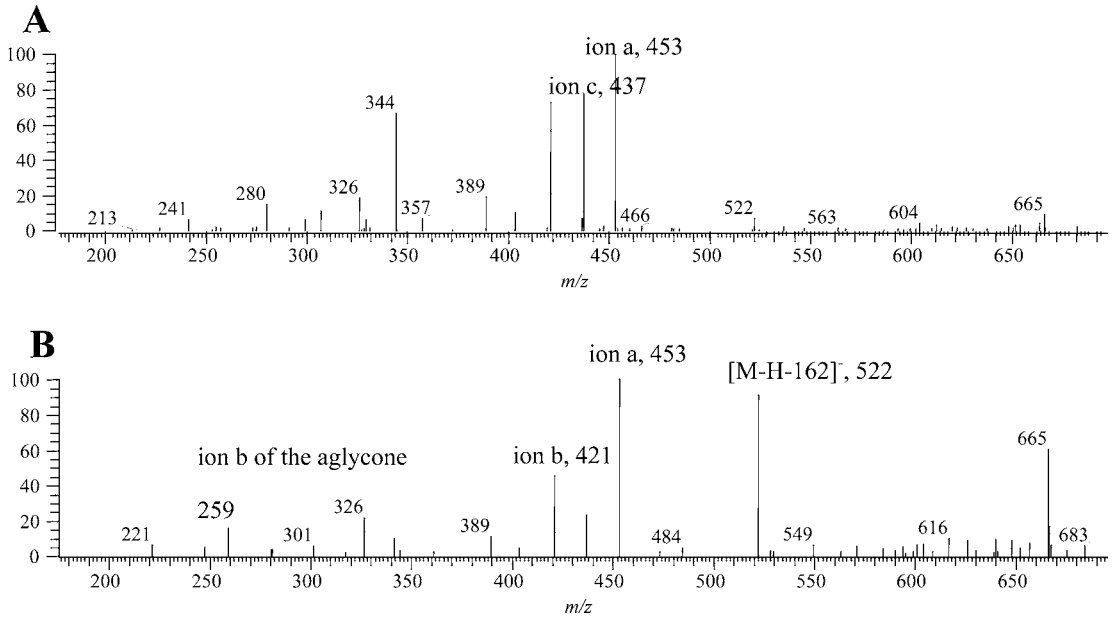

Figure 5. MS^2 spectra of the glucosides (A, GS-19; and B, GS-22) of 9-(methylsulfonyl)nonylglucosinolate.

GS-5, GS-6, GS-7, GS-8, GS-10, and GS-11) were previously reported, and GS-7, GS-8, and GS-11 were found in *Rorippa* plants.[4] Furthermore, the desulfoglucosinolates and/or isothiocyanates of the above glucosinolates (except GS-4) were previously isolated from the roots of this plant.[9] However, compounds GS-2, GS-3, and GS-9 were not known glucosinolates.[4−8]

The remaining 21 peaks were putatively identified as glucosinolates and will be discussed in detail. GS-12 (t_R = 33.33 min, $[M - H]^-$ = 488.1622 Da) had a deprotonated molecular ion of $C_{18}H_{34}O_{10}NS_2$ (error 0.49 ppm) and showed the classic glucosinolate MS^2 fragments at *m/z* 259 (100%), 275 (44%), and 291 (33%). After subtraction of ion b (*m/z* 259, $C_6H_{11}O_9S$) or ion a (*m/z* 291, $C_6H_{11}O_9S_2$) from the deprotonated molecule (Figure 3), the masses for R-NCS or R-CN were obtained. Each showed a formula for R = HO−$(CH_2)_{11}$, that is, $C_{11}H_{23}O$, the same as that obtained directly from R = $C_{18}H_{34}O_{10}NS_2$ − $C_7H_{11}O_9NS_2$ (Figure 3). In this way, the structures for the glucosinolates can be figured out easily. Thus, this compound was putatively identified as hydroxyundecyl glucosinolate. This glucosinolate was not among the predicted 180 new glucosinolates in the electronic database of Clarke because the number of CH_2 groups (*n*) is 11 and 10 was the largest considered in the prediction set.[8]

Two groups of the isomeric alkyl glucosinolates were observed. The first group (GS-13−GS-16) contained four isomers (t_R = 5.41, 6.47, 7.74, and 10.55 min, $[M - H]^-$ = 538.1081 Da). They showed product ions of *m/z* 291, 275, 259, and 97 and were identified as 9-(methylsulfonyl)-hydroxynonylglucosinolates. They had one more hydroxyl group than that of related 9-(methylsulfonyl)-nonylglucosinolate (GS-1) and its isomers (GS-2 and GS-3). The second group (GS-17 and GS-18) consisted of two isomers (t_R = 10.97 and 13.34 min, $[M - H]^-$ = 552.1236 Da). They showed the same diagnostic GS fragments and were putatively identified as 10-methylsulfonylhydroxydecylglucosinolates and to be the hydroxyl derivatives of 10-methylsulfonyldecylglucosinolate (GS-6) and its isomers. The R groups for the isomers can be determined in the same manner as described previously for GS-12. Among them, GS-13 and GS-17 (with suggested straight chains for the R group) were among the predicted 180 new glucosinolates in the electronic database of Clarke with code numbers 245 and 246, respectively.[8]

Four minor peaks (GS-19−GS-22) had different retention times (t_R = 17.68, 16.08, 16.84, and 20.92 min) but a similar mass ($[M - H]^-$ = 684.1658−684.1663 Da) corresponding to a formula of $C_{23}H_{42}O_{16}NS_3$ (errors less than −2.0 ppm). GS-19 had major MS^2 fragments at *m/z* 522 (77%, $[M - H] - 162$, loss of glucosyl), 453 (100%, 291 + 162, ion a_g, the "$_g$" means the fragment contained a glucosyl, $C_6H_{10}O_5$, Figure 3), 437 (23%, 275 + 162, ion c_g), 421 (94%, 259 + 162, ion b_g, Figure 3), and 259 (14%, ion b) (Figures 4 and 5 and Table 1). The detection of ions a, b, and c plus a glucosyl is reasonable, and $[M - H]^-$ = 421.0670 (error of 3.0 ppm) for ion b confirmed its composition as $C_{12}H_{21}O_{14}S$. Thus, the data suggest that these compounds are the glucosides of 9-(methylsulfonyl)nonyl glucosinolate (the glucoside of GS-1).

GS-20, GS-21, and GS-22 also showed the typical glucosinolate glucoside fragments at *m/z* 453, 437, and 421 (Figures 3 and 5 and Table 1). On the basis of both of the high-resolution mass values and the presence of the gluocosinolate glucoside characteristic fragments, they were identified as the glucosides of 9-(methylsulfonyl)nonylglucosinolates (the glucosides of GS-1−GS-3). Because there was no hydroxyl function on the R group, this glucosyl was most likely connected to the thioglucoside and most likely at the 6-position as that for a monoacylated glucosinolate.[6,7]

Similarly, four other compounds (GS-23−GS-26) were recognized as the glucosides of glucosinolates on the basis of the fact that they presented the same diagnostic fragments at *m/z* 453, 437, and 421. GS-23 (t_R = 22.55 min, $[M - H]^-$ = 654.1554 Da, $C_{22}H_{40}O_{15}NS_3$, error less than −2 ppm) was putatively identified as a glucoside of 9-(methylsulfinyl)-nonylglucosinolate (the glucoside of GS-8). GS-24−GS-26 (t_R = 23.37, 24.29, and 28.18 min, $[M - H]^-$ = 698.1915 Da, $C_{24}H_{44}O_{16}NS_3$, error −1.8 ppm) were putatively identified as the glucosides of 10-methylsulfonyldecylglucosinolates (the glucosides of GS-6 and its isomers).

dx.doi.org/10.1021/jf405538d | J. Agric. Food Chem. 2014, 62, 6118−6129

Table 1. Compound Code, Putative Identification, Retention Time, High-Resolution Mass of the Deprotonated Molecule, Formula, Error between Calculated and Measured Values, and MS^n Data of the Glucosinolates in *Rorippa indica*

code	glucosinolate putative identification[a]	t_R(min)	$[M-H]^-$ (Da)	formula	error (ppm)	MS^2 fragments (%)	MS^3 fragments (%)	MS^4 fragments (%)
GS-11	4-methoxyindol-3-ylmethylglucosinolate	11.85	477.0635	$C_{17}H_{21}O_{10})N_2S_2$	−1.697	459 (61), 291 (39), 275 (61), 259 (100), 235 (28)		
GS-12	hydroxyundecylglucosinolate	33.33	488.1624	$C_{18}H_{34}O_{10}NS_2$	−1.149	471 (90), 470 (60), 444 (50), 291 (40), 275 (40), 259 (100), 246 (30), 201 (30), 145 (30)	470 (89), 291 (33), 275 (44), 259 (100)	
GS-7	8-(methylsulfinyl)octylglucosinolate (glucohirsutin)	11.39	492.1031	$C_{16}H_{30}O_{10}N_{S3}$	−1.283	428 (100, −64)	275 (36), 259 (100)	
GS-4	7-(methylsulfonyl)heptylglucosinolate	6.67	494.0823	$C_{15}H_{28}O_{11}NS_3$	−1.409	476 (21), 291 (100), 275 (32), 259 (79), 252 (21)		
GS-8	9-(methylsulfinyl)nonylglucosinolate (glucoarabin)	17.66	506.1188	$C_{17}H_{32}O_{10}NS_3$	−0.951	442 (100, −64)	275 (46), 259 (100)	241 (12), 139 (100), 97 (44), 89 (8)
GS-9	isomer of GS-8	18.71	506.1189	$C_{17}H_{32}O_{10}NS_3$	−0.951	442 (100)		
GS-5	8-(methylsulfonyl)octylglucosinolate	12.24	508.0978	$C_{16}H_{30}O_{11}NS_3$	−1.665	291 (100), 275 (21), 259 (45),	97 (100)	
GS-10	10-(methylsulfinyl)decylglucosinolate	25.28	520.1347	$C_{18}H_{34}O_{10}NS_3$	−0.637	456 (100)	376 (16), 291 (18), 278 (16), 275 (47), 26 3(20), 259 (100)	241 (12), 223 (10), 139 (100), 97 (38)
GS-1	9-(methylsulfonyl)nonylglucosinolate	18.88	522.1134	$C_{17}H_{32}O_{11}NS_3$	−1.716	442 (12), 329 (16), 291 (100), 280 (27), 275 (30), 259 (73), 227 (6)	97 (100)	
GS-2	isomer of GS-1	21.00	522.1136	$C_{17}H_{32}O_{11}NS_3$	−1.333	522 (33), 504 (100), 478 (33), 476 (56), 450 (33), 444 (33), 291 (44), 259 (56)		
GS-3	isomer of GS-1	10.39	522.1138	$C_{17}H_{32}O_{11}NS_3$	−0.950	458 (100)	378 (39), 332 (35), 280 (26), 275 (30), 259(100), 235 (30)	
GS-6	10-(methylsulfonyl)decylglucosinolate	27.25	536.1301	$C_{18}H_{34}O_{11}NS_3$	1.125	456 (11), 343 (14), 340 (6), 294 (20), 291 (100), 275 (26), 259 (58)	97 (100)	
GS-13	9-(methylsulfonyl) hydroxynonylglucosinolate	5.41	538.1082	$C_{17}H_{32}O_{12}NS_3$	−1.878	520 (53), 494 (24), 458 (24), 291 (100), 275 (41), 259 (59)		
GS-14	isomer of GS-12	6.47	538.1082	$C_{17}H_{32}O_{12}NS_3$	−2.594	520 (45), 494 (36), 450 (27), 448 (27), 362 (27), 296 (45), 291(100), 259 (55)		
GS-15	isomer of GS-12	7.74	538.1060	$C_{17}H_{32}O_{12}NS_3$	0.298	296 (16), 291 (100), 275 (24), 259 (44)		
GS-16	isomer of GS-12	10.55	538.1080	$C_{17}H_{32}O_{12}NS_3$	−2.250	495 (26), 360 (21), 296 (26), 291 (100), 259 (21)		
GS-17	10-(methylsulfonyl) hydroxydecylglucosinolate	10.97	552.1238	$C_{18}H_{34}O_{12}NS_3$	−2.761	508 (17), 310 (11), 291 (100), 275 (20), 259 (37)		
GS-18	isomer of GS-16	13.34	552.1240	$C_{18}H_{34}O_{12}NS_3$	−1.559	534 (38), 340 (38), 310 (38), 291 (100)		
GS-30	glucoside of methylthioethylenylpentylglucosinolate	28.07	622.1300	$C_{21}H_{36}O_{14}NS_3$	−0.546	326 (100, −296), 299 (22)		
GS-31	glucoside of 7-methylthio-3-oxoheptylglucosinolate	22.16	638.1245	$C_{21}H_{36}O_{15}NS_3$	−1.182	620 (7), 522 (20), 326 (100, −312), 299 (22), 280 (33)	494 (14), 442 (11), 423 (7), 407 (25), 391 (100), 264 (7)	
GS-32	glucoside of 8-methylthiooctylglucosinolate	21.15	638.1608	$C_{22}H_{40}O_{14}NS_3$	−1.316	574 (100, −64)	423 (11), 407 (37), 391 (100), 191(16)	
GS-33	glucoside of 7-(methylsulfinyl) heptylglucosinolate	16.51	640.1403	$C_{21}H_{38}O_{15}NS_3$	−0.945	623 (62), 550 (62), 391 (100), 390 (38)		
GS-23	glucoside of 9-(methylsulfinyl) nonylglucosinolate	22.55	654.1554	$C_{22}H_{40}O_{15}NS_3$	−1.765	423 (88), 407 (42), 391 (100), 373 (12), 359 (21)		
GS-27	glucosides of 9-(methylsulfinyl) nonylglucosinolate	18.58	668.1708	$C_{23}H_{42}O_{15}NS_3$	−2.102	604 (100)	453 (25), 437 (100), 421 (100), 332 (38), 264 (100)	
GS-28	isomer of GS-27	16.70	668.1712	$C_{23}H_{42}O_{15}NS_3$	−1.504	604 (100)	528 (17), 453 (28), 437 (56), 421 (100), 403 (22)	

dx.doi.org/10.1021/jf405538d | J. Agric. Food Chem. 2014, 62, 6118−6129

Table 1. continued

code	glucosinolate putative identification[a]	t_R(min)	$[M - H]^-$ (Da)	formula	error (ppm)	MS^2 fragments (%)	MS^3 fragments (%)	MS^4 fragments (%)
GS-29	glucoside of (*R*)-10-(methylsulfinyl) decylglucosinolate	22.79	682.1868	$C_{24}H_{44}O_{15}NS_3$	−1.546	618 (100)		
GS-19	glucosides of 9-(methylsulfonyl) nonylglucosinolate	17.68	684.1663	$C_{23}H_{42}O_{16}NS_3$	−1.198	666 (59), 522 (91), 453 (100), 437 (23), 421 (45), 326 (23), 259 (14)		
GS-20	isomer of GS-19	16.08	684.1658	$C_{23}H_{42}O_{16}NS_3$	−1.928	453 (81), 437 (29), 421 (100)		
GS-21	isomer of GS-19	16.84	684.1630	$C_{23}H_{42}O_{16}NS_3$	2.563	643 (21), 453 (100, −231), 437 (42), 421 (96), 389 (42)		
GS-22	isomer of GS-19	20.92	684.1658	$C_{23}H_{42}O_{16}NS_3$	−1.928	453 (100), 437 (83), 421 (72), 389 (18), 344 (66), 326 (18), 307 (11), 280 (15)		
GS-24	glucosides of 10-(methylsulfonyl) decylglucosinolate	23.37	698.1812	$C_{24}H_{44}O_{16}NS_3$	−2.248	681 (31), 680 (23), 639 (23), 453 (100), 437 (31), 421 (23)		
GS-25	isomer of GS-31	24.29	698.1821	$C_{24}H_{44}O_{16}NS_3$	−0.959	680 (10), 662 (12), 453 (95), 437 (25), 421 (100), 389 (8), 343 (10)		
GS-26	isomer of GS-31	28.18	698.1815	$C_{24}H_{44}O_{16}NS_3$	−1.818	680 (100), 652 (45), 626 (27), 537 (27), 528 (27), 453 (64), 437 (36), 421 (64), 358 (64)		

[a]GS, glucosinolate.

One pair of isomers, GS-27 and GS-28 (t_R = 16.43 and 18.58 min, $[M - H]^-$ = 668.1712 Da, $C_{23}H_{42}O_{15}NS_3$, error −1.5 ppm) were putatively identified as glucosides of 9-(methylsulfinyl)nonylglucosinolate (the glucosides of GS-5 or its isomer). GS-29 (t_R = 22.79 min, $[M - H]^-$ = 682.1868 Da, $C_{23}H_{44}O_{15}NS_3$, error −1.5 ppm) was thought to be the glucoside of 10-(methylsulfinyl)decylglucosinolate (the glucosides of GS-10 or its isomer). The base MS^2 fragments (m/z 604 for GS-27 and GS-28 and m/z 618 for GS-29) showed a loss of 64 Da (loss of $CH_3 - SO - H$), indicating that these glucosinolates contained a methylsulfinyl ($CH_3{-}SO^-$) group in the side chain.[17,18] Both GS-27and GS-28 had MS^3 spectra containing the diagnostic gucosinolate glucoside fragments at m/z 453 (25 and 28%, respectively), 437 (100 and 56%), and 421 (both 100%) to confirm their identification. Similar fragments were not observed for GS-29. However, the MS^2 signal was very weak.

Four other compounds (GS-30−GS-33) also appeared to be analogues of the glucosides of glucosinolates on the basis of their masses and formulas. GS-30 (t_R = 28.07 min, $[M - H]^-$ = 622.1290 Da, $C_{21}H_{36}O_{14}NS_3$, error −0.5 ppm) might be the glucoside of methylthioethenylpentenyl (CH_3—S—C═C-$(CH_2)_5$) or an isomer of methylthioheptenyl. The aglycone with a methylthioethenylpentenyl group is among the 180 predicted new glucosinolates (no. 204) in the electronic database of Clarke.[8]

GS-31 and GS-32 (t_R = 22.16 and 21.15 min) have the same nominal masses, but have different high-accuracy masses. GS-31 ($[M - H]^-$ = 638.1245 Da, $C_{21}H_{36}O_{15}NS_3$, error −1.2 ppm) was putatively identified as the glucoside of 7-methylthio-3-oxoheptylglucosinolate or 7-methylsulfinylheptenylglucosinolate. GS-32 ($[M - H]^-$ = 638.1608 Da, $C_{22}H_{40}O_{14}NS_3$, error −1.3 ppm) might be the glucoside of 8-methylthiooctylglucosinolate.

GS-33 (t_R = 16.51 min, $[M - H]^-$ = 640.1403 Da, $C_{21}H_{38}O_{15}NS_3$, error −0.9 ppm) might be the glucoside of 7-(methylsulfinyl)heptyl glucosinolate. Instead of showing the typical glucosinolate glucoside fragment described above, three of them (GS-31−GS-33) had base MS^2 or MS^3 fragments at m/z 391 like GS-23. Consequently, the lack of definitive MS^2 fragments made it impossible to develop a molecular formula for this ion. The putative formula offered in Table 1 was based primarily on the close match of the experimentally measured high-resolution masses with calculated values. The aglycones of these three glucosides were known glucosinolates, but not detected in this plant.

The 14 glucosinolate glucosides mentioned above have not been previously reported in any other plants. They represent a new family of glucosinolates with a glucosyl connected to the thioglucosyl group. All of the observed MS^n fragments could be related to the structural elements of the glucosinolate skeleton. For examples, ions a, b, c, and d and thioglucosyl (m/z 195), as well as fragments obtained from further losses of oxygen, sulfur, or parts of the glucosyl were observed. However, not enough fragments were obtained to determine the structure of the R groups.[8,11−25] Of course, the R groups for the glucosinolates were not very large (containing fewer than 12 carbon atoms for the aliphatic GSs), but they can be arranged in several different ways to form the isomers. For example, the aliphatic structure can be linear or branched, the oxygen atom can be found in the oxo (keto) or hydroxy form, and the alkenyl double bond can be located at different positions.[3−8] As a result, nuclear

magnetic resonance (NMR) analysis is still the most accurate way to identify GSs structurally.[6,7]

The major glucosinolates of *R. montana* had similar side chains and were well separated, allowing for the measurement of their peak areas at 225 nm (Figure 3). Their concentrations were calculated relative to glucocheirolin using MRRF values of 1.0, on the basis of previous reports that the side chains were similar and did not alter the absorption coefficient of the molecules.[8,14,19,20] The relative peak area ratios for GS-1, GS-8, GS-6, GS-5, and GS-10 were 100.0, 15.5, 9.6, 5.1, and 4.6, respectively. The corresponding concentrations for GS-1, GS-8, GS-6, GS-5, and GS-10 were 0.51, 0.079, 0.049, 0.026, and 0.024% on a dry weight basis, and their total contents was 0.69% or 690 mg/100 g of dried plant materials. GS-1 constituted approximately 71% of the total glucosinolate content.

Identification of Phenolic and Other Common Compounds. Table 2 presents the retention times (recorded on the TIC chromatograms), HR masses, and formulas for deprotonated molecules $[M - H]^-$, diagnostic MS^2, MS^3, MS^4, and MS^5 product ions, and putative identities of 44 flavonol glycoside, 18 phenolic, and other common compounds. The listing is in order of molecular weight. The typical TIC and PDA (at 354 nm) chromatograms are shown in Figure 2. The strategy for identifying phenolic compounds in food samples has been described previously.[31,33] In this study, only the glycosides of flavonols were observed, and most are reported for the first time.

Two tetrahydroxyflavone 3-*O*-rhamnosylhexosides (t_R = 28.22 and 26.52 min, $[M - H]^-$ = 593.1491) provided the largest peaks (F-1 and F-2 in Figure 2A) in chromatograms of the *R. indica* extract. They had UV band I maximum absorbances at 265 and 346 nm and base MS^2 and MS^3 fragments of *m/z* 447 (by loss of 146) and *m/z* 284 (the radical anion species of kaempferol from the loss of 162 + 1 rather than the ion at *m/z* 285), suggesting that they might be kaempferol glycosides containing a rhamnosylhexose. This radical anion had base MS^4 and MS^5 fragments of *m/z* 255 (100%) and 221(100%), which suggested that this flavonol was most likely to be kaempferol. This identification was confirmed by the fact that kaempferol was the tetrahydroxyflavone (by direct comparison with kaempferol standards) in the acidic hydrolyzed extract (chromatogram not shown). The close retention times of the flavonol glycoside suggested that they might be kaempferol 3-*O*-rhamnosylglucosides with the rhamnosyl at the 6-position of hexosyl (glucosyl or galactosyl).[33] Their high-resolution mass confirmed their putative identification.

Four other peaks with different retention times (t_R = 17.35, 21.04, 30.80, and 32.13 min) had high-resolution masses close to 593.1500 Da, and all had similar fragments, suggesting they were also kaempferol rhamnosylhexosides. However, they were all minor components of the plant and did not provide sufficient UV data or MS^n fragments to allow identification of a specific isomeric structure. Thus, their position of attachment to the flavone and the type of hexose were not completely identified.

Similarly, flavonoid F-3 (t_R = 24.61 min, $[M - H]^-$ = 609.1470 Da) had a MS^2 fragment at *m/z* 447 (loss of 162) and an MS^3 fragment at *m/z* 301 (loss of 146) and was putatively identified as quercetin 3-*O*-hexosylrhamnoside. Its isomers (t_R = 23.42 and 25.84 min) had MS^2 fragments at *m/z* 463 (loss of 146) and MS^3 fragments at *m/z* 301 (loss of 162), suggesting they were quercetin 3-rhamnosylhexosides. The isomer with t_R = 23.42 min was further identified as rutin by direct comparison with an authentic standard. Another isomer (t_R = 34.50 min) had a MS^2 fragment at *m/z* 301, and its sugar connection could not be determined. The MS^4 and MS^5 fragments for *m/z* 301 were 255 (22−27%), 179 (41−71%), 151 (100%), and 107 (100) and suggested the aglycone was quercetin. This was confirmed by the fact that the pentahydroxyflavone in the acidic hydrolyzed extract was identified as quercetin.

One flavonoid (t_R = 30.31 min, $[M - H]^-$ = 623.1611 Da) had a base MS^2 fragment at *m/z* 477, a base MS^3 fragment at *m/z* 314, and MS^4 and MS^5 ions at *m/z* 285 and 270 to suggest it was isorhamnetin 3-*O*-rhamnosylhexoside. Two rhamnosides and three hexosides of kaempferol were detected. At least one of the rhamnosides and hexosides might have the glycosyl at the 3-position of kaempferol. Another flavonoid (t_R = 33.59 min, $[M - H]^-$ = 577.1555 Da, $C_{27}H_{29}O_{14}$) had a base MS^2 fragment at *m/z* 431 and a base MS^3 fragment at *m/z* 285 to suggest it was kaempferol 3-*O*-rhamnosylrhamnoside.

Similarly, six flavonoids conjugated with three monosaccharides were putatively identified. The first two flavonoids (t_R = 34.46 and 33.19 min, $C_{32}H_{37}O_{18}$) showed one pentosyl more than that of kaempferol 3-*O*-rhamnosylrhamnoside. The first one (F-6) had a base MS^2 fragment at *m/z* 563 (loss of 146 Da) and a base MS^3 fragment at *m/z* 284 (loss of 278 Da, i.e., 146 + 132) to indicate it was kaempferol 3-*O*-rhamnosylpentosylrhamnoside. The second one (t_R = 33.19) was very similar to F-6 but had a base MS^2 fragment at *m/z* 447 (loss of 294 Da) for a dirhamnosylpentoside. Another three flavonoids (t_R = 34.46, 33.19, 24.73, 26.21, and 27.94 min, $C_{33}H_{39}O_{20}$) had base MS^2 fragments at *m/z* 609 Da (loss of 146 Da), a base MS^3 fragment at *m/z* 285 Da (loss of 324 Da), and a base MS^4 fragment at *m/z* 151, suggesting them to be isomers of kaempferol 3-*O*-rhamnosyldihexosides. The last flavonoid (t_R = 22.95 min $[M - H]^-$ = 771.1971 Da, $C_{33}H_{39}O_{21}$) had a base MS^2 fragment at *m/z* 625 (loss of 146 Da), indicating it might be quercetin 3-*O*-rhamnosyldihexoside.

Acylation of the flavonol glycosides was determined by mass difference. An increased mass close to 146.0366, 162.0315, 176.0471, or 206.0576 Da was diagnostic of the presence of a *p*-coumaroyl, caffeoyl, feruloyl, or sinapoyl group. For example, two kaempferol acylglyocosides (t_R = 37.65 and 39.03 min, $[M - H]^-$ close to 755.1826 Da, $C_{36}H_{35}O_{18}$) had a base MS^2 fragment at *m/z* 609 Da (calculated as 609.1460, with error of −0.177 ppm for $C_{27}H_{29}O_{16}$, from loss of 146.0366 Da, $C_9H_6O_2$ for coumaroyl, instead of loss of 146.0576 Da, $C_6H_{10}O_4$, rhamnosyl) and base $MS^{3,4}$ fragments (*m/z* 447, 285, 257, 241, 229, 151 Da) identifying them as kaempferol 3-*O*-*p*-coumaroyldihexosides. Similarly, three acylated flavonoids (t_R = 30.24, 42.70, and 46.66 min, $[M - H]^-$ close to 769.1975 Da, $C_{37}H_{37}O_{18}$) had base MS^2 fragments at *m/z* 575 (loss of around 194.0576 Da for $C_{10}H_{10}O_4$, ferulic acid) suggesting they were kaempferol 3-*O*- feruloylrhamnosylhexosides. In the same way, four acylated glycosides were putatively identified as the 3-*O*-caffoeyldihexoside (t_R = 31.67 min, $[M - H]^-$ = 771.1797 Da), the 3-*O*-sinapoyldihexoside (t_R = 41.60 min, $[M - H]^-$ = 831.1974 Da), the 3-*O*-hexoside-7-*O*-methoxybenzoyldihexoside (t_R = 33.57 min, $[M - H]^-$ = 921.2290 Da), and the 3-*O*-sinapoylhydroxyferuoyldihexoside-7-*O*-hexoside (t_R = 39.84 min, $[M - H]^-$ = 1185.2914 Da) of quercetin, respectively. In the same manner, the remaining ones were identified as two 3-*O*-sinapoylhexoside-7-*O*-rhamnosides (t_R = 42.40 and 46.26 min, $[M - H]^-$ close to 799.2093 Da), the 3-*O*-

Table 2. Compound Name, Retention Time, High-Resolution Mass of the Deprotonated Molecule, Formula, Error between Calculated and Measured Values, and MS^n Data of the Flavonol Glycosides and Other Compounds in *Rorippa indica*

compound putative identification (code)[a]	t_R(min)	$[M-H]^-$ (Da)	formula	error (ppm)	MS^2 fragments (m/z) (%)	MS^3 fragments (m/z) (%)	MS^4 fragments (m/z) (%)	MS^5 fragments (m/z) (%)
malic acid[b]	2.02	133.0137	$C_4H_5O_5$	−4.109	115 (100)	71 (100)		
vanillic acid[b]	5.13	167.0349	$C_8H_70_4$	−0.491	152 (100), 123 (65), 108 (16)			
citric acid[b]	2.25	191.0193	$C_6H_70_7$	−3.276	173 (26), 111 (100)	67 (100)		
trans-ferulic acid[b]	23.48	193.0503	$C_{l0}H_9O_4$	−1.720	178 (26), 149 (56), 134 (100)	106 (100)		
cis-feruulic acid[b]	25.08	193.0503	$C_{10}H_9O_4$	−1.720	178 (26), 149 (56), 134 (100)	106 (100)		
trans-sinapic acid[b]	20.81	223.0241	$C_{10}H_7O_6$	−3.189	195 (8), 179 (100)	135 (100), 109 (66)		
cis -sinapic cid[b]	22.00	223.0241	$C_{10}H_7O_6$	−3.189	195 (8), 179 (100)	135 (100), 109 (66)		
dihydroxybenzoylpentose[b]	6.90	285.0611	$C_{12}H_{13}O_8$	−1.721	165 (6), 153 (100), 152 (33), 109 (7)	109 (100)		
dihydroxybenzoylpentose[b]	8.10	285.0611	$C_{12}H_{13}O_8$	−1.721	153 (100)	109 (100)		
dihydroxybenzoylpentose[b]	9.23	285.0611	$C_{12}H_{13}O_8$	−1.721	153 (100)	109 (100)		
p -coumaroylmalic acid[b]	20.59	279.0505	$C_{13}H_{11}O_7$	−1.885	163 (100), 133 (70)			
hydroxybenzoylhexose[b]	6.80	299.0767	$C_{13}H_{15}O_8$	−1.808	137 (100)	93 (100)		
hydroxybenzoylhexose[b]	8.44	299.0767	$C_{13}H_{15}O_8$	−1.808	137 (100)			
dihydroxybenzoylhexose[b]	4.27	315.0717	$C_{13}H_{15}O_9$	−1.445	225 (12), 165 (14), 163 (8), 153 (100), 152 (31)			
dihydroxybenzoylhexose[b]	5.62	315.0716	$C_{13}H_{15}O_9$	−1.762	153 (100)			
dihydroxybenzoylhexose[b]	6.33	315.0717	$C_{13}H_{15}O_9$	−1.445	169 (100), 151 (31)			
galloylquinic acids[b]	4.42	343.0665	$C_{14}H_{15}O_{10}$	−1.661	299 (28), 153 (100)			
km rhamnoside	47.97	431.0982	$C_{21}H_{19}O_{10}$	−0.394	285 (100), 284 (27)	257 (45), 241 (40), 213 (14), 151 (100)		
km rhamnoside	46.87	431.0984	$C_{21}H_{19}O_{10}$	0.070	285 (100), 284 (30)	257 (39), 241 (35), 213 (13), 151 (100)	107 (100), 83 (7)	65 (100), 63 (41)
sinapoylhexose + formic acid[b]	16.01	431.1919	$C_{20}H_{31}O_{11}$	−0.859	385 (100)	223 (80), 205 (77), 161 (28), 153 (100)		
km hexoside	32.80	447.0927	$C_{21}H_{19}O_{11}$	−1.307	327 (22), 301 (49), 300 (11), 285 (100), 284 (93)			
km 3-*O*-hexoside	30.58	447.0930	$C_{21}H_{19}O_{11}$	−0.636	327 (16), 285 (57), 284 (100), 255 (11)	255 (100), 227 (10)	255 (24), 227 (88), 211 (100)	
km 3-*O*-hexoside (F-5)[b]	32.17	447.0931	$C_{21}H_{19}O_{11}$	−0.413	327 (20), 285 (56), 284 (100), 255 (15)	255 (100), 227 (13)	255 (19), 227 (100), 211 (61)	227 (23), 199 (56), 183 (100)
laricresinol-4′-glucoside[b]	30.91	521.2023	$C_{26}H_{33}O_{11}$	−1.026	503 (11), 449 (9), 359 (18), 341 (100), 179 (49)			
km 3-*O*-dirhamnoside[b]	33.59	577.1555	$C_{27}H_{29}O_{14}$	−1.349	431 (100), 285 (25)	285 (100), 284 (14)	257 (77), 243 (100), 213 (93)	
km rhamnosylhexoside	17.35	593.1505	$C_{27}H_{29}O_{15}$	−1.169	503 (43), 473 (100), 383 (25), 353 (30)	383 (22), 353 (100)	325 (100), 297 (50)	297 (100)
km 3-*O*-hexoside-7-*O*-rhamnoside	21.04	593.1503	$C_{27}H_{29}O_{15}$	−1.506	447 (100), 431 (72)	285 (100), 284 (41)	257 (50), 241 (33), 151 (100)	107 (100)
km 3-*O*-rhamnosylhexoside (F-l)[b]	28.22	593.1491	$C_{27}H_{29}O_{15}$	−3.529	447 (100)	327 (16), 285 (41), 284 (100), 255 (12)	255 (100)	227 (100), 211 (63)
km 3-*O*-rhamnosylhexoside (F-2)[b]	26.52	593.1500	$C_{27}H_{29}O_{15}$	−2.012	447 (100), 431 (41), 285 (16)	327 (22), 285 (20)284 (100), 255 (15)	255 (100), 227 (11)	255 (13), 227 (100), 211 (57)
km 3-*O*-rhamnosylhexoside	30.80	593.1504	$C_{27}H_{29}O_{15}$	−1.337	473 (6), 447 (100), 43 1(37), 285 (12)			

dx.doi.org/10.1021/jf405538d | J. Agric. Food Chem. 2014, 62, 6118−6129

Table 2. continued

compound putative identification (code)[a]	t_R(min)	$[M-H]^-$ (Da)	formula	error (ppm)	MS^2 fragments (m/z) (%)	MS^3 fragments (m/z) (%)	MS^4 fragments (m/z) (%)	MS^5 fragments (m/z) (%)
km 3-*O*-rhamnosylhexoside	31.13	593.1504	$C_{27}H_{29}O_{15}$	−1.337	473 (8), 447 (100), 431 (35), 285 (18)			
km 3-*O*-hexoside-7-*O*-hexoside	16.92	609.1469	$C_{27}H_{29}O_{16}$	1.300	489 (14), 447 (100)	327 (17), 285 (42), 284 (100), 255 (14)		
km 3-*O*-hexoside-7-*O*-hexoside	18.79	609.1471	$C_{27}H_{29}O_{16}$	1.629	447 (100)	327 (20), 285 (49), 284 (100), 255 (17)	255 (100)	227 (100), 211 (69)
qn 3-*O*-hexosylrhamnoside	22.42	609.1470	$C_{27}H_{29}O_{16}$	1.465	463 (81), 447 (100), 446 (33), 301 (32)			
qn 3-*O*-rhamnosylhexoside (rutin)[b]	23.42	609.1472	$C_{27}H_{29}O_{16}$	1.793	463 (100), 447 (23), 301 (12)	301 (100), 300 (26)		
qn 3-*O*-hexosylrhamnoside (F-3)[b]	24.54	609.1470	$C_{27}H_{29}0_{16}$	1.465	463 (67), 447 (100), 446 (34), 301 (31)	301 (100), 299 (10)	255 (22), 179 (71), 151 (100)	107 (100)
qn 3-*O*-hexosylrhamnoside[b]	25.82	609.1470	$C_{27}H_{29}0_{16}$	1.465	463 (64), 447 (100), 446 (25), 301 (31), 285 (11)	301 (100)	255 (27), 179 (46), 151 (100)	
qn 3-*O*-hexosylrhamnoside[b]	26.17	609.1470	$C_{27}H_{29}0_{16}$	−1.467	463 (56), 447 (100), 301 (29)	301 (100)		
is 3-*O*-rhamnosylhexoside[b]	30.31	623.1611	$C_{28}H_{29}0_{17}$	−1.056	477 (100), 461 (41), 315 (9)	357 (19), 314 (100), 285 (8), 271 (6)	285 (100), 271 (75), 243 (27)	270 (100)
qn 3-*O*-hexoside-7-*O*-hexoside	15.60	625.1398	$C_{29}H_{31}O_{16}$	−1.956	463 (100), 301 (22)	301 (100), 300 (32)		
km 3-*O*-acetyl-hexosylrhamnoside	31.43	635.1605	$C_{29}H_{31}O_{16}$	−1.980	489 (57), 431 (100), 430 (12), 285 (73)			
km 3-*O*-rharnnosylpentasylrhamnoside (F-6)	34.46	709.1978	$C_{32}H_{37}O_{18}$	−1.040	563 (100)	413 (35), 285 (39), 284 (100), 255 (17)		
km 3-*O*-dirhamnosylpentoside	33.19	709.1972	$C_{32}H_{37}O_{18}$	−1.886	665 (14), 547 (8), 489 (7), 447 (100), 285 (20)			
km 3-*O*-(*p*-coumaroylhexosyl) rhamnoside	45.84	739.1877	$C_{36}H_{35}O_{17}$	−0.369	593 (100), 285 (7)	447 (6), 285 (100)	257 (68), 241 (37), 151 (100)	107 (100), 83 (10)
km 3-*O*-rhamnosylhexosylhexoside	24.73	755.2031	$C_{33}H_{39}O_{20}$	−1.479	609 (100)	285 (100)	267 (31), 257 (100), 229 (44), 151 (30)	
km 3-*O*-rhamnosylhexosylhexoside	26.21	755.2030	$C_{33}H_{39}O_{20}$	−1.346	609 (100)	285 (100)	267 (42), 257 (100), 239 (29), 229 (56)	
km 3-*O*-rhamnosylhexosylhexoside	27.94	755.2023	$C_{33}H_{39}O_{20}$	−2.273	609 (100), 431 (17), 285 (7)	285 (100)	267 (31), 257 (100), 229 (30), 151 (71)	
km 3-*O*-*p*-coumaroylhexosylhexoside[b]	37.65	755.1826	$C_{36}H_{35}O_{18}$	−0.380	609 (100)	447 (16), 323 (49), 285 (100), 221 (6)	257 (100), 241 (42), 229 (45), 151 (74)	
km 3-*O*-*p*-coumaroylhexosylhexoside[b]	39.03	755.1814	$C_{36}H_{35}O_{18}$	−1.969	609 (100)	447 (17), 323 (51), 285 (100)		
km 3-*O*-feruloylhexosylrhamnoside[b]	30.24	769.1975	$C_{37}H_{37}O_{18}$	−1.349	575 (100), 455 (12)	455 (100)	335 (100)	307 (100), 306 (19), 241 (10)
km 3-*O*-feruoylrhamnosylhexoside (F-4)	42.70	769.1974	$C_{37}H_{37}O_{18}$	−1.479	623 (100)	323 (100), 299 (66), 285 (68), 284 (15)	263 (46), 221 (100), 179 (82), 177 (36)	
km 3-*O*-feruloylrhamnosylhexoside	46\66	769.1972	$C_{37}H_{37}O_{18}$	−1.739	653 (7), 623 (100, −146), 285 (7)	447 (6), 299 (24), 285 (100)	257 (77), 241 (43), 213 (23) , 151 (100)	
km 3-*O*-caffeoyldihexoside	31.67	771.1797	$C_{36}H_{35}O_{19}$	2.461	609 (47), 608 (6), 447 (100), 327 (6), 285 (25)			
qn 3-*O*-rhamnosyldihexoside[b]	22.95	771.1971	$C_{33}H_{39}O_{21}$	−2.374	625 (100), 609 (68), 463 (40)			
km 3-*O* -sinapoylhexoside-7-*O* -rhamnoside	42.40	799.2093	$C_{38}H_{39}O_{19}$	0.248	653 (100)	353 (100), 339 (22), 299 (50), 285 (39)	251 (97), 209 (100), 207 (42), 191 (52)	
km 3-*O* -sinapoylhexosicle-7-*O* -rhamnoside	46.26	799.2080	$C_{38}H_{39}O_{19}$	−1.379	653 (100), 431 (10), 285 (15)			

dx.doi.org/10.1021/jf405538d | J. Agric. Food Chem. 2014, 62, 6118−6129

Table 2. continued

compound putative identification (code)[a]	t_R(min)	$[M - H]^-$ (Da)	formula	error (ppm)	MS^2 fragments (m/z) (%)	MS^3 fragments (m/z) (%)	MS^4 fragments (m/z) (%)	MS^5 fragments (m/z) (%)
qn 3-*O*-sinapoyldihexoside	41.60	831.1974	$C_{38}H_{39}O_{21}$	−1.842	787 (100), 641 (42), 625 (57), 607 (7), 479 (74)			
km 3-*O*-hydroxybenzoylhexoside-7-*O*-dihexoside	31.17	891.2185	$C_{40}H_{43}O_{23}$	−1.751	729 (96), 567 (100)			
qn3-*O*-hexoside-7-*O*-methoxybenzoyldihexoside	33.57	921.2290	$C_{41}H_{45}O_{24}$	−1.764	593 (25), 463 (100), 457 (37)			
km 3-*O* -caffeoyldihexoside-7-*O* -rhamnoside	32.85	917.2340	$C_{42}H_{45}O_{23}$	−1.865	771 (100), 755 (29), 609 (31)	609 (100)	447 (26), 323 (50), 285 (100), 221 (7)	
km 3-*O* -feruloyldihexoside-7-*O* -rhamnoside	34.95	931.2505	$C_{43}H_{47}O_{23}$	−0.924	785 (100), 623 (10)	623 (100), 447 (47), 285 (7)		
km 3-*O*-feruoyldihexoside-7-*O*-rhamnoside	38.95	931.2503	$C_{43}H_{47}O_{23}$	−1.139	785 (100), 769 (38), 623 (54), 447 (37), 431 (6)	623 (100, −162), 447 (72), 285 (13)		
km 3-*O*-sinapoyldihexoside-7-*O*-rhamnoside	34.46	961.2604	$C_{44}H_{49}O_{24}$	−1.587	815 (100), 799 (12), 653 (18), 447 (10)	653 (100), 447 (45), 285 (8)		
qn 3-*O*-sinapoylhydroxyferuoyl-dihexoside-7-*O*-hexoside	39.84	1185.2914	$C_{54}H_{57}O_{30}$	−2.205	1039 (23), 1023 (100), 893 (12), 877 (18)	877 (100), 861 (93), 861 (37), 731 (61)		

[a]is, isorhamnetin; km, kaempferol; qn, quercetin. [b]Identified using in-house database.

hydroxybenzoyldihexoside-7-*O*-hexoside (t_R = 31.17 min, $[M - H]^-$ = 891.2185 Da), the 3- *O*-caffeoyldihexoside-7-*O*-rhamnoside (t_R = 32.85 min, $[M - H]^-$ = 917.2340 Da), the 3-*O*-feruloyldihexoside-7-*O*-rhamnosides (t_R = 34.95 and 38.95 min, $[M - H]^-$ = 931.2504 Da), two 3-*O*-sinapoyldihexoside-7-*O*-rhamnosides (t_R = 34.46 min, $[M - H]^-$ = 961.2604 Da), and the 3-*O*-acetylhexosylrhamnoside (t_R = 31.43 min, $[M - H]^-$ = 635.1605 Da) of kaempferol, respectively.

As mentioned in a previous publication, dried rutin (at 354 nm) was used as the quantification standard and the MRRF values of two main flavonoids were used to determine their concentrations.[31] Concentrations of approximately 0.05 and 0.01% (or 50 and 10 mg/100 g of plant material on dry weight basis) were obtained for flavonoids F1 and F2, respectively. The total flavonoid content of this plant is <0.10% because the remaining flavonols were present at very low concentrations and UV peaks were not detectable for absorbance measurements.

In addition to the flavonoids, 1 lignan (lariciresinol 4-*O*-*β*-D-glucopyranoside) and 18 other common compounds, including the glucosides of hydroxybenzoic and hydroxycinnamic acids and their derivatives (e.g., bound to sugar, quinic acid, and malic acid) and organic acids, were identified by comparison of the chromatographic and MS data with those in our in-house flavonoid database. Most of the common compounds have previously been detected in other plants analyzed in this laboratory.

The results of this study showed that *R. indica* is a rich source of glucosinolates.[1−5,8] These compounds were reasonably separated using the UHPLC conditions described here and identified by their high-accuracy mass measurement and multistage mass fragments. The UV absorbance of the major glucosinolates was used to compute their concentration. In summary, 33 glucosinolates, over 40 flavonoids, and more than 20 other phenolic and organic compounds were identified.

AUTHOR INFORMATION

Corresponding Author

*(L.-Z.L.) Phone: (301) 504-9136. Fax: (301) 504-8314. E-mail: longze.lin@ars.usda.gov.

Funding

This research is supported by the Agriculture Research Service of the U.S. Department of Agriculture and an Interagency Agreement with the Office of Dietary Supplements of the National Institutes of Health.

Notes

The authors declare no competing financial interest.

REFERENCES

(1) Halkiel, B. A.; Gershenzon, J. Biology and biochemistry of glucosinolates. *Annu. Rev. Plant Biol.* **2006**, *57*, 303−333.

(2) Johnson, I. T. Glucosinolates: bioavailability and importance to health. *Int. J. Vitam. Nutr. Res.* **2002**, *72*, 26−31.

(3) Dinkova-Kostova, A. T.; Rumen, V.; Kostov, R. T. Glucosinolates and isothiocyanates in health and disease. *Trends Mol. Med.* **2012**, *18*, 337−347.

(4) Fahey, J. W.; Zalcmann, A. T.; Talalay, P. The chemical diversity and distribution of glucosinolates and isothiocyanates among plants. *Phytochemistry* **2001**, *6*, 5−51.

(5) Agerbirk, N.; Olsen, C. E. Glucosinolate structures in evolution. *Phytochemistry* **2012**, *77*, 16−45.

(6) Reichelt, M.; Brown, P. D.; Schneider, B.; Oldham, N. J.; Stauber, E.; Tokuhisa, J.; Kliebenstein, D. J.; Mitchell-Olds, T.; Gershenzon, J.

Benzoic acid glucosinolate esters and other glucosinolates from *Arabidopsis thaliana*. *Phytochemistry* **2002**, *59*, 663−671.
(7) Agerbirk, N.; Olsen, C. E. Isoferuloyl derivatives of five seed glucosinolates in the crucifer genus *Barbarea*. *Phytochemistry* **2011**, *72*, 610−623.
(8) Clarke, D. B. Glucosinolates, structures and analysis in food. *Anal. Methods* **2010**, *2*, 310−325.
(9) Yamane, A.; Fujikura, J.; Ogawa, H.; Mizutani, J. Isothiocyanates as alleopathic compounds from *Rorippa indica* Hiern. (Cruciferae) roots. *J. Chem. Ecol.* **1992**, *18*, 1941−1954.
(10) Kawabata, J.; Fukushi, Y.; Hayashi, R.; Suzuki, K.; Mishima, Y.; Yamane, A.; Mizutani, J. 8-Methylsufinyloctyl isothicyanate as an allelochemical candidate from *Rorippa sylvestris* Besser. *Agric. Biol. Chem.* **1989**, *53*, 3361−3362.
(11) Mellon, F. A.; Bennett, R. N.; Holst, B.; Williamson, G. Intact glucosinolate analysis in plant extracts by programmed cone voltage electrospray LC/MS: performance and comparison with LC/MS/MS methods. *Anal. Biochem.* **2002**, *306*, 83−91.
(12) Fabre, N.; Poinsot, V.; Debrauwer, L.; Vigor, C.; Tulliez, J.; Fourasté, I.; Moulis, C. Characterisation of glucosinolates using electrospray ion trap and electrospray quadrupole time-of-flight mass spectrometry. *Phytochem. Anal.* **2007**, *18*, 306−319.
(13) Rochfort, S. J.; Trenerry, V. C.; Imsic, M.; Panozzo, J.; Jones, R. Class targeted metabolomics: ESI ion trap screening methods for glucosinolates based on MS*n* fragmentation. *Phytochemistry* **2008**, *69*, 1671−1679.
(14) Francisco, M.; Moreno, D. A.; Cartea, M. E.; Ferreres, F.; García-Viguera, C.; Velasco, P. Simultaneous identification of glucosinolates and phenolic compounds in a representative collection of vegetable *Brassica rapa*. *J. Chromatogr., A* **2009**, *1216*, 6611−6619.
(15) Cataldi, T. R.; Lelario, F.; Orlando, D.; Bufo, S. A. Collision-induced dissociation of the A + 2 isotope ion facilitates glucosinolates structure elucidation by electrospray Ionization-tandem mass spectrometry with a linear quadrupole ion trap. *Anal. Chem.* **2010**, *82*, 5686−5696.
(16) Bianco, G.; Lelario, F.; Battista, F. G.; Bufob, S. A.; Cataldic, T. R. I. Identification of glucosinolates in capers by LC-ESI-hybrid linear ion trap with Fourier transform ion cyclotron resonance mass spectrometry (LC-ESI-LTQ-FTICR MS) and infrared multiphoton dissociation. *J. Mass Spectrom.* **2012**, *47*, 1160−1169.
(17) Glauser, G.; Schweizer, F.; Turlings, T. C.; Reymond, P. Rapid profiling of intact glucosinolates in *Arabidopsis* leaves by UHPLC-QTOFMS using a charged surface hybrid column. *Phytochem. Anal.* **2012**, *23*, 520−528.
(18) Maldini, M.; Baima, S.; Morelli, G.; Scaccini, C.; Natella, F. A liquid chromatography-mass spectrometry approach to study "glucosinoloma" in broccoli sprouts. *J. Mass Spectrom.* **2012**, *47*, 1198−1206.
(19) Mohn, T.; Cutting, B.; Ernst, B.; Hamburger, M. Extraction and analysis of intact glucosinolates − a validated pressurized liquid extraction/liquid chromatography−mass spectrometry protocol for *Isatis tinctoria*, and qualitative analysis of other cruciferous plants. *J. Chromatogr., A* **2007**, *1166*, 142−151.
(20) Kusznierewicz, B.; Iori, R.; Piekarska, A.; Namieśnik, J.; Bartoszek, A. Convenient identification of desulfoglucosinolates on the basis of mass spectra obtained during liquid chromatography-diode array-electrospray ionisation mass spectrometry analysis: method verification for sprouts of different Brassicaceae species extracts. *J. Chromatogr., A* **2013**, *1278*, 108−115.
(21) Bennett, R. N.; Carvalho, R.; Mellon, F. A.; Eagles, J.; Rosa, E. A. Identification and quantification of glucosinolates in sprouts derived from seeds of wild *Eruca sativa* L. (salad rocket) and *Diplotaxis tenuifolia* L. (wild rocket) from diverse geographical locations. *J. Agric. Food Chem.* **2007**, *55*, 67−74.
(22) Velasco, P.; Francisco, M.; Moreno, D. A.; Ferreres, F.; García-Viguera, C.; Cartea, M. E. Phytochemical fingerprinting of vegetable *Brassica oleracea* and *Brassica napus* by simultaneous identification of glucosinolates and phenolics. *Phytochem. Anal.* **2011**, *22*, 144−152.
(23) Ediage, E. N.; Di Mavungu, J. D.; Scippo, M. L.; Schneider, Y. J.; Larondelle, Y.; Callebaut, A.; Robbens, J.; Van Peteghem, C.; De Saeger, S. Screening, identification and quantification of glucosinolates in black radish (*Raphanus sativus* L. niger) based dietary supplements using liquid chromatography coupled with a photodiode array and liquid chromatography-mass spectrometry. *J. Chromatogr., A* **2011**, *1218*, 4395−4405.
(24) Argentieri, M. P.; Accogli, R.; Fanizzi, F. P.; Avato, P. Glucosinolates profile of "mugnolo", a variety of *Brassica oleracea* L. native to southern Italy (Salento). *Planta Med.* **2011**, *77*, 287−292.
(25) Hennig, K.; Verkerk, R.; Bonnema, G.; Dekker, M. Rapid estimation of glucosinolate thermal degradation rate constants in leaves of Chinese kale and broccoli (*Brassica oleracea*) in two seasons. *J. Agric. Food Chem.* **2012**, *60*, 7859−7865.
(26) Márton, M. R.; Krumbein, A.; Platz, S.; Schreiner, M.; Rohn, S.; Rehmers, A.; Lavric, V.; Mersch-Sundermann, V.; Lamy, E. Determination of bioactive, free isothiocyanates from a glucosinolate-containing phytotherapeutic agent: a pilot study with in vitro models and human intervention. *Fitoterapia* **2013**, *85*, 25−34.
(27) The Editorial Commission of Chinese Materia Medica. *Rorippa indica in Chinese Materia Medica*; Shanghai Science and Technology Press: Shanghai, China, 1999; Vol. 3, pp 731−734.
(28) Lee, K. C.; Cheuk, M. W.; Chan, W.; Lee, A. W.; Zhao, Z. Z.; Jiang, Z. H.; Cai, Z. Determination of glucosinolates in traditional Chinese herbs by high-performance liquid chromatography and electrospray ionization mass spectrometry. *Anal. Bioanal. Chem.* **2006**, *486*, 2225−2232.
(29) Tan, Z.-G.; Chen, Y.; Ji, G.-L. The study on the active components of *Rorippa indica*. *Chinese Sci.* **1974**, *No. 1*, 15−20.
(30) Ananthi, P.; Kumari, B. D. R. Gas chromatography-mass spectrometry analysis of methanolic seed and root extracts of *Rorippa indica* L. *Int. J. Chem. Technol. Res.* **2013**, *5*, 299−306.
(31) Lin, L.-Z.; Harnly, J. M. A screening method for the identification of glycosylated flavonoids and other phenolic compounds using a standard analytical approach for all plant materials. *J. Agric. Food Chem.* **2007**, *55*, 1084−1096.
(32) Lin, L.-Z.; Harnly, J. M.; Zhang, R.-Z.; Fan, X.-E.; Chen, H.-J. Quantitation of the hydroxycinnamic acid derivatives and the glycosides of flavonols and flavones by UV absorbance after identification by LC-MS. *J. Agric. Food Chem.* **2012**, *60*, 544−553.
(33) Lin, L.-Z.; Sun, J.; Chen, P.; Harnly, J. M. UHPLC-PDA-EIS/HRMS/MS^n analysis of anthocyanins, flavonol glycosides and hydroxycinnamic acid derivatives in red mustard green (*Brassica juncea* Coss variety). *J. Agric. Food Chem.* **2011**, *59*, 12059−12072.

JOURNAL OF AGRICULTURAL AND FOOD CHEMISTRY

Article

pubs.acs.org/JAFC

24(*S*)-Saringosterol from Edible Marine Seaweed *Sargassum fusiforme* Is a Novel Selective LXRβ Agonist

Zhen Chen,[†,∥] Jiao Liu,[§,∥] Zhifei Fu,[†] Cheng Ye,[§] Renshuai Zhang,[†] Yiyun Song,[§] Ying Zhang,[§] Haihua Li,[†] Hao Ying,*[,§] and Hongbing Liu*[,†]

[†]Key Laboratory of Marine Drugs, Chinese Ministry of Education, Institute of Marine Food and Drugs, School of Medicine and Pharmacy, Ocean University of China, Qingdao 266003, China

[§]Key Laboratory of Nutrition and Metabolism, Institute for Nutritional Sciences, Shanghai Institutes for Biological Sciences, Graduate School of the Chinese Academy of Sciences, Chinese Academy of Sciences, Shanghai 200031, China

ABSTRACT: Dietary phytosterols have been successfully used for lowering cholesterol levels, which correlates with the fact that some phytosterols are able to act as liver X receptor (LXR) agonists. *Sargassum fusiforme* is an edible marine seaweed well-known for its antiatherosclerotic function in traditional Chinese medicine. In this study, seven phytosterols including fucosterol (**1**), saringosterol (**2**), 24-hydroperoxy-24-vinyl-cholesterol (**3**), 29-hydroperoxy-stigmasta-5,24(28)-dien-3β-ol (**4**), 24-methylene-cholesterol (**5**), 24-keto-cholesterol (**6**), and 5α,8α-epidioxyergosta-6,22-dien-3β-ol (**7**) were purified and evaluated for their actions on LXR-mediated transcription using a reporter assay. Among these phytosterols, **2** was the most potent compound in stimulating the transcriptional activities of LXRα by (3.81 ± 0.15)-fold and LXRβ by (14.40 ± 1.10)-fold, respectively. Two epimers of **2**, 24(*S*)-saringosterol (**2a**) and 24(*R*)-saringosterol (**2b**), were subsequently separated by semipreparative high-performance liquid chromatography. Interestingly, **2a** was more potent than **2b** in LXRβ-mediated transactivation ((3.50 ± 0.17)-fold vs (1.63 ± 0.12)-fold) compared with control. Consistently, **2a** induced higher expression levels of LXR target genes including key players in reverse cholesterol transport in six cell lines. These data along with molecular modeling suggested that **2a** acts as a selective LXRβ agonist and is a potent natural cholesterol-lowering agent. This study also demonstrated that phytosterols in *S. fusiforme* contributed to the well-known antiatherosclerotic function.

KEYWORDS: *Sargassum fusiforme, phytosterols, 24(S)-saringosterol, selective LXRβ agonist, cholesterol metabolism*

INTRODUCTION

Sargassum fusiforme (Harvey) Setchell, a member of the genus *Sargassum* of the Sargassaceae family, is a common edible marine seaweed in China, Japan, and Korea.[1−4] In China, the seaweed is called "Chang Shou Cai", which is translated to "antiaging vegetable" in English.[1] *S. fusiforme* has also been widely used in traditional Chinese medicine (TCM) for thousands of years for treating atherosclerosis, hyperlipidemia, hypertension, thyroid diseases, and cancer.[1,3,5] In addition, several other species in *Sargassum* (*S. pallidum*, *S. thunbergii*, *S. muticum*, *S. horneri*, *S. siliquastrum*, *S. hemiphyllum*, *S. vachellianum*) are used as TCM for treating cardiovascular disease (CVD).[3] The active components and the underlying molecular mechanism of the antiatherosclerotic function of *Sargassum* have not been systematically investigated.

Polysaccharides, fatty acids, phytosterols, phlorotannins, and meroterpenoids were the major components previously described in *Sargassum*.[1,3] Recent studies on the antiatherosclerotic constituents of *S. fusiforme* were focused on polysaccharides and their derivatives, whereas investigations on nonpolar components such as phytosterols have not been done.[6,7] It is well-known that phytosterols, such as β-sitosterol, campesterol, and stigmasterol from terrestrial plants, are able to reduce plasma low-density lipoprotein (LDL) cholesterol levels and have been shown to be safe for half a century.[8−13] Phytosterols are abundant in *Sargassum*; however, the functions of its phytosterols are barely reported.[1,3,5]

Phytosterols are structurally related to cholesterol. They cannot be synthesized by humans and, therefore, are always obtained from diet. β-Sitosterol, campesterol, and stigmasterol account for >95% of phytosterol dietary intake,[9] and are known as "terrestrial lipid-rich food". Dietary phytosterols decrease intestinal cholesterol absorption, resulting in a reduction of both LDL and total cholesterol concentrations in plasma.[9] It has been shown recently that some phytosterols may regulate gene expressions in the cholesterol metabolism pathway through liver X receptor (LXR) activation.[14,15]

LXRs are ligand-dependent nuclear receptors that play critical roles in cholesterol homeostasis, inflammation, and lipogenesis. Their putative association with human diseases makes them promising pharmacological targets.[16,17] Functioning as chief regulators of cholesterol homeostasis, LXRs, the sterol-responsive transcription factors, control cholesterol influx, transport, and efflux. Studies have shown that local activation of LXRs have beneficial effects on atherosclerosis.[18] LXRs have two isoforms (LXRα and LXRβ) with distinct tissue distributions.[17,19] It has been suggested that hepatic lipogenesis is mainly mediated through LXRα and that LXRβ mediates the antiatherogenic effects.

Received: January 6, 2014
Revised: June 8, 2014
Accepted: June 13, 2014
Published: June 13, 2014

ACS Publications © 2014 American Chemical Society

dx.doi.org/10.1021/jf500083r | *J. Agric. Food Chem.* 2014, 62, 6130−6137

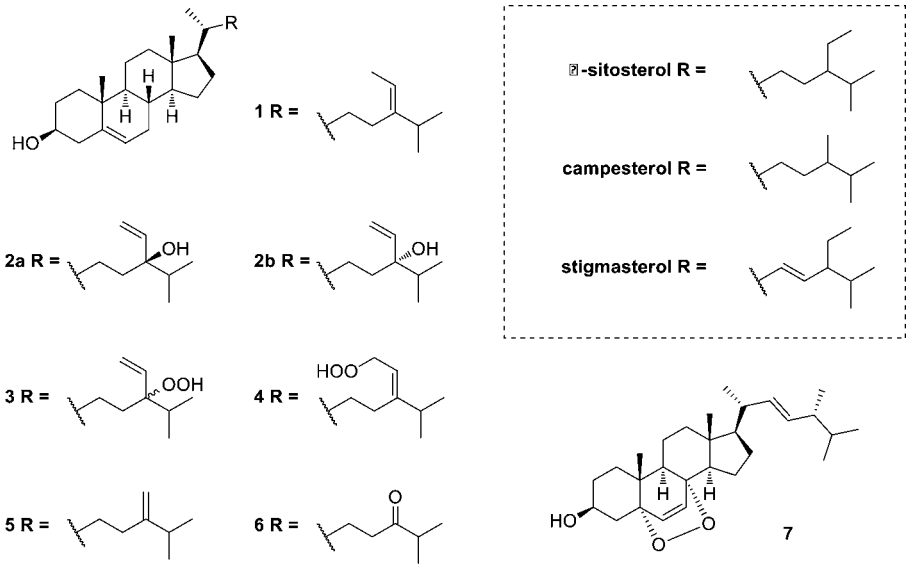

Figure 1. Marine phytosterols isolated and identified from *Sargassum fusiforme*. Three common terrestrial plant sterols are shown together.

Table 1. APCI-MS Data for Phytosterols 1−7

Compound	Side chain	Fomula	M.W.	APCI-MS fragment ions (*m/z*)
1		$C_{29}H_{48}O$	412	413 ([M+H]$^+$, 5), 411 ([M+H-2H]$^+$, 17), 409 ([M+H-4H]$^+$, 53), 395 ([M-H_2O+H]$^+$, 100)
2	OH	$C_{29}H_{48}O_2$	428	427 ([M+H-2H]$^+$, 18), 425 ([M+H-4H]$^+$, 31), 411 ([M-H_2O+H]$^+$, 23), 393 ([M-2H_2O+H]$^-$, 100)
2a	OH	$C_{29}H_{48}O_2$	428	411 ([M-H_2O+H]$^+$, 23), 393 ([M-2H_2O+H]$^+$, 100)
2b	OH	$C_{29}H_{48}O_2$	428	411 ([M-H_2O+H]$^+$, 23), 393 ([M-2H_2O+H]$^+$, 100)
3	OOH	$C_{29}H_{48}O_3$	444	443 ([M+H-2H]$^+$, 7), 441 ([M+H-4H]$^+$, 5), 427 ([M-H_2O+H]$^+$, 25), 393 (25), 367 (100)
4	HOO	$C_{29}H_{48}O_3$	444	443 ([M+H-2H]$^+$, 5), 441 ([M+H-4H]$^+$, 8), 427 ([M-H_2O+H]$^+$, 42), 409 (100), 393 (52)
5		$C_{28}H_{46}O$	398	399 ([M+H]$^+$, 16), 397 ([M+H-2H]$^+$, 18), 395 ([M+H-4H]$^+$, 31), 381 ([M-H_2O+H]$^+$, 100)
6	O	$C_{27}H_{44}O_2$	400	401([M+H]$^+$, 18), 399 ([M+H-2H]$^+$, 12),397 ([M+H-4H]$^+$, 33), 383 ([M-H_2O+H]$^+$, 100)
7		$C_{28}H_{44}O_3$	428	429 ([M+H]$^+$, 67), 411 ([M-H_2O+H]$^+$, 100), 393 (50), 377 (35)

Endogenous LXR ligands are oxysterols.[15,20] Phytosterols found in *Sargassum* possess similar structures.[1,3,5] Could these analogues of oxysterols activate LXRs and be responsible for the observed antiatherosclerotic effects? Little evidence has been afforded until now except for fucosterol, which inhibits cholesterol absorption in rats and activates LXRs.[21] In the current study, seven phytosterols from *S. fusiforme* were purified and characterized by NMR and MS. These compounds

dx.doi.org/10.1021/jf500083r | *J. Agric. Food Chem.* 2014, 62, 6130−6137

Table 2. ^{1}H NMR (600 MHz, δ, J in Hz) Data for 1−4 in $CDCl_3$

position	1	2	2a	2b	3	4
3	3.53 m	3.52 m	3.521 m	3.521 m	3.53 m	3.53 m
6	5.35 d (5.2)	5.35 m	5.347 br d	5.346 br d	5.35 br d (5.0)	5.36 br d (3.5)
18	0.69 s	0.67 s	0.668 s	0.666 s	0.68 s	0.68 s
19	1.01 s	1.00 s	1.001 s	1.000 s	1.01 s	1.01 s
21	0.99 d (7.0)		0.915 d (6.5)	0.920 d (6.3)	0.96 d (6.6)	0.99 d (6.4)
26	0.98 d (6.8)	0.87 d (7.0)	0.868 d (7.0)	0.867 d (6.8)	0.86 d (7.0)	1.03 d (6.9)
27	0.98 d (6.8)	0.89 m	0.895 d (6.9)	0.887 d (6.7)	0.88 d (6.7)	1.03 d (6.9)
28	5.18 q (6.8)	5.76−5.84 m	5.793 dd (17.2, 10.9)	5.807 dd (17.3, 10.8)	5.75 dd (17.4, 11.4)	5.31 t (7.1)
29	1.57 d (6.6)	5.16−5.21 m	5.181 d (17.2)	5.187 d (17.3)	5.28 dd (11.4, 1.2)	4.55 d (7.02)
		5.11−5.15 m	5.129 dd (10.9, 1.2)	5.135 dd (10.8, 1.2)	5.16 dd (18.0, 1.2)	

were then evaluated for their effects on LXR-mediated transactivation and target gene expression in six cell lines. Indeed, 24(*S*)-saringosterol, an analogue of oxysterols, acted as a selective LXRβ agonist. This study also demonstrated that phytosterols in *S. fusiforme* contributed to the well-known antiatherosclerotic function.

MATERIALS AND METHODS

Chemicals. Spectral grade solvents for spectroscopic measurements were obtained from Sigma-Aldrich. HPLC grade solvents were obtained from Merck Inc. (Merck KgaA, Darmstadt, Germany). All other solvents were of analytical grade (Yuwang Reagent Co., Shandong, China).

Cell culture materials such as Dulbecco's modified Eagle medium (DMEM), modified Eagle medium (MEM), fetal bovine serum (FBS), trypsin, glutamine, and penicillin/streptomycin (PES) were obtained from Gibco. Phorbol myristate acetate (PMA) and T0901317 were obtained from Sigma-Aldrich. Lipofectamine 2000 transfection reagent was obtained from Invitrogen. Dual-GloLuciferase Assay System was purchased from Promega. For RNA isolation, TRIzol reagent and M-MLV reverse transcriptase were obtained from Invitrogen. Regular PCR was performed with the TaKaRa Taq Kit (Takara). Power SYBR Green PCR Master Mix was purchased from Applied Biosystems.

General Experimental Procedures. NMR spectra were recorded on JEOL JNM-ECP 600 NMR spectrometers, using TMS as internal standard, and chemical shifts were recorded as δ values. APCI-MS analysis was performed on a Bruker amaZon SL mass spectrometer. High-performance liquid chromatography (HPLC) analysis was performed on an Agilent 1100 HPLC system coupled to a photodiode array detector with routine detection at 210 nm. The separation column (250 × 4.6 mm i.d., 5 μm) was prefilled with YMC ODS Pack-A, and a linear gradient of MeOH and H_2O was used. Semipreparative HPLC was performed on a Shimadzu LC-6AD using a C-18 column (YMC ODS Pack-A, 250 × 10 mm i.d., 5 μm; flow rate = 4.0 mL/min, UV detection at 210 nm). Silica gel (100−200 and 200−300 mesh; Qingdao Haiyang Chemical Co., Ltd., Qingdao, China), Sephadex LH-20 (GE Healthcare Bio-Sciences AB, Uppsala, Sweden) were used for column chromatography. Thin layer chromatography (TLC) silica gel GF_{254} plates (Yantai Zi Fu Chemical Co., Ltd., Yantai, China) were used for TLC analysis.

Plant Material. Fronds of *S. fusiforme* (Harvey) Setchell were collected from the Dongtou area in Zhejiang Provinice, China, in May 2012. The original seaweed was identified by Dr. Tao Liu (College of Marine Life Science, Ocean University of China), and a voucher specimen has been deposited at the School of Medicine and Pharmacy, Ocean University of China.

Isolation and Identification. Air-dried fronds of *S. fusiforme* (200 g) were powdered and repeatedly extracted with dichloromethane/methanol (1:2) three times to give a crude extract (12.4 g), which was fractionated by vacuum liquid chromatography over silica gel by gradient elution using dichloromethane/methanol to yield six fractions. The fourth fraction (CH_2Cl_2/MeOH 98:2, 1450 mg) was subsequently separated over Sephadex LH-20 with CH_2Cl_2/MeOH (1:1) followed by flash silica gel column chromatography with light petroleum/acetone (20:1 to 8:1) to achieve five subfractions. Compounds **1** (119 mg), **2** (60 mg), and **3** (7.6 mg) were crystallized as colorless needles from subfractions 1, 3, and 4, respectively. Subfraction 2 was further purified by semipreparative HPLC (MeOH/H_2O, 85:15) to afford compound **7** (3 mg). Subfraction 5 was further purified by semipreparative HPLC with MeOH/H_2O (85:15) to yield compounds **4** (4.1 mg), **5** (5 mg), and **6** (5.6 mg). The epimeric mixture **2** was separated into **2a** (2.4 mg) and **2b** (4.9 mg) by semipreparative HPLC (MeOH/acetonitrile/H_2O, 95:1:4).

Characterization of Purified Compounds. Fucosterol (**1**): colorless needles; APCI-MS data, see Table 1; ^{1}H NMR data, see Table 2.

Saringosterol (**2**): colorless needles; APCI-MS data, see Table 1; ^{1}H NMR data, see Table 2.

24(*S*)-Saringosterol (**2a**): colorless needles; APCI-MS data, see Table 1; ^{1}H NMR data, see Table 2.

24(*R*)-Saringosterol (**2b**): colorless needles; APCI-MS data, see Table 1; ^{1}H NMR data, see Table 2.

24-Hydroperoxy-24-vinyl-cholesterol (**3**): colorless needles; APCI-MS data, see Table 1; ^{1}H NMR data, see Table 2.

29-Hydroperoxy-stigmasta-5,24(28)-dien-3β-ol (**4**): colorless needles; APCI-MS data, see Table 1; ^{1}H NMR data, see Table 2.

24-Methylene-cholesterol (**5**): colorless needles; APCI-MS data, see Table 1; ^{1}H NMR (600 MHz, $CDCl_3$) δ 5.35 (1H, br d, J = 5.2 Hz, H-6), 4.71 (1H, br s, H-28), 4.65 (1H, br s, H-28), 3.52 (1H, m, H-3), 1.02 (6H, d, J = 6.8 Hz, H-26 and H-27), 1.00 (3H, s, H-19), 0.95 (3H, d, J = 6.6 Hz, H-21), 0.68 (3H, s, H-18).

24-Keto-cholesterol (**6**): colorless needles; APCI-MS data, see Table 1; ^{1}H NMR (600 MHz, $CDCl_3$) δ 5.35 (1H, br d, J = 3.5 Hz, H-6), 3.52 (1H, m, H-3), 2.61 (1H, m, H-25), 1.09 (6H, d, J = 6.9 Hz, H-26 and H-27), 1.00 (3H, s, H-19), 0.91 (3H, d, J = 6.5 Hz, H-21), 0.67 (3H, s, H-18).

5α,8α-Epidioxyergosta-6,22-dien-3β-ol (**7**): APCI-MS data, see Table 1; ^{1}H NMR (600 MHz, $CDCl_3$) δ 6.51 (1H, d, J = 8.6 Hz, H-6), 6.25 (1H, d, J = 8.5 Hz, H-7), 5.22 (1H, dd, J = 15.2, 7.7 Hz, H-22), 5.14 (1H, dd, J = 15.4, 8.6 Hz, H-23), 3.97 (3H, m, H-3), 1.00 (3H, d, J = 6.6 Hz, H-28), 0.88 (3H, s, H-19), 0.83 (3H, d, J = 6.8 Hz, H-27), 0.82 (3H, d, J = 6.7 Hz, H-26), 0.82 (3H, s, H-18).

Cell Culture. HEK293T, THP-1, HepG2, and Caco-2 cells were from ATCC. HEK293T and HepG2 cells were maintained in DMEM containing 10% heat-inactivated FBS and 1% PES. THP-1 cells were maintained in RPMI-1640 medium supplemented with 10% FBS and 1% PES. THP-1 cells were differentiated in the presence of PMA (50 ng/mL) for 72 h prior to treatment and RNA extraction. Caco-2 cells were maintained in MEM supplemented with 20% FBS and 1% PES. All cell lines were grown in 5% CO_2 at 37 °C. As for phytosterol treatment, cells were preincubated in a complete growth medium for 24 h and then were incubated for an additional 24 h in 2 mL of medium containing phytosterols (30 μM), T0901317 (20 μM), ethanol, or DMSO. Stock solutions of phytosterols were prepared in ethanol, whereas a stock solution of T0901317 (0.1 mM) was prepared in DMSO. Control cells were treated with the corresponding amount of ethanol (1%). Experiment was carried out in at least triplicate.

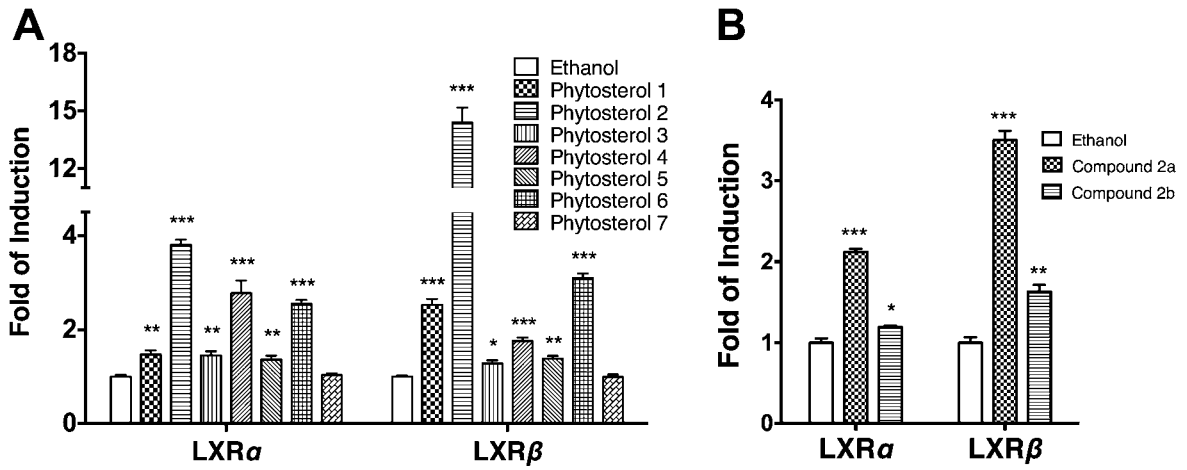

Figure 2. Effects of different phytosterols on LXR transcriptional activity. Luciferase assay was performed to compare the effects of phytosterols **1**-**7** (a and b), **2a** and **2b** (c and d), on LXR-mediated transcription. HEK-293T cells were transfected with expression plasmids pGal4-LXRα-LBD (a and c) or pGal4-LXRβ-LBD (b and d), together with reporter plasmid pTATA-LUC. Twelve hours after transfection, the cells were exposed to phytosterols **1**−**7** (30 μM), **2a** and **2b** (10 μM), or ethanol for 12 h. Data represent the means ± SEM ($n \geq 3$). (∗) $P < 0.05$, (∗∗) $P < 0.01$, and (∗∗∗) $P < 0.001$ versus control.

Transfection and Luciferase Assay. A dual-luciferase reporter assay system was utilized to examine the effect of phytosterols on the transactivation of LXRα/β. The vectors used in luciferase assays in the Gal4-LXR system include pGal4-LXRα/β-LBD (LBD, ligand-binding domain; amino acids 137−102 for LXRα and amino acids 209−468 for LXRβ, respectively), pTATA-LUC containing UAS element, and pRL-TK as control. A modified assay method was used in this study.[22] Briefly, HEK293T cells (1×10^5/mL) were plated in 48-well culture plates and then incubated in DMEM containing 10% FBS without antibiotics. After 24 h, cells were cotransfected with 0.075 μg/well of plasmid below: 0.05 μg of pTATA-luc, 0.005 μg of pRL-TK, and 0.02 μg of either pGal4-LXRα-LBD or pGal4-LXRβ-LBD, using Lipofectamine 2000 transfection reagent. Cells were cultured for 24 h post-transfection and then treated with phytosterols, T0901317, ethanol, or DMSO for an additional 12 h. After that, cells were lysed in 1× passive lysis buffer. The supernatant was assayed for Firefly luciferase activity and Renilla luciferase activity. Values were reported as relative Firefly luciferase to Renilla luciferase activity.

Quantitative RT-PCR. Total RNA was extracted with TRIzol reagent from THP-1, Caco-2, RAW264.7, HEK293T, and HepG2 cells, after treatment for 24 h with T0901317 and phytosterol or vehicle. After reverse transcription by M-MLV reverse transcriptase, regular PCR was performed with the TaKaRa Taq Kit. Quantitative real-time PCR was conducted with an ABI Prism 7500 sequence detection system, using Power SYBR Green PCR Master Mix according to the manufacturer's recommendations. Expression levels were normalized to those of glyceraldehyde 3-phosphate dehydrogenase or β-actin by the normalized expression (CT) method, according to the manufacturer's guidelines. The oligonucleotide primers for each target gene examined are as follows: h-ABCA1-F, ACCCACCCTATGAACAACATGA; h-ABCA1-R, GAGTCGGGTAACGGAAACAGG; h-ABCG1-F, ATTCAGGGACCTTTCCTATTCGG; h-ABCG1-R, CTCACCACTATTGAACTTCCCG; h-SREBF1-F, ACAGTGACTTCCCTGGCCTAT; h-SREBF1-R, GCATGGACGGGTACATCTTCAA.

Statistical Analysis. GraphPad Prism 5.0 was used for statistical analysis. All data are presented as the mean ± standard error of the mean (SEM). Statistical analysis was conducted using an unpaired two-tailed t test. $P < 0.05$ was considered to be statistically significant.

Molecular Modeling. Molecular docking analysis and visualization including other related work were performed with SYBYL-X 2.0 (Tripos Inc., St. Louis, MO, USA) running on Microsoft Windows 7. All of the ligand structures were drawn using the sketch tool in SYBYL-X with the default parameters. Then Gasteiger−Huckel charges were calculated and their geometric conformations minimized with the Tripos force field. The crystal structure of LXRβ with 24,25-epoxy-cholesterol (PDB ID 1P8D)[23] as ligand was used for docking study. Before docking, ligand and waters in the complex were removed, and the protein structure was standardized with the protein preparation processes in SYBYL-X.

RESULTS

Identification of Compounds. Phytosterols were isolated from the extract of *S. fusiforme*. On the basis of spectroscopic methods combined with comparison with the data of authentic compounds, they were identified as fucosterol (**1**),[24] saringosterol (**2**, as 1:1 mixture of epimers),[24] 24-hydroperoxy-24-vinyl-cholesterol (**3**),[25] 29-hydroperoxy-stigmasta-5,24(28)-dien-3β-ol (**4**),[25] 24-methylene-cholesterol (**5**),[25] 24-keto-cholesterol (**6**),[26] and 5α,8α-epidioxyergosta-6,22-dien-3β-ol (**7**).[27] Further separation of **2** offered 24(*S*)-saringosterol (**2a**)[28] and 24(*R*)-saringosterol (**2b**)[28] (Figure 1). Compounds **5**−**7** were isolated from *S. fusiforme* for the first time.

Effects of Compounds 1−7 on LXR Transcriptional Activity. Dual-luciferase reporter assay was utilized to investigate the effects of compounds **1**−**7** on LXR-mediated transcription. Consistent with a recent report by Dr. Hoang,[29] fucosterol (**1**) increased the transactional activity of both LXRα and LXRβ. Saringosterol (**2**) showed the strongest ability to activate LXRs compared with other active compounds **1**, **4**, and **6**, whereas **3**, **5**, and **7** exhibited little effects (Figure 2A). Our data demonstrated that various oxidized phytosterols had different abilities to activate LXRs, which was in agreement with the review on oxidized phytosterols by Hovenkamp.[20]

Saringosterol (**2**) at 30 μM increased the transcriptional activity of LXRα by (3.81 ± 0.15)-fold and that of LXRβ by (14.40 ± 1.10)-fold, indicating that **2** had a selective effect. Because **2** was a mixture of stereoisomers, 24(*S*)-saringosterol (**2a**) and 24(*R*)-saringosterol (**2b**) were separated and tested individually to clarify the influence of the orientation of 24-OH group on the LXR activation. With regard to the transcriptional activity of LXRα and LXRβ, **2a** was more potent than **2b** for LXRβ-mediated transactivation ((3.50 ± 0.17)-fold vs (1.63 ± 0.12)-fold) at 10 μM (Figure 2B). These results hinted that **2a** was a stronger LXR agonist than **2b**.

dx.doi.org/10.1021/jf500083r | J. Agric. Food Chem. 2014, 62, 6130−6137

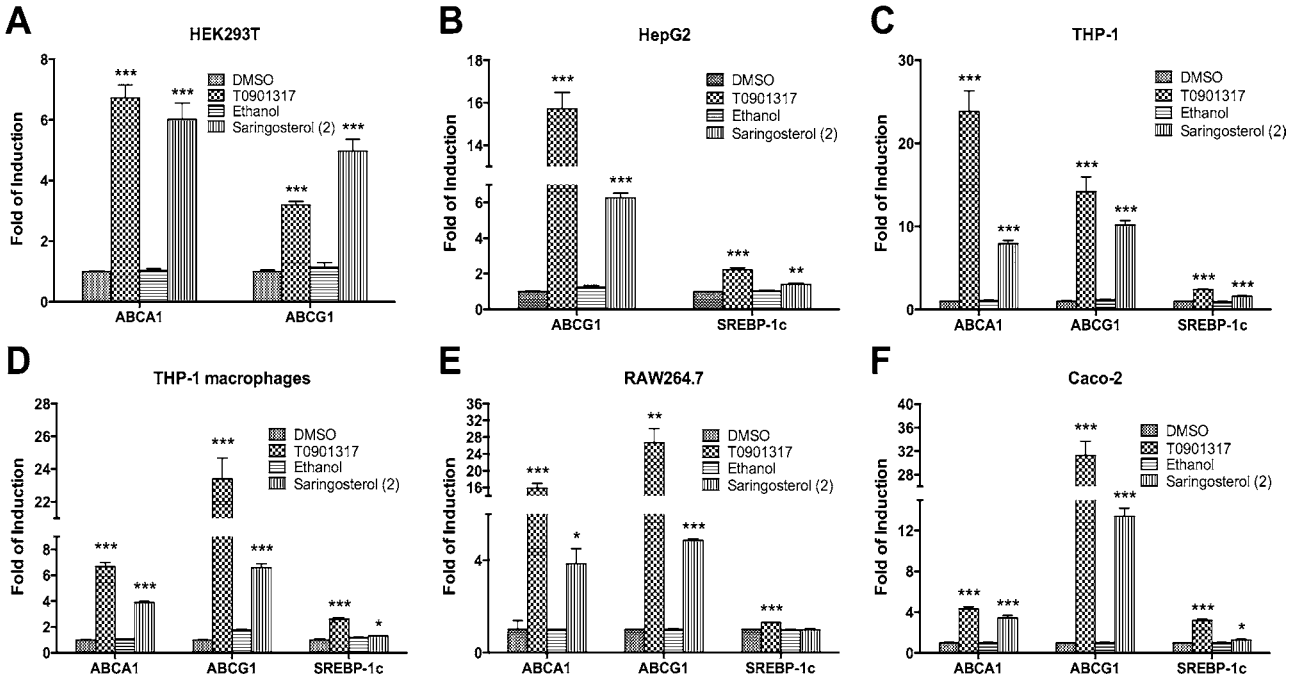

Figure 3. Effects of saringosterol (**2**) on LXR target genes expression in multiple cell types. The HEK293T (A), HepG2 (B), THP-1 monocytes (C), THP-1-derived macrophages (D), RAW264.7 (E), and intestinal Caco-2 (F) cells were cultured and then treated with **2** (30 μM), T0901317 (20 μM), or vehicle (DMSO, or ethanol) for 12 h. Total RNA was extracted and mRNA expression of ABCA1, ABCG1, and SREBP-1c was measured by qPCR. Data represent the means ± SEM ($n \geq 3$). (*) $P < 0.05$, (**) $P < 0.01$, and (***) $P < 0.001$ versus control.

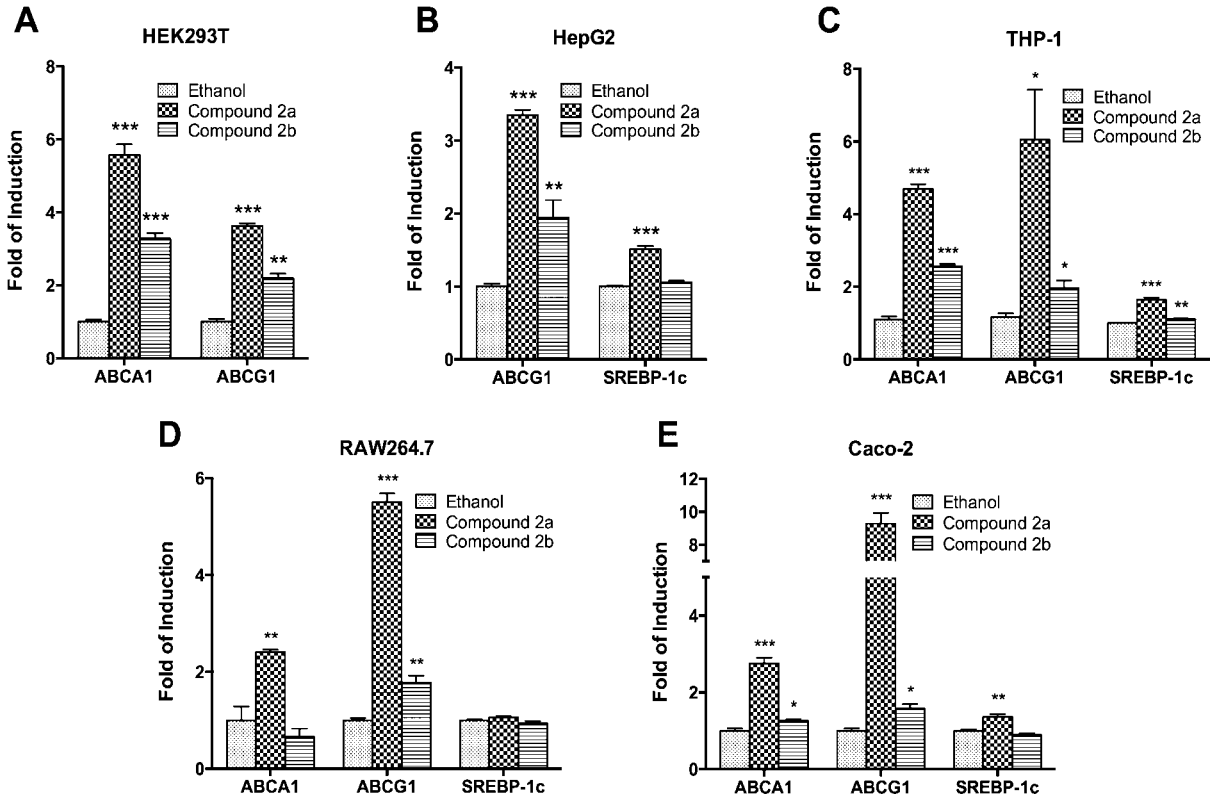

Figure 4. Induction of LXR-responsive genes by saringosterol isomers **2a** and **2b** in multiple cell types. The HEK293T (A), HepG2 (B), THP-1 monocytes (C), RAW264.7 (E), and intestinal Caco-2 (E) cells were treated with **2a** and **2b** (10 μM) or vehicle (ethanol) for 12 h. Total RNA was extracted, and mRNA expression of ABCA1, ABCG1, and SREBP-1c was measured by qPCR. Data represent the means ± SEM ($n \geq 3$). (*) $P < 0.05$, (**) $P < 0.01$, and (***) $P < 0.001$ versus control.

Effects of 2, 2a, and 2b on LXR Target Gene Expression in Multiple Cells Types. The regulation of LXR target genes by the epimer mixture **2** in different cell lines was examined subsequently. The LXR target gene expression in

dx.doi.org/10.1021/jf500083r | J. Agric. Food Chem. 2014, 62, 6130−6137

HEK293T cells was examined with real-time qRT-PCR. The mRNA expressions of two LXR target genes, ATP-binding cassette family transporter A1 (ABCA1) and ATP-binding cassette family transporter G1 (ABCG1),[17] were significantly increased by treatment with **2** (Figure 3A) as expected. The effects of **2** in HepG2 were also tested. The epimeric mixture **2** increased mRNA expression of ABCG1 and another LXR target gene, sterol regulatory element-binding protein-1c (SREBP-1c) (Figure 3B). In addition, **2** significantly enhanced the mRNA expression of ABCA1 and ABCG1 in THP-1 monocytes (Figure 3C), THP-1 derived macrophages (Figure 3D), RAW264.7 macrophages (Figure 3E), and Caco-2 cells (Figure 3F). Increased expression of SREBP-1c by **2** in THP-1, RAW264.7, Caco-2, and HepG2 cells was very limited compared to that of ABCA1 and ABCG1, but the increase was statistically significant (Figure 3B–F).

The abilities of compounds **2a** and **2b** to modulate LXR target gene expression in various cell lines were then compared. Consistent with the results obtained from luciferase assay, the induction fold of ABCA1 and ABCG1 by **2a** was greater than that of **2b** in HEK-293T cells (Figure 4A). Similarly, **2a** increased the mRNA expression of ABCG1 and SREBP-1c in HepG2 cells (Figure 4B). In agreement with the finding in luciferase assay, the mRNA expression of ABCA1 and ABCG1 was more sensitive to **2a** treatment as compared with **2b** in THP-1 monocytes and RAW264.7 macrophages (Figure 4C,D). A similar result was obtained in intestinal Caco-2 cells (Figure 4E). Consistent with the activity of **2**, the induction of SREBP-1c by **2a** was relatively small (Figure 4B–E). Thus, 24(*S*)-saringosterol (**2a**) was the major active component to stimulate LXR target gene expression.

24(*S*)-Saringosterol Acting As a Selective LXR*β* Agonist. Highest induction by the epimer mixture **2** was observed in the presence of LXR*β* (Figure 2A). This observation prompted us to test whether 24(*S*)-saringosterol (**2a**) was a selective LXR*β* agonist. To this end, dual luciferase assay using different doses of **2a** was performed. As shown in Figure 5, when the highest concentration of **2a** (40 *μ*M) was used, the LXR*β*-mediated transactivation increased 5-fold, whereas a <2-fold induction was seen for LXR*α*-mediated transactivation. Moreover, **2a** at a concentration lower than 5 *μ*M was still able to enhance LXR*β*-mediated transcription. In contrast, the transactivation of LXR*α* by **2a** was almost diminished when the concentration was lower than 5 *μ*M (Figure 5). These results clearly indicated that **2a** was a selective agonist for LXR*β*.

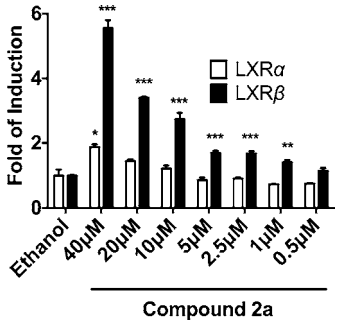

Figure 5. 24(*S*)-Saringosterol (**2a**) acts as a selective LXR*β* agonist. Luciferase assay were performed to compare the effect of compound **2a** on LXR*α*- and LXR*β*-mediated transcription. Compound **2a** at different concentrations was used as indicated.

A molecular docking approach was used to explore the interaction modes between the compounds and LXR*β*. After an energy minimization process, the lowest energy conformations of **2a** and **2b** were obtained, respectively (Figure 6). Both of the side chains of **2a** and **2b** were buried into the pocket, and the steroid nuclei were pushed outward. For **2a**, with a relatively higher docking scores, the hydroxyl group in C-3 position formed three hydrogen bonds with amino acid residues ARG319 and PHE329, which granted **2a** the binding affinity with LXR*β*. The equivalent hydroxyl group of **2b** formed only one hydrogen bond with amino acid residue GLU281. We inferred that the different docking modes of **2a** and **2b** were caused by the conformational difference in steroid nuclei A-ring, which showed an obvious difference after energy minimization. This result suggested that specific chirality is required in forming hydrogen bond indirectly. This observation agreed with the result of the luciferase assay and likely explained why **2a** showed better agonist activity than **2b**.

DISCUSSION

Phytosterols purified from *S. fusiforme* had more oxygen-containing groups than terrestrial plant phytosterols, especially on their side chain (Figure 1). Thus, marine phytosterols resembled the oxysterols, which are native LXR ligands, more than terrestrial plant phytosterols did. On the basis of this structural characteristic, we hypothesized that the marine phytosterols from *Sargassum* might be an excellent source for novel LXR agonist screening. As expected, phytosterols **2**, **4**, and **6** acted as LXR agonists, which could be correlated with their oxysterol-like structures, with **3** as an exception. Meanwhile, a peroxide bridge in steroid nucleus, such as in compound **7**, did not contribute to their effect on LXR-mediated transcription activation. Most importantly, our results indicated that 24(*S*)-saringosterol might be a selective LXR*β* agonist. Specific chiral configuration of C-24 position was a pivotal factor responsible for the activity, which was also supported by the molecular docking results. Further research is needed on the structure–activity relationship of *Sargassum* phytosterols, including natural or their synthetic analogues.

LXR*α* is highly expressed in the liver, adrenal gland, intestine, adipose tissue, macrophages, lung, and kidney, whereas LXR*β* is ubiquitously expressed.[29] LXR agonists stimulate reverse cholesterol transport and cholesterol excretion in the bile, but they can also activate lipogenesis at the same time. Lipogenesis could lead to hypertriglyceridemia and liver steatosis, which casts a shadow on the development of drugs based on LXR agonists.[30−32] Some studies have shown that it is the highly specific expression of LXR*α* in liver that causes hypertriglyceridemia.[29,31] Hence, selective LXR*β* activation could be a promising treatment for hypercholesteremia without side effects. Because natural selective LXR*β* agonists are rare, LXR*α*-null animals were usually used to test nonselective LXRs agonists on LXR*β* activation.[30,33] Thus, 24(*S*)-saringosterol would be a valuable agent to test if selective LXR*β* activation could be a promising way to treat hypercholesteremia.

ABCA1 and ABCG1 play important roles in atherosclerosis. Recent studies demonstrated that in humans, ABCA1 mutations can cause a severe HDL deficiency syndrome characterized by cholesterol deposition in tissue macrophages and prevalent atherosclerosis.[34] Similarly, ABCG1 has also been shown to have antiatherosclerotic activity in mice.[35] Here, our

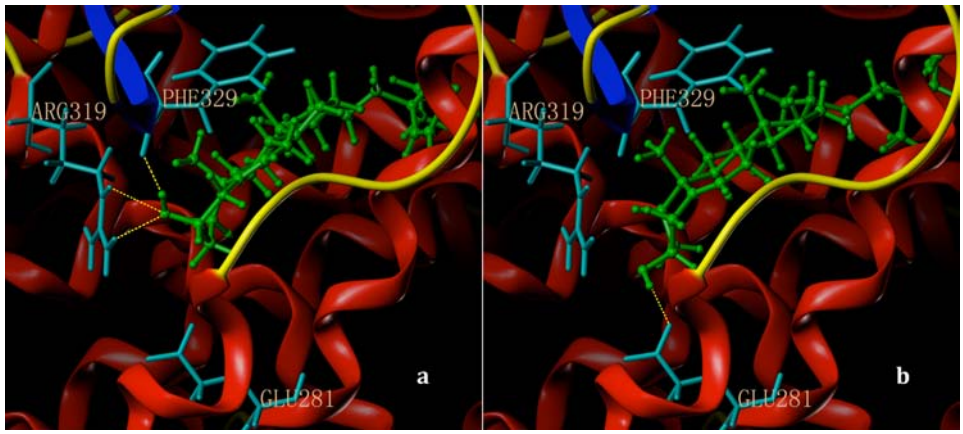

Figure 6. Predicted interaction modes of compounds **2a** and **2b** with LXRβ from molecular docking. Compounds **2a** (left) and **2b** (right) are shown as indicated. Only important residues (cyan) are shown for clarity. Hydrogen bonds are denoted by yellow dotted lines.

data indicated that compound **2a** might be a potential agent useful in treating atherosclerosis. In addition, SREBP-1c is responsible for lipogenesis in liver and may cause steatosis that develops in both leptin-deficient ob/ob mice and wild-type mice fed a lard-based high-fat diet.[36] In our study little effect of **2a** on the expression of SREBP-1c was seen in hepatocytes, implying that **2a**, not like other LXR agonists such as T0901317,[29,31,32] might not cause fatty liver.

Taken together, we investigated phytosterols from *S. fusiforme* and evaluated their effect on LXR-mediated transactivation and downstream target gene expression in various cell lines. On the basis of our findings, we concluded that 24(*S*)-saringosterol acted as a selective LXRβ agonist and is a potentially interesting natural cholesterol-lowering agent.

AUTHOR INFORMATION

Corresponding Authors

*(Hongbing Liu) Phone: +86-532-82032030. Fax: +86-532-82033054. E-mail: liuhongb@ouc.edu.cn.

*(Hao Ying) Phone: +86-21-54920247. Fax: +86-21-54920291. E-mail: yinghao@sibs.ac.cn

Author Contributions

‖Z.C. and J.L. contributed equally to this work.

Funding

Financial support by the NSFC (31271845) to Hongbing Liu is gratefully acknowledged.

Notes

The authors declare no competing financial interest.

ACKNOWLEDGMENTS

We thank Prof. Tao Jiang (School of Medicine and Pharmacy, Ocean University of China) for help with molecular modeling studies.

ABBREVIATIONS USED

LXRs, liver X receptors; TCM, traditional Chinese medicine; LDL, low-density lipoprotein; DMEM, Dulbecco's modified Eagle's medium; MEM, modified Eagle medium; FBS, fetal bovine serum; PES, penicillin/streptomycin; PMA, phorbol myristate acetate; HPLC, high-performance liquid chromatography; TLC, thin layer chromatography; SEM, standard error of the mean; ABCA1, ATP-binding cassette family transporter A1; ABCG1, ATP-binding cassette family transporter G1; SREBP-1c, sterol regulatory element-binding protein-1c

REFERENCES

(1) Liu, L.; Heinrich, M.; Myers, S.; Dworjanyn, S. Towards a better understanding of medicinal uses of the brown seaweed *Sargassum* in traditional Chinese medicine: a phytochemical and pharmacological review. *J. Ethnopharmacol.* **2012**, *142*, 591−619.

(2) Nisizawa, K.; Noda, H.; Kikuchi, R.; Watanabe, T. The main seaweed foods in Japan. *Hydrobiologia* **1987**, *151*−*152*, 5−29.

(3) Chen, Z.; Liu, H. B. Research progress in chemical components and biological activity of *Sargassum*. *Chin. J. Mar. Drugs* **2012**, *31*, 41−51.

(4) Fitzgerald, C.; Gallagher, E.; Tasdemir, D.; Hayes, M. Heart health peptides from macroalgae and their potential use in functional foods. *J. Agric. Food Chem.* **2011**, *59*, 6829−6836.

(5) Wang, W.; Li, H.; Wang, Y.; Xia, X. Chemical constituents from brown alga *Sargassum fusiforme*. *Chinese Tradit. Herb. Drugs* **2008**, *39*, 657−661.

(6) Yu, Z.; Shuai, L.; Li, X.; Duan, D.; Guo, Y. Regulating effect of *Sargassum fusiforme* (Harv.) Setch. on the level of blood lipid in experimental rats with hyperlipidemia. *Med. Plant* **2013**, *4*, 54−56.

(7) Mao, W.; Li, B.; Gu, Q.; Fang, Y.; Xing, H. Preliminary studies on the chemical characterization and antihyperlipidemic activity of polysaccharide from the brown alga *Sargassum fusiforme*. *Hydrobiologia* **2004**, *512*, 263−266.

(8) Kritchevsky, D.; Chen, S. C. Phytosterols − health benefits and potential concerns: a review. *Nutr. Res. (N.Y.)* **2005**, *25*, 413−428.

(9) Marangoni, F.; Poli, A. Phytosterols and cardiovascular health. *Pharmacol. Res.* **2010**, *61*, 193−199.

(10) He, W.-S.; Jia, C.-S.; Yang, Y.-B.; Ma, Y.; Zhang, X.-M.; Feng, B.; Jin, J. Cholesterol-lowering effects of plant steryl and stanyl laurate by oral administration in mice. *J. Agric. Food Chem.* **2011**, *59*, 5093−5099.

(11) Moran-Valero, M. I.; Martin, D.; Torrelo, G.; Reglero, G.; Torres, C. F. Phytosterols esterified with conjugated linoleic acid. In vitro intestinal digestion and interaction on cholesterol bioaccessibility. *J. Agric. Food Chem.* **2012**, *60*, 11323−11330.

(12) Eilat-Adar, S.; Sinai, T.; Yosefy, C.; Henkin, Y. Nutritional recommendations for cardiovascular disease prevention. *Nutrients* **2013**, *5*, 3646−3683.

(13) Silbernagel, G.; Genser, B.; Nestel, P.; März, W. Plant sterols and atherosclerosis. *Curr. Opin. Lipidol.* **2013**, *24*, 12−17.

(14) Calpe-Berdiel, L.; Escolà-Gil, J. C.; Blanco-Vaca, F. New insights into the molecular actions of plant sterols and stanols in cholesterol metabolism. *Atherosclerosis* **2009**, *203*, 18−31.

(15) Plat, J.; Nichols, J. A.; Mensink, R. P. Plant sterols and stanols: effects on mixed micellar composition and LXR (target gene) activation. *J. Lipid Res.* **2005**, *46*, 2468−2476.

(16) Repa, J. J.; Mangelsdorf, D. J. The liver X receptor gene team: potential new players in atherosclerosis. *Nat. Med.* **2002**, *8*, 1243−1248.

(17) Viennois, E.; Mouzat, K.; Dufour, J.; Morel, L.; Lobaccaro, J.; Baron, S. Selective liver X receptor modulators (SLiMs): what use in human health? *Mol. Cell. Endocrinol.* **2012**, *351*, 129−141.
(18) Bonamassa, B.; Moschetta, A. Atherosclerosis: lessons from LXR and the intestine. *Trends Endocrinol. Metab.* **2013**, *24*, 120−128.
(19) Calkin, A. C.; Tontonoz, P. Liver X receptor signaling pathways and atherosclerosis. *Arterioscler. Thromb. Vasc. Biol.* **2010**, *30*, 1513−1518.
(20) Hovenkamp, E.; Demonty, I.; Plat, J.; Lütjohann, D.; Mensink, R. P.; Trautwein, E. A. Biological effects of oxidized phytosterols: a review of the current knowledge. *Prog. Lipid Res.* **2008**, *47*, 37−49.
(21) Ikeda, I.; Tanaka, K.; Sugano, M.; Vahouny, G. V; Gallo, L. L. Inhibition of cholesterol absorption in rats by plant sterols. *J. Lipid Res.* **1988**, *29*, 1573−1582.
(22) Song, Y.; Shan, S.; Zhang, Y.; Liu, W.; Ding, W.; Ren, W.; Xia, H.; Li, X.; Zhang, Q.; Zhao, L.; Li, X.; Yan, J.; Ying, H. Ligand-dependent corepressor acts as a novel corepressor of thyroid hormone receptor and represses hepatic lipogenesis in mice. *J. Hepatol.* **2012**, *56*, 248−254.
(23) Williams, S.; Bledsoe, R. K.; Collins, J. L.; Boggs, S.; Lambert, M. H.; Miller, A. B.; Moore, J.; McKee, D. D.; Moore, L.; Nichols, J.; Parks, D.; Watson, M.; Wisely, B.; Willson, T. M. X-Ray crystal structure of the liver X receptor β ligand binding domain: regulation by a histidine-tryptophan switch. *J. Biol. Chem.* **2003**, *278*, 27138−27143.
(24) Wu, Z. H.; Liu, T.; Gu, C. X.; Shao, C. L.; Zhou, J.; Wang, C. Y. Steroids and triterpenoids from the brown alga *Kjellmaniella crassifolia*. *Chem. Nat. Compd.* **2012**, *48*, 158−160.
(25) Permeh, P.; Saeidnia, S.; Mashinchian-Moradi, A.; Gohari, A. R. Sterols from *Sargassum oligocystum*, a brown algae from the Persian Gulf, and their bioactivity. *Nat. Prod. Res.* **2012**, *26*, 774−777.
(26) Cui, J. G.; Lin, C. W.; Zeng, L. M.; Su, J. Y. Synthesis of polyhydroxysterols (III): synthesis and structural elucidation of 24-methylenecholest-4-en-3β,6α-diol. *Steroids* **2002**, *67*, 1015−1019.
(27) Yue, J. M.; Chen, S. N.; Lin, Z. W.; Sun, H. D. Sterols from the fungus *Lactarium volemus*. *Phytochemistry* **2001**, *56*, 801−806.
(28) Catalan, C. A. N.; Kokke, W. C. M. C.; Duque, C.; Djerassi, C. Synthesis of (24*R*)- and (24*S*)-5,28-stigmastadien-3β-ol and determination of the stereochemistry of their 24-hydroxy analogs, the saringosterols. *J. Org. Chem.* **1983**, *48*, 5207−5214.
(29) Hoang, M. H.; Jia, Y.; Jun, H. J.; Lee, J. H.; Lee, B. Y.; Lee, S. J. Fucosterol is a selective liver X receptor modulator that regulates the expression of key genes in cholesterol homeostasis in macrophages, hepatocytes, and intestinal cells. *J. Agric. Food Chem.* **2012**, *60*, 11567−11575.
(30) Degirolamo, C.; Moschetta, A. Casting a shadow on liver X receptor-mediated atheroprotection: is LXRβ to blame? *J. Intern. Med.* **2012**, *272*, 449−451.
(31) Schultz, J. R.; Tu, H.; Luk, A.; Repa, J. J.; Medina, J. C.; Li, L.; Schwendner, S.; Wang, S.; Thoolen, M.; Mangelsdorf, D. J.; Lustig, K. D.; Shan, B. Role of LXRs in control of lipogenesis. *Genes Dev.* **2000**, *14*, 2831−2838.
(32) García-Mediavilla, M. V.; Pisonero-Vaquero, S.; Lima-Cabello, E.; Benedicto, I.; Majano, P. L.; Jorquera, F.; González-Gallego, J.; Sánchez-Campos, S. Liver X receptor α-mediated regulation of lipogenesis by core and NS5A proteins contributes to HCV-induced liver steatosis and HCV replication. *Lab. Invest.* **2012**, *92*, 1191−1202.
(33) Hu, X.; Steffensen, K. R.; Jiang, Z.-Y.; Parini, P.; Gustafsson, J.-Å.; Gåfvels, M.; Eggertsen, G. LXRβ activation increases intestinal cholesterol absorption, leading to an atherogenic lipoprotein profile. *J. Intern. Med.* **2012**, *272*, 452−464.
(34) Fitzgerald, M. L.; Mujawar, Z.; Tamehiro, N. ABC transporters, atherosclerosis and inflammation. *Atherosclerosis* **2010**, *211*, 361−370.
(35) Jeon, T.-I.; Osborne, T. F. SREBPs: metabolic integrators in physiology and metabolism. *Trends Endocrinol. Metab.* **2012**, *23*, 65−72.
(36) Ye, D.; Lammers, B.; Zhao, Y.; Meurs, I.; Van Berkel, T. J.; Van Eck, M. ATP-binding cassette transporters A1 and G1, HDL metabolism, cholesterol efflux, and inflammation: important targets for the treatment of atherosclerosis. *Curr. Drug Targets* **2011**, *12*, 647−660.

JOURNAL OF AGRICULTURAL AND FOOD CHEMISTRY

Article

pubs.acs.org/JAFC

Purification, Characterization, and in Vitro Activity of 2,4-Di-*tert*-butylphenol from *Pseudomonas monteilii* PsF84: Conformational and Molecular Docking Studies

Seema Dharni,[†] Sanchita,[‡] Anupam Maurya,[#] Abdul Samad,[⊥] Santosh Kumar Srivastava,[#] Ashok Sharma,[‡] and Dharani Dhar Patra*[,†]

[†]Agronomy and Soil Science Division, [‡]Biotechnology Division, [#]Chemical Sciences Division, and [⊥]Crop Protection Division, CSIR−Central Institute of Medicinal and Aromatic Plants, Lucknow 226015, India

Supporting Information

ABSTRACT: A novel strain of *Pseudomonas monteilii*, PsF84, was isolated from tannery waste soil from Jajmau, Kanpur, India. 16S rRNA gene sequence phylogenetic analysis confirmed the taxonomic affiliation of PsF84 as *P. monteilii*. An antifungal volatile organic compound (VOC) active against hyphal growth of *Fusarium oxysporum* (CIMAP-IMI-357464) in vitro was isolated from strain PsF84 by using chromatographic techniques. The molecular formula of the antifungal VOC was deduced to be $C_{14}H_{22}O$ by EI-MS and 1D and 2D NMR spectral analysis. 2,4-Di-*tert*-butylphenol was found to be effective against an agriculturally important fungus, namely, *F. oxysporum*, in inhibiting spore germination and hyphal growth. Molecular docking analysis of 2,4-di-*tert*-butylphenol with β-tubulin further validated the potential of β-tubulin binding in *F. oxysporum*. Two residues of β-tubulin protein, HIS 118 and THR 117, showed hydrogen binding with ligand. To the authors' knowledge, this is the first report of antifungal VOC (2,4-di-*tert*-butylphenol) produced by *P. monteilii* PsF84 that can be a potent inhibitor of β-tubulin of *F. oxysporum*.

KEYWORDS: *Pseudomonas monteilii, 2, 4-di-tert-butylphenol, Fusarium oxysporum, molecular modeling, docking, β-tubulin*

INTRODUCTION

Fungal phytopathogens pose serious problems worldwide in the cultivation of economically important plants, especially in subtropical and tropical regions.[1] However, excessive use of chemical fungicides in agriculture has led to deterioration of the environment, impairing human health and increasing development. Because of the worsening problems in fungal disease control, serious efforts are required to identify alternative methods for plant protection that are less dependent on chemicals and are more environment friendly. Biological control using microbes or organic products in agriculture systems has been proposed as an environment friendly disease management strategy.[2−5] For successful biocontrol, searching for beneficial microbes that can prevent plant pathogens is a critical first step. Microbial antagonist strains are capable of producing a wide range of soluble secondary metabolites, many of which are volatile organic compounds (VOCs) exhibiting strong inhibitory activity against plant pathogens, and have received much attention.[6,7] All microbial species produce a unique reproducible profile of VOCs under specific conditions.[8] These antagonists include bacteria, such as *Pseudomonas* spp., *Streptomyces* spp., and *Bacillus* spp.[6,9,10] Strains of *Pseudomonas* spp. have been reported to produce several VOCs, such as benzothiazole, cyclohexanol, *n*-decanal, dimethyl trisulfide, 2-etyhl-1-hexanol, and nonanal, which directly inhibit mycelial growth and spore germination of pathogenic fungi and could be a mechanism of biocontrol against some soilborne fungal disease.[11,12] VOCs belong to several chemical classes (aldehydes, alcohols, esters, lactones, butylphenol, terpenes, and sulfur compounds) and are characterized by low molecular weight and the ability to interact with olfactory receptors.[13] Antifungal VOCs produced by *Pseudomonas chlororaphis*, *Pseudomonas corrugata*, *Pseudomonas fluorescence*, and *Pseudomonas. aurantiaca* inhibited the growth and spore germination of *Sclerotinia sclerotiorum* in vitro.[11] VOCs produced by bacteria or fungi could be a mechanism of biocontrol against some soilborne fungal diseases.[7,14] Antifungal VOCs produced from microorganisms with novel structures have the potential to provide insight to agricultural researchers as to which compounds could be used as fungicides. The relationship between soil microorganisms and VOCs is still unclear, and many fungistatic compounds remain to be identified. Recognizing the hazards of fungicides and pesticides to man and the environment, many countries in the world today are considering biological control as the best alternative to chemical control of plant diseases and pests.[15] *F. oxysporum* is well represented among the communities of soilborne fungi, in every type of soil all over the world.[16] Some strains of *F. oxysporum* are pathogenic to plants and are difficult to control; however, biological methods may be a reliable alternative to chemical methods for controlling soilborne fungal growth. Studies using in silico approaches such as targeted protein have begun to shed light on the mechanisms underlying some of these processes and their role in spore germination inhibition.[17]

Received: January 8, 2014
Revised: June 17, 2014
Accepted: June 17, 2014
Published: June 17, 2014

ACS Publications © 2014 American Chemical Society

dx.doi.org/10.1021/jf5001138 | J. Agric. Food Chem. 2014, 62, 6138−6146

Microtubules composed of heterodimers of α-tubulin and β-tubulin, which are present in all eukaryotic cells, play important roles in various cellular processes such as cell signaling, cell motility, separation of the duplicated centrosomes, cell division, and mitosis.[18] In fungal cells mitosis takes place without nuclear envelope breakdown in many organisms; cytoplasmic microtubules break down upon entry into mitosis, and tubulin molecules are transported into the nucleoplasm to establish an internuclear spindle. Therefore, one would assume that the loss of microtubules should negatively affect the growth rate of spore germination.[19] Loss of cytoplasmic microtubules should negatively affect tip growth rate, and if they disappear completely during mitosis, one should expect a reduction in fungal growth.

Despite its important role, β-tubulin has not yet been well characterized either functionally or structurally in *F. oxysporum*. In this study, the structure of the β-tubulin protein was predicted in silico on the basis of sequence similarity with protein having known structure. The sequence of β-tubulin is consistent with a conserved domain of the tubulin FtsZ superfamily. This domain family includes alpha (α), beta (β), gamma (γ), delta (λ), and epsilon (δ) tubulins as well as FtsZ, all of which are involved in polymer formation. Tubulin is the major component of microtubules, but also exists as a heterodimer and a curved oligomer. FtsZ can polymerize into tubes, sheets, and rings in vitro and is ubiquitous in eubacteria, archaea, and chloroplasts. Cellular microtubules are known to play an essential role in nuclear division as components of the mitotic spindle, and dimeric tubulin is their primary component. A key property of tubulin is its ability to assemble into microtubules via interaction between polymerized α- and β-tubulin monomers (heterodimer) and to undergo disassembly at appropriate times in the cell cycle. In this study, we have characterized the antifungal VOC produced by strain PsF84, a potential biocontrol agent, highly active against *F. oxysporum*. We used various chromatographic techniques, 1D and 2D nuclear magnetic resonance (NMR) spectral analysis and gas chromatography−mass spectroscopy (GC-MS), to identify antifungal VOC. The sequence-based prediction of 3D structure of β-tubulin was predicted to analyze the properties and function of the protein. In addition, a molecular docking study of 2,4-di-*tert*-butylphenol with β-tubulin has been carried out to explore binding to this antifungal relevant protein target as a possible mechanism of the antifungal activity of volatile compounds.

MATERIALS AND METHODS

Chemicals. All of the chemicals and organic solvents used for vacuum liquid chromatography (VLC) were of analytical grade and purchased from Merck (Mumbai, India). For thin layer chromatography (TLC) precoated silica gel 60_{254} plates (20 × 20 cm, Merck) were used. Hexane, dichloromethane (DCM, GR), methanol (MeOH, GR), and *p*-dimethylaminobenzaldehyde were also purchased from Merck. The conventional fungicide bavistin (methyl benzimidazol-2-ylcarbamate) was purchased from Sigma-Aldrich.

General Experimental Conditions. ^{1}H and ^{13}C NMR spectra were recorded at 400 MHz (Avance, Bruker, Switzerland). The GC-MS analysis was carried out on a Perkin- Elmer SQ8 mass spectrometer instrument using a DB-5 column (30 m × 0.25 mm i.d., film thickness = 0.25 μm). The carrier gas was helium with a flow rate of 1 mL/min column head pressure; temperature was programmed from 60 to 240 °C at a rate of 3 °C/min with a final hold for 10 min. The injector (250 °C), transfer line, and ion-source temperature were 220 °C. Mass spectra were prepared in EI-mode with 70 eV ionization energy between 40 and 450 amu mass range and 0.35 s scan time. Characterization was carried out by computer matching of the mass spectra of the peak with the Wiley and NIST libraries mass spectral databases.

Collection of Samples and Isolation of Bacterial Strain PsF84. Soil samples were collected from the tannery waste polluted area of Jajmau, a Research center of CSIR−Central Leather Research Institute, Chennai, India, located at latitude 26° 42′ N and longitude 80° 41′ E in the Kanpur district of Uttar Pradesh, India, in November 2012 and were dried at ambient temperature. Isolation was carried out on Pseudomonas Isolation Agar (PIA) following the serial dilution technique of Hammond and Lambert.[20] Colonies were further purified and screened for fluorescence under UV light (366 nm). For long-term maintenance, strain PsF84 was preserved in nutrient broth containing 20% (v/v) glycerol at −80 °C.

Phenotypic Characterization of *P. monteilii* PsF84. Bacterial isolates were characterized for phenotypic and biochemical traits according to *Bergey's Manual of Determinative Bacteriology*.[21] Grams reaction was determined by using the KOH technique.[22] The presence of cytochrome oxidase was determined using 1% *N,N,N′,N′*-tetramethyl-*p*-phenylenediamine dihydrochloride solution.[23] Catalase, levan formation, nitrate reduction, starch, casein, and gelatin liquefaction and growth at pH 5−7 and 4−42 °C were recorded following the methods described.[24] Substrate utilization profiles were tested using Hi-carbohydrate kits (Himedia Laboratories, Mumbai, India) according the instructions of the manufacturer.

16S rRNA Gene Amplification, Sequencing, and Phylogenetic Analysis. Isolation of genomic DNA, PCR amplification of 16S rRNA gene, and purification and sequencing of the PCR product were performed as previously described.[25] Phylogenetic molecular evolutionary analysis was conducted using MEGA version 5.05.[26] The nucleotide sequence of 16S rRNA was deposited as GenBank accession no. KC45055.

Extraction and Purification of Bioactive Volatile Compound. A single colony of *P. monteilii* PsF84 on a nutrient agar (NA agar) plate was transferred into 100 mL of modified pigment production medium (PPM) broth: peptone, 10.0 g; NaCl, 5.0 g; glycerol, 5.0 mL; and KNO_3, 1.0 g, in 1 L of distilled H_2O (pH 7.5). The PPM was used to recover antibiotics from the culture filtrate of strain PsF84. The fermentation was carried out in pigment production medium for 4 days at 28 °C on a rotary shaker at 150 rpm. The harvested broth (120 L) of *P. monteilii* strain PsF84 was centrifuged at 8000 rpm and the supernatant pooled. The culture filtrate (CF) was successively fractionated with hexane and dichloromethane (3 × 100 mL each).

Isolation and Characterization of Bioactive Constituent. The DCM extract (8 g) was subjected to Vacuum Liquid Chromatographic (VLC) separation over TLC grade silica gel H (250 g). Gradient elution of the VLC was carried out with mixtures of *n*-hexane, $CHCl_3$, and MeOH in increasing polarity as shown in the flowchart (Figure 1). A total of 125 fractions of 100 mL each were collected and pooled on the basis of their TLC (SiO_2) profile after spraying with Ehrlich reagent and heating the plate for 2 min at 100 °C.[27] The pooled fractions were marked as fractions 1−10 (F1), 4−7 (F2), 10−12 (F3), 13−16 (F4), 17−20 (F5), 21−25 (F6), 26−46 (F7), 47−115 (F8), and 116−125 (F9). Subfraction fraction 8 (F8) was further purified by preparative TLC [$CHCl_3$/MeOH (90:10)], which afforded a homogeneous compound **P1a** (75 mg). **P1a** was subjected to ^{1}H and ^{13}C NMR and GC-MS spectroscopic data as given below.

^{1}H NMR ($CDCl_3$) δ 7.34 (1H, d, J = 2.4 Hz, H-3), 7.11 (1H, dd, J = 8.2, 2.4 Hz, H-5) 6.63 (1H, d, J = 8.2 Hz, H-6), 1.46 (9H, s, H-9), 1.34 (9H, s, H-10); ^{13}C NMR δ 151.8 (C-1), 135.2 (C-2), 124.1 (C-3), 143.0 (C-4), 123.5 (C-5), 115.1 (C-6), 34.3 (C-7), 34.7 (C-8), 31.6 (C-9, 3 × CH_3), 29.7 (C-10, 3 × CH_3); GC-MS m/z 206 $[M]^+$, $C_{14}H_{22}O$.

In Vitro Disk Diffusion Assay against *F. oxysporum*. CF, DCM, F8, and **P1a** were subjected to evaluation of their antifungal activity in vitro against the wilt-causing pathogen, *F. oxysporum*, by using the standard agar disk diffusion technique of Kai et al.[28] A mycelial disk (5 mm), obtained from a 4-day-grown culture of *F. oxysporum*, was placed on one side of a 90 mm potato dextrose agar

dx.doi.org/10.1021/jf5001138 | J. Agric. Food Chem. 2014, 62, 6138−6146

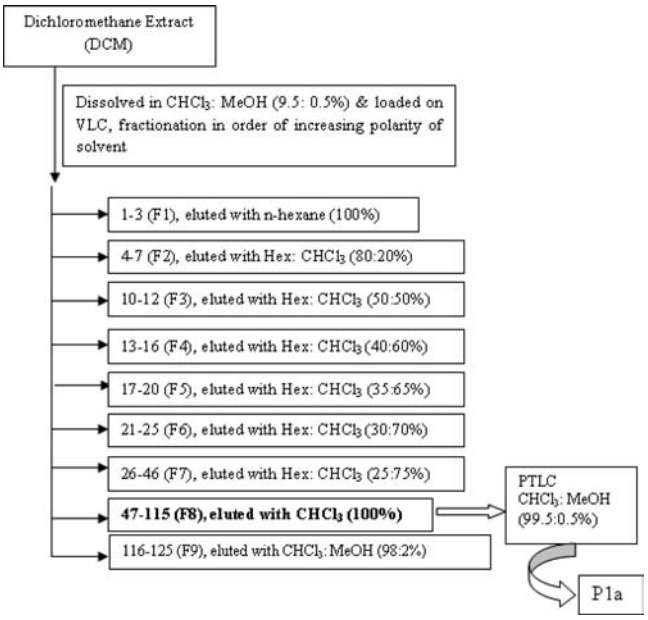

Figure 1. Schematic representation of vacuum liquid chromatography.

(PDA) medium containing Petri plate. The commercial fungicide bavistin (methyl benzimidazol-2-ylcarbamate), provided as technical grade material (Carbendazim 50% DF), was used to compare the antifungal activity in vitro. For evaluation of the antifungal activity of 2,4-di-*tert*-butylphenol and bavistin, both were dissolved in methanol and diluted with water containing Tween 20 (0.5 g/L; Himedia, India) to give concentrations of 1, 25, 50, 100, 200, and 500 μg/mL. Pure compound (2,4-di-*tert*-butylphenol) was applied on the paper disk and for the control set, and an equal volume of Tween 20 solution was also applied. The Petri dishes were sealed with sterile laboratory parafilm to avoid eventual evaporation of the volatile compound, and plates were incubated at 28 ± 2 °C for 72 h, measuring the size of growth inhibition in comparison to control plate. Each assay in these experiments was repeated three times, and the results (percent inhibition) were expressed as average values (± standard deviation).

Statistical Anlysis. Data from three independent replicate trials were subjected to analysis using one-way analysis of variance (ANOVA) techniques. The data are reported as the mean ± standard deviations, and significant differences between mean values were determined with Duncan's multiple-range tests (DMRT) performed by ASSISTAT software version 7.6 beta (2013) http://www.assistat.com. The significance of the data was analyzed at $p > 0.005$.

Effect of 2,4-Di-*tert*-butylphenol on Hyphal Morphology of *F. oxysporum*. To evaluate morphological changes with volatile compounds, fungal samples of *F. oxysporum* taken from areas showing inhibition levels were placed on the slides and were stained with lactophenol cotton blue (Fluka, Buchi, Switzerland). A sample from the control plate without volatile compound was also stained and observed under a light microscope (40× magnification) (Axio Scope A1, Zeiss, Germany).

Computational Analysis. Computational studies were carried out with different tools and software packages. The conserved domains were analyzed through a tool incorporated in a conserved domain database (http://www.ncbi.nlm.nih.gov/Structure/cdd/wrpsb.cgi).[29] Geno3d (http://geno3d-pbil.ibcp.fr) was used for structure prediction of the protein.[30] The spatial restraint (distances and dihedrals) satisfaction was performed for comparative protein structure modeling. The modeled protein was validated by PROCHECK for its stereochemical qualities through SAVES (Structure Analysis and Verification Server) (http://nihserver.mbi.ucla.edu/SAVES/).[31] The ProSA program was used to examine the validation of the model.[32] Protein visualization and superimposition were carried out using PyMol (http://www.pymol.org/). The secondary structure of tubulin protein was predicted by Polyview (http://polyview.cchmc.org/). Protein–ligand docking studies were carried out on the basis of the predicted structure of β- tubulin protein. Molecular docking calculations for 2,4-di-*tert*-butylphenol, considered as a ligand with β-tubulin, was undertaken using Autodock 4.2,[33] and different orientations of the ligands were searched and ranked on the basis of their energy scores. The RMSD threshold for multiple cluster poses was set at <1.00 Å. The docking algorithm was set at a maximum of 1500 iterations with a simple evolution population size of 50 and a minimum of 25 runs for the ligand.

RESULTS AND DISCUSSION

Isolation and Screening of Fluorescent Pseudomonas. Eight hundred fluorescent pseudomonas isolates were obtained on PIA from the tannery waste polluted soil samples, in which a unique fluorescent *Pseudomonas* strain, designated PsF84, was predominantly produced. The strain was further purified and maintained on Luria–Bertani (LB) slants at −20 °C for subsequent studies.

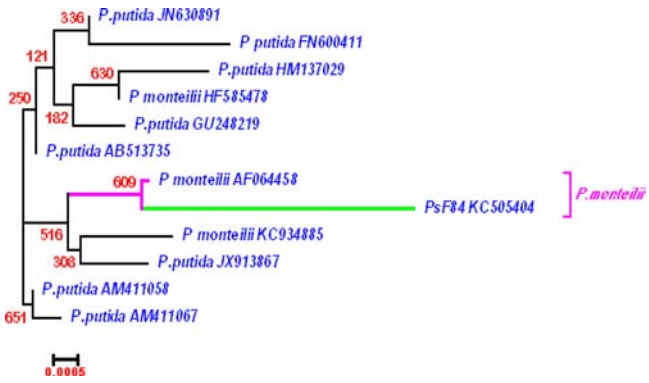

Figure 2. Phylogenetic tree based on 16S rRNA sequences, representing the relatedness among the *Pseudomonas monteilii* PsF84. Distance and clustering were performed by using the software package MEGA 5.05. Boot strap values based on 1000 replications are listed at the branching point. The sequence of the present study is dotted in red.

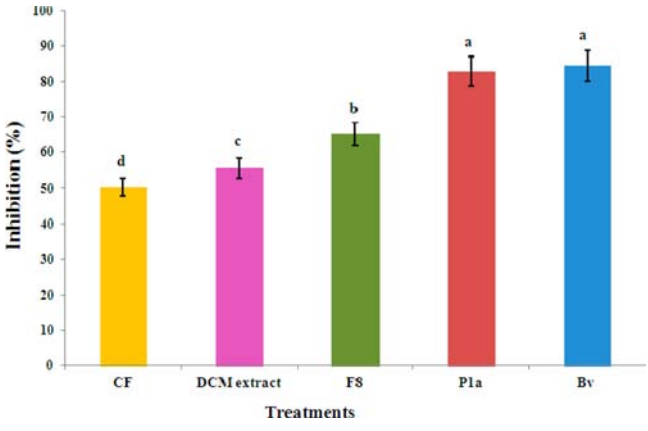

Figure 3. Antifungal activity of CF, culture filtrate; DCM, dichloromethane; F8, eighth fraction; P1a, 2,4-di-tert-butylphenol; Bv, Bavistin against *F. oxysporum*. Mean values followed by different letters are significantly different according to Duncan's multiple-range test ($P < 0.05$).

Identification of Bacterial Strain. PsF84 was found to be a Gram-negative, aerobic, motile, non-spore-forming bacterium. The strain grew at 15–37 °C but not at >40 °C. Growth was optimum at pH 5.5–10 but inhibited at pH <5.5. The strain

dx.doi.org/10.1021/jf5001138 | J. Agric. Food Chem. 2014, 62, 6138–6146

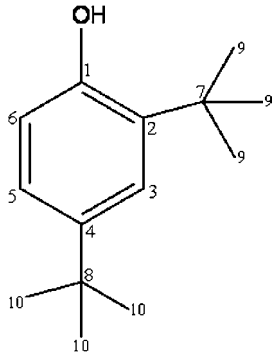

Figure 4. Molecular structure of 2,4-di-*tert*-butylphenol.

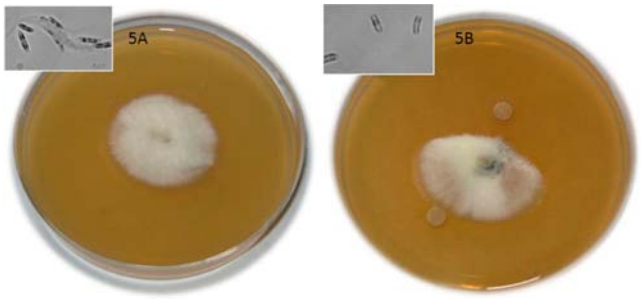

Figure 5. Antifungal activity of 2,4-di-*tert*-butylphenol against *Fusarium oxysporum*: (A) control showing normal growth; (B) potato dextrose plate containing filter disk loaded with 25 μg/mL of 2,4-di-*tert*-butylphenol showing growth inhibition.

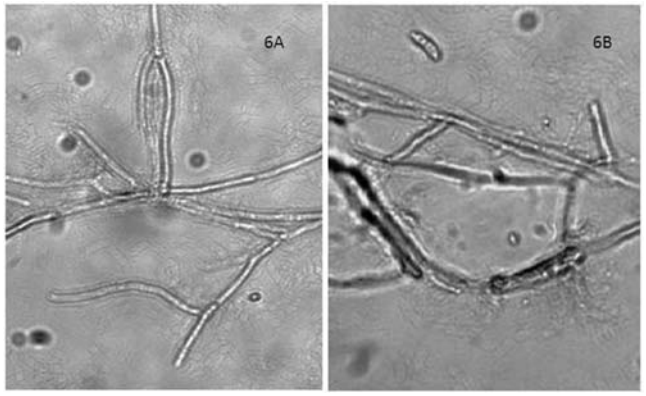

Figure 6. Microscopic examination of hyphal morphology of (A) *F. oxysporum* from PDA culture (40× magnification) and (B) effect of 2,4-di-*tert*-butylphenol showing deformed mycelia of *F. oxysporum* (40× magnification). Arrows indicate hyphal lysis.

tolerated well up to 7% NaCl in the basal medium. It utilized citrate and produced catalase and cytochrome oxidase. Nitrate reduction, urease, indole, levan, gelatin liquification, or hydrogen sulfides were not produced. Methyl red and Voges−Proskauer reactions were negative. PsF84 strain utilized L-arabinose, galactose, glucose, fructose, and xylose, but not mannitol, raffinose, salicin, sucrose, rhamanose, meso-inositol, and lactose.

16S rRNA Gene Amplification Sequencing and Phylogenetic Tree Analysis. The 16S rRNA sequence of starin PsF84 has been submitted to the GenBank database of NCBI (http://www.ncbi.nlm.nih.gov/) having the accession number KC45055. A phylogenetic tree is presented (Figure 2).

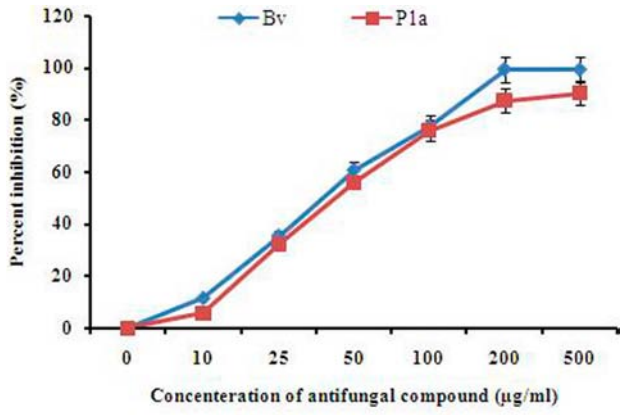

Figure 7. Antifungal spectrum of the metabolite 2,4-di-*tert*-butylphenol isolated from *P. monteilii* PsF84 against *F. oxysporum* under in vitro conditions (values are the mean of three replicates ± SD). Mean values followed by different letters are significantly different according to Duncan's multiple-range test ($P < 0.05$).

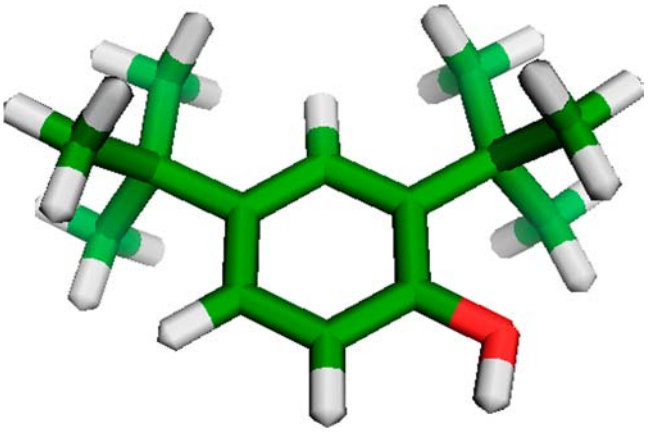

Figure 8. Three-dimensional visualization of 2,4-di-*tert*-butylphenol.

Activity-Guided Isolation and Characterization of Bioactive Constituents. The culture filtrate (CF) of *P. monteilii* PsF84 showed significant activity against *F. oxysporum* at 25 μg/mL (50.23 ± 1.48) (Figure 3), which prompted us to carry out activity-guided fractionation, isolation, and characterization of the bioactive compound. For this purpose, the CF was fractionated into *n*-hexane and DCM fractions, and both fractions were evaluated for their antifungal potential. The results showed that the DCM fraction was found to be most active at 25 μg/mL (55.46 ± 0.67) (Figure 3). Hence, the DCM fraction was subjected to chromatographic separation. Finally, the most active subfraction 8 (F8) at 25 μg/mL (65.23 ± 0.80) (Figure 3) was further purified by preparative TLC, which afforded a homogeneous compound, **P1a**. The ^{1}H NMR spectra of **P1a** showed the presence of a total 21 protons, of which 18 protons were present as six *tert*-methyls at δ 1.34 (9H, s, 3 × CH_3) and 1.46 (9H, s, 3 × CH_3). The remaining three protons were present in the downfield aromatic region at 6.63 (1H, d, J = 8.2 Hz), 7.11 (1H, dd, J = 8.2, 2.4 Hz), and 7.34 (1H, d, J = 2.4 Hz), suggesting that this compound is a trisubstituted aromatic compound. This was supported by its ^{13}C NMR spectra, which showed the presence of 10 carbon signals, of which six downfield carbon signals between 115.1and 151.8 ppm were in the aromatic region, whereas the remaining four carbon signals were in the upfield region between 29.7 and

dx.doi.org/10.1021/jf5001138 | J. Agric. Food Chem. 2014, 62, 6138−6146

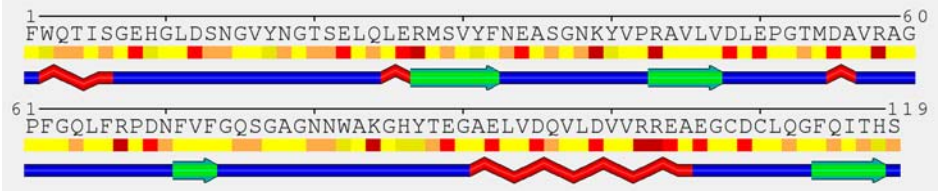

Figure 9. Predicted secondary structure of *F. oxysporum* β-tubulin amino acid sequence obtained by Polyview. Red, green, and blue indicate the helical domain, sheet domain, and coils, respectively.

```
4DRXB           MREIVHIQAGQCGNQIGAKFWEVISDEHGIDPTGSYHGDSDLQLERINVYYNEATGNKYV 60
4DRXD           MREIVHIQAGQCGNQIGAKFWEVISDEHGIDPTGSYHGDSDLQLERINVYYNEATGNKYV 60
beta-tubulin    ------------------FWQTISGEHGLDSNGVYNGTSELQLERMSVYFNEASGNKYV 41
                                  **:.**.***:*..* *:* *:*****:.**:***:*****

4DRXB           PRAILVDLEPGTMDSVRSGPFGQIFRPDNFVFGQSGAGNNWAKGHYTEGAELVDSVLDVV 120
4DRXD           PRAILVDLEPGTMDSVRSGPFGQIFRPDNFVFGQSGAGNNWAKGHYTEGAELVDSVLDVV 120
beta-tubulin    PRAVLVDLEPGTMDAVRAGPFGQLFRPDNFVFGQSGAGNNWAKGHYTEGAELVDQVLDVV 101
                ***:**********:**:*****:*******************************.***** 

4DRXB           RKESESCDCLQGFQLTHSLGGGTGSGMGTLLISKIREEYPDRIMNTFSVMPSPKVSDTVV 180
4DRXD           RKESESCDCLQGFQLTHSLGGGTGSGMGTLLISKIREEYPDRIMNTFSVMPSPKVSDTVV 180
beta-tubulin    RREAEGCDCLQGFQITHS------------------------------------------ 119
                *:*:*.********:***

4DRXB           EPYNATLSVHQLVENTDETYSIDNEALYDICFRTLKLTTPTYGDLNHLVSATMSGVTTCL 240
4DRXD           EPYNATLSVHQLVENTDETYSIDNEALYDICFRTLKLTTPTYGDLNHLVSATMSGVTTCL 240
beta-tubulin    ------------------------------------------------------------

4DRXB           RFPGQLNADLRKLAVNMVPFPRLHFFMPGFAPLTSRGSQQYRALTVPELTQQMFDSKNMM 300
4DRXD           RFPGQLNADLRKLAVNMVPFPRLHFFMPGFAPLTSRGSQQYRALTVPELTQQMFDSKNMM 300
beta-tubulin    ------------------------------------------------------------

4DRXB           AACDPRHGRYLTVAAIFRGRMSMKEVDEQMLNVQNKNSSYFVEWIPNNVKTAVCDIPPRG 360
4DRXD           AACDPRHGRYLTVAAIFRGRMSMKEVDEQMLNVQNKNSSYFVEWIPNNVKTAVCDIPPRG 360
beta-tubulin    ------------------------------------------------------------

4DRXB           LKMSATFIGNSTAIQELFKRISEQFTAMFRRKAFLHWYTGEGMDEMEFTEAESNMNDLVS 420
4DRXD           LKMSATFIGNSTAIQELFKRISEQFTAMFRRKAFLHWYTGEGMDEMEFTEAESNMNDLVS 420
beta-tubulin    ------------------------------------------------------------

4DRXB           EYQQYQDATAD 431
4DRXD           EYQQYQDATAD 431
beta-tubulin    -----------
```

Figure 10. Sequence alignment of β-tubulin with chains B and D of the template. Highly aligned regions are indicated by *. Residues are colored on the basis of physicochemical properties.

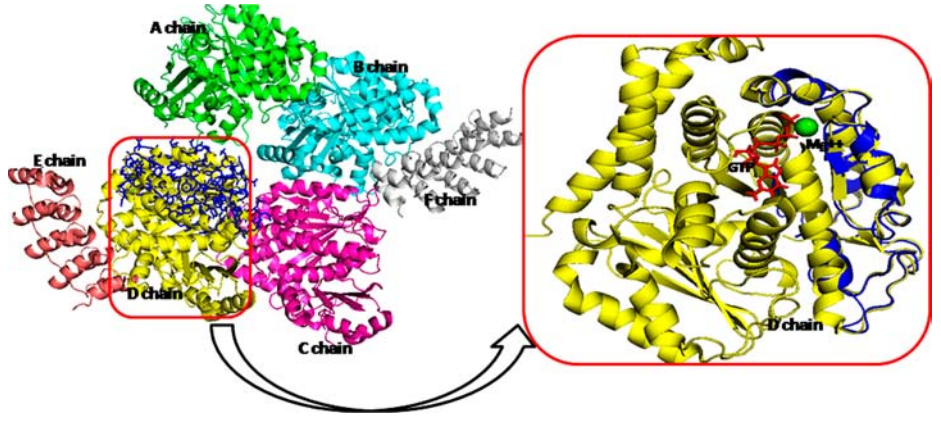

Figure 11. Superimposition of tubulin protein of *F. oxysporum* with chain D of the template. The highlighted image shows chain D in yellow and query protein in blue. GTP and Mg^{2+} are also shown to be bonded with chain D.

dx.doi.org/10.1021/jf5001138 | J. Agric. Food Chem. 2014, 62, 6138−6146

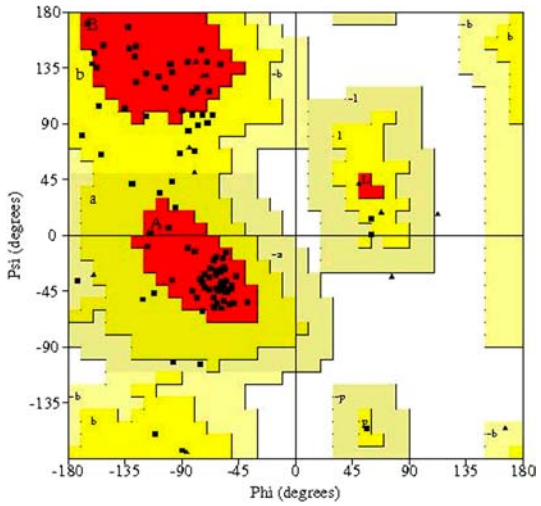

Figure 12. Ramachandran plot of the *F. oxysporum* β-tubulin model. The plot was calculated with the PROCHECK program.

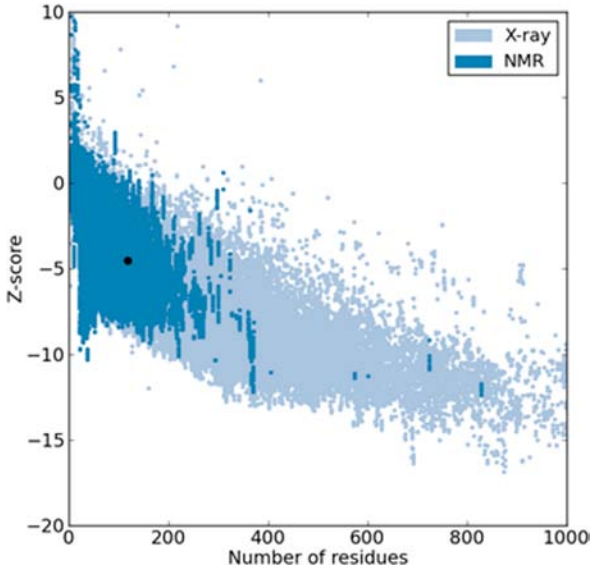

Figure 13. Z-plot of β-tubulin protein by ProSA.

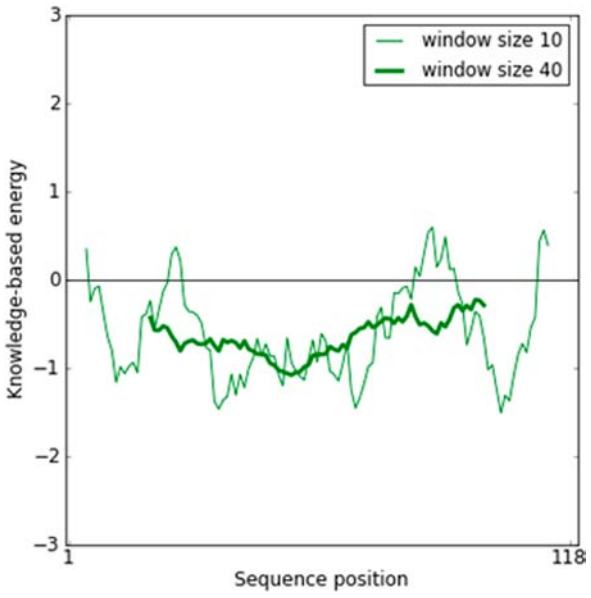

Figure 14. Energy plot for the predicted β-tubulin protein by ProSA.

34.7 ppm. Of six aromatic carbon signals, three were quaternary carbons (135.2, 143.0, and 151.8 ppm), suggesting that the aromatic substitutions were at these carbons. The most downfield quaternary carbon at 151.8 ppm indicated the presence of a phenolic OH group at this carbon in the molecule. Among the four upfield carbon signals, the two at 34.3 and 34.7 ppm were tertiary carbons and the remaining two at 29.7 and 31.6 ppm were methyl signals. This clearly suggested the presence of two *tert*-butyl substitutions on the two remaining quaternary carbons at 135.2 and 143.0 ppm in the aromatic ring. Finally, on the basis of the splitting patterns and coupling constants of the three aromatic protons, the structure of **P1a** was deduced as 2,4-di-*tert*-butylphenol. This was further confirmed from the GC-MS spectra of **P1a**, which showed a single peak at a retention time of 26.95 min with m/z 206, showing reverse and forward matching 915 and 890 for the 2,4-di-*tert*-butylphenol (Figure 4). Our results were in complete agreement with data reported by Yoon et al.[14] for **P1a**. To the best of our knowledge this is the first report of 2,4-di-*tert*-butylphenol in *P. monteilii* PsF84 (see ^{1}H and ^{13}C NMR and GC-MS spectra in the Supporting Information, Figure S1).

In Vitro Antifungal Activity of 2,4-Di-*tert*-butylphenol against *F. oxysporum*. Compound **P1a** inhibited the hyphal growth of *F. oxysporum* f. sp. (CIMAP-IMI-357464) (a soilborne pathogen causing vascular wilt/rot) under in vitro conditions at a concentration of 25 μg/mL (32.2 $\pm$ 1.2) (Figure 5). Nonvolatile antibiotics, including lipopeptides, have strong antifungal activities.[34−36] The light microscopic image of the treated *F. oxysporum* with 2,4-di-*tert*-butylphenol revealed a deformation of the fungal mycelia and growth inhibition (Figure 6). It is possible that application of 2,4-di-*tert*-butylphenol suppresses the assembly of spindle microtubules and disturbs the chromosomal alignment at the metaphase plate and microtubule−kinetochore interactions, causing chromatids loss, chromosome loss, or nondisjunction in target cells, which may reduce the mycelia growth and the germination of spores. A similar study reported on 2,4-di-*tert*-butylphenol to be an antifungal volatile compound from *Bacillus amyloliquefaciens* NJN-6 indicated that 2,4-di-*tert*-butylphenol strongly inhibited the growth of *F. oxysporum* f. sp. cubense.[37] The antifungal bioactive compound significantly inhibited the conidial suspension of *F. oxysporum* under in vitro conditions at a concentration of 100 μg/mL, whereas that of standard fungicide also exhibited inhibition action at the same level of 100 μg/mL, respectively (Figure 7). The result showed the effect of 2,4-di-*tert*-butylphenol on *F. oxysporum* occurred during spore germination, and it completely inhibited the germination of spores by preventing the emergence of a normal germ tube and led to abnormal branching and swelling of hyphae occurring after 72 h of incubation at 26 $\pm$ 2 °C. This compound has also been found in plant extracts or plant essential oils with antibacterial or antioxidant activities[14,38] because phenols had been described as antioxidants, growth regulators, or flavors.[39] Recently, an antifungal compound 2,4-di-*tert*-butylphenol isolated from *Flavobacterium johsoniae* strain GSE09 showed biocontrol activity against *Phytophthora capsici* in peppers.[40] The antifungal nature of the organic volatiles has been demonstrated in several pathogen systems, such as inhibition of hyphal extension and formation of arthrospore in

dx.doi.org/10.1021/jf5001138 | J. Agric. Food Chem. 2014, 62, 6138−6146

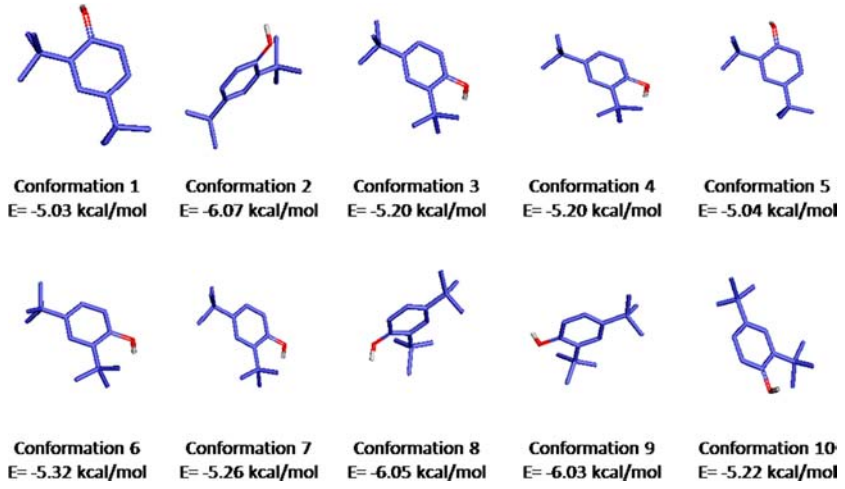

Figure 15. Low-energy and docked conformations of 2,4-di-*tert*-butylphenol.

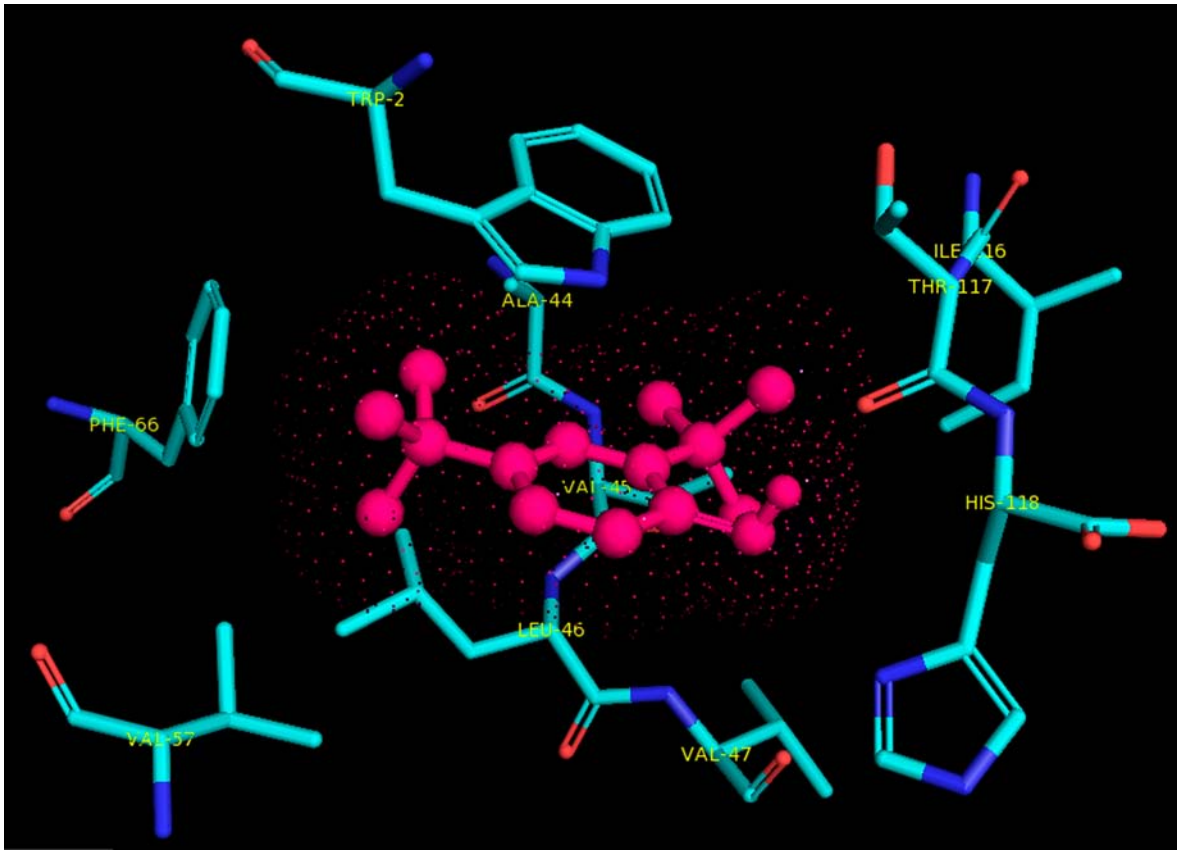

Figure 16. 2,4-Di-*tert*-butylphenol (pink) showing docking with active site residues (labeled in yellow).

Geotrichum candidum by trimethylamine,[41] inhibition of carpogenic germination of sclerotia of *S. sclerotiorum* in bean by allyl alcohol,[42] and control of root rot of tobacco by hydrogen cyanide produced by pseudomonads.[43] On the basis of the results from in vitro studies, 2,4-di-*tert*-butylphenol is assumed to play a major role in the inhibition of fungal growth and indicates that germination inhibition is one of the mechanisms by which a volatile compound (2,4-di-*tert*-butylphenol) might provide effective biocontrol activity against *F. oxysporum*.

Structure Prediction of β-Tubulin. The three-dimensional structure of 2,4-di-*tert*-butylphenol was retrieved from the pubchem database of NCBI (http://www.ncbi.nlm.nih.gov/) (Figure 8). The pubchem id of this compound is CID 7311. The protein sequence of β-tubulin of *F. oxysporum* was retrieved from the Genpept database of NCBI. The accession number of the sequence is AAU15035.1 and the length, 119 amino acids. The secondary structure of the sequence of *F. oxysporum* β-tubulin was assigned (Figure 9).

Model Building. The three-dimensional structure was predicted through homology modeling approach. The template for the prediction of structure was selected on the basis of identity with the sequence having known structure. The PDB blast search suggested *Ovis aries* tubulin protein crystal

dx.doi.org/10.1021/jf5001138 | J. Agric. Food Chem. 2014, 62, 6138−6146

structure at 2.22 Å resolution (PDB id 4DRX) for structure prediction. The selected protein is present in six chains. Of the six, chains B and D showed highest sequence similarity. The query and template identity and positives were 81 and 93% after pairwise alignment. The stretch 20−138 of the sequence of chains B and D showed alignment. The expected value and query coverage were 4e-74 and 99%, respectively. Multiple sequence alignment among β-tubulin sequence and B and D chains of template protein was performed to show the regions of identity (Figure 10). The percentage identity with chains A and C was 41% and with chains E and F was 32%. After finding the most appropriate template, three models were generated by Geno3D having their respective model energies. The model with lowest energy of −5050.22 kcal/mol was chosen as the best model and subjected to further analysis. The generated model was submitted to the PMDB database (http://mi.caspur.it/PMDB/main.php). The assigned PMDB id is PM0079294. Although the β-tubulin sequence showed highest identity with both chains B and D, the modeled structure was superimposed with chain D only (Figure 11).

Protein Model Validation. After modeling of the protein, several structure assessment methods including Ramachandran plot, *z* score, and energy plot were used to check the reliability of the 3D model. To validate the *F. oxysporum* β-tubulin model, a Ramachandran plot was drawn to analyze the stereochemical quality of the model by PROCHECK. It was found that the phi-psi angles of 71.1% of the residues were in the core regions, 25.8% in the additional allowed regions, 3.1% in generously allowed region, and no residues were in the disallowed regions (Figure 12). To determine the overall quality and measures of the deviation of the total energy of the structure, the ProSA program was used.[44] A *z* score of −4.52 of β-tubulin was in the acceptable range (−10 to 10) (Figure 13). A negative *z* score is good and depends on the length of the protein. The *z* score in this plot is displayed with a dark black point. The structure is displayed in two distinguishing regions, the dark blue and light blue representing NMR and X-ray, respectively. The energy plot analysis from the ProSA program showed that most of the residues of the protein were within the negative range of energy, indicating the stability of the protein (Figure 14).

Docking Analysis. The docking of ligand with modeled β-tubulin protein was performed by Autodock 4.2 using a genetic algorithm approach. Conformational analyses were carried out for 2,4-di-*tert*-butylphenol at the result of docking poses. Ten conformations were generated having different docking energies and numbers of hydrogen bonds (Figure 15). The docking energies were in the range from −5.86 to −6.40 kcal/mol. Conformation 4 was considered to be most suitable, binding with HIS 118 and THR 117 with two hydrogen bonds. Residues within a 5 Å radius of the ligand were selected as actively participating in binding (Figure 16). The following amino acid residues of β-tubulin played an active role in the interaction with ligand: PHE 66, VAL 57, TRP 2, ALA 44, VAL 45, LEU 46, VAL 47, ILE 116, HIS 118, and THR 117. The more negative value of the docking energy as well as the maximum number of hydrogen bonds showed strong and most favorable binding between protein and ligand molecules.

These findings are important as antifusarium activity of 2,4-di-*tert*-butylphenol from *P. monteilii* PsF84 significantly reduced the pathogen's mycelial growth and inhibited spore germination. It is assumed that 2,4-di-*tert*-butylphenol may be binding with β-tubulin in microtubules, inhibiting their proliferation and suppressing their dynamic instability as the microtubules are the cytoskeletal polymers in eukaryotic cells and thus play a vital role in many cellular functions.[18] Therefore, one would assume that the loss of microtubules should negatively affect the growth rate of spore germination and expect a reduction in fungal growth in vitro. Furthermore, docking results also supported that compound 2,4-di-*tert*-butylphenol is a potent inhibitor of *F. oxysporum*. These observations may be of great help in the QSAR-based design of fungicides from a very common, inexpensive, and nontoxic natural product, which is safe for humans, animals, and the environment. The current study may provide useful information regarding the antifungal activity of the bioactive compounds against the plant pathogenic fungi *F. oxysporum* from *P. monteilii* PsF84. We conclude that the *P. monteilii* strain PsF84 is a promising source of natural bioactive secondary metabolites, which may receive great benefit as potential sources in the agricultural and pharmacological industries. However, further evaluation of the effectiveness of 2,4-di-*tert*-butylphenol in vivo for disease control and formulations is required.

■ ASSOCIATED CONTENT

Supporting Information

Figure S1: Structure elucidation of metabolite produced by *P. putida*. This material is available free of charge via the Internet at http://pubs.acs.org.

■ AUTHOR INFORMATION

Corresponding Author

*(D.D.P.) Phone: +91-522-2718536. Fax: +91-522-2342666or 2357136. E-mail:ddpatra@rediffmail.com.

Funding

S., S.G., and A.M. are grateful to the Council of Scientific and Industrial Research (CSIR), New Delhi, India, for the award of a Senior Research fellowship, and S.D. is also grateful to the Academy of Scientific and Innovative Research (AcSIR) for Ph.D. registration.

Notes

The authors declare no competing financial interest.

■ ABBREVIATIONS USED

VOC, volatile organic compound; NMR, nuclear magnetic resonance; CF, culture filtrate; DCM, dichloromenthane; MeOH, methanol; F8, fraction 8; P1a, 2,4-di-*tert*-butylphenol; Bv, bavisitin; GC-MS, gas chromtography−masss spectrometry; VLC, vacuum liquid chromatography; TLC, thin layer chromatgraphy

■ REFERENCES

(1) Brimner, T. A.; Boland, G. J. A review of the non-target effects of fungi used to biologically control plant diseases. *Agric. Ecosyst. Environ.* **2003**, *100*, 3−16.

(2) Kim, H. S.; Sang, M. K.; Jeun, Y. C.; Hwang, B. K.; Kim, K. D. Sequential selection and efficacy of antagonistic rhizobacteria for controlling *Phytophthora* blight of pepper. *Crop Prot.* **2008**, *27*, 436−443.

(3) Kim, H. S.; Sang, M. K.; Jung, H. W.; Jeun, Y. C.; Myung, I. S.; Kim, K. D. Identification and characterization of *Chryseobacterium wanjuense* strain KJ9C8 as a biocontrol agent of *Phytophthora* blight of pepper. *Crop Prot.* **2012**, *32*, 129−137.

(4) Sang, M. K.; Do Kim, J.; Kim, B. S.; Kim, K. D. Root treatment with rhizobacteria antagonistic to phytophthora blight affects anthracnose occurrence, ripening and yield of pepper fruit in the plastic house and field. *Phytopathology* **2011**, *101*, 666−678.

(5) Sang, M. K.; Kim, J. G.; Kim, K. D. Biocontrol activity and induction of systemic resistance in pepper by compost water extracts against *Phytophthora capsici*. *Phytopathology* **2010**, *100*, 774−783.
(6) Fernando, W. G. D.; Linderman, R. G. Inhibition of *Phytophthora vignae* and stem and root-rot of cowpea by soil bacteria. *Biol. Agric Hortic.* **1995**, *12*, 1−14.
(7) Ryu, C. M.; Farag, M. A.; Hu, C. H.; Reddy, M. S.; Wei, H. X.; Pare, P. W.; Kloepper, J. W. Bacterial volatiles promote growth in *Arabidopsis*. *Proc. Natl. Acad. Sci. U.S.A.* **2003**, *100*, 4927−4932.
(8) Bruce, A.; Wheatley, R. E.; Humphris, S. N.; Hackett, C. A.; Florence, M. E. J. Production of volatile organic compounds by *Trichoderma* in media containing different amino acids and their effect on selected wood decay fungi. *Holzforschung* **2000**, *54*, 481−486.
(9) Scholler, C. E.; Gurtler, H.; Pedersen, R.; Molin, S.; Wilkins, K. Volatile metabolites from actinomycetes. *J. Agric. Food Chem.* **2002**, *50*, 2615−2621.
(10) Fiddaman, P. J.; Rossall, S. Effect of substrate on the production of antifungal volatiles from *Bacillus subtilis*. *J. Appl. Bbacteriol.* **1994**, *76*, 395−405.
(11) Fernando, W. G. D.; Ramarathnam, R.; Krishnamoorthy, A. S.; Savchuk, S. C. Identification and use of potential bacterial organic antifungal volatiles in biocontrol. *Soil Biol. Biochem.* **2005**, *37*, 955−964.
(12) Mckee, N. D.; Robinson, P. M. Production of volatile inhibitors of germination and hyphal extension by *Geotrichum candidum*. *Trans. Br. Mycol. Soc.* **1988**, *91*, 157−190.
(13) Cheetham, P. S. J. Combining the technical push and the business pull for natural flavours. *Biotechnol. Aroma Compds.* **1997**, *55*, 1−49.
(14) Yoon, M. A.; Jeong, T. S.; Park, D. S.; Xu, M. Z.; Oh, H. W.; Song, K. B.; Lee, W. S.; Park, H. Y. Antioxidant effects of quinoline alkaloids and 2,4-di-*tert*-butylphenol isolated from *Scolopendra subspinipes*. *Biol. Pharm. Bull.* **2006**, *29*, 735−739.
(15) Souto, G. I.; Correa, O. S.; Montecchia, M. S.; Kerber, N. L.; Pucheu, N. L.; Bachur, M.; Garcia, A. F. Genetic and functional characterization of a *Bacillus sp* strain excreting surfactin and antifungal metabolites partially identified as iturin-like compounds. *J. Appl. Microbiol.* **2004**, *97*, 1247−1256.
(16) Burgess, L. W. *General Ecology of the Fusaria*; Pennsylvania State University Press: State College, PA, USA,1981; pp 225−235.
(17) Dharni, S.; Sanchita; Samad, A.; Sharma, A.; Patra, D. D. the interaction pattern between a homology model of 40S ribosomal S9 protein of *Rhizoctonia solani* and 1-hydroxyphenaize by docking study. *Biomed. Res. Int.* **2014**, *2014*, 1−6.
(18) Kai, M.; Effmert, U.; Berg, G.; Piechulla, B. Volatiles of bacterial antagonists inhibit mycelial growth of the plant pathogen *Rhizoctonia solani*. *Arch. Microbiol.* **2007**, *187*, 351−360.
(19) Jung, M. K.; Prigozhina, N.; Oakley, C. E.; Nogales, E.; Oakley, B. R. Alanine-scanning mutagenesis of *Aspergillus* gamma-tubulin yields diverse and novel phenotypes. *Mol. Biol. Cell* **2001**, *12*, 2119−2136.
(20) Hammond, S. M.; Lambert, P. A. *Antimicrobial Action*; Edward Arnold: London, UK, 1978; Vol. 4, pp 4−9.
(21) Bergey, D. H.; Breed, R. S.; Murray, E. G. D.; Smith, N. R. *Bergey's Manual of Determinative Bacteriology*, 7th ed.; Williams & Wilkins: Baltimore, MD, USA, 1957; pp xviii, 1094.
(22) Ryu, E. A simple method of differentiating between gram positive and gram negative organism without staining. *Kitasato Arch. Exp. Med.* **1998**, *17*, 58−63.
(23) Gerhardt, P.; Murray, R. G. E.; Costilow, R. N.; Nester, E. W.; Wood, W. A.; Krieg, N. R.; Phillips, G. B. *Manual of Methods for General Bacteriology*; ASM Press: Washington, DC, USA, 1981.
(24) Bossis, E.; Lemanceau, P.; Latour, X.; Gardan, L. The taxonomy of *Pseudomonas fluorescens* and *Pseudomonas monteilii*: current status and need for revision. *Agronomie* **2000**, *20*, 51−63.
(25) Dharni, S.; Alam, M.; Kalani, K.; Khaliq, A.; Samad, A.; Srivastava, S. K.; Patra, D. D. Production, purification, and characterization of antifungal metabolite from *Pseudomonas aeruginosa* SD12, a new strain obtained from tannery waste polluted soil. *J. Microbiol. Biotechnol.* **2012**, *22*, 674−683.
(26) Tamura, K.; Peterson, D.; Peterson, N.; Stecher, G.; Nei, M.; Kumar, S. MEGA5: molecular evolutionary genetics analysis using maximum likelihood, evolutionary distance, and maximum parsimony methods. *Mol. Biol. Evol.* **2011**, *28*, 2731−2739.
(27) Oleszek, W.; Kapusta, I.; Stochmal, A. TLC of triterpenes (including saponins). In *Thin Layer Chromatography in Phytochemistry*; CRC Press, Taylor & Francis Group: New York, 2008; pp 519−541.
(28) Kai, M.; Effmert, U.; Berg, G.; Piechulla, B. Volatiles of bacterial antagonists inhibit mycelial growth of the plant pathogen *Rhizoctonia solani*. *Arch. Microbiol.* **2007**, *187*, 351−360.
(29) Marchler-Bauer, A.; Lu, S. N.; Anderson, J. B.; Chitsaz, F.; Derbyshire, M. K.; DeWeese-Scott, C.; Fong, J. H.; Geer, L. Y.; Geer, R. C.; Gonzales, N. R.; et al. CDD: a conserved domain database for the functional annotation of proteins. *Nucleic Acids Res.* **2011**, *39*, D225−D229.
(30) Combet, C.; Jambon, M.; Deleage, G.; Geourjon, C. Geno3D: automatic comparative molecular modelling of protein. *Bioinformatics* **2002**, *18*, 213−214.
(31) Laskowski, R. A.; Macarthur, M. W.; Moss, D. S.; Thornton, J. M. Procheck − a program to check the stereochemical quality of protein structures. *J. Appl. Crystallogr.* **1993**, *26*, 283−291.
(32) Wiederstein, M.; Sippl, M. J. ProSA-web: interactive web service for the recognition of errors in three-dimensional structures of proteins. *Nucleic Acids. Res.* **2007**, *35*, W407−W410.
(33) Morris, G. M.; Huey, R.; Lindstrom, W.; Sanner, M. F.; Belew, R. K.; Goodsell, D. S.; Olson, A. J. AutoDock4 and AutoDockTools4: automated docking with selective receptor flexibility. *J. Comput. Chem.* **2009**, *30*, 2785−2791.
(34) Nakano, M. M.; Marahiel, M. A.; Zuber, P. Identification of a genetic locus required for biosynthesis of the lipopeptide antibiotic surfactin in *Bacillus subtilis*. *J. Bacteriol.* **1988**, *170*, 5662−5668.
(35) Kim, P. I.; Bai, H.; Bai, D.; Chae, H.; Chung, S.; Kim, Y.; Park, R.; Chi, Y. T. Purification and characterization of a lipopeptide produced by *Bacillus thuringiensis* CMB26. *J. Appl. Microbiol.* **2004**, *97*, 942−949.
(36) Ahmad-Qasem, M. H.; Canovas, J.; Barrajon-Catalon, E.; Carreres, J. E.; Micol, V.; Garcia Perez, J. V. Influence of olive leaf processing on the bioaccessibility of bioactive polyphenols. *J. Agric. Food Chem.* **2014**, DOI: 10.1021/jf501414h.
(37) Yuan, J.; Raza, W.; Shen, Q.; Huang, Q. Antifungal activity of *Bacillus amyloliquefaciens* NJN-6 volatile compounds against *Fusarium oxysporum* f. sp. cubense. *Appl.Environ. Microbiol.* **2012**, *78*, 5942−5944.
(38) Patharakorn, T.; Arpornsuwan, T.; Wetprasit, N.; Promboon, A.; Ratanapo, S. Antibacterial activity and cytotoxicity of the leaf essential oil of *Morus rotunbiloba* Koidz. *J. Med. Plants Res.* **2010**, *4*, 837−843.
(39) Williamson, S. M.; Guzman, M.; Marin, D. H.; Anas, O.; Jin, X.; Sutton, T. B. Evaluation of *Pseudomonas syringae* strain ESC-11 for biocontrol of crown rot and anthracnose of banana. *Biol. Control* **2008**, *46*, 279−286.
(40) Sang, M. K.; Kim, K. D. The volatile-producing *Flavobacterium johnsoniae* strain GSE09 shows biocontrol activity against *Phytophthora capsici* in pepper. *J. Appl. Microbiol.* **2012**, *113*, 383−398.
(41) Robinson, P. M.; Mckee, N. D.; Thompson, L. A. A.; Harper, D. B.; Hamilton, J. T. G. Autoinhibition of germination and growth in *Geotrichum candidum*. *Mycol. Res.* **1989**, *93*, 214−222.
(42) Huang, H. C.; Huang, J. W.; Saindon, G.; Erickson, R. S. Effect of allyl alcohol and fermented agricultural wastes on carpogenic germination of sclerotia of *Sclerotinia sclerotiorum* and colonization by *Trichoderma* spp. *Can. J. Plant. Pathol.* **1997**, *19*, 43−46.
(43) Voisard, C.; Keel, C.; Haas, D.; Defago, G. Cyanide Production by *Pseudomonas fluorescens* helps suppress black root-rot of tobacco under gnotobiotic conditions. *EMBO J.* **1989**, *8*, 351−358.
(44) Sanchita; Chauhan, R.; Soni, G.; Sudhamalla, B.; Sharma, A. Docking and molecular dynamics studies of peptide inhibitors of ornithine decarboxylase: a rate-limiting enzyme for the metabolism of *Fusarium solani*. *J. Biomol. Struct. Dyn.* **2013**, *31*, 874−887.

JOURNAL OF AGRICULTURAL AND FOOD CHEMISTRY

Article

pubs.acs.org/JAFC

Bioactive Compounds from Culinary Herbs Inhibit a Molecular Target for Type 2 Diabetes Management, Dipeptidyl Peptidase IV

Allyson M. Bower,[†] Luis M. Real Hernandez,[‡] Mark A. Berhow,[§] and Elvira Gonzalez de Mejia*[,†,‡]

[†]Division of Nutritional Sciences and [‡]Department of Food Science and Human Nutrition, University of Illinois at Urbana-Champaign, 228 ERML, 1201 West Gregory Avenue, Urbana, Illinois 61801, United States

[§]United States Department of Agriculture Agricultural Research Service, 1815 North University Street, Peoria, Illinois 61604, United States

ABSTRACT: Greek oregano (*Origanum vulgare*), marjoram (*Origanum majorana*), rosemary (*Rosmarinus officinalis*), and Mexican oregano (*Lippia graveolens*) are concentrated sources of bioactive compounds. The aims were to characterize and examine extracts from greenhouse-grown or commercially purchased herbs for their ability to inhibit dipeptidyl peptidase IV (DPP-IV) and protein tyrosine phosphatase 1B (PTP1B), enzymes that play a role in insulin secretion and insulin signaling, respectively. Greenhouse herbs contained more polyphenols (302.7−430.1 μg of gallic acid equivalents/mg of dry weight of extract (DWE)) and flavonoids (370.1−661.4 μg of rutin equivalents/mg of DWE) compared to the equivalent commercial herbs. Greenhouse rosemary, Mexican oregano, and marjoram extracts were the best inhibitors of DPP-IV (IC_{50} = 16, 29, and 59 μM, respectively). Commercial rosemary, Mexican oregano, and marjoram were the best inhibitors of PTP1B (32.4−40.9% at 500 μM). The phytochemicals eriodictyol, naringenin, hispidulin, cirsimaritin, and carnosol were identified by LC−ESI-MS as being present in greenhouse-grown Mexican oregano and rosemary. Computational modeling indicated that hispidulin, carnosol, and eriodictyol would have the best binding affinities for DPP-IV. Biochemically, the best inhibitors of DPP-IV were cirsimaritin (IC_{50} = 0.43 ± 0.07 μM), hispidulin (IC_{50} = 0.49 ± 0.06 μM), and naringenin (IC_{50} = 2.5 ± 0.29 μM). Overall, herbs contain several flavonoids that inhibit DPP-IV and should be investigated further regarding their potential in diabetes management.

KEYWORDS: *hispidulin, marjoram, oregano, rosemary, type 2 diabetes mellitus, DPP-IV, PTP1B*

INTRODUCTION

Type 2 diabetes mellitus (T2DM) affects 8.3% of Americans and cost the United States $175 billion in 2012.[1] Currently, the only effective therapies for the management of T2DM are lifestyle intervention and treatment with pharmaceuticals; however, these approaches have poor adherence[2] and can be expensive to maintain.[1] Thus, there is a need to identify natural compounds that can aid in the management of this disease.

Plants produce bioactive compounds that inhibit the pharmaceutical targets related to T2DM, dipeptidyl peptidase IV (DPP-IV) and protein tyrosine phosphatase 1B (PTP1B).[3,4] DPP-IV is a serine protease responsible for the degradation of the insulinotropic incretin glucagon-like peptide 1 (GLP-1). Pharmaceutical inhibitors of this enzyme have successfully reduced hyperglycemia and hemoglobin A1C levels as a monotherapy and in combination with other antidiabetic agents.[5] PTP1B is a tyrosine phosphatase responsible for the reversal of insulin receptor autophosphorylation. Reducing the activity of this enzyme is hypothesized to prolong the insulin signaling cascade and thus increase insulin sensitivity.[6] A synthetic inhibitor of PTP1B reduced enzyme activity and plasma insulin levels in high-fat-diet-induced obese mice.[7]

A review of recent scientific publications on culinary herbs indicates that herbs from a traditional Mediterranean diet alleviate inflammation, hypertension, hyperlipidemia, and hyperglycemia in vivo.[8] Investigation of the hypoglycemic mechanisms showed that oregano (*Origanum vulgare*), marjoram (*Origanum majorana*), and rosemary (*Rosmarinus officinalis*) can inhibit α-glucosidase[9−11] and act as peroxisome proliferator-activated receptor γ (PPAR-γ) agonists in vitro;[12,13] however, there has been no investigation into the effect of these herbs on DPP-IV or PTP1B.

Mexican oregano (*Lippia graveolens*) is an herb from Latin cuisine that has traditional medicinal uses. In a comprehensive review of the traditional uses of 28 varieties of *Lippia* from around the world, only the use of *L. graveolens* had been reported as a therapy for diabetes.[14] Mexican oregano is also of specific interest in diabetes research because it contains one of the highest concentrations of flavonoids of all foods listed in the U.S. Deparment of Agriculture (USDA) database. Remarkably, there have been no studies examining its potential in diabetes management.

It is well-known that the concentration of phytochemicals such as polyphenols in plants can be impacted by growth conditions[15,16] and drying methods;[17] therefore, it is important to consider origin when examining the therapeutic potential of these herbs. Thus, the first aim of this study was to examine the differences in polyphenol concentration and antioxidant capacity of greenhouse-grown and commercial herbs and the ability of herb extracts from different sources to inhibit DPP-IV and PTP1B. Our second aim was to identify and quantify specific compounds responsible for DPP-IV inhibition in culinary herbs using bioassay-guided fractionation, LS−ESI-

Received: February 5, 2014
Revised: May 28, 2014
Accepted: June 1, 2014
Published: June 1, 2014

ACS Publications © 2014 American Chemical Society

MS, and HPLC. Our third aim was to examine these compounds for the ability to inhibit DPP-IV independently. To complement this work, computational modeling was used to provide insight into the theoretical enzyme−ligand interactions which identifies molecular targets for inhibition within the enzyme. Through these aims, we have systematically identified compounds that inhibit DPP-IV, an enzyme that plays a role in insulin secretion.

MATERIALS AND METHODS

Materials. Seeds for *O. majorana* and *O. vulgare* ssp. *hirtum* were purchased from Richter's Herbs (Goodwood, Ontario, Canada). Propagated cuttings of *L. graveolens* and *R. officinalis* were purchased from Companion Plants (Athens, OH). Commercial dry herbs were purchased at local grocery stores in the area of Urbana, IL. Fluorescein (S71283), *p*-nitrophenyl phosphate (≥98%, BP2534-1), and all solvents used in extraction, chromatography, and mass spectrometry were of HPLC grade and were purchased from Fisher Scientific (Pittsburgh, PA). Sitagliptin phosphate monohydrate (≥98%, S8576), sodium orthovanadate (≥90%, S6508), Trolox (97%, 238813), gallic acid (≥97.5%, G7384), rutin (≥94%, R5143), hispidulin (≥98%, SML0582), cirsimaritin (≥90%, SMB00174), naringenin (≥95%, N5893), rosmarinic acid (96%, 536954), porcine DPP-IV (D7052, EC 3.4.14.5), AAPH (97%, 440914), 2-aminoethyl diphenylborinate (D9754), and Folin−Ciocalteu phenol reagent (F9252) were purchased from Sigma Chemical Co. (St. Louis, MO). Carnosol (≥96%, 89800) was purchased from Cayman Chemical Co. (Ann Arbor, MI). Eriodictyol (95%, 20056) was purchased from Indofine Chemical Co. (Hillsburough, NJ). Human recombinant PTP1B (BML-SE332-0050, EC 3.1.3.48) was purchased from Enzo Life Sciences (Farmingdale, NY).

Greenhouse Herb and Extract Preparation. Fresh herbs were grown in the University of Illinois Plant Care Facility under greenhouse conditions (average temperature 24.0 ± 0.3 °C) between the months of March and June 2013 and were not exposed to any pesticides or fertilizers. After three months, leaves were removed from the plants, washed, frozen at −80 °C, and freeze-dried within 48 h using a Labconco Freezone 6L (Kansas City, MO) freeze-dryer with a collector temperature of −50 °C. The dried leaves were ground using a commercial coffee grinder and pulverized using a mortar and pestle until a fine powder developed. The powder was sifted through a 20 mesh sieve to remove any remaining large pieces of material. The herb powder was then extracted in an excess of 100% methanol using a Soxhlet exhaustive extraction apparatus for at least 24 h. The methanolic extract was filtered using no. 4 Whatman filter paper by gravity flow and concentrated by evaporation under a fume hood at room temperature overnight. An aliquot was removed and evaporated to near dryness (∼3 mL) using a Buchi rotoevaporator. After rotoevaporation, water was added, and the aliquot was freeze-dried to remove any residual water and methanol. The remaining methanolic extract was fractionated by flash chromatography.

Commercial Herb and Extract Preparation. Commercial dry herbs were ground into a fine powder using a commercial coffee grinder, pulverized with a mortar and pestle, and sifted. The herbs were then extracted in methanol at room temperature for 4 h, after which the extract was filtered using no. 4 Whatman filter paper by gravity flow, the methanol was reserved, and new methanol was added to the herbs for a second extract overnight at room temperature. After the extract was filtered once more, methanol from the 4 h extraction and that from the overnight extraction were pooled. Methanolic extract was evaporated to near dryness (∼3 mL) using a Buchi rotoevaporator (Newcastle, DE). After rotoevaporation, water was added, and the extracts were freeze-dried to remove any residual water and methanol.

Flash Chromatography and Fraction Preparation. Fractionation was performed using a Büchi Sepacore flash chromatography system (Newcastle, DE) with dual C-605 pump modules, a C-615 pump manager, a C-660 fraction collector, and a C-635 UV photometer, with SepacoreRecord chromatography software. The column used was a 40 × 150 mm flash column with approximately 90 g of preparative C18 reversed-phase bulk packing material (125 Å, 55−105 μm, Waters Corp., Milford, MA). The column was equilibrated with 20% methanol and 0.5% acetic acid in water for 10 min at a flow rate of 30 mL/min. After injection of the samples (20 mL), the column was developed with a binary gradient to 100% methanol over 45 min. The effluent was monitored at 280 nm, and fractions based on absorbance were collected in the fraction collector by the software program. Fractions containing each absorbance peak were then pooled. This procedure was repeated until all the extract was used. Fraction designations correspond to the following elution times (min): (Greek oregano) OA, 4−5; OB, 6−10; OC, 11−19; OD, 20−23; OE, 24−28; OF, 29−45; (Mexican oregano) LA, 4−5; LB, 6−10; LC, 11−13; LD, 14−17; LE, 18−20; LF, 21−25; LG, 26−28; LH, 29−31; LI, 32−45; (rosemary) RA, 4−6; RB, 7−15; RC, 16−22; RD, 23−26; RE, 27−30; RF, 31−32; RG, 33−35; RH, 36−39; RI, 40−45; (marjoram) MA, 4−6; MB, 7−13; MC, 14−19; MD, 20−21; ME, 22−23; MF, 24−25; MG, 26−27; MH, 28−45. The fraction pools were then concentrated by evaporation in the hood at room temperature, rotoevaporation, and then freeze-drying. The fraction extracts were then weighed and stored at −20 °C for future use.

Total Polyphenols. The total phenolic concentration was quantified on the basis of the principles introduced by Singleton and Rossi[18] adapted to a microassay. Samples (100 μg of extract/mL) or gallic acid standard and 1 N Folin−Ciocalteu phenol reagent were added to a 96-well flat-bottom plate and allowed to stand for 5 min before the addition of 20% Na_2CO_3. The mixture was allowed to stand for 10 min before the absorbance was read at 690 nm using a Synergy 2 multiwell plate reader (Biotek Instruments, Winooski, VT). The results are expressed as micrograms of gallic acid equivalents (GAE) per milligram of dry weight of extract (DWE) using a gallic acid standard curve: $y = 0.0195x + 0.0054$, $R^2 = 0.9997$.

Total Flavonoids. The total flavonoid concentration was quantified using an adaptation of the method used by Oohmah et al.[19] Briefly, 20 μL of sample (100 μg/mL) or rutin standard was added to a flat-bottom 96-well plate followed by the addition of 180 μL of distilled water. A solution of 2-aminoethyl diphenylborinate (10 mg/mL, 20 μL) was then added to each well, and the absorbance was read at 380 nm using a Synergy 2 multiwell plate reader (Biotek Instruments). The results are expressed as micrograms of rutin equivalents (RE) per milligram of DWE using a rutin standard curve: $y = 0.0028x + 0.0487$, $R^2 = 0.99$.

Oxygen Radical Absorbance Capacity. Antioxidant capacity was measured by the oxygen radical absorbance capacity (ORAC) assay previously described.[20] Trolox standard, blanks, or samples in assay buffer (75 mM phosphate buffer, pH 7.4) were added to the wells of a 96-well black-walled plate. Fluorescein (116.9 nM) was added to each well, and the plate was incubated at 37 °C for 15 min. AAPH (40 mM) was added to each well, and fluorescence was read at 485 and 582 nm every 2 min at sensitivity 60 at 37 °C using a Synergy2 multiwell plate reader (Biotek Instruments). The results are expressed as millimoles of Trolox equivalents (TE) per milligram of DWE.

DPP-IV Inhibition. DPP-IV inhibition was measured using the DPP-IV Glo protease assay (G8351, Promega, Madison, WI) following the manufacture's protocol. Briefly, 50 μL of DPP-IV Glo reagent was added to a white-walled 96-well plate containing 50 μL of blank, 40 μL of enzyme control, 40 μL of sample, 40 μL of positive control sitagliptin, or 40 μL of pure compounds. The samples were prepared in an assay buffer (100 mM Tris, 200 mM NaCl, 1 mM EDTA, pH 8.0) at a concentration of 100, 10, 1, or 0.1 μg of GAE/mL. A stock solution of sitagliptin was prepared by adding 10.48 mg of sitagliptin phosphate monohydrate to 10 mL of assay buffer, making a 2 mM solution which was then diluted to 10, 1, 0.1, and 0.01 μM. Pure compounds were prepared in assay buffer at a concentration of or 100, 10, 1, and 0.1 μM. The blank contained only assay buffer, while the enzyme control contained assay buffer and 10 μL of purified porcine DPP-IV enzyme (88% homology to the human enzyme)[21] at 0.075 U/nL. DPP-IV enzyme was also added to each sample. Luminescence was then measured after gentle mixing and incubation at 26 °C for 30 min

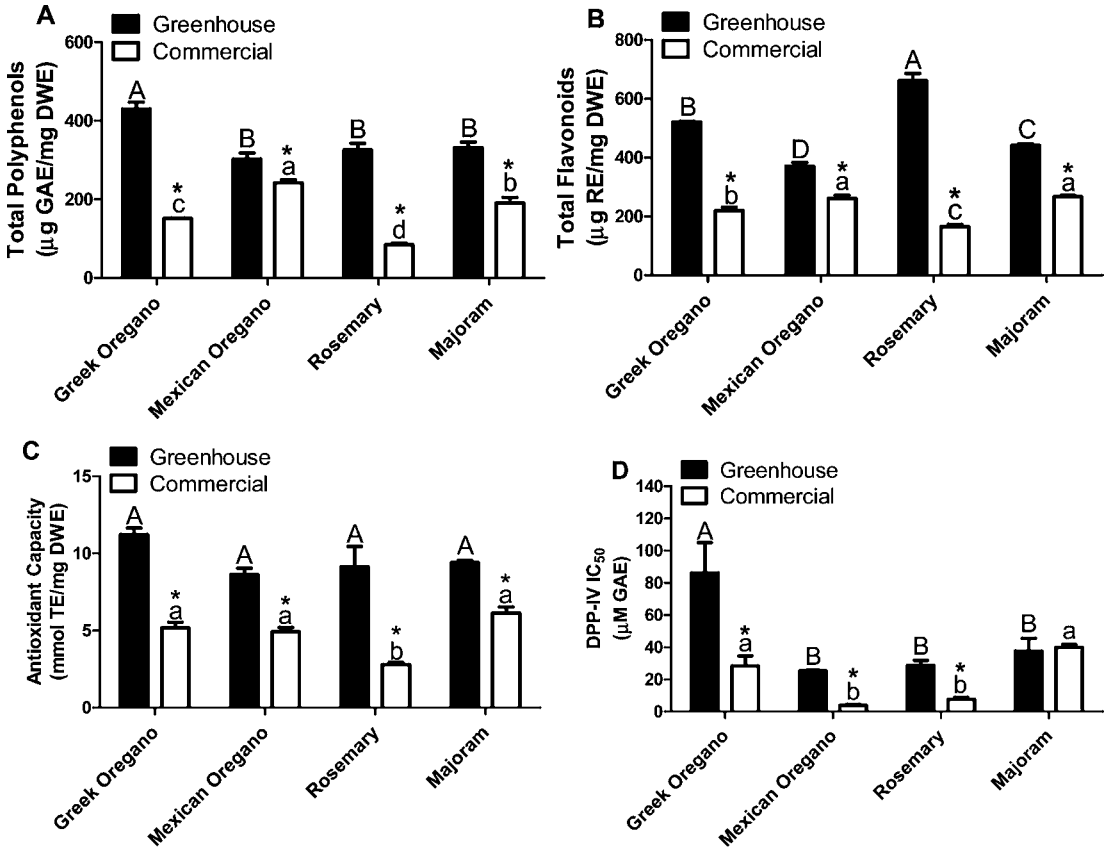

Figure 1. (A) Concentration of polyphenols, (B) concentration of flavonoids, (C) antioxidant capacity, and (D) DPP-IV IC_{50} for greenhouse and commercial herbs. The data represent the mean ± SEM from at least three independent studies done in triplicate. Capital letters indicate significant difference among greenhouse herbs. Lowercase letters indicate significant difference among commercial herbs. Asterisks indicate significant difference between greenhouse and commercial herbs. Significance is reported at $p < 0.05$. GAE = gallic acid equivalents, RE = rutin equivalents, and TE = Trolox equivalents.

using a Synergy2 multiwell plate reader (Biotek Instruments). Percent inhibition was calculated from the blank and enzyme control for each sample. IC_{50} was calculated from the quadratic formula generated from log(concentration) and percent inhibition, and the units were converted to micromolar.

PTP1B Inhibition. PTP1B inhibition was determined by analysis of *p*-nitrophenyl phosphate (*p*-NPP) degradation adapted from the methods of previous researchers.[22−24] Briefly, 50 μL of blank, 40 μL of enzyme control, 40 μL of sample, or 40 μL of positive control sodium orthovanadate was added to a flat-bottomed clear 96-well plate followed by the addition of 50 μL of *p*-NPP (10 mM). The samples and sodium orthovanadate were prepared in assay buffer (50 mm HEPES, 100 mm NaCl, 0.1% BSA, 1 mm DTT, pH 7.3) and contained 100, 10, 1, or 0.1 μg of GAE/mL on the basis of data obtained from the polyphenol analysis for the samples or 100, 10, 1, or 0.1 μM for sodium orthovanadate. The blank contained only assay buffer, while the enzyme control contained assay buffer and 10 μL of purified PTP1B enzyme (10 μg/mL). Purified PTP1B enzyme was also added to each sample. The plates were incubated at room temperature for 20 min, the reaction was terminated with the addition of 50 μL of 1.5 M NaOH, and the absorbance was read at 405 nm using a Synergy2 multiwell plate reader (Biotek Instruments). Each sample at each concentration was also run without enzyme in the same experiment to control for the inherent color present in each sample. Percent inhibition was calculated from the blank and enzyme control for each sample. IC_{50} was calculated from the quadratic formula generated from log(concentration) and percent inhibition, and the units were converted to micromolar.

LC−ESI-MS and HPLC Analysis. A turbo ion spray electrospray source and an Agilent 100 series HPLC system (G1379A degasser, G1357A binary capillary pump, G1389A autosampler, G1315B photodiode array detector, and G1316A column oven) running under Applied Biosystems Analyst 2.0 (build 1446) LC−MS software were utilized. The mass spectrometer was calibrated at least daily with a standard calibration mixture recommended by Applied Biosystems, and the signal detection was optimized as needed. The data were acquired in the MOF MS mode, negative. The MS parameters were as follows: accumulation time, 1 s; mass range, 200−1000 Da; source gas 1, 50 units; source gas 2, 35 units; curtain gas, 25 units; ion spray voltage, 4500; source heater, 400 °C; declustering potential 1, 80; focusing potential, 265; declustering potential 2, 15; ion release delay, 6; ion release width, 5. The column was a 3 mm × 150 mm Inertsil reversed-phase C-18, ODS-3, 3 μm column (Metachem, Torrance, CA). The initial solvent system was 20% methanol and 80% water with 0.25% formic acid at a flow rate of 0.25 mL/min. After injection (15 μL) the column was developed with a linear gradient to 100% methanol over 50 min. The column effluent was monitored at 280 nm in the PDA detector. The software package was set to collect mass data between 150 and 1000 amu.

Phenolic Compound Quantification by HPLC. HPLC analysis was conducted on a Shimadzu LC-20 HPLC system (LC-20AT quaternary pump, DGU-20A5 degasser, SIL-20A HT autosampler, and SPD M20A photodiode array detector) running under Shimadzu LCSolutions version 1.22 chromatography software (Columbia, MD). The column used was a 4.6 mm × 250 mm Inertsil ODS-3 reversed-phase C-18, 5 μm column from Varian. The initial conditions were 20% methanol and 80% water with 0.05 M phosphoric acid at a flow rate of 1 mL/min. The effluent was monitored at 280 nm. After injection of 25 μL, the column was held at the initial conditions for 2 min and then developed to 100% methanol in a linear gradient over 55 min. A standard curve based on nanomoles injected was prepared from rosmarinic acid, eriodictyol, naringenin, hispidulin, cirsimaritin, and

carnosol prepared at concentrations of 0.1, 0.2, 1, and 2 nmol/μL. The molar extinction coefficients for each standard were 1.702×10^{-3}, 1.375×10^{-3}, 1.686×10^{-3}, 1.254×10^{-3}, and 10.087×10^{-3} abs/nmol, respectively, and were used to quantify the concentrations of the compounds of interest.

Computational Modeling. Molecular files for the compounds tested were acquired from Chemical Book (www.chemicalbook.com). Structural hydrogens were added to the molecular files, and the CHARMm force field was applied using Accelrys Discovery Studio 3.5 Vizualizer (Discovery Studio 3.5, Accelrys Software Inc., San Diego, CA). The structure of DPP-IV was acquired from the Protein Data Bank (PDB ID 1X70, www.rcsb.org). Because DPP-IV exists as a homodimer in the crystal structure with sitagliptin and stabilizing water molecules, the ligands from the crystal structure, water molecules, and a monomer unit of DPP-IV were removed from PDB file 1X70 using Discovery Studio 3.5. Rotational bonds for each compound were assigned, and the amino acid TYR547 was made flexible in the DPP-IV structure using AutoDock Tools (version 1.5.6).[25] AutoDock Vina[26] search box parameters were determined using a rigid form of DPP-IV. The orientation of the search box was predetermined by AutoDock Tools; however, the dimensions in angstroms were changed to encapsulate DPP-IV as a whole (center $X = -8.425$, center $Y = 54.618$, center $Z = 33.543$, size $X = 68$, size $Y = 64$, size $Z = 78$). In a physiological system a ligand may have access to other regions of the enzyme beyond the catalytic site. Thus, the enzyme was encapsulated as a whole to model any potentially novel interactions between the ligands of interest and DPP-IV outside of its active site. A text configuration file was created detailing the search parameters, and the exhaustiveness of the search was set to 150. The exhaustiveness is proportional to the number of runs per search and was increased from the default setting of 8 to 150 due to the large search space used in this study, as such a low value may have given inconsistent results. Additionally, exhaustiveness was increased to 150 on the basis of the consistency of preliminary research modeling sitagliptin. The best binding conformation was determined by the lowest binding affinity (kcal/mol) of each computational docking for each compound tested. Interactions between the amino acids of DPP-IV and each compound were observed using Discovery Studio 3.5. AutoDock Vina provides the results based on the best docking conformation, which is given a root-mean-square deviation of zero. Since only the best docking conformation for each ligand was chosen, the root-mean-square deviations could not be compared.

Statistics. Data are expressed as the mean ± SEM of at least three replications. Statistical analysis was conducted using SAS Enterprise Guide (version 6.1, SAS Institute Inc., Cary, NC) and GraphPad Prism (version 5.02, GraphPad Software, Inc., San Diego, CA). One-way analysis of variance (ANOVA) with Tukey's post-test was used to evaluate the differences between group means. Regression analysis was used to evaluate associations between variables. Analyses were considered statistically significant at an α-level of $p < 0.05$.

RESULTS AND DISCUSSION

Characterization and Comparison of Greenhouse and Commercial Herbs. Figure 1A–C represents the total polyphenol concentration, total flavonoid concentration, and antioxidant capacity measured in greenhouse-grown and commercially available Greek oregano, Mexican oregano, rosemary, and marjoram. Greenhouse-grown herbs had significantly higher polyphenol concentrations (range 302.7–430.1 μg of GAE/mg of DWE), flavonoid concentrations (range 370.1–661.4 μg of RE/mg of DWE), and antioxidant capacity (range 8.62–11.22 mmol of TE/mg of DWE) compared to the commercially available products.

Of all greenhouse-grown herbs, extracts from Greek oregano contained the highest concentration of polyphenols (430.1 ± 17.1 μg of GAE/mg of DWE) and rosemary extract contained the highest concentration of flavonoids (661.4 ± 24.6 μg of RE/mg of DWE), while there was no statistical difference in antioxidant capacity among the extracts from the greenhouse grown herbs. Of all commercial herbs, Mexican oregano extract contained the highest concentration of polyphenols (241.5 ± 8.0 μg of GAE/mg of DWE) and Mexican oregano and marjoram extracts contained the highest concentration of flavonoids (260.9 ± 11.0 and 266.9 ± 3.8 μg of RE/mg of DWE). Rosemary extract had the lowest antioxidant capacity (2.8 ± 0.1 mmol of TE/mg of DWE) of the commercial herbs. There was a positive correlation ($R^2 = 0.70$, $P < 0.001$) between total polyphenol and total flavonoid concentrations, total polyphenol concentration and antioxidant capacity ($R^2 = 0.92$, $P < 0.001$), and total flavonoid and antioxidant capacity ($R^2 = 0.74$, $P < 0.01$) of the extracts.

Extraction in polar solvents results in a yield of approximately 15%.[27−30] Adjusting for extract yield, the total polyphenol concentration for the dry herbs ranged from 1266 mg of GAE/100 g of dry weight (DW) (commercial rosemary) to 6452 mg of GAE/100 g of DW (greenhouse Greek oregano). These values are consistent with those reported in the literature for culinary herbs.[31] The total flavonoid concentration ranged from 2474 mg/100 g of DW (commercial rosemary) to 9921 mg/100 g of DW (greenhouse rosemary), and the antioxidant capacity ranged from 41.9 mmol of TE/100 g of DW (commercial rosemary) to 168.3 mmol of TE/100 g of DW (greenhouse Greek oregano). These values are consistent with the reported antioxidant capacity of methanol extracts from culinary herbs.[32]

Previous reports indicated that field-grown herbs have significantly lower total polyphenol concentration and antioxidant capacity[16] than greenhouse-grown herbs. Drying temperatures can also negatively impact the total polyphenol concentration and antioxidant capacity.[17] Furthermore, the cultivar or plant origin can play an important role in dictating the concentrations of antioxidants.[32] All of the aforementioned factors may have contributed to the differences observed between greenhouse and commercial herbs.

DPP-IV and PTP1B Inhibition by Greenhouse and Commercial Herbs. Figure 1D indicates the concentration required to inhibit DPP-IV by 50%. Lower concentrations indicate a fraction is a more potent inhibitor. Among all greenhouse-grown herbs, rosemary (IC_{50} = 28.7 ± 3.1 μM), Mexican oregano (25.3 ± 0.3 μM), and marjoram (37.7 ± 7.9 μM) extracts were the most potent inhibitors of DPP-IV. For all commercially produced herbs, rosemary (6.5 ± 0.4 μM) and Mexican oregano (IC_{50} = 3.9 ± 0.6 μM) extracts were the most potent inhibitors of DPP-IV.

Commercial Greek oregano extract (28.4 ± 6.3 μM) was a better inhibitor of DPP-IV than greenhouse-grown Greek oregano extract (86.2 ± 18.8 μM), commercial Mexican oregano extract (3.9 ± 0.6 μM) was a better inhibitor of DPP-IV than greenhouse-grown Mexican oregano extract (25.3 ± 0.3 μM), and commercial rosemary extract (6.5 ± 0.4 μM) was a better inhibitor than greenhouse rosemary extract (28.7 ± 3.1 μM). There was no difference in DPP-IV inhibition between the extracts of commercially produced and greenhouse-grown sources for marjoram. The positive control sitagliptin had an IC_{50} of 0.05 ± 0.01 μM.

Percent inhibition of PTP1B by 500 μM herb extracts was measured from each greenhouse and commercial herb. Extracts from greenhouse herbs did not inhibit PTP1B; however, commercial Mexican oregano (37.3% ± 6.8%), rosemary (40.9% ± 7.2%), and marjoram (32.4% ± 17.5%) extracts inhibited PTP1B at this concentration (data not shown). The

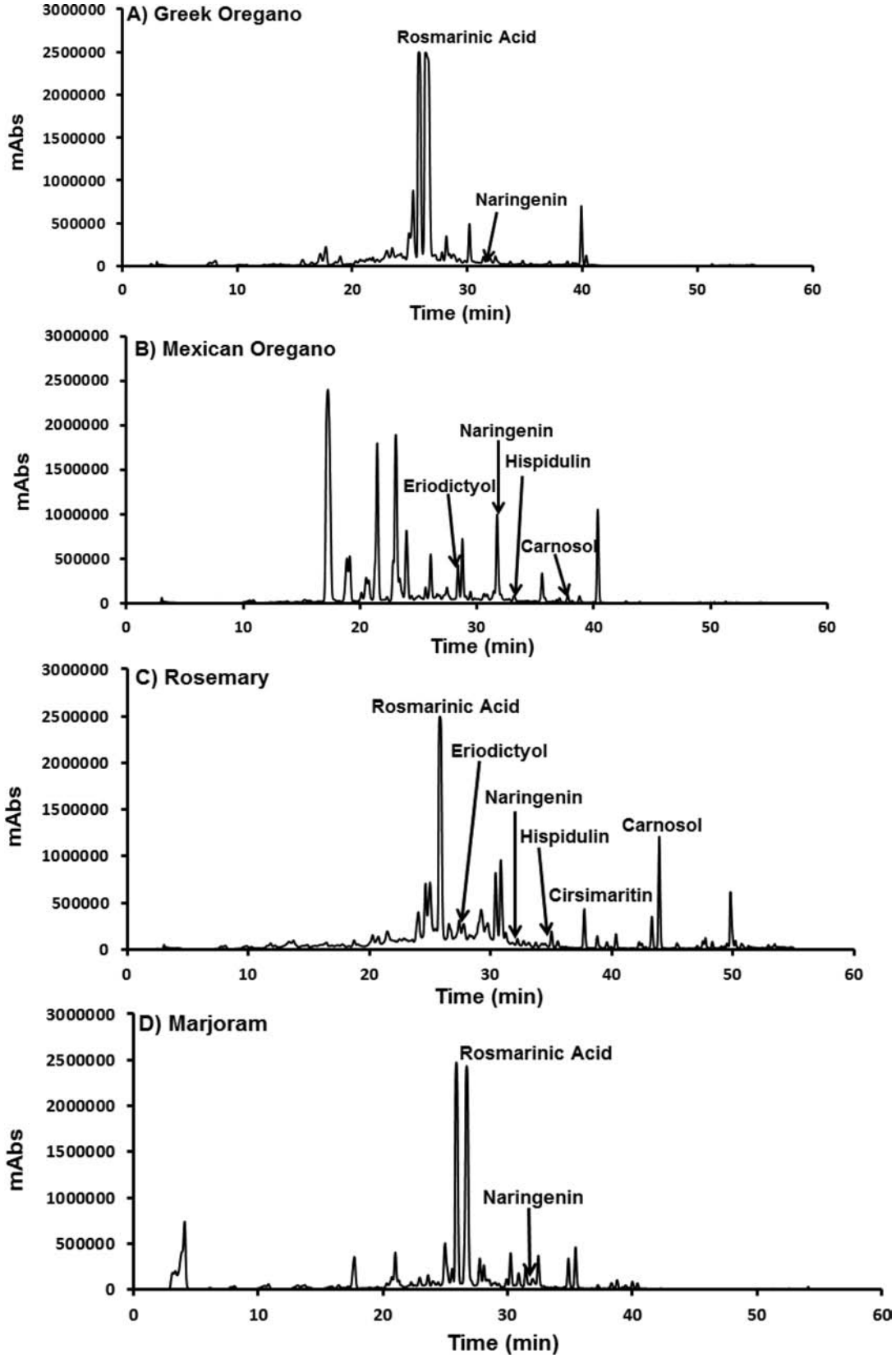

Figure 2. Representative HPLC chromatograms of the greenhouse-grown herbs. Positively identified compounds are indicated.

positive control sodium orthovanadate inhibited PTP1B by 100% at 500 μM and by 50% at 5.7 $\pm$ 2.7 μM. Comparison of the LC−ESI-MS chromatograms between commercial and greenhouse Greek oregano reveals many differences between the two in peak retention times and intensities (data not shown). We are currently performing further analysis to better understand the chemical differences in the composition of the commercial and greenhouse herb extracts.

dx.doi.org/10.1021/jf500639f | J. Agric. Food Chem. 2014, 62, 6147−6158

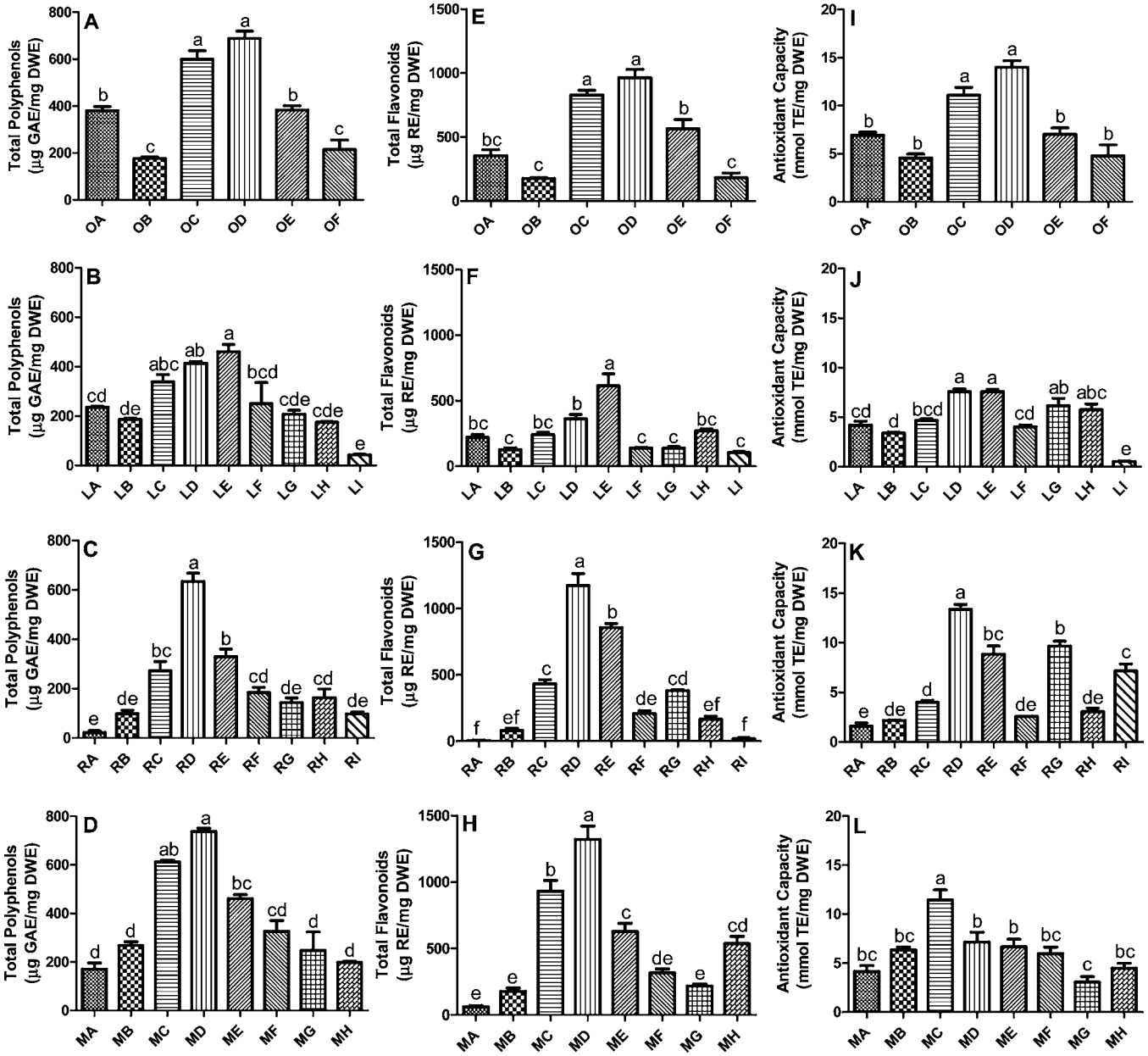

Figure 3. Total polyphenols (A–D), total flavonoids (E–H), and antioxidant capacity (I–L) for all fractions of greenhouse herbs: Greek oregano (A, E, I), Mexican oregano (B, F, J), rosemary (C, G, K), and marjoram (D, H, L). The data represent the mean ± SEM from at least three independent studies done in triplicate. Columns with differing letters are different with a significance of $p < 0.05$. GAE = gallic acid equivalents, RE = rutin equivalents, and TE = Trolox equivalents.

Jiang et al.[4] identified more than 200 natural compounds that were reported to inhibit PTP1B with IC_{50} < 100 μM; these included flavones, phenolic acids, and phenolic terpenoids. The natural compounds present in the herb extracts examined in this study did not inhibit PTP1B to the same extent. Jiang et al.[4] reported the values for pure compounds rather than whole extracts, and they reported natural compounds from a wide variety of sources such as plant roots, bark, and leaves as well as fungi and marine algae, and it is possible that the types of compounds that best inhibit PTP1B are not found in high concentrations in the leaves of culinary herbs.

Characterization of Fractions from Greenhouse Herbs. Figure 2 shows the comparative HPLC chromatograms of the greenhouse-grown herbs. Positively identified compounds are indicated. Figure 3 indicates the polyphenol concentration, flavonoid concentration, and antioxidant capacity of all fractions collected from each herb extract based on retention times using flash chromatography as indicated in the Materials and Methods. For Greek oregano (O), fractions C and D had the highest concentration of polyphenols and flavonoids and the highest antioxidant capacity. For Mexican oregano (L), fraction E had the highest of these three measurements, while, for rosemary (R), it was fraction D. For marjoram (M), fraction D had the highest concentration of polyphenols and flavonoids; however, fraction C had the highest antioxidant capacity. This could be due to the presence of nonphenolic antioxidants such as iridoid glycosides,[33] terpenoids, or saponins.[34]

DPP-IV and PTP1B Inhibition by Fractions from Greenhouse Herbs. Table 1 contains the IC_{50} values for

dx.doi.org/10.1021/jf500639f | J. Agric. Food Chem. 2014, 62, 6147–6158

Table 1. DPP-IV and PTP1B Inhibition for All Fractions of Greenhouse-Grown Herbs[a]

	DPP-IV IC_{50} (μM GAE)			
fraction	Greek oregano	Mexican oregano	rosemary	marjoram
A	>500	207.0 ± 52.3 ab	>500	>500
B	206.3 ± 47.2 a	130.3 ± 27.2 ab	>500	231.08 ± 52.0 a
C	>500	162.8 ± 37.0 a	>500	>500
D	317.4 ± 60.7 a	160.7 ± 9.3 a	>500	>500
E	**20.3 ± 3.9** b	56.5 ± 13.8 bc	65.3 ± 14.9 a	146.1 ± 49.3 ab
F	23.3 ± 1.9 b	19.0 ± 5.9 c	22.4 ± 11.9 bc	29.9 ± 1.1 b
G	NA	1.5 ± 0.7 c	**0.4 ± 0.1** c	47.3 ± 10.1 b
H	NA	1.3 ± 0.2 c	6.8 ± 1.5 bc	**1.9 ± 0.4** b
I	NA	**0.8 ± 0.3** c	30.1 ± 4.6 b	NA
	PTP1B inhibition (%) (500 μM)			
fraction	Greek oregano	Mexican oregano	rosemary	marjoram
A	7.0 ± 3.5 b	NI	NI	NI
B	13.3 ± 4.2 b	6.3 ± 3.3 c	NI	NI
C	1.3 ± 1.0 b	2.2 ± 2.1 c	NI	NI
D	NI	NI	NI	17.1 ± 10.4 b
E	32.1 ± 3.3 b	NI	NI	3.7 ± 3.1 b
F	**77.4 ± 18.4** a	NI	NI	4.7 ± 2.7 b
G	NA	12.1 ± 3.1 c	49.8 ± 20.6 a	NI
H	NA	**97.5 ± 1.0** a	NI	**77.7 ± 4.3** a
I	NA	78.9 ± 4.4 b	**87.2 ± 2.9** a	NA

[a]The data represent the mean ± SEM from at least three independent studies done in triplicate. Values within a column followed by different letters are significant at $p < 0.05$. GAE = gallic acid equivalents, and IC_{50} = concentration required to inhibit enzyme activity by 50%. NI = no inhibition at 500 μM. NA = not applicable. Bold numbers indicate the most potent fractions.

DPP-IV for the fractions of each herb extract. From Mexican oregano, fractions LF, LG, LH, and LI were the most potent inhibitors of DPP-IV (IC_{50} range 0.8−19.0 μM), from rosemary, fraction RG was the most potent inhibitor of DPP-IV (IC_{50} = 0.4 ± 0.1 μM), from marjoram, fraction MH was the most potent inhibitor of DPP-IV (IC_{50} = 1.9 ± 0.4 μM), and from Greek oregano, fractions OE and OF were the most potent inhibitors of DPP-IV (IC_{50} range 20.3−23.3 μM). Fractions from these herbs also inhibited PTP1B. At 500 μM, the most potent inhibitors of PTP1B were fractions LH (97.5% ± 1.0%), RI (87.2% ± 2.9%), MH (77.7% ± 4.3%), and OE (77.4% ± 18.4%).

LC−EIS-MS Composition Analysis. To identify specific compounds from these herbs that inhibit DPP-IV, the most potent fractions were analyzed by LC−ESI-MS. Figure 4 shows representative chromatograms and a mass spectrum for rosemary fraction RG. Table 2 indicates which compounds were identified in the most potent fractions for Mexican oregano and rosemary. Eriodictyol, naringenin, hispidulin, and cirsimaritin have been previously identified in Mexican oregano.[35] Other compounds previously found in Mexican oregano that were tentatively identified but not confirmed due to lack of an analytical standard were sakuranetin or scutellarein[36,37] and desmethoxycentaureidin.[38] Rosmarinic acid, hispidulin, cirsimaritin, carnosol, and 7-methylrosmanol have been previously reported in rosemary.[39−43] Rosmarinic acid glucoside[44] and rosmanol isomers[39−42] were tentatively identified in rosemary fractions on the basis of comparison to the literature.

Concentrations of Purified Compounds. The concentrations of compounds identified through bioassay-guided fractionation were quantified using HPLC. Table 3 indicates the concentrations of the compounds in each herb.

Naringenin was quantified in all four species of culinary herbs, ranging from 0.15 mg/g of DW in Greek oregano and marjoram to 4.49 mg/g of DW in Mexican oregano. On the basis of the literature, Mexican oregano (3.72 mg/g of DW)[35] and Greek oregano (2.20 mg/g of DW)[45] concentrations are comparable to these results. There have yet to be reports on the concentration of naringenin aglycon in rosemary or marjoram; however, the concentration of naringenin glycoside has been reported to be 7.16 mg/g of DW[46] in rosemary. In other species of the same family, thyme (*Thymus vulgaris*) contains 0.64 mg/g of DW[47] naringenin glycoside, while the aglycon has been identified in savory (*Satureja cuneifolia*) and thyme (*Thymbra spicata*) at 0.30 and 0.23 mg/g of DW, respectively.[48] Cirsimaritin was also identified in all four culinary herbs in concentrations ranging from 0.05 mg/g of DW in marjoram to 1.10 mg/g of DW in rosemary. The cirsimaritin concentration has previously been reported in rosemary and Mexican oregano to be 0.08 mg/g of DW[49] and 0.68 mg/g of DW,[35] respectively, agreeing with the results of this study.

Eriodictyol was quantified at concentrations ranging from 0.30 ± 0.02 mg/g in marjoram to 1.38 ± 0.02 mg/g in Mexican oregano. Lin et al.[35] measured the range of concentrations of eriodictyol in three samples of Mexican oregano at 0.72−0.91 mg/g, and eriodictyol has been identified as being present in Greek oregano at a concentration of 0.4 mg/g by Agiomyrgianaki et al.[45] There have been no reports on the concentration of eriodictyol in rosemary and marjoram; however, eriodictyol has been identified in thyme,[47] indicating its presence in other species of the Lamiaceae family.

Rosmarinic acid was present in Greek oregano, rosemary, and marjoram extracts at concentrations that ranged from 16.87 mg/g of DW in rosemary to 28.77 mg/g of DW in Greek oregano. Almela et al.[40] report that methanol extract from rosemary contains 32.6 mg/g of DW rosmarinic acid, while

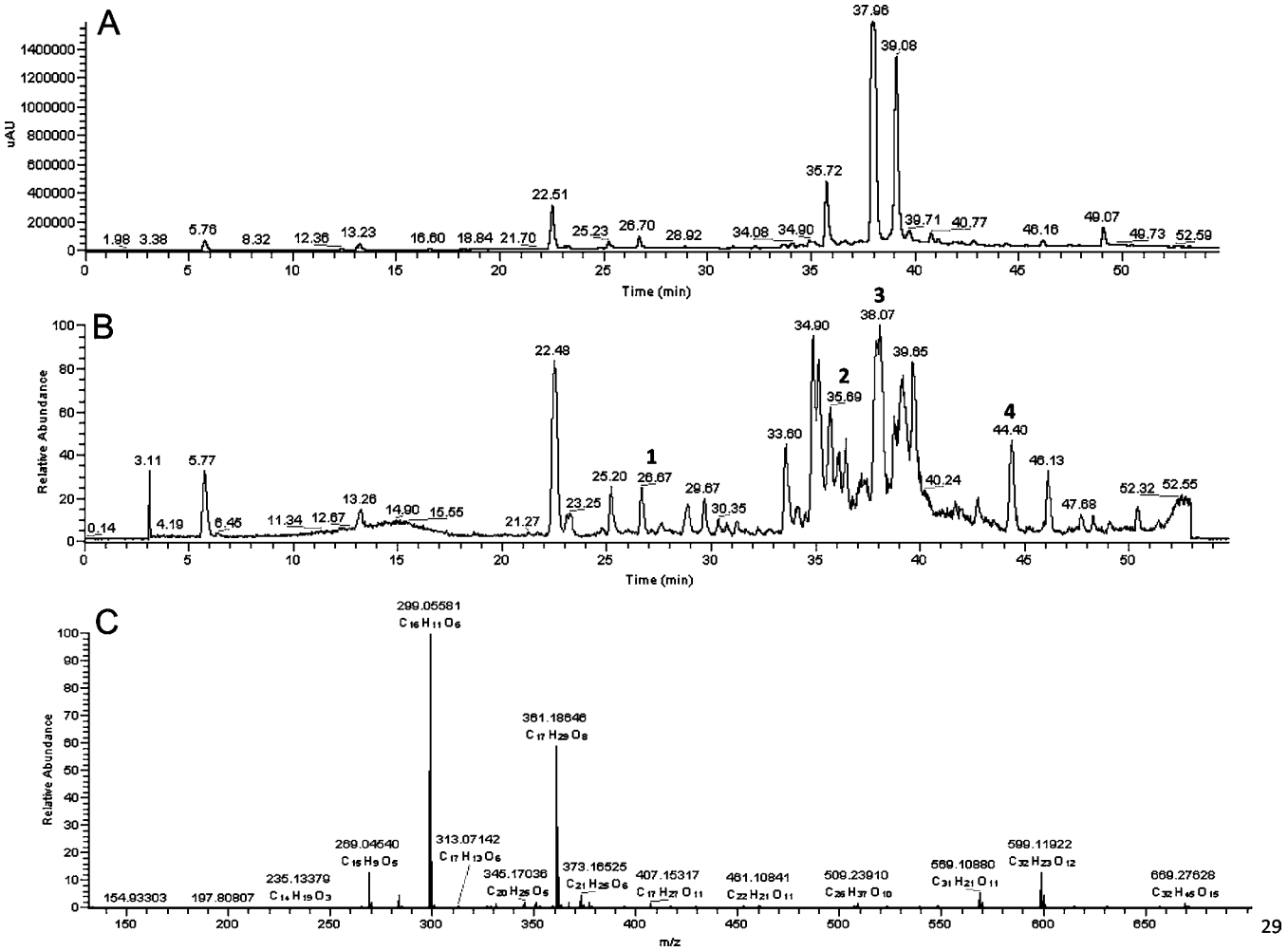

Figure 4. Representative chromatograms [(A) absorbance at 280 nm, (B) total ion current] and mass spectrum (C) from LC−ESI-MS for rosemary fraction RG: rosmarinic acid (**1**), hispidulin (**2**), cirsimaritin (**3**), carnosol (**4**).

Table 2. Composition As Determined by LC−ESI-MS of the Most Potent Fractions, Lowest DPP-IV IC_{50}, from Mexican Oregano and Rosemary

Mexican oregano				rosemary			
fraction	peak (t_R)	m/z	compound	fraction	peak (t_R)	m/z	compound
LF	28.48	287.06	eriodictyol	RF	32.64	345.17	rosmanol isomers[39−42]
	31.76	271.06	naringenin		38.63	520.14	rosmarinic acid 3-*O*-glucoside[44]
	35.72	299.06	hispidulin	RG	26.67	359.08	rosmarinic acid
LG	32.15	271.06	naringenin		33.6	345.17	rosmanol isomers[39−42]
	36.11	299.06	hispidulin		34.9	345.17	rosmanol isomers[39−42]
	38.26	313.07	cirsimaritin		35.69	299.06	hispidulin
	41.26	329.18	carnosol		38.07	313.07	cirsimaritin
LH	36.03	299.06	hispidulin		39.14	520.14	rosmarinic acid 3-*O*-glucoside[44]
	38.24	313.07	cirsimaritin		39.65	345.17	rosmanol isomers[39−42]
	39.28	285.08	sakuranetin,[36] scutellarein[36]		44.40	329.18	carnosol
	41.32	329.18	carnosol	RH	38.01	313.07	cirsimaritin
LI	40.24	329.03	desmethoxycentaureidin[38]		39.79	345.17	rosmanol isomers[39−42]
					44.51	329.18	carnosol
				RI	34.9	345.17	rosmanol isomers[39−42]
					44.40	329.18	carnosol

Shekarchi et al.[50] reported that ethanol extraction of Greek oregano yields a rosmarinic acid concentration of 25.0 mg/g of DW, concentrations which are comparable to those presented in this study.

Hispidulin was identified in Mexican oregano at 0.14 mg/g of DW and rosemary at 0.08 mg/g of DW. Previously, Mexican oregano has been reported to contain 1.00 mg/g of DW,[35] while rosemary has been reported to contain 0.02 mg/g of

dx.doi.org/10.1021/jf500639f | J. Agric. Food Chem. 2014, 62, 6147−6158

Table 3. Concentrations of Compounds (mg/g of DW) in Greek Oregano, Mexican Oregano, Rosemary, and Marjoram[a]

	rosmarinic acid	eriodictyol	naringenin	hispidulin	cirsimaritin	carnosol
Greek oregano	28.77 ± 0.42 a	0.38 ± 0.01 b	0.15 ± 0.03 b	ND	0.09 ± 0.01 c	0.04 ± 0.01 b
Mexican oregano	ND	1.38 ± 0.02 a	4.49 ± 0.29 a	0.14 ± 0.02 a	0.25 ± 0.00 b	0.29 ± 0.01 b
rosemary	16.92 ± 0.47 b	0.43 ± 0.02 b	0.36 ± 0.01 b	0.08 ± 0.00 b	1.10 ± 0.02 a	24.86 ± 1.27 a
marjoram	16.87 ± 0.69 b	0.30 ± 0.02 c	0.15 ± 0.01 b	ND	0.05 ± 0.00 c	0.04 ± 0.00 b

[a]The data represent the mean ± SEM from at least three independent extractions. Values within a column followed by different letters are significant at $p < 0.05$. ND = none detected. DW = dry weight.

Table 4. Binding Affinity and DPP-IV IC_{50} of the Compounds of Interest[a]

flavonoid	binding affinity (kcal/mol)	IC_{50} (μM)	functional group, location	fraction
hispidulin	−9.4	0.49 ± 0.1 b	OH, 4′, 5, 7; OCH_3, 6	LF, LG, LH, RG
eriodictyol	−8.9	10.9 ± 0.4 a	OH, 3′, 4′, 5, 7	LF
naringenin	−8.6	2.5 ± 0.3 b	OH, 4′, 5′, 7	LF, LG
cirsimaritin	−8.4	0.43 ± 0.07 b	OH, 4′, 5; OCH_3, 6, 7	LG, LH, RG, RH
other				
carnosol	−8.8	>100		LG, RG, RH, RI
rosmarinic acid	−7.8	14.1 ± 1.7 a		RG, MH
sitagliptin	−9.6	0.06 ± 0.03 b		control

[a]The data represent the mean ± SEM from at least three independent studies done in triplicate. Values within a column followed by different letters are significant at $p < 0.05$. Binding affinities were obtained through computational modeling. IC_{50} values were determined by biochemical assay.

DW[49] and 1.5 mg/g of DW[39] hispidulin. Carnosol was measured in all herbs; the highest concentration was 24.86 mg/g of DW in rosemary, which is similar to 21.5 mg/g of DW previously reported by Kontagianni et al.[39] While the values obtained in this study deviate some from the reported values, it is important to note that there is variation in the literature regarding the concentrations of secondary plant metabolites due to the differences in growth conditions, processing, and extraction.

DPP-IV Inhibition by Purified Compounds. Table 4 lists the IC_{50} of DPP-IV for the compounds of interest. Of the compounds identified, cirsimaritin (0.43 ± 0.07 μM), hispidulin (0.49 ± 0.1 μM), and naringenin (2.5 ± 0.3 μM) were the most potent inhibitors of DPP-IV. Eriodictyol (10.9 ± 0.4 μM) and rosmarinic acid (14.1 ± 1.7 μM) were also good inhibitors of DPP-IV. Carnosol was the least effective inhibitor, having an IC_{50} over 100 μM. These results are comparable to those published for flavonoids by Fan et al.,[3] where the IC_{50} values for luteolin, apigenin, and naringenin were 0.12, 0.14, and 0.24 μM, respectively.

Computational Modeling. Table 4 lists the calculated binding affinities between the compounds of interest and DPP-IV. Computational modeling indicates that hispidulin (−9.4 kcal/moL), eriodictyol (−8.9 kcal/mol), carnosol (−8.8 kcal/moL), and naringenin (−8.6 kcal/moL) have the most negative binding affinities for the DPP-IV enzyme, suggesting that they could easily bind to DPP-IV.

Figure 5A−E shows the theoretical ligand−amino acid interactions between DPP-IV and hispidulin, eriodictyol, naringenin, carnosol, and the pharmaceutical inhibitor sitagliptin. Hispidulin and eriodictyol interacted with amino acids in the catalytic region of DPP-IV.[51] The experimental conformation of sitagliptin was compared to the conformation of sitagliptin in the crystal structure of PDB file 1X70 through Discovery Studio 3.5 to validate the results of the computational model. Both conformations had 14 identical interactions and interacted with all three pockets of DPP-IV.

These flavonoids formed H-bonds to the amino acids Thr565 and Arg560. Hispidulin and naringenin formed H-bonds with Lys512, while only hispidulin formed an H-bond with Asn562. Figure 5F shows the relative positions of these flavonoids in the catalytic region of DPP-IV. The arrow in Figure 5G shows the location of the catalytic region relative to the whole enzyme.

Carnosol had electrostatic interactions with amino acids in the S1 and S2 pockets of DPP-IV and van der Waals interactions with the S3 pocket. The S1 pocket consists of the key catalytic amino acids Ser630, Asn710, and His740, the S2 pocket consists of Glu205 and Glu206, and the S3 pocket consists of Ser209, Phe357, and Arg358.[52] Sitagliptin interacted with all three pockets of DPP-IV and had the lowest binding affinity of all compounds tested (−9.6 kcal/mol), but does not interact with the catalytic region. Given that the best binding conformations of naringenin, hispidulin, and eriodictyol did not show interactions with the pockets of DPP-IV, these compounds may have synergistic effects with sitagliptin in the inhibition of DPP-IV.

Computational modeling of cirsimaritin (diagram not shown) revealed that this flavonoid also binds within the catalytic region and has several amino acid interactions in common with hispidulin, naringenin, and eriodictyol. In contrast to the computational modeling, carnosol was not a good inhibitor of DPP-IV. This could be due to the relatively weak electrostatic interactions predicted between carnosol and DPP-IV compared to the several hydrogen bonds predicted for the flavonoids. This may also be the result of competition between the substrate and carnosol for the binding pockets and access to the catalytic amino acids.

Our model was validated on the basis of the comparison of sitagliptin interactions between the crystal structure and experimental conformation. The two arrangements had most interactions in common and bonded to the active site in a similar manner. The experimental conformation and the crystal structure both have sitagliptin having electrostatic interactions with all the residues of the S1 and S2 pockets of DPP-IV, and both have interactions with the S3 pocket. The two arrangements deviated where the crystal structure has sitagliptin interacting electrostatically with Arg358 of DPP-IV while the

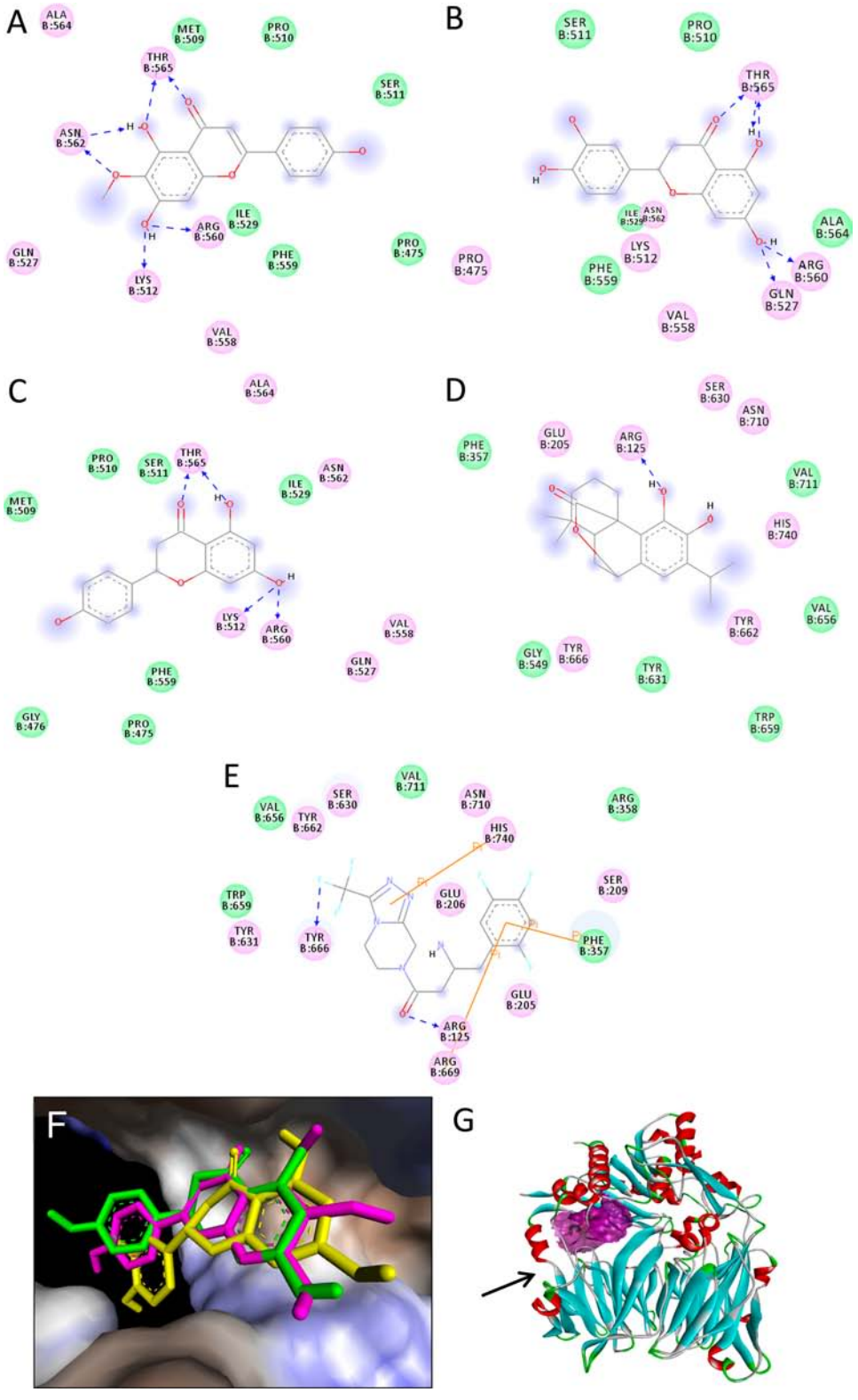

Figure 5. Computational amino acid–ligand interactions for (A) hispidulin, (B) eriodictyol, (C) naringenin, (D) carnosol, and (E) sitagliptin: electrostatic interactions (pink), van der Waals interactions (green), H-bonds (blue arrows), π-interactions (orange lines). (F) 3-D molecular docking of hispidulin (purple), eriodictyol (yellow), and naringenin (green) in DPP-IV. (G) Location of the catalytic pockets (arrow) relative to the region in which the flavonoids bind (purple).

experimental results have sitagliptin having only a van der Waals interaction with the same residue and the crystal structure has sitagliptin interacting with Val207 and Tyr547 while the experimental conformation does not. These deviations may be a result of the structure of sitagliptin being rotated in the final experimental conformation, rather than being planar as in the crystal structure. Furthermore, the experimental conformation for sitagliptin interactions with the

dx.doi.org/10.1021/jf500639f | J. Agric. Food Chem. 2014, 62, 6147–6158

S1, S2, and S3 subsites has been published by Nabeno et al.,[53] further validating this model.

Conclusion. In summary, extracts of greenhouse-grown herbs were a better source of flavonoids and polyphenols compared to commercially produced herbs; however, this did not impact the concentration required to inhibit DPP-IV. Commercially produced herbs inhibited PTP1B; however, this effect remained only in fractions of greenhouse-grown herbs. Extracts from rosemary and Mexican oregano were the most potent inhibitors of DPP-IV and contained the flavonoids cirsimaritin, hispidulin, and naringenin, which are potent inhibitors of DPP-IV independently. Future work in this area should focus on optimization of the growth and processing conditions for Mexican oregano and rosemary to increase their concentrations of these flavonoids. Overall, this research supports further investigation into the potential for rosemary and Mexican oregano and their flavonoids to be used in the management of T2DM.

AUTHOR INFORMATION

Corresponding Author

*E-mail: edemejia@illinois.edu. Fax: 217-265-0925.

Funding

We thank the Division of Nutritional Sciences at the University of Illinois at Urbana-Champaign for a Jonathan Baldwin Turner Fellowship, the National Science Foundation for a Mentoring in New Biology Fellowship, and the USDA for a Multicultural Advocates in Nutrition Needs and Agriculture Scholarship.

Notes

Mention of trade names or commercial products in this paper is solely for the purpose of providing specific information and does not imply recommendation or endorsement by the U.S. Department of Agriculture (USDA). The USDA is an equal opportunity provider and employer.

The authors declare no competing financial interest.

ABBREVIATIONS USED

DPP-IV, dipeptidyl peptidase IV; DW, dry weight; DWE, dry weight of extract; GAE, gallic acid equivalents; GLP-1, glucagon-like peptide 1; ORAC, oxygen radical absorbance capacity; PTP1B, protein tyrosine phosphatase 1B; RE, rutin equivalents; TE, Trolox equivalents; T2DM, type 2 diabetes mellitus

REFERENCES

(1) American Diabetes Association.. Economic costs of diabetes in the U.S. in 2012. *Diabetes Care* **2013**, *36*, 1033−1046.

(2) Magkos, F.; Yannakoulia, M.; Chan, J. L.; Mantzoros, C. S. Management of the metabolic syndrome and type 2 diabetes through lifestyle modification. *Annu. Rev. Nutr* **2009**, *29*, 223−256.

(3) Fan, J.; Johnson, M. H.; Lila, M. A.; Yousef, G.; de Mejia, E. G. Berry and citrus phenolic compounds inhibit dipeptidyl peptidase IV: implications in diabetes management. *Evidence-Based Complementary Altern. Med.* **2013**, *2013*, 479505.

(4) Jiang, C. S.; Liang, L. F.; Guo, Y. W. Natural products possessing protein tyrosine phosphatase 1B (PTP1B) inhibitory activity found in the last decades. *Acta Pharmacol. Sin.* **2012**, *33*, 1217−1245.

(5) Wu, D.; Li, L.; Liu, C. Efficacy and safety of dipeptidyl peptidase-4 inhibitors and metformin as initial combination therapy and as monotherapy in patients with type 2 diabetes mellitus: a meta-analysis. *Diabetes, Obes. Metab.* **2014**, *16*, 30−37.

(6) Carpino, P. A.; Hepworth, D. Beyond PPARs and metformin: new insulin sensitizers for the treatment of type 2 diabetes. *Annu. Rep. Med. Chem.* **2012**, *47*, 177−192.

(7) Lantz, K. A.; Hart, S. G.; Planey, S. L.; Roitman, M. F.; Ruiz-White, I. A.; Wolfe, H. R.; McLane, M. P. Inhibition of PTP1B by trodusquemine (MSI-1436) causes fat-specific weight loss in diet-induced obese mice. *Obesity* **2010**, *18*, 1516−1523.

(8) Bower, A. M.; Marquez, S.; De Mejia, E. G. The health benefits of selected culinary herbs and spices found in the traditional Mediterranean diet. *Crit. Rev. Food Sci. Nutr.* **2014**, BFSN-2013-1009.R1.

(9) Cazzola, R.; Camerotto, C.; Cestaro, B. Anti-oxidant, anti-glycant, and inhibitory activity against α-amylase and α-glucosidase of selected spices and culinary herbs. *Int. J. Food Sci. Nutr.* **2011**, *62*, 175−184.

(10) Koga, K.; Shibata, H.; Yoshino, K.; Nomoto, K. Effects of 50% ethanol extract from rosemary (*Rosmarinus officinalis*) on α-glucosidase inhibitory activity and the elevation of plasma glucose level in rats, and its active compound. *J. Food Sci.* **2006**, *71*, S507−S512.

(11) Kwon, Y. I.; Vattem, D. A.; Shetty, K. Evaluation of clonal herbs of Lamiaceae species for management of diabetes and hypertension. *Asia Pac. J. Clin. Nutr.* **2006**, *15*, 107−118.

(12) Ibarra, A.; Cases, J.; Roller, M.; Chiralt-Boix, A.; Coussaert, A.; Ripoll, C. Carnosic acid-rich rosemary (*Rosmarinus officinalis* L.) leaf extract limits weight gain and improves cholesterol levels and glycaemia in mice on a high-fat diet. *Br. J. Nutr.* **2011**, *106*, 1182−1189.

(13) Mueller, M.; Lukas, B.; Novak, J.; Simoncini, T.; Genazzani, A. R.; Jungbauer, A. Oregano: a source for peroxisome proliferator-activated receptor gamma antagonists. *J. Agric. Food Chem.* **2008**, *56*, 11621−11630.

(14) Pascual, M. E.; Slowing, K.; Carretero, E.; Sanchez Mata, D.; Villar, A. Lippia: traditional uses, chemistry and pharmacology: a review. *J. Ethnopharmacol.* **2001**, 201−214.

(15) Dixon, R. A.; Paiva, N. L. Stress-induced phenylpropanoid metabolism. *Plant Cell* **1995**, *7*, 1085−1097.

(16) Yi, W.; Wetzstein, H. Y. Biochemical, biological and histological evaluation of some culinary and medicinal herbs grown under greenhouse and field conditions. *J. Sci. Food Agric.* **2010**, *90*, 1063−1070.

(17) Yi, W.; Wetzstein, H. Y. Effects of drying and extraction conditions on the biochemical activity of selected herbs. *HortScience* **2011**, *46*, 70−73.

(18) Singleton, V. L.; Rossi, J. A. Colorimetry of total phenolics with phosphomolybdic- phosphotungstic acid reagents. *Am. J. Enol. Vitic.* **1965**, *16*, 144−158.

(19) Oomah, B. D.; Cardador-Martinez, A.; Loarca-Pina, G. Phenolics and antioxidative activities in common beans (*Phaseolus vulgaris* L). *J. Sci. Food Agric.* **2005**, *85*, 935−942.

(20) Prior, R. L.; Wu, X.; Schaich, K. Standardized methods for the determination of antioxidant capacity and phenolics in foods and dietary supplements. *J. Agric. Food Chem.* **2005**, *53*, 4290−4302.

(21) Bar, J.; Weber, A.; Hoffmann, T.; Stork, J.; Wermann, M.; Wagner, L.; Aust, S.; Gerhartz, B.; Demuth, H. U. Characterisation of human dipeptidyl peptidase IV expressed in *Pichia pastoris*. A structural and mechanistic comparison between the recombinant human and the purified porcine enzyme. *Biol. Chem.* **2003**, *384*, 1553−1563.

(22) Sun, T.; Wang, Q.; Yu, Z.; Zhang, Y.; Guo, Y.; Chen, K.; Shen, X.; Jiang, H. Hyrtiosal, a PTP1B inhibitor from the marine sponge *Hyrtios erectus*, shows extensive cellular effects on PI3K/AKT activation, glucose transport, and TGFβ/Smad2 signaling. *ChemBioChem* **2007**, *8*, 187−193.

(23) Lubben, T.; Clampit, J.; Stashko, M.; Trevillyan, J.; Jirousek, M. R. In vitro enzymatic assays of protein tyrosine phosphatase 1B. *Curr. Protoc. Pharmacol.* **2001**, Chapter 3, Unit 3.8.

(24) Yang, S.; Na, M. K.; Jang, J. P.; Kim, K. A.; Kim, B. Y.; Sung, N. J.; Oh, W. K.; Ahn, J. S. Inhibition of protein tyrosine phosphatase 1B by lignans from *Myristica fragrans*. *Phytother. Res.* **2006**, *20*, 680−682.

(25) Trott, O.; Olson, A. J. AutoDock Vina: improving the speed and accuracy of docking with a new scoring function, efficient optimization, and multithreading. *J. Comput. Chem.* **2010**, *31*, 455−461.

(26) Morris, G. M.; Huey, R.; Lindstrom, W.; Sanner, M. F.; Belew, R. K.; Goodsell, D. S.; Olson, A. J. AutoDock4 and AutoDockTools4: automated docking with selective receptor flexibility. *J. Comput. Chem.* **2009**, *30*, 2785−2791.
(27) Ozkan, G.; Baydar, H.; Erbas, S. The influence of harvest time on essential oil composition, phenolic constituents and antioxidant properties of Turkish oregano (*Origanum onites* L.). *J. Sci. Food Agric.* **2010**, *90*, 205−209.
(28) Bimakr, M.; Rahman, R. A.; Taip, F. S.; Ganjloo, A.; Salleh, L. M.; Selamat, J.; Hamid, A.; Zaidul, I. S. M. Comparison of different extraction methods for the extraction of major bioactive flavonoid compounds from spearmint (*Mentha spicata* L.) leaves. *Food Bioprod. Process.* **2011**, *89*, 67−72.
(29) Šliumpaitė, I.; Venskutonis, P. R.; Murkovic, M.; Pukalskas, A. Antioxidant properties and polyphenolics composition of common hedge hyssop (*Gratiola officinalis* L.). *J. Funct. Foods* **2013**, *5*, 1927−1937.
(30) Kadum Yakob, H.; Manaf Uyub, A.; Fariza Sulaiman, S. Toxicological evaluation of 80% methanol extract of *Ludwigia octovalvis* (Jacq.) P.H. Raven leaves (Onagraceae) in BALB/c mice. *J. Ethnopharmacol.* **2012**, *142*, 663−668.
(31) Neveu, V.; Perez-Jiménez, J.; Vos, F.; Crespy, V.; du Chaffaut, L.; Mennen, L.; Knox, C.; Eisner, R.; Cruz, J.; Wishart, D.; Scalbert, A. Phenol-Explorer: an online comprehensive database on polyphenol contents in foods. *Database* **2010**, DOI: 10.1093/database/bap024.
(32) Dragland, S.; Senoo, H.; Wake, K.; Holte, K.; Blomhoff, R. Several culinary and medicinal herbs are important sources of dietary antioxidants. *J. Nutr.* **2003**, *133*, 1286−1290.
(33) Kwak, J. H.; Kim, H. J.; Lee, K. H.; Kang, S. C.; Zee, O. P. Antioxidative iridoid glycosides and phenolic compounds from *Veronica peregrina*. *Arch. Pharmacal Res.* **2009**, *32*, 207−213.
(34) Craig, W. J. Health-promoting properties of common herbs. *Am. J. Clin. Nutr.* **1999**, *70*, 491S−499S.
(35) Lin, L.-Z.; Mukhopadhyay, S.; Robbins, R. J.; Harnly, J. M. Identification and quantification of flavonoids of Mexican oregano (*Lippia graveolens*) by LC-DAD-ESI/MS analysis. *J. Food Compost. Anal.* **2007**, *20*, 361−369.
(36) Funari, C. S.; Passalacqua, T. G.; Rinaldo, D.; Napolitano, A.; Festa, M.; Capasso, A.; Piacente, S.; Pizza, C.; Young, M. C.; Durigan, G.; Silva, D. H. Interconverting flavanone glucosides and other phenolic compounds in *Lippia salviaefolia* Cham. ethanol extracts. *Phytochemistry* **2011**, *72*, 2052−2061.
(37) Funari, C. S.; Eugster, P. J.; Martel, S.; Carrupt, P. A.; Wolfender, J. L.; Silva, D. H. High resolution ultra high pressure liquid chromatography-time-of-flight mass spectrometry dereplication strategy for the metabolite profiling of Brazilian Lippia species. *J. Chromatogr., A* **2012**, *1259*, 167−178.
(38) Abe, F.; Nagao, T.; Okabe, H. Antiproliferative constituents in plants 9. Aerial parts of *Lippia dulcis* and *Lippia canescens*. *Biol. Pharm. Bull.* **2002**, *25*, 920−922.
(39) Kontogianni, V. G.; Tomic, G.; Nikolic, I.; Nerantzaki, A. A.; Sayyad, N.; Stosic-Grujicic, S.; Stojanovic, I.; Gerothanassis, I. P.; Tzakos, A. G. Phytochemical profile of *Rosmarinus officinalis* and *Salvia officinalis* extracts and correlation to their antioxidant and anti-proliferative activity. *Food Chem.* **2013**, *136*, 120−129.
(40) Almela, L.; Sanchez-Munoz, B.; Fernandez-Lopez, J. A.; Roca, M. J.; Rabe, V. Liquid chromatograpic-mass spectrometric analysis of phenolics and free radical scavenging activity of rosemary extract from different raw material. *J. Chromatogr., A* **2006**, *1120*, 221−229.
(41) Hossain, M. B.; Rai, D. K.; Brunton, N. P.; Martin-Diana, A. B.; Barry-Ryan, C. Characterization of phenolic composition in Lamiaceae spices by LC-ESI-MS/MS. *J. Agric. Food Chem.* **2010**, *58*, 10576−81.
(42) Senorans, F. J.; Ibanez, E.; Cavero, S.; Tabera, J.; Reglero, G. Liquid chromatographic-mass spectrometric analysis of supercritical-fluid extracts of rosemary plants. *J. Chromatogr., A* **2000**, *870*, 491−499.
(43) Pukalskas, A.; van Beek, T. A.; de Waard, P. Development of a triple hyphenated HPLC−radical scavenging detection−DAD−SPE−NMR system for the rapid identification of antioxidants in complex plant extracts. *J. Chromatogr., A* **2005**, *1074*, 81−88.
(44) Lee, J. H.; Park, K. H.; Lee, M. H.; Kim, H. T.; Seo, W. D.; Kim, J. Y.; Baek, I. Y.; Jang, D. S.; Ha, T. J. Identification, characterisation, and quantification of phenolic compounds in the antioxidant activity-containing fraction from the seeds of Korean perilla (*Perilla frutescens*) cultivars. *Food Chem.* **2013**, *136*, 843−852.
(45) Agiomyrgianaki, A.; Dais, P. Simultaneous determination of phenolic compounds and triterpenic acids in oregano while in Greece by ^{31}P NMR spectroscopy. *Magn. Reson. Chem.* **2012**, 739−748.
(46) Koşar, M.; Dorman, H. J. D.; Hiltunen, R. Effect of an acid treatment on the phytochemical and antioxidant characteristics of extracts from selected Lamiaceae species. *Food Chem.* **2005**, *91*, 525−533.
(47) Fecka, I.; Turek, S. Determination of polyphenolic compounds in commercial herbal drugs and spices from Lamiaceae: thyme, wild thyme and sweet marjoram by chromatographic techniques. *Food Chem.* **2008**, *108*, 1039−1053.
(48) Dorman, H. J.; Bachmayer, O.; Kosar, M.; Hiltunen, R. Antioxidant properties of aqueous extracts from selected Lamiaceae species grown in Turkey. *J. Agric. Food Chem.* **2004**, *52*, 762−70.
(49) Luis, J. C.; Pérez, R. M.; González, F. V. UV-B radiation effects on foliar concentrations of rosmarinic and carnosic acids in rosemary plants. *Food Chem.* **2007**, *101*, 1211−1215.
(50) Shekarchi, M.; Hajimehdipoor, H.; Saeidnia, S.; Gohari, A.; Hamedani, M. Comparative study of rosmarinic acid content in some plants of Labiatae family. *Pharmacogn. Mag.* **2012**, *8*, 37−41.
(51) Engel, M.; Hoffmann, T.; Wagner, L.; Wermann, M.; Heiser, U.; Kiefersauer, R.; Huber, R.; Bode, W.; Demuth, H. U.; Brandstetter, H. The crystal structure of dipeptidyl peptidase IV (CD26) reveals its functional regulation and enzymatic mechanism. *Proc. Natl. Acad. Sci. U.S.A.* **2003**, *100*, 5063−5068.
(52) Jadav, P.; Bahekar, R.; Shah, S. R.; Patel, D.; Joharapurkar, A.; Kshirsagar, S.; Jain, M.; Shaikh, M.; Sairam, K. V. Long-acting peptidomimetics based DPP-IV inhibitors. *Bioorg. Med. Chem. Lett.* **2012**, *22*, 3516−21.
(53) Nabeno, M.; Akahoshi, F.; Kishida, H.; Miyaguchi, I.; Tanaka, Y.; Ishii, S.; Kadowaki, T. A comparative study of the binding modes of recently launched dipeptidyl peptidase IV inhibitors in the active site. *Biochem. Biophys. Res. Commun.* **2013**, 191−196.

JOURNAL OF AGRICULTURAL AND FOOD CHEMISTRY

Article

pubs.acs.org/JAFC

Essential Oil Alloaromadendrene from Mixed-Type *Cinnamomum osmophloeum* Leaves Prolongs the Lifespan in *Caenorhabditis elegans*

Chan-Wei Yu,[†] Wen-Hsuan Li,[†] Fu-Lan Hsu,[‡] Pei-Ling Yen,[§] Shang-Tzen Chang,*[,§] and Vivian Hsiu-Chuan Liao*[,†]

[†]Department of Bioenvironmental Systems Engineering, and [§]Department of Forestry and Resource Conservation, National Taiwan University, Number 1 Roosevelt Road, Section 4, Taipei 106, Taiwan

[‡]Forest Chemistry Division, Taiwan Forestry Research Institute, 53 Nanhai Road, Taipei 100, Taiwan

ABSTRACT: *Cinnamomum osmophloeum* Kaneh. is an indigenous tree species in Taiwan. The present study investigates phytochemical characteristics, antioxidant activities, and longevity of the essential oils from the leaves of the mixed-type *C. osmophloeum* tree. We demonstrate that the essential oils from leaves of mixed-type *C. osmophloeum* exerted *in vivo* antioxidant activities on *Caenorhabditis elegans*. In addition, minor (alloaromadendrene, 5.0%) but not major chemical components from the leaves of mixed-type *C. osmophloeum* have a key role against juglone-induced oxidative stress in *C. elegans*. Additionally, alloaromadendrene not only acts protective against oxidative stress but also prolongs the lifespan of *C. elegans*. Moreover, mechanistic studies show that DAF-16 is required for alloaromadendrene-mediated oxidative stress resistance and longevity in *C. elegans*. The results in the present study indicate that the leaves of mixed-type *C. osmophloeum* and essential oil alloaromadendrene have the potential for use as a source for antioxidants or treatments to delay aging.

KEYWORDS: *Cinnamomum osmophloeum, alloaromadendrene, antioxidant, lifespan, Caenorhabditis elegans, FOXO transcription factor DAF-16*

INTRODUCTION

Essential oils are considered to be secondary metabolites and important for plant defense because they often possess antimicrobial properties.[1] Today, many essential oils of plants have gained attention for various types of bioactivity, such as antibacterial,[2] antiviral,[3] antifungal,[4] and antioxidant[5] actions. For these reasons, essential oils from natural plants are considered to be important alternative source of drugs and natural food preservatives.[6]

Cinnamomum osmophloeum Kaneh. is an indigenous tree species in Taiwan.[7] *C. osmophloeum* contains essential oils showing multiple biological activities, including antibacterial,[8] antifungal,[9] anti-inflammatory,[10] and *in vivo* antioxidant[11] activities. Other beneficial properties of the essential oils of *C. osmophloeum*, however, remain further explored. Among essential oils, aromadendrene is one of a group of naturally occurring sesquiterpenes structurally characterized by the fusion of a cyclopropane ring to a hydroazulene skeleton. Several studies have reported that aromadendrene has biological properties, including antifungal,[12] antiviral,[13] antibacterial,[14] antifeedant and repellent,[15] and cytotoxic[16] properties. However, most of the potential beneficial effects, including the antioxidant and anti-aging properties of aromadendrene have not yet been evaluated.

Aging research has rapidly gained increased scientific interest. The causes of aging remain largely unknown, although they are probably related to radical and mitochondrial activities.[17] An increase in stress resistance has been linked with an increase in longevity in a variety of organisms, including the nematode *Caenorhabditis elegans*.[18,19] *C. elegans* has become an informative and popular model for stress and aging studies because of its small size, relatively short life cycle, and well-defined genetic and environmental factors that influence lifespan.[20] The Forkhead box O (FOXO) transcription factors are evolutionarily conserved and have important roles in diverse cellular functions, including metabolism, cellular proliferation, defense against oxidative stress, and probably lifespan.[21] Therefore, the association between oxidative stress and FOXO is of particular interest as a result of the possible role of FOXO in controlling lifespan, because aging has been suggested to result from cumulative free-radical-induced cellular and organismal damage.[17,22]

Herein, we use *C. elegans* as an *in vivo* model to determine whether extracts and bioactive compounds from *C. osmophloeum* leaves could (1) enhance oxidative stress resistance and also trigger mechanisms that lead to a longer lifespan in a whole organism and, if so, (2) what potential mechanism is involved.

MATERIALS AND METHODS

Plant Material and Essential Oil Preparation. Leaves of *C. osmophloeum* were collected, and the species was identified as previously described.[23] Fresh leaves from a single plant were divided into three batches (200 g/batch) and then hydrodistilled in a Clevenger-type apparatus for 6 h, followed by determination of the

Received: February 8, 2014
Revised: June 8, 2014
Accepted: June 11, 2014
Published: June 11, 2014

ACS Publications © 2014 American Chemical Society

dx.doi.org/10.1021/jf500417y | J. Agric. Food Chem. 2014, 62, 6159−6165

essential oil contents. The essential oils were stored in airtight containers prior to further analysis.

Gas Chromatography–Mass Spectrometry (GC–MS) and Gas Chromatography–Flame Ionization Detection (GC–FID) Analyses of Essential Oils. Essential oils were analyzed by a Trace GC Ultra (Thermo, Austin, TX) gas chromatograph coupled with a Polaris Q (Thermo) ion-trap mass spectrometer, equipped with a 30 m × 0.25 mm × 0.25 μm DB-5ms column (Agilent J&W Scientific, Santa Clara, CA). The mass spectrometer was operated in the electron-impact mode, with ionization energy of 70 eV. The oven temperature started at 60 °C for 1 min and then was programmed as follows: from 60 to 220 °C at 4 °C/min, held for 2 min, then increased to 250 °C at 20 °C/min, and held for 3 min. The injector temperature was 250 °C, and the flow rate of helium (the carrier gas) was 1.0 mL/min in a 1:10 split ratio. Samples were diluted (1.0 μL, 1:10^4, v/v, in ethyl acetate) and then manually injected in the split mode. Kovats indices were determined for all volatile constituents using a homologous series of C_9–C_{19} *n*-alkanes on the DB-5ms column. Quantification was determined by percentage peak area calculations using GC–FID, and the major constituents were identified by co-injection with standards (wherever possible) and confirmed by using the Wiley (version 7.0) and National Institute of Standards and Technology (NIST) version 2.0 GC–MS libraries and the Kovats indices provided in the literature.[24] The relative concentration of each compound was quantified by integrating the peak area of the chromatograms.

***C. elegans* Strains and Handling.** The nematodes used in this study were Bristol wild-type N2 and GR1307 *daf-16* (*mgDf50*). *C. elegans* strains and *Escherichia coli* OP50 were obtained from the *Caenorhabditis* Genetics Center (CGC), University of Minnesota, Minneapolis, MN. *C. elegans* were maintained and assayed (unless otherwise stated) at 20 °C on nematode growth medium (NGM) agar plates carrying a lawn of *E. coli* OP50. Phytochemicals were dissolved in dimethyl sulfoxide (DMSO). All chemicals in NGM plates and liquid are presented as the final concentrations.

***C. elegans* Oxidative Stress Assays.** Oxidative stress assays were performed essentially as previously described.[25] Briefly, synchronized L1 larvae were treated with chemical or 0.1% DMSO (Wako, Saitama, Japan) as the solvent control for 72 h, followed by 250 μM juglone (5-hydroxy-1,4-naphthoquinone) (Sigma, St. Louis, MO) exposure for 3 h,[11] and then scored for viability. The survival of nematodes was determined by touch-provoked movement as previously described.[19] At least three independent biological replicates were performed.

***C. elegans* Lifespan Assays.** *C. elegans* lifespan analyses were performed in the same manner for all treatments at 20 °C. Synchronized L1 larvae (wild-type N2 and *daf-16* mutant) were transferred to NGM plates in the absence or presence of 100 μM alloaromadendrene, and nematodes were allowed to develop to adulthood. Surviving and dead animals were counted daily (starting on the first day of adulthood) until all nematodes had died. Animals that did not move when gently prodded (with a platinum wire) were scored as dead. During the reproductive period, adult *C. elegans* was transferred to fresh NGM plates (in the absence or presence of 100 μM alloaromadendrene) every day during the progeny production period and then every other day thereafter. To examine antibacterial effects of alloaromadendrene, lifespan assays were performed with live and ultraviolet (UV)-killed *E. coli* OP50 according to Kaeberlein et al.[26] At least three independent biological replicates were performed.

Data Analysis. For the lifespan assay, animal survival was plotted using Kaplan–Meier survival curves and analyzed by log-rank test using GraphPad Prism (GraphPad Software, Inc., La Jolla, CA). Survival curves resulting in p values of < 0.05 relative to the untreated control were considered significantly different.

Statistical analysis was performed using SPSS Statistics 17.0 Software (SPSS, Inc., Chicago, IL). The results are presented as the mean ± standard error of the mean (SEM). The statistical significance of differences between the *C. elegans* populations was determined using one-way analysis of variation (ANOVA) and the least significant difference (LSD) post-hoc test. A two-factor analysis of variation (two-way ANOVA) was performed to determine significance and interactions between factors in the wild-type N2 lifespan assays. Differences were considered significant at $p < 0.05$ (see the figures).

RESULTS AND DISCUSSION

Chemical Constituents of the Essential Oils. Table 1 shows the main components and their relative contents of essential oils distilled from leaves of *C. osmophloeum*. The relative amounts of each component were determined by GC–FID analysis. At least 27 chemicals were identified, comprising about 78% of the total amount. The remaining was either unidentified or of very low amount. The major compounds were L-bornyl acetate (16.6%) with 95% purity, T-cadinol (14.2%) with > 95% purity, α-cadinol (8.8%) with > 95% purity, caryophyllene oxide (5.5%) with 95% purity, and alloaromadendrene (5.0%) with 97% purity (Table 1).

Table 1. Major Components from Mixed-Type *C. osmophloeum* Leaves

compound[a]	content (%)[a]	Kovats index[b]
L-bornyl acetate	16.6	1285
T-cadinol	14.2	1641
α-cadinol	8.8	1654
caryophyllene oxide	5.5	1581
alloaromadendrene	5.0	1461
coumarin	4.3	1433
cadalene	4.1	1671
(−)-α-copaene	2.8	1377
γ-muurolene	2.7	1475
4-allylanisole	1.9	1198
trans-calamenene	1.9	1520
γ-cadinene	1.9	1512
1,10-di-*epi*-cubenol	1.2	1613
α-muurolene	1.1	1497
spathulenol	1.0	1576
α-terpineol	0.7	1195
β-selinene	0.6	1488
α-calacorene	0.6	1541
(+)-cyclosativene	0.5	1370
L-borneol	0.4	1175
β-bourbonene	0.4	1385
(−)-nerolidol	0.4	1561
trans-cinnamyl acetate	0.3	1444
(+)-aromadendrene	0.3	1439
cis-verbenol	0.2	1144
D-(+)-camphor	0.2	1151
benzyl benzoate	0.2	1765

[a]Compounds presented here are the main components (%) in the mixed-type essential oils from *C. osmophloeum* leaves according to a GC–MS analysis. [b]Kovats index relative to *n*-alkanes (C_9–C_{19}) on a DB-5ms column.

It has been suggested that the constituents and their relative contents of essential oils from the same plant species may vary because of ecological and plant growth factors.[27] On the basis of the differences in the chemical constituents of leaf essential oils, *C. osmophloeum* was classified into nine types: cassia, cinnamaldehyde, coumarin, linalool, eugenol, camphor, terpineol-4-ol, linalool-terpineol, and mixed-type.[28] On the basis of this classification, the indigenous *C. osmophloeum* tree, which was analyzed in this study, belongs to the mixed-type *C. osmophloeum* because of the lack of a dominant compound.

In light of the existence of chemical polymorphisms of leaf essential oils from various geographical indigenous cinnamon (*C. osmophloeum*),[29] chemical compositions in mixed-type *C. osmophloeum* were varied. However, it is difficult to predict or conclude the chemical compositions in mixed-type *C. osmophloeum* simply based on geographical or environmental factors. Therefore, it is of great concern to use the plant extract instead of pure compounds because of the possible variability of the components in the same plant group.

Extracts from the Leaves of Mixed-Type *C. osmophloeum* Enhance the Oxidative Stress Resistance in Wild-Type *C. elegans*. Our previous study showed that essential oils from leaves of cinnamaldehyde- and camphor-type *C. osmophloeum* trees exhibited antioxidant activities in *C. elegans*.[11] To investigate whether essential oils from the leaves of the mixed-type *C. osmophloeum* tree have protective effects against oxidative stress in *C. elegans*, wild-type N2 nematodes were pretreated with extracts immediately followed by exposure to juglone-induced oxidative stresses. Wild-type N2 synchronized L1 larvae were pretreated with 0, 1, 5, 10, and 20 μg/mL extracts and 0.1% DMSO as the solvent control for 72 h before being exposed to juglone (250 μM) and then were incubated for 3 h. Juglone was used as the oxidative stress generator because it is a redox-active quinone capable of intracellular redox cycling with superoxide radical $O_2^{\bullet -}$ production in *C. elegans*[30] and is commonly used to generate the intracellular oxidative stress in *C. elegans*.[25,31]

The results show that pretreatment with 5, 10, and 20 μg/mL extracts from the leaves of the mixed-type *C. osmophloeum* tree significantly increased the survival of *C. elegans* exposed to juglone-induced oxidative stress (Figure 1). It was observed that 5 μg/mL extract exerted the maximal effect, whereas higher concentrations (10 and 20 μg/mL) of extract did not further enhance the antioxidant resistance of the nematodes. The extract contains various chemical compounds that might exert different biological activities. In addition, it is possible that higher concentrations of extracts might be toxic, thereby reducing the antioxidant effects.

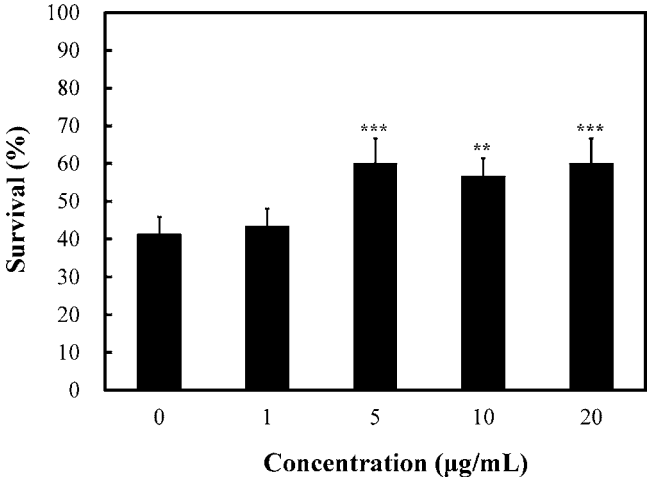

Figure 1. Essential oils from the leaves of mixed-type *C. osmophloeum* enhance the oxidative stress resistance of wild-type *C. elegans*. Synchronized wild-type L1 larvae were pretreated with 0, 1, 5, 10, and 20 μg/mL essential oils or 0.1% DMSO as the solvent control for 72 h. Adult worms were then immediately subjected to oxidative stress assays. Essential-oil-treated and untreated control adult nematodes were exposed to 250 μM juglone for 3 h and then scored for viability. At least three independent biological replicates were performed, and approximately 60−80 worms were scored in each experiment. Error bars represent the standard error, and differences compared to the control (0 μg/mL, 0.1% DMSO) were considered significant at (*) $p < 0.05$, (**) $p < 0.01$, and (***) $p < 0.001$ by one-way ANOVA and the LSD post-hoc test.

Alloaromadendrene Is the Key Compound That Contributes to the Oxidative Stress Resistance in *C. elegans*. We next examined which chemical constituents from the leaves of the mixed-type *C. osmophloeum* tree contributed to the observed oxidative stress resistance in Figure 1. Five major compounds (Figure 2A and Table 1), L-bornyl acetate, α-cadinol, T-cadinol, caryophyllene oxide, and alloaromadendrene, were selected for further oxidative stress resistance assays.

Initially, synchronized wild-type N2 L1 larvae were pretreated with 100 μM of each chemical and 0.1% DMSO (solvent control) for 72 h before juglone exposure. Except for alloaromadendrene, none of chemicals demonstrated significantly enhanced juglone-induced oxidative stress resistance in *C. elegans* (Figure 2B). Given that alloaromadendrene estimated at ∼5% in the extracts and as low as 5 μg/mL extracts from the leaves of mixed-type *C. osmophloeum* was able to protect *C. elegans* from juglone-induced oxidative stress, we tested levels of alloaromadendrene [molecular weight (MW) of 204.35] as low as 1.5 μM, which is approximately 0.3 μg of alloaromadendrene/mL of extracts. Figure 2C show that all examined concentrations of alloaromadendrene (1.5, 20, 100, and 200 μM) pretreatment produced a significant increase in the survival of nematodes exposed to juglone-induced oxidative stress (Figure 2C). This suggests that minor (alloaromadendrene, 5%) but not major chemical components in the extract might have played a key role in the observed oxidative stress resistance in Figure 1. This unexpected finding differed from *trans*-cinnamaldehyde and D-(+)-camphor, which represent the major compounds in the cinnamaldehyde- and camphor-type trees, respectively, and which exerted significant *in vivo* antioxidant activities against juglone-induced oxidative stress in *C. elegans*.[11]

Alloaromadendrene Prolongs the Lifespan of Wild-Type *C. elegans*. Aromadendrene is a member of a group of naturally occurring sesquiterpenes, and it has been shown to exhibit toxicity in a number of applications.[12−16] However, most of its potential beneficial effects remain largely unexplored. In addition, most of the biological activities of aromadendrene were examined in cell cultures or with *in vitro* systems and not with *in vivo* studies.

Stress resistance has been linked to an increase in lifespan in *C. elegans*.[18,19] Similarly, an increased lifespan has been shown to be closely associated with enhanced survival under conditions of oxidative stress or heat in *C. elegans*.[19] Moreover, oxidative stress has been shown to be a major determinant of the aging process.[32]

We evaluated whether alloaromadendrene has an effect on the lifespan of *C. elegans* by comparing the lifespan of untreated (control) and alloaromadendrene-treated wild-type N2 nematodes. Synchronized wild-type L1 larvae were transferred to alloaromadendrene-containing plates and exposed to alloaromadendrene throughout normal aging. In Figure 2C, because 100 μM alloaromadendrene exerted the most significantly oxidative stress resistance, 100 μM alloaromadendrene was chosen as the working concentration for further experiments.

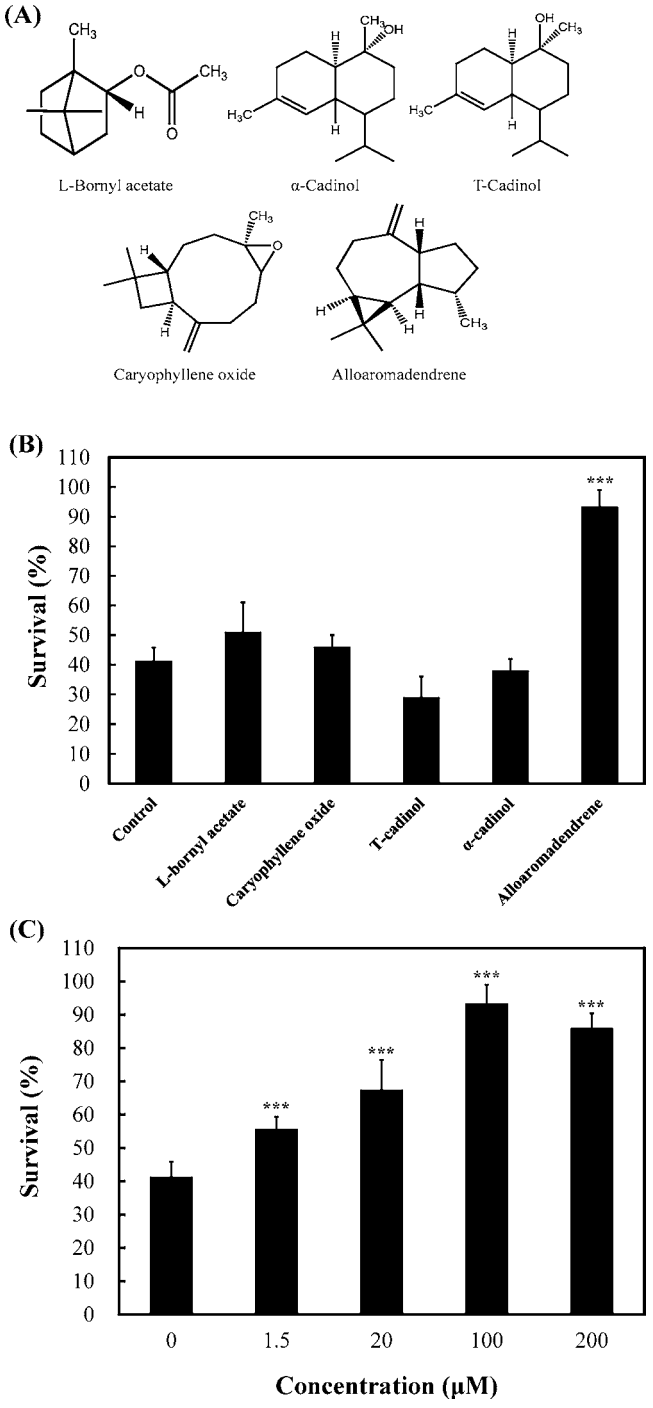

Figure 2. Effects of major compounds on the oxidative stress resistance in *C. elegans*. (A) Structure of five major compounds from leaves of *C. osmophloeum*. (B) Oxidative stress assays were performed as described in extracts, except that L1 larvae were pretreated with 100 μM L-bornyl acetate, α-cadinol, T-cadinol, caryophyllene oxide, and alloaromadendrene. (C) Oxidative stress assays were performed as described in extracts, except that L1 larvae were pretreated with 1.5, 20, 100, and 200 μM alloaromadendrene. At least three independent biological replicates were performed. Approximately 60–80 worms were scored in each experiment. Error bars represent the standard error, and differences compared to the control (0 μM, 0.1% DMSO) were considered significant at (*) $p < 0.05$, (**) $p < 0.01$, and (***) $p < 0.001$ by one-way ANOVA and the LSD post-hoc test.

The results showed that adult wild-type *C. elegans* fed with live *E. coli* OP50 and grown under our standard laboratory conditions at 20 °C have a mean lifespan of 12.0 ± 0.8 days, with a maximum lifespan of 18 days (age at death of the oldest animals) (Figure 3 and Table 2). On media containing 100 μM alloaromadendrene, the mean lifespan of wild-type animals was 13.4 ± 0.6 days, with a maximum lifespan of 20 days (log rank; $p = 0.047$; untreated versus treated) (Figure 3 and Table 2), indicating that alloaromadendrene is capable of extending the lifespan of wild-type *C. elegans*. This suggests that the observed delayed aging by alloaromadendrene might be due to its antioxidant activity in *C. elegans*.

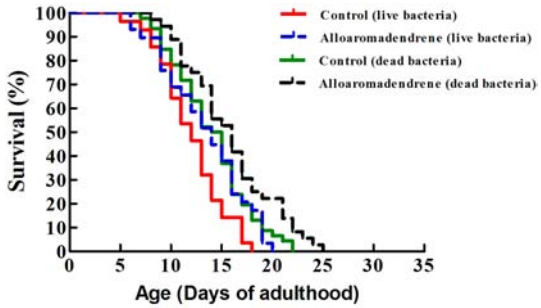

Figure 3. Alloaromadendrene prolongs the lifespan of wild-type *C. elegans*. Synchronized wild-type L1 larvae were incubated on NGM plates with dead or live *E. coli* OP50 in the absence (0 μM, 0.1% DMSO) or presence of alloaromadendrene (100 μM), and nematodes were allowed to develop to adulthood. Surviving and dead nematodes were counted daily until all nematodes had died. Survival curves are of the untreated control (0 μM, 0.1% DMSO) compared to alloaromadendrene-treated nematodes. Day 1 refers to the first day of adulthood. At least three independent biological replicates were performed. Approximately 60 worms were scored in each experiment. Statistical significance of the difference between the curves (treated versus untreated control) was demonstrated by the log-rank test using the Kaplan–Meier survival analysis. Differences at the $p < 0.05$ level were considered significantly different.

One factor contributing to late-age mortality in *C. elegans* is the adverse effect of proliferating bacteria that produce harmful metabolites.[33] To evaluate whether the lifespan extension by alloaromadendrene treatment was regulated by the inhibition of bacterial growth, nematodes were fed with UV-killed bacteria in the absence and presence of 100 μM alloaromadendrene. The results showed that UV-killed (non-proliferating) *E. coli* bacteria increased the mean lifespan from 12.0 ± 0.8 to 14.0 ± 0.3 days in the absence of alloaromadendrene, whereas exposure to 100 μM alloaromadendrene even further and significantly increased the lifespan to 16.1 ± 0.3 days (log rank; $p = 0.0265$; untreated versus treated) (Figure 3 and Table 2). We further performed a two-way ANOVA to determine significance and interaction between factors (with alloaromadendrene untreated versus treated and live versus dead bacteria as factors) in the wild-type N2 lifespan assays. Two-way ANOVA analysis showed that there is no statistically significant interaction between alloaromadendrene and the food source bacteria ($p = 0.663$), suggesting that the effect of alloaromadendrene on lifespan does not depend upon the bacterial load. Hence, the antibacterial property of alloaromadendrene is not an important factor for the lifespan extension. A summary of *C. elegans* lifespan data is present in Table 2.

Several studies have reported that *C. elegans* responds to various natural compounds with increased stress resistance and/or extended lifespan.[34,35] Although translation of lifespan extension from *C. elegans* to more complex organisms remains

Table 2. Lifespan of Alloaromadendrene Treatment on *C. elegans*

		median lifespan (day)	mean lifespan (day)	maximum lifespan (day)	log-rank test[a]
N2	control (live bacteria)	12	12.0 ± 0.8	18	$p = 0.047$[b] (untreated versus treated)
	alloaromadendrene (live bacteria)	14	13.4 ± 0.6	20	
	control (dead bacteria)	14.5	14.0 ± 0.3	22	$p = 0.0265$[b] (untreated versus treated)
	alloaromadendrene (dead bacteria)	16	16.1 ± 0.3	25	
daf-16	control (dead bacteria)	10	10.0 ± 0.7	17	$p = 0.9876$ (untreated versus treated)
	alloaromadendrene (dead bacteria)	9	9.8 ± 0.6	17	

[a]Statistical significance of the difference between the survival curves was demonstrated by the log-rank test using the Kaplan−Meier survival analysis. [b]$p < 0.05$.

to be elucidated, studies have shown that an increase in stress resistance has been linked with an increase in longevity in a variety of organisms, including the nematode *C. elegans*.[18,19] Moreover, several lines of experimental evidence suggest that drugs prolonging lifespan in *C. elegans* are very effective in the treatment of age-related diseases, such as cancer and neurodegenerative diseases.[36,37] Therefore, *C. elegans* provides a useful tool for identifying genes and compounds that can prolong lifespan in higher animals, perhaps including humans.

Alloaromadendrene Enhances Oxidative Stress Resistance and Longevity Depending upon DAF-16. One potential mechanism that might be involved in alloaromadendrene-mediated oxidative stress resistance and longevity was further explored. In *C. elegans*, many signaling pathways, including the insulin like/IGF-1, JNK, the sensory neurons signaling, and the germline signaling pathways, converge at the FOXO transcription factor DAF-16, which is the only FOXO in *C. elegans*.[38,39] DAF-16 integrates signals from multiple pathways and regulates its downstream target genes to control diverse cellular functions, including metabolism, stress resistance, and longevity.[38,39] Therefore, DAF-16 is regarded as a key regulator to enhance stress resistance and longevity in *C. elegans* and mammals.[38,39] Herein, to analyze the involvement of DAF-16 in alloaromadendrene-mediated oxidative stress resistance and longevity, we examined the loss of function of the *daf-16* mutant for its ability to resist oxidative stress and prolong lifespan during alloaromadendrene exposure. The premise of these experiments was that alloaromadendrene treatment would not increase oxidative stress resistance or extend lifespan in *daf-16* mutant nematodes.

Oxidative stress and lifespan assays for the *daf-16* mutant were performed essentially the same as those for wild-type nematodes. For the oxidative stress-resistance test, unlike wild-type N2 *C. elegans*, the survival of alloaromadendrene-treated (100 and 200 μM) *daf-16* mutants did not show a significant difference compared to untreated *daf-16* mutants (Figure 4A). This suggests that DAF-16 is required for alloaromadendrene-mediated oxidative stress resistance in *C. elegans*.

For lifespan assays, 100 μM alloaromadendrene-treated *daf-16* mutant nematodes did not exhibit a significant difference in lifespan in compared to that of untreated animals (log rank; $p = 0.9876$; Figure 4B and Table 2). The mean lifespans for both alloaromadendrene-treated and untreated *daf-16* mutant animals are 10.0 ± 0.7 and 9.8 ± 0.6 days, respectively, with a maximum lifespan of 17 days (Figure 4B and Table 2). This indicates that DAF-16 is required for alloaromadendrene-enhanced lifespan in *C. elegans*. Taken together, DAF-16 is required for alloaromadendrene-mediated oxidative stress resistance and longevity in *C. elegans*.

In conclusion, the results obtained from this study reveal that minor (alloaromadendrene, 5%) but not major chemical components from the leaves of mixed-type *C. osmophloeum* have key roles in oxidative stress resistance. We demonstrate that the essential oil alloaromadendrene not only acts protective against oxidative stress but also prolongs the lifespan of *C. elegans*. Additionally, DAF-16 is required for alloaromadendrene-mediated oxidative stress resistance and longevity in *C. elegans*. We show that alloaromadendrene can

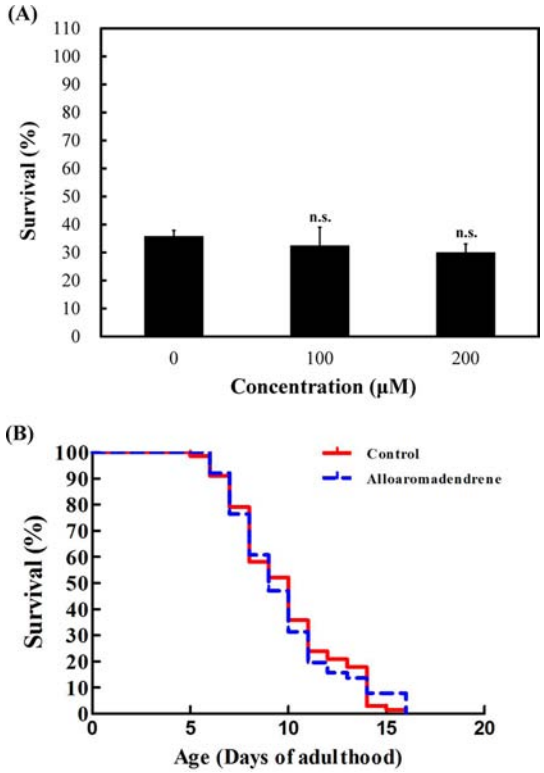

Figure 4. Alloaromadendrene enhances oxidative stress resistance and longevity depending upon DAF-16. Oxidative stress and lifespan assays for *daf-16* mutants were performed essentially the same as wild-type nematodes. (A) For oxidative stress assays, *daf-16* mutants were treated with 100 and 200 μM alloaromadendrene and at least three independent biological replicates were performed. Approximately 60−80 worms were scored in each experiment. Error bars represent the standard error, and differences compared to the control (0 μM, 0.1% DMSO) were considered significant at (∗) $p < 0.05$, (∗∗) $p < 0.01$, and (∗∗∗) $p < 0.001$ by one-way ANOVA and the LSD post-hoc test. n.s. = non-significant. (B) For lifespan assays, *daf-16* mutants were treated with 100 μM alloaromadendrene and at least three independent biological replicates were performed. Approximately 60 worms were scored in each experiment. Statistical significance of the difference between the curves (treated versus untreated control) was demonstrated by the log-rank test using the Kaplan−Meier survival analysis. Differences at the $p < 0.05$ level were considered statistically significant.

significantly prolong lifespan and enhance resistance to oxidative stress in a whole organism. Although further detailed investigations are needed, our results provide the first tantalizing insights on the alloaromadendrene function in longevity and antioxidative stress *in vivo*. The results in the present study indicate that alloaromadendrene has the potential for use as a source for antioxidants or treatments to delay aging.

AUTHOR INFORMATION

Corresponding Authors

*Telephone: +886-2-33664626; E-mail: peter@ntu.edu.tw.
*Telephone: +886-2-33665239. Fax: +886-2-33663462. E-mail: vivianliao@ntu.edu.tw.

Funding

This work was financially supported in part by grants (Career Development Project (101R7845/102R7845) from the National Taiwan University to Vivian Hsiu-Chuan Liao.

Notes

The authors declare no competing financial interest.

ACKNOWLEDGMENTS

All nematode strains used in this work were provided by the *Caenorhabditis* Genetics Center (CGC), which is funded by the National Center for Research Resources (NCRR), National Institutes of Health (NIH).

REFERENCES

(1) Tajkarimi, M. M.; Ibrahim, S. A.; Cliver, D. O. Antimicrobial herb and spice compounds in food. *Food Control* **2010**, *21*, 1199−1218.

(2) Oussalah, M.; Caillet, S.; Saucier, L.; Lacroix, M. Inhibitory effects of selected plant essential oils on the growth of four pathogenic bacteria: *E. coli* O157:H7, *Salmonella typhimurium*, *Staphylococcus aureus* and *Listeria monocytogenes*. *Food Control* **2007**, *18*, 414−420.

(3) Astani, A.; Reichling, J.; Schnitzler, P. Screening for antiviral activities of isolated compounds from essential oils. *J. Evidence-Based Complementary Altern. Med.* **2011**, *2011*, 253643.

(4) Silva, F.; Ferreira, S.; Duarte, A.; Mendonça, D. I.; Domingues, F. C. Antifungal activity of *Coriandrum sativum* essential oil, its mode of action against *Candida* species and potential synergism with amphotericin B. *Phytomedicine* **2011**, *19*, 42−47.

(5) Brenes, A.; Roura, E. Essential oils in poultry nutrition: Main effects and modes of action. *Anim. Feed Sci. Technol.* **2010**, *158*, 1−14.

(6) Ahmadi, F.; Sadeghi, S.; Modarresi, M.; Abiri, R.; Mikaeli, A. Chemical composition, in vitro anti-microbial, antifungal and antioxidant activities of the essential oil and methanolic extract of *Hymenocrater longiflorus* Benth., of Iran. *Food Chem. Toxicol.* **2010**, *48*, 1137−1144.

(7) Tung, Y. T.; Yen, P. L.; Lin, C. Y.; Chang, S. T. Anti-inflammatory activities of essential oils and their constituents from different provenances of indigenous cinnamon (*Cinnamomum osmophloeum*) leaves. *Pharm. Biol.* **2010**, *48*, 1130−1136.

(8) Chang, S. T.; Chen, P. F.; Chang, S. C. Antibacterial activity of leaf essential oils and their constituents from *Cinnamomum osmophloeum*. *J. Ethnopharmacol.* **2001**, *77*, 123−127.

(9) Cheng, S. S.; Liu, J. Y.; Hsui, Y. R.; Chang, S. T. Chemical polymorphism and antifungal activity of essential oils from leaves of different provenances of indigenous cinnamon (*Cinnamomum osmophloeum*). *Bioresour. Technol.* **2006**, *97*, 306−312.

(10) Chao, L. K.; Hua, K. F.; Hsu, H. Y.; Cheng, S. S.; Liu, J. Y.; Chang, S. T. Study on the antiinflammatory activity of essential oil from leaves of *Cinnamomum osmophloeum*. *J. Agric. Food Chem.* **2005**, *53*, 7274−7278.

(11) Hsu, F. L.; Li, W. H.; Yu, C. W.; Hsieh, Y. C.; Yang, Y. F.; Liu, J. T.; Shih, J.; Chu, Y. J.; Yen, P. L.; Chang, S. T.; Liao, V. H. C. *In vivo* antioxidant activities of essential oils and their constituents from leaves of the Taiwanese *Cinnamomum osmophloeum*. *J. Agric. Food Chem.* **2012**, *60*, 3092−3097.

(12) Moreira, I. C.; Lago, J. H. G.; Young, M. C. M.; Roque, N. F. Antifungal aromadendrane sesquiterpenoids from the leaves of *Xylopia brasiliensis*. *J. Braz. Chem. Soc.* **2003**, *14*, 828−831.

(13) Detommasi, N.; Pizza, C.; Conti, C.; Orsi, N.; Stein, M. L. Structure and *in vitro* antiviral activity of sesquiterpene glycosides from *Calendula arvensis*. *J. Nat. Prod.* **1990**, *53*, 830−835.

(14) Bukvicki, D. R.; Tyagi, A. K.; Gottardi, D. G.; Veljic, M. M.; Jankovic, S. M.; Guerzoni, M. E.; Marin, P. D. Assessment of the chemical composition and *in vitro* antimicrobial potential of extracts of the liverwort *Scapania aspera*. *Nat. Prod. Commun.* **2013**, *8*, 1313−1316.

(15) Messer, A.; McCormick, K.; Sunjaya; Hagedorn, H. H.; Tumbel, F.; Meinwald, J. Defensive role of tropical tree resins: Antitermitic sesquiterpenes from Southeast Asian Dipterocarpaceae. *J. Chem. Ecol.* **1990**, *16*, 3333−3352.

(16) Phongmaykin, J.; Kumamoto, T.; Ishikawa, T.; Suttisri, R.; Saifah, E. A new sesquiterpene and other terpenoid constituents of *Chisocheton penduliflorus*. *Arch. Pharm. Res.* **2008**, *31*, 21−27.

(17) Romano, A. D.; Serviddio, G.; de Matthaeis, A.; Bellanti, F.; Vendemiale, G. Oxidative stress and aging. *J. Nephrol.* **2010**, *23* (Suppl 15), S29−S36.

(18) Kapahi, P.; Boulton, M. E.; Kirkwood, T. B. L. Positive correlation between mammalian life span and cellular resistance to stress. *Free Radical Biol. Med.* **1999**, *26*, 495−500.

(19) Lithgow, G. J.; Walker, G. A. Stress resistance as a determinate of *C. elegans* lifespan. *Mech. Ageing Dev.* **2002**, *123*, 765−771.

(20) Guarente, L.; Kenyon, C. Genetic pathways that regulate ageing in model organisms. *Nature* **2000**, *408*, 255−262.

(21) van der Horst, A.; Burgering, B. M. Stressing the role of FoxO proteins in lifespan and disease. *Nat. Rev. Mol. Cell Biol.* **2007**, *8*, 440−450.

(22) Sanz, A.; Stefanatos, R. K. The mitochondrial free radical theory of aging: A critical view. *Curr. Aging Sci.* **2008**, *1*, 10−21.

(23) Cheng, S. S.; Liu, J. Y.; Tsai, K. H.; Chen, W. J.; Chang, S. T. Chemical composition and mosquito larvicidal activity of essential oils from leaves of different *Cinnamomum osmophloeum* provenances. *J. Agric. Food Chem.* **2004**, *52*, 4395−4400.

(24) Adams, R. P. In *Identification of Essential Oil Components by Gas Chromatography/Quadrupole Mass Spectroscopy*; Adams, R. P., Ed.; Allured Publishing Corp.: Carol Stream, IL, 2007.

(25) Yu, C. W.; Wei, C. C.; Liao, V. H. Curcumin-mediated oxidative stress resistance in *Caenorhabditis elegans* is modulated by *age-1*, *akt-1*, *pdk-1*, *osr-1*, *unc-43*, *sek-1*, *skn-1*, *sir-2.1*, and *mev-1*. *Free Radical Res.* **2014**, *48*, 371−379.

(26) Kaeberlein, T. L.; Smith, E. D.; Tsuchiya, M.; Welton, K. L.; Thomas, J. H.; Fields, S.; Kennedy, B. K.; Kaeberlein, M. Lifespan extension in *Caenorhabditis elegans* by complete removal of food. *Aging Cell* **2006**, *5*, 487−494.

(27) Deans, S. G.; Svoboda, K. P. Antibacterial activity of summer savory (*Satureja hortensis* L.) essential oil and its constituents. *J. Hortic. Sci.* **1989**, *64*, 205−210.

(28) Hu, T. W.; Lin, Y. T.; Ho, C. K. Natural variation of chemical components of the leaf oil of *Cinnamomum osmophloeum* Kaneh. *Bull. Taiwan For. Res. Ind. New Ser.* **1985**, 78.

(29) Lee, H. C.; Cheng, S. S.; Liu, J. Y.; Chang, S. T. Chemical polymorphism of leaf essential oils from different geographical clones of indigenous cinnamon (*Cinnamomum osmophloeum*). *Q. J. Chin. For.* **2003**, *36*, 411−422.

(30) Blum, J.; Fridovich, I. Superoxide, hydrogen peroxide, and oxygen toxicity in two free-living nematode species. *Arch. Biochem. Biophys.* **1983**, *222*, 35−43.

(31) de Castro, E.; Hegi de Castro, S.; Johnson, T. E. Isolation of long-lived mutants in *Caenorhabditis elegans* using selection for resistance to juglone. *Free Radical Biol. Med.* **2004**, *37*, 139−145.

(32) Wallace, D. C.; Melov, S. Radicals r'aging. *Nat. Genet.* **1998**, *19*, 105−106.

(33) Garigan, D.; Hsu, A. L.; Fraser, A. G.; Kamath, R. S.; Ahringer, J.; Kenyon, C. Genetic analysis of tissue aging in *Caenorhabditis elegans*: A role for heat-shock factor and bacterial proliferation. *Genetics* **2002**, *161*, 1101−1112.
(34) Pietsch, K.; Saul, N.; Menzel, R.; Stürzenbaum, S. R.; Steinberg, C. E. Quercetin mediated lifespan extension in *Caenorhabditis elegans* is modulated by *age-1*, *daf-2*, *sek-1* and *unc-43*. *Biogerontology* **2009**, *10*, 565−578.
(35) Wilson, M. A.; Shukitt-Hale, B.; Kalt, W.; Ingram, D. K.; Joseph, J. A.; Wolkow, C. A. Blueberry polyphenols increase lifespan and thermotolerance in *Caenorhabditis elegans*. *Aging Cell* **2006**, *5*, 59−68.
(36) Petrascheck, M.; Ye, X.; Buck, L. B. An antidepressant that extends lifespan in adult *Caenorhabditis elegans*. *Nature* **2007**, *450*, 553−556.
(37) Pinkston, J. M.; Garigan, D.; Hansen, M.; Kenyon, C. Mutations that increase the life span of *C. elegans* inhibit tumor growth. *Science* **2006**, *313*, 971−975.
(38) Jensen, V. L.; Gallo, M.; Riddle, D. L. Targets of DAF-16 involved in *Caenorhabditis elegans* adult longevity and dauer formation. *Exp. Gerontol.* **2006**, *41*, 922−927.
(39) Henderson, S. T.; Johnson, T. E. *daf-16* integrates developmental and environmental inputs to mediate aging in the nematode *Caenorhabditis elegans*. *Curr. Biol.* **2001**, *11*, 1975−1980.

JOURNAL OF AGRICULTURAL AND FOOD CHEMISTRY

Article

pubs.acs.org/JAFC

Relationship between the Acyl Chain Length of Paradol Analogues and Their Antiobesity Activity following Oral Ingestion

Akinori Haratake, Daisuke Watase,* Shuichi Setoguchi, Kazuki Terada, Kazuhisa Matsunaga, and Jiro Takata

Laboratory of Drug Design and Drug Delivery, Faculty of Pharmaceutical Sciences, Fukuoka University, 8-19-1 Nanakuma, Jonan-ku, Fukuoka 814-0180, Japan

ABSTRACT: 6-Paradol is known to activate thermogenesis in brown adipose tissue (BAT), and paradol analogues with different acyl chain lengths possess different pungency thresholds. In this study, the influence of the acyl chain length on the antiobesity activity of the paradol analogues was investigated. The antiobesity activity of 6-paradol in mice fed a high-fat diet for 8 weeks was greater than that of dihydrocapsiate. A comparison of the antiobesity activities of zingerone and 6-paradol showed that the length of the acyl chain in the paradol analogue was important for strong activity. Furthermore, the antiobesity activities of 6-, 8-, and 12-paradol appeared to decrease in an acyl chain length-dependent manner. The mechanism of the antiobesity activity of 6-paradol was enhanced by increasing levels of energy metabolism in the BAT, as well as an increase in the expression of uncoupling proteins 1 via the activation of sympathetic nerve activity.

KEYWORDS: *antiobesity activity, paradol analogue, acyl chain, oral ingestion, uncoupling protein*

INTRODUCTION

Obesity and related health issues represent a significant threat to human health in an increasing number of countries.[1] Obesity is the outcome of a prolonged positive energy balance, which can be caused by reduced energy expenditure and/or excessive calorie intake. A negative energy balance is needed to produce weight loss and can be achieved by a reduction in calorie intake or increased energy expenditure. Several tools are available for the management of obesity, including caffeine, ephedrine, capsaicin, and green tea, and materials of this type have been proposed as parts of strategies for weight loss and weight maintenance because their intake can lead to an increase in energy and could therefore counteract the decrease in metabolic rate that occurs during weight loss.[2]

Brown adipose tissue (BAT) acts as a major defense mechanism against obesity in rodents and human infants, where it serves to increase energy expenditure through dissipation in the form of heat (thermogenesis).[3] BAT tends to be localized in the intrascapular and paraspinal regions, and the amount present in rodents and humans appears to decrease as they develop from the neonatal to adult stage.[4] Increases in thermogenesis in BAT occur in response to cold or calorie intake, whereas the ablation of BAT resulting from the use of a toxigene results in hyperphagia and obesity.[5] The protein responsible for thermogenesis in BAT is uncoupling protein (UCP)-1,[6−8] which is the major endogenous stimulator of thermogenesis, and β_3-adrenergic receptor stimulation induces UCP-1 expression.[7] Knockout of UCP-1 in mice leads to a decrease in oxygen consumption following treatment with a β_3-adrenergic receptor agonist and also leads to increased cold sensitivity.[9] Two other UCPs, UCP-2 and UCP-3, are more widely expressed than UCP-1 and appear to play important roles in mitochondrial function in a limited number of tissues. Although it was initially thought that UCP-2 and UCP-3 might also allow tissues such as skeletal muscle to undergo thermogenesis and energy expenditure,[10] subsequent studies revealed this speculation to be unfounded.[11,12] Furthermore, the results of a recent study revealed that UCP-3 does not play a role in any thermogenic process, although the results of the same study did indicate that novel UCPs were involved in attenuating the production of reactive oxygen species, particularly during fatty acid oxidation.[13] The results of another recent study, however, showed that UCP-3 was not required for fatty acid oxidation or fatty acid anion export, but that it was essential for adaptation to fasting, where it may be involved in mitigating the formation of reactive oxygen species.[14] Finally, the overexpression of UCP-3 in mice leads to decreased body mass despite higher food intake.[15] Although the role of UCP-3 is currently unclear, evidence from the literature strongly suggests that an increase in UCP-3 expression leads to a reduction in body mass.

In their recent review, Bonet et al.[16] reported that dietary changes and chemicals including specific nutrients were strongly associated with BAT. There have been several reports in the literature suggesting that the activity of BAT was activated with dietary methionine restriction, dietary leucine restriction, high-fat diet, fucoxanthin, salmon protein hydrolysate, n-3 fatty acids of marine origin, and resveratrol. Furthermore, thermogenesis can be modified by macronutrient content in the different types of fat.[17] It has also been reported that olive leaf extracts can exert beneficial antiobesity effects by regulating the expression of genes involved in adipogenesis and thermogenesis in the visceral adipose tissue of mice fed a high-fat diet.[18] Spices and their principal pungent components have been reported to provide several potential benefits to human

Received: February 21, 2014
Revised: June 4, 2014
Accepted: June 8, 2014
Published: June 8, 2014

ACS Publications © 2014 American Chemical Society

dx.doi.org/10.1021/jf500873a | J. Agric. Food Chem. 2014, 62, 6166−6174

health, including antiobesity activity. Capsaicin, which is the major pungent component of hot red pepper,[19] has been reported to elevate body temperature,[20] stimulate the secretion of catecholamines,[21] promote energy expenditure,[22] and suppress body fat accumulation[23] in experimental animals. However, capsaicin is strongly pungent and neurotoxic,[24] and high capsaicin concentrations can be damaging to human health. Capsinoids (i.e., capsiate, dihydrocapsiate (Figure 1), and nordihydrocapsiate) are nonpungent analogues of capsaicin that are derived from CH-19 sweet pepper,[25] and have been shown to increase oxygen consumption and suppress body fat accumulation in mice to the same extent as capsaicin.[26,27] Capsaicin analogues bearing longer acyl chains than capsaicin, such as vanillyl tetradecanamide (C14) and vanillyl octadecanamide (C18), are not pungent, although some of these analogues do enhance the secretion of adrenaline from the adrenal medulla in rodents in the same way as capsaicin.[21,28] Vanillyl (*Z*)-9-octadecenamide (C18:1) possesses capsaicin-like biological and physiological properties without any noxious stimuli.[29]

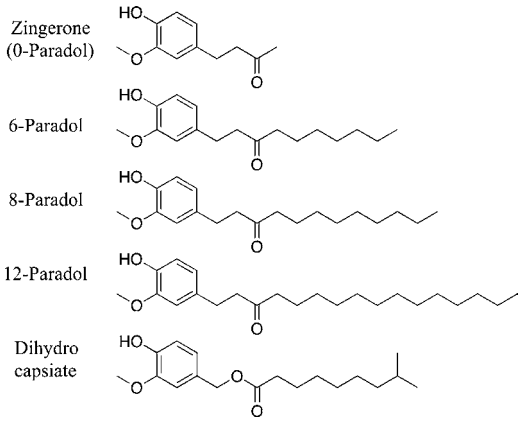

Figure 1. Structures of the paradol analogues and dihydrocapsiate tested for their antiobesity effects.

Paradols are a series of phenolic ketones that are structurally related to gingerols and shogaols.[30] Zingerone (Figure 1) is a 0-paradol of paradol analogues and is the major pungent component of ginger.[31] The oral administration of zingerone led to a significant reduction in the body weight and final parametrial adipose tissue weight in ovariectomized rats.[31] 6-Paradol (Figure 1) is the characteristic pungent component of the extract of the seeds of *Amomum melegueta* Roscoe (zingiberaceae), which are also known as grains of paradise, and is the only naturally occurring member of the paradol series to have been isolated to date exclusive of zingerone, although there are strong indications that other paradols also exist in nature.[30] Iwami et al.[32] recently demonstrated that an extract from the grains of paradise and 6-paradol activated thermogenesis in BAT, which could open up new avenues for the regulation of weight loss and weight maintenance. Furthermore, Sugita et al.[33] demonstrated that the oral ingestion of an extract of grains of paradise increased whole-body energy expenditure via the activation of BAT in human subjects. However, no studies have been reported in the literature to date pertaining to the antiobesity effects of 6-paradol following oral ingestion. Paradol analogues with different acyl chain lengths have been reported to have different pungency thresholds.[30] With this in mind, it was envisaged that the length of the acyl chains in different paradol analogues, which is related to their pungency strength, could also be related to the strength of their antiobesity effect following oral ingestion.

Table 1. Compositions (% wt) of the Different Diets Used in This Study

	diet groups						
	high-fat						normal
ingredient	control	zingerone	6-paradol	8-paradol	12-paradol	dihydro capsiate	AIN-93M
AIN-93 mix	67.0	66.9	66.9	66.9	66.9	66.9	100.0
milk casein	38.2	38.2	38.2	38.2	38.2	38.2	14.0
L-cysteine	0.5	0.5	0.5	0.5	0.5	0.5	0.2
maltodextrin	9.0	9.0	9.0	9.0	9.0	9.0	
corn starch							46.6
α-corn starch	23.9	23.9	23.9	23.9	23.9	23.9	15.5
sucrose	8.2	8.2	8.2	8.2	8.2	8.2	10.0
soybean oil	3.0	3.0	3.0	3.0	3.0	3.0	4.0
cellulose powder	9.9	9.9	9.9	9.9	9.9	9.9	5.0
AIN-93G-MX[a]	5.2	5.2	5.2	5.2	5.2	5.2	3.5
$CaCO_3$	0.3	0.3	0.3	0.3	0.3	0.3	
AIN-93-VM[b]	1.5	1.5	1.5	1.5	1.5	1.5	1.0
choline bitartrate	0.3	0.3	0.3	0.3	0.3	0.3	0.3
lard	33.0	33.0	33.0	33.0	33.0	33.0	
zingerone		0.1					
6-paradol			0.1				
8-paradol				0.1			
12-paradol					0.1		
dihydrocapsiate						0.1	
total	100.0	100.0	100.0	100.0	100.0	100.0	100.0

[a]Mineral mix. [b]Vitamin mix.

dx.doi.org/10.1021/jf500873a | J. Agric. Food Chem. 2014, 62, 6166−6174

In this study, the antiobesity activities of high-fat diets containing 6-paradol or zingerone were compared in mice. Furthermore, the antiobesity activities of a series of paradol analogues bearing acyl chains of different lengths were evaluated following their oral ingestion, and the antiobesity mechanism of 6-paradol was investigated.

MATERIALS AND METHODS

Animals. Five-week-old C57BL/6J mice (male) were purchased from Clea Japan (Tokyo, Japan) and 5-week-old Sprague−Dawley rats (male) were purchased from Charles River Laboratories Japan (Kanagawa, Japan). The animals were housed in standard cages (345 × 403 × 177 mm) under controlled conditions (i.e., ambient temperature, 23 ± 2 °C; relative humidity, 60 ± 10%; 12 h light/dark cycle). The mice were given AIN-93 M (Oriental Yeast, Tokyo, Japan) and water ad libitum, whereas the rats received CE-2 (Clea Japan) and water ad libitum. All of the procedures used in the current study regarding the care and use of the animals were carried out on the basis of the regulations dictated by the Experimental Animal Care and Use Committee of Fukuoka University.

Chemicals. Zingerone was purchased from Givaudan (Dubendorf, Switzerland). 6-, 8-, and 12-paradol (Figure 1) were synthesized from the reactions of vanillin (Tokyo Chemical Industry, Tokyo, Japan) with 2-nonanone (Wako Pure Chemical Industries, Osaka, Japan), 2-undecanone (Wako Pure Chemical Industries), and 2-pentadecanone (Tokyo Chemical Industry), respectively, using the methods reported by Locksley and Rauney.[30] Dihydrocapsiate was synthesized from vanillyl alcohol (Tokyo Chemical Industry) and methyl nonanoate (Tokyo Chemical Industry) according to the method described by Kobata et al.[34] The compounds synthesized in this study were characterized by NMR spectrometry (JNM-A500, JEOL, Tokyo, Japan) at 500 MHz, and their purities were confirmed by element analysis (MICRO CORDER JM10, J-Science, Kyoto, Japan) with an absolute error of <0.3% between the theoretical and experimentally determined values. All of the other reagents used in the current study were purchased from Wako Pure Chemical Industries. AIN-93 M and the high-fat diet (HFD-60) were obtained from Oriental Yeast.

Comparison of the Antiobesity Effects following the Oral Ingestion of Zingerone and 6-Paradol. The mice were randomly divided into five groups of 10 at 8 weeks old, including one normal group and four experimental groups. The compositions of the experimental diets are shown in Table 1. The normal group was fed a normal diet of AIN-93 M for 8 weeks, whereas the four experimental groups were fed a high-fat diet with or without 0.1% by weight of zingerone, 6-paradol, or dihydrocapsiate for 8 weeks, with the latter serving as a positive control. The total food intake for each group was recorded five times a week, and the body weight of each mouse was recorded once a week. After 8 weeks on their diet, the mice were euthanized without suffering, and their inguinal subcutaneous fat, epididymal fat, perirenal fat, and interscapular BAT were collected. Each fat specimen was weighed, with the result expressed as milligram of wet weight (mean ± SE). Each BAT specimen was stored at −80 °C prior to being subjected to Western blotting for UCP-1.

Comparison of Antiobesity Effects following Oral Ingestion of 6-, 8-, or 12-Paradol. The mice were randomly divided into five groups of 10 at 8 weeks old. The compositions of the experimental diets are shown in Table 1. The normal group was fed a normal diet (AIN-93M) for 8 weeks, whereas the four experimental groups were fed a high-fat diet with or without 0.1% by weight of 6-, 8-, or 12-paradol for 8 weeks. Thereafter, the mice were subjected to the same protocol as that described above.

Expression of UCP-3 in Femoral Muscle following Oral Ingestion of 6-Paradol. The mice were randomly divided into three groups of 10 at 8 weeks old. The normal group was fed a normal diet (AIN-93M) for 8 weeks, whereas the two experimental groups were fed a high-fat diet with or without 0.1% by weight of 6-paradol for 8 weeks. Thereafter, the mice were subjected to the same protocol as that described above. After 8 weeks, the mice were sacrificed and their femoral muscles were collected and stored at −80 °C prior to being subjected to Western blotting for UCP-3.

Immunoblotting. Mitochondria were isolated using the method reported by Hong et al.[35] The protein contents were determined in triplicate using the Bradford method (Bradford reagent, Sigma-Aldrich, St. Louis, MO, USA). BAT and muscle protein (4 μg) samples were subjected to gel electrophoresis using sodium dodecyl sulfate 10% polyacrylamide mini-gels and electroblotted onto polyvinylidene difluoride. Blocked polyvinylidene difluoride (Blocking One, Nacalai Tesque, Kyoto, Japan; 4 °C, overnight) was probed with rabbit anti-UCP-1 polyclonal antibody (Abcam, Cambridge, MA, USA) at a dilution of 1:100000, as well as rabbit anti-UCP-3 polyclonal antibody (Abcam) at a dilution of 1:5000. Horseradish peroxidase-conjugated mouse anti-rabbit IgG antibody (Cell Signaling Technology, Beverly, MA, USA) was used as the secondary antibody at a dilution of 1:50000. Each incubation was performed for 1 h at room temperature, with the resulting immune complexes being detected with Immunostar LD (Wako Pure Chemical Industries) and a Western blot imaging system (FluorChemQ, Palo Alto, CA, USA). The expression levels of UCP-1 and -3 have been shown as the ratio of the level of expression on the high-fat diet to the level of expression observed on the normal diet (mean ± SE).

Pharmacokinetics. The pharmacokinetic properties of the paradol analogues and their metabolites were investigated following their oral administration to determine their active sites.

At 8 weeks old, the rats were fasted for 14 h prior to the oral administration of olive oil (1 mL) containing zingerone or 6-, 8-, or 12-paradol (10 mg/kg). Three rats in each group were anesthetized with isoflurane, and samples (300 μL) of their blood were collected from their jugular vein using a heparinized needle and syringe at 0 (before administration), 0.25, 0.5, 1, 3, 6, and 24 h after oral administration. The samples were centrifuged, and the resulting plasma was harvested and frozen at −80 °C prior to its analysis. The plasma (50 μL) was incubated at 37 °C for 1 h with 50 μL of β-glucuronidase. Each component was then collected by sequential extraction with 100 μL of methanol and 300 μL of *n*-hexane using a combination of vortexing and centrifugation. The hexane extract was then evaporated to dryness under a gentle stream of N_2 gas to give a residue, which was dissolved in methanol and analyzed using an API4000 QTRAP LC-MS/MS system (Applied Biosystems API4000, Life Technologies, Carlsbad, CA, USA) and a Prominence UFLC system (Shimadzu) equipped with a reversed-phase C18 column (Capcell PAK C18 UG120, 3 μm particle size, 100 × 2.0 mm, i.d., Shiseido). The MS detector was equipped with an electrospray ionization source. Mass spectral data were obtained by electrospray in the positive ion mode. Quantization analyses were performed using the multiple reaction monitoring mode with an external standard. The following pairs of ions were monitored with values of 195 (Q1) and 137 (Q3) for zingerone; 279 (Q1) and 137 (Q3) for 6-paradol; 307 (Q1) and 137 (Q3) for 8-paradol; and 363 (Q1) and 137 (Q3) for 12-paradol. The maximum concentration in the plasma (C_{max}) and the time to reach C_{max} (t_{max}) were recorded as observed. The area under the plasma concentration−time curve from 0 to 24 h (AUC_{0-24h}) and the mean residence time (MRT) were calculated using the moment method.[36,37]

Measurement of Lipolysis. Mice at 8 weeks old were fed a high-fat diet for 8 weeks. The mice were then sacrificed, and their epididymal adipose tissue was quickly collected. Isolated fat cells were obtained from the collected epididymal adipose tissue using the method of Rodbell.[38] The fat cells (40 μL packed volume) were incubated at 37 °C for 1 h in 160 μL of Hanks' buffer (pH 7.4) supplemented with 2.5% (w/v) bovine serum albumin (Rockland Immunochemicals, Gilbertsville, PA, USA), 6-paradol (concentration of 10^{-6}, 10^{-5}, or 10^{-4} M), and norepinephrine (NE, 0.1 μg/mL). The free fatty acids (FFAs) were extracted, and the amount of FFAs was determined using the method of Zapf et al.[39] The amounts of FFAs are shown as microquivalents released per milliliter of packed fat cells per hour (mean ± SE).

Statistical Analysis. All of the values have been expressed as the mean ± SE. Data were analyzed using Student's *t* test or Tukey's

Table 2. Food Intake and Body and Adipose Tissue Weights of the Mice Given Zingerone, 6-Paradol, and Dihydrocapsiate[a]

	diet groups				
	high-fat				normal
parameter	control	zingerone	6-paradol	dihydrocapsiate	
n	10	10	10	10	10
food intake (g/mouse/day)	1.89 ± 0.03	1.98 ± 0.05	2.04 ± 0.05	2.06 ± 0.05	2.22 ± 0.03
initial body wt (g)	22.7 ± 1.0	23.2 ± 0.5	23.5 ± 0.7[b]	23.5 ± 1.1[b]	22.4 ± 0.7
final body wt (g)	36.1 ± 0.6	36.8 ± 0.5[e]	33.1 ± 0.5[c]	34.5 ± 0.8[d]	26.4 ± 0.3
subcutaneous fat (mg)	2042.7 ± 94.4	1821.7 ± 90.7[e]	1342.3 ± 72.4[c]	1329.7 ± 124.7[cd],	497.3 ± 49.7
epididymal fat (mg)	2211.7 ± 95.6	2283.6 ± 84.0[e]	1691.8 ± 89.8[c]	1855.5 ± 184.0[c]	573.5 ± 50.3
perirenal fat (mg)	934.3 ± 45.4	1047 ± 51.2[e]	622.2 ± 41.4[c]	825.2 ± 100.6[d]	178.4 ± 18.7

[a]Data are shown as the mean ± SE (n = 10). [b]$p < 0.05$. [c]$p < 0.01$ vs control. [d]$p < 0.01$ vs zingerone. [e]$p < 0.05$ vs 6-paradol, Tukey's multiple-range test.

multiple-range test, and differences were considered significant at $p < 0.05$.

RESULTS AND DISCUSSION

The antiobesity activities and UCP-1 expression levels in BAT were compared following oral ingestion of zingerone or 6-paradol. No differences were observed between the high-fat diet groups in terms of the food intake, which indicated that there were no differences in the energy intakes of the different groups (Table 2). Furthermore, the intake levels of zingerone, 6-paradol, and dihydrocapsiate were the same in each group (Table 2). Table 2 also shows the initial and final body weights for each group, as well as the adipose tissue weights. Significant differences were observed in the initial body weights of the 6-paradol and dihydrocapsiate groups compared with the control ($p < 0.05$ in both groups). The final body weight of the mice in the 6-paradol group was significantly lower than that of the control ($p < 0.01$). The dihydrocapsiate and zingerone groups did not show a significant difference in their final body weight compared with the control. The final body weights of the 6-paradol and dihydrocapsiate groups were significantly lower than that of the zingerone group ($p < 0.01$ and $p < 0.05$, respectively).

A comparison of the subcutaneous fat weights across the different groups revealed that the 6-paradol and dihydrocapsiate groups exhibit significantly lower weights than the control ($p < 0.01$ in both cases). In contrast, there was no significant difference between the subcutaneous fat weight of the zingerone group and the control, although there were significant differences between the zingerone group and the dihydrocapsiate and 6-paradol groups ($p < 0.05$ and $p < 0.01$, respectively). With regard to the epididymal fat weight, the 6-paradol group exhibited significantly lower levels of fat compared with those of the control and zingerone groups ($p < 0.01$ in both cases). The dihydrocapsiate group exhibited a significantly lower level of epididymal fat, which followed a similar tendency to that of the final body weight. With regard to the perirenal fat weight, the 6-paradol group exhibited significantly lower levels of fat compared with the control and zingerone groups ($p < 0.01$ in both cases). The dihydrocapsiate group exhibited a significantly lower level of perirenal fat weight compared with the zingerone group ($p < 0.05$).

The lowest overall body weight gain was observed in the 6-paradol group, followed by the dihydrocapsiate group, with the highest body weight gain being observed in the control group (Figure 2). Significant differences in body weight gain were observed between the control and 6-paradol groups from week 1 of the study, the control and dihydrocapsiate groups at weeks

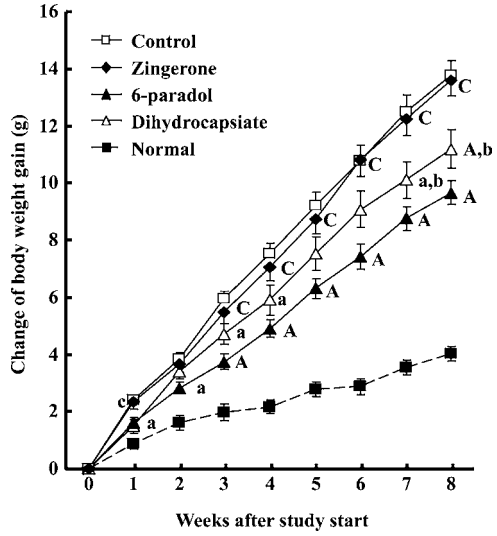

Figure 2. Changes in body weight gain following the oral ingestion of zingerone, 6-paradol, and dihydrocapsiate in mice. Normal group was fed AIN-93M, and the experimental groups were fed a high-fat diet with or without 0.1% (w/w) zingerone, 6-paradol, or dihydrocapsiate for 8 weeks. Data are shown as the mean ± SE (n = 10). There were significant difference between control and normal at all time points after the first week, $p < 0.01$, respectively, Student's t test. a, $p < 0.05$, and A, $p < 0.01$, versus control; b, $p < 0.05$ versus zingerone; c, $p < 0.05$, and C, $p < 0.01$, versus 6-paradol; Tukey's multiple-range test.

3, 4, and 7 of the study as well as at the end point of the study; the zingerone and dihydrocapsiate groups at week 7 as well as at the end point of the study, and the zingerone and 6-paradol groups from week 1 of the study, except at week 2.

Figure 3 shows changes in the expression levels of the UCP-1 protein in BAT mitochondria for all of the tested diets. The level of UCP-1 protein expression in the mice fed the high-fat diet with 6-paradol was about 2.6-fold greater than that found in the mice given the normal diet ($p < 0.01$). The level of UCP-1 expression in the dihydrocapsiate group (1.9-fold) was also significantly higher than that of the mice that received the normal diet ($p < 0.01$). These increases in the levels of UCP-1 expression in the control (1.4-fold) and zingerone (1.3-fold) groups were not significant relative to the normal diet. It has been reported that the level of UCP-1 expression in BAT increased significantly in mice fed a high-fat diet compared with a normal diet.[40] With this in mind, our current data were analyzed to identify any differences compared with the normal diet group. The results of this analysis revealed that the 6-paradol group had significantly higher levels of UCP-1 protein

dx.doi.org/10.1021/jf500873a | J. Agric. Food Chem. 2014, 62, 6166−6174

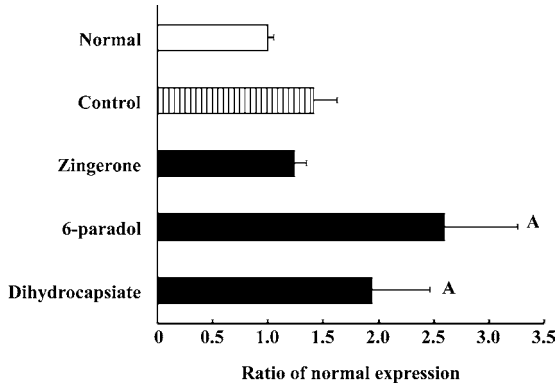

Figure 3. UCP-1 protein expression levels in murine interscapular brown adipose tissue following the oral ingestion of zingerone, 6-paradol, and dihydrocapsiate for 8 weeks. Data are shown as the mean ± SE (normal, n = 5, control; 6-paradol, n = 9, zingerone; dihydrocapsiate, n = 10). A, $p < 0.01$, versus normal; Tukey's multiple-range test.

expression compared with the normal diet group, whereas the levels of expression in the high-fat control group were similar to those of the control. Although there was no significant difference between the 6-paradol and control groups, it was concluded that the effect of 6-paradol was greater than that of the control. This result was similar to that of dihydrocapsiate, which was used as a positive control. The antiobesity activity of 6-paradol was found to be stronger than that of zingerone or dihydrocapsiate, with the latter used as a positive control. On the basis of these results, it was concluded that the length of the acyl chain of the paradol analogues was closely related to their antiobesity activity.

A separate experiment was then conducted to compare the antiobesity activities of 6-, 8-, and 12-paradol following their oral ingestion. Significant differences were observed in the food intake levels of the control group and the 8- and 12-paradol groups, and a similar difference was also observed between the 6- and 12-paradol groups (Table 3). These results indicated that the energy and intake levels of the test compounds were lower in the 8- and 12-paradol groups than they were in the control and 6-paradol groups. Although significant differences were observed in the food intake of the animals belonging to the high-fat diet groups, it was concluded that the antiobesity effects were limited, because both the calorie and test compound intake decreased. 6-Paradol was the most pungent of these compounds, followed sequentially by 8- and 12-paradol.[30] The latter two of these compounds may therefore have had an effect on appetite suppression, although their effects in this regard have not been clarified and further studies would be required.

Table 3 shows the initial and final body weights of the mice fed the different diets, as well as their adipose tissue weight. No differences were observed in the initial body weights of each high-fat diet group. The final body weight was lowest in the 6-paradol group, followed by the 12-paradol group, whereas the final body weight in the control group was found to be the highest of all of the groups tested. Significant differences were observed in body weight between the 6-paradol and control groups ($p < 0.01$) and between the control group and the 6-, 8-, and 12-paradol groups ($p < 0.01$, $p < 0.05$, and $p < 0.05$, respectively). The subcutaneous and epididymal fat weights were lowest in the 6-paradol group, followed by the 8- and 12-paradol groups, with the control group showing the highest subcutaneous and epididymal fat weights of all of the groups tested. Significant differences were also observed in the subcutaneous and epididymal fat weights between the control and 6-paradol groups ($p < 0.05$ and $p < 0.01$, respectively). In comparison to the 6-paradol group, the 8- and 12-paradol groups exhibited significantly higher epididymal fat weights ($p < 0.05$ and $p < 0.01$, respectively). The 6-paradol group showed the lowest level of perirenal fat weight of all the groups tested, followed by the 8-paradol and control groups, with the highest level of fat being observed in the 12-paradol group. A significant difference was also observed in the perirenal fat weights of the 6- and 12-paradol groups ($p < 0.05$).

The level of UCP-1 protein expression in mice fed the high-fat diet with 6-paradol was about 2.6-fold greater than that of the mice given the normal diet ($p < 0.05$, Figure 4). No significant differences were observed in the levels of UCP-1 protein expression between the control, 8-paradol (1.7-fold), and 12-paradol (1.5-fold) groups and the normal diet group. On the basis of these results, it was concluded that the antiobesity activities of the paradol analogues in this study were related to the length of their acyl chain, and 6-paradol was consequently identified as the most promising antiobesity candidate of all of the compounds tested.

It has been reported that the intragastric injection of 6-paradol in rats enhanced the efferent discharges of sympathetic nerves in a dose-dependent manner and also led to a significant increase in the tissue temperature of BAT.[32] A high caloric intake diet and a high-fat diet independent of caloric intake can both stimulate the sympathetic nervous system.[41−43] The activation of BAT by the sympathetic nervous system prevented the occurrence of obesity associated with a high-fat diet in rodents. Furthermore, capsaicin has been reported to activate

Table 3. Food Intake and Body and Adipose Tissue Weights of Mice for Paradol Analogues Study[a]

	diet groups				
	high-fat				normal
parameter	control	6-paradol	8-paradol	12-paradol	
n	9	9	9	9	9
food intake (g/mouse/day)	1.96 ± 0.05	1.89 ± 0.02	1.78 ± 0.03[c]	1.74 ± 0.03[c,e]	2.38 ± 0.06
initial body wt (g)	21.9 ± 0.7	21.8 ± 0.02	22.2 ± 0.2	22.5 ± 1.1	22.3 ± 0.4
final body wt (g)	33.4 ± 0.8	29.7 ± 0.4[c]	31.1 ± 0.6[b]	30.9 ± 0.8[b]	27.6 ± 0.3
subcutaneous fat (mg)	1105.9 ± 99.2	814.0 ± 58.8[b]	938.6 ± 57.1	1035.6 ± 44.7[c]	623.3 ± 49.7
epididymal fat (mg)	1387.4 ± 56.2	668.4 ± 143.1[c]	1180.8 ± 151.9[d]	1269.2 ± 93.3[e]	686.3 ± 50.9
perirenal fat (mg)	393.7 ± 38.7	277.3 ± 53.9	365.3 ± 39.9	455.5 ± 24.5[d]	159.0 ± 17.4

[a]Data are shown as the mean ± SE (n = 9). [b]$p < 0.05$. [c]$p < 0.01$ vs control. [d]$p < 0.05$. [e]$p < 0.01$, vs 6-paradol. Tukey's multiple-range test.

dx.doi.org/10.1021/jf500873a | J. Agric. Food Chem. 2014, 62, 6166−6174

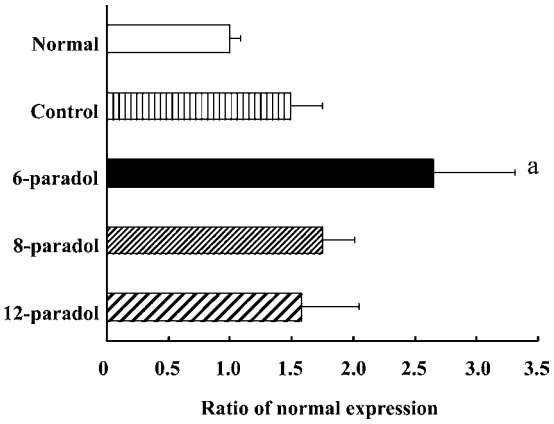

Figure 4. UCP-1 protein expression levels in murine interscapular brown adipose tissue following the oral ingestion of the paradol analogues for 8 weeks. Data are shown as the mean ± SE (n = 9). a, p < 0.05 versus normal; Tukey's multiple-range test.

the sympathetic nervous system.[44] On the basis of these findings, it was concluded that one of the possible mechanisms for the antiobesity effects of 6-paradol involved increased energy metabolism resulting from thermogenic activity in the BAT, as well as an increase in UCP-1 protein expression via the activation of the sympathetic nervous system.

Our understanding of white adipose tissue is currently changing with the realization that it is possible to induce the appearance of brown-like adipocytes in white adipose tissue depots and that these brown-like adipocytes are capable of expressing UCP-1 and activating uncoupled respiration in response to an appropriate stimulus. This process is referred to as the browning of white adipose tissue, and the brown-like cells that appear in white adipose tissue depots are known as brite or beige adipocytes.[45,46] Apart from browning, another manifestation of the metabolic plasticity of white adipose tissue that could be exploited in the context of the management of obesity and associated medical complications is the stimulation of mitochondrial oxidative capacity in a manner that is independent of UCP-1, but linked to the activation of a futile substrate cycle based on lipolysis of triacylglycerols and the re-esterification of the fatty acids in the adipocytes.[47] This approach would lead to increased energy expenditure and reduced adiposity while improving the deleterious conditions associated with mitochondrial dysfunction in white adipose tissue in obesity.[47,48] An increasing number of dietary and pharmacological agents capable of stimulating mitochondrial oxidative metabolism in white adipocytes are being reported in the literature as well as agents capable of modulating the browning of white fat, including UCP-1.[16] Capsaicin and capsinoids have been reported to induce the browning of white adipose tissue in rats fed a high-fat diet supplemented with these compounds.[49] Although the change in white adipose tissue has not been observed in this study, it remains likely that changes in the white adipose tissue were involved in the mechanism of the antiobesity activity of 6-paradol.

Figure 5 shows the mean concentrations of zingerone and 6-, 8-, and 12-paradol in the plasma following oral administration. Under the optimized conditions, linear relationships with good correlation coefficients (r = 0.999, n = 3, respectively) were observed between the peak area ratios and the concentrations of zingerone and 6-, 8-, and 12-paradol in the range of 10.0–1000.0 ng/mL. These experiments were performed using a

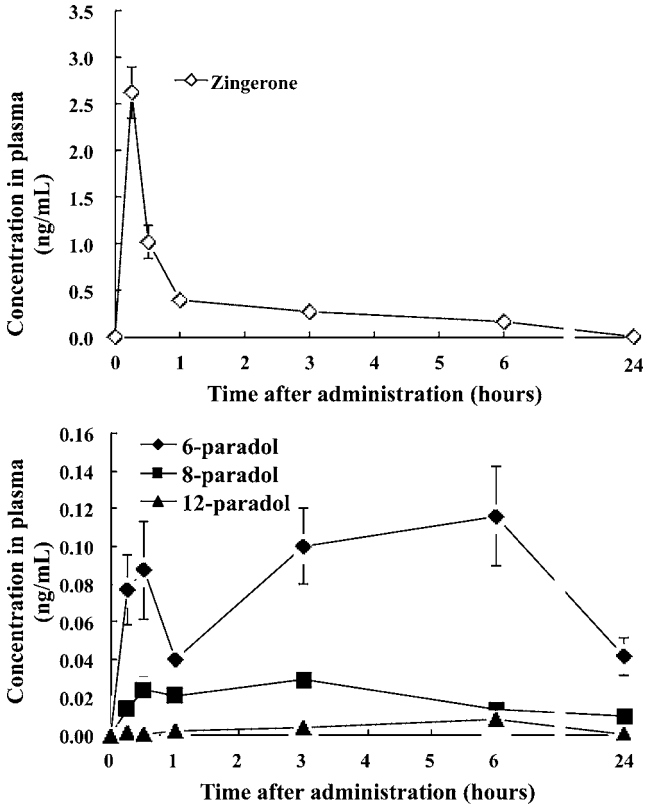

Figure 5. Mean plasma concentrations of the paradol analogues following their oral administration in rats. Rats were fasted for 14 h prior to the oral administration of olive oil (1 mL) containing zingerone or 6-, 8-, or 12-paradol (10 mg/kg). Data are shown as the mean ± SE (n = 3).

standard four-point series for each component. The limit of detection (LOD) and limit of quantitation (LOQ) were calculated according to the International Conference on Harmonization guidelines for the validation of analytical procedures based on the standard deviations of the responses and the slopes of the calibration curves. All four experiments were performed in triplicate and the results averaged to give LODs of 78.6, 0.551, 1.06, and 2.62 ng/mL and LOQs of 236, 1.65, 3.18, and 7.85 ng/mL for zingerone and 6-, 8-, and 12-paradol, respectively. In this study, the plasma concentrations of the tested compounds were determined from the sum of the concentration of the free compound and its glucuronide conjugate, because all of the compounds being tested for egestion were effectively metabolized to the corresponding glucuronides following their absorption. The pharmacokinetic parameters are summarized in Table 4. Zingerone was rapidly absorbed after oral administration, with C_{max} occurring at 0.25 h (t_{max}), whereas 6-, 8-, and 12-paradol were adsorbed at significantly slower rates. Furthermore, the C_{max} values of the paradols decreased as their acyl chain length increased and a significant difference was observed relative to zingerone (p < 0.01, respectively). The AUC_{0-24h} values also decreased as the acyl chain length of the paradols increased. The MRT of zingerone was the shortest of all of the compounds tested at 3.9 h, followed by 12- and 6-paradol, with that of 8-paradol being the longest at 9.5 h.

The water and lipid solubility properties of a drug compound are important factors for consideration in terms of the oral absorption of the material. The calculated logP (clogP) value of

dx.doi.org/10.1021/jf500873a | J. Agric. Food Chem. 2014, 62, 6166–6174

Table 4. Pharmacokinetic Parameters for the Paradol Analogues following Their Oral Administration in Rats[a]

parameter	zingerone	6-paradol	8-paradol	12-paradol
C_{max} (ng/mL)	2624.8 ± 393.4	126 ± 33.9[b]	32.9 ± 8.2[b]	9.5 ± 2.2[b]
t_{max} (h)	0.25	6	3	6
AUC_{0-24h} (ng·h/mL)	4191.7 ± 1132.5	1948.4 ± 504.5[b]	344.5 ± 43.1[b]	112.5 ± 0.8[b,c]
MRT (h)	3.9 ± 0.9	8.8 ± 0.6[b]	9.5 ± 0.4[b]	6.7 ± 0.1[b,c,d]

[a]Data are the sum of intrinsic paradols and their glucuronides and are shown as the mean ± SE (n = 3). [b]$p < 0.01$ vs zingerone. [c]$p < 0.01$ vs 6-paradol. [d]$p < 0.01$ vs 8-paradol, Tukey's multiple-range test.

a compound can be used to provide an index of its lipid solubility. The clogP values of 6-, 8-, and 12-paradol were 4.7, 5.5, and 7.2, respectively, with the increase in the clogP value reflecting the increase in lipid solubility of the compounds. This increase in lipid solubility was attributed to the increase in the length of the acyl chains of the paradol analogues, which reduced their solubility in the intestinal lumen, leading to a decrease in their bioavailability. These results clearly indicate that 6-paradol was effectively absorbed into the enterocyte following oral ingestion and, therefore, suggested that the difference in the absorption properties were related to the different effects of the paradol analogues.

The effect of 6-paradol on norepinephrine-induced lipolysis is shown in Figure 6. The administration of NE at a concentration of 0.1 μg/mL led to a significant increase in the amount of FFAs released by fat cells ($p < 0.05$). In contrast, 6-paradol at a concentration in the range of 10^{-6}–10^{-4} M had no discernible effect on the release of FFAs from fat cells. It was previously reported that capsiate is readily broken down in the intestinal tract to yield vanillyl alcohol and a fatty acid,[50] indicating that the active sites for the antiobesity effect of orally administered capsiate were located in the digestive canal prior to the small intestine. The bioactivity of capsaicin has been attributed to an increase in the secretion of catecholamine from the adrenal medulla, which occurs through the activation of the sympathetic nervous system,[44] as well binding to and activating specific transient receptor potential channels within the gastrointestinal tract.[51] The capsaicin-dependent selective activation of transient receptor potential channels in the upper gastrointestinal tract has been shown to trigger the thermogenic reflex by activating vagal afferents to the brain, as well as sympathetic efferents innervating BAT.[51] Taken together, these results indicated that the active sites for the antiobesity activity of the orally ingested paradol analogues were located in the small intestine.

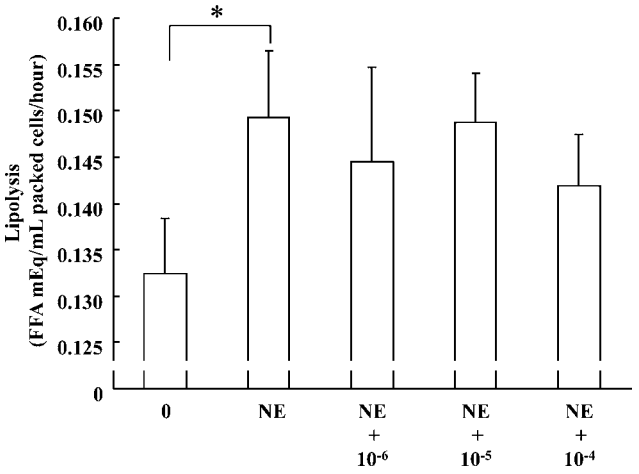

Figure 6. Effect of 6-paradol on lipolysis in fat cells derived from murine epididymal fat following oral ingestion of a high-fat diet for 8 weeks. Fat cells were incubated at 37 °C for 1 h with 6-paradol (10^{-6}, 10^{-5}, or 10^{-4} M) and/or norepinephrine (NE, 0.1 μg/mL). Data are shown as the mean ± SE (n = 4). (*) $p < 0.05$; Student's t test.

Although it has been reported that zingerone and 6-paradol possess similar levels of pungency,[30] the antiobesity activity of zingerone was found to be much lower than that of 6-paradol in the current study. It was reported in another study, however, that zingerone (170 mg/kg) exhibited pronounced antiobesity activity when it was administered to ovariectomized rats via a stomach tube.[31] The intake volumes of the compounds tested in the current study were in the range of 60–85 mg/kg/day. Furthermore, it was envisaged that the evanescent increase in the plasma concentration of zingerone observed as bioavailability would not occur in the present animals as a consequence of ingestion ad libitum. For this reason, it was considered that the intake of zingerone in the current study was too low to exhibit a significant antiobesity effect. Moreover, the results of the current study indicated that receptor related to the pungency of zingerone could be different from that of 6-paradol, although the precise nature of these receptors remains unclear at this stage, and further work would be needed to clarify any potential differences. The bioavailability of zingerone (AUC_{0-24h}) was found to be >2-fold greater than that of 6-paradol, and zingerone also had a faster absorption rate (t_{max}; Table 4; Figure 5). It has been reported that the accelerated effect of lipid decomposition led to a decrease in the adipose tissue weight of rats treated with zingerone via a stomach tube for 72 days.[31] However, 6-paradol did not have an effect on murine adiposities in the current study, as measured using the method of Han et al.[31] (Figure 6). Although the differences observed between zingerone and 6-paradol could be related to differences in the animal species studied,[31] it was speculated that they were most likely related to the active sites because of the differences in the physical properties of these compounds.

The level of UCP-3 expression in the femoral muscle following the oral ingestion of 6-paradol was also investigated. No differences were observed in the food intakes between the high-fat control and 6-paradol groups (Table 5). Table 4 also shows the initial and final body weights of the mice fed the different diets, as well as their adipose tissue weight. These data show that the final body weight of the 6-paradol group was significantly lower than that of the high-fat control group ($p < 0.01$). The amounts of subcutaneous, epididymal, and perirenal fat in the 6-paradol group were also significantly lower than those found in the high-fat control group ($p < 0.05$, $p < 0.01$, and $p < 0.05$, respectively).

Figure 7 shows the changes in the expression levels of UCP-3 protein in the femoral muscle mitochondria. The level of UCP-3 protein expression in mice fed the high-fat diet with 6-paradol was about 1.5-fold greater than that of those given the normal diet ($p < 0.05$). In contrast, the level of UCP-3 expression in

Table 5. Food Intake and Body and Adipose Tissue Weights[a]

parameter	diet groups		
	high-fat		normal
	control	6-pardol	
n	9	10	10
food intake (g/mouse/day)	1.96 ± 0.05	1.89 ± 0.02	2.14 ± 0.05
initial body wt (g)	22.0 ± 0.7	21.9 ± 0.2	22.6 ± 0.4
final body wt (g)	33.4 ± 0.8	30.1 ± 0.5[c]	27.9 ± 0.2
subcutaneous fat (mg)	1105.9 ± 99.2	851.6 ± 65.6[b]	603.4 ± 48.9
epididymal fat (mg)	1387.4 ± 72.8	632.1 ± 134.9[c]	669.3 ± 48.7
perirenal fat (mg)	393.7 ± 36.5	258.3 ± 51.9[b]	153.6 ± 16.5

[a]Data are shown as the mean ± SE (n = 9 or 10). [b]$p < 0.05$. [c]$p < 0.01$, Student's t test.

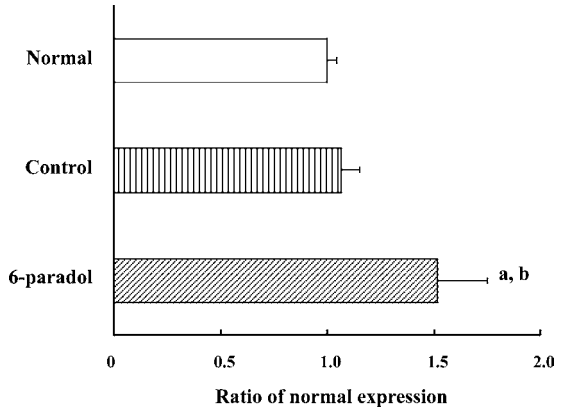

Figure 7. UCP-3 protein expression levels in murine femoral muscles following the oral ingestion of 6-paradol for 8 weeks. Data are shown as the mean ± SE (n = 9). a, $p < 0.05$ versus normal; b, $p < 0.05$ versus control; Tukey's multiple-range test.

the high-fat control group (1.1-fold) remained unchanged relative to the normal diet group, although it was significantly different from the 6-paradol diet group ($p < 0.05$). Although the role of UCP-3 remains unclear, it was concluded that the increase in UCP-3 expression was one of the mechanisms responsible for the antiobesity effects of 6-paradol.

In summary, the antiobesity activities of orally ingested paradols with different acyl chain lengths were investigated. The effect of 6-paradol was stronger than that of the positive control dihydrocapsiate. Our results also showed that the length of the acyl chain of the paradol analogues had a significant impact on the strength of their antiobesity activity. Furthermore, a comparison of the antiobesity activities of 6-, 8-, and 12-paradol revealed that the strength of their antiobesity activities was also related to the length of their acyl chain. On the basis of these results, it was concluded that the mechanisms of the antiobesity activity of 6-paradol involve increased energy metabolism in BAT, as well as an increase in UCP-1 protein expression, which occurred through the activation of the sympathetic nervous system.

AUTHOR INFORMATION

Corresponding Author

*(D.W.) E-mail: watase@fukuoka-u.ac.jp. Phone: +81-92-871-6631. Fax: +81-92-862-4431.

Notes

The authors declare no competing financial interest.

ABBREVIATIONS USED

BAT, brown adipose tissue; UCP, uncoupling protein; C_{max}, maximum concentration in plasma; t_{max}, time to reach C_{max}; AUC_{0-24h}, area under plasma concentration−time curve from 0 to 24 h; MRT, mean residence time; NE, norepinephrine; FFA, free fatty acid; LOD, limit of detection; LOQ, limit of quantitation; clogP, calculated logP

REFERENCES

(1) Obesity: preventing and managing the global epidemic. Report of a WHO consultation. *WHO Tech. Rep. Ser.* **2000**, *No. 894*, i−xii, 1−253.

(2) Diepvens, K.; Westerterp, K. R.; Westerterp-Plantenga, M. S. Obesity and thermogenesis related to the consumption of caffeine, ephedrine, capsaicin, and green tea. *Am. J. Physiol. Regul. Integr. Comp. Physiol.* **2007**, *292*, R77−R85.

(3) Spiegelman, B. M.; Flier, J. S. Obesity and the regulation of energy balance. *Cell* **2001**, *104*, 531−543.

(4) Himms-Hagen, J. Does brown adipose tissue (BAT) have a role in the physiology or treatment of human obesity? *Rev. Endocr. Metab. Disord.* **2001**, *2*, 395−401.

(5) Lowell, B. B.; S-Susulic, V.; Hamann, A.; Lawitts, J. A.; Himms-Hagen, J.; Boyer, B. B.; Kozak, L. P.; Flier, J. S. Development of obesity in transgenic mice after genetic ablation of brown adipose tissue. *Nature* **1993**, *366*, 740−742.

(6) Lowell, B. B. Adaptive thermogenesis: turning on the heat. *Curr. Biol.* **1998**, *8*, R517−R520.

(7) Lowell, B. B.; Spiegelman, B. M. Towards a molecular understanding of adaptive thermogenesis. *Nature* **2000**, *404*, 652−660.

(8) Nicholls, D. G.; Locke, R. M. Thermogenic mechanisms in brown fat. *Physiol. Rev.* **1984**, *64*, 1−64.

(9) Enerback, S.; Jacobsson, A.; Simpson, E. M.; Guerra, C.; Yamashita, H.; Harper, M. E.; Kozak, L. P. Mice lacking mitochondrial uncoupling protein are cold-sensitive but not obese. *Nature* **1997**, *387*, 90−94.

(10) Wolf, G. The uncoupling proteins UCP2 and UCP3 in skeletal muscle. *Nutr. Rev.* **2001**, *59*, 56−57.

(11) Erlanson-Albertsson, C. The role of uncoupling proteins in the regulation of metabolism. *Acta Physiol. Scand.* **2003**, *178*, 405−412.

(12) Fink, B. D.; Hong, Y. S.; Mathahs, M. M.; Scholz, T. D.; Dillon, J. S.; Sivitz, W. I. UCP2-dependent proton leak in isolated mammalian mitochondria. *J. Biol. Chem.* **2002**, *277*, 3918−3925.

(13) Affourtit, C.; Crichton, P. G.; Parker, N.; Brand, M. D. Novel uncoupling proteins. *Novartis Found. Symp.* **2007**, *287*, 70−80 (discussion 80−91).

(14) Seifert, E. L.; Bezaire, V.; Estey, C.; Harper, M. E. Essential role for uncoupling protein-3 in mitochondrial adaptation to fasting but not in fatty acid oxidation or fatty acid anion export. *J. Biol. Chem.* **2008**, *283*, 25124−25131.

(15) Clapham, J. C.; Arch, J. R.; Chapman, H.; Haynes, A.; Lister, C.; Moore, G. B.; Piercy, V.; Carter, S. A.; Lehner, I.; Smith, S. A.; Beeley, L. J.; Godden, R. J.; Herrity, N.; Skehel, M.; Changani, K. K.; Hockings, P. D.; Reid, D. G.; Squires, S. M.; Hatcher, J.; Trail, B.; Latcham, J.; Rastan, S.; Harper, A. J.; Cadenas, S.; Buckingham, J. A.; Brand, M. D.; Abuin, A. Mice overexpressing human uncoupling protein-3 in skeletal muscle are hyperphagic and lean. *Nature* **2000**, *406*, 415−418.

(16) Bonet, M. L.; Oliver, P.; Palou, A. Pharmacological and nutritional agents promoting browning of white adipose tissue. *Biochim. Biophys. Acta* **2013**, *1831*, 969−985.

(17) Rodriguez, V. M.; Portillo, M. P.; Pico, C.; Macarulla, M. T.; Palou, A. Olive oil feeding up-regulates uncoupling protein genes in rat brown adipose tissue and skeletal muscle. *Am. J. Clin. Nutr.* **2002**, *75*, 213−220.

(18) Shen, Y.; Song, S. J.; Keum, N.; Park, T. Olive leaf extract attenuates obesity in high-fat diet-fed mice by modulating the expression of molecules involved in adipogenesis and thermogenesis. *Evidence-Based Complement. Alternat. Med.* **2014**, *2014*, No. 971890.
(19) Nelson, E.; Dawson, L. The constitution of capsaicin, the pungent principle of *Capsicum*. III. *J. Am. Chem. Soc.* **1923**, *45*, 2179−2181.
(20) Dib, B. Effects of intrathecal capsaicin on autonomic and behavioral heat loss responses in the rat. *Pharmacol., Biochem. Behav.* **1987**, *28*, 65−70.
(21) Watanabe, T.; Kawada, T.; Kato, T.; Harada, T.; Iwai, K. Effects of capsaicin analogs on adrenal catecholamine secretion in rats. *Life Sci.* **1994**, *54*, 369−374.
(22) Kawada, T.; Sakabe, S.; Aoki, N.; Watanabe, T.; Higeta, K.; Iwai, K.; Sugimoto, E. Intake of sweeteners and pungent ingredients increases the thermogenin content in brown adipose tissue of rat. *J. Agric. Food Chem.* **1991**, *39*, 651−654.
(23) Kawada, T.; Hagihara, K.; Iwai, K. Effects of capsaicin on lipid metabolism in rats fed a high fat diet. *J. Nutr.* **1986**, *116*, 1272−1278.
(24) Jancso, G.; Kiraly, E.; Jancso-Gabor, A. Pharmacologically induced selective degeneration of chemosensitive primary sensory neurones. *Nature* **1977**, *270*, 741−743.
(25) Kobata, K.; Sutoh, K.; Todo, T.; Yazawa, S.; Iwai, K.; Watanabe, T. Nordihydrocapsiate, a new capsinoid from the fruits of a nonpungent pepper, *Capsicum annuum*. *J. Nat. Prod.* **1999**, *62*, 335−336.
(26) Ohnuki, K.; Haramizu, S.; Watanabe, T.; Yazawa, S.; Fushiki, T. CH-19 sweet, nonpungent cultivar of red pepper, increased body temperature in mice with vanilloid receptors stimulation by capsiate. *J. Nutr. Sci. Vitaminol. (Tokyo)* **2001**, *47*, 295−298.
(27) Ohnuki, K.; Haramizu, S.; Oki, K.; Watanabe, T.; Yazawa, S.; Fushiki, T. Administration of capsiate, a non-pungent capsaicin analog, promotes energy metabolism and suppresses body fat accumulation in mice. *Biosci., Biotechnol., Biochem.* **2001**, *65*, 2735−2740.
(28) Kim, K. M.; Kawada, T.; Ishihara, K.; Inoue, K.; Fushiki, T. Swimming capacity of mice is increased by oral administration of a nonpungent capsaicin analog, stearoyl vanillylamide. *J. Nutr.* **1998**, *128*, 1978−1983.
(29) Liu, L.; Lo, Y.; Chen, I.; Simon, S. A. The responses of rat trigeminal ganglion neurons to capsaicin and two nonpungent vanilloid receptor agonists, olvanil and glyceryl nonamide. *J. Neurosci.* **1997**, *17*, 4101−4111.
(30) Locksley, H.; Rainey, D.; Rohan, T. Pungent compounds. Part I. An improved synthesis of the paradols (alkyl 4-hydroxy-3-methoxyphenethyl ketones) and an assessment of their pungency. *J. Chem. Soc., Perkin Trans. 1* **1972**, 3001−3006.
(31) Han, L. K.; Morimoto, C.; Zheng, Y. N.; Li, W.; Asami, E.; Okuda, H.; Saito, M. [Effects of zingerone on fat storage in ovariectomized rats]. *Yakugaku Zasshi* **2008**, *128*, 1195−1201.
(32) Iwami, M.; Mahmoud, F. A.; Shiina, T.; Hirayama, H.; Shima, T.; Sugita, J.; Shimizu, Y. Extract of grains of paradise and its active principle 6-paradol trigger thermogenesis of brown adipose tissue in rats. *Auton. Neurosci.* **2011**, *161*, 63−67.
(33) Sugita, J.; Yoneshiro, T.; Hatano, T.; Aita, S.; Ikemoto, T.; Uchiwa, H.; Iwanaga, T.; Kameya, T.; Kawai, Y.; Saito, M. Grains of paradise (*Aframomum melegueta*) extract activates brown adipose tissue and increases whole-body energy expenditure in men. *Br. J. Nutr.* **2013**, *110*, 733−738.
(34) Kobata, K.; Kawaguchi, M.; Watanabe, T. Enzymatic synthesis of a capsinoid by the acylation of vanillyl alcohol with fatty acid derivatives catalyzed by lipases. *Biosci., Biotechnol., Biochem.* **2002**, *66*, 319−327.
(35) Hong, Y.; Fink, B. D.; Dillon, J. S.; Sivitz, W. I. Effects of adenoviral overexpression of uncoupling protein-2 and -3 on mitochondrial respiration in insulinoma cells. *Endocrinology* **2001**, *142*, 249−256.
(36) Yamaoka, K.; Nakagawa, T.; Uno, T. Statistical moments in pharmacokinetics. *J. Pharmacokinet. Biopharm.* **1978**, *6*, 547−558.
(37) Yamaoka, K.; Tanigawara, Y.; Nakagawa, T.; Uno, T. A pharmacokinetic analysis program (multi) for microcomputer. *J. Pharmacobiodyn.* **1981**, *4*, 879−885.
(38) Rodbell, M. Metabolism of isolated fat cells. I. Effects of hormones on glucose metabolism and lipolysis. *J. Biol. Chem.* **1964**, *239*, 375−380.
(39) Zapf, J.; Schoenle, E.; Waldvogel, M.; Sand, I.; Froesch, E. R. Effect of trypsin treatment of rat adipocytes on biological effects and binding of insulin and insulin-like growth factors: further evidence for the action of insulin-like growth factors through the insulin receptor. *Eur. J. Biochem.* **1981**, *113*, 605−609.
(40) Fink, B. D.; Herlein, J. A.; Almind, K.; Cinti, S.; Kahn, C. R.; Sivitz, W. I. Mitochondrial proton leak in obesity-resistant and obesity-prone mice. *Am. J. Physiol. Regul. Integr. Comp. Physiol.* **2007**, *293*, R1773−R1780.
(41) Schwartz, J. H.; Young, J. B.; Landsberg, L. Effect of dietary fat on sympathetic nervous system activity in the rat. *J. Clin. Invest.* **1983**, *72*, 361−370.
(42) Rothwell, N. J.; Stock, M. J.; Warwick, B. P. Energy balance and brown fat activity in rats fed cafeteria diets or high-fat, semisynthetic diets at several levels of intake. *Metabolism* **1985**, *34*, 474−480.
(43) Young, J. B.; Walgren, M. C. Differential effects of dietary fats on sympathetic nervous system activity in the rat. *Metabolism* **1994**, *43*, 51−60.
(44) Watanabe, T.; Kawada, T.; Yamamoto, M.; Iwai, K. Capsaicin, a pungent principle of hot red pepper, evokes catecholamine secretion from the adrenal medulla of anesthetized rats. *Biochem. Biophys. Res. Commun.* **1987**, *142*, 259−264.
(45) Petrovic, N.; Walden, T. B.; Shabalina, I. G.; Timmons, J. A.; Cannon, B.; Nedergaard, J. Chronic peroxisome proliferator-activated receptor gamma (PPARgamma) activation of epididymally derived white adipocyte cultures reveals a population of thermogenically competent, UCP1-containing adipocytes molecularly distinct from classic brown adipocytes. *J. Biol. Chem.* **2010**, *285*, 7153−7164.
(46) Wu, J.; Bostrom, P.; Sparks, L. M.; Ye, L.; Choi, J. H.; Giang, A. H.; Khandekar, M.; Virtanen, K. A.; Nuutila, P.; Schaart, G.; Huang, K.; Tu, H.; van Marken Lichtenbelt, W. D.; Hoeks, J.; Enerback, S.; Schrauwen, P.; Spiegelman, B. M. Beige adipocytes are a distinct type of thermogenic fat cell in mouse and human. *Cell* **2012**, *150*, 366−376.
(47) Flachs, P.; Rossmeisl, M.; Kuda, O.; Kopecky, J. Stimulation of mitochondrial oxidative capacity in white fat independent of UCP1: a key to lean phenotype. *Biochim. Biophys. Acta* **2013**, *1831*, 986−1003.
(48) Kusminski, C. M.; Scherer, P. E. Mitochondrial dysfunction in white adipose tissue. *Trends Endocrinol. Metab.* **2012**, *23*, 435−443.
(49) Joo, J. I.; Kim, D. H.; Choi, J. W.; Yun, J. W. Proteomic analysis for antiobesity potential of capsaicin on white adipose tissue in rats fed with a high fat diet. *J. Proteome Res.* **2010**, *9*, 2977−2987.
(50) Iida, T.; Moriyama, T.; Kobata, K.; Morita, A.; Murayama, N.; Hashizume, S.; Fushiki, T.; Yazawa, S.; Watanabe, T.; Tominaga, M. TRPV1 activation and induction of nociceptive response by a non-pungent capsaicin-like compound, capsiate. *Neuropharmacology* **2003**, *44*, 958−967.
(51) Ono, K.; Tsukamoto-Yasui, M.; Hara-Kimura, Y.; Inoue, N.; Nogusa, Y.; Okabe, Y.; Nagashima, K.; Kato, F. Intragastric administration of capsiate, a transient receptor potential channel agonist, triggers thermogenic sympathetic responses. *J. Appl. Physiol. (1985)* **2011**, *110*, 789−798.

JOURNAL OF AGRICULTURAL AND FOOD CHEMISTRY

Article

pubs.acs.org/JAFC

Isolation of the Sapogenin from Defatted Seeds of *Camellia oleifera* and Its Neuroprotective Effects on Dopaminergic Neurons

Yong Ye,* Fei Fang, and Yue Li

Department of Pharmaceutical Engineering, School of Chemistry and Chemical Engineering, South China University of Technology, Guangzhou 510640, People's Republic of China

ABSTRACT: Sasanqua saponin is a major active compound in the defatted seeds of *Camellia oleifera* but is always discarded without effective utilization. The sapogenin from hydrolysis of sasanqua saponin was purified, and its amination derivative was investigated on its neuroprotective effects, which were evaluated by animal models of Parkinson disease in mice induced by 1-methyl-4-phenyl-1,2,3,6-tetrahydropyridine (MPTP). The results showed that the sapogenin and its derivative increased dopamine content in striatum and tyrosine hydroxylase (TH) positive cells in substantia nigra and relieved inflammation and behavioral disorder, but the effect on movement was reversed by dopamine receptor antagonist haloperidol and was not intervened by adenosine receptor antagonist CGS 15943. Molecular simulation showed the interaction between dopamine receptor and the sapogenin or its derivative. It is proven that the sapogenin can protect dopamine neurons through antineuroinflammation and activation of dopamine receptor rather than adenosine receptor, and its amination improves the effects. This research provides the prospective prodrugs for Parkinson disease and a new medicinal application of sasanqua saponin.

KEYWORDS: *sasanqua saponin, amination, Camellia oleifera, neurodegeneration, Parkinson disease, dopaminergic neuron*

INTRODUCTION

Parkinson disease (PD) is a chronic neurodegenerative disease caused by extrapyramidal dysfunction, which is related to genetic factors, environmental factors, mitochondrial dysfunction, and so forth,[1] and is characterized with the loss of dopaminergic neurons in midbrain and the formation of Lewy body with the main component of α-synuclein.[2] Its clinical symptoms will appear since almost 50% of dopaminergic neurons located at substantia nigra compact (SNC) are lost and the concentration of dopamine in the striatum decreases to 80%,[3] including motor dysfunction of bradykinesia, tremor, rigidity, and gait disorders as well as movement unassociated symptoms such as the smell sense disorder, autonomic nerve dysfunction, depression, cognitive impairment, sleep disorders, and so forth. Currently, there is no perfect treatment for PD, and traditional treatment strategy is L-dopa replacement therapy. Although the clinical symptoms can be controlled, disease progression cannot be prevented. Moreover, long-term L-dopa treatment can lead to efficacy reduction and severe adverse effects, lowering the quality of patients' lives.[4] In recent years, medication therapy of PD has changed from direct dopamine supplement to multilevel therapy, aiming at reliving the symptoms and impeding the progression of the disease at the same time.[5] Natural medicines play an important role in therapy of PD.

Camellia oleifera, an edible oil plant, is mainly distributed in China, but the defatted seeds are discarded, leading to environmental pollution and waste of resource. Flavonoids, saponins, and polysaccharides are the main compounds in the defatted seeds of *C. oleifera*,[6] but flavonoids and polysaccharides are unstable in vivo and cannot take effect in the central system because it is difficult for them to pass through the blood brain barrier.[7,8] Sasanqua saponin is a safe compound with LD_{50} 4.5 g/kg and accumulation coefficient 5.3 in rats.[9] It has a stable block called sapogenin with a lot of pharmacological activities of antioxidation, anti-inflammation, immunomodulation, and antitumor,[10−12] and it may play a role in neuroprotection.

Saponin is one of the active ingredients in many herbs, and some have neuroprotective effects. It is found that ginsenoside Rg1 can reverse the changes of neurotransmitters caused by 1-methyl-4-phenyl-1,2,3,6-tetrahydropyridine (MPTP),[13] and ginsenoside Re has significant inhibition on apoptosis of nigra neurons in mouse caused by MPTP,[14] and gypenosides can cause neuroprotective effects through enhancing activity of antioxidative enzymes and inhibiting generation of hydroxyl radicals and lipid peroxide to reduce Glu-mediated oxidative nerve injury.[15] Unlike those saponins, sasanqua saponin from seeds of *C. oleifera* has a different structure of pentacyclic triterpenoids, whose main active block is sapogenin.[16] Our previous research proved the anti-inflammatory and analgesic activities of the sapogenin,[17] diclosing its central roles. The protective role of the sapogenin and its derivative on dopaminergic neurons is worth investigation.

MATERIALS AND METHODS

Materials. The defatted seeds of *Camellia oleifera* were collected from The Oil Factory in Meizhou of Guangdong province, China. Macroreticular resin AB-8 was purchased from Cangzhou Resin Company (Hebei, China). Reagents for synthesis were triphenyl chloromethane, triphenyl phosphine, and diethyl azodicarboxylate bought from J & K Scientific Ltd.

Received: March 10, 2014
Revised: May 16, 2014
Accepted: June 8, 2014
Published: June 9, 2014

ACS Publications © 2014 American Chemical Society

(Beijing, China). Drugs for animal tests were MPTP and CGS 15943 purchased from Sigma-Aldrich Company (St. Louis, MO, U.S.) and haloperidol from Shanghai Pharmaceutical Co. Ltd. (Shanghai, China). TNF-α, IL-1β, and tyrosine hydroxylase (TH) immunoassay kits were bought from Jiancheng Biotech. Co. (Nanjing, China). Other chemicals were purchased from Qianhui Reagent Company (Guangzhou, China).

Animals. The experiments were carried out on male Kunming mice of weight 30 ± 3 g. The animals were housed under conditions of 25 ± 2 °C, 50 ± 10% humidity with a 12 h light/dark cycle. Food and water were accessible ad libitum. The experiments were performed in accordance with the Chinese Guidelines for the use of laboratory animals, which conforms to the European Union Directive for the protection of experimental animals (2011/63/EU), and received approval (Permit No. 13910) from the Animal Experimentation Ethic Committee of South China University of Technology. All efforts were made to minimize animal suffering and to reduce the number of animals used.

Isolation of the Sapogenin. The seeds of *C. oleifera* were defatted with *n*-hexane in the Soxhlet apparatus for 8 h. One kilogram of the defatted seeds was extracted with 15 L of 70% (V/V) methanol aqueous solution under reflux at 80 °C for 2 h. The filtrate was vaporized to 5 L in reduced pressure, was flowed at 2 mL/min through the column (diameter 5 cm × height 30 cm) filled with macroreticular resin AB-8, and then was eluted by 2 L of 80% (V/V) ethanol aqueous solution. The eluent was added to 52 mL of hydrochloride acid and was refluxed at 80 °C for 5 h. The precipitate was collected and dissolved in 500 mL of 80% ethanol containing 25 g of sodium hydroxide and was refluxed for the second time at 80 °C for 5 h. The precipitate was collected and crystallized with diethyl ether and was dried in vacuum condition. Then, 82 g of the sapogenin was obtained. The scheme of extraction is illustrated in Figure 1.

Synthesis of Sapogenin Derivative. Fifty grams of the sapogenin was dissolved in 300 mL of pyridine, was mixed with triphenyl chloromethane (28.4 g), and was stirred at 50 °C for 8 h. Then, acetic anhydride (20.8 g) was added into the mixture and was stirred for 15 h. The solution was added to 4.7 mL of formic acid and was heated to 100−110 °C under reflux for 1 h and then was cooled to 20 °C. Five grams of ammonia, 0.5 g of triphenyl phosphine, and 0.5 g of diethyl azodicarboxylate were mixed into the solution, stirring for 9 h. Finally, 28 g of potassium carbonate was added, stirring for 1 h. Pyridine was distilled off under reduced pressure, and the soluble fractions in water and toluene were removed stepwise by 500 mL of water and toluene. The residue was dissolved in methanol to crystallize and was dried under vacuum condition. Twenty-six grams of the product was gained. The synthetic route is illustrated in Figure 2.

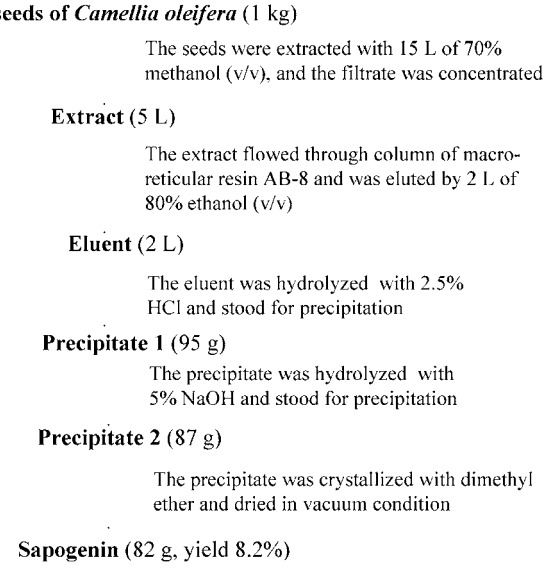

Figure 1. Scheme of sapogenin isolation from the defatted seeds of *Camellia oleifera*.

Structural Analysis. UV spectra analysis was carried out on UV-3010 ultraviolet spectrometer (Hitachi Company, Japan) scanning from 200 to 600 nm. IR spectra were measured on Nicolet 380 FT-IR spectrometer (Nicolet Apparatus Company, U.S.) with KBr tablets from 4000 to 400 cm^{-1} with resolution 2 cm^{-1}. Mass spectra were recorded on Bruker Esquire Hct Plus Mass spectrometer with electrospray ionization (ESI, Bruker Company, Germany) in m/z of cation model scanning from 150 to 1200 for 60 min. NMR spectra were determined on 400 MHz AM NMR (Bruker Company, Switzerland) in DMSO-d_6 operating at 101 MHz for ^{13}C NMR and at 400 MHz for ^{1}H NMR.

PD Model Induced by MPTP. The experiment was performed according to ref 18. Eighty mice were randomly divided into 10 groups of 8 mice for each: normal group, MPTP group, four medicated groups, and four antagonist groups. Medicated groups of mice were intragastricly administered once a day with the sapogenin and its derivative at 25 mg/kg (low dose) and 100 mg/kg (high dose), respectively, for 6 days; the antagonist groups received 1 mg/kg haloperidol or CGS 15 943 (intraperitoneal injection (i.p.)) plus a high dose of the sapogenin or the derivative (i.g.), and the other groups were fed with normal saline instead. Haloperidol, a dopamine receptor antagonist, can decrease dopamine neurotransmission in the striatum and can induce Parkinson disease-like symptoms in humans.[19] CGS 15943 is a competitive adenosine receptor antagonist and a behavioral stimulant in animals.[20] These drugs were used in this experiment to deduce whether the drugs took effect through the dopamine receptor pathway or through the adenosine receptor pathway. On the seventh day of administration, the mice except the normal group were intraperitoneally injected with 20 mg/kg MPTP once every 2 h for three consecutive times to prepare the PD mice model. The mice were reared for an additional 7 days and were decapitated after behavioral tests; the striatum of half the brain was quickly separated, and remain of the half was used to determine the levels of TNF-α and IL-1β with the ELISA method of the kit description. The other half of the brain was kept for immunohistochemical analysis. The striatum was homogenized in 1 mL 0.1 mol/L pH 7.4 PBS-EDTA buffer. The homogenate was centrifuged at 3000g for 10 min, and the content of dopamine (DA) in supernatant was measured by high-performance liquid chromatography-electron-capture detector (HPLC-ECD, Agilent Company, U.S.).[21] The operating conditions of HPLC were column, Diamonsil C18 (150 × 4.6 mm, 5 μm); mobile phase, 110 mM citrate buffer/100 mM EDTA/70 mM 1-octanesulfonate sodium solution and 20% (V/V) methanol; flow rate, 1 mL/min; temperature, 30 °C; and injection volume, 20 μL.

dx.doi.org/10.1021/jf501166w | J. Agric. Food Chem. 2014, 62, 6175−6182

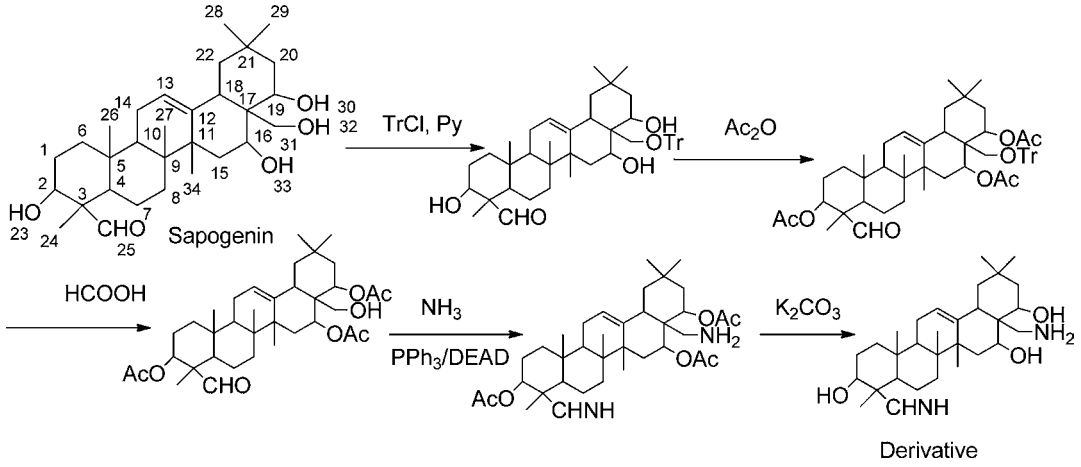

Figure 2. Synthetic route of the sapogenin derivative.

Behavioral Test. The locomotive activities of mice were monitored by a ZZ-6 spontaneous activity apparatus (Chengdu Taimeng Software Co., China). Moving counts were collected by computer with the infrared-sensitive motion-detection system. Each mouse was placed in the testing chamber for 10 min of adaptation, followed by a 10 min recording.[22] The rotarod test was used to detect the balance of mice. Mice were trained three times before the test, and the rotating speed was set to 15 r/min.[23] Latency to fall was calculated five times within 180 s. In the traction test, a horizontal metal rod with diameter of 1.5 mm was used as a hanging rod at a height of 30 cm from the ground. Latency to fall was recorded to evaluate their motor coordination.[24]

Assay of TH Expression. The test was carried out on the basis of the protocol.[25] The half brain of a mouse was sunk in paraformaldehyde solution (pH 7.4, 40 g/L) containing 300 g/L sucrose for 48 h and was cryostat sectioned to slices (60 mm thickness). Nigra slices were incubated in TH antibody with dilution of 1:5000, were stained by diaminobenzidine (DAB), and were mounted to slides for photograph and TH positive cell counting.

Simulation of Molecular Interaction. Molecular docking was simulated by Discovery Studio V2.5 software (Accelry Inc., CA, U.S.) in the following procedure.[26] Structural data of dopamine receptor was downloaded from Brookhaven Library.[27] The missing amino acids and hydrogens were supplemented, and excessive protein conformation was removed. Dopamine receptor was defined as the receptor, and the binding sites and coordinates were defined. A new plot window was opened to draw structures of the sapogenin and its derivative, to optimize 3D geometric structures, and to apply CHARMm force field to ensure correct bond length and bond angle in a state of energy stability.[28] CDOCKER Protocol was run to obtain binding parameters, which were used to evaluate the interaction. CDOCKER energy and CKOCKER interaction energy were two important parameters, and their absolute values were in accord with the affinity and action force between the receptor and the ligand.

Statistical Analysis. Data were expressed as mean ± standard deviation ($\bar{x} \pm s$) and were analyzed with SPSS13.0 software. Significant tests among the groups were based on one-way ANOVA and Student−Newman−Keuls (SNK) test.

RESULTS AND DISCUSSION

Structure of the Sapogenin and Its Derivative. Sasanqua saponin has certain antioxidative, anti-inflammatory, and analgesic effects, and the sapogenin from hydrolysis of the sasanqua saponin could increase cellular uptake and could promote its roles in vivo.[17] The amino group enhances the interaction of drugs with some receptors[29] and may be helpful to PD. Thus, the sapogenin was purified and was derived by amination in hydroxyl and aldehyde groups in order to improve its neuroprotective effects.

Table 1. Influence of the Sapogenin and Its Derivative on DA Content in Striatum of Mice Treated with MPTP ($\bar{x} \pm s$, $n = 8$)[a]

group	dose (mg/kg)	DA content (pmol)	TH^+ neurons number
normal saline		63.2 ± 8.1[b]	39.6 ± 8.1[b]
MPTP		23.4 ± 7.4	6.6 ± 3.7
sapogenin	25	30.4 ± 9.8	12.6 ± 5.8
sapogenin	100	40.9 ± 8.5[b]	35.8 ± 6.9[b]
derivative	25	33.2 ± 8.7	14.4 ± 8.0
derivative	100	42.8 ± 8.4[b]	36.2 ± 8.6[b]
DA antagonist/sapogenin	1/100	41.7 ± 6.2[b]	35.6 ± 5.8[b]
DA antagonist/derivative	1/100	42.7 ± 7.9[b]	36.4 ± 6.5[b]
adenosine antagonist/sapogenin	1/100	39.1 ± 4.6[b]	32.8 ± 6.6[b]
adenosine antagonist/derivative	1/100	41.3 ± 4.4[b]	34.2 ± 6.1[b]

[a]Mice were administered (i.g.) with sapogenin or derivative or were injected (i.p.) with haloperidol (dopamine antagonist) or CGS 15943 (adenosine antagonist) once a day for 6 days and then were injected (i.p.) with MPTP. Seven days later, striatum was taken for determination of dopamine by HPLC. TH positive neurons in nigra were counted under microscope in five visual fields (4 mm^2) for each of eight slices after immunostaining. [b]$p < 0.01$, compared with MPTP group.

The purified sapogenin was an amorphous powder and was insoluble in water, chloroform, petroleum ether, and dimethyl ether and was soluble in methanol, ethanol, acetone, and ethyl acetate. mp 251.2−251.7 °C. There was an absorption peak at 207 nm in UV spectra. IR spectra showed a smaller peak of hydroxyl groups at 3435 cm^{-1} and no characteristic absorption peak of α, β-unsaturated ester, and ether. In MS, m/z was 488 (M^+). ^1H NMR spectra had no Tig moiety signals but showed

dx.doi.org/10.1021/jf501166w | J. Agric. Food Chem. 2014, 62, 6175−6182

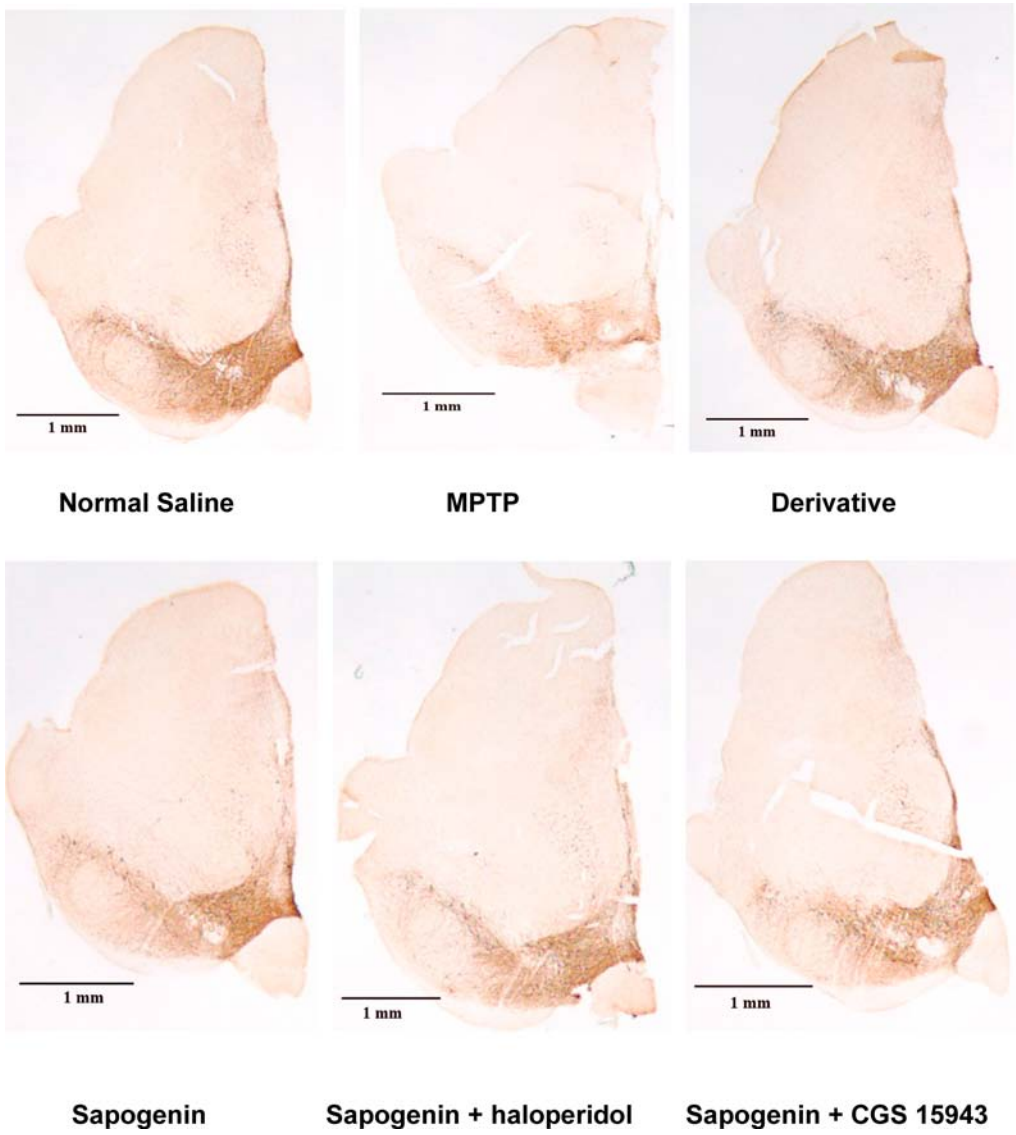

Figure 3. TH immunohistochemistry of substantia nigra sections in mice with different treatments. Sapogenin, 100 mg/kg, i.g.; derivative, 100 mg/kg, i.g.; MPTP, 20 mg/kg × 3 i.p.; haloperidol, 1 mg/kg, i.p.; CGS 15943, 1 mg/kg, i.p. Half brains were sectioned for determination of TH expression by immunohistochemistry. The photos were taken by camera in 50 times magnification.

one carbonyl (d 9.97, J = 12.48). ^{13}C NMR spectra had signals of one carbonyl carbon and two olefinic carbons. The signals in ^{13}C NMR spectra were assigned as follows: δ208.7 (C-25), 144.5 (C-12), 123.3 (C-13), 74.9 (C-2), 70.3 (C-19), 67.7 (C-16), 65.6 (C-31), 52.6 (C-3), 50.1 (C-4), 47.5 (10, 22), 45.9 (C-11, 20), 42.1 (C-17, 18), 38.4 (C-6, 9, 15), 36.1 (C-5, 8), 30.7 (C-21, C-28, 29), 27.1 (C-1), 24.9 (C-14, 34), 19.5 (C-7), 16.8 (C-24, 26, 27). Its property and structure are the same with camelliagenin ($C_{30}H_{48}O_5$) in the reference.[30]

The derivative of sapogenin had similar properties as the sapogenin. The maximum absorption peak was at 215 nm in UV spectra. IR spectra showed imino groups at 1640 cm^{-1}. MS: m/z 486 (M^+). There were signals of imino proton (d 9.61) and amino protons (d 2.71) in ^{1}H NMR spectra. ^{13}C NMR spectra also had no signal of carbonyl carbon. Its formula was speculated as $C_{30}H_{50}N_2O_3$. The structures of sapogenin and its derivative are shown in Figure 2.

Protection on Dopaminergic Neurons Damaged by MPTP. The MPTP model is one of the well-known animal models of PD and is used to appraise the neuroprotective effects of the sapogenin and its derivative. MPTP can cross the blood-brain barrier, transforms to 1-methyl-4-phenylpyridine radical with the oxidation of monoamine oxidase B, and then enters dopaminergic nerve cells and selectively destructs dopaminergic neurons, causing a significant reduction of dopamine neurotransmitters in neurons and behavioral changes.[31]

The result of animal tests showed that DA levels in striatum of mice treated by MPTP were significantly (p < 0.01) lower than the normal saline group, indicating that MPTP caused the damage of the dopaminergic neuron. However, mice fed with the sapogenin and its derivative increased the levels of DA in striatum, and especially, the high dose of the sapogenin and its derivative had significant effects (p < 0.01) on the increase of DA content. Mice treated with the dopamine receptor antagonist haloperidol and the adenosine receptor antagonist CGS 15943 also had higher DA levels in striatum (Table 1). This suggests that high doses of the sapogenin and its derivative can prevent dopaminergic neurons from damage induced by

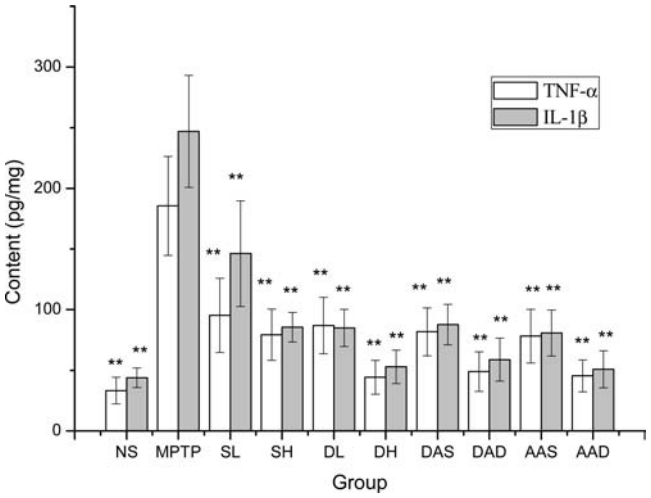

Figure 4. Levels of TNF-α and IL-1β in brain of mice in different treatments. The groups are normal (NS), MPTP (20 mg/kg × 3 i.p.), low dose of sapogenin (SL, 25 mg/kg, i.g.), high dose of sapogenin (SH, 100 mg/kg, i.g.), low dose of derivative (DL, 25 mg/kg, i.g.), high dose of derivative (DH, 100 mg/kg, i.g.), dopamine antagonist plus sapogenin (DAS, haloperidol 1 mg/kg i.p. and sapogenin 100 mg/kg i.g.), dopamine antagonist plus derivative (DAD, haloperidol 1 mg/kg i.p. and derivative 100 mg/kg i.g.), adenosine antagonist plus sapogenin (AAS, CGS15943 1 mg/kg i.p. and sapogenin 100 mg/kg i.g.), and adenosine antagonist plus derivative (AAD, CGS15943 1 mg/kg i.p. and derivative 100 mg/kg i.g.). Data are presented as mean ± standard deviation ($\bar{x} \pm s$, $n = 8$). **, $p < 0.01$, compared with MPTP group.

MPTP and that DA or adenosine receptor antagonist has no adverse effect on DA content.

Tyrosine hydroxylase (TH) is the key enzyme for dopamine synthesis in dopaminergic neurons, and its expression is lowered in substantia nigra of patients with Parkinson disease.[32] Immunostaining intensity of brain slices in immunohistochemistry can reflect the expression of TH. Compared with normal mice, MPTP treated mice had less staining in substantia nigra of brain slices, indicating that MPTP depressed the expression of TH. However, the intensity had no significant difference between normal control and high dose of the sapogenin or its derivative and between dopamine or adenosine receptor antagonist and sapogenin. This further proves that high dose of the sapogenin and its derivative has the protective effects on dopaminergic neurons and that the antagonists did not reduce the effects. The pictures are shown in Figure 3.

TH positive neurons were counted in five visual fields (4 mm^2) for each of eight slices, and the average cell number is listed in Table 1. Significant difference ($p < 0.01$) was found between MPTP group and high dose of sapogenin or its derivative but was not found between antagonist and no antagonist group, suggesting that the dopaminergic neurons' protection of the sapogenin and its derivative was not affected by dopamine or adenosine receptor antagonist.

Inhibition on the Inflammation in Brain. MPTP can induce neuroinflammation through an increase in the expression of TNF-α and IL-1β in the brain.[33] The anti-inflammatory effects of the sapogenin and its derivative on brain tissues were investigated. The results showed that TNF-α and IL-1β in mice brain of MPTP group were significantly ($p < 0.01$) increased but decreased in the groups treated with the sapogenin and its derivative. There was no significant difference

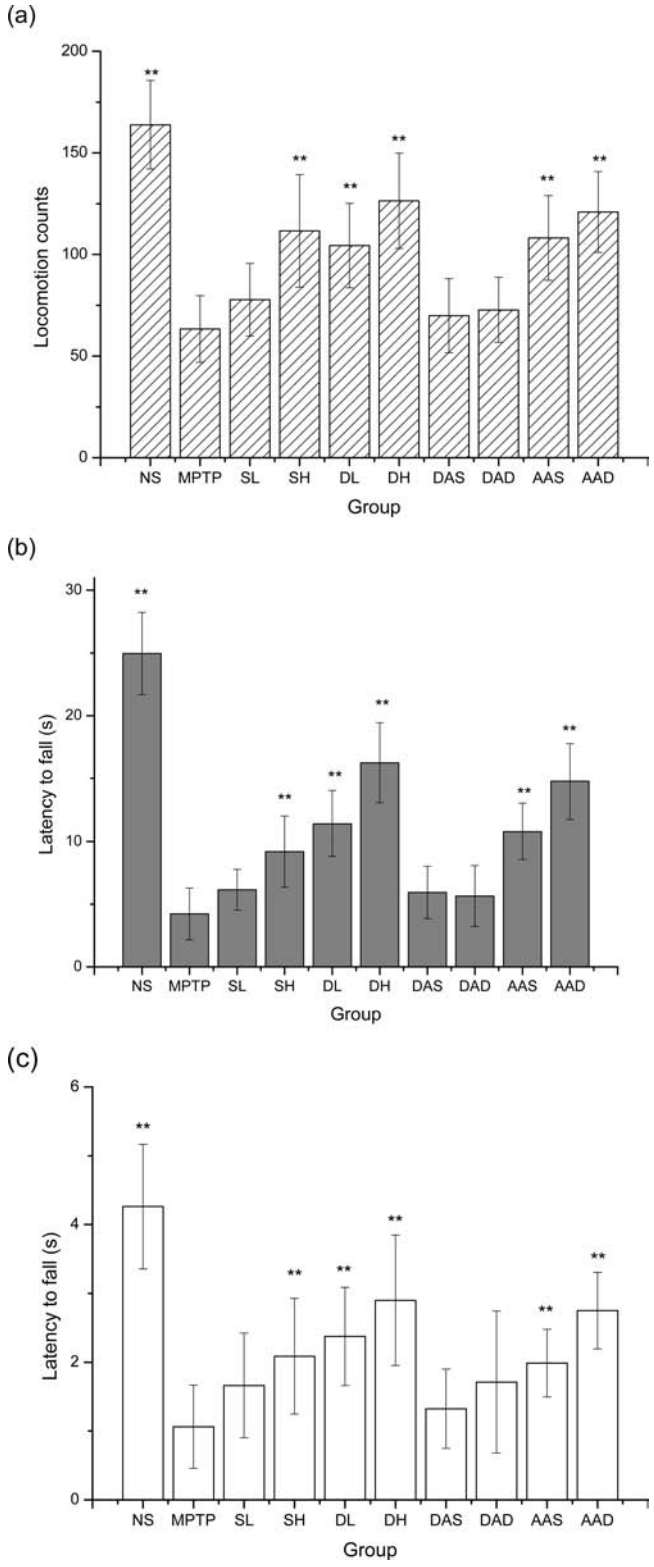

Figure 5. (a) Locomotive activity, (b) latency to fall by rotarod test, and (c) latency to fall by traction test in mice of different groups. The groups are NS (normal saline), MPTP (20 mg/kg × 3 i.p.), SL (low dose of sapogenin, 25 mg/kg), SH (high dose of sapogenin, 100 mg/kg), DL (low dose of derivative, 25 mg/kg), DH (high dose of derivative, 100 mg/kg), DAS (dopamine antagonist haloperidol 1 mg/kg plus sapogenin 100 mg/kg), DAD (dopamine antagonist haloperidol 1 mg/kg plus derivative 100 mg/kg), AAS (adenosine antagonist CGS 15943 1 mg/kg plus sapogenin 100 mg/kg), and AAD (adenosine antagonist CGS 15943 1 mg/kg plus derivative 100 mg/

dx.doi.org/10.1021/jf501166w | J. Agric. Food Chem. 2014, 62, 6175−6182

Figure 5. continued

kg). Mice were administered (i.g.) with sapogenin or its derivative or were injected (i.p.) with haloperidol or CGS 15943 for 6 days and then were administered (i.p.) with MPTP. Seven days later, locomotive activity and latency to fall were separately determined. Data are presented as mean ± standard deviation ($\bar{x} \pm s$, $n = 8$). **, $p < 0.01$, compared with MPTP group.

Table 2. Binding Energy of the Sapogenin and Its Derivative with Dopamine Receptor

compound	pose no.	CDOCKER energy (kcal/mol)	CDOCKER interaction energy (kcal/mol)
sapogenin	1	−83.46	47.53
	2	−84.62	41.96
	3	−85.11	45.76
	4	−85.19	45.82
	5	−85.3	41.58
	$\bar{x} \pm s$	−84.74 ± 0.76	44.53 ± 2.62
derivative	6	−85.8	48.85
	7	−86.31	48.1
	8	−86.71	48.12
	9	−86.86	48.66
	10	−87.03	48.63
	$\bar{x} \pm s$	−86.54 ± 0.49[a]	48.47 ± 0.34[a]

[a] $p < 0.01$, compared with sapogenin.

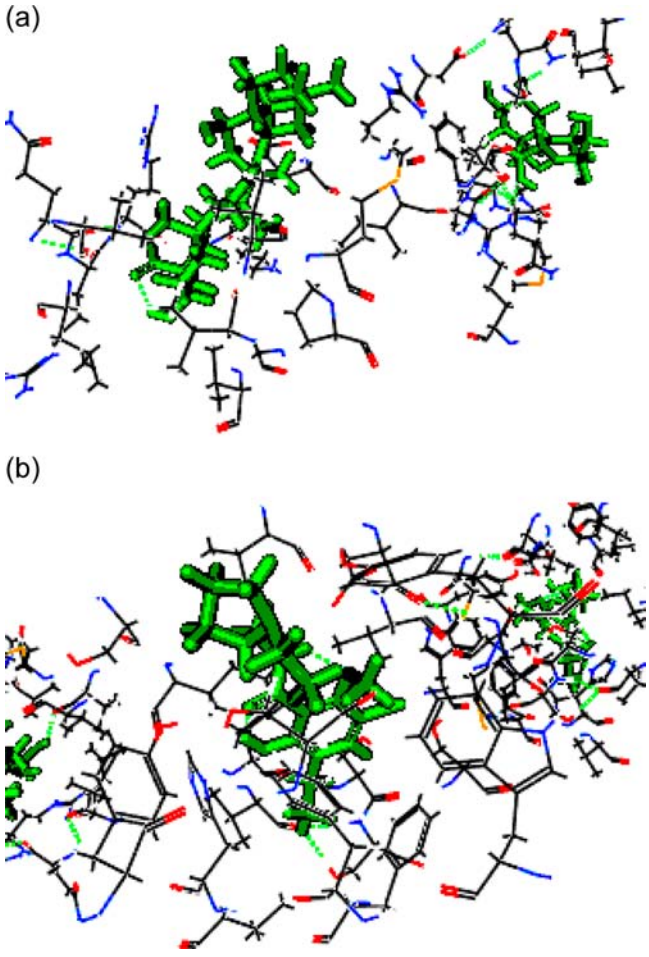

Figure 6. Group linkage of interaction of (a) the sapogenin and (b) its derivative with dopamine receptor.

between the group of derivative in high dose and normal group, suggesting that the derivative had better control of inflammation in brain. The antagonists had no significant effects on neuroinflammation. The results are illustrated in Figure 4.

TNF-α and IL-1β had obvious neurotoxicity on dopaminergic neurons.[34] High-level expression of TNF-α could induce great loss of dopaminergic neurons, accompanied by the proliferation of glial monocytes and macrophages.[35] TNF-α and IL-1β could also cause phosphorylation and degradation of IKK-β kinase, leading to translocation of NF-κB into the nucleus to promote expression of inflammatory genes.[36] This experiment shows that MPTP increases the expression of TNF-α and IL-1β in the brain, triggering inflammation and leading to neuron loss. The sapogenin and its derivative inhibit the expression of TNF-α and IL-1β in the mouse brain induced by MPTP and protect dopaminergic neurons in the brain from degeneration by antineuroinflammation.

Behavioral Improvement of PD Mice. PD patients not only have dopamine loss in striatum and substantia nigra of brain but also have a lot of motor dysfunction, which can be imitated by animal tests. Spontaneous activities of mice were determined by locomotion test, and the balances were measured by the rotarod test and the traction test. The results showed that MPTP significantly ($p < 0.01$) lessened the spontaneous activity and latency to fall, suggesting that it caused movement disorder and damaged the motion balance and coordination of mice. The locomotion counts and latency to fall were increased significantly ($p < 0.01$) after the administration of the sapogenin and its derivative but decreased after injection of haloperidol. This indicated that the sapogenin and its derivative improved the behavioral disorders induced by MPTP, but the effects were reversed by DA receptor antagonist. The derivative had better effects than the sapogenin on behavioral improvement. The results are shown in Figure 5.

The structures of sapogenin and its derivative are responsible for their effects on protection of dopaminergic neurons and behavior improvement. They do not have phenolic hydroxyl groups, and it is difficult for them to eliminate the MPTP radical. The neuroprotection contributes to their significant anti-inflammatory effects rather than to their antioxidant effect. They can relieve the motor dysfunction, and the effects are counteracted by dopamine receptor antagonist, indicating they might take effect by activating dopamine receptor rather than adenosine receptor, which is related to PD in many reports.[37] The amination of sapogenin shows better effects on amelioration of PD symptoms. It may be attributed to its stronger interaction with dopamine receptor.

Interaction with Dopamine Receptor. Molecular simulation is a good way to observe the interaction among groups. The protocol of semiflexible docking (CDOCKER) is proper for interaction of large molecule receptor and small molecule ligand. Major factors on binding stability of receptor and ligand are hydrophobicity and bonding force, which are calculated and judged by free energy. Docking simulation showed that both the sapogenin and its derivative could bind to the dopamine receptor. Each molecule successfully docked in five poses; the binding energy is shown in Table 2. The derivative had higher CDOCKER interactive energy and higher absolute value of CDOCKER energy than the sapogenin, suggesting that it is more powerful to bind to and interact with the dopamine receptor. The group linkage of the sapogenin and its derivative with dopamine receptor is shown in Figure 6, illustrating that one receptor can interact with many more derivatives. The

dx.doi.org/10.1021/jf501166w | J. Agric. Food Chem. 2014, 62, 6175−6182

interaction between the sapogenin or the derivative and the dopamine receptor contributes to their effects on behavioral improvement.

The sapogenin was isolated from the defatted seeds of *C. oleifera* and was used to synthesize a derivative by amination. By means of animal PD models induced by MPTP, it is found that the sapogenin and its derivative have significant effects on inhibition of DA loss, relieving motor deficits and protection of dopaminergic neurons. It is owing to their control of neuroinflammation in central tissues and interaction with dopamine receptor. The sapogenin and its derivative may become the prospective prodrugs for PD.

Although the MPTP animal model is widely used for PD therapeutic interventions, it has limitations and cannot produce sleep disturbances and cognitive deficits commonly seen in PD patients.[38] Because many factors are involved in PD including gene mutation, environmental impact, and so forth, the key mechanism of PD is still unknown. Therefore, other models such as transgenic animal model will be discussed in our next investigation so as to achieve the clinical application of the sapogenin and its derivative on PD.

AUTHOR INFORMATION

Corresponding Author

*Tel: +86-20-87110234. E-mail: yeyong@scut.edu.cn. Fax: +86-20-22236337.

Funding

The project is supported by National Science Funding of China (No. 81173646).

Notes

The authors declare no competing financial interest.

ACKNOWLEDGMENTS

The authors gratefully thank staff in South China University of Technology for data analysis and ethical committee for approval of animal tests.

ABBREVIATIONS

ANOVA, analysis of variance; CGS 15943, 9-Chloro-2- (2-furanyl)- [1,2,4] triazolo [1,5-*c*] quinazolin-5-amine; DA, dopamine; ELISA, enzyme-linked immuno sorbent assay; MPTP, 1-methyl-4-phenyl-1,2,3,6- tetrahydropyridine hydrochloride; PD, Parkinson disease; SNK, Student−Newman−Keuls; TH, tyrosine hydroxylase

REFERENCES

(1) Burch, D.; Sheerin, F. Parkinson's disease. *Lancet* **2005**, *365*, 622−627.

(2) Braak, H.; Del Tredici, K.; Rüb, U.; de Vos, R. A.; Jansen Steur, E. N.; Braak, E. Staging of brain pathology related to sporadic Parkinson's disease. *Neurobiol. Aging* **2003**, *24*, 197−211.

(3) Andre, L.; Sullivan, A. M. Progress in Parkinson's disease-where do we stand? *Prog. Neurobiol.* **2008**, *85*, 376−392.

(4) Wu, L.; Xu, X. H.; Chen, W. The clinical research on standardization of Parkinson's disease treated with a comprehensive treatment program of traditional Chinese and western medicine. *Liaoning J. Tradit. Chin. Med.* **2011**, *38*, 313−316.

(5) Baker, W. L.; Silver, D.; White, C. M.; Kluger, J.; Aberle, J.; Patel, A. A.; Coleman, C. I. Dopamine agonists in the treatment of early Parkinson's disease: a meta-analysis. *Parkinsonism Relat. Disord.* **2009**, *15*, 287−294.

(6) Lee, C. P.; Yen, G. C. Antioxidant activity and bioactive compounds of tea seed (*Camellia oleifera* Abel.) oil. *J. Agric. Food Chem.* **2006**, *54*, 779−784.

(7) Biasutto, L.; Zoratti, M. Prodrugs of quercetin and resveratrol: a strategy under development. *Curr. Drug. Metab.* **2014**, *15*, 77−95.

(8) Tsuji, A. Small molecular drug transfer across the blood-brain barrier via carrier-mediated transport systems. *NeuroRx* **2005**, *2*, 54−62.

(9) Hu, S. H.; Wei, J.; Yan, X. W.; Li, Q. M. The poisonous study of Sasanqua saponin-the acute poisonous and accumulated poisonous of Sasanqua saponin to SD mouse through its mouth and skin. *China Oils Fats* **1998**, *23*, 47−48.

(10) Chen, Y. F.; Yang, C. H.; Chang, M. S.; Ciou, Y. P.; Huang, Y. C. Foam properties and detergent abilities of the saponins from *Camellia oleifera*. *Int. J. Mol. Sci.* **2010**, *11*, 4417−4425.

(11) Sugimoto, S.; Chi, G. H.; Kato, Y.; Nakamura, S.; Matsuda, H.; Yoshikawa, M. Medicinal flowers. XXVI.1) structures of acylated oleanane-type triterpene oligoglycosides, yuchasaponins A, B, C, and D, from the flower Buds of *Camellia oleifera*—gastroprotective, aldose reductase inhibitory, and radical scavenging effects. *Chem. Pharm. Bull.* **2009**, *3*, 269−275.

(12) Sur, P.; Chaudhuri, T.; Vedasiromoni, J. R.; Gomes, A.; Ganguly, D. K. Anti-inflammatory and antioxidant property of saponins of tea *Camellia sinensis* (L) Kuntzeroot extract. *Phytother. Res.* **2001**, *15*, 174−176.

(13) Yang, D. H.; Jiang, H.; Song, L.; Wang, J.; Xie, J. X. Neuroprotective effects of ginsenoside Rg_1 on the dopaminergic neurons in the substantia nigra in MPTP-treated C_{57} BL_6 mice. *Med. Pharm. J. Chin. People's Liberation Army* **2007**, *23*, 17−21.

(14) Xu, P. P. The protective effects of ginsenoside Re from MPTP-induced Parkinson's disease C_{57} BL_6 Mice. *Chin. J. Nat. Med.* **2004**, *2*, 171−175.

(15) Han, Y. X.; Wei, X. B.; Li, X.; Ding, Y.; Xin, H.; Ding, H. Protective effects of gypenosides against glutamate-induced hippocampus injury in rats. *J. Shandong Univ.* **2008**, *46*, 449−452.

(16) Ye, Y.; Chen, X. L.; Xing, H. T. Hypolipidemic and antioxidant activities of hydrolyzed saponins from defatted seeds of *Camellia oleifera* Abel. *Lat. Am. J. Pharm.* **2013**, *32*, 409−417.

(17) Ye, Y.; Xing, H. T.; Chen, X. L. Anti-inflammatory and analgesic activities of the hydrolyzed sasanqua saponins from the defatted seeds of *Camellia oleifera*. *Arch. Pharm. Res.* **2013**, *36*, 941−951.

(18) Petroske, E.; Meredith, G. E.; Callen, S.; Totterdell, S.; Lau, Y. S. Mouse model of Parkinsonism: a comparison between subacute MPTP and chronic MPTP/probenecid treatment. *Neuroscience* **2001**, *106*, 589−601.

(19) Lazzarini, M.; Salum, C.; Del Bel, E. A. Combined treatment of ascorbic acid or alpha-tocopherol with dopamine receptor antagonist or nitric oxide synthase inhibitor potentiates cataleptic effect in mice. *Psychopharmacol. (Berlin, Ger.).* **2005**, *181*, 71−79.

(20) Stephen, G. H. Discriminative effects of CGS 15943, a competitive adenosine receptor antagonist, have a dopamine component in monkeys. *Eur. J. Pharmacol.* **1999**, *376*, 7−15.

(21) Wang, H.; Pan, Y.; Xue, B.; Wang, X.; Zhao, F.; Jia, J.; Liang, X.; Wang, X. The antioxidative effect of electro-acupuncture in a mouse model of Parkinson's disease. *PLoS One* **2011**, *6*, e19790.

(22) He, M.; Zhao, L.; Wei, M. J.; Yao, W. F.; Zhao, H. S.; Chen, F. J. Neuroprotective effects of (−)-epigallocatechin-3-gallate on aging mice induced by D-galactose. *Biol. Pharm. Bull.* **2009**, *32*, 55−60.

(23) Rozas, G.; Labandeira Garcia, J. L. Drug free evaluation of rat models of Parkinsonism and nigral grafts using a new automated rotarod test. *Brain Res.* **1997**, *749*, 188−199.

(24) Yao, Q. H.; Zhang, H.; Gao, G. D. Comparison of behavioral tests in MPTP-induced Parkinson's disease in mice. *Acta Lab. Anim. Sci. Sin.* **2006**, *14*, 264−270.

(25) Zhao, Y. M.; Li, J. Q.; Lv, F. Y. Activation of microglia and dopaminergic neurons degeneration following intraventricalar injection of LPS in the substantia nigra of rats. *Chin. J. Neuroimmunol. Neurol.* **2012**, *19*, 121−145.

(26) Uthaman, G.; Mannu, J.; Durai, S. Molecular docking studies of dithionitrobenzoic acid and its related compounds to protein disulfide isomerase: computational screening of inhibitors to HIV-1 entry. *BMC Bioinf.* **2008**, *9*, S14−16.

(27) Chien, E. Y.; Liu, W.; Zhao, Q.; Katritch, V.; Han, G. W.; Hanson, M. A.; Shi, L.; Newman, A. H.; Javitch, J. A.; Cherezov, V.; Stevens, R. C. Structure of the human dopamine D3 receptor in complex with a D2/D3 selective antagonist. *Science* **2010**, *330*, 1091−1095.
(28) Robinson, D. D.; Lyne, P. D.; Richards, W. G. Partial molecular alignment via local structure analysis. *J. Chem. Inf. Comput. Sci.* **2000**, *40*, 503−512.
(29) Carro, L.; Torrado, M.; Raviña, E.; Masaguer, C. F.; Lage, S.; Brea, J.; Loza, M. I. Synthesis and biological evaluation of a series of aminoalkyl-tetralones and tetralols as dual dopamine/serotonin ligands. *Eur. J. Med. Chem.* **2013**, *71C*, 237−249.
(30) Toshiyuki, M.; Junko, N.; Hisashi, M.; Masayuki, Y. Bioactive saponins and glycosides. XV.1) saponin constituents with gastroprotective effect from the seeds of tea plant, *Camellia sinensis* L. var. *assamica* PIERRE, Cultivated in Sri Lanka: structures of assamsaponins A, B, C, D, and E. *Chem. Pharm. Bull.* **1999**, *47*, 1759−1764.
(31) Ono, S.; Hirai, K.; Tokuda, E. Effects of pergolide mesilate on metallothionein mRNAs expression in a mouse model for Parkinson disease. *Biol. Pharm. Bull.* **2009**, *32*, 1813−1817.
(32) Kastner, A.; Hirsch, E. C.; Agid, Y.; Javoy-Agid, F. Tyrosine hydroxylase protein and messenger RNA in the dopaminergic nigral neurons of patients with Parkinson's disease. *Brain Res.* **1993**, *606*, 341−345.
(33) Khan, M. M.; Kempuraj, D.; Thangavel, R.; Zaheer, A. Protection of MPTP-induced neuroinflammation and neurodegeneration by Pycnogenol. *Neurochem. Int.* **2013**, *62*, 379−388.
(34) Wu, Y. P.; Mizukami, H.; Matsuda, J.; Saito, Y.; Proia, R. L.; Suzuki, K. Apoptosis accompanied by upregulation of TNF alpha death pathway genes in the brain of Niemann-Pick type C disease. *Mol. Genet. Metab.* **2005**, *84*, 9−17.
(35) Chertoff, M.; Di Paolo, N.; Schoeneberg, A.; Depino, A.; Ferrari, C.; Wurst, W.; Pfizenmaier, K.; Eisel, U.; Pitossi, F. Neuroprotective and neurodegenerative effects of the chronic expression of tumor necrosis factor in the nigrostriatal dopaminergic circuit of adult mice. *Exp. Neurol.* **2011**, *227*, 237−251.
(36) Litteljohn, D.; Mangano, E.; Clarke, M.; Bobyn, J.; Moloney, K.; Hayley, S. Inflammatory mechanisms of neurodegeneration in toxin-based models of Parkinson's disease. *Parkinsons Dis.* **2011**, DOI: 10.4061/2011/713517.
(37) Armentero, M. T.; Pinna, A.; Ferré, S.; Lanciego, J. L.; Müller, C. E.; Franco, R. Past, present and future of A(2A) adenosine receptor antagonists in the therapy of Parkinson's disease. *Pharmacol. Ther.* **2011**, *132*, 280−299.
(38) Fifel, K.; Dkhissi-Benyahya, O.; Cooper, H. M. Lack of long-term changes in circadian, locomotor, and cognitive functions in acute and chronic MPTP (1-methyl-4-phenyl-1,2,3,6-tetrahydropyridine) mouse models of Parkinson's disease. *Chronobiol. Int.* **2013**, *30*, 741−755.

JOURNAL OF AGRICULTURAL AND FOOD CHEMISTRY

Article

pubs.acs.org/JAFC

Increase in the Protein-Bound Form of Glutathione in Human Blood after the Oral Administration of Glutathione

Eun Young Park,[†] Nami Shimura,[†] Toru Konishi,[‡] Yusuke Sauchi,[‡] Sayori Wada,[†] Wataru Aoi,[†] Yasushi Nakamura,[†] and Kenji Sato*[,†]

[†]Division of Applied Life Sciences, Graduate School of Life and Environmental Sciences, Kyoto Prefectural University, 1-5 Hangi-cho, Shimogamo, Sakyo-ku, Kyoto 606-8522, Japan

[‡]KOHJIN Life Sciences Company, Ltd., 1-3 Yurakucho 1-chome, Chiyoda-ku, Tokyo 100-0006, Japan

ABSTRACT: The present study examined the impact of the supplementation of glutathione (GSH), γ-L-glutamyl-L-cysteinyl-glycine, on human blood GSH levels. Healthy human volunteers were orally supplemented with GSH (50 mg/kg body weight). Venous blood was collected from the cubital vein before and after ingestion. Plasma was mixed with 3 volumes of ethanol. The supernatant and precipitate were used for the deproteinized and protein fractions of plasma, respectively. Blood cell and plasma fractions were pretreated with 5% trichloroacetic acid−2% 2-mercaptoethanol to reduce the oxidized form of GSH and liberate protein-bound GSH. The 2-mercaptoethanol-pretreated GSH was determined by precolumn derivatization with 6-aminoquinolyl-*N*-hydroxy succinimidyl carbamate and liquid chromatography−tandem mass spectrometry. There was no significant difference in GSH contents in the deproteinized fraction of plasma and blood cell fraction after GSH ingestion. However, the GSH contents in the protein-bound fraction of plasma significantly ($P < 0.01$) increased from 60 to 120 min after GSH supplementation.

KEYWORDS: *glutathione, GSH, blood, supplementation, oral administration, human trial*

INTRODUCTION

Glutathione (GSH), γ-L-glutamyl-L-cysteinyl-glycine, is a ubiquitous compound found in humans, animals, plants, and microorganisms.[1] Within cells, GSH exists in both reduced and oxidized states. In healthy cells, the majority of GSH is present in the reduced form.[2] Most cells in the human body are capable of synthesizing GSH from glutamate, cysteine, and glycine. First, γ-glutamyl-cysteine is synthesized from L-glutamate and L-cysteine by γ-glutamyl-cysteine synthetase. Second, glycine is conjugated to the C-terminaus of γ-glutamyl-cysteine by GSH synthetase.[1,3]

GSH is a cofactor or substrate for GSH peroxidase and GSH *S*-transferase (GST), which are involved in very important antioxidant and detoxification systems, respectively.[4] The main function of GSH peroxidase is to reduce hydrogen peroxide to water and to reduce lipid hydroperoxides to their corresponding alcohols.[3,5] The reduced form of GSH, which is involved in these reactions as a cofactor, is converted to the oxidized form. Thus, the ratio of the oxidized form to the reduced form of GSH has been thought to reflect oxidative status in cells, organs, and individuals.[6] However, oxidized GSH is reduced by GSH reductase. The reduced form of nicotinamide adenine dinucleotide phosphate, which is a cofactor for GSH reductase, is supplied by the pentose phosphate pathway.[7] GST catalyzes the conjugation of reduced GSH to a wide variety of exogenous chemicals through a sulfhydryl group to make the compounds more soluble and to facilitate urinary excretion.[8,9]

Decreased GSH levels in cells have been demonstrated to increase the risks of diseases and poisoning.[1,10] GSH has therefore been used to treat chronic liver diseases and poisoning through intravenous injections.[11,12] In addition to intravenous injections of GSH, oral administration has been used for medical applications. Aside from medical applications, GSH has also been implicated in skin whitening. In vitro studies have revealed that GSH inhibits melanin synthesis in the reaction of tyrosinase and L-3,4-dihydroxyphenylalanine in a dose-dependent manner.[13,14] On the basis of these findings, GSH has been used as a supplement for skin whitening and improvement of liver function.

GSH supplementation has been prevalent worldwide. However, bioavailability and the metabolic fate of orally administered GSH have not been fully understood. It has been proposed that GSH is first degraded by γ-glutamyl transferase into γ-glutamyl-X (X = other amino acids) and cysteinyl-glycine. The cysteinyl-glycine is degraded into cysteine and glycine by peptidases.[6,15] Orally administered GSH could be degraded in this system. In addition, some human studies have demonstrated no significant increases in blood GSH levels in human volunteers after the oral administration of a relatively large dose of GSH.[16,17] These findings suggest that GSH supplementation has no impact on blood and organ GSH levels. However, GSH can potentially bind to proteins by disulfide bonds. Therefore, it is possible that orally administered GSH may be present and transported as a protein-bound form in the blood, and this has not been reported in previous studies.

The objective of the present study was to elucidate the impact of GSH supplementation on human blood GSH levels in the free and protein-bound forms.

Received: March 18, 2014
Revised: May 17, 2014
Accepted: May 30, 2014
Published: May 30, 2014

ACS Publications © 2014 American Chemical Society

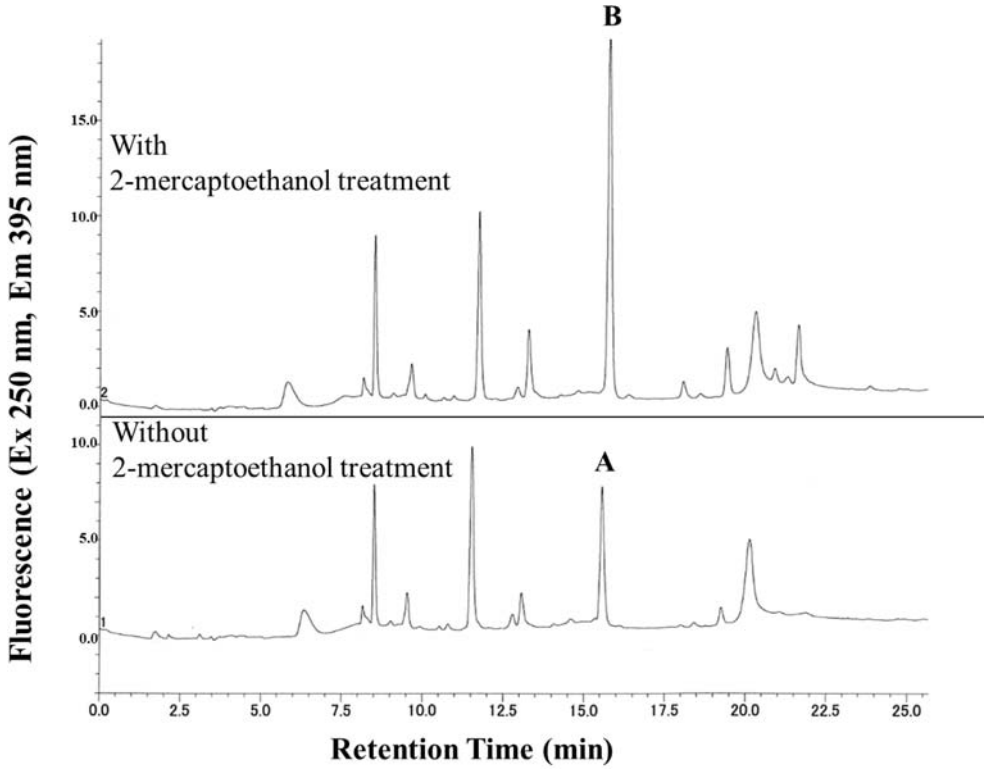

Figure 1. Elution profiles of the 6-aminoquinolyl-*N*-hydroxysuccinimidyl carbamate (AccQ) derivatives of 2-mercaptoethanol-pretreated or intact glutathione (GSH). Pretreated and intact GSH was dried in the presence of triethylamine (TEA) before derivatization with AccQ. Peaks marked A and B show GSH derivatives.

MATERIALS AND METHODS

Chemicals. The reduced form of L-glutathione was produced by fermentation with Torula yeast by KOHJIN Life Sciences, a subsidiary of Mitsubishi Corp. (Tokyo, Japan). This product has been qualified for Generally Recognized As Safe status by the U.S. Food and Drug Administration (U.S. FDA GRAS notified GRN000293). γ-L-Glutamyl-L-cysteine (γGlu-Cys) and L-cysteinyl-glycine (Cys-Gly) were obtained from Sigma-Aldrich (St. Louis, MO, USA). An amino acid labeling kit (AccQ Tag) that consisted of 6-aminoquinolyl-*N*-hydroxysuccinimidyl carbamate reagent (AccQ), acetonitrile, and 0.2 mM sodium borate buffer, pH 8.8, was purchased from Waters (Milford, MA, USA). Acetonitrile [high-performance liquid chromatography (HPLC) grade], triethylamine (TEA), formic acid, trichloroacetic acid (TCA), and 2-mercaptoethanol were obtained from Wako Pure Chemicals (Osaka, Japan). All other reagents were of analytical grade or higher.

Clinical Study Design. The experimental protocol was submitted to and approved by the experimental ethical committees of Kyoto Prefectural University (KPU no. 63) and KOHJIN Life Sciences. The human studies were performed according to the Helsinki Declaration and were under the control of medical doctors. The potential risks of the ingestion of GSH and the objective of the present study were revealed to the volunteers. After careful reading of a consent form, all subjects signed it. Seven healthy male subjects (mean age ± standard deviation 39.8 ± 15.1 years) were fasted for 12 h before the experiment and given the reduced form of L-glutathione at 50 mg/kg body weight and 100 mL of water, which was the same dose as used in the previous study.[17] Approximately 10 mL of venous blood was collected in the presence of heparin from the cubital vein before and 15, 30, 60, 90, and 120 min after ingestion.

Preparation of Blood Samples. One milliliter of the blood was centrifuged at 3700*g* for 5 min to prepare the plasma and blood cell fractions. Four hundred microliters of the plasma was mixed with 1.2 mL of ethanol and then centrifuged at 3700*g* for 5 min. Then, the supernatant was collected. Aliquots of the supernatant (300 μL) were dried under vacuum and added to 100 μL of 5% TCA containing 2% 2-mercaptoethanol, and the mixture was allowed to stand for 30 min at room temperature and used as the deproteinized plasma fraction in the following experiments. The ethanol precipitate of the plasma was washed with 200 μL of 75% (v/v) ethanol and then mixed with 160 μL of 10% (w/v) TCA and stirred vigorously. To this suspension were added another 320 μL of 5% (w/v) TCA and 10 μL of 10% (v/v) 2-mercaptoethanol. The mixture was allowed to stand for 30 min at room temperature and then centrifuged at 14800*g* for 5 min. The supernatant was collected and used as the protein-bound plasma fraction. The blood cell from 1 mL of blood was mixed with 500 μL of 10% TCA and 1 mL of 5% TCA and stirred for 3 min. The supernatant was collected after centrifugation at 14800*g* for 5 min. Fifty microliters of the 5% TCA extract of the blood cell was mixed with 450 μL of 5% TCA containing 2% 2-mercaptoethanol and allowed to stand for 30 min at room temperature and used as the blood cell fraction.

The weights of the blood cell and plasma ethanol precipitate were determined before the addition of TCA solutions. The samples were stored at −80 °C until use.

Derivatization of GSH with the AccQ Reagent. The reduced form of GSH was dissolved in 10 mM HCl to result in 2.5 μmol/mL and used as a stock solution. Suitable amounts of the standard stock solution were dried under vacuum in a glass tube (50 mm × 6 mm i.d.) with a KLV-CC-105 centrifugal concentrator (Tomy, Tokyo, Japan). Fifty microliters of 5% TCA containing 2% 2-mercaptoethanol was added to the tube and allowed to stand for 30 min, and the solution was then dried under vacuum in a hydrolysis/derivatization vial with a resealable valve (Waters). Twenty microliters of an alkaline solution, which consisted of methanol, water, and TEA at a ratio of 7:1:2 (v/v), was added to the tube, and the mixture was then dried under vacuum to increase the pH for derivatization with AccQ. In some cases, this treatment was deleted from the protocol. The dried standards were resolved in 20 μL of 20 mM HCl, and 20 μL of AccQ reagent and 60 μL of borate buffer were added in the AccQ Tag Kit and reacted at 50 °C for 10 min. The resultant AccQ derivatives were

dx.doi.org/10.1021/jf501338z | J. Agric. Food Chem. 2014, 62, 6183−6189

diluted with 5 mM sodium phosphate buffer, pH 7.4, containing 10% (v/v) acetonitrile. The solutions were filtered through a 0.45 μm filter (column guard LCR4; Millipore, Billerica, MA, USA).

Fifty microliters of the plasma deproteinized and protein-bound fractions and blood cell fraction were also dried under vacuum in the presence of TEA and then derivatized with AccQ, as described above.

Isolation of the AccQ Derivatives. The AccQ derivatives of GSH with and without 5% TCA−2% 2-mercaptoethanol and TEA pretreatments were isolated by reversed phase HPLC (RP-HPLC) with an Inertsil ODS-3 (4.6 mm i.d. × 250 mm, GL Sciences, Tokyo, Japan). Elution was performed with a binary gradient system with 0.1% formic acid (solvent A) and 60% (v/v) acetonitrile (solvent B). The gradient profile was as follows: 0−1 min, 5−10% B; 1−10 min, 10−20% B; 10−25 min, 20−40% B; 25−30 min, 40−45% B; 30−35 min, 45−50% B; 35−40 min, 50−100% B; 40−45 min, 100% B; 45−45.1 min, 100−5% B; and 45.1−55 min, 5% B. The column was equilibrated with 5% B at 1 mL/min. The column was maintained at 45 °C, and elution was monitored by fluorescence at 395 nm that was excited at 250 nm.

Mass Spectrometry Analysis. The isolated AccQ derivatives of GSH were analyzed by electrospray ionization ion trap mass spectrometry (ESI-MS) with an LCQ (Thermo Fisher Scientific, Waltham, MA, USA). The sample was delivered to the ion source by a syringe pump at 3 μL/min. Detection was conducted in positive mode and optimized and processed by Xcalibur version 2.07 (Thermo Fisher Scientific).

Determination of GSH by Liquid Chromatography−Tandem Mass Spectrometry (LC-MS/MS). The concentrations of GSH, γGlu-Cys, and Cys-Gly in the blood samples were determined by precolumn derivatization with AccQ that was followed by an LC-MS/MS analysis with a Q-TRAP 3200 (AB SCIEX, Framingham, MA, USA). The AccQ derivative was prepared as described above and clarified by passing through a filter (0.45 μm column guard; Millipore). The samples (10 μL) were injected onto an Inertsil ODS-3 column (2.1 mm i.d. × 250 mm; GL Sciences), and a binary gradient elution was performed with 0.1% formic acid (solvent A) and 60% acetonitrile (solvent B) at a flow rate of 0.2 mL/min. The column was equilibrated with 100% solvent A, and the gradient profile was as follows: 0−15 min, 0−50% B; 15−20 min, 50−100% B; 20−24 min, 100% B; 24−24.1 min, 100−0% B; and 24.1−30 min, 0% B. The column was maintained at 40 °C throughout. The multireaction monitoring (MRM) condition was optimized in positive mode with Analyst version 4.2 (AB SCIEX) in autoselect mode.

Statistics. Differences between the means were evaluated by analyses of variance (ANOVA) that were followed by one-way ANOVAs with StatView 4.11 (Abacus Concepts, Berkeley, CA, USA). Significant differences between the groups were evaluated by Scheffe's post hoc test.

RESULTS

Structures of the AccQ Derivatives. The AccQ derivatives of GSH, which had been pretreated with or without the 5% TCA−2% 2-mercaptoethanol solution, were resolved by RP-HPLC. In both cases, the GSH was pretreated by TEA before derivatization with AccQ. As shown in Figure 1, several peaks of fluorescence were observed. When different amounts of GSH were derivatized, only the peaks marked A and B changed in a dose-dependent manner, which indicated that these peaks corresponded to AccQ−GSH derivatives and that the other ones were reagent peaks. The derivative that had been pretreated without 2-mercaptoethanol (A) showed a similar but slightly different retention time and a smaller peak area compared to the counterpart (B). These peaks were collected and subjected to an ESI-MS analysis. As shown in Figure 2A, the AccQ derivative without 2-mercaptoethanol pretreatment showed a main peak with a m/z of 477 (full scan). A zoom scan analysis revealed that the difference in m/z between the adjacent isotopes was 0.5, which indicated that the charge

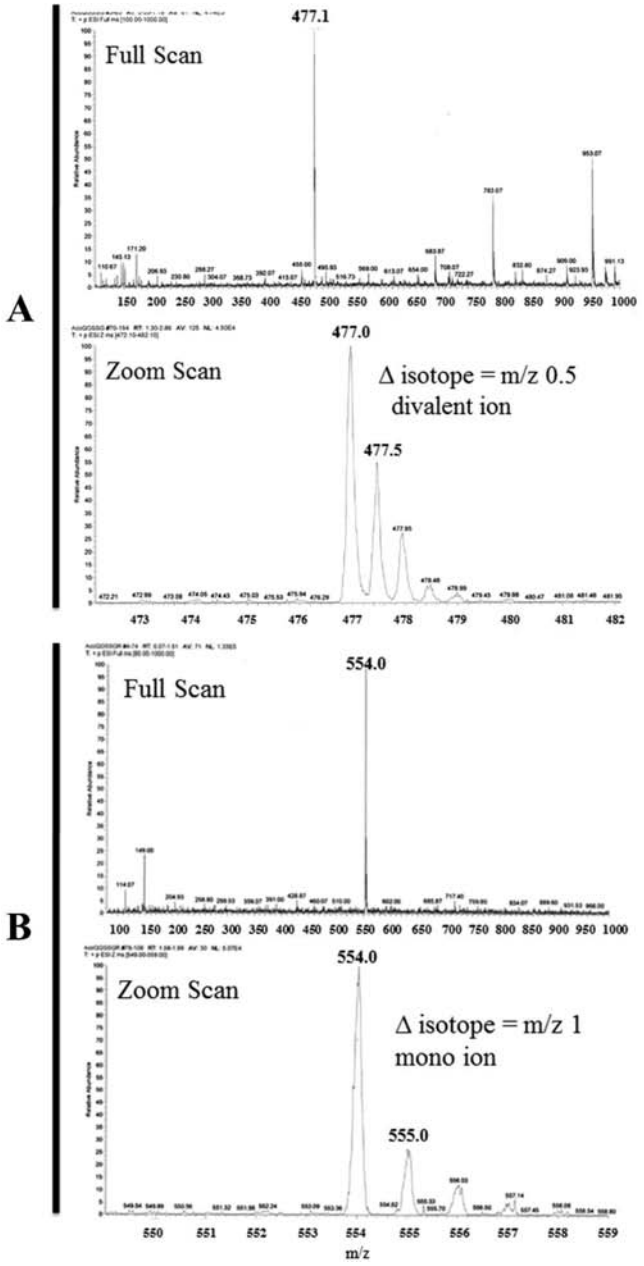

Figure 2. Mass spectrometry analyses of the GSH derivative that had been prepared without (A) and with (B) 2-mercaptoethanol pretreatment. Peaks marked A and B in Figure 1 were collected and analyzed by electrospray ionization (ESI) ion trap MS. The upper and lower panels represent full and zoom scan spectra, respectively.

number was 2. Assuming that this derivative had two protons, its molecular weight (x_1) can be calculated with the following formula: $(x_1 + 2)/2 = 477$, $x_1 = 952$. This value coincided with the molecular weight of the oxidized form of GSH that was coupled with two AccQ molecules through two amino groups, as shown in Figure 3A. However, the AccQ derivative with 2-mercaptoethanol pretreatment showed a main peak with a m/z of 554 (Figure 2B). The difference in m/z between the adjacent isotopes was 1.0. Then, its molecular weight (x_2) can be calculated as follows: $(x_2 + 1)/1 = 554$, $x_2 = 553$. This value did not coincide with the reduced form of AccQ-GSH that was conjugated through an amino group, but it corresponded to the AccQ−GSH−2-mercaptoethanol conjugate through an amino

dx.doi.org/10.1021/jf501338z | J. Agric. Food Chem. 2014, 62, 6183−6189

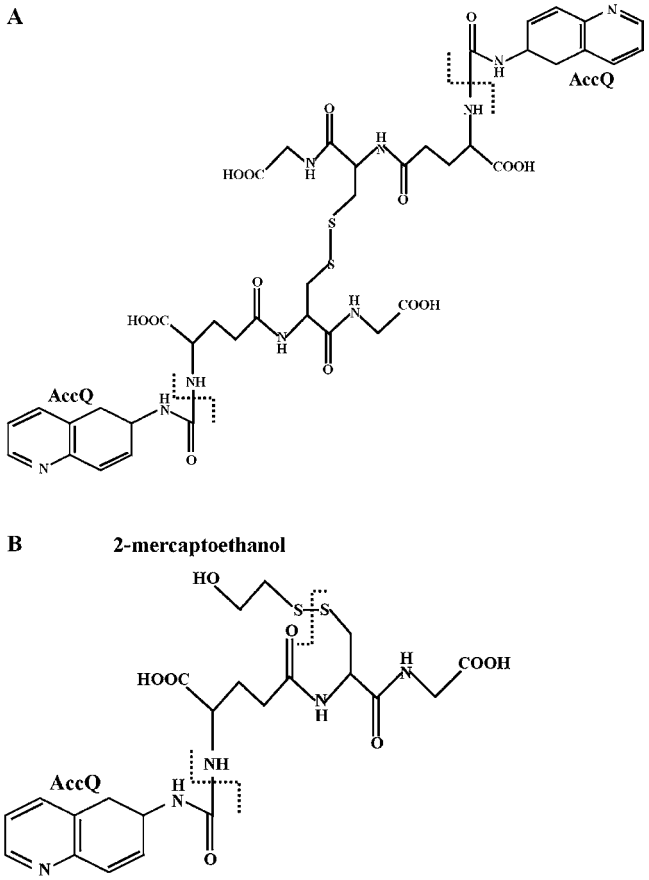

Figure 3. Estimated chemical structures of GSH derivatives that were prepared without (A) and with 2-mercaptoethanol pretreatment (B).

group and a sulfhydryl group, respectively, as shown in Figure 3B. The other peaks in Figure 1 could not be assigned to GSH derivatives, such as the AccQ−GSH conjugate with a free sulfhydryl group and the AccQ−GSH−AccQ conjugate through an amino and a sulfhydryl group. For preparation of these derivatives, the 5% TCA−2% 2-mercaptoethanol solution was removed by vacuum in the presence of TEA before reaction with the AccQ reagent. When this drying treatment with TEA was deleted, a similar chromatogram was obtained (Figure 4, upper) with a larger peak of the derivative (C) compared to the derivative with the drying treatment (A). The ESI-MS analysis of the derivative without the drying treatment with TEA (peak C) showed no significant peak of m/z 554, which was the protonated ion of the AccQ−GSH−2-mercaptoethanol conjugate (Figures 2B and 3B). However, two main peaks with m/z 171 and 249 were observed, and these corresponded to the AccQ fragment ion and the AccQ−2-mercaptoethanol protonated ion, respectively. These results indicated that the amino group of GSH was dissociated to the $-NH_3^+$ ion in the presence of a strong acid (TCA) and that it then could not react with the AccQ reagent. However, an excess amount of 2-mercaptoethanol reacted with AccQ through the sulfhydryl group under this condition. Therefore, the drying treatment with TEA was critical for the derivatization of GSH when the sample was pretreated with 5% TCA−2% 2-mercaptoethanol to liberate the protein-bound GSH.

On the basis of these findings, all of the blood samples were pretreated with 5% TCA−2% 2-mercaptoethanol, which was followed by the drying treatment with TEA before derivatization with AccQ for the determination of GSH by LC-MS/MS in the MRM mode. The fragment ions with the first and second high intensities (m/z 554.1 → 171.3 and m/z 554.1 → 145.2) were automatically selected.

Blood GSH Levels. Figure 5a shows the GSH contents in the deproteinized fraction of plasma before and after the ingestion of GSH. There was no significant difference in the GSH contents after the ingestion of GSH in this fraction. Much higher contents of GSH were contained in the blood cell fraction than in the deproteinized fraction of the plasma (Figure 5b). However, no significant difference was observed in the GSH contents in the blood cell fraction during the experimental period. However, the contents of GSH, γGlu-Cys, and Cys-Gly in the protein-bound fraction of plasma significantly increased 60−120 min after the supplementation of GSH (Figure 6). The protein-bound GSH and related compounds in plasma did not return to the initial level 2 h after supplementation.

DISCUSSION

GSH is present in high concentrations in liver and blood cells.[3,18] Generally, GSH concentrations have been determined in such samples with Ellman's reagent, which contains 5,5′-dithiobis(2-nitrobenzoic acid). To increase sensitivity, an enzyme recycling reaction using GSH reductase has been developed.[19,20] The GSH content in the blood cells, hepatic tissues, and other tissues has been determined with these methods. Allen et al. have reported that oral GSH supplementation did not improve blood cell GSH levels.[16] However, plasma GSH levels are lower (low μM levels) than those in blood cells. The plasma GSH levels have been determined by RP-HPLC with the precolumn derivatization of the sulfhydryl group or the enzyme recycling reaction method. Witschi et al. have observed no increase in plasma GSH levels after a single oral supplementation of GSH to healthy human volunteers at 0.15 mmol/kg body weight.[17] The present study confirmed these results (Figure 5). On the basis of these results, it has been suggested that the oral supplementation of GSH does not affect blood GSH levels.

It has been demonstrated that plasma proteins, including albumin, can bind to low molecular weight thiol compounds through a disulfide bond.[21,22] Therefore, there is the possibility that supplemented GSH may be transported as a conjugate of protein in the blood, and this has not been examined. In the present study, the effects of the supplementation of GSH on plasma protein-bound GSH levels were examined. To liberate GSH from protein conjugate, a reducing reagent is necessary. For this purpose, dithiothreitol has been frequently used,[23,24] but it is incompatible with the enzyme recycling reaction method. The dithiothreitol also reacts with labeling reagents for sulfhydryl and amino groups, which can interfere with the precolumn labeling reaction. In the present study, 2-mercaptoethanol was used to liberate GSH from the conjugates. The excess amount of 2-mercaptoethanol can be removed by vacuum in the presence of TEA. This drying treatment is, therefore, indispensable in the reaction between AccQ and an amino group of GSH. The final GSH derivative was double conjugated with AccQ and 2-mercaptoethanol through amino and sulfhydryl groups, respectively. As the final GSH derivative had no free sulfhydryl groups, it could not be oxidized to form a disulfide bond. A single GSH derivative was obtained, as shown by the MS analysis of the derivative peaks

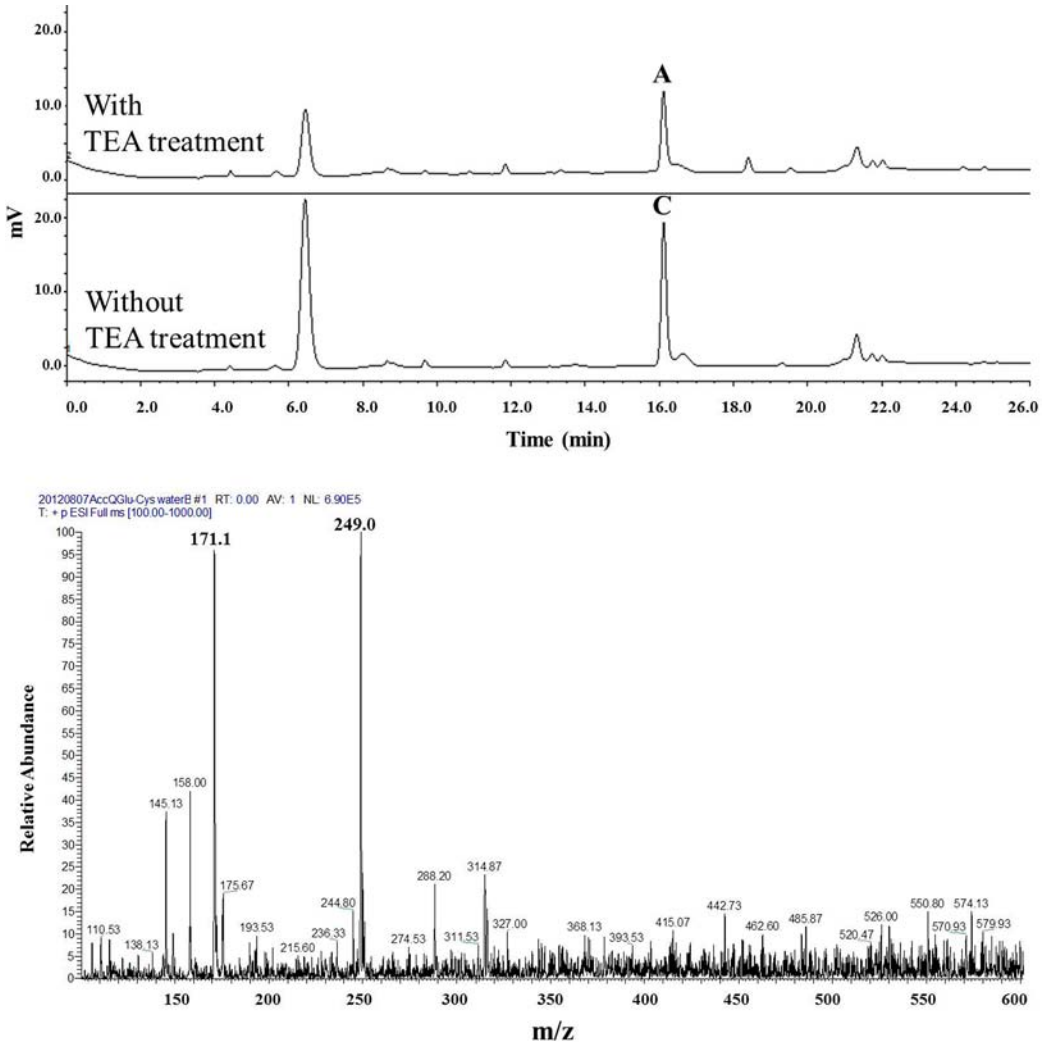

Figure 4. Effects of the drying pretreatment with TEA on the derivatization of 2-mercaptoethanol-pretreated GSH with AccQ: elution profiles of the derivatives with and without the TEA treatment (upper); ESI-MS analysis of the derivative without TEA treatment (lower).

(Figure 1). The GSH derivative could be resolved by RP-HPLC and detected by fluorescence. Other derivatives of thiol compounds, such as γGlu-Cy and Cys-Gly, however, show similar retention times (data not shown). These peaks may interfere with the determination of GSH by fluorescence detection.

Therefore, the MRM was used for the specific detection of the GSH and its fragment peptides (γGlu-Cys, Cys-Gly) by monitoring m/z 554 → 171.3 and m/z 554 → 145.2 (GSH), m/z 497 → 171.3 and m/z 497 → 145.2 (γGlu-Cys), and m/z 425 → 171.2 and m/z 425 → 116.1 (Cys-Gly), respectively, in the present study. By using this method, protein-bound GSH and its fragment peptides at a concentration of <1 μM in the plasma could be successfully determined.

Ikegaya et al. have demonstrated that cysteine and cysteinyl-glycine bind to human serum albumins through disulfide bonds, whereas no significant amount of GSH is bound to serum albumin that is obtained from human blood.[22] The present study also demonstrated that only a negligible amount of GSH was bound to plasma protein before the supplementation of GSH. However, the protein-bound GSH significantly (P < 0.01) increased from 60 to 120 min after the oral supplementation of GSH. This is the first report to demonstrate an increase in GSH in the human blood fraction by the oral supplementation of GSH. The protein-bound form GSH level in plasma after supplementation of GSH is much higher (>1000 times) than that of other food-derived peptides such as Val-Tyr[25] and Ile-Pro-Pro[26] but less than that of the food-derived collagen peptides in human blood.[27]

It has been thought that orally administered GSH is successively degraded to cysteinyl-glycine, cysteine, and glycine by γ-glutamyl-transferase and peptidase.[17,28,29] Cysteine could be used for GSH synthesis in cells. Increased levels of protein-bound GSH might be derived from the newly synthesized GSH. The present study also detected fragment peptide (Cys-Gly) and precursor peptide (γGlu-Cys) as protein-bound forms in human blood, which suggests some GSH is synthesized from degradation products of GSH.

However, an early study by Kubo that used ^{35}S-labeled GSH and paper electrophoresis has suggested that GSH could be directly absorbed from the small intestine into rat portal blood.[30] Therefore, there is a possibility that supplemented GSH is directly absorbed into human blood and bound to plasma protein. To solve these problems, further studies on the metabolic fate of supplemented GSH that use ^{13}C-labeled GSH are in progress. The procedure that was used in the present study for the determination of protein-bound GSH that was based on LC-MS/MS and precolumn label techniques can

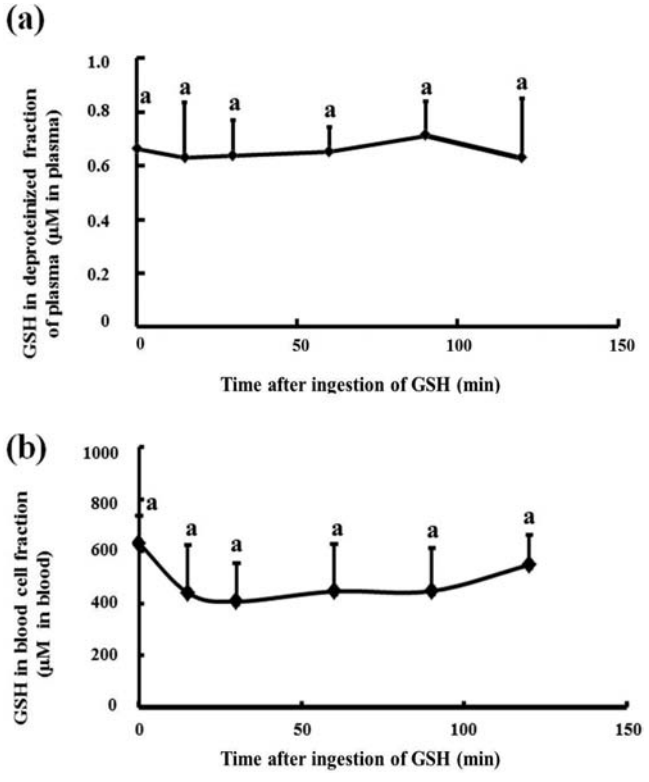

Figure 5. Total GSH contents in the deproteinized (ethanol-soluble) plasma fraction (a) and blood cell fraction (b) after the ingestion of GSH. No significant difference was observed between groups (P < 0.01).

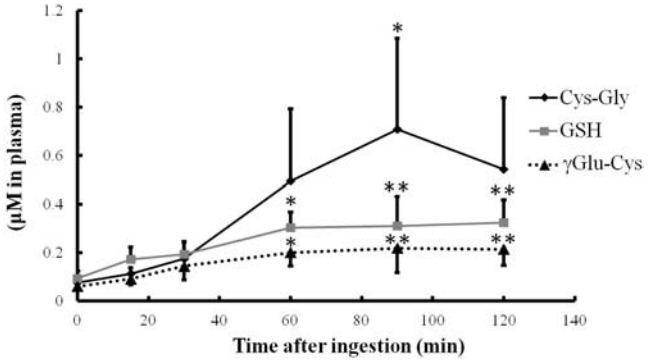

Figure 6. Contents of glutathione (GSH), γ-glutamyl-cysteine (γGlu-Cys), and cysteinyl-glycine (Cys-Gly) in the ethanol precipitate fraction of plasma after ingestion of GSH. (*, **) Significantly different from baseline P < 0.05 and 0.01, respectively, according to Scheffe's post hoc test.

distinguish food-derived (^{13}C-labeled) and endogenous GSH and their metabolites, such as γGlu-Cys, Cys-Gly, and cysteine, and this is a powerful tool for the elucidation of the absorption, metabolism, and transportation of food-derived GSH.

AUTHOR INFORMATION

Corresponding Author

*(K.S.) Mail (present address): Division of Applied Biosciences, Graduate School of Agriculture, Kyoto University, Kitashirakawa Oiwake-cho, Kyoto 606-8502, Japan. Phone: +81-75-753-6444. Fax: +81-75-723-3503. E-mail: kensato@kais.kyoto-u.ac.jp.

Notes

The authors declare no competing financial interest.

ACKNOWLEDGMENTS

We express our appreciation to the Kyoto Integrated Science and Technology Bio-Analysis Center for the use of their LC-MS/MS.

ABBREVIATIONS USED

GSH, glutathione; γGlu-Cys-Gly, γ-L-glutamyl-L-cysteinyl-glycine; Cys-Gly, L-cysteinyl-glycine; γGlu-Cys, γ-L-glutamyl-L-cysteine; AccQ, 6-aminoquinolyl-*N*-hydroxysuccinimidyl carbamate; TEA, triethylamine; TCA, trichloroacetic acid; RP-HPLC, reversed phase high-performance liquid chromatography; ESI-MS, electrospray ionization mass spectrometry; LC-MS/MS, liquid chromatography−tandem mass spectrometry; ESI-MS/MS, electrospray ionization tandem mass spectrometry

REFERENCES

(1) Anderson, M. E. Glutathione: an overview of biosynthesis and modulation. *Chem.−Biol. Interact.* **1998**, *112*, 1−14.
(2) Fahey, R. C. Novel thiols of prokaryotes. *Annu. Rev. Microbiol.* **2001**, *55*, 533−556.
(3) Meister, A. Glutathione metabolism and its selective modification. *J. Biol. Chem.* **1988**, *263*, 17205−17208.
(4) Mannervik, B.; Danielson, U. H. Glutathione transferases-structure and catalytic activity. *CRC Crit. Rev. Biochem.* **1988**, *23*, 283−337.
(5) Mannervik, B. The enzymes of glutathione metabolism: an overview. *Biochem. Soc. Trans.* **1987**, *15*, 717−718.
(6) Meister, A.; Anderson, M. E. Glutathione. *Annu. Rev. Biochem.* **1983**, *52*, 711−760.
(7) Nuray, N.; Ulusu, M. S.; Aslihan, A.; Orhan, C.; Gülgün, O.; Nuray, A.; Musa, B.; Milan, S.; Svorad, S.; Andrej, G.; Çimen, K. Pentose phosphate pathway, glutathione-dependent enzymes and antioxidant defense during oxidative stress in diabetic rodent brain and peripheral organs: effects of stobadine and vitamin E. *Neurochem. Res.* **2003**, *28*, 815−823.
(8) Douglas, K. T. Mechanism of action of glutathione-dependent enzymes. *Adv. Enzymol. Relat. Areas Mol. Biol.* **1987**, *59*, 103−167.
(9) Oakley, A. Glutathione transferases: a structural perspective. *Drug Metab. Rev.* **2011**, *43*, 138−151.
(10) White, A. C.; Thannickal, V. J.; Fanburg, B. L. Glutathione deficiency in human disease. *J. Nutr. Biochem.* **1992**, *5*, 218−226.
(11) Dentico, P.; Volpe, A.; Buongiorno, R.; Grattagliano, I.; Altomare, E.; Tantimonaco, G.; Scotto, G.; Sacco, R.; Schiraldi, O. Glutathione in the treatment of chronic fatty liver diseases. *Recent Prog. Med.* **1995**, *86*, 290−293.
(12) Altomare, E.; Colonna, P.; Dagostino, C.; Castellaneta, G.; Vendemiale, G.; Grattagliano, I.; Cirelli, F.; Bovenzi, F.; Colonna, L. High-dose antioxidant therapy during thrombolysis in patients with acute myocardial infarction. *Curr. Ther. Res.* **1996**, *57*, 131−141.
(13) Matsuki, M.; Watanabe, T.; Ogasawara, A.; Mikami, T.; Matsumoto, T. Inhibitory mechanism of melanin synthesis by glutathione. *Yakugaku Zasshi* **2008**, *128*, 1203−1207.
(14) Arjinpathana, N.; Asawanonda, P. Glutathione as an oral whitening agent: a randomized, double-blind, placebo-controlled study. *J. Dermatol. Treat.* **2012**, *23*, 97−102.
(15) Meister, A. Glutathione deficiency produced by inhibition of its synthesis, and its reversal; applications in research and therapy. *Pharmacol. Ther.* **1991**, *51*, 155−194.
(16) Allen, J.; Bradley, R. D. Effects of oral glutathione supplementation on systemic oxidative stress biomarkers in human volunteers. *J. Altern. Complement. Med.* **2011**, *17*, 827−833.

(17) Witschi, A.; Reddy, S.; Stofer, B.; Lauterburg, B. H. The systemic availability of oral glutathione. *Eur. J. Clin. Pharmacol.* **1992**, *43*, 667−669.
(18) Monks, T. J.; Anders, M. W.; Dekant, W.; Stevens, J. L.; Lau, S. S.; van Bladeren, P. J. Glutathione conjugate mediated toxicities. *Toxicol. Appl. Pharmacol.* **1990**, *106*, 1−19.
(19) Teitze, F. Enzymic method for quantitative determination of nanogram amounts of total and oxidized glutathione. *Anal. Biochem.* **1969**, *27*, 502−522.
(20) Rahman, I.; Kode, A.; Biswas, S. K. Assay for quantitative determination of glutathione and glutathione disulfide levels using enzymatic recycling method. *Nat. Protoc.* **2006**, *1*, 3159−3165.
(21) Sengupta, S.; Chen, H.; Togawa, T.; DiBello, P. M.; Majors, A. K.; Büdy, B.; Kettere, M. E.; Jacobsen, D. W. Albumin thiolate anion is an intermediate in the formation of albumin-S−S-homocysteine. *J. Biol. Chem.* **2001**, *276*, 30111−30117.
(22) Ikegaya, K.; Nokihara, K.; Yasuhara, T. Characterization of sulfhydryl heterogeneity in human serum albumin and recombinant human serum albumin for clinical use. *Biosci., Biotechnol., Biochem.* **2010**, *74*, 2232−2236.
(23) Griffith, O. W. Determination of glutathione and glutathione disulfide using glutathione reductase and 2-vinylpyridine. *Anal. Biochem.* **1980**, *106*, 207−212.
(24) Ates, B.; Ercal, B. C.; Manda, K.; Abraham, L.; Ercal, N. Determindation of glutathione disulfide levels in biological samples using thiol-disulfide exchanging agent, dithiothreitol. *Biomed. Chromatogr.* **2009**, *23*, 119−123.
(25) Matsui, T.; Tamaya, K.; Seki, E.; Osajima, K.; Matsumo, K.; Kawasaki, T. Absorption of Val-Tyr with *in vitro* angiotensin I-converting enzyme inhibitory activity into the circulating blood system of mild hypertensive subjects. *Biol. Pharm. Bull.* **2002**, *25*, 1228−1230.
(26) Foltz, M.; Meynen, E. E.; Bianco, V.; van Platerink, C.; Koning, T. M.; Kloek, J. Angiotensin converting enzyme inhibitory peptides from a lactotripeptide-enriched milk beverage are absorbed intact into the circulation. *J. Nutr.* **2007**, *137*, 953−958.
(27) Iwai, K.; Hasegawa, T.; Taguchi, Y.; Morimatsu, F.; Sato, K.; Nakamura, Y.; Higashi, A.; Kido, Y.; Nakabo, Y.; Ohtsuki, K. Identification of food-derived collagen peptides in human blood after oral ingestion of gelatin hydrolysates. *J. Agric. Food Chem.* **2005**, *53*, 6531−6536.
(28) Flagg, E. W.; Coates, R. J.; Eley, J. W.; Jones, D. P.; Gunter, E. W.; Byers, T. E.; Block, G. S.; Greenberg, R. S. Dietary glutathione intake in humans and the relationship between intake and plasma total glutathione level. *Nutr. Cancer* **1994**, *21*, 33−46.
(29) MacNee, W.; Rahman, I. Oxidants/antioxidants in idiopathic pulmonary fibrosis. *Thorax* **1995**, *50*, S53−S58.
(30) Kubo, Y. Absorption of ^{35}S-GSH and its incorporation into protein in rats. *Kurume Med. J.* **1968**, *15*, 113−125.

JOURNAL OF AGRICULTURAL AND FOOD CHEMISTRY

Article

pubs.acs.org/JAFC

Influence of Olive Leaf Processing on the Bioaccessibility of Bioactive Polyphenols

Margarita H. Ahmad-Qasem,[†] Jaime Cánovas,[†] Enrique Barrajón-Catalán,[§] José E. Carreres,[#] Vicente Micol,[§] and José V. García-Pérez*,[†]

[†]Grupo de Análisis y Simulación de Procesos Agroalimentarios (ASPA), Departamento de Tecnología de Alimentos, Universitat Politècnica de València, Valencia 46022, Spain

[§]Instituto de Biología Molecular y Celular, Universidad Miguel Hernández, Elche 03202, Spain

[#]AINIA Centro Tecnológico, Parque Tecnológico de Valencia, Benjamin Franklin, Paterna 46980, Spain

ABSTRACT: Olive leaves are rich in bioactive compounds, which are beneficial for humans. The objective of this work was to assess the influence of processing conditions (drying and extraction) of olive leaves on the extract's bioaccessibility. Thus, extracts obtained from dried olive leaves (hot air drying at 70 and 120 °C or freeze-drying) by means of conventional or ultrasound-assisted extraction were subjected to in vitro digestion. Antioxidant capacity, total phenolic content, and HPLC-DAD/MS/MS analysis were carried out during digestion. The dehydration treatment used for the olive leaves did not have a meaningful influence on bioaccessibility. The digestion process significantly ($p < 0.05$) affected the composition of the extracts. Oleuropein and verbascoside were quite resistant to gastric digestion but were largely degraded in the intestinal phase. Nevertheless, luteolin-7-*O*-glucoside was the most stable polyphenol during the in vitro simulation (43% bioaccessibility). Therefore, this compound may be taken into consideration in further studies that focus on the bioactivity of olive leaf extracts.

KEYWORDS: *Olea europaea, drying, in vitro digestion, antioxidant potential, byproduct*

INTRODUCTION

Although olives (*Olea europaea* L.) are cultivated in several parts of the world, the Mediterranean region is the major crop production area, accounting for about 98% of the world's olive cultivation.[1] Olive hydrophilic extracts contain a large number of phenolic compounds.[2] The most important source of these polyphenolic compounds is the olive fruit; however, they are also present in the leaves.[3] The most abundant polyphenols identified in olive leaf extracts have been oleuropein, hydroxytyrosol, verbascoside, apigenin-7-glucoside, and luteolin-7-glucoside.[4] These compounds confer bioactive properties on the olive leaf extracts, such as antioxidant,[4] antimicrobial,[5] and antitumor capacities.[6] Moreover, they are able to reduce the risk of coronary heart disease.[7]

Not only do olive leaves appear as a byproduct during oil processing in the olive oil industries (10% of the total weight of the olives), they are also a residue of olive tree pruning.[8] Despite the aforementioned bioactive potential of olive leaves, the large volumes generated of this byproduct have been traditionally used as animal feed.[9] The exploitation of olive leaves as a natural resource rich in antioxidant phenolic compounds would involve the valorization of this byproduct. However, it is essential to determine if the leaf processing (drying and extraction methods) used to obtain the extracts can affect not only the antioxidant potential but also the stability necessary for later applications. Hot air and freeze-drying are common dehydration techniques used in the food, chemical, and pharmaceutical industries. Nevertheless, although both methods reduce the water content of the raw material, improving the polyphenol extraction, the extracts obtained exhibit different compositions,[10] and their degree of stability could also vary. Moreover, the stability of extracts obtained by conventional maceration could also be different from those obtained by the use of new, emerging extraction technologies, such as ultrasound-assisted or supercritical CO_2 extraction. In the case of ultrasound (US), although its ability to speed the extraction process has already been stated, it is also well-known that it induces the formation of free radicals,[11] which even at low concentrations could affect extract behavior.

The aforementioned facts, together with the scarce amount of knowledge about the stability and behavior of olive leaf phenolic compounds under digestion conditions, open up a new line of research in the area of antioxidant extracts and their possible applications as natural remedies. Thus, to use the olive leaf polyphenols for the benefit of human health, it is important not only to extract and quantify these bioactive compounds but also to study their bioaccessibility. This term is defined as the amount of an ingested compound that is available for absorption in the gut after digestion.[12] Nowadays, there are two possible methods for the evaluation of the behavior of bioactive compounds during the digestive processes: in vivo and in vitro. On the one hand, in vivo methods simulate the digestion better, but are complex, expensive, and lengthy,[13] and the control of the process variables is complicated. On the other hand, in vitro digestion models simulate the release of compounds from the food matrix[14] and the gastrointestinal conditions, are relatively inexpensive, are technically simple,[13,15]

Received: March 26, 2014
Revised: June 3, 2014
Accepted: June 13, 2014
Published: June 13, 2014

ACS Publications © 2014 American Chemical Society

and allow for the accurate testing of several process variables. Moreover, considering that there exist some host-related factors, such as intestinal factors, gender, age, disorders, or physiological conditions which could influence bioaccessibility,[16] in vitro methods seem to be a suitable alternative to obtain proper simulation data. In fact, they are considered a proper alternative to animal experimentation by the European Directive on the protection of animals (2010/63/UE).[17]

Even so, the bioaccessibility study is a challenge because, apart from human factors, there are external, food, or processing factors that could affect bioactive compounds. Thus, there is ample evidence that the physical state of the matrix plays a key role in the release, mass transfer, accessibility, and biochemical stability of many food components.[18] Hence, nutrients located in natural cellular compartments or within assemblies produced during processing need to be released during digestion so they can be absorbed in the gut.[19] Therefore, removing the handicap of structural barriers could facilitate the extraction of the components and, consequently, it would improve their bioaccessibility. In this sense, obtaining extracts rich in bioactive compounds could be a suitable alternative.

The objective of this work was to assess the influence of the processing conditions (drying and extraction) of olive leaves on the bioaccessibility of the extracts. The study aims to evaluate not only the compositional but also the kinetic changes that take place in the extracts during in vitro gastrointestinal digestion.

MATERIALS AND METHODS

Olive Leaf Extracts. Olive leaf extracts were obtained from leaves (*O. europaea* var. Serrana) dried by following two different methods described in previous works:[10] hot air drying at 70 °C (HAD-70) and 120 °C (HAD-120) and freeze-drying using conventional freezing at −28 °C (FD).

The extraction of olive leaf phenolic compounds was carried out by using conventional[10] and US-assisted extraction.[20] Briefly, extractions were performed at 25 °C using milled olive leaves (Blixer 2, Robot Coupe USA, Inc., Jackson, MS, USA) and an 80:20 (v/v) ethanol/water solution as solvent (extracting medium). The ratio between the weight of olive leaves and the solvent volume used was different depending on the method: 0.125 and 0.031 g/mL for conventional and US-assisted extraction, respectively. In the ultrasonic experiments, the ultrasonic emitter, with a surface of 12.6 cm^2, was immersed 1 cm into the solution, and 100% electric power of the system (400 W) was supplied to the transducer. The extracts obtained were centrifuged for 10 min at 5000 rpm (Medifriger BL-S, J.P. Selecta, Barcelona, Spain), filtered (nylon filters of 0.45 μm), and stored in opaque vials at 4 °C until used. Thus, combining the drying (FD, HAD-70, and HAD-120) and the extraction methods (conventional or US-assisted), a total of four different extracts were obtained: FD, HAD-70, HAD-120, and HAD-120+US. At least three extraction replicates were made for each different processing condition.

Polyphenolic Standard Solutions. Standard solutions of the main polyphenols found in the olive leaf extracts were prepared in distilled water. Concentrations of the standard solutions were similar to the concentration (mg compounds/mL extract) of the polyphenols in the olive leaf extracts. The standard polyphenols used are described in the following sections.

In Vitro Digestion. In vitro digestion was simulated using a slightly modified version of previously described methods.[21,22] Ten grams of sample (olive leaf extract, polyphenolic standards solution, or blank) was diluted with distilled water (1:8, p/v) and acidified to pH 2.0 using 6 N HCl under vigorous stirring. The acidified sample was stirred for 15 min. Then, the pH value was checked and eventually corrected if necessary with 6 N HCl. The extract sample was then mixed with 3 mL of a solution (160 mg/mL) of pepsin from pig gastric mucosa (Sigma Chemical Co., 3.8 units/mg protein) in 0.1 N HCl. Subsequently, distilled water was added to reach a final volume of 100 mL. The mixture was stirred for 2 h at 37 °C. After gastric digestion, the pH of the digesta was increased to pH 5 with 0.9 M $NaHCO_3$, and 22.54 mL of pancreatin−bile solution (pancreatin 4 mg/mL, bile 25 mg/mL in 0.1 M $NaHCO_3$) was added. Then, to complete the intestinal digestion, the pH was increased to 7.0 with 0.1 M $NaHCO_3$, and the mixture was stirred for 2 h at 37 °C.

The digestion simulation was carried out in sealed containers protected from light and placed in an orbital incubator (Rotabit, J. P Selecta, Barcelona, Spain) at 120 rpm. To monitor the changes undergone by extracts during in vitro digestion, samples of 2 mL were taken at preset times (0, 1, 2, 3, and 4 h). All samples were immediately cooled and filtered (nylon filters of 0.45 μm), stored in opaque vials at 4 °C, and analyzed within 24 h. At least three digestion replicates were made for each different olive leaf extract.

Total Phenolic Content (TPC) Measurement. The phenolic content was determined by the Folin−Ciocalteu method.[23] Briefly, 100 μL of sample or blank was mixed with 200 μL of Folin−Ciocalteu's phenol reagent (Sigma-Aldrich, Madrid, Spain) and 2 mL of distilled water. After 3 min at 25 °C, 1 mL of Na_2CO_3 (Panreac, Barcelona, Spain) solution (Na_2CO_3/water 20:80, w/v) was added to the mixture. The reaction was kept in the dark at room temperature for 1 h. Finally, the absorbance was read at 765 nm using a spectrophotometer (Helios Gamma, Thermo Spectronic, Cambridge, UK). The measurements were carried out in triplicate, unless otherwise stated. The standard curve was previously prepared using solutions of a known concentration of gallic acid hydrate (Sigma-Aldrich) in water and ethanol/water (80:20, v/v). Results were expressed as milligrams of gallic acid (GAE) per gram of dry weight of olive leaves (g dw) or in the case of the standards as milligrams of gallic acid (GAE) per gram of compound.

Antioxidant Capacity (AC) Measurement. *Ferric Reducing Ability Power (FRAP).* The FRAP method, which is a simple method used to estimate the reduction of a ferric−tripyridyltriazine complex, was applied[24] with some modifications. Briefly, 900 μL of freshly prepared FRAP reagent was mixed with 30 μL of distilled water and 30 μL of test sample or blank and kept at 37 °C for 30 min. The FRAP reagent contained 2.5 mL of a 10 mM TPTZ (Fluka, Steinheim, Germany) solution in 40 mM HCl (Panreac, Barcelona, Spain) plus 2.5 mL of 20 mM $FeCl_3 \cdot 6H_2O$ (Panreac) and 2.5 mL of 0.3 M acetate buffer (Panreac), pH 3.6.[25] Readings at the maximum absorption level (595 nm) were taken using a spectrophotometer (Helios Gamma, Thermo Spectronic). Four replicates were made for each measurement. The antioxidant capacity was evaluated through a calibration curve, which was previously determined using water and ethanol solutions (ethanol/water 80:20, v/v) of known Trolox (Sigma-Aldrich) concentrations and expressed as milligrams of Trolox per gram of dry weight of olive leaves (g dw) or in the case of the standards as milligrams of Trolox per gram of compound.

Trolox Equivalent Antioxidant Capacity (TEAC). The TEAC method, which measures the reduction of the radical cation of ABTS by antioxidants, was performed.[26] Briefly, ABTS radical cation ($ABTS^{\bullet+}$) was produced by reacting ABTS (Sigma-Aldrich) stock solution with 2.45 mM potassium persulfate (final concentration) and allowing the mixture to stay in the dark at room temperature for 12−24 h before use. The $ABTS^{\bullet+}$ solution was diluted with distilled water until an absorbance value of 0.714 ± 0.02 at 734 nm was reached. For the photometric assay, the absorbance of 200 μL of the $ABTS^{\bullet+}$ solution or blank was measured (Spectrostar Omega, BMG Labtech, Offenburg, Germany). Afterward, 20 μL of the antioxidant extract or blank (water or ethanol/water 80:20, v/v) was added and, after 29 min at 734 nm, the final absorbance was measured (Spectrostar Omega, BMG Labtech). The antioxidant capacity was determined from the difference of absorbance, using a Trolox calibration curve (Sigma-Aldrich). Four replicates were made for each extract. The antioxidant capacity results were expressed as milligrams of Trolox per gram of dry weight of olive leaves (g dw) or in the case of the standards as milligrams of Trolox per gram of compound.

Table 1. Content (Milligrams per Gram Dry Weight) of the Main Identified Polyphenols and Antioxidant Activity of Olive Leaf Extracts

	initial extracts[a]			
extract characterization	HAD-70	HAD-120	FD	HAD-120+US
TPC (mg GAE/g dw)	42 ± 4 a	66 ± 3 b	33 ± 3 a	66 ± 9 b
AC (mg Trolox/g dw)				
FRAP	87 ± 6 a	102.2 ± 1.7 b	75 ± 4 c	112 ± 4 d
TEAC	4.96 ± 0.17 ab	6.3 ± 0.2 bc	4.4 ± 0.9 a	7.2 ± 1.4 c
verbacoside	6.48 ± 0.15 a	18.7 ± 0.3 b	4.2 ± 0.4 c	18.5 ± 0.8 b
oleuropein	47 ± 3 a	74.9 ± 0.4 b	22.9 ± 0.4 c	65 ± 3 d
oleuropein-glucoside[b]	3.7 ± 0.9 a	16.4 ± 0.5 b	3.6 ± 0.6 a	13.9 ± 0.3 c
luteolin-glucoside	8.4 ± 0.5 a	9.7 ± 0.4 b	9.9 ± 0.7 b	11 ± 4 c
luteolin[c]	0.9 ± 0.2 a	0.76 ± 0.07 a	0.9 ± 0.3 a	0.28 ± 0.03 b
luteolin-7-*O*-rutinoside[c]	2.7 ± 0.5 a	2.52 ± 0.13 ab	2.1 ± 0.4 bc	1.86 ± 0.19 c
apigenin-7-*O*-glucoside[d]	0.67 ± 0.12 ab	0.78 ± 0.02 a	0.62 ± 0.06 b	0.698 ± 0.014 ab
apigenin-6,8-diglucoside[d]	0.48 ± 0.07 a	0.40 ± 0.15 ab	0.25 ± 0.03 b	0.36 ± 0.06 ab
apigenin rutinoside[d]	0.92 ± 0.15 a	1.13 ± 0.03 b	0.71 ± 0.08 c	0.93 ± 0.02 a

[a]Letters following entries show homogeneous groups in the same row established from least significance difference intervals ($p < 0.05$). [b]Content expressed as equivalents of oleuropein (mg/g dw). [c]Content expressed as equivalents of luteolin-7-*O*-glucoside (mg/g dw). [d]Content expressed as equivalents of apigenin (mg/g dw).

Identification and Quantification of Polyphenols by HPLC-DAD/MS-MS. To identify and quantify the main polyphenols, olive leaf extracts were analyzed using an HPLC instrument (Agilent LC 1100 series; Agilent Technologies, Inc., Palo Alto, CA, USA) controlled by Chemstation software. The HPLC instrument was coupled to an Esquire 3000+ (Bruker Daltonics, GmbH, Bremen, Germany) mass spectrometer equipped with an ESI source and ion-trap mass analyzer and controlled by Esquire control and data analysis software. A Merck Lichrospher 100RP-18 (5 μm, 250 × 4 mm) column was used for analytical purposes.

Separation was carried out through a linear gradient method using 2.5% acetic acid (A) and acetonitrile (B), starting the sequence with 10% B and programming the gradient to obtain 20% B at 10 min, 40% B at 35 min, 100% B at 40 min, 100% B at 45 min, 10% B at 46 min, and 10% B at 50 min. For the LC-MS pump to perform accurately, 10% of organic solvent was premixed in the water phase. The flow rate was 1 mL/min, and the chromatograms were monitored at 240, 280, and 330 nm. Mass spectrometry operating conditions were optimized to achieve maximum sensitivity values. The ESI source was operated in negative mode to generate $[M - H]^-$ ions using the following conditions: desolvation temperature at 365 °C and vaporizer temperature at 400 °C; dry gas (nitrogen) and nebulizer were set at 12 L/min and 4.83 bar, respectively. The MS data were acquired as full scan mass spectra at m/z 50−1100 by using 200 ms for collection of the ions in the trap.

The main compounds were identified by HPLC-DAD analysis, comparing the retention time, UV spectra, and MS/MS data of the peaks in the samples with those of authentic standards or data reported in the literature. Only the main olive leaf polyphenols were quantified using commercial standards: oleuropein (Extrasynthese, Genay Cedex, France), luteolin-7-*O*-glucoside (Phytolab, Vestenbergsgreuth, Germany), and apigenin (Nutrafur, Murcia, Spain). A verbascoside standard (96.85%) purified from *Lippia citriodora* extract was kindly provided by Universidad Miguel Hernández (Elche, Spain). The quantitative evaluation of the compounds was performed with a calibration curve for each polyphenol, using ethanol (oleuropein) or methanol (verbascoside and luteolin) solutions of known concentration. The polyphenol concentrations were expressed as milligrams of polyphenol per gram of dry weight of olive leaves (g dw) or, in the case of the standards, as milligrams of compound per milliliter of initial solution.

Method accuracy for the determination of oleuropein, verbascoside, and luteolin-glucoside in samples was further assessed with recovery studies by spiking standard compounds into blank samples in triplicate. The linearity range of the responses was determined on seven concentration levels with three injections for each level. Calibration graphs for HPLC were recorded with sample amount ranging from 0.25 μg/mL to 0.25 mg/mL ($r^2 > 0.9999$). Quantitative evaluation of oleuropein, verbascoside, and luteolin-glucoside was performed by means of a six-point regression curve ($r^2 > 0.996$, 0.997, and 0.986, respectively) in a concentration range between 0.25 μg/mL and 10 mg/mL, using oleuropein, verbascoside, and luteolin-glucoside as reference external standard and evaluated by DAD signal. The limit of detection (LOD) was 0.10 μg/mL and the limit of quantification (LOQ), 0.25 μg/mL.

Statistical Analysis. Analysis of variance (ANOVA) was applied to determine the significant effects of in vitro digestion on extract composition taking a significance level of 95%. The statistical analysis was performed using Statgraphics-Plus software 5.1 (Statistical Graphics, Rockville, MD, USA).

RESULTS AND DISCUSSION

Initial Characterization of Olive Leaf Extracts. Previous studies have reported that the composition of olive leaf extracts is greatly influenced by processing conditions, namely, the drying and extraction. In such a way, a conventional extraction method[10] was used with leaves hot air-dried at 70 (HAD-70) and 120 °C (HAD-120) and freeze-dried (FD). Moreover, HAD-120 leaves were subjected to ultrasound-assisted extraction (HAD-120+US).[20]

As can be observed in Table 1, the TPC and AC of the extracts used were significantly ($p < 0.05$) influenced by the olive leaf drying technique, which confirms the previously reported results.[10] It is relevant to highlight that the HAD-120 and FD extracts showed the highest and lowest antioxidant potentials, respectively. With regard to the extraction method, ultrasonically assisted extraction provided extracts (HAD-120+US) with a bioactive content similar to that of the conventional procedure (HAD-120), as already reported.[20] Thus, although US did not involve a change in the initial polyphenolic composition of the extracts, the HAD-120+US extracts were included in the analysis due to the reported ability of US to promote the formation of free radicals.[27] These compounds, even at low concentrations, may induce compositional changes in the gastric/intestinal environment, a fact that has not been previously studied.

To gain insight into the differences in the antioxidant potential of olive leaf extracts, major polyphenolic compounds

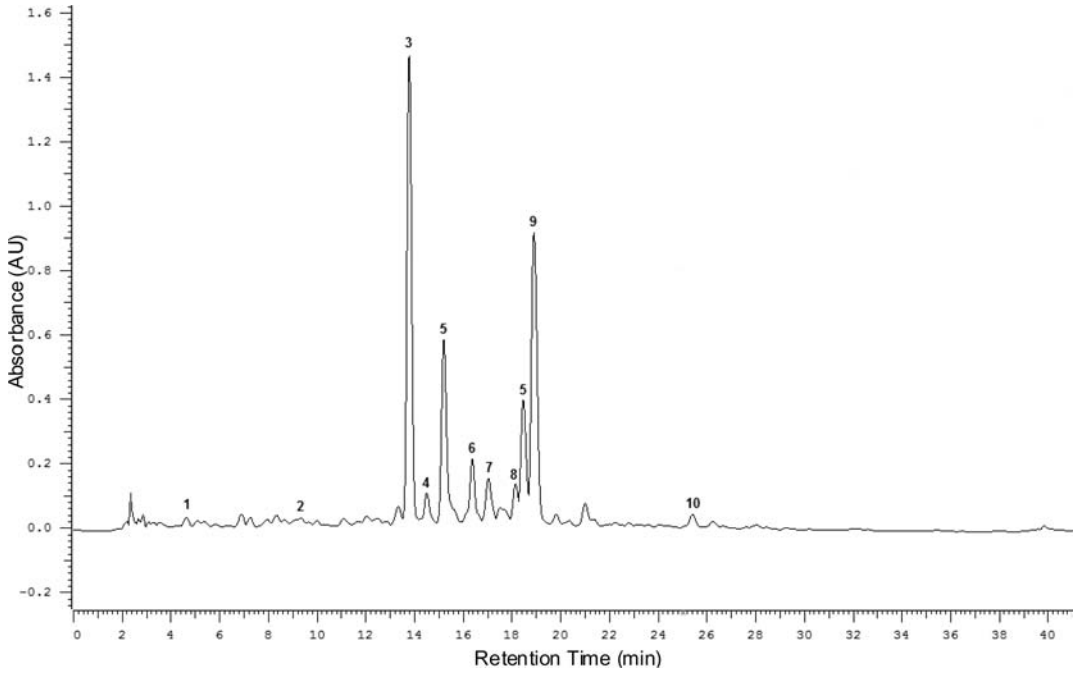

Figure 1. HPLC chromatograms at 280 nm of extracts obtained from fresh olive leaves dried by hot air drying at 120 °C using conventional extraction (HAD-120).

Table 2. Relevant Analytical Data of Compounds in Olive Leaf Extracts Identified by HPLC-ESI-MS/MS

peak	phenolic compound	mol mass (g/mol)	retention time (min)
1	caffeoyl	354.31	4.70
2	apigenin-6,8-diglucoside	594.52	9.41
3	verbascoside	624.6	13.85
4	luteolin-7-*O*-rutinoside	578.52	14.57
5	luteolin-7-*O*-glucoside	448.38	15.27
	luteolin-7-*O*-glucoside (isomer)	448.38	18.50
6	oleuropein-glucoside	702	16.45
7	apigenin-rutinoside	578.53	17.11
8	apigenin-7-*O*-glucoside	432.37	18.24
9	oleuropein	540.52	19.02
10	luteolin	286.24	25.50

were identified by HPLC-DAD/MS/MS (Figure 1 and Table 2). A similar phenolic profile was found in all of the extracts, with minor differences. However, significant ($p < 0.05$) differences were found (Table 1) for the concentration of the main polyphenols (verbascoside, oleuropein, luteolin-glucoside). In overall terms, the highest contents of these compounds were correlated with the highest levels of TPC and AC.

Influence of in Vitro Gastrointestinal Digestion on Antioxidant Potential. To simulate the stability of the main identified bioactive polyphenols, in vitro digestions of the olive leaf extracts and polyphenolic pure standards (oleuropein, verbascoside, and luteolin-glucoside) were carried out. During digestion, samples were taken at preset times (0, 1, 2, 3, and 4 h) and the TPC and AC determined.

A significant ($p < 0.05$) decrease in the TPC was observed for all extracts within the first hour of the gastric phase (Figure 2a), thereafter remaining practically constant for the rest of the intestinal digestion. This result indicates that a portion of the

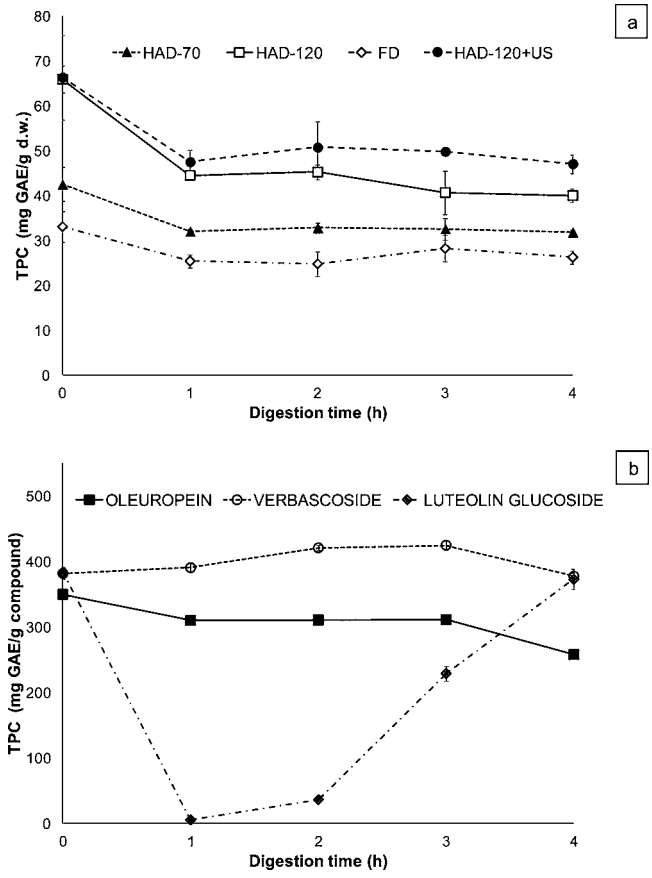

Figure 2. Kinetics of total phenolic content (TPC) during the in vitro digestion of olive leaf extracts (a) and standard compounds (b). Means ± standard deviation are plotted.

bioactive compounds may be degraded in the first steps of the digestion[28] due to the combined effect of the pH changes and

dx.doi.org/10.1021/jf501414h | J. Agric. Food Chem. 2014, 62, 6190−6198

the enzymatic activity, but a significant portion still reached the duodenum. Thus, after the gastric digestion (2 h), the TPC of HAD-120 extracts decreased by 31.4%, whereas the reduction in HAD-70 and FD extracts was smaller (22.9 and 25.1%, respectively). Grape bioaccessible polyphenols have been reported to behave differently during digestion.[29] Thus, after 2 h under gastric conditions, the TPC increased by 21.9% in the liquid fraction. These differences could be ascribed to the nature of the matrix being digested. The bioaccessibility study of grape polyphenols[29] was conducted in solid matrices (grapes); therefore, a release of polyphenols from the solid parts of the grape must take place during digestion. However, in our study, polyphenols were solubilized into the solution and, hence, directly exposed to gastric conditions from the beginning.

The kinetics showed that the intestinal phase, from 2 to 4 h, hardly influenced the TPC, because only slight changes were found (Figure 2a). The global balance of the TPC throughout the digestion showed a decrease of between 20.6% (FD) and 39.3% (HAD-120) when values were compared at 0 and 4 h. Although the HAD-120 extracts exhibited the highest TPC at the beginning of the digestion, they also showed a more significant decrease, indicating that these extracts were less resistant to gastrointestinal conditions. In contrast, FD and HAD-70 processed extracts were less affected by the digestion process.

On the other hand, when conventional and US extraction methods were compared, the US extracts exhibited a smaller reduction of TPC at the end of the in vitro digestion (29% for HAD-120+US and 39% for HAD-120). Consequently, the extraction method would have a significant influence ($p < 0.05$) on the TPC bioaccessibility; ultrasound application would be a good alternative to reduce olive leaf polyphenol extraction time[20] and ensure a better preservation of phenols during digestion.

To determine the contribution of the major compounds present in olive leaf to the TPC evolution under gastric digestion, their individual stability was studied (Figure 2b) by subjecting selected polyphenolic standard solutions to digestion and monitoring the TPC. The behavior observed during the digestion of the standard solutions was quite different compared to that of olive leaf extracts. Whereas oleuropein and verbascoside TPC values remained practically constant throughout the digestion process, the behavior of luteolin-glucoside standard solution was unexpected; that is, it dropped to a value of 0 after 1 h of digestion and increased to initial values after 4 h of digestion. The only reasonable explanation for this fact is that luteolin-glucoside shows a poor solubility or is complexed to proteins in the solutions for gastric digestion, so no TPC values were detected and its solubility recovered at the end of the intestinal digestion. This drop in the TPC of the luteolin-glucoside standard solution could contribute to the TPC reduction of the olive leaf extracts in the first hour of digestion (Figure 2).

The evolution of the AC of the extracts during digestion was determined by using two different methods, FRAP (Figure 3) and TEAC (Figure 4), which yielded different results. Whereas the TEAC kinetics of olive leaf extracts showed a behavior similar to that obtained for TPC (Figures 2a and 4a), the AC evolution measured by the FRAP method behaved totally differently (Figure 3a). The AC methods showed different trends, a fact that was also found in the case of in vitro tested

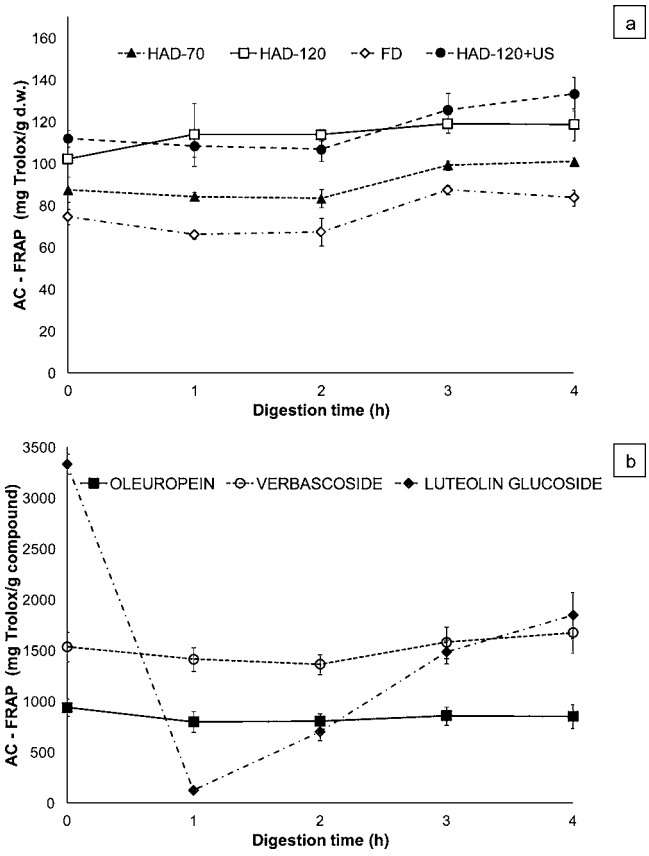

Figure 3. Kinetics of antioxidant capacity (AC) measured by FRAP method during the in vitro digestion of olive leaf extracts (a) and standard solution compounds (b). Means ± standard deviation are plotted.

wholegrain foods[30] and could be explained by the different chemical principles on which both AC methods are based.

The decrease in the TEAC values within the first hour of the extracts' digestion coincided with that observed for the TPC, and it may be related to the degradation of some compounds. We have reported that oleuropein is the major contributor to AC when measured by TEAC,[10] and it is also the most abundant compound in olive leaf extracts. The results of the evolution of the TEAC values for polyphenolic standard solutions under digestion (Figure 4b) also agree with this hypothesis, because the oleuropein and verbascoside TEAC values dropped dramatically after 1 h of digestion. Otherwise, the TEAC values for luteolin-glucoside recovered during intestinal digestion, coinciding with the behavior of the TPC and FRAP values during the same type of digestion (Figures 2b and 3b), indicating that this compound may resist the in vitro digestion process and may be considered for the subsequent intestinal absorption process. This negative impact of the digestion process on the TEAC values of the extracts has also been observed in the in vitro digestion of polyphenols deriving from extra virgin olive oils,[31] so the source of the compounds may not be the reason for this behavior.

However, although the FRAP values of olive leaf extracts remained almost constant during gastric digestion, despite the decrease in TPC and TEAC, a significant increase was observed during the intestinal digestion (Figure 3a). It has been reported that the reaction rates for the radical scavenging capacity of some flavonoids increase in correlation with their anionic

dx.doi.org/10.1021/jf501414h | J. Agric. Food Chem. 2014, 62, 6190−6198

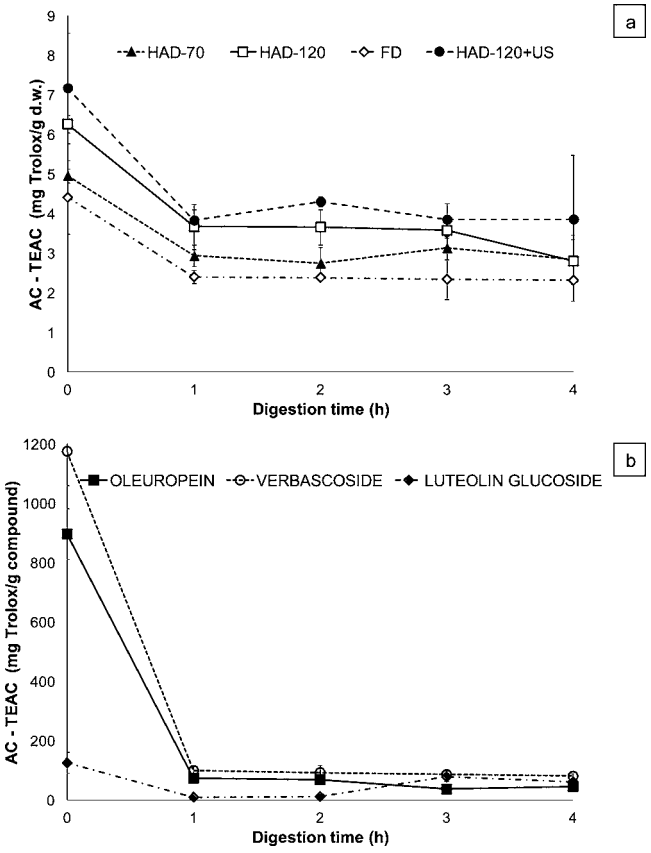

Figure 4. Kinetics of antioxidant capacity (AC) measured by TEAC method during the in vitro digestion of olive leaf extracts (a) and standard compounds (b). Means ± standard deviation are plotted.

character due to their higher electron-donating capacity. We postulate that at least luteolin may contribute to the greater capacity for reducing Fe^{3+} ions during the intestinal digestion process (Figures 3b, 3–4h) due to the fact that less protonation occurs at neutral pH.[32,33] We have previously reported that verbascoside and oleuropein are the main polyphenols contributing to the measurement of the FRAP values in the olive leaf extract.[10] This result would support the steady FRAP values of the extracts throughout the digestion (Figure 3a,b). However, although the luteolin-glucoside in the extracts is much less concentrated, its contribution to the final stages of the digestion process would be significant. Moreover, the formation of polyphenol derivatives during the digestion with enhanced AC, as well as potential synergistic effects among individual olive phenols, could contribute to keep the AC[34] measured by FRAP despite the observed reduction in the TPC.

In general terms, processing conditions did not largely affect the AC kinetic of the extracts during the in vitro digestion. However, as in the case of the TPC, both AC methods confirmed that the US extracts withstood the gastrointestinal digestion slightly better than the conventional extracts.

Considering that AC and TPC are global measurements of the extracts' antioxidant potential and taking into account that the polyphenolic composition may vary throughout the digestion, a more thorough characterization of the extracts was proposed during the digestion process. Hence, the HPLC-DAD/MS/MS was chosen as the most reliable alternative to understand how individual olive leaf polyphenols evolved during in vitro digestion.

Degradation Kinetics of the Individual Olive Leaf Polyphenols during in Vitro Digestion. With the aim of gaining insight into the stability of the major olive leaf polyphenols under gastric and intestinal conditions and to design strategies aimed at increasing their bioaccessibility in the gut, their contents were monitored during the in vitro digestion (0, 1, 2, 3, and 4 h) (Figure 5).

The content of the studied phenolic compounds underwent a significant ($p < 0.05$) decrease during the first hour of the gastric digestion. However, from 1 to 2 h the gastric conditions

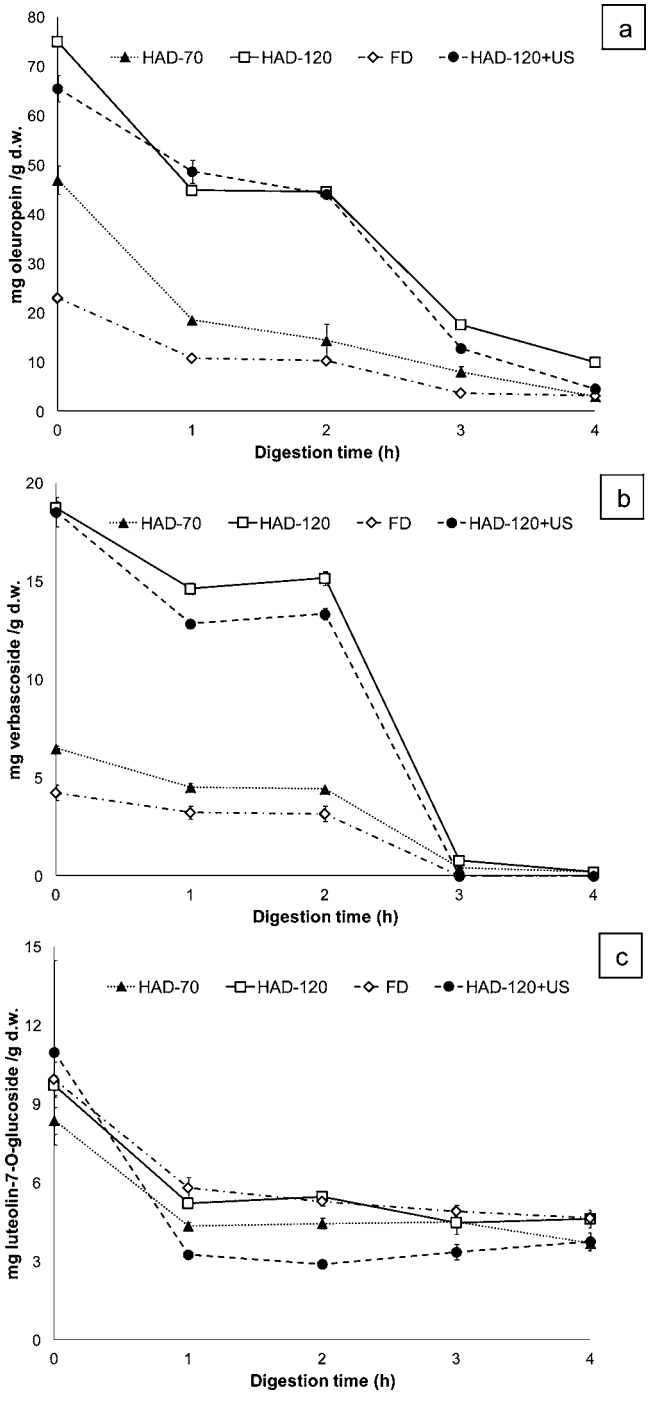

Figure 5. Kinetics of oleuropein (a), verbascoside (b), and luteolin-7-*O*-glucoside (c) content during the in vitro digestion of olive leaf extracts. Means ± standard deviation are plotted.

dx.doi.org/10.1021/jf501414h | J. Agric. Food Chem. 2014, 62, 6190–6198

did not promote significant changes in the polyphenol concentrations and the content of every compound was almost constant. Oleuropein degradations ranged from 26 to 61%, depending on the extract source (Figure 5a). The most resistant oleuropein was the one extracted from HAD-120 leaves by means of US-assisted extraction (HAD-120+US). As far as the verbascoside is concerned (Figure 5b), its degradation during the first hour under gastric conditions ranged from 22 to 31%. Thus, it could be stated that verbascoside was less affected during gastric incubation than oleuropein. The reduction in the luteolin-glucoside content after 1 h of digestion was around 45% for the extracts obtained by conventional extraction (Figure 5c). However, a significantly ($p < 0.05$) greater reduction (63%) was found in the US extract. Dietary polyphenols have been reported to enjoy a good degree of stability during gastric digestion,[28,35,36] including all of the major olive oil phenolics, such as tyrosol, hydroxytytrosol, and related secoiridoids.[13] Our results show that verbascoside is a little more resistant to gastric digestion than oleuropein and luteolin-glucoside.

The intestinal in vitro digestion hardly affected the luteolin-7-*O*-glucoside content (Figure 5c). However, the main part of the verbascoside degradation during in vitro simulation happened under intestinal conditions (Figure 5b), probably due to the fact that it is extremely susceptible at high pH.[37] As a consequence, the verbascoside practically disappeared, with its final content being close to 0 mg/g dw. Although the oleuropein reduction was less marked than that of verbascoside, the intestinal phase affected oleuropein more than the gastric period (Figure 5a). Thus, pancreatic enzymatic activity and alkaline pH contributed to a reduction in the bioaccessibility of oleuropein and verbascoside extracted from olive leaves, and both compounds almost disappeared from the medium. Some authors have also pointed to the possible interaction of pancreatic α-amylase and trypsin with phenolic compounds.[38] Therefore, the study of the degradation kinetics of polyphenols and the polyphenol−protein interactions would allow the bioaccessibility of these bioactive compounds to be improved through the design of pharmaceutical formulations aimed at increasing the amount of these compounds present at the site of intestinal absorption.

Cooked amaranth leaves have been reported to exhibit β-carotene bioaccessibility values of 18%.[39] Compared with this result, the percentage of bioaccessible luteolin-7-*O*-glucoside exhibited by olive leaf extracts was much higher, because 43 ± 6% of its initial content was recovered after digestion. However, only 10 ± 4% of oleuropein resisted the in vitro simulation, and most of the verbascoside practically disappeared in the extracts. Although oleuropein undergoes rapid hydrolysis under gastric conditions and it is rapidly degraded by the colonic microflora, leading to significant increases in the amount of tyrosol and hydroxytyrosol,[40,41] neither of these compounds was found in the HPLC-DAD/MS/MS analysis.

Another set of experiments was carried out to confirm if the stability of the compounds behaved in a similar manner when these were in the extract or in isolated form. Thus, oleuropein, verbascoside, and luteolin-glucoside standard solutions were subjected to complete digestions (Figure 6). Oleuropein and verbascoside solutions were quite resistant to gastric conditions and behaved similarly to the digestions of the extracts (Figure 6a,b). Thus, in both cases, the amount of these compounds at the end of the pancreatic digestion was almost negligible; therefore, their level of absorption must be even lower, as

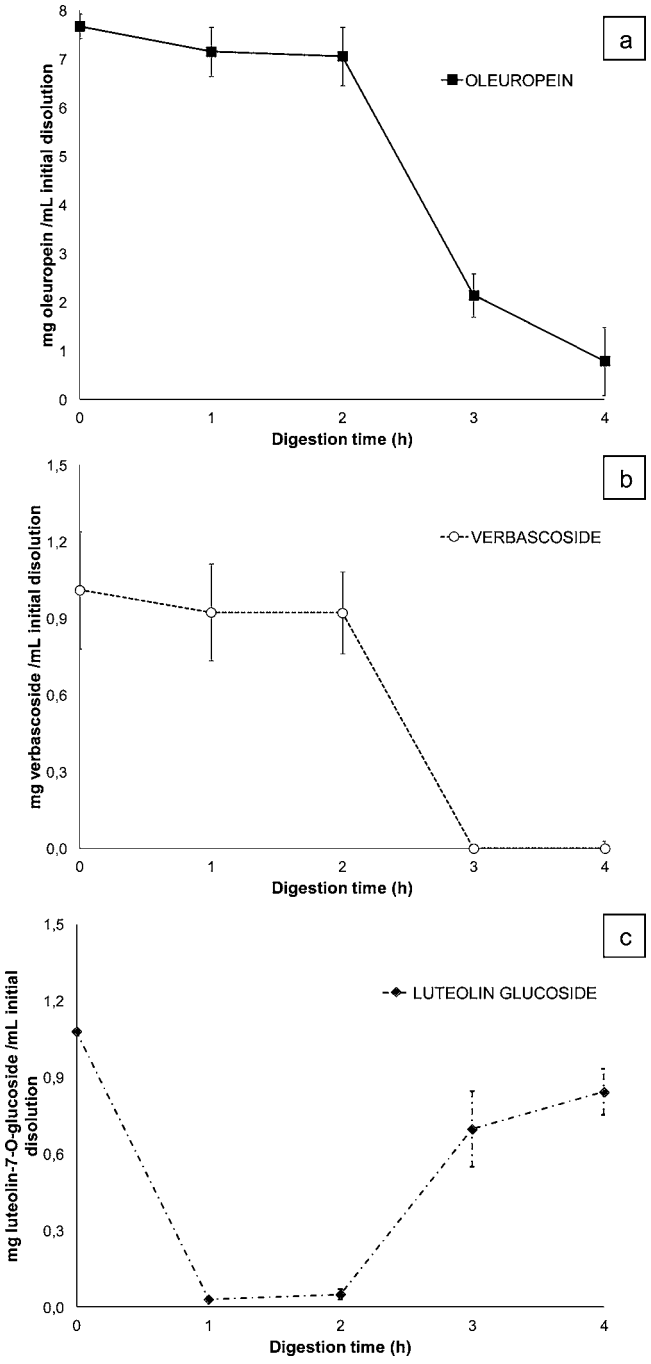

Figure 6. Kinetics of oleuropein (a), verbascoside (b), and luteolin-7-*O*-glucoside (c) content during the in vitro digestion of its standard solutions. Means ± standard deviation are plotted.

reported.[41,42] In contrast, isolated luteolin showed a completely different stability from that contained in the extract. Whereas the luteolin-glucoside in olive leaf extracts remained fairly stable after the first hour of digestion, it was not identified by HPLC in the standard solution during gastric digestion and was detected again during intestinal digestion, as shown in Figures 2b and 3b. As mentioned above, this effect could be due to the precipitation of this compound under acidic gastric conditions or its complexation with proteins under gastric conditions, a fact that may be enhanced when in pure form. Both digestions (Figures 5c and 6c) demonstrate the pancreatic−biliar resistance of luteolin.

dx.doi.org/10.1021/jf501414h | J. Agric. Food Chem. 2014, 62, 6190−6198

In conclusion, the degradation kinetics of the major bioactive compounds derived from olive leaf extracts was not dependent on the type of extract or source. Hence, neither the drying treatment of olive leaves nor the extraction method (conventional or US application) had a significant ($p < 0.05$) influence on oleuropein, verbacoside, and luteolin-7-*O*-glucoside behavior during in vitro digestion. The most relevant finding of our study is that the amounts of oleuropein and verbascoside at the end of the digestion processes are almost negligible, mainly due to their instability during intestinal digestion. Interestingly, luteolin-7-*O*-glucoside was fairly resistant to digestion and, therefore, must be considered as an interesting polyphenol for further absorption processes.

AUTHOR INFORMATION

Corresponding Author

*(J.V.G.-P.) Phone: +34 96 3879376. Fax: +34 96 3879839. E-mail: jogarpe4@tal.upv.es.

Funding

We thank the Generalitat Valenciana (PROMETEO/2010/062, PROMETEO/2012/007, and ACOMP/2013/93) for its financial support. M.H.A.-Q. was the recipient of a fellowship from the Ministerio de Educación, Cultura y Deporte of Spain (Programa de Formación de Profesorado Universitario del Programa Nacional de Formación de Recursos Humanos de Investigación), and J.C. was the recipient of a fellowship from Catedra AINIA (Universitat Politècnica de València). This investigation has also been supported by the Ministerio de Ciencia e Innovación (AGL2011-29857-C03-03) and CIBERobn (CB12/03/30038, Fisiopatología de la Obesidad y la Nutrición, CIBERobn, Instituto de Salud Carlos III).

Notes

The authors declare no competing financial interest.

ABBREVIATIONS USED

HAD, hot air drying; FD, freeze-drying; TPC, total phenolic content; GAE, gallic acid equivalents; AC, antioxidant capacity; FRAP, ferric-reducing ability power; TPTZ, 2,4,6-tri(2-pyridyl)-s-triazine; TEAC, trolox equivalent antioxidant capacity; ABTS, 2,2′-azinobis(3-ethylbenzothiazoline-6-sulfonic acid); HPLC-DAD, high-performance liquid chromatography with diode array detection; MS/MS, tandem mass spectrometry; ESI, electrospray ionization; UV, ultraviolet; US, ultrasound

REFERENCES

(1) Ryan, D.; Robards, K. Phenolic compounds in olives. *Analyst* **1998**, *123*, 31−44.

(2) Montedoro, G. F.; Servili, M.; Baldioli, M.; Selvaggini, R.; Miniati, E.; Maccchioni, A. Simple and hydrolyzable compounds in virgin olive oil. 3. Spectroscopic characterizations of the secoiridoid derivatives. *J. Agric. Food Chem.* **1993**, *41*, 2228−2234.

(3) Japón-Luján, R.; Luque de Castro, M. D. Small branches of olive tree: a source of biophenols complementary to olive leaves. *J. Agric. Food Chem.* **2007**, *55*, 4584−4588.

(4) Benavente-García, O.; Castillo, J.; Lorente, J.; Ortuño, A.; Del Río, J. A. Antioxidant activity of phenolics extracted from *Olea europaea* L. leaves. *Food Chem.* **2000**, *68*, 457−462.

(5) Micol, V.; Caturla, N.; Pérez-Fons, L.; Más, V.; Pérez, L.; Estepa, A. The olive leaf extract exhibits antiviral activity against viral haemorrhagic septicaemia rhabdovirus (VHSV). *Antiviral Res.* **2005**, *66* (2−3), 129−136.

(6) Taamalli, A.; Arráez-Román, D.; Barrajón-Catalán, E.; Ruiz-Torres, V.; Pérez-Sánchez, A.; Herrero, M.; Ibáñez, E.; Micol, V.; Zarrouk, M.; Segura-Carretero, A.; Fernández-Gutiérrez, A. Use of advanced techniques for the extraction of phenolic compounds from Tunisian olive leaves: phenolic composition and cytotoxicity against human breast cancer cells. *Food Chem. Toxicol.* **2012**, *50* (6), 1817−1825.

(7) Singh, I.; Mok, M. The effects of polyphenols in olive leaves on platelet function. *Nutr. Metab. Cardiovasc.* **2008**, *18*, 127−132.

(8) Tabera, J.; Guinda, A.; Ruiz-Rodríguez, A.; Señorans, J. F.; Ibáñez, E.; Albi, T.; Reglero, G. Countercurrent supercritical fluid extraction and fractionation of high-added-value compounds from a hexane extract of olive leaves. *J. Agric. Food Chem.* **2004**, *52*, 4774−4779.

(9) Martín-García, A. I.; Molina-Alcaide, E. Effect of different drying procedures on the nutritive value of olive (*Olea europaea* var. *europaea*) leaves for ruminants. *Anim. Feed Sci. Technol.* **2008**, *142*, 317−329.

(10) Ahmad-Qasem, M. H.; Barrajón-Catalán, E.; Micol, V.; Mulet, A.; García-Pérez, J. V. Influence of freezing and dehydration of olive leaves (var. Serrana) on extract composition and antioxidant potential. *Food Res. Int.* **2013**, *50*, 189−196.

(11) Paniwnyk, L.; Beaufoy, E.; Lorimer, J. P.; Mason, T. J. The extraction of rutin from flower buds of *Sophora japonica*. *Ultrason. Sonochem.* **2001**, *8*, 299−301.

(12) Hedrén, E.; Mulokozi, G.; Svanberg, U. *In vitro* accessibility of carotenes from green leafy vegetables cooked with sunflower oil or red palm oil. *Int. J. Food Sci. Nutr.* **2002**, *53*, 445−453.

(13) Soler, A.; Romero, M. P.; Macià, A.; Saha, S.; Furniss, C. S. M.; Kroon, P. A.; Motilva, M. J. Digestion stability and evaluation of the metabolism and transport of olive oil phenols in the human small-intestinal epithelial Caco-2/TC7 cell line. *Food Chem.* **2010**, *119*, 703−714.

(14) Gil-Izquierdo, A.; Zafrilla, P.; Tomás-Barberán, F. A. An *in vitro* method to simulate phenolic compound release from the food matrix in the gastrointestinal tract. *Eur. Food Res. Technol.* **2002**, *214*, 155−159.

(15) Failla, M. L.; Huo, T.; Thakkar, S. K. *In vitro* screening of relative bioaccessibility of carotenoids from foods. *Asia Pac. J. Clin. Nutr.* **2008**, *17*, 200−203.

(16) D'Archivio, M.; Filesi, C.; Varì, R.; Scazzocchio, B.; Masella, R. Bioavailability of the polyphenols: status and controversies. *Int. J. Mol. Sci.* **2010**, *11*, 1321−1342.

(17) Directive 2010/63/EU. *Off. J. Eur. Union*. **2010**, *L276*, 33.

(18) Aguilera, J. M. Why food microstructure? *J. Food Eng.* **2005**, *67*, 3−11.

(19) Parada, J.; Aguilera, J. M. Food microstructure affects the bioavailability of several nutrients. *J. Food Sci.* **2007**, *72*, 21−32.

(20) Ahmad-Qasem, M. H.; Cánovas, J.; Barrajón-Catalán, E.; Micol, V.; Cárcel, J. A.; García-Pérez, J. V. Kinetic and compositional study of phenolic extraction from olive leaves (var. Serrana) by using power ultrasound. *Innovative Food Sci. Emerging Technol.* **2013**, *17*, 120−129.

(21) Miller, D. D.; Schricker, B. R.; Rasmussen, R. R.; Van Campen, D. In vitro method for estimation of iron availability from meals. *Am. J. Clin. Nutr.* **1981**, *34*, 2248−2256.

(22) Garret, D. A.; Failla, M.; Sarama, R. J. Development of an in vitro digestion method to assess carotenoid bioavailability from meals. *J. Agric. Food Chem.* **1999**, *47*, 4301−4309.

(23) Singleton, V. L.; Ortholer, R.; Lamuela-Raventos, R. M. Analysis of total phenols and other oxidation substrates and antioxidants by means of Folin-Ciocalteu reagent. *Methods Enzymol.* **1999**, *299*, 152−178.

(24) Benzie, I. F. F.; Strain, J. J. The ferric reducing ability of plasma (FRAP) as a measure of "antioxidant power": The FRAP assay. *Anal. Biochem.* **1996**, *239*, 70−76.

(25) Pulido, R.; Bravo, L.; Saura-Calixto, F. Antioxidant activity of dietary polyphenols as determined by a modified ferric reducing/antioxidant power assay. *J. Agric. Food Chem.* **2000**, *48*, 3396−3402.

(26) Laporta, O.; Pérez-Fons, L.; Mallavia, R.; Caturla, N.; Micol, V. Isolation, characterization and antioxidant capacity assessment of the bioactive compounds derived from *Hypoxis rooperi* corm extract (African potato). *Food Chem.* **2007**, *101*, 1425−1437.

(27) Riesz, P.; Berdahl, D.; Christman, C. L. Free radical generation by ultrasound in aqueous and nonaqueous solutions. *Environ. Health Perspect.* **1985**, *64*, 233−253.
(28) McDougall, G. J.; Dobson, P.; Smith, P.; Blake, A.; Stewart, D. Assessing potential bioavailability of raspberry anthocyanins using an in vitro digestion system. *J. Agric. Food Chem.* **2005**, *53*, 5896−5904.
(29) Tagliazucchi, D.; Verzelloni, E.; Bertolini, D.; Conte, A. In vitro bio-accessibility and antioxidant activity of grape polyphenols. *Food Chem.* **2010**, *120*, 599−606.
(30) Nagah, A. M.; Seal, C. J. *In vitro* procedure to predict apparent antioxidant release from wholegrain foods measured using three different analytical methods. *J. Sci. Food Agric.* **2005**, *85*, 1177−1185.
(31) Dinnella, C.; Minichino, P.; D'Andrea, A. M.; Monteleone, E. Bioaccessibility and antioxidant activity stability of phenolic compounds from extra-virgin olive oils during in vitro digestion. *J. Agric. Food Chem.* **2007**, *55*, 8423−8429.
(32) Mukai, K.; Oka, W.; Watanabe, K.; Egawa, Y.; Nagaoka, S. Kinetic study of free-radical-scavenging action action of flavonoids in homogeneous and aqueous triton X-100 micellar solutions. *J. Phys. Chem. A* **1997**, *101*, 3746−3753.
(33) Tyrakowska, B.; Soffers, A. E. M.; Szymcsiak, H.; Boeren, S.; Boersma, M. G.; Lemanska, K.; Vervoort, J.; Rietjens, I. M. TEAC antioxidant activity of 4-hydroxybenzoates. *Free Radical Biol. Med.* **1999**, *27*, 1427−1436.
(34) Lavelli, V. Comparison of the antioxidant activities of extra virgin olive oils. *J. Agric. Food Chem.* **2002**, *50*, 7704−7708.
(35) Pérez-Vicente, A.; Gil-Izquierdo, A.; García-Viguera, C. In vitro gastrointestinal digestion study of pomegranate juice phenolic compounds, anthocyanins, and vitamin C. *J. Agric. Food Chem.* **2002**, *50*, 2308−2312.
(36) Bermúdez-Soto, M. J.; Tomás-Barberán, F. A.; García-Conesa, M. T. Stability of polyphenols in chokeberry (*Aronia melanocarpa*) subjected to *in vitro* gastric and pancreatic digestion. *Food Chem.* **2007**, *102*, 865−874.
(37) Cardinali, A.; Linsalata, V.; Lattanzio, V.; Ferruzzi, G. Verbascosides from olive mil waste water: assessment of their bioaccessibility and intestinal uptake using an in vitro digestion/Caco-2 model system. *J. Food Sci.* **2011**, *76*, 48−54.
(38) Rhon, S.; Rawel, H. M.; Kroll, J. Inhibitory effects of plant phenols on the activity of selected enzymes. *J. Agric. Food Chem.* **2002**, *50*, 3566−3571.
(39) Hedren, E.; Mulkozi, G.; Svanberg, U. In vitro accessibility of carotenes from green leafy vegetables cooked with sunflower oil or red palm oil. *Int. J. Food Sci. Nutr.* **2002**, *53*, 445−453.
(40) Corona, G.; Tzounis, X.; Assunta-Dessa, M.; Deiana, M.; Debnam, E. S.; Visioli, F.; Spencer, J. P. The fate of olive oil polyphenols in the gastrointestinal tract: implications of gastric and colonic microflora-dependent biotransformation. *Free Radical Res.* **2006**, *40*, 647−658.
(41) de Bock, M.; Thorstensen, E. B.; Derraik, J. G.; Henderson, H. V.; Hofman, P. L.; Cutfield, W. S. Human absorption and metabolism of oleuropein and hydroxytyrosol ingested as olive (*Olea europaea* L.) leaf extract. *Mol. Nutr. Food Res.* **2013**, DOI: 10.1002/mnfr.201200795.
(42) Funes, L.; Fernández-Arroyo, S.; Laporta, O.; Pons, A.; Roche, E.; Segura-Carretero, A.; Fernández-Gutierrez, A.; Micol, V. Correlation between plasma antioxidant capacity and verbascoside levels in rats after oral administration of lemon verbena. *Food Chem.* **2009**, *117*, 589−598.

JOURNAL OF AGRICULTURAL AND FOOD CHEMISTRY

Article

pubs.acs.org/JAFC

Using a Non-invasive Technique in Nutrition: Synchrotron Radiation Infrared Microspectroscopy Spectroscopic Characterization of Oil Seeds Treated with Different Processing Conditions on Molecular Spectral Factors Influencing Nutrient Delivery

Xuewei Zhang[†,‡] and Peiqiang Yu*[,†,‡]

[†]College of Animal Science and Animal Veterinary, Tianjin Agricultural University, Tianjin 300384, People's Republic of China

[‡]College of Agriculture and Bioresources, University of Saskatchewan, Saskatoon, Saskatchewan S7N 5A8, Canada

ABSTRACT: Non-invasive techniques are a key to study nutrition and structure interaction. Fourier transform infrared microspectroscopy coupled with a synchrotron radiation source (SR-IMS) is a rapid, non-invasive, and non-destructive bioanalytical technique. To understand internal structure changes in relation to nutrient availability in oil seed processing is vital to find optimal processing conditions. The objective of this study was to use a synchrotron-based bioanalytical technique SR-IMS as a non-invasive and non-destructive tool to study the effects of heat-processing methods and oil seed canola type on modeled protein structure based on spectral data within intact tissue that were randomly selected and quantify the relationship between the modeled protein structure and protein nutrient supply to ruminants. The results showed that the moisture heat-related processing significantly changed ($p < 0.05$) modeled protein structures compared to the raw canola (control) and those processing by dry heating. The moisture heating increased ($p < 0.05$) spectral intensities of amide I, amide II, α-helices, and β-sheets but decreased ($p < 0.05$) the ratio of modeled α-helices to β-sheet spectral intensity. There was no difference ($p > 0.05$) in the protein spectral profile between the raw and dry-heated canola tissue and between yellow- and brown-type canola tissue. The results indicated that different heat processing methods have different impacts on the protein inherent structure. The protein intrinsic structure in canola seed tissue was more sensitive and more response to the moisture heating in comparison to the dry heating. These changes are expected to be related to the nutritive value. However, the current study is based on limited samples, and more large-scale studies are needed to confirm our findings.

KEYWORDS: *protein structure, heat-induced processing, nutrient availability, yellow- and brown-type canola, synchrotron application, spectral modeling*

INTRODUCTION

Recently, it has been reported that using synchrotron radiation infrared microspectroscopy (SR-IMS) as a non-invasive and non-destructive tool for inherent molecular structure changes in different plant-based foods/seeds/feeds could be revealed within intact tissue at cellular and molecular levels.[1−3] The published results showed that the changes of protein, carbohydrate, and lipid molecular structure spectral profiles could be induced by bioethanol processing,[4] gene transformation,[5] and heating.[6,7] In these published studies, it was found that the inherent structure of the plant tissue within cellular or subcellular dimension could affect nutritive quality, fermentation, and degradation behavior. Different cultivars have different inherent structure characteristics. The relative percentage of protein secondary structure profiles may influence protein functionality and nutritive utilization. Different protein structure profiles affect the access of gastrointestinal digestive enzymes to the protein and subsequently affect digestibility.[8,9]

Oil seed canola is considered an important protein and energy source for animal and human food because of its high contents of both protein and oil. There are several different processing methods available for canola processing. To understand internal structure changes in relation to nutrient availability in canola processing is vital to find optimal processing conditions and prevent huge nutrient loss. However, any conventional "wet" chemical analytical method is unable to detect the structure changes within intact tissue after processing at cellular and molecular levels. In contrast to traditional "wet" chemical methods, which during processing for analysis often result in destruction of the intrinsic structures of feeds/seeds, to date, there has been little application of SR-IMS to study heat-induced molecular structure changes within intact tissue in different types of canola seeds with different processing methods in relation to digestive behavior and nutrient utilization.

The objectives of this study were to study the modeled protein structure changes (α-helices, β-sheets, and their ratio; amide I, amide II, and their ratios) induced by heat-related dry and moisture processing based on spectral data that were collected on the seed tissue and to investigate the relationship between protein structural changes (α-helix/β-sheet ratio) and protein chemical profiles, Cornell Net Carbohydrate and Protein System (CNCPS) protein fractions, truly digestible nutrients, energy value, *in situ* rumen degradation, and intestinal protein available in the raw (control) and heating of yellow- and brown-type canola seeds that were reported previously in a conventional

Received: April 1, 2014
Revised: June 6, 2014
Accepted: June 12, 2014
Published: June 12, 2014

ACS Publications © 2014 American Chemical Society

dx.doi.org/10.1021/jf501553g | *J. Agric. Food Chem.* 2014, 62, 6199−6205

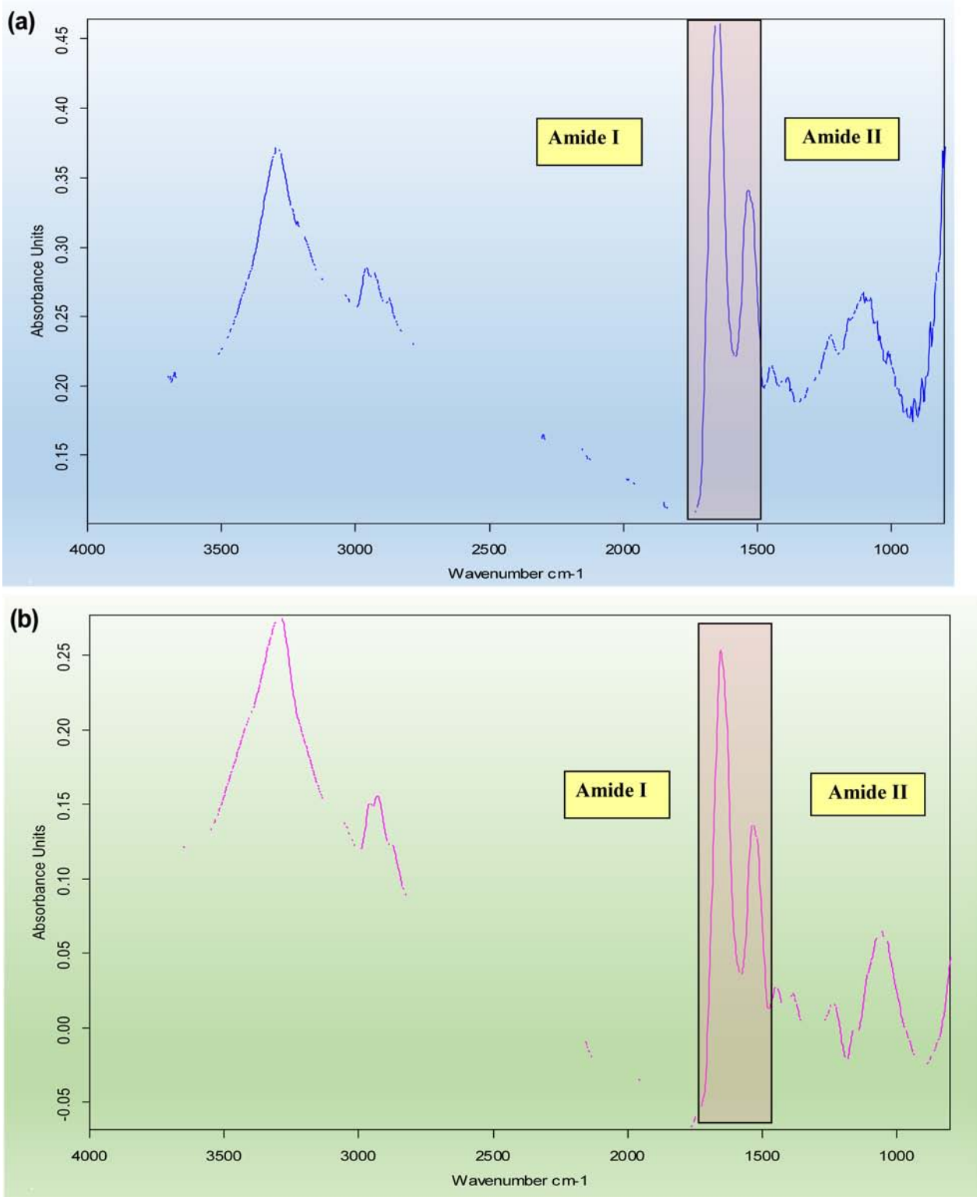

Figure 1. Typical synchrotron-based IMS spectrum in (a) yellow-type canola and (b) brown-type canola seed tissues after a section at 6 μm thickness.

nutrition study. In addition, hierarchical cluster analysis and principal component analysis of the synchrotron-based spectral data from randomly selected seed tissue were performed to classify treatment difference. The hypothesis of this study was that the sensitivity and response of oil seed canola to heating differed in the nutrient availability between different heating methods and between yellow- and brown-type oil seed canola. These structural changes and differences are expected to be associated with nutritive values.

MATERIALS AND METHODS

Canola Varieties and Processing Methods: Moisture Heating and Dry Heating. Two different types of canola samples: yellow-seeded canola (*Bassica rapa*) and dark-brown-seeded canola (*Bassica nupus*) were used in a synchrotron-based modeled protein structure

Table 1. Effect of the Heat Processing Method on the Molecular Structure Spectral Characteristics (Randomly Spot Samples) of Protein in Randomly Selected Canola Seed Tissues after Sectioning at ca. 6 μm Thickness Using Synchrotron-Based FTIR Microspectroscopy: Comparison of Raw (Control) versus Heat Treatments (Wet and Dry Heating) of Brown- and Yellow-Type Canola Seed Tissues[a]

	heat processing methods				contrast		yellow versus brown			
item	TRT0 control/raw	TRT1	TRT2	SEM	control versus TRTS	*p* value	yellow	brown	SEM	*p* value
modeled amides (AU)										
modeled amide I	16.77 b	24.67 a	14.86 b	1.781	0.1806	0.0013	19.54	17.98	1.812	0.5466
modeled amide II	5.64 b	8.15 a	4.93 b	0.672	0.2854	0.0055	6.69	5.79	0.642	0.3309
ratio of modeled amide I/II	3.01	3.13	3.06	0.056	0.2268	0.3353	2.98 b	3.15 a	0.041	0.0047
α-helix and β-sheet (AU)										
modeled α-helix (height)	0.25 ab	0.30 a	0.22 b	0.023	0.7678	0.0462	0.27	0.24	0.020	0.3755
modeled β-sheet (height)	0.22 b	0.33 a	0.19 b	0.025	0.1852	0.0014	0.26	0.24	0.025	0.5631
ratio of modeled α-helix/β-sheet	1.15 a	0.93 b	1.15 a	0.026	0.0022	<0.0001	1.10	1.05	0.034	0.3065

[a]Means within a row with different letters differ ($p < 0.05$). SEM, pooled standard error of means; TRT1, autoclaved at 121 °C for 1 h; and TRT2, dry heating at 120 °C for 1 h.

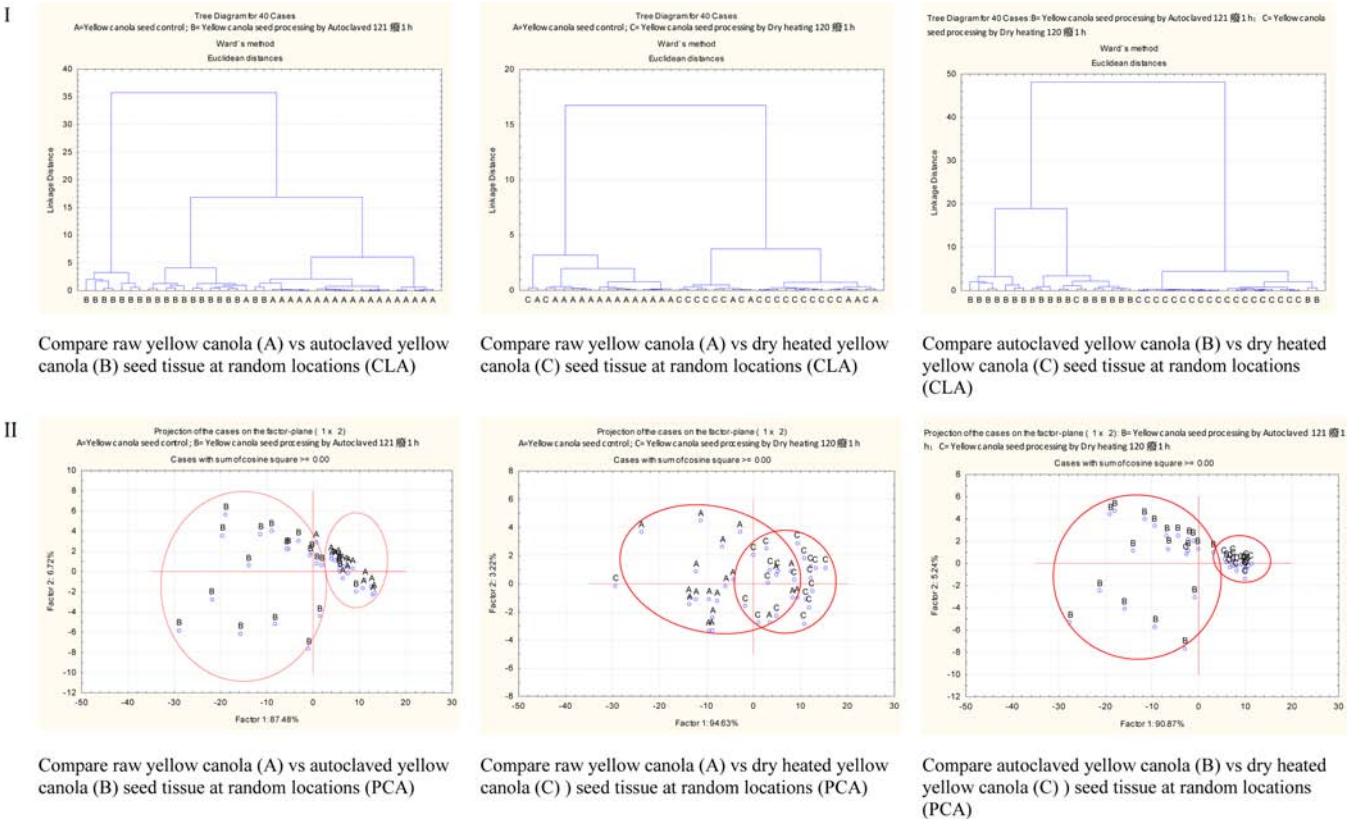

Figure 2. Multivariate spectral analyses of canola structures in the whole seed tissues at random locations using synchrotron-based FTIR microspectroscopy. Comparison of raw (control) and heated yellow-type canola seed: A, yellow-type canola (control); B, yellow-type canola autoclaved at 121 °C for 1 h; and C, yellow-type canola dry heated at 120 °C for 1 h. (I) CLA: (1) protein fingerprint spectral region, ca. 1724−1487 cm^{-1}; (2) distance method, Euclidean; and (3) cluster method, Ward's algorithm. (II) PCA: scatter plots of the first principal components (PC_1) versus the second principal components (PC_2). Protein spectral region, ca. 1724−1487 cm^{-1}.

study based on randomly selected seed tissues (spot samples). Each canola sample was previously heated by moisture (autoclave) and dry heating (Amsco Eagle SG-3031, Steris Corp., Mentor, OH) at the temperature of 120 °C for 1 h before nutrition and spectral studies. Control samples were kept raw. Heat-treated samples were subsequently cooled at room temperature. The detailed sampling structure, nutrient profiles, degradation kinetics, and metabolic characteristics of protein as well as Globar-source infrared (IR) spectroscopy work and functional group relationship to the nutrient value were reported previously.[7] In this study, we used the same samples for the synchrotron-based SR-IMS study to see what changes inside of the tissues after processing application and how these changes are related to nutritive values.

Canola Tissue and Synchrotron-Based IR Window Preparation. As reported before in synchrotron IR sample preparation methodology, the canola seed samples were cut into thin cross-sections (6 μm thickness) using a microtome. The cross-sections of the canola tissues were transformed to BaF2 windows (size of 13 × 1 mm disk) for transmission mode in SR-IMS work. Randomly selected five different seeds from each sample and randomly selected spot samples from each

dx.doi.org/10.1021/jf501553g | J. Agric. Food Chem. 2014, 62, 6199−6205

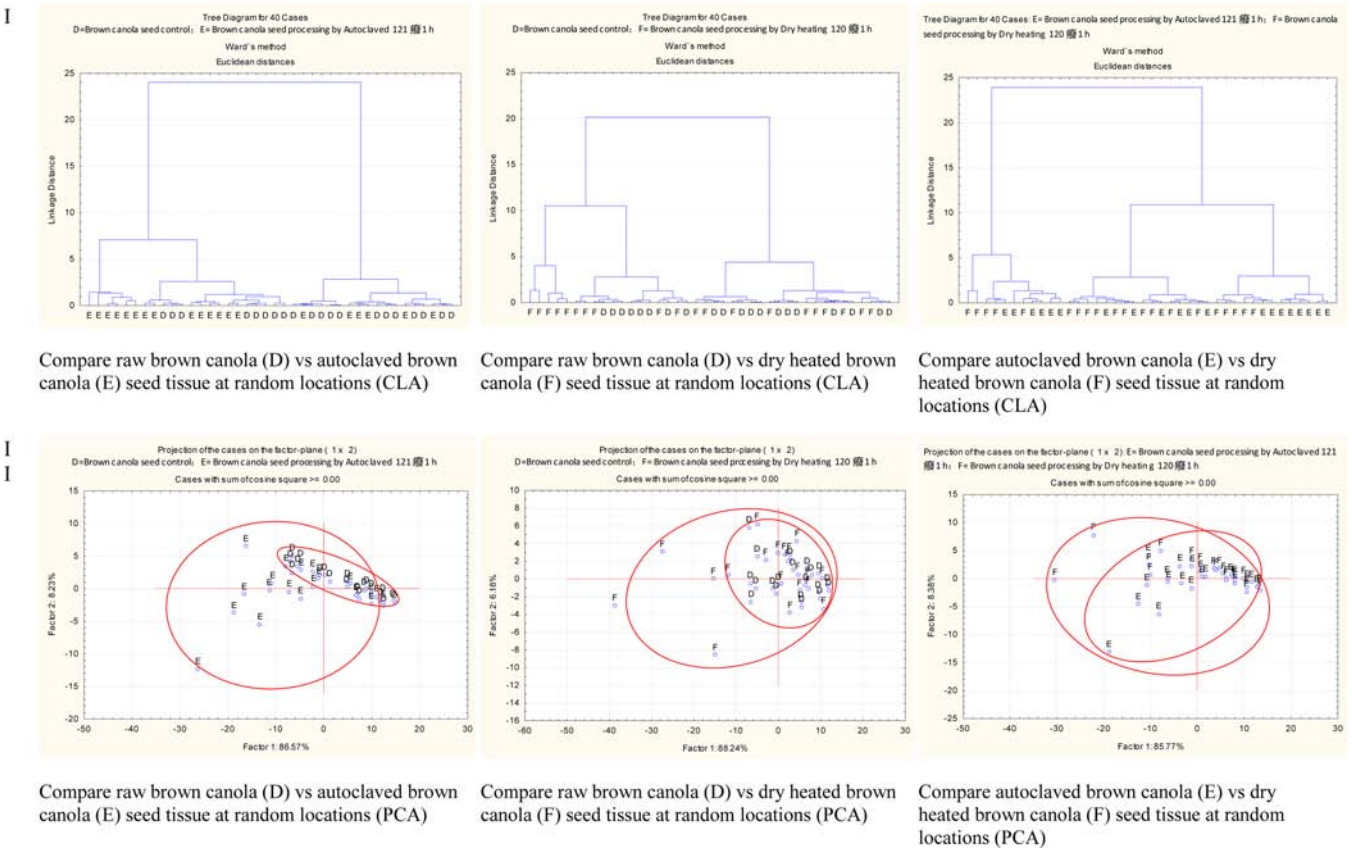

Figure 3. Multivariate spectral analyses of canola structures in the whole seed tissue at random locations using synchrotron-based FTIR microspectroscopy. Comparison of raw (control) and heated brown-type canola seeds: D, brown-type canola (control); E, brown-type canola autoclaved at 121 °C for 1 h; and F, brown-type canola dry heated at 120 °C for 1 h. (I) CLA: (1) protein fingerprint spectral region, ca. 1724−1487 cm^{-1}; (2) distance method, Euclidean; and (3) cluster method, Ward's algorithm. (II) PCA: scatter plots of the first principal components (PC_1) versus the second principal components (PC_2). Protein fingerprint spectral region, ca. 1724−1487 cm^{-1}.

seed tissue were used to investigate the modeled protein structural features. Each seed tissue was collected around 40 spot spectral samples from a relative pure protein tissue area (which means with high amide I and II peaks) in the tissue between ca. 100 and 600 μm as detected by SR-IMS. More detailed methodology on synchrotron window preparation was described by Yu et al.[10]

Canadian Light Source (CLS) and Synchrotron-Based IR Microspectroscopy. The experiment was performed at the mid-IR station in the CLS with a SR-IMS station. "A Bruker Vertex 70v/S spectrometer with a Hyperion 3000 microscope is attached to the synchrotron, providing diffraction limited spatial resolution with a variety of experimental techniques available" (see the CLS website for the detailed facility description). The spectroscopic data were recorded using Fourier transform infrared (FTIR) spectroscopy equipped with IR microscopy. The bench was configured with a synchrotron light beamline. The spectra were collected in the mid-IR range of ca. 4000−800 cm^{-1} at a resolution of 4 cm^{-1} with 128 scans co-added. To obtain an ideal signal-to-noise ratio, the aperture setting was set in ca. 10 × 10 μm. Scanned visible images were obtained using a charge-coupled device (CCD) camera linked to the IR images.

Synchrotron Spectral Data Analysis. The spectral data of the canola tissues were collected, corrected for background spectrum, displayed in the absorbance mode, and analyzed using the Bruker-OPUS 6.5 and OMNIC 7.2 (Spectra Tech, Madison, WI). Figure 1 shows typical tissue spectra of spot samples. Protein amide I and II peak areas, amide I and II peak heights, modeled α-helix and β-sheet peak height intensities, and their ratios were determined. Chemical functional groups related to the protein structure were identified on the basis of band assignments published in the literature.[11,12] The analysis amide spectral region in this study was approximately ca. 1725−1487 cm^{-1} because this region is mainly related to protein biopolymer. The analysis of protein spectral regions of amide I and II in this study were ca. 1725−1577 cm^{-1} and ca. 1577−1487 cm^{-1}, respectively. For the modeled α-helix and β-sheet, the peak falls within the range of ca. 1650−1660 cm^{-1} and ca. 1620−1640 cm^{-1}, respectively. The ratio of the amide I and II peak areas, the ratio of the amide I and II peak heights, and the ratio of modeled α-helix and β-sheet peak heights were calculated on the basis of respective spectral absorbance intensity values. The ratio data were obtained by the height or area under one functional group band (e.g., amide I) divided by the height or area under another functional group band (e.g., amide II) at each pixel (spot sample), which represents the biological component ratio intensity and distribution in the tissue. Because the protein amide I component band was overlapped, a secondary derivative function was used to identify component bands for estimating the relative intensity of modeled protein secondary structures, such as modeled α-helices, β-sheets, and their ratios. The FTIR protein fingerprint data of canola tissue were analyzed by agglomerative hierarchical cluster analysis (CLA) and principal component analysis (PCA) using Statistica 8.0 software (StatSoft, Inc., Tulsa, OK) to classify and distinguish inherent protein structural differences among different types of canola seeds and then identify the main sources of variation within the protein amide I and II fingerprint spectra (ca. 1724−1487 cm^{-1}).[5,13]

Statistical Analysis. Statistical analysis between different types of canola seeds and different heat processing were performed using the mixed procedure of SAS.[14] Correlation analysis between protein structure α-helix and β-sheet and nutrient profile in raw and heated brown- and yellow-type canola were analyzed using the SAS. The normality tests were used with the univariate procedure of SAS with options of normal and plot. Treatment means were compared using Fisher's protected least significant difference test. For all statistical analysis, significant was declared at $p < 0.05$ and trends at $p \leq 0.10$.

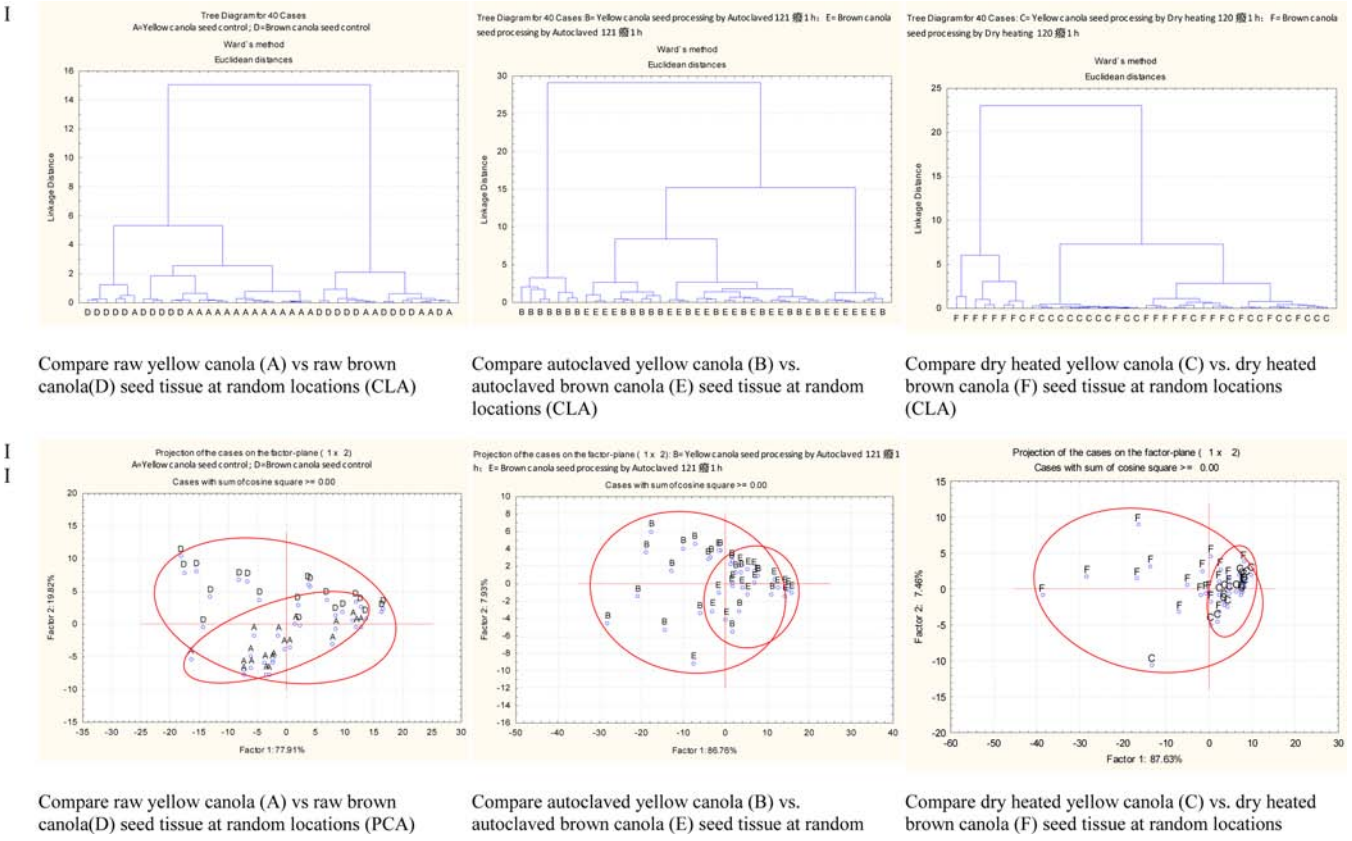

Figure 4. Multivariate spectral analyses of canola structures in the whole seed tissues at random locations using synchrotron-based FTIR microspectroscopy. Comparison of yellow- and brown-type canola and their heat treatments: A versus D, yellow- versus brown-type canola (control); B versus E, yellow- versus brown-type canola autoclaved at 121 °C for 1 h; and C versus F, yellow- versus brown-type canola dry heated at 120 °C for 1 h. (I) CLA: (1) protein fingerprint spectral region, ca. 1724−1487 cm^{-1}; (2) distance method, Euclidean; and (3) cluster method, Ward's algorithm. (II) PCA: scatter plots of the first principal components (PC_1) versus the second principal components (PC_2). Protein fingerprint spectral region, ca. 1724−1487 cm^{-1}.

RESULTS AND DISCUSSION

Effect of the Heat Treatment on the Physical Shape of Canola Seeds. The sensitivity of canola seeds to heating may differ among different heated treatments or between different types of canola. To investigate the physical−chemical changes, the entire images of raw (control) and heat treatments of canola seeds were scanned using the synchrotron-based SR-IMS equipped with a microscopy. From the images, it indicated that heat treatments may affect seed physical shape. Both yellow- and brown-type canola seeds were more sensitive to the moisture heat treatment because the physical shape had dramatic changes in terms of internal (the tissue swelled) or external (the seed coat split off) tissue. These results indicated that different processing methods had different impacts on physical structures and different types of seeds might have different sensitivity or response to different heat processing methods.

Effect of the Heat Treatment on Chemical Profiles, Protein Fractions, Digestible Nutrients, and *In Vitro* Intestinal Digestibility: Comparison of Raw (Control) versus Heat Treatments of Canola Seed, with a Summary of the Previous Study. Effects of heat treatments on chemical profiles, protein subfractions, digestible nutrient, and estimated intestinal digestibility of the raw and heat treatments of canola seed were reported by Samadi and Yu.[7] In summary, in the previous study, we found that moisture heating resulted in a significant increase in neutral detergent insoluble protein (NDIP), slowly degradable protein subfraction (PB_3), and estimated intestinal digestibility of rumen undegraded protein (dRUP, % of CP) but a decrease in soluble crude protein [SCP, % of crude protein (CP)], non-protein nitrogen (NPN, % of CP), protein PA fraction, rapidly degradable protein fraction (PB_1), and *in situ* dry matter (DM) and CP rumen degradation after 16 h of rumen incubation and resulted in increased more bypass protein and increased more protein availability in the small intestine. As a result, moisture heating greatly improved the nutrient value and the usage of canola seed in diets in dairy cattle. However, dry heating did not affect overall the content of chemicals and the degradability and availability of nutrient profiles. The results indicated that the sensitivity and response of canola seeds to heating differed between the moisture and dry heating. Moisture heating had a much greater effect on chemical and nutrient profiles than dry heating. To improved nutrient availability, moisture heating is a good potential method.[7] The data from the previous study were used in the following relationship study between the modeled protein structure and protein nutrient profiles and the protein utilization and availability.

Changes in Spectral Characteristics of Protein Induced by Heat-Related Processing, Revealed Using a Non-invasive Method (SR-IMS). The results of the structural spectral characteristics of protein between the raw and heat treatments of randomly selected canola seed tissue are presented in Table 1. The results showed that the heat-induced protein structure changes were able to be revealed and identified by the

dx.doi.org/10.1021/jf501553g | J. Agric. Food Chem. 2014, 62, 6199−6205

Table 2. Correlation between the Protein Molecular Structure α-Helix/β-Sheet Ratio and Protein Chemical and Nutrient Profiles in Raw (Control) and Heat Treatments (Wet and Dry Heating) of Brown- and Yellow-Type Canola Seed Tissues in Randomly Selected Spot Samples after Sectioning at ca. 6 μm Thickness

item	correlation with modeled protein α-helix/β-sheet ratios	
	correlation coefficient R	p value
protein profiles (% of CP)		
total CP (% of DM)	0.050	0.9681
soluble CP	0.962	0.1756
neutral detergent insoluble protein (NDIP)[a]	−0.998	0.0407
acid detergent insoluble protein (ADIP)[b]	−0.999	0.0256
protein fractions[c] (% of CP)		
PA	0.974	0.1446
PB1	0.937	0.2278
PB2	−0.867	0.3339
PB3	−0.997	0.0453
PC	0.115	0.9268
digestible nutrients (NRC-2001 summary approach)		
truly digestible CP (tdCP, % of DM)	0.412	0.7298
truly digestible FA (tdFA, % of DM)	−0.968	0.1600
$TDN_{1\times}$ (% of DM)	−0.954	0.1936
rumen and intestinal digestion		
in situ rumen degradation (% of DM)	0.971	0.1537
in situ rumen degradation (% of CP)	0.972	0.1514
intestinal digestibility of RUP (%)	−0.972	0.1512

[a]NDIP = 6.25 × neutral detergent insoluble nitrogen. [b]ADIP = 6.25 × acid detergent insoluble nitrogen. [c]Protein subfractions using CNCPS: PA, fraction of CP that is instantaneously solubilized at time zero; PB1, fraction of CP that is soluble in borate−phosphate buffer and precipitated with trichloroacetic acid; PB2, calculated as total CP minus the sum of fractions PA, PB1, PB3, and PC; PB3, calculated as the difference between the portions of total CP covered with NDF and ADF; and PC, fraction of CP recovered with ADF and considered to be undegradable. It contained protein associated with lignin and tannins and heat-damaged protein, such as the Millard reaction products.

non-invasive method (SR-IMS). In comparison to the raw, moisture heating significantly affected the spectral modeled protein structure profile and it increased ($p < 0.05$) amide I, amide II, modeled α-helices, and moldeled β-sheets while decreasing ($p < 0.05$) the ratio of modeled α-helices to modeled β-sheet; however, there was no change ($p > 0.05$) to the ratio of amide I/amide II. Similarly, dry heating did not change ($p > 0.05$) the protein structure spectral profiles, including amide I, amide II, modeled α-helices, and modeled β-sheets, as well as their ratios (both the modeled α-helix/modeled β-sheet ratio and the amide I/amide II ratio). The results in the present study were in agreement with our previous work using IR spectroscopy for soybean.[7] The moisture heating altered the inherent protein structures, subsequently, altered *in situ* rumen degradation of DM and CP, and further changed intestinal digestibility of rumen undegraded protein. However, dry heating did not change the molecular protein structures; thus, there were no differences in chemical characteristics and nutrient metabolic kinetics between dry heat treatment and the control. The change of the ratio of modeled α-helices/modeled β-sheets by moisture heating was reported by Doiron et al.[6] in Vimy flax. However, in their study, the ratio of modeled α-helices/modeled β-sheets of Vimy flaxseed was increased when the autoclaving temperature was increased from 40 to 60 min at 120 °C. The differences in the ratio of modeled α-helices/modeled β-sheets may be caused by heating processing conditions. These results indicated that different types of oil seeds (canola versus flaxseed versus soybean) had different sensitivities and responses to even the same heat processing. Generally, there was very little application of this novel advanced synchrotron radiation analytical technique to the study of internal structure changes in different plant-based feed samples with different heating methods for structure and nutrition interaction.

The protein structure spectral profiles between different types of canola seeds using the non-invasive method SR-IMS is presented in Table 1. The results showed that yellow-type canola was lower in the ratio of amide I/amide II than the dark-brown-type canola tissues that were randomly selected but there were no differences in amide I, amide II, modeled α-helices, modeled β-sheets, and the ratio of modeled α-helices/modeled β-sheets between yellow- and brown-type canola tissues.

Multivariate Spectral Analyses of Protein Spectral Profiles Using the Non-Invasive Method (SR-IMS): Comparison of the Control and Heat Treatments. The results of CLA and PCA of protein amide I and amide II spectra in the region of ca. 1724−1487 cm^{-1} obtained from different canola seed tissues with different heating are presented in Figures 2−4. From Figure 2, the results showed that yellow-type canola seed processing by moisture heating (B) was relatively different from the yellow-type canola seed processing by dry heating (C) and raw yellow-type canola seed (A), which could be discriminated into different clusters (CLA) and could be grouped into separate ellipses (PCA). However, the yellow-type canola seed processing by dry heating (C) and raw yellow-type canola seed (A) had similarities in their structure makeup, which could not be discriminated into different clusters (CLA) and could not be grouped into separate ellipses (PCA). However, the results showed that brown-type canola seed processed by moisture heating (E) was the same as the brown-type canola seed processed by dry heating (F) and raw brown-type canola seed (D) (Figure 3), which could not be discriminated into different clusters (CLA) and could not be grouped into separate ellipses (PCA). Likewise, the brown-type canola seed processed by dry heating (C) and raw brown-type canola seed (D) had similarities in their structure makeup, which could not be discriminated into different clusters (CLA) and could not be grouped into separate ellipses (PCA) (Figure 3). In Figure 4, it is again proven that there was no difference between yellow- and brown-type canola (both CLA and PCA) in vibrational pattern in amide I and II regions, which indicated that heating did not result in a significant impact on different types of canola seeds (yellow and brown). On the other side, maybe the heat condition in this study was not optimal and not enough to reveal the due changes or CLA and PCA are not sensitive enough to pick up subtle changes of the protein intrinsic structures.

Correlation between Protein Spectral Profiles and Protein Nutrient Profiles. Pearson correlations between protein secondary structure and chemical profiles, protein fractions, truly digestible nutrients, energy value, *in situ* rumen degradability, and intestinal protein availability in the control and heat treatments of canola seed tissues are presented Table 2. The results showed that the ratio of modeled α-helices/modeled β-sheets in the control and heat treatments had a strong negative correlation with NDIP ($R = -0.998$; $p < 0.05$), ADIP ($R =$

dx.doi.org/10.1021/jf501553g | J. Agric. Food Chem. 2014, 62, 6199−6205

−0.999; $p < 0.05$), and PB_3 ($R = -0.997$; $p < 0.05$). Our results are different from the flaxseed reported by Doiron et al.[6] The reason may also be different types of oil seeds (flaxseeds versus canola). The flaxseed results reported by Doiron et al.[6] were under the conditions of moisture heating at 120 °C from 20, 40, and 60 min. There was no significant correlation detected between the ratio of modeled α-helices/modeled β-sheets and other protein chemical and nutrient profiles. It needs to be mentioned that only moisture heating showed the significant effect on canola seed tissue but dry heating did not in this study. There is no published report on the protein spectral profile study on various feeds from other laboratories using our approaches. No comparison can be made. This is because previously we did not have an advanced non-invasive tool to detect molecular structure changes within intact tissue. Since the advanced synchrotron-based analytical technique has been developed, the structure spectral features can be revealed in relation to nutrient availability.

It was concluded that the effect of heating processing on the protein structure spectral profiles in canola seed tissues were detected using advanced the non-invasive method, synchrotron-radiation-based Fourier transform infrared microspectroscopy. Using moisture heat processing, the canola seeds were significantly changed in physical shape, protein structure spectral profile, protein nutrient profiles, utilization, and availability compared to the control and those processed by dry heating. The results partially supported our hypothesis that the sensitivity of canola seeds to heating methods differed between different types of canola seeds and the nutrient availability differed between different heating methods. Using an advanced synchrotron radiation technique, a non-invasive approach to evaluate protein quality could be further developed.

AUTHOR INFORMATION

Corresponding Author

*Telephone: +1-306-966-4132. E-mail: peiqiang.yu@usask.ca.

Funding

The authors are grateful to the SaskCanola, Natural Sciences and Engineering Research Council of Canada (NSERC), Agricultural Development Fund (ADF), Ministry Agriculture Strategic Research Chair Program, and Thousand-Talent-People Program in Tianjin for financial support in feed chair (to Peiqiang Yu) research programs.

Notes

The authors declare no competing financial interest.

ACKNOWLEDGMENTS

All of our synchrotron experiments were carried out at the Canadian Light Sources (CLS, Saskatoon, Saskatchewan, Canada) and the National Synchrotron Light Source, Brookhaven National Laboratory (NSLS−BNL, Upton, NY). The authors are grateful to Tim May, Ferenc Borondics, Liu Xia, etc. for helpful data collection at the 01B1-1 station, CLS, Lisa Miller, Randy Smith, etc. for helpful data collection at U2B experimental stations, NSLS−BNL. The authors especially thank Zhiyuan Niu, Arjan Jonker, and Bo Liu for lab analysis assistance.

REFERENCES

(1) Becker, P. M.; Yu, P. What makes protein indigestible from tissue, cellular and molecular structure aspects? *Mol. Nutr. Food Res.* **2013**, *57*, 1695−1707.

(2) Yang, L.; Yu, P. Synchrotron-based and globar-sourced molecular (micro)spectroscopy contributions to advances in new hulless barley (with structure alteration) research on molecular structure, molecular nutrition and nutrient delivery. *Crit. Rev. Food Sci. Nutr.* **2013**.

(3) Yang, L.; Christensen, D. A.; McKinnon, J. J.; Beattie, A. D.; Xin, H.; Yu, P. Investigating the molecular structure features of hulless barley (*Hordeum vulgare* L.) in relation to metabolic characteristics using synchrotron-based Fourier transform infrared microspectroscopy. *J. Agric. Food Chem.* **2013**, *61*, 11250−11260.

(4) Yu, P.; Nuez-Ortin, W. G. Relationship of protein molecular structure to metabolisable proteins in different types of dried distillers grains with solubles: A novel approach. *Br. J. Nutr.* **2010**, *104*, 1429−1437.

(5) Yu, P.; Jonker, A.; Gruber, M. Molecular basis of protein structure in proanthocyanidin and anthocyanin-enhanced *Lc*-transgenic alfalfa in relation to nutritive value using synchrotron-radiation FTIR microspectroscopy: A novel approach. *Spectrochim. Acta, Part A* **2009**, *73*, 846−853.

(6) Doiron, K.; Yu, P.; McKinnon, J. J.; Christensen, D. A. Heat-induced protein structure and subfractions in relation to protein degradation kinetics and intestinal availability in dairy cattle. *J. Dairy Sci.* **2009**, *92*, 3319−3330.

(7) Samadi; Yu, P. Dry and moist heating-induced changes in protein molecular structure, protein subfraction, and nutrient profiles in soybeans. *J. Dairy Sci.* **2011**, *94*, 6092−6102.

(8) Yu, P. Molecular chemical structure of barley proteins revealed by ultra-specially resolved synchrotron light sourced FTIR microspectroscopy: Comparison of barley varieties. *Biopolymers* **2006**, *85*, 308−317.

(9) Yu, P. Molecular chemistry of plant protein structure at a cellular level by synchrotron-based FTIR spectroscopy: Comparison of yellow (*Brassica rapa*) and brown (*Brassica napus*) canola seed tissues. *Infrared Phys. Technol.* **2008**, *51*, 473−481.

(10) Yu, P.; McKinnon, J. J.; Christensen, C. R.; Christensen, D. A.; Marinkovic, N. S.; Miller, L. M. Chemical imaging of micro-structures of plant tissues within cellular dimension using synchrotron infrared microspectroscopy. *J. Agric. Food Chem.* **2003**, *51*, 6062−6067.

(11) Wetzel, D. L.; Eilert, A. J.; Pietrzak, L. N.; Miller, S. S.; Sweat, J. A. Ultraspatially resolved synchrotron infrared microspetroscopy of plant tissue in situ. *Cell Mol. Biol.* **1988**, *44*, 145−167.

(12) Wetzel, D. L. When molecular causes of wheat quality are known, molecular methods will supercede traditional methods. *Proceedings of the International Wheat Quality Conference*; Manhattan, KS, May 20−24, 2001; pp 1−20.

(13) Yu, P.; Doiron, K.; Liu, D. Shining light on the differences in molecular structural chemical makeup and the cause of distinct degradation behavior between malting- and feed- type barley using synchrotron FTIR microspectroscopy: A novel approach. *J. Agric. Food Chem.* **2008**, *56*, 3417−3426.

(14) Statistical Analysis System (SAS). *User's Guide Statistics, Version 9.1.3*; SAS Institute, Inc.: Cary, NC, 2005.

JOURNAL OF AGRICULTURAL AND FOOD CHEMISTRY

Article

pubs.acs.org/JAFC

Simple and Sensitive Analysis of Histamine and Tyramine in Japanese Soy Sauces and Their Intermediates Using the Stable Isotope Dilution HILIC–MS/MS Method

Kenichiro Todoroki,[†] Yasuhiro Ishii,[†] Chiemi Miyauchi,[†] Sachiyo Kitagawa,[‡] Jun Zhe Min,[†] Koichi Inoue,[†] Tomoyuki Yamanaka,[‡] Kuniaki Suzuki,[‡] Yuko Yoshikawa,[§] Norio Ohashi,[§] and Toshimasa Toyo'oka*,[†]

[†]Laboratory of Analytical and Bio-Analytical Chemistry, School of Pharmaceutical Sciences, University of Shizuoka, 52-1 Yada, Suruga, Shizuoka 422-8526, Japan

[‡]Shizuoka Kensan Shoyu K. K., 80-1 Takashinden, Yaizu, Shizuoka 421-0204, Japan

[§]Laboratory of Microbiology, School of Food and Nutritional Sciences, University of Shizuoka, 52-1 Yada, Suruga, Shizuoka 422-8526, Japan

ABSTRACT: We established a simple, sensitive, and reproducible method to analyze the histamine and tyramine levels in Japanese soy sauce and its mash (called *moromi*) using hydrophilic interaction liquid chromatography with tandem mass spectrometry (HILIC–MS/MS). Histamine and tyramine quantification was performed using their stable isotopes for electrospray ionization–tandem mass spectrometry in the selected reaction monitoring mode. The sample pretreatment process was a simple, one-step liquid–liquid extraction. HILIC separation was performed with a gradient elution of aqueous ammonium formate and acetonitrile. Because of validation tests, the linearity, the accuracies, and precisions were sufficient. The limit of detection and the limit of quantification were 0.09 and 0.29 ppm for histamine and 0.13 and 0.42 ppm for tyramine, respectively. We successfully applied this method to histamine and tyramine determination in four kinds of commercial Japanese soy sauces and also in *moromi* samples during soy sauce production.

KEYWORDS: *histamine, tyramine, high-performance liquid chromatography, HILIC–MS/MS, soy sauce, moromi*

INTRODUCTION

Soy sauces are fermented condiments produced from soybeans, grain, brine, and *Aspergillus oryzae* or *Aspergillus sojae* molds. In the Japanese traditional soy sauce manufacturing process, the microbial fermentation occurs in soy sauce mash (commonly called *moromi*). Several aromatic components of soy sauces are generated during this process. Lactic acid is produced by halophilic lactic acid bacteria (*Tetragenococcus* spp., primarily *Tetragenococcus halophilus*) to acidify the *moromi*; alcoholic fermentation is subsequently caused by yeast (*Zygosaccharomyces rouxii*). Histamine (Him) and tyramine (Tym) are produced during the lactic acid fermentation in the mash by the *Tetragenococcus* spp. having histidine decarboxylase (HDC) and/or tyrosine decarboxylase (TDC) genes. The HDC gene is encoded on a 30-kb plasmid, and the plasmid can be transferred among *Tetragenococcus* bacteria, and the bacterium that acquire the transformable element become histamine-productive.[1] Excessive intake of Him and Tym can cause an allergy-like food poisoning.[2] Therefore, the maximum acceptable Him levels in foods has been established as less than 200 ppm in European Union (EU) countries, Switzerland, and Norway.[3−5] Although Him and Tym levels in foods have not yet been legally regulated in Japan, they will be regulated as in the EU in the near future. To manufacture soy sauces with low Him and/or Tym levels, it is necessary to use *Tetragenococcus* spp. without HDC and/or TDC genes during the lactic acid fermentation of the soy sauce mash. Therefore, a simple and sensitive monitoring method for Him and Tym during the production process of soy sauce is required.

Biogenic amines, including Him and Tym, analysis in foods by LC coupled in tandem with mass spectrometry (MS) using an ODS column[6−8] and a hydrophilic interaction liquid chromatography (HILIC) column[9−11] have been widely reported. In the HILIC mode, analytes interact with the hydrophilic stationary phase, and the elution is generated by the hydrophobic binary mobile phase, which uses water as a strong eluting solvent; therefore, polar substances such as Him and Tym are strongly retained to minimize the potential endogenous interferences and ion suppression. Unlike other food samples, however, soy sauces contain high concentrations of sodium chloride and many stained compounds such as melanoidins.[12] Time consuming pretreatments, such as ion-pair or cation-exchange solid-phase extraction, are required to remove these interfering compounds. Nevertheless, these pretreatments could not sufficiently prepare samples from soy sauce to be introduced into the mass spectrometer.

In this study, we established an HILIC–MS/MS method to analyze Him and Tym in soy sauces and their intermediates. This method enables highly selective Him and Tym detection,

Received: February 16, 2014
Revised: June 2, 2014
Accepted: June 5, 2014
Published: June 5, 2014

ACS Publications © 2014 American Chemical Society

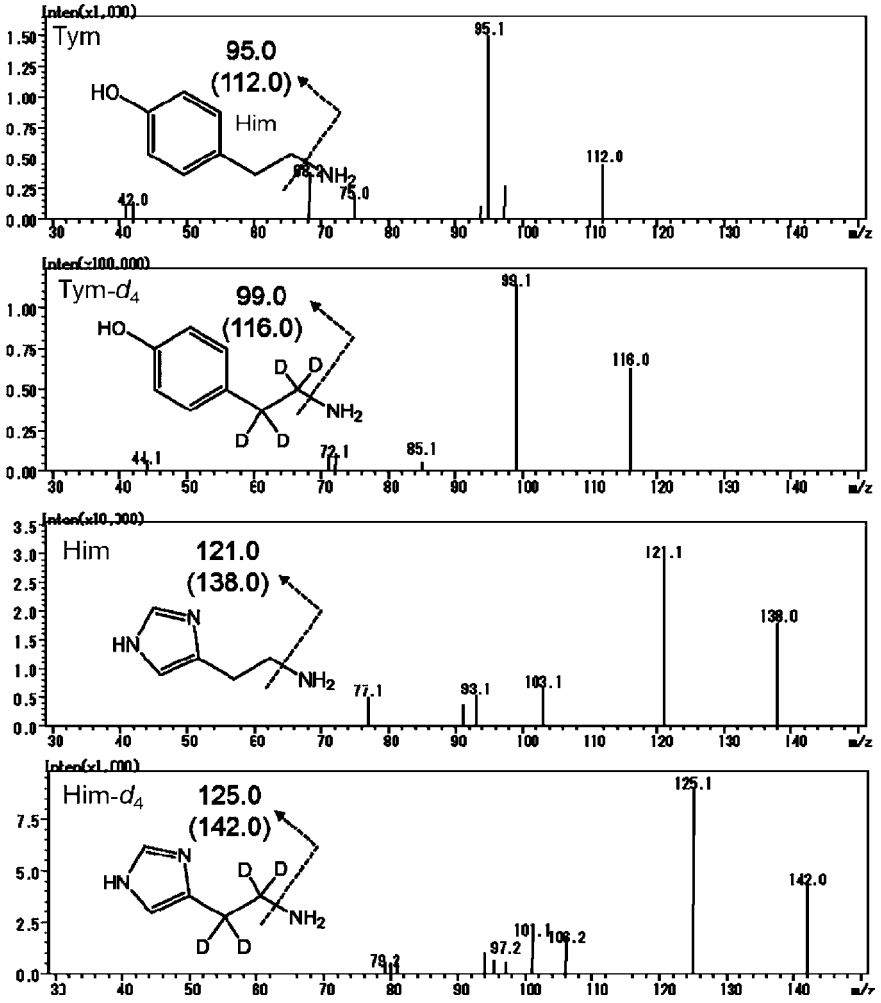

Figure 1. MS spectra of the 100 ppm standards of Tym, Tym-d_4, Him and Him-d_4.

and the sample pretreatment process has been simplified to a one-step liquid−liquid extraction (LLE). For Him and Tym quantification, the stable isotopes Him-d_4 and Tym-d_4 were used for the electrospray ionization−tandem mass spectrometry (ESI−MS/MS) in the selected reaction monitoring (SRM) mode. The developed method was validated with regard to linearity, sensitivity, precision, accuracy, and recovery. Furthermore, we successfully applied this method to sensitive and selective Him and Tym analysis in soy sauce and its *moromi* samples after lactic acid fermentation during soy sauce production.

MATERIAL AND METHODS

Reagents and Solutions. Deionized and distilled water purified using an Aquerius pwu-200 automatic water distillation apparatus (Advantec, Tokyo, Japan) was used to prepare all aqueous solutions. LC grade acetonitrile was purchased from Honeywell Burdick & Jackson (Muskegon, MI). Histamine dihydrochloride, tyramine hydrochloride, magnesium sulfate, and 1 M sodium hydroxide solution were purchased from Wako Pure Chemicals (Osaka, Japan). Histamine-d_4 sodium salt and tyramine-d_4 were purchased from Cambridge Isotope Laboratories (Andover, MA) and CDN Isotopes (Quebec, Canada), respectively. Other chemicals and solvents were of the highest purity available and were used as received. Individual stock solutions (1000 ppm) were prepared by dissolving 5 mg of each compound in 5 mL of water and stored in polypropylene test tubes at 4 °C. Various concentrations of standard working solutions were prepared daily by appropriate dilution with water just prior to use.

Sample Collection. Four kinds of Japanese soy sauces (*koikuchi*, *usukuchi*, *saishikomi*, and *tamari*)[13] were purchased from supermarkets in Shizuoka city (Japan). Two *moromi* samples after lactic acid fermentation with pH 4.68 and pH 5.04 were obtained from Shizuoka Kensan Shoyu K. K. (Yaizu, Shizuoka, Japan). In addition, an additional soy sauce mash was prepared as an example of lower contamination with Him and Tym after lactic acid fermentation by a *T. halophilus* 52−47C strain that was isolated from a soy sauce mash naturally fermented by a procedure previously described.[14] Polymerase chain reaction (PCR) was performed on the *T. halophilus* 52−47C strain in advance to confirm the absence of the genes HDC and TDC before starting the lactic acid fermentation of the soy sauce mash. PCR reactions were performed using primers of HmF (5′-TGTTTCGTATGACCGTGCGG-3′) and HmR (5′-CACCATTTTCGCCGGCAGTG-3′) for a partial 560 bp HDC gene[1] and using primers of TD5 (5′-CAAATGGAAGAAGAAGTAGG-3′) and TD2 (5′-ACATAGTCAACCATRTTGAA-3′) for a 1100 bp TDC gene.[15]

Instrumentation. Liquid chromatography was performed using a Shimadzu (Kyoto, Japan) Nexera system coupled with a Shimadzu LCMS 8040 triple quadrupole mass spectrometer with an ESI interface. Data acquisition was controlled using the LabSolution LCMS software ver. 5.53 (Shimadzu).

Chromatographic Conditions. The analytical column used was an Aeris HILIC column (2.1 mm i.d. × 150 mm, 5 μm, Phenomenex, Torrance, CA) maintained at 40 °C; the mobile phase consisted of 10 mM ammonium formate in water (solvent A) and a mixture of acetonitrile and 100 mM ammonium formate (9:1) (solvent B). The gradient profile was as follows: 85% solvent B at 0 min, 85% solvent B at 2.5 min, 50% solvent B at 4 min, 50% solvent B at 6 min, 85%

dx.doi.org/10.1021/jf500767p | J. Agric. Food Chem. 2014, 62, 6206−6211

solvent B at 6.01 min, and 85% solvent B at 12 min with a flow rate of 0.4 mL/min. The total run time was 12 min.

MS Conditions. The mass spectrometer was operated in the SRM mode using positive electrospray ionization. The parameters for the SRM analysis were as follows: drying N_2 gas flow at 15.0 L/min, nebulizing Ar gas flow at 2.0 L/min, desolvation line temperature at 250 °C, heat block temperature at 400 °C, interface voltage of 4.5 kV, and collision gas flow of 230 kPa. SRM transition of the precursor to product ions used for quantification were as follows: m/z 112.0 → 95.1 for Him, m/z 116.0 → 99.1 for Him-d_4, m/z 138.0 → 121.0 for Tym, and m/z 142.0 → 125.0 for Tym-d_4. The collision energy was 18 eV for Him and Him-d_4 and 14 eV for Tym and Tym-d_4.

Sample Preparation. A mixture of 100 ppm of Him-d_4 and Tym-d_4 (20 μL, for internal standard), 1 M sodium hydroxide (20 μL) and 100 mM magnesium sulfate (20 μL) were added to a 20-μL portion of each sample. After the addition of acetonitrile (320 μL), the solution was vigorously shaken for 1 min. An aliquot (20 μL) of the upper layer was transferred to another tube and then diluted 50 times with the initial mobile phase. The resulting solution (1 μL) was applied to the LC−MS/MS system.

Method Validation. To obtain the validation parameters, the peak areas were estimated by the LabSolution LCMS, and the baseline-to-baseline method was used for quantification. Him and Tym concentrations were calculated by the internal standard method. For quantitative analysis, calibration standard solutions (n = 6 each) with concentrations ranging from 0.5 to 500 ppm (0.5, 1, 5, 10, 50, 100, and 500 ppm) were prepared by diluting the stock solutions. The equations of the calibration curves were determined using least-squares linear prediction.

Precision of the assays was determined by the repeated measurement of four spiked samples at the lowest, low, middle, and high levels (0.5, 10, 100, and 500 ppm; n = 6). For intraday precision, these levels were analyzed six times each day, whereas for interday precision, specimens of the spiked samples at the same concentrations were analyzed twice per day for 6 days (n = 12). The spiked samples were pretreated and subsequently subjected to the HILIC−MS/MS. Him and Tym levels were determined from each calibration curve. Accuracy was defined as $F/(F_0 + A) \times 100$ (%), where F is the level of Him and Tym in the spiked sample, F_0 is the level of Him and Tym in the unspiked sample, and A is the spiked concentration.

RESULTS AND DISCUSSION

MS Analysis of Him and Tym. Figure 1 shows SRM chromatograms of the 100 ppm standard for Him and Tym and their MS spectra. We could observe ions regarding the major fragment ions at m/z = 138.0 → 121.0 (Tym), 142.0 → 125.0 (Tym-d_4), 112.0 → 95.0 (Him), and 116.0 → 99.0 (Him-d_4). The retention times of Tym, Tym-d_4, Him, and Him-d_4 were 1.6, 1.6, 5.4, and 5.4 min, respectively. Him and Him-d_4 as well as Tym and Tym-d_4 were eluted at almost the same retention times. Quantitative separation of Him and Tym was achieved within 6 min on the HILIC column at the given chromatographic conditions, and selective detection of Him and Tym was also achieved with the SRM mode.

Sample Pretreatment. Japanese soy sauces currently on the market are weakly acidic and contain approximately 16% sodium chloride. For the pretreatment process, soy sauce samples were alkalinized to a pH of ca. 10 by the addition of 1 M sodium hydroxide. These solutions were subsequently added to 100 mM magnesium sulfate and acetonitrile to form a bilayer. Water-soluble compounds, neutral and acidic amino acids, proteins, and melanoidins all remained in the aqueous layer. In contrast, positively charged, undissociated Him and Tym successfully partitioned into the acetonitrile phase.

Method Validation. Seven different concentrations in the range 0.5−500 ppm with six replicates were chosen to draw each calibration curve. The calibration curves for both Him and Tym were observed between the peak area and analyte concentration with good correlation coefficients (r^2 > 0.999).

Limit of detection (LOD) and limit of detection (LOQ) were determined from the signal-to-noise ratios of 3 and 10, respectively. LOD of Him and Tym was 0.09 and 0.13 ppm, respectively, LOQ of Him and Tym was 0.29 and 0.42 ppm, respectively. When analyzing the Him and Tym standard solution without the pretreatment process, 1000th of the above values were obtained as LOD and LOQ by the same HILIC−MS/MS system.

The results of precision and accuracy of intraday and interday assays are listed in Tables 1 and 2. The intraday assay precisions of Him and Tym were in the range 1.11−5.57% and 1.25−5.76%, respectively; the interassay precisions were in the range 1.76−7.17% and 4.66−9.72%, respectively. Accuracy of the method was determined by assessing the agreement between the observed and nominal concentrations of the analyzed samples. These values for Him and Tym were in the range 85.9−98.6% and 96.6−103.8%, respectively.

Recovery studies for the method were performed by spiking seven concentrations (0.5, 1, 5, 10, 50, 100, and 500 ppm) of Him and Tym into soy sauce samples. The recoveries were calculated from the slope of the calibration curve ratio of the peak areas of spiked soy sauce samples and those of standards

Table 1. Precision and Accuracy of Intra-day Assay for Him and Tym in Soy Sauce Samples (n = 6)

nominal concentration (ppm)	observed concentration (ppm)	precision[b] (%)	accuracy[c] (%)
	Him		
QC + 0.5 ppm (2.53)	2.42 ± 0.13 ppm	5.57	95.1
QC + 10 ppm (12.03)	11.1 ± 0.23 ppm	2.09	92.2
QC + 100 ppm (102.23)	100.5 ± 1.56 ppm	1.55	98.5
QC + 500 ppm (502.03)	495.0 ± 5.50 ppm	1.11	98.6
	Tym		
QC + 0.5 ppm (1.78)	1.54 ± 0.08 ppm	5.26	85.9
QC + 10 ppm (11.29)	10.0 ± 0.23 ppm	2.28	88.7
QC + 100 ppm (101.29)	94.2 ± 1.18 ppm	1.25	93.0
QC + 500 ppm (501.29)	472.6 ± 6.83 ppm	1.45	94.3

[a] n = 6 per day. [b] Expressed as relative standard deviation. [c] Accuracy % = Average of Observed concentration/(nominal concentration + concentration of QC sample) × 100.

Table 2. Precision and Accuracy of Inter-day Assay for Him and Tym in Soy Sauce Samples (n = 12)[a]

nominal concentration (ppm)	observed concentration (ppm)	precision[b] (%)	accuracy[c] (%)
	Him		
QC + 0.5 ppm (2.53)	2.48 ± 0.18 ppm	7.17	97.8
QC + 10 ppm (12.03)	12.5 ± 0.81 ppm	6.50	103.8
QC + 100 ppm (102.23)	104.2 ± 1.84 ppm	1.76	102.1
QC + 500 ppm (502.03)	518.0 ± 11.6 ppm	2.24	103.2
	Tym		
QC + 0.5 ppm (1.78)	1.73 ± 0.17 ppm	9.72	96.6
QC + 10 ppm (11.29)	11.3 ± 0.52 ppm	4.66	100.2
QC + 100 ppm (101.29)	100.5 ± 5.54 ppm	5.52	99.2
QC + 500 ppm (501.29)	508.8 ± 36.1 ppm	7.09	101.5

[a] n = 12 (2 × 6 days). [b] Expressed as relative standard deviation. [c] Accuracy % = Average of observed concentration/(nominal concentration + concentration of QC sample) × 100.

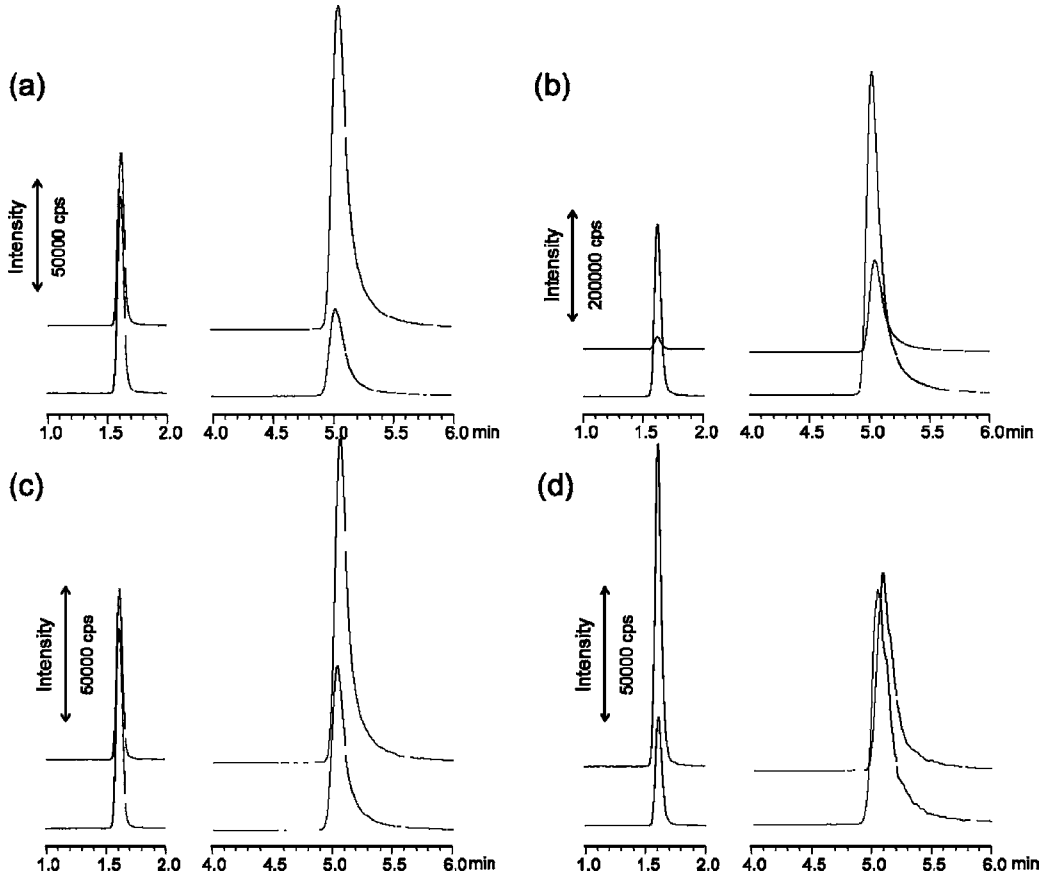

Figure 2. Typical SRM chromatograms obtained from commercially available Japanese soy sauces: (a) *koikuchi*, (b) *usukuchi* (10-fold diluted), (c) *saishikomi*, and (d) *tamari*. Upper, 100 ppm internal standards; lower, soy sauce samples.

(n = 3 each). Mean recoveries of Him and Tym were 47.7 and 59.9%, respectively.

Him and Tym Determination in Commercial Japanese Soy Sauces. This method was used for Him and Tym quantification in commercial Japanese soy sauces to investigate its applicability. Figure 2 shows typical SRM chromatograms of four kinds of commercial soy sauce samples: (a) *koikuchi*, (b) *usukuchi*, (c) *saishikomi*, and (d) *tamari*. The *koikuchi*, *usukuchi*, and *tamari*-type soy sauces are produced from *moromi*, which is fermented with rice malt and brine, whereas *nama shoyu* (raw soy sauce) is used in the production of the *saishikomi* soy sauce instead of brine. The *nama shoyu* is rich in color, taste, aroma, and nitrogen contents, and it may contain significant amounts of Him and Tym. Results of the Him and Tym levels obtained by the present method were summarized in Table 3. Him levels of the commercial soy sauce samples used were 1.2−775 (*koikuchi*), 1.9−364 (*usukuchi*), 46.2−173.9 (*saishikomi*), and 131 ppm (*tamari*). Tym levels of the above samples were 1.2−2040 (*koikuchi*), 4.3−1594 (*usukuchi*), 171−575 (*saishikomi*), and 336 ppm (*tamari*). Each sample was purchased from a different manufacturer; therefore, Him and Tym levels were significantly different because of differences in the manufacturers.

Him and Tym Analysis in *Moromi* Samples after Lactic Acid Fermentation. Figure 3 shows the SRM chromatograms of three *moromi* samples after lactic acid fermentation during the manufacturing process of *koikuchi* soy sauces. When the soy sauce mash was fermented at pH 4.68, 183.4 ppm of Him and 108.7 ppm Tym were detected (Figure 3a). When the mash was fermented at a slightly higher pH (5.04), 116.7 ppm of Him and 150.3 ppm Tym were observed (Figure 3b). Thus, lactic acid fermentations under different pHs appears to influence the production quantities of Him and Tym; this probably depends on the growth of contaminated *Tetragenococcus* spp. that contains HDC and TDC genes during the fermentation, although no significant difference was observed in the Him and Tym levels between the two pH samples.

We further analyzed Him and Tym levels in a soy sauce mash after lactic acid fermentation using a *T. halophilus* 52−47C strain that did not have HDC and TDC genes. Extremely low Him and Tym levels were detected (less than 8.29 and 14.3

Table 3. Him and Tym Contents in Commercial Japanese Soy Sauces

		concentration (ppm)	
sample no.	kind of soy sauce	Tym	Him
1	*koikuchi* (bland A)	2.0	1.2
2	*koikuchi* (bland B)	234.5	277.0
3	*koikuchi* (bland C)	14.1	29.0
4	*koikuchi* (bland D)	32.6	134.3
5	*koikuchi* (bland E)	774.6	2040
6	*koikuchi* (bland F)	1.2	11.4
7	*usukuchi* (bland B)	363.7	1594
8	*usukuchi* (bland G)	1.9	17.5
9	*usukuchi* (bland H)	11.1	4.3
10	*saishikomi* (bland B)	62.5	171.2
11	*saishikomi* (bland I)	173.9	575.1
12	*saishikomi* (bland G)	46.2	258.3
13	*tamari* (bland J)	131.1	336.0

dx.doi.org/10.1021/jf500767p | J. Agric. Food Chem. 2014, 62, 6206−6211

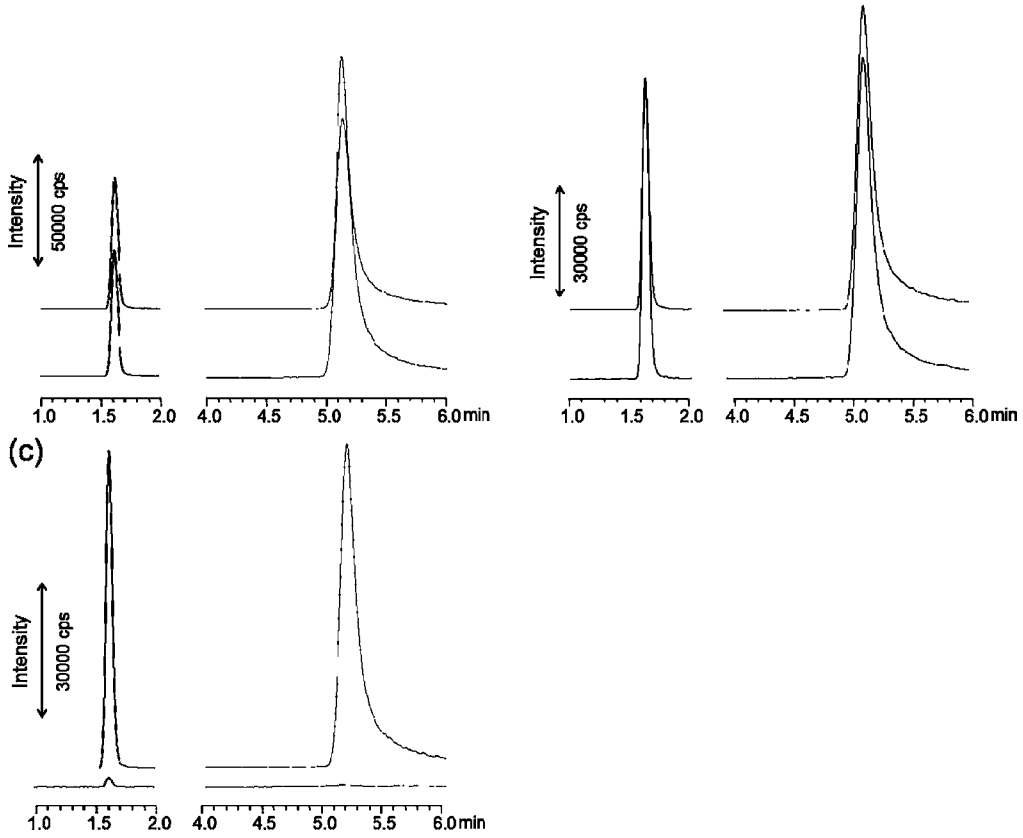

Figure 3. Chromatograms of three *moromi* samples after the lactic fermentation manufacturing process of *koikuchi* soy sauces. (a) Lactic acid fermentation at pH 4.68; (b) lactic acid fermentation at pH 5.04; (c) lactic acid fermentation using a *T. halophilus* 52−47C strain without HDC and TDC genes. Upper, 100 ppm internal standards; lower, *moromi* samples.

ppm, respectively) in the mash (Figure 3c), suggesting that *T. halophilus* without HDC and TDC genes available in lactic acid fermentation can be used to manufacture soy sauce with minimal Him and Tym contamination.

As mentioned above, our method would be useful for monitoring Him and Tym contaminations during the manufacturing of soy sauce.

CONCLUSION

This paper reports a simple and sensitive analysis method for Him and Tym in Japanese soy sauce and *moromi* samples. The total run time was satisfactorily short for the routine analyses. The sample pretreatment procedure was also simplified to a one-step LLE without concentration of the extract. In this procedure, solid-phase extraction cartridge was not necessary, and general-use reagents, which are magnesium sulfate, sodium hydroxide and acetonitrile, were only required for the LLE. Therefore, it would suppress the analytical cost and be useful in routine analyses. The developed method was validated and successfully applied for Him and Tym quantification in the four kinds of Japanese commercial soy sauces and *moromi* samples. The proposed method would be useful as a simple assay method for soy sauce manufacturers, quality control units in food companies, and related analytical laboratories. Our simple pretreatment procedure enabled the extraction of Him and Tym from high-salting and protein-containing matrices selectively and efficiently. In addition, the HILIC−MS/MS analysis provided simple and clean SRM chromatograms for Him and Tym with high sensitivity. Therefore, our proposed method would be applicable to Him and Tym analysis in various kinds of foods and beverages beside Japanese soy sauces, such as fish sauces, seafood, and lactic fermented foodstuffs.

AUTHOR INFORMATION

Corresponding Author

*Tel: +81-54-264-5656. Fax: +81-54-264-5593. E-mail: toyooka@u-shizuoka-ken.ac.jp.

Notes

The authors declare no competing financial interest.

ACKNOWLEDGMENTS

This work was supported in part by Shizuoka Foundation for Industry Promotion. The authors greatly thank to Shimadzu Corporation for useful technical assistance regarding an LC−MS/MS instrument.

REFERENCES

(1) Satomi, M.; Furushita, M.; Oikawa, H.; Yoshikawa-Takahashi, M.; Yano, Y. Analysis of a 30 kbp plasmid encoding histidine decarboxylase gene in *Tetragenococcus halophilus* isolated from fish sauce. *Int. J. Food Microbiol.* **2008**, *126*, 202−209.

(2) Taylor, S. L. Histamine food poisoning - Toxicology and clinical aspects. *CRC Cr. Rev. Toxicol.* **1986**, *17*, 91−128.

(3) Directive, E. U. Council Directive 91/493/EEC of 22 July 1991 laying down the health conditions for the production and the placing on the market of fishery products. *Official Journal L 268.24/09*, **1991**, 0015−0034.

(4) Fish, F. D. A. *Fishery Products Hazards Controls Guide* **1998**.

(5) Lehane, L.; Olley, J. Histamine fish poisoning revisited. *Int. J. Food Microbiol.* **2000**, *58*, 1−37.

(6) Ö nal, A. A review: Current analytical methods for the determination of biogenic amines in foods. *Food Chem.* **2007**, *103*, 1475−1486.
(7) Romero-Gonzalez, R.; Alarcon-Flores, M. I.; Vidal, J. L. M.; Frenich, A. G. Simultaneous determination of four biogenic and three volatile amines in anchovy by ultra-high-performance liquid chromatography coupled to tandem mass spectrometry. *J. Agric. Food Chem.* **2012**, *60*, 5324−5329.
(8) Mayr, C. M.; Schieberle, P. Development of stable isotope dilution assays for the simultaneous quantitation of biogenic amines and polyamines in foods by LC-MS/MS. *J. Agric. Food Chem.* **2012**, *60*, 3026−3032.
(9) Gianotti, V.; Chiuminatto, U.; Mazzuccoa, E.; Gosetti, F.; Bottaro, M.; Frascarolo, P.; Gennaro, M. C. A new hydrophilic interaction liquid chromatography tandem mass spectrometry method for the simultaneous determination of seven biogenic amines in cheese. *J. Chromatogr., A* **2008**, *1185*, 296−300.
(10) Kakigi, Y.; Yamashita, A.; Miyamoto, Y.; Icho, T.; Mochizuki, N. Quantification of non-volatile amines in beer using hydrophilic interaction liquid chromatograph-tandem mass spectrometer. *Bunseki Kagaku* **2011**, *60*, 157−162.
(11) Self, R. L.; Wu, W. H.; Marks, H. S. Simultaneous quantification of eight biogenic amine compounds in tuna by matrix solid-phase dispersion followed by HPLC−orbitrap mass spectrometry. *J. Agric. Food Chem.* **2011**, *59*, 5906−5913.
(12) Obretenov, T.; Vernin, G. Melanoidins in the Maillard reaction. *Dev. Food Sci.* **1998**, *40*, 455−482.
(13) Lioe, H. N.; Wada, K.; Aoki, T.; Yasuda, M. Chemical and sensory characteristics of low molecular weight fractions obtained from three types of Japanese soy sauce (shoyu)−Koikuchi, tamari and shiro shoyu. *Food Chem.* **2007**, *100*, 1669−1677.
(14) Justé, A.; Van Trappen, S.; Verreth, C.; Cleenwerck, I.; De Vos, P.; Lievens, B.; Willems, K. A. Characterization of *Tetragenococcus* strains from sugar thick juice reveals a novel species, *Tetragenococcus osmophilus* sp. nov., and divides *Tetragenococcus halophilus* into two subspecies, *T. halophilus* subsp. nov. and *T. halophilus* subsp. *flandriensis* subsp. nov. *Int. J. Syst. Evol. Micr.* **2012**, *62*, 129−137.
(15) Coton, M.; Coton, E.; Lucas, P.; Lonvaud, A. Identification of the gene encoding a putative tyrosine decarboxylase of *Carnobacterium divergens* 508. Development of molecular tools for the detection of tyramine-producing bacteria. *Food Microbiol.* **2004**, *21*, 125−130.

JOURNAL OF AGRICULTURAL AND FOOD CHEMISTRY

Article

pubs.acs.org/JAFC

Purification and Characterization of Parvalbumin Isotypes from Grass Carp (*Ctenopharyngodon idella*)

Zheng Li,[†,‡] Juan You,[†,‡] Yongkang Luo,*[,†] and Jianping Wu*[,‡]

[†]Beijing Higher Institution Engineering Research Center of Animal Product, College of Food Science and Nutritional Engineering, China Agricultural University, Beijing 100083, People's Republic of China

[‡]Department of Agricultural, Food and Nutritional Science, University of Alberta, Edmonton, Alberta T6G 2P5, Canada

ABSTRACT: The prevalence of fish allergy is rapidly increasing because of a growing fish consumption driven mainly by a positive image of the fish and health relationship. The purpose of this study was to characterize parvalbumin isotypes from grass carp (*Ctenopharyngodon idella*), one of the most frequently consumed freshwater fish in China. Three parvalbumin isotypes were purified using consecutive gel filtration and reverse-phase chromatography and denoted as PVI, PVII, and PVIII. The molecular weights of the isotypes were determined to be 11.968, 11.430, and 11.512 kDa, respectively. PVI showed 74% matched amino acids sequence with PV isotype 4a from *Danio rerio*, while PVII and PVIII showed 46% matched amino acids sequence with PV isotypes from *Hypophthalmichthys molitrix*. PVII is the dominant allergen, but it was liable to gastrointestinal enzymes as PVIII; however, PVI was resistant to pepsin digestion. A further study is to characterize the epitopes of PVII, the dominant allergen.

KEYWORDS: *parvalbumin isotypes, purification, characterization, IgG binding, IgE binding*

INTRODUCTION

Fish consumption has grown tremendously over the past several decades, driven mainly by a positive image of the fish and health relationship and as an alternative animal protein source over pork and beef.[1,2] Fish (including shellfish) allergies are common in both the western world and Asian countries, affecting 0.2−2.29% of the general population;[3] unlike other allergies, most of the children cannot outgrow fish allergy. Although fish allergies occur mainly via the gastrointestinal tract (eating fish), handling and inhalation of cooking vapors can also cause fish allergic reactions.[4,5] Fish allergies cause urticaria, rhino conjunctivitis, asthma, oral allergy syndrome, diarrhea, and even life-threatening anaphylaxis.[6]

Parvalbumin (PV), accounting for 90% of fish allergic reaction, was first identified as the major allergen in cod[7] and then from many different species.[8−10] As the major clinical cross-reactive fish allergen, PV is a subfamily of closely related three EF-hand calcium-binding proteins, with a molecular weight of 10−12 kDa and isoelectric points of 3.9−5.5.[11] PV is often subdivided into two distinct isoform lineages, α-PV and β-PV, with β-PV as the major allergen.[3] α-PV and β-PV consist of 109 and 108 amino acid residues, respectively. PV consisting of 110 amino acid residues was also reported in herring recently.[12] The pI value of α-PV is ∼5.0, while that of β-PV is more acidic, with an pI value ∼4.5.[13,14] The presence of isotypes with different levels of immunoglobulin G (IgG)- and immunoglobulin E (IgE)-binding capacities was reported in several kinds of fish species.[15−17] Cai et al. indicated that PVII (11.95 kDa) may be more allergenic than PVI (12.29 kDa) in red stingray.[15] However, two isotypes of PV with the same molecular weight (11.5 kDa) and similar IgG- and IgE-binding capacities but different isoelectric points (4.39 and 4.6, respectively) were reported from Alaska pollack.[16]

Grass carp (*Ctenopharyngodon idella*) is one of the most frequently consumed freshwater fish in China, with an annual harvest of 4.78 million metric tons in 2012.[18] There were reports about the main allergen in carp[9] and silver carp,[19] but PV from grass carp has not been characterized. Carp, grass carp, silver carp, and zebrafish are from the same family (Cyprinidae) but different genus. Liu et al. revealed that silver carp PV had 92.7 and 82.6% similarities with PVs from carp.[19] Therefore, it is important to investigate and characterize the main allergen in grass carp. The objectives of this study were to purify and characterize PV isotypes from grass carp, determine their IgG- and IgE-binding capacities, and compare their digestibility using a simulated gastrointestinal condition.

MATERIALS AND METHODS

Materials. Live grass carps were purchased from a local fish market (Beijing, China). After sacrifice, white muscle was collected and used for PV extraction. Human sera were purchased from Plasma Lab International (Everett, WA). According to the supplier, these patients were selected on the basis of their allergic symptoms, such as itchy mouth, hives, wheezing, swelling throat, and IgE levels, against codfish. The IgE levels were measured by the Thermo Fisher Scientific ImmunoCAP at levels of 68.4, 77.5, 84.4, and 44.7 kU/L for 17716 (female, age: 28), 21290 (male, age: 22), 21473 (female, age: 56), and 17485 (male, age: 38), respectively. Anti-grass carp PV sera from rabbit was prepared in the lab (China Agricultural University, China). Mouse anti-frog PV monoclonal antibody (PARV-19), *para*-nitrophenylphosphate (*p*-NPP) substrate solution, tetramethylbenzidine (TMB) substrate solution, anti-mouse IgG peroxidase-conjugated antibody produced in goat, anti-rabbit IgG peroxidase-conjugated antibody produced in goat, and anti-human IgE peroxidase-conjugated antibody produced in goat were from Sigma (St. Louis, MO). Molecular weight protein standard and 4−20% gel were purchased from Bio-Rad Laboratories,

Received: February 18, 2014
Revised: May 11, 2014
Accepted: May 27, 2014
Published: May 27, 2014

ACS Publications © 2014 American Chemical Society

Inc. (Hercules, CA). Trypsin used in gel digestion was purchased from Promega (Madison, WI). High-performance liquid chromatography (HPLC)-grade acetonitrile was from Acros Organics (Fair Lawn, NJ). Pepsin (from porcine gastric mucosa) and trypsin (from porcine pancreas) used in simulated gastrointestinal digestion were purchased from Sigma (St. Louis, MO).

Extraction and Purification of PV. For PV extraction, the white muscle was homogenized with three volumes of 20 mM Tris−HCl (pH 7.5). After centrifugation at 10000*g* for 20 min, the supernatant was incubated in a water bath at 95 °C for 30 min. The heated extract was subjected to gel filtration chromatography on a Superdex 75 column coupled with an ÄKTA explorer 10XT system (GE Healthcare, Uppsala, Sweden) and eluted with 0.15 M NaCl in 0.01 M phosphate buffer (pH 7.0). Fractions were collected every 7 min, and absorbance was measured at 220 and 280 nm. Cytochrome *c* from horse heart (molecular mass of 12.4 kDa) was run under the identical conditions as a standard. Fractions containing PV from gel filtration chromatography were further applied to a Waters XBridge C_{18} column (5 μm, 3.0 × 250 mm, Waters Corporation, Milford, MA) coupled with a guard column (40 × 10 mm, Waters Corporation, Milford, MA) attached with a Waters 600 HPLC system. Instrumental control and data collection were carried out by Empower, version 2. Samples were automatically injected by Waters 2707 autosampler at a volume of 25 μL. The column was eluted by two solvents, solvent A [HPLC-grade water containing 0.1% trifluoroacetic acid (TFA)] and solvent B (70% acetonitrile containing 0.1% TFA), at a flow rate of 0.5 mL/min using a gradient from 0 to 50% B within 5 min, to 50% B within 30 min, to 0% B over 5 min, and maintained for 10 min for the next injection. Fractions were collected every 0.5 min from 19 to 24 min, and elution was monitored by a Waters 2998 photodiode array at 220 nm. The fractions were concentrated by a vacuum rotary evaporator at 35 °C and then freeze-dried for further analysis.

Sodium Dodecyl Sulfate−Polyacrylamide Gel Electrophoresis (SDS−PAGE). SDS−PAGE was performed with 4−20% gel (Bio-Rad) according to the method by Laemmli.[20] The load volume was 15 μL at a protein concentration of 2 mg mL^{-1}. SDS−PAGE was performed in a Mini-PROTEAN tetra cell at a constant voltage of 200 V. Protein bands were stained using Brilliant Blue R-250. After destaining, the gel was scanned in an Alpha Innotech gel scanner (Alpha Innotech Corp., San Leandro, CA) with FluorChem SP software.

Matrix-Assisted Laser Desorption/Ionization Time-of-Flight Mass Spectrometry (MALDI-TOF-MS) Analysis of PV Isotypes. Molecular weight of the purified PV isotypes was analyzed by MALDI-TOF-MS according to the procedure of two-layer sample preparation.[21,22] For the first thin matrix layer, 0.7 μL of 10 mg mL^{-1} 3,5-dimethoxy-4-hydroxycinnamic acid (sinapinic acid) in 80% acetone/20% methanol (HPLC grade) (v/v) was loaded onto a clean MALDI target, and then the matrix layer was spread and dried immediately. A total of 2 μL of diluted PV isotype sample was mixed with 2 μL of saturated sinapinic acid in 50% acetonitrile/50% water (v/v). A total of 1 μL of treated sample was applied to the first layer of the matrix. After drying, 5 μL of water was added on top of the dry spot to desalt the sample, and after 10 s, the liquid was blown off by an air pulse; this was repeated 5 times. Each sample was applied to six spots. At least, three spots of each sample were analyzed. MALDI analysis was carried out on an Applied Biosystems Voyager Elite MALDI (Foster City, CA) time-of-flight mass spectrometer in a positive linear ion mode.

In-Gel Digestion of PV Isotypes and Liquid Chromatography (LC)−Tandem Mass Spectrometry (MS/MS) Analysis. Excised gel pieces containing PV isotypes were digested by trypsin, as Offengenden et al. described.[23] First, the protein in gel pieces were reduced with 10 mM dithiothreitol (DTT) and then alkylated with 50 mM iodoacetamide. After washing with 100 mM ammonium bicarbonate and acetonitrile, the gel pieces were dried in a SpeedVac. The dried gel pieces were digested by 0.8 μg of trypsin (20 ng μg^{-1} in 50 mM ammonium) at 37 °C. After overnight digestion, the peptides were extracted with 30 μL of 100 mM ammonium bicarbonate, followed by two steps of extraction with 30 μL of solution containing 5% formic acid and 50% acetonitrile in water. At last, the extracts were dried to about 15 μL in a SpeedVac. The sample after in-gel trypsin digestion was analyzed by a hybrid quadrupole orthogonal acceleration time-of-flight mass spectrometer, QToF Premier (Waters, Milford, MA), online connected to a Waters nanoAcquity ultrahigh-performance liquid chromatography (UPLC) system. A total of 5 μL of sample was loaded onto a nanoAcquity UPLC system with a peptide trap (180 μm × 20 mm, Symmetry C18 nanoAcquity column, Waters Corporation, Milford, MA) and a nano analytical column (75 μm × 100 mm, Atlantis dC18 nanoAcquity column, Waters Corporation, Milford, MA). A solution of 1% acetonitrile and 0.1% formic acid in water (solvent A) was used to flush the trap column at a flow rate of 10 μL min^{-1} for 3 min to desalt the trapped sample. Peptides were separated with a gradient of 1−65% solvent B (acetonitrile and 0.1% formic acid) over 35 min at a flow rate of 300 nL min^{-1}. The column was connected to a QToF Premier (Waters Corporation) for electrospray ionization−mass spectrometry (ESI−MS) and MS/MS analyses of the effluent. Then, analysis using the online search algorithm Mascot (Matrix Science) was carried out for peptide identification.

Preparation of Anti-grass Carp PV Antibodies in Rabbit. Anti-PV antibody was prepared from three female New Zealand rabbits by injection of purified PV from gel filtration chromatography, as described everywhere.[24] The first injection was 0.5 mL of PV solution (1 mg mL^{-1}) emulsified with an equal volume of Freund's complete adjuvant (Sigma, St. Louis, MO) to the hind leg muscle of a rabbit. After 2 weeks, 0.5 mL of PV solution (1 mg mL^{-1}) emulsified with an equal volume of incomplete Freund's complete adjuvant (Sigma, St. Louis, MO) was injected to the back muscle of a rabbit. After 2 weeks, the rabbits were injected with another 1 mL solution containing 2 mg of PV via the ear vein of a rabbit. After 1 week, the rabbit sera were collected and kept at −80 °C until use.

Indirect Enzyme-Linked Immunosorbent Assay (ELISA). IgG- and IgE-binding capacities of PVs from grass carp were analyzed by indirect ELISA using PARV-19, anti-grass carp PV produced in the sera of rabbits and fish allergic patients. Briefly, samples were coated on a 96-well high binding polystyrene plate and incubated at 4 °C overnight, and bovine serum albumin (BSA) was coated as the blank. After four steps of washing, 100 μL of phosphate-buffered saline (PBS) containing 0.1% Tween-20 and 1% BSA was added to each well to block the unoccupied space of the wells and incubated at 37 °C for 1 h. Then, 100 μL of antibodies was added to wells after four steps of washing. Four human serum diluted 1:10 with PBS contained 0.1% Tween-20 and 1% BSA. Mouse serum and rabbit serum were diluted 1:400 000 and 1:160 000 with the same dilution, respectively. After incubation at 37 °C for 1 h, 100 μL of the corresponding peroxidase-conjugated antibody produced in goat (anti-mouse IgG, anti-rabbit IgG, or anti-human IgE) was added to the plate after diluted 1:10 000 with PBS contained 0.1% Tween-20 and 1% BSA and incubated at 37 °C for 1 h. For anti-human IgE, the enzyme reactions was performed using *p*-NPP substrate solution at room temperature for 30 min and stopped by 3 mol L^{-1} sodium hydroxide, and the color that developed was measured by absorbance at 405 nm. For the anti-mouse IgG and anti-rabbit IgG, the enzyme reaction was performed using TMB substrate solution at 37 °C for 10 min, stopped by 2 mol L^{-1} sulfuric acid, and measured by absorbance at 450 nm.

Simulated Gastrointestinal Digestion. Simulated gastrointestinal digestion of purified PVs was performed according to a modified method by Majumder et al.[25] PVs were dispersed in 0.15 M KCl−HCl (pH 2.0) buffer at a concentration of 2 mg mL^{-1} and first digested with pepsin (E/S, 2%, w/w) at 37 °C for 1.5 h, and then the pH of the digest was raised to 7.4. Half of the pepsin digest was removed and heated in a 95 °C water bath for 15 min. The rest of the sample was further digested by trypsin (E/S, 2%, w/w) at 37 °C for 3 h and then was inactivated by heating the sample at 95 °C for 15 min. The digested samples were stored at −20 °C for further analysis.

Separation of Digested PV Isotypes by HPLC. The digested PV isotypes were applied to a Waters XBridge C_{18} column (5 μm, 3.0 × 250 mm, Waters Corporation, Milford, MA) coupled with a guard column (40 × 10 mm, Waters Corporation, Milford, MA) attached with a Waters 600 HPLC system for further separation. Instrumental control and data collection were carried out by Empower, version 2. Samples were automatically injected by a Waters 2707 autosampler at a volume of

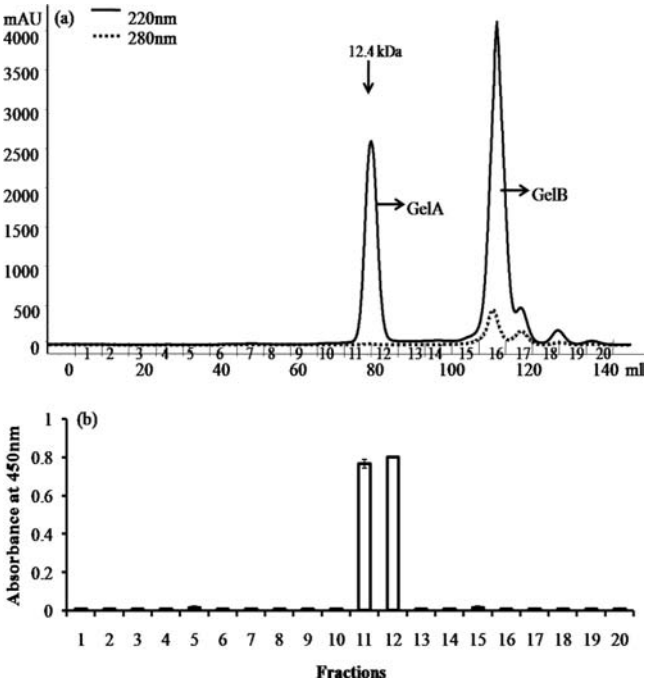

Figure 1. (a) Fractionation of PV, extracted from grass carp white muscle, by gel filtration chromatography on a Superdex 75 (1.6 × 60 cm) column. (b) IgG-binding capacity of fractions with mouse anti-frog PV monoclonal antibody (PARV-19). Data were expressed as the mean ± SD (n = 3).

25 μL. The column was eluted at a flow rate of 0.5 mL/min using a gradient consisting of solvent A (HPLC-grade water containing 0.1% TFA) and solvent B (70% acetonitrile containing 0.1% TFA) from 0 to 50% B within 5 min, to 50% B within 30 min, to 0% B over 5 min, and maintained for 10 min for the next injection. Fractions were collected every 1 min from 21 to 41 min, and elution was monitored by a Waters 2998 photodiode array at 220 nm. The fractions were concentrated by a vacuum rotary evaporator at 35 °C and then freeze-dried for further analysis.

Data Analysis. All sample determinations were performed in triplicate, and the results were expressed as the mean value ± standard deviation (SD). Analysis of variance (ANOVA) with Tukey's post-hoc test was used to determine statistical differences, and differences were considered significant with a p value of <0.05.

RESULTS AND DISCUSSION

Purification of PV Isotypes from Grass Carp White Muscle. PV extracted from grass carp was first purified by gel filtration chromatography, as shown in Figure 1a, where two major fractions, GelA and GelB, were collected. The GelA fraction displayed high binding capacity to PARV-19, whereas no binding activity was found in fraction GelB, indicating fraction GelA containing PV (Figure 1b). Furthermore, fraction GelA did not have absorbance at 280 nm because of the lack of Trp and Tyr residues in PV.[15,17] The retention time of fraction GelA was close to the protein standard, indicating that the molecular weight of fraction GelA was close to the molecular weight of the standard protein (12.4 kDa).

Fraction GelA was further purified by reverse-phase (RP)-HPLC. Three distinct peaks were collected and denoted as PVI, PVII, and PVIII (Figure 2a). PV samples were subjected to SDS–PAGE analysis (Figure 2b). GelA fraction revealed two bands, similar to the band of PVI, whereas PVII and III contain one band at a molecular weight of ~10 kDa. The presence of a lower molecular weight band in PVI was probably due to cross-contamination of PVII. Different isotypes of PV was previously reported in several fish species.[16,26] Hamada et al. purified two isotypes by reverse-phase HPLC from Janpanese flounder and Japanese eel but did not detect isotypes in red sea bream and skipjack.[27] Liu et al. purified three PV isotypes by DEAE-Sepharose chromatography and Superdex 75 gel filtration chromatography from silver carp with the molecular weights of 12, 11, and 14, respectively.[19]

Characterization of PV Isotypes. As shown in Figure 3, the molecular weights of PVI, PVII, and PVIII were 11.968, 11.430, and 11.516 kDa, respectively, which were in the range of PV molecular weight (10–12 kDa) as previously reported.[3] However, a 14 kDa isotype was recently reported in sea bream[17] and red sea bream.[28] The molecular weight of PVI was close to that of a PV isotype (11.954 kDa) in red stingray.[15] There are three small peaks that appeared in the MS spectrum of PVI as inserted, corresponding to the smaller band observed in Figure 2b of PVI, with the molecular weights of 11 430, 11 462, and 11 479 Da, respectively. The 11 430 kDa peak was the contamination of PV II, whereas the peak of 11 462 showed the same/similar molecular weight to isotypes of Atlantic cod, with the molecular weight of 11 462 Da[13] or 11 459 Da.[29] The peak

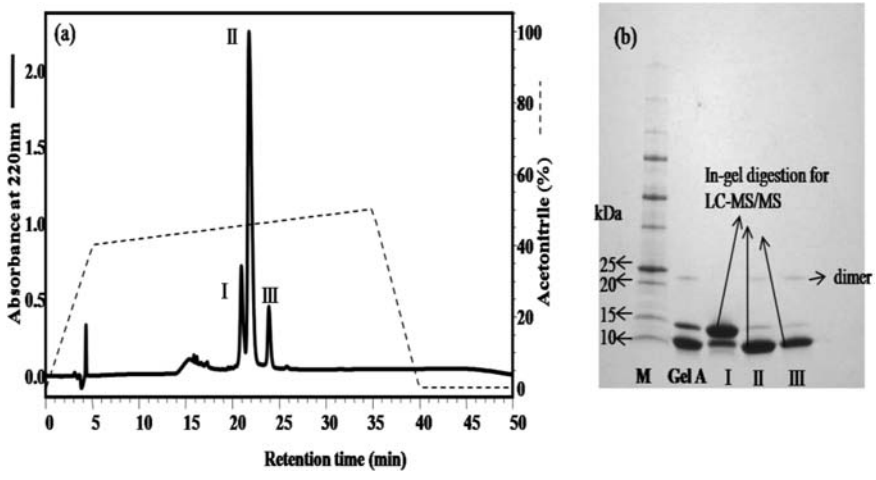

Figure 2. (a) Reverse-phase chromatogram of the PV GelA fraction obtained from gel filtration chromatography. (b) SDS–PAGE analysis of fractions. M, protein markers; GelA, a fraction prepared from Figure 1; PVI, PVII, and PVIII, fractions prepared from panel a.

dx.doi.org/10.1021/jf500817f | J. Agric. Food Chem. 2014, 62, 6212–6218

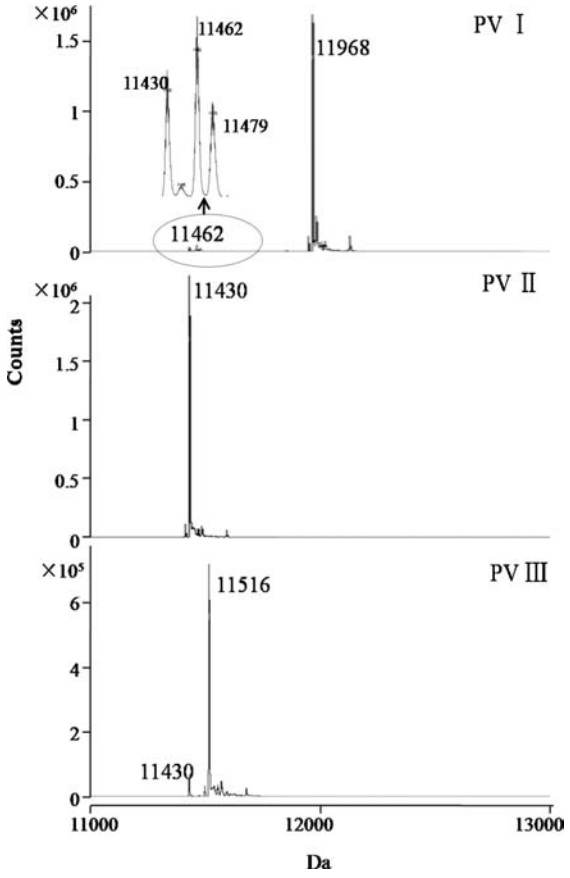

Figure 3. MALDI-TOF-MS analysis of molecular weights of PV isotypes.

of 11 479 Da showed a similar molecular weight to PV (11 487 Da) of carp.[9]

To characterize the sequences, three bands of PVI, PVII, and PVIII in Figure 2b were digested by trypsin and subjected to LC−MS/MS. As shown in Table 1, PVI showed 74% sequence coverage with the PV isoform 4a from *Danio rerio* (gil28194094), supporting that PVI was an isotype of PV. Perez-Gordo et al.[30] reported a 15 amino acid residue (DGKIGVDEFGAMIKA) of PV from Atlantic cod, which was considered as a major epitope of the protein. A 15 amino acid residue (DGKIGIDEFEALVHE) of PVI displayed 60% similarity with the major epitope of PV from Atlantic cod; it is to be determined if this epitope in PVI is the major epitope. PVII and PVIII showed 46% sequence coverage with PV isotypes from *Hypophthalmichthys molitrix* (gil209902357 and gil209902355). In addition, PVII and PVIII shared two epitopes, 51-65 (IDQDKSGFIEEDELK) and 89-103 (AG DSDGDGKIGVDEF). The 51-65 amino acid epitope was also reported in the PV isotype of crimson sea bream, Janpanese eel, carp, Atlantic salmon, cod, and horse mackerel.[17] The 89-103 amino acid epitope was identified in the PV isotype of cod, horse mackerel, and skipjack.[17] Therefore, these two epitopes are likely to be antigenic epitopes of PV.

IgG- and IgE-Binding Capacities of PV Isotypes. Absorbance of the immunosorbent assay was used to reflect the binding capacity of IgG or IgE. IgG-binding capacities with anti-frog and anti-grass carp PV antibodies increased dose-dependently at increasing concentrations of PVI, PVII, and PVIII, further supporting that the purified proteins are PV isotypes. PVI showed the highest IgG-binding capacity with anti-frog antibody (Figure 4a), whereas PVII displayed the highest IgG-binding capacity with anti-grass carp antibody (Figure 4b). The difference in IgG-binding capacities of fish PV with anti-frog PV antibody and anti-grass carp antibody was due to the difference in PV amino acid sequences between frog and grass carp PVs. Lee et al. also demonstrated that antibodies raised against fish and frog PVs displayed varying specificity for different fish species.[31]

The IgE-binding capacity of PV samples with sera from four allergic patients also increased dose-dependently with an increasing concentration of PVI, PVII, and PVIII, as shown in panels c−f of Figure 4. The PV isotypes were recognized as allergens by the sera of all four fish allergic patients. Three isotypes purified from pilchard PV and two isotypes from anchovy, yellowtail, and bake purified PVs were also reported to have an IgE-binding capacity with different sera of fish allergic patients.[32] When the coated protein concentration was 0.1 or 10 μg mL^{-1}, the IgE-binding capacity of the three isotypes showed no significant difference. At the coated protein concentration of 1 μg mL^{-1}, PVII showed the highest IgE-binding capacity, whereas PVIII showed the lowest IgE-binding capacity. Kuehn et al.[33] pointed out that, besides the difference in PV IgE epitopes in different fish species, variability in the PV content was likely to contribute to the variation in clinical reactivity to different fish species. In this study, PVII showed the highest content in grass carp PV (Figure 2a); therefore, PVII is the dominant allergen in PV isotypes. Cai et al. also reported that PVII from red stingray is more allergenic than PVI.[15] Guo et al. reported that the 14 kDa PV isotype showed lower antibody binding capacity than the 12 kDa PV isotype from crimson sea bream.[17]

Table 1. LC−MS/MS Analysis of the Amino Acid Identify of PV Isotypes

protein name	number	possible amino acid sequence[a]	sequence coverage (%)
PVI	1	MAMKNILKDD DIKKALDQFK AADSFDHKKF FDVVGLKALS ADNVKLVFKA	74
	51	LDVDASGFIE EEELKFVLKG FSADGRDLTD KETKAFLAAA DKDGDGKIGI	
	101	DEFEALVHE	
PVII	1	MAFAGILNDA DIAAALEACKAADSFNHKAF FAKVGLSAKS GDDVKKAFAI	46
	51	IDQDKSGFIE EDELKLFLQN FKAGARALTD AETKIFLKAG DSDGDGKIGV	
	101	DEFAALVKA	
PVIII	1	MAFAGILNEA DVTAALQACQ AADSFKYKDF FAKVGLSAKS PDDIKKAFAV	46
	51	IDQDKSGFIE EDELKLFLQD FSAGARALTD AETKAFLKAG DSDGDGKIGV	
	101	DEFAVLVKA	

[a]PVI was matched to PV isoform 4a from *D. rerio* (gil28194094), and PVII and PVIII were matched to PV isotypes from *H. molitrix* (gil209902357 and gil209902355).

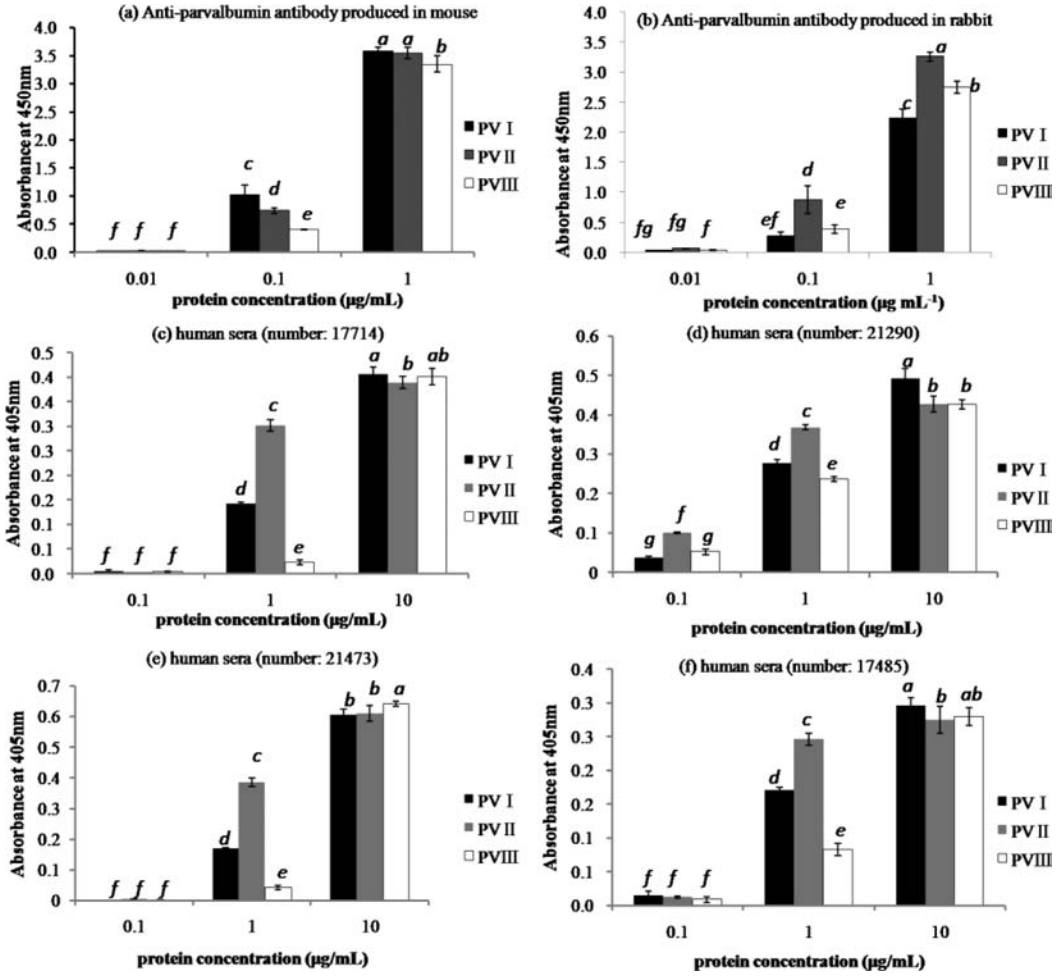

Figure 4. Analysis of IgG- and IgE-binding capacities of fractions PVI, PVII, and PVIII by ELISA. Data are the mean ± SD ($n = 3$). Means with different letters in the same panel are significantly different ($p < 0.05$): (a) IgG-binding capacity with anti-frog PV antibody produced in mouse, (b) IgG-binding capacity with anti-grass carp PV antibody produced in rabbit, and (c–f) IgE-binding capacity with four codfish allergic human sera.

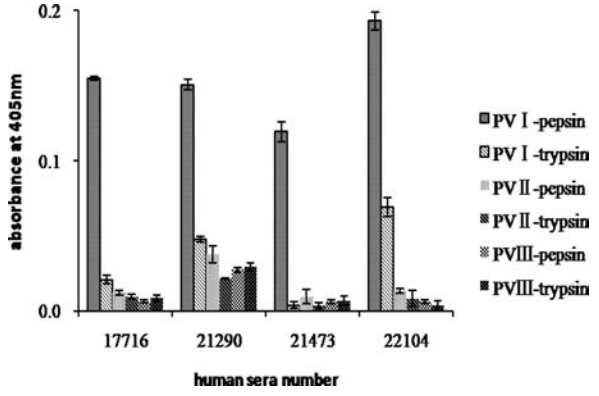

Figure 5. IgE-binding capacity of digested PVs by indirect ELISA. The concentration of samples coated on the plate was 10 μg mL^{-1}. Data are the mean ± SD ($n = 3$).

Simulated Digestibility of the Three PV Isotypes. Normally, primary food allergens present strong resistance to gastrointestinal degradation and are therefore believed to sensitize via the gut,[34] and an incomplete digestion of dietary protein may cause an inappropriate immune response in the gut.[35] Therefore, digestibility of allergens is one major factor that might affect the allergenic potential of an allergen. The effect of pepsin and trypsin digestion on IgE-binding capacity is shown in Figure 5. In comparison to the IgE-binding capacity of PV isotypes in panels c–f of Figure 4, it was apparent that digestion significantly decreased the IgE-binding capacity of the digested PV isotypes. Untersmayr et al. also reported that peptic digestion of codfish PV could significantly reduce allergenic potency probably because of the generation of small fragments.[36] The absorbance of pepsin-digested PVI was higher than 0.1, while the absorbance of pepsin-digested PVII and PVIII was less than 0.05; although the IgE-binding capacity of PVI was further decreased by trypsin digestion, the IgE-binding capacity of trypsin-digested PVI was still higher than those of pepsin-digested PVII and PVIII. Our results implied that PVI was resistant to digestion or there are IgE-binding sites after pepsin and trypsin digestions. A number of food allergens were also claimed to be resistant to simulating gastrointestinal digestion.[37−39]

To determine if there was residual PV or there were new peptides generated from digestion that could contribute to IgE-binding capacity of peptic and tryptic digests, these two digests were further fractionated by PR-HPLC (Figure 6a). Peptic digestion showed residual PVI in the digest, but most of the residual PVI can be further digested by trypsin. For the peptic digestion, 20 fractions were collected from 21 to 41 min, and each fraction was subjected to an IgE-binding capacity assay. As shown in Figure 6b, the two fractions collected from 39 to 41 min showed the highest IgE-binding capacity, suggesting that the undigested

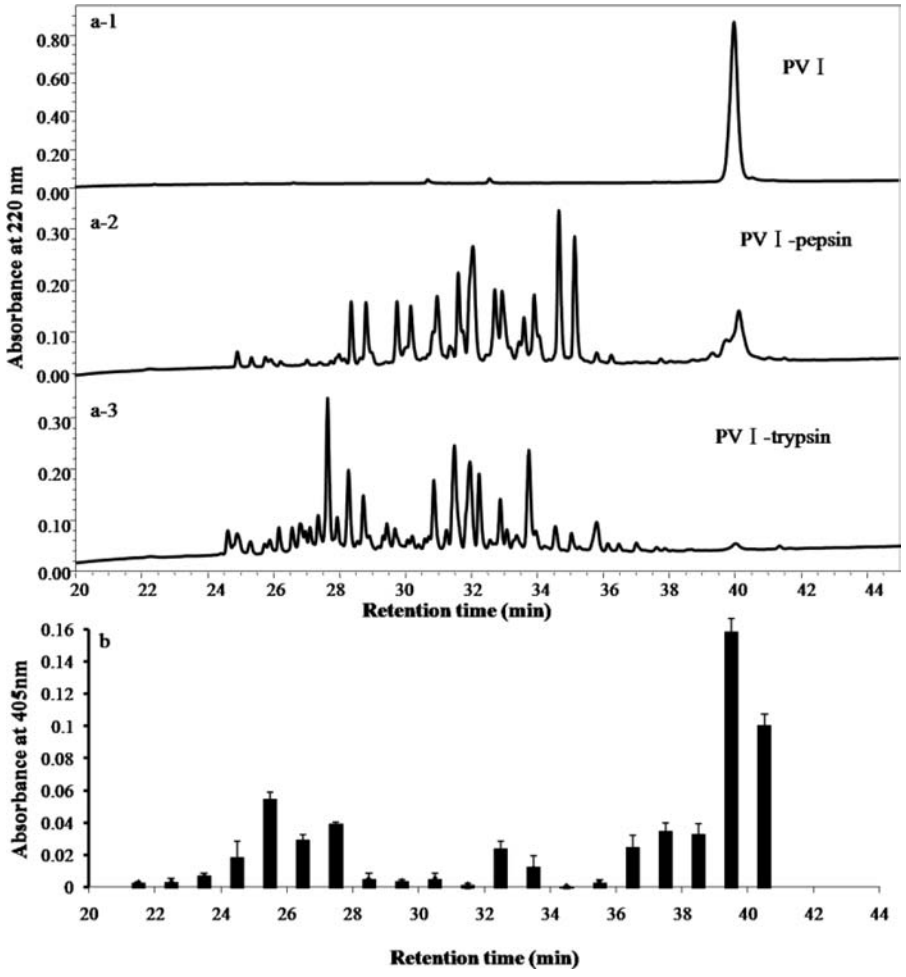

Figure 6. (a) Reverse-phase chromatogram of PVI and its pepsin and trypsin digests. (b) IgE-binding capacity of each fractions (collected every 1 min) from 21 to 41 min. Data were expressed as mean ± SD (n = 3).

PVI in the peptic digest was responsible for its IgE-binding capacity. RP-HPLC analysis was also perform on digested PVII and PVIII (data not shown), and almost all of the PVII and PVIII were digested by pepsin after 1.5 h. In summary, three PV isotypes were first purified from grass carp and identified by LC−MS/MS. These isotypes were different in molecular weight, amino acid sequence, IgG-binding capacity, IgE-binding capacity, and digestibility. PVII may be the main allergen but was liable to gastrointestinal enzymes, as well as PVIII; however, PVI was resistant to pepsin digestion.

AUTHOR INFORMATION

Corresponding Authors

*Telephone/Fax: +86-10-62737385. E-mail: luoyongkang@cau.edu.cn.

*Telephone: 780-492-6885. Fax: 780-492-4365. E-mail: jwu3@ualberta.ca.

Funding

The work was supported by the Natural Sciences and Engineering Research Council of Canada (NSERC), the China Scholarship Council, and the earmarked fund for the China Agriculture Research System (CARS-46).

Notes

The authors declare no competing financial interest.

REFERENCES

(1) Cho, J. H.; Kim, I. H. Fish meal—Nutritive value. *J. Anim. Physiol. Anim. Nutr.* **2011**, *95*, 685−692.

(2) Beveridge, M. C. M.; Thilsted, S. H.; Phillips, M. J.; Metian, M.; Troell, M.; Hall, S. J. Meeting the food and nutrition needs of the poor: The role of fish and the opportunities and challenges emerging from the rise of aquaculturea. *J. Fish Biol.* **2013**, *83*, 1067−1084.

(3) Sharp, M.; Lopata, A. Fish allergy: In review. *Clin. Rev. Allergy Immunol.* **2013**, 1−14.

(4) Dahlman-Höglund, A.; Renström, A.; Larsson, P. H.; Elsayed, S.; Andersson, E. Salmon allergen exposure, occupational asthma, and respiratory symptoms among salmon processing workers. *Am. J. Ind. Med.* **2012**, *55*, 624−630.

(5) Lopata, A.; Jeebhay, M. Airborne seafood allergens as a cause of occupational allergy and asthma. *Curr. Allergy Asthma Rep.* **2013**, *13*, 288−297.

(6) Helbling, A.; Haydel, R., Jr.; McCants, M. L.; Musmand, J. J.; El-Dahr, J.; Lehrer, S. B. Fish allergy: Is cross-reactivity among fish species relevant? Double-blind placebo-controlled food challenge studies of fish allergic adults. *Ann. Allergy Asthma Immunol.* **1999**, *86*, 517−523.

(7) Elsayed, S.; Aas, K. Isolation of purified allergens (cod) by isoelectric focusing. *Int. Arch. Allergy Appl. Immunol.* **1971**, *40*, 428−438.

(8) Arif, S. H.; Jabeen, M.; Hasnain, A.-U. Biochemical characterization and thermostable capacity of parvalbumins: The major fish-food allergens. *J. Food Biochem.* **2007**, *31*, 121−137.

(9) Bugajska-Schretter, A.; Grote, M.; Vangelista, L.; Valent, P.; Sperr, W. R.; Rumpold, H.; Pastore, A.; Reichelt, R.; Valenta, R.; Spitzauer, S. Purification, biochemical, and immunological characterisation of a major

food allergen: Different immunoglobulin E recognition of the apo- and calcium-bound forms of carp parvalbumin. *Gut* **2000**, *46*, 661−669.
(10) Perez-Gordo, M.; Cuesta-Herranz, J.; Maroto, A. S.; Cases, B.; Ibáñez, M. D.; Vivanco, F.; Pastor-Vargas, C. Identification of sole parvalbumin as a major allergen: Study of cross-reactivity between parvalbumins in a Spanish fish-allergic population. *Cli. Exp. Allergy* **2011**, *41*, 750−758.
(11) Moncrief, N. D.; Kretsinger, R. H.; Goodman, M. Evolution of EF-hand calcium-modulated proteins. I. Relationships based on amino acid sequences. *J. Mol. Evol.* **1990**, *30*, 522−562.
(12) Kuehn, A.; Hilger, C.; Graf, T.; Hentges, F. Protein- and DNA-based assays as complimentary methods for tracing of fish allergens in food. *Allergologie* **2012**, *35*, 343−350.
(13) Ma, Y.; Griesmeier, U.; Susani, M.; Radauer, C.; Briza, P.; Erler, A.; Bublin, M.; Alessandri, S.; Himly, M.; Vàzquez-Cortés, S.; Rincon de Arellano, I. R.; Vassilopoulou, E.; Saxoni-Papageorgiou, P.; Knulst, A. C.; Fernández-Rivas, M.; Hoffmann-Sommergruber, K.; Breiteneder, H. Comparison of natural and recombinant forms of the major fish allergen parvalbumin from cod and carp. *Mol. Nutr. Food Res.* **2008**, *52*, S196−S207.
(14) Goodman, M.; Pechére, J.-F. The evolution of muscular parvalbumins investigated by the maximum parsimony method. *J. Mol. Evol.* **1977**, *9*, 131−158.
(15) Cai, Q. F.; Liu, G. M.; Li, T.; Hara, K.; Wang, X. C.; Su, W. J.; Cao, M. J. Purification and characterization of parvalbumins, the major allergens in red stingray (*Dasyatis akajei*). *J. Agric. Food Chem.* **2010**, *58*, 12964−12969.
(16) Van Do, T.; Hordvik, I.; Endresen, C.; Elsayed, S. Characterization of parvalbumin, the major allergen in Alaska pollack, and comparison with codfish Allergen M. *Mol. Immunol.* **2005**, *42*, 345−353.
(17) Guo, F. F.; Kubota, H.; Shiomi, K. Purification, immunological properties and molecular cloning of two allergenic parvalbumins from the crimson sea bream, *Evynnis japonica*. *Food Chem.* **2012**, *132*, 835−840.
(18) Fishery Bureau of Ministry of Agriculture of the People's Republic of China. *China Fishery Statistical Yearbook*; China Agriculture Press: Beijing, China, 2013 (in Chinese).
(19) Liu, G. M.; Wang, N.; Cai, Q. F.; Li, T.; Sun, L. C.; Sua, W. J.; Cao, M. J. Purification and characterization of parvalbumins from silver carp (*Hypophthalmichthys molitrix*). *J. Sci. Food Agric.* **2010**, *90*, 1034−1040.
(20) Laemmli, U. K. Cleavage of structural proteins during the assembly of the head of bacteriophage T4. *Nature* **1970**, *227*, 680−685.
(21) Dai, Y.; Whittal, R. M.; Li, L. Two-layer sample preparation: A method for MALDI−MS analysis of complex peptide and protein mixtures. *Anal. Chem.* **1999**, *71*, 1087−1091.
(22) Li, S.; Offengenden, M.; Fentabil, M.; Gänzle, M. G.; Wu, J. Effect of egg white fermentation with lactobacilli on IgE binding ability of egg white proteins. *Food Res. Int.* **2013**, *52*, 359−366.
(23) Offengenden, M.; Fentabil, M.; Wu, J. N-glycosylation of ovomucin from hen egg white. *Glycoconjugate J.* **2011**, *28*, 113−123.
(24) Tong, P.; Gao, J.; Chen, H.; Li, X.; Zhang, Y.; Jian, S.; Wichers, H.; Wu, Z.; Yang, A.; Liu, F. Effect of heat treatment on the potential allergenicity and conformational structure of egg allergen ovotransferrin. *Food Chem.* **2012**, *131*, 603−610.
(25) Majumder, K.; Panahi, S.; Kaufman, S.; Wu, J. Fried egg digest decreases blood pressure in spontaneous hypertensive rats. *J. Funct. Foods* **2013**, *5*, 187−194.
(26) Gajewski, K. G.; Hsieh, Y.-H. P. Monoclonal antibody specific to a major fish allergen: Parvalbumin. *J. Food Prot.* **2009**, *72*, 818−825.
(27) Hamada, Y.; Tanaka, H.; Sato, A.; Ishizaki, S.; Nagashima, Y.; Shiomi, K. Expression and evaluation of IgE-binding capacity of recombinant Pacific mackerel parvalbumin. *Allergol. Int.* **2004**, *53*, 271−278.
(28) Kobayashi, A.; Tanaka, H.; Hamada, Y.; Ishizaki, S.; Nagashima, Y.; Shiomi, K. Comparison of allergenicity and allergens between fish white and dark muscles. *Allergy* **2006**, *61*, 357−363.
(29) De Jongh, H. H. J.; Robles, C. L.; Timmerman, E.; Nordlee, J. A.; Lee, P. W.; Baumert, J. L.; Hamilton, R. G.; Taylor, S. L.; Koppelman, S. J. Digestibility and IgE-binding of glycosylated codfish parvalbumin. *Biomed. Res. Int.* **2013**, *2013*, 756789.
(30) Perez-Gordo, M.; Pastor-Vargas, C.; Lin, J.; Bardina, L.; Cases, B.; Ibáñez, M. D.; Vivanco, F.; Cuesta-Herranz, J.; Sampson, H. A. Epitope mapping of the major allergen from Atlantic cod in Spanish population reveals different IgE-binding patterns. *Mol. Nutr. Food Res.* **2013**, *57*, 1283−1290.
(31) Lee, P.-W.; Nordlee, J. A.; Koppelman, S. J.; Baumert, J. L.; Taylor, S. L. Evaluation and comparison of the species-specificity of 3 antiparvalbumin IgG antibodies. *J. Agric. Food Chem.* **2011**, *59*, 12309−12316.
(32) Beale, J. E.; Jeebhay, M. F.; Lopata, A. L. Characterisation of purified parvalbumin from five fish species and nucleotide sequencing of this major allergen from Pacific pilchard, *Sardinops sagax*. *Mol. Immunol.* **2009**, *46*, 2985−2993.
(33) Kuehn, A.; Scheuermann, T.; Hilger, C.; Hentges, F. Important variations in parvalbumin content in common fish species: A factor possibly contributing to variable allergenicity. *Int. Arch. Allergy Immunol.* **2010**, *153*, 359−366.
(34) Schulten, V.; Lauer, I.; Scheurer, S.; Thalhammer, T.; Bohle, B. A food matrix reduces digestion and absorption of food allergens in vivo. *Mol. Nutr. Food Res.* **2011**, *55*, 1484−1491.
(35) Dupont, D.; Mandalari, G.; Molle, D.; Jardin, J.; Léonil, J.; Faulks, R. M.; Wickham, M. S. J.; Mills, E. N. C.; Mackie, A. R. Comparative resistance of food proteins to adult and infant in vitro digestion models. *Mol. Nutr. Food Res.* **2010**, *54*, 767−780.
(36) Untersmayr, E.; Poulsen, L. K.; Platzer, M. H.; Pedersen, M. H.; Boltz-Nitulescu, G.; Skov, P. S.; Jensen-Jarolim, E. The effects of gastric digestion on codfish allergenicity. *J. Allergy Clin. Immunol.* **2005**, *115*, 377−382.
(37) Chicón, R.; Belloque, J.; Alonso, E.; López-Fandiño, R. Antibody binding and functional properties of whey protein hydrolysates obtained under high pressure. *Food Hydrocolloids* **2009**, *23*, 593−599.
(38) Fujita, S.; Shimizu, Y.; Kishimura, H.; Watanabe, K.; Hara, A.; Saeki, H. In vitro digestion of major allergen in salmon roe and its peptide portion with proteolytic resistance. *Food Chem.* **2012**, *130*, 644−650.
(39) Moreno, F. J. Gastrointestinal digestion of food allergens: Effect on their allergenicity. *Biomed. Pharmacother.* **2007**, *61*, 50−60.

JOURNAL OF AGRICULTURAL AND FOOD CHEMISTRY

Article

pubs.acs.org/JAFC

Characterization of Phenolic Compounds in Brazilian Pepper (*Schinus terebinthifolius* Raddi) Exocarp

Michelle M. Feuereisen,[†] Julia Hoppe,[†] Benno F. Zimmermann,[†,§] Fabian Weber,[†] Nadine Schulze-Kaysers,[†] and Andreas Schieber*[,†]

[†]Department of Nutritional and Food Sciences – Chair of Food Technology and Food Biotechnology, University of Bonn, Römerstrasse 164, D-53117 Bonn, Germany

[§]Institut Prof. Dr. Georg Kurz GmbH, Eupener Strasse 161, D-50933 Köln, Germany

Supporting Information

ABSTRACT: The objective of this study was to characterize the phenolic composition of Brazilian pepper (*Schinus terebinthifolius* Raddi) exocarp extract. Using UHPLC-DAD-MS/MS analysis, four anthocyanins, three biflavonoids, gallic acid, and two types of hydrolyzable tannins (galloyl glucoses, galloyl shikimic acids) were tentatively identified. The structure of the so far unknown 7-*O*-methylpelargonidin 3-*O*-*β*-D-galactopyranoside was elucidated by 2D NMR. Within the group of gallotannins, galloyl shikimic acids with uncommon degrees of galloylation (tetra- to hexagalloyl shikimic acids) were detected. Among the biflavonoids, I3′,II8-biapigenin (amentoflavone), I6,II8-biapigenin (agathisflavone), and II-2,3-dihydro-I3′,II8-biapigenin were identified, which have already been described for Anacardiaceae. From the results of the present study together with previous findings on the phenolic profile of other Anacardiaceae plants, it is concluded that 7-methoxylated flavonoids are a chemotaxonomic trait frequently found in this family.

KEYWORDS: *Anacardiaceae, biflavones, chemotaxonomy, galloyl glucose, galloyl shikimic acid, methylated anthocyanidins, NMR, Schinus terebinthifolius, tandem mass spectrometry, UHPLC*

INTRODUCTION

The Brazilian pepper tree (*Schinus terebinthifolius* Raddi) belongs to the Anacardiaceae family, which also encompasses economically relevant species such as mango (*Mangifera indica* L.), pistachio (*Pistacia vera* L.), and cashew nut (*Anacardium occidentale* L.) as well as plants of regional importance such as jocote (*Spondias purpurea* L.) and marula (*Sclerocarya birrea* (A. Rich) Hochst.).[1−4] The fruits of *S. terebinthifolius* are commonly used as a spice, either alone or in mixtures with pepper. *S. terebinthifolius*, which is indigenous to Brazil, has meanwhile spread to other countries and is even classified as an invasive species in Florida.[5,6] Its success in foreign habitats and the aggressive expansion of *S. terebinthifolius* suggest that this plant harbors phytochemicals which protect it from biotic stress. There is ample evidence for the presence of allelopathic antimicrobial compounds in various plant parts. Among these, phenolics presumably contribute to the biological activity observed.[6−8]

Although some information is available on the chemical composition of different parts of *S. terebinthifolius*,[9] detailed studies on the nature of phenolic compounds are scarce. Our previous investigations into the phytochemical profile of mango and jocote have revealed the presence of a broad spectrum of various types of phenolic compounds, such as phenolic acids, hydrolyzable tannins, and anthocyanins.[10−12] In mango peels, a novel anthocyanin, namely, 7-*O*-methylcyanidin 3-*O*-*β*-D-galactopyranoside, has been found.[11] Because of the chemotaxonomic relationship between *Mangifera indica*, *Spondias purpurea*, and *S. terebinthifolius*, we hypothesized that Brazilian pepper contains phenolic compounds of similar composition. Therefore, the objective of this work was to characterize the phenolic composition of the exocarp from *S. terebinthifolius* by UHPLC-DAD-MS/MS. The structure of a so far unknown anthocyanin was elucidated by NMR spectroscopy.

MATERIALS AND METHODS

Chemicals. All solvents and reagents were of analytical grade and were purchased from Roth (Karlsruhe, Germany), Sigma-Aldrich (Steinheim, Germany), and VWR (Darmstadt, Germany). Technical grade ethanol was obtained from Hofmann (Düsseldorf, Germany). Unless noted otherwise, deionized water was used throughout. All solvents used as UHPLC-MS eluents were of LC-MS grade and obtained from the following suppliers: Optigrade water was from Promochem (Wesel, Germany), acetonitrile was from Mallinckrodt Baker (Deventer, The Netherlands), and formic acid was from Fluka/Sigma-Aldrich. Amentoflavone (I3′,II8-biapigenin) was purchased from Extrasynthèse (Lyon, France); pelargonidin 3-*O*-glucoside and cyanidin 3-*O*-glucoside were from PhytoLab (Vestenbergsgreuth, Germany).

Sample Preparation and Extraction of Phenolic Compounds. Air-dried fruits from *S. terebinthifolius* Raddi were obtained from Fuchs (Dissen, Germany). Most of the phenolic compounds are located in the outer layer (exocarp), especially the red pigments, which have been characterized here for the first time. Thus, the extraction of phenolic compounds is more efficient and selective when the exocarp is extracted separately. Therefore, the exocarp was manually separated from the rest of the fruit and ground using a model S100 ball mill

Received: February 28, 2014
Revised: May 27, 2014
Accepted: May 31, 2014
Published: May 31, 2014

ACS Publications © 2014 American Chemical Society

dx.doi.org/10.1021/jf500977d | J. Agric. Food Chem. 2014, 62, 6219−6226

(Retsch, Haan, Germany). Accelerated solvent extraction (ASE) was performed with a Dionex ASE 350 (Thermo Scientific, Idstein, Germany) system. The powdered exocarp (1.5 g) was mixed with diatomaceous earth (Thermo Scientific) and filled into 10 mL Dionex (ASE 350) stainless steel cells. For extraction, the cell was filled with extraction solvent (EtOH/water/acetic acid, 70:25:5, v/v/v), pressurized (1500 psi), and heated (to 160 °C). Then, the cell was rinsed with fresh extraction solvent (150% of the cell volume) and purged with a flow of nitrogen (100 psi, 60 s).

Purification of Anthocyanin Ac4. Because MS analysis was not sufficient for structure elucidation of anthocyanin Ac4, purification by SPE and preparative HPLC followed by structure elucidation by NMR spectroscopy was necessary. For this purpose, the extract obtained from ASE was evaporated in vacuo at 30 °C in a rotary evaporator (Büchi, Essen, Germany). After dilution with water (1:3, v/v), liquid−liquid extraction with ethyl acetate (1:1, v/v) was performed, followed by rotary evaporation of the aqueous phase. Subsequently, this fraction was purified[13] using a C18 (ec) SPE column (Macherey-Nagel, Düren, Germany). The solvents were removed from the eluate by evaporation and freeze-drying prior to storage in a vacuum desiccator.

For preparative HPLC, the lyophilisate was reconstituted (10 mg/mL) in acetonitrile/water/formic acid (18:80:2, v/v/v) and filtered through 0.2 μm Chromafil RC-20/15 MS filters (Macherey-Nagel).

The anthocyanins were separated on a semipreparative HPLC from Knauer (Berlin, Germany) consisting of a pump 1050, an autosampler 3950, a manager 5050, and a UV detector 2550. Using a reversed phase C18 column (Vertex, 250 × 16 mm Eurosphere II 100-5 C18, Knauer) with a C18 guard column (Vertex, 30 × 16 mm Eurospher 100-5 C18, Knauer), the compounds were eluted with 2.9% (v/v) formic acid in water (solvent A) and 2.9% (v/v) formic acid in acetonitrile (solvent B) at a constant flow rate of 6.0 mL/min. An isocratic separation with 18% of solvent B was performed for 20 min followed by conditioning and equilibration (0 min, 18% B; 4 min, 100% B; 8 min, 100% B; 10 min, 18% B; 20 min, 18% B). The injection volume was 500 μL. The peak recognition mode (500 nm, start/stop 70/100 AU) was used for collection of the anthocyanin fractions with a Foxy R1 fraction collector (Teledyne ISCO, Lincoln, NE, USA). During removal of the organic solvent and the following lyophilization, the fraction containing peak Ac4 was protected from light and temperatures above 30 °C. The lyophilisate was dissolved in deuterated methanol acidified with d_1-TFA (1%) for analysis by NMR spectroscopy. All samples were stored at −80 °C until further use.

UHPLC-DAD-MS/MS Analysis of Phenolic Compounds. For the analysis of phenolic compounds, an Acquity UPLC system (Waters, Milford, MA, USA) consisting of a binary pump (BSM), an autosampler (SM) cooled at 10 °C, a column oven (CM) set at 40 °C, a diode array detector (PDA) scanning from 190 to 500 nm, and an Acquity TQD triple-quadrupole mass spectrometer with an electrospray interface was used.

Anthocyanins were separated using an Acquity HSS-T3 RP18 column (150 mm × 2.1 mm; 1.8 μm particle size) from Waters with a guard column (5 mm × 2.1 mm). Eluent A was water/1% formic acid, and eluent B was acetonitrile/0.1% formic acid. The gradient program was as follows: 0 min, 0% B; 0.2 min, 5% B; 12 min, 16.9% B; 13 min, 98% B; 15 min, 98% B; 16 min, 5% B; 18 min, 5% B. The flow rate was 0.4 mL/min. The mass spectrometer was tuned using a solution of cyanidin 3-*O*-glucoside. The following parameters were used: capillary voltage, 1.6 kV; cone voltage, 32 V; extractor voltage, 3.0 V; RF voltage, 1.3 V; source temperature, 150 °C; desolvation temperature, 450 °C; cone gas (nitrogen) flow, 50 L/h; desolvation gas (nitrogen) flow, 800 L/h. The collision gas (argon) flow used in MS/MS experiments was 0.3 mL/min.

For the separation of nonanthocyanin phenolics, an Acquity BEH Shield RP18 column (150 mm × 2.1 mm, particle size = 1.7 μm) from Waters with a guard column (5 mm × 2.1 mm) was used. Eluent A was water/0.1% formic acid, and eluent B was acetonitrile/0.1% formic acid. The gradient program at a flow rate of 0.4 mL/min was as follows: 0 min, 2% B; 20 min, 60% B; 20.3 min, 100% B; 21.3 min, 100% B; 22 min, 2% B; 23.5 min, 2% B. The mass spectrometer was tuned using a solution of I3′,II8-biapigenin, resulting in the following parameters: capillary voltage, −1.0 kV; cone voltage, 25 V; extractor voltage, 2.0 V; RF voltage, 2.0 V; source temperature, 150 °C; desolvation temperature, 450 °C; cone gas (nitrogen) flow, 50 L/h; desolvation gas (nitrogen) flow, 800 L/h. Argon was used as the collision gas in tandem mass spectrometry experiments at a flow rate of 0.25 mL/min. The MS system was controlled by MassLynx 4.1 software.

The compounds were first detected using single MS scanning followed by fragment ion scans of the peaks showing major signals in the MS or UV−vis chromatogram. The UV−vis and mass spectra were used as a basis for structural assignments. To obtain more structural information about the anthocyanins, the cone voltage was set at 50 V for enhanced in-source fragmentation. The aglycones generated were then subjected to fragment ion scans. For the identification of gallic acid derivatives, fixed product ion scan (m/z 169) and neutral loss scans (152 u) were conducted. Furthermore, the cone voltage was set at 100 V, resulting in in-source fragmentation. The resulting fragment at m/z 169 was then used for fragment ion scan.

The exact masses of the glycosides and the corresponding aglycones were determined by HPLC-QToF-MS using a 6530 Accurate-Mass QToF mass spectrometer (Agilent, Waldbronn, Germany) connected to an Agilent 1260 series HPLC consisting of a degasser, binary pump, autosampler, and DAD. The mass spectrometer was used in positive ionization mode with the following settings: capillary voltage, 3000 V; fragmentor voltage, 200 V; and skimmer, 65 V. The separation was performed on a Kinetex C18 column (150 mm × 2.1 mm, 2.6 μm particle size) from Phenomenex (Aschaffenburg, Germany). The gradient program was as follows: 0 min, 0% B; 7 min, 5% B; 15 min, 15% B; 24 min, 50% B; 25 min, 100% B; 27 min, 100% B; 28 min, 0% B. Eluent A was 93% water, 5% acetonitrile, and 2% formic acid (v/v/v), and eluent B was 5% water, 93% acetonitrile, and 2% formic acid (v/v/v). The flow rate was 0.4 mL/min, and the column temperature was set to 40 °C.

NMR Spectroscopy. NMR experiments were carried out on a Bruker Avance DPX-300 spectrometer (Rheinstetten, Germany). The sample was dissolved in d_4-methanol (99.8% D, Deutero, Kastellaun, Germany) acidified with d_1-TFA (99.5% D, Sigma-Aldrich).

^{1}H NMR (300 MHz, CD_3OD wih CF_3COOD) δ 2.71 (d, H3″, 1H, J = 3.4 Hz), 3.83 (m, H6′, 1H), 3.86 (m, H5″, 1H), 3.99 (d, H4″, 1H, J = 3.4 Hz), 4.04 (m, H2″, 1H), 4.08 (s, H7a, 3H OCH_3), 5.34 (d, H1″, 1H, J = 7.5 Hz), 6.72 (s, H6, 1H), 7.09 (d, H3′ and H5′, 2H, J = 8.7 Hz), 7.25 (s, H8, 1H), 8.71 (d, H2′ and H6′, 2H, J = 8.7 Hz), 9.11 (s, H4, 1H); ^{13}C NMR (75 MHz CD_3OD wih CF_3COOD) δ 57.5 (C7a (OCH_3)), 62.4 (C6″), 70.1 (C4″), 72.4 (C2″), 74.1 (C3″), 77.8 (C5″), 92.9 (C8), 103.1 (C6), 104.3 (C1″), 114.4 (C4a), 117.9 (C3′ and C5′), 120.2 (C1′), 136.0 (C4), 136.2 (C2′ and C6′), 146.4 (C3), 157.2 (C8a), 158.4 (C5), 165.5 (C2), 167.1 (C4′), 170.7 (C7).

RESULTS AND DISCUSSION

Anthocyanins. The separation of phenolic compounds in exocarp extracts from *S. terebinthifolius* detectable at 500 nm is shown in Figure 1. Four peaks are designated Ac1, Ac2, Ac3, and Ac4, respectively.

Compound Ac1. Peak Ac1 showed a molecular ion at m/z 449 and a dominant fragment m/z 287 ($M^+ - 162$) in the MS^2 experiment, corresponding to a hexose attached to cyanidin. The standard of cyanidin 3-*O*-glucoside eluted later than Ac1. It is well-known that in reversed-phase chromatography, galactosides of a given aglycone elute prior to the glucosides.[14]

The product ion scan of the in-source fragment with m/z 287 of peak Ac1 gave rise to product ions at m/z 241, 213, 137, 121, and 109. Identical fragmentation was observed for the cyanidin reference (originating from cyanidin 3-*O*-glucoside). Because an authentic reference compound was not available, the identity of peak Ac1 was proven indirectly by analyzing extracts of mango (*Mangifera indica* L.) peels, chokeberry (*Aronia melanocarpa* [Michx.] Elliot) juice, and Cornelian cherry

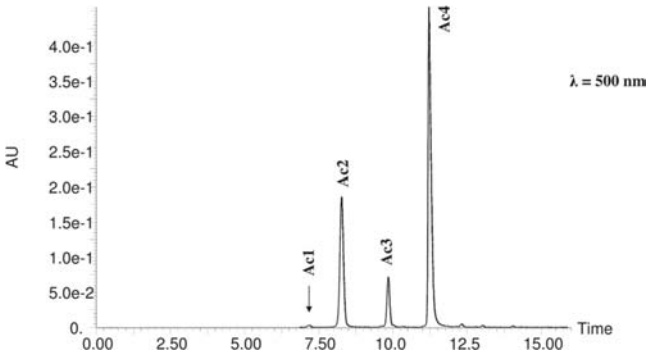

Figure 1. Separation of anthocyanins from Brazilian pepper exocarp extracts by UHPLC (detection wavelength = 500 nm). Ac1, cyanidin 3-*O*-galactoside; Ac2, pelargonidin 3-*O*-galactoside; Ac3, 7-*O*-methylcyanidin 3-*O*-galactoside; Ac4, 7-*O*-methylpelargonidin 3-*O*-galactoside.

(*Cornus mas* L.) fruit extracts. These plants have previously been demonstrated to contain cyanidin 3-*O*-galactoside.[15−18] By comparison of the retention time and the UV−vis and mass spectrometric data, compound Ac1 was identified as cyanidin 3-*O*-galactoside (Figure 2a).

Compound Ac2. Peak Ac2 showed a molecular ion at m/z 433 (M^+) and a dominant fragment at m/z 271 ($M^+ - 162$) in the MS^2 experiment, corresponding to a hexose attached to the pelargonidin aglycone. The standard of pelargonidin 3-*O*-glucoside eluted later than Ac2. As mentioned above, in reversed-phase chromatography, galactosides of a given aglycone elute prior to the glucosides.[14]

The product ion scan of the in-source fragment with m/z 271 of peak Ac2 gave rise to product ions at m/z 197, 169, 141, and 121, which matched the fragmentation of the pelargonidin 3-*O*-glucoside reference. Corresponding data have previously been reported in multistage mass spectrometric studies on black carrot anthocyanins.[15] A peak with the same retention time, UV−vis spectrum, and fragmentation pattern has been found in the above-mentioned extract from Cornelian cherry. Seeram and co-workers[16,17] had identified pelargonidin 3-*O*-galactoside in Cornelian cherry by NMR spectroscopy. On the basis of these findings, compound Ac2 was identified as pelargonidin 3-*O*-galactoside (Figure 2a).

Compound Ac3. The retention time of peak Ac3 matched that of the peonidin 3-*O*-glucoside standard. For both Ac3 and peonidin 3-*O*-glucoside, a molecular ion at m/z 463 (M^+) and a loss of 162 in MS/MS were obtained. In both cases, the product ion scan of the in-source fragment at m/z 301 showed three predominant product ions at m/z 301, 286, and 258, but several minor fragments were different (Table 1).

In mango peel extract, a compound with the same retention time, UV−vis spectrum, and fragmentation pattern as Ac3 has been described as 7-*O*-methylcyanidin 3-*O*-galactoside.[11] The fragmentation patterns of the in-source fragment with m/z 301 of Ac3 and the major anthocyanidin in a mango peel extract used in our study for comparison matched well, even regarding the minor fragments and the abundance of each fragment. On the basis of these data, compound Ac3 was identified as 7-*O*-methylcyanidin 3-*O*-galactoside (Figure 2a). Until recently, 7-*O*-methylcyanidin had been detected only in mango peels as its galactoside and in Madagascar rosy periwinkle (*Catharanthus roseus* (L.) G. Don) as its rhamnogalactoside.[18] However, a number of unusual anthocyanins including 7-*O*-methylcyanidin 3-*O*-galactoside have recently been identified in the fruits of Staghorn sumac (*Rhus typhina* L.).[19]

Compound Ac4. Prior to NMR analysis, compound Ac4 was isolated using SPE and semipreparative HPLC. These fractionation and purification processes were necessary because of the complex composition of the crude extract. The anthocyanins not only had to be concentrated, but some of the phenolic compounds, namely, hydrolyzable tannins, coeluted with the anthocyanins and therefore needed to be removed. The chromatographical purity of Ac4 was determined at 280 nm and was ≥96%.

The proton and carbon signals of Ac4 were attributed according to previously published data.[11,17,20] The ^{1}H NMR displays the typical AA′XX′ signal pattern with two doublets at δ 8.71, J = 8.6 Hz, and δ 7.06, J = 8.6 Hz, which is characteristic of a symmetric monosubstituted B-ring. The anomeric proton of the hexose moiety displays a doublet with a coupling constant of 7.5 Hz, confirming a β-glycosidic bond. The two A-ring protons exhibit two relatively broad singlets (δ 6.72 and 7.25), revealing a meta substitution. The H4 proton shows a typical high-field shifted singlet at δ 9.11. Besides the signals of the glycosyl moiety between δ 3.8 and 4.1, the spectrum includes a large singlet of a methyl group (δ 4.08). The identity of the galactosyl moiety may be deduced from the small coupling constant (J = 3.6 Hz) of the proton H4″ (δ 3.99), which is characteristic of an equatorial proton. The

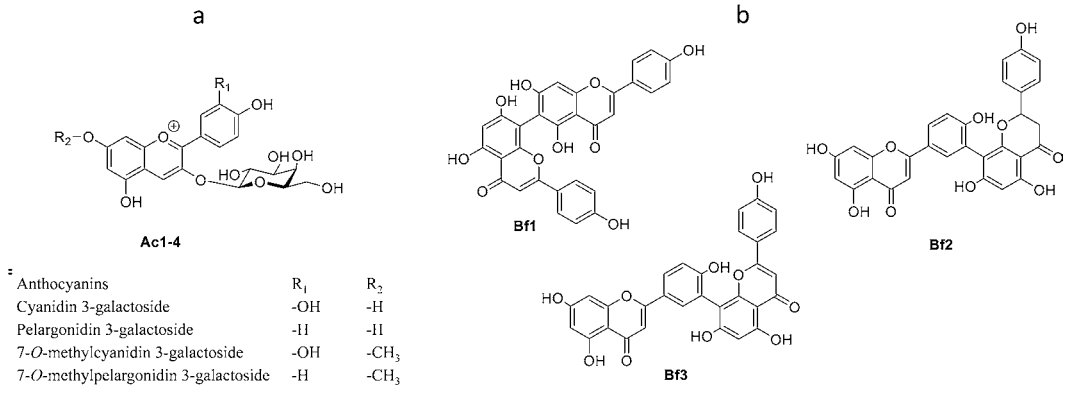

Anthocyanins	R_1	R_2
Cyanidin 3-galactoside	-OH	-H
Pelargonidin 3-galactoside	-H	-H
7-*O*-methylcyanidin 3-galactoside	-OH	-CH_3
7-*O*-methylpelargonidin 3-galactoside	-H	-CH_3

Figure 2. Structures of the anthocyanins (Ac1, cyanidin 3-*O*-galactoside; Ac2, pelargonidin 3-*O*-galactoside; Ac3, 7-*O*-methylcyanidin 3-*O*-galactoside; Ac4, 7-*O*-methylpelargonidin 3-*O*-galactoside) and biflavones (Bf1, I6,II8-biapigenin; Bf2, II-2,3-dihydro-I3′,II8-biapigenin; Bf3, I3′,II8-biapigenin) identified in *Schinus terebinthifolius* Raddi exocarp.

dx.doi.org/10.1021/jf500977d | *J. Agric. Food Chem.* 2014, 62, 6219−6226

Table 1. UV−Vis and Mass Spectrometric Characteristics (Observed and Theoretical Fragments) of Anthocyanidins Found in Exocarp Extracts from *Schinus terebinthifolius* Raddi[a] (after in-source fragmentation of the glycosides)

	peonidin	Ac3	Ac4	
	3′-*O*-methylcyanidin	7-*O*-methylcyanidin	7-*O*-methyl-pelargonidin	4′-*O*-methylpelargonidin (hypothetical)
vis max (nm)	526	513	499	
$[M]^+$	**301** (20)[b]	**301** (40)	**285** (40)	285
$[M - CH_3]^+$	**286** (100)	**286** (55)	**270** (55)	270
$[M - CH_3CO]^+$	**258** (70)	**258** (100)	**242** (100)	242
$1,3B^+ - CO$	137	**123** (10)	**107** (25)	121
$0,2B^+$	**151** (5)	**137** (15)	**121** (20)	135
$0,2B^+ - CO$	123	109	93	107
$0,3A^+$	121	135	135	121
$0,2A^+$	**151** (5)	165	165	151

[a]Nomenclature of the fragment ions according to Olivera et al.[47] Data of peonidin and the hypothetical 4′-*O*-methyl-pelargonidin are included for comparison. [b]*m*/*z* of observed product ions in bold face; relative abundance in parentheses.

corresponding proton in a glucose moiety would exhibit a larger coupling constant due to the larger dihedral angle to the adjacent protons.[21] Two-dimensional NMR experiments were conducted to determine the positions of the galactose moiety and the methyl group. HMBC correlations of both the methyl protons and the A ring protons H8 and H6 with the carbon at position C7 revealed that the methoxy group is located at C7. Furthermore, the 3-glycosidic bond was deduced from the correlation of the anomeric proton H1″ and the C4 carbon (Figure 3). The signal pattern of Ac4 is in agreement with the

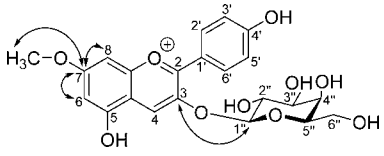

Figure 3. Structure of 7-*O*-methylpelargonidin 3-*O*-*β*-D-galactopyranoside identified in *Schinus terebinthifolius* Raddi exocarp. Arrows show important HMBC correlations.

data observed by Berardini et al.,[11] who isolated 7-*O*-methylcyanidin 3-*O*-*β*-D-galactopyranoside from mango peel. To our knowledge, 7-*O*-methylpelargonidin 3-*O*-*β*-D-galactopyranoside has not been described before.

Mass Spectrometric Considerations. Although the structure was elucidated by NMR spectroscopy, it is appropriate to discuss the mass spectrometric data of Ac4 together with those of Ac3 to confirm the proposed identity of Ac3 as 7-*O*-methylcyanidin 3-*O*-galactoside (Figure 2a). Compound Ac4 showed a molecular ion at *m*/*z* 447 (M^+) with a loss of 162 in the MS^2 experiment, resulting in a fragment with *m*/*z* 285 ($M^+ - 162$). The fragments of the aglycones match the theoretically possible fragments of 7-*O*-methylpelargonidin and also those of 4′-*O*-methylpelargonidin for Ac4 and 7-*O*-methylcyanidin or 4′- or 3′-*O*-methylcyanidin (peonidin) for Ac3 (Table 1).

Ac4 showed a molecular ion at *m*/*z* 447 (M^+) (exact mass of 447.12970) with a loss of 162 in the MS^2 experiment, resulting in a fragment with *m*/*z* 285 ($M^+ - 162$). The predominant fragments of the aglycones (formed by in-source fragmentation) at *m*/*z* 270 and 242 for Ac4 and at 286 and 258 for Ac3 correspond to the loss of a methyl group (M − 162 − 15) and of a CH_3CO moiety (M − 162 − 43), respectively (Table 1). The minor fragments may be used for the localization of the methyl moiety, but the fragments of the aglycones match the theoretically possible fragments of both conceivable structures 7-*O*-methylpelargonidin or 4′-*O*-methylpelargonidin for Ac4 and 7-*O*-methylcyanidin or 4′- or 3′-*O*-methylcyanidin (= peonidin) for Ac3.

Nevertheless, the 7-*O*-position of the methyl group on Ac4 can be deduced by comparison of the mass spectra of the aglycones of Ac3, Ac4, and the peonidin standard. Ac3 and peonidin are isomers and show partially the same fragments in the MS^2 spectra of the aglycones. The major fragments (*m*/*z* 286 and 258; loss of a methyl group (M − 162 − 15) and of a CH_3CO moiety (M − 162 − 43), respectively) match, whereas the minor fragments differ. Furthermore, the relative intensities of the major fragments and of the unfragmented aglycone (*m*/*z* 301) differ. These data indicate that the Ac3 aglycone is not peonidin and the methyl moiety is not attached at the 4′-*O* position.

The product ion scan of the in-source fragment with *m*/*z* 285 of peak Ac4 reveals a fragment pattern similar to that of Ac3, but Ac4 shows fragments that differ from those of Ac3 by 16 u. The relative intensities of all fragments match well considering the mass shift of 16 u, which is a clear indication of close structural similarity. The mass spectrometric data of Ac3 are consistent with those of 7-*O*-methylcyanidin 3-*O*-galactoside found in mango peel extract. Considering the pronounced similarity of the aglycone fragments of Ac3 and Ac4, it is convincing that also Ac4 has the methyl moiety at position 7-*O*. Additionally, it is observed that under the ionization and fragmentation conditions applied in this study, the positive charge of the aglycone fragments is always located on the B-ring and the $0,2B^+ - CO$ fragment, which would be of diagnostic value, is never detected (Table 1).

Chemotaxonomic Considerations. The occurrence of 7-*O*-methylated flavonoids in Brazilian pepper fruits is particularly remarkable in view of the results of previous investigations into the profile of flavonoids in members of the Anacardiaceae family. In mango peel extracts, 7-*O*-methylcyanidin 3-*O*-galactoside and cyanidin 3-*O*-galactoside have been described previously.[11] Mango peels have also been demonstrated to contain both quercetin 3-*O*-glycosides and 7-*O*-methylquercetin (rhamnetin) glycosides.[22,23] In peels of Costa Rican jocote fruits, several glycosides of quercetin and rhamnetin have also been found.[24] Interestingly, Kirby and colleagues detected 7-*O*-methyl derivatives of delphinidin and cyanidin, along with other unusual anthocyanins, in fruits of Staghorn sumac,[19] which is also a member of the Anacardiaceae family. However, the corresponding pelargonidin derivatives were not detected in the sumac fruits. Taking together these results, it becomes evident

that 7-methoxylated flavonoids, including anthocyanins, frequently occur in Anacardiaceae and might even be considered a chemotaxonomic trait of this family.

Gallotannins. Gallotannins often occur in complex mixtures, which renders their separation and characterization difficult. The separation by UHPLC of gallotannins and other phenolic compounds from Brazilian pepper exocarp is shown in Figure 4. The gallotannins were tentatively identified by their

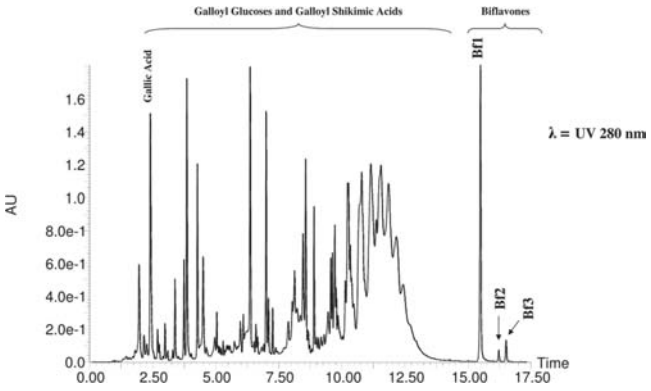

Figure 4. Separation of gallotannins (galloyl glucoses and galloyl shikimic acids) and biflavones by UHPLC (detection wavelength = 280 nm).

MS^2 spectra. There were a number of peaks showing a signal at the fixed product ion scan of m/z 169 and the neutral loss scan of 152 suggesting gallotannins. They gave rise to an in-source fragment at m/z 169 with the same product ion spectrum as gallic acid, confirming the galloyl moiety. These peaks were further examined. Two groups of compounds were distinguished: (1) Peaks showed mass differences of 152 between each other, starting at m/z 331 and ending at m/z 2155; this group was identified as mono- to tridecagalloyl glucoses (Supporting Information Tables S1 and S2). (2) Peaks showed mass differences of 152 between each other, starting at m/z 325 and ending at m/z 1085; this group was later tentatively identified as mono- to hexagalloyl shikimic acids (Supporting Information Tables S3 and S4).

In addition, gallic acid was identified by comparing retention time and mass spectrometric data with those of an authentic reference.

Galloyl Glucoses. Three peaks were detected with m/z 331 (at 2.7, 2.9, and 3.3 min) showing the same product ions differing in abundance (Supporting Information Tables S1 and S2) as reported by others for monogalloyl glucoses,[25−27] including fragments formed by the loss of water (313), the loss of hexose (169), and cross-ring fragmentation of the glucose (271, 241, 211). The loss of CO_2 was not observed for monogalloyl glucoses, indicating that the gallic acid moieties are attached to the sugar moiety via an ester linkage rather than an ether linkage.[27]

Five peaks were observed with m/z 483 (at 5.1, 5.4, 5.7, 5.8, and 6.1 min) showing the same product ions differing in abundance as reported by others for digalloyl glucoses.[25−27] The peaks with m/z 483 had the same product ions as monogalloyl glucose and an additional product ion with m/z 331. Furthermore, two of these peaks (eluting after 5.8 and 6.1 min) showed a product ion at m/z 439, corresponding to the loss of CO_2 and indicating at least one ether linkage between glucose and gallic acid. This series of peaks with m/z of 179 + ($n \times 152$) proceeded consistently until m/z 2155, that is, for n = 1−13.

Whereas there were three or five peaks with m/z 331 or 483, respectively, indicating several isomers of the mono- or digalloyl glucoses, the signals with m/z 635 and higher did not split into multiple peaks. It remains to be demonstrated whether this observation may be explained by coelution of isomers or by the absence of different isomers.

Starting from m/z 939 (n = 5), the doubly charged ion $[M - 2H]^{2-}$ was more abundant than the singly charged ion, resulting in a series of ions from m/z 469 to 1077 with m/z differences of 76. This behavior has already been described for galloyl glucoses.[28] In most cases, the fragment ions of the $[M - 2H]^{2-}$ precursor ions were interpreted also as doubly charged. Thus, this group was identified as mono- to tridecagalloyl glucoses. 1,2,3,4,6-*O*-Pentagalloylglucose has been reported to occur in *S. terebinthifolius*.[29] Although galloyl glucoses have been intensively investigated,[30] the presence of undeca-, dodeca- and tridecagalloyl glucose has only rarely been reported.[31,32]

Galloyl Shikimic Acids. Three peaks were detected with m/z 325 (at 3.4, 3.75, and 3.9 min) showing the same profile of product ions with dominant ions at m/z 169, 125 and 173 (Supporting Information Tables S3 and S4), as reported by others for monogalloyl shikimic acid.[33,34] The four peaks with m/z 477 (eluting after 6.7, 7.0, 7.6, and 7.75 min) showed the same product ions as monogalloyl shikimic acid and in two cases an additional product ion with m/z 325 corresponding to digalloyl shikimic acids. This series of peaks with m/z 173 + ($n \times 152$) proceeded consistently until m/z 1085, that is, for n = 1−6. The two heaviest compounds of this series with m/z 933 and 1085 showed equally abundant doubly charged ions $[M - 2H]^-$ with m/z 467 and 543, respectively. Thus, this group was tentatively identified as mono- to hexagalloyl shikimic acids. Monogalloyl,[35−37] digalloyl,[38,39] and trigalloyl[33,38] shikimic acids have been described before, whereas to our knowledge there is no literature precedent for the presence of tetra-, penta-, and hexagalloyl shikimic acids.

Biflavones. Three major peaks named Bf1, Bf2, and Bf3 were visible in the chromatogram recorded at 280 nm (Figure 4) in the time range from 15.0 to 17.5 min with UV absorption maxima close to 335 nm. Their UV and mass spectrometric data are shown in Table 2.

Compound Bf1. Compound Bf1 eluting at 15.6 min showed a UV spectrum similar to that of the I3′,II8-biapigenin standard, with the two maxima at 272 and 334 nm (I3′,II8-biapigenin, 269 and 335 nm). Identical fragments were found for Bf1 and the reference compound in the negative product ion scans. However, in the positive mode some differences are evident. In the mass spectrum of Bf1, m/z 387 and 153 are lacking and m/z 419 and 257 are present in significant intensity. The fragment at m/z 121 is about 4-fold more abundant in Bf1 than in I3′,II8-biapigenin. This fragmentation behavior can be explained by assuming the structure I6,II8-biapigenin.

In I6,II8-biapigenin, the C−C bond between the apigenin moieties links the two A-rings. Therefore, fissions of the C-ring leading to B^+ fragments form relatively light ions, for example, m/z 121 ($^{0,2}IB^+$ and $^{0,2}IIB^+$) and 163 ($^{0,4}IB^+$ and $^{0,4}IIB^+$). These ions are also formed from I3′,II8-biapigenin, but only when cleavage of part II occurs ($^{0,2}IIB^+$ and $^{0,4}IIB^+$). $^{1,3}IB^+$ fragmentation of I3′,II8-biapigenin yields a rather heavy ion (m/z 387) because part II is attached to the B-ring of part I. A fragment ion at m/z 387 is not observed in Bf1. The A^+

dx.doi.org/10.1021/jf500977d | J. Agric. Food Chem. 2014, 62, 6219−6226

Table 2. UV Maxima and Positive Product Ions (m/z, Relative Abundances in Parentheses; Collision Energy = 40 V) with Hypothetical Structures of the Biflavones Bf1, Bf2, and Bf3[a]

	Bf1	Bf2	Bf3
RT (min)	15.6	16.3	16.6
assigned identity	I6,II8-biapigenin	II-2,3-dihydro-I3′,II8-biapigenin	I3′,II8-biapigenin
UV max (nm)	272, 333	282, 328	269, 335
$[M + H]^+$	539 (6)	541 (2)	539 (55)
$[M + H - H_2O]^+$	521 (5)		521 (3)
$[M + H - C_2H_2O]^+$	497 (2)		497 (9)
$^{1,4}IB^+$		415 (9)	
$^{1,3}IIA^+$	421 (2)[b]		421 (4)
$^{0,2}IIA^+$	419 (49)[b]		419 (3)
$^{1,3}IIA^+ - H_2O$	403 (100)[b]		403 (100)
$^{0,2}IIA^+ - H_2O$	401 (29)[b]		401 (3)
$^{1,3}IB^+$		389 (86)	387 (19)
$^{0,4}IIA^+$	377 (82)[b]		377 (82)
$^{1,3}IIA^+ - H_2O - CO$	375 (45)[b]		375 (48)
$^{1,3}IB^+ - H_2O$		371 (2)	
$^{1,3}IIA^+ - H_2O - 2CO$	347 (50)[b]	347 (1)	347 (20)
$^{0,4}IIA^+ - C_2H_2O$	335 (16)[b]		335 (30)
$^{1,3}IIA^+ - C_2H_2O - C_3O_2$	311 (3)[b]		311 (15)
$^{0,4}IIA^+ - C_2H_2O - CO$	307 (16)[b]		307 (14)
$^{1,4}IB^+ - {}^{1,3}IIB$		297 (4)	
$^{1,3}IIA^+ - C_2H_2O - C_3O_2 - CO$	283 (15)[b]		283 (26)
$^{1,3}IB^+ - {}^{1,3}IIB$		271 (5)	
[flavone I or II]$^+$	270 (4)	270 (8)	270 (10)
$^{1,3}IB^+ - {}^{1,3}IIB$ (or $^{1,3}IIA^+ - {}^{1,3}IA$)			269 (4)
$^{0,4}IA^+ - {}^{0,2}IIB^+ + H^+$	257 (12)		
$^{0,4}IIB^+$	163 (7)[b]		163 (8)
$^{1,3}IA^+$		153 (100)	153 (32)
$^{0,4}IIB^+ - H_2O$	145 (3)[b]		145 (3)
$^{0,2}IIB^+$	121 (88)[b]	121 (10)	121 (23)
$^{1,3}IIB^+$	119 (3)[b]		119 (4)
$^{0,2}IIB^+ - CO$	93 (5)[b]	93 (4)	93 (1)
unknown	229 (4), 361 (15)	111 (6)	453 (3)

[a]Nomenclature of the fragment ions according to Zhang et al.[45] [b]In the case of Bf1 this ring fission in part I leads to the same fragment.

fragments of I6,II8-biapigenin always have the same m/z regardless of whether fission occurs in part I or II: m/z 421 ($^{1,3}IA^+$ and $^{1,3}IIA^+$) and m/z 377 ($^{0,4}IA^+$ and $^{0,4}IIA^+$). These ions are also formed from I3′,II8-biapigenin, but only when cleavage of part II occurs ($^{1,3}IIA^+$ and $^{0,4}IIA^+$). After $^{1,3}IA^+$ fragmentation of I3′,II8-biapigenin, an ion with m/z 153 is formed, which is not observed in Bf1. The fragment with m/z 257 in the mass spectrum of Bf1 can be explained by the two ring fissions $^{0,4}IA^+$ and $^{0,2}IIA^+$ if Bf1 is considered as I6,II8-biapigenin (Figure 2b).

Although the mass spectrometric data do not allow the distinction between 6,8-, 6,6- and 8,8-linkages, I6,II8-biapigenin (agathisflavone) confirms the structure, which has been described in *S. terebinthifolius*[9,40] as well as in other Anacardiaceae species (*Rhus* ssp.[41,42] and *Anacardium occidentale* (cashew)[43]).

Compound Bf2. Peak Bf2 eluting at 16.3 min with $[M - H]^-$ 539 shows UV maxima at 282 and 330 nm, which indicates the presence of a naringenin part. The MS^2 fragments in the positive ionization mode are in agreement with those of a II-2,3-dihydro-I3′,II8a biapigenin from *S. terebinthifolius*[44] and a 2,3-dihydro biapigenin from *Selaginella tamariscina*.[45] However, the mass spectrometric data do not allow the distinction between 3′,6- and 3′,8-linkages. We consider our findings as a confirmation of the II-2,3-dihydro-I3′,II8a biapigenin found by Skopp and Schwenker.[44] Therefore, peak Bf2 was tentatively identified as a II-2,3-dihydro-I3´,II8-biapigenin (I3',II8-naringeninyl-apigenin), Figure 2b).

Compound Bf3. Peak Bf3 eluting at 16.6 min with $[M - H]^-$ 537 shows the same retention time, UV spectrum, and MS fragments as the I3′,II8-biapigenin (amentoflavone) standard. The UV spectrum as well as MS^2 spectra in negative and positive mode are in agreement with published data of I3′,II8-biapigenin,[45,46] which has been described in *S. terebinthifolius*[44] as well as in other Anacardiaceae species (*Rhus* ssp.[41,42]). Therefore, peak Bf3 was identified as I3′,II8-biapigenin (Figure 2b).

In conclusion, this study contributes to the characterization of the phenolic compounds found in *S. terebinthifolius* fruits. The red pigments in the exocarp of *S. terebinthifolius* were characterized for the first time. Besides three anthocyanins, which are known from other Anacardiaceae, the novel anthocyanin 7-*O*-methylpelargonidin 3-*O*-*β*-D-galactopyranoside was identified. Furthermore, two groups of hydrolyzable tannins, namely, galloyl glucoses and galloyl shikimic acids, with partially uncommon degrees of galloylation and three biflavonoids were found.

The presence of 7-*O*-methylated anthocyanins confirms the assumed chemotaxonomic relationship to other Anacardiaceae

because 7-*O*-methylcyanidin 3-*O*-β-D-galactopyranoside was also found in mango and Staghorn sumac. These findings expand the knowledge about the phenolic profile of Anacardiaceae and enhance the chemotaxonomic understanding. Antimicrobial effects of extracts from leaves and bark of *S. terebinthifolius* have already been shown. Therefore, microbiological testing with exocarp extracts from *S. terebinthifolius* should be the focus of further investigations. The successful characterization of the phenolic profile facilitates the isolation and identification of promising antimicrobials and may thus enable the assignment of bioactivity to particular compounds. Thus, the present study provides a crucial basis for future research.

■ ASSOCIATED CONTENT

Supporting Information

Tables S1−S4. This material is available free of charge via the Internet at http://pubs.acs.org.

■ AUTHOR INFORMATION

Corresponding Author

*(A.S.) Phone: +49-228-73-4452. Fax: +49-228-73-4429. E-mail: schieber@uni-bonn.de.

Notes

The authors declare no competing financial interest.

■ ACKNOWLEDGMENTS

We thank Stefan Kehraus from the Institute of Pharmaceutical Biology, University of Bonn, Germany, for performing NMR analysis and Patrick Nickolaus from the Competence Center for Wine Research, DLR Rheinpfalz, Germany, for determining exact masses by LC-MS.

■ REFERENCES

(1) Miller, A. J.; Schaal, B. A. Domestication and the distribution of genetic variation in wild and cultivated populations of the Mesoamerican fruit tree *Spondias purpurea* L. (Anacardiaceae). *Mol. Ecol.* **2006**, *15*, 1467−1480.

(2) Rayne, S.; Mazza, G. Biological activities of extracts from sumac (*Rhus* spp.): a review. *Plant Foods Hum. Nutr.* **2007**, *62*, 165−175.

(3) Mariod, A. A.; Abdelwahab, S. I. *Sclerocarya birrea* (Marula), an African tree of nutritional and medicinal uses: A review. *Food Rev. Int.* **2012**, *28*, 375−388.

(4) Moyo, M.; Staden, J. Micropropagation of Anacardiaceae species of economic importance: advances and future prospects. *In Vitro Cell. Dev. Biol.−Plant* **2012**, *49*, 85−96.

(5) www.fleppc.org.

(6) Morgan, E. C.; Overholt, W. A. Potential allelopathic effects of Brazilian pepper (*Schinus terebinthifolius* Raddi, Anacardiaceae) aqueous extract on germination and growth of selected Florida native plants 1. *J. Torrey Bot. Soc.* **2005**, *132*, 11−15.

(7) Johann, S.; Pizzolatti, M. G.; Donnici, C. L.; de Resende, M. A. Antifungal properties of plants used in Brazilian traditional medicine against clinically relevant fungal pathogens. *Braz. J. Microbiol.* **2007**, *38*, 632−637.

(8) Rhouma, A.; Ben Daoud, H.; Ghanmi, S.; Ben Salah, H.; Romdhane, M.; Demak, M. Antimicrobial activities of leaf extracts of *Pistacia* and *Schinus* species against some plant pathogenic fungi and bacteria. *J. Plant Pathol.* **2009**, *91*, 339−345.

(9) Carvalho, M. G.; Melo, A.; Aragão, C.; Raffin, F. N.; Moura, T. *Schinus terebinthifolius* Raddi: chemical composition, biological properties and toxicity. *Rev. Bras. Planta Med.* **2013**, *15*, 158−169.

(10) Berardini, N.; Carle, R.; Schieber, A. Characterization of gallotannins and benzophenone derivatives from mango (*Mangifera indica* L. cv. 'Tommy Atkins') peels, pulp and kernels by high-performance liquid chromatography/electrospray ionization mass spectrometry. *Rapid Commun. Mass Spectrom.* **2004**, *18*, 2208−2216.

(11) Berardini, N.; Schieber, A.; Klaiber, I.; Beifuss, U.; Carle, R.; Conrad, J. 7-*O*-Methylcyanidin 3-*O*-β-D-galactopyranoside, a novel anthocyanin from mango (*Mangifera indica* L. cv. 'Tommy Atkins') peels. *Z. Naturforsch.* **2005**, *60*, 801.

(12) Engels, C.; Schieber, A.; Gänzle, M. G. Inhibitory spectra and modes of antimicrobial action of gallotannins from mango kernels (*Mangifera indica* L.). *Appl. Environ. Microbiol.* **2011**, *77*, 2215−2223.

(13) Wrolstad, R. E.; Acree, T. E.; Decker, E. A.; Penner, M. H.; Reid, D. S.; Schwartz, S. J.; Shoemaker, C. F.; Smith, D.; Sporns, P. Anthocyanins. In *Handbook of Food Analytical Chemistry*; Wrolstad/Handbook; Wiley: Hoboken, NJ, USA, 2005; pp 5−69.

(14) Wu, X.; Prior, R. L. Systematic identification and characterization of anthocyanins by HPLC-ESI-MS/MS in common foods in the United States: fruits and berries. *J. Agric. Food Chem.* **2005**, *53*, 2589−2599.

(15) Kammerer, D.; Carle, R.; Schieber, A. Detection of peonidin and pelargonidin glycosides in black carrots (*Daucus carota* ssp. *sativus* var. *atrorubens* Alef.) by high-performance liquid chromatography/electrospray ionization mass spectrometry. *Rapid Commun. Mass Spectrom.* **2003**, *17*, 2407−2412.

(16) Pawlowska, A. M.; Camangi, F.; Braca, A. Quali-quantitative analysis of flavonoids of *Cornus mas* L. (Cornaceae) fruits. *Food Chem.* **2010**, *119*, 1257−1261.

(17) Seeram, N. P.; Schutzki, R.; Chandra, A.; Nair, M. G. Characterization, quantification, and bioactivities of anthocyanins in *Cornus* species. *J. Agric. Food Chem.* **2002**, *50*, 2519−2523.

(18) Toki, K.; Saito, N.; Irie, Y.; Tatsuzawa, F.; Shigihara, A.; Honda, T. 7-O-Methylated anthocyanidin glycosides from *Catharanthus roseus*. *Phytochemistry* **2008**, *69*, 1215−1219.

(19) Kirby, C. W.; Wu, T.; Tsao, R.; McCallum, J. L. Isolation and structural characterization of unusual pyranoanthocyanins and related anthocyanins from Staghorn sumac (*Rhus typhina* L.) via UPLC-ESI-MS, (1)H, (13)C, and 2D NMR spectroscopy. *Phytochemistry* **2013**, *94*, 284−293.

(20) Pedersen, A. T.; Andersen, Ø. M.; Aksnes, D. W.; Nerdal, W. NMR of anthocyanins: assignments and effects of exchanging aromatic protons. *Magn. Reson. Chem.* **1993**, *31*, 972−976.

(21) Bjorøy, Ø.; Fossen, T.; Andersen, Ø. M. Anthocyanin 3-galactosides from *Cornus alba* 'Sibirica' with glucosidation of the B-ring. *Phytochemistry* **2007**, *68*, 640−645.

(22) Schieber, A.; Berardini, N.; Carle, R. Identification of flavonol and xanthone glycosides from mango (*Mangifera indica* L. Cv. 'Tommy Atkins') peels by high-performance liquid chromatography-electrospray ionization mass spectrometry. *J. Agric. Food Chem.* **2003**, *51*, 5006−5011.

(23) Berardini, N.; Fezer, R.; Conrad, J.; Beifuss, U.; Carle, R.; Schieber, A. Screening of mango (*Mangifera indica* L.) cultivars for their contents of flavonol *O*- and xanthone *C*-glycosides, anthocyanins, and pectin. *J. Agric. Food Chem.* **2005**, *53*, 1563−1570.

(24) Engels, C.; Gräter, D.; Esquivel, P.; Jiménez, V. M.; Gänzle, M. G.; Schieber, A. Characterization of phenolic compounds in jocote (*Spondias purpurea* L.) peels by ultra high-performance liquid chromatography/electrospray ionization mass spectrometry. *Food Res. Int.* **2012**, *46*, 557−562.

(25) Gordon, A.; Jungfer, E.; da Silva, B. A.; Maia, J. G. S.; Marx, F. Phenolic constituents and antioxidant capacity of four underutilized fruits from the Amazon region. *J. Agric. Food Chem.* **2011**, *59*, 7688−7699.

(26) Sandhu, A. K.; Gu, L. Antioxidant capacity, phenolic content, and profiling of phenolic compounds in the seeds, skin, and pulp of *Vitis rotundifolia* (Muscadine grapes) as determined by HPLC-DAD-ESI-MS^n. *J. Agric. Food Chem.* **2010**, *58*, 4681−4692.

(27) Meyers, K. J.; Swiecki, T. J.; Mitchell, A. E. Understanding the native Californian diet: Identification of condensed and hydrolyzable tannins in Tanoak acorns (*Lithocarpus densiflorus*). *J. Agric. Food Chem.* **2006**, *54*, 7686−7691.

(28) Engels, C.; Gänzle, M. G.; Schieber, A. Fractionation of gallotannins from mango (*Mangifera indica* L.) kernels by high-speed counter-current chromatography and determination of their antibacterial activity. *J. Agric. Food Chem.* **2010**, *58*, 775−780.
(29) Cavalher-Machado, S. C.; Rosas, E. C.; Brito, F. A. The antiallergic activity of the acetate fraction of *Schinus terebinthifolius* leaves in IgE induced mice paw edema and pleurisy. *Int. Immunopharmacol.* **2008**, *8*, 1552−1560.
(30) Arapitsas, P. Hydrolyzable tannin analysis in food. *Food Chem.* **2012**, *135*, 1708−1717.
(31) Sáyago-Ayerdi, S. G.; Moreno-Hernández, C. L.; Montalvo-González, E.; García-Magaña, M. L.; de Oca, M. M.-M.; Torres, J. L.; Perez-Jimenez, J. Mexican 'Ataulfo' mango (*Mangifera indica* L.) as a source of hydrolyzable tannins. Analysis by MALDI-TOF/TOF MS. *Food Res. Int.* **2013**, *51*, 188−194.
(32) Engels, C.; Knödler, M.; Zhao, Y.-Y.; Carle, R.; Gänzle, M. G.; Schieber, A. Antimicrobial activity of gallotannins isolated from mango (*Mangifera indica* L.) kernels. *J. Agric. Food Chem.* **2009**, *57*, 7712−7718.
(33) Pfundstein, B.; El Desouky, S. K.; Hull, W. E.; Haubner, R.; Erben, G.; Owen, R. W. Polyphenolic compounds in the fruits of Egyptian medicinal plants (*Terminalia bellerica*, *Terminalia chebula* and *Terminalia horrida*): characterization, quantitation and determination of antioxidant capacities. *Phytochemistry* **2010**, *71*, 1132−1148.
(34) Singab, A.-N.; Ayoub, N.; Al-Sayed, E.; Martiskainen, O.; Sinkkonen, J.; Pihlaja, K. Phenolic constituents of *Eucalyptus camaldulensis* Dehnh, with potential antioxidant and cytotoxic activities. *Rec. Nat. Prod.* **2011**, *5*, 271−280.
(35) Fecka, I.; Cisowski, W. Tannins and flavonoids from the *Erodium cicutarium* herb. *Z. Naturforsch.* **2005**, *60*, 555−560.
(36) Huang, Y.-L.; Tanaka, T.; Matsuo, Y.; Kouno, I.; Li, D.-P.; Nonaka, G.-I. Two new phenolic glucosides and an ellagitannin from the leaves of *Castanopsis sclerophylla*. *Phytochem. Lett.* **2012**, *5*, 158−161.
(37) Lee, M.-W.; Tanaka, T.; Nonaka, G.-I.; Nishioka, I. Dimeric ellagitannins from *Alnus japonica*. *Phytochemistry* **1992**, *31*, 2835−2839.
(38) Nonaka, G.-I.; Nishioka, I.; Nishizawa, M.; Yamagishi, T.; Kashiwada, Y.; Dutschman, G. E.; Bodner, A. J.; Kilkuskie, R. E.; Cheng, Y.-C.; Lee, K.-H. Anti-AIDS agents, 2: Inhibitory effect of tannins on HIV reverse transcriptase and HIV replication in H9 lymphocyte cells. *J. Nat. Prod.* **1990**, *53*, 587−595.
(39) Yokozawa, T.; Chen, C. P.; Dong, E.; Tanaka, T.; Nonaka, G. I.; Nishioka, I. Study on the inhibitory effect of tannins and flavonoids against the 1,1-diphenyl-2-picrylhydrazyl radical. *Biochem. Pharmacol.* **1998**, *56*, 213−222.
(40) Kassem, M.; El-Desoky, S. K.; Sharaf, M. Biphenyl esters and biflavonoids from the fruits of *Schinus terebenthefolus*. *Chem. Nat. Compd.* **2004**, *40*, 447−450.
(41) Lin, Y. M.; Chen, F. C. Agathisflavone from the drupes of *Rhus succedanea*. *Phytochemistry* **1974**, *13*, 657−658.
(42) Svenningsen, A. B.; Madsen, K. D.; Liljefors, T.; Stafford, G. I.; Staden, J. V.; Jäger, A. K. Biflavones from *Rhus* species with affinity for the $GABA_A$/benzodiazepine receptor. *J. Ethnopharmacol.* **2006**, *103*, 276−280.
(43) Konan, N. A.; Lincopan, N.; Collantes Díaz, I. E.; de Fátima Jacysyn, J.; Tanae Tiba, M. M.; Pessini Amarante Mendes, J. G.; Bacchi, E. M.; Spira, B. Cytotoxicity of cashew flavonoids towards malignant cell lines. *Exp. Toxicol. Pathol.* **2012**, *64*, 435−440.
(44) Skopp, G.; Schwenker, G. Biflavonoide aus *Schinus terebinthifolius* Raddi (Anacardiaceae). *Z. Naturforsch.* **1986**, *41*, 1479−1482.
(45) Zhang, Y.-X.; Li, Q.-Y.; Yan, L.-L.; Shi, Y. Structural characterization and identification of biflavones in *Selaginella tamariscina* by liquid chromatography-diode-array detection/electrospray ionization tandem mass spectrometry. *Rapid Commun. Mass Spectrom.* **2011**, *25*, 2173−2186.
(46) Michler, H.; Laakmann, G.; Wagner, H. Development of an LC-MS method for simultaneous quantitation of amentoflavone and biapigenin, the minor and major biflavones from *Hypericum perforatum* L., in human plasma and its application to real blood. *Phytochem. Anal.* **2011**, *22*, 42−50.
(47) Oliveira, M. C.; Esperança, P.; Almoster Ferreira, M. A. Characterisation of anthocyanidins by electrospray ionisation and collision-induced dissociation tandem mass spectrometry. *Rapid Commun. Mass Spectrom.* **2001**, *15*, 1525−1532.

JOURNAL OF AGRICULTURAL AND FOOD CHEMISTRY

Article

pubs.acs.org/JAFC

Comparative Analysis of Antioxidant Activity and Functional Components of the Ethanol Extract of Lotus (*Nelumbo nucifera*) from Various Growing Regions

Xu Zhao,[†] Jian Shen,[‡] Kyung Ja Chang,[†] and Sung Hoon Kim*[,‡]

[†]Department of Food and Nutrition, Inha University, Incheon 402-751, Korea

[‡]Department of Chemistry, Konkuk University, Seoul 143-701, Korea

Supporting Information

ABSTRACT: The variations in antioxidant activity and concentration of functional components in the ethanol extracts of lotus seeds and rhizomes based on the growing region and dryness were investigated. Free radical scavenging activity, total phenolic and flavonoid content, and concentration of several specific flavonoids and alkaloids in the ethanol extracts of lotus were measured. Antioxidant activity and its correlative total phenolic content varied characteristically depending on the growing region and dryness. High-perfomance liquid chromatography analysis showed that the ethanol extracts of lotus seeds from Vietnam (Ho Chi Minh City), raw rhizomes from Korea (Siheung), and dried rhizomes from Japan (Nigata) had the greatest specific flavonoid content. The ethanol extracts of seeds from China (Hubei), raw rhizomes from Japan (Nigata), and dried rhizomes from Korea (Siheung) had the greatest specific alkaloid content. Astragaline, rutin, isoquercetin, nuciferine, dauricine, isoliensinine, and neferine were identified in lotus rhizomes for the first time in this study.

KEYWORDS: *lotus (Nelumbo nucifera), seeds, rhizomes, ethanol extract, antioxidant, flavonoids, alkaloids*

INTRODUCTION

Lotus (*Nelumbo nucifera* Gaertn), a member of the Nymphaeaceae family, is an aquatic plant widely cultivated in Asia. Most parts of the lotus are utilized as the medicinal herbs in traditional medicine. Lotus seeds, rhizomes, leaves, and flowers are also food ingredients, especially in Korea, China, Indian, Japan, Vietnam, and Thailand. The important functional components of the lotus are flavonoids and alkaloids, and their physiological properties have been extensively reported. Flavonoids, a group of polyphenols in plants, are usually subdivided into anthoxanthins, flavanones, flavanonols, flavans, anthocyanidins, and isoflavonoids. The total flavonoid intake of an average American is ≈20 mg/day and for Japanese it is ≈63 mg/day in food originating from plants.[1] Flavonoids have been found to possess antiallergic,[2] anti-inflammatory,[3] antiviral,[4,5] antiproliferative,[6] anticarcinogenic,[7] and antioxidant[8] effects. Alkaloids, a group of compounds containing basic nitrogen atoms, are toxic to humans when consumed beyond a certain level. Previous studies have indicated that alkaloids possess antifibrotic,[9] sedative,[10] anti-HIV,[11] antioxidant, anti-inflammatory,[12] and antiobesity[13] properties.

Compared to the white lotus, which is distinguished by the color of the lotus flower, the red lotus is more commonly used as a food ingredient. The concentration of functional components differ in the red and white lotus.[14] The methanol extracts of different parts of the lotus also contain different concentrations of functional components.[15] Additionally, lotus leaves from different growing regions contain different concentrations of functional components and exert different levels of antioxidant effects.[16] Therefore, the concentration of functional components and antioxidant effect of the lotus varies with the lotus type and parts, as well as the geographic location where the lotus is grown. In addition, the concentration of functional components is also affected by the drying process.[17]

Recently, a lot of studies have been dedicated to the analysis of functional components of lotus leaves and embryos and their health-related properties. Lotus leaves and embryos are more commonly consumed as tea and medicines than as ingredients in meals. Lotus rhizomes, followed by lotus seeds, hold the largest market share as edible vegetables. Some previous studies indicated that lotus seeds and rhizomes possess antipyretic, antidiarrheal,[18] antidiabetic,[19] hepatoprotective,[20,21] anti-inflammatory,[12] and antioxidant[22,23] effects. Flavonoids (flavonols and flavanols) and several alkaloids (neferine, liensinine, isoliensinine, and nuciferine) in lotus seeds have been extensively studied.[24−27] However, only a few flavonoids such as catechin, quercetin, and gallocatechin and alkaloids from lotus rhizomes have been studied.[28−30] Therefore, determination of several specific flavonoid and alkaloid contents in lotus rhizomes and seeds may be valuable for the development of functional foods derived from the lotus.

In our preliminary studies, the ethanol extracts of lotus seeds and rhizomes showed an antiobesity effect.[31,32] The lipid components in the ethanol extracts of lotus seeds and rhizomes, which were analyzed by our group,[33] showed no antiobesity effect. Therefore, it was necessary to analyze the obesity-related functional components in the ethanol extracts of lotus seeds and rhizomes. In addition, the analysis of antioxidant activity and concentration of functional compounds, which vary with

Received: April 10, 2014
Revised: June 9, 2014
Accepted: June 16, 2014
Published: June 16, 2014

ACS Publications © 2014 American Chemical Society

Table 1. Growing Region, Part, and Storage Condition of Lotus Used in This Study

no.	growing region	type[a]	part	storage condition
1	Korea (Muan)	white	seeds with embryo and coat	dried[b]
2	China (Guangzhou)	red	seeds with embryo and coat	dried[b]
3	China (Hubei)	red	seeds with embryo and coat	dried[b]
4	Vietnam (Ho Chi Minh City)	red	seeds with embryo and coat	dried[b]
5	Thailand (Lamphun)	red	seeds with embryo and coat	dried[b]
6	Korea (Siheung)	red	rhizomes with knot	liquid nitrogen frozen raw
7	Korea (Daegu)	red	rhizomes with knot	liquid nitrogen frozen raw
8	Korea (Haman)	red	rhizomes with knot	liquid nitrogen frozen raw
9	Korea (Muan)	white	rhizomes with knot	liquid nitrogen frozen raw
10	Japan (Nigata)	white	rhizomes with knot	liquid nitrogen frozen raw
11	Korea (Siheung)	red	rhizomes with knot	dried[c]
12	Korea (Daegu)	red	rhizomes with knot	dried[c]
13	Korea (Haman)	red	rhizomes with knot	dried[c]
14	China (Guangxi)	red	rhizomes with knot	dried[b]
15	Vietnam (Ho Chi Minh City)	red	rhizomes with knot	dried[b]
16	Korea (Muan)	white	rhizomes with knot	dried[c]
17	Japan (Nigata)	white	rhizomes with knot	dried[c]

[a]Two types of lotus were distinguished by the color of the lotus flower. [b]Dried lotus samples were purchased from different lotus farms and the Internet. [c]Raw lotus rhizomes were dried with a fan for 1 day in our laboratory.

the growing region and drying process, may play an important role in utilizing lotus extracts and developing functional foods. Therefore, in this study, we compared the antioxidant activity and concentration of several specific functional compounds in the ethanol extracts of dried lotus seeds and raw and dried lotus rhizomes from various growing regions.

MATERIALS AND METHODS

Materials and Chemicals. Lotus samples were purchased from various lotus farms and via the Internet in September 2012 (Table 1). Dried lotus seeds were procured from Korea (Muan), China (Guangzhou and Hubei), Vietnam (Ho Chi Minh City), and Thailand (Lamphun) (Figure 1A). Raw lotus rhizomes were procured from Korea (Siheung, Daegu, Haman, and Muan), and Japan (Nigata) and frozen in liquid nitrogen (Figure 1B). Dried lotus rhizomes were obtained from China (Guangxi) and Vietnam (Ho Chi Minh City). Each raw rhizome from various growing regions was subdivided into two parts: one part for direct extraction and the other for drying. For the preparation of dried lotus rhizomes, air was fan-blown on the samples for 1 day at room temperature. The water content of the dried samples was normally less than 5%. The photographs of dried lotus rhizomes are shown in Figure 1C. All lotus samples were stored at −20 °C until they were used.

Astragaline, rutin, isoquercetin, nuciferine, dauricine, isoliensinine, and neferine (≥98%) were obtained from Shenzhen Sungening Bio-Tech Co. Ltd. (Shengzhen, China). Gallic acid (≥98%), (+)-catechin (≥98%), Folin-Ciocalteu's phenol reagent, and 2,2-diphenyl-1-picrylhydrazyl (DPPH) were purchased from Sigma-Aldrich (St. Louis, MO, USA). AB-8 macroporous adsorption resin was purchased from Anhui Sanxing Resin Technology Co. Ltd. (Anhui, China).

Extraction of Lotus Seeds and Rhizomes. Each lotus sample (200 g) was blended with 70% ethanol solvent (1 L), extracted at 50 °C for 2 h and then filtered over a short pad of Celite. The filter cake was extracted with 70% ethanol three times (1 L × 3) at 50 °C for 2 h. The combined ethanol extract was evaporated to complete dryness under reduced pressure at 40 °C. The ethanol extract is referred to hereafter as LE. The crushed LE was continuously extracted with hexane (0.05 g of sample/(mL of hexane)) five times at room temperature for separating lipids and pigment components from the LE fractions. The combined hexane extract and residual fraction after hexane extraction were evaporated to dryness under reduced pressure at 40 °C. The hexane extract and residual fraction after hexane extraction from the LE fraction are respectively referred to hereafter as LEa and LEb. Each LE and LEb fraction was assayed to determine

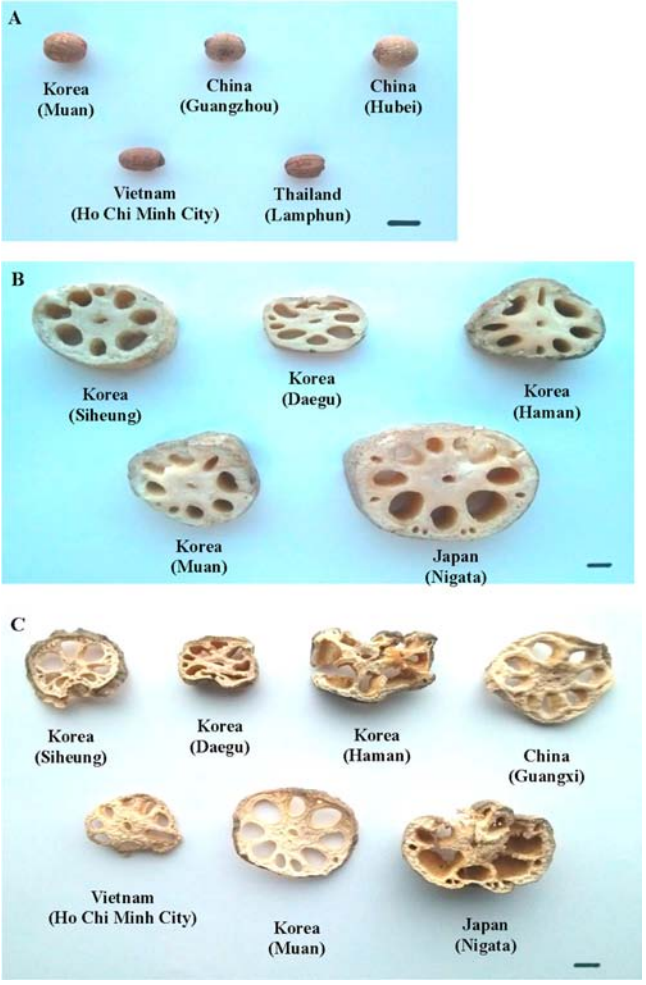

Figure 1. Photographs of lotus seeds and raw and dried rhizomes used in this study. (A): Dried lotus seeds used in this experiment. (B): Raw lotus rhizomes used in this experiment. (C): Dried lotus rhizomes used in this experiment. Bar: 1 cm.

DPPH radical scavenging activity and total phenolic and flavonoid content.

Determination of Free Radical Scavenging Activity. Free radical scavenging activity was assessed using a modified DPPH radical decoloration assay.[34] Various concentrations of samples (0−3.0 mg/mL, 0.6 mL) were reacted with a DPPH methanol solution (100 μmol/L, 5 mL) in the dark for 30 min. The absorbance was measured at 517 nm using a UV−vis spectrophotometer (Agilent Technologies, Santa Clara, CA, USA), and methanol without DPPH was used as the blank. The antioxidant activity of each sample was expressed as an EC_{50} value (the efficient concentration of the sample that decreases the initial DPPH radical formation by 50%), which was estimated using linear regression analysis. In this decoloration assay, higher EC_{50} value refers to a lower antioxidant activity.

Determination of Total Phenolic Content. The total phenolic content was analyzed using Folin-Ciocalteu assay.[34] The sample (5 mg/mL, 0.1 mL) was mixed with distilled water (2 mL) and Folin-Ciocalteu's phenol reagent (1 mL). After 5 min, a 20% aqueous sodium carbonate solution (5 mL) was added, and the mixture was incubated in the dark for 60 min. The absorbance was measured at 735 nm using a UV−vis spectrophotometer, and with distilled water was used as the blank. The total phenolic content was determined using gallic acid (0−0.8 mg/mL) as a calibration standard, and the results were expressed as milligrams of gallic acid equivalents (GAE) per gram of sample.

Determination of Total Flavonoid Content. Total flavonoid content was determined using a modified aluminum chloride coloration method.[34] Each sample (10 mg/mL, 0.6 mL) was mixed with distilled water (3.75 mL) and 5% aqueous sodium nitrite solution (0.225 mL). After 6 min, a 10% aqueous aluminum chloride solution (0.45 mL) was added, and the mixture was incubated for 5 min, after which a sodium hydroxide solution (1 mol/mL, 1.5 mL) and distilled water were added for a total volume of 7.5 mL. The absorbance was measured at 510 nm using a UV−vis spectrophotometer, and distilled water was used as the blank. Total flavonoid content was determined using catechin (0−0.8 mg/mL) as a calibration standard. The results were expressed as milligrams of catechin equivalents (CE) per gram of sample.

AB-8 Macroporous Adsorption Resin Column Chromatography. Each aliquot of the LEb fraction (1 g) was suspended in distilled water (10 mL) and centrifuged to the separate aqueous solution and precipitated fraction. The precipitated fraction was evaporated to complete dryness under reduced pressure. The aqueous solution was applied into an AB-8 macroporous adsorption resin column (190 mm × 30 mm i.d.) for 2 h and then eluted.[35] Elution was performed as follows: first, polar compounds such as amino acids and carbohydrates were eluted with distilled water (500 mL) at a flow rate of 3 mL/min; second, nonpolar compounds such as flavonoids and alkaloids were eluted with 95% ethanol (500 mL) at a flow rate of 5 mL/min; third, the rest of the compounds were eluted with 5% ammonia solution (300 mL) at a flow rate of 5 mL/min. Water and ammonia fractions eluted from the column are referred to hereafter as LEb-1 and LEb-3, respectively. The precipitated fraction of the LEb separated by centrifugation and the ethanol fraction eluted from the column were combined and designated as LEb-2. The LEb-1, LEb-2, and LEb-3 fractions were evaporated to dryness under reduced pressure. The LEb-2 fraction was analyzed by high-performance liquid chromatography (HPLC) to determine the concentration of specific flavonoids and alkaloids.

HPLC Analysis. Each LEb-2 fraction was dissolved in 50% aqueous methanol and filtered through a 0.45 μm filter. Analysis of flavonoids and alkaloids was performed by HPLC (Agilent Technologies 1200 series HPLC) using a Waters SYMMETRY C_{18} (T61421F) reverse-phase column (250 mm × 4.6 mm i.d., 5 μm particle size) with a column temperature of 30 °C. The flow rate was 1 mL/min, and the injection volume was 20 μL. For the flavonoid analysis, the mobile phase was composed of two solvents: 2% aqueous acetic acid solution (solvent A) and 0.5% aqueous acetic acid solution:acetonitrile (1:1, v/v, solvent B).[34] Gradient elution conditions were as follows: 0−10 min, 90% solvent A; 10−40 min, 90−60% solvent A; 40−55 min, 60−45% solvent A; 55−60 min, 45−20% solvent A; 60−65 min, 20−0% solvent A; 65−70 min, 0−50% solvent A; 70−75 min, 50−70% solvent A; and 75−80 min, 70−90% solvent A. Elution was monitored by UV detection at 270 and 350 nm. For the alkaloid analysis, the mobile phase was composed of two solvents: acetonitrile (solvent A) and 0.1% aqueous triethylamine solution (solvent B).[36] Gradient elution conditions were as follows: 0−15 min, 40−70% solvent A; 15−20 min, 70−100% solvent A; and 20−30 min, 100−40% solvent A. Elution was monitored by UV detection at 270 nm. The concentration of several specific flavonoids and alkaloids were calculated using the individual calibration curves.

Statistical Analysis. Statistical analysis was performed using SPSS version 17.0. Results from three independent experiments were used to calculate the mean ± SD values for each sample. Significant differences among dried seeds and raw or dried rhizomes were determined using the Student's *t* test and analysis of variance (ANOVA), respectively. Duncan's multiple range tests were performed when data differences were identified at $P < 0.05$ by ANOVA analysis. Pearson's correlation coefficient was used to analyze correlation between EC_{50} values and total phenolic and flavonoid content in the LE and LEb fractions.

RESULTS AND DISCUSSION

Descriptions of lotus samples, including growing region, lotus parts used, and storage conditions, are presented in Table 1. The growing regions in Korea, China, Japan, Vietnam, and Thailand represent the main lotus-producing and lotus-consumption areas in Asia. Since many factors such as oxidants and the presence of microorganisms can lower the quality of raw lotus, the shelf life of raw lotus is very short. A semidrying process is adopted for long-term storage and ease of transportation, although the drying process can increase the oxidative browning of some antioxidants, such as flavonoids, and reduce antioxidant capacity.[17] Dried lotus seeds and raw lotus rhizomes are commonly found in the market. In this study, raw lotus rhizomes from Korea (Siheung, Daegu, Haman, and Muan) and Japan (Nigata) were dried in order to compare the antioxidant effect and functional compound content of raw and dried rhizomes. The water content in raw lotus rhizomes was not statistically different (77.12%−81.60%, w/w).

In general, organic solvents such as ethyl acetate, *n*-butanol, and methanol are widely used to extract functional components from natural products. However, such solvents are toxic and harmful for humans. A previous report indicated that 70% alcoholic solvents (either ethanol or methanol) exhibit a higher extraction efficiency for flavonoids from lotus leaves than 100% alcoholic solvents.[37] Some of the hydrophilic functional compounds of lotus, such as certain alkaloids and polar phenolic content, are readily soluble in water and not organic solvents. Therefore, in this study, 70% aqueous ethanol was used as a nontoxic, safe, and highly efficient solvent to extract functional compounds from lotus seeds and rhizomes.

The variations in the extract yield are presented in Table 2. The large quantity of water in raw lotus samples is likely to result in a lower yield under similar extraction conditions. Accordingly, the yield of the LE fractions showed obvious variation between raw and dried lotus rhizomes (5.30%−34.85%, w/w), due to the variable water content and not the growing region. Lotus rhizomes are the richest in carbohydrates of all lotus parts studied, followed by the seeds.[38−40] The high water-absorbing capacity of carbohydrates may result in a higher yield than the actual yield of the LE fractions, especially from starch-rich lotus rhizomes. Residual ethanol, absorbed water, and other volatile compounds in the LE fraction were

Table 2. Yields of the LE, LEa, and LEb Fractions of Lotus Seeds and Rhizomes[a]

no.	LE fraction	LEa fraction	LEb fraction
dried seeds			
1	20.53	4.47	95.84
2	19.35	7.55	92.45
3	18.20	6.93	92.96
4	20.84	10.99	90.25
5	19.42	8.37	92.61
raw rhizomes			
6	5.30	2.87	94.09
7	5.51	2.23	93.75
8	6.49	1.23	94.32
9	5.85	2.15	97.83
10	6.84	1.79	95.31
dried rhizomes			
11	20.52	3.04	94.87
12	22.31	3.19	94.60
13	26.52	1.01	97.29
14	23.65	2.40	95.80
15	34.85	1.49	95.19
16	27.99	2.28	94.98
17	23.38	2.42	92.37

[a]Yields (%) of the LE, LEa, and LEb fractions were calculated as LE/lotus, LEa/LE, and LEb/LE, respectively. LE, the ethanol extract; LEa, hexane fraction of the ethanol extract; LEb, residual fraction after separating the hexane fraction from the ethanol extract.

Table 3. Yields of the Three Fractions of Lotus Seeds and Rhizomes Isolated by AB-8 Macroporous Adsorption Resin Column Chromatography[a]

no.	LEb-1 fraction	LEb-2 fraction	LEb-3 fraction
dried seeds			
1	95.59	6.41	3.25
2	93.76	4.87	2.49
3	97.33	6.75	2.83
4	94.73	5.11	2.69
5	94.35	6.94	2.16
raw rhizomes			
6	92.13	8.39	3.21
7	90.43	8.20	3.48
8	91.51	6.11	3.04
9	92.37	8.07	3.91
10	92.31	6.93	2.30
dried rhizomes			
11	89.22	10.24	3.25
12	91.36	7.86	2.01
13	91.76	6.90	2.93
14	96.62	5.53	2.69
15	95.89	5.92	1.88
16	87.77	9.42	3.93
17	89.23	6.94	3.16

[a]Yields (%) of the LEb-1, LEb-2, and LEb-3 fractions were calculated by LEb-1/LEb, LEb-2/LEb, and LEb-3/LEb, respectively. LEb-1, water fraction eluted from the AB-8 column; LEb-2, combined precipitated fraction of the LEb separated by centrifugation and the ethanol fraction eluted from the AB-8 column; LEb-3, ammonia fraction eluted from the AB-8 column.

eliminated by hexane extraction followed by vacuum drying. Therefore, the sum of the yields of LEa and LEb fractions was less than the yield of the LE fraction. The yields of the three fractions isolated by AB-8 macroporous resin column are shown in Table 3. Similarly, the total yield of all fractions, including the LEb-1, LEb-2, and LEb-3 fractions, appeared to be higher than 100% because the LEb-1 fraction contained most of the carbohydrates presented in the LE fraction.

DPPH radical scavenging activity varied significantly in the LE and LEb fractions of lotus seeds and rhizomes depending on the growing region and dryness (Table 4). The free radical scavenging activity was the highest in the LE fraction of lotus seeds from Vietnam and raw and dried rhizomes from Korea (Siheung). Phenolic compounds such as flavonoids are common plant antioxidants, and these are abundant in lotus seeds and rhizomes.[23,41] In this study, the total phenolic and flavonoid content differed significantly in the LE and LEb fractions of lotus seeds and rhizomes from different growing regions (Table 5). The total phenolic content was the highest in the LE fraction of lotus seeds from Vietnam and raw and dried rhizomes from Korea (Siheung). In addition, the total flavonoid content was the highest in the LE fraction of lotus seeds from Korea (Muan), raw rhizomes from Korea (Daegu), and dried rhizomes from Korea (Siheung). A previous report demonstrated that the polyphenolic content determined in apple cultivars was affected by the growing region.[42] Therefore, identical lotus parts may exhibit variations in antioxidant activity and total phenolic and flavonoid content depending on their growing region.

The EC_{50} values and total phenolic content, not total flavonoid content, in the LE and LEb fractions of most raw rhizomes obviously increased after drying. Compared with the results for dried rhizomes, the extraction efficiency for nonpolar phenolic compounds in raw rhizomes was lower because of the dilution of the ethanol solvent by the large water content in raw rhizomes. However, most of these nonpolar phenolic compounds (e.g., chlorogenic acid) exhibit low DPPH radical scavenging activity. The drying process led to an increase in oxidative browning, which in turn results in a decrease in antioxidant capacity.[17] Therefore, this may explain why the extracts of dried rhizomes exhibited a lower antioxidant activity than did raw rhizomes. In addition, DPPH radical scavenging capacity and total phenolic content were lower in oven-dried papaya than freeze-dried papaya because of the decomposition of functional compounds at high temperatures.[43] Dried brownish rhizomes purchased from China and Vietnam, which has been dried in a hot air oven, exhibited lower antioxidant activity and total phenolic content than other, less colored rhizomes dried under a fan in our laboratory. These results indicated that the drying process affects the antioxidant activity and total phenolic content of rhizome extract, not the total flavonoid content.

As for the lotus part, the DPPH radical scavenging activity of seeds was lower than that of rhizomes. In addition, the total phenolic content in the LE fraction of seeds was obviously lower than that of the rhizomes. However, the total flavonoid content in lotus seeds and rhizomes was similar. These results did not correspond with a previous report, which indicated that the extract of lotus seeds showed similar DPPH radical scavenging activity with rhizomes and had higher total phenolic and flavonoid content than rhizomes.[15] The ascorbic acid content in raw lotus seeds is under the detection limit,[40] but its concentration in raw rhizomes is 0.44 mg/g[39] and in dried rhizomes of Korea is from 15.5 to 22.5 mg/g.[44] Other than phenolic compounds, ascorbic acid is a well-known potent

Table 4. DPPH Radical Scavenging Activities of the LE and LEb Fractions of Lotus Seeds and Rhizomes[a]

	EC_{50} value (μg/mL)	
no.	LE fraction	LEb fraction
dried seeds		
1	211.88 ± 10.06a	145.56 ± 5.27a
2	255.76 ± 18.88b	237.21 ± 15.22b
3	191.67 ± 10.19c	162.62 ± 6.02c
4	134.92 ± 4.11d	103.26 ± 1.57d
5	138.40 ± 5.98d	137.99 ± 5.08a
raw rhizomes		
6	45.79 ± 2.25a	35.57 ± 1.04a[d]
7	45.89 ± 0.28a[d]	41.83 ± 3.80b
8	82.07 ± 3.22b[c]	73.63 ± 3.99d[b]
9	74.99 ± 3.72c[d]	58.22 ± 1.81c[c]
10	63.63 ± 3.36d[b]	57.30 ± 0.67c[d]
dried rhizomes		
11	48.34 ± 3.12a	45.94 ± 1.03a
12	69.32 ± 3.28b	45.72 ± 1.70a
13	108.80 ± 0.69c	87.97 ± 4.49bc
14	98.89 ± 0.63d	92.88 ± 3.40c
15	110.35 ± 4.99c	86.91 ± 3.81b
16	111.69 ± 2.56c	80.32 ± 3.44d
17	73.28 ± 3.83b	71.23 ± 0.35e
ascorbic acid	5.79 ± 0.11	

[a]Data shown are mean ± standard deviation (SD) from SPSS; each data point was derived from three independent repetitions. LE, the ethanol extract; LEb, residual fraction after separating hexane fraction from the ethanol extract. Values with different letters within the column were significantly different ($P < 0.05$) as observed by Duncan's multiple range test for dried seeds and raw and dried rhizomes. Values with characters within raw and dried lotus rhizomes from the same growing region were significantly different as observed by the Student's t test (see P values in footnotes b, c, and d). [b]$P < 0.05$. [c]$P < 0.01$. [d]$P < 0.001$.

antioxidant, and its EC_{50} value of DPPH in this study was 5.79 μg/mL. Folin-Ciocalteu's phenol reagent is sensitive to not only phenolic compounds but also nonphenolic compounds such as vitamins and certain amino acids.[45] Studies in our laboratory showed that the Folin-Ciocalteu assay is very sensitive toward ascorbic acid while the aluminum chloride assay is not. In the Folin-Ciocalteu assay, 1 g of ascorbic acid shows 596.19 mg of GAE, but in the aluminum chloride assay, 1 g of ascorbic acid shows only 1.12 mg of CE. Therefore, the higher DPPH radical scavenging activity and total phenolic content may be attributed to a higher concentration of ascorbic acid in lotus rhizomes. In addition, the differences in the results between the current and previous study[15] may be due to potential differences in dryness and extraction conditions, which can affect the degree of oxidation and extraction efficiency of phenolic compounds and ascorbic acid.

Because the aluminum chloride coloration method is specific only for the analysis of anthoxanthins, including flavones and flavonols, estimation of total flavonoid content using this method likely underestimates the actual content.[46] In this study, similar total flavonoid content in lotus seeds and rhizomes indicated similarity in the concentration of anthoxanthins, not of other flavonoids.

Similar correlation coefficients were observed for DPPH radical scavenging activity and total phenolic and flavonoid content in the extracts of dried seeds and raw and dried rhizomes (Tables S1−S3, Supporting Information), respectively. The EC_{50} value significantly negatively correlated with the total phenolic content in lotus. A previous report also indicated that the total phenolic content in plant extracts significantly correlated with their free radical scavenging activity.[47] Therefore, our finding indicated that the total phenolic content in lotus extracts contributes to their antioxidant potential.

The HPLC analysis showed significant differences in the special flavonoids content for the LEb-2 fractions of dried lotus seeds and raw and dried rhizomes from various growing regions (Table 6). The highest concentrations of flavonoids identified in the LEb-2 fractions of lotus were as follows: catechin in seeds from Vietnam and raw and dried rhizomes from Japan; astragaline in seeds from China (Guangzhou), raw rhizomes from Korea (Muan), and dried rhizomes from Korea (Daegu); rutin in seeds from Vietnam, raw rhizomes from Japan, and dried rhizomes from China (Guangxi); and isoquercetin in seeds from Thailand, raw rhizomes from Korea (Siheung), and dried rhizomes from China (Guangxi). These results suggest that the variations in the concentration of special flavonoids in the LE fraction of lotus can be partly attributed to different growing conditions (e.g., weather and soil) and dryness. After drying, the concentration of catechin obviously increased and the concentration of other flavonoids obviously decreased in the LEb-2 fractions of rhizomes. A previous study showed that the concentration of special flavonoids such as catechin and isoquercetin in *Ziziphus jujuba* fruit was affected by the growing region, and the concentrations decreased after drying.[17]

Catechin in lotus embryos was determined by Geng et al.[48] A previous study showed that fresh seed coats from China (Wuhan) contained astragaline (7.2 mg/kg), rutin (11.8 mg/kg), and isoquercetin (55.8 mg/kg); while dried embryos contained rutin (4079.0 mg/kg) and isoquercetin (637.8 mg/kg).[24] However, in this study, the concentrations of astragaline, rutin, and isoquercetin (1.0−3.3 mg/kg, 81.7−166.5 mg/kg, and 17.8−36.1 mg/kg, respectively) were measured in dried lotus seeds, which included the seed coat, embryo, and endosperm. In dried lotus rhizomes from China (Hubei), the concentration of catechin was 25 mg/kg in rhizomes and 110 mg/kg in knots of rhizomes.[49] In this study, the concentration of catechin in dried rhizomes with knots varied from 13.2 to 133.7 mg/kg depending on the growing region and dryness. Lotus seeds that include the seed coat, embryo, and endosperm are rich in starch, lipids, and protein, and lotus rhizomes with knots contain more carbohydrates than isolated knots. This may be one of the reasons for the differences in specific flavonoid content between current and previous studies; the differences in the lotus-growing regions and analysis methods could also have contributed to the observed differences. Although many flavonoids found in lotus leaves and seeds have been previously reported,[24,34,49] the presence of astragaline, rutin, and isoquercetin in lotus rhizomes was first identified in this study. Because of the lower flavonoids contents in lotus rhizomes,[15] the levels of special flavonoids in rhizomes obtained from some growing regions were under the detection limit. In future studies, the unknown peaks in HPLC chromatograms are expected to be identified.

There were significant differences in alkaloid contents in the LEb-2 fraction of lotus seeds and raw and dried rhizomes from various growing regions (Table 7). After drying, the concentration of dauricine significantly increased and the concentration of neferine decreased in the LEb-2 fractions of rhizomes. The concentration of specific alkaloids in the LEb-2

Table 5. Total Phenolic and Flavonoid Content of the LE and LEb Fractions of Lotus Seeds and Rhizomes[a]

	total phenolic content		total flavonoid content	
no.	LE fraction (mg of GAE/(g of LE))	LEb fraction (mg of GAE/(g of LEb))	LE fraction (mg of CE/(g of LE))	LEb fraction (mg of CE/(g of LEb))
dried seeds				
1	21.63 ± 0.57a	23.27 ± 0.81a	13.88 ± 0.35a	16.52 ± 0.36a
2	13.99 ± 0.18b	14.61 ± 0.63b	8.21 ± 0.22b	8.18 ± 0.14b
3	18.65 ± 0.75c	19.67 ± 0.33c	8.51 ± 0.37b	8.57 ± 0.32b
4	31.22 ± 0.70d	32.57 ± 1.01d	13.34 ± 1.30a	14.62 ± 0.48c
5	24.70 ± 0.73e	28.04 ± 0.85e	10.91 ± 0.90c	10.48 ± 0.59d
raw rhizomes				
6	70.01 ± 5.94a[b]	74.72 ± 2.46a[b]	12.71 ± 1.23a	13.39 ± 0.62a
7	61.64 ± 0.75b[b]	67.24 ± 0.54b	13.21 ± 0.69b[b]	15.96 ± 0.67b[c]
8	41.65 ± 0.88c	41.94 ± 0.48c[d]	8.16 ± 0.15c	8.81 ± 0.66c
9	31.63 ± 1.37d[d]	38.68 ± 1.23d[d]	7.33 ± 0.18d	7.27 ± 0.02d
10	49.69 ± 1.43e	50.19 ± 1.54e[c]	11.34 ± 0.66a[c]	12.21 ± 0.30e
dried rhizomes				
11	82.21 ± 4.28a	80.05 ± 1.43a	13.05 ± 0.62a	14.24 ± 0.41a
12	64.63 ± 0.95b	65.70 ± 3.43b	11.41 ± 0.27b	11.60 ± 0.82b
13	43.19 ± 1.99c	54.47 ± 1.25c	7.83 ± 0.53c	9.25 ± 0.54c
14	29.20 ± 0.64d	33.41 ± 1.17d	7.94 ± 0.41c	13.44 ± 0.60a
15	31.21 ± 0.26d	31.14 ± 0.85d	8.74 ± 0.38d	9.02 ± 0.59c
16	52.17 ± 1.19e	51.81 ± 1.53c	6.82 ± 0.16e	7.12 ± 0.23d
17	53.38 ± 2.37e	60.46 ± 1.11e	9.33 ± 0.22d	12.11 ± 0.51b
ascorbic acid	596.19 ± 21.44		1.12 ± 0.09	

[a]Data shown are mean ± SD from SPSS; each data point was derived from three independent repetitions. LE, the ethanol extract; LEb, residual fraction after separating hexane fraction from the ethanol extract. Values with different letters within the column were significantly different ($P < 0.05$) as observed by Duncan's multiple range test of dried seeds and raw and dried rhizomes. Values with characters within raw and dried lotus rhizomes from the same growing region were significantly different as observed by the Student's *t* test (see *P* values given in footnotes *b*, *c*, and *d*). [b]$P < 0.05$. [c]$P < 0.01$. [d]$P < 0.001$.

Table 6. Concentrations of Individual Flavonoids in the LEb-2 Fractions of Lotus Seeds and Rhizomes (mg/(g of LEb-2))[a]

no.	catechin	astragaline	rutin	isoquercetin	total
dried seeds					
1	3.48 ± 0.78ab	0.08 ± 0.01a	11.29 ± 0.62a	2.58 ± 0.16a	17.43 ± 1.39a
2	3.89 ± 0.55b	0.38 ± 0.10b	14.76 ± 1.25b	2.71 ± 0.80a	21.74 ± 1.59b
3	0.79 ± 0.04c	0.11 ± 0.01a	7.15 ± 0.51c	1.56 ± 0.23b	9.60 ± 0.74c
4	9.16 ± 0.45d	0.26 ± 0.01c	17.32 ± 2.74b	2.66 ± 0.66a	29.40 ± 3.53d
5	2.70 ± 0.34a	0.15 ± 0.02a	7.14 ± 0.79c	2.89 ± 0.38a	12.88 ± 0.91c
raw rhizomes					
6	3.02 ± 0.01a	0.07 ± 0.01a		0.54 ± 0.14[b]	3.64 ± 0.15ab
7	3.23 ± 0.44a[d]				3.23 ± 0.44a[d]
8	1.43 ± 0.03b[d]	0.06 ± 0.01a[c]			1.49 ± 0.04c[d]
9	1.65 ± 0.10b[d]	0.11 ± 0.02b			1.76 ± 0.11c[d]
10	3.25 ± 0.46a[d]		0.22 ± 0.06	0.49 ± 0.02[d]	3.96 ± 0.46b[d]
dried rhizomes					
11	3.71 ± 0.45a	0.05 ± 0.01ab	0.10 ± 0.01a	0.03 ± 0.01a	3.89 ± 0.45a
12	8.06 ± 0.30b	0.09 ± 0.01c			8.15 ± 0.29b
13	6.83 ± 0.30c	0.03 ± 0.01d		0.07 ± 0.01b	6.93 ± 0.30c
14	1.45 ± 0.08d	0.08 ± 0.01c	0.43 ± 0.09b	0.18 ± 0.02c	2.15 ± 0.16d
15	0.67 ± 0.05e	0.04 ± 0.01ad	0.30 ± 0.01c	0.12 ± 0.01d	1.13 ± 0.05e
16	2.98 ± 0.14f	0.07 ± 0.03bc			3.05 ± 0.14f
17	9.53 ± 0.52g	0.06 ± 0.01ab	0.22 ± 0.03c	0.16 ± 0.01c	9.96 ± 0.50g

[a]Data shown are mean ± SD from SPSS; each data point was derived from three independent repetitions. Values with different letters (a~g) within the column were significantly different ($P < 0.05$) as observed by Duncan's multiple range test for dried lotus seeds and raw and dried lotus rhizomes, respectively. Values with characters within raw and dried lotus rhizomes from the same growing region were significantly different as observed by the Student's *t* test (see P values given in footnotes *c* and *d*). [b]$P < 0.05$. [cb]$P < 0.01$. [d]$P < 0.001$.

fraction of seeds was higher than that of rhizomes. This finding may be because of the higher concentration of alkaloids detected in lotus embryos.[12,50] The highest concentrations of alkaloids identified in the LEb-2 fractions of lotus were as follows: nuciferine in seeds from Korea (Muan), raw rhizomes from Japan, and dried rhizomes from China (Guangxi); dauricine in seeds from China (Guangzhou) and raw and dried rhizomes from Japan; isoliensinine in seeds from

Table 7. Concentrations of Individual Alkaloids in the LEb-2 Fractions of Lotus Seeds and Rhizomes (mg/(g of LEb-2))

no.	nuciferine	dauricine	isoliensinine	neferine	total
dried seeds					
1	4.97 ± 0.13a	3.55 ± 0.21a	1.49 ± 0.15a	14.24 ± 0.56a	24.24 ± 0.77a
2	2.06 ± 0.03b	3.91 ± 0.05a	19.37 ± 0.50b	20.14 ± 1.01b	45.48 ± 1.52b
3	0.99 ± 0.02c	1.93 ± 0.13b	19.02 ± 1.39b	27.35 ± 0.27c	49.29 ± 1.06c
4	1.58 ± 0.06d	2.18 ± 0.71b	19.48 ± 0.95b	28.40 ± 1.39c	51.64 ± 3.06c
5	1.48 ± 0.16d	3.53 ± 0.99a	9.61 ± 1.62c	8.58 ± 0.29d	23.20 ± 2.89a
raw rhizomes					
6		2.87 ± 0.04a[c]		1.59 ± 0.32a	4.46 ± 0.29a
7	0.25 ± 0.09	1.64 ± 0.17b[b]	1.49 ± 0.03	2.21 ± 0.15a[c]	5.60 ± 0.35b[c]
8		1.37 ± 0.34b[b]		3.07 ± 0.27b	4.44 ± 0.26a
9		1.33 ± 0.21b			1.33 ± 0.21c[d]
10	0.26 ± 0.03	5.43 ± 0.08c[b]		4.09 ± 0.06c[c]	9.78 ± 0.14d
dried rhizomes					
11	0.15 ± 0.01a	2.60 ± 0.06a		2.16 ± 0.39a	4.91 ± 0.45a
12	0.22 ± 0.03b	2.13 ± 0.14bc	1.53 ± 0.06a	2.69 ± 0.07ab	6.57 ± 0.25b
13		2.26 ± 0.20ac		2.54 ± 0.56ab	4.80 ± 0.68a
14	0.48 ± 0.01c	1.77 ± 0.26bd	1.40 ± 0.17a	3.78 ± 0.23c	7.43 ± 0.26b
15	0.29 ± 0.04d	2.37 ± 0.40ac	4.69 ± 0.80b	7.13 ± 0.89d	14.48 ± 2.12c
16		1.44 ± 0.02d		1.93 ± 0.06a	3.36 ± 0.06a
17	0.27 ± 0.01d	6.00 ± 0.21e		3.23 ± 0.25bc	9.50 ± 0.41d

[a]Data shown are mean ± SD from SPSS; each data point was derived from three independent repetitions. Values with different letters (a~e) within the column were significantly different ($P < 0.05$) as observed by Duncan's multiple range test for dried lotus seeds and raw and dried lotus rhizomes, respectively. Values with characters within raw and dried lotus rhizomes from the same growing region were significantly different as observed by the Student's t test (see P values in footnotes b, c, and d). [b]$P < 0.05$. [c]$P < 0.01$. [d]$P < 0.001$.

Vietnam, raw rhizomes from Korea (Daegu), and dried rhizomes from Vietnam; and neferine in seeds from Vietnam, raw rhizomes from Japan, and dried rhizomes from Vietnam. These results suggested that the concentration of special alkaloids in the lotus extracts can vary depending on the growing region and dryness.

The presence of dauricine in lotus embryos was first reported in 1961.[51] In previous reports from China, the concentration of nuciferine in dried lotus embryos from Hubei was reported to be 10.2 mg/kg,[52] while the concentrations of isoliensinine and neferine in dried lotus embryos from Shanghai were reported as 2466.7 and 226.4 mg/kg, respectively.[26] These concentrations were different from those obtained in this study for nuciferine, isoliensinine, and neferine in dried lotus seeds (11.3−62.7, 18.8−217.2, and 93.7−312.4 mg/kg). These differences between current and previous studies may be attributed to the fact that we used whole lotus seeds containing endosperm rich in starch, lipids, and protein, and this may have affected the concentration of alkaloids. Moreover, the concentration of alkaloids in lotus seeds may vary depending on the growing region and analysis methods. In addition, the presence of dauricine, nuciferine, isoliensinine, and neferine in lotus rhizomes was first identified in this study. The concentrations of special alkaloids in rhizomes from some growing regions were under the detection limit because lotus rhizomes generally have lower levels of alkaloids. There were some unknown peaks in the HPLC chromatograms that need further analysis.

In conclusion, the antioxidant activity and total phenolic and flavonoid content in lotus seeds and rhizomes varied characteristically depending on the growing region and dryness. Total phenolic content in the LE fraction positively correlated with the antioxidant activity. In addition, the LE fractions of lotus seeds and rhizomes contained several specific flavonoids and alkaloids, and their concentrations also varied depending on the growing region and dryness. The HPLC analysis showed that the LE fractions of lotus seeds from Vietnam, raw rhizomes from Korea (Siheung), and dried rhizomes from Japan have the highest flavonoid content, and they were 2.25, 3.34, and 10.07 times more than the flavonoid content in samples with the lowest levels, that is, the seeds from China (Hubei), raw rhizomes from Korea (Haman), and dried rhizomes from Vietnam, respectively. However, the LE fractions of seeds from China (Hubei), raw rhizomes from Japan, and dried rhizomes from Korea (Siheung) had the highest alkaloid content. The HPLC analysis indicated that these samples contained 2.08, 6.15, and 6.41 times more alkaloid content than the samples with the lowest alkaloid levels which were the seeds and raw and dried rhizomes from Korea (Muan), respectively. Therefore, these results indicated that the conditions in the growing region may significantly affect the antioxidant activity and concentration of functional components in the extracts of lotus seeds and rhizomes. The antioxidant activity and concentration of functional components in rhizomes were also sensitive to dryness. Moreover, this study is the first to detect the presence of astragaline, rutin, isoquercetin, dauricine, nuciferine, isoliensinine, and neferine in lotus rhizomes and to provide novel data regarding these functional components. Therefore, the lotus part, i.e., seeds or rhizomes, obtained from different growing regions can be selected based on the antioxidant activity and concentration of functional components for specific applications as functional foods.

■ ASSOCIATED CONTENT

Ⓢ Supporting Information

Correlation coefficients among EC_{50} values and total phenolic and flavonoid content of lotus seeds (Table S1) and raw (Table S2) and dried rhizomes (Table S3). This material is available free of charge via the Internet at http://pubs.acs.org.

AUTHOR INFORMATION

Corresponding Author

*E-mail: shkim@konkuk.ac.kr. Tel.: +82-02-450-3420. Fax: +82-02-3436-5382.

Funding

This work was supported by Konkuk University in 2011.

Notes

The authors declare no competing financial interest.

ACKNOWLEDGMENTS

We express warm thanks to Dr. Sung Wha Seok of K&S Medical Center for his kind comments on this manuscript.

REFERENCES

(1) Beecher, G. R. Overview of dietary flavonoids: Nomenclature, occurrence and intake. *J. Nutr.* **2003**, *133* (10), 3248S−3254S.

(2) Toyoda, M.; Tanaka, K.; Hoshino, K.; Akiyama, H.; Tanimura, A.; Saito, Y. Profiles of potentially antiallergic flavonoids in 27 kinds of health tea and green tea infusions. *J. Agric. Food Chem.* **1997**, *45* (7), 2561−2564.

(3) Hämäläinen, M.; Nieminen, R.; Vuorela, P.; Heinonen, M.; Moilanen, E. Anti-inflammatory effects of flavonoids: Genistein, kaempferol, quercetin, and daidzein inhibit STAT-1 and NF-κB activations, whereas flavone, isorhamnetin, naringenin, and pelargonidin inhibit only NF-κB activation along with their inhibitory effect on iNOS expression and NO production in activated macrophages. *Mediators Inflammation* **2007**, *2007*, 1−10.

(4) Kaul, T. N.; Middleton, E.; Ogra, P. L. Antiviral effect of flavonoids on human viruses. *J. Med. Virol.* **1985**, *15* (1), 71−79.

(5) Nagai, T.; Suzuki, Y.; Tomimori, T.; Yamada, H. Antiviral activity of plant flavonoid, 5, 7, 4′-trihydroxy-8-methoxyflavone, from the roots of Scutellaria baicalensis against influenza A (H3N2) and B viruses. *Biol. Pharm. Bull.* **1995**, *18* (2), 295−299.

(6) Ferguson, P. J.; Kurowska, E.; Freeman, D. J.; Chambers, A. F.; Koropatnick, D. J. A flavonoid fraction from cranberry extract inhibits proliferation of human tumor cell lines. *J. Nutr.* **2004**, *134* (6), 1529−1535.

(7) Cui, Y.; Morgenstern, H.; Greenland, S.; Tashkin, D. P.; Mao, J. T.; Cai, L.; Cozen, W.; Mack, T. M.; Lu, Q. Y.; Zhang, Z. F. Dietary flavonoid intake and lung cancer—A population-based case-control study. *Cancer* **2008**, *112* (10), 2241−2248.

(8) Cho, E. J.; Yokozawa, T.; Rhyu, D. Y.; Kim, S. C.; Shibahara, N.; Park, J. C. Study on the inhibitory effects of Korean medicinal plants and their main compounds on the 1,1-diphenyl-2-picrylhydrazyl radical. *Phytomedicine* **2003**, *10* (6−7), 544−551.

(9) Xiao, J. H.; Zhang, J. H.; Chen, H. L.; Feng, X. L.; Wang, J. L. Inhibitory effects of isoliensinine on bleomycin-induced pulmonary fibrosis in mice. *Planta Med.* **2005**, *71* (3), 225−230.

(10) Sugimoto, Y.; Furutani, S.; Itoh, A.; Tanahashi, T.; Nakajima, H.; Oshiro, H.; Sun, S.; Yamada, J. Effects of extracts and neferine from the embryo of *Nelumbo nucifera* seeds on the central nervous system. *Phytomedicine* **2008**, *15* (12), 1117−1124.

(11) Kashiwada, Y.; Aoshima, A.; Ikeshiro, Y.; Chen, Y.-P.; Furukawa, H.; Itoigawa, M.; Fujioka, T.; Mihashi, K.; Cosentino, L. M.; Morris-Natschke, S. L.; Lee, K.-H. Anti-HIV benzylisoquinoline alkaloids and flavonoids from the leaves of *Nelumbo nucifera*, and structure-activity correlations with related alkaloids. *Bioorg. Med. Chem.* **2005**, *13* (2), 443−448.

(12) Jung, H. A.; Jin, S. E.; Choi, R. J.; Kim, D. H.; Kim, Y. S.; Ryu, J. H.; Kim, D.-W.; Son, Y. K.; Park, J. J.; Choi, J. S. Anti-amnesic activity of neferine with antioxidant and anti-inflammatory capacities, as well as inhibition of ChEs and BACE1. *Life Sci.* **2010**, *87* (13−14), 420−430.

(13) Bin, X.; Jin, W.; Wenqing, W.; Chunyang, S.; Xiaolong, H.; Jianguo, F. *Nelumbo nucifera* alkaloid inhibits 3T3-L1 preadipocyte differentiation and improves high-fat diet-induced obesity and body fat accumulation in rats. *J. Med. Plant. Res.* **2011**, *5* (10), 2021−2028.

(14) Chen, S.; Xiang, Y.; Deng, J.; Liu, Y. L.; Li, S. H. Simultaneous analysis of anthocyanin and non-anthocyanin flavonoid in various tissues of different lotus (*Nelumbo*) cultivars by HPLC-DAD-ESI-MS^n. *PloS One* **2013**, *8* (4), 1−13.

(15) Jung, H. A.; Jung, Y. J.; Yoon, N. Y.; Jeong, D. M.; Bae, H. J.; Kim, D.-W.; Na, D. H.; Choi, J. S. Inhibitory effects of *Nelumbo nucifera* leaves on rat lens aldose reductase, advanced glycation endproducts formation, and oxidative stress. *Food Chem. Toxicol.* **2008**, *46* (12), 3818−3826.

(16) Huang, B.; Ban, X.; He, J.; Tong, J.; Tian, J.; Wang, Y. Comparative analysis of essential oil components and antioxidant activity of extracts of *Nelumbo nucifera* from various areas of China. *J. Agric. Food Chem.* **2010**, *58* (1), 441−448.

(17) Chen, J.; Li, Z.; Maiwulanjiang, M.; Zhang, W. L.; Zhan, J. Y.; Lam, C. T.; Zhu, K. Y.; Yao, P.; Choi, R. C.; Lau, D. T. Chemical and biological assessment of *Ziziphus jujuba* fruits from China: Different geographical sources and developmental stages. *J. Agric. Food Chem.* **2013**, *61* (30), 7315−7324.

(18) *Encyclopedia of Chinese traditional medicine*; Shanghai Science and Technology Press: Shanghai, 1977, vol. *2*, 1803−1804, 2690.

(19) Mani, S. S.; Subramanian, I. P.; Pillai, S. S.; Muthusamy, K. Evaluation of hypoglycemic activity of inorganic constituents in *Nelumbo nucifera* seeds on streptozotocin-induced diabetes in rats. *Biol. Trace. Elem. Res.* **2010**, *138* (1−3), 226−237.

(20) Sohn, D. H.; Kim, Y. C.; Oh, S. H.; Park, E. J.; Li, X.; Lee, B. H. Hepatoprotective and free radical scavenging effects of *Nelumbo nucifera*. *Phytomedicine* **2003**, *10* (2−3), 165−169.

(21) Tsuruta, Y.; Nagao, K.; Kai, S.; Tsuge, K.; Yoshimura, T.; Koganemaru, K.; Yanagita, T. Polyphenolic extract of lotus root (edible rhizome of *Nelumbo nucifera*) alleviates hepatic steatosis in obese diabetic db/db mice. *Lipids Health Dis.* **2011**, *10* (1), 202−230.

(22) Yen, G. C.; Duh, P. D.; Su, H. J.; Yeh, C. T.; Wu, C. H. Scavenging effects of lotus seed extracts on reactive nitrogen species. *Food Chem.* **2006**, *94* (4), 596−602.

(23) Hu, M.; Skibsted, L. H. Antioxidative capacity of rhizome extract and rhizome knot extract of edible lotus (*Nelumbo nuficera*). *Food Chem.* **2002**, *76* (3), 327−333.

(24) Chen, S.; Fang, L. C.; Xi, H. F.; Guan, L.; Fang, J. B.; Liu, Y. L.; Wu, B. H.; Li, S. H. Simultaneous qualitative assessment and quantitative analysis of flavonoids in various tissues of lotus (*Nelumbo nucifera*) using high performance liquid chromatography coupled with triple quad mass spectrometry. *Anal. Chim. Acta* **2012**, *724* (29), 127−135.

(25) Wu, S.; Sun, C.; Cao, X.; Zhou, H.; Hong, Z.; Pan, Y. Preparative counter-current chromatography isolation of liensinine and its analogues from embryo of the seed of *Nelumbo nucifera* Gaertn. using upright coil planet centrifuge with four multilayer coils connected in series. *J. Chromatogr. A* **2004**, *1041* (1−2), 153−162.

(26) Chen, Y.; Fan, G.; Wu, H.; Wu, Y.; Mitchell, A. Separation, identification and rapid determination of liensine, isoliensinine and neferine from embryo of the seed of *Nelumbo nucifera* Gaertn. by liquid chromatography coupled to diode array detector and tandem mass spectrometry. *J. Pharm. Biomed. Anal.* **2007**, *43* (1), 99−104.

(27) Yang, T. H.; Chen, C. M. On the alkaloids of *Nelumbo nucifera* Gaertn. Studies on the alkaloids of loti embryo. *J. Chin. Chem. Soc.* **1970**, *17* (4), 113−120.

(28) Xu, J.; Guo, C. J.; Wei, J. Y.; Yang, J. J.; Cheng, S.; Wu, J. Q. The method of HPLC for determination of major flavomoids in vegetables [J]. *Acta Nutr. Sin.* **2005**, *27* (4), 276−279.

(29) Cao, J.; Chen, W.; Zhang, Y.; Zhang, Y.; Zhao, X. Content of selected flavonoids in 100 edible vegetables and fruits. *Food Sci. Technol. Res.* **2010**, *16* (5), 395−402.

(30) Kim, J. S.; Cho, S. M.; Kim, J. H.; Lee, M. W. Phenolic compounds from the node of lotus rhizome (*Nelumbo nucifera* Gaerth). *Yakhak Hoechi* **2001**, *45* (6), 599−603.

(31) You, J. S.; Lee, Y. J.; Kim, K. S.; Kim, S. H.; Chang, K. J. Anti-obesity and hypolipidaemic effects of *Nelumbo nucifera* seed ethanol extract in human pre-adipocytes and rats fed a high-fat diet. *J. Sci. Food Agric.* **2013**, DOI: 10.1002/jsfa.6297.

(32) Chang, K. J. *A preclinical study of lotus and development of individualized program for healthy weight control and publicity contents using lotus for globalization of Korean food*; Ministry of Food, Agriculture, Forestry and Fisheries: Seoul, Republic of Korea, 2013.
(33) Zhao, X.; Shen, J.; Chang, K. J.; Kim, S. H. Analysis of fatty acids and phytosterols in ethanol extracts of *Nelumbo nucifera* seeds and rhizomes by GC-MS. *J. Agric. Food Chem.* **2013**, *61* (28), 6841−6847.
(34) Lin, H. Y.; Kuo, Y. H.; Lin, Y. L.; Chiang, W. Antioxidative effect and active components from leaves of Lotus (*Nelumbo nucifera*). *J. Agric. Food Chem.* **2009**, *57* (15), 6623−6629.
(35) Deng, S.; Deng, Z.; Fan, Y.; Peng, Y.; Li, J.; Xiong, D.; Liu, R. Isolation and purification of three flavonoid glycosides from the leaves of *Nelumbo nucifera* (Lotus) by high-speed counter-current chromatography. *J. Chromatogr. B* **2009**, *877* (24), 2487−2492.
(36) Zhenjia, Z.; Minglin, W.; Daijie, W.; Wenjuan, D.; Xiao, W.; Chengchao, Z. Preparative separation of alkaloids from *Nelumbo nucifera* leaves by conventional and pH-zone-refining counter-current chromatography. *J. Chromatogr. B* **2010**, *878* (19), 1647−1651.
(37) Chen, S.; Wu, B. H.; Fang, J. B.; Liu, Y. L.; Zhang, H. H.; Fang, L. C.; Guan, L.; Li, S. H. Analysis of flavonoids from lotus (*Nelumbo nucifera*) leaves using high performance liquid chromatography/photodiode array detector tandem electrospray ionization mass spectrometry and an extraction method optimized by orthogonal design. *J. Chromatogr. A* **2012**, *1227*, 145−153.
(38) Xu, S. Y.; Shoemaker, C. F. Gelatinization properties of Chinese water chestnut starch and lotus root starch. *J. Food Sci.* **1986**, *51* (2), 445−449.
(39) United States Department of Agriculture. Basic Report: 11254, Lotus root, raw http://ndb.nal.usda.gov/ndb/foods/show/3051.
(40) United States Department of Agriculture. Basic Report: 12205, Seeds, lotus seeds, raw http://ndb.nal.usda.gov/ndb/foods/show/3755.
(41) Yen, G. C.; Duh, P. D.; Su, H. J. Antioxidant properties of lotus seed and its effect on DNA damage in human lymphocytes. *Food Chem.* **2005**, *89* (3), 379−385.
(42) McGhie, T. K.; Hunt, M.; Barnett, L. E. Cultivar and growing region determine the antioxidant polyphenolic concentration and composition of apples grown in New Zealand. *J. Agric. Food Chem.* **2005**, *53* (8), 3065−3070.
(43) Annegowda, H.; Bhat, R.; Joon, Y. K.; Min-Tze, L.; Karim, A.; Mansor, S. Influence of drying treatments on polyphenolic contents and antioxidant properties of raw and ripe papaya (*Carica Papaya L.*). *Int. J. Food Prop.* **2014**, *17* (2), 283−292.
(44) Park, Y. S.; Towantakavanit, K.; Kowalska, T.; Jung, S. T.; Ham, K. S.; Heo, B. G.; Cho, J. Y.; Yun, J. G.; Kim, H. J.; Gorinstein, S. Bioactive compounds and antioxidant and antiproliferative activities of Korean white lotus cultivars. *J. Med. Food* **2009**, *12*, 1057−1064.
(45) Everette, J. D.; Bryant, Q. M.; Green, A. M.; Abbey, Y. A.; Wangila, G. W.; Walker, R. B. Thorough study of reactivity of various compound classes toward the Folin-Ciocalteu reagent. *J. Agric. Food Chem.* **2010**, *58* (14), 8139−8144.
(46) Chang, C. C.; Yang, M. H.; Wen, H. M.; Chern, J. C. Estimation of total flavonoid content in propolis by two complementary colorimetric methods. *J. Food Drug Anal.* **2002**, *10* (3), 178−182.
(47) Dudonné, S.; Vitrac, X.; Coutière, P.; Woillez, M.; Mérillon, J. M. Comparative study of antioxidant properties and total phenolic content of 30 plant extracts of industrial interest using DPPH, ABTS, FRAP, SOD, and ORAC assays. *J. Agric. Food Chem.* **2009**, *57* (5), 1768−1774.
(48) Geng, C. H.; Wang, W. Y.; Lin, M.; Ye, J. N. Determination of flavonoids in Plumula Nelumbini by micellar electrokinetic capillary electrophoresis with electrochemical detection. *J. Capillary Electrophor. Microchip Technol.* **2006**, *10* (3−4), 57−61.
(49) Yan, S. L.; Wang, Q. Z.; Peng, G. H. Determination of catechin in lotus rhizomes by high-performance liquid chromatography. *Int. J. Food Sci. Nutr.* **2009**, *60* (5), 432−438.
(50) Huang, Y.; Zhao, L.; Bai, Y.; Liu, P.; Wang, J.; Xiang, J. Simultaneous determination of liensinine, isoliensinine and neferine from seed embryo of *Nelumbo nucifera* Gaertn. in rat plasma by a rapid HPLC method and its application to a pharmacokinetic study. *Arzneimittel Forschung* **2011**, *61* (6), 347−352.
(51) Tomita, M.; Furukawa, H.; Yang, T. H. Alkaloids of *Nelumbo nucifera* Gaertn. *Yakugaku Zasshi* **1961**, *81*, 469−473.
(52) Wang, J. L.; Hu, X. M.; Yin, W. H.; Cai, H. S. Analysis of alkaloids in lotus embryo. *J. Chin. Med. Mater.* **1991**, *14* (6), 36−38.

JOURNAL OF AGRICULTURAL AND FOOD CHEMISTRY

Article

pubs.acs.org/JAFC

Analysis of Different European Hazelnut (*Corylus avellana* L.) Cultivars: Authentication, Phenotypic Features, and Phenolic Profiles

Loredana F. Ciarmiello,[†,‡] Maria F. Mazzeo,[‡,§] Paola Minasi,[§] Angela Peluso,[§] Antonio De Luca,[†] Pasquale Piccirillo,[†] Rosa A. Siciliano,*[,§] and Virginia Carbone[§]

[†]Unità di Ricerca per la Frutticoltura (Fruit Tree Research Unit), Consiglio per la Ricerca e la Sperimentazione in Agricoltura, Via Torrino, 3, 81100 Caserta, Italy

[§]Centro di Spettrometria di Massa Proteomica e Biomolecolare, Istituto di Scienze dell'Alimentazione, Consiglio Nazionale delle Ricerche, Via Roma, 64, 83100 Avellino, Italy

Supporting Information

ABSTRACT: Hazelnuts exhibit functional properties due to their content in fatty acids and phenolic compounds that could positively affect human health. The food industry requires precise traits for morphological, chemical, and physical kernel features so that some cultivars could be more suitable for specific industrial processing. In this study, agronomical and morphological features of 29 hazelnut cultivars were evaluated and a detailed structural characterization of kernel polyphenols was performed, confirming the presence of protocatechuic acid, flavan-3-ols such as catechin, procyanidin B2, six procyanidin oligomers, flavonols, and one dihydrochalcone in all the analyzed cultivars. In addition, an innovative methodology based on the MALDI-TOF mass spectrometric analysis of peptide/protein components extracted from kernels was developed for the authentication of the most valuable cultivars. The proposed method is rapid, simple, and reliable and holds the potential to be applied in quality control processes. These results could be useful in hazelnut cultivar evaluation and choice for growers, breeders, and food industry.

KEYWORDS: *European hazelnut, bioagronomical characterization, polyphenols, MALDI-TOF-MS, cultivar authentication*

INTRODUCTION

European hazelnut (*Corylus avellana* L.) is a diploid ($2n = 2x = 22$), monoecious, open pollinated tree. It has self-incompatibility, due to negative chemical interaction between pollen and style tissue, which enforces cross-pollination.[1]

Hazelnut kernels are rich in fats, proteins, and vitamins and play a relevant role in the agricultural market, mainly because of their use to provide flavor in dairy, bakery, confectionery, candy, and chocolate products. In fact, the aroma is considered to be among the primary determinants of nut quality and is improved by the roasting process. Therefore, the majority of the world hazelnut crop is roasted, thus developing a unique aroma that depends on the cultivar used and on the roasting conditions applied. The volatile profiles of fresh and roasted products were characterized by integrating sensory evaluation, nuclear magnetic resonance (NMR), high-resolution gas chromatography-olfactometry (HRGC-O), high-resolution gas chromatography-mass spectrometry (HRGC-MS), and two-dimensional gas chromatography-mass spectrometry.[2] More recently a new discipline, named sensomics, has been introduced that was aimed to perform a quantitative analysis of the entire set of aroma compounds of a given food, thus defining its sensometabolome. This methodology was applied to the analysis of odorant compounds in raw and roasted hazelnuts of different cultivars.[3,4]

European hazelnut is one of the most cultivated nut crops worldwide. This species spread from Asia Minor and Caucasus region to Europe and North Africa. Italian hazelnut production is 85.232 tons yearly for in-shell product.[5] Particularly, Campania, Lazio, Piemonte, and Sicilia account for 98% of the national production. About 90% of the world crop is sold as kernels and processed in the food industry (i.e., chocolates, bakery, dairy), and the remaining 10% is sold as in-shell product and consumed fresh, blanched, or roasted.[6] The food industry requires uniform high-quality nuts and precise morphological, chemical, and physical kernel characteristics, as well as absence of defects.[7,8] European hazelnut includes several cultivars, biotypes, and accessions, and many of these come from Europe and Turkey. These cultivars show a high level of genetic diversity for traits such as vigor, growth habits, suckering, nut size and shape, and shell thickness.[1] Cultivars more used in the food industry are Tonda Gentile delle Langhe, also named Tonda Gentile Trilobata, Tonda Gentile Romana, Tonda di Giffoni, S. Giovanni, Mortarella, and Riccia di Talanico, cultivated in Italy; Tombul, Sivri, Palaz, and Fosa, cultivated in Turkey; Negret and Pauetet produced in Spain. Among Italian cultivars, Tonda di Giffoni and Tonda Gentile delle Langhe gained the Protected Geographical Indication (PGI) European marks "Nocciola di Giffoni" and "Nocciola Piemonte", respectively. These cultivars are particularly appreciated for their agronomic traits such as resistance to pathogens and pests, round kernels of excellent quality, and consistent yields, and for their processing qualities such as

Received: April 16, 2014
Revised: June 12, 2014
Accepted: June 13, 2014
Published: June 13, 2014

 © 2014 American Chemical Society

sweetness, low burnt aroma, and cooked bread aroma.[9,10] Other minor Italian cultivars such as Tonda Bianca, Tonda Rossa, Camponica, and Riccia di Talanico are mainly destined to be sold in shelled form as snacks for direct consumption (fresh consumption).[7,11] USA production, especially that from Oregon, is principally destined for fresh consumption and only recently has been directed to industrial use.[12]

Hazelnut consumption may have a positive influence on human health,[13,14] as kernels are rich in unsaturated fatty acids (i.e., oleic, palmitic, stearic, linoleic, and linolenic acids)[15] and in α-tocopherol (vitamin E) and polyphenols.[16,17] Furthermore, the presence of Fe, Zn, and Cu and a high K/Na ratio make hazelnut interesting for human diets, and especially for electrolyte balance.[17] The bioaccessibility of essential and toxic elements in hazelnut kernels has been also evaluated.[18]

In this context, the analysis of nut and kernel phenotypic traits and polyphenolic content could lead to define genotype specific features, providing information useful to growers, breeders, and the food industry for cultivar evaluation and choice. The agronomical and morphological features of 29 hazelnut cultivars originating from different geographical areas were characterized in this study. In addition, a comprehensive study of the phenolic composition of extracts from hazelnut kernels was conducted.

The authentication of different cultivars is also crucial in the definition of hazelnut quality. Traditional methods to identify hazelnut cultivars were based on phenotypic observations that may be affected by environmental and developmental factors, making cultivar differentiation difficult. Therefore, the development of innovative analytical methodologies that could suitably integrate well-established protocols for cultivar authentication is clearly desirable. DNA-typing methods such as random amplification of polymorphic DNA (RAPD), inter-simple sequence repeat (ISSR), restriction fragment length polymorphism (RFLP), amplification refractory mutation system (ARMS-PCR), and simple sequence repeat (SSR) were known to be useful for revealing genetic polymorphisms among different cultivars and accurately identifying hazelnut cultivars. However, these methods were laborious and time-consuming and were mainly applied on leaf material.[19−21]

Other approaches used for hazelnut cultivar identification were based on the analysis of volatile constituents and metabolites using chromatographic and/or spectroscopic techniques such as gas chromatography coupled to mass spectrometry (GC-MS)[22] and NMR[10,23] as well as on the analysis of trace elements such as lanthanides by means of inductively coupled plasma mass spectrometry (ICP-MS).[24] In addition, a few papers describe the application of molecular profiling strategies based on matrix-assisted laser desorption ionization time-of-flight mass spectrometry (MALDI-TOF-MS) in food science,[25,26] and novel methodologies have been developed for authentication and detection of fraud in different food matrices.[27,28] In this study, a similar approach has been developed, based on the MALDI-TOF-MS analysis of the peptide/protein fraction extracted from kernels, and, for the first time, has been applied to hazelnut cultivar authentication.

MATERIALS AND METHODS

Plant Material. Twenty-nine hazelnut cultivars originating from different geographical areas were used (Table 1). Three plants per cultivar were maintained in the same agronomical and pedoclimatical conditions, in the Fruit Tree Research Unit's collection field (CRA-FRC) located in Pignataro Maggiore (Caserta province, Italy). All plants were about seven years old.

Chemicals. High performance liquid chromatography (HPLC) grade methanol, HPLC grade acetonitrile, and formic acid were obtained from Merck (Darmstadt, Germany). HPLC grade *n*-hexane and chloroform were obtained from Carlo Erba (Milan, Italy). Protocatechuic acid, quercetin-3-*O*-rhamnoside (quercitrin), phloretin-2′-*O*-glucoside (phloridzin), myricetin, sodium carbonate, sinapinic acid, and ribonuclease A (Rnase A) and trifluoroacetic acid (TFA) were purchased from Sigma Chemical Company (St. Louis, MO, USA). (+)-Catechin, procyanidin B2, and myricetin-3-*O*-rhamnoside (myricitrin) were purchased from Extrasynthese (Genay, France). HPLC grade water (18.2 mΩ) was prepared using a Millipore Milli-Q purification system (Millipore Corp., Bedford, MA, USA).

Agronomical and Pomological Characterization. Agronomical and pomological traits were evaluated for each cultivar for three years (2010−2012), according to the guidelines provided by Bioversity International in the "Descriptor for Hazelnut".[29] The investigated plants were taken from the Fruit Tree Research Unit's collection field (Pignataro Maggiore-Caserta, Campania, South Italy). Nut samples from the selected cultivars were collected at the ripening time optimum for each cultivar, i.e., when nut falling, observed at maturity, occurred.[29] Nut samples were dried at 43 °C to prevent quality deterioration and rancidity, frozen with carbon dioxide to destroy insect pests, and stored according to good handling practices in clean, closed vials at room temperature. Twelve standard descriptors were evaluated.[29] Agronomical traits, such as growth habit, vigor, and suckering, were evaluated on three plants per cultivar. Pomological traits, such as nut shape, nut weight, kernel weight, and yield, were estimated on 50 nuts per cultivar for each year (Table 1). These characters were monitored following previously reported guidelines.[30,31] The percentage of pellicle removal was estimated after blanching kernels at 115 °C for 20 min and skin was removed by mechanical brushing.[32]

Sample Treatment and Polyphenol Extraction. Kernels (with skin) were ground with an electric blender, and, for each cultivar, 5 g of these samples was defatted three times with 10 mL of *n*-hexane, with the help of an ultrasonic bath, and then filtered through filter paper. The defatted samples were extracted with 15 mL of methanol in an ultrasonic bath for 60 min. Extracts were then dried in a rotary evaporator (LaboRota 4000/HB Efficient, Heidolph, Schwabach, Germany) and stored at −20 °C until analysis.

HPLC-UV Analysis. Extracts from different hazelnut cultivars were analyzed by HPLC-UV using a HP 1110 series HPLC (Agilent, Palo Alto, CA, USA) equipped with a binary pump (G-1312A) and a UV detector (G-1314A). Compounds were separated on an XBridge BEH C18 column (130 Å, 5 μm, 4.6 mm × 150 mm) (Waters, Milford, MA, USA) at a flow rate of 1 mL/min; solvent A was 0.1% formic acid, and solvent B was 0.1% formic acid in acetonitrile. After an 8 min hold at 2% solvent B, elution was performed according to the following conditions: from 2% (B) to 35% (B) in 42 min, from 35% (B) to 95% (B) in 2 min, followed by 10 min of maintenance. Extracts were reconstituted in HPLC solvent A prior to injection into the HPLC, and chromatograms were acquired at 280 nm. Standard curves for each polyphenol standard were prepared over a concentration range of 2.5−30 μg/mL with five different concentration levels and duplicate injections at each level. Peak area ratios between the areas of each polyphenol standard and those of myricetin, used as internal standard, were calculated and plotted against the corresponding standard concentration, using weighted linear regression to generate standard curves. All samples were prepared and analyzed in duplicate. Results were expressed as mg/kg of fresh weight (FW).

ESI-ITMS^n Analysis. Identification of phenolic compounds present in the different HPLC separated fractions was carried out by electrospray ionization multistage ion trap mass spectrometry (ESI-ITMS^n) using a Finnigan LCQ DECA XP Max ion trap mass spectrometer (Thermo Finnigan, San Jose, CA, USA) equipped with Xcalibur system manager data acquisition software (Thermo Finnigan, San Jose, CA, USA). Mass spectra were recorded from mass/charge (m/z) 50 to 1200 in negative ionization mode. The capillary voltage

Table 1. Geographic Origin and Values of Representative Agronomic and Carpological Traits[a] for 29 Cultivars of Hazelnut *Corylus avellana* L.[b]

cultivar name	locally origin	growth habit	vigor	suckering	bud break[c]	nut shape	shell color	shell thickness	nut wt (g)	kernel wt (g)	kernel yield (%)	pellicle removal (%)	kernel fiber texture
Amandi	Spain	intermediate	Medium-high	strong	late	subcylindrical short	auburn	relatively thin	1.85	0.86	46.3	39.9	medium corky
Apolda	Italy	spreading	intermediate	strong	intermediate	suboval	light brown striated	medium	3.30	1.40	42.4	19.8	light corky
Avellana sp	Italy	semierect	intermediate	strong	intermediate	subspheroidal	light brown	medium	2.12	0.91	43.1	65.3	strongly corky
Badem	Turkey	semierect	low	medium	intermediate	subcylindrical long	brown	medium	2.28	0.88	38.6	40	light corky
Barcelona	USA-Oregon	intermediate	intermediate	weak	intermediate	subspherical	dark brown	high	3.30	1.50	45.5	61.1	medium corky
Bearn	France/Spain	spreading	medium-low	strong	intermediate	ovate	light brown striated	high	2.16	0.89	41.5	43.5	light corky
Comen	Greece	spreading	intermediate	medium	intermediate	subcylindrical short	dark brown	thin	1.36	0.57	41.9	51.3	medium corky
Cosford	England	intermediate	medium-high	weak	late	subcylindrical short	light brown striated	thin	1.55	0.69	45	42.3	strongly corky
Endrix	USA	intermediate	high	weak	medium-late	subcylindrical elongated	brown	medium	1.67	0.66	39.3	28	strongly corky
Fructo Rubro	Turkey	spreading	intermediate	strong	intermediate	subcylindrical elongated	light brown striated	medium	2.95	1.31	44.3	60.9	strongly corky
Ghirara	Italy	spreading	medium-high	strong	early	subelliptic	light brown	medium	2.84	1.34	47.2	38.4	medium corky
Gironell	Spain	erect	high	medium	early	subcylindrical short	brown	medium	1.82	0.73	41.2	26.3	medium corky
Grifoll	Spain	spreading	medium-high	strong	intermediate	subcylindrical short	dark brown	medium	1.95	0.82	42	19.6	medium corky
Grossal	Spain	upright	high	weak	late	subspheroidal	light brown striated	high	2.08	0.84	40.3	32.3	medium corky
Jeans	Italy	spreading	intermediate	strong	intermediate	ovate	brown	high	2.28	0.88	38.6	51	light corky
Locale di Piazza Armerina	Italy	intermediate	medium-high	strong	medium-early	elliptic	brown	high	2.22	0.83	37.5	30.6	strongly corky
Minnolara	Italy	intermediate	intermediate	medium	intermediate	elliptic	light brown striated	high	2.51	1.02	40.6	37	medium corky
Montebello	Italy	spreading	intermediate	weak	late	ovate	light brown striated	high	2.46	1.00	40.6	61.9	medium corky
Napoletana II	Italy	semierect	high	strong	intermediate	subspheroidal	brown	high	2.36	0.98	41.3	61.6	medium corky
Nocchione	Italy	intermediate	high	medium	intermediate	subelliptic	light brown striated	high	2.70	1.10	40.7	31.5	strongly corky
Nociara	Italy	intermediate	high	strong	intermediate	subspheroidal	light brown striated	high	2.67	1.01	38	48.7	medium corky
Riccia di Talanico	Italy	intermediate	medium high	medium	intermediate	subspheroidal	auburn	thin	2.10	1.10	52.4	72.5	medium corky
Royal	USA-Oregon	erect	high	strong	intermediate	subcylindrical short	light brown striated	medium	3.40	1.41	41.3	51.2	stronglycorky
S. Maria del Gesù	Italy	intermediate	medium-high	medium	intermediate	subelliptic	light brown	medium	2.42	0.99	41.1	56.8	medium corky
Segorbe	France	erect	very high	medium	intermediate	subspheroidal	light brown striated	relatively high	2.00	0.76	37.9	59.5	medium corky
Sivri	Turkey	semispreading	low	strong	early	ovate	brown fawn striated	relatively thin	1.41	0.67	47.8	76.3	medium corky
Tonda di Giffoni	Italy	semierect	intermediate	strong	early	subspheroidal	brown striated	relatively thin	3.00	1.50	50	87.8	light corky

dx.doi.org/10.1021/jf5018324 | J. Agric. Food Chem. 2014, 62, 6236−6246

Table 1. continued

cultivar name	locally origin	growth habit	vigor	suckering	bud break[c]	nut shape	shell color	shell thickness	nut wt (g)	kernel wt (g)	kernel yield (%)	pellicle removal (%)	kernel fiber texture
Tonda Gentile Romana	Italy	semierect	low	medium	early	subspheroidal	light brown striated	thin	2.70	1.30	48	55.3	light corky
Willamette	USA-Oregon	intermediate	medium-high	strong	intermediate	subcylindrical short	light brown striated	medium	2.22	0.98	44.5	56.1	strongly corky

[a] According to the "Descriptors for hazelnut (*Corylus avellana* L.)", Bioversity, FAO and CIHEAM. 2008. [b] Phenological and carpological traits were calculated from three-yearly data. The investigated plants were from the Fruit Tree Research Unit's collection field. [c] Early: < 02/28. Medium-early: 03/01−03/10. Intermediate: 03/11−03/20. Medium-late: 03/21−03/30. Late: >03/30.

was set at −10 V, the spray voltage was at 3.0 kV, and the tube lens offset was at −10 V. The capillary temperature was 275 °C. Data were acquired in MS, MS/MS, and MS^n scanning mode.

Statistical Analysis. Data were analyzed in the R environment,[33] using Packages FactoMineR,[34] ade4,[35] and ggplot2[36] (R version 3.1.0). R is a software environment for statistical computing and graphics that provides a wide variety of statistical (linear and nonlinear modeling, classical statistical tests, classification, clustering, etc.) and graphical techniques.[33] FactoMineR is a package dedicated to multivariate data analysis. The main feature of this package is the possibility to take into account different types of variables (quantitative or categorical), data structures, and supplementary information.[34] The ade4 package (Data Analysis functions to analyze Ecological and Environmental data in the framework of Euclidean Exploratory methods) is dedicated to multivariate analyses for the identification and the understanding of structures of ecological communities.[35] Finally, ggplot2 is a data visualization package for the statistical programming language R.[36]

Individual and total polyphenol content as well as nut shape (length/width) and kernel weight were used for cultivar ordination by clustering. Other traits (kernel yield, growth habit, plant vigor, plant suckering, and bud break) were introduced as supplementary variables. A range score was calculated in order to make comparable variables with different ranges and to focus on distributions. Range score values for $n(x)$ are obtained as the ratio between each value (x) minus the minimum and the difference between maximum and minimum: $[X - \min(x)]/[\max(x) - \min(x)]$ for x from 1 to n. Score distributions were summarized in quartiles for graphical presentation. Hierarchical clustering was performed on principal components using Euclidean distances with the complete-linkage method.

Extraction of the Protein Fraction. 0.06 g of ground kernels (with skin) was suspended in 0.8 mL of chloroform and vortexed for 5 min. 0.8 mL of 0.1% TFA, containing 1% protease inhibitor cocktail (Sigma, St. Louis, MO, USA), was added, and protein extraction was carried out for 5 min. The mixture was then centrifuged for 10 min at 13000 rpm, and the aqueous fraction was recovered. Protein concentration was determined using the Bradford method.[37]

MALDI-TOF-MS Analyses and Processing of Mass Spectra. Two separated aliquots (0.2 μg) of the protein extract were concentrated and desalted by solid phase extraction using μZipTipC18 tips (Millipore, Billerica, MA, USA). Tips were washed and equilibrated with 0.1% TFA and eluted in 1 μL of sinapinic acid (10 mg/mL in 0.1% TFA/acetonitrile (1:1 v:v), containing 1 pmol/μL of Rnase A) used as matrix for MALDI-TOF-MS analyses. Three spectra were acquired from each well, so that six mass spectra were generated for each sample.

MALDI-TOF-MS analyses were carried out on a Voyager DE PRO mass spectrometer (AB SCIEX, Foster City, CA, USA) operating in linear positive-ion mode. Mass spectra, acquired in the m/z range 3500−15000, were calibrated using the average peaks (doubly charged ion at m/z 6841 and singly charged ion at m/z 13682) originating from the internal standard Rnase A. Mass spectra were processed and transformed in a list containing the m/z values of all the signals and the corresponding intensity, using the DataExplorer 5.1 software (AB SCIEX).

Peak intensities were normalized by considering 100 the intensity of the most intense signal in the mass spectrum, and signals having intensity <2% were excluded from the peak list. For each cultivar, peak lists obtained from the six mass spectra were aligned along the m/z axis using the NEAPOLIS software developed in-house (www.bioinformatics.org/bioinfo-af-cnr/NEAPOLIS).[38] The threshold value to align signals was fixed to 1000 ppm, so that, among the aligned signals, the minimum and maximum m/z values differed for <1000 ppm. Signals present in at least four of the six replicate mass spectra were included in the mean peak list. This processing allowed calculating the mean m/z value and the corresponding mean intensity for each signal, leading to the mean peak list of each cultivar. Mean peak lists from all the hazelnut cultivars were further aligned by NEAPOLIS to obtain the total data set. Data processed by NEAPOLIS were subjected to a visual inspection to resolve any mass spectral ambiguities.

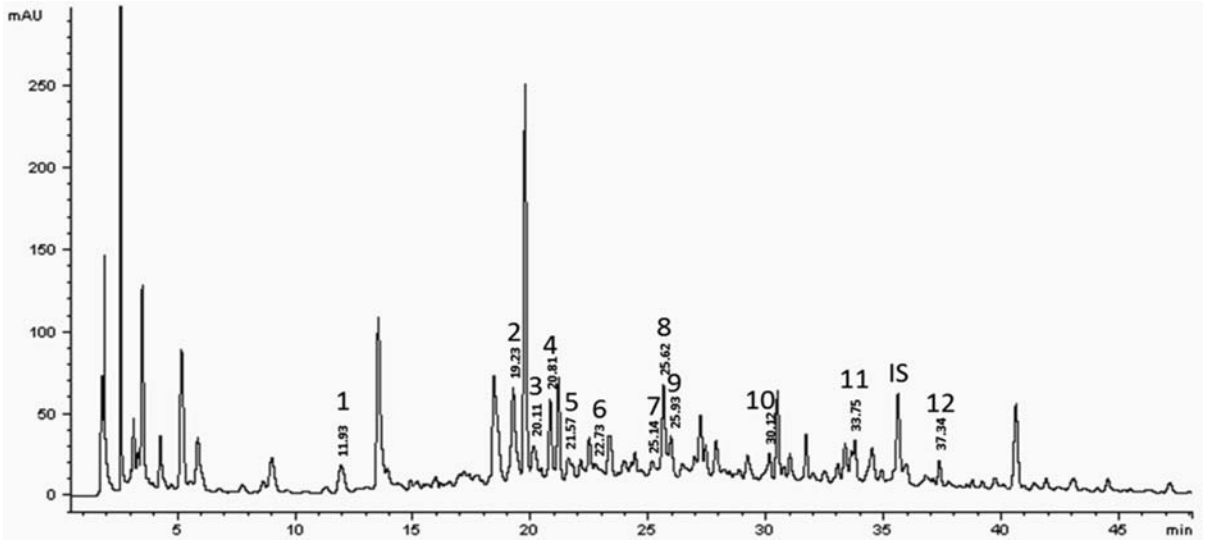

Figure 1. HPLC chromatogram of hazelnut extract (Grossal cultivar) recorded at 280 nm. Peaks are labeled according to Table 2

RESULTS AND DISCUSSION

Plants used in the present study (29 cultivars) were grown in the CRA-FRC collection field, and some of them were phenotypically and genetically characterized in previous studies.[1,39] In addition, as plants were grown in the same field, the effects of agronomical and pedoclimatical conditions on fruit characteristics were minimized and it could be assumed that the reported results are mainly related to differences in genetic traits of the cultivars.

Bioagronomical and Pomological Analysis. According to the guidelines provided by Bioversity, 12 agronomical and pomological traits were selected to describe the 29 hazelnut cultivars.[29−31] The selected traits represent well-defined characteristics of economic interest and, consequently, could act as target traits for selection by growers, breeders, and the food-processing industry. Agronomical and pomological traits are depicted in Table 1.

Significant differences among cultivars were observed for all the examined nut and kernel traits. Pellicle removal, one of the most important practices for nut quality preservation, was evaluated after roasting.[40] Percentage of pellicle removal ranged from 19.6% for Grifoll to 87.5% for Tonda di Giffoni. Other cultivars that showed good score for pellicle removal (value higher than 55%) were Avellana sp, Barcelona, Fructo Rubro, Montebello, Napoletana II, Riccia di Talanico, S. Maria del Gesù, Segorbe, Sivri, Tonda Romana, and Willamette. The most common shapes were short subcylindrical (24.14%) and subspherical (31.03%). The kernel yield ranged from 37.5% for Locale di Piazza Armerina to 50% for Tonda di Giffoni. Apolda, Barcelona, Fructo Rubro, Ghirara, Nocchione, Royal, Tonda di Giffoni, and Tonda Gentile Romana were characterized by higher nut weights, associated with kernel yield higher than 40% and lower than 50%, and Tonda di Giffoni showed the highest kernel yield (50%) (Table 1). In particular, Barcelona, Tonda di Giffoni, and Tonda Gentile Romana showed high kernel yield and subspheroidal nut shape, which are the most important traits required by the food-processing industry, as also reported by Cristofori et al.[41]

Identification and Quantification of Polyphenols and Their Correlation with Agronomical and Pomological Traits. The polyphenol fraction of each cultivar was analyzed by HPLC. The characterization of phenolic compounds was carried out by ESI-ITMS^n. Identification was achieved on the basis of pseudomolecular $[M - H]^-$ ions, together with the interpretation of their collision induced dissociation (CID) fragments. When authentic standards were available, identification was conducted by comparing retention times and MS^n fragmentation spectra with those of standards. Twelve compounds were characterized, and the classes of polyphenols detected were in agreement with those already reported in previous studies on phenolic composition of hazelnut.[42,43] As an example, the HPLC chromatogram of hazelnut extract (Grossal cultivar) recorded at 280 nm is shown in Figure 1 and the list of compounds identified in the polyphenol hazelnut extract of Grossal cultivar is reported in Table 2.

Table 2. List of Compounds Identified in Hazelnut Extract (Grossal Cultivar) Including Corresponding HPLC Retention Times, Quasi-Molecular Ions, and Fragment Ions

peak	t_R (min)	$[M - H]^-$ m/z	MS/MS ions m/z	identification
1	11.93	153	109	protocatechuic acid
2	19.23	577	451, 407, 289	procyanidin dimer (D1)
3	20.11	577	451, 407, 289	procyanidin dimer (D2)
4	20.81	865	577	procyanidin trimer (T1)
5	21.57	289	245	(+)-catechin
6	22.73	865	577	procyanidin trimer (T2)
7	25.14	577	451, 407, 289	procyanidin dimer (D3)
8	25.62	577	451, 407, 289	procyanidin B2
9	25.93	865	577	procyanidin trimer (T3)
10	30.12	463	317	myricetin-3-*O*-rhamnoside (myricitrin)
11	33.75	447	301	quercetin-3-*O*-rhamnoside (quercitrin)
12	37.34	435	273	phloretin-2′-*O*-glucoside (phloridzin)

Total and individual polyphenol content of each cultivar is summarized in Figure 2 and in Supplementary Table 1 in the Supporting Information. The total polyphenol content varied among the different cultivars and ranged from 84.80 ± 3.10 mg/kg of FW in Fructo Rubro to 32.29 ± 0.11 mg/kg of FW in Cosford. ESI-ITMS^n identification of individual phenolics in

dx.doi.org/10.1021/jf5018324 | J. Agric. Food Chem. 2014, 62, 6236−6246

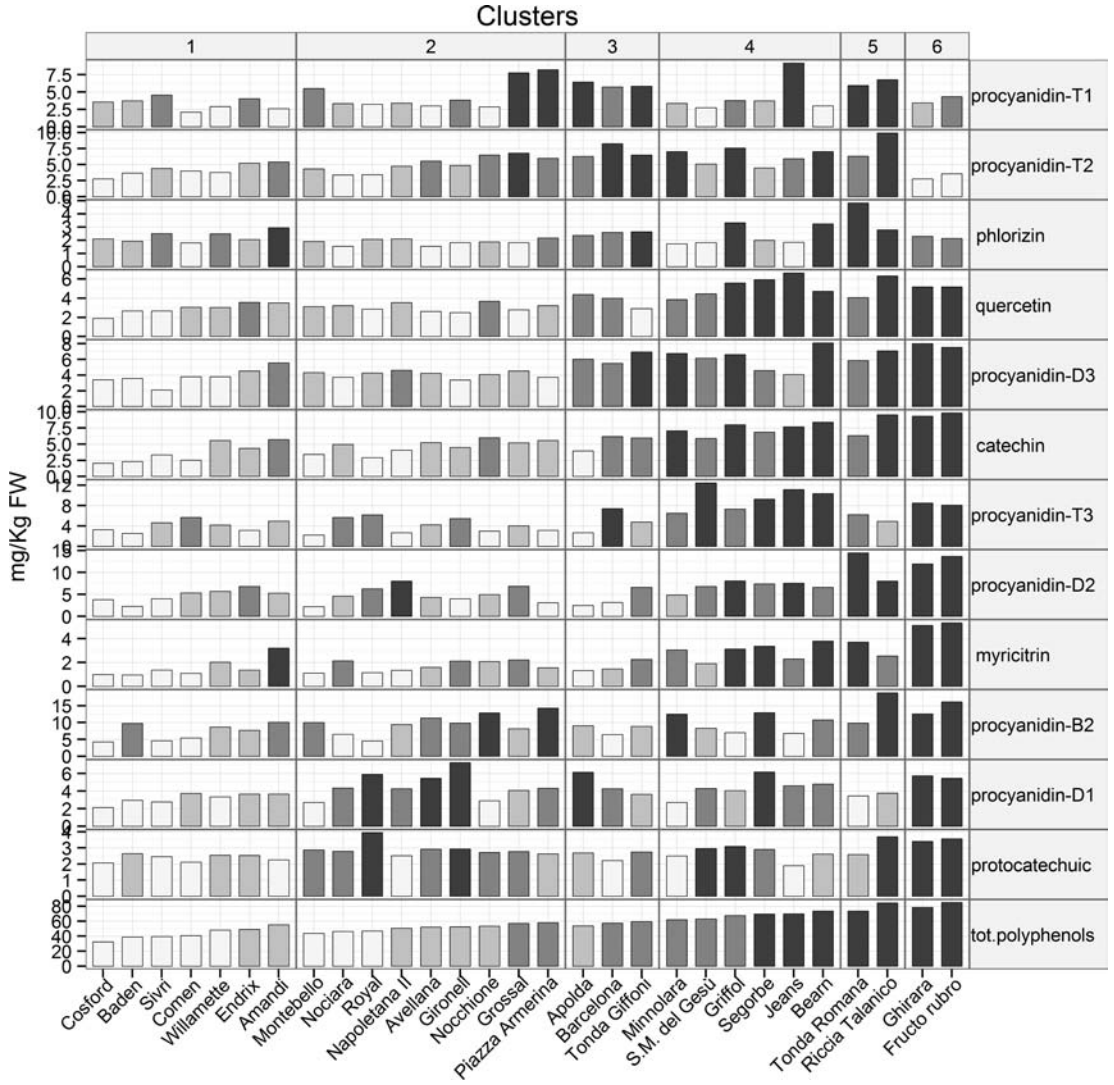

Figure 2. Medium score for total and individual polyphenolic content in kernels. Parameters are subdivided into four quartiles, depicted with different colors: white (lower quartile), light gray (second quartile), dark gray (third quartile), and black (upper quartile).

the different hazelnut extracts confirmed the presence of protocatechuic acid, flavan-3-ols such as catechin, procyanidin B2, six procyanidin oligomers (three other unidentified procyanidin dimers (indicated as D1, D2, D3), and three unidentified procyanidin trimers (indicated as T1, T2, T3)), flavonols (quercetin-3-*O*-rhamnoside and myricetin-3-*O*-rhamnoside), and one dihydrochalcone (phloretin-2-*O*-glucoside) in all the analyzed cultivars. Among the detected flavonols, quercetin-3-*O*-rhamnoside was present in highest content in whole kernels, ranging from 1.89 ± 0.04 mg/kg of FW in Cosford to 6.62 ± 0.42 mg/kg of FW in Jeans (Supplementary Table 1 in the Supporting Information).

Based on kernel polyphenolic content, cultivars were divided into six clusters, and this division reflected the clustering obtained by correlating the total polyphenolic content with the agronomical and pomological features (Figures 2 and 3).

Some agronomical and pomological features, such as kernel weight and yield, nut shape (as length/width ratio), plant vigor, suckering, bud break, and growth habit were summarized and correlated to total polyphenol content in kernels (Figure 3). A negative correlation between nut shape and kernel weight and yield was observed, and plant vigor and suckering were negatively correlated with kernel weight and yield. Tonda di Giffoni and Riccia di Talanico showed the higher kernel yield, while the higher total polyphenol content was registered in Riccia di Talanico, Tonda Gentile Romana, Fructo Rubro, and Ghirara (Figure 3, Supplementary Table 1 in the Supporting Information). Based on these features, cultivars can be divided into six clusters:

- Cluster 1 containing cultivars with small, elongated nuts and low polyphenol levels (Table 1, Figure 3). In this cluster Willamette was the most typical and Cosford was the most specific.
- Cluster 2 containing 9 of the 29 cultivars with high vigor, erect branches, low kernel yield, and low levels of procyanidin trimer (T3), phlorizin, procyanidin dimer (D3), and quercetin (Table 1, Figures 2 and 3, Supplementary Table 1 in the Supporting Information). In this cluster, Napoletana II was the most typical and Royal was the most specific.
- Cluster 3 including cultivars with round nuts and high kernel weight (Table 1, Figure 3). In this cluster Barcelona was the most typical, Apolda was the most

dx.doi.org/10.1021/jf5018324 | J. Agric. Food Chem. 2014, 62, 6236−6246

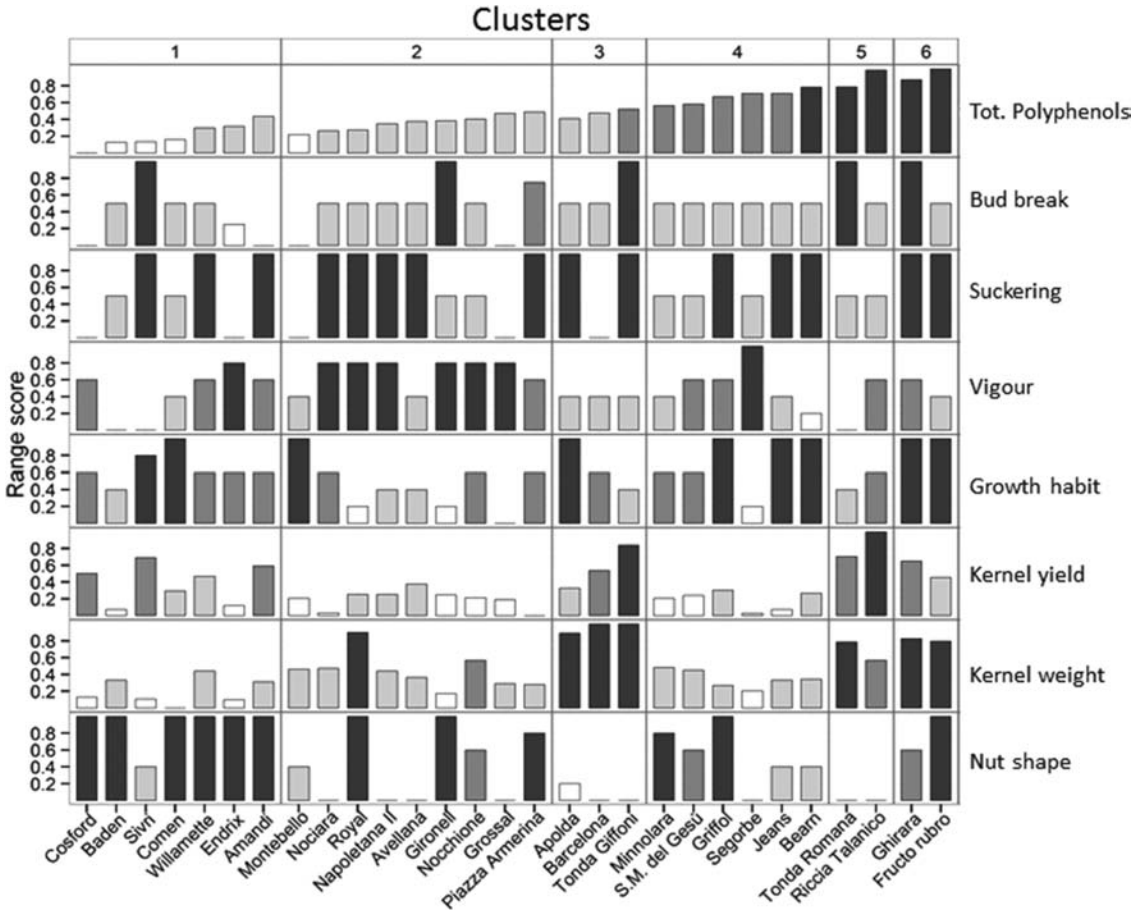

Figure 3. Medium score for morphological and pomological traits combined with total polyphenolic content in kernels. Parameters are subdivided into four quartiles, depicted with different colors: white (lower quartile), light gray (second quartile), dark gray (third quartile), and black (upper quartile).

specific, and Tonda di Giffoni showed the better combination of features of this cluster (Figure 3).

- Cluster 4 including cultivars whose nuts showed high levels of quercetin, catechin, and procyanidin trimer (T3) (Figure 2, Supplementary Table 1 in the Supporting Information). In this cluster, S. Maria del Gesù was the most typical and Jeans was the most specific.
- Cluster 5 containing two cultivars, Tonda Romana and Riccia di Talanico, that showed high kernel yield and high levels of phlorizin, procyanidin B2, procyanidin dimer (D2), and trimer (T2) (Figures 2 and 3, Supplementary Table 1 in the Supporting Information).
- Cluster 6 including two cultivars, Ghirara and Fructo Rubro, whose nuts showed the higher total polyphenol content and high levels of myricitrin, catechin, protocatehuic acid, procyanidin B2, and procyanidin dimers (D2) and (D3) (Figure 2, Supplementary Table 1 in the Supporting Information).

In order to better observe the relationship among traits of the hazelnut cultivars, a dendrogram based on Euclidean distances was constructed (Figure 4). Clustering cannot be related to geographical origin of cultivars. This is likely due to plant species domestication that resulted in a narrowing of the gene pool.[44] Two major clusters were recognized; about 67% of cultivars included in cluster 1 originated from Italy, while the others had different geographic origin (see Table 1). Cluster 2 was composed of European cultivars, excepted for Fructo

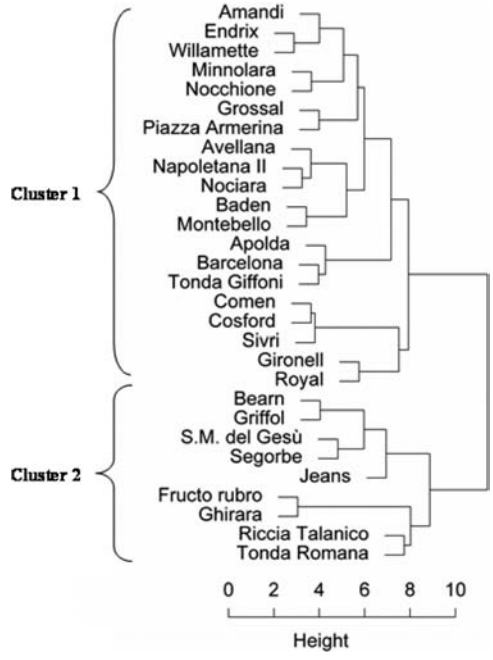

Figure 4. Dendrogram depicting the relationship among different *C. avellana* cultivars based on quantitative and qualitative features. Dendrogram was inferred using Euclidean distances with complete-linkage method.

dx.doi.org/10.1021/jf5018324 | J. Agric. Food Chem. 2014, 62, 6236−6246

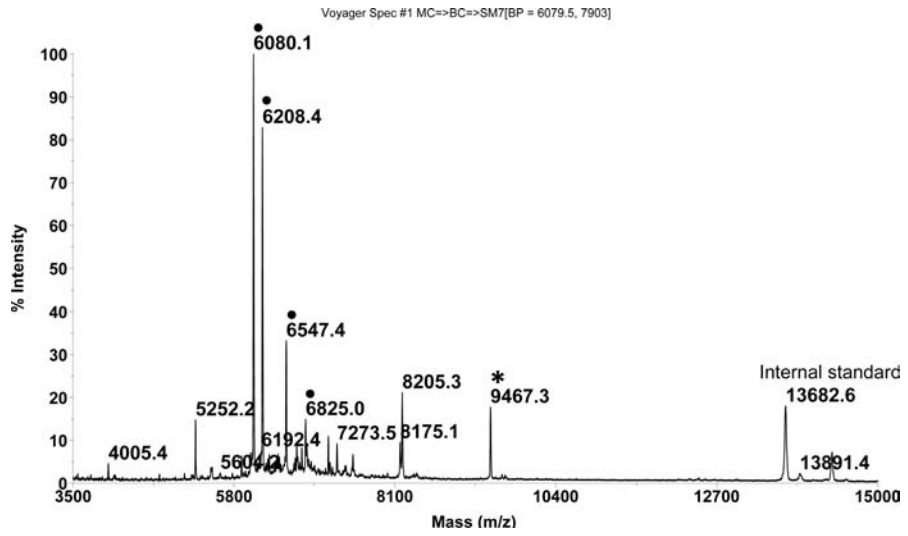

Figure 5. MALDI-TOF mass spectrum obtained from the analysis of the protein fraction extracted from kernels of the Tonda di Giffoni cultivar. The four signals present in the molecular profiles of all the cultivars are indicated by dots. The signal originating from the allergen Cor a 8 (nonspecific-lipid transfer protein) is indicated by an asterisk.

Rubro, a cultivar originating from Turkey (Figure 4). The two clusters reflected cultivar features such as kernel weight and yield, nut shape, and content of polyphenols. Cultivars included in cluster 2 showed higher content of polyphenols than those included in cluster 1, but lower kernel yield, except for Tonda Gentile Romana and Riccia di Talanico (Table 1, Figures 2, 3, and 4).

MALDI-TOF-MS Analyses and Processing of Mass Spectra. The present study was also aimed to develop an innovative strategy based on the MALDI-TOF-MS suitable for discriminating different hazelnut cultivars. The applicability of the method was ascertained by analyzing the 29 selected cultivars. Protein extracts from kernels were analyzed by MALDI-TOF-MS and mass spectra were acquired in the m/z range 3500−15000 in linear positive-ion mode, as no significant peaks were detected outside the selected m/z range (data not shown). The mass spectrum obtained from the analysis of Tonda di Giffoni is shown in Figure5.

The 29 mean peak lists were aligned by the NEAPOLIS software, and a data set that included about 270 m/z values and their corresponding mean intensity was thus generated. This data set highlighted a high variability in the molecular profile of different samples. To increase data reliability, m/z values having mean intensity less than 10% in all the cultivars were excluded from this data set. Unfortunately, only a few signals had intensity higher than 10% in the mean peak lists of Grossal and Willarmette. Therefore, these cultivars were not further included in this analysis.

Four intense signals in the m/z range 6000−7000 (m/z 6825.3, 6547.9, 6209.0, 6080.5) were present in the acquired molecular profiles, regardless of the cultivar (Supplementary Table 2 in the Supporting Information, Figure 5). Interestingly, these signals were absent in the mass spectra of protein extracts from walnuts, peanuts, and almonds (data not shown). Therefore, it could be suggested to consider this cluster as a specific signature of hazelnut presence in nut mixtures or in nut containing products.

Furthermore, a signal at m/z 9468.3 was present in the mean peak lists of 20 cultivars and it could be originated from the nonspecific-lipid transfer protein (ns-LTP), also called Cor a 8 (theoretical molecular weight 9468.0 Da), described as one of the predominant hazelnut allergens (Figure 5). Due to the presence of four disulfide bridges, the protein structure of ns-LTPs is particularly stable and resistant to proteolysis, harsh pH changes, or thermal treatments.[45] As these proteins are usually not affected by technological processes, they have been also proposed as biomarkers for in vitro diagnosis of potentially severe hazelnut allergy.[46]

The main goal of the molecular profiling analyses was to discriminate the analyzed cultivars. Specific signals among the ones having the highest mean intensity for at least one cultivar (>10%) were selected as putative biomarkers, thus leading to the data set of 35 signals reported in Supplementary Table 2 in the Supporting Information. Due to the high specificity of the acquired molecular profiles, the 27 different hazelnut cultivars could be unambiguously discriminated on the basis of specific biomarker patterns (presence and/or absence of m/z values). The obtained data could be also used for the identification of unknown samples.

In this context, in order to automate the authentication method, a four-step process that used the NEAPOLIS software was set up, as reported in the flowchart (Figure 6). At first, the mean peak list of a putative unknown sample should be aligned with a list containing the selected biomarkers of each cultivar of Group I using 500 ppm as threshold for aligning values (Sheet Group I in Supplementary File 1 in the Supporting Information) and 2 as the minimum number of aligned signals. This step would allow us to rapidly identify the unknown sample (if it is one of these 12 cultivars) on the basis of a biomarker pattern including from two to five signals, as indicated in Supplementary File 1 in the Supporting Information. In case the identification would not been achieved, as following steps, this process should be reiterated using the lists of Group II (that is defined based on the presence of the m/z value 3661, Sheet Group II in Supplementary File 1 in the Supporting Information), Group III (whose peculiar features were the absence of the m/z value 3661 and the presence of the m/z value 14345, Sheet Group III in Supplementary File 1 in the Supporting Information), Group IIIA (that included Nociara and Locale Piazza Armerina, Sheet Group IIIA in

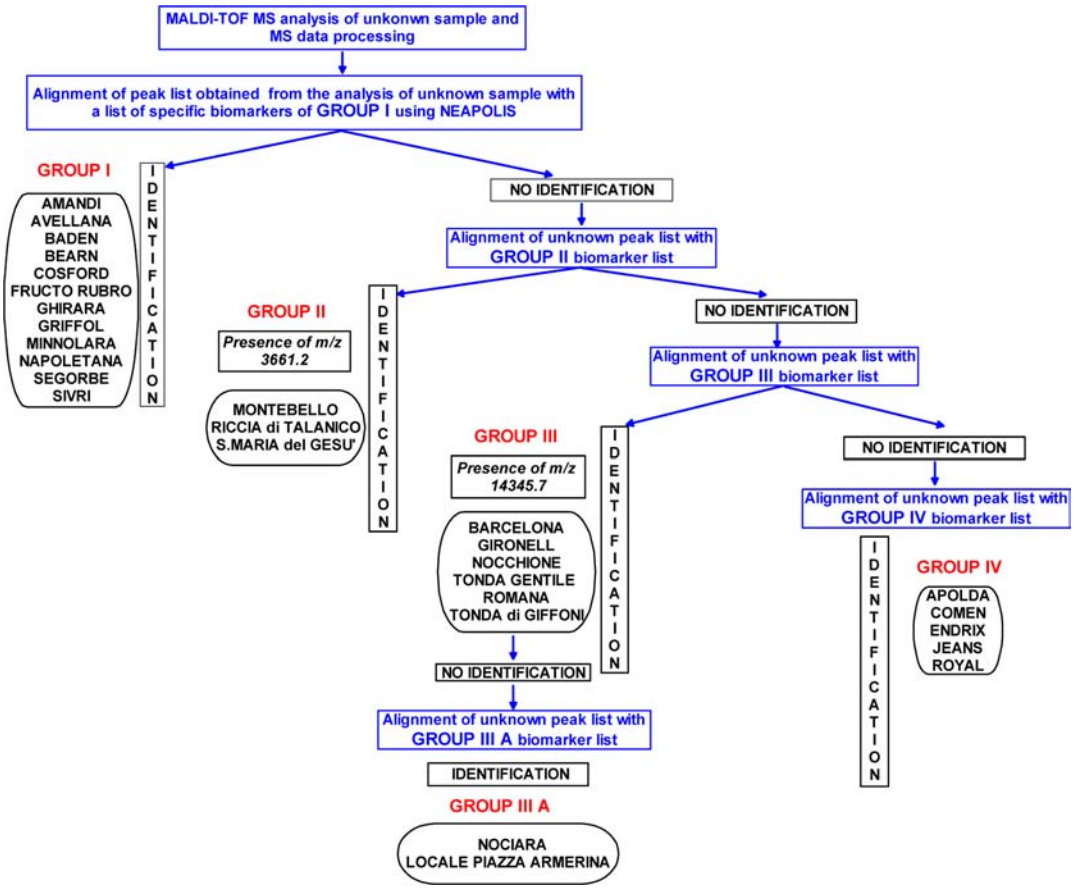

Figure 6. Flowchart of the four-step process developed in order to automate the authentication method based on the MALDI-TOF-MS molecular profiles of the different cultivars.

Supplementary File 1 in the Supporting Information), and Group IV (whose peculiar feature was the absence of the m/z values 3661 and 14345, Sheet Group IV in Supplementary File 1 in the Supporting Information). It is worth stressing that the biomarker data set could be easily updated as more mass spectrometric data on other cultivars will be gathered and bioinformatic tools could be further developed to simplify and speed the identification process.

In conclusion, although the analysis of a larger number of cultivars of different geographic origins could further validate the method, these results clearly highlight that the developed molecular profiling strategy is able to discriminate hazelnut cultivars and strongly suggest the applicability of the method to the analysis of other foods of plant origin. Furthermore, as the method is rapid, simple, and reliable, it holds the potential to be routinely applied in quality control processes.

■ ASSOCIATED CONTENT

Supporting Information

Supplementary Table 1: Concentration of individual and total polyphenolics determined by HPLC (mg/kg of FW) extracted from different hazelnut cultivars. Results were expressed as average (mean) concentration ± SD of duplicate analyses (HPLC method). Supplementary Table 2: Data set obtained from the MALDI-TOF-MS molecular profiles of the protein fraction extracted from the 27 cultivars. Specific signals among the ones having the highest mean intensity for at least one cultivar (>10%) were included in the data set. The mean intensity values of signals selected as biomarkers are indicated in red. Supplementary File 1: Lists containing the selected biomarkers of cultivars included in the defined Groups. The lists, as reported, can be directly uploaded in the NEAPOLIS software, together with the list of an unknown sample to achieve cultivar identification. The absence of signals at m/z 3661 and 14345 is crucial for discriminating the different groups. This material is available free of charge via the Internet at http://pubs.acs.org.

■ AUTHOR INFORMATION

Corresponding Author

*Tel: +39-0825-299363. Fax: +39-0825-781585. E-mail: rsiciliano@isa.cnr.it.

Author Contributions

‡These authors equally contributed to the present paper.

Funding

This work was supported by a dedicated grant from the Italian Ministry of Economy and Finance to CNR and ENEA for the Project "Innovazione e Sviluppo del Mezzogiorno e Conoscenze Integrate per Sostenibilità ed Innovazione del Made in Italy Agroalimentare (CISIA)" Legge n.191/2009. This work has been also supported by Regione Campania in the framework of the "Rete di Spettrometria di Massa della Campania" (RESMAC).

Notes

The authors declare no competing financial interest.

■ ACKNOWLEDGMENTS

The authors are grateful to Dr. Filippo Piro (C.R.A.-Research Institute of Horticolture, Pontecagnano, Italy) for improving the manuscript.

■ ABBREVIATIONS USED

ESI-ITMS^n, electrospray ionization multistage ion trap mass spectrometry; FW, fresh weight; HPLC, high performance liquid chromatography; MALDI-TOF-MS, matrix-assisted laser desorption ionization time-of-flight mass spectrometry; m/z, mass/charge; Rnase A, ribonuclease A; TFA, trifluoroacetic acid

■ REFERENCES

(1) Boccacci, P.; Aramini, M.; Valentini, N.; Bacchetta, L.; Rovira, M.; Drogoudi, P.; Silva, A. P.; Solar, A.; Calizzano, F.; Erdoğan, V.; Cristofori, V.; Ciarmiello, L. F.; Contessa, C.; Ferreira, J. J.; Marra, F. P.; Botta, R. Molecular and morphological diversity of on-farm hazelnut (*Corylus avellana* L.) landraces from southern Europe and their role in the origin and diffusion of cultivated germplasm. *Tree Genet. Genomes* **2013**, *9*, 1465−1480.

(2) Burdack-Freitag, A.; Schieberle, P. Changes in the key odorants of Italian Hazelnuts (*Coryllus avellana* L. var. Tonda Romana) induced by roasting. *J. Agric. Food Chem.* **2010**, *58*, 6351−6359.

(3) Kiefl, J.; Pollner, G.; Schieberle, P. Sensomics analysis of key hazelnut odorants (*Corylus avellana* L. 'Tonda Gentile') using comprehensive two-dimensional gas chromatography in combination with time-of-flight mass spectrometry (GC×GC-TOF-MS). *J. Agric. Food Chem.* **2013**, *61*, 5226−5235.

(4) Kiefl, J.; Schieberle, P. Evaluation of process parameters governing the aroma generation in three hazelnut cultivars (*Corylus avellana* L.) by correlating quantitative key odorant profiling with sensory evaluation. *Agric. Food Chem.* **2013**, *61*, 5236−5244.

(5) FAOstat Agriculture data. Available from: http://faostat.fao.org/site/408/default.aspx. 2012. Accessed 08 Apr 2014.

(6) Valentini, N.; Rolle, L.; Stévigny, C.; Zeppa, G. Mechanical behaviour of hazelnuts used for table consumption under compression loading. *J. Sci. Food Agric.* **2006**, *86*, 1257−1262.

(7) Mehlenbacher, S. A. Hazelnuts (*Corylus*). *Acta Hortic.* **1991**, *290*, 791−838.

(8) Hosseinpour, A.; Seifi, E.; Javadi, D.; Ramezanpour, S. S.; Molnar, T. J. Nut and kernel characteristics of twelve hazelnut cultivars grown in Iran. *Sci. Hortic.* **2013**, *150*, 410−413.

(9) Petriccione, M.; Ciarmiello, L. F.; Boccacci, P.; De Luca, A.; Piccirillo, P. Evaluation of 'Tonda di Giffoni' hazelnut (*Corylus avellana* L.) clones. *Sci. Hortic.* **2010**, *124*, 153−158.

(10) Caligiani, A. C.; Coisson, J. D.; Travaglia, F.; Acquotti, D.; Palla, G.; Palla, L.; Arlorio, M. Application of ^{1}H NMR for the characterisation and authentication of "Tonda Gentile Trilobata" hazelnuts from Piedmont (Italy). *Food Chem.* **2014**, *148*, 77−85.

(11) Piccirillo, P. Attualità e problematiche della coltura del nocciolo in Campania. In *Atti II Convegno Nazionale sul Nocciolo*; Giffoni Valle Piana (SA): Italy, 2002; 5−6 October; pp 113−121.

(12) Tombesi, A.; Limongelli, F. Varietà e miglioramento genetico del nocciolo. In *Atti II Convegno Nazionale sul Nocciolo*; Giffoni Valle Piana (SA): Italy, 2002; 5−6 October; pp 11−27.

(13) Mercanligil, S. M.; Arslan, P.; Alasalvar, C.; Okut, E.; Akgül, E.; Pinar, E.; Geyik, P. O.; Tokgözoglu, L.; Shahidi, F. Effects of hazelnut-enriched diet on plasma cholesterol and lipoprotein profiles in hypercholesterolemic adult men. *Eur. J. Clin. Nutr.* **2007**, *61*, 212−220.

(14) Ros, E. Health Benefits of Nut Consumption. *Nutrients* **2010**, *2*, 652−682.

(15) Amaral, J. S.; Cunha, S. C.; Santos, A.; Alves, M. R.; Seabra, R. M.; Oliveira, B. P. Influence of cultivar and environment conditions on the triacylglycerol profile of hazelnut (*Corylus avellana* L.). *J. Agric. Food Chem.* **2006**, *54*, 449−456.

(16) Özdemir, M.; Açkurt, F.; Kaplan, M.; Yildiz, M.; Löker, M.; Gürkan, T.; Biringen, G.; Okay, A.; Seyhan, F. G. Evalutation of new Turkish hybrid hazelnut (*Corylus avellana* L.) varieties: fatty acid composition, α-tocopherol content, mineral composition and stability. *Food Chem.* **2001**, *73*, 411−415.

(17) Köksal, A.İ.; Artik, N.; Şimşek, A.; Güneş, N. Nutrient composition of hazelnut (*Corylus avellana* L.) varieties cultivated in Turkey. *Food Chem.* **2006**, *99*, 509−515.

(18) Arpadjan, S.; Momchilova, S.; Venelinov, T.; Blagoeva, E.; Nikolova, M. Bioaccessibility of Cd, Cu, Fe, Mn, Pb, and Zn in hazelnut and walnut kernels investigated by an enzymolysis approach. *J. Agric. Food Chem.* **2013**, *61*, 6086−6091.

(19) Gokirmak, T.; Mehlenbacher, S. A.; Bassil, N. V. Characterization of European hazelnut (*Corylus avellana*) cultivars using SSR markers. *Genet. Resour. Crop Evol.* **2009**, *56*, 147−172.

(20) Ciarmiello, L. F.; Piccirillo, P.; Pontecorvo, G.; De Luca, A.; Woodrow, P. A PCR based SNPs marker for specific characterization of English walnut (*Juglans regia* L.) cultivars. *Mol. Biol. Rep.* **2011**, *38*, 1237−1249.

(21) Ciarmiello, L. F.; Pontecorvo, G.; Piccirillo, P.; De Luca, A.; Carillo, P.; Kafantaris, I.; Woodrow, P. Use of nuclear and mitochondrial single nucleotide polymorphisms to characterize English walnut (*Juglans regia* L.) genotypes. *Plant Mol. Biol. Rep.* **2013**, *31*, 1116−1130.

(22) Cordero, C.; Liberto, E.; Bicchi, C.; Rubiolo, P.; Schieberle, P.; Reichenbach, S. E.; Tao, Q. Profiling food volatiles by comprehensive two-dimensional gas chromatography coupled with mass spectrometry: advanced fingerprinting approaches for comparative analysis of the volatile fraction of roasted hazelnuts (*Corylus avellana* L.) from different origins. *J. Chromatogr. A* **2010**, *1217*, 5848−5858.

(23) Cevallos-Cevallos, J. M.; Reyes-De-Corcuera, J. I.; Etxeberria, E.; Danyluk, M. D.; Rodrick, J. E. Metabolomic analysis in food science: A review. *Trends Food Sci. Technol.* **2009**, *20*, 557−566.

(24) Oddone, M.; Aceto, M.; Baldizzone, M.; Musso, D.; Osella, D. Authentication and traceability study of hazelnuts from piedmont, Italy. *J. Agric. Food Chem.* **2009**, *57*, 3404−3408.

(25) Herrero, M.; Simó, C.; García-Cañas, V.; Ibáñez, E.; Cifuentes, A. Foodomics: MS-based strategies in modern food science and nutrition. *Mass Spectrom. Rev.* **2012**, *31*, 49−69.

(26) Nunes-Miranda, J. D.; Igrejas, G.; Araujo, E.; Reboiro-Jato, M.; Capelo, J. L. Mass spectrometry-based fingerprinting of proteins & peptides in wine quality control: a critical overview. *Crit. Rev. Food Sci. Nutr.* **2013**, *53*, 751−759.

(27) Cozzolino, R.; Passalacqua, S.; Salemi, S.; Malvagna, P.; Spina, E.; Garozzo, D. Identification of adulteration in milk by matrix-assisted laser desorption/ionization time-of-flight mass spectrometry. *J. Mass Spectrom.* **2001**, *36*, 1031−1037.

(28) Mazzeo, M. F.; De Giulio, B.; Guerriero, G.; Ciarcia, G.; Malorni, A.; Russo, G. L.; Siciliano, R. A. Fish authentication by MALDI-TOF mass spectrometry. *J. Agric. Food. Chem.* **2008**, *56*, 11071−11076.

(29) Bioversity, FAO. *CIHEAM. Descriptor for Hazelnut (Corylus avellana L.)*; Bioversity International/Food and Agriculture Organization of the United Nations/International Centre for Advanced Mediterranean Agronomic Studies: Rome, Italy/Rome, Italy/Zaragoza, Spain, 2008.

(30) Thompson, M. M.; Romisondo, P.; Germani, E.; Vidal-Barraquer, R.; Tasias Valls, J. An evaluation system for filberts (*Corylus avellana* L.). *Hort. Sci.* **1978**, *13*, 514−517.

(31) UPOV. Guidelines for the conduct of test for distinctness, homogeneity and stability Hazelnut (*Corylus avellana* L. & *Corylus maxima* Mill.) TG/71/3 [online], 1979, http://www.upov.int/en/publications/tg-rom/tg_index_numerical.html. 11 May 2012.

(32) Ciarmiello, L. F.; Piccirillo, P. V.; Gerardi, C.; Piro, F.; De Luca, A.; D'Imperio, F.; Rosito, V.; Poltronieri, P.; Santino, S. Microwave irradiation for dry-roasting of hazelnuts and evaluation of microwave treatment on hazelnuts peeling and fatty acid oxidation. *J. Food Res.* **2013**, *2*, 22−35.

(33) R Core Team. *R: A language and environment for statistical computing*; R Foundation for Statistical Computing: Vienna, Austria, 2013; http://www.R-project.org/.

(34) Husson, F.; Josse, J.; Le, S.; Mazet, J. *FactoMineR: Multivariate Exploratory Data Analysis and Data Mining with R*; R package version 1.25; 2013; http://CRAN.R-project.org/package=FactoMineR.
(35) Dray, S.; Dufour, A. B. The ade4 package: implementing the duality diagram for ecologists. *J. Stat. Software* **2007**, *22*, 1−20.
(36) Wickham, H. *ggplot2: elegant graphics for data analysis*; Springer: New York, 2009.
(37) Bradford, M. M. A rapid and sensitive method for the quantitation of microgram quantities of protein utilizing the principle of protein-dye binding. *Anal. Biochem.* **1976**, *72*, 248−254.
(38) Mangerini, R.; Romano, P.; Facchiano, A.; Damonte, G.; Muselli, M.; Rocco, M.; Boccardo, F.; Profumo, A. The application of atmospheric pressure matrix-assisted laser desorption/ionization to the analysis of long-term cryopreserved serum peptidome. *Anal. Biochem.* **2011**, *417*, 174−181.
(39) Campa, A.; Trabanco, E.; Pérez-Vega, E.; Rovira, M.; Ferreira, J. J. Genetic relationship between cultivated and wild hazelnuts (*Corylus avellana* L.) collected in northern Spain. *Plant Breed.* **2011**, *130*, 360−366.
(40) Basaran, P.; Akhan, Ü. Microwave irradiation of hazelnuts for the control of aflatoxin producing *Aspergillus parasiticus*. *Innovative Food Sci. Emerging Technol.* **2010**, *11*, 113−117.
(41) Cristofori, V.; Ferramondo, S.; Bertazza, G.; Bignami, C. Nut and kernel traits and chemical composition of hazelnut (*Corylus avellana* L.) cultivars. *J. Sci. Food Agric.* **2008**, *88*, 1091−1098.
(42) Jakopic, J.; Petkovsek, M. M.; Likozar, A.; Solar, A.; Stampar, F.; Veberic, R. HPLC-MS identification of phenols in hazelnut (*Corylus avellana* L.) kernels. *Food Chem.* **2011**, *124*, 1100−1106.
(43) Schmitzer, V.; Slatnar, A.; Veberic, R.; Stampar, F.; Solar, A. Roasting affects phenolic composition and antioxidative activity of hazelnuts (*Corylus avellana* L.). *J. Food Sci.* **2011**, *76*, S14−19.
(44) Gatesy, J.; DeSalle, R.; Wahlberg, N. How many genes should a systematist sample? Conflicting insights from a phylogenomic matrix characterized by replicated incongruence. *Syst. Biol.* **2007**, *56*, 355−363.
(45) Breiteneder, H.; Mills, E. N. Molecular properties of food allergens. *J. Allergy Clin. Immunol.* **2005**, *115*, 14−23.
(46) Schocker, F.; Lüttkopf, D.; Scheurer, S.; Petersen, A.; Cisteró-Bahima, A.; Enrique, E.; San Miguel-Moncín, M.; Akkerdaas, J.; van Ree, R.; Vieths, S.; Becker, W. M. Recombinant lipid transfer protein Cor a 8 from hazelnut: a new tool for in vitro diagnosis of potentially severe hazelnut allergy. *J. Allergy Clin. Immunol.* **2004**, *113*, 141−147.

Overcautionary and unsubstantiated precautionary labeling however unnecessarily limits the freedom of choice for allergic consumers in a given product range and can thus negatively affect their quality of life.[18]

It is therefore important to have reliable and sensitive methods at hand to accurately determine the allergenic residues' concentration and the resulting health hazard. Recent analytical approaches toward detecting lysozyme include chromatographic methods with either fluorescence or mass spectrometric detection,[19,20] DNA aptamer-based methods,[21] and competitive ELISA methods for use in wine[22] and cheese matrices.[23] Since all of these methods may be prone to severe matrix interactions,[24] a noncompetitive, indirect ELISA method to be specifically used in wine analysis was developed and validated.

Furthermore, in order to assess the contamination risk of the final product and to evaluate the possibilities for effective allergen management by technical measures, the lysozyme depletion efficiencies of an array of different filtration regimes and other enological procedures were compared. To gain knowledge about the fate of lysozyme throughout the wine making process, trial wines were treated with lysozyme, further processed according to the respective enological procedures, and successively analyzed for allergen content.

MATERIALS AND METHODS

Reagents and Materials. Antibodies were produced by immunizing rabbits with enological grade lysozyme by Eurogentecs (Seraing, Belgium) as described by Weber et al.[25]

Goat anti-rabbit antibody-horseradish peroxidase (HRP) conjugate was purchased from Dako (Glostrup, Denmark). 3,3′,5,5′-Tetramethylbenzidine (TMB) was purchased from Serva (Heidelberg, Germany). Analytical grade lysozyme, ovomucoid, and ovalbumin were purchased from Sigma (St. Louis, MO, USA), and enological grade lysozyme used for treatment of the wines was purchased from Begerow (Langenlonsheim, Germany). Further enological grade lysozyme qualities from several European producers were supplied by Oenoppia (Paris, France). Gradient grade acetonitrile for HPLC-F analysis was purchased from VWR (Radnor, PA, USA). Citric buffer, pH 4.0 (210 mM citric acid monohydrate, 300 mM potassium hydroxide), carbonate buffer, pH 9.6 (75 mM sodium carbonate, 175 mM sodium bicarbonate), Tris/Tween20 buffer, pH 9.6 (50 mM tris(hydroxymethyl)aminomethane, 150 mM sodium chloride, 0.5% Tween 20), and phosphate buffered saline (PBS)/Tween20, pH 7.4 (10 mM sodium phosphate monobasic monohydrate, 70 mM sodium phosphate dibasic, 150 mM sodium chloride, 0.5% Tween 20), for ELISA were prepared according to Weber et al.[25] All other chemicals were of analytical grade if not stated otherwise.

Wines. Wine fining and processing was performed at pilot scale size at the Geisenheim cellars using a Rheingau region Müller-Thurgau as white wine and a Nahe region Regent as red wine. Musts were inoculated with cultured yeast strains and kept in stainless steel tanks after vinification. The physicochemical characteristics of the wines are given in Table 1.

Treatment with enological grade lysozyme was carried out at the maximum permissible concentration of 0.5 g/L and, to mimic the case of a potential accidental overdose, at a double concentration of 1.0 g/L. Twenty-four hours after initial lysozyme treatment, the following filtration regimes and enological procedures were employed to evaluate their respective lysozyme depletion potentials:

- sheet filtration using SEITZ-K 200 200 × 200 mm filter sheets from Pall Corporation (Port Washington, NY, USA)
- membrane filtration using a Type 419A, grade B (beverage version) SEITZ-MEMBRAcart cartridge with 0.45 μm pore size from Pall Corporation (Port Washington, NY, USA)

Table 1. Analytical Characterization of the Trial Wines

	white wine (Müller-Thurgau)	red wine (Regent)
alcoholic strength by volume	90.7 g/L (11.5% vol)	97.2 g/L (12.3% vol)
total alcoholic strength	90.7 g/L (11.5% vol)	97.8 g/L (12.4% vol)
total dry extract	23.2 g/L	22.1 g/L
reduced extract	23.2 g/L	20.7 g/L
residual extract	8.8 g/L	8.5 g/L
reducing sugars	1.0 g/L	2.4 g/L
reducing sugars after inversion	1.0 g/L	2.4 g/L
pH value	3.5	3.6
total acidity	3.5 g/L	5.2 g/L
tartaric acid	1.7 g/L	2 g/L
lactic acid	1.4 g/L	1.8 g/L
malic acid	0.3 g/L	0.2 g/L
volatile acid	0.4 g/L	0.6 g/L
glycerol	6.6 g/L	8.5 g/L

- cross-flow filtration using a Sartoflow Compact system from Sartorius (Göttingen, Germany) at a flow of 15−20 m^3/h at a pressure of 2.5 bar
- precoat/alluviation filtration using fine diatomaceous earth (kieselguhr) from Pall Corporation (Port Washington, NY, USA) as filter aid
- centrifugation using a SB14 disk separator from GEA Westfalia (Oelde, Germany) at 7500 rounds per minute, separating 1500 L/h at a pressure of 3.5 bar
- flash-pasteurization at 72 °C for 20 s
- fining with the inorganic fining agent silica, using Klar-Sol 30 silica colloid from Erbslöh (Geisenheim, Germany) at a concentration of 0.5 mL/L
- fining with the inorganic fining agent bentonite using Aktivit bentonite from Erbslöh (Geisenheim, Germany) at a concentration of 2 g/L.

Immediately after secondary treatments, sterilizing filtration was performed on all wines, using SEITZ-EK 200 × 200 mm depth filter sheets from Pall Corporation (Port Washington, NY, USA), and wines were bottled into 0.7 L screw cap bottles. Samples were drawn after every production step and kept at 8 °C until analysis.

Electrophoresis and Immunoblotting. Electrophoresis and successive immunoblotting were carried out following the protocol laid down by Steinhoff et al.[26] Proteins were separated with precast NuPAGE Bis-Tris 12% gels and MOPS SDS running buffer from Invitrogen (Karlsruhe, Germany) after reduction with dithiothreitol (DTT) and lithium dodecyl sulfate (LDS). For unspecific detection of the separated proteins, silver staining was carried out as described by Heukeshoven and Dernick.[27]

For immunoblotting, proteins were transferred to a 2 mm nitrocellulose membrane from Whatman (Maidstone, U.K.) by semidry-Western blot and incubated overnight at room temperature with rabbit anti-lysozyme antibodies, diluted 1:20000 in Tris/Tween20 buffer, pH 9.6. Successively, the membranes were incubated with goat anti-rabbit antibody-HRP conjugate, diluted 1:20000 in Tris/Tween20 buffer, pH 9.6, and staining solution, as described by Steinhoff et al.[26]

ELISA. For ELISA analysis, analytical grade lysozyme stock solutions of 5000 mg/L were prepared in citric buffer, pH 4.0, and diluted with carbonate buffer, pH 9.6, to the respective calibration standard concentrations. Wine samples were diluted with carbonate buffer, pH 9.6, at least 1:10 or higher, if required to match the calibration range. For matrix calibration and determination of repeatability and recovery rates, untreated red and white wines were diluted 1:10 and spiked with ascending lysozyme concentrations to reach the corresponding calibration standard concentrations. Measurements were performed on two separate assays on 3 consecutive days (n = 6). For the determination of dilution linearity, wines were spiked

with 300 mg/L and diluted 1:30, 1:300, and 1:3000. For ELISA analysis of wines, 3 measurements from 2 discrete bottles of each sample were performed on 3 consecutive days (n = 6) and values confirmed by HPLC-F analysis. The measured lysozyme concentrations were calculated as % of the theoretical lysozyme concentrations. All measurements were carried out in triplicate by pipetting 3 × 200 μL per sample in Nunc MaxiSorb 96-well microplates (Thermo Fisher Scientific, Waltham, MA, USA) and leaving the plates for 16 h for incubation at 4 °C. All samples and calibration standards were prepared immediately before incubation, and stock solutions were prepared freshly at least every 5 days and kept at 4 °C.

After incubation, wells were washed three times with Tris/Tween20 buffer, pH 9.6, and blocked for 2 h with 300 μL of Tris/Tween20 buffer, pH 9.6, at room temperature under gentle agitation. After blocking, wells were washed three times with PBS/Tween20, pH 7.4, and 200 μL of rabbit anti-lysozyme antibodies diluted 1:10000 in PBS/Tween20, pH 7.4, was added to each well. After incubation for 1 h at room temperature under gentle agitation, wells were washed three times with PBS/Tween20, pH 7.4, and 200 μL of goat anti-rabbit antibody-HRP conjugate, diluted 1:2000 in PBS/Tween20, pH 7.4, was added to each well. Wells were left for incubation for 1 h at room temperature under gentle agitation again and washed three times with PBS/Tween20, pH 7.4, before rebuffering by washing three times with 300 μL of citric buffer, pH 4.0. All washing procedures were carried out using a Biotek Elx50 plate washer with 8-tube manifold (Biotek, Winooski, VT, USA).

For the detection step, HRP substrate solutions were prepared immediately before incubation as described by Holzhauser and Vieths,[28] resulting in a final organic solvent content of no more than 5%.

Incubation was started by adding 200 μL of substrate solution to each well, and color development was stopped by addition of 100 μL of stopping solution consisting of 2 M sulfuric acid after 2 min. Incubation times were intentionally kept short in order to minimize TMB autoxidation, especially with regard to the blanks and low concentration standards. Increased signal intensity deviations caused by autoxidation could otherwise augment detrimental effects on the assays sensitivity.

Photometric measurements were carried out on a Dynex MRX plate reader (Dynex, Chantilly, VA, USA) at 450 nm with a reference wavelength of 630 nm. Calculation of regression curves was accomplished using the nonweighted 4 parameter logistic regression logarithm of the SoftMax Pro v5.4 software (Molecular Devices, Sunnyvale, CA, USA).

HPLC-F. HPLC analysis was performed on a Agilent 1100 series HPLC equipped with a G1321A fluorescence detector (Agilent, Santa Clara, CA) using a Phenomenex Jupiter C4 column (250 × 4.6 mm), 5 μm particle size with 300 Å pore size (Phenomenex, Torrance, CA, USA), held at 36 °C. Mobile phase was a gradient of solvent A (0.1% formic acid in bidistilled water) and solvent B (acetonitrile). The gradient program started with 18% solvent B for the first 1.5 min, then a ramp toward 40% solvent B at minute 3 and back to 18% at minute 4.5, with a gradient flow of 2.5 mL/min. Total run time was 7 min, and lysozyme retention time was at 0.8 min. Fluorescence detection was performed at 280 nm excitation wavelength and 340 nm emission wavelength. Wine samples were diluted 1:1 with a mix of solvent A and solvent B (82/18, v/v) prior to analysis.

RESULTS AND DISCUSSION

Antibody Characterization and Lysozyme Preparation Characterization. By choosing enological grade lysozyme actually intended for enological application as sensitizing agent instead of highly purified analytical grade lysozyme, it was facilitated to raise antibodies that show specificity not only against intact lysozyme but also against partially denatured, modified, or fragmented lysozyme molecules potentially formed during production and handling of the enological product, which could still possess allergenic properties, but potentially exhibit different solubility or depletion resistance patterns than intact lysozyme.

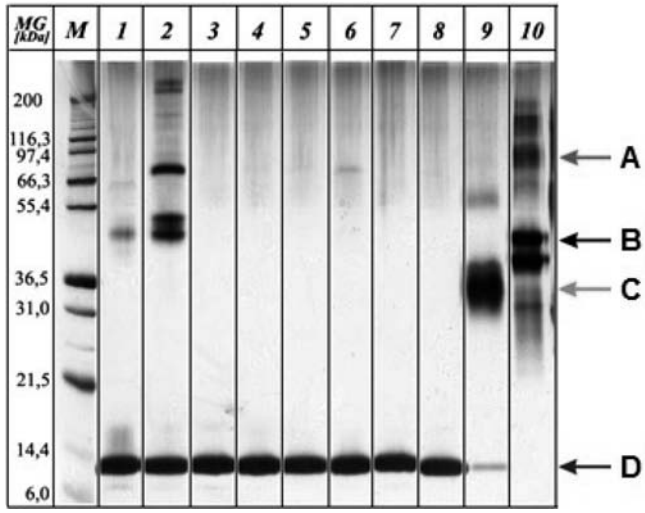

Figure 1. Antibody characterization, LDS−PAGE (M, molecular weight marker; 1−7, enological grade lysozyme preparations from different suppliers, with 7, enological grade lysozyme used for wine treatments; 8, analytical grade lysozyme; 9, analytical grade ovomucoid; 10, analytical grade ovalbumin; A, conalbumin (77−78 kDa); B, ovalbumin (42.7 kDa); C, ovomucoid (28 kDa); D, lysozyme (14.4 kDa)).

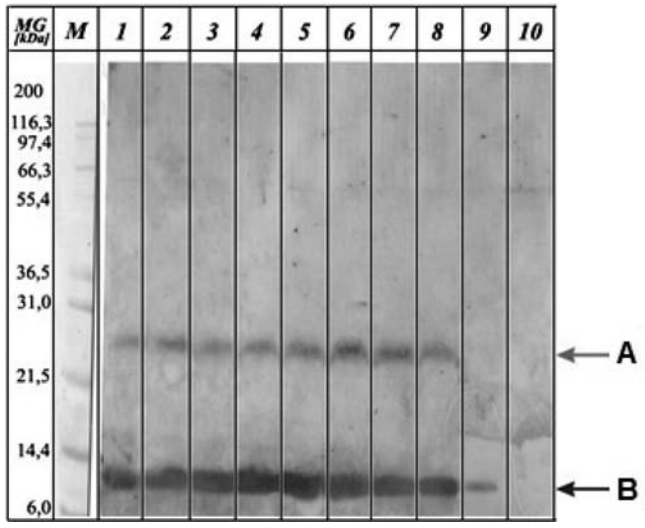

Figure 2. Antibody characterization, immunoblot (M, molecular weight marker; 1−7, enological grade lysozyme preparations from different suppliers, with 7, enological grade lysozyme used for wine treatments; 8, analytical grade lysozyme; 9, analytical grade ovomucoid; 10, analytical grade ovalbumin; A, unknown/artifact?; B, lysozyme (14.4 kDa)).

To show specific affinity and exclude potential cross-reactivities, antibodies were characterized by electrophoresis and immunoblotting of analytical grade lysozyme, enological grade lysozyme from different suppliers, and contiguous egg allergens ovomucoid and ovalbumin (Figures 1 and 2). It could be shown that the antibodies specifically detect lysozyme and show no cross-reactivity toward ovomucoid or ovalbumin (Figure 2, lanes 9 and 10). Furthermore, in all lysozyme preparations including analytical grade lysozyme, they are

dx.doi.org/10.1021/jf405319j | J. Agric. Food Chem. 2014, 62, 6247−6253

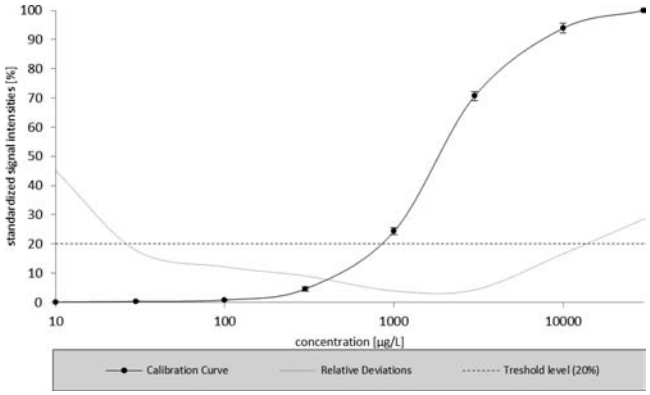

Figure 3. ELISA calibration curve and according precision profile.

Table 2. Statistical Characteristics of the Developed Indirect ELISA Method

LOD (blank + 3 × SD_{blank})	5 μg/L
LOD (blank + 3 × SD_{blank} < x − SD_x)	6 μg/L
LLOQ (blank + 10*SD_{blank})	10 μg/L
LLOQ (precision profile)	30 μg/L
ULOQ (precision profile)	10 mg/L
repeatability (n = 6)	5.2−14.7%
recovery rate	69.8−105.1%

Table 3. Performance Characteristics of HPLC-F Methods

	HPLC-F method as described	OIV-MA-AS315-14[30]
linearity range	5−400 mg/L	1−250 mg/L
correlation coeff	0.9998	0.9990
LOD	0.46 mg/L	0.18 mg/L
LOQ	1.38 mg/L	0.59 mg/L
repeatability (n = 5)		
buffer	0.98%	2.61%
white wine	1.78%	0.68%
red wine	2.54%	2.37%
recovery rate	94.4−101.3%	97.7−102.2%
retention time	0.8 min	25.5 min
total run time	7 min	40 min

capable of detecting an additional protein band of a higher molecular weight than native lysozyme (Figure 2, lanes 1−8, indicator A), possibly a lysozyme artifact or dimerized lysozyme. Since this protein has only been detected by immunoblotting and not by silver staining, specificity seems to be high and concentrations low. Immunostaining intensities suggest that the concentration is lowest in analytical grade lysozyme and may vary in enological grade lysozyme preparations, indicating a potential influence of the production protocol on its presence. Furthermore, residues of ovalbumin could be detected in some preparations (lanes 1, 2, and 6), but not in others. Low molecular weight lysozyme fragments could not be detected in either of the lysozyme preparations.

Development of the ELISA Method. Comparison of different enological grade lysozyme preparations showed a significant degree of variability in composition. In order to have a more reliably defined calibrator, calibration and validation of the ELISA method were carried out using analytical grade lysozyme. Signal response intensities of the analytical grade lysozyme used for calibration and the enological grade lysozyme used for treatments of the wines showed a correlation of 97.4−106.0% over the entire quantification range, averaging

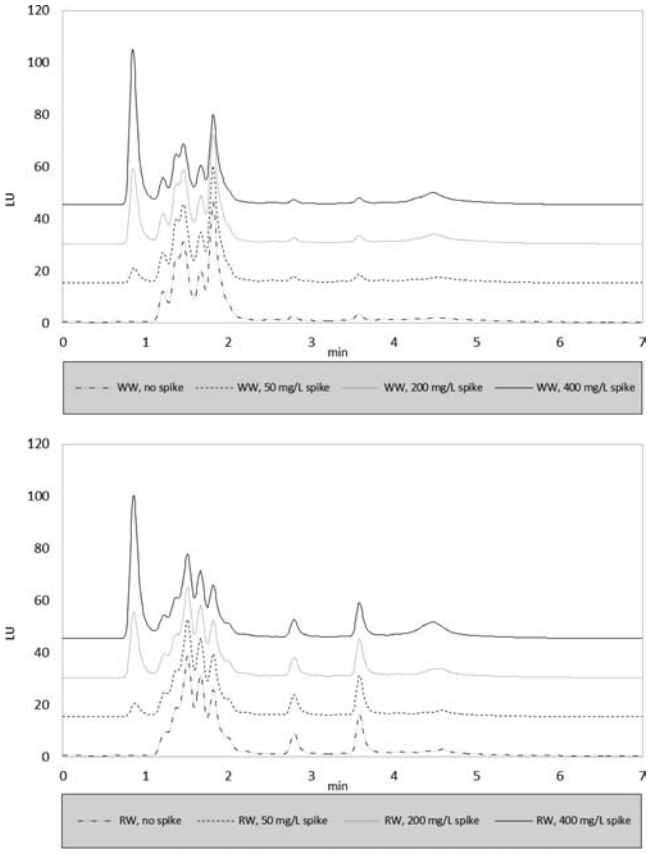

Figure 4. HPLC-F analysis of untreated white and red wines spiked with lysozyme.

101.1%. Therefore, signal responses of this enological grade lysozyme can be regarded as equivalent to the analytical grade lysozyme signal responses. In order to estimate the limit of detection (LOD) and limit of quantification (LOQ), it is a well-established approach to calculate the concentration value corresponding to the matrix blank signal plus a respective multiple (usually n = 3 for the LOD, n = 10 for the LOQ) of the standard deviation of the matrix blank signal. This approach is based on the presumption of homogeneity of variances over the complete calibration range and does not take into account the actual signal variations of the calibration standards. However, in an analytical system like an ELISA, relying on a cascade of interrelated principles for signal generation and amplification, a heteroscedastic distribution of signal deviations over the calibration range may be assumed, even more so when employing a calibration range covering multiple orders of magnitude. The relevance of this consideration for determining the LOD/LOQ is further enhanced by the nonlinear, logistic nature of the signal curve in an ELISA. With the decreasing slope on both ends of the curve, it becomes increasingly difficult to reliably distinguish between discrete calibration standard concentrations on the fringes of the calibration range. Depending on the calibration range, this may lead to the necessity to determine not only a lower but also an upper LOQ.

To account for these characteristics, an alternative approach toward establishing potentially more meaningful LOQs for ELISA methods has been pursued by employment of a precision profile as proposed by Ekins.[29] This approach aims to take both the steepness of the slope and the standard deviation of the matrix calibration standard signal over the

Table 4. Analysis of Wines[a]

			before StF				after StF			
EnP	matrix	dosage [mg/L]	c(LYZ) [mg/L]	SD [mg/L]	CV [%]	% (c_{theo})	c(LYZ) [mg/L]	SD [mg/L]	CV [%]	% (c_{theo})
ShF	WW	500.0	251.5	47.3	18.8	50.3	257.5	57.2	22.2	51.5
		1000.0	593.9	147.3	24.8	59.4	304.7	76.5	25.1	30.5
	RW	500.0	245.8	27.9	11.3	49.2	218.1	30.8	14.1	43.6
		1000.0	505.3	64.5	9.5	50.5	517.7	8.8	1.2	51.8
MeF	WW	500.0	297.7	49.2	16.5	59.5	304.0	78.6	25.9	60.8
		1000.0	586.8	196.6	33.5	58.7	642.8	164.0	25.5	64.3
	RW	500.0	297.3	28.6	9.6	59.5	223.1	14.1	6.3	44.6
		1000.0	596.0	68.6	9.9	59.6	602.0	114.6	14.1	60.2
CrF	WW	500.0	282.4	64.6	22.9	56.5	255.4	59.2	23.2	51.1
	RW	500.0	283.1	21.9	7.7	56.6	256.1	37.8	14.7	51.2
		1000.0	477.9	442.2	30.5	47.8	561.1	0.7	3.1	56.1
KiF	WW	500.0	325.8	72.7	22.3	65.2	265.9	85.2	32.0	53.2
		1000.0	622.7	140.0	22.5	62.3	776.4	147.0	18.9	77.6
	RW	500.0	199.7	9.6	4.8	39.9	198.0	8.4	4.2	39.6
		1000.0	492.8	36.9	8.8	49.3	540.0	183.9	16.6	54.0
Cen	WW	500.0	321.6	46.4	14.4	64.3	316.3	72.1	22.8	63.3
		1000.0	570.6	135.7	23.8	57.1	612.8	182.1	29.7	61.3
	RW	500.0	313.5	20.3	6.5	62.7	199.9	14.0	7.0	40.0
		1000.0	666.3	0.2	1.1	66.6	670.6	29.8	3.9	67.1
FlP	WW	500.0	292.8	60.4	20.6	58.6	256.3	79.0	30.8	51.3
		1000.0	586.1	149.9	25.6	58.6	672.9	167.5	24.9	67.3
	RW	500.0	276.8	8.9	3.2	55.4	170.8	16.1	9.4	34.2
		1000.0	577.8	7.0	1.4	57.8	585.1	101.0	11.2	58.5
SiF	WW	500.0	402.0	57.9	14.4	80.4	385.6	125.2	32.5	77.1
		1000.0	511.8	47.5	9.3	51.2	647.0	183.1	28.3	64.7
	RW	500.0	257.2	23.6	9.2	51.4	213.9	23.0	10.8	42.8
		1000.0	574.8	33.4	3.5	57.5	588.4	34.4	3.4	58.8
BeF	WW	500.0	36.0	8.1	22.5	7.2	n.d.			
		1000.0	101.8	25.1	24.6	10.2	90.8	27.2	29.9	9.1
	RW	500.0	57.6	8.2	14.2	11.5	n.d.			
		1000.0	221.7	46.6	6.8	22.2	212.3	12.0	3.5	21.2

[a]WW: white wine. RW: red wine. EnP: enological procedure. c(LYZ): lysozyme concentration. SD: standard deviation (n = 6). CV: coefficient of variation (n = 6). % (c_{theo}): recovery of theoretical lysozyme concentration. StF: sterilizing filtration. ShF: sheet filtration. MeF: membrane filtration (0.45 μm). CrF: cross-flow filtration. KiF: kieselguhr filtration. Cen: centrifugation. FlP: flash-pasteurization. SiF: silica fining. BeF: bentonite fining. n.d.: not detected.

whole range of the calibration curve into consideration for determining a lower and an upper LOQ (LLOQ, ULOQ). Relative deviations of the calibration standard signal intensities are calculated by dividing the standard deviations of the calibration standard signals by the product of the calibration standard concentration and the steepness of the slope at the calibration standard concentration value in question. These relative deviations are plotted against a set threshold level that provides a cutoff value to warrant a defined quantitative significance of the signal read-out. Thus, the LLOQ and ULOQ are respectively considered the lowest and highest matrix calibration standard concentrations yielding a relative deviation below the threshold level. Figure 3 shows the calibration curve and the according precision profile.

Furthermore, for the estimation of an LOD taking both the standard deviation of the blank and the standard deviations of the calibration standards into account, the lowest calibration standard concentration for which the matrix blank signal plus 3-fold its standard deviation is smaller than the matrix calibration standard signal minus 3-fold its standard deviation is considered the LOD.

Table 2 summarizes the statistical characteristics of the ELISA with a relative deviation of 20% defined as the threshold value determining the LLOQ and ULOQ. The proposed alternative approaches toward establishing an LOD and LLOQ bring forth higher values than with the commonly applied method. This comes as no surprise, taking into consideration that these alternative approaches aim to address more elements of uncertainty than only the standard deviation of the blank. With regard to the presumed higher reliability of these values, however, this appears acceptable. Recovery rates for matrix calibration standards calculated on the calibration curves obtained from calibration standards in buffer were between 69.8 and 105.1% over the entire quantification range. Repeatability is reflected in the coefficients of variation ranging from 5.2 to 14.7% for n = 6. Dilution linearity for dilutions 1:30, 1:300, and 1:3000 was considered satisfying with recovery rates of 86.7−99.8%.

For analysis of the wines, ELISA results were confirmed by additional HPLC-F analysis. With a LOD < 0.5 mg/L (calculated as blank + 3 × SD_{blank}), linearity range from 5 to 400 mg/L, and correlation coefficient of 0.9998, the HPLC method shows good correlation with the statistical characteristics defined in the official OIV method for the measurement of lysozyme in wine by HPLC OIV-MA-AS315-14,[30] but with a total run time of 7 min as compared to 40 min in OIV-MA-

dx.doi.org/10.1021/jf405319j | J. Agric. Food Chem. 2014, 62, 6247−6253

AS315-14, it gives an almost 6-fold increase in sample throughput. Table 3 gives a brief comparison of the performance characteristics of the two methods. Chromatograms of untreated white and red wine spiked with ascending lysozyme concentrations are shown in Figure 4. Upon comparison, the congruency of the ELISA and the HPLC-F method was considered very satisfying. Lysozyme concentrations measured by HPLC-F in the spiked wines were on average 98% of the concentrations measured by ELISA.

Analysis of Wines and Comparison of Enological Procedures. For the assessment of the depletion efficiencies, the wines were subjected to the respective enological procedures and samples drawn directly after the procedure and after sterilizing filtration. As can be seen from Table 4, all enological procedures under scrutiny are capable of reducing the detectable lysozyme amount. However, except for bentonite fining, the detectable amounts are still very high. This shows that most of these procedures are not capable of satisfactorily reducing the lysozyme content and thus do not represent suitable tools for allergen depletion. This may at least in part be attributed to the good solubility and low molecular weight of lysozyme. For both red and white wines treated with 500 mg/L lysozyme, bentonite fining is effective enough to deplete the lysozyme amounts to levels below 100 mg/L. While the effect of sterilizing filtration on depletion efficiencies generally appears to be negligible, for bentonite-treated wines, this last filtration step serves to lower lysozyme levels below the LOD. Potentially, the remaining lysozyme adsorbs to bentonite particles still in suspension, forming aggregates big enough to be removed by sterilizing filtration. For wines treated with 1000 mg/L lysozyme, however, not even bentonite fining and successive sterilizing filtration proved sufficient for total depletion. This spotlights the general limitation of the capability of a given amount of bentonite to reduce a given amount of lysozyme present in wine. On the other hand, employed amounts of bentonite cannot be continuously increased, without severely affecting the sensory and organoleptic characteristics of the wine. Excessive use of bentonite may impair both the aroma profile and the color intensity of the wine, resulting in quality deterioration and thus economic loss. Differences in bentonite quality used for treatment of wines may effect different results regarding their respective potential to deplete lysozyme or to affect the overall quality and taste of the wine being treated.

Hence, it may be concluded that, depending on the production technique employed, lysozyme used as a microbial stabilizer in the wine making process may potentially be present in the final product at concentrations that could pose a thread toward sensitized individuals..

This is relevant information for winemakers intending to establish a good manufacturing practice guideline to be able to utilize lysozyme in their cellars and still provide wines free of allergenic residues. Since in the case of wine, the labeling of allergenic ingredients is only statutory if the wines were positively tested for allergenic residues, bentonite fining might offer a viable opportunity to enable lysozyme treatment of musts and wines, and still provide products that can safely be enjoyed by allergic individuals.

Overall, it can be concluded that allergen management of lysozyme in wine should always include analytical control for product safety. Regarding future developments, there are also intentions not to rely on dissolved lysozyme in the wine but rather to use lysozyme immobilized on supportive beads.[31] Uncertainties regarding the durability of the attachment of the lysozyme to the beads and the release rates encountered in commercial application would of course create sufficient necessity for sensitive lysozyme analysis of the final product just as if the wine was treated with the native enzyme and then subjected to filtration or other further processing.

AUTHOR INFORMATION

Funding

The research project (AiF 16330 N) was funded under the program to promote Industrial Joint Research (IGF) of the Federal Ministry of Economics and Technology (via AiF) by the Research Association of the German Food Industry (FEI).

Notes

The authors declare no competing financial interest.

REFERENCES

(1) Santos, M. C.; Nunes, C.; Saraiva, J. A.; Coimbra, M. A. Chemical and Physical Methodologies for the Replacement/reduction of Sulfur Dioxide Use During Winemaking: Review of Their Potentialities and Limitations. *Eur. Food Res. Technol.* **2012**, *234*, 1−12.

(2) Sonni, F.; Cejudo Bastante, M. J.; Chinnici, F.; Natali, N.; Riponi, C. Replacement of Sulfur Dioxide by Lysozyme and Oenological Tannins During Fermentation: Influence on Volatile Composition of White Wines. *J. Sci. Food Agric.* **2009**, *89*, 688−696.

(3) Vocadlo, D. J.; Davies, G. J.; Laine, R.; Withers, S. G. Catalysis by Hen Egg-white Lysozyme Proceeds via a Covalent Intermediate. *Nature* **2001**, *412*, 835−838.

(4) Masschalck, B.; Michiels, C. W. Antimicrobial Properties of Lysozyme in Relation to Foodborne Vegetative Bacteria. *Crit. Rev. Microbiol.* **2003**, *29*, 191−214.

(5) Gerbaux, V.; Villa, A.; Monamy, C.; Bertrand, A. Use of Lysozyme to Inhibit Malolactic Fermentation and to Stabilize Wine After Malolactic Fermentation. *Am. J. Enol. Vitic.* **1997**, *48*, 49−54.

(6) Gao, Y. C.; Zhang, G.; Krentz, S.; Darius, S.; Power, J.; Lagarde, G. Inhibition of Spoilage Lactic Acid Bacteria by Lysozyme During Wine Alcoholic Fermentation. *Aust. J. Grape Wine Res.* **2002**, *8*, 76−83.

(7) Gendel, S. M. The Regulatory Challenge of Food Allergens. *J. Agric. Food Chem.* **2013**, *61*, 5634−5637.

(8) Walsh, B. J.; Hill, D. J.; Macoun, P.; Cairns, D.; Howden, M. E. H. Detection of Four Distinct Groups of Hen Egg Allergens Binding IgE in the Sera of Children with Egg Allergy. *Allergol. Immunopathol.* **2005**, *33*, 183−191.

(9) Jacobsen, B.; Hoffmann-Sommergruber, K.; Have, T. T.; Foss, N.; Briza, P.; Oberhuber, C.; Radauer, C.; Alessandri, S.; Knulst, A. C.; Fernandez-Rivas, M.; Barkholt, V. The Panel of Egg Allergens, Gal d 1−Gal d 5: Their Improved Purification and Characterization. *Mol. Nutr. Food Res.* **2008**, *52*, S176−S185.

(10) Frémont, S.; Kanny, G.; Nicolas, J. P.; Moneret-Vautrin, D. A. Prevalence of Lysozyme Sensitization in an Egg-allergic Population. *Allergy* **1997**, *52*, 224−228.

(11) Poulsen, L. K.; Hansen, T. K.; Nørgaard, A.; Vestergaard, H.; Stahl Skov, P.; Bindslev-Jensen, C. Allergens from Fish and Egg. *Allergy* **2001**, *56*, 39−42.

(12) Everberg, H.; Brostedt, P.; Oman, H.; Bohman, S.; Movérare, R. Affinity Purification of Egg-white Allergens for Improved Component-resolved Diagnostics. *Int. Arch. Allergy Immunol.* **2011**, *154*, 33−41.

(13) Sampson, H. A. Update on Food Allergy. *J. Allergy Clin. Immunol.* **2004**, *113*, 805−819 quiz 820.

(14) Savage, J. H.; Matsui, E. C.; Skripak, J. M.; Wood, R. A. The Natural History of Egg Allergy. *J. Allergy Clin. Immunol.* **2007**, *120*, 1413−1417.

(15) Benhamou, A. H.; Zamora, S. A.; Eigenmann, P. A. Correlation Between Specific Immunoglobulin E Levels and the Severity of Reactions in Egg Allergic Patients. *Pediatr. Allergy Immunol. Off. Publ. Eur. Soc. Pediatr. Allergy Immunol.* **2008**, *19*, 173−179.

(16) European Union. *Directive 2003/89/EC of the European Parliament and of the Council of 10 November 2003 Amending Directive 2000/13/EC as Regards Indication of the Ingredients Present in Foodstuffs (1)*, 2003.
(17) European Union. *Commission Implementing Regulation (EU) No 579/2012 of 29 June 2012 Amending Regulation (EC) No 607/2009 Laying down Certain Detailed Rules for the Implementation of Council Regulation (EC) No 479/2008 as Regards Protected Designations of Origin and Geographical Indications, Traditional Terms, Labelling and Presentation of Certain Wine Sector Products*; 2012.
(18) Schnadt, S. Problematik "versteckter Allergene" in Lebensmitteln Aus Sicht Des Allergischen Verbrauchers. *Bundesgesundheitsblatt - Gesundheitsforschung - Gesundheitsschutz* **2012**, *55*, 385−393.
(19) Riponi, C.; Natali, N.; Chinnici, F. Quantification of Hen's Egg White Lysozyme in Wine by an Improved HPLC-FLD Analytical Method. *Am. J. Enol. Vitic.* **2007**, *58*, 405−409.
(20) Schneider, N.; Becker, C.-M.; Pischetsrieder, M. Analysis of Lysozyme in Cheese by Immunocapture Mass Spectrometry. *J. Chromatogr. B: Anal. Technol. Biomed. Life Sci.* **2010**, *878*, 201−206.
(21) Tran, D. T.; Janssen, K. P. F.; Pollet, J.; Lammertyn, E.; Anné, J.; Van Schepdael, A.; Lammertyn, J. Selection and Characterization of DNA Aptamers for Egg White Lysozyme. *Molecules* **2010**, *15*, 1127−1140.
(22) Weber, P.; Kratzin, H.; Brockow, K.; Ring, J.; Steinhart, H.; Paschke, A. Lysozyme in Wine: A Risk Evaluation for Consumers Allergic to Hen's Egg. *Mol. Nutr. Food Res.* **2009**, *53*, 1469−1477.
(23) Schneider, N.; Weigel, I.; Werkmeister, K.; Pischetsrieder, M. Development and Validation of an Enzyme-linked Immunosorbent Assay (ELISA) for Quantification of Lysozyme in Cheese. *J. Agric. Food Chem.* **2010**, *58*, 76−81.
(24) Cucu, T.; Jacxsens, L.; De Meulenaer, B. Analysis To Support Allergen Risk Management: Which Way To Go? *J. Agric. Food Chem.* **2013**, *61*, 5624−5633.
(25) Weber, P.; Steinhart, H.; Paschke, A. Investigation of the Allergenic Potential of Wines Fined with Various Proteinogenic Fining Agents by ELISA. *J. Agric. Food Chem.* **2007**, *55*, 3127−3133.
(26) Steinhoff, M.; Fischer, M.; Paschke-Kratzin, A. Comparison of extraction conditions for milk and hen's egg allergens. *Food Addit. Contam., Part A* **2011**, *28*, 373−383.
(27) Heukeshoven, J.; Dernick, R. Neue Ergebnisse zum Mechanismus der Silberfärbung. Paper presented at *Electrophoresis Forum '86, Technical University Munich*;1986, pp 22−27.
(28) Holzhauser, T.; Vieths, S. Indirect Competitive ELISA for Determination of Traces of Peanut (Arachis Hypogaea L.) Protein in Complex Food Matrices. *J. Agric. Food Chem.* **1999**, *47*, 603−611.
(29) Ekins, R. The "Precision Profile": Its Use in RIA Assessment and Design. *Ligand Q.* **1981**, *4*, 33−44.
(30) OIV (International Organisation of Vine and Wine) Method OIV-MA-AS315−14: Measurement of Lysozyme in Wine by High Performance Liquid Chromatography. In *Compendium of International Analysis of Methods—OIV*; Resolution Oeno; 2007.
(31) Liburdi, K.; Straniero, R.; Benucci, I.; Vittoria Garzillo, A. M.; Esti, M. Lysozyme Immobilized on Micro-Sized Magnetic Particles: Kinetic Parameters at Wine pH. *Appl. Biochem. Biotechnol.* **2012**, *166*, 1736−1746.

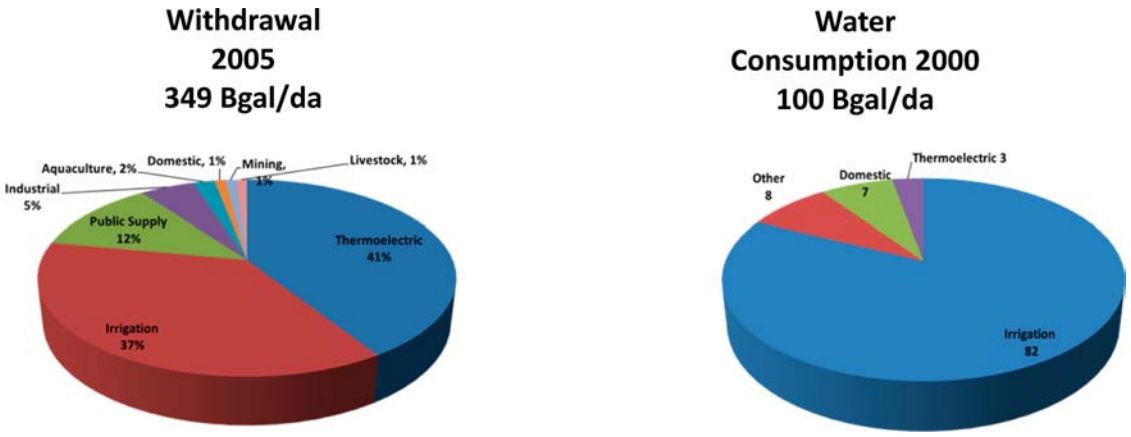

Figure 1. Fresh water withdrawals and consumption in the United States. Adapted from Faeth.[5]

Table 1. Agricultural, Industrial, and Domestic Use of Water Withdrawals in Regions of the World in Cubic Meters per Year Based on 2000 Data[6,10]

region	renewable water resources	total water withdrawals	agriculture amount	industry amount	domestic urban	% renewable resources
Africa	3936	217	186	9	22	5.5
Asia	11594	2378	1939	270	172	20.5
Latin America	13447	252	178	26	47	1.9
Caribbean	93	13	9	1	3	14
North America	6253	525	203	252	70	8.4
Oceana	1703	26	18	3	5	1,5
Europe	6603	418	132	223	63	6.3
world	43559	3829	2663	784	382	8.8

including irrigation or public water needs. Much of this water is returned for use in agriculture or municipal uses downstream. For this reason thermoelectric power plants are located near rivers, lakes, or oceans. The power plant needs for water are vulnerable to fluctuating water supplies, and when water is not adequate, there is increased risk of environmental damage or forced shutdown if there is not sufficient water for cooling requirements.

The water demands for food production and processing are enormous. Agricultural crop irrigation accounts of 82% of all water withdrawals in the United States.[5] Irrigation directly competes with water uses such as power-plant cooling, municipal needs, and fossil fuel production and transportation. When we face drought conditions, irrigation restrictions are by state and county governments, which can negatively affect food production. Food production also can have an impact on water quality because of water runoff from agriculture, which contains fertilizers, pesticides, herbicides, and manure from agricultural production and wastewater from food-processing facilities. More efficient use of water, through drip irrigation and other conservation practices, is an ongoing need in agricultural.

Figure 1 illustrates the water withdrawals and water consumption in the United States. Electricity generation and irrigation account for the largest withdrawals of water in the United States. However, electricity generation returns most of the water withdrawn, whereas irrigation does not. This water use is critical for the production of agricultural commodities including both domestic needs and economically important exported agricultural products.[5] Major concerns exist as we see more areas of drought from global climate change (GCC). If we use irrigated biomass for energy production, our already limited water system becomes further strained. GCC estimates are that drier areas will become drier and wetter areas will become wetter. Therefore, water redistribution might be the biggest challenge for the future.

Increases in demand for food and energy have made clear the concerns about sufficient water availability. Renewable water resources throughout the world are used to various degrees for agriculture, industry, and domestic uses. In all cases agriculture is the largest user of water worldwide as summarized in Table 1. It is worth noting that Asia is the largest user of agricultural water, whereas Asia, North America, and Europe use similar amounts of water for industrial purposes. This supports the demand for more efficient use of water in agriculture and the need for plants that require less water for food or biofuel production.

Water is a key component in energy production; it is used in power generation, cooling thermal power plants, and the extraction, transportation, and processing of fuels. Water also is required for irrigation and for processing of biomass crops. Energy is also required for the collection, transport, treatment, and distribution of fresh potable water. Both fresh water and seawater are critically important for transportation of raw materials and products in most parts of the world.[7]

Continuing droughts and demands for irrigation to support food production are requiring greater reliance on underground water aquifers. To meet these needs, water wells must be drilled deeper and deeper. Energy is required for groundwater delivery. As we drill deeper for groundwater sources, more energy is required to bring the water to the surface. The need for current and expanding populations for clean water and sewage treatment will require energy to move water to the needed sites economically and without the addition of more environmental stress.

If desalination becomes economical, it could provide an important source of water at least in coastal areas. The technology for desalination of seawater and/or brackish water has improved significantly in the past 10 years; as a result, the capacity has grown rapidly. Cost remains a significant figure in desalination. The cost of desalinated water ranges from U.S. $0.50/m^3$ to U.S. $1.00/m^3$ depending on location. Recent developments including the increase of unit capacity, process design and materials, improved membrane technology, and hybrid systems are offering promise for decreased cost and reduced energy consumption in the desalination processes. The developments of low-energy desalination technologies, such as adsorption desalination, provide promise for low cost and energy demand in the future.[8,9]

The relative amounts of water used in the energy sectors differ among the various sectors. Table 2 provides a comparison of the amounts of water required to produce a million British thermal units (BTU) of energy. The data provide interesting comparisons of the amounts of water required for enhanced recovery techniques. It also must be kept in mind that currently it is difficult to recycle that water. The biofuels comparisons are important to consider, but it must be recognized that rainwater is not considered in the estimates.

Table 2. Average Water Consumption for Production of Transportation Fuels[10]

source	water for material recovery (gal/million BTU)	transformation (gal/million BTU)	total gal/million BTU
traditional oil	1.4	12.5	13.9
conventional natural gas	0	2	2
shale natural gas	12.5	2	14.5
oil sands	260	12.5	272.5
enhanced oil recovery (fracking)	1257	172	1429
irrigated corn (ethanol)	15750	9	15759
irrigated soy biodiesel	44500	9	44509

Traditional oil and gas production use less water than production from tar sands and fracturing. Developing agricultural-based bioenergy substitutes produces additional stress on water resources. The need for water posts a significant constraint on corn-based ethanol production in the United States. Water demand for ethanol fuel production ranges widely. For example, to produce a gallon of ethanol, from 995 to 2967 gal of water is required.[10] These differences are due to variations in climate and irrigation requirements. Switch grass requires from 1.9 to 9.8 gal of water per gallon of ethanol.[11] Gasoline production requirements range from 2.8 to 6.6 gal of water per gallon of gasoline.[12] In 2001, 707 million bushels of grain were used for ethanol production. By 2010, 5020 million bushels of corn were utilized for ethanol production. The 2010 figure represents about 40% of the 12447 bushels of corn produced.[5,13] To put water use and energy use in perspective, it requires about 2 million BTU to drive an automobile on a round trip from New York City to Washington, DC. Table 3 presents the amount of water necessary to produce the various fuels required for such a trip.

Table 3. Gallons of Water Consumed To Produce Fuel for a Round Trip Drive from New York City to Washington DC

fuel type	gal of water to produce fuel
natural gas (as on land)	5
shale natural gas	33
traditional oil	32
oil sands mining	616
irrigated corn (ethanol)	35616
irrigated soy	100591

Hydraulic fracturing, or "fracking," is used to extract gas and oil from rock formations where oil and gas are not normally accessible. However, after fractures are developed in the rock formations using horizontal drilling and high levels of hydraulic pressure, gas and oil can move through the fractures and become accessible. These more accessible oil and gas reserves can then be exploited by wells.[14] The Marcellus shale basin, one of the largest, extends from northern Georgia to New York. Various other formations are found in Texas, Oklahoma, Indiana, Michigan, Arkansas, Louisiana, and the Rockies.[15] Other areas of the country offer similar opportunities for oil and gas production, including North Dakota, Pennsylvania, Wyoming, and Montana[5,17] Fracking has resulted in the ability to recover vast new quantities of petroleum and natural gas, lowered energy costs, and improved energy independence for the United States. Production estimates for the Eagle Ford area in Texas are expected to reach 2−3 million barrels of oil per day by 2035. This would represent as much as 1.5−2% of current gasoline production from this single area. To accomplish this, water demand in the Eagle Ford region will increase 10-fold by 2020.[17]

It is anticipated that shale gas will make up 46% of the total energy supply of the United States by 2035. Fracking raises a major concern because of the volumes of water required and the risk of contamination of aquifers needed for food production and domestic drinking water needs. The average shale gas well requires 3−4 million gallons of water and will yield 800 million cubic feet of gas over the 7.5 year lifetime of a well.[15]

The large volumes of water required by the fracking process pose particular problems in semiarid areas where water tables are receding. This generates a competition with agricultural irrigation and domestic water needs.[16] In addition to the vast quantities of water required for fracking, the wastewater from fracking contains a variety of compounds that make it unsuitable for irrigation or domestic use. Fracking fluid contains hundreds of chemical compounds. Companies involved in fracking reported to a Congressional committee that up to 750 different chemicals are used and/or formed in the fracking process. They range from the innocuous such as sodium chloride, citric acid, coffee, and walnut hulls to toxic ones such as lead, benzene, and methanol. Twenty-nine known or possible carcinogens have been reported in fracking wastewater.[15]

A major challenge for the industry is to develop processes to clean this water enough that it can be used for other purposes, such as irrigation, potable water, or environmentally benign release to the environment. There is rising public concern about water competition where fracking is conducted in arid regions.[17]

Thermoelectric power consumption whether coal, oil, or gas requires cooling water, which comes from surface water.

Table 4. Cost and Environmental Factors for Electricity-Generating Technologies[26]

energy technology	av levelized cost of electricity ($/MWh)	median water withdrawal by cooling type (gal/MWh)	median water consumption by cooling type (gal/MWh)	CO_2 (lb/MWh)
existing technology				
conventional coal	62	531−36350	250−471	1886
natural gas combined cycle	57	253−11380	100−198	797
nuclear	59	1101−44350	269−672	
new technology				
conventional coal	95	531−17914	493−779	1886
advanced coal	109	390	372	1755
advanced coal + carbon capture and sequestration (CCS)	126	596	540	206
natural gas combined cycle (NGCC)	66	253−5950	198−240	797
NGCC + CCS	89	496	378	86
advanced nuclear	104	1101−7050	610−672	
hydroelectric	86		4491	
wind, onshore	97		0	
wind, offshore	243		0	
solar thermal	312		8−1000	
photovoltaic	211		26	

Currently, cooling for thermoelectric power withdraws up to 75% of the surface water in some areas, however, much of it is returned for other uses.[18]

When greenhouse gases are sequestered, their cooling water demand could double because of the energy and water required for compressing the carbon dioxide.[19]

Water is very likely to become the most limiting resource in the nexus scenario. More work is needed to improve the efficiency of our water use, enhance our ability to provide clean water where needed, and purify wastewater from domestic use, energy production, and agriculture. We also need to continue development of drought- and heat-resistant crops.

■ ENERGY

The energy system, as defined by Hanlon et al.,[1] includes operations necessary to generate, transport, and distribute electricity and the steps required to produce and distribute fuels required for transportation and industry. Electrical energy is generated in a variety of power plants, which operate through the combustion of fossil fuels (coal or natural gas) or nuclear fission. These processes all generate heat, which is converted to steam, which turns turbines and ultimately generates electricity. Electricity is also generated from flowing water, wind, sunlight, and the Earth's heat (e.g., geothermal). Most electricity-generating facilities consume water either to process the raw materials used in the facility for fuel, to cool thermoelectric generation plants (fossil fuel and nuclear), or to generate the electricity itself (i.e., hydroelectric).

Thermal power plants require large amounts of water to remove excess heat. Up to 39% of all freshwater withdrawals in the United States are used for thermoelectric energy production. The needs for cooling water frequently are in competition with agriculture and municipal demands. If drought conditions increase as predicted with continuing GCC, some river flows will be very low in the summer, putting additional strain on power production and waterway transportation.[20]

In thermoelectric power plants in the United States, 1 kilowatt hour (kWh) of electricity requires the evaporation of about 2 U.S. gal (7.6 L) of water to eliminate waste heat from the process. In hydroelectric plants an average of 18 gal (68 L) of water is evaporated to generate 1 kWh of electricity. In practical terms, this means that 8−16 gal of water IS required to burn one 60 W light bulb for 12 h. This would mean that annually one incandescent light bulb would consume 3999−6300 gal of water. If it is assumed that the 111 million occupied housing units (U.S. Census Bureau 2005) burned one 60 W light bulb for 12 h a day for a year, it would require between 336 and 656 billion gallons of water use.[21]

Extraction and pumping water from ground and surface sources to sites of use requires electrical energy. The energy intensity of treatment required for different types of water source varies, depending on water sources. Fresh surface waters use energy mainly for pumping over long distances. Use of seawater adds the energy requirements for desalination. The energy required for residential end use water is very high relative to other parts of the water supply cycle. Processes such as heating water, washing clothes and dishes, and cooking all require intense energy input. Hot water usage is responsible for making end use the most energy-intensive stage of the water cycle.[22] Potable water must be pumped from its source (underground or surface) to the treatment plant, pretreated, and then pumped to consumers. In areas without adequate fresh water, it may be necessary to bring water from very long distances, making the energy footprint for this water extremely high.

Table 4 compares the cost of energy to the amount of water (withdrawals and consumption) and carbon dioxide emissions produced by various means of power generation. The data provide insight into the trade-offs of different means of energy production. Nuclear power has no carbon dioxide emissions but requires large amounts of cooling water. This water (like water for hydroelectric power generation) is suitable for reuse in agriculture or domestic use. Coal uses relatively modest amounts of water but generates high levels of carbon dioxide, which is a significant contributor to greenhouse gas and related global warming.

Southern California receives potable water from the Sacramento−San Joaquin Delta, which requires pumping water over hundreds of miles over low-lying mountains using 9200 kWh per million gallons.[23] In California the conveyance, storage, treatment, distribution, wastewater collection, and

discharge of water consumes 19% of the state's electricity, 30% of its natural gas, and 88 billion U.S. gallons (330,000,000 m^3) of diesel fuel annually. The River Network reports that the United States consumes at least 521 million megawatt-hours a year for water-related purposes, which is equivalent to 13% of the nation's electricity consumption.[24−26]

FOOD

From a global perspective food security would exist "when all people at all times have physical, social and economic access to sufficient, safe, nutritious food to meet dietary needs and food preferences".[27] Increases in demand for food and energy have made clear the concerns for sufficient water. Table 5 summarizes the amount of water required to bring selected foods to market. The water demand for animal protein foods is much higher than that for plant-based foods. This begs the question as to the sustainability of high animal protein production under ever-increasing population growth.

Table 5. Water Requirements for Food Commodities[27]

product	unit	equivalent water (m^3/unit)
cattle	head	4000
sheep and goats	head	500
fresh beef	kg	15
fresh lamb	kg	10
fresh poultry	kg	6
cereals	kg	1.5
citrus fruits	kg	1
palm oil	kg	2
pulses, roots, and tubers	kg	1

The production and processing of food are the largest users of fresh water, consuming an average of 70% of the human use of fresh water. Modern agriculture and food production requires large amounts of energy and also affects the water resources because of land degradation, changes in runoff, disruption of groundwater recharge, water quality, and availability of water and land for other purposes such as natural habitat. Modern agriculture, which is required to feed the current population, uses approximately 30% of total global energy. Fuels are required for land preparation, fertilizer production, irrigation and sowing, harvesting, transportation of crops, and processing and distribution of foods.[27]

All food production requires significant amounts of water. The quantities are determined by growing conditions and the nature of the food. Animal production, because of the inherent inefficiencies, utilizes relatively large amounts of water compared to cereals and pulses. Table 5 illustrates the range of water required to produce some basic agricultural commodities. To produce a kilogram of beef requires 15500 L of water, the same amount required to produce 12 kg of wheat or 118 kg of carrots. Making a hamburger requires >2400 L of water, not including the bun.

Table 6 contains the water requirements to produce some processed foods and fruits. This offers an interesting perspective on how much water is required for various foods. The values include production as well as processing requirements.

The Food and Agricultural Organization of the United Nations (FAO) projects that to feed the 9 billion people anticipated in 2050, global food production will need to rise by 70% and in the developing world will need to double. Currently we are not providing sufficient food to prevent global hunger. The FAO reports that in the past decade the number of chronically hungry people rose to one billion. The FAO estimated the number of people suffering from chronic hunger at 642 million in Asia and the Pacific, 265 million in sub-Saharan Africa, 53 million in Latin America and the Caribbean, and 42 million in the Near East and North Africa.[27]

Table 6. Water Requirements for Processed Foods[27]

product	quantity	equivalent water (L)
glass of beer	250 mL	75
glass of wine	125 mL	120
glass of milk	200 mL	200
glass of apple juice	200 mL	190
cup of coffee	125 mL	140
glass of orange juice	200 mL	170
cup of tea	250 mL	35
bag of chips	200 g	185
slice of bread	30 g	40
egg	40 g	135
slice of bread with cheese	30 g + 10 g	90
hamburger	150 g	2400
potato	100 g	25
tomato	70 g	13
apple	100 g	70
orange	100 g	50

The use of agricultural land for biofuels will further stress food production agriculture. The FAO projected that biofuel production by 2030 will require 35 million hectares of land, an area about the size of France and Spain combined. The projected 70% increase in food production is challenged by rising energy prices, depletion of aquifers available for water withdrawal, and the continuing loss of farmland to urbanization.

Energy conversion from solar energy to food products is inherently inefficient. Photosynthesis converts <2% of incoming solar radiation to biomass. Conversion of that biomass to food by feeding animals compounds the inefficiency, because only 5−10% of feed is converted to edible beef. Poultry is only slightly better with a 10−15% conversion. The United States expends approximately 10 units of fossil or other energy to recover one unit of food energy. To put this in perspective, a healthy male might expend 2500 kcal/day, which equates to 10000 BTU per day or 125 W.[28] If one extrapolates these numbers to the 9 billion mouths to feed in 40 years, energy for food production must be considered to be equally challenging to the water issues. In addition to developing more energy-efficient production practices from farm to fork, we also need to improve efficiency by reducing food waste. Wasted food not only does no good from a nutritional point of view, but requires energy to dispose of it. Table 7 summarizes estimated food wasted in the United States. Clearly reducing waste will

Table 7. Food Wasted in the United States[28]

food group	% ultimately wasted
grains	32
vegetables	25
fruit	23
tree nuts, peanuts	16
dairy	33
meat, poultry, fish	16
eggs	31

dx.doi.org/10.1021/jf501496r | J. Agric. Food Chem. 2014, 62, 6255−6262

ultimately improve sustainability and total food supply. However, we need to consider the entire food system, including the consumption and use of animals and the inherent inefficiencies of current animal food production.

In recent years there has been a growing interest in "eating local". Consuming locally produced foods reduces transportation and frequently addresses freshness and quality issues with produce. In some cases the locally produced products have a larger energy input than foods imported from miles away. For example, when marginal land is used, it may require more chemical input (fertilizers and pesticides), where yields per acre still remain much less.[28] Locally produced food is often labor-intensive and does not provide the efficiencies of large farming operations. It is an important niche in food production, but not likely to substantially affect food production for the 9 billion population of the future.

Establishing a model or simple measure of energy requirements to move food from farm to dinner plate is difficult because of the wide diversity of agriculture and the inherent variability of locale and climate. The cost of energy to produce food products can be extremely high, particularly when we consider production of animal protein foods.[29]

From Tables 8−10 it is clear that animal production is far less efficient than the production of corn. The efficiency also translates to other commodity crops. It is unlikely that we can convince meat-eating societies to switch to vegetarian diets in the near future. In addition, as low-consumption meat-eating societies become wealthier, it is likely that they will demand more meat protein in their diet. One approach would be to produce ground meat and sausage products that are blends of meat with pulse crops (dry beans and lentils). Pulse crops maintain protein levels, contribute fiber, and lower fat and cholesterol. Pulses are efficient crops to produce, requiring relative low levels of water and energy for production. Therefore, pulse/meat blends could provide energy-efficient and healthier options.

Table 8. Energy Use at Various Stages of Food Production[30]

use segment	energy use (quads[a])
farm fuel	1.0
farm chemicals	1.5
farm machinery	0.6
farm irrigation	0.5
processing	1.2
packaging	2.3
transportation	1.4
retail and commercial	2.5
residential	7.1

[a]A quad is 10^{15} BTU.

Table 9. Energy Required To Produce 1 lb of Various Foods[30]

food	energy (kWh) to produce 1 lb
corn	0.43
milk	0.75
apples	1.67
eggs	4
chicken	4.4
cheese	6.75
pork	12.6
beef	31.5

Table 10. Energy Efficiency of Various Foods Measured as Food Calories per Energy Used in Production[30]

food	cal/lb	energy efficiency (%)
corn	390	102
milk	291	45
cheese	1824	31
eggs	650	19
apples	216	15
chicken	573	15
pork	480	8.5
beef	1176	4.3

SOLUTIONS MUST BE SUSTAINABLE

The solutions to the water, energy, and food crisis must be carefully integrated to meet the needs to produce resources for the 9 billion inhabitants in the next 40 years. Without joint solutions the entire system will fail. Sustainable food production requires optimizing health, safety, quality, and consumer appeal of sufficient foods to sustain the growing world population. Agricultural food production has helped sustain this growth by increasing food production 20% from 1990 to 2010. If we are to meet the food needs of the anticipated population growth, this rate of increased production must continue for the next 25 years.[31] In addition to increasing population, improved nutrition and health care are extending life expectancy, further increasing the need for more high-quality food. These increases must continue in the face of limited energy supplies, limited water supplies, and increased global warming, which results in lower production using current practices.

To meet the growing need for food production, we must face the following considerations:

1 − production of more food on less desirable land using less water;
2 − decreasing energy required for production;
4 − sufficient water in the proper location at a low cost;
3 − increased globalization of best means to provide energy and water resources for food;
4 − globalization of compliance regulations.

Within the food system sustainability is regarded quite differently depending on the particular segment. For example, for food producers sustainability relates to land, water, and energy management. In addition to these macroconcerns, producers must consider fertilization and pest management, focusing on the sustainable environmental factors as well as energy resources for production of the chemicals. To help address these concerns, in recent years the U.S. Environmental Protection Agency (EPA) registration of new pesticides is now largely devoted to biorational or biopesticides, rather than further modification of synthetics from the 20th century.[32] This should help improve overall water quality by reducing residual agricultural chemicals. When food sustainability is considered from the food health and nutrition viewpoint, consumer health and nutrition are particularly important (e.g., vitamin, antioxidant, and mineral balance and avoiding undue levels of fats, carbohydrates, sodium, and synthetic additives).[33−37] Food processors' sustainability issues are focused on preserving and distributing foods, including maximizing shelf life for quality and safety.

dx.doi.org/10.1021/jf501496r | J. Agric. Food Chem. 2014, 62, 6255−6262

There is growing momentum demonstrating the benefits of new biopesticides, biofuels, and biobased products used in the production, processing, and distribution of foods.[38] Food processing results in the production of considerable waste, but much of the waste material could be recovered and used as an energy source as summarized in Table 7. Food waste needs to be minimized and value captured whenver possible. Capturing and using the energy from processing and food wastes through approaches such as anaerobic fermentation to biogas and recovering the energy as electricity would make use of biomass and result in net energy savings.[39]

The "9 Billion Problem" has implications for the way research, education, and outreaches are supported at the National Institute of Food and Agriculture (NIFA). The science, policies, and regulations must align with addressing the global challenges in a sustainable manner, including food security, hunger, food safety, health and nutrition, childhood obesity, energy, water, and climate change.

The nexus between food, water, energ,y and health is critical as to how we deploy resources to address the same because of the need to consider them collectively, rather than individually. The increase in population will contribute to escalating the scarcity of land, water, energy, and food.[40]

Addressing these complex issues will take a commitment to seeking collaborative efforts between federal and state agencies, private enterprise, and nongovernmental organizations. Investing in enabling sound science and policies that address these complex issues and investments in ensuring food security and sustainable bioenergy and water will be a significant part of NIFA's portfolio. NIFA along with other federal agencies including the National Science Foundation, the Department of Energy, and the Bureau of Land Management must continue to support the best and brightest scientists at academic institutions and in private and nongovernmental sectors to find innovative solutions to these challenges. By making the right investments in science, our expectation is that NIFA-supported reseach will enable the scientific community to make great discoveries that can be translated into innovations beneficial to the lives of the American people, and for that matter, globally.[40] For example, drought-resistant and heat-tolerant crops produced through biotechnology could help maintain or increase usable production land for commodity crops such as corn. The corn would lower food production costs and potentially provide feed for production of more animal protein for the growing population. Improving the feed efficiency for milk and meat production also provides challenging but potentially impactful means to provide desirable foods for the growing population.

The dilemma of food, energy, and water present us with a worldwide multidimensional problem that links resources, politics, and quality of life for all on the planet now and for the 9 billion that will inhabit the plant in the next 40 years.

IMPLICATIONS

We must adopt a nexus approach to deal with the relationships of food, energy, and water. None of these issues can be effectively resolved in isolation. Development of new technology in any of the sectors must consider the impact on the other sectors as well as the environment. Specifically, the development of a new energy or food crop must consider water use, energy consumption, and waste or byproduct production during the process. Government and international policy needs to be developed to ensure integrated implementation of technologies considering growing population stresses, the associated energy and food needs, and how these affect the environment and potential for global warming. We must avoid isolated silo approaches and consider broad effects of new technologies and their impact on the food, water, and energy systems. The nexus must involve individuals, policy makers, and thought leaders. As scientists we need to take leadership in communicating the issues clearly and bring forth new technologies that solve problems while also considering the broad implications of these new technologies.

In summary, it is critical that we develop environmentally sustainable sources of energy. The use of carbon-based energy sources needs to be restricted in favor of lower carbon emission sources including solar, wind, and nuclear energy. Water use and protection are major concerns. It is imperative that groundwater pollution be restricted and water used in processes such as fracking be purified to a degree that it can be used for agricultural or domestic applications. Agriculture is the largest user of water, and thus improved practices to minimize water use are needed. Biotechnology should continue to develop drought-tolerant crops for use throughout the world. With GCC the need for drought-tolerant crops will become even greater. With the potential problem of feeding 9 billion people in 40 years, we must seriously consider how much agricultural land should be used for biofuels. Land not suitable for agriculture can be used for crops such as switchgrass that may be viable alternatives for biofuel production. As part of this consideration, however, the impact on the local environment and the habitats of wildlife must be assessed. In addition, sugar cane could be a sustainable source for biofuels. The decreased consumption of sugar from antiobesity campaigns may result in increased sugarcane supplies at prices favorable for biofuels. A major concern is the sustainability of animal products. As discussed, animal production requires large amounts of water and energy compared to grain- and pulse-based products. It is important that we consider greater use of plant-based foods to meet long-term needs for the growing population.

The pressures on energy, water, and food for the growing population are being exacerbated by climate change. At the current pace of growth of food, water, and energy needs, the planet will not be able to provide sufficient resources to meet these demands. There is no one simple solution to resolve these complex issues. Additional investment is needed by government, universities, and industry to identify, fund, and develop integrated and sustainable solutions to address our current and future needs for food, energy, and water. Solutions must include environmentally benign approaches through continued research on sustainable processes. Alternative solutions that provide greener processes need to be encouraged with tax incentives. Assessments and metrics need to be based on long-term solutions that reflect their true impact.

AUTHOR INFORMATION

Corresponding Author

*(J.W.F.) Phone: (225) 578-5085. E-mail: jfinley@agcenter.lsu.edu.

Notes

The authors declare no competing financial interest.

REFERENCES

(1) Hanlon, P.; Madel, R.; Olson-Sawyer, K.; Rabin, K.; Rose, J. *Food, Water and Energy: Know the Nexus*; Grace Communications: New York, 2013; programs@gracelinks.org.

(2) Watersheds; Water.epa.gpv/type/watersheds/ (accessed June 6, 2014).
(3) Vickers, A. *The Handbook of Water Use and Conservation*; WaterPlow Press: Amherst, MA, USA, 2001; ISBN 1-931579-07-5.
(4) Barber, N. L. *Summary of Estimated Water Use in the United States in 2005*; U.S. Geological Survey Fact Sheet 2009-3098; 2009; 2 pp.
(5) Faeth, P. U.S. energy security and water: the challenges we face. *Environ.: Sci. Policy Sustainable Dev.* **2012**, *54* (1), 4−19, DOI: 10.1080/00139157.2012.639595.
(6) Agricultural water withdrawals as share of total water withdrawals; http://webworld.unesco.org/water/wwap/wwdr/indicators/pdf/G5_Agriculture_water_withdrawals.pdf (accessed June 6, 2014).
(7) Aquastat; http://www.fao.org/nr/water/aquastat/main/index.stm, www.fao.org/faostat/.
(8) Ghaffour, N.; Missimer, T. M.; Amy, G. L. Technical review and evaluation of the economics of water desalination: current and future challenges for better water supply sustainability. *Desalination* **2013**, *309*, 197−207.
(9) Subramani, A.; Badruzzaman, M.; Oppenheimer, J.; Jacangelo, J. G. Energy minimization strategies and renewable energy utilization for desalination: a review. *Water Res.* **2011**, *45* (5), 1907−1920.
(10) Mckenna, P. *Measuring Corn Ethanol'S Thirst for Water*; MIT Technology Review; MIT: Cambridge, MA, USA, April 14, 2009.
(11) Glassman, D.; Wucker, M.; Isaacman, T.; Champilou, C. *The Water-Energy Nexus: Adding Water to the Energy Agenda*; World Policy Papers; World Policy Institute: New York, 2011.
(12) Consumptive Water Use in the Production of Bioethanol and Petroleum Gasoline; http://www.acs.org/content/dam/acsorg/policy/acsonthehill/briefings/energywaternexus/12-08-anl-water-use-in-bioethanol-gas.pdf (accessed June 6, 2014).
(13) Corn; http://www.ers.usda.gov/topics/crops/corn/background.aspx#.U5cA_HJdWf8 (accessed June 6, 2014).
(14) Hydraulic Fracturing 101; http://www.earthworksaction.org/FracingDetails.cfm (accessed June 6, 2014).
(15) U.S. Department of Energy, Office of Fossil Energy and the National Energy Technology Laboratory. *Modern Shale Gas Development in the United States: Primer*; http://frack.mixplex.com/content/us-department-energy-doe-office-fossil-energy-and-national-energy-technology-laboratory-mode (accessed June 6, 2014).
(16) U.S. House of Representatives Committee on Energy and Commerce. Minority Staff, Chemicals Used in Hydraulic Fracturing, April (2011); http://democrats.energycommerce.house.gov/sites/default/files/documents/Hydraulic%20Fracturing%20Report%204.18.11.pdf (accessed June 6, 2014).
(17) South Texas Enjoys Major Boom From Oil Fracking; http://www.huffingtonpost.com/huff-wires/20110612/us-gas-drilling-boom-towns/ (accessed June 6, 2014).
(18) Jenicek, E. M.; Myers, N.; Fournier, D. F.; Miller, K.; Hessel, M.; Carroll, R.; Holmes, R. *Army Installations Water Sustainability Assessment: An Evaluation of Vulnerability to Water Supply*; U.S. Army Corps of Engineers, Engineer Research and Development Center, ERDC/CERL TR-09-38; Sept (2009), map D3, 2009.
(19) U.S. Energy Security and Water: The Challenges We Face; http://www.netl.doe.gov/energy-analyses/pubs/Bituminous_Performance_Tool_Rev4.swf (accessed June 6, 2014).
(20) Energy-Water Nexus Overview; http://www.sandia.gov/energy-water/nexus_overview.htm (accessed June 6, 2014).
(21) Consumptive Water Use for U.S. Power Production; Technical Report National Renewable Energy Laboratory NREL/TP-550-33905; http://www.nrel.gov/docs/fy04osti/33905.pdf (accessed June 6, 2014).
(22) Hill, R.; Younos, T. *Water Cooler, The Intertwined Tale of Energy and Water*; Virginia Water Resources Research Center, Virginia Tech, Blacksburg, VA, 2008; http://vwrrc.vt.edu/watercooler/watercooler_apr08.html (accessed June 6, 2014).
(23) Plappally, A. K.; Lienhard, J. H., V. Energy requirements for water production, treatment, end use, reclamation, and disposal. *Renew. Sustain. Energy Rev.* **2012**, *16*, 4818−4848.
(24) The Carbon Footprint of Water; http://www.rivernetwork.org/resource-library/carbon-footprint-water (accessed June 6, 2014).
(25) Water-Related Energy Use in California; http://www.energy.ca.gov/2007publications/CEC-999-2007-008/CEC-999-2007-008.PDFAccessed (accessed June 6, 2014).
(26) Macknick, J.; Newmark, R.; Heath, G.; Hallet, K. C. *A Review of Operational Water Consumption and Withdrawal Factors for Electricity Generating Technologies*; National Renewable Energy Laboratory Technical Report NREL/TP-6A20-50900; National Renewable Energy Laboratory: Golden, CO, USA, 2011.
(27) Use of Water in Agriculture; http://www.lenntech.com/water-food-agriculture (accessed June 6, 2014).
(28) Breckel, A.; Fyffe, J. R.; Webber, M. E. Trash to treasure: turning non-recycled waste into low-carbon fuel. *Earth Mag.* **2012**, Aug.
(29) List of Foods by Environmental Impact and Energy Efficiency; http://truecostblog.com/2010/02/24/list-of-foods-by-environmental-impact-and-energy-efficiency/ (accessed June 6, 2014).
(30) Alter, L. Energy to produce a pound of food. *Living Green* March 2010; http://www.treehugger.com/green-food/energy-required-to-produce-a-pound-of-food.html
(31) World population from http://simple.wikipedia.Org/wiki/World_population.
(32) Cantrell, C. L.; Dayan, F. E.; Duke, S. O. Natural products as sources for new pesticides. *J. Nat. Prod.* **2012**, *75*, 1231−1242.
(33) *JAFC Selects Virtual Issue: Food Quality Traits for Sustaining Agriculture* 2011, http://pubs.acs.org/page/vi/2011/food-quality.html (accessed June 6, 2014). Editorial summary: Seiber , J. N. *J. Agric. Food Chem.* **2011**, *59*, 2127−2130, DOI: 10.1021/jf200629j.
(34) Frankel, E. N. Nutritional and biological properties of extra virgin olive oil. *J. Agric. Food Chem.* **2011**, *59*, 785−792.
(35) Hafer, T. J.; Howard, L. R.; Prior, R. L. processing and storage effects on ellagitannin composition of processed blackberry products. *J. Agric. Food Chem.* **2010**, *58*, 11749−11750.
(36) Sharma, G. M.; Su, M.; Joshi, A. U.; Roux, K. H.; Sathe, S. K. Functional properties of select edible oilseed proteins. *J. Agric. Food Chem.* **2010**, *58*, 5457−5464.
(37) Argov-Araman, N.; Smilowicz, J. T.; Bricarello, D. A.; Barboza, M.; Lerno, L.; Froehlich, J. W.; Lee, H.; Zivkovic, A. M.; Lemay, D. G.; Freeman, S.; Lebrilla, C. B.; Parikh, A. N.; German, J. B. Lactosomes: structural and compositional classification of unique nanometer-sized protein lipid particles of human milk. *J. Agric. Food Chem.* **2010**, *58*, 11234−11242.
(38) Orts, W. J.; Holtman, K. M.; Seiber, J. N. Agricultural chemistry and bioenergy. *J. Agric. Food Chem.* **2008**, *56*, 3892−3899.
(39) Zhang, R.; Zhang, Z. Biogasification of solid waste with an anaerobic-phased solids-digester system. U.S. Patent 6342378 B1, 2002.
(40) Ramaswamy, S. Nexus between food, water and energy. *Abstracts of Papers*, 245th ACS National Meeting and Exposition, New Orleans, LA, USA; American Chemical Society: Washington, DC, USA, 2013.

herbicide, formulation, and related adjuvants; or the tank mix herbicide spray solution.[26] Vegetable oils have been used as adjuvant to increase the performance of sethoxydim,[27] but so far, they have received little attention on their effect on photosensitivity or photoquenching of sethoxydim. The purposes of this project were (i) to study the effects of vegetable oils on photodecomposition of sethoxydim, (ii) to assess the effect of vegetable oil viscosity on photodecomposition of sethoxydim, and (iii) to study the saturation status of vegetable oils on photodecomposition of sethoxydim.

MATERIALS AND METHODS

Chemicals and Vegetable Oils. Oils of soybean, cotton, canola, sesame (*Sesamum indicum* L.), castor (*Ricinus communis* L.), corn (*Zea mays* L.), sunflower (*Helianthus annuus* L.), and turnip (*Eruca sativa* L.) were extracted from grains via the mechanical extraction method.[28] Olive oil (*Olea europaea* L.) was extracted from fruit with the Decanter centrifugation (horizontal centrifuge rotating at 3 000 rpm) method.[29] The reference of fatty acid methyl esters in methylene chloride (ampule containing 10 mg/mL) was obtained from Supelco (grain fatty acid methyl ester mix 99−100%).The standard of sethoxydim [(RS)-(EZ)-2-[1-(ethoxyimino)butyl]-5-[2-(ethylthio)propyl]-3-hydroxycyclohex-2-enone] with 99.3% purity was supplied by BASF Ltd. (Limburgerhof, Germany). All solvents were of high-performance liquid chromatography (HPLC) and gas chromatography (GC) grade. N-Hexane and methanol were of chromatography grade (99.9% purity, Merck); potassium hydroxide (pellets/certified ACS) and sodium lauryl sulfate powder were purchased from Fisher Chemicals.

Sample Preparation. *Oil Composition.* To determine the chemical nature of fatty acid oils, 15 drops of each vegetable oil were added to 7 mL N-hexane plus 2 mL of potassium hydroxide in methanol (11.2% m/v). Then, four replications of the supplied compounds were shacked for 1 min and heated to 55 °C for 5 min until the solution was separated into two phases. The upper phase was desiccated with sodium lauryl sulfate and filtered to analyze with gas chromatography.

Herbicide Solution. A nonionic emulsifier, Citogate (100% alkylarylpolyglycol ether prepared from Zarnegaran Pars Company, Karaj, Iran) was added to the vegetable oils at 10% (v/v). This compound (90% vegetable oil +10% emulsifier) was added to the recommended rate of sethoxydim (375 g ai ha^{-1}) at 0.5% (v/v). Herbicide preparation solutions (100 mL) were placed into 250 mL Erlenmeyer flasks. Then they were shacked for a period of 1 h.

Oil Viscosity. A K100 tensiometer was used to determine the viscosity of vegetable oils with ring method. The measurement was determined via the buoyancy of the solid in the liquid and the weight difference of the solid in the air and in the liquid. The mass of the volume of liquid displaced by the measuring probe corresponds exactly to the difference in weight. If the viscosity of the measuring probe is known, then the viscosity of the liquid is obtained by differential weighting using the following equation

$$\rho_L = \rho_{MP}\frac{G_{MPA} - G_{MPL}}{G_{MPA}} \quad (1)$$

where ρ_L is the viscosity of the liquid; ρ_{MP} is the viscosity of the measuring probe; G_{MPA} is the weight of the measuring probe in air; and G_{MPL} is the weight of the measuring probe in liquid.

Photodecomposition Experiments. Irradiation experiments were carried out under sunlight at the College of Agriculture, Ferdowsi University of Mashhad, Mashhad, Iran, with latitude 36°, 17′, 44″ N, longitude 59°, 36′, 42″ E, and altitude of 985 m, on April 11, 2013 (mean temperature 30 °C, light intensity 16.407 MJ/M2/day, and UV index 8), from 11:10 a.m. to 3:10 p.m.

The experiment was conducted as completely randomized factorial design with three replications including nine vegetable oil and eight time course study. Time course study for each herbicide solution (with and without vegetable oil) was 0, 5, 10, 20, 30, 60, 120, and 240 min. After each interval, 15 mL of each solution was sampled and placed in an amber vial and immediately stored in a refrigerator (at 5 °C) until being used for HPLC analysis.

Analytical Equipment and Methods. *Gas Chromatography Mass Spectroscopy.* The fatty acid content was determined using gas chromatography Acme 6000 (Younglin, South Korea) equipped with a flame ionization detector and a CP-Sil 88 Wcot fused silica column (100 m × 0.25 mm i.d. × 0.2 μm film thickness; Chrompack, Middleburg, Netherlands). The carrier gas was ultrahigh-purity helium; we used a 1:100 split mode and a flame-ionization detector. The GC oven temperature was maintained at 140 °C for 5 min, then ramped to 240 °C at the rate of 4 °C/min and maintained at 240 °C for 15 min. The flow rate of helium was 20 mL/min. The injector and detector temperatures were 250 and 280 °C, respectively. The volume of injected sample was 1 μL. Fatty acids were identified by matching their retention times with those of their relative standards.

High-Performance Liquid Chromatography. Photodecomposition kinetics was performed in an HPLC system (Shimadzu) coupled to a RF-10A_{XL} fluorescence detector (280 nm excitation and 425 nm emission), equipped with a pump (6000A). This HPLC system was furnished with a degassing tool (DGU-14A). The analytical column was a perfect sil target, C18column (5 μm particle size, 4.6 mm 250 mm, back pressure 5.7 MPa) with a octadecylsilane (ODS) precolumn (3−5 μm particle size). The mobile phase was methanol/water (80:20, v/v), degassed by placing in an ultrasonic bath (Camlab UK) before using them. For determining the kinetic parameters, an isocratic method of 80% methanol was applied. The flow rate was 1 mL min^{-1}; the injection volume was 20 μL. All samples were filtered through a 0.45 μm Millex filter (Millipore, HV-4, Beford, MA) before injecting into the chromatograph. The limit of detection by HPLC for sethoxydim was 0.01 ppm.

Data Processing. Quantitative analysis was performed using the standard curve method,[10] with the detection mode of full scan, setting up a standard curve of sethoxydim (peak height) at the concentration of 2, 4, 8, 16, 32, 81, 162, 324, 405, 810, 1215, and 1620 mg/L (Figure 1). A linear association was obtained ($y = 0.164x + 4.190$, $R^2 = 0.999$)

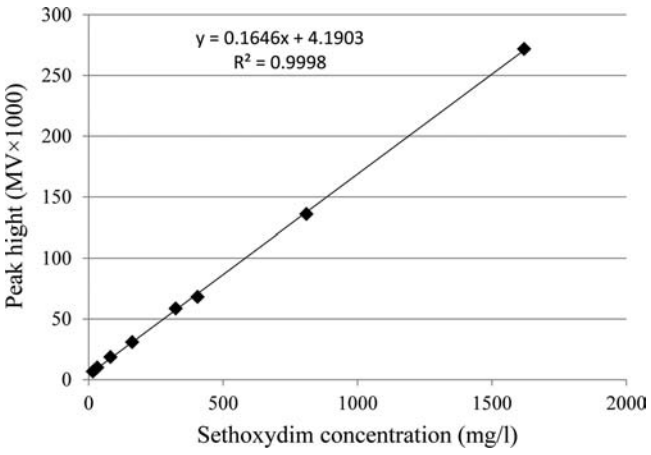

Figure 1. Standard curve of sethoxydim.

by peak height. The peak height was used as a model to determine the concentration of the other sample injection.

The constant rate of photodecomposition of sethoxydim (k) and half-life ($t_{1/2}$) were estimated by fitting the concentration of sethoxydim on eqs 1 and 2,

$$c_t = c_0\, e^{-kt} \quad (2)$$

where c_t is the herbicide concentration at irradiation time t, c_0 is the initial concentration, and k is the first-order rate constant. The half-life $t_{1/2}$ of sethoxydim was calculated using the following equation:

$$t_{1/2} = \frac{\ln 2}{k} \quad (3)$$

dx.doi.org/10.1021/jf501447x | J. Agric. Food Chem. 2014, 62, 6263−6268

Analysis of variance (ANOVA) was conducted to determine the differences between types of vegetable oils, at the 0.05 significance level. The results were analyzed using LSD statistical procedure (Sigma plot 11).

RESULTS AND DISCUSSION

Photodecomposition in the Presence of Vegetable Oils. Sethoxydim is a photochemicaly unstable herbicide (Figure 2). Under the irradiation experiment, in contrast light

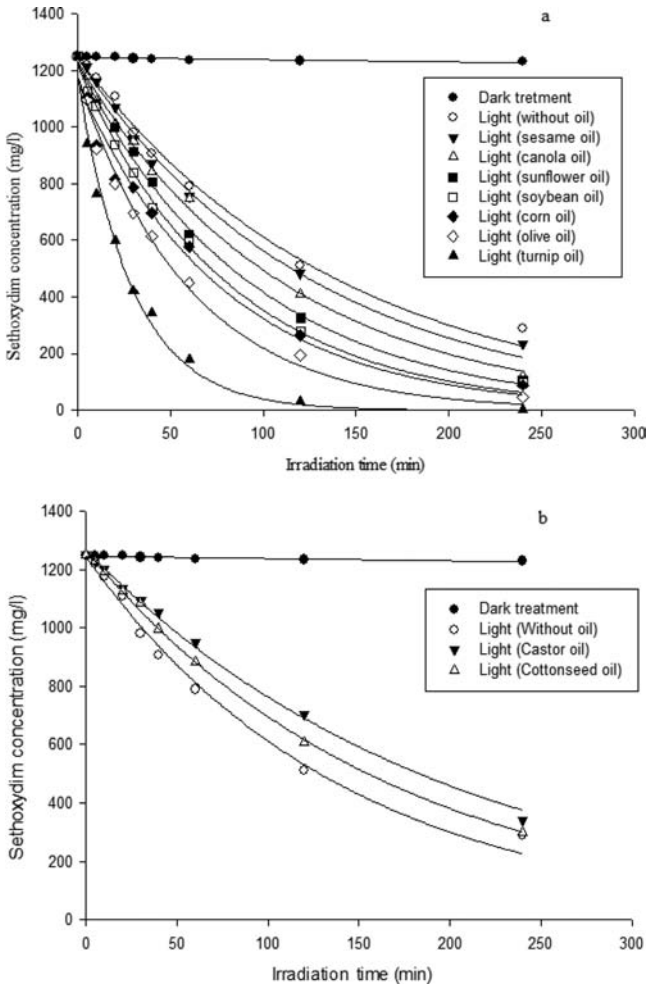

Figure 2. Photodecomposition rate of sethoxydim in the presence of vegetable oils: (a) decrease half-life and (b) increase half-life to compare without oil.

sethoxydim decomposed very fast, whereas the concentration of it remained constant in dark control experiments during the same irradiation time (Figure 2). The effects of vegetable oils on photodecomposition of sethoxydim are illustrated in Figure 2. Sethoxydim photodecomposition was enhanced in the presence of turnip, olive, corn, soybean, sunflower, canola, and sesame oils, and the photodecomposition values were considerably increased. However, in the presence of castor and cottonseed oils, photodecomposition of sethoxydim was retarded (Figure 2 and Table 1).

When turnip, olive, corn, soybean, sunflower, canola, and sesame oils were added to sethoxydim solution, the half-life of sethoxydim was decreased down to 4.74-, 2.38-, 1.81-, 1.75-, 1.52-, 1.28-, and 1.11-fold, respectively (a significant difference was observed between vegetable oils), compared to non-

Table 1. Kinetic Parameters of Sethoxydim Photolysis with Vegetable Oils under Natural Sunlight

vegetable oil	$k^{a,b}$ (10^{-3} min^{-1})	$t_{1/2}$ (min)	R^2
castor	5.1 ± 0.2 a	135.91 ± 5.13	0.9964
cottonseed	6.0 ± 0.1 b	115.52 ± 1.9	0.9964
none	7.1 ± 0.4 c	97.62 ± 5.2	0.9911
sesame	7.9 ± 0.3 d	87.74 ± 5.2	0.9948
canola	9.1 ± 0.3 e	76.17 ± 2.4	0.9970
sunflower	10.8 ± 0.4 f	64.18 ± 2.2	0.9969
soybean	12.4 ± 0.1 g	55.90 ± 0.4	0.9978
corn	12.9 ± 0.2 h	53.73 ± 0.8	0.9969
olive	16.9 ± 1.2 i	41.01 ± 2.7	0.9878
turnip	34.0 ± 2.4 j	20.39 ± 1.3	0.9889

[a] k is the first-order rate constant. [b] Different letters show significant differences according to LSD test at $\alpha = 0.01$.

vegetable oil solution. The half-life of sethoxydim was increased in the presence of castor and cottonseed oils by 1.39- and 1.18-fold, respectively (a significant difference was observed between vegetable oils), compared to nonvegetable oil solution (Table 1). Among vegetable oils, turnip oil and castor oil had the highest photosensitivity and photoquenching impact on sethoxydim, respectively. An acceptable fit to the first-order kinetics reaction was obtained for the photodecomposition of sethoxydim in the presence of all vegetable oils over the irradiation time as indicated by the regression coefficient ranging from 0.97 to 0.99 (Table 1). Kinetic parameters of sethoxydim photolysis revealed that a significant difference among vegetable oils existed (Table 1).

Previous studies[3,4] provided the evidence for the early photodecomposition of the sethoxydim under synthetic light and sunlight conditions. This herbicide was highly sensitive to the light. Characteristics of the herbicide, formulation, and adjuvants added to their formulations affected the photodecomposition of sethoxydim. The disappearance of sethoxydim upon irradiation with sunlight largely depends on the presence of total organic carbon (TOC) in herbicide solution.[4] Harrison and Wax[25] reported that, with the addition of soybean oil to 2,4-D and haloxyfop, their photodecomposition effect increased.

According to Izadi-Darbandi et al.,[27] turnip oil alone did not have the phytotoxic potential on wild oat, whereas in combination with sethoxydim, the performance on fresh and dry weight of wild oat was increased by 4.13 and 5.85 times, respectively. These findings were also observed for olive, soybean, canola, and sesame oils. It may be concluded that not only does the application of turnip oil improve the performance of sethoxydim but also it may increase the amount of sethoxydim photodecomposition. Therefore, the use of proper vegetable oils with sethoxydim provides bilateral benefits: (i) an increase in performance and/or (ii) an increase in photodecomposition.

Vegetable Oils' Viscosities. The values of vegetable oils' viscosities are shown in Table 2. Our finding indicated a positive relationship between the half-life of sethoxydim in the presence of each vegetable oil and the viscosity of the vegetable oils (Figure 3). The half-life of sethoxydim was increased by increasing the viscosity with a determination coefficient (R^2) of 0.8951 ($y = 3369.6x - 3021.7$). When vegetable oils with high density were added to the sethoxydim solution, an increase in half-life of sethoxydim was observed as compared to adding vegetable oils with low density (Figure 3). In general, an

dx.doi.org/10.1021/jf501447x | J. Agric. Food Chem. 2014, 62, 6263−6268

Table 2. Fatty Acid Composition of Vegetable Oils

	saturates					monounsaturates					polyunsaturates			
oil	16:0	18:0	20:0	22:0	24:0	16:1	18:1	20:1	22:1	24:1	18:2	18:3	unsat/sat ratio	viscosity (g/mL)
turnip	3.85	1.13	0.75	1.01	0.56	0.27	15.38	9.34	43.99	2.19	8.96	10.65	12.4	0.907
soybean	5.63	3.26	0.83	0.49	0.14	0.14	54.11	1.68	0.67		25.75	7.3	8.66	0.916
cottonseed	20.87	3.19	0.37			0.55	20.1				53.78	0.21	2.94	0.933
sunflower	6.54	3.92	0.32	1.13	0.50	0.26	51.68	0.32			35.23		6.99	0.916
olive	7.1	2.05	0.24			0.5	69.84	0.14			19.85		9.64	0.909
castor	9.54	10.52	0.92				34.05	2.73			37.94	4.29	3.76	0.937
sesame	9.90	5.95	0.82	0.22	0.07	0.20	40.55	0.29			41.19	0.54	4.83	0.911
corn	4.92	2.95	0.91	0.52	0.22	0.25	60.54	2.15		0.26	18.41	8.04	8.66	0.915
canola	12.32	2.49	0.75	0.20	0.37	0.14	30.89	0.29			50.70	0.86	4.84	0.913

[a]Percentages may not add to 100% due to rounding and other constituents not listed.

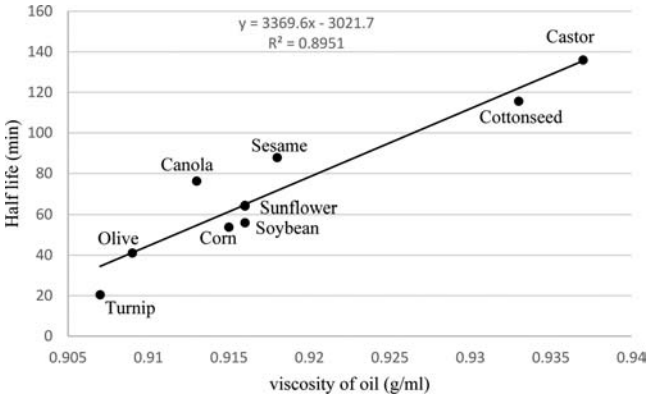

Figure 3. Relationship between viscosity of vegetable oils and half-life of sethoxydim.

increase in viscosity led to a high half-life of sethoxydim for all vegetable oils.

Apparently, enhancing vegetable oil viscosity depends on fatty acid chain length and degree of saturation. Theoretically, herbicides applied with a highly saturated vegetable oil could be too viscous for a good deposit of spray droplets on the leaf surface and reduced efficacy, especially when applied under cool conditions.[30] Beattie et al.[31] declared that, with the reduction of vegetable oils' viscosity and increasing solubility of the herbicide with methylation, the penetration of the herbicide solution within the plants increased. Therefore, decreasing the half-life of the aqueous solution of sethoxydim in the presence of vegetable oil with low viscosity will be compensated by fast penetration through the leaf surface. Izadi-Darbandi et al.[27] showed that sethoxydim performance for wild oat control was increased in the presence of turnip oil with low viscosity mainly due to fast penetration of the herbicide solution through the epicuticular wax layer.

Vegetable Oils' Fatty Acids Compositions. Fatty acids compositions of vegetable oils are summarized in Table 2. Equation 2 determined the k parameter and eq 3 determined the half-life ($t_{1/2}$) values of the sethoxydim in the presence of each vegetable oil (Table 1). Turnip oil and castor oil had the highest increasing and decreasing on the rate of sethoxydim photodecomposition, respectively (Table 1).

The reason for these differences may be attributed to differences in saturation status of fatty acids composition (Table 2). There was a negative relationship between monounsaturated (Figure 4a) and unsaturated/saturated fatty acids ratios (Figure 4b) with determination coefficient (R^2) of 0.73 and 0.85 half-life, respectively. Moreover, there was a positive relationship between the half-life of sethoxydim in the presence of each vegetable oil with saturation status of vegetable oils: saturated fatty acids (Figure 4c), polyunsaturated fatty acids (Figure 4d), palmitic acids (Figure 4e), and linoleic acids (Figure 4f) with coefficient determinations (R^2) of 0.86, 0.62, 0.75, and 0.60, respectively.

It means that the half-life was enhanced with increasing saturated fatty acids, polyunsaturated fatty acids, palmitic acid, or linoleic acids. Half-life was also reduced with increasing monounsaturated and unsaturated/saturated fatty acids ratio (Figure 4a and b). A correlation existed between the half-life of sethoxydim in the presence of each vegetable oil with the content of palmitic acid (C 16:0) and linoleic acid (C 18:2). A correlation between the half-life of stearic acid (C 18:0), palmitoleic acid (C 16:1), oleic acid (C18:1), and linolenic acid (C 18:3) of each vegetable oil was not observed.

The results indicated that the rate of photodecomposition of sethoxydim mainly depended on the kind of vegetable oil added to the sethoxydim solution. Adding vegetable oils with high unsaturated/saturated ratio increased the half-life of sethoxydim less than the low unsaturated/saturated ratio. Vegetable oils were ranked in the following order based on the decrease of half-life reduction, turnip oil > olive oil > corn oil > soybean oil > sunflower oil > canola oil > sesame oil, and based on the increase of half-life, castor oil > cottonseed oil compared with the sethoxydim solution without oil (Table 1)

In general, oil plants grown at high latitudes (cool conditions) have more unsaturated fatty acids than those grown in lower latitudes (warm conditions).[31] Therefore, to obtain accurate results in any given experiment, determination of oils' characteristics, such as the amount of fatty acids and viscosity, is indispensable. The large variation in the composition of vegetable oils imposes different effects on the modification of the herbicide efficacy. Izadi-Darbandi et al.[27] showed that, with increasing oleic acid (C 18:1) or decreasing palmitic acid volume, the relative potency of sethoxydim to control wild oat was decreased with coefficient of determination (R^2) of 0.80 and 0.76, respectively. They also reported that, with increasing unsaturated/saturated fatty acids ratio, the sethoxydim performance was decreased. On the basis of our results, this may be due to enhanced photodecomposition and decreased half-life of sethoxydim in the presence of vegetable oils with a high level of unsaturated fatty acids on the leaf surface but increasing through to the cuticular wax in the presence of vegetable oils with a high level of unsaturated fatty acids before photodecomposition, which improved herbicide performance.

dx.doi.org/10.1021/jf501447x | J. Agric. Food Chem. 2014, 62, 6263−6268

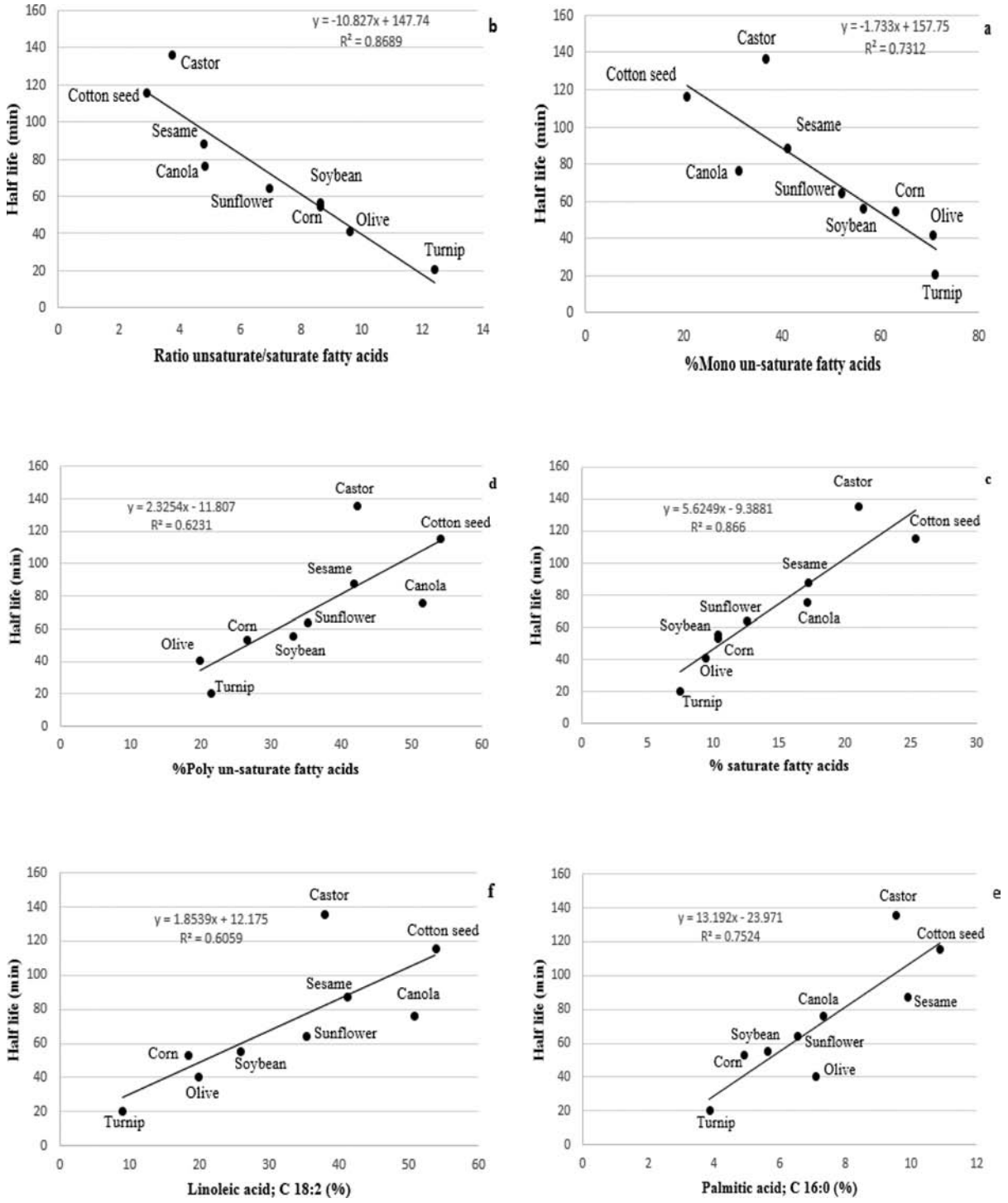

Figure 4. Relationship between half-life of sethoxydim plus vegetable oils in the presence of sunlight: (a) % monounsaturated fatty acids of vegetable oils; (b) ratio of unsaturated/saturated fatty acid; (c) saturated fatty acid; (d) % polyunsaturated fatty acids ratio of vegetable oils; (e) palmitic acid; and (f) linoleic acid.

Selecting the proper adjuvant is a key factor in weed management mainly because of reducing the dosage of herbicide. On the other hand, vegetable oils are less phytotoxic compared with mineral oils, and due to fast degradation,[32] they are a better choice for the environment. Therefore, the application of vegetable oil is a proper ecological method to enhance herbicide performance and decrease its dosage. Our results revealed that vegetable oils can enhance photodecomposition effects of the herbicide sethoxydim. Careful selection of adjuvants in formulation or tank mix is very important because it will alter photodecomposition of sethoxydim after spraying. The fatty acid compositions of vegetable oils are clearly effective in their impact on the photodecomposition of sethoxydim. Our findings also revealed that a negative correlation existed between quantities of monounsaturated or unsaturated/saturated fatty acids ratio with half-life. Moreover, there was a positive relationship between viscosity and saturate status with half-life. Therefore,

dx.doi.org/10.1021/jf501447x | J. Agric. Food Chem. 2014, 62, 6263−6268

the importance of viscosity and fatty acids composition of vegetable oils on the photodecomposition of sethoxydim was proved.

AUTHOR INFORMATION

Corresponding Author

*Tel.: 9157995166. E-mail: homamihossein@gmail.com.

Notes

The authors declare no competing financial interest.

ACKNOWLEDGMENTS

This work was conducted in partial fulfilment of requirements for the Ph.D. degree (Project No. 17489) in Weed Science at Ferdowsi University of Mashhad that was funded by a grant from the College of Agriculture. Appreciation is also extended to Dr. Akbar Aliverdi, Mrs. Reyhaneh Haghdoost, and Mr. Sajad Hammami who provided invaluable assistance in conducting this research.

REFERENCES

(1) Payraudeau, S.; Gregoire, C. Modelling pesticides transfer to surface water at the catchment scale: A multi-criteria analysis. *Agron. Sustainable Dev.* **2012**, *32*, 479−500.

(2) Schnoor, J. L. *Fate of Pesticides and Chemicals in the Environment*; Wiley-Interscience: New York, 1991.

(3) Shoaf, A. R.; Carlson, W. C. Analytical techniques to measure sethoxydim and breakdown products. *Weed Sci.* **1986**, *34*, 745−751.

(4) Sevilla-Morána, B.; Mateo-Mirandaa, M. M.; Alonso-Pradosa, J. L.; García-Baudína, J. M.; Sandín-Españaa, P. Sunlight transformation of sethoxydim−lithium in natural waters and effect of humic acids. *Int. J. Environ. Anal. Chem.* **2010**, *90*, 487−496.

(5) Sevilla-Moran, B.; Sandín-Españaa, P.; Vicente-Arana, M. J.; Alonso-Prados, J. L.; Garcia-Baudina, J. M. Study of alloxydim photodecomposition in the presence of natural substances: Elucidation of transformation products. *J. Photochem. Photobiol., A* **2008**, *198*, 162−168.

(6) Falb, L. N.; Bridges, D. C.; Smith, A. E. Effects of pH and adjuvants on clethodim photodecomposition. *J. Agric. Food Chem.* **1990**, *38*, 875−878.

(7) Sun, X.; Liu, H.; Zhang, Y.; Zhao, Y.; Quan, X. Effects of Cu(II) and humic acid on atrazine. *J. Environ. Sci.* **2011**, *23*, 773−777.

(8) Quivet, E.; Faure, R.; Georges, J.; Pai-ssea, J. O.; Herbreteau, B. P.; Lanteri, J. Photochemical Degradation of Imazamox in Aqueous Solution: Influence of Metal Ions and Anionic Species on the Ultraviolet Photolysis. *J. Agric. Food Chem.* **2006**, *54*, 3641−3645.

(9) Eyheraguibel, B.; Ter-halle, A.; Richard, C. Photodecomposition of Bentazon, Clopyralid, and Triclopyr on Model Leaves: Importance of a Systematic Evaluation of Pesticide Photostability on Crops. *J. Agric. Food Chem.* **2009**, *57*, 1960−1966.

(10) Lu, Z.; Hou, Z.; Wang, X.; Wang, S.; Shang, Y.; Yuan, X. Photodecomposition of new herbicide HW-02 in organic solvents. *J. Environ. Sci.* **2010**, *22*, 1774−1778.

(11) Bhattacharjeel, A. K.; Dureja, P. Light induced transformation of tribenuronmethyl on glass, soil and plant surface. *J. Environ. Sci. Health, Part B* **2002**, *37*, 131−140.

(12) Vulliet, E.; Emmelin, C.; Scrano, L.; Bufo, S. A.; Chovelon, J. M.; Meallier, P.; Grenier-Loustalot, M. F. Photochemical Degradation of Acifluorfen in Aqueous Solution. *J. Agric. Food Chem.* **2001**, *49*, 4795−4800.

(13) Zertal, A.; Jacquet, M.; Lavedrine, B.; Sehili, T. Photodecomposition of chlorinated pesticides dispersed on sand. *Chemosphere* **2005**, *58*, 1431−1437.

(14) Abu-Qare, A. W.; Duncan, H. J. Photodecomposition of the herbicide EPTC and the safener dichlormid, alone and in combination. *Chemosphere* **2002**, *46*, 1183−1189.

(15) Massad, W.; Criado, S.; Bertolotti, S.; Pajares, A.; Gianotti, J.; Escalada, J. P.; Amat-Guerri, F.; Garcia, N. A. Photodecomposition of the herbicide Norflurazon sensitized by Riboflavin. A kinetic and mechanistic study. *Chemosphere* **2004**, *57*, 455−461.

(16) Wiszniowski, J.; Ter Halle, A.; Richard, C.; Hitmi, A.; Ledoigt, G. Photodecomposition product of sulcotrione and the physiological response of maize (*Zea mays*) and white mustard (*Sinapis alba*). *Chemosphere* **2009**, *74*, 1224−1230.

(17) Halladja, S.; Amine-Khodja, A.; Halle, A.; Boulkamh, A.; Richard, C. Photolysis of fluometuron in the presence of natural water constituents. *Chemosphere* **2007**, *69*, 1647−1654.

(18) Miller, G. C.; Zepp, R. G. Extrapolating photolysis rates from the laboratory to the environment. *Residue Rev.* **1983**, *85*, 89−110.

(19) Pinna, M. V.; Pusino, A. Direct and indirect photolysis of cyhalofop in aqueous systems. *Chemosphere* **2011**, *82*, 817−821.

(20) Kamiya, M.; Kameyama, K. Effect of select meal ions on photodegradation of organophosphorus pesticides sensitized by humic acid. *Chemosphere* **2001**, *45*, 231−235.

(21) Hazen, J. L. Adjuvants: Terminology, classification, and chemistry. *Weed Technol.* **2000**, *14*, 773−784.

(22) Nutahara, M.; Murai, T. Accelerating effect of natural unsaturated fatty acids on photodecomposition of chinomethionat (Morestan). *J. Pestic. Sci.* **1984**, *9*, 667−674.

(23) Thomas, S. M.; Harrison, S. K. Surfactant-altered rates of chlorimuron and metsulfuron Photolysis in sunlight. *Weed Sci.* **1990**, *38*, 602−606.

(24) Tanaka, F. S.; Wien, R. G.; Mansager, E. R. Survey for surfactant effects on the photodecomposition of herbicides in aqueous media. *J. Agric. Food Chem.* **1981**, *29*, 227−230.

(25) Harrison, S. K.; Wax, L. M. The effect of adjuvants and oil carriers on photodecomposition of 2,4-D, bentazon and haloxyfop. *Weed Sci.* **1985**, *34*, 81−87.

(26) Fred, F. Pesticides and the environment. *Agricultural M U Guide*; University Extension, University of Missouri-Columbia: Columbia, MO, 1997; pp 1−6.

(27) Izadi-Darbandi, E.; Aliverdi, A.; Hammami, H. Behavior of vegetable oils in relation to their influence on herbicides' effectiveness. *Ind. Crops Prod.* **2013**, *44*, 712−717.

(28) Kemper, T. G. Industrial Oil and Fat Products. *Oil Extraction*, sixth ed.; John Wiley & Sons, Inc.: New York, 2005.

(29) Rubio, J. C. Olive Oil History and Facts. *Aceites Toledo SA* **2008**, 20.

(30) Matysiak, R.; Nalewaja, J. D. Temperature, Adjuvants, and UV Light Affect Sethoxydim Phytotoxicity. *Weed Technol.* **1999**, *13*, 94−99.

(31) Beattie, A.; Watson, D.; Stevens, M.; Rae, D.; Spooner, H. Spray Oils Beyond 2000. *Sustain. Pest Dis. Manage.* **2002**, 290−300.

(32) Cabanne, F.; Gaudry, J.; Streibig, J. C. Influence of alkyl oleates on efficacy of phenmedipham applied as an acetone:water solution on *Galium aparine*. *Weed Res.* **1999**, *39*, 57−67.

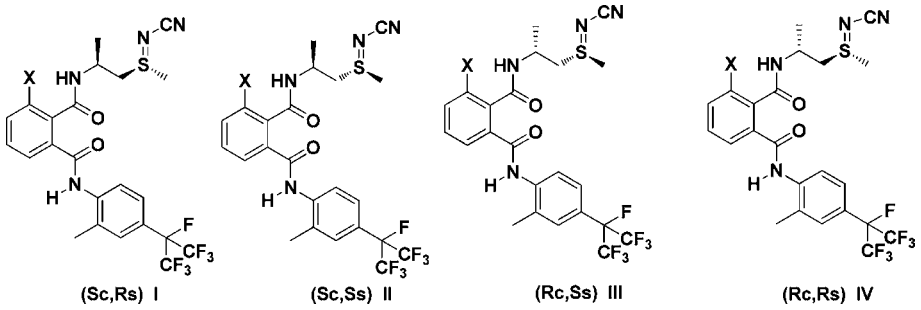

Figure 2.

field analysis (CoMFA) calculation was also undertaken. The structure−activity relationship (SAR) was concluded.

MATERIALS AND METHODS

Instruments and Materials. The melting points were determined on an X-4 binocular microscope melting point apparatus (Beijing Tech Instrument Co., Beijing, China) and are uncorrected. ^{1}H NMR and ^{13}C NMR spectra were recorded at 300 MHz (Bruker AC-P 300 spectrometer) or 400 MHz (Bruker AV 400 spectrometer) in $CDCl_3$ or DMSO-d_6 solution with tetramethylsilane as internal standard, and chemical shift (δ) were recorded in parts per million. Elemental analyses were performed on a Vario EL elemental analyzer. HRMS data were obtained by Varian QFT-ESI. Optical rotations were measured with a PerkinElmer 341 polarimeter at 20 °C. GC-MS was recorded on HP 5973 MSD with 6890 GC flash chromatography with silica gel (200−300 mesh). All reagents were analytically pure. All solvents and liquid reagents were dried according to standard methods and distilled before use. Commercial insecticide flubendiamide was used only as contrast compound and synthesized according to the literature.[19] 3-Substituted anhydride compounds **4a**−**f**,[20,21] 2-methyl-4-(perfluoropropan-2-yl)aniline **6a**,[22] (*S*)-1-(methylthio)propan-2-amine **3**, and (*R*)-1-(methylthio)propan-2-amine **10**[23] were synthesized according to the methods reported in the cited literature.

Synthesis of Intermediate Compounds. Synthesis of 1-(methylthio)propan-2-amine **3**: pale yellow liquid; yield 57.8%; ^{1}H NMR (400 MHz, $CDCl_3$-d_6) δ 2.90 (dqd, J = 8.4, 6.3, 4.5 Hz, 1H, −CHNH$_2$), 2.42 (dd, J = 13.2, 4.4 Hz, 1H, −SCH$_2$−), 2.19 (dd, J = 13.2, 8.4 Hz, 1H, −SCH$_2$−), 1.95 (s, 3H, −SCH$_3$), 0.99 (d, J = 6.4 Hz, 3H, −C−CH$_3$).

(*S*)-1-(Methylthio)propan-2-amine **12**: $[\alpha]^{20}_D$ +30.13 (c = 53.7, $CHCl_3$).

(*R*)-1-(Methylthio)propan-2-amine **13**: $[\alpha]^{20}_D$ = −29.79 (c = 53.2, $CHCl_3$).

General Synthetic Procedure for Compounds ***7a*****−*****f*****.** These phthalamide derivatives were synthesized in moderate yield according to the method reported in the literature. The melting point and ^{1}H NMR data were consistent with the literature.[24]

(*S*)-N^1-(1-(Methylthio)propan-2-yl)-N^2-(3-(trifluoromethyl)-phenyl)phthalamide, **7f**: ^{1}H NMR (400 MHz, DMSO-d_6) δ 10.65 (s, 1H, Ar−NH), 8.36 (d, J = 7.7 Hz, 1H, −CNH), 8.22 (s, 1H, Ar−H), 7.90 (d, J = 7.1 Hz, 1H, Ar−H), 7.58 (m, 5H, Ar−H), 7.44 (d, J = 7.0 Hz, 1H, Ar−H), 4.08−3.98 (m, 1H, −N−CH), 2.66 (dd, J = 13.0, 6.3 Hz, 1H, −SCH$_2$), 2.54 (m, 1H, −SCH$_2$), 2.05 (s, 3H, −SCH$_3$), 1.19 (d, J = 6.3 Hz, 3H, −CCH$_3$).

General Synthetic Procedure for Compounds ***Ia*****−*****e*****,** ***IIa*****−*****e*****,** ***IIIa*****−*****d*****, and** ***IVa*****−*****d*****.** A mixture of 1.0 mmol of **7a**−**f** and 0.046 g (1.1 mmol) of cyanamide in 20 mL of acetonitrile was cooled below 0 °C. To this solution was added 0.322 g (1 mmol) of iodobenzene diacetate all at once. The reaction mixture was allowed to stir below 0 °C for 10 min and slowly warmed to room temperature over 1.5 h; the progress of the reaction was followed by TLC. Excess oxidant was destroyed by adding 5 mL of 2.5% aqueous sodium metabisulfite. The solution was washed with dilute hydrochloric acid, water, an aqueous sodium carbonate solution, and water, respectively, and dried over anhydrous sodium sulfate. The solvent was removed under reduced pressure, and the residue was purified by silica gel column chromagraphy.[25−28]

(*S*,*R*)-3-Iodo-N^2-(1-(*N*-cyano-*S*-methylsulfinimidoyl)propan-2-yl)-N^1-(2-methyl-4-(perfluoropropan-2-yl)phenyl)phthalamide, **Ia**: white solid; yield 70.3%; mp 116−119 °C; ^{1}H NMR (400 MHz, DMSO-d_6) δ 9.95 (s, 1H, Ar−NH), 8.83 (d, J = 7.8 Hz, 1H, −CNH), 8.05 (d, J = 7.9 Hz, 1H, Ar−H), 7.79−7.75 (m, 2H, Ar−H), 7.54 (d, J = 7.3 Hz, 2H, Ar−H), 7.31 (t, J = 7.8 Hz, 1H, Ar−H), 4.24 (dt, J = 13.6, 6.8 Hz, 1H, −N−CH), 3.29 (dd, J = 12.7, 5.9 Hz, 1H, −SCH$_2$), 3.18 (dd, J = 7.9, 4.9 Hz, 1H, −SCH$_2$), 2.66 (s, 3H, −SCH$_3$), 2.36 (s, 3H, ArCH$_3$), 1.26 (d, J = 6.7 Hz, 3H, −CCH$_3$); ^{13}C NMR (101 MHz, DMSO-d_6) δ 167.68, 165.45, 141.54, 140.92, 139.25, 135.59, 133.63, 130.31, 127.38, 127.20, 125.79, 123.33, 121.80, 120.48, 95.32, 54.77, 41.27, 32.01, 18.67, 17.94. Aanl. Calcd for $C_{23}H_{20}F_7IN_4O_2S$: C, 40.75; H, 3.01; N, 8.13. Found: C, 40.84; H, 2.98; N, 8.28. HRMS calcd for $C_{23}H_{20}F_7IN_4O_2SH$ ([M + H]$^+$): 677.0313. Found: 677.0310. $[\alpha]^{20}_D$ = −8.2 (c = 10, EtOAc).

(*S*,*R*)-3-Fluoro-N^2-(1-(*N*-cyano-*S*-methylsulfinimidoyl)propan-2-yl)-N^1-(2-methyl-4-(perfluoropropan-2-yl)phenyl)phthalamide, **Ib**: white solid; yield 59.6%; mp 103−105 °C; ^{1}H NMR (400 MHz, DMSO-d_6) δ 10.13 (s, 1H, Ar−NH), 8.96 (d, J = 7.9 Hz, 1H, −CNH), 7.75 (d, J = 8.1 Hz, 1H, Ar−H), 7.64 (m, 2H, Ar−H), 7.56 (d, J = 8.3 Hz, 2H, Ar−H), 7.53−7.46 (m, 1H, Ar−H), 4.40−4.22 (m, 1H, −N−CH), 3.43−3.27 (m, 1H, −SCH$_2$), 3.20 (dd, J = 12.6, 6.9 Hz, 1H, −SCH$_2$), 2.74 (s, 3H, −SCH$_3$), 2.39 (s, 3H, ArCH$_3$), 1.28 (d, J = 6.6 Hz, 3H, −CCH$_3$); ^{13}C NMR (101 MHz, DMSO-d_6) δ 165.31, 163.06, 159.62, 157.17, 139.28, 136.62, 134.00, 130.95, 127.25, 126.20, 123.80, 123.34, 120.43, 118.18, 117.95, 54.90, 32.07, 18.90, 17.98. HRMS calcd for $C_{23}H_{20}F_8N_4O_2SH$ ([M + H]$^+$): 569.1252. Found: 569.1256. $[\alpha]^{20}_D$ = −31.6 (c = 10, EtOAc).

(*S*,*R*)-3-Chloro-N^2-(1-(*N*-cyano-*S*-methylsulfinimidoyl)propan-2-yl)-N^1-(2-methyl-4-(perfluoropropan-2-yl)phenyl)phthalamide, **Ic**: white solid; yield 61.2%; mp 120−122 °C; ^{1}H NMR (300 MHz, DMSO-d_6) δ 10.05 (s, 1H, Ar−NH), 8.91 (s, 1H, −CNH), 7.72 (m, 3H, Ar−H), 7.58 (m, 3H, Ar−H), 4.28 (m, 1H, −N−CH), 3.19 (m, 2H, −SCH$_2$), 2.70 (s, 3H, −SCH$_3$), 2.37 (s, 3H, ArCH$_3$), 1.25 (d, J = 6.0 Hz, 3H, −CCH$_3$); ^{13}C NMR (101 MHz, DMSO-d_6) δ 165.31, 164.85, 139.23, 135.97 (d, J = 16.3 Hz), 133.85, 131.49, 130.69, 130.19, 127.16, 126.52, 126.01, 123.29, 121.84, 120.46, 54.84, 41.22, 31.96, 18.80, 17.96. HRMS calcd for $C_{23}H_{20}ClF_7N_4O_2SH$ ([M + H]$^+$): 585.0957. Found: 585.0951. $[\alpha]^{20}_D$ = −28.0 (c = 10, EtOAc).

(*S*,*R*)-3-Nitro-N^2-(1-(*N*-cyano-*S*-methylsulfinimidoyl)propan-2-yl)-N^1-(2-methyl-4-(perfluoropropan-2-yl)phenyl)phthalamide, **Id**: white solid; yield 69.8%; mp 121−123 °C; ^{1}H NMR (400 MHz, DMSO-d_6) δ 10.22 (s, 1H, Ar−NH), 9.04 (d, J = 7.6 Hz, 1H, −CNH), 8.25 (d, J = 8.1 Hz, 1H, Ar−H), 8.12 (d, J = 7.4 Hz, 1H, Ar−H), 7.82 (dd, J = 16.2, 8.4 Hz, 2H, Ar−H), 7.57 (m, 2H, Ar−H), 4.22 (dt, J = 13.4, 6.6 Hz, 1H, −N−CH), 3.26 (dd, J = 12.8, 6.0 Hz, 1H, −SCH$_2$), 3.15 (dd, J = 12.7, 6.7 Hz, 1H, −SCH$_2$), 2.69 (s, 3H, −SCH$_3$), 2.39 (s, 3H, ArCH$_3$), 1.22 (d, J = 6.7 Hz, 3H, −CCH$_3$); ^{13}C NMR (101 MHz, DMSO-d_6) δ 165.56, 164.14, 147.10, 139.58, 137.61, 135.84 (d, J = 354.8 Hz), 135.84 (d, J = 354.8 Hz), 138.43−131.64 (m), 131.19 (d, J = 85.7 Hz), 130.42−127.83 (m), 130.42−123.89 (m), 122.37, 120.37, 55.03, 41.82, 33.13, 19.91, 18.49. HRMS calcd for $C_{23}H_{20}F_7N_5O_4SH$

dx.doi.org/10.1021/jf501727k | J. Agric. Food Chem. 2014, 62, 6269−6277

([M + H]$^+$): 596.1197. Found: 596.1194. $[\alpha]^{20}_D$ = −18.8 (*c* = 3, MeOH).

(*S*,*R*)-3-Bromo-*N*^{2}-(1-(*N*-cyano-*S*-methylsulfinimidoyl)propan-2-yl)-*N*^{1}-(2-methyl-4-(perfluoropropan-2-yl)phenyl)phthalamide, **Ie**: white solid; yield 71.2%; mp 116−118 °C; ^{1}H NMR (400 MHz, DMSO-d_6) δ 10.02 (s, 1H, Ar−NH), 8.89 (d, *J* = 8.0 Hz, 1H, −CNH), 7.85 (d, *J* = 8.0 Hz, 1H, Ar−H), 7.78 (dd, *J* = 13.7, 8.2 Hz, 2H, Ar−H), 7.55 (d, *J* = 7.7 Hz, 2H, Ar−H), 7.51 (t, *J* = 7.9 Hz, 1H, Ar−H), 4.26 (dt, *J* = 13.7, 6.9 Hz, 1H, −N−CH), 3.30 (dd, *J* = 12.7, 5.9 Hz, 1H, $-SCH_2$), 3.18 (dd, *J* = 12.7, 7.1 Hz, 1H, $-SCH_2$), 2.69 (s, 3H, $-SCH_3$), 2.37 (s, 3H, $ArCH_3$), 1.26 (d, *J* = 6.8 Hz, 3H, $-CCH_3$); ^{13}C NMR (101 MHz, DMSO-d_6) δ 165.77, 165.31, 139.24, 137.80, 136.15, 134.60, 133.75, 130.36, 127.55−126.83 (m), 125.91, 123.32 (d, *J* = 10.2 Hz), 121.79 (d, *J* = 20.5 Hz), 121.59−121.53 (m), 120.47, 120.06, 118.98, 118.71, 54.80, 41.24, 31.95, 18.75, 17.96. HRMS calcd for $C_{23}H_{20}BrF_7N_4O_2SH$ ([M + H]$^+$): 629.0452. Found: 629.0453. $[\alpha]^{20}_D$ = −4.0 (*c* = 1.5, MeOH).

(*S*,*R*)-*N*^{2}-(1-(*N*-Cyano-*S*-methylsulfinimidoyl)propan-2-yl)-*N*^{1}-(3-(trifluoromethyl)phenyl)phthalamide, **If**: white solid; yield 79.7%; mp 74−78 °C; ^{1}H NMR (400 MHz, DMSO-d_6) δ 10.69 (s, 1H, Ar−NH), 8.75 (s, 1H, −CNH), 8.21 (s, 1H, Ar−H), 7.91 (d, *J* = 7.8 Hz, 1H, Ar−H), 7.66−7.57 (m, 5H, Ar−H), 7.44 (d, *J* = 7.4 Hz, 1H, Ar−H), 4.35−4.25 (m, 1H, −N−CH), 3.38−3.36 (m, 1H, $-SCH_2$), 3.29−3.21 (m, 1H, $-SCH_2$), 2.83 (s, 3H, $-SCH_3$), 1.29 (d, *J* = 5.6 Hz, 3H, $-CCH_3$); ^{13}C NMR (101 MHz, DMSO-d_6) δ 167.39, 167.34, 140.14, 136.33, 135.58, 129.92, 129.67 (d, *J* = 32.5 Hz), 129.20, 127.67 (d, *J* = 18.9 Hz), 125.49, 123.06, 122.78, 120.55, 119.69, 115.54, 55.35, 41.27, 32.24, 19.44. HRMS calcd for $C_{20}H_{19}F_3N_4O_2SH$ ([M + H]$^+$), 437.1254. Found: 437.1252. $[\alpha]^{20}_D$ = −29.8 (*c* = 10, MeOH).

(*S*,*S*)-3-Iodo-*N*^{2}-(1-(*N*-cyano-*S*-methylsulfinimidoyl)propan-2-yl)-*N*^{1}-(2-methyl-4-(perfluoropropan-2-yl)phenyl)phthalamide, **IIa**: white solid; yield 29.7%; mp 116−118 °C; ^{1}H NMR (400 MHz, DMSO-d_6) δ 9.96 (s, 1H, Ar−NH), 8.70 (d, *J* = 6.6 Hz, 1H, −CNH), 8.04 (d, *J* = 6.8 Hz, 1H, Ar−H), 7.82−7.74 (m, 2H, Ar−H), 7.55 (m, 2H, Ar−H), 7.31 (m, 1H, Ar−H), 4.23 (m, 1H, -N−CH), 3.28−3.20 (m, 1H, $-SCH_2$), 3.16 (d, *J* = 11.1 Hz, 1H, $-SCH_2$), 2.67 (s, 3H, $-SCH_3$), 2.37 (s, 3H, $ArCH_3$), 1.28 (d, *J* = 5.1 Hz, 3H, $-CCH_3$); ^{13}C NMR (101 MHz, DMSO-d_6) δ 167.72, 165.51, 140.77, 141.58, 139.29, 135.86, 133.52, 130.29, 127.36, 125.67, 123.34, 121.50, 120.12, 95.101, 54.76, 41.15, 32.80, 19.62, 17.98. HRMS calcd for $C_{23}H_{20}F_7IN_4O_2SH$ ([M + H]$^+$): 677.0313. Found: 677.0310. $[\alpha]^{20}_D$ = +51.2 (*c* = 10, EtOAc).

(*S*,*S*)-3-Fluoro-*N*^{2}-(1-(*N*-cyano-*S*-methylsulfinimidoyl)propan-2-yl)-*N*^{1}-(2-methyl-4-(perfluoropropan-2-yl)phenyl)phthalamide, **IIb**: white solid; yield 40.4%; mp 106−107 °C; ^{1}H NMR (400 MHz, DMSO-d_6) δ 10.11 (s, 1H, Ar−NH), 8.79 (d, *J* = 7.6 Hz, 1H, −CNH), 7.75 (d, *J* = 7.9 Hz, 1H, Ar−H), 7.61 (m, 2H, Ar−H), 7.54 (d, *J* = 9.2 Hz, 2H, Ar−H), 7.49 (d, *J* = 8.0 Hz, 1H, Ar−H), 4.27 (m, 1H, −N−CH), 3.23 (m, 2H, $-SCH_2$), 2.76 (s, 3H, $-SCH_3$), 2.38 (s, 3H, $ArCH_3$), 1.27 (d, *J* = 6.4 Hz, 3H, $-CCH_3$); ^{13}C NMR (101 MHz, DMSO-d_6) δ 165.38, 163.01, 159.54, 159.09, 139.32, 136.98, 133.91, 130.92 (d, *J* = 32.0 Hz), 127.18 (d, *J* = 44.0 Hz), 126.09, 124.91 (d, *J* = 79.6 Hz), 123.28 (d, *J* = 37.6 Hz), 121.78 (d, *J* = 80.4 Hz), 119.91, 117.91 (d, *J* = 87.6 Hz), 54.48, 41.20, 32.67, 19.90, 18.00. HRMS calcd for $C_{23}H_{20}F_8N_4O_2SH$ ([M + H]$^+$): 569.1252. Found: 569.1256. $[\alpha]^{20}_D$ = +42.0 (*c* = 10, EtOAc).

(*S*,*S*)-3-Chloro-*N*^{2}-(1-(*N*-cyano-*S*-methylsulfinimidoyl)propan-2-yl)-*N*^{1}-(2-methyl-4-(perfluoropropan-2-yl)phenyl)phthalamide, **IIc**: white solid; yield 38.8%; mp 83−86 °C; ^{1}H NMR (400 MHz, DMSO-d_6) δ 10.05 (s, 1H, Ar−NH), 8.76 (d, *J* = 7.8 Hz, 1H, −CNH), 7.76 (dd, *J* = 14.4, 7.9 Hz, 2H, Ar−H), 7.70 (d, *J* = 7.9 Hz, 1H, Ar−H), 7.61−7.53 (m, 3H, Ar−H), 4.26 (m, 1H, −N−CH), 3.22 (m, 2H, $-SCH_2$), 2.72 (s, 3H, $-SCH_3$), 2.38 (s, 3H, $ArCH_3$), 1.26 (d, *J* = 6.7 Hz, 3H, $-CCH_3$); ^{13}C NMR (101 MHz, DMSO-d_6) δ 165.38, 164.88, 139.26, 136.32, 135.91, 133.76, 131.31, 130.62, 130.16, 127.19 (d, *J* = 11.2 Hz), 126.46, 125.87, 123.35, 121.83, 121.63, 120.04, 54.53, 41.06, 32.75, 19.73, 17.99. Aanl. Calcd for $C_{23}H_{20}ClF_7N_4O_2S$: C, 47.23; H, 3.45; N, 9.58. Found: C, 46.98; H, 3.48; N, 9.68. HRMS calcd for $C_{23}H_{20}ClF_7N_4O_2SH$ ([M + H]$^+$): 585.0957. Found: 585.0951. $[\alpha]^{20}_D$ = +68.4 (*c* = 10, MeOH).

(*S*,*S*)-3-Nitro-*N*^{2}-(1-(*N*-cyano-*S*-methylsulfinimidoyl)propan-2-yl)-*N*^{1}-(2-methyl-4-(perfluoropropan-2-yl)phenyl)phthalamide, **IId**: white solid; yield 30.2%; mp 99−102 °C; ^{1}H NMR (400 MHz, DMSO-d_6) δ 10.22 (s, 1H, Ar−NH), 8.88 (d, *J* = 7.1 Hz, 1H, −CNH), 8.26 (d, *J* = 7.7 Hz, 1H, Ar−H), 8.10 (d, *J* = 7.0 Hz, 1H, Ar−H), 7.84 (d, *J* = 7.6 Hz, 2H, Ar−H), 7.57 (m, 2H, Ar−H), 4.19 (m, 1H, −N−CH), 3.26−3.18 (m, 1H, $-SCH_2$), 3.14 (m, 1H, $-SCH_2$), 2.68 (s, 3H, $-SCH_3$), 2.40 (s, 3H, $ArCH_3$), 1.25 (d, *J* = 5.7 Hz, 3H, $-CCH_3$); ^{13}C NMR (101 MHz, DMSO-d_6) δ 166.25, 164.84, 147.80, 140.27, 138.30, 134.77, 134.28, 132.31, 131.46, 128.43 (d, *J* = 10.5 Hz), 126.91 (d, *J* = 19.0 Hz), 124.47, 122.98 (d, *J* = 20.5 Hz), 121.07, 55.73, 42.53, 33.84, 20.60, 19.18. HRMS calcd for $C_{23}H_{20}F_7N_5O_4SH$ ([M + H]$^+$): 596.1197. Found: 596.1194. $[\alpha]^{20}_D$ = +23.6 (*c* = 2, MeOH).

(*S*,*S*)-3-Bromo-*N*^{2}-(1-(*N*-cyano-*S*-methylsulfinimidoyl)propan-2-yl)-*N*^{1}-(2-methyl-4-(perfluoropropan-2-yl)phenyl)phthalamide, **IIe**: white solid; yield 28.8%; mp 94−96 °C; ^{1}H NMR (400 MHz, DMSO-d_6) δ 10.05 (d, *J* = 12.5 Hz, 1H, Ar−NH), 8.76 (t, *J* = 8.1 Hz, 1H, −CNH), 7.74−7.69 (m, 3H, Ar−H), 7.60−7.47 (m, 3H, Ar−H), 4.25 (m, 1H, −N−CH), 3.27−3.16 (m, 2H, $-SCH_2$), 2.71 (d, *J* = 5.9 Hz, 3H, $-SCH_3$), 2.37 (s, 3H, $ArCH_3$), 1.25 (d, *J* = 6.7 Hz, 3H, $-CCH_3$); ^{13}C NMR (101 MHz, DMSO) δ 165.61, 164.89, 139.28, 137.83, 136.34, 135.93, 134.43, 133.77, 131.32, 130.63, 130.17, 127.25−126.47 (m), 125.88, 123.35, 121.73 (d, *J* = 20.7 Hz), 121.53−121.35 (m), 120.06, 54.52, 41.07, 32.79 (d, *J* = 8.3 Hz), 19.74, 18.00. HRMS calcd for $C_{23}H_{20}BrF_7N_4O_2SH$ ([M + H]$^+$): 629.0452. Found: 629.0453. $[\alpha]^{20}_D$ = +2.6 (*c* = 0.5, MeOH).

(*S*,*S*)-*N*^{2}-(1-(*N*-Cyano-*S*-methylsulfinimidoyl)propan-2-yl)-*N*^{1}-(3-(trifluoromethyl)phenyl)phthalamide, **IIf**: white solid; yield 20.3%; mp 85−87 °C; ^{1}H NMR (400 MHz, DMSO-d_6) δ 10.68 (s, 1H, Ar−NH), 8.58 (d, *J* = 7.2 Hz, 1H, −CNH), 8.20 (m, 1H, Ar−H), 7.89 (m, 1H, Ar−H), 7.59 (d, *J* = 5.9 Hz, 5H, Ar−H), 7.44 (d, *J* = 7.2 Hz, 1H, Ar−H), 4.27 (m, 1H, −N−CH), 3.29 (d, *J* = 9.6 Hz, 2H, $-SCH_2$), 2.81 (s, 3H, $-SCH_3$), 1.27 (d, *J* = 6.6 Hz, 3H, $-CCH_3$); ^{13}C NMR (101 MHz, DMSO-d_6) δ 167.43, 167.23, 140.17, 136.43, 135.62, 129.84 (d, *J* = 10.9 Hz), 129.50, 129.19, 127.70 (d, *J* = 23.9 Hz), 125.50, 123.05, 120.08, 119.63, 115.54, 54.24, 41.01, 32.67, 19.88. HRMS calcd for $C_{20}H_{19}F_3N_4O_2SH$ ([M + H]$^+$): 437.1254. Found: 437.1252. $[\alpha]^{20}_D$ = +45.1 (*c* = 10, MeOH).

(*R*,*S*)-3-Iodo-*N*^{2}-(1-(*N*-cyano-*S*-methylsulfinimidoyl)propan-2-yl)-*N*^{1}-(2-methyl-4-(perfluoropropan-2-yl)phenyl)phthalamide, **IIIa**: white solid; yield 70.3%; mp 116−118 °C; ^{1}H NMR (400 MHz, DMSO-d_6) δ 9.95 (s, 1H, Ar−NH), 8.83 (d, *J* = 7.8 Hz, 1H, −CNH), 8.05 (d, *J* = 7.9 Hz, 1H, Ar−H), 7.79−7.75 (m, 2H, Ar−H), 7.54 (d, *J* = 7.3 Hz, 2H, Ar−H), 7.31 (t, *J* = 7.8 Hz, 1H, Ar−H), 4.24 (dt, *J* = 13.6, 6.8 Hz, 1H, −N−CH), 3.29 (dd, *J* = 12.7, 5.9 Hz, 1H, $-SCH_2$), 3.18 (dd, *J* = 7.9, 4.9 Hz, 1H, $-SCH_2$), 2.66 (s, 3H, $-SCH_3$), 2.36 (s, 3H, $ArCH_3$), 1.26 (d, *J* = 6.7 Hz, 3H, $-CCH_3$); ^{13}C NMR (101 MHz, DMSO-d_6) δ 167.68, 165.45, 141.54, 140.92, 139.25, 135.59, 133.63, 130.31, 127.38, 127.20, 125.79, 123.33, 121.80, 120.48, 95.32, 54.77, 41.27, 32.01, 18.67, 17.94. Anal. Calcd for $C_{23}H_{20}F_7IN_4O_2S$: C, 40.75; H, 3.01; N, 8.13. Found: C, 40.84; H, 2.98; N, 8.28. HRMS calcd for $C_{23}H_{20}F_7IN_4O_2SH$ ([M + H]$^+$): 677.0313. Found: 677.0310. $[\alpha]^{20}_D$ = +8.3 (*c* = 10, EtOAc).

(*R*,*S*)-3-Fluoro-*N*^{2}-(1-(*N*-cyano-*S*-methylsulfinimidoyl)propan-2-yl)-*N*^{1}-(2-methyl-4-(perfluoropropan-2-yl)phenyl)phthalamide, **IIIb**: white solid; yield 59.6%; mp 106−108 °C; ^{1}H NMR (400 MHz, DMSO-d_6) δ 10.13 (s, 1H, Ar−NH), 8.96 (d, *J* = 7.9 Hz, 1H, −CNH), 7.75 (d, *J* = 8.1 Hz, 1H, Ar−H), 7.64 (m, 2H, Ar−H), 7.56 (d, *J* = 8.3 Hz, 2H, Ar−H), 7.53−7.46 (m, 1H, Ar−H), 4.40−4.22 (m, 1H, −N−CH), 3.43−3.27 (m, 1H, $-SCH_2$), 3.20 (dd, *J* = 12.6, 6.9 Hz, 1H, $-SCH_2$), 2.74 (s, 3H, $-SCH_3$), 2.39 (s, 3H, $ArCH_3$), 1.28 (d, *J* = 6.6 Hz, 3H, $-CCH_3$); ^{13}C NMR (101 MHz, DMSO-d_6) δ 165.31, 163.06, 159.62, 157.17, 139.28, 136.62, 134.00, 130.95, 127.25, 126.20, 123.80, 123.34, 120.43, 118.18, 117.95, 54.90, 32.07, 18.90, 17.98. HRMS calcd for $C_{23}H_{20}F_8N_4O_2SH$ ([M + H]$^+$): 569.1252. Found: 569.1256. $[\alpha]^{20}_D$ = +30.9 (*c* = 10, EtOAc).

(*R*,*S*)-3-Chloro-*N*^{2}-(1-(*N*-cyano-*S*-methylsulfinimidoyl)propan-2-yl)-*N*^{1}-(2-methyl-4-(perfluoropropan-2-yl)phenyl)phthalamide, **IIIc**: white solid; yield 61.2%; mp 121−122 °C; ^{1}H NMR (300 MHz, DMSO-d_6) δ 10.05 (s, 1H, Ar−NH), 8.91 (s, 1H, −CNH), 7.72 (m,

Scheme 1

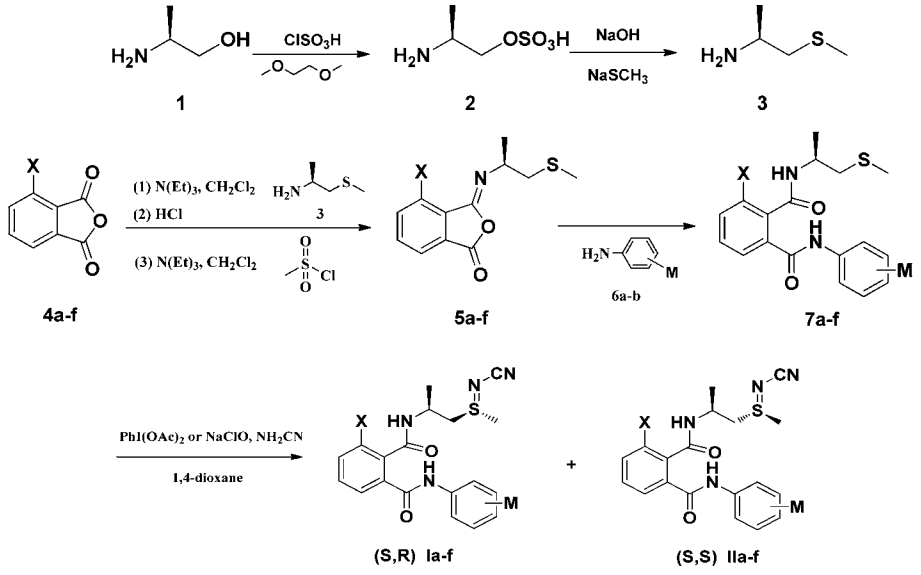

4a: X=I; 4b: X=F; 4c: X=Cl; 4d: X=NO_2; 4e: X=Br; 4f: X=H;

6a: M=2-CH_3-C_3F_7; 6b: M=3-CF_3;

7a: X=I, M=2-CH_3-C_3F_7; 7b: X=F, M=2-CH_3-C_3F_7; 7c: X=Cl, M=2-CH_3-C_3F_7;

7d: X=NO_2, M=2-CH_3-C_3F_7; 7e: X=Br, M=2-CH_3-C_3F_7; 7f: X=H, M=3-CF_3.

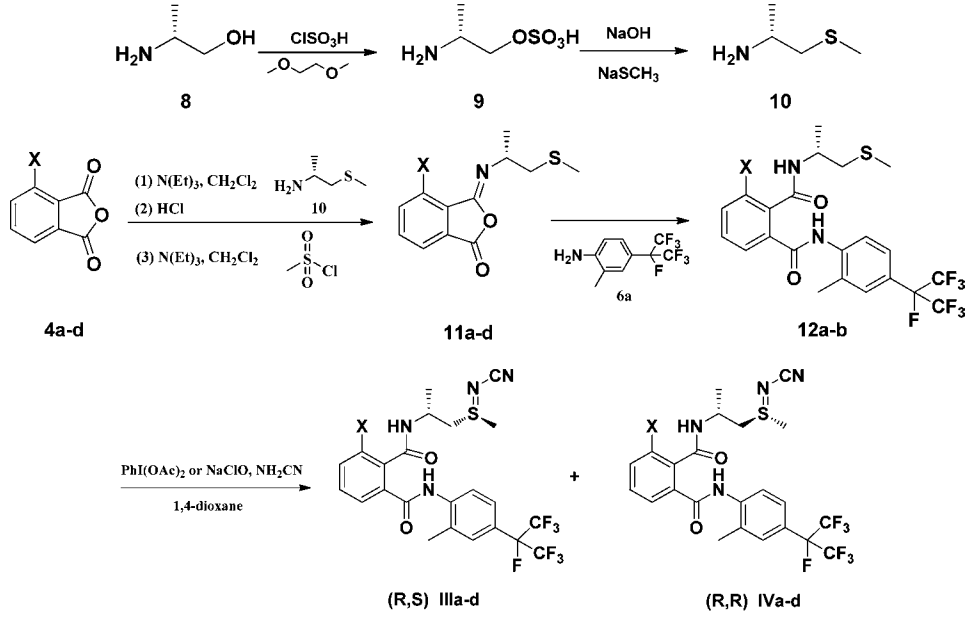

a: X=I, b: X=F, c: X=Cl, d: X=NO_2, e: X=Br.

3H, Ar−H), 7.58 (m, 3H, Ar−H), 4.28 (m, 1H, −N−CH), 3.19 (m, 2H, $-SCH_2$), 2.70 (s, 3H, $-SCH_3$), 2.37 (s, 3H, $ArCH_3$), 1.25 (d, J = 6.0 Hz, 3H, $-CCH_3$); ^{13}C NMR (101 MHz, DMSO-d_6) δ 165.31, 164.85, 139.23, 135.97 (d, J = 16.3 Hz), 133.85, 131.49, 130.69, 130.19, 127.16, 126.52, 126.01, 123.29, 121.84, 120.46, 54.84, 41.22, 31.96, 18.80, 17.96. HRMS calcd for $C_{23}H_{20}ClF_7N_4O_2SH$ ($[M + H]^+$): 585.0957. Found: 585.0951. $[\alpha]^{20}_D$ = +28.1 (c = 10, EtOAc).

(*R*,*S*)-3-Nitro-*N*^{2}-(1-(*N*-cyano-*S*-methylsulfinimidoyl)propan-2-yl)-*N*^{1}-(2-methyl-4-(perfluoropropan-2-yl)phenyl)phthalamide, **IIId**: white solid; yield 69.8%; mp 119−121 °C; ^{1}H NMR (400 MHz, DMSO-d_6) δ 10.22 (s, 1H, Ar−NH), 9.04 (d, J = 7.6 Hz, 1H, −CNH), 8.25 (d, J = 8.1 Hz, 1H, Ar−H), 8.12 (d, J = 7.4 Hz, 1H, Ar−H), 7.82 (dd, J = 16.2, 8.4 Hz, 2H, Ar−H), 7.57 (m, 2H, Ar−H), 4.22 (dt, J = 13.4, 6.6 Hz, 1H, −N−CH), 3.26 (dd, J = 12.8, 6.0 Hz, 1H, $-SCH_2$), 3.15 (dd, J = 12.7, 6.7 Hz, 1H, $-SCH_2$), 2.69 (s, 3H, $-SCH_3$), 2.39 (s, 3H, $ArCH_3$), 1.22 (d, J = 6.7 Hz, 3H, $-CCH_3$); ^{13}C NMR (101 MHz, DMSO-d_6) δ 165.56, 164.14, 147.10, 139.58, 137.61, 135.84 (d, J = 354.8 Hz), 135.84 (d, J = 354.8 Hz), 138.43−131.64 (m), 131.19 (d, J = 85.7 Hz), 130.42−127.83 (m), 130.42−123.89 (m), 122.37, 120.37, 55.03, 41.82, 33.13, 19.91, 18.49. HRMS calcd for $C_{23}H_{20}F_7N_5O_4SH$

dx.doi.org/10.1021/jf501727k | J. Agric. Food Chem. 2014, 62, 6269−6277

([M + H]$^+$): 596.1197. Found: 596.1194. $[\alpha]^{20}_D$ = +19.2 (c = 3, MeOH).

(*R*,*R*)-3-Iodo-N^2-(1-(*N*-cyano-*S*-methylsulfinimidoyl)propan-2-yl)-N^1-(2-methyl-4-(perfluoropropan-2-yl)phenyl)phthalamide, **IVa**: white solid; yield 29.7%; mp 116−118 °C; ^{1}H NMR (400 MHz, DMSO-d_6) δ 9.96 (s, 1H, Ar−NH), 8.70 (d, J = 6.6 Hz, 1H, −CNH), 8.04 (d, J = 6.8 Hz, 1H, Ar−H), 7.82−7.74 (m, 2H, Ar−H), 7.55 (m, 2H, Ar−H), 7.31 (m, 1H, Ar−H), 4.23 (m, 1H, −N−CH), 3.28−3.20 (m, 1H, $-SCH_2$), 3.16 (d, J = 11.1 Hz, 1H, $-SCH_2$), 2.67 (s, 3H, $-SCH_3$), 2.37 (s, 3H, $ArCH_3$), 1.28 (d, J = 5.1 Hz, 3H, $-CCH_3$); ^{13}C NMR (101 MHz, DMSO-d_6) δ 167.72, 165.51, 140.77, 141.58, 139.29, 135.86, 133.52, 130.29, 127.36, 125.67, 123.34, 121.50, 120.12, 95.101, 54.76, 41.15, 32.80, 19.62, 17.98. HRMS calcd for $C_{23}H_{20}F_7IN_4O_2SH$ ([M + H]$^+$): 677.0313. Found: 677.0310. $[\alpha]^{20}_D$ = −50.9 (c = 10, EtOAc).

(*R*,*R*)-3-Fluoro-N^2-(1-(*N*-cyano-*S*-methylsulfinimidoyl)propan-2-yl)-N^1-(2-methyl-4-(perfluoropropan-2-yl)phenyl)phthalamide, **IVb**: white solid; yield 40.4%; mp 105−106 °C; ^{1}H NMR (400 MHz, DMSO-d_6) δ 10.11 (s, 1H, Ar−NH), 8.79 (d, J = 7.6 Hz, 1H, −CNH), 7.75 (d, J = 7.9 Hz, 1H, Ar−H), 7.61 (m, 2H, Ar−H), 7.54 (d, J = 9.2 Hz, 2H, Ar−H), 7.49 (d, J = 8.0 Hz, 1H, Ar−H), 4.27 (m, 1H, −N−CH), 3.23 (m, 2H, $-SCH_2$), 2.76 (s, 3H, $-SCH_3$), 2.38 (s, 3H, $ArCH_3$), 1.27 (d, J = 6.4 Hz, 3H, $-CCH_3$); ^{13}C NMR (101 MHz, DMSO-d_6) δ 165.38, 163.01, 159.54, 159.09, 139.32, 136.98, 133.91, 130.92 (d, J = 32.0 Hz), 127.18 (d, J = 44.0 Hz), 126.09, 124.91 (d, J = 79.6 Hz), 123.28 (d, J = 37.6 Hz), 121.78 (d, J = 80.4 Hz), 119.91, 117.91 (d, J = 87.6 Hz), 54.48, 41.20, 32.67, 19.90, 18.00 (s). HRMS calcd for $C_{23}H_{20}F_8N_4O_2SH$ ([M + H]$^+$): 569.1252. Found: 569.1256. $[\alpha]^{20}_D$ = −41.5 (c = 10, EtOAc).

(*R*,*R*)-3-Chloro-N^2-(1-(*N*-cyano-*S*-methylsulfinimidoyl)propan-2-yl)-N^1-(2-methyl-4-(perfluoropropan-2-yl)phenyl)phthalamide, **IVc**: white solid; yield 38.8%; mp 85−87 °C; ^{1}H NMR (400 MHz, DMSO-d_6) δ 10.05 (s, 1H, Ar−NH), 8.76 (d, J = 7.8 Hz, 1H, −CNH), 7.76 (dd, J = 14.4, 7.9 Hz, 2H, Ar−H), 7.70 (d, J = 7.9 Hz, 1H, Ar−H), 7.61−7.53 (m, 3H, Ar−H), 4.26 (m, 1H, −N−CH), 3.22 (m, 2H, $-SCH_2$), 2.72 (s, 3H, $-SCH_3$), 2.38 (s, 3H, $ArCH_3$), 1.26 (d, J = 6.7 Hz, 3H, $-CCH_3$); ^{13}C NMR (101 MHz, DMSO-d_6) δ 165.38, 164.88, 139.26, 136.32, 135.91, 133.76, 131.31, 130.62, 130.16, 127.19 (d, J = 11.2 Hz), 126.46, 125.87, 123.35, 121.83, 121.63, 120.04, 54.53, 41.06, 32.75, 19.73, 17.99. Aanl. Calcd for $C_{23}H_{20}ClF_7N_4O_2S$: C, 47.23; H, 3.45; N, 9.58. Found: C, 46.98; H, 3.48; N, 9.68. HRMS calcd for $C_{23}H_{20}ClF_7N_4O_2SH$ ([M + H]$^+$): 585.0957. Found: 585.0951. $[\alpha]^{20}_D$ = −67.9 (c = 10, EtOAc).

(*R*,*R*)-3-Nitro-N^2-(1-(*N*-cyano-*S*-methylsulfinimidoyl)propan-2-yl)-N^1-(2-methyl-4-(perfluoropropan-2-yl)phenyl)phthalamide, **IVd**: white solid; yield 30.2%; mp 99−101 °C; ^{1}H NMR (400 MHz, DMSO-d_6) δ 10.22 (s, 1H, Ar−NH), 8.88 (d, J = 7.1 Hz, 1H, −CNH), 8.26 (d, J = 7.7 Hz, 1H, Ar−H), 8.10 (d, J = 7.0 Hz, 1H, Ar−H), 7.84 (d, J = 7.6 Hz, 2H, Ar−H), 7.57 (m, 2H, Ar−H), 4.19 (m, 1H, −N−CH), 3.26−3.18 (m, 1H, $-SCH_2$), 3.14 (m, 1H, $-SCH_2$), 2.68 (s, 3H, $-SCH_3$), 2.40 (s, 3H, $ArCH_3$), 1.25 (d, J = 5.7 Hz, 3H, $-CCH_3$); ^{13}C NMR (101 MHz, DMSO-d_6) δ 166.25, 164.84, 147.80, 140.27, 138.30, 134.77, 134.28, 132.31, 131.46, 128.43 (d, J = 10.5 Hz), 126.91 (d, J = 19.0 Hz), 124.47, 122.98 (d, J = 20.5 Hz), 121.07, 55.73, 42.53, 33.84, 20.60, 19.18. HRMS calcd for $C_{23}H_{20}F_7N_5O_4SH$ ([M + H]$^+$): 596.1197. Found: 596.1194. $[\alpha]^{20}_D$ = −22.9 (c = 2, MeOH).

X-ray Diffraction. The crystal structure of compound **If** was determined, and X-ray intensity data were recorded on a Bruker SMART 1000 CCD diffraction meter using graphite monochromated Mo Kα radiation (λ = 0.71073 Å). All calculations were refined anisotropically. All hydrogen atoms were located from a difference Fourier map and were placed at calculated positions and were included in the refinements in the riding mode with isotropic thermal parameters.

Biological Assay. All bioassays were performed on representative test organisms reared in the laboratory. The bioassay was repeated at 25 ± 1 °C according to statistical requirements. Assessments were made on a dead/alive basis, and mortality rates were corrected using Abbott's formula.[29] Evaluations were based on a percentage scale of 0−100, in which 0 = no activity and 100 = total kill. The standard deviations of the tested biological values were ±5%. LC_{50} and LC_{95} values were calculated by probit analysis.[30]

Larvicidal Activity against Oriental Armyworm (*Mythimna separata* Walker). The larvicidal activity of the title compounds and commercial flubendiamide against oriental armyworm was tested according to the leaf-dip method using the reported procedure.[31] Leaf disks (about 5 cm) were cut from fresh corn leaves and were dipped into the test solution for 3−5 s. After drying, the treated leaf disks were placed individually into a glass-surface vessel (7 cm). Each dried treated leaf disk was infested with 10 third-instar oriental armyworm larvae. Percentage mortalities were evaluated 4 days after treatment. Leaves treated with acetone were provided as controls. Each treatment was performed three times. The larvicidal activities of **Ia**, **IIIa**, **Va**, and flubendiamide against oriental armyworm are listed in Table 2. The insecticidal activity is summarized in Table 3. LC_{50} values of compounds **Ia**,**b**, **IIa**,**b**, **IId**, **IIIa**,**b**, and **IVa**,**b** and flubendiamide against oriental armyworm are listed in Table 4.

Larvicidal Activity against Diamondback Moth (*Plutella xylostella* L.). The larvicidal activity of the title compounds and flubendiamide against diamondback moth was tested by the leaf-dip method using the reported procedure.[32,33] Leaf disks (5 cm × 3 cm) were cut from fresh cabbage leaves and then dipped into the test solution for 3 s. After air-drying, the treated leaf disks were placed individually into boxes (80 cm). Each dried treated leaf disk was infested with 30 second-instar diamondback moth larvae. Percentage mortalities were evaluated 3 days after treatment. Each treatment was performed three times. The insecticidal activity is summarized in Table 5.

RESULTS AND DISCUSSION

Synthesis. The method of oxidative imination based on a sulfide was followed to prepare these sulfilimines. Cyanogen amine was used as a nitrogen source, and hypervalent iodinane such as $PhI(OAc)_2$ was used as a mild oxidant. The reaction of the sulfide with cyanogen amine in the presence of $PhI(OAc)_2$ was carried out in 1,4-dioxane. The preferred reaction temperature ranged from −5 to 0 °C. *N*-Cyanosulfilimines were obtained in 95−99% yield with the ratio of diastereoselectivity 7:3. The title compounds were synthesized as shown in Scheme 1.

The title compounds have been characterized by melting point, ^{1}H NMR, ^{13}C NMR, elemental analyses (or high-resolution mass spectrometry), and optical polarimetry. All spectral and analytical data were consistent with the assigned structures. Physical parameters of each pair of enantiomers were alike, except with the opposite specific optical rotation signs. Compared with each diastereoisomer in **I** and **II**, the value of HRMS was the same, whereas differences were found in the melting points and proton signals of −NHCO− in the aliphatic amide moiety. As shown in Table 1, the melting point of isomer in **I** was approximately equal to or lower than that of the corresponding diastereoisomer in **II**. As for the proton signals of −NHCO− in the aliphatic amide moiety, the former was 0.14−0.16 ppm higher than the later, as well as in **III** and **IV**. Specific optical rotation values were negative (**I**), positive (**II**), positive (**III**), and negative (**IV**), respectively (Table 1). In ^{1}H NMR spectra of all title compounds, the proton signals of −NHCO− on the amide bridge were observed at δ 8.26−10.84 and 7.96−8.90 as a singlet or doublet, respectively. In all title compounds, the methyne proton appeared at δ 4.23−4.53 as a multiplet, and the methylene protons attached to the sulfur atom appeared at δ 3.52−4.16 and 2.97−3.89 as a couple of doublets due to respective chemical environment. Meanwhile, in the ^{1}H NMR of aliphatic amide moiety, methyl protons attached to tertiary carbon were observed as a doublet as well.

dx.doi.org/10.1021/jf501727k | J. Agric. Food Chem. 2014, 62, 6269−6277

Table 1. Some Physical Parameters of Ia−e, IIa−e, IIIa−d, and IVa−d

	Ia	Ib	Ic	Id	IIa	IIb	IIc	IId
mp (°C)	117–119	103–105	120–122	121–123	116–118	104–106	84–86	99–102
$[\alpha]_D^{20}$	−8.2 (c = 10)	−31.6 (c = 10)	−28.0 (c = 10)	−18.8 (c = 3)	+51.2 (c = 10)	+42.0 (c = 10)	+68.4 (c = 10)	+23.6 (c = 3)
HMRS (M + H)	677.0313	569.1252	585.0957	596.1197	677.0313	569.1252	585.0957	596.1197
	IIIa	**IIIb**	**IIIc**	**IIId**	**IVa**	**IVb**	**IVc**	**IVd**
mp (°C)	116–118	106–108	121–122	119–121	116–117	105–106	85–86	99–101
$[\alpha]_D^{20}$	+8.3 (c = 10)	+30.9 (c = 10)	+28.1 (c = 10)	+19.2 (c = 3)	−50.9 (c = 10)	−41.5 (c = 10)	−67.9 (c = 10)	−22.9 (c = 3)
HMRS (M + H)	677.0313	569.1252	585.0957	596.1197	677.0313	569.1252	585.0957	596.1197

Crystal Structure Analysis. To identify the chiral characteristic of each isomer, the colorless crystal (0.20 mm × 0.10 mm × 0.10 mm) structure of compound **If** was obtained in DMSO, which was suitable for X-ray single-crystal diffraction as shown in Figure 3 with the following crystallographic

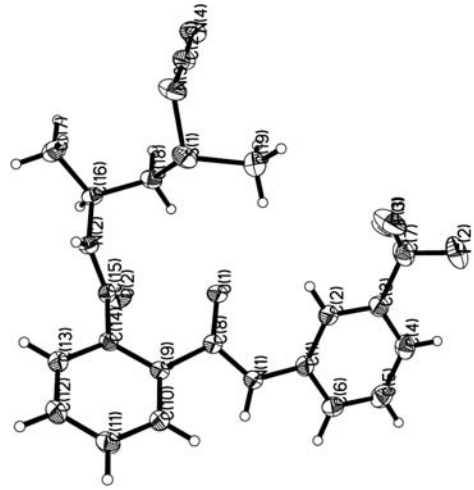

Figure 3. Crystal structure of compound **If**.

parameters: a = 5.0807(10) Å, b = 21.298 (4) Å, c = 19.011(4) Å, α = 90°, β = 90.17 (3)°, γ = 90°, V = 2057.1(7) Å^3, Z = 4, D_c = 1.409 mg m^{-3}, μ = 0.208 mm^{-1}, F (100) = 904, R = 0.0717, wR = 0.0908, final R factor = 4.37%, final wR factor = 7.98%, absolute structure parameter = 0.02 (7).

Structure−Activity Relationship (SAR). *Larvicidal Activity against Oriental Armyworm.* To explore the impact of carbon chirality on larvicidal activity, **Va** (the racemic compound of **Ia** and **IIIa**) was evaluated against oriental armyworm for its insecticidal activity. As shown in Table 2, **Va** displayed 60, 40, and 20% larvicidal activities at concentration of 0.5, 0.25, and 0.1 mg L^{-1}, respectively, which showed better activity than **IIIa** (0.5 mg L^{-1}, 20%) and weaker activity than **Ia** (0.1 mg L^{-1}, 60%). These observations clearly revealed that the Sc configuration of **Ia** improved the bioactivity greatly. Furthermore, carbon chirality resulted from the aliphatic amine, which can easily be derived from the obtained (L)-alanine.

The larvicidal activities of compounds **Ia−e**, **IIa−e**, **IIIa−d**, and **IVa−d** and flubendiamide against oriental armyworm are listed in Tables 3 and 4. Most compounds exhibited good to excellent activity against oriental armyworm. Generally, the sequence of each configuration's biological activity is (Sc, Ss) ≥ (Sc, Rs) ≫ (Rc, Ss) > (Rc, Rs). For example, **IId** (Sc, Ss) showed 60% insecticidal activity at 0.25 mg L^{-1} (0.5 mg L^{-1}, 100%), whereas **Id** (Sc, Rs) gave a death rate of 60% at only 1 mg L^{-1}. It is worth noting that the Sc configurations showed much better than Rc configurations. At a higher concentration of 10 mg L^{-1}, we can see that **IIId** (Rc, Ss) (50%) showed better activity than **IVd** (Rc, Rs) (30%). As seen for other substituents in the phthaloyl moiety, (Sc, Ss) **II** was most active followed by (Sc, Rs) **I** and (Rc, Ss) **III**, and the (Rc, Rs) **IV** was almost inactive. The results indicated that the improvement of insecticidal activity required a reasonable coordination of both carbon and sulfur chirality and that a probable synergistic effect was involved.

In comparison, Sc configurations (**Ia** vs **IIa**, **Ib** vs **IIb**, **Ie** vs **IIe**) and Rc configurations (**IIIb** vs **IVb**, **IIIc** vs **IVc**, **IIId** vs

dx.doi.org/10.1021/jf501727k | J. Agric. Food Chem. 2014, 62, 6269−6277

Table 2. Insecticidal Activities of Compounds Ia, IIIa, and Va and Flubendiamide against Oriental Armyworm

	larvicidal activity (%) at concn of										
compd	200 mg L^{-1}	100 mg L^{-1}	50 mg L^{-1}	25 mg L^{-1}	10 mg L^{-1}	5 mg L^{-1}	2.5 mg L^{-1}	1 mg L^{-1}	0.5 mg L^{-1}	0.25 mg L^{-1}	0.1 mg L^{-1}
Ia	100	100	100	100	100	100	100	100	100	100	60
IIIa	100	100	100	100	100	100	100	100	20	0	
Va	100	100	100	100	100	100	100	100	60	40	20
fubendiamide			100	100	100	100	100	100	100	100	50

Table 3. Insecticidal Activities of Ia−e, IIa−e, IIIa−d, IVa−d, and Flubendiamide against Oriental Armyworm

	larvicidal activity (%) at concn of										
compd	200 mg L^{-1}	100 mg L^{-1}	50 mg L^{-1}	25 mg L^{-1}	10 mg L^{-1}	5 mg L^{-1}	2.5 mg L^{-1}	1 mg L^{-1}	0.5 mg L^{-1}	0.25 mg L^{-1}	0.1 mg L^{-1}
Ia	100	100	100	100	100	100	100	100	100	100	60
Ib	100	100	100	100	100	100	100	40			
Ic	100	100	100	100	100	100	100	60			
Id	100	100	100	100	100	100	100	40			
Ie	100	100	100	100	100	100	100	60			
IIa	100	100	100	100	100	100	100	100	100	100	48
IIb	100	100	100	100	100	100	100	70			
IIc	100	100	100	100	100	100	100	100	100	60	
IId	100	100	100	100	100	100	100	100	100	60	
IIe	100	100	100	100	100	100	100	100	60		
IIIa	100	100	100	100	100	100	100	100	20	0	
IIIb	100	100	100	100	20						
IIIc	100	100	100	100	60						
IIId	100	100	100	100	50						
IVa	100	100	100	100	100	100	60				
IVb	100	100	100	100	10						
IVc	100	100	100	100	40						
IVd	100	100	100	100	30						
flubendiamide			100	100	100	100	100	100	100	100	50

Table 4. LC_{50} Values of Compounds Ia,b, IIa,b, IId, IIIa,b, and IVa,b and Flubendiamide against Oriental Armyworm

	LC_{50} (mg L^{-1})			
compd	$y = a + bx$	R	LC_{50}	LC_{95}
Ia	$y = 7.4089 + 1.8566x$	0.9885	0.0504 (0.0326−0.0699)	0.3877 (0.2400−1.0199)
Ib	$y = 5.2469 + 1.8142x$	0.9331	0.7310	5.8963
IIa	$y = 7.5886 + 2.2397x$	0.9402	0.0699 (0.0536−0.0878)	0.3790 (0.2488−0.8174)
IIb	$y = 5.6952 + 2.2259x$	0.9939	0.4872	2.6709
IId	$y = 7.5067 + 3.9160x$	0.9541	0.2290	0.6024
IIIa	$y = 6.5079 + 3.5344x$	0.9351	0.3744	1.0933
IIIb	$y = 2.2365 + 1.9655x$	0.9882	25.4675	174.9238
IVa	$y = 4.2267 + 3.5772x$	0.9282	1.6450	4.7423
IVb	$y = 1.2531 + 2.4626x$	0.9688	33.2304	154.6959
flubendiamide	$y = 7.4237 + 2.6428x$	0.9945	0.1230 (0.0958−0.1503)	0.5160 (0.3733−0.8966)

IVd), these diastereoisomers reached the same activity level. For example, **Ia** and **IIa** showed similar activity at 0.1 mg L^{-1}. **IIc** displayed 60% insecticidal activity at 0.25 mg L^{-1}, whereas **Ic** gave a death rate of only 60% at 1 mg L^{-1}, as did **Id** and **IId**. These observations showed that chiral sulfur had an influence on the larvicidal activity. However, carbon chirality influenced the activities more strongly than sulfur, as seen in comparison of compounds in Rs configurations such as **Ia** versus **IIIa**, **Ib** versus **IIIb**, **Ic** versus **IIIc**, and **Id** versus **IIId**) and in Ss configurations such as **IIa** versus **IVa**, **IIb** versus **IVb**, **IIc** versus **IVc**, and **IId** versus **IVd**.

As shown in Table 3, all compounds showed a mortality of 100% at 10 mg L^{-1}, except **IIIb−d**, **IVb**, **IVd**. Particularly (Sc, Rs) **Ia−e**, (Sc, Ss) **IIa−e**, (Rc, Ss) **VIIa**, and (Rc, Rs) **VIIIa** exhibited 100% larvicidal activities at 2.5 mg L^{-1}. **Ia** and **IIa** showed excellent activities comparable to that of flubendiamide. These results indicated that compounds with the iodine substituent in each configuration showed the best larvicidal activity, which was consistent with the previous study.[19] A Cl substituent as well as NO_2, Br, and F possessed inferior insecticidal activity against oriental armyworm.

From Table 4, it is worth noting that the LC_{50} values of **Ia** and **IIa** were 0.0504 and 0.0699 mg L^{-1}, respectively, lower than that of flubendiamide (0.1230 mg L^{-1}). In addition, the LC_{50} values of compounds **IIb**, **IId**, and **IIIa** were 0.4872, 0.2290, and 0.3744 mg L^{-1}, respectively.

Larvicidal Activity against Diamondback Moth. The larvicidal activities of compounds **Ib−e**, **IIa−e**, and **IVa** and flubendiamide against diamondback moth are listed in Table 5. Most compounds possessed excellent activities. In comparison

dx.doi.org/10.1021/jf501727k | J. Agric. Food Chem. 2014, 62, 6269−6277

Table 5. Insecticidal Activities of Compounds Ib−e, IIa−e, IVa, Va, Ve , and VIa−c and Flubendiamide against Diamondback Moth

	larvicidal activity (%) at							
compd	100 mg L^{-1}	10 mg L^{-1}	1 mg L^{-1}	10^{-1} mg L^{-1}	10^{-2} mg L^{-1}	10^{-3} mg L^{-1}	10^{-4} mg L^{-1}	10^{-5} mg L^{-1}
Ib	100	100	100	100	90	40		
Ic	100	100	100	100	90	75		
Id	100	100	100	100	60	40		
Ie	100	100	100	100	100	60		
IIa	100	100	100	100	90	50		
IIb	100	100	100	100	40	0		
IIc	100	100	100	100	100	80		
IId	100	100	100	100	100	80		
IIe	100	100	100	100	100	100	90	40
IVa	100	100	100	100	70	30		
flubendiamide		100	100	100	100	50	0	

of Sc configurations **I** and **II**, the sequence of activity was (Sc, Ss) > (Sc, Rs), except in the case of **Ib** (10^{-2} mg L^{-1}, 90%), which displayed better activity than **IIb** (10^{-2} mg L^{-1}, 40%). For the pair of enantiomers, it is worth noting that **IIa** and **IVa** reached similar activity levels. We conclude that in these cases the sulfur chirality influenced the activities more greatly than carbon. When different substituents in the phthaloyl scaffold were compared, it was found that Br showed the best activity. **Ie** and **IIc**,**d** reached the same activity as flubendiamide. In particular, **IIe** gave higher activity than flubendiamide with a mortality of 40% at low 10^{-5} mg L^{-1}, whereas flubendiamide showed only 50% at 10^{-3} mg L^{-1}.

CoMFA Analysis by SYBYL. A brief CoMFA analysis for compounds **Ia**,**b**, **IIa**,**b**, **IId**, **IIIa**,**b**, and **IVa**,**b** was performed with SYBYL.[34] The conformations with minimum energy were calculated with Tripos force field and Gasteiger−Hukel charges in advance. The activity data were reported as pLC_{50}, and the negative logarithms of the LC_{50} data are in Table 2. Thus, a larger number of pLC_{50} indicates a higher activity. Details are shown in Figure 4.

From the results of CoMFA, the green area near the I substituent suggests a bulkier group is favorable, as Cl or F declines in larvicidal activity. The yellow area indicates a less bulky substituent enhances activity. It is worth noting that the chiral carbon atom is located near the yellow area, and chirality (Rc or Sc) causes a difference in the orientation of the methyl group, which is bulkier than H atom. Thus, the methyl groups with Rc configurations (**III** and **IV**) come closer to the yellow area and have a poorer activity than Sc configurations. Finally, the red area surrounding the CN group indicates more electronegativity is favorable here, whereas Rc configurations on chiral carbon atoms cause the CN group to stay out of the red area, which leads to a decrease in activity. This is in accordance with SARs described in this paper.

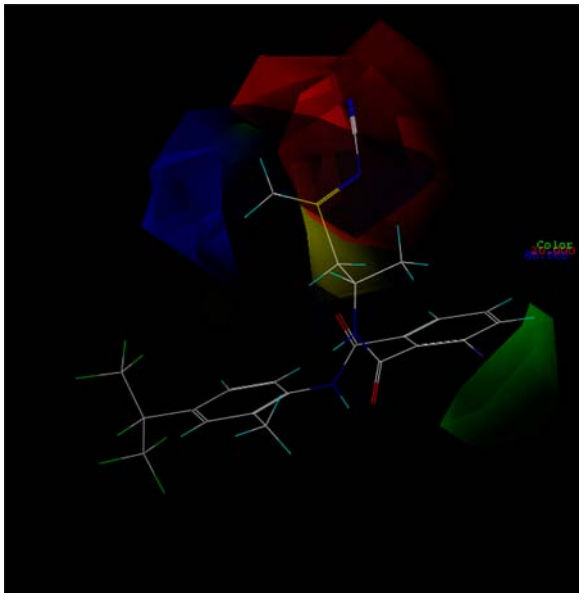

Figure 4. CoMFA results for **Ia**.

Partial least-squares analysis gives an excellent linear relationship between predicted and actual activities (R_2 = 1.000), which indicates a valid CoMFA model.

In summary, this is the first report of the novel optically active configuration incorporated into dicarboxamides containing *N*-cyano sulfiliminyl moieties. Four chiral series of novel phthalamide derivatives with sulfur-containing groups were designed, synthesized, and evaluated against oriental armyworm and diamondback moth for their insecticidal activities. All structures were characterized by ^{1}H NMR, ^{13}C NMR, and HRMS (or elemental analysis), and their relative absolute configurations were confirmed by optical polarimetry. For oriental armyworm, these stereoisomers exhibited different impacts on biological activity following the sequence (Sc, Ss) ≥ (Sc, Rs) ≫ (Rc, Ss) > (Rc, Rs); carbon chirality influenced the activities more strongly than sulfur. Compounds **Ia** and **IIa** reached activity as high as that of commercial flubendiamide, with LC_{50} values of 0.0504 and 0.0699 mg L^{-1}, respectively, lower than that of flubendiamide (0.1230 mg L^{-1}). For diamondback moth, the sequence of activity was (Sc, Ss) > (Sc, Rs), and the sulfur chirality influenced the activities greater to a greater extent than carbon. Compound **IIe** had an even higher activity than flubendiamide, whereas **Ie** and **Ic**,**d** reached the activity of the latter. The results indicated that the improvement of insecticidal activity required a reasonable coordination of both carbon and sulfur chirality. Probable synergistic influence was involved. CoMFA calculation indicated that stereoisomers with Sc configurations containing a strong electron-withdrawing group such as CN are important to retain their high activity. The *N*-cyano sulfiliminyl substituent was also essential for high larvicidal activity. Our research indicated that some of the title compounds could be potential candidates as ryanodine receptor activators.

AUTHOR INFORMATION

Corresponding Author

*(Z.L.) Phone: +86-22-23503732. E-mail: nkzml@vip.163.com.

Funding

This work was supported by the project supported by the National Basic Research Program of China (No. 2010CB126106) and the National Key Technologies R&D Program (No. 2011BAE06B05) .

Notes

The authors declare no competing financial interest.

REFERENCES

(1) Lahm, G. P.; Selby, T. P.; Frendenberger, J. H.; Stevenson, T. M.; Myers, B. J.; Seburyamo, G.; Smith, B. K.; Flexner, L.; Clark, C. E.; Cordova, D. Insecticidal anthranilicdiamides: a new class of potent ryanodine receptor activators. *Bioorg. Med. Chem. Lett.* **2005**, *15*, 4898−4906.

(2) Feng, Q.; Liu, Z. L.; Xiong, L. X.; Wang, M. Z.; Li, Y. Q.; Li, Z. M. Synthesis and insecticidal activities of novel anthranilicdiamides containing modified *N*-pyridylpyrazoles. *J. Agric. Food Chem.* **2010**, *58*, 12327−12336.

(3) Nakao, H.; Harayama, H.; Yamaguchi, M.; Tohnishi, M.; Morimoto, M.; Fujioka, S. *Preparation of phthalamide derivatives as insecticides*. WO 2002088074, 2002.

(4) Harayama, H.; Tohnishi, M.; Morimoto, M.; Fujioka, S. *Preparation of phthalamide derivatives as insecticides*. WO 2002088075, 2002.

(5) Mochizuki, K.; Inoue, S.; Hatanaka, T. *Optically active phthalamide derivative, agricultural or horticultural insecticide, and method of using the same*. U.S. 2008260440, 2008.

(6) Tohnishi, M.; Nakao, H.; Kohno, E.; Nishida, T.; Furuya, T.; Shimizu, T.; Seo, A.; Sakata, K.; Fujioka, S.; Kanno, H. *Preparation of phthalic acid diamides as agricultural and horticultural insecticides*. EP 0919542, 1999.

(7) Tohnishi, M.; Nakao, H.; Kohno, E.; Nishida, T.; Furuya, T.; Shimizu, T.; Seo, A.; Sakata, K.; Fujioka, S.; Kanno, H. *Preparation of phthalamides as agrohorticultural insecticides*. EP 1006107, 2000.

(8) Tozai, M.; Morimoto, M.; Fujioka, N.; Seo, A. *Preparation of phthalic diamides and insecticides for agriculture and horticulture*. JP 2001335559, 2001.

(9) Wada, K.; Gomibuchi, T.; Yoneta, Y.; Otsu, Y.; Shibuya, K.; Matsuo, H.; Fischer, R. *Preparation of phthalamide derivatives as insecticides*. WO 2004000796, 2003.

(10) Wada, K.; Gomibuchi, T.; Yoneta, Y.; Otsu, Y.; Shibuya, K.; Nakakura, N.; Fischer, R. *Preparation of pyrazolylmethylmethylphenyl phthalamides and related compounds as insecticides*. WO 2005095351, 2005.

(11) Seo, A.; Tohnishi, M.; Nakao, H.; Furuya, T.; Kodama, H.; Tsubata, K.; Fujioka, S.; Kodama, H.; Nishimatsu, T.; Hirooka, T. Flubendiamide, a new insecticide characterized by its novel chemistry and biology. In *Pesticide Chemistry: Crop Protection, Public Health, Environmental Safety*; Ohkawa, H., Miyagawa, H., Lee, P. W., Eds.; Wiley-VCH Verlag: Weinheim, Germany, 2007; pp 127−135.

(12) Zhu, Y.; Loso, M. R.; Watson, G. B.; Sparks, T. C.; Rogers, R. B.; Hunag, J. X.; Gerwick, B. C.; Babcock, J. M.; Kelley, D.; Hegde, V. B.; Nugent, B. M.; Renga, J. M.; Denholm, I.; Gorman, K.; DeBoer, G. J.; Hasler, J.; Meade, T.; Thomas, J. D. Discovery and characterization of sulfoxaflor, a novel insecticide targeting sap-feeding pests. *J. Agric. Food Chem.* **2011**, *59*, 2950−2957.

(13) Sparks, T. C.; Watson, G. B.; Loso, M. R.; Geng, C.; Babcock, J. M.; Thomas, J. D. Sulfoxaflor and the sulfoximine insecticides: chemistry, mode of action and basis for efficacy on resistant insects. *Pestic. Biochem. Physiol.* **2013**, *107*, 1−7.

(14) Babcock, J. M.; Gerwick, B.; Hunag, J. X.; Loso, M. R.; Nakamura, G.; Nolting, S. P.; Rogers, R. B.; Sparks, T. C.; Thomas, J.; Watson, G. B.; Zhu, Y. Biological characterization of sulfoxaflor, a novel insecticide. *Pest Manag. Sci.* **2011**, *67*, 328−334.

(15) Babcock, J. M.; Gerwick, C. B.; Huang, J. X.; Loso, M. R.; Nakamura, G. E.; Nolting, S.; Rogers, R. B.; Sparks, T. C.; Thomas, J.; Watson, G. B.; Zhu, Y. Biological characterization of sulfoxaflor, a novelinsecticide. *Pest Manag. Sci.*. **2011**, *67*, 328−334.

(16) Furukawa, N.; Oae, S. Sulfilimines. Synthetic applications and potential utilizations. *Ind. Eng. Chem. Prod. Res. Dev.* **1981**, *20*, 260−270.

(17) Lamberth, C.; Jeanmart, S.; Luksch, T.; Plant, A. Current challenges and trends in the discovery of agrochemicals. *Science* **2013**, *134*, 742−746.

(18) Nakao, H.; Matsuzaki, Y.; Fujioka, S.; Morimoto, M.; Tohnishi, M.; Fisher, R.; Funke, C.; Malsam, O. WO 2006022225, 2006.

(19) Tohnishi, M.; Nakao, H.; Furuya, T.; et al. Flubendiamide, a novel insecticide highly active against lepidopterous insect pests. *J. Pestic. Sci.* **2005**, *30*, 354−360.

(20) Soucy, C.; Favreau, D.; Kayser, M. M. The regioselectivity of metal hydride reductions of 3-substituted phthalic anhydrides. *J. Org. Chem.* **1987**, *52*, 129−134.

(21) Wei, R. B.; Li, S. W.; Lu, J. K.; Zheng, S. H.; Hu, W. H. Synthesis of organic pigment intermediate *N,N′*-bisacetylaceto-2,5-dimethyl-1,4-phenylenediamine. *Dyestuff Ind.* **2000**, *37*, 16−18.

(22) Masanobu, O.; Akihiko, Y.; Eiji, K. *Process for the Production of perfluoroalkylated aniline derivatives*. EP 1006102, 2000.

(23) Pazenok, S. *Preparation of thioalkylamines with high yields*. WO 2007022900, 2007.

(24) Blaschke, H.; Pazenok, S. *Chiral 3-halophthalic acid derivatives*. WO 2006024402, 2006.

(25) Loso, M. R.; Nugent, B. M.; Huang, J. X.; Rogers, R. B.; Zhu Y.; Rogers, R. B.; et al. *Preparation of insecticidal N-substituted (6-haloalkylpyridin-3-yl) alkyl sulfoximines*. WO 2007095229, 2007.

(26) Podhorez, D. E.; Ross, R., Jr.; McConnell, J. R. *Process for the preparation of certain substituted sulfilimines*.U.S. 20080207910, 2008.

(27) Bland, D. C.; Adaway, T. J.; Podhorez, D. E. *Process for the preparation of certain substituted sulfilimines*. U.S. 819322, 2012.

(28) Huang, J. X.; Rogers, R. B.; Orr, N.; Sparks, T. C.; Clifford, J. M.; Loso, M. R.; Zhu Y.; Meade, T. *A method to control insects resistant to common insecticides*. WO 2007149134, 2007.

(29) Abbott, W. S. A method of computing the effectiveness of an insecticide. *J. Econ. Entomol.* **1925**, *18*, 265−267.

(30) Raymond, M. Presentation d'un programme Basic d'analyse log-probit pour miero-ordinateur. *Cah. ORSTOM Ser. Ent. Med. Parasitol.* **1985**, *23*, 117−121.

(31) Wu, Y. D.; Shen, J. L.; Chen, J.; Lin, X. W.; Li, A. M. Evaluation of two resistance monitoring methods in *Helicoverpa armigera*: topical application method and leaf dipping method. *Plant Prot.* **1996**, *22* (5), 3−6.

(32) Ma, H.; Wang, K. Y.; Xia, X. M.; Zhang, Y.; Guo, Q. L. The toxicity testing of five insecticides to different instar larvae of *Spodoptera exigua*. *Modern Agrochem.* **2006**, *5*, 44−46.

(33) Busivine, J. R. Recommended methods for measurement of pest resistance to pesticides. *FAO Plant Production and Protection Paper 21*; FAO: Rome, Italy, 1980; pp 3−13 and 119−122.

(34) SYBYL 6.9, Tripos Associates, St. Louis, MO, USA.

NOTE ADDED AFTER ASAP PUBLICATION

In the third from last sentences of both the abstract and final paragraph of the text, the stereoisomer configuration has been corrected from Rs in the original publication of June 26, 2014, to Sc, as corrected on June 27, 2014.

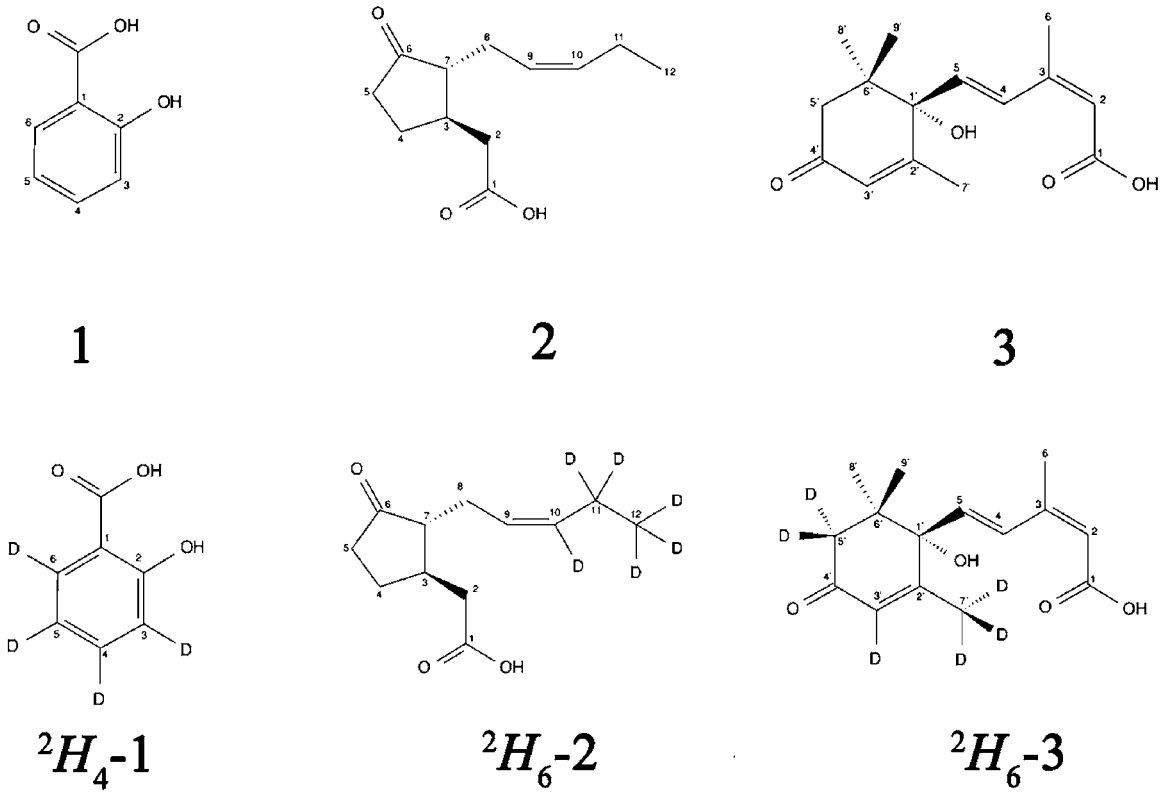

Figure 1. Chemical structures of salicylic acid (**1**), (−)-jasmonic acid (**2**), (±)-2-*cis*-4-*trans*-abscisic acid (**3**), and deuterium-labeled internal standards [$^2H_4$]-salicylic acid ($^2H_4$-**1**), [$^2H_6$]-(±)-jasmonic acid ($^2H_6$-**2**), and [$^2H_6$]-(+)-2-*cis*-4-*trans*-abscisic acid ($^2H_6$-**3**).

Sensitivity of these analytical approaches is often not sufficient to provide hormone content information on specific plant tissue in small samples. GC−MS is routinely applied for the multiplex analysis of various hormones in plant tissues.[19] However, the hydrophilic groups need to be derivatized to obtain the high analyte volatility for proper GC separation. Besides this relatively time-consuming step, another disadvantage is the need for at least 300 mg of fresh plant material to reach the dynamic range of the mass spectrometer even with the modern GC−MS approaches.[21] An elegant way to overcome the limitations of GC−MS is the use of reversed-phase high-performance liquid chromatography (RP-HPLC)−electrospray ionization (ESI)−MS. This technique offers a high separation efficiency and selectivity and minimal ESI matrix effects, and it ensures the sensitive detection of analytes without the need for derivatization.[22,23] Sensitivity is improved by tandem mass spectrometry (MS/MS) with triple quadrupole instruments operating in multiple reaction monitoring (MRM) mode by fast duty cycles and reduced chemical noise.[24] A rapid analysis of multiple hormones is possible through the relatively short dwell times typical for modern mass spectrometers.[25] In addition, the application of ultrahigh-performance liquid chromatography (UHPLC)[26] as well as solid-phase extraction (SPE)-based enrichment[27] may lead to the further improvement of sensitivity of phytohormone analysis.

The aim of this study was to develop a selective and sensitive analytical method for the simultaneous quantitation of (±)-2-*cis*-4-*trans*-abscisic acid (**3**), (−)-jasmonic acid (**2**), and salicylic acid (**1**) in rose leaves based on SPE purification and UHPLC−MS/MS analysis. [$^2H_4$]-salicylic acid ($^2H_4$-**1**), [$^2H_6$]-(±)-jasmonic acid ($^2H_6$-**2**), and [$^2H_6$]-(+)-2-*cis*-4-*trans*-abscisic acid ($^2H_6$-**3**) were used as internal standards (Figure 1). The method developed was validated according to Commission Decision 2002/657/EC.[28]

MATERIALS AND METHODS

Reagents and Chemicals. Analytical-reagent-grade chemicals were used. Water was HPLC-grade, generated by a Milli-Q gradient purification system (Millipore, Billerica, MA). Methanol (MeOH, LC−MS absolute) and acetic acid (99%, ULC−MS) were supplied by Biosolve B.V. (Biosolve B.V., Valkenswaard, Netherlands). Phytohormones **1**, **2**, and **3** and the deuterium-labeled internal standards $^2H_4$-**1**, $^2H_6$-**2**, and $^2H_6$-**3** were all purchased from OlChemIm (OlChemIm, Olomouc, Czech Republic).

Stock and Working Solution Preparation. Stock standard solutions (1 mg/mL) of compounds **1**, **2**, and **3** were prepared using methanol/water (75:25, v/v). Working standard solutions were prepared by dilution of the stock solution to obtain concentrations ranging between 0 and 60.0 μg/g for compound **3** and between 0 and 20.0 μg/g for compounds **1** and **2**.

Rose Leaf Samples and Sample Preparation. Rose plants were grown in the greenhouse of the Institute for Agricultural and Fisheries Research (ILVO, Melle, Belgium) and were subjected to standard cultural practices. The rose genotype used was a F1 hybrid of 'Yesterday' × *Rosa wichurana*. For the method development and validation, young (just unfolded) leaves were used. The collected rose leaves were free from any damage and were immediately frozen in liquid nitrogen to prevent enzymatic and thermal degradation of the phytohormones. They were stored at −80 °C until analysis. Prior to extraction, the leaf material was homogenized by removing the biggest veins and grinding with liquid nitrogen, using a mortar and pestle. In total, 20 mg of each homogenized sample was transferred to a 10 mL glass tube.

Extraction buffer containing the internal standard (IS) was prepared with final concentrations of 20 ng/mL $^2H_4$-**1**, 1 ng/mL $^2H_6$-**2**, and 400 ng/mL $^2H_6$-**3**.

dx.doi.org/10.1021/jf5023884 | J. Agric. Food Chem. 2014, 62, 6278−6284

Table 1. Optimized ESI−MS/MS Conditions with Indication of the Precursor Ion (m/z), Cone Voltage (V), Product Ions (m/z), Collision Energy (eV), and Chromatographic Retention Time (min) of Salicylic Acid (1), (−)-Jasmonic Acid (2), (±)-2-*cis*-4-*trans*-Abscisic Acid (3), and Deuterium-Labeled Internal Standards [$^2H_4$]-Salicylic Acid ($^2H_4$-1), [$^2H_6$]-(±)-Jasmonic Acid ($^2H_6$-2), and [$^2H_6$]-(+)-2-*cis*-4-*trans*-Abscisic Acid ($^2H_6$-3)

compound	precursor ion (m/z)	cone voltage (V)	product ions (m/z)	collision energy (eV)	retention time (min)
1	137.00	40	64.95/92.96[a]	22/14	4.86
2	209.15	25	58.77[a]/165.00	12/17	5.65
3	263.02	25	153.19[a]/219.00	17/17	5.28
$^2H_4$-**1**	140.74	35	96.84	17	4.84
$^2H_6$-**2**	215.11	30	58.77	12	5.63
$^2H_6$-**3**	269.12	35	159.10	30	5.26

[a]Product ion used in the screening program.

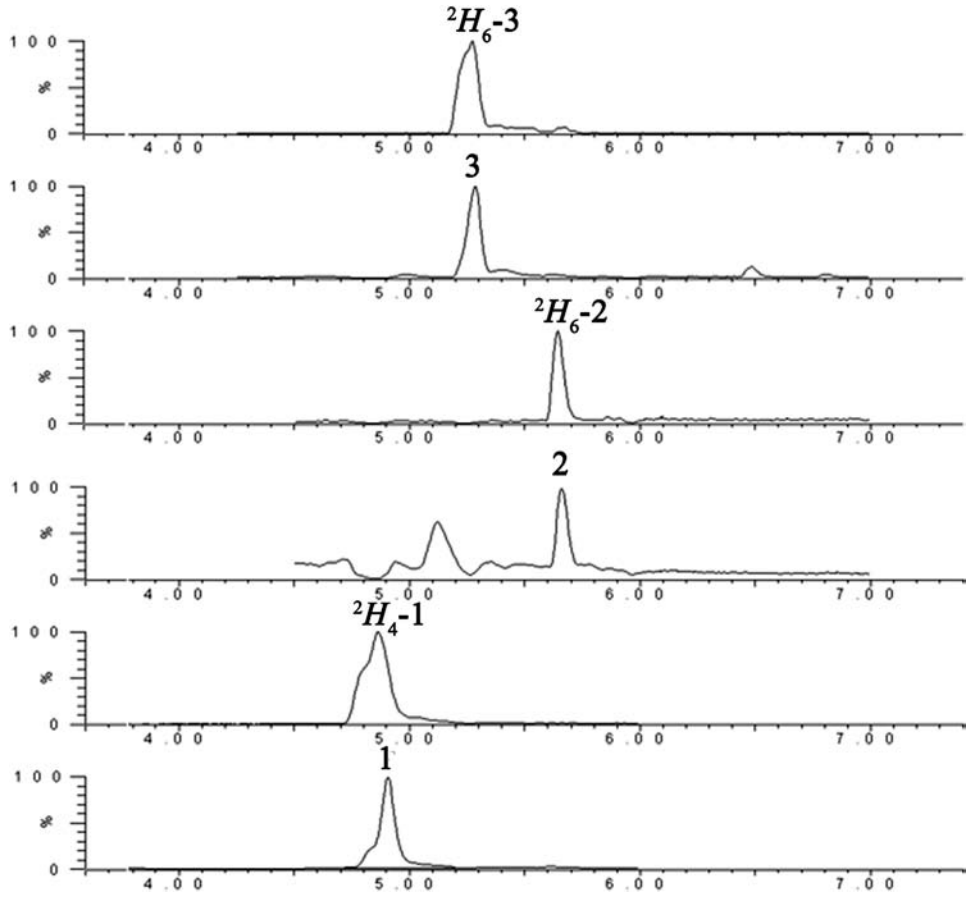

Figure 2. Representative total ion chromatograms (TIC) of the rose leaf matrices analyzed using the method developed (the concentrations of the peaks in the chromatogram correspond to endogenous concentrations, with the addition of 1.25 μg/g of compounds **1** and **2** and 3.75 μg/g of compound **3**, with the intensities of the signals at 4.26×10^6, 1.11×10^6, and 1.36×10^6, respectively).

Extraction was performed using 2 mL of methanol/water/acetic acid (10:89:1) for 16 h at 4 °C in the dark on an orbital shaker rotating at 210 rpm. The extract was filtered through a 0.22 μm Millex-GV filter (Millipore, Billerica, MA). Before loading 1 mL of this eluate onto Oasis MCX 1 cm^3 SPE cartridges (Waters, Milford, MA), these cartridges were first conditioned with 1 mL of methanol (100%), followed by 1 mL of water for equilibration. The acidic hormones bound onto the column were washed with 0.5 mL of H_2O and then eluted with a total of 1 mL of methanol (100%), applied in two consecutive steps of 0.5 mL each. Subsequently, the total eluate was evaporated to dryness using nitrogen gas at 35 °C, and the residues were redissolved in 0.5 mL of methanol/water (75:25, v/v). This extract was transferred to a microvial and stored at 4 °C prior to injection (10 μL) into the UHPLC−MS/MS system.

UHPLC−MS/MS Analyses. An Acquity UHPLC system coupled to a Xevo TQ-S triple quadrupole MS detector (Waters, Milford, MA) was used for analytical determination of the target compounds in the leaf samples. Chromatographic separation was achieved using a 100 × 2.1 mm inner diameter, 1.7 μm, Acquity UHPLC BEH C_{18} column (Waters, Milford, MA) at 30 °C. The mobile phase consisted of 0.3% acetic acid in water (A) and 0.3% acetic acid in methanol (B). The flow rate was set at 0.3 mL/min. The gradient was adapted from a previous report[29] as follows: 0 min, 2% B; 1.0−2.5 min, 2−40% B; 2.5−4.0 min, 40−50% B; 4.0−5.0 min, 50−80% B, held for 2.0 min; 7.0−7.1 min, 80−100% B, held for 0.9 min; and 8.0−11.0 min, 100−2% B.

The mass spectrometer operated in the ESI negative mode with MRM. Desolvation gas was set at 1000 L/h and a temperature of 600 °C. The MRM settings in the MS/MS function with corresponding

dx.doi.org/10.1021/jf5023884 | J. Agric. Food Chem. 2014, 62, 6278−6284

cone voltage and collision energy were optimized for each compound (Table 1). Data were acquired and processed using MassLynx, version 4.1 (Waters, Milford, MA). A standard mix at a concentration of 100 μg/g was prepared and injected into the LC−MS/MS system prior to each experiment to check the system sensitivity and reproducibility.

Method Validation. Because of the absence of specific guidelines for the analysis of phytohormones in plant tissue, the Commission Decision 2002/657/EC was used as a guideline for the validation of the extraction and detection method developed for compounds **1**, **2**, and **3**. Appropriate deuterium-labeled internal standards, $^2H_4$-**1**, $^2H_6$-**2**, and $^2H_6$-**3**, were used to correct the data obtained for the extraction of the corresponding phytohormones from rose leaf tissue. Matrix-matched calibration curves making use of these deuterium-labeled internal standards were used for quantitation. The validation parameters considered were specificity, linearity (R^2), matrix effect by signal suppression/enhancement (SSE), apparent recovery (R_A), repeatability through the relative standard deviation (RSD_r), intra-laboratory reproducibility [also through calculation of the relative standard deviation (RSD_R)], and the limits of decision (LOD) and quantitation (LOQ).

RESULTS AND DISCUSSION

Method Development. By infusion of pure standards into the UHPLC mass spectrometer, the analyte-dependent mass spectrometric parameters were optimized for both the precursor ion and product ions (Table 1). The shortest analysis time with good resolution and peak shapes was observed using the Acquity UHPLC BEH C_{18} column. The effect of the column temperature on analyte separation within the range of 25−45 °C was investigated, with the most optimal results obtained at 30 °C. Representative chromatograms for compounds **1**, **2**, and **3** in rose leaves are shown in Figure 2. The retention times of compounds **1**, **2**, and **3** were 4.86, 5.65, and 5.28 min, respectively.

After optimization of the LC−MS/MS conditions, a suitable extraction procedure for the three phytohormones **1**, **2**, and **3** from rose leaves was developed. Although the cleanup of raw extracts can theoretically be kept to a minimum when applying analytical methods as sensitive and specific as UHPLC−MS/MS, the "dilute-and-shoot" principle was not tested in this study. Given the complexity of the plant material considered and the yet to be proven long-term suitability of such methods without cleanup step(s) in terms of minimally polluting the MS equipment, we chose to test a SPE cleanup method. When searching for suitable SPE columns, several factors should be taken into account: the sample matrix, analyte-specific physicochemical properties, and the nature of the bonded phase. Besides enrichment, SPE-based procedures also provide a reduction in sample complexity and help to minimize the matrix effect by SSE. To select an appropriate SPE column capable of retaining the analytes of interest, which are characterized by different hydrophobicities and pK_a values, a screening experiment with five commercially available solid-phase materials was conducted using a standard mixture of the three hormones **1**, **2**, and **3**. In this experiment, Oasis mixed-mode ion-exchange chemistry MAX (strong anion exchanger), WAX (weak anion exchanger), MCX (strong cation exchanger), WCX (weak cation exchanger), and Oasis HLB (universal polymeric reversed-phase sorbent) were evaluated. For the three hormones **1**, **2**, and **3**, the average recovery percentage of three repetitions was determined. This experiment showed that the anion-exchange cartridges MAX and WAX can be used for the purification of compounds **2** and **3** but not for compound **1** because the latter is not retained by the stationary phase (data not shown). In contrast, cation-exchange cartridges MCX and WCX and the generic cartridge HLB retained all three phytohormones examined. Balcke et al.[30] developed a purification method similar to the method presented in this paper. They tested 11 types of SPE devices and found strong cation-exchange solid-phase material to give the best recovery results. Our findings are in agreement with these results and the choice of the MCX cartridge as the best SPE cartridge for the purification of the phytohormones **1**, **2**, and **3** from plant material. The method currently presented offers a more effective extraction protocol when compared to the method by Balcke et al.[30] The amount of leaf material used was reduced to 20 mg and combined with an easier analysis procedure. Furthermore, the method was tested on a woody plant. It is known that interference of secondary metabolites makes woody plants more recalcitrant.

At present, extraction with organic solvents is the most widely used method for plant hormones. Many procedures and solvents have been developed and used for plant hormone extraction.[29,30] The polarity of the extraction solvent is chosen to closely match that of the target compounds; thus, the ratio of organic solvent/water is defined according to the polarity of hormones. Nonpolar solvents, such as ether, are rarely used to extract plant hormones. Instead, methanol is the preferred solvent, allowing for efficient plant cell penetration during extraction.[31,32] Because methanol produced the best recoveries in preliminary experiments (data not shown), experiments were performed using methanol alone[30] and with different proportions of ultrapure water [methanol/water, 75:25;[20] methanol/water/formic acid, 75:20:5;[29] and methanol/water/acetic acid, 10:89:1[33]). The results obtained are summarized in Table 2. The extraction solvent methanol/water/acetic acid (10:89:1) resulted in the highest recovery for compound **1** and a good recovery for compounds **2** and **3**, whereas the other extraction solvents led to a significantly lower recovery of compound **1**. For the optimization of the extraction time, three situations were tested: 1, 2, and 16 h. These data indicated that 1 h of extraction was sufficient for the recovery of compound **3** (100%), but the recovery of compounds **1** and **2** was only 70%. An extraction of 2 h yielded a recovery of 100% for the phytohormones **2** and **3** and 83% for phytohormone **1**. After 16 h of extraction, the recovery of compound **1** was 100%. On the basis of these data and logistical issues, the analyzes were carried out after 16 h of extraction.

Table 2. Percentage of Recovery with Different Solvents and Solvent Combinations Used for Extraction of Salicylic Acid (1), (−)-Jasmonic Acid (2), and (±)-2-*cis*-4-*trans*-Abscisic Acid (3)

	phytohormone (% recovery)		
solvent	1	2	3
100% methanol	29	100	93
75:25% methanol/water	46	72	100
75:20:5% methanol/water/formic acid	42	78	78
10:89:1% methanol/water/acetic acid	100	68	98

Method Validation. *Specificity.* When pure phytohormone standards were injected separately, the obtained UHPLC−MS/MS signals clearly did not interfere with the traces of the other phytohormones, baseline separation of all analytes could be achieved, and no crosstalk between different mass ranges of the MRM experiment was observed.

dx.doi.org/10.1021/jf5023884 | J. Agric. Food Chem. 2014, 62, 6278−6284

Table 3. Overview of the Percentage of Apparent Recovery (R_A), Repeatability by Calculation of the Relative Standard Deviation (RSD_r), and Interday Precision over 3 Days also Calculated as the Relative Standard Deviation (RSD_R) at the Three Concentrations Used for Validation, LOD (μg/g), LOQ (μg/g), and SSE (%) for Salicylic Acid (1), (−)-Jasmonic Acid (2), (±)-2-*cis*-4-*trans*-Abscisic Acid (3)

		low concentration			medium concentration			high concentration					
phytohormone	concentrations (μg/g)	R_A (%)	RSD_r (%)	RSD_R (%)	R_A (%)	RSD_r (%)	RSD_R (%)	R_A (%)	RSD_r (%)	RSD_R (%)	LOD (μg/g)	LOQ (μg/g)	SSE (%)
1[a]	1.25, 5, and 10	109	11	11	103	7	6	100	3	13	0.0089	0.017	+130
2	1.25, 5, and 10	104	3	8	106	3	4	103	4	6	0.00015	0.00030	+202
3	3.75, 15, and 30	105	3	11	103	2	6	100	2	4	0.0075	0.015	+140

[a] n = 4 for first day of validation. For the second and third days, n = 6.

Linearity. Linearity was evaluated by preparing seven-point calibration curves in the matrix for the different phytohormones (in triplicate). The "blank" samples were fortified with concentrations ranging from 0.00 to 60.0 μg/g for compound **3** and from 0.00 to 20.0 μg/g for compounds **1** and **2**. Correlation coefficients (R^2) obtained for these compounds were all >0.99, which indicated good linearity within the considered concentration ranges.

Matrix Effect. SSE is common in LC−ESI−MS/MS because of competition of charge carriers between analytes and co-eluting compounds during the ionization process. Matrix effect (SSE), ionization suppression or enhancement, in liquid chromatography/electrospray ionization mass spectrometry (LC/ESI−MS) is caused by matrix components co-eluting with the analytes. The matrix effect is also highly variable from sample to sample, making it difficult to compensate. To determine possible matrix effects, calibration curves of spiked extracts (i.e., matrix-matched calibration curves) were compared to the corresponding calibration curves of the pure standards. These effects were expressed in terms of SSE and calculated as follows: SSE (%) = 100 × (slope of the matrix-matched standard/slope of the pure standard). The values of SSE shown in Table 3 indicate that all phytohormones considered suffered from signal enhancement (≥100%), with the most profound enhancement observed for compound **2** (202% SSE). The observed SSE emphasized the need to quantitate these analytes by means of matrix-matched calibration curves.

Recovery, Precision, LOD, and LOQ. Table 3 gives an overview of the percentage of apparent recovery (R_A), intraday precision (RSD_r), interday precision over three non-consecutive days (RSD_R), LOD (μg/g), and LOQ (μg/g) for each phytohormone. R_A percentages were within an acceptable range (80−110%). Intralaboratory reproducibility and repeatability were all considered acceptable according to Commission Decision 2002/657/EC ("performance criteria"). For the phytohormones, the LOD and LOQ were theoretically calculated on the basis of calibration curves in the matrix: LOD = 3(seb/slope) and LOQ = 6(seb/slope), with seb being the standard deviation on the intercept of the calibration curve with the y axis and slope being the slope of the calibration curve (Table 3). The LOD and LOQ for compounds **1**, **2**, and **3** were 0.00015 and 0.015 μg/g, 0.0075 and 0.018 μg/g, and 0.0089 and 0.00030 μg/g, respectively. In our method, LOD and LOQ values show that hormones can be analyzed at endogenous concentrations. One can conclude that the values for the LOD and LOQ obtained with the multi-phytohormones method developed in this study were below typical endogenous concentrations.[34]

Analysis of Leaf Samples. In this study, concentrations of compounds **1**, **2**, and **3** measured in leaves were 0.68 ± 0.014, 0.17 ± 0.009, and 0.65 ± 0.032 μg/g, respectively (n = 3). The resulting values agreed with the ranges found in previous studies.

Knowledge of the compound **3** concentration in leaves is of particular interest to understand plant responses to abiotic stresses. Compound **3** is involved in the adaptability toward drought, salinity, cold, and other environmental stresses. A recent study[35] in roses under dark/light conditions and moderate/high humidity indicated compound **3** leaf quantitation levels in rose leaves ranging from ca. 1.00 to ca. 5.00 μg/g using UHPLC−ESI−MS/MS. The data obtained by our method for compound **3** (0.4−0.9 μg/g) showed comparable results to those by Giday et al.,[36] but no data were shown in the latter study on the concentrations of compounds **1** and **2** in rose leaves.

Plant matrix complexity complicates the analysis of phytohormones. Accurate quantitation of amounts of these compounds depends upon a robust method. We have developed a highly specific protocol for simultaneous determination of compounds **1**, **2**, and **3** in rose leaf material. The method is a rapid, sensitive, and accurate way to simultaneously determine the amount of compounds **1**, **2**, and **3** in rose leaves based on SPE purification and UHPLC separation, coupled with MS detection in MRM mode. The procedure described allows for quantitation of endogenous plant hormones in plants, without the need of a derivatization step. The compounds studied are representative of three groups of acidic plant hormones with several important biological properties. This method offers the possibility to incorporate other plant hormones and related metabolites into one single analysis. The simultaneous determination of phytohormones could support scientific efforts in plant functional genomics and hormone signal transduction. Using matrix-matched calibration curves for quantitation, we worked with a woody plant species. We assume that the method is also applicable and improves the analysis of phytohormones proposed earlier[30] in other plant material (e.g., tomato, rice, etc.) as well.

AUTHOR INFORMATION

Corresponding Author

*Telephone: +32-9-272-28-84. Fax: +32-9-272-29-01. E-mail: leen.leus@ilvo.vlaanderen.be.

Notes

The authors declare no competing financial interest.

■ ACKNOWLEDGMENTS

The authors are grateful to Marijke Hunninck and to all of the staff of ILVO for their excellent technical assistance.

■ ABBREVIATIONS USED

MRM, multiple reaction monitoring; SPE, solid-phase extraction; SSE, signal suppression/enhancement

■ REFERENCES

(1) Vogler, H.; Kuhlemeier, C. Simple hormones but complex signaling. *Curr. Opin. Plant Biol.* **2003**, *6*, 51−56.
(2) Yu, B.; Fuyou, D.; Huwei, L. Determination strategies of phytohormones: Recent advances. *Anal. Meth.* **2010**, *2*, 1867−1873.
(3) Kumar, A. R.; Sivakumar, D. Role of hormones on seed germination—A review. *Agric. Rev.* **2008**, *29*, 281−289.
(4) Glazebrook, J. Contrasting mechanisms of defense against biotrophic and necrotrophic pathogens. *Annu. Rev. Phytopathol.* **2005**, *43*, 205−227.
(5) Robert-Seilaniantz, A.; Navarro, L.; Bari, R.; Jones, J. D. G. Pathological hormone imbalances. *Curr. Opin. Plant Biol.* **2007**, *10*, 372−379.
(6) Loake, G.; Grant, M. Salicylic acid in plant defence the players and protagonists. *Curr. Opin. Plant Biol.* **2007**, *10*, 466−472.
(7) Mur, L. A.; Kenton, P.; Atzorn, R.; Miersch, O.; Wasternack, C. The outcomes of concentration-specific interactions between salicylate and jasmonate signaling include synergy, antagonism, and oxidative stress leading to cell death. *Plant Physiol.* **2006**, *140*, 249−262.
(8) Forcat, S.; Bennett, M. H.; Mansfield, J. W.; Grant, M. R. A rapid and robust method for simultaneously measuring changes in the phytohormones ABA, JA and SA in plants following biotic and abiotic stress. *Plant Meth.* **2008**, *4*, 16−23.
(9) Buell, C. R.; Joardar, V.; Lindeberg, M.; Selengut, J.; Paulsen, I. T.; Gwinn, M. L.; Dodson, R. J.; Deboy, R. T.; Durkin, A. S.; Kolonay, J. F.; Madupu, R.; Daugherty, S.; Brinkac, L.; Beanan, M. J.; Haft, D. H.; Nelson, W. C.; Davidsen, T.; Zafar, N.; Zhou, L.; Liu, J.; Yuan, Q.; Khouri, H.; Fedorova, N.; Tran, B.; Russell, D.; Berry, K.; Utterback, T.; Van Aken, S. E.; Feldblyum, T. V.; D'Ascenzo, M.; Deng, W. L.; Ramos, A. R.; Alfano, J. R.; Cartinhour, S.; Chatterjee, A. K.; Delaney, T. P.; Lazarowitz, S. G.; Martin, G. B.; Schneider, D. J.; Tang, X.; Bender, C. L.; White, O.; Fraser, C. M.; Collmer, A. The complete genome sequence of the *Arabidopsis* and tomato pathogen *Pseudomonas syringae* pv. tomato DC3000. *Proc. Natl. Acad. Sci. U. S. A.* **2003**, *100*, 10181−10186.
(10) DebRoy, S.; Thilmony, R.; Kwack, Y. B.; Nomura, K.; He, S. Y. A family of conserved bacterial effectors inhibits salicylic acid-mediated basal immunity and promotes disease necrosis in plants. *Proc. Natl. Acad. Sci. U. S. A.* **2004**, *101*, 9927−9932.
(11) Nomura, K.; Melotto, M.; He, S. Y. Suppression of host defense incompatible plant—*Pseudomonas syringae* interactions. *Curr. Opin. Plant Biol.* **2005**, *8*, 361−368.
(12) Nishimura, N.; Yoshida, T.; Kitahata, N.; Asami, T.; Shinozaki, K.; Hirayama, T. Hypersensitive Germination1 encodes a protein phosphatase 2C, an essential component of abscisic acid signaling in *Arabidopsis* seed. *Plant J.* **2007**, *50*, 935−949.
(13) Adie, B. A.; Perez-Perez, J.; Perez-Perez, M. M.; Godoy, M.; Sanchez-Serrano, J. J.; Schmelz, E. A.; Solano, R. ABA is an essential signal for plant resistance to pathogens affecting JA biosynthesis and the activation of defenses in *Arabidopsis*. *Plant Cell* **2007**, *19*, 1665−1681.
(14) de Torres-Zabala, M.; Truman, W.; Bennett, M. H.; Lafforgue, G.; Mansfield, J. W.; Rodriguez Egea, P.; Bogre, L.; Grant, M. *Pseudomonas syringae* pv. tomato hijacks the *Arabidopsis* abscisic acid signalling pathway to cause disease. *EMBO J.* **2007**, *26*, 1434−1443.
(15) Hernandez-Blanco, C.; Feng, D. X.; Hu, J.; Sanchez-Vallet, A.; Deslandes, L.; Llorente, F.; Berrocal-Lobo, M.; Keller, H.; Barlet, X.; Sanchez-Rodriguez, C.; Anderson, L. K.; Somerville, S.; Marco, Y.; Molina, A. Impairment of cellulose synthases required for *Arabidopsis* secondary cell wall formation enhances disease resistance. *Plant Cell* **2007**, *19*, 890−903.
(16) Mohr, P. G.; Cahill, D. M. Suppression by ABA of salicylic acid and lignin accumulation and the expression of multiple genes, in *Arabidopsis* infected with *Pseudomonas syringae* pv. tomato. *Funct. Integr. Genomics* **2007**, *7*, 181−191.
(17) Anderson, J. P.; Badruzsaufari, E.; Schenk, P. M.; Manners, J. M.; Desmond, O. J.; Ehlert, C.; Maclean, D. J.; Ebert, P. R.; Kazan, K. Antagonistic interaction between abscisic acid and jasmonate−ethylene signaling pathways modulates defense gene expression and disease resistance in *Arabidopsis*. *Plant Cell* **2004**, *16*, 3460−3479.
(18) Fujita, M.; Fujita, Y.; Noutoshi, Y.; Takahashi, F.; Narusaka, Y.; Yamaguchi-Shinozaki, K.; Shinozaki, K. Crosstalk between abiotic and biotic stress responses: A current view from the points of convergence in the stress signaling networks. *Curr. Opin. Plant Biol.* **2006**, *9*, 436−442.
(19) Mueller, M. J.; Mène-Saffrané, L.; Grun, C.; Karg, K.; Farmer, E. E. Oxylipin analysis methods. *Plant J.* **2006**, *45*, 472−489.
(20) Bosco, R.; Caser, M.; Vanara, F.; Scariot, V. Development of a rapid LC−DAD/FLD method for the simultaneous determination of auxins and abscisic acid in plant extracts. *J. Agric. Food Chem.* **2013**, *61*, 10940−10947.
(21) Chehab, E. W.; Kaspi, R.; Savchenko, T.; Rowe, H.; Negre-Zakharov, F.; Kliebenstein, D. Distinct roles of jasmonates and aldehydes in plant-defense responses. *PLoS One* **2008**, *3*, No. e1904.
(22) Taylor, P. J. Matrix effects: The Achilles heel of quantitative high-performance liquid chromatography−electrospray−tandem mass spectrometry. *Clin. Biochem.* **2005**, *38*, 328−334.
(23) Glauser, G.; Grata, E.; Dubugnon, L.; Rudaz, S.; Farmer, E. E.; Wolfender, J. L. Spatial and temporal dynamics of jasmonate synthesis and accumulation in *Arabidopsis* in response to wounding. *J. Biol. Chem.* **2008**, *283*, 16400−16407.
(24) Tamogami, S.; Kodama, O. Quantification of amino acid conjugates of jasmonic acid in rice leaves by high-performance liquid chromatography−turboionspray tandem mass spectrometry. *J. Chromatogr. A* **1998**, *822*, 310−315.
(25) Ma, Z.; Ge, L.; Lee, A. S. Y.; Yong, J. W. H.; Tan, S. N.; Ong, E. S. Simultaneous analysis of different classes of phytohormones in coconut (*Cocos nucifera* L.) water using high-performance liquid chromatography and liquid chromatography−tandem mass spectrometry after solid-phase extraction. *Anal. Chim. Acta* **2008**, *610*, 274−281.
(26) Flores, M. I.; Romero-Gonzalez, R.; Frenich, A. G.; Vidal, J. L. QuEChERS-based extraction procedure for multifamily analysis of phytohormones in vegetables by UHPLC−MS/MS. *J. Sep. Sci.* **2011**, *34*, 1517−1524.
(27) Fan, S.; Wang, X.; Li, P.; Zhang, Q.; Zhang, W. Simultaneous determination of 13 phytohormones in oilseed rape tissues by liquid chromatography−electrospray tandem mass spectrometry and the evaluation of the matrix effect. *J. Sep. Sci.* **2011**, *34*, 640−650.
(28) European Union. Commission Decision 2002/657/EC Implementing Council Directive 96/23/EC 533 concerning the performance of analytical methods and the interpretation of results. 534. *Off. J. Eur. Communities: Legis.* **2002**, *L221*, 8−36.
(29) Van Meulebroek, L.; Vanden Bussche, J.; Steppe, K.; Vanhaecke, L. Ultra-high performance liquid chromatography coupled to high resolution Orbitrap mass spectrometry for metabolomic profiling of the endogenous phytohormonal status of the tomato plant. *J. Chromatogr. A* **2012**, *1260*, 67−80.
(30) Balcke, G. U.; Handrick, V.; Bergau, N.; Fichtner, M.; Stellmach, A. H. H.; Tissier, A. B.; Frolov, A. An UPLC−MS/MS method for highly sensitive high-throughput analysis of phytohormones in plant tissues. *Plant Methods* **2012**, *8*, 47.
(31) Rozhon, W.; Petutschnig, E.; Wrzaczek, M.; Jonak, C. Quantification of free and total salicylic acid in plants by solid-phase extraction and isocratic high-performance anion-exchange chromatography. *Anal. Bioanal. Chem.* **2005**, *382*, 1620−1627.
(32) Eshita, S. M. 3-Hydroxybenzoic acid as an internal standard for the high-pressure liquid chromatography quantitation of salicylic acid in plants. *Anal. Biochem.* **2001**, *289*, 99−102.

(33) Forcat, S.; Bennett, M. H.; Mansfield, J. W.; Grant, M. R. A rapid and robust method for simultaneously measuring changes in the phytohormones ABA, JA and SA in plants following biotic and abiotic stress. *Plant Methods* **2008**, *4*, 16.
(34) Van Pamel, E.; Verbeken, A.; Vlaemynck, G.; De Boever, J.; Daeseleire, E. Ultrahigh-performance liquid chromatographic−tandem mass spectrometric multimycotoxin method for quantitating 26 mycotoxins in maize silage. *J. Agric. Food Chem.* **2011**, *59*, 9747−9755.
(35) Arve, L. E.; Terfa, M. T.; Gislerod, H. R.; Olsen, J. E.; Torre, S. High relative air humidity and continuous light reduce stomata functionality by affecting the ABA regulation in rose leaves. *Plant, Cell Environ.* **2013**, *36*, 382−392.
(36) Giday, H.; Fanourakis, D.; Fomsgaard, I. S.; K, H. K; Ottosen, C. O. Foliar abscisic acid content underlies genotypic variation in stomatal responsiveness after growth at high relative air humidity. *Ann. Bot.* **2013**, *10*, 1093−1104.

(renal inflammation, tissue necrosis, and renal apoptosis).[10] In addition, the International Agency for Research on Cancer (IARC) has now classified nanosized TiO_2 as a potential carcinogen on the basis of the rate of incidence of respiratory tract cancer in rats after prolonged inhalation of TiO_2 dust particles.[11] This indicates the need to evaluate the possible carcinogenicity of nanosized TiO_2 following other exposure routes.

A Monte Carlo human exposure analysis indicated that U.S. adults are exposed to about 1 mg Ti/kg bw per day.[8] These authors indicate that in the assessed food and consumer products approximately 36% of the TiO_2 particles were <100 nm in one dimension. Although TiO_2 has been authorized as a food additive,[7] no recent risk assessment is available. In general, the risk assessment of oral exposure to nanoparticles is difficult because of a number of uncertainties and a general lack of data.[12] Specifically for TiO_2, knowledge about the particle sizes and size distribution of TiO_2 particles in E171, let alone food and consumer products containing E171, is limited. The European Commission adopted a recommendation for the definition of nanomaterials, Commission Recommendation 2011/696/EU, stating that a material is a nanomaterial if 50% or more of the particles in a number-based size distribution have one or more external dimension in the size range of 1−100 nm. In specific cases the number-based size distribution threshold of 50% may be replaced by a threshold between 1 and 50%.[13] Currently the recommendation is under review; the discussion is focused on the percentage of the number-based size distribution below the 100 nm to classify a material as nanomaterial. Yet no internationally agreed upon method to determine the number-based size distribution has been proposed. Therefore, we used a combination of analytical methods as suggested by Linsinger.[14]

In this study we aimed to provide more information on the number-based size distribution of food grade TiO_2 ingredients and their occurrence in consumer products because this is required to increase the reliability of the human food exposure studies as part of the risk assessment. We used a combination of methods for this: asymmetric flow field-flow fractionation online with inductively coupled plasma mass spectrometry (AF4-ICP-MS) and two methods that provide number-based size distributions, scanning electron microscopy (SEM) and single-particle ICP-MS (sp-ICP-MS). Comparable size distributions were found, indicating that these methods can reliably be used to enforce food labeling in line with the recommendation of the EU definition of nanomaterials.

EXPERIMENTAL PROCEDURES

Samples. In this study three types of samples were involved: first, several types of TiO_2 food additive E171; second, food products such as cakes, candy, and chewing gum; and last, personal care products such as toothpaste. In total seven E171 materials, all food grades and four labeled as E171, were received from suppliers in China, Germany, Italy, The Netherlands, and the United Kingdom and consisted of fine white powders. In total 24 food products and 3 personal care products were investigated. All of these products were purchased in 2012 from regular shops in The Netherlands. Because food labeling for titanium dioxide may be imprecise, 20 products that listed "E171", "TiO_2", or "titanium dioxide" on the package were selected, as well as 7 products without this labeling but with a typical white color. Samples were stored in a clean, dry, and dark location and analyzed before the expiration data.

Determination of Total Titanium Content. For the determination of the total titanium content of the TiO_2 materials, a suspension of these materials was prepared according to the method of Jensen.[15] In short, ca. 15 mg of bovine serum albumin (BSA) is dissolved and diluted in Milli-Q water to reach a final concentration of 10 mg/mL. This solution is filtered over a 0.2 μm pore size filter and diluted 20-fold with Milli-Q water to a final concentration of 0.5 mg/mL BSA. An accurately weighed sample of ca. 15 mg of finely powdered TiO_2 material is brought into a 30 mL vial. Then 30 μL of 96% ethanol is added and distributed equally over the TiO_2 material followed by 970 μL of the 0.5 mg/mL BSA solution. The mixture is shaken manually, another 5 mL of the 0.5 mg/mL BSA solution is added, and the final suspension is shaken manually to obtain a homogeneous suspension. While the sample vial is cooled in ice water, the suspension is sonicated with a Misonix XL-2000 sonicator with a CML-4 needle probe for 16 min at 22.5 kHz and 4 W power. The final suspension is used as such or after further dilution to the desired concentration with the 0.5 mg/mL BSA solution. Suspensions prepared in this way showed to be stable for at least 3 days. From each suspension a subsample was collected in a perfluoroalkoxy (PFA) digestion vial to which 8 mL of nitric acid (70% HNO_3) and 2 mL of hydrogen fluoride (50% HF) were added. For the determination of the total titanium content of the food and personal care products, the whole sample was cut into small pieces and ground, and a representative subsample was used for analysis. An analytical sample of ca. 0.5 g was collected from each sample and brought into a PFA digestion vial to which 6 mL of nitric acid (70% HNO_3), 2 mL of hydrofluoric acid (50% HF), and 2 mL of hydrogen peroxide (30% H_2O_2) were added. All samples were digested in a MARS microwave system for 50 min. The temperature program was as follows: at 1200 W power from 20 to 150 °C in 15 min, then to 180 °C in 15 min, and finally constant at 180 °C for 20 min. Following digestion and cooling to room temperature, Milli-Q water was added to a total volume of 50 mL. The extracts were shaken manually, diluted to 100 mL, and analyzed with a Thermo X series-2 ICP-MS equipped with an autosampler and a conical glass concentric nebulizer and operated at an RF power of 1400 W. Data acquisition was performed in the selected ion monitoring mode at m/z ratios of 48 and 49 that are characteristic for titanium. Quantification was based on ionic titanium standard diluted in the same acidic matrix. The recovery of the total Ti method was determined by spiking three products of different matrices in triplicate with known amounts of a TiO_2 reference material, NM-103.

Determination of the Size Distribution in TiO_2 Materials Using Electron Microscopy. To determine the size distribution of the titanium oxide nanoparticles in the TiO_2 materials, suspensions of these materials were studied using electron microscopy. TiO_2 suspensions (2.5 mg/mL) were filtered over an Anopore aluminum oxide filter with a pore size of 20 nm. The filters were mounted on aluminum specimen holders with double-sided adhesive carbon tape and were coated with a 5 nm layer of chromium using an Emitech K575X turbo sputter coater. The filters were analyzed with a high-resolution field emission gun scanning electron microscopy in combination with X-ray analysis (FEG-SEM/EDX). The microscope is a Tescan MIRA-LMH FEG-SEM at an accelerating voltage of 15 kV, working distance of 10 mm, spot size of 5 nm. The EDX spectrometer is a Bruker AXS spectrometer with a Quantax 800 workstation and an XFlash 4010 detector. The SEM is equipped with the Scandium SIS software package (Olympus Soft Imaging Solutions, Germany) for automated particle analysis. With this system the filter area is automatically inspected on a field-by-field basis. In each field of view particles are recognized using a preselected grayscale video threshold (detection threshold level) to discriminate between particles and filter background. The analysis is conducted using the backscattered electron (BE) mode. From each particle/cluster of particles the projected area equivalent diameter (dpa) is measured. Magnifications were chosen so that their measurable size ranges overlap slightly and cover the particle sizes of interest. To measure dpa values from 25 to 1600 nm, three magnifications of 10000×, 25000×, and 75000× were selected. These three magnifications cover eight size bins: 25−40, 40−65, 65−100, 100−160, 160−250, 250−400, 400−650, 650−1000, and 1000−1600 nm. Per size bin a minimum of 10 particles were measured, and in total approximately 1000 particles were measured

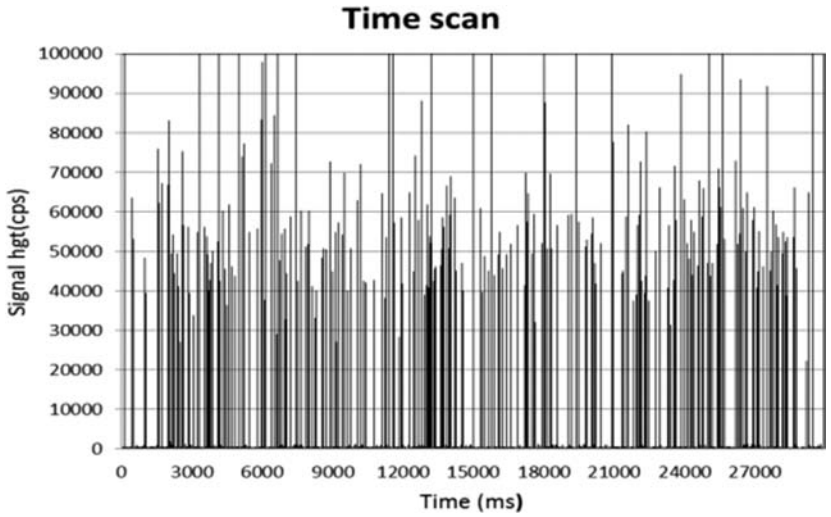

Figure 1. Single-particle ICPMS time scan of a diluted sample extract. Each peak represents one particle. The number of peaks is proportional to the particle concentration in the sample, whereas the peak height is proportional to the particle's diameter to the third power.

per sample. To ensure that there is no overlap of particles, the total loading of the filter with particles was always <10%. Per size bin the mean diameter and the 95% confidence interval are calculated on the basis of the Poisson distribution.

Quantification and Size Determination of TiO_2 Particles Using AF4-ICP-MS. For quantification and size determination of particulate TiO_2 in TiO_2 materials, a suspension of these materials was prepared as described before. For quantification and size determination of particulate TiO_2 in food and personal care products a representative subsample was prepared, and 0.5 g of this sample was brought into a 50 mL glass beaker together with 20 mL of hydrogen peroxide (30% H_2O_2). The content of the beaker was heated to about 100 °C and kept just below the boiling point of the H_2O_2 matrix. When most of the organic matrix is consumed, the content is evaporated until a residue of about 1 mL remains. The content is allowed to cool to room temperature and is diluted to 10 mL with the 0.5 mg/mL BSA solution. Prepared suspensions and extracts are analyzed with asymmetric flow field-flow fractionation (AF4) online coupled with ICP-MS. The AF4 consisted of a metal-free Wyatt Eclipse Dualtec separation system equipped with a 153 × 22 mm flow cell containing a Nadir regenerated cellulose separation membrane with a 10 kDa molecular weight cutoff and a spacer of 350 μm. The AF4 system was further coupled to an Agilent 1100 system with an autoinjector and a binary pump for eluent flow delivery and degassing. Prior to injection, samples were thoroughly mixed to ensure homogeneous distribution of suspended particles. The injection volume was 10 μL, and a 7 min focusing time was used. A constant cross-flow of 0.1 mL/min was applied, and the flow rate to the detector was kept at 0.5 mL/min. After 57 min, the cross-flow was reduced to 0 mL/min within 5 min and kept at 0 mL/min for 5 min to remove any residual particles from the separation channel. The outlet flow of the AF4 system passed through a UV detector and was directly coupled with the ICP-MS system for the selective determination of titanium. The ICP-MS system and settings were as described before. Because no well-characterized titanium oxide particles were available for calibration purposes, particle size calculation was based on FFF theory using the Boltzmann constant, the column temperature, the eluent viscosity, and the instrumental settings.[16,17] In short, the AF4 separation channel consists of an impermeable top block and a bottom block holding a semipermeable ultrafiltration membrane on top of a porous frit. The perpendicular field is caused by restricting the channel flow at the outlet. This restriction will force part of the carrier liquid to leave the channel through the bottom block, thus causing the cross-flow. Prior to elution, the analyte is concentrated at a position close to the injection port during a focusing step. Particle equilibrium heights above the membrane in AF4 depend on the diffusion coefficient of the particles and the applied cross-flow rate with larger particles being driven closer to the membrane. Retention times are dependent on the equilibrium height at which the particles travel in the parabolic flow profile of the channel flow and are expressed by

$$t_r = \frac{\pi \eta d \omega^2}{2kT} \times \frac{V_{cross}}{V_{channel}} \quad (1)$$

where t_r is the retention time of the analyte, η the viscosity of the eluent, d the hydrodynamic diameter of the particle, ω the channel thickness, k the Boltzmann constant, T the absolute temperature, V_{cross} the cross-flow rate, and $V_{channel}$ the channel flow rate. With this equation the particle's hydrodynamic diameter can be calculated directly from its retention time. This relationship was confirmed by calibration with polystyrene particles. Mass calibration of the ICP-MS was performed with one of the TiO_2 materials for which it was established that the TiO_2 content of this material was close to 100%.

Transformation of Mass-Based to Number-Based Size Distributions. The signal measured by ICP-MS in standard mode is a mass-based signal, and the size distribution determined with AF4-ICP-MS is thus also a mass-based distribution. The conversion of a mass- to a particle number-based distribution is carried out by placing the detected mass in size bins and calculating the number of particles as

$$N = \frac{M}{\rho \frac{4}{3}\pi (r \times 10^{-7})^3 \times 10^9} \quad (2)$$

where N is the number of particles, M is the mass detected in a certain particle size bin in ng, ρ is the density of the particle material in g/cm^3 (4.23 g/cm^3 was used for TiO_2), and r is the radius of the particle in that size bin in nm. The numbers are conversion factors to get the units right.

Size Determination of TiO_2 Particles Using Single-Particle ICP-MS. Single-particle ICP-MS is a relatively new approach for the detection and characterization of nanoparticles, and the principle has been described previously.[18−21] The ICP-MS instrument and settings used were as described before, only in this case data acquisition was done in the time-resolved analysis (TRA) mode. The dwell time was set at 3 ms with a typical acquisition time of 60 s per measurement. Because of the short dwell time, it is not possible to switch between different isotopes (switching itself takes ∼50 ms), and therefore only one titanium isotope, m/z 48, is monitored during measurement. Note that polyatomic interferences are possible, for example, $^{32}S^{16}O$ and $^{36}Ar^{12}C$, and also isobaric interference by ^{48}Ca. However, these interferences result in a continuous background, whereas TiO_2 particles will result in discontinuous signals (peaks) and can thus be distinguished from the background. Because only a part of the

dx.doi.org/10.1021/jf5011885 | J. Agric. Food Chem. 2014, 62, 6285−6293

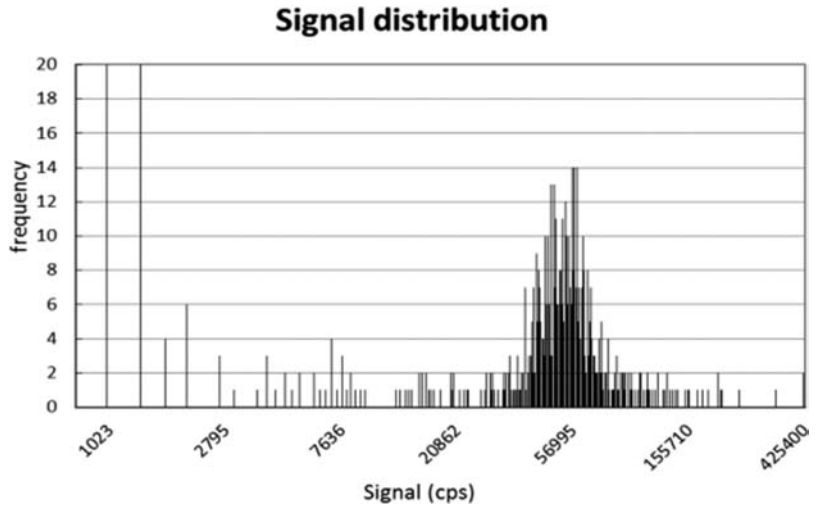

Figure 2. Signal distribution graph plotting the frequency of the ICP-MS response in data points as a function of the ICP-MS response. ICP-MS responses to the left of the minimum depict background and ions, those to the right the minimum particles.

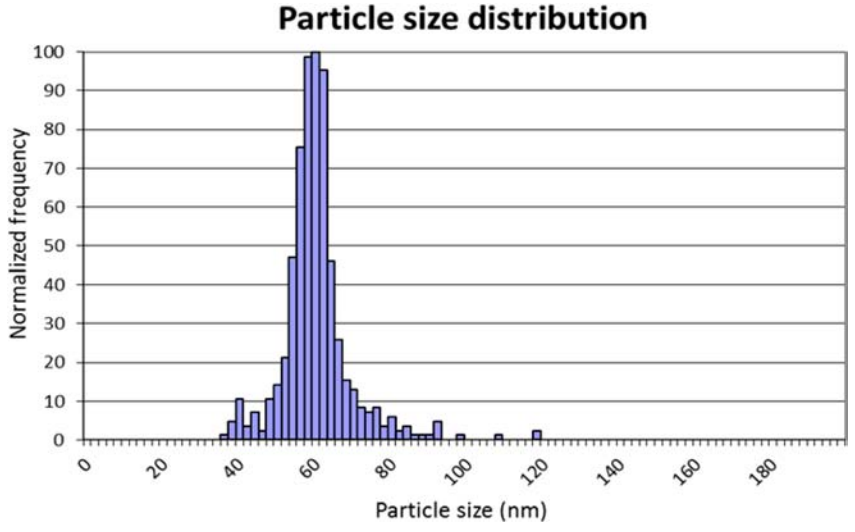

Figure 3. Typical example of a particle size distribution as produced by single-particle ICP-MS analysis.

nebulized droplets reaches the plasma, the nebulization efficiency needs to be known to determine the actual particle number concentration in the extract. The nebulization efficiency is determined by the analyses of a NIST material, SRM8013, a suspension of 60 nm gold nanoparticles in a citrate buffer, under the same instrumental conditions as the samples but monitoring m/z 197 for gold. The nebulization efficiency is calculated from the observed number of particles in the time scan and the particle flux into the ICP-MS system using eq 3. Single-particle data are transferred to and processed in Microsoft Excel for the calculation of particle sizes, particle size distributions, and particle concentrations. Acquiring data for 60 s at a dwell time of 3 ms results in 20000 data points consisting of background signals and signals with a much higher intensity originating from particles (Figure 1). These particle signals are isolated from the background by plotting a signal distribution, that is, the frequency with which a signal height occurs as a function of that signal height. This allows the determination of a cutoff point to separate particle signals from the background (Figure 2). From the number of the particle signals in the time scan and the nebulization efficiency determined previously with the gold nanoparticles, the particle number concentration in the diluted sample suspension is calculated as

$$C_p = \frac{N_p}{\eta_n} \times \frac{1000}{V} \quad (3)$$

where C_p = particle number concentration (L^{-1}), N_p = number of particles detected in the time scan (min^{-1}), η_n = nebulization efficiency, and V = sample input flow (mL/min). The same formula is used to calculate the nebulization efficiency after measurement of the 50 ng/L 60 nm gold nanoparticle suspension. In that case the particle number concentration C_p is known (50 ng/L of a 60 nm gold particle results in 2×10^7 particles/L) and the nebulization efficiency is calculated from the observed number of particles N_p in the time scan. From the intensity of the particle signals and the response factor calculated from a series of ionic titanium calibration standards that are analyzed under the same conditions, the mass of the individual particles is calculated as

$$m_p = \frac{I_p t_d}{RF_{ion}} \times \frac{V\eta_n}{60} \quad (4)$$

where m_p = particle mass (ng), I_p = particle signal intensity in the sample (cps), RF_{ion} = ICP-MS response factor from the calibration curve of the ionic titanium standards (cps/μg/L), t_d = dwell time (s), and V = sample flow (mL/min). To calculate the particle mass concentration in the diluted sample suspension, the masses of all

dx.doi.org/10.1021/jf5011885 | J. Agric. Food Chem. 2014, 62, 6285−6293

individual particles are summed and corrected for nebulization efficiency and sample flow:

$$C_m = \frac{\sum m_p}{\eta_n \times V \times 1000} \quad (5)$$

In eq 5 C_m = particle mass concentration (ng/L). Finally, the particle size, expressed as the particle's diameter (and assuming a spherical particle shape), is calculated for each particle as

$$d_p = \sqrt[3]{\frac{6m_p}{\pi\rho_p}} \times 10^4 \quad (6)$$

where d_p = particle diameter in the sample (nm) and ρ_p = particle density (g/mL). The individual particle sizes can be used to produce a size distribution graph (Figure 3). For all of these calculations a template in Microsoft Excel was produced and used throughout.

RESULTS AND DISCUSSION

We compared the size distributions of TiO_2 particles as determined with three different analytical approaches in three types of samples. First we characterized TiO_2 powders that, according to the manufacturers, are E171 food additives; second, we characterized food products (cakes, candy, and chewing gum); and, finally, personal care products (toothpaste) were examined.

Titanium Content and Particle Size Determination of TiO_2 Materials. *Total Titanium Content of TiO_2 Materials.* The total TiO_2 content of the E171 materials was determined as total titanium using HNO_3/HF digestion and ICP-MS analysis of the extracts followed by recalculation of results to titanium dioxide. The results show that the total TiO_2 content is in the range of 90−99% for five of the seven E171 materials and is 74 and 83% for the other two materials. Taking into account the measurement uncertainty of the total-Ti method (±6%) and the fact that these materials may contain some water, five of the seven E171 materials consist of pure TiO_2. It is known that some TiO_2 materials are coated with aluminum and silicon oxides or polymers to increase photostability and prevent aggregation.[22,23] Only the packaging of one of the two samples with a lower TiO_2 content declares that the material may contain aluminum hydroxide, amorphous silica, aluminum phosphate, and water. No further information about the chemical composition of these two TiO_2 materials was available.

Size Distributions of TiO_2 Materials Determined with SEM. The size distribution of the particles in the TiO_2 materials was determined by SEM. For this the materials were suspended in water and stabilized by BSA.[15] Representative SEM images of the TiO_2 materials are shown in Figure 4. The images on the left side in Figure 4 give a good picture of the large agglomerates that are encountered in the samples, whereas the images on the right side allow the estimation of the primary particle sizes. Detected particles were automatically counted using image analyses software and divided into size bins of 25−40, 40−65, 65−100, 100−160, 160−250, 250−400, 400−650, 650−1000, and 1000−1600 nm. The number percentage of the particles in each bin is then plotted against the mean particle size of the size bin to produce a number-based size distribution (Figure 4). In general, the size distributions of the seven TiO_2 materials are very alike and range from 30 to 600 nm, with the apex in all size distributions between 200 and 400 nm. About 10% of the particles have dimensions below 100 nm. The actual percentage of particles with at least one dimension <100 nm will be higher because the image analysis software determines an area equivalent diameter (diameter projected area; dpa) for the particles. As a consequence, particles with an aspect ratio different from 1 will be "averaged" into round particles, leading to an underestimation of the number of particles with one dimension <100 nm. From the image analysis it appears that for >80% of the particles, large and small, the aspect ratio is in the range of 0.8−1.2. As a consequence, it is expected that the underestimation of the number of particles with one dimension <100 nm is limited to 10−20%. That all materials appear to be more or less identical probably reflects the production process of this material. The most common production method for TiO_2 particles is the chloride process or the sulfate process.[24] In industrialized countries chloride processes appear to be favored over sulfate processes for environmental, economic, and qualitative reasons.[25] Therefore, there is a reasonable chance that all investigated TiO_2 materials are produced by the same process.

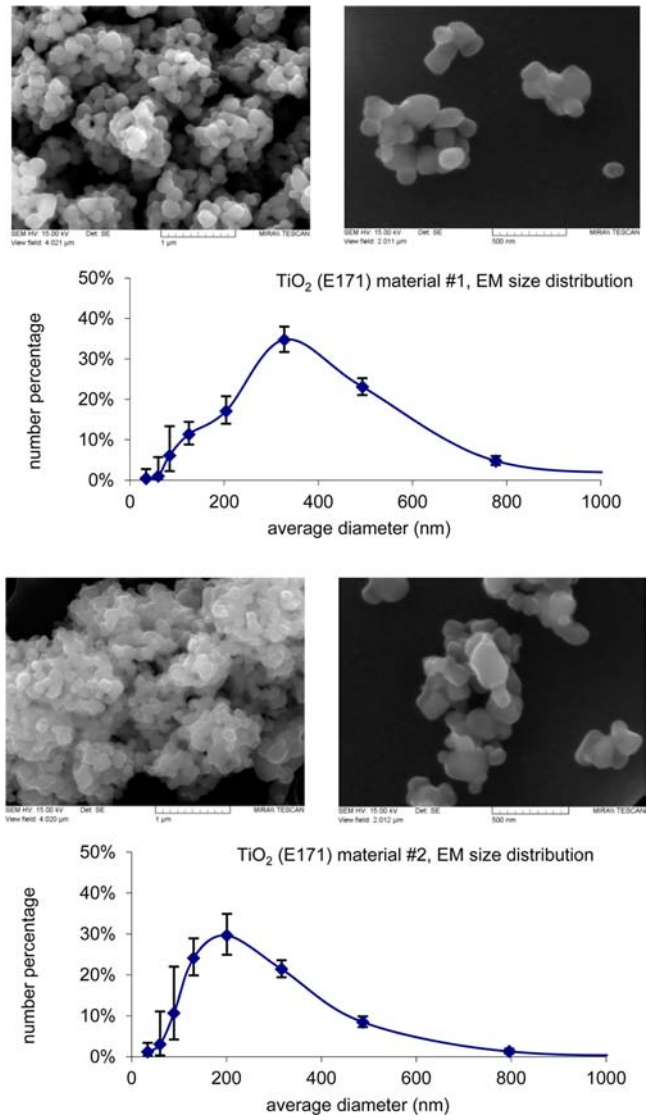

Figure 4. Representative SEM images of TiO_2 materials. The image on the left shows the agglomerates, whereas the image on the right shows the individual particles. The number-based size distributions produced by image analysis of the SEM images are shown below the SEM images (the error bars indicate the 95% confidence intervals of the number percentage in each particular size bin).

dx.doi.org/10.1021/jf5011885 | J. Agric. Food Chem. 2014, 62, 6285−6293

The smallest size bin used in our measurements was 25−40 nm. Particles in that size range could still be detected, identified, and counted by the image analysis software. TiO_2 particles <20 nm cannot be reliably identified and counted by the image analysis software. Manually, the operator can detect TiO_2 particles with diameters down to 10−20 nm in clean suspensions. However, manually detecting small particles is not a reasonable option because many fields have to be viewed to produce a reliable particle number. Thus, our measurements show that the lower size limit of detection for routine SEM analysis is around 20 nm for TiO_2 particles.

Size Distributions of TiO_2 Materials Determined with AF4-ICP-MS. Strictly speaking, AF4 is a separation technique and is not able to determine size, or a number-based size distribution. As there are no well-characterized TiO_2 particles of different sizes (i.e., reference materials for size calibration), we used a theoretical approach based on the well-established theory of flow field-flow fractionation for size calibration as explained under Experimental Procedures.

The result of the AF4-ICP-MS analysis is a chromatogram in which the signal height is a measure for the mass of titanium detected at a certain retention time. Following mass calibration this signal height is expressed as the mass of Ti or TiO_2, and with the time scale recalculated as a particle size scale based on an equation from flow field-flow fractionation theory described under Experimental Procedures, this results in a mass-based size distribution. However, to apply the EU definition for nanomaterials this mass-based distribution has to be transformed into a number-based distribution. Therefore, this mass-based size distribution is transformed into a number-based size distribution using the equation under Experimental Procedures and assuming that particles have a spherical shape. However, if the mass is converted into a number of particles, this number depends on particle size. If the mass remains constant, as shown in Figure 5, the number of particles increases strongly when

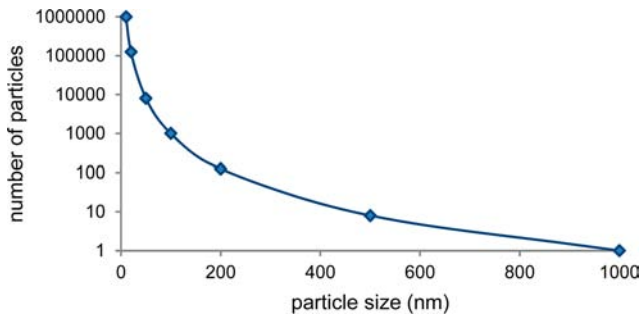

Figure 5. When the mass remains constant, the number of particles rapidly increases, especially at smaller particle sizes.

going to smaller particle (notice that the *y*-scale is a log scale), especially at small particle sizes, because particle size and mass are related by d^3 (see eq 6 under Experimental Procedures). This means that mass to number transformations have large conversion factors for small particles that easily lead to erroneous results. In practice, the beginning of chromatograms tends show small spikes, noise, nonparticle peaks or small electrical offsets. If these phenomena are also transformed from mass- to number-based, small particle sizes will completely and erroneously dominate the number-based distribution, resulting in a dramatic shift of the size distribution to smaller particle sizes. From the chromatograms in this study it was concluded that the smallest TiO_2 particle size that can be determined and reliably transformed from mass- to number-based distributions is around 20 nm.

Comparing the Measured Size Distributions of TiO_2 Materials. Conversion of the retention time into particle size and the mass-based distribution into a number-based distribution allows us to derive number-based size distributions for the TiO_2 materials. The AF4 size distribution of the materials for which the EM size distribution is shown in Figure 4 is shown in Figure 6. In general, the number-based size

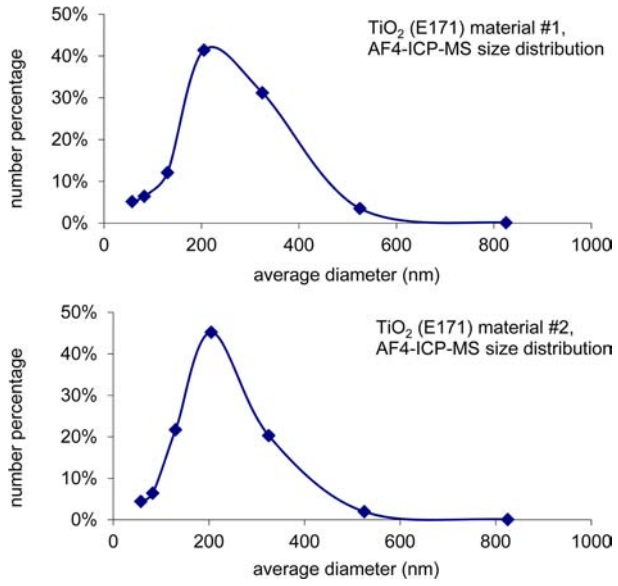

Figure 6. Number-based size distribution of two TiO_2 materials as determined with AF4-ICP-MS and after recalculation from mass-based to number-based.

distribution as determined by EM and AF4 shows two types of differences. First, the apex of the size distributions originating from AF4 generally is between 200 and 300 nm, whereas in EM size distributions it is between 200 and 400 nm. Second, the EM size distributions contain larger particles (diameter > 600 nm) than the AF4 size distributions. In AF4 large particles (diameter > 400 nm) may actually drop on, and roll over, the membrane surface at velocities that are higher than normal elution.[26] As a result these large particles elute at shorter retention times, thereby simulating smaller sized particles. In the number-based size distribution this will become visible as a shift to smaller particle sizes. As before, the percentage of particles with a size <100 nm is determined. In the AF4 analysis this ranges from 10 to 15% with an average of 12%. This is comparable with the 10% of particles with sizes below 100 nm that were found in the EM analyses.

Titanium Content and Size Distributions in Food and Personal Care Products. In addition to the TiO_2 materials, food and personal care products were also analyzed for total titanium content and with AF4-ICP-MS for titanium content as well as size distribution. An attempt was made to determine the size distribution of the TiO_2 particles in the extracts of these products with SEM. However, matrix constituents that were still present made it impossible to make a proper image analysis of the particle sizes. As an alternative, the extracts were analyzed using single-particle ICP-MS (sp-ICPMS) because this technique also produces a number-based size distribution. In total 24 food products and 3 personal care products were purchased in regular shops in The Netherlands. Products that

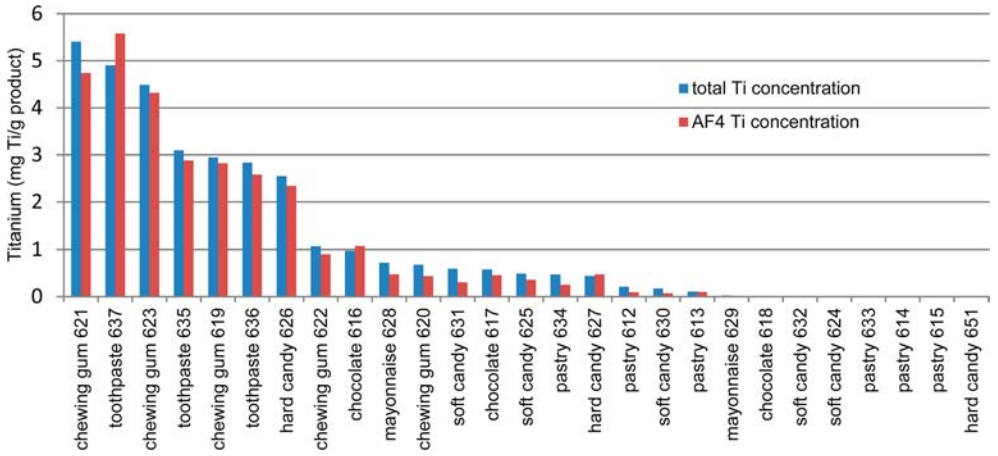

Figure 7. Total Ti content in food and personal care products determined with ICP-MS (blue, left-side bars) and the particle-based Ti content in the same products determined with AF4-ICP-MS analysis (red, right-side bars). The numbers after the product description refer to sample codes.

listed "E171" or "titanium dioxide" on the package, as well as a few products with a typical "white color", were selected for this study.

Total Titanium Content of Food and Personal Care Products. All 27 products were digested with a combination of HNO_3, HF, and H_2O_2, and the total Ti content was determined using ICP-MS. Total Ti recovery was determined by spiking three products of different matrices in triplicate with known amounts of a TiO_2 reference material NM-103. The total Ti recovery ranged from 92 to 109% with an average of 96 ± 6%. Method blanks showed only low amounts of titanium, that is, on average <2 μg of Ti, which corresponds to <0.005 mg Ti/g product. The quantification limit of the digestion and detection method was set to 0.01 mg Ti/g product. The total Ti content of the products ranges from 5.4 mg Ti/g product for a chewing gum to 0.01 mg Ti/g for a white-topped cookie. Four products had total Ti levels that were below the quantification limit of the method. The highest levels of total Ti are found in chewing gums and in toothpastes and the lowest in bakery products such as cookies and cupcakes (Figure 7). The results are comparable to the total Ti content in food items reported recently by Weir et al.[8]

Titanium Content of Food and Personal Care Products Determined by AF4-ICP-MS. All food and consumer products with a detectable amount of total Ti have been analyzed with AF4-ICP-MS for particle-based Ti content as well as the particle size distribution. For this purpose a separate sample preparation was set up using H_2O_2 to oxidize the sample matrix. The use of strong acids was avoided because these are not compatible with the AF4 analysis. H_2O_2 oxidation worked for all samples with the exception of the chewing gums, where debris of the guar gum remained. Because the TiO_2 particles are expected to be present in the outer, water-soluble coating of the chewing gum,[8] the removal of this debris probably does not influence the result. The time between sample preparation and measurement with AF4-ICP-MS was kept as short as possible and was no more than 4 h. After sonication of the sample extract, the extract was kept in constant movement on a roller bank until analysis. Prior to injection, the sample was thoroughly mixed to ensure homogeneous distribution of suspended particles. Because ions are removed in AF4 separation during the focusing of the analyte on the semipermeable membrane, mass calibration can be done only with a particle-based standard. In the absence of a reliable, well-characterized TiO_2 particle standard, one of the TiO_2 powders characterized as pure, 99% TiO_2, was used for this purpose. The particle-based Ti content of the food and personal care products as determined with AF4 and expressed as milligrams of Ti particle per gram of product is presented as the red, right-side, bars in Figure 7. The side-by-side comparison of the total Ti content and the particle-based Ti content as determined with AF4-ICP-MS in each product shows that they are comparable, certainly at Ti concentrations >0.5 mg Ti/g product. At lower concentration the results from the AF4 determination are generally lower than those from the total ICP-MS method. This can be explained by adsorption processes in the AF4 separation that become visible in the lower concentration range. Another reason may be that very large particles, aggregates, or agglomerates (>1600 nm) may be present in the samples and are lost in the AF4 determination. For products containing >0.5 mg Ti/g the results show that most of the total Ti originates from particles, that is, TiO_2 particles, and that no large amounts of titanium are unaccounted for in the AF4 analysis.

Number-Based Size Distributions in Food and Personal Care Products. Next to the particle-based Ti content of the samples, number-based size distributions were determined (Figure 8). From products containing <0.1 mg Ti/g product no reliable number-based size distributions could be produced. In general, the calculated number-based size distributions in food items and personal care products based on AF4-ICP-MS analysis are comparable with the number-based size distribution as determined for TiO_2 in E171 materials with EM. The apex of the size distribution was mostly found around 200 nm, which is in the size range of the primary particle sizes found with EM. The results indicate that a part of the TiO_2 particles have diameters below 100 nm. On a number-based basis the average percentage of particles with diameters <100 nm is around 8%, comparable with the 12 and 10% that were found for the number-based size distributions of TiO_2 in E171 with AF4-ICPMS and EM analyses.

Size Distributions Determined Using Single-Particle ICPMS. Because EM analysis was not feasible in products, sp-ICP-MS was used to determine a number-based size distribution of the TiO_2 particles in food and personal care products. The sample extracts that were used for the AF4 analysis were diluted 10000 times to get in the proper working range of the sp-ICP-MS method. Counting between 300 and

dx.doi.org/10.1021/jf5011885 | J. Agric. Food Chem. 2014, 62, 6285−6293

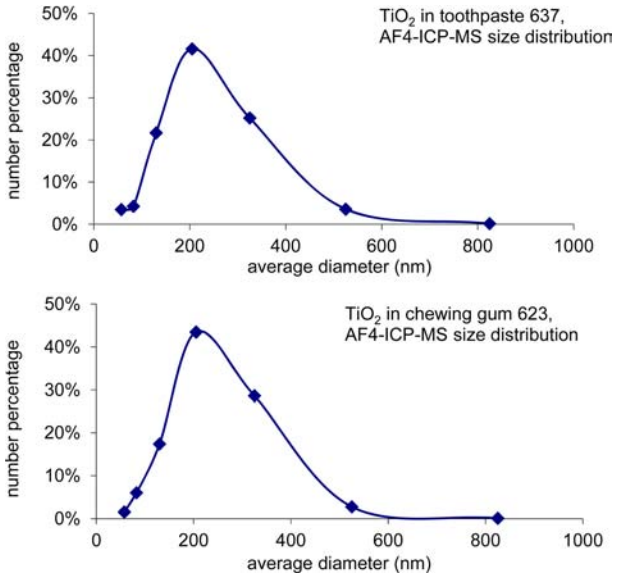

Figure 8. Number-based size distribution of the TiO_2 material in a toothpaste and chewing gum sample as determined with AF4-ICP-MS and after transformation of the mass-based to a number-based distribution.

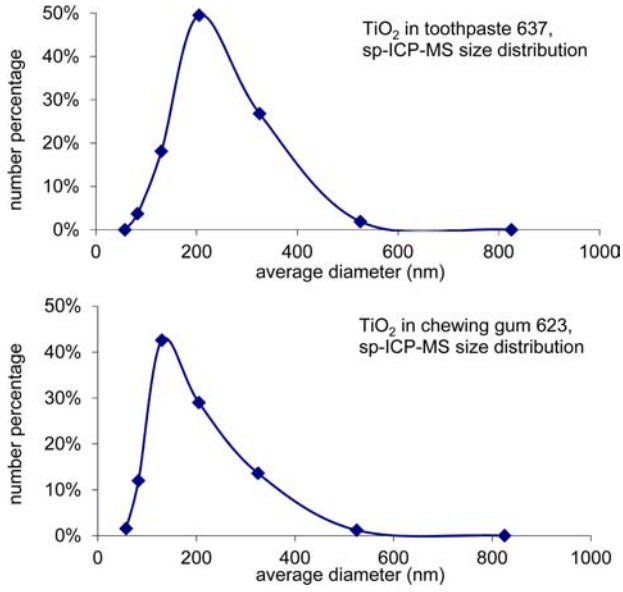

Figure 9. Number-based size distribution of the TiO_2 material in toothpaste as determined directly with sp-ICPMS.

3000 particle peaks in each time scan gives enough information to produce a reliable number-based size distribution. Whereas TiO_2 particles produce discontinuous signals (peaks) in sp-ICP-MS, small particle peaks will disappear in the background noise and can no longer be distinguished. Ti is measured at m/z 48 or 49, which is not that specific or sensitive, respectively. The presence of biatomic ions such as $^{32}S^{16}O$ and $^{36}Ar^{12}C$ and isobaric interference by ^{48}Ca result in a continuous background. This background noise for Ti measured at m/z 48 is substantially higher than that for silver (m/z 107) or gold (m/z 197), and therefore the minimum particle size that can be determined for titanium is also higher. Whereas for gold and silver 20 nm nanoparticles can be determined, the particle size detection limit for TiO_2 particles in the sp-ICP-MS method is 50 nm. The use of a collision cell did not improve the situation because not only the background noise but also the Ti particle peaks were reduced, resulting in no improvement of the signal/noise ratio.

Comparing the Measured Size Distributions of TiO_2 Materials. Compared to the calculated AF4-ICP-MS number-based size distribution (Figure 8), the measured sp-ICP-MS number-based size distributions (Figure 9) generally are shifted to the left, that is, toward smaller particle sizes, as illustrated by the results for chewing gum 623 in Figure 9. Nevertheless, the AF4-ICP-MS and sp-ICP-MS number-based size distributions of TiO_2 particles in the products are comparable. Furthermore, the distributions of the TiO_2 particles in the products are also comparable with the number-based size distributions of the TiO_2 (E171) materials as determined with AF4-ICP-MS and with EM. In all cases the apex of the size distribution is found around 200 nm within the size range of the primary particle sizes found with EM. The sp-ICP-MS results indicate that 5−10% of the TiO_2 particles have diameters below 100 nm. This is comparable to, or somewhat lower than, what was found in the EM and AF4-ICP-MS analysis and may in part be explained by the difference in the smallest particle that can be detected. For EM in the analysis of the TiO_2 materials the smallest TiO_2 particle that could be detected was around 20 nm; for AF4-ICP-MS in the analysis of TiO_2 materials and food and personal care products it was also around 20 nm, whereas in the sp-ICP-MS analysis of the food and personal care products the smallest detectable TiO_2 particle had a diameter of 50 nm.

These practical size detection limits for TiO_2 particles introduce a certain and perhaps significant bias because the size range between 1 and 20 nm is excluded. Whereas Figure 7 shows that >95% of the total titanium (mass-based) concentration is explained by TiO_2 particles >20 nm, if even only 1% of the total titanium (mass-based) concentration exists of TiO_2 particles <20 nm, this will change the determined number-based particle size distribution significantly. As a consequence, it is not clear whether TiO_2 in food products is a nanomaterial, and the results especially show the inability of current state of the art methods to support the EU recommendation for the definition of nanomaterials.

Potential for Consumer Exposure Assessment. In this study 7 TiO_2 materials, 24 food products, and 3 personal care products were studied for their titanium dioxide content and the number-based size distribution of TiO_2 particles therein. Three principally different methods have been used to determine the number-based size distribution of TiO_2 particles in E171 materials and food and personal care products. Comparable size distributions were found, and from these it was determined that 5−12% of the TiO_2 particles in these materials and products were <100 nm. These data are suitable to be used in an exposure study, further refining the exposure assessment by Weir et al. for the U.S. population.[8] Previously we assessed the SiO_2 content of food products[27] and subsequently assessed its fate during in vitro digestion.[28] There we concluded that the intestinal epithelium is exposed to nanoscale material. The fate of TiO_2 particles while in the human digestive tract is unknown and should be evaluated to allow a comparison with the existing oral toxicity studies using different forms of the TiO_2 NPs. Although the applied analytical methods showed practical size limits, all of these methods, and especially sp-ICP-MS, can be elegantly employed for further studies on the fate of food grade TiO_2 to bridge the

dx.doi.org/10.1021/jf5011885 | J. Agric. Food Chem. 2014, 62, 6285−6293

gap between our findings and recent oral toxicity studies to guarantee consumer safety.

AUTHOR INFORMATION

Corresponding Author

*(R.J.B.P.) E-mail: ruudj.peters@wur.nl. Phone: +31 317 48 06 71.

Funding

This research was commissioned and financed by The Netherlands Food and Consumer Product Safety Authority.

Notes

The authors declare no competing financial interest.

REFERENCES

(1) Johnson, R. W.; Thiele, E. S.; French, R. H. Light-scattering efficiency of white pigments: an analysis of model core−shell pigments vs. optimized rutile TiO_2. *TAPPI J.* **1997**, *11*, 233−239.

(2) Braun, J. H. Titanium dioxide—a review. *J. Coatings Technol.* **1997**, *69*, 59−72.

(3) Linak, E.; Schlag, S.; Kishi, A. *Chemical Economics Handbook: Titanium Dioxide, (Marketing Research Report)*; SRI International: Menlo Park, CA, USA, 2002.

(4) Swiler, D. R. Pigments, inorganic. In *Kirk-Othmer Encyclopedia of Chemical Technology*; Wiley: New York, 2005.

(5) Robichaud, C. O.; Uyar, A. E.; Darby, M. R.; Zucker, L. G.; Wiesner, M. R. Estimates of upper bounds and trends in nano-TiO_2 production as a basis for exposure assessment. *Environ. Sci. Technol.* **2009**, *43*, 4227−4233.

(6) Hendren, C. O.; Mesnard, X.; Droge, J.; Wiesner, M. R. Estimating production data for five engineered nanomaterials as a basis for exposure assessment. *Environ. Sci. Technol.* **2011**, *45*, 2562−2569.

(7) European Commission.. European Parliament and Council Directive 94/36/EC of 30 June 1994 on colours in foodstuffs. *Off. J. Eur. Communities* **1994**, *L237*, 13−29.

(8) Weir, A.; Westerhoff, P.; Fabricius, L.; Hristovski, K.; van Goetz, N. Titanium dioxide nanoparticles in food and personal care products. *Environ. Sci. Technol.* **2012**, *46*, 2242−2250.

(9) Tassinari, R.; Cubadda, F.; Moracci, G.; Aureli, F.; D'Amato, M.; Valeri, M.; De Berardis, B.; Raggi, A.; Mantovani, A.; Passeri, D.; Rossi, M.; Maranghi, F. Oral, short-term exposure to titanium dioxide nanoparticles in Sprague-Dawley rat: focus on reproductive and endocrine systems and spleen. *Nanotoxicology* **2013**, DOI: 10.3109/17435390.2013.822114.

(10) Gui, S.; Sang, X.; Zheng, L.; Ze, Y.; Zhao, X.; Sheng, L.; Sun, Q.; Cheng, Z.; Cheng, J.; Hu, R.; Wang, L.; Hong, F.; Tang, M. Intragastric exposure to titanium dioxide nanoparticles induced nephrotoxicity in mice, assessed by physiological and gene expression modifications. *Part. Fibre Toxicol.* **2013**, *10*, 4−10.

(11) IARC. *Carbon Black, Titanium Dioxide and Talc*; IARC Monograph 93 on the Evaluation of Carcinogenic Risks to Humans; IARC: Lyon, France, 2010; downloadable from http://monographs.iarc.fr/ENG/Monographs/vol93/mono93.pdf.

(12) Bouwmeester, H.; Dekkers, S.; Noordam, M. Y.; Hagens, W. I.; Bulder, A. S.; De Heer, C.; Ten Voorde, S. E. C. G.; Wijnhoven, S. W. P.; Marvin, H. J. P.; Sips, A. J. A. M. Review of health safety aspects of nanotechnologies in food production. *Regul. Toxicol. Pharmacol.* **2009**, *53*, 52−62.

(13) European Commission. Commission Recommendation of 18 October 2011 on the definition of nanomaterial. 2011/696/EU. European Commission, Luxembourg, 2011.

(14) Linsinger, T.; Roebben, G.; Gilliland, D.; Calzolai, L.; Rossi, F.; Gibson, N.; Klein, C. *Requirements for the Implementation of the European Commission Definition of the Term "Nanomaterial"*; JRC Reference report EUR 25404 EN, EUR Scientific and Technical research series; 2012; ISSN 1831-9424, DOI: 10.2787/63490.

(15) Jensen, K. A.; Kembouche, Y.; Christiansen, E.; Jacobson, N. R.; Wallin, H.; Guiot, C.; Spalla, O.; Witschger, O. *Final Protocol for Producing Suitable Manufactured Nanomaterial Exposure Media*; NANOGENOTOX deliverable report 3; July 2011; downloadable from http://www.nanogenotox.eu/files/PDF/web%20nanogenotox%.

(16) Moon, M. H.; Park, I.; Kim, Y. Size characterization of liposomes by flow field-flow fractionation and photon correlation spectroscopy. *J. Chromatogr., A* **1998**, *813*, 91−100.

(17) Park, I.; Paeng, K. J.; Yoon, Y.; Song, J. H.; Moon, M. H. Separation and selective detection of lipoprotein particles of patients with coronary artery disease by frit-inlet asymmetrical flow field-flow fractionation. *J. Chromatogr., B* **2002**, *780*, 415−422.

(18) Degueldre, C.; Favalgar, P. Y.; Wold, S. Gold colloid analysis by inductively coupled plasma-mass spectrometry in a single particle mode. *Anal. Chim. Acta* **2006**, *555*, 263−268.

(19) Laborda, F.; Lamanna, J. J.; Bolea, E.; Castillo, J. R. Selective identification, characterization and determination of dissolved silver(I) and silver nanoparticles based on single particle detection by inductively coupled plasma mass spectrometry. *J. Anal. At. Spectrom.* **2011**, *26*, 1362−1371.

(20) Pace, H. E.; Rogers, N. J.; Jarolimek, C.; Coleman, V. E.; Higgins, C. P.; Ranville, J. F. Determining transport efficiency for the purpose of counting and sizing nanoparticles via single particle inductively coupled plasma mass spectrometry. *Anal. Chem.* **2011**, *83*, 9361−9369.

(21) Peters, R. J.; Herrera Rivera, Z.; van Bemmel, G.; Marvin, H. J.; Bouwmeester, H. Development and validation of single particle ICP-MS for sizing and quantitative determination of nano-silver in chicken meat. *Anal. Bioanal. Chem.* **2014**, DOI: 10.1007/s00216-013-7571-0.

(22) Labille, J.; Feng, J. H.; Botta, C.; Borscgneck, D.; Sammutt, M.; Cabie, M.; Auffan, M.; Rose, J.; Bottero, J. Y. Aging of TiO_2 nanocomposites used in sunscreen. Dispersion and faste of the degradation products in aqueous environment. *Environ. Pollut.* **2010**, *158*, 3482−3489.

(23) Carlotti, M. E.; Ugazio, E.; Sapino, S.; Fenoglio, I.; Greco, G.; Fubini, B. Role of particle coating in controlling skin damage photoinduced by titania nanoparticles. *Free Radical Res.* **2009**, *43*, 312−322.

(24) Macwan, D. P.; Dave, P. N.; Chaturvedi, S. A review on nano-TiO_2 sol-gel type synthesis and its applications. *J. Mater. Sci.* **2011**, *46*, 3669−3686.

(25) Linak, E.; Inoguchi, Y. In *Chemical Economics Handbook: Titanium Dioxide*; SRI Consulting: Menlo Park, CA, USA, 2005.

(26) Schimpf, M. E.; Caldwell, K.; Giddings, J. C. In *Field-Flow Fractionation Handbook*; Wiley: New York, 2000.

(27) Dekkers, S.; Krystek, P.; Peters, R. J.; Lankveld, D. X.; Bokkers, B. G.; Van Hoeven-Arentzen, P. H.; Bouwmeester, H.; Oomen, A. G. Presence and risks of nanosilica in food products. *Nanotoxicology* **2011**, *5*, 393−405.

(28) Peters, R.; Kramer, E.; Oomen, A. G.; Herrera Rivera, Z. E.; Oegema, G.; Tromp, P. C.; Fokkink, R.; Rietveld, A.; Marvin, H. J. P.; Weigel, S.; Peijnenburg, A. A. C. M.; Bouwmeester, H. Presence of nano-sized silica during in vitro digestion of foods containing silica as a food additive. *ACS Nano* **2012**, *6*, 2441−2451.

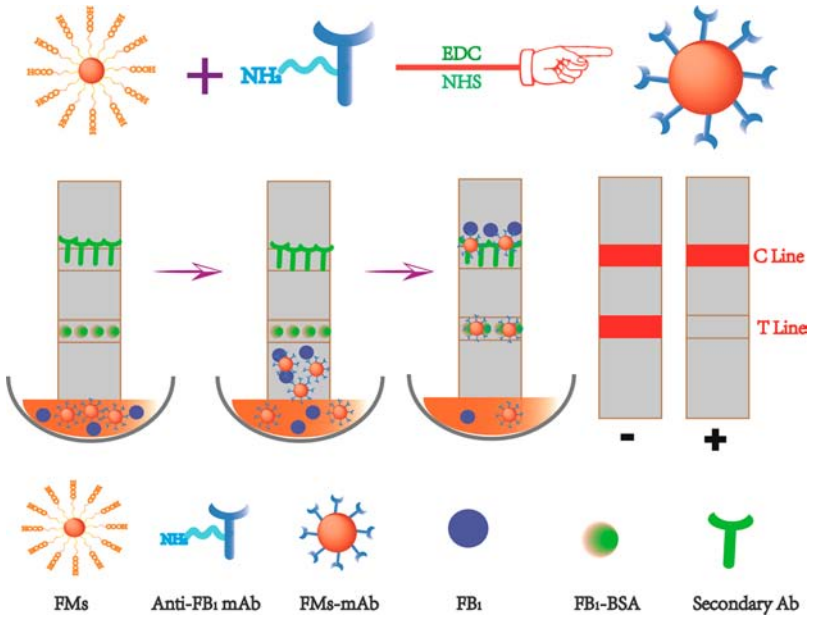

Figure 1. Fabrication process of the prepared FM−mAbs and the schematic illustration of the ICA. The ICA shows two lines on the vertical strip; the test line (T Line) is coated with coating antigen (FB_1-BSA), whereas the control line (C Line) is coated with secondary antibody that is specific to anti-FB_1 mAb.

(580/605, $\lambda_{ex}/\lambda_{em}$), 2% solids, were purchased from Invitrogen (Carlsbad, CA, USA). Bovine serum albumin (BSA), 1-ethyl-3-(3-(dimethylamino)propyl) carbodiimide hydrochloride (EDC), and 2-(*N*-morpholino)ethanesulfonic acid (MES) were purchased from Sigma-Aldrich (St. Louis, MO, USA). All other reagents were of analytical grade or better and were purchased from Beijing Reagent Corp. (Beijing, People's Republic of China). The nitrocellulose filter membrane (HF13520s25) was obtained from Millipore Corp. (Bedford, MA, USA). The sample pad (CH37K) and the absorbance pad (SB08) were supplied by Shanghai Liangxin Co., Ltd. (Shanghai, China). White opaque 96-well polystyrene microtiter plates were purchased from Costar, Inc. (Milpitas, CA, USA). The mAb 2D7 to FB_1 and the coating antigen were prepared previously and were purified using protein A prior to use.[22]

MES buffer was prepared as follows: 9.76 g of MES was dissolved in 1000 mL of purified water. The pH value of the MES buffer was adjusted by using 1 M NaOH.

Apparatus. The NanoDrop ND-1000 spectrophotometer was purchased from Gene Co., Ltd. (Hong Kong, People's Republic of China). The ZX1000 dispensing platform and the CM4000 guillotine cutting module used to prepare the ICA were purchased from BioDot, Inc. (Irvine, CA, USA). The ESE Quant LFR fluorescence reader was purchased from QIAGEN (Dusseldorf, Germany). The UV spectrometer was provided by Qiangyun Co. (Shanghai, People's Republic of China).

Preparation of FM-Labeled FB_1-mAbs. The FM−mAb conjugates were prepared as follows: anti-FB_1 mAb (7 μg) was dissolved in 1 mL of 50 mM MES (pH 6.5), and FMs (10 μL) were added dropwise. After 15 min, EDC (0.5 mg) was added and maintained on a shaker for 2 h at room temperature. The pH of the reaction mixture was adjusted to 6.5 using 1 M $NaHCO_3$. To quench the reaction, 100 μL of 0.1 M glycine was added and incubated for 30 min. The FM-labeled mAbs were obtained after centrifugation at 8076*g* for 15 min at room temperature to remove any unreacted mAbs. The pellets were resuspended in 100 μL of 0.05 M PBS containing 0.2% BSA and 0.4% poly(ethylene glycol). The suspension was dispersed and blended by supersonic vibration for 10 min and stored at 4 °C in the dark until use.

Fluorescence-Based ICA. Suspensions of 0.1 mg/mL FB_1-BSA and 1 mg/mL goat anti-mouse IgG were dispensed onto nitrocellulose filter membranes to produce the test (0.7 μL/cm) and control (0.9 μL/cm) lines, respectively. The membrane was dried for 2 h at 37 °C in an air oven. The sample pad was soaked in 0.01 M PBS (containing 0.05% Tween 20 and 0.05% sodium azide) and dried at 40 °C for 24 h. The absorbent pad was pasted onto the top side of the backing pad by overlapping a 2 mm section with the membrane. The sample pad was also pasted onto the other side of the backing pad by overlapping a 2 mm section with the membrane. Finally, the whole assembled plate was cut into 4 mm wide strips and stored under dry conditions at room temperature. A total of 120 μL of sample solution (or standard buffer) was transferred into a 96-well microtiter plate and homogenized with 2 μL of FM−mAbs at room temperature. After 5 min of shaking, the strip was added to the microwell to absorb the mixture. The capillary migration process lasted approximately 15 min, and the strip was then removed and fully dried for 5 min at 40 °C in an air oven prior to measuring the fluorescence signal. The results of the test and control lines were either qualitatively estimated by eye under a UV light or quantitatively measured by measuring the signal intensities using an ESE Quant lateral flow reader set at 580 and 605 nm for the excitation and emission wavelengths, respectively.

To test the specificity of the ICA for FB_2, FB_3, T-2 toxin, DON, ochratoxin A, zearalenone, and aflatoxin B_1, standard solutions of these mycotoxins with concentrations of 0.1, 0.5, 1, 1.5, 2.0, 4.0, and 10 ng/mL were prepared by diluting the corresponding stock solutions (1 mg/mL) with 0.01 M PBS. The following ICA experiments were carried out in the same way as mentioned above for FB_1. The cross-reactivity values were calculated according to the following equation:

$$[IC_{50}\ (FB_1,\ ng/mL)/IC_{50}\ (mycotoxins,\ ng/mL)] \times 100\%$$

Analysis of Maize Samples. Maize flour samples were provided by a local company in Belgium and stored at −20 °C. The concentration of mycotoxins was determined by HPLC-MS/MS, as previously described.[23] In spike and recovery studies, 10 g of FB_1-negative maize flour samples was spiked with FB_1, which was dissolved in methanol, with 500, 1000, and 1500 μg/kg. The samples were thoroughly mixed and then allowed to stand at room temperature overnight. Maize flour (1 g) was vigorously mixed and extracted with 20 mL of methanol/water (4:6, v/v) for 5 min before ultrasonic dispersion for 5 min and centrifugation at 8076*g* for 5 min. A total of 20 μL of supernatant was diluted with 980 μL of sample diluent prior to analysis by the ICA as described before.

dx.doi.org/10.1021/jf5017219 | J. Agric. Food Chem. 2014, 62, 6294−6298

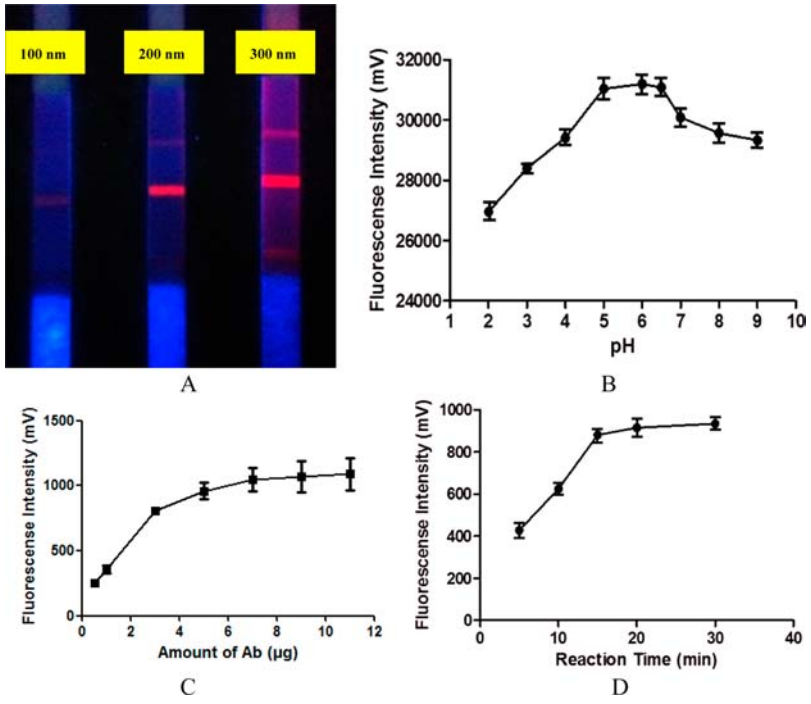

Figure 2. (A) Effect of the FM diameter on the fluorescence signal and mobility on the test line. (B) Effect of the pH on the fluorescence signals of FMs and FM−mAbs. The signals of FMs alone (pH values outside 5.0−6.5) and the signal of FM−mAb conjugates (pH values between 5.0 and 6.5) are shown. (C) Effect of the antibody loading amount on the fluorescence signal of FM−mAbs. (D) Effect of the immunoreaction time on the fluorescence signal in the ICA. Error bars = ±SD, n = 5.

RESULTS AND DISCUSSION

Detection Principle of the FM-Based ICA. In this study, the detector reagent consisted of anti-FB_1 mAb-functionalized FMs. The carboxyl groups of fluorescent microsphere were covalently coupled to the amino group of mAb in the presence of carbodiimide to ensure the stability of the detector (Figure 1). The detection principle of the FM-based ICA was based on the competitive binding between the FB_1-BSA (test line) and the mycotoxin FB_1 to combine with the limited mAbs on the fluorescence reporter. As shown in Figure 1, when FB_1 was present in the sample solution, the FB_1-FM−mAbs were formed in a microwell, diminishing the formation of FB_1-BSA−FM−mAbs at the test line, causing its fluorescence intensity to become weaker. Regardless of the presence of FB_1 in the sample, secondary antibody in the control line would bind to the anti-FB_1 mAbs ensuring the validity of the detection. According to the principle described above, the fluorescence intensity on the test line would be inversely proportional to FB_1 concentrations in the sample, which could be used for quantitation of FB_1 in samples. Quantitative analysis was realized by reading the fluorescence intensities of test line with a portable strip reader.

FM-Labeled mAbs. The activity of the FM−mAbs primarily guaranteed assay speed and sensitivity; thus, we first optimized the FM−mAb preparation conditions. Figure 2A shows the influence of the FM diameter on the fluorescence intensity of the test line. In the presence of 300 nm FMs, the signal generation was rather slow, and it took >30 min to accomplish the procedure. Although the 300 nm FMs produced strong signals, this duration is not appropriate for a rapid assay (Figure 2A). Besides, the significant residue of FM−mAb conjugates in the membrane pores could affect the accurate detection of the target (Figure 2A). It took <10 min to accomplish the procedure in the presence of 100 nm FMs; however, the signal response was very weak, as shown in Figure 2A, indicating that the small-diameter FMs were not appropriate for application with the ICA. The 200 nm FMs represented a compromise between speed and sensitivity in the assay and were selected for further experiments (Figure 2A).

The pH of the buffer has a great influence on the fluorescence of the FMs alone and on the FM−mAb conjugates, for example, through their dissolution and stability properties; therefore, the effect of several buffers with different pH values on these FM properties was evaluated. The fluorescence signal of FMs alone has been tested at pH values outside 5.0−6.5 and the signal of FM−mAb conjugates at pH values between 5.0 and 6.5 (Figure 2B). Thus, we evaluated the effect of buffers with pH values of 5.0, 6.0, and 6.5 on the performance of the FM−mAb conjugates. The FM−mAb conjugates clogged the membrane at pH values of 5.0 and 6.0. The pH 6.5 coupling buffer was thus selected as the most suitable condition for the subsequent experiments.

Figure 2C shows the results of the mAb loading onto the FMs. The fluorescence intensity of the FMs increased as increasing amounts of mAb were added onto the FMs until asymptotically approaching a maximum value. As the increase of intensity is very limited for amounts of added mAb above 7 μg (Figure 2C), this quantity has been selected as the most appropriate for an adequate signal sensitivity in the ICA.

One of the main characteristics of ICA is rapid detection, which is an important advantage over other immunoassays. A time−intensity curve was constructed by measuring the signal of the test line as a function of incubation time. The signal increased rapidly during the first 15 min, and the signal asymptotically reached a maximum for longer incubation time plateaued between 15 and 30 min (Figure 2D), indicating that the signal was already relatively stable for analysis at 15−30

dx.doi.org/10.1021/jf5017219 | J. Agric. Food Chem. 2014, 62, 6294−6298

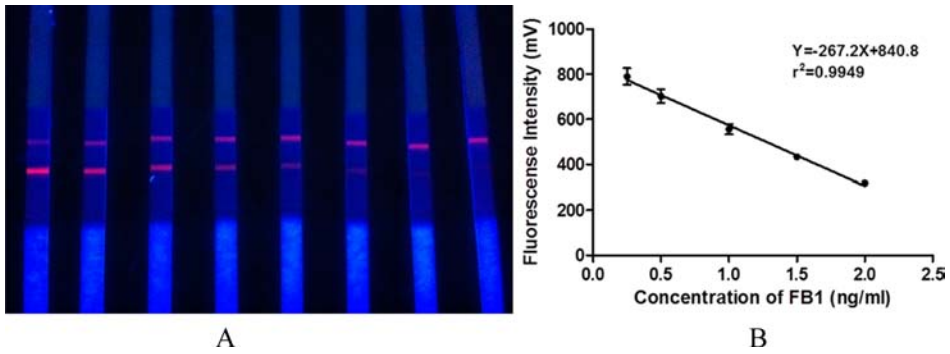

Figure 3. (A) Fluorescent image of the ICA acquired under UV light for 0, 0.25, 0.5, 1, 1.5, 2.0, 2.5, and 3 ng/mL FB_1 (from left to right). (B) Standard curve for quantitative detection by the fluorescence ICA. Error bars = ±SD, n = 5.

min. With consideration of finding the shortest time for an optimal detection, the best incubation time was considered as 15 min.

Analytical Performance of the ICA. The fluorescence ICA is based on competitive binding of the FB_1 in the samples and the FB_1-BSA immobilized on the test line to the FM−mAb conjugates flowing through the membrane. Analytical parameters of the ICA for FB_1 were obtained under the previously determined optimal conditions. Concentrations of FB_1 from 0 to 3.0 ng/mL were applied to the ICA, and the corresponding inhibition fluorescence intensity of the test line was observed under an ultraviolet light source or recorded by a fluorescence reader. As shown in Figure 3A, the red fluorescence intensity of the test line clearly decreased as the concentration of FB_1 increased. The fluorescence intensity was barely detectable at 2.5 ng/mL of FB_1; thus, 2.5 ng/mL FB_1 was considered the cutoff value for the assay (corresponding to 25 μg/kg in maize flour samples according to the extraction procedure used in the study). A calibration curve was generated using FB_1 in the range of 0.25−2.0 ng/mL (250−2000 μg/kg in maize flour samples) with an IC_{50} value of 1.32 ng/mL, as shown in Figure 3B (r^2 = 0.9949). The LOD for the quantitative detection was estimated from the concentration that corresponded to the blank test line value minus 3 times the standard deviation of the blank, which was calculated as 0.12 ng/mL (1.2 μg/kg in maize flour samples). This LOD is lower than that of the ELISA method employing the same immunoreagents (5.4 μg/kg in maize flour samples).[22]

The specificity of the ICA was determined by evaluating cross-reactivity with frequently occurring mycotoxins, including FB_2, FB_3, T-2 toxin, DON, ochratoxin A, zearalenone, and aflatoxin B_1. The ICA exhibited cross-reactivities with FB_2 and FB_3 of 1.5 and 67.3%, respectively, and negligible cross-reactivities with other mycotoxins (<1%).

Maize Sample Analysis. Results for the analytical recovery of FB_1 spiked to maize sample are given in Table 1. As observed in Table 1, the average recovery values (n = 5) ranged from 91.4 to 118.2% with CV values between 6.01 and 12.02%. Ten naturally contaminated maize samples were subjected to both the ICA and an HPLC-MS/MS method. The data obtained by the two methods were in good agreement (r^2 = 0.93), as shown in Table 2. The content of DON in the maize samples did not appear to affect the quantification of FB_1 in the maize samples by the ICA.

Table 1. Recoveries of FB_1 Added to Maize Flour Samples

added concn (μg/kg)	measured concn (μg/kg)	recovery (%)	CV[a] (%)
500	591	118.2	6.01
1000	914	91.4	6.82
1500	1527	101.8	12.02

[a]Coefficient of variation.

Table 2. Naturally Contaminated Maize Flour Samples

sample	HPLC-MS/MS[a] (μg/kg)	ICA[b] (μg/kg)	CV (%)
1 (FB_1 + DON[c])	297 + 2197	314	7.62
2 (FB_1 + DON)	291 + 213	320	8.96
3 (FB_1 + DON)	742 + 705	427	5.68
4 (FB_1 + DON)	236 + 913	281	7.79
5 (FB_1 + DON)	0 + 78		
6 (FB_1 + DON)	1686 + 535	1479	12.71
7 (FB_1 + DON)	308 + 990	306	6.87
9 (FB_1+DON)	2285 + 0		

[a]High-performance liquid chromatography−mass spectrometry. [b]Immunochromatographic assay. [c]Deoxynivalenol.

Comparison with Colloidal Gold-Based ICA. ICA provides a simple, rapid, and robust technique for the screening detection of mycotoxins in cereals, and colloidal gold is the most frequently used reporter system. Shiu et al. developed an ICA for the detection of FB_1 in grain-based food and feed samples. This strip had a cutoff value of 5 ng/mL for FB_1.[24] Wang et al. also described an ICA for FB_1 and obtained a cutoff value of 1.0 μg/L.[25] A lateral flow dual immunoassay for the quantitative detection of zearalenone and FB_1 in corn and wheat samples was recently reported. The LODs were 5.23 ng/mL for FB_1 in the dual ICA format.[26] Anfossi et al. developed a quantitative ICA for simultaneous detection of both FB_1 and FB_2 in maize because the employed FB_1-antiserum provided a cross-reactivity of 97% to FB_2. The LOD of the quantitative ICA was 12 μg/L.[27] In the study, we employed FMs as a reporter to develop a fluorescence ICA for FB_1. Compared to the colloidal gold reporter, we found that the sensitivity of the fluorescence ICA is greater than or comparable to those of most currently available ICAs.

In conclusion, we demonstrated that FMs are a promising practical reporter for ICAs. The FM-based ICA for FB_1 was capable of detecting a minimum of 0.12 ng/mL FB_1 within 15 min. The assay was simple, rapid, and sensitive and provided not only qualitative results for rapid assessment but also quantitative results for the accurate determination of FB_1 in maize samples. Therefore, the FM-based ICA has great potential to improve detection sensitivity to enable more

dx.doi.org/10.1021/jf5017219 | J. Agric. Food Chem. 2014, 62, 6294−6298

sensitive and quantitative bioassays. The application of FMs can be easily extended to other contaminants by using the corresponding specific antibody.

AUTHOR INFORMATION

Corresponding Author

*(J.S.) Phone: +86-10-6273 3289. Fax: +86-10-6273 1032. E-mail: sjz@cau.edu.cn.

Funding

This work was supported by grants from the International Science and Technology Cooperation Program of China (2012DFG31840), the National Natural Science Foundation of China (31372475), and the Key Projects in the National Science and Technology Pillar Program during the t12th Five-Year Plan Period (2012BAK17B16, 2011BAK10B01).

Notes

The authors declare no competing financial interest.

ACKNOWLEDGMENTS

We thank Shupeng Yang, Shaoqin Ma, and Chao Wu for excellent technical assistance and discussion.

REFERENCES

(1) Maragos, C. M.; Busman, M. Rapid and advanced tools for mycotoxin analysis: a review. *Food Addit. Contam.* **2010**, *27*, 688−700.

(2) Krska, R.; Becalski, A.; Braekevelt, E.; Koerner, T.; Cao, X. L.; Dabeka, R.; Godefroy, S.; Lau, B.; Moisey, J.; Rawn, D. F.; Scott, P. M.; Wang, Z.; Forsyth, D. Challenges and trends in the determination of selected chemical contaminants and allergens in food. *Anal. Bioanal. Chem.* **2012**, *402*, 139−162.

(3) Lattanzio, V. M.; Nivarlet, N.; Lippolis, V.; Della Gatta, S.; Huet, A. C.; Delahaut, P.; Granier, B.; Visconti, A. Multiplex dipstick immunoassay for semi-quantitative determination of *Fusarium* mycotoxins in cereals. *Anal. Chim. Acta* **2012**, *718*, 99−108.

(4) Anfossi, L.; Baggiani, C.; Giovannoli, C.; D'Arco, G.; Giraudi, G. Lateral-flow immunoassays for mycotoxins and phycotoxins: a review. *Anal. Bioanal. Chem.* **2013**, *405*, 467−480.

(5) Mirasoli, M.; Buragina, A.; Dolci, L. S.; Simoni, P.; Anfossi, L.; Giraudi, G.; Roda, A. Chemiluminescence-based biosensor for fumonisins quantitative detection in maize samples. *Biosens. Bioelectron.* **2012**, *32*, 283−287.

(6) Kolosova, A. Y.; De Saeger, S.; Sibanda, L.; Verheijen, R.; Van Peteghem, C. Development of a colloidal gold-based lateral-flow immunoassay for the rapid simultaneous detection of zearalenone and deoxynivalenol. *Anal. Bioanal. Chem.* **2007**, *389*, 2103−2107.

(7) Molinelli, A.; Grossalber, K.; Krska, R. A rapid lateral flow test for the determination of total type B fumonisins in maize. *Anal. Bioanal. Chem.* **2009**, *395*, 1309−1316.

(8) Posthuma-Trumpie, G. A.; Korf, J.; van Amerongen, A. Lateral flow (immuno)assay: its strengths, weaknesses, opportunities and threats. A literature survey. *Anal. Bioanal. Chem.* **2009**, *393*, 569−582.

(9) Liu, C.; Jia, Q.; Yang, C.; Qiao, R.; Jing, L.; Wang, L.; Xu, C.; Gao, M. Lateral flow immunochromatographic assay for sensitive pesticide detection by using Fe_3O_4 nanoparticle aggregates as color reagents. *Anal. Chem.* **2011**, *83*, 6778−6784.

(10) Beloglazova, N. V.; Shmelin, P. S.; Goryacheva, I. Y.; De Saeger, S. Liposomes loaded with quantum dots for ultrasensitive on-site determination of aflatoxin M_1 in milk products. *Anal. Bioanal. Chem.* **2013**, *405*, 7795−7802.

(11) Beloglazova, N. V.; Shmelin, P. S.; Speranskaya, E. S.; Lucas, B.; Helmbrecht, C.; Knopp, D.; Niessner, R.; De Saeger, S.; Goryacheva, I. Y. Quantum dot loaded liposomes as fluorescent labels for immunoassay. *Anal. Chem.* **2013**, *85*, 7197−7204.

(12) Pyo, D.; Yoo, J. New trends in fluorescence immunochromatography. *J. Immun. Immunochem.* **2012**, *33*, 203−222.

(13) Suarez-Pantaleon, C.; Wichers, J.; Abad-Somovilla, A.; van Amerongen, A.; Abad-Fuentes, A. Development of an immunochromatographic assay based on carbon nanoparticles for the determination of the phytoregulator forchlorfenuron. *Biosens. Bioelectron.* **2013**, *42*, 170−176.

(14) Goryacheva, I. Y.; Lenain, P.; De Saeger, S. Nanosized labels for rapid immunotests. *Trends Anal. Chem.* **2013**, *46*, 30−43.

(15) Xia, X.; Xu, Y.; Zhao, X.; Li, Q. Lateral flow immunoassay using europium chelate-loaded silica nanoparticles as labels. *Clin. Chem.* **2009**, *55*, 179−182.

(16) Chen, R.; Li, H.; Zhang, H.; Zhang, S.; Shi, W.; Shen, J.; Wang, Z. Development of a lateral flow fluorescent microsphere immunoassay for the determination of sulfamethazine in milk. *Anal. Bioanal. Chem.* **2013**, *405*, 6783−6789.

(17) Langenhorst, R. J.; Lawson, S.; Kittawornrat, A.; Zimmerman, J. J.; Sun, Z.; Li, Y.; Christopher-Hennings, J.; Nelson, E. A.; Fang, Y. Development of a fluorescent microsphere immunoassay for detection of antibodies against porcine reproductive and respiratory syndrome virus using oral fluid samples as an alternative to serum-based assays. *Clin. Vaccine Immunol.* **2012**, *19*, 180−189.

(18) Vilarino, N.; Louzao, M. C.; Fraga, M.; Rodriguez, L. P.; Botana, L. M. Innovative detection methods for aquatic algal toxins and their presence in the food chain. *Anal. Bioanal. Chem.* **2013**, *405*, 7719−7732.

(19) Wang, Y.; Ning, B.; Peng, Y.; Bai, J.; Liu, M.; Fan, X.; Sun, Z.; Lv, Z.; Zhou, C.; Gao, Z. Application of suspension array for simultaneous detection of four different mycotoxins in corn and peanut. *Biosens. Bioelectron.* **2013**, *41*, 391−396.

(20) Czeh, A.; Mandy, F.; Feher-Toth, S.; Torok, L.; Mike, Z.; Koszegi, B.; Lustyik, G. A flow cytometry based competitive fluorescent microsphere immunoassay (CFIA) system for detecting up to six mycotoxins. *J. Immunol. Methods* **2012**, *384*, 71−80.

(21) International Agency for Research on Cancer. *Some Traditional Herbal Medicines, Some Mycotoxins, Naphthalene and Styrene* ; IARC monograph 82 on the evaluation of carcinogenic risks to humans; IARC: Lyon, France, 2002; pp 301−366.

(22) Sheng, Y.; Jiang, W.; De Saeger, S.; Shen, J.; Zhang, S.; Wang, Z. Development of a sensitive enzyme-linked immunosorbent assay for the detection of fumonisin B_1 in maize. *Toxicon* **2012**, *60*, 1245−1250.

(23) Monbaliu, S.; Van Poucke, C.; Detavernier, C.; Dumoulin, F.; De Velde, M.; Schoeters, E.; Van Dyck, S.; Averkieva, O.; Van Peteghem, C.; De Saeger, S. Occurrence of mycotoxins in feed as analyzed by a multi-mycotoxin LC-MS/MS method. *J. Agric. Food Chem.* **2009**, *58*, 66−71.

(24) Shiu, C. M.; Wang, J. J.; Yu, F. Y. Sensitive enzyme-linked immunosorbent assay and rapid one-step immunochromatographic strip for fumonisin B_1 in grain-based food and feed samples. *J. Sci. Food Agric.* **2010**, *90*, 1020−1026.

(25) Wang, S.; Quan, Y.; Lee, N.; Kennedy, I. R. Rapid determination of fumonisin B_1 in food samples by enzyme-linked immunosorbent assay and colloidal gold immunoassay. *J. Agric. Food Chem.* **2006**, *54*, 2491−2495.

(26) Wang, Y. K.; Yan, Y. X.; Ji, W. H.; Wang, H. A.; Li, S. Q.; Zou, Q.; Sun, J. H. Rapid simultaneous quantification of zearalenone and fumonisin B_1 in corn and wheat by lateral flow dual immunoassay. *J. Agric. Food Chem.* **2013**, *61*, 5031−5036.

(27) Anfossi, L.; Calderara, M.; Baggiani, C.; Giovannoli, C.; Arletti, E.; Giraudi, G. Development and application of a quantitative lateral flow immunoassay for fumonisins in maize. *Anal. Chim. Acta* **2010**, *682*, 104−109.

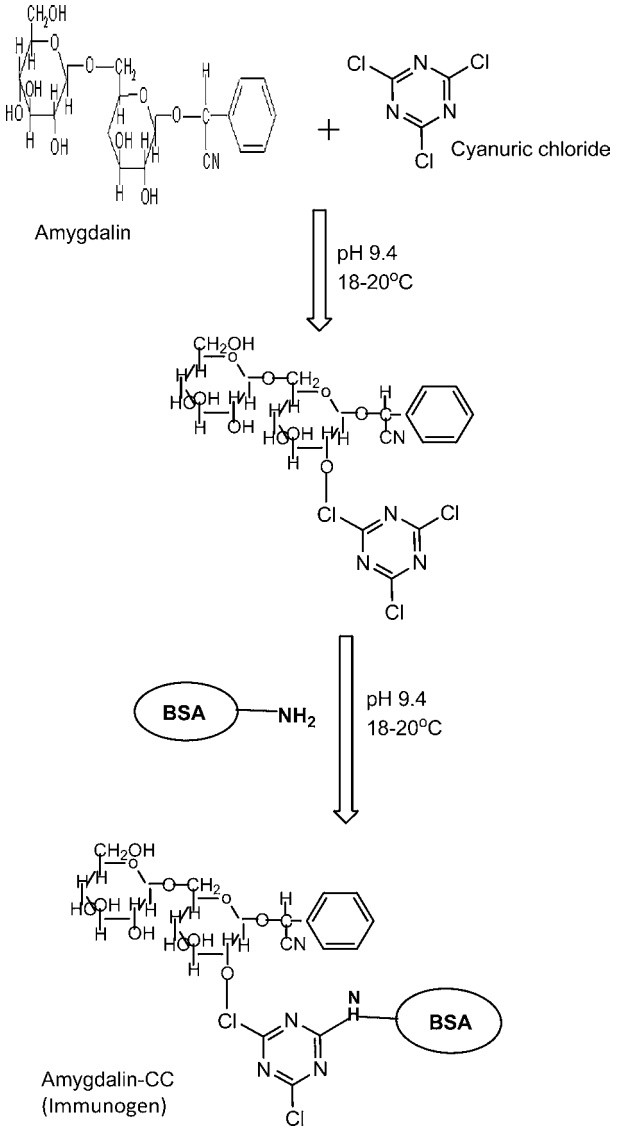

Figure 1. Structure of amygdalin and the synthetic approach to immunogen production.

food analysis for the determination of food contaminants and in the agrochemical industry for the detection of chemical residues in plants, water, and soil.[19−21] Different types of immunoassay techniques have been developed for the detection and quantification of hazardous compounds in foods. Quan et al.[22] developed a sensitive enhanced chemiluminescence enzyme-linked immunosorbent assay (ECL-ELISA) for the detection of fumonisin B_1 (FB_1) in foods and animal feeds. An ELISA developed by Pastor-Navarro et al.[23] was able to detect different tetracycline residues in honey. ELISA methods have also been developed for monitoring the levels of herbicides in water,[24] pesticides, and estrogenic compounds in agricultural products.[25,26] Antibodies against amygdalin have been described previously[27,28] but have not been fully characterized or used quantitatively. We describe the development, characterization, and application (for the first time) of an ELISA for the specific quantification of amygdalin in commercially available food products.

MATERIALS AND METHODS

Chemicals. Amygdalin, dhurrin, TMB (ready-to-use ELISA substrate), acetone, cyanuric chloride, Tween 20, gelatin, casein, and buffer salts were all purchased from the Sigma Chemical Co., Poole, Dorset, UK. Prunasin, mandelonitrile and linamarin were purchased from Santa Cruz Biotechnology, Dallas, TX, USA. 2,4,6-Trinitrobenzenesulfonic acid (TNBS; 5%, w/v) was obtained from VWR International Ltd., Leicestershire, UK. Keyhole limpet hemocyanin (KLH) was from Merck Chemicals Ltd., Nottingham, UK. Bovine serum albumin (BSA) was purchased from Fisher Scientific Ltd., Leicestershire, UK. Goat anti-rabbit IgG (H+L) horseradish peroxidase conjugate was obtained from Invitrogen Life Technology, Paisley, UK. Microtitration plates (96-well, MaxiSorp) were purchased from Nunc, Rosklide, Denmark. Microtitration plate washing was carried out using a Labsystem 4MK2 Wellwash (Labsystems, Uxbridge, UK), and the optical densities at 405 nm were recorded using a plate reader (ThermoFisher Scientific, Vantaa, Finland). Phosphate-buffered saline (PBS, 0.01 M, pH 5.5 and 7.4), phosphate-buffered saline (pH 7.4) containing 0.05% Tween 20 (PBST), sodium carbonate−bicarbonate buffer (0.05 M, pH 9.4 and 9.6) were used.

Food Samples. All fruits and processed products used in this study were purchased from local supermarkets in Leeds, UK. The products were toasted almond kernels (produced in the United States, packaged in the United Kingdom by Sainsbury's), EcoMil almond cocoa dessert (8% almond) produced in Spain, Tesco own-brand almond flour (produced in the United States, packaged in the United Kingdom by Tesco), Morrison's own-brand white marzipan (25% almond) produced in the United Kingdom, Sainsbury's own-brand apple juice (produced in the United Kingdom), Copella apple juice (hand-picked English apples, produced in the United Kingdom), Del Monte quality long life apple juice (100% concentrate), squashes, melons, and black cherries (from the United Kingdom), black plums (from Chile), yellow plums (from South Africa), apples (from Brazil), pears (from The Netherlands), courgettes and cucumbers (from Spain), peaches (from Argentina), and marrows (from Egypt). Three packs from different batches were purchased for each brand or product. All products were stored at 4 °C for 2 days after purchase and extracted as soon as possible.

Synthesis of Hapten−Protein Conjugates. The hapten−protein synthesis route is illustrated in Figure 1. Amygdalin was first activated with cyanuric chloride (CC) using a modification of the method of Abuknesha et al.[29] used for antibody−enzyme conjugations. CC (1 mg) was dissolved in acetone (1 mL), and 0.3 mL of the solution was measured into a glass vial. The content of the vial was allowed to evaporate. Amygdalin was activated by adding a solution of amygdalin (2.3 mg in 0.5 mL sodium carbonate−bicarbonate buffer, pH 9.4) to the CC residue. The mixture was stirred for 6 h at room temperature (20 ± 2 °C) to produce the activated hapten (amygdalin-CC). BSA (0.1 μmol, 6.6 mg in 0.5 mL sodium carbonate−bicarbonate buffer, pH 9.4) was added to the hapten, and the mixture was incubated overnight at 37 °C and then dialyzed for 6 h against 0.01 M phosphate buffer (pH 5.5). The resulting material (amygdalin−BSA conjugate, Figure 1) was freeze-dried to obtain a white powder. The conjugate was stored at −20 °C until use. The synthesized amygdalin−BSA conjugate was used as the immunogen. Amygdalin−KLH conjugate used for the immobilized phase of the ELISA was synthesized using the same method as for immunogen production.

Assessment of Hapten−Protein Conjugates. The ratios of coupled hapten to protein in the conjugates were assessed by both spectrophotometric and chemical methods.[130−] First, verification of conjugate synthesis and estimation of the number of moles of hapten conjugated per mole of protein were estimated by UV−visible spectrometry. Amygdalin (1 mg), BSA (1 mg), or amygdalin−BSA conjugate (1 mg) was dissolved in sodium carbonate−bicarbonate buffer (0.05 M, pH 9.6, 1 mL). Absorption over 200−400 nm was determined, and the number of moles of hapten in the conjugate was calculated using the maximum absorbance for amygdalin at 262 nm to calculate the molar extinction coefficient. The number of moles of conjugated hapten was calculated using $A = \varepsilon cl$.

Second, the trinitrobenzenesulfonic acid assay (TNBS; Habeeb[30]) was used to estimate the molar conjugation ratios of amygdalin−BSA and amygdalin−KLH conjugates. The method is based on the determination of available amino acid groups present in carrier protein before and after hapten conjugation following its reaction with TNBS. The end product of the reaction of TNBS produces trinitophenyl derivatives, which can be measured spectrophotometrically. The assay protocol used was as modified by Kemp and Morgan.[31] Carrier protein or conjugate (1 mg) was dissolved in 1 mL of 0.05 M sodium carbonate−bicarbonate buffer, pH 9.4. Standard curves for the proteins were constructed using a total volume of 200 μL in the wells of a microtitration plate. To each of the wells was added 50 μL of TNBS (0.1%) in carbonate buffer (4%). The plate was incubated for 2 h at 37 °C for color development, and the absorbance was read at 405 nm on a plate reader. The percentage substitution of amino acid in the carrier protein was used to estimate the conjugation ratio of hapten to carrier protein.

$$\%\ \text{substitution} \equiv \frac{\text{OD of carrier protein} - \text{OD of hapten−protein conjugate}}{\text{OD of carrier protein}} \times 100$$

Immunization Protocol and Polyclonal Antibody Production. Antibodies were raised by Covalab Ltd., Cambridge, UK. Two female New Zealand White rabbits (2−2.5 kg) were immunized with the immunogen (amygdalin−BSA conjugate) to generate polyclonal antibodies. The first injection consisted of the immunogen (50 μg in 0.5 mL of phosphate-buffered saline) emulsified with 0.5 mL of Freund's complete adjuvant and injected intradermally on multiple sites on the rabbits' back. The rabbits were further boosted by injecting intradermally the immunogen (50 μg) dissolved in 0.5 mL of Freund's incomplete adjuvant three times at 3 week intervals, with the final booster injection administered subcutaneously. The antisera were stored at −20 °C until use.

Enzyme-Linked Immunosorbent Assay. For determination of antibody titer, each well of the 96-well microtitration plate was coated with amygdalin−KLH overnight at 4 °C using 300 μL of a solution of conjugate dissolved in 0.05 M carbonate−bicarbonate buffer, pH 9.6. The plate was then washed three times with water and twice with 0.01 M PBST. Antibody titer was determined by incubating serial dilutions of antisera and preimmune sera in PBST (200 μL per well, in triplicate). The plate was incubated overnight at 4 °C, washed five times with PBST, and dried. A species-specific secondary antibody, goat anti-rabbit horseradish peroxidase IgG conjugate (diluted 1/1000 in PBST, v/v; 200 μL per well), was added. The plate was incubated at 37 °C for 2 h, washed and dried as before, and then TMB substrate (200 μL) was added to each well. The plate was further incubated for 30 min at 37 °C, and the reaction was stopped with sulfuric acid (2 M, 50 μL per well). The absorbance of each well was determined at 405 nm. The development of yellow color was proportional to the amount of antibody present. The mean absorbance values of triplicate determinations were plotted against antiserum dilutions.

For the indirect competitive ELISA (icELISA), standard curves were constructed with 100 μL of solution containing amygdalin standard (10 pg/well−10 μg/well) dispensed into appropriate wells of the coated plates prior to adding antibody (100 μL). The plate was then processed for the antibody titer curve determination. The limit of detection of the assay was estimated as the concentration that corresponds to the optical density at zero binding minus 3 times the standard deviation of the mean of zero binding.

To optimize the ELISA, the sensitivity of the immunoassay was improved by varying the antiserum dilution, the incubation time, and the concentration of the coating antigen and by using different protein buffers. The protein buffers that were evaluated were PBST containing 1% BSA, 1% gelatin, or 1% casein. Evaluation of the optimization process was based on the IC_{50} value and the coefficient of evaluation of the linear equation (R^2) as described by Qian et al.[32]

Cross-Reactions. The optimized assays were applied to cross-reactivity studies using standard solutions of amygdalin and other cyanogenic glycosides. The cross-reactivity of the antibody with some closely related cyanogenic glycosides such as prunasin, dhurrin, mandelonitrile, and linamarin was determined by icELISA. The specificity of the polyclonal antibody was determined using

$$\%\ \text{cross-reactivity (CR)} = (IC_{50}\ \text{of amygdalin}/IC_{50}\ \text{of analogue}) \times 100$$

Application of the icELISA to Quantification of Amygdalin in Commercially Available Food Products. The extraction method described previously[18] was used for the extraction of amygdalin from food samples. Solid samples (2 g) were ground in a blender (20 s; Moulinex Optiblend 2000, France), and 1 g was weighed into a round-bottom flask (500 mL). In the case of liquid samples, ethanol (50 mL) was added to the samples (10 mL) in a round-bottom flask, and the mixture was boiled under reflux for 100 min. The extracts were filtered (Whatman no. 1 filter paper) and transferred into plastic polypropylene tubes (50 mL). Ethanol was completely evaporated from the filtrate with a rotary evaporator (low boiling point, 35 °C, 7 mbar). Diethyl ether (10 mL) was added to the dried sample, and the mixture was vortexed (1 min) at room temperature (20 ± 2 °C) to precipitate amygdalin. The diethyl ether was allowed to evaporate overnight in a fume hood, and the extracted amygdalin was dissolved in 1% BSA−PBST (1 mL). The food extract (100 μL) was then incubated with antibody on a coated plate as previously described for setting up the standard curve. Quantification of amygdalin in the sample was by reference to standard curves. Samples were also analyzed by HPLC as described previously to show the correlation of the results from the two methods. The HPLC extraction method was, however, different from the ELISA method. In the HPLC method, extracted amygdalin was further purified by dissolving it in water followed by centrifugation (14000 rpm, 22 °C, 10 min) and filtration with 0.45 μm PTFE filters prior to HPLC analysis.

RESULTS AND DISCUSSION

Immunoassays are now widely used in quantitative analysis for agri-food components for their advantages of cost-effectiveness and simplicity, which arise directly from the affinity of the antibody interaction with its target. Surprisingly, perhaps, given that immunoassays can be used away from fully equipped laboratories to monitor food processing, only two previous papers have described antibody production against cyanogenic glycosides, both against amygdalin.[27,28] No antibody characterization was carried out and no assay validation reported, nor were any quantitative data provided. The present paper provides antibody characterization, assay validation, and quantitative data on commercially available food products.

Hapten Synthesis. Methods for the production of hapten−protein conjugates need to be efficient, carried out under mild conditions, and effective. To produce the amygdalin immunogen, we used a method previously used by Abuknesha et al.[29] to synthesize antibody−enzyme conjugates. Cyanuric chloride has reactivity toward hydroxyl groups under mild conditions, and the coupling method did not affect the structure of the target analyte (amygdalin). Figure 1 shows the synthetic scheme followed. To provide the immobilized phase of the assay, a KLH−amygdalin conjugate was produced using the same chemistry.

Estimation of Hapten−Protein Ratios. Amygdalin exhibited a UV maximum at 262 nm and BSA at 278 nm. The BSA−amygdalin conjugate had a peak at 278 nm and a significant shoulder at 262 nm. Similar results were seen with KLH. The magnitude of the 262 nm absorption was used to calculate hapten−protein ratios, which were found to be 23:1 and 19:1 for the BSA−amygdalin and KLH−amygdalin conjugates, respectively.

dx.doi.org/10.1021/jf501978d | J. Agric. Food Chem. 2014, 62, 6299−6305

Reaction of the proteins with TNBS generated standard curves at 405 nm. Theoretically, 59 lysine residues of BSA are available for coupling to hapten.[1] The percentage substitution of amygdalin calculated from the standard curves was 34.4%, giving a hapten−protein ratio for the immunogen of 20:1. The same procedure was employed for the KLH coating conjugate, and the ratio was calculated to be 17:1.

The hapten−protein ratios obtained for the BSA conjugate (23 and 20:1) and the coating conjugate (19 and 17:1) using the spectrophotometric and chemical methods were very close. This is an indication that the use of cyanuric chloride as a coupling agent for conjugate production was efficient and that the procedure merits wider utilization in the future. The hapten−protein ratios obtained in this study were in line with recommended ratios for good antibody production. Kemp and Morgan[31] reported that a conjugate with a high hapten−protein ratio is good as an immunogen, whereas the one with a low ratio may be desirable as a coating antigen. Hapten densities of 15−30 molecules per carrier protein were also reported to be good for the production of high antibody titers.[1]

Antibody Titer. The BSA−amygdalin conjugate was used in antibody production in rabbits. The presence of anti-amygdalin antibodies was observed through production of titer curves using KLH−amygdalin as the immobilized phase on microtitration plates. Antibody binding as measured by optical density was 2.1 at a dilution of 1:10000 (v/v) compared to that given by preimmune serum (0.03 at 1:10000). Even at dilutions of 1:100,000, the antisera showed significant binding above that of the preimmune serum. The antiamygdalin antiserum was used at a dilution of 1:30000 for subsequent experiments unless otherwise stated. For antihapten antisera, such a dilution is at the high end of what is achievable.

Optimization of the ELISA. The antibody dilution, incubation time, coating conjugate concentration, and use of protein buffers were each investigated for ELISA optimization (Table 1). Antibody dilution significantly influenced the sensitivity of the ELISA. A lower dilution (1:10000) of antibody resulted in higher IC_{50} (7 μg/well) than a 1:30000 dilution, which gave an IC_{50} of 0.80 μg mL^{-1}. When the antibody dilution was increased beyond 1:30000, the IC_{50} increased significantly. Consequently, an antibody dilution of 1:30000 in PBST was used throughout.

The incubation time for anti-amygdalin antibody and amygdalin on the microtitration plate was varied from 1 to 5 h (at 37 °C) and overnight at 4 °C. A higher IC_{50} (5.51 μg/mL) and lower R^2 (0.97) resulted from a 1 h incubation at 37 °C. As the incubation time increased, the IC_{50} decreased and R^2 values increased. Overnight incubation at 4 °C resulted in the lowest IC_{50} with $R^2 > 0.9$. Subsequent assays utilized an overnight incubation at 4 °C.

The concentration of the coating conjugate, KLH−amygdalin, strongly influenced ELISA performance. As the concentration of the coating conjugate was decreasing, the concentration of the free hapten (unconjugated amygdalin) was increasing. Consequently, an increase in the binding of the antibody to the unconjugated amygdalin was evidenced for coating conjugate concentrations of 0.01−0.05 μg mL^{-1}. The IC_{50} of the standard curve decreased with decreased coating conjugate concentration and the associated R^2 value increased. The assay was most sensitive with a coating conjugate concentration of 0.05 μg mL^{-1}. The assay sensitivity was good at this concentration (50 ng mL^{-1}), possibly because antibody bivalent binding was prevented at this lower concentration of conjugate.[31] A coating conjugate concentration of 0.05 μg mL^{-1} was used for subsequent assays.

Table 1. Effect of Antibody Dilution, Incubation Time, Coating Antigen Concentration, and Protein Buffers on ELISA Sensitivity

factor	IC_{50}[a] (μg/mL)	R^2 of linear equation
antibody dilution		
1:10000	7.00	0.96
1:20000	5.52	0.98
1:30000	0.80	0.99
1:40000	5.10	0.99
1:60000	8.91	0.99
incubation time (h)		
1	5.51	0.97
2	5.82	0.97
3	2.00	0.97
4	1.00	0.99
5	1.00	0.99
overnight	0.80	0.99
coating antigen concentration (μg/mL)		
0.01	0.08	0.90
0.05	0.39	0.99
0.1	0.75	0.98
1	0.80	0.99
protein buffers		
PBST	0.39	0.99
1% casein−PBST	0.81	0.98
1% gelatin−PBST	0.75	0.99
1% BSA−PBST	0.05	0.99

[a] IC_{50} = concentration of the analyte required for 50% inhibition of the antibody binding to the coating antigen.

The ELISA absorbance and sensitivity were greatly enhanced by using 1% (w/v) BSA−PBST as buffer. A significantly lower IC_{50} value was observed when 1% BSA−PBST was used as buffer compared to when PBST only or 1% casein−PBST or 1% gelatin−PBST was used as buffer. On the basis of the IC_{50} values, R^2 values and the ratios of the maximum and minimum absorbances for the amygdalin standard curves, 1% BSA−PBST was selected as the buffer for subsequent experiments.

Indirect Competitive ELISA. The optimized conditions were used to obtain an indirect competitive standard curve for amygdalin (Figure 2), represented by $Y = A_2 + (A_1 - A_2)/(1 + (x/x_0)_p)$, $R^2 = 0.9995$. The curve was fitted using OriginPro 8.6 software. The IC_{50} of the assay was estimated to be 50 ± 0.02 ng/mL with a detection limit of 200 ± 0.05 pg mL^{-1} (as determined by the concentration that corresponded to the optical density of zero binding reduced by 3 times the standard deviation of the mean zero binding). The working concentration range of the icELISA was 10 ng mL^{-1} (IC_{20}) and 1 μg mL^{-1} (IC_{80}). The detection limit of the ELISA reported here was significantly lower than previously reported limits using a polyclonal antibody (100 μg mL^{-1})[27] or a recombinant antibody (500 pg mL^{-1}).[28]

Cross-Reactivity. The specificity of the assay was investigated by testing the cross-reactivity of the antibody with other cyanogenic glycosides that are closely related to amygdalin. The results obtained (Table 2) showed that the antibody was very specific for amygdalin, with cross-reactions of 1.3% for prunasin, 0.1% for mandelonitrile, and <0.01% for linamarin and dhurrin. The differences in structure between amygdalin and prunasin occur at the point farthest from the

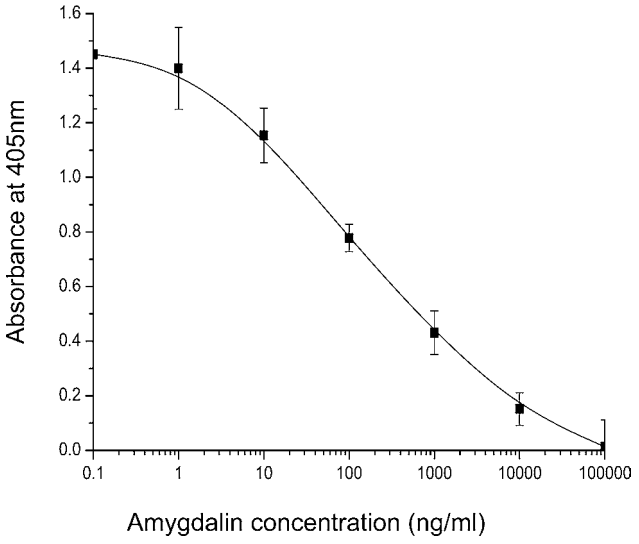

Figure 2. ELISA standard curve for amygdalin.

hydroxyl group used for coupling of hapten to protein. Even prunasin, a metabolite of amygdalin, did not inhibit antibody binding despite the close structural similarity to amygdalin. There was also a lack of reaction of the antibody with dhurrin (0.01%), where the additional hydroxyl group has a significant effect on antibody recognition. It can be assumed that the two sugar residues are key factors in antibody recognition. Other slight changes in other parts of amygdalin structure dramatically reduced antibody recognition for the other cyanogenic glycosides tested.

Quantification of Amygdalin in Commercially Available Food Products. Fruit kernels and processed products were analyzed by icELISA and HPLC after extraction of amygdalin. Figure 3 shows the correlation of the results with the two methods. The correlation is excellent ($r = 0.983$) across the whole range of amygdalin contents. The sample extraction procedure used for the ELISA is considerably simplified compared to that employed for HPLC. In addition, the batchwise nature of the ELISA further contributes to the high rate of sample throughput compared to HPLC.

Table 3 shows the values for amygdalin concentrations as determined by ELISA. Among the food samples analyzed in this study, fruit juices had the lowest amygdalin content (0.001−0.07 mg g^{-1}) followed by products (0.04−0.15 mg g^{-1}) and squashes (0.05−0.17 mg g^{-1}). However, high levels of amygdalin were detected in fruit seeds (0.04−4.52 mg g^{-1}) and kernels (2.14−9.75 mg g^{-1}). Lower levels of amygdalin observed in juices and processed products could be a result of the effect of processing on amygdalin. Processing methods have been reported to reduce the toxicity of cyanogenic glycosides (see the Introduction). Although low levels of cyanide would be generated from fruit juices, products, and squashes, the levels of cyanide that would be generated from fruit seeds (0.005−0.6 mg of equivalent HCN) and kernels

Table 2. Cross-Reactivity of the Anti-amygdalin Antiserum[a]

Compound	Chemical structure	IC_{50} (μg mL^{-1})	CR (%)
Amygdalin	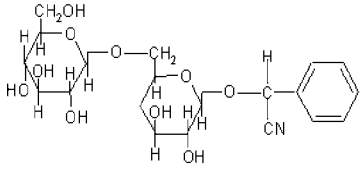	0.05	100
Prunasin	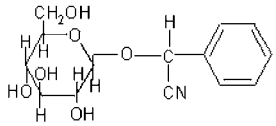	3.75	1.3
Dhurrin	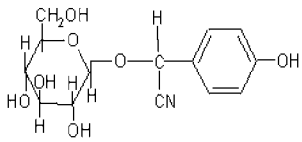	>500	<0.01
Mandelonitrile	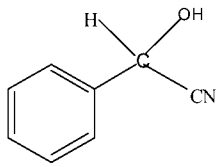	50	0.1
Linamarin	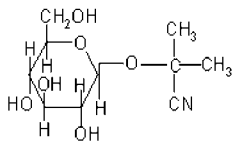	>500	<0.01

[a] IC_{50} = concentration of analyte required for 50% inhibition of antibody binding to the coating antigen.

dx.doi.org/10.1021/jf501978d | J. Agric. Food Chem. 2014, 62, 6299−6305

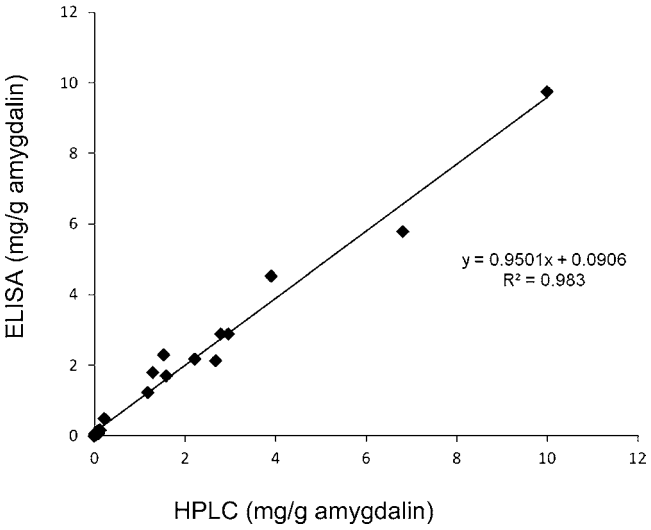

Figure 3. Correlation of results obtained by ELISA and HPLC analysis of food products.

Table 3. Quantification of Amygdalin in Commercially-Available Food Samples As Determined by ELISA

sample	amygdalin content[a] (mg g^{-1})
juices	
Del Monte apple	0.001 ± 0.001
Tesco pressed apple	0.017 ± 0.003
Copella apple	0.030 ± 0.004
Sainsbury's pressed apple	0.034 ± 0.002
Tropicana apple	0.038 ± 0.002
Sun-Grown cloudy apple	0.041 ± 0.005
Bramley apple	0.070 ± 0.003
products	
almond flour	0.040 ± 0.010
almond milk	0.061 ± 0.012
marzipan	0.060 ± 0.004
almond kernel (toasted)	0.152 ± 0.031
squashes	
butternut	0.051 ± 0.012
acorn	0.090 ± 0.022
Red Kabocha	0.131 ± 0.030
Crown Prince	0.172 ± 0.050
fruit seeds	
marrow	0.041 ± 0.003
melon (honeydew)	0.170 ± 0.041
cucumber	0.110 ± 0.041
courgette	0.501 ± 0.020
Braeburn apple	1.221 ± 0.510
Cox apple	1.711 ± 0.151
Conference pear	1.812 ± 0.760
Jazz apple	2.180 ± 0.681
Royal Gala apple	2.881 ± 0.911
Red Delicious apple	2.892 ± 0.621
Golden Delicious apple	4.521 ± 1.201
fruit kernels	
black cherry	2.140 ± 0.151
yellow plum	2.303 ± 0.901
peach	5.792 ± 0.831
black plum	9.751 ± 1.322

[a]Each value is expressed as the mean ± standard deviation (n = 3 determinations).

(0.3−1.3 mg of equivalent HCN) are relatively high. The lethal dose of cyanide is 0.5−3.5 mg kg^{-1} body weight.[4] Cyanide toxicity could easily occur from the consumption of fruit seeds and kernels, unless appropriate processing techniques are used and monitored.

Application of the icELISA to Cyanogenic Plants. Extracts of apricot kernels (a natural cyanogenic plant) having a high amygdalin content showed linearity (R^2 = 0.998) of the icELISA assay (result not shown). This further illustrates the detection of amygdalin by the developed ELISA method.

The reliability of the icELISA method was assessed by repeated ELISA analysis of amygdalin standard and food extract, 10 times on the same day (intraday variations) and 10 times on different days (interday variations). The coefficients of variation of both interday and intraday analyses were <1.0. The mean recovery of amygdalin (10 μg) added in triplicate to each of the 30 food samples analyzed in this study was determined to be 99 ± 1.2% (results not shown). The developed icELISA is a sensitive, cost-effective, and simple method for the quantification of amygdalin in food, capable of high sample throughputs.

Further research will investigate the efficiencies of processing techniques used with cyanogenic plants.

AUTHOR INFORMATION

Corresponding Author

*(I.F.B.) E-mail: m.morgan@food.leeds.ac.uk.

Notes

The authors declare no competing financial interest.

REFERENCES

(1) Ganjewala, D.; Kumar, S.; Asha, D. S.; Ambika, K. Advances in cyanogenic glycosides biosynthesis and analyses in plants: a review. *Acta Biol. (Szeged)* **2010**, *54*, 1−14.

(2) Zagrobelny, M.; Bak, S.; Rasmussen, A. N.; JØrgensen, B.; Naumann, C. M.; Møller, B. L. Cyanogenic glycosides and plant-insect interactions. Review. *Phytochemistry* **2004**, *65*, 293−306.

(3) Carter, J. H.; McLafferty, M. A.; Goldman, P. Role of the gastrointestinal microflora in amygdalin (laetrile)-induced cyanide toxicity. *Biochem. Pharmacol.* **1980**, *29*, 301−304.

(4) Speijers, G. *Cyanogenic Glycosides*; JECFA; WHO Food Additives Series 30; Geneva, Switzerland, 1993.

(5) Suchard, J. R.; Wallace, K. L.; Gerkin, R. D. Acute cyanide toxicity caused by apricot kernel ingestion. *Ann. Emerging Med.* **1998**, *32*, 742−744.

(6) Geller, R. J.; Barthold, C.; Saier, J. A.; Hall, A. H. Pediatric cyanide poisoning: causes, manifestations, management, and unmet needs. A review. *Pediatrics* **2006**, *118*, 2146−2158.

(7) Akyildiz, B. N.; Kurtoğlu, S.; Kondolot, M.; Tunç, A. Cyanide poisoning caused by ingestion of apricot seeds. *Ann. Trop. Paediatr.* **2010**, *30*, 39−43.

(8) Sahin, S. Cyanide poisoning in children caused by apricot seeds. *J. Health Med. Inform.* **2011**, *2*, 106.

(9) Sanchez-Verlaan, P.; Geeraerts, T.; Buys, S.; Riu-Poulenc, B.; Cabot, C.; Fourcade, O.; Mégarbane, B.; Genestal, M. An unusual cause of severe lactic acidosis:cyanide poisoning after bitter almond ingestion. *Intensive Care Med.* **2011**, *37*, 168−169.

(10) Jones, D. A. Why are so many food plants cyanogenic? *Phytochemistry* **1998**, *47*, 155−162.

(11) Francisco, I. A.; Pinitto, M. H. P. Cyanogenic glycosides in plants. *Braz. Arch. Biol. Technol.* **2000**, *43*, 487−492.

(12) Donald, G. B. Cyanogenic foods (cassava, fruit kernels, and cycad seeds). Review. *Med. Toxicol. Nat. Substances* **2009**, *55*, 336−352.

(13) Montagnac, J. A.; Davis, C. R.; Tanumihardjo, S. A. Processing techniques to reduce toxicity and antinutrients of cassava for use as a staple food. *Compr. Rev. Food Sci. Food Saf.* **2009**, *8*, 17−27.

(14) Voldřich, M.; Kyzlink, V. Cyanogenesis in canned stone fruits. *J. Food Sci.* **1992**, *57*, 161−162.
(15) Wasserkrug, K.; Rassi, Z. E. High performance liquid phase separation of glycosides. I. Reversed phase chromatography of cyanogenic glycosides with UV and pulsed amperometric detection. *J. Liq. Chromatogr. Relat. Technol.* **1997**, *20*, 335−349.
(16) Sornyotha, S.; Kyu, K. L.; Ratanakhanokchai, K. Purification and detection of linamarin from cassava root cortex by high performance liquid chromatography. *Food Chem.* **2007**, *104*, 1750−1754.
(17) Chassagne, D.; Crouzet, J. C.; Bayonove, C. L.; Baumes, R. L. Identification and quantification of passion fruit cyanogenic glycosides. *J. Agric. Food Chem.* **1996**, *44*, 3817−3820.
(18) Bolarinwa, I. F.; Orfila, C.; Morgan, M. R. A. Amygdalin content of seeds, kernels and food products commercially-available in the UK. *Food Chem.* **2013**, *152*, 133−139.
(19) Meulenberg, E. P. Immunochemical detection of environmental and food contaminants: development, validation and application − review. *Food Technol. Biotechnol.* **1997**, *35*, 153−163.
(20) Ramesh, A.; Thirugnanam, P. E.; Balakrishnamurthy, P. Hapten synthesis, generation of polyclonal antibodies and development of ELISA for determination of thiamethoxam residues in food and environmental samples. *Indian J. Biotechnol.* **2007**, *6*, 365−371.
(21) Sathe, M.; Ghorpade, R.; Merwyn, S.; Agarwal, G. S.; Kaushik, M. P. Direct hapten-linked competitive inhibition enzyme-linked immunosorbent assay (CIELISA) for the detection of *O*-pinacolyl methylphosphonic acid. *Analyst* **2012**, *137*, 406−413.
(22) Quan, Y.; Zhang, Y.; Wang, S.; Lee, N.; Kennedy, I. R. A rapid and sensitive chemiluminescence enzyme-linked immunosorbent assay for the determination of fumonisin B_1 in food samples. *J. Anal. Chim. Acta* **2006**, *580*, 1−8.
(23) Pastor-Navarro, N.; Morais, S.; Maquieira, A.; Puchades, R. Synthesis of haptens and development of a sensitive immunoassay for tetracycline residues application to honey samples. *J. Anal. Chim. Acta* **2007**, *594*, 211−218.
(24) Watanabe, E.; Hoshino, R.; Kanzaki, Y.; Tokumoto, H.; Kubo, H.; Nakazawa, H. New approach to immunochemical determinations for triclopyr and 3,5,6-trichloro-2-pyridinol by using a bifunctional hapten, and evaluation of polyclonal antiserum. *J. Agric. Food Chem.* **2002**, *50*, 3637−3646.
(25) Shinkaruk, S.; Lamothe, V.; Schmitter, J.-M.; Fructus, A.; Sauvant, P.; Vergne, S.; Degueil, M.; Babin, P.; Bennetau, B.; Bennetau-Pelissero, C. Synthesis of haptens and conjugates for ELISA of glycitein: development and validation of an immunological test. *J. Agric. Food Chem.* **2008**, *56*, 6809−6817.
(26) Kondo, M.; Tsuzuki, K.; Hamada, H.; Yamaguchi, Y.; Uchigashima, M.; Saka, M.; Watanabe, E.; Iwasa, S.; Narita, H.; Miyake, S. Development of an enzyme-linked immunosorbent assay (ELISA) for residue analysis of the fungicide azoxystrobin in agricultural products. *J. Agric. Food Chem.* **2011**, *60*, 904−911.
(27) Cho, A.-Y.; Yi, K. S.; Rhim, J.-H.; Kim, K.-I.; Park, J.-Y.; Keum, E.-H.; Chung, J.; Oh, S. Detection of abnormally high amygdalin content in food by an enzyme immunoassay. *Mol. Cells* **2006**, *21*, 308−313.
(28) Cho, A.-Y.; Shin, K.-J.; Chung, J.; Oh, S. A sensitive enzyme immunoassay for amygdalin in food extracts using a recombinant antibody. *J. Food Prot.* **2008**, *71*, 2048−2052.
(29) Abuknesha, R. A.; Luk, C. Y.; Griffith, H. H. M.; Maragkou, A.; Lakovaki, D. Efficient labelling of antibodies with horseradish peroxidase using cyanuric chloride. *J. Immunol. Methods* **2005**, *306*, 211−217.
(30) Habeeb, A. Determination of free amino groups in proteins by trinitrobenzenesulfonic acid. *Anal. Biochem.* **1966**, *14*, 328−336.
(31) Kemp, H. A.; Morgan, M. R. A. Studies on the detrimental effects of bivalent binding in a microtitration plate ELISA and possible remedies. *J. Immunol. Methods* **1986**, *94*, 65−72.
(32) Qiant, G. L.; Wang, L. M.; Wu, Y. R.; Zhang, Q.; Sun, Q.; Liu, Y.; Liu, F. A monoclonal antibody-based sensitive enzyme-linked immunosorbent assay (ELISA) for the analysis of the organophosphorous pesticsides chlorpyrifos-methyl in real samples. *Food Chem.* **2009**, *117*, 364−370.

Few studies on carotenoid content of bee pollen are published worldwide,[1,13,16,26,27] and, to the best of our knowledge, no studies related to carotenoid and also fatty acid composition of multifloral bee-collected pollen from Romanian (Transylvania) have been done, although pollen is often consumed as a food supplement. With respect to adopting the European Regulations regarding bee product labeling, the present work aims to offer new important information about the lipid classes present in pollen samples and also about total and individual carotenoid composition of multifloral pollen loads collected by bees in different regions from Transylvania (Romania). For the first time, a classification of pollen samples was achieved by subjecting the data obtained in chemical analysis to principal component analysis (PCA) with cross-validation (full model size and center data).

MATERIALS AND METHODS

Pollen Samples. Sixteen bee pollen samples (0.5 kg each) were collected between May and August 2010 from three different counties in the Transylvania region (Romania) (Supporting Information Table S1). The areas were characterized by rich spontaneous and also cultivated plants. Bee pollen was obtained with a bottom fitting pollen trap placed in the front of the hives, daily harvested, cleaned of impurities, and stored immediately at −18 °C until analysis.

Physicochemical analyses of pollen samples were made according to literature studies[1] and existing pollen regulations, and results were published previously.[24]

Palynological Origin. The bases of palynological analysis were the methods described by Almeida-Muradian et al.,[1] Morais et al.,[6] and Louvreaux et al.[28] adapted for pollen load.

A sample of 2 g, corresponding to approximately 200 pollen pellets, was considered to be representative for botanical origin determination. The pellets were grouped into subsamples according to their color, and each subsample was weighed to calculate the percentage from the main bee-collected pollen samples.[1,6] From each subsample, one microscopic slide was prepared without acetolysis, by dissolving and washing the pollen in diluted H_2SO_4 (5‰) and colored using a mixture of glycerin−gelatin−fuxine for permanent preparation.[28]

Slide examination was performed using a Nikon Eclipse 50i optic microscope at 1000× magnification (for identification) and 400× magnification for counting. Five hundred pollen grains were counted from every slide, and percentages of different botanical species were calculated. For the identification of pollen type, reference pollen collection slides from the Beekeeping Department, University of Agricultural Sciences and Veterinary Medicine from Cluj Napoca, were used, as well as different pollen guides.[29,30]

Chemicals and Reagents. All reagents (used for the lipid extraction and fatty acid methyl esters (FAMEs) preparation) were of chromatographic grade (Sigma-Aldrich, St. Louis, MO, USA). The FAMEs standard (37 component FAME Mix) were purchased from Supelco (Bellefonte, PA, USA).

Methanol, ethyl acetate, petroleum ether, diethyl ether, sodium chloride, triethylamine, and anhydrous sodium sulfate were purchased from Sigma Chemical Co. The purity of carotenoid standards (98% for β-cryptoxanthin, 96% for β-carotene, and 97.5% for lutein) was estimated by UV−vis spectra and by an individual HPLC analysis. Solvents used for carotenoid analysis (ethyl acetate, and acetonitrile) were purchased from Merck.

Analytical Methods. *Carotenoids Identification. (a) Carotenoids Extraction.* Total carotenoids were extracted from 5 g of fresh bee pollen with a mixture of methanol/ethyl acetate/petroleum ether (1:1:1, v/v/v) containing BHT as antioxidant, following the procedure described by Breithaupt and Schwack.[31] Extraction was carried out under agitation and diminished light and was repeated until the bee pollen became colorless. The combined extracts were washed in a separation funnel with sodium chloride and diethyl ether, and the upper collected phase was evaporated to drynes.

(b) Saponification. Every sample of obtained oleoresin was dissolved in 20 mL of diethyl ether and divided for further analysis. Ten milliliters of extract was saponified with 30% methanolic KOH, at room temperature, in the dark, for 24 h. For the removal of soaps and alkalis, the solution was washed three to four times with a sodium chloride saturated solution and distilled water. The organic layer containing carotenoids was dried over anhydrous sodium sulfate and evaporated to dryness.[32] Samples were kept under nitrogen at −20 °C until further utilization.

Total carotenoids content was estimated spectrophotometrically from saponified samples, at 450 nm, using a Shimadzu UV-2102 PC scanning spectrophotometer.

HPLC Analysis. HPLC-DAD of all samples was performed on a system with a Waters 990 PDA detector, Kontron pumps and controller, and a reversed phase C 18 column Zorbax ODS (250 × 4.6 mm), 5 μm. The mobile phase consisted of mixtures of acetonitrile/water (9:1, v/v) with 0.25% triethylamine (solvent A) and ethyl acetate with 0.25% triethylamine (solvent B). The gradient started from 20% B to 50% B at 3 min. The percent of B increased to 75% at 12 min and continued isocratically up to 25 min. The flow rate was 1 mL/min. The chromatograms were monitored at 450 nm.

The carotenoids identification was made by comparing the retention times of sample compounds with available standards and according to UV−vis spectra recorded by PDA detector.

Calibration curves for lutein, β-cryptoxanthin, and β-carotene were used for quantitative analysis. The results were expressed as micrograms per gram of pollen (fresh and dry weight).

Fatty Acid Analysis. (a) Lipids Extraction. The total lipids (TLs) of the honeybee-collected pollen samples were extracted using a chloroform/methanol mixture.[33,34] The sample (5 g pollen) was homogenized in methanol (20 mL) for 1 min with a high-power homogenizer (MICCRA D-9, Germany), then chloroform (40 mL) was added, and homogenization was continued for 2 min. The mixture was filtered, and the solid residue was resuspended in chloroform/methanol mixture (2:1, v/v, 60 mL) and homogenized again for 3 min. The mixture was again filtered, and the residue was washed with 60 mL chloroform/methanol (2:1, v/v). The filtrates and washings were combined and cleaned with an 0.88% potassium chloride water solution and a methanol/water solution (1:1, v/v). The purified lipid layer (bottom) was filtered and dried over anhydrous sodium sulfate, and the solvent was removed in a rotary evaporator. The recovered total lipid fractions were transferred to vials with 4 mL of chloroform, forming the stock solution, and stored at −18 °C for further analysis.

(b) GC Analysis of FAMEs. The fatty acid methyl esters (FAMEs) were prepared from TLs using the acid-catalyzed transesterification procedure described by Christie.[35] The FAMEs were determined by gas chromatography−mass spectrometry (GC-MS).[34] A PerkinElmer Clarus 600 T GC-MS (PerkinElmer, Inc., Shelton, CT, USA) equipped with a Supelcowax 10 (60 m × 0.25 mm i.d., 0.25 μm film thickness; Supelco Inc., Bellefonte, PA, USA) capillary column was used. The injector temperature was set at 210 °C. The temperature program for the column was as follows: initial temperature, 140 °C; increase by 7 °C/min to 220 °C; and hold for 23 min. The flow rate of the carrier gas (helium) was 0.8 mL/min, and the split value was a ratio of 1:24. The injected volume was 0.5 μL. The positive ion electron impact (EI) mass spectra was recorded at an ionization energy of 70 eV and a trap current of 100 μA with a source temperature of 150 °C. The mass scans were performed within the range of m/z 22−395 at a rate of 0.14 scan/s with an intermediate time of 0.02 s between the scans. Identification of FAMEs was achieved by comparing their retention times with those of known standards (37 component FAME Mix, Supelco no. 47885-U) and the resulting mass spectra to those in our database (NIST MS Search 2.0). The amount of fatty acids was expressed as percent of total fatty acids.

Statistical Analysis. Three different replicates of each honeybee-collected pollen were assayed. The analytical results reported for the fatty acid compositions are the average of triplicate measurements of three independent total lipid fractions ($n = 3 \times 3$). Results reported for carotenoid determination represent the mean of three independent analyses. Statistical differences among samples were estimated using ANOVA (one-way analysis of variance; Tukey's multiple-comparison test; GraphPad Prism version 4.0, Graph Pad Software Inc., San Diego, CA, USA). A probability value of $p < 0.05$ was considered to be statistically significant.

Table 1. Plant Species Giving the Predominant, Secondary, and Minor Pollen in the Analyzed Samples

	predominant pollen (>45%)		secondary pollen (16−45%)		important minor pollen (3−15%)		minor pollen (<3%)	
sample	family	species	family	species	family	species	family	species
P1	Rosaceae	*Crataegus monogyna*	Fagaceae	*Quercus* sp.	Brassicaceae	*Brassica* sp.	Asteraceae	*Taraxacum officinale*
							Fabaceae	*Onobrychis viciifolia*
P2	Rosaceae	*Filipendula ulmaria*	Hypericaceae	*Hypericum* sp.	Lamiaceae	*Thymus* sp.	Fabaceae	*Trifolium pratense*
					Asteraceae	*Artemisia* sp.	Ericaceae	*Calluna vulgaris*
							Onagraceae	*Epilobium* sp.
P3	Rosaceae	*Filipendula ulmaria*	Ericaceae	*Calluna* sp.	Asteraceae	*Artemisia* sp.	Onagraceae	*Epilobium* sp.
					Hypericaceae	*Hypericum* sp.	Asteraceae	*Taraxacum officinale*
							Geraniaceae	*Geranium* sp.
P4	Rosaceae	*Malus domestica*	Brassicaceae	*Brassica* sp.	Asteraceae	*Taraxacum officinale*		
P5	Fabaceae	*Trifolium repens*	Hypericaceae	*Hypericum* sp.	Fabaceae	*Anthillis* sp.	Asteraceae	*Taraxacum officinale*
						Medicago sativa		
					Asteraceae	*Artemisia* sp.	Fabaceae	*Onobrychis viciifolia*
							Onagraceae	*Epilobium* sp.
P6	Rosaceae	*Prunus* sp.	Brassicaceae	*Brassica* sp.			Asteraceae	*Taraxacum officinale*
P7	Asteraceae	*Calendula officinalis*	Tiliaceae	*Tilia* sp.	Brassicaceae	*Brassica* sp.	Asteraceae	*Taraxacum officinale*
			Fabaceae	*Trifolium pratense*			Fabaceae	*Vicia sativa*
							Asteraceae	*Artemisia* sp.
								Matricaria chamomilla
							Rosaceae	*Filipendula ulmaria*
P8	Asteraceae	*Taraxacum officinale*	Rosaceae	*Prunus* sp.	Asteraceae	*Cichorium* sp.	Fabaceae	*Anthillis* sp.
							Brassicaceae	*Brasica* sp.
							Rosaceae	*Malus domestica*
P9	Rosaceae	*Filipendula ulmaria*	Hypericaceae	*Hypericum* sp.	Lamiaceae	*Thymus* sp.	Fabaceae	*Medicago sativa*
					Asteraceae	*Artemisia* sp.		*Onobrychis viciifolia*
					Onagraceae	*Epilobium* sp.	Rosaceae	*Rubus* sp.
							Asteraceae	*Taraxacum officinale*
							Ericaceae	*Calluna* sp.
P10	Fabaceae	*Anthilis* sp.	Fabaceae	*Medicago sativa*	Asteraceae	*Calendula officinalis*	Fabaceae	*Onobrychis viciifolia*
			Asteraceae	*Taraxacum officinale*	Rosaceae	*Carduus* sp.	Lamiaceae	*Thymus* sp.
						Rubus sp.	Geraniaceae	*Geranium* sp.
						Filipendula ulmaria		
					Salicaceae	*Salix* sp.		
P11	Rosaceae	*Rosa canina*	Hypericaceae	*Hypericum* sp.	Asteraceae	*Taraxacum officinale*	Fabaceae	*Onobrychis viciifolia*
			Scrophulariaceae	*Verbascum*sp.		*Matricaria chamomilla*		*Amorpha fruticosa*
							Rosaceae	*Filipendula ulmaria*
P12			Fabaceae	*Anthillis* sp.	Rosaceae	*Rubus* sp.	Asteraceae	*Taraxacum officinale*

dx.doi.org/10.1021/jf5020318 | J. Agric. Food Chem. 2014, 62, 6306−6316

Table 1. continued

	predominant pollen (>45%)		secondary pollen (16−45%)		important minor pollen (3−15%)		minor pollen (<3%)	
sample	family	species	family	species	family	species	family	species
				Medicago sp.	Ericaceae	*Vaccinum* sp.		
			Asteraceae	*Carduus* sp.	Fabaceae	*Trifolium* sp.		*Helianthus annuus*
							Lamiaceae	*Thymus* sp.
							Fabaceae	*Vicia sativa*
P13	Brasicaceae	*Brassica* sp.	Rosaceae	*Rubus* sp.	Rosaceae	*Prunus* sp.	Fagaceae	*Quercus* sp.
					Fabaceae	*Anthyllis* sp.	Fabaceae	*Medicago sativa*
P14	Ericaceae	*Calluna vulgaris*	Rosaceae	*Filipendula ulmaria*	Geraniaceae	*Geranium* sp.	Asteraceae	*Taraxacum officinale*
					Asteraceae	*Matricaria chamomilla*		
						Artemisia sp.		*Helianthus annuus*
P15	Salicaceae	*Salix* sp.	Betulaceae	*Carpinus betulus*	Rosaceae	*Prunus* sp.	Asteraceae	*Taraxacum officinale*
P16	Fabaceae	*Robinia pseudoacacia*			Asteraceae	*Taraxacum officinale*	Fabaceae	*Onobrychis viciifolia*
						Anthyllis sp.	Ericaceae	*Vaccinum* sp.
					Fabaceae	*Trifolium pratense*		
						Vicia faba		
					Salicaceae	*Salix* sp.		

Table 2. Individual Carotenoids Concentration in Bee Pollen Samples (HPLC Determination) and Total Carotenoid Content (Spectrophotometric Determination), Expressed as Micrograms per Gram Sample[a]

	lutein		β-cryptoxanthin		β-carotene		total carotenoid content	
sample	fresh wt	dry wt	fresh wt	dry wt	fresh wt	dry wt	fresh wt	dry wt
P1	50.89 k	64.17 j,k	1.04 j	1.31 m	0.17 h	0.21 i	58.30 h,i	73.52 j,k
P2	239.37 d	329.67 d	13.29 c	18.30 d	13.20 a	18.18 a	295.40 c	406.84 b
P3	51.26 k	65.80 j,k	1.78 i,j	2.28 l,m	tr	tr	59.30 h,i	76.12 j,k
P4	178.39 e,f	229.62 f	5.51 f	7.09 i	tr	tr	183.90 e,f	236.71 f
P5	151.31 g	235.88 e,f	6.88 e	10.73 g	7.20 c	11.22 c	177.90 f	277.33 e
P6	44.52 k	57.04 k	2.49 h,i	3.19 k,l	2.89 f	3.70 f,g	49.90 i	63.94 k
P7	255.04 c,d	346.90 c,d	14.55 c	19.79 c,d	nd	nd	269.60 d	366.71 c
P8	392.52 a	476.30 a	13.31 c	16.15 e	0.59 h	0.72 h,i	425.32 a	516.08 a
P9	157.5 f,g	208.25 f	8.63 d	11.41 f,g	10.57 b	13.98 b	207.31 e	274.10 e
P10	317.11 b	433.84 b	21.04 b	28.78 b	12.56 a	17.18 a	385.44 b	527.27 a
P11	52.89 k	72.47 j,k	3.37 g,h	4.62 j	0.18 h	0.25 i	65.31 h,i	89.47 j,k
P12	153.96 g	218.53 f	24.96 a	35.43 a	tr	tr	198.82 e,f	282.17 d,e
P13	49.06 k	66.53 j,k	1.02 j	1.38 m	tr	tr	54.80 h,i	74.31 j,k
P14	94.92 i	130.28 g,h	5.22 f	7.14 h,i	5.08 d	6.97 d	113.05 g	155.13 g,h
P15	65.90 j,k	85.33 i,j	2.13 h,i,j	2.76 l,m	2.09 g	2.71 g	77.62 h	100.48 i,j
P16	95.63 h,i	116.29 h	4.59 f,g	5.58 i,j	4.17 e	5.07 e	104.39 g	126.94 h,i

[a]Different letters in each column denote statistical difference at $p < 0.05$. The values represent the mean of three replicates, separately analyzed. nd, not detected; tr, traces.

The classification of pollen samples was achieved by subjecting the data obtained for palynological analysis, fatty acids, total lipids content, lutein, β-cryptoxanthin, β-carotene, and total carotenoids to PCA with cross-validation (full model size and center data). All of the statistical analyses were performed using Unscrambler X software version 10.1 (CAMO Software AS, Oslo, Norway).

RESULTS AND DISCUSSION

Palynological Identification. Table 1 presents the identified plant families and species giving the predominant, secondary, and minor pollen in the analyzed samples.

According to palynological analysis, all pollen samples were found to be heterofloral, having different pollen types and percentages as constituents. Six plant families were found in the 16 pollen samples as predominant pollen constituents (>45% from the total content): Rosaceae (*Crataegus monogyna*, *Filipendula ulmaria*, *Malus domestica*, *Prunus* sp.,*Rosa canina*); Fabaceae (*Trifolium repens*, *Anthilis* sp., *Robinia pseudoacacia*); Asteraceae (*Calendula officinalis*, *Taraxacum officinale*); Brassicaceae (*Brassica* sp.); Ericaceae (*Calluna vulgaris*); and Salicaceae (*Salix* sp.); another 10 botanical species were found to be secondary pollens for bee pollen samples (Table 1).

The Rosaceae family was dominant (>45%) in sevem pollen samples and was present as secondary pollen (16−45%) in another three samples, whereas the Fabaceae family was the

dx.doi.org/10.1021/jf5020318 | J. Agric. Food Chem. 2014, 62, 6306−6316

predominant pollen for three samples and the secondary pollen for another three samples. The Asteraceae family with *Taraxacum officinale*, *Calendula officinalis* and *Carduus* sp. was present in three different samples.

Pollen botanical origin from the pollen pellets may vary according to the region of collection, vegetation available for bees at the collecting moment, and climatic conditions.[36]

Carotenoid Determination. The total carotenoid content in saponified honeybee-collected pollen samples was determined using UV−vis spectrophotometry.

Quantitative analysis showed a wide range of concentrations for total carotenoid content: 49.90−425.32 μg/g in freshly collected bee pollen and 63.94−527.27 μg/g when reported to each sample's dry weight (Table 2). The highest carotenoid concentration was found in sample P8, having *Taraxacum officinale* as predominant pollen, and the lowest in sample P6, *Prunus spinosa* predominant pollen. In *Filipendula ulmaria* bee pollen (samples P2, P3, and P9) total carotenoid content was quantified as 295.40, 59.30, and 207.31 μg/g fresh weight, respectively. The results obtained for samples P2 and P9 are significantly different and also significantly different from P3 (lower catorenoid content), this fact being attributed to the secondary pollen found in this sample. In P2 and P9 *Hypericum* sp. is the secondary pollen (high content of total carotenoids quantified) and *Calluna* sp. the secondary pollen in P3, where low amounts of carotenoids were found.

Taraxacum officinale is reported to be the richest natural vegetable source of β-carotene,[37] above carrots, broccoli, and spinach.[38] *Filipendula ulmaria* is also a rich source of β-carotene (36.32 μg/g plant).[39] These data are additional proof of the results obtained in our study. No statistical differences on total carotenoid content were found between samples P1, P3, P11, and P13, reported as either fresh or dry weight.

HPLC-PDA analysis of carotenoids from bee pollen allows the separation, identification, and quantification of individual carotenoids present in the samples. Obtained results are presented in Table 2.

Lutein and β-cryptoxanthin were identified in all analyzed samples.

Lutein was the major carotenoid found in pollen samples. The concentration varied between 44.52 and 392.52 μg/g fresh weight (57.04 and 476.30 μg/g dry weight). The highest concentration was found in sample P8 (392.52 μg/g), followed by sample P10 (317.11 μg/g). The lowest lutein concentration was found in sample P6 (44.52 μg/g). Lutein concentration showed no significant statistical difference for samples P1, P3, P6, P11, P13, and P15.

The concentration of β-cryptoxanthin ranged between 1.02 and 24.96 μg/g fresh weight; the highest concentration (found in sample P12) is significantly different from that of sample P10, in which the concentration was 21.04 μg/g. The lowest concentration of β-cryptoxanthin was found in samples P1 and P13 with no statistical differences between the mentioned samples (1.04 and 1.02 μg/g fresh weight).

With regard to β-carotene content, in some of the samples only traces were detected, whereas the highest contents were found in samples P2 and P10 (13.20 and 12.56 μg/g fresh weight and 18.18 and 17.18 μg/g dry weight). No statistical differences between these two pollen samples was observed.

Most of the papers published on carotenoid determination from bee pollen (either total carotenoids or individual) report their results as micrograms per gram of fresh or dehydrated sample. To have a better comparison with literature data, our

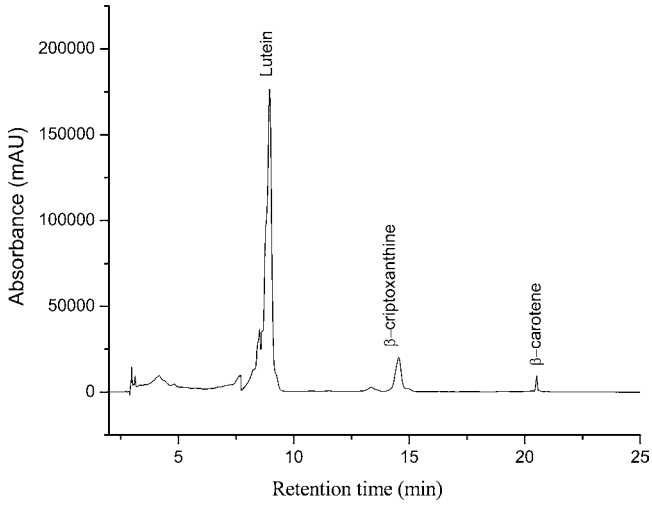

Figure 1. Chromatogram of identified carotenoids from saponified extract of bee pollen P2.

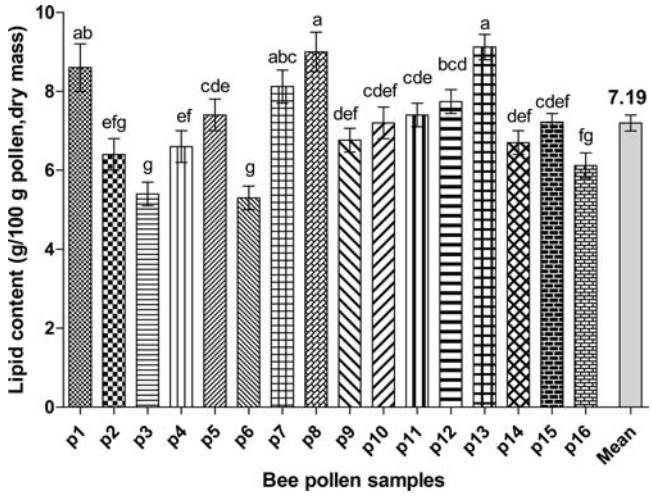

Figure 2. Total lipid content of honeybee-collected pollen samples from Romania (Transylvania). Results are given as the mean ± SD (n = 3). Values with different letters (a−g) are significantly different ($p < 0.05$), using ANOVA Tukey's multiple-comparison test. P1−P16, samples of multifloral pollen.

results regarding carotenoids are also reported on fresh and dry weight bases.

Almeida-Muradian et al.,[1] analyzing 10 Brazilian bee pollen samples, found a wide range of total carotenoid content: from "traces" (in 2 of the samples) to 451.50 μg/g fresh weight (489.20 μg/g dry weight). Although pollen samples were designated by the producers as monofloral pellets, botanical origin analysis showed the presence of 17 plant taxa in the 10 samples. The authors concluded that botanical origin is directly connected with carotenoid content; the highest value was obtained in pellets with high contents of *Senecio* and *Vernonia* pollen grains. The lack of β-carotene in all samples was attributed to the drying process of the samples.

Pereira de Melo and Almeida-Muradian,[27] analyzing fresh and dehydrated pollen samples from Brazil, found total carotenoid contents in fresh bee pollen ranging from 27.08 to 344.6 μg/g. β-Carotene content, quantified by HPLC by the same authors, varied from 3.77 to 99.27 μg/g fresh bee pollen samples. With regard to total carotenoid content, the results obtained from Romanian samples are in agreement with amounts determined

dx.doi.org/10.1021/jf5020318 | J. Agric. Food Chem. 2014, 62, 6306−6316

Table 3. Fatty Acid Composition (Percent of Total Fatty Acids)[a] of Total Lipids in the Honeybee-Collected Pollen from Transylvania, Romania

	pollen sample[b]																
fatty acid[c]	P1	P2	P3	P4	P5	P6	P7	P8	P9	P10	P11	P12	P13	P14	P15	P16	mean
1. 6:0	0.05	0.03	0.08	0.05	0.05	0.04	0.11	0.15	0.03	0.10	0.02	0.08	0.12	0.07		0.04	0.06
2. 8:0		0.01	0.04	0.08	0.03	0.02	1.74	0.34	0.01	0.29	0.06	0.19	0.12	0.02		0.16	0.19
3. 10:0	0.05	0.97	1.68	0.17	0.98	0.11	2.23	0.16	0.87	0.79	0.29	0.20	0.20	0.34	0.04	0.08	0.57
4. 12:0	0.60	1.96	3.65	3.39	2.14	1.53	2.06	8.51	1.98	2.67	1.56	2.30	0.13	3.59	0.49	0.63	2.33
5. 14:0	1.10	2.26	3.62	1.21	2.46	0.77	1.13	0.18	2.08	1.69	0.62	0.83	1.86	0.89	0.69	0.35	1.36
6. 16:0	24.28	28.99	23.30	23.01	25.58	22.29	27.00	18.39	27.92	23.88	30.93	30.00	28.05	27.58	24.46	27.32	25.81
7. 18:0	3.25	1.99	2.21	4.32	2.07	3.24	2.51	8.99	2.17	3.32	1.63	2.67	3.09	2.01	3.50	1.62	3.04
8. 18:1n-9	14.41	4.18	8.06	8.51	3.86	15.34	8.78	8.60	4.61	9.52	5.23	6.81	5.15	6.54	14.28	5.55	8.09
9. 18:1(9*t*)n-9	0.99	0.52	0.34	0.42	0.54	0.36	0.56	0.46	0.67	0.33	1.02	0.42	0.60	0.42	0.36	0.88	0.56
10. 18:2n-6	33.21	20.86	24.68	26.99	25.31	30.75	13.50	22.06	19.85	20.28	7.62	14.79	11.44	23.63	30.65	29.10	22.17
11. 18:3n-3	20.28	35.87	28.44	29.25	33.77	22.48	35.15	29.58	37.04	34.76	49.37	38.43	46.93	29.40	24.26	32.33	32.96
12. 20:0	0.73	1.23	2.09	0.97	1.34	0.96	0.83	1.30	1.32	0.72	0.58	1.47	0.84	3.18	0.55	0.67	1.17
13. 20:1n-9	0.19	0.26	0.25	0.33	0.28	0.45	3.63	0.53	0.33	0.38	0.22	0.35	0.11	0.51	0.23	0.23	0.52
14. 22:0	0.87	0.88	1.56	1.30	1.58	1.66	0.77	0.74	1.13	1.26	0.85	1.46	1.37	1.83	0.49	1.02	1.17
∑n-3 PUFAs	20.28	35.87	28.44	29.25	33.77	22.48	35.15	29.58	37.04	34.76	49.37	38.43	46.93	29.40	24.26	32.33	32.96
∑n-6 PUFAs	33.21	20.86	24.68	26.99	25.31	30.75	13.50	22.06	19.85	20.28	7.62	14.79	11.44	23.63	30.65	29.10	22.17
∑n-9 PUFAs	15.59	4.96	8.65	9.26	4.69	16.15	12.97	9.59	5.61	10.24	6.47	7.59	5.87	7.46	14.87	6.67	9.16
n-6/n-3	1.64	0.58	0.87	0.92	0.75	1.37	0.38	0.75	0.54	0.58	0.15	0.38	0.24	0.80	1.26	0.90	0.76

[a]The values represent the means of three samples, analyzed individually in triplicate ($n = 3 \times 3$). [b]P1−P16, samples of beepollen. [c]PUFAs, polyunsaturated fatty acids; caproic acid (6:0); caprylic acid (8:0); capric acid (10:0); lauric acid (12:0); myristic acid (14:0); palmitic acid (16:0); stearic acid (18:0); oleic acid (18:1n-9); elaidic acid [18:1(9*t*)n-9]; linoleic acid (18:2n-6); α-linolenic acid (18:3n-3); arachidic acid (20:0); 11-eicosenoic acid (20:1n-9); behenic acid (22:0).

dx.doi.org/10.1021/jf5020318 | J. Agric. Food Chem. 2014, 62, 6306−6316

from Brazilian fresh samples, but β-carotene content was significantly lower in Romanian samples (from traces to 13.2 μg/g fresh bee pollen). This can be attributed to different flora and climatic conditions between the samples.

Muniategui et al.[26] found 50−150 μg/g of carotene and 140−400 μg/g xanthophylls in four samples of fresh pollen. The same authors reported that total carotene content varied widely between samples. The small number of pollen samples analyzed in this case is not very conclusive, due to the fact that multifloral bee pollen is very different in composition because of the botanical origin of floral pollen. Also in this study, the high variability of total and individual carotenoids found could be attributed to climatic differences and the floral contribution to the pollen.

The HPLC-PDA chromatogram for one pollen sample (P2) is presented in Figure 1.

Besides carotenoids, other classes of biologically active compounds make important contributions to the nutritional and therapeutic properties of bee pollen. From previous research,[3,25] it is obvious that bee pollen can compete with other important sources of polyphenols,[32,39−43] having also high amounts of polyphenols and different classes of flavonoids.

Lipid Contents. The TLs contents in 16 honeybee-collected pollen samples are presented in Figure 2. Generally, the yields varied significantly ($p < 0.05$) within the analyzed pollen samples, with the highest levels of fats in P13 (9.12 g/100 g bee-collected pollen) and the lowest in P6 (5.30 g/100 g bee-collected pollen). Correlation with botanical origin is again confirmed, the highest amount of lipids being found in the sample having *Brassica* sp. as predominant pollen. Bee pollen samples having high amounts of total lipids (P7, P1, and P8) have in their botanical compositions different amounts of *Brassica* sp. pollen. It is known that *Brassica* sp. are rich sources of oleic, linoleic, and linolenic acids.[44] Pollens with high lipid concentrations are considered attractive to bees.[45] Previous studies have shown that the cytoplasm of pollen can contain twice as much lipids as found on the outermost layer of the pollen wall (pollenkitt).[2,18,22] The values obtained in this work were similar to those observed in the samples of honeybee-collected pollen originating from Poland (ranged from 6.74 to 10.99% dry matter), but higher, on average, than those determined for Korean (5.5% dw) and Chinese (6.2% dw) samples.[21] Differences in the lipid content of bee pollen may be attributed to the geographical and climate conditions, apicultural practices, and, last but not least, the genetic composition of plant species.[21]

Fatty Acid Composition. The fatty acid compositions, total n-3, n-6, n-9 polyunsaturated fatty acids (PUFAs) and the n-6/n-3 ratios of TLs from the Romanian honeybee-collected pollen are presented in Table 3. There were no qualitative differences in the fatty acid profiles of the TLs in all samples, except for the caproic acid (6:0) and caprylic acid (8:0), which are absent in the TLs of P1 and P15, respectively. Fourteen fatty acids were identified in the pollen extracts (Figure 3), from which the most abundant was α-linolenic (18:3n-3) acid, ranging between 20.28% (P1) and 49.37% (P11). The next most abundant fatty acids were linoleic acid (18:2n-6) (from 7.62%, P11, to 33.21% P1), followed by palmitic (16:0) (from 18.39%, P8, to 30.93%, P11) and oleic acids (18:1n-9) (from 3.86%, P5, to 15.34%, P6). Small and very small amounts (<3%) of stearic (18:0), myristic (14:0), lauric (12:0), arachidic (20:0), 11-eicosenoic (20:1n-9), behenic (22:0), elaidic [18:1(9 *t*)n-9), caproic (6:0), caprylic (8:0), and capric (10:0) acids were also determined. The ratios of n-6 to n-3 PUFAs ranged from 0.15 (P11) to 1.64 (P1) (Table 3). The average value of these ratios (0.76) is close to the values

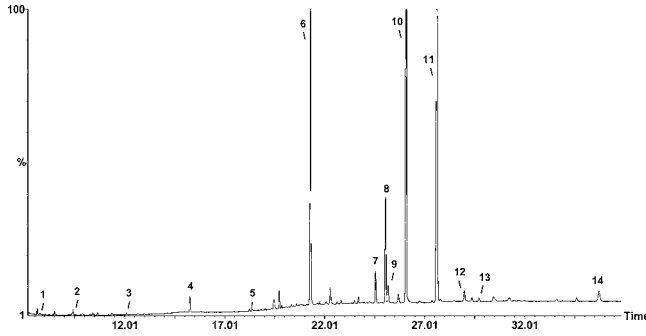

Figure 3. GC-MS chromatogram of FAMEs in the TLs of the honeybee-collected multifloral pollen (P16) from Romania (Transylvania) analyzed with a Supelcowax 10 capillary column. Peak identification: (1) caproic (6:0); (2) caprylic (8:0); (3) capric (10:0); (4) lauric (12:0); (5) myristic (14:0); (6) palmitic (16:0); (7) stearic (18:0); (8) oleic (18:1n-9); (9) elaidic [18:1(9*t*)n-9]; (10) linoleic (18:2n-6); (11) α- linolenic (18:3 n-3); (12) arachidic (20:0); (13) 11-eicosenoic (20:1(n-9); (14) behenic (22:0) acids.

recommended by Simopoulos[46] (n-6/n-3 = 1−5/1) as beneficial for good health.

Several studies suggest that lowering the dietary n-6/n-3 fatty acid ratio may reduce the risk of coronary heart disease and cancer.[47,48]

It is generally known that the dominant fatty acids present in pollens are palmitic, oleic, linoleic, and α-linolenic acids.[21] Significant differences were reported by different authors for compositions of myristic and arachidic acids.[21,44] It is interesting to note that the study of Bastos et al.,[49] carried out on 14 pollen samples from Brazil, demonstrated that one of the predominating fatty acids appeared to be arachidic acid (ranging from 8.90 to 42.7%). In contrast, the content of this long-chain saturated fatty acid estimated in our study and those of other researchers did not exceed even 1.50%.[21]

Manning[22] mentioned that pollen lipids, dominated by long-chain unsaturated (linoleic and linolenic) and saturated (myristic and lauric) fatty acids, have bactericidal and antifungal properties, playing an important role in inhibiting the growth of the spore-forming bacteria *Paenibacillus* (American foulbrood), *Melissococcus pluton* (European larvae larvae foulbrood) and other microorganisms that inhabit the brood combs of beehives. For larvae and young adult bees the fatty acids and other lipid classes are important sources of energy. The honeybees use the lipids for the synthesis of fat reserve and glycogen and for the production of royal jelly.[2]

The statistical analysis of fatty acid classes showed significant differences ($p < 0.05$) between pollen samples (Figure 4). The highest values of saturated fatty acids (SFAs) ($p < 0.05$) were registered in the TLs of P12 and P14 (~39%) (Figure 4A), whereas P6 (16.15%), P1 (15.59%), and P15 (14.90%) were the richest sources of monounsaturated fatty acids (MUFAs) (Figure 4B). On the other hand, small variations ($p < 0.05$) were found in PUFAs contents (Figure 4C), with the highest proportions in P16 (61.43%) and the lowest in P7 (48.65%). Different ratios of saturated and unsaturated fatty acids as quality index for pollen loads were determined. As shown in Figure 4D, the levels of the PUFAs/SFAs ratios were significantly higher ($p < 0.05$) in TLs of P16 (due to the high values of 18:3 (32.33%) and 18:2 (29.10%) fatty acids) than in the TLs of the other 15 pollen samples. The UFAs (unsaturated fatty acids)/SFAs ratio, considered as a quality index of bee pollen, determined in the present study was similar to the values reported by Serra Bonvehi

dx.doi.org/10.1021/jf5020318 | J. Agric. Food Chem. 2014, 62, 6306−6316

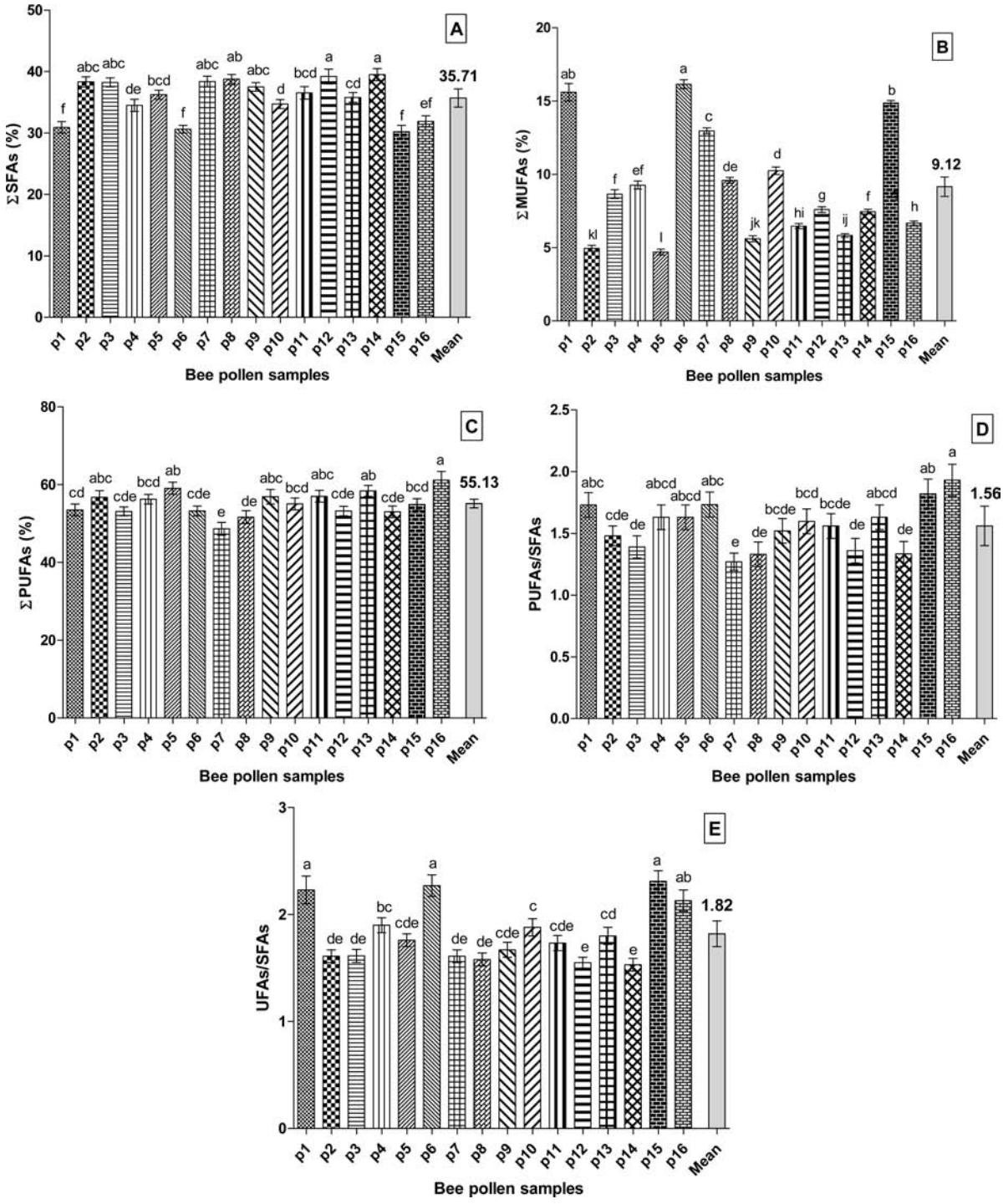

Figure 4. Comparative representation of fatty acid classes from total lipids of honeybee-collected pollen samples from Romania: (A) SFAs, saturated fatty acids; (B) MUFAs, monounsaturated fatty acids; (C) PUFAs, polyunsaturated fatty acids; ratio of polyunsaturated fatty acids to saturated fatty acids (D) and unsaturated fatty acids to saturated fatty acids (E) from multifloral bee collected pollen. Values are the mean ± SD of three samples, analyzed individually in triplicate ($n = 3 \times 3$). Values with different letters (a–l) are significantly different ($p < 0.05$), using ANOVA Tukey's multipl-comparison tes". P1–P16, samples of multifloral pollen

and Escora Jorda[50] and Szczęsna[21] and accounted for about 1.82 on average (Figure 4E).

According to PCA, the botanical origin of pollen samples was correlated with the amount of total lipids and fatty acid profile.

High levels of total carotenoids were found in some of the samples, demonstrating the direct link of botanical species rich in carotenoids (*Taraxacum*, *Calendula*, and *Filipendula* sp.) and bee pollen, these pollen types being important providers of provitamin A.

The major carotenoids found in the samples were lutein, β-cryptoxanthin, and β-carotene. Lutein was present in all samples as the major carotenoid. In contrast, β-carotene was identified and quantified only in some of the analyzed samples, and there detected just in traces or very small amounts.

dx.doi.org/10.1021/jf5020318 | J. Agric. Food Chem. 2014, 62, 6306–6316

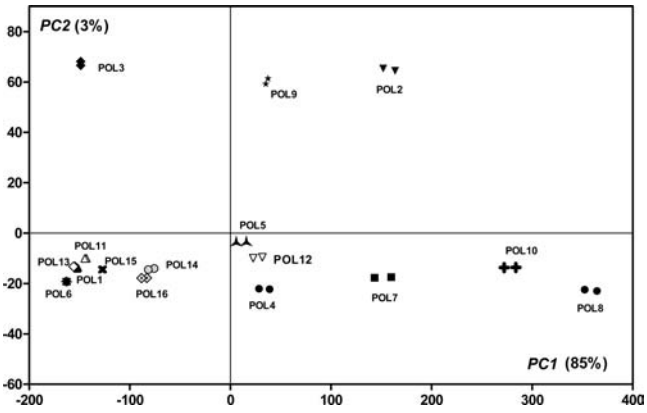

Figure 5. Principal component analysis biplot for the analyzed pollen samples. Two dimensions together explained 88% of the data variance.

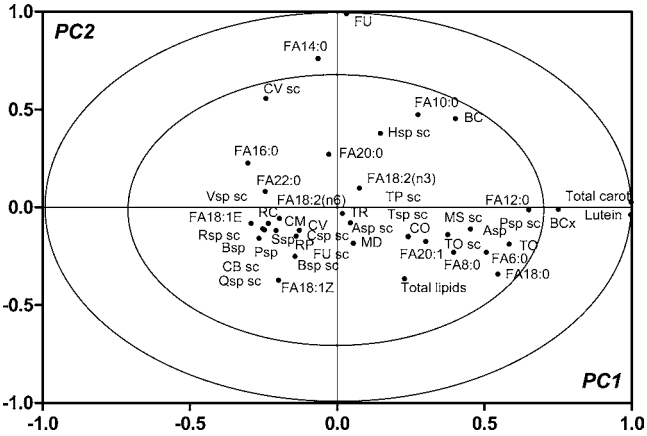

Figure 6. Correlation loading biplot for the analyzed pollen samples.

Lipid and carotenoid amounts in bee-collected pollen presented great variability between samples, which can be explained by the various botanical origins of those samples. In general, the investigated samples were characterized by high levels of α-linolenic (32.96% on average), palmitic (25.80, on average), and linoleic (22.17% on average) acids. Well-known is the beneficial effect of n-3 fatty acids in the prevention and management of cardiovascular disease, hyperinsulinemia, and possibly type 2 diabetes.[46] Bee-collected pollen with high levels of α-linolenic (n-3) acid together with a near 1:1 ratio of n-6 to n-3 PUFAs represents also a very balanced source of essential PUFAs for human health.

The PCA is a chemometric method that can be used to establish interrelationships between different sample variables, leading to the detection of similarities or differences between the patterns of the analyzed samples. On the basis of the PCA of the palynological analysis data, the pollen samples studied were not clearly discriminated, the first two principal components explaining only 31% of the variance of data. Instead, introducing also the fatty acid profile, total lipids content, lutein, β-cryptoxanthin, β-carotene, and total carotenoids contents as variables in PCA, a good discrimination of the pollen samples was achieved (the first two principal components explaining 89% of the variance of data). As shown in Figure 5, all analyzed pollen samples can be clearly differentiated on the basis of the above-mentioned parameters. Samples 2, 3, and 7−10 had a very distinctive pattern, whereas samples 1, 6, 11, 13, and 15 showed pattern similarities, as well as samples 5 and 12, respectively, and samples 14 and 16. The importance of individual variables can be assessed by computing the correlation loadings plot (Figure 6). The compounds from the inner ellipse indicate 50% of the explained variance, whereas those found in the outer ellipse indicate 100% of explained variance. Variables with loading values near zero have similar concentrations in all samples. Thus, it can be noted that total carotenoid content, lutein content, β-cryptoxanthin content, myristic acid (14:0) concentration, and *Filipendula ulmaria* predominant pollen significantly contribute to sample discrimination. According to the correlation loading plot, pollen samples 2, 3, and 9 are characterized by a high content in *Filipendula ulmaria* pollen and also in myristic acid compared to the other samples, whereas samples 7, 8, and 10 are richer in lutein, β-cryptoxanthin, and total carotenoids. With regard to carotenoid compounds, it has to be mentioned that a correlation loading plot showed that there is a strong positive correlation between total carotenoids and lutein.

■ ASSOCIATED CONTENT

Supporting Information

Table S1: Place of Origin and Harvesting Period for Bee-Collected Pollen Samples. This material is available free of charge via the Internet at http://pubs.acs.org.

■ AUTHOR INFORMATION

Corresponding Author

*(F.D.) Phone: 0040- 264-596384. Fax: 0040-264-593792. E-mail: francisc_dulf@yahoo.com.

Author Contributions

All authors contributed equally to this paper

Funding

This work was supported by a grant of the Romanian Ministry of Education, CNCS − UEFISCDI, Project PNII-RU-PD-2012-3-0245 (Contract 92/25.06.2013), POS CCE project RoBeeTech, no. 206/2010 and is a part of R.M.'s Ph.D. thesis.

Notes

The authors declare no competing financial interest.

■ ABBREVIATION USED

HPLC-DAD, high-performance liquid chromatography with photodiode array detection; GC-MS, gas chromatography with mass spectrometry detection; PUFAs, polyunsaturated fatty acids; SFAs, saturated fatty acids; UFAs, unsaturated fatty acids; UV, ultraviolet; PCA, principal component analysis; FAMEs, fatty acid methyl esters; BHT, butylated hydroxytoluene; TLs, total lipids; MUFAs, monounsaturated fatty acids

■ REFERENCES

(1) Almeida-Muradian, L. B.; Pamplona, L. C.; Coimbra, S.; Barth, O. M. Chemical composition and botanical evaluation of dried bee pollen pellets. *J. Food Compos. Anal.* **2005**, *18*, 105−111.

(2) Human, H.; Nicolson, S. W. Nutritional content of fresh, bee-collected and stored pollen of *Aloe greatheadii* var. *davyana* (Asphodelaceae). *Phytochemistry* **2006**, *67*, 1486−1492.

(3) Mărghitaş, L. A.; Stanciu, O. G.; Dezmirean, D. S.; Bobiş, O.; Popescu, O.; Bogdanov, S.; Campos, M. G. *In vitro* antioxidant capacity of honeybee-collected pollen of selected floral origin harvested from Romania. *Food Chem.* **2009**, *115*, 878−883.

(4) Szczesna, T.; Rybak-Chmielewska, H.; Chmielewski, W. Sugar composition of pollen loads harvested at different periods of the beekeeping season. *J. Apic. Sci.* **2002**, *46*, 107−115.

(5) Kleinschmidt, G. J.; Kondos, A. C. The effect of dietary protein on colony performance. *Aust. Beekeeper* **1978**, *80*, 251−257.

(6) Morais, M.; Moreira, L.; Feas, X.; Estevinho, L. M. Honeybee-collected pollen from five Portuguese natural Parks: plynological origin, phenolic content, antioxidant properties and antimicrobial activity. *Food Chem. Toxicol.* **2011**, *49*, 1096−1101.
(7) Yang, K.; Wu, D.; Ye, X.; Liu, D.; Chen, J.; Sun, P. Characterization of chemical composition of bee pollen in China. *J. Agric. Food Chem.* **2013**, *61*, 708−718.
(8) Tomás-Barberán, F. A.; Tomás-Lorente, F.; Ferreres, F.; Garcia-Viguera, C. Flavonoids as biochemical markers of the plant origin of bee pollen. *J. Sci. Food Agric.* **1989**, *47*, 337−340.
(9) Yasumoto, R.; Kawanishi, H.; Tsujino, T.; Tsujita, M.; Nishisaka, N.; Horii, A.; Kishimoto, T. Clinical evaluation of long term treatment using cernitin pollen extract in patients with benign prostatic hyperplasia. *Clin. Ther.* **1995**, *17*, 82−87.
(10) Haro, A.; López-Aliaga, I.; Lisbona, F.; Barrionuevo, M.; Alférez, M. J.; Campos, M. S. Beneficial effect of pollen and/or propolis on the metabolism of iron, calcium, phosphorus and magnesium in rats with nutritional ferropenic anemia. *J. Agric. Food Chem.* **2000**, *48*, 5715−5722.
(11) Eraslan, G.; Kanbur, M.; Silici, S. Effect of carbaryl on some biochemical changes in rats: the ameliorative effect of bee pollen. *Food Chem. Toxicol.* **2009**, *47*, 86−91.
(12) Pinto, B.; Cagiagli, F.; Riccio, E.; Reali, D.; Saric, A.; Balog, T.; Likic, S.; Scarpato, R. Antiestrogenic and antigenotoxic activity of bee pollen from *Cystus incanus* and *Salix alba* as evaluated by the yeast estrogen screen and the micronucleus assay in human lymphocytes. *Eur. J. Med. Chem.* **2010**, *45*, 4122−4128.
(13) Szczęsna, T.; Rybak-Chmielewska, H.; Skowronek, W. Zmiany wskladzie chemicznym obnózy pylkowych zachodzace podczas ich przechowywania w róznych warunkach. III. witamina C i prowitamina A (μ-karoten) [Alterations in the chemical composition of the pollen loads stored under various conditions. III vitamin C and provitamin A (μ-carotene)]. *Pszczelnicze Zeszyty Naukowe* **1995**, *40*, 171−189.
(14) Bogdanov, S. Quality and standards of pollen and beeswax. *Apiacta* **2004**, *38*, 334−341.
(15) Kritchevsky, S. B. β-Carotene, carotenoids and the prevention of coronary heart disease. *J. Nutr.* **1999**, *129*, 5−8.
(16) Montenegro, G.; Avila, G.; Rougier, D.; Timmermann, B. Pollen loads: source of carotenoids originating from the mediterranean plant communities of the central zone of Chile. *Rev. Chil. Hist. Nat.* **1997**, *70*, 91−99.
(17) Herbert, E. W. Chapter 6. Honey bee nutrition. In *The Hive and the Honey Bee*; Graham, J. M., Ed.; Dadant: Hamilton, IL, USA, 1997.
(18) Roulston, T. H.; Cane, J. H. Pollen nutritional content and digestibility for animals. *Plant Syst. Evol.* **2000**, *222*, 187−209.
(19) Nicolson, S. W. Bee food: the chemistry and nutritional value of nectar, pollen and mixtures of the two. *Afr. Zool.* **2011**, *46*, 197−204.
(20) Muniategui, S.; Sancho, M. T.; Lopez, J.; Huidobro, J. F.; Simal, J. Separación de las clases de lípidos neutros de polen apícola mediante cromatografía líquida de alta resolución (HPLC). *Grasas y Aceites* **1991**, *42*, 277−280.
(21) Szczęsna, T. Long-chain fatty acids composition of honeybee-collected pollen. *J. Apic. Sci.* **2006**, *50*, 65−79.
(22) Manning, R. Fatty acids in pollen: a review of their importance for honey bees. *Bee World* **2001**, *82*, 60−75.
(23) Stanciu, O. G.; Mărghitaş, L. Al.; Dezmirean, D.; Campos, M. G. A comparison between the mineral content of flower and honeybee collected pollen of selected plant origin (*Helianthus annuus* L. and *Salix* sp.). *Rom. Biotechnol. Lett.* **2011**, *16*, 6291−6296.
(24) Mărgăoan, R.; Mărghitaş, L. Al.; Dezmirean, D. S.; Bobiş, O.; Mihai, C. M. Physicochemical composition of fresh bee pollen from Transylvania. *Bull. USAMV C-N.* **2012**, *69*, 351−355.
(25) Mărgăoan, R.; Mărghitaş, L. Al.; Dezmirean, D. S.; Bobiş, O.; Tomoş, L.; Mihai, C. M.; Bonta, V. Honeybee-collected pollen from Transylvania: palynological origin, phenolic content and antioxidant activity. *Bull.USAMV C-N.* **2013**, *70*, 311−315.
(26) Muniategui, S.; Sancho, M. T.; Lopez, J.; Huidobro, J. F.; Simal, J. Determination of carotenes from bee-collected by high performance liquid chromatography. *J. Apic. Res.* **1990**, *29*, 147−150.
(27) Pereira de Melo, I. L.; Almeida-Muradian, L. B. Stability of antioxidants vitamins in bee pollen samples. *Quim. Nova* **2010**, *33*, 514−518.
(28) Louveaux, J.; Maurizio, A.; Vorwohl, G. Methods of melissopalynology. *Bee World* **1978**, *59*, 139−157.
(29) Sawyer, R. *Pollen Identification for Beekeepers*; Northern Bee Books, CLE Print: West Yorkshire, UK, 2006; pp24−30, 33−44.
(30) http://www.geo.arizona.edu/palynology.
(31) Breithaupt, D. E.; Schwack, W. Determination of free and bound carotenoids in paprika (*Capsicum annuum* L.) by LC/MS. *Eur. Food Res.Technol.* **2000**, *211*, 52−55.
(32) Bunea, C. I.; Pop, N.; Babeş, A. C.; Matea, C.; Dulf, F. V.; Bunea, A. Carotenoids, total polyphenols and antioxidant activity of grapes (*Vitis vinifera*) cultivated in organic and conventional systems. *Chem. Cent. J.* **2012**, *6*, 66−74.
(33) Yang, B. R.; Kallio, H. P. Fatty acid composition of lipids in sea buckthorn (*Hippophaë rhamnoides* L.) berries of different origins. *J. Agric. Food Chem.* **2001**, *49*, 1939−1947.
(34) Dulf, F. V. Fatty acids in berry lipids of six sea buckthorn (*Hippophae rhamnoides* L., subspecies *carpatica*) cultivars grown in Romania. *Chem. Cent. J.* **2012**, *6*, 106−117.
(35) Christie, W. W. Preparation of methyl ester and other derivatives. In *Gas Chromatography and Lipids. A Practical Guide*, 1st ed.; Christie, W. W., Ed.; Oily Press:: Glasgow, UK, 1989; pp 36−44.
(36) Luz, C.; Bacha, G., Jr.; Fonseca, R. L. E.; Sousa, P. Comparative pollen preferences by Africanized honeybees *Apis mellifera* L. of two colonies in Pará de Minas, Minas Gerais, Brazil. *An. Acad. Bras. Cienc.* **2010**, *82*, 293−304.
(37) Gail, P. A. *The Dandelion Celebration: A Guide to Unexpected Cuisine*; Goosefoot, AcresPress: Cleveland, OH, USA, 1994; pp155.
(38) Steward-Wade, S. M.; Neuman, S.; Collins, L. L.; Boland, G. J. The biology of Canadian weeds. 117. *Taraxacum officinale* G.H. Weber ex Wiggers. *Can. J. Plant Sci.* **2002**, 825−853.
(39) Barros, L.; Cabrita, L.; Boas, V. M.; Calvalho, A. M.; Ferreira, I. C. F. R. Chemical, biochemical and electrochemical assays to evaluate phytochemicals and antioxidant activity of wild plants. *Food Chem.* **2011**, *127*, 1600−1608.
(40) Figueiredo-González, M.; Martínez-Carballo, E.; Cancho-Grande, B.; Santiago, J. L.; Martínez, M. C.; Simal-Gandara, J. Pattern recognition of three *Vitis vinifera* L red grapes varieties based on anthocyanion and flavonol profiles, with correlations between their biosynthesis pathways. *Food Chem.* **2012**, *130*, 9−19.
(41) Vodnar, D. M.; Socaciu, C. Selenium enriched green tea increase stability of *Lactobacillus casei* and *Lactobacillus plantarum* in chitosan coated alginate microcapsules during exposure to simulated gastro-intestinal and refrigerated conditions. *LWT-Food. Sci. Technol.* **2014**, *57*, 406−411.
(42) Pugliese, G. A.; Tomás-Barberán, F. A.; Truchado, P.; Genovese, M. I. Flavonoids, proanthocyanidins, vitamin C, and antioxidant activity of *Theobroma grandiflorum* (cupuassu) pulp and seeds. *J. Agric. Food Chem.* **2013**, *61*, 2720−2728.
(43) Dezmirean, G. I.; Mărghitaş, L. Al.; Bobiş, O.; Dezmirean, D. S.; Bonta, V.; Erler, S. Botanical origin cause changes in nutritional profile and antioxidant activity of fermented products obtained from honey. *J. Agric. Food Chem.* **2012**, *60*, 8028−8035.
(44) Barissova, M.; Palk, K.; Vaher, M. Rapid analysis of free fatty acid composition in *Brassica rapa* L. and *Brassica napus* L. extracts by surface-assisted laser desorption/ionization time-of-flight mass spectrometry. *Proc. Chem. 2* **2010**, 174−179.
(45) Nicolson, S. W.; Human, H. Chemical composition of the 'low quality' pollen of sunflower (*Helianthus annuus,* Asteraceae). *Apidologie* **2013**, 144−152.
(46) Simopoulos, A. P. The importance of the omega-6/omega-3 fatty acid ratio in cardiovascular disease and other chronic diseases. *Exp. Biol. Med. (Maywood)* **2008**, *233*, 674−688.
(47) Goodstine, S. L.; Zheng, T.; Holford, T. R.; Ward, B. A.; Carter, D.; Owens, P. H.; Mayne, S. T. Dietary (n-3)/ (n-6) fatty acid ratio: possible relationship to premenopausal but not postmenopausal breast cancer risk in U.S. women. *J. Nutr.* **2003**, *133*, 1409−1414.

(48) Lee, S. P.; Dart, A. M.; Walker, K. Z.; O'Dea, K.; Chin-Dusting, J. P.; Skilton, M. R. Effect of altering dietary n-6:n-3 PUFA ratio on cardiovascular risk measures in patients treated with statins: a pilot study. *Br. J. Nutr.* **2012**, *108*, 1280−1285.
(49) Bastos, M. D. H.; Barth, O. M.; Rocha, C. I.; Silva Cunha, I. B.; Oliveira Carvahlo, P.; Silva Torres, E.; Michelan, M. Fatty acid composition and palynological analysis of bee (*Apis*) loads in the state of Sao Paulo and Minas Gerais, Brazil. *J. Apic. Res.* **2004**, *43*, 35−39.
(50) Serra Bonvehi, J.; Escola, J. R. Nutrient composition and microbiological quality of honeybee-collected pollen. *J. Agric. Food Chem.* **1997**, *45*, 725−732.

Furthermore, recent studies have demonstrated a genotype effect on retention[9] and bioefficacy,[10] underscoring the importance to conduct studies in the varieties ready for release.

Therefore, the purpose of this study was to evaluate the retention of provitamin A carotenoids in biofortified maize hybrids from the National Performance Trials (NPTs) in Zambia taking into consideration the local conditions of processing, cooking and storage.

MATERIALS AND METHODS

Biofortified Provitamin A Maize. Four medium maturing three-way hybrids with levels ranging from 6 to 8 μg/g DW of provitamin A were evaluated for their provitamin A retention after storage, milling, and cooking: two, GV662A (HP1002) and GV665A (HP1005), were hybrids released in Zambia in 2012, and two, HP1001 and HP1003, were advanced genotypes.

Harvesting and Storage of Maize. The four biofortified maize genotypes were planted in November 2010 at the Golden Valley Agriculture Research Trust (GART) in Chisamba, Zambia. In April 2011, the maize was harvested at the "green" stage (60% moisture content), which were immediately boiled and roasted; two months later, the "dry maize" (12% moisture content) was harvested. On the day of harvest, ears of all four genotypes were labeled and transported to ZARI in Lusaka where half of them were shelled (kernels) and the other half kept unshelled (ears) for six months in a traditional storage bin at ambient temperature. The temperature and humidity inside the storage bin were recorded on a weekly basis during the duration of the study.

Maize samples were collected at several intervals from the storage bin, and raw, processed, and cooked samples were kept in a liquid nitrogen tank until the samples were shipped for analysis. The baseline value (i.e., control) of provitamin A for all four genotypes was obtained from maize samples that were tested within 24 h of harvest. Subsequently, maize samples, stored as kernels and ears, were analyzed every two weeks (HP1002 and HP1005) and three and six months after storage (HP1001 and HP1003).

Retention of Provitamin A. All processing and cooking of maize samples were performed at the National Institute of Scientific and Industrial Research (NISIR) in Lusaka. Samples were stored in liquid nitrogen until shipped to the laboratory at the University of Wisconsin—Madison for analysis.

Processing of Green Maize. Green maize is commonly eaten either roasted or boiled. Before roasting or boiling, three rows of kernels of the raw green ear were removed and mixed to form the pool of maize kernels for the baseline values of the "raw roasted" or "raw boiled". The maize kernels were mixed and divided into four quarters from which two opposite quarters were combined, discarding the other two quarters. This procedure was repeated, and 10 to 15 kernels were selected and packed in 5 mL vials with screw caps and stored in the freezer at −30 °C.

After removing the kernels to obtain the "raw samples", three ears from each genotype were placed on a brazier without the husk and roasted for 15−20 min until all sides had turned brown. After roasting, three rows of kernels were removed from each ear and mixed to obtain a sample of roasted maize.

After removing three rows of kernels to obtain the "raw samples", three ears for each variety containing a thin layer of husk were put in an aluminum pot with 1200 mL of tap water. The pots were covered with lids and the ears were boiled for 35 min at 95 °C. After boiling, three rows of kernels were removed from each ear and mixed to obtain a sample of boiled maize.

Processing of Dry Maize. Most of the maize consumed in Zambia is in the form of "dry maize", which is usually milled and cooked into mainly three products for consumption: porridge, *nshima* (thick porridge), and *samp*. Dry maize can be stored for long periods of time. In order to study the retention of provitamin A during milling and cooking, 25 maize ears of each genotype were shelled, producing about 2.6−3.1 kg of kernels. Approximately 250 g of kernel was sampled per genotype to form the baseline pool.

Milling Methods. From the remaining maize kernels, about 2/3 was milled into *samp* and 1/3 was milled into maize meal using a local hammer mill. Approximately 250 g from each of the milled products was collected and formed the *raw samp* and *raw whole maize meal* samples. The effect of milling on retention was evaluated at baseline and three and six months.

Raw Maize *Samp*. First, 1700 g of whole dry kernels with 12% moisture (as-is-basis) was conditioned by steeping in cold water for 3−5 min to loosen the bran for decortication by a PRL dehuller (380 V, 50 Hz, 250−500 g/h, Canada) using abrasive carborundum disks, revolving at high speed in a barrel, and then bran was removed by aspiration. The dehulled kernels were collected as maize *samp* and bran as byproduct.

Whole Maize Meal (Mealie Meal). Whole maize kernels (400−900 g, 12% moisture) was put on a hopper through the hammer mills (Model-Commercial, 50T/24 Hr 380 V, 50 Hz, China) fitted with sieve no. 2 (8 mm opening) to produce fine whole maize meal for use in cooking porridge and/or *nshima*.

Cooking Methods. Three local women prepared the traditional Zambian maize dishes: porridge, *nshima*, and *samp* at NISIR in Lusaka. Their cooking methods were very similar; the recipes were standardized and each woman prepared only one dish in duplicate. Cooked products were prepared at baseline (time zero) and after the maize had been stored for three and six months. The cooking methods were standardized as follows:

Porridge. First, 100 g of maize meal was added to 700 mL of water at 50 °C in an aluminum pot. Then the mixture was continuously stirred with a wooden spoon until it started boiling and formed a gel at 95 °C. The pot was then covered with a lid, and the boiling continued for about 15 min. Total cooking time was 20 min.

Nshima. First, 150 g of maize meal was weighed and about 85 to 90 g was added to 600 mL of water at 50 °C in an aluminum pot. Then the mixture was continuously stirred with a wooden spoon until it started boiling and formed a gel at 95 °C and boiling was continued for 10 to 15 min. The remaining maize meal (60−65 g) was added to the pot with continuous stirring until a thick gel (*nshima*) was formed. The pot, covered with a lid, was allowed to simmer for about 5 min (total cooking time was 25 min).

Cooked Samp. First, 250 g of *samp* was weighed, washed with tap water, and transferred to an aluminum pot with 2000 mL of tap water (enough to cover the *samp*). Then the *samp* was boiled at 97 °C with occasional stirring and replenishing with tap water as needed. The total cooking time was 180 min.

Determination of Moisture. The moisture content of stored and processed samples was determined at baseline and three and six months by using a standard method (AOAC, 1984).

Extraction and Analysis of Carotenoids. The carotenoid extraction method from maize flour and maize porridge was based on a previously published procedure[11] with minor modifications. Whole maize samples were ground using a Knifetec 1095 sample mill (FOSS, Eden Prairie, MN, US). For all samples, 500 μL of 80% potassium hydroxide (w/v) was used for saponification. Saponification was performed to reduce the amount of lipid in the extract, which interferes with clean chromatography of carotenoids. Porridge samples were physically broken up after weighing but prior to the addition of ethanol and saponified for 45 min at room temperature. β-Apo-8′-carotenal (Sigma-Aldrich, St. Louis, MO, US) was used as an internal standard. Samples were reconstituted in 500 μL of 50:50 methanol:dichloroethane (v/v) and 50 μL injected into the HPLC system for quantification. The HPLC system was composed of a 1525 binary pump, a 717 autosampler, and a 2996 PDA detector (Waters, Milford, MA, US). Two mobile phases were used in a 40 min gradient system run through a C30 carotenoid column (3 μm, 4.6 mm × 250 mm) (YMC America, Allentown, PA). Solvent A, methanol:water (92:8, v/v) with 10 mmol/L ammonium acetate, and solvent B, 100% methyl-tertiary-butyl ether, were used. The gradient was run at 1 mL/min starting with 70% solvent A and transitioning to 40% within 30 min. The flow returned to 70% solvent A over 2 min, and then the column was equilibrated for 8 min prior to the next injection. Chromatograms were generated at 450 nm for quantification. β-

Carotene (Sigma-Aldrich, St. Louis, MO), α-carotene (isolated from freeze-dried carrots), β-cryptoxanthin (CaroteNature, GmbH, Lupsingen, Switzerland), lutein (GNC, Inc., Pittsburgh, PA), and zeaxanthin (GNC, Inc., Pittsburgh, PA) were identified using HPLC-purified standards. The β-carotene equivalents (BCE) were computed as follows: all-*trans*-β-carotene + 1/2 α-carotene + 1/2 β-cryptoxanthin + 1/2 13-*cis*-β-carotene + 1/2 9-*cis*-β-carotene.

Statistical Analysis. All data were analyzed using STATA version 13.0 (StataCorp, 2013). Descriptive statistics including mean and SD from duplicate analyses were calculated for the retention of carotenoids from processed maize. Means were compared using Student *t* tests and one-way ANOVA. Differences were considered significant at $P < 0.05$.

RESULTS AND DISCUSSION

Carotenoid Profile of Biofortified Maize. *Green versus Dry Maize.* The total carotenoid content, on DW basis, ranged from 19.0 to 36.4 μg/g in the green maize and from 24.4 to 30.8 μg/g in the dry maize among all four genotypes (Table 1); the values in fresh weight are provided in Table 1A of the Supporting Information. As expected, the green maize had a higher (3−33%) total carotenoid content than the dry maize, except for genotype HP1003, which presented a 26% increase in the total carotenoid content in the dry maize. This was mainly due to the average decrease in the zeaxanthin and lutein levels from 14.8 to 9.2 μg/g DW and 5.0 to 3.87 μg/g DW, respectively. On the other hand, β-cryptoxanthin increased from 1.7 to 6.3 μg/g DW between the green and dry maturity stages among all four genotypes. Therefore, the BCE was higher in the dry maize compared to the green maize for most genotypes. The green maize is available during a short season and is consumed roasted or boiled, while the dry maize is consumed throughout the year on a daily basis. Unless specified, the results presented in the following sections refer to the dry maize.

Dry Maize. Several carotenoids are present in maize (Table 1). The non-provitamin A carotenoids, lutein and zeaxanthin, are the major carotenoids in all four biofortified genotypes. Among the different genotypes, zeaxanthin and lutein accounted for 35% (28−46%) and 15% (11−20%) of total carotenoids, respectively. Although these carotenoids do not have vitamin A activity, they have an important role in maintaining good eye health and are associated with a reduced risk for age-related macular degeneration (AMD), the leading cause of blindness among elderly people.[12−15]

β-Cryptoxanthin and all-*trans*-β-carotene, were the main provitamin A carotenoids in the dry maize, accounting for 24% (19−28%) and 16% (10−23%) of total carotenoids, respectively. Collectively, the two provitamin A carotenoids accounted for 40% (33−49%) of total carotenoids. The amounts of α-carotene were negligible, accounting for only 1.5% (0.1−2.9%) of total carotenoids, while the *cis*-isomers of β-carotene, 9-*cis* and 13-*cis*, accounted for 4.3% and 4.9%, respectively. Overall, the β-carotene equivalents among all four genotypes ranged from 7.5 to 10.3 μg/g DW (7.0−9.5 μg/g FW). Genotype HP1005 (released in Zambia as variety GV665A) had the highest BCE (10.3 μg/g DW). Genotype HP1002 (released in Zambia as variety GV662A) presented BCE of 8.0 μg/g DW, not significantly different from either genotype HP1001 (8.9 μg/g DW) or HP1003 (7.5 μg/g DW). However, the genotypes showed different levels of all-*trans*-β-carotene and its *cis*-isomers as reported in the literature.[26]

It is important to note that high levels of β-cryptoxanthin in the biofortified maize were twice as high as all-*trans*-β-carotene

Table 1. Baseline Carotenoid Content (μg/g DW) of Four Genotypes of Biofortified Maize at Two Harvesting Stages[a,b]

variety/genotype	lutein	zeaxanthin	β-cryptoxanthin	α-carotene	all-*trans*-β-carotene	13-*cis*-β- carotene	9-*cis*-β-carotene	β-carotene equivalent[e]
Green Maize[c]								
all varieties	5.00 ± 1.18^{A}	14.83 ± 4.54^{A}	1.65 ± 0.45^{B}	0.39 ± 0.11^{A}	4.58 ± 2.22^{A}	1.30 ± 0.53^{A}	1.25 ± 0.48^{A}	6.87 ± 2.83^{A}
HP1001	4.03 ± 0.12^{cA}	14.30 ± 0.41^{bA}	1.19 ± 0.06^{cB}	0.36 ± 0.02^{aA}	5.84 ± 0.69^{bA}	1.68 ± 0.09^{bA}	1.58 ± 0.22^{aA}	8.24 ± 0.57^{bA}
HP1002	6.11 ± 0.68^{aA}	19.78 ± 0.61^{aA}	1.43 ± 0.16^{bcB}	0.36 ± 0.05^{aB}	2.50 ± 0.20^{cB}	0.77 ± 0.08^{cB}	0.70 ± 0.10^{bB}	4.13 ± 0.38^{cB}
HP 1003	4.16 ± 0.70^{bcA}	8.42 ± 2.94^{cA}	1.74 ± 0.10^{bB}	0.31 ± 0.14^{aA}	2.57 ± 0.39^{cA}	0.83 ± 0.15^{cA}	0.93 ± 0.12^{bA}	4.47 ± 0.61^{cB}
HP1005	5.70 ± 1.23^{abA}	16.83 ± 0.82^{abA}	2.25 ± 0.37^{aB}	0.50 ± 0.11^{aA}	7.41 ± 0.40^{aA}	1.92 ± 0.09^{aA}	1.78 ± 0.13^{aA}	10.64 ± 0.25^{aA}
Dry Maize[d]								
all varieties	3.87 ± 0.94^{B}	9.21 ± 3.02^{B}	6.26 ± 1.06^{A}	0.40 ± 0.30^{A}	4.18 ± 1.31^{A}	1.26 ± 0.25^{A}	1.12 ± 0.19^{A}	8.69 ± 1.16^{A}
HP1001	3.82 ± 0.33^{bA}	7.70 ± 0.47^{bB}	4.64 ± 0.25^{bA}	0.34 ± 0.01^{bA}	5.03 ± 0.04^{bA}	1.47 ± 0.02^{aB}	1.37 ± 0.06^{aA}	8.94 ± 0.21^{bA}
HP1002	3.83 ± 0.06^{bB}	14.03 ± 0.09^{aB}	6.89 ± 0.10^{aA}	0.88 ± 0.02^{aA}	3.13 ± 0.06^{cA}	1.08 ± 0.020^{bA}	0.95 ± 0.03^{bA}	8.02 ± 0.09^{bcA}
HP 1003	5.13 ± 0.15^{aA}	8.16 ± 0.22^{bA}	7.14 ± 0.03^{aA}	0.22 ± 0.08^{bcA}	2.83 ± 0.08^{cA}	0.99 ± 0.01^{bA}	0.99 ± 0.06^{bA}	7.50 ± 0.08^{cA}
HP1005	2.68 ± 0.12^{cB}	6.96 ± 0.29^{bB}	6.35 ± 0.44^{aA}	0.16 ± 0.10^{cB}	5.72 ± 0.27^{aB}	1.50 ± 0.14^{aB}	1.17 ± 0.09^{abB}	10.30 ± 0.61^{aA}

[a]Data are means ± SD of duplicated analyses. [b]Different lowercase letters indicate a statistically significant difference among the genotypes/varieties for the same harvesting stage. Different uppercase letters indicate a statistically significant difference between the two harvesting stages for the same genotype/variety. [c]Green maize was harvested after 5 months of planting with a moisture content of 61% on average. [d]Dry maize was harvested two months after the green maize with a final moisture content of 12% on average. [e]β-carotene equivalent = [all-*trans*-β-carotene + 1/2 α-carotene + 1/2 β-cryptoxanthin + 1/2 13-*cis*-β-carotene + 1/2 9-*cis*-β-carotene].

dx.doi.org/10.1021/jf501233f | J. Agric. Food Chem. 2014, 62, 6317−6325

(HP1002 and HP1003) or at equal levels with HP1001 and HP1005. During the germplasm screening for genetic variation, the sources of high provitamin A were found among maize from temperate regions, which were then bred into varieties suitable for tropical conditions. Moreover, these tropical varieties contain more β-cryptoxanthin and less β-carotene, and the emphasis was to enhance the β-carotene, which provides two vitamin A molecules per carotenoid molecule.[2] However, animal studies have shown that β-cryptoxanthin is absorbed and stored in many tissues[16] and it maintains the vitamin A status of gerbils as efficiently or better than β-carotene.[17]

Most of the yellow maize grown and consumed throughout the world has less than 2.0 μg/g DW of provitamin A carotenoids in kernels.[2] The first wave of biofortified maize grown in Zambia contained 7.5 to 10.3 μg/g DW BCE and higher levels of β-cryptoxanthin, which is as efficient as β-carotene as a source of vitamin A. Most importantly was that the increase in β-cryptoxanthin and β-carotene did not compromise the levels of lutein and zeaxanthin, which have similar concentrations to those reported for yellow maize accounting for 30−50% of total carotenoids.[18]

Effect of Storage. At a household level, in Zambia, maize is harvested during the months of April−May, it is usually stored "as harvested" on the ears or shelled into kernels, and stored in bags under shelter for up to eight months at 16−27 °C and relative humidity 40 to 65%.[27] These postharvest storage methods are practiced in specific regions of the country. For example, in Nyimba district in the Eastern Province, the majority of households (84%) stored maize on ears, covered with leaves and in a barn, while in Mkushi district in the Central Province, the majority of households (92%) store shelled maize in bags (F. F. De Moura, personal communication). Therefore, both postharvest storage practices were evaluated during storage (kernels and ears) on carotenoid retention over a period of 6 months. Weekly records of humidity and temperature inside the storage bin were taken and are provided in Table 2A of the Supporting Information. In general, the retention of the provitamin A carotenoids for all four genotypes did not differ significantly according to the postharvest storage method in which the maize was stored, either as ears or kernels (data not shown). Therefore, only kernel retention data over a 6-month period are presented herein.

Figure 1 shows the retention of BCE in biofortified maize measured in 15-day intervals up to six months for stored ears of genotypes HP1002 and HP1005. All four genotypes followed a similar decay pattern for BCE with a 40% decrease occurring within the first 15 days of storage. A further 10% reduction within the next 15 days (total 30 days of storage) was observed, followed by a stabilization at 50% retention until 120 days of storage, thereafter declining to 40% retention between 120 and 180 days. The retention of BCE for genotypes HP1001 and HP1003 measured at baseline, 90 and 180 days of storage, followed a similar pattern achieving, respectively, 51.5% and 62.9% retention at 90 days and 40% and 63.1% retention at 180 days of storage.

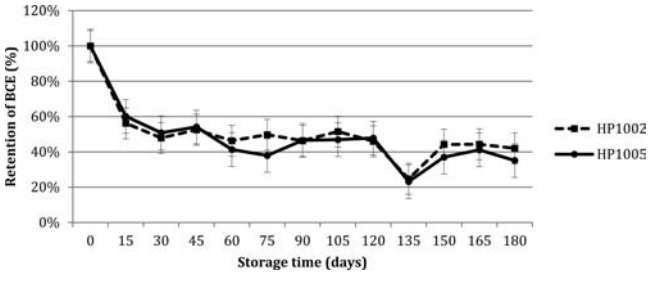

Figure 1. Effect of storage on BCE retention of maize when stored as kernels for six months under ambient conditions in Zambia for genotypes HP1002 and HP1005 at 15-day intervals. Day 135 did not follow the projected decay line.

Weber[19] reported an average total carotenoid retention of 58% among four inbred lines after 6 months of storage. Other provitamin A biofortified crops (e.g., sorghum, rice) also showed a comparable pattern of 40% degradation of provitamin A within the first few days of storage. Further postharvest research is needed to optimize storage conditions in order to minimize provitamin A degradation during storage, particularly immediately after harvest.

A similar better performance of some genotypes was observed by Burt et al.,[8] which reported an overall 25−60% decay of provitamin A among six genotypes after drying and four months of dark storage at 25 °C; total carotenoid loss ranged from 15 to 45% and 0 to 50% due to drying and storage, respectively. In this particular study, the researchers were able to categorize the genotypes into three groups, i.e., those with high losses due to drying and low loss due to storage, those with low losses due to drying, but high loss due to storage, and the intermediate genotypes with moderate losses due to both drying and storage. Another study showed a wide range of provitamin A degradation (7−45%) among six maize genotypes within the first four months of storage (unpublished data from Natalia Palacios).

Effect of Milling. *Milling into Mealie Meal.* Maize kernels are usually milled into whole maize meal (named mealie meal), which is a fine flour used for making *nshima* and porridge. Most of the carotenoids were retained during this process except for β-cryptoxanthin, which showed a consistent 60% retention across all genotypes (Table 3). These findings were contrary to those reported by Pillay et al.,[9] where a higher retention of β-cryptoxanthin (95.3−113.5%) was observed in milled maize. Different maize genotypes and milling processes could be a source of variation with reported studies. Moreover, Pillay et al.[20] reported that β-cryptoxanthin is the most abundant provitamin A carotenoid present in some biofortified varieties, and their range was higher than those reported by Li et al.[7]

Although lower β-cryptoxanthin retention was constant among genotypes in this study, Li et al.[7] reported small significant losses (7−10%) of provitamin A carotenoids after soaking and milling to produce wet-milled flour. It was not surprising to observe degradation because the maize was soaked for 24 h prior to milling. Traditionally, Zambians mill the maize kernels directly, limiting exposure to oxygen and light. Although not significantly different, the β-carotene levels were higher in the mealie meal than in the intact raw maize kernels, which is a reason for figures above 100% BCE retention in some genotypes (HP1003 and HP1005). The higher carotenoid levels in the final milled products than those found in the raw samples could be due to extraction efficiency from processed samples compared with those of raw fresh foods as elaborated by Rodriguez-Amaya and Kimura Rodriguez.[21] Overall, the BCE retention ranged from 80 to 110% among all four genotypes with HP1005 being the highest.

Milling into Samp. Maize kernels can also be milled into *samp* after conditioning or tempering (soaking in water) for 5

Table 2. Carotenoid Content (μg/g DW) of Four Genotypes of Biofortified Green Maize in Raw Kernels and Boiled and Roasted Products[a,b]

variety/genotype	final product	lutein	zeaxanthin	β-cryptoxanthin	α-carotene	all-*trans*-β-carotene	13-*cis*-β-carotene	9-*cis*-β-carotene	BCE	BCE retention rate (%)
all varieties	raw-B	5.33 ± 1.12^{a}	15.30 ± 3.58^{ab}	1.69 ± 0.59^{b}	0.43 ± 0.11^{b}	4.39 ± 2.02^{a}	1.33 ± 0.55^{a}	1.27 ± 0.50^{a}	6.75 ± 2.74^{a}	
	boiled	5.72 ± 0.68^{a}	19.81 ± 2.53^{a}	3.00 ± 1.13^{a}	1.22 ± 0.48^{a}	3.57 ± 1.11^{a}	1.48 ± 0.47^{a}	1.22 ± 0.45^{a}	7.03 ± 1.78^{a}	104
	raw-R	4.68 ± 1.22^{a}	14.36 ± 5.55^{b}	1.61 ± 0.28^{b}	0.34 ± 0.10^{b}	4.77 ± 2.54^{a}	1.27 ± 0.55^{a}	1.22 ± 0.49^{a}	6.99 ± 3.10^{a}	
	roasted	4.61 ± 0.61^{a}	10.94 ± 3.40^{b}	1.85 ± 0.33^{b}	0.30 ± 0.08^{b}	3.83 ± 1.53^{a}	1.62 ± 0.66^{a}	1.47 ± 0.59^{a}	6.44 ± 2.05^{a}	92.1
HP1001	raw-B	4.11 ± 0.05^{cB}	14.00 ± 0.02^{bC}	1.14 ± 0.03^{bC}	0.38 ± 0.10^{bB}	5.26 ± 0.07^{bB}	1.75 ± 0.04^{bA}	1.77 ± 0.06^{bA}	7.78 ± 0.04^{cB}	
	boiled	6.16 ± 0.19^{aA}	22.49 ± 1.32^{aA}	1.44 ± 0.05^{aC}	1.69 ± 0.03^{aA}	4.12 ± 0.03^{cB}	1.59 ± 0.04^{cB}	1.64 ± 0.20^{bA}	7.30 ± 0.13^{cB}	93.9
	raw-R	3.95 ± 0.11^{cB}	14.59 ± 0.41^{bB}	1.24 ± 0.04^{abC}	0.35 ± 0.02^{bA}	6.41 ± 0.30^{aB}	1.61 ± 0.02^{cB}	1.40 ± 0.10^{bB}	8.71 ± 0.32^{bB}	
	roasted	4.60 ± 0.02^{bB}	9.56 ± 1.06^{cB}	1.50 ± 0.11^{aB}	0.40 ± 0.02^{bA}	6.15 ± 0.11^{aA}	2.60 ± 0.01^{aA}	2.29 ± 0.05^{aA}	9.54 ± 0.15^{aA}	110
HP1002	raw-B	5.72 ± 0.66^{aAB}	20.12 ± 0.29^{aA}	1.29 ± 0.04^{dC}	0.33 ± 0.04^{bB}	2.35 ± 0.15^{bD}	0.70 ± 0.03^{cB}	0.62 ± 0.02^{bC}	3.82 ± 0.15^{cD}	
	boiled	4.68 ± 0.21^{aB}	21.26 ± 0.51^{aAB}	2.60 ± 0.07^{aB}	0.90 ± 0.04^{aA}	2.15 ± 0.07^{bD}	0.88 ± 0.01^{bD}	0.63 ± 0.02^{bB}	4.65 ± 0.09^{abC}	122
	raw-R	6.50 ± 0.58^{aA}	19.44 ± 0.75^{aA}	1.56 ± 0.05^{cBC}	0.40 ± 0.03^{bA}	2.66 ± 0.03^{abC}	0.84 ± 0.01^{bcC}	0.77 ± 0.06^{bC}	4.45 ± 0.06^{bcC}	
	roasted	5.53 ± 0.11^{aA}	15.47 ± 0.11^{bA}	2.17 ± 0.06^{bA}	0.30 ± 0.00^{bB}	2.98 ± 0.19^{aC}	1.24 ± 0.08^{aC}	1.03 ± 0.10^{aBC}	5.34 ± 0.31^{aBC}	120
HP1003	raw-B	4.73 ± 0.37^{bB}	10.94 ± 0.54^{bD}	1.76 ± 0.08^{bcB}	0.43 ± 0.03^{bAB}	2.91 ± 0.10^{aC}	0.96 ± 0.10^{bB}	1.02 ± 0.08^{aB}	4.99 ± 0.17^{bC}	
	boiled	6.27 ± 0.00^{aA}	16.43 ± 0.13^{aC}	3.92 ± 0.12^{aA}	1.22 ± 0.02^{aA}	3.11 ± 0.06^{aC}	1.34 ± 0.00^{aC}	1.04 ± 0.03^{aB}	6.87 ± 0.11^{aB}	138
	raw-R	3.58 ± 0.06^{cB}	5.89 ± 0.18^{cC}	1.71 ± 0.14^{cAB}	0.19 ± 0.01^{cB}	2.24 ± 0.04^{bC}	0.70 ± 0.04^{cC}	0.84 ± 0.08^{aC}	3.95 ± 0.10^{cC}	
	roasted	4.24 ± 0.10^{bcB}	6.87 ± 0.36^{cC}	2.14 ± 0.04^{bA}	0.21 ± 0.02^{cC}	2.41 ± 0.06^{bC}	0.97 ± 0.08^{bC}	0.94 ± 0.02^{aC}	4.54 ± 0.00^{bC}	115
HP 1005	raw-B	6.74 ± 0.51^{a}	16.14 ± 0.12^{cB}	2.56 ± 0.15^{bA}	0.58 ± 0.06^{aA}	7.06 ± 0.04^{bA}	1.91 ± 0.12^{abA}	1.67 ± 0.02^{aA}	10.42 ± 0.07^{aA}	
	boiled	5.79 ± 0.16^{abA}	19.05 ± 0.47^{aBC}	4.03 ± 0.02^{A}	1.07 ± 0.97^{aA}	4.91 ± 0.02^{cA}	2.10 ± 0.04^{aA}	1.57 ± 0.13^{aA}	9.29 ± 0.60^{aA}	89.2
	raw	4.67 ± 0.07^{bcB}	17.52 ± 0.35^{bA}	1.95 ± 0.09^{cA}	0.42 ± 0.05^{aA}	7.75 ± 0.01^{a}	1.93 ± 0.09^{abA}	1.89 ± 0.01^{aA}	10.85 ± 0.03^{aA}	
	roasted	4.09 ± 0.25^{cB}	11.86 ± 0.29^{B}	1.58 ± 0.08^{cB}	0.30 ± 0.02^{aB}	3.78 ± 0.27^{dB}	1.66 ± 0.11^{bB}	1.61 ± 0.29^{aB}	6.35 ± 0.51^{bB}	58.6

[a]Data are means ± SD for three independent experiments of green raw maize and green roasted maize. [b]Different lowercase letters indicate a statistically significant difference among final products (raw-B vs boiled uses "a" and "b"; raw-R vs roasted uses "c" and "d") within each genotype/variety. Different uppercase letters indicate a statistically significant difference among the genotypes/varieties for the same final product.

dx.doi.org/10.1021/jf501233f | J. Agric. Food Chem. 2014, 62, 6317−6325

Table 3. Baseline Carotenoid Content (μg/g DW) of Four Genotypes of Biofortified Dry Maize in Raw Kernels and Processed Products[a,b]

variety/genotype	final product[c]	lutein	zeaxanthin	β-cryptoxanthin	α-carotene	all-*trans*-β-carotene	13-*cis*-β-carotene	9-*cis*-β-carotene	BCE	BCE retention (%)
all varieties	raw kernel	3.87 ± 0.94^{c}	9.21 ± 3.02^{b}	6.26 ± 1.06^{a}	0.40 ± 0.30^{bc}	4.18 ± 1.31^{b}	1.26 ± 0.25^{ab}	1.12 ± 0.19^{b}	8.69 ± 1.16^{ab}	NA
	raw meal	4.95 ± 1.10^{bc}	9.99 ± 2.09^{b}	3.69 ± 0.70^{b}	0.25 ± 0.11^{c}	5.12 ± 1.68^{ab}	1.53 ± 0.28^{ab}	1.28 ± 0.30^{ab}	8.50 ± 1.91^{ab}	97.8
	nshima	9.64 ± 3.82^{a}	19.88 ± 6.71^{a}	1.72 ± 0.59^{c}	0.67 ± 0.21^{ab}	8.40 ± 3.61^{a}	1.83 ± 0.51^{a}	1.79 ± 0.46^{a}	11.40 ± 4.11^{a}	131
	porridge	7.33 ± 3.21^{ab}	16.30 ± 3.12^{a}	0.80 ± 0.18^{c}	0.84 ± 0.33^{a}	7.08 ± 2.75^{ab}	1.37 ± 0.56^{ab}	1.30 ± 0.53^{ab}	9.23 ± 3.32^{ab}	106
	raw *samp*	4.30 ± 0.98^{bc}	9.44 ± 2.23^{b}	6.90 ± 1.03^{a}	0.25 ± 0.10^{c}	4.54 ± 1.30^{b}	1.25 ± 0.25^{ab}	1.26 ± 0.32^{ab}	9.36 ± 1.33^{ab}	108
	cooked *samp*	3.98 ± 1.60^{bc}	9.34 ± 3.71^{b}	1.11 ± 0.27^{c}	0.37 ± 0.13^{bc}	4.49 ± 1.95^{b}	1.15 ± 0.38^{b}	1.53 ± 0.35^{ab}	6.56 ± 2.34^{b}	75.5
HP1001	raw kernel	3.82 ± 0.33^{abcB}	7.70 ± 0.47^{bcB}	4.64 ± 0.25^{bB}	0.34 ± 0.01^{aB}	5.03 ± 0.04^{abB}	1.47 ± 0.02^{aA}	1.37 ± 0.06^{aA}	8.94 ± 0.21^{aB}	NA
	raw meal	4.89 ± 1.22^{abcA}	9.93 ± 1.36^{abcB}	2.66 ± 0.16^{cB}	0.23 ± 0.08^{aB}	5.48 ± 0.44^{abB}	1.58 ± 0.14^{aAB}	1.44 ± 0.08^{aAB}	8.44 ± 0.58^{aB}	94.3
	nshima	6.62 ± 0.34^{abB}	13.56 ± 0.38^{abA}	0.97 ± 0.04^{dA}	0.61 ± 0.01^{aA}	7.36 ± 0.16^{abA}	1.55 ± 0.05^{aA}	1.75 ± 0.08^{aA}	9.80 ± 0.25^{aA}	110
	porridge	6.78 ± 1.43^{aB}	15.97 ± 4.14^{aA}	0.66 ± 0.14^{dA}	0.83 ± 0.47^{aA}	8.90 ± 2.51^{aA}	1.74 ± 0.61^{aA}	1.67 ± 0.81^{aA}	11.35 ± 3.52^{aA}	127
	raw *samp*	3.43 ± 0.24^{bcB}	6.40 ± 0.00^{bcC}	5.29 ± 0.22^{aB}	0.31 ± 0.03^{aA}	5.24 ± 0.21^{abAB}	1.42 ± 0.07^{aA}	1.39 ± 0.02^{aB}	9.44 ± 0.36^{aB}	106
	cooked *samp*	2.87 ± 0.12^{cA}	5.12 ± 0.99^{cC}	0.69 ± 0.01^{dB}	0.33 ± 0.11^{aAB}	4.12 ± 0.55^{bB}	1.07 ± 0.07^{aB}	1.71 ± 0.34^{aA}	6.02 ± 0.80^{aB}	67.3
HP1002	raw kernel	3.83 ± 0.06^{bB}	14.03 ± 0.09^{aA}	6.89 ± 0.01^{aA}	0.88 ± 0.02^{aA}	3.13 ± 0.06^{aC}	1.08 ± 0.02^{aB}	0.95 ± 0.02^{aB}	8.02 ± 0.09^{aBC}	NA
	raw meal	4.59 ± 0.11^{abA}	13.10 ± 0.27^{aA}	4.23 ± 0.04^{bA}	0.16 ± 0.01^{cB}	3.29 ± 0.02^{aD}	1.13 ± 0.02^{aC}	0.83 ± 0.01^{aC}	6.47 ± 0.01^{aC}	80.6
	nshima	9.27 ± 2.90^{aAB}	27.07 ± 9.85^{aA}	2.02 ± 0.75^{cA}	0.67 ± 0.24^{abA}	5.43 ± 2.02^{aA}	1.42 ± 0.56^{aA}	1.48 ± 0.56^{aA}	8.23 ± 3.08^{aA}	103
	porridge	5.42 ± 0.18^{abB}	18.23 ± 0.12^{aA}	0.77 ± 0.00^{cA}	0.50 ± 0.03^{abcA}	3.44 ± 0.12^{aA}	0.66 ± 0.02^{aA}	0.66 ± 0.02^{aA}	4.73 ± 0.10^{aA}	58.9
	raw *samp*	3.97 ± 0.22^{bB}	12.22 ± 0.01^{aA}	7.77 ± 0.26^{aA}	0.21 ± 0.10^{cA}	2.89 ± 0.06^{aC}	0.86 ± 0.01^{aB}	0.75 ± 0.01^{aC}	7.68 ± 0.24^{aC}	95.7
	cooked *samp*	3.78 ± 0.09^{bA}	14.20 ± 1.41^{aA}	1.30 ± 0.10^{cA}	0.28 ± 0.00^{bcB}	2.53 ± 0.08^{aB}	0.74 ± 0.09^{aC}	1.07 ± 0.08^{aA}	4.22 ± 0.21^{aB}	52.6
HP1003	raw kernel	5.13 ± 0.15^{bA}	8.16 ± 0.22^{bB}	7.14 ± 0.02^{aA}	0.22 ± 0.08^{cBC}	2.83 ± 0.08^{cC}	0.99 ± 0.01^{bB}	0.99 ± 0.06^{aB}	7.50 ± 0.08^{abC}	NA
	raw meal	6.42 ± 0.24^{bA}	8.50 ± 0.10^{bB}	4.01 ± 0.08^{bA}	0.20 ± 0.01^{cB}	4.25 ± 0.01^{bcC}	1.53 ± 0.02^{abB}	1.31 ± 0.01^{aB}	7.77 ± 0.02^{abB}	104
	nshima	15.09 ± 2.04^{aA}	20.76 ± 2.56^{aA}	2.07 ± 0.32^{cA}	0.90 ± 0.17^{abA}	7.32 ± 1.22^{aA}	2.11 ± 0.39^{aA}	1.66 ± 0.42^{aA}	10.69 ± 1.86^{aA}	143
	porridge	12.14 ± 2.07^{aA}	18.17 ± 3.05^{aA}	1.04 ± 0.19^{dA}	1.13 ± 0.34^{aA}	6.73 ± 1.38^{abA}	1.78 ± 0.45^{abA}	1.60 ± 0.01^{aA}	9.51 ± 1.87^{abA}	127
	raw *samp*	5.82 ± 0.16^{bA}	9.21 ± 0.17^{bB}	7.46 ± 0.02^{aA}	0.17 ± 0.01^{cA}	3.99 ± 0.11^{bcBC}	1.31 ± 0.05^{abA}	1.49 ± 0.01^{aA}	9.20 ± 0.09^{abB}	123
	cooked *samp*	6.26 ± 1.71^{bA}	10.56 ± 0.53^{bAB}	1.21 ± 0.10^{dA}	0.29 ± 0.03^{bcB}	3.89 ± 0.12^{bcB}	1.09 ± 0.02^{bB}	1.49 ± 0.14^{aA}	5.93 ± 0.15^{bB}	79.1
HP1005	raw kernel	2.68 ± 0.20^{bC}	6.96 ± 0.29^{bB}	6.35 ± 0.44^{aA}	0.16 ± 0.01^{bC}	5.72 ± 0.27^{bA}	1.50 ± 0.14^{aA}	1.17 ± 0.09^{bAB}	10.30 ± 0.61^{aA}	NA
	raw meal	3.89 ± 0.012^{bA}	8.42 ± 0.02^{bB}	3.87 ± 0.05^{bA}	0.43 ± 0.01^{bA}	7.47 ± 0.02^{abA}	1.86 ± 0.02^{aA}	1.55 ± 0.02^{abA}	11.32 ± 0.04^{aA}	110
	nshima	7.59 ± 1.68^{aAB}	18.14 ± 4.50^{aA}	1.83 ± 0.46^{cA}	0.48 ± 0.19^{abA}	13.47 ± 3.48^{aA}	2.23 ± 0.62^{aA}	2.28 ± 0.53^{aA}	16.88 ± 4.38^{aA}	164
	porridge	4.96 ± 0.54^{abB}	12.83 ± 1.74^{abA}	0.72 ± 0.06^{dA}	0.91 ± 0.02^{aA}	9.25 ± 1.37^{abA}	1.30 ± 0.11^{aA}	1.28 ± 0.22^{bA}	11.36 ± 1.57^{aA}	110
	raw *samp*	3.99 ± 0.31^{bB}	9.91 ± 0.53^{bB}	7.08 ± 0.07^{aA}	0.30 ± 0.18^{bA}	6.03 ± 0.611^{bA}	1.40 ± 0.156^{aA}	1.41 ± 0.00983^{abB}	11.12 ± 0.567^{aA}	108
	cooked *samp*	3.00 ± 0.40^{bA}	7.48 ± 0.40^{bBC}	1.23 ± 0.03^{cdA}	0.56 ± 0.03^{abA}	7.42 ± 0.699^{abA}	1.70 ± 0.085^{aA}	1.83 ± 0.177^{abA}	10.08 ± 0.654^{aA}	97.8

[a]Data are means ± SD, n = 2 independent analyses. [b]Different lowercase letters indicate a statistically significant difference among final products within each genotype/variety. Different uppercase letters indicate a statistically significant difference among the genotypes/varieties for the same final product. [c]Moisture content (as percentage of wet weight) of raw maize kernels (12%), raw whole maize meal (12%), raw samp (13%), cooked samp (70%), *nshima* (75%), and porridge (86%).

dx.doi.org/10.1021/jf501233f | J. Agric. Food Chem. 2014, 62, 6317−6325

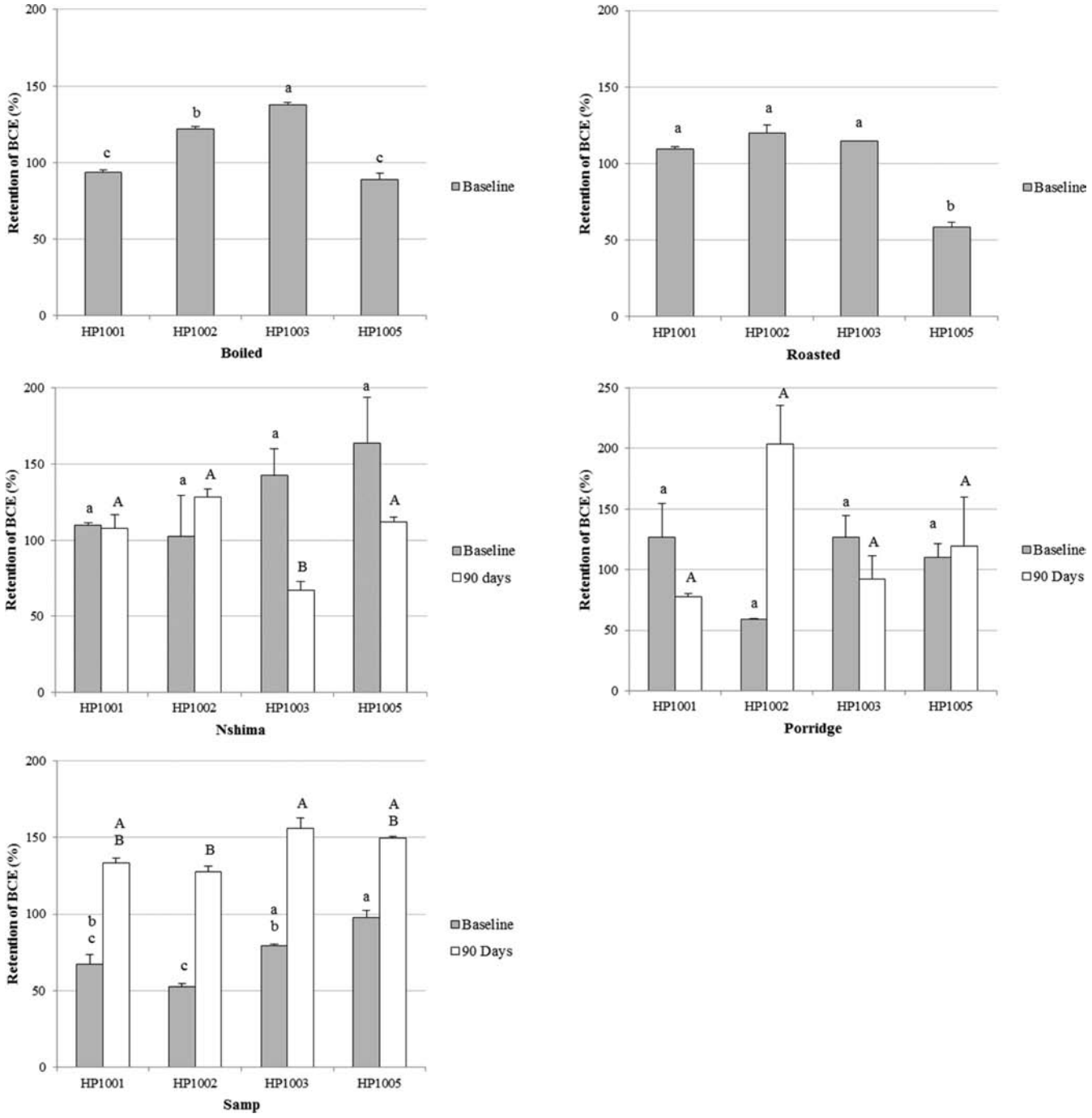

Figure 2. Retention of BCE of traditional Zambian cooked products from four genotypes of biofortified provitamin A maize (HP1001, HP 1002, HP1003, and HP1005) at baseline and after the maize was stored for 90 days at room temperature before cooking. For each cooking method, the different letters among genotypes indicates significant difference ($P < 0.05$) at baseline (lower case letters) and after 90 days (upper case letters). The error bars indicate standard deviations.

min for ease of bran removal to obtain the dehulled kernels. No significant carotenoid losses were observed after milling into *samp*, resulting in retention of BCE, in most cases, higher than 100%. Both β-carotene and β-cryptoxanthin were maintained in *samp*; therefore, yielding a final product with a higher retention range (95.7−154.7%) compared to maize milled into mealie meal (91.6−130.7%), although these values showed no significant difference at ($P < 0.05$) (Table 3). On the other hand, Pillay et al.,[9] reported that maize milled into mealie meal resulted in higher retention of zeaxanthin, β-carotene, and β-cryptoxanthin compared with milling into *samp*.

Effect of Cooking. *Green Maize.* After roasting the green maize for 20 min, the retention of BCE was above 100%, except for genotype HP1005, yielding a 59% BCE retention. This lower retention can be attributed to the reduction of almost 50% in all-*trans*-β-carotene content of raw green maize (Table 2). The *cis*-isomers of β-carotene increased after roasting, the 13-*cis* increased by 65% among genotypes HP1001, HP1002, and HP1003, and the 9-*cis* increased by 60% in genotype HP1001.

Similar retention was obtained after boiling the green maize for 35 min at 95 °C. Genotypes HP1002 and HP1003 obtained

dx.doi.org/10.1021/jf501233f | J. Agric. Food Chem. 2014, 62, 6317−6325

100% of the BCE retention and 90% of the BCE retention for genotypes HP1001 and HP1005 (Table 2). HP1005 lost almost 50% of the all-*trans*-β-carotene after boiling. No consistent trend was observed for the *cis*-isomers after boiling. Muzhingi et al.[22] also reported similar results on retention levels above 100% for all individual carotenoids, except for β-cryptoxanthin (92%), for yellow maize boiled for 1 h at 100 °C.

Dry Maize. The retention of individual carotenoids and BCE of all three cooked products, *nshima*, porridge, and cooked *samp*, are shown in Table 3. *Nshima*, by far the most popular maize dish consumed in Zambia, showed high BCE retention levels (103−164%) despite the lower retention (21−29%) of β-cryptoxanthin. Lutein and zeaxanthin were also significantly higher in *nshima* than raw maize. Porridge, which is consumed mostly by children at breakfast, likewise had high BCE retention (110−127%) except for genotype HP1002 (59%). The lower BCE retention observed in genotype HP1002 can be attributed to the drastic drop in the levels of β-cryptoxanthin from 6.9 to 0.8 μg/g DW. Similar results of high retention (>100%) of individual carotenoids were reported by Muzhingi et al.[22] for cooked products of yellow maize for "*sadza*", which is Zimbabwe's version of *nshima*, as well as porridge.[23−25] In particular in porridge, but not in *sadza*, the β-cryptoxanthin was significantly lower than in the raw kernels while the all-*trans*-β-carotene was constant in both products. Additionally, the muffins, which were baked for 25 min at 232 °C, showed significantly lower retention for all individual carotenoids, including 25% and 51% retention for all-*trans*-β-carotene and β-cryptoxanthin, respectively. Lastly, the cooked *samp* in the current study showed higher BCE retention when the maize was milled into *samp* (96−155%), although the combination of high temperature with prolonged cooking (3 h) resulted in a lower BCE retention range (53−98%) among the four genotypes.

Retention of β-Carotene Equivalents (BCE) among All Cooked Products. In this study, the BCE retention of cooked products from just harvested maize was compared with those of cooked products from maize stored for 90 and 180 days. The BCE retention did not differ significantly between the cooked products made from maize stored either at 90 or 180 days. Therefore, Figure 2 shows the BCE retention of different cooked products of maize that have just been harvested, including green and dry maize, and cooked products made from dry maize that had been stored for 90 days. On average, the genotypes, HP1001 and HP1003, showed high BCE retention among the different maize cooked products, except for a lower BCE retention in cooked *samp* as discussed in the previous section. Furthermore, genotype HP1002, besides lower BCE retention for *samp*, had 60% retention in cooked porridge. Interestingly, genotype HP1005 was the only type that showed a 60% BCE retention for roasted product, while the other three genotypes had BCE retention higher than 100%; however, it had the highest BCE retention, almost 100% when cooked as *samp*. The BCE retention of the cooked product was not affected by the maize being stored for 90 days, although the carotenoid levels decreased substantially (see the previous section on the Effects of Storage).

In summary, the carotenoids in the provitamin A biofortified maize showed virtually no degradation when the maize was cooked into *nshima* and porridge, for most of the maize genotypes. When the maize was cooked into *samp*, the degradation was more significant but still showed a wide range among genotypes from 50% to 100% retention. After an initial drop, the retention of provitamin A was maintained consistent throughout the six months of storage. Therefore, the 50% of provitamin A degradation assumed in the original calculation of the target levels for provitamin A for maize was somewhat accurate, concluding that the values for retention were satisfactory in ultimately providing adequate amounts of vitamin A through biofortification. In addition, we recognize the need for upstream research identifying genotypes with higher provitamin A retention during storage in order to achieve the maximum benefit of biofortified maize. Further research could also identify the mechanisms that make one genotype more resistant to provitamin A degradation than another. An effort to optimize postharvest storage methods is also recognized in order to minimize provitamin A degradation, particularly soon after harvest where the decay pattern for BCE is in excess of 40-50% in the first 15 days. More improvements and optimization of cooking methods could also increase retention of carotenoids in provitamin A biofortified maize for the benefit of populations who consume maize in the rural settings in Africa. Overall, these results are very encouraging for the biofortification program in Zambia.

■ ASSOCIATED CONTENT

Ⓢ Supporting Information

Baseline carotenoid content (μg/g FW) of four genotypes of biofortified maize at two harvesting stages. Weekly humidity and temperature readings. This material is available free of charge via the Internet at http://pubs.acs.org.

■ AUTHOR INFORMATION

Corresponding Author

*Phone: 1-202-862-5693. Fax: 1-202-467-4439. E-mail: f.moura@cgiar.org.

Funding

Funding was provided by HarvestPlus (www.HarvestPlus.org), a global alliance of agriculture and nutrition research institutions working to increase the micronutrient density of staple food crops through biofortification.

Notes

The authors declare no competing financial interest.

■ ACKNOWLEDGMENTS

We are greatly thankful to Eliab Simpungwe for his assistance and support.

■ ABBREVIATIONS USED

BCE, β-carotene equivalents = [all-*trans*-β-carotene + 1/2 α-carotene +1/2 β-cryptoxanthin +1/2 13-*cis*-β-carotene +1/2 9-*cis*-β-carotene]; DW, dry weight basis; FW, fresh weight basis

■ REFERENCES

(1) Saltzman, A.; Birol, E.; Bouis, H.; Boy, E.; De Moura, F.; Islam, Y.; Pfeiffer, W. Biofortification: progress toward a more nourishing future. *Global Food Secur.* **2013**, *2*, 9−17.

(2) Pixley, K.; Palacios-Rojas, N.; Babu, R.; Mutale, R.; Surles, R.; Simpungwe, E. Biofortification of Maize with Provitamin A Carotenoids. *In Carotenoids and Human Health*; Tanumihardjo, S. A., Ed.; Springer Science: New York, 2013.

(3) Hotz, C.; McClafferty, B. From harvest to health: challenges for developing biofortified staple foods and determining their impact on micronutrient status. *Food Nutr. Bull.* **2007**, *28*, S271−279.

(4) Hotz, C.; Chileshe, J.; Siamusantu, W.; Palaniappan, U.; Kafwembe, E. Vitamin A and infection are associated with plasma

retinol among pre-school children in rural Zambia. *Public Health Nutr.* **2012**, *15*, 1688−1696.
(5) Li, S.; Nugroho, A.; Rocheford, T.; White, W. Vitamin A equivalence of the β-carotene in β-carotene biofortified maize porridge consumed by women. *Am. J. Clin. Nutr.* **2010**, *92*, 1105−1112.
(6) Food and Nutrition Board, Institute of Medicine. *Dietary Reference Intakes: Vitamin A, Vitamin K, Arsenic, Boron, Chromium, Copper, Iodine, Iron, Manganese, Molybdenum, Nickel, Silicon, Vanadium and Zinc*; National Academy Press: Washington, DC, 2001; pp 65−126.
(7) Li, S.; Tayie, F.; Young, M.; Rocheford, T.; White, W. Retention of provitamin A carotenoids in high β-carotene maize (*Zea mays* L.) during traditional African household processing. *J. Agric. Food Chem.* **2007**, *55*, 10744−10750.
(8) Burt, A.; Grainger, C.; Young, C.; Shelp, B.; Lee, E. Impact of postharvest handling on carotenoid concentration and composition in high-carotenoid maize (*Zea mays* L.) kernels. *J. Agric. Food Chem.* **2010**, *58*, 8286−8292.
(9) Pillay, K.; Siwela, M.; Derera, J.; Veldman, F. Provitamin A carotenoids in biofortified maize and their retention during processing and preparation of South African maize foods. *J. Food Sci. Technol.* **2011**, *48*, 1−11.
(10) Schmaelzle, S.; Gannon, B.; Crawford, S.; Arscott, S. A.; Goltz, S.; Palacios-Rojas, N.; Pixley, K.; Simon, P.; Tanumihardjo, S. A. Maize genotype and food matrix affect the provitamin A carotenoid bioefficacy from staple and carrot-fortified feeds in Mongolian gerbils (*Meriones unguiculatus*). *J. Agric. Food Chem.* **2014**, *62*, 136−143.
(11) Kurilich, A. C.; Juvik, J. A. Quantification of carotenoid and tocopherol antioxidants in *Zea mays*. *J. Agric. Food Chem.* **1999**, *47*, 1948−1955.
(12) Seddon, J. M.; Ajani, U. A.; Sperduto, R. D.; Hiller, R.; Blair, N.; Burton, T. C.; Farber, M. D.; Gragoudas, E. S.; Haller, J.; Miller, D. T.; Yannuzzi, L. A.; Willet, W. Dietary carotenoids, vitamins A, C, E and advanced age-related macular degeneration. *JAMA, J. Am. Med. Assoc.* **1994**, *272*, 1413−20.
(13) Schalch, W.; Dayhaw-Barker, P.; Barker, F. M. The carotenoids of the human retina. In *Nutritional and Environmental Influences on the Eye*; Taylor, A., Ed.; CRC Press: Boca Raton, FL, 1999.
(14) Snodderly, D. M. Evidence for protection against age-related macular degeneration by carotenoids and antioxidant vitamins. *Am. J. Clin. Nutr.* **1995**, *62* (Suppl.), 1448S−1461S.
(15) Schalch, W. Carotenoids in the retina—a review of their possible role in preventing or limiting damage caused by light and oxygen. In *Free Radicals and Aging*; Emerit, I., Chance, B., Eds.; Birkhauser Verlag: Basel, Switzerland, 1992; pp 280−298.
(16) La Frano, M. R.; Zhu, C.; Burri, B. J. Assessment of tissue distribution and concentration of β-cryptoxanthin in response to varying amounts of dietary β-cryptoxanthin in the Mongolian gerbil. *Br. J. Nutr.* **2014**, *111*, 968−978.
(17) Davis, C.; Jing, H.; Howe, J. A.; Rocheford, T.; Tanumihardjo, S. A. β-Cryptoxanthin from supplements or carotenoid-enhanced maize maintains liver vitamin A in Mongolian gerbils (*Meriones unguiculatus*) better than or equal to β-carotene supplements. *Br. J. Nutr.* **2008**, *100*, 786−793.
(18) Brenna, O. V.; Berardo, N. Application of near-infrared reflectance spectroscopy (NIRS) to the evaluation of carotenoids content in maize. *J. Agric. Food Chem.* **2004**, *52*, 5577−5582.
(19) Weber, E. Carotenoids and tocols of corn grain determined by HPLC. *J. Am. Oil Chem. Soc.* **1987**, *64*, 1129−1134.
(20) Pillay, K. Nutritional quality and consumer acceptability of provitamin A-biofortified maize. Ph.D. Thesis. University of Kwazulu-Natal, 2011.
(21) Rodriguez-Amaya, D.; Kimura, M. *HarvestPlus Handbook for Carotenoid Analysis*; HarvestPlus Technical Monograph 2; Technical Report for International Food Policy Research Institute (IFPRI) and International Center for Tropical Agriculture (CIAT): Washington, DC, 2004.
(22) Muzhingi, T.; Yeum, K. J.; Russell, R. M.; Johnson, E. J.; Qin, J.; Tang, G. Determination of carotenoids in yellow maize, the effects of saponification and food preparations. *Int. J. Vitam. Nutr. Res.* **2008**, *78*, 112−120.
(23) De Moura, F.; Miloff, A.; Boy, E. Retention of provitamin A carotenoids in staple crops targeted for biofortification in Africa: Cassava, maize and sweet potato. *Crit. Rev. Food Sci. Nutr.*. **2013** DOI: 10.1080/10408398.2012.724477.
(24) De la Parra, C.; Saldivar, S. O.; Liu, R. H. Effect of processing on the phytochemical profiles and antioxidant activity of corn for production of masa, tortillas, and tortilla chips. *J. Agric. Food Chem.* **2007**, *55*, 4177−4183.
(25) Lozano-Alejo, N.; Carrillo, G. V.; Pixley, K. Physical properties and carotenoid content of maize kernels and its nixtamalized snacks. *Innovative Food Sci. Emerging Technol.* **2007**, *8*, 385−389.
(26) Harjes, C. E.; Rocheford, T.; Bai, L.; Brutneil, P. T.; Kandianis, B. C.; Sowinski, G. S.; Stapleton, E. A.; Vallabhaneni, R.; Williams, M.; Wurtzel, T. E.; Yan, J.; Buckler, S. E. Natural genetic variation in lycopene epsilon cyclase tapped for maize biofortification. *Science* **2008**, *319*, 330−333.
(27) *Aquastat. Food and Agricultural Organisations's (FAO) Information Systems on Water and Agriculture*; Food and Agriculture Organization of the United Nations: Rome, 2005; http://www.fao.org/ag/agl/aglw/aquastat/countries/zambia/index.stm.

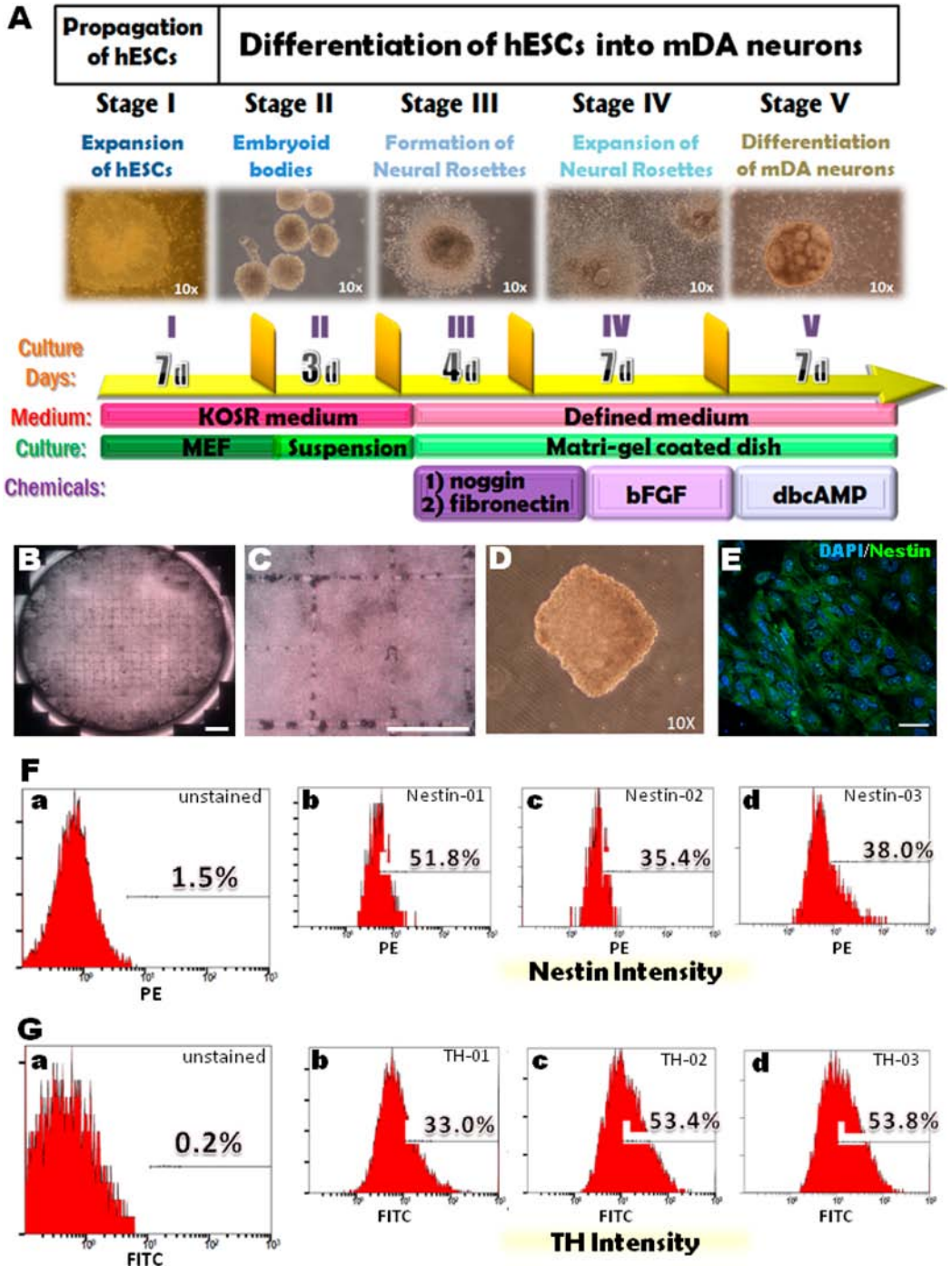

Figure 1. In vitro midbrain dopaminergic (mDA) differentiation of human embryonic stem cells (hESCs). (A) Differentiation process of hESC H9 cell line into dopaminergic (DAergic) neurons. (B, C) Morphology of hESC colonies after dissection using LEAP: (B) scale bar = 2.5 mm; (C) scale bar = 1 mm. (D) Morphology of cell aggregates lifted by collagenase type IV after LEAP dissection. (E) Immunofluorescence detection for nestin (green) as the phenotypic marker in stage III differentiated neural progenitors and plus DAPI nucleic staining (blue). Scale bar = 100 μm. (F) The differentiation rate of stage-III cells analyzed by the flow cytometer: (a) the unstained control group; (b–d) the percentage of stage-III nestin-positive neural rosettes from three independent samples. (G) The differentiation rate of stage-V cells analyzed by flow cytometer: (a) the unstained control group; (b–d) the percentage of stage-V TH-positive DAergic neurons from three independent samples.

model system due to their unlimited self-renewal and pluripotency.[9] Consequently, the primary objective of the present study was to establish an in vitro differentiation platform derived from hESCs to enhance the preclinical predictable values. To reach the goal, the utility of the established cell-based model was first verified, and we sought evidence that the final differentiated cells were functional midbrain DAergic (mDA) neurons with SN-A9 neuron phenotypes and special voltage-gated ion channel expression for dopamine release. Then, two neurogenic DR drugs (bromocriptine and 7-OH-DPAT) were used to illustrate that the cell model can be used as a platform for screening neurogenic compounds. Finally, since the neuroprotective effects of tea catechins[18] and ginsenosides[19] have been verified

dx.doi.org/10.1021/jf501640a | J. Agric. Food Chem. 2014, 62, 6326–6336

Table 1. Primers Used for Reverse-Transcriptase PCR

gene[a]	size (bp)	primer sequence F (top), R (bottom)
Primers for Internal Control		
GADPH	474	5′-GCTCAGACACCATGGGGAAGGT-3′
		5′-GTGGTGCAGGAGGCATTGCTGA-3′
Primers for Undifferentiated hESC Markers		
Oct3/4	320	5′-CGTTCTCTTTGGAAAGGTGTTC-3′
		5′-ACACTCGGACCACGTCTTTC-3′
Primers for DAergic Differentiation-Related Phenotype		
Nestin	167	5′-GAAACAGCCATAGAGGGCAAA-3′
		5′-TGGTTTTCCAGAGTCTTCAGTGA-3′
En1	357	5′-CTGGGTGTACTGCACACGTTAT-3′
		5′-TACTCGCTCTCGTCTTTGTCCT-3′
Lmx1a	150	5′-CAGCCTCAGACTCAGGTAAAAGTG-3′
		5′-TGAATGCTCGCCTCTGTTGA-3′
Lmx1b	561	5′-TCCTGATGCGAGTCAACGAGTC-3′
		5′-CTGCCAGTGTCTCTCGGACCTT-3′
TH	331	5′-GTCCCCTGGTTCCCAAGAAAAGT-3′
		5′-TCCAGCTGGGGGATATTGTCTTC-3′
Pitx3	175	5′-GTGGGTGGAGAGGAGAACAA-3′
		5′-TTCCTCCCTCAGGAAACAATG-3′
AADC	145	5′-GGGACCACAACATGCTGCTC-3′
		5′-CCACTCCATTCAGAAGGTGCC-3′
GIRK2	162	5′-GCTACCGGGTCATCACAGAT-3′
		5′-ACTGCATGGGTGGAAAAGAC-3′
Primers for Three Germ Markers		
AFP	253	5′-GAATGCTGCAAACTGACCACGCTGGAAC-3′
		5′-TGGCATTCAAGAGGGTTTTCAGTCTGGA-3′
PDX-1	193	5′- ATCTCCCCATACGAAGTGCC-3′
		5′- CGTGAGCTTTGGTGGATTTCAT-3′
GATA-4	183	5′-TCCAAACCAGAAAACGGAAGC-3′
		5′-GCCCGTAGTGAGATGACAGG-3′
BRACHYURY	248	5′-GCCCTCTCCCTCCCCTCCACGCACAG-3′
		5′-CGGCGCCGTTGCTCACAGACCACAG-3′
MAP2	186	5′-AATAGACCTAAGCCATGTGACATCC-3′
Primers for Three Germ Markers		
		5′-AGAACCAACTTTAGCTTGGGCC-3′
GFAP	161	5′-CCTCTCCCTGGCTCGAATG-3′
		5′-GGAAGCGAACCTTCTCGATGTA-3′
Primers for Voltage-Gated Ion Channels		
Kv1.4	270	5′-ACGAGGGCTTTGTGAGAGAA-3′
		5′-CACGATGAAGAAGGGGTCAT-3′
Kv4.2	326	5′-ACCGTGACCCAGACATCTTC-3′
		5′-CACTGTTTCCACCACATTCG-3′
Kv4.3	272	5′-GCCTCCGAACTAGGCTTTCT-3′
		5′-CCCTGCGTTTATCAGCTCTC-3′
Kv10.1	437	5′-TGGATTTTGCAAGCTGTCTG-3′
		5′-GAGTCTTTGGTGCCTCTTGC-3′
Nav1.5	165	5′-CCTAATCATCTTCCGCATCC-3′
		5′-TGTTCATCTCTCTGTCCTCATC-3′
Nav1.7	408	5′-GCTCCGAGTCTTCAAGTTGG-3′
		5′-GGTTGTTTGCATCAGGGTCT-3′
Cav1.2	431	5′-AACATCAACAACGCCAACAA-3′
		5′-AGGGCAGGACTGTCTTCTGA-3′
Cav3.1	348	5′-CTGCCACTTAGAGCCAGTCC-3′
		5′-TCTGAGTCAGGCATTTCACG-3′

[a]Abbreviations: Oct-4, octamer-binding transcription factor 4; En1, engrailed-1; Lmx1a/b, LIM/homeobox protein 1 a/b; TH, tyrosine hydrolase; Pitx3, paired-like homeobox transcription factor 3; AADC, aromatic amino acid decarboxylase; GIRK2, G-protein-regulated inward-rectifier potassium channel 2; AFP, alpha-fetoprotein; PDX-1, pancreatic and duodenal homeobox gene 1; GATA-4, GATA-binding protein 4; MAP2, microtubule-associated protein 2; GFAP, glial fibrillary protein; Kv1.4, potassium voltage-gated channel, shaker-related subfamily, member 4; Kv4.2, potassium voltage-gated channel, Shal-related subfamily, member 2; Kv4.3, potassium voltage-gated channel, Shal-related subfamily, member 3; Kv10.1/Eag1, potassium voltage-gated channel, subfamily H (eag-related), member 1; Nav1.5, sodium channel, voltage-gated, type V, alpha subunit; Nav1.7, sodium channel, voltage-gated, type IX, alpha subunit; Cav1.2, calcium channel, voltage-dependent, L type, alpha 1C subunit; Cav3.1, calcium channel, voltage-dependent, T type, alpha 1G subunit.

using animal model, these two phytochemicals were also investigated using our in vitro model for their mDA differentiation-boosting abilities.

MATERIALS AND METHODS

Culturing Undifferentiated hESCs. The NIH-registered H9 (WA-09, karyotype XX) cell line was used in this study. The culture and maintenance of undifferentiated hESC cell line H9 (passage 40−55) were performed at the National Taiwan University (NTU) Stem Cell Core (NTU Center of Genomic Medicine, Taipei, Taiwan) according to National Stem Cell Bank (NSCB) protocols. Briefly, undifferentiated hESC cells were cultured on γ-irradiated mouse embryonic fibroblasts (MEFs) in 3.5 mm dishes containing 20% knockout serum replacer (KOSR; Invitrogen Life Technologies, Grand Island, NY, USA) medium. This medium consisted of Dulbecco's modified Eagle's medium/nutrient mixture F-12 (DMEM/F12; Invitrogen) supplemented with 1% nonessential amino acid (NEAA; Invitrogen), 0.1 mM 2-mercaptoethanol, 1 mM L-glutamine (Invitrogen), 4 ng/mL basic fibroblast growth factor (bFGF; BD Biosciences, Sparks, MD, USA), and 20% KOSR. Fresh medium was replaced every 2 d. For continual propagation of cells, hESC colonies were manually lifted, dissected into small clumps, and then replated on fresh γ-irradiated MEFs every 7 d. The propagation of undifferentiated hESC cells was regarded as the first stage of our differentiation process (as shown in Figure 1A).

Induction and Differentiation of mDA Neurons. The induction and differentiation of hESC cells followed the procedures reported by Iacovitti et al.[20] with modification; the complete procedure is presented in Figure 1A. First, hESC colonies were grown on a monolayer of γ-irradiated MEF feeder cells in 12-well plates with 20% KOSR medium until 80−90% confluence. To induce the differentiation, hESC colonies were dissected with a Laser Enabled Analysis and Processing (LEAP; Cyntellect, San Diego, CA, USA) workstation to obtain a uniform hESC colony size distribution with diameter ∼1 mm. After they were gently dissociated with 1 mg/mL type IV collagenase (Invitrogen; dissolved in DMEM/F12 medium) from feeder layers, hESC colony clumps were suspended on 10 cm bacterial-grade Petri dishes in 20% KOSR medium at 37 °C for 3 days to form embryoid bodies (EBs) in stage II. Medium was renewed on the second day of this stage. During stage III, EBs were then cultured on Matrigel (BD; diluted 1:2 in DMEM/F12 medium) coated 12-well plates in defined medium supplemented with 5 μg/mL fibronectin (Sigma-Aldrich Chemicals, St. Louis, MO, USA) and 200 ng/mL recombinant human noggin (BioVision Inc., Milpitas, CA, USA) at 37 °C for 4 d to induce formation of neural progenitor rosettes. The defined medium was composed of DMEM/F12, 100 U/mL penicillin/streptomycin, 1.5 mM L-glutamine, 6 mg/mL glucose, and 1% ITS premix (Invitrogen; containing human recombinant insulin, human

transferrin, and selenous acid, all at 5 μg/mL). Medium was also changed on the second day of stage III. Neural rosettes were further expanded in stage IV on Matrigel-coated plates containing defined medium with 20 ng/mL bFGF at 37 °C for 7 d. Medium was replaced every 2−3 d. For differentiation of dopaminergic neurons in stage V, expanded rosettes were gently lifted with 0.5 mg/mL dispase (dissolved in DMEM/F12 medium) and reseeded on Matrigel-coated 12-well plates in defined medium with 1 mM dibutyryl cyclic adenosine monophosphate (dbcAMP; Santa Cruz Biotechnology Inc., Santa Cruz, CA, USA) at 37 °C for 7 days.

Immunostaining of Cultured Cells. For immunostaining analysis, cells were cultured on Matrigel-coated glass coverslips in 12-well plates under the same culture conditions during stage III or V. After washing cells in phosphate buffered saline (PBS), they were fixed with 4% formaldehyde (in PBS) at room temperature for 20 min. Thereafter, they were washed twice with PBS containing 0.05% Tween 20, and the fixed cells were then permeabilized with 0.1% Triton X-100 (in PBS) at room temperature for 10 min, washed twice with 0.05% Tween 20 (in PBS), and blocked with blocking solution containing goat serum (GeneTex Inc., Irvine, CA, USA) at room temperature for 30 min to minimize the nonspecific binding. Subsequently, the samples were incubated at room temperature for 1 h with appropriate primary antibodies, including anti-nestin, 1:50 (#MAB353; EMD Millipore Corp., Billerica, MA, USA), anti-tyrosine hydroxylase (TH), 1:50 (#AB152 and #AB9702; Millipore), anti-β-III-tubulin, 1:50 (#04−1049; Millipore), and anti-dopamine transporter (DAT), 1:50 (#MAB369; Millopore). The cells were then incubated at room temperature for 1 h with appropriate 488- or 549-fluorescence-tagged secondary Dylight antibodies (Rockland Immunochemicals Inc., Gilbertsville, PA, USA) after being washed twice with 0.05% Tween 20 (in PBS). Finally, 0.4 ng/mL 4′,6-diamidino-2-phenylindole (DAPI) was added to the cells for nuclear staining. The immunostained cells were observed using a LEICA TCS SP5 II confocal microscope system (Leica Microsystems Inc., Buffalo Grove, IL, USA) with Leica Application Suite Advanced Fluorescence (LAS AF) software.

Reverse-Transcriptase PCR (Polymerase Chain Reaction) and Real-Time PCR. Total RNA was isolated from cells at various stages by using Rezol C&T reagent (Protech Technology, Taipei, Taiwan) according to the manufacturer's instructions, and cDNA was synthesized from 5 ng of total RNA in a 20 μL reaction using iScript cDNA Synthesis kit (Bio-Rad Laboratories, Inc., Hercules, CA, USA.). Reverse-transcriptase PCR was carried out using EconoTaq PLUS GREEN 2X Master Mix kit (Lucigen Corp., Middleton, WI, USA). Primers used in reverse-transcriptase PCR are shown (Table 1). Amplification conditions were as follows: denaturation at 94 °C for 20 s, annealing at 55 or 60 °C for 20 s, and extension at 72 °C for 7 min. The number of cycles varied from 30 to 45, and the length of the amplified products is shown (Table 1). Real-time PCR was performed using iQ SYBR Green Supermix (Bio-Rad) reagent kit and an Applied Biosystems StepOne real-time PCR system (Life Technologies Corp., Carlsbad, CA, USA). The thermal parameters were 95 °C for 2 min, followed by 45 cycles of 95 °C for 15 s and 60 °C for 1 min. The relative gene (mDA marker *TH* and *GIRK2*; neurotrophin *BDNF* and *NT-3/4*) quantities were obtained using the comparative Ct method after normalization to an internal control (*G3PDH*). Primers included the following: *TH* (5′-CGTGCTAAACCTGCTCTT-3′, 5′-CGTCTCAAACACCTTCACA-3′), *GIRK2* (5′-CTCAGTTATTCAGATTGACAAGGT-3′, 5′-GTACAACACATGCAGGTAAGT-3′), brain-derived neurotrophic factor (*BDNF*) (5′-GAGTATTACCTCCGCCATGC-3′, 5′-ATTCACGCTCTCCAGAGTCC-3′), neurotrophin-3 (*NT-3*) (5′-TGGCATCCAAGGTAACAACA-3′, 5′-CTCTGTTGTCGCAGCAGTTC-3′), *NT-4* (5′-AGCGAAACTGCACCAGCGAG-3′, 5′-CACCTTCCTCAGCGTTATCA-3′), and *G3PDH* (5′-GCTCAGACACCATGGGGAAGGT-3′, 5′-GTGGTGCAGGAGGCATTGCTGA-3′).

Flow Cytometry. Differentiation rates of stage-III and stage-V cells were determined using flow cytometry. Briefly, cells were centrifuged, resuspended in PBS, fixed with BD Cytofix Fixation Buffer (BD), and permeabilized with ice-cold BD Phosflow Perm Buffer III (BD) at room temperature for 20 min in the dark. Nestin expression in differentiated stage-III neural rosettes was labeled using a direct immunofluorescence method. Permeabilized stage-III cells were then rinsed and incubated with nestin phycoerythrin (PE)-conjugated antibody (#561230; BD) at room temperature for 30 min. Conversely, TH expression in differentiated stage-V cells was detected using an indirect method. Permeabilized stage-III cells were reacted with rabbit anti-TH polyclonal antibody (#GTX61717; GeneTex) at room temperature for 30 min. Thereafter, cells were washed and treated with fluorescein isothiocyanate (FITC)-conjugated goat anti-rabbit antibody (#GTX77059; GeneTex) at room temperature for 30 min in the dark. Finally, the fluorescence analysis of the labeled cells was performed using a Cytomics FC500 flow cytometer (Beckman-Coulter Inc., Brea, CA, USA). Approximately 10,000 events per sample were analyzed for $n = 3$ independent cultures. The percentages of nestin-PE and TH-FITC positive cells were respectively determined with CXP software version 2.2 (Beckman). The unstained stage-III and stage-V cells were taken as the control groups.

Ratiometric Calcium Ion Imaging. Stage-V cells grown on Matrigel-coated glass coverslips were treated with 1 μM acetoxymethyl-ester Fura-2 (fura-2 AM) (TefLabs, Austin, TX, USA) at 37 °C for 1 h in the dark. Fura-2 AM, as a fluorophore, rapidly binds to calcium ion (Ca^{2+}) and shifts its absorption spectrum to lower wavelengths upon binding, enabling determination of intracellular calcium concentrations. After washing three times with Hanks balanced salt solution (HBSS) buffer, the stage-V cells on coverslips were mounted on the imaging chamber. To perform real-time microscopic ratiometric fluorescence imaging, the light from a xenon lamp (Lambda DG-4; Sutter Instrument Co., Novato, CA, USA) was directed through narrowband fluorescence filters (Chroma Technology, Brattleboro, VT, USA) centered at 340 nm (for Ca^{2+}-bound fura-2; F_{340}) and 380 nm (for Ca^{2+}-unbound fura-2; F_{380}). The excitation light was then passed into an inverted Zeiss Axiovert 200 M microscope (Carl Zeiss Axiovert, Göttingen, Germany) with 20× objective lens (Carl Zeiss Axiovert). Subsequently, emitted light from the mounted stage-V cells with fura-2 fluorescence was passed through an appropriate dichroic filter and an emission filter centered at 510 nm. The resulting photomicrographic series were obtained with a cooled charge-couple device (CCD) camera (CoolsnapFx; Roper Scientific, Tucson, AZ, USA) every 300 ms as controlled by MetaFlour software (Molecular Devices, Downingtown, PA, USA), which was also used for postexperiment image and data analysis. The ratio was computed as $R = F_{340}/F_{380}$, and the change of ratio reflected the change in $[Ca^{2+}]_i$. To depolarize the stage-V cells for observing the transient Ca^{2+}, a high-potassium solution ([KCl] = 150 mM) was applied around the 35th second. The HBSS solution contained 138 mM NaCl, 5.6 mM glucose, 4 mM $NaHCO_3$, 0.3 mM Na_2HPO_4, 0.5 mM $MgCl_2$, 0.41 mM $MgSO_4$, 5.33 mM KCl, 1.26 mM $CaCl_2$, and 0.44 mM KH_2PO_4 (pH 7.3).

Dopamine Determination. Dopamine (DA) release was determined using reversed-phase HPLC. At the end of 21 d culture, stage V differentiated cells in 12-well plates were rinsed with Hanks balanced salt solution (HBSS) twice, and then incubated in 0.5 mL of HBSS or HBSS supplemented with 56 mM KCl solution for 15 min to induce depolarization. After that, the medium was collected and stabilized with 0.1 mM ethylenediaminetetraacetic acid (EDTA) for further analysis. DA contents were analyzed at 0.5 V by HPLC system coupled to an amperometric detector LC-4C (BASi, West Lafayette, IN, USA). Samples (20 μL) were injected by an autosampler (LaChrom Elite autosampler L-2200; Hitachi HTA, Inc., Schaumburg, IL, USA) into an Apollo C-18 reverse-phase column (5 μm; particle size, 250 × 4.6 mm; Alltech Associates, Inc., Deerfield, IL, USA). The mobile phase (per liter) consisted of 20.5 g of NaH_2PO_4, 185 mg of EDTA, 130 mg of 1-octanesulfonic sodium salt (SOS), 2 mM KCl, and 200 mL of methanol (pH 3.11, adjusted with H_3PO_4), and was pumped at a flow rate of 0.5 mL/min. DA levels were calculated by external DA standard curve.

Sample Treatment. Dopamine receptor (DR) agonist and antagonist drugs used in the present study included bromocriptine (Sigma), 7-hydroxy-2-(dipropylamino)tetralin (7-OH-DPAT; Sigma),

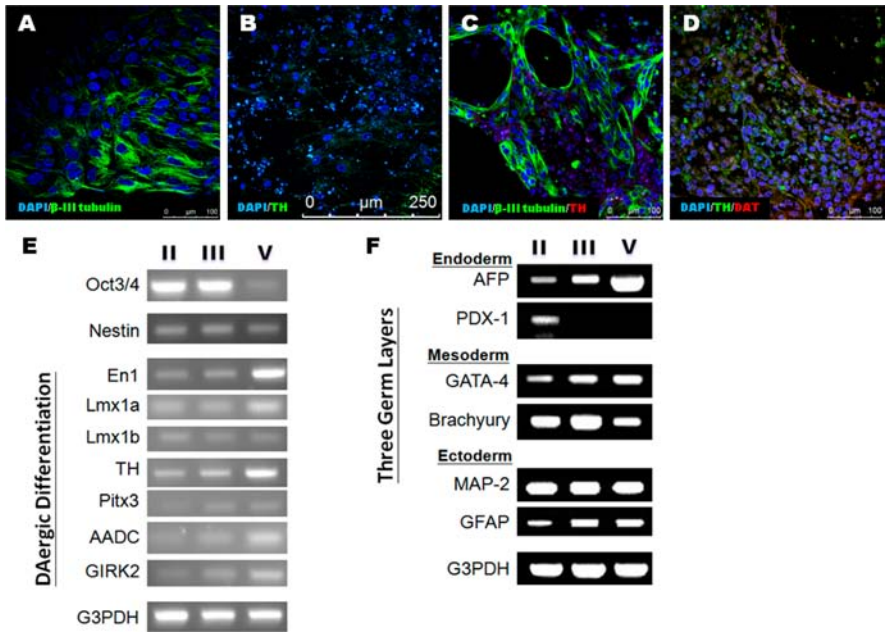

Figure 2. Characterization of differentiated hESCs. (A–D) Immunofluoroscence staining results of stage-V differentiated DAergic neurons. (A) β-III tubulin-positive neurons (green) and merge with DAPI nucleic acid staining (blue). Scale bar = 100 μm. (B) TH-positive neurons (green) and merge with DAPI nucleic acid staining (blue). Scale bar = 250 μm. (C, D) Double-label staining results for β-III tubulin (green) and TH (red) (C); TH (green) and DAT (red) (D) and all merged with DAPI nucleic staining (blue). Scale bar = 100 μm. (E, F) Gene expression profile during hESC differentiation. Semiquantitative reverse-transcriptase PCR analyses from stage-II embryoid bodies (EBs), stage-III neural progenitors (NPs), and stage-V DAergic neurons. (E) Markers specific to undifferentiated hESCs (Oct3/4), neural progenitors (nestin), and DAergic differentiation (En1, Lmx1a, Lmx1b, TH, Pitx3, AADC, and GIRK2). (F) Markers of other germ layers. Abbreviations: TH, tyrosine hydroxylase; DAT, dopamine transporter; AADC, aromatic L-amino acid decarboxylase; AFP, alpha-fetoprotein; PDX-1, pancreatic and duodenal homeobox gene 1; GATA-4, GATA-binding protein 4; MAP2, microtubule-associated protein 2; GFAP, glial fibrillary protein.

and sulpiride (Sigma), while the phytochemicals included epigallocatechin-3-gallate (EGCG; Sigma), epicatechin-3-gallate (ECG; Sigma), epicatechin (EC; Sigma), ginsenoside Rg1 (ChromaDex Inc., Santa Ana, CA, USA), ginsenoside Rg3 (ChromaDex), and ginsenoside Rb1 (ChromaDex). All samples were prepared in water as 1000 μM stock solutions and subsequently diluted to the appropriate concentrations. These prepared samples were added into the medium at the beginning of stage-V cultivation. After cultivation for 7 d, the cells were collected and analyzed for mRNA expression of TH and GIRK2 for evaluating the respective effects of these samples on differentiation of mDA neurons.

Statistical Analysis. Statistical significance was determined by one-way analysis of variance (ANOVA), and the comparisons between means were performed by Duncan's multiple range test. Differences were considered significant $p < 0.05$. All statistical analyses were performed with a SAS 9.2 software package (SAS Institute Inc., Cary, NC, USA).

RESULTS AND DISCUSSION

Differentiation of hESCs into mDA Neurons. To overcome the limitation of PD medicine, stimulation of endogenous DAergic neurogenesis in SN by exogenous factors seems to be a feasible approach.[21] The human-derived cells, especially human pluripotent stem (PS) cells such as embryonic stem cells (ESCs) and induced pluripotent stem cells (iPSCs), provide an opportunity to create more relevant and accurate cellular models than the low-efficacy or propagation restrictions of traditional models, e.g., recombinant immortalized cells or primary cells. Thus, the main purpose of this study was to establish a reliable cellular model for screening potential neurogenic candidates. However, the pluripotent state, transcribed genes, differentiation abilities, epigenetic memories, and mutation loading of iPSCs have also been questioned as being distinctly different from native ESCs.[9] Therefore, we chose ESCs to develop the in vitro platform for screening mDA neurogenesis-boosting compounds with potential to relieve clinical signs of PD.

The mDA differentiation process is shown (Figure 1A). In stage I, hESC H9 cells were cultured on MEFs. The MEFs acted as feeder cells to support the hESC growth and maintained the hESC in an undifferentiated state. To initiate neural differentiation, propagated hESC colonies were then lifted by LEAP workstation to obtain uniform sized cell aggregates around 1 mm (Figure 1B–D). The cell aggregates were then allowed to grow in suspension using bacterial-grade dishes for 3 d to form EBs in stage II. General methods to induce ESC differentiation include feeder-dependent coculture of ESCs with stromal cells and spheroid-shaped EB formation from ESCs. Although the culture of hESC on feeder monolayers tends to simplify culture conditions and reduce steps, the 3-D EB aggregation technique is more capable to recapitulate the situation of early embryogenesis because hESCs will spontaneously differentiate into three-germ layer derivatives during EB formation.

For neural induction, cells were further seeded onto Matrigel-coated dishes with noggin and fibronectin (in stage III). Although type IV collagen-coated dishes have been used in our experience, it is difficult to make EBs attach on these dishes. Therefore, mouse sarcoma-secreted matrigel was used because it has a three-dimensional structure which could facilitate cell attachment, and it comprises extracellular matrix (ECM) components which promote cell growth. Noggin in the system has neural-inducing properties through inhibiting the bone morphogenic protein (BMP) signal.[22] Furthermore, fibronec-

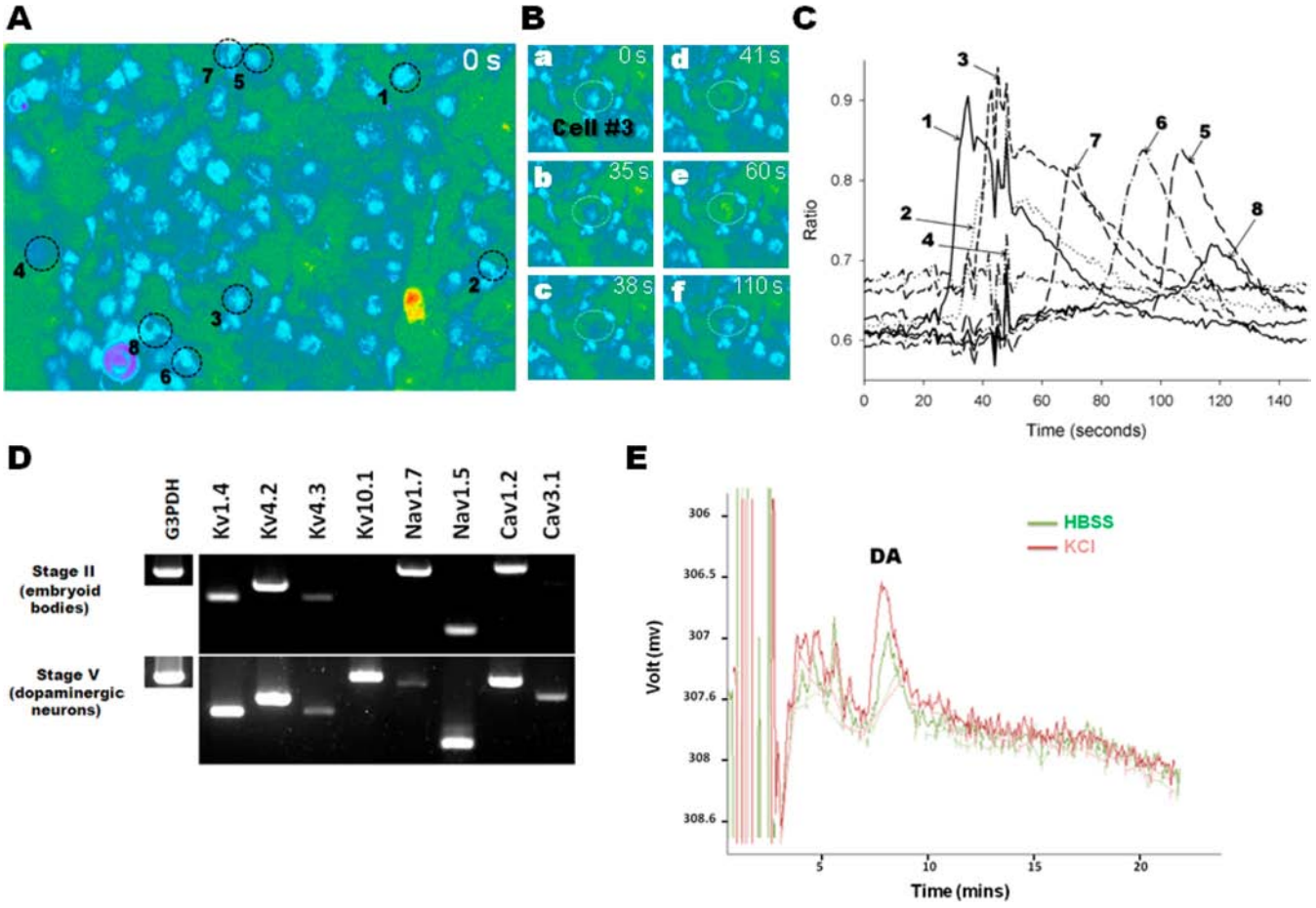

Figure 3. Ion channel related expression of stage-V differentiated DAergic neurons. (A) Image of selected stage-V cells before stimulation with high potassium solution ([KCl] = 150 mM). (B) Time-lapse images showing intracellular calcium ion transients induced by KCl solution in cell 3. (C) Calcium ion transients of all selected cells (cells 1 to 8) over 140 s. The transients are plotted in terms of the fura-2 fluorescence intensity ratio $R = F_{340}/F_{380}$. (D) Voltage-gated ion channel mRNA expression in stage-II EBs and stage-V differentiated DAergic neurons. (E) Retention time of dopamine peak in a representative HPLC chromatogram (red line, a sample treated with 56 mM KCl solution; green line, a control sample without KCl treatment).

tin, a kind of ECM, contributes to the enhancement of cell attachment, growth, and differentiation.[23] The differentiated neural progenitor rosettes with nestin-positive expression (Figure 1E) were formed after 4 d of culture, and the percentage of nestin-positive cells was 33.9−50.3%, suggesting the neural induction (Figure 1F). Then, the expansion of neural rosettes was achieved by culturing cells with bFGF for 7 d in stage IV, which relied on the mitogenic effects of bFGF.[24] To complete the final differentiation of mDA neurons after 7 d, the medium was replaced with defined medium (DM) containing dbcAMP. The DAergic proliferation and differentiation effects of dbcAMP are well-established.[25] As a rate-limiting enzyme during the synthesis of DA, TH is often used as a marker of DAergic neurons, but it should be noted that the TH staining could only verify the existence of catecholamine neurons here. As shown in Figure 1G, the percentage of TH-positive cells was 32.8−53.6%. Compared to previous reports, the predominant points of our protocol included a higher DAergic differentiation rate[26,27] and shorter differentiation periods.[26,28−30] Although higher differentiation rates have been claimed, those studies only counted colonies rather than single cells as used in our study.[20,31]

Characterization of hESC-Derived Cells. Since our differentiation process of hESC into mDA neuron tried to recapitulate the development of mDA neurons, specific transcriptional or nuclear factors would be expressed in distinct stages. Thus, after establishing in vitro mDA differentiation process, expression of DAergic neuronal markers including β-III-tubulin, TH, and DAT in stage-V cells were determined with an immunofluorescence assay. Differentiated DAergic neurons derived from hESCs indeed expressed β-III-tubulin (Figure 2A) and TH (Figure 2B). Results of double staining confirmed not only expression of β-III-tubulin and TH (Figure 2C) but also expression of DAT and TH (Figure 2D). In addition, during the process of differentiation of hESCs into mDA neurons, several other markers were detected by semiquantitative reverse-transcriptase PCR (RT-PCR) (Figure 2E). Oct-3/4 is an essential regulator for maintenance of self-renewal and pluripotency in undifferentiated stem cells,[27] and we found a significant decrease in Oct-3/4 (Figure 2E). Our results further indicated that the early mDA neuron marker En1 and Lmx1a expression kept increasing until the stage-V final differentiation, whereas neural progenitor marker nestin slightly diminished (Figure 2E). The A9 clusters of DAergic neurons in ventral midbrain (VM) ultimately give rise to the SNpc, resulting in a close association with PD. Consequently, GIRK2 was also adopted as a phenotypic marker in SN-A9 DAergic neurons because of its specific expression. Based on RT-PCR results in

dx.doi.org/10.1021/jf501640a | J. Agric. Food Chem. 2014, 62, 6326−6336

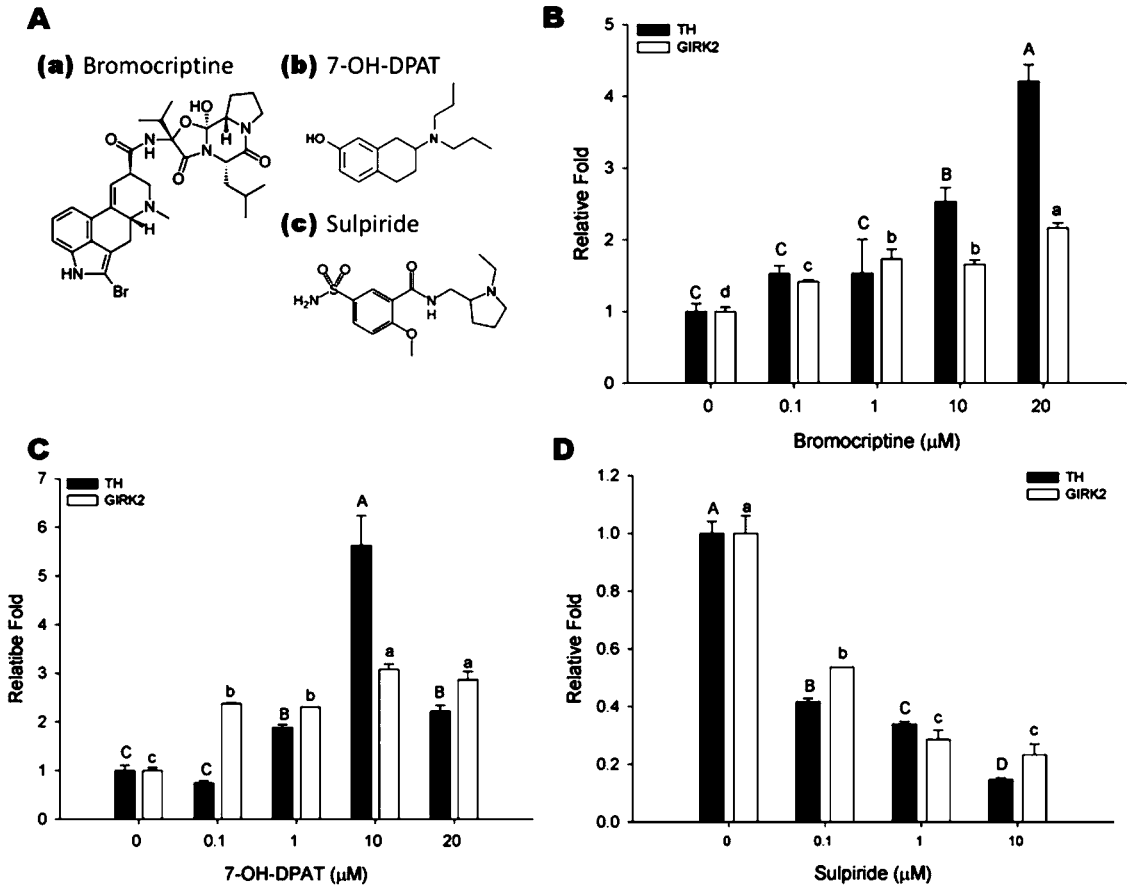

Figure 4. (A) Structure of dopamine receptor (DR) agonist, bromocriptine (a), 7-OH-DPAT (b), and DR antagonist, sulpiride (c). (B–D) TH and GIRK2 mRNA expression in stage-V cells incubated without/with bromocriptine (0.1, 1, 10, and 20 μM) (B); 7-OH-DPAT (0.1, 1, 10, and 20 μM) (C); or sulpiride (0.1, 1, and 10 μM) (D). Each value presents mean ± SD (n = 3). Means without a common uppercase letter A–C differed in TH expression ($p < 0.05$). Means without a common lowercase letter a–c differed in GIRK2 expression ($p < 0.05$).

the present study, enhancements in DA synthesis enzyme TH, AADC, and SN-A9 marker GIRK2 were clearly apparent in the differentiated stage-V cells with mild upregulation in mature mDA marker Pitx3 (Figure 2E). Other germ layer and astrocyte-related (glial fibrillary acidic protein; GFAP) markers were also examined. The PDX-1 (endoderm pancreatic marker) completely disappeared at stage III, whereas brachyury (mesoderm marker) gradually reduced during the course of differentiation (Figure 2F). The mRNA analyses of the three germ layers confirmed the heterogeneous cell populations of the differentiated stage-V cells.

Functional Analysis of hESC-Derived Dopaminergic Neurons. Rapid Ca^{2+} influx through voltage-dependent calcium channels (VDCC) upon membrane depolarization results in neurotransmitter release and other neuronal activities. To further clarify the functional differentiation of stage-V cells, Ca^{2+} dynamics of specific cells were investigated under depolarization induced with a high-potassium solution (cells 1 to 8; Figure 3A). A series of time-lapse images (Figure 3B) reflected transient Ca^{2+} concentrations within the specific cell (cell 3). Furthermore, the fura-2A emissions ratios of all selected cells (cells 1 to 8; Figure 3A) are shown (Figure 3C). It was noteworthy that cell 1 responded immediately after KCl stimulation, whereas other cells had delayed responses. In addition for real-time Ca^{2+} influx detection, the mRNA expression of various common neuronal voltage-gated ion channels including voltage-gated potassium (Kv), voltage-gated sodium (Nav), and voltage-gated calcium (Cav) channels was investigated in stage-II EBs and stage-V differentiated DAergic neurons (Figure 3D). The strong upregulated expression of most ion channels in stage-V cells was prominent, and strikingly, expression of Cav3.1 and Kv10.1 was only detected in stage-V cells (Figure 3D). The Cav3.1 channel has been demonstrated to cooperatively modulate motor function in essential tremor (ET),[32] whereas the Kv10.1 channel is able to maintain the electrophysiological activity of mDA neurons due to its colocalization with DAergic neurons and its reduction induced by a neurotoxin lesion.[33]

Besides, the ability of dopamine (DA) release of differentiated cells was examined by reverse-phase HPLC. Higher DA levels (red line: 7.28 ± 1.30 ng/mL, n = 3) were detected in KCl-evoked samples as compared with control samples (green line: 2.89 ± 0.34 ng/mL, n = 3) (Figure 3E). The combined characterization of differentiated cells following the protocol developed in this study strongly indicated the presence of functional mDA neurons after 21 d of culture.

Validation of the hESC-Derived Model by Dopamine Receptor Agonists and Antagonist. Involvement of DR agonists in adult neurogenesis has been proven in recent studies.[21] The D2L agonists, e.g., bromocriptine (Figure 4A-a) and 7-OH-DPAT (Figure 4A-b), significantly increased neurogenesis of SVZ precursors, whereas the D2L antagonist sulpiride (Figure 4A-c) inhibited the neurogenic effect of bromocriptine.[5] Moreover, 7-OH-DPAT infusion induced cell

dx.doi.org/10.1021/jf501640a | J. Agric. Food Chem. 2014, 62, 6326–6336

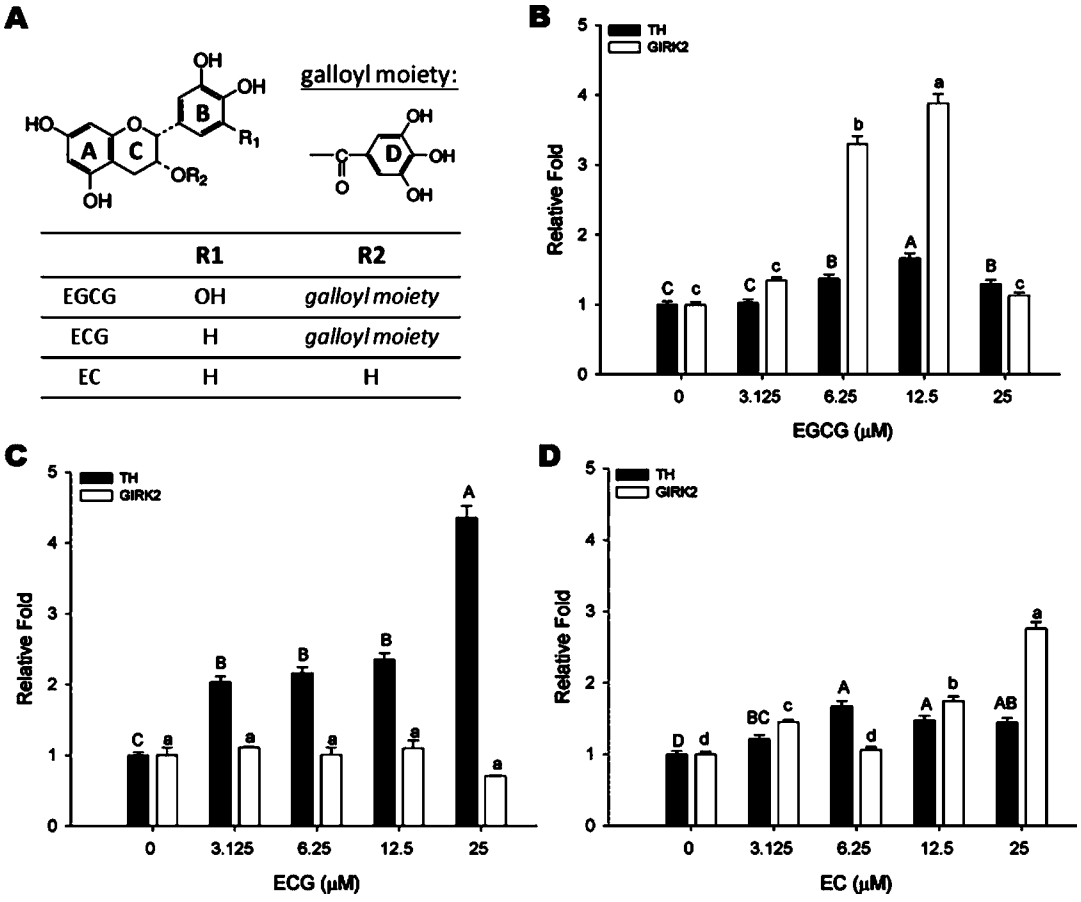

Figure 5. (A) Structure of tea polyphenols, including epigallocatechin gallate (EGCG), epicatechin gallate (ECG), and epicatechin (EC). (B–D) TH and GIRK2 mRNA expression in stage-V cells incubated without/with EGCG (3.125, 6.25, 12.5, and 25 μM) (B); ECG (3.125, 6.25, 12.5, and 25 μM) (C); or EC (3.125, 6.25, 12.5, and 25 μM) (D). Each value presents mean ± SD (n = 3). Means without a common uppercase letter A–C differed in TH expression ($p < 0.05$). Means without a common lowercase letter a–c differed in GIRK2 expression ($p < 0.05$).

proliferation in the striatum,[6] even in SN,[7] and 7-OH-DPAT also recovered locomotor functions of 6-hydroxydopamine (6-OHDA) PD rats.[8] These findings demonstrated that activation of D2/D3 receptors could stimulate SN neurogenesis. Therefore, the present study also investigated the effect of bromocriptine, 7-OH-DPAT, and sulpiride on the expression of SN-A9 markers (TH and GIRK2) to validate the established in vitro differentiated model. As predicted, the D2L agonist bromocriptine (0.1–20 μM) upregulated TH and GIRK2 expression in a concentration-dependent manner; their highest expression all appeared at 20 μM with a 4.5- and 2-fold increase ($p < 0.05$), respectively (Figure 4B). Furthermore, ≥0.1 μM bromocriptine in the culture medium of stage-V cells increased expression of GIRK2 ($p < 0.05$) (Figure 4B). However, bromocriptine concentrations ≥10 μM were required to enhance expression of TH as compared to the control ($p < 0.05$) (Figure 4B). In addition, GIRK2 expression was also significantly enhanced upon treatment with 0.1 μM 7-OH-DPAT (Figure 4C). Expression of TH dramatically increased due to 7-OH-DPAT treatment at doses of 1, 10, and 20 μM; the highest increase, approximately 6-fold, was also at the dose of 10 μM ($p < 0.05$; Figure 4C). Interestingly, 7-OH-DPAT activation reached its highest expression at a lower concentration (10 μM) than that in the bromocriptine-treated group (20 μM; Figures 4B and 4C). This result might be caused by the crucial role of D3 receptor in neurogenesis suggested by its long-term presence in the nervous system, and in contrast to bromocriptine, 7-OH-DPAT has a greater affinity for D3 receptors compared to D2 receptors.[34] Conversely, the D2L antagonist sulpiride (0.1–10 μM) decreased expression of TH and GIRK2 at all concentrations ($p < 0.05$) (Figure 4D). The highest reduction in TH expression was with 10 μM sulpiride (Figure 4D). These observations confirmed the neurogenic potentials of bromocriptine and 7-OH-DPAT in our model.

Screening of Phytochemicals with DAergic Differentiation-Boosting Potential by the Established Model. Although so far there is still no preclinical model able to recapitulate pathological features of PD, 6-hydroxydopamine (6-OHDA), 1-methyl-4-phenyl-1,2,3,6-tetrahydropyridine (MPTP), and rotenone are three commonly used neurotoxins to induce DAergic neurodegeneration in vitro and in vivo.[10] By using these neurotoxin-based models, tea cathechins and ginsenosides are identified as two natural anti-PD compounds. Individual polyphenolic catechins and crude tea extracts all have protective effects on 6-OHDA-treated PC12 cells[35]/SD rats[36] and MPTP-induced C57BL6 mice[37] by inhibition of ROS-nitrogen oxygen (NO) synthetic pathway. Blocking of MPP^+ uptake through dopamine transporter (DAT) is another identified function of green tea polyphenols.[38] Ginseng and ginsenosides can also prevent primary and PC12 cells from oxidative injury from glutamate[14] and rotenone.[12] Ginsenosides can recover the inhibition of neurite growth caused by MPP^+ damage in primary cell model[13] and decrease overload of iron in MPTP-induced C57BL6 mice.[16] Prevention of DAergic

dx.doi.org/10.1021/jf501640a | J. Agric. Food Chem. 2014, 62, 6326–6336

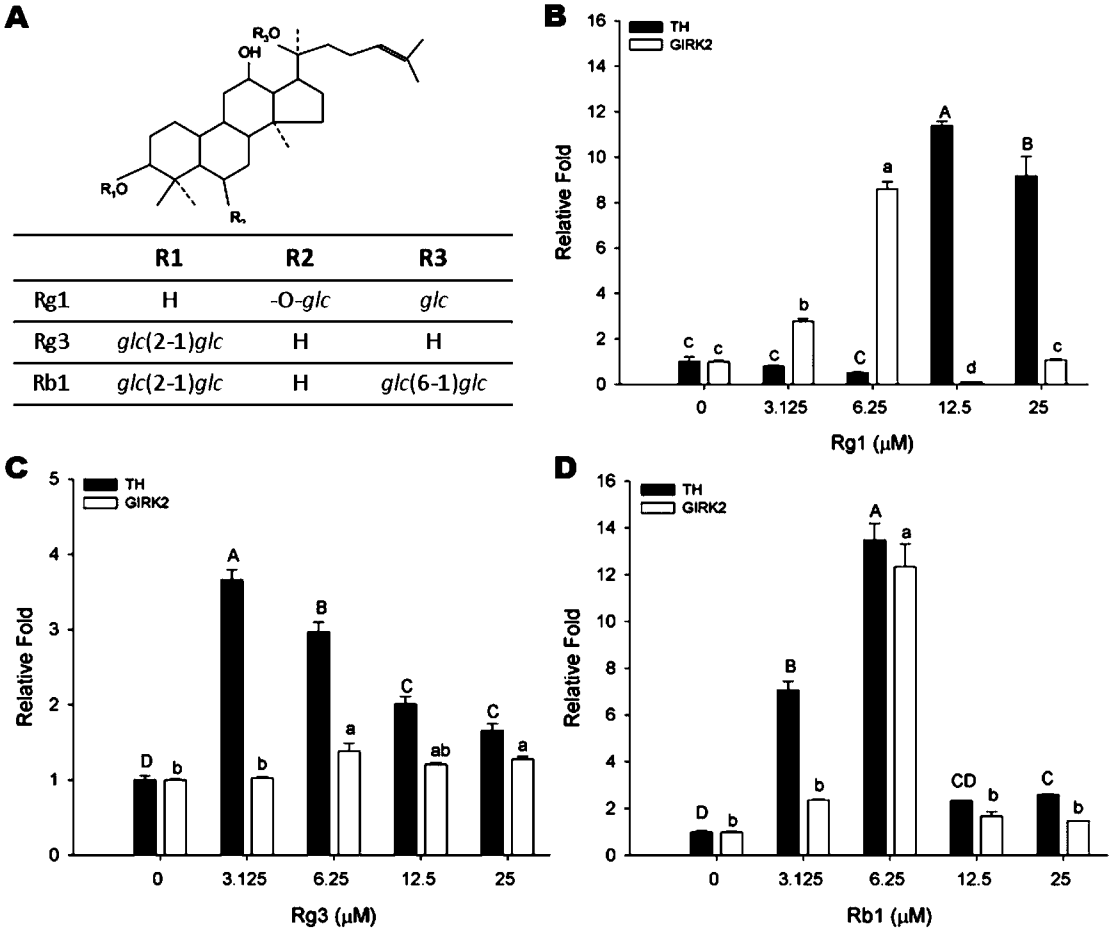

	R1	R2	R3
Rg1	H	-O-*glc*	*glc*
Rg3	*glc*(2-1)*glc*	H	H
Rb1	*glc*(2-1)*glc*	H	*glc*(6-1)*glc*

Figure 6. (A) Structure of ginsenosides, including Rg1, Rg3, and Rb1. (B–D) TH and GIRK2 mRNA expression in stage-V cells incubated without/with Rg1 (3.125, 6.25, 12.5, and 25 μM) (B); Rg3 (3.125, 6.25, 12.5, and 25 μM) (C); or Rb1 (3.125, 6.25, 12.5, and 25 μM) (D). Each value presents mean ± SD (n = 3). Means without a common uppercase letter A–C differed in TH expression ($p < 0.05$). Means without a common lowercase letter a–c differed in GIRK2 expression ($p < 0.05$).

neuron loss by ginseng and ginsenosides has been clarified in MPTP-parkinism C57BL6 mice[15] and 6-OHDA-treated Wistar rats.[17] Moreover, ginsenoside Rg1 has been found to induce glucocorticoid receptor (GR)-dependent neural differentiation in mouse ESC model,[19] while green tea activates neuronal survival and plasticity via enhancement of brain-derived neurotrophic factor (BDNF) and antiapoptotic B-cell lymphoma-2 (Bcl-2) levels in aged rats.[18]

Different from aforementioned studies, our model is for screening phytochemicals with mDA differentiation-boosting potential. As shown in Figure 5B, EGCG significantly enhanced the expression of TH and GIRK2 at dose ≥6.25 μM ($p < 0.05$), and the highest increases of TH and GIRK2 were 1.5- and 4-fold, respectively, which were both at the dose of 12.5 μM. In contrast, ECG had no effect on the enhancement of GIRK2 expression ($p > 0.05$), but it upregulated TH expression, and the highest (4-fold) upregulation occurred at the dose of 25 μM (Figure 5C). Although EC significantly increased both TH and GIRK2 expression as compared with the control group ($p < 0.05$), the levels of increases were rather low (Figure 5D). The mDA differentiation-boosting order of tea catechins might be correlated with their structure (Figure 5A). EGCG, with 3,4,5-trihydroxyl group at B ring as well as D ring galloyl moiety, was the most potent one among the tested tea catechins. The possible antioxidative neuroprotective mechanism contributed from different parts of EGCG structure has been proposed.[39]

Better than tea catechins, ginsenoside Rg1 and Rb1 dramatically induced the expression of A9-SN markers in differentiated stage-V cells, which was even higher than 14-fold (Figures 6B and 6D). However, the enhancement of TH and GIRK2 by Rg1 had a controversial trend. Increase of TH expression appeared at lower doses (3.125 and 6.25 μM), but GIRK2 expression was upregulated at higher doses (12.5 and 25 μM) (Figure 6B). Upon Rg3 treatment, the GIRK2 expression had no obvious enhancement, while the TH expression was significantly increased at all Rg3 concentrations ($p < 0.05$) (Figure 6C). The highest increase of TH expression was at 3.125 μM and gradually decreased when Rg3 concentration increased (Figure 6C). Among tested ginsenosides, Rb1 induced the highest increases of TH and GIRK2 expression at 6.25 μM (Figure 6D). Ginsenosides Rg1, Rg3, and Rb1 all contain a dammarane skeleton with various sugar moieties attached to the C-3 and C-20 positions (Figure 6A). The diversity of ginsenoside structure might contribute to the differences of mDA differentiation abilities. However, we found that Rb1 treatment increased several neurotrophin mRNA levels probably derived from surrounding supporting cells such as astrocytes. In fact, the cross-talk interaction of mDA neurons and astrocytes or microglia has been extensively discussed recently to explain the neural survival, growth, and differentiation.[40] Moreover, brain-derived neurotrophic factor (BDNF), neurotrophin-3 (NT-3), and neurotrophin-4 (NT-

dx.doi.org/10.1021/jf501640a | J. Agric. Food Chem. 2014, 62, 6326–6336

4) secreted by astrocytes are crucial neurotrophins responsible for neuronal survival and differentiation.[41] As shown in Figure 7, the significant upregulation of BDNF and NT-3 consistently

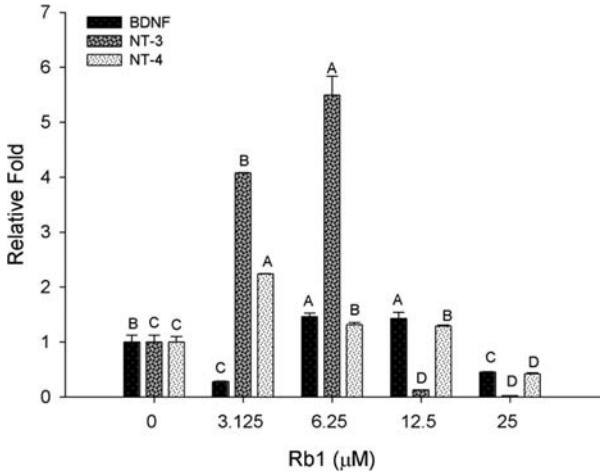

Figure 7. BDNF, NT-3, and NT-4 mRNA expression in stage-V cells incubated without/with Rb1 (3.125, 6.25, 12.5, and 25 μM). Means without a common uppercase letter A–C differed in BDNF, NT-3, or NT-4 expression ($p < 0.05$).

appeared at 6.25 μM ($p < 0.05$), and particularly, NT-3 had a 6-fold increase, thus neurotrophin might also play a vital role in mDA differentiation effects of Rb1.

Although the existence of neural stem cells (NSCs) in SN is debatable, or it is rarely proliferative in SN,[42] stimulation of NSCs resident in active SVZ and SGZ to migrate and differentiate into mDA neurons in SN by drugs or certain phytochemicals to compensate the loss of mDA neurons in damaged PD brains seems to be possible. In addition, induction of protective neurotrophin secretion by surrounding astrocytes or microglia by phytochemicals may be also possible. In this report, we described a five-stage mDA differentiation process that combined D2/D3 agonist bromocriptine, 7-OH-DPAT, and D2L blockade sulpiride respectively as positive and negative controls. Their working concentrations were 20 μM bromocriptine, 10 μM 7-OH-DPAT, and 10 μM sulpiride. The final differentiated cells were functional mDA neurons with SN-A9 neuron phenotypes and special voltage-gated ion channel expression including Cav3.1 and Kv10.1. DA release was also detected in response to K^+ depolarization. Compared to other differentiation protocols, our differentiation period (21 d) was much shorter, with an acceptable differentiation rate between 32.8 and 53.6%. These results manifested the predictive potential of our model for screening phytochemicals with mDA neurogenesis-boosting abilities. Using this model, we found that Rb1 is a very potent phytochemical for relieving PD, and it might induce mDA differentiation and upregulate the expression of BDNF and NT-3 from surrounding cells like astrocytes.

AUTHOR INFORMATION

Corresponding Author

*E-mail: bhchiang@ntu.edu.tw. Tel: +886-2-33664120. Fax: +886-2-23620849.

Funding

This research is funded by the Ministry of Science and Technology of Republic of China (Taiwan) under project No. 101-2313-B-002-064.

Notes

The authors declare no competing financial interest.

ACKNOWLEDGMENTS

We gratefully acknowledge Professor Chung-Liang Chien and his laboratory assistants at Stem Cell Core (NTU Genomic Medicine Center, Taipei, Taiwan) and the technical support from Professor Chien-Yua Pan of the Institute of Zoology and the Joint Center for Instruments and Researches (College of Bioresources and Agriculture, NTU, Taipei, Taiwan).

REFERENCES

(1) Kalinderi, K.; Fidani, L.; Katsarou, Z.; Bostantjopoulou, S. Pharmacological treatment and the prospect of pharmacogenetics in Parkinson's disease. *Int. J. Clin. Pract.* **2011**, *65*, 1289–1294.

(2) Ming, G. L.; Song, H. Adult neurogenesis in the mammalian brain: significant answers and significant questions. *Neuron* **2011**, *70*, 687–702.

(3) Marxreiter, F.; Regensburger, M.; Winkler, J. Adult neurogenesis in Parkinson's disease. *Cell. Mol. Life Sci.* **2013**, *70*, 459–473.

(4) Coronas, V.; Bantubungi, K.; Fombonne, J.; Krantic, S.; Schiffmann, S. N.; Roger, M. Dopamine D3 receptor stimulation promotes the proliferation of cells derived from the post-natal subventricular zone. *J. Neurochem.* **2004**, *91*, 1292–1301.

(5) Höglinger, G. U.; Rizk, P.; Muriel, M. P.; Duyckaerts, C.; Oertel, W. H.; Caille, I.; Hirsch, E. C. 2004. Dopamine depletion impairs precursor cell proliferation in Parkinson disease. *Nat. Neurosci.* **2004**, *7*, 726–735.

(6) Van Kampen, J. M.; Hagg, T.; Robbertson, A. Induction of neurogenesis in the adult rat subventricular zone and neostriatum following dopamine D3 receptor stimulation. *Eur. J. Neurosci.* **2004**, *19*, 2377–2387.

(7) Van Kampen, J. M.; Robertson, H. A. A possible role for dopamine D3 receptor stimulation in the induction of neurogenesis in the adult rat substantia nigra. *Neuroscience* **2005**, *136*, 381–386.

(8) Van Kampen, J. M.; Eckman, C. B. 2006. Dopamine D3 receptor agonist delivery to a model of Parkinson's disease restores the nigrostriatal pathway and improves locomotor behavior. *J. Neurosci.* **2006**, *26*, 7272–7280.

(9) Liu, W.; Deng, Y.; Liu, Y.; Gong, W.; Deng, W. Stem cell models for drug discovery and toxicology studies. *J. Biochem. Mol. Toxicol.* **2013**, *27*, 17–27.

(10) Beal, M. F. 2001. Experimental models of Parkinson's disease. *Nat. Rev. Neurosci.* **2001**, *2*, 325–334.

(11) Chen, X. C.; Zhu, Y. G.; Zhu, L. A.; Huang, C.; Chen, Y.; Chen, L. M.; Fang, F.; Zhou, Y. C.; Zhao, C. H. 2003. Ginsenoside Rg1 attenuates dopamine-induced apoptosis in PC12 cells by suppressing oxidative stress. *Eur. J. Pharmacol.* **2003**, *473*, 1–7.

(12) Leung, K. W.; Yung, K. K.; Mak, N. K.; Chan, Y. S.; Fan, T. P.; Wong, R. N. Neuroprotective effects of ginsenoside-Rg1 in primary nigral neurons against rotenone toxicity. *Neuropharmacology* **2007**, *52*, 827–835.

(13) Radad, K.; Gille, G.; Moldzio, R.; Saito, H.; Ishige, K.; Rausch, W. D. Ginsenosides Rb1 and Rg1 effects on survival and neurite growth of MPP^+-affected mesencephalic dopaminergic cells. *J. Neural Transm.* **2004**, *111*, 37–45.

(14) Radad, K.; Gille, G.; Moldzio, R.; Saito, H.; Rausch, W. D. Ginsenosides Rb1 and Rg1 effects on mesencephalic dopaminergic cells stressed with glutamate. *Brain Res.* **2004**, *1021*, 41–53.

(15) Chen, X. C.; Zhou, Y. C.; Chen, Y.; Zhu, Y. G.; Fang, F.; Chen, L. M. 2009. Ginsenoside Rg1 reduces MPTP-induced substantia nigra neuron loss by suppressing oxidative stress. *Acta Pharmacol. Sin.* **2009**, *26*, 56–62.

(16) Wang, J.; Xu, H. M.; Yang, H. D.; Du, X. X.; Jiang, H.; Xie, J. X. Rg1 reduces nigral iron levels of MPTP-treated C57BL6 mice by regulating certain iron transport proteins. *Neurochem. Int.* **2009**, *54*, 43−48.
(17) Xu, L.; Chen, W. F.; Wong, M. S. Ginsenoside Rg1 protects dopaminergic neurons in a rat model of Parkinson's disease through the IGF-I receptor signalling pathway. *Br. J. Pharmacol.* **2009**, *158*, 738−748.
(18) Assunção, M.; Santos-Marques, M. J.; Carvalho, F.; Andrade, J. P. Green tea averts age-dependent decline of hippocampal signaling systems related to antioxidant defenses and survival. *Free Radical Biol. Med.* **2010**, *48*, 831−838.
(19) Wu, J.; Pan, Z.; Cheng, M.; Shen, Y.; Yu, H.; Wang, Q.; Lou, Y. Ginsenoside Rg1 facilitates neural differentiation of mouse embryonic stem cells via GR-dependent signaling pathway. *Neurochem. Int.* **2013**, *62*, 92−102.
(20) Iacovitti, L.; Donaldson, A. E.; Marshall, C. E.; Suon, S.; Yang, M. A protocol for the differentiation of human embryonic stem cells into dopaminergic neurons using only chemically defined human additives: studies *in vitro* and *in vivo*. *Brain Res.* **2007**, *1127*, 19−25.
(21) van den Berge, S. A.; van Strien, M. E.; Hol, E. M. Resident adult neural stem cells in Parkinson's disease-The brain's own repair system? *Eur. J. Pharmacol.* **2013**, *719*, 117−127.
(22) Dhara, S. K.; Stice, S. L. Neural differentiation of human embryonic stem cells. *J. Cell. Biochem.* **2008**, *105*, 633−640.
(23) Erceg, S.; Ronaghi, M.; Stojković, M. Human embryonic stem cell differentiation toward regional specific neural precursors. *Stem Cells* **2009**, *27*, 78−87.
(24) Park, S.; Lee, K. S.; Lee, Y. J.; Shin, H. A.; Cho, H. Y.; Wang, K. C.; Kim, Y. S.; Lee, H. T.; Chung, K. S.; Kim, E. Y.; Lim, J. Generation of dopaminergic neurons in vitro from human embryonic stem cells treated with neurotrophic factors. *Neurosci. Lett.* **2004**, *359*, 99−103.
(25) Michel, P. P.; Agid, Y. Chronic activation of the cyclic AMP signaling pathway promotes development and long-term survival of mesencephalic dopaminergic neurons. *J. Neurochem.* **1996**, *67*, 1633−1642.
(26) Park, C. H.; Minn, Y. K.; Lee, J. Y.; Choi, D. H.; Chang, M. Y.; Shim, J. W.; Ko, J. Y.; Koh, H. C.; Kang, M. J.; Kang, J. S.; Rhie, D. J.; Lee, Y. S.; Son, H.; Moon, S. Y.; Kim, K. S.; Lee, S. H. *In vitro* and *in vivo* analyses of human embryonic stem cell-derived dopamine neurons. *J. Neurochem.* **2005**, *92*, 1265−1276.
(27) Rizzino, A. 2009. Sox2 and Oct-3/4: a versatile pair of master regulators that orchestrate the self-renewal and pluripotency of embryonic stem cells. *Wiley Interdiscip. Rev.: Syst. Biol. Med.* **2009**, *1*, 228−236.
(28) Cho, M. S.; Lee, Y. E.; Kim, J. Y.; Chung, S.; Cho, Y. H.; Kim, D. S.; Kang, S. M.; Lee, H.; Kim, M. H.; Kim, J. H.; Leem, J. W.; Oh, S. K.; Choi, Y. M.; Hwang, D. Y.; Chang, J. W.; Kim, D. W. Highly efficient and large-scale generation of functional dopamine neurons from human embryonic stem cells. *Proc. Natl. Acad. Sci. U.S.A.* **2008**, *105*, 3392−3397.
(29) Ko, J. Y.; Park, C. H.; Koh, H. C.; Cho, Y. H.; Kyhm, J. H.; Kim, Y. S.; Lee, I.; Lee, Y. S.; Lee, S. H. Human embryonic stem cell-derived neural precursors as a continuous, stable, and on-demand source for human dopamine neurons. *J. Neurochem.* **2007**, *103*, 1417−1429.
(30) Perrier, A. L.; Tabar, V.; Barberi, T.; Rubio, M. E.; Bruses, J.; Topf, N.; Harrison, N. L.; Studer, L. Derivation of midbrain dopamine neurons from human embryonic stem cells. *Proc. Natl. Acad. Sci. U.S.A.* **2004**, *101*, 12543−12548.
(31) Brederlau, A.; Correia, A. S.; Anisimov, S. V.; Elmi, M.; Paul, G.; Roybon, L.; Morizane, A.; Bergquist, F.; Riebe, I.; Nannmark, U.; Carta, M.; Hanse, E.; Takahashi, J.; Sasai, Y.; Funa, K.; Brundin, P.; Eriksson, P. S.; Li, J. Y. Transplantation of human embryonic stem cell-derived cells to a rat model of Parkinson's disease: effect of *in vitro* differentiation on graft survival and teratoma formation. *Stem Cells* **2006**, *24*, 1433−1440.
(32) Chang, K. Y.; Park, Y. G.; Park, H. Y.; Homanics, G. E.; Kim, J.; Kim, D. Lack of CaV3.1 channels causes severe motor coordination defects and an age-dependent cerebellar atrophy in a genetic model of essential tremor. *Biochem. Biophys. Res. Commun.* **2011**, *410*, 19−23.
(33) Ferreira, N. R.; Mitkovski, M.; Stühmer, W.; Pardo, L. A.; Del Bel, E. A. *Ether-à-go-go* 1 (Eag1) potassium channel expression in dopaminergic neurons of basal ganglia is modulated by 6-hydroxydopamine lesion. *Neurotox. Res.* **2012**, *21*, 317−333.
(34) Levant, B. The D3 dopamine receptor: neurobiology and potential clinical relevance. *Pharmacol. Rev.* **1997**, *105*, 317−327.
(35) Jin, C. F.; Shen, S. R., Sr.; Zhao, B. L. Different effects of five catechins on 6-hydroxydopamine-induced apoptosis in PC12 cells. *J. Agric. Food Chem.* **2001**, *49*, 6033−6038.
(36) Guo, S.; Yan, J.; Bezard, E.; Yang, T.; Yang, X.; Zhao, B. Protective effects of green tea polyphenols in the 6-OHDA rat model of Parkinson's disease through inhibition of ROS-NO pathway. *Biol. Psychiatry* **2007**, *62*, 1353−1362.
(37) Levites, Y.; Weinreb, O.; Maor, G.; Youdim, M. B.; Mandel, S. Green tea polyphenol epigallocatechin-3-gallate prevents MPTP induced dopaminergic neurodegeneration. *J. Neurochem.* **2001**, *78*, 1073−1082.
(38) Pan, T.; Fei, J.; Zhou, X.; Jankovic, J.; Le, W. Effects of green tea polyphenols on dopamine uptake and on MPP^+-induced dopamine neuron injury. *Life Sci.* **2003**, *72*, 1073−1083.
(39) Mähler, A.; Mandel, S.; Lorenz, M.; Ruegg, U.; Wanker, E. E.; Boschmann, M.; Paul, F. Epigallocatechin-3-gallate: a useful, effective and safe clinical approach for targeted prevention and individualised treatment of neurological diseases? *EPMA J.* **2013**, *4*, 5.
(40) Marchetti, B.; L'Episcopo, F.; Morale, M. C.; Tirolo, C.; Testa, N.; Caniglia, S.; Serapide, M. F.; Pluchino, S. Uncovering novel actors in astrocyte-neuron crosstalk in Parkinson's disease: the Wnt/β-catenin signaling cascade as the common final pathway for neuroprotection and self-repair. *Eur. J. Neurosci.* **2013**, *37*, 1550−1563.
(41) Oliveira, S. L.; Pillat, M. M.; Cheffer, A.; Lameu, C.; Schwindt, T. T.; Ulrich, H. Functions of neurotrophins and growth factors in neurogenesis and brain repair. *Cytometry, Part A* **2013**, *83*, 76−89.
(42) Kim, H. J.; Sun, W. Adult neurogenesis in the central and peripheral nervous systems. *Int. Neurourol. J.* **2012**, *16*, 57−61.

disease, antidementia, anti-inflammation, antitumor, antiaging, and free radical scavenging.[13,14] EGb761 has been one of the most commonly used herbal dietary remedies in many countries, including China, the United States, France, and Germany. In rats with osteoarthritis on the knee and LPS-treated chondrocytes, EGb761 was found to reduce the inflammatory effects by production of prostaglandin (PG)E2 and nitric oxide (NO), expression of cyclooxygenase (COX)-2 and inducible nitric oxide synthase (iNOS), and phosphorylation of NFκB.[15] In murine macrophages, *Ginkgo biloba* extract reduces LPS-induced production of NO and PGE2 through expression of iNOS and COX-2 via NFκB phosphorylation.[16] Previously, we have demonstrated that EGb761 attenuates LPS-induced ALI via inhibition of oxidative stress and the NFκB-dependent matrix metalloproteinase-9 pathway.[17] In the present study, we aimed to verify the protective mechanism of EGb761 via MAPK and Akt pathways on LPS-induced ALI in an in vivo animal model.

MATERIALS AND METHODS

Materials. EGb761 was obtained from the laboratory of Dr. Willmar Schwabe (Karlsruhe, Germany). Antibodies against p38 MAPK, ERK, JNK, Akt, IκB, phospho-Akt (Ser473), phospho-IκB (Ser32), phospho-ERK (Thr212/Tyr204), phospho-JNK (Thr183/Tyr185), COX-2, iNOS, and β-actin were purchased from Santa Cruz Biotechnology (Santa Cruz, CA, USA). The antibody against phospho-p38 MAPK (Thr180/Tyr182) was purchased from Cell Signaling Technology (Danvers, MA, USA). Secondary antibodies were obtained from Jackson Immuno Research Laboratories (Baltimore, MD, USA). NFκB p65 Transcription Factor Kit was obtained from Thermo Fisher Scientific (Waltham, MA, USA). Enzyme-linked immunosorbent assay (ELISA) kits were obtained from Cayman (Ann Arbor, MI, USA). LPS from *Escherichia coli* Serotype 0111:B4, dimethyl sulfoxide (DMSO), and other reagents, unless specifically stated elsewhere, were purchased from Sigma-Aldrich (St. Louis, MO, USA). The concluding volume of DMSO in the reaction mixture was <0.5%.

Animals. Adult male ICR mice weighing 25−30 g were purchased from BioLASCO Taiwan (Taipei, Taiwan). All mice were housed under standard laboratory conditions and fed a standard laboratory diet and water ad libitum. All mice were cared for following guidelines provided by the Institutional Animal Ethics Committee of Chung Shan Medical University.

Murine Model of LPS-Induced ALI. The ALI induced by LPS was performed as described in previous studies.[8,9] Sixty mice were randomly subdivided into six groups: a sham operation group and five treatment groups. The sham operation group received vehicle intraperitoneally (IP) for 30 min followed by intratracheal (IT) administration of 50 μL of saline, while the five treatment groups were pretreated with 0, 10, 100, and 1000 μg/kg of EGb761 or 1000 μg/kg of dexamethasone (DEX) IP for 30 min, respectively, before administration of 100 μg/50 μL of LPS IT. After 6 h, the mice were sacrificed, and samples were collected.

Bronchoalveolar Lavage Fluid (BALF) Collection. The collection of BALF was performed as previously described.[8,9] The airways and lungs were flushed with sterile saline three times through a tracheal cannula, installed up to a total volume of 1 mL. The pooled BALF was collected on ice and centrifuged at 700*g* for 10 min at 4 °C. The cell-free supernatant was subsequently stored at −20 °C for cytokine and chemokine concentration analysis, the sediment cells were stained with Giemsa stain solution, and the numbers of neutrophils were counted.

Blood Gas Analysis of Arterial Blood. After euthanasia, blood samples were collected from the abdominal aorta. Partial pressures of oxygen (PaO_2) and carbon dioxide ($PaCO_2$) and acidity (pH) in arterial blood were measured immediately by a blood gas analyzer (Radiometer ABL 700 blood gas analyzer, Copenhagen, Denmark).

Histopathological Studies of Lung Tissues. After midsternal thoracotomy, the lungs were removed rapidly, fixed in 4% isotonic paraformaldehyde, embedded in paraffin, sliced into 3 μm sections with a microtome, and stained with hematoxylin and eosin (H&E) for histopathological studies.

Wet to Dry Weight Ratio of Lung Tissues. The lungs were dissected immediately, and the wet weight was recorded. Then the tissues were baked in an incubator at 80 °C for 24 h to obtain the dry weight. The ratio of wet weight to dry weight was calculated to evaluate the extent of lung edema.

Measurement of Cytokines and Chemokines. Measurement of cytokines and chemokines, such as tumor necrosis factor (TNF)α, macrophage inflammatory protein (MIP)-2, and interleukin (IL)-6, in BALF was performed with commercially available ELISA assay kits. The quantification of cytokines and chemokines was performed according to the manufacturer's instructions.

Western Blot Analysis of Lung Tissue. As previously described, lungs were harvested, rinsed with saline, and frozen in liquid nitrogen immediately until homogenization.[17] Tissue extracts were homogenized in a tissue protein extraction solution (T-PER; Pierce, Rockford, IL, USA) containing 1% proteinase inhibitor cocktail and phosphatase inhibitor cocktail. Protein samples, 100 μg each, were separated by SDS-PAGE and electrophoretically transferred to polyvinylidene difluoride membranes. The membranes were blocked with phosphate-buffered saline (PBS) containing 0.1% Tween-20 (PBST) and 5% nonfat milk (w/v) for 1 h at room temperature. After they were washed with PBST, the membranes were probed with antibodies including iNOS, COX-2, β-actin, phosphory-IκB, and phosphorylated and nonphosphorylated forms of JNK, ERK, p38 MAPK, and Akt. The membranes were washed again with PBST, then a 1/10000 (v/v) dilution of horseradish peroxidase labeled IgG was added at room temperature for 1 h, and the blots were developed using ECL Western blotting reagents.

NFκB Activation. The preparation of nuclear extract from lung homogenates and measurement of NFκB activation in nuclear extract were performed with a nuclear extraction kit and NFκB p65 Transcription Factor Kit (both from NEPER Nuclear and Cytoplasmic Extraction Reagents, Thermo Science), respectively, according to the manufacturer's instructions.

Statistical Analysis. Statistical analyses were performed using ANOVA followed by the Bonferroni *t* test for multigroup comparisons; $p < 0.05$ was considered significant for all tests. Data are expressed as mean ± standard deviation (SD).

RESULTS

Effects of EGb761 on Arterial Blood Gas in LPS-Induced ALI. To study the effects of EGb761 on LPS-induced ALI, the mice were pretreated with EGb761 for 30 min before LPS administration. As shown in Figure 1, pH and PaO_2 were significantly decreased while $PaCO_2$ was significantly increased in the LPS-treated group. However, all these effects were attenuated by EGb761 in a dose-dependent manner; a significant inhibitory effect began at 100 μg/kg ($p < 0.05$).

Effects of EGb761 on Histopathological Changes in the Lung of LPS-Induced ALI. Severe lung damage, including diffuse hemorrhage, edema, thickening of the alveolar septum, formation of hyaline membranes, and infiltration of inflammatory cells into the lung parenchyma and alveolar spaces, occurred after LPS administration for 6 h (Figure 2B). In contrast, no pathohistological change was observed in the control group (Figure 2A). However, administration of EGb761 significantly attenuated these pathohistological changes in a concentration-dependent manner (Figure 2C−E).

Effects of EGb761 on LPS-Induced Neutrophils Infiltration and Lung Edema. Neutrophil infiltration was significantly increased in LPS-treated mice in comparison with the control group ($p < 0.05$). Pretreatment with EGb761 reduced LPS-induced neutrophil infiltration in a concentration-dependent manner starting at 10 μg/kg ($p < 0.05$, Figure 3A). Neutrophil infiltration results in increasing vascular permeability, which leads to edema formation in LPS-treated lung tissue. As shown in Figure 3B, lung edema was significantly increased in LPS-treated

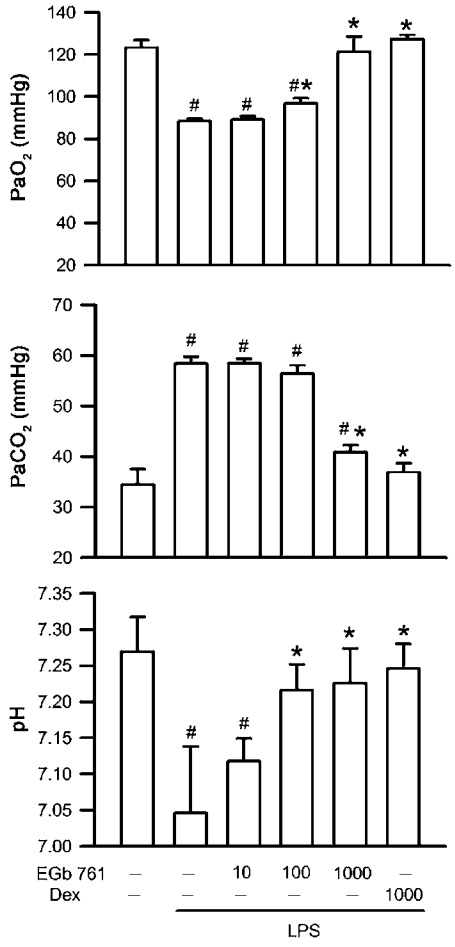

Figure 1. Effect of EGb761 in changes of arterial blood gas in LPS-induced ALI. # represents a significant difference between the indicated and control group, and * represents a significant difference between the indicated and LPS groups, $p < 0.05$. The represented parameters are PaO_2, $PaCO_2$, and pH. Values are expressed as mean ± SD of 5 mice per group.

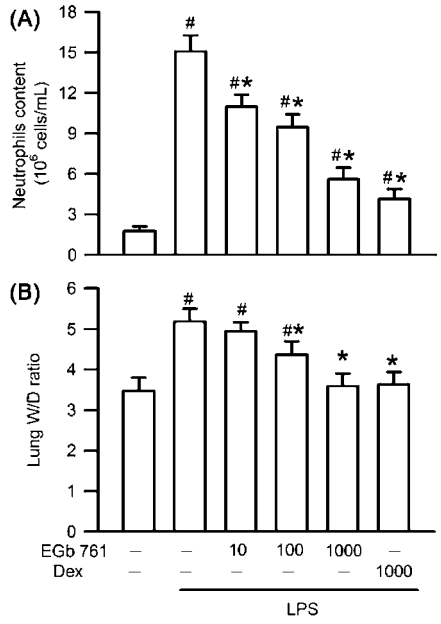

Figure 3. Effects of EGb761 on LPS-induced neutrophil infiltration and lung edema: (A) neutrophil infiltration determined by leukocyte counts in BALF; (B) lung edema determined by quantifying the wet to dry weight ratio. Values are expressed as mean ± SD ($n = 4$ in each group). * represents a significant difference between the indicated and normal control group, and # represents a significant difference between the indicated and LPS groups, $p < 0.05$.

mice in comparison to the control group ($p < 0.05$). Pretreatment with EGb761 reduced LPS-induced lung edema in a concentration-dependent manner starting at 100 μg/kg ($p < 0.05$, Figure 3A).

Effects of EGb761 on LPS-Induced TNFα, IL-6, and MIP-2 Generation. TNFα, IL-6, and MIP-2 are important proinflammatory cytokines and chemokines participating in the recruitment of leukocytes into the lungs in LPS-induced ALI.[17−19] The effect of EGb761 on TNFα, IL-6, and MIP-2 generation in the BALF was analyzed by ELISA. The concentration of TNFα, IL-6, and MIP-2 increased significantly after the mice were treated with LPS for 6 h in comparison with the control group ($p < 0.05$). Pretreatment of EGb761 at 100 μg/kg

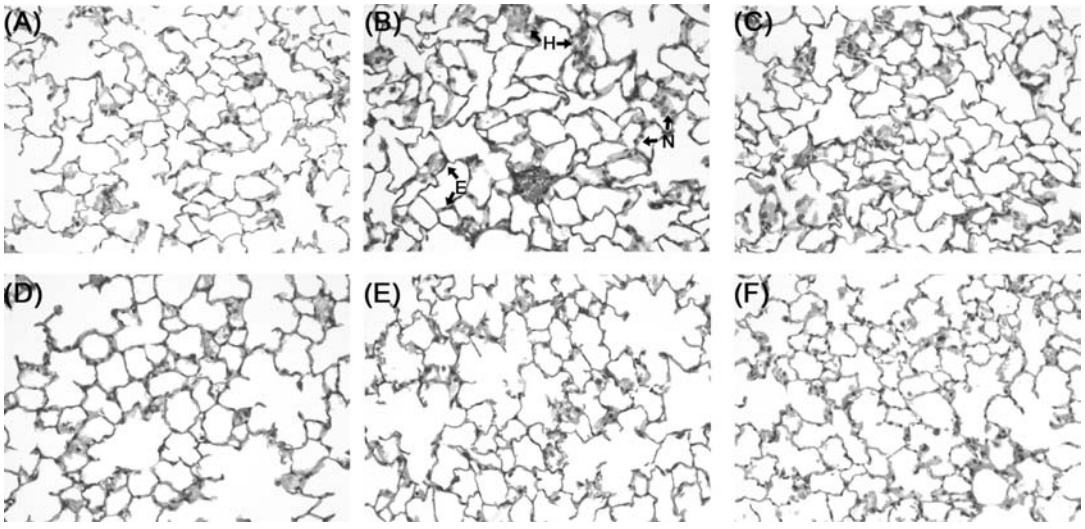

Figure 2. Effect of EGb761 on pathohistological changes of the lung in LPS-induced ALI (100×): (A) control; (B) LPS; (C) 10 μg/kg of EGb761 + LPS; (D) 100 μg/kg of EGb761 + LPS; (E) 1000 μg/kg of EGb761 + LPS; (F) 1000 μg/kg of dexamethasone (Dex) + LPS. Arrows point to hyaline membranes (H), interstitial edema (E), and neutrophils (N).

dx.doi.org/10.1021/jf501913b | J. Agric. Food Chem. 2014, 62, 6337−6344

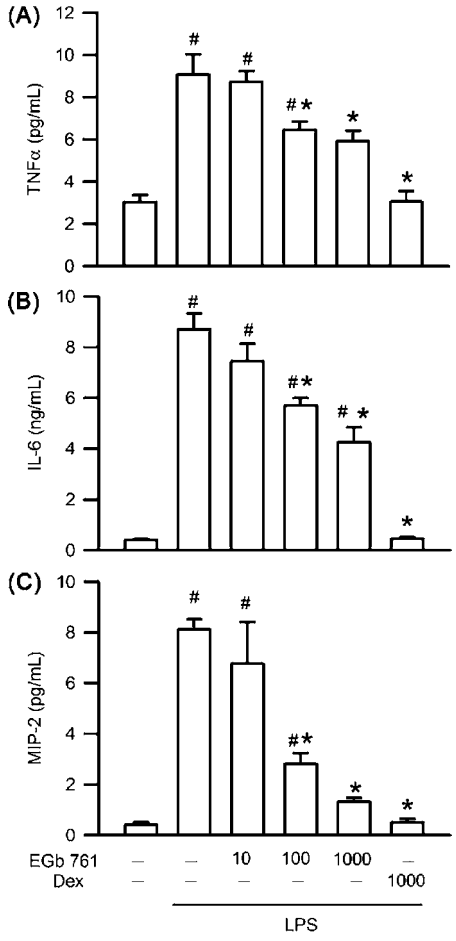

Figure 4. Effect of EGb761 on LPS-induced generation of TNFα, IL-6, and MIP-2 in BALF. Values are expressed as mean ± SD of 4 mice per group. # represents a significant difference between the indicated and control group, and * represents a significant difference between the indicated and LPS groups, $p < 0.05$.

and up reduced the generation of TNFα, IL-6, and MIP-2 significantly in a concentration-dependent manner ($p < 0.05$, Figure 4).

Effects of EGb761 on LPS-Induced COX-2 and iNOS Expression. Expression of COX-2 and iNOS in lung tissue is a critical sign of LPS-induced ALI.[20,21] After LPS treatment, COX-2 and iNOS were dramatically expressed in lung tissues in comparison to the control group ($p < 0.05$). Pretreatment with EGb761 reduced LPS-induced COX-2 and iNOS expression in a concentration-dependent manner starting at 100 μg/kg ($p < 0.05$, Figure 5).

Effects of EGb761 on LPS-Induced NFκB Activation and IκB Phosphorylation. The activation of NFκB is critically required for the generation of proinflammatory cytokines and chemokines in LPS-induced ALI.[7] After LPS treatment, NFκB activation was significantly expressed in lung tissues in comparison with the control group ($p < 0.05$). Pretreatment with EGb761 reduced the expression of LPS-induced NFκB activation in a concentration-dependent manner starting at 100 μg/kg ($p < 0.05$, Figure 6A). Phosphorylation and degradation of IκB participate in NFκB activation.[7] After LPS treatment, phosphorylation of IκB was significantly expressed in lung tissues in comparison with the control group ($p < 0.05$). Pretreatment with EGb761 reduced LPS-induced phosphorylation of IκB in a concentration-dependent manner starting at 100 μg/kg ($p < 0.05$, Figure 6B).

Effects of EGb761 on LPS-Induced Phosphorylation of JNK, ERK, p38 MAPK, and Akt. JNK, ERK, p38 MAPK, and Akt have been demonstrated as the upstream factors in NFκB activation in LPS-induced ALI.[10−12,22] LPS stimulation significantly increased JNK, ERK, p38 MAPK, and Akt phosphorylation in comparison to the control group ($p < 0.05$). EGb761 suppressed LPS-induced phosphorylation of JNK and Akt pathways in a concentration-dependent manner starting at 100 μg/kg ($p < 0.05$, Figure 7A,D). However, significant inhibition on the phosphorylation of ERK and p38 MAPK by

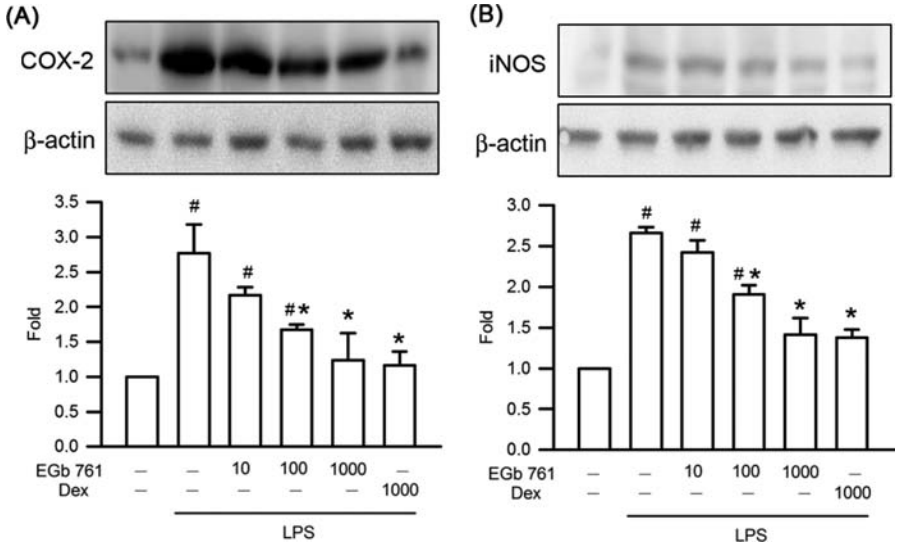

Figure 5. Effect of EGb761 on LPS-induced COX-2 and iNOS expression in lung. Lung tissues harvested from post-treated mice were analyzed by Western blotting. The fold of COX-2 (A) and iNOS (B) expressions between the treated and control groups was calculated. Values are expressed as mean ± SD ($n = 3-5$ in each group). * represents a significant difference between the indicated and normal control group, and # represents a significant difference between the indicated and LPS groups, $p < 0.05$.

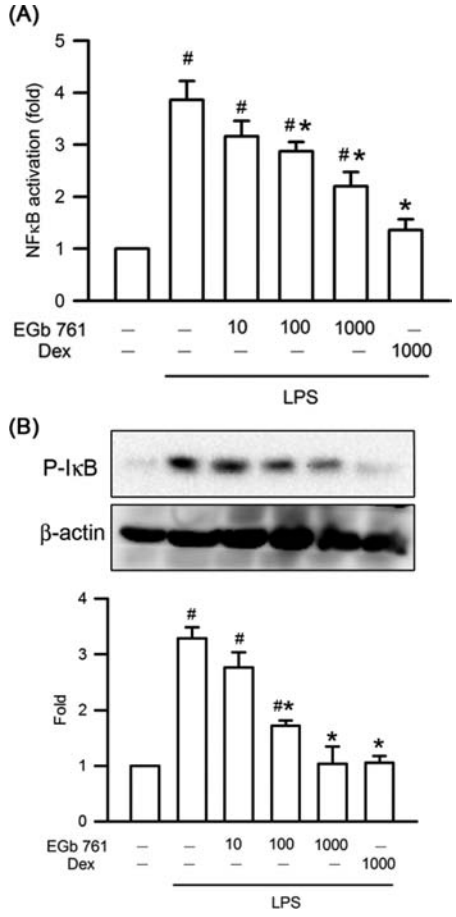

Figure 6. Effect of EGb761 on LPS-induced NFκB activation and IκB phosphorylation in lung. (A) Lungs were harvested from post-treated mice, and nuclear extracts from whole lung tissues were analyzed by p65 transcription factor assay to study the activation levels of NFκB. The fold of NFκB activation between the treatment and control groups was calculated. In addition, lung tissues harvested from post-treated mice were analyzed by Western blotting. (B) The fold of IκB phosphorylation between the treated and control groups was calculated. Values are expressed as mean ± SD (n = 3−5 in each group). * represents a significant difference between the indicated and normal control group, and # represents a significant difference between the indicated and LPS groups, $p < 0.05$.

EGb761 was not observed until the concentration was up to 1000 μg/kg ($p < 0.05$, Figure 7B,C).

DISCUSSION

In the present investigation, evidence had shown that pretreatment with EGb761 prevented the pathological changes occurring in response to the endotoxin, LPS, induced ALI in the murine model. EGb761 not only effectively prevented LPS-induced changes in blood gas parameters and lung histopathology, neutrophils infiltration, lung edema, and generation of proinflammatory cytokines and chemokines, such as TNFα, IL-6, and MIP-2, but also reduced the LPS-induced expression of COX-2 and iNOS, phosphorylation of p38 MAPK, ERK, JNK, Akt, and IκB, and activation of NFκB.

The progression of ALI is related to the systemic inflammatory responses due to direct or sequential injury, such as sepsis.[1] The major causal factor in the development of sepsis is mediated in part by endotoxin. LPS is one of the prototypical endotoxins and a component of the Gram-negative bacteria cell wall. The characteristics of ALI induced by LPS administered intratracheally in mice are the most similar in pathological features to those of human patients.[23] In the early stage, ALI is represented by the disruption of the alveolar−capillary barrier, which results in neutrophil infiltration and protein-rich fluid leakage into the alveolar space.[6] Typical pathophysiological appearances include gas exchange damage, dyspnea, hypoxemia, bilateral infiltrates on chest radiograph, and noncardiogenic pulmonary edema.[24] Pathohistological appearances contain the hyaline membrane formation, hemorrhage, alveolar septal thickening, and neutrophil infiltration.[25] In a previous study, we have demonstrated that EGb761 suppresses the LPS-induced ALI in mice via reduction of leukocyte infiltration and protein leakage.[17] With the present study, our investigation on the protective effect of EGB761 in LPS treated mice was extended further to the verification of its ability to improve the blood gas exchange. Moreover, we found that LPS-induced pathohistological changes were reduced by EGb761. These results indicated EGb761 was able to prevent and ameliorate the ALI induced by endotoxin.

Neutrophils are on the first line of innate immune defense against invading bacteria through the generation of proinflammatory mediators, such as superoxide anions and its related active metabolites, nitric oxide, and proteolytic enzymes. Excessive generation of proinflammatory mediators by activated neutrophils induces peripheral normal tissue injury.[26] In clinical trials, neutrophil infiltration is an important hallmark in the pathogenesis of ALI.[6] In animal studies, intratracheal administration of LPS induces activation or injury of alveolar macrophages and respiratory membrane which contained alveolar epithelial cells, capillary endothelial cells, and basement membrane. Generation of proinflammatory cytokines and chemokines from respiratory membrane results in neutrophil activation in peripheral tissue followed by transmigration into alveolar space due to broken respiratory membranes. Previous studies have demonstrated that LPS induces neutrophil infiltration in the mouse model.[8,17] At present, we also found neutrophil infiltration in LPS-treated mice. Ginkgolide B, a component of *Ginkgo biloba* extracts, significantly decreases neutrophil infiltration in ovalbumin-challenged mice.[27] Recently, we proposed that EGb761 significantly suppressed the number of infiltrating leukocytes in BALF caused by LPS.[17] In the present study, the data collected had further confirmed our earlier hypothesis that EGb761 significantly decreased neutrophil infiltration caused by LPS in BALF. These results strongly suggested that EGb761 was capable of improving LPS-induced ALI via reducing the neutrophil infiltration.

Activation of alveolar macrophages and respiratory membranes can be induced by LPS administration, which leads to the generation of proinflammatory cytokines and chemokines such as TNF-α, IL-6, and MIP-2.[17−19] However, TNF-α and IL-6 induce the expression of adhesion molecules on capillary endothelial cells. MIP-2, a homologue of human IL-8 in mice, is a potent chemokine for neutrophils.[19] Together, they induced the infiltration of peripheral neutrophils into the alveolar space.[17−19] *Ginkgo biloba* extracts are found to protect against mercury(II)-induced TNF-α in rat serum and LPS-induced TNF-α in RAW264.7 macrophages.[16,28] In rats with trinitrobenzenesulfonic acid induced colitis, *Ginkgo biloba* extract reduces the generation of TNF-α and IL-6 in colon tissues.[29] When LPS is administered intratracheally, EGb761 reduced the generation of TNF-α, IL-6, and MIP-2 in BALF. The parallel trends between cytokine and chemokine generation and neutrophil infiltration can both be inhibited by EGb761.

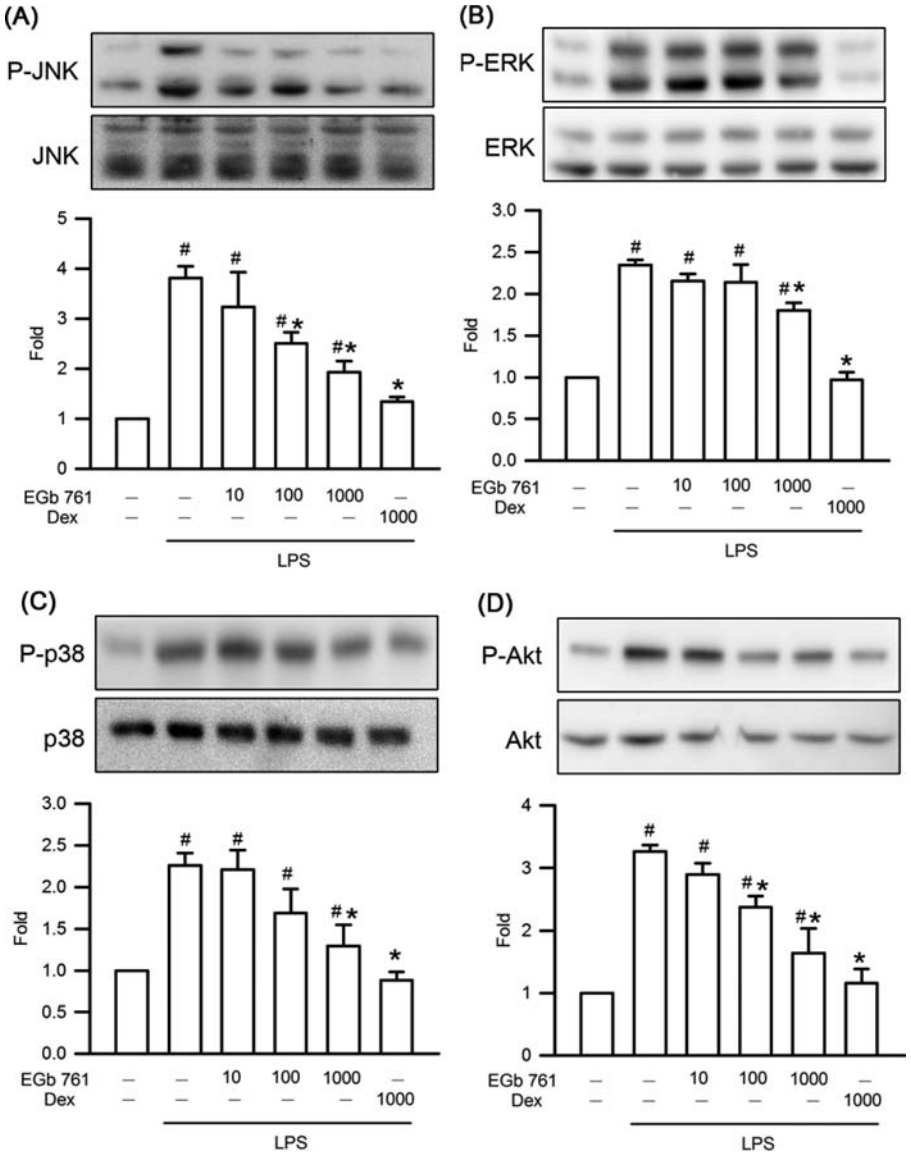

Figure 7. Effect of EGb761 on LPS-induced JNK, ERK, p38 MAPK, and Akt phosphorylation in lung. Lung tissues harvested from post-treated mice were analyzed by Western blotting. The fold of JNK (A), ERK (B), p38 MAPK (C), and Akt (D) phosphorylation between the treated and control groups was calculated. Values are expressed as mean ± SD (n = 3–5 in each group). * represents a significant difference between the indicated and normal control group, and # represents a significant difference between the indicated and LPS groups, $p < 0.05$.

Therefore, the reduction of neutrophil infiltration by EGb761 was partially due to its inhibitory effect on the production of proinflammatory cytokines and chemokines.

PGE2 and NO are involved in the lung tissue damage of LPS-induced ALI.[30,31] After LPS administration, PGE2 and NO are reflected in BALF.[9] In addition, TNF-α and IL-6 can amplify and accelerate the process of LPS-induced ALI by stimulating the expression of PGE2 and NO.[32,33] NO and PGE2 are produced by iNOS and COX-2. The inflammatory responses caused by LPS, production of PGE2 and NO, and protein expression of COX-2 and iNOS are reversed by EGb761 in human chondrocytes.[15] In RAW264.7 macrophages, *Ginkgo biloba* extract inhibits LPS-induced production of PGE2 and NO and protein and mRNA expression of COX-2 and iNOS.[16] On the basis of the present results, we conclude with fair certainty that EGb761 suppresses LPS-induced expression of iNOS and COX-2 in lung tissues.

NFκB, a transcription factor that is a key component of the inflammatory responses in ALI, is involved in the production of proinflammatory cytokines and chemokines, generation of PGE2 and NO, and expression of COX2 and iNOS.[34,35] In the inactive state, NFκB is bound to IκB, an inhibitor of NFκB, and remains in cytosol through masking nuclear localization signals of NFκB.[35] LPS, TNF-α, and IL-6 can trigger the activation of IκB kinase complex, which results in its phosphorylation, ubiquitination, and degradation. NFκB, which is liberated from phosphorylated IκB, translocates to the nucleus and activates transcription genes for proinflammatory mediators.[34] After LPS administration, *Ginkgo biloba* extract reduces NFκB activation and IκB degradation in RAW264.7 macrophages.[16] In a previous study, we demonstrated that pretreatment with EGb761 prevents NFκB phosphorylation and IκB degradation in LPS-induced ALI.[17] The present study further demonstrates that, while intratracheal administration of LPS results in phosphorylation of IκB and activation of NFκB in lung tissue, EGb761 reduces these phenomena significantly in a concentration-dependent manner. These results indicated that the generation of proinflammatory

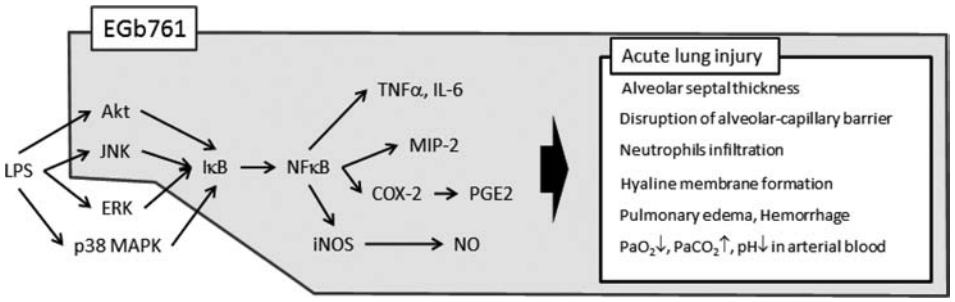

Figure 8. Schemes of the protective mechanism of EGb761 on LPS-induced ALI. The gray area indicates the molecules reduced by EGb761.

mediators reduced by EGb761 was due to inhibition of NFκB activation via IκB phosphorylation.

Akt and MAPK pathways participate in the activation of NFκB in LPS-induced ALI.[8−12] Akt is a downstream factor of phosphoinositol 3 kinase, involved in LPS-stimulated activation of alveolar macrophages, peripheral neutrophils, and the cells in the respiratory membrane in the lung.[36] The three different MAPKs p38 MAPK, ERK, and JNK also play a critical role in the inflammatory responses from innate immunity and respiratory membrane caused by LPS administration.[10−12] In RAW264.7 macrophages treated with LPS, EGb761 had no effect on the phosphorylation of JNK but inhibited the phosphorylation of p38 MAPK and ERK.[37] In mice with ovalbumin-induced asthma, ginkgolide B attenuates the phosphorylation of ERK but not p38 and JNK in lung.[27] When SH-SY5Y human neuroblastoma cells are cotreated with Aβ (1−42) and EGb761, the phosphorylation of ERK, JNK, and Akt is completely inhibited.[38] In our present study, Western blot assays showed that the phosphorylation of JNK and Akt inhibited by various concentrations of EGb761 was in direct correlation with the generation of inflammatory responses induced by LPS. However, inhibition of the marker on the phosphorylation of ERK and p38 required higher concentration of EGb761 than that of JNK and Akt. On the basis of these results, we suggested that phosphorylation of JNK and Akt reduced by EGb761 was a primary signal pathway in LPS-induced ALI.

As shown in Figure 8, we demonstrated that EGb761 significantly improved the histopathological changes and inflammatory responses, such as neutrophils infiltration, pulmonary edema, hyaline membrane formation, and arterial blood exchanges, in the mouse model of LPS-induced ALI. The molecular mechanisms involved in the protective effect of EGb761 were (1) decreased generation of proinflammatory cytokines and chemokines, such as TNF-α, IL-6, and MIP-2, (2) decreased expression of COX-2 and iNOS, (3) decreased IκB phosphorylation and NFκB activation, (4) downregulation of Akt and JNK phosphorylation as the primary pathway, and (5) downregulation of ERK and p38 MAPK phosphorylation as the secondary pathway. These results suggested the possibility of EGb761 as a preventive agent against ALI associated with infection caused by LPS via reversing the pathway of JNK- and Akt-dependent NFκB activation.

AUTHOR INFORMATION

Corresponding Author

*Y.-H.K.: tel, +886-4-24730022, ext. 11662; fax, +886-4-24739030; e-mail, kuanyh@csmu.edu.tw.

Notes

The authors declare no competing financial interest.

ACKNOWLEDGMENTS

The authors thank the National Science Council of the Republic of China, Taiwan, for financially supporting this research under Contract No. NSC102-2320-B-040-009-. We also thank the Chung Shan Medical University Hospital of the Republic of China, Taiwan, for financially supporting this research under Contract No. CSH-2013-C-027

REFERENCES

(1) Wheeler, A. P.; Bernard, G. R. Acute lung injury and the acute respiratory distress syndrome: a clinical review. *Lancet* **2007**, *369*, 1553−1564.

(2) Rubenfeld, G. D.; Herridge, M. S. Epidemiology and outcomes of acute lung injury. *Chest* **2007**, *131*, 554−562.

(3) Varisco, B. M. The pharmacology of acute lung injury in sepsis. *Adv. Pharmacol. Sci.* **2011**, *2011*, 254619.

(4) Iscimen, R.; Cartin-Ceba, R.; Yilmaz, M.; Khan, H.; Hubmayr, R. D.; Afessa, B.; Gajic, O. Risk factors for the development of acute lung injury in patients with septic shock: an observational cohort study. *Crit. Care Med.* **2008**, *36*, 1518−1522.

(5) Rojas, M.; Woods, C. R.; Mora, A. L.; Xu, J.; Brigham, K. L. Endotoxin-induced lung injury in mice: structural, functional, and biochemical responses. *Am. J. Physiol. Lung Cell. Mol. Physiol.* **2005**, *288*, L333−L341.

(6) Grommes, J.; Soehnlein, O. Contribution of neutrophils to acute lung injury. *Mol. Med.* **2011**, *17*, 293−307.

(7) Fan, J.; Ye, R. D.; Malik, A. B. Transcriptional mechanisms of acute lung injury. *Am. J. Physiol. Lung Cell. Mol. Physiol.* **2001**, *281*, L1037−L1050.

(8) Kuo, M. Y.; Liao, M. F.; Chen, F. L.; Li, Y. C.; Yang, M. L.; Lin, R. H.; Kuan, Y. H. Luteolin attenuates the pulmonary inflammatory response involves abilities of antioxidation and inhibition of MAPK and NFκB pathways in mice with endotoxin-induced acute lung injury. *Food Chem. Toxicol.* **2011**, *49*, 2660−2666.

(9) Li, Y. C.; Yeh, C. H.; Yang, M. L.; Kuan, Y. H. Luteolin suppresses inflammatory mediator expression by blocking the Akt/NFκB pathway in acute lung injury induced by lipopolysaccharide in mice. *Evid. Based Complement Alternat. Med.* **2012**, *2012*, 383608.

(10) Liu, S.; Feng, G.; Wang, G. L.; Liu, G. J. p38 MAPK inhibition attenuates LPS induced acute lung injury involvement of NF-kappaB pathway. *Eur. J. Pharmacol.* **2008**, *584*, 159−165.

(11) Lee, H. S.; Kim, H. J.; Moon, C. S.; Chong, Y. H.; Kang, J. L. Inhibition of c-Jun NH2-terminal kinase or extracellular signal-regulated kinase improves lung injury. *Respir. Res.* **2004**, *5*, 23.

(12) Schuh, K.; Pahl, A. Inhibition of the MAP kinase ERK protects from lipopolysaccharide-induced lung injury. *Biochem. Pharmacol.* **2009**, *77*, 1827−1834.

(13) Chan, P. C.; Xia, Q.; Fu, P. P. Ginkgo biloba leave extract: biological, medicinal, and toxicological effects. *J. Environ. Sci. Health, Part C: Environ. Carcinog. Ecotoxicol. Rev.* **2007**, *25*, 211−244.

(14) Diamond, B. J.; Shiflett, S. C.; Feiwel, N.; Matheis, R. J.; Noskin, O.; Richards, J. A.; Schoenberger, N. E. Ginkgo biloba extract: mechanisms and clinical indications. *Arch. Phys. Med. Rehabil.* **2000**, *81*, 668−678.

(15) Chen, Y. J.; Tsai, K. S.; Chiu, C. Y.; Yang, T. H.; Lin, T. H.; Fu, W. M.; Chen, C. F.; Yang, R. S.; Liu, S. H. EGb761 inhibits inflammatory responses in human chondrocytes and shows chondroprotection in osteoarthritic rat knee. *J. Orthop. Res.* **2013**, *31*, 1032−1038.
(16) Park, Y. M.; Won, J. H.; Yun, K. J.; Ryu, J. H.; Han, Y. N.; Choi, S. K.; Lee, K. T. Preventive effect of Ginkgo biloba extract (GBB) on the lipopolysaccharide-induced expressions of inducible nitric oxide synthase and cyclooxygenase-2 via suppression of nuclear factor-kappaB in RAW 264.7 cells. *Biol. Pharm. Bull.* **2006**, *29*, 985−990.
(17) Huang, C. H.; Yang, M. L.; Tsai, C. H.; Li, Y. C.; Lin, Y. J.; Kuan, Y. H. Ginkgo biloba leaves extract (EGb 761) attenuates lipopolysaccharide-induced acute lung injury via inhibition of oxidative stress and NFκB-dependent matrix metalloproteinase-9 pathway. *Phytomedicine* **2013**, *20*, 303−309.
(18) Reutershan, J.; Morris, M. A.; Burcin, T. L.; Smith, D. F.; Chang, D.; Saprito, M. S.; Ley, K. Critical role of endothelial CXCR2 in LPS-induced neutrophil migration into the lung. *J. Clin. Invest.* **2006**, *116*, 695−702.
(19) Li, L. F.; Huang, C. C.; Lin, H. C.; Tsai, Y. H.; Quinn, D. A.; Liao, S. K. Unfractionated heparin and enoxaparin reduce high stretch ventilation-augmented lung injury - a prospective, controlled animal experiment. *Crit. Care* **2009**, *13*, R108.
(20) Shang, Y.; Li, X.; Prasad, P. V.; Xu, S.; Yao, S.; Liu, D.; Yuan, S.; Feng, D. Erythropoietin attenuates lung injury in lipopolysaccharide treated rats. *J. Surg. Res.* **2009**, *155*, 104−110.
(21) Fukunaga, K.; Kohli, P.; Bonnans, C.; Fredenburgh, L. E.; Levy, B. D. Cyclooxygenase 2 plays a pivotal role in the resolution of acute lung injury. *J. Immunol.* **2005**, *174*, 5033−5039.
(22) He, Z.; Zhu, Y.; Jiang, H. Inhibiting toll-like receptor 4 signaling ameliorates pulmonary fibrosis during acute lung injury induced by lipopolysaccharide: an experimental study. *Respir. Res.* **2009**, *10*, 126.
(23) Chen, H.; Bai, C.; Wang, X. The value of the lipopolysaccharide-induced acute lung injury model in respiratory medicine. *Expert Rev. Respir. Med.* **2010**, *4*, 773−783.
(24) Ware, L. B. Pathophysiology of acute lung injury and the acute respiratory distress syndrome. *Semin. Respir. Crit. Care Med.* **2006**, *27*, 337−349.
(25) Johnson, E. R.; Matthay, M. A. Acute lung injury: epidemiology, pathogenesis, and treatment. *J. Aerosol Med. Pulm. Drug Delivery* **2010**, *23*, 243−252.
(26) Moraes, T. J.; Zurawska, J. H.; Downey, G. P. Neutrophil granule contents in the pathogenesis of lung injury. *Curr. Opin. Hematol.* **2006**, *13*, 21−27.
(27) Chu, X.; Ci, X.; He, J.; Wei, M.; Yang, X.; Cao, Q.; Li, H.; Guan, S.; Deng, Y.; Pang, D.; Deng, X. A novel anti-inflammatory role for ginkgolide B in asthma via inhibition of the ERK/MAPK signaling pathway. *Molecules* **2011**, *16*, 7634−7648.
(28) Sener, G.; Sehirli, O.; Tozan, A.; Velioğlu-Ovunç, A.; Gedik, N.; Omurtag, G. Z. Ginkgo biloba extract protects against mercury(II)-induced oxidative tissue damage in rats. *Food Chem. Toxicol.* **2006**, *45*, 543−550.
(29) Zhou, Y. H.; Yu, J. P.; Liu, Y. F.; Teng, X. J.; Ming, M.; Lv, P.; An, P.; Liu, S. Q.; Yu, H. G. Effects of Ginkgo biloba extract on inflammatory mediators (SOD, MDA, TNF-alpha, NF-kappaBp65, IL-6) in TNBS-induced colitis in rats. *Mediators Inflamm.* **2006**, *2006*, 92642.
(30) Ejima, K.; Layne, M. D.; Carvajal, I. M.; Kritek, P. A.; Baron, R. M.; Chen, Y. H.; Vom Saal, J.; Levy, B. D.; Yet, S. F.; Perrella, M. A. Cyclooxygenase-2-deficient mice are resistant to endotoxin-induced inflammation and death. *FASEB J.* **2003**, *17*, 1325−1327.
(31) Farley, K. S.; Wang, L. F.; Razavi, H. M.; Law, C.; Rohan, M.; McCormack, D. G.; Mehta, S. Effects of macrophage inducible nitric oxide synthase in murine septic lung injury. *Am. J. Physiol. Lung Cell. Mol. Physiol.* **2006**, *290*, L1164−L1172.
(32) Goldring, S. R.; Goldring, M. B. The role of cytokines in cartilage matrix degeneration in osteoarthritis. *Clin. Orthop. Relat. Res.* **2004**, *427* (Suppl), S27−S36.
(33) Mastbergen, S. C.; Lafeber, F. P.; Bijlsma, J. W. Selective COX-2 inhibition prevents proinflammatory cytokine-induced cartilage damage. *Rheumatology* **2002**, *41*, 801−808.
(34) Said, S. I.; Dickman, K. G. Pathways of inflammation and cell death in the lung: modulation by vasoactive intestinal peptide. *Regul. Pept.* **2000**, *93*, 21−29.
(35) Baeuerle, P. A.; Baltimore, D. NF-kappa B: ten years after. *Cell* **1996**, *87*, 13−20.
(36) Ci, X.; Chu, X.; Wei, M.; Yang, X.; Cai, Q.; Deng, X. Different effects of farrerol on an OVA-induced allergic asthma and LPS-induced acute lung injury. *PLoS One* **2012**, *7*, e34634.
(37) Wadsworth, T. L.; McDonald, T. L.; Koop, D. R. Effects of Ginkgo biloba extract (EGb 761) and quercetin on lipopolysaccharide-induced signaling pathways involved in the release of tumor necrosis factor-alpha. *Biochem. Pharmacol.* **2001**, *62*, 963−974.
(38) Shi, C.; Zhao, L.; Zhu, B.; Li, Q.; Yew, D. T.; Yao, Z.; Xu, J. Protective effects of Ginkgo biloba extract (EGb761) and its constituents quercetin and ginkgolide B against beta-amyloid peptide-induced toxicity in SH-SY5Y cells. *Chem. Biol. Interact.* **2009**, *181*, 115−123.

MATERIALS AND METHODS

General Experimental Procedures. Optical rotations were measured on a JASCO P-2200 polarimeter. NMR spectra were recorded on a Bruker AVANCE-500 instrument (^{1}H NMR, 500 MHz; ^{13}C NMR, 125 MHz) using TMS as an internal standard. High resolution electrospray ionization mass spectra (HRESIMS) were obtained on a Waters LCT Premier. CD spectra were run on a CD-J600 spectropolarimeter (JASCO). Column chromatography was performed with silica gel 60N (63-210 μm, Kanto Kagaku), Sephadex LH-20 (25−100 μm, GE Healthcare Bioscience), and MCI gel CHP20P (75−150 μm, Mitsubishi Chemical Corporation). HPLC was performed on a JASCO apparatus consisting of a PU-980 prep pump, UV-970 UV/VIS (at the wavelength of 280 nm), and Cosmosil 5C$_{18}$-AR-II (5 μm, φ20 × 250 mm^2, nacalai tesque), or Cosmosil π-NAP (5 μm, φ20 × 250 mm^2, nacalai tesque). TLC was conducted on precoated silica gel 60 F$_{254}$ (0.20 mm, Merck), and spots were detected by UV illumination and by spraying $FeCl_3$ reagent or cerium sulfate reagent followed by heating.

Plant Material. The stems and leaves of *Desmodium caudatum* (Thunb.) H. Ohashi were collected in Tokushima, Japan, in December 2011. The plant was identified by one of the authors (K.I.), and a voucher specimen (MSO08001) was deposited at the herbarium of Faculty of Pharmaceutical Sciences, The University of Tokushima.

Extraction and Isolation of Compounds. The stems (1.9 kg) of *D. caudatum* were extracted three times with MeOH (5 L × 3) at room temperature for 3 days. The MeOH extracts were concentrated in vacuo to give a residue (132 g), which was partitioned between EtOAc and H_2O. The EtOAc layer was concentrated to give a residue (15 g). The EtOAc-soluble fraction was dissolved in EtOH, loaded onto a Sephadex LH-20 column (4.2 × 27 cm^2), and eluted with EtOH (4L) to give eight fractions (frs.1−8). The spots of fraction 3 and 4 on the TLC plate (TLC solvent; $CHCl_3$/MeOH = 10:1) were yellow and orange, detected by UV illumination and by spraying with $FeCl_3$ reagent. Fraction 3 (1.3 g) was subjected to chromatography over MCI gel CHP20P (3.0 × 30 cm^2) [eluted with H_2O−MeOH gradient (1:1, 2:3, 3:7, 1:4, 1:9, 0:1), each solvent volume 200 mL] to give 15 further fractions (frs. 3.1−3.15). Sephadex LH-20 chromatography (3.0 × 30 cm^2) [eluted with H_2O−MeOH gradient (4:1, 7:3, 1:1, 2:3, 3:7, 1:4, 1:9, 0:1), each solvent volume 100 mL] of fr. 3.6 (136.6 mg) gave **10** (13.9 mg) [R_f 0.35 ($CHCl_3$/MeOH =10:1)]. Fr. 3.8 was subjected to chromatography over Sephadex LH-20 (3.0 × 30 cm^2) [eluted with H_2O−MeOH gradient (7:3, 3:2, 1:1, 2:3, 3:7, 1:4, 1:9, 0:1), each solvent volume 100 mL] to give **2** (8.4 mg) [R_f 0.35 ($CHCl_3$/MeOH = 10:1)] and **5** (97.3 mg) [R_f 0.38 ($CHCl_3$/MeOH = 10:1)], together with 16 fractions (frs. 3.8.1−3.8.16). Fraction 3.8.9 (2.1 mg) was purified by HPLC on 5C$_{18}$-AR-II [MeOH−H_2O (7:3), flow rate 3.5 mL/min, UV at 280 nm, eluted at 70 min] to furnish **15** (1.0 mg) [R_f 0.18 ($CHCl_3$/MeOH = 10:1)]. Fr. 3.8.10 was separated by HPLC on 5C$_{18}$-AR-II [MeOH−H_2O (7:3), flow rate 3.5 mL/min, UV at 280 nm, eluted at 100 min] and then purified by HPLC on π-NAP [MeOH−H_2O (7:3), flow rate 3.5 mL/min, UV at 280 nm, eluted at 88 min] to give **13** (2.3 mg) [R_f 0.35 ($CHCl_3$/MeOH = 10:1)]. Fraction 3.9 (61.7 mg) was fractionated by Sephadex LH-20 (2.5 × 27 cm^2) [eluted with H_2O−MeOH gradient (3:2, 1:1, 2:3, 3:7, 1:4, 1:9, 0:1), each solvent volume 100 mL] into 12 fractions (frs. 3.9.1−3.9.12). Fr. 3.9.7 (6.8 mg) was purified by HPLC on 5C$_{18}$-AR-II [MeOH−H_2O (1:1), flow rate 3.5 mL/min, UV at 280 nm, eluted at 78 min] to furnish **1** (3.2 mg) [R_f 0.38 ($CHCl_3$/MeOH = 10:1)]. Fr. 3.9.11 was separated by HPLC on 5C$_{18}$-AR-II [MeOH−H_2O (1:1), flow rate 3.5 mL/min, UV at 280 nm, eluted at 128 min] to give **6** (1.7 mg) [R_f 0.25 ($CHCl_3$/MeOH = 10:1)]. Fr. 3.10 was subjected to Sephadex LH-20 chromatography (3.0 × 30 cm^2) [eluted with H_2O−MeOH gradient (7:3, 3:2, 1:1, 2:3, 3:7, 1:4, 1:9, 0:1), each solvent volume 100 mL] to afford **8** (41.0 mg) [R_f 0.48 ($CHCl_3$/MeOH = 10:1)] and a fraction that was further purified by HPLC on 5C$_{18}$-AR-II [MeOH−H_2O (45:55), flow rate 3.5 mL/min, UV at 280 nm, eluted at 98 min] to give **19** (0.5 mg) [R_f 0.33 ($CHCl_3$/MeOH = 10:1)]. Fr. 3.11 (93.2 mg) was chromatographed over Sephadex LH-20 (3.0 × 30 cm^2) [eluted with H_2O−MeOH gradient (3:2, 1:1, 2:3, 3:7, 1:4, 1:9, 0:1), each solvent volume 100 mL] to furnish **7** (2.2 mg) [R_f 0.45 ($CHCl_3$/MeOH = 10:1)] and a fraction that was further purified by HPLC on 5C$_{18}$-AR-II [MeOH−H_2O (45:55), flow rate 3.5 mL/min, UV at 280 nm, eluted at 122 min] to give **25** (0.7 mg) [R_f 0.35 ($CHCl_3$/MeOH = 10:1)]. Fr. 3.12 (45.4 mg) was subjected to chromatography over Sephadex LH-20 (2.5 × 27 cm^2) [eluted with H_2O−MeOH gradient (3:2, 1:1, 2:3, 3:7, 1:4, 1:9, 0:1), each solvent volume 100 mL] and then purified by HPLC on 5C$_{18}$-AR-II [MeOH−H_2O (3:7), flow rate 3.0 mL/min, UV at 280 nm, eluted at 164 min] to yield **3** (0.7 mg) [R_f 0.28 ($CHCl_3$/MeOH = 10:1)]. Chromatography of Fr. 3.13 (187.3 mg) over Sephadex LH-20 (2.1 × 13 cm^2) [eluted with H_2O−MeOH gradient (1:1, 2:3, 3:7, 1:4, 1:9, 0:1), each solvent volume 100 mL] furnished **14** (83.8 mg) [R_f 0.40 ($CHCl_3$/MeOH = 10:1)] and a fraction that was further purified by HPLC on 5C$_{18}$-AR-II [MeOH−H_2O (3:7), flow rate 3.0 mL/min, UV at 280 nm, eluted at 84 min] giving **9** (0.4 mg) [R_f 0.48 ($CHCl_3$/MeOH = 10:1)]. Sephadex LH-20 chromatography (2.5 × 27 cm^2) [eluted with H_2O−MeOH gradient (1:1, 2:3, 3:7, 1:4, 1:9, 0:1), each solvent volume 100 mL] of fr. 3.14 (47.6 mg) gave **11** (14.0 mg) [R_f 0.55 ($CHCl_3$/MeOH = 10:1)] and **12** (4.3 mg) [R_f 0.60 ($CHCl_3$/MeOH = 10:1)]. Fraction 4 (781.2 mg) was applied to a MCI gel CHP20P column (3.0 × 24 cm^2) with a gradient of H_2O−MeOH (7:3, 3:2, 1:1, 2:3, 3:7, 1:4, 1:9, 0:1, each solvent volume 200 mL) to give 22 further fractions (frs. 4.1−4.22). Fr. 4.7 (123.7 mg) was chromatographed over Sephadex LH-20 (3.0 × 30 cm^2) [eluted with H_2O−MeOH gradient (7:3, 3:2, 1:1, 2:3, 3:7, 1:4, 1:9, 0:1), each solvent volume 100 mL] to afford **20** (3.5 mg) [R_f 0.58 ($CHCl_3$/MeOH/H_2O = 8:2:0.2)]. Sephadex LH-20 chromatography (2.1 × 15 cm^2) [eluted with H_2O−MeOH gradient (7:3, 3:2, 1:1, 2:3, 3:7, 1:4, 1:9, 0:1), each solvent volume 100 mL] of fr. 4.12 gave **23** (1.2 mg) [R_f 0.65 ($CHCl_3$/MeOH/H_2O = 8:2:0.2)]. Fr. 4.15 was subjected to Sephadex LH-20 chromatography (2.6 × 28 cm^2) [eluted with H_2O−MeOH gradient (7:3, 3:2, 1:1, 2:3, 3:7, 1:4, 1:9, 0:1), each solvent volume 100 mL] to furnish **21** (9.8 mg) [R_f 0.63 ($CHCl_3$/MeOH/H_2O = 8:2:0.2)], **22** (3.6 mg) [R_f 0.65 ($CHCl_3$/MeOH/H_2O = 8:2:0.2)], and 11 fractions (frs. 4.15.1−4.15.11). Fr. 4.15.9 (5.5 mg) was purified by HPLC on 5C$_{18}$-AR-II [MeOH−H_2O (3:2), flow rate 3.5 mL/min, UV at 280 nm, eluted at 51 min] to furnish **26** (0.9 mg) [R_f 0.71 ($CHCl_3$/MeOH/H_2O = 8:2:0.2)]. Sephadex LH-20 chromatography (2.6 × 26 cm^2) [eluted with H_2O−MeOH gradient (7:3, 3:2, 1:1, 2:3, 3:7, 1:4, 1:9, 0:1), each solvent volume 100 mL] of fr. 4.13 (26.0 mg) gave **4** (3.7 mg) [R_f 0.60 ($CHCl_3$/MeOH/H_2O = 8:2:0.2)].

The leaves (0.5 kg) of *D. caudatum* were extracted three times with MeOH (3 L × 3) at room temperature for 3 days. The MeOH extracts were concentrated in vacuo to give a residue (116 g), which was partitioned between EtOAc and H_2O. The EtOAc layer was concentrated to give a residue (25 g). The EtOAc-soluble fraction was dissolved in EtOH, loaded onto a Sephadex LH-20 column (6.0 × 20 cm^2), and eluted with EtOH (4 L) to give ten fractions (frs. 1−10). The spots of fraction 2 on the TLC plate (TLC solvent; $CHCl_3$/MeOH = 10:1) were yellow and orange, detected by UV illumination and by spraying with $FeCl_3$ reagent. Fraction 2 (1.7 g) was subjected to chromatography over MCI gel CHP20P (3.6 × 24 cm^2) [eluted with H_2O−MeOH gradient (7:3, 3:2, 1:1, 2:3, 3:7, 1:4, 1:9, 0:1), each solvent volume 200 mL] to give 20 further fractions (frs. 2.1−2.20). Fr. 2.9 was subjected to chromatography over Sephadex LH-20 (2.6 × 27 cm^2) [eluted with H_2O−MeOH gradient (7:3, 3:2, 1:1, 2:3, 3:7, 1:4, 1:9, 0:1), each solvent volume 100 mL] to give **13** (1.6 mg) [R_f 0.65 ($CHCl_3$/MeOH/H_2O = 8:2:0.2)] and **5** (4.0 mg) [R_f 0.58 ($CHCl_3$/MeOH/H_2O = 8:2:0.2)]. Fr. 2.10 (69.1 mg) was rechromatographed over Sephadex LH-20 (2.0 × 16 cm^2) [eluted with H_2O−MeOH gradient (7:3, 3:2, 1:1, 2:3, 3:7, 1:4, 1:9, 0:1), each solvent volume 100 mL] to furnish **1** (6.0 mg) [R_f 0.59 ($CHCl_3$/MeOH/H_2O = 8:2:0.2)]. Sephadex LH-20 chromatography (2.6 × 27 cm^2) [eluted with H_2O−MeOH gradient (7:3, 3:2, 1:1, 2:3, 3:7, 1:4, 1:9, 0:1), each solvent volume 100 mL] of fr. 2.11 (78.9 mg) gave **8** (10.6 mg) [R_f 0.40 ($CHCl_3$/MeOH = 10:1)]. Fr. 2.12 (59.7 mg) was subjected to chromatography over Sephadex LH-20 (2.0 × 16 cm^2) [eluted with H_2O−MeOH gradient (7:3, 3:2, 1:1, 2:3, 3:7, 1:4, 1:9,

dx.doi.org/10.1021/jf5020439 | J. Agric. Food Chem. 2014, 62, 6345−6353

Table 1. ^{1}H and ^{13}C-NMR Data for 1, 16, and 18 in Acetone-d_6

	1		16		18	
position	δ_H [a]	δ_C [b]	δ_H [a]	δ_C [b]	δ_H [a]	δ_C [b]
2	5.13 (1H, d, 11.5)	84.5	5.10 (1H, d, 11.5)	84.7	5.43 (1H, d, 11.5)	83.6
3	4.66 (1H, d, 11.5)	73.2	4.65 (1H, d, 11.5)	73.6	4.97 (1H, d, 11.5)	72.5
4		198.7		199.2		198.4
5		164.3		158.0		163.5
6	5.90 (1H, s)	97.9		106.2	6.31 (1H, s)	97.3
7		163.6		161.1		161.9
8		102.8		102.6		101.7
9		157.8		156.1		156.7
10		102.0		101.8		101.6
1′		129.0		129.4		129.6
2′,6′	7.43 (2H, d, 8.5)	130.4	7.43 (2H, d, 8.5)	130.6	7.75 (2H, d, 8.5)	129.3
3′,5′	6.90 (2H, d, 8.5)	116.1	6.89 (2H, d, 8.5)	116.3	7.09 (2H, d, 8.5)	113.8
4′		159.0		159.2		160.0
1″	6.52 (1H, d, 10.5)	117.7	6.45 (1H, d, 10.0)	116.5	6.58 (1H, d, 10.5)	115.2
2″	5.54 (1H, d, 10.5)	124.6	5.59 (1H, d, 10.0)	127.6	5.49 (1H, d, 10.5)	126.2
3″		82.4		79.3		77.8
4″	3.60 (1H, d, 12.0) 3.53 (1H, d, 12.0)	68.7	1.42 (3H, s)	29.0	1.40 (3H, s)	27.7
5″	1.38 (3H, s)	23.9	1.45 (3H, s)	28.8	1.40 (3H, s)	27.5
6-Me			1.95 (3H, s)	7.2		
5-OH					12.6 (1H, s)	
4′-OMe					3.70 (3H, s)	54.7

[a] δ_H, ppm (mult., J in Hz); 500 MHz. [b] δ_C, ppm; 125 MHz.

Table 2. ^{1}H and ^{13}C-NMR Data for 2, 3, 15, and 17 in Acetone-d_6

	2		3		15		17	
position	δ_H [a]	δ_C [b]	δ_H [a]	δ_C [b]	δ_H [a]	δ_C [b]	δ_H [a]	δ_C [b]
2	5.63 (1H, d, 2.0)	79.1	5.47 (1H, d, 11.5)	79.4	5.46 (1H, d, 11.5)	79.3	5.14 (1H, d, 11.5)	85.0
3	4.24 (1H, d, 2.0)	71.5	4.82 (1H, d, 11.5)	72.5	4.77 (1H, d, 11.5)	72.5	4.72 (1H, d, 11.5)	73.4
4		196.6		199.6		199.0		199.0
5		163.4		163.3		162.7		163.2
6	5.06 (1H, s)	96.4	6.17 (1H, s)	93.3	6.03 (1H, s)	97.0	5.92 (1H, s)	98.1
7		165.1		165.0		165.9		164.4
8		108.4		109.7		110.0		102.2
9		161.2		158.3		161.6		158.2
10		101.6		101.6		101.8		100.2
1′		114.8		115.0		115.9		129.6
2′		156.2		159.0		158.2	7.23 (1H, d, 2.0)	112.6
3′	6.44 (1H, d, 2.0)	103.3	6.46 (1H, d, 2.5)	103.8	6.46 (1H, d, 2.5)	104.0		148.5
4′		159.3		160.7		159.9		148.4
5′	6.40 (1H, dd, 8.5, 2.0)	107.5	6.42 (1H, dd, 8.5, 2.5)	107.9	6.41 (1H, dd, 8.5, 2.5)	107.9	6.88 (1H, d, 8.0)	115.8
6′	7.40 (1H, d, 8.5)	131.0	7.31 (1H, d, 8.5)	130.6	7.34 (1H, d, 8.5)	130.4	7.05 (1H, dd, 2.0, 8.0)	122.4
1″	3.28 (2H, d, 7.0)	22.3	3.15 (2H, d, 7.5)	22.2	2.57 (2H, t, 8.0)	18.2	6.44 (1H, d, 10.0)	116.1
2″	5.21 (1H, t, 7.0)	123.8	5.11 (1H, t, 7.5)	123.5	1.61 (2H, t, 8.0)	43.8	5.59 (1H, d, 10.0)	127.9
3″		131.2		131.7		70.9		79.3
4″	1.60 (3H, s)	26.0	1.55 (3H, s)	26.1	1.13 (3H, s)	29.5	1.42 (3H, s)	28.9
5″	1.64 (3H, s)	17.9	1.56 (3H, s)	17.9	1.28 (3H, s)	29.6	1.40 (3H, s)	28.7
5-OH	11.9 (1H, s)		11.8 (1H, s)		11.6 (1H, s)			
7-OMe			3.90 (3H, s)	56.8				
3′-OMe							3.87 (3H, s)	56.6

[a] δ_H, ppm (mult., J in Hz); 500 MHz. [b] δ_C, ppm; 125 MHz.

0:1), each solvent volume 100 mL] to yield 19 fractions (frs. 4.8.1−4.8.19) and then purified by HPLC on π-NAP [MeOH−H_2O (7:3), flow rate 3.5 mL/min, UV at 280 nm, eluted at 58 min] to afford **7** (0.7 mg) [R_f 0.75 ($CHCl_3$/MeOH/H_2O = 8:2:0.2)]. Fr. 2.14 (50.3 mg) was chromatographed over Sephadex LH-20 (2.0 × 16 cm^2) [eluted with H_2O−MeOH gradient (7:3, 3:2, 1:1, 3:2, 1:1, 2:3, 3:7, 1:4, 1:9, 0:1), each solvent volume 100 mL] to furnish **9** (3.6 mg) [R_f 0.48 ($CHCl_3$/MeOH = 10:1)] and a fraction that was further purified by HPLC on π-NAP [MeOH−H_2O (7:3), flow rate 3.5 mL/min, UV at 280 nm, eluted at 100 min] to yield **14** (12.6 mg) [R_f 0.35 ($CHCl_3$/MeOH = 10:1)]. Fraction 2.15 (100.7 mg) was fractionated by Sephadex LH-20 (2.6 × 27 cm^2) [eluted with H_2O−MeOH gradient (7:3, 3:2, 1:1, 2:3, 3:7, 1:4, 1:9, 0:1), each solvent volume 100 mL] into eight fractions (frs. 2.15.1−2.15.8). Fr. 2.15.6 was purified by

dx.doi.org/10.1021/jf5020439 | J. Agric. Food Chem. 2014, 62, 6345−6353

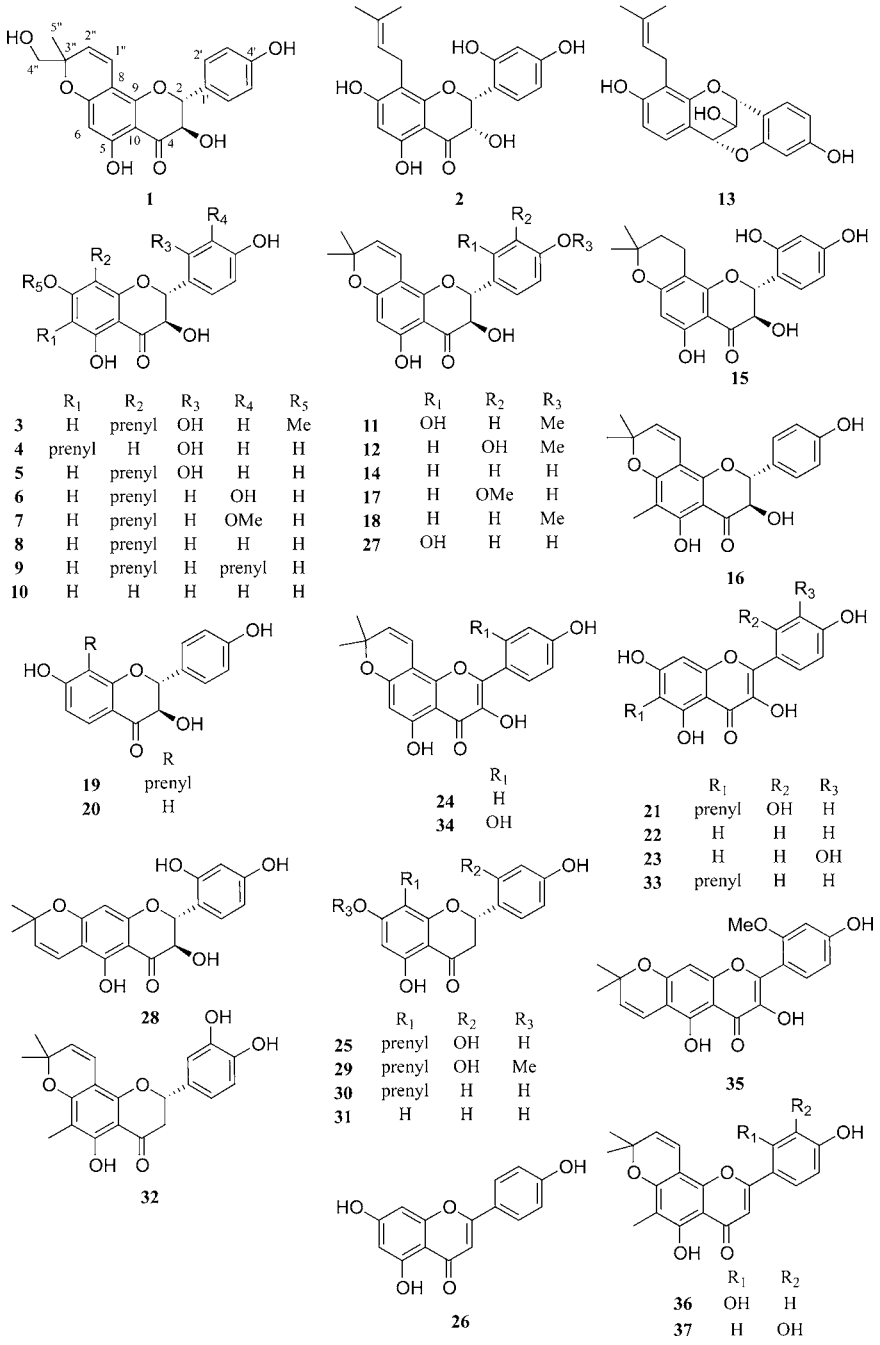

	R_1	R_2	R_3	R_4	R_5
3	H	prenyl	OH	H	Me
4	prenyl	H	OH	H	H
5	H	prenyl	OH	H	H
6	H	prenyl	H	OH	H
7	H	prenyl	H	OMe	H
8	H	prenyl	H	H	H
9	H	prenyl	H	prenyl	H
10	H	H	H	H	H

	R_1	R_2	R_3
11	OH	H	Me
12	H	OH	Me
14	H	H	H
17	H	OMe	H
18	H	H	Me
27	OH	H	H

Figure 1. Structures of flavonoids (**1**−**26**) isolated from the stems and leaves of *D. caudatum* and previously isolated flavonoids (**27**−**37**) evaluated for anti-film-forming activities.

HPLC on π-NAP [MeOH−H_2O (7:3), flow rate 3.5 mL/min, UV at 280 nm, eluted at 128 and 160 min, respectively] to furnish **11** (7.9 mg) [R_f 0.45 ($CHCl_3$/MeOH = 10:1)] and **16** (1.3 mg) [R_f 0.31 ($CHCl_3$/MeOH = 10:1)]. Fr. 2.15.2 (9.8 mg) was purified by HPLC on π-NAP [MeOH−H_2O (7:3), flow rate 3.5 mL/min, UV at 280 nm, eluted at 138 and 145 min, respectively] to afford **17** (0.5 mg) [R_f 0.65 ($CHCl_3$/MeOH = 10:1)] and **12** (2.7 mg) [R_f 0.68 ($CHCl_3$/MeOH = 10:1)]. Fr. 2.16 (32.3 mg) was chromatographed over Sephadex LH-20 (2.0 × 16 cm^2) [eluted with H_2O−MeOH gradient (1:1, 2:3, 3:7, 1:4, 1:9, 0:1), each solvent volume 100 mL] to furnish **24** (6.2 mg) [R_f 0.50 ($CHCl_3$/MeOH = 10:1)]. Fr. 2.17 (78.9 mg) was rechromatographed over Sephadex LH-20 (2.6 × 27 cm^2) [eluted with H_2O−MeOH gradient (7:3, 3:2, 1:1, 2:3, 3:7, 1:4, 1:9, 0:1), each solvent volume 100 mL] and by crystallization (aqueous acetone) to give **18** (5.6 mg) [R_f 0.80 ($CHCl_3$/MeOH = 10:1)].

Compound ***1***. Yellow amorphous powder; $[\alpha]^{20}_D$ +10.0 (*c* 0.11, MeOH). CD (MeOH; *c* 2.7 × 10^{-4} M; $\Delta\varepsilon$ λ_{max}): 321 (+2.19), 295 (−4.83), 278 (−3.57), 252 (+4.55), 238 (+2.28), 221 (+6.91). HRESIMS: *m*/*z* 393.0939, $[M + Na]^+$ (calcd for $C_{20}H_{18}O_7Na$, 393.0950). ^1H NMR (acetone-d_6) and ^{13}C NMR (acetone-d_6) spectroscopic data, see Table 1.

Acetylation of ***1***. Compound **1** (1.0 mg) was treated with dry pyridine (500 μL) and Ac_2O (500 μL) overnight at room temperature. The reaction mixture was worked up as usual, and the product was purified by silica chromatography [benzene/acetone (30:1)] to furnish **1a** (1.0 mg) as a yellow amorphous powder; $[\alpha]^{20}_D$ +2.7 (*c* 0.10, MeOH). HRESIMS: *m*/*z* 561.1384, $[M + Na]^+$ (calcd for $C_{20}H_{18}O_7Na$, 561.1373). ^1H NMR ($CDCl_3$, 500 MHz): δ 7.49 (2H, d, *J* = 8.5 Hz, H-2′, 6′), 7.17 (2H, d, *J* = 8.5 Hz, H-3′, 5′), 6.68 (1H, d, *J* = 10.5 Hz, H-1″), 6.26 (1H, s, H-6), 5.66 (1H, d, *J* = 12.0 Hz, H-3),

dx.doi.org/10.1021/jf5020439 | J. Agric. Food Chem. 2014, 62, 6345−6353

5.49 (1H, d, J = 10.5 Hz, H-2″), 5.40 (1H, d, J = 12.0 Hz, H-2), 4.23 (1H, d, J = 12.0 Hz, H-4″a), 4.12 (1H, d, J = 12.0 Hz, H-4″b), 2.38 (3H, s, 5-OAc), 2.33 (3H, s, 4′-OAc), 2.05 (3H, s, 4″-OAc), 2.02 (3H, s, 3-OAc), 1.47 (3H, s, H-5″).

Compound **2**. Yellow amorphous powder; $[\alpha]^{20}_{D}$ −75.4 (c 0.23, MeOH). CD (MeOH; c 2.7 × 10^{-4} M; $\Delta\varepsilon$ λ_{max}): 340 (+3.23), 295 (−6.95), 238 (+0.75), 211 (+6.98). HRESIMS: m/z 395.1109, $[M + Na]^+$ (calcd for $C_{20}H_{20}O_7Na$, 395.1109). ^{1}H NMR (acetone-d_6) and ^{13}C NMR (acetone-d_6) spectroscopic data, see Table 2.

Compound **3**. Yellow amorphous powder; $[\alpha]^{20}_{D}$ +2.5 (c 0.10, MeOH). CD (MeOH; c 2.6 × 10^{-4} M; $\Delta\varepsilon$ λ_{max}): 317(−0.33), 295 (−1.24), 248 (−0.47), 202 (+4.20). HRESIMS: m/z 409.1253, $[M + Na]^+$ (calcd for $C_{21}H_{22}O_7Na$, 409.1263). ^{1}H NMR (acetone-d_6) and ^{13}C NMR (acetone-d_6) spectroscopic data, see Table 2.

Compound **6**. Yellow amorphous powder; $[\alpha]^{20}_{D}$ +5.0 (c 0.20, MeOH). CD (MeOH; c 2.7 × 10^{-4} M; $\Delta\varepsilon$ λ_{max}): 326 (+1.76), 295 (−4.40), 247 (+1.92), 223 (+6.30), 210 (+2.55). HRESIMS: m/z 371.1136, $[M - H]^-$(calcd for $C_{20}H_{19}O_7$, 371.1131). ^{1}H NMR (acetone-d_6, 500 MHz): δ 7.08 (1H, d, J = 2.0 Hz, H-2′), 6.93 (1H, dd, J = 8.5, 2.0 Hz, H-6′), 6.86 (1H, d, J = 2.0 Hz, H-5′), 6.06 (1H, s, H-6), 5.16 (1H, t, J = 5.5 Hz, H-2″), 4.98 (1H, d, J = 11.5 Hz, H-2), 4.55 (1H, d, J = 11.5 Hz, H-3), 3.17 (2H, d, J = 5.5 Hz, H-1″), 1.59 (3H, s, H-4″), 1.56 (3H, s, H-5″).

Compound **15**. Yellow amorphous powder; $[\alpha]^{20}_{D}$ +34.9 (c 0.12, MeOH). HRESIMS: m/z 371.1113, $[M - H]^-$ (calcd for $C_{20}H_{19}O_7$ 371.1131). CD (MeOH; c 2.7 × 10^{-4} M; $\Delta\varepsilon$ λ_{max}): 317(+1.13), 295 (−1.78), 224 (+3.99). ^{1}H NMR (acetone-d_6) and ^{13}C NMR (acetone-d_6) spectroscopic data, see Table 2.

Compound **16**. Yellow amorphous powder; $[\alpha]^{20}_{D}$ −7.1 (c 0.11, MeOH). CD (MeOH; c 2.7 × 10^{-4} M; $\Delta\varepsilon$ λ_{max}): 325 (+0.27), 300 (−3.79), 286 (−2.53), 258(+1.93), 221(+2.96). HRESIMS: m/z 391.1117, $[M + Na]^+$ (calcd for $C_{21}H_{20}O_6Na$, 391.1158). ^{1}H NMR (acetone-d_6) and ^{13}C NMR (acetone-d_6) spectroscopic data, see Table 1.

Compound **17**. Yellow amorphous powder; $[\alpha]^{20}_{D}$ +3.9 (c 0.10, MeOH). CD (MeOH; c 2.6 × 10^{-4} M; $\Delta\varepsilon$ λ_{max}): 330 (+0.31), 293 (−0.94), 254 (+0.70). HRESIMS: m/z 407.1091, $[M + Na]^+$ (calcd for $C_{21}H_{20}O_7Na$ 407.1107). ^{1}H NMR (acetone-d_6) and ^{13}C NMR (acetone-d_6) spectroscopic data, see Table 2.

Compound **18**. Yellow granules, mp 132−138 °C; $[\alpha]^{20}_{D}$ −10.6 (c 0.54, MeOH). HRESIMS: m/z 391.1150, $[M + Na]^+$ (calcd for $C_{21}H_{20}O_6Na$ 391.1158). CD (MeOH; c 2.7 × 10^{-4} M; $\Delta\varepsilon$ λ_{max}): 320 (+2.33), 298 (−6.22), 248 (+5.50), 232 (+2.23). ^{1}H NMR (acetone-d_6) and ^{13}C NMR (acetone-d_6) spectroscopic data, see Table 1.

Biological Evaluation. *Test Microorganisms and Media.* Two osmophilic yeasts of *Z. rouxii* K122 and F51 were kindly provided from Tokushima Prefectural Industrial Technology Center, Tokushima, Japan. *Z. rouxii* K122, which has been industrially used for miso-making, was used as a typical non-film-forming strain and F51 as a film-forming strain. Both strains of *Z. rouxii* were cultured in slant agar media of Sabouraud dextrose agar (SDA; Difco) supplemented with 10% NaCl [NaCl 8.4 g] and a soy sauce [10 mL (salt conversion 1.6 g) per 100 mL SDA] and 50 μg/mL chloramphenicol at 25 °C for 2 weeks.

MIC Measurement. The MICs of Tween 80 and the isolated compounds (purity >95%) against the film-forming growth of *Z. rouxii* F51 were determined by the broth microdilution method in 96-well microtiter plates (Well Plate; Becton Dickinson Labware) using Sabouraud dextrose broth (SDB; Difco) supplemented with 10% NaCl [NaCl 8.4 g] and a soy sauce [10 mL (salt conversion 1.6 g) per 100 mL SDB]. The compounds were serially diluted with DMSO to prepare the solutions, which contained from 5000 to 4.8 μg/mL of the samples. Aliquots (5 μL) of the test compound solution were added to wells of the plate, which contained 50 μL of double-strength SDB and 35 μL of water. The 2-week cultures of the test strains were harvested and suspended into saline and finally adjusted to obtain the concentration of 10^6 CFU/mL. Aliquots (10 μL) of the suspensions were then added into wells of the plate. The plate was incubated at 25 °C for 2 weeks. Optical density (OD) at 540 nm was measured with a microplate reader (Sunrise; TECAN Group Ltd.) on the start day and after 2-week cultivation. The effects of compounds were evaluated by the difference of OD values on the start day and the 2-week cultivation. When the OD value was increased more than 0.1, compound was considered to have no inhibitory activity against the film-forming growth of *Z. rouxii* F51. Five microliters of DMSO did not inhibit the film-forming growth of *Z. rouxii* F51 at all. In contrast, the tested compounds, Tween 80, and DMSO have no effects on the growth of non-film-forming strain K122 on the same evaluation procedure as for *Z. rouxii* F51.

RESULTS AND DISCUSSION

Structure Elucidation and Identification. The stems of *D. caudatum* were extracted with MeOH at room temperature, and the MeOH extract was partitioned between EtOAc and H_2O. Repeated chromatography of the EtOAc-soluble fraction over Sephadex LH-20 and MCI gel CHP20P and purification by HPLC afforded four new flavonoids (**1**−**3**, **15**), together with 18 known flavonoids (**4** −**14**, **19**−**23**, **25**, **26**) (Figure 1).

The MeOH extract of leaves of *D. caudatum* was partitioned between EtOAc and H_2O. Repeated chromatography of the EtOAc-soluble fraction over Sephadex LH-20, MCI gel CHP20P, and SiO_2 and purification by HPLC afforded four new flavonoids (**1**, **16**−**18**), together with nine known compounds (**5**, **7**−**9**, **11**−**14**, **24**) (Figure 1). The known compounds were identified as 6-*C*-prenyl-5,7,2′,4′-tetrahydroxydihydroflavanonol (**4**),[2] 8-*C*-prenyl-5,7,2′,4′-tetrahydroxydihydroflavanonol (**5**),[2] 8-*C*-prenyldihydroisohamnetin (**7**),[8] 3-hydroxy-8-*C*-prenylnaringenin (**8**),[9] lespedezaflavanone C (**9**),[10] dihydrokaempferol (**10**),[11] 7,8-(2,2-dimethyl-2*H*-pyran)-5,2′-dihydroxy-4′-methoxyflavanonol (**11**),[2] glysapinol (**12**),[12] 8-*C*-prenyl-chromanochroman (**13**),[2] yukovanol (**14**),[13] lespecyrtin A1 (**19**),[14] garbanzol (**20**),[15] 6-*C*-prenyl-5,7,2′,4′-tetrahydroxydihydroflavonol (**21**),[3] kaempferol (**22**),[16] luteoline (**23**),[17] citrusinol (**24**),[18] leachianone G (**25**),[19] and apigenin (**26**)[20] by comparison of their physical and spectral data with those reported in the literature. The structure of compound **6** was assigned as 8-*C*-prenyldihydroquercetin by analysis of the spectral data. Since the spectroscopic data of this compound has not been reported previously, the data are shown in the experimental section. Compounds **6**, **9**, **12**, **19**, **20**, **22**, **23**, and **26** were isolated from *D. caudatum* for the first time.

The molecular formula of compound **1** was assigned as $C_{20}H_{18}O_7$ by HRESIMS (m/z 393.0950 $[M + Na]^+$). The ^{1}H and ^{13}C NMR spectra showed signals due to a 1,4-disubstituted benzene ring, a 1,2,3,4,5-pentasubstituted benzene ring, two oxygenated methines, a tertiary-methyl, an oxymethylene, a pair of *cis*-coupled olefinic doublets, and an oxygen-bearing quaternary sp^3 carbon (Table 1). These spectroscopic data were similar to those of the flavanonol derivatives with a 2,2-dimethyl-2*H*-pyran ring either at C-6,7 or C-7,8, except for the absence of the signal due to one of the tertiary methyl groups of a 2,2-dimethyl-2*H*-pyran moiety. The HMBC correlations of the tertiary methyl signal with the oxygen-bearing quaternary sp^3 carbon, one of the sp^2 methines (δ_C 124.6), and the oxymethylene suggested that one of methyl groups of 2,2-dimethyl-2*H*-pyran moiety was replaced by a hydroxymethyl group. This was further supported by the fact that acetylation of **1** with Ac_2O/pyridine yielded a tetraacetate of **1**. The positions of the 2-hydroxymethyl-2-methyl-2*H*-pyran ring were concluded to be at C-7 and C-8 from the HMBC correlations of H-1″ with C-7, C-8, and C-9 and of H-2″ with C-8. The 2,3-*trans* configuration was assigned from the coupling constant value of H-2/H-3 (11.5 Hz). In addition, the absolute configuration at

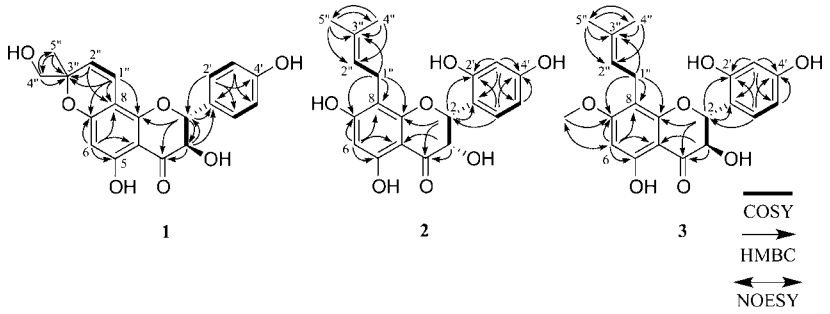

Figure 2. Selected COSY and HMBC correlations for compounds **1**, **2**, and **3**.

C-2 was assigned as 2*R* by the CD spectral analysis; the positive Cotton effect at 321 nm and the negative one at 295 nm were similar to those of the related compounds.[21−23] However, the configuration of C-3″ could not to be determined by spectral analyses. On the basis of this observation, the structure of **1** was established as shown (Figure 1).

Compound **2** gave a $[M + Na]^+$ ion peak at *m*/*z* 395.1107 in the HRESIMS, indicating the molecular formula of $C_{20}H_{20}O_7$. The ^1H NMR spectrum of **2** quite resembled those of 8-*C*-prenyl-(+)-dihydromorin (**5**), except for the signals due to H-2 and H-3 with small coupling constant values. The $^1H-^1H$ COSY and HMBC correlations shown in Figure 2 were in good agreement with the positions of the prenyl group at C-8 and the hydroxyl groups at C-5, C-2′, and C-4′. The 2,3-*cis* configuration was judged from the small coupling constant value of H-2/H-3 (2.0 Hz), and the absolute configuration at the C-2 was assigned as 2*R* by the CD spectral analysis, in which the positive Cotton effect at 340 nm and the negative one at 295 nm were similar to those of the related compounds.[21−23] On the basis of this observation, the structure of **2** was characterized as shown (Figure 1).

Compound **3** gave a quasi-molecular ion peak at *m*/*z* 409 $[M + Na]^+$ in the ESIMS, and its molecular formula was confirmed as $C_{21}H_{20}O_7$ by HRESIMS. The ^1H and ^{13}C NMR spectra of compound **3** were quite similar to those of **5** except for the observation of a methoxy signal [δ_H 3.90 (3H, s), δ_C 56.8]. Taking its molecular formula into account, compound **3** was considered to be a monomethyl ether of **5**. The location of the methoxy group in **3** was assigned to be at C-7 by the analysis of HMBC and NOESY spectra. The OMe resonance only showed a NOESY correlation with H-6. A planar structure for **3** was assigned by the $^1H-^1H$ COSY and HMBC analyses (Figure 2). The 2*R* configuration in **3** was assigned by the analysis of CD spectra, which showed similar Cotton effects to those found in **1**. From this examination, the structure of **3** was assigned as shown (Figure 1).

The molecular formula of compound **15** was assigned as $C_{20}H_{20}O_7$ by HRESIMS (*m*/*z* 371.1113 $[M - H]^-$). The ^1H and ^{13}C NMR spectra were correlated to those of **27** except for the absence of the *cis*-coupled olefinic signals, but instead signals due to two methylenes [δ_H 2.57, 1.61 (each 2H, t, *J* = 8.0 Hz), δ_C 18.2, 43.8] were observed. This spectral data, coupled with the molecular formula of **3**, implied the presence of a 2,2-dimethyl-dihydro-2*H*-pyran ring. The HMBC correlations of tertiary methyl signals with C-3″ and C-2″, H-2″ with C-8, and H-1″ with C-7, C-8, C-9, and C-3″ indicate that the 2,2-dimethyl-dihydro-2*H*-pyran ring was attached to C-7 and C-8 (Figure 3). The 2,3-*trans* configuration was assigned from the *J* value of H-2/H-3 (11.5 Hz), and the 2*R* configuration was elucidated by analysis of the CD spectrum.

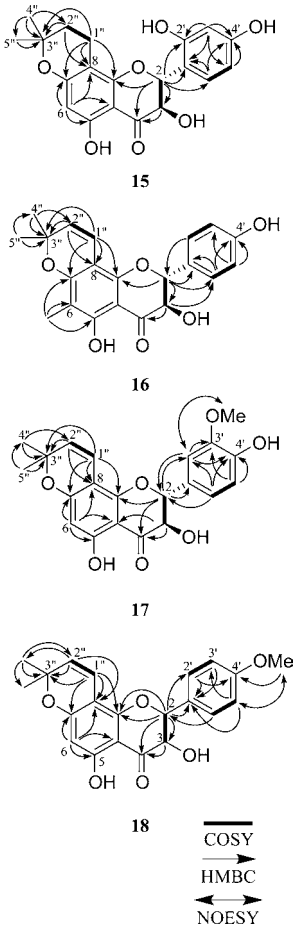

Figure 3. Selected COSY and HMBC correlations for compounds **15**−**18**.

Based on this examination, the structure of **15** was elucidated as shown (Figure 1).

The molecular formula of **16** was determined as $C_{21}H_{20}O_6$ by HRESIMS (*m*/*z* 391.1117 $[M + Na]^+$). The ^1H and ^{13}C NMR spectra were well correlated with those of **14**. However, an aromatic signal due to the A-ring of flavonoid was absent, but instead a *C*-methyl proton signal [δ_H 1.95 (3H, s), δ_C 7.2] was observed, suggesting compound **16** to be a *C*-methyl-flavanonol derivative with a 2,2-dimethyl-2*H*-pyran ring. The HMBC correlations of the H-1″ with C-7, C-8, and C-9 indicated that the 2,2-dimethyl-2*H*-pyran ring was attached to C-7 and C-8, while the location of the methyl group was concluded to be at C-6 from the HMBC correlations of the methyl signal with C-5, C-6, and C-7 (Figure 3). The *trans*-configuration of H-2 and H-3 was assigned from the *J*-value of H-2 and Hax-3 (11.5 Hz),

dx.doi.org/10.1021/jf5020439 | J. Agric. Food Chem. 2014, 62, 6345−6353

Table 3. MIC Values of Compounds against Film-Forming Growth of *Zygosaccharomyces rouxii* F51, CLog *P* Values, and Their Isolated Yields (%) From *D. caudatum*

compd	systematic name	MIC (μg/mL)	log P^a (ACD)	yields (%) isolated from *D. caudatum*		
				stems	leaves	roots
1	2″-hydroxymethyl-2″-methylpyran-(5″,6″:7,8)-5,4′-(2*R*,3*R*)-dihydroxydihydroflavonol	125.0	3.10	0.00017	0.00108	
2	8-(γ,γ-dimethylallyl)-5,7,2′,4′-tetrahydroxy-(2*R*,3*S*)-dihydroflavonol	62.5	3.79	0.00075		
4	6-(γ,γ-dimethylallyl)-5,7,2′,4′-tetrahydroxy-(2*R*,3*R*)-dihydroflavonol	62.5	3.79	0.00019		0.00122
5	8-(γ,γ-dimethylallyl)-5,7,2′,4′-tetrahydroxy-(2*R*,3*R*)-dihydroflavonol	31.3	3.79	0.01066	0.00072	0.02842
7	8-(γ,γ-dimethylallyl)-5,7,4′-trihydroxy-3′-methoxy-(2*R*,3*R*)-dihydroflavonol	125.0	4.22	0.00012	0.00013	0.00041
8	8-(γ,γ-dimethylallyl)-5,7,4′-trihydroxy-(2*R*,3*R*)-dihydroflavonol	125.0	4.51	0.00223	0.00203	0.00294
9	8,3′-di(γ,γ-dimethylallyl)-5,7,4′-trihydroxy-(2*R*,3*R*)-dihydroflavonol	>125.0	6.60	0.00002	0.00065	
10	5,7,4′-trihydroxy-(2*R*,3*R*)-dihydroflavonol	125.0	2.42	0.00713		0.00372
11	2″,2″-dimethylpyran-(5″,6″:7,8)-5,2′-dihydroxy-4′-methoxy-(2*R*,3*R*)-dihydroflavonol	7.8	4.71	0.00109	0.00142	0.00185
12	2″,2″-dimethylpyran-(5″,6″:7,8)-5,3′-dihydroxy-4′-methoxy-(2*R*,3*R*)-dihydroflavonol	31.3	4.39	0.00023	0.00065	
13	10-(γ,γ-dimethylallyl)-3,9,13-trihydroxy-6,12-metano-6*H*,12*H*-dibenzo[*b*,*f*][1,5]dioxocin	>125.0	3.61	0.00012	0.00029	0.00068
14	2″,2″-dimethylpyran-(5″,6″:7,8)-5,4′-dihydroxy-(2*R*,3*R*)-dihydroflavonol	15.6	4.68	0.00490	0.00474	0.00827
20	7,4′-dihydroxy-(2*R*,3*R*)-dihydroflavonol	125.0	1.99	0.00023		
21	6-(γ,γ-dimethylallyl)-5,7,2′,4′-tetrahydroxyflavonol	62.5	3.70	0.00052		0.00140
22	5,7,4′-trihydroxyflavonol	15.6	2.05	0.00019		
24	2″,2″-dimethylpyran-(5″,6″:7,8)-5,4′-dihydroxyflavonol	125.0	4.55		0.00136	0.00074
25	8-(γ,γ-dimethylallyl)-5,7,2′,4′-tetrahydroxy- (2*R*)-flavanone	62.5	4.56	0.00004		0.00012
27	2″,2″-dimethylpyran-(5″,6″:7,8)-5,2′,4′-trihydroxy-(2*R*,3*R*)-dihydroflavonol	62.5	3.96			0.00256
28	2″,2″-dimethylpyran-(5″,6″:6,7)-5,2′,4′-trihydroxy-(2*R*,3*R*)-dihydroflavonol	31.3	4.15			0.00212
29	8-(γ,γ-dimethylallyl)-5,7,2′-trihydroxy-4′-methoxy-(2*R*)-flavanone	125.0	4.74			0.00023
30	8-(γ,γ-dimethylallyl)-5,7,4′-trihydroxy-(2*R*)-flavanone	>125.0	5.29			0.00008
31	5,7,4′-trihydroxy-(2*R*)-flavanone	125.0	3.19			0.00011
32	2″,2″-dimethylpyran-(5″,6″:7,8)-5,3′,4′-trihydroxy-6-methyl-(2*R*)-flavanone	31.3	5.31			0.00039
33	6-(γ,γ-dimethylallyl)-5,7,4′-trihydroxyflavonol	62.5	4.15			0.00039
34	2″,2″-dimethylpyran-(5″,6″:7,8)-5,2′,4′-trihydroxyflavonol	31.3	4.11			0.00109
35	2″,2″-dimethylpyran-(5″,6″:6,7)-5,4′-dihydroxy-4′-methoxy-flavonol	15.6	4.83			0.00024
36	2″,2″-dimethylpyran-(5″,6″:7,8)-5,2′,4′-trihydroxy-6-methyl-flavone	125.0	4.37			0.00018
37	2″,2″-dimethylpyran-(5″,6″:7,8)-5,3′,4′-trihydroxy-6-methyl-flavone	>125.0	5.10			0.00052
	Tween 80	<0.5				

[a]The log *P* values were calculated using ACD software.

and the absolute configurations at the C-2 were determined to be *R* from the positive Cotton effect at 325 nm, and a negative one at 286 nm in the CD spectrum, being similar to those found in the related compound.[21−23] On the basis of this examination, the structure of **16** was characterized as shown in Figure 1.

The ^{1}H NMR spectra of compounds **17** and **18** were well correlated to each other except for the signals due to the B-ring moiety; compound **17** gave a ^{1}H NMR spectrum quite similar to that of **12**, but the signals arising from the B-ring moiety were slightly different, while that of **18** showed the presence of a 1,4-disubstituted B-ring moiety. This observation suggested that the position of the methoxy group in compound **17** is different from that in **12**. The oxygen functions at C-3′ and C-4′ were indicated by the HMBC correlations of H-2′ and H-6′ with C-2, while the methoxy group was assigned to be at C-3′ from the NOESY correlation of the OMe resonance with H-2′. In contrast, the ^{1}H NMR spectrum of **18** was similar to that of **17** except for the appearance of A_2B_2-type aromatic signals instead of signals due to a 1,3,4-trisubstituted benzene ring, suggesting that the oxygen function of the B-ring is present only at C-4′. This was consistent with the HRESIMS of **18**, which showed an $[M + Na]^+$ peak at *m*/*z* 391.1158, being 16 mass units less than that of **17**, and was further confirmed by the HMBC correlations of H-2′,6′ with C-2 and C-4′ (Figure 3). Besides, the position of the methoxy group was assigned to be at C-4′ based on the HMBC and NOESY correlations; the OMe resonance only showed a NOESY correlation with H-3′,5′ (Figure 3). The HMBC correlations shown in Figure 3 were in good agreement with the structures for **17** and **18**. From these examinations, the structures of **17** and **18** were characterized as shown in Figure 1.

Biological Evaluation. Seventeen flavonoids (**1**, **2**, **4**, **5**, **7**−**14**, **20**−**22**, **24**, **25**) obtained in this study, together with 11 flavonoids (**27**−**37**) previously isolated from the roots of this plant, were evaluated for their effect on the film-forming growth of a film-forming strain (F51) of *Z. rouxii*. The film-forming growth inhibitory activity of nine compounds (**3**, **6**, **15**−**19**, **23**, and **26**) could not be evaluated owing to the small amount of samples. Under the cultivation conditions in the present work, not only *Z. rouxii* K122 but also F51 grew well in the presence of the tested flavonoids. Therefore, the effect of these flavonoids on the characteristic film-forming property of *Z. rouxii* F51 was examined by the broth microdilution method in 96-well microtiter plates (Table 3).

Compound **11** demonstrated potent inhibitory activity against the film-forming growth of *Z. rouxii* F51 with an MIC value of 7.8 μg/mL. Compounds **5**, **12**, **14**, **28**, **32**, **33**, and **35** also showed moderate inhibitory activity with MIC values ranging from 15.6 to 31.3 μg/mL. Compounds **2**, **4**, **21**, **25**, **27**,

dx.doi.org/10.1021/jf5020439 | J. Agric. Food Chem. 2014, 62, 6345−6353

28, and **33** were weak inhibitors (MIC value of 62.5 μg/mL), while compounds **1**, **7**−**10**, **13**, **20**, **24**, **29**−**31**, **36**, and **37** did not show inhibition at 125 μg/mL. Regarding the active flavanonol derivatives, the compounds possessing a 2,2-dimethyl-2*H*-pyran group in the A-ring (**11**, **12**, **14**, **27**, and **28**) were more potent (MIC values ranging from 7.8 to 62.5 μg/mL) compared with those (MIC values ranging from 31.5 to 62.5 μg/mL) having a prenyl group (**2**, **4**, and **5**), suggesting that the 2,2-dimethyl-2*H*-pyran group in the A-ring may contribute more critically to the film-forming growth of a film-forming strain (F51) of *Z. rouxii*. Flavonols possessing a 2,2-dimethyl-2*H*-pyran group (MIC values ranging from 15.6 to 62.5 μg/mL) also tend to show more potent activity than those having a prenyl group, except for compound **24**. In contrast, flavones and flavanones were less active compared with flavanonols and flavonols. Therefore, the hydroxyl group at C-3 might be important for the activity, whereas a double bond at C-2−C-3 seems to be not essential, since flavanonols and flavonols showed similar activities. In addition, compounds having hydroxyl groups at C-2′ and C-4′ tend to show better activity. Overall, flavonoids possessing either a prenyl or a 2,2-dimethyl-2*H*-pyran group in the A-ring or oxygen functions at C-2′ and C-4′ in the B-ring or both, which were the typical structural features of the constituents in *D. caudatum*, showed inhibitory activity against film-forming growth of *Z. rouxii* F51.

Compounds that possess an amphiphilic character, like Tween, are considered to interact with membrane altering the properties of membranes of cells.[24] Since the cell surface of *Z. rouxii* F51 has higher hydrophobicity than non-film-forming strain K122, amphiphilies were also considered to decrease surface tension of culture solution resulting in inhibition of the film-forming growth.[7] However, the active flavonols with a 2,2-dimethyl-2*H*-pyran group had higher CLog *P* values than the less active ones. In contrast, a trend of relationship between inhibitory activity and CLog *P* values in the flavonols with a prenyl group was opposite. In the case of flavonol, flavanone, and flavone, the relationship between inhibitory activity and CLog *P* values was not found. Therefore, the inhibitory activity of flavonoids against the film-forming growth of *Z. rouxii* F51 could not be explained only by amphiphilic character. Since the ATPase activity of *Z. rouxii* F51 was more than twice the activity of *Z. rouxii* K122,[25] flavonoids might have effects on the ATPase activity of plasma membrane.

Considering the fact that 9 of 15 active compounds were isolated as new compounds from *D. caudatum*, they are characteristic compounds of this plant. Since the contents of compounds **11** and **14** are higher than the other flavonoids in roots, leaves, and stems, they especially play important roles for inhibiting the film-forming growth of *Z. rouxii* F51. In consideration of the biological activity coupled with yields of the compounds from leaves and stems, compounds **2**, **4**, **5**, **11**, and **14** were considered to be mainly involved in the application as well as the Japanese name of this plant. In addition, compounds **27** and **28**, which were isolated only from the roots of this plant, were found to have similar inhibitory activity against the film-forming growth of *Z. rouxii* F51.

AUTHOR INFORMATION

Corresponding Author

*Tel: +81-88-633-7276. Fax: +81-88-633-9501. E-mail: kasiwada@tokushima-u.ac.jp.

Notes

The authors declare no competing financial interest.

ACKNOWLEDGMENTS

We are most grateful to Mr. S. Yamamoto (Industrial Technology Center of Tokushima, Japan) for the generous supply of Z. *rouxii* F51 and K122, as well as valuable advice. We also express our thanks to Dr. K. Murakami (Sojo University, Japan) for the plant collection and identification.

REFERENCES

(1) *Chinese Materia Medica*; Shanghai People's Publishing House, Jiangsu New Medical College: Shanghai, 1985; pp 1384−1385.

(2) Sasaki, H.; Kashiwada, Y.; Shibata, H.; Takaishi, Y. Prenylated flavonoids from *Desmodium caudatum* and evaluation of their anti-MRSA activity. *Phytochemistry* **2012**, *82*, 136−142.

(3) Sasaki, H.; Kashiwada, Y.; Shibata, H.; Takaishi, Y. Prenylated flavonoids from the roots of *Desmodium caudatum* and evaluation of their antifungal activity. *Planta Med.* **2012**, *78*, 1851−1856.

(4) Makino, T. *Makino's New Illustrated Flora of Japan*; Hokuryu-kan Publishing Co., Ltd.: Tokyo, 1998; pp 209.

(5) Sujaya, I.; Tamura, Y.; Tanaka, T.; Yamaki, T.; Ikeda, T.; Kikushima, N.; Yata, H.; Yokota, A.; Asano, K.; Tomita, F. Development of Internal Transcribed Spacer Regions Amplification Restriction Fragment Length Polymorphism Method and Its Application in Monitoring the Population of *Zygosaccharomyces rouxii* M2 in Miso Fermentation. *J. Biosci. Bioeng.* **2003**, *96*, 438−447.

(6) Kreger-van Rij, N. J. W. (ed.). *The Yeasts, A Taxonomic Study*; Elsevier Science Publishers B. V.: Amsterdam, the Netherlands, 1984; pp 462−465.

(7) Tomita, M.; Yamamoto, S.; Yamaguchi, K.; Ohigashi, H.; Koshimizu, K. Physiological characteristics of a film-forming strain of *Zygosaccharomyces rouxii*, and its cellular fatty acid synthesis. *Biosci., Biotechnol., Biochem.* **1997**, *61*, 51−55.

(8) McCormick, S.; Robson, K.; Bohm, B. Flavonoids of *Wyethia angustifolia* and *W. helenioides*. *Phytochemistry* **1986**, *25*, 1723−1726.

(9) Souza, M. P.; Machado, M. I. L.; Braz-Filho, R. Six flavonoids from *Bursera leptophloeos*. *Phytochemistry* **1989**, *28*, 2467−2470.

(10) Li, J.; Wang, M. Two flavanones from the root bark of *Lespedeza davidii*. *Phytochemistry* **1989**, *28*, 3564−3566.

(11) Taira, J.; Nanbu, H.; Ueda, K. Nitric oxide-scavenging compounds in *Agrimonia pilosa* Ledeb on LPS-induced RAW264.7 macrophages. *Food Chem.* **2009**, *115*, 1221−1227.

(12) Lukaseder, B.; Vajrodaya, S.; Hehenberger, T.; Seger, C.; Nagl, M.; Lutz-Kutschera, G.; Robien, W.; Greger, H.; Hofer, O. Prenylated flavanones and flavanonols as chemical markers in *Glycosmis* species (Rutaceae). *Phytochemistry* **2009**, *70*, 1030−1037.

(13) Ito, C.; Sato, K.; Oka, T.; Inoue, M.; Ju-ichi, M.; Omura, M.; Furukawa, H. Two flavanones from *Citrus* species. *Phytochemistry* **1989**, *28*, 3562−3564.

(14) Mori-Hongo, M.; Yamaguchi, H.; Warashima, T.; Miyase, T. Melanin Synthesis Inhibitors from *Lespedeza cyrtobotrya*. *J. Nat. Prod.* **2009**, *72*, 63−71.

(15) Zhang, D.-W.; Dai, S.-J.; Li, G.-H.; Dai, J.-G. Chemical constituents in cane of *Pueraria lobata*. *Chin. Trad. Herb. Drugs* **2011**, *42*, 649−651.

(16) Hadizadeh, F.; Khalili, N.; Hosseinzadeh, H.; Khair-Aldine, R. Kaempferol from *Saffron petals*. *Iran. J. Pharm. Res.* **2003**, *2*, 251−252.

(17) Ozgen, U.; Mavi, A.; Terzi, Z.; Kazaz, C.; Asci, A.; Kaya, Y.; Secen, H. Relationship between chemical structure and antioxidant activity of luteolin and its glycosides isolated from *Thymus sipyleus subsp. sipyleus var. sipyleus*. *Rec. Nat. Prod.* **2011**, *5*, 12−21.

(18) Wu, T. S. A 2,2-dimethylpyranoflavonol from *Citrus nobilis*. *Phytochemistry* **1987**, *26*, 3094−3095.

(19) Jung, H. A.; Jeong, D.-M.; Chung, H. Y.; Lim, H. A.; Kim, J. Y.; Yoon, N. Y.; Choi, J. S. Re-evaluation of the antioxidant prenylated flavonoids from the roots of *Sophora flavescens*. *Biol. Pharm. Bull.* **2008**, *31*, 908−915.

(20) Shen, C.-C.; Chang, Y.-S.; Ho, L.-K. Nuclear magnetic resonance studies of 5,7-dihydroxyflavonoids. *Phytochemistry* **1993**, *34*, 843−845.

(21) Gaffield, W. Circular dichroism, optical rotatory dispersion and absolute configuration of flavanones, 3-hydroxyflavanones and their glycosides. Determination of aglycone chirality in flavanone glycosides. *Tetrahedron* **1970**, *26*, 4093−4108.
(22) Slade, D.; Ferreira, D.; Marais, J. P. J. Circular dichroism, a powerful tool for the assessment of absolute configuration of flavonoids. *Phytochemistry* **2005**, *66*, 2177−2215.
(23) Sutthivaiyakit, S.; Thongnak, O.; Lhinhatrakool, T.; Yodchun, O.; Srimark, R.; Dowtaisong, P.; Chuankamnerdkarn, M. Cytotoxic and antimycobacterial prenylated flavonoids from the roots of *Eriosema chinense*. *J. Nat. Prod.* **2009**, *72*, 1092−1096.
(24) Schreier, S.; Malheiros, S. V. P.; de Paula, E. Surface active drugs: self-association and interaction with membranes and surfactants. Physicochemical and biological aspects. *Biochim. Biophys. Acta* **2000**, *1508*, 210−234.
(25) Tomita, M.; Yamamoto, S.; Yamaguchi, K.; Ohigashi, H.; Yagi, T.; Kohata, K.; Berden, J. A. Theasaponin E1 destroys the salt tolerance of yeasts. *J. Biosci. Bioeng.* **2000**, *90*, 637−642.

Table 1. Effect of the Calcium Concentration and Source on the Gelation Characteristics and CaP Yield

CaP type	concn (g/100 g of pectin) abbrev	gelling behavior	CaP yield (mean ± SD) (%)
C-CaP	$CaCl_2$ 10	The mixture became viscous flowable and did not gel at all after 0.5 h of standing.	
	$CaCl_2$ 12	The mixture became viscous and initiated a certain gel formation after 0.5 h of standing	68.2 ± 1.61
	$CaCl_2$ 14	A gel formed immediately as $CaCl_2$ solution was added; however, it was not strong enough for a real gelation.	77.6 ± 1.14
	$CaCl_2$ 16	A compact gel was formed as $CaCl_2$ solution was added.	79.1 ± 1.53
	$CaCl_2$ 18	A compact gel was formed before all of the $CaCl_2$ solution was added.	
HO-CaP	$Ca(OH)_2$ 10.8	The mixture became viscous flowable with addition of $Ca(OH)_2$. Bits of broken gel could be found in the bottom of the solution.	
	$Ca(OH)_2$ 11.6	The mixture became viscous and initiated a certain gel formation.	52.8 ± 1.08
	$Ca(OH)_2$ 12.5	A gel formed when $Ca(OH)_2$ suspension was added.	81.6 ± 1.74
	$Ca(OH)_2$ 13.3	A compact gel was formed when $Ca(OH)_2$ suspension was added.	83.9 ± 0.29
	$Ca(OH)_2$ 14.1	A compact gel formed when $Ca(OH)_2$ suspension was added. Undissolved $Ca(OH)_2$ was observed in the gel.	

pectin (abbreviated as $CaCl_2$ 10, $CaCl_2$ 12, $CaCl_2$ 14, $CaCl_2$ 16, and $CaCl_2$ 18) and 10.8, 11.6, 12.5, 13.3, and 14.1 g of $Ca(OH)_2$/100 g of pectin [abbreviated as $Ca(OH)_2$ 10.8, $Ca(OH)_2$ 11.6, $Ca(OH)_2$ 12.5, $Ca(OH)_2$ 13.3, and $Ca(OH)_2$ 14.1]. A gel was formed after the mixture stood for 0.5 h. The end product (C-CaP or HO-CaP) was then separated through filtration, washed with deionized water, and lyophilized. The yield of CaP was calculated using the following equation:

$$X\ (\%) = \frac{m_{\mathrm{CaP}}}{m_{\mathrm{pectin}}} \times 100 \quad (1)$$

where X is the yield of CaP (%), m_{CaP} is the mass of CaP (g), and m_{pectin} is the mass of pectin (g).

Decalcification Process. To obtain the decalcified pectin (DC-pectin), C-CaP ($CaCl_2$ 14) and HO-CaP [$Ca(OH)_2$ 12.5] were suspended in a 60% acidified ethanol–water solution (the pH was adjusted to 0.5 with 37% HCl) in a ratio of 1:40 (w/v), and the resulting suspension was homogenized for 2 min. The suspension was filtered, washed with 95% ethanol, and then heated at 35 °C in an air-circulated oven for 4 h. To separate the soluble pectin and insoluble CaP, DC-pectin was again suspended in deionized water in a ratio of 1:100 (w/v) with stirring. Five replications were performed. The pectin recovery was calculated as

$$Y\ (\%) = \frac{m_{\text{DC-pectin}} - m_{\text{I-CaP}}}{m_{\text{DC-pectin}}} \times 100 \quad (2)$$

where Y refers to pectin recovery (%), $m_{\text{DC-pectin}}$ is the mass of DC-pectin (g), and $m_{\text{I-CaP}}$ is the mass of insoluble CaP (g).

FTIR. An FTIR analysis was carried out to investigate the CaP and DC-pectin functional groups. These functional groups included free carboxyl, an ionized carboxyl group, and a carbomethoxy group. Frequently, functional group changes will cause a measurable change in the infrared spectrum of the molecule. According to Table 1, CaP was generated only when the calcium concentration fell within the range of 12–16 g of $CaCl_2$/100 g of pectin or 11.6–13.3 g of $Ca(OH)_2$/100 g of pectin. Therefore, only the CaPs formed in the above concentration ranges were then used for FTIR analysis. Moreover, the DC-pectins prepared from C-CaP ($CaCl_2$ 14) and HO-CaP [$Ca(OH)_2$ 12.5] were also used for the FTIR analysis.

For the spectroscopic measurements, a 2% (w/w) sample was mixed with KBr before compression into a disk[20] and then ground into a fine powder using an agate mortar. Each disk was scanned at a resolution of 4 cm^{-1} over a spectral range of 400–4000 cm^{-1} using an Equinox 55 FTIR spectrometer (Bruker, Germany). FTIR spectral parameters, including band frequency and band area, were acquired by a software package (OMNIC FTIR software, version 6.0, Thermo Fisher Scientific, Madison WI). The data represent the mean of triplicate experiments.

Rheology. The rheological properties of the C-CaP gel ($CaCl_2$ 14) and HO-CaP gel [$Ca(OH)_2$ 12.5] were characterized using a Kinexus Pro rheometer (Malven, Worcestershire, U.K.) equipped with a parallel plate geometry (diameter 20 mm, gap size 0.5 mm, temperature 20 ± 0.1 °C). To assess the viscoelastic properties, a frequency sweep test was performed over a range of 0.01–10 Hz at a strain of 1%. A strain sweep test was carried out over a range of 0.1–100% at 1 Hz. The storage modulus (G') and loss modulus (G'') were measured as a function of the frequency and strain. Each experiment was conducted in three replicates.

SEM. To examine the internal microstructure of CaP, lyophilized CaP gels [$CaCl_2$ 14 or $Ca(OH)_2$ 12.5] were scanned with scanning electron microscopy (Philips XL-30 ESEM, Royal Philips, Holland). Before scanning, the lyophilized CaP gel sample was fixed on the conductive material of the copper vector and then sputter coated with gold–palladium under argon. The photographs were recorded using an accelerating voltage of 20 kV.[15,21]

XRD. The structure of the egg-box junction zone was investigated with a Bruker MSAL-XD2 Discovery X-ray diffractometer (Germany) equipped with a Cu Kα source and Ni filter. The X-ray diffractometer was operated under the following conditions: voltage 36 kV, current 20 mA, scanning regions of the diffraction angle 2θ = 10–30°, and scanning rate 0.05 deg (2θ) min^{-1}.[22] Standard sample holders were carefully filled with approximately 0.5 g of CaP powder [$CaCl_2$ 14 or $Ca(OH)_2$ 12.5]. The relative crystallinity was measured according to Nara and Komiya,[23] and the separation methods of the crystalline and amorphous portions are shown in Figure 1. The diffractogram was smoothed using the fit Gaussian method with Origin 7.0 (OriginLab Corp., Northampton MA). The relative crystallinity was calculated using the following formula:

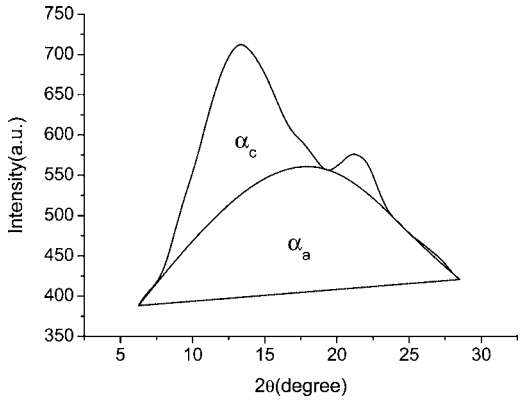

Figure 1. Calculation of the relative degree of crystallinity in the X-ray diffractogram. α_c (upper area) and α_a (lower area) indicate the crystalline and amorphous portions, respectively.

dx.doi.org/10.1021/jf5004545 | J. Agric. Food Chem. 2014, 62, 6354–6361

$$X_c = \frac{\alpha_c}{\alpha_a + \alpha_c} \quad (3)$$

where X_c is the crystallinity, α_a is the area of the amorphous region, and α_c is the area of the crystalline region.

RESULTS

Effect of the Calcium Concentration and Source on the CaP Yield. Table 1 provides a summary of the CaP gelling state and yield obtained under varied calcium concentrations and sources. A CaP gel formed when the calcium concentration was in the range of 12−16 g of $CaCl_2$/100 g of pectin or 11.6−13.3 g of $Ca(OH)_2$/100 g of pectin. The rate of CaP gel coagulation accelerated with increased calcium concentration, regardless of the calcium source. At 14 g of $CaCl_2$/100 g of pectin and 12.5 g of $Ca(OH)_2$/100 g of pectin, a better gelling quality and greater yield were achieved. In addition, at all concentrations investigated, the yield of CaP from $Ca(OH)_2$ was significantly higher than it was from $CaCl_2$.

As indicated from earlier studies, pectin can form a gel in the presence of calcium by the formation of the egg-box junction zones. Thus, the gel strength increases with increasing calcium concentration, since the number of junction zones formed is also increased.[3,24] If the calcium concentration were too low, the egg-box junctions would be insufficient to form the gel, but if the calcium concentration were too high, inferior gels would form due to instant gel formation in some areas, which would not only lower the CaP yield, but also negatively affect the gel structure. Therefore, the calcium concentration was a critical factor in the formation of the egg-box structure.

Calcium Binding Stability of CaP. The calcium binding stability of CaP was determined by the pectin recovery (eq 2). Higher pectin recovery indicates easier decalcification and less stability for CaP. During decalcification, H^+ in acidified alcohol can displace Ca^{2+} and thus convert CaP into pectin.[25] As shown in Table 2, the average pectin recovery from HO-CaP (90.9%) was significantly higher than that from C-CaP (72.6%). Thus, C-CaP exhibited a higher calcium binding stability due to difficult decalcification.

Table 2. Pectin Recovery from Calcium Pectinate during Decalcification

	pectin recovery (%)						
CaP type	1	2	3	4	5	mean (%)	SD
C-CaP	71.8	72.5	72.1	73.8	72.7	72.6	0.76
HO-CaP	90.5	89.8	91.7	92.4	90.1	90.9	1.11

Overall, HO-CaP exhibited a higher yield (Table 1) and weaker calcium binding affinity (Table 2) than did C-CaP. To explain these differences, the structural variability between HO-CaP and C-CaP was evaluated by using FTIR, rheology, SEM, and XRD.

FTIR Spectra of CaP. FTIR spectra of C-CaP ($CaCl_2$ 14) and HO-CaP [$Ca(OH)_2$ 12.5] are illustrated in Figure 2. The spectra are divided into two wavenumber areas: A (3500−1350 cm^{-1}) and B (<1350 cm^{-1}). The broad and intense band at 3450 cm^{-1} corresponds to the absorption due to stretching vibration of the O−H groups from carboxylic acid and polysaccharides,[26,27] while the band at a lower wavenumber of 2930 cm^{-1} corresponds to the infrared C−H stretching of the methyl group. The C═O stretching band of the carbomethoxy group at 1740 cm^{-1} was partially overlapped by the strong COO− band. Therefore, the change in the carbomethoxy group could be elucidated by analysis of the C═O and $-CH_3$ bands. Two strong absorptions at 1610 and 1420 cm^{-1} indicate antisymmetric and symmetric stretching vibrations of the ionized COO− in CaP.[28] Since both wavenumber areas could reflect the change of COO-Ca content simultaneously, the absorption at 1610 cm^{-1} was selected for subsequent analysis. Area B (Figure 2) is considered to be a fingerprint region which reflects the stretching vibration absorption of C−C, C−O−C, C−OH, and glycosidic bonds in pectin.[16] There are many absorption bands in this region; therefore, area B is not suitable for functional group analysis. In contrast, special interest is focused on area A, where two groups, carbomethoxy ($-CH_3$, 2930 cm^{-1}; C═O, 1740 cm^{-1}) and carboxylate (asymmetric stretching vibration at 1610 cm^{-1}), are observed.

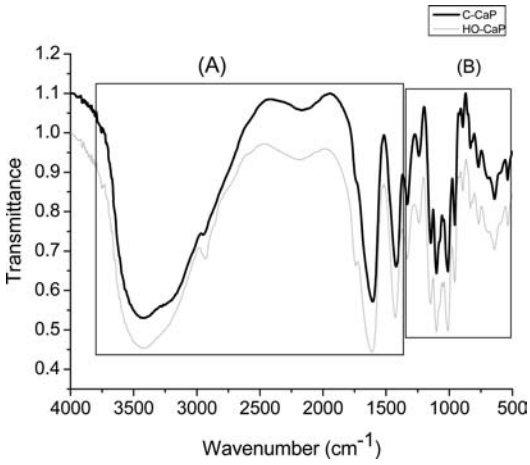

Figure 2. FTIR spectra of C-CaP and HO-CaP. Two areas, A (3500−1350 cm^{-1}) and B (<1350 cm^{-1}), are divided according to wavenumber.

The structural variation could be reflected by the wavenumber, peak area, and peak intensity of the functional groups, including $-CH_3$, C═O, and COO−. The spectral characteristics of three bands ($-CH_3$, C═O, COO−) in C-CaP and HO-CaP are summarized as a function of the calcium concentration and source (Figures 3−5, Table 3). There are two main aspects shown in the results.

1. The Wavenumber Values of the Functional Groups [$-CH_3$, C═O (Esterified), COO−] Changed with the Calcium Concentration and Source. The carbomethoxy group (C═O, $-CH_3$) wavenumber values for the two CaPs shifted significantly with increasing calcium concentration (Figure 4a,b). This shift may be due to the addition of calcium and a modification of the functional group environment.[29] The changes of carbomethoxy wavenumbers in HO-CaP ($\Delta\nu_{-CH_3}$ = 5; $\Delta\nu_{C=O}$ = 2) were less than those in C-CaP ($\Delta\nu_{-CH_3}$ = 15; $\Delta\nu_{C=O}$ = 8) (Table 3), which indicated that the effect of calcium on carbomethoxy from HO-CaP was weaker than it was on carbomethoxy from C-CaP.[16] The wavenumbers for COO− from the two CaPs (Figure 4c) were apparently decreased compared to that from pectin. This finding indicated that calcium binding with pectin could change the wavenumber for COO−.[29,30] From early studies, electrostatic interactions exist between Ca^{2+} and COO− in the egg-box model.[31,32] As an electron-withdrawing ion, calcium induces a charge deviation, which results in a change of the band vibration.[26] In addition,

dx.doi.org/10.1021/jf5004545 | J. Agric. Food Chem. 2014, 62, 6354−6361

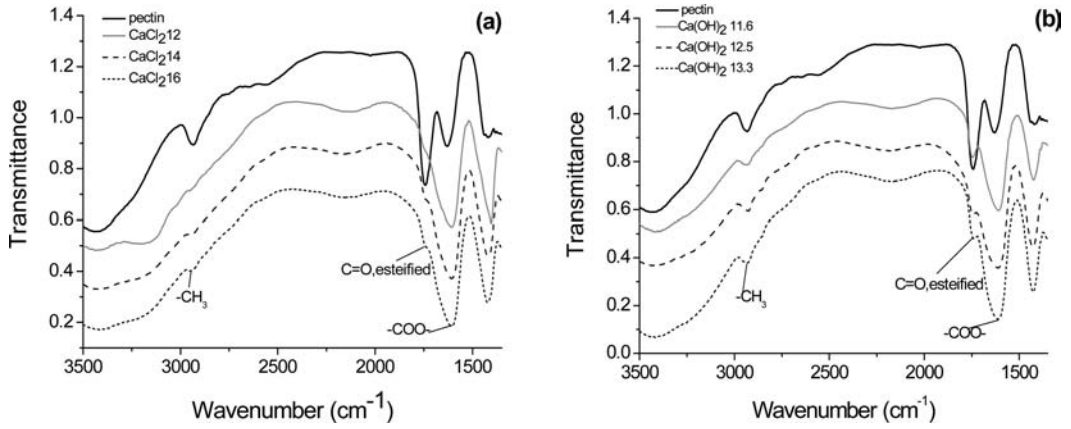

Figure 3. FTIR spectra for (a) C-CaP and (b) HO-CaP at different calcium concentrations.

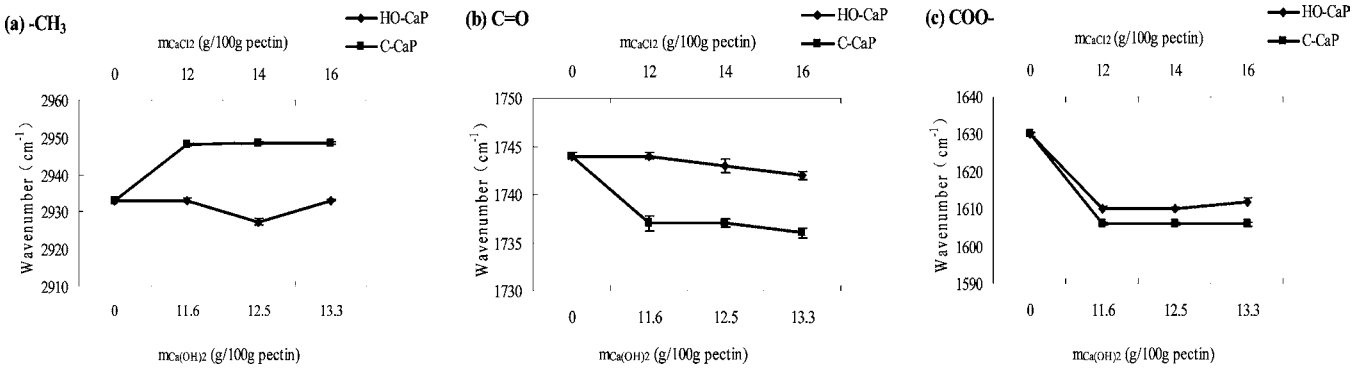

Figure 4. Calcium concentration dependence of the wavenumber values of (a) $-CH_3$, (b) C═O (esterified), and (c) COO− for C-CaP (■) and HO-CaP (◆).

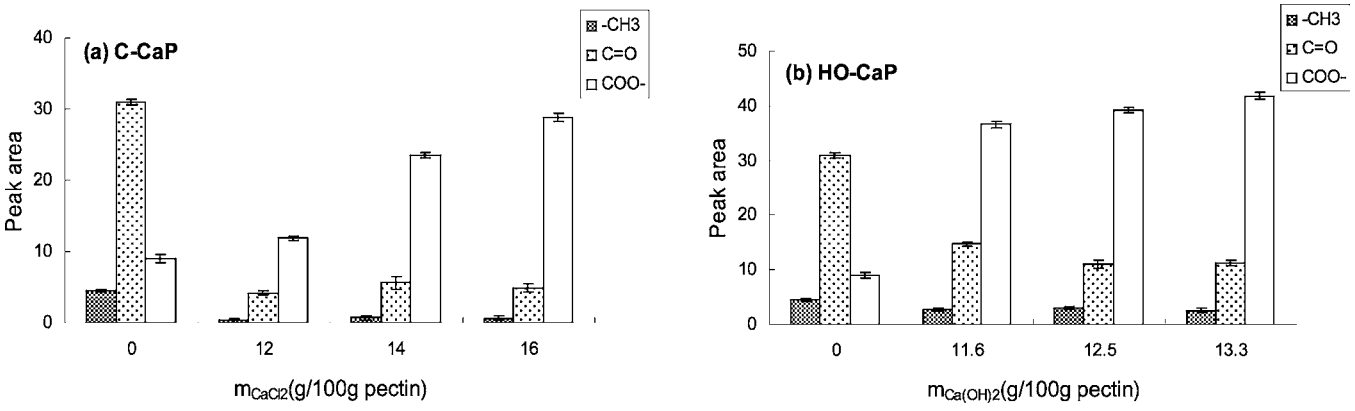

Figure 5. Calcium concentration dependence of the absorption area of the functional groups ($-CH_3$, C═O, COO−) for (a) C-CaP and (b) HO-CaP.

Table 3. Change of Wavenumber for Three Functional Groups in C-CaP and HO-CaP[a]

CaP type	$\Delta\nu_{-CH_3}$ (cm^{-1})	$\Delta\nu_{C=O}$ (cm^{-1})	$\Delta\nu_{COO-}$ (cm^{-1})
C-CaP	15	8	24
HO-CaP	5	2	20

[a] $\Delta\nu = |\nu_{max} - \nu_{min}|$.

$\Delta\nu_{COO-}$ from HO-CaP ($\Delta\nu_{COO-} = 20$) was smaller than it was from C-CaP ($\Delta\nu_{COO-} = 24$) (Table 3). This result indicates a weaker electrostatic interaction between Ca^{2+} and COO− in HO-CaP than in C-CaP. In summary, the changes in the wavenumber for the three functional groups indicate that the interaction between calcium and pectin is much stronger in C-CaP than it is in HO-CaP. This result is consistent with the decalcification result.

2. The Peak Areas of the Functional Groups [$-CH_3$, C═O (Esterified), COO-] Changed with the Calcium Concentration and Source. As shown in Figure 5, the COO− function quantity increased gradually with increasing calcium concentration. The COO− peak area is one index to reflect the yield of CaP. HO-CaP had a larger COO− quantity than C-CaP, which indicated a higher yield than that of C-CaP. This finding

dx.doi.org/10.1021/jf5004545 | J. Agric. Food Chem. 2014, 62, 6354−6361

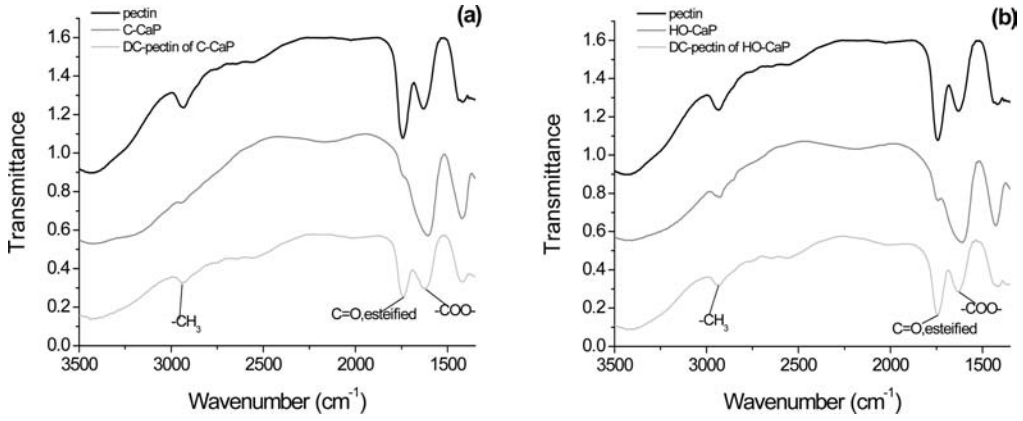

Figure 6. Effect of decalcification on the FTIR spectra of (a) C-CaP ($CaCl_2$ 14) and (b) HO-CaP [$Ca(OH)_2$ 12.5]. Pectin (black curve), CaP (gray curve), and DC-pectin (light gray curve) are measured.

is consistent with the result seen for the CaP yield, as evident in Table 1.

The carbomethoxy (C═O, $-CH_3$) quantities fell sharply after C-CaP formed (Figure 5a), whereas for HO-CaP, they did not have such an obvious change. To identify whether calcium binding caused this reduction, FTIR analysis of DC-pectin was further investigated. As shown in Figure 6, the absorptive intensity of carbomethoxy disappeared with the addition of Ca^{2+}; however, it reappeared after Ca^{2+} was removed by decalcification. Therefore, incorporation of Ca^{2+} into pectin resulted in the disappearance of the FTIR absorptive intensity for carbomethoxy.[16] Ravanat and Rinaudo[33] previously demonstrated that Ca^{2+} induces chain−chain associations to form stable egg-box junction zones. The ordering and arrangement of junction zones may be different under various gel conditions.[22] For C-CaP, the sharp decrease in carbomethoxy intensity might be because this functional group was embedded into the highly ordered or compact egg-box junction zones, and thus, its infrared absorption was masked. For HO-CaP, carbomethoxy was exposed and its infrared absorption was easier to detect because the egg-box junction zones became less well organized or were in a metastable form.

Rheological Properties of CaP. The rheological behaviors of C-CaP gel ($CaCl_2$ 14) and HO-CaP gel [$Ca(OH)_2$ 12.5] were evaluated. Figure 7 shows the frequency dependence of the storage modulus G' and loss modulus G'' for C-CaP and HO-CaP. C-CaP showed higher G' and G'' values than did HO-CaP, which means that C-CaP was more elastic and viscous. Moreover, the higher difference in magnitude between G' and G'' of C-CaP indicates that C-CaP has a stronger cross-linked network structure compared with HO-CaP.[34,35] The values of G' and G'' were also plotted as a function of strain in Figure 8. C-CaP had a greater range of elastic behavior than did HO-CaP. Both G' and G'' values tended to decrease beyond the crossover point, consistent with the large deformation. Therefore, the rheological properties were clearly different in the C-CaP and HO-CaP gels. The C-CaP gel showed a broader range of elastic behavior and needed a higher force to break down its structure, indicating a predominant cross-linking network and more stable junction zones.[17]

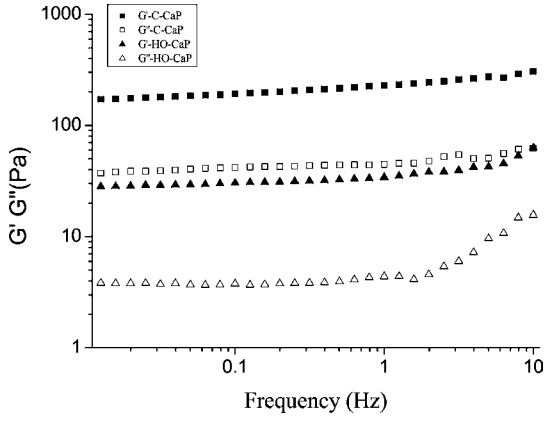

Figure 7. Frequency dependence of G' (filled symbols) and G'' (open symbols) measured at 1% strain for the C-CaP gel ($CaCl_2$ 14, squares) and HO-CaP gel [$Ca(OH)_2$ 12.5, triangles].

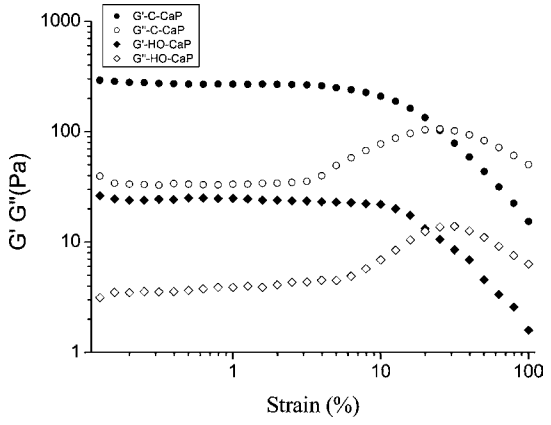

Figure 8. Strain dependence of G' (filled symbols) and G'' (open symbols) measured at 1 Hz for the C-CaP gel ($CaCl_2$ 14, circles) and HO-CaP gel [$Ca(OH)_2$ 12.5, tilted squares].

Morphology of CaP under SEM. The morphologies of C-CaP ($CaCl_2$ 14) and HO-CaP [$Ca(OH)_2$ 12.5] lyophilized gels were examined by SEM and showed some differences (Figure 9). Generally, two CaPs were made up by irregular membranes, but HO-CaP was more porous. For C-CaP, the membranes were relatively even and the surface was quite smooth (Figure 9a), which suggested a tight structure. On the contrary, for HO-CaP, the whole structure was loose and the membranes were rolled with more pores. The surface of HO-CaP was rough with

dx.doi.org/10.1021/jf5004545 | J. Agric. Food Chem. 2014, 62, 6354−6361

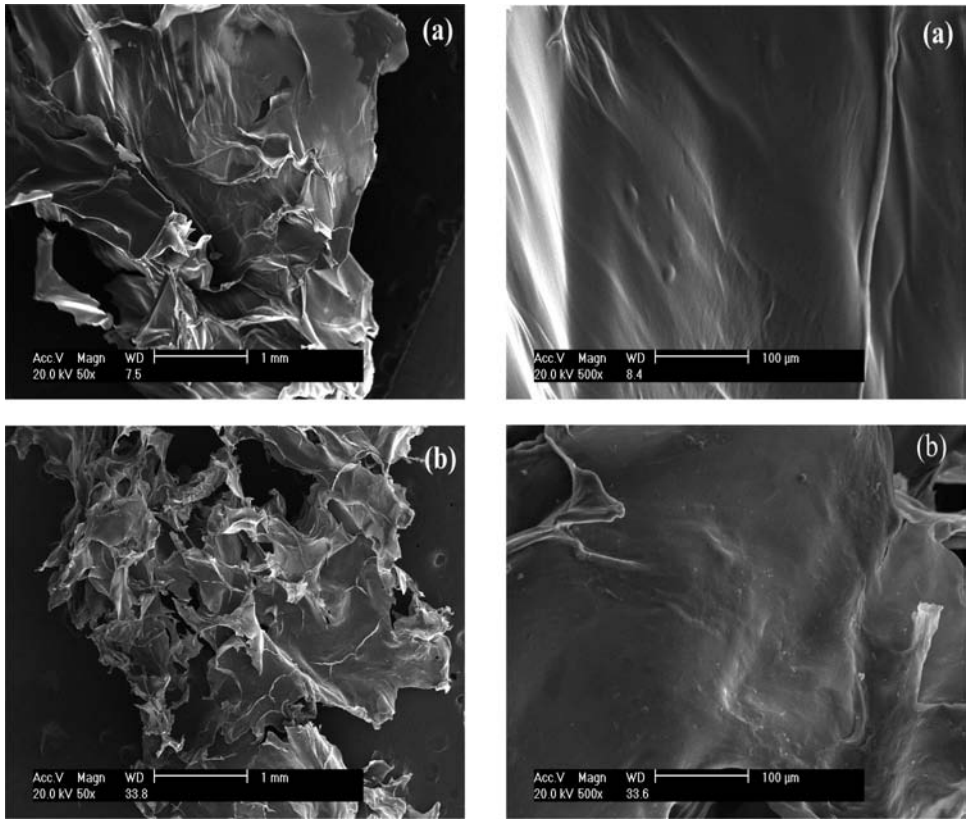

Figure 9. SEM photographs of lyophilized CaP gels for (a) C-CaP ($CaCl_2$ 14) and (b) HO-CaP [$Ca(OH)_2$ 12.5] at 50× (left) and 500× (right) magnification.

some particles, which were more likely undissolved $Ca(OH)_2$, scattered on it (Figure 9b).

Morphology is the macroreflection of molecular permutations in a material. Thus, it is inferred that the morphological differences between C-CaP and HO-CaP are ascribed to the different arrangements of the egg-box junction zones in CaP. When egg-box junction zones present an orderly and stable arrangement, CaP will show a smooth surface and form a gel too strong to break during lyopilization. Thus, it may be concluded that C-CaP maintains more orderly and stable junction zones than HO-CaP. This result is in agreement with decalcification, FTIR, and rheological analysis findings that the calcium binding of C-CaP is stronger than that of HO-CaP.

XRD Patterns of CaP. To determine whether the ordering of the egg-box junction zone had an effect on the functional groups and morphological structure, the structures of the junction zones were further investigated by X-ray diffraction. Figure 10 shows X-ray diffraction patterns of C-CaP ($CaCl_2$ 14) and HO-CaP [$Ca(OH)_2$ 12.5]. The XRD intensity curves of the egg-box junction zones of CaP exhibited patterns similar to those of calcium alginate which were reported by Li et al.[22] Because the junction zones are relatively regular, two main peaks appeared at ∼13° and ∼21.5° (2θ) and can be detected by XRD. Li et al. fitted the two peaks into the egg-box model.[22] According to eq 3, the crystallinities of the C-CaP and HO-CaP samples were 0.49 and 0.41, respectively. These results indicated that the arrangements of the junction zones in the two CaPs were different. Compared to HO-CaP, the egg-box junction zone in C-CaP was more regular and tighter. Therefore, the distinction of the junction zones could be responsible for the differences in the calcium binding stability,

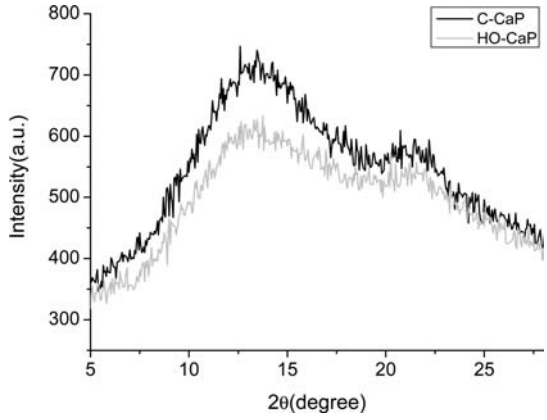

Figure 10. X-ray diffraction patterns of C-CaP ($CaCl_2$ 14) and HO-CaP [$Ca(OH)_2$ 12.5].

FTIR spectra, rheological properties, and morphological structure.

DISCUSSION

The egg-box junction zone conformation of calcium alginate was used as a reference to identify the junction zone of CaP. In the present study, using the same XRD operating conditions as those of Li et al.,[22] we found that the diffraction peaks of CaP were identical with those of calcium alginate. Alginate is a polysaccharide consisting of 1,4-linked D-guluronate and L-mannuronate that can appear in homopolymeric blocks of each monomer.[36] The egg-box junction zone in calcium alginate is formed due to the binding of Ca^{2+} with poly(guluronic acid), while in CaP it is formed due to the binding of Ca^{2+} with

dx.doi.org/10.1021/jf5004545 | J. Agric. Food Chem. 2014, 62, 6354−6361

poly(galacturonic acid). Poly(guluronic acid) and poly-(galacturonic acid) are nearly mirror images in their structure (with the only exception being at C3)[37] and solid circular dichroism spectra. Furthermore, the same egg-box model was proposed for the junction zones of calcium alginate and CaP.[38,39] Therefore, the egg-box junction zone in CaP could be confirmed on the basis of the diffraction peaks.

In the current study, CaPs were prepared with high methoxyl pectin under alkaline conditions. C-CaP was formed when the pH value was 9.75. For HO-CaP, the pH value was stable at 9.77 after $Ca(OH)_2$ addition. Generally, under alkaline conditions, demethylation often occurs and a great number of egg-box junction zones may be formed, which could improve the crystallinity of CaP. Considering the gelling pH of CaP in the current study, demethylation and β-elimination may occur. However, on the basis of the previous report, less than 5% methyl ester had been saponified in 1/2 h at room temperature.[40] The initial reaction rate of β-elimination is very low at pH 9.5−10.[41] Thus, there was limited demethylation and β-elimination in the process of CaP formation.

The results from decalcification, FTIR, rheology, and SEM indicated that there were significant differences between C-CaP and HO-CaP in certain aspects of calcium binding stability, functional group, gel strength, and microstructure. These differences were mainly caused by the distinction of the egg-box junction zones. It was observed that the infrared absorption of the functional groups, gel strength, and microstructure were changed with the quantity of the junction zones. A higher crystallinity (XRD) indicated that C-CaP preserved a more organized structure than HO-CaP (Figure 10). The difference between the two CaP structures could be ascribed to the calcium sources used and the process of gel formation. When preparing C-CaP, the pH was adjusted before the addition of the calcium reagent. However, for HO-CaP, pH adjustment and addition of the calcium reagent were performed simultaneously. Thus, further investigations are needed to explain the kinetic and structural differences during gel formation.

Investigation of different properties of these two CaPs is valuable for their potential application in related areas. Currently, pectin is mostly extracted from citrus peel and apple pomace by the traditional ethanol method, which has a high energy and ethanol cost. With a loose structure, a high yield, and fast decalcification, HO-CaP is therefore suitable for pectin production. However, the pectin obtained by this method may preserve different properties compared with pectin obtained by the traditional method. Further investigation is therefore necessary to characterize the molecular weight, the DE, and the gelling behavior. In addition, considering HO-CaP has a weaker binding with calcium, it may be used as a calcium supplement with further study. Due to its compact structure and chemical stability, C-CaP is not easily degraded and is more suitable as a carrier of active ingredients or some oral drugs to provide protection or control release.[13,42] It also has been used as the outer membrane to maintain the moisture and increase the thermal stability of fried food.[11]

AUTHOR INFORMATION

Corresponding Author

*Phone: +86 20 85226630. Fax: +86 20 85226630. E-mail: thxs@jnu.edu.cn.

Author Contributions

†X.G. and H.D. contributed equally to this work.

Funding

We are grateful for financial support from the Special Fund for Agro-Scientific Research in the Public Interest (Grant 201303077) and National Natural Science Foundation of China (Grant 31171722).

Notes

The authors declare no competing financial interest.

ACKNOWLEDGMENTS

We thank Dr. William W. Riley for excellent writing assistance.

ABBREVIATIONS USED

CaP, calcium pectinate; C-CaP, calcium pectinate prepared by calcium chloride; HO-CaP, calcium pectinate prepared by calcium hydroxide; DE, degree of esterification; FTIR, Fourier transform infrared spectroscopy; SEM, scanning electron microscopy; XRD, X-ray diffractometry; DC-pectin, decalcium pectin; G', storage modulus; G'', loss modulus

REFERENCES

(1) Thakur, B. R.; Singh, R. K.; Handa, A. K. Chemistry and uses of pectin—a review. *Crit. Rev. Food Sci.* **1997**, *37*, 47−73.

(2) Ralet, M. C.; Bonnin, E.; Thibault, J. F. Pectin. In *Biopolymers. Volume 6: Polysaccharides II: Polysaccharide from Eukaryotes*; Baets, S. D., Vandamme, E. J., Steinbüchel, A., Eds.; Wiley-VCH Verlag GmbH & Co. KGaA: Weinheim, Germany, 2002; p 312.

(3) Powell, D. A.; Morris, E. R.; Gidey, M. J.; Rees, D. A. Conformation and interactions of pectins: II. Influence of residue sequences on chain association in calcium pectate gels. *J. Mol. Biol.* **1982**, *155*, 517−531.

(4) Walkinsshaw, M. D.; Arnott, S. Conformations and interactions of pectins: II. Models for junction zones in pectinic acid and calcium pectate gels. *J. Mol. Biol.* **1981**, *153*, 1075−1085.

(5) Morris, E. R.; Powell, D. A.; Gidley, M. J.; Rees, D. A. Conformations and interactions of pectins: I. Polymorphism between gel and solid states of calcium polygalacturonate. *J. Mol. Biol.* **1982**, *155*, 507−516.

(6) FDA. Select committee on GRAS substances (SCOGS) opinion: pectin, amidated. http://www.fda.gov/food/ingredientspackaginglabeling/gras/scogs/ucm260947.htm (accessed May 2, 2014).

(7) Tiwari, A.; Ramteke, S.; Dahima, R. Preparation and characterization of satranidazole loaded calcium pectinate microbeads for colon specific delivery; application of response surface methodology. *Curr. Nanosci.* **2011**, *7*, 608−615.

(8) Jain, A.; Gupta, Y.; Jain, S. K. Potential of calcium pectinate beads for target specific drug release to colon. *J. Drug Targeting* **2007**, *15*, 285−294.

(9) Xu, C.; Tan, R. X.; Zhang, J. S.; Mo, Y. Calcium pectinate capsules for colon-specific drug delivery. *Drug Dev. Ind. Pharm.* **2005**, *31*, 127−134.

(10) Oidtmann, J.; Schantz, M.; Mäder, K.; Baum, M.; Berg, S.; Betz, M.; Kulozik, U.; Leick, S.; Rehage, H.; Schwarz, K.; Richling, E. Preparation and comparative release characteristics of three anthocyanin encapsulation systems. *J. Agric. Food Chem.* **2012**, *60*, 844−851.

(11) Gerrish, T.; Higgins, C.; Kresl, K. Method of making battered and breaded food composition using calcium pectins. U.S. Patent 5,601,861, 1995.

(12) Huang, X. S. Calcium pectinate and its production method and applications. CN Patent 103,130,913 A, 2013.

(13) Olsen, A. G. Method of preparing pectin. U.S. Patent 2132577, 1934.

(14) Guo, X. J.; Huang, X. S. Effect of some technology factors on yield of calcium pectinate from orange peel. *Sci. Technol. Food Ind.* **2013**, *34*, 258−261.

(15) Sriamornsak, P.; Thirawong, N.; Cheewatanakornkool, K.; Burapapadh, K.; Sae-Ngow, W. Cryo-scanning electron microscopy (cryo-SEM) as a tool for studying the ultrastructure during bead formation by ionotropic gelation of calcium pectinate. *Int. J. Pharm.* **2008**, *352*, 115−122.
(16) Assifaoui, A.; Loupiac, C.; Chambin, O.; Cayot, P. Structure of calcium and zinc pectinate films investigated by FTIR spectroscopy. *Carbohydr. Res.* **2010**, *345*, 929−933.
(17) Vithanage, C. R.; Grimson, M. J.; Wills, P. R.; Harrison, P.; Smith, B. G. Rheological and structural properties of high-methoxyl esterified, low-methoxyl esterified and low-methoxyl amidated pectin gels. *J. Texture Stud.* **2010**, *41*, 899−927.
(18) Xu, P. J.; Liu, J. J. Research on technology of extracting pectin from pericarp of orange. *Sci. Technol. Food Ind.* **2008**, *29*, 208−209.
(19) FCC. *Food Chemical Codex*, 2nd ed.; National Academy of Sciences: Washington, DC, 1972; p 580.
(20) Wong, T. W.; Nurjaya, S. Drug release property of chitosan-pectinate beads and its changes under the influence of microwave. *Eur. J. Pharm. Biopharm.* **2008**, *69*, 176−188.
(21) Maestrelli, F.; Cirri, M.; Corti, G.; Mennini, N.; Mura, P. Development of enteric-coated calcium pectinate microspheres intended for colonic drug delivery. *Eur. J. Pharm. Biopharm.* **2008**, *69*, 508−518.
(22) Li, L. B.; Fang, Y. P.; Vreeker, R.; Appelqvist, I. Reexamining the egg-box model in calcium-alginate gels with X-ray diffraction. *Biomacromolecules* **2007**, *8*, 464−468.
(23) Nara, S.; Komiya, T. Studied on the relationship between water saturated state and crystallinity by the diffraction method for moistened potato starch. *Starch/Stärke* **1983**, *35*, 407−410.
(24) Fraeye, I.; Duvetter, T.; Doungla, E.; Van Loey, A.; Hendrickx, M. Fine-tuning the properties of pectin-calcium gels by control of pectin fine structure, gel composition and environmental conditions. *Trends Food Sci. Technol.* **2010**, *21*, 219−228.
(25) Xu, J. R.; Liu, X. H.; Ren, Y. M. Studies on the salting-out technology of pectin from apple pomace. *J. Chin. Inst. Food Sci. Technol.* **2006**, *6*, 95−99.
(26) Li, R. Q. *Spectral Analysis of Organic Structures*; Tianjin University Press: Tianjin, China, 2002; pp 55−104.
(27) Silverstein, R. M.; Bassler, G. C.; Morril, T. C. *Infrared spectroscopy spectrometric identification of organic compounds*, 6th ed.; John Wiley & Sons, Inc.: New York, 1996; pp 91−164.
(28) Gnanasambandam, R.; Proctor, A. Determination of pectin degree of esterification by diffuse reflectance Fourier transform infrared spectroscopy. *Food Chem.* **2000**, *68*, 327−332.
(29) Tajmir-Riahi, H. A. Sugar complexes with calcium ion: infrared spectra of crystalline D-glucuronic acid and its calcium complexes. *Carbohydr. Res.* **1983**, *122*, 241−248.
(30) Nurjaya, S.; Wong, T. W. Effects of microwave on drug release properties of matrices of pectin. *Carbohydr. Polym.* **2005**, *65*, 245−257.
(31) Thibault, J. F.; Rinaudo, M. Chain association of pectic molecules during calcium-induced gelation. *Biopolymers* **1986**, *25*, 455−468.
(32) Braccini, I.; Perez, S. Molecular basis of Ca^{2+}-induced gelation in alginates and pectins: the egg-box model revisited. *Biomacromolecules* **2001**, *2*, 1089−1096.
(33) Ravanat, G.; Rinaudo, M. Investigation on oligo- and polygalacturonic acids by potentiometry and circular dichroism. *Biopolymers* **1980**, *19*, 2209−2222.
(34) Evageliou, V.; Richardson, R. K.; Morris, E. R. Effect of pH, sugar type and thermal annealing on high-methoxy pectin gels. *Carbohydr. Polym.* **2000**, *42*, 245−259.
(35) Tsoga, A.; Richardson, R. K.; Morris, E. R. Role of cosolutes in gelation of high-methoxy pectin. Part 1. Comparison of sugars and polyols. *Food Hydrocolloids* **2004**, *18*, 907−919.
(36) Rees, D. A. Structure, conformation, and mechanism in the formation of polysaccharide gels and networks. *Adv. Carbohydr. Chem. Biochem.* **1969**, *24*, 267−332.
(37) Rees, D. A. Polysaccharide shapes and their interactions—some recent advances. *Pure Appl. Chem.* **1981**, *53*, 1−14.
(38) Atkins, E. D. T.; Nieduszynski, I. A.; Mackie, W.; Parker, K. D.; Smolko, E. E. Structural components of alginic acid. II. The crystalline structure of poly-α-L-guluronic acid. Results of X ray diffraction and polarized infrared studies. *Biopolymers* **1973**, *12*, 1879−1887.
(39) Morris, E. R.; Rees, D. A.; Robinson, G.; Young, G. A. Competitive inhibition of interchain interactions in polysaccharide systems. *J. Mol. Biol.* **1980**, *138*, 363−374.
(40) Renard, C. M. G. C.; Thibault, J. F. Degradation of pectins in alkaline conditions: kinetics of demethylation. *Carbohydr. Res.* **1996**, *286*, 139−150.
(41) Renard, C. M. G. C.; Thibault, J. F. Pectins in mild alkaline conditions: β-elimination and kinetics of demethylation. *Prog. Biotechnol.* **1996**, *14*, 603−608.
(42) Borzelleca, J. F.; Filer, L. J., Jr.; Kinoshita, F. K.; Gerrish, T. C.; Kuo, P. K.; La Du, B. N. Evaluation of the safety of sodium pectate as a food ingredient. *Food Chem. Toxicol.* **1996**, *34*, 21−25.

to ^{14}C-protein contamination.[20] Advances in high resolution nuclear magnetic resonance spectroscopy (NMR) and the development of methodologies to completely solubilize the entire plant cell wall[21] make it possible to observe structural transformations of lignocellulose components. For example, this approach has been previously employed to look for evidence of lignin decomposition by brown rot fungi[22] and in the structural characterization of thermochemically treated plant biomass.[23]

The objective of this study was to look for evidence of chemical changes in lignin during anaerobic decomposition of different woody plant materials under mesophilic and thermophilic conditions. To our knowledge, this is the first time that high resolution 2D NMR of completely dissolved cell walls has been used to look for evidence of chemical transformations during anaerobic decomposition of lignocellulosic materials in their native state (i.e., when the natural complex associations between cellulose, hemicelluloses, and lignin are retained).

MATERIALS AND METHODS

Experimental Design. Anaerobic decomposition experiments were conducted with lignocellulosic materials (HW, hardwood *Quercus rubra*; SW, softwood *Pinus taeda*; and ONP, old newsprint Washington Post) at mesophilic (37 °C) and thermophilic (55 °C) temperatures. ONP was selected to represent a pulp and paper product in which the lignin remains in the product. Copy paper was selected as a positive control because it contains primarily cellulose and very little lignin.

Each material was incubated under conditions optimal for anaerobic decomposition in 160 mL serum bottles containing an inoculum and biological growth medium. Decomposition was allowed to proceed until no significant methane production was measured so as to allow the bioavailable substrates to be consumed. In order of preference, lignin degradation will not proceed unless readily degradable substrates such as cellulose and hemicelluloses have been depleted. The incubation period for different materials ranged from 467 days to 585 days. At the completion of incubation, the solid residue was recovered by drying the entire contents of the bottle at 50 °C. The solid residue was subjected to the wet chemical and spectroscopic analyses described below.

Sample Collection and Preparation. Mature wood samples (oven-dried at 105 °C for 48 h and stored at room temperature) were obtained from the collection of Dr. Ilona Peszlen of the Department of Forest Biomaterials at NC State University. The copy paper used in the experiments is a commercially available white paper. The ONP was represented by the Washington Post and was collected in August 2011. Samples were dried at 50 °C, then ground to pass a 60-mesh screen (0.251 mm opening) in a Wiley mill, and then redried at 50 °C to constant weight. This temperature is well below the predicted glass transition temperature of lignin.[24] Samples were stored in Mason jars at room temperature until used.

Preparation of Anaerobically Decomposed Materials. The goal of the preparation of decomposed materials was to generate solids for subsequent analysis with negligible background lignin, cellulose, and hemicelluloses. Anaerobically decomposed materials were prepared following the biochemical methane potential (BMP) test with some modifications.[9] Test material weighing 2 g was incubated in a 160 mL serum bottle with 80 mL of reduced medium and 20 mL of inoculum according to Wang et al.[9] The bottle was capped with a butyl rubber stopper and then sealed with an aluminum crimp. The head space was flushed with a mixture of CO_2/N_2 (20:80, v/v). Flushing was done for about 10 min at a flow rate of at least 100 mL/min. This was sufficient to replace the headspace gases with CO_2/N_2 (20:80, v/v). The BMP inoculum described in Wang et al.[9] is rich in humic materials that could interfere with lignin analyses. Thus, it was necessary to prepare mesophilic and thermophilic inocula with negligible background lignin.

The mesophilic inoculum has been maintained on ground (<1 mm) residential MSW in our laboratory for over 15 years at 37 °C. The thermophilic inoculum was obtained from a thermophilic anaerobic sludge digester (Carrboro, NC) operated at 55 °C and was collected in March 2011. Serial transfer (1:1, v/v) of the inoculum was done every 2 weeks into a fresh mixture of reduced medium with copy paper as the growth substrate until no significant lignin was detected by CuO analysis, a process that required about 14 transfers over 7 months. The copy paper was initially tested for methane potential (~250 mL of CH_4/g) to ensure that the paper does not contain inhibitory substances. Copy paper used in the experiments contained less than 1% Klason lignin. The viability of the inoculum was monitored by measuring gas production.[9]

Analytical Methods. *CuO Digestion and HPLC Detection.* A sample containing 2−5 mg of C equivalent was placed in a 25 mL Teflon vial with 0.5 g of CuO powder, 0.1 g of $Fe(NH_4)_2(SO_4)_2 \cdot 6H_2O$, and 5 mL of 2 M NaOH ($O_2$-free), sealed, and locked under a N_2 headspace in an anaerobic hood. Digestion was conducted in a furnace at 150 °C for 3 h. After digestion and cooling, the liquid portion of the digestate was separated by centrifugation and then acidified (pH ≤ 2). An aliquot of this solution was diluted as necessary to obtain a concentration within the calibration range (0.05−25 μM for each phenolic monomer) and was analyzed using a LC-20AT high performance liquid chromatograph (HPLC) equipped with a degasser (DGU-20A5) and a SPD 20A photodiode array detector (PDA) (Shimadzu, Canby, OR). Chromatographic analyses were conducted using a gradient program at 55 °C with a Kinetex 2.6u C18 100A column (Phenomenex, Torrance, CA) as described previously.[25,26]

Peak integration for each lignin phenol (LP) was done at its respective maximum wavelength using LC solutions software (Shimadzu, Canby, OR). The 11 LP liberated during CuO oxidation that were analyzed are as follows with the corresponding chemical structure number and are illustrated in Figure 1: [4-hydroxybenzaldehyde (**1**); 4-hydroxyacetophenone (**2**); 4-hydroxybenzoic acid (**3**); 4-hydroxy-3-methoxybenzaldehyde (vanillin, **4**); 4-hydroxy-3-methoxyacetophenone (acetovanillone, **5**); 4-hydroxy-3-methoxybenzoic acid (vanillic acid, **6**); 3,5-dimethoxy-4-hydroxybenzaldehyde (syringaldehyde, **7**); 3,5-dimethoxy-4-hydroxyacetophenone (acetosyringone, **8**); 3,5-dimethoxy-4-hydroxybenzoic acid (syringic acid, **9**); 4-hydroxycinnamic acid (*p*-coumaric acid, **10**); 4-hydroxy-3-methoxycinnamic acid (ferulic acid, **11**)]. All HPLC samples and standard solutions were filtered through 0.2 μm Millex Teflon filter (Millipore, Billerica, MA) prior to injection. Aqueous solutions were prepared using filtered (0.2 μm) and UV-treated deionized water. Standard LPs were purchased from Sigma-Aldrich (St. Louis, MO) at the highest purity available.

Cellulose, Hemicelluloses, Klason, and Acid-Soluble Lignin. A ~1 g sample was extracted with 140 mL of toluene/ethanol (2:1, v/v) and then dried. A known weight (~0.1−0.3 g) of ground sample was subjected to a two-stage acid hydrolysis.[27,28] Sugars (arabinose, galactose, glucose, mannose, and xylose) liberated from acid digestion were then analyzed by HPLC using an ICS 2500 pulsed electrochemical detector (Dionex, Sunnyvale, CA).[27,28] Anhydro correction was done to convert glucose to cellulose and the other sugars to hemicelluloses. Klason lignin was measured from the solids remaining after acid hydrolysis as the weight loss on ignition at 550 °C for 2 h. Acid-soluble lignin was determined from UV absorbance at 205 nm (extinction coefficient of 110) of the filtered (0.45 μm) acid hydrolysate from the second stage digestion.[19,29]

Total Organic Carbon (TOC). Total organic carbon (TOC) was measured with a PE 2400 CHN analyzer (PerkinElmer, Akron, OH). All samples were acid washed (1 M HCl) to eliminate inorganic carbon prior to analysis.[30]

Methoxyl Group Determination. The lignin methoxyl group content of the samples was determined by gas chromatography as developed previously with some modifications.[31] Briefly, a 10 mg sample was digested with 0.5 mL of 57% HI in a Tekmar 22 mL Teflon septum-sealed headspace vial (Teledyne, Thousand Oaks, CA) at 130 °C for 35 min. The digestate was allowed to cool to room

1	*p*-hydroxybenzaldehyde 4-hydroxybenzaldehyde	
2	*p*-hydroxyacetophenone 4'-Hydroxyacetophenone	
3	*p*-hydroxybenzoic acid	
4	Vanillin 4-Hydroxy-3-methoxybenzaldehyde	
5	Acetovanillone 4'-Hydroxy-3'-methoxyacetophenone	
6	Vanillic Acid 4-Hydroxy-3-methoxybenzoic acid	
7	Syringaldehyde 4-Hydroxy-3,5-dimethoxybenzaldehyde	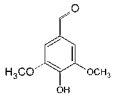
8	Acetosyringone 4'-Hydroxy-3',5'-dimethoxyacetophenone	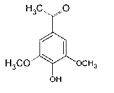
9	Syringic Acid 4-Hydroxy-3,5-dimethoxy-benzoic acid	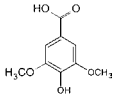
10	*p*-coumaric acid *trans*-4-Hydroxycinnamic acid	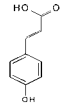
11	Ferulic acid *trans*-4-Hydroxy-3-methoxycinnamic acid	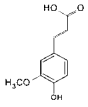

Figure 1. Suites of lignin phenols (LP) liberated during CuO oxidation of lignin.[45]

temperature and neutralized by addition of 0.5 mL of 6 M NaOH. The headspace was analyzed for methyl iodide using an 7890A GC (Agilent, Santa Clara, CA) equipped with a model 7000 headspace auto sampler (Teledyne, Thousand Oaks, CA), capillary column (30 m × 0.25 mm × 0.1 μm), and flame ionization detector (FID) at 250 °C. The carrier gas was 3.8 mL of He/min. Headspace gas concentration was determined from an external calibration curve constructed by the full evaporation technique, injecting 0.1 to 10 μL of pure methyl iodide as previously described.[31]

Cell Wall Dissolution. Complete dissolution of plant cell walls for subsequent high resolution solution state nuclear magnetic resonance (NMR) spectroscopy has been described.[21,32,33] A ground sample (<60 mesh) weighing 2 g was ball-milled in toluene using alumina fortified porcelain jars charged with zirconia grinding medium (6.4 × 6.4 mm) in a 0.4 L jar mill (Cole-Parmer, Vernon Hills, IL) rotating at 30 rpm under a N_2 headspace.[34,35] Optimal charging of 45−55% (v/v) was used as per the manufacturer's instructions. A ball-milling experiment showed that complete dissolution is possible after 14−28 days depending on the sample. Studies have shown that ball-milling results in only a minor increase in detectable cleaved lignin structures, and ball-milling in toluene is recommended as it serves to regulate temperature and acts as a radical scavenger.[34,35] After ball-milling, the sample suspended in toluene was centrifuged at 2850 rpm for 15 min. The toluene layer was aspirated and the remaining solvent was removed by evaporation at 50 °C under vacuum.

A ball-milled sample weighing 600 mg was dissolved in 10 mL of dimethyl sulfoxide (DMSO) and 5 mL of *N*-methylimidazole. A clear amber color solution was produced after stirring for at least 4 h. The solution was acetylated in situ by addition of 3 mL of acetic anhydride and stirred for 1.5 h, after which a dark brown solution was formed. The acetylated cell wall solution was precipitated in 2 L of deionized water, stirred overnight, recovered by vacuum filtration (0.2 μm nylon filter), washed with 250 mL of DI water, and then dried under vacuum (50 °C). The yield of acetylated cell wall was about 136% of the initial weight of material, which is typical for sample acetylation.[21] After drying, 90 mg of acetylated cell wall was dissolved in 0.75 mL of DMSO-d_6 (Cambridge Isotope Laboratories, Tewksbury, MA) and then transferred to a 5 mm NMR tube for analysis.

Nuclear Magnetic Resonance (NMR) Spectroscopy. One-bond $^{1}H-^{13}C$ heteronuclear single quantum coherence (HSQC) NMR spectra were obtained at the Bio-NMR facility of the Department of Molecular and Structural Biochemistry, NC State University, using an Avance III 700 MHz spectrometer (Bruker, The Woodlands, TX) equipped with QNP cryoprobe implementing the Bruker's hsqcetgpsisp2.2 pulse sequence program at 30 °C. HSQC is a 2D NMR

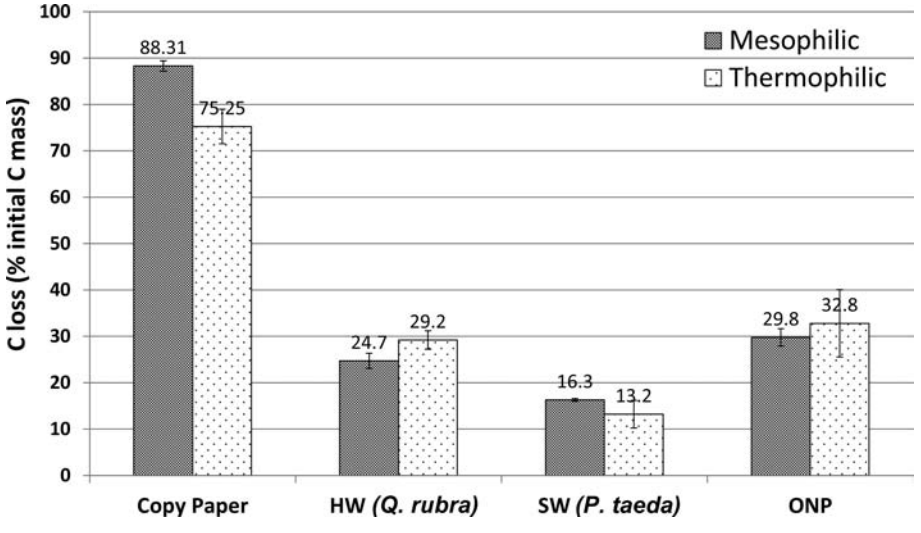

Figure 2. Carbon loss during anaerobic decomposition of different lignocellulosic materials under mesophilic and thermophilic conditions. HW, hardwood; SW, softwood; ONP, old newsprint. Error bar represents ± sd (n = 3).

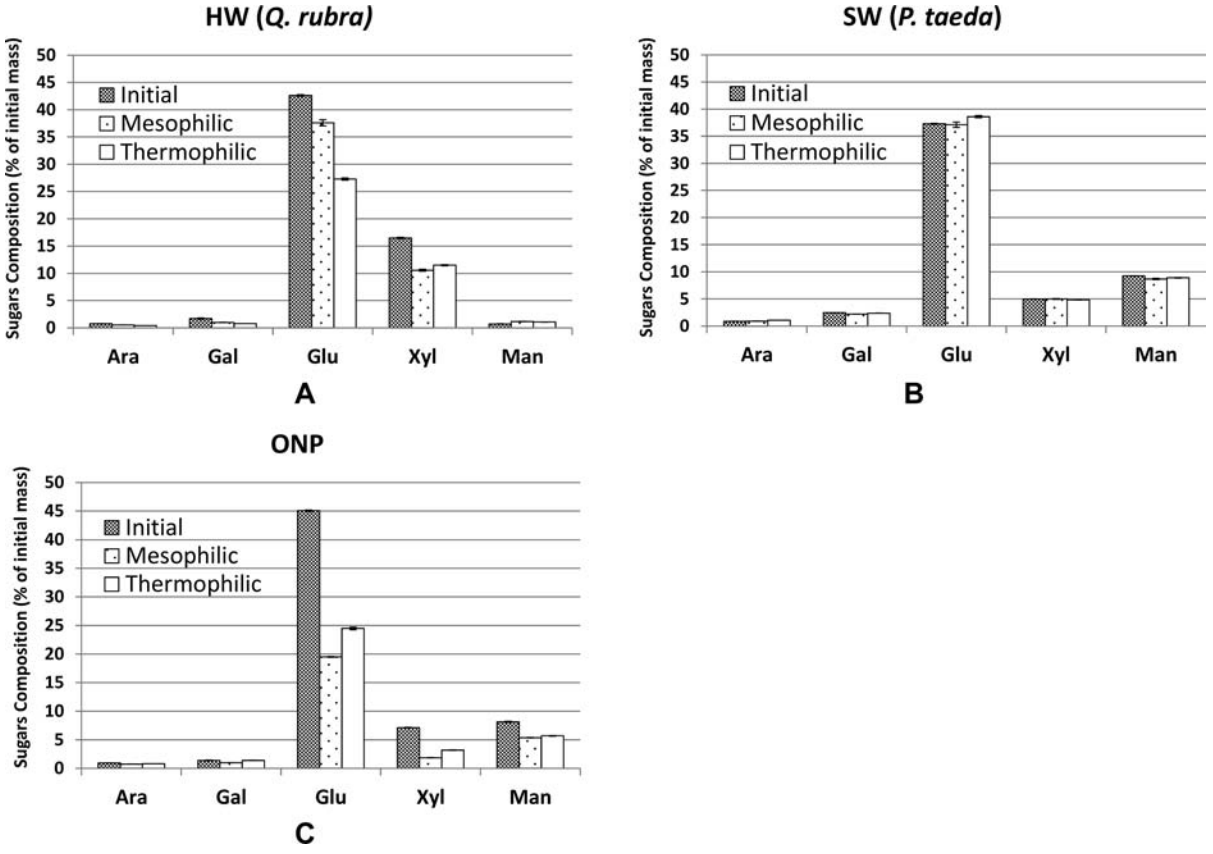

Figure 3. Changes in composition of sugars during decomposition under mesophilic and thermophilic conditions normalized to the initial mass of the sample. Ara, arabinose; Xyl, xylose; Man, mannose; Gal, galactose; Glu, glucose. Error bar represents ± sd (n = 3).

experiment which creates cross peaks that correlate the hydrogen in a molecule with its directly attached carbon.[36] The F_2 acquisition time for these NMR experiments were about 8 h with about 1 h for F_1 acquisition time. The DMSO-d_6 peak (δ_H/δ_C = 2.49 ppm/39.5 ppm) was used for internal calibration reference. Data processing and integration were done using Topspin 3.2. No attempts were made to conduct NMR experiments using nonacetylated samples. Acetylation of the whole cell wall does result in the loss of information on the natural acetates found on mannan and xylan.

NMR Quantitation. Peak assignment was performed using the lignin NMR database[37] and comparison with previously published lignin spectra for different lignin preparations.[33,38−41] Calculations to obtain absolute quantitation of different substructures were done as follows (eq 1) using the methoxyl group content obtained from wet chemical analyses as a reference.[22]

$$C_{\text{linkage}}\left[\frac{\text{mmol}}{\text{g of sample}}\right] = 2D_{\text{linkage}} \times \frac{C_{-\text{OCH}_3}\left[\frac{\text{mmol}}{\text{g of sample}}\right]}{2D_{-\text{OCH}_3}} \quad (1)$$

where C_{linkage} [mmol/(g of sample)] = concentration of a given linkage or substructure; $2D_{\text{linkage}}$ = HSQC volume integral of a given linkage or substructure; $C_{-\text{OCH}_3}$ [mmol/(g of sample)] = concentration of methoxyl group in the sample as determined by wet chemistry; $2D_{-\text{OCH}_3}$ = HSQC volume integral of the methoxyl group. Since the intensity of the HSQC regions are dependent on a coupling constant, comparisons of the different substructures were done on the basis of their Hα−Cα correlations having a similar chemical environment. The resinol volume was divided by 2 as two correlations are involved in each linkage unit. To quantitate the C_9 units of lignin, the volume integral for $H_{2/6}$−$C_{2/6}$ correlations of the HSQC spectra was used for *p*-hydroxyphenyl (H) and syringyl (S) units while H_2−C_2 was used for guaiacyl (G) units. The volume integral of H_2−C_2 correlation of G units was logically doubled because it involves a single correlation.[32] The different lignin substructures were normalized to C_9 units assuming a molecular weight of 220 mg/mmol and 198 mg/mmol for HW and SW, respectively. The molecular weight of ONP was assumed to be equal to that of SW.

RESULTS AND DISCUSSION

Carbon Loss. Variation in carbon loss from anaerobic decomposition of different lignocellulosic materials representative of MSW components was observed (Figure 2). The high carbon losses in the copy paper positive control demonstrate the viability and the suitability of the anaerobic inocula to anaerobically convert substrate to methane. While methane yields were not measured, the gas composition data over the entire incubation period showed that the gas produced was methane and carbon dioxide. The carbon losses observed in HW and ONP were comparable, while the lowest carbon loss was recorded in SW. The carbon losses presented in Figure 2 are higher than previously reported using laboratory-scale decomposition experiments.[42,43] The differences in carbon loss are perhaps a result of the smaller particle size and lower solids to liquid ratio in BMP tests conducted here relative to reactor studies designed to measure methane yields under simulated landfill conditions in which materials were shredded (3 × 4 cm) and had a higher solids to liquid ratio.

The inoculum used in this study was enriched on copy paper which does not contain significant amounts of lignin. This may have promoted changes in the relative abundance of different microbial communities in the culture. However, the carbon losses measured in this study for lignocellulosic substrates are comparable to values reported previously in tests with an inoculum enriched on MSW that would contain lignocellulosic

dx.doi.org/10.1021/jf501653h | J. Agric. Food Chem. 2014, 62, 6362−6374

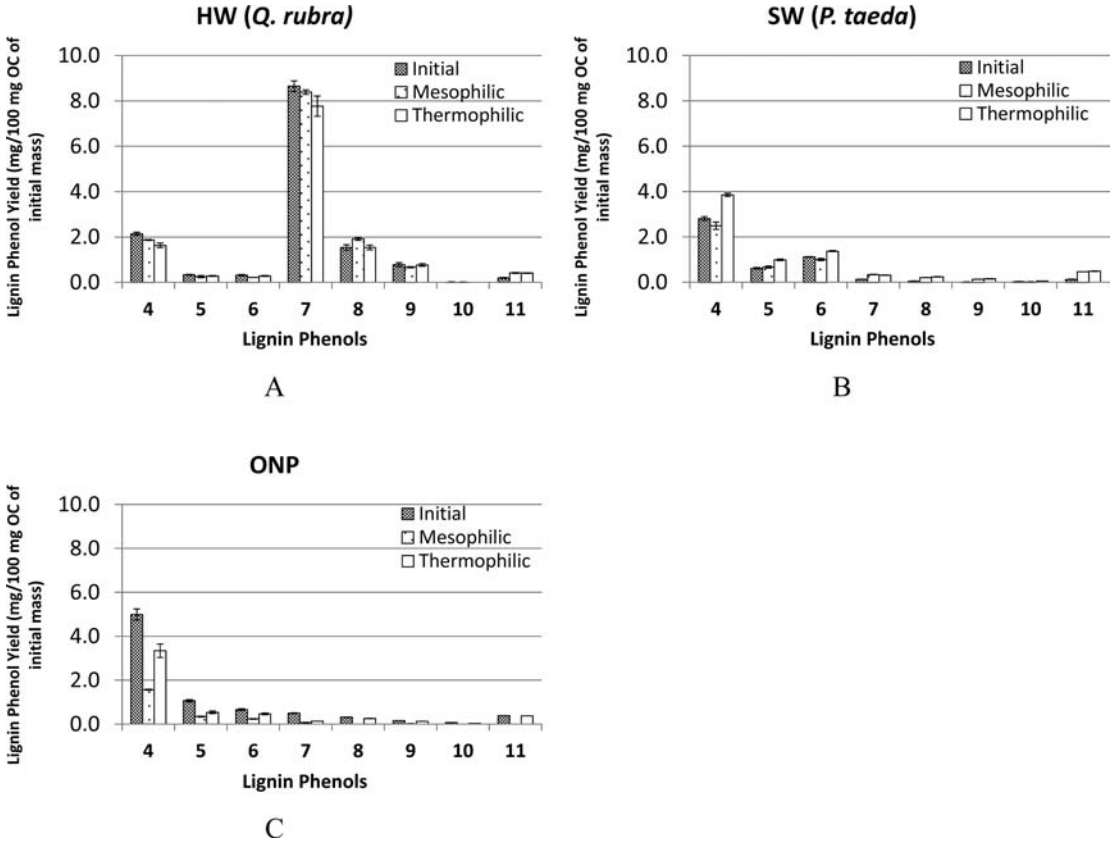

Figure 4. Changes in CuO lignin composition during anaerobic decomposition under mesophilic and thermophilic conditions normalized to the initial mass of the sample. Error bar represents ± sd (n = 3).

substrates.[9,42,43] Thus, the use of a lignin-free inoculum did not influence the extent of decomposition and the measured C conversions. This suggests that all of the readily degradable substrates have been depleted or that the accessibility to the readily degradable substrates is limited by the lignin in which the polysaccharides are encased, putting pressure on microorganisms to utilize more recalcitrant substrates such as lignin.

Structural Carbohydrates. The plant cell wall is composed of the structural carbohydrates cellulose and hemicelluloses, which account for the majority of its dry mass. Cellulose is a homopolymer of glucose linked together by β (1→4) glycosidic linkages. The linear structure of cellulose makes up its crystalline tertiary structure, which is the building block of cellulose microfibril. Hemicelluloses are heteropolymers of different sugar residues, the composition of which varies according to tissue type. Evidence has shown that hemicelluloses link cellulose microfibrils and lignin together, making up the cell wall lignocellulose composite.[44] The plant cell wall's rigidity and chemical reactivity is attributed to these intricate and complex associations between lignin and structural carbohydrates.

The changes in sugar residues after anaerobic decomposition of different lignocellulosic materials could provide insights on the reactivity and the preferential attack of anaerobic microorganisms to the different cell wall carbohydrates (Figure 3). For HW, the major sugar residues are glucose from cellulose and xylose from xylan, with xylan being a major component in angiosperms. About 12% and 36% of the initial glucose and about 36% and 30% of the initial xylose were lost after mesophilic and thermophilic anaerobic decomposition, respectively.

No significant change in sugars was observed in SW (Figure 3). This result is surprising because we observed relatively small but significant C losses in SW for both mesophilic and thermophilic decomposition (Figure 2). The result of the sugars analysis suggests that the methane and carbon dioxide mineralization in softwood did not come from cellulose and hemicelluloses.

In contrast, in ONP, a SW mechanical pulp based on CuO oxidation products (Figure 4), the glucose loss was 57% and 46%, while mannose loss was about 34% and 30% for mesophilic and thermophilic decomposition, respectively. Mannose sugar residue comes from glucomannan, which is a major component of SW hemicelluloses. The data suggests that the conversion of cell wall sugars is highly correlated to bioavailability rather than the differences in the reactivity of individual sugars.

While ONP was derived from SW pulp, its decomposition behavior is significantly different from the SW that was tested. Significant carbon loss from cellulose and hemicelluloses was recorded in ONP. This demonstrates the effect of mechanical pulping as well as the role of lignin on the accessibility/bioavailability of cellulose and hemicelluloses in SW. Mechanical pulping could involve mechanical, thermal, and some chemical processes, resulting in chemical modifications of lignin leading to disruption of the S2 layer and releasing the cellulose fiber. This process is different from Wiley milling used during sample preparation, which is a mechanical process of particle size reduction.

Lignin CuO Oxidation Products. The CuO oxidation products of initial and anaerobically decomposed samples are presented in Figure 4. For HW, the sum of 8 LP (Figure 1), Λ_8

[Λ_8 = LP **4** + LP **5** + LP **6** + LP **7** + LP **8** + LP **9** + LP **10** + LP **11**, mg/100 mg of organic carbon (OC)], after mesophilic and thermophilic decomposition is not significantly different when compared with the initial material (14.0 ± 0.6 mg/100 mg of OC). The Λ_8 is a measure of total releasable CuO lignin monomers normalized to OC and could indicate degradation/repolymerization of lignin during decomposition. The *p*-hydroxy phenols (LP **1**, **2**, and **3** in Figure 1) could have nonlignin sources such as amino acids tyrosine and phenylalanine and therefore were excluded from the sum of LP. Similarly, for HW, the acid (LP **6**) to aldehyde (LP **4**) ratios of vanillyl phenols $(Ad/Al)_V$ of the initial material (0.15) and after mesophilic (0.12) and thermophilic (0.17) decomposition are not significantly different ($p > 0.05$) from each other. The $(Ad/Al)_V$ is a measure of the extent of degradation of lignin. The result suggests that HW lignin was not significantly degraded after anaerobic decomposition.

For SW, the Λ_8 of mesophilic decomposed substrate (5.3 ± 0.3 mg/100 mg of OC) is not significantly different when compared with the initial material (4.9 ± 0.2 mg/100 mg of OC). The Λ_8 increase in thermophilic (7.5 ± 0.2 mg/100 mg of OC) is anomalous, and there is no indication that it is a result of decomposition as indicated by the constant $(Ad/Al)_V$ of 0.4 for SW initial material, after mesophilic and after thermophilic decomposition.

The CuO oxidation products of lignin can also be used as a biomarker to fingerprint the plant tissue source of lignin in an unknown sample.[45] The ratio of S (S = LP **7** + LP **8** + LP **9**) to vanillyl (V) (V = LP **4** + LP **5** + LP **6**) (S/V) has been used to discriminate between angiosperm (HW, leaves, and grasses) and gymnosperm (SW and needles) tissues while the ratio of cinnamyl (C) (C = LP **10** + LP **11**) to V phenols (C/V) has been used to discriminate between woody (HW and SW) and nonwoody (leaves, grasses, and needles) tissues.[45] The low C/V and low S/V ratios indicate that the source of lignin in ONP is softwood.

While the lignin CuO oxidation products of ONP are similar to those of SW, their decomposition behaviors are different. Significant loss of VAL phenols was recorded in ONP for both mesophilic and thermophilic decomposition. The $(Ad/Al)_V$ of fresh ONP (0.13) is not significantly different from those of materials decomposed under mesophilic (0.15) and thermophilic (0.14) conditions ($p > 0.05$). This indicates that the lignin polymer has not been significantly depolymerized during decomposition. The loss of VAL without a corresponding increase in $(Ad/Al)_V$ is an indication that no significant lignin cleavage occurred during anaerobic decomposition of ONP. This result suggests that reaction of VAL is limited to side chain oxidation without destruction of the aromatic structure.

Lignin Methoxyl Group. Losses in lignin methoxyl group were observed after anaerobic decomposition (Figure 5). The C_9 normalized methoxyl group contents of initial materials were 1.74, 1.00, and 0.54 mmol $-OCH_3$/mmol of C_9 unit for HW, SW, and ONP, respectively. As SW is dominated by G units, with minute amounts of S units,[44,46] it contains one methoxyl group per C_9 unit. Similarly, since HW is a combination of both S (that contains two methoxyl groups per C_9 unit) and G units, the methoxyl group content per C_9 unit is between one and two. The methoxyl group content of ONP confirms the SW character of this material having one methoxyl group per C_9 unit.

After anaerobic decomposition, the loss of methoxyl group was 23% and 13% for HW, and 35% and 20% for ONP, for mesophilic and thermophilic decomposition, respectively. The loss in the methoxyl group content of SW for both mesophilic and thermophilic decomposition was not statistically significant ($p > 0.05$). The loss of methoxyl group content in ONP is statistically similar between mesophilic and thermophilic conditions. In contrast, the methoxyl group loss in HW was significantly greater under mesophilic conditions ($p < 0.05$).

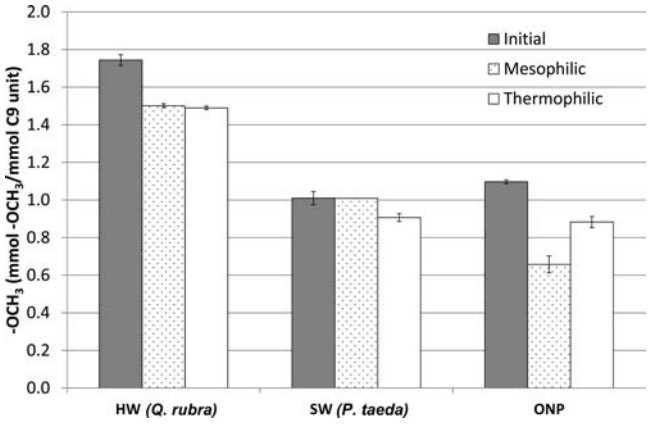

Figure 5. Changes in lignin methoxyl group composition during decomposition under mesophilic and thermophilic conditions normalized to the initial mass of the sample. Error bar represents ± sd ($n = 3$).

Evidence of the demethoxylation of lignin-derived molecules under anaerobic conditions has been reported previously where ^{14}C-labeled aromatic $-OCH_3$ was metabolized to CO_2 and acetates.[13] The results of this study support the notion that one of the first steps in the metabolism of aromatic molecules is the removal of aromatic substituents such as methoxyl groups,[14,15] which in turn can be metabolized by acetogens.[13] Perhaps because of the complexity of SW lignin polymer, these initial steps in SW lignin decomposition are more difficult compared to other lignocellulosic substrates.

Klason and Acid Soluble Lignin. The Klason and acid-soluble lignin (ASL) contents of initial and anaerobically decomposed samples are presented in Figure 6. While Klason lignin is operationally defined as the volatile fraction of the acid-insoluble material remaining after acid hydrolysis, it is widely used to measure the total lignin of a sample.[19,44]

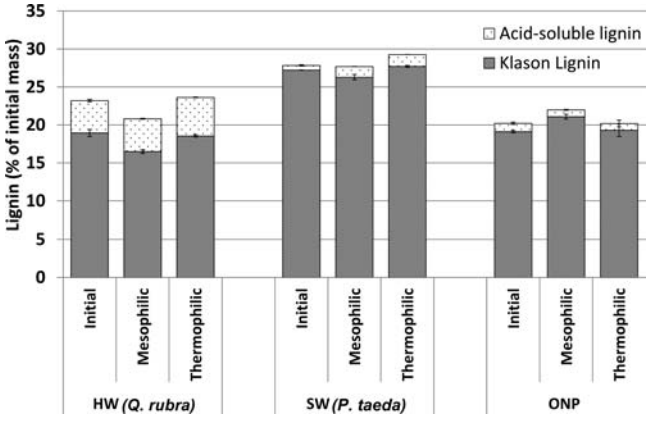

Figure 6. Changes in Klason and acid-soluble lignin composition during decomposition under mesophilic and thermophilic conditions normalized to the initial mass of the sample. Error bar represents ± sd ($n = 3$).

dx.doi.org/10.1021/jf501653h | J. Agric. Food Chem. 2014, 62, 6362−6374

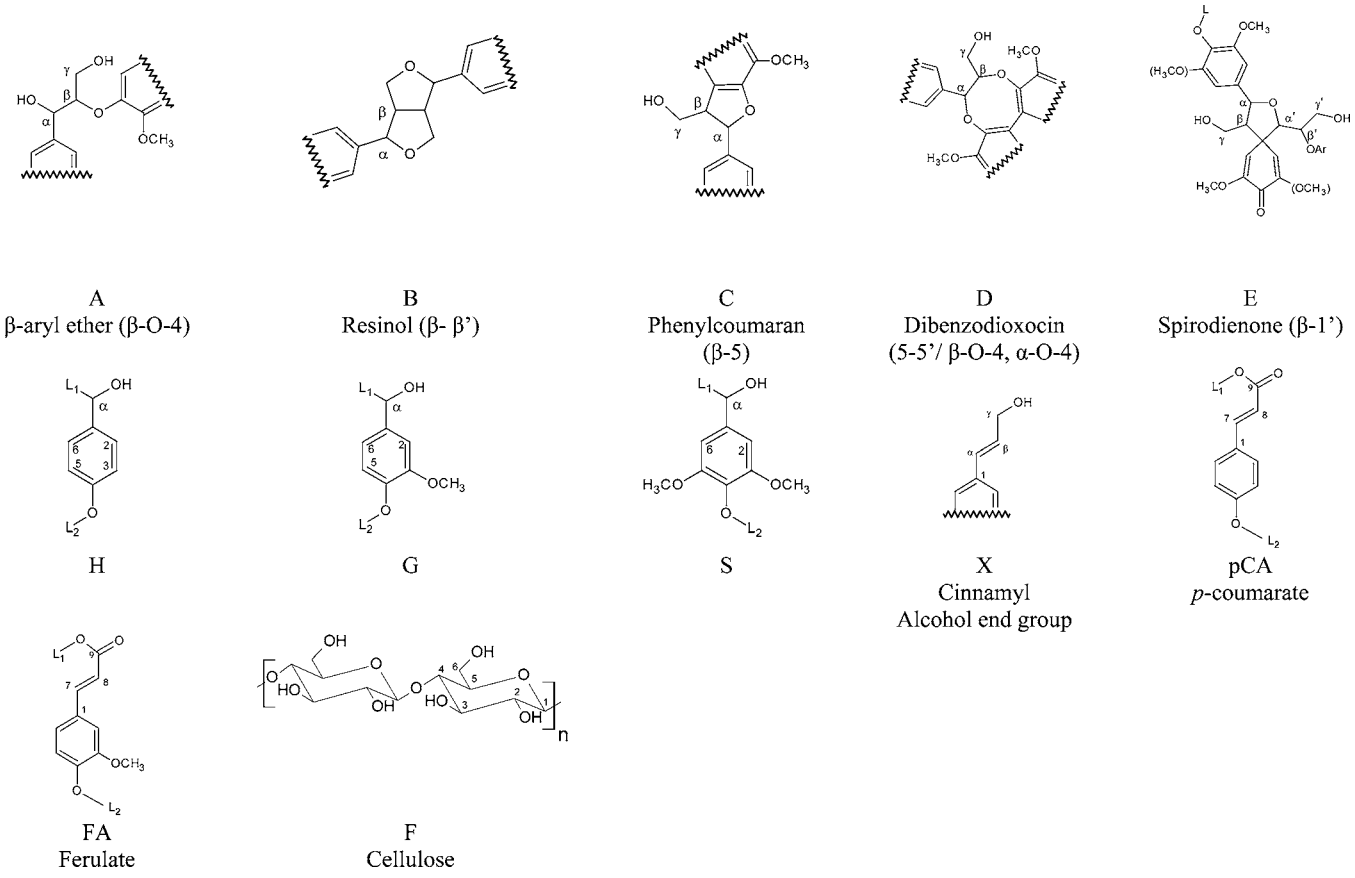

Figure 7. Linkages and substructures in lignin and lignocellulose. L, lignin polymer.

The loss of HW Klason lignin under mesophilic conditions (13%) was significant ($p < 0.05$) while no significant difference was observed under thermophilic conditions. In contrast, losses of HW ASL were significant only under thermophilic conditions. In some tissues such as in nonwoody angiosperms, the amount of ASL can be significant. Moreover, the amount of ASL could also be an indicator of the extent of decomposition as some lignin can be broken down to lower molecular weight fractions and then to soluble fractions rendering them more amenable to anaerobic decomposition. There was no significant change in either Klason lignin or ASL in ONP.

There were no significant losses in either Klason lignin or ASL for SW. As noted above, anaerobic decomposition of SW resulted in a small but significant carbon loss. It is interesting to note, however, that, based on chemical analyses, the carbon loss recorded in SW was not due to the cellulose, hemicelluloses, or lignin but from other components. To evaluate whether this observation is plausible, the amount of carbon that can be attributed to these major lignocellulosic components was estimated assuming empirical formulas for cellulose, hemicelluloses, and lignin as $(C_6H_{10}O_5)_n$, $(C_5H_8O_4)_n$, and $C_{(9)}H_{(7.92)}O_{(2.40)}(OCH_3)_{(0.92)}$, respectively. Based on the empirical formulas and their corresponding compositions, about 85% of the carbon in SW can be attributed to cellulose, hemicelluloses, and lignin. Thus, the uncharacterized cell components of SW (e.g., proteins, tannins, extractives, etc.), amounting to about 15% of the total carbon (estimated by difference), in theory could explain the observed carbon loss. This possibility is supported by the result of extractives in the softwood sample which was determined to be 17 ± 0.73% of the initial mass.

It is well-documented that SW lignin is dominated by G units. This lignin unit is more complex because of more branching as a result of the availability of the 5-position in lignin phenolic units to cross-link, making the SW lignin polymer more difficult to depolymerize.[19,44] Moreover, the complex structure of SW lignin hinders microbial enzyme access to structural carbohydrates, resulting in minor mineralization of cellulose, hemicelluloses, and lignin.

Lignin Substructures. Decomposition of lignocellulose components may not necessarily result in mass loss due to mineralization to CH_4 and CO_2. The ability of lignin to depolymerize and repolymerize makes the study of the transformation of lignin complicated.[47] In this section, evidence of lignin transformations was examined using HSQC NMR spectroscopy. The different lignin and carbohydrates substructures are illustrated in Figure 7. Figures 8 to 10 show the aliphatic and the aromatic regions of the HSQC spectra of different test materials. The spectra for initial and decomposed materials are quite similar, and the only difference was the intensities of different contours. As such, only the spectra of the initial material are presented. The difference between the initial and decomposed material is reflected in the volume integrations of different contours corresponding to different lignin substructures as summarized in Table 1. The HSQC spectra were color referenced for easy comparison.

Quantitative comparisons of the absolute amount of different substructures normalized to C_9 unit are presented in Table 1 for different materials (initial material, and after mesophilic and thermophilic decomposition). The relative abundance of different lignin substructures has been reported for different types of tissues. The majority of inter C_9 unit linkages in lignin

dx.doi.org/10.1021/jf501653h | J. Agric. Food Chem. 2014, 62, 6362−6374

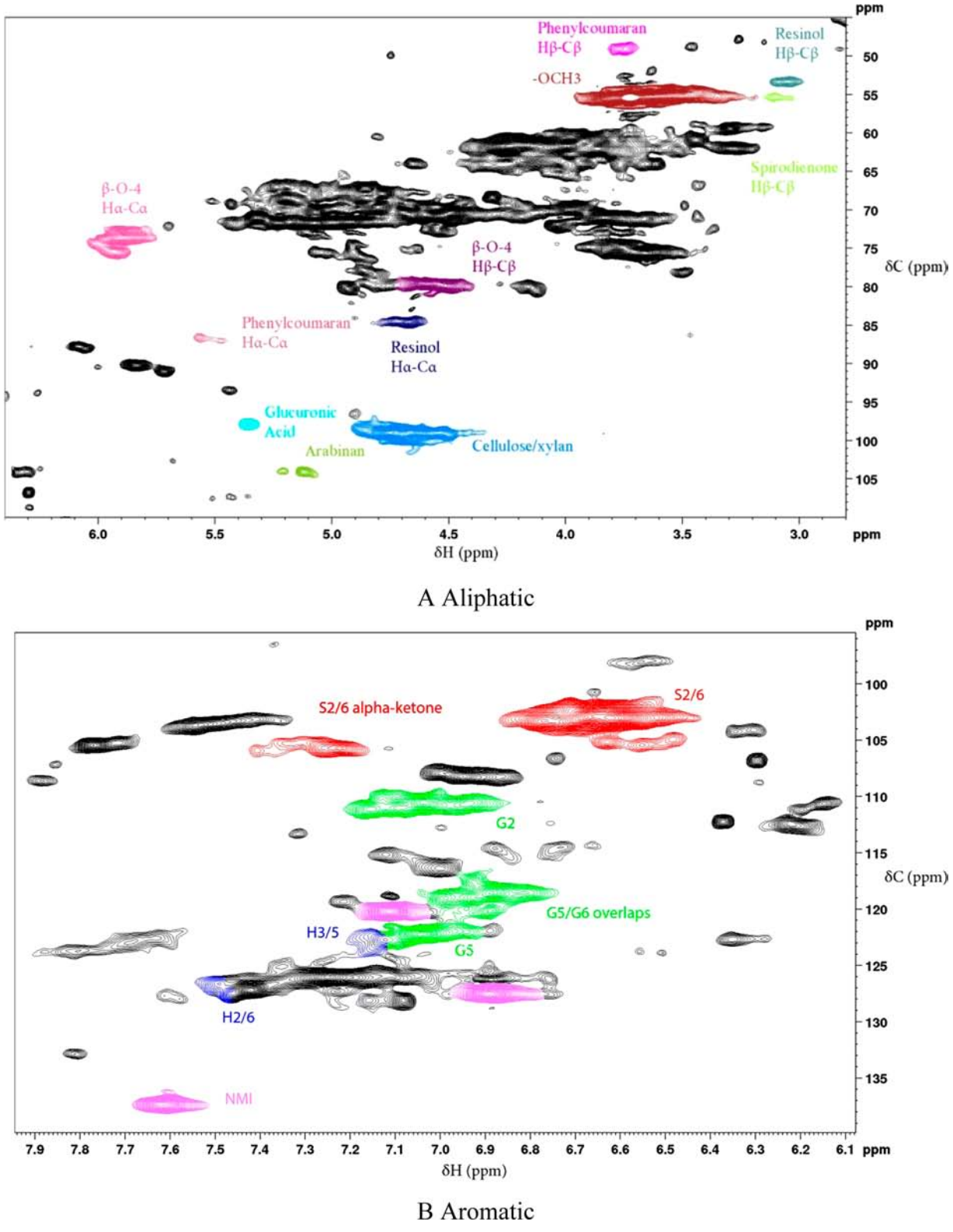

Figure 8. HSQC spectra of HW (*Quercus rubra*): (A) aliphatic region; (B) aromatic region.

are *β-O*-4, followed by significantly smaller and varying amounts of resinol, phenylcoumaran, spirodienone, and dibenzodioxocin structures (Figure 7). For example, in white birch (*Betula pendula* Roth) MWL, the relative abundance of lignin inter C_9 unit linkages is about 69% *β-O*-4, 17% resinol, 3% phenylcoumaran, and 4% spirodienone estimated from 2D HSQC spectra.[48]

The HSQC spectrum of the HW aliphatic region (Figure 8A) illustrates the well-resolved peak corresponding to the H*α*−C*α* (δ_H/δ_C = 5.91 ppm/74.3 ppm) correlation in the *β-O*-4 linkage with distinct separation between the *threo* and *erythro* diastereomers. Figure 8A also shows the intense methoxyl group peak (δ_H/δ_C = 3.60 ppm/55.3 ppm). Three of the major inter C_9 unit linkages in lignin were quantified as presented in

dx.doi.org/10.1021/jf501653h | J. Agric. Food Chem. 2014, 62, 6362−6374

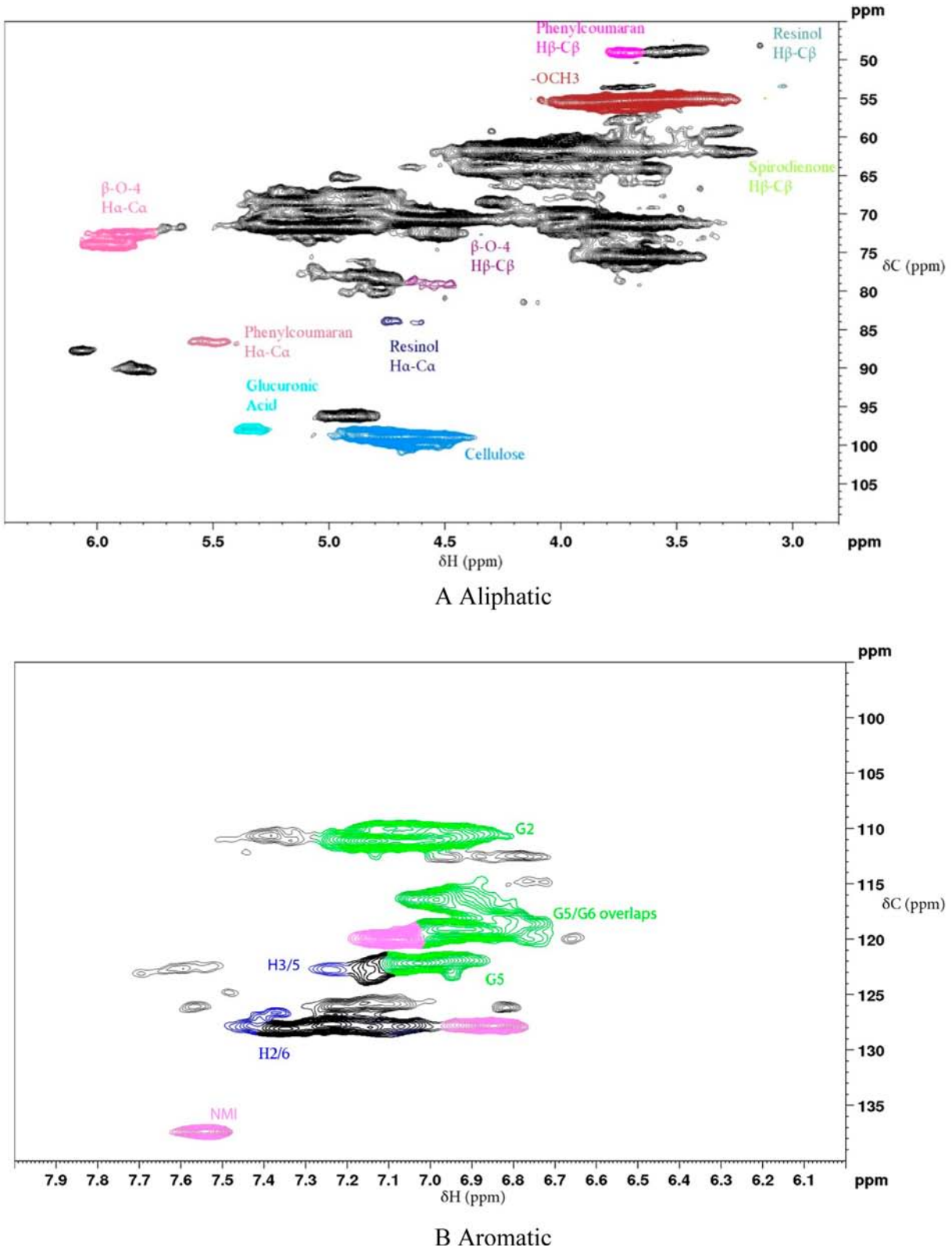

Figure 9. HSQC spectra of SW (*Pinus taeda*): (A) aliphatic region; (B) aromatic region.

Table 1. While other lignin substructures have been identified, their quantities were not calculated because the relative amounts are small and are subject to high uncertainty. In addition to lignin substructures, Figures 8−10 show the different structures found in cellulose and hemicelluloses. The black regions in the aliphatic regions of HSQC spectra are unidentified overlapping peaks primarily due to carbohydrates.

In the aromatic regions (Figure 8B), the intense $H_{2/6}$−$C_{2/6}$ (δ_H/δ_C = 6.65 ppm/102.7 ppm) contour region is due to S units, which are the major C_9 unit in angiosperms such as HW. In a majority of the HSQC spectra, *N*-methylimidazole

dx.doi.org/10.1021/jf501653h | *J. Agric. Food Chem.* 2014, 62, 6362−6374

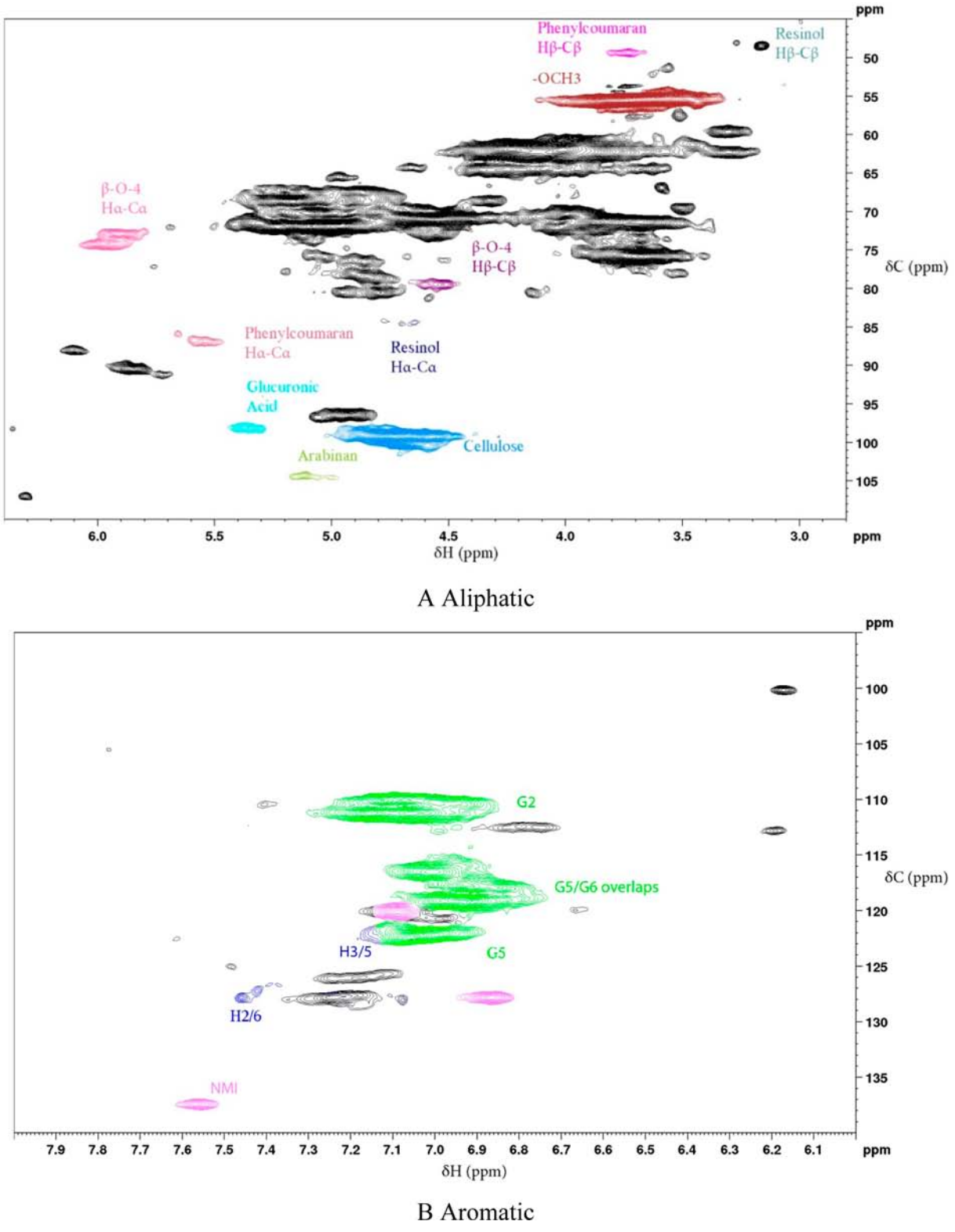

Figure 10. HSQC spectra of ONP: (A) aliphatic region; (B) aromatic region.

contamination due to incomplete washing was detected. This did not affect the NMR quantification as *N*-methylimidazole peaks did not overlap with regions that were used for quantification. The H_2-C_2 correlation in G units is also well-resolved in the HW aromatic region of the HSQC spectra. The low proportion of H is a characteristic of woody tissues.

As expected, the major lignin inter C_9 unit linkage is *β-O*-4. A slight reduction in the amount of this linkage in HW for mesophilic and thermophilic decomposition respectively was observed (Table 1). Anaerobic decomposition resulted in a decrease in the amount of *β-O*-4 linkage brought about by *α*-oxidation. For both mesophilic and thermophilic anaerobic

dx.doi.org/10.1021/jf501653h | J. Agric. Food Chem. 2014, 62, 6362−6374

Table 1. Structural Characteristics of Initial and Anaerobically Decomposed Lignocellulose Calculated from Volume Integration of the $^{1}H-^{13}C$ Correlation Signals in the HSQC Spectrum Normalized to Lignin C_9 Unit

		linkage amount (mmol/mmol of C_9 unit)								
		HW (*Q. rubra*)			SW (*P. taeda*)			ONP		
linkage/lignin substructures	H−C correlation	I[a]	M[a]	T[a]	I[a]	M[a]	T[a]	I[a]	M[a]	T[a]
β-O-4 structures (A)	$H_\alpha-C_\alpha$	0.136	0.124	0.112	0.080	ND	ND	0.085	0.059	0.077
resinol (B)	$H_\alpha-C_\alpha$	0.015	0.012	0.012	0.003	ND	ND	0.006	0.005	0.007
phenylcoumaran (C)	$H_\alpha-C_\alpha$	0.010	0.004	0.006	0.014	ND	ND	0.018	0.014	0.019
aromatic methoxyl group[b]	H−C	1.744	1.480	1.490	1.010	1.008	0.906	1.097	0.658	0.883
H	$H_{2/6}-C_{2/6}$	0.002	0.001	0.001	0.007	ND	ND	0.002	0.002	0.001
G	H_2-C_2	0.167	0.103	0.099	0.348	ND	ND	0.311	0.195	0.133
S	$H_{2/6}-C_{2/6}$	0.249	0.236	0.220	0.007	ND	ND	0.002	0.002	0.001
S/G ratio		1.5	2.3	2.4	0.01	ND	ND	0.04	0.02	0.02

[a]I = initial material; M = mesophilic decomposition; T = thermophilic decomposition; ND = no data was acquired for SW degraded samples. [b]Determined by wet chemistry.

decomposition of HW, α-carbonyl ($S_{2/6}$ α-ketone) slightly increased (data not shown).

The NMR spectra of decomposed SW were not acquired because there is no evidence of lignin degradation observed using degradative methods as described previously. The spectrum of the initial material is presented here for completeness (Figure 9).

The aliphatic region of the ONP HSQC spectrum (Figure 10A) is quite similar to that of SW with the well-resolved H_2-C_2 correlation of the G aromatic peak (δ_H/δ_C = 7.01 ppm/110.8 ppm). The majority of the lignin inter C_9 unit linkages are *β-O*-4, which was observed to decrease for mesophilic and thermophilic decomposition (Table 1). Decrease in resinol and phenylcoumaran content was observed in mesophilic anaerobic decomposition of ONP.

In the aromatic region (Figure 10B), the absence of the $S_{2/6}$ peak confirms that the ONP sample was made from SW pulp. The low proportion of the H group is a characteristic of woody tissues as observed in HW and SW. It is interesting to note that, similar to HW, the amount of G decreased when compared with the initial material (Table 1).

The HSQC spectra showed only slight reductions in *β-O*-4 linkage, suggesting no significant lignin depolymerization for any substrate. The loss of H_2-C_2 of G units in HW and ONP is surprising as it is well-documented that the S units are more reactive than G units. This could be a subject of further research. Nonetheless, the Klason and acid soluble lignin data as well as CuO lignin data indicate no substantial depolymerization of lignin. It is possible that the loss of the G_2 region in HW and ONP is primarily a result of side chain reactions with no destruction of the aromatic structure. The study suggests that the presence of lignin in its natural form will result in carbon storage from plant biomass in a strictly anaerobic environment such as the deep layer of soil and marine sediments. In addition, the varying reactivity of different plant tissues has implications on the estimates of life cycle emissions of forest products where wood and similar tissues are treated as having the same decomposition rates under current greenhouse gas reporting protocols.[49]

■ ASSOCIATED CONTENT

Supporting Information

Details of the CuO oxidation, a summary of the chemical characteristics of the initial materials tested, and cellulose and hemicellulose loss during anaerobic decomposition of different lignocellulosic materials. This material is available free of charge via the Internet at http://pubs.acs.org.

■ AUTHOR INFORMATION

Corresponding Author

*Phone: (919)513-4421. Fax: (919)515-7908. E-mail: fbdelacr@ncsu.edu.

Funding

Funding for this research was provided by the U.S. National Science Foundation and Waste Management Inc.

Notes

The authors declare no competing financial interest.

■ ACKNOWLEDGMENTS

The authors would like to thank David Black, Michael Mondou, and Yinglong Guan for their help in wet analytical chemistry; Dr. Ilona Peszlen of the Department of Forest Biomaterials, NCSU for providing the wood samples; and the four anonymous reviewers for their valuable suggestions for the improvement of this manuscript.

■ REFERENCES

(1) Hedges, J. I. Global biogeochemical cycles: progress and problems. *Mar. Chem.* **1992**, *39*, 67−93.

(2) Colberg, P. Anaerobic microbial degradation of cellulose, lignin, oligolignols and monoaromatic lignin derivatives. In *Biology of Anaerobic Microorganisms*; Zehnder, A. J. B., Ed.; Wiley-Interscience: New York, 1988; Vol. *28*, pp 886−889.

(3) *U.S. Environmental Protection Agency Municipal Solid Waste Generation, Recycling, and Disposal in the United States: Facts and Figures for 2011*. 2013, EPA530-R-13-001, available at URL http://www.epa.gov/osw/nonhaz/municipal/pubs/MSWcharacterization_fnl_060713_2_rpt.pdf (accessed May 27, 2014).

(4) Bogner, J.; Spokas, K.; Burton, E.; Sweeney, R.; Corona, V. Landfills as atmospheric methane sources and sinks. *Chemosphere* **1995**, *31*, 4119−4130.

(5) Barlaz, M. A. Carbon storage during biodegradation of municipal solid waste components in laboratory-scale landfills. *Global Biogeochem. Cycles* **1998**, *12*, 373−380.

(6) De la Cruz, F. B.; Chanton, J. P.; Barlaz, M. A. Measurement of carbon storage in landfills from the biogenic carbon content of excavated waste samples. *Waste Manage.* **2013**, *33*, 2001−2005.

(7) Benner, R.; Maccubbin, A. E.; Hodson, R. E. Anaerobic biodegradation of the lignin and polysaccharide components of lignocellulose and synthetic lignin by sediment microflora. *Appl. Environ. Microbiol.* **1984**, *47*, 998−1004.

(8) Benner, R.; Hodson, R. E. Thermophilic anaerobic biodegradation of [C-14] lignin, [C-14] cellulose, and [C-14] lignocellulose preparations. *Appl. Environ. Microbiol.* **1985**, *50*, 971−976.
(9) Wang, Y. S.; Byrd, C. S.; Barlaz, M. Anaerobic biodegradability of cellulose and hemicellulose in excavated refuse samples using a biochemical methane potential assay. *J. Ind. Microbiol.* **1994**, *13*, 147−153.
(10) Zeikus, J.; Wellstein, A.; Kirk, T. Molecular basis for the biodegradative recalcitrance of lignin in anaerobic environments. *FEMS Microbiol. Lett.* **1982**, *15*, 193−197.
(11) Colberg, P.; Young, L. Anaerobic degradation of soluble fractions of [C-14-lignin] lignocellulose. *Appl. Environ. Microbiol.* **1985**, *49*, 345.
(12) Stinson, J. A.; Ham, R. K. Effect of lignin on the anaerobic decomposition of cellulose as determined through the use of a biochemical methane potential method. *Environ. Sci. Technol.* **1995**, *29*, 2305−2310.
(13) Young, L. Y.; Frazer, A. C. The fate of lignin and lignin-derived compounds in anaerobic environments. *Geomicrobiol. J.* **1987**, *5*, 261.
(14) Heider, J.; Fuchs, G. Anaerobic metabolism of aromatic compounds. *Eur. J. Biochem.* **1997**, *243*, 577−596.
(15) Harwood, C. S.; Burchhardt, G.; Herrmann, H.; Fuchs, G. Anaerobic metabolism of aromatic compounds via the benzoyl-CoA pathway. *FEMS Microbiol. Rev.* **1998**, *22*, 439−458.
(16) Crawford, R. L. *Lignin biodegradation and transformation*; Wiley: New York, 1981; pp 154.
(17) Lai, Y. Z.; Sarkanen, K. V. Isolation and structural studies. In *Lignins: occurrence, formation, structure and reactions*, 1st ed.; Sarkanen, K. V., Ludwig, C. H., Eds.; Wiley-Interscience: New York, 1971; Vol. *1*, pp 165−240.
(18) Santos, R. B.; Capanema, E. A.; Balakshin, M. Y.; Chang, Hou-Min; Jameel, H. Effect of hardwoods characteristics on Kraft pulping process: emphasis on lignin structure. *BioResources* **2011**, *6*, 3623−3637.
(19) Lin, S. Y.; Dence, C. W. *Methods in lignin chemistry*; Springer-Verlag: Berlin, New York, 1992; pp 578.
(20) Benner, R.; Mccubbin, A. E.; Hodson, R. E. Preparation, characterization, and microbial-degradation of specifically radiolabeled [C14] lignocelluloses from marine and fresh-water macrophytes. *Appl. Environ. Microbiol.* **1984**, *47*, 381.
(21) Lu, F.; Ralph, J. Non-degradative dissolution and acetylation of ball-milled plant cell walls: high-resolution solution-state NMR. *Plant J.* **2003**, *35*, 535−544.
(22) Yelle, D. J.; Ralph, J.; Lu, F.; Hammel, K. E. Evidence for cleavage of lignin by a brown rot *Basidiomycete*. *Environ. Microbiol.* **2008**, *10*, 1844−1849.
(23) Chundawat, S. P. S.; Donohoe, B. S.; da Costa Sousa, L.; Elder, T.; Agarwal, U. P.; Lu, F.; Ralph, J.; Himmel, M. E.; Balan, V.; Dale, B. E. Multi-scale visualization and characterization of lignocellulosic plant cell wall deconstruction during thermochemical pretreatment. *Energy Environ. Sci.* 973−984.
(24) Glasser, W. G., Sarkanen, S., Eds. *Lignin: properties and materials*; ACS Symposium Series; American Chemical Society: Washington, DC, 1989; Vol. *397*, 545 pp.
(25) Lobbes, J.; Fitznar, H.; Kattner, G. High-performance liquid chromatography of lignin-derived phenols in environmental samples with diode array detection. *Anal. Chem.* **1999**, *71*, 3008−3012.
(26) Steinberg, S.; Venkatesan, M. I.; Kaplan, I. R. Analysis of the products of the oxidation of lignin by CuO in biological and geological samples by reversed-phase high-performance liquid chromatography. *J. Chromatogr. A* **1984**, *298*, 427−434.
(27) Petterson, R. C.; Schwandt, V. H. Wood sugar analysis by anion chromatography. *J. Wood Chem. Technol.* **1991**, *11*, 495−501.
(28) Davis, M. W. A Rapid modified method for compositional carbohydrate analysis of lignocellulosics by high pH anion-exchange chromatography with pulsed amperometric detection (HPAEC/PAD). *J. Wood Chem. Technol.* **1998**, *18*, 235−252.
(29) Maekawa, E.; Ichizawa, T.; Koshijima, T. An evaluation of the acid-soluble lignin determination in analyses of lignin by the sulfuric acid method. *J. Wood Chem. Technol.* **1989**, *9*, 549−567.
(30) Ryba, S. A.; Burgess, R. M. Effects of sample preparation on the measurement of organic carbon, hydrogen, nitrogen, sulfur, and oxygen concentrations in marine sediments. *Chemosphere* **2002**, *48*, 139−147.
(31) Li, H.; Chai, X.; Liu, M.; Deng, Y. Novel method for the determination of the methoxyl content in lignin by headspace gas chromatography. *J. Agric. Food Chem.* **2012**, *60*, 5307−5310.
(32) Mansfield, S. D.; Kim, H.; Lu, F.; Ralph, J. Whole plant cell wall characterization using solution-state 2D NMR. *Nat. Protoc.* **2012**, *7*, 1579−1589.
(33) Yelle, D. J.; Ralph, J.; Frihart, C. R. Characterization of nonderivatized plant cell walls using high-resolution solution-state NMR spectroscopy. *Magn. Reson. Chem.* **2008**, *46*, 508−517.
(34) Ikeda, T.; Holtman, K.; Kadla, J. F.; Chang, H.; Jameel, H. Studies on the effect of ball milling on lignin structure using a modified DFRC method. *J. Agric. Food Chem.* **2002**, *50*, 129−135.
(35) Holtman, K. M.; Chang, H.; Jameel, H.; Kadla, J. F. Quantitative ^{13}C NMR characterization of milled wood lignins isolated by different milling techniques. *J. Wood Chem. Technol.* **2006**, *26*, 21−34.
(36) Claridge, T. D. *High-resolution NMR Techniques in Organic Chemistry*; Elsevier Ltd.: Amsterdam, The Netherlands, 2009; Vol. *27*, 383 pp.
(37) Ralph, S. A.; Ralph, J.; Landucci, L. L. NMR Database of Lignin and Cell Wall Model Compounds. Available at URL http://ars.usda.gov/Services/docs.htm?docid=10491. 2004 (accessed April 1, 2014).
(38) Ralph, J.; Marita, J. M.; Ralph, S. A.; Hatfield, R. D.; Lu, F.; Ede, R. M.; Peng, J.; Quideau, S.; Helm, R. F.; Grabber, J. H.; Kim, H.; Jimenez- Monteon, G.; Zhang, Y.; Jung, H. G.; Landucci, L. L.; MacKay, J. J.; Sederoff, R. R.; Chapple, B.; Clint, A. M. Solution-State NMR of Lignins. In *Advances in Lignocellulosics characterization*; Argyropoulos, D. S., Williams, P. A., Eds.; TAPPI Press: Atlanta, GA, 1999; pp 55−108.
(39) Ralph, J.; Lundquist, K.; Brunow, G.; Lu, F.; Kim, H.; Schatz, P.; Marita, J.; Hatfield, R.; Ralph, S.; Christensen, J.; Boerjan, W. Lignins: Natural polymers from oxidative coupling of 4-hydroxyphenyl-propanoids. *Phytochem. Rev.* **2004**, *3*, 29−60.
(40) Ibarra, D.; Chávez, M. I.; Rencoret, J.; del Río, J. C.; Gutiérrez, A.; Romero, J.; Camarero, S.; Martínez, M. J.; Jiménez-Barbero, J.; Martínez, Á. T. Structural modification of eucalypt pulp lignin in a totally chlorine-free bleaching sequence including a laccase-mediator stage. *Holzforschung* **2007**, *61*, 634.
(41) Rencoret, J.; Marques, G.; Gutiérrez, A.; Nieto, L.; Santos, I. J.; Jiménez-Barbero, J.; Martínez, Á. T.; del Río, J. C. HSQC-NMR analysis of lignin in woody (*Eucalyptus globulus* and *Picea abies*) and non-woody (*Agave sisalana*) ball-milled plant materials at the gel state. *Holzforschung* **2009**, *63*, 691−698.
(42) Wang, X.; Padgett, J. M.; De la Cruz, F. B.; Barlaz, M. A. Wood biodegradation in laboratory-scale landfills. *Environ. Sci. Technol.* **2011**, *45*, 6864−6871.
(43) Eleazer, W. E.; Odle, W. S.; Wang, Y. S.; Barlaz, M. A. Biodegradability of municipal solid waste components in laboratory-scale landfills. *Environ. Sci. Technol.* **1997**, *31*, 911−917.
(44) Sarkanen, K. V.; Ludwig, C. H. *Lignins: occurrence, formation, structure and reactions*; Wiley-Interscience: New York, 1971; 916 pp.
(45) Hedges, J. I.; Mann, D. C. The characterization of plant tissues by their lignin oxidation products. *Geochim. Cosmochim. Acta* **1979**, *43*, 1803−1807.
(46) Obst, J. R.; Landucci, L. L. The syringyl content of softwood lignin. *J. Wood Chem. Technol.* **1986**, *6*, 311−327.
(47) Li, J.; Henriksson, G.; Gellerstedt, G. Lignin depolymerization/repolymerization and its critical role for delignification of aspen wood by steam explosion. *Bioresour. Technol.* **2007**, *98*, 3061−3068.
(48) Rencoret, J.; del Rio, J. C.; Gutierrez, A.; Martinez, A. T.; Li, S.; Parkas, J.; Lundquist, K. Origin of the acetylated structures present in white birch (*Betula pendula* Roth) milled wood lignin. *Wood Sci. Technol.* **2012**, *46*, 459−471.

(49) IPCC Intergovernmental Panel on Climate Change: 2006 IPCC Guidelines for National Greenhouse Gas Inventories: Reference Manual (Volume 3). IPCC National Greenhouse Gas Inventory Program. 2006.

Table 1. Transesterification of Soybean Oil with Different Alcohols in *n*-Heptane Using Different Naturally Immobilized *Carica papaya* Lipases

		conversion[a] (%)									
		pCPL-GX[b]					pCPL-GD[c]				
alcohol	no. of steps	4 h	8 h	12 h	16 h	24 h	4 h	8 h	12 h	16 h	24 h
methanol	one[d]	0.8	2.2	3.3	4.6	6.4	1.7	2.1	5	5.8	10.8
	three	19.9	22.7	24.2	24.8	25.2	28.7	29.6	30.1	32	36.5
ethanol	one	25.7	32	35.3	35.8	35.9	23.8	28.8	33.5	33.7	36.6
	three	27.7	28.3	30.1	31.1	32.3	30.7	32.8	34.9	35.2	36.9
n-propanol	one	33.5	38	39.4	42.6	43.5	31.1	41.2	45.1	46.4	50.4
	three	35.6	36.4	37.2	37.7	38.5	41.5	42.8	43.3	49.7	52.1
isopropanol	one	10.6	14.1	20.7	22.3	26.6	9.2	13.7	19.3	22.5	30.1
	three	17.6	20.1	24.1	26.8	30.9	12.8	14.6	19.1	23	31.6
n-butanol	one	38.7	41	45.7	46.4	47.3	44.4	54.5	54.8	55.3	55.8
	three	40.3	42.9	43.2	45.2	46.8	43.5	49.8	50.5	53.7	54.6
isobutanol	one	39.8	40.5	41.2	42.1	42.7	46.7	50.4	54.1	55.6	56.4
	three	35.8	37.8	41.3	42	43.3	44.8	54.7	56.8	57.3	57.6
n-pentanol	one	39.8	43.3	46.2	49.1	49.6	46.5	56.7	57.1	57.6	58.4
	three	42.8	43.6	45.7	48.8	49.3	44.3	51.3	54.8	55.6	57
isopentanol	one	42.1	43.4	45.9	48.1	49.3	46.8	53.5	54.8	55.9	56.8
	three	41.2	44.3	45.2	48.4	49.5	44.5	54.1	54.4	55.2	56.1

[a]Reaction conditions: 4 mL of reaction mixture containing 0.4 mmol of soybean oil and 1.6 mmol of different alcohols, *n*-heptane used as the solvent, 50 °C, 150 rpm, 10% enzyme based on oil weight, a_w = 0.225. [b]pCPL-GX: partially purified lipase prepared from the crude *Carica papaya* latex bought from Guangxi province. [c]pCPL-GD: partially purified lipase prepared from the crude *Carica papaya* latex bought from Guangdong province. [d]"One" represents one step addition of alcohol at 0 h; "three" represents three step addition of alcohol at 0 h, 6 h, and 14 h, respectively.

the *Carica papaya* latex is needed. In other words, the insoluble substance is treated as a waste during papain purification. However, the CPL is attached to the insoluble substance. Recovering the waste insoluble substance can be used as a new product (CPL) and play a role in waste recycling. According to the preliminary estimate, the price of CPL is approximately about one-third that of crude *Candida rugosa* lipase and 1/30 that of Novozym 435.[12,13] In this work, this low cost CPL was investigated as a catalyst to catalyze the FABE production. The cost of enzymatic butyl-biodiesel production would be considerably reduced by using this low cost plant lipase.

MATERIALS AND METHODS

Materials. Crude *Carica papaya* latex was bought from Guangzhou Huaqi Biotech Co., Ltd. (Guangdong province, China) and Biology Institute, Guangxi Academy of Sciences (Guangxi province, China). *Pistacia chinensis* Bunge oil, *Jatropha curcas* L. oil, sunflower oil, corn oil, cottonseed oil, castor oil, olive oil, soybean oil, rapeseed oil, and peanut oil were all purchased locally. Standard alkyl esters of palmitic acid, stearic acid, oleic acid, linoleic acid, linolenic acid, erucic acid, ricinoleic acid, and heptadecanoic acid were bought from Sigma and were chromatographically pure. All other chemicals and reagents were obtained commercially and were of analytical grade. All the organic solvents were treated with 3 Å molecular sieves for several days before being used.

Preparation of Partially purified *Carica papaya* Lipase. The partially purified *Carica papaya* lipase was prepared according to the reported method with modification.[14] To 20 g of the crude *Carica papaya* latex was added 200 mL of deionized water at 4 °C with gentle stirring for 30 min. The resultant solution was centrifuged at 10000 rpm for 15 min, and the supernatant was discarded. This procedure was repeated three times. The remaining precipitate was then collected and fast frozen using liquid nitrogen and then lyophilized for 8 h. This preparation was used as partially purified *Carica papaya* lipase (pCPL) in this work. Notations pCPL-GX and pCPL-GD refer to pCPL prepared from the crude *Carica papaya* latex bought from Guangxi province and Guangdong province, respectively.

Water Activity (a_w) Equilibration. In order to control the initial a_w of the CPL catalyzed reaction, the CPL, substrates and reaction solvents were separately adjusted to the desired a_w in sealed containers for at least 2 days, at 25 °C, with the vapor phase of saturated salt solutions of known a_w: KNO_3 (a_w 0.936), KCl (a_w 0.843), NaCl (a_w 0.753), $Mg(NO_3)_2$ (a_w 0.528), K_2CO_3 (a_w 0.432), $MgCl_2$ (a_w 0.328), CH_3COOK (a_w 0.225), LiCl (a_w 0.113), and 3 Å molecular sieves (a_w 0.02).

General Procedure for CPL Catalyzed Biodiesel Production in Batch Reactor. A certain molar ratio of vegetable oil and alcohol in an organic solvent (4 mL) was mixed with appropriate amount of pCPL in a 25 mL screw capped vial. The average molecular weight of different oil was calculated according to the formula M (g/mol) = 56.1 × 1000 × 3/(SV − AV), where SV is the saponification value (mg KOH/g oil) of the oil and AV is the acid value (mg KOH/g oil) of the oil. SV and AV can be obtained by the methods of Chinese National Standard GB5534-85 and GB/T5530-1998, respectively. The average molecular weight of different oil obtained in this method was used to calculate the molar ratio in each experiment. The alcohol may be added by a one-step method (at 0 h) or a three-step method (at 0 h, 6 h, and 14 h). The reactions were carried out at different temperatures and 150 rpm in a thermostated shaker. Aliquots (50 μL) of the reaction mixture were taken at intervals and centrifuged at 10000 rpm for 5 min. Samples (6 μL) were withdrawn and mixed with 7.5 μL of 20 mM heptadecanoic acid methyl ester (served as internal standard) and 136.5 μL of *n*-heptane, and were analyzed by gas chromatography.

Continuous Biodiesel Production in the CPL Packed-Bed Reactor. Figure S1 in the Supporting Information shows the schematic diagram of the packed-bed reactor (PBR) experimental apparatus. A column (1.5 cm × 25 cm) with a water jacket was packed with a mixture of pCPL-GD and glass beads (1:1.5, w/w) as the CPL packed-bed reactor. The upper and lower ends of the column were layered with glass wool. The substrate mixture was mixed by a stirrer in the substrate reservoir and preheated by a constant temperature bath. Then the substrate mixture was fed upward through the column by a peristaltic pump. The system temperature was maintained by a circulating water bath. The reaction progress was monitored by analyzing regular samples with gas chromatography.

Gas Chromatography. Samples prepared as described above were analyzed by injecting 1 μL of *n*-heptane solution and internal standard

into an Agilent 6890 gas chromatograph, equipped with a HP-5 capillary column (5% phenyl methyl siloxane capillary, 30.0 m × 320 μm × 0.25 μm nomimal). The column temperature was kept at 180 °C for 1 min, heated to 300 °C at 10 °C/min, and then maintained for 2 min. The temperatures of the injector and detector were set at 260 and 280 °C, respectively. All samples were measured in triplicate, with reproducibility always within 3%. The qualitative analysis of different fatty acid alkyl esters was based on the retention time of standard fatty acid alkyl ester on the GC. Because the standard fatty acid isobutyl ester, amyl ester, and isopentyl ester could not be obtained from commercial suppliers, some assumptions in qualitative analysis of these fatty acid alkyl esters were made based on the fatty acid composition of different oils and the retention time of different standard fatty acid methyl esters and/or fatty acid ethyl esters.

RESULTS AND DISCUSSION

Comparison of Different CPL Source and Alcohol Acyl Acceptor. *Carica papaya* is a soft-stemmed and unbranched tree able to grow up to 20 m in height. As a native to the Central America, the papaya tree has been successfully established in many ecological niches in tropical and subtropical climates. China is now one of the papaya distribution centers. Papaya mainly is distributed in the south provinces of China such as Guangdong, Guangxi, Hainan, Yunnan, Fujian, Sichuan, Guizhou, and Taiwan. The largest papaya output is produced in Guangdong and Guangxi. Therefore, the crude *Carica papaya* latex produced in Guangdong and Guangxi was chosen as the source of different CPL in this work. Gandhi et al.[15−17] and Caro et al.[18] reported that the crude papaya lipase showed strict selectivity toward the alcohol acyl acceptor in catalyzing esterification or transesterification reaction. In order to achieve the naturally immobilized CPL catalyzed alcoholysis of vegetable oil for biodiesel production, the selectivity of pCPL-GX and pCPL-GD toward different alcohol acyl acceptor was first investigated. The results are shown in Table 1. As for the primary alcohols, the conversion increased along with the increase of carbon chain length. This result was consistent with previous works.[15−18] When making comparison between primary alcohols and secondary alcohols, it could be found that using secondary alcohols except isopropanol as acyl acceptors resulted in conversions similar to those of primary alcohols. These results were not in accordance with the previous works, which reported that the conversions obtained by using secondary alcohols as acyl acceptors were lower than those obtained by using primary alcohols as acyl acceptors.[15−18] Comparison between one-step addition and three-step addition of alcohol acyl acceptor showed that the inhibition of methanol on CPL activity was the largest, followed by the ethanol. Step addition of methanol and ethanol to reduce their amount in the reaction system could decrease their inhibition on CPL activity. Alcohol acyl acceptor with a carbon chain length more than three would not impair the CPL activity because one-step and three-step addition of the alcohol gave almost the same conversions. As far as the CPL source is concerned, the pCPL-GD catalyzed alcoholysis gave rise to higher conversions than those of pCPL-GX catalyzed alcoholysis. The pCPL-GD was chosen for the following study. The *n*-butanol can be produced by fermentation, and its boiling point is moderate. In order to fulfill complete renewable biodiesel production, the *n*-butanol was chosen as the acyl acceptor in the following experiments.

Effect of Reaction Solvents. Lipases are diverse in their sensitivity to solvents with different polarity. Log *P* is an index of the polarity of the solvent and is generally used to correlate solvent polarity with enzyme activity and stability in non-aqueous media. According to log *P* trends, the less hydrophobic the organic solvent, the lower the activity of enzyme in the solvent.[19] Organic solvents with various log *P* values were taken as reaction solvents to investigate their effects on the CPL catalyzed butanolysis. The results are shown in Figure 1. In the presence of organic solvents having log *P* greater than 3, the conversions were all high. The highest conversion was attained in *n*-heptane solvent. Solvents with log *P* values below 3 were not suitable for CPL catalyzed butanolysis. The CPL catalyzed alcoholysis activities (conversions) were better correlated with the log *P* values of the reaction solvents. Only the acetonitrile was an exception. Similar activity correlation was also found in CPL catalyzed alcoholysis resolution of amino esters in our previous work.[20]

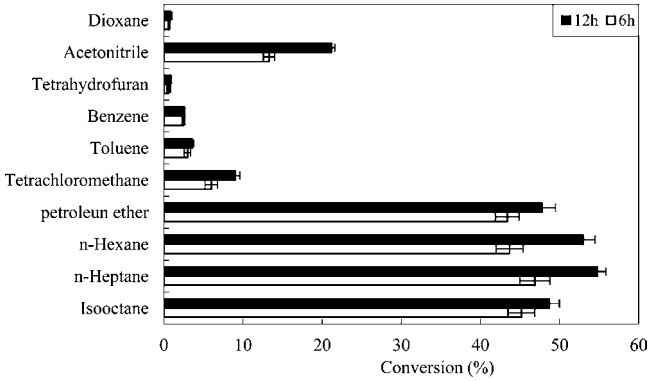

Figure 1. Effect of reaction solvents on the pCPL-GD-catalyzed alcoholysis of soybean oil with *n*-butanol. Reaction conditions: 50 °C, 150 rpm, *n*-butanol/soybean oil molar ratio of 4:1, 10% pCPL-GD based on oil weight, a_w = 0.225.

Effect of Substrate Molar Ratio. In Table 1, the conversions of CPL catalyzed alcoholysis reactions remained almost the same after 12 h. This showed that the reactions reached equilibrium at 12 h. In Figure 1, the conversions attained at 12 h were only a little higher than those attained at 6 h. This showed that the conversions increased slowly after 6 h. Caro et al. reported that the optimal alcohol/triacylglycerol molar ratio for crude papain lipase catalyzed interesterification was as high as 40:1.[18] Therefore, we hold that the conversions not increasing or increasing slowly along with the reaction time resulted from low molar ratio of alcohol/oil (4:1) used in our experiments. The molar ratio used was so low that the CPL catalyzed alcoholysis reaction reached equilibrium at lower substrate conversion. Various substrate molar ratios were performed to test their effects on the CPL catalyzed butanolysis reaction. As showed in Figure 2, the conversion increased along with the increase of alcohol/oil molar ratio until 12:1, attained the maximum at 12:1, and then decreased with the increase of alcohol/oil molar ratio. On one hand, the CPL catalyzed butanolysis reaction required excessive *n*-butanol to drive the reaction forward. Alcohol/oil molar ratio less than 12:1 could not satisfy this requirement, and thus led to low conversion. On the other hand, along with the increase of *n*-butanol addition the log P_{mix} of mixed solvent formed between *n*-heptane and *n*-butanol would decline gradually.[21] The low log P_{mix} of mixed solvent affected the CPL activity adversely (Figure 1), which could explain the reason that the conversion would decrease when alcohol/oil molar ratio was more than 12:1.

dx.doi.org/10.1021/jf501993v | J. Agric. Food Chem. 2014, 62, 6375−6381

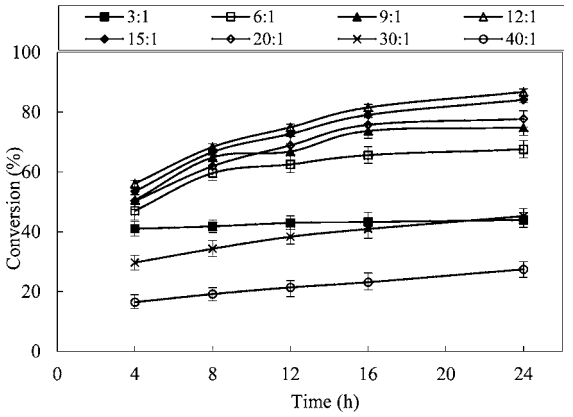

Figure 2. Effect of the alcohol/oil molar ratio on pCPL-GD-catalyzed alcoholysis of soybean oil with *n*-butanol. Reaction conditions: 50 °C, 150 rpm, 10% pCPL-GD based on oil weight, a_w = 0.225.

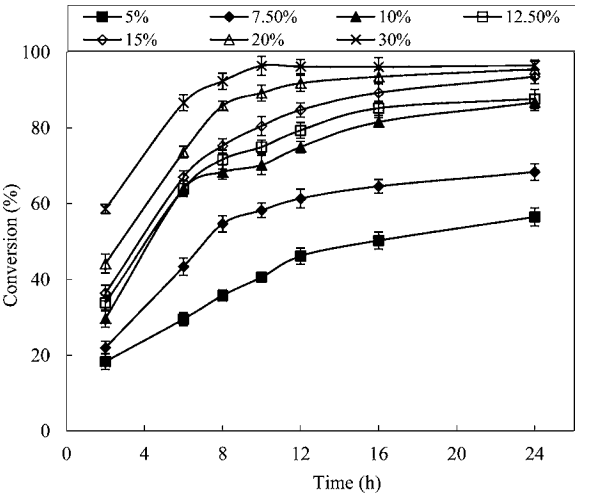

Figure 3. Effect of the pCPL-GD amount on the alcoholysis of soybean oil with *n*-butanol. Reaction conditions: 50 °C, 150 rpm, alcohol/oil molar ratio of 12:1, a_w = 0.225, reaction time 24 h.

In addition to being an important chemical raw material, *n*-butanol can also be used as solvent for the extraction of oilseeds, herbs, and spices. In this work, the optimal alcohol/oil molar ratio for CPL catalyzed butanolysis reaction was 12:1, at which the amount of *n*-butanol had exceeded that of oil. Therefore, the *n*-butanol was taken as both the reaction solvent and acyl acceptor for further investigation. As shown in Figure S2 in the Supporting Information, the CPL could catalyze the biodiesel production with *n*-butanol as the reaction solvent and acyl acceptor at the same time. However, the conversions attained were obviously lower than those obtained in the organic solvents at the same alcohol/oil molar ratio. The *n*-butanol is a medium polar solvent with a log *P* value of 0.8, which could impair the CPL activity to some degree just as in the discussion in Effect of Reaction Solvents.

Effect of CPL Amount. The previous work reported that the reaction rate of crude papain lipase catalyzed alcoholysis increased along with the increase of CPL addition amount until 15%.[17] Foglia and Villeneuve found that 15% of crude papain could lead to the best transesterification effect.[22] In this work, the CPL used was partially purified from the crude *Carica papaya* latex, and free from the water-soluble matter such as the proteases. Therefore, the effect of CPL amount was examined with amount ranging from 5% to 30% on the weight base of oil. The results are shown in Figure 3. There was a gradual increase in the conversion with the CPL amount increasing from 5% to 15%, and the conversion increased continuously with the lengthening of reaction time during 24 h. The conversion increased unobviously when the CPL amount was more than 15%. The alcoholysis reaction equilibrated at 12 h when 20% of CPL amount was used, and equilibrated at 10 h when 30% of CPL amount was used. In contrast, 15% was the optimal CPL addition amount. At first glance, the results obtained in this work were very inconsistent with the previous works.[18,22] In their works the optimal enzyme amount was 15% when the crude papain lipase was used. In this work the partially purified CPL was used, and thus the optimal enzyme amount should be much lower than 15%. Through analyzing their works in detail, it was found that the enzyme addition amount was calculated on the basis of all the substrates. However, the CPL addition amount was calculated only on the basis of oil not including the *n*-butanol in this work. According to the same addition amount of 15%, the enzyme amount used in their work was about 40 times higher than that used in this work. From Figure 3, it was also found that the conversion exceeded 80% at 24 h when more than 10% of CPL amount was used. The CPL shows sn-3 stereoselectivity in hydrolysis or interesterification of triacylglycerols.[8,11,18,22] In theory, the conversion should not surpass 67% in the CPL catalyzed alcoholysis reaction. However, more than 80% conversions were obtained in this work. Therefore, acyl transfer had been thought to occur during the CPL catalyzed alcoholysis.[23]

Effect of Temperature. Temperature has a clear impact on the catalytic activity of lipases. Some plant lipases derived from plant extracts can be catalytically active at temperatures above their physiological activity temperature.[24] Optimum temperature determined for various plant lipases used in biosynthesis generally ranges between 30 and 55 °C.[24] The effect of temperature on CPL catalyzed butanolysis reaction was investigated in the range from 45 to 70 °C. As showed in Figure 4, the CPL showed high catalytic activity between 50 and 60 °C with the 55 °C as the optimum temperature. This result was consistent with the previous works.[18,20] The optimum temperature range of CPL catalyzed biodiesel production is similar to that of commercial Novozym 435.[25]

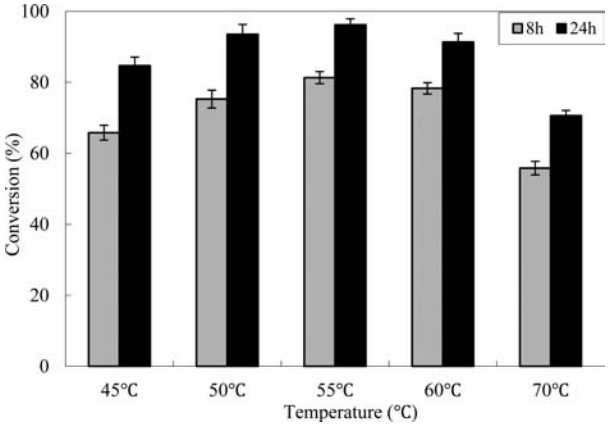

Figure 4. Effect of the temperature on the pCPL-GD-catalyzed alcoholysis of soybean oil with *n*-butanol. Reaction conditions: 150 rpm, alcohol/oil molar ratio of 12:1, 15% pCPL-GD based on oil weight, a_w = 0.225.

dx.doi.org/10.1021/jf501993v | J. Agric. Food Chem. 2014, 62, 6375−6381

Effect of Water Activity. The water thermodynamic activity (a_w) is conditioning the lipase spatial structure and thus its catalytic activity either toward synthesis or hydrolysis. For each lipase catalyzed synthesis reaction performed in nonaqueous system, an initial hydration level ruled by the initial a_w, for which the best synthesis performance is obtained, does exist.[4] The effect of a_w on the CPL catalyzed butanolysis reaction was investigated at various initial a_w (from 0.02 to 0.936). As shown in Figure 5, the conversion exhibited a bell

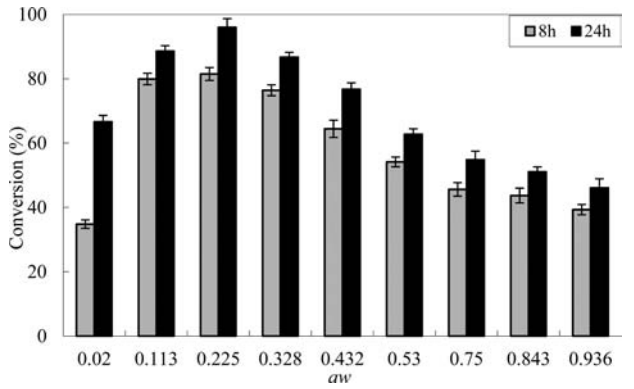

Figure 5. Effect of the water activity on the pCPL-GD-catalyzed alcoholysis of soybean oil with *n*-butanol. Reaction conditions: 55 °C, 150 rpm, alcohol/oil molar ratio of 12:1, 15% pCPL-GD based on oil weight.

shape, when the reaction conversion was plotted as a function of water activity. The CPL showed the maximum catalytic activity at 0.225 water activity, which generated a conversion of 96%. The conversion was about 2 times lower than the maximum at higher water activity of 0.936. These results suggested that water activity strongly influenced the hydration level of the CPL, which in turn affected the catalytic activity. At lower water activity the CPL showed lower catalytic activity due to the shortage of water to form enough oil−water interfaces. However, at higher water activity the CPL showed lower conversion, and this could be due to aggregation of enzyme or increased reverse hydrolysis reaction.

CPL Catalyzed Butanolysis of Other Vegetable Oils. In the above the soybean oil was taken as a model substrate to investigate the CPL catalyzed butanolysis for biodiesel production. Several key parameters had been optimized. In order to further investigate the capacity of CPL catalyzed biodiesel production, some other vegetable oils were chosen as the substrates. The result is shown in Figure 6. All the vegetable oils tested attained high conversion (about 90%), which showed that the CPL could catalyze the butanolysis of different oils, and could be used as a promising lipase for biodiesel production.

Continuous Biodiesel Production in the CPL Packed-Bed Reactor. The selection of a proper reactor type is critical to bioprocesses and plays a major role in large-scale production. The bioreactors widely used in today's bioindustry are mainly those developed in the past decades purely for chemical reactions. Among them, batch stirred tank reactor (BSTR) and packed-bed reactor (PBR) find the widest application. Batch reactor is often used in the laboratory for experiments of reaction kinetics, thermodynamics, and small scale production. It has the disadvantages of high labor costs per batch, the variability of products from batch to batch, and the difficulty of

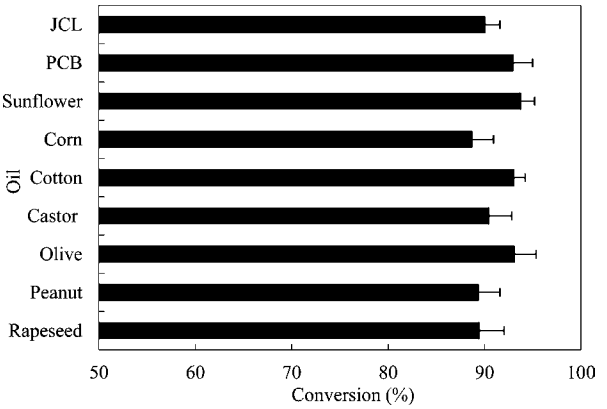

Figure 6. pCPL-GD-catalyzed alcoholysis of different oils with *n*-butanol. Reaction conditions: 55 °C, 150 rpm, alcohol/oil molar ratio of 12:1, 15% pCPL-GD based on oil weight, a_w = 0.225; JCL, *Jatropha curcas* L. seed oil; PCB, *Pistacia chinensis* Bunge seed oil.

large-scale production. Continuous PBR may be a way to solve the problems mentioned. The PBR can offer low cost, high efficiency, high stability of enzyme, automatic separation of product from enzyme, and ease of operation.[26] It may provide many opportunities for transferring the protocols of enzyme-catalyzed synthesis from the laboratory to an industrial scale. After systematic investigation of the CPL catalyzed butanolysis in the batch reactor, a CPL packed-bed reactor was further developed for the continuous biodiesel production.

Effect of Residence Time. The residence time of the reactants inside the reactor is one of the most important factors in the PBR, and it is defined as the average time that the reactants spend in a PBR. The effect of residence time on the CPL catalyzed butanolysis in PBR was investigated by varying the substrate feed flow rate. As shown in Figure S3 in the Supporting Information, the conversion increased fast with the decrease of flow rate because of the long residence time of substrates in the PBR. The conversion reached about 96% at the residence time of 40 min, and remained almost the same after 40 min. The residence time determined the contact time between the substrates (soybean oil and *n*-butanol) and the CPL. At the shorter residence time, the CPL did not have enough time to catalyze the alcoholysis of soybean oil with *n*-butanol, and thus generated lower conversion.

Long-Term Operation of PBR System. The long-term operational stability of the enzyme is an important characteristic of the PBR. For the CPL catalyzed butanolysis in the PBR, the long-term operational stability was examined under the operational parameters optimized at batch reactor. As shown in Figure 7, the operational stability of the PBR system was longer than 150 h, and the conversion was maintained almost the same during this continuous reaction time. When calculating on the basis of the optimal residence time of 40 min, 150 h was equivalent to 225 batches. The high operational stability of this CPL packed-bed reactor mainly resulted from the high stability of CPL. The cost of lipase necessary for the biodiesel production plays a decisive role in determining whether a process could possibly be considered by the industry. For a certain amount of lipase, the cost could be reduced by improving its operational stability. In this work, the CPL showed a very high operational stability in the PBR. Hence, the alcoholysis continuously catalyzed by CPL in the PBR has the potential for being applied in the large-scale production of biodiesel. Furthermore, the PBR system developed in this work

dx.doi.org/10.1021/jf501993v | J. Agric. Food Chem. 2014, 62, 6375−6381

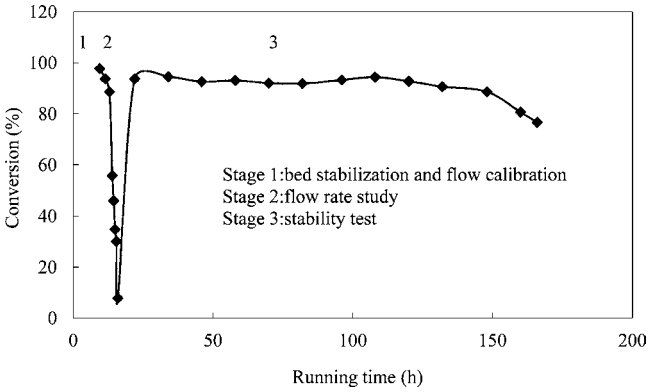

Figure 7. Operational stability of the pCPL-GD packed-bed reactor for continuous alcoholysis of soybean oil with *n*-butanol. Reaction conditions: 55 °C, alcohol/oil molar ratio of 12:1, residence time of 40 min, a_w = 0.225.

held another advantage, namely, the glycerol produced in the alcoholysis could dissolve in the *n*-butanol, and thus an auxiliary glycerol-separating system integrated with the PBR was not necessary.[27]

In conclusion, the alcohol acyl acceptor, reaction solvent, alcohol/oil molar ratio, enzyme amount, reaction temperature, and water activity all affected the CPL catalyzed alcoholysis process. Under the optimized conditions, the highest conversion of about 96% could be attained in 24 h. The CPL packed-bed reactor could stably operate for more than 150 h, which showed obvious potential for large-scale production. Therefore, the low cost naturally immobilized *Carica papaya* lipase was successfully used to catalyze butanolysis for butyl-biodiesel production in this work.

■ ASSOCIATED CONTENT

Supporting Information

Schematic diagram of naturely immobilized CPL packed-bed reactor for continuous biodiesel production, figure depicting pCPL-GD-catalyzed alcoholysis of soybean oil with butanol as the solvent and acyl acceptor at the same time, and figure depicting residence time course of the pCPL-GD-catalyzed alcoholysis of soybean oil with *n*-butanol in the packed-bed reactor. This material is available free of charge via the Internet at http://pubs.acs.org.

■ AUTHOR INFORMATION

Corresponding Authors

*E.S. Tel: +86 25 85428906. Fax: +86 25 85428906. E-mail: ezhsu@njfu.edu.cn.

*D.W. Tel: +86 21 64252078. Fax: +86 21 64250068. E-mail: dzhwei@ecust.edu.cn.

Funding

This work was supported by "A Project Funded by the Priority Academic Program Development of Jiangsu Higher Education Institutions, PAPD", the "Scientific Research Fund of Nanjing Forestry University for the Introduction of High-level talents" (G2014024), and the "Program for the Top Young Talents of Nanjing Forestry University". E.S. thanks China Scholarship Council and Nanjing Forestry University for an Overseas Visiting Scholarship.

Notes

The authors declare no competing financial interest.

■ REFERENCES

(1) Köse, Ö.; Tüter, M.; Aksoy, A. H. Immobilized *Candida antarctica* lipase-catalyzed alcoholysis of cottonseed oil in a solvent-free medium. *Bioresour. Technol.* **2002**, *83*, 125−129.

(2) Tüter, M.; Aksoy, H. A.; Gilbaz, E. E.; Kursun, E. Synthesis of fatty acid esters from acid oils using lipase B from *Candida Antarctica*. *Eur. J. Lipid Sci. Technol.* **2004**, *106*, 513−517.

(3) Li, L. L.; Du, W.; Liu, D. H.; Wang, L.; Li, Z. B. Lipase-catalyzed transesterification of rapeseed oils for biodiesel production with a novel organic solvent as the reaction medium. *J. Mol. Catal. B: Enzym.* **2006**, *43*, 58−62.

(4) Caro, Y.; Pina, M.; Turon, F.; Guilbert, S.; Mougeot, E.; Fetsch, D. V.; Attwool, P.; Graille, J. Plant lipases: biocatalyst aqueous environment in relation to optimal catalytic activity in lipase-catalyzed synthesis reactions. *Biotechnol. Bioeng.* **2002**, *77*, 693−703.

(5) Caro, Y.; Villeneuve, P.; Pina, M.; Reynes, M.; Graille, J. Investigation of crude latex from various *Carica papaya* varieties for lipid bioconversions. *J. Am. Oil Chem. Soc.* **2000**, *77*, 891−901.

(6) Giordani, R.; Moulin, A.; Verger, R. Tributyroylglycerol hydrolase activity in *Carica papaya* and other latices. *Phytochemistry* **1991**, *30*, 1069−1072.

(7) Ng, I.; Tsai, S. W. Partially purified *Carica papaya* lipase: a versatile biocatalyst for the hydrolytic resolution of (R, S)-2-arylpropionic thioesters in water-saturated organic solvents. *Biotechnol. Bioeng.* **2005**, *91*, 106−113.

(8) Domínguez, D. M. P.; Sinisterra, J. V.; Tsai, S. W.; Alcántara, A. R. *Carica papaya* lipase (CPL): an emerging and versatile biocatalyst. *Biotechnol. Adv.* **2006**, *24*, 493−499.

(9) Chen, H. M.; Wang, P. Y.; Tsai, S. W. *Carica papaya* lipase-catalyzed transesterification resolution of secondary alcohols in organic solvents. *J. Taiwan Inst. Chem. Eng.* **2009**, *40*, 549−554.

(10) Pinyaphong, P.; Sriburi, P.; Phutrakul, S. Biodiesel fuel production by methanolysis of fish oil derived from the discarded parts of fish catalyzed by *Carica papaya* lipase. *WASET* **2011**, *5*, 418−424.

(11) Gonzalo, C. A.; Ricardo, T. M. Recent advances and applications of the lipolytic activity of *Carica papaya* latex. *J. Mol. Catal. B: Enzym.* **2013**, *90*, 49−60.

(12) Ng, I. S.; Tsai, S. W. Hydrolytic resolution of (R, S)-naproxen 2, 2, 2-trifluoroethyl thioester by *Carica papaya* lipase in water-saturated organic solvents. *Biotechnol. Bioeng.* **2005**, *89*, 88−95.

(13) Gandhi, N. N.; Mukherjee, K. D. Specificity of papaya lipase in esterification of aliphatic alcohols-A comparison with microbial lipases. *J. Am. Oil Chem. Soc.* **2001**, *78*, 161−165.

(14) Ng, I. S.; Tsai, S. W. Investigation of lipases from various *Carica papaya* varieties for hydrolysis of olive oil and kinetic resolution of (R,S)-Profen 2, 2, 2-trifluoroethyl thioesters. *Process Biochem.* **2006**, *41*, 540−546.

(15) Gandhi, N. N.; Mukherjee, K. D. Specificity of papaya lipase in esterification with respect to the chemical structure of substrates. *J. Agric. Food Chem.* **2000**, *48*, 566−570.

(16) Gandhi, N. N.; Mukherjee, K. D. Synthesis of designer lipids using papaya (*Carica papaya*) latex lipase. *J. Mol. Catal. B: Enzym.* **2001**, *11*, 271−277.

(17) Gandhi, N. N.; Mukherjee, K. D. Reactivity of medium-chain substrates in the interesterification of tripalmitin catalyzed by papaya lipase. *J. Am. Oil Chem. Soc.* **2001**, *78*, 965−968.

(18) Caro, Y.; Turon, F.; Villeneuve, P.; Pina, M.; Graille, J. Enzymatic synthesis of medium-chain triacylglycerols by alcoholysis and interesterification of copra oil using a crude papain lipase preparation. *Eur. J. Lipid Sci. Technol.* **2004**, *106*, 503−512.

(19) Yang, C. F.; Wang, F. H.; Lan, D. M.; Whiteley, C.; Yang, B.; Wang, Y. H. Effects of organic solvents on activity and conformation of recombinant *Candida antarctica* lipase A produced by *Pichia pastoris*. *Process Biochem.* **2012**, *47*, 533−537.

(20) You, P. Y.; Qiu, J.; Su, E. Z.; Wei, D. Z. *Carica papaya* Lipase catalysed resolution of *β*-amino esters for the highly enantioselective synthesis of (*S*)-Dapoxetine. *Eur. J. Org. Chem.* **2013**, 557−565.

(21) Su, E. Z.; Wei, D. Z. Improvement in lipase-catalyzed methanolysis of triacylglycerols for biodiesel production using a solvent engineering method. *J. Mol. Catal. B: Enzym.* **2008**, *55*, 118−125.
(22) Foglia, T. A.; Villeneuve, P. *Carica papaya* latex-catalyzed synthesis of structured triacylglycerols. *J. Am. Oil Chem. Soc.* **1997**, *74*, 1447−1450.
(23) Oda, M.; Kaieda, M.; Hama, S.; Yamaji, H.; Kondo, A.; Izumoto, E.; Fukuda, H. Facilitatory effect of immobilized lipase-producing *Rhizopus oryzae* cells on acyl migration in biodiesel-fuel production. *Biochem. Eng. J.* **2005**, *23*, 45−51.
(24) Mounguengui, R. W. M.; Brunschwig, C.; Barea, B.; Villeneuve, P.; Blin, J. Are plant lipases a promising alternative to catalyze transesterification for biodiesel production? *Prog. Energy Combust. Sci.* **2013**, *39*, 441−456.
(25) Su, E. Z.; Zhang, M. J.; Zhang, J. G.; Gao, J. F.; Wei, D. Z. Lipase-catalyzed irreversible transesterification of vegetable oils for fatty acid methyl esters production with dimethyl carbonate as the acyl acceptor. *Biochem. Eng. J.* **2007**, *36*, 167−173.
(26) Rønne, T. H.; Yang, T. K.; Mu, H. L.; Jacobsen, C.; Xu, X. B. Enzymatic interesterification of butterfat with rapeseed oil in a continuous packed bed reactor. *J. Agric. Food Chem.* **2005**, *53*, 5617−5624.
(27) Hama, S.; Tamalampudi, S.; Yoshida, A.; Tamadani, N.; Kuratani, N.; Noda, H.; Fukuda, H.; Kondo, A. Enzymatic packed-bed reactor integrated with glycerol-separating system for solvent-free production of biodiesel fuel. *Biochem. Eng. J.* **2001**, *55*, 66−71.

Table 1. Yield and Thiolysis Results of Different Kiwifruit Pericarp PA Fractions Eluted from a Sephadex LH-20 Column

			contents[a] (mg/g PAs)					
fraction	yield (%)	mDP	catechin	epicatechin	gallo catechin	epigallo catechin	catechin gallate	epicatechin gallate
FA	0.93 ± 0.10	4.30 ± 0.30c	16.5 ± 0.80a	8.78 ± 0.30a	1.74 ± 0.80	0.66 ± 0.01	1.99 ± 0.02a	6.20 ± 0.60a
FB	1.43 ± 0.20	9.10 ± 0.60b	5.70 ± 0.60b	1.98 ± 0.05b			0.31 ± 0.01b	2.90 ± 0.30b
FC	0.28 ± 0.05	13.60 ± 0.70a	4.50 ± 0.40c	0.88 ± 0.01c			0.21 ± 0.01c	1.90 ± 0.10c

[a]Values are expressed as the mean of triplicate determinations ± standard deviation. Different letters (a−c) in the same column show significant differences from each other at the $P < 0.05$ level.

damage or injury because of insects or fungal infection. They were manually separated into pulp and pericarp. The latter was immediately washed and freeze-dried for 72 h, and then they were ground into fine powders. These fine powders were stored at −20 °C before analyses.

Extraction and Fractionation of PAs. Freeze-dried powders (10.0 g) were ultrasonically extracted with 7:3 (v/v) acetone/water solution containing 0.05% ascorbic acid (3 × 250 mL) at room temperature. Each extract was filtered and pooled, and the acetone was removed by evaporation under vacuum (40 °C). The remaining aqueous residue was subsequently extracted three times with petroleum ether (3 × 150 mL) and ethyl acetate (3 × 150 mL), yielding dried crude tannin extracts. The crude tannin fraction was chromatographed on a 50 × 1.5 cm i.d. Sephadex LH-20 column (Pharmacia Biotech, Uppsala, Sweden), the column was washed with 500 mL of methanol/water (50:50, v/v) to remove sugars, glycosides, and monomeric polyphenols and then eluted with methanol/H_2O (80:20, v/v), acetone/methanol/H_2O (40:40:20, v/v/v), and acetone/water (70:30, v/v) to obtain fraction A (FA), fraction B (FB), and fraction C (FC) (each 500 mL), respectively. Organic solvents were removed, and the remaining aqueous fractions were freeze-dried. Their yields were calculated and are listed in Table 1. Three fractions were freeze-dried after the organic solvents were eliminated and stored at −20 °C before analyses. The fractionation experiment was repeated three times. In addition, UV−vis spectra of three fractions showed a pronounced and symmetrical peak near 280 nm with no band broadening beyond 300 nm. This kind of spectrum is typical of the PAs.

MALDI-TOF MS Analysis. MALDI-TOF MS analysis was performed by using a Bruker Reflex III MALDI-TOF mass spectrometer (Bruker, Bremen, Germany). The parameters for positive mode spectra in the reflectron mode and linear mode were set according to our previous study.[15] Parameters for positive pattern spectra in the reflectron pattern were as follows: accelerating voltage, 20 kV; reflectron voltage, 23.0 kV; delayed extraction voltage, 16.32 kV; lens voltage, 9.45 kV. Parameters for positive pattern spectra in the linear pattern were as follows: accelerating voltage, 20.0 kV; delayed extraction voltage, 16.25 kV; lens voltage, 10.0 kV. Cs^+ was used as the cationization and 2,5-dihydroxybenzoic acid was selected as the matrix. Amberlite IRP-64 cation-exchange resins (Sigma-Aldrich, USA) were used to deionize the analyte and matrix solution. An aqueous solution of cesium chloride (1.5 μL, 1.52 mg/mL in aqueous) was added to the sample solution (1.5 μL, 10 mg/mL in 30% aqueous acetone) followed by the addition of an equal volume of 2,5-dihydroxybenzoic acid (10 mg/mL in aqueous). The mixture (1 μL) was spotted to a steel target and introduced into the mass spectrometer.

Thiolysis of Polymeric PAs for Reversed-phase HPLC-ESI-MS Analysis. A thiolysis method based on that described by Guyot et al.[16] was carried out with a minor modification. Degradation products of thiolysis were analyzed by reversed-phase HPLC-ESI-MS. PAs used for thiolysis were 5 mg/mL. The high-performance liquid chromatograph (HPLC) was performed on an Agilent 1200 system (USA). The thiolysis medium was further analyzed using LC-MS (QTRAP 3200, USA). Two solvents, 0.5% trifluoroacetic acid (A) and acetonitrile (B), were used. The linear gradient elution process was as follows: 0−45 min, 12−80% B; 45−50 min, 80−12% B. The column temperature was 25 °C, and the flow rate was 1 mL/min. The detection wavelength was set at 280 nm. Degradation products were identified on chromatograms according to their retention times and LC-MS. The calculation of the mean degree of polymerization (mDP) was based on the following equation:

$$\text{mDP} = (\text{total area of the extender units}) / (\text{total area of the terminal units}) + 1$$

Normal-Phase HPLC-ESI-MS Analysis. The HPLC equipment consisted of an Agilent 1200 liquid chromatograph system as described above. Concentration values of the solutions used for analysis were 5 mg/mL. The column temperature was 35 °C, and the injection volume was 20 μL. The mobile phase consisted of A, dichloromethane/methanol/water/acetic acid (41:7:1:1, v/v/v/v), and B, dichloromethane/methanol/water/acetic acid (5:43:1:1, v/v/v/v). The 60 min linear gradient was as follows: 0−13.5% B (0−20 min); 13.5−29.2% B (20−50 min); 29.2−100% B (50−55 min); 100% B (55−60 min).[17] Then the eluting stream (1 mL/min) was introduced into a QTRAP 3200 mass spectrometer. Peaks were identified on chromatograms according to their retention times and LC-MS.

Enzyme Assay. *Inhibitory Effects Assay.* Enzyme reaction was performed by using a 3 mL system established by our laboratory.[18] In brief, L-tyrosine was selected as substrate for the monophenolase reaction assay and 3,4-dihydroxyphenylalanine was selected as substrate for the diphenolase reaction assay. The reaction medium (3 mL) contained 12 mM L-tyrosine or 0.5 mM 3,4-dihydroxyphenylalanine in 50 mM sodium phosphate buffer (pH 6.8). The final concentrations of tyrosinase were 33.33 μg/mL for the monophenolase reaction and 6.67 μg/mL for the diphenolase reaction. Absorption was detected by using a Beckman UD-800 spectrophotometer (USA). The extent of inhibition by the addition of the sample was expressed as the percentage necessary for 50% inhibition (IC_{50}) for the enzyme activity assay. A lower value of IC_{50} indicates better anti-tyrosinase activity. Controls, without inhibitor but containing equal H_2O, were routinely carried out. All measurements were carried out at 30 °C.

Inhibitory Mechanism and Type Assay. An inhibitory mechanism assay was carried out by changing the enzyme concentration in the reaction medium. The plots of the remaining enzyme activity versus the concentrations of enzyme in the presence of inhibitors with diffierent concentrations gave a family of straight lines. If the inhibition is reversible, all straight lines intersect at the origin; when the inhibition is irreversible, these straight lines are parallel. An inhibition type assay was achieved by changing the substrate concentration in the reaction medium. The inhibition type was assayed by using a Lineweaver−Burk plot.

Fluorescence Emission Spectra of Mushroom Tyrosinase in Solutions with Different Concentration of PAs. The fluorescence assay was measured with a Varian Cary Eclipse fluorescence spectrophotometer. The reaction medium (3 mL) contained 600 μL of mushroom tyrosinase solution, 2.1 mL of 50 mM sodium phosphate buffer (pH 6.8), and 300 μL of sample solution with different concentrations. The experiment was performed with an excitation wavelength of 290 nm at a constant temperature of 25 °C.

Fluorescence Emission Spectra of L-Tyrosine or 3,4-Dihydroxyphenylalanine in Solutions with Different Concentrations of PAs. The fluorescence assay was carried out on a Varian Cary Eclipse fluorescence spectrophotometer. In brief, L-tyrosine (12 mM) or 3,4-dihydroxyphenylalanine (0.5 mM) solution (200 μL) was added into 50 mM sodium phosphate buffer (pH 6.8), and sample solution was then added at a constant temperature of 25 °C (the final

medium is 1 mL), preincubated for 30 s before fluorescence spectra measurements with an excitation wavelength of 290 nm.

DPPH Radical Scavenging Capacity. The DPPH method was achieved in compliance with the study of Brand-Williams et al.[19] with minor modification. Mainly, sample solution (0.1 mL) was mixed with 3 mL of DPPH solution (25 mg/L in methanol). Methanol (0.1 mL) and 3 mL of DPPH served as the control. After the mixture was shaken and kept at room temperature for 30 min, the absorbance at 517 nm was measured. The calculated equation for scavenging percentage of DPPH was

$$\text{DPPH \% inhibition} = [(A_1 - A_2)/A_1] \times 100$$

where A_1 = the absorbance of the control reaction and A_2 = the absorbance in the presence of the sample. The quality of the antioxidants about the PAs was determined by the IC_{50} values (the concentration that led to a 50% decrease in absorbance). A lower value of IC_{50} indicates better antioxidant activity. In addition, Trolox and ascorbic acid were selected as reference. All fractions were analyzed in three replicates.

ABTS Radical Scavenging Activity. ABTS assay was conducted in accordance with the procedure described by Re et al.[20] $ABTS^+$ was generated by reacting 7 mM ABTS and 2.45 mM potassium persulfate after incubation at room temperature in the dark for 16 h. The $ABTS^+$ solution was then diluted with 80% ethanol to an absorbance of 0.700 ± 0.050 at a wavelength of 734 nm. Tested sample solution (0.1 mL) was added to $ABTS^+$ solution (3.9 mL), and the mixture was mixed well. The absorbance of the reactive mixture was recorded at 734 nm on a Beckman UD-800 spectrophotometer after being kept at room temperature for 6 min. The results were expressed the same as for the DPPH assay described previously, with ABTS % inhibition and IC_{50} value.

Ferric Reducing Antioxidant Power (FRAP). The FRAP assay was performed according to the method of Benzie and Strain[21] with slight modification. Mainly, 3 mL of FRAP reagent (10 mM TPTZ, 20 mM ferric chloride, and 300 mM sodium acetate buffer were mixed at a ratio of 1:1:10) was mixed with test sample solution (0.1 mL) or methanol (blank). The absorbance of the reaction mixture at 593 nm was measured after incubation at room temperature for 10 min. The FRAP values, expressed in millimoles of ascorbic acid equivalents (AAE) per gram fraction, were derived from a standard curve. A higher absorbance corresponds to a higher ferric reducing power.

Statistical Analysis. All data were expressed as means ± standard deviation of three independent determinations. One-way analysis of variance was used, and the differences were considered to be significant at $P < 0.05$. All statistical analyses were performed with SPSS 13.0 for Windows.

RESULTS AND DISCUSSION

MALDI-TOF MS Analysis. Reflectron MALDI-TOF MS spectra (Figure 1) of three fractions were obtained when 2,5-dihydroxybenzoic acid was selected as the matrix and Cs^+ was used as the cationization. The results indicated that the studied polymeric mixture exhibited mass spectra with a dominating set of peaks with differences of 288 Da, corresponding to the mass difference of one (epi)catechin monomer unit. Other repeated patterns within each main set of peaks were the signals separated by the subset of masses 16 Da difference. These masses were produced by propelargonidin-type (which lack one hydroxyl group at the 3′-position of the B-ring compared to procyanidin-type flavan-3-ol units) and prodelphinidin-type flavan-3-ol units (which possess one hydroxyl group at the 5′-position of the B-ring compared to procyanidin-type flavan-3-ol units). It was further suggested that the PAs from fruit pericarps of kiwifruit contain prodelphinidin, procyanidin, and prodelphinidin when the absolute masses corresponding to each peak were obtained. Procyanidins were the dominating constituent of kiwifruit pericarp PAs. A series of peaks with additional 132

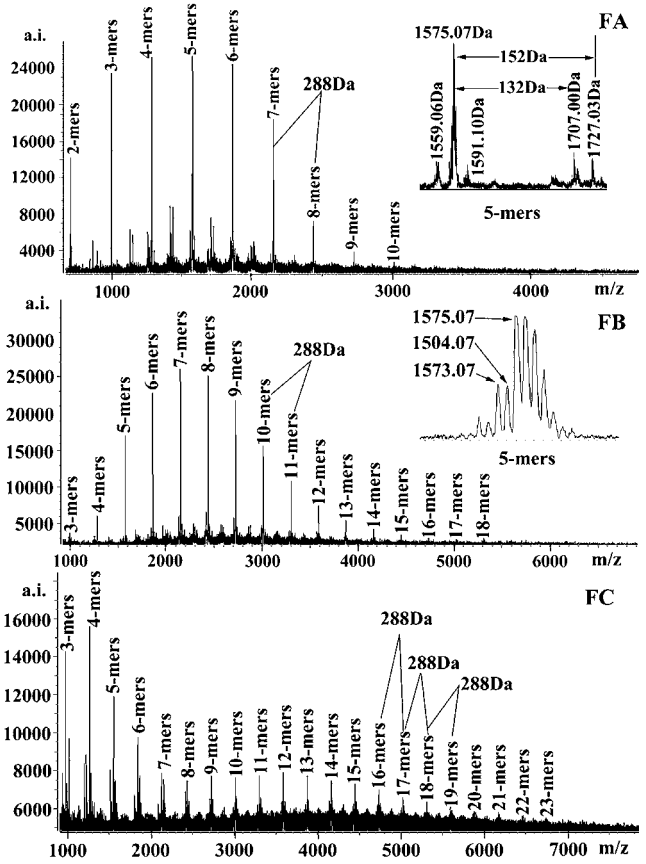

Figure 1. MALDI-TOF positive-ion (Cs^+) mode mass spectra of polymeric kiwifruit pericarp PAs in the reflectron mode.

Da (which are produced by synchronous attachment of two Cs^+ and the absence of a proton $[M + 2Cs^+ - H]^+$)[22] and 152 Da (corresponding to the addition of one galloyl group at the heterocyclic C-ring)[23] were also detected. Additionally, the A-type interflavan linkages with characteristic signals 2 Da smaller than the B-type linked PAs (due to the loss of two hydrogen atoms with the formation of the ether bond) were not detected in the mass spectra.

The distributions of polymerization degree and predominant polymers were clearly different among the three fractions, the DP varying from 2-mers to 10-mers, from 3-mers to 18-mers, and from 3-mers to 23-mers for FA, FB, and FC, respectively. MALDI-TOF mass spectra provided evidence that PAs from kiwifruit pericarp possessed structural heterogeneity and distinct DP distribution in each fraction. In this study, up to 23-mers were present in the spectra of FC, which might be attributed to the improvement of fractionation in the MALDI-TOF MS analysis as stated in a previous paper.[24] Therefore, fractionation of lower oligomers (FA) on the Sephadex LH-20 column would significantly enhance the sensitivity of the detection of larger polymers (FB) under MALDI-TOF MS analysis.

PA polymers extracted from kiwifruit pericarp were then characterized by MALDI-TOF MS in the positive-ion (Cs^+) linear mode (Figure 2). In the mass spectra, an equispaced series of signal groups corresponding to the polymeric distribution of the PAs was observed. The distance between each degree of polymerization was 288 Da. This agreed well with the results obtained from reflectron mode. PAs with DP up to 29-mers could be detected working in the linear mode.

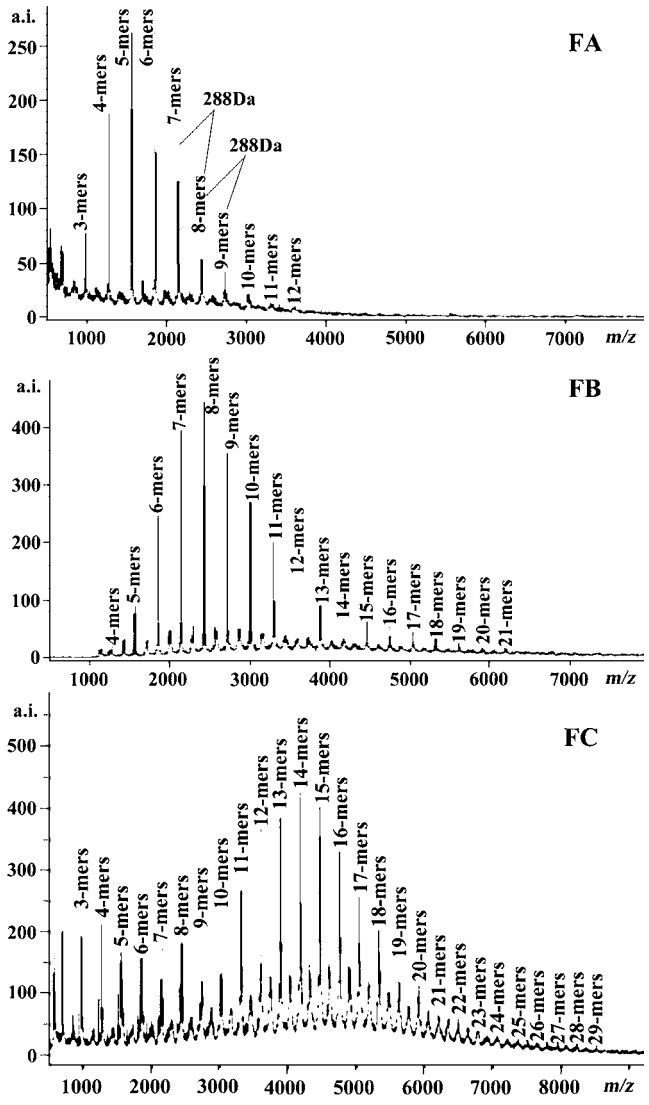

Figure 2. MALDI-TOF positive-ion (Cs^+) mode mass spectra of polymeric PAs extracted from kiwifruit pericarp in the linear mode.

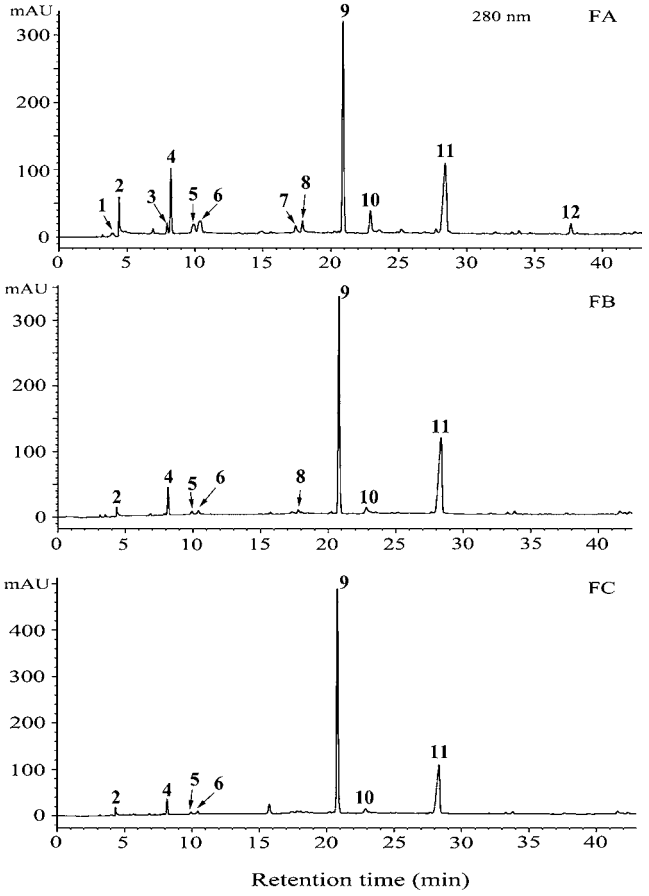

Figure 3. Reversed-phase HPLC chromatograms of polymeric PAs extracted from kiwifruit pericarp after thiolytic degradation. Peaks: 1, gallocatechin (305 Da, $[M - H]^-$); 2, catechin (289 Da, $[M - H]^-$); 3, epigallocatechin (305 Da, $[M - H]^-$); 4, epicatechin (289 Da, $[M - H]^-$); 5, catechin gallate (441 Da, $[M - H]^-$); 6, epicatechin gallate (441 Da, $[M - H]^-$); 7, gallocatechin benzylthioether (427 Da, $[M - H]^-$); 8, epigallocatechin benzylthioether (427 Da, $[M - H]^-$); 9, epicatechin benzylthioether (411 Da, $[M - H]^-$); 10, (epi)afzelechin benzylthioether (395 Da, $[M - H]^-$); 11, benzyl mercaptan.

Therefore, the linear mode provided better information about the DP distribution of the PAs present in the sample. However, high mass resolution power in the reflectron spectrum allowed the mass of the isotopic peaks to be distinguished with enough accuracy (Figure 1).

Reversed-Phase HPLC-ESI-MS Analysis followed Thiolysis Reaction. The chromatograms of thiolytic products of FA, FB, and FC are illustrated in Figure 3. The results showed that the terminal units contained catechin (peak 2), epicatechin (peak 4), gallocatechin (peak 1), epigallocatechin (peak 3), catechin gallate (peak 5), and epicatechin gallate (peak 6) for the FA. However, gallocatechin and epigallocatechin were not detected in FB and FC. The extension units of FA contained (epi)afzelechin (peak 10), epicatechin (peak 9), gallocatechin (peak 7), and epigallocatechin (peak 8), with the epicatechin dominating. However, gallocatechin benzylthioether and epigallocatechin benzylthioether were not found in FB and FC. A-type PAs could not be detected in the chromatogram. The profile after thiolysis demonstrated that PAs extracted from kiwifruit pericarp are B-type procyanidin (the most abundant type of PAs in plants), propelargonidin, and prodelphinidin. B-type procyanidin dominates. These results confirmed the findings obtained from MALDI-TOF MS analysis. In addition, the mDP for the polymers was estimated by thiolysis to be in a range from 4.3 ± 0.3 to 13.6 ± 0.7 (Table 1). The contents of terminal units decreased in the order FA > FB > FC (Table 1).

Normal-Phase HPLC-ESI-MS Analysis. The normal-phase HPLC profile of kiwifruit pericarp PAs is illustrated in Figure 4. The result indicated the presence of PAs with different degrees of polymerization. The good resolution between each oligomeric class suggested that the PAs are quite homogeneous, showing only minor differences in their constituent units and the linkages between them. HPLC performance implied the precise separation of PAs from monomers to 6-mers and the presence of isomers. However, the polymers could not be resolved by normal-phase HPLC. They showed a profile with a single broad peak at the end of the run with a retention time of approximately 55.7 min. No PAs with DP higher than 10-mers could be separated. Our results agreed well with the finding of Gu et al.[17] on the analysis of PAs from lowbush blueberry.

Inhibition Effect, Mechanism, and Type of Kiwifruit Pericarp PAs on the Monophenolase Activity and Diphenolase Activity of Mushroom Tyrosinase. The monophenolase and diphenolase activity may be both

dx.doi.org/10.1021/jf501009v | J. Agric. Food Chem. 2014, 62, 6382−6389

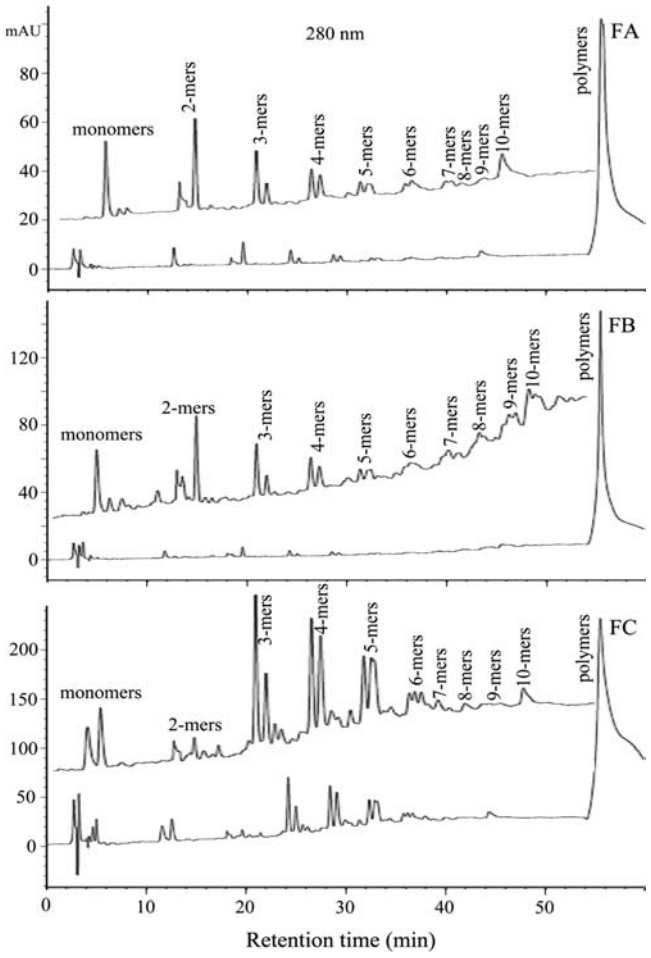

Figure 4. Normal-phase HPLC chromatograms of PAs from kiwifruit pericarp. The degree of polymerization of the peaks is labeled in expanded insets.

negatively affected by adding of kiwifruit pericarp PAs as shown in Table 2. The IC_{50} values for the monophenolase activity were estimated to be 180.2 ± 6.5, 80.1 ± 4.1, and 48.9 ± 4.6 μg/mL for FA, FB, and FC, respectively. As for diphenolase activity, the inhibitor concentrations leading to 50% (IC_{50}) enzyme activity decrease were estimated to be 390.2 ± 12.6, 192.6 ± 10.3, and 64.9 ± 3.2 μg/mL for FA, FB, and FC, respectively. In previous studies, the methanol extracts from sorghum distillery residue[25] and red koji extracts[26] (containing a high percentage of PAs) showed inhibitory effect with IC_{50} values of 580 and 5570 μg/mL on mushroom tyrosinase activity, respectively. Therefore, PAs from kiwifruit pericarp in this study were potent inhibitors on tyrosinase. In the present study, we further found that DP, that is, molecular weight, had an obvious effect on the inhibition of mushroom tyrosinase activity. The PAs with higher DP possessed a better inhibition on the activity of tyrosinase. This revealed the possible use of these compounds (especially FB and FC) as whitening agents, insect control agents, and food additives.

The inhibitory mechanism and type of the three fractions on the monophenolase and diphenolase enzyme reactions were then investigated. The results obtained from inhibitory mechanism analysis showed that the inhibition was reversible. It could be concluded that the presence of inhibitor did not bring down the amount of enzyme, but led to a decrease in activity of the enzyme for oxidation of L-tyrosine and 3,4-dihydroxyphenylalanine. This further indicated that DP had no effect on the inhibitory mechanism. Inhibition type analysis indicated that they were mixed-type inhibitors of the enzyme. The results revealed that these fractions combined with free enzymes as well as enzyme−substrate complexes. The results also displayed that the three fractions had the same type of inhibition on the enzyme.

Fluorescence Quenching Analysis. The fluorescence of tryptophan, which existed in tyrosinase molecules, has been frequently examined to obtain information about conformational changes.[27] The interaction of tyrosinase with PAs and its conformational alteration were evaluated by measuring the intrinsic fluorescence intensity of the protein in the presence or absence of PAs. The fluorescence emission spectra were collected from a range of 300−500 nm with the excitation wavelength set at 290 nm. The result showed that the addition of fractions caused a dramatic decrease in the fluorescence emission spectra. The fluorescence intensity decreased by 51.3, 80.0, and 85.6% (Figure 5A) for FA, FB, and FC, respectively, at 100 μg/mL. Undoubtedly, FC had better interaction with the tryptophan residue in the enzyme than did FA and FB. This indicated that PAs with high DP combined with the tryptophan residue more effectively. Therefore, these findings may be one reason for the strong inhibition of PAs on the tyrosinase. In addition, an obvious blue shift was also present in the spectra of FB and FC. These results indicated that PAs induced the change of enzyme conformation and also led to inactivation of the enzyme after binding to the enzyme molecule. Moreover, the interaction of PAs with the tryptophan of tyrosinase implied that the tyrosinase became disagglomerated and its structure got loosened. It was concluded that the tryptophan residue is one of the essential groups of the enzyme activity and it is situated on the surface of the enzyme and easily influenced by PAs. However, the results showed that PAs of FA did not affect the conformation of tyrosinase. Further study should be carried out to illustrate this. Tyrosinase possesses two copper ions in the active center, and they are of great importance for tyrosinase activity.[28] The inhibitory effects of PAs on the tyrosinase might be due to binding with copper ions (which is

Table 2. Effects of PA Fractions from Kiwifruit Pericarp on the Activity of Mushroom Tyrosinase for the Oxidation of L-Tyrosine and 3,4-Dihydroxyphenylalanine

	monophenolase			diphenolase		
sample	IC_{50}[a] (μg/mL)	inhibition	inhibition type	IC_{50}[a] (μg/mL)	inhibition	inhibition type
FA	180.2 ± 6.5c	reversible	mixed	390.2 ± 12.6c	reversible	mixed
FB	80.1 ± 4.1b	reversible	mixed	192.6 ± 10.3b	reversible	mixed
FC	48.9 ± 4.6a	reversible	mixed	64.9 ± 3.2a	reversible	mixed

[a]Values are expressed as the mean of triplicate determinations ± standard deviation. Different letters (a−c) in the same column show significant differences from each other at the $P < 0.05$ level.

dx.doi.org/10.1021/jf501009v | J. Agric. Food Chem. 2014, 62, 6382−6389

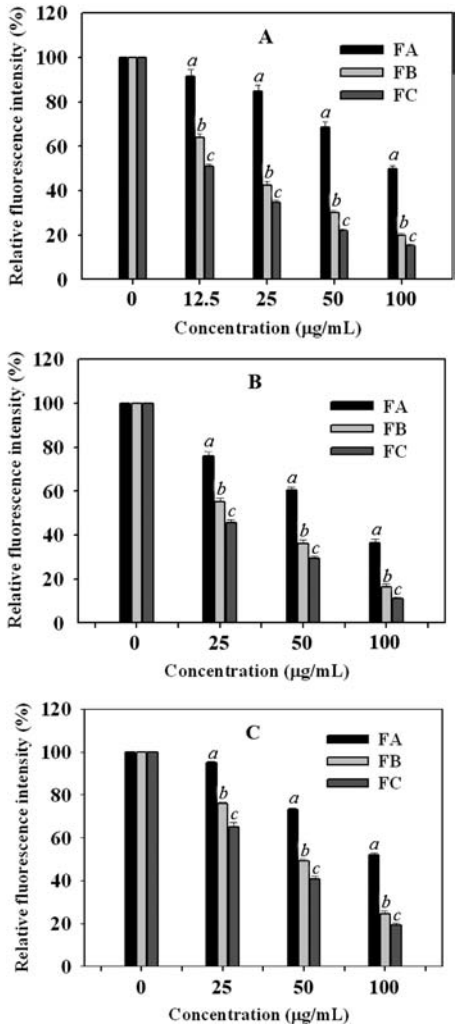

Figure 5. (A) Relative fluorescence intensity of tyrosinase in solution with different concentrations of PAs. The concentrations of PAs were 0, 12.5, 25, 50, and 100 μg/mL, respectively. (B) Relative fluorescence intensity of L-tyrosine in solution with different concentrations of PAs. The concentrations of PAs were 0, 25, 50, and 100 μg/mL. (C) Relative fluorescence intensity of 3,4-dihydroxyphenylalanine in solution with different concentrations of PAs. The concentrations of PAs were 0, 25, 50, and 100 μg/mL, respectively. The excitation wavelength for fluorescence analyses was set at 290 nm. Different letters (a–c) in the same column show significant differences from each other at the $P < 0.05$ level.

the metal at the center of the active site of tyrosinase) with their −OH group. Because the −OH group of PAs presents an anionic form at pH 6.8, they might interact electrostatically with copper ions in the mushroom tyrosinase. The copper-chelating properties of the PAs were thought to be another reason for their strong inhibitory activity on tyrosinase.[29]

Fluorescence Emission Spectra of L-Tyrosine or 3,4-Dihydroxyphenylalanine in Solutions with Different Concentrations of PAs. The interaction of three fractions with L-tyrosine, which was used as a substrate of monophenolase, was first investigated by the fluorescence quenching method. The fluorescence emission spectra were recorded in the range of 300–400 nm with excitation wavelength set at 290 nm. The results showed that fluorescence intensity decreased distinctly with the increase of PA concentration. The fluorescence intensity decreased by 63.7, 83.7, and 89.1% (Figure 5B) for FA, FB, and FC, respectively, at 100 μg/mL.

Then fluorescence emission spectra of 3,4-dihydroxyphenylalanine, which used as a substrate of diphenolase, were recorded in the presence of PAs with different concentrations. The excitation was the same as L-tyrosine assay. The results showed that fluorescence intensity decreased distinctly with the increase of PA concentration. The fluorescence intensity decreased by 47.9, 75.5, and 80.7% (Figure 5) for FA, FB, and FC, respectively, at 100 μg/mL.

These results provided the first evidence that PAs are the effective binding agent of L-tyrosine and 3,4-dihydroxyphenylalanine. Obviously, PAs could effectively stop the reaction of substrate and tyrosinase in this way. It could be another reason for the strong inhibition of PAs on the tyrosinase catalytic reaction. These findings were significant in both designing and screening of potent novel tyrosinase inhibitiors. The results also indicated that combining capacities with L-tyrosine and 3,4-dihydroxyphenylalanine decreased in the order FC > FB > FA. These were also proof that DP is an important factor for the inhibition of PAs on the enzyme.

Determination of Antioxidant Capacity. DPPH, ABTS, and FRAP assays were simultaneously used for measuring the antioxidant properties of three fractions to better reflect their potential protective effects. Table 3 shows the scavenging effect

Table 3. Antioxidant Activities of the PAs Fractionated from Kiwifruit Pericarp Using the DPPH Free Radical Scavenging Assay, the ABTS Free Radical Scavenging Assay, and the FRAP Assay

	antioxidant activity[a]		
sample	IC_{50}/DPPH (μg/mL)	IC_{50}/ABTS (μg/mL)	FRAP (mmol AAE/g)
FA	105.3 ± 1.8b	74.7 ± 2.5c	7.4 ± 0.2c
FB	67.7 ± 1.5a	60.1 ± 1.8b	9.5 ± 0.3a
FC	69.3 ± 0.9a	39.5 ± 1.2a	9.6 ± 0.9a
ascorbic acid	102.6 ± 3.9b	82.5 ± 0.6d	
Trolox	111.9 ± 2.9c	89.1 ± 2.7e	8.3 ± 0.4b

[a]Values are expressed as the mean of duplicate determinations ± standard deviation. Different letters (a–e) in the same column show significant differences from each other at the $P < 0.05$ level.

on the DPPH radical decreased in the order FC ≈ FB > FA ≈ ascorbic acid >Trolox. The order for the ABTS radical scavenging activity was FC > FB > FA > ascorbic acid > Trolox. The antioxidant activity of kiwifruit pericarp PAs was also measured by FRAP assay. The FRAP values for FA, FB, and FC were 7.4 ± 0.2, 9.6 ± 0.3, and 9.6 ± 0.9 mmol AAE/g (Table 3), respectively. At each concentration, FB and FC exhibited distinctly higher reducing power than that of Trolox. In addition, with increasing concentration of the compounds, the antioxidant activity of PAs was observably increased in a concentration-dependent pattern.

Yokozawa et al.[30] confirmed that an increase of galloyl groups, molecular weight (DP), and o-hydroxyl structure enhanced the scavenging activity of tannins. In this study, the results obtained from three antioxidant analyses revealed that PAs were potent antioxidants. This can be explained by the fact that PAs possessed abundant hydroxyl groups. FB and FC possessed obviously higher antioxidant properties than FA. The result revealed that DP was a key factor for the antioxidant capacity of PAs. Hagerman et al.[31] provided insights into the

mechanism of procyanidin as a potential antioxidant, which showed that high molecular weight and hydroxyl groups were important factors for free radical scavenging by tannins. Our results agreed well with Hagerman's findings. In conclusion, our results indicated for the first time that PAs from kiwifruit pericarp might be a good resource for further development as antioxidants. This indicated the possible use of these compounds (especially FB and FC) in medical, cosmetic, food, and agricultural industries.

Structure−Activity of PAs from Kiwifruit Pericarp. Fractions FA, FB, and FC, with distinguishing DP ranges, were selected for discussing the structure−activity relation of PAs. In previous studies, many researchers had focused on the relationship between DP and antioxidant activity. Ariga et al.[32] found that the ability to scavenge peroxyl radicals was proportional to DP after testing several oligomeric flavonoids. Zhou et al.[33] thought that 9−10 mDP PAs should be considered as a dividing point for predicting the structure−activity of mangosteen pericarp PAs. In the present study, the antioxidant activity of kiwifruit pericarp PAs increased from mDP = 4.3 (fraction F1) to 9.1 (fraction F2), but remained stable after that when using DPPH and FRAP assays. However, an increasing antioxidant activity of PAs was displayed following the increase of mDP when using the ABTS assay. Our results partly agreed with the findings of Zhou et al.[33] As for anti-tyrosinase activity, our results revealed that activities (the monophenolase activity and the diphenolase activity) increased following the increase of PAs mDP. However, Shoji et al.[34] fractionated the procyanidins according to the DP using normal-phase chromatography, and no correlation between the DP and tyrosinase inhibitory activity was observed. It was suggested that methods are used to separate PAs from other polyphenols and to fractionate them according to the DP important. In a word, appropriate fractionation might be a feasible way to screen better antioxidant and anti-tyrosinase agents.

In conclusion, the structures of proanthocyanidin fractions (FA, FB, and FC) from kiwifruit pericarp were successfully characterized and elucidated. They possessed structural heterogeneity in monomer units and polymer length. Furthermore, the PAs exhibited excellent efficiency in inhibiting the activities of the mushroom tyrosinase, including the monophenolase activity and the diphenolase activity. The anti-tyrosinase activity of kiwifruit PAs increased with mDP. PAs were found to be reversible and mixed-type inhibitors of the enzyme. Moreover, the inhibition was carried out mainly through the interaction of the hydroxyl groups of the condensed tannins with the active center of the enzyme and the substrate of the enzymatic reaction. Additionally, these proanthocyanidin fractions, especially FB and FC, could effectively scavenge DPPH, ABTS radical, and Fe^{3+}−TPTZ. The antioxidant activity of kiwifruit pericarp PAs increased from mDP = 4.3 (fraction F1) to 9.1 (fraction F2), but remained stable after that when using DPPH and FRAP assays. However, the antioxidant activity of these compounds increased with mDP when using the ABTS assay. The elucidation of the anti-tyrosinase mechanisms and antioxidant activity of the PAs is significant in both designing and screening of novel tyrosinase inhibitiors and potent antioxidant.

AUTHOR INFORMATION

Corresponding Author

*(Q.-X.C.) E-mail: chenqx@xmu.edu.cn.

Funding

The present investigation was supported by the Natural Science Foundation of China (Grants 31071611 and 31070522), the National Science Foundation for Fostering Talents in Basic Research of the National Natural Science Foundation of China (Grant J1310027/J0106), the Science and Technology Foundation of Fujian Province (Grant 2010N5013), and the National Natural Science Fund of China (No. 31371988).

Notes

The authors declare no competing financial interest.

ABBREVIATIONS USED

PAs, proanthocyanidins; MALDI-TOF MS, matrix-assisted laser desorption/ionization time-of-flight mass spectrometry; HPLC-ESI-MS, high-performance liquid chromatography electrospray ionization mass spectrometry; DP, degree of polymerization; ABTS, 2,2-azinobis(3-ethylbenzothiazoline-6-sulfonic acid) diammonium salt; DPPH, 2,2-diphenyl-1-picrylhydrazyl; FRAP, ferric reducing antioxidant power

REFERENCES

(1) Mayer, A. M.; Harel, E. Polyphenol oxidases in plants. *Phytochemistry* **1979**, *18*, 193−215.

(2) Korner, A.; Pawelek, J. Mammalian tyrosinase catalyzes three reactions in the biosynthesis of melanin. *Science* **1982**, *217*, 1163−1165.

(3) Pan, Z. Z.; Li, H. L.; Yu, X. J.; Zuo, Q. X.; Zheng, G. X.; Shi, Y.; Liu, X.; Lin, Y. M.; Liang, G.; Wang, Q. Synthesis and antityrosinase activities of alkyl 3,4-dihydroxybenzoates. *J. Agric. Food Chem.* **2011**, *59*, 6645−6649.

(4) Friedman, M. Food browning and its prevention: an overview. *J. Agric. Food Chem.* **1996**, *44*, 631−653.

(5) Chai, W. M.; Shi, Y.; Feng, H. L.; Qiu, L.; Zhou, H. C.; Deng, Z. W.; Yan, C. L.; Chen, Q. X. NMR, HPLC-ESI-MS, and MALDI-TOF MS analysis of condensed tannins from *Delonix regia* (Bojer ex Hook.) Raf. and their bioactivities. *J. Agric. Food Chem.* **2012**, *60*, 5013−5022.

(6) Gomez-Cordoves, C.; Bartolomé, B.; Vieira, W.; Virador, V. Effects of wine phenolics and sorghum tannins on tyrosinase activity and growth of melanoma cells. *J. Agric. Food Chem.* **2001**, *49*, 1620−1624.

(7) Serrano, J.; Puupponen Pimiä, R.; Dauer, A.; Aura, A. M.; Saura Calixto, F. Tannins: current knowledge of food sources, intake, bioavailability and biological effects. *Mol. Nutr. Food Res.* **2009**, *53*, S310−S329.

(8) Aron, P. M.; Kennedy, J. A. Flavan-3-ols: nature, occurrence and biological activity. *Mol. Nutr. Food Res.* **2008**, *52*, 79−104.

(9) Cai, Y. Z.; Sun, M.; Xing, J.; Luo, Q.; Corke, H. Structure-radical scavenging activity relationships of phenolic compounds from traditional Chinese medicinal plants. *Life Sci.* **2006**, *78*, 2872−2888.

(10) Dixon, R. A.; Xie, D. Y.; Sharma, S. B. Proanthocyanidins − a final frontier in flavonoid research? *New Phytol.* **2005**, *165*, 9−28.

(11) Hümmer, W.; Schreier, P. Analysis of proanthocyanidins. *Mol. Nutr. Food Res.* **2008**, *52*, 1381−1398.

(12) Kim, J. G.; Beppu, K.; Kataoka, I. Varietal differences in phenolic content and astringency in skin and flesh of hardy kiwifruit resources in Japan. *Sci. Hortic.−Amsterdam* **2009**, *120*, 551−554.

(13) Park, Y.-S.; Leontowicz, H.; Leontowicz, M.; Namiesnik, J.; Suhaj, M.; Cvikrová, M.; Martincová, O.; Weisz, M.; Gorinstein, S. Comparison of the contents of bioactive compounds and the level of antioxidant activity in different kiwifruit cultivars. *J. Food Compos. Anal.* **2011**, *24*, 963−970.

(14) Dawes, H. M.; Keene, J. B. Phenolic composition of kiwifruit juice. *J. Agric. Food Chem.* **1999**, *47*, 2398−2403.

(15) Chai, W. M.; Chen, C. M.; Gao, Y. S.; Feng, H. L.; Ding, Y. M.; Shi, Y.; Zhou, H. T.; Chen, Q. X. Structural analysis of proanthocyanidins isolated from fruit stone of Chinese hawthorn

with potent antityrosinase and antioxidant activity. *J. Agric. Food Chem.* **2014**, *62*, 123−129.
(16) Guyot, S.; Marnet, N.; Laraba, D.; Sanoner, P.; Drilleau, J. F. Reversed-phase HPLC following thiolysis for quantitative estimation and characterization of the four main classes of phenolic compounds in different tissue zones of a French cider apple variety (*Malus domestica* var. Kermerrien). *J. Agric. Food Chem.* **1998**, *46*, 1698−1705.
(17) Gu, L.; Kelm, M.; Hammerstone, J. F.; Beecher, G.; Cunningham, D.; Vannozzi, S.; Prior, R. L. Fractionation of polymeric procyanidins from lowbush blueberry and quantification of procyanidins in selected foods with an optimized normal-phase HPLC-MS fluorescent detection method. *J. Agric. Food Chem.* **2002**, *50*, 4852−4860.
(18) Li, Z. C.; Chen, L. H.; Yu, X. J.; Hu, Y. H.; Song, K. K.; Zhou, X. W.; Chen, Q. X. Inhibition kinetics of chlorobenzaldehyde thiosemicarbazones on mushroom tyrosinase. *J. Agric. Food Chem.* **2010**, *58*, 12537−12540.
(19) Brand-Williams, W.; Cuvelier, M.; Berset, C. Use of a free radical method to evaluate antioxidant activity. *LWT−Food Sci. Technol.* **1995**, *28*, 25−30.
(20) Re, R.; Pellegrini, N.; Proteggente, A.; Pannala, A.; Yang, M.; Rice-Evans, C. Antioxidant activity applying an improved ABTS radical cation decolorization assay. *Free Radical Biol. Med.* **1999**, *26*, 1231−1237.
(21) Benzie, I. F. F.; Strain, J. The ferric reducing ability of plasma (FRAP) as a measure of "antioxidant power": the FRAP assay. *Anal. Biochem.* **1996**, *239*, 70−76.
(22) Xiang, P.; Lin, Y.; Lin, P.; Xiang, C.; Yang, Z.; Lu, Z. Effect of cationization reagents on the matrix-assisted laser desorption/ionization time-of-flight mass spectrum of Chinese gallotannins. *J. Appl. Polym. Sci.* **2007**, *105*, 859−864.
(23) Li, C.; Leverence, R.; Trombley, J. D.; Xu, S.; Yang, J.; Tian, Y.; Reed, J. D.; Hagerman, A. E. High molecular weight persimmon (*Diospyros kaki* L.) proanthocyanidin: a highly galloylated, A-linked tannin with an unusual flavonol terminal unit, myricetin. *J. Agric. Food Chem.* **2010**, *58*, 9033−9042.
(24) Monagas, M.; Quintanilla-López, J. E.; Gómez-Cordovés, C.; Bartolomé, B.; Lebrón-Aguilar, R. MALDI-TOF MS analysis of plant proanthocyanidins. *J. Pharm. Biomed.* **2010**, *51*, 358−372.
(25) Wang, C. Y.; Ng, C. C.; Lin, H. T.; Shyu, Y. T. Free radical-scavenging and tyrosinase-inhibiting activities of extracts from sorghum distillery residue. *J. Biosci. Bioeng.* **2011**, *111*, 554−556.
(26) Wu, L.; Chen, Y.; Ho, J. A.; Yang, C. Inhibitory effect of red koji extracts on mushroom tyrosinase. *J. Agric. Food Chem.* **2003**, *51*, 4240−4246.
(27) Kim, D.; Park, J.; Kim, J.; Han, C.; Yoon, J.; Kim, N.; Seo, J.; Lee, C. Flavonoids as mushroom tyrosinase inhibitors: a fluorescence quenching study. *J. Agric. Food Chem.* **2006**, *54*, 935−941.
(28) Matoba, Y.; Kumagai, T.; Yamamoto, A.; Yoshitsu, H.; Sugiyama, M. Crystallographic evidence that the dinuclear copper center of tyrosinase is flexible during catalysis. *J. Biol. Chem.* **2006**, *281*, 8981−8990.
(29) Maisuthisakul, P.; Gordon, M. H. Antioxidant and tyrosinase inhibitory activity of mango seed kernel by product. *Food Chem.* **2009**, *117*, 332−341.
(30) Yokozawa, T.; Chen, C. P.; Dong, E.; Tanaka, T.; Nonaka, G. I.; Nishioka, I. Study on the inhibitory effect of tannins and flavonoids against the 1,1-diphenyl-2-picrylhydrazyl radical. *Biochem. Pharmacol.* **1998**, *56*, 213−222.
(31) Hagerman, A. E.; Riedl, K. M.; Jones, G. A.; Sovik, K. N.; Ritchard, N. T.; Hartzfeld, P. W.; Riechel, T. L. High molecular weight plant polyphenolics (tannins) as biological antioxidants. *J. Agric. Food Chem.* **1998**, *46*, 1887−1892.
(32) Ariga, T.; Hamano, M. Radical scavenging action and its mode in procyanidins B-1 and B-3 from Azuki beans to peroxyl radicals (food and nutrition). *Agric. Biol. Chem.* **1990**, *54*, 2499−2504.
(33) Zhou, H. C.; Lin, Y. M.; Wei, S. D.; Tam, N. F. Y. Structural diversity and antioxidant activity of condensed tannins fractionated from mangosteen pericarp. *Food Chem.* **2011**, *129*, 1710−1720.
(34) Shoji, T.; Masumoto, S.; Moriichi, N.; Kobori, M.; Kanda, T.; Shinmoto, H.; Tsushida, T. Procyanidin trimers to pentamers fractionated from apple inhibit melanogenesis in B16 mouse melanoma cells. *J. Agric. Food Chem.* **2005**, *53*, 6105−6111.

tion is available on the oxidation and physicochemical changes in frozen pork dumpling filler. In our previous study, the influence of the storage temperature and temperature oscillation on lipid and protein oxidation and flavor changes in frozen pork dumpling filler was evaluated.[18] The aim of the present study is to assess the influence of the fat content on the oxidation and physicochemical changes in pork dumpling filler at various frozen durations. In particular, protein thermal stability, dynamic rheological properties, and sensory attributes were investigated.

MATERIALS AND METHODS

Materials and Chemicals. Six Landrace × Large white × Duroc crossbred pigs (90−100 kg body weight, 6 months old) were harvested at a local processing plant. The animals were reared intensively and fed until they reached a commercial slaughter weight. Animals were humanely slaughtered in a commercial abattoir (Beidahuang Meat Corp., Harbin, Heilongjiang, China) following standard industry procedures. After evisceration, carcasses were split immediately and chilled at 4 °C. At 12 h after slaughter, 40 kg of pork neck and shoulder lean meat and 10 kg of backfat (thickness = 2−2.5 cm) were obtained. The samples were kept on ice and transported to the laboratory and used on the same day. Bovine serum albumin and 2,4-dinitrophenylhydrazine (DNPH) were purchased from Sigma Chemical Co. (St. Louis, MO, USA). All other chemicals were purchased from Wantai Biomedicals Inc. (Harbin, China) and were of at least analytical grade.

Sample Preparation. Three batches of dumplings were manufactured in a pilot plant (10−12 °C), and each batch was used as a replicate. Pork shoulder and neck meat were ground through a 4 mm plate and mixed with porcine back fat and ingredients according to the product formulations (Table 1). Four fat levels (0, 10, 20, and 30% w/w, i.e., back fat/lean ratios of 0:100, 10:90, 20:80, and 30:70) of dumpling filler were prepared. In the dumpling filler preparation, fresh pork trims and ingredients were mixed by blending for 5 min with a KitchenAid mixer (SYM-10, Guangzhou Shanyou Machinery Equipment Co., Ltd., Guangdong, China) at a speed of 160 rpm. Dumplings with 10 g of filling each were shaped by hand with wheat dough as the dumpling wrapper. Then they were frozen at −25 °C for at least 20 h to ensure the core temperature of dumplings was below −18 °C. The dumplings were placed in styrene foam trays, wrapped with an oxygen-permeable polyvinyl chloride film (8 μm thickness and 18500 $cm^3/m^2/24$ h/atm of oxygen permeability; Weiguang Plastic Co., Ltd., Jiangsu, China), and stored for 0, 30, 60, 90, and 180 days at −18 °C. To determine the cooking loss and breaking strength accurately, some of the raw dumpling filler (30 samples for each treatment and 40 g of raw filler for each sample) were directly stuffed into polyvinyl chloride (PVC) casing (20 mm of diameter) to obtain shape-consistent "casing dumpling" samples, and then they were stored at −18 °C. A strict sanitation procedure was followed to avoid microbial contamination by implementing sanitation standard operating procedures. All equipment and tools were cleaned and sanitized with hot water (>82 °C), and the personnel hand disinfection was in accordance with standard procedures. For each fat level, 230 dumplings were used. At 0 days, 50 dumplings (44 ordinary dumplings and 6 casing dumplings) from each fat level were used for analysis. Among them, 5 raw dumplings were peeled off for proximate composition, 19 raw dumplings were peeled off for physicochemical analysis, 6 casing dumplings were cooked and used for cooking loss and breaking strength, and 20 dumplings were cooked for a sensory panel evaluation. At 30, 60, 90, and 180 days, only 45 dumplings (39 ordinary dumplings and 6 casing dumplings) were used, because there was no need to analyze proximate composition at these storage times.

Table 1. Formulations (in Grams) for Dumpling Fillers with Different Levels of Fat

	fat level[a]			
ingredient	0%	10%	20%	30%
lean meat	1000	900	800	700
fat	0	100	200	300
soy oil	6	6	6	6
salt	30	30	30	30
soy sauce	40	40	40	40
water	100	100	100	100
fresh ginger	20	20	20	20
green onion	20	20	20	20
spices	8	8	8	8
total	1224	1224	1224	1224

[a]The fat level (%) means the percentage of fat added to the total meat amount.

Proximate Composition. The proximate composition was analyzed according to the method of Hou.[19] The moisture in the fillers was determined by drying the samples in a 105 °C oven to a constant weight. Crude lipid was extracted by petroleum ether in a Soxhlet apparatus for 2.5 h at 60 °C. Protein was measured by the Kjeldahl method (KDN-F, FOSS Corp., Slangerupgade, Hilleroed, Denmark), and a 6.25 nitrogen-to-protein conversion factor was used for the calculation. The ash content was measured as the residue after overnight heating of the samples in a 550 °C muffle furnace (SX2-25-10, Zhonghuan Experimental Stove Corp., Tianjin, China) for 5 h.

Preparation of Myofibrillar Protein (MP). MP was prepared from dumpling filler according to the procedure of Xia et al.[8] Thawed dumpling filler was homogenized by blending for 30 s in a Waring Blendor with 4 volumes (w/v) of an isolation buffer (0.1 M NaCl, 10 mM sodium phosphate, 1 mM EGTA, and 2 mM $MgCl_2$, pH 7.0). The filler homogenate was centrifuged at 2000*g* for 20 min, and the supernatant was discarded. The pellet was washed two more times with 4 volumes of the same isolation buffer using the same centrifugation and blending conditions as mentioned above. The myofibril suspension was filtered through four layers of cheesecloth to remove connective tissue, and its pH was adjusted to 6.0 with 0.1 M HCl prior to centrifugation. The MP was stored in a tightly capped bottle and utilized within 24 h. The protein concentration of the myofibril pellet was measured according to the biuret method. The MP solution was used for carbonyl content determination and dynamic rheological testing.

Thiobarbituric Acid-Reactive Substances (TBARS). TBARS were determined according to the method of Wang and Xiong.[20] The TBARS value, expressed as milligrams of malonaldehyde per kilogram of dumpling filler sample, was calculated using the equation

$$\text{TBARS [mg malondialdehyde (MDA)/kg meat]} = (A_{532}/W_s) \times 9.48$$

where A_{532} is the absorbance (532 nm) of the assay solution, W_s is the dumpling filler weight (g), and 9.48 is a constant derived from the dilution factor and the molar extinction coefficient (152,000 M^{-1} cm^{-1}) of the red thiobarbituric acid reaction product. The assay was carried out with three samples, and each sample was analyzed in triplicate.

Carbonyl Content Determination. The carbonyl groups were detected by reaction with DNPH to form protein hydrazones according to the method of Xia et al.[8] Absorbance was measured at 370 nm for the DNPH-treated sample against HCl control. The amount of carbonyl is expressed as nanomoles of DNPH fixed per milligram of protein using an absorption coefficient of 22000 M^{-1} cm^{-1} for protein hydrazones.

Differential Scanning Calorimetry (DSC). In dumpling filler, the pork was ground through a 4 mm plate, so it existed in the form of small muscle particles. The minced muscle particles were separated from dumpling filler and were used for DSC analyses for thermal denaturation on a PerkinElmer DSC system 6 device (PerkinElmer Co. Ltd., Waltham, MA, USA) according to the method of Srinivasan

dx.doi.org/10.1021/jf5008083 | J. Agric. Food Chem. 2014, 62, 6390−6399

Table 2. Proximate Analysis of Dumpling Fillers with Different Added Fat Levels (Mean Value ± SD)[a]

fat level[b] (%)	protein	lipid	moisture	ash
0	18.09 ± 0.13a	5.13 ± 0.84d	70.50 ± 0.57a	3.44 ± 0.01a
10	15.32 ± 0.11b	12.14 ± 2.52c	64.38 ± 0.43b	3.07 ± 0.20a
20	14.53 ± 0.01c	20.53 ± 3.05b	56.45 ± 1.97c	2.98 ± 0.14a
30	13.71 ± 0.01d	28.09 ± 2.52a	52.86 ± 2.88d	2.89 ± 0.22a

[a]Means (n = 3) in the same column with different letters differ significantly ($P < 0.05$). [b]The fat level (%) means the percentage of fat added to the total meat amount.

et al.[21] The muscle samples (15−18 mg) were weighed accurately into aluminum pans and hermetically sealed. An empty pan was used as reference. The instrument was calibrated for temperature and enthalpy using indium and naphthalene as standards. DSC scans were recorded from 30 to 100 °C at a constant rate of 10 °C/min. The transition temperature (T_{max}) was recorded, and the total transition enthalpy change (ΔH) associated with protein denaturation was calculated from the peak area using PerkinElmer software and expressed in joules per gram of sample material. All DSC scanning was performed in triplicate.

Dynamic Thermomechanical Analysis (DTMA). The DTMA of the prepared MP solution during thermal gelation was performed using a Bohlin Gemini2 rheometer (Malvern Corp., UK) as described by Xia et al.[9] The MP samples (40 mg/mL protein in 0.1 M NaCl) were loaded in the 1 mm gap between the two parallel plates (diameter of upper plate = 6 cm) by shearing the sample in an oscillatory mode at a fixed frequency of 1 Hz with a maximum strain of 0.02 and heated at a rate of 2 °C/min from 20 to 85 °C. Distilled water was filled to a groove fixed on the upper parallel plate, and then the samples were coated with a stainless cover to prevent drying. The dynamic rheological properties of myofibril samples were described in terms of the shear storage modulus (G', the elastic response of the gelling material), and tan δ values (the ratio of G''/G') ae presented to demonstrate the relative viscosity to elasticity, which was also continuously recorded during the rheological testing.

Cooking Loss Determination. The frozen casing dumplings were weighed (W_0) individually and then cooked directly in boiling water (100 °C) for exactly 10 min and chilled to equilibrate to room temperature (20 °C). Then, a needle was inserted into the casing of the casing dumpling; the juice in the wrapper was released, and then the filler was weighed again (W_1). The cooking loss (%) of the samples was calculated as follows:

$$\text{cooking loss (\%)} = \frac{W_0 - W_1}{W_0} \times 100\%$$

All measurements were made in six replicates, and the mean values from these replicates are reported. After cooking loss measurement, the fillers were subjected to breaking strength analysis.

Breaking Strength Determination. The breaking strength of the cooked fillers was measured by compression tests using a texture analyzer (Stable Micro System; TA: XT2i, UK) with a flat-surface cylindrical probe (P/50) 50 mm in diameter attached to a 25 kg load cell with a 60 mm/min crosshead speed of the probe. From each cooked filler, 25 × 20 mm (high × diameter) cores were compressed until the structure was disrupted. Both the break force (B) and distance (D) of the first break point were recorded automatically by the software, and the breaking strength was expressed as

$$\text{breaking strength (N/m)} = B/D$$

All measurements were made in six replicates, and the mean values from these replicates are reported.

Sensory Evaluation. The sensory qualities of the cooked dumplings were evaluated by eight persons (selected staff, faculty, and graduate students) who had prior experience with meat product evaluation. The panel was trained to identify the specific sensory traits of dumplings using 20 other cooked dumplings in preliminary sessions. A total of five panel sessions, corresponding to 0, 30, 60, 90, and 180 days of frozen storage, were conducted. At the beginning of every panel session, a "warm-up" sample (cooked dumplings) was assessed as a reminder of the score range for each sensory trait. During the sensory sessions, no visible signs of psychological or physical anomaly were observed in any of the panelists. The number of dumplings sampled from each treatment at each frozen storage time was 20, and the total number of samples per session was 80. The sensory evaluation room contained partitioned booths each illuminated with normal lights. The juiciness, texture, rancid odor, and overall acceptability were assessed. Each assessor was served two dumplings on hot plates from the same group immediately after cooking. The samples were assigned random numbers and given to the panelists randomly. The panelists scored the dumplings using a 10-point scale as follows: for texture, 1 = rough, 10 = smooth; for rancid odor, 1 = undetectable, 10 = sharply pungent smell; for juiciness, 1 = dry, 10 = juicy; and for overall acceptability, 1 = low and 10 = high. Between sample evaluations, the panelists were given water to rinse their mouths.

Statistical Analyses. The effects of fat addition levels (0, 10, 20, and 30%) and storage duration (0, 30, 60, 90, and 180 days) at −18 °C on the oxidation and physicochemical changes of frozen pork dumpling filler were evaluated. Three batches of dumplings were prepared, and all specific experiments were repeated at least three times to test the quality changes in the dumplings. Data were analyzed using the General Linear Model procedure of Statistix software 8.1 (Analytical Software, St. Paul, MN, USA). Analysis of variance (ANOVA) was conducted to determine the significance of the main effects. Significant differences ($P < 0.05$) between means were identified using Tukey's HSD test for multiple comparisons.

RESULTS AND DISCUSSION

Proximate Composition. Proximate analyses for raw dumpling fillers in four formulations are given in Table 2. There were significant differences in the percentages of moisture, protein, and lipid among different fat level groups. As the fat level increased from 0 to 30%, the lipid content increased from 5.13 to 28.09% ($P < 0.05$), and the percentages of protein and moisture decreased from 18.09 and 70.50% to from 13.71 and 52.86%, respectively ($P < 0.05$). The results are in agreement with those reported by Serdaroğlu and Değırmencioğlu,[22] who reported that the fat content of raw meatballs increased from 5.8 to 22.2%, whereas the moisture and protein percentages decreased from 67.8 and 19.8 to 58.1 and 16.2%, respectively. Guerra et al.[23] also found in goat mortadella that the protein and moisture levels decreased with increased fat percentages.

Lipid Oxidation. As shown in Figure 1a, the TBARS in the frozen dumpling filler steadily increased from 0.18, 0.30, 0.33, and 0.43 mg MDA/kg meat (0 days) to 1.60, 1.98, 2.41, and 3.29 mg/kg for 0, 10, 20, and 30% fat addition ($P < 0.05$), respectively, over 180 days of storage. TBARS production was significantly enhanced with increased fat levels, which indicated that high fat contents could significantly increase the formation of malonaldehyde or other secondary products. The influence of the frozen storage duration on TBARS was significantly higher than that of the fat levels ($P < 0.05$). The results of the present study were in good agreement with the results of Soyer

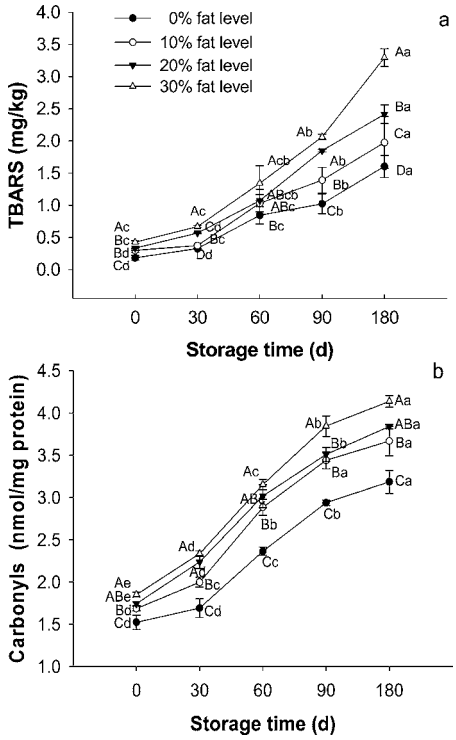

Figure 1. Influence of different fat levels on TBARS and carbonyl content in frozen dumpling fillers. The fat level (%) means the percentage of added fat to the total meat amount. Means (n = 3) for the same storage time with different upper case letters (A–D) differ significantly (P < 0.05); means for the same fat level with different lower case letters (a–e) differ significantly (P < 0.05).

et al.,[24] who suggested that the fat level increased the frozen storage effect on lipid oxidation.

Oxidation is a major cause of the reduction of the quality and acceptability of meats and meat products, leading to the development of rancidity, off-flavor compounds, polymerization, and other reactions resulting in the reduction of shelf life.[25] During frozen storage, lipids in the dumpling filler are oxidized, and unsaturated fatty acids form hydroperoxides that subsequently decompose to generate various secondary products, such as aldehydes, and other carbonyl compounds that cause rancidity flavors.[18] The dumpling filler in this experiment consisted mainly of comminuted pork meat and fat; the pro-oxidants in comminuted meat are released and diffused from various broken cellular organelles, and oxygen from the air also can be an accelerator of lipid oxidation processes by enabling oxygen to react with muscle components.[26,27] Lipid oxidation is commonly linked to the textural attribute of meat products, leading to increasing cooking loss and weakening springiness and cohesiveness of the gel matrix.[8] In our previous study, the free fatty acid (FFA) composition and FFA content in the dumpling filler were determined. The results showed that the total FFA concentration generally increased and the percentage of unsaturated fatty acids in total lipids decreased with increasing frozen storage time in the dumpling samples at −18 °C (P < 0.05).[18] The formation of FFAs is attributed to lipid oxidation and lipid hydrolysis occurring in the dumplings during frozen storage, and FFAs may also have interacted with other constituents during storage.

Protein Oxidation. An increase in the carbonyl contents during frozen storage for all products was observed (Figure 1b). Similar to the fat level and storage duration effect on lipid

Table 3. Influence of Different Added Fat Levels on Maximum Transition Temperatures (T_{max}) and Enthalpies of Denaturation (ΔH) of Muscle Particle from Frozen Dumpling Fillers at −18 °C for Various Times (Mean Value ± SD)[a]

		transition temperature (°C)			enthalpy
fat level[b] (%)	storage time (days)	T_{max-1}	T_{max-2}	T_{max-3}	ΔH^c (J/g)
0	0	58.48 ± 0.10a	67.42 ± 0.53a	80.82 ± 0.45a	0.52 ± 0.02a
	30	57.80 ± 0.17abc	65.92 ± 0.60bcde	80.79 ± 0.66a	0.51 ± 0.01a
	60	57.65 ± 0.16bc	65.32 ± 0.25cdef	79.29 ± 0.13ab	0.48 ± 0.01abc
	90	56.86 ± 0.13defg	64.63 ± 0.24efgh	78.32 ± 0.25ab	0.44 ± 0.01abcd
	180	57.49 ± 0.09cde	63.73 ± 0.09fgh	78.02 ± 0.74ab	0.34 ± 0.01fg
10	0	58.48 ± 0.10a	67.42 ± 0.53a	80.82 ± 0.45a	0.52 ± 0.02a
	30	57.81 ± 0.04abc	65.39 ± 0.35cde	80.19 ± 1.50a	0.49 ± 0.01ab
	60	57.55 ± 0.12cd	66.73 ± 0.33abc	79.68 ± 0.10ab	0.44 ± 0.01abcd
	90	57.44 ± 0.04cde	64.88 ± 0.39defg	78.21 ± 0.55ab	0.41 ± 0.01cdef
	180	56.86 ± 0.16defg	63.09 ± 0.34h	76.85 ± 1.07b	0.34 ± 0.02fg
20	0	58.48 ± 0.10a	67.42 ± 0.53a	80.82 ± 0.45a	0.52 ± 0.02a
	30	58.34 ± 0.08ab	66.50 ± 0.23abcd	80.55 ± 1.13a	0.44 ± 0.02abcd
	60	57.54 ± 0.34cd	65.20 ± 0.57cdef	79.43 ± 0.05ab	0.43 ± 0.04bcdef
	90	56.78 ± 0.06efg	65.95 ± 0.10bcde	76.87 ± 1.04b	0.37 ± 0.01defg
	180	56.34 ± 0.20g	63.48 ± 0.24gh	77.84 ± 1.13b	0.35 ± 0.02efg
30	0	58.48 ± 0.10a	67.42 ± 0.53a	80.82 ± 0.45a	0.52 ± 0.02a
	30	57.46 ± 0.11cde	66.12 ± 0.17ab	80.25 ± 0.54a	0.43 ± 0.02bcde
	60	57.31 ± 0.10cdef	65.57 ± 0.16bcde	79.36 ± 0.74ab	0.41 ± 0.02bcdef
	90	56.62 ± 0.13fg	64.14 ± 0.53cdef	78.84 ± 0.20ab	0.29 ± 0.03g
	180	56.16 ± 0.10g	63.20 ± 0.03gh	76.87 ± 0.48b	0.19 ± 0.01h

[a]Means (n = 3) in the same column with different letters differ significantly (P < 0.05). [b]The fat level (%) means the percentage of fat added to the total meat amount. [c]ΔH value represents the total enthalpy change for all the transitions.

dx.doi.org/10.1021/jf5008083 | J. Agric. Food Chem. 2014, 62, 6390–6399

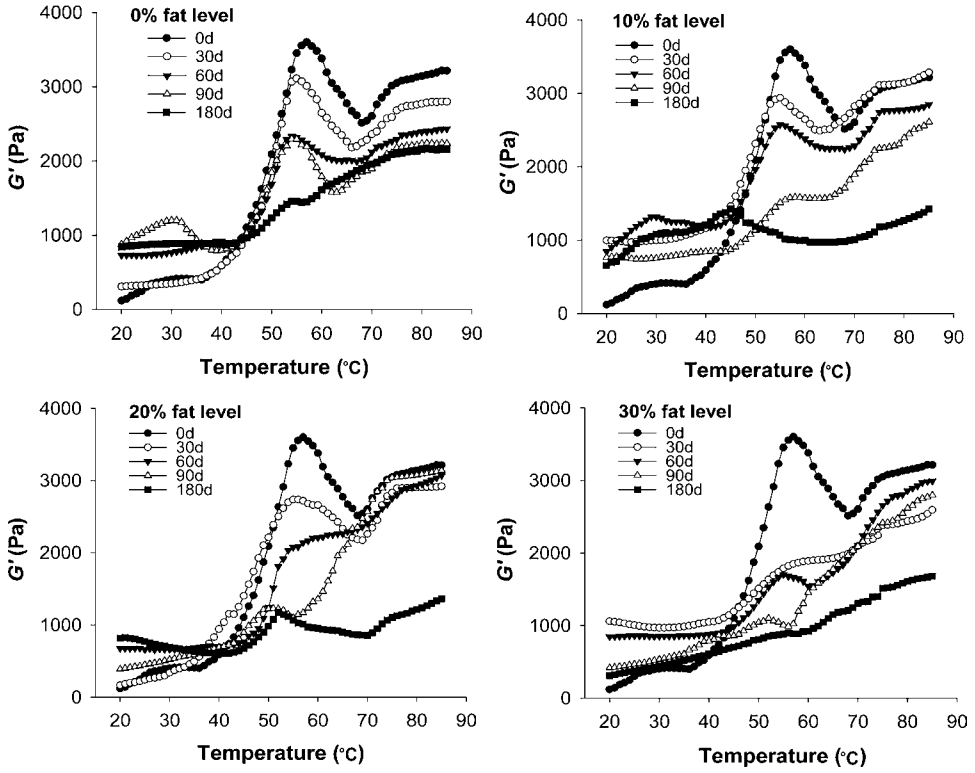

Figure 2. Influence of different fat levels on shear storage modulus (G') of porcine myofibrillar protein in frozen dumpling fillers. The fat level (%) means the percentage of fat added to the total meat amount. Each data point represents the mean from three replications (n = 3).

oxidation, protein oxidation progressed strikingly in four formulations (P < 0.05). At 0 days, the protein carbonyl contents were 1.52, 1.68, 1.74, and 1.85 nmol/mg protein and significantly increased to 3.18, 3.69, 3.84, and 4.14 nmol/mg protein for samples with 0, 10, 20, and 30% fat levels (P < 0.05), respectively, over 180 days of storage. The protein carbonyl contents in 10, 20, and 30% fat levels were all significantly higher than that in the 0% fat level, and carbonyl groups in the 30% fat level were significantly higher than that in 10% fat level (P < 0.05). There were no significant differences between 20 and 30% fat levels over the 180 days of storage except at 90 days. The results were in good agreement with Soyer et al.,[24] who reported significant increases of the total amount of protein carbonyls in chopped chicken meat after 6 months of frozen storage at −18 °C. The increase of protein carbonyls showed that muscle proteins in dumpling fillers were susceptible to oxidative reactions leading to carbonyl gain.

Many of the amino acid side-chain groups, such as those with NH_2 or NH−, are well-known to be sensitive to hydroxyl radical attack. These groups are easily converted to carbonyls when oxidized.[28] Protein carbonyls can also be produced by peptide bond cleavages. Additionally, exogenous carbonyls may be introduced into proteins by reaction with lysine residues.[29] Oxidation causes quality losses in frozen meat products characterized by discoloration, flavor deterioration, destruction of nutrients, and the possible formation of toxic compounds.[30] Formation of carbonyl compounds is one of the most marked changes occurring during the oxidation of proteins. In the present experiments, mincing and the low temperatures applied during storage could have disrupted the tissues, thereby promoting protein oxidation in the dumpling fillers. Muscle proteins are susceptible to oxidative reactions initiated by secondary products of lipid oxidation, such as malonaldehyde.[20,31] The aldehydes formed by lipid oxidation can react with the side-chain amino groups of proteins, such as lysine, in myofibrils to produce Schiff bases, which may cause deterioration in the flavor, texture, and overall quality of muscle foods.[24]

Changes in Protein Thermal Stability. DSC is a suitable method for studying the protein thermal stability during processing and storage. As shown in Table 3, transition temperatures in the muscle protein conformation were assayed to occur within different temperature ranges such as 56.2−58.5 °C for myosin, 63.1−67.4 °C for collagen and sarcoplasmic proteins, and 76.9−80.8 °C for actin, which were similar to the literature reports.[32] The temperature maxima for transitions (T_{max}) of lean meat from frozen dumpling fillers shifted to lower temperatures with increased frozen storage duration. The fat level nearly has no significant effect on transition temperatures except the $T_{max\text{-}1}$ in 20 and 30% fat levels were significantly higher than that in the 0% fat level (P < 0.05). The $T_{max\text{-}1}$, $T_{max\text{-}2}$, and $T_{max\text{-}3}$ of frozen dumplings (0 days) were 58.5, 67.4, and 80.8 °C, and they decreased to 57.5, 63.7, and 78.0 °C, respectively, for the 0% fat level group and to 56.2, 63.2, and 76.9 °C, respectively, for the 30% fat level group after 180 days. A remarkable decrease (P < 0.05) in T_{max} indicated that the thermal stability of the protein reduced, which was possibly because of the dissociation of subunits and protein denaturation.[33] The T_{max} of an endothermic peak designates the maximum transition temperature during the thermal denaturation of a protein. Thus, the smaller the T_{max}, the lower the thermal stability of the protein. Similarly, the total enthalpy (ΔH) of the protein denaturation was substantially reduced during storage. It decreased from 0.52 J/g (0 days) to 0.34 J/g for the 0% fat level group and to 0.19 J/g for the 30% fat level group (P < 0.05) after 180 days. The ΔH was significantly

dx.doi.org/10.1021/jf5008083 | J. Agric. Food Chem. 2014, 62, 6390−6399

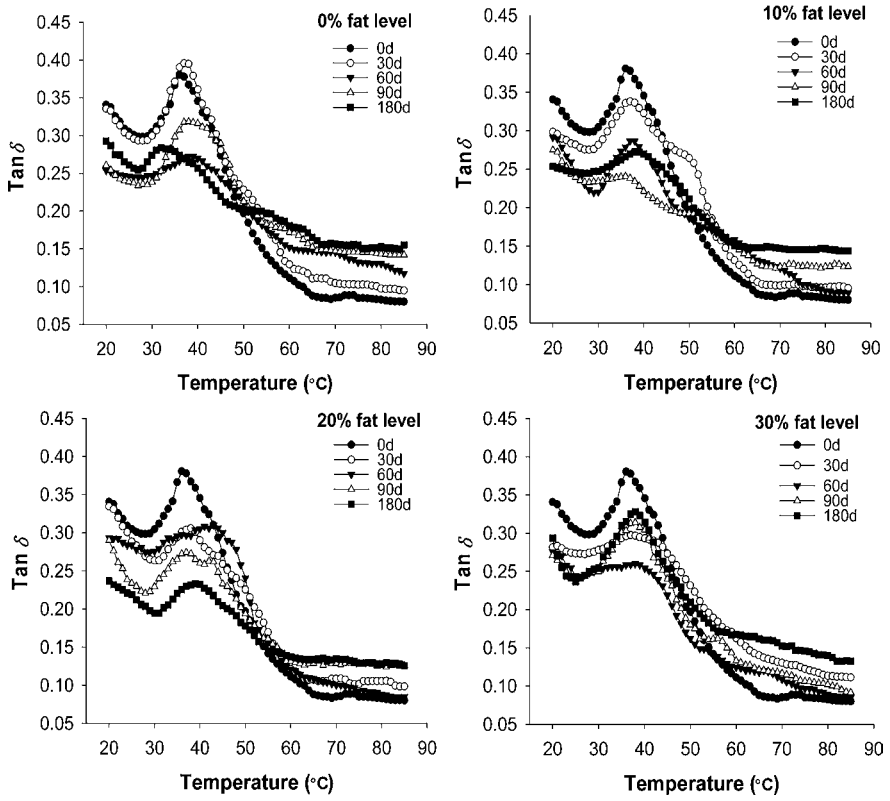

Figure 3. Influence of different fat levels on tangent δ of porcine myofibrillar protein in frozen dumpling fillers. The fat level (%) means the percentage of fat added to the total meat amount. Each data point represents the mean from three replications (n = 3).

decreased only in the products with 30% fat after 90 days of storage ($P < 0.05$). This suggests that protein destabilization in dumping fillers occurred more seriously for a long time of frozen storage, and the higher fat level (30%) further destabilized the proteins.

It is postulated that a possible cause of quality loss was a partial loss of the native structure of meat protein in the dumpling fillers during frozen storage. The reduced conformational stability of muscle protein would also affect negatively the physical attributes of cooked dumpling fillers, such as sensory texture and juiciness. The muscle in dumpling filler was in a minced state, and most likely the previous processing and some ingredients induced a greater alteration of protein structures. A decrease in the thermal stability of protein was also a presumable consequence of oxidative modifications to their primary structures, which were demonstrated by protein oxidation (Figure 1b). Moreover, it is also worth mentioning the possible contribution of some ingredients to the protein thermal stability because of the proportion of some ingredients present in the formulation, such as NaCl, for example. Salt plays an important role in decreasing the hydrogen bonds or augmenting protein aggregation and, consequently, the protein is expected to need lower denaturation energies.[34]

Changes in Dynamic Rheological Properties. The dynamic rheological properties monitored the transformation of a protein solution to a three-dimensional gel network. Curves of storage modulus (G') of MP extracted from dumpling fillers are depicted in Figure 2. For 0% fat level samples at 0 days, the G' started to increase from the beginning of heating to a maximum value (3602 Pa) when the temperature reached approximately 57 °C. From 57 to 68 °C, the G' dropped rapidly and then rose again until 85 °C. This observation was in agreement with other reported findings[35] and is typical of muscle protein rheological patterns and reflects the transitions of heavy meromyosin and light meromyosin. When the dumpling was stored for up to 30, 60, 90, and 180 days, the first peak G' values of the MP gel were decreased to 3109, 2331, 1825, and 1527 Pa, respectively, and the peak temperature was reduced by 2−4 °C. The G' for MP samples from the other three fat levels had a similar reducing trend, and the G' and peak temperature decreased more rapidly with increased fat levels. The transition temperatures of the subfragments of myosin suggested the stability of protein; thus, the decreases in transition temperatures indicated that the reduction in stability of MP was affected by oxidation or denaturation. The rheological changes were also illustrated by the temperature-dependent shifts in tan δ, which describes the relative distribution of "viscosity" compared with "elasticity" during the protein gel matrix formation. As shown in Figure3, the samples (0 days) produced a rheogram composed of a tan δ peak (0.38) at 37 °C followed by a sharp decline to the final heating temperature. The increase in tan δ at the initial heating stage resulted from the formation of a more viscous sol by myosin upon heating to >30 °C. The "viscous" feature of the gelling system outweighs the "elastic" component of the pregel; thus, there is an overall increase in tan δ. As the temperature was increased from 67 to 85 °C, the tan δ dropped steadily, and all gels showed a phase shift angle of <8°, which suggested that the conformation of the myosin molecule changed further and formed a firm, irreversible, and thermal gel. A similar rheological pattern of MP was obtained in the samples at each fat level stored for 30, 60, 90, and 180 days. With increased frozen storage time, the tan δ decreased at the initial heating stage (30−50 °C) and increased at the final heating

dx.doi.org/10.1021/jf5008083 | J. Agric. Food Chem. 2014, 62, 6390−6399

stage (>60 °C). The increase in tan δ at the final heating stage was referred to as "gel weakening", leading to a loose network gel formation.

A possible explanation for the deleterious effect of the high fat level on dynamic rheological properties of MP is that the high content of fat can cause more severe lipid oxidation (proven by TBARS, Figure 1), and the aldehydes formed by lipid oxidation can react with the amino groups of proteins, causing protein structural changes, protein denaturation, and a decrease in the protein stability, which essentially agreed with the DSC results (Table 3). The decrease in G' and increase in tan δ indicated a decrease in the gel-forming ability of MP, which is the most important functional property of comminuted meat products. As displayed in Figure 2, the viscoelasticity of MP decreased as frozen storage time was prolonged and fat level increased, which contributed to explaining the reduction in breaking strength and cooking loss as seen below (Figure 3).

Cooking Loss. Cooking loss of dumpling fillers was affected by the fat level ($P < 0.05$) (Figure 4a). In dumpling fillers of 0, 10, 20, and 30% fat levels, the cooking losses were 17.8, 19.4, 20.4, and 21.5% at 0 days and increased to 22.0, 23.1, 24.3, and 27.0%, respectively, after 180 days ($P < 0.05$). The cooking losses in all products increased during storage, but their increasing rate in each fat level during storage was similar. The fat content in dumpling filler was positively related to the total cooking losses, which was probably due to an insufficient amount of meat proteins to hold all of this added fat and water.

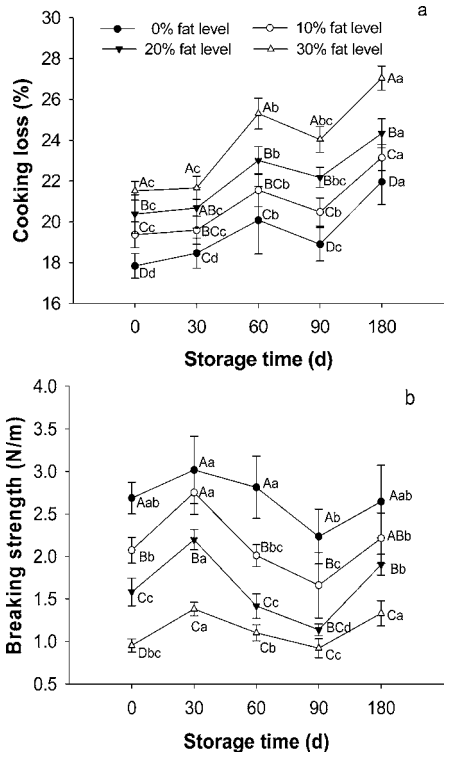

Figure 4. Influence of different fat levels on cooking loss and breaking strength of frozen dumpling fillers. Means ($n = 6$) for the same storage time with different upper case letters (A–D) differ significantly ($P < 0.05$); means for the same fat level with different lower case letters (a–d) differ significantly ($P < 0.05$).

Water loss affects meat and meat product appearance, texture, and sensory properties, and it is most relevant to water-binding capacity.[36] The cooking loss of muscle can lead to less acceptability because of the loss of some taste constituents, such as some nucleotides or amino acids. The liquid of cooking loss comes mainly from constitutive water and fat that melts during heating because of the effect of freezing and frozen storage on muscle structure; hence, its capacity to retain water could be attenuated with increased frozen storage time. The increased cooking loss of filler samples during frozen storage may also be construed as a result of increased protein oxidation as demonstrated above (Figure 1) and possibly the weakening of the myofibril lattices because of protein denaturation (Table 2 and Figure 2). Muscle proteins play a key role in the three-dimensional gel matrix development in meat products; the denatured and reduced protein decreased the gel-forming ability of fillers, so the poorly formed gel matrix possessed lower water- and lipid-holding capacities,[37] which resulted in an increase in loss of water as the frozen storage time increased. McCord et al.[38] suggested that the addition of the higher fat content apparently led to a weaker and more deformable gel structure and decreased the binding between meat particles. Additionally, increasing cooking losses were observed with increasing fat levels, which suggested that a larger fat to protein ratio would also generate a much less stable gel matrix with reduced binding properties and would most likely lead to a greater release of water and fat.[39]

Breaking Strength. The fat addition levels had a remarkable effect on the breaking strength of the dumpling fillers. The increase of fat level significantly lowered the breaking strength ($P < 0.05$) (Figure 4b). No change of breaking strength was observed during 180 days of storage in products except for the products with 20 and 30% fat, in which the breaking strength slightly increased after 180 days of storage. In dumpling fillers of the 0, 10, 20, and 30% fat levels, the breaking strengths were 2.69, 2.07, 1.58, and 0.95 N/m on 0 days and changed to 2.65, 2.21, 1.90, and 1.33 N/m, respectively, after 180 days. There was a significant increase ($P < 0.05$) at 30 days of storage in the breaking strength in all of the filler samples except that in 0% fat addition, and then they decreased until 90 days, which may be attributed to the modest protein oxidation of MP as proven by the carbonyl content measurement (Figure 1b). This observation was in agreement with the findings of Bess et al.,[40] who reported that the breaking strength of ground pork patties stored frozen for 6 weeks was higher than that of patties stored for 9 weeks. Liu et al.[41] confirmed that slow and mild-to-moderate oxidation could facilitate the formation of disulfide cross-links in myofibrils, resulting in the formation of a stronger gel. An increase of the damage to the three-dimensional network structure of the dumpling filler could result in a decrease in the breaking strength of the dumpling filler. The pronounced decrease in breaking strength might be related to the fact that cohesiveness tended to decrease as animal fat content increased in the meat treatments, as suggested by Youssef and Barbut.[42] An increase in the fat content and a decrease in the protein content will lower the ability to form a stronger and denser gel/emulsion matrix, which can affect the internal structure of the product, resulting in weakened binding properties. Furthermore, freezing and frozen storage can cause chemical and structural changes of muscle protein, which negatively affects the quality attributes of meat products, that is, texture, water- and fat-binding properties, sensory characteristics, and others.[43]

Sensory Evaluation. The sensory panel results on the dumpling fillers with different fat levels stored at −18 °C for

dx.doi.org/10.1021/jf5008083 | J. Agric. Food Chem. 2014, 62, 6390–6399

Table 4. Sensory Evaluation of Frozen Dumplings Stored with Different Fat Levels (Mean Value ± SD)[a]

		sensory attribute[b]			
fat level[c](%)	storage time (days)	texture	rancidity	juiciness	overall acceptability
control	0	6.27 ± 0.25efg	1.00 ± 0.01i	4.87 ± 0.11fg	6.23 ± 0.25fg
	30	6.10 ± 0.36fgh	1.17 ± 0.15hi	4.70 ± 0.26fgh	6.00 ± 0.20fgh
	60	5.43 ± 0.40hi	1.43 ± 0.12fghi	4.07 ± 0.12gh	5.23 ± 0.25hi
	90	4.50 ± 0.30jk	1.67 ± 0.31efgh	3.80 ± 0.26hi	4.27 ± 0.25j
	180	3.77 ± 0.25k	2.03 ± 0.15def	2.90 ± 0.10i	3.33 ± 0.41k
10	0	7.23 ± 0.25cd	1.00 ± 0.01i	6.13 ± 0.15de	7.30 ± 0.17de
	30	6.63 ± 0.15def	1.20 ± 0.10ghi	5.80 ± 0.20e	6.80 ± 0.20ef
	60	6.03 ± 0.25fgh	1.57 ± 0.20fghi	5.37 ± 0.32ef	6.07 ± 0.25fgh
	90	5.57 ± 0.21ghi	2.23 ± 0.25cde	4.43 ± 0.40gh	5.90 ± 0.10gh
	180	4.77 ± 0.25ij	2.70 ± 0.36bc	3.80 ± 0.26hi	4.97 ± 0.21ij
20	0	8.90 ± 0.36a	1.03 ± 0.05hi	9.03 ± 0.45a	9.13 ± 0.32a
	30	8.43 ± 0.21ab	1.30 ± 0.20ghi	8.41 ± 0.40ab	8.63 ± 0.32ab
	60	7.77 ± 0.25bc	1.83 ± 0.15efg	8.10 ± 0.36b	8.07 ± 0.21bcd
	90	6.93 ± 0.11de	2.07 ± 0.15cdef	7.10 ± 0.36c	7.43 ± 0.40cde
	180	5.77 ± 0.25gh	3.00 ± 0.20b	6.23 ± 0.25cde	6.77 ± 0.25ef
30	0	9.23 ± 0.25a	1.10 ± 0.10hi	9.20 ± 0.40a	9.27 ± 0.30a
	30	9.13 ± 0.20a	1.43 ± 0.15fghi	8.77 ± 0.25a	8.80 ± 0.26ab
	60	8.73 ± 0.25a	1.97 ± 0.15efg	8.17 ± 0.35ab	8.43 ± 0.41ab
	90	8.47 ± 0.42gh	2.60 ± 0.46bcd	7.93 ± 0.31ab	8.00 ± 0.20bc
	180	7.23 ± 0.25cd	4.10 ± 0.36a	7.03 ± 0.25cd	6.77 ± 0.25e

[a]Means (n = 8) in the same column with different letters differ significantly ($P < 0.05$). [b]Texture = 1 (rough) to 10 (smooth); rancidity = 1 (slight) to 10 (sharply pungent smell); juiciness = 1 (dry) to 10 (juicy); overall acceptability = 1 (low) to 10 (high). [c]The fat level (%) means the percentage of fat added to the total meat amount.

Table 5. Correlation Coefficients (r) between Oxidation and Physicochemical Properties of Dumpling Filler[a]

	cooking loss	breaking strength	$T_{max\text{-}1}$	ΔH	G'	tan δ
TBARS	0.83**	−0.16	−0.90**	−0.92**	−0.67*	0.81*
carbonyl content	0.75*	−0.13	−0.97**	−0.97**	−0.85**	0.88**

[a]**, correlations are significant ($P < 0.01$); *, correlations are significant ($P < 0.05$). $T_{max\text{-}1}$ represents the transition temperature of myosin. ΔH value represents the total enthalpy change for all transitions. G' and tan δ are the values at the end of thermal gelation at the highest temperature (Figures 2 and 3).

180 days are presented in Table 4. During frozen storage, the dumplings with a 30% fat level had significantly higher texture, juiciness, and overall acceptability scores ($P < 0.05$) and also had higher rancidity scores ($P < 0.05$) than those with a 0% fat level and lower fat level samples, indicating that the fat addition was able to improve the texture and juiciness. Independent of the fat level, all of the samples exhibited sensory quality deteriorations with extended frozen storage time. Juiciness is the amount of perceived juices in the meat during chewing or mastication; thus, it is one of the major meat attributes influencing eating quality.[44] From the results of the present study, the juiciness scores decreased with increased frozen storage time, which was consistent with the results of Huff-Lonergan et al.[45] The rancidity change was very significant in all samples ($P < 0.05$) and followed a tendency similar to that of the TBARS value (Figure 1a). As storage time increased, the rancid flavor of the dumpling filler with a 30% fat level developed to a higher extent, whereas the samples with a 0% fat level deteriorated more severely in texture and juiciness. Although rancidity scores of samples with a 30% fat level stored for 180 days developed to a higher level, they were still in the sensory acceptable range. The juiceless and waxy qualities of dumplings may have some relationship to protein denaturation and the increase in ice crystal size during frozen storage.

Relationship between Oxidative and Physicochemical Properties. The relationships between oxidation (TBARS and carbonyl content) and physicochemical properties (cooking loss, breaking strength, transition temperature $T_{max\text{-}1}$, enthalpy, G', and tan δ) of dumpling filler were determined through regression analyses (Table 5). Most of the oxidative and physicochemical indices were all significantly correlated ($P < 0.01$ or $P < 0.05$) except between oxidation indices (TBARS and carbonyl content) and breaking strength, indicating that the oxidative modifications of protein were ultimately responsible for the observed physicochemical property changes including cooking loss, protein thermal stability, and dynamic rheological properties. However, the breaking strength, an index expressing the degree of cohesiveness of the filler mixture, was not significantly affected by the oxidation ($P > 0.05$). In dumpling fillers, salt-soluble myofibrillar proteins exert a cohesive force to bind meat particles together and stabilize fat particles in the matrix,[46] and fat content significantly affects the binding properties as observed in Figure 4. Jost et al.[47] claimed that some large fat globules may disturb protein reticulation and were likely to be excluded from a protein gel

matrix, which may result in poor protein-binding properties. Therefore, fat levels may play vital roles in decreasing the breaking strength of dumpling fillers.

In conclusion, the results of this study demonstrated that the frozen dumplings stored at −18 °C underwent lipid and protein oxidation and exhibited deterioration in physicochemical and sensory properties. The fat level and frozen storage duration have strong effects on lipid and protein oxidation, protein thermal stability, gel-forming ability, cooking loss, breaking force, and sensory attributes. Lipid and protein oxidation was closely related to protein denaturation and gel-forming ability deterioration. The dumplings with a high fat level stored for long periods of time had significantly enhanced lipid and protein oxidation and cooking loss and lowered protein thermal stability, viscoelasticity, and breaking strength. The sensory qualities revealed that the dumplings with a high fat level had significantly higher texture, juiciness, and overall acceptability scores but also had higher rancidity scores. Therefore, considering the palatability brought about by fat, it is imperative to add proper fat into dumpling fillers. Additional experiments are needed to evaluate whether the addition of natural antioxidants to pork dumpling filler will help to keep its quality during frozen storage.

AUTHOR INFORMATION

Corresponding Author

*(B.K.) Phone: +86 451 55191794. Fax: +86 451 55190577. E-mail: kongbh63@hotmail.com.

Funding

This research has been supported by the Science Foundation of National Public Beneficial Vocation in China (Grant 201303082), the National 12th Five-Year Science and Technology Supporting Grant (Grant 2012BAD28B02), and the Foundation of Science and Technology in Heilongjiang (Grant GC13B212).

Notes

The authors declare no competing financial interest.

REFERENCES

(1) Zhang, Y.; Ye, Y.; Liu, J.; Xiao, Y.; Sun, Q.; He, Z. The relationship between chinese raw dumpling quality and flour characteristics of Shandong winter wheat cultivars. *Agric. Sci. China* **2011**, *10*, 1792−1800.

(2) Gurjral, H. S.; Kaur, A.; Singh, N.; Sodhi, N. S. Effect of liquid whole egg, fat and textured soy protein on the textural and cooking properties of raw and baked patties from goat meat. *J. Food Eng.* **2002**, *53*, 377−385.

(3) Keeton, J. T. Low-fat meat products-technological problems with processing. *Meat Sci.* **1994**, *36*, 261−276.

(4) Pietrasik, Z.; Janz, J. A. M. Influence of freezing and thawing on the hydration characteristics, quality, and consumer acceptance of whole muscle beef injected with solutions of salt and phosphate. *Meat Sci.* **2009**, *81*, 523−532.

(5) Filgueras, R. S.; Gatellier, P.; Zambiazi, R. C.; Santé-Lhoutellier, V. Effect of frozen storage duration and cooking on physical and oxidative changes in *M. Gastrocnemius parsinterna* and *M. Iliofiburalis* of *Rhea americana*. *Meat Sci.* **2011**, *88*, 645−651.

(6) Vieira, C.; Diaz, M. T.; Martínez, B.; García-Cachán, M. D. Effect of frozen storage conditions (temperature and length of storage) on microbiological and sensory quality of rustic crossbred beef at different states of ageing. *Meat Sci.* **2009**, *83*, 398−404.

(7) Farouk, M. M.; Swan, J. E. Effect of rigor temperature and frozen storage on functional properties of hot-boned manufacturing beef. *Meat Sci.* **1998**, *49*, 233−247.

(8) Xia, X.; Kong, B.; Liu, Q.; Liu, J. Physicochemical change and protein oxidation in porcine longissimus dorsi as influenced by different freeze−thaw cycles. *Meat Sci.* **2009**, *83*, 239−245.

(9) Xia, X.; Kong, B.; Xiong, Y. L.; Ren, Y. Decreased gelling and emulsifying properties of myofibrillar protein from repeatedly frozen-thawed porcine longissimus muscle are due to protein denaturation and susceptibility to aggregation. *Meat Sci.* **2010**, *85*, 481−486.

(10) Losada, V.; Barros-Velázquez, J.; Aubourg, S. P. Rancidity development in frozen pelagic fish: influence of slurry ice as preliminary chilling treatment. *Food Sci. Technol.* **2007**, *40*, 991−999.

(11) Kanner, J. Oxidative processes in meat and meat products: quality implications. *Meat Sci.* **1994**, *36*, 169−189.

(12) Ladikos, D.; Lougovois, V. Lipid oxidation in muscle foods: a review. *Food Chem.* **1990**, *35*, 295−314.

(13) Obanu, Z.; Ledward, D.; Lawrie, R. Lipid-protein interactions as agents of quality deterioration in intermediate moisture meats: an appraisal. *Meat Sci.* **1980**, *4*, 79−88.

(14) Santé-Lhoutellier, V.; Astruc, T.; Marinova, P.; Greve, E.; Gatellier, P. Effect of meat cooking on physicochemical state and in vitro digestibility of myofibrillar proteins. *J. Agric. Food Chem.* **2008**, *56*, 1488−1494.

(15) Estévez, M.; Ventanas, S.; Cava, R. Protein oxidation in frankfurters with increasing levels of added rosemary essential oil: effect on color and texture deterioration. *J. Food Sci.* **2005**, *70*, c427−c432.

(16) Chen, H. C.; Kung, H. F.; Chen, W. C.; Lin, W. F.; Hwang, D. F.; Lee, Y. C.; Tsai, Y. H. Determination of histamine and histamine-forming bacteria in tuna dumpling implicated in a food-borne poisoning. *Food Chem.* **2008**, *106*, 612−618.

(17) Lee, Y. C.; Kung, H. F.; Lin, C. S.; Hwang, C. C.; Lin, C. M.; Tsai, Y. H. Histamine production by *Enterobacter aerogenes* in tuna dumpling stuffing at various storage temperatures. *Food Chem.* **2012**, *131*, 405−412.

(18) Huang, L.; Xiong, Y. L.; Kong, B.; Huang, X. G.; Li, J. Influence of storage temperature and duration on lipid and protein oxidation and flavour changes in frozen pork dumpling. *Meat Sci.* **2013**, *95*, 295−301.

(19) Hou, M. Determination of moisture, lipid, protein and ash content in foods. In *Food Analysis*; Hou, M., Ed.; Chemical Industry Press: Beijing, China, 2005; pp27−125.

(20) Wang, L. L.; Xiong, Y. L. Inhibition of lipid oxidation in cooked beef patties by hydrolyzed potato protein is related to its reducing and radical scavenging ability. *J. Agric. Food Chem.* **2005**, *53*, 9186−9192.

(21) Srinivasan, S.; Xiong, Y. L.; Blanchard, S. P.; Tidwell, J. H. Physicochemical changes in prawns (*Machrobrachium rosenbergii*) subjected to multiple freeze−thaw cycles. *J. Food Sci.* **1997**, *62*, 123−127.

(22) Serdaroğlu, M.; Değrmencioğlu, Ö. Effects of fat level (5%, 10%, 20%) and corn flour (0%, 2%, 4%) on some properties of Turkish type meatballs (koefte). *Meat Sci.* **2004**, *68*, 291−296.

(23) Guerra, I.; Félex, S.; Meireles, B.; Dalmás, P.; Moreira, R.; Honório, V.; Morgano, M.; Milani, R.; Benevides, S.; Queiroga, R. Evaluation of goat mortadella prepared with different levels of fat and goat meat from discarded animals. *Small Ruminant Res.* **2011**, *98*, 59−63.

(24) Soyer, A.; Özalp, B.; Dalmıs, Ü.; Bilgin, V. Effects of freezing temperature and duration of frozen storage on lipid and protein oxidation in chicken meat. *Food Chem.* **2010**, *120*, 1025−1030.

(25) Morrissey, P. A.; Sheehy, P. J. A.; Galvin, K.; Kerry, J. P.; Buckley, D. J. Lipid stability in meat and meat products. *Meat Sci.* **1998**, *49*, S73−S86.

(26) Ladikos, D.; Lougovois, V. Lipid oxidation in muscle foods: a review. *Food Chem.* **1990**, *35*, 295−314.

(27) O'Grady, M. N.; Monahan, F. J.; Brunton, N. P. Oxymyoglobin oxidation and lipid oxidation in bovine muscle-mechanistic studies. *J. Food Sci.* **2001**, *66*, 386−392.

(28) Sante-Lhoutellier, V.; Aubry, L.; Gatellier, P. Effect of oxidation on in vitro digestibility of skeletal muscle myofibrillar proteins. *J. Agric. Food Chem.* **2007**, *55*, 5343−5348.

(29) Butterfield, D. A.; Stadtman, E. R. Protein oxidation processes in aging brain. *Adv. Cell Aging Gerontol.* **1997**, *2*, 161−191.
(30) Shahidi, F.; Zhong, Y. Lipid oxidation and improving the oxidative stability. *Chem. Soc. Rev.* **2010**, *39*, 4067−4079.
(31) Kikugawa, K.; Beppu, M. Involvement of lipid oxidation products in the formation of fluorescent and cross-linked proteins. *Chem. Phys. Lipids* **1987**, *44*, 277−296.
(32) Tornberg, E. Effects of heat on meat proteins-implications on structure and quality of meat products. *Meat Sci.* **2005**, *70*, 493−508.
(33) Aktaş, N.; Aksu, M. I.; Kaya, M. Changes in myofibrillar proteins during processing of pastirma (Turkish dry meat product) produced with commercial starter cultures. *Food Chem.* **2005**, *90*, 649−654.
(34) Pighin, D.; Sancho, A.; Gonzalez, C. Effect of salt addition on the thermal behavior of proteins of bovine meat from Argentina. *Meat Sci.* **2008**, *79*, 549−556.
(35) Ferris, J.; Sandoval, A.; Barreiro, J.; Sánchez, J.; Müller, A. Gelation kinetics of an imitation-mortadella emulsion during heat treatment determined by oscillatory rheometry. *J. Food Eng.* **2009**, *95*, 677−683.
(36) Huff-Lonergan, E.; Lonergan, S. M. Mechanisms of water-holding capacity of meat: the role of postmortem biochemical and structural changes. *Meat Sci.* **2005**, *71*, 194−204.
(37) Benjakul, S.; Visessanguan, W.; Thongkaew, C.; Tanaka, M. Effect of frozen storage on chemical and gel-forming properties of fish commonly used for surimi production in Thailand. *Food Hydrocolloids* **2005**, *19*, 197−207.
(38) McCord, A.; Smyth, A. B.; O'Neill, E. E. Heat-induced gelation properties of salt-soluble muscle proteins as affected by non-meat proteins. *J. Food Sci.* **1998**, *63*, 580−583.
(39) Carballo, J.; Mota, N.; Baretto, G.; Colmenero, F. J. Binding properties and colour of bologna sausage made with varying fat levels, protein levels and cooking temperatures. *Meat Sci.* **1995**, *41*, 301−313.
(40) Bess, K. N.; Boler, D. D.; Tavárez, M. A.; Johnson, H. K.; McKeith, F. K.; Killefer, J.; Dilger, A.C. Texture, lipid oxidation and sensory characteristics of ground pork patties prepared with commercially available salts. *Food Sci. Technol.* **2013**, *50*, 408−413.
(41) Liu, G.; Xiong, Y. L. Thermal transitions and dynamic gelling properties of oxidatively modified myosin, β-lactoglobulin, soy 7S globulin and their mixtures. *J. Sci. Food Agric.* **2000**, *80*, 1728−1734.
(42) Youssef, M. K.; Barbut, S. Fat reduction in comminuted meat products-effects of beef fat, regular and pre-emulsified canola oil. *Meat Sci.* **2011**, *87*, 356−360.
(43) Colmenero, F. J.; Barreto, G.; Fernández, P.; Carballo, J. Frozen storage of Bologna sausages as a function of fat content and of levels of added starch and egg white. *Meat Sci.* **1996**, *42*, 325−332.
(44) Maltin, C. A.; Warkup, C. C.; Matthews, K. R.; Grant, C. M.; Porter, A. D.; Delday, M. I. Pig muscle fibre characteristics as a source of variation in eating quality. *Meat Sci.* **1997**, *47*, 237−248.
(45) Huff-Lonergan, E.; Baas, T. J.; Malek, M.; Dekkers, J. C.; Prusa, K.; Rothschild, M. F. Correlations among selected pork quality traits. *J. Anim. Sci.* **2002**, *80*, 617−627.
(46) Xiong, Y. L. Structure-function relationship of muscle protein. In *Food Proteins and Their Applications*; Damodaran, S., Paraf, A., Eds.; Dekker: New York, 1997; pp 341−392.
(47) Jost, R.; Beachler, R.; Masson, G. Heat gelation of oil-in-water emulsions stabilized by whey protein. *J. Food Sci.* **1986**, *51*, 440−449.

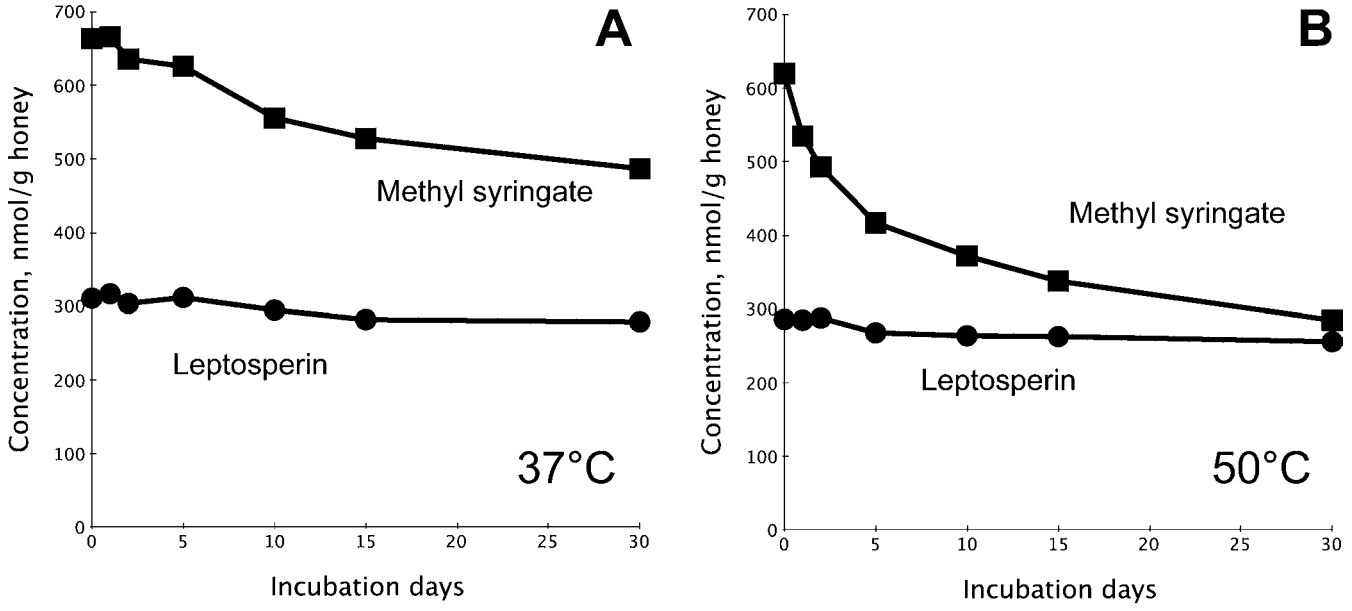

Figure 1. Time-dependent changes in the amounts of leptosperin or methyl syringate in manuka honey during incubation under warm conditions [37 °C (A) or 50 °C (B)].

mL of water, stirred at room temperature (r.t.) for 30 min, and filtered to remove impurities. The filtrate and 400 mL of (wet) Diaion Sepabeads HP20 resins (Mitsubishi Chemical Co., Tokyo, Japan), pretreated with methanol and then water, were mixed in a bottle and incubated with gentle shaking for 3 h at r.t. and subsequently filtered. HP20 resins were washed with water (500 mL) and 20% methanol (500 mL). Subsequently, the materials were eluted with methanol (2 L). Following the evaporation of methanol, materials were dissolved in 100 mL of water and transferred to a separating funnel. An equal volume of ethyl acetate was added, and the mixture washed three times. The water fraction was collected and concentrated. The concentrate was applied to an open column filled with HP20 resin and preequilibrated with water. The column was washed with 200 mL of water and 20% methanol, and elution performed with 50% methanol (500 mL). The eluate was fractionated, and absorbance at 262 nm was measured. The fractions containing leptosperin were pooled in a flask and evaporated. The concentrate was purified using reversed-phase HPLC with Develosil Combi-RP (20 × 100 mm, Nomura Chemical Co., Ltd., Aichi, Japan) containing 0.1% acetic acid/CH_3CN = 85/15 at a flow rate of 5 mL/min with monitoring at 262 nm. The peak was collected and repurified under the same conditions.

Honey and Related Samples. Twenty certified samples of manuka honey were obtained from the Unique Manuka Factor Honey Association. Information on NPA (phenol equivalent) and methylglyoxal contents of the 20 samples was provided by Hill Laboratories. Other kinds of honey and samples were obtained from retail stores between 2011 and 2014 in Japan, China, Brazil, and New Zealand. The samples were dissolved in water at a concentration of 0.1 g/mL and centrifuged. The supernatant was collected and directly used for HPLC or diluted 100-fold with water before application of liquid chromatography tandem mass spectrometry (LC/MS/MS), as described below. In addition, in the case of sample no. 26 (Table 2), the original honey solution (0.1 g/mL) was directly analyzed using LC/MS/MS. Samples of candy, cosmetics, or toothpaste were dissolved in 0.1% formic acid/CH_3CN (9/1) at a concentration of 0.1 g/mL. In some cases, in particular for candy, samples were crushed into small pieces and dissolved at 60 °C for 30 min. After centrifugation, the supernatant was collected and diluted 2−100 fold, which was estimated by preliminary analysis of each sample. Vodka was eightfold diluted with water and then used. Tea samples were extracted with 500 mL of boiled water for 5 min using two bags and directly used for mass analyses.

HPLC Measurement. The honey solution (0.1 g honey/mL) was analyzed using a HPLC-photodiode-array detector (PDA), as described previously,[9] with some modifications. In brief, a 5 μL sample was injected into the HPLC connected to a Develosil ODS-HG-5 column (4.6 × 150 mm, Nomura Chemical Co., Ltd.). The separation was performed with gradient elution using a two-solvent system (solvent A, 0.1% formic acid; solvent B, CH_3CN) at a flow rate of 0.8 mL/min with the following gradient program: 0 min (A90%), 10 min (A60%), 11 min (A90%), 25 min (A90%). Leptosperin and methyl syringate were quantified at 262 and 275 nm, respectively.

LC/MS/MS Measurement. Analyses were performed using the API3000 tandem mass spectrometer (AB Sciex Instruments, Foster City, CA) connected with a HPLC system using a Develosil ODS-HG-3 column (2 × 50 mm, Nomura Chemical Co., Ltd.). The flow rate was 0.2 mL/min, and 0.1% formic acid (A) and CH_3CN (B) were used as solvents. The time program was as follows: 0 min (A90%), 6 min (A60%), 6.4 min (A90%), 15 min (A90%). The leptosperin content in honeys and samples was measured using electrospray ionization (ESI) with multiple reaction monitoring (MRM) negative mode (ESI-MS/MS). Simultaneous measurement of leptosperin and methyl syringate was accomplished using atmospheric pressure chemical ionization (APCI) with MRM negative mode (APCI-MS/MS). For APCI-MS/MS, the duration time was divided into two periods (6 and 9 min) for effective ionization settings of the respective compounds. Prior to MS analyses, internal standards (100 nM PNPG and 250 nM TMBZ) were added to both samples and standard cocktails. The MRM transitions by collision-induced fragmentation were as follows: leptosperin, 581.0/323.2 (APCI), 581.0/210.9 (ESI); methyl syringate, 211.1/181.1; PNPG, 346.2/138.1; TMBZ, 211.1/152.1. In addition, $[M-HCOO^-]^-$ (581.10) was selected for Q1 transition of leptosperin (M.W. 536).

Marker Stability. Honey samples (raw) were directly aliquoted into screw-capped microtubes, which were sealed tightly and incubated at 37 or 50 °C. At various intervals, tubes were individually removed and stored at −80 °C until analysis. The samples were dissolved in water at a concentration of 0.1 g/mL, and the changes in the leptosperin and methyl syringate contents were analyzed using HPLC as described above.

Statistical Analysis. The relationship between the two markers was calculated using SPSS Statistics ver. 17.0 with Spearman's correlation.

Table 1. Quantitation of Leptosperin and Methyl Syringate in 20 Certified Manuka Honey Samples

			leptosperin (nmol/g honey)			methyl syringate (nmol/g honey)	
sample no.	methylglyoxal (MGO) (mg/kg honey)	NPA	HPLC	ESI-MS	APCI-MS	HPLC	APCI-MS
A	261	9.5	380	347	131	511	301
B	361	11.7	1069	999	217	325	156
C	631	17.2	997	1090	293	636	395
D	830	20.7	753	671	205	293	154
E	131	6.4	343	245	132	122	60
F	289	10.1	568	491	191	360	240
G	196	8.0	631	502	219	183	111
H	162	7.2	592	591	181	409	219
I	611	16.8	599	490	232	479	332
J	761	19.5	863	760	268	503	295
K	686	18.2	729	576	297	365	252
L	135	6.5	314	265	130	283	157
M	416	12.9	877	935	194	327	144
N	562	15.8	626	474	210	420	300
O	739	19.2	1268	851	423	525	324
P	1207	26.3	782	723	296	381	273
Q	109	5.9	339	244	129	146	64
R	535	15.3	761	584	262	403	257
S	315	10.7	472	465	175	681	520
T	999	23.4	928	851	321	314	197

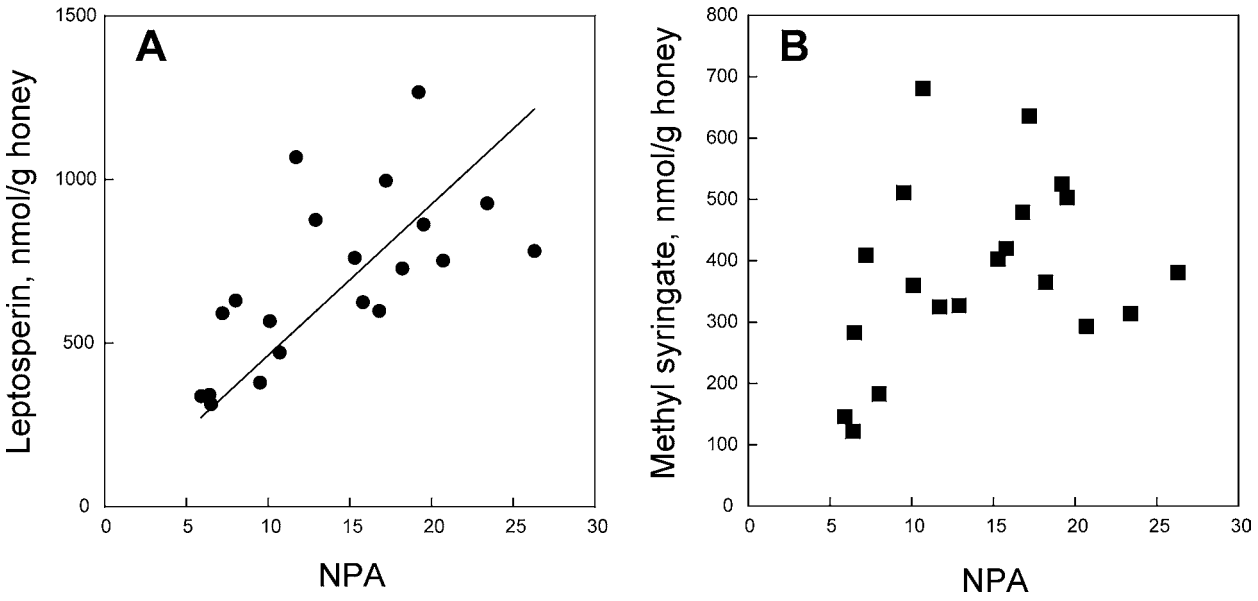

Figure 2. Correlation of the amount of leptosperin (A) or methyl syringate (B) with nonperoxide antibacterial activity (NPA). Methyl syringate and leptosperin contents were measured using HPLC.

RESULTS

Heat Stability of Leptosperin and Its Aglycone, Methyl Syringate. Stabilities of leptosperin and methyl syringate in manuka honey were examined. As shown in Figure 1, methyl syringate was significantly decreased with increasing incubation times. We observed a loss of approximately 30% of methyl syringate over a period of 30 days at 37 °C. At a higher temperature of 50 °C, approximately 50% of methyl syringate was lost over the 30 day period. In contrast, leptosperin was relatively stable at the same temperatures.

Correlation of Leptosperin and Methyl Syringate with Antibacterial Activity. Leptosperin and methyl syringate contents in 20 certified manuka honey samples were analyzed using HPLC. Leptosperin and methyl syringate amounts varied from 314 to 1268 and 122 to 681 μmol/g of honey, respectively (Table 1). NPA of honey samples were independently determined by an authentic organization, as described in Materials and Methods. NPA has a high correlation with leptosperin content (r = 0.732, p < 0.001) but not significant with that of methyl syringate (Figure 2A, B). Our results are similar to those reported in a previous study.[9]

Establishment of LC/MS/MS Analyses for Leptosperin and/or Methyl Syringate. Leptosperin can be measured using the negative mode of ESI with MRM using 581/211 or 581/323 transitions. MRM chromatograms of a standard and typical honey sample using ESI (MRM 581.10/210.9) are shown in Figure 3A. The limit of detection (LOD) for

dx.doi.org/10.1021/jf501475h | J. Agric. Food Chem. 2014, 62, 6400−6407

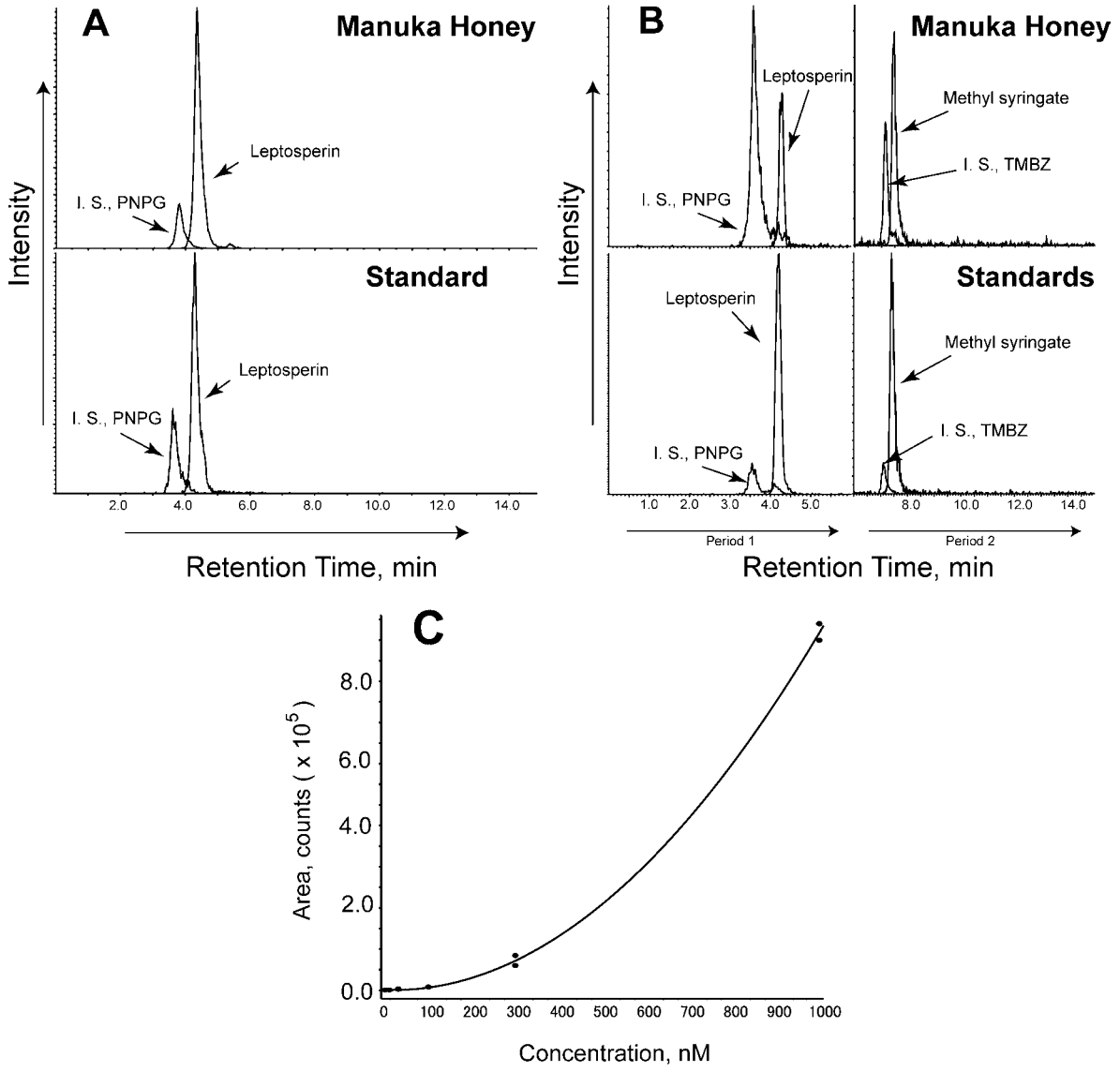

Figure 3. Electrospray ionization (ESI) with multiple reaction monitoring (MRM) negative mode (ESI-MS/MS) or atmospheric pressure chemical ionization (APCI) with MRM negative mode (APCI-MS/MS) analyses of standards and honey sample. (A) Chromatograms of ESI-MS/MS analysis of leptosperin with internal standard (I.S.), *p*-nitrophenyl-*β*-D-glucopyranoside (PNPG). Upper chart, manuka honey; lower chart, standard leptosperin. (B) Chromatograms of APCI-MS/MS analysis of leptosperin or methyl syringate with internal standards, PNPG or 3,4,5-trimethoxybenzoic acid (TMBZ). Upper chart, manuka honey; lower chart, standard of leptosperin and methyl syringate. (C) Quadratic standard curve of leptosperin using APCI-MS/MS.

leptosperin was 3 nM (1.5 fmol/injection), and the peak area linearly increased up to 2000 nM. PNPG was used as the internal standard for leptosperin measurement. However, methyl syringate was barely detected using ESI-MS/MS at a concentration lower than approximately 1 μM. Leptosperin contents in the 20 manuka samples were analyzed using ESI (Table 1). High linearity of leptosperin data was observed between HPLC and ESI-MS/MS (r = 0.947, p < 0.001). In addition, APCI-MS/MS negative mode was developed to analyze methyl syringate with leptosperin (Figure 3B). In this ionization mode, methyl syringate could be analyzed at concentrations of 10−1000 nM, but LOD of leptosperin (30 nM) was lower than that of ESI ionization (3 nM). TMBZ was selected as the internal standard for methyl syringate (Figure 3B). The standard curve of leptosperin was not linear and was then adapted using a quadratic curve fitting (Figure 3C). Leptosperin and methyl syringate contents in the 20 samples were also analyzed using APCI-MS/MS. Each correlation of leptosperin and methyl syringate between APCI-MSMS and HPLC was significantly high (r = 0.812 and 0.949, respectively). However, the amount of leptosperin detected with LC/MS/MS methods, in particular APCI-MS/MS, was lower than that observed with HPLC-PDA, indicating that the reliability of APCI-MS/MS for determining leptosperin content is relatively lower compared with that of the other two methods. Similar to the HPLC analyses, the correlation between leptosperin and NPA observed using both LC/MS/MS methods was significant. On the other hand, the methyl syringate content was not correlated with antibacterial activity.

Plausible Authentication of Manuka Honey by Measuring Leptosperin. We analyzed the leptosperin and methyl syringate contents in commercial manuka honey samples, along with some nonmanuka honey samples (Table 2). Manuka honey authenticated using UMF, MGO, or Active

dx.doi.org/10.1021/jf501475h | J. Agric. Food Chem. 2014, 62, 6400−6407

Table 2. Quantitation of Leptosperin and Methyl Syringate in Honey[a]

sample no., information	certified	purchased	origin	leptosperin[a] (nmol/g honey)	methyl syringate[a] (nmol/g honey)
UMF (Manuka Honey)					
01	UMF 15+	China	NZ	860	432
02	UMF 15+	China	NZ	530	243
03	UMF 15+	China	NZ	758	369
04, similar label with no. 26, 27	UMF 15+	Japan	NZ	835	382
05	UMF 15+	Japan	NZ	414	335
06	UMF 15+	Japan	NZ	579	335
07	UMF 12+	Japan	NZ	487	316
08, beech trees blended, Southern Alps	UMF 5+	NZ	NZ	852	485
Active + (Manuka Honey or Jelly Bush Honey)					
09	Active 15+	China	NZ	396	185
10, certified chloramphenicol-free	Active 15+	China	NZ	262	152
11, stick type	Active 13+	Japan	NZ	483	603
12	Active 12+	NZ	NZ	294	90
13	Active 10+	NZ	NZ	147	303
14, 100% raw unpasteurized	Active 5+	NZ	NZ	1044	343
15, Jelly bush honey	Active 5+	Japan	Australia	58	N.D.
MGO (Manuka Honey)					
16	MGO 250+	Japan	NZ	690	329
17	MGO 250+	China	NZ	386	260
Noncertified (Or Self-Certified) Manuka Honey (or Jelly Bush Honey)					
18	–	Japan	NZ	113	346
19, "self-rigid inspection passed"	–	Japan	NZ	372	1048
20, bottled in Japan, liquid type	–	Japan	NZ	438	433
21	–	Japan	NZ	767	572
22, with kiwi fruit (2%)	–	Japan	NZ	74	224
23, South Island	–	Japan	NZ	592	345
24, "high-grade manuka honey, 92.5%"	–	Japan	NZ	720	587
25, with 0.25% propolis, 5+ certificated by a laboratory	–	Japan	NZ	258	307
26, same jar and label with no. 27	–	Japan	NZ	22[b]	27
27, same jar and label with no. 26	–	NZ	NZ	164	85
28, squeeze type, Jelly bush honey	–	Japan	Australia	35	27
Other Honeys (Nonmanuka Honey)					
29, Scottish heather honey	–	Japan	U.K.	N.D.	N.D.
30	–	Brazil	Brazil	N.D.	N.D.
31, buckwheat	–	Japan	Japan	N.D.	N.D.
32, multifloral honey, Awaji island	–	Japan	Japan	N.D.	N.D.
33, multifloral honey	–	Japan	Japan	N.D.	N.D.
34, kiawe tree	–	Japan	U.S.	N.D.	N.D.

[a]N.D., not detected. [b]Quantified by ESI-MS/MS.

contained high concentrations of leptosperin (664, 383, or 538 nmol leptosperin/g honey on average, respectively), whereas the leptosperin contents in noncertified manuka honey were lower (on average, 323 nmol leptosperin/g honey). However, some noncertified honey samples (no. 21 and 24) were also rich in leptosperin. As shown in Figure 4 and Table 2, one nonauthenticated manuka honey sample (no. 26) obtained at an online store by a Japanese agent contained only trace amounts of leptosperin (22 nmol/g of honey), which could be quantified using ESI-MS/MS without 100-fold dilution but not using HPLC (Figure 4, trace line B′). The leptosperin level was only 1.7%−2.5% compared with the relatively high content in manuka honey "O" (Table 1, ESI or HPLC). Manuka honey (no. 27), which had the same label as sample no. 26, except for the expiration date and was purchased at a retail store in New Zealand, contained 164 nmol leptosperin per g of honey [Figure 4, trace line B, and Table 2 (HPLC)]. The leptosperin content in no. 27 was calculated as 13% of the manuka honey "O" and 7.5 fold richer than that of no.26. Certified UMF15+ honey (no. 03, Table 2) showed strong signals derived from leptosperin and methyl syringate (Figure 4, trace line A).

Plausible Authentication of Manuka Honey Products by Measuring Leptosperin with Methyl Syringate. Manuka honey is added to commercial foods, cosmetics, and toothpaste for expected medicinal purposes, which may not be expressed on the label or attached brochure. We then investigated the detection of leptosperin using ESI-MS/MS and methyl syringate using APCI-MS/MS from some market products. As shown in Tables 3 and 4, leptosperin was detected in the examined samples, including manuka honey, but not in the toothpaste containing manuka honey. In addition, no leptosperin signals from nonmanuka candies were observed. The methyl syringate pattern was similar to that of leptosperin, although one nonmanuka candy contained trace amounts of methyl syringate. These results collectively validate the

dx.doi.org/10.1021/jf501475h | J. Agric. Food Chem. 2014, 62, 6400−6407

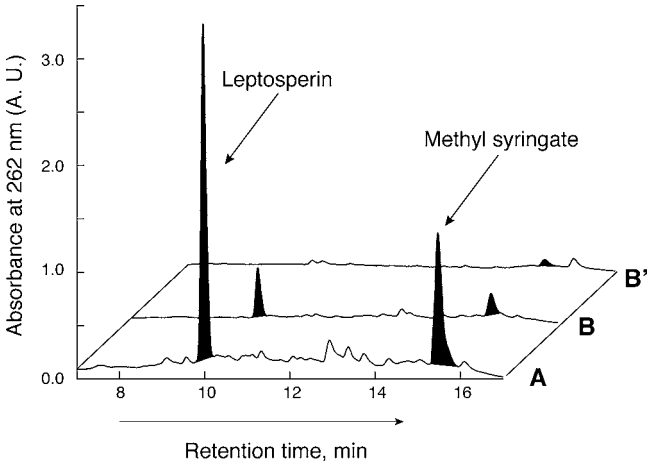

Figure 4. Different contents of leptosperin and methyl syringate in the same manuka honey product. Product A was UMF 15+ honey as a positive control. Honey samples B (no. 27) and B′ (no. 26) were filled into the same type of bottle with the same label and sealed. Honey sample B was purchased in New Zealand (NZ) and B′ in Japan. Leptosperin appeared at 10 min and methyl syringate at 15.5 minutes.

Table 3. Detection of Leptosperin and Methyl Syringate in Solid-Type Honey-Related Products[a]

samples (origin)	leptosperin (nmol/g sample)[a] (ESI-MS)	methyl syringate (nmol/g sample)[a] (APCI-MS)
manuka honey lozenges with blackcurrant, UMF10+ (NZ)	43	19
manuka lozenges, NPA 12+, 100% manuka honey (NZ)	589	417
manuka honey nuglets (NZ)	44	22
manuka honey candy with propolis, MGO 400+ (NZ)	52	28
manuka's cosmet-cleansing	3	3
manuka's cosmet-soap, 15% manuka honey	32	41
manuka's cosmet-drop lotion	22	13
manuka's cosmet-gel cream	19	15
manuka and propolis toothpaste with tea tree oil (NZ)	N.D.	8
tablet type of manuka honey, for portable, 100% (NZ)	135	923
manuka honey candy with green tea powder, UMF15+ (JP)	36	31.5
candy with honey and lemon with vitamin C (JP)[b]	N.D.	0.03
candy with honey and apple (JP)[b]	N.D.	N.D.
mint candy with milk and xylitol (JP)[b]	N.D.	N.D.
fruit candy with Chinese quince and orange oil (JP)[b]	N.D.	N.D.

[a]N.D., not detected. [b]Manuka honey was not included.

application of leptosperin as a preferable chemical marker for manuka honey authentication.

DISCUSSION

Manuka honey is one of the most premium kinds of honey worldwide. On the basis of its unique antibacterial activity, the quality of manuka honey is certified and ranked for consumers using UMF, Active, or MGO. The honey is applied for medicinal purposes, such as treatment of wounded skin. Honey intake/treatment is also expected to promote health; therefore, not only manuka honey but also products containing manuka honey such as candies and cosmetics have been available in the market.

Table 4. Detection of Leptosperin and Methyl Syringate in Liquid-Type Honey-Related Products

samples (origin)	leptosperin (pmol/mL sample) (ESI-MS)	methyl syringate (pmol/mL sample) (APCI-MS)
manuka honey vodka (NZ)	3792	1900
chamomile with lemon balm and manuka honey tea (U.K.)	240	9

Methylglyoxal is the key compound underlying the antibacterial activity of honey. Twenty certified honey samples displayed a high correlation between NPA and methylglyoxal contents (Table 1). Methylglyoxal is probably generated from the predicted precursor molecule, dihydroxyacetone, in the honey.[3] This is consistent with the finding that the UMF rating is enhanced by storage, which is known to the beekeeper/honey industry.[12] Moreover, because both methylglyoxal and dihydroxyacetone are available as reagents, artificial addition of these compounds into manuka or nonmanuka honey to increase antibacterial activity is possible. Supplementation with chemicals is often used for preparation of manuka honey mimics.[13,14] That is, it is possible to disguise other kinds of honey, including multifloral honeys, as manuka honey. The association of UMF is setting up traceability of UMF-certified manuka honey from the marketplace to ensure that the products are from the stated origin to protect the consumer from counterfeiting.

The main purpose of this study was to evaluate the application of leptosperin[9] as a potential chemical marker for authentication of manuka honey. Stability and reliability are important characteristics of an effective chemical marker. The leptosperin level remained constant during incubation at both 37 °C and higher temperatures of 50 °C (Figure 1A, B). This is probably because leptosperin has less reactive moieties than phenolics, such as methyl syringate, which has phenolic hydroxyl. Methylation of phenolic components in honey has been suggested.[12] As discussed above, the amount of the other major key component, methylglyoxal, is known to be nonconstant because methyglyoxal is generated from dihydroxyacetone and could be lost during further incubation/storage.[3] These findings suggest that either methylglyoxal or dihydroxyacetone is not suitable as chemical markers for manuka honey.

As shown in Figure 2A, B, NPA is highly correlated with leptosperin (r = 0.732, p < 0.001) but not with methyl syringate. Oelschlaegel et al. also reported that the leptosperin content in manuka honey has good correlation with that of methylglyoxal (r = 0.848, p = 0.000), which is a well-known strong germinant.[11] On the other hand, leptosperin only displays antibacterial activity at a high concentration range.[9] The underlying reason for the strong association of leptosperin content with antibacterial activity remains to be established.

A number of plausible chemical candidates have been identified for manuka honey authentication. A recent study showed that 2-formyl-5-(2-methoxyphenyl)pyrrole, a unique compound in manuka honey, is correlated with NPA (r^2 = 0.364).[15] Another study also reported that 2-methoxybenzoic acid in fresh honey (n = 10) is highly correlated with

dx.doi.org/10.1021/jf501475h | J. Agric. Food Chem. 2014, 62, 6400−6407

methylglyoxal (r^2 = 0.7968).[12] Fearney et al. identified a novel glycoside of TMBZ in honey, but its correlation with NPA (UMF) or methylglyoxal (MGO) is yet to be established.[16] In this study, we developed a plausible authentication method on the basis of leptosperin measurement, which is a specific compound of manuka honey.[9]

Apart from the reports on manuka honey, few studies focused on authentication of different kinds of honey. For example, over 100 chemicals in lavandin honey, a monofloral product of recent proliferation obtained from a hybrid of *Lavandula angustifolia* and *L. latifolia* species, were assessed as possible markers for authentication, with the aim of distinguishing it from the more common Lavender honey (*L. latifolia*).[16] Authentication of monofloral Yemeni Sidr honey using ultraviolet spectroscopy and chemometric analysis has also been proposed.[17]

As shown in Figure 4, one sample of manuka honey (no. 26) obtained from an online shop in Japan contained an extremely low level of leptosperin (22 nmol/g honey), which could be only analyzed using ESI-MS/MS. However, the honey sample (no. 27) with the same label, obtained from a retail store in New Zealand, displayed relatively low amount of leptosperin. We suspected that sample no. 26 was produced and sold improperly. In a masked study, five of six volunteers felt that the taste of "manuka honey" in no. 27 was more prominent compared with no. 26 (unpublished observation). In addition, UMF 15+ honey (no. 04), made by the same maker as no. 26 and no. 27 products, contained significant amounts of leptosperin and methyl syringate (Table 2). Therefore, the quantification of leptosperin with methyl syringate as a supplement may serve as an effective authenticator of manuka honey.

Few cosmetics or foods in the market indicate additional inclusions of manuka honey as a component. However, there is no simple way to chemically validate supplementation of honey by consumers and even producers at the present time. In our study, leptosperin (or methyl syringate) was detected in vodka, soap, or candy using mass spectrometry. Some of the samples contained trace amounts of leptosperin and methyl syringate, which could be detected using mass spectrometry.

Gaps in data were observed between HPLC and mass spectrometry analyses (Table 1), but mass spectrometry was suitable for detection of trace leptosperin and methyl syringate. In this study, we have also selected PNPG as the internal standard for leptosperin analyses using the MS/MS, but the PNPG is the substrate for β-glycosidase. Therefore, if active β-glycosidase is contaminated in the sample, it may interfere with the quantitation of leptosperin. On the other hand, TMBZ, the internal standard for quantitation of methyl syringate, is a possible component of manuka honey.[12] In the future, stable isotopic leptosperin and methyl syringate should be synthesized as the preferable internal standards.[18]

In summary, we investigated the possible application of leptosperin with methyl syringate for authentication of premium manuka honey using HPLC, ESI-MSMS, and APCI-MS/MS. The detection and quantitation of leptosperin with methyl syringate as an adjunct would be applicable for manuka honey authentication.

AUTHOR INFORMATION

Corresponding Author

*Tel.: +81-79-292-9413. Fax: +81-79-293-5710. E-mail: yojikato@shse.u-hyogo.ac.jp.

Notes

The authors declare no competing financial interest.

ACKNOWLEDGMENTS

We are grateful to Mr. John Rawcliffe, UMF Honey Association, for providing honey samples and Hill laboratories in New Zealand for providing analytical data.

ABBREVIATIONS USED

UMF, unique manuka factor; TRPA1, transient receptor potential channel ankryn 1; PNPG, *p*-nitrophenyl-β-D-glucopyranoside; TMBZ, 3,4,5-trimethoxybenzoic acid; NPA, nonperoxide antibacterial activity; LC/MS/MS, liquid chromatography tandem mass spectrometry; ESI, electrospray ionization; MRM, multiple reaction monitoring; APCI, atmospheric pressure chemical ionization; I.S, internal standard

REFERENCES

(1) Mavric, E.; Wittmann, S.; Barth, G.; Henle, T. Identification and quantification of methylglyoxal as the dominant antibacterial constituent of manuka (*Leptospermum scoparium*) honeys from New Zealand. *Mol. Nutr. Food Res.* **2008**, *52*, 483−9.

(2) Atrott, J.; Henle, T. Methylglyoxal in manuka honey—Correlation with antibacterial properties. *Czech J. Food Sci.* **2009**, *27*, S163−S165.

(3) Adams, C. J.; Manley-Harris, M.; Molan, P. C. The origin of methylglyoxal in New Zealand manuka (*Leptospermum scoparium*) honey. *Carbohydr. Res.* **2009**, *344*, 1050−3.

(4) Inoue, K.; Murayama, S.; Seshimo, F.; Takeba, K.; Yoshimura, Y.; Nakazawa, H. Identification of phenolic compound in manuka honey as specific superoxide anion radical scavenger using electron spin resonance (ESR) and liquid chromatography with coulometric array detection. *J. Sci. Food Agric.* **2005**, *85*, 872−878.

(5) Jermnak, U.; Yoshinari, T.; Sugiyama, Y.; Tsuyuki, R.; Nagasawa, H.; Sakuda, S. Isolation of methyl syringate as a specific aflatoxin production inhibitor from the essential oil of Betula alba and aflatoxin production inhibitory activities of its related compounds. *Int. J. Food Microbiol.* **2012**, *153*, 339−44.

(6) Kim, M. J.; Son, H. J.; Song, S. H.; Jung, M.; Kim, Y.; Rhyu, M. R. The TRPA1 agonist, methyl syringate suppresses food intake and gastric emptying. *PLoS One* **2013**, *8*, e71603.

(7) Son, H. J.; Kim, M. J.; Park, J. H.; Ishii, S.; Misaka, T.; Rhyu, M. R. Methyl syringate, a low-molecular-weight phenolic ester, as an activator of the chemosensory ion channel TRPA1. *Arch. Pharmacal Res.* **2012**, *35*, 2211−8.

(8) Tuberoso, C. I.; Bifulco, E.; Jerkovic, I.; Caboni, P.; Cabras, P.; Floris, I. Methyl syringate: A chemical marker of asphodel (*Asphodelus microcarpus* Salzm. et Viv.) monofloral honey. *J. Agric. Food Chem.* **2009**, *57*, 3895−900.

(9) Kato, Y.; Umeda, N.; Maeda, A.; Matsumoto, D.; Kitamoto, N.; Kikuzaki, H. Identification of a novel glycoside, leptosin, as a chemical marker of manuka honey. *J. Agric. Food Chem.* **2012**, *60*, 3418−23.

(10) Fujimatu, E.; Ishikawa, T.; Kitajima, J. Aromatic compound glucosides, alkyl glucoside, and glucide from the fruit of anise. *Phytochemistry* **2003**, *63*, 609−16.

(11) Oelschlaegel, S.; Gruner, M.; Wang, P. N.; Boettcher, A.; Koelling-Speer, I.; Speer, K. Classification and characterization of manuka honeys based on phenolic compounds and methylglyoxal. *J. Agric. Food Chem.* **2012**, *60*, 7229−37.

(12) Stephens, J. M.; Schlothauer, R. C.; Morris, B. D.; Yang, D.; Fearnley, L.; Greenwood, D. R.; Loomes, K. M. Phenolic compounds and methylglyoxal in some New Zealand manuka and kanuka honeys. *Food Chem.* **2010**, *120*, 78−86.

(13) Jervis-Bardy, J.; Foreman, A.; Bray, S.; Tan, L.; Wormald, P. J. Methylglyoxal-infused honey mimics the anti-Staphylococcus aureus biofilm activity of manuka honey: Potential implication in chronic rhinosinusitis. *Laryngoscope* **2011**, *121*, 1104−7.

(14) Rogers, K.; Grainger, M.; Manley-Harris, M. The unique manuka effect: Why New Zealand manuka honey fails the AOAC 998.12 C-4 sugar method. Part 2. *J. Agric. Food Chem.* **2014**, DOI: 10.1021/jf404767b.
(15) Chan, C. W.; Deadman, B. J.; Manley-Harris, M.; Wilkins, A. L.; Alber, D. G.; Harry, E. Analysis of the flavonoid component of bioactive New Zealand manuka (*Leptospermum scoparium*) honey and the isolation, characterisation and synthesis of an unusual pyrrole. *Food Chem.* **2013**, *141*, 1772−81.
(16) Castro-Vázquez, L.; Leon-Ruiz, V.; Alañon, M. E.; Pérez-Coello, M. S.; González-Porto, A. V. Floral origin markers for authenticating Lavandin honey (*Lavandula angustifolia x latifolia*). Discrimination from Lavender honey (*Lavandula latifolia*). *Food Control* **2014**, *37*, 362−370.
(17) Roshan, A.-R. A.; Gad, H. A.; El-Ahmady, S. H.; Khanbash, M. S.; Abou-Shoer, M. I.; Al-Azizi, M. M. Authentication of monofloral Yemeni Sidr honey using ultraviolet spectroscopy and chemometric analysis. *J. Agric. Food Chem.* **2013**, *61*, 7722−7729.
(18) Aitken, H. M. R.; Johannes, M.; Loomes, K. M.; Brimble, M. A. Synthesis of leptosin, a glycoside isolated from mānuka honey. *Tetrahedron Lett.* **2013**, *54*, 6916−6919.

85-23, 1996), and all procedures were approved by the Animal Care Review Committee (Animal application approval number 0064257), Nanchang University, China.

Porridge Preparation. Porridges were prepared according to the recipes in Table 1 in a stainless steel pot. For white rice porridge, 1 L of distilled water was boiled to 98 ± 2 °C in the pot, and then 75 g of white rice was dropped into the pot. For mixed grain porridge, 75 g of mixed grains was soaked in 500 mL of distilled water for 6 h first. Another 500 mL of distilled water was boiled to 98 ± 2 °C in the pot. After that, the mixed grains together with the water used for soaking were poured into the pot. For white rice porridge added with gum arabic, 10 g of gum arabic was dissolved in 1 L of distilled water in the pot first, then boiled to 98 ± 2 °C. After that, 75 g of white rice was dropped into the pot. For mixed grain porridge added with gum arabic, mixed grains were soaked in 500 mL of distilled water for 6 h first. Ten grams of gum arabic was dissolved in another 500 mL of distilled water in the pot, then boiled to 98 ± 2 °C. After that, the mixed grains together with the water used for soaking were poured into the pot. For all of the porridges, the pot was boiled with frequent stirring for 60 min after water boiling again to cause full gelatinization of starches. The cooked porridge was then transferred to a glass container and left to cool at room temperature.

Table 1. Preparations of Different Porridges

porridges	recipes
porridge 1[a]	white rice (75 g) boiled in 1 L of water
porridge 2	mixed grains (75 g) boiled in 1 L of water[b]
porridge 3	white rice (75 g) and gum arabic (10 g) boiled in 1 L of water
porridge 4	mixed grains (75 g) and gum arabic (10 g) boiled in 1 L of water

[a]Porridge 1, white rice porridge; porridge 2, mixed grain porridge; porridge 3, white rice porridge fortified with gum arabic; porridge 4, mixed grain porridge fortified with gum arabic. [b]Mixed grains: oat (15 g), buckwheat (15 g), brown rice (15 g), corn dregs (6 g), peanut (6 g), red bean (6 g), kidney bean (6 g), and coix seed (6 g).

Determination of Apparent Viscosity of Porridges. Apparent viscosity of each porridge was measured at 25 °C with a Brookfield DV-Ultra Programmable rheometer (Brookfield, Stoughton, MA), equipped with a CP52 spindle (spindle multiplier constant = 9.83, shear rate constant = 2).[19]

Simulated Gastric and Intestinal Digestion of Porridges in Vitro. *Digestion Media Used Throughout the Digestion Experiments.* All chemicals and enzymes were obtained from Sigma Chemical Co. (St. Louis, MO) and Amano Enzyme Inc. (Nagoya, Japan). The simulated gastric and intestinal fluids were prepared according to the protocol used by a model gastrointestinal system (TNO Intestinal Model 1, TIM1 from TNO Zeist, The Netherlands), which simulates the physiological conditions of the human stomach and small intestine.[20,21]

Gastric Medium Preparation. The gastric medium was prepared according to the method by Tedeschi et al. with some modifications.[22] The gastric electrolyte solution (GES) consisted of 3.1 g L^{-1} NaCl, 1.1 g L^{-1} KCl, 0.15 g L^{-1} $CaCl_2{\cdot}2H_2O$, and 0.6 g L^{-1} $NaHCO_3$. The final pH was adjusted to 3 by addition of HCl (0.1 N). Next, 37.5 mg of gastric lipase (Lipase DF Amano 15, Amano Enzyme Inc., Japan) and 35.4 mg of pepsin from porcine gastric mucosa (Sigma) were added to a solution of 150 g of GES and 1.5 mL of CH_3COONa (1 M, pH 5). The solution was gently mixed for 10 min on a magnetic stirrer at room temperature, and simultaneously the pH was adjusted to 3 by additions of HCl (0.1 N). The solution was stored on ice before use.

Small Intestinal Alkaline Medium. The small intestinal medium was prepared according to the method by Tedeschi et al.[22] The simulated small intestinal electrolyte solution (SIES) consisted of 5.4 g L^{-1} NaCl, 0.65 g L^{-1} KCl, and 0.33 g L^{-1} $CaCl_2{\cdot}2H_2O$. The pH was adjusted to 7 using NaOH (0.1 M). To simulate a duodenum residue solution, bile salt was added to a SIES containing the enzymes pancreatine and trypsin. A SIES with enzymes and bile salts was first prepared (SIENZY). The SIENZY solution contained 100 g of SIES, 100 g of pancreatin solution (7%, w/w, Sigma), 13 mg of trypsin (Sigma), and 200 g bile salt solution (4%, w/w). For the pancreatin solution, 14 g of pancreatin was dissolved in 200 g of water, and the solution was mixed for 10 min with a magnetic stirrer and centrifuged for 10 min at 2800*g*. The supernatant (100 g) was used for the preparation of the SIENZY solution. The dilution was performed using SIES as dilution medium, and the pH was adjusted to 7.5 by NaOH (0.1 M).

Simulated Digestion. Digestion studies were performed using an RC806 flow-through dissolution system (Tianfa Corp., Tianjing, China), equipped with a temperature circulator-controller, which allowed one to maintain the temperature at 37 °C throughout all of the experiments. Stirring paddles (Tianfa Corp., Tianjing, China), which were at the top of sample cells, were also equipped with a flow-through dissolution system for simulating the gastric peristalsis. In addition, several pumps (HL-2D, Qingpu Corp., Shanghai, China) were connected to the dissolution system to pump in the gastric and intestinal medium for digestion. Further, a pH meter (XB89-PH-2612, XG Corp., Beijing, China) was also connected to the dissolution system for controlling the pH in digestion system. The pH was monitored and continuously controlled by adding either water or 1 M HCl into the stomach, and either electrolytes or 1 M $NaHCO_3$ into the small intestine. Before each experiment, the system was washed with detergent and rinsed with water. For the gastric digestion tests of porridges, cells were loaded with 100 mL of porridge, and 150 mL of gastric medium was pumped through the cells at a constant flux of 0.4 mL min^{-1}. For the intestinal digestion of porridges, porridges that were predigested by gastric medium were placed inside another sample cells. Around 200 mL of small intestinal medium was pumped at a constant flux of 0.56 mL min^{-1}. For all of the experiments, a fraction collector (BSZ-100, Jingke Corp., Shanghai, China) was used to withdraw 3 mL samples at specified time intervals. The collected samples were used for the determination of glucose concentration and the calculation of glucose amount.

The gastric digestion of the porridges was followed for 6 h. Samples were analyzed before and after digestion. Glucose concentration was determined at 0, 0.5, 1, 2, 3, 4, 5, and 6 h according to the hexokinase method of Yokoyama et al.[2] Three independently replicated extractions were performed for each sample. The intestinal digestion of the porridge was also followed for 6 h. Samples were analyzed after digestion, and the glucose concentration was determined after 0.5, 1, 2, 3, 4, 5, and 6 h according to the hexokinase method.[2] Three independently replicated extractions were performed for each sample. The maximum producing velocity of glucose (V_{max1}) for porridges during intestinal digestion was calculated as follows. The experimental data were fitted with an equation of parabola:

$$Y = ax^2 + bx + c$$

where Y is the glucose concentration (mM); x is time (min); and a, b, and c are coefficients. The equation to calculate the producing rate (Y') at any time is $Y' = 2ax + b$. When x is close to 0, $Y' = V_{max1} = b$.

Determination of Glucose Diffusion. The residue digestion mixtures of porridges after digestion were used to determine diffusion of glucose according to the method by Ou et al. with some modifications.[23] Briefly, a total of 12 samples (3 replicates of 4 different porridges), 25 mL each, were dialyzed in dialysis bags with a molecular weight cutoff of 8000−14 000 against 200 mL of deionized water at 37 °C. The glucose concentration in 2.0 mL of the dialysate was determined after 10, 20, 30, 60, 90, 120, 150, 180, 240, 300, and 360 min (the results at 12 h proved 360 min was enough for equilibrium) according to the hexokinase method.[2]

The maximum diffusion velocity of glucose (V_{max2}) was calculated as follows. The experimental data were fitted with an equation of parabola:

$$Y = ax^2 + bx + c$$

where Y is the glucose diffusion concentration (mM); x is time (min); and a, b, and c are coefficients. The equation to calculate the diffusion

dx.doi.org/10.1021/jf501557b | J. Agric. Food Chem. 2014, 62, 6408−6416

rate (Y') at any time is $Y' = 2ax + b$. When x is close to 0, $Y' = V_{max2} = b$.

Animal Study. Male 6-week-old Kunming mice (20.0 ± 2.0 g) were individually housed in stainless steel cages in a room with controlled temperature (25.0 ± 0.5 °C), relative humidity (50 ± 5%), and 12 h/12 h light/dark cycle. All mice were fed with the same amount of basal diet, which was prepared according to the published formula,[24] and water was provided ad libitum. Food was stopped to the mice 12 h before the experiment. All mice were randomly divided into four groups: (1) porridge 1 group, mice were given oral administration of white rice porridge at 25 mL/kg body weight (solid content = 1.875 g solid/kg body weight); (2) porridge 2 group, mice were given mixed grain porridge at 25 mL/kg body weight (solid content = 1.875 g solid/kg body weight); (3) porridge 3 group, mice were given white rice porridge fortified with gum arabic at 25 mL/kg body weight (solid content = 2.125 g solid/kg body weight; gum arabic content = 0.25 g/kg body weight); (4) porridge 4 group, mice were given mixed grain porridge fortified with gum arabic at 25 mL/kg body weight (solid content = 2.125 g solid/kg body weight; gum arabic content = 0.25 g/kg body weight). Each group had 12 mice, and 6 mice were put in one cage. The blood glucose of each mouse was determined before oral administration (0 h) and also 0.5, 1, 2, and 3 h after being given oral administration of porridge. Blood glucose levels were obtained by using an Accu-Chek Performa blood glucose meter (Roche, Mannheim, Germany).

In Vitro Fermentation of Porridges. *Fecal Slurry Preparation.* The fresh fecal samples were collected from four healthy donors who never had large bowel disease before. The donors also had followed normal diets and had not been treated with antibiotics for at least 3 months. Collected fecal samples were mixed with an equal amount of feces from each donor. The mixed fecal samples were immediately stored in an anaerobic jar before use.[25]

Preculture. Mixed fecal samples (120 g) was precultured in 1 L of preculture medium (10 g of tryptone, 5 g of yeast, 10 g of NaCl, 5 g of glucose, and 6 g of maltose) anaerobically. After overnight growth, 120 mL of the preculture was filtered through sterile gauze sponges to remove large particles and stored in an anaerobic jar before use.[26]

Fermentation. The composition of 1 L growth medium was: 4.5 g of NaCl, 4.5 g of KCl, 1.5 g of $NaHCO_3$, 0.69 g of $MgSO_4 \cdot H_2O$, 0.8 g of L-cysteine $HCl \cdot H_2O$, 0.5 g of KH_2PO_4, 0.5 g of K_2HPO_4, 0.4 g of bile salt, 0.08 g of $CaCl_2$, 0.005 g of $FeSO_4 \cdot 7H_2O$, 1 mL of Tween 80, and 4 mL of resazurin solution (0.025%, w/v) as anaerobic indicator.[25] Growth medium was sterilized at 121 °C for 15 min before use and divided into sterile anaerobic vessels.

The porridge samples (after gastrointestinal digestion) were subjected to the in vitro fermentation with the precultured human fecal microbiota. The total volume of the fermentation slurry was 50 mL. For the tested samples, the final fermentation volume was 40% growth medium, 40% human fecal preculture, and the last 20% was porridge or distilled water (control). All samples and the fecal preculture were introduced in different anaerobic sealed tubes containing growth medium, under the condition of 10% H_2, 10% CO_2, and 80% N_2 in Forma Anaerobic System (Thermo Electron Corp., Marietta, OH).[27] Separated tubes were prepared for each replicate at each time point (0, 6, 12, and 24 h during fermentation). The anaerobic sealed tubes were then incubated at 37 °C for 24 h in a TC-2112B Thermostat shaker (160 rpm, Shanghai Nuoji Corp., Shanghai, China).

SCFA Measurement. The fermentation cultures were centrifuged at 4800*g* for 15 min. The supernatants were used for determination of SCFA. Chromatographic analysis was carried out using the Agilent 6890 N GC system according to our published method.[28] A GC column (HP-INNOWAX, 190901N-213, J & W Scientific, Agilent Technologies Inc., U.S.) of 30 m × 0.32 mm i.d. coated with 0.50 μm film thickness was used. Nitrogen was supplied as the carrier gas at a flow rate of 19.0 mL/min with a split ratio of 1:10. An initial column temperature was held at 100 °C for 0.5 min, then programmed at a rate of 4 °C/min to 180 °C. The temperature of the FID and injection port was 240 °C. The flow rates of hydrogen and air were 30 and 300 mL/min, respectively. The volume of injected standard SCFA and sample for GC analysis was 0.2 μL, and the running time for each analysis was 20.5 min. The independently replicated determinations were performed three times for each sample. Data handling was carried out with HP Chem Station Plus software (A.09.xx, Agilent).

Statistical Analysis. All of the experiments were done in triplicate. Statistical analysis was carried out using SPSS (version 16.0, Chicago, IL). The results were expressed as mean ± standard deviations and compared using the Tukey test at 5% confidence level.

RESULTS AND DISCUSSION

Apparent Viscosity of Porridges. There was some difference in the apparent viscosity among porridges (Table 2). The apparent viscosity level (shear rate = 30 or 50 s^{-1}) of white rice porridge was higher than that of mixed grain porridge. The difference in the apparent viscosity between white rice porridge and mixed grain porridge may be due to the difference of the materials in the porridges. This was consistent with previous result reported by Wood et al.[29] However, apparent viscosity of the two porridges was significantly increased after addition of gum arabic ($p < 0.05$). The apparent viscosity of white rice porridge was improved from 633 ± 3 to 720 ± 4 mPa s^{-1} at shear rate = 30 s^{-1} and increased from 342 ± 4 to 435 ± 2 mPa s^{-1} at shear rate = 50 s^{-1}. Meanwhile, the apparent viscosity of mixed grain porridge increased from 602 ± 2 to 683 ± 2 mPa s^{-1} at shear rate = 30 s^{-1} and increased from 303 ± 2 to 410 ± 3 mPa s^{-1} at shear rate = 50 s^{-1}. This may result from the addition of gum arabic to porridges. Viscous water-soluble dietary fibers could affect the apparent viscosity of solution.[30] A higher viscosity of solution could be provided by gum arabic.[31] In addition, gum arabic was reported to belong to the family of dietary fiber, and our results agreed well with those of other dietary fibers, which could improve the values of apparent viscosity.[30,32] The increase in the apparent viscosity may have an effect on the glucose production and diffusion, which affect the blood sugar response.[29]

Table 2. Apparent Viscosities of Different Porridges at Different Shear Rates (s^{-1})[a]

sample	apparent viscosity (mPa s^{-1})	
	30 s^{-1}	50 s^{-1}
porridge 1[b]	633 ± 3 a[c]	342 ± 4 a
porridge 2	602 ± 2 b	303 ± 2 b
porridge 3	720 ± 4 c	435 ± 2 c
porridge 4	683 ± 2 d	410 ± 3 d

[a]Data are presented as means ± standard deviations of triplicate measurements. [b]Porridge 1, white rice porridge; porridge 2, mixed grain porridge; porridge 3, white rice porridge fortified with gum arabic; porridge 4, mixed grain porridge fortified with gum arabic. [c]Mean values in the same column with different letters are significantly different (Tukey test, $p < 0.05$).

Glucose Production of Porridges during Gastric Digestion. As shown in Table 3, the total amount of glucose in white rice porridge was 40 mmol at the beginning and then increased to 460 mmol at 6 h. These amounts of the glucose may result from hydrolysis of the starch in the white rice porridge, which may be due to the acid environment of the gastric medium (pH = 3) because there was no enzyme in gastric medium that could hydrolyze the whole starch in white rice porridge to glucose. In addition, the glucose amount of white rice porridge fortified with gum arabic was significantly lower than that of the white rice porridge at the same time point throughout the whole gastric digestion ($p < 0.05$). This

dx.doi.org/10.1021/jf501557b | J. Agric. Food Chem. 2014, 62, 6408−6416

Table 3. Glucose Amount of Different Porridges during Gastric and Intestinal Digestion[a]

	glucose amount							
samples	0 h	0.5 h	1 h	2 h	3 h	4 h	5 h	6 h
Gastric Digestion (mmol)								
porridge 1[b]	40 ± 6 a[c]	298 ± 18 a	377 ± 22 a	395 ± 24 a	417 ± 20 a	438 ± 18 a	440 ± 16 a	460 ± 22 a
porridge 2	5 ± 1 b	45 ± 5 b	74 ± 10 b	89 ± 6 b	113 ± 5 b	128 ± 16 b	142 ± 18 b	160 ± 15 b
porridge 3	38 ± 5 a	222 ± 25 c	274 ± 12 c	348 ± 14 c	384 ± 10 c	388 ± 16 c	399 ± 15 c	410 ± 15 c
porridge 4	5 ± 1 b	22 ± 2 d	37 ± 4 d	44 ± 6 d	52 ± 4 d	59 ± 5 d	67 ± 9 d	80 ± 8 d
Intestinal Digestion (mol)								
porridge 1		3.0 ± 0.2 a	6.7 ± 0.6 a	11.5 ± 0.7 a	13.2 ± 0.7 a	16.7 ± 1.0 a	18.9 ± 1.0 a	22.6 ± 1.2 a
porridge 2		2.0 ± 0.3 b	5.0 ± 0.5 b	6.9 ± 0.6 b	8.5 ± 0.5 b	10.6 ± 1.0 b	13.6 ± 0.5 b	14.8 ± 1.1 b
porridge 3		2.5 ± 0.2 b	5.2 ± 0.4 b	8.6 ± 0.5 c	9.9 ± 0.2 c	13.1 ± 1.0 c	14.8 ± 0.5 c	16.8 ± 1.2 c
porridge 4		1.4 ± 0.1 c	4.2 ± 0.5 c	5.2 ± 0.5 d	6.4 ± 0.2 d	8.3 ± 0.9 d	10.8 ± 0.8 d	11.7 ± 1.0 d

[a]Data are presented as means ± standard deviations of triplicate measurements. [b]Porridge 1, white rice porridge; porridge 2, mixed grain porridge; porridge 3, white rice porridge fortified with gum arabic; porridge 4, mixed grain porridge fortified with gum arabic. [c]Mean values in the same column (from the same digestion) with different letters are significantly different (Tukey test, $p < 0.05$).

may be because the gum arabic coated on the surface of grains, which could affect the starch in the white rice porridge to get in touch with the gastric medium and delay the glucose production. Furuta et al. also found the coating of another dietary fiber, water-soluble soybean polysaccharides, on the surface of cooked rice grains.[33]

The glucose amount in mixed grain porridge at 0 h was only 5 mmol, and the amount increased to 160 mmol at 6 h (Table 3). The lower initial glucose amount of mixed grain porridge would be due to less rice in the formula. The increase of glucose amount would also result from weak hydrolysis of the carbohydrates in mixed grain porridge, which was due to the acid environment of the gastric medium (pH = 3). The glucose amount of mixed grain porridge fortified with gum arabic was significantly lower than those of mixed grain porridge at the same time points during gastric digestion ($p < 0.05$), and very little glucose was produced in mixed grain porridge fortified with gum arabic during gastric digestion (22−80 mmol). This may be also because the gum arabic could inhibit the carbohydrates in mixed grain porridge to get in touch with the gastric medium and thus reduce the glucose production.

Glucose Production of Porridges during Intestinal Digestion. The glucose amounts of porridges during intestinal digestion were also shown in Table 3. The glucose amount of white rice porridge was high (approximately 3.0 mol) in the initial time point (0.5 h), and the glucose amount differed significantly from 0.5 to 6 h. The glucose amount of white rice porridge increased along with the digestion time, with the maximum level of 22.6 mol at 6 h, for there was an enzyme, amylase, which could hydrolyze the starch in white rice to glucose. However, after addition of gum arabic, the level of glucose amount in the white rice porridge was significantly decreased at all time points ($p < 0.05$), with a maximum level of around 16.8 mol at 6 h. The maximum glucose producing velocity (V_{max1}) of white rice porridge fortified with gum arabic (0.2233 ± 0.0010 mM min^{-1}) was significantly lower than that of white rice porridge (0.2880 ± 0.0015 mM min^{-1}) (Table 4, $p < 0.05$).

As presented in Table 3, the glucose amount of mixed grain porridge was approximately 2.0 mol at the initial time point (0.5 h), and it differed significantly from 0.5 to 6 h. The glucose amount of mixed grain porridge increased along with the digestion time, with the maximum level of around 14.8 mol at 6 h. However, after addition of gum arabic, the level of glucose amount in the mixed grain porridge was significantly decreased

Table 4. Maximum Producing Velocity of Glucose (V_{max1}) and Maximum Diffusion Velocity of Glucose (V_{max2}) for Different Porridges[a]

	V_{max} (mM min^{-1})	
samples	V_{max1}	V_{max2}
porridge 1[b]	0.2880 ± 0.0015 a[c]	0.0348 ± 0.0007 a
porridge 2	0.1779 ± 0.0008 b	0.0250 ± 0.0010 b
porridge 3	0.2233 ± 0.0010 c	0.0297 ± 0.0005 c
porridge 4	0.1350 ± 0.0005 d	0.0196 ± 0.0008 d

[a]Data are presented as means ± standard deviations of triplicate measurements. [b]Porridge 1, white rice porridge; porridge 2, mixed grain porridge; porridge 3, white rice porridge fortified with gum arabic; porridge 4, mixed grain porridge fortified with gum arabic. [c]Mean values in the same column with different letters are significantly different (Tukey test, $p < 0.05$).

at all time points ($p < 0.05$), with a maximum level of around 11.7 mol at 6 h. The maximum glucose producing velocity (V_{max1}) of mixed grain porridge fortified with gum arabic (0.1350 ± 0.0005 mM min^{-1}) was significantly lower than that of mixed grain porridge (0.1779 ± 0.0008 mM min^{-1}) (Table 4, $p < 0.05$).

Annison and Topping reported that dietary fibers can be adsorbed to starch and thus decreased hydrolysis of starch by α-amylase in the intestinal digestion.[34] The activity of α-amylase was also influenced to some extent by the kind of dietary fiber. However, further studies are needed to investigate whether the gum arabic is a competent inhibitor of α-amylase or simply acts as a barrier between the enzyme and starch.[23]

Diffusion of the Glucose. Diffusion of glucose was different for different porridges (Table 5). Diffused glucose for white rice porridge was significantly higher than that for white rice porridge fortified with gum arabic at all of the time points ($p < 0.05$). The maximum diffusion velocity (V_{max2}) of white rice porridge fortified with gum arabic was (0.0297 ± 0.0005) mM min^{-1}, which was significantly lower than that of white rice porridge (0.0348 ± 0.0007 mM min^{-1}) (Table 4, $p < 0.05$). Diffused glucose for mixed grain porridge was also significantly higher than that for mixed grain porridge fortified with gum arabic at all of the time points (Table 5, $p < 0.05$). The maximum diffusion velocity (V_{max2}) of mixed grain porridge fortified with gum arabic was 0.0196 ± 0.0008 mM min^{-1} and was notably lower than that of mixed grain porridge (0.0250 ± 0.0010 mM min^{-1}) (Table 4, $p < 0.05$).

dx.doi.org/10.1021/jf501557b | J. Agric. Food Chem. 2014, 62, 6408−6416

Table 5. Glucose Diffusion of Different Porridges after Digestion[a]

samples	glucose concentration of dialysate (mM)											
	10 min	20 min	30 min	60 min	90 min	120 min	150 min	180 min	240 min	300 min	360 min
porridge 1[b]	0.54 ± 0.01 a[c]	0.91 ± 0.01 a	1.20 ± 0.03 a	2.12 ± 0.02 a	2.99 ± 0.01 a	3.73 ± 0.02 a	4.45 ± 0.01 a	5.13 ± 0.01 a	6.17 ± 0.02 a	6.82 ± 0.02 a	7.50 ± 0.01 a
porridge 2	0.47 ± 0.01 b	0.74 ± 0.01 b	0.95 ± 0.01 b	1.68 ± 0.04 b	2.29 ± 0.01 b	2.53 ± 0.03 b	3.28 ± 0.03 b	3.95 ± 0.05 b	4.24 ± 0.05 b	4.61 ± 0.03 b	5.33 ± 0.04 b
porridge 3	0.47 ± 0.01 b	0.71 ± 0.01 c	0.97 ± 0.01 b	1.55 ± 0.02 c	2.05 ± 0.03 c	2.94 ± 0.04 c	3.85 ± 0.04 c	4.34 ± 0.05 c	5.02 ± 0.03 c	5.53 ± 0.05 c	5.85 ± 0.04 c
porridge 4	0.44 ± 0.01 c	0.62 ± 0.01 d	0.86 ± 0.03 c	1.42 ± 0.03 d	1.92 ± 0.02 d	2.32 ± 0.02 d	2.37 ± 0.01 d	3.23 ± 0.04 d	3.43 ± 0.04 d	4.12 ± 0.02 d	4.44 ± 0.03 d

[a]Data are presented as means ± standard deviations of triplicate measurements. [b]Porridge 1, white rice porridge; porridge 2, mixed grain porridge; porridge 3, white rice porridge fortified with gum arabic; porridge 4, mixed grain porridge fortified with gum arabic. [c]Mean values in the same column with different letters are significantly different (Tukey test, $p < 0.05$).

The viscosity of porridge may influence the diffusion of glucose. For example, Wood et al. reported that the rates of glucose diffusion from the high viscous solution were considerably less than diffusion in low viscous solution.[29] Thus, the increase of the apparent viscosity of porridges due to addition of gum arabic (Table 2) may have some effects on the glucose diffusion. Water-soluble dietary fibers were also reported to have the effects of hampering the diffusion of glucose and postponing the absorption.[2] Thus, the addition of gum arabic in porridges may also have the ability of slowing the diffusion of glucose, which was similar to other dietary fibers, such as guar gum, xanthan gum, and oat gum.[23,29]

Mouse Blood Glucose Rise after Oral Administration of Porridges. As shown in Figure 1, the initial glucose level of all groups of mice was near 4.5 mmol/L. The blood glucose levels of all of the mice then increased from 0 to 0.5 h after oral administration of porridges and reached the maximum levels at 0.5 h. However, the blood glucose level of mice in white rice porridge fortified with gum arabic group (10.7 ± 0.4 mmol/L) was notably less than that in the white rice porridge group at 0.5 h (13.0 ± 0.8 mmol/L, $p < 0.05$). The blood glucose level of mice in mixed grain porridge fortified with gum arabic group (7.5 ± 0.3 mmol/L) was also obviously lower than that of the mixed grain porridge group at 0.5 h (9.9 ± 0.4 mmol/L, $p < 0.05$). The blood glucose levels of mice in these porridge groups decreased from 0.5 to 1 h, and porridges fortified with gum arabic group mice had significantly lower blood glucose level than that of the unfortified porridges group of mice at 1 h ($p < 0.05$). The blood glucose levels of these porridge groups returned to the normal level at 2 and 3 h, and there was no significant difference among them ($p > 0.05$).

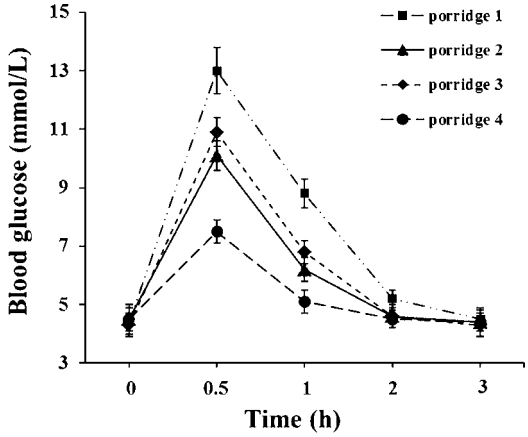

Figure 1. Changes of blood glucose level in mice orally given different porridges.

It can be recognized that the response of blood glucose rise after oral administration of porridges could be significantly lowered due to the addition of gum arabic ($p < 0.05$). This was consistent with our results for the glucose production (Table 3) and glucose diffusion (Table 5) in this study. It may be also because the gum arabic carried out some effects on the blood glucose rise after oral administration of the porridge. This was similar to the results reported by Schweizer et al.,[35] and they compared the serum glucose response of a study group with low dietary fiber intake and a group with high dietary fiber intake. They found that the glucose index of the former was 100% higher than that of the latter. Furthermore, dietary fibers

dx.doi.org/10.1021/jf501557b | J. Agric. Food Chem. 2014, 62, 6408−6416

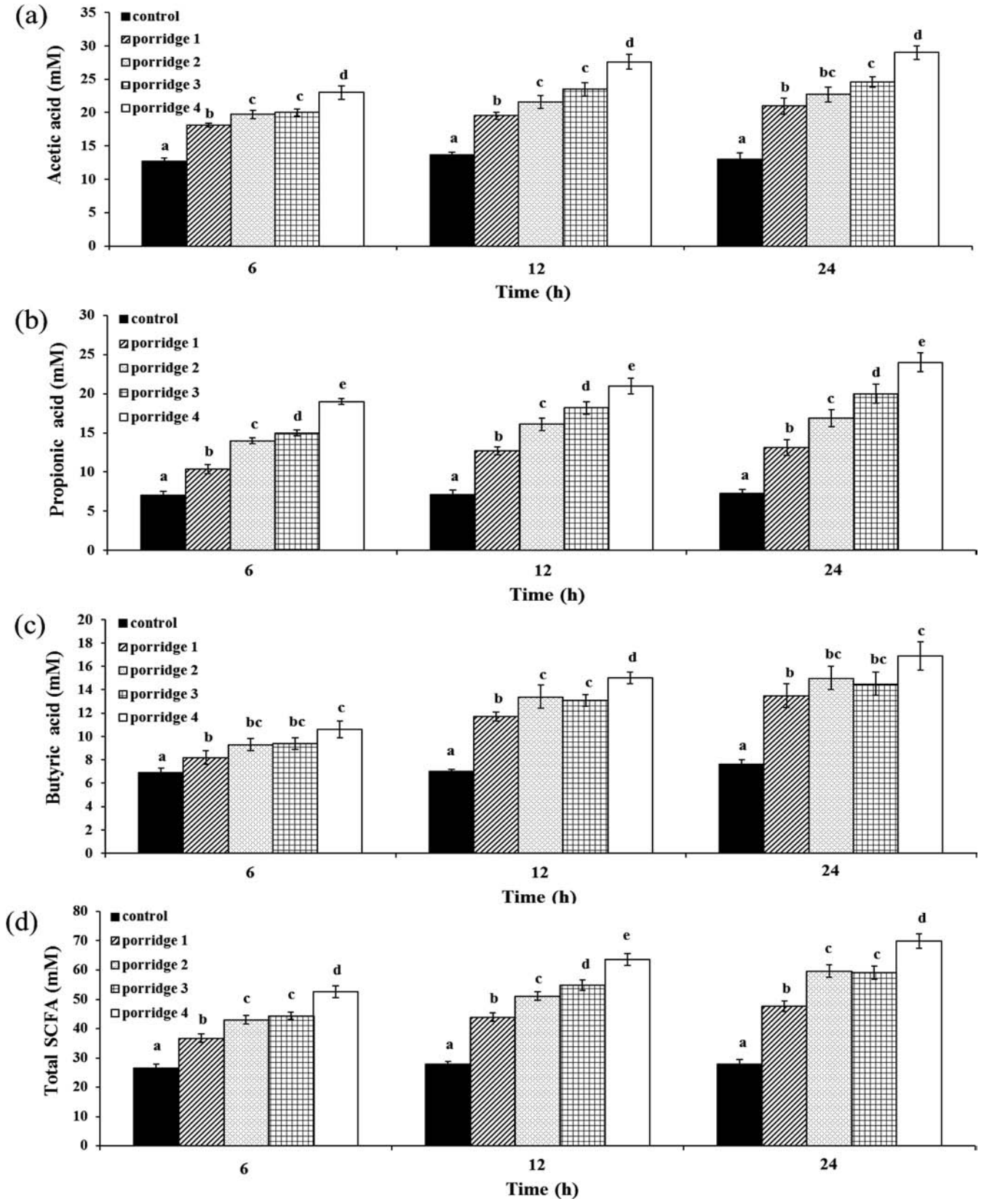

Figure 2. Changes in acetic acid (a), propionic acid (b), butyric acid (c), and total SCFA (d) concentrations after 6, 12, and 24 h of fermentation (37 °C, anaerobic) of different porridge samples (after gastrointestinal digestion) and the control (distilled water). Porridge 1, white rice porridge; porridge 2, mixed grain porridge; porridge 3, white rice porridge fortified with gum arabic; porridge 4, mixed grain porridge fortified with gum arabic. Data are expressed as means ± standard deviations. Values from the same time point differ significantly ($p < 0.05$) when not sharing a common letter. Values for the start of the fermentation experiment (time 0 h) are 9.5 ± 0.3, 4.1 ± 0.2, 3.7 ± 0.3, and 17.3 ± 1.0 mM for (a), (b), (c), and (d), respectively.

dx.doi.org/10.1021/jf501557b | J. Agric. Food Chem. 2014, 62, 6408−6416

have been reported to help lower the blood glucose rise and glycemic level in serum by increasing the function of the upper gastrointestinal tract as well as the plasma levels of the intestinotrophic factor,[36] lowering the insulin response,[37] and slowing glucose absorption through an effect on gastric emptying and/or entrapment of materials in the viscous digesta.[38]

Microbial SCFA Production of Porridge Fermentation. In this study, mixed fresh fecal samples from four donors were used to minimize the difference of the feces from different people.[25] In addition, according to the references, the intestinal anaerobic species, *Bacteroides*, *Eubacterium*, *Clostridium*, *Lactobacillus*, and *Bifidobacterium*, were found in high numbers and were considered to be the main anaerobic microbes in the stools of normal adults and children. These anaerobic species were also found as the main species in the precultured human fecal slurry that may degrade and ferment carbohydrates.[26,39] During the fermentation of porridges, acetic, propionic, and butyric acids were found as the dominant components in total SCFA (Figure 2). As shown in Figure 2a, acetic acid concentrations were strongly increased for all porridge samples upon incubation with human fecal microbiota, the increase being the strongest in the first 6 h of incubation. After 24 h, acetic acid concentrations of the porridge fermented cultures were always significantly higher than that at the time of 0 h (9.5 ± 0.3 mM). At all time points, fermentation of porridges fortified with gum arabic resulted in significantly ($p < 0.01$) higher concentrations of acetic acid than fermentation of the unfortified porridges. This may result from the addition of the gum arabic, which is a kind of soluble dietary fiber. It was reported that acetic acid is a SCFA that is produced as a result of colonic bacterial fermentation of dietary fiber, and acetic acid exerts beneficial effects on glucose homeostasis in diabetes.[40] Several reports have reported that increased acetic acid production in the bowel might, in part, account for the reduction of the postprandial glycemic response, which is one of the beneficial metabolic effects of dietary fiber. Acetic acid was also considered to be beneficial in enhancing glycogen repletion after fasting.[41]

It has been demonstrated that propionic acid could lower fatty acids content in liver and plasma, and improve tissue insulin sensitivity. Thus, increased production of propionic acid by the microbiota might be considered beneficial in the context of reducing postprandial glycemic response. The concentration of propionic acid was presented in Figure 2b, and it was increased for all porridges with incubation time. Values after 6, 12, and 24 h incubation differed significantly ($p < 0.05$) from that at the start (4.1 ± 0.2 mM), and the highest level (at 24 h) was 3.5−6.0 times higher than that at time 0 h. At all time points, fermentation of porridges fortified with gum arabic resulted in significantly ($p < 0.05$) higher concentrations of propionic acid than fermentation of the responding unfortified porridges. Research indicated that dietary fiber had a profound effect on general health, which included the increase of postmeal satiety and the decrease of body weight, fat mass, and the severity of diabetes.[41,42] These effects may be contributed via the fermentation of dietary fiber by the colonic microbiota and in turn the production of propionic acid production.[43,44] Good evidence exists that systemically relevant concentrations of propionic acid might exert a beneficial effect on insulin sensitivity, and thus propionic acid may well form the link for prebiotics supplementation and their beneficial effects on diabetes and related diseases.[5]

Butyric acid was also considered to have some beneficial effects on diabetes. In this study, butyric acid concentration differed significantly ($p < 0.05$) from that at the start of the experiment (3.7 ± 0.3 mM) for all porridges after 6 h incubation (Figure 2c). It continued to increase upon further incubation, and values after 12 and 24 h of incubation were 3−4 times and 4−5 times higher than that at time 0 h, respectively. Fermentation of porridges fortified with gum arabic resulted in significantly higher concentrations of butyric acid than fermentation of the responding unfortified porridges at the time point of 12 h ($p < 0.05$). This may be also due to the addition of the gum arabic to the porridges. As a product of the dietary fiber fermentation, the butyric acid was found to have some effects on preventing and treating diet-induced diabetes and insulin resistance in mouse models. The mechanism of the butyric acid action is related to the promotion of energy expenditure and induction of mitochondria function.[5]

In addition, concentrations of total SCFA at 6, 12, and 24 h during fermentation are presented in Figure 2d. The fermentation cultures for porridges fortified with gum arabic contained significantly higher concentrations of total SCFA than the responding unfortified porridges at all time points ($p < 0.05$).

There have been extensive studies on the health benefit of gum arabic on glucose level and SCFA production. Because of the physical properties of gum arabic, such as viscosity, it was found to be a good in vitro glucosidase inhibitor and have effects on the retardation and delay of carbohydrate and glucose absorption.[45−47] Gum arabic was also reported to reach the large intestine without digestion in the small intestine, and it can be mostly fermented by intestinal bacteria to SCFA, particularly propionic acid, in large intestine and feces.[46−48] Previous studies mainly focused on the gum arabic itself on glucose level and SCFA production. Limited information is available for the effects of gum arabic on glucose levels and microbial SCFA production in food models.

Therefore, our results showed in vitro and in vivo information about the effects of gum arabic on glucose levels and microbial SCFA productions in food model (white rice porridge model and mixed grain porridge model) for the first time. Apparent viscosity of the two porridges was significantly increased after addition of gum arabic, and the glucose productions of porridges were both notably lowered at the same time points during gastrointestinal digestion. Diffused glucose amount was also significantly decreased after gum arabic addition. Furthermore, blood glucose rise after oral administration of porridges fortified with gum arabic in mice was considerably lower than the responding unfortified porridges. Microbial short-chain fatty acid production of porridges during in vitro fermentation was also significantly increased after addition of gum arabic. Therefore, gum arabic may be a helpful ingredient, which could be added in porridges to have benefits for the reduction of postprandial glycemic response.

AUTHOR INFORMATION

Corresponding Author

*Tel./fax: +86-791-88304452. E-mail: spnie@ncu.edu.cn.

Funding

This study is financially supported by the National Key Technology R&D Program of China (2012BAD33B06), the Key Program of National Natural Science Foundation of China (no. 31130041), the Program for New Century Excellent

Talents in University (NCET-12-0749), the Project of Science and Technology of Jiangxi Provincial Education Department (KJLD13004), the Research Project of State Key Laboratory of Food Science and Technology (SKLF-ZZA-201301, SKLF-KF-201202), and the Jiangxi Provincial Postgraduate Innovation Fund (YC2011-B004), which we gratefully acknowledge.

Notes

The authors declare no competing financial interest.

■ ABBREVIATIONS USED

GI, glycemic index; SCFA, short-chain fatty acid; GC, gas chromatography; FID, flame ionization detector

■ REFERENCES

(1) Fu, Z.; Yuskavage, J.; Liu, D. Dietary flavonol epicatechin prevents the onset of Type 1 diabetes in nonobese diabetic mice. *J. Agric. Food Chem.* **2013**, *61*, 4303−4309.

(2) Yokoyama, W. H.; Hudson, C. A.; Knuckles, B. E.; Chiu, M. C. M.; Sayre, R. N.; Turnlund, J. R.; Schneeman, B. O. Effect of barley β-glucan in durum wheat pasta on human glycemic response. *Cereal Chem.* **1997**, *74*, 293−296.

(3) Yang, Z.-C.; Liang, J.; Liu, Y.-q.; Liu, Y.-t.; Ma, K.; Jin, L.-M.; Hu, W.-z. Component analysis of coix seeds. *J. Anhui Agric. Sci.* **2011**, *39*, 756−756.

(4) Ebihara, K.; Masuhara, R.; Kiriyama, S. Effect of konjac mannan, a water-soluble dietary fiber on plasma glucose and insulin responses in young men undergone glucose tolerance test. *Nutr. Rep. Int.* **1981**, *23*, 577−583.

(5) Gao, Z.; Yin, J.; Zhang, J.; Ward, R. E.; Martin, R. J.; Lefevre, M.; Cefalu, W. T.; Ye, J. Butyrate improves insulin sensitivity and increases energy expenditure in mice. *Diabetes* **2009**, *58*, 1509−1517.

(6) Williams, P. A.; Phillips, G. O. Gum arabic. In *Handbook of Hydrocolloids*, 1st ed.; Phillips, G. O., Williams, P. A., Eds.; CRC Press: Boca Raton, FL, 2000; pp 155−168.

(7) Verbeken, D.; Dierckx, S.; Dewettinck, K. Exudate gums: occurrence, production, and applications. *Appl. Microbiol. Biotechnol.* **2003**, *63*, 10−21.

(8) Rehman, K.; Wingertzahn, M. A.; Harper, R. G.; Wapnir, R. A. Proabsorptive action of G.A.: regulation of nitric oxide metabolism in the basolateral potassium channel of the small intestine. *J. Pediatr. Gastroenterol. Nutr.* **2001**, *32*, 529−533.

(9) Gamal el-din, A. M.; Mostafa, A. M.; Al-Shabanah, O. A.; Al-Bekairi, A. M.; Nagi, M. N. Protective effect of arabic gum against acetaminophen-induced hepatotoxicity in mice. *Pharmacol. Res.* **2003**, *48*, 631−635.

(10) Ali, A. A.; Ali, K. E.; Fadlalla, A.; Khalid, K. E. The effects of G.A. oral treatment on the metabolic profile of chronic renal failure patients under regular haemodialysis in Central Sudan. *Nat. Prod. Res.* **2008**, *22*, 12−21.

(11) Benton, D.; Sargent, J. Breakfast, blood glucose and memory. *Biol. Psychol.* **1992**, *33*, 207−210.

(12) Chan, E. M. Y.; Cheng, W. M. W.; Tiu, S. C.; Wong, L. L. L. Postprandial glucose response to Chinese foods in patients with type 2 diabetes. *J. Am. Diet. Assoc.* **2004**, *104*, 1854−1858.

(13) Sugiyama, M.; Tang, A.; Wakaki, Y.; Koyama, W. Glycemic index of single and mixed meal foods among common Japanese foods with white rice as a reference food. *Eur. J. Clin. Nutr.* **2003**, *57*, 743−752.

(14) Murakami, K.; Sasaki, S.; Okubo, H.; Takahashi, Y.; Hosoi, Y.; Itabashi, M. Dietary fiber intake, dietary glycemic index and load, and body mass index: a cross-sectional study of 3931 Japanese women aged 18−20 years. *Eur. J. Clin. Nutr.* **2007**, *61*, 986−995.

(15) Gilbertson, H. R.; Brand-Miller, J. C.; Thorburn, A. W.; Evans, S.; Chondros, P.; Werther, G. A. The effect of flexible low glycemic index dietary advice versus measured carbohydrate exchange diets on glycemic control in children with type 1 diabetes. *Diabetes Care* **2001**, *24*, 1137−1143.

(16) Jenkins, D.; Wolever, T.; Taylor, R. H.; Barker, H.; Fielden, H.; Baldwin, J. M.; Bowling, A. C.; Newman, H. C.; Jenkins, A. L.; Goff, D. V. Glycemic index of foods: a physiological basis for carbohydrate exchange. *Am. J. Clin. Nutr.* **1981**, *34*, 362−366.

(17) Wolever, T. M. S.; Boume, G. H. The glycemic index. Aspects of some vitamins, minerals and enzymes in health and diseases. *World Rev. Nutr. Diet.* **1990**, *62*, 120−185.

(18) Kim, S. O.; Yun, S. J.; Jung, B.; Lee, E. H.; Hahm, D. H.; Shim, I.; Lee, H. J. Hypolipidemic effects of crude extract of adlay seed (*Coix lachrymajobi var. mayuen*) in obesity rat fed high fat diet: Relations of TNF-α and leptin mRNA expressions and serum lipid levels. *Life Sci.* **2004**, *75*, 1391−1404.

(19) Chen, J.; Liang, R. H.; Liu, W.; Liu, C. M.; Li, T.; Tu, Z. C.; Wan, J. Degradation of high-methoxyl pectin by dynamic high pressure microfluidization and its mechanism. *Food Hydrocolloids* **2012**, *28*, 121−129.

(20) Blanquet, S.; Zeijdner, E.; Beyssac, E.; Meunier, J. P.; Denis, S.; Havenaar, R.; Alric, M. A dynamic artificial gastrointestinal system for studying the behavior of orally administered drug dosage forms under various physiological conditions. *Pharm. Res.* **2004**, *21*, 585−591.

(21) Salovaara, S.; Alminger, M. L.; Eklund-Jonsson, C.; Andlid, T.; Sandberg, A. S. Prolonged transit time through the stomach and small intestine improves iron dialyzability and uptake in vitro. *J. Agric. Food Chem.* **2003**, *51*, 5131−5136.

(22) Tedeschi, C.; Clement, V.; Rouvet, M.; Valles-Pamies, B. Dissolution tests as a tool for predicting bioaccessibility of nutrients during digestion. *Food Hydrocolloids* **2009**, *23*, 1228−1235.

(23) Ou, S.; Kwok, K.; Li, Y.; Fu, L. In vitro study of possible role of dietary fiber in lowering postprandial serum glucose. *J. Agric. Food Chem.* **2001**, *49*, 1026−1029.

(24) Adachi, T.; Ono, Y.; Koh, K. B.; Takashima, K.; Tainaka, H.; Matsuno, Y.; Nakagawa, S.; Todaka, E.; Sakurai, K.; Fukata, H. Long-term alteration of gene expression without morphological change in testis after neonatal exposure to genistein in mice: toxicogenomic analysis using cDNA microarray. *Food Chem. Toxicol.* **2004**, *42*, 445−452.

(25) Bianchi, F.; Dall'Asta, M.; Del Rio, D.; Mangia, A.; Musci, M.; Scazzina, F. Development of a headspace solid-phase microextraction gas chromatography-mass spectrometric method for the determination of short-chain fatty acids from intestinal fermentation. *Food Chem.* **2011**, *129*, 200−205.

(26) Ruiz-Perez, F.; Sheikh, J.; Davis, S.; Boedeker, E. C.; Nataro, J. P. Use of a continuous-flow anaerobic culture to characterize enteric virulence gene expression. *Infect. Immun.* **2004**, *72*, 3793−3802.

(27) Hughes, S.; Shewry, P.; Li, L.; Gibson, G.; Sanz, M.; Rastall, R. In vitro fermentation by human fecal microflora of wheat arabinoxylans. *J. Agric. Food Chem.* **2007**, *55*, 4589−4595.

(28) Hu, J.-L.; Nie, S.-P.; Min, F.-F.; Xie, M.-Y. Polysaccharide from seeds of *Plantago asiatica* L. increases short-chain fatty acid production and fecal moisture along with lowering pH in mouse colon. *J. Agric. Food Chem.* **2012**, *60*, 11525−11532.

(29) Wood, P. J.; Braaten, J. T.; Scott, F. W.; Riedel, D.; Poste, L. M. Comparisons of viscous properties of oat and guar gum and the effects of these and oat bran on glycemic index. *J. Agric. Food Chem.* **1990**, *38*, 753−757.

(30) Dikeman, C. L.; Murphy, M. R.; Fahey, G. C., Jr. Dietary fibers affect viscosity of solutions and simulated human gastric and small intestinal digesta. *J. Nutr.* **2006**, *136*, 913−919.

(31) Eichner, K.; Karel, M. Influence of water content and water activity on the sugar-amino browning reaction in model systems under various conditions. *J. Agric. Food Chem.* **1972**, *20*, 218−223.

(32) Staffolo, M.; Bertola, N.; Martino, M. Influence of dietary fiber addition on sensory and rheological properties of yogurt. *Int. Dairy J.* **2004**, *14*, 263−268.

(33) Furuta, H.; Nakamura, A.; Ashida, H.; Asano, H.; Maeda, H.; Mori, T. Properties of rice cooked with commercial water-soluble soybean polysaccharides extracted under weakly acidic conditions from soybean cotyledons. *Biosci., Biotechnol., Biochem.* **2003**, *67*, 677−683.

(34) Annison, G.; Topping, D. L. Nutritional role of resistant starch: chemical structure vs physiological function. *Annu. Rev. Nutr.* **1994**, *14*, 297−320.
(35) Schweizer, T.; Andersson, H.; Langkilde, A.; Reimann, S.; Torsdottir, I. Nutrients excreted in ileostomy effluents after consumption of mixed diets with beans or potatoes. II. Starch, dietary fibre and sugars. *Eur. J. Clin. Nutr.* **1990**, *44*, 567−575.
(36) Thulesen, J.; Hartmann, B.; Nielsen, C.; Holst, J. J.; Poulsen, S. S. Diabetic intestinal growth adaptation and glucagon-like peptide 2 in the rat: effects of dietary fibre. *Gut* **1999**, *45*, 672−678.
(37) Jarvi, A. E.; Karlstrom, B. E.; Granfeldt, Y. E.; Bjorck, I. E.; Asp, N.; Vessby, B. Improved glycemic control and lipid profile and normalized fibrinolytic activity on a low-glycemic index diet in type 2 diabetic patients. *Diabetes Care* **1999**, *22*, 10−18.
(38) Baghurst, P. A.; Baghurst, K.; Record, S. Dietary fibre, non-starch polysaccharides and resistant starch: a review. *Food Aust.* **1996**, *48*, S3−S35.
(39) Berg, R. D. The indigenous gastrointestinal microflora. *Trends Microbiol.* **1996**, *4*, 430−435.
(40) Kondo, S.; Tayama, K.; Tsukamoto, Y.; Ikeda, K.; Yamori, Y. Antihypertensive effects of acetic acid and vinegar on spontaneously hypertensive rats. *Biosci., Biotechnol., Biochem.* **2001**, *65*, 2690−2694.
(41) Fushimi, T.; Tayama, K.; Fukaya, M.; Kitakoshi, K.; Nakai, N.; Tsukamoto, Y.; Sato, Y. Acetic acid feeding enhances glycogen repletion in liver and skeletal muscle of rats. *J. Nutr.* **2001**, *131*, 1973−1977.
(42) Cani, P. D.; Knauf, C.; Iglesias, M. A.; Drucker, D. J.; Delzenne, N. M.; Burcelin, R. Improvement of glucose tolerance and hepatic insulin sensitivity by oligofructose requires a functional glucagon-like peptide 1 receptor. *Diabetes* **2006**, *55*, 1484−1490.
(43) Chen, W. J.; Anderson, J. W. D. Propionate may mediate the hypocholesterolemic effects of certain soluble plant fibers in cholesterol-fed rats. *Proc. Soc. Exp. Biol. Med.* **1984**, *175*, 215−218.
(44) Thacker, M. O.; Salomons, F. X.; Aherne, L. P.; Milligan, J. P. Influence of propionic acid on the cholesterol metabolism of pigs fed hypercholesterolemic diets. *Can. J. Anim. Sci.* **1981**, *61*, 961−975.
(45) Bisht, S.; Kant, R.; Kumar, V. α-D-Glucosidase inhibitory activity of polysaccharide isolated from *Acacia tortilis* gum exudate. *Int. J. Biol. Macromol.* **2013**, *59*, 214−220.
(46) Adiotomre, J.; Eastwood, M. A.; Edwards, C. A.; Brydon, W. G. Dietary fiber: *in vitro* methods that anticipate nutrition and metabolic activity in humans. *Am. J. Clin. Nutr.* **1990**, *52*, 128−134.
(47) Annison, G.; Trimble, R. P.; Topping, D. L. Feeding Australian acacia gums and gum arabic leads to non-starch polysaccharide accumulation in the cecum of rats. *J. Nutr.* **1995**, *125*, 283−292.
(48) May, T.; Mackie, R. I.; Fahey, G. C., Jr.; Cremin, J. C.; Garleb, K. A. Effect of fiber source on short-chain fatty acid production and on the growth and toxin production by *Clostridium difficile*. *Scand. J. Gastroenterol.* **1994**, *29*, 916−922.

between the phenolic compounds present in the PGJ and milk proteins and its impact on the antioxidant activity of the yogurt.

MATERIALS AND METHODS

Materials and Chemicals. Commercial starter cultures of *Streptococcus thermophilus* and *Lactobacillus delbrueckii* subsp. *bulgaricus* (Ezal MY900, Rhodia Food-Danisco A/S, Sassenage, France) were used at the concentrations recommended by the suppliers. For all the study, the same batch of skim milk powder was used (34% protein, 52% lactose, 1% fat, 6.8% ash, 5.2% moisture) (Central Lechera Asturiana, CAPSA, Granada-Siero, Spain).

2,2-Diphenyl-1-picrylhydrazyl (DPPH$^{\bullet}$), Folin−Ciocalteu reagent, gallic acid, iron(III) chloride, trichloroacetic acid (TCA), aluminum chloride, Trolox, and formic acid were from Sigma Chemical Company (Germany). Methanol of HPLC ultragradient grade, HCl, potassium chloride, sodium acetate, dibasic potassium phosphate, sodium nitrite (II), sodium hydroxide, sodium carbonate, and dibasic sodium phosphate were from Merck (Darmstadt, Germany). Potassium hexacyanoferrate was from Fluka BioChemika (Germany). Ellagic acid was from Tocris Bioscience (Ellisville, MO, USA), and pure punicalagins were from Chengdu Biopurity Phytochemicals Ltd. (Sischuan, China). Cyanidin-3,5-*O*-diglucoside and -glucoside, pelargonidin-3-*O*-glucoside, and delphinidin-3-*O*-glucoside, were from Extrasynthese (Genay, France). Acetonitrile for HPLC-DAD and LC/MS (Gradient grade) was from Merck (Darmstadt, Germany). LC grade water, prepared by using an HLP SMART 1000s system (Hydrolab, Gdańsk, Poland), was additionally filtered through a 0.22 μm membrane filter immediately before use.

Plant Material. Mature PG fruit cultivar "Mollar de Elche", with no visible external cuts or spoilage was purchased from a local market. The PG fruits were peeled manually, and the arils were introduced in a blender Ju2000 Vitae (Moulinex, Barcelona, Spain) to obtain PGJ. PGJ was filtered through cotton gauze to remove particles and was kept frozen until use.

Yogurt Manufacture. Set-type yogurt was produced following the manufacture method developed by Trigueros et al.[10] Briefly, skim milk powder (SMP) was reconstituted with deionized water at 15% w/v total solids to serve as control. SMP was reconstituted at 25% w/v total solids to be further completed with PGJ to have a final solid content of 15% w/v after pasteurization. PGJ, 15% reconstituted skim milk (RSM), and 25% RSM were separately pasteurized at 80 °C for 30 min. After cooling to 43 °C, PGJ was added to the RSM to a final concentration of 40% v/v. At this point, the starter culture was added and the inoculated mix was incubated at 43 °C for 4 h and then cooled and stored at 4 °C for 28 days.

Colorimetric Analysis. The CIE LAB color space of yogurts was studied, and the following color coordinates were determined: lightness (L^*), redness (a^*, ± red−green), and yellowness (b^*, ± yellow−blue). Color determinations were made at 12 ± 2 °C by means of a Minolta CM-2002 (Minolta Camera Co., Osaka, Japan) spectrophotometer, with a liquid accessory CR-A70 (Minolta Camera Co., Osaka, Japan), with illuminant D_{65} and an observer of 10°.

Preparation of the Free-Protein Phase (Permeate). To quantitatively estimate the interaction of phenolic compounds with proteins, a protein-free phase (permeate) was obtained with a laboratory scale ultrafiltration (UF) cartridge (Amicon Ultra-15; Merck Millipore Ltd., Ireland), with a nominal cutoff of 10000 Da and a nominal area of 7.6 cm^2 was used. To remove caseins, 30 g of yogurt were centrifuged at 7000 rpm for 30 min, at 4 °C. The supernatant was ultrafiltrated through the cartridge at 5500 rpm for 30 min, at 4 °C, and permeate was collected for further analysis.

Extraction of Phenolics from PJ and Yogurt Permeate. PGJ and permeates (10 mL) were extracted with 30 mL of acidified methanol (methanol containing 100 μL concd HCl) for 30 s at 12000 rpm (IKA T25 digital ULTRA-TURRAX, IKA Werke Staufen, Germany). Then, the mixtures were centrifuged at 5000 rpm for 10 min at 4 °C. Then 5 mL of the extract was separated for determining anthocyanin content. The remaining portions were evaporated to dryness using a rotary evaporator R-205 (Büchi, Flawil, Switzerland) under reduced pressure (<100 mbar) at 50 °C and used for determining total phenolics, total flavonoids, antioxidant activities, and HPLC analysis.

Extraction of Phenolics from PJ Yogurt. Yogurt samples (20 g) were mixed with 30 mL of acidified methanol. Then the mixture was left at 4 °C for overnight incubation. The mixture was filtered by using no. 1 Whatman filter paper, and residue was washed with acidified methanol until it became colorless.[14] Ten milliliters of the extract were separated for determining anthocyanin content. The remaining portions were concentrated as previously described and used for determining total phenolics, total flavonoids, antioxidant activities, and LC and HPLC analysis.

HPLC-DAD Analysis (Nonanthocyanin Phenolics). Phenolic compounds were analyzed by high performance liquid chromatography coupled with a diode array detector (HPLC-DAD) as previously described by Benavente-García et al.[15] Samples (20 μL) were injected into a Hewlett-Packard HPLC series 1200 instrument (Woldbronn, Germany) equipped with a C18 Teknokroma column (Mediterranean sea$_{18}$ 25 cm × 0.4 cm, Teknokroma, Barcelona, Spain) and detected by absorbance at 280 and 360 nm. UV spectra of individual peaks were recorded in the range of 200−600 nm. The separation columns were controlled thermostatically at 35 °C. Phenolic compounds were analyzed in standard and sample solutions using a gradient elution at 1 mL/min with the following gradient program (0−20 min 95−75% A, 20−40 min 75−50% A, 40−45 min 50−95% A) with 4.5% formic acid in water (v/v) as solvent A and 100% of acetonitrile as solvent B. Peaks were identified by comparing retention times and photodiode array spectra with analytical standards. The phenolic compounds were quantified by the absorbance of their corresponding peaks with calibration curves of standard compounds. For this purpose, stock solutions were diluted to concentrations of 10−160 mg/L (ellagic acid) and 25−800 mg/L (punicalagins isomers).

LC-PDA/MS Analysis (Anthocyanins). Identification of phenolic compounds was carried out using an ACQUITY Ultra Performance LC system (UPLC) with binary solvent manager and photo diode array (PDA) detector (Waters Corporation, Milford, MA, USA) and a Micromass Q-TOF Micro mass spectrometer (Waters, Manchester, UK) equipped with an electrospray ionization (ESI) source operating in negative and positive mode. Separations of individual phenolic compounds were carried out using a UPLC BEH C18 column (1.7 μm, 2.1 mm × 100 mm; Waters Corporation) at 30 °C. Samples (10 μL juice and 2 μL yogurt and permeate extracts) were injected and elution completed in 20 min with a sequence of linear gradients and isocratic flow rates of 0.45 mL/min. The mobile phase was composed of solvent A (4.5% formic acid in water, v/v) and solvent B (100% of acetonitrile). The program began with isocratic elution with 99% A (0−1 min), and then a linear gradient was used until 15 min, lowering A to 75%, and then 2.5 min for 0% of solvent A and 2.5 min, returned to the initial composition (99% A) and then held constant to re-equilibrate the column. Analysis was carried out using full-scan, data-dependent MS scanning from m/z 100 to 1500. The mass tolerance was 0.001 Da, and the resolution was 5000. Leucine enkephalin was used as the internal reference compound during ESI-MS accurate mass experiments and was permanently introduced via the LockSpray channel using a Hamilton pump. The lock mass correction was ±1000 for Mass Window. All TOF-MS chromatograms are displayed as base peak intensity (BPI) chromatograms and scaled to 12400 counts per second (cps) (= 100%). The effluent was led directly to an electrospray source with a source block temperature of 130 °C, desolvation temperature of 350 °C, capillary voltage of 2.5 kV, and cone voltage of 30 V. Nitrogen gas used as desolvation gas at a flow rate of 300 L/h.

The characterization of the single components was carried out via the retention time and the accurate molecular masses. Each compound was optimized to its estimated molecular mass in the negative and positive mode before and after fragmentation. The data obtained from LC/MS were subsequently entered into the MassLynx 4.0 ChromaLynx Application Manager software. On the basis of these data, the software is able to scan different samples for the characterized substances.

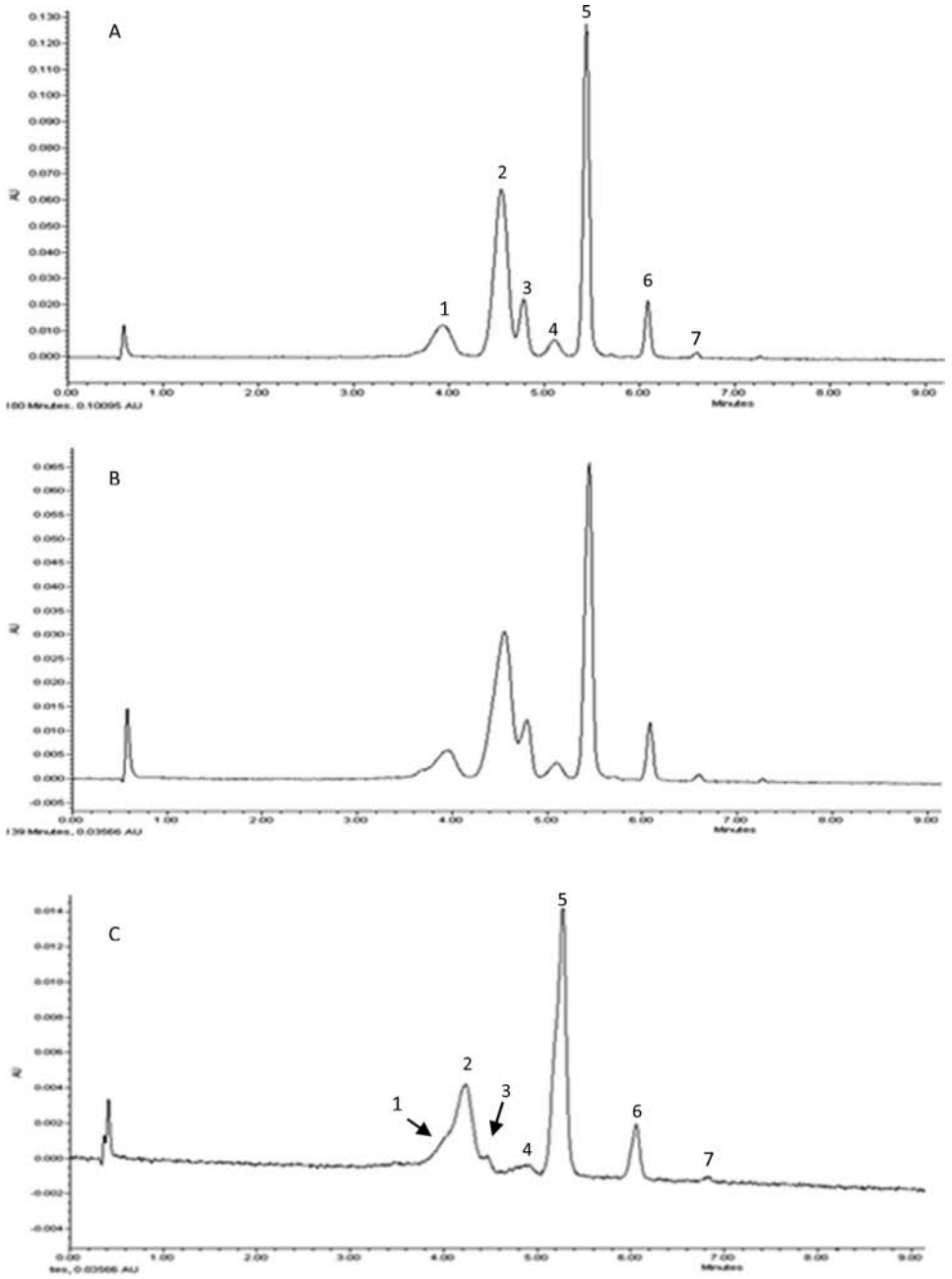

Figure 1. Chromatograms of anthocyanins in (A) pomegranate juice, (B) pomegranate juice yogurt, and (C) permeate from pomegranate yogurt at 520 nm.

For quantification of anthocyanin compounds spectra were measured over the range 200−600 nm in steps of 2 nm. The run was monitored at 520 nm. Calibration curves at concentration ranging from 0.05 to 5 mg/L ($r^2 \leq 0.9997$) were made from cyanidin-3,5-*O*-diglucoside and -glucoside, pelargonidin-3-*O*-glucoside, and delphinidin-3-*O*-glucoside. Delphinidin-3,5-*O*-diglucoside was expressed as delphinidin-3-*O*-glucoside, pelargonidin-3,5-*O*-diglucoside as pelargonidin-3-*O*-glucoside, and cyanidin-pentoside as cyanidin-3-*O*-glucoside. All determinations were done in triplicate. Results were expressed as milligrams per L.

Determination of Total Phenol Content, Total Flavonoid Content, and Total Anthocyanin Content by Colorimetric Methods. The total phenol content (TPC) in the yogurts, PGJ, and permeates was determined using the Folin−Ciocalteu's reagent.[16] Volumes of 0.3 mL of the methanolic extracts were introduced into test tubes followed by 2.5 mL of Folin−Ciocalteu's reagent (diluted 10 times with water) and 2 mL of sodium carbonate (7.5% w/v). The tubes were vortexed and incubated at 50 °C for 5 min. Absorption at 760 nm was measured with a HP 8451 spectrophotometer (Hewlet Packard, Cambridge, UK) and compared to a gallic acid calibration curve. The results were expressed as mg gallic acid equivalents (GAE)/g sample. Samples were analyzed in triplicate.

For total flavonoid content (TFC) the method based on Blasa et al.[17] with some modifications, was used. One milliliter of the methanolic extracts of yogurts, PGJ, and permeates was mixed with 0.3 mL of $NaNO_2$ (5%), and 0.3 mL of $AlCl_3$ (10%) were added after 5 min. Samples were mixed and after 6 min, were neutralized with 2 mL of NaOH solution (1 M). Absorbance was read at 510 nm, and the quantification was carried out using a calibration curve. Different concentrations of rutin (8.5−170 μg/mL) were used for calibration. The results were expressed in mg rutin equivalents (RE)/100 g of sample as mean of three replicates.

Total anthocyanin content (TAC) in the yogurts and PGJ were determined by the pH differential method described by Wrolstad[18]

dx.doi.org/10.1021/jf501503h | J. Agric. Food Chem. 2014, 62, 6417−6425

using a UV−vis HP 8451 spectrophotometer. Absorbance of the samples in 0.2 N potassium chloride buffer (pH 1.0) and 1 M sodium acetate buffer (pH 4.5) were measured at 520 and 700 nm. Anthocyanin content was determined using the equation: $A = (A_{\lambda 520} - A_{\lambda 700})_{\text{pH 1.0}} - (A_{\lambda 520} - A_{\lambda 700})_{\text{pH 4.5}}$ with a molar extinction coefficient of 29600. Results were expressed as mg of cyanindin-3-glucoside equivalent/L of sample as mean of three replicates.

Quantification of Antioxidant Activity by (i) DPPH• Radical Scavenging Method and (ii) Ferric Reducing Antioxidant Power Assay. Free radical scavenging activities of the PGJ, yogurts, and permeates were determined by DPPH• (2,2-diphenyl-1-picrylhydrazyl) assay with minor modifications as described by Brand-Williams et al.[19] A 0.1 mM solution of DPPH• in ethanol was prepared. A volume of 0.1 mL of various concentrations of the PGJ and yogurt methanolic extracts diluted in methanol was added to 2.9 mL of DPPH• solution. The mixtures were well shaken in a Vortex (2500 rpm) for 1 min and then placed in a dark room. The decrease in absorbance at 517 nm was determined with a HP 8451 spectrophotometer after 1 h for all samples. Methanol was used to zero the spectrophotometer. Absorbance of the radical without extract was used as control. The amount of sample necessary to decrease the absorbance of DPPH• by 50% (IC_{50}) was calculated graphically. The inhibition percentage of the DPPH• was calculated from the following equation: $\%I = [(A_C - A_S)/A_C] \times 100$, where I = DPPH• inhibition %, A_C = absorbance of control sample (t = 0 h) and , A_S = absorbance of a tested sample at the end of the reaction (t = 1 h).

The ferric reducing antioxidant power (FRAP) of PGJ, yogurts, and permeates was determined by using the potassium ferricyanide−ferric chloride method.[20] One mL of the PGJ, yogurt, and permeate methanolic extracts of four different concentrations (2.5, 5.0, 7.5, and 10.0 g/100 mL) was added to 2.5 mL of phosphate buffer (0.2 M, pH 6.6) and 2.5 mL of potassium ferricyanide (1%). The mixtures were incubated at 50 °C for 20 min, after which 2.5 mL of trichloroacetic acid (10%) was added. An aliquot of the mixture (2.5 mL) was taken and mixed with 2.5 mL of water and 0.5 mL of 0.1% $FeCl_3$. The absorbance at 700 nm was measured after allowing the solution to stand for 30 min. The FRAP of a sample is estimated in terms of Trolox equivalent antioxidant capacity (TEAC) in mmol Trolox/L. Each essay was carried out in triplicate.

Statistical Analysis. Statistical analysis and comparison among means were carried out using the statistical package SPSS 20.0 (IBM SPSS Statistics, Chicago, IL, USA). ANOVA test was used to evaluate factors: sample type (pomegranate yogurts and permeates) and storage time (days 1, 14, 28). Tukey's pair wise comparisons test was used for means comparison (95% confidence level). The whole experiment was independently run three times.

RESULTS AND DISCUSSION

Individual Phenolic Compounds Content from Pomegranate Juice, Yogurts, and Permeates. Pomegranate anthocyanins were characterized by comparison of their UV−vis spectra (λ_{max}), retention times (R_t), and mass spectra (MS) before and after fragmentation (MS/MS) with standards, if available, and published data. Figure 1 shows a typical UPLC chromatogram of pomegranate juice (A), pomegranate yogurt (B), and yogurt permeate (C) anthocyanins recorded at 520 nm. The retention times, UV−vis, and mass spectral characteristics as well as peak assignments for all compounds are specified in Table 1.

The anthocyanin profiles of the pomegranate juice (PGJ) and pomegranate yogurts (PGY) were similar; however, the amount of individual compounds differed. A total of seven anthocyanins were detected, three cyanidins and two delphinidins and two pelargonidins. Each of these anthocyanins were associated by monoglucoside or diglucoside. The anthocyanins revealed the typical mass spectrometric behavior in ESI(+) experiments, i.e., they showed M^+ ions in the MS experiments and the sequential loss of their saccharide moieties, releasing the aglycones in the MS/MS experiments (Table 1). These results agreed quite well with recently published data.[21,22] In accordance with our results, previous analysis of juices produced from arils alone[21,23,24] reported that anthocyanins were identified as the most abundant phenolic compounds; other phenolics including ellagic acid and punicalagins were also present.[24] Ellagic acid (EA) has exhibited both antioxidant[25] and anticarcinogenic[26] properties together that it combines with proteins to form insoluble sediments.[27] EA content was 21.17 mg/L in PGJ, 8.58 in PGY at first day and 11.75 mg/L in PGY at 28th day. Our findings for EA in PGJ were in the range detected by Mena et al.[28] (3.6−152.8 mg/L) and Gil et al.[23] (33.2 mg/L) and slightly higher than those reported by Qu et al.[24] (2.1−15.3 mg/L) in juices made solely from arils. Regarding punicalagins ($\alpha + \beta$) content in PGJ was 46.35 mg/L, 31.90 mg/L in PGY at first day, and 31.37 mg/L in PGY at 28th day of storage, being the content for all samples tested higher in the β anomer (data not shown), which is typical of noncommercial juices.[28] In this sense, our results are in accordance to those reported by Mena et al.[28] ($\alpha + \beta$, 2.0−44.1 mg/L) and higher than the amounts reported by Gil et al.[23] (22.8 mg/L) and Qu et al.[24] (4.1−22.8 mg/L). Many authors attribute the high antioxidant capacity of pomegranate juice to hydrolyzable tannins including punicalagins.[23,29] In permeates, EA remained stable, showing values of 9.95 mg/L at the first day of storage and 10.87 mg/L at the 28th day of the storage, meaning that EA did not bind to milk proteins. However, no punicalagin content was detected in yogurt permeates, indicating a high affinity to milk proteins. Hence, only EA remained in free form in yogurt. The increase of EA during 28th days of storage PGY and permeate is the result of the transformation of ellagitannins to ellagic acid. Ellagic acid is transformed by human gut bacteria to the dibenzopyranone type urolithins that are much better absorbed because of the higher lipophilicity of the resulting components compared to intact form of punicalagins and ellagitannins.[30]

Table 2 shows the content of anthocyanins previously identified in pomegranate juice, yogurts, and permeates. Anthocyanins have been associated with prevention of cardiovascular disease, obesity, and diabetes,[31] and they are phenolic compounds responsible for pomegranate juice color.

Table 1. LC/MS Analysis of Anthocyanin Compounds in Pomegranate Juices and Pomegranate Yogurt

peak	compd	R_t (min)	λ_{max} (nm)	$[M + H]^+$ (m/z)	MS/MS (m/z)
1	delphinidin-3,5-*O*-diglucoside	5.70	277; 519	627	465/303/186
2	cyanidin-3,5-*O*-diglucoside	6.82	277; 513	611	449/287/186
3	delphinidin-3-*O*-glucoside	7.25	277; 522	465	303/186
4	pelargonidin-3,5-*O*-diglucoside	7.99	274; 499	595	433/274/303/186
5	cyanidin-3-*O*-glucoside	8.49	280; 516	449	287
6	pelargonidin-3-*O*-glucoside	9.77	274; 503	433	271
7	cyanidin-pentoside	10.80	277; 513	419	287

dx.doi.org/10.1021/jf501503h | J. Agric. Food Chem. 2014, 62, 6417−6425

Table 2. Content of Individual Anthocyanins (mg/L) in Pomegranate Juice, Yogurts, and Protein-Free Permeates[a]

	anthocyanins							
sample[b]	Dp 3,5-diglc	Cy 3,5-diglc	Dp 3-glc	Pg 3,5-diglc	Cy 3-glc	Pg 3-glc	Cy-pent	total anthocyanins
PGJ	78.41 ± 0.78	190.03 ± 1.88	62.85 ± 0.65	21.55 ± 0.25	221.00 ± 2.20	64.65 ± 0.65	3.00 ± 0.10	641.48 ± 1.25
PGY d1	61.80 ± 0.60	162.70 ± 1.60	49.35 ± 0.45	16.45 ± 0.15	125.65 ± 1.25	24.45 ± 0.25	1.75 ± 0.05	442.15 ± 3.05
PGY d14	59.85 ± 0.55	149.65 ± 1.45	43.45 ± 0.45	15.75 ± 0.15	110.40 ± 1.10	23.05 ± 0.25	1.55 ± 0.05	403.70 ± 0.10
PGY d28	31.40 ± 0.30	103.10 ± 1.00	33.10 ± 0.30	9.85 ± 0.25	80.60 ± 0.80	16.35 ± 0.15	1.25 ± 0.05	275.65 ± 0.85
permeate d1	47.55 ± 1.45	0.00 ± 0.00	0.00 ± 0.00	3.45 ± 0.05	12.85 ± 015	3.65 ± 0.05	0.00 ± 0.00	67.50 ± 1.20
permeate d28	16.85 ± 1.15	0.00 ± 0.00	0.00 ± 0.00	1.25 ± 0.05	7.25 ± 0.15	2.05 ± 0.05	0.00 ± 0.00	27.40 ± 0.90

[a]Values expressed as means of duplicate ± standard error. Significant differences between values in the same column are indicated by different small letters ($p < 0.05$) according to Tukey's multiple range test. [b]Dp-3,5-diglc, delphinidin-3,5-*O*-diglucoside; Cy-3,5-diglc, cyanidin-3,5-*O*-diglucoside; Dp-3-glc, delphinidin-3-*O*-glucoside; Pg-3,5-diglc, pelargonidin-3,5-*O*-diglucoside; Cy-3-glc, cyanidin-3-*O*-glucoside; Pg-3-glc, pelargonidin-3-*O*-glucoside; Cy-pent, cyanidin-pentoside; PGJ, pomegranate juice; PGY, pomegranate juice yogurt.

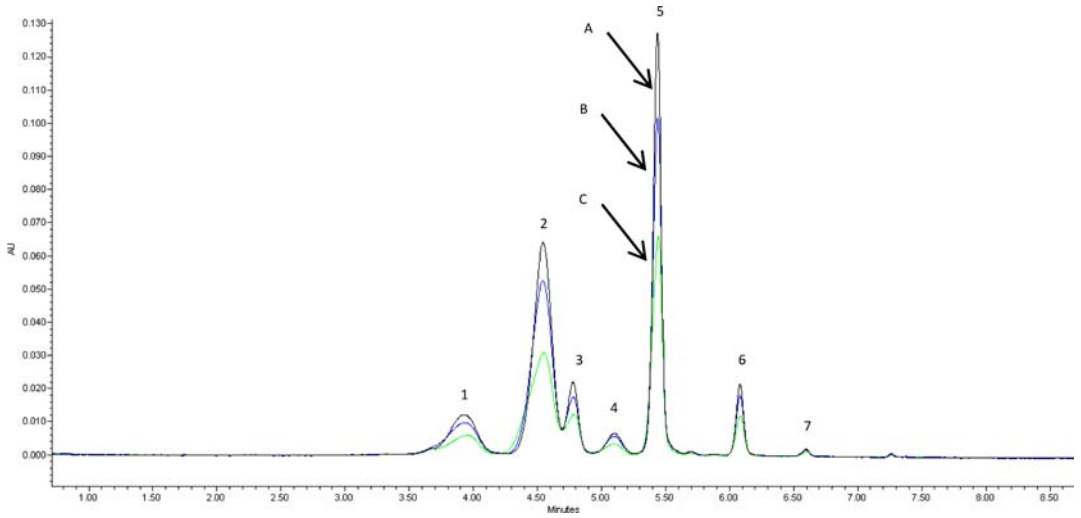

Figure 2. Chromatograms of anthocyanins in pomegranate yogurts after 1 (A), 14 (B), and 28 (C) days of cold storage.

In contrast to the other phenolic compounds identified, PGJ was extremely rich in anthocyanins (641.48 mg/L). Similar to our data, Fischer et al.[21] reported an anthocyanin content of 558 mg/L in a handmade juice from arils. Cyanidin-3-*O*-glucoside was the predominant anthocyanin in juice; that predominance is characteristic for "Mollar de Elche" varieties.[32,33] In yogurts, the relative quantitative distribution of the individual anthocyanins was slightly different from PGJ. In yogurt samples, the predominant anthocyanin was cyanidin-3,5-*O*-glucoside followed by cyanidin-3-*O*-glucoside at all days analyzed. In other PGJ fermentation processes, it has been studied for losses up to 61% in the anthocyanin content, mainly occurring during the initial fermentation. The structure influenced the stability in the way that monoglucosides were less stable than diglucosides.[32] In the present study, both cyanidin-3-*O*-glucoside and pelargonidin-3-*O*-glucoside were the most affected anthocyanins in the fermentation process whereas cyanidin-3,5-*O*-diglucoside was the most stable one. A similar trend has also been displayed in the pomegranate winemaking process described by Mena et al.[32] Additionally, the yogurt polymer network and gel matrix might have protected the polyphenols to some extent, through reducing the oxidation rates of these sensitive components.[34] During the storage period, significant losses in the individual anthocyanin content were observed especially at the end of the storage (Figure 2). Degradation of anthocyanins has been widely studied, and it is well-known that most anthocyanin follow a first-order reaction kinetics[35−37] and even bacterial culture could affect the anthocyanin content during storage probably associated with the production of antimicrobial compounds by the starter culture.[38] Results from permeates revealed that most of the anthocyanins remained bound to milk proteins; cyanidin-3,5-*O*-diglucoside, the main anthocyanin present in the yogurts, was not detected in the permeate, neither delphinidin-3-*O*-glucoside and cyanidin-pentoside did it. Delphinidin-3,5-*O*-diglucoside was found to be the most stable anthocyanin and showed the lowest interaction rate with milk proteins. The 84.73% of total anthocyanins remained bound to proteins at first day of storage and 90.06% after 28 days of cold storage. Indeed, retentates (proteic phase) had a more pronounced reddish color than their corresponding permeates. That could be explained due to the monoglucosides of flavonoids showing stronger binding affinities with milk proteins than their polyglucoside forms.[39] It has been demonstrated that antioxidant activity of polyphenols decreases as interactions of milk proteins−polyphenol complexes increase.[39] As far as we know, no previous studies have been conducted on the extent of interaction between individual anthocyanins and milk proteins, so results from this study would provide a first overview about the degree of anthocyanin−milk protein interaction, giving knowledge about which anthocyanins are available to exert the beneficial action. On the other hand, the interactions between other flavonoids such as tea catechins have widely studied[7,8,40] and moreover the effect of such interaction on antioxidant activity.[41] Arts et al.[41] found that the antioxidant activity of tea components was masked due to the

addition of proteins, i.e., assessing separately the antioxidant activity of flavonoid and protein yields higher values than the antioxidant activity of the mixture tea−milk. Additionally, they proved that masking not only depends on the type of protein but also on the type of flavonoid; proteins which contains more proline groups and flavonoids such as epigallocatechin gallate (EGCG) and epicatechin gallate in green tea and gallic acid in black tea are responsible for the masking. However, the protein−polyphenol interaction could be both reversible and irreversible depending on pH, temperature, and protein and flavonoid concentration.[42] Nevertheless, new findings have pointed out to a protective role of milk as a carrier of bioactive molecules such as flavonoids, arguing that binding of flavonoids such as EGCG to the casein micelles did not affect the bioefficacy of EGCG.[43]

Total Phenol Content, Total Flavonoid Content, and Total Anthocyanin Content. Figure 3 shows total phenol content (TPC), total flavonoid content (TFC), and total anthocyanin content (TAC) of pomegranate juice, pomegranate yogurts, pomegranate yogurt permeates, and control yogurts. As expected, among the assayed samples the higher phenolic content was observed in the PGJ (707.25 mg GAE/L). We found lower phenolic substances than did previous reports[10,28] for the same pomegranate cultivar group. Both aril composition and differing textural properties of fruit tissues may influence the transfer of phenolic compounds into the juices upon processing.[11] PGY contained 40% of juice and presented 241.44 mg GAE/L of total phenolic substances, which means 85.35% of the theoretically expected. On the first day of storage, the TPC in JY permeates was 111.92 mg GAE/L, which means that nearly 54% of the total phenolic substances remained in the proteic phase interacting with milk proteins. At the end of the storage period, this percentage decreased (40.50%), the TPC in PGY and yogurt permeates being 142.60 mg GAE/L and 111.92 mg GAE/L, respectively. PGY exhibited the most remarkable decrease (40.94%) in phenolic concentration ($p < 0.05$) during the storage period followed by yogurt permeates (24.19%), CY being the most stable (4.32%) sample. Other studies showed the same tendency in phenolic content reducing in enriched yogurts with phenolic compounds stored during 14 days[14] and 7 days.[44] The stability of pigments and phenolics in yogurts is affected by storage temperature, pH, phenolic content, fat,[38,44] and the type of bacterial culture used.[38] Taking into account the TFC in the juice (75.50 mg RE/100 g), that observed in JY was higher than expected (34.13 mg RE/100 g). Permeates retained the 65.78% and 90% of the flavonoids on the first day and 28th day, respectively. So we have estimated by colorimetric methods that flavonoids have less affinity to proteins than other phenolic compounds. Interestingly, although yogurt is not being considered as a significant source of phenolic compounds,[13] CY presented 39.08 mg GAE/L and 3.78 mg RE/100 g on the first day of storage for TPC and TFC. During the storage period, TFC decreased 39.93%, 17.82%, and 23.28% in PGY, yogurt permeates, and CY, respectively (Figure 3), although such decrease was only statistically significant for PGY. The phenolic and flavonoid contents can be used as important indicators of antioxidant capacity in the screening of natural sources of antioxidants.[45]

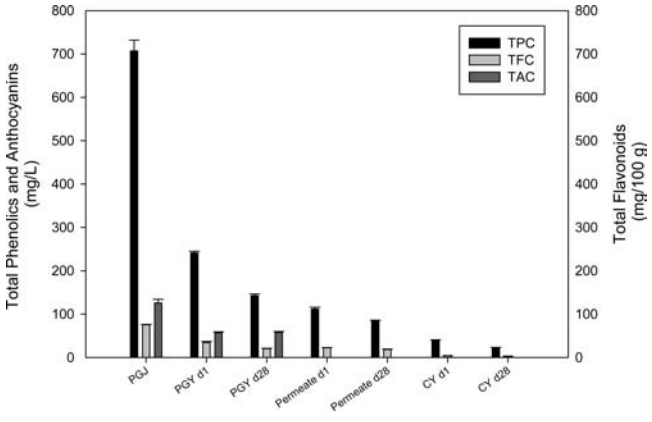

Figure 3. Total phenol content (TPC; mg GAE/L), total flavonoid content (TFC; mg RE/100 g), and total anthocyanin content (TAC; mg cyanidin-3-glucoside/L) of pomegranate juice and yogurts and permeates over 28 days of storage at 4 °C.

PGJ presented a total anthocyanin content of 126.04 mg of cyanidin-3-glucoside equivalents/L. Quantitatively, our results are higher than those reported by Elfalleh et al.[46] (39.19 mg CGE/L) and Ozgen et al.[47] (60.0 mg CGE/L) as analyzed by the same method, but lower than our own LC-MS results an those of by Gil et al.[23] (306.0 mg/L) as assessed by chromatographic method. Chromatographic methods and results are considered more accurate than colorimetric methods given their limitations and expression under an individual representative compound. However, colorimetric methods may be still of interest where more sophisticated chromatographic methods are not available.

Because naturally neither milk nor control yogurts provide anthocyanins, we found that such content was relatively high in PGY during the storage period (56.91 and 57.60 mg of cyanidin-3-glucoside equivalents/L at first and 28th day, respectively). Anthocyanin concentrations of PGY as assessed by colorimetric methods were not affected ($p > 0.05$) by storage time, which is not correlated with the previous HPLC results. But these results were in accordance with those obtained from color determinations in yogurt (Table 3).

Table 3. Color Characteristics of Yogurts during 28 Days of Cold Storage[a]

type of yogurt	L^*	a^*	b^*
control	84.61 ± 1.16^{b}	-2.73 ± 0.06^{a}	5.27 ± 0.17^{c}
PGY d1	66.65 ± 0.41^{a}	5.61 ± 0.10^{b}	4.93 ± 0.11^{b}
PGY d14	65.95 ± 0.05^{a}	5.78 ± 0.02^{b}	$4.83 \pm 0.05^{a,b}$
PGY d28	65.24 ± 0.52^{a}	6.26 ± 0.04^{c}	4.56 ± 0.04^{a}

[a]Values expressed as means of triplicate ± standard error. Significant differences between values in the same column are indicated by different small letters ($p < 0.05$) according to Tukey's multiple range test.

During the storage period, the recorded a^* and b^* values showed significant variations: redness (a^*) increased and yellowness (b^*) decreased, meaning that the reddish color was reinforced. Although not statistically, lightness (L^*) decrease during storage was also a clear sign of pigment stabilization. This stabilization could be due to intermolecular/intramolecular, copigmentation, and self-association reactions.[42] Furthermore, Jing and Giusti[48] found that anthocyanins were more stable in milk matrices than in a phosphate buffer solution used as control. In the study carried out by Srivastava et al.,[49] a relatively superior content of malvidin glucosides was observed

Table 4. Antioxidant Activity of Pomegranate Juice and Yogurts and Protein-Free Permeates during Storage at 4 °C Measured by the DPPH• Assay and the FRAP Method at Different Concentrations (A = 2.5 g/100 mL, B = 5 g/100 mL, C = 7.5 g/100 mL, D = 10 g/100 mL)[e]

			FRAP TEAC[b] (mM Trolox/L)			
sample	storage time (day)	DPPH• IC_{50}[a]	A	B	C	D
juice		10.45	0.254 ± 0.006^{aD}	0.479 ± 0.001^{bE}	0.710 ± 0.011^{cD}	0.870 ± 0.011^{dD}
PGY[c]	1st	2.51	0.090 ± 0.003^{aC}	$0.132 \pm 0.002^{a,bD}$	$0.215 \pm 0.036^{b,cC}$	0.279 ± 0.030^{cC}
	28th	2.45	0.060 ± 0.002^{aB}	0.115 ± 0.001^{bC}	$0.163 \pm 0.002^{cB,C}$	0.202 ± 0.009^{dB}
PGY permeate	1st	70.62	0.061 ± 0.001^{aB}	0.111 ± 0.001^{bC}	$0.164 \pm 0.001^{cB,C}$	0.208 ± 0.004^{dB}
	28th	85.46	0.049 ± 0.001^{aB}	0.089 ± 0.003^{bB}	0.132 ± 0.001^{cB}	0.162 ± 0.002^{dB}
CY[d]	1st	5.38	0.023 ± 0.002^{aA}	0.036 ± 0.000^{bA}	0.048 ± 0.000^{cA}	0.062 ± 0.001^{dA}
	28th	6.96	0.022 ± 0.000^{aA}	$0.028 \pm 0.004^{a,bA}$	$0.044 \pm 0.000^{b,cA}$	0.054 ± 0.004^{cA}

[a]IC_{50}, concentration (g/100 mL) for a 50% of inhibition. [b]TEAC, Trolox equivalent antioxidant capacity. [c]PGY, pomegranate yogurt. [d]CY, control yogurt. [e]Values expressed as means of duplicate ± standard error. Significant differences between values in the same line are indicated by different small letters ($p < 0.05$) according to Tukey's multiple range test. Significant differences between values in the same column are indicated by different capital letters ($p < 0.05$) according to Tukey's multiple range test.

in a stored blueberry extract. In yogurt permeates, non-anthocyanin content was detected by colorimetric quantitative methods.

Antioxidant Activity in Pomegranate Juice, Yogurts, and Permeates. In this study, the in vitro antioxidant activity (AA) of pomegranate juice and yogurts and permeates during 28 days of storage was measured by two different analytical methods: DPPH• and FRAP (results shown in Table 4). The free radical scavenging activity of the samples were reported as the amount of the juice, yogurt, or permeate (g/100 mL) required to scavenge 50% of DPPH• (IC_{50}), and the lower the IC_{50} values the higher the antioxidant power. PGY displayed the highest AA in comparison to the other samples. PGJ showed a poor free radical scavenging activity by DPPH• method, similar to the reported in a previous own study, 7.47.[10] Considering the results obtained for CY, it is possible that a synergistic action is taking place when the pomegranate yogurt is produced. Indeed, we analyzed the unfermented mix of milk and PGJ (data not presented), resulting in a IC_{50} value of 4.72. During the storage time, enriched yogurts slightly increased the radical scavenging activity, and the same pattern was found in the study carried out by Jiménez et al.[50] Nonetheless, at the end of the storage, TPC and TFC decreased significantly (Figure 3), anthocyanins (TAC) being the phenolic compound which remained stable. Hence, is it possible that the radical scavenging activity of the PGY could be done by the anthocyanins. Oppositely, studies carried out in yogurts fortified in phenolic extracts showed a tendency in decreasing the AA during the storage period.[14]

According to the FRAP values, a concentration-dependent ferric reducing capacity was found for all the samples analyzed. PGJ showed by far the highest ($p < 0.05$) ferric reducing capacity in terms of Trolox concentrations. In juice, FRAP was strongly correlated with TPC and TAC (Table 6). In PGY at day 1 of storage, results from FRAP assay corresponded to nearly 40% of those of PGJ, so due to the low AA of CY detected by this method, the AA of PGY was done by PGJ. In Table 5, we could easily intuit how the same potentially antioxidant sample behaves differently in the face of different antioxidant methods. Only the ferric reducing capacity was affected ($p < 0.05$) by the storage time in PGY. At the end of the storage, no difference were found between PGY and permeates. Furthermore, the AA in CY was correlated with TPC (Table 6).

Table 5. Relative Antioxidant Activity of Pomegranate Juice and Yogurts and Protein-Free Permeates[a]

sample	DPPH•	FRAP
juice	++	++++
PGY	++++	++
PGY permeate	−	++
CY	+++	+

[a]PGY, pomegranate yogurt; CY, control yogurt; .

Table 6. Correlation Matrix between Antioxidant Capacity Methods and Total Phenol Content (TPC), Total Flavonoid Content (TFC), and Total Anthocyanin Content (TAC) in Pomegranate Juice, Pomegranate Yogurts, Protein-Free Permeates, and in Control Yogurts[d]

		TPC	TFC	TAC
PGJ[a]	DPPH•	0.98	0.10	1
	FRAP	0.99	0.45	0.92
PGY[b]	DPPH•	0.64	0.88	0.24
	FRAP	0.89	0.77	0.72
PGY permeates	DPPH•	0.90	0.99	
	FRAP	0.99	0.98	
CY[c]	DPPH•	0.57	0.01	
	FRAP	0.84	0.42	

[a]PGJ, pomegranate juice. [b]PGY, pomegranate yogurt. [c]CY, control yogurt. [d]The r value of the correlation is given. All correlations were significant at $p < 0.05$.

A point worth mentioning is the poor correlation between phenolic compounds and antioxidant activity in PGY in comparison to juice and permeates (Table 6). Permeates and juices are free of proteins, so phenolics are mainly in free form. However, yogurt is a complex matrix where several interactions could occur, so it is not clear whether the antioxidant capacity of the PGY is given by phenolics alone or by a multifactorial cause. This fact may mean that other components naturally present in PGJ, such as ascorbic acid or vitamin E, need to be investigated for their contribution to the AA.[12]

In conclusion, yogurts enriched in pomegrante juice are especially rich in anthocyanins, and also other phenolic compounds such ellagic acid and punicalagins are present at significant levels. Fermentation process affects the anthocyanin profile; the content in cyanidin-3-*O*-glucoside, the main anthocyanin present in the juice, is significantly reduced

dx.doi.org/10.1021/jf501503h | J. Agric. Food Chem. 2014, 62, 6417−6425

whereas cyanidin-3,5-*O*-diglucoside remains much more stable, pointing out that structure (mono or diglucoside form) affects the anthocyanin stability. During the storage period, the individual anthocyanin content is diminished, which is not detected in color measurements of yogurt. Results from permeates reveal that the interaction of phenolic compounds with milk proteins occurs at different levels depending on the type of phenolic; ellagic acid and delphinidin-3,5-*O*-diglucoside show the lowest affinity to bind proteins.

Considerable variation in antioxidant activity is observed depending on the antioxidant assay. Pomegranate juice shows the strongest ferric reducing capacity, whereas pomegranate yogurts display the highest radical scavenging activity. The presence of PGJ in yogurt enhanced radical scavenging performance, whereas all the observed ferric reducing power ability of PGY was strictly due to the PGJ present. Pomegranate yogurt can be considered a good antioxidant dairy product and also during the storage period in terms of scavenging activity. Permeates in general had a poor antioxidant activity. The interaction of PG phenolics with milk proteins does not affect the antioxidant activity of yogurts.

AUTHOR INFORMATION

Corresponding Author

*Phone: 34966749735. Fax: 966749677. E-mail: esther.sendra@umh.es.

Notes

The authors declare no competing financial interest.

ACKNOWLEDGMENTS

We thank Dr. Francisca Hernández for gently providing ellagic acid and punicalagins standards for the study.

ABBREVIATIONS USED

PG, pomegranate; PGJ, pomegranate juice; PGY, pomegranate yogurt; CY, control yogurt; HPLC, high performance liquid chromatography; *L**, lightness; *a**, redness; *b**, yellowness; TPC, total phenol content; TFC, total flavonoid content; TAC, total anthocyanin content; AA, antioxidant activity; DPPH, 2,2-diphenyl-1-picrylhydrazyl; FRAP, ferric reducing antioxidant power

REFERENCES

(1) Miguel, M. G.; Neves, M. A.; Antunes, M. D. Pomegranate (*Punica granatum* L.): a medicinal plant with myriad biological properties—a short review. *J. Med. Plants Res.* **2010**, *4*, 2836−2847.

(2) Teixeira da Silva, J. A.; Rana, T. S.; Narzary, D.; Verma, N.; Meshram, D. T.; Ranade, S. A. Pomegranate biology and biotechnology: a review. *Sci. Hort.* **2013**, *160*, 85−107.

(3) Syed, D. N.; Afaq, F.; Mukhtar, H. Pomegranate derived products for cancer chemoprevention. *Semin. Cancer Biol.* **2007**, *17*, 377−385.

(4) Wang, R.; Ding, Y.; Liu, R.; Xiang, L.; Du, L. Pomegranate: constituents, bioactivities and pharmacokinetics. *Fruit, Veg. Cereal Sci. Biotechnol.* **2010**, *4*, 77−87.

(5) Johanningsmeier, S. D.; Harris, G. K. Pomegranate as a functional food and nutraceutical source. *Annu. Rev. Food Sci.* **2011**, *2*, 181−201.

(6) Mena, P.; Calani, L.; Dall'Asta, C.; Galaverna, G.; García-Viguera, C.; Bruni, R.; Crozier, A.; Del Rio, D. Rapid and comprehensive evaluation of (poly)phenolic compounds in pomegranate (*Punica granatum* L.) juice by UHPLC-MS^n. *Molecules* **2012**, *17*, 14821−14840.

(7) Jöbstl, E.; Howse, J. R.; Fairclough, J. P. A.; Williamson, M. P. Noncovalent cross-linking of casein by epigallocatechin gallate characterized by single molecule force microscopy. *J. Agric. Food Chem.* **2006**, *54*, 4077−4081.

(8) Yuksel, Z.; Avci, E.; Erdem, Y. K. Characterization of binding interactions between green tea flavonoids and milk proteins. *Food Chem.* **2010**, *121*, 450−456.

(9) Yazdi, S. R.; Corredig, M. Heating of milk alters the binding of curcumin to casein micelles. A fluorescence spectroscopy study. *Food Chem.* **2012**, *132*, 1143−1149.

(10) Trigueros, L.; Viuda-Martos, M.; Pérez-Álvarez, J. A.; Sendra, E. Low fat set yoghurt rich in pomegranate juice: a new antioxidant dairy product. *Milchwissenschaft* **2012**, *67*, 177−180.

(11) Fischer, U. A.; Jaksch, A. V.; Carle, R.; Kammerer, D. R. Influence of origin source, different fruit tissue and juice extraction methods on anthocyanin, phenolic acid, hydrolysable tannin and isolariciresinol contents of pomegranate (*Punica granatum* L.) fruits and juices. *Eur. Food Res. Technol.* **2013**, *237*, 209−221.

(12) Viladomiu, M.; Hontecillas, R.; Lu, P.; Bassaganya-Riera, J. Preventive and prophylactic mechanisms of action of pomegranate bioactive constituents. *Evidence-Based Complementary Altern. Med.* **2013**, http://dx.doi.org/10.1155/2013/789764.

(13) O'Connell, J. E.; Fox, P. F. Significance and applications of phenolic compounds in the production and quality of milk and dairy products: a review. *Int. Dairy J.* **2001**, *11*, 103−120.

(14) Karaaslan, M.; Ozden, M.; Vardin, H.; Turkoglu, H. Phenolic fortification of yogurt using grape and callus extracts. *LWT−Food Sci. Technol.* **2011**, *44*, 1065−1072.

(15) Benavente-García, O.; Castillo, J.; Lorente, J.; Ortuño, A.; Del Río, J. A. Antioxidant activity of phenolics extracted from *Olea europea* L. leaves. *Food Chem.* **1999**, *68*, 457−462.

(16) Singlenton, V. L.; Rossi, J. A. Colorimetry of total phenolics with phosphomolybdic−phosphotungstic acid reagents. *Am. J. Enol. Vitic.* **1965**, *16*, 144−158.

(17) Blasa, M.; Candiracci, M.; Accorsi, A.; Piacentini, P. M.; Albertini, M. C.; Piatti, E. Raw Millefiori honey is packed full of antioxidants. *Food Chem.* **2005**, *97*, 217−222.

(18) Wrolstad, R. E. In *Color and Pigments Analyses in Fruit Products*; Station Bulletin; Agricultural Experiment Station, Oregon State University, Corvallis, Oregon, 1976, reprinted 1993; Vol. *624*, pp 1−17.

(19) Brand-Williams, W.; Cuvelier, M. E.; Berset, C. Use of a free radical method to evaluate antioxidant activity. *LWT−Food Sci. Technol.* **1995**, *28*, 25−30.

(20) Oyaizu, M. Studies on products of browning reactions: antioxidative activities of products of browning reaction prepared from glucosamine. *Jpn. J. Nutr.* **1986**, *44*, 307−315.

(21) Fischer, U. A.; Carle, R.; Kammerer, D. R. Identification and quantification of phenolic compounds from pomegranate (*Punica granatum* L.) peel, mesocarp, aril and differently produced juices by HPLC-DAD−ESI/MSn. *Food Chem.* **2011**, *127*, 807−821.

(22) Gil, M.; Garcia-Viguera, C.; Artés, F.; Tomás-Barberán, F. Changes in pomegranate juice pigmentation during ripening. *J. Sci. Food Agric.* **1995**, *68*, 77−81.

(23) Gil, M. I.; Tomás-Barberán, F. A.; Hess-Pierce, B.; Holcroft, D. M.; Kader, A. A. Antioxidant activity of pomegranate juice and its relationship with phenolic composition and processing. *J. Agric. Food Chem.* **2000**, *48*, 4581−4589.

(24) Qu, W.; Breksa, A. P., III; Pan, Z.; Ma, H. Quantitative determination of major polyphenol constituents in pomegranate products. *Food Chem.* **2012**, *132*, 1585−1591.

(25) Falsaperla, M.; Morgia, G.; Tartarone, A.; Ardito, R.; Romano, G. Support ellagic acid therapy in patients with hormone refractory prostate cancer (HRPC) on standard chemotherapy using vinorelbine and estramustine phosphate. *Eur. Urol.* **2005**, *47*, 449−454.

(26) Hassoun, E. A.; Vodhanel, J.; Abushaban, A. The modulatory effects of ellagic acid and vitamin E succinate on TCDD-induced oxidative stress in different brain regions of rats after subchronic exposure. *J. Biochem. Mol. Toxicol.* **2004**, *18*, 196−203.

(27) Niino, H.; Sakane, I.; Okanoya, K.; Kuribayashi, S.; Kinugasa, H. Determination of mechanism of flock sediment formation in tea beverages. *J. Agric. Food Chem.* **2005**, *53*, 3995−3999.
(28) Mena, P.; García-Viguera, C.; Navarro-Rico, J.; Moreno, D. A.; Bartual, J.; Saura, D.; Martí, N. Phytochemical characterisation for industrial use of pomegranate (*Punica granatum* L.) cultivars grown in Spain. *J. Sci. Food Agric.* **2011**, *91*, 1893−1906.
(29) Hagerman, A. E.; Riedl, K. M.; Jones, G. A.; Sovik, K. N.; Ritchard, N. T.; Hartfield, P. W.; Riechel, T. L. High molecular weight plant polyphenolics (tannins) as biological antioxidants. *J. Agric. Food Chem.* **1998**, *46*, 1887−1892.
(30) Bialońska, D.; Ramnani, P.; Kasimsetty, S. G.; Muntha, K. R.; Gibson, G. R.; Ferreira, D. The influence of pomegranate by-product and punicalagins on selected groups of human intestinal microbiota. *Int. J. Food Microbiol.* **2010**, *140*, 175−182.
(31) Jurenka, J. Therapeutic applications of pomegranate (*Punica granatum* L.): a review. *Altern. Med. Rev.* **2008**, *13*, 128−144.
(32) Mena, P.; Gironés-Vilaplana, A.; Martí, N.; García-Viguera, C. Pomegranate varietal wines: phytochemical composition and quality parameters. *Food Chem.* **2012**, *133*, 108−115.
(33) Pérez-Vicente, A.; Serrano, P.; Abellán, P.; García-Viguera, C. Influence of packaging material on pomegranate juice color and bioactive compounds during storage. *J. Sci. Food Agric.* **2004**, *84*, 639−644.
(34) Sun-Waterhouse, D.; Zhou, J.; Wadhwa, S. S. Drinking yoghurts with berry polyphenols added before and after fermentation. *Food Control* **2013**, *32*, 450−460.
(35) Giusti, M. M.; Wrolstad, R. E. Radish anthocyanin extract as a natural red colorant for maraschino cherries. *J. Food Sci.* **1996**, *61*, 688−694.
(36) Iversen, C. K. Black currant nectar: effect of processing and storage on anthocyanin and ascorbic acid content. *J. Food Sci.* **1999**, *64*, 37−41.
(37) Wang, W. D.; Xu, S. Y. Degradation kinetics of anthocyanins in blackberry juice and concentrate. *J. Food Eng.* **2007**, *82*, 271−275.
(38) Ścibisz, I.; Ziarno, M.; Mitek, M.; Zaręba, D. Effect of probiotic cultures on the stability of anthocyanins in blueberry yoghurts. *LWT−Food Sci. Technol.* **2012**, *49*, 208−212.
(39) Xiao, J.; Mao, F.; Yang, F.; Zhao, Y.; Zhang, C.; Yamamoto, K. Interaction of dietary polyphenols with bovine milk proteins: molecular structure−affinity relationship and influencing bioactivity aspects. *Mol. Nutr. Food Res.* **2011**, *55*, 1637−1645.
(40) Kanakis, C. D.; Hasni, I.; Bourassa, P.; Tarantilis, P. A.; Polissiou, M. G.; Tajmir-Riahi, H.-A. Milk β-lactoglobulin complexes with tea polyphenols. *Food Chem.* **2011**, *127*, 1046−1065.
(41) Arts, M. J. T. J.; Haenen, G. R. M. M.; Wilms, L. C.; Beetstra, S. A. J. N.; Heijnen, C. G. M.; Voss, H.-P.; Bast, A. Interactions between flavonoids and proteins: effect on the total antioxidant capacity. *J. Agric. Food Chem.* **2002**, *50*, 1184−1187.
(42) Luck, G.; Liao, H.; Murray, J.; Grimmer, H.; Warminski, E.; Williamson, M.; Lilley, E. H.; Haslam, E. Polyphenols, astringency and proline-rich proteins. *Phytochemistry* **1994**, *37*, 357−371.
(43) Haratifar, S.; Meckling, K. A.; Corredig, M. Antiproliferative activity of tea catechins associated with casein micelles, using HT29 colon cancer cells. *J. Dairy Sci.* **2014**, *97*, 672−678.
(44) Wallace, T. C.; Giusti, M. M. Determination of color, pigment, and phenolic stability in yogurt systems colored with nonacylated anthocyanins from *Berberis boliviana* L. as compared to other natural/synthetic colorants. *J. Food Sci.* **2008**, *73*, C241−C248.
(45) Viuda-Martos, M.; Ruiz-Navajas, Y.; Fernández-López, J.; Sendra, E.; Sayas-Barberá, E.; Pérez-Álvarez, J. A. Antioxidant properties of pomegranate (*Punica granatum* L.) bagasses obtained as co-product in the juice extraction. *Food Res. Int.* **2011**, *44*, 1217−1223.
(46) Elfalleh, W.; Tlili, N.; Nasri, N.; Yahia, Y.; Hannachi, H.; Chaira, N.; Ying, M.; Ferchichi, A. Antioxidant capacities of phenolic compounds and tocopherols from Tunisian pomegranate (*Punica granatum*) fruits. *J. Food Sci.* **2011**, *76*, C707−C713.
(47) Ozgen, M.; Durgaç, C.; Serçe, S.; Kaya, C. Chemical and antioxidant properties of pomegranate cultivars grown in the Mediterranean region of Turkey. *Food Chem.* **2008**, *111*, 703−706.
(48) Jing, P.; Giusti, M. M. Characterization of anthocyanin-rich waste from purple corncobs (*Zea mays* L.) and its application to color milk. *J. Agric. Food Chem.* **2005**, *53*, 8775−8781.
(49) Srivastava, A.; Akoh, C. C.; Yi, W.; Fischer, J.; Krewer, G. Effects of storage conditions on the biological activity of phenolic compounds of blueberry extract packed in glass bottles. *J. Agric. Food Chem.* **2007**, *55*, 2705−2713.
(50) Jiménez, A. M.; Murcia, M. A.; Parras, P.; Martínez-Tomé, M. On the importance of adequately choosing the ingredients of yoghurt and enriched milk for their antioxidant activity. *Int. J. Food Sci. Technol.* **2008**, *43*, 1464−1473.

The influence of different processing methods on preservation of bioactive compounds in strawberry has been studied,[21,22] and color stability of fruits has been reported.[23] However, sensory evaluation of strawberry juice based on processing methods is seldom mentioned. The simultaneous utilization of E-nose and E-tongue will make it possible to clearly show and assess how processing methods influence a juice's sensory and quality indirectly.

Conventional heat treatments ensure safety and extend the shelf life of the juices but can lead to undesirable changes both in sensorial and in nutritional properties. This study applied processing approaches (i.e., microwave pasteurization, steam blanching, HTST, and frozen−thawed) as alternative preservations and focused on exploring the influences of processing approaches on strawberry juice quality changes. An E-nose and an E-tongue were utilized as a new detection system to discriminate juice types and to predict quality parameters. The main objectives of this study is (1) to characterize five types of strawberry juices based on different processing approaches (i.e., microwave pasteurization, steam blanching, frozen−thawed, HTST, and freshly squeezed) by E-nose and E-tongue and to measure juice quality parameters (vitamin C, pH, TSS, TA, and sugar/acid ratio) by traditional measuring methods; (2) to solve classification and regression problems based on Random Forest (RF) and Support Vector Machine (SVM), including searching the best parameters for RF and SVM, and contrasting two networks according to cross-validation performance; (3) to explore if the simultaneous utilization of the two instruments will increase the extent of information or, on the contrary, will they lead to data redundancy.

MATERIALS AND METHODS

Experimental Conditions. Strawberries (*Fragaria* × *ananassa* Duch.) were picked at a strawberry garden in southeast Hangzhou city of China, and the picking time was in the morning on 13 May 2011. Strawberries were selected for this experiment based on uniform size, weight, and color. After being cleaned, the strawberry fruits were divided into five groups randomly. Five different kinds of processing approaches were chosen: microwave pasteurization, steam blanching, HTST, frozen−thawed, and freshly squeezed. The details of the five approaches were as follows:

1. Microwave Pasteurization. Microwaves have the ability to destroy the microbes or enzymes at sublethal temperatures according to following theories: selective heating, electroporation, and cell membrane.[24] Samples in beakers were put into the microwave oven (G80F23N1P-M8, Guangdong Galanz Group Co., Ltd.) under the power of 240 W for 1 min.

2. Steam Blanching. Steam blanching is an excellent tool for inactivating enzymes as well as to prevent microorganism growth without considering the reduction of sensory and nutrient quality in foods.[25] Samples were put in the steamer above boiling water and steamed for 3 min.

3. High Temperature Short Time Pasteurization. HTST, which is commonly used for heat treatment in the juice industry, is quite efficient in preventing microbial spoilage of juice.[26] Samples were put into the hot water directly at 90 °C for 2 min.

4. Frozen−Thawed. Freezing is used to maintain product quality over long storage and results in a slower rate of most deteriorative reactions such as senescence, enzymatic decay, chemical decay, and microbial growth.[27] Samples were packed in plastic bags, frozen at −23 °C (BD(C)-238N, Qindao AUCMA Co., Ltd., China) for 1 day to have sufficient time to be frozen, and then thawed at room temperature next day.

5. Freshly Squeezed. Fresh strawberry samples were squeezed directly without any process, and this group was regarded as a reference for the quality assessment.

After being processed, all the strawberry fruits were squeezed into juice by the juicer (JYL-C051, Joyoung Co., Ltd., China), and then the juice was filtered through four and eight layers of 120 mesh cotton respectively in order to remove the solid particles. Four groups (microwave pasteurization, steam blanching, HTST, and freshly squeezed) were measured by the E-nose and E-tongue immediately to minimize the quality losses, except the group of frozen−thawed, which needed 1 day to be completely frozen. Twenty replicates were prepared in each group both for E-nose and E-tongue detection. The environment temperature during samples preparation was at 20 °C ± 3 °C. The samples were juiced by a juicer without any heating or refrigerating apparatus.

The Instrument Systems and Sampling Procedure. *Electronic Nose System and Sampling Procedure.* The headspace analysis was performed with the E-nose (PEN2, Airsense Analytics, Germany). The PEN2 system consists of a sampling apparatus, a detector unit containing the array of sensors and pattern-recognition software for data recording and elaboration. The sensor array system was composed of 10 metal oxide semiconductors (MOS) of different chemical compositions and thicknesses to provide selectivity toward volatile compound. The details of sensor array have already been introduced in previous work of Hong.[20]

A 10 mL of sample juice was taken into a 500 mL beaker, and the beaker was sealed by plastic wrap for a headspace generation time of 30 min to ensure that the headspace volatiles could be enough for detection. According to previous work,[20] employing hydrous sodium carbonate as desiccant to remove the moisture in the headspace does not improve the performance in the qualitative and quantitative analysis. Samples (20 samples × 5 groups) were detected by E-nose immediately. The measurement phase lasted for 80 s, which was long enough for the sensors to reach stable signal values. After each experiment, cleaning gas (nitrogen) was pumped into the sample gas path for 60 s, which was long enough to normalize sensor signals. During the sampling process, the sample gas was transferred into the sensor chamber at a flow rate of 200 mL min^{-1} and per second a signal was collected. All the samples were detected at 20 °C ± 3 °C.

Electronic Tongue System and Sampling Procedure. An E-tongue (α-Astree, Alpha MOS Company, France) was employed to classify and characterize the strawberry juices. This instrument mainly consists of seven potentiometer chemical sensors (ZZ, BA, BB, CA, GA, HA, and JB), a reference electrode of Ag/AgCl, data acquisition system, and basic data analysis software. The sensitivity of the seven chemical sensors is different from that of the five tastes (sourness, saltiness, sweetness, bitterness, and savory). The details of sensor array have already been introduced in the previous work of Tian.[28]

Experiment was carried out with filtrated strawberry juice to avoid the influence caused by solid particles. The amount of strawberry sample was 80 mL to ensure that the sensors could be fully immersed in the liquid. The measurement time was set to 120 s for each sample, which was long enough for the sensors to reach stable signal values, and the sensors were rinsed for 10 s using deionized water to minimize and correct the drift of sensors. All the samples were detected at 20 ± 3 °C, and the number of samples was the same as in the E-nose experiment.

Determination of Quality Parameters. Fruit juice quality parameters were determined according to the methods proposed by Chinese national standardd. Vitamin C was estimated by titration with a colored oxidation/reduction indicator, 2,6-dichloroindophenol.[29] The value of pH was measured by a titrimeter (Ti-Touch-916, Metrohm, Switzerland). Total soluble solid (TSS), expressed as °Brix, was determined by using a temperature compensating refractometer (digital refractometer 2WA-J 0−32% Shanghai, China). Total acid (TA), expressed as percentage of citric acid, was determined by titration to pH 8.2 ± 0.1 with 0.1 M NaOH.[30]

In fruit juice quality properties analysis, three replicates were carried out for each group, and the mean values of vitamin C, pH, TSS, and TA were expressed as the original values, respectively.

Data Processing. *Linear Discriminant Analysis.* Linear discriminant analysis (LDA) was used as a supervised learning technique to extract features which preserve class separability. LDA explicitly

Table 1. Average Values and Standard Deviation for Strawberry Juice Quality Parameters in Different Pretreatments

pretreatment method	vitamin C (g kg^{-1})	pH	TSS (°Brix)	TA (%)	TSS/TA ratio
microwave pasteurization	0.581 (± 0.025)	3.86 (± 0.40)	8.4 (± 0.5)	0.68 (± 0.03)	12.35 (± 1.34)
steam blanching	0.406 (± 0.025)	3.76 (± 0.40)	8.4 (± 0.5)	0.64 (± 0.03)	13.12 (± 1.47)
HTST	0.483 (± 0.035)	3.80 (± 0.35)	7.9 (± 0.5)	0.67 (± 0.04)	11.79 (± 1.54)
frozen−thawed	0.360 (± 0.025)	3.84 (± 0.35)	7.8 (± 0.5)	0.69 (± 0.03)	11.3 (± 1.27)
freshly squeezed	0.400 (± 0.035)	3.74 (± 0.42)	8.0 (± 0.5)	0.70 (± 0.03)	11.42 (± 1.27)

models the difference between the classes of data, and tries to maximize the variance between categories and minimize the variance within categories.[31] The LDA is a robust statistical technique that can be applied even when small violations of the above-mentioned requirements are observed.[32] It provides a classification model, characterized by a linear dependence of the classification scores with respect to the descriptors.

Partial Least Squares Regression. Partial least squares regression (PLSR) technique is based on multiple linear regression (MLR), which is suitable for large problems where the amount of computation with standard methods of matrix inversion or diagonalization becomes prohibitive.[33] PLSR produces a technique that is able to accept collinear data and separate out the sample noise in order to make linear combinations in the dependent concentration matrix.[34]

Random Forest. RFs are a nonparametric and nonlinear classification and regression algorithm first proposed by Ho[35] and further developed by Breiman.[36] RF is a method based on a kind of learning strategy, "ensemble learning", with generating many classifiers and aggregating their results. According to its algorithm, RF does not need any data preprocessing which is one of its main advantages. This approach materialized the "bootstrap strategies" put forward by L. Breiman[37] combining "random subspace" method proposed by Ho[38] successfully. RF runs very fast, and that is a very important factor in the field of online and in situ measurements especially in the field of E-nose and E-tongue detections.

The RF ensemble grows multiple unpruned trees (*mtree*) on bootstrap samples of the original data.[31] Each tree is grown on a bootstrap sample ($^2/_3$ of the original data known as "in-bag" data for training, and $^1/_3$ of the original data known as "out of bag" data for testing) taken with replacement from the original data. Trees are split to many nodes using random subsets of variables (*mtry*); the default *mtry* value is the square root of the total number of variables.[39] A single tree in RF is a weak classifier because a random subset sample is used to train a tree, while the aggregation from all trees is considered as a strong classifier. The measure of classification accuracy is based on an internal estimate known as "out of bag" data (OOB) error, which is calculated from the prediction of the data that is not used for growing the classification trees.[31]

Support Vector Machine. SVM is the hot issue accompanying artificial neural network in machine learning which involves any practical problems such as classification and regression estimation. Originally as an effective classification method, SVM has been proposed on the basis of statistical learning theory (SLT) by Cortes and Vapnik.[40] SVM is a linear machine working in the high dimensional feature space formed by the nonlinear mapping of the n-dimensional input vector x into a K-dimensional feature space ($K > n$) through the use of a function. SVM neural network applies one hidden layer of nonlinear neurons, one-output linear neuron, and a specialized learning procedure leading to the global minimum of the error function and excellent generalization ability of the trained network.[41]

Distribution of Data Sets and Cross-Validation. Before data treatment, the E-nose and E-tongue signal values were normalized by setting the mean value at the origin of each variable and then dividing them by their standard deviation in order to eliminate the effect of index dimension from this two detection system except for RF models. In this paper, data treatments included two parts: qualitative classification and quantitative regression.

For qualitative classification, a stepwise LDA was applied for visual classification. Leave-one-out (LOO) cross-validation was used to verify stepwise LDA classification model. For neural networks (RF and Lib-SVM), data sets (E-nose system, E-tongue system, and the fusion of E-nose and E-tongue system) were divided into two subsets (15 samples of each pretreatment were randomly selected as the training set, and 5 samples of each pretreatment were considered as the testing set). Generally, the larger accuracy rates both in the training set and testing set are, the better classification model is.

For quantitative regression, PLSR, Lib-SVM, and RF were utilized. Data set was designed into two subsets (15 samples of each group were randomly selected as the training set, and the remaining 5 samples as the testing set). Prediction performance of PLSR, Lib-SVM, and RF were estimated using the parameters obtained from the fitted equation: correlation coefficient (R^2) and root-mean-square error (RMSE) between predicted and experimental values. The larger R^2 and the lower RMSE are, the better the prediction model is.

The data processing method LDA was performed by Statistical Product and Service Solutions v16.0 (International Business Machines Corporation, USA). PLSR was analyzed by Minitab 15 software (Minitab Inc. USA). RF and Lib-SVM[42] were performed by MATLAB 2012a software (MathWorks, USA).

RESULTS AND DISCUSSION

Quality Parameters of Strawberry Juices. The average values of the quality parameters of strawberry juice were represented in Table 1. The group processed by freshly squeezed was taken as a reference. The proportion of vitamin C was raised dramatically when processed by microwave pasteurization due to microwave technology is an appropriate means of achieving the required level of enzyme inactivation to prevent food deterioration. In frozen−thawed, vitamin C was much lower than the reference. Accordingly, freezing results in cell decompartmentalization which allows reactions between genuine enzyme activities and their corresponding substrates. Therefore, ascorbic acid may already be degraded during thawing due to their interaction with oxidative enzyme activities such as polyphenoloxidases (PPO) and ascorbic acid oxidases (AAO).[43] The TSS content of those five types strawberry juices varied from 8.4 to 7.8 °Brix. The amounts of TSS obtained from microwave pasteurization group and steam blanching group were the highest.

Organic, nonvolatile acids are the second most important component of strawberry flavor, after soluble sugars. The main compound accounting for TA is citric acid, which is predominant in strawberry. Those acids regulate the value of pH and may influence the nutrition stability. The values of TA declined no matter what kind of processing approach was (range from 0.64% to 0.7%). So, the quality parameter of pH raised no matter what kind of processing approach was, but the changes of TA and pH were not significant.

The ratio of TSS/TA was chosen as another criterion because this ratio is generally considered to reflect flavor quality and may be more important for quality and perceived sweetness by a sensory panel than soluble solids alone.[44] As shown in Table 1, the highest TSS/TA ratio was detected in the steam blanching group (13.12), whereas the lowest was in frozen−thawed group (11.3), but the difference between frozen−

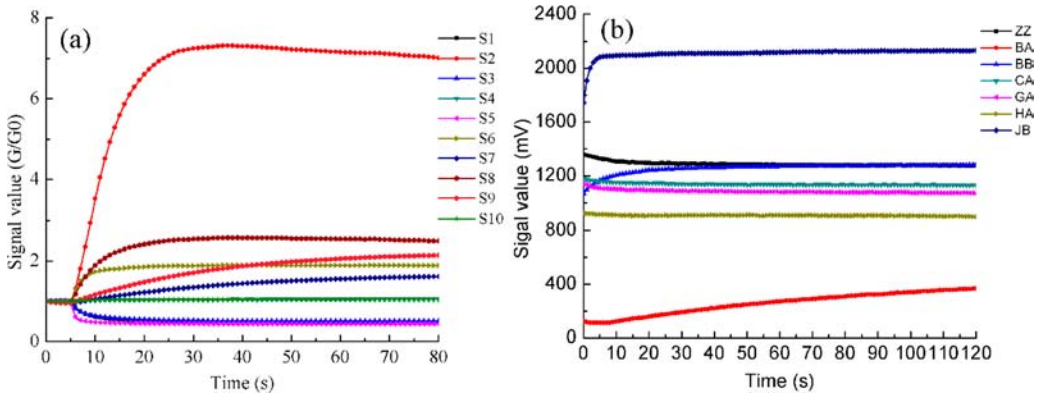

Figure 1. Typical responses of a juice sample obtained by (a) E-nose measurement, (b) E-tongue measurement.

Table 2. Results of RSD and One-Way ANOVA of the Sensor Value of Strawberry Juice Samples[a]

						one-way ANOVA	
no.	microwave pasteurization (%)	steam blanching (%)	HTST (%)	frozen−thawed (%)	freshly squeezed (%)	*F*	*P*
S1	4.4	3.6	4.4	4.2	1.4	385.5	<0.001
S2	6.6	6.8	15.3	8.9	2.8	428.8	<0.001
S3	3.2	3.5	4.5	4.2	1.3	207.2	<0.001
S4	0.4	0.7	0.5	1.1	0.9	17.0	<0.001
S5	3.3	4.3	6.0	4.2	1.7	157.3	<0.001
S6	3.5	2.8	5.5	4.1	2.7	105.3	<0.001
S7	5.7	7.8	3.8	5.1	3.4	97.3	<0.001
S8	5.2	4.6	7.6	6.1	3.8	105.2	<0.001
S9	6.8	6.6	3.1	8.3	3.4	214.0	<0.001
S10	0.6	0.9	0.4	0.5	0.4	46.9	<0.001
ZZ	5.83	0.33	0.37	0.62	0.69	17.0	<0.001
BA	6.76	12.90	7.86	6.33	7.93	157.3	<0.001
BB	6.70	0.87	0.64	0.72	0.95	105.6	<0.001
CA	6.37	1.54	0.42	1.11	2.73	97.3	<0.001
GA	1.33	7.30	5.09	4.70	6.26	105.2	<0.001
HA	6.04	2.29	0.60	1.91	0.81	214.0	<0.001
JB	0.40	0.19	0.08	0.29	0.24	46.9	<0.001

[a]Twenty samples of each group were tested, and the RSD of sensor values demonstrated high stability of the test. Significant ($P < 0.001$) obtained from one-way ANOVA of sensors values measured in 100 samples in total. S1−S10 sensors belong to E-nose, and sensors (ZZ, BA, BB, CA, GA, HA, and JB) belong to E-tongue.

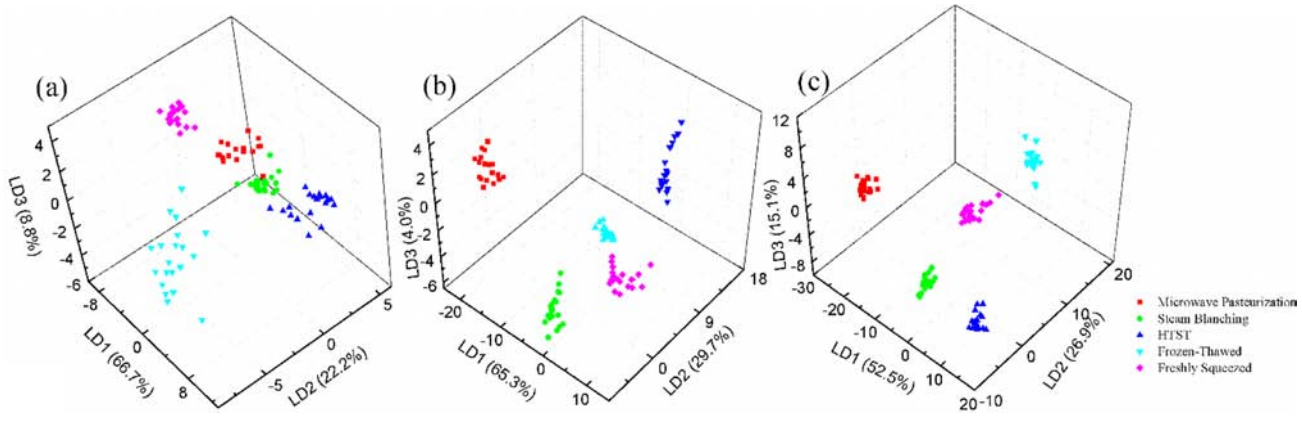

Figure 2. LDA discrimination of five strawberry juices with pretreatment: (a) is obtained by E-nose measurement, (b) is obtained by E-tongue measurement, and (c) is obtained by the fusion of E-nose data and E-tongue data.

thawed group (11.3) and freshly squeezed (11.43) was not obvious.

ANOVA Results. Parts a and b of Figure 1 are typical responses of E-nose and E-tongue during the measurement of a strawberry juice sample. Figure 1a shows that the responses of E-nose sensors reached dynamic balance after 30 s. The responses at the 60th second were selected as an original data. In Figure 1b, significant changes took place in 0−10 s and then

dx.doi.org/10.1021/jf501468b | J. Agric. Food Chem. 2014, 62, 6426−6434

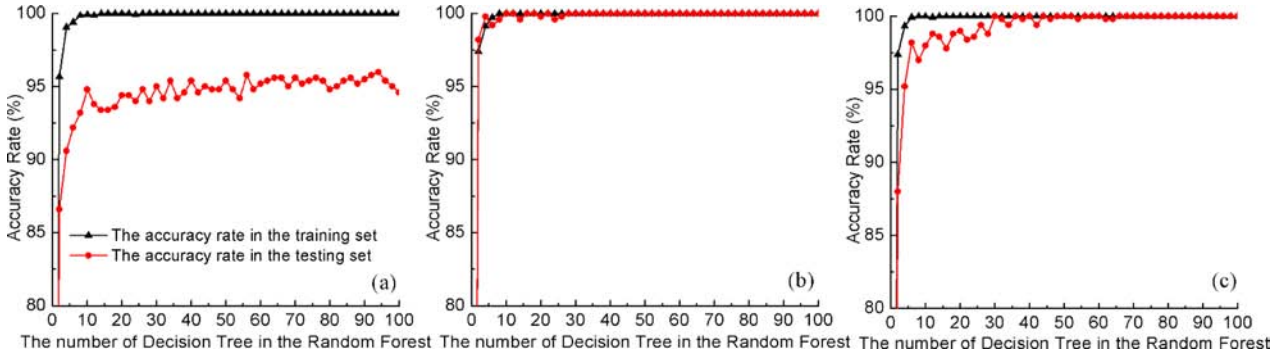

Figure 3. Performance of RF network according to the number of Decision Tree: (a) based on E-nose data set, (b) based on E-tongue data set, (c) based on the fusion of E-nose data set and E-tongue.

achieved dynamic balance except for sensor BA, whose signals had showed a slight increase during the subsequent period. The signal values of E-tongue sensors at 120th second were chosen as the original data. The stability of sensors' responses (E-nose at 60th second and E-tongue at 120th second) was analyzed by calculating the relative standard deviation (RSD). Only those sensors that exhibit good stability (small RSD) in the target matrix were included in the sensor array used for evaluation employing that matrix.[45] The result indicates a high stability of each sensor in Table 2. The result of one-way ANOVA for 17 sensors is presented in Table 2, and the values mean that significant difference was found ($p < 0.001$) between different strawberry juice samples.

The Classification Result Based on Linear Discriminant Analysis. A stepwise LDA procedure with leave-one-out cross-validation was carried out to visualize distribution of strawberry juice samples. The stepwise technique, using the Wilks' lambda method with the usual probabilities of F (0.05) for a variable to be included and F (0.10) to be removed from the model, was applied for variable selection. To verify which canonical discriminant functions were significant, the Wilks' Lambda test was applied. A leaving-one-out cross-validation procedure was carried out to avoid overoptimistic data modulation.

In the E-nose data treatment, the use of the stepwise LDA resulted in a discriminant model with four discriminant functions, and those four discriminant functions were significant according to Wilks' Lambda test ($P < 0.001$); 99% of samples were correctly classified for the original groups, and 98% for the cross-validation procedure. Figure 2a shows the effect of the first three discriminant functions in the classification of the strawberry juices. These three functions explained 97.7% of the total variance of the E-nose data (the first explaining 66.7%, the second 20.6%, and the third 8.8%).

In the E-tongue LDA analysis, all variables were selected into the model by the stepwise procedure. Four discriminant functions ($P < 0.001$ for the Wilks' Lambda test) were found in the discriminant model. The model showed a very satisfactory classification performance, allowing correct classification of 100% of samples for the original groups, and 98% for the cross-validation procedure. These three functions explained 99.0% of the total variance of the E-nose data (the first explaining 65.3%, the second 29.7%, and the third 4.0%) as shown in Figure 2b.

E-nose data and E-tongue data were combined directly after the data were preprocessed, so 17 variables were included (10 variables from E-nose and 7 variables from E-tongue). Finally, 15 variables were selected into the coalescent model by the stepwise procedure, thus sensor S4 and S6 from E-nose were excluded. Four discriminant functions ($P < 0.001$ for the Wilks' Lambda test) were found in the discriminant model. The model showed an excellent classification performance with 100% accuracy both for the original groups and the cross-validation procedure. Figure 2c shows the distribution of samples according to the first three discriminant functions. These three functions explained 94.5% of the total variance of the E-nose data (the first explaining 52.5%, the second 26.9%, and the third 15.1%).

In summary, the results show that the simultaneous utilization of both the instruments from perceptual knowledge could be a better performance than individual utilization of E-nose or E-tongue in the stepwise LDA procedure.

The Classification Results Based on Random Forest. *Model Design and Parameter Optimization for Random Forest.* In this section, a base scenario is presented to analyze the model design and parameter according to its behavior and performance. RF is an ensemble of unpruned classification and regression tree (CART) and adds an additional layer of randomness to Bagging (i.e., first drawing a bootstrap sample through Bagging method and then selecting the best split among a randomly chosen subset of *mtry* rather than all descriptor variables at each node). So the main parameters for RF network design are the value of *mtry* and the number of decision trees. The default *mtry* value is the square root of the total number of variables, so the values of *mtry* for three analysis systems (E-nose, E-tongue, and the simultaneous utilization) were 3, 3, and 4, respectively. Experiment was carried out according to the number of decision trees from 0 to 100 at 2 trees intervals, and the training accuracy rate and testing accuracy rate were considered as evaluation criteria. In Figure 3a, the testing accuracy rate of RF network based on E-nose data set could not reach to 100% no matter how large of the number of decision trees was. Parts b and c of Figure 3 show that when the number of decision trees was large enough, the training accuracy rate and testing accuracy rate could both reach to 100%. Comparing Figure 3b with Figure 3c, RF network based on E-tongue data set could achieve better results with less decision tree, which might mean that the fusion of E-nose data set and E-tongue data set lead to information redundancy.

The Classification Results of E-Nose, E-Tongue, and the Fusion of E-Nose and E-Tongue. According to the preparative work, the RF network design is that the number of decision tree was 100 and the values of *mtry* for three analysis systems (E-nose, E-tongue, and the simultaneous utilization) were 3, 3, and

4 respectively. Results of this analysis are shown in Table 3 including training accuracy rate, OOB error rate, and testing rate. OOB error is calculated from the prediction of the data that are not used for growing the classification trees. For E-nose date treatment, classification results based on RF was not perfect (100% accuracy rate for training set, 96% accuracy rate for testing set, and 4% error rate for OOB). Both the E-tongue system and the simultaneous system classified the strawberry juice samples based on different pretreatments successfully (100% accuracy rate both for training testing sets, 0% error rate for OOB).

Table 3. Comparative Classification Results of RF Network

data set	training rate (%)	OOB error (%)	testing rate (%)
E-nose	100	4	96
E-tongue	100	0	100
fusion of E-nose and E-tongue	100	0	100

The Classification Results Based on Support Vector Machines. In the approach of Lib-SVM, 5-fold cross-validation was applied to get the best performance of classification, and radial basis function (RBF) was chosen as the core function. The first step is to optimize penalty parameter C and kernel parameter gamma (γ) in Lib-SVM model for obtaining the optimal Lib-SVM models. Best combination of C and γ is often selected by a grid search method with exponentially growing sequences of C and γ. Here, log 2C and log 2 (γ) range from $[-10, 10]$ at an interval of 1. Each combination of parameter choices (C, γ) is checked using cross-validation, and the parameters with best cross-validation accuracy are picked. Results of this analysis are shown in Table 4. In the E-nose data treatment, the classification results based on Lib-SVM were not perfect (98.67% accuracy rate in 5-fold cross-validation, and 84% accuracy rate in the testing set) with best parameter choices (1, 0.125). The E-tongue system classified the strawberry juice samples successfully both in the training set and testing set (100% accuracy rate) with best parameter choices (0.00097656, 0.25). After searching the best parameter choices (0.00097656, 0.0039), the simultaneous system of E-nose and E-tongue classified the strawberry juice samples successfully in the training set (100% accuracy rate). However, the testing set were only correct about 88%, thus might combined pattern caused data redundancy.

Table 4. Using of Lib-SVM for the Classification of Strawberry Juices Based on Different Data Sets

	parameter			
data set	best C	best γ	5-fold cross-validation rate (%)	testing rate (%)
E-nose	1	0.125	98.67	84
E-tongue	9.7656×10^{-4}	0.2500	100	100
fusion of E-nose and E-tongue	9.7656×10^{-4}	0.0039	100	88

Quantitative Regression of Quality Indices Based on E-Nose, E-Tongue, and the Fusion of E-Nose and E-Tongue, Respectively. *Quantitative Regression of Quality Parameters Based on Partial Least Squares Regression.* PLSR was used to establish a correlation between sensor signals and the strawberry juice quality parameters (vitamin C, pH, TSS, TA, and TSS/TA ratio), which were obtained by conventional analytical methods.

Fifteen sets of independent regression models were performed. The first five sets of models correlated the results of the E-nose with five quality parameters, and the second five sets of models correlated the results of the E-tongue with parameters. The last five sets of models merge the information obtained from both the E-nose and E-tongue with quality parameters. Table 5 summarizes the statistical parameters for the PLSR regression models and shows the value of RMSE and R^2 at calibration and testing sets. The relations found between the E-nose output and the values of five juice quality parameters were not good, which might mean that E-nose can provide global information on the composition of the headspace, however, fail to be related to the chemical composition of liquid phase based on PLSR. The regression models based on E-tongue signals had good performance ($R^2 >$ 0.95 in calibration sets, except for TA) but were not good in the validation sets ($R^2 < 0.87$). Furthermore, performances based on fusion were much better than based on sole usage of E-nose or E-tongue ($R^2 > 0.97$ in calibration sets, $R^2 > 0.85$ in calibration sets). Figure 4 visualizes the distributions between predicted and experimental values. As shown in Figure 4a1, Figure 4a2, Figure 4a3, Figure 4a4, and Figure 4a5, the unorganized data points might mean that E-nose sensors can not build good correlation with specific substances which are dissolving in the solutions not as gas in the headspace. As it is

Table 5. Comparison of Three Predictive Models Built on the Responses of the E-Nose Data Set, E-Tongue Data Set, and the Fusion of E-Nose and E-Tongue by PLSR

		calibration		validation	
data set	quality parameters	R^2	RMSE	R^2	RMSE
E-nose	vitamin C	0.8592	0.2606 (g/kg)	0.5769	0.2800 (g/kg)
	pH	0.7938	0.1793	0.4440	0.2748
	TSS	0.8659	0.0926 (°Brix)	0.8195	0.1165 (°Brix)
	TA	0.7887	0.0095 (%)	0.4403	0.0156 (%)
	TSS/TA ratio	0.7258	0.3111	0.8622	0.3829
E-tongue	vitamin C	0.9504	0.1513 (g/kg)	0.8304	0.1913 (g/kg)
	pH	0.9606	0.0784	0.8741	0.0833
	TSS	0.9586	0.0415 (°Brix)	0.8377	0.1101 (°Brix)
	TA	0.7362	0.0106 (%)	0.5344	0.0159 (%)
	TSS/TA ratio	0.9527	0.1400	0.8622	0.3829
fusion of E-nose and E-tongue	vitamin C	0.9627	0.1312 (g/kg)	0.8959	0.1808 (g/kg)
	pH	0.9795	0.0065	0.8903	0.0879
	TSS	0.9721	0.0341 (°Brix)	0.8553	0.1190 (°Brix)
	TA	0.9795	0.0029 (%)	0.8592	0.0103 (%)
	TSS/TA ratio	0.9834	0.0858	0.8895	0.3174

dx.doi.org/10.1021/jf501468b | J. Agric. Food Chem. 2014, 62, 6426−6434

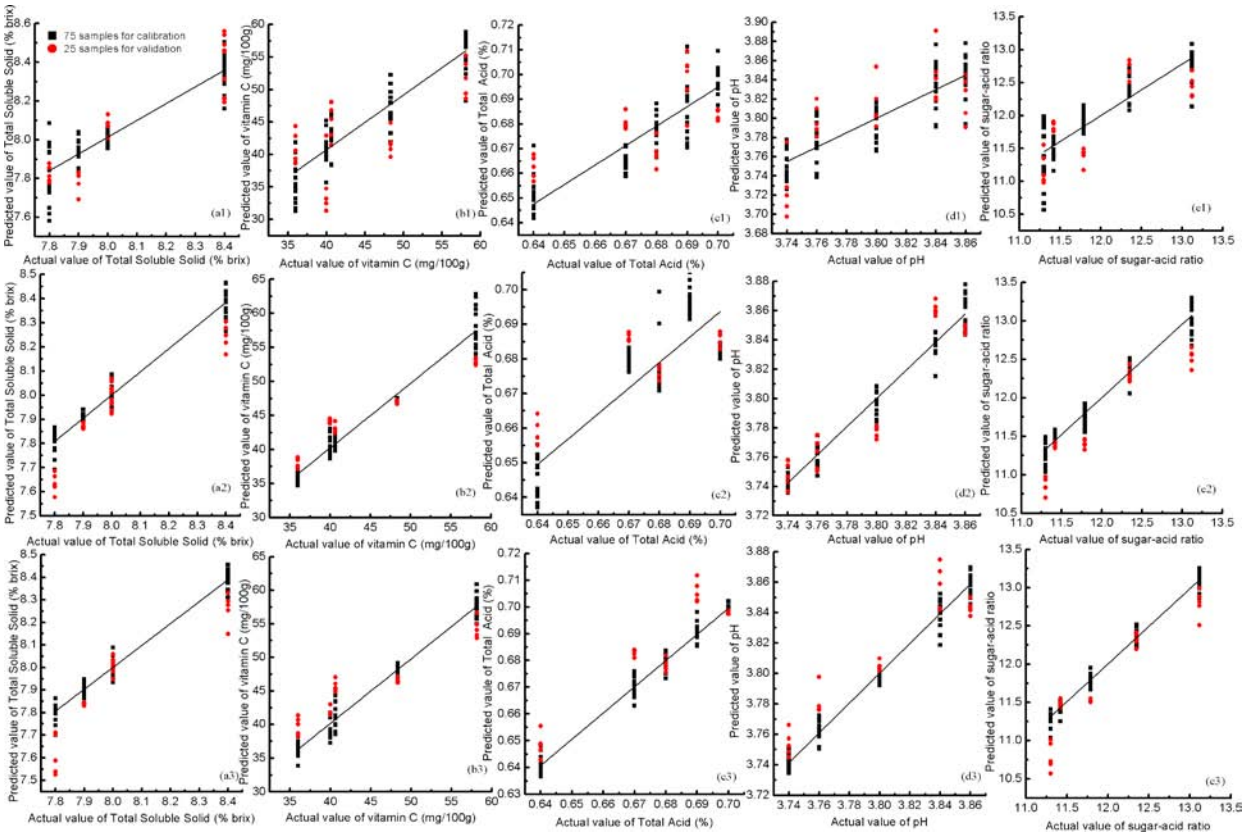

Figure 4. Estimated strawberry juice quality parameters (vitamin C and pH) using PLSR versus experimental data: (a), (b), (c), and (d) are for total soluble solid, vitamin C, total acid, pH and sugar/acid ratio respectively; (1), (2), and (3) based on data set of E-nose, E-tongue, and the fusion of E-nose and E-tongue, respectively.

Table 6. Comparison of Three Predictive Models Built on the Responses of the E-Nose Data Set, E-Tongue Data Set, and the Fusion of E-Nose and E-Tongue by Lib-SVM

		parameter		calibration		validation	
data set	quality index	best C	best γ	R^2	RMSE	R^2	RMSE
E-nose	vitamin C	16	0.0039	0.8882	0.3385(g/kg)	0.5222	0.7397(g/kg)
	pH	16	0.0039	0.8545	0.3879	0.7224	0.6351
	TSS	11.3137	0.0039	0.8600	0.1465 (°Brix)	0.6022	0.4395 (°Brix)
	TA	16	0.0055	0.9086	0.0940 (%)	0.7106	0.3077 (%)
	TSS/TA ratio	16	0.0078	0.9262	0.0758	0.7272	0.2873
E-tongue	vitamin C	11.3137	0.0039	0.8892	0.3364(g/kg)	0.5256	0.7251(g/kg)
	pH	16	0.0039	0.8551	0.3869	0.4064	0.8459
	TSS	1	0.1768	0.8620	0.1440 (°Brix)	0.6332	0.3813 (°Brix)
	TA	1.4143	0.0625	0.9100	0.0923 (%)	0.7193	0.2937 (%)
	TSS/TA ratio	1	0.0625	0.9266	0.0751	0.7351	0.2760
fusion of E-nose and E-tongue	vitamin C	16	0.0039	0.8945	0.3276(g/kg)	0.5290	0.7066(g/kg)
	pH	4	0.0039	0.8592	0.3766	0.3915	0.8203
	TSS	16	0.0039	0.8620	0.1443 (°Brix)	0.6204	0.4151 (°Brix)
	TA	8	0.0078	0.9127	0.0893 (%)	0.7261	0.2822 (%)
	TSS/TA ratio	8	0.0039	0.9288	0.0725	0.7261	0.2862

shown in Figure 4c1, Figure 4c2, Figure 4c3, Figure 4c4, and Figure 4c5, there are close relationship between quality parameters from conventional analytical methods and those estimated by the PLSR models based on the fusion. In this way, a good prediction of these variables could be performed from the fusion of E-nose and E-tongue.

Quantitative Regression of Quality Parameters Based on Support Vector Machines. For Lib-SVM regression models, the E-nose data set, and E-tongue data set, the fusion and the quality parameters were processed same as Lib-SVM classification did. Then 5-fold cross-validation was applied to get the best performance of classification, and radial basis function (RBF) was chosen as the core function. Parameter C

dx.doi.org/10.1021/jf501468b | J. Agric. Food Chem. 2014, 62, 6426−6434

and kernel parameter gamma (γ) in SVM model were also optimized in the Lib-SVM regression models. Results of this analysis are shown in Table 6. On the whole, regression models based on Lib-SVM were not good as regression models based on PLSR were according to R^2 in this strawberry juice case. Better predictions of these variables were performed from the fusion of E-nose and E-tongue, compared to an individual apparatus utilization.

Quantitative Regression of Quality Parameters Based on Random Forest. The regression results based on RF are summarized in Table 7. The overall level of regression based on RF is higher than models established by PLSR and Lib-SVM. The predictive models, built on the responses of the E-nose, have higher value of R^2 in the calibration and in the validation sets than models by Lib-SVM did. In this section, the result of the fusion data is slightly higher than models built by E-tongue data. The RF algorithm may be able to extract useful information more effectively than Lib-SVM and PLSR do in the field of E-nose and E-tongue data processing.

Table 7. Comparison of Three Predictive Models Built on the Responses of the E-Nose Data Set, E-Tongue Data Set, and the Fusion of E-Nose and E-Tongue by RF

		calibration		validation	
data set	quality parameters	R^2	RMSE	R^2	RMSE
E-nose	vitamin C	0.9969	0.1052 (g/kg)	0.7823	0.1511 (g/kg)
	pH	0.9845	0.0855	0.8873	0.1109
	TSS	0.9220	0.0285 (°Brix)	0.9876	0.0305 (°Brix)
	TA	0.9888	0.0033 (%)	0.9693	0.0055 (%)
	TSS/TA ratio	0.9834	0.0833	0.9946	0.1296
E-tongue	vitamin C	0.9980	0.0450 (g/kg)	0.9931	0.0528 (g/kg)
	pH	0.9974	0.0349	0.9889	0.0479
	TSS	0.9963	0.0196 (°Brix)	0.9954	0.0315 (°Brix)
	TA	0.9979	0.0015 (%)	0.9558	0.0057 (%)
	TSS/TA ratio	0.9956	0.0496	0.9977	0.0711
fusion of E-nose and E-tongue	vitamin C	0.9992	0.0315 (g/kg)	0.9987	0.0309 (g/kg)
	pH	0.9979	0.0327	0.9966	0.0252
	TSS	0.9964	0.0222 (°Brix)	0.9895	0.0269 (°Brix)
	TA	0.9665	0.0021 (%)	0.9939	0.0024 (%)
	TSS/TA ratio	0.9980	0.0490	0.9888	0.1161

This work presented a comprehensive and systematic experimental analysis of the performance of E-nose and E-tongue to discriminate processed strawberry juices and to predict juice quanlity changes. Conclusions were reached here: (1) E-tongue system reached higher accuracy rate compared to E-nose system both in the classification and regression, and the combination did have a slight advantage in the LDA classification and PLSR regression. (2) The network design and parameter optimization adjusted RF and SVM to perfection for classification and regression, and RF has shown outstanding and indisputable performances in the qualitative and quantitative analysis when compared with Lib-SVM in this experiment. To our knowledge, there has been no previous study to RF analysis in the E-nose or E-tongue data processing for regression, and future work may consider the utilization of data sampling with respect to the RF learner. This work indicates that the simultaneous utilization of E-nose and E-tongue with appropriate algorithm can discriminate between processed fruit juices and predict quality changes successfully for the beverage industry in replacement of existing detection systems.

AUTHOR INFORMATION

Corresponding Author

*Phone: +86-571-88982178. Fax: +86-571-88982192. E-mail: jwang@zju.edu.cn.

Funding

We acknowledge the financial support of the National Key Technology R&D Program 2012BAD29B02-4, the Chinese National Foundation of Nature and Science through projects 31071548 and 31370555, and the Doctoral Program of the Ministry of Education project 2010010110133.

Notes

The authors declare no competing financial interest.

REFERENCES

(1) Aaby, K.; Mazur, S.; Nes, A.; Skrede, G. Phenolic compounds in strawberry (*Fragaria* × *ananassa* Duch.) fruits: composition in 27 cultivars and changes during ripening. *Food Chem.* **2012**, *132*, 86−97.

(2) Seeram, N. P.; Lee, R.; Scheuller, H. S.; Heber, D. Identification of phenolic compounds in strawberries by liquid chromatography electrospray ionization mass spectroscopy. *Food Chem.* **2006**, *97*, 1−11.

(3) Peinado, I.; Rosa, E.; Heredia, A.; Escriche, I.; Andres, A. Influence of processing on the volatile profile of strawberry spreads made with isomaltulose. *Food Chem.* **2013**, *138*, 621−629.

(4) Piyasena, P.; McKellar, R.; Bartlett, F. Thermal inactivation of *Pediococcus* sp. in simulated apple cider during high-temperature short-time pasteurization. *Int. J. Food Microbiol.* **2003**, *82*, 25−31.

(5) Ancos, B. d.; Cano, M. P.; Hernandez, A.; Monreal, M. Effects of microwave heating on pigment composition and colour of fruit purees. *J. Sci. Food Agric.* **1999**, *79*, 663−670.

(6) Odriozola-Serrano, I.; Soliva-Fortuny, R.; Martín-Belloso, O. Phenolic acids, flavonoids, vitamin C and antioxidant capacity of strawberry juices processed by high-intensity pulsed electric fields or heat treatments. *Eur. Food Res. Technol.* **2008**, *228*, 239−248.

(7) Cruz, R.; Vieira, M. C.; Silva, C. L. Effect of heat and thermosonication treatments on watercress (*Nasturtium officinale*) vitamin C degradation kinetics. *Innovative Food Sci. Emerging Technol.* **2008**, *9*, 483−488.

(8) Montero, T. M.; Mollá, E. M.; Esteban, R. M.; López-Andréu, F. J. Quality attributes of strawberry during ripening. *Sci. Hortic.* **1996**, *65*, 239−250.

(9) Berna, A. Z.; Lammertyn, J.; Saevels, S.; Natale, C. D.; Nicolaï, B. M. Electronic nose systems to study shelf life and cultivar effect on tomato aroma profile. *Sens. Actuators, B* **2004**, *97*, 324−333.

(10) Escuder-Gilabert, L.; Peris, M. Review: Highlights in recent applications of electronic tongues in food analysis. *Anal. Chim. Acta* **2010**, *665*, 15−25.

(11) Rizzolo, A.; Bianchi, G.; Vanoli, M.; Lurie, S.; Spinelli, L.; Torricelli, A. Electronic Nose To Detect Volatile Compound Profile and Quality Changes in 'Spring Belle' Peach (*Prunus persica* L.) during Cold Storage in Relation to Fruit Optical Properties Measured by Time-Resolved Reflectance Spectroscopy. *J. Agric. Food Chem.* **2012**, *61*, 1671−1685.

(12) Farnworth, E. R.; Mckellar, R. C.; Chabot, D.; Lapointe, S.; Chicoine, M.; Knight, K. P. Use of an electronic nose to study the contribution of volatiles to orange juice flavor. *J. Food Qual.* **2002**, *25*, 569−576.
(13) Shaw, P. E.; Rouseff, R. L.; Goodner, K. L.; Bazemore, R.; Nordby, H. E.; Widmer, W. W. Comparison of headspace GC and electronic sensor techniques for classification of processed orange juices. *LWT−Food Sci. Technol.* **2000**, *33*, 331−334.
(14) Karlshøj, K.; Nielsen, P. V.; Larsen, T. O. Prediction of *Penicillium expansum* spoilage and patulin concentration in apples used for apple juice production by electronic nose analysis. *J. Agric. Food Chem.* **2007**, *55*, 4289−4298.
(15) Ciosek, P.; Augustyniak, E.; Wróblewski, W. Polymeric membrane ion-selective and cross-sensitive electrode-based electronic tongue for qualitative analysis of beverages. *Analyst* **2004**, *129*, 639−644.
(16) Beullens, K.; Kirsanov, D.; Irudayaraj, J.; Rudnitskaya, A.; Legin, A.; Nicolaï, B. M.; Lammertyn, J. The electronic tongue and ATR−FTIR for rapid detection of sugars and acids in tomatoes. *Sens. Actuators, B* **2006**, *116*, 107−115.
(17) Kovács, Z.; Szöllősi, D.; Yoshida, K.; Fekete, A.; Ishikawa, E.; Isz, S.; Bonnefille, M., Taste attributes profiling in carrot juice using an electronic tongue. In *Proceedings of the First Indo−Japan Conference on Perception and Machine Intelligence*; Springer-Verlag: Kolkata, India, 2012; pp 180−186.
(18) Wide, P.; Winquist, F.; Bergsten, P.; Petriu, E. M. The human-based multi-sensor fusion method for artificial nose and tongue sensor data. In*Instrumentation and Measurement Technology Conference, 1998, IMTC/98, Conference Proceedings*; IEEE: New York, 1998; pp 531−536.
(19) Bleibaum, R. N.; Stone, H.; Tan, T.; Labreche, S.; Saint-Martin, E.; Isz, S. Comparison of sensory and consumer results with electronic nose and tongue sensors for apple juices. *Food Qual. Preference* **2002**, *13*, 409−422.
(20) Hong, X.; Wang, J. Detection of adulteration in cherry tomato juices based on electronic nose and tongue: comparison of different data fusion approaches. *J. Food Eng.* **2014**, *126*, 89−97.
(21) Hartmann, A.; Patz, C. D.; Andlauer, W.; Dietrich, H.; Ludwig, M. Influence of processing on quality parameters of strawberries. *J. Agric. Food Chem.* **2008**, *56*, 9484−9489.
(22) Terefe, N. S.; Kleintschek, T.; Gamage, T.; Fanning, K. J.; Netzel, G.; Versteeg, C.; Netzel, M. Comparative effects of thermal and high pressure processing on phenolic phytochemicals in different strawberry cultivars. *Innovative Food Sci. Emerging Technol.* **2013**, *19*, 57−65.
(23) Gössinger, M.; Moritz, S.; Hermes, M.; Wendelin, S.; Scherbichler, H.; Halbwirth, H.; Stich, K.; Berghofer, E. Effects of processing parameters on colour stability of strawberry nectar from puree. *J. Food Eng.* **2009**, *90*, 171−178.
(24) Chen, L.; Dai, G. The influence on the preservation rate of vitamin C with different measures in the process of strawberry juice. *Food Res. Dev.* **2007**, *2*, 115−117.
(25) Ndiaye, C.; Xu, S. Y.; Wang, Z. Steam blanching effect on polyphenoloxidase, peroxidase and colour of mango (*Mangifera indica*) slices. *Food Chem.* **2009**, *113*, 92−95.
(26) Aguilar-Rosas, S.; Ballinas-Casarrubias, M.; Nevarez-Moorillon, G.; Martin-Belloso, O.; Ortega-Rivas, E. Thermal and pulsed electric fields pasteurization of apple juice: effects on physicochemical properties and flavour compounds. *J. Food Eng.* **2007**, *83*, 41−46.
(27) Bahçeci, K. S.; Serpen, A.; Gökmen, V.; Acar, J. Study of lipoxygenase and peroxidase as indicator enzymes in green beans: change of enzyme activity, ascorbic acid and chlorophylls during frozen storage. *J. Food Eng.* **2005**, *66*, 187−192.
(28) Tian, X.; Wang, J.; Zhang, X. Discrimination of preserved licorice apricot using electronic tongue. *Math. Comput. Model.* **2012**, *58*, 743−751.
(29) *Determination of Vitamin C in Vegetables and Fruits (2,6-Dichloro-indophenol Titration Method)*, GB 6195-86, Standard of the people's Republic of China, 1986.
(30) *Determination of Total Acid in Foods*, GB/T 12456-2008, National Standard of the People's Republic of China, 2008.
(31) Versari, A.; Parpinello, G. P.; Mattioli, A. U.; Galassi, S. Characterisation of Italian commercial apricot juices by high-performance liquid chromatography analysis and multivariate analysis. *Food Chem.* **2008**, *108*, 334−340.
(32) Dias, L.; Peres, A. M.; Barcelos, T. P.; Sá Morais, J.; Machado, A. A. Semiquantitative and quantitative analysis of soft drinks using an electronic tongue. *Sens. Actuators, B* **2011**, *154*, 111−118.
(33) Wold, S.; Ruhe, A.; Wold, H.; Dunn, I. W. J. The collinearity problem in linear regression. The partial least squares (PLS) approach to generalized inverses. *SIAM J. Sci. Comput.* **1984**, *5*, 735−743.
(34) Lozano, J.; Santos, J. P.; Arroyo, T.; Aznar, M.; Cabellos, J. M.; Gil, M.; Horrillo, M. d. C. Correlating e-nose responses to wine sensorial descriptors and gas chromatography−mass spectrometry profiles using partial least squares regression analysis. *Sens. Actuators, B* **2007**, *127*, 267−276.
(35) Ho, T. K. Random Decision Forests. In *Proceedings of the Third International Conference on Document Analysis and Recognition*, 1995; pp 278−282.
(36) Breiman, L. Random forests. *Machine Learn.* **2001**, *45*, 5−32.
(37) Breiman, L. Bagging predictors. *Mach. Learning* **1996**, *24*, 123−140.
(38) Ho, T. K. The random subspace method for constructing decision forests. *IEEE Trans. Pattern Anal. Mach. Intell.* **1998**, *20*, 832−844.
(39) Abdel-Rahman, E. M.; Mutanga, O.; Adam, E.; Ismail, R. Detecting *Sirex noctilio* grey-attacked and lightning-struck pine trees using airborne hyperspectral data, random forest and support vector machines classifiers. *ISPRS J. Photogrammetry Remote Sens.* **2014**, *88*, 48−59.
(40) Cortes, C.; Vapnik, V. Support-vector networks. *Machine Learn.* **1995**, *20*, 273−297.
(41) Brudzewski, K.; Osowski, S.; Markiewicz, T. Classification of milk by means of an electronic nose and SVM neural network. *Sens. Actuators, B* **2004**, *98*, 291−298.
(42) Chang, C. C.; Lin, C. J. LIBSVM: a library for support vector machines. *ACM Trans. Intell. Syst. Technol.* **2011**, *2*, 27.
(43) Holzwarth, M.; Korhummel, S.; Carle, R.; Kammerer, D. R. Evaluation of the effects of different freezing and thawing methods on color, polyphenol and ascorbic acid retention in strawberries (*Fragaria × ananassa* Duch.). *Food Res. Int.* **2012**, *48*, 241−248.
(44) Shaw, D. Genotypic variation and genotypic correlations for sugars and organic acids of strawberries. *J. Am. Chem. Soc.* **1988**, *113*, 770−774.
(45) Sadrieh, N.; Brower, J.; Yu, L.; Doub, W.; Straughn, A.; Machado, S.; Pelsor, F.; Saint Martin, E.; Moore, T.; Reepmeyer, J. Stability, dose uniformity, and palatability of three counterterrorism drugs—human subject and electronic tongue studies. *Pharm. Res.* **2005**, *22*, 1747−1756.

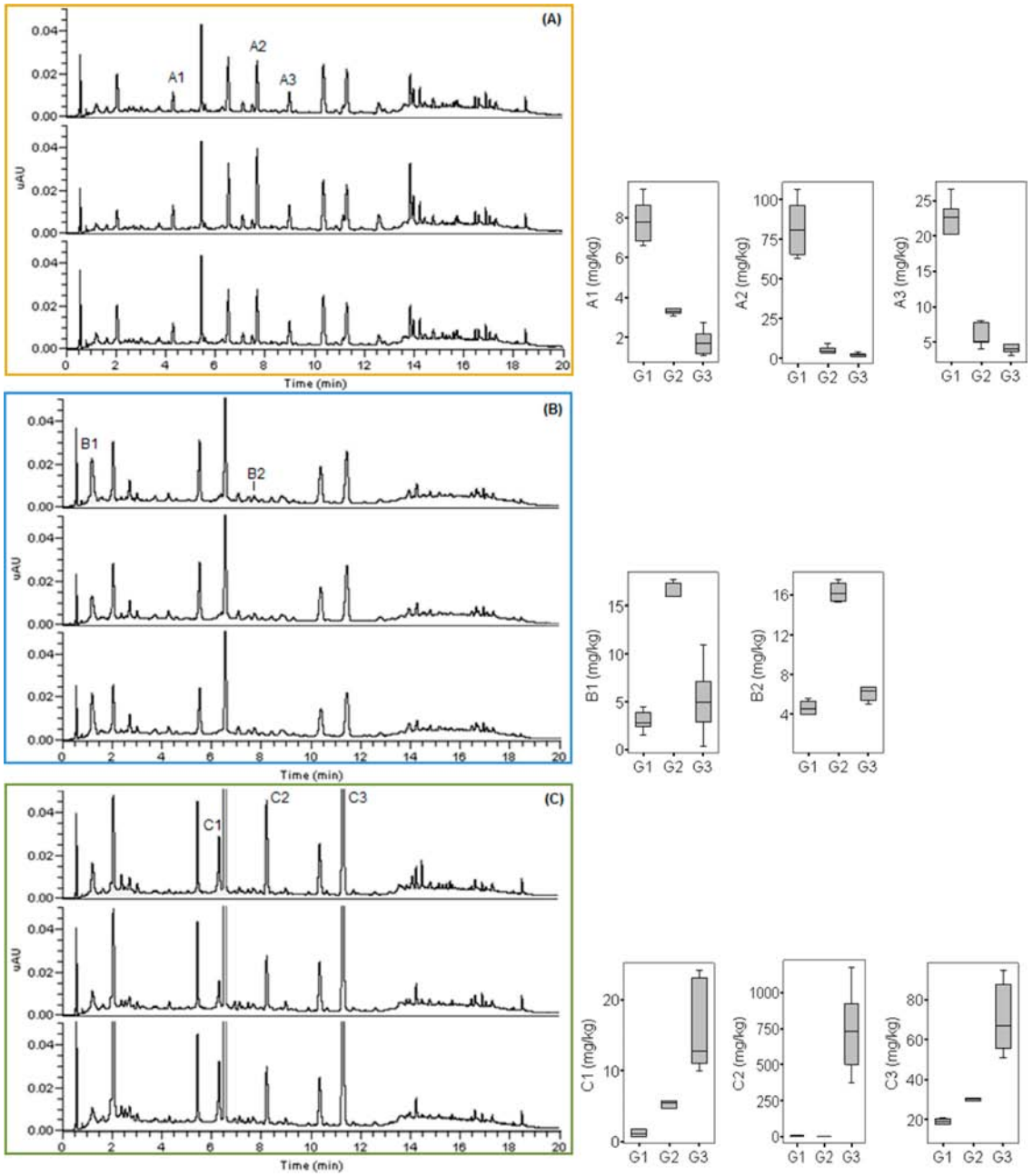

Figure 1. UHPLC-PDA-MS/MS example profiles, λ = 272 nm: group classification extracted from the publication by Oelschlaegel et al.[11] of commercially available manuka honeys; numbered peaks are characteristic compounds of each group. (A) group 1 (25%), (B) group 2 (25%), (C) group 3 (50%); (A1) 4-hydroxybenzoic acid, (A2) dehydrovomifoliol, (A3) benzoic acid; (B1) kojic acid, (B2) 2-methoxybenzoic acid; (C1) syringic acid, (C2) 4-methoxyphenyllactic acid, (C3) methyl syringate.

isophorone, 3,4,5-trimethylphenol, benzoic acid, and phenylacetic acid were specific for group 1 (Figure 2). The honeys of group 2 contained the highest intensities of 2-methylbenzofuran, 2′-hydroxyacetophenone, and 2′-methoxyacetophenone, and group 3 honeys contained a high intensity of *cis*-linalool oxide. Because of the high MGO content determined for group 2, which strongly differed from the two other groups, Oelschlaegel et al.[11] assumed that group 2 represents pure manuka honeys. For kanuka honey, 4-methoxyphenyllactic acid is said to be characteristic according to Stephens et al.[14]

The Australian native jelly bush (*Leptospermum polygalifolium* Salisb.) honey or berringa honey whose nectar plant is classified to the same genus as the manuka shrub needs to be considered as well. Its nonperoxide antibacterial activity caused by approximately the same quantities of MGO has already been noted as a New Zealand equivalent.[15,16] The fact of the same botanical classification but a different geographical origin constitutes a very important distinction. In the literature, only Yao et al.[17] investigated the two different manuka species concerning flavonoids and phenolic acids. They described myricetin, luteolin, and tricetin as main flavonoids for jelly bush honey and quercetin, isorhamnetin, luteolin, and an unknown flavanon for manuka honey. In regard to the phenolic acids, gallic acid was measured to be dominant in manuka honey, jelly bush honey should additionally contain coumaric acid.

dx.doi.org/10.1021/jf501818f | J. Agric. Food Chem. 2014, 62, 6435−6444

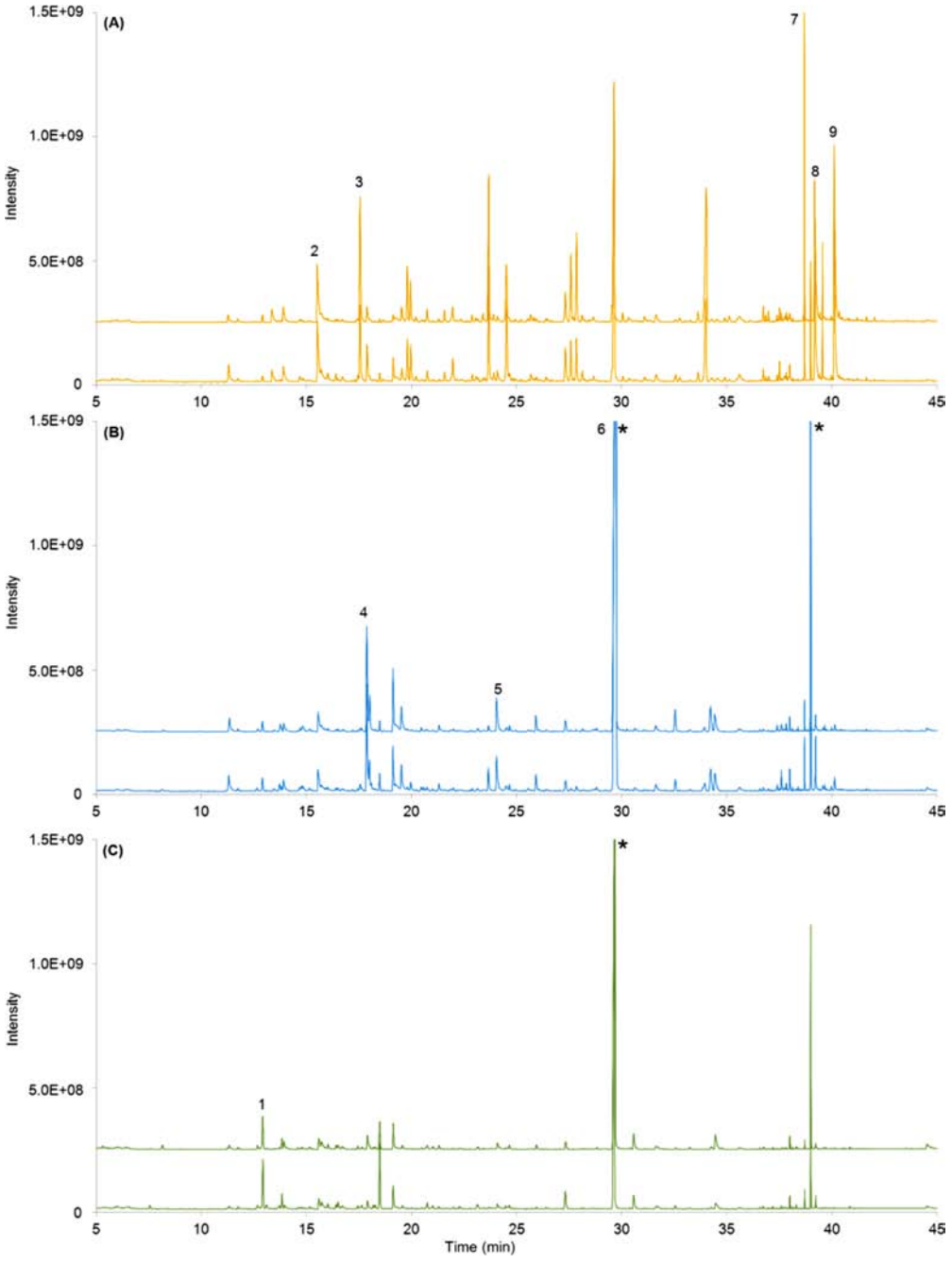

Figure 2. HS-SPME-GC/MS example profiles: group classification of commercially available manuka honeys according to Oelschlaegel et al.[13] (A) group 1 (25%), (B) group 2 (50%), (C) group 3 (25%); (1) *cis*-linalool oxide, (2) benzaldehyde, (3) α-isophorone, (4) 2-methylbenzofuran, (5) 2′-hydroxyacetophenone, (6) 2′-methoxyacetophenone, (7) 3,4,5-trimethylphenol, (8) benzoic acid, (9) phenylacetic acid; * peak cut.

The aim of this study was to establish chemical marker compounds for the three different monofloral honeys in order to differentiate between them. This was achieved by analyzing both the nonvolatile compounds such as phenolic substances or norisoprenoides obtained by UHPLC-PDA-MS/MS and the volatile compounds by HS-SPME-GC/MS. By a subsequent comparison of the resulting PDA- and GC-MS-profiles, marker compounds could be worked out for the first time allowing for a clear differentiation of the three honeys derived from monocultures among themselves on the basis of chemometrics.

MATERIAL AND METHODS

Honey Samples. Eight monofloral manuka honeys (New Zealand), seven monofloral kanuka honeys (New Zealand), and one jelly bush honey (Australia) were received from UMFHA, which also performed pollen-analytical studies. According to the information obtained from UMFHA, the monofloral honeys were harvested in regions with only one of the three honey cultivars in 2012. All the samples were stored in a refrigerator at 6 °C.

Chemicals. Methanol (HPLC grade and LC-MS grade) and acetonitrile (HPLC grade) were purchased from Fisher Scientific (Schwerte, Germany). Daidzein standard, 2′-hydroxyacetophenone, 2′-methoxyacetophenone, and 2,6,6-trimethyl-2-cyclohexene-1,4-dione were acquired from Alfa Aesar (Karlsruhe, Germany). The 4-methoxy-^{13}C, d_3-benzoic-2,3,5,6-d_4 acid as internal standard for LC-

dx.doi.org/10.1021/jf501818f | J. Agric. Food Chem. 2014, 62, 6435−6444

Table 1. HS-SPME-GC/MS: Characteristic Compounds of Monofloral Honey Samples, Including LRI and Identification Method (via Reference Standard, STD; via NIST Library, MS)[a]

compound	LRI FFAP	identification	manuka (n = 7)	kanuka (n = 2)	jelly bush (n = 1)
cis-linalool oxide	1443	STD, LRI	+	++	+++
2-methylbenzofuran	1579	STD	++	−	−
2,6,6-trimethyl-2-cyclohexene-1,4-dione	1676	STD, LRI	∓	++	+
2′-hydroxyacetophenone	1785	STD	+	−	−
phenethyl alcohol	1892	STD, LRI	∓	++	−
2′-methoxyacetophenone	1979	STD	+++	+	+
p-anisaldehyde	2013	STD, LRI	∓	+++	−
unknown	2056		−	+++	−
3,4,5-trimethylphenol	>2100	STD	∓	+	+++

[a]Percentage of peak area in total peak area, average of n samples (− not detected; + 0−1%; ++ >1−5%, +++ >5−45%).

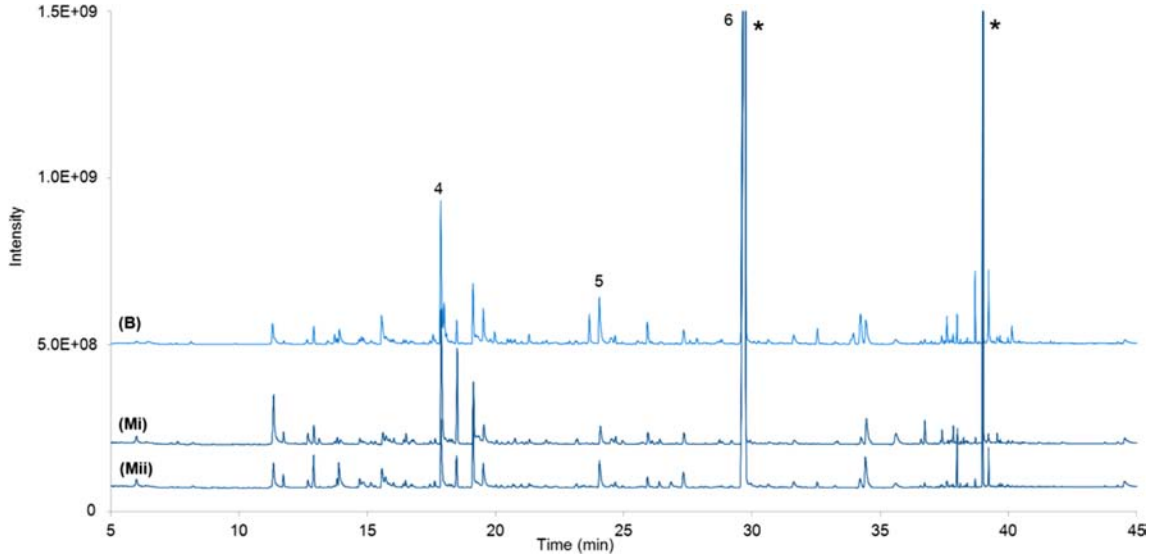

Figure 3. HS-SPME-GC/MS profiles: comparison of Oelschlaegel's group 2[13] (B) with pure manuka honeys (Mi), (Mii); (4) 2-methylbenzofuran, (5) 2′-hydroxyacetophenone, (6) 2′-methoxyacetophenone; * peak cut.

MS/MS was supplied by Isotec via Sigma-Aldrich (Steinheim, Germany). Acetic acid 100% glacial was from Fluka via Sigma-Aldrich (Steinheim, Germany). Sodium chloride was purchased from VWR International (Darmstadt, Germany) and benzaldehyde-d_6, phenethyl alcohol, *cis*-linalool oxide, *p*-anisaldehyde, and 2-methyl-6-propyl phenol from Sigma-Aldrich (Steinheim, Germany). 3,4,5-Trimethylphenol and 2-methylbenzofuran were purchased from Dr. Ehrenstorfer GmbH via VWR International (Darmstadt, Germany). All the chemicals used in this study were of analytical grade. Bidistilled water was generated by the Bi-Distilling Apparatures Bi 18E QSC GmbH (Maintal, Germany).

Head Space Solid Phase Microextraction (HS-SPME). The HS-SPME-GC/MS was carried out as described by Oelschlaegel et al.[12] Briefly, honey was homogenized with sodium chloride and water in a SPME vial. Deuterated benzaldehyde was used as internal standard. Before measuring, the DVB/CAR/PDMS fiber which is described as the most suitable fiber for honey volatiles was conditioned.[18] Subsequently, the analytes were desorbed in the PTV injector. The HS-SPME holder was part of a Combi PAL (CTC Analytics, Zwingen, Swiss).

GC/MS Detection. A Thermo Scientific Trace GC Ultra interfaced with a Thermo Scientific DSQ II (Thermo Fisher, Dreieich, Germany) was used. The MS was operated in the positive EI mode at 70 eV, and the mass range was m/z 50−600. EI source temperature was set at 200 °C. Spectral data recording started only after 4 min due to the huge solvent peak. Identification of the compounds based on a comparison of the MS spectra with those of the NIST-08-mass spectral library, with linear retention indices (LRI) and with reference substances (retention time, MS spectrum).

UHPLC-PDA-MS/MS Detection. Prior to the UHPLC analyses, a solid phase extraction was carried out and has already been described.[11] Briefly, 2 g of honey were dissolved in 2% sodium chloride (pH 2−3) with subsequent SPE cleanup using Chromabond cartridges. Chromatographic analyses were performed with an Acquity Ultra Performance UPLC-PDA system (Waters, Eschborn, Germany) on a Nucleodur C18 column with a water/methanol/formic acid gradient within 20 min. Mass spectrometric investigations were carried out using a coupled TSQ Quantum Access MAX (Thermo Fisher, Dreieich, Germany). The identification of the compounds was realized via retention time, UV maxima, and also timed SRM (single reaction monitoring).

Statistical Analyses. The data matrix consists of rows representing the different honeys (objects) and columns, which includes SPE-UHPLC-PDA-MS/MS data of the substances (variables) previously described as characteristic. For PCA and k-means, the matrix covered 16 objects × 13 variables. For this, SPSS 22.0 was used. All data were standardized (z-values) before chemometrics.

RESULTS AND DISCUSSION

Comparison of the HS-SPME-GC/MS Profiles. The volatiles were examined in seven manuka, two kanuka, and one jelly bush honey using the HS-SPME-GC/MS method by Oelschlaegel et al.[12] Because of the rather small sample size, this investigation comprised less honeys than those analyzed by

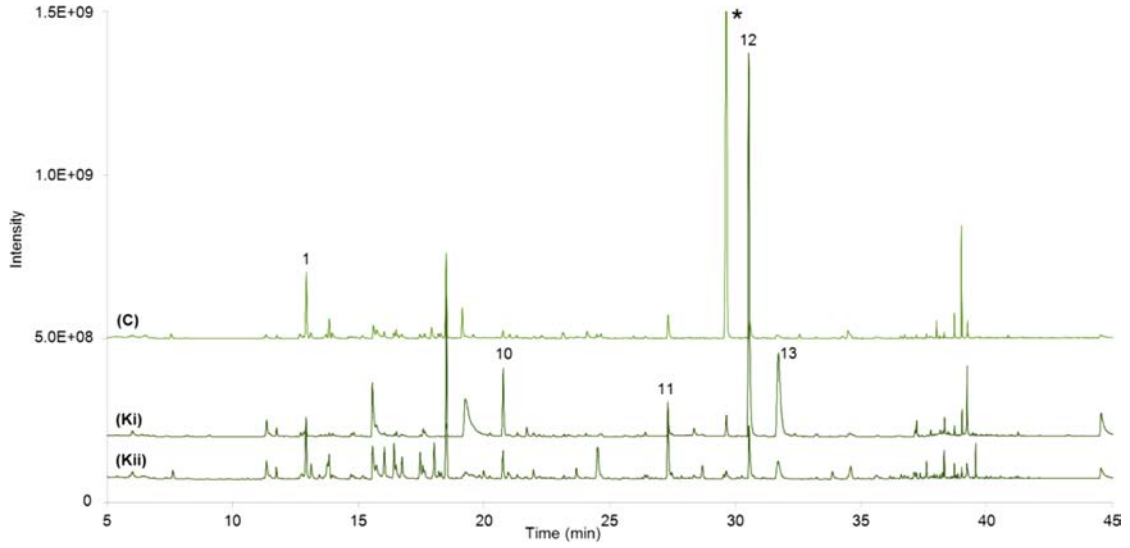

Figure 4. HS-SPME-GC/MS profiles: comparison of Oelschlaegel's group 3[13] (C) with pure kanuka honeys (Ki), (Kii); (1) *cis*-linalool oxide, (10) 2,6,6-trimethyl-2-cyclohexene-1,4-dione, (11) phenethyl alcohol, (12) *p*-anisaldehyde, (13) unknown; * peak cut.

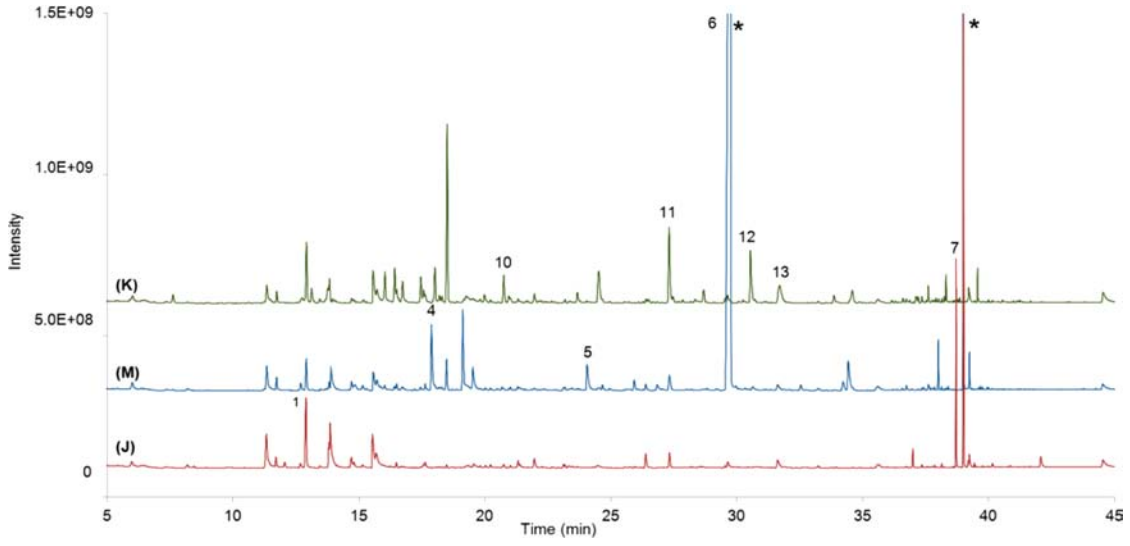

Figure 5. HS-SPME-GC/MS profiles: comparison of pure kanuka honey (K), pure manuka honey (M), and pure jelly bush honey (J); (1) *cis*-linalool oxide, (4) 2-methylbenzofuran, (5) 2′-hydroxyacetophenone, (6) 2′-methoxyacetophenone, (7) 3,4,5-trimethylphenol, (10) 2,6,6-trimethyl-2-cyclohexene-1,4-dione, (11) phenethyl alcohol, (12) *p*-anisaldehyde, (13) unknown; * peak cut.

the UHPLC-PDA-MS/MS method. The chromatographic profiles of the three honey sorts were compared; the resulting characteristic compounds are listed in Table 1.

In the samples of the monofloral manuka honey, mostly the compounds of Oelschlaegel's group 2 were detected as well (Figure 3).[13] The following volatile substances could be confirmed as characteristic for manuka honey: 2-methylbenzofuran, 2′-hydroxyacetophenone, and 2′-methoxyacetophenone. In contrast, for kanuka honey, subsequent compounds proved to be prominent: 2,6,6-trimethyl-2-cyclohexene-1,4-dione, phenethyl alcohol, *p*-anisaldehyde, and an unknown compound, which refers to a similarity to Oelschlaegel's group 3 (Figure 4).[13] 2,6,6-Trimethyl-2-cyclohexene-1,4-dione and phenethyl alcohol, although already known in honey in general, were now described for kanuka honey for the first time.

2′-Methoxyacetophenone as characteristic for manuka honey has already been reported by Daher et al.,[19] whereas Tan et al.[20] described this compound for manuka/kanuka honeys without differentiation. In one Portuguese multifloral honey, 2′-methoxyacetophenone was analyzed with an equivalent high peak intensity as well, however, this honey showed a completely different MS-profile.[21] Because of our findings that this compound could only be detected in negligible intensities for kanuka honey under the chosen conditions, 2′-methoxyacetophenone can be used as a criterion distinguishing manuka honey from kanuka honey. Nevertheless, 2-methylbenzofuran and 2′-hydroxyacetophenone are present exclusively in manuka honey in reference to the three monofloral honeys. For kanuka honeys, there are two characteristic peaks which are present in other honeys, especially in European ones, in definitely small quantities: one has been identified as anisaldehyde, the second is unknown.[22−29] The latter was first assumed to be *p*-propyl anisole, which was proposed by Visser et al.[29] and later by Daher et al.[19] as a marker for manuka honey. However, both groups of authors identified this component solely via the NIST

dx.doi.org/10.1021/jf501818f | J. Agric. Food Chem. 2014, 62, 6435−6444

Table 2. UHPLC-PDA-MS/MS: Characteristic Compounds of Monofloral Honey Samples, Including Retention Time and UV Maxima[a]

compound[b]	t_R (min)	UV_{max} (nm)	manuka $n = 8$	kanuka $n = 7$	jelly bush $n = 1$
kojic acid	1.13	266	+++	+	++
5-methyl-3-furancarboxylic acid[c]	2.68	266	+	∓	++
leptosin[d,f]	6.52	263	++++	++	++++
unknown M4	6.90	252, 309	+	−	−
2-methoxybenzoic acid[f]	7.53	295	++	+	++++
acetyl-2-hydroxy-4-(2-methoxyphenyl)-4-oxobutanate[e]	8.02	249, 309	+	−	−
4-methoxyphenyllactic acid	8.18	274	∓	++++	−
3-hydroxy-1-(2-methoxyphenyl)-penta-1,4-dione[e,f]	9.32	249, 309	++	−	−
unkown J2	10.55	245	−	−	+++
p-anisic acid	10.73	256	−	+++	−
methyl syringate	11.50	274	+++	++++	+++
lumichrome[g]	12.79	259, 349	−	+++	−
unkown M7	13.96	245, 306	++	−	−

[a]Percentage of peak area in total peak area at $\lambda = 254$ nm, average of n samples (− not detected, + 0−1%; ++ >1−2%, +++ >2−6%, ++++ >6−35%). [b]Identification via reference standard. [c]Identification via isolated standard was proven by NMR and MS. [d]MS/MS identification via m/z 559 = $[M + Na + H]^+$. [e]MS/MS identification via 225 = $[M\text{-}Ac + H]^+$. [f]Described as prevalent for manuka honey and jelly bush honey by Analytical Laboratories Ltd., Waikato, New Zealand. [g]Described as prevalent for kanuka honey by Analytical Laboratories Ltd., Waikato, New Zealand.

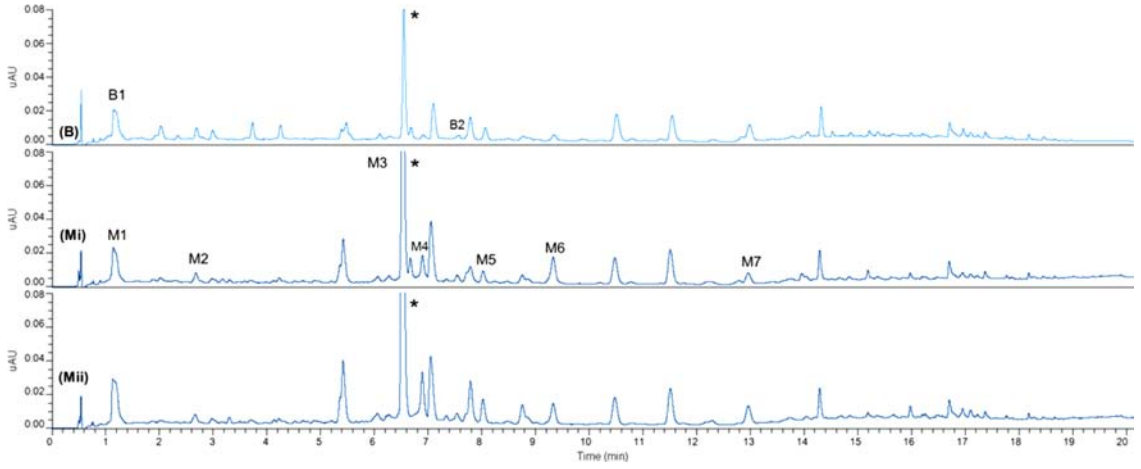

Figure 6. UHPLC-PDA-MS/MS profiles (254 nm): comparison of Oelschlaegel's group 2[11] (B) with pure manuka honeys (Mi), (Mii); (B1 = M1) kojic acid, (B2) benzoic acid; (M2) 5-methyl-3-furancarboxylic acid, (M3) leptosin, (M4) unknown, (M5) acetyl-2-hydroxy-4-(2-methoxyphenyl)-4-oxobutanate, (M6) 3-hydroxy-1-(2-methoxyphenyl)-penta-1,4-dione, (M7) unknown; * peak cut.

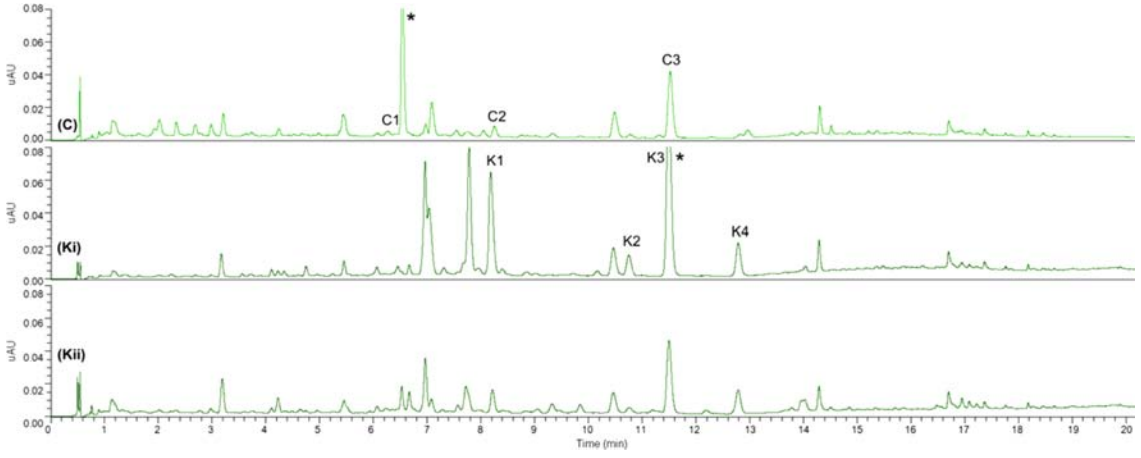

Figure 7. UHPLC-PDA-MS/MS profiles (254 nm): comparison of Oelschlaegel's group 3[11] (C) with pure kanuka honeys (Ki), (Kii); (C1) syringic acid, (C2 = K1) 4-methoxyphenyllactic acid, (C3 = K3) methyl syringate, (K2) *p*-anisic acid, (K4) lumichrome; * peak cut.

database; Visser et al.[29] analyzed one manuka honey, Daher et al.[19] two commercial manuka honeys.

Because of our investigations using a reference standard, *p*-propyl anisole could not be confirmed neither as a component

dx.doi.org/10.1021/jf501818f | J. Agric. Food Chem. 2014, 62, 6435−6444

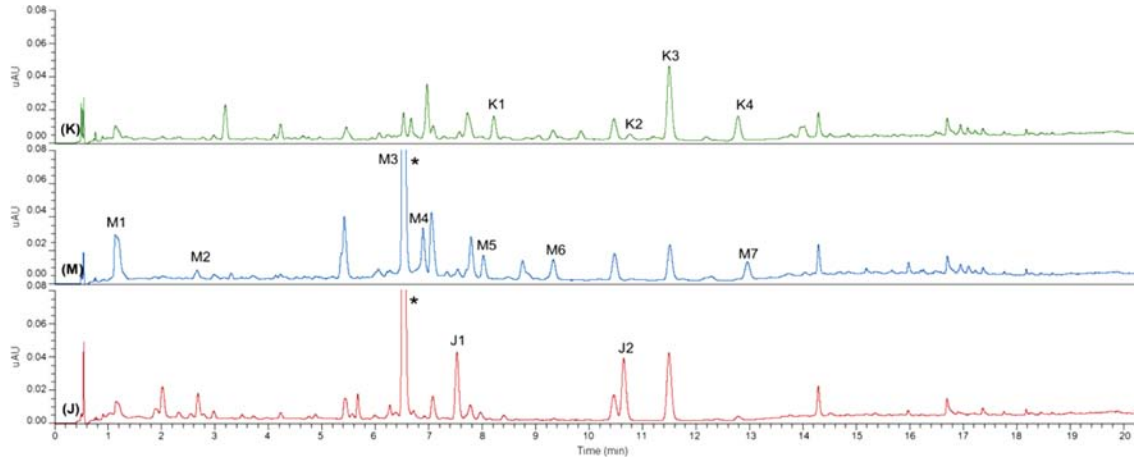

Figure 8. UHPLC-PDA-MS/MS profiles (254 nm): comparison of pure kanuka honey (K) with pure manuka honey (M) and pure jelly bush honey (J); (K1) 4-methoxyphenyllactic acid, (K2) *p*-anisic acid, (K3) methyl syringate, (K4) lumichrome; (M1) kojic acid, (M2) 5-methyl-3-furancarboxylic acid, (M3) leptosin, (M4) unknown, (M5) acetyl-2-hydroxy-4-(2-methoxyphenyl)-4-oxobutanate, (M6) 3-hydroxy-1-(2-methoxyphenyl)-penta-1,4-dione, (M7) unknown; (J1) 2-methoxybenzoic acid, (J2) unknown; * peak cut.

in manuka nor in kanuka honey. Subsequent studies with a further suggested compound by the NIST database, with 2-methyl-6-propyl phenol as a reference substance, also failed, although the MS spectrum was the same. The investigations concerning the identification are still ongoing.

An Australian jelly bush honey also provided by UMFHA was analyzed to do a profile matchup with manuka honey as well (Table 1). Because of the notably lower intensities of 2′-methoxyacetophenone and higher concentrations of *cis*-linalool oxide and 3,4,5-trimethylphenol in the jelly bush honey profile, a differentiation toward manuka honey was possible (Figure 5). However, a confirmation of the distinctive features would require further analyses of more jelly bush honeys.

Comparison of the UHPLC-PDA Profiles. In all, eight manuka, seven kanuka, and one jelly bush honey were investigated according to the UHPLC-PDA-MS/MS method described by Oelschlaegel et al.[11] (Table 2). Comparing the PDA profiles (λ = 254 nm), an unambiguous distinction among the pure manuka and pure kanuka honeys can immediately be recognized. Additionally, all the investigated samples of manuka, kanuka, and jelly bush honey were analyzed by UHPLC-HRMS and evaluated by Braggins et al. (Analytica Laboratories Ltd., Waikato, New Zealand).[30] Results are noted in Table 2.

Leptosin was detected as the principal analyte of manuka honey (Figure 6). In contrast, kanuka honey profiles were dominated by 4-methoxyphenyllactic acid and also by methyl syringate (Figure 7). Leptosin, a glycoside of methyl syringate, was already described exclusively for the *Leptospermum* species by Kato and cowriters[31] and, therefore, could be confirmed as a marker for manuka honey. 4-Methoxyphenyllactic acid was found in manuka/kanuka honeys by Tan et al.[20] and in one of six commercial manuka honeys analyzed by Le Gresley et al.[32] According to Stephens et al.,[14] the substance is uniquely characteristic for kanuka honey which, in turn, corresponds to our results. A large number of other characteristic substances in the profiles of pure monofloral honeys were worked out as follows: acetyl-2-hydroxy-4-(2-methoxyphenyl)-4-oxobutanate, 3-hydroxy-1-(2-methoxyphenyl)-penta-1,4-dione, and still unknown compounds M4 and M7 for manuka honey and, for kanuka honey, *p*-anisic acid and lumichrome (Figure 8). Kojic acid and 5-methyl-3-furancarboxylic acid which are well-marked for manuka may be a further distinction criteria. Acetyl-2-hydroxy-4-(2-methoxyphenyl)-4-oxobutanate and 3-hydroxy-1-(2-methoxyphenyl)-penta-1,4-dione were proved exclusively for manuka honey and had been isolated and subsequently identified via NMR-spectroscopy by Oelschlaegel et al.[11] Although lumichrome is currently discussed controversially as a marker substance, both for the country-specific Italian thistle honey (*Galactites tomentosa* Moench) and for the cornflower honey (*Centaurea cynaus L.*) (recent studies reported 2−3-fold higher contents in cornflower honey), the compound constitutes an important distinguishing criterion in the manuka/kanuka comparison due to its uniqueness to kanuka honey.[33−36] With a retention time similar to lumichrome, the unknown peak M7 existing in manuka honey with UV maxima at λ = 245 and 306 nm compared to lumichrome (λ = 259, 349 nm) has a markedly deviating UV spectrum and, after its identification, could serve as a further marker substance for manuka honey.

p-Anisic acid as well as methyl syringate could be used as differentiation criteria in the profile matchup for kanuka honey versus manuka honey due to the uniqueness or to the tendentially higher peak intensities. Their comparatively low occurrence in honeys from Europe and other honey from New Zealand can be neglected.[14,26,37−41] Senanayake[42] divided his manuka honeys into active and inactive samples on the basis of their UMF contents. The inactive samples contained higher 4-methoxyphenyllactic acid and methyl syringate than the active samples. On the basis of our results, kanuka honey, which verifiably does not have any nonperoxide antibacterial activity, might be contained in these honeys in larger quantities. In accordance with Oelschlaegel et al.,[11] group 2 represents the true manuka honeys (Figure 6). In contrast, group 3 includes honeys with a higher proportion of kanuka honey, and honeys of group 1 very probably contain only low proportions of both manuka honey and kanuka honey (Figure 7).

Distinguishing the so-called Australian manuka honey (jelly bush honey) from the New Zealand manuka honey is also of interest. Although both honey sorts show a giant leptosin peak, the PDA profiles are characterized by distinct differences (Figure 8). Whereas acetyl-2-hydroxy-4-(2-methoxyphenyl)-4-oxobutanate, 3-hydroxy-1-(2-methoxyphenyl)-penta-1,4-dione, and two unknown peas M4 and M7 are present in New

Zealand manuka honey, the Australian manuka honey is characterized by 2-methoxybenzoic acid and an unknown substance J2 (Figure 8). On the basis of these substances, it is possible to achieve a differentiation of these two kinds of honey, however, the prominent compounds of jelly bush honey would have to be ascertained by additional samples. The results reported by Yao et al.[17] who had analyzed honeys of both kinds of manuka honey could not be confirmed as already demonstrated by Oelschlaegel et al.[11] Neither could any high contents of abscisic acid nor gallic acid, which was declared as prominent for manuka honey, nor any different flavonoids be detected.

Final Assessment of Honey Characterization by Chemometrics. A PCA was calculated with the results of UHPLC-PDA-MS/MS. So, the marker potential of the above-mentioned characteristic substances for each of the three honeys was investigated. About 82% of the variation could be explained by the first two principal components (PC). Thereby, the first PC in negative is loading with lumichrome, 4-methoxyphenyllactic acid, and *p*-anisic acid, in positive through kojic acid, acetyl-2-hydroxy-4-(2-methoxyphenyl)-4-oxobutanate, 3-hydroxy-1-(2-methoxyphenyl)-penta-1,4-dione, unknown M4, and unknown M7 (Figure 9). If moving to the higher values of PC 2, 2-methoxybenzoic acid and unknown J2 are located. Looking at the scatter plot, the individual honeys are separated from each other. Negative values of PC 1 present the characteristic substances of kanuka honey, while positive values mark the typical manuka honey compounds. The analytes which are explained by PC 2 are referring to jelly bush honey (Figure 10). A few substances, which are listed below, do not permit a clear allocation: methyl syringate, leptosin, and 5-methyl-3-furancarboxylic acid. This is caused by the fact that the compounds are not clearly assigned only to one honey and, therefore, this kind of behavior in the loading plot was to be expected (Figure 9). Nonetheless, due to their huge peak height and individuality, a further consideration is indispensable in profile matchup. These results confirm that potential marker suitability is assured.

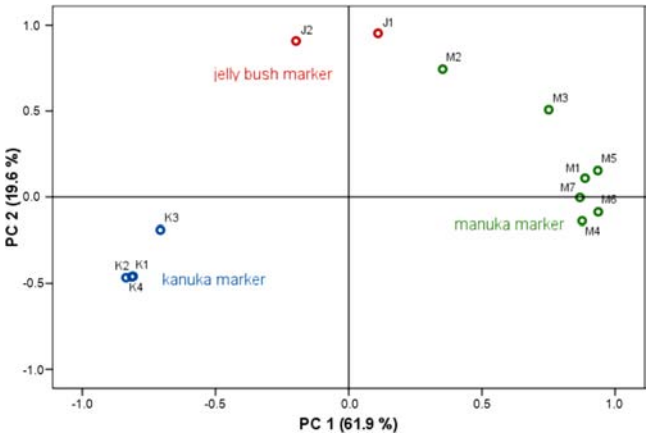

Figure 9. Loading plot (varimax rotation) for the first two principal components (PC1 with 61.9% of the total variance and PC2 19.6% of the total variance) of the determined UHPLC-PDA-MS/MS data; (K1) 4-methoxyphenyllactic acid, (K2) *p*-anisic acid, (K3) methyl syringate, (K4) lumichrome; (M1) kojic acid, (M2) 5-methyl-3-furancarboxylic acid, (M3) leptosin, (M4) unknown 1, (M5) acetyl-2-hydroxy-4-(2-methoxyphenyl)-4-oxobutanate, (M6) 3-hydroxy-1-(2-methoxyphenyl)-penta-1,4-dione, (M7) unknown 3; (J1) 2-methoxybenzoic acid, (J2) unknown 2.

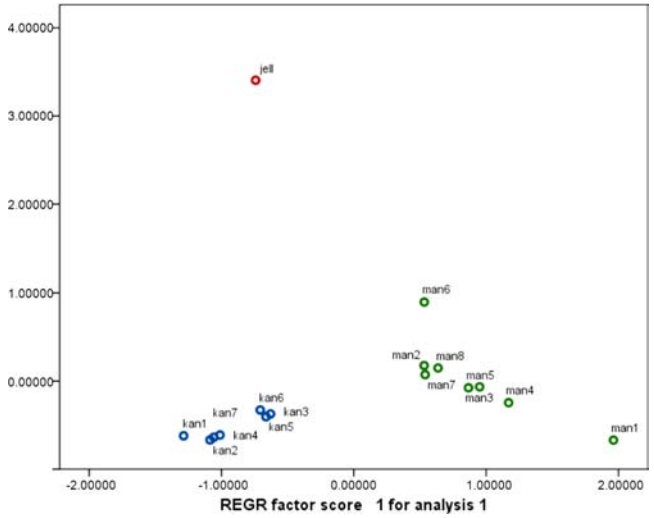

Figure 10. PCA score plot of manuka honeys (man), kanuka honeys (kan), and the jelly bush honey (jell) of the determined UHPLC-PDA-MS/MS data; number = sample number.

By means of the 13 declared substances, a cluster analysis was carried out to cluster the investigated honeys on the basis of their measured data. For this, a *k*-means with the requirement of 3 clusters was used. Before clustering, a successful test of dissimilarity was carried out. On the basis of Euclidean distance and subsequent iteration, a corresponding classification after cluster membership was generated. The aim to classify similar honeys in one cluster was achieved. Therefore, all manuka honeys were assigned to cluster 1, all kanuka honeys were assigned to cluster 2, and the last one, cluster 3, contains only the jelly bush honey. Chemometrics confirmed the characteristic substances for each honey that had already been worked out by profile matchup, allowing for a classification in three clusters to which only one kind of honey was assigned. A definite classification of the kind of honey requires numerous further investigations with a larger number of samples as well as with samples from different years and the various areas of New Zealand.

This is now a first approach to differentiating the manuka honeys from New Zealand and Australia as well as distinguishing the kanuka honeys among themselves by UHPLC-PDA-MS/MS and HS-SPME-GC/MS profile matchup.

AUTHOR INFORMATION

Corresponding Authors

*E-mail: Nicole.Beitlich@chemie.tu-dresden.de.

*Phone: +4935146333132. Fax: +4935146433132. E-mail: Karl.Speer@chemie.tu-dresden.de.

Notes

The authors declare no competing financial interest.

ACKNOWLEDGMENTS

We thank UMFHA for providing the samples. Our sincere thanks go to Gesa Heuser (TU Dresden, Germany) for sample preparation.

ABBREVIATIONS USED

jell, jelly bush honey; kan, kanuka honey; man, manuka honey; MGO, methylglyoxal; PC, principal component

REFERENCES

(1) Molan, P. C. The antibacterial activity of honey 1. The nature of the antibacterial activity. *Bee World* **1992**, *73*, 5−28.

(2) Adams, C. J.; Boult, C. H.; Deadman, B. J.; Farr, J. M.; Grainer, M. N. C.; Manley-Harris, M.; Snow, M. J. Isolation by HPLC and characterisation of the bioactive fraction of New Zealand manuka (*Leptospermum scoparium*) honey. *Carbohydr. Res.* **2008**, *343*, 651−659.

(3) Mavric, E.; Wittmann, S.; Barth, G.; Henle, T. Identification and quantification of methylglyoxal as the dominant antibacterial constituent of manuka (*Leptospermum scoparium*) honeys from New Zealand. *Mol. Nutr. Food Res.* **2008**, *52*, 483−489.

(4) Kwakman, P. H. S.; te Velde, A. A.; de Boer, L.; Vandenbroucke-Grauls, C. M. J. E.; Zaat, S. A. J. Two major medicinal honeys have different mechanisms of bactericidial activity. *PloS One* **2011**, *6*, e17709.

(5) Kwakman, P. H. S.; te Velde, A. A.; de Boer, L.; Speijer, D.; Vandenbroucke-Grauls, C. M. J. E.; Zaat, S. A. J. How honey kills bacteria. *FASEB J.* **2010**, *24*, 2576−2582.

(6) Allen, K. L.; Molan, P. C.; Reid, G. M. A survey of the antibacterial activity of some New Zealand honeys. *J. Pharm. Pharmacol.* **1991**, *43*, 817−822.

(7) Stephens, J. M. The factors responsible for the varying levels of UMF in mānuka (*Leptospermum scoparium*) honey. Ph.D. Dissertation. The Waikato University, Hamilton, New Zealand, 2006.

(8) *Options for defining monofloral manuka honey*; MPI Discussion Paper No: 2013/38; New Zealand Government, Ministry for Primary Industries, 2013.

(9) *What is Manuka Honey?* Unique Manuka Factor Honey Association, 2014; http://www.umf.org.nz/what-is-umf-honey (Accessed Apr 15, 2014).

(10) Manriquez, A. New Zealand—Project to Avoid the Fake Manuka Honey. *ApiNews* March 23, 2013; http://www.apinews.com/en/news/item/21356-new-zealand-project-to-avoid-the-fake-manuka-honey (Accessed April 15, 2014).

(11) Oelschlaegel, S.; Gruner, M.; Wang, P.-N.; Boettcher, A.; Koelling-Speer, I.; Speer, K. Classification and characterization of manuka honeys based on phenolic compounds and methylglyoxal. *J. Agric. Food Chem.* **2012**, *60*, 7229−7237.

(12) Oelschlaegel, S.; Speer, K. Characterization of unifloral honeys using HS-SPME/GC/MS. *ApiNews* **2011**; oral presentation Apimondia.

(13) Oelschlaegel, S. Charakterisierung und Differenzierung von Sortenhonigen. Ph.D. Dissertation. Technische Universität Dresden, Dresden, Germany, 2013.

(14) Stephens, J. M.; Schlothauer, R. C.; Morris, B. D.; Yang, D.; Fearnley, L.; Greenwood, D. R.; Loomes, K. M. Phenolic compounds and methylglyoxal in some New Zealand manuka and kanuka honeys. *Food Chem.* **2010**, *120*, 78−86.

(15) Irish, J.; Blair, S.; Carter, D. A. The antibacterial activity of honey derived from Australian flora. *PLoS One* **2011**, *6*, e18229.

(16) Windsor, S.; Pappalardo, M.; Brooks, P.; Williams, S.; Manley-Harris, M. A convenient new analysis of dihydroxyacetone and methylglyoxal applied to Australian *Leptospermum* honeys. *J. Pharmacogn. Phytother.* **2012**, *4*, 6−11.

(17) Yao, L.; Datta, N.; Tomás-Barberán, F. A.; Ferreres, F.; Martos, I.; Singanusong, R. Flavonoids, phenolic acids and abscisic acid in Australian and New Zealand *Leptospermum* honeys. *Food Chem.* **2003**, *81*, 159−169.

(18) Manyi-Loh, C. E.; Ndip, R. N.; Clarke, A. M. Volatile compounds in honey: a review on their involvement in aroma, botanical origin determination and potential biomedical activities. *Int. J. Mol. Sci.* **2011**, *12*, 9514−9532.

(19) Daher, S.; Gülaçar, F. O. Identification of new aromatic compounds in the New Zealand manuka honey by gas chromatography−mass spectrometry. *E-J. Chem.* **2010**, *7*, S7−S14.

(20) Tan, S.-T.; Holland, P. T.; Wilkins, A. L.; Molan, P. C. Extractives from New Zealand honeys. 1. White clover, manuka, and kanuka unifloral honeys. *J. Agric. Food Chem.* **1988**, *36*, 453−460.

(21) Pontes, M.; Marques, J. C.; Câmara, J. S. Screening of volatile composition from Portuguese multifloral honeys using headspace solid-phase microextraction-gas chromatography−quadrupole mass spectrometry. *Talanta* **2007**, *74*, 91−103.

(22) Guyot, C.; Scheirman, V.; Collin, S. Floral origin markers of heather honeys: *Calluna vulgaris* and *Erica arborea*. *Food Chem.* **1999**, *64*, 3−11.

(23) Alissandrakis, E.; Tarantilis, P. A. Ultrasound-assisted extraction gas chromatography−mass spectrometry analysis of volatile compounds in unifloral thyme honey from Greece. *Eur. Food Res. Technol.* **2009**, *229*, 365−373.

(24) Piasenzotto, L.; Gracco, L.; Conte, L. Solid phase microextraction (SPME) applied to honey quality control. *J. Sci. Food Agric.* **2003**, *83*, 1037−1044.

(25) Shimoda, M.; Wu, Y.; Osajima, Y. Aroma compounds from aqueous solution of haze (*Rhus succedanea*) honey determined by adsorptive column chromatography. *J. Agric. Food Chem.* **1996**, *44*, 3913−3918.

(26) Guyot, C.; Bouseta, A.; Scheirman, V.; Collin, S. Floral origin markers of chestnut and lime tree honeys. *J. Agric. Food Chem.* **1998**, *46*, 625−633.

(27) Jerković, I.; Mastelić, J.; Marijanović, Z. A. Variety of volatile compounds as markers in unifloral honey from Dalmatian sage (*Salvia officinalis* L.). *Chem. Biodiversity* **2006**, *30*, 1307−1316.

(28) Bouseta, A.; Scheirman, V.; Collin, S. Flavor and free amino acid composition of lavender and eucalyptus honeys. *J. Food Sci.* **1996**, *4*, 683−687.

(29) Visser, F. R.; Allen, J. M.; Shaw, G. J. The effect on the volatile flavour fraction from a unifloral honey. *J. Apicult. Res.* **1988**, *27*, 175−181.

(30) Braggins, T. J.; Jaine, J. Analytica Laboratories Ltd.: Waikato, New Zealand; personal communication.

(31) Kato, Y.; Umeda, N.; Maeda, A.; Matsumoto, D.; Kitamoto, N. Identification of a novel glycoside, leptosin, as a chemical marker of manuka honey. *J. Agric. Food Chem.* **2012**, *60*, 3418−3423.

(32) Le Gresley, A.; Kenny, J.; Cassar, C.; Kelly, A.; Sinclair, A.; Fielder, M. D. The application of high resolution diffusion NMR to the analysis of manuka honey. *Food Chem.* **2012**, *135*, 2879−2886.

(33) Tuberoso, C. I. G.; Bifulco, E.; Caboni, P.; Sarais, G.; Cottiglia, F.; Floris, I. Lumichrome and phenyllactic acid as chemical markers of thistle (*Galactitis tomentosa* Moench) honey. *J. Agric. Food Chem.* **2011**, *76*, 364−369.

(34) Oelschlaegel, S.; Pieper, L.; Staufenbiel, R.; Gruner, M.; Zeippert, L.; Pieper, B.; Koelling-Speer, I.; Speer, K. Floral markers of cornflower (*Centaurea cyanus*) honeys and its peroxide antibacterial activity for an alternative treatment of digital dermatitis. *J. Agric. Food Chem.* **2012**, *60*, 11811−11820.

(35) Kuś, P. M.; Jerković, I.; Tuberoso, C. I. G.; Marijanović, Z.; Congiu, F. Cornflower (*Centaurea cyanus* L.) honey quality parameters: chromatographic fingerprints, chemical biomarkers, antioxidant capacity and others. *Food Chem.* **2014**, *142*, 12−18.

(36) Beitlich, N.; Speer, K. Lumichrome as a marker for unifloral honeys? Proceedings 43rd International Apicultural Congress APIMONDIA, Kyiv, Ukraine, September 29−October 4, 2013, Scientific Program, Beekeeping Technology and Quality , Poster 18.

(37) Alissandrakis, E.; Kibaris, A. C.; Tarantilis, P. A.; Harizanis, P. C.; Polissiou, M. Flavour compounds of Greek cotton honey. *J. Sci. Food Agric.* **2005**, *85*, 1444−1452.

(38) Tuberoso, C. I. G.; Jerković, I.; Sarais, G.; Congiu, F.; Marijanović, Z.; Kuś, P. M. Color evaluation of seventeen European unifloral honey types by means of spectrophotometrically determined CIE $L^*C^*_{ab}h^\circ_{ab}$ chromaticity coordinates. *Food Chem.* **2014**, *145*, 284−291.

(39) Jerković, I.; Tuberoso, C. I. G.; Gugić, M.; Bubalo, D. Composition of sulla (*Hedysarum coronarium* L.) honey solvent extractives determined by GC/MS: norisoprenoids and other volatile organic compounds. *Molecules* **2010**, *15*, 6375−6385.
(40) Schievano, E.; Morelato, E.; Facchin, C.; Mammi, S. Characterization of markers of botanical origin and other compounds from unifloral honeys. *J. Sci. Food Agric.* **2013**, *61*, 1747−1755.
(41) Weston, R. J.; Mitchell, K. R.; Allen, K. L. Antibacterial phenolic components of New Zealand manuka honey. *Food Chem.* **1999**, *64*, 295−301.
(42) Senanayake, M. J. *A Chemical Investigation of New Zealand Unifloral Honeys*; The University of Waikato: New Zealand, 2006.

100 g pin mixer (National Manufacturing, Lincoln, NE, USA) with 57.0 mL of deionized water (mixograph-derived water absorption), 6.0 g of sucrose, 5.3 g of compressed yeast (Bruggeman, Ghent, Belgium), and 1.5 g of salt. The mixed dough was transferred to a lightly greased bowl and put in a fermentation cabinet (National Manufacturing) at 90% relative humidity and 30 °C. Fermentation took 90 min, with intermediate punching after 52 and 77 min using a dough sheeter (National Manufacturing). After 90 min, dough was punched a last time and molded. It was then either placed in a lightly greased metal baking pan for conventional baking or put in a plexiglass ERO baking chamber. In both cases, dough was then transferred to the fermentation cabinet for a final proof stage of 36 min.

Conventional Baking. Proofed dough was baked at 215 °C for 24 min in a National Manufacturing rotary oven. After baking, depanning, and 120 min of cooling to room temperature, breads were weighed, packed in a hermetically sealed plastic bag to prevent moisture loss, and stored at room temperature until further analysis.

Baking in an Electrical Resistance Oven. Heating of dough by an ERO is based on the principle of Joule's first and Ohm's laws. Joule's first law expresses the relationship between the heat (Q) generated by the current (I) flowing through a resistance (R) for a time (t): $Q = I^2 \times R \times t$. Joule heating, also known as ohmic or resistive heating, is the process by which the passage of an electric current through a resistance releases heat. According to Ohm's law, the applied voltage (V) equals the current (I) × the resistance (R). In line with the above, at a given dough resistance, the intensity of the current rises and, as a result, the temperature in dough increases at a higher rate when the applied voltage is increased. Evidently, the heating rate also depends on dough/bread resistance. The ERO was based on a model described by Hoseney[1] with slight modifications (baking chamber made of plexiglass plates of 10 mm thickness with internal dimensions of 12.5 × 10.0 × 22.0 cm). Figure 1 shows the system, with indications of the positions of the thermocouples (see below). Dough was placed between two stainless steel plates (distance between the plates = 6.5 cm, plate thickness = 1.5 mm), which were coupled to a variable transformer (Hossoni, Hongbao, China; 0−250 V). A perforated (126 holes, each with a diameter of 1.5 mm) plexiglass plate (12.4 × 6.4 cm, plate thickness 10 mm), which could easily slide upward when the dough/bread expanded, was placed on top of the dough during proofing and baking to keep the surface of the bread flat. This ensured good contact of the baking dough/bread with the electrode plates and reproducible baking.

ERO baking was programmed to simulate the temperature profile of the center of dough/bread during conventional baking. The heating rate, and thus also dough temperature, was controlled by adjusting the applied voltage by a variable transformer. Temperature was monitored by thermocouples (see below) inserted into dough through a hole in the baking chamber 4.0 cm above the bottom of the oven or through holes in the perforated plate. The voltage−time profile applied during baking was chosen to simulate the temperature profile in the center of conventionally baked dough/bread and was as follows: 50 V (0−1 min), 100 V (1−8 min), 120 V (8−14 min). After baking, bread was removed from the oven and allowed to cool for 120 min. Afterward, it was weighed and packed individually in a hermetically sealed plastic bag to prevent moisture loss. It was then stored at room temperature for 7 days. Analyses at day 0 were those on breads cooled to room temperature and stored for 2 h.

Temperature Measurements during Baking. Temperature measurements were performed using a Datapaq (Cambridge, UK) temperature data logger (MultiPaq 21) with type T thermocouples. In conventional baking, a stainless steel thermal barrier (Datapaq) protected the MultiPaq temperature data logger. Temperature measurements were performed in triplicate.

Determination of Moisture Contents. Moisture contents were measured for samples withdrawn at eight different places (indicated in Figure 5) in fresh and aged bread according to AACC International method 44-15A.[11]

Differential Scanning Calorimetry (DSC). DSC was carried out with a Q1000 differential scanning calorimeter (TA Instruments, New Castle, DE, USA). Bread crumb samples were freeze-dried, ground,

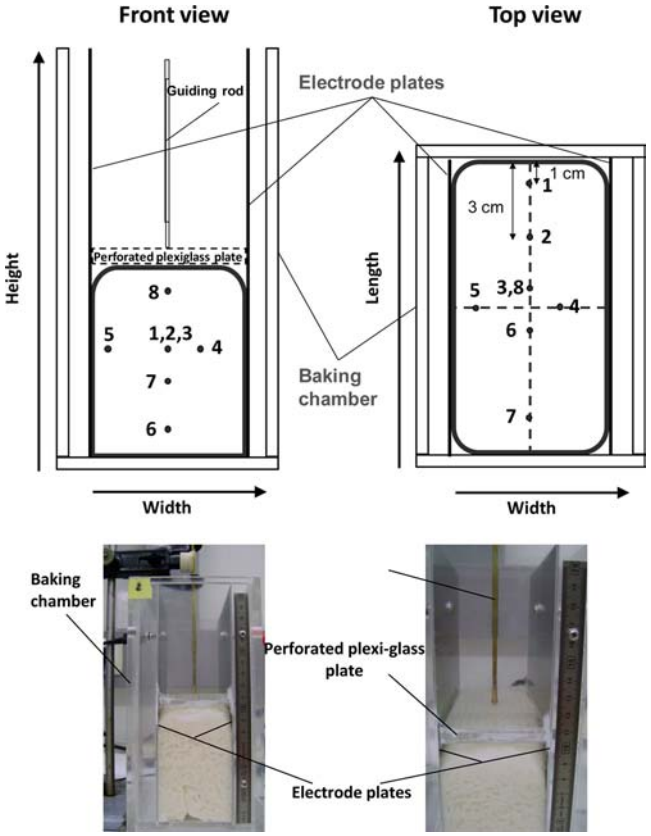

Figure 1. Schematic representation of baking chamber of the electrical resistance oven (ERO). The baking chamber is made from plexiglass. The voltage is applied by a variable transformer over the two electrode plates. A perforated plexiglass plate is used to keep the surface of the bread flat during final proof and oven rise. The produced gases can escape from the system through the pores. The numbers indicate the places where the thermocouples are placed.

and accurately (2.5−4.0 mg) weighed in three separate aluminum pans (PerkinElmer, Waltham, MA, USA). An excess of deionized water was added [1:3 w/w sample dry matter (dm)/water]. The pans were hermetically sealed. After equilibration at room temperature for at least 20 min, the pans were heated from 0 to 120 °C at 4 °C/min. An empty pan was used as reference. Calibration was with indium. TA Universal Analysis software was used to determine the onset (T_o), peak (T_p), and conclusion (T_c) temperatures and melting enthalpy (ΔH) of retrograded amylopectin.

Polarized Light Microscopy. The gelatinization process during baking using both conventional and ERO technologies was visualized using polarized light microscopy. For these analyses, samples obtained from dough before baking and from fully baked bread were prepared by putting a small piece of dough/crumb collected from the center of the dough/bread on a carrier glass. After the addition of a drop of deionized water, a cover glass was placed on it, and the samples were examined with an Olympus BH2 microscope (Olympus, Tokyo, Japan) in the polarization mode.

Proton Nuclear Magnetic Resonance Measurements. Measurements of proton distribution in fresh and stored bread crumbs were performed with a low-resolution proton nuclear magnetic resonance (^{1}H NMR) spectrometer (Minispec mq 20, Bruker BioSpin, Ettlingen, Germany) at an operating resonance frequency of 20 MHz for ^{1}H (magnetic field strength of 0.47 T) according to the method of Bosmans et al.[12] This technique detects differences in mobility of protons that are in different environments.[13−16] During measurements, the probe head was kept at 25 °C using an external water bath. Samples (approximately 0.3 g) were accurately weighed in a Bruker NMR tube (10 mm external diameter) and sealed to prevent moisture

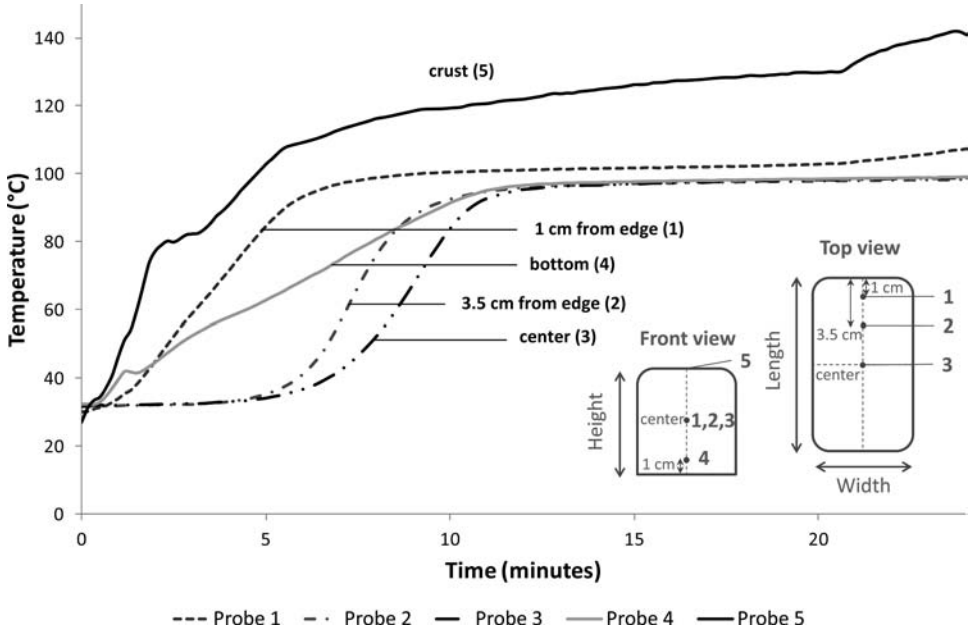

Figure 2. Temperature evolution of dough/bread during baking in a conventional rotary oven, measured at five different places.

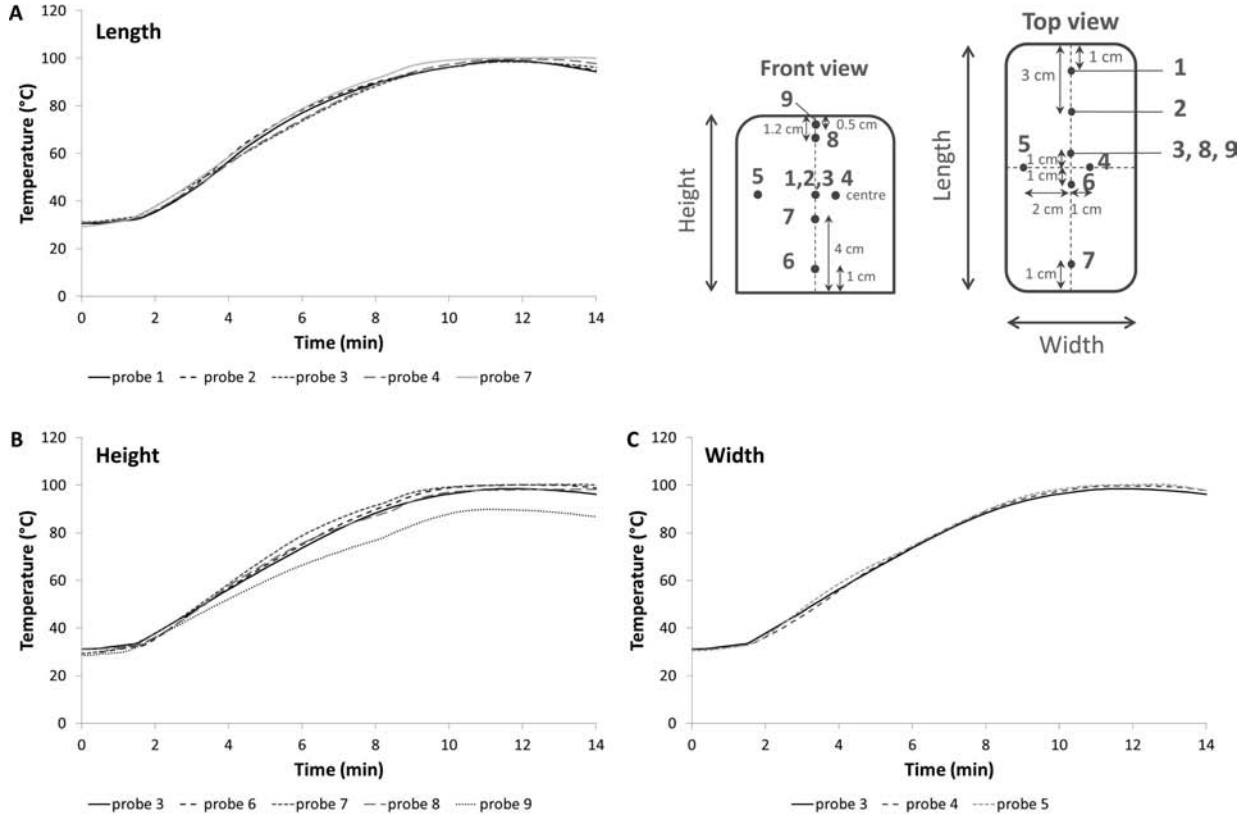

Figure 3. Temperature evolution in dough/bread during baking in an ERO, measured at nine different places in dough/bread, differing in length (A), height (B), and width (C).

loss. Three NMR tubes were filled to about 8 mm height with tightly compressed bread crumb (extracted from the loaf center) to avoid large air holes. Triplicate measurements were performed on each NMR tube. Transverse relaxation times (T_2) were measured. The transverse relaxation curves were developed using a single 90° pulse [free induction decay (FID)] and the Carr−Purcell−Meiboom−Gill (CPMG) pulse sequence. The pulse lengths were 2.86 and 5.42 μs, respectively. An acquisition period of 0.5 ms was used for FID measurements, and 500 data points were collected. The inhomogeneity of the static magnetic field affected the output for the most mobile FID population (around 0.5 ms). Therefore, this fraction was excluded from the analyses. The CPMG sequence had an interpulse spacing of 0.1 ms, and 2500 data points were acquired during the measurements. To increase the signal-to-noise ratio, 32 scans were performed with a recycle delay of 3.0 s for both measurements. The transverse relaxation curves were transformed with an inverse Laplace

dx.doi.org/10.1021/jf501856s | J. Agric. Food Chem. 2014, 62, 6445−6453

transformation to continuous distributions of T_2's using the Contin algorithm of Provencher (Bruker software).[17] Fast-relaxing protons, for example, protons of solids or protons strongly associated with solids, have a short transverse relaxation time. These can be observed in FID measurements. CPMG measurements are used to study protons with higher transverse relaxation times, such as water protons and solid protons in strong interaction with water.[14,16,18] The areas under the curves of the different proton populations are proportional to the quantity of protons in these populations for both FID and CPMG measurements. The areas were calculated by taking into account the exact weight of the bread crumb samples. Measurements were performed in triplicate to confirm the reproducibility.

RESULTS AND DISCUSSION

Breadmaking: From Dough to Fresh Bread. *Temperature Changes during Baking.* Monitoring the temperature at different places in dough/bread during conventional baking revealed that there were large gradients from the outside to the center of the dough (Figure 2). The closer to the dough center, the longer is the lag phase and the longer the temperature rise is postponed. In crumb, a maximum temperature of about 100 °C is reached. In contrast, the temperature increases to above 100 °C at the surface, when water vaporization has finished.

For ERO baking, He and Hoseney[8] observed that the resistance of dough changes during the baking process. At about 65 °C, the resistance of yeasted dough increases gradually. This is caused by starch gelatinization, which makes less free water available to the ionic solution to conduct the electric current.[7,8] In the present case, the total baking time (14 min) was shorter than in conventional baking (24 min) by omitting the isothermal phase around 30 °C (0−5 min) in the center of the bread crumb, which exists during conventional baking, and by shortening the final isothermal phase. The latter was done to avoid shrinking of the breads in the ERO and thereby losing contact with the electrode plates. Nevertheless, the baking process was considered to be complete because the bread crumb structure was set and no crumb collapse ("key-holing") was observed.

The temperature gradients during conventional baking are much larger than those during ERO baking. They were measured in the length, width, and height, as shown in Figure 3. Nearly no temperature gradients at points differing in height (measuring points 3, 6, and 7; Figure 3B) were noted. The differences in temperature between these measuring points were limited to maximally 2.3 °C. However, temperature gradients ran up to 13.1 °C near the surface (measuring point 9, Figure 3B). The differences were much lower (3.0 ± 0.7 °C) when the temperature was measured approximately 12 mm under the surface (measuring point 8, Figure 3B). In the length axis of the bread (measuring points 1−4 and 7, Figure 3A) and across the width (measuring points 3−5, Figure 3C), temperature gradients were limited to maximum differences of 2.8 and 2.5 °C, respectively. These small differences showed that ERO baking is almost gradient-free. At the end of baking (e.g., probes 1, 2, and 9, Figure 3), the temperature decreased when shrinking occurred and caused the bread to lose contact with the electrode plates at some places.

Starch Gelatinization during Baking As Visualized by Polarized Light Microscopy. Starch granules in dough are present as native semicrystalline granules with a typical Maltese cross when viewed under polarized light.[19] During the initial stages of both conventional and ERO baking, starch granules are still present as native granules (Figure 4A,B). Irrespective of the heating mode, at some point during baking, starch granules lost their Maltese crosses (Figure 4C,D) and thus were gelatinized.

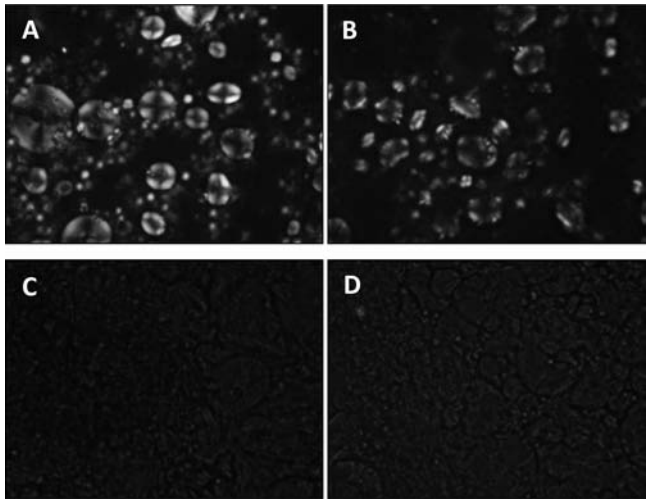

Figure 4. Polarized light microscope images of conventional (A, C) and ERO dough/bread (B, D) before baking (A, B) and after finishing the baking process (C, D).

Bread Moisture Content after Baking. During conventional baking, water evaporation occurs at the surface. Water vapor is lost through the crust into the surrounding hot air while another part of the water moves toward the cooler regions inside the crumb and condenses there.[20,21] In general, conventional bread had a lower weight than ERO bread, that is, 135.7 (±0.6) and 149.8 (±0.9) g, respectively. In conventional bread, the moisture content in the different parts of the crumb was relatively constant (approximately 43%). Possibly, moisture had redistributed during cooling. The moisture content in the crust of conventional bread was much lower, that is, approximately 12.9% (Figure 5). During ERO baking, water vapor condenses on the relatively cold surface of the bread and the plexiglass plates in contact with the ERO bread, whereas the air in a conventional oven is warmer and water vapor stays in the gas phase during the entire baking process. As a result, a small, relatively wet, and leathery layer was formed on top of ERO bread rather than a dry and crisp crust, as observed in conventional baking. Furthermore, the baking time of ERO bread is slightly shorter than that in conventional baking, which shortened the time span over which water could evaporate. Although the total amount of water was higher in ERO breads, the moisture contents in the different parts of the bread crumb were generally lower for ERO bread than for conventional bread. In addition the water was unequally distributed (Figure 5). The moisture content ranged from 33.0% (long side, bottom) to 41.0% (center, top). Overall, the center of ERO bread had a slightly higher moisture content than its outer parts. However, moisture content was higher in the "crust" of ERO breads, as described earlier by Martin et al.,[9] who reported that the exterior 5−10 mm of ERO bread contains approximately 47% moisture.[9] These observations can be explained by differences in water transport during ERO and conventional baking due to the differences in temperature gradient. In ERO bread, temperature gradients are small and the outer parts of the bread are in contact with relatively cooler surfaces (plexiglass and metal electrode plates). Water evaporation and subsequent condensation occur on the colder

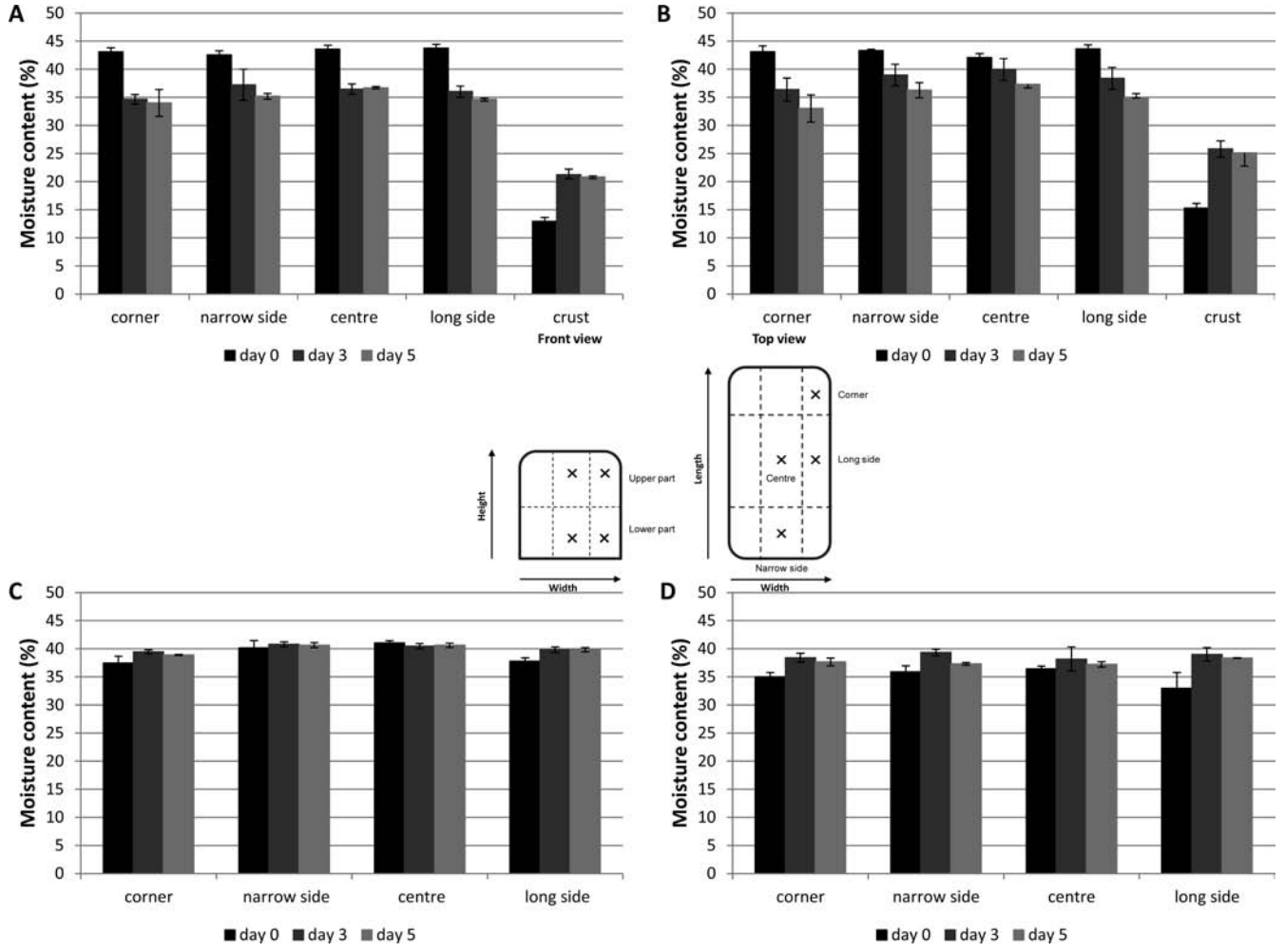

Figure 5. Moisture content during storage (days 0, 3, and 5) of conventional (A, B) and ERO (C, D) baked breads measured at four different places in the upper (A, C) and lower parts (B, D) of the breads.

plexiglass plates of the baking chamber or water evaporates and escapes to the surrounding air. In this way, a water distribution opposite that in a conventional bread (i.e., high moisture content on top of the ERO bread) was reached, similar to what has been observed earlier.[8,9] As a result, the moisture content of the upper part of ERO bread was higher than that of the lower parts.

Changes during Storage of Breads. *Macroscopic Changes in Moisture Gradient during Storage of Breads.* During storage of conventional bread, water migrates from the crumb to the crust. Figure 5 shows the evolution of the moisture content in different parts of the bread during storage. Moisture content decreased in every part of the crumb, whereas that of the crust increased. The largest shifts occurred during the first days of storage. After 5 days of storage, the moisture content of the crust seemed to have stabilized. In contrast to what one might expect on the basis of these data, only a slight weight loss occurred, that is, approximately 1.7 g on a total of 136 g. In contrast to conventional bread, freshly baked ERO bread does not have a dry and crisp crust. Previous studies showed the exterior layer (5−10 mm) of ERO bread to have a moisture content of approximately 47%,[9] whereas the moisture content of the crust in a conventional bread is <15% (Figure 5). As a result, water redistribution in ERO breads was less pronounced, as shown in Figure 5.

Amylopectin Retrogradation during Storage of Bread. Retrogradation of amylopectin was monitored by DSC analysis of crumb samples. Recrystallized amylopectin melted between 40 and 65 °C (peak temperatures around 50 °C). Figure 6 shows the increase in enthalpy of recrystallized amylopectin melting in crumb during storage of conventional and ERO baked breads. For both samples, very low enthalpy values were

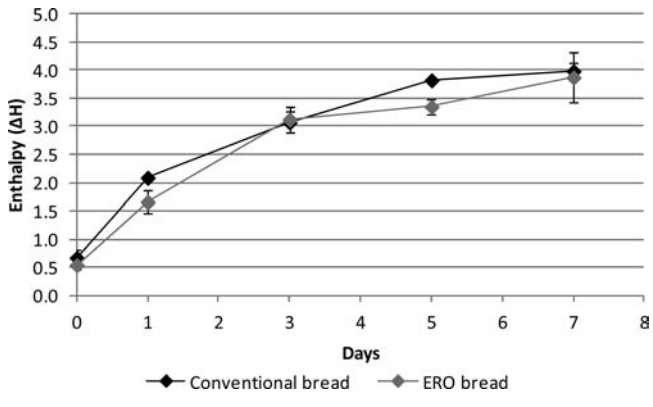

Figure 6. Melting enthalpy of retrograded amylopectin of crumb of conventional and ERO breads, measured by differential scanning calorimetry (DSC) and plotted as a function of bread storage time.

dx.doi.org/10.1021/jf501856s | J. Agric. Food Chem. 2014, 62, 6445−6453

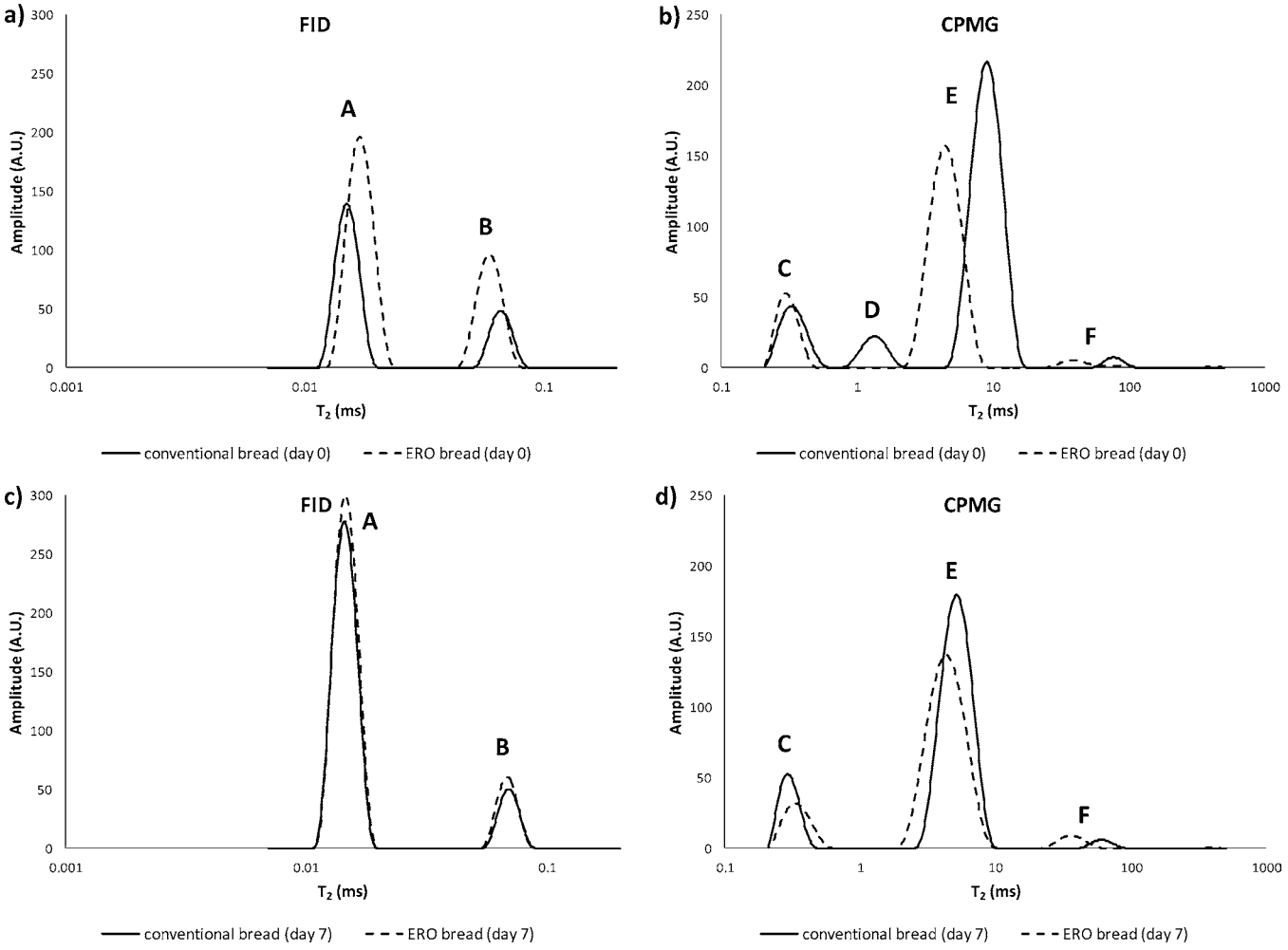

Figure 7. Distribution of transverse relaxation times of protons in the crumbs of ERO and conventionally baked bread on days 0 (a, b) and 7 (c, d), obtained by the inverse Laplace transformation of the free induction decay (FID) (a, c) and Carr−Purcell−Meiboom−Gill (CPMG) pulse sequence (b, d). Amplitudes are given in arbitrary units (A.U.).

obtained on day 0. This observation is in line with previous studies showing a very small endotherm corresponding to melting of retrograded amylopectin a few hours after baking.[22−24] During further bread storage, no significant changes were observed between melting enthalpies for ERO and conventional breads. The levels of recrystallized amylopectin increased in a very similar way in both the conventional and ERO breads (Figure 6).

Changes in Molecular Water Mobility of Bread during Storage. Water migration in conventional and ERO bread was studied using low-resolution ^{1}H NMR spectrometry. Conventionally and ERO baked breads were stored during 7 days in hermetically sealed plastic bags at room temperature. ^{1}H NMR measurements on bread crumb were carried out at different points in time. The large differences in moisture content of conventional bread crumb and crust cause water to migrate from the crumb to the crust. Next to crumb-to-crust water migration, redistribution of water also occurs in bread crumb. This may include incorporation of water in starch crystals.[12]

(a) ^{1}H NMR Analysis of Fresh ERO and Conventional Bread Crumb. Figure 7 compares the distribution of the transverse relaxation time curves of the crumb of ERO and conventional bread. In fresh conventional bread crumb, two FID proton populations (A and B) could be distinguished. Protons in FID population A were assigned to rigid nonexchanging CH protons of starch, that is, those of amylopectin crystals and densely packed amorphous starch not in contact with water, and rigid protons of gluten.[16] The protons in population B have been suggested to correspond to protons of a more mobile amorphous starch fraction in interaction with water.[16] Much as for conventional breads, two FID proton populations could be differentiated for ERO breads. However, the areas of proton populations A and B of ERO bread crumb were initially higher than those of the conventionally baked breads, suggesting lower proton mobility. The moisture content of ERO bread crumb was generally lower than that of crumb from conventional bread. This presumably explains the increase in FID proton populations A and B and hence the lower mobility of the protons in the ERO bread crumb at day 0. This higher initial area could not have resulted from amylopectin retrogradation because on day 0 hardly any amylopectin retrogradation had occurred and the levels of retrograded amylopectin were similar in both conventional and ERO bread crumb (Figure 6). Also, the observed higher initial value of FID population A in the crumb from ERO bread could not be ascribed to incomplete starch gelatinization because its starch had been completely gelatinized.

dx.doi.org/10.1021/jf501856s | J. Agric. Food Chem. 2014, 62, 6445−6453

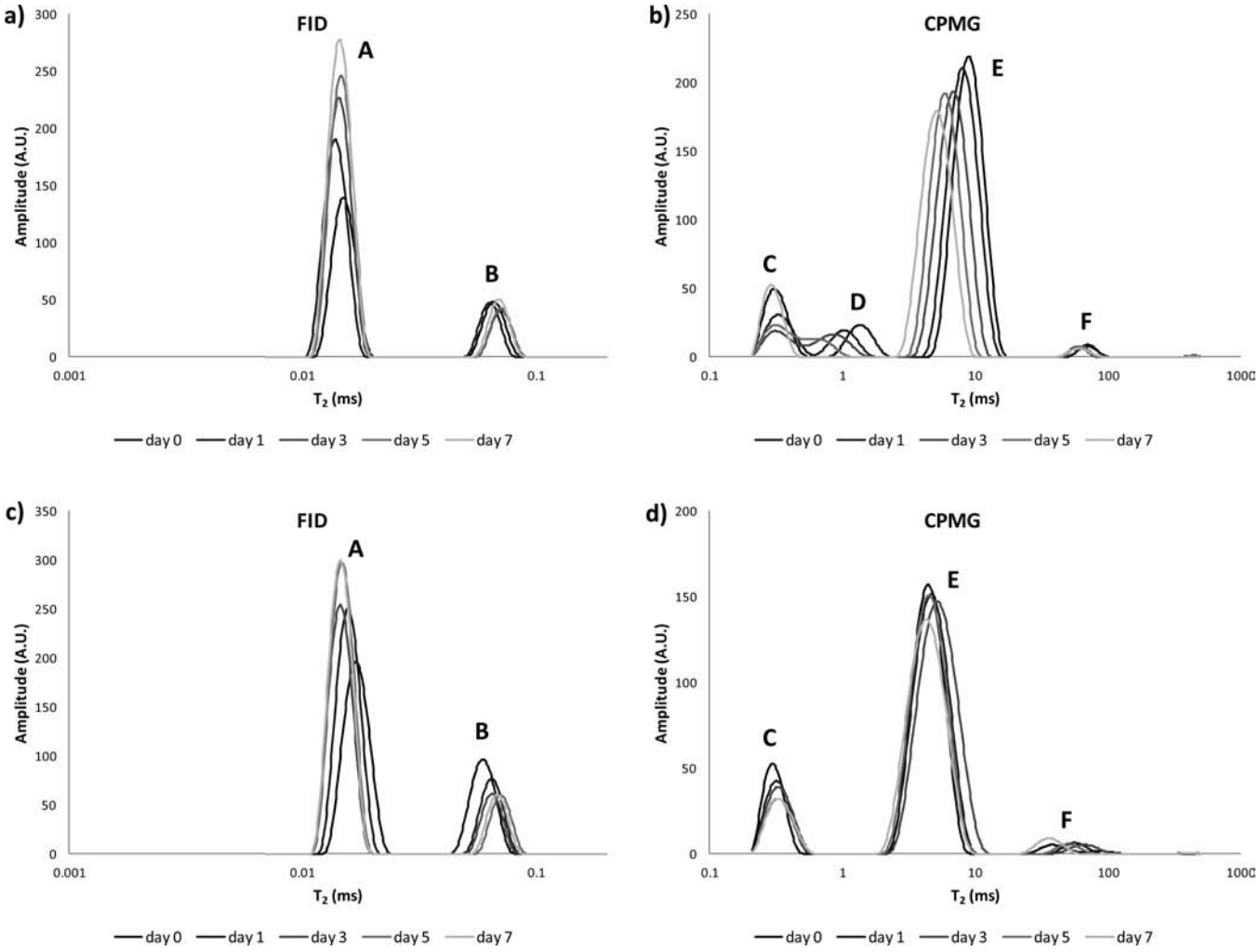

Figure 8. Distribution of transverse relaxation times of crumb from conventionally (a, b) and ERO baked bread (c, d) during storage for 7 days, obtained by the inverse Laplace transformation of the free induction decay (FID) and Carr−Purcell−Meiboom−Gill (CPMG) pulse sequence. Amplitudes are given in arbitrary units (A.U.).

The CPMG measurements of crumb from conventionally baked fresh bread showed four different proton populations (C, D, E, and F). Bosmans et al.[16] suggested that the protons in CPMG population C correspond to those in FID proton population B, because this population is affected in a similar way by heat treatment. Proton population D has been suggested to contain protons such as those of confined water exchanging with starch hydroxyl protons in the intragranular space.[16] Besides proton populations C and D, a very large CPMG proton population E was observed. Its protons are presumably mobile water protons in exchange with starch hydroxyl protons in the extragranular space.[16] In contrast to what was observed in CPMG measurements of conventional bread, in the crumb of ERO breads only three (instead of four) distinct proton populations (C, E, and F) were distinguished. Possibly, protons from proton population D shifted to proton population C or had merged with protons of population E. Furthermore, the proton populations (E in particular) of ERO bread crumb appeared at lower T_2 values than those of crumb from conventional bread. The lower mobility of this proton fraction is probably due to lower moisture content. In general, the observed differences between ERO and conventional bread crumb were presumably mainly due to the lower moisture content of the crumb of ERO breads on day 0 and, associated with this, an overall decrease in proton mobility.

(b) Changes in Water Mobility of Bread Crumb during Storage of Conventional Breads. Figure 8 (a, b) shows the distributions of the transverse relaxation times of protons of crumb from conventional bread during storage for 7 days. These were obtained by inverse Laplace transformation of the FID and CPMG pulse sequences. During storage of conventional bread, the area of FID proton population A increased due to both amylopectin crystallization and loss of water from crumb to crust. Additional experiments in which moisture migration from crumb to crust was prevented by storage of crumb rather than bread itself showed that this increase occurred to a lesser extent in the former case (results not shown). These observations suggest that both amylopectin crystallization and loss of water from crumb to crust reduce mobility in the bread matrix, as suggested earlier by Curti et al.[15] The area of FID population B did not change during storage of bread (thus allowing moisture migration from crumb to crust) (Figure 8a), whereas it decreased during storage of bread crumb as such (results not shown). Possibly, when both amylopectin retrogradation and moisture migration from crumb to crust occur, the decrease in the area of FID proton population B is compensated by an increase due to decreased

dx.doi.org/10.1021/jf501856s | J. Agric. Food Chem. 2014, 62, 6445−6453

proton mobility as bread crumb loses moisture. The decrease in area of FID proton population B is partly caused by amylopectin retrogradation. It seems likely that the amorphous amylopectin CH protons of population B become incorporated into crystal structures and lose mobility, and consequently part of this population appears in proton population A. This has also been observed by Bosmans et al.[12]

As a result of storage of bread, the areas of both CPMG proton populations C and D decreased. After 3 days of storage of conventional bread, its proton populations C and D had merged (Figure 8b). This was also noted after 5 days when crumb rather than bread had been stored (results not shown). Thus, both moisture migration from crumb to crust and other changes in the crumb (including starch retrogradation) contribute to the decrease in proton mobility.

Probably, the decrease in crumb moisture content also contributes to these changes in proton mobility. The simultaneous decrease in the areas of both FID proton population B and CPMG proton population C as a result of bread storage is in line with earlier suggestions that FID proton population B and CPMG proton population C correspond to the same proton population.[16] Besides proton populations C and D, also a large CPMG proton population E was observed. These protons are suggested to correspond to mobile water protons in exchange with starch hydroxyl protons in the extragranular space.[16] When moisture migration from crumb to crust was allowed to occur, the area of proton population E gradually decreased and shifted to lower T_2 values during further storage. The area of proton population E hardly changed during storage of bread crumb from which the crust had been detached (results not shown). Only a small decrease in T_2 was noted in samples stored for 5 and 7 days. The migration of water molecules from crumb to crust over time explained the decrease in the area of proton population E such as observed in Figure 8b. Also, proton population E shifted to lower T_2 values, indicating reduced mobility. Lastly, a small proton population (F) was observed at high T_2. This population presumably corresponded to protons of shortening used to grease mixing bowls, sheeter, and baking pans during breadmaking, as lipid protons usually appear at higher T_2 values.[16,25]

(c) Changes in Water Mobility of Bread Crumb during Storage of ERO Breads. Figure 8 (c, d) shows the distribution of the transverse relaxation times of ERO baked breads stored during 7 days. These were obtained by inverse Laplace transformation of FID and CPMG pulse sequences. The relative intensities of FID proton populations A and B increased and decreased, respectively, during storage for 7 days. Protons in FID population A were assigned to rigid CH protons of starch and gluten, whereas those in population B have been suggested to correspond to protons of a more mobile amorphous starch fraction in interaction with water.[16] The area of FID proton population A increased by almost 60% during storage of ERO breads. This increase is associated with amylopectin retrogradation.[16] As noted above, amylopectin retrograded to similar extents in both ERO and conventional breads during storage (Figure 6). Figure 7 (c, d) compares the transverse relaxation curves of ERO and conventional breads on day 7. The FID profiles of ERO or conventional bread that had been stored for 7 days were very similar. This may well be due to the comparable moisture contents of ERO and conventional breads on day 7 (Figure 5).

With CPMG measurements, three different proton populations (C, E, and F) were observed in ERO bread. As a result of storage, similar to what was observed for FID proton population B, the area of proton population C decreased. The area of proton population E was hardly affected by storage. In general, the CPMG profiles of ERO and conventional bread were more comparable on day 7 than on day 0 (Figure 7). These observations emphasize again the importance of bread moisture content and moisture migration.

In conclusion, this study compared the starch populations and moisture contents of bread baked in a conventional oven with those of bread baked in an ERO. ERO allows imposing specific temperature/time profiles during baking as well as only small temperature gradients in the different parts of the dough/bread during baking and produces crustless bread. ERO breads generally had a lower moisture content than conventional breads (39 vs 43%). The upper parts of ERO breads had a higher moisture content than the lower parts, whereas, in conventional bread, the moisture content increases from crust to crumb.

Over time, the moisture contents in the different parts of bread change more in conventional than in ERO breads. That of conventional bread decreases throughout the crumb and, concomitantly, the crust moisture content rapidly increases. Due to the absence of crust in ERO bread, the moisture content did not significantly decrease throughout the crumb. Large differences in moisture migration during storage of ERO and conventional breads were not reflected in differences in the retrogradation of amylopectin.

Finally, the use of proton NMR measurements to compare the water mobility in both conventional and ERO bread revealed a lower proton mobility in ERO than in conventional bread.

In conclusion, ERO baking technology allows the study of temperature-dependent transitions during baking. It is also a powerful tool to straightforwardly change the heating rate of dough/bread in a controlled way and to interrupt the baking process at specific and uniform temperatures.

AUTHOR INFORMATION

Corresponding Author

*(L.J.D.) E-mail: liesbeth.derde@biw.kuleuven.be. Phone: +32 16 32 16 34. Fax: +32 16 32 19 97.

Funding

This research was conducted within the framework of research project G.0427.07 financed by the Fund for Scientific Research, Brussels, Belgium. It is also a part of the Flemish government Methusalem project "Food for the Future" at KU Leuven. J.A.D. is the W. K. Kellogg Chair in Cereal Science and Nutrition at KU Leuven.

Notes

The authors declare no competing financial interest.

ACKNOWLEDGMENTS

We thank Dr. Geertrui Bosmans for fruitful discussions.

REFERENCES

(1) Hoseney, R. C. Component interaction during heating and storage of baked products. In *Chemistry and Physics of Baking*; Blanshard, J. M. V., Frazier, P. J., Galliard, T., Eds.; Royal Society of Chemistry: London, UK, 1986; pp 216–226.

(2) Baker, J. C. A method and apparatus for testing doughs. *Cereal Chem.* **1939**, *16*, 513–517.

(3) Hayman, D.; Hoseney, R. C.; Faubion, J. M. Effect of pressure (crust formation) on bread crumb grain development. *Cereal Chem.* **1998**, *75*, 581−584.
(4) He, H.; Hoseney, R. C. Gas retention in bread dough during baking. *Cereal Chem.* **1991**, *68*, 521−525.
(5) He, H.; Hoseney, R. C. Differences in gas retention, protein solubility and rheological properties between flours of different baking quality. *Cereal Chem.* **1991**, *68*, 526−530.
(6) Junge, R. C.; Hoseney, R. C. A mechanism by which shortening and certain surfactants improve loaf volume in bread. *Cereal Chem.* **1981**, *58*, 408−412.
(7) Baker, J. C.; Mize, M. D. Effect of temperature on dough properties, I. *Cereal Chem.* **1939**, *16*, 517−533.
(8) He, H.; Hoseney, R. C. A critical look at the electric resistance oven. *Cereal Chem.* **1991**, *68*, 151−155.
(9) Martin, M. L.; Zeleznak, K. J.; Hoseney, R. C. A mechanism of bread firming. 1. Role of starch swelling. *Cereal Chem.* **1991**, *68*, 498−503.
(10) Finney, K. F. An optimized, straight dough bread making method after 44 years. *Cereal Chem.* **1984**, *61*, 20−27.
(11) AACC International. *Approved Methods of Analysis*, 11th ed.; Method 44-15.02. Moisture − air-oven methods. Approved Nov 3, 1999; AACC International: St. Paul, MN, USA, 2012; DOI: 10.1094/AACCIntMethod-44-15.02.
(12) Bosmans, G. M.; Lagrain, B.; Ooms, N.; Fierens, E.; Delcour, J. A. Biopolymer interactions, water dynamics and bread crumb firming. *J. Agric. Food Chem.* **2013**, *61*, 4646−4654.
(13) Ruan, R. R.; Wang, X.; Chen, P. L.; Fulcher, R. G.; Pesheck, P.; Chakrabarti, S. Study of water in dough using nuclear magnetic resonance. *Cereal Chem.* **1999**, *76*, 231−235.
(14) Chen, P. L.; Long, Z.; Ruan, R.; Labuza, T. P. Nuclear magnetic resonance studies of water mobility in bread during storage. *LWT−Food Sci. Technol.* **1997**, *30*, 178−183.
(15) Curti, E.; Bubici, S.; Carini, E.; Baroni, S.; Vittadini, E. Water molecular dynamics during bread staling by nuclear magnetic resonance. *LWT−Food Sci. Technol.* **2011**, *44*, 854−859.
(16) Bosmans, G. M.; Lagrain, B.; Deleu, L. J.; Fierens, E.; Hills, B. P.; Delcour, J. A. Assignments of proton populations in dough and bread using NMR relaxometry of starch, gluten, and flour model systems. *J. Agric. Food Chem.* **2012**, *60*, 5461−5470.
(17) Provencher, S. W. Contin − a general-purpose constrained regularization program for inverting noisy linear algebraic and integral-equations. *Comput. Phys. Commun.* **1982**, *27*, 229−242.
(18) Engelsen, S. B.; Jensen, M. K.; Pedersen, H. T.; Norgaard, L.; Munck, L. NMR-baking and multivariate prediction of instrumental texture parameters in bread. *J. Cereal Sci.* **2001**, *33*, 59−69.
(19) Delcour, J. A.; Hoseney, R. C. *Principles of Cereal Science and Technology*, 3rd ed.; AACC International Press: St. Paul, MN, USA, 2010.
(20) Eliasson, A. C.; Larsson, K. *Cereals in Breadmaking: A Molecular Colloidal Approach*; Dekker: New York, 1993.
(21) Vanin, F. M.; Lucas, T.; Trystram, G. Crust formation and its role during bread baking. *Trends Food Sci. Technol.* **2009**, *20*, 333−343.
(22) Krog, N.; Olesen, S. K.; Toernaes, H.; Joensson, T. Retrogradation of the starch fraction in wheat bread. *Cereal Foods World* **1989**, *34*, 281−285.
(23) Léon, A.; Durán, E.; de Barber, C. B. A new approach to study starch changes occurring in the dough-baking process and during bread storage. *Z. Lebensm. Unters. Forsch. A* **1997**, *204*, 316−320.
(24) Inagaki, T.; Seib, P. A. Firming of bread crumb with cross-linked waxy barley starch substituted for wheat starch. *Cereal Chem.* **1992**, *69*, 321−325.
(25) Assifaoui, A.; Champion, D.; Chiotelli, E.; Verel, A. Characterization of water mobility in biscuit dough using a low-field ^{1}H- NMR technique. *Carbohydr. Polym.* **2006**, *64*, 197−204.

However, whether H_2 plays a specific role in the modulation of UV-A-induced anthocyanin accumulation is largely unknown, and the molecular mechanisms underlying interactions between UV and H_2 signaling remain to be elucidated in anthocyanin regulation. In this paper, we report that hydrogen-rich water (HRW) reestablishes reactive oxygen species homeostasis but exerts differential effects on anthocyanin synthesis in two contrasting varieties of radish sprouts under UV-A irradiation.

MATERIALS AND METHODS

Plant Materials and Growth Conditions. Seeds of two contrasting radish (*Raphanus sativus* L.), i.e., cv. Qingtou (low level of anthocyanin, LA) and cv. Yanghua (high level of anthocyanin, HA), were soaked in either distilled water or hydrogen-rich water (HRW) for 12 h and then germinated for 1 d at 25 °C in darkness. Uniform gemmiparous seeds were then chosen and transferred to plastic chambers and cultured in nutrient medium (quarter-strength Hoagland's solution) prepared with HRW or distilled water. Four treatments with 3 replicates each were established, i.e., white light (W + Con), white light plus HRW (W + HRW), UV-A (UVA + Con), and UV-A plus HRW (UVA + HRW), respectively. The nutrient medium was replaced every 12 h. Radish sprouts were grown in the incubator at 25 °C in the dark for 2 d, and then transferred to a white or UV-A illuminating incubator (Ningbo Haishu Safe Instrument Experimental Factory, Zhejiang, China) at 25 °C for 24 h. The light intensity of white light was set at 50 ± 5 $\mu mol \cdot m^{-2} \cdot s^{-1}$, while the UV-A dose was set at 5.5 $W \cdot m^{-2}$ measured with a pocket UV light meter (UV-340A, Lutron, Taiwan).

Preparation of HRW. Purified hydrogen gas (99.99%, v/v) generated from a hydrogen gas generator (SHC-300; Saikesaisi Hydrogen Energy Co., Ltd., Shandong, China) was bubbled into 4000 mL of distilled water (pH 5.87, 25 °C) at a rate of 150 $mL \cdot min^{-1}$ for 1 h, a sufficient duration to saturate the solution with H_2 (about 0.22 mM).[28,30] Then, the corresponding HRW (pH 6.32, 25 °C) was immediately diluted to the required concentrations [1, 10, and 100% concentration (v/v)]. In our experimental conditions, the H_2 concentration in freshly prepared HRW analyzed by gas chromatography (GC) was 0.22 mM, which was defined as 100% HRW. The H_2 concentrations were about 22 μM in 10% HRW, 2.2 μM in 1% HRW, and maintained at a relatively constant level in 25 °C for at least 12 h.

Observation of the Hypocotyl Cross Section. The hypocotyls of radish sprouts were transected with a blade, then observed under a light microscope (model Stemi 2000-C; Carl Zeiss, Germany), and photographed on color film (Powershot A620, Canon Photo Film, Japan).

Determination of Thiobarbituric Acid Reactive Substances (TBARS). Lipid peroxidation was estimated by measuring the amount of TBARS as previously described.[31] About 500 mg of fresh tissues was ground in 0.25% 2-thiobarbituric acid (TBA) in 10% trichloroacetic acid (TCA) using a mortar and pestle. After heating at 95 °C for 30 min, the mixture was quickly cooled in an ice bath and centrifuged at 10000*g* for 10 min. The absorbance of the supernatant was read at 532 nm and corrected for unspecific turbidity by subtracting the absorbance at 600 nm. The blank was 0.25% TBA in 10% TCA. The concentration of lipid peroxides, together with oxidatively modified proteins of plants, was thus quantified in terms of TBARS amount using an extinction coefficient of 155 mM^{-1} $cm^{-1}$and expressed as nmol g^{-1} fresh weight (FW).

Antioxidant Enzyme Assays. The activity of antioxidant enzymes was determined as described by Jin et al. (2013).[28] Frozen radish plants (approximately 200 mg) were homogenized in 5 mL of 50 mM potassium phosphate buffer (pH 7.0) containing 1% polyvinylpyrrolidone for superoxide dismutase (SOD), peroxidase (APX), and catalase (CAT) assay. The homogenate was centrifuged at 12000*g* for 20 min at 4 °C, and the supernatant was used as the crude enzyme extract. Total SOD activity was measured on the basis of its ability to reduce nitroblue tetrazolium (NBT) by superoxide anion generated by the riboflavin system under illumination. One unit of SOD was defined as the amount of crude enzyme extract required to inhibit the reduction rate of NBT by 50%. APX activity was measured by monitoring the decrease in absorbance at 290 nm as ascorbic acid (AsA) was oxidized for at least 1 min in 3 mL of reaction mixture. CAT activity was spectrophotometrically measured by monitoring the consumption of hydrogen peroxide (H_2O_2) at 240 nm for at least 3 min.

Real-Time RT-PCR Analysis. Total RNA was isolated from 100 mg (fresh weight) of excised radish hypocotyls by grinding with mortar and pestle in liquid nitrogen until a fine powder appeared and using TRIzol reagent (Invitrogen, Gaithersburg, MD) according to the manufacturer's instructions. DNA-free total RNA (5 μg) from different treatments was used for first-strand cDNA synthesis in a 20 μL reaction volume containing 1 μL of RevertAid M-MuLV reverse transcriptase (Thermo Fisher Scientific Inc., USA) and 1 μL of oligo $(dT)_{18}$ primer. Real-time quantification RT-PCR reactions were performed using a Mastercycler ep *realplex* real-time PCR system (Eppendorf, Hamburg, Germany) with Bestar SybrGreen qPCR Mastermix (DBI, Bioscience Inc., Germany) according to the manufacturer's instructions. The cDNA was amplified using the primers as described as Table S1 in the Supporting Information.

Histochemical Staining. Stress-induced generation of O_2^- in situ was detected by nitroblue tetrazolium (NBT) staining.[32] Seedling leaves were stained with 0.1% solution of NBT in K-phosphate buffer (pH 6.4), containing 10 mM sodium azide (NaN_3) until a purple-blue color became visible, and the chlorophyll of the treated leaves was removed with 95% ethanol. Hydrogen peroxide (H_2O_2) production was detected by 3,3′-diaminobenzidine (DAB) staining.[27] Leaves were stained with 0.1% DAB solution for 6 h, and then chlorophyll was removed with 95% ethanol. After washing extensively, all the decolorized leaves were observed under a light microscope (model Stemi 2000-C; Carl Zeiss, Jena, Germany) and photographed on a color film (Powershot A620; Canon Photo Film, Tokyo, Japan).

Extraction and Assay of Anthocyanins, Total Phenolic, and DPPH Radical Scavenging Activity Assay. Anthocyanin measurement was performed according to the method reported by Zhou et al. (2013)[33] with some modifications. Briefly, 0.5 g samples were cut up and incubated in 10 mL of 1% HCl in methanol at room temperature in the dark for 24 h. Tubes were shaken with a vortex mixer every 6 h. The anthocyanins in the aqueous phase were then quantified by spectrophotometry ($A_{530}-A_{600}$) (UV-5200 spectrophotometer, Shanghai Metash Instruments Co., Ltd., Shanghai, China), and one unit (U) of anthocyanin was defined as the amount of 0.01 difference value. In the end, the quantity was normalized to the total fresh mass of tissue used for each sample.

Determination of total phenols was performed according to the method reported by George et al. (2005)[34] with some modifications. Samples (~0.5 g) were homogenized in 50% (w/v) acetone and shaken in ultrasonic wave cleaner for 30 min, and then centrifuged at 4000*g* for 20 min at 4 °C. One milliliter of extract was added to 2 mL of Folin−Ciocalteu reagent. The mixture was incubated for 2 min at room temperature, and 10 mL of 10% sodium carbonate was added. The mixture was incubated for 1 h at 50 °C and finally cooled in a water−ice bath. The specific absorbance at 765 nm was immediately measured.

The DPPH radical scavenging activity assay was performed according to the method reported by Chen et al. (2013).[35] Briefly, standard solutions or DMSO (control) was prepared and added to a 70 μmol/L DPPH methanolic solution; the mixtures were shaken vigorously and left to stand in the dark for 30 min at room temperature, and then absorbance was read at 517 nm. Radical scavenging capacity was expressed as percentage effect (%) and calculated using the following equation:

$$\text{percentage effect (\%)} = \left(\frac{\text{Abs}_{\text{control}} - \text{Abs}_{\text{sample}}}{\text{Abs}_{\text{control}}}\right) \times 100$$

Identification and Quantification of Anthocyanidins. *Sample Preparation.* Fresh samples (1.0 g) were homogenized in 3 mL of 70% (w/v) ethanol containing 1% methanoic acid. The mixtures were

dx.doi.org/10.1021/jf5019593 | J. Agric. Food Chem. 2014, 62, 6454−6462

shaken in ultrasonic wave cleaner for 10 min and then centrifuged at 6000*g* for 20 min, and finally 2 mL of supernate was taken out. The residue was combined with 1 mL of 70% ethanol and then shaken and centrifuged as done above. Another 2 mL of supernate was taken out and merged with the supernate above. Daidzein standard samples (20 μL, 25 μM) were added into the extract and used as internal standard. After mixture and centrifugation, 5 μL was taken out for injection. The relative abundance of anthocyanidins was estimated as the ratios of peak areas of samples to peak areas of Daidzein standard samples.

LC-MS/MS Analysis. The anthocyanidins were detected by a UHPLC system (Dionex, Thermo, USA) connected to a LTQ-Orbitrap XLhybrid mass spectrometer (Thermo Fisher Scientific). The instrument was controlled through Tune 2.6.0 and Chromeleon programs. The UHPLC column was Hypersil GOLD C18 (100 mm × 2.10 mm, 3 μm particle size, Thermo Fisher Scientific). Solvent A was 0.1% formic acid in water, B was 0.1% formic acid in acetonitrile, and separation was carried out in 30 min at a flow rate of 0.2 mL/min under the following conditions: 0−4 min, 5% B; 4−21 min, 5−95% B; 21−25 min, 95% B; 25.2−30 min, 5% B. Column oven temperature was set at 35 °C, and autosampler temperature was set at 10 °C. The capillary temperature was 300 °C, and the source voltage was set at 4 kV. Accurate mass spectra were recorded from 150 to 1200 m/z. The external mass calibration of the Orbitrap was performed once a week to ensure a working mass accuracy <5 ppm. Data dependent scan mode was applied for MS/MS fragmentation. Ion source was equipped with a heated electrospray ionization (HESI) source. The product ions were generated by the LTQ ion trap at normalized collision energy of 35%, q-activation of 0.25 using an isolation width of 2 Da. Data was processed using the Xcalibur software.

Statistical Analyses. Values presented are means ± standard deviation (SD) of three replicates. Data were subjected to analysis of variance (ANOVA), and mean values were compared by Duncan's multiple range test ($p < 0.05$). All the statistical analysis was performed using SPSS 19.0 for Windows.

RESULTS

UV-A Induced Inhibition of Hypocotyl Elongation and Increase of Anthocyanin Accumulation. The inhibition of hypocotyl elongation and accumulation of anthocyanin are two widely characterized phenotypic parameters in UV photomorphogenic responses of seedlings.[36] To assess the stress caused by exposure to UV-A, the hypocotyl elongation and anthocyanin content of radish sprouts at 0, 3, 6, 12, and 24 h were determined after exposure to UV-A (Figure 1). As shown in Figure 1B, the hypocotyl elongation of LA sprouts was generally longer than that of HA sprouts. In addition, compared with that under white light, the inhibition of hypocotyl elongation by exposure to UV-A for 3, 6, 12, and 24 h was in a time course dependent manner in the two radish varieties tested, exhibiting a 30% inhibition at 24 h. As expected, the anthocyanin content in the hypocotyls of HA was very high, about 40−60 U·g^{-1} FW, compared to 2 U·g^{-1} FW in LA. Higher anthocyanin accumulation in hypocotyls was observed under UV-A compared with white light in the two varieties at 24 h (Figure 1A,C). Above all, we performed the following experiments by exposing sprouts to white light or UV-A for 24 h.

HRW Alleviated UV-A-Induced Oxidative Damage and Increased Antioxidant Enzyme Activity. To investigate whether UV-A-mediated phenotypic parameters are influenced by HRW, HA sprouts were grown in the presence of various concentrations of HRW (1, 10, 50, and 100%). The results showed that treatments with different concentrations of HRW (10, 50, and 100%) increased anthocyanin contents, especially 100% of HRW (by 25%). However, the hypocotyl elongation was not dose-dependently influenced by HRW (see Figure S1 in the Supporting Information). Based on these, we chose 100% HRW as the following experimental concentration.

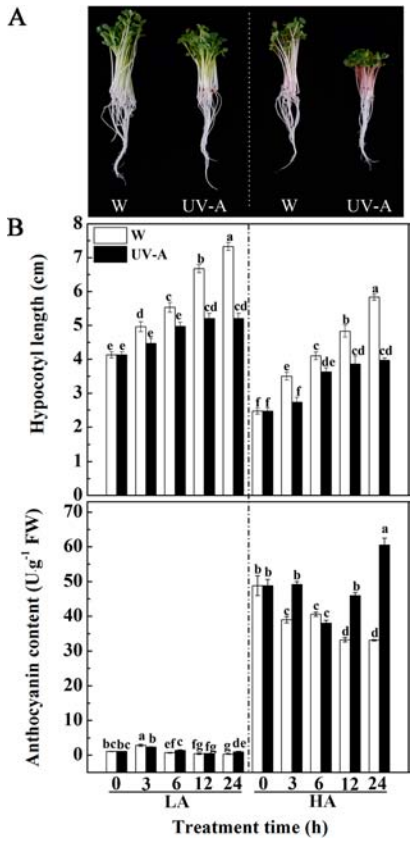

Figure 1. Effects of 24 h UV-A treatment on the morphology of radish sprouts (A), bar = 2 cm. Changes in hypocotyls elongation (B) and anthocyanin content (C) in the hypocotyls of two radish (*Raphanus sativus* L.) varieties' (LA and HA) sprouts upon UV-A stress. Seedlings were incubated under UV-A, and hypocotyl elongation and anthocyanin content were measured after 0 h, 3 h, 6 h, 12 h, and 24 h incubation. Values are the means ± standard error of three independent experiments with at least three replicates for each. Measurements in the same column followed by different letters are significantly different at the $P < 0.05$ level.

Abiotic stress-induced ROS has been demonstrated to cause oxidative damage to plants, and O_2^- and H_2O_2 are believed to be the most important components.[37] Figure 2 showed that leaves of radish sprouts under white light produced low production of O_2^- (NBT staining) and H_2O_2 (DAB staining), while those under UV-A were stained extensively. Compared to UV-A, fewer stains were observed in the leaves under UV-A + HRW treatment. To confirm the cytoprotective role of HRW in UV-A-induced oxidative stress in radish sprouts, we measured the content of TBARS, which was used as an indicator for lipid peroxidation in vitro. Interestingly, exposure to UV-A for 24 h failed to increase the TBARS content in the hypocotyls of LA sprouts; HRW had no effect either. But in HA sprouts, exposure to UV-A for 24 h caused an increase in levels of TBARS, while HRW significantly blocked this increase (Figure 3A).

To further assess whether there is a close link between oxidative stress and HRW-induced alleviation of UV-A stress, changes in several antioxidant enzyme activities in the hypocotyls in radish sprouts were compared. The activities of SOD and APX were increased under UV-A, especially APX

dx.doi.org/10.1021/jf5019593 | J. Agric. Food Chem. 2014, 62, 6454−6462

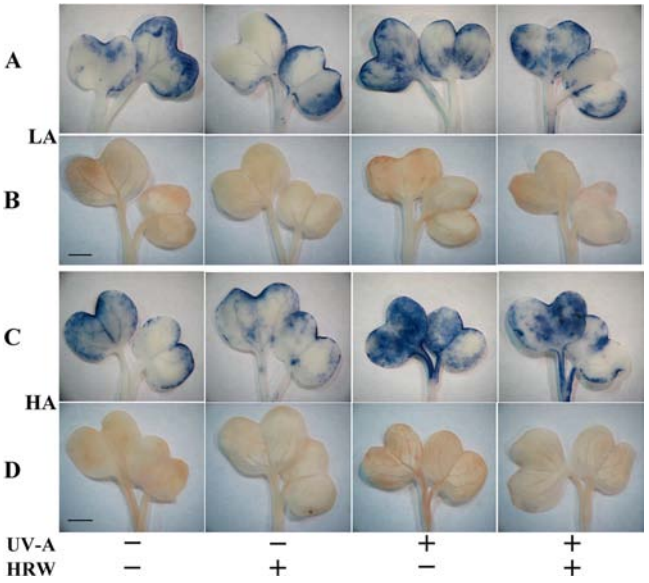

Figure 2. Effects of HRW on the ROS homeostasis in the leaves of radish sprouts. To detect O_2^- and H_2O_2, leaves of LA sprouts were stained with NBT (A) and DAB (B); leaves of HA sprouts were also stained with NBT (C) and DAB (D), respectively. Sprouts cultivated in distilled water (H_2O) or 100% HRW were exposed to white light or UV-A for 24 h. Bar = 1 cm.

(nearly 3-fold higher than that under white light). With the exception of APX in HA, this UV-A-induced increase was apparently enhanced by HRW (Figure 3B,D). However, no consistent changes in the activity of POD were observed (Figure 3C).

HRW Enhanced the UV-A-Induced Total Phenols and Anthocyanin Accumulation in HA. Besides the antioxidant enzymes, nonenzymic components are also involved in antioxidant responses. To investigate whether HRW influences the phenolic biosynthesis, the phenols content and DPPH scavenging effect were determined. As shown in Figure 4,

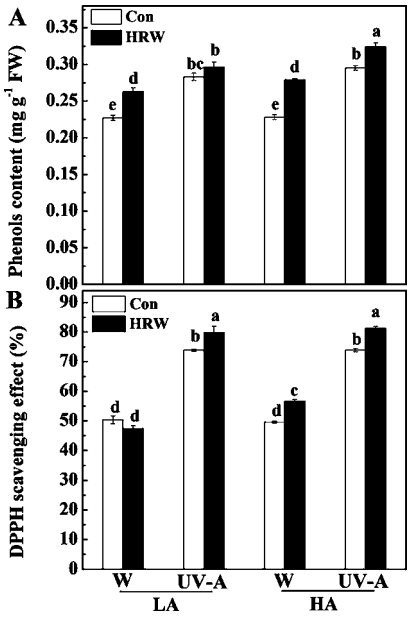

Figure 4. Total phenols content (A) and DPPH scavenging effect (%) (B) in the hypocotyls of radish sprouts. Sprouts cultivated in distilled water (H_2O) or 100% HRW were exposed to white light or UV-A for 24 h. Error bars represent SD with three repeats performed. For each repeat, more than 30 sprouts were analyzed. Measurements in the same column followed by different letters are significantly different at the $P < 0.05$ level.

exposure to UV-A for 24 h significantly increased the phenolics content and DPPH scavenging effect in both varieties tested. HRW treatment further enhanced them, though no significant difference was observed in LA sprouts (Figure 4A). Consistent

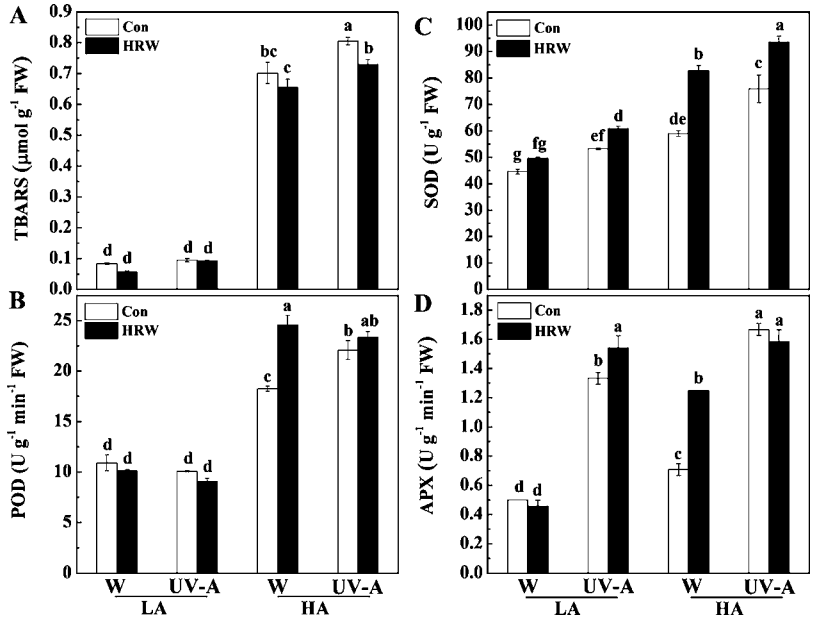

Figure 3. Lipid peroxidation, measured as TBARS content (A), SOD (B), POD (C), and APX (D) activities in the hypocotyls of LA and HA sprouts. Sprouts cultivated in distilled water (H_2O) or 100% HRW were exposed to white light or UV-A for 24 h. Error bars represent SD with three repeats performed. For each repeat, more than 30 sprouts were analyzed. Measurements in the same column followed by different letters are significantly different at the $P < 0.05$ level.

dx.doi.org/10.1021/jf5019593 | J. Agric. Food Chem. 2014, 62, 6454−6462

with this finding, HRW also significantly enhanced UV-A-induced increase of DPPH scavenging effect (Figure 4B).

Results of Figure 5 showed that the anthocyanin content in the hypocotyls of HA sprouts treated with HRW was increased

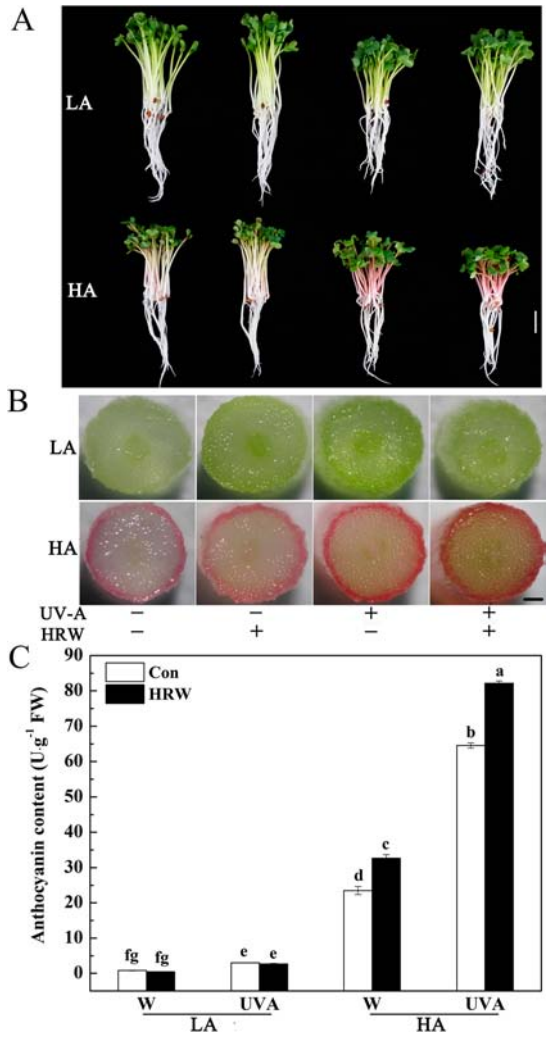

Figure 5. Phenotypes (A) and the transection (B) and anthocyanin accumulation (C) of the hypocotyls of two radish sprouts. Sprouts cultivated in distilled water (H_2O) or 100% HRW were exposed to white light or UV-A for 24 h. Error bars represent SD with three repeats performed. For each repeat, more than 30 sprouts were analyzed. Bar in A was 2 cm, in B was 0.3 mm. Measurements in the same column followed by different letters are significantly different at the $P < 0.05$ level.

significantly (by about 25%) compared with the control, but no changes of anthocyanin accumulation existed in LA sprouts (Figure 5C). These results were in accordance with the observation of the transection of the radish hypocotyls (Figure 5B). In addition, anthocyanin accumulation was observed mainly in the epidermis of hypocotyls of HA sprouts (Figure 5B).

HRW Increased the Main Anthocyanidin (Cyanidin) Content in HA. There are mainly six anthocyanidins, namely, cyanidin (Cy), delphinidin (Dp), pelargonidin (Pg), peonidin (Pn), petunidin (Pt), and malvidin (Mv) in plants.[5] To understand which anthocyanidin was predominant in radish sprouts and if this anthocyanidin was influenced by HRW, we detected the anthocyanidins in LA and HA sprouts using LC-MS. Five kinds of anthocyanidins were identified in HA sprouts, while only two were detected in LA sprouts with cyanidin (Cy) being the main anthocyanin monomer in radish sprouts. As expected, the Cy content in HA sprouts was above 10-fold higher than that in LA sprouts. Additionally, HRW treatment had neither effect on Cy content in the hypocotyls of LA sprouts exposed to both white light and UV-A, nor in HA sprouts exposed to white light, but significantly enhanced the Cy accumulation in the hypocotyls of HA sprouts exposed to UV-A for 24 h (Table 1).

HRW Upregulated the Expression Levels of Anthocyanin Biosynthesis-Related Genes. The findings obtained prompted further investigation into the mechanism of the increase of anthocyanin induced by HRW. To examine whether anthocyanin biosynthesis-related genes were influenced by H_2, quantitative real-time PCR analyses were performed on the hypocotyls of radish sprouts (Figures 6 and 7). As shown in Figures 6 and 7, the transcript levels of *PAL*, *CHS*, *CHI*, *F3H*, *DFR*, and *ANS* were all in a time-dependent manner. In LA sprouts, exposure to UV-A for 12, 24, or 36 h all significantly increased the transcriptions of *PAL*, *CHS*, *CHI*, *F3H*, *DFR*, and *ANS* compared to those under white light. With the exception of *CHI*, a combination of UV-A + HRW upregulated intensely the transcript levels of *PAL* at 24 h, *CHS* at 12 h, *F3H* at 24 and 36 h, *DFR* at 24 h, and *ANS* at 12, 24, and 36 h, respectively (Figure 6).

Similarly, UV-A significantly increased the transcriptions of these six genes in HA sprouts, but to a larger extent. Despite its different effect on LA sprouts, UV-A + HRW upregulated the transcript levels of *PAL*, *CHS*, *CHI*, *F3H*, *DFR*, and *ANS* at almost all time points and more intensely in HA. We also noticed that the responses of related genes to HRW appeared at different treatment times. The expressions of *PAL*, *CHS*, and *F3H* were upregulated by more than 1.5- to 2-fold under the combination of UV-A + HRW than under UV-A alone at 12 h after treatment. The transcript level of *CHI*, *DFR*, and *ANS* was higher under the combination of UVA + HRW than that under UV-A alone at 36 h, especially *DFR*, which was 5-fold higher (Figure 7). These results indicated that there was a time sequence in the response of different genes to HRW.

Though the expression of genes under UVA + HRW was all much higher than that under UVA + Con in the two varieties of radish sprouts tested, the expression level was 5- to 10-fold higher in HA sprouts than in LA sprouts (Figure S2 in the Supporting Information).

DISCUSSION

In recent years, the roles of H_2 in plant physiology, especially in abiotic stress, immediately drew widespread attention. Xu et al. (2013)[38] and Xie et al. (2012)[29] discovered that hydrogen-rich water could alleviate salt stress in rice and *Arabidopsis*. Jin et al. (2013)[28] reported that HRW was able to enhance plant tolerance to paraquat-induced oxidative stress. Furthermore, Zeng et al. (2013)[39] reported that hydrogen is involved in phytohormone signaling and stress responses in mung bean and rice. In the present study, we observed that hydrogen-rich water (HRW) enhanced radish sprout tolerance to UV-A, but the two radish varieties exhibited different sensitivities to HRW.

In higher plants, it is well-known that UV damage is mediated by oxidative stress and that UV not only inhibits hypocotyl elongation and seedling growth but also affects redox homeostasis.[40] Consequently, we investigated the effects of HRW on lipid peroxidation, the activity of some representative

dx.doi.org/10.1021/jf5019593 | J. Agric. Food Chem. 2014, 62, 6454−6462

Table 1. Varieties and Relative Abundance of Anthocyanidins in the Hypocotyls of HA and LA Sprouts under Different Treatments[a]

anthocyanidin	HA				LA			
	W + Con	W + HRW	UVA + Con	UVA + HRW	W + Con	W + HRW	UVA + Con	UVA + HRW
cyanidin	0.1643 ± 0.0230 c	0.1507 ± 0.0078 c	0.2967 ± 0.0110 b	0.6545 ± 0.0670 a	0.0049 ± 0.0005 d	0.0024 ± 0.0003 d	0.0309 ± 0.0004 d	0.0272 ± 0.0018 d
cyanidin-3-glucoside	0.0379 ± 0.0047 b	0.0390 ± 0.0034 b	0.0443 ± 0.0034 b	0.0877 ± 0.0059 a	0.0003 ± 0.0001 c	0.0003 ± 0.0000 c	0.0083 ± 0.0004 c	0.0025 ± 0.0002 c
cyanidin-3-rutinoside-5-glucoside	0.0038 ± 0.0001 a	0.0042 ± 0.0002 a	0.0062 ± 0.0019 a	0.0111 ± 0.0045 a				
malvidin-3-(6-coumaroylglucoside)	0.0090 ± 0.0007 c	0.0044 ± 0.0014 c	0.0274 ± 0.0026 b	0.0460 ± 0.0086 a				
peonidin-3′,5-*O*-glucoside	0.0052 ± 0.0008 b	0.0073 ± 0.0026 ab	0.0065 ± 0.0007 ab	0.0103 ± 0.0002 a				

[a]Values followed by a different letter were significantly different according to Duncan's one way test at $P < 0.05$.

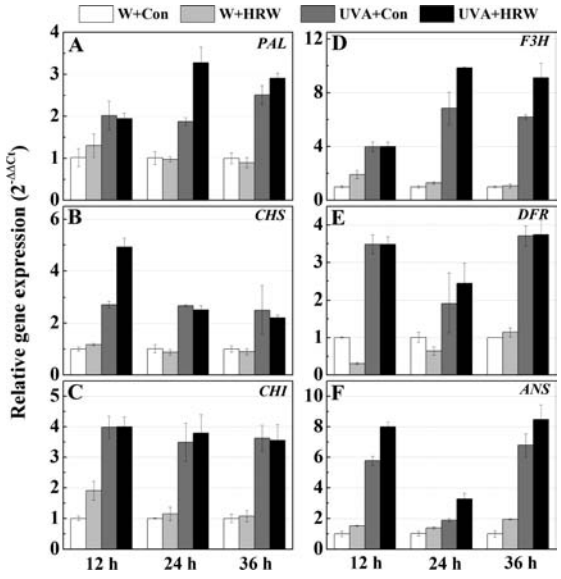

Figure 6. Transcript abundance of the *PAL* (A), *CHS* (B), *CHI* (C), *F3H* (D), *DFR* (E), and *ANS* (F) expression in the hypocotyls of LA sprouts exposed to white light or UV-A for 12 h, 24 h, and 36 h. Sprouts cultivated in distilled water (H_2O) or 100% HRW were exposed to white light or UV-A for 12 h, 24 h, or 36 h. Columns represent mean (+SD) values of independent experiments (n = 3), based on transcript level data normalized to W + Con at 12 h, 24 h, and 36 h.

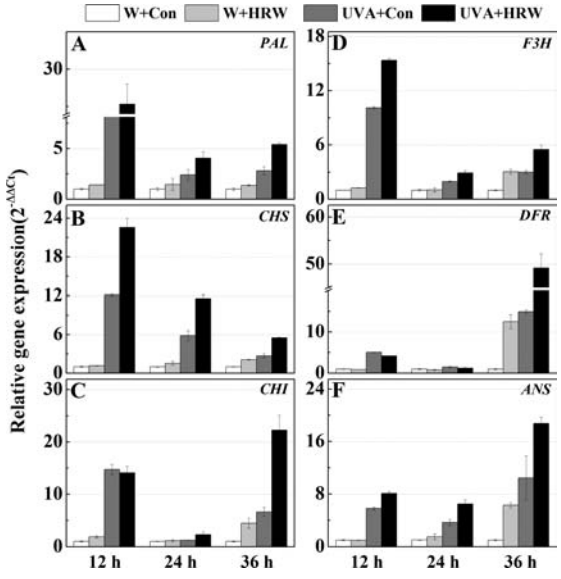

Figure 7. Transcript abundance of the *PAL* (A), *CHS* (B), *CHI* (C), *F3H* (D), *DFR* (E), and *ANS* (F) expression in the hypocotyls of HA sprouts exposed to white light or UV-A for 12 h, 24 h, and 36 h. Sprouts cultivated in distilled water (H_2O) or 100% HRW were exposed to white light or UV-A for 12 h, 24 h, or 36 h. Columns represent mean (+SD) values of independent experiments (n = 3), based on transcript level data normalized to W + Con at 12 h, 24 h, and 36 h.

enzymes, and the ROS content in radish sprouts. Low level of TBARS content detected in the hypocotyls of LA sprouts (nearly 6-fold lower than that in HA sprouts) (Figure 3A) confirmed that LA sprouts might be more tolerant to UV-A radiation. In HA sprouts, we noticed that UV-A treatment resulted in a significant increase in the level of TBARS content,

dx.doi.org/10.1021/jf5019593 | J. Agric. Food Chem. 2014, 62, 6454−6462

however, HRW significantly blocked this increase (Figure 3A). These results were supported by upactivation of SOD and APX (Figure 3B,D). In agreement with these, we also observed that UV-A radiation for 24 h resulted in a distinct increase in the level of O_2^- and H_2O_2 in the leaves of both LA and HA sprouts, while HRW treatment blocked this increase partly (Figure 2). All of this information suggests that HRW protected radish sprouts from UV-A by reestablishing reactive oxygen species homeostasis.

Radish sprouts have been recognized as richer sources of healthy phytochemicals than radishes. Red radishes contain anthocyanins which are very effective antioxidants, and are the most characteristic bioactive nutrients in berries and other "red−purple healthy food".[41] To better understand the relationship between anthocyanin biosynthesis and HRW, we chose two contrasting varieties of radish sprouts, LA sprouts (white hypocotyls, low level anthocyanin content, about 1 U g^{1-}) and HA sprouts (red hypocotyls, high level anthocyanin content, about 30 U g^{1-}), to study anthocyanin accumulation influenced by HRW. We found that HRW only increased anthocyanin accumulation in the hypocotyls of HA sprouts, but not in LA sprouts (Figure 5C). However, the anthocyanin biosynthesis-related structural genes were all upregulated in both LA and HA sprouts treated with UV-A + HRW compared to the UV-A treatment, although the gene expression level of LA was much lower than that of HA (Figures 6 and 7 and Figure S2 in the Supporting Information). This apparent paradox may be explained if the anthocyanidins produced in LA sprouts were used immediately (through coupled or channeled reactions) for the production of flavonoid compounds using endogenous modification and polymerization enzymes in vivo.

Among the six anthocyanidins in plants, we observed that Cy was the main anthocyanidin in radish sprouts and it was strongly enhanced when treated with UV-A + HRW (Table 1). These results indicated that HRW mainly enhanced the Cy accumulation in the hypocotyls of radish sprouts to increase the anthocyanin content.

Anthocyanin accumulation in the hypocotyls promotes the photoprotection to allow seedling survival during early development,[42] and to protect the plant's DNA from damage by ultraviolet (UV) light.[43] So, the anthocyanin content in the hypocotyls of HA sprouts under UV-A was increased significantly compared with that under W (about 2-fold) (Figure 5). However, the anthocyanin accumulation under HRW + UV-A was more than that under UV-A. This prompted us to hypothesize that HRW enhanced the tolerance of HA sprouts to UV-A. To confirm this hypothesis, the total phenols content and the DPPH scavenging effect of the total content in the hypocotyls of radish sprouts were first measured. As expected, HRW increased the total phenols content and the DPPH scavenging effect in radish sprouts under the combination of UV-A + HRW, though no significant difference was noted between the total phenols content in the hypocotyls of LA sprouts (Figure 4). All these results indicate that HRW has different effects on anthocyanin biosynthesis in LA and HA sprouts, though it has consistent impacts on antioxidant response.

In conclusion, we first reported that, in the present study, HRW alleviated UV-A induced oxidant damage via increasing the activity of SOD and APX, and reducing the ROS and TBARS content of radish sprouts (Figures 2 and 3). More importantly, we presented experimental evidence showing that HRW enhanced UV-A-induced anthocyanin accumulation in the hypocotyls of HA sprouts, while no effect was noted in LA sprouts, by upregulating the anthocyanin biosynthesis-related genes in HA sprouts (Figures 5−7). Anthocyanins belong to a diverse group of ubiquitous secondary metabolites known as flavonoids,[44] which are involved in protection against UV-light and pathogens. Cryptochromes perceive UV-A[45] and interact with COP1 to prevent the MYB from being ubiquitinated and degraded, so that MYB directly binds to the promoters of anthocyanin biosynthetic genes and activates their expression, finally increasing the anthocyanin accumulation.[46] In this paper, we observed that HRW enhanced the UV-A-induced anthocyanin increase. Carvalho et al. (2010)[42] reported that hormones modulated photomorphogenesis-controlled anthocyanin accumulation in tomato hypocotyls, and later, Zeng et al. (2013)[39] discovered that hydrogen was involved in phytohormone signaling. These prompted us to hypothesize that the HRW-induced increase of anthocyanin accumulation in the hypocotyls of radish sprouts in the present study may be mediated by phytohormone. On the other hand, as HRW significantly upregulated the expression of anthocyanin biosynthesis-related genes, HRW may influence MYB or COP1 transcriptional factors to enhance the anthocyanin accumulation. All these hypotheses need further complementary genetic approaches to support. A model summarizing these points is presented in Figure 8.

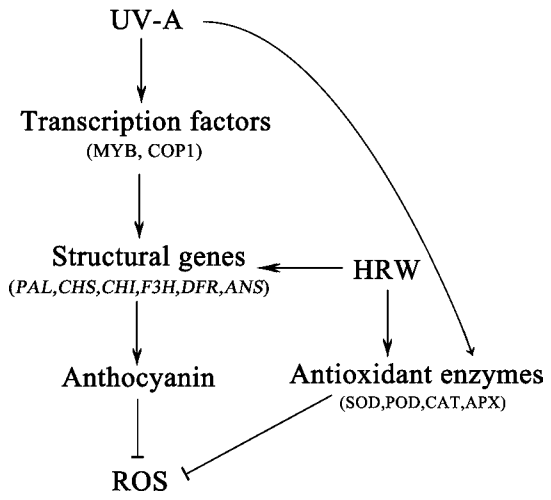

Figure 8. Model of HRW regulation of UV-A-induced increase of anthocyanin accumulation in the hypocotyls of radish sprouts. As a stress environment, UV-A incurs generation of active oxygen species (ROS), which eventually results in lipid peroxidation, leading to high concentration of thiobarbituric acid reactive substances (TBARS). On the other hand, when the photoreceptors of UV-A were activated, they acted to suppress COP1 and activated MYB upregulating the anthocyanin biosynthesis-related structural genes (*PAL*, *CHS*, *CHI*, *F3H*, *DFR*, and *ANS*) to enhance the anthocyanin accumulation, while hydrogen-rich water (HRW) act on the structural genes or antioxidant enzymes to participate in the UV-A-regulated anthocyanin metabolic pathway.

Recent studies revealed that hydrogen may serve as a modulator of signal transduction in the human body[47] and has a huge potential as a safe and potent therapeutic medical gas, as well as several potential advantages over current pharmacological therapies.[26] In addition, the safety of hydrogen for humans had been demonstrated by its application in driving.[48] In this study, we observed that exogenous hydrogen donor

(HRW) could enhance UV-A-induced anthocyanin accumulation in HA sprouts, suggesting that HRW will provide practical applications for enhancing the nutritional quality of radish sprouts in the sprout industry or commercially after further research on food quality and safety assessments.

■ ASSOCIATED CONTENT

Supporting Information

Figure S1, effects of different concentration of hydrogen-rich water (HRW) treatments on UV-A-induced inhibition of hypocotyls elongation and promotion of anthocyanin accumulation in HA radish sprouts. Figure S2, transcript abundance of the *PAL* (A), *CHS* (B), *CHI* (C), *F3H* (D), *DFR* (E), and *ANS* (F) in the hypocotyls of LA and HA sprouts exposed to white light or UV-A for 12 h, 24 h, and 36 h. Table S1, the nucleotide sequence of primers used in the RT-PCR. This material is available free of charge via the Internet at http://pubs.acs.org.

■ AUTHOR INFORMATION

Corresponding Author

*E-mail: cuijin@njau.edu.cn.

Notes

The authors declare no competing financial interest.

■ REFERENCES

(1) Takaya, Y.; Kondo, Y.; Furukawa, T.; Niwa, M. Antioxidant constituents of radish sprout (Kaiware-daikon), Raphanus sativus L. *J. Agric. Food Chem.* **2003**, *51*, 8061−8066.

(2) Zielinski, H.; Bucinski, A.; Kozłowska, H. Monitoring of the vitamin C content in germinating cruciferae seeds by HPLC. *Pol. J. Food Nutr. Sci.* **2002**, *11*, 142−146.

(3) Barillari, J.; Cervellati, R.; Paolini, M.; Tatibouet, A.; Rollin, P.; Iori, R. Isolation of 4-methylthio-3-butenyl glucosinolate from Raphanus sativus sprouts (kaiware daikon) and its redox properties. *J. Agric. Food Chem.* **2005**, *53*, 9890−9896.

(4) Tian, Q. G.; Rosselot, R. A.; Schwartz, S. J. Quantitative determination of intact glucosinolates in broccoli, broccoli sprouts, brussels sprouts, and cauliflower by high-performance liquid chromatography-electrospray ionization-tandem mass spectrometry. *Anal. Biochem.* **2005**, *343*, 93−99.

(5) Jaakola, L. New insights into the regulation of anthocyanin biosynthesis in fruits. *Trends Plant Sci.* **2013**, *18*, 477−483.

(6) He, J. A.; Giusti, M. M. Anthocyanins: Natural Colorants with Health-Promoting Properties. *Annu. Rev. Food Sci. Technol.* **2010**, *1*, 163−187.

(7) Chalker-Scott, L. Environmental significance of anthocyanins in plant stress responses. *Photochem. Photobiol.* **1999**, *70*, 1−9.

(8) Zhang, K. M.; Yu, H. J.; Shi, K.; Zhou, Y. H.; Yu, J. Q.; Xia, X. J. Photoprotective roles of anthocyanins in Begonia semperflorens. *Plant Sci.* **2010**, *179*, 202−208.

(9) Buer, C. S.; Imin, N.; Djordjevic, M. A. Flavonoids: New Roles for Old Molecules. *J. Integr. Plant Biol.* **2010**, *52*, 98−111.

(10) Mazza, C. A.; Battista, D.; Zima, A. M.; Szwarcberg-Bracchitta, M.; Giordano, C. V.; Acevedo, A.; Scopel, A. L.; Ballare, C. L. The effects of solar ultraviolet-B radiation on the growth and yield of barley are accompanied by increased DNA damage and antioxidant responses. *Plant, Cell Environ.* **1999**, *22*, 61−70.

(11) Apel, K.; Hirt, H. Reactive oxygen species: Metabolism, oxidative stress, and signal transduction. *Annu. Rev. Plant Biol.* **2004**, *55*, 373−399.

(12) Albert, K. R.; Mikkelsen, T. N.; Ro-Poulsen, H. Effects of ambient versus reduced UV-B radiation on high arctic Salix arctica assessed by measurements and calculations of chlorophyll a fluorescence parameters from fluorescence transients. *Physiol. Plant.* **2005**, *124*, 208−226.

(13) Kakani, V. G.; Reddy, K. R.; Zhao, D.; Sailaja, K. Field crop responses to ultraviolet-B radiation: a review. *Agric. For. Meteorol.* **2003**, *120*, 191−218.

(14) Boccalandro, H. E.; Mazza, C. A.; Mazzella, M. A.; Casal, J. J.; Ballare, C. L. Ultraviolet B radiation enhances a phytochrome-B-mediated photomorphogenic response in Arabidopsis. *Plant Physiol.* **2001**, *126*, 780−788.

(15) Eisinger, W. R.; Bogomolni, R. A.; Taiz, L. Interactions between a blue-green reversible photoreceptor and a separate UV-B receptor in stomatal guard cells. *Am. J. Bot.* **2003**, *90*, 1560−1566.

(16) Suesslin, C.; Frohnmeyer, H. An Arabidopsis mutant defective in UV-B light-mediated responses. *Plant J.* **2003**, *33*, 591−601.

(17) Chappell, J.; Hahlbrock, K. Transcription of plant defense genes in response to UV light or fungal elicitor. *Nature* **1984**, *311*, 76−78.

(18) Hirner, A. A.; Seitz, H. U. Isoforms of chalcone synthase in Daucus carota L. and their differential expression in organs from the European wild carrot and in ultraviolet-A-irradiated cell cultures. *Planta* **2000**, *210*, 993−998.

(19) Wang, Y.; Zhou, B.; Sun, M.; Li, Y. H.; Kawabata, S. UV-A Light Induces Anthocyanin Biosynthesis in a Manner Distinct from Synergistic Blue plus UV-B Light and UV-A/Blue Light Responses in Different Parts of the Hypocotyls in Turnip Seedlings. *Plant Cell Physiol.* **2012**, *53*, 1470−1480.

(20) Jeong, S. W.; Das, P. K.; Jeoung, S. C.; Song, J. Y.; Lee, H. K.; Kim, Y. K.; Kim, W. J.; Il Park, Y.; Yoo, S. D.; Choi, S. B.; Choi, G.; Park, Y. I. Ethylene Suppression of Sugar-Induced Anthocyanin Pigmentation in Arabidopsis. *Plant Physiol.* **2010**, *154*, 1514−1531.

(21) Lubitz, W.; Reijerse, E. J.; Messinger, J. Solar water-splitting into H-2 and O-2: design principles of photosystem II and hydrogenases. *Energy Environ. Sci.* **2008**, *1*, 15−31.

(22) Melis, A.; Happe, T. Hydrogen production. Green algae as a source of energy. *Plant Physiol.* **2001**, *127*, 740−748.

(23) Melis, A.; Melnicki, M. R. Integrated biological hydrogen production. *Int. J. Hydrogen Energy* **2006**, *31*, 1563−1573.

(24) Pinske, C.; Sawers, R. G., Delivery of Iron-Sulfur Clusters to the Hydrogen-Oxidizing [NiFe]-Hydrogenases in Escherichia coli Requires the A-Type Carrier Proteins ErpA and IscA. *PLoS One* **2012**, *7*.

(25) Tamagnini, P.; Axelsson, R.; Lindberg, P.; Oxelfelt, F.; Wunschiers, R.; Lindblad, P. Hydrogenases and hydrogen metabolism of cyanobacteria. *Microbiol. Mol. Biol. Rev.* **2002**, *66*, 1−+.

(26) Huang, C. S.; Kawamura, T.; Toyoda, Y.; Nakao, A. Recent advances in hydrogen research as a therapeutic medical gas. *Free Radical Res.* **2010**, *44*, 971−982.

(27) Zheng, X. F.; Sun, X. J.; Xia, Z. F. Hydrogen resuscitation, a new cytoprotective approach. *Clin. Exp. Pharmacol. Physiol.* **2011**, *38*, 155−163.

(28) Jin, Q. J.; Zhu, K. K.; Cui, W. T.; Xie, Y. J.; Han, B.; Shen, W. B. Hydrogen gas acts as a novel bioactive molecule in enhancing plant tolerance to paraquat-induced oxidative stress via the modulation of heme oxygenase-1 signalling system. *Plant Cell Environ.* **2013**, *36*, 956−969.

(29) Xie, Y. J.; Mao, Y.; Lai, D. W.; Zhang, W.; Shen, W. B., H-2 Enhances Arabidopsis Salt Tolerance by Manipulating ZAT10/12-Mediated Antioxidant Defence and Controlling Sodium Exclusion. *PLoS One* **2012**, *7*.

(30) Bernardi, C.; Chiesa, L. M.; Soncin, S.; Passero, E.; Biondi, P. A. Determination of carbon monoxide in tuna by gas chromatography with micro-thermal conductivity detector. *J. Chromatogr. Sci.* **2008**, *46*, 392−394.

(31) Han, Y.; Zhang, J.; Chen, X. Y.; Gao, Z. Z.; Xuan, W.; Xu, S.; Ding, X.; Shen, W. B. Carbon monoxide alleviates cadmium-induced oxidative damage by modulating glutathione metabolism in the roots of Medicago sativa. *New Phytol.* **2008**, *177*, 155−166.

(32) Sung, C. H.; Hong, J. K. Sodium nitroprusside mediates seedling development and attenuation of oxidative stresses in Chinese cabbage. *Plant Biotechnol. Rep.* **2010**, *4*, 243−251.

(33) Zhou, B.; Zhang, Z.; Wang, X. H. Anthocyanin-Rich Maize Purple Plant Pigment Stimulated the Proliferation and Differentiation

of Osteoblastic Mc3t3-E1 Cells. *Ann. Nutr. Metab.* **2013**, *63*, 1148−1149.
(34) George, S.; Brat, P.; Alter, P.; Amiot, M. J. Rapid determination of polyphenols and vitamin C in plant-derived products. *J. Agric. Food Chem.* **2005**, *53*, 1370−1373.
(35) Chen, Z.; Bertin, R.; Froldi, G. EC50 estimation of antioxidant activity in DPPH center dot assay using several statistical programs. *Food Chem.* **2013**, *138*, 414−420.
(36) Jiang, L.; Wang, Y.; Li, Q. F.; Bjorn, L. O.; He, J. X.; Li, S. S. Arabidopsis STO/BBX24 negatively regulates UV-B signaling by interacting with COP1 and repressing HY5 transcriptional activity. *Cell Res.* **2012**, *22*, 1046−1057.
(37) Lv, W. T.; Lin, B.; Zhang, M.; Hua, X. J. Proline Accumulation Is Inhibitory to Arabidopsis Seedlings during Heat Stress. *Plant Physiol.* **2011**, *156*, 1921−1933.
(38) Xu, S.; Zhu, S. S.; Jiang, Y. L.; Wang, N.; Wang, R.; Shen, W. B.; Yang, J. Hydrogen-rich water alleviates salt stress in rice during seed germination. *Plant Soil* **2013**, *370*, 47−57.
(39) Zeng, J. Q.; Zhang, M. Y.; Sun, X. J., Molecular Hydrogen Is Involved in Phytohormone Signaling and Stress Responses in Plants. *PLoS One* **2013**, *8*.
(40) Kataria, S.; Guruprasad, K. N. Solar UV-B and UV-A/B exclusion effects on intraspecific variations in crop growth and yield of wheat varieties. *Field Crop Res.* **2012**, *125*, 8−13.
(41) Matera, R.; Gabbanini, S.; De Nicola, G. R.; Iori, R.; Petrillo, G.; Valgimigli, L. Identification and analysis of isothiocyanates and new acylated anthocyanins in the juice of Raphanus sativus cv. Sango sprouts. *Food Chem.* **2012**, *133*, 563−572.
(42) Carvalho, R. F.; Quecini, V.; Peres, L. E. P. Hormonal modulation of photomorphogenesis-controlled anthocyanin accumulation in tomato (Solanum lycopersicum L. cv Micro-Tom) hypocotyls: Physiological and genetic studies. *Plant Sci.* **2010**, *178*, 258−264.
(43) Winkel-Shirley, B. Flavonoid biosynthesis. a colorful model for genetics, biochemistry, cell biology, and biotechnology. *Plant Physiol.* **2001**, *126*, 485−493.
(44) Sancar, A. Structure and function of DNA photolyase and cryptochrome blue-light photoreceptors. *Chem. Rev.* **2003**, *103*, 2203−2237.
(45) Tanaka, Y.; Sasaki, N.; Ohmiya, A. Biosynthesis of plant pigments: anthocyanins, betalains and carotenoids. *Plant J.* **2008**, *54*, 733−749.
(46) Li, Y. Y.; Mao, K.; Zhao, C.; Zhao, X. Y.; Zhang, H. L.; Shu, H. R.; Hao, Y. J. MdCOP1 Ubiquitin E3 Ligases Interact with MdMYB1 to Regulate Light-Induced Anthocyanin Biosynthesis and Red Fruit Coloration in Apple. *Plant Physiol.* **2012**, *160*, 1011−1022.
(47) George, J. F.; Agarwal, A. Hydrogen: another gas with therapeutic potential. *Kidney Int.* **2010**, *77*, 85−87.
(48) Abraini, J. H.; Gardettechauffour, M. C.; Martinez, E.; Rostain, J. C.; Lemaire, C. Psychophysiological Reactions in Humans during an Open Sea Dive to 500 M with a Hydrogen-Helium-Oxygen Mixture. *J. Appl. Physiol.* **1994**, *76*, 1113−1118.

kernels.[6,8,9] Insect-injured, infected kernels are often highly contaminated with fumonisins or other mycotoxins. Kernel-feeding insects are most effectively controlled through the use of transgenic maize hybrids expressing insecticidal proteins (*Bt* maize)[7] which have been shown to have reduced fumonisin levels.[10]

Bt maize has been grown in the United States since 1996, and, as of 2013, 76% of all maize planted in the U.S. expressed some form of *Bt*-derived insect protection.[11] *Bt* maize hybrids produce insecticidal proteins derived from the soil bacterium *Bacillus thuringiensis* which confer resistance to select lepidopteran insects, but are nontoxic to humans and other nontarget species. *Bt* maize plants have an important advantage over foliar insecticides in that they produce insecticidal proteins for targeted insect control in desired plant tissues during the entire growing season. Management with foliar insecticides is costly, often requiring multiple applications that must be timed around larval hatching. Insects in the class Lepidoptera are common targets of the insecticidal proteins produced by *Bt* maize as these insects are some of the most significant pests of maize worldwide. Commercial maize hybrids that express either Cry1Ab or Cry1F proteins target European corn borer (*Ostrinia nubilalis* (Hübner)) (ECB), the most notable lepidopteran pest in maize, and are available in the U.S. and other countries.

Prior to the cultivation of *Bt* maize, annual yield losses attributable to ECB alone have been estimated near US$ 1 billion.[12] In addition to ECB control, the Cry1F protein also is effective against Western bean cutworm (*Striacosta albicosta* (Smith)) (WBC), southwestern corn borer (*Diatraea grandiosella* Dyar), fall armyworm (*Spodoptera frugiperda* (J.E. Smith)), and black cutworm (*Agrotis ipsilon* (Hufnagel)), and mildly effective against corn earworm (*Helicoverpa zea* (Boddie)) (CEW). *Bt* maize has shown high efficacy against ECB feeding, reducing overall ECB populations in areas of high *Bt* adoption.[13] This is a significant benefit to maize growers in the U.S., however, maize pests which had previously been considered secondary to ECB are now competing for this viable food source. The arrival of WBC in the Midwest U.S. in the early 1990s has posed a new threat in this maize-intensive region. Catangui and Berg[14] observed that naturally infested fields of Cry1Ab maize experienced higher WBC infestation than ECB. In a laboratory setting, WBC has displayed increased survival on Cry1Ab maize in comparison with its two primary competitors for this food source, ECB and CEW.[15] Intraguild competition for this food source is currently changing hands with WBC as a potential candidate, but minimal study has been conducted on the influence of WBC on fumonisins in various *Bt* hybrids, especially in the field. The contribution of *Bt* maize to reducing insect injury is paramount to management of *Fusarium* infection and fumonisin contamination of grain. There is a considerable lack of data with regard to impacts of WBC infestation on both *Fusarium* infection of maize and fumonisin contamination as well as the ability of various *Bt* proteins to control this species and mitigate these issues.

MATERIALS AND METHODS

Safety. Fumonisin B_1, **1**, is a group 2B carcinogen, and sodium cyanide is highly toxic. Both should be handled with appropriate caution and personal protective equipment.

Field Trials. Field experiments were conducted in Story County, IA, in 2007 (preliminary), 2008, 2009, and 2010 to assess the effects of *Bt* transformation of maize hybrids on fumonisin contamination of grain manually infested with ECB and WBC. Six commercial maize hybrids were grown; four hybrids expressed *Bt* genes which produced insecticidal proteins. Two hybrids, with maturities of 109 and 113 d, were genetically engineered to produce Cry1F insecticidal proteins (Pioneer brand hybrids 33D14 and 34A20, DuPont Pioneer, Des Moines, IA); two, with maturities of 107 and 111 d, produced Cry1Ab insecticidal proteins (DEKALB hybrids DKC57-79 and DKC61-69, Monsanto Co., St. Louis, MO); and two, with maturities of 108 and 111 d, were near-isogenic, non-*Bt* hybrids not engineered to produce any insecticidal proteins (Pioneer 34A14 and DEKALB DKC61-72). In all experiments, plots were approximately 3 m by 6.1 m and contained 4 rows. Only the middle two rows of the plot were used for insect infestation treatment and grain harvest. Plots were arranged in a randomized complete block design, and the experiment included 5 replications of each combination of maize hybrid and insect infestation treatment.

ECB infestation was performed using a volumetric dispenser to apply neonatal larvae (reared in-house) mixed with maize cob grits (Table 1).[16] All plants in the middle two rows of the assigned plots were infested. In 2007, approximately 50 neonates were applied at the base of the primary ear, near the collar, and 50 on the silks of the primary ear. In 2008, plants were infested with approximately 50 neonatal larvae on two consecutive days, the first day on the silks of the primary ear and the second day on the silks of the second-highest ear on the plant. If there was only one ear on the plant, it was infested again. In 2009 and 2010, approximately 100 neonatal larvae were applied on the primary ear, 50 at the base (near the collar) and 50 on the silks.

Table 1. Summary of 2007−2010 Field Trials

insect infestation treatments[a]	planting date	ECB infest	WBC infest	harvest date
		2007		
ECB natural WBC	May 14	July 19	July 18, 23	Oct 19
		2008		
ECB natural	May 14	July 30, 31	n/a	Oct 28
		2009		
ECB natural WBC	May 8	July 30, 31, Aug 6	July 28	Oct 30
		2010		
ECB natural WBC	April 21	July 14, 16	July 20	Oct 5

[a]Insect infestation treatment abbreviations are as follows: ECB, European corn borer (*Ostrinia nubilalis*); WBC, Western bean cutworm (*Striacosta albicosta*); natural, no insects applied.

WBC infestation methods differed by year. In 2008, three second- or third-instar larvae (hatched out of egg masses collected from naturally infested fields) were applied to the silks of each primary ear on ten ears per plot with a small painter's brush. In 2009 and 2010, egg masses on maize leaf tissue, which were collected from naturally infested fields, were attached at the base of the primary ear of 20 plants per plot, on 10 consecutive ears in each of the treatment rows. In 2009 the maize leaves were first fixed to a section of plastic screen and then attached at the base of the ear, but in 2010 the screen was not used.

Sampling. In all experiments, harvest entailed collecting ten ears per plot by hand from infested plants or, in the case of naturally infested plots, the ears were taken from the middle two rows of the plot. Ears were stored in a cold room (~4 °C) until drying to inhibit fungal metabolism and further fumonisin production. Postharvest, ears were visually assessed for insect injury and *Fusarium* ear rot severity and then dried at approximately 38 °C to below 15% moisture. In

dx.doi.org/10.1021/jf5011897 | J. Agric. Food Chem. 2014, 62, 6463−6472

2008 the maize was shelled prior to drying on Nov 18. In 2009 and 2010, maize was dried on-the-cob on Nov 10 and Oct 14, respectively, followed by shelling. Shelled kernels from the ten harvested ears per plot were combined and ground using a Romer Laboratories mill (Romer Laboratories, Inc., Union, MO).

Mycotoxin Analyses. *Enzyme-Linked Immunosorbent Assay (ELISA).* In 2007, fumonisin analysis was conducted by the Pioneer Hi-Bred Grain Analysis Laboratory (DuPont Pioneer, Johnston, IA) using a quantitative, competitive enzyme-linked immunosorbent assay (ELISA) with proprietary antibodies for the detection of FB_1, **1**. Samples were finely ground, and a 3 g subsample was extracted for analysis. Precoated, stabilized plates were prepared by Beacon Analytical Systems, Inc. (Saco, ME). Maize extract samples and horseradish peroxidase conjugated fumonisin B_1 were coincubated at 20−25 °C for 60−62 min with shaking in the dark. Substrate was added following washing of the plates. The substrate reaction was allowed to proceed for 30−32 min at 20−25 °C with shaking in the dark. The reaction was stopped, and the resulting color intensity of the wells was read at 450 nm. The measuring range of the fumonisin ELISA was 0.8 mg/kg to 2000 mg/kg. This method has been validated in comparison to HPLC[17] using AOAC-approved methods.[18]

In 2008 and 2009, total fumonisin concentration (FB_1 + FB_2 + FB_3), **1**−**3**, in a 10 g subsample of ground maize was determined for each plot using AgraQuant Total Fumonisin Assay 0.25/5.0 (Romer Laboratories Inc., Union, MO), a direct-competitive ELISA capable of measuring fumonisins in solution at concentrations between 0.25 and 5 mg/kg. Samples exceeding 5 mg/kg were subject to additional extract dilution to bring it within range of the ELISA test. At the time of analysis, this method was among the USDA-GIPSA performance-verified rapid test kits for the determination of total fumonisins in ground maize.

HPLC. In the preliminary experiment (2007), only the ELISA method was used. HPLC was used in 2008, 2009, and 2010.

Reagents. Fumonisin standards in 50:50 acetonitrile:water were obtained from BioPure (Tulln, Austria) and stored at 4 °C. Naphthalene 2,3-dicarboxaldehyde (NDA) was purchased from Sigma-Aldrich (Buchs, Switzerland). All other chemicals were purchased from Fisher Scientific (Fair Lawn, NJ). Unless otherwise noted, 0.2 μm filtered Barnstead Nanopure deionized water (Thermo Fisher Scientific, Waltham, MA) was used in solution and sample preparation. Reagents were prepared monthly according to Bennett and Richard[19] with the modification of pH adjustment of 0.05 M phosphate buffer to 7.4 with phosphoric acid.

Sample Preparation. Sample extraction was adapted from European Standard EN 14352,[20] with modification. Briefly, 10 g of ground sample was extracted with 25 mL of methanol/acetonitrile/distilled water (25:25:50, v/v/v) by shaking on an orbital shaker for 20 min and then centrifuged at 2500*g* for 10 min. The supernatant was filtered through Fisherbrand G6 glass fiber filter paper (Thermo Fisher Scientific, Waltham, MA) and the supernatant collected in a 50 mL conical centrifuge tube. The solids were extracted in the same manner with a second 25 mL volume of extraction solution, and the collected filtrates were combined. Filtrates were stored at −23 °C prior to cleanup and analysis. Fumonisins were purified from sample extracts using Fumonistar immunoaffinity columns (Romer Laboratories, Inc., Union, MO, USA) and evaporated to dryness with a Visiprep SPE vacuum manifold (Supelco, Sigma-Aldrich, St. Louis, MO) according to package instructions.

Derivatization. Samples were derivatized with NDA reagent according Bennett and Richard[19] with some modification. Sample residues were reconstituted with 0.5 mL of methanol, followed by the sequential addition of 0.5 mL of 0.05 M sodium borate buffer, 0.25 mL of sodium cyanide reagent, and 0.25 mL of NDA reagent. Samples were heated in a 60 °C water bath for 20 min and then transferred to 4 °C for 4 min. Samples were diluted with 3.5 mL of 0.05 M phosphate buffer (pH 7.4)/acetonitrile (40:60, v/v) and transferred to 1 mL amber autosampler vials. Postderivatization, samples were stored at −23 °C for up to 24 h until transfer to the autosampler for injection, and sample analysis was completed within 2 h of this transfer.[21]

HPLC Instrumentation and Parameters. The LC system consisted of a Varian ProStar 210 pump, 410 AutoSampler (run with tray cooling at 4 °C and column oven 30 °C), and 363 fluorescence detector. The LC column was a Zorbax Eclipse Plus-C18, 3.5 μm (4.6 × 100 mm), and was preceded by a Zorbax Eclipse Plus-C18, 5 μm (4.6 × 12.5 mm), guard column (Agilent Technologies, Santa Clara, CA). Fumonisins were eluted isocratically in a mobile phase consisting of filtered deionized water/acetonitrile/glacial acetic acid (52:47:1, v/v/v) at a flow rate of 2.0 mL/min. Fumonisin−NDA derivatives were detected using 420 nm excitation and 500 nm emission wavelengths.

Method Quality Control. Limits of detection (LOD) were determined by dividing the standard deviation of the calibration curve residuals by the slope of the calibration curve at levels approaching the LOD and multiplying the result by 3.3. Limits of quantitation were calculated by multiplying 3 times the calculated LOD.[22] Method accuracy was tested by artificially contaminating duplicate ground maize samples with known amounts of fumonisin at 2 levels of contamination and testing the recoveries. Low level artificial contamination in ground maize was equivalent to 4.1, 1.2, and 0.51 μg/g FB_1, FB_2, and FB_3, respectively, and high level artificial contamination was equivalent to 6.8, 2.0, and 0.82 μg/g for FB_1, FB_2, and FB_3, respectively (Table 2). Method precision was measured by analyzing extracts of the same maize sample performed 4 times over a period of 2 weeks.

Table 2. Percent Recoveries by HPLC of FB_1, 1; FB_2, 2; and FB_3, 3; and Total Fumonisins for Low and High Spike Levels[a]

	FB_1 (%)	FB_2 (%)	FB_3 (%)	total FB recovery (%)
low spike	92.8, 104.8	81.0, 89.5	99.7, 117.6	90.9, 102.7
high spike	76.5, 85.5	71.6, 76.5	82.6, 92.2	76.0, 84.2

[a]Results are listed as repetition 1, repetition 2.

Statistical Analysis. Analysis of variance (ANOVA) was performed on log-transformed data using the PROC GLIMMIX procedure in SAS Version 9.3 software (SAS Institute Inc., Cary, NC) fitting the data to a gamma distribution. Insect feeding injury, severity of *Fusarium* ear rot symptoms, and total fumonisin concentration (FB_1 + FB_2 + FB_3) in grain were evaluated. Factorial analysis was used to determine simple effects of maize event, insect infestation treatment, and their interaction. Where interactions were present, multiple comparison analysis was performed using a Tukey−Kramer adjustment. ANOVA analysis revealed significant treatment differences among years of the study with regard to insect injury and *Fusarium* ear rot. As a result, data for these dependent effects were analyzed separately by year. Treatment effects among years of the study did not differ significantly for grain fumonisin contamination as measured by both ELISA and HPLC. The independent variable "hybrid" used for analysis combines results from each pair of hybrids used in the study which produced the same *Bt* insecticidal protein, either Cry1F, Cry1Ab, or none.

RESULTS AND DISCUSSION

Influences of Hybrid and Insect Infestation on Kernel Injury. In the 2007 preliminary study, hybrid and insect infestation significantly affected insect injury ($F_{2,77}$ = 5.93, P = 0.0040, and $F_{2,77}$ = 4.41, P = 0.0154, respectively). In 2008 and 2009, hybrid, insect treatment, and their interaction were significant factors (P < 0.0001 to P = 0.0169). In 2010, hybrid had a significant effect on insect injury ($F_{2,77}$ = 11.22, P < 0.0001). In 2007, WBC-infested plots suffered more kernel injury than either ECB (P = 0.0122) or naturally infested plots (P = 0.0123). In 2008, WBC were not available for infestations, and ECB-infested, non-*Bt* plots suffered more kernel injury (mean 6.5%) than any other hybrid/insect combination (P <

dx.doi.org/10.1021/jf5011897 | J. Agric. Food Chem. 2014, 62, 6463−6472

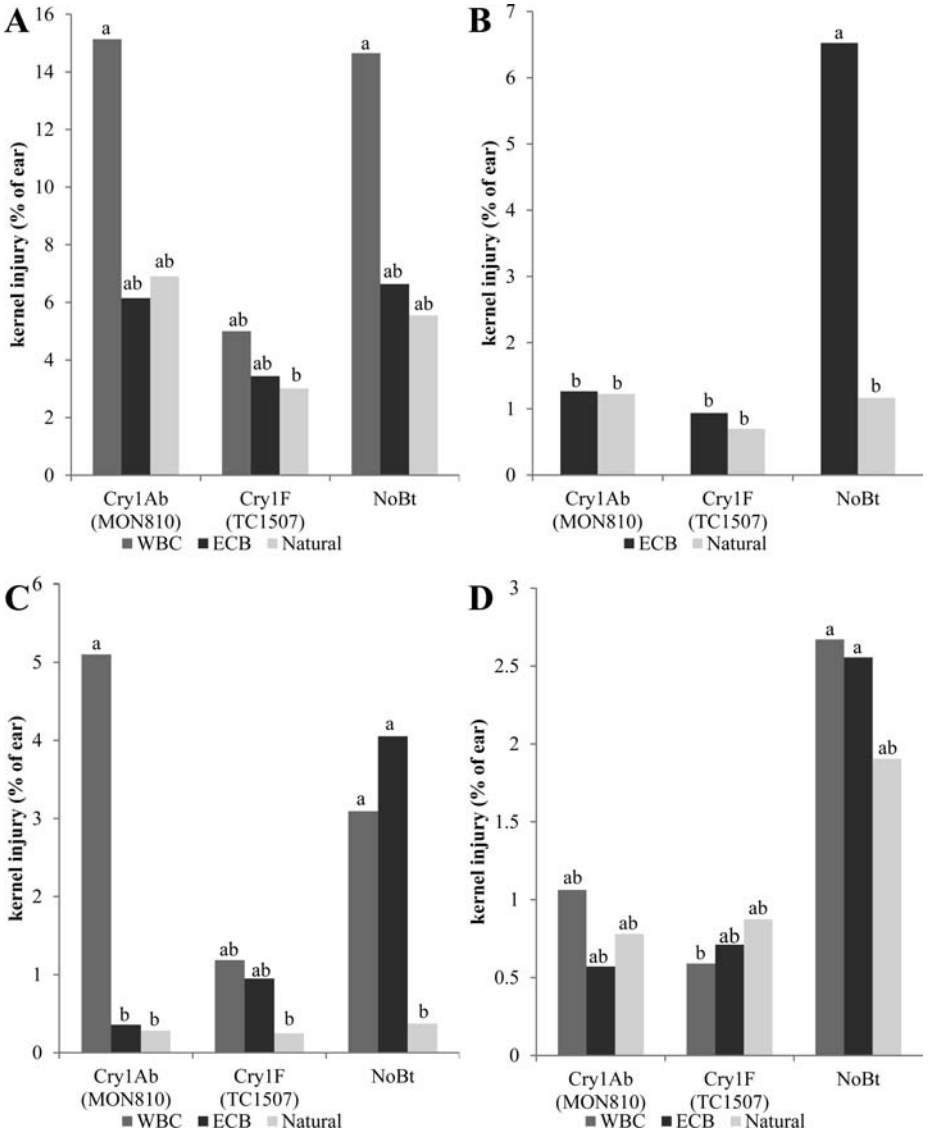

Figure 2. Insect injury (average percentage of kernels per ear) by *Bt* event for (A) 2007; (B) 2008; (C) 2009; and (D) 2010. Data are means of five replications each of two hybrids. Letters denote significant differences ($P < 0.05$) between hybrid/insect infestations within years.

0.0001 to $P = 0.0023$) (Figure 2B). In 2009, non-*Bt* hybrids infested with WBC and ECB exceeded naturally infested non-*Bt* plots ($P = 0.0035$ and $P = 0.0003$) in injury, and WBC infested Cry1Ab hybrids exceeded ECB or naturally infested Cry1Ab hybrids ($P < 0.0001$) (Figure 2C).

The susceptibility of Cry1Ab hybrids to WBC was marked in 2007 and 2009. In these years, WBC-infested Cry1Ab hybrids suffered the most kernel injury (mean 15.1% and 5.1%, respectively) (Figures 2A and 2C). Cry1F maize hybrids (*Bt* event TC1507), protected against both ECB and WBC, had very little kernel injury. In 2007, Cry1Ab hybrids and non-*Bt* hybrids experienced similar levels of kernel injury, but Cry1F hybrids suffered less injury than either Cry1Ab ($P = 0.0077$) or non-*Bt* hybrids ($P = 0.0142$). In both 2008 and 2009, non-Bt hybrids suffered more kernel injury than either Cry1Ab ($P = 0.0143$ and $P = 0.0179$) or Cry1F ($P = 0.0001$ and $P = 0.0053$) hybrids. In 2010, there were higher levels of injury in non-*Bt* as compared with either Cry1Ab ($P = 0.0005$) or Cry1F hybrids ($P = 0.0002$), and WBC incited more injury in non-*Bt* as compared to Cry1F plots (Figure 2D).

Manual insect infestations were used in this study to ensure that populations were present in the field with relatively uniform distribution. Their presence increases the likelihood of fungal infection in maize tissues affected by feeding injury and fungal spore dispersal by active larvae.[6,8] In 2007, 2008, and 2009, manual infestation significantly increased levels of kernel damage, indicating survival of manually infested insects. Insect infestations were chosen based on their traditional (ECB) and recent (WBC) significance in the growing area as well as the spectra of control provided by the *Bt* hybrids used in the study. Feeding patterns differ between ECB and WBC; WBC feeding is typically isolated at the tip of the ear and results in complete kernel destruction. ECB feeding is generally more widespread throughout the ear; the larvae leave partially intact kernels in their path as they migrate through the ear. "Railroading" is also common in ECB-infested maize, as small larvae move along a silk channel causing small amounts of injury to many kernels.[23]

Research has revealed a decline in natural ECB populations in several Midwest states as a result of the high adoption of *Bt* maize.[13] Historically, ECB has been the predominant lepidopteran pest of Midwest maize. In the years of this

dx.doi.org/10.1021/jf5011897 | J. Agric. Food Chem. 2014, 62, 6463−6472

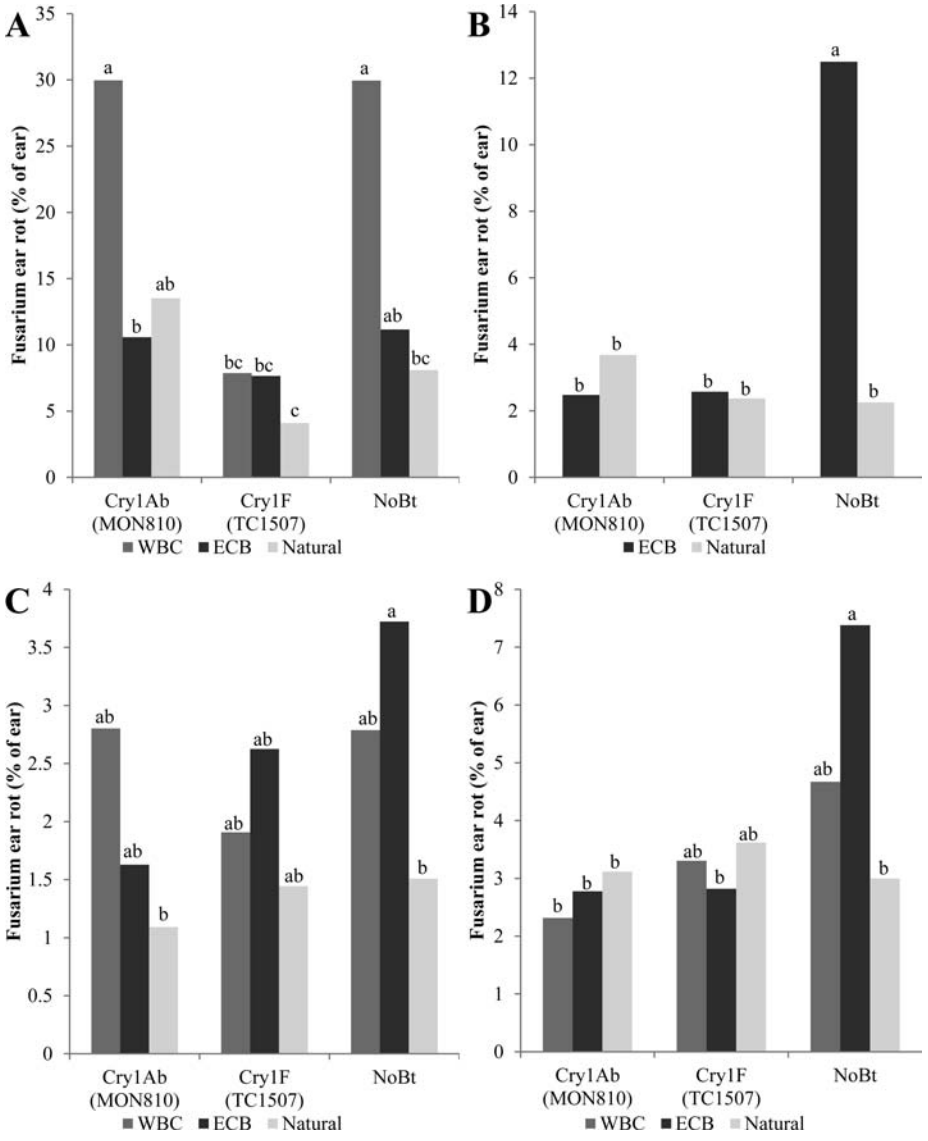

Figure 3. *Fusarium* ear rot (shown as average percent of kernels displaying visible symptoms of *Fusarium* infection per ear) by *Bt* event for (A) 2007; (B) 2008; (C) 2009; and (D) 2010. Data are means of five replications each of two hybrids. Letters denote significant differences ($P < 0.05$) between hybrid/insect infestations within years.

study, naturally infested plots did not differ in injury between susceptible and *Bt*-protected hybrids, indicating that natural ECB populations were low and injury was due to other endemic insects such as CEW. In maize-intensive regions of the U.S., regional suppression of ECB may result in predominance of pests that have historically been considered secondary to the ECB. WCB is a candidate, whose range has recently expanded from its recorded origin, Arizona,[24] all the way to Michigan, Ohio, and Pennsylvania in the U.S. as well as into Quebec.[25−27] WBC has also displayed a competitive advantage over another potential pest, CEW, when fed a diet of Cry1Ab (MON810) maize.[15] Reduced competition from ECB for maize in the Midwest will increase the need for WBC population monitoring for effective pest management, and hybrid selection will become even more important. The use of "stacked" Bt genes with different spectra of control and different modes of action may be necessary. In Puerto Rico, planting of Cry1F hybrids has been halted due to *Spodoptera frugiperda* (Lepidoptera: Noctuidae) resistance development.[28] A number of unique factors may have contributed to resistance development: little insect species migration into or off of the island; year-round maize cultivation; poor compliance with insect resistance management (IRM) requirements; and concurrent use of *Bt*-derived foliar insecticides; but this highlights the need for population monitoring and proactive resistance prevention and management in all regions where *Bt* maize is grown. Resistance has not spread to the mainland U.S.[29] and has not been noted in other lepidopteran species. In the U.S., the IRM strategy was developed to prevent resistance and, employed along with planting of *Bt* hybrids that produce different or multiple stacked *Bt* genes, can help reduce resistance development to any single gene on its own. IRM compliance is likely to improve significantly with the widespread commercialization of hybrid mixtures that include transgenic and non-transgenic (refuge) seeds in the same bag.

Influences of Hybrid and Insect Infestation on *Fusarium* Ear Rot. Hybrid and insect infestation effects on *Fusarium* ear rot were similar to those for kernel injury. Completely destroyed kernels were considered in the insect injury scores but were not physically present to contribute to

dx.doi.org/10.1021/jf5011897 | J. Agric. Food Chem. 2014, 62, 6463−6472

Table 3. Total Fumonisin Concentration (FB_1 + FB_2 + FB_3), 1−3, in Maize (mg/kg) As Determined by HPLC Analysis for 2008−2010 (Mean and Standard Deviation)

	mean ± SD[a]			
insect infestation	Cry1Ab (MON810)	Cry1F (TC1507)	non-*Bt*	overall mean by year or by insect infestation within year
			2008	
	1.42 ± 1.98	**1.62 ± 2.07**	**6.60 ± 8.62**	**3.22 ± 5.69**
ECB	1.40 ± 2.31	1.99 ± 1.99	12.34 ± 9.08	5.24 ± 7.39
natural	1.45 ± 1.73	1.26 ± 2.18	0.87 ± 1.08	1.19 ± 1.68
			2009	
	0.40 ± 0.69	**0.16 ± 0.25**	**0.67 ± 1.08**	**0.40 ± 0.75**
ECB	0.30 ± 0.47	0.20 ± 0.21	1.25 ± 1.40	0.55 ± 0.91
WBC	0.78 ± 1.05	0.23 ± 0.37	0.64 ± 1.04	0.55 ± 0.87
natural	0.15 ± 0.21	0.04 ± 0.02	0.12 ± 0.15	0.11 ± 0.16
			2010	
	0.51 ± 0.52	**0.43 ± 0.66**	**0.76 ± 0.93**	**0.57 ± 0.73**
ECB	0.69 ± 0.68	0.56 ± 0.59	1.00 ± 1.27	0.75 ± 0.89
WBC	0.55 ± 0.40	0.12 ± 0.11	0.86 ± 0.79	0.51 ± 0.59
natural	0.29 ± 0.39	0.61 ± 0.94	0.42 ± 0.60	0.44 ± 0.67
hybrid means	0.70 ± 1.19	0.66 ± 1.28	2.33 ± 5.22	

[a]Means within rows are either by year (boldface type) or by insect infestation within year (lightface type). Means within columns are grouped by *Bt* insecticidal protein produced with the corresponding (*Bt* event).

Fusarium ear rot scores or fumonisin contamination; nevertheless, a strong correlation was evident between insect injury and *Fusarium* ear rot (R = 0.74, P < 0.0001). In 2007, hybrid and insect infestation treatment were both significant factors influencing *Fusarium* ear rot severity ($F_{2,77}$ = 16.46 and $F_{2,77}$ = 15.26, respectively, P < 0.0001 for both). Hybrid, insect infestation treatment, and their interaction were all significant factors in 2008 ($F_{2,50}$ = 5.48 and P = 0.0071, $F_{1,50}$ = 7.64 and P = 0.0080, $F_{2,50}$ = 7.96 and P = 0.0010, respectively). In 2009, *Fusarium* ear rot severity was influenced by insect infestation treatment ($F_{2,77}$ = 5.18, P = 0.0077), and, in 2010, it was significantly influenced by hybrid ($F_{2,77}$ = 6.43, P = 0.0026) and the interaction of hybrid and insect infestation treatment ($F_{4,77}$ = 3.69, P = 0.0084). In 2007−2009, manual insect infestations resulted in higher levels of ear rot as compared with natural (P < 0.0001 to P = 0.0213), with the exception of 2007 ECB infestation. Cry1F hybrids suffered less ear rot than Cry1Ab and non-*Bt* maize hybrids (P < 0.0001 for both) in 2007 or non-*Bt* hybrids in 2008 (P = 0.0060). Non-*Bt* hybrids subject to ECB infestation in 2008 experienced higher levels of ear rot (mean 12.5%) than any other hybrid/insect combination (P < 0.0001 to P = 0.0106) (Figure 3B). Mean ear rot levels were low among all hybrids in 2009 (2.7%, 1.8%, and 2.0% for non-*Bt*, Cry1Ab, and Cry1F hybrids, respectively) and did not differ significantly (Figure 3C). The highest level was found in ECB infested, non-*Bt* plots at 3.7%. In 2010, Cry1Ab hybrids experienced the lowest level of ear rot (mean 2.7%), which was less than that of non-*Bt* hybrids (mean 5.0%, P = 0.0019). In 2010, ECB infested non-*Bt* hybrids experienced more ear rot (mean 7.4%) than naturally infested non-*Bt* hybrids (mean 3.0%, P = 0.0072), ECB infested Cry1F hybrids (mean 2.8%, P = 0.0078), or Cry1Ab hybrids under any insect infestation treatment (P = 0.0008 to P = 0.0059) (Figure 3D).

Fumonisin Contamination. *HPLC and ELISA Method Performance.* Accurate and repeatable determination of maize fumonisin content is a crucial step in commodity management. ELISA kits are used in grain-handling industries because of their ease-of-use, rapid results, minimal sample preparation, and affordability. In this industry, overestimation of mycotoxin contamination can result in false rejections, unnecessary limitations on grain usage, and subsequent economic loss. It also restricts marketability and impacts profitability, possibly affecting maize prices and available supplies. The AgraQuant Total Fumonisin ELISA used in years 2008 and 2009 of this study has limits of detection quantitation of 0.20 mg/kg and 0.25 mg/kg, respectively. This is less sensitive than results from the HPLC method used, for which the performance characteristics follow. HPLC calibration curves for FB_1, FB_2, and FB_3 had linear regression coefficients (R) of 0.999, 0.996, and 0.998. The limits of detection for FB_1, FB_2, and FB_3 were 0.11 ng, 0.18 ng, and 0.18 ng injected, respectively, which correspond to 40 μg/kg, 65 μg/kg, and 67 μg/kg in the maize sample (at 15% grain moisture). The limits of quantitation for FB_1, FB_2, and FB_3 were 0.33 ng, 0.54 ng, and 0.54 ng, respectively, which correspond to 120 μg/kg, 195 μg/kg, 200 μg/kg in maize (at 15% grain moisture).

Recoveries for FB_1 and FB_2 were within the acceptable range established by the European Commission, but ranges for FB_3 were not established in the EC directive.[30] The mean and standard deviations for FB_1, FB_2, and FB_3 in recovery samples were 1575 ± 121, 388 ± 27, and 70 ± 1.3 ng/g, respectively. The coefficients of variation for FB_1, FB_2, and FB_3, which are representative of precision and were obtained from independent extracts of the same maize sample, were 7.7%, 7.0%, and 1.9%, respectively. For fumonisin levels determined by HPLC and samples with FB_1, FB_2, and FB_3 levels all within their respective ranges of quantitation, FB_1 constituted 69.3 ± 4.7% of the total fumonisin contamination in the grain samples (N = 24).

Occurrence of Fumonisins and Range of Concentrations in Maize Samples. ELISA determinations of fumonisin B_1, **1**, in grain from 2007 indicated a range of FB_1 sample contamination from LOD to 80.62 mg/kg with a mean of 9.98 mg/kg. Fumonisin levels were below 2 mg/kg in 19 samples, 20 samples were between 2 and 4 mg/kg, and 51 samples exceeded 4 mg/kg. Hybrid and insect infestation treatment were significant influences on FB_1 concentrations in maize ($F_{2,77}$ = 4.76, P = 0.0112, and $F_{2,77}$ = 15.70, P < 0.0001). Non-*Bt*, Cry1Ab, and Cry1F hybrids averaged 13.14 mg/kg, 11.96 mg/kg, and 4.84 mg/kg FB_1, respectively. ELISA determi-

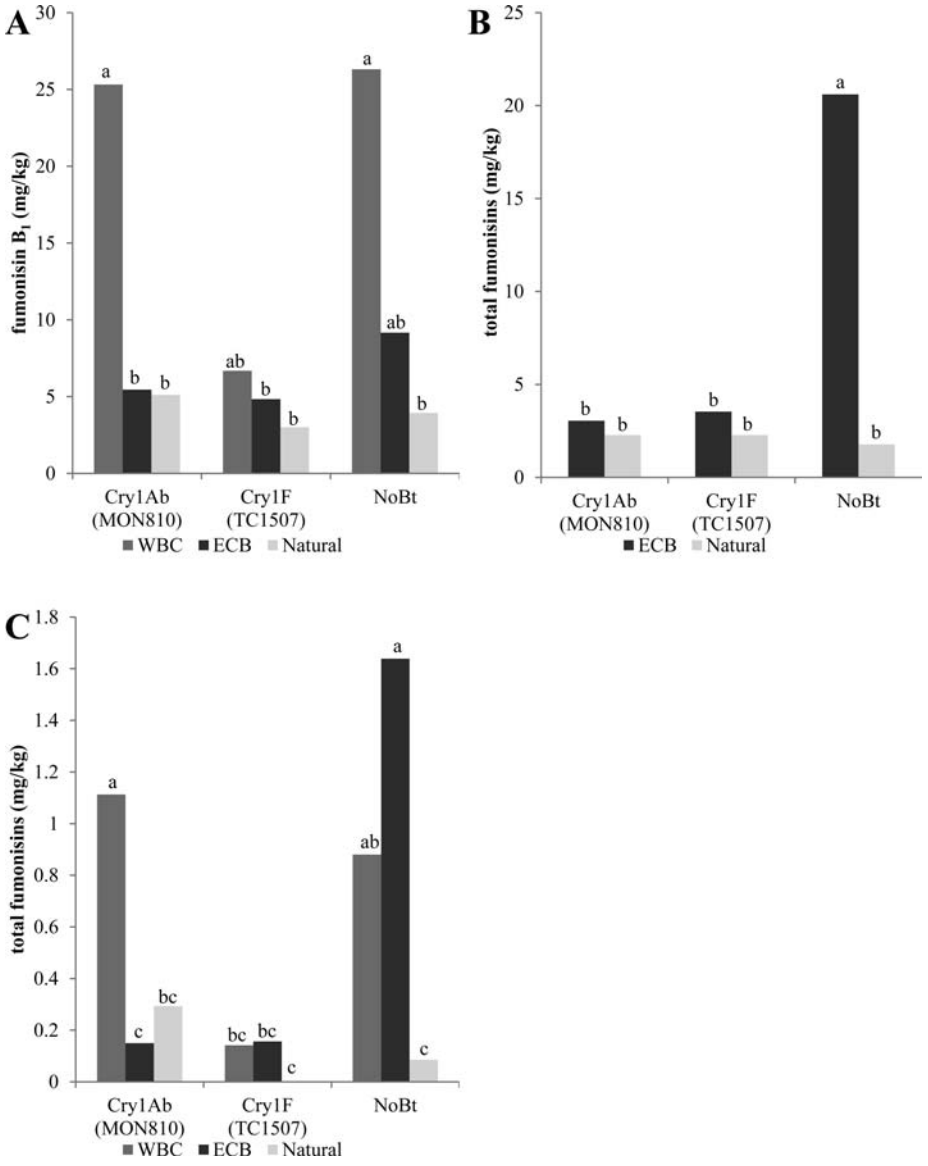

Figure 4. Fumonisin contamination in maize (mg/kg) as determined by ELISA. FB_1 contamination, **1**, is depicted for (A) 2007; total fumonisin contamination (FB_1 + FB_2 + FB_3), **1**−**3**, is depicted for (B) 2008 and (C) 2009. Data are means of five replications each of two hybrids. Letters denote significant differences ($P < 0.05$) between hybrid/insect infestations within years.

nations of total fumonisin levels (FB_1 + FB_2 + FB_3), **1**−**3**, in 2008−2009 ranged in samples from 0 to 48 mg/kg with a mean of 2.55 mg/kg. 109 samples had total fumonisin levels below 2 mg/kg, 20 samples were between 2 and 4 mg/kg, and 21 samples exceeded 4 mg/kg. ANOVA analysis revealed significant differences between years of the study ($F_{1,132}$ = 51.43 and $P < 0.0001$) with mean fumonisin levels higher in 2008 (5.59 mg/kg) than 2009 (0.50 mg/kg). In 2008, hybrid, insect infestation treatment, and their interaction were all significant factors contributing to the severity of total fumonisin contamination as determined by ELISA ($F_{2,50}$ = 4.31 and P = 0.0187, $F_{1,50}$ = 17.47 and $P = 0.0001$, $F_{2,50}$ = 5.15 and P = 0.0092, respectively) and likewise, in 2009 ($F_{2,77}$ = 15.55 and $P < 0.0001$, $F_{2,77}$ = 14.24 and $P < 0.0001$, $F_{4,77}$ = 8.11 and $P <$ 0.0001, respectively).

Total fumonisin levels as determined by HPLC ranged in individual samples from LOD to 34.87 mg/kg with a mean and standard deviation of 1.28 ± 3.19 mg/kg. A total of 197 samples had total fumonisin levels below 2 mg/kg, 17 samples were between 2 and 4 mg/kg, and 13 samples exceeded 4 mg/kg. Fumonisin contamination in maize grain (as determined by HPLC) was highest in 2008 (3.22 mg/kg), followed by 2010 (0.57 mg/kg), and lowest in 2009 (0.40 mg/kg) (Table 3).

Hybrids susceptible to WBC, namely, Cry1Ab and non-*Bt* hybrids, were significantly more contaminated with FB_1 than Cry1F hybrids which expressed insecticidal proteins against this insect. In 2007, ELISA results showed that Cry1F hybrids had less FB_1 contamination than Cry1Ab (P = 0.0423) or non-*Bt* hybrids (P = 0.0154). WBC infested plots had the highest mean FB_1 content in 2007 (19.44 mg/kg), greater than either ECB (6.48 mg/kg, P = 0.0019) or naturally infested plots (4.01 mg/kg, $P < 0.0001$) (Figure 4A). ECB infestation exacerbated total fumonisin contamination in comparison to naturally infested plots in 2008 ($P = 0.0001$ and $P = 0.0005$ for ELISA and HPLC, respectively). In 2008, non-*Bt* hybrids had higher levels of contamination than Cry1Ab hybrids or Cry1F hybrids. Among all hybrid/insect combinations in 2008, ECB infested non-*Bt* hybrids suffered this highest level of fumonisin

dx.doi.org/10.1021/jf5011897 | J. Agric. Food Chem. 2014, 62, 6463−6472

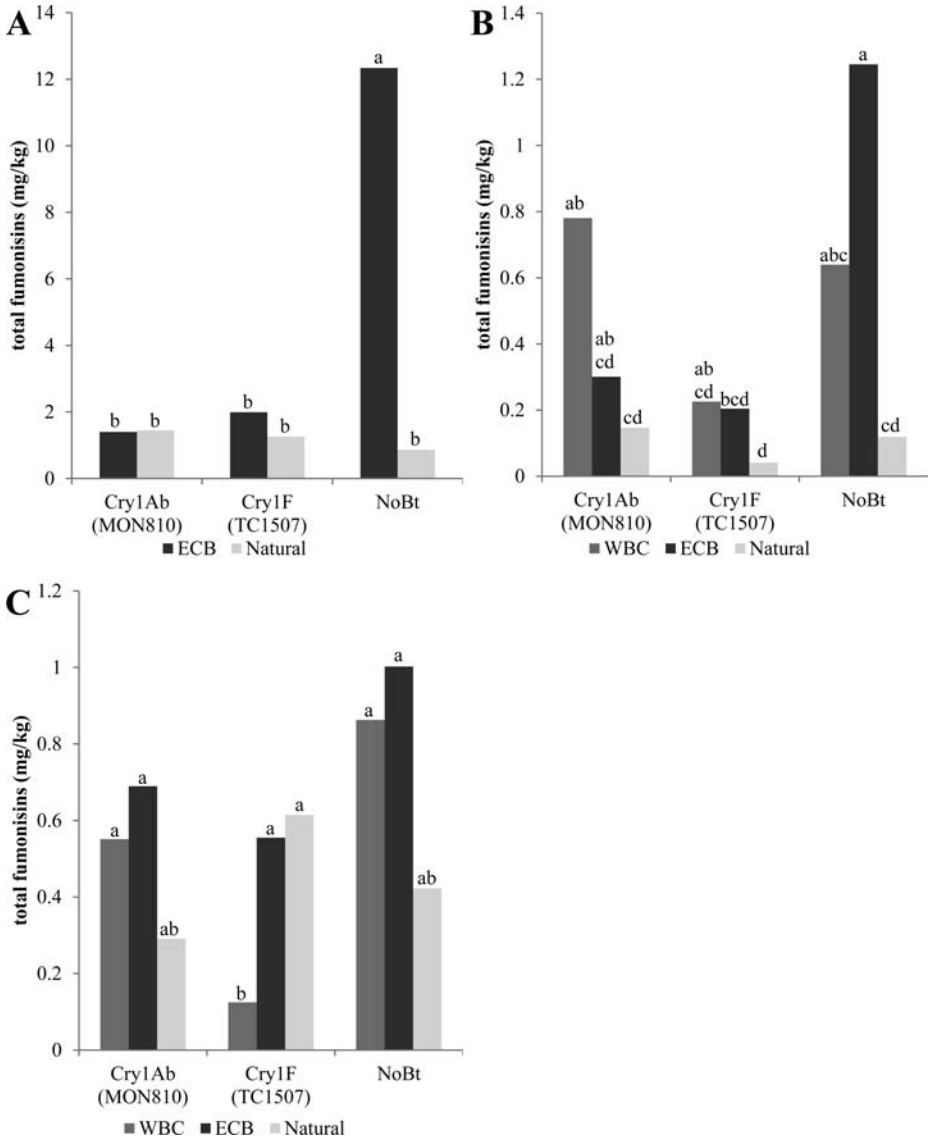

Figure 5. Fumonisin contamination, **1**−**3**, in maize (mg/kg) as determined by HPLC for (A) 2008, (B) 2009, and (C) 2010. Data are means of five replications each of two hybrids. Letters denote significant differences ($P < 0.05$) between hybrid/insect infestations within years.

contamination ($P < 0.0001$ to $P = 0.0062$) (Figure 4B and Figure 5A). In 2009, plots infested with WBC or ECB suffered higher levels of fumonisin contamination than naturally infested plots ($P < 0.0001$ and $P = 0.0012$, respectively (ELISA); $P < 0.0001$ and $P = 0.0002$, respectively (HPLC)). Cry1F hybrids in 2009 had less fumonisin contamination than Cry1Ab ($P = 0.0003$ by ELISA, $P = 0.0064$ by HPLC) or non-*Bt* hybrids ($P < 0.0001$ by ELISA, $P = 0.0005$ by HPLC) (Figure 4C and Figure 5B).

ELISA was not performed in 2010; HPLC results show that Cry1F hybrids were less contaminated than non-*Bt* hybrids ($P = 0.0101$) while Cry1Ab hybrids suffered an intermediate level of contamination relative to these, which did not differ from Cry1F or non-*Bt* hybrids. Averaged over all hybrids 2010, fumonisin contamination was the most severe in ECB infested plots, least in naturally infested plots ($P = 0.0146$), and WBC did not differ from either of these treatments. Cry1F plots infested with WBC in 2010 suffered the lowest levels of fumonisin contamination, less than either non-*Bt* or Cry1Ab plots infested with WBC ($P = 0.0002$ and $P = 0.0065$, respectively), or Cry1F plots subject to ECB or natural insect infestation treatment ($P = 0.0224$ and $P = 0.0277$, respectively) (Figure 5C). Overall, hybrids with *Bt* genes yielded grain with less kernel injury, *Fusarium* ear rot, and fumonisins compared to non-*Bt*, near-isogenic hybrids. Expression of *Bt* genes *cry1F* and *cry1Ab* in maize hybrids prevented insect feeding, thereby reducing the capability of toxigenic fungi to colonize the ear and produce mycotoxins. As a result, they experienced reduced contamination with fumonisins, compared to non-*Bt* hybrids, when grown under conditions of insect infestation. Total fumonisin contamination in maize obtained from *Bt* hybrids measured in 2008−2010 was consistently below FDA guidance levels.[31] In 2008, non-*Bt* grain would have suffered market limitations as a result of its fumonisin contamination, which exceeded 6 mg/kg as determined by HPLC and 11 mg/kg by ELISA.

In addition to the prevention of insect feeding by *Bt* maize that can result in reduced fumonisins, recent evidence also points to direct effects of *Bt* gene expression on fumonisin-producing *Fusarium* species. Rocha et al.[32] and Reis et al.[33] found that expression of genes in the fumonisin biosynthesis pathways was reduced when *F. verticillioides* fungus was grown

dx.doi.org/10.1021/jf5011897 | J. Agric. Food Chem. 2014, 62, 6463−6472

on maize kernels which express either Cry1Ab[32] or Cry1F[33] as compared with near-isogenic controls. In the current study, hybrids expressing Cry1Ab and Cry1F had reduced fumonisin contamination when exposed to pest pressures for which they expressed insecticidal proteins. Cry1F hybrids had the lowest fumonisin levels in 2007, 2009, and 2010, the three years in which WBC insect infestation was used. In all years of the study, Cry1F and Cry1Ab performed similarly under ECB infestation. Under nontarget pest pressures, *Bt* hybrids did not display a significant advantage over non-*Bt* hybrids. The rise of pests vying for maize as a secure food source will increase the need for planting hybrids which target a broader spectrum of pests. This will aid in reducing kernel injury and subsequently reducing toxigenic fungi colonization and mycotoxin accumulation in maize hybrids.

HPLC versus ELISA Results. There was a strong correlation ($r = 0.95$, $P < 0.0001$, $N = 138$) between total fumonisin results of HPLC and ELISA methods obtained for 2008−2009, the two years of the study for which both methods were used (Figure 6). ELISA results were, on average, higher than HPLC

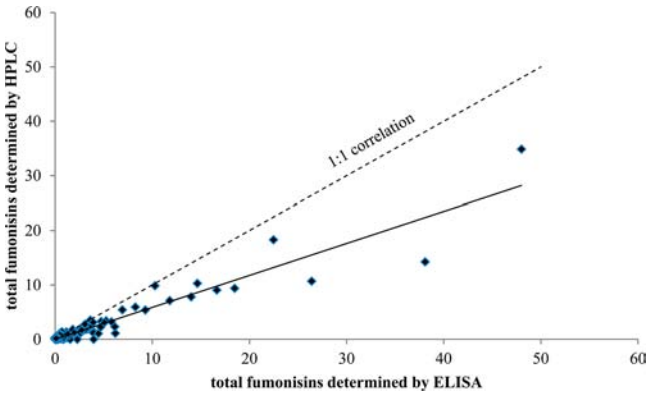

Figure 6. Correlation between total fumonisin concentration (FB_1 + FB_2 + FB_3) (mg/kg), **1**−**3**, determined by HPLC and ELISA (n = 138). Data are from 2008 and 2009.

results for the same sample, but the difference was not constant. Fumonisin contamination as determined by ELISA was correlated with insect injury ($R = 0.52$, $P < 0.0001$) and *Fusarium* ear rot ($R = 0.70$, $P < 0.0001$). These correlations were weaker when HPLC results were used to determine correlations with both insect injury ($R = 0.47$, $P < 0.0001$) and *Fusarium* ear rot ($R = 0.52$, $P < 0.0001$). Statistical significance of hybrid and insect infestation effects were generally the same for both HPLC and ELISA methods except for one case, a significant interaction effect in the 2009 ELISA data which was not significant for the HPLC data (Figures 4B and 5A, and Figures 4C and 5B). In this particular year, however, means calculated by hybrid-insect treatment combinations did not exceed 2 mg/kg for either method; it is, therefore, unlikely that market implications would have arisen from this discrepancy. Ghali et al.[34] also reported fumonisin contamination in maize by both HPLC and direct-competitive ELISA. In all commodities tested, ELISA gave more fumonisin-positive samples than HPLC. For samples detected as positive by both methods they found a significant coefficient of determination, $r^2 = 0.978$ ($N = 25$). Adoption and use of rapid test kits like ELISA in commercial settings is valuable to ensure that the mycotoxin contamination does not exceed market needs imposed by end-users. It may be appropriate to apply a correction factor to results obtained by rapid test kits, if their results differ from a validated analytical technique by a predictable factor. It is crucial, however, to use these techniques in the appropriate manner, ideally with regular check samples performed with validated analytical techniques.

AUTHOR INFORMATION

Corresponding Author

*Tel: 515-294-6383. E-mail: erin@iastate.edu.

Funding

This project was supported by the Biotechnology Risk Assessment Program competitive Grant No. 2008-33120-19543 from the USDA National Institute of Food and Agriculture Program. The project also was supported by a Crop Management Research Award from DuPont Pioneer, Inc., Des Moines, IA.

Notes

The authors declare no competing financial interest.

ACKNOWLEDGMENTS

The authors would like to thank Patricia Murphy (Iowa State University) for assistance with HPLC method validation and Jeanette Dyer (USDA-ARS Corn Insects and Crop Genetics Research Unit) and Larry Appel for providing insect eggs or larvae for infestation treatments. We also thank Clara Alarcon and Kelli Van Waus (DuPont Pioneer) for performing ELISA analysis for grain harvested from the 2007 preliminary study.

REFERENCES

(1) Munkvold, G. P.; Desjardins, A. E. Fumonisins in maize: can we reduce their occurrence? *Plant Dis.* **1997**, *81*, 556−565.

(2) Wu, F. Measuring the economic impacts of *Fusarium* toxins in animal feeds. *Anim. Feed Sci. Technol.* **2007**, *137*, 363−374.

(3) Sydenham, E. W.; Shephard, G. S.; Thiel, P. G.; Bird, C.; Miller, B. M. Determination of fumonisins in corn: evaluation of competitive immunoassay and HPLC techniques. *J. Agric. Food Chem.* **1996**, *44*, 159−164.

(4) Sutikno; Abouzied, M. M.; AzconaOlivera, J. I.; Hart, L. P.; Pestka, J. J. Detection of fumonisins in Fusarium cultures, corn, end corn products by polyclonal antibody-based ELISA: relation to fumonisin B_1 detection by liquid chromatography. *J. Food Prot.* **1996**, *59*, 645−651.

(5) Ono, E. Y. S.; Kawamura, O.; Ono, M. A.; Ueno, Y.; Hirooka, E. Y. A comparative study of indirect competitive ELISA and HPLC for fumonisin detection in corn of the state of Parana, Brazil. *Food Agric. Immunol.* **2000**, *12*, 5−14.

(6) Dowd, P. F., Involvement of arthropods in the establishment of mycotoxigenic fungi under field conditions. In *Mycotoxins in Agriculture and Food Safety*; Sinha, K. K., Bhatagnar, D., Eds.; Marcel Dekker: New York, 1998; pp 307−350.

(7) Dowd, P. F. Insect management to facilitate preharvest mycotoxin management. *Toxin Rev.* **2003**, *22*, 327−350.

(8) Sobek, E. A.; Munkvold, G. P. European corn borer (*Lepidoptera*: Pyralidae) larvae as vectors of *Fusarium moniliforme*, causing kernel rot and symptomless infection of maize kernels. *J. Econ. Entomol.* **1999**, *92*, 503−509.

(9) Christensen, J. J.; Schneider, C. L. European corn borer (*Pyrausta-Nubilalis* Hbn) in relation to shank, stalk, and ear rots of corn. *Phytopathology* **1950**, *40*, 284−291.

(10) Munkvold, G.; Hellmich, R.; Rice, L. Comparison of fumonisin concentrations in kernels of transgenic *Bt* maize hybrids and nontransgenic hybrids. *Plant Dis.* **1999**, *83*, 130−138.

(11) United States Department of Agriculture. Adoption of GE crops in the US. In *USDA-ERS National Agricultural Statistics Survey: 2013*; U.S. Dept. of Agriculture: 2013.

(12) Mason, C. E. *European corn borer: ecology and management*; Iowa State University: 1996; Vol. *327*.
(13) Hutchison, W. D.; Burkness, E. C.; Mitchell, P. D.; Moon, R. D.; Leslie, T. W.; Fleischer, S. J.; Abrahamson, M.; Hamilton, K. L.; Steffey, K. L.; Gray, M. E.; Hellmich, R. L.; Kaster, L. V.; Hunt, T. E.; Wright, R. J.; Pecinovsky, K.; Rabaey, T. L.; Flood, B. R.; Raun, E. S. Areawide suppression of European corn borer with Bt maize reaps savings to non-Bt maize growers. *Science* **2010**, *330*, 222−225.
(14) Catangui, M.; Berg, R. Western bean cutworm, *Striacosta albicosta* (Smith) (Lepidoptera: Noctuidae), as a potential pest of transgenic Cry1Ab *Bacillus thuringiensis* corn hybrids in South Dakota. *Environ. Entomol.* **2006**, *35*, 1439−1452.
(15) Dorhout, D.; Rice, M. Intraguild competition and enhanced survival of Western bean cutworm (*Lepidoptera*: Noctuidae) on transgenic Cry1Ab (MON810) Bacillus thuringiensis corn. *J. Econ. Entomol.* **2010**, *103*, 54−62.
(16) Guthrie, W. D. In *Advances in rearing the European corn borer in meridic diet*, Toward Insect Resistant Maize for the Third World. Proceedings of the International Symposium on Methodologies for Developing Host Plant Resistance to Maize Insects. International Maize and Wheat Improvement Center (CIMMYT), Mexico City, Mexico, 1987; pp 46−59.
(17) Kulisek, E. S.; Hazebroek, J. P. Comparison of extraction buffers for the detection of fumonisin B_1 in corn by immunoassay and high-performance liquid chromatography. *J. Agric. Food Chem.* **2000**, *48*, 65−69.
(18) Rice, L. G.; Dejong, J.; Ross, P. F.; Plattner, R. D.; Coats, J. R. Evaluation of a liquid chromatographic method for the determination of fumonisins in corn, poultry feed, and *Fusarium* culture material. *J. AOAC Int.* **1995**, *78*, 1002−1009.
(19) Bennett, G. A.; Richard, J. L. Liquid chromatographic method for analysis of the naphthalene dicarboxaldehyde derivative of fumonisins. *J. AOAC Int.* **1994**, *77*, 6.
(20) European Committee for Standardization (CEN), Determination of fumonisins B_1 and B_2 in maize based foods - HPLC method with immunoaffinity column clean up. CEN 14352:2005, 2005.
(21) Ndube, N.; van der Westhuizen, L.; Green, I. R.; Shephard, G. S. HPLC determination of fumonisin mycotoxins in maize: A comparative study of naphthalene-2,3-dicarboxaldehyde and *o*-phthaldialdehyde derivatization reagents for fluorescence and diode array detection. *J. Chromatogr., B: Anal. Technol. Biomed. Life Sci.* **2011**, *879*, 2239−2243.
(22) Konieczka, P.; Namiesnik, J., Method Validation. In *Quality assurance and quality control in the analytical chemical laboratory: a practical approach*; CRC Press: Boca Raton, 2009. http://www.fda.gov/food/guidanceregulation/guidancedocumentsregulatoryinformation/chemicalcontaminantsmetalsnaturaltoxinspesticides/ucm109231.htm (accessed 5/20/2014).
(23) Dowd, P. F. Biotic and abiotic factors limiting efficacy of Bt corn in indirectly reducing mycotoxin levels in commercial fields. *J. Econ. Entomol.* **2001**, *94*, 1067−1074.
(24) Smith, J. B. North American noctuidae. *Proc. U.S. Natl. Mus.* **1887**, *10*, 454.
(25) DiFonzo, C. D.; Hammond, R. Range expansion of Western bean cutworm, *Striacosta albicosta* (Noctuidae), into Michigan and Ohio. *Crop Manage. Online* **2008**, DOI: 10.1094/CM-2008-0519-01-BR.
(26) Tooker, J. F.; Fleischer, S. J. First report of Western bean cutworm (*Striacosta albicosta*) in Pennsylvania. *Crop Manage.* **2010**, DOI: 10.1094/CM-2010-0616-01-RS.
(27) Michel, A. P.; Krupke, C. H.; Baute, T. S.; Difonzo, C. D. Ecology and management of the Western bean cutworm (Lepidoptera: Noctuidae) in corn and dry beans. *J. Integr. Pest Manage.* **2010**, *1*, A1−A10.
(28) Storer, N.; Babcock, J.; Schlenz, M.; Meade, T.; Thompson, G.; Bing, J.; Huckaba, R. Discovery and characterization of field resistance to Bt maize: *Spodoptera frugiperda* (Lepidoptera: Noctuidae) in Puerto Rico. *J. Econ. Entomol.* **2010**, *103*, 1031−1038.
(29) Storer, N.; Kubiszak, M.; King, J. E.; Thompson, G.; Santos, A. Status of resistance to Bt maize in *Spodoptera frugiperda*: lessons from Puerto Rico. *J. Invertebr. Pathol.* **2012**, *110*, 294−300.
(30) European Commission, Commission Regulation (EC) No 401/2006 of 23 February 2006 laying down the methods of sampling and analysis for the official control of the levels of mycotoxins in foodstuffs. *Off. J. Eur. Union* **2006**, *L 70*, 12−34.
(31) United States Food and Drug Administration. *Guidance for industry: fumonisin levels in human foods and animal feeds; final guidance*; 2001.
(32) Rocha, L. O.; Reis, G. M.; Barroso, V. M.; Andrade, L. J.; Corrêa, B. Effect of Cry 1Ab toxins on FUM gene cluster expression and on fumonisin production by *Fusarium verticillioides*. *Proc., 12th Eur.* Fusarium *Semin.,* Bordeaux, France, 2013; INRA UR1264 MycSA, Ed. Bordeaux, France, 2013, 110.
(33) Reis, G. M.; Rocha, L. O.; Barroso, V. M.; Andrade, L. J.; Corrêa, B. Different levels of fumonisin production and FUM gene cluster expression on 2B710Hx corn hybrid. *Proc., 12th Eur.* Fusarium *Semin.,* Bordeaux, France, 2013; INRA UR1264 MycSA, Ed. Bordeaux, France, 2013; p 121.
(34) Ghali, R.; Ghorbel, H.; Hedilli, A. Fumonisin determination in Tunisian foods and feeds. ELISA and HPLC methods comparison. *J. Agric. Food Chem.* **2009**, *57*, 3955−3960.

fluorescence spontaneously when exposed to an allergen antigen. CD63 glycoprotein can be easily found on basophilic granular membranes in many cells, such as basophils, mast cells, and platelets.[22,23] The integration of cytoplasmic granules with the plasma membrane occurs when the basophils or mast cells are activated along with the successive release of inflammatory mediators, such as histamine,[24,25] although CD63 antigen expression on mast cell surfaces has always been detected by flow cytometric analysis.[26] However, the real-time expression of CD63 in individual cells cannot be observed.[27] Therefore, this study employed confocal fluorescence microscopy to examine CD63 surface expression on RBL mast cells stimulated with antigen, resulting in a rapid quantification method for fish PVs.

This study developed a novel, mast-cell-based, fluorescent sensor to quantify fish PV and evaluate IgE-mediated hypersensitivity. We contructed and transfected CD63−EGFP plasmid into RBL cells, to obtain stable genetically fluorescent cell lines. We also explored the use of the real-time surface expression of CD63−EGFP in anti-2,4-dinitrophenyl (DNP) IgE pre-sensitized RBL-2H3 cells exposed to DNP−bovine serum albumin (BSA) as a model for fluorescence detection by confocal laser scanning microscopy (CLSM). We measured changes in fluorescence intensity induced by the fish PV on mast cells and analyzed the relationship between different allergen concentrations and impedance signals. These RBL cell sensors successfully detected and identified target allergens within minutes, and the allergic reaction process was monitored in real time by CLSM.

EXPERIMENTAL PROCEDURES

Reagents and Chemicals. Mouse monoclonal anti-DNP IgE antibody, DNP−BSA, sulforhodamine B (SRB), bromochloroindolyl phosphate, nitro blue tetrazolium, and trichloroacetic acid were obtained from Sigma-Aldrich, Inc. (St. Louis, MO). Purified fish PV and mouse monoclonal anti-fish PV IgE antibody were purchased from Novus Biologicals (Littleton, CO). RBL cells were obtained from the Cell Bank of Chinese Academy of Sciences (Shanghai, China). RPMI 1640 medium and fetal bovine serum (FBS) was obtained from Gibco Laboratories (Gaithersburg, MD). Glass-bottomed dishes (35 mm) were purchased from Shengyou Biotechnology Co., Inc. (Hangzhou, China). Other conventional reagents were purchased from Sinopharm Chemical Reagent Co., Ltd. (Shanghai, China). All solutions were prepared with deionized water, and all reagents were of analytical grade.

Instrumentation. Fluorescence signals were recorded by CLSM (LSM 710, Carl Zeiss Microscopy GmbH, Göttingen, Germany). A FACS Calibur flow cytometer (BD Biosciences, San Jose, CA) was used to evaluate cell apoptosis. RBL cells were incubated in a CO_2 incubator (Thermo Scientific Forma Series II Water Jacket, Thermo Fisher Scientific, Inc., Waltham, MA).

Construction of a CD63−EGFP Prokaryotic Expression System. The complete coding sequence of mouse CD63 (NM_001042580) was retrieved from the National Center for Biotechnology Information (NCBI) GenBank database and amplified from mouse liver cDNA. The primers employed were mCD63, 5′-cgc gtc gac atg gcg gtg gaa gga g-3′ (forward) and 5′-gcg gga tcc cat tac ttc ata gcc ac-3′ (reverse). The mCD63 PCR products and apEGFP-N1 vector were digested with *Bam*HI and *Sal*I, and the resulting fragments were purified and ligated with T4 DNA ligase. The ligated product was transformed into DH5a competent cells and an isolated positive clone named pEGFP-N1-mCD63.

Transfection of Plasmid DNAs. At 1 day before transfection, plates were prepared containing 2×10^5 RBL mast cells in 500 μL of growth medium without antibiotics, such that the cells were 90−95% confluent at the time of transfection. The ratio of cationic carrier/DNA was optimized on the basis of the instructions of the manufacturer. Briefly, 4 μg of DNA were diluted in 50 μL of Opti-MEM I reduced serum medium without serum (Gibco Invitrogen, Life Technologies) and mixed gently. A total of 10 μL of Lipofectamine2000 (Invitrogen, Life Technologies, Grand Island, NY) was mixed gently before use and added to 50 μL of Opti-MEM I medium. After a 5 min incubation at room temperature, diluted DNA was combined with the diluted Lipofectamine 2000 (total volume of 100 μL) and incubated for 20 min at room temperature. Then, the mixture was added to RBL cell plates. After 4 h for DNA transfection, the transfection medium was replaced with fresh culture medium and these cells with CD63−GFP plasmid DNA were cultured in 35 mm dishes for a few days. Then, stable transfectants were obtained by selection with the antibiotic G418 (Gibco Invitrogen) and a stable transfectant RBL cell line with EGFP selected.

Western Blot Analysis for CD63−EGFP Expression. To each tube of harvested cells (in 20 μL), 180 μL of radio-immunoprecipitation assay (RIPA) lysis buffer containing phenylmethylsulfonyl fluoride (PMSF) was added and incubated for 10 min at room temperature (RT). Equal amounts of proteins were separated using 10% sodium dodecyl sulfate−polyacrylamide gel electrophoresis (SDS−PAGE) after boiling for 5 min in 4× loading buffer and transferred onto Immobilon-P membranes (Millipore Corp., Billerica, MA). The membranes were then incubated with anti-EGFP antibody and a second antibody immunoglobulin G (IgG horseradish peroxidase (HRP) (Santa Cruz Biotechnology, Santa Cruz, CA). Immunoreactivity was detected using the enhanced chemiluminescence (ECL) detection system (GE Healthcare Bio-Sciences Corp., Piscataway, NJ). The target protein bands were quantified by scanning densitometry using ImageJ processing software and normalized to the signal intensity of GAPDH.

***In Vitro* Cell Proliferation and Apoptosis Assay.** RBL cells seeded on a 96-well plate at 2×10^5 cells/well were infected with CD63−EGFP using the procedures described above or received only changes with fresh media, as controls. At 1, 2, or 3 days post-infection, SRB assays were performed as described by Cung at al.[28] In brief, cells were fixed at 4 °C and in 3.3% (w/v) trichloroacetic acid for 1 h without removing the culture media. After removal of the fixation solution by tapping until the plates were completely dry, each well of cells was incubated with 100 μL of 0.057% (w/v) SRB at RT for 30 min. The wells were then rinsed 4 times with 1% (v/v) aqueous acetic acid and dried, and the stained cells were dissolved in 200 μL of 10 mM Tris base (pH 10.5) with shaking for 5 min. Finally, the 510 nm absorbance was measured on a microplate reader (BioTek Instruments, Inc., Winooski, VT). The influence of EGFP gene transfer on cell survival was examined by evaluating apoptosis via fluorescence-activated cell-sorting analysis, including an annexin-V−EGFP apoptosis detection kit (Nanjing KeyGen Biotech Co., Ltd., Shanghai, China). Briefly, RBL cells on 12-well plates were harvested by trypsinization at 3 day after infection with CD63−EGFP plasmid. After neutralization by washing with culture media containing FBS and phosphate-buffered saline, the cells were resuspended in 100 μL of annexin-V binding buffer and stained in the dark with 4 μL of annexin-V−EGFP (an apoptosis marker) and 4 μL of propidium iodide (PI, a necrosis marker) for 15 min at room temperature as a control. After 400 μL of annexin-V binding buffer was added, 10 000 cells per sample were analyzed by flow cytometry and CellQuest software. Fluorescent signals from EGFP and PI were distinguished by three color detectors.

PV Purification. The PV from crucian carp, bream, and silver carp was extracted as described previously.[29] Briefly, 2 g of white muscle of each sample was extracted with 10 mL of 20 mM Tris−HCl (pH 7.5), using a homogenizer (NS1001 L2K, Niro Soavi, Italy). Supernatants were obtained as PV crude extracts after centrifugation at 8000*g* for 30 min. To achieve a clear solution for test, crude extracts were purified by taking advantage of their thermostability, heating at 70 °C for 5 min, and then immediately cooled in ice water, followed by centrifugation at 40000*g* for 30 min. Supernatants composed mainly of PV were analyzed by SDS−PAGE. Then, the extract solutions were subjected to anti-PV antibody pre-sensitized RBL cells, which were monitored by a confocal laser scanning (CLS) microscope for fluorescence analysis.

Scheme 1. Schematic Illustration of the Working Principle of a RBL Cell Sensor[a]

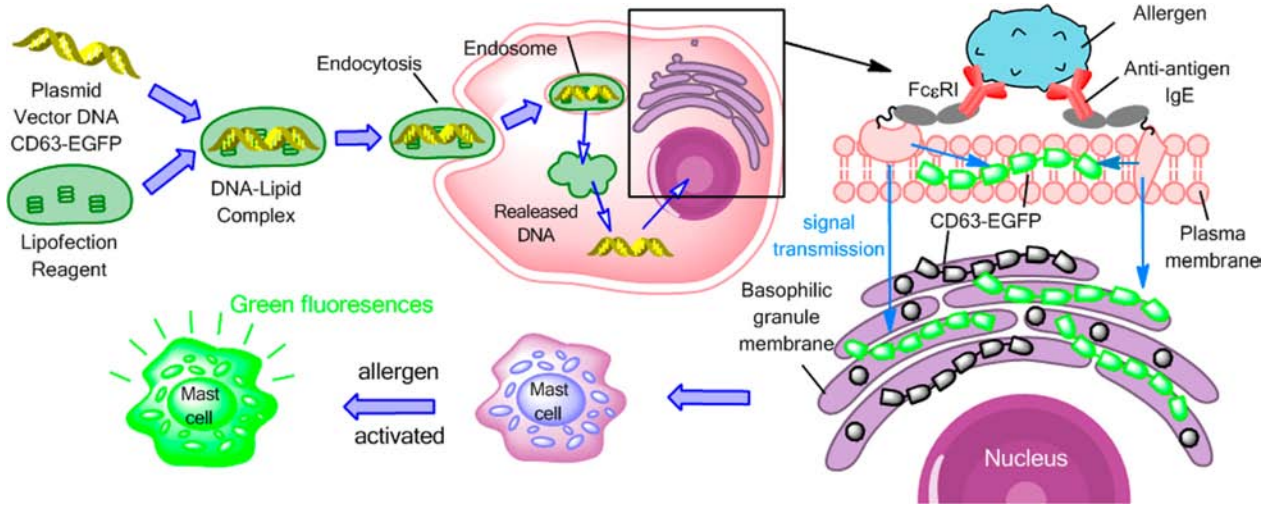

[a]Fusion plasmid CD63−EGFP was introduced into RBL cells to obtained stable transfectant fluorescent RBL cells. When allergen antigen bound to the antibody pre-sensitized mast cells, cytoplasmic granules would be fused with the plasma membrane and trigger the expression of CD63 and fluorescent protein on the cell surface. Therefore, allergen antigen would be detected by the elevation of intracellular fluorescence emitted by EGFP expression in RBL cells.

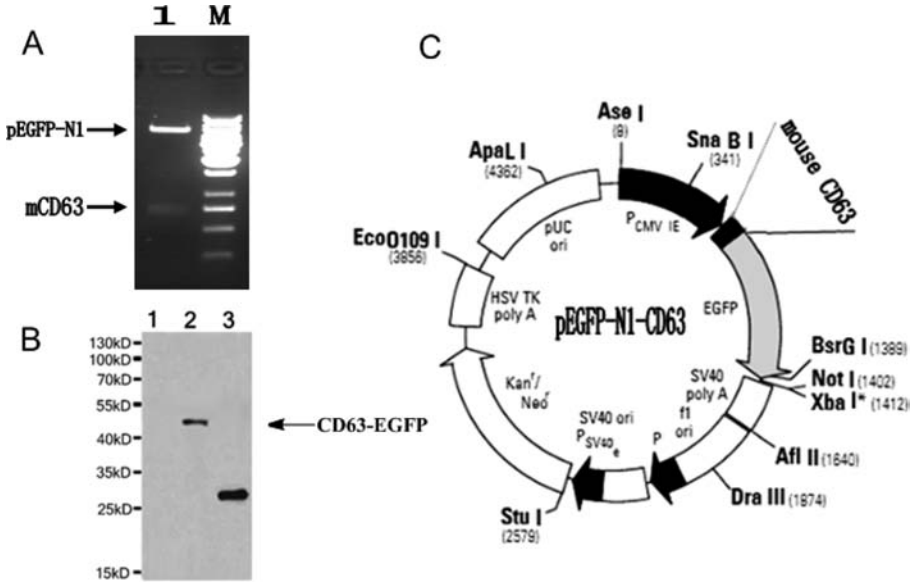

Figure 1. Construction of the pEGFP-N1-mCD63 vector and expression of the CD63−EGFP protein. (A) pEGFP-N1-mCD63 plasmid double-digested results, where M represents DNA markers (250, 500, 750, 1000, 1500, 2000, 2500, 3000, 3500, 4000, 45000, 5000, 6000, and 7000 bp) and 1 represents the pEGFP-N1-mCD63 plasmid double digested with *Bam*HI and *Sal*I. (B) Western blotting of lysates prepared from RBL cells at 24 and 48 h after transfection with the pEGFP-N1-mCD63 vector with anti-EGFP antibodies: 1, negative control (non-transfection cell); 2, CD63−EGFP fusion protein; 3, positive control (cell transfected with pEGFP-N1). (C) Map of the pEGFP-N1-CD63 plasmid. Mouse CD63 gene (not including the stop codon) was introduced at the *Sal*I and *Bam*HI restriction sites of the multiple cloning site (MCS) region of the pEGFP-N1 (Clontech, PT3027-5) vector.

RBL Cell Sensor Assay. RBL-2H3 cells were cultured in a flask in RPMI 1640 medium supplemented with 10% fetal calf serum, penicillin (100 μg mL^{-1}), and streptomycin (100 μg mL^{-1}) at 37 °C in a humidified atmosphere containing 5% CO_2. At the growth retardation stage after 3 days, cells reached the logarithmic growth phase, after which they were plated onto 35 mm glass-bottomed dishes (2×10^5 cells/dish) to form a monolayer overnight. Cells were then washed with Tyrode's buffer (Maishi BioTech, Suzhou, China) and pre-sensitized by incubation with Tyrode's buffer containing 10 mg/mL antibodies and 2.5 mM probenecid at 37 °C for 30 min. The resulting cells were then washed and maintained in Tyrode's buffer. A volume of 50 μL of serially diluted samples containing DNP−BSA or fish PV antigen was prepared in Tyrode's buffer and subjected to the prepared RBL sensor cells. The cell responses were monitored using a LSM 710 CLS microscope (Carl Zeiss Microscopy GmbH). Time-lapse sequences of RBL cells, recorded every 30 s, were collected, and the total fluorescence intensity for each image was calculated using Scion Image software (Scion Corp., Frederick MD). Cells not exposed to DNP−BSA (or fish PV antigen) served as controls.

β-Hexosaminidase Assay for Measurements of Cell Degranulation. A β-hexosaminidase assay was performed to validate the result of fluorescence analysis by IgE-mediated allergic response.[30] Cells growing in 96-well plates were washed, incubated in Tyrode's buffer, and stimulated with medium containing different allergen

dx.doi.org/10.1021/jf501382t | J. Agric. Food Chem. 2014, 62, 6473−6480

concentrations. After 1 h, the supernatant was removed and the cell monolayer was lysed in Tyrode's buffer containing 0.5% TX-100 to obtain the total cellular β-hexosaminidase activity. This activity was measured in both supernatant and lysates by adding 50 μL of substrate *p*-nitrophenyl-*N*-acetyl-β-glucopyranoside (1 mg/mL) to each well. After incubation at 37 °C for 1 h, the reaction was quenched by the addition of 150 μL of 0.4 M glycine at pH 10.7 and the 405 nm absorbance was read in an ELISA reader (BioTek Instruments, Inc.). The ratio of β-hexosaminidase release was calculated using the following formula: β-hexosaminidase release (%) = 100 × [(supernatant/blank supernatant)/(supernatant/blank supernatant) + (total cell lysate/blank total cell lysate)]. Cells incubated in medium without allergen served as blanks.

RESULTS AND DISCUSSION

Working Principles of RBL Cell Sensors. Scheme 1 illustrates the working principle by which a RBL cell sensor recognizes and quantifies a target antigen. In this study, we fused EGFP to mouse CD63, in which the C terminus of CD63 was conjugated with EGFP. Then, we introduced the fusion plasmid CD63−EGFP into RBL cells through a highly efficient, lipid-mediated, DNA-transfection procedure. DNA−lipid complexes were fused with the membrane by endocytosis, and the fluorescent protein gene was diffused throughout the intracellular membranes, thus entering the nucleus. Next, RBL cells were selected with the antibiotic G418 to obtained stable transfectant cells. Results show that CD63 expression on cell surfaces increased, along with the successive expression of fluorescent protein upon antibody activation in RBL mast cells pre-sensitized with allergen antigen (see the enlarged drawing on the right of Scheme 1). In this way, we monitored cell responses and quantified the allergen antigen through intracellular fluorescence changes observed under a CLS microscope.

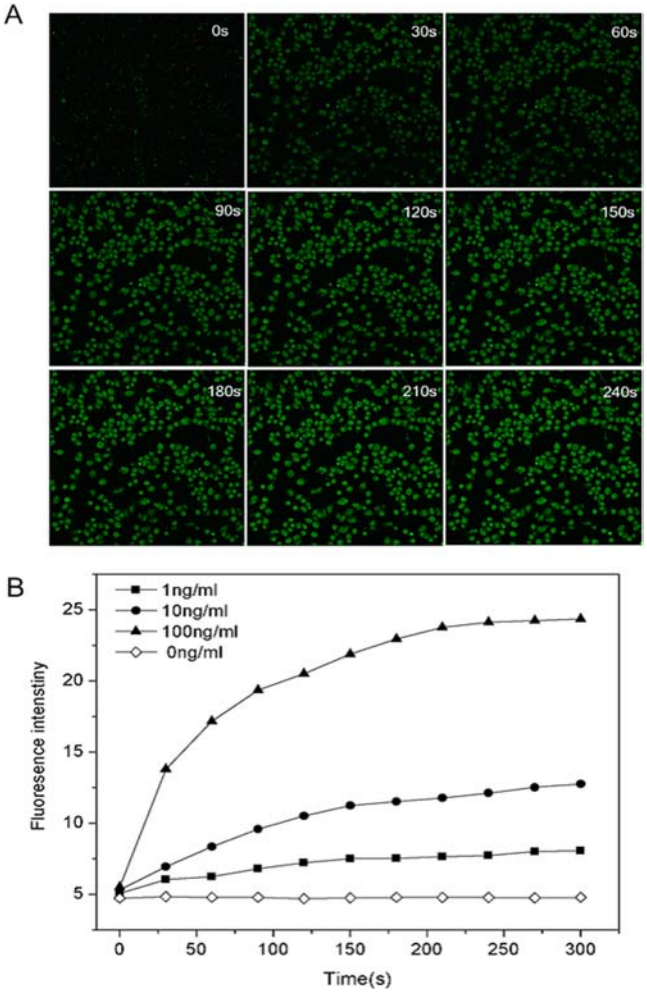

Figure 2. Fluorescence intensity changes of mast cells exposed to various concentrations of DNP−BSA. (A) Time-dependent images of cell fluorescence intensity responses. DNP−BSA (100 ng/mL) was employed to stimulate anti-DNP IgE pre-sensitized RBL cells. The images were recorded every 5 s and displayed every 30 s. (B) Quantification of fluorescence intensity in RBL cells after sensitization with 10-fold serial dilutions of DNP−BSA.

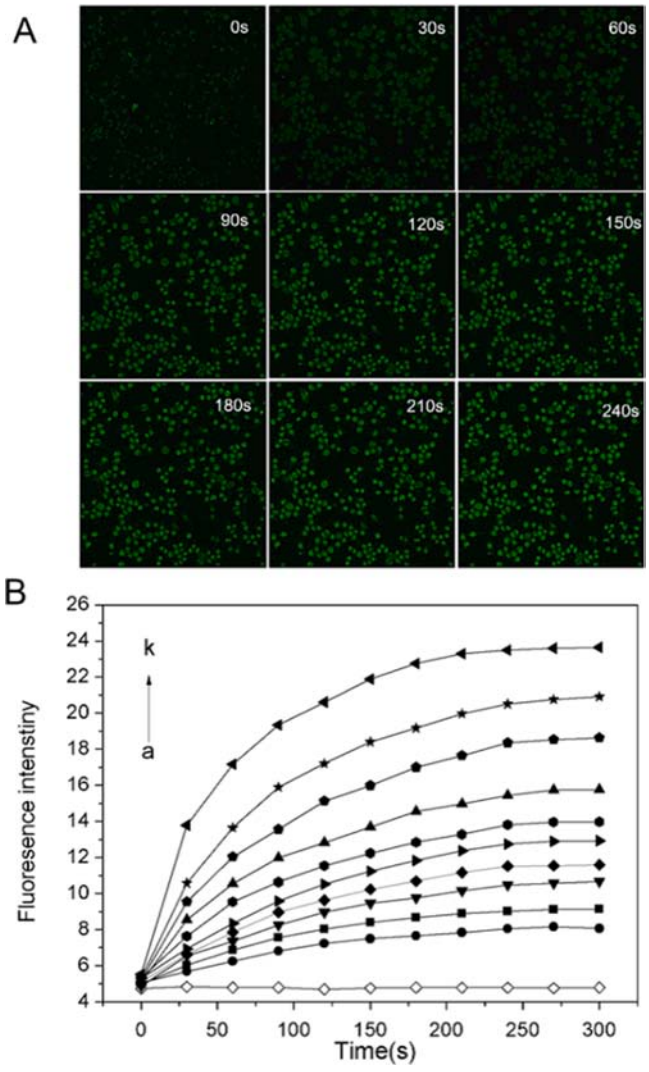

Figure 3. Fluorescence intensity changes of RBL cells with different concentrations of fish PV. (A) Time-dependent images of cell fluorescence intensity variation. PV (100 ng/mL) was used to stimulate RBL cells that pre-sensitized with anti-PV antibodies. The images were recorded at an interval of 5 s and exhibited every 30 s. (B) Quantification of fluorescence intensity in RBL cells exposed to 10 different concentrations of PV (from a to k: 0, 1, 2.5, 5, l0, 20, 40, 60, 80, and 100 ng/mL).

Successful Construction and Expression of CD63−EGFP Chimera Proteins. We amplified the CD63 gene from cDNA of mouse liver tissue with oligonucleotides, so that *Sal*I and *Bam*HI restriction sites were introduced at the 5′ and 3′

dx.doi.org/10.1021/jf501382t | J. Agric. Food Chem. 2014, 62, 6473−6480

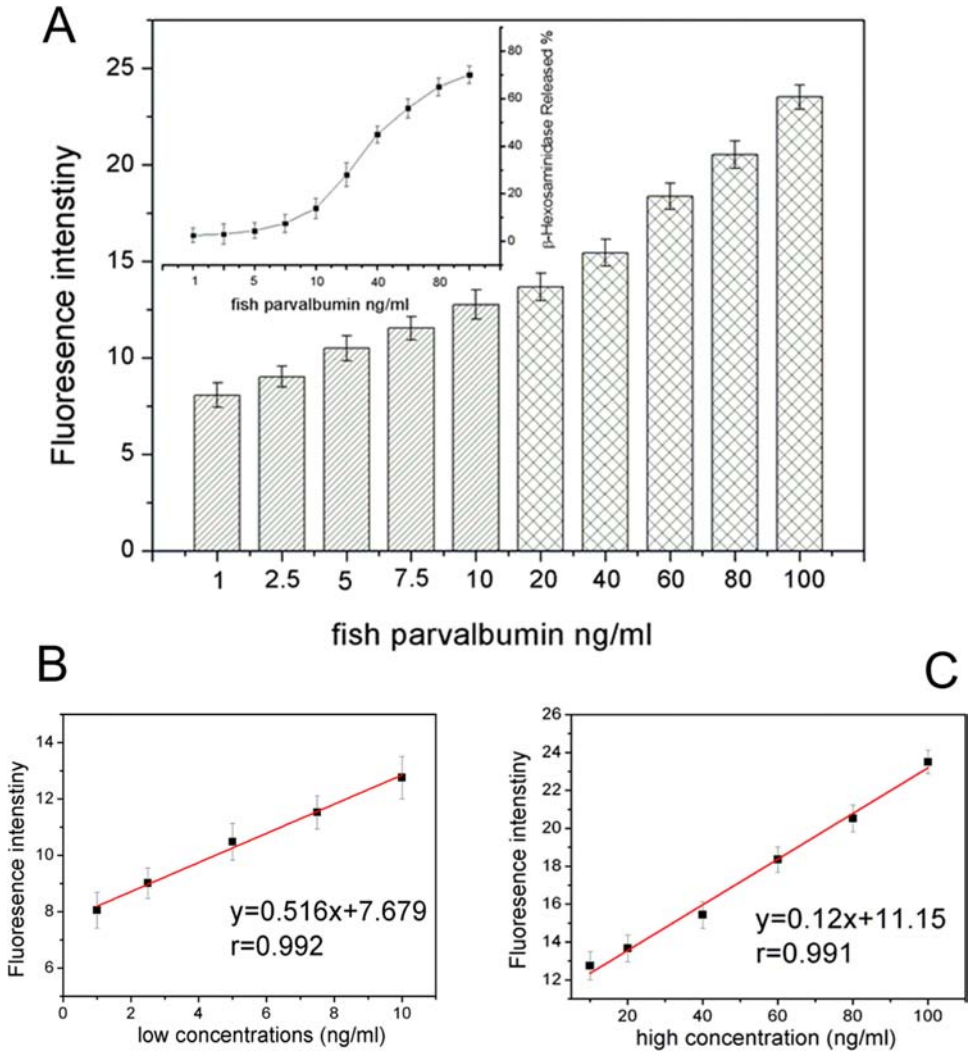

Figure 4. Quantification of fish allergen PV by RBL-2H3-cell-based sensor. (A) Fluorescence intensity spectroscopy for RBL-2H3 cells treated with different doses of fish allergen PV: 1, 2.5, 5, 7.5, 10, 20, 40, 60, 80, and 100 ng/mL. (Inset) β-Hexosaminidase assay for confirmation of the cell activated by fish allergen PV. (B) Linear regression of fluoresence intensity versus low concentrations of PV (1−10 ng/mL). (C) Linear regression of fluoresence intensity versus high concentrations of PV (10−100 ng/mL). Data represent the mean ± SE of three different experiments under similar conditions.

ends, respectively. The PCR products and pEGFP-N1 plasmids were also double-digested with *Bam*HI and *Sal*I, ligated with T4 DNA ligase, and transfected into DH5a competent cells (Figure 1A). The recombinant plasmids were double-digested with *Bam*HI and *Sal*I, and the positive clone was named pEGFP-N1-mCD63 (Figure 1C). The anti-EGFP antibody was used to detect CD63−EGFP fusion protein expression. One major band, ~46 kDa (the CD63 and EGFP fusion protein), was observed (Figure 1B), which was in good agreement with the sum of the molecular sizes of CD63 and EGFP. The RBL cells infected with CD63−EGFP showed strong fluorescence signals from EGFP expression at day 3 after antigen stimulation, indicating a high transfection efficiency of about 83.27 ± 1.45% through fluorescent observation and flow analysis (see Figure S1A of the Supporting Information).

SRB-based proliferation assays were performed to investigate potential adverse effects during the transfection process. Results show no difference in RBL cell numbers at 1, 2, and 3 days between the CD63−EGFP-infected and control groups (see Figure S1B of the Supporting Information). Flow cytometric analyses were conducted at day 3 for the CD63−EGFP-infected and control groups, using annexin V−EGFP and PI as markers for apoptosis and necrosis, respectively. Results show similar low rates of early apoptosis (0.86 ± 0.21 versus 0.72 ± 0.18%, respectively) and necrosis (0.17 ± 0.13 versus 0.23 ± 0.15%, respectively; see Figure S1C of the Supporting Information).

Quantification of Fish Allergen PV by RBL Cell Sensors. Naive RBL cells cannot recognize any antigens. They can only recognize antigens when anti-antigen IgE antibodies bind tightly to the high-affinity receptors (FcεRI) on their cell surfaces. This binding allows them to be stimulated by cross-linking with protein allergens to initiate a sequence of biochemical events, including cellular degranulation and release of inflammatory molecules.[31] We verified the use of cell sensors to recognize allergen antigen recognition with DNP−BSA, a multivalent model antigen, to stimulate RBL cells pre-sensitized with anti-DNP IgE.

We also used time-lapse imaging of cell responses after stimulation with DNP−BSA (100 ng/mL) and measured fluorescence intensity changes over time to determine the amplitude and speed of cell responses. Results show that both declined with a decreased DNP−BSA concentration (panels A

dx.doi.org/10.1021/jf501382t | J. Agric. Food Chem. 2014, 62, 6473−6480

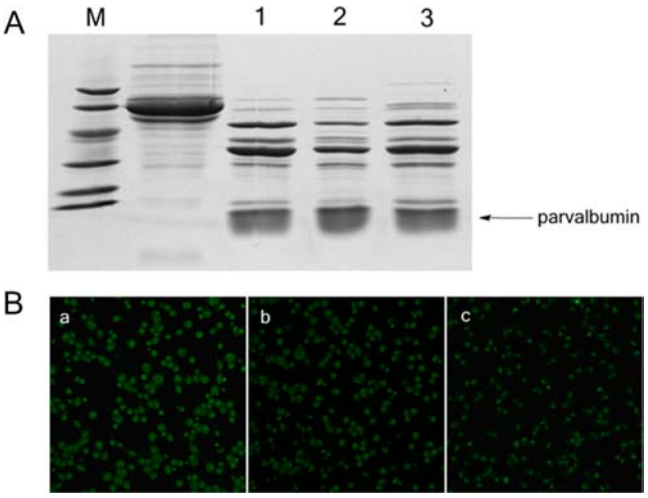

Figure 5. (A) SDS–PAGE analysis for PV from three kinds of different fish purifications: M, protein marker (97, 66, 44, 29, 20, and 14 kDa); 1, crucian carp; 2, silver carp; and 3, bream. (B) Quantification of three kinds of fish PV by a RBL-2H3-cell-based sensor: (a) crucian carp, (b) silver carp, and (c) bream.

Table 1. Concentration and Content of PV in Three Kinds of Fish[a]

sample	crucian carp	silver carp	bream
fluorescence intensity (mean ± SD)	18.84 ± 0.08	14.88 ± 0.14	13.68 ± 0.16
PV concentration (ng/mL ± SD)	64.08 ± 0.22	31.08 ± 0.35	21.08 ± 0.33
PV content (mg/g ± SD)	1.92 ± 0.23	0.93 ± 0.28	0.63 ± 0.26

[a]SD = standard deviation (n = 5).

and B of Figure 2, respectively). These results are in accordance with previous reports. They indicate the presence of target antigens and demonstrate that RBL cell sensor responses can be monitored in real time with CLSM.[19]

Next, fish PV standards were applied to evaluate the feasibility of RBL cell sensors. We prepared cell sensors using pre-sensitized RBL cells with anti-fish PV antibodies. We monitored the resulting cell fluorescence changes with CLSM in real time. Time-lapse images of RBL cell sensors responding to fish PV (100 ng/mL) reveal that activating mast cells with antigens led to a rapid and robust increase in cell fluorescence intensity (Figure 3A). We also measured the response of sensors to different PV concentrations in terms of the fluorescence intensity versus time (Figure 3B). PV samples were added after a stable fluorescence signal was obtained. At low PV concentrations (1–100 ng/mL), from the time of addition (at 0 s), RBL cells showed a slow increase in fluorescence intensity. This indicates the initiation of CD63–EGFP chimera protein expression on cytoplasmic granular and plasma membranes. This, in turn, created a non-uniform distribution of fluorescence on the cell surface and in the cytoplasm, leading to a lower fluorescence intensity.

At high PV concentrations, cell fluorescence intensity rose rapidly, reaching a plateau of sustained saturation within 60 s after stimulation. Further investigation of the allergic responses of these cells reveals that high activation of mast cells induced fusion of cytoplasmic granular membranes with plasma membranes. This resulted in the degranulation of secretory vesicles and release of inflammatory molecules, such as histamine and β-hexosaminidase.[32] We also examined fluorescence changes on the surface of single cells, and the result is in accordance with previous results (see Figure S2 of the Supporting Information).

A histogram of the linear relationship between the fish PV concentrations and fluorescence intensity clearly shows that fluorescence signals follow the same trend as that of DNP–BSA-activated cells (Figure 4A). Fluorescence intensity was proportional to PV, ranging from 1 to 100 ng/mL. A β-hexosaminidase assay was performed to confirm the fluorescence analysis results (inset of Figure 4A). This indicates that the β-hexosaminidase release rate increased gradually at low PV concentrations, while it grew rapidly at high concentrations. These data agreed well with the dose–response curve obtained from fluorescence measurements.

At both low and high PV concentrations, fluorescence intensities exhibited good linear relationships with fish PV concentrations, with correlation coefficients of 0.992 and 0.991 (low and high PV concentrations in panels B and C of Figure 4, respectively). The limit of detection (LOD) calculated from Figure 4B was 0. 35 ng/mL, according to the formula: LOD = $3s/m$, where s represents the blank sample standard deviation (n = 3) and m represents the slope of the related PV calibration curve. These measurements were performed in triplicate to assess the reproducibility and precision of freshly fabricated cell sensors. The relative standard deviation (RSD) of the detection results were all <5%, showing acceptable performance.

Real Sample Measurements. To assess the utility of these sensors for rapidly recognizing target allergens from the complex food matrix, we used crucian carp, bream, and silver carp extra to test the performance of this sensor. As shown in Figure 5A, purified PV was applied to the gel and SDS–PAGE was performed. There was a major protein band at 12 kDa, which was identified by Coomassie Brilliant Blue staining (arrow in Figure 5A). This indicated substantial purification on PV. Then, the activation of cell sensors with three kinds of fish extracts also led to a rapid and robust increase in cell fluorescence intensity (Figure 5B). The concentrations and contents of PV in three fish samples calculated from the standard curve of the fluorescence intensity versus PV standards in Figure 4B are shown in Table 1. The results obtained using the RBL sensors were similar to those reported methods, which confirms that this biosensor can be applied effectively for the detection and prediction in real allergen samples.

Investigation of RBL Cell Sensor Specificity and Reproducibility. We also assessed the effectiveness of this new sensor for recognition of fish PV by challenging RBL sensor cells that were pre-sensitized with anti-fish PV antibodies, fish PV, shrimp allergen Pen a 1, and peanut allergen Ara h 1 (prepared in-house). Non-specific interactions between cells and antigens were excluded by challenging naive, unsensitized RBL sensor cells in parallel with pre-sensitized cells. Shrimp allergen Pen a 1 or peanut allergen Ara h 1 produced few observable responses (see Figure S3 of the Supporting Information). Therefore, it can be assumed that contamination with shrimp and peanut allergens would not influence sensor recognition of fish PV in heterogeneous mixed-food samples containing various allergens.

To demonstrate the reproducibility of this cell-based sensor, measurements were performed in triplicate with the same prepared RBL cells to assess reproducibility and precision (SD = 0.446 ± 0.04). Moreover, RBL cells were repeatedly activated

by anti-PV IgE and PV antigens within a 24 h interval. Results of fluorescence analysis show that reactivated RBL cells in response to PV levels retained 80% of the original value (as seen in Figure S6 of the Supporting Information), which well illustrates the reproducible characteristics of the sensor.

■ ASSOCIATED CONTENT

Supporting Information

Efficiency of CD63−EGFP transfection and influence on cell proliferation and survival (Figure S1), time-lapse imaging of single cell fluorescence intensity change challenged with 100 ng/mL PV (Figure S2), specific detection of fish PV by RBL cell sensors (Figure S3), time-dependent antigen-stimulated increases in cytoplasmic Ca^{2+} detected by Fluo-4 fluorescence (Figure S4), time-dependent increases in stimulated production of reactive oxygen detected by DCDHF cytoplasmic fluorescence (Figure S5), and reproducibility of cell-based sensors activated with 100 ng/mL PV (Figure S6). This material is available free of charge via the Internet at http://pubs.acs.org.

■ AUTHOR INFORMATION

Corresponding Authors

*Telephone: +86-510-85329015. Fax: +86-510-85328726. E-mail: sxlzzz@jiangnan.edu.cn.

*Telephone: +86-510-85329015. Fax: +86-510-85328726. E-mail: genyiz@gmail.com.

Funding

This work has been supported by the National Research Program (2011BAK10B03), the "973" National Basic Research Program of China (2012CB720804), the Program for New Century Excellent Talents in Jiangnan University, the Commonwealth Project of the Ministry of Agriculture (201203069-1), and the Priority Academic Program Development of Jiangsu Higher Education Institutions.

Notes

The authors declare no competing financial interest.

■ REFERENCES

(1) Cai, Q. F.; Wang, X. C.; Liu, G. M.; Zhang, L.; Ruan, M. M.; Liu, Y.; Cao, M. J. Development of a monoclonal antibody-based competitive enzyme linked-immunosorbent assay (c-ELISA) for quantification of silver carp parvalbumin. *Food Control* **2013**, *29*, 241−247.

(2) Sampson, H. A. Food anaphylaxis. *Br. Med. Bull.* **2000**, *56*, 925−935.

(3) Lim, D. L. C.; Neo, K. H.; Yi, F. C.; Chua, K. Y.; Goh, D. L. M.; Shek, L. P. C.; Giam, Y. C.; Van Bever, H. P.; Lee, B. W. Parvalbumin—The major tropical fish allergen. *Pediatr. Allergy Immunol.* **2008**, *19*, 399−407.

(4) Jeebhay, M.; Robins, T.; Lehrer, S.; Lopata, A. Occupational seafood allergy: A review. *Occup. Environ. Med.* **2001**, *58*, 553−562.

(5) Griesmeier, U.; Vázquez Cortés, S.; Bublin, M.; Radauer, C.; Ma, Y.; Briza, P.; Fernández Rivas, M.; Breiteneder, H. Expression levels of parvalbumins determine allergenicity of fish species. *Allergy* **2010**, *65*, 191−198.

(6) Swoboda, I.; Bugajska-Schretter, A.; Verdino, P.; Keller, W.; Sperr, W. R.; Valent, P.; Valenta, R.; Spitzauer, S. Recombinant carp parvalbumin, the major cross-reactive fish allergen: A tool for diagnosis and therapy of fish allergy. *J. Immunol.* **2002**, *168*, 4576−4584.

(7) Carrera, M.; Cañas, B.; Piñeiro, C.; Vázquez, J.; Gallardo, J. M. Identification of commercial hake and grenadier species by proteomic analysis of the parvalbumin fraction. *Proteomics* **2006**, *6*, 5278−5287.

(8) Carrera, M.; Cañas, B.; Gallardo, J. M. Rapid direct detection of the major fish allergen, parvalbumin, by selected MS/MS ion monitoring mass spectrometry. *J. Proteomics* **2012**, *75*, 3211−3220.

(9) Sun, M.; Liang, C.; Gao, H.; Lin, C.; Deng, M. Detection of parvalbumin, a common fish allergen gene in food, by real-time polymerase chain reaction. *J. AOAC Int.* **2008**, *92*, 234−240.

(10) Li, Z.; Zhang, Y.; Pawar, R.; Wang, G.; Lin, H. Development of an optimized protein chip for the detection of fish parvalbumin allergen. *Curr. Anal. Chem.* **2011**, *7*, 349−356.

(11) Fæste, C. K.; Plassen, C. Quantitative sandwich ELISA for the determination of fish in foods. *J. Immunol. Methods* **2008**, *329*, 45−55.

(12) Shibahara, Y.; Uesaka, Y.; Wang, J.; Yamada, S.; Shiomi, K. A sensitive enzyme-linked immunosorbent assay for the determination of fish protein in processed foods. *Food Chem.* **2013**, *136*, 675−681.

(13) Matsubara, Y.; Murakami, Y.; Kobayashi, M.; Morita, Y.; Tamiya, E. Application of on-chip cell cultures for the detection of allergic response. *Biosens. Bioelectron.* **2004**, *19*, 741−747.

(14) Rider, T. H.; Petrovick, M. S.; Nargi, F. E.; Harper, J. D.; Schwoebel, E. D.; Mathews, R. H.; Blanchard, D. J.; Bortolin, L. T.; Young, A. M.; Chen, J. AB cell-based sensor for rapid identification of pathogens. *Science* **2003**, *301*, 213−215.

(15) Curtis, T. M.; Widder, M. W.; Brennan, L. M.; Schwager, S. J.; van der Schalie, W. H.; Fey, J.; Salazar, N. A portable cell-based impedance sensor for toxicity testing of drinking water. *Lab Chip* **2009**, *9*, 2176−2183.

(16) Pradhan, R.; Mandal, M.; Mitra, A.; Das, S. Assessing cytotoxic effect of ZD6474 on MDA-MB-468 cells using cell based sensor. *IEEE Sens. J.* **2014**, *14*, 1476−1478.

(17) Xing, J. Z.; Zhu, L.; Gabos, S.; Xie, L. Microelectronic cell sensor assay for detection of cytotoxicity and prediction of acute toxicity. *Toxicol. In Vitro* **2006**, *20*, 995−1004.

(18) Qu, M.; Boruah, B. M.; Zhang, W.; Li, Y.; Liu, W.; Bi, Y.; Gao, G. F.; Yang, R.; Liu, D.; Gao, B. A rat basophilic leukaemia cell sensor for the detection of pathogenic viruses. *Biosens. Bioelectron.* **2013**, *43*, 412−418.

(19) Curtis, T.; Naal, R. M. Z.; Batt, C.; Tabb, J.; Holowka, D. Development of a mast cell-based biosensor. *Biosens. Bioelectron.* **2008**, *23*, 1024−1031.

(20) Passante, E.; Frankish, N. The RBL-2H3 cell line: Its provenance and suitability as a model for the mast cell. *Inflammation Res.* **2009**, *58*, 737−745.

(21) Enoksson, M.; Lyberg, K.; Möller-Westerberg, C.; Fallon, P. G.; Nilsson, G.; Lunderius-Andersson, C. Mast cells as sensors of cell injury through IL-33 recognition. *J. Immunol.* **2011**, *186*, 2523−2528.

(22) Metzelaar, M.; Wijngaard, P.; Peters, P.; Sixma, J. J.; Nieuwenhuis, H. K.; Clevers, H. CD63 antigen. A novel lysosomal membrane glycoprotein, cloned by a screening procedure for intracellular antigens in eukaryotic cells. *J. Biol. Chem.* **1991**, *266*, 3239−3245.

(23) Nieuwenhuis, H. K.; Van Oosterhout, J.; Rozemuller, E.; van Iwaarden, F.; Sixma, J. J. Studies with a monoclonal antibody against activated platelets: Evidence that a secreted 53,000-molecular weight lysosome-like granule protein is exposed on the surface of activated platelets in the circulation. *Blood* **1987**, *70*, 838−845.

(24) Amano, T.; Furuno, T.; Hirashima, N.; Ohyama, N.; Nakanishi, M. Dynamics of intracellular granules with CD63-GFP in rat basophilic leukemia cells. *J. Biochem.* **2001**, *129*, 739−744.

(25) Furuno, T.; Teshima, R.; Kitani, S.; Sawada, J.-i.; Nakanishi, M. Surface expression of CD63 antigen (AD1 antigen) in P815 mastocytoma cells by transfected IgE receptors. *Biochem. Biophys. Res. Commun.* **1996**, *219*, 740−744.

(26) Knol, E. F.; Mul, F. P.; Jansen, H.; Calafat, J.; Roos, D. Monitoring human basophil activation via CD63 monoclonal antibody 435. *J. Allergy Clin. Immunol.* **1991**, *88*, 328−338.

(27) Mahmudi-Azer, S.; Downey, G. P.; Moqbel, R. Translocation of the tetraspanin CD63 in association with human eosinophil mediator release. *Blood* **2002**, *99*, 4039−4047.

(28) Quach, C. H. T.; Jung, K.-H.; Paik, J.-Y.; Park, J.-W.; Lee, E. J.; Lee, K.-H. Quantification of early adipose-derived stem cell survival:

Comparison between sodium iodide symporter and enhanced green fluorescence protein imaging. *Nucl. Med. Biol.* **2012**, *39*, 1251−1260.
(29) Kobayashi, A.; Tanaka, H.; Hamada, Y.; Ishizaki, S.; Nagashima, Y.; Shiomi, K. Comparison of allergenicity and allergens between fish white and dark muscles. *Allergy* **2006**, *61*, 357−363.
(30) Abassi, Y. A.; Jackson, J. A.; Zhu, J.; OConnell, J.; Wang, X.; Xu, X. Label-free, real-time monitoring of IgE-mediated mast cell activation on microelectronic cell sensor arrays. *J. Immunol. Methods* **2004**, *292*, 195−205.
(31) Dearman, R.; Skinner, R.; Deakin, N.; Shaw, D.; Kimber, I. Evaluation of an in vitro method for the measurement of specific IgE antibody responses: The rat basophilic leukemia (RBL) cell assay. *Toxicology* **2005**, *206*, 195−205.
(32) Furuno, T.; Nakanishi, M. Live cell imaging to study signaling molecules in allergic reactions. *Biol. Pharm. Bull.* **2005**, *28*, 1551.

compound, the Maillard reaction leads to brown color melanoidins and flavor compounds including pyrazines, pyrroles, furans, oxazoles, and so on.[16,17] There have been many research studies into the Maillard reaction's products in terms of color and flavor.

Various analytical methods to determine the presence of 4-MI have been developed, based on gas chromatography−mass spectrometry (GC−MS), high-performance liquid chromatography (HPLC), and liquid chromatography−tandem mass spectrometry (LC−MS/MS).[17−19] These methods require expensive equipment and specialized technical skills. Therefore, development of an index such as color parameters or volatile compounds would be useful for determining the presence of 4-MI.

The specific aim of this study was to examine the effect of food additives in the formation of 4-MI and determine the correlation among color parameters, pyrazines as dominant flavor compounds, and 4-MI. A caramel model system was chosen that consisted of glucose and ammonium hydroxide (as class III) with food additives such as metal ions (Fe^{2+}, Ca^{2+}, Zn^{2+}, Mg^{2+}) and amino acids (cysteine, tryptophan), each at different levels.

MATERIALS AND METHODS

Reagents. 4-Methylimidazole (4-MI, purity ≥98%), 2-ethylimidazole (2-EI, purity ≥98%), D-glucose (purity ≥99.5%), sodium sulfite (purity ≥98%), ammonium hydroxide solution (purity ≥29%), acetic acid (purity ≥99.7%), bis-2-ethylhexylphosphate (BEHPA, purity ≥97%), and isobutyl chloroformate (IBCF, purity ≥98%) were purchased from Sigma-Aldrich Chemical Co. (St. Louis, MO). Isooctane, acetonitrile (MeCN), pyridine, and isobutyl alcohol (purity ≥99%) were Lichrosolv quality and purchased from Merck (Darmstadt, Germany). Magnesium sulfate ($MgSO_4{\cdot}7H_2O$) and zinc sulfate ($ZnSO_4{\cdot}7H_2O$) were purchased from Junsei Chemical Co. (Tokyo, Japan), and iron sulfate ($FeSO_4$) was purchased from Kanto Chemical Co. (Tokyo, Japan). Calcium sulfate ($CaSO_4{\cdot}0.5H_2O$) was purchased from Yukari Pure Chemical Co. (Osaka, Japan), and tryptophan (purity ≥99%) and cysteine (purity ≥99.5%) were purchased from Junsei and Fluka (Neu-Ulm, Germany), respectively. All reagents were analytical grade.

Standard stock solutions of 4-MI and 2-EI used as an internal standard (IS) were prepared in 0.1 M HCl at a concentration of 20 and 1 mg/kg, respectively. All the solutions were kept at 4 °C until used.

Sample Preparations of the Caramel Model Systems. Glucose and ammonium hydroxide both were dissolved in 30 mL of HPLC-grade water in a swing top bottle, each at a concentration of 1 M. To compare the influences of food additives on the formation of 4-MI, all additives were added to glucose/ammonium solution individually at three distinct concentrations: 0.1, 0.05, and 0.01 M. The food additives were Fe^{2+} (as $FeSO_4$), Ca^{2+} (as $CaSO_4$), Zn^{2+} (as $ZnSO_4{\cdot}7H_2O$), Mg^{2+} (as $MgSO_4{\cdot}7H_2O$), cysteine, sodium sulfite, and tryptophan. The caramel model system solutions were heated at 100 °C for 2 h in an oven to instigate the Maillard reaction and cooled under running cold water to room temperature immediately in order to stop the reaction progress. All samples were stored at 4 °C, until they were analyzed.

Analysis of 4(5)-Methylimidazole. The procedure to extract 4-MI from a sample was carried out in the manner specified in a previous study.[17] Each sample (100 μL) was added to 4 mL of phosphate buffer that was extracted from 8 mL of 0.1 M BEHPA in chloroform by mixing for 1 min and centrifugation at 3500 rpm for 10 min. A 7.5 mL portion of the chloroform phase was transferred to a second vial containing 4 mL of 0.1 M HCl and mixed again by vortexing for 1 min. After centrifugation at 3500 rpm for 5 min, a 1 mL aliquot of the aqueous phase was added with 100 μL of 2-EI used as IS, which was placed into a vial and mixed with 1 mL of MeCN−isobutyl alcohol−pyridine (50:30:20, v/v) and 120 μL of IBCF for derivatization by hand for 30 s. Subsequently, 500 μL of a 1.0 M sodium bicarbonate solution and 500 μL of isooctane were added, and the mixture was mixed for 4−5 s. Then, 2 μL of the upper layer was injected into the GC−MS system.

The determination of 4-MI was conducted using an Agilent gas chromatograph interfaced to an inert 5975 mass selective detector (Palo Alto, CA) with an electron impact (EI) ionization chamber and equipped with a 7683B Series injector/autosampler. A DB-5 ms column (30 m × 0.25 mm i.d. × 0.25 μm film thickness; J&W Scientific, Folsom, CA) was used. The injection was carried out in splitless mode at 270 °C. Helium was applied as a carrier gas with a constant flow of 1.3 mL/min. The oven temperature was programmed as follows: An initial temperature of 80 °C was maintained for 1 min and then elevated to 280 °C at 30 °C/min and then held for 1.83 min. The temperature of the MS transfer line was 280 °C. The mass spectrometer was operated by electron impact at 70 eV, in selective ion monitoring (SIM) mode. Ions at m/z 68, 82, 109, and 182 were used for 4-MI and those at 95, 109, and 196 for 2-EI with a dwell time of 100 ms each. The temperatures of the ion source and quadrupole were 230 and 150 °C, respectively. Agilent Chemstation was used to control the GC−MS system.

Color Measurement from the Caramel Model System. Color parameters of the prepared solutions from various caramel model systems were monitored by a Nippon Denshoku NE 4000 colorimeter, using the 1976 CIELAB system. The sample solution (200 μL) was diluted with 10 mL of distilled water, and the colors were measured in transmittance mode. The parameters were L^* (brightness; $L^* = 0$ for black, and $L^* = 100$ for white), a^* (red-green component; $-a^*$ = greenness and $+a^*$ = redness) and b^* (yellow−blue component; $-b^*$ = blueness and $+b^*$ = yellowness). The color differences were calculated by the expression: $\Delta E = [(\Delta L^*)^2 + (\Delta a^*)^2 + (\Delta b^*)^2]^{1/2}$.[20] To evaluate color changes, ΔE was calculated with L^*, a^*, and b^* values of the caramel model systems with different food additives added, with respect to those in glucose/ammonium hydroxide 1 M model system.

Analysis of Pyrazines in the Caramel Model System. Each sample (3 g) was weighed into a 20 mL headspace vial and sealed with an unlined crimp cap containing polytetrafluoroethylene (PTFE)/silicone septa (Agilent). The assayed SPME device was divinylbenzene/carboxen/polydimethylsiloxane (DVB/CAR/PDMS, 50/30 μm thickness) fiber (Supelco, Bellefonte, PA). After the samples were equilibrated for 5 min at 50 °C, the SPME fiber was inserted to extract chemicals for 30 min at 50 °C under magnetic stirring.

Analyses were performed using a GC−MS system equipped with a DB-Wax column (60 m × 0.25 mm i.d. × 0.25 μm film thickness; J&W Scientific, Folsom, CA). The SPME fiber was inserted into the injection port of the GC, which was in splitless mode, and maintained at 260 °C for 5 min. The oven temperature program started at 50 °C, increased by 3 °C/min to 220 °C, and stayed at 220 °C for 10 min. The temperature of the transfer line was 280 °C, and the mass spectrometer was operated by electron impact at 70 eV. Quantification was performed by a GC that was equipped with a flame ionization detector under the same conditions that were described for the GC−MS system. The quantitation of identified pyrazines was carried out with undecane as the internal standard.

Pyrazines were identified through comparison with the Kovats gas chromatographic retention index I, by comparing the mass spectra with their authentic compound and through Wiley 275 libraries.

Statistical Analysis. All experiments were performed in triplicate. The data were analyzed using one-way ANOVA tests, and Duncan's new multiple range test was used for comparison of significant differences ($p < 0.05$) between the replicates ($n = 3$).

RESULTS AND DISCUSSION

Measurement of 4-MI in Caramel Model System Solution. As mentioned earlier, 4-MI was not detected in caramel colors I or II but was identified in both colors III and IV. Thus, glucose and ammonium hydroxide, which create

Table 1. Level and Reduction Rate of 4(5)-Methylimidazole Formed in Caramel Model System Solutions (n = 3)[a]

model systems		concn of additives (M)	amount of 4-MI (μg/mL)	reduction (%)
1 M glucose/1 M ammonium hydroxide			556 ± 1.3 g	0
1 M glucose/1 M ammonium hydroxide	sodium sulfite	0.1	583 ± 2.6 gh	−5
	iron sulfate	0.1	110 ± 0.7 a	80
		0.05	269 ± 1.8 b	52
		0.01	452 ± 2.9 de	19
	magnesium sulfate	0.1	483 ± 2.0 ef	13
		0.05	506 ± 1.4 f	9
		0.01	576 ± 1.3 gh	−3
	calcium sulfate	0.1	656 ± 3.4 j	−18
		0.05	552 ± 1.7 g	1
		0.01	652 ± 2.6 ij	−17
	zinc sulfate	0.1	460 ± 2.0 e	17
		0.05	507 ± 0.5 f	9
		0.01	581 ± 5.7 gh	−4
	tryptophan	0.1	409 ± 4.4 cd	26
		0.05	457 ± 2.3 e	18
		0.01	556 ± 1.8 g	0
	cysteine	0.1	397 ± 1.7 c	29
		0.05	444 ± 0.8 de	20
		0.01	609 ± 0.6 hi	−10

[a]Values followed by the same letter in a given column are not significantly different at $p < 0.05$.

Table 2. Color Measurement of Caramel Model System Solution by Colorimetry[a]

model system		concn of additives (M)	L^*	a^*	b^*	ΔE^b
1 M glucose/1 M ammonium hydroxide			17.9 o	1.3 g	22.7 ij	0
1 M glucose/1 M ammonium hydroxide	sodium sulfite	0.1	15.9 g	3.6 m	22.6 i	3.1
	iron sulfate	0.1	12.0 d	3.8 m	17.2 e	8.5
		0.05	15.5 f	2.3 i	20.2 g	3.7
		0.01	14.6 e	3.0 l	20.6 g	4.3
	magnesium sulfate	0.1	20.4 s	−0.8 d	18.8 f	5.0
		0.05	21.2 t	−1.6 c	16.2 d	7.9
		0.01	18.7 q	0.6 f	21.8 h	1.4
	calcium sulfate	0.1	16.4 i	2.6 jk	23.3 k	2.1
		0.05	16.5 j	2.7 k	23.3 k	2.1
		0.01	17.4 m	1.9 h	23.2 k	1.0
	zinc sulfate	0.1	10.1 c	3.9 m	15.2 c	11.2
		0.05	16.0 h	2.0 h	21.9 h	2.2
		0.01	16.9 l	2.4 i	22.9 ijk	1.5
	tryptophan	0.1	16.8 k	2.0 h	22.7 ij	1.4
		0.05	17.7 n	1.2 g	22.4 i	0.4
		0.01	17.4 m	1.8 h	23.2 jk	0.9
	cysteine	0.1	19.1 r	−0.1 e	20.4 g	2.9
		0.05	18.6 q	0.5 f	21.7 h	1.5
		0.01	18.2 p	1.0 f	22.7 ij	0.3

[a]Values followed by the same letter in a given column are not significantly different at $p < 0.05$. [b]Glucose/ammonium hydroxide model system was used as a control group for calculation of color differences.

colors III through heating, were used as a control group of the caramel model system in the present study. In a previous study, the Maillard reaction was investigated by using a model system that consisted of a sugar and an amine compound, and 4-MI was found in the glucose/ammonium hydroxide model system at a level that ranged from 490 to 710 μg/mL.[21]

An absolute calibration curve was obtained (y = 0.7958x + 2.6264, R^2 = 0.9937) using 4-MI standard solutions with various concentrations (1, 5, 10, 20, 50, and 100 μg/mL). The recovery and precision of the caramel model system solution of glucose/ammonium hydroxide (1 M) with added sodium sulfite (0.1 M) were determined, and each test was replicated five times. The recoveries that were measured for samples spiked with 4-MI at two concentration levels (20 and 100 μg/mL) ranged from 84 to 111%. The precision of the interday and intraday analysis, expressed as the relative standard deviation (RSD), were 0.9% and 4.9−6.5%, respectively.

Table 1 shows the amount of 4-MI formed in the caramel model system solutions that include each food additive at a level of 0.1, 0.05, and 0.01 M. A glucose and ammonium hydroxide (1 M) model system was used as a control. As each group was compared to the glucose/ammonium hydroxide model system, a reduction of 4-MI was observed in most caramel model systems with the 0.1 M food additives. In

dx.doi.org/10.1021/jf502008q | J. Agric. Food Chem. 2014, 62, 6481−6486

particular, there was a significant reduction of 4-MI formation in the caramel model system with 0.1 M Fe^{2+}, but the amount of 4-MI increased in the caramel model system with the addition of 0.1 M Ca^{2+}.

When the D-glucose and ammonium hydroxide were heated, the amount of 4-MI formed was 556 ± 1.3 μg/mL. The addition of 0.1 M sodium sulfite increased the 4-MI formation by up to 583 ± 2.6 μg/mL (5%), whereas the formation level and reduction rate of 4-MI through the addition of food additives were 110 ± 0.7 (80%) in 0.1 M Fe^{2+}, 483 ± 2.0 (13%) in 0.1 M Mg^{2+}, 460 ± 2.0 (17%) in 0.1 M Zn^{2+}, 409 ± 4.4 (26%) in 0.1 M tryptophan, and 397 ± 1.7 μg/mL (29%) in 0.1 M cysteine. The degree of contribution to the reduction of 4-MI from food additives had the following order: Fe^{2+} > cysteine > tryptophan > Zn^{2+} > Mg^{2+}. The formation levels of 4-MI ranged from 110 ± 0.7 (0.1 M Fe^{2+}) to 452 ± 2.9 (0.01 M Fe^{2+}), from 483 ± 2.0 (0.1 M Mg^{2+}) to 576 ± 1.3 (0.01 M Mg^{2+}), from 656 ± 3.4 (0.1 M Ca^{2+}) to 652 ± 2.6 (0.01 M Ca^{2+}), from 460 ± 2.0 (0.1 M Zn^{2+}) to 581 ± 5.7 (0.01 M Zn^{2+}), from 409 ± 4.4 (0.1 M tryptophan) to 556 ± 1.8 (0.01 M tryptophan), and from 397 ± 1.7 (0.1 M cysteine) to 444 ± 0.8 μg/mL (0.01 M cysteine). As a higher concentration of food additive was added, apart from the case of Ca^{2+}, the amount of 4-MI created by the Maillard reaction solution decreased, while an especially low concentration of food additive was not sufficient to reduce the formation of 4-MI. Furthermore, the addition of 0.01 M of Ca^{2+}, Mg^{2+}, Zn^{2+}, cysteine, and tryptophan led to a higher level of 4-MI than the control caramel model system, which was the Maillard reaction solution of 1 M glucose and 1 M ammonium hydroxide without additives. These results clearly suggest that some food additives at an appropriate concentration have a positive effect on the reduction of 4-MI in the Maillard reaction. This effect of the food additives on the formation of 4-MI in the Maillard reaction system was not previously reported. As food additives could be used in the manufacturing of foods, adding these food additives may be useful for reducing the formation of 4-MI during the Maillard reaction process.

Color Differences in the Caramel Model System Solutions. Since the Maillard reaction induces a brown color with formation of melanoidins, color is one of the important factors when considering how much 4-MI is formed during the Maillard reaction. Table 2 shows the results obtained for three series of color differences: L^*, a^*, and b^*. Significant differences according to the Duncan post hoc test are indicated by superscript letters. The L^* values of the caramel model systems with added 0.1 M food additives including 0.1 M sodium sulfite decreased compared to glucose/ammonium hydroxide (1 M) model system, except for Mg^{2+} and cysteine. Contrarily, values of a^* increased in the same caramel model systems, denoting the rise of redness characteristics when adding food additives. The b^* values did not show a significant change for any caramel model system. Although the measurement of color from the Maillard reaction model systems has not been reported, the decrease of L^* and the increase of a^* were observed in the foods due to the brown pigment formation that was induced by the Maillard reaction.[22,23] In the studies of Wang et al. and Ramonaitytė et al., the absorbance of the Maillard reaction model system showed increases at 420 and 450 nm, respectively, with addition of metal ions as a result of the Maillard reaction, indicating that the addition of metal ions accelerated the formation of the final browning compounds.[24,25]

In order to determine the correlation between the 4-MI concentration and color, a linear regression analysis was performed on each L^*, a^*, b^*, and ΔE. The total color difference, expressed as ΔE, showed a lack of negative correlation with the 4-MI concentration ($r = -0.4826$). On the other hand, L^*, a^*, and b^* values had no significant correlation with 4-MI ($p < 0.05$).

Pyrazines Formed in Caramel Model System Solutions. Table 3 lists the 12 kinds of pyrazine detected in the study of the caramel model system solutions. The majority of the pyrazines detected were 2-methylpyrazine, with a peak area ratio (PAR) ranging from 2.27 to 6.29, followed by 2,6-dimethylpyrazine ranging from 0.84 to 2.56 and 2,3-dimethylpyrazine ranging from 0.10 to 0.33. It is generally known that pyrazines are among the typical products of the Maillard reaction between amino compounds and carbonyl compounds.[26] All of the 12 pyrazine compounds confirmed in the present study were consistent with the previous literature that had investigated the pyrazines that could be derived from the Maillard reaction.[26−29]

It was difficult to find a relatively substantial relationship between 4-MI and the pyrazines formed in the greatest amounts, whereas 2-ethyl-6-methylpyrazine was among the 12 kinds of pyrazine compounds that showed a correlation with the concentration of 4-MI. Figure 1 showed a negative correlation ($r = -0.8239$) between 4-MI and 2-ethyl-6-methylpyrazine, indicating that 2-ethyl-6-methylpyrazine is formed in inverse proportion to the 4-MI concentration ($p < 0.05$). When the 4-MI declined by 80% with the addition of Fe^{2+} into the glucose/ammonium hydroxide 1 M solution, the content of 2-ethyl-6-methylpyrazine increased from 0.03 to 0.21 PAR.

Figure 2 shows the proposed formation pathway of 4-MI and 2-ethyl-6-methylpyrazine from methylglyoxal on the basis of the previous studies.[13,21,26,30,31] Methylglyoxal, as the sugar-derived reactive intermediate during the Maillard reaction, reacts with ammonia. Interestingly, the nitrogen-containing reactive intermediates formed from methylglyoxal with ammonia can produce either 4-MI by interacting with formaldehyde or 2-ethyl-6-methylpyrazine by reacting with ethylglyoxal. Therefore, if the nitrogen-containing reactive intermediates generated 4-MI with formaldehyde, the formation of 2-ethyl-6-methylpyrazine might be reduced. Further study that elucidates a more accurate correlation between 4-MI and 2-ethyl-6-methylpyrazine will be needed.

4-MI investigated in the present study has received much attention from regulatory agencies as a possible carcinogenic compound. Therefore, it is important to find a way to reduce the 4-MI produced by the Maillard reaction. The results of the present study demonstrate that the addition of food additives such as metal ions and amino acids at an appropriate level could reduce the formation of 4-MI. With current results various food products such as a bakery product could be applied to reduce the amount of 4-MI. However, more detail application study would be carried out in the future. In addition, a correlation between 2-ethyl-6-methylpyrazine and the 4-MI concentration was determined. Since the analysis of 4-MI requires expensive technology and specialized knowledge, the correlation between color, pyrazine levels, and 4-MI levels could be useful for the evaluation of the 4-MI formed during the Maillard reaction.

Table 3. Amounts of Pyrazine Compounds Identified in Caramel Model Systems

		peak area ratio[a]																			
		glucose/ammonium hydroxide	sodium sulfite	iron sulfate			calcium sulfate			magnesium sulfate			zinc sulfate			cysteine			tryptophan		
no.	pyrazines		0.1[b]	0.1	0.05	0.01	0.1	0.05	0.01	0.1	0.05	0.01	0.1	0.05	0.01	0.1	0.05	0.01	0.1	0.05	0.01
1	unsubstituted	0.15	0.11	0.12	0.10	0.11	0.20	0.19	0.21	0.18	0.18	0.18	0.24	0.27	0.27	0.12	0.15	0.15	0.25	0.29	0.25
2	2-methyl	3.11	2.27	4.33	3.26	2.72	4.19	4.13	3.88	4.38	4.25	4.12	5.77	6.29	5.95	3.30	3.38	3.02	5.41	6.11	5.06
3	2,5-dimethy-	0.30					0.37	0.36	0.37		0.32		0.34	0.34	0.27		0.25	0.26			
4	2,6-dimethyl	0.84	0.95	2.56	2.07	1.55	1.04	1.02	0.96	1.04	0.96	1.04	2.47	2.30	1.85	0.86	0.89	0.85	2.41	2.41	1.72
5	2-ethyl														0.02	0.01		0.02	0.01		0.01
6	2,3-dimethyl	0.10	0.11	0.33	0.23	0.17	0.14	0.14	0.13	0.10	0.11	0.09	4.25	1.42	0.37	0.08	0.10	0.10	0.21	0.23	0.18
7	2-ethyl-6-methyl	0.03	0.04	0.21	0.13	0.07	0.05	0.05	0.05	0.02	0.03	0.02	0.12	0.11	0.09	0.01	0.03	0.03	0.06	0.08	0.06
8	2-ethyl-5-methyl	0.01	0.01	0.05	0.05	0.03	0.02	0.02	0.02		0.01	0.02	0.05	0.04	0.04		0.01	0.01		0.03	
9	2-ethyl-3-methyl	0.12	0.15	0.57	0.39	0.25	0.19	0.19	0.18	0.11	0.13	0.10	0.51	0.42	0.33	0.10	0.13	0.13	0.32	0.34	0.23
10	ethenyl	0.05	0.03	0.09	0.07	0.04	0.06	0.05	0.07	0.07	0.06	0.07	0.15	0.12	0.10	0.03	0.04	0.04	0.05	0.07	0.05
11	2,5-dimethyl-3-ethyl		0.01	0.04	0.03	0.02	0.01	0.00	0.01			0.03	0.02	0.02	0.02						
12	2,6-diethyl		0.01	0.05	0.04	0.02	0.01	0.01	0.01			0.04	0.03	0.02				0.01			

[a]Compounds content = peak area of each compound/peak area of undecane (internal standard). [b]Concentration of food additives (M).

Figure 1. Correlation between 4(5)-methylimidazole and 2-ethyl-6-methylpyrazine.

Figure 2. Proposed formation pathway of 4(5)-methylimidazole and 2-ethyl-6-methylpyrazine.

AUTHOR INFORMATION

Corresponding Author

*Phone: 82-2-2260-3370. Fax: 82-2-2285-3370. E-mail: kwglee@dongguk.edu.

Funding

This research was supported by Basic Science Research Program through the National Research Foundation of Korea (NRF) funded by the Ministry of Education, Science and Technology (Grant No.: 2012R1A1A2007551) and R&D Convergence Center Support Program, Ministry for Food, Agriculture, Forestry and Fisheries, Republic of Korea

Notes

The authors declare no competing financial interest.

REFERENCES

(1) Tsuchida, H.; Komoto, M. Chemical studies on the reaction products of methylpentose and ammonia. *Agric. Biol. Chem.* **1967**, *31*, 185−189.

(2) National Toxicology Program (NTP, 2007). *Toxicology and Carcinogenesis of 4-Methylimidazole (CAS No. 822-36-6) in F344/N Rats ad B6C3F1Mice (Fee Studies); NTP Technical Report Series, No. 535, NIH Publication No. 07-4471*; U.S. Department of Health and Human Service, NTP: Research Triangle Park, NC, 2007; pp 1−274.

(3) Office of Environmental Health Hazard Assessment (OEHHA). Notice of amendment of text title 27, California code of regulations amendment of section 25705 specific regulatory levels: No significant 12; http://oehha.ca.gov/prop65/law/adopt020812.html (accessed Aug 20, 2013).

(4) Chan, P.; Mahler, J.; Travlos, G.; Nyska, A.; Wenk, M. Induction of thyroid lesions in 14-week toxicity studies of 2- and 4-methylimidazole in Fischer 344/N rats and B6C3F1 mice. *Arch. Toxicol.* **2006**, *80*, 169−180.
(5) Chan, P. C.; Hills, G. D.; Kissling, G. E.; Nyska, A. Toxicity and carcinogenicity studies of 4-methylimidazole in F344/N rats and B6C3F1 mice. *Arch. Toxicol.* **2008**, *82*, 45−53.
(6) Patey, A. L.; Shearer, G.; Knowles, M. E.; Denner, W. H. B. Ammonia caramel: Specifications and analysis. *Food Addit. Contam.* **1985**, *2*, 107−112.
(7) Hargreaves, M. B.; Jones, B. C.; Smith, D. A.; Gescher, A. Inhibition of p-nitro-phenolhydroxylase in rat liver microsomes by small aromatic and heterocyclic molecules. *Drug Metab. Dispos.* **1994**, *22*, 806−810.
(8) IARC Monographs. 4-Methylimidazole. Monographs.iarc.fr/ENG/Monographs/vol101/mono101-015.pdf (accessed Oct 16, 2012).
(9) WHO. *Toxicological Evaluation of Some Food Colours, Enzyme, Flavour Enhancers, Thickening Agents, And Certain Food Additives*; International Program on Chemical Safety World Health Organization, 1975; http://www.inchem.org/documents/jecfa/jecmono/v06je13.htm (accessed Aug 31, 2012).
(10) EFSA Panel on Food Additives and Nutrient Sources added to Food (ANS). Scientific opinion on the reevaluation of caramel colours (E 150a,b,c,d) as food additives. *EFSA J.* **2011**, *9* (3), 2004.
(11) Nursten, H. The chemistry of nonenzymic browning. *The Maillard Reaction: Chemistry, Biochemistry and Implications*; Royal Society of Chemistry: London, UK, 2005; pp 5−30.
(12) Komoto, M. Chemical studies on the reaction products of glucose and ammonia. III. Behaviors of glucosylamine in browning reaction of glucose and aqueous ammonia. *Nippon Nogei Kagaku Kaishi* **1962**, *36*, 403−407.
(13) Jang, H. W.; Jiang, Y.; Hengel, Matt.; Shibamoto, T. Formation of 4(5)-methylimidazole and its precursors, α-dicarbonyl compounds, in Maillard systems. *J. Agric. Food Chem.* **2013**, *61*, 6865−6872.
(14) Horikawa, H.; Okada, M.; Nikamura, Y.; Sato, A.; Iwamoto, N. Production of hydroxyl radicals and alpha-dicarbonyl compounds associated with Amadori compound−Cu^{2+} complex degradation. *Free Radical Res.* **2002**, *36*, 1059−1065.
(15) Keller, C.; Wedzicha, B. L.; Leong, L. P.; Berger, J. Effect of glyceraldehyde on the kinetics of Maillard browning and inhibition by sulphite species. *Food Chem.* **1999**, *66*, 495−501.
(16) Serpen, A.; Gökmen, V. Evaluation of the Maillard reaction in potato crisps by acrylamide, antioxidant capacity and color. *J. Food Compos. Anal.* **2009**, *22*, 589−595.
(17) Cunha, S. C.; Barrado, A. I.; Faria, M. A.; Fernandes, J. O. Assessment of 4-(5-)methylimidazole in soft drinks and dark beer. *J. Food Compos. Anal.* **2011**, *24*, 609−614.
(18) Thosen, M.; Willumsen, D. Quantitative ion-pair extraction of 4(5-)methylimidazole from caramel colour and its determination by reversed-phase ion-pair liquid chromatography. *J. Chromatogr., A* **1987**, *211*, 213−221.
(19) Yanaguchi, H.; Masuda, T. Determination of 4(5)-methylimidazole in soy sauce and other foods by LC−MS/MS after solid-phase extraction. *J. Agric. Food Chem.* **2011**, *59*, 9770−9775.
(20) Calvo, C. Physical characterization and nutrient analysis. Optical properties. In *Handbook of Food Analysis*; Nollet, L. M. L. , Ed.; Marcel Dekker: New York, 2004; Vol. *1*, pp 1−19.
(21) Moon, J. G.; Shibamoto, T. Formation of carcinogenic 4(5)-methylimidazole in Maillard reaction systems. *J. Agric. Food Chem.* **2011**, *59*, 615−618.
(22) Bosch, L.; Alegría, A.; Farré, R.; Clemente, G. Fluorescence and color as markers for the Maillard reaction on milk−cereal based infant foods during storage. *Food Chem.* **2007**, *105*, 1135−1143.
(23) Farroni, A.; Buera, M. P. Colour and surface fluorescence development and their relationship with Maillard reaction markers as influenced by structural changes during cornflakes production. *Food Chem.* **2012**, *135*, 1685−1691.
(24) Wang, H.; Zhou, Y.; Ma, J.; Zhou, Y.; Jiang, H. The effects of phytic acid on the Maillard reaction and the formation of acrylamide. *Food Chem.* **2013**, *141*, 18−22.
(25) Ramonaitytė, D. T.; Keršienė, M.; Adams, A.; Tehrani, K. A. The interaction of metal ions with Maillard reaction products in a lactose−glycine model system. *Food Res. Int.* **2009**, *42*, 331−336.
(26) Hwang, H.; Hartman, T. G.; Rosen, R. T.; Lech, J.; Ho, C. Formation of pyrazines from the Maillard reaction of glucose and lysine-α-amine-15N. *J. Agric. Food Chem.* **1994**, *42*, 1000−1004.
(27) Lee, K. G.; Jang, H.; Shibamoto, T. Formation of carcinogenic 4(5)-methylimidazole in caramel model systems: A role of sulphite. *Food Chem.* **2013**, *136*, 1165−1168.
(28) Shibamoto, T. Heterocyclic compounds in browning and browning/nitrite model systems: Occurrence, formation mechanisms, flavor characteristics and mutagenic activity. *Instrum. Anal. Foods* **1983**, *1*, 229−278.
(29) Yu, A.; Tan, Z.; Wang, F. Mechanistic studies on the formation of pyrazines by Maillard reaction between L-ascorbic acid and L-glutamic acid. *LWT-Food Sci. Technol.* **2013**, *50*, 64−71.
(30) Hengel, M.; Shibamoto, T. Carcinogenic 4(5)-methylimidazole found in beverages, sauces, and caramel colors: Chemical properties, analysis, and biological activities. *J. Agric. Food Chem.* **2013**, *61*, 780−789.
(31) Yaylayan, V. A.; Haffenden, L. W. Mechanism of imidazole and oxazole formation in [^{13}C-2]-labelled glycine and alanine model systems. *Food Chem.* **2003**, *81*, 403−409.

compounds and as the chelating agent of alkoxides. As a bioactive compound, it shows great potential in microbiology, botany, and pest control as well.[5]

Because acetoin has broad usages, it is valuable to study its production. Although there is industrial natural acetoin available from several small fermentation plants, current commercial acetoin is mainly produced by chemical synthesis from fossil-based raw materials and then added into our foods as a flavor enhancer.[5] There are currently three main routes that can be used for the synthesis of acetoin: route A, exploiting the transformation processes from structural analogues such as diacetyl and 2,3-butanediol; route B, utilizing the hydrolysis processes from halogenated butanone; and route C, seeking a direct synthesis from aldehyde.

Route A. The main disadvantage of using diacetyl as the raw material for the production of acetoin is the high cost as diacetyl or related compounds are fine chemical products. There are also additional issues associated with high equipment requirements and more stringent reaction conditions and controls. If over-reduced, acetoin can be further converted to 2,3-butanediol, decreasing the reaction yield. Similar issues would occur if 2,3-butanediol is used as the raw material. For these reasons there has been no report of industrial uptake of this route.[6]

Route B. In this route butanone is usually used as the starting material, involving the first step of halogenation to make 3-halogenated butanone and the second step of hydrolysis to make acetoin (Figure 1, top). Methyl ethyl ketone is a commonly used raw material. Route B thus has much reduced raw material cost. In addition, it has milder reaction conditions, lower equipment specifications, and no special catalysts required either. It is thus not surprising to see its extensive uses in industry. However, the hydrogens on the α-position of butanone tend to have greater reactivity. Apart from the target halogen-substituted ketone, other reactions also occur to produce 1-substituted butanone, 3,3-dihalobutanone, and other derivatives, causing the yield reduction of the 3-halogenated product. Furthermore, under the alkali hydrolysis in step 2, byproducts such as 1-hydroxy-2-butanone make separation and purification more difficult.[7]

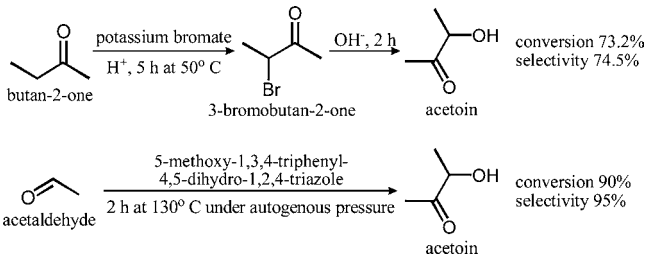

Figure 1. Industrial chemical synthesis routes of acetoin.

Route C. Acetaldehyde is used as the starting material, and the product is produced from condensation reaction under the catalysis of triazolium ylide or thiazolium ylide (Figure 1, bottom). This method also benefits from the lower cost of the starting material, less demanding equipment, fewer byproducts, higher yield, and simpler separation and purification, thereby enjoying more widespread industrial applications than route B. The main disadvantage lies in the complicated process of the catalyst preparation. Furthermore, acetaldehyde has a low boiling point. It is volatile and flammable and is difficult to transport and store. It can become easily lost during handling, resulting in environmental pollution and compromising safety. Most of these issues can be resolved by using paraldehyde but require the extra step of paraldehyde depolymerization, increasing the complexity and decreasing the yield.[8]

NATURAL ORIGINS OF ACETOIN

In contrast to the organic chemistry routes, however, acetoin can be generated by various natural or "green" routes. Generally speaking, natural acetoin has three origins, microorganisms, plants, and animals, and exists widely in some fermented products, fruits, crops, insects, mammals, and so on. Table 2 gives some examples of the natural origins of acetoin.

Table 2. Some Natural Origins of Acetoin

material	origin of acetoin
artisanal Spanish cheese[9]	microbial fermentation
French blue cheeses[10]	microbial fermentation
Chinese vinegars[11]	microbial fermentation
European vinegars[12]	microbial fermentation
beers[13]	microbial fermentation
wines from different countries[3]	microbial fermentation
young red wines[14]	microbial fermentation
Garnacha Tintorera-based sweet wines[15]	microbial fermentation
sherry wines[16]	microbial fermentation
palm wine[17]	microbial fermentation
pawpaw[18]	fruit, plant synthesis
dekopon[19]	fruit, plant synthesis
durian[20]	fruit, plant synthesis
banana[21]	fruit, plant synthesis
lychee[22]	fruit, plant synthesis
coconut[23]	fruit, plant synthesis
oil palm[23]	fruit, plant synthesis
guar bean[24]	vegetable, plant synthesis
ash gourd[25]	vegetable, plant synthesis
corn tortillas[26]	corn, plant synthesis
rice cakes[27]	rice, plant synthesis
honeys[28]	flower, plant synthesis
Avicennia marina[29]	flower, plant synthesis
sweet olive[30]	flower, plant synthesis
red clover[31]	flower, plant synthesis
kiwi fruit flowers[32]	flower, plant synthesis
Solomon's lily[33]	flower, plant synthesis
summer chafer[34]	insect, animal synthesis
rhinoceros beetle[35]	insect, animal synthesis
cockroaches[36]	insect, animal synthesis
liver homogenate and perfused liver of rats[37]	mammal, animal synthesis
blood and urinary from normal male students after ethanol ingestion[38]	mammal, animal synthesis
human sweat[39]	mammal, animal synthesis

PHYSIOLOGICAL ROLES

Acetoin biogenesis has different physiological roles in different biological species. Current knowledge on the physiological functions of acetoin biogenesis can be summarized into three categories: biological functions in microorganisms, semiochemical functions in higher plants and insects, and biological functions in higher animals.

dx.doi.org/10.1021/jf5013902 | J. Agric. Food Chem. 2014, 62, 6487−6497

The biogenesis of acetoin in bacteria and yeasts has been well investigated partly because acetoin is tightly related to many traditional fermentative dietary products. Furthermore, just like acetic acid, ethanol, and lactic acid, acetoin/2,3-butanediol is another popular primary metabolite in bacteria. The ability to secrete acetoin is a routine classification marker (i.e., the Voges−Proskauer test) used in bacterial identification. In a sugar-rich culture medium, the fast assimilation of carbon source and accumulation of 2,3-butanediol other than organic acids can avoid cellular acidification. When the fermentable sugars are depleted, 2,3-butanediol is transformed back to acetoin, regenerating the reducing force (NADH or NADPH).[40] Acetoin is further reutilized as an alternative carbon and energy source.[41] In addition, acetoin biosynthesis is closely related to the branched-chain amino acid pathway and the regulation of cell life in certain bacteria.[4]

In higher organisms, the secretion ability of acetoin/2,3-butanediol is substantially weakened or completely abolished. However, due to its moderate volatile ability, characteristic odor, and chemical structure, acetoin has great potential as a semiochemical, especially in some insects (Table 3), flowers, and fruits (Table 2). Acetoin and some other characteristic fermentative products such as acetic acid and isovaleric acid convey a selective message of fermentation and sugar-rich substrates,[48] which is highly attractive to ants, bugs, beetles, flies, wasps, honeybees, and moths. Acetoin synthesis in plant cells was confirmed,[49] and together with other odorous compositions, acetoin gives these plants rich fragrances, attracting insects and higher animals to help their pollination, breeding, and propagation. However, on the opposite side, pests are attracted. Mass-trapping techniques have been developed using acetoin as an active component of artificial lures against the corresponding pests (as some references in Table 3).

Table 3. Acetoin as a Semiochemical in Insects

species	function
cockroaches *Nauphoeta cinerea*,[42] *Henschoutedenia flexivitta*,[36] and *Leucophaea maderae*[43]	male pheromone
summer chafer *Amphimallon solstitiale*[34]	female pheromone
white-spotted flower chafer *Protaetia brevitarsis*[44]	attractant
rhinoceros beetle *Scapanes australis*[35]	male pheromone
American palm weevil *Rhynchophorus palmarum*[23]	attractant
fruit fly *Drosophila melanogaster*[45]	attractant
fly[46]	attractant
nymphalid butterflies *Kaniska canace* and *Vanessa indica*[47]	attractant
African fruit chafer *Pachnoda marginata*[48]	attractant

In the model organism fruit fly *Drosophila melanogaster*, acetoin has been recognized as a natural ligand for an olfactory sensory neuron[50] and the strongest known stimulus for the glomerulus VA2, which is associated with the close-range attraction of this fly to vinegar.[51] As a male pheromone, acetoin has been well studied in cockroaches. *Nauphoeta cinerea*, *Leucophaea maderae*, and *Henschoutedenia flexivitta* all belong to Oxyhaloinae and have the same mating behavior pattern. However, acetoin is the only compound common to the pheromone blends of the three species.[36] Acetoin is attractive to female *L. maderae* at low dosages (0.1−5 ng).[43] In *N. cinerea*, males must have the ability to secrete acetoin; otherwise, physiologically defective individuals without this ability will not be successful in female mate choice.[52] In male−male interactions, the secretion of acetoin plays an important role as well. Microgram levels of acetoin are released by aggressive cockroaches at high rates in strong attacks.[53] The dominant males release acetoin strategically to flaunt their dominance.[42] Therefore, acetoin is multifunctional in the world of cockroaches.

Acetoin is a well-known fermentative product, but it is perhaps less well-known to be the third most abundant volatile compound in fresh human sweat (ethanol, 15.1%; acetic acid, 10.9%; acetoin, 9.5%).[39] Acetoin was also detected in blood and urinary samples from normal male students after ethanol ingestion.[38] A pathway with acetoin as a key metabolite was proposed to explain the detoxication mechanism of acetaldehyde in mammals.[37,38] Under pathological conditions, acetoin has a role in regulating intermediate metabolism in mammalian systems.[54] However, the underlying mechanisms of acetoin biogenesis in higher organisms are largely unknown.

■ ACETOIN BIOSYNTHESIS

As shown in Table 2, acetoin biosynthesis widely exists in various food materials. In contrast, bacteria have very efficient acetoin biosynthesis systems.[5] Although the production of acetoin by eukaryotic cells is relatively less efficient, it is important due to its relationships with our foods. Acetoin biogenesis and dissimilation were seldom reported in archaea. Thus, the following discussion will focus on acetoin biosynthesis in eukaryotic systems with emphasis on enzymatic aspects by comparative study.

Currently, acetoin's precursor 2-acetolactate can be synthesized by five enzymes: α-acetolactate synthase (ALS, EC 2.2.1.6), acetohydroxy acid synthase (AHAS, EC 2.2.1.6), pyruvate oxidase (POX, EC 1.2.3.3), pyruvate decarboxylase (PDC, EC 4.1.1.1), and pyruvate dehydrogenase (PDH, EC 1.2.4.1). These enzymes share substantial similarities not only in amino acid sequences (Figure 2) but also in protein structures and catalytic mechanisms. All five enzymes are thiamin pyrophosphate (TPP)-dependent, and they all need a divalent metal ion such as Mg^{2+} to work properly. Furthermore, all five enzymes except ALS contain flavin adenine dinucleotide (FAD) in their structures. However, ALS replaced the position of FAD with reorientated amino acid side chains, and the overall structure of ALS remained unchanged.[55] Another good example of structural and functional similarity among the enzymes is that the D28A and D28N variants of yeast PDC resemble ALSs, which synthesize 2-acetolactate as a major product.[56]

All five enzymes follow a common mechanism of 2-acetolactate synthesis. Presumably, a pyruvate and an enzyme form an initial intermediate, an enzyme-bound lactyl-TPP (lactyl-TPP-E). Then the initial intermediate decarboxylates to form hydroxyethyl-TPP-E ("active acetaldehyde"). The active acetaldehyde reacts with another pyruvate to form 2-acetolactate (the so-called carboligase reaction).[49] POX, PDC, and PDH can also perform the carboligation of hydroxyethyl-TPP-E with an acetaldehyde moiety to direct yield acetoin.

However, although these five enzymes retain much commonality, evolution has taken place to fit differentiation and refinement functions. ALS exists only in some bacteria. The five genera in the ALS clade in Figure 1 are representatives of the most efficient acetoin producers.[5] ALS serves as the first key enzyme of the acetoin/2,3-butanediol biosynthesis pathway in these bacteria. Its sole duty is the condensation of pyruvate to

dx.doi.org/10.1021/jf5013902 | J. Agric. Food Chem. 2014, 62, 6487−6497

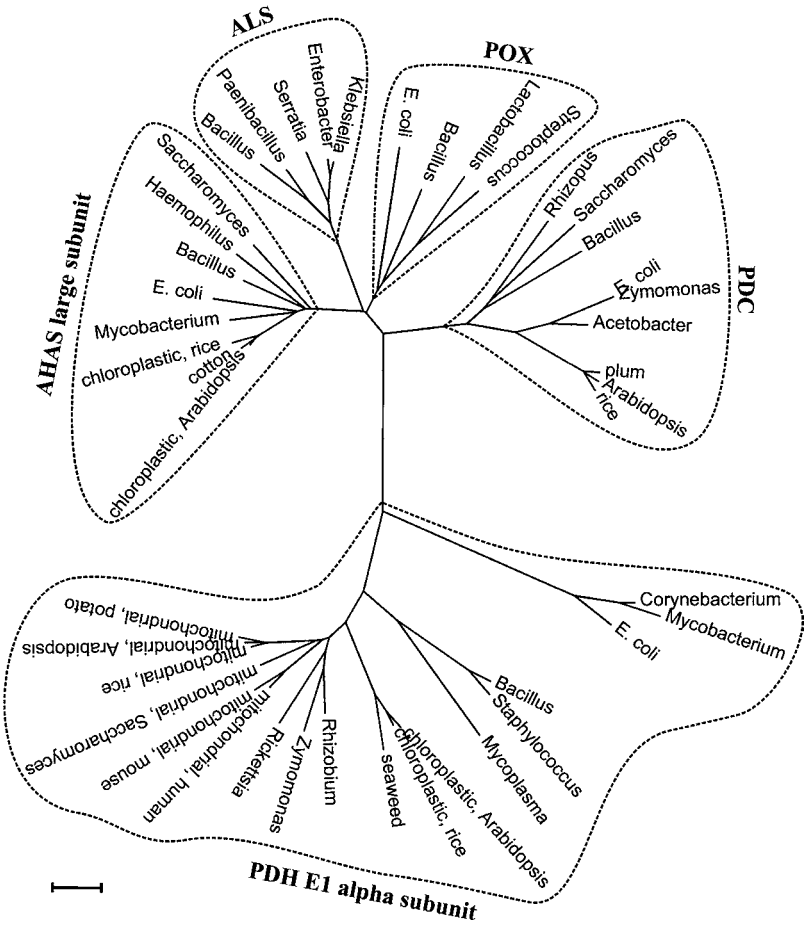

Figure 2. Simplified phylogenetic tree based on typical amino acid sequences of putative acetoin and/or 2-acetolactate biosynthesis enzymes. Representative sequences from typical species were extracted from the UniProt database. Accession numbers: AHAS large subunit, P17597 chloroplastic *Arabidopsis*, Q42768 cotton, Q6K2E8 chloroplastic rice, P0A622 *Mycobacterium*, P08142 *E. coli*, P37251 *Bacillus*, P45261 *Haemophilus*, P07342 *Saccharomyces*; ALS, Q04789 *Bacillus*, G0VU08 *Paenibacillus*, D4E3C0 *Serratia*, V5AYP9 *Enterobacter*, B5XWE0 *Klebsiella*; POX, Q8X6L4 *E. coli*, E0U346 *Bacillus*, P37063 *Lactobacillus*, Q54970 *Streptococcus*; PDC, Q8NK64 *Rhizopus*, P06169 *Saccharomyces*, M1QLG2 *Bacillus*, E8Y3L9 *E. coli*, P06672 *Zymomonas*, Q8L388 *Acetobacter*, B0ZS79 plum, Q9FFT4 *Arabidopsis*, A2XFI3 rice; PDH E1 α subunit, Q8NNF6 *Corynebacterium*, Q10504 *Mycobacterium*, P0AFG8 *E. coli*, P21881 *Bacillus*, P60089 *Staphylococcus*, P75390 *Mycoplasma*, O24457 chloroplastic *Arabidopsis*, Q7XTJ3 chloroplastic rice, P51267 seaweed, Q9R9N5 *Rhizobium*, O66112 *Zymomonas*, Q68XA9 *Rickettsia*, P08559 mitochondrial human, P35487 mitochondrial mouse, P16387 mitochondrial *Saccharomyces*, Q6Z5N4 mitochondrial rice, P52901 mitochondrial *Arabidopsis*, P52903 mitochondrial potato. The tree was constructed with the MEGA5 program using the neighbor-joining cluster algorithm (1000 bootstrap replicates). Scale bar, 0.2 substitutions/site.

yield 2-acetolactate with highest biological efficiency. Another major enzymatic reason for efficient acetoin biosynthesis in these bacteria is that they apply a specific enzyme, 2-acetolactate decarboxylase (ALDC, EC 4.1.1.5), to catalyze the yield of acetoin from 2-acetolactate. Similarly, ALDC has not been found in eukaryotes or archaea. To avoid 2-acetolactate accumulation during beer brewing, ALDC genes were often integrated into the chromosomes of brewer's yeasts.

AHASs were mainly found in bacteria, fungi, and plants. It has vital roles in the branched-chain amino acids (BCAAs) biosynthetic pathway. Each AHAS has a larger subunit and a smaller subunit, which perform catalysis and regulation functions, respectively. AHAS catalyzes the same reaction as ALS does but with comparatively much lower efficiency. The product 2-acetolactate is then channelled into the synthesis pathway of leucine and valine. AHAS also turns pyruvate and 2-oxobutyrate into 2-aceto-2-hydroxybutyrate, which is an intermediate of the isoleucine biosynthesis pathway.

Although AHAS evolved from an FAD-dependent POX-like ancestor,[57] FAD works purely for structural integrity in AHAS. The ALS sequences form a close cluster, and they belong to a larger group that includes AHAS and POX in the phylogenetic tree (Figure 1), indicating that ALS came from the same POX-like ancestor as AHAS did.[55] However, mutations occurred in ALS; that is, amino acid substitutions took place and ALS became dispensed with the requirement for FAD, after separation from the AHAS evolutionary lineage. By structural evolution, ALS achieved great activity enhancement. For example, the turnover number of the ALS from *Klebsiella pneumoniae* is 533 s^{-1}. This speed is about 10-fold faster than that of any other AHAS.[58]

POX, PDC, and PDH have their own main functions in different organisms. Acetoin and 2-acetolactate are only the byproducts of the three enzymes under certain circumstances. This side reaction has been well studied, for example, POX from *Escherichia coli* and *Pediococcus pseudomonas*;[59] PDC from *Zymomonas mobilis*,[60] yeast,[56] mammalian liver,[61] and very likely plant cells;[49] PDH from *Streptococcus mutans*,[62] animal tissues,[63] and mammalian tumor mitochondria.[64] Therefore, it is the general consensus from these studies that probably most,

dx.doi.org/10.1021/jf5013902 | J. Agric. Food Chem. 2014, 62, 6487−6497

if not all, TPP-dependent enzymes have the ability to form acetoin by condensing the hydroxyethyl group of the active acetaldehyde intermediate with an acetaldehyde acceptor molecule to give acetoin.[59]

The rate of acetoin formation by POX of *E. coli* is much slower than the oxidative reaction (approximately $^{1}/_{10}$ of the oxidative rate).[59] In yeast, the formation of acetoin and 2-acetolactate was estimated to be about 1% of the total reaction catalyzed by PDC.[56] Even though this kind of side reaction takes place at very low levels, the apparent widespread presence may account for important roles as discussed under Physiological Roles.

INTERCONVERSIONS AND DERIVATIVES

As discussed above, acetoin can be generated from 2-acetolactate by ALDC or the direct carboligation of pyruvate and acetaldehyde by POX, PDC, or PDH. 2-Acetolactate is not a stable molecule, and it can decarboxylate spontaneously to yield acetoin at acid pH or high temperature. Acetoin can also be generated from diacetyl by reductase. The formation of diacetyl in vivo is generally accepted to be the nonenzymatic oxidative decarboxylation result of 2-acetolactate.[4] As a central intermediate, acetoin plays important roles in the production of various types of derivatives: diols, esters, glycosides, heterocyclic compounds, etc. (Figure 3). Most of the derivatives are of importance in foods due to their rich odors and potential dietotherapy functions.

Diols, Esters, Glycosides, and Other Possible Enzymatic Derivatives. 2,3-Butanediol, the reduced form of acetion, is another regular product of the acetoin pathway in bacteria.[5] The reversible transformation of acetoin and 2,3-butanediol is catalyzed by acetoin reductase (2,3-butanediol dehydrogenase) in vivo. Acetoin's precursor, 2-acetolactate, can be spontaneously decarboxylated to diacetyl. Even though this spontaneous decarboxylation remains in very low levels in different cultures, diacetyl can be easily detected, for example, by scent or odor due to its very low perceptible threshold (0.001 ppm in Emmentaler cheese).[9] Therefore, it is not surprising that acetoin, 2,3-butanediol, and diacetyl often occur simultaneously in fermented foods, for example, in cheese[9] and wine.[17]

In acetoin-degrading bacteria, diacetyl could have another choice of transformation other than the production of acetoin by reductase. In this case diacetyl is catalyzed by the acetoin dehydrogenase enzyme system (AoDH ES) to yield 3-hydroxy-3-methyl-2,4-pentanedione (common name, acetylacetoin), which could be further reduced to a diol product, 3,4-dihydroxy-3-methylpentan-2-one (common name, acetylbutanediol).[4] Xiao et al. proposed a new biosynthetic method of acetylbutanediol from acetoin using *Bacillus pumilus*, a safe industrial species.[65] Thereafter, a novel diol, butyrylbutanediol (2,3-dihydroxy-3-methylheptan-4-one), was discovered during a thermophilic fermentation study of acetoin and 2,3-butanediol.[66] Butyrylbutanediol was postulated to be the synthetic product of acetoin and butyryl-CoA, following a similar synthetic mechanism as acetylbutanediol. However, the biosynthesis mechanisms of these diols largely remained unclear. These small molecular diols may have multiple usages in chemical synthesis, foods, and cosmetics due to their reactive hydroxyl groups, high water solubility, and hygroscopic properties.[65]

Dietary fruits usually have pleasant odors, and volatile esters account for a large portion of the aroma compounds. Alcohol

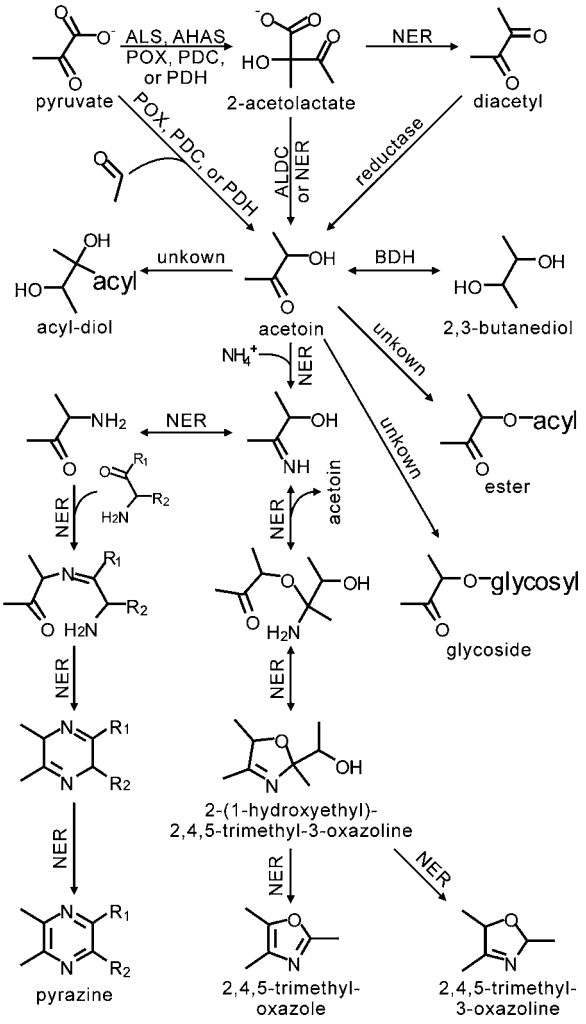

Figure 3. Generation pathways of acetoin and its derivatives. ALS, α-acetolactate synthase, which catalyzes the conversion of pyruvate to 2-acetolactate, was found only in bacteria. AHAS, acetohydroxy acid synthase, which catalyzes the synthesis of 2-acetolactate and 2-aceto-2-hydroxybutyrate, was mainly found in bacteria, fungi, and plants. POX, pyruvate oxidase, which converts pyruvate to acetate and carbon dioxide as its main catalytic function, was reported only in bacteria. PDC, pyruvate decarboxylase, which converts pyruvate to acetaldehyde as its main catalytic function, was found from microorganisms to higher plants. PDH, pyruvate dehydrogenase complex, which catalyzes the decarboxylation of pyruvate to acetyl-CoA as its main catalytic function, exists from lower prokaryotes to higher organisms including human beings. POX, PDC, and PDH can transfer pyruvate to 2-acetolactate and/or acetoin as a side reaction. NER, nonenzymatic reaction.

acyltransferases usually link alcohols to acyl moieties in the last step of ester biosynthesis. The hydroxyl groups of acetoin and 2,3-butanediol are also ready for the esterification reaction in some fruits. For example, plentiful acetoin esters and 2,3-butanediol esters were detected in pawpaw fruit,[18] and 2,3-butanediol acetates were also detected in banana extracts.[21] The odors and tastes of acetoin and 2,3-butanediol esters[18] support the popular characteristics of these fruits. Acetoin acetate and 2,3-butanediol acetate are sometimes present in some particular flowers, vinegars, and wines as well.[33]

Acetoin was found to be capable of acting as an aglycone and exist in glycosidically bound form in some vegetables and fruits. These glycosides are nonvolatile but may contribute to the

dx.doi.org/10.1021/jf5013902 | J. Agric. Food Chem. 2014, 62, 6487−6497

tastes. For example, acetoin was revealed as the major and key odor active aroma constituent (7.6 μg/kg) of ash gourd. Acetoin was also found to be the major constituent (24.00 mg/kg) existing as glycosidic conjugate in ash gourd.[25] In guar beans, the proportion of acetoin in free aroma constituents is even up to 95%, and acetoin is also the major component among the glycosidically bound aglycones in both guar beans (50%) and French beans (54%).[24] In lychee fruit acetoin was postulated to be a major characteristic aroma compound, but only a trace amount of glycosidically bound acetoin was detected.[22] Even until now, the formation mechanisms of these glycosides remain unknown. However, 2,3-butanediol-glucuronide was postulated to be the conjugation result of 2,3-butanediol and uridine diphosphate glucuronide by glucuronyltransferase in rats[37] and humans.[38] Therefore, the glycosidic bound reaction of acetion might be an enzymatic process in plant cells.

Acetoin could be precursors of other biological products. Speranza et al. postulated that the 2-butanol existing in distillates and wines most likely originated from 2,3-butanediol by the action of lactobacilli.[67] Yokota and Sasajima studied the enzymatic transformation of acetoin and D-ribose 5-phosphate to a monosaccharide, 1-deoxy-D-*altro*-heptulose 7-phosphate, by a transketolase mutant of *Bacillus pumilus*.[68] However, these two examples have no further or closely relevant reports.

Heterocyclic Compounds. Acetoin-derived heterocyclic derivatives include alkylpyrazines, oxazolines, oxazoles, and their homologues. Pyrazines are extensively used in food, agriculture, and medicine. Their occurrence is nearly ubiquitous in nature, and the alkylated ones are the most abundant among pyrazines.[69] According to the nature of the alkyl substituents, alkylpyrazines possess different flavors, but these flavors can be generally described as nutty, roasty, and toasty aroma.[70] Oxazolines and oxazoles are responsible for green, sweet, and nutty aromas and have strong sensory quality even at low concentrations. They have wide occurrence in processed foods such as coffee, soy sauce, wheat, and cooked beef.[71]

2,3,5,6-Tetramethylpyrazine (TTMP) is one of the main pyrazines found in Chinese vinegars,[73] tortillas,[26] rice cakes,[27] cocoa bean- or soybean-based fermented foods,[72] etc. In these foods, acetoin, sometimes with 2,3-butanediol and diacetyl, will always appear accompanied by the emergence of TTMP. TTMP is also a GRAS substance with FEMA No. 3237. Furthermore, TTMP is a biologically active ingredient in the medicinal plant *Ligusticum wallichii*. In addition to the flavoring contribution to foods, TTMP has potential dietotherapy functions. For example, TTMP is held to be good for cardiovascular and cerebrovascular health[74] and has a possible cognitive enhancement effect.[75] Therefore, research on TTMP has attracted widespread interests.

The formation mechanism of alkylpyrazines in vivo has two main controversial viewpoints:

(I) The enzymatic condensation biogenic pathway. This viewpoint is supported by only a few authors.[69] However, the enzymes or genes responsible for the condensation reaction have never been reported.

(II) The "Biochem-Chem" route. The precursors of alkyl pyrazines are prepared by biosynthesis pathways in vivo, but the subsequent condensation is a nonenzymic process. This route has gained convincing experimental support and obtained wider approval.

As early as 1988, Rizzi reviewed the possible formation mechanisms of food-related pyrazines and expressed his preference for the second mechanism.[76] In the same period, he observed the spontaneous formation of TTMP from acetoin and ammonium salts in water solution under mild conditions.[77] If other kinds of acyloins were supplied, other kinds of alkylpyrazines would be produced. During further studies on the reactions between acetoin and ammonia precursors under mild conditions, another major product, 2-(1-hydroxyethyl)-2,4,5-trimethyl-3-oxazoline (HE-TM-oxazoline), was identified.[78] The dynamic processes of TTMP and HE-TM-oxazoline were recorded in a 3 week storage study, and the mechanisms were postulated (Figure 3). Mechanistic studies of Fu and Ho supported these postulates, and another two heterocyclic derivatives, 2,4,5-trimethyl-3-oxazoline and 2,4,5-trimethyloxazole, were identified from an acetoin/ammonium acetate aqueous system.[79] Le Quéré et al. also hypothesized a chemical synthesis route of 2-alkyl-2,4,5-trimethyl-2,5-dihydrooxazole homologues in cheese from the precursors including acetoin, ammonia, and methyl ketones, which are abundant in cheeses.[10] If sulfide is present in acetoin/ammonium reaction systems, similar sulfur-containing heterocyclic compounds will be produced.[80]

HE-TM-oxazoline was manifested to be relatively unstable, and TTMP would be the main product either under an elevated reaction temperature[79] or in a prolonged storage time.[78] The dynamics of TTMP and its precursors during the industrial production process of a Chinese vinegar were investigated using GC-MS.[73] The results indicated that the main precursor of TTMP, that is, acetoin, was accumulated in the fermentation process, and then it condensed to TTMP during the subsequent storage period. The phenomenon is consistent with the "Biochem-Chem" route and the previous result of the 3 week storage dynamic study by Shu and Lawrence.[78]

Other kinds of alkylpyrazines and pentaheterocyclic compounds were often detected in acetoin-containing fermentation systems. For example, 2,3-dimethylpyrazine was found in tortillas[26] and rice cakes,[27] and 2,3,5-trimethylpyrazine was found in rice cakes[27] and Chinese vinegars.[11] During TTMP formation in a *Bacillus* fermentation process using glucose as the carbon source (actually the "Biochem-Chem" process), 2,3,5-trimethylpyrazine, 2-ethyl-3,5,6-trimethylpyrazine,[72] and a homologous product of 2,4,5-trimethyloxazole, 2,4,5-trimethylimidazole, were detected.[81] An extreme example is that a dozen kinds of alkylpyrazines, along with a very complex mixture of other volatile compounds, were also detected in a *Bacillus subtilis* fermentation process when cooked, roasted soybean cotyledons were applied as the substrate.[82] These diverse products might be closely related to the selection and pretreatment of raw materials for fermentation. Soybean cotyledons are rich in complex compounds, and the cooking and roasting processes will increase the complexity significantly. Shu used acetoin to react with amino acids at 250 °C and showed that all reactions between acetoin and α-amino acids generate TTMP and the corresponding Strecker aldehydes, indicating that alkylpyrazines could also be generated during food processing.[83]

Then, acetoin, sometimes with diacetyl, could be responsible for the generation of many kinds of heterocyclic derivatives, but these derivatives should share a common characteristic: each molecule has at least two adjacent methyl groups, a clear hallmark from the molecular structure of acetoin. Other kinds of alkyl heterocyclic compounds could be the derivatives of

Table 4. Electron Ionization (EI) and Chemical Ionization (CI) Mass Spectrometry Data of Acetoin and Its Derivatives[a]

common name or abbrev	IUPAC systematic name	ionization source	m/z (relative intensity)
acetoin	3-hydroxybutan-2-one	EI, 70 eV[b]	88 (10), 73 (2), 55 (3), 45 (100), 43 (56)
acetoin	3-hydroxybutan-2-one	CI, methane[65]	89 (100), 71 (61), 45 (6), 43 (33)
acetylbutanediol	3,4-dihydroxy-3-methylpentan-2-one	CI, methane[65]	133 (8), 115 (8), 89 (100), 87 (13), 73 (9), 71 (24), 45 (54), 43 (31)
butyrylbutanediol	2,3-dihydroxy-3-methylheptan-4-one	CI, methane[66]	161 (4), 143 (6), 115 (100), 89 (79), 73 (58)
diacetyl	butane-2,3-dione	EI, 70 eV[b]	86 (19), 43 (100)
acetoin acetate	3-acetoxy-2-butanone	EI, 70 eV[33]	130 (<1), 87 (8), 43 (100)
acetoin acetate	3-acetoxy-2-butanone	EI, 20 eV[18]	130 (3), 87 (19), 86 (2), 45 (2), 43 (100)
acetoin butanoate	3-oxobutan-2-yl butyrate	EI, 20 eV[18]	115 (12), 114 (2), 71 (100), , 45 (7), 43 (77), 41 (7)
acetoin hexanoate	3-oxobutan-2-yl hexanoate	EI, 20 eV[18]	143 (9), 100 (5), 99 (100), 88 (5), 71 (40), 55 (4), 45 (4), 43 (58), 41 (4)
acetoin octanoate	3-oxobutan-2-yl octanoate	EI, 20 eV[18]	171 (5), 130 (4), 128 (7), 127 (91), 98 (4), 88 (5), 84 (3), 72 (3), 71 (7), 57 (100), 55 (4), 45 (3), 43 (19), 41 (5)
2,3-butanediol	butane-2,3-diol	EI, 70 eV[b]	90 (1), 75 (3), 57 (9), 45 (100), 43 (10)
2,3-butanediol monoacetate	3-acetoxy-2-butanol	EI, 70 eV[33]	117 (1), 88 (41), 72 (8), 45 (63), 43 (100)
2,3-butanediol diacetate	2,3-diacetoxybutane	EI, 70 eV[33]	131 (3), 130 (6), 114 (2), 87 (32), 72 (13), 43 (100)
2,3-butanediol monobutanoate	3-hydroxybutan-2-yl butyrate	EI, 20 eV[18]	116 (9), 101 (3), 89 (9), 88 (5), 73 (9), 72 (9), 71 (100), 55 (4), 45 (30), 43 (42)
2,3-butanediol monohexanoate	3-hydroxybutan-2-yl hexanoate	EI, 20 eV[18]	144 (19), 115 (7), 101 (9), 100 (8), 99 (100), 89 (21), 88 (19), 73 (30), 72 (14), 71 (37), 60 (5), 57 (19), 45 (26), 43 (44)
2,3-butanediol monooctanoate	3-hydroxybutan-2-yl octanoate	EI, 20 eV[18]	172 (9), 127 (95), 101 (12), 89 (23), 88 (19), 73 (58), 72 (14), 57 (100), 55 (16), 45 (30), 43 (21), 41 (9)
2,4,5-trimethyl-3-oxazoline	2,4,5-trimethyl-2,5-dihydrooxazole	EI, 70 eV[79]	113 (23), 98 (30), 72 (100), 71 (24), 70 (12), 69 (21), 68 (13), 60 (8), 54 (6)
2,4,5-trimethyloxazole	2,4,5-trimethyloxazole	EI, 70 eV[79]	111 (100), 96 (1), 82 (16), 70 (3), 68 (33), 55 (50), 43 (94), 42 (74)
HE-TM-oxazoline	2-(1-hydroxyethyl)-2,4,5-trimethyl-3-oxazoline	EI, 70 eV[79]	157 (1), 113 (16), 112 (100), 98 (7), 72 (10), 71 (62)
HE-TM-oxazoline	2-(1-hydroxyethyl)-2,4,5-trimethyl-3-oxazoline	CI, methane[79]	198 (6), 186 (16), 158 (100), 140 (7), 112 (8), 98 (2), 71 (2)

[a]Acetoin's alkylpyrazine derivatives are not included here. [b]Data from the National Institute of Standards and Technology (http://webbook.nist.gov/chemistry/).

amino ketones, acyloins (hydroxyketones) other than acetoin, or diketones other than diacetyl. Amino ketones could be generated from cellular processes, for example, the metabolism of threonine.[70] Less common hydroxyketones and diketones could be produced by certain organisms.

ANALYSIS OF ACETOIN AND ITS DERIVATIVES IN FOOD MATERIALS

As discussed above, acetoin has various types of derivatives, but, generally speaking, these derivatives are not very difficult to identify and quantify because most of them are volatiles and can be determined using GC-MS techniques. Those nonvolatile derivatives, mainly glycosides per current knowledge, can also be determined by GC-MS after enzymatic[22] or acidic[25] hydrolysis of the glycosidic bonds. The identification of acetoin's alkylpyrazine derivatives, such as TTMP, is straightforward because the corresponding pure chemical standards are easily available and they have reference mass spectra in GC-MS workstations. However, the other derivatives are more complicated for confirmation, but representative ones have been synthesized or extracted from complex samples. Here, we show some of their MS data in Table 4.

The mass spectra of acetion, 2,3-butanediol, and diacetyl are also presented in Table 4 to provide comparison of the complex derivatives with these basic structures. Most of the molecules, except for the heterocyclic compounds, contain high abundance m/z 43 and/or 45. They are the characteristic fragments of acetoin, that is, $[CH_3CO]^+$ and $[CH_3CHOH]^+$, respectively. The diols and esters share another molecular fragmentation characteristic pattern in common; that is, these molecules are rather fragile in EI MS even when the ionization voltage is set at 20 eV.[18] To get the corresponding molecular ion peak and meanwhile rich fragments, CI MS has been proved to be useful from the results shown in Table 4. Of particular note is that some intermediates and products are very active due to the hydroxyl and/or carbonyl group(s). The components of the samples containing acetoin may change during storage.[78]

The analysis methods and quantitative results of acetoin and its derivatives in typical food materials are presented in Table 5. The overall feature is that no reliable clues can be drawn about the amount of acetoin or its derivatives in various foods. Even in the same food category, the differences are large. This mainly arises from uncertainties in the sources of raw materials and differences in processing methods, stages, etc.

In summary, great advances have been achieved in acetoin research, especially in microorganisms, during the past decades.[4,5] Current knowledge of acetoin and its derivatives in higher organisms is very limited and is mainly confined to the analysis of products using relatively simple methods, for example, GC-MS. However, due to the limitation of the gas chromatographic method, nonvolatile derivatives may have been overlooked. Still, the existing diverse results have led us into many unknown fields. The range of possible physiological roles and dietary functions of acetoin and its derivatives should not be underestimated. New experimental work should

dx.doi.org/10.1021/jf5013902 | J. Agric. Food Chem. 2014, 62, 6487−6497

Table 5. Amounts of Acetoin and Its Derivatives in Typical Food Materials

food material	sample preparation and analysis methods	compound	concentration (ppm)
artisanal Spanish cheese during ripening period[9]	headspace sampling, GC-MS	acetoin	248.1 ± 2.06 (3 days), 146.9 ± 44.18 (7 days), 65.15 ± 28.94 (15 days), 27.16 ± 18.14 (30 days)
		diacetyl[a]	2.60 ± 1.24 (3 days), 4.53 ± 1.23 (7 days), 1.66 ± 0.16 (15 days), 0.51 ± 0.18 (30 days)
opaque beer during manufacturing process[13]	headspace sampling, GC	acetoin	2.6 (1 days), 6.5 (3 days), 15.5 (5 days), 6.1 (7 days), 2.1 (10 days), 1.9 (15 days), 1.9 (20 days)
		diacetyl	0.064 (1 days), 0.248 (3 days), 0.175 (5 days), 0.073 (7 days), 0.012 (10 days), 0.008 (15 days), 0.005 (20 days)
11 Chinese vinegars[11]	headspace solid-phase microextraction, GC-MS	acetion	av[b] 2.420, min[c] 0.088, max[d] 7.280
		diacetyl	av 0.316, min nd[e], max 1.156
		2,3-butanediol	av 0.693, min nd, max 2.302
		trimethylpyrazine	ave 0.076, min nd, max 0.302
balsamic vinegar of Modena[12]	solid phase extraction, GC-MS	acetoin	av 5.960, min 1.786, max 14.997
sherry vinegar[12]			av 6.992, min 1.789, max 11.042
52 1- or 2-year-old Spanish red wines[14]	solvent extraction, GC-MS	acetoin	av 33.207, min 0.598, max 159.331
		diacetyl	av 0.350, min 0.200, max 1.840
Garnacha base wine from Spain[15]	solid phase extraction, GC-MS	acetoin	0.0066
Garnacha naturally sweet wine from Spain[15]			0.122
Garnacha sweet fortified wine from Spain[15]			nd
ordinary fino sherry wine from Spain[16]	solvent extraction, GC	acetoin	35.8 ± 4.8 (30 days), 50.9 ± 2.9 (120 days), 48.6 ± 1.5 (250 days)
accelerated aged fino sherry wine from Spain[16]			47.4 ± 7.6 (30 days), 125 ± 13.9 (120 days), 118 ± 4.2 (250 days)
palm wine from Nigeria[17]	solvent extraction, GC, GC-MS, stable isotope dilution assay	acetoin	663.500
pawpaw fruit from Japan[18]	simultaneous distillation and extraction, GC, GC-MS	acetoin	unripe nd, ripe 0.227, overripe 3.123
		acetoin esters	unripe nd, ripe 3.579, overripe 5.712
		2,3-butanediol monoesters	unripe nd, ripe 2.520, overripe 2.399
dekopon fruit from USA[19]	vacuum distillation followed by solvent extraction, GC, GC-MS	acetoin	peel nd, flesh 7.23
3 bananas from the French West Indies[21]	accelerated solvent extraction, adsorption chromatography, enzymatic hydrolysis and solvent extraction, GC-MS	diacetyl	av 0.054, min 0, max 0.161
		acetoin	av 1.426, min 0.035, max 3.387
		2,3-butanediol	av 1.314, min 0.161, max 3.194
		2,3-butanediol monoacetate	av 0.056, min 0.007, max 0.125
		2,3-butanediol diacetate	av 0.085, min 0.005, max 0.227
		glycosidically bound acetoin	av 0.003, min 0.0004, max 0.0066
		glycosidically bound 2,3-butanediol monoacetate	av 0.0005, min 0, max 0.0016
lychee fruit from Taiwan[22]	adsorption chromatography, enzymatic hydrolysis and solvent extraction, GC, GC-MS	acetoin	874 ± 80.3
		glycosidically bound acetoin	0.09 ± 0.01
ash gourd from India[25]	simultaneous distillation extraction, acid hydrolysis and solvent extraction, GC-MS	acetoin	0.007618 ± 0.00118
		acetoin glucoside	24.00 ± 1.945

dx.doi.org/10.1021/jf5013902 | J. Agric. Food Chem. 2014, 62, 6487−6497

Table 5. continued

food material	sample preparation and analysis methods	compound	concentration (ppm)
tortilla flour from USA[26]	high-flow dynamic headspace trapping, GC, GC-MS	acetoin	0.04
		diacetyl	0.06
corn tortilla from USA[26]	high-flow dynamic headspace trapping, GC, GC-MS	acetoin	0.31
		diacetyl	0.006
taco shell from USA[26]	high-flow dynamic headspace trapping, GC, GC-MS	acetoin	0.08
		diacetyl	nd
2 rice cakes from USA[27]	high-flow dynamic headspace trapping, GC, GC-MS	acetoin	av 0.675
		2,3-butanediol	av 0.050
		2,3-dimethylpyrazine	av 0.130
		trimethylpyrazine	av 0.245
Eucalyptus honey from Spain[28]	steam distillation, simultaneous distillation extraction, GC, GC-MS	acetoin	av 1.34, min 0.43, max 2.4
5 other monofloral honeys from Spain[28]			nd

[a]To be precise, diacetyl is not one of the derivatives, but one of the precursors of acetoin (Figure 3). However, because diacetyl belongs to the acetoin reaction system and has flavor importance, it is included in this table. [b]av, average. [c]min, minimum. [d]max, maximum. [e]nd, not detected.

investigate the acetoin series products in more categories of higher organisms using more kinds of analytical techniques, but, importantly, more attention should be paid to enzymes, genes, synthesis mechanisms, and the possible biological roles of these acetoin derivatives to achieve the goal of better control and use.

AUTHOR INFORMATION

Corresponding Authors

*(Z.X.) E-mail zjxiao@upc.edu.cn.
*(J.R.L.) E-mail: j.lu@manchester.ac.uk

Funding

We thank the National Natural Science Foundation of China (No. 21376264) for funding support and the Royal Society (London) for the Sino-British Fellowship and UK−China International Cooperation Award.

Notes

The authors declare no competing financial interest.

REFERENCES

(1) Haukeli, A. D.; Lie, S. Formation and removal of acetoin during yeast fermentation. *J. Inst. Brew.* **1975**, *81*, 58−64.
(2) Hall, R. L.; Oser, B. L. Recent progress in the consideration of flavor ingredients under the Food Additives Amendment. 3. GRAS Substances. *Food Technol.* **1965**, *19*, 151−197.
(3) Romano, P.; Suzzi, G. Origin and production of acetoin during wine yeast fermentation. *Appl. Environ. Microbiol.* **1996**, *62*, 309−315.
(4) Xiao, Z.; Xu, P. Acetoin metabolism in bacteria. *Crit. Rev. Microbiol.* **2007**, *33*, 127−140.
(5) Xiao, Z.; Lu, J. R. Strategies for enhancing fermentative production of acetoin: a review. *Biotechnol. Adv.* *32*, 492−503.
(6) Studer, M.; Okafor, V.; Blaser, H. U. Hydrogenation of butane-2,3-dione with heterogeneous cinchona modified platinum catalysts: a combination of an enantioselective reaction and kinetic resolution. *Chem. Commun.* **1998**, 1053−1054.
(7) Zhu, Z.; Yang, H.; Zhao, Y.; Chen, X.; Su, L. Method for preparing acetoin by butanone. China Tobacco Hunan Industrial Corp., Patent CN101357882 B, 2011.
(8) Ebel, K.; Schneider, R.; Melder, J. P.; Teles, J. H. Process for the preparation of acyloins. BASF Aktiengesellschaft, Patent US5831097 A, 1998.
(9) Fernandez-Garcia, E. Use of headspace sampling in the quantitative analysis of artisanal Spanish cheese aroma. *J. Agric. Food Chem.* **1996**, *44*, 1833−1839.
(10) Le Quéré, J. L.; Fournier, N.; Langlois, D.; Henry, R. Chapter 10. Identification of new odorous heterocyclic compounds in French blue cheeses. *Heteroatomic Aroma Compounds*; ACS Symposium Series 826; American Chemical Society: Washington, DC, USA, 2002; pp 166−178
(11) Xiao, Z.; Dai, S.; Niu, Y.; Yu, H.; Zhu, J.; Tian, H.; Gu, Y. Discrimination of Chinese vinegars based on headspace solid-phase microextraction-gas chromatography mass spectrometry of volatile compounds and multivariate analysis. *J. Food Sci.* **2011**, *76*, C1125−C1135.
(12) Chinnici, F.; Guerrero, E. D.; Sonni, F.; Natali, N.; Marin, R. N.; Riponi, C. Gas chromatography-mass spectrometry (GC-MS) characterization of volatile compounds in quality vinegars with protected European geographical indication. *J. Agric. Food Chem.* **2009**, *57*, 4784−4792.
(13) Tian, J. Determination of several flavours in beer with headspace sampling−gas chromatography. *Food Chem.* **2010**, *123*, 1318−1321.
(14) Ferreira, V.; Lopez, R.; Cacho, J. F. Quantitative determination of the odorants of young red wines from different grape varieties. *J. Sci. Food Agric.* **2000**, *80*, 1659−1667.
(15) Noguerol-Pato, R.; González-Álvarez, M.; González-Barreiro, C.; Cancho-Grande, B.; Simal-Gándara, J. Aroma profile of Garnacha Tintorera-based sweet wines by chromatographic and sensorial analyses. *Food Chem.* **2012**, *134*, 2313−2325.
(16) Cortes, M. B.; Moreno, J. J.; Zea, L.; Moyano, L.; Medina, M. Response of the aroma fraction in sherry wines subjected to accelerated biological aging. *J. Agric. Food Chem.* **1999**, *47*, 3297−3302.
(17) Lasekan, O.; Buettner, A.; Christlbauer, M. Investigation of important odorants of palm wine (*Elaeis guineensis*). *Food Chem.* **2007**, *105*, 15−23.
(18) Shiota, H. Volatile components of pawpaw fruit (*Asimina triloba* Dunal.). *J. Agric. Food Chem.* **1991**, *39*, 1631−1635.
(19) Umano, K.; Hagi, Y.; Shibamoto, T. Volatile chemicals identified in extracts from newly hybrid citrus, dekopon (*Shiranuhi mandarin* Suppl. J.). *J. Agric. Food Chem.* **2002**, *50*, 5355−5359.
(20) Weenen, H.; Koolhaas, W. E.; Apriyantono, A. Sulfur-containing volatiles of durian fruits (*Durio zibethinus* Murr.). *J. Agric. Food Chem.* **1996**, *44*, 3291−3293.
(21) Aurore, G.; Ginies, C.; Ganou-parfait, B.; Renard, C. M. G. C.; Fahrasmane, L. Comparative study of free and glycoconjugated volatile compounds of three banana cultivars from French West Indies: Cavendish, Frayssinette and Plantain. *Food Chem.* **2011**, *129*, 28−34.

(22) Chyau, C. C.; Ko, P. T.; Chang, C. H.; Mau, J. L. Free and glycosidically bound aroma compounds in lychee (*Litchi chinensis* Sonn.). *Food Chem.* **2003**, *80*, 387−392.
(23) Rochat, D.; Le Meillour, P. N.; Esteban Duran, J. R.; Malosse, C.; Perthuis, B.; Morin, J. P.; Descoins, C. Identification of pheromone synergists in American palm weevil, *Rhynchophorus palmarum*, and attraction of related *Dynamis borassi*. *J. Chem. Ecol.* **2000**, *26*, 155−187.
(24) Chatterjee, S.; Sharma, J.; Variyar, P. S.; Sharma, A. Free and glycosidically bound volatiles of some common Indian vegetables. *Electron. J. Environ. Agric. Food Chem.* **2009**, *8*, 613−620.
(25) Sharma, J.; Chatterjee, S.; Kumar, V.; Variyar, P. S.; Sharma, A. Analysis of free and glycosidically bound compounds of ash gourd (*Benincasa hispida*): identification of key odorants. *Food Chem.* **2010**, *122*, 1327−1332.
(26) Buttery, R. G.; Ling, L. C. Volatile flavor components of corn tortillas and related products. *J. Agric. Food Chem.* **1995**, *43*, 1878−1882.
(27) Buttery, R. G.; Orts, W. J.; Takeoka, G. R.; Nam, Y. Volatile flavor components of rice cakes. *J. Agric. Food Chem.* **1999**, *47*, 4353−4356.
(28) Bonvehí, J. S.; Coll, F. V. Flavour index and aroma profiles of fresh and processed honeys. *J. Sci. Food Agric.* **2003**, *83*, 275−282.
(29) Azuma, H.; Toyota, M.; Asakawa, Y.; Takaso, T.; Tobe, H. Floral scent chemistry of mangrove plants. *J. Plant Res.* **2002**, *115*, 47−53.
(30) Ding, D.; Zhu, M.; Huang, Z.; Zhao, J. Headspace analysis of *Osmanthus fragrans* Lour. *J. Essent. Oil Res.* **1989**, *1*, 295−297.
(31) Light, D. M.; Kamm, J. A.; Buttery, R. G. Electroantennogram response of alfalfa seed chalcid, *Bruchophagus roddi* (Hymenoptera: Eurytomidae) to host- and nonhost-plant volatiles. *J. Chem. Ecol.* **1992**, *18*, 333−352.
(32) Tatsuka, K.; Suekane, S.; Sakai, S.; Sumitani, H. Volatile constituents of kiwi fruit flowers: simultaneous distillation and extraction versus headspace sampling. *J. Agric. Food Chem.* **1990**, *38*, 2176−2180.
(33) Stökl, J.; Strutz, A.; Dafni, A.; Svatos, A.; Doubsky, J.; Knaden, M.; Sachse, S.; Hansson, B. S.; Stensmyr, M. C. A deceptive pollination system targeting drosophilids through olfactory mimicry of yeast. *Curr. Biol.* **2010**, *20*, 1846−1852.
(34) Tolasch, T.; Solter, S. R.; Toth, M.; Ruther, J.; Francke, W. (*R*)-Acetoin-female sex pheromone of the summer chafer *Amphimallon solstitiale* (L.). *J. Chem. Ecol.* **2003**, *29*, 1045−1050.
(35) Rochat, D.; Morin, J. P.; Kakul, T.; Beaudoin-Ollivier, L.; Prior, R.; Renou, M.; Malosse, I.; Stathers, T.; Embupa, S.; Laup, S. Activity of male pheromone of Melanesian rhinoceros beetle *Scapanes australis*. *J. Chem. Ecol.* **2002**, *28*, 479−500.
(36) Sreng, L. Seducin, male sex pheromone of the cockroach *Nauphoeta cinerea*: isolation, identification, and bioassay. *J. Chem. Ecol.* **1990**, *16*, 2899−2912.
(37) Otsuka, M.; Mine, T.; Ohuchi, K.; Ohmori, S. A detoxication route for acetaldehyde: metabolism of diacetyl, acetoin, and 2,3-butanediol in liver homogenate and perfused liver of rats. *J. Biochem.* **1996**, *119*, 246−251.
(38) Otsuka, M.; Harada, N.; Itabashi, T.; Ohmori, S. Blood and urinary levels of ethanol, acetaldehyde, and C-4 compounds such as diacetyl, acetoin, and 2,3-butanediol in normal male students after ethanol ingestion. *Alcohol* **1999**, *17*, 119−124.
(39) Meijerink, J.; Braks, M. A. H.; Brack, A. A.; Adam, W.; Dekker, T.; Posthumus, M. A.; Van Beek, T. A.; Van Loon, J. J. A. Identification of olfactory stimulants for *Anopheles gambiae* from human sweat samples. *J. Chem. Ecol.* **2000**, *26*, 1367−1382.
(40) Xiao, Z.; Lv, C.; Gao, C.; Qin, J.; Ma, C.; Liu, Z.; Liu, P.; Li, L.; Xu, P. A novel whole-cell biocatalyst with NAD^+ regeneration for production of chiral chemicals. *PLoS One* **2010**, *5*, No. e8860.
(41) Xiao, Z.; Qiao, S.; Ma, C.; Xu, P. Acetoin production associated with the increase of cell biomass in *Bacillus pumilus* ATCC 14884. *Afr. J. Microbiol. Res.* **2010**, *4*, 1997−2003.
(42) Chen, S. C.; Yang, R. L.; Ho, H. Y.; Chou, S. Y.; Kou, R. Strategic 3-hydroxy-2-butanone release in the dominant male lobster cockroach, *Nauphoeta cinerea*. *Naturwissenschaften* **2007**, *94*, 927−933.
(43) Farine, J. P.; Sirugue, D.; Abed-Vieillard, D.; Everaerts, C.; Le Quéré, J. L.; Bonnard, O.; Brossut, R. The male abdominal glands of *Leucophaea maderae*: chemical identification of the volatile secretion and sex pheromone function. *J. Chem. Ecol.* **2007**, *33*, 405−415.
(44) Chen, R.; Li, Y. A novel plant volatile attractant scheme to protect corn in China from the white-spotted flower chafer (Coleoptera: Scarabaeidae: Cetoniinae). *J. Pest Sci.* **2011**, *84*, 327−835.
(45) Becher, P. G.; Bengtsson, M.; Hansson, B. S.; Witzgall, P. Flying the fly: long-range flight behavior of *Drosophila melanogaster* to attractive odors. *J. Chem. Ecol.* **2010**, *36*, 599−607.
(46) Negishi, T.; Okano, T.; Yamamoto, T.; Kawamoto, S. Fly attractant and trap for catching fly. *Earth Chem.*, Japan patent 2001-233709, 2001.
(47) Ômura, H.; Honda, K.; Hayashi, N. Identification of feeding attractants in oak sap for adults of two nymphalid butterflies, *Kaniska canace* and *Vanessa indica*. *Physiol. Entomol.* **2000**, *25*, 281−287.
(48) Larsson, M. C.; Stensmyr, M. C.; Bice, S. B.; Hansson, B. S. Attractiveness of fruit and flower odorants detected by olfactory receptor neurons in the fruit chafer *Pachnoda marginata*. *J. Chem. Ecol.* **2003**, *29*, 1253−1268.
(49) Forlani, G.; Mantelli, M.; Nielsen, E. Biochemical evidence for multiple acetoin-forming enzymes in cultured plant cells. *Phytochemistry* **1999**, *50*, 255−262.
(50) Stensmyr, M. C.; Giordano, E.; Balloi, A.; Angioy, A. M.; Hansson, B. S. Novel natural ligands for *Drosophila* olfactory receptor neurones. *J. Exp. Biol.* **2003**, *206*, 715−724.
(51) De Bruyne, M.; Baker, T. C. Odor detection in insects: volatile codes. *J. Chem. Ecol.* **2008**, *34*, 882−897.
(52) Moore, A. J.; Moore, P. J. Balancing sexual selection through opposing mate choice and male competition. *Proc. R. Soc. London* **1999**, *266*, 711−716.
(53) Kou, R.; Chen, S. C.; Chen, Y. R.; Ho, H. Y. 3-Hydroxy-2-butanone and the first encounter fight in the male lobster cockroach, *Nauphoeta cinerea*. *Naturwissenschaften* **2006**, *93*, 286−291.
(54) Baggetto, L. G.; Testa-Parussini, R. Role of acetoin on the regulation of intermediate metabolism of Ehrlich ascites tumor mitochondria: its contribution to membrane cholesterol enrichment modifying passive proton permeability. *Arch. Biochem. Biophys.* **1990**, *283*, 241−248.
(55) Pang, S. S.; Duggleby, R. G.; Schowen, R. L.; Guddat, L. W. The crystal structures of *Klebsiella pneumoniae* acetolactate synthase with enzyme-bound cofactor and with an unusual intermediate. *J. Biol. Chem.* **2004**, *279*, 2242−2253.
(56) Sergienko, E. A.; Jordan, F. Catalytic acid-base groups in yeast pyruvate decarboxylase. 2. Insights into the specific roles of D28 and E477 from the rates and stereospecificity of formation of carboligase side products. *Biochemistry* **2001**, *40*, 7369−7381.
(57) Chang, Y. Y.; Cronan, J. E., Jr. Common ancestry of *Escherichia coli* pyruvate oxidase and the acetohydroxy acid synthases of the branched-chain amino acid biosynthetic pathway. *J. Bacteriol.* **1988**, *170*, 3937−3945.
(58) Störmer, F. C. Isolation of crystalline pH 6 acetolactate-forming enzyme from *Aerobacter aerogenes*. *J. Biol. Chem.* **1967**, *242*, 1756−1759.
(59) Bertagnolli, B. L.; Hager, L. P. Role of flavin in acetoin production by two bacterial pyruvate oxidases. *Arch. Biochem. Biophys.* **1993**, *300*, 364−371.
(60) Wu, Y. G.; Chang, A. K.; Nixon, P. F.; Li, W.; Duggleby, R. G. Mutagenesis at asp27 of pyruvate decarboxylase from *Zymomonas mobilis*. Effect on its ability to form acetoin and acetolactate. *Eur. J. Biochem.* **2000**, *267*, 6493−6500.
(61) Gabriel, M. A.; Jabara, H.; al-Khalidi, U. A. Metabolism of acetoin in mammalian liver slices and extracts. Interconversion with butane-2,3-diol and biacetyl. *Biochem. J.* **1971**, *124*, 793−800.

(62) Hillman, J. D.; Andrews, S. W.; Dzuback, A. L. Acetoin production by wild-type strains and a lactate dehydrogenase-deficient mutant of *Streptococcus mutans*. *Infect. Immun.* **1987**, *55*, 1399−1402.
(63) Montgomery, J. A.; Jetté, M.; Huot, S.; Des Rosiers, C. Acyloin production from aldehydes in the perfused rat heart: the potential role of pyruvate dehydrogenase. *Biochem. J.* **1993**, *294*, 727−733.
(64) Baggetto, L. G.; Lehninger, A. L. Formation and utilization of acetoin, an unusual product of pyruvate metabolism by Ehrlich and AS30-D tumor mitochondria. *J. Biol. Chem.* **1987**, *262*, 9535−9541.
(65) Xiao, Z.; Ma, C.; Xu, P.; Lu, J. R. Acetoin catabolism and acetylbutanediol formation by *Bacillus pumilus* in a chemically defined medium. *PLoS One* **2009**, *4*, No. e5627.
(66) Xiao, Z.; Wang, X.; Huang, Y.; Huo, F.; Zhu, X.; Xi, L.; Lu, J. R. Thermophilic fermentation of acetoin and 2,3-butanediol by a novel *Geobacillus* strain. *Biotechnol. Biofuels* **2012**, *5*, 88.
(67) Speranza, G.; Corti, S.; Fontana, G.; Manitto, P. Conversion of meso-2,3-butanediol into 2-butanol by lactobacilli. Stereochemical and enzymatic aspects. *J. Agric. Food Chem.* **1997**, *45*, 3476−3480.
(68) Yokota, A.; Sasajima, K. Enzymatic formation of a new monosaccharide, 1-deoxy-D-altro-heptulose phosphate, from DL-acetoin and D-ribose 5-phosphate by a transketolase mutant of *Bacillus pumilus*. *Agric. Biol. Chem.* **1983**, *47*, 1545−1553.
(69) Rajini, K. S.; Aparna, P.; Sasikala, Ch.; Ramana, Ch. V. Microbial metabolism of pyrazines. *Crit. Rev. Microbiol.* **2011**, *37*, 99−112.
(70) Larroche, C.; Besson, I.; Gros, J. B. High pyrazine production by *Bacillus subtilis* in solid substrate fermentation on ground soybeans. *Process Biochem.* **1999**, *34*, 667−674.
(71) Maga, J. A. Oxazoles and oxazolines in foods. *CRC Crit. Rev. Food Sci. Nutr.* **1981**, *14*, 295−307.
(72) Xiao, Z. J.; Xie, N. Z.; Liu, P. H.; Hua, D. L.; Xu, P. Tetramethylpyrazine production from glucose by a newly isolated *Bacillus* mutant. *Appl. Microbiol. Biotechnol.* **2006**, *73*, 512−518.
(73) Xu, W.; Xu, Q.; Chen, J.; Lu, Z.; Xia, R.; Li, G.; Xu, Z.; Ma, Y. Ligustrazine formation in Zhenjiang aromatic vinegar: changes during fermentation and storing process. *J. Sci. Food Agric.* **2011**, *91*, 1612−1617.
(74) Guo, S. K.; Chen, K. J.; Qian, Z. H.; Weng, W. L.; Qian, M. Y. Tetramethylpyrazine in the treatment of cardiovascular and cerebrovascular diseases. *Planta Med.* **1983**, *47*, 89.
(75) Watanabe, H. Candidates for cognitive enhancer extracted from medicinal plants: paeoniflorin and tetramethylpyrazine. *Behav. Brain Res.* **1997**, *83*, 138−141.
(76) Rizzi, G. P. The biogenesis of food-related pyrazines. *Food Rev. Int.* **1988**, *4*, 375−400.
(77) Rizzi, G. P. Formation of pyrazines from acyloin precursors under mild conditions. *J. Agric. Food Chem.* **1988**, *36*, 349−352.
(78) Shu, C. K.; Lawrence, B. M. Formation of 2-(1-hydroxyalkyl)-3-oxazolines from the reaction of acyloins and ammonia precursors under mild conditions. *J. Agric. Food Chem.* **1995**, *43*, 2922−2924.
(79) Fu, H. Y.; Ho, C. T. Mechanistic studies of 2-(1-hydroxyethyl)-2,4,5-trimethyl-3-oxazoline formation under low temperature in 3-hydroxy-2-butanone/ammonium acetate model systems. *J. Agric. Food Chem.* **1997**, *45*, 1878−1882.
(80) Xi, J.; Huang, T. C.; Ho, C. T. Characterization of volatile compounds from the reaction of 3-hydroxy-2-butanone and ammonium sulfide model system. *J. Agric. Food Chem.* **1999**, *47*, 245−248.
(81) Xiao, Z.; Lu, J. R.; Ma, C.; Xu, P. Formation and identification of trimethylimidazole during tetramethylpyrazine production from glucose by *Bacillus* strains. *Biotechnol. Lett.* **2009**, *31*, 1421−1425.
(82) Owens, J. D.; Allagheny, N.; Kipping, G.; Ames, J. M. Formation of volatile compounds during *Bacillus subtilis* fermentation of soya beans. *J. Sci. Food Agric.* **1997**, *74*, 132−140.
(83) Shu, C. K. Pyrazine formation from amino acids and reducing sugars, a pathway other than strecker degradation. *J. Agric. Food Chem.* **1998**, *46*, 1515−1517.

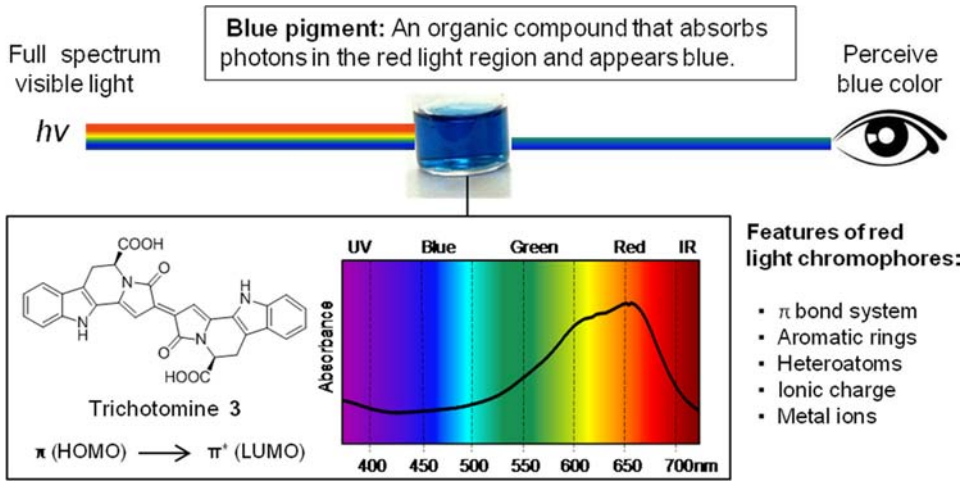

Figure 2. Color perception for a blue pigment using the visible absorbance spectrum of trichotomine (**3**) (λ_{max}, methanol, 660 nm) as an example. The typical properties of red light absorbing molecules are listed.

not absorbed, photons. Color can also result from diffraction or scattering of light. Only pigmentation by the absorptive processes of organic molecules is within the scope of this review. A *blue pigment* is defined as an organic molecule that absorbs red light (600 nm region) and appears blue by ordinary color perception (Figure 2). The origin of color in molecules, electron spectroscopic theory, and the processes of color perception are well-known.[10−12]

Why are blue pigments (red light absorbing molecules) relatively uncommon in nature? The answer lies in electronic absorption theory. When the energy of an incident photon matches an energy gap ($\Delta E = h\nu$) between molecular orbitals (σ, n, or π), the photon is absorbed by an electron that is promoted to the next higher energy orbital. Most molecules absorb ultraviolet photons by $\sigma \rightarrow \sigma^*$ and $\sigma \rightarrow \pi^*$ transitions. Far fewer molecules exhibit the lower energy $\pi \rightarrow \pi^*$ and n $\rightarrow \pi^*$ transitions that are required to absorb visible light, and these molecules appear to have color. Conjugation of π-bond systems can lower the HOMO → LUMO energy gap for $\pi \rightarrow \pi^*$ transitions to occur into the blue light region (400−500 nm, ΔE = 3.1−2.5 eV) and this produces red, orange, and yellow colors as in carotenoids.

Linear π-bond conjugation alone does not lead to absorption in the red light range (600−700 nm, ΔE = 2.1−1.8 eV). Blue pigments (red light absorbers) typically possess π-bond conjugation, aromatic ring systems, heteroatoms, and ionic charges. Also, organometallic and transition metal complexes are often brightly colored because their *d*-orbitals afford many lower energy electronic transitions. Heteroatom groups (−NH_2, −OH, =O, −Cl, etc.), sometimes called auxochromic groups, can further reduce the transition energies to produce the required bathrochromic shift. For example, red carotenoids can appear blue when complexed with iodine or converted to cations or through interactions with amino acid side chains such as those in blue carotenoproteins.[13] All of the blue pigments reviewed here contain two or more of these features. Compared with other pigments, natural blue pigments are uncommon because a more complex combination of molecular features is required to absorb red light.

IDEAL COLORANT PROPERTIES

Whether from natural or synthetic sources, all new color additives must meet stringent requirements before use. Gaining regulatory approval is the most critical step. The U.S. Code of Federal Regulations[14] provides details of the petitioning process. In addition, new colorants must meet targets for hue, stability, suitability for the target application, and cost. Natural colorants rarely match the intensity of FD&C dyes. Most natural and synthetic color additives have ε_{max} values on the order of 10^5 or 10^6.[7] Colorants with lower ε_{max} values must be used at higher levels to achieve the desired appearance, thereby increasing costs and the risk of off-flavors. Colorants must also be stable enough to avoid significant degradation throughout distribution and sales of both the ingredient and the food or beverage, which might include storage from days to years at refrigerated or ambient conditions. Common causes of instability include heat, light, oxygen, acid, and exposure to oxidants such as ascorbic acid and trace metals. Product developers might have additional requirements such as water- or oil-soluble formulations for specific applications. Insoluble forms may be necessary to prevent colorant migration. Finally, new natural colorants must be sourced from raw materials with a commercial supply and at levels that make extraction economically feasible.

NATURAL BLUE PIGMENTS

Blue colors are not uncommon in nature. Although brilliant blue shades can be seen in flowers, berries, bird feathers, and mushrooms, these colors derive from very different sources. Blue color in animals is typically caused by reflection of blue light from nanoscale structures (schemochromes). Examples include blue bird feathers (*Sialia* sp.) and iridescent butterfly wings (*Morpho* sp.). This effect is not limited to the animal kingdom. Quandong fruits (*Santalum acuminatum*) appear bright blue but contain no blue pigments.[15] Anthocyanins are the sources of most blue, red, and purple colors in plant leaves, berries, and roots. Plants may also contain blue copper metalloproteins for redox functions. Cyanobacteria often contain blue light harvesting proteins for photosynthesis such as phycocyanin. Some fungi and microorganisms produce a wide variety of blue secondary metabolites, which are often made in response to environmental stress or predators. Blue chromophores from underexplored sources such as marine microorganisms have been reviewed previously.[16]

Searching natural products databases for blue pigments is not straightforward, because they are organized by attributes such as molecular weight and composition instead of color. Publications often neglect to report the absorbance spectra or colors of newly identified natural products. In addition, the color of a given

dx.doi.org/10.1021/jf501419q | J. Agric. Food Chem. 2014, 62, 6498−6511

compound may vary with conditions such as pH, solvent, and the presence of trace metals or other compounds. Given these challenges, no review can be comprehensive. This review organizes organic blue chromophores by structural class. Inorganic blue compounds, such as copper salts, are not included.

Flavanoids. Anthocyanidins (Figure 3) and their glycosides, anthocyanins, are ubiquitous in the plant world and are

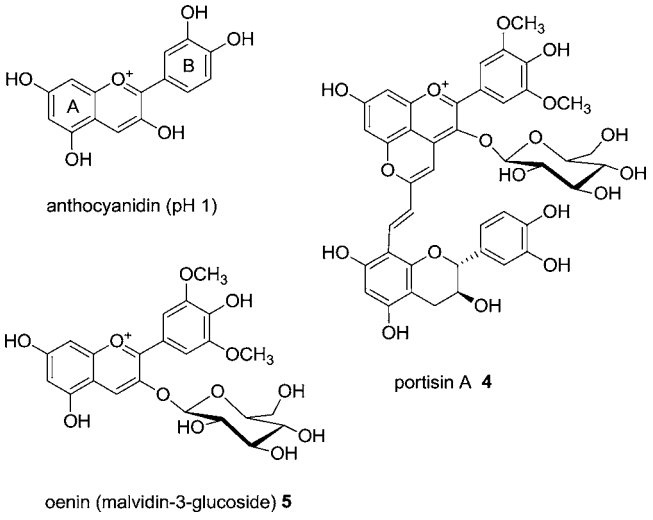

Figure 3. Chemical structures of blue flavanoid-derived natural products.

responsible for many of the colors of flowers and fruits.[15,17,18] Anthocyanins from fruits and vegetables are commonly used as food colorants, but their color is highly pH dependent. The blue quinoidal form predominates under neutral or alkaline conditions, whereas the red flavylium cation forms under acidic conditions (Figure 3). At least six pH-dependent structural forms are known.[1,19−21] Stability is a function of both structure and complex interactions such as acylation and copigmentation.[21]

Research into the biosynthesis and modification of anthocyanins is extensive and has been driven by the desire for blue cultivars of flowers such as roses and carnations. A recent review summarizes these complex pathways.[22] Anthocyanin color is influenced by its structure, intra- and intermolecular interactions, and pH. Increasing hydroxylation of the B-ring shifts anthocyanins to bluer shades, as seen with delphinidin, the pigment responsible for the blue color of delphiniums.[21,23] The formation of complexes with copigments such as flavones and with metal cations can also shift the hue.[21] A familiar example is the use of aluminum compounds to shift the color of hydrangea blossoms from pink to blue.

After synthesis, anthocyanins are transported to vacuoles for storage. The color of anthocyanins within the vacuole is a function of the anthocyanin type, its structural form when complexed with other components, and the vacuolar pH. These vacuoles have been suggested as food colorants.[23] The internal pH of the vacuole is higher than that of typical foods, so the anthocyanins will appear blue. It is not clear if anthocyanin vacuolar inclusions can survive the rigors of food processing and storage or if they can be produced efficiently on a commercial scale.

Complex blue anthocyanin-derived compounds such as portisin A (**4**) have been isolated from aged red wine.[24−26] At low pH, the portisins show a bathochromically shifted absorption maximum (portisin A (**4**), λ_{max} pH 1, 587 nm) relative to common anthocyanins such as oenin (malvidin-3-glucoside) (**5**) (λ_{max} pH 1, 538 nm). Portisins are purple rather than pink at low pH values.[24,26] These compounds face the same challenges as other new food colorants. Additional studies will be required to determine solubility and stability. These compounds are present at such low levels that isolation from wine is not feasible; new processes for commercial production will be required.

A thorough discussion of the structural variety and stability of anthocyanins is beyond the scope of this review. The chemistry, structural diversity, biosynthesis, distribution, safety, and stability of these compounds have been reviewed extensively.[1,27−29] The structures of some of these anthocyanin pigments are shown in Figure 3.

Quinones and Quinoids. The inclusion of carbonyl groups within an aromatic ring system can lead to the absorption of the lower energy visible spectrum photons required to produce absorption in the visible spectrum. Dyes based upon the 9,10-anthraquinone skeleton (Figure 4) were first isolated and synthesized for commercial use in the 19th century.[30,31] Varying substitutions on this skeleton for specific auxochromic effects have resulted in dyes of every color. Not all quinoid dyes are suitable for food use due to biological activity, and few are blue under acidic conditions.

Many natural blue anthraquinone or quinoid dyes are blue at alkaline pH but red or orange at neutral or acidic pH. One example is the chemotherapeutic anthraquinone drug daunorubicin (**6**). Isolated in 1964 from *Streptomyces peucetius*,[32] daunorubicin was among the first chemotherapeutic compounds derived from soil microbes. Daunorubicin interchelates between DNA strands and is prescribed for acute myeloid and lymphocytic leukemia.[33]

Streptomyces coelicolor excretes the benzoisochromaquinone actinorhodin (**7**) and its analogues at yields of up to 3 g L^{-1} of fermentation medium.[34−36] The actinorhodins have been proposed as food colorants, but as with most anthraquinones, they are blue only under alkaline conditions, limiting their use in foods and beverages. The actinorhodins show weak antibiotic activity but are not cytotoxic. For example, the MIC of actinorhodin against *Staphylococcus aureus* is 30 μg mL^{-1},[36] whereas its LD_{50} in mice is >15 g kg^{-1}.[34] Other blue benzoisochromaquinone-like antibiotics include granaticin B (**8**) and related analogues isolated from various *Streptomyces* species.[37−39] The granaticins are cytotoxic and not blue at low pH. Diosindigo A (**9**) is a blue bis(quinone) that has been isolated from the heartwood of at least seven *Diospyros* botanical species, but little additional information such as stability is available.[40,41]

Natural anthraquinoid compounds are rarely blue under acidic conditions, but there are a few exceptions for those with an extended aromatic ring system. These include the dark blue microbial metabolites anthracyclinone-blue B (**10**) from a *Streptomyces galilaeus* mutant[42] and kyanomycin (λ_{max} methanol, 600 nm, ε = 11480), from *Nonomuria* sp. NN22303.[43] Another blue compound with an extended quinone structure, ventilein A (**11**) (λ_{max} methanol, 645 nm), was isolated as a minor constituent from *Ventilago calyculata* root bark[44] and from *Ventilago goughii*.[45] Blepharismin and stentorin are red photosensory pigments from the protists *Blepharisma japonicum*[46] and *Stentor coeruleus*[47] with a fused eight-ring conjugated quinone system identical to hypericin (bright red). Photoreaction products of the blepharismins, such as oxyblepharismin A (**12**) and analogues, are blue.

Quinoid pigments are responsible for the blue colors of many fungi such as Basidiomycetes.[48] The bluing reactions of several mushroom species are due to the oxidation of conjugated

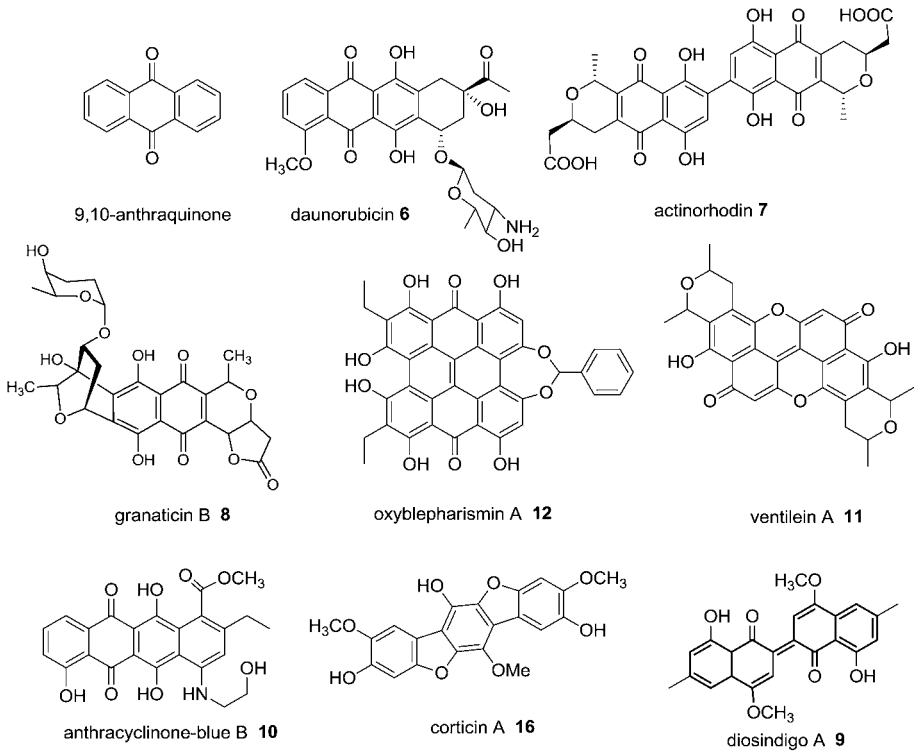

Figure 4. Chemical structures of some blue-colored natural quinoids and quinones.

furanoquinones to blue anionic compounds such as gyrocyanin,[49] variegatic acid (**13**),[50] xerocomic acid,[51] and chamonixin.[52] Although relatively little research has been reported on these furanoquinone oxidation products, anecdotal evidence of subsequent fading of blue-bruising fungi suggests that these oxidation products are unstable. The variegatic acid anion (**14**) fades to brown in <60 min.[50] The meroterpenoid quinone albatrellin (**15**) was identified as the source of blue color in the skin of *Alabtrellus flettii* (Basidiomycete) fruiting bodies.[53] The pigment is blue in chloroform or dichloromethane, but violet in methanol (λ_{max} methanol, 535 nm, ε = 3200). Corticin A (**16**), a derivative of the benzofuranoquinone fungal pigment thelephoric acid, was determined to be the blue pigment of the fungus *Corticium caeruleum*.[54] A bis(quinoid) fungal metabolite containing an imine linkage, scleroderris blue (**17**), was isolated from the canker fungus *Gremmeniella abietina*[55,56] and later from *Penicillium herquei* as a zinc complex.[57] The compound is intensely blue colored (λ_{max} CH_2Cl_2, 612 nm; ε = 50000) but relatively unstable; scleroderris blue can be converted to scleroderris green with a weak reducing agent.[56] Popolohuanone B (**18**), a pigment containing an aminoquinone chromophore, was isolated from a blue-purple *Dysidea* sp. sponge.[58] Structures of blue pigments of the quinoid or quinone class are shown in Figures 4 and 5.

Linear Tetrapyrrole Alkaloids. Tetrapyrroles cover every color of the visible spectrum. Blue tetrapyrroles are responsible for the blue coloration of bruises.[59] Biliverdins, heme degradation products found in bile, are among the few natural blue compounds in the animal kingdom. The bile pigment biliverdin-IX_a (oocyan) (**20**) is responsible for the pigmentation of bird egg shells.[60,61] The light harvesting protein phycocyanin in *Cyanobacteria* contains a bound linear tetrapyrrole phycocyanobilin (**19**) as the blue chromophore.[62,63] The difference between the intense blue phycocyanobilin and the heme byproduct urochrome, the source of yellow color in urine, is extended conjugation across four pyrrole rings via one additional unsaturation. Phycocyanin is commercially extracted from the alga *Spirulina platensis* and is used as a colorant in confections. However, phycocyanin is not stable enough for most food and beverage applications.

Bactobilin (**21**),[64,65] isolated from *Clostridium tetanomorphum* and *Propionibacterium shermanii* (used in Swiss cheese production), is one of the few known bacterial bile pigments.[66] Bactobilin shares the same blue chromophore as phycocyanobilin but has eight methyl ester side chains. The stability of bactobilin has not been reported, but because alkylation or acylation enhances the stability of chromophores such as anthocyanins, bactobilin should be more stable than phycocyanobilin.

A blue prodigiosin tetrapyrrole (**22**) analogue of the cytotoxic microbial red pigment prodigiosin has been isolated from a variety of sources including a mutant *Serratia marcescens* strain,[67] the marine bacterium *Hahella chejuensis* KCTC 2396,[68] some blue marine ascidians,[69,70] a blue bryozoan,[71] and the nudibranch *Nembrotha kubaryana*.[72] *N. kubaryana* might derive its color from feeding on blue ascidians and bryozoans. The prodigiosin tetrapyrrole is distinguished from bile pigments by having directly coupled pyrrole rings rather than methine spacers. Unlike the bile tetrapyrroles, prodigiosin and its analogues usually exhibit cytotoxic and antimicrobial activities.[73] Structures of these blue tetrapyrrole pigments are shown in Figure 6.

Phenazine Alkaloids. Hundreds of natural phenazine molecules have been isolated and characterized, primarily from *Pseudomonas* and *Streptomyces* species.[74,75] The colors of these compounds span the entire visible spectrum. One of the first identified and best known phenazines is the blue compound pyocyanin (**23**), the highly cytotoxic cystic fibrosis virulence factor from *Pseudomonas aeruginosa*.[76,77] Other blue phenazines include the *N*-terpenoid-substituted metabolites phenazinomycin (**24**) isolated from *Streptomyces* sp. WK-2057 mycelia[78,79]

dx.doi.org/10.1021/jf501419q | J. Agric. Food Chem. 2014, 62, 6498−6511

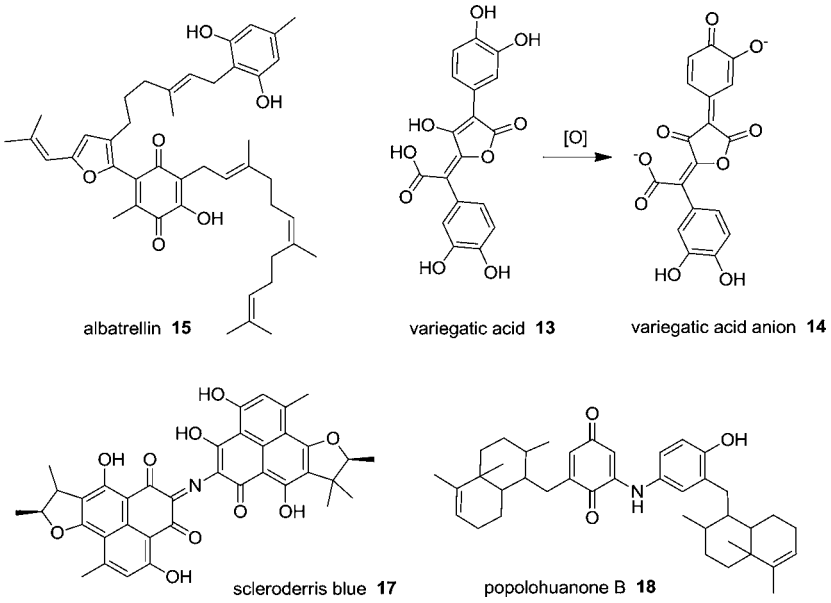

Figure 5. Chemical structures of some additional blue natural quinoids and quinones.

and lavanducyanin (**25**) from *Streptomyces aeriouvifer*.[80,81] The absorption maxima and molar absorptivities of phenazinomycin (λ_{max} methanol, 745 nm, ε = 6600) and lavanducyanin (λ_{max} methanol, 705 nm, ε = 1700) are similar to those of pyocyanin (λ_{max} methanol, 746 nm, ε = 5800). Both show broad visible absorbance in the far-red light region with relatively low molar absorptivity. Benthocyanin A (**26**) from *Streptomyces pruni-color*[82,83] contains an additional lactone ring and has a higher molar absorptivity in the red light region presumably due to the larger chromophore surface area (λ_{max} methanol + HCl, 638 nm, ε = 16200; λ_{max} methanol + NaOH, 616 nm, ε = 18400). Although many blue pigments of the phenazine class are blue under acidic conditions, they are usually cytotoxic or otherwise biologically active,[75,79,81] thereby excluding them from consideration as food colorants. Structures of these blue phenazines are shown in Figure 7.

Indole Alkaloids. A small fraction of the thousands of known indole alkaloids are blue. Indigo dyes from the tropical plants woad (*Isatis tinctoria*) and true indigo (*Indigofera tinctoria*) have a long history of use in textiles.[30,84] The bis(indole) indigotin (**27**) is responsible for the blue color of indigo-based dyes[85] and today is produced synthetically. Its disulfonate sodium salt, FD&C blue no. 2, is produced for the food and cosmetic industries.[7] Indigotin and its derivatives lack the pH and light stability often required for food and beverage products. Blue 5,5′-dichlorinated analogues of indigotin, akashins A (**28**), B, and C, were recently isolated from the marine *Streptomyces* sp. GW48/1497.[86,87] Whereas indigotin is not cytotoxic, the akashins showed activity against cancer cell lines with IC_{50} values near 3 μg mL^{-1}.[87] Candidine (**29**), a blue alkaloid originally isolated from *Candida lipolytica*,[88,89] is a constituent of the traditional Chinese medicinal herb qing-dai (*Indigo naturalis*).[90] Its bis(indole) chromophore is similar to indigotin.

Kusagi berries from the Asian shrub *Clerodendron trichotomum* have a bright blue skin.[91] Extracts of these berries have been used to dye textiles.[92,93] The berry skin contains the blue bis(indole) alkaloid trichotomine (**3**) and its glycosides,[94−96] which are structurally more complex and intensely colored than indigotin (Figure 8). The larger absorptive surface area of the compound imparts a blue color with a molar absorptivity similar to that of

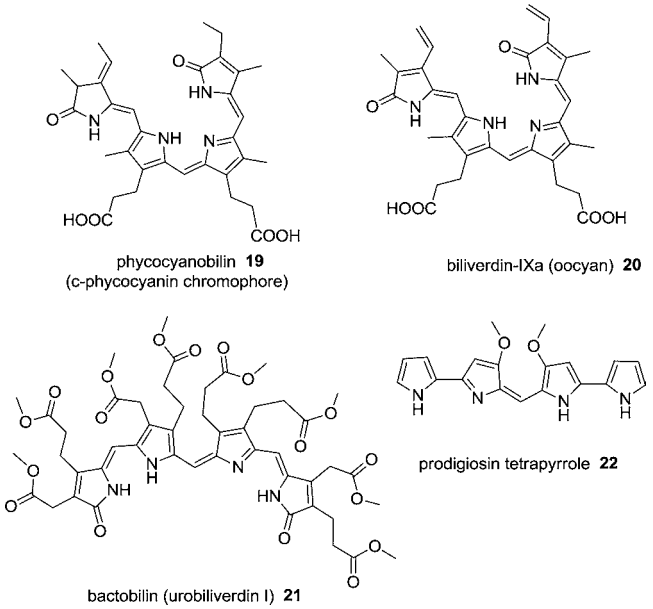

Figure 6. Chemical structures of some blue-pigmented linear tetrapyrroles.

FD&C blue no. 1 (**1**). Trichotomine and its derivatives are among the very few compounds that produce the same shade of blue as FD&C blue no. 1.

Violacein, a deep violet indole alkaloid first reported 1888, was isolated from *Chromobacterium violaceum*, a species native to the Amazon River.[97] It has been studied extensively for its biological activities[98] and as a textile dye.[99] Prodeoxyviolacein (**30**), a biosynthetic precursor of violacein, is blue in acid and red under neutral or alkaline conditions.[100,101] Deep red or violet microbial and sponge pyrroloquinoline metabolites containing the indole moiety have been reported.[102] Ammosamide A (**31**), isolated from the marine *Streptomyces* CNR-698, is similar in structure but contains an unusual thio-γ-lactam group contributing to its deep blue color.[103] The thionyl group ammosamide A slowly oxidizes in air to form a carbonyl group and the red compound ammosamide B. Both compounds are active against a variety of

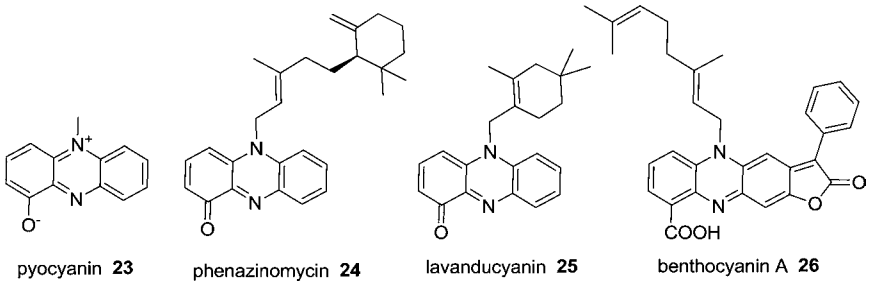

Figure 7. Chemical structures of natural blue phenazine molecules.

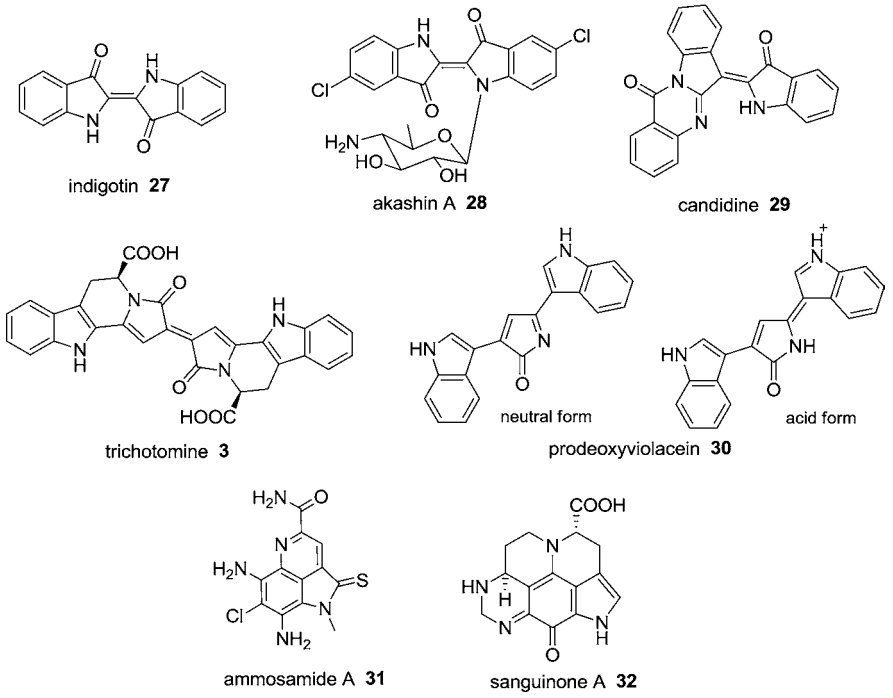

Figure 8. Chemical structures of indole-derived blue natural products.

cancer cell lines with IC_{50} values from 1 μM to 20 nM. The structurally related blue alkaloid sanguinone A (**32**) has been isolated and characterized from the mushroom *Mycena sanguinolenta*.[104] Data on its biological activity and stability have not been reported. See Figure 8 for the chemical structures of these indole-derived blue pigments.

Pyridine Alkaloids. Blue pigments containing 3,3′-bipyridyl chromophores (Figure 9) have been isolated from a variety of microbial sources. Indigoidine (**33**) and indochrome A (**34**) (also known as amylocyanin) were isolated in the 1960s as part of studies on the structurally related blue pigments of *Arthrobacter* sp., *Erwinia* sp., and *Corynebacterium* sp.[105−107] An unnamed blue pigment (**36**), a 3,3′-bipyridyl uncatalyzed oxidation product of 2,3,6-trihydroxypyridine, was identified as a side product of 2-hydroxypyridine metabolism in *Nocardia* sp.[108,109] Compound **36** was shown to be identical to the acidic hydrolysis product of indigoidine (**33**).[110] Similar but unidentified blue pigment byproducts such as "nicotine blue"[111] have been observed during the metabolism of various pyridine compounds by *Arthrobacter* sp.,[110−112] *Pseudomonas* sp.,[107] *Corynebacterium* sp.,[113] and *Bacillus* sp.[114] More recently, an *N*,*N*-dialkylated indigoidine analogue (**35**) was isolated and characterized from the deep sea marine microorganism *Shewanella violacea* DSS12.[115] Lemonnierin (**37**), a blue metabolite produced by *Pseudomonas lemonnieri*, contains a similar 3,3′-bipyridal blue chromophore.[116,117] Glaukothalin (**38**), isolated from the marine microorganism *Rheinheimera* sp. HP1,[118,119] contains a rare bis(oxazepinone) chromophore reminiscent of the 3,3′-bipyridyl chromophores. Glaukothalin has a LD_{100} of 0.1 mg mL^{-1} against brine shrimp. Little information is available concerning the stabilities and biological activities of most of the 3,3′-bipyridyl pigments.

Gardenia blue and huito juice are iridoid-derived mixtures with limited approval as food colorants. Colorless iridoids from *Genipa americana* and *Gardenia jasminoides* extracts can be converted to blue colorants by reacting the aglycones with a primary amine in the presence of oxygen.[1,120−122] The resulting mixture of polymeric pigments is not well-defined, but characterizations of some brown-red intermediates[123,124] and of a blue dimer product genipocyanin G_1 (**39**)[125] have been reported. The reaction converts the iridoid scaffold (**40**) into an aromatic 2-pyridine [5 + 6] scaffold (**41**) that has visible absorbance properties distinct from the indole ring.[126] Structures of these pyridine-derived compounds are shown in Figure 9.

Azulenes. The azulene (**42**) [5 + 7] ring system (Figure 10) is the only reported blue organic chromophore found in nature that does not contain heteroatoms. Guaiazulene (**43**) and related blue sesquiterpenes such as lactarazulene (**44**) and

dx.doi.org/10.1021/jf501419q | J. Agric. Food Chem. 2014, 62, 6498−6511

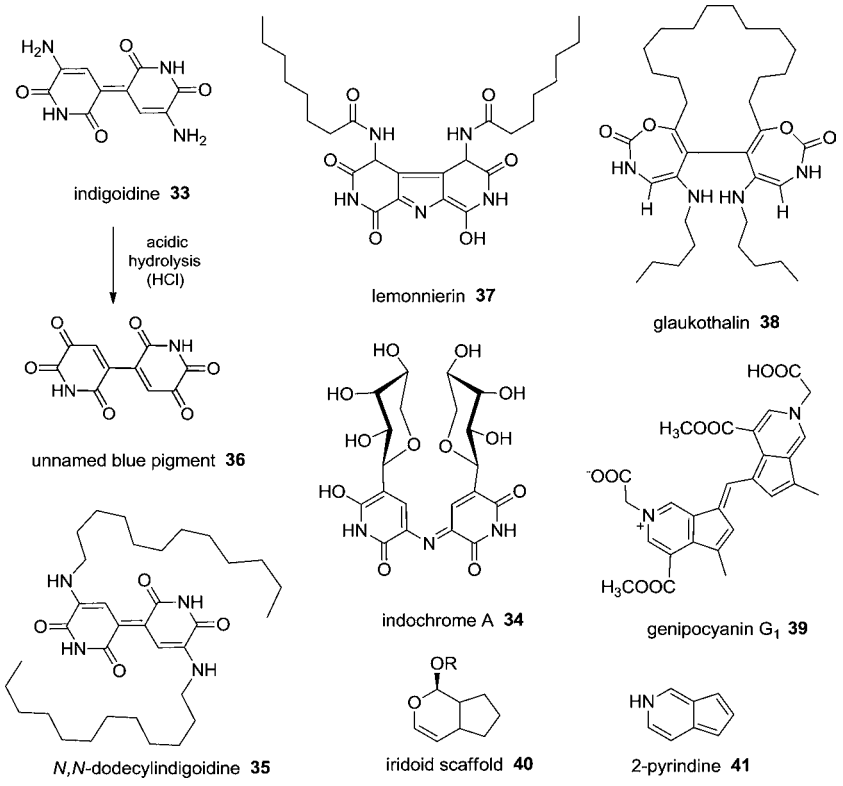

Figure 9. Chemical structures of blue pyridine-derived natural products.

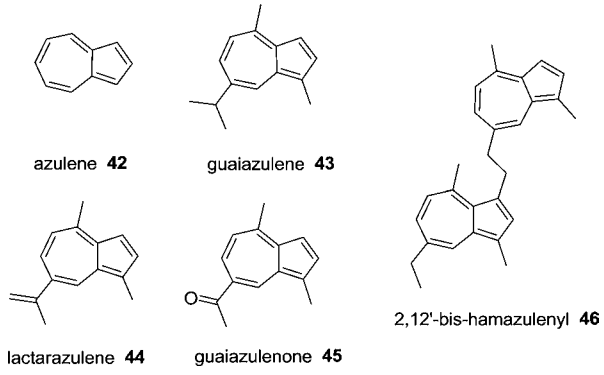

Figure 10. Chemical structures of some natural blue azulenes.

guaiazuleneone (**45**) have been isolated from various fungi (*Lactarius* sp.) and plant essential oils (*Matricaria* sp., *Artemisia* sp.).[127−129] Blue chlorinated and brominated analogues of guaiazulene and dimeric guaiazulene derivatives (anthogorgienes A−O) have been isolated from marine Gorgonian species.[130,131] Most dimeric azulene derivatives are not blue but purple or green. The 2,12′-bis(hamazulenyl) (**46**) dimer isolated from *Ajania fruticulosa*[132] is blue because the saturated ethyl linkage does not significantly alter the azulene chromophore. Azulene and its derivatives tend to be lipophilic, have low molar absorptivities, and poor stabilities.[127,131,134,135] Guaiazulene is approved for use in cosmetics by the U.S. FDA.[136] Structures of some blue azulene natural products are shown in Figure 10.

Organometallics and Metalloproteins. Blue metalloproteins and organometallic complexes have been identified in natural sources. A ferric ceratenolone complex (**47**) is thought to be responsible for the blue color of the pine rot fungus *Ceratocystis minor*[137] and a pale blue colored vanadium V^{4+} complex, amavadin (**48**) (Figure 11), has been isolated from

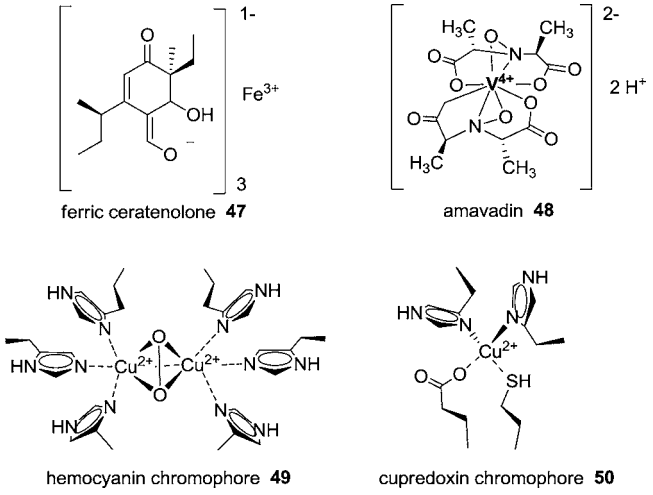

Figure 11. Chemical structures of some natural blue organometallic complexes.

Amanita muscaria, which is known to accumulate vanadium.[48,138] Crustaceans and arthropods have blue blood due to the respiratory protein hemocyanin instead of the iron-based hemoglobin.[139] The hemocyanin chromophore (**49**) contains a binuclear copper active site that reversibly binds O_2 molecules (Figure 11). Each copper is coordinated by three histidyl residues. Other blue copper proteins occur in some plants and bacteria, where they usually serve biosynthetic functions involving electron transfer.[140] Stellacyanin[141] and plastocyanin[142,143] are type I copper binding proteins (cupredoxins) common to vascular plants. The blue cupredoxin chromophore (**50**) found in stellacyanin contains a cupric ion coordinated by one cysteine and two histidines (Figure 11).[141] Other type I copper binding proteins include cuscacyanin and phytocyaninin

dx.doi.org/10.1021/jf501419q | J. Agric. Food Chem. 2014, 62, 6498−6511

Table 1. Natural Blue Compound Molecular Formula, Absorbance Data, Predicted Solubility, and Number of Literature Citations

no.	compound name	formula	MW (Da)	λ_{max}[a] (nm)	ε (M^{-1} cm^{-1})	sol.[b] (mg L^{-1})	no. of citations[c]	refs
				Synthetic				
1	FD&C blue no. 1	$C_{37}H_{36}N_2O_9S_3Na_2$	792.9	629 (w)	134000	na[e]	1447	7[d]
2	FD&C blue no. 2	$C_{16}H_{10}N_2O_8S_2Na_2$	466.4	607 (w)	7920	na[e]	2530	8[d]
				Flavanoid				
4	portisin A	$C_{42}H_{39}O_{18}^+$	831.8	587 (m) (B)	82900	na[e]	4	21, 24,[d] 26
5	oenin	$C_{23}H_{25}O_{12}^+$	493.4	538 (m) (A)	16000	na[e]	1571	21, 24,[d] 26
				Quinoid				
6	daunorubicin	$C_{27}H_{29}N_1O_{10}$	527.5	530 (dmf)	6000	20000	9848	32, 33, 169[d]
7	actinorhodin	$C_{32}H_{26}O_{14}$	634.5	640 (w) (B)	25 300	0.025	419	34,[d] 36
8	granaticin B	$C_{28}H_{30}O_{12}$	558.5	630 (et) (B)	8910	6.7	18	37,[d] 39
9	diosindigo A	$C_{24}H_{20}O_6$	404.4	697 (dcm)	28180	0.5	27	40,[d] 41
10	anthracyclinone-blue B	$C_{24}H_{21}N_1O_8$	451.4	608 (m)	28890	0.014	1	42,[d] 43
11	ventilein A	$C_{30}H_{24}O_8$	512.5	645 (m)	na	0.004	2	44,[d] 45
12	oxyblepharismin A	$C_{39}H_{24}O_{11}$	668.6	592 (et)	na	4×10^{-10}	2	46,[d] 47
14	variegatic acid anion	$C_{18}H_{12}O_9$	372.3	605 (w) (B)	na	63000	19	48, 50[d]
15	albatrellin	$C_{44}H_{56}O_6$	680.9	535 (m)	3162	0.001	2	53[d]
16	corticin A	$C_{21}H_{16}O_8$	396.4	565 (et)	6900	0.062	1	54[d]
17	scleroderris blue	$C_{38}H_{33}N_1O_{10}$	663.7	612 (dcm)	50000	0.2	8	55,[d] 57
18	popolohuanone B	$C_{42}H_{57}N_1O_3$	623.9	512 (hex)	2290	0.0004	1	58[d]
				Tetrapyrrole				
19	phycocyanobilin	$C_{33}H_{38}N_4O_6$	586.7	604 (m)	17100	6	395	62, 63, 170[d]
20	biliverdin-IX_a	$C_{33}H_{34}N_4O_6$	582.7	674 (w) (B)	12200	200	1281	60,[d] 61
21	bactobilin	$C_{39}H_{38}N_4O_{18}$	850.7	633 (chl)	na	73000	5	64,[d] 66
22	prodigiosin tetrapyrrole	$C_{19}H_{18}N_4O_2$	334.4	588 (et) (A)	na	87	8	67,[d] 68–72
				Phenazine				
23	pyocyanin	$C_{13}H_{10}N_2O$	210.2	746 (m)	5800	150	758	74–77, 78[d]
24	phenazinomycin	$C_{27}H_{32}N_2O$	400.6	745 (m)	6600	0.06	17	78,[d] 79
25	lavanducyanin	$C_{22}H_{24}N_2O$	332.4	705 (m)	1700	1.2	14	80,[d] 81
26	benthocyanin A	$C_{31}H_{28}N_2O_4$	492.6	638 (m) (A)	16200	0.026	6	82,[d] 83
				Indole				
27	indigotin	$C_{16}H_{10}N_2O_2$	262.3	610 (dmf)	22140	0.55	2574	30, 84, 85[d]
28	akashin A	$C_{22}H_{19}Cl_2N_3O_5$	476.3	619 (m)	10232	210	2	86, 87[d]
29	candidine	$C_{23}H_{13}N_3O_2$	363.4	573 (chl)	12880	13	13	88,[d] 90
3	trichotomine	$C_{30}H_{20}N_4O_6$	532.5	658[f] (chl)	70000	24000	15	91–94,[d] 96
30	prodeoxyviolacein	$C_{20}H_{13}N_3O$	311.3	609 (et) (A)	25000	1.5	9	97–100, 101[d]
31	ammosamide A	$C_{12}H_{10}Cl_1N_5O_1S_1$	307.8	584[g] (m)	5200	160	6	103
32	sanguinone A	$C_{15}H_{14}N_4O_3$	298.3	578 (w)	437	330	1	104[d]
				Pyridyl				
33	indigoidine	$C_{10}H_8N_4O_4$	248.2	602 (dmf)	23400	4500	35	105, 107[d]
34	indochrome A	$C_{20}H_{23}N_3O_{12}$	497.4	570 (w) (A)	38100	15000	3	105–107, 171[d]
35	*N,N*-dodecylindigoidine	$C_{36}H_{56}N_4O_4$	584.8	636 (chl)	na	0.00042	1	115[d]
36	unnamed blue pigment	$C_{10}H_4N_2O_6$	248.2	648 (dmf)	17380	14000	2	107,[d] 108, 112
37	lemonnierin	$C_{26}H_{37}N_5O_6$	515.6	625 (dmf)	56230	2.6	2	116,[d] 117
38	glaukothalin	$C_{34}H_{56}N_4O_4$	584.8	636 (chl)	32360	0.59	1	118,[d] 119
39	genipocyanin G_1	$C_{27}H_{24}N_2O_8$	504.2	595 (w)	43700	na[e]	3	120–124, 125[d]
				Azulene				
42	azulene	$C_{10}H_8$	128.2	576 (et)	362	140	3588	127, 133,[d] 134
43	guaiazulene	$C_{15}H_{18}$	198.3	648 (acn)	407	0.12	995	127–129, 135[d]
44	lactarazulene	$C_{15}H_{16}$	196.3	604 (m)	871	0.27	20	127–129, 134[d]
46	2,12′-bis(hamazulenyl)	$C_{28}H_{30}$	366.5	657 (chl)	132	0.00016	1	132[d]

[a](A), acidic conditions; (B), alkaline conditions; (w), water; (m), methanol; (et), ethanol; (chl), chloroform; (dcm), dichloromethane; (hex), hexane; (dmf), dimethylformamide; (acn), acetonitrile. [b]Solubility in water, pH 3, 25 °C. Calculated using ACD/Laboratories Software V11.02 or ACD/Percepta Build 2254. [c]Number of citations currently associated with the compound in CAS SciFinder scholar. [d]This reference is the source of the λ_{max} and ε values. [e]Species is ionic or charged. Solubility cannot be calculated. [f]For trichotomine dimethyl ester. [g]Authors' unpublished research.

from cucumber,[144,145] umecyanin from horseradish root,[146] and allergen Ra3 from ragweed.[147]

Bacterial type I copper-binding proteins include amicyanin from *Thiobacillus versutus*[148] and *Paracoccus denitrificans*[149] as well as halocyanin from the halophilic archaea *Natronomonas pharaonis*.[150] Halocyanin is one of the few pigmented compounds known from the Archaea. The blue arsenate reductase enzyme azurin (14 kDa) found in some *Pseudomonas* sp. and *Alcaligenes* sp. also contains the blue cupredoxin chromophore (Figure 11).[151,152] Auracyanin (12.8 kDa) from

Table 2. Natural Blue Compounds According to Biological Source

compound name (no.)	compound class	biological sources
	Synthetic	
FD&C blue no. 1 (**1**)	triphenylaryl	none
FD&C blue no. 2 (**2**)	bis(indole)	derivative of natural indigo dye
	Animal	
biliverdin-IX$_a$ (**20**)	linear tetrapyrrole	*Aves* (egg shell); mammal bile pigment
oxyblepharismin A (**12**)	naphthodianthrone	*Blepharisma japonicum* (protist)
popolohuanone B (**18**)	diterpene azaquinone	*Dysidea* sp. (marine sponge)
	Plant	
oenin (**5**)	anthocyanin	*Vitis vinifera* skin, aged wine
portisin A (**4**)	pyranoanthocyanin	*Vitis vinifera*; aged wine
diosindigo A (**9**)	benzoisochromaquinone	*Diospyros sp.* (tree; heartwood)
ventilein A (**11**)	naphthodianthrone	*Ventilago goughii* (root bark)
indigotin (**27**)	bis(indole)	*Indigofera tinctoria* (Indigo plant)
trichotomine (**3**)	bis(indoloid)	*Clerodendron trichotomum* (fruit callus)
genipocyanin G$_1$ (**39**)	2-pyrindine	*Gardenia jasminoides, Genipa americana*
azulene (**42**)	azulene	*Artemisia* sp. (oil), *Lactarius* sp. (fungi)
guaiazulene (**43**)	sesquiterpene	*Matricaria chamomilla* (oil), various fungi
lactarazulene (**44**)	sesquiterpene	*Artemisia* sp. (oil), *Lactarius* sp. (fungi)
2,12′-bis(hamazulenyl) (**46**)	bis(azulene)	*Ajania fruticulosa* (essential oil)
	Fungal	
variegatic acid anion (**14**)	benzofuranoquinone	Basidiomycete fungi
albatrellin (**15**)	meroterpenoid quinone	*Alabtrellus flettii* (Basidiomycete)
corticin A (**16**)	bis(benzofuranone)	*Corticium caeruleum* (fungus)
candidine (**29**)	bis(indoloid)	*Candida lipolytica* (yeast)
	Fungal	
sanguinone A (**32**)	indoloquinone	*Mycena sanguinolenta* (fungus)
scleroderris blue (**17**)	azobisquinone	*Gremmeniella abietina* (fungus)
	Microbial	
daunorubicin (**6**)	anthraquinone	*Streptomyces peucetius*
actinorhodin (**7**)	benzoisochromaquinone	*Streptomyces coelicolor*
granaticin B (**8**)	benzoisochromaquinone	*Streptomyces violaceoruber*
anthracyclinone-blue B (**10**)	tetracyclic quinone	*Streptomyces galilaeus* mutant
phycocyanobilin (**19**)	linear tetrapyrrole	*Spirulina* sp., common among cyanobacteria
bactobilin (**21**)	linear tetrapyrrole	*Clostridium tetanomorphum*
prodigiosin tetrapyrrole (**22**)	linear tetrapyrrole	*Serratia marcescens, Hahella* sp. (marine)
pyocyanin (**23**)	phenazine	*Pseudomonas aeruginosa*
phenazinomycin (**24**)	phenazine	*Streptomyces* sp. WK-2057 mycelia
lavanducyanin (**25**)	phenazine	*Streptomyces aeriouvifer*
benthocyanin A (**26**)	phenazine	*Streptomyces prunicolor*
akashin A (**28**)	bis(indole)	*Streptomyces* sp. GW 48/1497 (marine)
prodeoxyviolacein (**30**)	bis(indoloid)	*Chromobacterium violaceum*
ammosamide A (**31**)	thiopyrroloquinoline	*Streptomyces* CNR-698 (marine)
indigoidine (**33**)	3,3′-bipyridoid	*Corynebacterium insidiosum*
indochrome A (**34**)	3,3′-bipyridoid	*Arthrobacter polychromogenes*
N,N-dodecylindigoidine (**35**)	3,3′-bipyridoid	*Shewanella violacea* DSS12 (marine)
blue pigment (unnamed) (**36**)	3,3′-bipyridoid	*Arthrobacter* sp., *Nocardia* sp.
lemonnierin (**37**)	3,3′-bipyridoid	*Pseudomonas lemonnieri*
glaukothalin (**38**)	bis(oxazepinone)	*Rheinheimera* sp. HP1 (marine)

Chloroflexus aurantiacus is similar in structure to azurin but serves a role in photosynthesis.[153] Rusticyanin (16.5 kDa) from *Thiobacillus ferrooxidans* has the highest redox potential and best acid stability among the cupredoxin proteins.[154,155] Nevertheless, rusticyanin showed a color loss of 50% after 2 weeks at pH 2.0 and 4 °C.[154] Consequently, none of these copper proteins has sufficient stability for use as a food colorant.

Unidentified Blue Pigments. The source of blue coloration of many marine animals remains underexplored. A novel class of blue chromoprotein was recently isolated from the barrel jellyfish *Rhizostoma pulmo*, but the structure of the chromophore has not been determined.[156] Studies of the blue pigmentation of *Pollicopora* sp. and *Acropora* sp. corals led to the isolation of still unidentified chromoproteins.[157] An investigation of abalone shells in Japan has resulted in the partial characterization of a novel blue compound (electrospray MS m/z 581.8, $[M - H]^-$), but the structure remains unknown.[158] Investigations of the consumer preferred greening of cultured oyster[159] led to the isolation and partial characterization of a blue polyphenolic substance, marennine (λ_{max} water pH 8, 672 nm, $\varepsilon = 7200$) from an associated marine diatom, *Haslea ostrearia*.[160,161] Although its structure has not yet been determined, marennine (~10 kDa) is not composed of peptide, flavanoid, anthocyanin, or hydrolyzable tannin units and is not a metal complex.

Blue pigments observed in some fungi such as *Penicillin* sp. and *Hypocrea* sp. have been investigated but remain unidentified[162,163] due to challenges in isolating sufficient material for analysis. Some *Psilocybe* sp. fungi bruise blue when the tissue is broken and exposed to air, and the pigment structure is unknown but thought to be a psilocybin-related or indole oxidation product.[164] An unidentified water-soluble and unstable pigment reported from a soil strain of *Pantoea agglomerans* remains uncharacterized.[165] *Bacillus subtilis* var. *aterrimus* ATCC 6461 excretes an unidentified blue-black substance that is believed to be melanin related.[166] Our attempted characterization found the pigment too unstable for isolation. Future work to isolate and characterize blue compounds from natural sources will certainly continue to reveal novel blue chromophores.

Potential New Colorant Additives. The challenges of developing a new blue colorant cannot be overstated. The colorant must meet targets for hue, color intensity, and solubility. Ideally, it should be stable to heat, acid, light, and oxygen. The pigment should not contribute flavor or interact with other ingredients. Raw materials and processes must be in place for commercial production. Even if all of these criteria are met, the new colorant must be safe and go through the petitioning process for new color additives to get regulatory approval for use. This may require extensive safety and toxicity testing. Petitioning

Table 3. Summary of Leading Blue Colorants and Natural Colorant Candidates

compound name	compound class	λ_{max} (nm)	ε (M^{-1} cm^{-1})	acid color	commercial colorant applications
		Synthetic			
FD&C blue no. 1 (**1**)	triphenylaryl	629 (w)[a]	134000	blue	widespread commercial use in beverages and food
FD&C blue no. 2 (**2**)	bis(indole)	607 (w)	7920	blue	commercial textile dye; limited food applications
		Natural			
trichotomine (**3**)	bis(indoloid)	658[b] (chl)[a]	70000	blue	textile dye and natural ink (Japan)
guaiazulene (**43**)	azulene	648 (acn)[a]	407	blue	cosmetics
phycocyanobilin (**19**)	tetrapyrrole	604 (m)[a]	17100	blue	solid packaged food formulations
gardenia blue (**39**)	2-pyrindine	595[c] (w)	43700	blue	used in food (Asia); skin and hair dye (South America)
portisin A (**4**)	pyranoanthocyanin	587 (m) (A)	82900	purple	none
actinorhodin (**7**)	benzoisochromaquinone	640 (w) (B)	25300	red	none

[a](A), acidic conditions; (B), alkaline conditions; (w), water; (m), methanol; (chl), chloroform; (acn), acetonitrile. [b]For trichotomine dimethyl ester. [c]For the genipocyanin G_1 dimer.

must be repeated in every region with a separate regulatory process.

Table 1 summarizes the published information on the blue pigments covered in this review. Table 2 provides additional information on the sources of these natural blue pigments. As previously discussed, these compounds must meet stringent criteria before being considered for use in foods. Ideally, the natural blue pigment should have a shade and brilliance similar to those of FD&C blue no. 1. Visible λ_{max} and ε_{max} data are provided in Table 1 for comparison. New color additives must be safe, stable, and effective in the target application. Commercial production requires an abundant supply of the raw material and high pigment concentrations for economical extraction. Most of the reviewed pigments have not been investigated as potential colorants, and so specific data on human safety, application stability, and commercial production are not available. Nonetheless, it is apparent from published data that none of the blue pigments cited in this review are likely to meet all of these criteria.

Table 3 lists the most promising candidates in the opinion of the authors. Very few of the compounds listed in Table 1 have extinction coefficients approaching that of FD&C blue no. 1, so higher concentrations would be required to achieve the same appearance in food applications. In general terms for the structure classes, the phenazines are toxic, the azulenes and tetrapyrroles lack robust stability, and many of the quinoids and flavanoids are not blue in acid. The indole alkaloids are blue in acidic conditions but tend to have bioactivity or toxicity. Scarce data exist for the bipyridal pigments. Fungal and microbial secondary metabolites show great structural diversity and are good candidates for production on an industrial scale.[167,168] Unfortunately, compounds from these sources are often produced as part of a defense mechanism and have biological activities that render them unsuitable for food use.

The portisins come close to providing the desired color, but additional information about their stabilities and solubilities is required. Furthermore, portisins are found at only very low levels in wine, so an alternate pathway for commercial production will be required. Trichotomine is among the few pigments considered a good match for FD&C blue no. 1 in terms of shade and intensity in acidic solutions. Trichotomine has limited water solubility and stability, but its glycosylated derivatives are far more soluble and may be more stable. Research is currently limited by the limited supply of kusagi berries and the low concentration of pigment in these berries. It will be challenging to develop an alternate method of production because the biosynthetic pathway has not been identified. Anthocyanin and trichotomine derivatives are among the best candidates for new blue colorants.

Food and beverage producers continue to look for a naturally derived alternative to FD&C blue no. 1. The previous sections reviewed known naturally derived organic blue compounds. These compounds fall into seven structural classes and are derived from a broad range of sources. Blue colors in nature often arise from optical effects of reflected light rather than from blue pigment molecules. Anthocyanins are the primary source of blue in fruits, vegetables, and flowers, but as their color is pH dependent, they appear pink in most foods and beverages. Fungi and microorganisms produce a diverse array of blue compounds, often in response to environmental stress or predators. The associated biological activities of these compounds so far have rendered them unsuitable for food use. The best candidates for new blue color additives, anthocyanin and trichotomine derivatives, will require significant investment for development and regulatory approval.

AUTHOR INFORMATION

Corresponding Author

*E- mail: breemen@uic.edu. Telephone: 312-996-9353.

Funding

R.v.B. and A.N. thank PepsiCo for financial support for research on microbe-sourced blue pigments. The views expressed in this review are solely those of the authors and should not be construed as PepsiCo's statements of position, intention, or strategy.

Notes

The authors declare no competing financial interest.

ACKNOWLEDGMENTS

We thank San-Ei Gen, F.F.I., for informative discussions. We thank Brian Murphy for discussion and access to marine-derived microbial strains.

ABBREVIATIONS USED

HOMO, highest occupied molecular orbital; LUMO, lowest unoccupied molecular orbital; FD&C, Food Drug and Cosmetic; FDA, Food and Drug Administration; λ_{max}, visible wavelength of maximum absorption; ε, molar extinction coefficient (or molar absorptivity) in M^{-1} cm^{-1}; IC_{50}, half-maximal inhibitory concentration; LD_{50}, median lethal dose; MIC, minimum inhibitory concentration; kDa, kilodaltons; DNA, deoxyribonucleic acid

REFERENCES

(1) Wrolstad, R. E.; Culver, C. A. Alternatives to those FD&C food colorants. *Annu. Rev. Food Sci. Technol.* **2012**, 3, 59−77.

(2) Marmion, D. M. *Handbook of US Colorants*; Wiley: New York, 1991; 573 pp.

(3) Burrows, J. D. Palette of our palates: a brief history of food coloring and its regulation. *Compr. Rev. Food Sci. Food Saf.* **2009**, *8*, 394−408.
(4) Mortensen, A. Carotenoids and other pigments as natural colorants. *Pure Appl. Chem.* **2006**, *78*, 1477−1491.
(5) Downham, A.; Collins, P. Colouring our foods in the last and next millennium. *Int. J. Food Sci. Technol.* **2000**, *35*, 5−22.
(6) Sodium copper chlorophyllin. *Code of Federal Regulations* [online], Part 73.125 Title 21, 2002; http://www.ecfr.gov/cgi-bin/textidx?SID=6ffd146f772f44d1b7b76af13be18518&node=21:1.0.1.1.27.1.31.12&rgn=div8 (accessed March 3, 2014).
(7) Sharma, V.; McKone, H. T.; Markow, P. G. A global perspective on the history, use, and identification of synthetic food dyes. *J. Chem. Educ.* **2010**, *88*, 24−28.
(8) Gandra, N.; Frank, A. T.; Le Gendre, O.; Sawwan, N.; Aebisher, D.; Liebman, J. F.; Houk, K. N.; Greer, A.; Gao, R. Possible singlet oxygen generation from the photolysis of indigo dyes in methanol, DMSO, water, and ionic liquid, 1-butyl-3-methylimidazolium tetrafluoroborate. *Tetrahedron* **2006**, *62*, 10771−10776.
(9) Spirulina extract. *Code of Federal Regulations* [online], Part 73.530, Title 21, 2013; http://www.ecfr.gov/cgi-bin/text-idx?SID=6ffd146f772f44d1b7b76af13be18518&node=21:1.0.1.1.27&rgn=div5#21:1.0.1.1.27.1.31.33 (accessed March 3, 2014).
(10) Berns, R. S. *Billmeyer and Saltzman's Principles of Color Technology*, 3rd ed.; Wiley: New York, 2000; pp 1−30.
(11) Hunter, R. S.; Harold, R. W. *The Measurement of Appearance*, 2nd ed.; Wiley: New York, 1987; pp 51−67.
(12) Kalsi, P. S. Ultraviolet (UV) and visible spectroscopy. In *Spectroscopy of Organic Compounds*, 6th ed.; New Age International Publishers: New Delhi, India, 2004; pp 9−63.
(13) Liaaen-Jensen, S.; Kildahl-Andersen, G. Blue carotenoids. *ARKIVOC* **2008**, *6*, 5−25.
(14) Color additive petitions. *Code of Federal Regulations* [online], Part 71.1−71.37, Title 21, 2014; http://www.ecfr.gov/cgi-bin/retrieveECFR?gp=&SID=6ffd146f772f44d1b7b76af13be18518&r=PART&n=21y1.0.1.1.26 (accessed March 3, 2014).
(15) Lee, D. *Nature's Palette: The Science of Plant Color*, 1st ed.; The University of Chicago Press: Chicago, IL, USA, 2007; 432 pp.
(16) Newsome, A. G.; Murphy, B. T.; van Breemen, R. B. Isolation and characterization of natural blue pigments from underexplored sources. In *Physical Methods in Food Analysis*; Tunick, M. H., Onwulata, C. I., Eds.; ACS Symposium Series 1138; American Chemical Society: Washington, DC, USA, 2013; pp 105−125.
(17) Mazza, G.; Miniati, E. *Anthocyanins in Fruits, Vegetables, and Grains*; CRC Press: Boca Raton, FL, USA, 1993; 362 pp.
(18) Markakis, P. *Anthocyanins as Food Colors*, 1st ed.; Academic Press: New York, 1982.
(19) Castañeda-Ovando, A.; Pacheco-Hernández, M. D. L.; Páez-Hernández, M. E.; Rodríguez, J. A.; Galán-Vidal, C. A. Chemical studies of anthocyanins: a review. *Food Chem.* **2009**, *113*, 859−871.
(20) Wrolstad, R. E.; Durst, R. W.; Lee, J. Tracking color and pigment changes in anthocyanin products. *Trends Food Sci. Technol.* **2005**, *16*, 423−428.
(21) Mateus, N.; de Freitas, V. Anthocyanins as food colorants. In *Anthocyanins: Biosynthesis, Functions, and Applications*; Gould, K., Davies, K., Winefield, C., Eds.; Springer: New York, 2009; pp 283−304.
(22) Davies, K. Modifying anthocyanin production in flowers. In *Anthocyanins: Biosynthesis, Functions, and Applications*; Gould, K., Davies, K., Winefield, C., Eds.; Springer: New York, 2009; pp 49−84.
(23) Deroles, S.; Zhang, H.; Davies, K. Pigment composition comprising anthocyanic vacuolar inclusions. U.S. Patent Application 2011/0263723, Oct 27, 2011.
(24) Oliveira, J.; Santos-Buelga, C.; Silva, A. M. S.; de Freitas, V.; Mateus, N. Chromatic and structural features of blue anthocyanin-derived pigments present in Port wine. *Anal. Chim. Acta* **2006**, *563*, 2−9.
(25) Mateus, N.; Silva, A. M. S.; Rivas-Gonzalo, J. C.; Santos-Buelga, C.; de Freitas, V. A new class of blue anthocyanin-derived pigments isolated from red wines. *J. Agric. Food Chem.* **2003**, *51*, 1919−1923.
(26) Mateus, N.; de Freitas, V. Evolution and stability of anthocyanin-derived pigments during Port wine aging. *J. Agric. Food Chem.* **2001**, *49*, 5217−5222.
(27) *Anthocyanins: Biosynthesis, Functions, and Applications*; Gould, K., Davies, K., Winefield, C., Eds.; Springer: New York, 2009; 329 pp.
(28) Giusti, M. M.; Wrolstad, R. E. Unit F1.2: Characterization and measurement of anthocyanins by UV-visible spectroscopy. In *Current Protocols in Food Analytical Chemistry*; Wiley: New York, 2001; pp F1.2.1−F1.2.13.
(29) Holton, T. A.; Cornish, E. C. Genetics and biochemistry of anthocyanin biosynthesis. *Plant Cell* **1995**, *7*, 1071−1083.
(30) Ferreira, E. S. B.; Hulme, A. N.; McNab, H.; Quye, A. The natural constituents of historical textile dyes. *Chem. Soc. Rev.* **2004**, *33*, 329−336.
(31) Zollinger, H. *Color Chemistry: Syntheses, Properties, and Applications of Organic Dyes and Pigments*; Wiley VCH: Weinheim, Germany, 2003; 623 pp.
(32) Di Marco, A.; Gaetani, M.; Orezzi, P.; Scarpinato, B. M.; Silvestrini, R.; Soldati, M.; Dasdia, T.; Valentini, L. Daunomycin, a new antibiotic of the rhodomycin group. *Nature* **1964**, *201*, 706−707.
(33) Gewirtz, D. A. Critical evaluation of the mechanisms of action proposed for the antitumor effects of the anthracycline antibiotics adriamycin and daunorubicin. *Biochem. Pharmacol.* **1999**, *57*, 727−741.
(34) Zhang, H.; Zhan, J.; Su, K.; Zhang, Y. A kind of potential food additive produced by *Streptomyces coelicolor*: characteristics of blue pigment and identification of a novel compound, λ-actinorhodin. *Food Chem.* **2006**, *95*, 186−192.
(35) Bystrykh, L. V.; Fernández-Moreno, M. A.; Herrema, J. K.; Malpartida, F.; Hopwood, D. A.; Dijkhuizen, L. Production of actinorhodin-related "blue pigments" by *Streptomyces coelicolor* A3 (2). *J. Bacteriol.* **1996**, *178*, 2238−2244.
(36) Wright, L. F.; Hopwood, D. A. Actinorhodin is a chromosomally-determined antibiotic in *Streptomyces coelicolor* A3 (2). *J. Gen. Microbiol.* **1976**, *96*, 289−297.
(37) Gilpin, M. L.; Box, S. J.; Elson, A. L. New quinone antibiotics of the granaticin type, isolated from *Streptomyces lateritius*. II. Structure determination. *J. Antibiot.* **1988**, *41*, 512−518.
(38) Elson, A. L.; Box, S. J.; Gilpin, M. L. New quinone antibiotics of the granaticin type, isolated from *Streptomyces lateritius*. I: Production, isolation and properties. *J. Antibiot.* **1988**, *41*, 570−572.
(39) Chang, C. J.; Floss, H. G.; Soong, P.; Chang, C. T. Identity of the antitumor antibiotic litmomycin with granaticin A. *J. Antibiot.* **1975**, *28*, 156.
(40) Sankaram, A. V.; Narayana Reddy, V. V.; Sidhu, G. S. A pentacyclic quinone diosindigo B from the heartwood of *Diospyros melanoxylon*. *Phytochemistry* **1981**, *20*, 1093−1096.
(41) Musgrave, O. C.; Skoyles, D. Ebenaceae extractives. Part IV. Diosindigo A, a blue pigment from several *Diospyros* species. *J. Chem. Soc., Perkin Trans.* **1974**, 1128−1131.
(42) Eckardt, K.; Tresselt, D.; Ihn, W.; Schumann, G.; Eritt, I.; Sedmera, P.; Novak, J. Anthracyclinone-blue A and B, new natural anthracyclinones containing nitrogen in the molecules: Isolation, chemical structures and biosynthesis. *J. Basic Microbiol.* **1991**, *31*, 371−376.
(43) Pfefferle, C. M.; Breinholt, J.; Olsen, C. E.; Kroppenstedt, R. M.; Wellington, E. M.; Gürtler, H.; Fiedler, H. P. Kyanomycin, a complex of unusual anthracycline-phospholipid hybrids from *Nonomuria* species. *J. Nat. Prod.* **2000**, *63*, 295−298.
(44) Hanumaiah, T.; Marshall, D. S.; Rao, B. K.; Rao, J. U. M.; Rao, K. V. J.; Thomson, R. H. Naphthoquinone-lactones and extended quinones from *Ventilago calyculata*. *Phytochemistry* **1985**, *24*, 2669−2672.
(45) Jammula, S. R.; Pepalla, S. B.; Rao, K. V. J.; Rao, P. P. Chemical components from *Ventilago goughii*, gamble. *Acta Cienc. Indica Chem.* **1993**, *19*, 36.
(46) Spitzner, D.; Höfle, G.; Klein, I.; Pohlan, S.; Ammermann, D.; Jaenicke, L. On the structure of oxyblepharismin and its formation from blepharismin. *Tetrahedron Lett.* **1998**, *39*, 4003−4006.
(47) Checcucci, G.; Shoemaker, R. S.; Bini, E.; Cerny, R.; Tao, N.; Hyon, J. S.; Gioffre, D.; Ghetti, F.; Lenci, F.; Song, P. S. Chemical

structure of blepharismin, the photosensor pigment for *Blepharisma japonicum*. *J. Am. Chem. Soc.* **1997**, *119*, 5762−5763.
(48) Velisek, J.; Cejpek, K. Pigments of higher fungi: a review. *Czech J. Food Sci.* **2011**, *29*, 87−102.
(49) Besl, H.; Bresinsky, A.; Steglich, W.; Zipfel, K. Pilzpigmente, XVII. Über Gyrocyanin, das blauende Prinzip des Kornblumenröhrlings (*Gyroporus cyanescens*), und eine oxidative Ringverengung des Atromentins. *Chem. Ber.* **1973**, *106*, 3223−3229.
(50) Edwards, R. L.; Elsworthy, G. C. Variegatic acid, a new tetronic acid responsible for the blueing reaction in the fungus *Suillus* (boletus) *variegatus* (Swartz ex Fr.). *Chem. Commun. (London)* **1967**, *8*, 373−374.
(51) Kahner, L.; Dasenbrock, J.; Spiteller, P.; Steglich, W.; Marumoto, R.; Spiteller, M. Polyene pigments from fruit-bodies of *Boletus laetissimus* and *B. rufo-aureus* (basidiomycetes). *Phytochemistry* **1998**, *49*, 1693−1697.
(52) Besl, H.; Bresinsky, A.; Herrmann, R.; Steglich, W. Chamonixin und Involutin, zwei chemosystematisch interessante Cyclopentandione aus *Gyrodon lividus* (Boletales). *Z. Naturforsch. C: Biosci.* **1980**, *9/10*, 824−825.
(53) Koch, B.; Steglich, W. Meroterpenoid pigments from *Albatrellus flettii* (Basidiomycetes). *Eur. J. Org. Chem.* **2007**, 1631−1635.
(54) Briggs, L. H.; Cambie, R. C.; Dean, I. C.; Hodges, R.; Ingram, W. B.; Rutledge, P. S. Chemistry of fungi. XI. Corticins A, B, and C, benzobisbenzofurans from *Corticium caeruleum*. *Aust. J. Chem.* **1976**, *29*, 179−190.
(55) Ayer, W. A.; Hoyano, Y.; Pedras, M. S.; Altena, I. V. Metabolites produced by the Scleroderris canker fungus, *Gremmeniella abietina*. Part 1. *Can. J. Chem.* **1986**, *64*, 1585−1589.
(56) Ayer, W. A.; Pedras, M. S. Metabolites produced by the Scleroderris canker fungus, *Gremmeniella abietina*. Part 3. Some further metabolites. *Can. J. Chem.* **1987**, *65*, 754−759.
(57) Robinson, N.; Wood, K.; Hylands, P. J.; Gibson, T. M.; Weedon, C. J.; Covill, N. Blue pigments of *Penicillium herquei*. *J. Nat. Prod.* **1992**, *55*, 814−817.
(58) Rodriguez, A. D.; Yoshida, W. Y.; Scheuer, P. J. Popolohuanone A and B: two new sesquiterpenoid aminoquinones from a pacific sponge *Dysidea* sp. *Tetrahedron* **1990**, *46*, 8025−8030.
(59) Frankenberg, N.; Lagarias, J. C. Biosynthesis and biological functions of bilins. In *The Porphyrin Handbook: Chlorophylls And Bilins: Biosynthesis, Synthesis And Degradation*; Kadish, K. M., Smith, K. M., Guilard, R., Eds.; Academic Press: San Diego, CA, USA, 2003; Vol. 13, pp 211−236.
(60) Anglada, C.; Claret, J.; Crusats, J.; Farrera, J. A.; Ribó, J. M.; Trull, F. R. Reactivity of pyrrole pigments, part 13. Identification of the reaction product generated from bile pigments by the superoxide anion. *Monatsh. Chem.* **1990**, *121*, 653−663.
(61) Lemberg, R. Bile pigments. VI. Biliverdin, uteroverdin and oocyan. *Biochem. J.* **1934**, *28*, 978−987.
(62) Sidler, W. A. Phycobilisome and phycobiliprotein structures. In *The Molecular Biology of Cyanobacteria*; Springer: Dordrecht, The Netherlands, 2004; pp 139−216.
(63) Cole, W. J.; Chapman, D. J.; Siegelman, H. W. The structure of phycocyanobilin. *J. Am. Chem. Soc.* **1967**, *89*, 3643−3645.
(64) Valasinas, A.; Sambrotta, L.; Diaz, L. E.; Frydman, B. Total synthesis of the urobiliverdin and coprobiliverdin isomers. *J. Org. Chem.* **1986**, *51*, 3001−3006.
(65) Valasinas, A.; Diaz, L.; Frydman, B.; Friedmann, H. C. Total synthesis of the urobiliverdin isomers. Identification of bactobilin as urobiliverdin I. *J. Org. Chem.* **1985**, *50*, 2398−2400.
(66) Brumm, P. J.; Fried, J.; Friedmann, H. C. Bactobilin: blue bile pigment isolated from *Clostridium tetanomorphum*. *Proc. Natl. Acad. Sci. U.S.A.* **1983**, *80*, 3943−3947.
(67) Wasserman, H. H.; Friedland, D. J.; Morrison, D. A. A novel dipyrrolyldipyrromethene prodigiosin analog from *Serratia marcescens*. *Tetrahedron Lett.* **1968**, *9*, 641−644.
(68) Kim, D.; Lee, J. S.; Park, Y. K.; Kim, J. F.; Jeong, H.; Oh, T. K.; Lee, C. H. Biosynthesis of antibiotic prodiginines in the marine bacterium *Hahella chejuensis* KCTC 2396. *J. Appl. Microbiol.* **2007**, *102*, 937−944.
(69) Kazlauskas, R.; Marwood, J. F.; Murphy, P. T.; Wells, R. J. A blue pigment from a compound ascidian. *Aust. J. Chem.* **1982**, *35*, 215−217.
(70) Paul, V. J.; Lindquist, N.; Fenical, W. Chemical defenses of the tropical ascidian *Atapozoa* sp. and its nudibranch predators *Nembrotha* spp. *Mar. Ecol. Progr. Ser. Oldendorf* **1990**, *59*, 109−118.
(71) Matsunaga, S.; Fusetani, N.; Hashimoto, K. Bioactive marine metabolites. VIII. Isolation of an antimicrobial blue pigment from the bryozoan *Bugula dentata*. *Cell. Mol. Life Sci.* **1986**, *42*, 84.
(72) Karuso, P.; Scheuer, P. J. Natural products from three nudibranchs: *Nembrotha kubaryana*, *Hypselodoris infucata* and *Chromodoris petechialis*. *Molecules* **2002**, *7*, 1−6.
(73) Fürstner, A. Chemistry and biology of roseophilin and the prodigiosin alkaloids: a survey of the last 2500 years. *Angew. Chem., Int. Ed.* **2003**, *42*, 3582−3603.
(74) Price-Whelan, A.; Dietrich, L. E.; Newman, D. K. Rethinking 'secondary' metabolism: physiological roles for phenazine antibiotics. *Nat. Chem. Biol.* **2006**, *2*, 71−78.
(75) Laursen, J. B.; Nielsen, J. Phenazine natural products: biosynthesis, synthetic analogues, and biological activity. *Chem. Rev.* **2004**, *104*, 1663−1685.
(76) Lau, G. W.; Hassett, D. J.; Ran, H.; Kong, F. The role of pyocyanin in *Pseudomonas aeruginosa* infection. *Trends Mol. Med.* **2004**, *10*, 599−606.
(77) Wilson, R.; Pitt, T.; Taylor, G.; Watson, D.; MacDermot, J.; Sykes, D.; Roberts, D.; Cole, P. Pyocyanin and 1-hydroxyphenazine produced by *Pseudomonas aeruginosa* inhibit the beating of human respiratory cilia *in vitro*. *J. Clin. Invest.* **1987**, *79*, 221.
(78) Omura, S.; Eda, S.; Funayama, S.; Komiyama, K.; Takahashi, Y.; Woodruff, H. B. Studies on a novel antitumor antibiotic, phenazinomycin: taxonomy, fermentation, isolation, and physicochemical and biological characteristics. *J. Antibiot.* **1989**, *42*, 1037−1042.
(79) Otoguro, K.; Ishiyama, A.; Iwatsuki, M.; Namatame, M.; Nishihara-Tukashima, A.; Nakashima, T.; Shibahara, S.; Kondo, S.; Yamada, H.; Omura, S. *In vitro* and *in vivo* anti-*Trypanosoma brucei* activities of phenazinomycin and related compounds. *J. Antibiot.* **2010**, *63*, 579−581.
(80) Imai, S.; Furihata, K.; Hayakawa, Y.; Noguchi, T.; Seto, H. Lavanducyanin, a new antitumor substance produced by *Streptomyces* sp. *J. Antibiot.* **1989**, *42*, 1196−1197.
(81) Kondratyuk, T. P.; Park, E.-J.; Yu, R.; van Breemen, R. B.; Asolkar, R. N.; Murphy, B. T.; Fenical, W.; Pezzuto, J. M. Novel marine phenazines as potential cancer chemopreventive and anti-inflammatory agents. *Mar. Drugs* **2012**, *10*, 451−464.
(82) Shinya, K.; Furihata, K.; Teshima, Y.; Hayakawa, Y.; Seto, H. Benthocyanins B and C, new free radical scavengers from *Streptomyces prunicolor*. *J. Org. Chem.* **1993**, *58*, 4170−4172.
(83) Shin-ya, K.; Furihata, K.; Hayakawa, Y.; Seto, H.; Kato, Y.; Clardy, J. The structure of benthocyanin A. A new free radical scavenger of microbial origin. *Tetrahedron Lett.* **1991**, *32*, 943−946.
(84) Clark, R. J.; Cooksey, C. J.; Daniels, M. A.; Withnall, R. Indigo, woad, and Tyrian Purple: important vat dyes from antiquity to the present. *Endeavour* **1993**, *17*, 191−199.
(85) Seixas de Melo, J.; Moura, A. P.; Melo, M. J. Photophysical and spectroscopic studies of indigo derivatives in their keto and leuco forms. *J. Phys. Chem. A* **2004**, *108*, 6975−6981.
(86) Maskey, R. P.; Grün-Wollny, I.; Laatsch, H. Isolation and structure elucidation of diazaquinomycin C from a terrestrial *Streptomyces* sp. and confirmation of the akashin structure. *Nat. Prod. Res.* **2005**, *19*, 137−142.
(87) Maskey, R. P.; Grün-Wollny, I.; Fiebig, H. H.; Laatsch, H. Akashins A, B, and C: novel chlorinated indigoglycosides from *Streptomyces* sp. GW 48/1497. *Angew. Chem., Int. Ed.* **2002**, *41*, 597−599.
(88) Bergman, J. The identity of candidine and qingdainone. *Phytochemistry* **1989**, *28*, 3547.
(89) Bergman, J.; Tilstam, U. Structure determination of candidine, a violet indolic constituent from culture solutions of *Candida lipolytica*. *Tetrahedron* **1985**, *41*, 2883−2884.

(90) Tucker, A. M.; Grundt, P. The chemistry of tryptanthrin and its derivatives. *ARKIVOC* **2012**, *1*, 546−569.
(91) Koda, T.; Ichi, T.; Odake, K.; Furuta, H.; Sekiya, J. Blue pigment formation by *Clerodendron trichotomum* callus. *Biosci., Biotechnol., Biochem.* **1992**, *56*, 2020−2022.
(92) Matsumoto, Y. Weaving cloth from 'tosa-washi' (Japanese Paper from Kochi in Shikoku), Connection and Expansion of Area and People [online]; http://digitalcommons.unl.edu/tsaconf/114/ (accessed Feb 22, 2014).
(93) Ichi, T.; Shimizu, T.; Yoshihira, K. *Clerodendron trichotomum* Thunb.: blue pigment production for food color. In *Medicinal and Aromatic Plants IX*; Springer: Berlin, Germany, 1996; pp 108−126.
(94) Iwadare, S.; Shizuri, Y.; Sasaki, K.; Hirata, Y. Isolation and structure of trichotomine. *Tetrahedron Lett.* **1974**, *15*, 1051−1054.
(95) Iwadare, S.; Shizuri, Y.; Sasaki, K.; Hirata, Y. Isolation and structure of trichotomine and trichotomine G_1. *Tetrahedron* **1974**, *30*, 4105−4111.
(96) Sasaki, K.; Iwadare, S.; Hirata, Y. Structure and absolute configuration of trichotomine. *Tetrahedron Lett.* **1974**, *15*, 1055−1058.
(97) Rettori, D.; Durán, N. Production, extraction and purification of violacein: an antibiotic pigment produced by *Chromobacterium violaceum*. *World J. Microbiol. Biotechnol.* **1998**, *14*, 685−688.
(98) Duran, N.; Justo, G. Z.; Ferreira, C. V.; Melo, P. S.; Cordi, L.; Martins, D. Violacein: properties and biological activities. *Biotechnol. Appl. Biochem.* **2007**, *48*, 127−133.
(99) Shirata, A.; Tsukamoto, T.; Yasui, H.; Hata, T.; Kato, H.; Kojima, A. Isolation of bacteria producing bluish-purple pigment and use for dyeing. *Jpn. Agric. Res. Q.* **2000**, *34*, 131−140.
(100) Balibar, C. J.; Walsh, C. T. *In vitro* biosynthesis of violacein from L-tryptophan by the enzymes VioA-E from *Chromobacterium violaceum*. *Biochemistry* **2006**, *45*, 15444−15457.
(101) Hoshino, T.; Hayashi, T.; Odajima, T. Biosynthesis of violacein: oxygenation at the 2-position of the indole ring and structures of proviolacein, prodeoxyviolacein and pseudoviolacein, the plausible biosynthetic intermediates of violacein and deoxyviolacein. *J. Chem. Soc., Perkin Trans. 1* **1995**, 1565−1571.
(102) Antunes, E. M.; Copp, B. R.; Davies-Coleman, M. T.; Samaai, T. Pyrroloiminoquinone and related metabolites from marine sponges. *Nat. Prod. Rep.* **2005**, *22*, 62−72.
(103) Hughes, C. C.; MacMillan, J. B.; Gaudêncio, S. P.; Jensen, P. R.; Fenical, W. The ammosamides: structures of cell cycle modulators from a marine-derived *Streptomyces* species. *Angew. Chem., Int. Ed.* **2009**, *48*, 725−727.
(104) Peters, S.; Spiteller, P. Sanguinones A and B, blue pyrroloquinoline alkaloids from the fruiting bodies of the mushroom *Mycena sanguinolenta*. *J. Nat. Prod.* **2007**, *70*, 1274−1277.
(105) Knackmuss, H. J.; Cosens, G.; Starr, M. P. The soluble blue pigment, indochrome, of *Arthrobacter polychromogenes*. *Eur. J. Biochem.* **1969**, *10*, 90−95.
(106) Starr, M. P.; Cosens, G.; Knackmuss, H. J. Formation of the blue pigment indigoidine by phytopathogenic *Erwinia*. *Appl. Microbiol.* **1966**, *14*, 870−872.
(107) Kuhn, R.; Starr, M. P.; Kuhn, D. A.; Bauer, H.; Knackmuss, H. J. Indigoidine and other bacterial pigments related to 3,3′-bipyridyl. *Arch. Mikrobiol.* **1965**, *51*, 71−84.
(108) Kaiser, J. P.; Feng, Y.; Bollag, J. M. Microbial metabolism of pyridine, quinoline, acridine, and their derivatives under aerobic and anaerobic conditions. *Microbiol. Rev.* **1996**, *60*, 483−498.
(109) Shukla, O. P.; Kaul, S. M. Microbiological transformation of pyridine *N*-oxide and pyridine by *Nocardia* sp. *Can. J. Microbiol.* **1986**, *32*, 330−341.
(110) Ensign, J. C.; Rittenberg, S. C. The formation of a blue pigment in the bacterial oxidation of isonicotinic acid. *Arch. Mikrobiol.* **1965**, *51*, 384−392.
(111) Holmes, P. E.; Rittenberg, S. C.; Knackmuss, H. J. The bacterial oxidation of nicotine VIII. Synthesis of 2,3,6-trihydroxypyridine and accumulation and partial characterization of the product of 2,6-dihydroxypyridine oxidation. *J. Biol. Chem.* **1972**, *247*, 7628−7633.
(112) Kolenbrander, P. E.; Weinberger, M. 2-Hydroxypyridine metabolism and pigment formation in three *Arthrobacter* species. *J. Bacteriol.* **1977**, *132*, 51−59.
(113) Shukla, O. P.; Kaul, S. M. A constitutive pyridine degrading system in *Corynebacterium* sp. *Indian J. Biochem. Biophys.* **1974**, *11*, 201−207.
(114) Ensign, J. C.; Rittenberg, S. C. The pathway of nicotinic acid oxidation by a *Bacillus* species. *J. Biol. Chem.* **1964**, *239*, 2285−2291.
(115) Kobayashi, H.; Nogi, Y.; Horikoshi, K. New violet 3,3′-bipyridyl pigment purified from deep-sea microorganism *Shewanella violacea* DSS12. *Extremophiles* **2007**, *11*, 245−250.
(116) Ferguson, G.; Pollard, D. R.; Robertson, J. M.; Doherty, G. O.; Haynes, N. B.; Mathieson, D. W.; Whalley, W. B.; Simpson, T. H. The bacterial pigment from *Pseudomonas lemonnieri*. Part 1. Structure of a degradation product, 3-*n*-octanamidopyridine-2,5,6-trione, by X-ray crystallography. *J. Chem. Soc., Perkin Trans. 1* **1980**, 1782−1787.
(117) Jain, K. C.; Whalley, W. B. The bacterial pigment from *Pseudomonas lemonnieri*. Part 2. The synthesis of 3-*n*-octanamidopyridine-2,5,6-trione: the structure and synthesis of lemonnierin. *J. Chem. Soc., Perkin Trans. 1* **1980**, 1788−1794.
(118) Grossart, H. P.; Thorwest, M.; Plitzko, I.; Brinkhoff, T.; Simon, M.; Zeeck, A. Production of a blue pigment (glaukothalin) by marine *Rheinheimera* spp. *Int. J. Microbiol.* **2009**, 1−7.
(119) Plitzko I. Zur biosynthese des borrelidins sowie isolierung und strukturaufklärung vonsekundärmetaboliten aus marinen und terrestrischen mikroorganismen. Ph.D. thesis, University of Gottingen, 2007.
(120) Echeverry, L. F.; Torres, L. F.; Zapata, S. P. Blue colorant derived from *Genipa americana* fruit. U.S. Patent 7,927,637, April 19, 2011.
(121) Paik, Y. S.; Lee, C. M.; Cho, M. H.; Hahn, T. R. Physical stability of the blue pigments formed from geniposide of gardenia fruits: effects of pH, temperature, and light. *J. Agric. Food Chem.* **2001**, *49*, 430−432.
(122) Sadano, S. Method for producing gardenia blue pigment. U.S. Patent Application 13/822,742, Sept 7, 2011.
(123) Park, J. E.; Lee, J. Y.; Kim, H. G.; Hahn, T. R.; Paik, Y. S. Isolation and characterization of water-soluble intermediates of blue pigments transformed from geniposide of *Gardenia jasminoides*. *J. Agric. Food Chem.* **2002**, *50*, 6511−6514.
(124) Touyama, R.; Inoue, K.; Takeda, Y.; Yatsuzuka, M.; Ikumoto, T.; Moritome, N.; Shingu, T.; Yokio, T.; Inouye, H. Studies on the blue pigments produced from genipin and methylamine. II. On the formation mechanisms of brownish-red intermediates leading to the blue pigment formation. *Chem. Pharm. Bull.* **1994**, *42*, 1571−1578.
(125) Fujikawa, S.; Fukui, Y.; Koga, K.; Iwashita, T.; Komura, H.; Nomoto, K. Structure of genipocyanin G_1, a spontaneous reaction product between genipin and glycine. *Tetrahedron Lett.* **1987**, *28*, 4699−4700.
(126) Evleth, E. M. Systematics of the electronic absorption spectra of fused 5−6 ring heterocyclics. *Theor. Chim. Acta* **1970**, *16*, 22−32.
(127) Wang, L.; Yan, J.; Fu, P. P.; Parekh, K. A.; Yu, H. Photomutagenicity of cosmetic ingredient chemicals azulene and guaiazulene. *Mutat. Res.* **2003**, *530*, 19−26.
(128) Alberto-Marco, J.; Sanz-Cervera, J. F.; García-Lliso, V.; Vallès-Xirau, J. Sesquiterpene lactones and lignans from *Artemisia arborescens*. *Phytochemistry* **1997**, *44*, 1133−1137.
(129) Bergendorff, O.; Sterner, O. The sesquiterpenes of *Lactarius deliciosus* and *Lactarius deterrimus*. *Phytochemistry* **1988**, *27*, 97−100.
(130) Chen, D.; Yu, S.; van Ofwegen, L.; Proksch, P.; Lin, W. Anthogorgienes A−O, new guaiazulene-derived terpenoids from a Chinese gorgonian *Anthogorgia* species, and their antifouling and antibiotic activities. *J. Agric. Food Chem.* **2011**, *60*, 112−123.
(131) Li, M. K.; Scheuer, P. J. Halogenated blue pigments of a deep sea gorgonian. *Tetrahedron Lett.* **1984**, *25*, 587−590.
(132) Tikhonova, E. V.; Atazhanova, G. A.; Raldugin, V. A.; Bagryanskaya, I. Y.; Gatilov, Y. V.; Shakirov, M. M.; Adekenov, S. M. 2,12′-Bis-hamazulenyl from *Ajania fruticulosa* essential oil. *Chem. Nat. Compd.* **2006**, *42*, 298−300.
(133) Shevyakov, S. V.; Li, H.; Muthyala, R.; Asato, A. E.; Croney, J. C.; Jameson, D. M.; Liu, R. S. Orbital control of the color and excited state

properties of formylated and fluorinated derivatives of azulene. *J. Phys. Chem. A* **2003**, *107*, 3295−3299.
(134) Takekuma, S. I.; Matsubara, Y.; Yamamoto, H.; Nozoe, T. Autoxidation of solid guaiazulene and of the solution in DMF in the presence of base or acid: a comparative study of the product distribution. *Bull. Chem. Soc. Jpn.* **1988**, *61*, 475−481.
(135) Takekuma, S. I.; Mizutani, K.; Inoue, K.; Nakamura, M.; Sasaki, M.; Minematsu, T.; Sugimoto, K.; Takekuma, H. Reactions of azulene and guaiazulene with all-*trans*-retinal and *trans*-cinnamaldehyde: comparative studies on spectroscopic, chemical, and electrochemical properties of monocarbenium-ions stabilized by expanded π-electron systems with an azulenyl or 3-guaiazulenyl group. *Tetrahedron* **2007**, *63*, 3882−3893.
(136) Guaiazulene. *Code of Federal Regulations* [online], Part 73.2180, Title 21, 2014; http://www.ecfr.gov/cgi-bin/retrieveECFR?gp=&SID=6ffd146f772f44d1b7b76af13be18518&r=PART&n=21y1.0.1.1.27#21:1.0.1.1.27.3.31.10 (accessed March 3, 2014).
(137) Ayer, W. A.; Attah-Poku, S. K.; Browne, L. M.; Orszanska, H. The chemistry of the blue stain fungi. Part 3. Some metabolites of *Ceratocystis minor* (Hedgcock) Hunt. *Can. J. Chem.* **1987**, *65*, 765−769.
(138) Kneifel, H.; Bayer, E. Stereochemistry and total synthesis of amavadin, the naturally occurring vanadium compound of *Amanita muscaria*. *J. Am. Chem. Soc.* **1986**, *108*, 3075−3077.
(139) Magnus, K. A.; Ton-That, H.; Carpenter, J. E. Recent structural work on the oxygen transport protein hemocyanin. *Chem. Rev.* **1994**, *94*, 727−735.
(140) Nersissian, A. M.; Valentine, J. S.; Immoos, C.; Hill, M. G.; Hart, P. J.; Williams, G.; Herrmann, R. G. Uclacyanins, stellacyanins, and plantacyanins are distinct subfamilies of phytocyanins: plant-specific mononuclear blue copper proteins. *Protein Sci.* **1998**, *7*, 1915−1929.
(141) Hart, P. J.; Eisenberg, D.; Nersissian, A. M.; Valentine, J. S.; Herrmann, R. G.; Nalbandyan, R. M. A missing link in cupredoxins: crystal structure of cucumber stellacyanin at 1.6 Å resolution. *Protein Sci.* **1996**, *5*, 2175−2183.
(142) Guss, J. M.; Freeman, H. C. Structure of oxidized poplar plastocyanin at 1.6 A resolution. *J. Mol. Biol.* **1983**, *169*, 521−563.
(143) Katoh, S.; Shiratori, I.; Takamiya, A. Purification and some properties of spinach plastocyanin. *J. Biochem.* **1962**, *51*, 32−40.
(144) Guss, J. M.; Merritt, E. A.; Phizackerley, R. P.; Freeman, H. C. The structure of a phytocyanin, the basic blue protein from cucumber, refined at 1.8 Å resolution. *J. Mol. Biol.* **1996**, *262*, 686−705.
(145) Markossian, K. A.; Aikazyan, V. T.; Nalbandyan, R. M. Two copper-containing proteins from cucumber (*Cucumis sativus*). *Biochim. Biophys. Acta (Protein Struct.)* **1974**, *359*, 47−54.
(146) Paul, K. G.; Stigbrand, T. Umecyanin, a novel intensely blue copper protein from horseradish root. *Biochim. Biophys. Acta (Protein Struct.)* **1970**, *221*, 255−263.
(147) Rydén, L. G.; Hunt, L. T. Evolution of protein complexity: the blue copper-containing oxidases and related proteins. *J. Mol. Evol.* **1993**, *36*, 41−66.
(148) Lommen, A.; Canters, G. W. pH-dependent redox activity and fluxionality of the copper site in amicyanin from *Thiobacillus yersutus* as studied by 300- and 600-MHz ^{1}H NMR. *J. Biol. Chem.* **1990**, *265*, 2768−2774.
(149) Durley, R.; Chen, L.; Mathews, F. S.; Lim, L. W.; Davidson, V. L. Crystal structure analysis of amicyanin and apoamicyanin from *Paracoccus denitrificans* at 2.0 Å and 1.8 Å resolution. *Protein Sci.* **1993**, *2*, 739−752.
(150) Scharf, B.; Engelhard, M. Halocyanin, an archaebacterial blue copper protein (type I) from *Natronobacterium pharaonis*. *Biochemistry* **1991**, *32*, 12894−12900.
(151) Salgado, J.; Jiménez, H. R.; Moratal, J. M.; Kroes, S.; Warmerdam, G. C.; Canters, G. W. Paramagnetic cobalt and nickel derivatives of *Alcaligenes denitrificans* azurin and its M121Q mutant. A ^{1}H NMR study. *Biochemistry* **1996**, *35*, 1810−1819.
(152) Nar, H.; Messerschmidt, A.; Huber, R.; van de Kamp, M.; Canters, G. W. Crystal structure analysis of oxidized *Pseudomonas aeruginosa* azurin at pH 5.5 and pH 9.0: a pH-induced conformational transition involves a peptide bond flip. *J. Mol. Biol.* **1991**, *221*, 765−772.
(153) McManus, J. D.; Brune, D. C.; Han, J.; Sanders-Loehr, J.; Meyer, T. E.; Cusanovich, M. A.; Tollin, G.; Blankenship, R. E. Isolation, characterization, and amino acid sequences of auracyanins, blue copper proteins from the green photosynthetic bacterium *Chloroflexus aurantiacus*. *J. Biol. Chem.* **1992**, *267*, 6531−6540.
(154) Cox, J. C.; Boxer, D. H. The purification and some properties of rusticyanin, a blue copper protein involved in iron (II) oxidation from *Thiobacillus ferro-oxidans*. *Biochem. J.* **1978**, *174*, 497−502.
(155) Olsson, M. H.; Hong, G.; Warshel, A. Frozen density functional free energy simulations of redox proteins: computational studies of the reduction potential of plastocyanin and rusticyanin. *J. Am. Chem. Soc.* **2003**, *125*, 5025−5039.
(156) Bulina, M. E.; Lukyanov, K. A.; Yampolsky, I. V.; Chudakov, D. M.; Staroverov, D. B.; Shcheglov, A. S.; Gurskaya, N. G.; Lukyanov, S. New class of blue animal pigments based on Frizzled and Kringle protein domains. *J. Biol. Chem.* **2004**, *279*, 43367−43370.
(157) Dove, S. G.; Takabayashi, M.; Hoegh-Guldberg, O. Isolation and partial characterization of the pink and blue pigments of pocilloporid and acroporid corals. *Biol. Bull.* **1995**, *189*, 288−297.
(158) Cai, Z.; Wu, J.; Chen, L.; Guo, W.; Li, J.; Wang, J.; Zhang, Q. Purification and characterisation of aquamarine blue pigment from the shells of abalone (*Haliotis discus hannai* Ino). *Food Chem.* **2011**, *128*, 129−133.
(159) Turpin, V.; Robert, J. M.; Goulletquer, P.; Massé, G.; Rosa, P. Oyster greening by outdoor mass culture of the diatom *Haslea ostrearia* Simonsen in enriched seawater. *Aquacult. Res.* **2001**, *32*, 801−809.
(160) Pouvreau, J.-B.; Morançais, M.; Taran, F.; Rosa, P.; Dufossé, L.; Guérard, S. P.; Fleurence, J.; Pondaven, P. Antioxidant and free radical scavenging properties of marennine, a blue-green polyphenolic pigment from the diatom *Haslea ostrearia* (Gaillon/Bory) Simonsen responsible for the natural greening of cultured oysters. *J. Agric. Food Chem.* **2008**, *56*, 6278−6286.
(161) Pouvreau, J. B.; Morançais, M.; Fleury, F.; Rosa, P.; Thion, L.; Cahingt, B.; Pondaven, P. Preliminary characterisation of the blue-green pigment "marennine" from the marine tychopelagic diatom *Haslea ostrearia* (Gaillon/Bory) Simonsen. *J. Appl. Phycol.* **2006**, *18*, 757−767.
(162) Jaklitsch, W. M.; Stadler, M.; Voglmayr, H. Blue pigment in *Hypocrea caerulescens* sp. nov. and two additional new species in sect. *Trichoderma*. *Mycologia* **2012**, *104*, 925−941.
(163) Mapari, S. A.; Nielsen, K. F.; Larsen, T. O.; Frisvad, J. C.; Meyer, A. S.; Thrane, U. Exploring fungal biodiversity for the production of water-soluble pigments as potential natural food colorants. *Curr. Opin. Biotechnol.* **2005**, *16*, 231−238.
(164) Benedict, R. G.; Tyler, V. E.; Watling, R. Blueing in *Conocybe, Psilocybe* and a *Stropharia* species and the detection of psilocybin. *Lloydia* **1967**, *30*, 150−157.
(165) Fujikawa, H.; Akimoto, R. New blue pigment produced by *Pantoea agglomerans* and its production characteristics at various temperatures. *Appl. Environ. Microbiol.* **2011**, *77*, 172−178.
(166) Nakamura, L. K. Taxonomic relationship of black-pigmented *Bacillus subtilis* strains and a proposal for *Bacillus atrophaeus* sp. nov. *Int. J. Syst. Bacteriol.* **1989**, *39*, 295−300.
(167) Dufosse, L. Microbial production of food grade pigments. *Food Technol. Biotechnol.* **2006**, *44*, 313−321.
(168) Sogin, M. L.; Morrison, H. G.; Huber, J. A.; Welch, D. M.; Huse, S. M.; Neal, P. R.; Arrieta, J. M.; Herndl, G. J. Microbial diversity in the deep sea and the underexplored "rare biosphere". *Proc. Natl. Acad. Sci. U.S.A.* **2006**, *103*, 12115−12120.
(169) Fiallo, M. M.; Tayeb, H.; Suarato, A.; Garnier-Suillerot, A. Circular dichroism studies on anthracycline antitumor compounds. Relationship between the molecular structure and the spectroscopic data. *J. Pharm. Sci.* **1998**, *87*, 967−975.
(170) Knipp, B.; Kneip, K.; Matysik, J.; Gärtner, W.; Hildebrandt, P.; Braslavsky, S. E.; Schaffner, K. Regioselective deuteration and resonance Raman spectroscopic characterization of biliverdin and phycocyanobilin. *Chem.−Eur. J.* **1997**, *3*, 363−367.
(171) Habermehl, G.; Christ, B. G. Amylocyanin, the blue pigment of *Streptomyces coelicolor*. *Naturwissenschaften* **1977**, *64*, 97−98.

Table 2. Characteristics of Grape-Derived Odorants Important to Chardonnay Wine Typicity[a]

name and structure	aroma descriptor(s)	threshold (μg/L)	reported content in Chardonnay (μg/L)
linalool 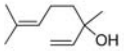	fruit, citrus[28,29]	25[30b]	2.0 – 142[31,32]
α-terpineol 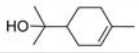	floral, musty, orange[33]	250[30b]	0.3 – 181[31,34]
1,1,6-trimethyl-1,2-dihydronaphthalene (TDN) 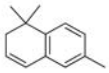	kerosene, petrol[35]	2[36c]	1 – 30[37]
β-damascenone 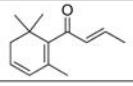	stewed fruit, apple, peach[28,33]	0.05[38d]	66 –170[39]
3-oxo-α-ionol 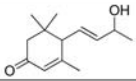	spicy[40]	N.A.[e]	19 – 2674[32,40]
3-sulfanylhexan-1-ol 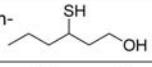	passionfruit, grapefruit[41]	0.06[41f]	0.010 – 0.148[42]
3-sulfanylhexyl acetate 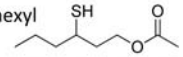	box tree, passion fruit[43]	0.004[43f]	0.006 – 0.100[42]
4-methyl-4-sulfanyl-pentan-2-one	box tree[41]	0.0008[41f]	0.0007 – 0.023[42]
4-ethylguaiacol 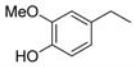	spice, phenolic[44]	33[30b]	0.2 – 50[40,45]
4-ethylphenol 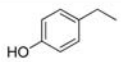	horse stable, medicinal, leather, phenolic[46,47]	440[48g]	<1 – 1194[49,50]
4-vinylphenol 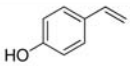	spicy, pharmaceutical[29]	180[51g]	44 – 638[29]
4-vinylguaiacol 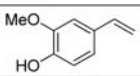	smoke, phenolic[52]	40[38d]	2.9 – 410.6[34,53]
methyl vanillate 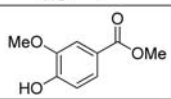	vanillin[46]	3,000[54f]	N.A.[e]

[a]Compounds are included in this table on the basis that they are present in grape berries or, more often, have precursors which are present in berries that are modified during fermentation or aging; that is, they are not produced de novo by winemaking microorganisms. Nonetheless, they may also be associated with other aspects of wine production, for example, storage in oak barrels. [b]11% aqueous ethanol solution containing 7 g/L glycerol and 5 g/L tartaric acid; pH adjusted to 3.4. [c]Calculated in a Chardonnay wine. [d]10% aqueous ethanol solution. [e]N.A., data not available. [f]10% aqueous ethanol solution; pH adjusted to 3.5. [g]Model aqueous alcohol solution.

means that the pathway for water to move back from the berry to the vine closes as cell vitality decreases, effectively stopping water backflow and late-ripening weight loss (shriveling).[16] Due to its anisohydric character, Chardonnay possesses a higher hydraulic conductance, which enables it to recover more rapidly from water stress after irrigation. Under water stress conditions, the decrease in stomatal conductance that Chardonnay undergoes is lower when compared to that of isohydric varieties, which in turn enables this variety to sustain a higher photosynthetic level and capacity.[18]

Chardonnay is undoubtedly a commercially important variety for the world's wine-producing nations, and its popularity among consumers is driven by the underlying chemical composition of the wines. In particular, aromas and flavors, resulting from volatile compounds derived from grapes, fermentation, and aging, are important to the quality of Chardonnay wines and, therefore, contribute to consumer liking.[19−22] The reported impacts of different viticultural and production practices that influence the aroma and flavor profiles and perceived quality of Chardonnay wines are summarized in this review. Future directions for research into factors that contribute to the differences in Chardonnay aroma composition are also outlined.

WINE AROMA AS AN INDICATOR OF QUALITY

Quality is a very subjective notion that, among other factors, drives the price a bottle of wine might fetch in the market. Wine quality depends not only on the physicochemical composition of the wine but also on what the consumer expects from it. Expectation will vary depending on the type of wine and from which standpoint quality is viewed from: young wine versus aged wine; producer versus consumer; low involvement versus high involvement level consumer.[23] Individual consumers will define this concept differently depending on their expectations and needs.[24] Various authors describe wine quality in terms of its fitness for purpose and the absence of faults,[19,23,25−27] but these terms are more related to production and establish only a very basic level of quality.

dx.doi.org/10.1021/jf501945s | J. Agric. Food Chem. 2014, 62, 6512−6534

Table 3. Characteristics of Odorants Important to Chardonnay Wine Typicity Formed during Alcoholic and Malolactic Fermentation

name and structure	aroma descriptor(s)	threshold (μg/L)	reported content in Chardonnay (μg/L)
acetic acid	vinegar[68]	200000[38a]	6460 – 925000[40,62]
hexanoic acid 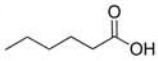	rancid, pungent, green[28,52]	420[30b]	50 – 10430[67]
octanoic acid 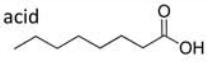	animal, spicy, cheese[29,44]	500[30b]	1150 – 50600[40,67]
decanoic acid 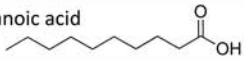	vinegar, animal, fatty[29]	1000[30b]	40 – 14150[40,60]
benzyl alcohol 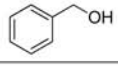	fruity, floral[29]	10000[69c]	12 – 679[53,70]
1-propanol	alcohol, ripe fruit[71]	306000[71d]	40 – 149000[40,67]
3-methyl-1-butanol (isoamyl alcohol) 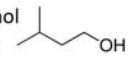	alcohol, harsh[72]	30000[38a]	50300 – 394900[59,67]
2-methylpropan-1-ol (isobutanol)	green, fresh, fusel[73]	40000[38a]	160 – 45400[74,75]
2-phenylethanol 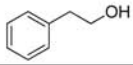	rose[28,33]	14000[30b]	930 – 153800[40,70]
methional 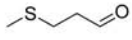	cooked vegetables[76]	0.5[76e]	N.A.[f]
phenylacet-aldehyde 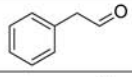	green, honey, floral, spicy[29,77]	1.0[78e]	4 – 28[29]
hexyl acetate 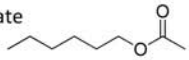	apple[79]	1500[79a]	24 – 1590[63,80]
2-methylpropyl acetate 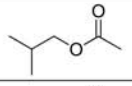	strawberry[44]	1600[28b]	25 – 4600[59,62]
2-methylbutyl acetate 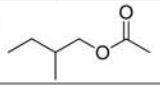	banana, pear[81]	N.A.[f]	33 – 671[62,82]
3-methylbutyl acetate (isoamyl acetate) 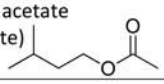	banana[29]	30[38a]	59 – 14900[63,67]
2-phenylethyl acetate 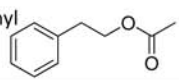	floral, rose[73]	250[38a]	40 – 2000[67,82]
ethyl 2-methyl-butanoate 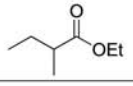	strawberry, berry[44]	18[30b]	0.5 – 3.6[82]
ethyl 3-methyl-butanoate 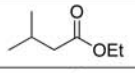	red fruit[33]	3[30b]	1.5 – 92[40,82]
ethyl propanoate 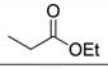	sweet, ethereal, fruity[83]	1800[79a]	3 – 546[80,82]
ethyl butanoate 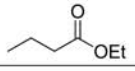	fruity, strawberry[29,44]	20[38,84a]	60 – 1970[67]
ethyl hexanoate 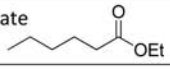	green apple, fruity, strawberry[29,33,44]	14[30b]	30 – 3960[63,70]
ethyl octanoate 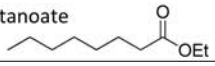	fruity, sweet[44]	5[30,38b]	30 – 3700[63,80]

dx.doi.org/10.1021/jf501945s | J. Agric. Food Chem. 2014, 62, 6512–6534

Table 3. continued

name and structure	aroma descriptor(s)	threshold (μg/L)	reported content in Chardonnay (μg/L)
ethyl decanoate 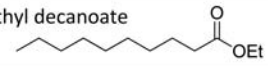	oily, fruity, floral[83]	200[30b]	17 – 496[63,70]
ethyl dodecanoate 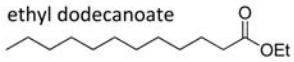	oily, fruity, floral[83]	500[85g]	1 – 3100[62,63]
diethyl succinate 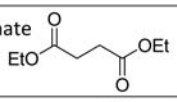	caramel[29]	200000[79a]	90 – 4580[67]
γ-hexalactone 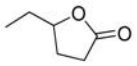	coconut, fruit[86]	13000[79a]	N.A.[f]
δ-decalactone 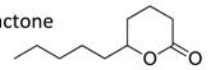	coconut, floral[29]	386[30b]	3 – 53[29]
diacetyl (2,3-butanedione)	butter, cream[28,73]	100[38a]	173[87]
acetoin (3-hydroxy-2-butanone)	fatty, wet, flowery, butter, cream[28,44,46,88]	150000[79a]	250 – 4800[40]
acetophenone 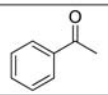	flower, almond, fruity[33,89]	65[69h]	N.A.[f]

[a]10% aqueous ethanol solution. [b]11% aqueous ethanol solution containing 7 g/L glycerol and 5 g/L tartaric acid; pH adjusted to 3.4. [c]Hydroalcoholic solution. [d]10% hydroalcoholic solution, pH 3.5. [e]10% aqueous ethanol solution containing 5 g/L tartaric acid; pH adjusted to 3.2. [f]N.A., data not available. [g]14% aqueous ethanol solution; pH adjusted to 3.5 with tartaric acid. [h]Aqueous ethanol solution.

Consumers also rate quality according to how much pleasure it affords them[23] (which is too subjective to use as a parameter for production), ongoing trends, and wine flavor in particular.[23]

The flavor or "style" of a wine depends on its chemical composition; this relates to perceptions of astringency, bitterness, and acidity, among others, due to nonvolatile components, but relies particularly on the type and concentration of volatile molecules contributing to wine aroma. For Chardonnay wines, the most relevant aroma compounds are listed in Tables 2–4. A recent, but somewhat limited, study by Saliba et al.[21] of 21 commercial Australian Chardonnay wines identified at least five distinct styles (A–E), which are outlined in Figure 1. The presence of particular odorants such as diacetyl, thiols, and esters above their aroma thresholds allows the perception of attributes such as "butter", "tropical fruit", and "citrus" (Tables 2–4). These attributes in turn characterize the different styles described by Saliba et al.[21] and consequently have a major impact on Chardonnay quality and acceptance by consumers. However, the identification of strong links between Chardonnay grape and wine composition remains a holy grail. If wine producers are to fully exploit the capability of producing wines of a targeted style and quality for a specific market segment, a detailed understanding of Chardonnay impact odorants and the contribution of grape precursors and winemaking inputs is paramount in helping to address this need.

The advancement in extraction and analytical techniques has allowed scientists to delve further into the precursors and volatile molecules that contribute to the aroma of most wine varieties. However, given the wide array of existing styles and production techniques available to winemakers, the makeup of Chardonnay wine aroma and its relationship to quality have yet to be completely comprehended. Nonetheless, despite all of the possible combinations of enological techniques, studies by authors such as Jaffre et al.[55] and Ballester et al.[56] have demonstrated that a common olfactory representation (or prototype, as Ballester et al.[56] described it), independent of vintage and origin, does exist for Chardonnay wines among industry experts. It should be remembered, however, that it is the opinions and perceptions of consumers that matter in the marketplace, and these are underpinned by their notions of quality.

Ongoing research appears to be delving deeper into the understanding of Chardonnay wine quality and the different factors that affect it. The literature covers an array of fields, from studies on how quality is perceived by consumers[55,57,58] to the effect of winemaking techniques to incorporate more flavor, character, and uniqueness, such as the use of new yeast strains and sequential inoculation and thermotreatment of grapes, among others.[59−63] Particular interest exists among researchers in understanding "minerality", which is an essential (although somewhat poorly characterized) attribute of some of the most famous Chardonnay wines in the world such as those from Chablis and Burgundy.[64] Given the changes in global climate, studies are also required into the adaptation of viticultural practices and clone selection to continue producing high-quality wines, particularly as related to a drive to reduce alcohol levels. Even though anecdotal knowledge exists among producers as to the quality and style of fruit that can be obtained from each different Chardonnay clone available, there is a lack of scientific information as to the characteristics of these clones, and studies are needed on how they adapt to different terroirs and rootstocks.

Table 4. Odorants Derived from Oak Contact or Formed during Aging That Are Important to the Typicity of Chardonnay Wines

name and structure	aroma descriptor(s)	threshold (μg/L)	reported content in Chardonnay (μg/L)
vanillin 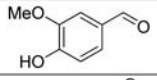	vanilla[33]	200[38a]	3.9 – 1223[40,53]
acetovanillone 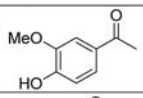	floral, clove, vanilla[46]	1000[54b]	N.A.[c]
ethyl cinnamate 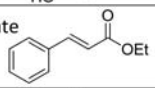	cinnamon, sweet, floral, strawberry, plum[28,44,99]	1.1[30d]	1 – 33[40]
furfural 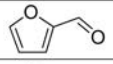	almond[48]	14100[46d]	1 – 21190[40,45]
5-methyl-furfural 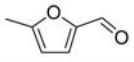	warm, spicy[100]	20000[101]	trace – 37.5[45]
guaiacol 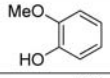	phenolic, chemical, spice[28,33,44]	9.5[30d]	1.6 – 284[40,45]
tyrosol 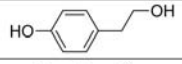	N.A.	N.A.[c]	600 – 17040[59,70]
cis-oak lactone 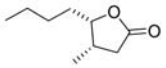	coconut[77]	24[102e]	33 – 382[40]
trans-oak lactone 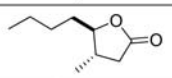	coconut, oak[103]	172[102e]	10.2 – 1355[40,45]
eugenol 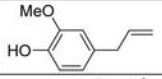	clove[48]	6[30d]	10 – 362[40,49]
2-methyltetrahydro-thiophen-3-one	metallic, natural gas[104]	0.09[105a]	18000[106g]
2-furan-methanethiol 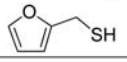	roasted coffee[107]	0.0004[107f]	0.014[108]
benzene-methanethiol 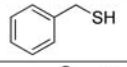	smoky, gunflint[109]	0.0003[109f]	0.03 – 0.04[109]
sotolon 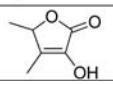	burnt, curry[28,33]	5[38a]	1.1 – 4.7[110]

[a]10% aqueous ethanol solution. [b]10% aqueous ethanol solution; pH adjusted to 3.5. [c]N.A., data not available. [d]11% aqueous ethanol solution containing 7 g/L glycerol and 5 g/L tartaric acid; pH adjusted to 3.4. [e]Neutral white wine. [f]12% aqueous ethanol solution containing 5 g/L tartaric acid; pH adjusted to 3.5. [g]As 1-octanol equivalents.

CHARDONNAY AROMA PROFILES

The headspace of Chardonnay wines has been tentatively determined to contain 243 volatiles detected through GC×GC-time-of-flight-mass spectrometry (TOF-MS),[65] which belong to a complex mixture of diverse chemical families including, but not restricted to, C_{13}-norisoprenoids, esters, alcohols, polyfunctional thiols, lactones, monoterpenoids, phenols, and acids.[39] Of these, the compounds derived from the grapes, winemaking, and aging listed in Tables 2–4 have been reported as having a positive relationship to the typicity of Chardonnay wines (i.e., the extent to which a wine is typical of the variety and is a good example of the Chardonnay wine concept), and some can be considered as character-relevant compounds for this variety.[29,55,56,66,67]

Not all of the compounds present in Tables 2–4 have an odor activity value (OAV) >1, which is normally taken as the value required for a compound to be a likely contributor to characteristic aroma. Their apparent importance to typical Chardonnay wine aroma highlights the fact that OAVs based on threshold values in a specific matrix (e.g., neutral white wine or 10% v/v aqueous ethanol) act merely as a guide when determining the importance of a compound to wine aroma, due to a significant effect of the matrix.[90–92]

When dealing with the typicity of a wine, with Sauvignon blanc being a good example, rather than search for impact compounds alone, researchers are also looking for those odorants that are essential for the wine to fit within a perceptual concept for that variety.[93] Similarly to quality, defining typicity requires a sensory analysis of samples; a number of sensory techniques are available for this purpose such as requiring the panelists to rate how well a wine belongs to a certain category and descriptive analysis or sorting of the samples, culminating with pairing and discrimination of the results based on the volatile composition of good and bad samples.[55,56,93] Other strategies to target relevant compounds include reconstitution analysis, which reveals the importance of certain volatiles to the overall aroma of the wine in question.[40] Consideration also needs to be given to the interactions among odorants, where differing concentrations of compounds in a mixture may have

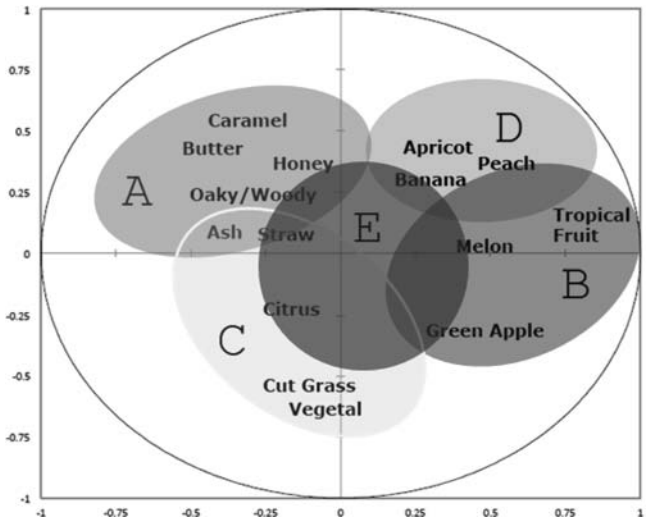

Figure 1. Representation of Chardonnay flavor profiles. A–E denote different commercial wine styles (based on data from Saliba et al.[21]).

synergistic or antagonistic effects and aromas may be enhanced or suppressed or odor quality altered as a result.[94−98]

Along the lines of seeking a perceptual concept for varietals, Louw et al.[67] analyzed 125 young unoaked Chardonnay wines, among other monovarietals from South Africa, using liquid−liquid extraction (LLE) and GC-flame ionization detection (FID), together with multivariate analysis and a "most used subset" of compounds to determine characteristic molecules that could be used to discriminate among cultivars. They showed that Chardonnay wines can be discriminated (with 74% correctly classified) by using the following eight volatile compounds: 2-phenylethanol, decanoic acid, diethyl succinate, ethyl hexanoate, ethyl decanoate, ethyl octanoate, hexyl acetate, and 1-propanol (Table 3). This prediction model, however, remains to be used to classify other sets of Chardonnay wines, particularly more developed ones, and the links between grape and wine composition for these eight specific compounds need clarification. They also observed that unlike most yeast-derived compounds (i.e., alcohols, acids, and esters such as those in Table 3), 2-phenylethanol, acetic acid, ethyl hexanoate, hexanoic acid, isoamyl alcohol, and 1-propanol were not affected by vintage, which could signify that their concentrations are characteristic of the Chardonnay cultivar. More work has to be done to confirm this, however.

Chardonnay juice does not possess any distinct aroma; however, certain precursors can be found in the must as well as the following volatile hydrolysis products: C_{13}-norisoprenoids, benzene derivatives, monoterpenoids, and aliphatic compounds as isolated by Sefton et al.[111] by reverse-phase chromatography followed by LLE and GC-MS. Although monoterpenoids (such as linalool and α-terpineol, Table 2) characterize the aroma of grape varieties such as Gewürztraminer and Muscats, Chardonnay is mostly deficient in these compounds, instead being dominated by C_{13}-norisoprenoids.[111] Studies by Lee and Noble,[40] Sefton et al.,[111] and Simpson et al.[39] suggest that the most relevant C_{13}-norisoprenoids to this variety's overall aroma are β-damascenone, 3-oxo-α-ionol, 1,1,6-trimethyl-1,2-dihydronaphthalene (TDN), and vitispirane.

C_{13}-Norisoprenoids such as β-damascenone and TDN are formed downstream from the oxidative cleavage of carotenoids (particularly lutein and β-carotene, with minor amounts of violaxanthin, neoxanthin, and several others), which occurs during grape berry ripening (e.g., Figure 2).[112−114] Although C_{13}-norisoprenoids can be found in their free form in the juice, they are usually present as glycoconjugates and easily degraded under acidic conditions.[115] β-Damascenone is a powerful odorant (odor threshold in model wine of 50 ng/L, Table 2) and aroma enhancer that, depending on concentration, can exhibit different odor qualities. At perithreshold concentrations, β-damascenone exhibits a "lemon balm" aroma, whereas at a concentration some 2 orders of magnitude higher it can be characterized as having "apple", "rose", and "honey" nuances.[116] Although β-damascenone is a ubiquitous wine component,[117] TDN, which possesses a "kerosene" aroma (Table 2), is typically associated with aged Riesling wines.[118] As determined by Lee and Noble[40] using GC−olfactometry (GC-O), 3-oxo-α-ionol possesses "spicy" notes at the concentrations found in Chardonnay wines (Table 2).

Polyfunctional thiols such as 3-sulfanylhexan-1-ol (3-SH), 3-sulfanylhexyl acetate (3-SHA), and 4-methyl-4-sulfanylpropan-2-one (4-MSP) are extremely potent odorants with very low aroma thresholds (60, 4.2, and 0.8 ng/L, respectively; Table 2) and aromas reminiscent of "box-tree", "grapefruit", and "passion fruit".[119,120] Both 3-SH and 4-MSP occur naturally in grapes as odorless glutathione and cysteine conjugates, which are released by yeast during alcoholic fermentation; 3-SHA is formed during alcoholic fermentation by esterification of 3-SH by alcohol acetyltransferase (AAT).[43,121,122] Although of particular significance to the typicity of Sauvignon blanc wines, these compounds are not as abundant in Chardonnay, yet still appear to be important.[42,119,123,124] The presence of other thiols such as benzenemethanethiol (BM) and 2-furanmethanethiol (FFT) at concentrations above their perception thresholds (0.3 ng/L[109] and 0.4 ng/L,[107] respectively) must also be noted (Table 4). BM has been described as having "flinty" and "smoky" (i.e., empyreumatic) notes, which may be related to Chardonnay wines' "mineral" character[64] and has an inconclusive formation

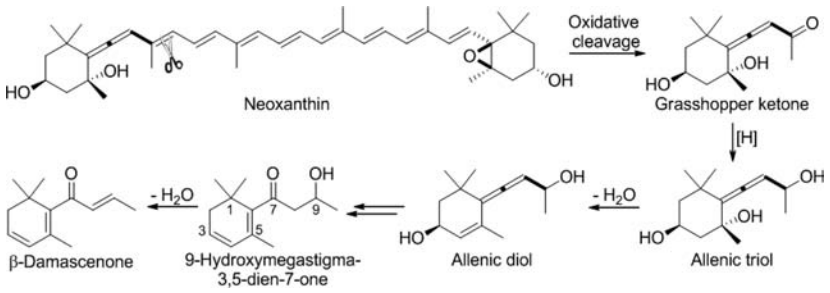

Figure 2. Formation of C_{13}-norisoprenoid β-damascenone from the carotenoid neoxanthin via oxidative cleavage, carbonyl reduction [H], and acid-catalyzed reactions. Although not depicted, glycosylated intermediates are also featured in this pathway.

pathway. On the other hand, FFT, with its strong "roast coffee" aroma, is formed from the furfural released by oak barrels and hydrogen sulfide formed during alcoholic fermentation.[125] Using a specific thiol extraction method (*p*-hydroxymercuribenzoate) together with GC-MS analysis, Tominaga et al.[109] determined that among wines from several appellation regions in France, Chardonnay possessed the highest concentrations of BM (30−32 ng/L), at 100 times above its detection threshold and 2−3 times more than all other assayed varieties. Mateo-Vivaracho et al.[42] have also confirmed the presence of suprathreshold concentrations of BM in Chardonnay (0.6−1.4 ng/L) through solid-phase extraction (SPE) and GC-MS analysis with negative chemical ionization (NCI). The different methodologies as well as the different origins of the wines employed by both research groups may account for the differences in quantities of BM found and in the hierarchy between Sauvignon blanc and Chardonnay in terms of these compounds. Comparison of Sauvignon blanc wines from different origins by Mateo-Vivaracho et al.[42] emphasized the importance that origin has on the content of all polyfunctional thiols (3-SH, 3-SHA, 4-MSP, BM, and FFT); BM concentration was highest in New Zealand wines, and FFT contents were found to be highest in French wines and lowest in those from Chile. However, these differences may be also due to viticultural and enological practices in each region. These two compounds have also been found at concentrations well above their perception thresholds in aged French Champagnes and have been shown to increase during aging.[126] Unfortunately, as with other polyfunctional thiols, analysis of BM and FFT is not a trivial undertaking (e.g., low abundance and reactive), and this may account for the fact that they have not been reported as characteristic of certain Chardonnay styles as yet.

Other important compounds are the esters (Table 3), which constitute the second most significant chemical group in the volatile fraction of Chardonnay wines. The esters are formed in excess during alcoholic fermentation by yeast metabolism and are responsible for "fruity" and "floral" aromas.[127,128] Wines contain two main types of odor-active esters: acetates of higher alcohols (formed by yeast AAT enzymes Atf1p and Atf2p, via condensation of their corresponding higher alcohols and acetyl CoA[129−131]) and ethyl esters of fatty acids (thought to be formed by esterification of the activated fatty acids (acyl CoA) during lipid biosynthesis mediated by acyl CoA:ethanol *O*-acyltransferase (EAT) enzymes Eeb1 and Eht1 together with other as yet unidentified enzymes[132]). Acetates are synthesized at higher concentrations than ethyl esters, and the ratio between both, as well as the concentration at which acetates are produced, is affected particularly by fermentation temperature, must nutrient content, and yeast strain rather than grape variety. Although both acetates and ethyl esters are liposoluble, excretion of ethyl esters through the yeast cell membrane becomes more difficult as chain length increases (only 8−17% of all ethyl decanoate produced by yeast is excreted into wine during alcoholic fermentation),[133] whereas 100% of all acetates produced are released.

The production of esters is modulated by the presence of cosubstrates and the activity of related synthesis and hydrolysis enzymes (esterases).[134] Formation of acetates depends on the concentration of unsaturated fatty acids (which inhibit AAT activity) available in the medium and carbon-to-nitrogen ratio.[134] A dynamic equilibrium exists between acetates and their corresponding acids and alcohols, which depends on the conditions of the medium.[135] Ethyl esters respond to the modification of most winemaking parameters in a similar way as acetates (albeit increases in nitrogen content or fermentation temperature have more pronounced effects on acetate formation). Higher concentrations of unsaturated fatty acids decreased ethyl ester production; however, inclusion of an additional carbon source to the medium increased only acetate production. Unlike acetates, synthesis of ethyl esters depends more on the availability of substrate (medium-chain fatty acids) rather than on enzyme expression level;[134] in turn, the amount and type of fatty acids available[136] depend on agricultural conditions and grape variety, making ethyl ester profiles more variety-dependent than that of acetates (except for hexyl acetate).[137] According to Smyth,[66] the most relevant esters for unwooded Chardonnay aroma appear to be ethyl hexanoate, ethyl octanoate, ethyl decanoate, ethyl 2-methylpropanoate, ethyl 2-methylbutanoate, ethyl 3-methylbutanoate, hexyl acetate, 2-methylbutyl acetate, and 3-methylbutyl acetate.

Moio,[138] Lorrain,[29] and Lee and Noble[40] all agree on the importance of volatile compounds such as guaiacol, *cis*- and *trans*-oak lactones, 4-ethylphenol, 4-ethylguaiacol, 4-vinylphenol, vanillin, methyl vanillate, and 5-methylfurfural (Tables 2 and 4) to the typicity of Chardonnay wines. These compounds derive mainly from aging in oak barrels, and some of them are even considered to be off-odors if they are present at concentrations above their perception threshold, as they are commonly associated with the metabolism of *Brettanomyces/Dekkera*.[47] However, some of these compounds, such as 4-vinylguaiacol, can also be found in wines that have had no contact with oak. 4-Vinylguaiacol is responsible for "smoke" and "phenolic" notes,[79] and although usually associated with aging in barrels, higher concentrations of this compound have been detected in some Chardonnay wines aged in stainless steel.[40] Spillman et al.[49] refer to 4-vinylguaiacol, 4-ethylguaiacol, 4-ethylphenol, and 4-vinylphenol as fermentation products rather than as compounds derived from oak contact. They are formed through decarboxylation of natural grape components ferulic and *p*-coumaric acids by *Saccharomyces cerevisiae* enzymatic activity[139] (hence their inclusion in Table 2). The concentration of these compounds appears to depend more on factors such as higher fermentation temperature and contact with lees than on the influence of oak wood.[140]

In their assessment of Australian Chardonnay wines, Saliba et al.[21] observed that five distinct styles resulted from the sensory analysis (Figure 1); among these, style A (a more "traditional/oaky" Chardonnay style, marked by "caramel", "butter", "honey", and "oak" attributes) and style B (a "crisp/fruity" style, with "tropical fruit", "melon", and "green apple" notes) seem to dominate the current market. From a volatile compound perspective, style A wines were marked by "woody", "smoky", "vanilla", "spicy", and "clove" odors, which are attributed to the presence of vanillin, guaiacol, 4-vinylguaiacol, furfural, and *cis*- and *trans*-oak lactones (Tables 2 and 4).[40,87] From the correlation matrix by Spillman et al.,[49] it can be inferred that the "smoky" notes present in Chardonnay wines aged in oak barriques are caused by the combined presence of guaiacol, 4-methylguaiacol, furfural, 5-methylfurfural, and, to a lesser extent, 4-ethylguaiacol and vanillin. Other oak-related aromas such as "cinnamon" and "coconut" were positively correlated to vanillin and *cis*-oak lactone (followed by guaiacol), respectively.

Unlike what might have been expected, the difference in resulting overall aroma between such A and B styles is not necessarily due to a different composition of characteristic

Table 5. Concentration (Micrograms per Liter) and Comparison of Volatile Compounds in Two Styles of Chardonnay Wines ("Fruity" and "Oaky") As Determined in Separate Studies

	Buettner et al.[87]			Lee and Noble[40]		
	fruity	oaky	factor of difference	fruity	oaky	factor of difference
ethyl isobutyrate	72.2	99.9	1.4	31		
ethyl butanoate	263	341.5	1.3	844	1040	1.2
ethyl isovalerate	9.2	19.9	2.2	42	41	1.0
3-methylbutyl acetate	943.7	163.5	0.2	519	349	0.7
ethyl hexanoate	757.2	737.5	1.0	843	600	0.7
linalool				50	31	0.6
2-phenylethanol	12415	24971	2.0	153840	116850	0.8
acetic acid	434232	489370	1.1	10000	11290	1.1
butanoic acid	1839	1611	0.9	1824	1505	0.8
trans-oak lactone	7.1	131.1	18.5	173	996	5.8
cis-oak lactone	17	214.8	12.6	33	382	11.6
2-methoxyphenol	2.7	9.9	3.7	25	284	11.4
ethyl cinnamate	1.5	3.1	2.1	3	6	2.0
eugenol	1.6	8.9	5.6	21	362	17.2
4-vinylguaiacol	50.5	49.3	1.0	1356	380	0.3
vanillin	48.5	241.6	5.0	107	1223	11.4

volatile molecules. A study by Buettner[87] of the potent odorants identified in two Chardonnay wines representative of a "traditional/oaky" and a "crisp/fruity" style (i.e., styles A and B according to Saliba et al.[21] in Figure 1) showed that they were both composed of the same volatiles, but each contained different amounts, leading to different time persistence levels for each attribute. Retronasal sensory assessment of both samples showed that the notes related to "oak" in style A were more persistent when judged by time−dilution analysis than the "fruity" ones in style B. Table 5 shows some of the results of this study, revealing that the concentration of *cis*-oak-lactone ("coconut" notes, Table 4) as measured by high-resolution (HR) GC-MS using stable isotope dilution analysis (SIDA) was almost 13 times higher in the A style wine than in the B style wine, and 3-methylbutyl acetate ("banana" notes, Table 3) was 6 times more abundant in the B style wine.

Lee and Noble[40] studied an array of California Chardonnay wines, two of which were characterized as belonging to the "crisp/fruity" and "traditional/oaky" styles (Figure 3). A comparison of their results to those obtained by Buettner[87] demonstrates similarities for certain compounds (Table 5). Both studies found concentrations of *cis*-oak lactone in the A styles that were approximately 13 times higher than in style B, as well as twice the concentration of ethyl cinnamate in the woodier styles than in the fruitier ones. The differences observed in the content of compounds related to fruity attributes were not as high as expected, and in some cases the difference found between both styles was not significant (i.e., ethyl hexanoate and ethyl butanoate). The use of aroma models and similarity tests by Lee and Noble[31] showed that even when trying to replicate wines with a high intensity of "fruity" aroma attributes, it was also necessary to incorporate "oak/spicy" volatiles (e.g., vanillin, furfural, 2-acetylfuran, *cis*- and *trans*-oak lactone, eugenol). The wines to which only "fruity" related aroma molecules (ethyl butanoate, 3-methylbutyl acetate, linalool, α-terpineol, and 2-phenylethyl acetate) were added were less representative and closer in profile to the base wine rather than the original "crisp/fruity" wine sample.

This highlights the potential importance of "oak" and "spicy" attributes to Chardonnay aroma even for "crisp/fruity" styles and explains the predominance of "woody" and "spicy" notes in

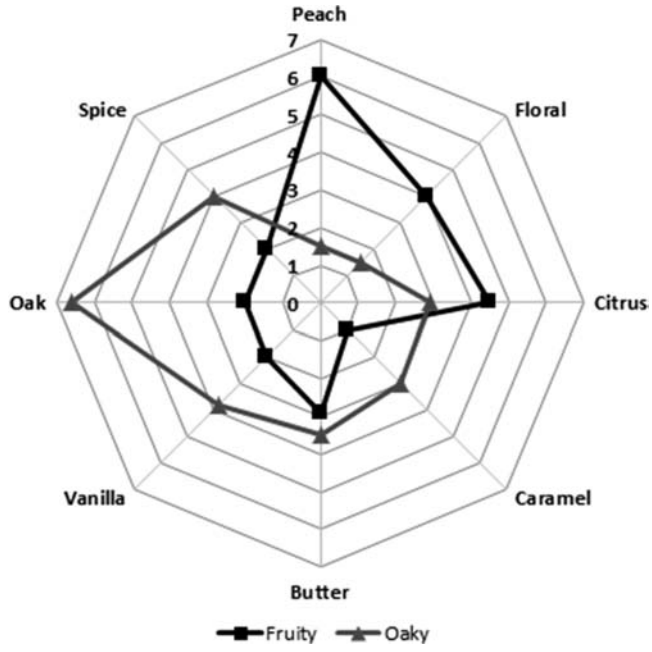

Figure 3. Aroma profiles of "fruity" and "oaky" Chardonnay wines (data from Lee and Noble[40]).

the "oaky" wine and lack thereof in the "fruity" style in the study by Buettner et al.[87] The only compounds not detected by tasters in the "fruity" sample were *cis*- and *trans*-oak lactone and eugenol; likewise, 3-methybutyl acetate was not detected by the tasters in the "oaky" wine and was, in fact, less abundant in the "oaky" style by a factor of 5.[87] The "fruity" style was also characterized by a higher detection frequency of linalool and α-terpineol,[40] which have been described as having "citrus" and "floral" notes.[40,79] Wines described as being "oaky" are seldom described as "fruity", and the work of Arrhenius et al.[37] showed a very significant negative correlation existed between the attributes "citrus" and "caramel/pumpkin" (this term is positively correlated to the presence of TDN). On the other hand, esters, which contribute "fruity" aromas, are often present in Chardonnay wines at concentrations well above their

dx.doi.org/10.1021/jf501945s | J. Agric. Food Chem. 2014, 62, 6512−6534

detection thresholds; therefore, no significant differences have been observed in the detection frequency of most of these compounds between both wine styles.[40]

FACTORS AFFECTING AROMA DEVELOPMENT

A range of factors determine the aroma composition of a wine, including but not limited to grape maturity, vine nutrition, harvest method, alcoholic and malolactic fermentation, and aging. Among these, grape maturity and alcoholic fermentation are considered the most critical stages.[26] Compounds related to grape variety and typicity, such as monoterpenoids, C_{13}-norisoprenoids, pyrazines, and polyfunctional thiols, which derive from the berry itself, can vary in concentration and can be found either in free form or bound as glycosides or amino acid conjugates, depending on the grape variety.[141−143] During fermentation, *S. cerevisiae* metabolism produces many of the olfactory compounds identified as being important to wine, such as esters and fusel alcohols, from the nutrients, elements, and different compounds present in the juice or must.[141,144,145]

Juice Composition and Nutrient Content. A balanced content of nutrients in the juice (nitrogen, amino acids, lipids, vitamins, and metal cations), as well as optimum oxygen and pH levels before the start of fermentation,[62] are determinant of yeast biomass formation, yeast metabolism, and alcoholic fermentation rate. Chardonnay appears to be the variety with the most reported cases of difficult fermentations in Australia as per Schmidt et al.,[146] most probably due to low pH and, in some cases, low potassium (K) concentration. The pH of juice appears to affect yeast performance in one of three ways; either the strain is unaffected, or its performance is affected (negatively) but can be corrected by adding K to the medium, or it is affected and K cannot correct the problem. A low pH combined with a low K concentration alters the redox potential of the medium, which is then corrected by an excess production of acetic acid, which is itself inhibitory for yeast metabolism and thereby further compromises the progression of fermentation.[146]

Nutrient deficiencies increase the risk of incomplete fermentations, leading to the appearance of off-odors (e.g., H_2S and other sulfur compounds) and unstable wines prone to bacterial spoilage. By supplementing a juice deficient in yeast assimilable nitrogen (YAN), usually in the form of diammonium phosphate (DAP) as an ammonium source, lower amounts of higher alcohols (for example, those in Table 3) and branched-chained acids (isoacids) are produced, and a higher concentration of esters is synthesized, improving overall sensory quality.[75] However, an excessive addition of DAP will tend to produce wines with an undesirable "solvent" character and higher ethyl acetate and acetic acid contents.[82,147]

In terms of the type of nitrogen supplement used, Torrea et al.[82] demonstrated that the addition of inorganic ammonium nitrogen (as NH_4Cl) to Chardonnay juices resulted in an increased concentration of acetic acid in the corresponding wines, but lower quantities of higher alcohols than with other forms of nitrogen (i.e., amino acids and ammonium). When the amount of ammonium supplementation was increased, the final wine had low fruit-related aromas and high "acetic" and "nail polish remover" notes, due to acetic acid and ethyl acetate, respectively; of 16 aroma descriptors evaluated, 14 changed significantly when different types and quantities of nitrogen were supplied.[82] These results can be explained on the basis of yeast metabolism, in which amino acids may play a role in certain metabolic pathways or may act as precursors to esters.[148]

If nitrogen is supplied in the form of amino acids, greater amounts of esters will be produced and higher alcohol concentrations will decrease.[75,82] In general, higher amino acid content improves the capacity of yeast to adapt to and/or work under anaerobic conditions, activating the synthesis of fatty acids and increasing the amount of ethyl esters produced.[75] However, there appears to be no correlation between higher alcohol acetates and amino acid levels; the extent of utilization of a particular amino acid by yeast will depend on the nature of the amino acid. As an example, greater amounts of leucine (a precursor to 3-methyl-1-butanol) were utilized in fermentations in which it was supplemented, but the final concentration of 3-methylbutyl acetate was similar to that of control fermentations.[149]

It should be mentioned that not all yeasts are equally sensitive to every nitrogen source. Certain strains were revealed to be insensitive to specific sources, whereas strain 254D, which is a moderate ester producer, was very responsive to changes in nitrogen source. For example, the content of ethyl and 3-methylbutyl acetates produced by 254D was significantly higher when using DAP than when nitrogen was incorporated as amino acids. Furthermore, use of amino acids when working with 254D yielded the lowest maximum and final concentrations of acetate esters and fatty acid ethyl esters determined in the study when compared to DAP-supplemented and control fermentations.[149]

Nutrients other than nitrogen are important to fermentation performance and metabolite profile. Varela et al.[62] demonstrated that aroma composition can be affected through lipid and oxygen supplementation, thereby influencing ester and higher alcohol production in Chardonnay wines while limiting production of fatty acids, especially of acetic acid, as well as lowering acetaldehyde concentrations.[62] Furthermore, supplementation of musts with these nutrients not only stimulated yeast growth and metabolism but improved fermentation rates significantly and diminished the amount of residual sugar in the final product. Addition of either oxygen or lipids changed the proportions of acetate to ethyl esters and of branched-chain to medium-chain fatty acids while, unfortunately, also increasing, by approximately 2-fold, the amount of higher alcohols to levels oscillating between 320 and 400 mg/L. This means higher alcohols were above the value indicated by Rapp and Mandery[68] as contributing positively to wine complexity (300 mg/L). These authors also suggested that concentrations of higher alcohols in excess of 400 mg/L no longer contribute positively to the overall aroma of a wine but rather detract from it. Addition of lipids (as unsaturated fatty acids) and sterol yielded Chardonnay wines with more esters overall, whereas incorporation of oxygen (with and without addition of lipids) increased acetate esters but strongly diminished the total content of ethyl esters. In either case there was a reduction in hexanoic acid but an increase in 3-methylpropanoic acid and variable effects on the other volatile acids (excluding acetic acid, which was reduced as mentioned above). Addition of lipids can also improve the fermentation progress of overly clarified juices and avoid stuck fermentations and high acetic acid concentrations.[62,146,150]

Use of Enzymatic Preparations. Endogenous grape glycosidases have a low enzymatic activity at the pH and/or sugar content of most grape juices and are therefore capable of only a limited level of aroma release through glycoside

cleavage.[151,152] In addition, different enzymes are required to release bound volatiles such as monoterpenoids and C_{13}-norisoprenoids from their different glycosidic forms (i.e., β-D-glucosides and disaccharides).[153,154] Winemaking yeasts possess glycosidase activity[155] as highlighted by Chassagne et al.,[152] who revealed differences in the extent of glycoside hydrolysis during fermentation of a Chardonnay must. Model fermentations containing a Chardonnay glycosidic extract also showed that yeast glycosidases exhibited different extents of hydrolysis depending on the type of sugar involved (mostly glucose, arabinose, and rhamnose); by the end of fermentation 47% of glucose contained within the glycoside pool had been hydrolyzed, whereas glycosides containing rhamnose and arabinose had been almost completely metabolized.[61]

The use of enzymatic preparations with glycosidase activity has been demonstrated to increase the content of total monoterpenoids and C_{13}-norisoprenoids,[153,154] and enological preparations (of fungal origin) are available for use in winemaking to help improve aroma profiles.[155,156] Enzymes are typically added prior to fermentation during commercial winemaking (i.e., preparations used for juice extraction and clarification containing glycosidase side activities), but in a study of Chardonnay wines, glycosidases were added postfermentation, leading to increases of around 50% or more in total monoterpenoids and C_{13}-norisoprenoids.[32] Unlike grape glycosides, fungal glycosides are not inhibited under normal wine conditions[151] and have even been shown to enhance aroma characteristics when applied to dealcoholized wine containing grape aroma precursors.[157]

Winemaking Techniques. In response to current market trends and the popularity of certain wines, two marked tendencies exist now for Chardonnay aroma profiles: fruity and light styles are opposed by more flavored and complex (and possibly more evolved) styles. These disparate styles are targeted through choices made during winemaking, which have a strong influence on the overall aromas of Chardonnay wine, perhaps more so than any other white wine variety. Yeast produces esters during alcoholic fermentation, and given that they constitute one of the main groups of sensorially important compounds in Chardonnay, the choice of fermentation conditions and yeast strain will play a major role in overall wine aroma.[145] This explains why some non-Chardonnay wines, produced in the same style as a Chardonnay, have been confused by experts as belonging to the latter category during tasting.[55] In particular, Chardonnay aroma is marked by the presence of the ethyl esters of fatty acids (i.e., butanoate, hexanoate, octanoate, and decanoate) along with hexyl acetate (Table 3); the "fruity" nuances derived from variation in the concentrations of these compounds will be dependent on yeast strain, providing uniqueness to wine aroma.[158]

Chardonnay is one of the few white varieties that can endure a prolonged maceration.[159] This is fortuitous, because as shown with various grape varieties, a number of aroma compounds and precursors are located preferentially in grape skins; among them are monoterpenoids and their glycosides and precursors to β-damascenone and polyfunctional thiols.[53,160−163] Extended skin contact increases the total aroma content both in terms of concentrations of volatile molecules and as evaluated by sensory analysis.[34,164,165] Increased concentrations of linoleic and linolenic acids (precursors to C_6 compounds such as hexenals and, ultimately, 1-hexanol) have also been revealed through extended skin contact of Chardonnay musts,[166] and maceration with skins produced wines that were described as being more intense and "fruitier".[34,164] Macerated wines were also shown to be richer in C_6 compounds, particularly 1-hexanol.[34] According to Colagrande et al.,[167] the effect of C_6 alcohols and aldehydes depends on their concentration; when at low concentrations (<0.5 mg/L) their contribution is actually positive, adding to the typical aroma of Chardonnay wines, but they are also responsible for herbaceous flavors when their content is higher. The production of fruitier wines can be partly explained by the results of Dennis et al.,[137] which confirmed the role of certain C_6 compounds (1-hexanol, hexanal, (*E*)-2-hexenal, (*E*)-2-hexen-1-ol, and (*Z*)-3-hexen-1-ol) as precursors to hexyl acetate after the respective reduction and/or acetylation. Hexyl acetate, with its pleasant "apple" aroma (Table 3), is typical of unwooded Chardonnay wines.[66]

It is worth noting that skin maceration will necessarily increase the extraction of grape phenolic compounds (i.e., nonvolatiles associated with taste, mouthfeel, and color (browning of white wine)), potentially having an adverse effect on white wine sensory properties. However, despite total phenolics being increased linearly with maceration time, no significant differences in bitterness or astringency of Chardonnay wines were found in studies employing different times for maceration treatments. After 16 or 24 h of maceration, the sensory effect of an increased level of phenolics was no different from the wines that did not undergo skin contact.[164,165] Temperature plays an important role, however, such that cooler temperatures minimize the extraction of phenols without overly affecting the extraction of aroma components.[168] Furthermore, maceration affected the pH, titrable acidity, total nitrogen and amino acid contents, and potassium, calcium, and magnesium levels.[164,165] Some of these parameters will influence fermentation performance and contribute to differences in aroma profiles.

Thermotreatment of grapes is usually reserved for red wines, where higher polyphenol and anthocyanin contents are sought for their effects on color and mouthfeel. Chardonnay juices or wines may also benefit from thermotreatments to improve the extraction of determinate compounds from grapes and accelerate the level of hydrolysis of glycosylated aroma precursors. A study by Francis et al.[61] showed that heat treatments of Chardonnay wines at around 45 °C for several weeks resulted in wines with sensory properties similar to those of wines that had been bottle-aged for several years. Thermal treatment reduced "floral", "pineapple", and "grassy" characters of the resulting wines and intensified their "oak", "honey", and "smoky" characteristics. On the contrary, heating of juices or wines for a short time (i.e., around 2−12 min) at 90 °C on a pilot scale (250 L) was shown not to produce any discernible sensory differences when compared to the unheated control wine. In either case, there were no oxidized, cooked, or maderized aromas. Thermal treatment of Chardonnay juice or wine using mild temperatures could be envisaged as a more rapid and economical alternative to ordinary aging of wines to obtain a more "evolved" profile.

A choice of fermentation vessels is available to winemakers when producing Chardonnay wines. Tanks constructed of steel, cement, or plastic as well as oak barrels and vats may be used, depending on the desired style, available infrastructure, and budget. Unlike stainless steel, barrels are not inert and interact with the juice during fermentation, resulting in higher concentrations of certain volatile compounds. According to González-Marco et al.[70] the total concentration of about 186 mg/L for higher alcohols in wines produced in new French oak

barrels was 42% greater than for stainless steel, but below the 400 mg/L total suggested as detrimental to wine aroma.[68] Ethyl acetate formed in oak barrels was approximately 32% higher, whereas other esters totaled almost 18 mg/L and were up to 4 times higher, particularly those of short- and medium-chain fatty acids, 3-methylbutyl acetate, and diethyl and monoethyl succinate, compared to stainless steel tanks. Hexanoic, octanoic, and decanoic acids were up to 6 times higher in oak barrel fermentations as well.

These outcomes can be rationalized by considering compositional differences between the fermentations in each type of vessel. Wood contains even-numbered saturated fatty acids (C2:0−C26:0), among a range of other volatile and nonvolatile compounds, which are extracted during fermentation, thus increasing the amount of esters and acids in the wine. The improved production of higher alcohols seemed to relate to a reduced consumption of amino acids in barrel-fermented wines, with the biggest differences being observed for 2-phenylethanol, benzyl alcohol, 1-hexanol, 1-propanol, 3-(methylthio)-1-propanol, methanol, tyrosol, and tryptophol.[70] Fermentation of wines in oak barrels also favors the extraction of typical oak-related volatiles such as oak lactones and furfurals, which undergo reduction to the corresponding furan alcohols because of a prolonged contact with lees.[140]

Yeast Influences. Yeasts affect the aroma composition and therefore quality of a wine in a number of ways. They synthesize odorant molecules de novo, such as esters and higher alcohols, release odorless precursors, and alter wine perception and flavor through the production of ethanol and the release of yeast constituents such as mannoproteins.[169] As well, the level of stress a yeast strain may tolerate will influence the amount of sulfur-containing malodorous compounds that will be formed in low-nitrogen situations. As outlined earlier, esters formed during fermentation comprise an important class of "fruity" aroma compounds in Chardonnay wine. Genetic variation between wine yeast strains and must composition leads to differences in expression of genes related to ester synthesis and hydrolysis.[149,169] Yeasts are also responsible for the cleavage of cysteinyl and glutathionyl conjugates and release of the corresponding polyfunctional thiols 3-SH, 3-SHA, and 4-MSP (see Table 2).[169] Typically, winemakers inoculate with selected strains of *Saccharomyces cerevisiae*, but a large diversity of yeast genera which can affect ester production exist as indigenous microflora.[170] A quick analysis of Australia's and America's major fine Chardonnay producers (based on wines with scores above 92 points as defined by James Halliday[171] and *Wine Spectator*) shows that many winemakers are choosing "natural" (i.e., wild or spontaneous) fermentations with indigenous yeasts (dominated initially by non-*Saccharomyces* yeast)[172] as a vehicle to incorporate more complexity and uniqueness into their wines. Wines from "natural" fermentations are not always scored better than inoculated wines, despite often possessing a higher aromatic intensity. This is because the use of non-*Saccharomyces* yeasts produces higher intensities of both positive and negative aromas, so scoring of the wine will depend on the balance between these compounds and the preference of the wine judge or consumer.[173]

Medina et al.[59] found that the use of commercial yeasts together with highly standardized procedures results in wines with uniform characteristics. Richter et al.[158] studied and characterized the metabolic footprint of 69 commercial yeast strains in Chardonnay wines. Despite the large number of strains studied, only four clusters, and therefore four wine aroma profiles, were identified through hierarchical clustering of their metabolites. Each cluster was identified by its particular ratio of acetate to ethyl esters, primarily due to a fluctuation in acetates. Each type of ester arises from discrete sets of precursors and enzymes, highlighting phenotypic differences among the clusters as a result of potential genetic variations. The final concentrations of esters in the wine depend on the maximum level attained during alcoholic fermentation, and the rate of formation, volatilization, and hydrolysis thereafter.[149] Esters are formed at different rates during fermentation, in particular, hexyl acetate and ethyl hexanoate, which derive from the modification of C_6 compounds by yeast. The earlier onset of production of these esters was suggested to depend on yeast cell growth, which relates to both the yeast strain and the medium conditions;[174] concentrations of hexyl acetate and ethyl hexanoate dropped significantly as fermentation progressed and ester degradation or volatilization overcame formation.[149]

New yeasts are still being selected and/or developed to provide winemakers with greater options to introduce complexity and increase diversity in aroma profiles. Strategies for the development of new strains include hybridization, mutagenesis, directed evolution, and genetic modification techniques such as the overexpression and introgression of genes related to the formation of specific aroma molecules or specific metabolic pathways.[169,175] Although genetically modified organisms are not currently permitted for use in the majority of wine-producing countries, and are anyhow met with high reticence by the public, they do constitute a very useful research tool. Gene deletions allow for metabolic pathways involved in the formation of key metabolites to be identified and comprehended, as has been the case in the elucidation of the mechanisms leading to the formation of polyfunctional thiols.[176] Even under the most favorable conditions (optimum fermentation temperature, extended skin maceration[177,178]), commercial yeast strains are able to release only 10% of all polyfunctional thiol precursors available. In response to this limitation, both Swiegers et al.[179] and Holt et al.[180] have developed yeast strains capable of releasing higher amounts of polyfunctional thiols due to enhanced carbon−sulfur (CS) lyase activity, through the insertion of the *Escherichia coli tna*A gene and by overexpressing the yeast gene *STR3*, respectively, in the commercial yeast VIN13 (considered to impart a high yield of thiols). Swiegers et al.[179] achieved a strain capable of releasing up to 25 times more 4-MSP and 3-SH than the original VIN13 strain, and Holt et al.[180] were able to confirm the CS β-lyase role of *STR3* gene product as well as design a yeast strain capable of releasing close to 10 times as much 3-SH as the original strain. Unfortunately, neither of these strains can be commercially applied.

Saberi et al.[63] isolated and studied two unique Burgundian strains individually and in cofermentations using Chardonnay juice, showing they were similar to each other and generally produced intermediate levels of higher alcohols, and ethyl and acetate esters, compared to the six commercial strains, which were more disparate to one another. The sensory profiles of the wines were estimated from descriptors and OAVs, showing the Burgundian strains produced higher alcohols (in particular, 1-butanol, 1-hexanol, and isobutanol) with OAVs of much less than 1 (minimizing fusel characters) and ethyl esters, responsible for pleasant "fruity" aromas, above their perception threshold (OAV > 1). Fermentations with mixed Burgundian strains tended to produce greater diversity in their profile of

volatile compounds, indicating some form of metabolic interaction.

Likewise, Orlic et al.[60] isolated seven indigenous strains of *Saccharomyces paradoxus* from the Zagreb region in Croatia. These strains have the capacity to produce higher levels of glycerol than *S. cerevisiae* and lower total amounts of higher alcohols. When used to ferment Chardonnay juice, *S. paradoxus* produced wines of similar or better organoleptic quality than those in which *S. cerevisiae* was used, with higher concentrations of 1-propanol and 1-hexanol and lower concentrations of isobutanol, capric acid, and ethyl acetate. However, they also produced lower amounts of 3-methylbutyl acetate and total volatile esters. Cell−cell communication and modification of gene expression through quorum sensing have been raised previously and may explain this phenomenon.[172] The results of Miller et al.[149] showed that no one yeast strain possesses a higher rate of accumulation for all of the desirable esters, so a choice has to be made according to the compounds that are to be maximized. Fermentations with mixed yeast populations therefore provide a potential means to better achieve the desired aroma outcome.

Unlike inoculated fermentations in which a single *S. cerevisiae* strain dominates throughout the whole process, spontaneous fermentations resemble more a relay course where different species and strains of yeast succeed one another as alcohol content increases and nutrients become scarcer. Sequential inoculations with chosen strains seek to imitate this progression while affording the winemaker more control over the process than in spontaneous fermentations; however, these schemes rarely incorporate more than two different yeasts. Medina et al.[59] used the apiculate yeast *Hanseniaspora vineae* (as a starter culture) together with *S. cerevisiae* to barrel ferment Chardonnay; this approach produced wines with more intense "fruity" characters and flavors than the wines fermented with only *S. cerevisiae*. Similarly, Soden et al.[181] produced Chardonnay wines with more intense desirable attributes such as "floral", "honey", and "apricot" when including *Candida stellata*. However, in both cases the concentration of ethyl acetate in the wine resulting from the sequential inoculation was almost double that of the control fermented with only *S. cerevisiae*, at levels above the perception threshold of this compound. When above its perception threshold, ethyl acetate possess a "solvent"/"varnish" aroma that is considered a fault and decreases wine quality. Contreras et al.[182] proved that sequential inoculation of Chardonnay musts with *Metschnikowia pulcherrima* and *S. cerevisiae* produced wines with lower ethanol contents as well as higher contents of esters (particularly the "pear" and "banana" smelling 2- and 3-methylbutyl acetate; see Table 3). Sequential inoculation with *M. pulcherrima* increased the concentration of higher alcohols, however, although these remained below their perception threshold, and augmented ethyl acetate 6.5-fold to a level above its perception threshold, at which it is negative to overall wine quality. As observed above, sequential inoculations can be used for a number of purposes, be it to incorporate more aroma complexity into the wine or to produce a wine with a certain desired characteristic, such as reduced ethanol content.

Unlike *S. cerevisiae*, where strains have been isolated, selected, and industrialized to minimize the production of off-odors and negative secondary products such as higher alcohols, acetic acid, and ethyl acetate, while ensuring the consumption of all fermentable sugars, similar work is still being undertaken for alternative yeasts. When using yeasts other than *S. cerevisiae*, a compromise is usually made by the winemaker in favor of the desired characteristic (e.g., trade-off with suboptimal fermentation performance). Parameters such as the optimum ratio between yeast strains and the ideal moment of inoculation with *S. cerevisiae*, depending on the desired style, have yet to be determined, and any possible synergistic effects among the different yeast species requires study. Ciani et al.[183] stated that using more than one yeast species may have unpredictable results, such as unexpected compounds or anomalous levels of components that can alter the final aroma of the wine; all of which must be tested before they can be commonly applied industrially.

White wine fermentations are typically conducted at cool temperatures (i.e., 10−18 °C), and bisulfite is a common winemaking additive used to eliminate indigenous yeasts on grapes prior to inoculation with *S. cerevisiae*. Fermentation temperature and sulfite addition are crucial when indigenous yeasts are used, however, as they are more sensitive to higher temperatures and the presence of sulfite than *S. cerevisiae*. At 21 °C, *S. cerevisiae* is 10 times more viable than any indigenous yeast, whereas an addition of 50 mg SO_2/L (as bisulfite) reduces any non-*Saccharomyces* population by a factor of 10.[173] Furthermore, for inoculated fermentations, ester formation will be affected by the level of inoculum and the sugar content (total soluble solids, TSS) of the must. When lower TSS are present, yeast should be inoculated at a higher level to maximize the ester formation potential. Due to a higher cell count and maximum percentage of viable cells, a high level of inoculation doubles the amount of esters produced in a low TSS situation compared to a low level of inoculation; however, this means that no differences can be detected from a per cell point of view. When TSS is higher and carbon energy sources sufficient, higher inoculation levels do not produce any significant effects on ester production.[127]

Despite the interesting aroma characteristics that may be obtained from using autochthonous yeasts, widespread preference for commercial options can be easily explained by the certainty they give the winemaker for the strain being inoculated and the favorable characteristics they will impart to the wine. Indigenous microflora can include a number of yeasts that produce undesired characteristics (i.e., elevated quantities of acetic acid and ethyl acetate, haziness, off-odors, etc.), that can induce wine spoilage such as *Kloeckera apiculata*, *Metschnikowia pulcherrima*, and *Brettanomyces* spp. For example, *Zygosaccharomyces bailli* produces elevated quantities of acetoin and *Saccharomyces prostoserdovii*, *Saccharomyces bayanus*, and *Zygosaccharomyces fermentati* generate flor-like films under aerobic conditions.[184]

Good hygiene and sound enological practices together with inoculation with selected commercial yeasts have basically eradicated problems with any of the aforementioned yeasts. However, given their resistance to high alcohol and SO_2 levels and low sugar content, *Brettanomyces* spp. pervade all winemaking regions. Contamination with *Brettanomyces* spp. results in higher concentrations of volatile phenols and isobutyric, isovaleric, and 2-methylbutyric acids (sweaty and cheesy aromas). Volatile phenols possess "smoky", "barnyard", "horse sweat", and "spicy" odors and arise from the decarboxylation of hydroxycinnamic acids into vinylphenols, which are then reduced into their corresponding ethylphenols.[47,184] Some strains such as *Brettanomyces intermedius* and *Brettanomyces lambicus* also have the ability to produce "mousy"-smelling 2-acetyltetrahydropyridine/pyrroline from

amino acid precursors;[185] others may produce high amounts of octanoic and decanoic acids (also known as "toxic fatty acids") that inhibit *S. cerevisiae* metabolism when present at the start of alcoholic fermentation.[184]

Bacterial Influences. Malolactic fermentation (MLF) of Chardonnay wines is a common practice in regions such as Burgundy and contributes the typical "buttery", "hazelnut", and "fresh bread" notes (and diminishes the intensity of "fresh" varietal odors such as "apple" and "grapefruit−orange")[186] associated with this variety from lactic acid bacteria (LAB) metabolites, particularly diacetyl and acetoin (Table 3). The contributions from MLF can differ due to grape variety[186] and, to some extent, the relative amounts of diacetyl and acetoin also relate to variety (thus, wine composition), with work by Flamini et al.[187] showing Chardonnay had a higher acetoin/diacetyl ratio than Cabernet Sauvignon. The desirability of this process depends on the style of wine being produced; winemakers have the choice of completely suppressing MLF, allowing it to occur only partially or on a portion of the wine, letting it take place naturally or encouraging it by adding LAB in the form of strains of *Oenococcus oeni*. In addition to deacidifying and helping stabilize wine by transforming malic acid into lactic acid, LAB also possess enzymatic activity, which further modifies wine aroma during MLF.[188] Grimaldi et al.,[189] D'Incecco et al.,[190] and Hernandez-Orte et al.[191] have confirmed the existence of glycosidase activity in *O. oeni* and its ability to release terpenes, C_{13}-norisoprenoids, and other glycoconjugates in model wine, even when MLF does not take place. This means that LAB not only contribute to the aroma of a wine through the production of diacetyl and acetoin but can also increase the amount of desirable compounds that are related to its typicity.[189]

As with yeast, development of indigenous bacteria can also have detrimental effects on the quality of the wine if production is not properly monitored and hygiene is not strictly observed. Several factors contribute to the spoilage of wines by bacteria such as high wine pH, elevated storage temperatures, insufficient SO_2, duration of MLF, strain of LAB present, and presence of residual sugar or O_2 during storage and aging.[184,192] Certain LAB, in particular *Pediococci* and *O. oeni*, possess enzymes that can decarboxylate amino acids into biogenic amines in wines with a high pH; these enzymes remain active even after the bacteria die.[193,194] These two strains are also responsible for the occurrence of "ropiness", in which high amounts of mucilaginous exopolysaccharides such as β-1,3-glucans are produced, conferring to the wine an oily appearance and a viscous texture, albeit no anomalous tastes or smells.[184,192] *Lactobacillus brevis* and *O. oeni* can cause what is known as "Tourne" disorder by fermenting tartaric acid into oxaloacetic acid, and subsequently succinic acid, or acetic acid and CO_2, causing a rise in pH, off-odors ("sauerkraut" and "mousy"), and a flat taste.[184] "Mousy" odors can also appear when 2-acetyltetrahydropyridine, 2-acetyl-1-pyrroline, and 2-ethyltetrahydropyridine are metabolized from ornithine and lysine.[195,196]

Of the eight known acetic acid bacteria (AAB) species, only *Acetobacter* sp. and *Gluconobacter* sp. are commonly found in grapes and wines.[184] These bacteria oxidize glucose and ethanol into acetic acid, acetaldehyde, and ethyl acetate.[192] Spoilage of musts occurs during pressing, when grapes are moldy and exhibit high levels of AAB.[184] Wines exposed to oxygen during aging (under *ullage* or with insufficient SO_2) are also susceptible to the development of AAB.

Contributions from Oak, Aging, and Lees. Chardonnay allows winemakers more stylistic choices than any other white wine variety; depending on the desired style, wines can be aged in oak and stored after bottling for long periods of time. Storage encompasses a number of variables (temperature, time, storage vessel, exposure to light, and closure) of which time and temperature are the most important ones,[74] because these promote and accelerate determinate chemical reactions among the different volatile and nonvolatile molecules in the wine. Unlike most other white wine varieties that are not aged, Chardonnay wines commonly spend a period of time, which may vary between several weeks and a year, in oak barrels. During barrel aging, furfural, 5-methylfurfural, furfuryl alcohol, guaiacol, 4-methylguaiacol, 4-propylguaiacol, eugenol, syringol, and oak lactone (both isomers) are extracted into wine from barrels (Table 4); the contents of 2-phenylethanol, 4-vinylguaiacol, and diethyl succinate also increase.[197]

Freshly cut oak does not contain the compounds that are desired in barrels and has too high a percentage of water; therefore, it must be seasoned and toasted before it can come into contact with wine.[198] Seasoning allows the wood to dry and prevents any shrinkage once the barrel has been formed. Compounds such as oak lactone and eugenol are formed during seasoning, and their concentration will depend on the wood's origin and where and for how long the wood is dried.[199,200] Furan aldehydes (furfural, 5-methylfurfural), vanillin, guaiacol, eugenol, and 4-methylguaiacol are degradation products formed by heat during wood cooperage from cellulose, hemicellulose, and lignin.[199] All of these oak compounds are responsible for the "smoky" and "spicy" aromas associated with barrel-aged Chardonnay wines.[140] Moio et al.[138] determined that guaiacol, derived from contact with oak, is one of Chardonnay's main impact odorants, denoting the relevance if this treatment for the typicity of certain styles of wine for this grape variety.

The amount of volatiles extracted from oak will vary according to the pH and ethanol content of the wine, as well as the barrel lot, its origin, and the number of years in use.[140] Although new French oak possesses on average 2−4 times more total volatile phenols than American oak, these compounds are formed during toasting and will depend on the degree of toasting rather than the origin of the wood. Certain compounds such as syringol, eugenol, and 4-methylguaiacol can decrease drastically between new and 2-year-old barrels to the point where no eugenol or 4-methylguaiacol may be found in wines aged in second-use barrels. Oak lactones are mainly formed from (3*S*,4*S*)-3-methyl-4-*O*-(6′-*O*-galloyl)-β-D-glucopyranosyloctanoic acid (galloylglucoside) and (3*S*,4*S*)-*cis*- and (3*S*,4*R*)-*trans*-3-methyl-4-*O*-β-D-glucopyranosyloctanoic acid during toasting and wine aging.[201] Oak lactones seem to be the exception to the general trend observed for most oak-derived compounds in wines, as the concentration of both isomers increased after 1 year of barrel use, with a more pronounced augmentation of the *cis*- rather than the *trans*-isomer. The ratio at which the *cis*- and *trans*-isomers are present will primarily depend on the origin of the wood, although seasoning can also play a role.[199] Among the oak lactones, the *cis*-isomer is more relevant to wine aroma and represents 57−90% of all oak lactones present,[202] and as highlighted by Maga,[203] only one enantiomer of each isomer can be found naturally in oak, that is, (4*S*,5*S*)-*cis*- and (4*S*,5*R*)-*trans*-oak lactones. *cis*-Oak lactone has been correlated with the intensity of "coconut" aroma in Chardonnay wine;[204] it is usually extracted at concentrations above its perception

Table 6. Concentration (Micrograms per Liter) and Standard Deviation (in Parentheses) of Odorants Relevant to Chardonnay Wine Typicity (Young, Bottle-Stored, and under Accelerated Aging Conditions)[a]

compound	young wine			stored wine (1 year; 18 °C)			accelerated aging		
hexyl acetate	72.7	(23)	a	5.6	(0.6)	b	14.1	(0.06)	c
ethyl butyrate	87.1	(7.9)		103	(11)		92.7	(1.7)	
ethyl hexanoate	674	(27)		871	(82)		830	(3.8)	
ethyl octanoate	1247	(199)		763	(48)		864	(2.7)	
ethyl decanoate	479	(35)	a	96.7	(16)	b	36.3	(1)	c
ethyl 4-oxopentanoate			a	4.52	(0.3)	b	3.40	(0.13)	a
ethyl dodecanoate	605	(47)	a	123	(10)	b	125	(14)	b
diethyl succinate	828	(47)	a	8930	(846)	b	4331	(135)	c
2-phenylethyl acetate	446	(117)	a	27.5	(9.1)	b	6.24	(3.4)	c
2-methyl-1-propanol	155	(11)	a	205	(38)	ab	286	(8.2)	b
1-butanol	15.2	(2.1)		18.4	(3.1)		22	(2.3)	
3-methyl-3-buten-1-ol	0.74	(0.2)							
1-hexanol	268	(88)		401	(98)		299	(0.9)	
(*E*)-3-hexen-1-ol	13.6	(2.7)		13.1	(4.7)		18.1	(0.4)	
(*Z*)-2-hexen-1-ol	1.56	(0.6)	a			a	4.13	(0.4)	b
linalool	5.93	(1.2)		3.35	(0.96)		2.16	(0.3)	
citronellol	4.33	(0.3)	a			b			b
geranic acid	67.1	(9.9)	a			b			b
benzaldehyde	11.5	(2.7)		4.91	(0.92)		12.9	(1.7)	
benzyl alcohol	112	(13)	a	169	(20)	b	108	(2.1)	ab
phenylethyl alcohol	5353	(13)	a	7876	(715)	b	6136	(250)	c
benzofuran			a	8.55	(1.34)	b	9.71	(0.25)	b
4-vinylguaiacol	126	(15)	a	226	(20)	b	212	(10)	b
γ-butyrolactone	19.9	(0.7)	a	18.3	(3)	a	0.06	(0.01)	b
γ-caprolactone			a	13.1	(1.49)	b	9.09	(0.42)	b
δ-decalactone	21	(2.8)	a	15.5	(2)	a	4.94	(1.2)	b
γ-undecalactone	226	(30)	a	436	(31)	b	552	(1.9)	b
furfural	5.52	(0.1)	a	69.2	(13)	b	92.8	(1.8)	b
5-methylfurfural			a	13.4	(1.8)	b	13.9	(3.0)	b
hexanoic acid	694	(8.1)	a	1019	(66)	b	827	(25)	c
octanoic acid	2545	(6.2)		2635	(7.8)		2718	(8.7)	
decanoic acid	558	(1.4)	a	381	(32)	b	400	(8.9)	b
dodecanoic acid	148	(0.7)	a	41.5	(13)	b	65.6	(2.4)	b
β-damascenone	13	(3.7)	a	14.4	(2.9)	a	45	(3.6)	b
3-oxo-α-ionol	154	(27)	a			b	99.5	(0.2)	a
3-hydroxy-β-damascenone	28.1	(5.4)	a			b	9.68	(0.28)	c
TDN			a	6.15	(0.86)	b	16.5	(0.8)	c

[a]Data from Cejudo-Bastante et al.[74] Where present, different letters across a row indicate significant differences ($p < 0.05$).

threshold (24 μg/L in white wine[102]) and at a low concentration is responsible for the "oaky" and "vanilla" aromas and of "coconut" notes when its concentration increases. The *trans*-isomer possesses a higher detection threshold of 172 μg/L (in white wine) and even when present at high levels does not seem to have an important influence on the overall aroma of the wine.[102,140,205]

As can be observed in Figure 1, Chardonnay wines can either have "smoky", "caramel", and "butter" attributes characteristic of a wine aged in oak or a more "fruity/crisp" character, dominated by "green apple" and "tropical fruit" notes. The Spearman rank-order correlation matrix by Spillman et al.[49] appears to support this claim. From the ranking of attributes the "green apple" attribute appears as very negatively correlated to guaiacol, 4-ethylguaiacol, furfural + furfuryl alcohol, and maltol and less significantly negatively correlated to 4-methylguaiacol, 5-methylfurfural, and furfuryl alcohol. "Green apple" was found to be highest in the control wine that had no contact with oak and exhibited a particularly significant negative correlation to "smoky"; the degree to which the "green apple" attribute was suppressed depended directly on the level of toasting of the barrel.

It is worth mentioning that oak barrel alternatives[45,206−208] (i.e., powders, chips, staves, plastic tanks lined with new or reclaimed oak staves) and different woods[209,210] (e.g., chestnut, beech, pine, cherry) have received attention from researchers. Although not specific to Chardonnay alone, as a whole, the use of oak barrel alternatives in particular offers an economical means of incorporating some of the desirable aroma compounds from oak without the time or expense associated with storing wine in oak barrels. The main factors to be considered when employing oak alternatives are the amount and surface area (shape and size) of the materials used. Chip-treated and barrel-aged wines differ in their contents of a range of volatiles, including vanillin, guaiacol, and furfural,[211] which translates accordingly into different aromas and flavors such as more pronounced "coconut" and "vanilla" together with more bitterness and astringency in white wines treated with chips.[45,212] Use of chips may also decrease the amount of perceived "fresh" and "unripe fruit" aromas and increase the

overall concentration of esters and wood-related compounds as well as the intensity of "oak" aromas in the treated wine.[213] In general, relative to unoaked wines, the use of oak chips improved the liking of wines by the assessors in a number of studies,[45,211,213] which makes it a useful and cost-effective technique for incorporation of oak into certain Chardonnay wines.

Unlike oak, glass is inert, and once a wine is bottled, it is deemed ready to be consumed. Nonetheless, bottle-aging encompasses a different set of changes from those taking place when wine is stored in barrels. For instance, from studies performed on Champagne wines, it is known that the concentration of FFT increases proportionally to the time spent in the bottle, whereas BM reaches a peak at 13−15 years, after which its concentration falls.[126] With regard to other aging phenomena, esters are particularly affected due to their acid−ester equilibria;[214,215] for a wine that had spent 1 year stored in a bottle at 18 °C, Cejudo-Bastante et al.[74] found a significant decrease in the concentration of acetates and certain short-chain fatty acid ethyl esters (C_8−C_{12}) responsible for "fruity" aromas of Chardonnay wines. As evidenced by those results (Table 6), time (storage period) and temperature (accelerated aging) introduced several of these changes in the aromatic profile of Chardonnay wines. Modifications included a decrease in acetates and short-chain fatty acid ethyl esters of octanoic, decanoic, and dodecanoic acid, and the disappearance of 3-methyl-3-buten-1-ol, citronellol, geranic acid, (*Z*)-2-hexen-1-ol, 3-hydroxy-*β*-damascenone, and 3-oxo-*α*-ionol (for the latter three the disappearance was true only in the case of storage time), thereby changing the aromatic profile of the wine. Storage time and accelerated aging induced the appearance of benzofuran, ethyl 4-oxopentanoate, 4-hydroxyhexanoic acid lactone (i.e., *γ*-caprolactone), 5-methyl-2-furancarboxaldehyde (i.e., 5-methylfurfural), and TDN. These compounds are responsible for some of the tertiary aromas of wine, and therefore wines containing high quantities of these volatiles are referred to as more "evolved".

Aging can take place in the presence or absence of yeast lees (autolyzed yeast cells). Aging on lees (often in barrel, but also in tank or bottle as is the case for Champagne) improves the organoleptic score of wines (including overall quality, persistence, color, and taste, as well as aroma) and attenuates the impact of wood on the wine's aroma.[106] During yeast autolysis, polysaccharides (mainly mannoproteins), amino acids, assimilable nitrogen, and other cell contents are released into the wine.[216,217] The presence of lees contributes to the formation of "floral" and "fruity" scented ketones and lactones and to an increase in monoterpenoid concentrations due to the release of *β*-glucosidase enzymes acting on precursors.[106] However, this technique also results in wines with a lower global ester content as yeast autolysis releases esterases, which hydrolyze some of the esters present, into the medium.

During aging, lees both adsorb positive compounds such as esters and glycosylated compounds and strip the wine of off-odors such as volatile phenols and malodorous sulfur compounds (e.g., methanethiol and ethanethiol; however, hydrogen sulfide, dimethyl sulfide, and thiophene were not absorbed).[218,219] In general, aging on lees creates a highly reductive environment that both protects the wine from oxidation and increases the possibility that these negative sulfur volatiles will be formed. This latter effect can be countered by frequent stirring to resuspend lees and create a limited oxidation, as well as by performing an early racking of the gross lees before any reduction odors appear. With time, lees do lose their ability to generate foul-smelling sulfur volatiles as sulfitoreductase activity progressively subsides.[220] Furthermore, both adsorption and hydrolysis reactions are enhanced when lees are stirred.[152,217] When volatile compounds are present at low concentrations, mannoproteins have been observed to enhance the perceived intensity of a number of aroma attributes in Chardonnay wines.[216] However, this effect on overall aroma and individual aroma attributes is not discernible when volatile compound concentrations are high.[106]

The presence of lees also affects the absorption of wood volatiles. Towey and Waterhouse[197] showed that during the last 60 days of a 150 day aging trial, the adsorption on lees of oak volatiles exceeded that of extraction by the wine. This implies that aging on lees decreased the overall oak volatile content in wine, which can be either positive or negative depending on the style of wine sought, the degree of toasting, and the age of the barrel.

Terroir: Regional and Environmental Effects. Terroir has been proven to be an important element in wine aroma profiles. Enological variables aside, each wine-producing region will impart certain aromatic characteristics to the wines produced through the unique combination of weather, soil composition, latitude, longitude, altitude, and viticulture practices.

Fruit set, ripening, and the accumulation and concentration of aroma precursors and free compounds in the berry are affected by environmental and agronomic practices such as canopy management, fertilization, and yield.[26,221−224] Berry development is very susceptible to changes in solar radiation, temperature, rainfall, irrigation, soil composition, and altitude.[225] In particular, sunlight seems to have the most impact on monoterpenoid and C_{13}-norisoprenoid concentrations among all cited parameters; an increase in sun exposure increases the amount of glycosidic aroma precursors present.[116,226] As mentioned previously, C_{13}-norisoprenoids arise from the enzymatic breakdown of carotenoids; if the berry receives a higher amount of sun exposure before veraison, the concentration of carotenoids will increase. If exposure to sunlight is higher after veraison, it will generally accelerate carotenoid breakdown and induce an increase in the amount of glycosylated C_{13}-norisoprenoids present.[227,228] Likewise, higher sunlight exposure increases monoterpenoid concentrations, with this effect being more pronounced in cooler years.[229] It must be noted, however, that the opposite seems to be true for the ubiquitous C_{13}-norisoprenoid *β*-damascenone, at least in the case of Cabernet Sauvignon. As Lee et al.[228] observed, concentrations of *β*-damascenone were highest and those of TDN, lowest, at lower sunlight exposure and temperature.

Arrhenius et al.[37] showed that within wines of a higher quality, sensory attributes were significantly correlated to the wine's origin. In turn, they found that aroma attributes were correlated only to secondary volatiles, such as 3-methylbutyl acetate with the term "green-apples/pears", TDN with "honey", and ethyl 2-hydroxypropanoate with "buttery". In fact, high-quality Chardonnay wines from the Carneros and Napa regions in California could be discriminated from other California wines on the basis of the concentration of 3-methylbutyl acetate, the level of which is unique to each of these regions. Environmental factors could be responsible for differentiating the regions; for example, the Carneros region has a different photoperiod from the Central Coast of California that may affect the rate of formation and accumulation of certain

compounds. This region could further be differentiated from the rest because of higher linalool content.[37] Williams et al.[230] and Marais et al.[231] observed that certain degradation products of carotenoids can be used as geographic markers for Chardonnay wines, because their concentrations vary depending on the temperature of the region; this is likely to be true of Australian Chardonnays, which seem to possess a distinct concentration of C_{13}-norisoprenoids that yield characteristic sensory attributes.[111,230]

Changes in environmental conditions between different vintages also affect the volatile composition of wines from a single vineyard (i.e., vintage effect). Louw et al.[67] showed that, with the exception of 2-phenylethanol, acetic acid, ethyl hexanoate, hexanoic acid, 3-methyl-1-butanol, and propanol, the level of 20 of 26 volatiles varied significantly during three consecutive South African vintages. That is, changes to fatty acids and their ethyl esters, along with higher alcohols and their acetates, were deemed to be caused by vintage effects. These compounds are associated with the volatiles derived from fermentation, implying an underlying change in grape composition (e.g., differences in amino acids and other nutrients) that was materialized upon fermentation.

Depending on intensity and timing, water deficit induces a reduction in Chardonnay wine quality, generating wines with high pH and low acidity and prone to atypical aging (i.e., wines with a lower intensity of varietal aromas and evident faults reminiscent of "acacia blossom", "furniture polish", "medicinal", and "naphthalene").[232,233] Atypical aging can be caused by suprathreshold levels of 2-aminocetophenone and other compounds such as sotolon that remain to be conclusively identified.[233−235] Research conducted by Reynolds et al.[236] showed that Chardonnay wines made from vines irrigated for different lengths of the season possessed higher intensities of "apple" and "citrus" compared to the nonirrigated controls and lower "earthy" aromas in three of four cases; however, consistent with the controls, wines showed greater atypical aging potential when the vines were subjected to irrigation up until lag phase or veraison. From their results, water stress could have interfered with the ability of grape berries to synthesize and accumulate monoterpenoids and ester precursors and may have promoted accumulation of compounds responsible for the atypical age character depending on the timing of water stress.

The characteristics of the soil where vines are planted is another environmental variable to consider when effects on wine composition are evaluated.[237] Soil properties can influence the depth that roots can penetrate, the availability of micronutrients, the retention of water, and therefore the level of hydric stress the plant is subjected to. All of these variables can affect the overall aroma of the subsequent wines. As Reynolds et al.[238] demonstrated, vineyards with high clay textures tended to yield Chardonnay wines with "vegetal", "earthy", and "citrus" characteristics, whereas wines made from grapes grown in sandy soils had "floral" and "melon" aromas. Although this study provides some guidance, at times there was a relationship between vine size and soil texture, and it was possible that vines in high-clay zones experienced some level of water stress. However, the results highlight the need to consider the impacts of the multiple facets of terroir on wine quality.

Weather can be partly countered through different agricultural techniques such as leaf removal and crop thinning. Leaf removal is particularly recommended in cold and cool climates to decrease the presence of "green" and "unripe" sensory attributes in the wine.[239] Under these conditions, leaf removal has been shown to increase the positive "floral" and "fruity" attributes. The effect of this treatment depends on when in the berry development cycle it is practiced; when applied during fruit set and veraison, the results are similar.[239] In areas with a high luminosity and potential for sunburn, a shaded bunch zone is preferable because a combination of high light intensity and temperature of the berry surface between 40 and 43 °C for only 5 min is enough to cause sunburn of mature Chardonnay berries. Sunburn damages the skin of the berry, decreasing quality and increasing concentrations of total phenolics, hydroxycinnamates, flavonoids, and tannins,[240−242] whereas under high light intensity and temperature conditions, shading can lead to crisper and more elegant wines that have more "citrus", "apple", and "quince" aromas.[16,224]

FUTURE DIRECTIONS

Given the popularity of Chardonnay wines and the global economic relevance of this variety, producers are always striving to produce better wines that cater to the current market trends. Understandably then, much work has been done to comprehend the volatile compounds present and the impact of each production step on the final aroma of Chardonnay wines. Over the years, quality has improved such that, for consumers, finding a good-quality wine is now extremely easy, but at the same time a certain homogeneity of flavor has appeared in the market, with two dominant styles arguably being responsible for most Chardonnays available in the market. In an industry where brand recognition goes only so far, uniqueness of the product is necessary. Determining whether this uniqueness is achieved at the vineyard level or via increased extraction of grape aroma compounds or through the use of different winemaking techniques requires more emphasis and understanding of the terroir dimension as well as a search for originality through the use of different yeast strains while preserving the typicity of Chardonnay.

Despite the definite existence of a typicity concept for Chardonnay, this has only started to be comprehended and requires deeper studies as this is a variety that can express itself in a multitude of profiles; Chardonnay is not as straightforward as other varieties (i.e., Sauvignon blanc or Muscats), which are dominated by distinct varietal compounds. Tackling its typicity requires multidisciplinary studies that analyze a number of variables responsible for the final product, rather than a one-directional focus.

Excellent advances in compositional knowledge have been detailed above, yet studies need to be carried out to confirm whether vintage-related changes between fatty acids and higher alcohols and their corresponding esters also occur in Chardonnay produced in different parts of the world and whether a trend can be determined. A better comprehension of the fate of aroma compound precursors extracted from the grapes is still required, as is the combined effect of the many components of terroir and how the most important ones are best manipulated and controlled. More work is therefore needed to correlate viticulture management with aroma/sensory profiles of the wines. In addition, very little is known of the potential of currently available Chardonnay clones, their interrelation with rootstocks, and any new clones that might be in development as related to other parameters such as yield, salt and drought tolerance, and vigor. Climate change will demand transformation and adaptation to new weather conditions with new choices that preserve the current quality standards.

Due to health concerns and taxation implications, as well as in response to the augmentation of alcoholic strength due to global warming and opting for riper fruit, low-alcohol wines and dealcoholization techniques have become a prime concern for the industry. Viable and cost-effective techniques that yield palatable and high-quality wines need to be formulated and tested on Chardonnay to determine the best alternative for producers. In a similar way, higher rates of individuals being susceptible to SO_2 and other industry additives, as well as dietary restrictions, pose new challenges for the wine industry, which will require the help of researchers to be solved.

AUTHOR INFORMATION

Corresponding Author

*(D.W.J.) Phone: +61 8 8313 6649. Fax: +61 8 8313 7116. E-mail: david.jeffery@adelaide.edu.au.

Funding

J.M.G. acknowledges financial support provided by the Turner Family Scholarship from the University of Adelaide and by the Grape and Wine Research and Development Corporation. S.E.P.B, D.C., and D.W.J. acknowledge financial support from the School of Agriculture, Food and Wine, University of Adelaide.

Notes

The authors declare no competing financial interest.

ABBREVIATIONS USED

T, tonnes; ha, hectares; TDN, 1,1,6-trimethyl-1,2-dihydronaphthalene; GC, gas chromatography; GC-O, gas chromatography−olfactometry; TOF, time-of-flight; OAV, odor activity value; LLE, liquid−liquid extraction; SPE, solid phase extraction; NCI, negative chemical ionization; FID, flame ionization detector; HR, high resolution; SIDA, stable isotope dilution analysis; 3-SH, 3-sulfanylhexan-1-ol; 3-SHA, 3-sulfanylhexyl acetate; 4-MSP, 4-methyl-4-sulfanylpropan-2-one; BM, benzenemethanethiol; FFT, 2-furanmethanethiol; YAN, yeast assimilable nitrogen; DAP, diammonium phosphate; TSS, total soluble solids; MLF, malolactic fermentation; LAB, lactic acid bacteria; AAB, acetic acid bacteria

REFERENCES

(1) U.S. Department of Agriculture. National Agricultural Statistics Service Web Site, grape acreage report overview, crop year 2012; http://www.nass.usda.gov/Statistics_by_State/California/Publications/Grape_Acreage/ (accessed March 29, 2014).

(2) U.S. Department of Agriculture. National Agricultural Statistics Service Web Site, White wine type grapes: acreage standing by variety, by year planted, California; http://www.nass.usda.gov/Statistics_by_State/California/Publications/Grape_Acreage/201204gabnarr.pdf (accessed March 29, 2014).

(3) Australian Bureau of Statistics Web Site, Vineyards, Australia, 2011−12; http://www.abs.gov.au/AUSSTATS/abs@.nsf/DetailsPage/1329.0.55.0022011-12?OpenDocument (accessed March 29, 2014).

(4) California Agricultural Statistics Service Web Site, California Chardonnay, Wine fact sheets; http://www.wineinstitute.org/resources/ (accessed March 29, 2014).

(5) Gobierno de Chile, Ministerio de Agricultura, Oficina de Estudios y Políticas Agrarias (ODEPA) Web Sit,. Catastro Vitícola Nacional; http://www.odepa.cl/documentos_informes/catastro-viticola-nacional/ (accessed Feb 6, 2014).

(6) Abele, E. Deutches Weininstitut Web Site, Deutscher wein 2012/2013 statistik; http://www.deutscheweine.de/icc/Internet-DE/nav/d0a/d0a40b54-13f9-0401-be59-267b48205846 (accessed March 29, 2014).

(7) Fresh Logic Web Site, Wine market profile; www.freshlogic.com.au (accessed March 29, 2014).

(8) Whitehead, C.; Uren, N. South African Wine Industry Statistics (SAWIS) Web Site, Statistics of wine-grape vines; http://www.sawis.co.za/info/statistics.php (accessed March 29, 2014).

(9) Díaz-Ambrona, A.; Seoane, P.; Rábade, M. T.; López, J. J., Ministerio de Agricultura, Alimentación y Medio Ambiente, Gobierno de España Web Site, Encuesta base de viñedo 2009; http://www.magrama.gob.es/es/estadistica/temas/estadisticas-agrarias/agricultura/encuestas-de-vinedo/ (accessed March 29, 2014).

(10) France-AgriMer, Etablissment national des produits de l'agriculture et de la mer Web Site, Les chiffres de la filière viti-vinicole, Données statistiques 2001/2011; www.franceagrimer.fr (accessed March 29, 2014).

(11) Instituto Nacional de Vitivinicultura Web Site, Operativo de actualización del Registro Nacional de Viñedos 2010−2011; www.inv.gov.ar (accessed April 22, 2014).

(12) Riaz, S.; Garrison, K. E.; Dangl, G. S. Genetic divergence and chimerism within ancient asexually propagated winegrape cultivars. *J. Am. Soc. Hortic. Sci.* **2002**, *127*, 508−514.

(13) Bowers, J.; Boursiquot, J.-M.; This, P.; Chu, K.; Johansson, H.; Meredith, C. Historical genetics: the parentage of Chardonnay, Gamay, and other wine grapes of northeastern France. *Science* **1999**, *285*, 1562−1565.

(14) Winkler, A. J.; Cook, J. A.; Kliewer, W. M.; Lider, L. A. *General Viticulture*, 2nd ed.; University of California Press: Davis, CA, USA, 1974; p 710.

(15) Coombe, B. G.; Dry, P. R. *Viticulture Vol. 2 − Practices*; Winetitles: Adelaide, Australia, 1992.

(16) Iland, P.; Dry, P.; Proffit, T.; Tyerman, S. *The Grapevine − From the Science to the Practice of Growing Vines for Wine*; Patrick Iland Wine Promotions: Adelaide, Australia, 2011.

(17) Kerridge, G.; Antcliff, A. *Wine Grape Varieties*; CSIRO Publishing: Victoria, Australia, 1999.

(18) Pou, A.; Medrano, H.; Tomàs, M.; Martorell, S.; Ribas-Carbó, M.; Flexas, J. Anisohydric behaviour in grapevines results in better performance under moderate water stress and recovery than isohydric behaviour. *Plant Soil* **2012**, *359*, 335.

(19) San Juan, F.; Cacho, J.; Ferreira, V.; Escudero, A. Aroma chemical composition of red wines from different price categories and its relationship to quality. *J. Agric. Food Chem.* **2012**, *60*, 5045−5056.

(20) Curtin, C. D.; Bellon, J. R.; Bartowsky, E. J. Harnessing AWRI's yeast and bacterial research to shape 'Next-Gen' Chardonnay. Part 1: 'Wild' and 'non-conventional' yeast. *Wine Vitic. J.* **2011**, 15−20.

(21) Saliba, A.; Heymann, H.; Blackman, J.; Macdonald, J. B. Consumer-sensory evaluation of Australian Chardonnay. *Wine Vitic. J.* **2013**, *28*, 64−66.

(22) Lesschaeve, I.; Bowen, A.; Bruwer, J. Determining the impact of consumer characteristics to project sensory preferences in commercial white wines. *Am. J. Enol. Vitic.* **2012**, *63*, 487−493.

(23) Charters, S.; Pettigrew, S. The dimensions of wine quality. *Food Qual. Pref.* **2007**, *18*, 997−1007.

(24) Verdú, A. J.; Lloréns, F.; Fuentes, M. Measuring perceptions of quality in food products: the case of red wine. *Food Qual. Pref.* **2004**, *15*, 453−469.

(25) Ferreira, V.; San Juan, F.; Escudero, A.; Culleré, L.; Fernández-Zurbano, P.; Sáenz-Navajas, M. P.; Cacho, J. Modeling quality of premium Spanish red wines from gas chromatography-olfactometry data. *J. Agric. Food Chem.* **2009**, *57*, 7490−7498.

(26) Jackson, D. I.; Lombard, P. B. Environmental and management practices affecting grape composition and wine quality − a review. *Am. J. Enol. Vitic.* **1993**, *44*, 409−430.

(27) D'Alessandro, S.; Pecotich, A. Evaluation of wine by expert and novice consumers in the presence of variations in quality, brand and country of origin cues. *Food Qual. Pref.* **2013**, *28*, 287−303.

(28) Ferreira, V.; Ortín, N.; Escudero, A.; Lopez, R.; Cacho, J. Chemical characterization of the aroma of grenache rosé wines: aroma

extract dilution analysis, quantitative determination, and sensory reconstitution studies. *J. Agric. Food Chem.* **2002**, *50*, 4048−4054.
(29) Lorrain, B.; Ballester, J.; Thomas-Danguin, T.; Blanquet, J.; Meunier, J. M.; Le Fur, Y. Selection of potential impact odorants and sensory validation of their importance in typical Chardonnay wines. *J. Agric. Food Chem.* **2006**, *54*, 3973−3981.
(30) Ferreira, V.; López, R.; Cacho, J. F. Quantitative determination of the odorants of young red wines from different grape varieties. *J. Sci. Food Agric.* **2000**, *80*, 1659−1667.
(31) Lee, S.; Noble, A. Use of partial least squares regression and multidimensional scaling on aroma models of California Chardonnay wines. *Am. J. Enol. Vitic.* **2006**, *57*, 363−370.
(32) Codresi, C.; Rapeanu, G.; Alexe, P. Effect of β-glucosidases in the making of Chardonnay wines. *Annals of the University "Dunarea de Jos" of Galati − Fascicle VI − Food Technology* **2012**, *36*, 9−17.
(33) Bailly, S.; Jerkovic, V.; Marchand-Brynaert, J.; Collin, S. Aroma extraction dilution analysis of sauternes wines. Key role of polyfunctional thiols. *J. Agric. Food Chem.* **2006**, *54*, 7227−7234.
(34) Baumes, R.; Bayonove, C.; Barillere, J. M.; Samson, A.; Cordonnier, R. La maceration pelliculaire dans la vinification en blanc − incidence sur la composition volatile des vins. *Vitis* **1989**, *28*, 31−48.
(35) Simpson, R. F. 1,1,6-Trimethyl-1,2-dihydronaphthalene: an important contributor to the bottle aged bouquet of wine. *Chem. Ind.* **1978**, 37.
(36) Sacks, G. L.; Gates, M. J.; Ferry, F. X.; Lavin, E. H.; Kurtz, A. J.; Acree, T. E. Sensory threshold of 1,1,6-trimethyl-1,2-dihydronaphthalene (TDN) and concentrations in young Riesling and non-Riesling wines. *J. Agric. Food Chem.* **2012**, *60*, 2998−3004.
(37) Arrhenius, S.; Mccloskey, M.; Sylvan, M. Chemical markers for aroma of *Vitis vinifera* var. Chardonnay regional wines. *J. Agric. Food Chem.* **1996**, *44*, 1085−1090.
(38) Guth, H. Quantitation and sensory studies of character impact odorants of different white wine varieties. *J. Agric. Food Chem.* **1997**, *45*, 3027−3032.
(39) Simpson, R. F.; Miller, G. C. Aroma composition of Chardonnay wine. *Vitis* **1984**, *23*, 143−158.
(40) Lee, S.; Noble, A. Characterization of odor-active compounds in Californian Chardonnay wines using GC-olfactometry and GC-mass spectrometry. *J. Agric. Food Chem.* **2003**, *51*, 8036−8044.
(41) Tominaga, T.; Furrer, A.; Henry, R.; Dubourdieu, D. Identification of new volatile thiols in the aroma of *Vitis vinifera* L. var. Sauvignon blanc wines. *Flavour Fragrance J.* **1998**, *13*, 159−162.
(42) Mateo-Vivaracho, L.; Zapata, J.; Cacho, J.; Ferreira, V. Analysis, occurrence, and potential sensory significance of five polyfunctional mercaptans in white wines. *J. Agric. Food Chem.* **2010**, *58*, 10184−10194.
(43) Tominaga, T.; Darriet, P.; Dubourdieu, D. Identification of 3-mercaptohexyl acetate in Sauvignon wine, a powerful aromatic compound exhibiting box-tree odor. *Vitis* **1996**, *35*, 207−210.
(44) Aznar, M.; López, R.; Cacho, J. F.; Ferreira, V. Identification and quantification of impact odorants of aged red wines from Rioja. GC-olfactometry, quantitative GC-MS, and odor evaluation of HPLC fractions. *J. Agric. Food Chem.* **2001**, *49*, 2924−2929.
(45) Guchu, E.; Díaz-Maroto, M. C.; Pérez-Coello, M. S.; González-Viñas, M. A.; Ibáñez, M. D. C. Volatile composition and sensory characteristics of Chardonnay wines treated with American and Hungarian oak chips. *Food Chem.* **2006**, *99*, 350−359.
(46) Culleré, L.; Escudero, A.; Cacho, J.; Ferreira, V. Gas chromatography-olfactometry and chemical quantitative study of the aroma of six premium quality Spanish aged red wines. *J. Agric. Food Chem.* **2004**, *52*, 1653−1660.
(47) Chatonnet, P.; Dubourdie, D.; Boidron, J.-N.; Pons, M. The origin of ethylphenols in wines. *J. Sci. Food Agric.* **1992**, *60*, 165−178.
(48) Boidron, J.-N.; Chatonnet, P.; Pons, M. Influence du bois sur certaines substances odorantes des vins. *Connaiss. Vigne Vin* **1988**, *22*, 275−293.
(49) Spillman, P. J.; Sefton, M.; Gawel, R. The contribution of volatile compounds derived during oak barrel maturation to the aroma of a Chardonnay and Cabernet Sauvignon wine. *Aust. J. Grape Wine Res.* **2004**, *10*, 227−235.
(50) Smit, A.; Cordero Otero, R. R.; Lambrechts, M. G.; Pretorius, I. S.; Van Rensburg, P. Enhancing volatile phenol concentrations in wine by expressing various phenolic acid decarboxylase genes in *Saccharomyces cerevisiae*. *J. Agric. Food Chem.* **2003**, *51*, 4909−4915.
(51) Chatonnet, P.; Dubourdieu, D.; Boidron, J.-N.; Lavigne, V. Synthesis of volatile phenols by *Saccharomyces cerevisiae* in wines. *J. Sci. Food Agric.* **1993**, *62*, 191−202.
(52) Baumes, R.; Cordonnier, R.; Nitz, S.; Drawert, F. Identification and determination of volatile constituents in wines from different vine cultivars. *J. Sci. Food Agric.* **1986**, *37*, 927−943.
(53) Castro Vázquez, L.; Pérez-Coello, M. S.; Cabezudo, M. D. Effects of enzyme treatment and skin extraction on varietal volatiles in Spanish wines made from Chardonnay, Muscat, Airén, and Macabeo grapes. *Anal. Chim. Acta* **2002**, *458*, 39−44.
(54) López, R.; Aznar, M.; Cacho, J.; Ferreira, V. Determination of minor and trace volatile compounds in wine by solid-phase extraction and gas chromatography with mass spectrometric detection. *J. Chromatogr., A* **2002**, *966*, 167−177.
(55) Jaffré, J.; Valentin, D.; Meunier, J.-M.; Siliani, A.; Bertuccioli, M.; Le Fur, Y. The Chardonnay wine olfactory concept revisited: a stable core of volatile compounds, and fuzzy boundaries. *Food Res. Int.* **2011**, *44*, 456−464.
(56) Ballester, J.; Dacremont, C.; Le Fur, Y.; Etievant, P. The role of olfaction in the elaboration and use of the and use of the Chardonnay wine concept. *Food Qual. Pref.* **2005**, *16*, 351−359.
(57) Saliba, A.; Blackman, J.; Bullock, J.; Schmidtke, L. M. The position of Australian Chardonnay in the world-wide flavour map. *Wine Vitic. J.* **2013**, *28*, 67−70.
(58) Sáenz-Navajas, M. P.; Campo, E.; Sutan, A.; Ballester, J.; Valentin, D. Perception of wine quality according to extrinsic cues: the case of Burgundy wine consumers. *Food Qual. Pref.* **2013**, *27*, 44−53.
(59) Medina, K.; Boido, E.; Fariña, L.; Gioia, O.; Gomez, M. E.; Barquet, M.; Gaggero, C.; Dellacassa, E.; Carrau, F. Increased flavour diversity of Chardonnay wines by spontaneous fermentation and co-fermentation with *Hanseniaspora vineae*. *Food Chem.* **2013**, *141*, 2513−2521.
(60) Orlic, S.; Redzepovic, S.; Jeromel, A.; Herjavec, S.; Iacumin, L. Influence of indigenous *Saccharomyces paradoxus* strains on Chardonnay wine fermentation aroma. *Int. J. Food Sci. Technol.* **2007**, *42*, 95−101.
(61) Francis, I. L.; Sefton, M. A.; Williams, P. J. The sensory effects of prefermentation or postfermentation thermal-processing on Chardonnay and Semillon wines. *Am. J. Enol. Vitic.* **1994**, *45*, 243−251.
(62) Varela, C.; Torrea, D.; Schmidt, S. A.; Ancin-Azpilicueta, C.; Henschke, P. A. Effect of oxygen and lipid supplementation on the volatile composition of chemically defined medium and Chardonnay wine fermented with *Saccharomyces cerevisiae*. *Food Chem.* **2012**, *135*, 2863−2871.
(63) Saberi, S.; Cliff, M. A.; Van Vuuren, H. J. J. Impact of mixed *S. cerevisiae* strains on the production of volatiles and estimated sensory profiles of Chardonnay wines. *Food Res. Int.* **2012**, *48*, 725−735.
(64) Ballester, J.; Mihnea, M.; Peyron, D.; Valentin, D. Exploring minerality of Burgundy Chardonnay wines: a sensory approach with wine experts and trained panellists. *Aust. J. Grape Wine Res.* **2013**, *19*, 140−152.
(65) Welke, J. E.; Zanus, M.; Lazzarotto, M.; Alcaraz, C. Quantitative analysis of headspace volatile compounds using comprehensive two-dimensional gas chromatography and their contribution to the aroma of Chardonnay wine. *Food Res. Int.* **2014**, *59*, 85−99.
(66) Smyth, H. E. *The Compositional Basis of the Aroma of Riesling and Unwooded Chardonnay Wine*. University of Adelaide, 2005.
(67) Louw, L.; Tredoux, A. G. J.; Van Rensburg, P.; Kidd, M.; Naes, T.; Nieuwoudt, H. H. Fermentation-derived aroma compounds in varietal young wines from South Africa. *S. Afr. J. Enol. Vitic.* **2010**, *31*, 213−225.
(68) Rapp, A.; Mandery, H. Wine aroma. *Experientia* **1986**, *42*, 873−884.

(69) Buttery, R. G.; Turnbaugh, J. G.; Ling, L. C. Contribution of volatiles to rice aroma. *J. Agric. Food Chem.* **1988**, *36*, 1006−1009.
(70) González-Marco, A.; Jiménez-Moreno, N.; Ancín-Azpilicueta, C. Concentration of volatile compounds in Chardonnay wine fermented in stainless steel tanks and oak barrels. *Food Chem.* **2008**, *108*, 213−219.
(71) Peinado, R.; Moreno, J.; Bueno, J.; Moreno, J.; Mauricio, J. Comparative study of aromatic compounds in two young white wines subjected to pre-fermentative cryomaceration. *Food Chem.* **2004**, *84*, 585−590.
(72) Ferreira, V.; López, R.; Escudero, A.; Cacho, J. F. The aroma of Grenache red wine: hierarchy and nature of its main odorants. *J. Sci. Food Agric.* **1998**, *77*, 259−267.
(73) Gómez-Míguez, M. J.; Cacho, J. F.; Ferreira, V.; Vicario, I. M.; Heredia, F. J. Volatile components of Zalema white wines. *Food Chem.* **2007**, *100*, 1464−1473.
(74) Cejudo-Bastante, M. J.; Hermosin-Gutierrez, I.; Perez-Coello, M. S. Accelerated aging against conventional storage: effects on the volatile composition of Chardonnay white wines. *J. Food Sci.* **2013**, *78*, C507−C5013.
(75) Guitart, A.; Hernández, P.; Ferreira, V.; Peña, C. Some observations about the correlation between the amino acid content of musts and wines of the Chardonnay variety and their fermentation aromas. *Am. J. Enol. Vitic.* **1999**, *50*, 253−258.
(76) Escudero, A.; Hernandez-Orte, P.; Cacho, J.; Ferreira, V. Clues about the role of methional as character impact odorant of some oxidized wines. *J. Agric. Food Chem.* **2000**, *48*, 4268−4272.
(77) Campo, E.; Ferreira, V.; Escudero, A.; Marques, J. C.; Cacho, J. Quantitative gas chromatography−olfactometry and chemical quantitative study of the aroma of four Madeira wines. *Anal. Chim. Acta* **2006**, 180−187.
(78) Culleré, L.; Cacho, J.; Ferreira, V. An assessment of the role played by some oxidation-related aldehydes in wine aroma. *J. Agric. Food Chem.* **2007**, *55*, 876−881.
(79) Etiévant, P. Wine. In *Volatile Compounds in Foods and Beverages*, 1st ed.; Maarse, H., Ed.; Dekker: New York, 1991; pp 483−546.
(80) Navarro, M.; Arozarena, I.; Marín, R.; Casp, A. The use of multivariate statistical analysis in determining the sensory quality of white monovarietal wines. *J. Food Qual.* **2002**, *25*, 541−551.
(81) Ferrari, G.; Lablanquie, O.; Cantagrel, R.; Ledauphin, J.; Payot, T.; Fournier, N.; Guichard, E. Determination of key odorant compounds in freshly distilled cognac using GC-O, GC-MS, and sensory evaluation. *J. Agric. Food Chem.* **2004**, *52*, 5670−5676.
(82) Torrea, D.; Varela, C.; Ugliano, M.; Ancin-Azpilicueta, C.; Leigh Francis, I.; Henschke, P. A. Comparison of inorganic and organic nitrogen supplementation of grape juice − effect on volatile composition and aroma profile of a Chardonnay wine fermented with *Saccharomyces cerevisiae* yeast. *Food Chem.* **2011**, *127*, 1072−1083.
(83) Bakker, J.; Clarke, R. J. *Wine Flavour Chemistry*; Wiley-Blackwell: Oxford, UK, 2004; p 326.
(84) Guth, H. Identification of character impact odorants of different white wine varieties. *J. Agric. Food Chem.* **1997**, *45*, 3022−3026.
(85) Moyano, L.; Zea, L.; Moreno, J.; Medina, M. Analytical study of aromatic series in sherry wines subjected to biological aging. *J. Agric. Food Chem.* **2002**, *50*, 7356−7361.
(86) Perestrelo, R.; Fernandes, A.; Albuquerque, F. F.; Marques, J. C.; Câmara, J. S. Analytical characterization of the aroma of Tinta Negra Mole red wine: identification of the main odorants compounds. *Anal. Chim. Acta* **2006**, *563*, 154−164.
(87) Buettner, A. Investigation of potent odorants and afterodor development in two Chardonnay wines using the buccal odor screening system (BOSS). *J. Agric. Food Chem.* **2004**, *52*, 2339−2346.
(88) Bartowsky, E. J.; Pretorius, I. S. Microbial formation and modification of flavor and off-flavor compounds in wine. In *Biology of Microorganisms on Grapes, in Must and in Wine*; König, H., Unden, G., Fröhlich, J., Eds.; Springer-Verlag: Berlin, Germany, 2009; pp 209−231.
(89) Bowen, A. J.; Reynolds, A. G. Odor potency of aroma compounds in Riesling and Vidal blanc table wines and icewines by gas chromatography−olfactometry−mass spectrometry. *J. Agric. Food Chem.* **2012**, *60*, 2874−2883.
(90) Villamor, R. R.; Evans, M. A.; Mattinson, D. S.; Ross, C. F. Effects of ethanol, tannin and fructose on the headspace concentration and potential sensory significance of odorants in a model wine. *Food Res. Int.* **2013**, *50*, 38−45.
(91) Robinson, A. L.; Ebeler, S. E.; Heymann, H.; Boss, P. K.; Solomon, P. S.; Trengove, R. D. Interactions between wine volatile compounds and grape and wine matrix components influence aroma compound headspace partitioning. *J. Agric. Food Chem.* **2009**, *57*, 10313−10322.
(92) Voilley, A.; Lubbers, S. Flavor-matrix interactions in wine. In *Chemistry of Wine Flavor*; Waterhouse, A. L., Ebeler, S. E., Eds.; American Chemical Society: Washington, DC, USA, 1998; Vol. 714, pp 217−229.
(93) Parr, W. V.; Green, J.; White, K. G.; Sherlock, R. The distinctive flavour of New Zealand Sauvignon blanc: sensory characterisation by wine professionals. *Food Qual. Pref.* **2007**, *18*, 849−861.
(94) Pineau, B.; Barbe, J.-C.; Van Leeuwen, C.; Dubourdieu, D. Examples of perceptive interactions involved in specific "red-" and "black-berry" aromas in red wines. *J. Agric. Food Chem.* **2009**, *57*, 3702−3708.
(95) Ferreira, V. Revisiting psychophysical work on the quantitative and qualitative odour properties of simple odour mixtures: a flavour chemistry view. Part 2: Qualitative aspects. A review. *Flavour Fragrance J.* **2012**, *27*, 201−215.
(96) Ferreira, V. Revisiting psychophysical work on the quantitative and qualitative odour properties of simple odour mixtures: a flavour chemistry view. Part 1: Intensity and detectability. A review. *Flavour Fragrance J.* **2012**, *27*, 124−140.
(97) Pineau, B.; Barbe, J.-C.; Van Leeuwen, C.; Dubourdieu, D. Which impact for β-damascenone on red wines aroma? *J. Agric. Food Chem.* **2007**, *55*, 4103−4108.
(98) Lytra, G.; Tempere, S.; Revel, G. D.; Barbe, J.-C. Impact of perceptive interactions on red wine fruity aroma. *J. Agric. Food Chem.* **2012**, *60*, 12260−12269.
(99) López, R.; Ferreira, V.; Hernández, P.; Cacho, J. Identification of impact odorants of young red wines made with Merlot, Cabernet Sauvignon and Grenache grape varieties: a comparative study. *J. Sci. Food Agric.* **1999**, *79*, 1461−1467.
(100) Gürbüz, O.; Rouseff, J. M.; Rouseff, R. L. Comparison of aroma volatiles in commercial Merlot and Cabernet sauvignon wines using gas chromatography−olfactometry and gas chromatography−mass spectrometry. *J. Agric. Food Chem.* **2006**, *54*, 3990−3996.
(101) Etievant, P. *Volatile Compounds in Food and Beverages*; Dekker: New York, 1991; p 764.
(102) Brown, R. C.; Sefton, M.; Taylor, D. K.; Elsey, D. G. An odour detection threshold determination of all four possible stereoisomers of oak lactone in a white and a red wine. *Aust. J. Grape Wine Res.* **2008**, *12*, 115−118.
(103) Chatonnet, P.; Dubourdieu, D.; Boidron, J. N. Incidence of fermentation and aging conditions of dry white wines in barrels on their composition in substances yielded by oak wood. *Sci. Aliments* **1992**, *12*, 665−685.
(104) Moreira, N.; Mendes, F.; Hogg, T.; Vasconcelos, I. Alcohols, esters and heavy sulphur compounds production by pure and mixed cultures of apiculate wine yeasts. *Int. J. Food Microbiol.* **2005**, *103*, 285−294.
(105) Moreira, N.; Guedes De Pinho, P.; Santos, C.; Vasconcelos, I. Volatile sulphur compounds composition of monovarietal white wines. *Food Chem.* **2010**, *123*, 1198−1203.
(106) Liberatore, M. T.; Pati, S.; Del Nobile, M. A.; La Notte, E. Aroma quality improvement of Chardonnay white wine by fermentation and ageing in barrique on lees. *Food Res. Int.* **2010**, *43*, 996−1002.
(107) Tominaga, T.; Blanchard, L.; Darriet, P.; Dubourdieu, D. A powerful aromatic volatile thiol, 2-furanmethanethiol, exhibiting roast coffee aroma in wines made from several *Vitis vinifera* grape varieties. *J. Agric. Food Chem.* **2000**, *48*, 1799−1802.

(108) Tominaga, T.; Dubourdieu, D. A novel method for quantification of 2-methyl-3-furanthiol and 2-furanmethanethiol in wines made from *Vitis vinifera* grape varieties. *J. Agric. Food Chem.* **2006**, *54*, 29−33.
(109) Tominaga, T.; Guimbertau, G.; Dubourdieu, D. Contribution of benzenemethanethiol to smoky aroma of certain *Vitis vinifera* L. wines. *J. Agric. Food Chem.* **2003**, *51*, 1373−1376.
(110) Lavigne, V.; Pons, A.; Darriet, P.; Dubourdieu, D. Incidence of some oenological parameters on the content of sotolon in white wines. *Wine Vitic. J.* **2013**, *28*, 25−29.
(111) Sefton, M. A.; Francis, I. L.; Williams, P. J. The volatile composition of Chardonnay juices: a study by flavor precursor analysis. *Am. J. Enol. Vitic.* **1993**, *44*, 359−370.
(112) Baumes, R.; Wirth, J.; Bureau, S.; Gunata, Z.; Razungles, A. Biogeneration of C13-norisoprenoid compounds: experiments supportive for an apo-carotenoid pathway in grapevines. *Anal. Chim. Acta* **2002**, *458*, 3−14.
(113) Young, P. R.; Lashbrooke, J. G.; Alexandersson, E.; Jacobson, D.; Moser, C. The genes and enzymes of the carotenoid metabolic pathway in *Vitis vinifera* L. *BMC Genomics* **2012**, *13*, 243−260.
(114) Razungles, A.; Bayonove, C.; Cordonnier, R.; Baumes, R. Etude des caroténoïdes du raisin à maturité. *Vitis* **1987**, *26*, 183−191.
(115) Strauss, C. R.; Wilson, B.; Anderson, R.; Williams, P. J. Development of precursors of C13-norisoprenoid flavorants in Riesling grapes. *Am. J. Enol. Vitic.* **1987**, *38*, 23−27.
(116) Fischer, U. Wine aroma. In *Flavours and Fragrances: Chemistry, Bioprocessing and Sustainability*; Berger, R. G., Ed.; Springer-Verlag: Berlin, Germany, 2007; pp 241−267.
(117) Sefton, M. A.; Skouroumounis, G. K.; Elsey, G. M.; Taylor, D. K. Occurrence, sensory impact, formation, and fate of damascenone in grapes, wines, and other foods and beverages. *J. Agric. Food Chem.* **2011**, *59*, 9717−9746.
(118) Cox, A.; Capone, D. L.; Elsey, G. M.; Perkins, M. V.; Sefton, M. A. Quantitative analysis, occurrence, and stability of (*E*)-1-(2,3,6-trimethylphenyl)buta-1,3-diene in wine. *J. Agric. Food Chem.* **2005**, *53*, 3584−3591.
(119) Dubourdieu, D.; Tominaga, T. Polyfunctional thiol compounds. In *Wine Chemistry and Biochemistry*; Moreno-Arribas, M. V., Polo, M. C., Eds.; Springer: New York, 2009; pp 275−293.
(120) Darriet, P.; Tominaga, T.; Lavigne, V.; Boidron, J.-N.; Dubourdieu, D. Identification of a powerful aromatic component of *Vitis vinifera* L. var. Sauvignon wines: 4-mercapto-4-methylpentan-2-one. *Flavour Fragrance J.* **1995**, *10*, 385−392.
(121) Swiegers, J. H.; Pretorius, I. S. Modulation of volatile sulfur compounds by wine yeast. *Appl. Microbiol. Biotechnol.* **2007**, *74*, 954−960.
(122) Tominaga, T.; Niclass, Y.; Frérot, E.; Dubourdieu, D. Stereoisomeric distribution of 3-mercaptohexan-1-ol and 3-mercaptohexyl acetate in dry and sweet white wines made from *Vitis vinifera* (var. Sauvignon Blanc and Semillon). *J. Agric. Food Chem.* **2006**, *54*, 7251−7255.
(123) Kobayashi, H.; Matsuyama, S.; Takase, H.; Sasaki, K.; Suzuki, S.; Takata, R.; Saito, H. Impact of harvest timing on the concentration of 3-mercaptohexan-1-ol precursors in *Vitis vinifera* berries. *Am. J. Enol. Vitic.* **2012**, *63*, 544−548.
(124) Mateo-Vivaracho, L.; Ferreira, V.; Cacho, J. Automated analysis of 2-methyl-3-furanthiol and 3-mercaptohexyl acetate at ng L^{-1} level by headspace solid-phase microextraction with on-fibre derivatisation and gas chromatography-negative chemical ionization mass spectrometric determination. *J. Chromatogr. A* **2006**, *1121*, 1−9.
(125) Blanchard, L.; Tominaga, T.; Dubourdieu, D. Formation of furfurylthiol exhibiting a strong coffee aroma during oak barrel fermentation from furfural released by toasted staves. *J. Agric. Food Chem.* **2001**, *49*, 4833−4835.
(126) Tominaga, T.; Guimbertau, G.; Dubourdieu, D. Role of certain volatile thiols in the bouquet of aged champagne wines. *J. Agric. Food Chem.* **2003**, *51*, 1016−1020.
(127) Lee, S.; Rathbone, D.; Asimont, S.; Adden, R.; Ebeler, S. E. Dynamic changes in ester formation during Chardonnay juice fermentations with different yeast inoculation and initial Brix conditions. *Am. J. Enol. Vitic.* **2004**, *55*, 346−354.
(128) Welke, J. E.; Zanus, M.; Lazarotto, M.; Schmitt, K. G.; Zini, C. A. Volatile characterization by multivariate optimization of headspace-solid phase microextraction and sensorial evaluation of Chardonnay base wines. *J. Braz. Chem. Soc.* **2012**, *23*, 678−687.
(129) Verstrepen, K. J.; Stijn, D. M.; Van Laere, S. D. M.; Vanderhaegen, B. M. P.; Derdelinckx, G.; Dufour, J.-P.; Pretorius, I. S.; Winderickx, J.; Thevelein, J. M.; Delvaux, F. R. Expression levels of the yeast alcohol acetyltransferase genes ATF-1, Lg-ATF1, and ATF2 control the formation of a broad range of volatile esters. *Appl. Environ. Microbiol.* **2003**, *69*, 5228−5237.
(130) Mason, A. B.; Jean-Pierre, D. Alcohol acetyltransferases and the significance of ester synthesis in yeast. *Yeast* **2000**, *16*, 1287−1298.
(131) Lilly, M.; Bauer, F. F.; Lambrechts, M. G.; Swiegers, J. H.; Cozzolino, D.; Pretorius, I. S. The effect of increased yeast alcohol acetyltransferase and esterase activity on the flavour profiles of wine and distillates. *Yeast* **2006**, *23*, 641−659.
(132) Saerens, S. M. G.; Vestrepen, K. J.; Van Laere, S. D. M.; Voet, A. R. D.; Van Dicjk, P.; Delvaux, F. R.; Thevelein, J. M. The *Saccharomyces cerevisiae* EHT1 and EEB1 genes encode novel enzymes with medium-chain fatty acid ethyl ester synthase and hydrolysis capacity. *J. Biol. Chem.* **2006**, *281*, 4446−4456.
(133) Swiegers, J. H.; Bartowsky, E. J.; Henschke, P. A.; Pretorius, I. S. Yeast and bacterial modulation of wine aroma and flavour. *Aust. J. Grape Wine Res.* **2005**, *11*, 139−173.
(134) Saerens, S. M. G.; Delvaux, F.; Verstrepen, K. J.; Van Dijck, P.; Thevelein, J. M.; Delvaux, F. R. Parameters affecting ethyl ester production by *Saccharomyces cerevisiae* during fermentation. *Appl. Environ. Microbiol.* **2008**, *74*, 454−461.
(135) Vianna, E.; Ebeler, S. E. Monitoring ester formation in grape juice fermentations using solid phase microextraction coupled with gas chromatography-mass spectrometry. *J. Agric. Food Chem.* **2001**, *49*, 589−595.
(136) Yunoki, K.; Hirose, S.; Ohnishi, M. Ethyl esterification of long-chain unsaturated fatty acids derived from grape must by yeast during alcoholic fermentation. *Biosci., Biotechnol., Biochem.* **2007**, *71*, 3105−3109.
(137) Dennis, E. G.; Keyzers, R. A.; Kalua, C. M.; Maffei, S. M.; Nicholson, E. L.; Boss, P. K. Grape contribution to wine aroma: production of hexyl acetate, octyl acetate, and benzyl acetate during yeast fermentation is dpendent upon precursors in the must. *J. Agric. Food Chem.* **2012**, *60*, 2638−2646.
(138) Moio, L.; Schlich, P.; Etiévant, P. Acquisition and analysis of aromagrams of Chardonnay burgundy wines. *Sci. Aliments* **1994**, *14*, 601−608.
(139) Shinohara, T.; Kubodera, S.; Yanagida, F. Distribution of phenolic yeasts and production of phenolic off-flavors in wine fermentation. *J. Biosci. Bioeng.* **2000**, *90*, 90−97.
(140) Towey, J. P.; Waterhouse, A. L. The extraction of volatile compounds from French and American oak barrels in Chardonnay during three successive vintages. *Am. J. Enol. Vitic.* **1996**, *47*, 163−172.
(141) Ribéreau-Gayon, P.; Dubourdieu, D.; Donèche, B.; Lonvaud, A. The grape and its maturation. In *Handbook of Enology − The Microbiology of Wine and Vinifications*, 2nd ed.; Wiley: Wiltshire, UK, 2006; Vol. 1, p 497.
(142) Martínez-Gil, A. M.; Garde-Cerdán, T.; Lorenzo, C.; Félix Lara, J.; Pardo, F.; Rosario Salinas, M. Volatile compounds formation in alcoholic fermentation from grapes collected at 2 maturation stages: influence of nitrogen compounds and grape variety. *J. Food Sci.* **2012**, *77*, C71−C79.
(143) Kang, W. H.; Xu, Y.; Qin, L.; Wang, Y. X. Effects of different β-D-glycosidases on bound aroma compounds in Muscat grape determined by HS-SPME and GC-MS. *J. Inst. Brew.* **2010**, *116*, 70−77.
(144) Morakul, S.; Mouret, J. R.; Nicolle, P.; Aguera, E.; Sablayrolles, J. M.; Athès, V. A dynamic analysis of higher alcohol and ester release during winemaking fermentations. *Food Bioprocess Technol.* **2013**, *6*, 818−827.

(145) Ugliano, M.; Henschke, P. A. Yeasts and wine flavour. In *Wine Chemistry and Biochemistry*; Moreno-Arribas, M. V., Polo, M. C., Eds.; Springer: New York, 2009; pp 313−392.
(146) Schmidt, S. A.; Dillon, S.; Kolouchova, R.; Henschke, P. A.; Chambers, P. J. Impacts of variations in elemental nutrient concentration of Chardonnay musts on *Saccharomyces cerevisiae* fermentation kinetics and wine composition. *Appl. Microb. Cell Physiol.* **2011**, *91*, 365−375.
(147) Curtin, C. D.; Bellon, J. R.; Bartowsky, E. J.; Henschke, P. A.; Chambers, P. J.; Herderich, M. J.; Pretorius, I. S. Harnessing AWRI's yeast and bacterial research to shape 'Next-Gen' Chardonnay. Part 2: Influence of yeast, nutritional management and malolactic fermentation. *Wine Vitic. J.* **2011**, *26*, 15−24.
(148) Nykanen, L.; Suomalainen, H. *Aroma of Beer, Wine and Distilled Alcoholic Beverages*; Reidel Publishing: Dordrecht, The Netherlands, 1983; 424 pp.
(149) Miller, A.; Wolff, S.; Bisson, L.; Ebeler, S. E. Yeast strain and nitrogen supplementation: dynamics of volatile ester production in Chardonnay juice fermentations. *Am. J. Enol. Vitic.* **2007**, *58*, 470−483.
(150) Larue, F.; Lafon-Lafourcade, S.; Ribereau-Gayon, P. Relationship between the sterol content of yeast cells and their fermentation activity in grape must. *Appl. Environ. Microbiol.* **1980**, *39*, 808−811.
(151) Pogorzelski, E.; Wilkowska, A. Flavour enhancement through the enzymatic hydrolysis of glycosidic aroma precursors in juices and wine beverages: a review. *Flavour Fragrance J.* **2007**, *22*, 251−254.
(152) Chassagne, D.; Vernizeau, S.; Nedjmac, M.; Alexandre, H. Hydrolysis and sorption by *Saccharomyces cerevisiae* strains of Chardonnay grape must glycosides during fermentation. *Enzyme Microb. Technol.* **2005**, *37*, 212−217.
(153) Schneider, R.; Razungles, A.; Augier, C.; Baumes, R. Monoterpenic and norisoprenoidic glycoconjugates of *Vitis vinifera* L. cv. Melon B. as precursors of odorants in Muscadet wines. *J. Chromatogr., A* **2001**, *936*, 145−157.
(154) Gunata, Z.; Bitteur, S.; Brillouet, J.-M.; Bayonove, C.; Cordonnier, R. Sequential enzymic hydrolysis of potentially aromatic glycosides from grape. *Carbohydr. Res.* **1988**, *184*, 139−149.
(155) Maicas, S.; Mateo, J. J. Hydrolysis of terpenyl glycosides in grape juice and other fruit juices: a review. *Appl. Microbiol. Biotechnol.* **2005**, *67*, 322−335.
(156) Cabaroglu, T.; Selli, S.; Canbas, A.; Lepoutre, J. P.; Günata, Z. Wine flavor enhancement through the use of exogenous fungal glycosidades. *Enzyme Microb. Technol.* **2003**, *33*, 581−587.
(157) Rodríguez-Bencomo, J. J.; Selli, S.; Muñoz-González, C.; Martín-Alvarez, P. J.; Pozo-Bayón, M. A. Application of glycosidic aroma precursors to enhance the aroma and sensory profile of dealcoholised wines. *Food Res. Int.* **2013**, *51*, 450−457.
(158) Richter, C.; Dunn, B.; Sherlock, G.; Pugh, T. Comparative metabolic footprinting of a large number of commercial wine yeast strains in Chardonnay fermentations. *FEMS Microbiol. Lett.* **2013**, *13*, 394−410.
(159) Singleton, V. L.; Zaya, J.; Trousdale, E. White table wine quality and polyphenol composition as affected by must SO_2 content and pomace contact time. *Am. J. Enol. Vitic.* **1980**, *31*, 14−20.
(160) Wilson, B.; Strauss, C. R.; Williams, P. J. The distribution of free and glycosidically-bound monoterpenes among skin, juice, and pulp fractions of some white grape varieties. *Am. J. Enol. Vitic.* **1986**, *37*, 107−111.
(161) Park, S. K.; Morrison, J. C.; Adams, D. O.; Noble, A. C. Distribution of free and glycosidically bound monoterpenes in the skin and mesocarp of Muscat of Alexandria grapes during development. *J. Agric. Food Chem.* **1991**, *39*, 514−518.
(162) Braell, P. A.; Acree, T. E.; Butts, R. M.; Zhou, P. G. Isolation of nonvolatile precursors of β-damascenone from grapes using charm analysis. In *Biogeneration of Aromas*; American Chemical Society: Washington, DC, USA, 1986; Vol. 317, pp 75−84.
(163) Roland, A.; Schneider, R.; Charrier, F.; Cavelier, F.; Rossignol, M.; Razungles, A. Distribution of varietal thiol precursors in the skin and the pulp of Melon B. and Sauvignon blanc grapes. *Food Chem.* **2011**, *125*, 139−144.
(164) Arnold, R. A.; Noble, A. C. Effect of pomace contact on the flavor of Chardonnay wine. *Am. J. Enol. Vitic.* **1979**, *30*, 179−181.
(165) Test, S.; Noble, A.; Schmidt, R. H. Effect of pomace contact on Chardonnay musts and wines. *Am. J. Enol. Vitic.* **1987**, *37*, 133−136.
(166) Ferreira, B.; Hory, C.; Bard, M. H.; Taisant, C.; Olsson, A.; Le Fur, Y. Effects of skin contact and settling on the level of the C18:2, C18:3 fatty acids and C6 compounds in Burgundy Chardonnay musts and wines. *Food Qual. Pref.* **1995**, *6*, 35−41.
(167) Colagrande, O. Génèse des odeurs et de goûts anormaux des vins. *Rev. Oenol.* **1989**, *53*, 25−27.
(168) Ramey, D.; Bertrand, A.; Ough, C. S.; Singleton, V. L.; Sanders, E. Effects of skin contact temperature on Chardonnay must and wine composition. *Am. J. Enol. Vitic.* **1986**, *37*, 99−106.
(169) Bisson, L.; Karpel, J. Genetics of yeast impacting wine quality. *Annu. Rev. Food Sci. Technol.* **2010**, *1*, 139−162.
(170) Ugliano, M. Enzymes in winemaking. In *Wine Chemistry and Biochemistry*; Moreno-Arribas, M. V., Polo, M. C., Eds.; Springer: New York, 2009; pp 103−126.
(171) Halliday, J. *James Halliday Australian Wine Companion*; Hardie Grant Books: Victoria, Australia, 2013.
(172) Fleet, G. H. Yeast interactions and wine flavour. *Int. J. Food Microbiol.* **2003**, *86*, 11−22.
(173) Egli, C. M.; Edinger, W. D.; Mitrakul, C. M.; Henick-Kling, T. Dynamics of indigenous and inoculated yeast populations and their effect on the sensory character of Riesling and Chardonnay wines. *J. Appl. Microbiol.* **1998**, *85*, 779−789.
(174) Boulton, R. B., Singleton, V. L.; Bisson, L. F.; Kunkee, R. E. *Principles and Practices of Winemaking*; Aspen Publishers: Gaithersburg, MD, USA, 1996.
(175) Cordente, A.; Curtin, C.; Varela, C.; Pretorius, I. Flavour-active wine yeasts. *Appl. Microbiol. Biotechnol.* **2012**, *96*, 601−618.
(176) Harsch, M.; Gardner, R. Yeast genes involved in sulfur and nitrogen metabolism affect the production of volatile thiols from Sauvignon blanc musts. *Appl. Microbiol. Biotl.* **2013**, *97*, 223−235.
(177) Murat, M.-L.; Tominaga, T.; Dubourdieu, D. Assessing the aromatic potential of Cabernet Sauvignon and Merlot musts used to produce rose wine by assaying the cysteinylated precursor of 3-mercaptohexan-1-ol. *J. Agric. Food Chem.* **2001**, *49*, 5412−5417.
(178) Masneuf-Pomarède, I.; Mansour, C.; Murat, M. L.; Tominaga, T.; Dubourdieu, D. Influence of fermentation temperature on volatile thiols concentrations in Sauvignon blanc wines. *Int. J. Food Microbiol.* **2006**, *108*, 385−390.
(179) Swiegers, J. H.; Capone, D. L.; Pardon, K. H.; Elsey, G. M.; Sefton, M. A.; Francis, I. L.; Pretorius, I. S. Engineering volatile thiol release in *Saccharomyces cerevisiae* for improved wine aroma. *Yeast* **2007**, *24*, 561−574.
(180) Holt, S.; Cordente, A. G.; Williams, S. J.; Capone, D. L.; Jitjaroen, W.; Menz, I. R.; Curtin, C.; Anderson, P. A. Engineering *Saccharomyces cerevisiae* to release 3-mercaptohexan-1-ol during fermentation through overexpression of an *S. cerevisiae* gene, *STR3*, for improvement of wine aroma. *Appl. Environ. Microbiol.* **2011**, *77*, 3626−3632.
(181) Soden, A.; Francis, I. L.; Oakey, H.; Henschke, P. A. Effects of co-fermentation with *Candida stellata* and *Saccharomyces cerevisiae* on the aroma and composition of Chardonnay wine. *Aust. J. Grape Wine Res.* **2008**, *6*, 21−30.
(182) Contreras, A.; Hidalgo, C.; Henschke, P. A.; Chambers, P. J.; Curtin, C.; Varela, C. Evaluation of non-*Saccharomyces* yeast for the reduction of alcohol content in wine. *Appl. Environ. Microbiol.* **2014**, *80*, 1670−1678.
(183) Ciani, M.; Comitini, F.; Mannazzu, I.; Domizio, P. Controlled mixed culture fermentation: a new perspective on the use of non-Saccharomyces yeasts in winemaking. *FEMS Yeast Res.* **2009**, *10*, 123−133.
(184) Jackson, R. Wine spoilage In *Wine Science − Principles and Applications*, 3rd ed.; Elsevier: London, UK, 2008; pp 493−504.
(185) Grbin, P.; Henschke, P. A. Mousy off-flavour production in grape juice and wine by *Dekkera* and *Brettanomyces* yeasts. *Aust. J. Grape Wine Res.* **2000**, *6*, 255−262.

(186) Sauvageot, F.; Vivier, P. Effects of malolactic fermentation on sensory properties of four burgundy wines. *Am. J. Enol. Vitic.* **1997**, *48*, 187−192.
(187) Flamini, R.; De Luca, G.; Di Stefano, R. Changes in carbonyl compounds in Chardonnay and Cabernet Sauvignon wines as a consequence of malolactic fermentation. *Vitis* **2002**, *2*, 107−112.
(188) Ribéreau-Gayon, P.; Dubourdieu, D.; Donèche, B.; Lonvaud, A. Metabolism of lactic acid bacteria. In *Handbook of Enology: The Microbiology of Wine and Vinifications*, 2nd ed.; Ribéreau-Gayon, P., Ed.; Wiley: West Sussex, UK, 2006; Vol. 1, pp 150−151.
(189) Grimaldi, A.; Mclean, H.; Jiranek, V. Identification and partial characterization of glycosidic activities of commercial strains of the lactic acid bacterium, *Oenococcus oeni*. *Am. J. Enol. Vitic.* **2000**, *51*, 362−369.
(190) D'Incecco, N.; Bartowsky, E. J.; Kassara, S.; Lante, A.; Spettoli, P.; Henschke, P. A. Release of glycosidically bound flavour compounds of Chardonnay by *Oenococcus oeni* during malolactic fermentation. *Food Microbiol.* **2004**, *21*, 257−265.
(191) Hernandez-Orte, P.; Cersosimo, M.; Loscos, N.; Cacho, J.; Garcia-Moruno, E.; Ferreira, V. Aroma development from non-floral grape precursors by wine lactic acid bacteria. *Food Res. Int.* **2009**, *42*, 773−781.
(192) Bartowsky, E. J. Bacterial spoilage of wine and approaches to minimize it. *Lett. Appl. Microbiol.* **2009**, *48*, 149−156.
(193) Lonvaud-Funel, A. Biogenic amines in wines: role of lactic acid bacteria. *FEMS Microbiol. Lett.* **2001**, *199*, 9−13.
(194) Coton, E.; Rollan, G.; Bertrand, A.; Lonvaud-Funel, A. Histamine-producing lactic acid bacteria in wines: early detection, frequency, and distribution. *Am. J. Enol. Vitic.* **1998**, *49*, 199−204.
(195) Costello, P.; Lee, T. H.; Henschke, P. A. Ability of lactic acid bacteria to produce N-heterocycles causing mousy off-flavour in wine. *Aust. J. Grape Wine Res.* **2001**, *7*, 160−167.
(196) Costello, P. J.; Henschke, P. A. Mousy off-flavour of wine: precursors and biosynthesis of the causative N-heterocycles 2-ethyltetrahydropyridine, 2-acetyltetrahydropyridine, and 2-acetyl-1-pyrroline by *Lactobacillus hilgardii* DSM 20176. *J. Agric. Food Chem.* **2002**, *50*, 7079−7087.
(197) Towey, J. P.; Waterhouse, A. L. Barrel-to-barrel variation of volatile oak extractives in barrel-fermented Chardonnay. *Am. J. Enol. Vitic.* **1996**, *47*, 17−20.
(198) Fernández De Simón, B.; Cadahía, E.; Del Álamo, M.; Nevares, I. Effect of size, seasoning and toasting in the volatile compounds in toasted oak wood and in a red wine treated with them. *Anal. Chim. Acta* **2010**, *660*, 211−220.
(199) Spillman, P. J.; Sefton, M. A.; Gawel, R. The effect of oak wood source, location of seasoning and coopering on the composition of volatile compounds in oak-matured wines. *Aust. J. Grape Wine Res.* **2004**, *10*, 216−226.
(200) Chatonnet, P.; Boidron, J.-N.; Pons, M. Incidence du traitement thermique du bois de chêne sur sa composition chimique, 2e partie: évolution de certains composés en fonction de l'intensité de brûlage. *Connaiss. Vigne Vin* **1989**, *23*, 223−250.
(201) Wilkinson, K. L.; Elsey, G. M.; Prager, R. H.; Tanaka, T.; Sefton, M. A. Precursors to oak lactone. Part 2: Synthesis, separation and cleavage of several β-D-glucopyranosides of 3-methyl-4-hydroxyoctanoic acid. *Tetrahedron* **2004**, *60*, 6091−6100.
(202) Wilkinson, K. L.; Prida, A.; Hayasaka, Y. Role of glycoconjugates of 3-methyl-4-hydroxyoctanoic acid in the evolution of oak lactone in wine during oak maturation. *J. Agric. Food Chem.* **2013**, *61*, 4411−4416.
(203) Maga, J. A. Oak lactones in alcoholic beverages. *Food Rev. Int.* **1996**, *12*, 105−130.
(204) Spillman, P. J.; Sefton, M. A.; Gawel, R. The contribution of volatile compounds derived during oak barrel maturation to the aroma of a Chardonnay and Cabernet Sauvignon wine. *Aust. J. Grape Wine Res.* **2004**, *10*, 227−235.
(205) Chatonnet, P.; Boidron, J.-N.; Pons, M. Maturation of red wines in oak barrels: evolution of some volatile compounds and their aromatic impact. *Sci. Aliments* **1990**, *10*, 565−587.
(206) Campbell, J. I.; Pollnitz, A. P.; Sefton, M.; Herderich, M.; Pretorius, I. S. Factors affecting the influence of oak chips on wine flavour. *Wine Ind. J.* **2006**, *21*, 38−42.
(207) Garde-Cerdán, T.; Ancín-Azpilicueta, C. Review of quality factors on wine ageing in oak barrels. *Trends Food Sci. Technol.* **2006**, *17*, 438−447.
(208) Wilkinson, K. L.; Li, S.; Grbin, P.; Warren, P. Barrel reclamation: everything that's old can be new again. *Aust. N.Z. Grapegrower Winemaker* **2013**, 71−72.
(209) Young, O. A.; Kaushal, M.; Robertson, J. D.; Burns, H.; Nunns, S. J. Use of species other than oak to flavor wine: an exploratory survey. *J. Food Sci.* **2010**, *75*, S490−S498.
(210) Fernández De Simón, B.; Esteruelas, E.; Muñoz, A.; Cadahía, E.; Sanz, M. Volatile compounds in acacia, chestnut, cherry, ash, and oak woods, with a view to their use in cooperage. *J. Agric. Food Chem.* **2009**, *57*, 3217−3227.
(211) Arapitsas, P.; Antonopoulos, A.; Stefanou, E.; Dourtoglou, V. G. Artificial aging of wines using oak chips. *Food Chem.* **2003**, *86*, 563−570.
(212) Gutiérrez-Alfonso, V. L. Sensory descriptive analysis between white wines fermented with oak chips and in barrels. *J. Food Sci.* **2003**, *67*, 2415−2419.
(213) Pérez-Coello, M. S.; Sánchez, M.-T.; Gónzales-Viñas, M. A.; Sanz, J.; Cabezudo, M. D. Fermentation of white wines in the presence of wood chips of American and french oak. *J. Agric. Food Chem.* **2000**, *48*, 885−889.
(214) Ramey, D. D.; Ough, C. S. Volatile ester hydrolysis or formation during storage of model solutions and wines. *J. Agric. Food Chem.* **1980**, *28*, 928−934.
(215) Díaz-Maroto, M. C.; Schneider, R.; Baumes, R. Formation pathways of ethyl esters of branched short-chain fatty acids during wine aging. *J. Agric. Food Chem.* **2005**, *53*, 3503−3509.
(216) Jones, P. R.; Gawel, R.; Francis, I. L.; Waters, E. J. The influence of interactions between major white wine components on the aroma, flavour and texture of model white wine. *Food Qual. Pref.* **2008**, *19*, 596−607.
(217) Ancín-Azpilicueta, C.; González-Marco, A.; Jiménez-Moreno, N. Evolution of esters in aged Chardonnay wines obtained with different vinification methods. *J. Sci. Food Agric.* **2009**, *89*, 2446−2451.
(218) Chassagne, D.; Guilloux-Benatier, M.; Alexandre, H.; Voilley, A. Sorption of wine volatile phenols by yeast lees. *Food Chem.* **2005**, *91*, 39−44.
(219) Palacios, S.; Vasserot, Y.; Maujean, A. Evidence for sulfur volatile products adsorption by yeast lees. *Am. J. Enol. Vitic.* **1997**, *48*, 525−526.
(220) Ribéreau-Gayon, P.; Dubourdieu, D.; Donèche, B.; Lonvaud, A. White winemaking. In *Handbook of Enology, Vol. 1: The Microbiology of Wines and Vinifications*, 2nd ed.; Ribéreau-Gayon, P., Ed.; Wiley: West Sussex, UK, 2006; Vol. 1, pp 397−443.
(221) Bureau, S. M.; Baumes, R. L.; Razungles, A. J. Effects of vine or bunch shading on the glycosylated flavor precursors in grapes of *Vitis vinifera* L. cv. Syrah. *J. Agric. Food Chem.* **2000**, *48*, 1290−1297.
(222) Basile, B.; Girona, J.; Behboudian, M. H.; Mata, M.; Rosello, J.; Ferre, M.; Marsal, J. Responses of "Chardonnay" to deficit irrigation applied at different phenological stages: vine growth, must composition, and wine quality. *Irrig. Sci.* **2012**, *30*, 397−406.
(223) Roland, A.; Schneider, R.; Razungles, A.; Cavelier, F. Varietal thiols in wine: discovery, analysis and applications. *Chem. Rev.* **2011**, *111*, 7355−7376.
(224) Zoecklin, B. W.; Wolf, T. K.; Duncan, S. E.; Marcy, J. E.; Jasinski, Y. Effect of fruit zone leaf removal on total glycoconjugates and conjugate fraction concentration of Riesling and Chardonnay (*Vitis vinifera* L.) grapes. *Am. J. Enol. Vitic.* **1998**, *49*, 259−265.
(225) Des Gachons, C. P.; Leeuwen, C. V.; Tominaga, T.; Soyer, J.-P.; Gaudillère, J.-P.; Dubourdieu, D. Influence of water and nitrogen deficit on fruit ripening and aroma potential of *Vitis vinifera* L cv Sauvignon blanc in field conditions. *J. Sci. Food Agric.* **2005**, *85*, 73−85.
(226) Boido, E.; Fariña, L.; Carrau, F.; Dellacassa, E.; Cozzolino, D. Characterization of glycosylated aroma compounds in Tannat grapes

and feasibility of the near infrared spectroscopy application for their prediction. *Food Anal. Methods* **2013**, *6*, 100−111.
(227) Razungles, A.; Bayonove, C. L.; Cordonnier, R. E.; Sapis, J. C. Grape carotenoids: changes during the maturation period and localization in mature berries. *Am. J. Enol. Vitic.* **1988**, *39*, 44−48.
(228) Lee, S.; Seo, M.; Riu, M.; Cotta, J.; Block, D.; Dokoozlian, N.; Ebeler, S. E. Vine microclimate and norisoprenoid concentration in Cabernet sauvignon grapes and wines. *Am. J. Enol. Vitic.* **2007**, *58*, 291−301.
(229) Skinkis, P. A.; Bordelon, B. P.; Butz, E. M. Effects of sunlight exposure on berry and wine monoterpenes and sensory characteristics of Traminette. *Am. J. Enol. Vitic.* **2010**, *61*, 147−156.
(230) Williams, P. J.; Sefton, M. A.; Francis, I. L. Glycosidic precursors of varietal grape and wine flavor. In *Flavor Precursors*; Teranishi, R., Takeoka, G. R., Güntert, M., Eds.; American Chemical Society: Washington, DC, USA, 1992; Vol. 490, pp 74−86.
(231) Marais, J.; Wyk, C. J. V.; Rapp, A. Effect of sunlight and shade on norisoprenoid levels in weisser Riesling and Chenin blanc grapes and Weisser wines. *S. Afr. J. Enol. Vitic.* **1992**, *13*, 23−32.
(232) Lakso, A. N.; Pool, R. M. The effects of water stress on vineyards and wine quality in Eastern vineyards. *Wine East* **2001**, *29*, 12−20.
(233) Fan, W.; Tsai, I. M.; Qian, M. C. Analysis of 2-amino-acetophenone by direct-immersion solid-phase microextraction and gas chromatography-mass spectrometry and its sensory impact in Chardonnay and Pinot gris wines. *Food Chem.* **2007**, *105*, 1144−1150.
(234) Lavigne, V. Laffort Web Site, Affinamento di vini bianchi sulle fecce, seconda parte: impatto sull'evoluzione e sulla tipicità dei vini; http://www.laffort.com/it/downloads/laffort-info (accessed June 18, 2014).
(235) Schneider, V. Atypical aging defect: sensory discrimination, viticultural causes, and enological consequences. A review. *Am. J. Enol. Vitic.* **2014**, DOI: 10.5344/ajev.2014.14014.
(236) Reynolds, A.; Lowrey, W.; Tomek, L.; Hakimi, J.; De Savigny, C. Influence of irrigation on vine performance, fruit composition, and wine quality of Chardonnay in a cool, humid climate. *Am. J. Enol. Vitic.* **2007**, *58*, 217−228.
(237) De Andrés-De Prado, R.; Yuste-Rojas, M.; Sort, X.; Andrés-Lacueva, C.; Torres, M.; Lamuela-Raventós, R. Effect of soil type on wines produced from *Vitis vinifera* L. cv. Grenache in commercial vineyards. *J. Agric. Food Chem.* **2007**, *55*, 779−786.
(238) Reynolds, A.; Taylor, G.; De Savigny, C. Defining Niagara terroir by chemical and sensory analysis of Chardonnay wines from various soil textures and vine sizes. *Am. J. Enol. Vitic.* **2013**, *64*, 180−194.
(239) Reynolds, A.; Schlosser, J.; Power, R.; Roberts, R.; Willwerth, J.; De Savigny, C. Magnitude and interaction of viticultural and enological effects I. Impact of canopy management and yeast strain on sensory and chemical composition of Chardonnay musqué. *Am. J. Enol. Vitic.* **2007**, *58*, 12−24.
(240) Nuzzo, V.; Genovese, M.; Schackel, K. A.; Matthews, M. In *Preliminary Investigations on Sunburn in Chardonnay Grapevine Variety*, 16th International GiESCO Symposium, California, July 2009; University of California: Davis, CA, USA, 2009; pp 183−187.
(241) Crothers, N. J. *The Effect of Increased Sun Exposure and Sun-Induced Browning on Chardonnay (Vitis vinifera L.) Grape and Wine Composition and Quality*. Victoria University, 2005.
(242) Crothers, J.; Downey, M. Effect of sun exposure on Chardonnay grapes and wines. In *Australian Viticulture − Practical Vineyard Management*; Coombe, B. G., Dry, P. R., Eds.; Winetitles: Adelaide, Australia, 2006.

■ NOTE ADDED AFTER ASAP PUBLICATION

This article published July 7, 2014 with errors in Tables 2, 3, and 4. The correct version published July 8, 2014.

Declaration and approved by the Ethics Committee from CSIC (Madrid, Spain) (Table 1). All volunteers gave their written informed consent prior to participation, and they had not taken antibiotics during 4 weeks before the trials. In the three intervention trials, volunteers consumed their usual diet but avoided ellagitannin-containing food products during the study and 1 week before starting.

In the first intervention study, healthy volunteers (n = 20, 11 men and 9 women) aged between 21 and 55 years consumed 30 g of walnuts (edible part)/day for 3 days. Walnuts were purchased in a local supermarket. After the last intake, 24 h urine samples were collected. Urinary volume was measured, and the samples were immediately stored at −20 °C.

In the second intervention study, healthy volunteers (n = 20, 10 men and 10 women) aged between 18 and 23 years ingested four capsules of pomegranate extract in a single intake (total dose = 1.8 g of extract). Urine samples were also collected for 24 h after the intake and were immediately stored at −20 °C.

In the third trial, overweight healthy subjects (n = 49, 32 men, 17 women; body mass index (BMI) > 27 kg/m^2) aged between 40 and 65 years ingested two daily capsules of pomegranate extract (0.9 g/day) for 3 days. Urine samples were collected for 24 h after the last intake, and the urine was stored at −20 °C until further analysis. In both interventions 2 and 3 capsules containing pomegranate extract were kindly supplied by Laboratorios Admira S.L. (Alcantarilla, Murcia, Spain).

Extraction Protocol of Urolithin Metabolites. Urine and feces samples were processed as previously reported.[4,5]

LC-MS Analysis. Samples were analyzed by HPLC-DAD-ESI-MS/MS or UPLC-ESI-QTOF-MS as previously reported.[4]

RESULTS AND DISCUSSION

We report here that human subjects can be consistently clustered within three phenotypes, that is, "phenotype A", "phenotype B", or "phenotype 0" according to their different capacities for excreting urolithins, independent of their demographic characteristics, health status, or ellagitannin-containing food product (Table 1). This has been observed in three dietary interventions in healthy volunteers (present study) as well as after re-examining available data for urinary profiles from previous studies.

Urolithins are mainly detected either as aglycones in feces or as phase II metabolites in systemic organs or biological fluids (glucuronide or sulfate derivatives). Overall, urolithin A (**1**) is the main metabolite produced in humans and previously identified as a urinary biomarker after consumption of ellagitannins/ellagic acid from different food products.[6] In the present study (Table 1), interventions 1−3 with healthy volunteers, some volunteers excreted only urolithin A metabolites (phenotype A), whereas other subjects, in addition to urolithin A (**1**), also excreted urolithin B (**3**) and isourolithin A (**2**) showing a more complex urinary metabolite profile (phenotype B) (Figure 2). Furthermore, a third group that did not excrete urolithins in urine was also identified (phenotype 0). The same three phenotypes were observed after intake of walnuts (intervention 1) or pomegranate extracts (interventions 2 and 3).

This observation prompted us to re-examine the excretion profiles observed in previous studies that we had previously completed in our laboratory or in collaboration with other research groups, as well as data available from other published studies. These three phenotypes were also found in intervention studies either with healthy volunteers or with those volunteers having some disease situations, confirming that these three phenotypes are quite robust and consistent (Table 1). In accordance with the three interventions described here, the three phenotypes were also observed no matter the

Table 1. Urolithin Urinary Phenotype Distribution in Different Human Trials

trial	food (quantity ingested, total ellagic acid content after hydrolysis/day)	analytical technique	N	age	BMI (kg/m^2)	health status	phenotype		
							A	B	0
intervention 1 (this study)	walnuts (30 g/day, 162.8 mg of total ellagic acid)	HPLC-DAD-ESI-IT-MS/MS	20 (10 men, 10 women)	21−55	23.8 ± 2.3	healthy	13 (65%)	4 (20%)	3 (15%)
intervention 2 (this study)	pomegranate extract (1.8 g, 220 mg of total ellagic acid)	UPLC-ESI-QTOF-MS	20 (10 men, 10 women)	18−23	20.5 ± 2.1	healthy	16 (80%)	2 (10%)	2 (10%)
intervention 3 (this study)	pomegranate extract (0.9 g/day, 110 mg of total ellagic acid)	UPLC-ESI-QTOF-MS	49 (32 men, 17 women)	40−65	30.4 ± 3.4	healthy-overweight	30 (60%)	15 (30%)	4 (10%)
González-Sarrías et al.[7]	walnuts (35 g/day, 190 mg of total EA), pomegranate juice (200 mL/day, 165.7 mg of total ellagic acid)	HPLC-DAD-ESI-IT-MS/MS	28 (men)	56−90	27.7 ± 3.6	prostate cancer or benign prostate hyperplasia	17 (60%)	4 (15%)	7 (25%)
Truchado et al.[8]	strawberry (200 g of fresh strawberries or the equivalent in puree, 150 mg of total ellagic acid)	HPLC-DAD-ESI-IT-MS/MS	20 (8 men, 12 women)	25−30	not available	healthy	16 (80%)	3 (15%)	1 (5%)
Puuponen-Pimia et al.[9]	strawberry (100 g/day, 75 mg total EA) + raspberry (100 g/day, 147 mg of total ellagic acid) + cloudberry (100 g/day)	HPLC-DAD-ESI-IT-MS/MS	20 (10 men, 10 women)	50−65	31.8 ± 4.4	metabolic syndrome	5 (25%)	10 (50%)	5 (25%)
Tulipani et al.[11]	nuts (unpeeled), (30 g/day, 81.4 mg of total ellagic acid) (15 g of walnuts + 7.5 g of almonds + 7.5 g of hazelnuts)	HPLC-DAD/ESI-QqQ-MS/MS and HPLC-ESI-IT-MS	22 (13 men, 9 women)	31−63	31.0 ± 2.9	metabolic syndrome	11 (50%)	9 (41%)	2 (9%)
Núñez-Sánchez et al.[4]	pomegranate extract (0.9 g/day, 110 mg of total ellagic acid)	UPLC-ESI-QTOF-MS	26 (14 men, 12 women)	52−89	28.9 ± 3.9	colorectal cancer	11 (42.3%)	11 (42.3%)	4 (15.4%)

dx.doi.org/10.1021/jf5024615 | J. Agric. Food Chem. 2014, 62, 6535−6538

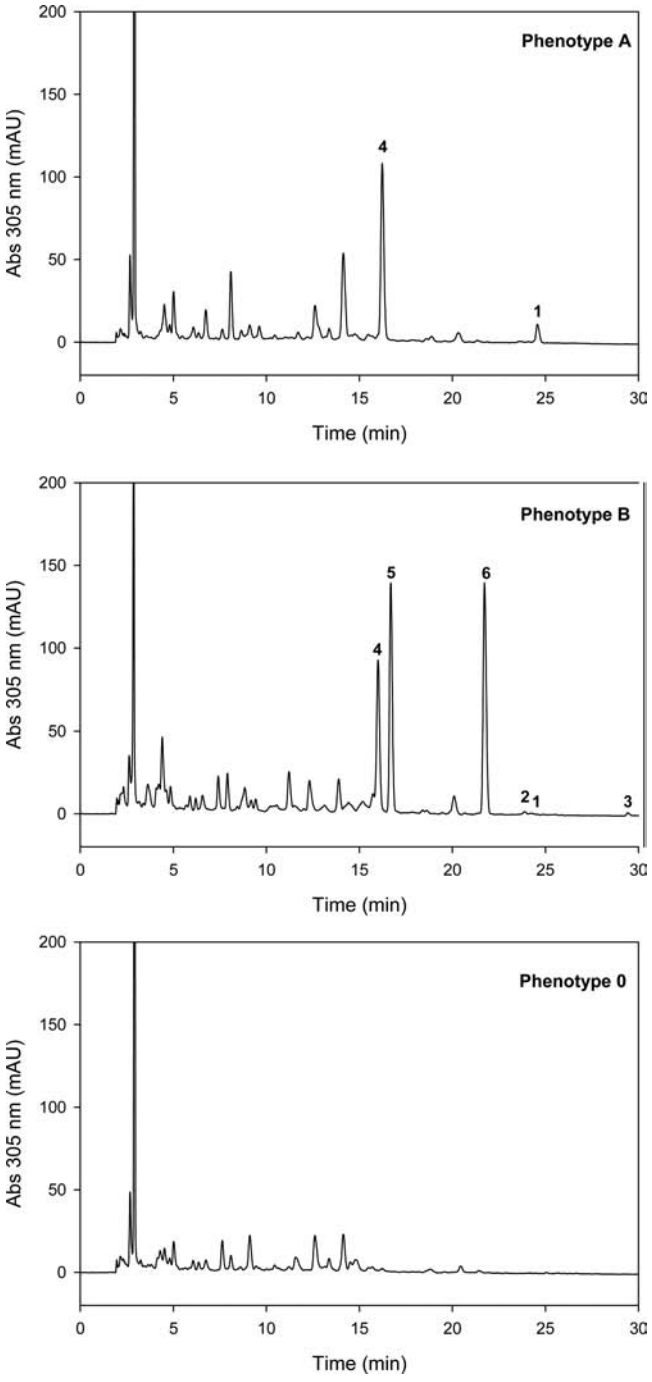

Figure 2. Characteristic HPLC-UV chromatograms showing the urolithin metabolite profiles corresponding to the three urinary phenotypes observed after the intake of walnuts.

source of ellagitannins and the amount of ellagic acid ingested. They were identified after the intake of walnuts, pomegranate juice,[7] pomegranate extracts,[4] strawberries,[8,9] raspberries,[9,10] cloudberries,[9] and unpeeled nuts.[11]

In healthy volunteers as well as in those patients with illnesses that are not characterized by gut dysbiosis (prostate cancer or benign hyperplasia), phenotype A was the main urinary profile (Table 1; Figure 3). In this regard, phenotype A was also the most abundant profile in patients with chronic obstructive pulmonary disease (age 60 ± 11 years) that consumed pomegranate juice for 5 weeks,[12] although data were not available for quantitative re-examination of the urinary

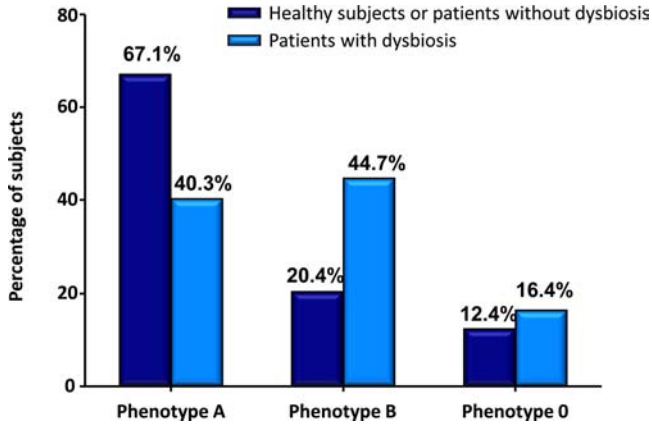

Figure 3. Mean distribution of the three phenotypes present in healthy subjects and patients without dysbiosis (n = 137) as well as in those patients with illnesses associated with gut dysbiosis (metabolic syndrome, n = 42; and colorectal cancer, n = 26).

profiles (results not shown). In contrast, the ratio between phenotypes A and B changed in patients with illness associated with gut dysbiosis such as metabolic syndrome or colorectal cancer, where phenotype B gained increasing relevance (Table 1; Figure 3). Age, gender, BMI, and geographical location did not affect urolithin urinary profiles (Table 1). We hypothesize that gut dysbiosis is the cause of the increase in the abundance of isourolithin A and urolithin B (phenotype B) in the patients with colon cancer and metabolic syndrome (Table 1). Therefore, a urolithin production test could be a useful biomarker to monitor certain gut microbial imbalances or to assess treatment efficacy.

Previous studies from other groups also showed the presence of these three phenotypes, which were within the ranges shown here. For example, a previous study of the urinary urolithins produced after the intake of raspberries by healthy volunteers (n= 10) showed that 70% were only urolithin A excreters (phenotype A), 20% excreted in addition isourolithin A and urolithin B (phenotype B), and 10% were nonexcreters (phenotype 0).[10] Interestingly, despite the relatively low number of volunteers, the distribution of the three phenotypes was similar to that observed in the three trials with healthy subjects shown here. A recent study[13] has reported the presence of three urinary urolithin excretion patterns after the intake of tropical highland blackberry juice by healthy volunteers that is also consistent with our results. However, demographic characteristics (age, gender, BMI) of volunteers were not described, and the ratio between phenotypes A and B was closer to that found in patients with gut dysbiosis than that observed in healthy subjects. In addition, in this previous study, the correlation of the production of urolithin B with that of isourolithin A was not described, as isourolithin A was not analyzed.

Our results show that stratification of subjects according to their urolithin phenotype should be considered in ellagitannin and ellagic acid intervention trials. Three consistent enterotypes, with different gut microbiota communities, have been described in humans.[14] In line with the trend highlighted by a previous study,[15] the challenge now is to investigate the correlation between these enterotypes, the three urolithin phenotypes, and the possible impact on human health.

Urolithins seem to be responsible for some health effects after ellagitannin intake;[2] therefore, volunteers in phenotype 0

dx.doi.org/10.1021/jf5024615 | J. Agric. Food Chem. 2014, 62, 6535−6538

will probably not benefit from them, and this should be demonstrated in further studies. Ellagic acid either remains unmetabolized in these volunteers or could be metabolized in a different way, leading to compounds different from urolithins that need to be further investigated.

Francisco A. Tomás-Barberán*
Rocío García-Villalba
Antonio González-Sarrías
María V. Selma
Juan C. Espín

Research Group on Quality, Safety and Bioactivity of Plant Foods, CEBAS-CSIC, P.O. Box 164, 30100 Espinardo, Murcia, Spain

AUTHOR INFORMATION

Corresponding Author

*(F.A.T.-B.) E-mail: fatomas@cebas.csic.es. Phone: +34-968 39 6334.

Funding

This work has been funded by the Fundación Séneca de la Región de Murcia (Grupo de Excelencia GERM 06, 04486), the program Consolider INGENIO 2010 (Project FUN-C-FOOD CSD2007-00063), and Projects CICYT-AGL2011-22447 (MINECO, Spain) and BACCHUS (FP7 European Commission Grant Agreement, 312090). R.G.-V. is the holder of a JAE-DOC contract from Consejo Superior de Investigaciones Científicas (CSIC, Spain), cofinanced by the European Social Fund (ESF), and A.G.-S. is the holder of a Juan de la Cierva contract (MINECO, Spain).

Notes

The authors declare no competing financial interest.

REFERENCES

(1) Larrosa, M.; García-Conesa, M. T.; Espín, J. C.; Tomás-Barberán, F. A. Ellagitannins, ellagic acid and vascular health. *Mol. Aspects Med.* **2010**, *31*, 513−39.

(2) Espín, J. C.; Larrosa, M.; García-Conesa, M. T.; Tomás-Barberán, F. A. Biological significance of urolithins, the gut microbial ellagic acid-derived metabolites: the evidence so far. *Evidence-Based Complement. Altern. Med.* **2013**, DOI:10.1155/2013/270418.

(3) Seeram, N. P.; Henning, S. M.; Zhang, Y.; Suchard, M.; Li, Z.; Heber, D. Pomegranate juice ellagitannin metabolites are present in human plasma and some persist in urine for up to 48 h. *J. Nutr.* **2006**, *136*, 2481−2485.

(4) Núñez-Sánchez, M. A.; García-Villalba, R.; Monedero-Saiz, T.; García-Talavera, N. V.; Gómez-Sánchez, M. B.; Sánchez-Alvarez, C.; García-Albert, A. M.; Rodríguez-Gil, F. J.; Ruiz-Marín, M.; Pastor-Quirante, F. A.; Martínez-Díaz, F.; Yáñez-Gascón, M. J.; González-Sarrías, A.; Tomás-Barberán, F. A.; Espín, J. C. Targeted metabolomics profiling of pomegranate polyphenols and urolithins in plasma, urine and colon tissues from colorectal cancer patients. *Mol. Nutr. Food Res.* **2014**, *58*, 1199−1211.

(5) García-Villalba, R.; Beltrán, D.; Espín, J. C.; Selma, M. V.; Tomás-Barberán, F. A. Time course production of urolithins from ellagic acid by human gut microbiota. *J. Agric. Food Chem.* **2013**, *61*, 8797−8806.

(6) Cerdá, B.; Tomás-Barberán, F.; Espín, J. C. Metabolism of chemopreventive and antioxidant ellagitannins from strawberries, raspberries, walnuts and oak-aged wines in humans: identification of biomarkers and individual variability. *J. Agric. Food Chem.* **2005**, *53*, 227−235.

(7) González-Sarrías, A.; Giménez-Bastida, J.; García-Conesa, M. T.; Gómez-Sánchez, M. B.; García-Talavera, N.; Gil-Izquierdo, A.; Sánchez-Alvarez, C.; Fontana-Compiano, L. O.; Morga-Egea, J. P.; Pastor-Quirante, F. A.; Martinez-Diaz, F.; Tomas-Barberan, F. A.; Espín, J. C. Occurrence of urolithins, gut microbiota ellagic acid metabolites, and proliferation markers expression response in human prostate gland upon consumption of walnuts and pomegranate juice. *Mol. Nutr. Food Res.* **2010**, *54*, 311−322.

(8) Truchado, P.; Larrosa, M.; García-Conesa, M. T.; Cerdá, B.; Vidal-Guevara, M. L.; Tomás-Barberán, F. A.; Espín, J. C. Strawberry processing does not affect the production and urinary excretion of urolithins, ellagic acid metabolites, in humans. A cross-over study. *J. Agric. Food Chem.* **2012**, *60*, 5749−5754.

(9) Puupponen-Pimiä, R.; Seppänen-Laakso, T.; Kankainen, M.; Maukonen, J.; Törrönen, R.; Kolehmaninen, M.; Leppänen, T.; Moilanen, E.; Nohynek, L.; Aura, A. M.; Poutanen, K.; Tomás-Barberán, F. A.; Espín, J. C.; Oksman-Caldentey, K. M. Effects of ellagitannin-rich berries on blood lipids, gut microbiota and urolithin production in human subjects with symptoms of metabolic syndrome. *Mol. Nutr. Food. Res.* **2013**, *57*, 2258−2263.

(10) González-Barrio, R.; Borges, G.; Mullen, W.; Crozier, A. Bioavailability of anthocyanins and ellagitannins following consumption of raspberries by healthy humans and subjects with an ileostomy. *J. Agric. Food Chem.* **2010**, *58*, 3933−3939.

(11) Tulipani, S.; Urpí-Sardá, M.; García-Villalba, R.; Rabassa, M.; López-Uriarte, P.; Bulló, M.; Jáuregui, O.; Tomás-Barberán, F. A.; Salas-Salvadó, J.; Espín, J. C.; Andrés-Lacueva, C. Urolithins are the main urinary microbial-derived phenolic metabolites discriminating a moderate consumption of nuts in free-living subjects with diagnosed metabolic syndrome. *J. Agric. Food Chem.* **2012**, *60*, 8930−8940.

(12) Cerdá, B.; Soto, M. C.; Albaladejo, M. D.; Martínez, P.; Sánchez-Gascón, F.; Tomás-Barberán, F. A.; Espín, J. C. Pomegranate juice supplementation in COPD: a 5-week randomised, double blind, placebo-controlled trial. *Eur. J. Clin. Nutr.* **2006**, *60*, 245−253.

(13) García-Muñoz, C.; Hernández, L.; Pérez, A.; Vaillant, F. Diversity of urinary excretion patterns of the main ellagitannins' colonic metabolites after ingestion of tropical highland blackberry (*Rubus adenotrichus*) juice. *Food Res. Int.* **2014**, *55*, 161−169.

(14) Arumugam, M.; Raes, J.; Pelletier, E.; Le Paslier, D.; Yamada, T.; Mende, D. R.; Fernandes, G. R.; Tap, J.; Bruls, T.; Batto, J. M.; Bertalan, M.; Borruel, N.; Casellas, F.; Fernandez, L.; Gautier, L.; Hansen, T.; Hattori, M.; Hayashi, T.; Kleerebezem, M.; Kurokawa, K.; Leclerc, M.; Levenez, F.; Manichanh, C.; Nielsen, H. B.; Nielsen, T.; Pons, N.; Poulain, J.; Qin, J.; Sicheritz-Ponten, T.; Tims, S.; Torrents, D.; Ugarte, E.; Zoetendal, E. G.; Wang, J.; Guarner, F.; Pedersen, O.; de Vos, W. M.; Brunak, S.; Doré, J.; MetaHIT Consortium; Antolín, M.; Artiguenave, F.; Blottiere, H. M.; Almeida, M.; Brechot, C.; Cara, C.; Chervaux, C.; Cultrone, A.; Delorme, C.; Denariaz, G.; Dervyn, R.; Foerstner, K. U.; Friss, C.; van de Guchte, M.; Guedon, E.; Haimet, F.; Huber, W.; van Hylckama-Vlieg, J.; Jamet, A.; Juste, C.; Kaci, G.; Knol, J.; Lakhdari, O.; Layec, S.; Le Roux, K.; Maguin, E.; Mérieux, A.; Melo-Minardi, R.; M'rini, C.; Muller, J.; Oozeer, R.; Parkhill, J.; Renault, P.; Rescigno, M.; Sánchez, N.; Sunagawa, S.; Torrejon, A.; Turner, K.; Vandemeulebrouck, G.; Varela, E.; Winogradsky, Y.; Zeller, G.; Weissenbach, J.; Ehrlich, S. D.; Bork, P. Enterotypes of the human gut microbiome. *Nature* **2011**, *473*, 174−180.

(15) Tomás-Barberán, F. A.; Mine, Y. A key to understanding the effects of food bioactives in health. Gut microbiota. *J. Agric. Food Chem.* **2013**, *61*, 9755−9757.

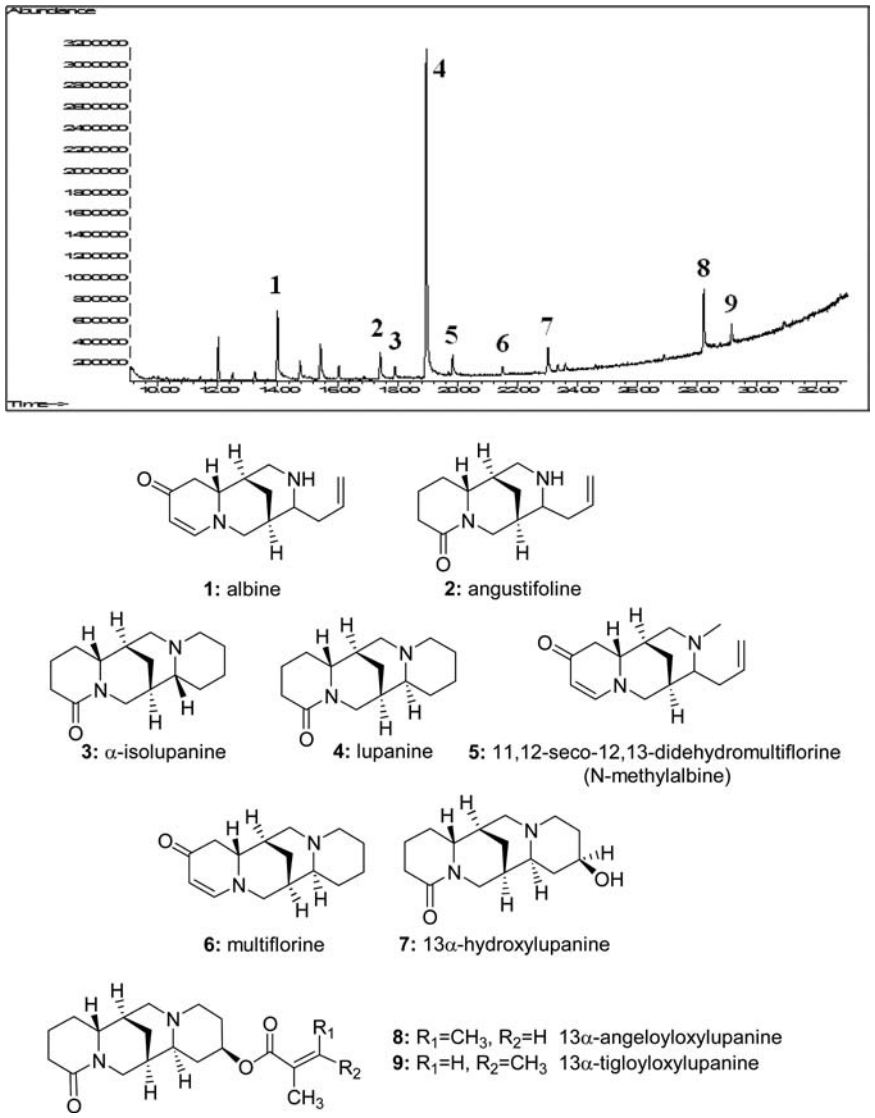

Figure 1. Total ion chromatogram of GC-MS analyses and QA chemical structure; **1**, albine; **2**, angustifoline; **3**, α-isolupanine; **4**, lupanine; **5**, 11,12-seco-12,13-didehydromultiflorine (formerly *N*-methylalbine); **6**, multiflorine; **7**, 13α-hydroxylupanine; **8**, 13α-angeloyloxylupanine; **9**, 13α-tigloyloxylupanine.

climate site compared with a subcontinental climate location (i.e., a location where autumn-sown crops undergo severe low-temperature stress during winter).[19] A second study, including some varieties and one ecotype grown in two climatically contrasting Italian sites, revealed large genotypic variation for various seed quality traits, along with large genotype × environment interaction variation for grain yield.[7] Subcontinental climate conditions determined higher QA content than Mediterranean conditions, leading various low-alkaloid varieties to exceed the limit of 200 mg/kg.[20]

The objective of this study is providing a thorough assessment of the relative contribution of genotypic, environmental, and genotype × environment interaction effects to variation in key production and quality traits of white lupin seeds. Our study included eight elite, phenotypically contrasting genotypes, which were grown in two climatically contrasting Italian locations for two cropping years, and we assessed grain yield, seed weight, and the content of oil, TOC, and QA.

MATERIALS AND METHODS

Chemicals. Hexane, dichloromethane, and 2-propanol were purchased from Baker (Deventer, The Netherlands); 36% hydrochloric acid was from Merck (Darmstadt, Germany); 25% NH_4OH was from Carlo Erba (Rodano, Italy); and standards of tocopherols were from Calbiochem (EMD Biosciences, Merck, Darmstadt, Germany).

Plant Material and Growing Environments. The test white lupin genotypes were (i) Multitalia, which is the only commercial variety of white lupin registered in Italy; (ii) seven advanced breeding lines produced by a joint selection program of CRA and Jouffray-Drillaud, coded hereafter as P2, P3, 4-3, 7-44, 7-7, 8-28, and 8-483. These lines were selected from a large number of breeding lines on the ground of wide or specific adaptation to subcontinental and Mediterranean climate locations of Italy, with the further objective of ensuring the presence of large morphophysiological variation within the set of tested material.[21] Modern white lupin varieties can be classified according to their phenological characteristics as spring (S) or autumn (A) types (which recall their suitability for spring or autumn sowing in cool temperate regions such as France); as tall (t), semidwarf (sd), or dwarf (d) types, according to genes affecting internode length and plant stature; and as indeterminate (I) or

dx.doi.org/10.1021/jf405615k | J. Agric. Food Chem. 2014, 62, 6539−6545

determinate (D) types, depending on the presence or absence of genetically determined ability to flower on secondary and higher-order branches.[22,23] The breeding lines exhibited the following combinations of traits: (i) lines P2 and P3, S/t/I; (ii) lines 4-3 and 7-44, A/sd/I; (iii) line 7-7, A/t/I; (iv) lines 8-28 and 8-483, A/d/D. Multitalia is t/I/ phenologically intermediate between S and A.

The eight genotypes were grown in Lodi (Lombardy, Italy, 45° 19′ N, 9° 03′ E) and Sanluri (Sardinia, Italy, 39° 30′ N, 8° 50′ E) in rain-fed autumn-sown field experiments, which were repeated in the seasons 2006−2007 and 2007−2008. Lodi has a subcontinental climate with cold winters and more favorable rainfall pattern than Sanluri, which has a Mediterranean climate (Table 1). The soils of both locations, featuring pH < 7.5 and active lime below 0.4%, were favorable for lupin cropping. Each experiment was designed as a randomized complete block with three replications. Each plot included 54 sown seeds arranged on three rows. Before sowing, the seeds were treated with Germipro UFB (BASF Agro, Ecully, France; 350 g/L iprodione + 177 g/L carbendazim) at the rate of 2.6 mL/kg, to limit possible damage by anthracnose (*Colletotrichum gloeosporioides*). They were inoculated with NPPL HiStick (Becker Underwood, Toulouse, France), to ensure proper nodulation and N fixation by *Bradyrhizobium* strains. The experiment in Lodi was fertilized with 40 kg/ha N and 120 kg/ha P_2O_5 and K_2O, whereas soil analyses suggested no fertilization requirement for Sanluri. Chemical weed control was performed in both sites by applying 4 L/ha Stomp 330 (BASF Agro; pendimentalin 32%). Individual plots were harvested individually when they reached crop maturity, which occurred in the first two weeks of July in Lodi and the second and third week of June in Sanluri. Grain yield was expressed at 13% seed moisture, after moisture determination on a random sample of 200 seeds per field replicate. These seed samples were also used for assessing the individual seed weight, expressed on a dry matter basis. Another random sample of 20 g of seed/replicate was used for assessing oil, TOC, and QA contents.

Extraction of Oil. Impurities were removed from the seeds, and the cleaned seeds were hand-dehulled, ground in a household mill (Braun, Germany), and sieved through a 60-mesh sieve. The oil was extracted with hexane for 6 h with a Soxhlet apparatus using cellulose extraction thimbles (123 mm × 43 mm i.d.; Whatman International, Brentford, U.K.); its content was gravimetrically determined and expressed as milligrams per gram of flour.[7,19] Each sample was independently extracted three times.

Extraction and Determination of Tocopherols. Tocopherols (TOC) were determined as previously reported.[6] Briefly, the oil was diluted in hexane, filtered through a 0.45 μm filter (Grace, Milan, Italy), and analyzed by a 1100 series HPLC (Agilent Technologies, Santa Clara, CA) equipped with an autosampler and a fluorometric detector (λ_{assn} = 295 nm, λ_{exc} = 290 nm, λ_{em} = 330 nm, frequency 55 Hz, gain 10). The analyses were performed on a Lichrosorb Si60 column with *n*-hexane/2-propanol (99:1 v/v) as mobile phase; the injection volume was 10 μL and the flow rate was 1 mL/min. The relative amounts of TOC were calculated by comparing their peak areas with standard curves, as previously reported.[6] The total TOC content was calculated by summing up the values of each detected isomer. TOC concentration was expressed as milligrams per gram of flour. Each sample was independently analyzed three times.

Extraction and Determination of Quinolizidine Alkaloids. Quinolizidine alkaloid (QA) extraction was performed as previously reported.[20,24] Briefly, 1 g of defatted flour was suspended in 8 mL of 0.1 N HCl and stirred at room temperature for 17 h; the mixture was centrifuged at 6000*g* for 50 min at 4 °C, the supernatant was collected, and the solid was washed twice with 5 mL of 0.1 N HCl. The gathered extracts were alkalinized with 5% NH_4OH to pH 10−11 and then applied onto an Extrelut NT 20 column (Merck, Darmstadt, Germany). The alkaloids were eluted with CH_2Cl_2 (4 × 20 mL), and the solvent was evaporated to dryness under vacuum. The residue was diluted in dichloromethane and analyzed by gas chromatography−mass spectrometry (GC-MS). Each sample was independently extracted at least three times. The GC-MS analyses were performed on a Shimadzu QP-5000 GC-MS instrument equipped with an AOC20i autosampler (Shimadzu) using an AT-1 ms capillary column 30 m × 0.25 mm i.d., 0.25 μm (Supelco, Milan, Italy). The temperature program was as follows: 150 °C for 5 min, from 150 to 300 °C at 5 °C/min, and then 300 °C for 15 min. Analyses were performed in split mode (split ratio 1:25), the injection volume was 1 μL, the injection temperature was 250 °C, the interface temperature was 300 °C, and the acquisition was in the range 50−450 *m*/*z*. The source operated in electron ionization (EI) mode. Each analysis was repeated three times. The identification and quantification of QA was performed as previously reported.[20,24] The total content, expressed as milligrams per gram of flour, is the sum of nine alkaloids (reported here in elution order): albine, angustifoline, α-isolupanine, lupanine, 11,12-seco-12,13-didehydromultiflorine (formerly *N*-methylalbine), multiflorine, 13α-hydroxylupanine, 13α-angeloyloxylupanine, and 13α-tigloyloxylupanine. Figure 1 reports a typical GC-MS chromatogram and chemical structures of QA. Each sample was independently analyzed three times. In Supporting Information, the main analytical features of the detected QA (Table S1) and composition of single QA (Table S2) are available.

Statistical Analysis. Chemical analysis replications belonging to same field plot were averaged prior to statistical analyses, which were performed on the three field plot replications available for each genotype−environment combination (considered more representative of treatment variation due to environmental effects than chemical replications). An analysis of variance (ANOVA) including the fixed factors genotype, location and year and the random factor experiment block was performed on plot values of grain yield, individual seed weight, oil content, TOC content, and QA content, to assess the significance of all genotypic, environmental, and GE interaction sources of variation. A second ANOVA including the fixed factors genotype and cropping environment (as defined from the four location−year combinations) and the random factor block aimed to compare mean values of genotypes and environments using Duncan's multiple range test at $p < 0.05$. The size of genotypic, environmental, and GE interaction effects was assessed by estimating the respective ANOVA components of variance through a restricted maximum likelihood method, assuming in this case that genotypes and environments were a random sample of the genetic and environmental variation relevant to a breeding program. ANOVAs were also carried out for each trait in each experiment, reporting least significance difference (LSD) values for genotype mean comparison at $p < 0.05$. All analyses were performed with Statistical Analysis System (SAS) software (1999).

RESULTS

Climatic information for test years and the long term at the test locations, particularly that with a bearing on the extent of winter cold stress and terminal drought stress, is given in Table 1. As expected, the subcontinental climate site (Lodi) was characterized by colder winters (in terms of number of frost days and absolute minimum temperature) and more rainy springs than the Mediterranean climate site (Sanluri). However,

Table 1. Climatic Characteristics of Test Locations of *Lupinus albus* Genotypes in the Cropping Years and the Long Term

period	frost days	winter abs min temp (°C)	mean daily temp October−June (°C)	rainfall April−June (mm)
Lodi (Subcontinental Climate)				
season 2006−2007	18	−2.5	11.0	202
season 2007−2008	38	−6.8	11.0	239
long-term value	56	−7.7	9.3	218
Sanluri (Mediterranean Climate)				
season 2006−2007	0	0.5	14.6	151
season 2007−2008	10	−4.0	13.8	117
long-term value	2	0.1	15.0	88

dx.doi.org/10.1021/jf405615k | J. Agric. Food Chem. 2014, 62, 6539−6545

Table 2. Mean Values of Grain Yield and Seed Quality Traits for Eight *Lupinus albus* Genotypes Grown in Four Environments[a]

genotype	Lodi		Sanluri		mean[b]
	2006−2007	2007−2008	2006−2007	2007−2008	
			Grain Yield (t/ha)		
Multitalia	8.106	6.850	1.764	2.760	4.870 ab
P2	7.563	3.583	2.322	2.560	4.007 b
P3	9.779	3.875	4.264	2.650	5.142 a
4-3	5.917	6.368	1.211	1.777	3.818 b
7-44	7.715	6.828	2.136	1.840	4.630 ab
7-7	6.318	6.342	2.099	1.700	4.115 b
8-28	5.969	3.639	1.225	1.230	3.016 c
8-483	4.314	3.766	2.475	1.317	2.968 c
mean[b]	6.960 a	5.156 b	2.187 c	1.979 c	4.071
LSD	3.283	1.092	1.971	0.649	0.941
			Seed Weight (mg)		
Multitalia	0.479	0.374	0.351	0.361	0.391 a
P2	0.354	0.283	0.257	0.315	0.302 c
P3	0.349	0.271	0.342	0.336	0.325 b
4-3	0.380	0.301	0.286	0.273	0.310 bc
7-44	0.358	0.256	0.304	0.319	0.309 bc
7-7	0.381	0.322	0.269	0.309	0.320 b
8-28	0.317	0.234	0.269	0.301	0.280 d
8-483	0.355	0.257	0.248	0.260	0.280 d
mean[b]	0.372 a	0.287 c	0.291 bc	0.309 b	0.315
LSD	0.027	0.023	0.042	0.039	0.015
			Oil Content (mg/g)		
Multitalia	117.2	102.1	101.5	113.3	108.5 a
P2	107.5	103.9	110.2	118.2	110.0 a
P3	98.5	88.7	109.6	112.3	102.3 b
4-3	92.5	92.3	99.2	107.8	98.0 c
7-44	123.0	92.2	116.5	105.4	109.3 a
7-7	97.4	109.1	110.7	114.7	108.0 a
8-28	88.6	86.1	97.6	97.5	92.4 d
8-483	94.0	87.2	94.7	103.2	94.8 cd
mean[b]	102.3 ab	95.2 b	105.0 ab	109.1 a	102.9
LSD	6.9	13.8	6.2	10.1	4.2
			Tocopherol Content (mg/g)		
Multitalia	0.1180	0.1200	0.1380	0.1070	0.1208 d
P2	0.1400	0.1240	0.1230	0.1250	0.1280 abc
P3	0.1110	0.1280	0.1380	0.1180	0.1238 cd
4-3	0.1360	0.1210	0.1490	0.1170	0.1308 ab
7-44	0.1160	0.1520	0.1340	0.1160	0.1295 abc
7-7	0.1260	0.1150	0.1450	0.1120	0.1245 bcd
8-28	0.1130	0.1210	0.1340	0.1160	0.1210 d
8-483	0.1240	0.1320	0.1530	0.1220	0.1328 a
mean[b]	0.1230 bc	0.1266 b	0.1393 a	0.1166 c	0.1264
LSD	0.0117	0.0172	0.0129	0.0099	0.0057
			Alkaloid Content (mg/g)		
Multitalia	6.392	4.820	2.448	3.467	4.282 a
P2	0.090	0.228	0.121	0.130	0.142 d
P3	0.169	0.159	0.047	0.092	0.117 d
4-3	0.329	0.291	0.082	0.181	0.221 c
7-44	0.320	0.275	0.108	0.225	0.232 c
7-7	0.614	0.441	0.240	0.339	0.409 b
8-28	0.175	0.300	0.117	0.310	0.226 c
8-483	0.623	0.323	0.146	0.389	0.370 b
mean[b]	1.089 a	0.855 b	0.414 d	0.642 c	0.750
LSD	0.193	0.052	0.196	0.136	0.067

[a]Environments were formed by the combination of one subcontinental (Lodi) or Mediterranean (Sanluri) climate location by each of two cropping years (2006−2007 and 2007−2008). Least significant difference (LSD) at $p < 0.05$ for genotype mean comparison within and across environments is also shown. [b]Environment row means, or genotype column means across environments, that are followed by different letters differ at $p < 0.05$ according to Duncan's test.

dx.doi.org/10.1021/jf405615k | J. Agric. Food Chem. 2014, 62, 6539−6545

milder winters and higher mean temperatures than the long term in Lodi (particularly in the first year), and wetter springs (particularly in the first year) and lower winter and mean temperatures (in the second year) than the long term in Sanluri, made the two locations less climatically contrasting over the test years than in the long term (Table 1).

Mean values of grain yield and seed quality traits for the eight lupin genotypes grown in the four environments formed by the combination of two climatically contrasting sites (Lodi or Sanluri) and two cropping years (2006−2007 and 2007−2008) are reported in Table 2, whereas ANOVA results for genotype, location and year factors and their interactions are given in Table 3. Significant variation among genotypes was detected

Table 3. Analysis of Variance *F*-Test Results for Grain Yield and Grain Quality Traits of Eight *Lupinus albus* Genotypes[a]

source of variation	grain yield	seed weight	oil content	total TOC	total QA
genotype	**	**	**	**	**
location	**	**	*	NS	**
year	*	**	NS	*	NS
genotype × location	**	**	**	**	**
genotype × year	**	*	**	**	**
location × year	*	**	NS	**	**
genotype × location × year	*	NS	*	**	**

[a]Grown in one subcontinental and one Mediterranean climate location for two cropping years. **Significant at $p < 0.01$; *significant at $p < 0.05$; NS, not significant.

both across and within environments for all traits. Genotype responses, however, interacted significantly with location and year in all cases (Table 3).

Averaged across genotypes, the lupin crop in the subcontinental climate site exhibited, in comparison with the Mediterranean location, almost 3-fold higher grain yield, larger seed (actually only in the first year), about 8% lower oil content, and definitely higher QA content (Table 2). The grain yield advantage of the former site over the latter was about 2-fold when the genotypes capable of maximizing the crop yield in each location are considered, that is, 7-44 in Lodi (site mean yield 7.27 t/ha), and P3 in Sanluri (site mean yield 3.46 t/ha) (Table 2). The mean crop response across environments tended to be more consistent and predictable for oil content (location factor was significant at $p < 0.05$; year, and location × year interaction were not significant) than for the other variables (Table 3). In contrast, site variation for TOC was inconsistent across years due to large location × year interaction (Table 3), since the Mediterranean location exhibited both the highest (first year) and the lowest (second year) environment mean value for this variable (Table 2).

The relative size of genotypic, environmental and GE interaction components of variance differed depending on the trait (Table 4). Grain yield variation was outstandingly affected by the cropping environment on the basis of the much greater size of the environmental component of variance relative to the genotypic and GE interaction variance components. Genotype yield responses were more affected by GE interaction than by purely genetic effects (as indicated by the almost 4-fold greater size of GE interaction variance relative to genotypic variance). Seed weight was affected by the environment and, to a lesser extent, by the genotype, in a fairly consistent manner (as indicated by the relatively smaller size of the GE interaction

Table 4. Estimates of Genotypic and Environmental Components of Variance for Grain Yield and Grain Quality Traits of Eight *Lupinus albus* Genotypes[a]

source of variation	grain yield $(t/ha)^2$	seed weight $(mg)^2$	oil content $(mg/g)^2$	total TOC $(mg/g)^2 \times 1000$	total QA $(mg/g)^2$
genotype	0.263	0.00106	0.384	0.0039	1.963
environment	5.608	0.00143	0.211	0.0759	0.046
genotype × environment	0.937	0.00051	0.366	0.0788	0.334

[a]Environments are combinations of two climatically contrasting locations by two cropping years. All variance components different from zero at $p < 0.01$.

variance component relative to the genotypic and environmental components of variance). Oil content variation was mainly affected by genotypic differences, which were partly inconsistent across environments (as indicated by comparable genotype and GE interaction variance). Purely genetic variation for TOC content had negligible size (although being statistically significant in Table 3) when compared with the outstanding variance of cropping environment and GE interaction (Table 4). Finally, QA content variation in this data set was largely affected by the genotype (Table 4), as further discussed later on.

Grain yield responses of the cultivars were heavily influenced by their phenological characteristics, as highlighted in greater detail in an analysis of adaptation that is reported elsewhere.[21] Spring types (lines P2 and P3) were top-yielding in the Mediterranean site, performed fairly well in the mild winter year of the subcontinental climate site, and yielded very poorly in the cold winter year of the same site (Table 2) because of severe winter mortality. Autumn types, including the remaining breeding lines, displayed the opposite adaptation pattern, whereas Multitalia (phenologically intermediate) was moderately adapted to any test environment (Table 2). Multitalia also featured larger seed than any breeding line (Table 2).

The genetic variation for mean value of oil content was sizable (range of genotype means across environments 9.2−11%), whereas that for TOC was modest (range of genotype means across environments: 0.121−0.133 mg/g) (Table 2). In both cases, they were unrelated to phenological types (Table 2). In absolute terms, the highest recorded values for these quality traits were 12.3% for oil content (line 7-44 in the first cropping year at Lodi) and 0.153 mg/g for TOC content (line 8-483 in the first year at Sanluri) (Table 2).

Multitalia exhibited extremely high QA content, exceeding by at least 12-fold the limit of 200 mg/kg even in the most suitable environment for producing low-QA lupins (Table 2). All breeding lines except for line P3 exceeded the 200 mg/kg limit in at least one test environment (Table 2).

DISCUSSION

Our results can contribute to choices and strategies of product supply for seed lupin processing industries, as well as to variety selection strategies, for production areas of southern Europe. This region includes Mediterranean climate areas (represented here by Sanluri) that are widespread in central and southern Italy and in coastal areas of the Iberian and Balkan peninsulas and southern France, as well as subcontinental climate areas (represented by Lodi) placed in northern Italy and in inland areas of the Iberian and Balkan peninsulas and southwestern France. However, conclusive indications for these climatic

regions, especially for areas outside Italy, would require verification from experiments in a larger sample of test environments.

Assessing also site crop production, as in the current study, has great practical importance for the seed market, particularly with respect to plant material with locally highest yielding ability and in case a trade-off existed between grain yield and quality. The Mediterranean climate growing site offered two seed quality advantages, namely, consistently higher oil content and much lower risk of exceeding the safety QA level of 200 mg/kg, compared with the subcontinental climate site. These results confirm earlier findings relative to other white lupin cultivars.[7,19,20] These advantages may justify the attribution of somewhat higher market price to seeds produced in Mediterranean environments, which could partly counterbalance the much lower grain yield of these environments relative to subcontinental climate ones.

Besides its use as a traditional or functional food, white lupin could be used as a dual-purpose crop for oil extraction and for use of the residual from extraction as a high-protein feed (as ordinarily done for soybean). This option would be reinforced by the excellent food quality of its oil.[6,7] This study confirmed that Mediterranean environments are more suitable than subcontinental climate ones to produce oil-rich seeds. However, the oil content of locally adapted material (lines P3 and P2 and Multitalia) never exceeded 12% (Table 2). Although their oil contents were higher than those reported for other white lupin material in the United States (highest value 8.2%)[25,26] and Turkey (highest value 10.7%),[27,28] they might be too low to justify the oil extraction. Higher oil content (up to 13.6%) was previously observed in another Mediterranean climate Italian site, which featured, however, extremely low grain yield.[19] On the whole, these results emphasize the potential interest of screening large germplasm collections with the aim to identify material with outstanding oil content. The selection from such material of improved varieties is encouraged by the current finding that about half the genetic variation for oil content is not subject to GE interaction and can, therefore, be expressed consistently across cropping environments. This finding agrees with previous results for different cultivars of white lupin,[7] as well as with results for narrow-leafed lupin (*L. angustifolius*) in Australia.[29]

This study confirms the large GE interaction for grain yield across south-European environments that had already emerged for other sweet-seeded cultivars[30] and for a world collection of ecotypes of white lupin.[31] This GE interaction depends to a large extent on the site-specific importance of flowering time, as early material is more susceptible to winter frost but more tolerant to terminal drought than late material, and vice versa.[31] More generally, white lupin breeding for European regions needs to cope with particularly large specific-adaptation effects.[32]

The amount of QA in white lupin cultivars is genetically controlled by one major recessive gene and various minor genes.[22] The current content of QA referred to the sum of albine, angustifoline, multiflorine, 11,12-seco-12,13-didehydro-multiflorine, lupanine, α-isolupanine, 13α-hydroxylupanine, 13α-angeloyloxylupanine, and 13α-tigloyloxylupanine. The lower QA content exhibited by seed produced in the Mediterranean environments agrees with the finding by Christiansen et al.[33] that terminal drought stress tends to decrease the white lupin seed content of QA. Large environmental effects that were substantially unrelated to rainfall were reported for narrow-leafed lupin in Australia.[29] The outstanding QA seed content of Multitalia is probably due to extensive contamination, which may have arisen at first from pollen of neighboring bitter-seed plants and then built up in the cultivar stock across the many cycles of multiplication of this 25-year old cultivar. The average QA value of Multitalia in Lodi (5.6 mg/g) may imply over 30% bitter seeds, considering that the most bitter-seed Italian ecotypes displayed around 15 mg/g QA in the same location.[20] A contamination of 3% bitter seeds may lead to 25% bitter seeds after eight generations of seed multiplication, owing to the advantage of high QA plants under natural selection.[22] Although much lower, the QA content of most current breeding lines occasionally exceeded the limit of 200 mg/kg, probably because of slight contamination that arose at some stage of the selection process.

Tocopherols exist in four different congeners (vitamers) called α, β, γ, and δ. The most abundant are α, which is the main contributor to vitamin E activity, and γ, which shows the highest antioxidant activity in foods.[10] White lupin seeds contains α-, γ-, and δ-TOC (unlike narrow-leafed lupin, which lacks the third one).[6] The occurrence of fairly wide variation for TOC values had already been reported.[34,35] While confirming that (absolute range 0.107−0.153 mg/g; Table 2), our study also shows that this variation is substantially unpredictable and not exploitable, being largely inconsistent both across locations in different years and across genotypes in different environments.

Large seed is important essentially for direct lupin utilization as a traditional food. No tested material featured seed large enough for that use. Our results suggest, however, that genetically based differences for seed weight are largely repeatable across environments and, hence, selectable through breeding. The environmental effect is larger than the genetic one but is partly predictable, as somewhat larger seed can be obtained from more favorable growing environments.

In conclusion, the different white lupin traits object of our study offer different challenges and opportunities for breeders and crop production stakeholders. Some traits, such as oil content, alkaloid content, and to a lesser extent seed size, are affected by the agroclimatic area in a fairly consistent manner across cropping years and could be selected for on the basis of the relative size of purely genetic effects. The reverse is true for the total content of TOC, despite its fairly wide range of variation across genotypes and cropping environments. Grain yield is largely affected by the cropping site, and it would require the selection of different cultivars for climatically contrasting regions.

■ ASSOCIATED CONTENT

Supporting Information

Two tables showing main analytical features of the detected QA and composition of single QA in white lupin seeds. This material is available free of charge via the Internet at http://pubs.acs.org.

■ AUTHOR INFORMATION

Corresponding Author

*Telephone +39-0371-404751; fax +39-0371-31853; e-mail paolo.annicchiarico@entecra.it.

Funding

The field experiments were carried out within the project Plant Genetic Resources/FAO Treaty, funded by the Ministry of Agricultural, Food and Forestry Policies of Italy.

Notes

The authors declare no competing financial interest.

■ ACKNOWLEDGMENTS

We are grateful to Nathalie Harzic for the initial multiplication of plant material; to Antonio Carroni and Sandro Proietti for scientific and technical contributions, respectively, to the field trials; to Marta Caglioni, Cristina Rutigliano, and Laura Vaccaro for valuable help in laboratory work; and to Donatella Resta for precious discussions.

■ ABBREVIATIONS USED

GE, genotype × environment; MW, molecular weight; QA, quinolizidine alkaloids; TOC, tocopherols

■ REFERENCES

(1) About lupin, global production & trade. http://www.lupins.org/lupins (Accessed 25 March 2014).

(2) D'Agostina, A.; Antonioni, C.; Resta, D.; Arnoldi, A.; Bez, J.; Knauf, U.; Waesche, A. Optimization of a pilot-scale process for producing lupin protein isolates with valuable technological properties and minimum thermal damage. *J. Agric. Food Chem.* **2006**, *54*, 92−98.

(3) Sirtori, C. R.; Triolo, M.; Bosisio, R.; Bondioli, A.; Calabresi, L.; De Vergori, V.; Gomaraschi, M.; Mombelli, G.; Pazzucconi, F.; Zacherl, C.; Arnoldi, A. Hypocholesterolaemic effects of lupin protein and pea protein/fibre combinations in moderately hypercholesterolaemic individuals. *Br. J. Nutr.* **2012**, *107*, 1176−1183.

(4) Boschin, G.; Scigliuolo, G. M.; Resta, D.; Arnoldi, A. Optimization of the enzymatic hydrolysis of lupin (*Lupinus*) proteins for producing ACE-inhibitory peptides. *J. Agric. Food Chem.* **2014**, *62*, 1846−1851.

(5) Sujak, A.; Kotlarz, A.; Strobel, W. Compositional and nutritional evaluation of several lupin seeds. *Food Chem.* **2006**, *98*, 711−719.

(6) Boschin, G.; Arnoldi, A. Legumes are valuable sources of tocopherols. *Food Chem.* **2011**, *127*, 1199−1203.

(7) Boschin, G.; D'Agostina, A.; Annicchiarico, P.; Arnoldi, A. Effect of genotype and environment on fatty acid composition of *Lupinus albus* L. seed. *Food Chem.* **2008**, *108*, 600−606.

(8) Dillard, C. J.; German, J. B. Phytochemicals: Nutraceuticals and human health. *J. Sci. Food Agric.* **2000**, *80*, 1744−1756.

(9) Cho, Y.-S.; Yeum, K.-J.; Chen, C.-Y.; Beretta, G.; Tang, G.; Krinsky, N. I.; Yoon, S.; Lee-Kim, Y. C.; Blumberg, J. B.; Russell, R. M. Phytonutrients affecting hydrophilic and lipophilic antioxidant activities in fruits, vegetables and legumes. *J. Sci. Food Agric.* **2007**, *87*, 1096−1107.

(10) Bramley, P. M.; Elmadfa, I.; Kafatos, A.; Kelly, F. J.; Manios, Y.; Roxborough, H. E.; Schuch, W.; Sheehy, P. J. A.; Wagner, K. H. Vitamin E. *J. Sci. Food Agric.* **2000**, *80*, 913−938.

(11) Duranti, M. Grain legume proteins and nutraceutical properties. *Fitoterapia* **2006**, *77*, 67−82.

(12) Wink, M.; Meissner, C.; Witte, L. Patterns of quinolizidine alkaloids in 56 species of the genus *Lupinus*. *Phytochemistry* **1995**, *38*, 139−153.

(13) Boschin, G.; Resta, D., Alkaloids derived from lysine: Quinolizidine, a focus on lupin alkaloids. In *Natural Products: Phytochemistry, Botany and Metabolism of Alkaloids, Phenolics and Terpenes*; Ramawat, K. G., Merillon, J. M., Eds.; Springer: Berlin and Heidelberg, Germany, 2013; pp 381−403.

(14) Muzquiz, M.; Cuadrado, C.; Ayet, G.; de la Cuadra, C.; Burbano, C.; Osagie, A. Variation of alkaloid components of lupin seeds in 49 genotypes of *Lupinus albus* from different countries and locations. *J. Agric. Food Chem.* **1994**, *42*, 1447−1450.

(15) Erbas, M. The effects of different debittering methods on the production of lupin bean snack from bitter *Lupinus albus* L. seeds. *J. Food Qual.* **2010**, *33*, 742−757.

(16) *Lupin Alkaloids in Food. A Toxicological Review and Risk Assessment*; Technical Report Series 3; Australia New Zealand Food Authority: Canberra, Australia, 2001; pp 1−21.

(17) Advisory Committee on Novel Foods and Processes. *ACNFP Report on Seeds from Narrow Leafed Lupin*, Appendix IX; MAFF Publications: London, 1996; p 107.

(18) CSHPF. *Bulletin Officiel 98/27*; Conseil Superieur d'Hygiene Publique de France: Paris, 1998.

(19) Boschin, G.; D'Agostina, A.; Annicchiarico, P.; Arnoldi, A. The fatty acid composition of the oil from *Lupinus albus* cv. Luxe as affected by environmental and agricultural factors. *Eur. Food Res. Technol.* **2007**, *225*, 769−776.

(20) Boschin, G.; Annicchiarico, P.; Resta, D.; D'Agostina, A.; Arnoldi, A. Quinolizidine alkaloids in seeds of lupin genotypes of different origins. *J. Agric. Food Chem.* **2008**, *56*, 3657−3663.

(21) Annicchiarico, P.; Manunza, P.; Proietti, S. White lupin tolerance to winter cold, terminal drought and soil lime: patterns of genetic variation and their exploitation in breeding for Southern Europe. In *Lupin crops: An Opportunity for Today, a Promise for the Future*; Naganowska, B., Kachlicki, P., Wolko, B., Eds.; Proceedings of the XIII International Lupin Conference, International Lupin Association, Canterbury, New Zealand, 2011; pp 99−103.

(22) Papineau, J.; Huyghe, C. *Le Lupin doux Protéagineux*. Editions France Agricole: Paris, 2004.

(23) Huyghe, C. White lupin (*Lupinus albus* L.). *Field Crops Res.* **1997**, *53*, 147−160.

(24) Resta, D.; Boschin, G.; D'Agostina, A.; Arnoldi, A. Evaluation of total quinolizidine alkaloids content in lupin flours, lupin-based ingredients, and foods. *Mol. Nutr. Food Res.* **2008**, *52*, 490−495.

(25) Bhardwaj, H. L.; Hamama, A. A.; Merrick, L. C. Genotypic and environmental effects on lupin seed composition. *Plant Foods Hum. Nutr.* **1998**, *53*, 1−13.

(26) Bhardwaj, H. L.; Hamama, A. A.; van Santen, E. Fatty acids and oil content in white lupin seed as affected by production practices. *J. Am. Oil Chem. Soc.* **2004**, *81*, 1035−1038.

(27) Erbas, M.; Certel, M.; Uslu, M. K. Some chemical properties of white lupin seeds (*Lupinus albus* L.). *Food Chem.* **2004**, *89*, 341−345.

(28) Uzun, B.; Arslan, C.; Karhan, M.; Toker, C. Fat and fatty acids of white lupin (*Lupinus albus* L.) in comparison to sesame (*Sesamum indicum* L.). *Food Chem.* **2007**, *102*, 45−49.

(29) Cowling, W. A.; Tarr, A. Effect of genotype and environment on seed quality in sweet narrow-leafed lupin (*Lupinus angustifolius* L.). *Aust. J. Agric. Res.* **2004**, *55*, 745−751.

(30) Annicchiarico, P.; Carroni, A. M. Diversity of white and narrow-leafed lupin genotype adaptive response across climatically-contrasting Italian environments and implications for selection. *Euphytica* **2009**, *166*, 71−81.

(31) Annicchiarico, P.; Harzic, N.; Carroni, A. M. Adaptation, diversity, and exploitation of global white lupin (*Lupinus albus* L.) landrace genetic resources. *Field Crops Res.* **2010**, *119*, 114−124.

(32) Annicchiarico, P.; Harzic, N.; Huyghe, C.; Carroni, A. M. Ecological classification of white lupin landrace genetic resources. *Euphytica* **2011**, *180*, 17−25.

(33) Christiansen, J. L.; Jornsgard, B.; Buskov, S.; Olsen, C. E. Effect of drought stress on content and composition of seed alkaloids in narrow-leafed lupine, *Lupinus angustifolius* L. *Eur. J. Agron.* **1997**, *7*, 307−314.

(34) Martinez-Villaluenga, C.; Frias, J.; Vidal-Valverde, C. Functional lupin seeds (*Lupinus albus* L. and *Lupinus luteus* L.) after extraction of α-galactosides. *Food Chem.* **2006**, *98*, 291−299.

(35) Frias, J.; Miranda, M. L.; Doblado, R.; Vidal-Valverde, C. Effect of germination and fermentation on the antioxidant vitamin content and antioxidant capacity of *Lupinus albus* L. var. Multolupa. *Food Chem.* **2005**, *92*, 211−220.

Fourier transform/infrared-attenuated total reflectance (FT/IR-ATR) molecular spectroscopy can be used as a rapid, direct, nondestructive bioanalytical technique to detect heat-induced changes in protein molecular structures.[7,15] The objectives of the present study were to reveal MIR induced changes in protein molecular structures of hulless and hulled barley and to correlate these structural changes to changes in (1) chemical profile, (2) CP subfraction composition, and (3) in situ rumen CP degradation and intestinal digestibility of RUP. We hypothesized that MIR for different durations (3 or 5 min) will alter protein molecular structures to different extents in hulled and hulless barley, which will correspond to different levels of alteration in protein nutritive value and digestibility.

MATERIALS AND METHODS

Samples Preparation and Treatment. Grains from two newly developed hulless cultivars (CDC Fibar and HB08302) with altered starch composition (amylose/amylopectin ratio) and a normal hulled cultivar (Copeland) of barley were evaluated in the present study. The samples were provided by Dr. Aaron D. Beattie (Crop Development Center, University of Saskatchewan, Saskatoon, Canada). The CDC Fibar is a zero-amylose (0% amylose and 100% amylopectin) waxy cultivar, and HB08302 is a high-amylose (40% amylose and 60% amylopectin) cultivar. Copeland is a normal two-row malting barley cultivar. Grains were sampled (~2 kg) from four replicate plots of each cultivar grown at the Kernen Crop Research Fields (52°9′ N and 106°32′ W) of the Crop Development Center (CDC; University of Saskatchewan, Saskatoon, SK, Canada) during two consecutive years (2009 and 2010). For each cultivar, eight samples were used for heat processing. A subsample (~500 g) of each sample was heated in a microwave oven (DMW904W, Findlay, OH, US), operated at a power of 900 W (1.33 W/g) and an irradiation frequency of 2450 MHz for 3 min (MIR3) or 5 min (MIR5) in two replicate runs. Raw grains (MIR0) were used as control.

The control and heat-treated samples were ground (Retsch ZM-1, Brinkmann Instruments Ltd., Mississauga, ON, Canada) through a 0.25 mm screen for molecular spectral analysis; through a 2 mm screen for in situ rumen incubation studies, and through a 1 mm screen for all other wet chemical analysis.

Chemical Analysis. The ground (1 mm) samples of barley were analyzed for the contents of DM (method 930.15), ash (method 942.05), CP (method 984.13; using a Kjeltec 2400 autoanalyzer; Foss Analytical A/S, Hillerød, Denmark), and ether extract (EE; method 920.39) according to the standard procedures of the AOAC.[16] The contents of neutral detergent insoluble CP (NDICP) and acid detergent insoluble CP (ADICP) were analyzed according to the method of Licitra et al.[17] The content of SCP was analyzed according to the method of Roe et al.[18] with slight modification as described by Peng et al.[7] The non-protein nitrogen (NPN) content was analyzed according to the method of Licitra et al.[17] The true protein in feeds was precipitated with tungstic acid, and the NPN content was calculated as the difference between total CP content and CP content of the residues after filtration.

Fractionation of Crude Protein. The CP content of the feeds was fractionated into immediately solubilized protein (PA), potentially degradable true protein (PB), and unavailable true protein (PC) according to the Cornell Net Carbohydrate Protein System (CNCPS).[19] The subfraction PB was further fractionated into three subfractions that are believed to have different rates of ruminal degradation. PB1 is the rapidly degradable subfraction with a degradation rate of 120−400%/h, PB2 is the intermediately degradable subfraction with a degradation rate of 3−16%/h, and PB3 is the slowly degradable subfraction with a degradation rate of 0.06−0.55%/h.[21] PA is calculated as NPN × 6.25; subfraction PB1 is the buffer-soluble protein and calculated as SCP − PA; subfraction PB2 is calculated as CP − (PA + PB1 + PB3 + PC); subfraction PB3 is calculated as NDICP − ACDIP; and subfraction PC is the ADICP.

In Situ Rumen Incubation. Three lactating Holstein dairy cows, each fitted with flexible rumen cannula with an internal diameter of 10 cm (Bar Diamond Inc., Parma, ID, USA), were used for the in situ rumen incubation studies. The fistulated cows were handled according to the guidelines of the Canadian Council on Animal Care.[20] The cows were individually fed a balanced TMR (15 kg/head/day on DM basis), containing 510 g of barley silage, 150 g of chopped alfalfa hay, and 340 g of concentrate per kg DM. The concentrate contained 560 g of barley, 50 g of wheat, 50 g of oats, 330 g of dairy supplement pellets, and 10 g of molasses per kg DM, whereas the pellet dairy mixture contained 316 g of soybean meal, 270 g of canola meal, 100 g of peas, 85 g of premix (University of Saskatchewan), 55 g of corn gluten meal, 55 g of corn grain, 47 g of sodium bicarbonate, 30 g of ground barley, 20 g of canola oil, 16 g of salt, and 7 g of Dynamate (K and Mg sulfate, University of Saskatchewan) per kg DM. The TMR was formulated according to NRC requirements for dairy cows[21] and fed twice daily (8:00 a.m. and 4:00 p.m.) in equal portions. All cows had 24 h/day access to fresh drinking water.

The in situ nylon bag technique as described by Peng et al.[7] was used to determine the rumen degradation kinetics of the feeds. Briefly, 7 g of the coarsely ground (2 mm) sample of each treatment of each barley cultivar was weighed into preweighed and coded nylon bags (10 × 20 cm) with a pore size of 41 μm (Nitex 03-41/31 monofilament open mesh fabric, Screentech Corp., Mississauga, ON, Canada). The ratio of sample size to bag surface area was 19 mg/cm^2. The gradual addition, all-out method was used. The bags were randomly incubated for 48, 24, 12, 8, 4, 2, and 0 h in rumen of the three fistulated cows in two replicate runs. To get enough residues for chemical analysis, multiple bags were used. The multiple bags for 48, 24, 12, 8, 4, 2, and 0 h incubation periods were 5, 4, 4, 2, 2, 2, and 2, respectively. A large polyester mesh bag (45 × 45 cm, fixed to rumen cannula with a 90 cm long rope) was used to hold the bags in rumen. To hold the bags in bottom liquid phase of the rumen, a 250 mL plastic bottle filled with gravel was placed in the polyester mesh bag. The bags were removed from the rumen at the end of incubation period and immediately gently rinsed (six times) in a bucket with cold tap water to remove adhering ruminal contents and stop microbial/enzymatic degradation. The 0 h samples were washed under similar conditions without rumen incubation. The bags were subsequently dried at 55 °C for 48 h, cooled, and reweighed. Residues were pooled together per incubation time for each run. The dried residues were ground and stored at 4 °C for chemical analysis.

Rumen Degradation Kinetics. The rumen degradation characteristics of DM and CP were computed according to the first-order kinetics equation of Ørskov and McDonald[22] with slight modifications as proposed by Tamminga et al.[23]

$$Y(t) = U + (100 - S - U) \times e^{-kd(t-T_0)}$$

where $Y(t)$ is the DM/CP (%) present in the residues at t hours of incubation; S is the soluble subfraction (%); U is the rumen undegradable subfraction (%); K_d is the degradation rate of potentially degradable subfraction (%/ h); and T_0 is lag time (h). The in situ parameters were analyzed using the nonlinear (PROC NLIN) procedure with iterative least-squares regression (Gauss−Newton method) of the Statictical Analysis System (SAS).[24] The effective degradability of DM (EDDM) and CP (EDCP) was computed according to the NRC-2001 dairy model[21] as

$$\text{ED (DM/CP)} = S + D \times \left[\frac{K_d}{(K_d + K_p)}\right]$$

where D is the potentially degradable subfraction (%) and estimated as $D = 100 - S - U$ and K_p is the estimated outflow rate of digesta from rumen, which was assumed to be 6%/h.[23] The rumen undegraded DM and CP was calculated as follows:

$$\text{RU (DM/CP)} = U + D \times \left[\frac{K_p}{(K_d + K_p)}\right]$$

dx.doi.org/10.1021/jf501024j | J. Agric. Food Chem. 2014, 62, 6546−6555

Table 1. Microwave Irradiation Induced Changes in Chemical Profiles of Hulless (CDC Fibar and HB08302) and Hulled (Copeland) Barley[a]

	microwave irradiation (MIR)[b,c]				barley variety[d]				*P* value[e]		contrasts[e]	
item	MIR0	MIR3	MIR5	SEM[f]	CDC Fibar	HB08302	Copeland	SEM	MIR	feed	control vs MIR	hulless vs hulled
basic chemical profile[g]												
DM, %	91.38c	94.66b	96.22a	0.088	94.08AB	94.33A	93.84B	0.088	***	**	***	**
EE, % DM	2.51	2.44	2.51	0.070	2.61A	2.79A	2.06B	0.070	ns	***	ns	***
ash, % DM	2.41	2.40	2.36	0.127	2.33B	2.18B	2.66A	0.127	ns	***	ns	***
protein profile[h]												
CP, % DM	13.62	13.49	13.35	0.165	16.00A	13.51B	10.94C	0.166	ns	***	ns	***
NDICP, % CP	13.32b	14.53b	26.20a	2.138	14.56B	24.25A	15.25B	2.139	**	*	*	ns
ADICP, % CP	0.97b	1.67b	5.32a	0.739	1.48B	4.62A	1.86AB	0.740	**	*	*	ns
SCP,[i] % CP	50.84	26.04	17.56	0.724	29.46	30.33	34.65	0.725	***	**	***	***
NPN, % CP	5.62b	12.31a	11.19a	0.677	9.34	9.95	9.83	0.678	***	ns	***	ns
NPN, % SCP	11.04c	47.61b	65.54a	3.236	43.53	45.99	34.66	3.236	***	†	***	*

[a]Means within a row with different lower case (a–c) or capital (A–C) letters differ at $P < 0.05$. [b]For each treatment (MIR0, MIR3, and MIR5) each sample was run two times. [c]Heated treated by microwave irradiation for 0 (MIR0), 3 (MIR03) or 5 (MIR05) min. [d]For each barley cultivar eight replicate samples were analyzed. [e]ns, not significant; †, $P < 0.1$; *, $P < 0.05$; **, $P < 0.001$; ***, $P < 0.001$. [f]SEM, standard error of the mean. [g]DM, dry matter; EE, ether extract. [h]CP, crude protein; NDICP, neutral detergent-insoluble protein; ADICP, acid detergent-insoluble protein; SCP, soluble CP; NPN, non-protein nitrogen. [i]The interactions of irradiation time and barley cultivar were significant ($P < 0.05$); therefore, no letter is given for the treatment means.

Intestinal Digestibility of Rumen Undegraded Protein. The three-step in vitro procedure as described by Calsamiglia and Stern[25] was used to determine the intestinal digestibility of RUP. Briefly, a calculated amount of dried ground residues of 16 h rumen incubation, containing approximately 15 mg of N, was transferred to 15 mL centrifuge tubes. Subsequently, 10 mL of 0.1 N HCl solution containing 1 g/L pepsin was added to the residues. The mixtures were then vortexed and incubated in a shaking water bath at 38 °C for 1 h. After incubation, 0.5 mL of 1 N NaOH was added to the mixture to neutralize the pH. Subsequently, 13.5 mL of phosphate buffer (pH 7.8) containing 37.5 mg of pancreatin was added to the mixture, vortexed, and further incubated at 38 °C for 24 h. After incubation, 3 mL of 100% (w/v) TCA solution was immediately added to precipitate the undigested protein and stop enzymatic reactions. The mixtures were vortexed and then centrifuged at 10000*g* for 15 min at a room temperature (20–22 °C). The supernatant was collected and analyzed for (soluble/digested) N content. Duplicate blank (without sample) tubes were run to correct for background effect of the solutions and enzyme mixtures used during the analysis. The intestinal digestibility of RUP was computed by dividing the content of TCA-soluble N by total N in the residue sample.

Molecular Spectroscopy. The protein molecular spectral analyses were carried out at the molecular spectroscopy laboratory of the Department of Animal and Poultry Science, University of Saskatchewan (Saskatoon, Canada). The molecular spectral profiles were generated using a JASCO FT/IR-ATR-4200 (Jasco Inc., Easton, MD, USA), equipped with a deuterated L-alanine doped triglycine sulfate detector and a ceramic IR light source and fitted with a MIRacle ATR accessory module with a ZnSe crystal and pressure clamp (Pike Technologies, Madison, WI, USA). The spectra were generated in a transmission mode in the mid-IR (ca. 4000–800 cm^{-1}) and amide fingerprint (ca. 1732–1483 cm^{-1}) regions, with 128 co-added scans and a spectral resolution of 4 cm^{-1}. Each sample was run five times. The spectra were collected and corrected for background and CO_2 noise using Jasco Spectra Manager II software. The protein primary and secondary structure related molecular spectral features from the FT/IR spectra were quantified using Ominic 7.3 software (Spectra-Tech Inc., Madison, WI, USA). The spectral bands of the protein functional groups (C═O, C—N, and N—H), representing the primary molecular structures, were identified and assigned using published information.[7,26] Briefly, amide I (~80% C═O and ~10% C—N stretching vibration and 10% N—H bending vibration; centered at a wavelength of ca. 1655 cm^{-1}) and amide II (~60% N—H bending vibration, ~40% C—N stretching vibration; centered at ca. 1565 cm^{-1}) were quantified for the characterization of protein primary structures. For characterization of protein secondary structures, the FSD spectrum was generated using Fourier self-deconvolution (FSD) or the secondary derivative functions in the OMNIC software. The FSD spectrum was further resolved into several multicomponent peaks in the protein amide I region, where α- helices (centered at ca. 1653 cm^{-1}) and β-sheets (centered at ca. 1630 cm^{-1}) were identified. Peak area, height of the spectral intensities of amide I and amide II, and α-helix and β-sheet were measured and ratios were calculated.

Statistical Analysis. Data on chemical profiles, CP subfractions, digestible nutrients, energy values of FT/IR spectra, in situ rumen degradation characteristics, and intestinal digestibility of RUP were analyzed according to the PROC MIXED procedure of the Statistical Analysis System (SAS).[24] The model used for analysis was

$$Y_{ijk} = \mu + \mathrm{MIR}_i + \mathrm{BC}_j + e_{ijk}$$

where Y_{ijkl} is an observation on the dependent variable *ijkl*; μ is the overall population mean; MIR_i is the fixed effect of MIR (control and 3 and 5 min of irradiation); BC_j is the fixed effect of the barley cultivars (CDC Fibar, HB08302, and Copeland); and e_{ijk} is random error associated with the observation *ijk*. Except for a few parameters, the interactions of MIR and barley variety were nonsignificant and hence removed from the final model. Significant ($P < 0.05$) interactions are reported in the footnotes of the tables. Post hoc analyses were carried out using the Tukey–Kramer test to compute pairwise differences in the means. Means with different letters were obtained with "pdmix 800 SAS macro".[27] The PROC CCORR of SAS[24] was used to determine the strength of relationship between protein molecular structural characteristics and chemical profiles, CP subfractions, in situ rumen degradation characteristics, and intestinal digestibility of RUP.

The agglomerative hierarchical cluster analysis (CLA) and principal component analysis (PCA) were performed on the spectral data at the fingerprint region og ca. 1732–1483 cm^{-1} (representing amide I and II bands) to visualize and classify the difference in intrinsic protein molecular structures of the feeds using Statistica software (version 8, StatSoft Inc., Tulsa, OK, USA). The detailed concepts and procedure of using CLA and PCA for FTIR/ATR spectral analysis were described earlier.[13]

RESULTS AND DISCUSSION

Microwave Irradiation Induced Changes in Chemical Profile. Results of the MIR induced changes in the mean chemical profile of different cultivars of barley are shown in Table 1. Compared with the raw grains, MIR increased ($P <$

Table 2. Effects of Microwave Irradiation on Cornell Net Carbohydrate and Protein System (CNCPS) Subfractions of Hulless (CDC Fibar and HB08302) and Hulled (Copeland) Barley[a]

	microwave irradiation (MIR)[b]				barley variety				*P* valuue[c]		contrasts[c]	
item	MIR0	MIR3	MIR5	SEM[d]	CDC Fibar	HB08302	Copeland	SEM	MIR	feed	control vs MIR	hulless vs hulled
CP subfractions[e] (% of CP)												
PA	5.62b	12.31a	11.19a	0.678	9.34	9.95	9.83	0.678	***	ns	***	ns
PB1	45.22a	13.73b	6.36c	0.686	20.11B	20.39B	24.82A	0.686	***	*	***	***
PB2	35.84b	59.43a	56.24a	1.970	55.99A	45.43B	50.11AB	1.970	***	*	***	ns
PB3	12.36b	12.86b	20.88a	1.751	13.08	19.62	13.39	1.751	*	*	ns	ns
PC	0.97b	1.67b	5.32a	0.739	1.48B	4.62A	1.86AB	0.739	**	*	*	ns
true protein (% of true protein)												
PB1	48.20a	15.69b	7.13c	0.741	21.83B	22.06B	27.13A	0.741	***	**	***	**
PB2	38.19b	67.77a	63.26a	2.240	62.18A	50.89B	56.15AB	2.240	***	*	***	ns
PB3	13.19b	14.64ab	23.56a	1.951	14.55B	21.99A	14.85B	1.951	**	*	*	ns

[a]Means within a row with different lower case (a–c) or capital (A–B) letters differ at $P < 0.05$. [b]Heated treated by microwave irradiation for 0 (MIR0), 3 (MIR03), or 5 (MIR05) min. [c]ns, not significant; *, $P < 0.05$; **, $P < 0.001$; ***, $P < 0.001$. [d]SEM, standard error of the mean. [e]PA = NPN, the subfraction of CP that is instantaneously solubilized at time zero; PB1 = SCP-NPN, the rapidly degradable CP subfraction; PB2 = CP − (PA + PB1 + PB3 + PC), the intermediately degradable CP subfraction; PB3 = NDIP − ADIP, the slowly degradable CP subfraction; PC = ADIP, the undegradable subfraction of CP (it contains protein associated with lignin and tannins and heat-damaged protein such as the Maillard reaction products).

0.001) the content of DM, indicating that MIR decreased the moisture-holding capacity of barley grains. Previous studies have shown a decrease in DM content with dry heating of Camelina[7] and moist heating of flaxseed.[14] Compared with the raw grains, the contents of NDICP and ADICP increased with increasing duration of the MIR. Samadi and Yu[15] and Penge et al.[7] also observed an increase in cell wall bound CP with moist heating (60 min at 120 °C) of soybean and camelina seeds, respectively. The increase in fiber-bound CP could be related to the heat-induced cross-linkages between amino acids and reducing sugars such as during Maillard reactions.[7] The MIR markedly decrease (from 50.84 to 17.56% CP) the SCP content of barley. This is in agreement with previous findings of a marked decrease in the SCP subfractions of camelina seeds (from 52.73 to 20.41% CP),[7] soybeans (from 43.38 to 11.35% CP),[15] and flaxseeds (from 51.88 to 8.82% CP)[14] with moist heating (at 120 °C for 60 min). In contrast, the NPN content increased ($P < 0.001$) with MIR. The present result is supported by the findings of Doiron et al.[14] and Peng et al.[7] However, Mustafa et al.[28] and Samadi and Yu[15] observed a decrease in NPN content during heat processing. This discrepancy may be related to the differences in heating methods (MIR vs dry toasting, moist heating) or to the inherent differences in seed types (cereal grains vs oilseeds) and NPN methodologies (tungstic acid vs TCA, differences in filter papers pore size, etc.). Overall, our present findings suggest that a short-term (5 min) MIR induces more or less similar changes in the CP profiles of feed as have been reported for other feeds after 60 min of dry/moist heating at 120 °C. Except SCP for which the interaction was significant (results not shown), the MIR induced changes in chemical profile were independent of barley type. As discussed in detail earlier,[5] the hulless barley cultivars had higher ($P < 0.001$) contents of CP and EE than the hulled barley.

Microwave Irradiation Induced Changes in Crude Protein Subfractions. Results on the MIR-induced changes in CP subfractions are presented in Table 2. The contents of all CP subfractions in barley grains altered ($P < 0.05$) with MIR, and PB1 was the only subfraction that decreased ($P < 0.05$) in concentration. The MIR for 3 min increased ($P < 0.05$) the PA (soluble) subfraction, whereas further irradiation for 5 min had no significant effect on PA subfraction. The major changes in CP subfractions, however, occurred in the contents of PB1 and PB2. The PB1 (rapidly degradable) subfraction markedly decreased from 45.22 to 6.36% (% CP), whereas the PB2 (intermediately degradable) subfraction markedly increased from 35.84 to 59.43% (% CP). The increase (from 5.62 to 11.19% of CP) in the PA (NPN × 6.25) subfraction with MIR was quantitatively small. Therefore, the shift from the ruminally degradable PB1 subfraction to a partially ruminally degradable PB2 subfraction demonstrates an overall decrease in ruminal CP degradation rate in the irradiated barley grains. The changes in CP subfractions with MIR have not been evaluated previously. The changes in PB1 and PB2 subfractions after MIR (for 5 min) were comparable with the changes produced by moist heating at 120 °C for 60 min.[7,14] The moist heating decreased the PB1 subfraction of flaxseed from 45.9 to 10.5% CP with a concomitant increase in the PB2 subfraction from 43.0 to 73.3% CP.[14] Similarly the moist heating of camelina seeds decreased the PB1 subfraction from 45.06 to 16.69% CP and increased the PB2 subfraction from 45.28 to 70.58% CP.[29] Compared to raw grains, MIR for 3 min did not change the PB3 and PC subfractions. However, MIR for 5 min significantly increased ($P < 0.05$) the PB3 and PC subfractions. PB3 is believed to be more slowly degraded in the rumen, and a large portion of this subfraction escapes ruminal degradation and is digested in the small intestine. Therefore, the increase in the PB3 subfraction will contribute to the digestible RUP supply to the small intestine. Subfraction PC is considered nondegradable in the rumen, and CP in this subfraction is heat damaged or bound to other compounds such as lignin, tannins, and Maillard reaction products.[19] MIR for 3 min decreased ($P < 0.05$) the PB1 subfraction and increased ($P < 0.05$) the PB2 subfraction but did not alter the PC subfraction (Table 2). These results suggest that MIR for 3 min decreased CP degradability in the rumen but did not overprotect the CP from digestion in the small intestine. However, MIR for 5 min significantly increased (from 0.97 to 5.32% CP) the PC subfraction, suggesting an overheating and protection of protein from intestinal digestion. These results show that MIR can decrease the ruminal degradation of feed CP in a

dx.doi.org/10.1021/jf501024j | J. Agric. Food Chem. 2014, 62, 6546–6555

Table 3. Microwave Irradiation Induced Changes in Rumen Degradation Kinetics of DM and CP in Hulless (CDC Fibar and HB08302) and Hulled (Copeland) Barley[a]

	microwave irradiation time (MIR)[b]				barley variety				P value[c]		contrasts[c]	
item	MIR0	MIR3	MIR5	SEM[d]	CDC Fibar	HB08302	Copeland	SEM	MIR	feed	control vs MIR	hulless vs hulled
in situ rumen degradation kinetics of dry matter[e] (DM)												
K_d, %/h	13.08a	12.07a	7.37b	0.798	11.05B	6.78C	14.69A	0.798	**	***	**	***
lag time (T_0, h)	0.20ab	0.65a	0.13b	0.130	0.36	0.32	0.30	0.130	*	ns	ns	ns
S subfraction, % DM	5.97	6.04	5.36	0.541	5.69AB	4.13B	7.56A	0.541	ns	**	ns	**
D subfraction, % DM	80.42b	84.55a	85.47a	0.857	83.01	83.83	83.61	0.857	**	ns	ns	ns
U subfraction, % DM	13.61a	9.40b	9.17b	0.650	11.30AB	12.05A	8.83B	0.650	**	*	***	**
RUDM, % DM	39.72b	39.38b	49.52a	2.070	41.79B	52.81A	34.02B	2.070	*	***	†	***
EDDM, % DM	60.28a	60.62a	50.48b	2.070	58.21A	47.19B	65.98A	2.070	*	***	†	***
in situ rumen degradation kinetics of crude protein (CP)												
K_d, %/h	8.16a	8.12a	3.53b	0.484	6.93B	4.35C	8.53A	0.484	***	***	**	***
lag time (T_0, h)	0.33	0.65	0.09	0.149	0.48	0.19	0.40	0.149	†	ns	ns	ns
S subfraction, % CP	6.45a	0.28b	0.00b	0.624	3.19A	1.27B	2.26AB	0.624	***	*	***	ns
D subfraction, % CP	86.32b	93.94a	95.98a	1.690	92.00AB	93.72A	90.53B	1.690	***	†	***	*
U subfraction, % CP	7.23	5.78	4.02	1.362	4.82	5.01	7.21	1.362	ns	ns	ns	ns
RUP, % CP	44.31b	47.57b	65.92a	1.909	49.64B	61.52A	46.63B	1.909	***	**	***	***
RUP, g/kg DM	60.42b	64.61b	88.06a	2.684	79.15A	83.04A	50.90B	2.684	***	***	***	***
EDCP, % CP	55.70a	52.44a	34.08b	1.909	50.36A	38.48B	53.37A	1.909	***	***	***	**
EDCP, g/kg DM	75.74a	70.23a	45.42b	3.376	80.83A	52.08B	58.48B	3.376	***	***	**	†
intestinal CP digestion												
IDCP, % RUP	79.35a	75.12ab	67.86b	2.334	77.10	74.58	70.65	2.333	**	ns	**	*
IDCP, % CP	35.01b	35.84b	44.74a	1.459	38.74B	44.91A	31.95C	1.459	**	***	*	***
IDCP, % DM	4.80b	4.94b	6.00a	0.194	6.19A	6.06A	3.49B	0.194	**	***	*	***

[a]Means within a row with different lower case (a, b) or capital (A–C) letters differ at $P < 0.05$. [b]Heated treated by microwave irradiation for 0 (MIR0), 3 (MIR03), or 5 (MIR05) min. [c]ns, not significant; †, $P < 0.1$; *, $P < 0.05$; **, $P < 0.001$; ***, $P < 0.001$. [d]SEM, standard error of the mean. [e]K_d = rate of degradation of D subfraction (%/h); S, soluble subfraction in the in situ incubation; D, degradable subfractions; U, undegradable subfractions; RUDM, rumen undegraded DM; EDDM, effecting degradability of DM in the rumen; RUP, rumen undegraded feed crude protein; EDCP, effective degradability of crude protein in the rumen; IDCP, intestinal digestibility of protein.

relatively shorter time with much less energy inputs compared to conventional heating systems.

The MIR induced changes in CP subfractions were independent of barley type. Except PB1, which was lower ($P < 0.001$) in hulless barley, the mean contents of all other CP subfractions did not significantly differ due to barley type (hulless vs hulled). Across the barley varieties, CDC Fibar had a higher ($P < 0.05$) PB2 subfraction and a lower ($P < 0.05$) PC subfraction. These findings are in general agreement with Yang et al.,[5] who observed no significant differences in the S and D subfractions of hulless and hulled barley, whereas the degradation rate was higher for the hulled (Copeland) cultivar.

Microwave Irradiation Induced Changes in Rumen Degradation and Intestinal Digestibility. Results of MIR induced changes in ruminal DM and CP degradation kinetics and intestinal digestibility of CP are presented in Table 3. MIR5 decreased ($P < 0.05$) the EDDM and increased ($P < 0.05$) rumen undegraded DM. The S subfraction of DM did not significantly change, and the D subfraction increased ($P < 0.01$) with MIR5. Therefore, the decrease in EDDM of the irradiated barely could mainly be related to the marked decrease (from 13.08 to 7.37%/h) in the K_d of the D subfraction. In agreement with our findings, a 6 min MIR markedly decreased the K_d of canola seeds (from 10.2 to 5.5%/h),[10] cottonseed meal (from 7.6 to 4.7%/h),[11] corn grain (from 5.1 to 4.3%/h),[12] and canola meal (from 7.0 to 4.9%/h).[9] MIR3 did not significantly alter any of the DM and CP degradation parameters. In contrast, there was a significant shift from PB1 to PB2 the CP subfraction after MIR3. This discrepancy may be, partly, explained by the higher K_d of barley grain in the rumen. Although the S subfraction of DM did not change with MIR5, the S subfraction of CP consistently decreased (from 6.45 to 0.00%; $P < 0.05$) with MIR. This means that the S subfraction of nutrients other than CP increased with MIR. Starch represents the bulk of non-CP DM of barley grains, and previous studies have shown that MIR for 5 min increased the S subfraction of starch in cereal grains,[12,30] partly due to gelatinization of starch with heating.[6] Decreases in the S subfraction of CP with 6 min MIR of corn grains,[12] canola seeds,[10] and cottonseed meal[11] have been reported. MIR5 decreased ($P < 0.001$) the EDCP with a concomitant increase ($P < 0.001$) in the supply of RUP to the postruminal tract (Table 3). The lower ruminal EDCP of the irradiated barley could be related to both lower S subfraction and lower K_d of D subfraction. Moreover, changes in CP subfractions such as the decrease in the rapidly degradable (PB1) subfraction and the increase in the intermediately degradable (PB2) and slowly degradable (PB3) subfractions could explain the lower ruminal EDCP.[7,15] These results demonstrate that a short-term (5 min) MIR induced a major shift in the site of CP digestion from the rumen to the postruminal tract. Digestion of feed protein in the small intestine results in lower losses of protein and essential amino acids. Moreover, the gradual degradation of the D subfraction in the irradiated barley can optimize the efficiency of rumen microbial protein synthesis with a consequent decrease in NH_3-N losses to the environment. However, overheating can reduce protein digestion in the postruminal tract.[15] In the present study, MIR for 5 min significantly

Table 4. Microwave Irradiation Induced Changes in the Molecular Structural Characteristics of Protein in Different Varieties (Hulless vs Hulled) of Barley As Revealed by Fourier Transform/Infrared-Attenuated Total Reflectance (FT/IR-ATR) Molecular Spectroscopy[a]

	microwave irradiation time (MIR)[b]				barley variety				*P* value[c]		contrasts[c]	
item	MIR0	MIR3	MIR5	SEM[d]	CDC Fibar	HB08302	Copeland	SEM	MIR	feed	control vs MIR	hulless vs hulled
protein primary structure characteristics[e,f]												
amide I height	0.036a	0.027b	0.023c	0.001	0.033A	0.028B	0.026B	0.001	***	***	***	***
amide II height	0.013a	0.009b	0.008c	0.000	0.011A	0.009B	0.008C	0.000	***	***	***	***
height ratio amide I:II	2.861b	3.230a	3.102a	0.042	3.092	3.010	3.093	0.042	***	ns	***	ns
amide I area	2.501a	1.804b	1.567c	0.071	2.255A	1.878B	1.739B	0.071	***	***	***	***
amide II area	0.699a	0.402b	0.379b	0.014	0.558A	0.485B	0.437C	0.014	***	***	***	***
area ratio amide I:II	3.596c	4.523a	4.155b	0.099	4.175	4.015	4.085	0.099	***	ns	***	ns
protein secondary structure α-helix and β-sheet[f,g]												
α-helix height	0.004a	0.003b	0.002c	0.001	0.033A	0.028B	0.026B	0.001	***	***	***	***
β-sheet height	0.033a	0.022b	0.019c	0.001	0.028A	0.024B	0.021C	0.001	***	***	***	***
ratio of α-helix: β-sheet	1.081b	1.258a	1.255a	0.012	1.183B	1.168B	1.242A	0.012	***	***	***	***

[a]Means within a row with different lower case (a–c) or capital letters (A–C) differ at $P < 0.05$. [b]Heat treated by microwave irradiation for 0 (MIR0), 3 (MIR03), or 5 (MIR05) min. [c]ns, not significant; ***, $P < 0.001$. [d]SEM, standard error of the mean. [e]Protein amide bands were measured at ca. 1715–1482 cm^{-1}, and the measurements are expressed in IR absorbance units. [f]Measurements of the protein structural bands are expressed in IR absorbance units. [g]α-Helix and β-sheet bands were measured in amide I region, centered at 1,653 and 1,630 cm^{-1}, respectively

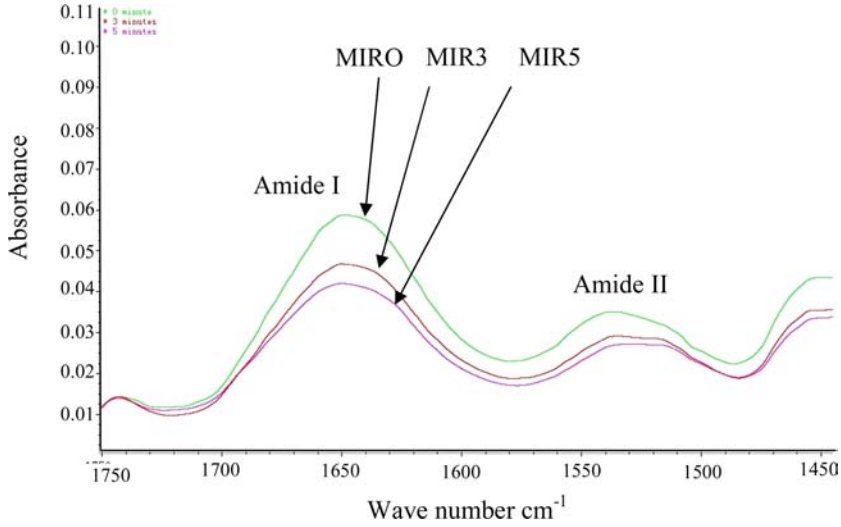

Figure 1. Biomolecular spectral parameters of protein (baseline region, ca. 1732–1483 cm^{-1}) of barley grains heat treated by microwave irradiation for 0 (MIR0), 3 (MIR03), or 5 (MIR05) min.

decreased (from 79.35 to 67.86%; $P < 0.05$) the intestinal digestibility of RUP. The lower intestinal digestibility of RUP is supported by the significant increase in the PC subfraction (Table 3), which is considered as nondigestible in the whole digestive tract. The lower intestinal digestibility offset some of the positive effects of MIR5 on the ruminal degradation characteristics of barley. However, the overall supply of digestible RUP as a percentage of feed CP increased to the small intestine. These results demonstrate that it is important to quantify the intestinal digestibility of RUP when heat-induced changes in the ruminal degradation of feed CP are evaluated to more accurately establish optimal heating regimens.

Microwave Irradiation Induced Changes in Protein Molecular Structure. Any temperature change in the environment of the protein that can modify the noncovalent interactions in protein molecules can lead to an alteration of the protein internal structures.[13] Heat processing of plant-derived protein feeds decreases ruminal CP degradation by altering the protein molecular structures such as by the uncoiling of the pleated structures or by denaturing the whole protein molecule.[7,13] The subsequent liberation of hydrophobic amino acids, racemization, and establishment of cross-linkages among the uncoiled peptides and between amino acids and reducing sugars can all reduce CP solubility.[29−32] Heating at a higher temperature or for a longer duration can denature the whole protein molecule, leading to more complex cross-linkages and advanced Maillard products. Thus, the protein molecules become more resistant to rumen microbial degradation and enzymatic hydrolysis.[13,31] Recent investigations have shown that FTIR molecular spectroscopy can be used to quantitatively evaluate the heat-induced changes in protein primary and secondary molecular structures.[7,15,26] The amide I and amide II spectral intensities in terms of peak area and height can be used to reveal changes in the primary structures of protein.[33,34] In this study, MIR for 3 and 5 min consistently decreased ($P < 0.05$) the amide I and amide II heights and areas. Our results are consistent with the findings of

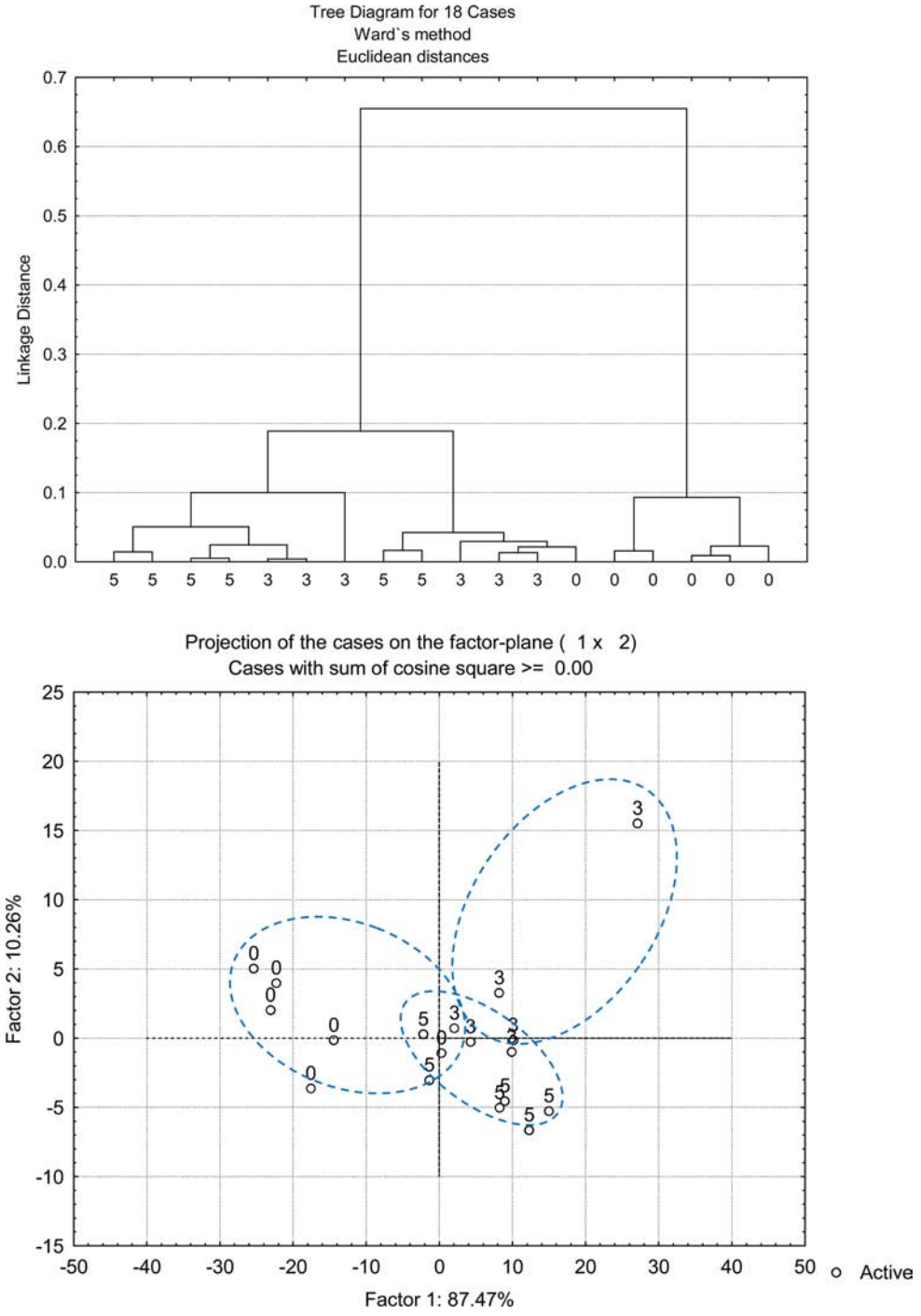

Figure 2. Agglomerative hierarchical cluster analysis (CLA) dendograms (top) and PCA scatter plot (bottom) visualizing the overall spectral differences in the protein primary structures in the amide regions (ca. 1732−1483 cm^{-1}) of untreated and heat-treated barley grains (untreated = 0; heat treated by microwave irradiation for 3 min = 3; or heat treated by microwave irradiation for 5 min = 5).

Samadi and Yu.[15] The decreases in amide peak bands were associated with a decrease in CP solubility and ruminal degradation. The protein secondary structures affect access to gastrointestinal digestive enzymes,[13,33] and heat-induced changes in protein secondary structures can alter protein digestibility in the rumen and intestine of dairy cattle.[7,33] The α-helix and β-sheet heights consistently decreased ($P < 0.05$) with increasing duration of MIR, whereas the ratio of α-helix to β-sheet increased with MIR. The changes in α-helix:β-sheet ratios show changes in structural makeup of the whole protein molecules and strongly reflect the difference in digestibility and utilization of protein molecules.[13,33] Although no study could be found on the molecular structures of the hulled barley cultivars (Copeland), the pattern of differences in molecular structural parameters of the hulless barely cultivars (CDC Fibar vs HB08302; Table 4) are consistent with the findings of Dariman and Yu.[33] The varietal differences in barley protein molecular structures in relation to ruminal CP degradation have been discussed in detail earlier.[13,33]

Multivariate Analysis. CLA and PCA were performed on the overall spectral data from the fingerprint region (ca. 1732−1483 cm^{-1}; Figure 1) to classify and visualize the MIR induced

Table 5. Coefficient of Correlation (Pearson) between Protein Molecular Structural Characteristics and Nutrient Availability and Utilization in the Rumen and Intestine of Dairy Cows[a]

	protein primary structure characteristics[b,c]				protein structure characteristics[c,d]		ratio	
item	amide I area	amide I peak height	amide II area	amide II peak height	α-helix height	β-sheet height	area ratio amide I:II	α-helix to β-sheet height ratio
protein profile[e]								
CP, % DM	0.62**	0.63**	0.58*	0.67**	0.66**	0.61**	−0.18	−0.39
NDICP, % CP	−0.41†	−0.45†	−0.49*	−0.37	−0.45†	−0.41†	0.29	0.10
ADICP, % CP	−0.71***	−0.73***	−0.66**	−0.68**	−0.71***	−0.72***	0.30	0.46†
SCP, % CP	0.62**	0.64**	0.65**	0.58*	0.59**	0.66**	−0.53*	−0.56*
NPN, % CP	−0.68**	−0.67**	−0.73***	−0.68**	−0.63**	−0.72***	0.73***	0.72***
CP subfractions[f] (% of CP)								
PA	−0.68**	−0.67**	−0.73***	−0.68**	−0.63**	−0.72***	0.73***	0.72***
PB1	0.62**	0.63**	0.65**	0.57*	0.59*	0.66**	−0.55*	−0.53*
PB2	−0.49*	−0.48*	−0.48*	−0.46†	−0.43†	−0.56*	0.57*	0.76***
PB3	−0.38	−0.42†	−0.44†	−0.33	−0.43†	−0.36	0.22	0.02
PC	−0.71***	−0.73***	−0.66**	−0.68**	−0.71***	−0.72***	0.30	0.46†
in situ rumen CP degradation[g]								
K_d (%/h)	0.54*	0.55*	0.50*	0.43†	0.54*	0.49*	−0.13	−0.09
S subfraction, % CP	0.81***	0.81***	0.81***	0.79***	0.77***	0.85***	−0.66**	−0.83***
U subfraction, % CP	0.22	0.22	0.16	0.14	0.22	0.22	−0.19	−0.15
D subfraction, % CP	−0.69**	−0.68**	−0.64**	−0.61**	−0.66**	−0.70**	0.50*	0.63**
RUP, % CP	−0.61**	−0.62**	−0.59*	−0.52*	−0.61**	−0.57*	0.24	0.21
RUP g/kg DM	−0.20	−0.20	−0.20	−0.10	−0.17	−0.18	0.15	0.04
EDCP, % CP	0.61**	0.62**	0.59*	0.52*	0.61**	0.57*	−0.24	−0.21
EDCP, g/kg DM	0.78***	0.81***	0.73***	0.75***	0.82***	0.74***	−0.26	−0.31
intestinal CP digestion[h]								
IDCP, % RUP	−0.38	−0.40†	−0.43†	−0.30	−0.39	−0.34	0.21	0.00
IDCP, g/kg DM	−0.02	−0.03	−0.09	0.06	−0.01	0.01	0.17	−0.15

[a]Correlation coefficients with no symbol are not significant; †, $P < 0.1$; *, $P < 0.05$; **, $P < 0.001$; ***, $P < 0.001$. [b]Protein amide bands were measured at ca. 1715−1482 cm^{-1}, and the measurements are expressed in IR absorbance units. [c]Protein structural bands were measured in IR absorbance units. [d]α-Helix and β-sheet bands were measured in amide I region, centered at 1653 and 1630 cm^{-1}, respectively. [e]CP, crude protein; NDICP, neutral detergent-insoluble protein; ADICP, acid detergent-insoluble protein; SCP, soluble CP; NPN, non-protein nitrogen [f]PA = NPN; PB1 = SCP − NPN; PB2 = CP − (PA + PB1 + PB3 + PC); PB3 = NDIP − ADIP; PC = ADIP. [g]K_d = rate of degradation of D subfraction (%/h); S, soluble subfraction in the in situ incubation; D, degradable subfractions; U, undegradable subfractions; RUP, rumen undegraded feed crude protein; EDCP, effective degradability of crude protein in the rumen. [h]IDCP, intestinal digestibility of CP.

changes in protein molecular structural characteristics. The CLA dendrograms (Figure 2, top) showed that protein molecular spectral data of irradiated barley grains could be separated from raw grains at a linkage distance of <0.7, demonstrating structural differences between the raw and irradiated grains. Only one spectrum of raw grains and irradiated grains was similar. The mixed dendograms show that the molecular spectral data of 3 and 5 min irradiated barley grains could not be distinguished from each other. Results of the PCA are visualized in a scatter plot between the first two principal components (Figure 2, bottom). The first and second principal components explained 97.73% of the total variation in protein molecular structures of the raw and irradiated barley grains. The PCA results show that the protein molecular spectra of raw grains could be almost completely distinguished from the irradiated (3 and 5 min) barley. Like CLA dendograms, only on spectrum was common between the raw and irradiated feeds, indicating some similarity in protein intrinsic molecular structures. The results of the present study showed that CLA and PCA analyses were able to classify differences in protein structural−chemical makeup.

Correlations between Protein Molecular Structural Characteristics and Crude Protein Availability and Utilization. Table 5 shows the coefficients of correlation (Pearson) and their significance levels between protein molecular spectral band characteristics and CP chemical profiles, CP subfraction, and CP digestion in the rumen and intestine of dairy cows. The MIR induced changes in all measured structural bands intensities (area and height) of protein primary and secondary structures had significant ($P < 0.05$) negative correlations with ADICP ($r \geq -0.66$) and significant positive correlations with SCP ($r \geq 0.58$). This means that protein denaturation during heating decreased the SCP and increased the nondegradable protein (ADICP). Our results are consistent with the findings of Dorion et al.[14] Moreover, the measured structural band intensities had significant ($P < 0.05$) positive correlations ($r \geq 0.57$) with the PB1 subfraction and strong negative correlations with PA ($r \geq -0.63$), PB2 ($r \geq -0.43$), and PC ($r \geq -0.66$) subfractions (Table 5). With the in situ parameter, changes in protein primary and secondary structural band intensities during MIR were positively correlated to the S subfraction ($r \geq 0.77$) and EDCP ($r \geq 0.52$) and negatively correlated to the D subfraction and the RUP contents. Except for amide II peak height, all other primary and secondary spectral bands showed a significant ($P < 0.05$) positive correlation with K_d. These

dx.doi.org/10.1021/jf501024j | J. Agric. Food Chem. 2014, 62, 6546−6555

results demonstrate that there is a close relationship between MIR-induced changes in inherent protein molecular structures and changes in CP chemical profile, CP subfractions, and ruminal degradation kinetics. There was, however, no correlation between the spectral band intensity and intestinal digestibility of RUP (Table 5). Yu and Nuez-Ortín[35] suggested that the spectral band intensities can be used as indicators for the changes in nutritive value of protein during heat processing, which is supported by the findings of the present study. However, it needs to be mentioned here that only limited numbers of samples and irradiation durations (3 or 5 min) were evaluated in this study, and further studies will be required to establish this relationship and develop regression equations.

In summary, MIR of barley grains for 5 min significantly changed CP chemical profiles, CP subfractions, rumen degradability, intestinal digestibility, and protein molecular structures compared to raw grains. MIR for 5 min significantly decreased SCP and K_d of the D subfraction, causing a marked decrease in CP degradation in the rumen. As a consequence, the total supply of digestible RUP to the postruminal tract increased. These changes in CP chemical profile and digestion were strongly associated with the alteration in protein intrinsic molecular structures. In contrast, MIR for 3 min did not alter protein molecular structures and did not induce significant changes in rumen CP degradation, RUP content, and intestinal digestibility compared with raw grains. These results showed that MIR for a short period and lower energy input can improve the nutritive value and utilization of CP in barely grains.

AUTHOR INFORMATION

Corresponding Author

*(P.Y.) Mail: Department of Animal and Poultry Science, College of Agriculture and Bioresources, University of Saskatchewan, Saskatoon, SK, Canada S7N 5A8. Phone: (306) 966-4132. E-mail: peiqiang.yu@usask.ca.

Present Address

⊥(N.A.K.) Department of Animal Nutrition, University of Agriculture Peshawar, Pakistan.

Funding

Research projects of the chair group (P.Y.) have been supported by grants from the Ministry of Agriculture Strategic Research Chair Program, Natural Sciences and Engineering Research Council of Canada (NSERC), SaskCanola, and Saskatchewan Agricultural Development Fund (ADF). X.Y.'s postdoctoral fellowship was financially supported by the China Scholarship Council (CSC) for research work in P.Y's laboratory at the University of Saskatchewan, Canada.

Notes

The authors declare no competing financial interest.

ACKNOWLEDGMENTS

We thank Dr. Aaron D. Beattie (Crop Development Center, University of Saskatchewan, Saskatoon, Canada) for providing hulless and hulled barley samples and Zhiyuan Niu (research assistant in the Department of Animal and Poultry Science, University of Saskatchewan) for providing assistance and arranging samples.

REFERENCES

(1) Damiran, D.; Yu, P. Metabolic characteristics in ruminants of the proteins in newly developed hull-less barley varieties with altered starch traits. *J. Cereal Sci.* **2012**, *55*, 351−360.

(2) FAOSTAT. Production and trade. Food and agriculture organization statistical database; FAO: Rome, Italy, 2012; http://faostat.fao.org/site/339/default.aspx (accessed Feb 5, 2014).

(3) Hart, K. J.; Rossnagel, B. G.; Yu, P. Chemical characteristics and in situ ruminal parameters of barley for cattle: comparison of the malting cultivar AC Metcalfe and five feed cultivars. *Can. J. Anim. Sci.* **2008**, *88*, 711−719.

(4) Yang, W. Z.; Beauchemin, K. A.; Farr, B. I.; Rode, L. M. Comparison of barley, hull-less barley, and corn in the concentrate of dairy cows. *J. Dairy Sci.* **1997**, *80*, 2885−2895.

(5) Yang, L.; Christensen, D. A.; McKinnon, J. J.; Beattie, A. D.; Yu, P. Effect of altered carbohydrate traits in hulless barley (*Hordeum vulgare* L.) on nutrient profiles and availability and nitrogen to energy synchronization. *J. Cereal Sci.* **2013**, *58*, 182−190.

(6) Prestløkken, E. In situ ruminal degradation and intestinal digestibility of dry matter and protein in expanded feedstuffs. *Anim. Feed Sci. Technol.* **1999**, *77*, 1−23.

(7) Peng, Q.; Khan, N. A.; Wang, Z.; Yu, P. Moist and dry heating-induced changes in protein molecular structure, protein subfractions, and nutrient profiles in camelina seeds. *J. Dairy Sci.* **2014**, *97*, 446−457.

(8) Yu, P.; Tamminga, S.; Egan, A. R.; Christensen, D. A. Probing equivocal effects of heat processing of legume seeds on performance of ruminants − a review. *Asian−Aust. J. Anim. Sci.* **2004**, *17*, 869−876.

(9) Sadeghi, A. A.; Shawrang, P. Effects of microwave irradiation on ruminal degradability and in vitro digestibility of canola meal. *Anim. Feed Sci. Technol.* **2006**, *127*, 45−54.

(10) Ebrahimi, S. R.; Nikkhah, A.; Sadeghi, A. A. Changes in nutritive value and digestion kinetics of canola seed due to microwave irradiation. *Asian−Aust. J. Anim. Sci.* **2010**, *23*, 347−354.

(11) Sadeghi, A. A.; Shawrang, P. Effects of microwave irradiation on ruminal protein degradation and intestinal digestibility of cottonseed meal. *Livest. Sci.* **2007**, *106*, 176−181.

(12) Sadeghi, A. A.; Shawrang, P. Effects of microwave irradiation on ruminal protein and starch degradation of corn grain. *Anim. Feed Sci. Technol.* **2006**, *127*, 113−123.

(13) Yu, P. Protein molecular structures, protein subfractions, and protein availability affected by heat processing: a review. *Am. J. Biochem. Biotechnol.* **2007**, *3*, 70−90.

(14) Doiron, K.; Yu, P.; McKinnon, J. J.; Christensen, D. A. Heat-induced protein structure and subfractions in relation to protein degradation kinetics and intestinal availability in dairy cattle. *J. Dairy Sci.* **2009**, *92*, 3319−3330.

(15) Samadi; Yu, P. Dry and moist heating-induced changes in protein molecular structure, protein subfraction, and nutrient profiles in soybeans. *J. Dairy Sci.* **2011**, *94*, 6092−6102.

(16) AOAC. *Officials Methods of Analysis*, 15th ed.; Association of Official Analytical Chemists: Arlington, VA, USA, 1990.

(17) Licitra, G.; Hernandez, T. M.; Van Soest, P. J. Standardization of procedures for nitrogen subfractionation of ruminant feeds. *Anim. Feed Sci. Technol.* **1996**, *57*, 347−358.

(18) Roe, M. B.; Sniffen, C. J.; Chase, L. E. *Techniques for Measuring Protein Subfractions in Feedstuffs*; Proceedings, Cornell Nutrition Conference; Cornell University: Ithaca, NY, USA, 1990; pp 81−85.

(19) Sniffen, C. J.; O'Connor, J. D.; Van Soest, P. J.; Fox, D. G.; Russell, J. B. A net carbohydrate and protein system for evaluating cattle diets: II. Carbohydrate and protein availability. *J. Anim. Sci.* **1992**, *70*, 3562−3577.

(20) CCAC. *Guide to the Care and Use of Experimental Animals*, Vol. 1, 2nd ed.; Canadian Council on Animal Care: Ottawa, ON, Canada, 1993.

(21) NRC. *Nutrient Requirements of Dairy Cattle*, 7th rev. ed.; National Research Council, Academies Press: Washington, DC, USA, 2001.

(22) Ørskov, E. R.; McDonald, I. The estimation of protein degradability in the rumen from incubation measurements weighted according to rate of passage. *J. Agric. Sci.* **1979**, *92*, 499−503.
(23) Tamminga, S.; Van Straalen, W. M.; Subnel, A. P. J.; Meijer, R. G. M.; Steg, A.; Wever, C. J. G.; Blok, M. C. The Dutch protein evaluation system: the DVE/OEB-system. *Livest. Prod. Sci.* **1994**, *40*, 139−155.
(24) SAS. *User's Guide: Statistics*, 8th ed.; SAS Institute: Cary, NC, USA, 2009.
(25) Calsamiglia, S.; Stern, M. D. A three-step in vitro procedure for estimating intestinal digestion of protein in ruminants. *J. Anim. Sci.* **1995**, *73*, 1459−1465.
(26) Theodoridou, K.; Yu, P. Application potential of ATR-FT/IR molecular spectroscopy in animal nutrition: revelation of protein molecular structures of canola meal and presscake, as affected by heat-processing methods, in relationship with their protein digestive behavior and utilization for dairy cattle. *J. Agric. Food Chem.* **2013**, *61*, 5449−5458.
(27) Saxton, A. M. A macro for converting mean separation output to letter groupings in Proc Mixed. In *Proceedings of the 23rd SAS Users Group International*; SAS Institute: Cary, NC, USA, 1998; pp 243−1246.
(28) Mustafa, A. F.; Chouinard, Y. P.; Ouellet, D. R.; Soita, H. Effects of moist heat treatment on ruminal nutrient degradability of sunflower seed. *J. Sci. Food Agric.* **2003**, *83*, 1059−1064.
(29) Peng, Q.; Khan, N. A.; Wang, Z.; Christensen, D. A.; Yu, P. Relationship of feeds protein structural makeup in common prairie feeds with protein solubility, in situ ruminal degradation and intestinal. *Anim. Feed Sci. Technol.* **2014**, DOI: 10.1016/j.anifeedsci.2014.05.004.
(30) Sadeghi, A. A.; Shawrang, P. Effects of microwave irradiation on ruminal dry matter, protein and starch degradation characteristics of barley grain. *Anim. Feed Sci. Technol.* **2008**, *141*, 184−194.
(31) Mustafa, A. F.; McKinnon, J. J.; Christensen, D. A. Protection of canola (low glucosinolate rapeseed) meal and seed protein from ruminal degradation − review. *Asian−Aust. J. Anim. Sci.* **2000**, *13*, 535−542.
(32) Khan, N. A.; Peng, Q.; Xin, H.; Yu, P. Vibrational spectroscopic investigation of heat-induced changes in functional groups related to protein structural conformation in camelina seeds and their relationship to digestion in dairy cows. *Anim. Prod. Sci.* **2014**, in press.
(33) Damiran, D.; Yu, P. Molecular basis of structural makeup of hulless barley in relation to rumen degradation kinetics and intestinal availability in dairy cattle: a novel approach. *J. Dairy Sci.* **2011**, *94*, 5151−5159.
(34) Liu, B.; Yu, P. Application of advanced synchrotron radiation-based and conventional molecular techniques in recent research on molecular structure, metabolic characteristics, and nutrition in coproducts from biofuel processing. *Appl. Spectrosc. Rev.* **2013**, *48*, 589−608.
(35) Yu, P.; Nuez-Ortín, W. G. Relationship of protein molecular structure to metabolisable proteins in different types of dried distillers grains with solubles: a novel approach. *Br. J. Nutr.* **2010**, *104*, 1429−1437.

the (1) chemical profile; (2) CP subfractions according to Cornell Net Carbohydrate and Protein System (CNCPS); (3) ruminal CP degradation characteristics and intestinal digestibility of rumen nondegraded protein (RUP); and (4) the protein's molecular structural features using Fourier transform/infrared-attenuated total reflectance (FT/IR-ATR) molecular spectroscopy of newly developed CDC yellow flaxseed in comparison with that of brown flaxseed. The fifth objective was to quantify the relationship between the protein's molecular structural features and their chemical profiles and digestive behavior in the rumen and intestine of dairy cattle.

MATERIALS AND METHODS

Flaxseeds, Samples Collection, and Heat Processing. Four varieties of flaxseed (*Linum usitatissimum* L.), including two brown oilseed flax varieties (CDC Bethune and CDC Sorrel) and two newly developed yellow oilseed flax breeding lines (coded as FY11140 and F08×425) were selected for this study. Seeds (∼2 kg) from each genotype were sampled from two replicate plots at two different locations, namely, from the crop grown on a clay-loam soil at Kernen Crop Research Farm (52°9′ N and 106°32′ W; University of Saskatchewan, Saskatoon, SK, Canada) and from the crop gown on a silty-clay soil at Melfort Research Station (52°8′ N and 104°59′ W; Melfort, SK, Canada) of Agriculture and Agri-Food Canada. The samples of each genotype were pooled by location and mixed, and subsamples of ∼1 kg were collected and stored at −20 °C for laboratory analysis. Subsequently, the seeds were ground through a 2 mm screen for in situ studies and through a 1 mm screen for wet chemical analysis using a laboratory mill (Retsch ZM-1, Brinkmann Instruments Ltd., Mississauga, ON, Canada). The seeds were ground through a 0.25 mm screen for molecular spectral analyses. Because of high oil content of the seeds, the samples were kept cool and gradually fed to the grinder to avoid sticking and clumping and to make sure that the seeds were cracked and not extruded.

Molecular Spectroscopy. The samples were analyzed for the protein's molecular spectral profiles using a JASCO FT/IR-ATR-4200 (Jasco Inc., Easton, MD) at the molecular spectroscopy laboratory of the Department of Animal and Poultry Science, University of Saskatchewan (Saskatoon, SK, Canada). The spectrometer was outfitted with a ceramic IR light source, a deuterated L-alanine doped triglycine sulfate detector, and a MIRacle ATR (Pike Technologies, Madison, WI, USA) sampling accessory equipped with a pressure clamp and ZnSe crystal plates. The molecular spectrum was generated in the mid-IR region (ca. 4,000−800 cm^{-1}) at a spectral resolution of 4 cm^{-1}. For each sample, five spectra were obtained, and each spectrum was generated with 128 co-added scans. Jasco Spectra Manager II software (Jasco Inc., Easton, MD) was used to collect, correct (against background and CO_2 noise), and process the molecular spectral data. Ominic 7.3 software (Spectra-Tech Inc., Madison, WI, USA) was used to identify and quantify the absorbance bands associated with the protein's primary and secondary structures. The protein's primary structural characteristics were quantified from two bands at the amide I (1712−1580 cm^{-1}; Figure 1) and amide II (1,580−1482 cm^{-1}; Figure 1) regions using literature information as reported earlier.[14] The protein's secondary structural characteristics were quantified from the absorption peak height of the α-helix (centered at ca. 1,653 cm^{-1}) and β-sheet (centered at ca. 1,630 cm^{-1}) in the amide I region. The α-helix and β-sheet peaks were indentified using Fourier self-deconvolution spectra, obtained with the second-derivative function of OMNIC 7.2 as described by Yu.[13]

In Situ Rumen Incubation. Four rumen fistulated (10 cm internal diameter; Bar Diamond Inc., Parma, ID, USA) lactating Holstein dairy cows (body weight, 680 ± 10 kg) were used for in situ incubation. The cows were handled and cared for according to the recommendations of CCAC.[17] A balanced TMR was individually fed to the dairy cows twice daily (8:00 and 16:00 h) in equal portions. The TMR contained 53% dairy concentrate, 31% barley silage, and 16% chopped alfalfa hay. Detailed information on the ingredients and chemical composition of the concentrates, barley silage, and alfalfa hay has been reported earlier.[18] All cows had 24 h/d access to fresh drinking water.

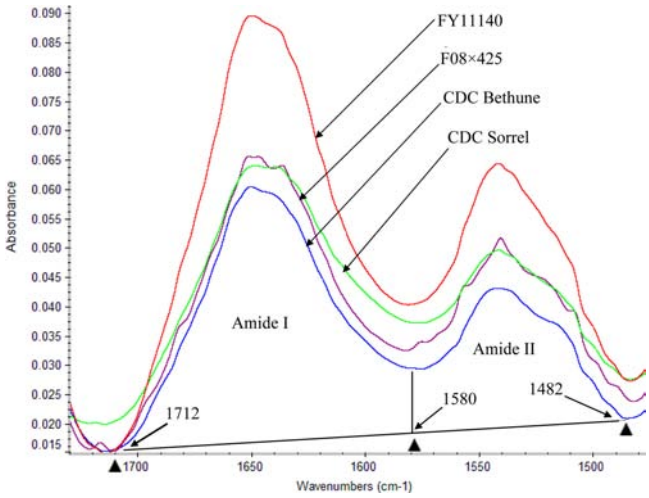

Figure 1. Protein molecular spectra of raw brown flaxseed varieties (CDC Bethune and CDC Sorrel) and newly developed yellow flaxseed breeding lines (FY11140 and FO8×425) in the amide I and amide II regions (1712−1482 cm^{-1}).

The standard in situ nylon bag protocol described by Peng et al.[14] was used to determine the rumen degradation kinetics of DM and CP. Briefly, 7 g of ground (2 mm) sample of each feed was randomly incubated for 48, 24, 12, 8, 4, 2, and 0 h in rumen of the four cows, using preweighed and coded nylon bags (10 × 20 cm) with a pore size of 41 μm (Nitex 03-41/31 monofilament open mesh fabric, Screentec Corp., Mississauga, ON, Canada). All samples were incubated in two replicated runs, and multiple bags were used for each incubation time to obtain more representative data and enough residues for chemical analysis. For 48, 24, 12, 8, 4, 2, and 0 h incubation periods, the replicate bags were 4, 4, 4, 2, 2, 2, and 2, respectively. The gradual addition, all out method was used. A maximum of 20 bags were incubated in the rumen at any given time. All bags were removed from the rumen at the end of 48 h of incubation and immediately washed (6 times) in a bucket with cold tap water to remove adhering ruminal contents and stop enzymatic and microbial degradation. The bags were subsequently dried (55 °C for 48 h), cooled to room temperature (20−22 °C), and reweighed. Residues were pooled together as per incubation time and run, ground to 1 mm particle size, and stored at 4 °C for chemical analysis.

Rumen Degradation Kinetics. Rumen degradation kinetics of DM and CP was computed according to the first-order kinetics equation of Ørskov and McDonald[19] with a slight modification on lag time.[20,21]

$$Y(t) = U + (100 - S - U) \times e^{-kd(t-T_0)}$$

where $Y(t)$ was the residues at t h of incubation; S was the soluble fraction; U was the rumen nondegradable fraction; kd was the ruminal degradation rate (%/h) of the potentially degradable fraction, and T_0 was the lag time (h). The kd, U fraction, and T_0 were estimated from the in situ data using the nonlinear (PROC NLIN) procedure of SAS[22] with iterative least-squares regression (Gauss−Newton method). The rumen nondegraded DM (RUDM) and RUP were computed according to the NRC-2001[23] as follows:

$$\text{RUDM/RUP} = U + D \times \left[\frac{K_p}{(K_d + K_p)}\right]$$

where D is the potentially rumen degradable fraction and calculated as D = 100 − S − U, and K_p is the passage rate of digesta from the rumen, which was supposed to be 0.06/h.[21] The rumen degradable DM (RDDM) and CP (RDP) were calculated as

dx.doi.org/10.1021/jf501284a | J. Agric. Food Chem. 2014, 62, 6556−6564

Table 1. Chemical Profiles of Flaxseed: Comparison of the Brown Seed Type vs Yellow Seed Type[a]

Item	brown seed type		yellow seed type		SEM[b]	contrast[c]	
	CDC Bethune	CDC Sorrel	FY11 140	F08×425		brown vs yellow	*P*- value[c]
Basic Chemical Profile							
DM (%)	94.28 ab	94.25 b	95.46 a	95.47 a	0.206	**	*
ether extract (EE) (% of DM)	42.88 b	39.96 c	42.60 b	46.49 a	0.351	***	***
ash (% of DM)	3.70 a	3.69 a	3.82 a	3.38 b	0.041	†	**
crude protein (CP) (% of DM)	22.04 ab	19.79 b	25.70 a	24.18 ab	0.960	***	**
NDIP[d] (% of CP)	15.89 ab	17.02 a	11.39 b	11.49b	0.793	**	*
ADIP[e] (% of CP)	2.56 b	4.20 b	5.05 b	10.54 a	0.811	**	**

[a]a−c: means within a row with different letters differ at the $P < 0.05$ level. [b]SEM = standard error of the mean. [c]†, $P < 0.1$; *, $P < 0.05$; **, $P < 0.01$; ***, $P < 0.001$. [d]NDIP = neutral detergent-insoluble protein. [e]ADIP = acid detergent-insoluble protein.

$$\text{RDDM/RDP} = \text{S} + \text{D} \times \left[\frac{K_\text{d}}{(K_\text{d} + K_\text{p})}\right]$$

Chemical Analysis. The standard methods of the AOAC[24] were used to analyze the contents of DM (method 930.15), CP (method 984.13; adopted for Kjeltec 2400 autoanalyzer; Foss Analytical A/S, Hillerød, Denmark), ash (method 942.05), and ether extract (EE, method 920.39). The content of SP was analyzed according to the method of Roe et al.[25] with slight modifications as described by Peng et al.[14] The contents of acid detergent-insoluble protein (ADIP), neutral detergent-insoluble protein (NDIP), and nonprotein N (NPN) were analyzed according to the methods described by Licitra et al.[26] The 3-step in vitro method of Calsamiglia and Stern[27] was adopted to analyze the digestibility of RUP in air-dried rumen residues of 16 h rumen incubation as described by Peng et al.[18]

Fractionation of Crude Protein. The CP subfractions were computed according to the Cornell Net Carbohydrate and Protein System (CNCPS).[28,29] The CP was partitioned into NPN (PA), true protein (PB), and ADIP (PC). The PA fraction contains peptides, free amino acids, ammonia, amides, amines, ureides, nucleotides, and nitrates, and is considered to degrade in the rumen at the rate of 200%/h.[30] The PB fraction was further fractionated into a rapidly (10 to 40%/h) degradable fraction (PB1); a moderately (3 to 20%/h) degradable fraction (PB2); and slowly (0.06 to 0.55%/h) degradable fraction (PB3).[30] PB1 was computed as SP − PA; PB2 as CP − (PA + PB1 + PB3 + PC); and PB3 as NDIP − ADIP. These CP fractions were computed from the data obtained with wet-chemical analysis using the following approach, the trichloroacetic acid precipitated CP = PB1 + PB2 + PB3 + PC; borate-phosphate buffer insoluble CP = PB2 + PB3 + PC; NDIP = PB3 + PC; and ADIP = PC.[26]

Statistical Analysis. The data on chemical composition, CP subfractions, and the protein's molecular spectral characteristics were analyzed using the PROC MIXED procedure of SAS.[22] The model used for analysis was

$$Y_{ijk} = \mu + V_i + L_j + e_{ijk}$$

where Y_{ijk} is an observation on the dependent variable *ijk*; μ is the population mean; V_i was the fixed effect of flaxseed variety (CDC Bethune, CDC Sorrel, FY11140 and F08×425), L_j is the random effect of crop location (Kernen and Melfort) and e_{ijk} is the random error associated with the observation *ijk*.

The data on in situ rumen degradation parameters and intestinal digestibility were analyzed with the following model:

$$Y_{ijk} = \mu + V_i + R_k + e_{ijk}$$

where Y_{ijk} is an observation on the dependent variable *ijk*; μ is the population mean; V_i is the fixed effect of flaxseed variety, R_k is the random effect of in situ experimental run, and e_{ijk} is the random error associated with the observation *ijk*. When significant ($P < 0.05$) effects were observed, posthoc analyses were conducted on the least-squares means to compute pairwise differences among the means, using the Tukey-Kramer test adjusted for multiple comparisons.

The PROC CORR procedure of SAS[22] was used to compute the strength of relationships between the protein's molecular structural characteristics and CP chemical profile, subfractions, in situ degradation parameters, and intestinal digestibility of RUP. The PROC REG procedure of SAS[22] with stepwise selection at $P < 0.05$ was used to obtain multiple regression equations for the prediction of the chemical profile, CP subfractions, in situ degradation parameters, and intestinal digestibility of RUP. The independent variables tested in the model were amide I area, amide II area, and their ratio; amide I height, amide II height, and their ratios; and α-helix and β-sheet height and their ratios. Only equations contributing significantly ($P < 0{\cdot}05$) to the estimation of dependent variables are reported.

Multivariate analysis, the agglomerative hierarchical cluster analysis (CLA), and principal component analysis (PCA) were performed on the entire spectral data (n = 249 spectral bands), obtained from the amide fingerprint region (ca. 1732−1483 cm^{-1}), to classify and visualize varietal differences in intrinsic protein molecular structures. The concepts and procedure of using CLA and PCA for FT/IR-ATR spectral data are described earlier.[31]

RESULTS AND DISCUSSION

Chemical Profiles. The results of chemical profiles of the brown flaxseed varieties and yellow flaxseed breeding lines are shown in Table 1. Except for ash, the contents of all nutrients varied ($P < 0.05$) among the four genotypes. On average, the yellow-seeded lines had higher ($P < 0.001$) contents of EE (44.54 vs 41.42% DM) and CP (24.94 vs 20.91% DM) compared to those of the brown-seeded varieties. The higher contents of CP and EE in the yellow-seeded lines could be related to their larger seed size[32] and thinner and translucent seed coat[32,33] that results in a relatively greater proportion of oil and protein containing mass (cotyledons and endosperm) and smaller proportion of fiber containing mass (seed coat) compared to those of the brown seeded varieties.[11] In agreement with our findings, higher contents of CP and EE have been reported for yellow-seeded canola meal compared to that of its brown-seeded counterpart.[11,34] Within the yellow-seeded lines, FO8×425 had a higher ($P < 0.05$) content of EE; and within the brown-seeded varieties, CDC Bethune had a higher ($P < 0.05$) content of EE and CP. The latter findings suggest some genotype differences in the chemical profiles of flaxseed within the yellow and brown seed types.

The CP chemical profile revealed that on average the CP in yellow flaxseed lines had a higher ($P < 0.01$) content of ADIP (7.80 vs 3.38% CP). The ADIP is believed to be nondegradable in rumen and nondigestible in the postruminal tract. In contrast to our findings, previous studies have reported lower contents of ADIP in yellow-seeded carinata strains and canola meal compared to their brown-seeded counterparts.[11,12] This discrepancy may be related to the inherent genetic variation

dx.doi.org/10.1021/jf501284a | J. Agric. Food Chem. 2014, 62, 6556−6564

Table 2. Cornell Net Carbohydrate and Protein System (CNCPS) CP Subfraction Profiles of Flaxseed: Comparison of the Brown Seed Type vs Yellow Seed Type[a]

	brown seed type		yellow seed type			contrast[c]	
item	CDC Bethune	CDC Sorrel	FY11 140	F08×425	SEM[b]	brown vs yellow	*P* value[c]
Crude Protein Subfraction[d] (% of CP)							
PA	4.71 b	3.12 b	7.98 ab	13.77 a	1.537	**	*
PB1	56.18 a	49.00 b	51.57 b	49.60 b	0.700	*	**
PB2	23.23 b	30.90 a	29.05 a	25.13 b	1.208	ns	*
PB3	13.33 a	12.83 a	6.34 b	0.95 b	0.978	***	**
PC	2.56 b	4.20 b	5.05 b	10.55 a	0.811	**	**
total true protein	92.74 a	92.69 a	86.96 a	75.69 b	1.456	**	**
True Protein[e] (% of True Protein)							
PB1	60.59 ab	52.83 b	59.34 ab	65.59 a	1.519	*	*
PB2	25.05 b	33.34 a	33.41 a	33.19 a	1.299	*	*
PB3	14.35 a	13.84 a	7.26 b	1.22 b	1.083	***	**

[a]a–b: means within a row with different letters differ at the $P < 0.05$ level. [b]SEM = Standard error of the mean. [c]ns, not significant; *, $P < 0.05$, **; $P < 0.01$; ***, $P < 0.001$. [d]PA = NPN, fraction of CP that is instantaneously solubilized at time zero; PB1 = fraction of CP that is rapidly degraded in the rumen and calculated as soluble protein − NPN; PB2, intermediately degradable fraction and calculated as CP − (PA + PB1+ PB2 + PB3 + PC); PB3, slowly degradable crude protein fraction and calculated as (NDIP − ADIP); and PC, fraction of CP recovered with ADF and is considered to be nondegradable. [e]True protein = PB1 (% of CP) + PB2 (% of CP) + PB3 (% of CP).

Table 3. In Situ Rumen Degradation Kinetics and Intestinal Digestibility of Flaxseeds: Comparison of the Brown Seed Type vs Yellow Seed Type[a]

	brown seed type		yellow seed type			contrast[c]	
item	CDC Bethune	CDC- Sorrel	FY11 140	F08×425	SEM[b]	brown vs yellow	*P* value[c]
In Situ Rumen Degradation Kinetics of Dry Matter (DM)[d]							
K_d, %/h	7.90 b	8.10 b	8.470 ab	9.66 a	0.286	**	**
lag time (T_0, h)	0.40	0.33	0.08	1.05	0.245	ns	*
S fraction, % DM	20.72 b	7.56 d	25.52 a	15.74 c	0.628	***	***
D fraction, % DM	68.15 b	82.39 a	67.17 b	80.18 a	1.097	ns	***
U fraction, % DM	11.13 a	10.07 ab	7.31 bc	4.09 c	0.782	***	***
RDDM, % DM	59.40 b	54.77 c	64.79 a	65.18 a	0.372	***	***
RUDM, % DM	40.60 b	45.16 a	35.20 c	34.82 c	0.372	***	***
In Situ Rumen Degradation Kinetics of Crude Protein (CP)[d]							
K_d, %/h	10.67 a	9.38 b	10.62 a	11.28 a	0.462	**	**
lag time (T_0, h)	0.70 ab	0.94 ab	0.04 b	1.19 a	0.230	ns	*
S fraction, % CP	26.71 b	10.96 d	30.78 a	19.93 c	0.881	***	***
D fraction, % CP	65.92 c	81.92 a	64.63 c	76.07 b	1.101	**	***
U fraction, % CP	7.38 a	7.13 a	4.59 b	4.00 b	0.551	***	***
RDP, % CP	68.85 b	60.90 c	72.04 a	69.57 b	0.462	***	***
RUP, % CP	31.14 b	39.12 a	27.96 c	30.43 b	0.707	***	***
Intestinal Digestibility of RUP[e]							
IDCP, % RUP	56.31 ab	51.05 b	67.38 a	68.75 a	3.391	***	**

[a]a–d: means within a row with different letters differ at the $P < 0.05$ level. [b]ns, not significant; *, $P < 0.05$, **; $P < 0.01$; ***, $P < 0.001$. [c]SEM = standard error of the mean. [d]K_d = the degradation rate of the D fraction (%/h); S = soluble fraction; D = rumen degradable fraction; U = rumen nondegradable fraction; RDDM, effective degradability of DM in the rumen; RUDM, rumen nondegraded DM; and RUP, rumen nondegraded protein. [e]IDCP, intestinal digestibility of CP.

in these seeds. Compared to brown-seeded varieties, the content of NDIP was lower ($P < 0.01$; 16.45 vs 11.44% CP) in the yellow-seeded lines, which is in line with literature findings.[11,12] Among the yellow-seeded lines, the content of ADIP was higher ($P < 0.05$) in F08×425, whereas no significant differences were observed in the CP chemical profile among the brown-seeded varieties. Overall, the results of chemical profiles showed that the yellow-seeded lines had higher contents of EE and CP; however, the CP in the yellow-seeded lines may not be optimally utilized by dairy cows due to the relatively high proportion of rapidly degradable SP (data not shown) and nondigestible ADIP fractions.

Crude Protein Subfractions. Results of the CNCPS CP subfractions of the brown-seeded and yellow-seeded flax are presented in Table 2. The contents of all CP subfractions varied ($P < 0.05$) among the four genotypes. The yellow-seeded lines had significantly ($P < 0.01$) higher contents of the nonprotein fractions, namely, the instantaneously solublilized (PA) fraction (10.88 vs 3.91% CP). In contrast, Theodoridou and Yu,[11] found lower content of the PA fraction (0.24 vs 3.1%) in yellow-seeded canola meal compared to that in brown-seeded canola meal. Whereas, Xin et al.[12] found no differences in the PA content of yellow- and brown-seeded carinata strains. Moreover, the yellow-seeded lines contained a high content of nonavailable (PC) fraction (7.80 vs 3.38% CP) compared to

dx.doi.org/10.1021/jf501284a | J. Agric. Food Chem. 2014, 62, 6556–6564

Table 4. Protein's Inherent Molecular Structural Characteristics Revealed by FT/IR-ATR Molecular Spectroscopy: Comparison of Brown Seed Type vs Yellow Seed Type[a]

	brown seed type		yellow seed type			contrast[d]	
item	CDC Bethune	CDC Sorrel	FY11 140	F08×425	SEM[c]	brown vs yellow	*P* value[d]
Protein Amide[b] (ca. 1715−1482 cm^{-1})[e]							
amide I height	0.059 b	0.054 c	0.064 a	0.058 b	0.0004	ns	***
amide II height	0.030 b	0.024 d	0.033 a	0.029 c	0.0246	*	***
amide I/II height ratio	1.975 b	2.296 a	1.956 b	2.018 b	0.0393	*	**
amide I area	3.639 b	3.447 c	3.940 a	3.547 bc	0.0571	**	***
amide II area	1.365 b	1.074 c	1.558 a	1.360 b	0.0133	**	***
amide I/II area ratio	2.667 b	3.240 a	2.558 c	2.655 b	0.0239	***	***
Protein Structure[b] α-Helix and β-Sheet[f]							
α-helix (height)	0.0580 b	0.0515 c	0.0625 a	0.0565 b	0.0004	ns	***
β-sheet (height)	0.0480 b	0.0455 c	0.0515 a	0.048 b	0.0004	ns	**
α-helix/β-sheet ratio	1.193 ab	1.135 c	1.120 a	1.184 b	0.0023	***	***

[a]a−d: means within a row with different letters differ at the $P < 0.05$ level. [b]The measurements are expressed in IR absorbance units. [c]SEM = standard error of the mean. [d]ns, not significant; *, $P < 0.05$; **, $P < 0.01$; ***, $P < 0.001$. [e]Protein amide bands were measure at ca. 1712−1482 cm^{-1}. [f]α-Helix and β-sheet bands were measured in the amide I region second derivative and Fourier self deconvolution spectra. The α-helix and β-sheet were centered at 1,653 and 1,630 cm^{-1}, respectively.

that in brown-seeded varieties. As a consequence of high PA and PC fractions, the true protein fraction of the yellow-seeded lines was markedly lower ($P < 0.01$; 81.31 vs 92.71% CP) than that in the brown-seeded varieties. The PA fraction very rapidly (200%/h)[31] degrades to NH_3-N in the rumen and often contributes to NH_3-N losses in the environment. Whereas, the PC fraction neither degrades in the rumen nor is digested in the postruminal tract and excreted in feces to the environment.[28] These results suggest that CP in the yellow flaxseed genotypes is not optimally digested and utilized in the gastrointestinal tract of dairy cows compared brown flaxseed varieties. However, the brown flaxseed varieties had a markedly higher (13.13 vs 3.65% CP) PB3 subfraction. The PB3 slowly (0.06 to 0.55%/h)[29,31] degrades in the rumen, and a large fraction of PB3 bypasses the rumen and is digested in the small intestine. Indeed, the in situ results showed higher RUP (35.1 vs 29.2% CP) contents for the brown-seeded varieties. Among the brown-seeded varieties, CDC Sorrel had lower ($P < 0.05$) PB1 and higher ($P < 0.05$) PB2 and PB3 fractions (Table 2), suggesting that CP in CDC Sorrel will be more gradually broken down to NH_3-N in the rumen and that a higher fraction of CP will bypass the rumen. This was confirmed by the in situ results, which showed high RUP values for CDC Sorrel (Table 3).

Rumen Degradation and Intestinal Digestibility. Results on the ruminal DM and CP degradation kinetics and intestinal digestibility of RUP in the yellow-seeded lines and brown-seeded varieties are shown in Table 3. The yellow-seeded lines had lower ($P < 0.001$) content of RUDM compared to that of the brown-seeded varieties. The D fraction of DM did not significantly change among the two seed coat types. Therefore, the lower content of RUDM of the yellow-seeded lines could be related to its higher ($P < 0.05$) S fraction and *kd* of the D fraction. The lower proportion of fiber (hull), higher proportion of CP and EE,[11,32] and higher *kd* of CP (Table 3) can all contribute to the lower RUDM of the yellow seed coat genotypes. Within the yellow seed coat genotypes, FY11140 had higher ($P < 0.05$) S fraction and lower ($P < 0.05$) D fraction; however, no significant differences were observed in the RUDM among the two yellow-seeded lines. In the brown flaxseed varieties, CDC Sorrel had higher ($P < 0.05$) RUDM. As the *kd* was not significantly different among the two brown-seeded varieties, the higher RUDM of CDC Sorrel was mainly caused by its markedly lower S-fraction (7.56 vs 20.72% CP) compared to that of CDC Bethune.

Except for lag time, all ruminal CP degradation parameters varied ($P < 0.05$) between the brown-seeded and yellow-seeded genotypes. The brown-seeded varieties had a higher ($P < 0.001$) content of RUP compared to that of the yellow-seeded genotypes. The higher RUP content of brown-seeded varieties could be related to their lower S fraction and lower *kd* of the D fraction compared to those of the yellow-seeded genotypes. However, there were significant differences in the in situ CP degradation parameters within the yellow- and brown-seeded genotypes. Among the brown-seeded flax, CDC Sorrel had a higher ($P < 0.05$) content of RUP. The higher RUP content of CDC Sorrel could be related to its markedly lower S fraction and lower *kd* of the D fraction compared to those of CDC Bethune (Table 3). In the yellow-seeded lines, FY08×425 had a significantly higher content of RUP. As the *kd* was not different between the two genotypes, the higher RUP content of FY08×425 was mainly caused by its markedly lower S fraction and higher lag time. The RUP in the yellow flaxseed lines were more ($P < 0.001$) digestible in the small intestine compared to that in the brown flaxseed varieties.

These results are consistent with earlier findings.[11] The high intestinal digestibility of RUP in yellow-seeded genotypes was, however, not supported by its significantly higher content of PC subfraction. Previous studies have shown a strong negative correlation ($r = -0.81$) between the PC (ADIP) subfraction and the total tract digestibility of CP,[35] and a strong positive correlation ($r = 0.84$) between the content of PC and the content of N excreted in the feces.[36] Nevertheless, the (in vitro)-intestinal digestibility of RUP in the brown flaxseed varieties was close to the reported values of intestinal digestibility for the brown flaxseed measured with the mobile nylon bag technique.[7] The lower digestibility of RUP in the brown flaxseed could be partly explained by the presence of condensed tannins in the brown seed coat.[11,37,38] Condensed tannins can make bonds with protein as well as with digestive enzymes and can decrease protein digestibility.[39,40] Overall, these results suggest that the CP in yellow-seeded lines was more extensively degraded in the rumen causing a lower supply of RUP to the small intestine compared to that in brown-

seeded varieties. However, the RUP in the former seeds were more digestible in the small intestine. These findings also demonstrate that it is important to determine the intestinal digestibility of RUP in order to more accurately estimate the metabolizable protein supply to dairy cattle.

Protein's Molecular Structures. Recently, advance molecular spectroscopy methods have been developed to quantitatively evaluate the primary and secondary molecular makeups of feed protein.[31,41] In general, the amide I and amide II spectral intensities in terms of peak area and height reveal information about the concentration of protein in feed.[18,42] Table 4 shows that the yellow seed coat FY11140 line had greater ($P < 0.05$) amide I and II height and amide I and II peak area among the four genotypes, which correspond to the higher concentration of CP in this variety. In agreement with our findings, Dariman and Yu[42] found that greater amide I and II height and area in zero-amylose waxy cultivar of barley were associated with a higher content of CP compared to those of waxy, high amylose and normal cultivars. However, the ratios of amide I/II and α-helix/β-sheet reveal information about the protein's molecular makeup.[42,43] The molecular makeup of feed protein strongly influences CP degradation in the rumen and the digestibility of RUP by affecting their solubility and access to microbes and proteolytic enzymes.[16,31] Among the four genotypes, CDC Sorrel had the highest amide I/II area ratio and lowest α-helix/β-sheet ratio, which were associated with the lowest contents of PA and PB1, and the highest content of RUP. Our results are consistent with the findings of Samadi and Yu[15] and Peng et al.[18] The correlation analysis (Table 5) showed that the amide I/II area ratio had a significant ($P < 0.05$) negative correlation to SP ($r = -0.77$) and the in situ S fraction ($r = -0.94$) and significant positive correlations to the D fraction ($r = 0.88$), RUP ($r = 0.96$), and intestinal digestibility of RUP ($r = 0.63$). The α-helix/β-sheet ratio had significant ($P < 0.05$) positive correlation to the content of SP ($r = 0.85$), kd ($r = -0.82$), S fraction ($r = 0.91$), and RDP ($r = -0.92$), and had significant negative correlations to the D fraction ($r = -0.88$), RUP ($r = -0.92$), and intestinal digestibility of RUP (-0.71). These results demonstrate that there is a strong relationship between the protein's molecular structures and CP chemical profiles, ruminal degradation characteristics, and intestinal digestibility of RUP.

Multivariate Analysis. Figure 2 shows the results of multivariate CLA and PCA analyses that classify and visualize the overall differences in the protein's inherent molecular makeup of brown-seeded and yellow-seeded genotypes. The CLA dendrograms (Figure 2a) show that the protein's molecular spectral data of CDC Sorrel can be distinguished from the other genotypes at a linkage distance of <0.18. CDC Bethune could also be distinguished from CDC Sorrel and FY11140 at a linkage distance of 0.02. The mixed dendograms of the two yellow-seeded lines (FY11140 and F08×425) demonstrate similarity in the structural makeup of their protein. Results of the PCA are visualized in a scatter plot between the first two principal factors (Figure 2, panel b). The scatter plot explained 90.14% of the total variation in the protein's molecular structures of the brown and yellow flaxseed. The protein's molecular spectra of CDC Bethune, CDC Sorrel, and FY11140 were clustered together into separate groups, demonstrating similarities within their molecular makeup. At the same time, these groupings show that CDC Bethune, Sorrel, and FY11140 could be completely distinguished from each other as demonstrated by CLA dendograms. These results confirm genotype differences in the protein's molecular makeup.

Table 5. Coefficient of Correlation (Pearson)[a] and Its Level of Significance between Protein Molecular Structural Characteristics and Nutrients Profile, Crude Protein Subfraction Profile, in Situ Degradation Kinetics, and Intestinal Availability in Yellow- and Brown-Seeded Flaxseed

	amide I/II height ratio		amide I/II area ratio		α-helix/β-sheet ratio	
item	r	P value[b]	r	P value	r	P value
Chemical Profile						
crude protein (CP), % of DM	−0.60	ns	−0.78	*	0.68	*
soluble protein (SP), % CP	−0.65	ns	−0.77	*	0.85	**
Protein Subfractions[c]						
PB1	0.01	ns	0.02	ns	0.65	*
PB2	0.04	ns	0.06	ns	−0.64	*
In Situ Rumen DM Degradation						
soluble fraction (S)	0.01	ns	0.00	ns	0.89	**
rumen degradable fraction (D)	0.01	ns	0.01	ns	−0.79	*
effective degradability of DM	0.24	ns	0.11	ns	0.71	*
rumen nondegraded DM	0.24	ns	0.11	ns	−0.71	*
In Situ Rumen CP Degradation						
degradation rate (K_d), %/h	−0.73	*	−0.81	*	0.82	**
soluble fraction (S)	−0.94	***	−0.94	***	0.91	***
rumen degradable fraction (D)	0.93	***	0.88	***	−0.88	***
rumen nondegraded protein (RUP)	0.90	***	0.96	***	−0.92	***
intestinal digestibility of RUP	0.72	*	0.63	†	−0.71	*

[a]Only variables with significant ($P < 0.05$) correlation are shown. [b]*, $P < 0.05$; **, $P < 0.01$; ***, $P < 0.01$. [c]PB1, the rapidly degraded CP fraction and is calculated as soluble protein − NPN; PB2, intermediately degradable CP fraction and is calculated as CP − (PA + PB1 + PB2 + PB3 + PC.

Multiple Regression Equations. Table 6 shows the multiple regression equations, based on the protein's spectral parameters, and their predictive power for the estimation of the contents of chemical components, CP subfractions, in situ CP degradation parameters, and intestinal digestibility. The results showed that the contents of CP ($R^2 = 0.87$) and SP ($R^2 = 0.92$) can be predicted from the amide I/II height and area ratios and α-helix height. Similarly, the protein spectral parameters could be used to estimate the in situ CP degradation parameters such as kd ($R^2 = 0.62$), S fraction ($R^2 = 0.88$), D fraction ($R^2 = 0.85$), RUP ($R^2 = 0.97$), and intestinal digestibility of RUP ($R^2 = 0.71$). The relatively good predictive powers of the regression equations, based on the protein's spectral parameters, for the estimation of total CP, SP, and RUP could have important practical implications in feed evaluation. FT/IR-ATR molecular spectroscopy is a fully established, noninvasive, and non-destructive analytical technique that can analyze the molecular structures of the proteins of a large number of feed samples in a relatively short time. Yu and Nuez-Ortín[16] and Becker and Yu[44] suggested that the ratios of amide I/II and α-helix/β-sheet can be used as an indicator for the changes in CP nutritive value during heat-related processing or among different feed types,

dx.doi.org/10.1021/jf501284a | J. Agric. Food Chem. 2014, 62, 6556−6564

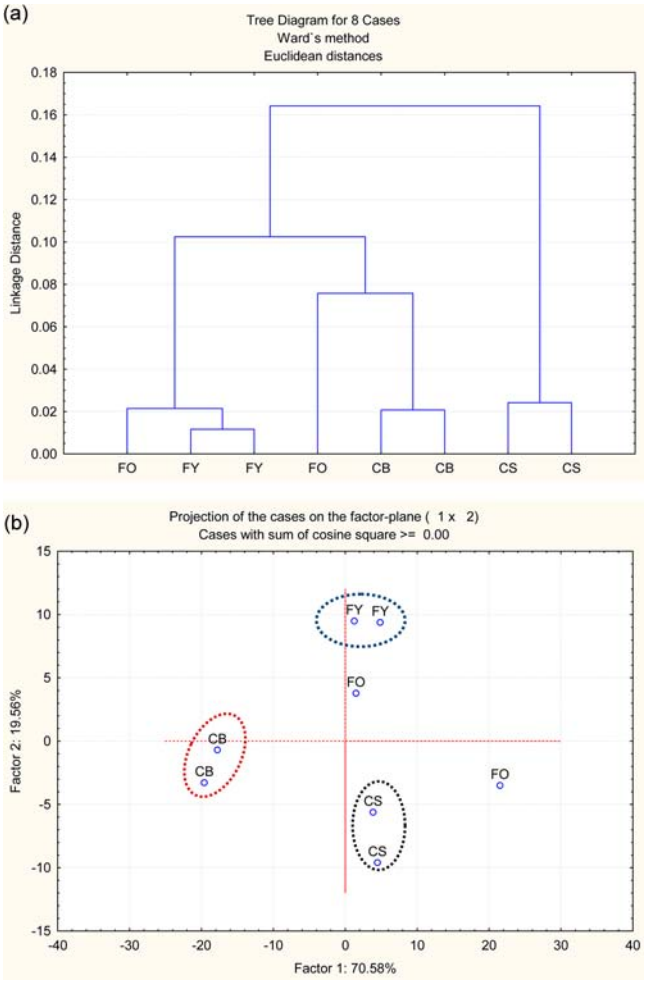

Figure 2. Agglomerative hierarchical cluster analysis (CLA) dendograms (a) and principal component analysis (PCA) scatter plot (b) visualizing the overall spectral (n = 249 spectral bands; collected at ca. 1712−1482 cm^{-1}) differences in the protein molecular makeup of brown seeded (CB = CDC Bethune; CS = CDC Sorrel) and newly developed yellow seeded (FY = FY11140; FO = FO8×425) flaxseed genotypes. (a) Agglomerative hierarchical cluster analysis (CLA) dendograms. (b) PCA scatter plot of the 1st principal factor versus 2nd principal factor.

which is supported by the findings of the present study. However, it is pertinent to mention here that these prediction equations were derived from limited samples based on one type of oilseed. Prediction equations based on a large number of samples with diverse sources will be required to illustrate the actual relationship between spectral parameters of protein and CP subfraction composition and digestive behavior.

In conclusion, the newly developed yellow flaxseed breeding lines had significantly higher contents of oil and CP compared to those of the brown flaxseed varieties. However, the CP in yellow-seeded lines had higher contents of PA and PC subfractions. As a consequence, the true protein subfraction was significantly lower in yellow-seeded lines. Moreover, the CP in the yellow-seeded lines was more extensively degraded in rumen resulting in the lower content of RUP than that in the brown-seeded varieties. However, the RUP in yellow-seeded lines was more digestible in the small intestine than that in the brown-seeded varieties tested; as a result, the total supply of digestible RUP was not different between the two seed color types. The molecular spectroscopy study revealed significant differences in the inherent molecular structures of protein, and these structural differences were strongly correlated to the CP chemical profile, ruminal degradation kinetics, and intestinal digestibility. The multiple regression equations showed that the protein's molecular spectral features can be used to estimate the contents of total CP, SP, RUP, and intestinal digestibility of RUP with relatively good predictive power. FT/IR-ATR spectroscopy can characterize feed molecular structures within cellular dimension, and the spectral parameters can be used as predictors for the estimation of CP subfractions, rumen degradation, and intestinal digestibility.

AUTHOR INFORMATION

Corresponding Author

*Dr. Peiqiang Yu, Professor Ministry of Agriculture Strategic Research Chair, Department of Animal and Poultry Science, College of Agriculture and Bioresources, University of Saskatchewan, 6D10 Agriculture Building, 51 Campus Drive, Saskatoon, S7N 5A8, SK, Canada. Tel: +1 306-966-4132. E-mail: Peiqiang.yu@usask.ca.

Present Address

§(N.A.K.) Department Animal Nutrition, The University of Agriculture Peshawar, Pakistan.

Table 6. Multiple Regression Equations, Degrees of Fit (R^2), and Standard Error of Estimation (SEE) for the Prediction of Crude Protein Chemical Profile and Ruminal Degradation Characteristics from the Protein's Spectral Parameters Analyzed by FT/IR-ATR Molecular Spectroscopy

predicted variable (Y)	regression equations: $Y = a$ (±SE) + b (±SE) × x	R^2	SEE	P value[a]
Crude Protein Chemical Profile				
crude protein (CP, % DM)	Y = 95.98 (±14.53) −13.59 (±2.15) × amide I/II area ratio −627.61 (±160.77) × α-helix height	0.87	0.948	**
soluble protein, % DM	Y = 15.58 (±3.87) + 13.61 (±3.99) × amide I/II height ratio −11.25712 (±1.85652) amide I/II area ratio	0.92	0.509	***
In Situ Rumen CP Degradation[b]				
K_d, %/h	− 15.87(±7.52) + 22.38 (±6.38) × α-helix/β-sheet ratio	0.62	0.462	*
S fraction, % CP	129.50 (±15.25) −51.70 (±7.32) × amide I/II area ratio	0.88	2.856	***
D fraction, % CP	−29.47 (±15.84) + 48.91 (±7.61) × amide I/II height ratio	0.85	2.956	***
RUP, % CP	−36.79 (±9.99) − 6.58 (±2.02) × amide I − 16.43 (±1.27) × amide I/II area ratio	0.97	0.796	***
IDCP[c], % of CP	64.79 (±10.76) −12.45 × amide I area	0.71	1.544	**

[a]†, P < 0.1; *, P < 0.05; **, P < 0.01; ***, P < 0.001. [b]K_d = the degradation rate of the D fraction (%/h); S = soluble fraction; D = rumen degradable fraction; and RUP, rumen nondegraded protien. [c]Intestinal digestibility of RUP.

Funding

Research projects of the Feed Research Chair group of Professor Dr. Peiqiang Yu have been supported by grants from Ministry of Agriculture Strategic Research Chair Program, Natural Sciences and Engineering Research Council of Canada (NSERC), SaskCanola, and Agricultural Development Fund (ADF; Saskatchewan).

Notes

The authors declare no competing financial interest.

■ ACKNOWLEDGMENTS

We thank Zhiyuan Niu for assistance in seed sampling and laboratory analysis.

■ REFERENCES

(1) FCC. *Canadian Flax*; Flax Council of Canada: Winnipeg, Canada. http://www.flaxcouncil.ca/english/index.jsp?p=what2&mp=what (accessed Feb 05, 2014).

(2) FAOSTAT. *Production and Trade*; Food and Agriculture Organization Statistical Database; FAO: Rome, Italy, 2012. http://faostat.fao.org/site/339/default.aspx (accessed Feb 05, 2014). .

(3) Petit, H. V.; Twagiramungu, H. Conception rate and reproductive function of dairy cows fed different fat sources. *Theriogenology* **2006**, *66*, 1316−1324.

(4) Ambrose, D. J.; Kastelic, J. P.; Corbett, R.; Pitney, P. A.; Petit, H. V.; Small, J. A.; Zalkovic, P. Lower pregnancy losses in lactating dairy cows fed a diet enriched in α−linolenic acid. *J. Dairy Sci.* **2006**, *89*, 3066−3074.

(5) Petit, H. V. Review: Feed intake, milk production and milk composition of dairy cows fed flaxseed. *Can. J. Anim. Sci.* **2010**, *90*, 115−127.

(6) Khan, N. A.; Tewoldebrhan, T. A.; Zom, R. L. G.; Cone, J. W.; Hendriks, W. H. Effect of corn silage harvest maturity and concentrate type on milk fatty acid composition of dairy cows. *J. Dairy Sci.* **2012**, *95*, 1472−1483.

(7) Mustafa, A. F.; McKinnon, J. J.; Christensen, D. A.; He, T. Effects of micronization of flaxseed on nutrient disappearance in the gastrointestinal tract of steers. *Anim. Feed Sci. Technol.* **2002**, *95*, 123−132.

(8) Oomah, B. D.; Mazza, G. Flaxseed proteins-a review. *Food Chem.* **1993**, *48*, 109−114.

(9) Mueller, K.; Eisner, P.; Yoshie-Stark, Y.; Nakada, R.; Kirchhoff, E. Functional properties and chemical composition of fractionated brown and yellow linseed meal (Linum usitatissimum L.). *J. Food Eng.* **2010**, *98*, 453−460.

(10) Petit, H. V.; Dewhurst, R. J.; Proulx, J. G.; Khalid, M.; Haresign, W.; Twagiramungu, H. Milk production, milk composition, and reproductive function of dairy cows fed different fats. *Can. J. Anim. Sci.* **2001**, *81*, 263−271.

(11) Theodoridou, K.; Yu, P. Effect of processing conditions on the nutritive value of canola meal and presscake. Comparison of the yellow and brown-seeded canola meal with the brown-seeded canola presscake. *J. Sci. Food Agric.* **2013**, *93*, 1986−1995.

(12) Xin, H.; Falk, K. C.; Yu, P. Studies on brassica carinata seed. 1. protein molecular structure in relation to protein nutritive values and metabolic characteristics. *J. Agric. Food Chem.* **2013**, *61*, 10118−10126.

(13) Yu, P. Protein secondary structures (α-helix and β-sheet) at a cellular level and protein fractions in relation to rumen degradation behaviours of protein: A new approach. *Br. J. Nutr.* **2005**, *94*, 655−665.

(14) Peng, Q.; Khan, N. A.; Wang, Z.; Yu, P. Relationship of feeds protein structural makeup in common prairie feeds with protein solubility, in situ ruminal degradation and intestinal digestibility. *Anim. Feed Sci. Technol.* **2014**, DOI: 10.1016/j.anifeedsci.2014.05.004.

(15) Samadi; Yu, P. Dry and moist heating-induced changes in protein molecular structure, protein subfraction, and nutrient profiles in soybeans. *J. Dairy Sci.* **2011**, *94*, 6092−6102.

(16) Yu, P.; Nuez-Ortín, W. G. Relationship of protein molecular structure to metabolisable proteins in different types of dried distillers grains with solubles: A novel approach. *Br. J. Nutr.* **2010**, *104*, 1429−1437.

(17) CCAC. *Guide to the Care and Use of Experimental Animals*, 2nd ed.; Vol. *1*, Canadian Council on Animal Care: Ottawa, Canada, 1993.

(18) Peng, Q.; Khan, N. A.; Wang, Z.; Yu, P. Moist and dry heating-induced changes in protein molecular structure, protein subfractions, and nutrient profiles in camelina seeds. *J. Dairy Sci.* **2014**, *97*, 446−457.

(19) Øskov, E. R.; McDonald, I. The estimation of protein degradability in the rumen from incubation measurements weighted according to rate of passage. *J. Agric. Sci.* **1979**, *92*, 499−503.

(20) Robinson, P. H.; Fadel, J. G.; Tamminga, S. Evaluation of mathematical models to describe neutral detergent residue in terms of its susceptibility to degradation in the rumen. *Anim. Feed Sci. Technol.* **1986**, *15*, 249−271.

(21) Tamminga, S.; Van Straalen, W. M.; Subnel, A. P. J.; Meijer, R. G. M.; Steg, A.; Wever, C. J. G.; Blok, M. C. The Dutch protein evaluation system: the DVE/OEB-system. *Livest. Prod. Sci.* **1994**, *40*, 139−155.

(22) SAS Institute. *User's Guide: Statistics*, 8th ed.; SAS Institute Inc.: Cary, NC., 2009.

(23) NRC. *Nutrient Requirements of Dairy Cattle*, 7th ed.; National Research Council, NRC; Academies Press: Washington, DC, 2001.

(24) AOAC. *Officials Methods of Analysis*, 15th ed.; Association of Official Analytic Chemists: Arlington, VA, 1990.

(25) Roe, M. B.; Sniffen, C. J.; Chase, L. E. Techniques for Measuring Protein Fractions in Feedstuffs. In *Proceedings of the Cornell Nutrition Conference*, Ithaca, NY; Cornell University: Ithaca, NY, 1990; pp 81−85.

(26) Lacitra; Lacitra, G.; Hernandez, T. M.; Van Soest, V. J. Standardization of procedures for nitrogen fractionation of ruminant feeds. *Anim. Feed Sci. Technol.* **1996**, *57*, 347−358.

(27) Calsamiglia, S.; Stern, M. D. A three-step in vitro procedure for estimating intestinal digestion of protein in ruminants. *J. Anim. Sci.* **1995**, *73*, 1459−1465.

(28) Sniffen, C. J.; O'Connor, J. D.; Van Soest, P. J.; Fox, D. G.; Russell, J. B. A net carbohydrate and protein system for evaluating cattle diets: II. Carbohydrate and protein system availability. *J. Anim. Sci.* **1992**, *70*, 3562−3577.

(29) Tylutki, T. P.; Fox, D. G.; Durbal, V. M.; Tedeschi, L. O.; Russell, J. B.; VanAmburgh, M. E.; Overton, T. R.; Chase, L. E.; Pell, A. N. Cornell Net Carbohydrate and Protein System: A model for precision feeding of dairy cattle. *Anim. Feed. Sci. Technol.* **2008**, *143*, 174−202.

(30) Van Amburgh, M. E., Chase, L. E.; Overton, T. R.; Ross, D. A.; Recktenwald, E. B.; Higgs, R. J.; Tylutki, T. P. Updates to the Cornell Net Carbohydrate and Protein System v6.1 and Implications for Ration Formulation. In *Proceedings of the Cornell Nutrition Conference*; Feed Manufacturers, Syracruse, NY, 2010; pp 144−159.

(31) Yu, P. Protein molecular structures, protein subfractions, and protein availability affected by heat processing: A review. *Am. J. Biochem. Biotechnol.* **2007**, *3*, 70−90.

(32) Diederichsen, A.; Raney, J. P. Seed colour, seed weight and seed oil content in Linum usitatissimum accessions held by Plant Gene Resources of Canada. *Plant Breed.* **2006**, *125*, 372−377.

(33) Sood, S. P.; Bhateria, S.; Sood, S. Inheritance of flower & seed colour in flax (Linum usitatissimum L.) over environments in North Western Himalaya. *National Acad. Sci. Lett.* **2012**, *35*, 127−130.

(34) Simbaya, J.; Slominski, B. A.; Rakow, G.; Campbell, L. D.; Downey, R. K.; Bell, J. M. Quality characteristics of yellow-seeded Brassica seed meals: Protein, carbohydrates, and dietary fiber components. *J. Agric. Food Chem.* **1995**, *43*, 2062−2066.

(35) Moshtaghi, N. S. A.; Ingalls, J. R. Effect of heating canola meal protein degradationin the rumen and digestion in the lower gastrointestinal tract of steers. *Can. J. Anim. Sci.* **1992**, *72*, 83−88.

(36) Van Soest, P. J.; Mason, V. C. The influence of the Maillard reaction upon the nutritive value of fibrous feeds. *Anim. Feed Sci. Technol.* **1991**, *32*, 45−53.
(37) Plahar, W. A.; Annan, N. T.; Nti, C. A. Cultivar and processing effects on the pasting characteristics, tannin content and protein quality and digestibility of cowpea (Vigna unguiculata). *Plant Foods Human Nutr.* **1997**, *51*, 343−356.
(38) Sedghi, M.; Golian, A.; Soleimani-Roodi, P.; Ahmadi, A.; Aami-Azghadi, M. Relationship between color and tannin content in sorghum grain: Application of image analysis and Artificial Neural Network. *Rev. Bras. Cienc. Avic.* **2012**, *14*, 57−62.
(39) Imran, M.; Anjum, F. M.; Butt, M. S.; Sheikh, M. A. Influence of extrusion processing on tannin reduction and oil loss in flaxseed (Linum usitatissimum L.) meal. *J. Food Proc. Pres.* **2014**, *38*, 622−629.
(40) Khan, N. A.; Habib, G.; Ullah, G. Chemical composition, rumen degradability, protein utilization and lactation response to selected tree leaves as substitute of cottonseed cake in the diet of dairy goats. *Anim. Feed Sci. Technol.* **2009**, *154*, 160−168.
(41) Khan, N. A.; Peng, Q.; Xin, H.; Yu, P. Vibrational spectroscopic investigation of heat-induced changes in functional groups related to protein structural conformation in camelina seeds and their relationship to digestion in dairy cows. *Anim. Prod. Sci.* **2014**, in press.
(42) Damiran, D.; Yu, P. Molecular basis of structural makeup of hulless barley in relation to rumen degradation kinetics and intestinal availability in dairy cattle: A novel approach. *J. Dairy Sci.* **2011**, *94*, 5151−5159.
(43) Yu, P.; Niu, Z.; Damiran, D. Protein molecular structures and protein fraction profiles of new coproducts from bioethanol production: a novel approach. *J. Agric. Food Chem.* **2010**, *58*, 3460−3464.
(44) Becker, P. M.; Yu, P. What makes protein indigestible from tissue-related, cellular, and molecular aspects? *Mol. Nutr. Food Res.* **2013**, *57*, 1695−1707.

show three-dimensional variability with highly complex relationships between bioavailability and biodegradation in both subsoil and topsoil.[12] Understanding the extent of this three-dimensional variation and its controlling factors is essential in the risk assessment of environmental exposure. Additionally, pesticide quantitative-diversely distributes at different parts of plants (cuticle and internal parts or above-ground and underground parts, etc.), which results in differences in human intake risk. It is necessary to discuss the distribution of pesticides in the different parts of the plant. Wang et al. reported that the plasma of tomato initially accumulated the highest pesticide concentration, and the concentrations of chlorothalonil and chlorpyrifos in tomato followed the order cuticle > plasma > pulp.[13] However, few studies thoroughly focused on the distribution of pesticides in soils and plants. Another purpose of this work is to determine the time-dependent dynamic distribution of CHP in different parts of bamboo area (bamboo shoots and soil) and the influencing factors. This study would help to provide basic information for developing regulations to safeguard the use of CHP in bamboo shoot cultivation and to prevent health problems in consumers. This may further lead to the development of optimized pesticide removal procedures.

MATERIALS AND METHODS

Reagents and Solutions. Pesticide analytical standards were purchased from National Information Center for Certified Reference Materials (Beijing, China), certified quality. Individual pesticide stock solutions (100 mg/L) were prepared in methanol or acetonitrile and stored at −20 °C. Then, a series of dilutions containing the mixture of standards were prepared (10 mg/L) in methanol. HPLC-grade acetonitrile and methanol were obtained from Merck (Darmstadt, Germany). A Milli-Q-Plus ultrapure water system from Millipore (Milford, MA, USA) was used throughout the study to obtain the HPLC-grade water used during the analyses. Other solvents were from Shanghai Sanying Chemical Reagents (Shanghai, China), pesticide residue analysis quality.

HPLC-MS/MS. The LC system consists of a high-performance liquid chromatograph (Waters, Milford, MA, USA) with an HSS T3 column (5 μm, 100 mm × 2.1 mm, i.d., Waters). A mobile phase consisting of solvent A (0.1% formic acid, in water) and solvent B (methanol) was used with the following gradient program: 80:20 A:B (initial), 10−90% A with 90−10% B (0−5 min), 10:90 A:B (5−10 min), 10−80% A with 90−20% B (10−14 min), 80:20 A:B (14−15 min). A subsequent requilibration time (3 min) was performed after each injection. The flow rate was 0.3 mL/min, and the injection volume was 10 μL. The column and sample temperatures were maintained at 35 °C.

MS/MS was performed on a Waters Quattro Premier triple-quadruple mass spectrometer equipped with an ESI source (Waters, Milford, MA, USA). MS/MS detection was performed in positive ion mode for CHP and in negative mode for TCP separately. The monitoring conditions were optimized for target compounds. Acquisition parameters were as follows: capillary voltage 3.5 kV, cone voltage 45 V, source block temperature 80 °C, cone gas 50 L/h, desolvation temperature 450 °C, desolvation gas (nitrogen gas) 550 L/h, respectively. As the precursor ion for CHP, 352 (m/z) was selected, and its quantitative and qualitative product ions were 97 (m/z) and 198 (m/z), respectively, when the collision energies were both 30 V. As for TCP, 196/35 was selected as the quantification ion transition, and 198/37 were selected as the confirmatory ion transition with all the collision energies at 15 V. Multireaction monitoring mode was selected as the scan mode. Under the described conditions, the retention times of CHP and TCP were approximately 9.92 and 7.88 min, respectively.

Pesticide Analysis. A portion (20.0 g) of prehomogenized sample (bamboo shoot) was weighed in a 250 mL glass breaker. The sample was extracted with 50 mL of acetonitrile by homogenization with a high-speed blender (Ultra-Turrax T18, IKA, Germany) for 2 min. After the addition of 6 g of $MgSO_4$ and 4 g of NaCl, each mixture was shaken intensively for 1 min and centrifuged for 5 min at 8000 rpm. An aliquot of the organic phase (25.0 mL) was transferred and concentrated by a rotatory evaporator at 40 °C to near dryness, then dissolved in 1.0 mL of methanol. Prior to analysis, the methanolic analyte was filtered through a 0.22 μm PTFE filter (Milford, MA, USA).

A 2.0 g sample of soil (sieved through a 2 mm mesh) was mixed with 1 mL of distilled water for 5 min. Then methanol (5 mL) was added and vortexed for 2 min, and the sample was centrifuged for 5 min (4000 rpm). A 2.0 mL portion of the superstratum was transferred and filtered through a 0.22 μm PTFE filter.

Chemical and Biological Analyses of Soils. Soil characteristics were examined including moisture content, pH, and organic carbon. Moisture content was measured according to Bending et al.[12] Soil pH was measured in water with a soil to water ratio of 1:5 (w/v). Organic carbon was determined by dichromate oxidation and titrated with ferrous ammonium sulfate, followed by converting to soil organic matter content using the Van Bemmelen factor 1.724.[14]

Field Experiments and Sampling Procedure. The trial field (red soil) was located in Fuyang, Zhejiang Province, China. The recommended dosage is 120 kg/ha for 3% chlorpyrifos granules (Tianyi Agriculture Chemistry Company, Zhejiang, China). The field experiment was started on Nov 6, 2012. After the pesticide application, the surface soil was turned to mix uniformly. On the next day, compound fertilizer was applied by hand (1000 kg/ha), and the soil surface was covered by straw (20 cm in thickness). Representative soil samples were collected by random sampling, and CHP and its metabolic residues were measured using the method described above. The soil (0−20 cm) was divided into three layers (0−5, 5−10, and 10−20 cm) and collected (1 kg). Samples were collected randomly from each plot at 0, 6, 13, 21, 29, 38, 62, 83, 111, 140, 170, 201, 250, and 300 day intervals after pesticide application. The bamboo shoot samples were collected randomly from each plot at 83, 111, 115, 119, 125, 129, 132 day intervals after pesticide application. Each sample (1 kg) was chopped and divided into two samples.

Data Analysis. To determine the kinetics of the degradation, plots of concentration against time were made, and an exponential regression analysis (first-order rate equation) was then performed on each data set.

$$c = c_0 e^{-kt}$$

where c represents the concentration of pesticide at time t, c_0 represents the initial concentration, and k is the rate constant.

RESULTS AND DISCUSSION

Efficiency of Analysis Method. The accuracy and precision of the method were obtained with recovery studies by spiking tested compound-free soil and bamboo shoots at three levels (Table 1). The control samples from untreated plots and reagent blanks were also processed in the same way so as to find out the interferences, if any, due to the substrate and reagents, respectively. The peaks of CHP and its metabolic TCP were free from interfering peaks of soil and bamboo shoots. For the blank sample substrate, there was no peak detectable in the range of runtime. The recovery of CHP and TCP from soil and bamboo shoots ranged from 70.5% to 108.2% with RSD (relative standard deviation) ranging from 3.4% to 10.5%. The lowest spiked concentration of the analyte, which could be determined with acceptable precision and accuracy, was considered as the limit of detection (LOD) of the method. From the validation data presented in Table 1, it can be observed that the LODs were 0.10 mg/kg (soil) and 0.01 mg/kg (bamboo shoot), respectively.

Table 1. Recoveries and RSD of Fortified Soil and Bamboo Shoot Samples

matrix	compound	fortified level (mg/kg)	recoveries (%)			RSD (%)
soil	CHP	0.1	85.2	89.6	80.3	5.5
		0.25	93.2	95.7	105.6	6.7
		0.5	93.2	98.7	106.7	6.8
bamboo shoot	CHP	0.01	100.2	95.7	93.4	3.6
		0.05	91.3	86.7	92.5	3.4
		0.1	108.2	100.7	99.3	4.7
soil	TCP	0.1	93.6	82.3	85.1	6.8
		0.25	73.2	86.7	89.6	10.5
		0.5	89.4	96.3	87.2	5.2
bamboo shoot	TCP	0.01	79.3	70.5	85.4	9.6
		0.05	88.2	76.8	85.1	7.1
		0.1	92.4	88.6	83.7	4.9

Dynamics of CHP in Soil. The subsoil represents a very different physical, chemical, and biological environment from the topsoil. Previous studies showed that pesticide degradation rates declined with soil depth.[15] In this study, the soil layer (0−20 cm, the cultivation soil layer for bamboo root growing) was divided into three parts: top layer (Tl, 0−5 cm), middle layer (Ml, 5−10 cm), and bottom layer (Bl, 10−20 cm). The dynamic curves of CHP in the covered (CP) and noncovered cultivation (NCP) are shown in Figure 1. The original deposits

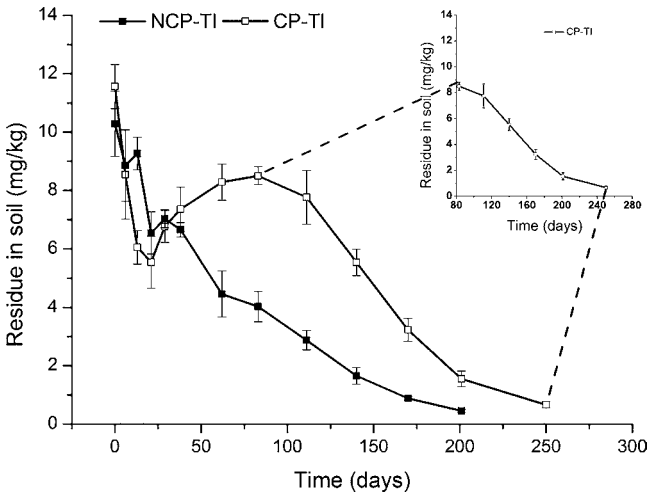

Figure 1. Dissipation curves of CHP residues (mg/kg), fitted to the first-order kinetics model, in the top layer of soil (0−5 cm). Data are means ± SD (n = 3).

in the soils in two cultivation patterns were 11.57 mg/kg (CP) and 10.29 mg/kg (NCP), respectively. The degradation dynamic in NCP-Tl could be fitted to a first-order exponential decay model.[16] The equation was $C_t = 10.84e^{-0.0144t}$ (R^2 = 0.96), and the half-life was 48.1 days. However, the degradation dynamics in CP-Tl could not be fitted to any decay model. CHP degraded rapidly in Tl by more than 52% in 21 days. Then the dissipation curve pattern in Tl showed a fluctuant ascent until 83 days and a subsequent descent. This performance was due to the character of granule formulation of CHP, which was slowly released during the experiment, and then the quantity of CHP residue in the soil increased. After 83 days, the slow-release effect weakened or disappeared. From 83 to 250 days, the degradation equation in Tl was $C_t = 11.52e^{-0.0164t}$ (R^2 = 0.87), with a half-life 42.3 days. From 29 to 140 days, the CHP residue could be detected in Ml (Table 2), with the concentrations ranging from 1.25 to 0.15 mg/kg.

Table 2. Distribution of CHP in the Middle Layer (Ml) and Bottom Layer (Bl) of CP Soil

time (day)	Ml (±SD, mg/kg)	Bl (±SD, mg/kg)
0−21	<LOD	<LOD
29	1.25 ± 0.12	<LOD
38	0.79 ± 0.07	0.54 ± 0.07
62	1.03 ± 0.08	0.78 ± 0.08
83	0.56 ± 0.06	0.31 ± 0.03
111	0.34 ± 0.04	0.11 ± 0.02
140	0.15 ± 0.02	<LOD
170−250	<LOD	<LOD

Between day 38 and 111, the CHP residues in Bl ranged from 0.78 to 0.11 mg/kg. The appearance of CHP residue in Ml and Bl demonstrated that CHP could gradually migrate from the top layer of soil to the bottom, which is likely to result in some risk for underground water or other species in the subsoil. However, in the NCP soil, the CHP residue could be detected only in Tl, which meant that CHP was fixed in the topsoil with reduced risk. In addition, there was almost no slow-release effect in NCP, and CHP degraded rapidly. Obviously, the soil surface mulching cultivation could lead to the slow release and migration of CHP. The previous studies have suggested the half-life of CHP (emulsifiable concentrate) in soil was 36.5 days.[17] In other studies where CHP was applied directly to bare tropical field soils (23−25 °C), shorter half-lives in the range 0.6−5.4 days were found,[18] and the residue of CHP in the soil could range up to 120 days,[16] even one year, depending on soil type, insecticide dose, climate, and other environmental factors.[19,20] The slower CHP (granule formulation) degradation under bamboo shoot soil may also be attributed to shading of the soil, resulting in less photodegradation and volatilization.

CHP Residue in Bamboo Shoots. The bamboo shoot samples (edible part, with average length 15−20 cm) were divided into two parts: an upper part (10−15 cm length) and a bottom part (5 cm). For CP bamboo shoots, the residues at harvest time were found mainly in the bottom part: the residues at harvest time were 38.3 μg/kg (83 d), 20.5 μg/kg (111 d), and 10.9 μg/kg (115 d), respectively (Table 3). The concentration in the upper part was only detected at 83 and 111 days, with 24.2 and 12.8 μg/kg, respectively. The maximum residue limits (MRLs) of CHP and TCP in bamboo shoot have not established in China. However, China established 50 μg/kg as the MRL for asparagus. The EU and USA set 50 μg/kg as the MRL for CHP in bamboo shoots, and the MRL for bamboo shoots in Japan (Positive List System) is 500 μg/kg. All the quantities for CHP detected in this work were below the MRLs mentioned above. It is worth noting that the total quantity of residue in 83 days was 62.5 μg/kg, which was above the MRLs (except for Japan). However, bamboo shoots could be found only sporadically before 111 days and could not be put on the market. So there is no risk for consumers. Obviously, the concentration in the bamboo shoot was higher for CP compared with NCP. The CHP residues in NCP bamboo shoots were below the LOD of the method (10 μg/kg). This result might be due to the immobility of CHP in the topsoil;

dx.doi.org/10.1021/jf501540e | J. Agric. Food Chem. 2014, 62, 6565−6570

Table 3. Distribution of CHP in Bamboo Shoots

time after pesticide application (d)	residues in bamboo shoot of CP (±SD, μg/kg) upper	bottom	time after pesticide application (d)	residues in bamboo shoot of NCP (±SD, μg/kg) upper	bottom
83	24.2 ± 3.32	38.3 ± 5.47	132	<LOD	<LOD
111	12.8 ± 1.88	20.5 ± 2.10	136	<LOD	<LOD
115	<LOD	10.9 ± 1.39	139	<LOD	<LOD
119	<LOD	<LOD	145	<LOD	<LOD
125	<LOD	<LOD	148	<LOD	<LOD
129	<LOD	<LOD	153	<LOD	<LOD
132	<LOD	<LOD	160	<LOD	<LOD

the CHP could not reach the root of the bamboo and adsorb into the bamboo shoot. In addition, the harvest time for NCP is behind the CP by almost 30 days, and the total quantity of CHP residue in the soil is relatively less in that period.

Metabolism of CHP in Soil and Bamboo Shoots. When a pesticide is applied, it enters a hostile environment and is subjected to a wide range of biological (enzymes), chemical (hydrolysis), and physical (photolysis) reactions, which may change its chemical nature.[21] The degradation products (metabolites) have different inherent properties from their parent pesticides, and the effects of these changes need to be assessed in terms of both environmental and human safety. Metabolism studies are conducted to provide a detailed understanding of the fate and behavior of the pesticide in the environment.[22,23] Liang et al. found TCP was most likely to leach through paddy soil into groundwater.[24] In this work, the results showed that CHP could be degraded into TCP in bamboo shoot soil (Figure 2). The rainfall had a notable effect

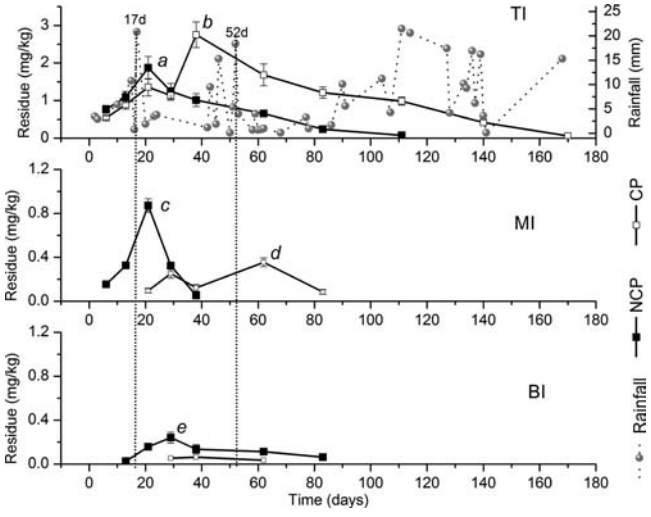

Figure 2. Distribution of TCP in different layers of soil.

on the leaching of TCP in the soil. After a rainfall, TCP in Tl could leach into Ml, and even Bl. This was especially obvious when a large-scale rainfall occurred. In NCP soil, the CHP degraded rapidly between day 17 and 21 (rainfall capacity was 20.7 mm on day 17); residue peaks of TCP in Tl (point *a*) and Ml (point *c*) were reached on day 21. The rainfall accelerated the degradation of CHP; on the other hand, a strong leaching effect occurred. However, in CP soil, the residue peaks occurred relatively late. TCP residues in Tl and Ml were 2.75 mg/kg on day 38 (point *b*) and 0.35 mg/kg on day 62 (point *d*), respectively. The leaching delay resulted from the adsorption of rain from the covering materials, which led to the slow leaching effect for TCP. In CP soil, the leaching of TCP was a gradual process. In addition, most of TCP residues gathered and degraded in Tl before the migration process occurred. Although the TCP residue levels in the topsoil (Tl) were higher in CP than that in NCP, the latter had higher residue values in the subsoil (Ml and Bl). The concentration of the degradation product TCP did not exceed 3 mg/kg during the 180-day experimental period. For bamboo shoots, there were no TCP residues detected. The high hydrophilicity of TCP made it diffcult to penetrate the hydrophobic shell of bamboo shoots. In addition, the nonresidue detected in bamboo shoots was also closely related to the minor residue of TCP in the root layer (Bl).

pH Change of Soil and Its Effect on Pesticide Behaviors. Soil pH is known to play a key role in controlling the structure of soil microbial communities, which could influence pesticide metabolism indirectly. In addition, the soil pH could influence pesticide hydrolysis directly. The degradation rate of several pesticides has been found to be related to pH.[25] In a study of Canadian and French soils, the soils with a pH over 6.5 typically showed growth-linked metabolism of atrazine, and those with a pH lower than 6.5 showed slower co-metabolic degradation.[12] Additionally, pH is known to affect the extent to which some pesticides adsorb to soil organic matter and, therefore, determine the bioavailability of such pesticides to the degradative community. From Figure 3, in 0−5 cm surface soil, the pH in the CP treatment increased

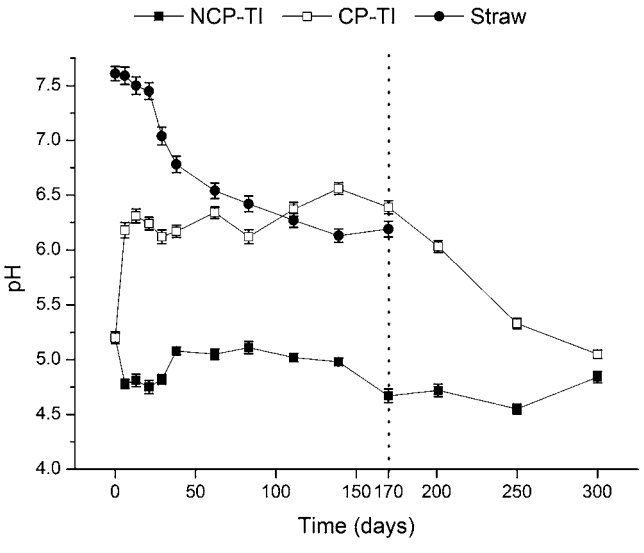

Figure 3. pH changes of the topsoil in different treatments.

dx.doi.org/10.1021/jf501540e | J. Agric. Food Chem. 2014, 62, 6565−6570

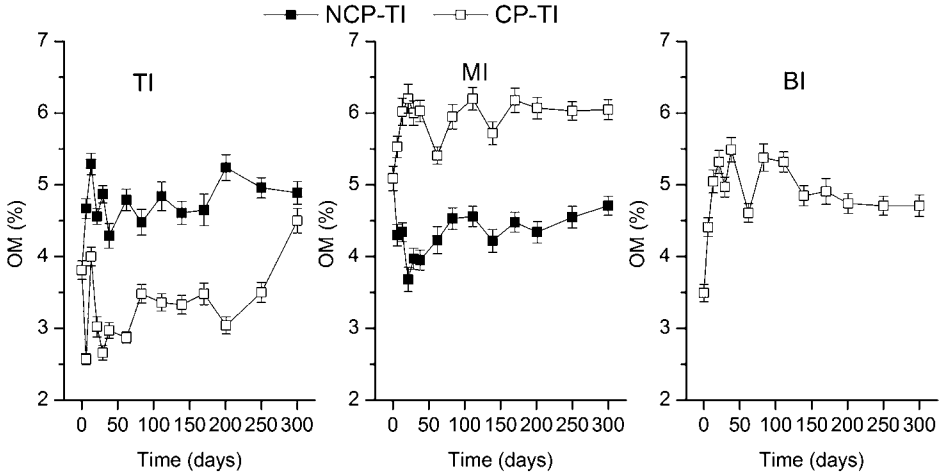

Figure 4. OM changes of soils in different treatments.

from 5.2 to 6.18 after the experiment was carried out for 6 days, while the NCP treatment reduced the pH from 5.2 to 4.78. The reduction of pH from NCP surface soil might be induced by acid rain. There was a small amount of precipitation on days 2 and 3 after the experiment's beginning. The pH of the rain ranged from 4.7 to 5.2. In the CP treatment, the rain washed the straw, and then the leachate (pH above 6.0) of the straw leached into the soil surface, leading to a higher pH value. During the experiment period, 0−170 days, the pH of the CP treatment of the topsoil was significantly higher than that of the NCP treatment; after 170 days, the pH difference between the two treatments was significantly smaller with the cover material removed, which indicated that the alkalinity or acidity of covering material itself could affect the pH value of the topsoil. In the subsoil, there were little differences in pH between the CP and NCP treatments (not exceeding 0.3 unit of pH), which illustrated that the leachate of the covering material was mainly in the 0−5 cm of surface soil, and the leachate containing some substance capable of changing the soil pH did not readily leach into the soil below 5 cm. The pH value of the surface soil in the CP treatment was higher than that in the NCP treatment, and the pH of the 0−5 cm surface layer was higher than that of the 5−10 and 10−20 cm soil layers. The higher pH can directly accelerate the degradation of pesticides, which explained the fast degradation of CHP from day 0 to 21 in the CP treatment.

OM Change of Soil and Its Effect on Pesticide Behaviors. Pesticide adsorption can also show significant spatial variability at both the catchment and field level. Several authors have shown that adsorption of pesticides decreases with soil depth, with the pattern governed by soil organic matter (OM) content.[12,26] Since adsorption can be an indicator of bioavailability, a change in the amount or variability of adsorption with depth could affect patterns of biodegradation, even though the significance of any changes would be expected to depend on the strength of adsorption of individual compounds. One of the factors for the high persistence of fipronil in soil was the high organic carbon level and low pH.[22] CHP was strongly adsorbed to soil particles, which may retard its degradation.[27] The results from NCP obtained in the present investigation seem to be in agreement with the above studies. In the three stratified soil types of the NCP treatment, soil OM content significantly decreased with depth, ranging between 2.24% and 5.89% in topsoil and from 0.78% to 2.80% at 5−20 cm depth (Figure 4). However, in the three stratified soil types of the CP treatment, the OM of the subsoil layer (5−20 cm) was obviously higher. Compared with the NCP treatment, OM decreased in topsoil and increased in subsoil from the CP treatment, which may be due to the insulation of the covering material (the OM of straw was 36.1%) or the leachate from the straw into the subsoil.

Usually, there is a negative correlation between OM and pH.[14] In this work, the topsoil performed in agreement with the principle. The OM of topsoil in the CP treatment was lower than that in the NCP treatment, and the former had a higher pH over the latter. The topsoil with a low pH and high OM could absorb more CHP in the NCP treatment, which explained why CHP was fixed in the 0−5 cm soil layer. Correspondingly, the topsoil with lower OM in the CP treatment had less adsorption capacity for CHP than that in the NCP treatment, so CHP in CP treatment will produce significant leaching effects. However, TCP did not show a significant positive correlation with OM values. The high hydrosolublity of TCP led to its notable leaching effect in the NCP treatment.

Effect of Soil Surface Mulching on Pesticide Behaviors. Due to the slow-release effect from the granule formulation of CHP, its degradation process could result in a degradation rate of CHP that is slower than the other formulations with a non-slow-release effect. This difference is particularly evident in the soil surface mulching cultivation and may cause persistence of pesticides and long-term environmental risks. In the soil surface mulching cultivation, the straw used as the mulched material, with higher OM and pH, had some regulatory role in changing the pH and OM characteristics of the soil. Thus, the straw could indirectly affect the adsorption and degradation behavior of CHP and TCP in soil. CHP was more easily fixed in the 0−5 cm soil layer of the NCP treatment; thus it was difficult to produce a leaching effect and cause further effects. The rain leaching delay performance from the mulched materials led to the slow-leaching effect for TCP. TCP could generate an obvious leaching capacity to enter into the subsoil. In contrast, CHP was easy to leach in the CP treatment, and the leaching capacity of TCP in the CP treatment was not more obvious than that in the NCP treatment. Although the CHP and TCP residues in the harvested bamboo shoot samples from mulched ground did not basically exceed the MRLs, a sample close to the MRL value still existed. This deserved our attention regarding food safety

dx.doi.org/10.1021/jf501540e | J. Agric. Food Chem. 2014, 62, 6565−6570

issues. In general, although CHP granule formulation leads to high efficiency for insect control under soil surface mulching, additional risks for consumers, agriculture workers, and the environment should be taken into account due to prolonged persistence and leaching of high residue levels in the soil.

AUTHOR INFORMATION

Corresponding Author

*Tel: 86-0571-63122616. Fax: 86-0571-63122616. E-mail: yalin_zj@163.com.

Funding

We gratefully acknowledge financial support from the Fundamental Research Funds for the Central Nonprofit Research Institution of CAF (RISF61252), Special Fund for Forestry Scientific Research in the Public Interest (201304705), and the Applied Research Project in the Public Interest of Zhejiang Province (2013C32106).

Notes

The authors declare no competing financial interest.

ABBREVIATIONS USED

CHP, chlorpyrifos; TCP, 3,5,6-trichloro-2-pyridinol; CP, soil surface mulching conditions; NCP, noncovered cultivation conditions; LC-MS/MS, liquid chromatography−mass/mass spectrometry; RSD, relative standard deviation; LOD, limit of detection; Tl, top layer of soil (0−5 cm); Ml, middle layer (5−10 cm); Bl, bottom layer (10−20 cm)

REFERENCES

(1) Ostwal, P.; Dabadghao, V. S.; Sharma, S. K.; Dhakane, A. B. Chlorpyrifos toxicity causing delayed myeloneuropathy. *Ann. Indian Acad. Neurol.* **2013**, *16*, 736−736.

(2) Liu, Y. H.; Chen, J. A.; Guo, Y. R.; Wang, C. M.; Liang, X. A.; Zhu, G. N. A sensitive monoclonal antibody-based enzyme-linked immunosorbent assay for chlorpyrifos residue determination in chinese agricultural samples. *J. Environ. Sci. Health B* **2011**, *46*, 313−320.

(3) Han, Y. T.; Li, W. M.; Dong, F. S.; Xu, J.; Liu, X. G.; Li, Y. B.; Kong, Z. Q.; Liang, X. Y.; Zheng, Y. Q. The behavior of chlorpyrifos and its metabolite 3,5,6-trichloro-2-pyridinol in tomatoes during home canning. *Food Control* **2013**, *31*, 560−565.

(4) Delgado-Moreno, L.; Lin, K.; Veiga-Nascimento, R.; Gan, J. Occurrence and toxicity of three classes of insecticides in water and sediment in two Southern California coastal watersheds. *J. Agric. Food Chem.* **2011**, *59*, 9448−9456.

(5) Maya, K.; Upadhyay, S. N.; Singh, R. S.; Dubey, S. K. Degradation kinetics of chlorpyrifos and 3,5,6-trichloro-2-pyridinol (TCP) by fungal communities. *Bioresour. Technol.* **2012**, *126*, 216−223.

(6) Pareja, L.; Colazzo, M.; Perez-Parada, A.; Besil, N.; Heinzen, H.; Bocking, B.; Cesio, V.; Fernandez-Alba, A. R. Occurrence and distribution study of residues from pesticides applied under controlled conditions in the field during rice processing. *J. Agric. Food Chem.* **2012**, *60*, 4440−4448.

(7) Fan, S. F.; Deng, K. L.; Yu, C. S.; Zhao, P. Y.; Bai, A. J.; Li, Y. J.; Pan, C. P.; Li, X. S. Influence of different planting seasons of six leaf vegetables on residues of five pesticides. *J. Agric. Food Chem.* **2013**, *61*, 9036−9044.

(8) Liu, C. Y.; Wang, S. L.; Li, L.; Ge, J.; Jiang, S. R.; Liu, F. M. Dissipation and residue of cyprodinil in strawberry and soil. *Bull. Environ. Contam. Toxicol.* **2011**, *86*, 323−325.

(9) Liang, Y.; Wang, W.; Shen, Y.; Liu, Y.; Liu, X. J. Dynamics and residues of chlorpyrifos and dichlorvos in cucumber grown in greenhouse. *Food Control* **2012**, *26*, 231−234.

(10) Zhang, X.; Shen, Y.; Yu, X. Y.; Liu, X. J. Dissipation of chlorpyrifos and residue analysis in rice, soil and water under paddy field conditions. *Ecotoxicol. Environ. Saf.* **2012**, *78*, 276−280.

(11) Fantke, P.; Juraske, R. Variability of pesticide sissipation half-lives in plants. *Environ. Sci. Technol.* **2013**, *47*, 3548−3562.

(12) Bending, G. D.; Lincoln, S. D.; Edmondson, R. N. Spatial variation in the degradation rate of the pesticides isoproturon, azoxystrobin and diflufenican in soil and its relationship with chemical and microbial properties. *Environ. Pollut.* **2006**, *139*, 279−287.

(13) Wang, Z. W.; Huang, J. X.; Chen, J. Y.; Li, F. L. Time-dependent movement and distribution of chlorothalonil and chlorpyrifos in tomatoes. *Ecotoxicol. Environ. Saf.* **2013**, *93*, 107−111.

(14) Liu, Y. H.; Xu, Z. Z.; Wu, X. G.; Gui, W. J.; Zhu, G. N. Adsorption and desorption behavior of herbicide diuron on various Chinese cultivated soils. *J. Hazard. Mater.* **2010**, *178*, 462−468.

(15) Rodriguez-Cruz, M. S.; Jones, J. E.; Bending, G. D. Field-scale study of the variability in pesticide biodegradation with soil depth and its relationship with soil characteristics. *Soil Biol. Biochem.* **2006**, *38*, 2910−2918.

(16) Alvarez, M.; du Mortier, C.; Sokolic, T.; Cirelli, A. F. Studies on the persistence of a commercial formulation of chlorpyrifos on an agricultural soil from provincia de buenos aires, republica argentina. *Water Air Soil Pollut.* **2013**, *224*.

(17) Singh, B. K.; Walker, A.; Wright, D. J. Degradation of chlorpyrifos, fenamiphos, and chlorothalonil alone and in combination and their effects on soil microbial activity. *Environ. Toxicol. Chem.* **2002**, *21*, 2600−2605.

(18) Chai, L. K.; Wong, M. H.; Hansen, H. C. B. Degradation of chlorpyrifos in humid tropical soils. *J. Environ. Manage.* **2013**, *125*, 28−32.

(19) Xiong, J. F.; Tang, X. Y.; Zhou, G. M.; Guan, Z.; Wu, L. M. Dispersive solid phase extraction coupled with HPLC-UV for simultaneous determination of chlorpyrifos and 3,5,6-trichloro-2-pyridinol in soil samples. *Anal. Methods* **2013**, *5*, 536−540.

(20) Karpuzcu, M. E.; Sedlak, D. L.; Stringfellow, W. T. Biotransformation of chlorpyrifos in riparian wetlands in agricultural watersheds: Implications for wetland management. *J. Hazard. Mater.* **2013**, *244−245*, 111−120.

(21) Imfeld, G.; Lefrancq, M.; Maillard, E.; Payraudeau, S. Transport and attenuation of dissolved glyphosate and AMPA in a stormwater wetland. *Chemosphere* **2013**, *90*, 1333−1339.

(22) Mandal, K.; Singh, B. Persistence of fipronil and its metabolites in sandy loam and clay loam soils under laboratory conditions. *Chemosphere* **2013**, *91*, 1596−1603.

(23) Placido, A.; Paiga, P.; Lopes, D. H.; Correia, M.; Delerue-Matos, C. Determination of methiocarb and its degradation products, methiocarb sulfoxide and methiocarb sulfone, in bananas using QuEChERS extraction. *J. Agric. Food Chem.* **2013**, *61*, 325−331.

(24) Liang, B.; Yang, C. L.; Gong, M. B.; Zhao, Y. F.; Zhang, J.; Zhu, C. X.; Jiang, J. D.; Li, S. P. Adsorption and degradation of triazophos, chlorpyrifos and their main hydrolytic metabolites in paddy soil from Chaohu Lake, China. *J. Environ. Manage.* **2011**, *92*, 2229−2234.

(25) Rodrigues, E. T.; Lopes, I.; Pardal, M. A. Occurrence, fate and effects of azoxystrobin in aquatic ecosystems: A review. *Environ. Int.* **2013**, *53*, 18−28.

(26) Zhao, C. C.; Xie, H. J.; Zhang, J.; Xu, J. T.; Liang, S. Spatial distribution of organochlorine pesticides (OCPs) and effect of soil characters: A case study of a pesticide producing factory. *Chemosphere* **2013**, *90*, 2381−2387.

(27) Alvarez, M.; du Mortier, C.; Cirelli, A. F. Behavior of insecticide chlorpyrifos on soils and sediments with different organic matter content from provincia de buenos aires, republica argentina. *Water Air Soil Pollut.* **2013**, *224*.

antibacterial,[14] and antifungal[15] properties and so on. The compound can be used to treat several ailments.[16]

Another natural product, stelladerol (Figure 2), is a strong inhibitor of cyclooxygenase enzyme and phospholipid oxidation.[17] The compound 2-hydroxynaphthalene-1-carbaldehyde itself is known to possess moderate antibacterial property.[18] Naphthol is a precursor for a variety of insecticides and is a well-known component with contact insecticidal properties.[19]

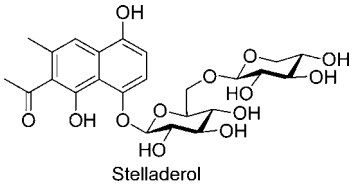

Figure 2. Structure of naphthalene glycoside, stelladerol, which has potential biological activities.

As our group is involved in the synthesis of β-naphthol-based synthetics,[20] we designed and synthesized a series of naphthalene-based hybrid molecules using a novel green protocol to screen them for their dual inhibitory activity as angiotensin converting enzyme inhibitors and calcium channel blockers in treating resistant hypertension. In a recent study Venugopala et al. reported that these compounds show good antimosquito properties.[21] The existing literature and recent studies drove us to screen our compounds for their antifeedant and toxic properties against major agricultural pests. In the present paper we describe the synthesis of 2-aminobenzothiazolomethylnaphthol derivatives using a green protocol and their influence on the feeding behavior and toxicity effects against a major polyphagous pest, *Spodoptera litura*, and a monophagous pest, *Achaea janata* (L).

MATERIALS AND METHODS

Instruments. Commercially available reagent grade chemicals and solvents were used in all reactions and purification processes. All of the reactions were monitored by TLC on E. Merck Kieselgel 60 F_{254}, with detection by UV light, charring with PMA charring solution, or exposure to I_2 vapors. The ^{1}H (300 MHz) and ^{13}C NMR (75 MHz) were recorded on Avance-300 in DMSO-d_6. The spectra were acquired with sufficiently long relaxation delay to ensure quaternary carbon relaxation. Also, more scans were used to obtain reasonable sensitivity of the ^{13}C NMR spectra. Multiplicities arising from ^{13}C−^{19}F couplings were low in intensity and present over a large area, so they were counted independently. Chemical shift values are reported in parts per million relative to DMSO as internal reference. Coupling constant value J is measured in hertz. s (singlet), d (doublet), t (triplet), brs (broad singlet), dd (double doublet), m (multiplet). Mass spectra were recorded on an Agilent LC/MSD trap SL 1100 series spectrometer with a 70 eV ESI probe, and high-resolution mass spectra were obtained by using ESI-QTOF mass spectrometry. Infrared spectra were recorded on a Thermo Nicolet Nexus 670 FT-IR spectrometer.

General Synthesis. To a 10 mL RB flask were added aldehyde (1.0 mmol), 2-aminobenzothiazole (1.0 mmol), and β-naphthol (1.0 mmol); these were mixed thoroughly and heated in preheated oil bath at 110−120 °C for an appropriate time (Table 1). After completion of reaction as indicated by TLC, the reaction mixture was allowed to cool. The so-formed solid was powdered, washed with methanol (8 mL × 3 times for compounds except fluoro and methoxy derivatives, 4 mL × 3 times in the case of fluoro and methoxy derivatives), and dried under vacuum to obtain the corresponding pure 2-aminobenzothiazolomethylnaphthol derivative. However, in the case of fluoro- and methoxy-substituted derivatives, care must be taken during washing or unreacted material present in the reaction mixture may dissolve in methanol and help methanol to dissolve the product, resulting in a decrease in the overall yield. Moreover, the solubility of fluoro and methoxy derivatives is better in methanol when compared to other derivatives. A schematic representation of the reaction is given in Scheme 1.

Table 1. Optimized Reaction Conditions for the Synthesis of Compounds 4a−4q

no.	compd	time, min	temp, °C	yield, %
1	**4a**	40	110	94
2	**4b**	50	120	92
3	**4c**	40	110	93
4	**4d**	45	110	91
5	**4e**	50	110	94
6	**4f**	40	110	95
7	**4g**	45	110	92
8	**4h**	45	110	90
9	**4i**	45	110	91
10	**4j**	45	110	88
11	**4k**	40	110	93
12	**4l**	40	110	92
13	**4m**	50	120	92
14	**4n**	40	110	94
15	**4o**	40	110	94
16	**4p**	40	110	93
17	**4q**	45	110	90

Scheme 1. Schematic Representation for the Synthesis of Compounds 4a−4q

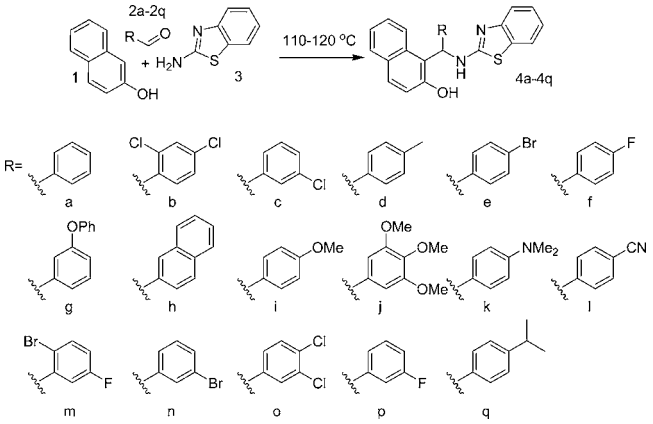

*1. 1-((Benzo[d]thiazol-2-ylamino)(phenyl)methyl)naphthalen-2-ol (**4a**):* white solid; mp = 200−202 °C; ^{1}H NMR (300 MHz, DMSO-d_6) δ 10.17 (brs, 1H), 8.78 (d, 1H, J = 7.6 Hz), 7.94−7.74 (m, 3H), 7.66 (d, 1H, J = 7.6 Hz), 7.40−7.13 (m, 10H), 7.0 (t, 1H, J = 7.4 Hz); ^{13}C NMR (75 MHz, DMSO-d_6) δ 166.3, 153.2, 152.1, 142.5, 132.1, 130.8, 129.6, 128.6, 128.6, 128.1, 126.2, 126.0, 125.4, 123.8, 122.4, 121.0, 120.9, 118.7, 118.4, 118.1, 53.1; IR (KBr) ν_{max} 3376, 3060, 1598, 1547, 1514, 1444, 1331, 1263, 744 cm^{-1}; ESI-MS m/z 383 (M + H). HRMS calcd for $C_{24}H_{19}N_2OS$, 383.1218; found, 383.1206.

*2. 1-((Benzo[d]thiazol-2-ylamino)(2,4-dichlorophenyl)methyl)-naphthalen-2-ol (**4b**):* white solid; mp = 190−192 °C; ^{1}H NMR (300 MHz, DMSO-d_6) δ 10.02−9.91 (brs, 1H), 8.88 (d, 1H, J = 7.0 Hz), 8.02 (d, 1H, J = 8.5 Hz), 7.79 (t, 2H, J = 9.3 Hz), 7.70−7.63 (m, 2H), 7.49 (d, 1H, J = 2.1 Hz), 7.46−7.35 (m, 3H), 7.27 (t, 1H, J = 7.6 Hz), 7.23−7.12 (m, 3H), 7.01 (t, 1H, J = 7.6 Hz); ^{13}C NMR (75 MHz, DMSO-d_6) δ 165.2, 153.8, 152.1, 139.0, 133.0, 132.7, 131.8, 131.1, 130.7, 130.0, 128.7, 128.3, 126.6, 126.5, 125.5, 122.6, 122.4, 121.1, 120.9, 118.5, 118.3, 115.9, 52.3; IR (KBr) ν_{max} 3378, 3068, 1592, 1542, 1438, 1371, 1331, 1268, 751 cm^{-1}; ESI-MS m/z 451 (M + H). HRMS calcd for $C_{24}H_{17}N_2OSCl_2$, 451.0438; found, 451.0451.

dx.doi.org/10.1021/jf501705u | J. Agric. Food Chem. 2014, 62, 6571−6576

*3. 1-((Benzo[d]thiazol-2-ylamino)(3-chlorophenyl)methyl)-naphthalen-2-ol (**4c**):* white solid; mp = 193−194 °C; ^{1}H NMR (300 MHz, DMSO-d_6) δ 10.23 (s, 1H), 8.81 (d, 1H, J = 7.6 Hz), 7.94−7.77 (m, 3H), 7.67 (d, 1H, J = 7.6 Hz), 7.45−7.15 (m, 10H), 7.02 (t, 1H, J = 7.4 Hz); ^{13}C NMR (75 MHz, DMSO-d_6) δ 166.1, 153.1, 151.9, 145.3, 132.8, 131.9, 130.8, 130.0, 129.8, 128.6, 128.5, 126.5, 126.1, 125.6, 125.4, 124.8, 123.3, 122.5, 121.1, 120.9, 118.3, 118.2, 118.0, 52.6; IR (KBr) ν_{max} 3360, 3062, 1596, 1573, 1548, 1515, 1444, 1332, 1268, 749 cm^{-1}; ESI-MS m/z 417 (M + H). HRMS calcd for $C_{24}H_{18}N_2OSCl$, 417.0828; found, 417.0809.

*4. 1-((Benzo[d]thiazol-2-ylamino)(p-tolyl)methyl)naphthalen-2-ol (**4d**).* white solid; mp = 180−182 °C; ^{1}H NMR (300 MHz, DMSO-d_6) δ 10.18−10.11 (brs, 1H), 8.78 (d, 1H, J = 7.6 Hz), 7.91−7.73 (m, 3H), 7.66 (d, 1H, J = 7.4 Hz), 7.39−6.96 (m, 11H), 2.22 (s, 3H); ^{13}C NMR (75 MHz, DMSO-d_6) δ 166.2, 153.1, 152.1, 139.4, 135.1, 132.1, 130.7, 129.4, 128.6, 128.5, 126.1, 125.9, 125.4, 123.9, 122.4, 120.9, 120.8, 118.7, 118.3, 118.0, 52.9, 20.5; IR (KBr) ν_{max} 3307, 1535, 1441, 1317, 1261, 744 cm^{-1}; ESI-MS m/z 397 (M + H). HRMS calcd for $C_{25}H_{21}N_2OS$, 397.1374; found, 397.1373.

*5. 1-((Benzo[d]thiazol-2-ylamino)(4-bromophenyl)methyl)-naphthalen-2-ol (**4e**):* white solid; mp = 202−204 °C; ^{1}H NMR (300 MHz, DMSO-d_6) δ 10.24−10.16 (brs, 1H), 8.82 (d, 1H, J = 7.0 Hz), 7.89−7.75 (m, 3H), 7.67 (d, 1H, J = 7.6 Hz), 7.49−7.36 (m, 4H), 7.30−7.12 (m, 6H), 7.02 (t, 1H, J = 7.6 Hz); ^{13}C NMR (75 MHz, DMSO-d_6) δ 166.1, 153.1, 151.9, 142.1, 131.9, 130.9, 130.8, 129.7, 128.5, 128.2, 126.3, 125.3, 123.5, 122.4, 121.0, 120.8, 119.1, 118.3, 118.1, 52.6; IR (KBr) ν_{max} 3373, 1627, 1541, 1442, 1332, 1267, 1206, 1070, 749, 571 cm^{-1}; ESI-MS m/z 461 (M + H). HRMS calcd for $C_{24}H_{18}N_2OSBr$, 461.0323; found, 461.0320.

*6. 1-((Benzo[d]thiazol-2-ylamino)(4-fluorophenyl)methyl)-naphthalen-2-ol (**4f**):* white solid; mp = 178−180 °C; ^{1}H NMR (300 MHz, DMSO-d_6) δ 1.22−10.13 (brs, 1H), 8.81 (d, 1H, J = 7.4 Hz), 7.93−7.76 (m, 3H), 7.67 (d, 1H, J = 7.7 Hz), 7.42−7.32 (m, 2H), 7.31−7.15 (m, 6H), 7.93−6.95 (m, 3H); ^{13}C NMR (75 MHz, DMSO-d_6) δ 166.1, 162.2, 159.0, 153.1, 151.9, 138.4, 131.9, 130.7, 129.5, 128.5, 127.9, 127.8, 126.2, 125.3, 123.5, 122.3, 120.9, 120.8, 118.3, 118.0, 114.8, 114.5, 52.6; IR (KBr) ν_{max} 3308, 1537, 1436, 1319, 1286, 1060, 810, 746 cm^{-1}; ESI-MS m/z 401 (M + H). HRMS calcd for $C_{24}H_{18}FN_2OS$, 401.1123; found, 401.1115.

*7. 1-((Benzo[d]thiazol-2-ylamino)(3-phenoxyphenyl)methyl)-naphthalen-2-ol (**4g**):* white solid; mp = 171−173 °C; ^{1}H NMR (300 MHz, DMSO-d_6) δ 10.16 (s, 1H), 8.78 (d, 1H, J = 7.4 Hz), 7.89−7.73 (m, 3H), 7.66 (d, 1H, J = 7.0 Hz), 7.43−7.16 (m, 9H), 7.06−6.93 (m, 4H), 6.87 (d, 2H, J = 7.6 Hz), 6.79 (dd, 1H, J_1 = 7.6 Hz, J_2 = 2.1 Hz); ^{13}C NMR (75 MHz, DMSO-d_6) δ 166.1, 156.5, 156.0, 153.1, 152.0, 145.0, 132.0, 130.7, 129.7, 128.6, 128.5, 126.2, 125.4, 123.0, 122.4, 121.3, 121.0, 120.8, 118.3, 118.1, 117.9, 116.6, 116.3, 52.7; IR (KBr) ν_{max} 3314, 3052, 1541, 1511, 1451, 1267, 814, 749 cm^{-1}; ESI-MS m/z 475 (M + H). HRMS calcd for $C_{30}H_{23}N_2O_2S$, 475.1480; found, 475.1471.

*8. 1-((Benzo[d]thiazol-2-ylamino)(naphthalen-2-yl)methyl)-naphthalen-2-ol (**4h**):* white solid; mp = 190−192 °C; ^{1}H NMR (300 MHz, DMSO-d_6) δ 10.21−10.16 (brs, 1H), 8.91 (d, 1H, J = 7.4 Hz), 7.95 (d, 1H, J = 7.9 Hz), 7.89−7.74 (m, 6H), 7.68 (d, 1H, J = 7.9 Hz), 7.53−7.40 (m, 3H), 7.38−7.15 (m, 6H), 7.02 (m, 1H); ^{13}C NMR (75 MHz, DMSO-d_6) δ 166.2, 153.1, 152.0, 140.1, 132.6, 132.1, 131.7, 130.7, 129.6, 128.5, 128.4, 127.5, 127.3, 126.1, 126.0, 125.4, 125.3, 124.9, 123.8, 123.6, 122.3, 120.9, 120.8, 118.5, 118.3, 118.0, 53.3; IR (KBr) ν_{max} 3313, 3052, 1541, 1442, 1264, 814, 749 cm^{-1}; ESI-MS m/z 433 (M + H). HRMS calcd for $C_{28}H_{21}N_2OS$, 433.1374; found, 433.1387.

*9. 1-((Benzo[d]thiazol-2-ylamino)(4-methoxyphenyl)methyl)-naphthalen-2-ol (**4i**):* white solid; mp = 190−192 °C; ^{1}H NMR (300 MHz, DMSO-d_6) δ 10.19−10.11 (brs, 1H), 8.79 (d, 1H, J = 7.4 Hz), 7.94−7.84 (brs, 1H), 7.79 (t, 2H, J = 8.7 Hz), 7.66 (d, 1H, J = 7.6 Hz), 7.42−7.12 (m, 9H), 7.0 (t, 1H, J = 7.9 Hz), 6.83 (d, 1H, J = 8.7 Hz), 3.68 (s, 3H); ^{13}C NMR (75 MHz, DMSO-d_6) δ 166.2, 157.7, 153.0, 152.1, 134.1, 132.1, 130.6, 129.4, 128.6, 128.5, 127.2, 126.1, 125.3, 123.8, 122.3, 120.9, 120.8, 118.7, 118.4, 118.0, 113.5, 54.9, 52.8; IR (KBr) $_{\nu max}$ 3313, 3052, 1541, 1442, 1264, 814, 749 cm^{-1}; ESI-MS m/z 413 (M + H). HRMS calcd for $C_{25}H_{21}N_2O_2S$, 413.1323; found, 413.1319.

*10. 6.1.1.20. 1-((Benzo[d]thiazol-2-ylamino)(3,4,5-trimethoxyphenyl)methyl)naphthalen-2-ol (**4j**):* white solid; mp = 170−172 °C; ^{1}H NMR (300 MHz, DMSO-d_6) δ 10.42−10.30 (brs, 1H), 8.63−8.37 (brs, 1H), 7.98−7.87 (brs, 1H), 7.75−7.63 (m, 2H), 7.52−7.31 (m, 3H), 7.28−7.15 (m, 3H), 7.11−6.94 (m, 2H), 6.58 (s, 2H), 3.70 (s, 3H), 3.66 (s, 6H); ^{13}C NMR (75 MHz, DMSO-d_6) δ 166.3, 153.3, 152.4, 137.0, 136.1, 132.0, 129.9, 129.1, 128.6, 128.1, 125.8, 125.1, 123.0, 122.2, 120.8, 120.1, 119.1, 118.8, 117.9, 103.6, 95.6, 59.8, 55.4, 54.3; IR (KBr) ν_{max} 3317, 2923, 2833, 1590, 1538, 1441, 1315, 1248, 1171, 1030, 813, 745 cm^{-1}; ESI-MS m/z 473 (M + H). HRMS calcd for $C_{27}H_{25}N_2O_4S$, 473.1535; found, 473.1527.

*11. 1-((Benzo[d]thiazol-2-ylamino)(4-(dimethylamino)phenyl)-naphthalen-2-ol (**4k**):* white solid; mp = 156−158 °C; ^{1}H NMR (300 MHz, DMSO-d_6) δ 10.22−10.04 (brs, 1H), 8.71 (d, 1H, J = 7.4 Hz), 7.93 (d, 1H, J = 7.5 Hz), 7.77 (t, 2H, J = 9.1 Hz), 7.64 (d, 1H, J = 7.4 Hz), 7.39−7.29 (m, 2H), 7.28−7.11 (m, 4H), 7.07 (d, 2H, J = 8.5 Hz), 6.99 (t, 1H, J = 7.9 Hz), 6.63 (d, 2H, J = 8.9 Hz), 2.80 (s, 6H); ^{13}C NMR (75 MHz, DMSO-d_6) δ 166.2, 153.0, 152.1, 149.0, 132.1, 130.5, 129.5, 129.1, 128.6, 128.4, 126.8, 125.9, 125.3, 122.2, 120.7, 118.9, 118.4, 117.9, 112.2, 53.1, 40.1; IR (KBr) ν_{max} 3315, 2849, 1602, 1538, 1446, 1318, 1264, 1165, 810, 745 cm^{-1}; ESI-MS m/z 426 (M + H). HRMS calcd for $C_{26}H_{24}N_3OS$, 426.1640; found, 426.1639.

*12. 4-((Benzo[d]thiazol-2-ylamino)(2-hydroxynaphthalen-1-yl)-methyl)benzonitrile (**4l**):* white solid; mp = 213−215 °C; ^{1}H NMR (300 MHz, DMSO-d_6) δ 10.31−10.20 (brs, 1H), 8.85 (d, 1H, J = 7.0 Hz), 7.89−7.78 (m, 3H), 7.76−7.65 (m, 3H), 7.46−7.33 (m, 5H), 7.31−7.17 (m, 3H), 7.03 (t, 1H, J = 7.4 Hz); ^{13}C NMR (75 MHz, DMSO-d_6) δ 166.1, 153.2, 151.9, 148.8, 132.0, 130.8, 130.0, 128.6, 128.5, 127.0, 126.5, 125.4, 123.2, 122.5, 121.2, 120.9, 118.8, 118.3, 117.8, 108.9, 53.0; IR (KBr) ν_{max} 3379, 3056, 2226, 1573, 1541, 1437, 1329, 1270, 1026, 751 cm^{-1}; ESI-MS m/z 408 (M + H). HRMS calcd for $C_{25}H_{18}N_3OS$, 408.1170; found, 408.1163.

*13. 1-((Benzo[d]thiazol-2-ylamino)(2-bromo-5-fluorophenyl)-methyl)naphthalen-2-ol (**4m**):* white solid; mp = 198−200 °C; ^{1}H NMR (300 MHz, DMSO-d_6) δ 9.92 (brs, 1H), 8.90 (d, 1H, J = 7.4 Hz), 8.05 (d, 1H, J = 8.7 Hz), 7.80 (t, 2H, J = 9.3 Hz), 7.66 (d, 1H, J = 7.7 Hz), 7.61−7.54 (m, 1H), 7.39−7.34 (m, 3H), 7.28 (t, 1H, J = 7.4 Hz), 7.20 (t, 1H, J = 7.6 Hz), 7.14−6.97 (m, 4H); ^{13}C NMR (75 MHz, DMSO-d_6) δ 165.0, 162.6, 159.4, 153.7, 152.0, 144.2, 144.1, 134.1, 134.0, 132.8, 130.6, 129.9, 128.5, 128.1, 126.5, 125.3, 122.4, 122.3, 121.0, 120.8, 118.5, 118.2, 116.9, 116.7, 116.6, 115.6, 115.3, 54.7; IR (KBr) ν_{max} 3383, 1598, 1543, 1512, 1453, 1431, 1265, 812, 752 cm^{-1}; ESI-MS m/z 479 (M + H). HRMS calcd for $C_{24}H_{17}BrFN_2OS$, 479.0204; found, 479.0190.

*14. 1-((Benzo[d]thiazol-2-ylamino)(3-bromophenyl)naphthalen-2-ol (**4n**):* white solid; mp = 201−203 °C; ^{1}H NMR (300 MHz, DMSO-d_6) δ 10.27−10.20 (brs, 1H), 8.84 (d, 1H, J = 7.4 Hz), 7.92−7.77 (m, 3H), 7.68 (d, 1H, J = 7.6 Hz), 7.45−7.15 (m, 11H), 7.02 (t, 1H, J = 7.6 Hz); ^{13}C NMR (75 MHz, DMSO-d_6) δ 166.0, 153.1, 151.9, 145.5, 131.9, 130.7, 130.2, 129.8, 129.0, 128.5, 126.4, 125.4, 125.1, 123.3, 122.4, 121.4, 121.0, 120.8, 118.3, 118.1, 118.0, 52.6; IR (KBr) ν_{max} 3377, 3058, 1543, 1511, 1435, 1327, 1268, 747 cm^{-1}; MS-ESI m/z 461 (M + H). HRMS calcd for $C_{24}H_{18}BrN_2OS$, 461.0323; found, 461.0312.

*15. 1-((Benzo[d]thiazol-2-ylamino)(3,4-dichlorophenyl)-naphthalen-2-ol (**4o**):* white solid; mp = 212−214 °C; ^{1}H NMR (300 MHz, DMSO-d_6) δ 10.28−10.24 (brs, 1H), 8.87 (d, 1H, J = 7.2 Hz), 7.93−7.79 (m, 3H), 7.69 (d, 1H, J = 7.6 Hz), 7.53 (d, 1H, J = 8.3 Hz), 7.47−7.37 (m, 3H), 7.32−7.15 (m, 5H), 7.03 (t, 1H J = 7.7 Hz); ^{13}C NMR (75 MHz, DMSO-d_6) δ 166.0, 153.2, 151.8, 144.0, 131.9, 130.8, 130.6, 130.2, 130.0, 128.6, 128.4, 127.7, 126.6, 126.5, 125.4, 123.1, 122.5, 121.1, 120.9, 118.3, 118.2, 117.6, 52.3; IR (KBr) ν_{max} 3379, 1577, 1540, 11461, 1328, 1268, 1205, 1028, 816, 747 cm^{-1}; ESI-MS m/z 451 (M + H). HRMS calcd for $C_{24}H_{17}Cl_2N_2OS$, 451.0438; found, 451.0439.

*16. 1-((Benzo[d]thiazol-2-ylamino)(3-fluorophenyl)naphthalen-2-ol (**4p**):* white solid; mp = 179−181 °C; ^{1}H NMR (300 MHz, DMSO-d_6) δ 10.26−10.19 (brs, 1H), 8.84 (d, 1H, J = 7.4 Hz), 7.90−

7.78 (m, 3H), 7.68 (d, 1H, J = 7.7 Hz), 7.43−7.17 (m, 7H), 7.07−6.96 (m, 4H); ^{13}C NMR (75 MHz, DMSO-d_6) δ 166.1, 163.7, 160.5, 153.1, 151.9, 145.8, 145.8, 131.9, 130.7, 130.0, 129.9, 129.7, 128.5, 126.3, 125.4, 123.4, 122.4, 122.1, 121.0, 120.8, 118.3, 118.1, 113.0, 112.8, 112.5, 52.7; IR (KBr) ν_{max} 3387, 1587, 1536, 1482, 1439, 1329, 1244, 1053, 749 cm^{-1}; ESI-MS m/z 401 (M + H). HRMS calcd for $C_{24}H_{18}FN_2OS$, 401.1123; found, 401.1118.

*17. 1-((Benzo[d]thiazol-2-ylamino)(4-isopropylphenyl)-naphthalen-2-ol (**4q**):* white solid; mp = 191−193 °C; ^{1}H NMR (300 MHz, DMSO-d_6) δ 10.17−10.09 (brs, 1H), 8.78 (d, 1h, J = 7.6 Hz), 7.98−7.87 (brs, 1H), 7.79 (t, 2H, J = 7.8 Hz), 7.66 (d, 1H, J = 7.6 Hz), 7.4−7.32 (m, 2H), 7.30−7.10 (m, 8H), 7.00 (t, 1H, J = 8.1 Hz), 2.89−2.74 (m, 1H), 1.14 (dd, 6H, J_1 = 7.0 Hz, J_2 = 1.5 Hz); ^{13}C NMR (75 MHz, DMSO-d_6) δ 166.2, 153.0, 152.1, 146.1, 139.6, 132.1, 130.6, 129.3, 128.5, 128.4, 126.1, 126.0, 125.9, 125.3, 123.7, 122.3, 120.8, 120.8, 118.7, 118.4, 118.0, 53.0, 32.9, 23.8, 23.7; IR (KBr) ν_{max} 3314, 3055, 2957, 1540, 1450, 1268, 1060, 746 cm^{-1}; ESI-MS m/z 425 (M + H). HRMS calcd for $C_{27}H_{25}N_2OS$, 425.1687; found, 425.1704.

Test Insects. *S. litura* and *A. janata* larvae used in this study were obtained from a laboratory colony maintained in the Biology and Biotechnology Division, IICT, Hyderabad, India. The culture has been continuously maintained on castor leaves (*Ricinus communis*) at room temperature (26 ± 2 °C), 65 ± 5% relative humidity, and 16:8 L:D photoperiod in the laboratory.

Antifeedant Bioassay. The antifeedant activity of the compounds was tested against tobacco caterpillar, *S. litura* (F.), and castor semilooper, *A. janata* (L.). The experiments were conducted according to the classical no-choice leaf disk method described earlier by Akhtar et al.[22] To study the antifeedant activity of the test compounds, a small circular disk of 4 cm diameter was cut from fresh castor leaves. The leaf disks were treated on their upper surface with individual concentrations of the test compounds; after that, the leaf disks were air-dried at room temperature, and each leaf disk was transferred to a separate Petri plate of 15 cm diameter containing wet filter paper. Control leaf disks were treated with the same volume of the DMSO only. The third-instar larvae of *S. litura* and *A. janata* (starved for 4−5 h prior to the experiment) were allowed to feed to assess antifeedant activity. Progress of the consumption of the leaf area was measured at 6, 12, and 24 h period intervals in both treated and control leaf disks. Areas of control and treated leaf disks consumed were measured after 24 h using a leaf area meter (AM-300, ADC Bioscientific Limited, Hoddesdon, UK). The antifeedant index was then calculated as $(C - T)/(C + T) \times 100$, where C is the consumption of control leaf disks and T is consumption of treated leaf disks.[23] For each concentration, 10 experimental sets were assayed. All tests were replicated three times. The mean of the 30 sets was taken for each compound. Means were subjected to probit analysis.[24]

Topical Bioassay. Toxicity of the test compounds was determined by topical application to the third instar larvae of test insects.[25] Two micrograms of compounds was applied directly to the dorsum of the larva in a 1 μL drop of DMSO using a micro applicator. Insects treated with solvent alone were considered as controls. The treated and control larvae were treated on fresh castor leaves. Mortality was measured daily until 2 days after treatment. Larvae that lost elasticity and heavy water loss from their body and showed no responses when their tails were pinched with forceps were regarded as dead. On the basis of three independent trials, each experiment was conducted in five replicates, leading to 15 replicates with each concentration of compounds. The mean of 15 replicates was taken for each compound, and the percentage of mortality with standard deviation was calculated.

Data Analysis. Antifeedant index was calculated using five different concentrations of each test compound, and data were subjected to probit analysis[24] to determine the ED_{50} value representing the concentrations that caused 50% feeding deterrence along with the 95% fiducial limits. The data were analyzed by completely randomized, one-way analysis of variance (ANOVA), and the means were separated using the Tukey HSD test (Biostat 2008).

RESULTS AND DISCUSSION

Scheme 1 illustrates the general procedure for the synthesis of 2-aminobenzothiazolomethylnaphthol derivatives. The synthesis procedure is completely green, economic, and high-yielding. A total of 17 derivatives were synthesized and screened for their antifeedant effect (Table 2) and toxicity (Table 3) against *S. litura* and *A. janata*.

Table 2. Antifeedant Effect of 2-Aminobenzothiazolomethylnaphthol Derivatives 4a−q against *S. litura* and *A. janata* by No-Choice Leaf Disk Bioassay Method

	antifeedant ED_{50}, μg/cm^2 (95% FL[a])	
compd	*S. litura*	*A. janata*
4a	>300	185.2 (175.0−192.3)
4b	109.9 (96.7−123.1)	204.7 (204.5−204.9)
4c	59.2 (53.9−63.0)	31.7 (21.0−37.6)
4d	**16.4 (16.1−16.7)**	**13.9 (12.7−14.8)**
4e	>300	>300
4f	**19.3 (19.1−19.6)**	**17.2 (13.8−19.6)**
4g	>300	219.0 (216.9−220.8)
4h	201.7 (197.0−205.2)	265.2 (257.6−271.6)
4i	**7.0 (6.3−7.8)**	**10.2 (8.6−10.8)**
4j	**5.2 (4.3−5.8)**	**7.7 (4.0−11.9)**
4k	103.9 (100.0−107.0)	111.2 (58.4−138.4)
4l	31.7 (19.0−38.9)	21.9 (20.9−22.5)
4m	28.0 (27.8−28.2)	43.4 (43.1−43.6)
4n	46.7 (39.7−53.7)	33.4 (29.8−37.3)
4o	73.6 (62.4−80.2)	81.7 (79.23−83.88)
4p	89.2 (80.9−94.4)	76.7 (73.6−79.2)
4q	>300	230.9 (228.8−232.9)
azadirachtin	3.1 (2.0−4.0)	4.7 (3.5−6.0)

[a]Fiducial limits.

The antifeedant activity of the 2-aminobenzothiazolomethylnaphthol derivatives was studied using the no-choice leaf disk method. The results are summarized in Table 2. It is interesting to note that most of the derivatives synthesized have good antifeedancy against *S. litura* and *A. janata*. A few of them, **4d**, **4f**, **4i**, and **4j**, show a high level of antifeedancy even at lower concentrations (5−100 μg/cm^2) against both insects. Derivatives **4d**, **4f**, **4i**, and **4j** showed significant antifeedant activity (ED_{50}) at lower doses of 16.4, 19.3, 7.0, and 5.2 μg/cm^2 against *S. litura* and lower doses of 13.9, 17.2, 10.2, and 7.7 μg/cm^2 against *A. janata*, respectively.

Compounds **4a−q** were primarily screened for their toxicity using topical bioassay method at a dosage of 0.5 μg/insect (Table 3). Compounds **4d**, **4f**, **4i**, and **4j** showed 100% mortality against both species. Interestingly, two compounds, **4l** and **4m**, showed 100% mortality against *A. janata* but were least toxic to *S. litura*. To estimate the mortality rate at a lower dose, we again screened the compounds at a dosage of 0.2 μg/insect (Table 3). Derivative **4j** produced high mortality >95% against the larvae of both *S. litura* and *A. janata*, whereas derivative **4i** showed high mortality, that is, >95%, against *S. litura* but only moderate mortality, that is, >85% and <95% against *A. janata*. On the contrary, derivatives **4d** and **4m** showed moderate mortality against *A. janata*, leaving them least toxic to *S. litura*. Larval death took place soon after exposure to the treatment. Derivatives **4i** and **4j** are very potent in penetrating the larval body through cuticle and cause lethal effects because in these

Table 3. Toxicity Effects of 2-Aminobenzothiazolomethylnaphthol Derivatives 4a−q against *S. litura* and *A. janata* by Topical Bioassay Method

	mortality,[a] %, ± SE		mortality,[b] %, ± SE	
compd	*S. litura*	*A. janata*	*S. litura*	*A. janata*
4a	13.6 ± 0.3	16.6 ± 0.5	6.4 ± 0.5	7.8 ± 0.6
4b	16.0 ± 0.8	14.1 ± 0.4	4.4 ± 0.7	0.0 ± 0.0
4c	67.7 ± 0.8	70.5 ± 1.0	42.2 ± 2.3	56.4 ± 2.7
4d	**100 ± 0.0**	**100 ± 0.0**	84.7 ± 1.1	**88.1 ± 0.9**
4e	3.7 ± 0.3	5.5 ± 0.4	0.0 ± 0.0	0.0 ± 0.0
4f	**100 ± 0.0**	**100 ± 0.0**	70.5 ± 0.8	63.5 ± 1.6
4g	10.5 ± 0.8	6.5 ± 0.4	0.0 ± 0.0	0.0 ± 0.0
4h	27.4 ± 0.5	67.6 ± 0.5	13.2 ± 0.8	47.1 ± 2.0
4i	**100 ± 0.0**	**100 ± 0.0**	**98.6 ± 0.5**	**89.1 ± 1.0**
4j	**100 ± 0.0**	**100 ± 0.0**	**96.3 ± 1.6**	**99.3 ± 0.5**
4k	64.6 ± 2.0	32.3 ± 1.2	43.0 ± 2.7	20.6 ± 1.8
4l	77.7 ± 2.3	**100 ± 0.0**	59.4 ± 1.3	61.6 ± 1.0
4m	80.0 ± 0.9	**100 ± 0.0**	45.5 ± 1.4	**89.1 ± 1.2**
4n	78.8 ± 0.6	69 ± 0.7	60.2 ± 0.9	50.1 ± 1.3
4o	64.2 ± 1.7	**99.7 ± 0.4**	42.5 ± 0.8	64.5 ± 1.3
4p	24.33 ± 1.3	31.7 ± 1.3	0.0 ± 0.0	19.4 ± 1.4
4q	13.3 ± 0.4	17.4 ± 0.3	0.0 ± 0.0	4.3 ± 0.4
azadirachtin	100 ± 0.0	100 ± 0.0	100 ± 0.0	100 ± 0.0

[a]Mortality at a dosage of 0.5 μg/insect. [b]Mortality at a dosage of 0.2 μg/insect.

treatments the feeding was absolutely prevented. It appears, from the results, that derivative **4j** is a strong feeding deterrent and strongly toxic, where as **4i** is a strong feeding deterrent but strongly toxic against *S. litura* and moderately toxic against *A. janata*. On the other hand, compound **4f** is a strong feeding deterrent but least toxic against both *S. litura* and *A. janata*. The treatments could cause desirable impact on larval feeding and survival and could totally achieve the management of these two major crop pests under laboratory conditions. Therefore, these compounds can be used as both antifeedants and pesticides.

It is clear from their structures that the compounds were differently substituted on the phenyl ring, leaving naphthyl and benzothiazole rings unsubstituted. Even though it may not be appropriate to draw a precise structure−activity relationship with the present data, we can observe from the results that the 4-bromophenyl (**4e**) and 4-phenoxyphenyl (**4g**) derivatives are completely nontoxic at a dosage of 0.2 μg/insect, whereas the 3,4,5-trimethoxyphenyl (**4j**) derivative is strongly toxic, leaving the others in between. Fused and bulky substituted phenyl derivatives **4b**, **4e**, **4g**, **4h**, **4k**, and **4q** are inactive or least active along with unsubstituted phenyl derivative **4a**, whereas 3,4,5-trimethoxy-substituted (**4j**) phenyl has strong antifeedancy and toxicity. However, in the case of the 4-methoxy (**4i**) phenyl derivative toxicity increases for *S. litura* and decreases for *A. janata*. The derivatives substituted with chloro, cyano, dimethylamino, dichloro, and fluoro substituents have comparatively low antifeedancy and are least toxic. From the above results we may conclude that the 3,4,5-trimethoxy derivative is strongly antifeedant and toxic, but 4-methoxy derivatives are strong antifeedants with selective toxicity against *S. litura*.

Overall, we identified a novel class of synthetic molecules that do not belong to organochlorides, organophosphates, carbamates, neonicotinoids, and anthranilamides as potent antifeedants and insecticides. These results may enlighten a way to search for natural product inspired synthetic antifeedants and insecticides. Compounds **4i** and **4j** may be useful in protecting crops from the above insects. Derivatives **4d** and **4m** are worth considering as feeding deterrents along with moderate insecticidal properties, and derivative **4f** can be considered as a strong feeding deterrent with least toxicity. Their potential field applicability is yet to be explored.

■ ASSOCIATED CONTENT

Ⓢ Supporting Information

Additional experimental details. This material is available free of charge via the Internet at http://pubs.acs.org.

■ AUTHOR INFORMATION

Corresponding Author

*(Ravirala Narender) E-mail: ravindra@iict.res.in, raviralanarender@gmail.com. Phone: +91-40-27191538. Fax: +91-40-27193382.

Funding

P.K.K. is thankful to CSIR and R.P. is thankful to ICMR for the award of senior research fellowships.

Notes

The authors declare no competing financial interest.

■ ACKNOWLEDGMENTS

The support of A. V. Subrahmanya Sarma and T. Prabhakar Rao, Centre for NMR and Structural Chemistry, CSIR-IICT, is greatly acknowledged. Without their support, obtaining a good-quality ^{13}C NMR spectrum might have been difficult. We are also thankful to V. J. Rao, Head, CPC Division, CSIR-IICT, for his constant support and encouragement throughout the work.

■ REFERENCES

(1) Clothianidin − Registration Status and Related Information; http://www.epa.gov/pesticides/about/intheworks/clothianidin-registration-status.html (updated July 27, 2012) (accesssed March 21, 2014).

(2) EXTOXNET − Extension Toxicology Network. A Pesticide Information Project of Cooperative Extension Offices of Cornell University, Michigan State University, Oregon State University, and University of California at Davis; http://pmep.cce.cornell.edu/

profiles/extoxnet/carbaryl-dicrotophos/chlorpyrifos-ext.html (accessed March 21, 2014).
(3) Hayden, K. M.; Norton, M. C.; Darcey, D.; Ostbye, T.; Zandi, P. P.; Breitner, J. C. S.; Welsh-Bohmer, K. A. For the Cache County Study Investigators. Occupational exposure to pesticides increases the risk of incident AD: the Cache County study. *Neurology* **2010**, *74* (19), 1524−1530.
(4) Bouchard, M. F.; Bellinger, D. C.; Wright, R. O.; Weisskopf, M. G. Attention-deficit/hyperactivity disorder and urinary metabolites of organophosphate pesticides. *Pediatrics* **2010**, *125* (6), e1270−e1277.
(5) Velmurugan, G.; Venkatesh, B. D. D.; Ramasamy, S. Prolonged monocrotophos intake induces cardiac oxidative stress and myocardial damage in rats. *Toxicology* **2013**, *307*, 103−108.
(6) Mahendra, P. K.; Abhishek, K. S.; Vivek, K.; Vinay, K. T.; Ritesh, K. S.; Megha, A.; Vinay, K. K.; Sanjay, Y.; Swatantra, K. J.; Aditya, B. P. Monocrotophos induced apoptosis in PC12 cells: role of xenobiotic metabolizing cytochrome P450s. *PLoS One* **2011**, *6*, e17757.
(7) Gill, R. J.; Ramos-Rodriguez, O.; Raine, N. Combined pesticide exposure severely affects individual- and colony-level traits in bees. *Nature* **2012**, *491* (7422), 105−108.
(8) McDonald-Gibson, C. 'Victory for bees' as European Union bans neonicotinoid pesticides blamed for destroying bee population; http://www.independent.co.uk/environment/nature/victory-for-bees-as-european-union-bans-neonicotinoid-pesticides-blamed-for-destroying-bee-population-8595408.html (accesses June 17, 2014).
(9) Mineau, P.; Palmer, C. The impact of the nation's most widely used insecticides on birds; http://www.abcbirds.org/abcprograms/policy/toxins/Neonic_FINAL.pdf (accessed June 17, 2014).
(10) Daniel, W. S. Altacor WG Insecticide (DPX-E2Y45) Introducing a Novel Anthranilic Diamide Insecticide from DuPont; http://ncc.confex.com/ncc/viewHandout.cgi?uploadid=246 (accessed June 17, 2014).
(11) The United States of America as represented by the Secretary of Agriculture. US6773727, 2004.
(12) Puckhaber, L. S.; Dowd, M. K.; Stipanovic, R. D.; Howell, C. R. Toxicity of (+)- and (−)-gossypol to the plant pathogen *Rhizoctonia solani*. *J. Agric. Food Chem.* **2002**, *50*, 7017−7021.
(13) Ilkevych, N. S.; Schroeder, G.; Rybachenko, V. I.; Chotiy, K. Y.; Makarova, R. A. Vibrational spectra, structure and antioxidant activity of gossypol imine derivatives. *Spectrochim. Acta Mol. Biomol. Spectrosc.* **2012**, *86*, 328−335.
(14) Tegos, G.; Stermitz, F. R.; Lomovskaya, O.; Lewis, K. Multidrug pump inhibitors uncover remarkable activity of plant antimicrobials. *Antimicrob. Agents Chemother.* **2002**, *46*, 3133−3141.
(15) Mellon, J. E.; Dowd, M. K.; Beltz, S. B.; Klich, M. A.; Zelaya, C. A. Inhibitory effects of gossypol, gossypolone, and apogossypolone on a collection of economically important filamentous fungi. *J. Agric. Food Chem.* **2012**, *60*, 2740−2745.
(16) Ascenta Therapeutics Inc. WO2008/150506, 2008.
(17) Cichewicz, R. H.; Nair, M. G. Isolation and characterization of stelladerol, a new antioxidant naphthalene glycoside, and other antioxidant glycosides from edible daylily (*Hemerocallis*) flowers. *J. Agric. Food Chem.* **2002**, *50*, 87−91.
(18) Patel, M. N.; Patel, S. H.; Chhasatia, M. R.; Desai, C. R. *Nucleosides Nucleotides Nucleic Acids* **2010**, *29*, 200−215.
(19) Swaine, W. Organic contact insecticide and its use. U.S. Patent Office, New York, 2283471, 1942.
(20) Praveen, K. K.; Satyanarayana, S.; Lakshmi, R. P.; Narasimhulu, G.; Narender, R.; Subba Reddy, B. V. Iodine-catalyzed three-component one-pot synthesis of naphthopyranopyrimidines under solvent-free conditions. *Tetrahedron Lett.* **2012**, *53*, 1738−1741.
(21) Venugopala, K. N.; Krishnappa, M.; Nayak, S. K.; Subrahmanya, B. K.; Vaderapura, J. P.; Chalannavar, R. K.; Gleiser, R. M.; Odhav, B. Synthesis and antimosquito properties of 2,6-substituted benzo[*d*]-thiazole and 2,4-substituted benzo[*d*]thiazole analogues against *Anopheles arabiensis*. *Eur. J. Med. Chem.* **2013**, *65*, 295−303.
(22) Akhtar, Y.; Isman, M. B. Feeding responses of specialist herbivores to plant extracts and pure allelochemicals: effects of prolonged exposure. *Entomol. Exp. Appl.* **2004**, *111*, 201−208.
(23) Murray, B. I.; Opender, K.; Anna, L.; Jerzy, K. Insecticidal and antifeedant bioactivities of neem oils and their relationship to azadirachtin content. *J. Agric. Food Chem.* **1990**, *38*, 1406−1411.
(24) Finney, D. J. In *Probit Analysis*; Cambridge University Press: London, UK, 1971; pp 68−72.
(25) Jamil, K.; Usha Rani, P.; Tyagarajan, G. Water hyacinth a potential new juvenile hormone mimic. *Int. Pest Control* **1984**, *26*, 106−108.

sulfate (4.9 mg/L), total chloride (6.3 mg/L), total magnesium (2.7 mg/L), total calcium (25 mg/L), and total sodium (4.4 mg/L). Natural water was also filtered through a 0.2 μm filter for sterilization.

For each aqueous photolysis experiment, 20 or more incubation vessels were prepared for irradiation and an equal number were prepared for use as nonirradiated (dark) controls. Individual test systems were composed of either pH 4 buffer or natural water spiked with (CN−^{14}C)-CNAP or (PC−^{14}C)-CNAP in separate incubation vessels. Likewise, the BC- and PC-labeled materials were used for CLAP degradations. The two sites of radiolabel served as replicates for both test compounds. Reactions were conducted at 1 and 0.6 ppm concentrations for CNAP and CLAP, respectively, with a maximum 1% acetonitrile as cosolvent. Samples were collected at various time intervals and analyzed by HPLC for determination of component amounts.

Test vessels for soil photolysis consisted of glass cuvettes (dimensions $L-W-D$ = 52 mm−31 mm−60 mm) with quartz lids, which were connected to a series of three traps; a safety trap, an ethanediol trap for collection of ^{14}C-organic volatiles, and a NaOH trap for collection of $^{14}CO_2$. The test soil (Nambsheim Clay Loam) originated from a field site in Nambsheim, France. Soil was characterized as sand (21%), silt (47.8%), clay (31.2%), pH in 0.01 M $CaCl_2$ (7.5), organic matter (3.5%), total nitrogen (1796 mg/kg). The soil was stored at ca. 20 °C until air dried and passed through a 2 mm sieve after which it was stored at ambient temperature. Aliquots of soil (ca. 5 g oven dry equivalents) were weighed into borosilicate glass incubation vessels, and sufficient Milli-Q water (3 mL) was added to produce water−soil slurry. The entire slurry was poured into a glass cuvette to prepare one of many samples generated in a similar manner. Each sample was then air dried at ambient temperature. Moisture content was adjusted to a soil moisture of 50% field capacity (75% of 1/3 bar, moisture content 20.03%) with a soil depth of ca. 2 mm. Once each sample was at the target moisture level the total weight was recorded and this weight used as the target for all subsequent moisture adjustments. The test substance was applied dropwise as a 100 μL aliquot of a solution containing 50 μg/mL of the test substance (for CNAP). Soil photolysis experiments were conducted in alternating light and dark cycles, with 12 h of irradiation followed by 12 h of dark over each 1 day period.

Agilent 1100 series HPLC System (Agilent Technologies, Palo Alto, CA) equipped with a photodiode array detector and a radiochemical detector attached in tandem. Column: Luna C18, 250 mm × 4.6 mm; 5 μm particle size (Phenomenex). Guard column: Securiguard C18, 3.0 × 4.0 mm (Phenomenex). Column temperature: 40 °C. Injection volume: 20 μL to 1.0 mL. Autosampler temperature: 10 °C. Flow rate: 1.0 mL/min. UV detection wavelength: 210 and 254 nm. For HPLC gradient program: solvent A 0.1% formic acid in water; solvent B 0.1% formic acid in acetonitrile. Gradient started at 38% B, increasing to 51% over 10 min, and then to 100% over 20 min. Separation of the observed degradates is illustrated by sample chromatograms for CLAP in Figure 2. Similar separation was observed for CNAP degradates, although retention times were different as expected.

LC/MS System: Micromass (Waters) LCT Mass Spectrometer equipped with MassLynx version 3.5 software controller (Micromass, Manchester, UK). Ionization method: electrospray positive (ESI±). Cone voltage: 30 V. Capillary voltage: 3 kV. Source temperature: 125 °C. Desolvation temperature: 300 °C. NMR (^{1}H NMR) data was collected using a Bruker BioSpin Avance 600 MHz Digital NMR Spectrometer.

Product Identification. Prior to the start of photolysis work for CLAP, three degradates observed in preliminary experiments had been isolated in larger quantities and their structures elucidated. Samples of all three CLAP photoproducts were available for identification by cochromatography. Preparation and structure identification of all three degradates for CLAP have been independently verified[6] and therefore not repeated here. For identification of CNAP degradate structures, larger amounts needed for structure elucidation were prepared as described below. Synthetic standards of CNAP_M1−M6 and CLAP_M1−M5 were also generated by unambiguous synthetic routes, and they were used to confirm the degradate identities via cochromatography experiments. Identification of degradate CNAP_M1 has been published previously in our work.[11]

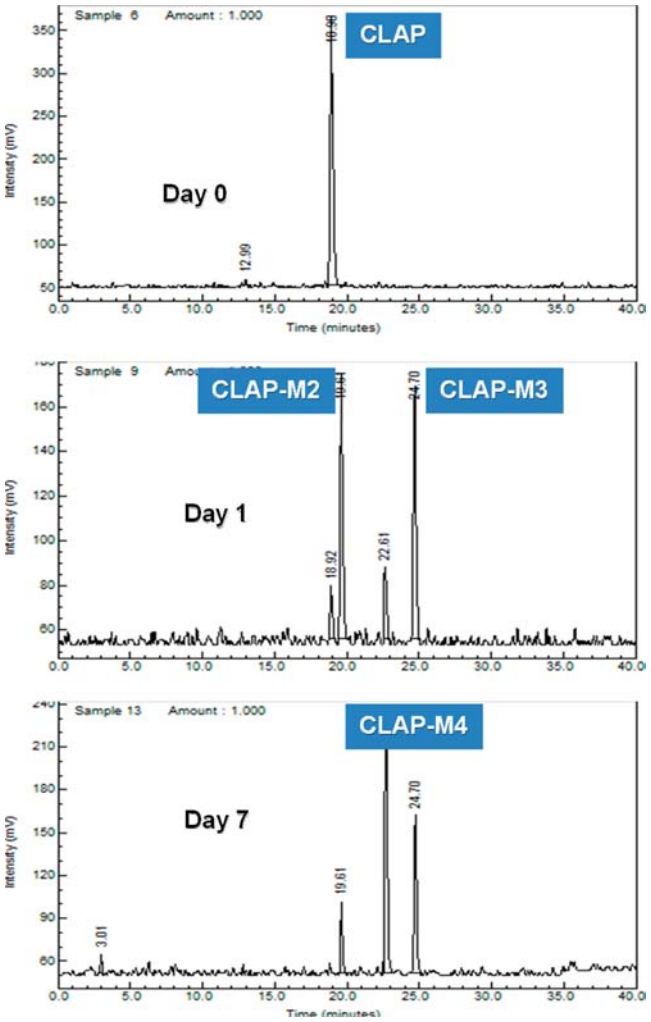

Figure 2. Chromatograms for chlorantraniliprole photolysis in natural water.

Identification of CNAP_M2. A 300 mL amount of sterilized 0.01 M pH 5 acetate buffers was added to a water-jacketed beaker, and the solution was treated with 2.25 mL of the 2000 ppm stock solution of CNAP. The beaker was covered with a quartz lid and placed in a Heraeus Suntest unit, and the beaker was connected to a water bath set at 20 °C. The sample was irradiated for 5 days until there was approximately >85% conversion to CNAP_M2 as measured by HPLC-UV. The solution containing CNAP_M2 was acidified to pH 3 with acetic acid to prevent its degradation. The acidified solution was applied to a 2 g, 12 cc C18 Mega Bond Elut SPE cartridge (Varian Inc., Lake Forest, CA) and washed with 2 mL of 0.1% formic acid. The column was flushed dry with hexane and vacuum dried. The product was eluted with 10 mL of ethyl acetate with 0.1% formic acid.

LC/MS analysis of the sample, in ESI positive mode, gave a molecular weight of 437 and molecular formula $C_{19}H_{13}BrN_6O_2$, and the isotope cluster was consistent with a molecule containing one bromine. LC-IR analysis of the sample showed absorption bands for CN at 2228, benzamide C═O at 1695, and C═N at 1651 cm^{-1}, which were characteristic of functional groups in the structure. Additional heterocycle and benzene double bonds were also present at 1591, 1518, and 1453 and C−O at 1195 cm^{-1}. A portion of the sample was loaded on to SPE cartridge, and the degradate was recovered in acetonitrile-d_3 to acquire ^{1}H NMR data.

Identification of CNAP_M3. A 300 mL aliquot of the solution containing CNAP_M2 was transferred to a 1 L Erlenmeyer flask, an

dx.doi.org/10.1021/jf5017175 | J. Agric. Food Chem. 2014, 62, 6577−6584

CNAP_M2

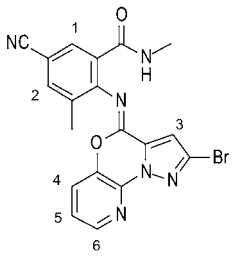

Phenyl-CH_3 observed at δ 2.20 s, NH-CH_3 at 2.70 d, Pyridine H6 at 7.39 dd and H5 at 8.33 dd, H4 at 7.49 as broad s; Phenyl-H1 at 7.73 and H2 at 7.90; broad s for NH at 7.13, H3 as s at 7.38. These assignments were confirmed with a COrrelation SpectroscopY (COSY) experiment, at 2°C.

equal volume of 0.01 M pH 9 borate buffer was added, and the mixture was stored under ambient conditions of temperature and light for 2 days, until there was approximately 89% conversion to CNAP_M3 as measured by HPLC-UV analysis. The solution containing M3 was concentrated using a 2 g, 12 cc C18 Mega Bond Elut SPE cartridge using pH 5 acetate buffer for preconditioning instead of 0.01% formic acid. The photoproduct was eluted with acetonitrile and reduced to dryness by nitrogen evaporation. The dry solid containing 87% M3 was analyzed by LC-MS/MS, LC-IR, and LC/^{1}H NMR-MS. The solid was dissolved in deuterated acetonitrile prior to LC/^{1}H NMR analysis.

LC/MS analysis of the sample in ESI positive mode gave a molecular weight consistent with structure of M3 (molecular weight 437) and isotope cluster pattern consistent with a molecule containing one bromine. The IR spectrum showed a cyano stretch at 2229 cm^{-1}, cyclic amide C═O at 1683, C−O stretch at 1250, and ring double bonds at 1461, 1592, and 1528 cm^{-1}. ^{1}H NMR further verified the assigned structure.

CNAP_M3

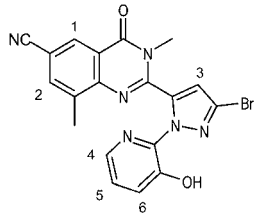

Phenyl-CH_3 observed at δ 2.33 s, N-CH_3 at 3.36 s, Pyridine H6 at 7.43 d and H5 at 7.19 dd, H4 at 7.63 as d; Phenyl-H1 at 7.87 and H2 at 8.47; broad s for OH at 9.64, H3 as s at 6.96. These assignments were confirmed with a COrrelation SpectroscopY (COSY) experiment, at 2°C, of the aromatic region.

Identification of CNAP_M4. The 600 mL solution containing CNAP_M3 was transferred to a water-jacketed beaker covered with a quartz lid and placed in a Heraeus Suntest unit in a water bath set at 20 °C. The sample was irradiated for 2 days until there was approximately 88% conversion to M4 as measured by HPLC-UV. The solution containing CNAP_M4 was concentrated using a 2 g, 12 cc C18 Mega Bond Elut SPE cartridge. The cartridge was preconditioned with one column volume of acetonitrile followed by one column volume of 1:1 pH 5 acetate buffer/pH 9 borate buffers. The solution was applied to the column and washed with 5 mL of H_2O. The column was then flushed dry using house vacuum. The photoproduct was eluted with acetonitrile. The eluate was reduced to dryness by nitrogen evaporation. The dry solid was analyzed by LC-MS/MS, LC-IR, and LC/^{1}H NMR-MS. The sample generated contained approximately 93% of M4 by HPLC analysis.

LC/MS analysis of the sample, in ESI positive mode, gave a molecular weight consistent with that of CNAP_M4 (molecular weight 344, with acetate adduct at mass 387). The isotope cluster pattern is consistent with a molecule containing one bromine atom. LC-IR of the sample gave an IR spectrum which showed cyano functionality at 2227 cm^{-1}, cyclic amide C═O at 1678, and ring double bonds at 1581, 1471, and 1476 cm^{-1}.

CNAP_M4

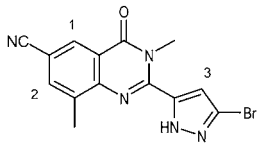

Phenyl-CH_3 observed at δ 2.66 s, N-CH_3 at 3.73 s, Phenyl-H1 at 7.91 and H2 at 8.42; H3 as s at 7.02. NH was not observed possibly due to rapid tautomeric shift. Spectrum of the aromatic region is illustrated below

Identification of CNAP_M5. The solution containing CNAP_M2 was acidified to a pH of approximately 2−3 with formic acid and the container placed in a water bath at 70 °C for 2 days. The container was then stored under ambient conditions of temperature and light for 5 days, until there was approximately 30% conversion to M5 as measured by HPLC-UV analysis. The solution containing M5 was concentrated using a 2 g, 12 cc C18 Mega Bond Elut SPE cartridge preconditioned with one column volume of methanol followed by one column volume of water containing 0.1% formic acid. The solution was applied to the column and washed with 15−20 mL of 0.1% formic acid. The photoproduct was eluted with a 40/60 acetonitrile/water−0.1% formic acid. The eluate was reduced to a small volume by nitrogen evaporation and quick frozen using the shelling technique in a dry ice−acetone bath. Remaining solvents were removed on a lyophilizer overnight. The lyophilized sample was stored in a freezer. Final purification was conducted by HPLC prior to recording the spectra. An aliquot of the sample was analyzed by LC-MS/MS, LC-IR, and LC/^{1}H NMR.

LC/MS analysis of the sample, in ESI positive mode, gave a molecular ion at 455/457 (1:1) consistent with the structure of M5. Prominent fragments at 424/426 and 266/268 (both showing peak cluster ratios of 1:1 indicative of Br atom in structure) resulted from acylium ion formed from loss of CH_3NH and the pyrazole acylium ion moiety after cleavage of the benzamide side. The IR spectrum showed CN at 2232, two amide C═O peaks at 1670 and 1639 cm^{-1}, and C−O stretch at 1266 cm^{-1}.

CNAP_M5

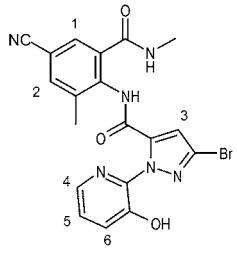

Phenyl-CH_3 observed at δ 2.21 s, NH-CH_3 at 2.73 s, Pyridine H4 at 7.94 dd and H5 at 7.41 dd, H6 at 7.36 as dd; Ph-H1 at 7.75 and H2 at 7.66; pyrazole H3 as s at 7.02, signals for OH and NH protons were not detected due to deuterium exchange. These assignments were confirmed with a COSY experiment, at 2°C.

dx.doi.org/10.1021/jf5017175 | J. Agric. Food Chem. 2014, 62, 6577−6584

Identification of CNAP_M6. LC/MS analysis of the sample, in ESI positive mode, gave a molecular weight consistent with that of CNAP_M6 (molecular weight 436). The exact mass suggested a molecular formula of $C_{19}H_{13}BrN_6O_2$, and the isotope cluster pattern was consistent with a molecule containing one bromine atom. The molecule was clearly an isomer of CNAP_M2 and M3 but quite different in HPLC retention time, and it was stable to base. Stability to base ruled out the possibility of *E*/*Z* isomers of M2. Structure assignment was based on the MS fragmentation; NMR of an isolated sample was obtained by aqueous photolysis of CNAP_M1 (ca. 20% yield). NMR spectra for this sample verified the structure.

CNAP_M6

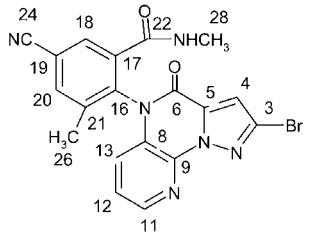

^{1}H-NMR in CD_3CN: Phenyl-CH_3 observed at δ 2.16 s, NH-CH_3 at 2.58 s, Pyrazole H4 at 7.33 s, Pyridine H11 at 8.43 d, H12 at 7.38 dd, H13 at 7.03 d; Ph-H18 at 7.95 d, and H20 at 8.02; signals for NH proton at 6.83 br. These assignments were confirmed with COSY experiments.

^{13}C-NMR: Carbonyl C22 at 165.8, C6 at 153.3, Pyridine ring: C8 at 126.7, C9 at 136.3, C11 at 144.9, C12 at 124.1, C13 at 126.0, Phenyl ring: C16 at 141.7, C17 at 137.1, C18 at 131.6, C19 at 114.7, C20 at 137.9, C21 at 137.8, Cyano C24 at 118.4, Pyrazole: C3 at 132.2, C4 at 111.8, C5 at 136.5, Methyl C26 at 17.6, C28 at 26.6 ppm

Determination of Rate Constants. Optimization of kinetics and rate constant calculations was conducted by building a first-order kinetics model in ModelMaker (software purchased from apbenson.com). The models represented by the sequence of transformations are discussed in the Results and Discussion section. In each case alternative models with a different order of transformations, which appeared to be logical based on chemistry, were also tested. The models presented gave the best optimization fit for the observed data. The rate constants generated for optimized kinetics of all experiments are summarized in Table 1, and the data fit is illustrated in various figures.

RESULTS AND DISCUSSION

CLAP and CNAP have a water solubility of 1.2 and 14.6 μg/mL, respectively. It has been shown in our previous work[11] that both compounds are vulnerable to hydrolytic degradation at alkaline pH, therefore, photodegradations were conducted in buffers of either pH 4 (CNAP) or 7 (CLAP) because the contribution from hydrolysis reactions was expected to be minimal and photodegradation reactions were anticipated to dominate. A generalized photodegradation pathway applicable to both compounds is displayed in Figure 3. All products displayed in the figure were not necessarily observed for both compounds under various conditions, and the degradations observed were consistent with those reported earlier.[4,6] The similarities and differences between the experiments for both test compounds are discussed.

Photodegradation of Chlorantraniliprole. Photolysis of CLAP in pH 7 buffer generated three products which appeared to have been formed sequentially. Degradation initially led to formation of M2, which reached a peak quickly by day 1. As M2 declined, the concentration of M3 increased, which also started to decline during the study period, leading to progressively

Table 1. Rate Constants and DT_{50} Values for CNAP and CLAP[a]

		chlorantraniliprole		cyantraniliprole	
media	reaction	K (day^{-1})	DT_{50} (day^{-1})	K (day^{-1})	DT_{50} (day^{-1})
buffer	P to M1(c)	NA		0.003 ± 0.001	231.0
	P to M2	1.696 ± 0.069	0.41	4.01 ± 0.094	0.17
	M2 to M3	0.659 ± 0.034	1.00	0.011 ± 0.002	64.8
	M3 to M4	0.313 ± 0.016	2.25	0.234 ± 0.051	3.0
	M4 to sink	0.004 ± 0.002	165.0	0.357 ± 0.125	1.9
	M2 to M5	NA		0.007 ± 0.002	
nat-water	P to M1(c)	0.003 ± 0.001	218.0	0.379 ± 0.010	1.8
	P to M3	2.311 ± 0.096	0.31	2.946 ± 0.136	0.24
	P to M5	NA		0.090 ± 0.025	7.7
	M3 to M4	1.166 ± 0.055	0.59	1.003 ± 0.038	0.7
	M4 to sink	0.010 ± 0.003	66.65	0.030 ± 0.002	23.3
	M1 to sink	NA		0.33 ± E	2.1
	M5 to sink	NA		0.001 ± E	693.1
soil	P to M1(c)			0.043 ± 0.006	16.0
	M1 to sink(c)			0.024 ± 0.012	28.5
	P to M1			0.064 ± 0.006	7.1[b]
	P to M3			0.034 ± 0.007	[b]
	M1 to M6			0.027 ± 0.007	25.8
	M3 to M4			0.457 ± 0.249	1.5
	M4 to sink			0.091 ± 0.036	7.7
	M6 to sink			0.065 ± 0.046	10.7

[a]P = parent compound (CLAP or CNAP), NA = not observed, E = rate constant not optimized, (c) = dark control. [b]DT_{50} of parent calculated using sum of rate constants for P to M1 and P to M3

dx.doi.org/10.1021/jf5017175 | J. Agric. Food Chem. 2014, 62, 6577−6584

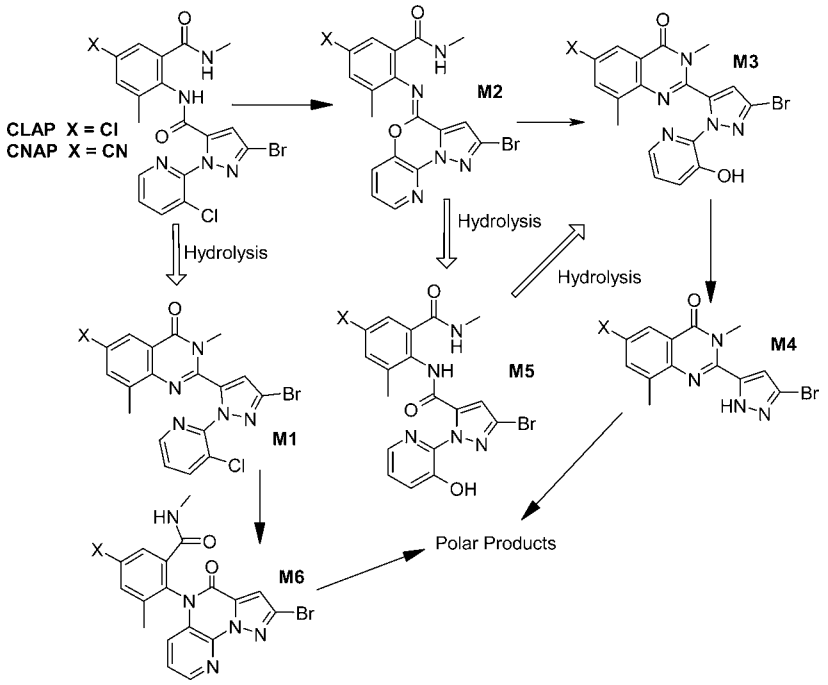

Figure 3. Transformations of chlorantraniliprole and cyanantraniliprole under photolysis conditions.

higher amounts of M4 (Figure 4). A similar incubation in the absence of light showed no degradation of CLAP.

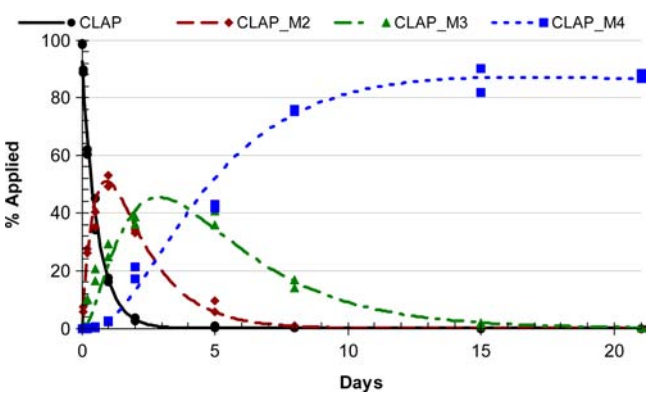

Figure 4. Chlorantraniliprole photolysis, pH 7 buffer.

The observed data for degradation in buffer were fitted to a kinetics model, illustrated below, in which each successive transformation product is generated as a result of first-order reaction from the preceding component and the last degradate leading to minor unknown products. Optimized kinetics parameters resulting from such a degradation scheme showed a good fit for all significant components (Figure 4), which verified that the products were indeed generated in succession. Even though degradates M2 and M3 had identical molecular weights and mechanistically it was possible to rationalize transformations leading to formation of both compounds directly from the parent, kinetics modeling verified that these two products were indeed formed in succession. Lack of stability of M2 and its hydrolytic transformation to M3 further supported the sequential transformations. Optimized rate constants for each step are listed in Table 1.

Photolysis of CLAP in natural water (pH 7.4) also produced the same degradates as the buffer, except degradate M2, which

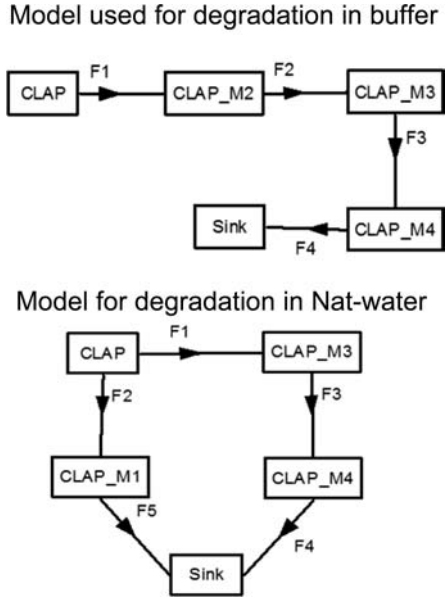

was not observed. Instead, degradation proceeded directly to M3, which again declined rapidly, leading to increasing amounts of M4. There was a gradual decline in the amount of M4 as the photolysis period progressed. A parallel incubation in the absence of light showed slow degradation of CLAP and formation of a small amount of M1. However, conversion of CLAP to M1 was too slow to make a meaningful contribution to the degradation observed in the presence of light. Therefore, inclusion of degradation to M1 in natural water as a parallel hydrolytic degradation did not alter the kinetics optimization of the photodegradation process. For model optimization in natural water, degradate M2 was ignored, since it was not observed. Instead, direct transformation of CLAP to M3 followed by M4 was optimized to derive the rate constants. The optimized model provided a good fit for the observed data. Figure 5 illustrates the result of inclusion of a simultaneous

dx.doi.org/10.1021/jf5017175 | J. Agric. Food Chem. 2014, 62, 6577−6584

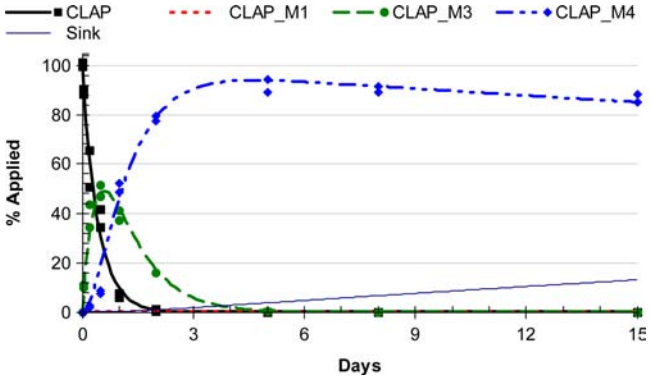

Figure 5. Chlorantraniliprole photolysis, nat-water.

degradation to M1 using a CLAP to M1 rate constant of 0.0032 day^{-1} (calculated from dark control experiment). A good data fitting (Figure 5) verified that partial hydrolysis due to increased pH played no significant role in the photodegradation of CLAP. Nevertheless, constituents of natural water did alter the overall photodegradation in two ways. First, the degradation rate increased, and second, a key degradate M2 was no longer detected.

Even though M2 was not observed in natural water photodegradation, it was presumed that M2 was a transient intermediate. Apparently, M2 underwent hydrolytic degradation in natural water too rapidly (possibly due to higher pH) to have been detected. Degradation of M2 to M3 under alkaline conditions was noted while attempting to isolate samples of M2, and indeed, it showed rapid conversion to M3 under slightly alkaline conditions. Some hydrolytic conversion of M2 to M3 even in pH 7 buffer cannot be ruled out, since stable isolation of M2 required acidic pH of 5 or less. However, the increase in photolysis rate in natural water probably was not merely due to the higher pH of natural water, because all subsequent transformations were also expedited. The transient behavior of M2 became even more obvious when the analogous product CNAP was investigated, as discussed later. It appeared more likely that faster photochemical reactions were due to dissolved ions and/or organic matter, a phenomenon noted by others as well.[7,8] Conversion of parent compound (P) to M3, which was controlled by P to M2 rate constant in buffer, increased by a factor of about 1.5 in natural water (2.3 vs 1.7 day^{-1}, data in Table 1). A faster degradation rate of CLAP was observed in natural water not only for the parent compound but each subsequent transformation M3 to M4 as well as M4 to unknown products. The presence of carbonate, nitrates, sulfates, and dissolved organic carbon has been reported to enhance generation of OH radicals or hydroperoxide radicals.[9] Other investigators have also reported quenching of radicals by the same species;[10] therefore, it cannot be stated with certainty as to which constituents of natural water facilitated the phototransformation rates. While the transformation mechanism for M2 to M3 (displayed in figure below) is believed to occur with OH anion (pH effect), the same reaction could just as well be triggered by OH radical (photodegradation). In reality, both mechanisms may have been operative to expedite this transformation so much that its degradation in natural water was faster than its formation; hence, M2 was not observed.

A comparison of the rate constants for transformation of M3 to M4 (data in Table 1) shows that this reaction was nearly 4-

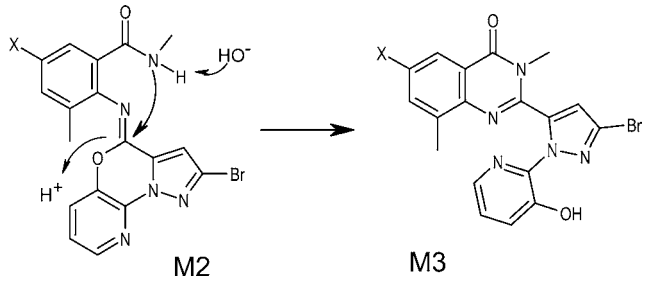

fold faster in natural water as compared to buffer. Even degradation of M4 to minor unknown products (sink) was faster by a factor of 2.5, indicating that degradation of CLAP as well as all photodegradates accelerated in natural water. If pH alone was the primary factor, enhanced degradation of M3 and M4 would not be expected.

Degradation of CLAP in soil was not significant over the 30 day duration of the experiment.

Photodegradation of Cyantraniliprole. Degradation of CNAP showed many similarities with CLAP photodegradations, but there were substantial differences. A lower pH buffer was chosen for CNAP degradation because only at pH 4 was photodegradation with the least contribution from hydrolytic degradations. Control solutions of CNAP in pH 4 buffer kept in the dark showed minimal conversion to M1. However, unlike CLAP, substantial degradation to cyclodehydration product, CNAP_M1, was noted in natural water dark control (Figure 6).

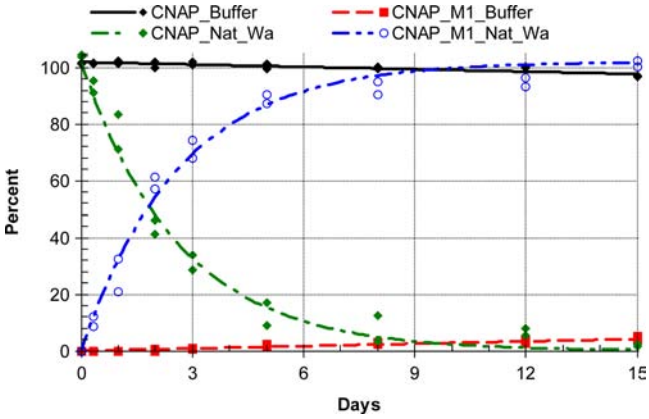

Figure 6. Cyantraniliprole, dark controls.

This clearly was due to the higher pH (7.4) of natural water. A faster hydrolytic degradation of CNAP in alkaline water, especially when compared with CLAP, has been discussed in detail previously;[11] therefore, hydrolytic degradation was anticipated to compete with photodegradation for CNAP in alkaline natural water.

Since cyantraniliprole is hydrolytically stable in pH 4 buffer, photodegradation was expected to occur with little contribution from hydrolytic reactions. As noted in Figure 7, degradation was faster than degradation of CLAP, resulting in formation of one main product M2. This product M2 degraded slowly, but it did degrade to three other products. Two of these, M3 and M4, were analogous to those found in CLAP degradation, while M5 was new to CNAP photolysis. Optimization of data using kinetics modeling suggested that M5 was derived from M2 and not from CNAP. It was surprising that CNAP_M2 was slower to degrade photochemically, as compared to CLAP_M2. In part, slower degradation of M2 may have been due to lower pH

dx.doi.org/10.1021/jf5017175 | J. Agric. Food Chem. 2014, 62, 6577−6584

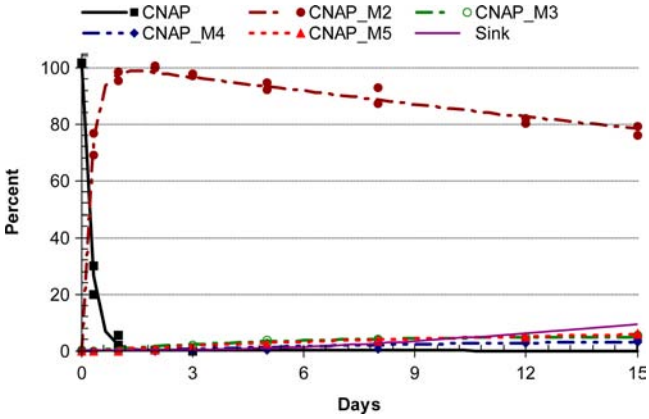

Figure 7. Cyantraniliprole photolysis in pH 4 buffer.

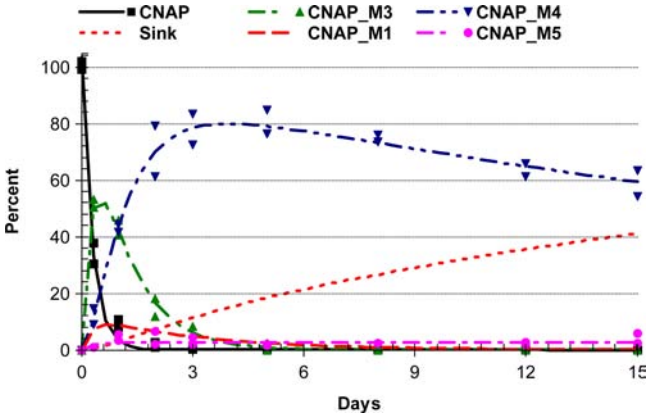

Figure 8. Cyantraniliprole photolysis, nat-water.

of the buffer used, which provided stability toward hydrolytic degradation of M2 to M3. Additional stability toward photodegradation of M2 may also have been caused by the "CN" group due to the extended conjugation of the phenyl and pyrazole rings. Such stabilization possibly made CNAP_M2 somewhat reluctant toward further degradation at pH 4 and allowed it the opportunity to generate an additional degradate M5 in small amounts.

Conversion of CNAP_M2 to M3 and M5 is probably due to hydrolytic reactions, even though a photolytic reaction mechanism due to OH radicals can be envisioned equally well. During degradate purification work it was noted that both M2 and M5 were easily converted to M3 in the presence of base or even at pH 7. Therefore, it was not surprising that photodegradation in natural water showed no CNAP_M2 and only a small amount, seldom exceeding 3−4%, for CNAP_M5. Initial formation of M2 undoubtedly did occur in natural water, but its further degradation to M3 was too rapid to allow detection of M2, just as it was noted for CLAP. A small portion did, however, manage to transform to M5 even in natural water. Similar to CLAP, further degradations, such as M3 to M4 and M4 to other unknown products, were observed in buffer as well as natural water, except that these transformations were again accelerated in natural water even for CNAP.

In the case of CNAP it was anticipated that formation of M1 via hydrolysis should compete with photolysis in natural water. Since CNAP_M1 was not actually observed during photolysis, we decided to explore this issue via kinetic modeling. While all observed degradates in natural water were optimized for their formation/degradation rates, the rate constant for hydrolysis in natural water was added to the kinetic model (figure below) using a rate constant computed from the dark control experiment. Such modeling for CNAP suggested that nearly 5−10% of total residue should have been observed as M1 in early stages of the study (Figure 8). After all, the presence of light would not be expected to shut down the hydrolytic degradation. Given that this hydrolytic pathway to CNAP_M1 occurs without light, not finding it means that M1 must be photodegrading just as it is formed via hydrolysis. This indeed was found to be the case when a new photodegradate CNAP_M6 was detected and identified. M6 was only observed at a few sampling intervals and accounted for ∼3−4% of the total mixture. Formation of M6 from M1 was verified by direct photolysis of CNAP_M1 in a separate experiment, albeit yielding a maximum of ∼20% only. The small amount of M6 being observed was attributed to its instability under photodegradation conditions. Due to the small amount observed, optimization of its formation rates via modeling was not feasible. Hence, it was not included in kinetics and treated as part of a "sink", a normal practice in kinetics modeling to deal with all minor and unknown products.

CNAP Degradation Model in Buffer

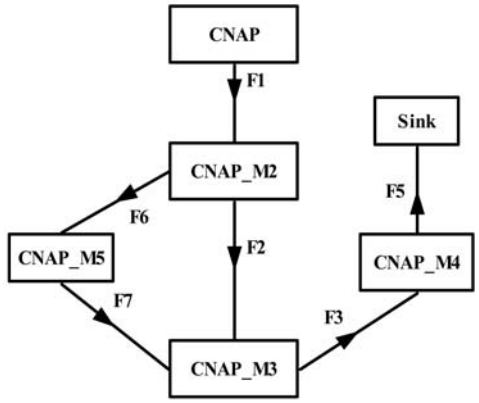

CNAP Degradation Model in Natural Water

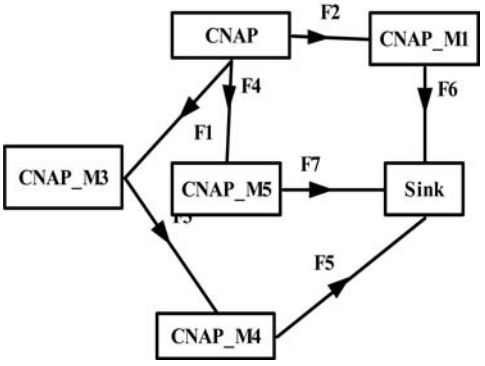

Degradation of cyantraniliprole in air-dried soil was slow, and the degradation rates in the presence as well as in the absence of light showed no meaningful differences. However, its degradation in moist soil, which was maintained at approximately 50% of maximum water-holding capacity, did display significant degradation. CNAP degradation in soil kept in the dark led primarily to formation of CNAP_M1 (Figure 9) along with numerous minor products. Photolysis in moist soil

dx.doi.org/10.1021/jf5017175 | J. Agric. Food Chem. 2014, 62, 6577−6584

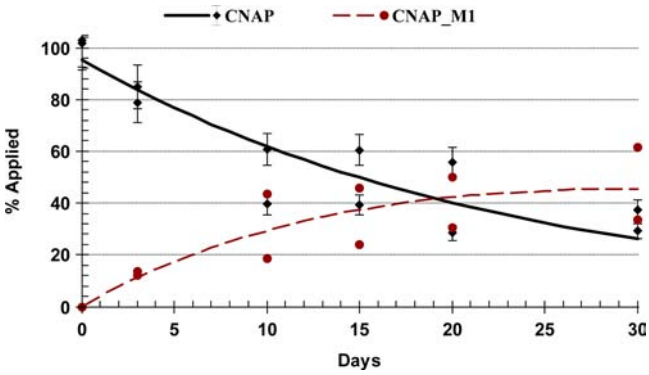

Figure 9. Cyantraniliprole soil photolysis, dark control.

enhanced the overall degradation rate of CNAP, and formation of most aqueous photolysis products was noted. Degradation occurred via two distinct pathways. One pathway proceeded via initial formation of CNAP_M1, the hydrolysis product, and its subsequent degradation to M6, while the other followed the natural water photolysis sequence. A kinetics assessment using a model similar to that employed for natural water degradation showed a good fit for all observed components, and the kinetics fits are displayed in Figure 10. Photodegradation in a moist soil

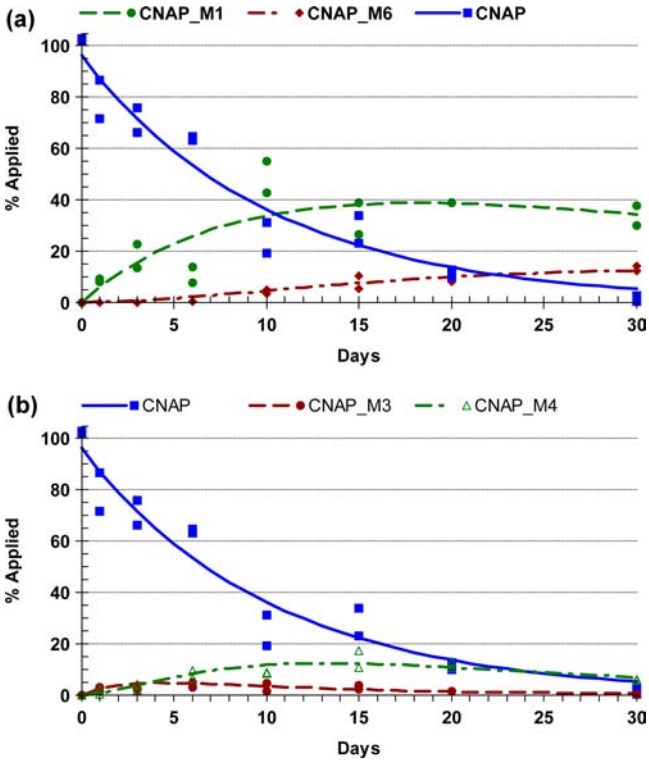

Figure 10. (a) Cyantraniliprole soil photolysis. (b) Cyantraniliprole soil photolysis.

surface was clearly faster than degradation in moist soil maintained in the dark due to participation of photolysis reactions. However, the rate of photodegradation even in moist soil was much slower than photodegradation in water itself. This experiment implies that photodegradation of CNAP on the soil surface may not be a significant degradation pathway in the environment because moist soils tend to dry out quickly in sunlight.

One can conclude from this investigation that both CLAP and CNAP are degraded by light essentially along the same pathway in water, leading primarily to formation of degradates M3 and M4. M2 may be encountered in water under acidic pH, but it is unlikely to be observed in significant quantity in natural water or soil. The degradation reactions observed were consistent with those reported previously, except for minor additional products observed for CNAP. Kinetics modeling of the data not only served to compute the degradation rates but also undoubtedly helped clarify the degradation pathway as well.

AUTHOR INFORMATION

Corresponding Author

*E-mail: ashok.k.sharma@dupont.com.

Present Address

§(K.M.) Smithers Viscient, 790 Main Street, Wareham, MA 02571, USA.

Notes

The authors declare no competing financial interest.

ACKNOWLEDGMENTS

Contributions of Steve Cheatham and Boiana Budevska for spectral data are sincerely acknowledged.

REFERENCES

(1) Cordova, D.; Benner, E. A.; Sacher, M. D.; Rauh, J. J.; Sopa, J. S.; Lahm, G. P.; Selby, T. P.; Stevenson, T. M.; Flexner, L.; Gutteridge, S.; Rhoades, D. F.; Wu, L.; Smith, R. M.; Tao, Y. *Pestic. Biochem. Physiol.* **2006**, *84*, 196−214.

(2) Selby, T. P.; Lahm, G. P.; Stevenson, T. M.; Hughes, K. A.; Cordova, D.; Annan, B.; Barry, J. D.; Benner, E. A.; Curries, M. J.; Pahutski, T. F. *Bioorg. Med. Chem. Lett.* **2013**, *23*, 6341−6345.

(3) Caboni, P.; Sarais, G.; Angioni, A.; Vargiu, S.; Pagnozzi, D.; Cabras, P.; Casida, J. E. *J. Agric. Food Chem.* **2008**, *56*, 7679−7699.

(4) Zhang, J. M.; Hai, W. G.; Wu, Y. L. *Chemosphere* **2012**, *87*, 132−136.

(5) Malhat, F.; Abdallah, H.; Hegazy, I. *Bull. Environ. Contam. Toxicol.* **2012**, *88*, 349−351.

(6) Lavtizar, V.; van Gestel, C. A. M.; Dolenc, D.; Trebse, P. *Chemosphere* **2014**, *95*, 408−414.

(7) Wallace, D. F.; Hand, L. H.; Oliver, R. G. *Environ. Toxicol. Chem.* **2010**, *29*, 575−581.

(8) Wols, B. A.; Hofman-Caris, C. H. M. *Water Res.* **2012**, *46*, 2815−2827.

(9) Dong, M. M.; Rosaio-Ortiz, F. L. *Environ. Sci. Technol.* **2012**, *46*, 3788−3794.

(10) Wenger, J. C. *Environ. Sci. Technol.* **2004**, *38*, 831−837.

(11) Sharma, A. K.; Zimmerman, W. T.; Lowrie, C.; Chapleo, S. *J. Agric. Food Chem.* **2014**, *62*, 3531−3536.

of immature fruit.[24] Juice from asymptomatic and symptomatic fruit has also been shown to contain more bitter compounds, but in concentrations lower than taste threshold values.[14,24]

The value of Florida's sweet orange crop for 2011−2012 alone is reported to be $1.2 billion. Hamlin and Valencia varieties make up 42.6% and 55%, respectively, of this value.[25] In our previous study, we evaluated the juices prepared from Valencia oranges of varying stages of CLas infection and harvested from a single location.[21] Additionally, we have examined the impact of environmental differences such as variations in elevation and soil depth on the metabolome of Mandarin oranges.[26] Recognizing that the state of HLB infection, as well as varietal and regional differences, could influence the metabolome of citrus juices, this study was undertaken to investigate the metabolite differences between healthy and infected fruit of two different citrus varieties grown in different regions. It is important to understand the impact of regional and varietal variation on the juice metabolome during infection, as this may provide insight into differences in response to infection depending on location or cultivar, and therefore help determine if these variables may confound the ability to detect disease using this method.

MATERIALS AND METHODS

Plant Materials. *Citrus sinensis* cultivars Valencia and Hamlin fruit samples were used in this study. The presence of CLas bacteria in symptomatic and asymptomatic trees, and its absence in control trees, was confirmed by polymerase chain reaction (PCR) using standard methods as described.[27] Control Hamlin fruit samples were collected from CLas$^-$ (PCR negative), and asymptomatic and symptomatic Hamlin fruit were collected from different CLas$^+$ (PCR positive) trees. Asymptomatic fruit were visually indistinguishable from control (CLas$^-$) fruit. A total of 54 Hamlin samples were collected: 18 control, 18 asymptomatic, and 18 symptomatic. Control Valencia fruit samples were collected from CLas$^-$ (PCR negative) trees; symptomatic Valencia fruit were collected from CLas$^+$ (PCR positive) trees and showed visual symptoms of HLB. A total of 36 Valencia samples were collected: 18 control and 18 symptomatic.

All samples were collected from mature trees approximately 20 years old. In each region, fruit were gathered from up to three different blocks, and in each block, samples were taken from three different trees. The per-tree sample size consisted of 15−20 fruits that were juiced, aliquoted, and stored at −20 °C until used for analysis. Sampling of Valencia fruits was conducted from May 2009 to June 2009 and Hamlin fruits from December 2009 to January 2010. For each cultivar, trees were from commercial orchards in south and east Florida. For the Hamlin oranges, 36 samples came from east Florida (12 samples from each infection stage), and 18 came from south Florida (6 samples from each infection stage). For the Valencia oranges, 18 samples came from east Florida, and 18 came from south Florida (9 samples from each infection stage for both locations).

°Brix and Limonin Measurements and NMR Data Collection. °Brix, limonin measurements, and NMR data collection were performed as previously described by Slisz et al.[21] Briefly, °Brix was determined by measuring total soluble solids with a Rudolph Research model J257 automatic refractometer (Hackettstown, NJ). Limonin was measured by high-performance liquid chromatography (HPLC) and represents limonin concentration after a 48 h thaw at 4 °C to allow conversion of limoninoate A-ring lactone into limonin. A 50 × 2.0 mm Phenomenex Phenosphere-Next-4 μm phenyl column with a guard column of the same material was used with solvent flow rate at 1.0 mL/min comprised of 70% 10 mM formic acid and 30% ACN.

For NMR analysis, juice samples were thawed, centrifuged, and then filtered (Nanosep Omega-3 3000 molecular weight cutoff (Pall Life Sciences, Ann Arbor, MI)). Internal standard containing 5 mM 3-(trimethylsilyl)-1-propanesulfonic acid-d_6 (DSS-d_6) in >98% D_2O and 0.2% NaN_3 (for a final DSS-d_6 concentration of 0.5 mM, 0.02% NaN_3, and approximately 10% D_2O in each sample) was added to a mixture of 400 μL of juice filtrate and 185 μL of ultrapure H_2O to ensure a sample volume of 600 μL required for NMR analysis. Sample pH was adjusted to 6.8 ± 0.1 using NaOH, and then 600 μL of sample was transferred to 5 mm NMR tubes. NMR spectra were acquired at 298 K using the Bruker "noesypr1d" experiment on a Bruker Advance 600 MHz NMR spectrometer equipped with a SampleJet with the following acquisition parameters: 12 ppm sweep width, 2.5 s acquisition time with 2.5 s relaxation delay, and 100 ms mixing time. Water saturation was applied during the relaxation delay and mixing time. The resulting spectra were zero-filled to 128 000 data points, and an exponential apodization function corresponding to a line-broadening of 0.5 Hz was applied. Spectra were processed in Chenomx NMRSuite Processor v7.6.

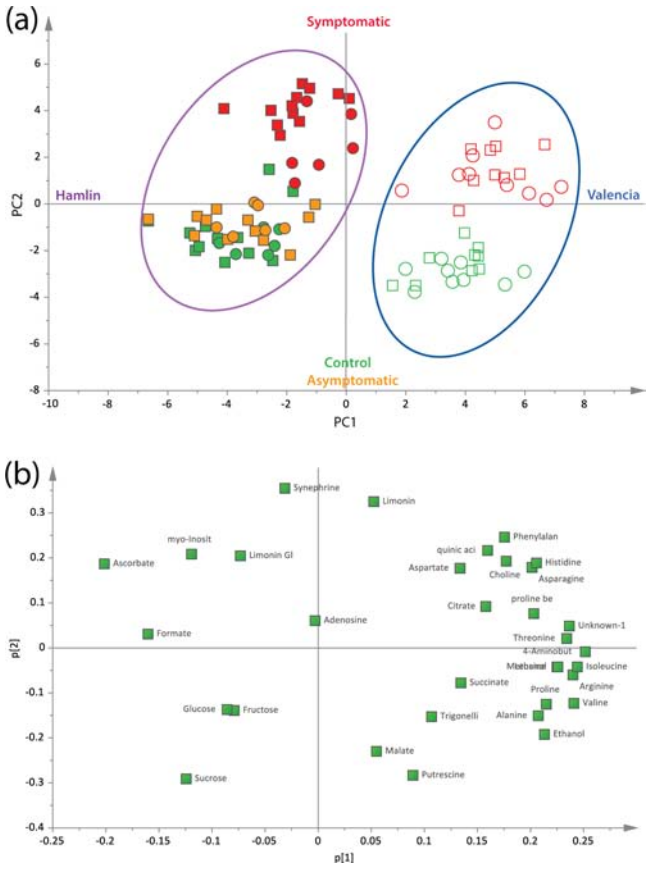

Figure 1. Comparison of composition of both Hamlin (filled) and Valencia (open) orange juice samples. (a) PCA scores plot comparing control (green), asymptomatic (orange), and symptomatic (red) samples. Circle and square markers indicate south or east Florida origin, respectively. Principal component 1 (PC1) explains 45.1% of the variation, and PC2 explains 17.9% of the variation. R^2X = 0.787; Q^2 = 0.658. (b) Loadings plot corresponding to panel a.

Data Analysis. Metabolites in orange juice samples were identified and quantified using targeted profiling[28] with Chenomx NMR suite v7.6 (Chenomx Inc., Edmonton, Alberta, Canada). In total, 32 metabolites were assigned and quantified as previously described[21] and included sugars (fructose, glucose, sucrose, and myo-inositol), amino acids (alanine, arginine, asparagine, aspartate, histidine, isoleucine, leucine, phenylalanine, proline, threonine, and valine), organic acids (citrate, succinate, malate, formate, ascorbate, and γ-aminobutyric acid (GABA), and others (adenosine, choline, ethanol, limonin glucoside, methanol, proline betaine, putrescine, quinic acid, trigonelline, synephrine, and an unknown metabolite with peaks at 0.8, 1.1, and 1.4 ppm). The concentration of limonin was determined using HPLC and was included in statistical analysis. For NMR measured metabolites, the profiled concentrations were corrected for dilution by multiplying the measured concentration by the final volume (650 μL)

dx.doi.org/10.1021/jf5017434 | J. Agric. Food Chem. 2014, 62, 6585−6591

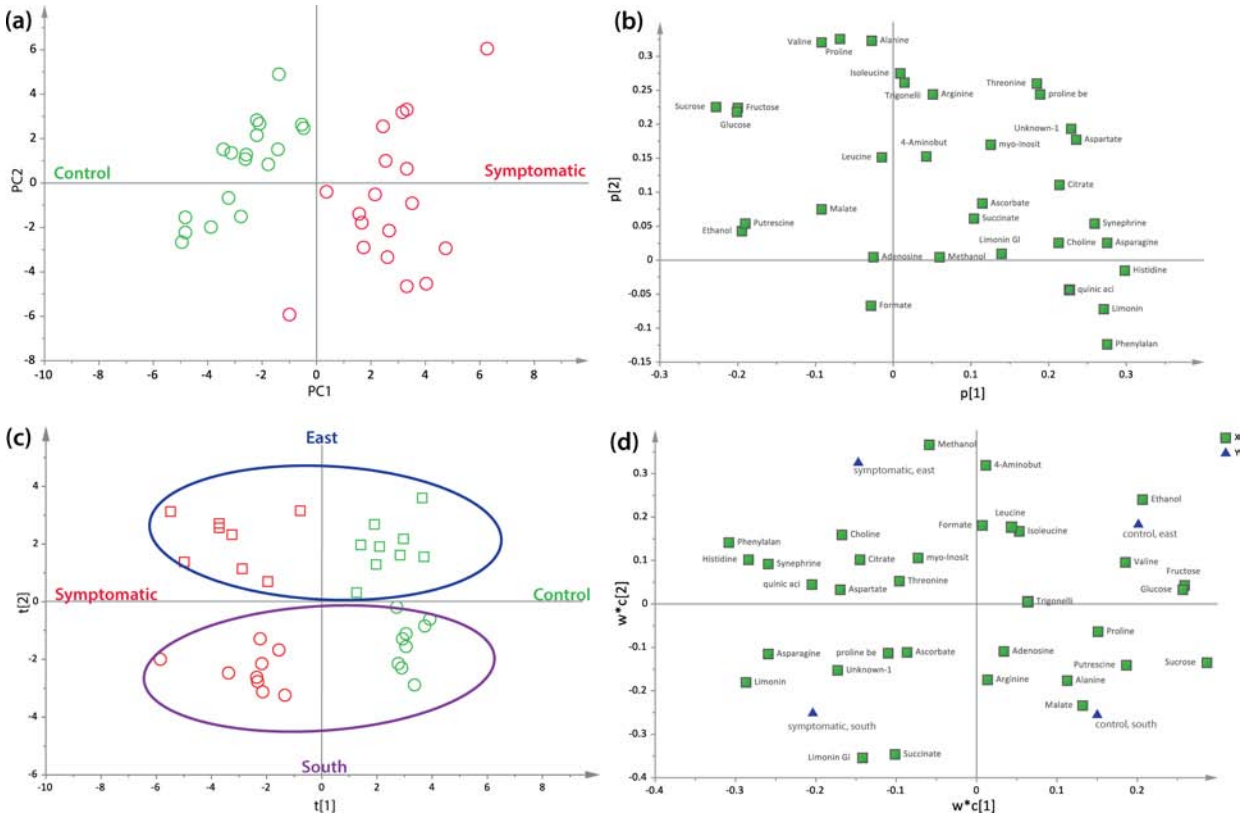

Figure 2. Comparison of composition of Valencia oranges. (a) PCA scores plot of control (green) and symptomatic (red) Valencia orange juice samples. PC1 explains 29% of the variation and PC2 23.3%. $R^2X = 0.812$; $Q^2 = 0.496$. (b) Loadings plot corresponding to panel a. (c) PLS-DA scores plot of Valencia samples classified by both region and infection status. Square and circle markers represent fruit from east and south Florida, respectively. R^2 and Q^2 were 0.587 and 0.532, respectively, and validation by random permutation (100 permutations) had y-intercepts for R^2 and Q^2 of 0.111 and −0.238, respectively, and both had positive slopes. (d) Loadings plot corresponding to panel c.

and dividing by the volume of juice used (400 μL). Final metabolite concentrations were subjected to $\log_{10}$ transformation to ensure normal distribution as described by Zhang et al.[26] Multivariate statistical data analyses, including principal component analysis (PCA) and partial least-squares-discriminant analysis (PLS-DA), were performed using SIMCA-P with mean centering and unit variance scaling. The quality of the models was judged by the goodness-of-fit parameter (R^2X or R^2Y) and predictive ability parameter (Q^2), as well as permutation testing (for the PLS-DA models), where each data point was randomly assigned a class 100 times, and the corresponding R^2Y and Q^2 calculated and compared to the original model. From the PLS-DA models, variable influence in projection (VIP), which is a weighted sum of squares of the PLS loading weights that takes into account the amount of explained Y-variation in each dimension, was used to assess those variables of significance for further scrutiny. Metabolites with a VIP value greater than 1 were selected for further discussion.[29] Significance testing, using Mann−Whitney test for Valencia samples, and Kruskal−Wallis test and Dunn's multiple comparison test for Hamlin samples, was performed on raw untransformed data using GraphPad Prism with significance set at $\alpha = 0.05$. Kruskal−Wallis test and Dunn's multiple comparison test were selected for the Hamlin samples due to unbalanced numbers in the selected sample groups.

RESULTS

We previously published on the metabolite composition of control and asymptomatic Valencia fruit.[21] However, that study only examined one variety of fruit from one location in Florida. Here, we analyzed the composition of two citrus varieties from different growing regions in the context of infection by CLas (control (PCR CLas$^-$), asymptomatic (PCR CLas$^+$), and symptomatic (PCR CLas$^+$) Hamlin fruit, as well as control (PCR CLas$^-$) and symptomatic (PCR CLas$^+$) Valencia fruit). The contributions of variety and growing region (south or east Florida) were assessed to evaluate the impact of these variables on tree metabolic response to infection by CLas.

All Orange Samples. Multivariate analysis of all of the Hamlin and Valencia samples (Figure 1) showed clear separation by principal components analysis (PCA) (R^2X = 0.787 ; Q^2 = 0.658) based on their cultivar and infection status (healthy, HLB-asymptomatic or HLB-symptomatic). Samples were discriminated by cultivar along principal component 1 (PC1), and were separated by infection status along principal component 2 (PC2). These data show that orange cultivar represents the major difference in the fruit metabolome, followed by infection status. Many metabolites were higher in the Valencia juice samples including GABA, isoleucine, arginine, valine, and threonine. Ascorbate and formate were higher in the Hamlin juice samples (Figure 1b). To understand and compare the impact of CLas infection on each cultivar, statistical analyses were conducted independently on each variety and are shown below.

Valencia Samples. Figure 2a shows a PCA for Valencia fruit samples (R^2X = 0.812; Q^2 = 0.496). Sucrose, glucose, fructose, proline, ethanol, and putrescine were higher in concentration in control fruit as compared to symptomatic fruit (Figure 2b). Sucrose concentration was over 2-fold higher in control. Phenylalanine, histidine, limonin, synephrine, quinic acid, and asparagine were higher in symptomatic fruit (Figure 4 and Supporting Information Figure S1). The symptomatic fruit had over 2-fold higher phenylalanine and asparagine, and 2.6-fold higher limonin concentration. °Brix content was significantly

dx.doi.org/10.1021/jf5017434 | J. Agric. Food Chem. 2014, 62, 6585−6591

Table 1. °Brix for Hamlin and Valencia Juice Samples, Grouped by Infection Status[a]

Hamlin				Valencia	
group 1	group 2	group 3	symptomatic	control	symptomatic
10.66 ab	12.05 a	12.90 a	8.73 b	12.18	8.79[b]

[a]Comparisons are within each cultivar. For Hamlin, values with different letters are significant at $p < 0.05$. [b]For Valencia, denotes significance at $p < 0.0001$.

lower in symptomatic Valencia oranges as compared to control oranges (Table 1).

To determine the impact of the growing region on metabolite composition, fruit classified by both their region and their infection status were compared using PLS-DA. Figure 2c shows the scores plot, and Figure 2d shows the loadings plot. Interestingly, although regional differences could be observed, the ability to differentiate fruit on the basis of infection status was clearly evident, as metabolites responsible for regional variation differed from those responsible for variation due to infection (Figure 2d).

Hamlin Samples. To investigate the influence of infection and growing region on metabolite composition of Hamlin orange samples, PLS-DA was employed (Figure 3a). A similar trend was observed for Hamlin oranges as was observed for Valencia oranges. The control and CLas$^+$ symptomatic samples separated along component 1. The control and CLas$^+$ asymptomatic samples clustered together on component 1, but some differentiation could be observed along component 2. The low Q^2 value (0.436), which represents the predictive ability of the model, reflects the overlap between the control and asymptomatic samples; however, permutation testing revealed a valid model. Although separation was not complete, a pattern emerged that appeared as mainly control fruit in the lower right-hand quadrant that transitioned to mostly CLas$^+$ asymptomatic fruit in the upper right-hand quadrant. Proposed groupings based on this clustering are circled and labeled as groups 1−3 in Figure 3a. Distinctions in metabolite composition included higher ethanol and malate in group 1 (mostly control), and higher fructose, glucose, proline, and sucrose in group 3 (mostly asymptomatic) fruit (Figure 4). Malate and ethanol exhibited a stepwise decrease in concentration from group 1 to group 3 fruit (Supporting Information Figure S2). Fructose, glucose, sucrose, °Brix, and proline initially increased from group 2 (mixture of control and asymptomatic) to group 3 (mostly asymptomatic) fruit, and then decreased in symptomatic fruit. Sucrose was approximately 2-fold higher in group 3 fruit as compared to symptomatic fruit. Phenylalanine, histidine, synephrine, asparagine, GABA, choline, limonin, and quinic acid were higher in symptomatic fruit as compared to control and group 3 fruit (Supporting Information Figure S2). Phenylalanine was approximately 3.8-fold higher, histidine 3-fold higher, and asparagine 2-fold higher in symptomatic fruit as compared to group 3 fruit. °Brix was significantly lower in symptomatic fruit as compared to fruit classified as groups 2 and 3 (Table 1).

To understand how different growing regions contribute to Hamlin fruit metabolite composition during infection, the fruit were classified based on the combination of infection status and growing region (Figure 3b). As with the Valencia juice samples, juice samples from Hamlin oranges discriminated by infection status along component 1, and by region along component 2, and metabolites that characterized growing regions differed from those that characterized infection stage (Figure 3c).

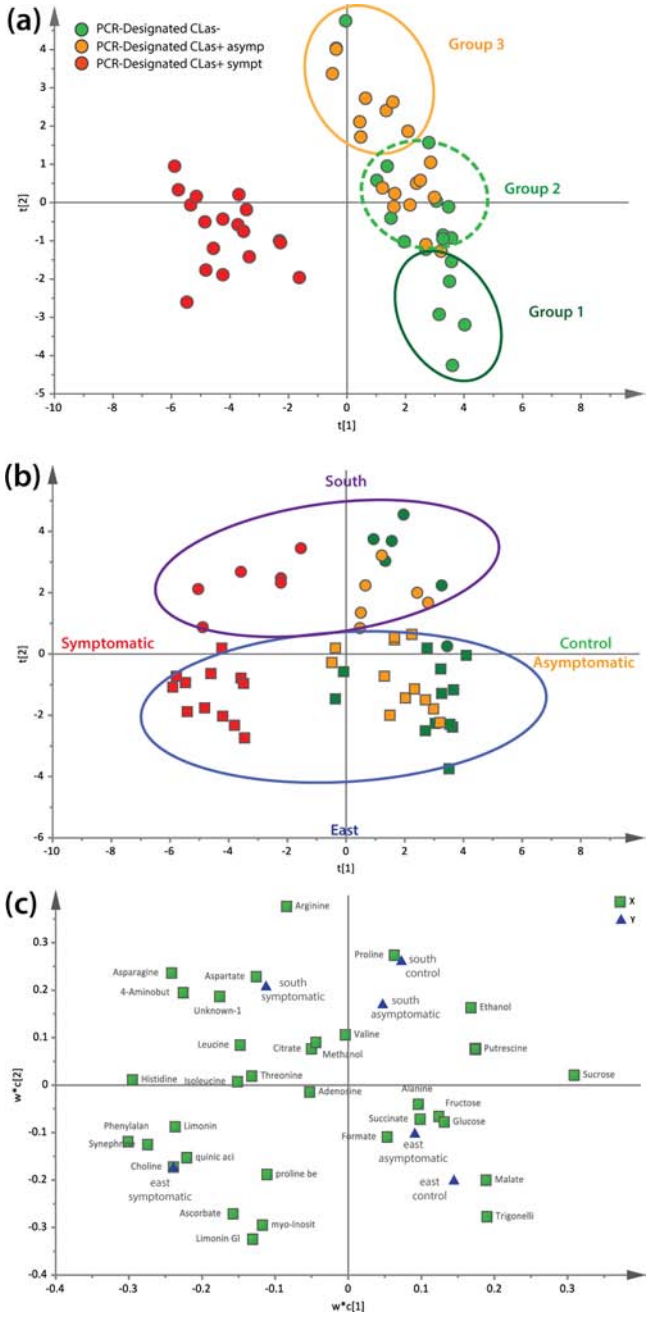

Figure 3. Comparison of composition of Hamlin orange juice samples. (a) PLS-DA scores plot of control (green), asymptomatic (orange), and symptomatic (red) Hamlin samples. $R^2 = 0.537$ and $Q^2 = 0.436$; validation by random permutation (100 permutations) showed positive slopes for R^2 and Q^2, and intercepts of 0.118 and −0.187, respectively. (b) PLS-DA scores plot of Hamlin samples based on infection status (control (green), asymptomatic (orange), and symptomatic (red)) and the sample's growing region (south (circle) and east (square) Florida). R^2 and Q^2 are 0.33 and 0.292, respectively, and random permutation (100 permutations) revealed positive slopes with R^2 and Q^2 intercepts of 0.054 and −0.147, respectively. (c) Loadings plot corresponding to panel b.

DISCUSSION

Analysis of Hamlin and Valencia oranges revealed that the two varieties are distinguishable from one another on the basis of their metabolite composition. Although the samples originated from varying locations and were from two cultivars, the ability

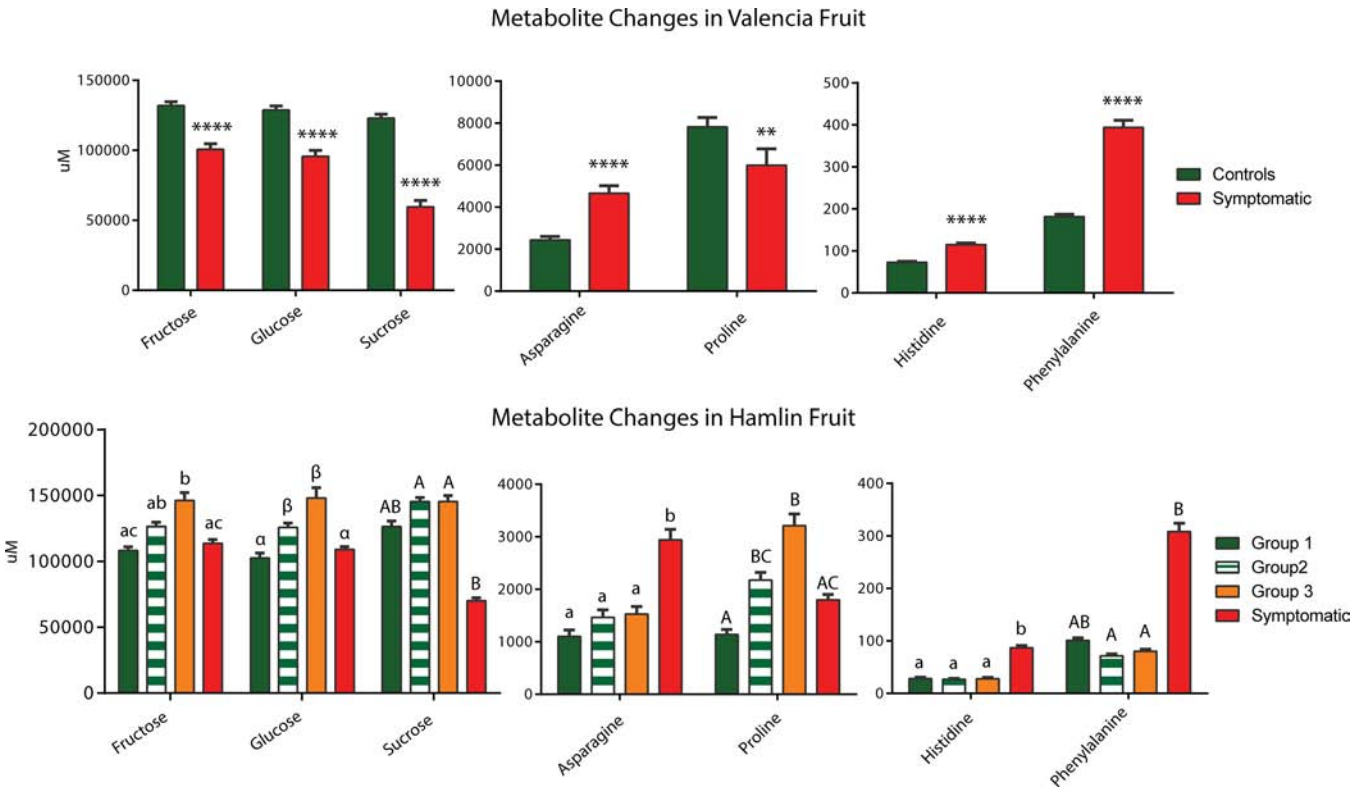

Figure 4. Metabolite concentration (average ± SEM) at varying states of CLas infection in Hamlin and Valencia orange juice samples. Valencia samples are grouped according to whether they are control or symptomatic ($CLas^-$ or $CLas^+$ via PCR, respectively). $^{**}p < 0.01$ and $^{****}p < 0.0001$. Hamlin samples are classified as group 1, group 2, group 3, and symptomatic. Samples with shared letters/symbols indicate no significant difference between those samples at $p < 0.05$.

to discriminate samples on the basis of infection status was not impaired. The concentrations of phenylalanine, histidine, asparagine, and limonin were lower in the control and asymptomatic Valencia or Hamlin fruit as compared to symptomatic fruit in both varieties (Figure 4). This is in agreement with another study on juice,[14] as well as our previous study in which we reported increases in amino acids such as asparagine, histidine, and phenylalanine in symptomatic Valencia oranges as compared to healthy and asymptomatic Valencia oranges.[21]

Examination of the PLS-DA (Figure 3a) of Hamlin fruit revealed a cluster of samples delineated as control fruit (PCR $CLas^-$) in the lower right quadrant, and a cluster of mostly asymptomatic fruit (PCR $CLas^+$) in the upper right quadrant. A mixture of control and asymptomatic samples was between the two. Similarity in metabolite composition among samples in groups 2 and 3 suggests that some of the controls were possible false negatives by PCR. PCR is a nucleic acid-based method that can be used to determine the presence or absence of a bacterium by testing for the presence of its genetic material. Indeed, PCR is prone to false negatives, as it requires a minimum bacterial titer for detection, and bacteria are not evenly distributed throughout the tree.[30,31] Since detection of HLB in Florida in 2005, the entire state is now under quarantine for HLB and ACP.[15] It is unknown how many truly $CLas^-$ trees remain in Florida. These results suggest a potential role for metabolomics to detect infection earlier than PCR. Detecting infection early and understanding the tree response to infection is important for developing treatment plans. These results will need to be further investigated with a broader range of citrus varieties to establish global metabolite biomarkers of CLas infection.

Fructose, glucose, sucrose, and proline concentrations were significantly lower in symptomatic fruit as compared to control Valencia. However, differences in these metabolite concentrations between group 1 (primarily control fruit) and symptomatic Hamlin failed to reach significance. There may be different reasons for this discrepancy. First, there is a difference in sample size, with fewer samples in group 1 as compared to symptomatic fruit. Second, not all Valencia control samples may be truly control, and some could come from trees not yet testing positive for CLas. While Hamlin fruit are harvested from October to January, Valencia fruit are late season fruit and harvested from March to June. Indeed, lower amplification of CLas during the spring months has been reported,[32] and thus the difference in harvest time may contribute to the presence of false negatives by PCR. However, because there are no asymptomatic Valencia samples in this study, we cannot attempt to tease out possible PCR false-negatives based on similarities in metabolite composition as we have done with the Hamlin samples, and it is unknown if the Valencia control samples may contain samples that are analogous to Hamlin groups 2 and 3.

Comparison of fructose, glucose, sucrose, and proline concentrations between group 3 and symptomatic Hamlin and control and symptomatic Valencia revealed similar trends (Figure 4). In the asymptomatic Hamlin samples (groups 2 and 3), these metabolites increase. Symptoms of HLB include starch accumulation in the leaves and phloem impairment.[20,33,34] The decrease in sugars during symptomatic infection could reflect altered carbohydrate transport. Fructose and glucose have been shown to increase in tomatoes subjected to water and nematode stress,[35] and sucrose, fructose, and glucose accumulated in strawberries infected

dx.doi.org/10.1021/jf5017434 | J. Agric. Food Chem. 2014, 62, 6585−6591

with *Colletotrichum nymphaeae*.[36] Defensive mechanisms are costly,[37] and the influx of sugars during asymptomatic infection could indicate mobilization of plant defenses prior to symptom development. Thus, these metabolite concentrations measured in Hamlin group 1 could reflect true control concentrations, and those measured in groups 2 and 3 reflect changes in plant metabolism with early infection. Because there are no asymptomatic Valencia samples, however, it is unknown if a similar pattern can be observed during early infection in Valencia oranges.

Although we previously reported decreases in the concentrations of fructose, glucose, sucrose, and proline when comparing healthy and asymptomatic Valencia fruit,[21] it is important to note that there were differences in the appearance of the asymptomatic fruit as compared to this study. This may explain why the results presented here for asymptomatic Hamlin fruit differ from those of asymptomatic Valencia fruit in the Slisz et al. paper.[21] Indeed, the fruit in that article showed minor signs of HLB such as a slight reduction in average size and small amounts of greening. Here, the asymptomatic Hamlin fruit were visually indistinguishable from control fruit, although they were $CLas^+$ by PCR. Unfortunately, no asymptomatic Valencia fruit were available for this study, and thus a difference between cultivars in how asymptomatic fruit differ in terms of metabolite content cannot be ruled out. Nonetheless, this brings to light a need for standardization of the term "asymptomatic" because it currently relies on subjective interpretation of visual symptoms. A chemical profile that classifies the fruit may be desirable to promote sampling uniformity and to reduce possible misunderstandings.

Although Hamlin and Valencia oranges are two distinct orange varieties harvested during different parts of the year, the presence of CLas has a substantial effect on the metabolite composition of the fruit. The overall pattern for change in many metabolites remained consistent in both Hamlin and Valencia cultivars. Asymptomatic Hamlin oranges revealed more details about nuances in metabolite changes during early infection. Although differences due to the tree location can be detected, this does not impair our ability to discriminate the fruit on the basis of their infection status.

In summary, the present data suggest that metabolomics may be useful to detect trees in the early stage of infection (asymptomatic), and differentiate from those in later stages (symptomatic).

■ ASSOCIATED CONTENT

Supporting Information

Comparisons of additional metabolites for control and symptomatic Valencia juice samples (Figure S1); comparison of additional metabolites for Hamlin juice samples based on infection status (Figure S2). This material is available free of charge via the Internet at http://pubs.acs.org.

■ AUTHOR INFORMATION

Corresponding Author

*Tel.: (530) 752-6804. E-mail: cslupsky@ucdavis.edu.

Funding

This work was supported in part by The California Citrus Research Board, and Roll Global (Fellowship to E.L.C.). Support for the Bruker Advance 600 MHz NMR comes from NIH grant RR011973.

Notes

The authors declare no competing financial interest.

■ ACKNOWLEDGMENTS

We thank Anne Slisz and Yaqi Lan for their help with sample preparation.

■ ABBREVIATIONS USED

HLB, Huanglongbing; CLas, *Candidatus* Liberibacter asiaticus; ACP, Asian Citrus Psyllid; NMR, nuclear magnetic resonance; PCA, principal component analysis; PLS-DA, partial least-squares-discriminant analysis

■ REFERENCES

(1) CDFA Asian Citrus Psyllid (ACP) Fact Sheet. http://www.cdfa.ca.gov/plant/factsheets/ACP_FactSheet.pdf (accessed December 16, 2013).

(2) Gottwald, T. R. Current epidemiological understanding of citrus Huanglongbing. *Annu. Rev. Phytopathol.* **2010**, *48*, 119−139.

(3) Xu, C.; Xia, Y.; Li, K.; Ke, C. Further study of the transmission of citrus huanglongbing by a psyllid, Diaphorina citri Kuwayama. *Proc. 10th Conference of the International Organization of Citrus Virologists*; Riverside, CA, 1988; pp 243−248.

(4) Gottwald, T.; da Graca, J.; Bassanezi, R. Citrus huanglongbing: the pathogen and its impact. *Plant Health Prog.* **2007**, DOI: 10.1094/PHP-2007-0906-01-RV.

(5) McClean, A.; Oberholzer, P. Greening disease of the sweet orange: evidence that it is caused by a transmissible virus. *S. Afr. J. Agric. Sci.* **1965**, *8*, 253−275.

(6) Lopes, S.; Bertolini, E.; Frare, G.; Martins, E.; Wulff, N.; Teixeira, D.; Fernandes, N.; Cambra, M. Graft transmission efficiencies and multiplication of 'Candidatus Liberibacter americanus' and 'Ca. Liberibacter asiaticus' in citrus plants. *Phytopathology* **2009**, *99*, 301−306.

(7) Cevallos-Cevallos, J. M.; Futch, D. B.; Shilts, T.; Folimonova, S. Y.; Reyes-De-Corcuera, J. I. GC-MS metabolomic differentiation of selected citrus varieties with different sensitivity to citrus huanglongbing. *Plant Physiol. Biochem.* **2012**, *53*, 69−76.

(8) Bové, J. M. Huanglongbing: a destructive, newly-emerging, century-old disease of citrus. *J. Plant Pathol.* **2006**, *88*, 7−37.

(9) Polek, M. *Citrus Bacterial Canker Disease and Huanglongbing (Citrus Greening)*; UCANR Publications: 2007.

(10) Gottwald, T.; Graham, J.; Irey, M.; McCollum, T.; Wood, B. Inconsequential effect of nutritional treatments on huanglongbing control, fruit quality, bacterial titer and disease progress. *Crop Prot.* **2012**, *36*, 73−82.

(11) Folimonova, S. Y.; Robertson, C. J.; Garnsey, S. M.; Gowda, S.; Dawson, W. O. Examination of the responses of different genotypes of citrus to Huanglongbing (citrus greening) under different conditions. *Phytopathology* **2009**, *99*, 1346−1354.

(12) Lopes, S.; Frare, G.; Bertolini, E.; Cambra, M.; Fernandes, N.; Ayres, A.; Marin, D.; Bové, J. Liberibacters associated with citrus Huanglongbing in Brazil: 'Candidatus Liberibacter asiaticus' is heat tolerant, 'Ca. L. americanus' is heat sensitive. *Plant Dis.* **2009**, *93*, 257−262.

(13) Plotto, A.; Baldwin, E. A.; McCollum, T. G.; Narciso, J.; Irey, M. Effect of early detection Huanglongbing on juice flavor and chemistry. *Proc. Fla. State Hortic. Soc.* **2008**, *121*, 265−269.

(14) Baldwin, E.; Plotto, A.; Manthey, J.; McCollum, G.; Bai, J.; Irey, M.; Cameron, R.; Luzio, G. Effect of Liberibacter infection (Huanglongbing disease) of citrus on orange fruit physiology and fruit/fruit juice quality: Chemical and physical analyses. *J. Agric. Food Chem.* **2010**, *58*, 1247−1262.

(15) Quarantined Areas: Citrus Greening and Asian Citrus Psyllid. *Code of Federal Regulations*, Part 301, Title 76-3, 2014.

(16) Stokstad, E. Dread citrus disease turns up in California, Texas. *Science* **2012**, *336*, 283−284.

(17) Schilmiller, A. L.; Howe, G. A. Systemic signaling in the wound response. *Curr. Opin. Plant Biol.* **2005**, *8*, 369−377.

(18) Durrant, W.; Dong, X. Systemic acquired resistance. *Annu. Rev. Phytopathol.* **2004**, *42*, 185−209.
(19) Ryals, J. A.; Neuenschwander, U. H.; Willits, M. G.; Molina, A.; Steiner, H.-Y.; Hunt, M. D. Systemic acquired resistance. *Plant Cell* **1996**, *8*, 1809.
(20) Kim, J.-S.; Sagaram, U. S.; Burns, J. K.; Li, J.-L.; Wang, N. Response of sweet orange (Citrus sinensis) to 'Candidatus Liberibacter asiaticus' infection: microscopy and microarray analyses. *Phytopathology* **2009**, *99*, 50−57.
(21) Slisz, A. M.; Breksa, A. P., III; Mishchuk, D. O.; McCollum, G.; Slupsky, C. M. Metabolomic analysis of citrus infection by 'Candidatus Liberibacter' reveals insight into pathogenicity. *J. Proteome Res.* **2012**, *11*, 4223−4230.
(22) Dixon, R. A.; Paiva, N. L. Stress-induced phenylpropanoid metabolism. *Plant Cell* **1995**, *7*, 1085.
(23) Lee, H.-I.; León, J.; Raskin, I. Biosynthesis and metabolism of salicylic acid. *Proc. Natl. Acad. Sci. U.S.A.* **1995**, *92*, 4076−4079.
(24) Dagulo, L.; Danyluk, M. D.; Spann, T. M.; Valim, M. F.; Goodrich-Schneider, R.; Sims, C.; Rouseff, R. Chemical characterization of orange juice from trees infected with citrus greening (Huanglongbing). *J. Food Sci.* **2010**, *75*, C199−207.
(25) USDA. NASS Florida Citrus Statistics 2011−2012. http://www.nass.usda.gov/Statistics_by_State/Florida/Publications/Citrus/fcs/2011-12/fcs1112.pdf (accessed January 11, 2014).
(26) Zhang, X.; Breksa, A. P., III; Mishchuk, D. O.; Slupsky, C. M. Elevation, rootstock, and soil depth affect the nutritional quality of mandarin oranges. *J. Agric. Food Chem.* **2011**, *59*, 2672−2679.
(27) Li, W.; Hartung, J. S.; Levy, L. Quantitative real-time PCR for detection and identification of *Candidatus Liberibacter* species associated with citrus huanglongbing. *J. Microbiol. Methods* **2006**, *66*, 104−115.
(28) Weljie, A. M.; Newton, J.; Mercier, P.; Carlson, E.; Slupsky, C. M. Targeted profiling: Quantitative analysis of ^{1}H NMR metabolomics data. *Anal. Chem.* **2006**, *78*, 4430−4442.
(29) Eriksson, L.; Johansson, E.; Kettaneh-Wold, N.; Trygg, J.; Wikström, C.; Wold, S. *Multi- and Megavariate Data Analysis: Part II: Advanced Applications and Method Extensions*, 2nd ed.; Umetrics AB: Umea, Sweden, 2006; pp 63−102.
(30) Cevallos-Cevallos, J. M.; Rouseff, R.; Reyes-De-Corcuera, J. I. Untargeted metabolite analysis of healthy and Huanglongbing-infected orange leaves by CE-DAD. *Electrophoresis* **2009**, *30*, 1240−1247.
(31) Tatineni, S.; Sagaram, U. S.; Gowda, S.; Robertson, C. J.; Dawson, W. O.; Iwanami, T.; Wang, N. In planta distribution of 'Candidatus Liberibacter asiaticus' as revealed by polymerase chain reaction (PCR) and real-time PCR. *Phytopathology* **2008**, *98*, 592−599.
(32) Gopal, K.; Pradeepthi, E.; Gopi, V.; Khayum Ahammed, S.; Sreenivasulu, Y.; Reddy, M.; Baranwal, V.; Purushotham, K. Occurrence, molecular diagnosis and suitable time of detection of citrus greening disease in sweet orange. *Acta Phytopathol. Entomol. Hung.* **2007**, *42*, 49−58.
(33) Fan, J.; Chen, C.; Brlansky, R.; Gmitter, F., Jr.; Li, Z. G. Changes in carbohydrate metabolism in Citrus sinensis infected with 'Candidatus Liberibacter asiaticus'. *Plant Pathol.* **2010**, *59*, 1037−1043.
(34) Etxeberria, E.; Gonzalez, P.; Achor, D.; Albrigo, G. Anatomical distribution of abnormally high levels of starch in HLB-affected Valencia orange trees. *Physiol. Mol. Plant Pathol.* **2009**, *74*, 76−83.
(35) Atkinson, N. J.; Dew, T. P.; Orfila, C.; Urwin, P. E. Influence of combined biotic and abiotic stress on nutritional quality parameters in tomato (Solanum lycopersicum). *J. Agric. Food Chem.* **2011**, *59*, 9673−9682.
(36) Mikulic-Petkovsek, M.; Schmitzer, V.; Slatnar, A.; Weber, N.; Veberic, R.; Stampar, F.; Munda, A.; Koron, D. Alteration of the content of primary and secondary metabolites in strawberry fruit by *Colletotrichum nymphaeae* infection. *J. Agric. Food Chem.* **2013**, *61*, 5987−5995.
(37) Bolton, M. D. Primary metabolism and plant defense-fuel for the fire. *Mol. Plant-Microbe Interact.* **2009**, *22*, 487−497.

chemiluminescence,[28,29] and electrochemical methods.[30,31] However, most of them have some limitations such as poor selectivity, insufficient sensitivity, and time-consuming procedure, which limit their applications to real sample analysis. Especially, although fluorescence analysis can provide high sensitivity and good selectivity, those developed fluorescent measurements based on oxidation-enhanced fluorescence,[23,24] lanthanide-sensitized fluorescence,[25,26] and quantum dots,[27] remained poorly sensitive for FA. Consequently, further research is needed to develop a highly sensitive fluorescence sensor for folic acid.

Metal nanoclusters, especially Au and Ag nanoclusters, have received much attention during the past decades due to their ultrasmall size, nontoxicity, biocompatibility, and high fluorescence properties, and various fluorescence sensors using metal nanoclusters have been developed.[32−45] However, until now, fluorescence sensors for detecting FA on the basis of metal nanoclusters have not been reported. Herein, polyethylenimine-capped silver nanoclusters (PEI-AgNCs) were introduced as a new fluorescent platform for sensing FA. The interactions between PEI and FA bring FA and AgNCs into close proximity, and a two-step electron transfer from FA to AgNCs through PEI results in the decrease in fluorescence (Scheme 1). A two-step electron-transfer quenching mechanism was proposed and discussed. As expected, this sensing system has been applied successfully to the detection of FA in real samples. Those substances coexisting with FA could not lead to any significant fluorescence decrease of AgNCs. Consequently, our research would be a promising candidate for practical application.

MATERIALS AND METHODS

Chemicals. Silver nitrate ($AgNO_3$), hyperbranched polyethylenimine (PEI, Mw = 10000, 99%), formaldehyde (35 wt %), 4-(2-hydroxyethyl)-1-piperazineethanesulfonic acid (HEPES), and folic acid as well as all amino acids were purchased from Aladdin Reagent Co., Ltd., Shanghai, China. Saccharides, vitamins, creatine, creatinine, uric acid, and urea were obtained from Shanghai Sangon Biotechnology Co., Ltd., Shanghai, China. Other reagents were of analytical reagent grade, and all chemicals were used as received without further purification. The PEI-AgNCs stock solution was synthesized according to the previous paper from our group.[42] This stock solution was diluted 10-fold with ultrapure water (18.2 MΩ cm), and the diluted AgNCs was used as the probe to measure the concentration of FA in this assay. The FA stock solution was prepared daily by adding 0.10 M NaOH solution to an opaque system containing FA and ultrapure water until clear. Then, the clear FA solution was serially diluted to required concentrations with ultrapure water. The stock Britton−Robinson (BR) buffer solutions were prepared with 0.20 M NaOH solution and the mixed acid solution containing 0.04 M phosphate solution, 0.04 M boric acid solution, and 0.04 M acetate solution. All solutions were freshly prepared before use, and ultrapure water was used throughout the experiments.

Detection of Folic Acid. In the quenching studies, 900 μL of ultrapure water, 50 μL of BR buffer solution (pH 11.0), 10 μL of diluted AgNCs, and 40 μL of FA solution at different concentrations were vortex mixed for 1 min. After 20 min of incubation at room temperature, the fluorescence emission spectra of PEI-AgNCs were recorded on a Hitachi F-4500 fluorescence spectrophotometer (Tokyo, Japan) at an excitation wavelength of 375 nm, and the fluorescence intensity at an emission wavelength of 452 nm was monitored. Three trials for each sample were performed, and the results represent the average of measurements. In addition, 10 μL of diluted AgNCs and 6 μM FA were used in the optimization of the sensing system.

Sample Preparation. One tablet of folic acid was fully dissolved in 5 mL of 0.10 M NaOH solution,[46] and the resulting mixture was centrifuged for 10 min at 12000 rpm. The supernatant was used as sample solution.

Wheat flour was obtained from a local market. The sample preparation was done as described by Xiao,[47] with a slight modification. First, wheat flour (0.5 g) or wet fermented dough (1.0 g) was dispersed in 5.0 mL of 0.1 M NaOH solution. Then, 10 min of centrifugation was performed at 12000 rpm. Finally, the supernatant was filtered using a 0.22 μm micropore filter membrane, and the filtrate was collected and used as the sample solution.

A urine sample was stored in a refrigerator immediately after collection.[48] After 10 min of centrifugation at 12000 rpm at 10 °C, an appropriate volume of 0.1 M $AgNO_3$ solution was added to the supernatant and the mixture was shaken well. Another centrifugation later, the pH value of the supernatant was adjusted to 12 with NaOH solution. The pH-adjusted system was further centrifuged, and the supernatant was filtered using a 0.22 μm micropore filter membrane.

Liquid milk and milk powder were first deproteinized according to the literature.[49] Milk powder (0.5 g) or liquid milk (1.0 g) was uniformly dispersed in 0.05 M HAc solution, and the mixture was centrifuged for 20 min at 12000 rpm at 10 °C. The supernatant was collected, in which appropriate amounts of 0.1 M $BaCl_2$ and $AgNO_3$ solutions were added in turn. After thorough shaking, the following treatments, including centrifuging, pH-adjusting, centrifuging, and filtering, were the same as those for the urine sample.

RESULTS AND DISCUSSION

Establishment of the Fluorescence Sensing System for Folic Acid. The fact that the fluorescence of PEI-AgNCs is quenched by FA was observed in an exploratory experiment. To achieve the best sensing performance, several conditions such as pH, buffer system, concentration of buffer solution, and reaction time were optimized, respectively. The effect of the pH value on the sensing system was investigated first because the fluorescence quenching efficiency ($1 - F/F_0$) of PEI-AgNCs is pH-dependent (Supporting Information Figure S1). F_0 and F denote the fluorescence intensity of PEI-AgNCs in the absence and presence of FA, respectively. To cover a wide pH range, BR buffer solutions were used as the medium for optimizing the pH value. Figure S1 in the Supporting Information shows that, in the presence of FA, high-efficiency fluorescence quenching was observed at pH >7.0, and the highest quenching efficiency was obtained at pH 11.0. Therefore, a basic medium at pH 11.0 would ensure the sensitive detection of FA.

The influence of different buffer systems on FA analysis was studied as the result of the influence of the ionic species on the stability of PEI-AgNCs.[42] Apart from BR buffer solution (50 μL mL^{-1}: 1 mL of solution contains 50 μL of stock BR buffer solution), another four buffer solutions, including $Na_2B_4O_7$−NaOH (10 mM), $Na_2B_4O_7$−Na_2CO_3 (10 mM), Na_2HPO_4−NaOH (10 mM), and NH_2CH_2COOH−NaOH (20 mM), were employed to test the quenching of the PEI-AgNCs fluorescence by FA. In consideration of the better stability of the diluted PEI-AgNCs and almost zero ionic strength of ultrapure water as well as the low ionic strength of sodium hydroxide solution at pH 11.0, ultrapure water and sodium hydroxide solution at pH 11.0 were also used as the medium for investigating the changes in fluorescence intensity of PEI-AgNCs (Supporting Information Figure S2). The quenching efficiencies of PEI-AgNCs are higher, and only a little difference was observed for ultrapure water, sodium hydroxide solution, and BR buffer. Therefore, the other four buffers were excluded at first. Meanwhile, the BR buffer can give a greater ability to resist interference than ultrapure water and the pure acid or

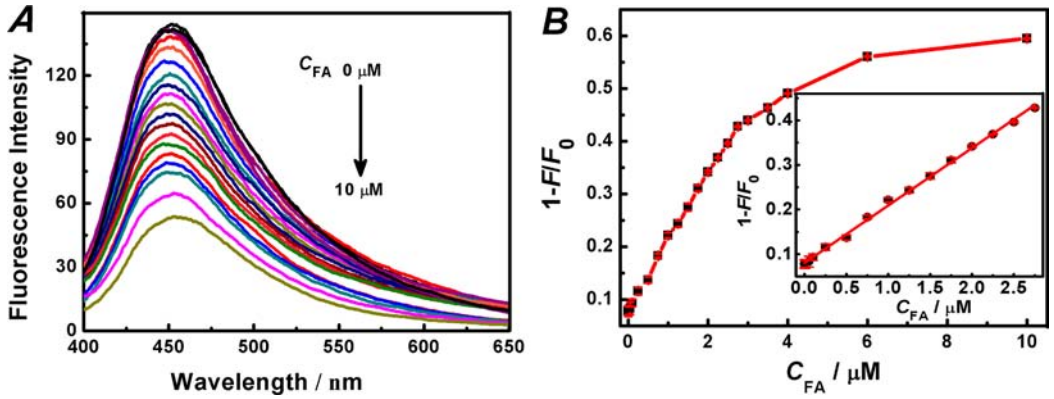

Figure 1. Fluorescence emission spectra (A) and fluorescence quenching efficiencies (B) of PEI-AgNCs upon addition of different concentrations of FA: 0, 0.1, 1.0, 10 nM; 0.1, 0.25, 0.5, 0.75, 1.0, 1.25, 1.5, 1.75, 2.0, 2.25, 2.5, 2.75, 3.0, 3.5, 4.0, 6.0, 10.0 μM. The inset in panel B displays the linear relationship between the fluorescence quenching efficiency $(1 - F/F_0)$ and the concentration of FA from 0.1 nM to 2.75 μM. F_0 and F denote the fluorescence intensity of PEI-AgNCs in the absence and presence of FA, respectively.

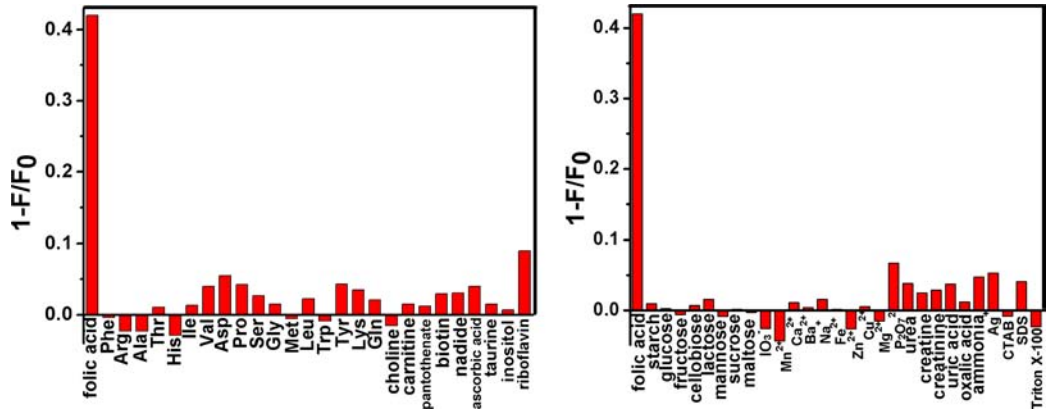

Figure 2. Selectivity of PEI-AgNCs for the detection of FA over other potential coexisting constituents. The concentration of FA is 2.75 μM; the concentration of saccharides is 5 mM; the concentrations of amino acids, carnitine, pantothenate, biotin, taurine, inositol, urea, creatine, creatinine, uric acid, oxalic acid, Ba^{2+}, Ca^{2+}, Na^+, NO_3^-, CH_3COO^-, $P_2O_7^{2-}$, IO_3^-, and $NH_3{\cdot}H_2O$ are 1 mM; the concentrations of choline, nadide, and ascorbic acid are 100 μM; the concentrations of riboflavin, Cu^{2+}, Mg^{2+}, Zn^{2+}, Ag^+, and Fe^{2+} are 1 μM, respectively; the concentrations of CTAB, SDS, and Triton X-100 are 0.2, 0.2, and 1 mM, respectively. F_0 and F represent the fluorescence intensity of PEI-AgNCs in the absence and presence of FA (or other species), respectively; $(1 - F/F_0)$ is the fluorescence quenching efficiency of PEI-AgNCs by FA or other species.

basic solution. Therefore, to gain more outstanding sensing performance, BR buffer is the only medium that can be adopted in this work.

According to the literature,[42] not only do the ionic species have different influences on the stability of PEI-AgNCs, but also the ionic strength has a nonnegligible effect. The ionic strength is tied to the concentration of ions, so the effect of the concentration of BR buffer on sensing performance was also investigated. Figure S3 in the Supporting Information indicates that the fluorescence quenching efficiencies of PEI-AgNCs in the presence of FA were decreased by increasing the concentration of BR buffer solution (pH 11.0). To gain the most satisfactory results, 50 μL mL^{-1} BR buffer solution was used for sensing FA.

Finally, under the optimum conditions mentioned above, the effect of reaction time on the fluorescence intensity of the system was investigated. The fluorescence intensity of PEI-AgNCs in the presence of FA was monitored for 60 min. The maximum quenching and stable fluorescence intensity was observed after 20 min of interaction (Supporting Information Figure S4), indicating that the interaction between FA and PEI-AgNCs was complete within 20 min and the fluorescence of PEI-AgNCs/FA was stable for at least 40 min. Consequently, all measurements were carried out after the FA solution or real sample solution was incubated with PEI-AgNCs in the BR buffer (pH 11.0) for 20 min.

Sensitivity of the Sensing System. The linearity and detection limit of this measurement were evaluated by varying the concentration of FA under optimum conditions discussed above. The fluorescence of PEI-AgNCs was quenched proportionately over the FA concentration range of 0.1 nM–2.75 μM (Figure 1). A good linear correlation (R^2 = 0.9981) was found, and a detection limit of 0.032 nM (3σ/slope) was obtained. Compared to other FA sensors reported in recent years (Supporting Information Table S1), our method provides a better linear range and a lower detection limit.

Selectivity of the Sensing System. To investigate whether this sensing system is specific for FA, the fluorescence response of PEI-AgNCs to other potential coexistent substances was studied under optimum conditions. Figure 2 shows that 5 mM saccharides, 1 mM amino acids, carnitine, pantothenate, biotin, taurine, inositol, urea, creatine, creatinine, uric acid, oxalic acid, Ba^{2+}, Ca^{2+}, Na^+, NO_3^-, CH_3COO^-, $P_2O_7^{2-}$, IO_3^-, and $NH_3{\cdot}H_2O$, 100 μM choline, nadide, and ascorbic acid, 1 μM riboflavin, and 1 μM Cu^{2+}, Mg^{2+}, Zn^{2+}, and Fe^{2+} (according to the solubility product constants (K_{sp}^{θ}) of the

dx.doi.org/10.1021/jf4054534 | J. Agric. Food Chem. 2014, 62, 6592–6599

Table 1. Detection of FA in Real Samples (n = 3)

sample	specified	measured	original (μM)	spiked (μM)	found (μM)	recovery (%)	RSD %
tablet	0.400 mg tablet^{-1}	0.401 mg tablet^{-1}					1.8
			0.50	0.50	1.00	100.0	0.4
			0.50	1.00	1.51	100.1	1.9
			0.50	1.50	2.02	101.3	0.3
wheat flour		74.8 mg 100 g^{-1}					2.6
			1.26	0.50	1.74	96.0	1.3
			1.26	1.00	2.23	97.0	3.1
			0.36	1.00	1.41	105.0	2.0
wet fermented dough		53.2 mg 100 g^{-1}					1.4
			0.24	1.50	1.70	97.33	3.4
			0.62	0.50	1.10	96.0	3.5
			1.05	1.00	2.10	105.0	1.3
human urine		1.86 μg mL^{-1}					2.0
			1.68	1.0	2.65	97.0	2.5
			1.68	0.5	2.20	104.0	0.7
			0.81	1.0	1.79	98.00	2.6
liquid milk		2.18 μg mL^{-1}					2.3
			0.89	0.5	1.40	102.0	0.5
			0.89	1.0	1.93	104.0	1.1
			0.89	1.5	2.41	101.3	2.2
milk powder 1		545 μg 100 g^{-1}					1.8
			0.31	0.5	0.83	104.0	1.5
			0.31	1.0	1.34	103.0	2.1
			0.31	1.5	1.78	98.0	1.7
milk powder 2		68.8 μg 100 g^{-1}					2.0
			0.03	0.5	0.55	104.0	2.4
			0.03	1.0	1.05	102.0	1.1
			0.03	1.5	1.51	98.67	2.0

corresponding hydroxides, the concentrations of these metal ions are not higher than 1 μM in this testing system) could not lead to any significant fluorescence decrease of PEI-AgNCs. The surfactants, including 0.2 mM hexadecyltrimethylammonium bromide (CTAB, cationic), 0.2 mM sodium dodecyl sulfonate (SDS, anionic), and 1 mM Triton X-100 (nonionic), also show only little effect on the determination of FA. These results indicate that the proposed assay has a good selectivity for FA.

Analytical Applications in Real Sample. To assess the applicability of the sensing system, the proposed method was used for the analysis of FA in tablet, human urine, wheat flour, wet fermented dough, liquid milk, and milk powder samples. The results are listed in Table 1. The recovery from 96.0 to 105.0% and the relative standard deviation (RSD) smaller than 5% were satisfactory. Furthermore, the measured result of 205 μg FA 100 g^{-1} milk powder is in good agreement with the testing value of 183 μg 100 g^{-1} by official method[50] in the Comprehensive Test Center of China Academy of Inspection and Quarantine. The found values of 0.407 mg tablet^{-1} and 1.68 μg mL^{-1} human urine according to the ref 25 also show a good correspondence with the values found by the proposed method (0.401 mg tablet^{-1} and 1.55 μg mL^{-1} human urine, respectively). Therefore, the proposed design is feasible for FA detection in practical applications.

Mechanism for the Recognition of Folic Acid. To understand the mechanism of the fluorescence quenching of PEI-AgNCs by FA, the absorption and the fluorescence spectra of PEI-AgNCs, FA, and PEI-AgNCs/FA were studied. Figure 3A shows three similar fluorescence excitation wavelengths and three similar fluorescence emission wavelengths, suggesting that fluorescence resonance energy transfer as a possible mechanism for AgNCs fluorescence quenching is ruled out. Moreover, the absorption spectrum of PEI-AgNCs/FA exhibits no new peak (Figure 3B) compared to those of both AgNCs and FA, which implies that the decrease in fluorescence intensity was not induced by the change in the excitation wavelength or the aggregation of AgNCs, thereby excluding possible mechanisms including static quenching upon formation of the ground-state complex and AgNCs aggregation-induced self-quenching.[44,52] In addition, evidence from the IR spectral data and the high-resolution transmission electron microscopy (HRTEM) image also support the above inference, because IR spectra of PEI-AgNCs/FA were almost a simple superposition of those of both PEI-AgNCs and FA (Figure 3C) and AgNCs remained dispersed upon addition of FA, which were similar to the original PEI-AgNCs (Figure 3D).

As for the quenching mechanism, theoretically, fluorescence quenching in this system could occur by the nonfluorescent ground-state complex, aggregation of AgNCs, energy transfer,

dx.doi.org/10.1021/jf4054534 | J. Agric. Food Chem. 2014, 62, 6592−6599

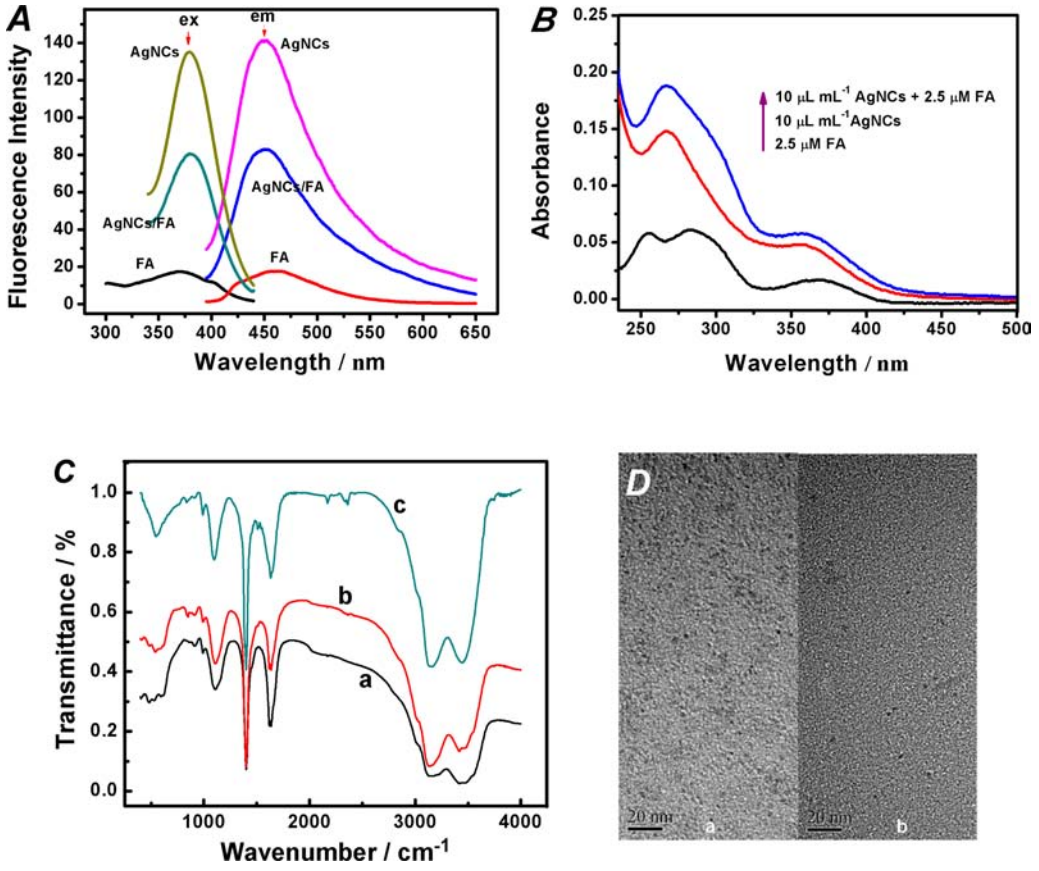

Figure 3. (A) Fluorescence emission and excitation spectra of PEI-AgNCs, FA, and PEI-AgNCs/FA. Concentration: 10 μL mL^{-1} diluted PEI-AgNCs; 2.5 μM FA. (B) Absorption spectra of PEI-AgNCs, FA, and PEI-AgNCs/FA. (C) IR spectra of (a) PEI-AgNCs, (b) FA, and (c) PEI-AgNCs/FA. (D) HRTEM image of (a) PEI-AgNCs and (b) PEI-AgNCs/FA.

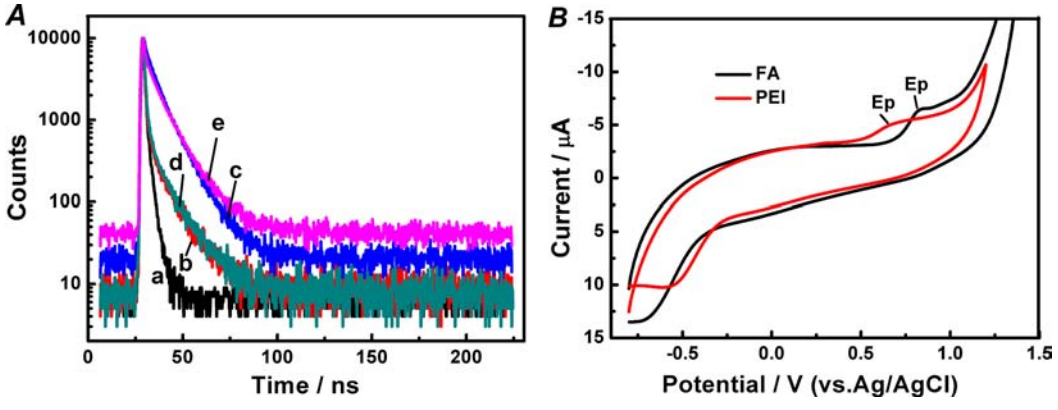

Figure 4. (A) Decay time profiles of (a) PEI-AgNCs, (b) PEI-AgNCs/FA, (c) FA, (d) FA/PEI-AgNCs, and (e) FA/PEI. Concentration: 10 μL mL^{-1} diluted PEI-AgNCs; 10 μM FA. The concentration of PEI was the same as that of PEI in 10 μL mL^{-1} diluted PEI-AgNCs. λ_{ex} = 375 nm and λ_{em} = 452 nm for (a) and (b); λ_{ex} = 367 nm and λ_{em} = 462 nm for (c), (d), and (e). (B) Cyclic voltammogram of FA and PEI in BR buffer solution (pH 11.0) on the glassy carbon electrode.

Table 2. Fitting Results Using Global Analysis for the Data of Figure 4[a]

sample	a_1	τ_1 (ns)	a_2	τ_2 (ns)	a_3	τ_3 (ns)	$\bar{\tau}$ (ns)
PEI-AgNCs	0.755	0.294	0.133	1.108	7.72×10^{-3}	3.34	0.798
PEI-AgNCs/FA	6.17×10^{-2}	1.543	0.753	0.35	7.19×10^{-3}	10.38	2.45
FA	7.82×10^{-2}	4.59	6.24×10^{-2}	9.719	0.132	0.6589	7.22
FA/PEI-AgNCs	3.95×10^{-2}	1.924	0.495	0.554	7.79×10^{-3}	10.806	2.78
FA/PEI	5.42×10^{-2}	4.485	5.43×10^{-3}	10.607	0.285	0.529	3.94

[a] a_i represents the amplitudes of components i at t = 0; τ_i is the decay time of component i; $\bar{\tau}$ is the average fluorescence lifetime.

dx.doi.org/10.1021/jf4054534 | J. Agric. Food Chem. 2014, 62, 6592−6599

or electron transfer. As discussed above, only the electron transfer is expected in the quenching process. The proposed electron-transfer quenching mechanism was further examined using fluorescence decay kinetics. The fluorescence decay profiles of PEI-AgNCs in the absence and presence of FA together with FA in the absence and presence of PEI-AgNCs are shown in Figure 4A, respectively. The fluorescence decay of all samples could be fitted using a three-exponential function, and the fitted results are given in Table 2. The average fluorescence lifetime ($\bar{\tau}$) was estimated using the equation[51]

$$\bar{\tau} = \frac{\sum a_i \tau_i^2}{\sum a_i \tau_i} \quad (1)$$

where a_i represents the amplitude of the component i at $t = 0$ and τ_i is the decay time of the component i. As shown in Table 2, the average fluorescence lifetime estimated for FA was approximately 7.22 ns. In the presence of PEI-AgNCs, the average lifetime for FA decreased to 2.78 ns. On the basis of the literature,[52] we can deduce that the decrease in lifetime is due to the efficient electron transfer from FA to PEI-AgNCs, wherein FA acts as an electron donor. In addition, before and after the addition of FA, the lifetime of PEI-AgNCs increased from 798 ps to 2.54 ns. This opposite change provided evidence for electron-transfer sequence from FA to PEI-AgNCs.

Interestingly, the fluorescence of FA could also be quenched by PEI. The fluorescence quenching mechanism based on electron transfer is speculated because we did not observe any absorption band in the absorption spectrum of PEI, and the absorption spectrum of FA did not vary after PEI was added (Supporting Information Figure S5). The feasibility of the electron-transfer quenching was examined by further measuring the fluorescence decay dynamics of FA solution in the presence of PEI (plot e in Figure 4A). An average lifetime of 3.94 ns was obtained, and considering the average lifetime of 7.22 ns for FA, we conclude that the excited electrons of FA can be transferred to PEI. Meanwhile, the oxidation potential of both PEI and FA was further adopted to confirm the direction of electron transfer. The oxidation potential of PEI was measured to be +0.68 V versus Ag/AgCl (saturated KCl) [0.90 V vs normal hydrogen electrode (NHE)], and FA exhibited a more positive oxidation potential of +0.83 V versus Ag/AgCl (1.05 V vs NHE), as shown in Figure 4B. According to the test results, the electron transfer from FA to PEI can also be concluded.

On the basis of the conclusions of the foregoing discussion and the sequence of 7.22 ns (the average lifetime of FA) > 3.94 ns (the average lifetime of FA with addition of PEI) > 2.54 ns (the average lifetime of FA in the presence of PEI-AgNCs), we put forward a two-step electron-transfer process in the system comprising FA and PEI-AgNCs, in which an electron is transferred from FA to AgNCs through the PEI molecule. Moreover, we note that a similar energy transfer mechanism has been proposed for ethidium bromide in the complex comprising a cationic conjugated polymer, a fluorescein molecule linked to one terminus of the DNA, and ethidium bromide.[53] FA is brought into close proximity to the template molecule PEI for AgNCs through the electrostatic interactions between FA and PEI, and electron transfer from FA to PEI changes the electronic properties of PEI. As metal nanoclusters are both excellent electron donors and acceptors, the fluorescence of the nanoclusters can be quenched by electron acceptors or donors.[54] Therefore, electron transfer from PEI to AgNCs quenched the fluorescence of AgNCs. Although interactions between FA and PEI shortened the distance between FA and AgNCs, the distance was still longer than that between PEI and AgNCs. To our knowledge, electron transfer is distance-dependent,[55] so electrons are more easily transferred from PEI to AgNCs. Consequently, the two-step electron-transfer process was reasonably proposed, in which FA served as an electron donor, AgNCs as an electron acceptor, and PEI as an electron-transfer bridge.

In conclusion, a highly sensitive method for the detection of FA based on the fluorescence quenching of PEI-AgNCs was developed in this study, and the mechanism of fluorescence quenching through a two-step electron-transfer process was proposed. We believe that the research is of importance in the development of metal nanoclusters and FA detection in real samples.

■ ASSOCIATED CONTENT

Supporting Information

Figures S1−S5 and Table S1. This material is available free of charge via the Internet at http://pubs.acs.org.

■ AUTHOR INFORMATION

Corresponding Authors

*(H.Q.L.) Phone: +86 23 68253237. Fax: +86 23 68253237. E-mail: luohq@swu.edu.cn.

*(N.B.L.) Phone: +86 23 68253237. Fax: +86 23 68253237. E-mail: linb@swu.edu.cn.

Funding

This work was supported by the National Natural Science Foundation of China (No. 21273174, 20975083), the Municipal Science Foundation of Chongqing City (No. CSTC-2013jjB00002), and the Fundamental Research Funds for the Central Universities of China (No. XDJK2013C064).

Notes

The authors declare no competing financial interest.

■ ABBREVIATIONS USED

FA, folic acid; PEI-AgNCs, polyethylenimine-capped silver nanoclusters; AgNCs, silver nanoclusters

■ REFERENCES

(1) Mi, Y.; Liu, Y.; Feng, S. S. Formulation of docetaxel by folic acid-conjugated D-α-tocopheryl polyethylene glycol succinate 2000 (vitamin E $TPGS_{2k}$) micelles for targeted and synergistic chemotherapy. *Biomaterials* **2011**, *32*, 4058−4066.

(2) Hoegger, D.; Morier, P.; Vollet, C.; Heini, D.; Reymond, F.; Rossier, J. S. Disposable microfluidic ELISA for the rapid determination of folic acid content in food products. *Anal. Bioanal. Chem.* **2007**, *387*, 267−275.

(3) Guo, H. X.; Li, Y. Q.; Fan, L. F.; Wu, X. Q.; Guo, M. D. Voltammetric behavior study of folic acid at phosphomolybdic-polypyrrole film modified electrode. *Electrochim. Acta* **2006**, *51*, 6230−6237.

(4) Mulinare, J.; Cordero, J. F.; Erickson, J. D.; Berry, R. J. Periconceptional use of multivitamins and the occurrence of neural tube defects. *JAMA, J. Am. Med. Assoc.* **1988**, *260*, 3141−3145.

(5) Milunsky, A.; Jick, H.; Jick, S. S.; Bruell, C. L.; MacLaughlin, D. S.; Rothman, K. J. Multivitamin/folic acid supplementation in early pregnancy reduces the prevalence of neural tube defects. *JAMA, J. Am. Med. Assoc.* **1989**, *262*, 2847−2852.

(6) Gujska, E.; Kuncewicz, A. Determination of folate in some cereals and commercial cereal-grain products consumed in poland using

trienzyme extraction and high-performance liquid chromatography methods. *Eur. Food Res. Technol.* **2005**, *221*, 208−213.
(7) Xiao, F.; Ruan, C.; Liu, L.; Yan, R.; Zhao, F.; Zeng, B. Single-walled carbon nanotube-ionic liquid paste electrode for the sensitive voltammetric determination of folic acid. *Sens. Actuators B* **2008**, *134*, 895−901.
(8) Lucock, M. Folic acid: nutritional biochemistry, molecular biology, and role in disease processes. *Mol. Genet. Metab.* **2000**, *71*, 121−138.
(9) Duthie, S. J. Folic acid deficiency and cancer: mechanisms of DNA instability. *Br. Med. Bull.* **1999**, *55*, 578−592.
(10) Jennings, E. Folic acid as a cancer-preventing agent. *Med. Hypotheses* **1995**, *45*, 297−303.
(11) Food and Drug Administration, Food standards: amendment of standards of identity for enriched grain products to require addition of folic acid. *Food and Drug Administration, Rockville, MD, USA*, 1996.
(12) Wright, A. J. A.; Finglas, P. M.; Southon, S. Proposed mandatory fortification of the UK diet with folic acid: have potential risks been underestimated. *Trends Food Sci. Technol.* **2001**, *12*, 313−321.
(13) Zhang, T. C.; Xue, H. Y.; Zhang, B.; Zhang, Y.; Song, P.; Tian, X.; Xing, Y.; Wang, P.; Meng, M.; Xi, R. M. Determination of folic acid in milk, milk powder and energy drink by an indirect immunoassay. *J. Sci. Food Agric.* **2012**, *92*, 2297−2304.
(14) Hoegger, D.; Morier, P.; Vollet, C.; Heini, D.; Reymond, F.; Rossier, J. S. Disposable microfluidic ELISA for the rapid determination of folic acid content in food products. *Anal. Bioanal. Chem.* **2007**, *387*, 267−275.
(15) Nelson, B. C.; Sharpless, K. E.; Sander, L. C. Quantitative determination of folic acid in multivitamin/multielement tablets using liquid chromatography/tandem mass spectrometry. *J. Chromatogr., A* **2006**, *1135*, 203−211.
(16) Pawlosky, R. J.; Flanagan, V. P. A quantitative stable-isotope LC−MS method for the determination of folic acid in fortified foods. *J. Agric. Food Chem.* **2001**, *49*, 1282−1286.
(17) Zhao, S. L.; Yuan, H. Y.; Xie, C.; Xiao, D. Determination of folic acid by capillary electrophoresis with chemiluminescence detection. *J. Chromatogr., A* **2006**, *1107*, 290−293.
(18) Aurora-Prado, M. S.; Sliva, C. A.; Tavares, M. F. M.; Altria, K. D. Determination of folic acid in tablets by microemulsion electrokinetic chromatography. *J. Chromatogr., A* **2004**, *1051*, 291−296.
(19) Rodriguez Bernaldo de Quiros, A.; Castro de Ron, C.; Lopez Hernandez, J.; Lage Yusty, M. A. Determination of folates in seaweeds by high-performance liquid chromatography. *J. Chromatogr., A* **2004**, *1032*, 135−139.
(20) Ginting, E.; Arcot, J. High-performance liquid chromatographic determination of naturally occurring folates during tempe preparation. *J. Agric. Food Chem.* **2004**, *52*, 7752−7758.
(21) Patring, J. D. M.; Jastrebova, J. A.; Hjortmo, S. B.; Andlid, T. A.; Jägerstad, I. M. Development of a simplified method for the determination of folates in baker's yeast by HPLC with ultraviolet and fluorescence detection. *J. Agric. Food Chem.* **2005**, *53*, 2406−2411.
(22) Wang, Y.; Zhu, P. H.; Tian, T.; Tang, J.; Wang, L.; Hu, X. Y. Synchronous fluorescence as a rapid method for the simultaneous determination of folic acid and riboflavin in nutritional beverages. *J. Agric. Food Chem.* **2011**, *59*, 12629−12634.
(23) Ouyang, H. X.; Wang, L. S.; Tian, J. N.; Liang, A. H.; Jiang, Z. L. A simple and sensitive nanocatalytic fluorescence method for the determination of folic acid in foods using Fe_3O_4 nanoparticle-$K_2S_2O_8$ system. *Food Anal. Methods* **2013**, *6*, 76−81.
(24) Huang, Z. B.; Chen, H. W.; He, Q. H. Flow injection on-line photochemically spectrofluorimetric determination of folic acid in pharmaceutical preparations. *Chin. J. Anal. Chem.* **2003**, *31*, 229−231.
(25) Manzoori, J. L.; Jouyban, A.; Amjadi, M.; Soleymani, J. Spectrofluorimetric determination of folic acid in tablets and urine samples using 1,10-phenanthroline-terbium probe. *Luminescence* **2011**, *26*, 106−111.
(26) Alam, A. M.; Kamruzzaman, M.; Lee, S. H.; Kim, Y. H.; Min, K. Europium-enoxacin complexas fluorescence probe for the determination of folic acid in pharmaceutical and biological samples. *Bull. Korean Chem. Soc.* **2012**, *33*, 3055−3060.
(27) Zhan, X. S.; Shang, Y.; Wu, F. Y. Determination of folic acid using Mn^{2+} doped ZnS quantum dots capped with L-cysteine. *J. Instrum. Anal.* **2012**, *31*, 564−569.
(28) Zhang, B. T.; Zhao, L. X.; Lin, J. M. Determination of folic acid by chemiluminescence based on peroxomonosulfate-cobalt(II) system. *Talanta* **2008**, *74*, 1154−1159.
(29) Zhao, S. H.; Zhang, P. P.; Liang, X. H.; Hua, D. L.; Ma, T. S.; Pei, G. L. A new potassium tetrabromoaurate(III)−luminol chemiluminescence system for the determination of folic acid in milk powder. *J. Food Sci.* **2012**, *71*, 102−106.
(30) Beitollahi, H.; Sheikhshoaie, I. Electrocatalytic and simultaneous determination of isoproterenol, uric acid and folic acid at molybdenum(VI) complex-carbon nanotube paste electrode. *Electrochim. Acta* **2011**, *56*, 10259−10263.
(31) Zarea, H. R.; Shishehboreb, M. R.; Nematollahi, D. A highly sensitive and selective sensor on the basis of 4-hydroxy-2-(triphenylphosphonio)phenolate and multi-wall carbon nanotubes for electrocatalytic determination of folic acid in presence of ascorbic acid and uric acid. *Electrochim. Acta* **2011**, *58*, 654−661.
(32) Peyser, L. A.; Vinson, A. E.; Bartko, A. P.; Dickson, R. M. Photoactivated fluorescence from individual silver nanoclusters. *Science* **2001**, *291*, 103−106.
(33) Lin, C. A. J.; Yang, T. Y.; Lee, C. H.; Huang, S. H.; Sperling, R. A.; Zanella, M.; Li, J. K.; Shen, J. L.; Wang, H. H.; Yeh, H. I.; Parak, W. J.; Chang, W. H. Synthesis, characterization, and bioconjugation of fluorescent gold nanoclusters toward biological labeling applications. *ACS Nano* **2009**, *3*, 395−401.
(34) Shang, L.; Dong, S. J.; Nienhaus, G. U. Ultra-small fluorescent metal nanoclusters: synthesis and biological applications. *Nano Today* **2011**, *6*, 401−418.
(35) Patel, S. A.; Richards, C. I.; Hsiang, J. C. Water-soluble Ag nanoclusters exhibit strong two-photon-induced fluorescence. *J. Am. Chem. Soc.* **2008**, *130*, 11602−11603.
(36) Xie, J. P.; Zheng, Y. G.; Ying, J. Y. Protein-directed synthesis of highly fluorescent gold nanoclusters. *J. Am. Chem. Soc.* **2009**, *131*, 888−889.
(37) Xu, H. X.; Suslick, K. S. Water-soluble fluorescent silver nanoclusters. *Adv. Mater.* **2010**, *22*, 1078−1082.
(38) Xu, H. X.; Suslick, K. S. Sonochemical synthesis of highly fluorescent Ag nanoclusters. *ACS Nano* **2010**, *4*, 3209−3214.
(39) Xie, J. P.; Zheng, Y. G.; Ying, J. Y. Highly selective and ultrasensitive detection of Hg^{2+} based on fluorescence quenching of Au nanoclusters by Hg^{2+}−Au^{+} interactions. *Chem. Commun.* **2010**, *46*, 961−963.
(40) Wen, F.; Dong, Y.; Feng, L.; Wang, S.; Zhang, S.; Zhang, X. Horseradish peroxidase functionalized fluorescent gold nanoclusters for hydrogen peroxide sensing. *Anal. Chem.* **2011**, *83*, 1193−1196.
(41) Yang, S. W.; Vosch, T. Rapid detection of microRNA by a silver nanocluster DNA probe. *Anal. Chem.* **2011**, *83*, 6935−6939.
(42) Qu, F.; Li, N. B.; Luo, H. Q. Polyethyleneimine-templated Ag nanoclusters: a new fluorescent and colorimetric platform for sensitive and selective sensing halide ions and high disturbance-tolerant recognitions of iodide and bromide in coexistence with chloride under condition of high ionic strength. *Anal. Chem.* **2012**, *84*, 10373−10379.
(43) Wen, T.; Qu, F.; Li, N. B.; Luo, H. Q. Polyethyleneimine-capped silver nanoclusters as a fluorescence probe for sensitive detection of hydrogen peroxide and glucose. *Anal. Chim. Acta* **2012**, *749*, 56−62.
(44) Zhang, N.; Qu, F.; Luo, H. Q.; Li, N. B. Sensitive and selective detection of biothiols based on target-induced agglomeration of silver nanoclusters. *Biosens. Bioelectron.* **2013**, *42*, 214−218.
(45) Qu, F.; Li, N. B.; Luo, H. Q. Highly sensitive fluorescent and colorimetric pH sensor based on polyethylenimine-capped silver nanoclusters. *Langmuir* **2013**, *29*, 1199−1205.

(46) Bandžuchová, L.; Šelešovská, R.; Navrátil, T.; Chýlková, J. Electrochemical behavior of folic acid on mercury meniscus modified silver solid amalgam electrode. *Electrochim. Acta* **2011**, *56*, 2411−2419.
(47) Xiao, F.; Ruan, C. P.; Liu, L. H.; Yan, R.; Zhao, F. Q.; Zeng, B. Z. Single-walled carbon nanotube-ionic liquid paste electrode for the sensitive voltammetric determination of folic acid. *Sens. Actuators B* **2008**, *134*, 895−901.
(48) Zhu, Z. Y.; Wu, H. W.; Wu, S. C.; Huang, Z. P.; Zhu, Y.; Xi, L. L. Determination of methotrexate and folic acid by ion chromatography with electrochemical detection on a functionalized multi-wall carbon nanotube modified electrode. *J. Chromatogr., A* **2013**, *1283*, 62−67.
(49) Ding, X. J.; Yang, Y. Y.; Li, Y.; Zhao, S.; Wang, Z. Investigation of removal of proteins in raw milk, infant formula and yogur. *Chin. J. Anal. Chem.* **2010**, *38*, 77−81.
(50) AOAC Official Method 992.05: Total folate (pteroylglutamic acid) in infant formula. *Microbiological Methods, First Action 1992, Final Action 1995*; AOAC International: Arlington, VA, USA, 2006.
(51) Al Attar, H. A.; Monkman, A. P. Effect of surfactant on FRET and quenching in DNA sequence detection using conjugated polymers. *Adv. Funct. Mater.* **2008**, *18*, 2498−2509.
(52) Zhang, L. B.; Zhu, J. B.; Guo, S. J.; Li, T.; Li, J.; Wang, E. K. Photoinduced electron transfer of DNA/Ag nanoclusters modulated by G-quadruplex/hemin complex for the construction of versatile biosensors. *J. Am. Chem. Soc.* **2013**, *135*, 2403−2406.
(53) Xu, Q. H.; Wang, S.; Korystov, D.; Mikhailovsky, A.; Bazan, G. C.; Moses, D.; Heeger, A. J. The fluorescence resonance energy transfer (FRET) gate: a time-resolved study. *Proc. Natl. Acad. Sci. U.S.A.* **2005**, *102*, 530−535.
(54) Su, B.; Eugster, N.; Girault, H. H. Reactivity of monolayer-protected gold nanoclusters at dye-sensitized liquid/liquid interfaces. *J. Am. Chem. Soc.* **2005**, *127*, 10760−10766.
(55) Wu, M. Y.; Mukherjee, P.; Lamont, D. N.; Waldeck, D. H. Electron transfer and fluorescence quenching of nanoparticle assemblies. *J. Phys. Chem. C* **2010**, *114*, 5751−5759.

Table 1. Information about Rice Accessions

sample ID	accession	moisture content (%)	apparent amylose (%)	comment
R01	Yunanheixiannuo	10.73 ± 0.02	0.9 ± 0.1	waxy
R02	Youzaonuo	10.82 ± 0.05	1.2 ± 0.1	waxy
R03	Zhefu 504	10.74 ± 0.08	13.1 ± 0.1	low amylose
R04	Yixiang B	10.94 ± 0.20	14.2 ± 0.1	low amylose
R05	Ce 482	11.10 ± 0.39	14.8 ± 0.6	low amylose
R06	Zheda 104	10.84 ± 0.21	17.2 ± 0.5	low amylose
R07	Xiushui 110	11.06 ± 0.31	18.0 ± 0.5	low amylose
R08	Lemont	11.07 ± 0.06	22.8 ± 0.4	intermediate
R09	II32B	11.47 ± 0.12	24.8 ± 0.4	high amylose
R10	Guangluai 4	10.86 ± 0.09	25.5 ± 0.2	high amylose
R11	Xinnong 170	10.39 ± 0.12	25.7 ± 0.1	high amylose
R12	Zhaiyeqing 8	10.99 ± 0.03	25.9 ± 0.1	high amylose
R13	Longtefu B	11.13 ± 0.15	26.4 ± 0.2	high amylose

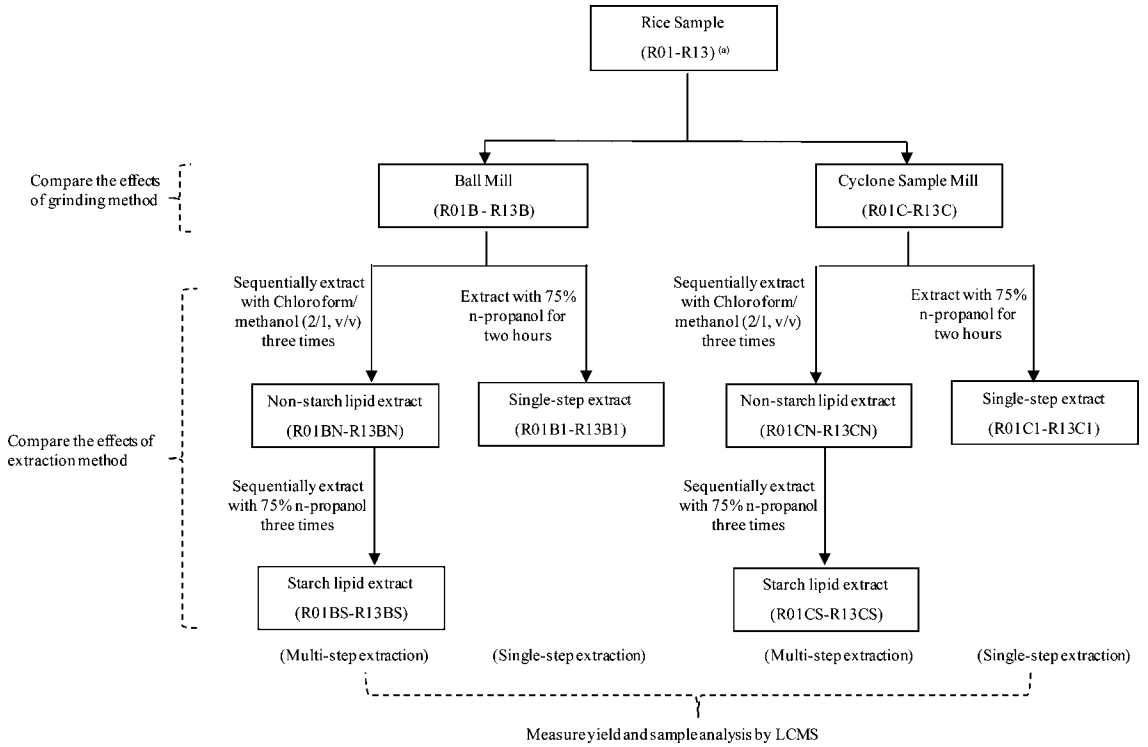

Figure 1. Rice samples and their grinding, extraction, and LC-MS analysis of rice lipids. [a]Rice sample numbers are the same as in Table 1.

mass detector (LC-MS) has become significantly cheaper and more accessible to many researchers. We have accumulated considerable experience in successfully analyzing metabolites in cereal grains using this approach.[15,16] The aim of this research was to develop a fast, reliable, and low-cost LC-MS method to analyze starch LPLs in rice grain. Because starch LPLs form inclusion complexes with amylose and require a different procedure for extraction,[6] we also investigated the effects of different grinding and extraction methods on total rice starch LPL content. This extraction and analytical strategy is most likely suitable for analyzing starch LPLs in cereals other than rice.

MATERIALS AND METHODS

Plant Materials, Reagents, and Standards. Rice accessions (Table 1) were obtained from the Key Laboratory of Zhejiang Province and Chinese Ministry of Agriculture for Nuclear-Agricultural Sciences, Zhejiang University, China. The rice grains were harvested in October 2012. The rice grains were air-dried, stored at room temperature for 2 months until the physiochemical properties of the rice grain stablized,[17,18] and then stored at 4 °C until analyzed in March 2013.

All organic solvents used were of HPLC or LC-MS grade. The LPL standards, 1-oleoyl-2-hydroxy-*sn*-glycero-3-phosphoethanolamine (LPE 18:1), 1-palmitoyl-2-hydroxy-*sn*-glycero-3-phosphoethanolamine (LPE 16:0), 1-oleoyl-2-hydroxy-*sn*-glycero-3-phosphocholine (LPC 18:1), and 1-palmitoyl-2-hydroxy-*sn*-glycero-3-phosphocholine (LPC 16:0), were purchased from Avanti Polar Lipids Inc. (Alabaster, AL, USA).

Sample Grinding and Amylose Content Determination. Rice samples were milled to white rice using a Satake rice machine (Satake Corp., Japan). A laboratory ball mill (Mixer Mill MM301, Retsch) and a cyclone sample mill (UDY Corp., Fort Collins, CO, USA) were used separately to produce rice flour samples (Figure 1). For the cyclone grinding, the milled rice was ground into flour and passed through a 0.5 mm mesh sieve. For the ball mill, the grinding jar was filled with about 8 g of white rice each time and shaken at 30 r/s for 15 s to produce the rice flour samples. The moisture content of the flour was measured by loss on drying; the flour samples were dried under vacuum (6 kPa) and at 60 °C overnight until constant weight.

dx.doi.org/10.1021/jf500585j | J. Agric. Food Chem. 2014, 62, 6600−6607

Apparent amylose content was determined using the iodine staining method.[19] The absorbance of the solution was measured at 620 nm against the blank solution using a spectrophotometer. The apparent amylose content was determined in duplicate for each sample.

Multistep Extractions. The multistep extraction was carried out in triplicate for each sample. In the first step of extraction, rice flour (0.5 g) from each sample was weighed accurately and placed in a 16 × 125 mm, Pyrex culture tube. Chloroform/methanol (2:1, v/v; 8 mL) was added to each tube, and the tubes were capped with rubber liners and placed on ice; the supernatant was removed after 15 min[20] (Figure 1). This extraction was repeated two times for each sample (a total of three extractions). The supernatants from each of the three sequential extractions were combined and dried under N_2. This concentrated extract (R01BN−R13BN and R01CN−R13CN, Figure 1) was dissolved in isopropanol/acetonitrile (50:50, v/v) for LC-MS analysis. The chloroform/methanol extracted rice flour was carefully dried under N_2 in the culture tube before the next extraction step.

In the second step of extraction, the chloroform/methanol extracted rice flour above was extracted with 75% *n*-propanol (*n*-propanol/water, 75:25, v/v; 8 mL) for 2 h under nitrogen at 100 °C in the same culture tube following the method of Morrison and Coventry[21] (Figure 1). The supernatant was removed and the extraction repeated, once for 2 h and once for 1 h. The supernatants from each sequential extractions were combined in a 25 mL volumetric flask, and a 1 mL aliquot was transferred to a vial for LC-MS analysis. The remaining 24 mL of extract (Figure 1; R01BS−R13BS and R01CS−R13CS) was dried using a rotational vacuum concentrator (CHRiST, Osterode am Harz, Germany) and redissolved in 1 mL of 75% *n*-propanol for LC-MS analysis.

Single-Step Extraction. Rice flour (~0.15 g) from each sample was weighed accurately, placed in a culture tube and extracted for 2 h under nitrogen at 100 °C with 75% *n*-propanol (8 mL). The culture tubes were weighed before and after heat extraction to ensure there was no loss of solvent, which would have affected the solvent/sample ratio (w/w). A 1 mL aliquot of the extract (Figure 1; R01B1−R13B1 and R01C1−R13C1) was transferred to a vial for the LC-MS analyses. Triplicate extractions of each sample were undertaken.

LC-MS Analysis. The analysis of extracts was undertaken using an Agilent HPLC (series 1290) equipped with a vacuum degasser, binary pump, autoinjector, and diode array detector (DAD, 1260), coupled to an Agilent quadrupole mass detector (MSD, 6120). A Phenomenex Luna C18 column (5 μm; 150 × 4.6 mm internal diameter) was used for analysis of rice grain lipids. Column temperature was set at 40 °C. Absorbance was monitored between 190 and 600 nm. The injection volume was set at 5 μL per injection. The LC-MS system was controlled using ChemStation software.

Two linear gradient elution programs based on our previous research of the lipophilic components in wheat grain[15,16,22] were used for the qualitative analysis of concentrated rice lipid extracts (Figure 1; R01BN−R13BN, R01CN−R13CN, R01BS−R13BS, and R01CS−R13CS). The first linear gradient contained methanol with 0.005% trifluoroacetic acid (TFA) and 2-propanol with 0.005% TFA. The solvent gradient was programmed from 10 to 95% 2-propanol with 0.005% TFA in 15 min with a flow rate of 1.0 mL/min. The second linear gradient contained acetonitrile with 0.005% TFA and water with 0.005% TFA. The solvent gradient was programmed from 10 to 99% acetonitrile in 30 min with a flow rate of 1.0 mL/min and held at 99% acetonitrile for 5 min.

The MSD was carried out in two ionization modes: atmospheric pressure chemical ionization (APCI) and electrospray ionization (ESI). The APCI mode used the following parameters: scan mass range, 100−1200; fragmentor, 150; capillary voltage, 3000 V (positive); corona current, 4.0 μA; drying gas flow, 5.0 L/min; drying gas temperature, 350 °C; vaporizer temperature, 350 °C; nebulizer pressure, 35 psig. The ESI mode used the following parameters: scan mass range, 100−1200; fragmentor, 150; capillary voltage, 3000 V (positive); drying gas flow, 12.0 L/min; drying gas temperature, 350 °C; vaporizer temperature, 350 °C; nebulizer pressure, 35 psig. All LC-MS settings and parameters above were optimized on the basis of the manufacturer's recommendations and a number of flow injection experiments.

Quantification of Starch LPLs. The same Agilent LC-MS equipment above was used to quantify LPLs. A much shorter and lower volume Agilent Eclipse Plus C18 RRHD column (1.8 μm; 50 × 2.1 mm internal diameter) was used for the quantitative analysis of rice starch LPLs. A shorter linear gradient elution program was used for the quantitative analysis, with a mobile phase containing water and 0.005% TFA and acetonitrile with 0.005% TFA programmed from 10 to 99% acetonitrile in 10 min with a flow rate of 0.3 mL/min and held at 99% acetonitrile for 1.5 min. For this quantitative analysis, the injection volume was set at 3 μL per injection.

The rice starch LPLs were quantified using an external standard method. The MSD was operated using the same parameters as for the ESI method above except that single ion monitoring (SIM) mode was used rather than scan mode. Four available MSD signal channels were employed to detect 10 ions simultaneously as shown in Table 2.

Table 2. LC-MS Single Ion Monitoring (SIM) Mode Setting for Quantification of Starch Lysophospholipids in Rice

time (min)	group	SIM ion	fragmentor	gain	dwell (ms)	% rel dwell
	Signal 1 (% Cycle Time, 25); Mode, SIM; Polarity, Positive					
5.00	LPC 18:3[a]	518	150	1.00	20	100.0
6.15	LPC 18:2[b]	520	150	1.00	20	100.0
6.75	LPC 18:1[c]	522	150	1.00	110	100.0
	Signal 2 (% Cycle Time, 25); Mode, SIM; Polarity, Positive					
5.00	LPC 14:0[d]	468	150	1.00	20	100.0
6.25	LPC 16:0[e]	496	150	1.00	20	100.0
	Signal 3 (% Cycle Time, 25); Mode, SIM; Polarity, Positive					
5.00	LPE 18:3[f]	476	150	1.00	20	100.0
6.15	LPE 18:2[g]	478	150	1.00	20	100.0
6.70	LPE 18:1[h]	480	150	1.00	50	100.0
	Signal 4 (% Cycle Time, 25); Mode, SIM; Polarity, Positive					
5.00	LPE 14:0[i]	426	150	1.00	20	100.0
6.25	LPE 16:0[j]	454	150	1.00	20	100.0

[a]LPC 18:3 for 1-linolenoyl-2-hydroxy-*sn*-glycero-3-phosphocholine. [b]LPC 18:2 for 1-linoleoyl-2-hydroxy-*sn*-glycero-3-phosphocholine. [c]LPC 18:1 for 1-oleoyl-2-hydroxy-*sn*-glycero-3-phosphocholine. [d]LPC 14:0 for 1-myristoyl-2-hydroxy-*sn*-glycero-3-phosphocholine. [e]LPC 16:0 for 1-palmitoyl-2-hydroxy-*sn*-glycero-3-phosphocholine. [f]LPE 18:3 for 1-linolenoyl −2-hydroxy-*sn*-glycero-3-phosphoethanolamine. [g]LPE 18:2 for 1-linoleoyl −2-hydroxy-*sn*-glycero-3-phosphoethanolamine. [h]LPE 18:1 for 1-oleoyl-2-hydroxy-*sn*-glycero-3-phosphoethanolamine. [i]LPE 14:0 for 1-myristoyl-2-hydroxy-*sn*-glycero-3-phosphoethanolamine. [j]LPE 16:0 for 1-palmitoyl-2-hydroxy-*sn*-glycero-3-phosphoethanolamine.

Standards were prepared at concentrations of 32, 160, 800, 4000, 20,000, 100,000, and 200,000 pM. LPLs eluted at similar retention times were allocated to different signal channels (Table 2). The LPLs without commercially available standards were quantified using LPLs of similar structure (Table 2). The method was validated for linearity, precision, limit of detection, limit of quantification, and working concentration range prior to quantification.

Statistical Analysis. All of the LPLs data were measured at least in triplicate. Data analyses were performed with the SAS program version 9.1 (SAS Institute Inc., Cary, NC, USA). The analysis of variance (ANOVA) was performed to determine the effects of grinding methods and extraction methods on the starch lipids and nonstarch lipids with the general linear model procedure (Proc GLM). The multiple comparisons of different mean values for test of significance were determined with Proc means. The correlation coefficients between the parameters were conducted with Proc corr.

RESULTS AND DISCUSSION

Sample Grinding and Multistep Extraction. Ball and cyclone sample mills were chosen for this experiment as they are

the two most commonly used sample grinding methods for plant material prior to solvent extraction and instrumental analysis. Ball mills are widely available in most analytical laboratories, where they are used for general purpose plant sample preparation, whereas cyclone sample mills are often used for grain quality assessment, such as Rapid Visco-Analyzer (RVA) test of pasting viscosity. In this experiment, we used a very gentle ball mill method (30 r/s for 15 s) as severe ball-milling may destroy starch granule structure and affect quantitative extraction of lipids.[21] The rice flour produced by this gentle ball mill method has visibly larger particle size than flour generated by the cyclone sample mill. The moisture content of the flour was between 10.39 and 11.47% (Table 1).

The multistep extraction conditions were chosen carefully on the basis of our previous review.[6] The first step of the multistep extraction with chloroform/methanol was designed to extract nonstarch lipids, and it is a classic method for lipid extraction. The second step of the multistep extraction with *n*-propanol aqueous solution was designed to extract starch lipids. As rice starch lipids (including the LPLs) are protected by the impermeable starch granules and form inclusion complexes with amylose, they are not readily extracted by organic solvent at room temperature. Efficient extraction of internal starch LPLs requires both water and heat to swell or gelatinize the native starch granule to permit the alcohol to penetrate and extract the lipids.[21] The starch lipids were initially suspected to be an artifact formed during starch isolation. Later, ^{13}C cross-polarization/magic angle spinning nuclear magnetic resonance (^{13}C CP/MAS NMR) analysis confirmed that the LPLs exist in vivo in native rice starch granules.[23]

The multistep extraction procedure included three repeated extractions for each step to exhaustively extract and separate nonstarch and starch lipids in rice endosperm. The extraction of nonstarch lipid was carried out at low temperature (0 °C) as a precautionary measure to slow enzymatic reactions during extraction and to reduce the coextraction of nonlipid components.[6] These preventative measures were proven to be effective to reduce the action of lipase and phosphatase as no degradation products (such as phosphatidic acids) were found by subsequent LC-MS analysis. Through the multistep extraction, <1% of starch LPLs was found in the nonstarch lipid fraction by subsequent LC-MS analysis, suggesting the multistep sequential extraction of rice flour was capable of separating the nonstarch lipids from starch lipids.

The yields (%) of nonstarch lipids extracted by chloroform/methanol (2:1, v/v) varied from 0.10% (R04CN) to 1.34% (R02CN) (Table 1; Figures 1 and 2). For some samples such as R02, R03, R07, R08, and R09, the yields (%) of nonstarch lipid extracts of cyclone-milled samples were significantly higher than those of ball-milled samples ($P < 0.001$), which may be due to the effects of different grinding methods. The yields (%) of starch lipids extracted by 75% *n*-propanol were higher than the nonstarch lipids extracted by chloroform/methanol ($P < 0.05$) and varied from 0.70% (R01BS) to 2.24% (R12CS) (Figure 2). In general, the yields of extracted lipids are higher from the cyclone-milled flour than from the ball-milled flour, which may be attributed to the finer flour generated by the cyclone mill, which has higher contact surface with the extraction solutions. However, the two grinding methods were shown to have no significant effects on the quantification of total LPLs by subsequent LC-MS analysis ($P = 0.363$). As yield (%) calculations were based on extraction from a very small quantity of rice flour (0.5 g for each extraction), these results should be considered only as a preliminary indication of the relative nonstarch lipid and starch lipid content in rice grain. Although different rice samples were used, the yields obtained are higher than those reported by Juliano[24] for nonstarch lipid (0.41−0.81%) and starch lipid (0.12−0.57%) ($P < 0.05$), suggesting a possible coextraction of nonlipid components in our experiment.

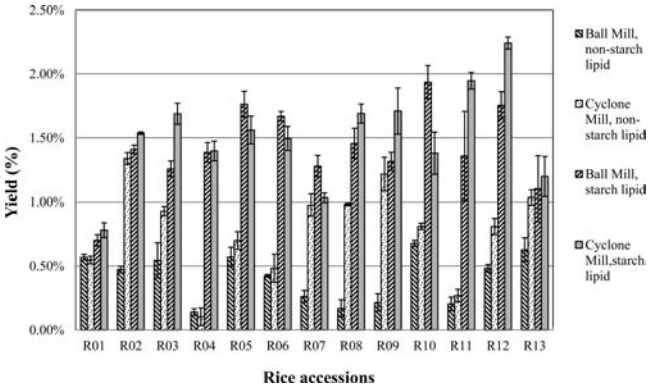

Figure 2. Extraction yields (%) of nonstarch and starch lipids of rice by multistep extraction.

LC-MS Analysis of Lipids Extracted from Multistep Extraction. The concentrated extracts from multistep extraction (Figure 1; R01BN−R13BN, R01CN−R13CN, R01BS−R13BS, and R01CS−R13CS) were analyzed using the 2-propanol/methanol LC-MS method. The total ion chromatograph (TIC) clearly indicated that the major components in the first-step extract of multistep extraction (nonstarch lipids) were the relatively nonpolar triglycerides (eluted at 8−11 min) as discussed in our previous papers (Figure 3a; TIC of R10BN was used as an example).[15,16] The extract (starch lipids) from the second step of the multistep extraction contained relatively more polar lipids (Figure 3a; TIC of R10BS was used as an example), which are further investigated using the acetonitrile/water gradient (Figure 3b).

The extracts (starch lipids) from the second step of the multistep extraction were better separated in the acetonitrile/water gradient than in the 2-propanol/methanol gradient (Figure 3b; TIC of R10BS was used as an example). There was little response observed for the starch lipid samples with the mass detector (MSD) working in the atmospheric pressure chemical ionization (APCI) mode (Figure 3b), with only two LPEs (LPE 18:2, m/z 478 [M + H$^+$] and LPE 16:0, m/z 454 [M + H$^+$]) identified in the TIC of starch lipids (Figure 3b). We explored many parameters in the APCI mode but were unable to detect any LPC. A method using electrospray ionization (ESI) mode was developed and optimized, on the basis of the method of Xia and Jemal.[25] It is apparent that LPLs, including LPEs and LPCs, have a much stronger response in the ESI mode than in the APCI mode (Figure 3b). Seven peaks including both LPCs and LPEs were identified between 19 and 26 min in the ESI mode (Figure 3b), and so this was used for all subsequent experiments (see Supporting Information for the mass spectra).

The LPL composition of rice grains was analyzed on the basis of the starch LPLs reported by Maningat and Juliano[7] using an extract ion method in the TIC of starch lipids (Figure 3c). Ten major LPLs, including five LPCs and five LPEs, were clearly identified, and coelution of some LPLs was observed (Figure 3c). Different mobile phases and columns were used in an attempt to separate the coeluted components. However, we were unable to

dx.doi.org/10.1021/jf500585j | J. Agric. Food Chem. 2014, 62, 6600−6607

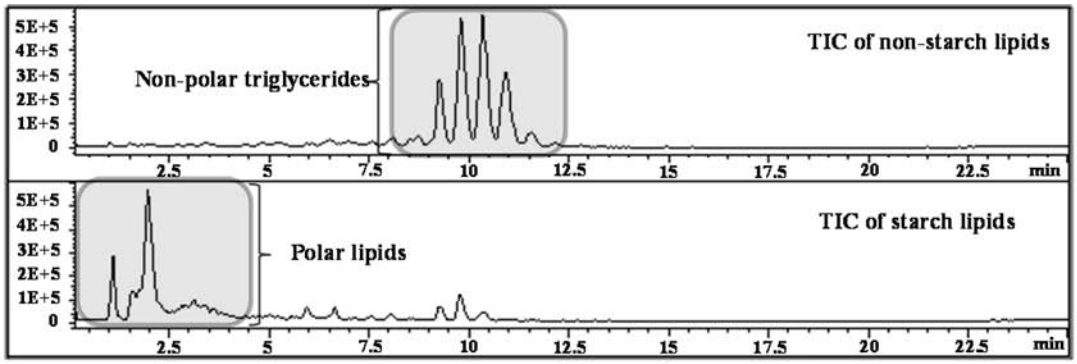

(a) TIC of non-starch (R10BN) and starch (R10BS) lipids using 2-propanol/methanol gradient (APCI, Scan).

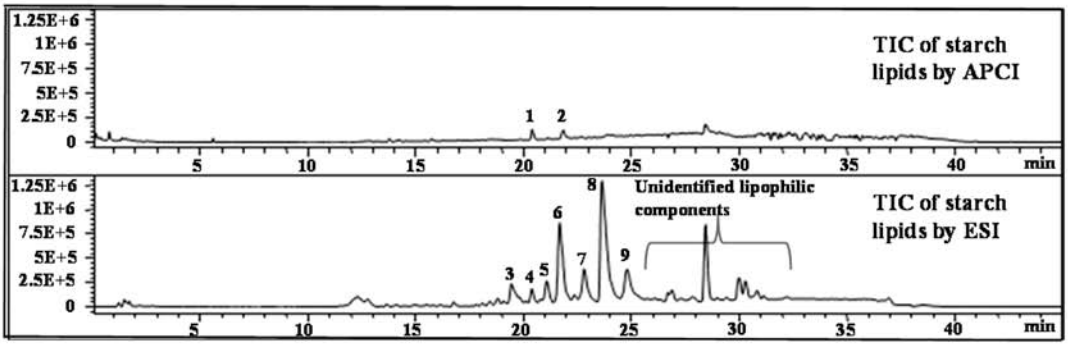

(b) TIC of starch lipids (R10BS) using acetonitrile/water gradient in APCI and ESI modes (Scan).
Peak-1: LPE18:2; Peak-2: LPE16:0; Peak-3: LPC 14:0;Peak-4: LPE18:2; Peak-5 and 6: LPC 18:2; Peak-7 and 8: LPC16:0; Peak-9: LPC 18:1.

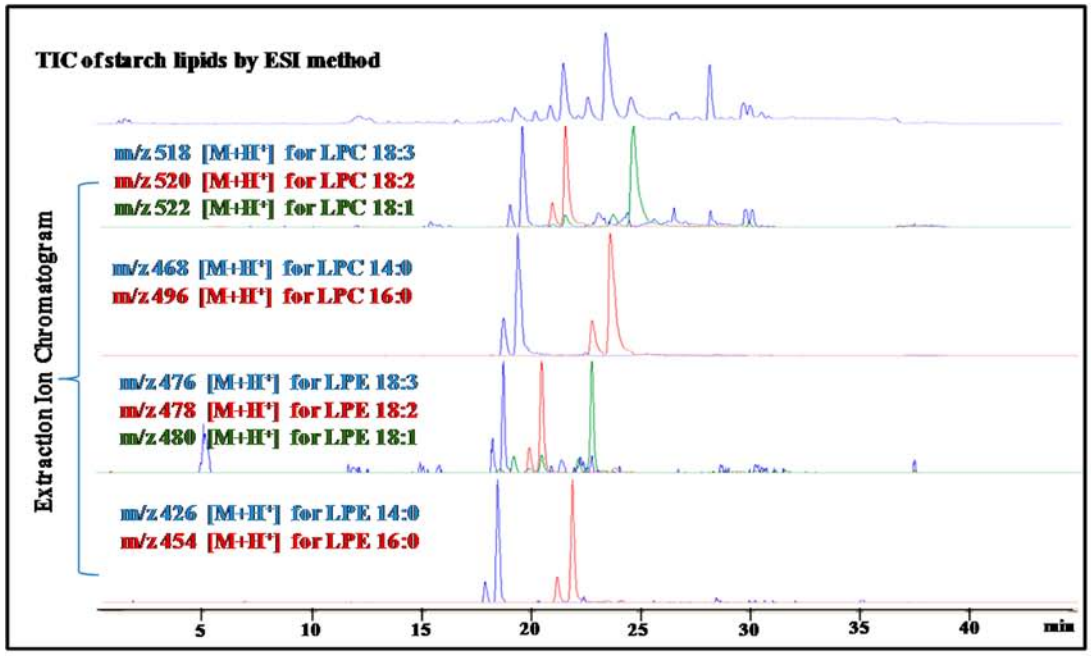

(c) Extracted ions chromatograms for LPC and LPE (R10BS, ESI, Scan).

Figure 3. LC-MS profiles of rice nonstarch (R10BN) and starch (R10BS) lipids.

obtain an improved separation, indicating that SIM may be the only option to quantify this class of LPLs.

Interestingly, Figure 3c shows two peaks for each of the LPCs or LPEs, whereas to date there has been no mention of this phenomenon in the literature on the quantification of LPLs using LC-MS. The standards purchased from Avanti also displayed two peaks for the same compounds, suggesting the two peaks for one compound could result from the amphoteric or zwitterionic nature of the LPLs, containing both $-O-P(O_2^-)-O-$ (anionic phosphate) and $-N^+(CH_3)_3$ (cationic quaternary ammonium

dx.doi.org/10.1021/jf500585j | J. Agric. Food Chem. 2014, 62, 6600−6607

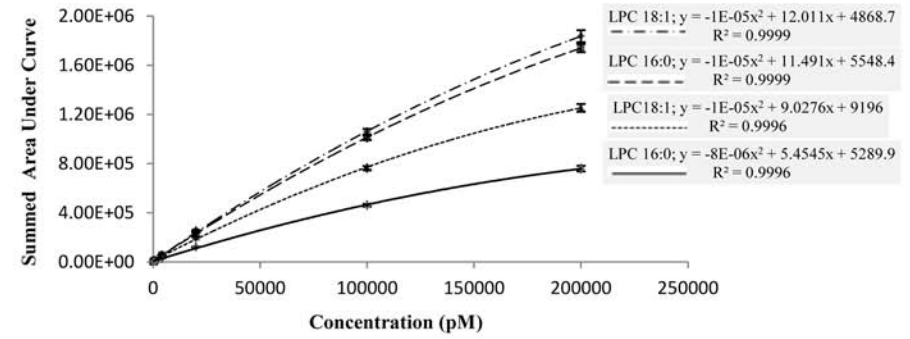

(a) Standard curves for LPCs and LPEs.

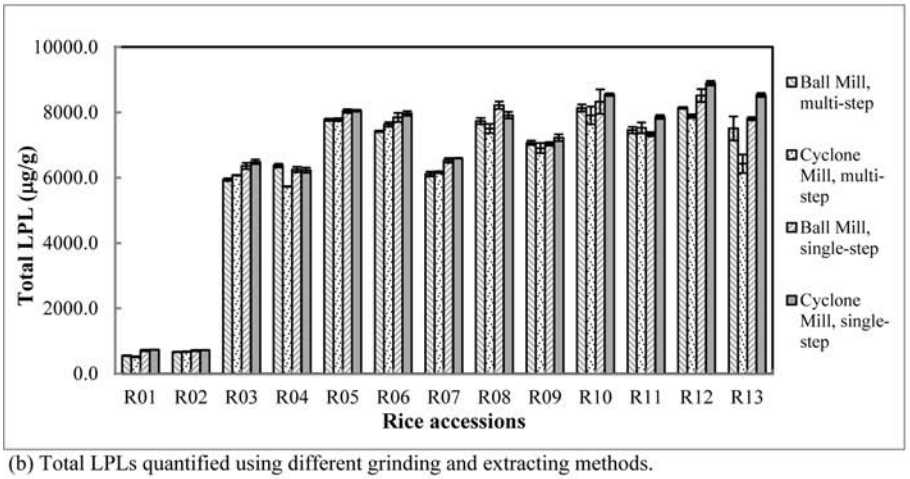

(b) Total LPLs quantified using different grinding and extracting methods.

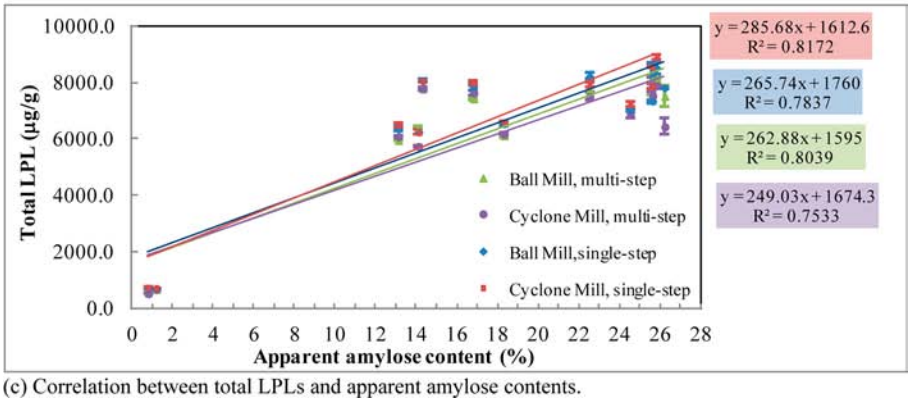

(c) Correlation between total LPLs and apparent amylose contents.

Figure 4. Quantification of total LPLs using different grinding and extracting methods.

for LPC) or $-NH_3^+$ (ammonium ion for LPE). On the basis of the study by Xia and Jemal,[25] we attempted to run the samples and standards at different pH values (2.7, 3.2, 4.4 and 9.3) and at different column temperatures (30, 40, 50, and 60 °C), but the two peaks for each LPL remained in all conditions. Subsequent ^{1}H NMR analysis (see the Supporting Information) demonstrated that the two peaks were actually positional isomers of 1-acyl-2-hydroxy and 2-acyl-1-hydroxy LPLs, which were formed via acyl migration.[26] We tried to isolate pure 1-acyl-2-hydroxy LPC/LPE, the thermodynamically favored isomer,[26] using preparative HPLC. However, it underwent migration during separation attempts, forming a mixture of 1-acyl-2-hydroxy and 2-acyl-1-hydroxy isomers and so we were unable to obtain pure 1-acyl-2-hydroxy or 2-acyl-1-hydroxy LPC/LPE within the scope of this study. The ^{1}H NMR analysis indicated that the isomer mixtures generally contained up to 10% 2-acyl-1-hydroxy isomer.

LC-MS Quantification of LPLs. The LC-MS method used for the qualitative analysis could also be used to quantify LPLs with modification of mass detection from scan mode to SIM mode. However, this method was not suited for testing a large number of samples as it took 45 min and consumed approximately 25 mL of acetonitrile and 540 L of high-purity N_2 for each analysis. Therefore, an ultraperformance liquid chromatography (UPLC) approach was introduced, with the optimized method involving about 30% of the time (a decrease from 45 to 15 min) and 10% of the cost (e.g., a decrease from 25 to 2.5 mL of acetonitrile) for each analysis. In this UPLC method, the effect of column length reduction (from 150 to 50 mm) on chromatography resolution was compensated by the finer column packing particles (a decrease from 5 to 1.8 μm).

As some LPL standards are not commercially available and every LPL standard has two positional isomers, quantification has to be based on the assumption that LPLs with similar

dx.doi.org/10.1021/jf500585j | J. Agric. Food Chem. 2014, 62, 6600−6607

structures have similar response factors (area/concentration) in our LC-MS analysis. The area under each peak was integrated by the ChemStation software, and the areas of two positional isomers were summed and considered as one LPL. Plots of the LPL concentrations and the areas were used to obtain second-order polynomial regression equations (Figure 4a). The response factors of LPCs are larger than LPEs. Compared to the LPE, the two LPCs have very similar response factors (Figure 4a).

In this study, the limit of detection (LOD) was defined as the concentration of LPL that was required to produce a signal >3 times the standard deviation of the noise level (S/N > 3). The limit of quantification (LOQ) was defined as the concentration of LPL that was required to produce a signal >10 times the standard deviation of the noise level (S/N > 10). The signal-to-noise ratio (S/N) was calculated using Agilent Chemstation software (rev. B04.03). Under the LC-MS conditions used in this study, the LOD was about 6 pM (about 3 pg/mL) and the LOQ was about 30 pM (about 15 pg/mL). On the basis of the current extraction and sample preparation methods, we can detect and quantify each LPL when its concentration in the rice grain is >0.75 ng/g (about 1 ppb).

The R^2 values of the LPL standard curves were all >0.9996 over the working concentration range (between 32 and 200,000 pM). The precision of the instrument was determined by injecting a standard mix solution six times (n = 6). The average of the relative standard deviation (RSD) values for each LPL was about 1% of the six repeated analyses.

Total Starch LPLs by Multistep Extraction. The 10 major starch LPLs extracted by the second-step extraction of the multistep extraction were quantified using the LC-MS method above and added together as the total starch LPLs. The total starch LPLs (from R01CS−R02CS and R01BS−R02BS, Figure 1) varied between 516 and 675 μg/g for the waxy rice (or glutinous rice, amylose content <2%) and 5733−8139 μg/g for the nonwaxy rice (R03CS−R12BS) (Figure 4b). Our starch LPL results were greater (P < 0.05) than those (~3 mg/g for nonwaxy rice) reported by Choudhury and Juliano[27] but similar to those (4070−8110 μg/g for nonwaxy rice) reported by Morrison et al.[9] Our method could quantify low levels of starch LPLs in waxy rice with <2% amylose content, which is more sensitive than the TLC-GC method used by Morrison et al.[9] The lower starch LPL values for the nonwaxy rice reported by Choudhury and Juliano[27] may be due to the limitation of column chromatography (CC) and gravimetric method used at that time. However, the difference may be also due to the nature of the samples themselves, as different rice samples have been used in this study.

Total starch LPLs were well correlated with apparent amylose content (P < 0.001) when waxy and nonwaxy rice samples were considered together (Figure 4c), similar to the finding reported by Morrison et al.[9] However, this correlation did not exist when the nonwaxy rice was considered alone. The correlation between total LPLs and amylose content has been found in other waxy and nonwaxy cereal grains, such as barley.[28] This correlation is possibly affected by both varietal and environmental factors in rice.[9] Therefore, such a correlation, if it exists, can be revealed only by investigating a sufficient number of rice samples grown in controlled environments.

Individual Starch LPLs by Multistep Extraction. We found that LPL16:0 is the single most abundant (45.4−63.2%) starch LPL in both waxy and nonwaxy rices, followed by LPC 18:2 (10.5−23.4%) (Table 3), in agreement with Maniñgat and Juliano.[7] Palmitic acid (16:0) (up to ~76%) and linoleic acid (18:2) (up to ~29%) are the two major fatty acids within both starch LPC and LPE. The fatty acids of LPLs in waxy rice were more saturated than those found in nonwaxy rice. Although the minor LPLs in waxy rice, such as LPC 18:3 and LPE 18:1, are below the limit of quantification, their presence can still be clearly identified in the chromatogram.

Table 3. Individual Starch LPL/Total Starch LPLs in Waxy and Nonwaxy Rice[a]

individual LPL[b]	% of total LPLs in waxy rice	% of total LPLs in nonwaxy rice
LPC 18:3	n/a[c]	0.2−0.7
LPC 18:2	10.5−15.0	14.7−23.4
LPC 18:1	5.9−7.1	4.9−12.7
LPC 14:0	5.6−11.6	3.1−7.6
LPC 16:0	56.5−63.2	45.4−53.4
LPE 18:3	n/a	0−0.1
LPE 18:2	0.6−0.9	3.6−5.9
LPE 18:1	0−0.3	0.7−1.9
LPE 14:0	0.1−0.6	0.4−1.0
LPE 16:0	9.1−12.3	8.8−13.3

[a]The data are obtained from ball-milled samples with multistep extraction for the starch LPLs. [b]LPL codes are the same as in Table 2. [c]Lower than quantification limit.

The percentage of individual LPLs can sometimes vary by almost 4-fold between different rice genotypes. For example, LPC 14:0 varied from 3.1 to 11.6% among the rice accessions analyzed (Table 3). As reported by Chang et al.,[14] the individual LPL differences observed in this study may be caused by the combination of varietal and environmental effects. To unravel how environmental variation contributes to the rice starch LPLs, growing environments should be studied at different stages of rice development.

Increased Sample Throughput with the Single-Step Extraction Method. The 10 major starch LPLs extracted by the single-step extraction were quantified using the LC-MS method above and added together as the total LPLs in rice. ANOVA analysis indicated that extraction methods had a significant effect on total LPLs (P < 0.001). In most cases, total LPLs were slightly higher in the single-step extraction than total starch LPLs in the multistep extraction (Figure 4b). This difference is possibly due to the minimal amount of nonstarch LPLs in rice,[10] which represented only <1% of starch LPLs in our study and were included in the total LPLs by the single-step extraction but not included for the total starch LPLs by the multistep extraction. However, the difference may be also due to loss through the extended multistep extraction.

To analyze a large number of samples for genetic and metabolomics studies, reducing the time for a single sample preparation is paramount. The multistep extraction method (6 samples in triplicate for 2 days) takes about 6−8 times longer compared to the single-step extraction (24 samples in triplicate for 1 day) for each sample prepared. The simplification from multistep to single-step extraction can significantly reduce the sample preparation time as well as the risk of human error in removing and combining supernatants. As the total LPLs are almost the same as total starch LPLs, we recommend the single-step extraction method for screening large numbers of samples followed by a multistep extraction of samples of particular interest identified by the initial screening.

This is the first report of the determination of starch LPLs in rice using LC-MS. Compared to previous TLC-GC methods, the

LC-MS method developed here is more efficient and sensitive and can simultaneously quantify individual LPLs. The comparison of grinding methods indicates that ball or cyclone mills are equally effective for determination of total starch LPLs. The rapid single-step extraction method significantly simplifies sample preparation, improves consistency, and increases throughput for lower cost. The combination of efficient extraction and LC-MS method for the first time provides an opportunity to analyze starch LPLs within extensive collections of rice grain samples and should contribute to unravelling genetic and environmental contributions to variation in starch LPLs and may also help to improve the understanding of the effects of starch LPLs on rice grain quality. Starch LPLs in other cereal grains may be also determined using this strategy, and this should be further explored for grain research and development.

■ ASSOCIATED CONTENT

Supporting Information

Mass spectra and compound structures. This material is available free of charge via the Internet at http://pubs.acs.org.

■ AUTHOR INFORMATION

Corresponding Authors

*(L.L.) E-mail: lliu@scu.edu.au. Phone: 61-2-66223211. Fax: 61-2-66223459. Mail: Southern Cross Plant Science, Southern Cross University, P.O. Box 157, Lismore, NSW 2480, Australia. *(J.B.) E-mail: jsbao@zju.edu.cn. Phone: 86-571-86971932. Fax: 86-571-86971421. Mail: Institute of Nuclear Agricultural Sciences, Zhejiang University, Huajiachi Campus, Hangzhou 310029, China.

Notes

The authors declare no competing financial interest.

■ ACKNOWLEDGMENTS

We are grateful for the support and NMR analysis provided by Avanti Polar Lipids Inc. (Alabaster, AL, USA).

■ REFERENCES

(1) Morrison, W. R. Lipids in cereal starches: a review. *J. Cereal Sci.* **1988**, *8*, 1−15.

(2) Morrison, W. R. Starch lipids and how they relate to starch granule structure and functionality. *Cereal Foods World* **1995**, *40*, 437−446.

(3) Blazek, J. *Role of Amylose in Structure-Function Relationship in Starches from Australian Wheat Varieties*. The University of Sydney, Sydney, Australia, 2008.

(4) Putseys, J. A.; Derde, L. J.; Lamberts, L.; Östman, E.; Björck, I. M.; Delcour, J. A. Functionality of short chain amylose−lipid complexes in starch−water systems and their impact on in vitro starch degradation. *J. Agric. Food Chem.* **2009**, *58*, 1939−1945.

(5) Putseys, J. A.; Lamberts, L.; Delcour, J. A. Amylose-inclusion complexes: formation, identity and physico-chemical properties. *J. Cereal Sci.* **2010**, *51*, 238−247.

(6) Liu, L.; Waters, D. L. E.; Rose, T. J.; Bao, J.; King, G. J. Phospholipids in rice: significance in grain quality and health benefits: a review. *Food Chem.* **2013**, *139*, 1133−1145.

(7) Maniñgat, C. C.; Juliano, B. O. Starch lipids and their effect on rice starch properties. *Starch/Stärke* **1980**, *32*, 76−82.

(8) Azudin, M. N.; Morrison, W. R. Non-starch lipids and starch lipids in milled rice. *J. Cereal Sci.* **1986**, *4*, 23−31.

(9) Morrison, W. R.; Milligan, T. P.; Azudin, M. N. A relationship between the amylose and lipid contents of starches from diploid cereals. *J. Cereal Sci.* **1984**, *2*, 257−271.

(10) Choudhury, N. H.; Juliano, B. O. Effect of amylose content on the lipids of mature rice grain. *Phytochemistry* **1980**, *19*, 1385−1389.

(11) Christie, W. Chromatographic analysis of phospholipids. *Chem. Mater. Sci.* **1985**, *181*, 171−182.

(12) Hu, C.; van Dommelen, J.; van der Heijden, R.; Spijksma, G.; Reijmers, T. H.; Wang, M.; Slee, E.; Lu, X.; Xu, G.; van der Greef, J.; Hankemeier, T. RPLC-ion-trap-FTMS method for lipid profiling of plasma: method validation and application to p53 mutant mouse model. *J. Proteome Res.* **2008**, *7*, 4982−4991.

(13) Rectra, K. *Schistosomal Lysophosphatidylserine: An Immunomodulatory Factor*. Utrecht University, The Netherlands, 2007.

(14) Chang, Y.; Zhao, C.; Zhu, Z.; Wu, Z.; Zhou, J.; Zhao, Y.; Lu, X.; Xu, G. Metabolic profiling based on LC/MS to evaluate unintended effects of transgenic rice with cry1Ac and sck genes. *Plant Mol. Biol.* **2012**, *78*, 477−87.

(15) Liu, L.; Deseo, M. A.; Morris, C.; Winter, K. M.; Leach, D. N. Investigation of α-glucosidase inhibitory activity of wheat bran and germ. *Food Chem.* **2011**, *126*, 553−561.

(16) Liu, L.; Winter, K. M.; Stevenson, L.; Morris, C.; Leach, D. N. Wheat bran lipophilic compounds with in vitro anticancer effects. *Food Chem.* **2012**, *130*, 156−164.

(17) Juliano, B. O. Criteria and tests for rice grain qualities. In *Rice Chemistry and Technology*; Juliano, B. O., Ed.; American Association of Cereal Chemists: St. Paul, MN, USA, 1985; p 403.

(18) Juliano, B. O. Rice: overview. In *Encyclopedia of Grain Science*; Wrigley, C., Corke, H., Walker, C., Eds.; Academic Press: San Diego, CA, 2004; Vol. 3, pp 41−48.

(19) Bao, J. S.; Shen, S. Q.; Sun, M.; Corke, H. Analysis of genotypic diversity in the starch physicochemical properties of nonwaxy rice: apparent amylose content, pasting viscosity and gel texture. *Starch/Stärke* **2006**, *58*, 259−267.

(20) Yoshida, H.; Tanigawa, T.; Yoshida, N.; Kuriyama, I.; Tomiyama, Y.; Mizushina, Y. Lipid components, fatty acid distributions of triacylglycerols and phospholipids in rice brans. *Food Chem.* **2011**, *129*, 479−484.

(21) Morrison, W. R.; Coventry, A. M. Extraction of lipids from cereal starches with hot aqueous alcohols. *Starch/Stärke* **1985**, *37*, 83−87.

(22) Liu, L. *Phytochemical and Pharmacological Perspectives of Wheat Grain and Lupin Seed*. Southern Cross University, Lismore, NSW, Australia, 2009.

(23) Morrison, W. R.; Law, R. V.; Snape, C. E. Evidence for inclusion complexes of lipids with V-amylose in maize, rice and oat starches. *J. Cereal Sci.* **1993**, *18*, 107−109.

(24) Juliano, B. O. Lipids in rice and rice processing. In *Lipids in Cereal Technology*; Barnes, P. J., Ed.; Academic Press: London, UK, 1983; pp 305−330.

(25) Xia, Y. Q.; Jemal, M. Phospholipids in liquid chromatography/mass spectrometry bioanalysis: comparison of three tandem mass spectrometric techniques for monitoring plasma phospholipids, the effect of mobile phase composition on phospholipids elution and the association of phospholipids with matrix effects. *Rapid Commun. Mass Spectrom.* **2009**, *23*, 2125−38.

(26) Plueckthun, A.; Dennis, E. A. Acyl and phosphoryl migration in lysophospholipids: importance in phospholipid synthesis and phospholipase specificity. *Biochemistry* **1982**, *21*, 1743−1750.

(27) Choudhury, N. H.; Juliano, B. O. Lipids in developing and mature rice grain. *Phytochemistry* **1980**, *19*, 1063−1069.

(28) Morrison, W. R.; Tester, R. F.; Snape, C. E.; Law, R.; Gidley, M. J. Swelling and gelatinization of cereal starches. IV. Some effects of lipid-complexed amylose and free amylose in waxy and normal barley starches. *Cereal Chem.* **1993**, *70*, 385−391.

studies focused primarily on the changes in fatty acid composition, but rarely report complete fatty acid composition of TAG and phospholipid (PL) species.[19] Composition of TAG and PL species in conjunction with fatty acid composition of CLA-rich egg yolks would provide a more complete description of the deposition and the nutritional significance of CLA-rich soy oil in poultry diets.

Rapid matrix-assisted laser desorption ionization time-of-flight mass spectrometry (MALDI-TOF-MS) characterization methods have been used to qualitatively determine fatty acid composition of specific lipids, such as TAG and PL, in crude samples. Yolk lipids have a combination of TAG and PL, but direct MALDI-TOF-MS biased the detection of PL species over TAG.[22] Decreased TAG detection is a result of suppression by phosphatidylcholine (PC).[20−22] Fuchs et al.[23] reported an alternative method that couples thin-layer chromatography (TLC) with MALDI-TOF-MS to avoid suppression of other lipid classes by PC. However, this method only described the egg yolk PL and disregarded the detection of the more abundant TAG. Emerson et al.[24] addressed suppression by applying solid-phase extraction (SPE) to separate TAG and PL species from beef and yolk lipid samples that could be then be analyzed by direct MALDI-TOF-MS analysis. However, analytical replications using this approach were found to be extremely difficult due to inherent heterogeneity in matrix crystallization in the MALDI MS preparation.

Direct flow infusion electrospray ionization MS (DFI ESI-MS) is an alternative method that has been used for PL and TAG lipid identification and characterization. However, only free fatty acids and small PL molecules are analyzed, while major TAG species remain undetected.[25] Also, lipids that have different molecular elemental compositions may actually yield ions with the same ionic elemental compositions, depending on the ionic adduct that is formed upon ESI-MS. To solve this problem, Fhaner et al.[25] dissolved a lipid extract mixture of various PLs and TAGs in a Folch solvent system modified with 20 mM ammonium formate to enable ESI-MS identification and quantification of each PL and TAG species. This technique decreased molecular species containing sodium ions in the crude lipid extract and lessened the possibility of isobaric mass overlap. Combining lipid profiling analysis using direct flow infusion ESI/MALDI MS along with fatty acid methyl esters (FAMEs) will provide a thorough description of the effect of CLA-rich soy oil on the lipid composition in egg yolks.

Eggs enriched with 140 mg of CLA per egg were produced at The University of Arkansas Poultry Farm using CLA-rich soy oil in a standard commercial hen diet and subsequently used in the following study. The goal of this study was to quantify differences in the fatty acid and lipid composition in CLA-rich eggs relative to control eggs. Fatty acid compositions were determined using FAMEs by gas chromatography with flame ionization detection (GC-FID). FAME studies by GC-FID were carried out directly from total lipid extracts and also from individual classes of lipids separated by TLC to estimate fatty acid composition differences. Lipid extracts were analyzed by direct MALDI-TOF-MS, DFI ESI-MS, and TLC-UV-MALDI-MS to obtain fatty acid composition using the intact lipid form.

In summary the objectives of the investigation were to (1) determine the fatty acid composition of total lipids in CLA-rich egg yolks relative to control eggs; (2) quantify the CLA content in TAG and PL fractions of CLA-rich egg yolks; and (3) compare TAG and PL species in CLA-rich egg yolks and control yolks.

MATERIALS AND METHODS

Materials. Control eggs were produced by adding 10% (wt) refined, bleached, deodorized (RBD) soy oil to a standard commercial diet for six commercial white leghorn hens, 25 weeks old. (Riceland Foods, Stuttgart, AR). CLA-rich eggs were produced by adding 10% (wt) CLA-rich soy oil to a standard commercial feed for six additional commercial leghorns. The CLA oil contained 15% CLA. Diets were prepared by combining oil and feed in a Hobart stand mixer and mixing at speed level 2 for 5 min (Hobart Legacy HL-200). CLA-rich eggs were collected after 12 days of treatment administration. CLA feeding was approved by the University's Institutional Animal Care and Use Committee.

All solvents used for sample preparation were analytical grade, and solvents used for TLC-UV-MALDI-MS, direct MALDI-MS, and DFI ESI-MS were HPLC grade. The PL standards, including PC, phophatidyl ethanolamine (PE), lyso-phosphatidyl choline (LPC), and sphingomyelin (SM), were purchased from Cayman Chemical Co (Ann Arbor, MI). The FAME standards used were purchased from Supelco (Bellefonte, PA). Primuline dye was purchased from Sigma−Aldrich (cat. no. 206865-1G, St. Louis, MO).

Methods. *Fatty Acid Composition of Total Lipids. Yolk Lipid Extractions.* Nine eggs were randomly collected from each of the CLA-rich eggs and control eggs. Three eggs from each egg type were pooled. This was performed three times to produce triplicate pooled samples. Eggs were carefully broken, and a stainless steel yolk separator was used to separate the egg yolks for each replicate. Yolks were combined in 50 mL plastic centrifuge tubes and vortexed for 3 min to homogenize the pooled samples.

Lipids were extracted using a rapid hexane/isopropanol (IPA) solvent extraction protocol.[26] Duplicate 5 g samples from each yolk replicate were dissolved in 10 times hexane/IPA (1:1, v/v), vortexed for 5 min, and filtered using Whatman #4 filter paper; the solvent was evaporated using a rotoevaporator (Buchi Rotavapor R-210). The extract was weighed, and the yield was recorded. These extracts were used to determine the yolk total fatty acid composition, the fatty acid composition of individual lipid classes, and the lipid composition.

Fatty Acid Analysis from Total Lipids by GC-FID. FAMEs were prepared from all yolk extractions using a rapid, micro FAMEs preparation method.[27] Samples of 0.1 g were weighed (Mettler Toledo Classic AB204-S) in 50 mL centrifuge tubes. A 1% heptadecanoic acid methyl ester (HME, C17:0; Sigma−Aldrich) solution in hexane was prepared. HME equivalent to 5% of the extract weight was added to each centrifuge tube as an internal standard. A 1 mL amount of toluene and 4 mL of 0.5 M sodium methoxide in methanol were added to each tube. The tubes were heated to 50 °C in a water bath for 10 min and then cooled at ambient temperature for 5 min. To inhibit sodium hydroxide formation, 0.2 mL of glacial acetic acid was added to each centrifuge tube. FAMEs were efficiently extracted in to hexane by a solvent-extraction procedure. The tubes were vortexed for 2 min and then placed on the benchtop for phase separation. The upper hexane layer was pipetted out and dried over anhydrous sodium sulfate for 15−20 s. Fatty acid profiles were obtained by measuring FAMEs in duplicate by GC using an SP 2560 fused silica capillary column (100 m × 0.25 mm i.d. × 0.2 μm film thickness; Supelco Inc., Bellefonte, PA) with FID (model 3800, Varian, Walnut Creek, CA). Samples of 2.0 μL were injected by an auto sampler (Varian). The GC-FID settings were as follows: oven temperature, 250 °C; sensitivity, 12; He gas, 30 mL/min; H_2, 31 mL/min; air, 296 mL/min; and oven program time, 111 min. Fatty acid concentrations were calculated by the following equation:

$$[\%\text{fatty acid}] = ([\text{HME}] \times \text{sample peak area} \times \text{relative response factor})/\text{HME peak area}$$

dx.doi.org/10.1021/jf501100y | J. Agric. Food Chem. 2014, 62, 6608−6615

Statistical analysis was performed using JMP 10.1 software. Relative percentages of fatty acids were analyzed using a studentized t test (α level = 0.05).

Fatty Acid Composition of TAG and PL Fractions. TLC-FAMEs-GC-FID. Lipids were fractionated from yolk extraction samples using 20 cm × 20 cm TLC silica plates (T_{254}, Merck, Darmstadt, Germany). Samples of 0.3 g (±0.005) were dissolved in 100 μL and applied to a TLC plate as 20 μL aliquots, carefully to prevent smearing. Four TLC plates were placed into a closed chamber with chloroform, ethanol, water, and triethylamine (5:5:1:5) for approximately 2 h to perform chromatographic separation of all lipid classes. After separation, the TLC plates were allowed to dry under the hood. Then, one of the TLC plates was sprayed with 0.05% Primuline dye to visualize individual classes using Gel Logic GL2200 (Carestream Health, Inc., Rochester, NY).[28] Once the locations of the TAG and PL on the TLC were determined, on the basis of the Primuline spray, TAG and PL fractions were scraped into separate 50 mL disposable centrifuge tubes, and the lipid extracts were converted to FAMEs using the method described above.[26] Autosampler injection volume was increased to 8.0 μL to account for the lower sample concentration. Statistical analysis was performed using JMP 10.1 software. Relative percentages of fatty acids among egg yolk types were analyzed using a studentized t test (α level = 0.05).

Intact Lipid Composition. TLC-UV-MALDI-MS Analysis Determination of TAG and PL Species. Triplicate pooled samples from all three egg types plus a standard TAG and PL solution with a concentration of 50 mg/mL in $CHCl_3$ were applied to a TLC plate (TLC Silica Gel 60 5 cm × 7.5 cm, T_{254}, Merck, Darmstadt, Germany) as 1 μL droplets to avoid smearing during the TLC loading. The mass of the dried sample loaded onto a TLC plate did not exceed 80 μg. TLC plates were developed using chloroform, ethanol, water, and triethylamine (5:5:1:5) for 45 min. After the separation was completed, the TLC plate was allowed to dry under the hood. An airbrush sprayer attached to a high-purity nitrogen tank was used to homogeneously coat the entire TLC plate with a 0.05% Primuline dye solution.[28] The dye allowed visualization and quantification of lipid classes on the TLC plate using UV excitation followed by monitoring 535 nm emission using Gel Logic GL2200.

A separate TLC plate developed simultaneously with plates for UV analysis, as described above, was used for direct TLC-MALDI-MS analysis. An airbrush sprayer attached to a nitrogen tank was used to homogeneously coat the entire TLC plate with a MALDI-MS matrix aerosol (10 mL of 100 mg/mL DHB in acetonitrile/water, 4:1 v/v). After complete drying, the plate was fitted to a 5 × 7.5 MALDI TLC plate holder. The TLC plate was imaged by an Ultraflex II MALDI-TOF/TOF with a 200 Hz smart beam laser in the reflector mode. The extraction voltage was set to 25 kV, and matrix suppression was set to m/z < 200. Data were acquired using FlexControl (FC 3.0) and FlexImaging 2.0 software under Compass 1.2 settings. A pixel raster of 600 μm × 600 μm spots was set during the imaging run on the entire TLC lane area. For each pixel, 200 laser shots were accumulated. Certain colors were assigned based on the m/z to each lipid, and the spatial distribution of lipids across the TLC plate was extracted from the MALDI-MS total ion count and displayed as a heat map. The data were processed using Bruker FlexImaging 2.0, Flex Analysis 2.4/3.0, and ClinProTools 2.2 software. Lipid species were identified by submitting both low- and high-resolution monoisotopic m/z peaks, and the fatty acid composition information, was obtained from FAMEs analysis to the www.lipidmaps.org database.

Direct Infusion ESI-MS and Direct MALDI-MS Quantification of Major TAG and PL Species. A Bruker Esquire 2000 (Billerica, MA) LC ion trap mass spectrometer (Bruker, Daltonics Corp., Germany) was used to acquire all the mass spectra in this study. Triplicate pooled lipid extracts from each egg type were dissolved in chloroform to reach a final concentration of 50 mg/mL. A 5 μL amount of lipid extract was mixed with 200 μL of IPA/MeOH/$CHCl_3$ (4:2:1, v/v/v) containing 20 mM ammonium formate.[26] A 5 μL sample was directly infused into the ESI source for MS analysis using a syringe. The mass spectrometer was scanned from 400 to 1500 Da at a spectral averaging rate of 10 s^{-1} with low skimmer voltage optimized for ions at m/z 800. The mass spectrometer was operated in both positive and negative ion modes with a nebulizing gas pressure (N_2) of 12 psi and a drying gas flow of 7 mL/min maintained at 150 °C. The spectra data were analyzed by Bruker Daltonics Data Analysis 3.0 software (Bruker Daltonik GmbH, Germany). Statistical analysis was performed using JMP 10.1 software. Relative percentages of lipid species among egg types were compared using a studentized t test (α level = 0.05).

RESULTS AND DISCUSSION

Fatty Acid Composition of Total Lipids. *Fatty Acid Analysis from Total Lipids by GC-FID.* Extractions resulted in a total lipid content of 34.7 ± 0.05% per volume of yolk with no significant difference in egg type. Table 1 shows the fatty acid composition of the control and CLA-rich egg yolk lipid extracts. Administration of the CLA-rich diet resulted in 2.02 ± 0.08% CLA of total fatty acids, equating to 120 mg of CLA in the egg yolk. Myristic, palmitic, and stearic acid concentrations, all saturated fatty acids (SFAs), were significantly higher in CLA-rich eggs, relative to the control eggs (p < 0.001). Palmitoleic and oleic acid concentrations were significantly lowered in CLA-rich eggs. These changes in SFA and monounsaturated fatty acid (MUFA) concentrations in response to dietary CLA have been reported multiple times.[12−17] Linoleic and linolenic acid, both 18 carbon polyunsaturated fatty acids (PUFAs), were significantly higher in CLA-rich eggs. This increase corresponds to the increased linoleic and linolenic acid amounts in the CLA-rich diet. Eicosenoic acid concentration was significantly higher in control yolks (p < 0.001).

Table 1. Fatty Acid Composition of Yolk Lipids from Control and CLA-Rich Eggs[a]

fatty acid	control yolk fatty acid (% FA)	CLA-rich yolk fatty acid (% FA)
myristic acid (C14:0)	0.33 ± 0.00b	0.39 ± 0.03a
palmitic acid (C16:0)	24.46 ± 0.09b	26.21 ± 1.17a
palmitoleic acid (C16:1)	1.33 ± 0.05a	0.84 ± 0.09b
stearic acid (C18:0)	10.36 ± 0.05b	14.50 ± 1.16a
oleic acid (C18:1)	32.49 ± 0.49b	27.32 ± 1.22b
linoleic acid (C18:2)	24.27 ± 0.61b	26.24 ± 0.90a
linolenic acid (C18:3)	0.72 ± 0.03b	0.93 ± 0.09a
CLA (C18:2 *c*-9,*t*-11)	0.00	0.13 ± 0.01a
CLA (C18:2 *t*-9,*c*-11 and *c*-10,*t*-12)	0.00	0.34 ± 0.01a
CLA (C18:2 *t*-10,*c*-12)	0.00	0.31 ± 0.02a
CLA (C18:3 other isomer)	0.00	0.08 ± 0.00a
CLA (C18:2 *t*,*t*)	0.00	1.17 ± 0.02a
total CLA	0.00	2.02 ± 0.02a
eicosenoic acid (C20:1)	1.69 ± 0.05a	1.57 ± 0.08b
eicosatrienoic acid (C20:3)	0.18 ± 0.00a	0.17 ± 0.00a
arachidonic acid (C20:4)	1.27 ± 0.05a	1.01 ± 0.03b
docosahexaenoic acid (C22:6)	0.72 ± 0.01a	0.53 ± 0.10b

[a]Values are expressed as % of total fatty acids in crude lipid extracts. Values in the same row with the same letter are not significantly different (α level = 0.05).

Figure 1 shows the fatty acid type composition for each treatment yolk. CLA-rich eggs contain 43.1% SFA, which is significantly higher than control eggs at 36.0% SFA (p < 0.001). The PUFA concentrations in CLA-rich yolk was also significantly lower in comparison to both commercial egg types (p < 0.001). The CLA-rich yolk MUFA concentration was 31.5%, which was significantly lower than both commercial egg types (p < 0.001). The PUFA concentration was highest in

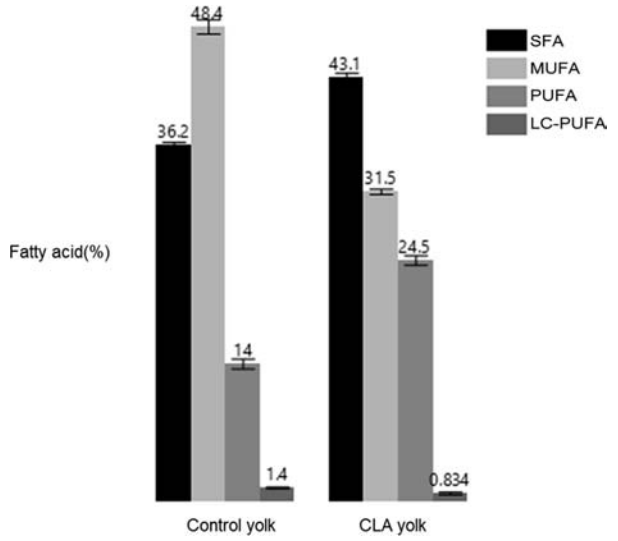

Figure 1. Total fatty acid composition of yolk lipids from control eggs and CLA-rich eggs. Fatty acids are grouped by degree of unsaturation: saturated fatty acid (SFA), monounsaturated fatty acid (MUFA), polyunsaturated fatty acids (PUFA), long-chain polyunsaturated fatty acid (LC-PUFA). Error bars are one standard error from the mean.

CLA-rich yolks at 24.5%, while control eggs contained 14.0%. Long-chain PUFA (LC-PUFA) concentrations were highest in control yolks at 1.4% while CLA-rich yolks contained only 0.8%.

Fatty Acid Composition of TAG and PL Fractions. *TLC-FAMEs-GC-FID.* Table 2 shows the fatty acid composition of the TAG fraction of the control and CLA-rich yolks. Yolk lipids are generally composed of 62% TAG, 33% PL, and 5% cholesterol.[29] The TAG fraction CLA content was 0.9% of the total fatty acids. The relative proportions of CLA isomers in TAG reflected total lipid CLA isomers. CLA TAG had significantly more myristic, palmitic, and stearic acid, relative to control TAG fractions ($p < 0.001$). Control yolk TAG had the highest concentration of C24:0 at 3%, which was significantly higher than CLA-rich yolk TAG.

Table 2. TAG Fatty Acid Composition of Control and CLA-Rich Yolks[a]

fatty acid	control yolk TAG fatty acid (%)	CLA-rich yolk TAG fatty acid (%)
myristic acid (C14:0)	0.21 ± 0.01b	0.49 ± 0.07a
palmitic acid (C16:0)	23.15 ± 1.62b	32.07 ± 1.22a
palmitoleic acid (C16:1)	1.61 ± 0.08b	1.1 ± 0.08c
stearic acid (C18:0)	11.09 ± 1.04b	14.3 ± 0.49a
oleic acid (C18:1)	43.23 ± 1.02a	34.2 ± 0.96b
linoleic acid (C18:2)	13.42 ± 2.12b	16.06 ± 0.04b
linolenic acid (C18:3)	0.33 ± 0.06b	0.46 ± 0.01b
CLA (C18:2 *c*-9,*t*-11)	0	0.18 ± 0.01a
CLA (C18:2 *t*-9,*c*-11 and *c*-10,*t*-12)	0	0.12 ± 0.02a
CLA (C18:2 *t*-10,*c*-12)	0	0.14 ± 0.02a
CLA (C18:2 *t*,*t*)	0	0.41 ± 0.07a
total CLA	0	0.86 ± 0.11a
eicosenoic acid (C20:1)	0.10 ± 0.04a	0.15 ± 0.01a
eicosatrienoic acid (C20:3)	0.1 ± 0.03a	0.06 ± 0.01a
arachidonic acid (C20:4)	0.42 ± 0.04a	0.16 ± 0.01b
tetracosanoic acid (C24:0)	3.23 ± 0.18a	0.08 ± 0.004b
docosahexaenoic acid (C22:6)	3.1 ± 0.79a	0.02 ± 0.002b

[a]Values are expressed as % of total fatty acids. Values in the same row with the same letter are not significantly different (α level = 0.05).

Figure 2 presents TAG fatty acid concentration for control and CLA-rich yolks, grouped by degree of unsaturation. The relative proportions of fatty acid groups closely resemble what was seen in the total lipid fatty acid composition. SFA concentration in CLA-rich yolk TAG was 46.9%, which was significantly higher than the control commercial yolk at 37.7%. CLA-rich yolk TAG had a significantly lower MUFA concentration at 35.4%, while control yolk TAG had 45%. Regular eggs yolks contained the highest levels of LC-PUFA in TAG at 3.6%, relative to CLA-rich yolk at 0.2%.

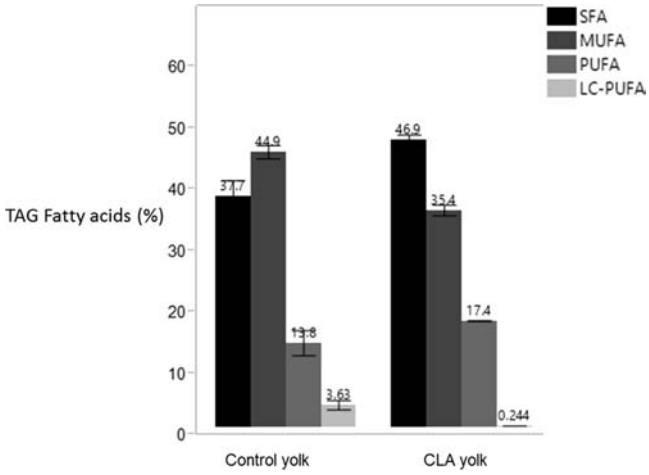

Figure 2. Triacylglycerol (TAG) fatty acid composition of yolk lipids from control and CLA-rich yolks. Fatty acids are grouped by degree of unsaturation: saturated fatty acid (SFA), monounsaturated fatty acids (MUFA), polyunsaturated fatty acids (PUFA), and long-chain polyunsaturated fatty acids (LC-PUFA). Error bars are one standard error from the mean.

Table 3 shows the fatty acid composition of the PL fraction of control and CLA-rich yolks. Yolk lipids contained approximately 33% PL.[29] The CLA contained in the PL fraction was 1.7% of the total fatty acids. CLA-rich yolk PL contained 20% stearic acid, which is significantly higher than control yolk PL at 16%. However, CLA-rich and control PL had no other significant differences in individual fatty acid concentrations.

Figure 3 depicts the PL fatty acid concentration for control and CLA-rich yolks, grouped by degree of unsaturation. CLA-rich yolk PL total SFA concentration was 45.8%, significantly higher than control yolk PL at 42.6%. Control yolk PL had significantly less SFA. The amount of MUFA in control regular yolk PL is surprisingly higher in control eggs at 59%.

Intact Lipid Composition. *TLC-UV-MALDI MS Analysis Determination of TAG and PL Species.* Figure 4 depicts the separation and visualization of lipid classes by TLC-UV, including LPC, SM, PC, PI, PE and total TAG, which were validated by TLC-MALDI imaging mass spectrometry (image not shown), identifying 2 LPC species, 1 SM species, 17 PC species, 19 TAG species, and 9 PE species (Table 4) based on observed m/z values. PI species had relatively low ion intensities in positive ion mode as expected due to its ability to easily form a negative ion rather than a positive ion under the MALDI positive reflector mode analysis and could not be

dx.doi.org/10.1021/jf501100y | J. Agric. Food Chem. 2014, 62, 6608−6615

Table 3. PL Fatty Acid Composition of Control and CLA-Rich Yolks[a]

fatty acid	control yolk PL fatty acid (%)	CLA-rich yolk PL fatty acid (%)
myristic acid (C14:0)	0.13 ± 0.01a	0.09 ± 0.02ab
palmitic acid (C16:0)	15.29 ± 0.50b	23.83 ± 1.76a
palmitoleic acid (C16:1)	1.86 ± 0.07a	0.35 ± 0.07c
stearic acid (C18:0)	8.77 ± 0.10c	20.22 ± 0.41a
oleic acid (C18:1)	56.67 ± 0.59a	25.61 ± 1.43b
linoleic acid (C18:2)	15.25 ± 0.16b	18.82 ± 0.81a
linolenic acid (C18:3)	0.36 ± 0.01a	0.33 ± 0.09a
CLA (C18:2 *c*-9,*t*-11)	0	0.34 ± 0.08a
CLA (C18:2 *t*-9,*c*-11 and *c*-10,*t*-12)	0	0.17 ± 0.06a
CLA (C18:2 *t*-10,*c*-12)	0	0.19 ± 0.03a
CLA (C18:2 *t*,*t*)	0	0.96 ± 0.01a
total CLA	0	1.66 ± 0.06a
eicosenoic acid (C20:1)	0.13 ± 0.01b	0.27 ± 0.03a
eicosatrienoic acid (C20:3)	0.13 ± 0.01b	0.54 ± 0.13a
arachidonic acid (C20:4)	0.9 ± 0.04b	4.94 ± 1.58a
tetracosanoic acid (C24:0)	0.31 ± 0.02b	1.61 ± 0.52a
docosahexaenoic acid (C22:6)	0.21 ± 0.01c	1.73 ± 0.59b

[a]Values are expressed as % of total fatty acids. Values in the same row with the same letter are not significantly different (α level = 0.05).

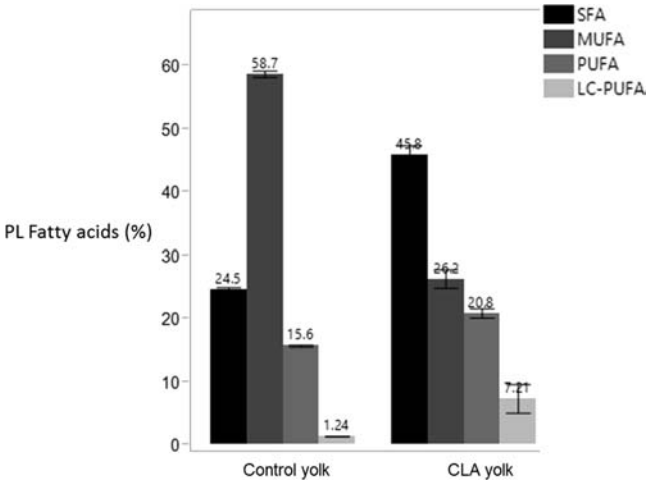

Figure 3. Phospholipid (PL) fatty acid composition of control commercial egg yolk, CLA-rich yolk, and omega-3 commercial yolk. Fatty acids are grouped by degree of unsaturation: saturated fatty acid (SFA), monounsaturated fatty acids (MUFA), polyunsaturated fatty acids (PUFA), and long-chain polyunsaturated fatty acids (LC-PUFA). Error bars are one standard error from the mean.

identified. We did not see overall changes in lipids in CLA-rich egg yolk compared to both commercial eggs.

Direct Infusion ESI-MS and Direct MALDI MS Quantification of Major TAG and PL Species. Both direct infusion ESI-MS and direct MALDI MS results lead to similar conclusions. Figure 5 shows representative average spectra for yolk lipid extracts. In the direct MALDI-TOF-MS spectra, TAG were not detected due to PC suppression.[22] When the lipid samples were fractionated by SPE before MALDI MS analysis, PL species intensities were much greater than TAG, although TAG are the more abundant in egg yolk lipids. ESI-MS resulted in a spectra of both TAG and PL species with an intensity ratio that was representative of the TAG and PL abundances. Direct flow Infusion ESI-MS in general had less peak intensity variation

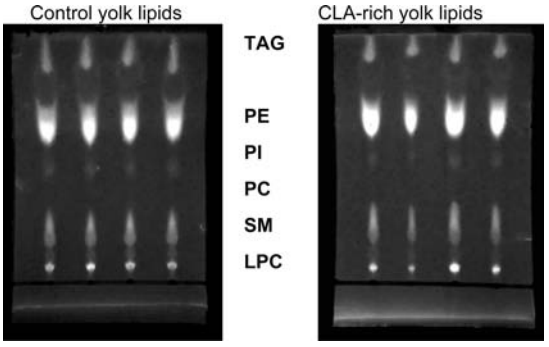

Figure 4. Lipid species separations from three yolk types: control regular commercial yolk, CLA-rich yolk, and omega-3 commercial yolk. These images were developed from the primuline sprayed TLCs as described in the Methods section.

leading to lower standard deviation in estimating relative composition. Therefore, we used only the DFI ESI-MS data to calculate yolk lipid relative composition, shown in Table 4.

Lysophosphatidylcholine and Sphingomyelin. LPC 16:0 and LPC 18:0 were significantly higher in CLA-rich yolks, relative to both controls ($p < 0.001$). Higher C16:0 and C18:0 levels were observed in CLA-rich yolk PL fractions, reported in Table 3. SM intensities were highest in control egg yolks ($p < 0.001$).

Phosphatidylcholine Species. ESI-MS relatively quantified 13 PC species in the positive ion mode and 4 additional species in the negative ion mode. CLA-rich yolks had significantly higher PC C34:2, which contains linoleic and palmitic fatty acid chains. Palmitic and linoleic acid concentrations were higher in the CLA PL fraction, which explains this higher intensity. The PC C34:1 levels were not significantly different among CLA-rich and control yolks. This is despite the fact that oleic acid concentrations were significantly lower in CLA yolks. The PC C34:0 was highest in control yolk. This species was expected to be at higher concentrations in CLA due to the elevated SFA levels seen in the PL fatty acid profiles (Figure 3), but this was not the case. PC C36:4 contains two linoleic acid chains, and PC C36:3 and C36:2 both contain one. It was not surprising that these three species were at highest concentration in CLA-rich yolks, in response to the elevated total linoleic acid levels in the CLA-rich soy oil. The C36:2 concentration was even more elevated in CLA-rich yolks due to increased stearic, linoleic, and possibly CLA concentrations observed in the PL fraction. PC C36:1 had two possible species identifications, one containing C16:0 and C20:1 chains and the other containing C18:0 and C18:1. By using the FAMEs profiles for the PL fractions, it seems that the control yolk C36:1 contains only C18:0 and C18:1, while CLA-rich yolks have elevated C16:0 and C20:1 levels and could contain a mixture of both species. There were no significant differences between PC C38:6 and C38:5 among yolk types ($p = 0.3$). There were two PC species containing one docosahexaenoic acid chain. PC38:6 was identified in both positive and negative ion modes.

Triacylglycerols. CLA-rich yolk contained elevated levels of all TAG species containing only SFA (C48:0, C50:0, C52:0, and C54:0). This again coincides with the elevated saturated fat concentrations observed in CLA-rich yolks. A substantial amount of variation was found between species with 52 carbon chains. C52:5 and C52:4 were elevated in CLA-rich yolks. By using FAMEs data with the www.lipidmaps.org mass spectra analysis tool, C52:5 and C52:4 were identified differently for

Table 4. Lipid Species Identified by TLC-MALDI MS and Intensities Quantified by ESI-MS, Including LPC, SM, PC, TAGs, and PE[a]

LPC and SM lipid species	m/z	control yolk	CLA yolk
LPC 16:0	496.3	0.48 ± 0.03b	0.95 ± 0.23a
LPC 18:0	524.3	0.29 ± 0.03b	0.84 ± 0.12a
SM 16:0	703.6	0.71 ± 0.04a	0.61 ± 0.06ab
PC lipid species	m/z	control yolk	CLA yolk
C34:2 [PC(16:0/18:2)]	758.57	5.98 ± 0.09a	7.99 ± 1.03a
C34:1 [PC16:0/18:1)]	760.58	13.97 ± 0.23a	12.06 ± 1.59a
C34:0 [PC(16:0/18:0)]	762.60	1.78 ± 0.06a	1.59 ± 0.04b
C36:4 [PC(18:2/18:2)]	782.57	1.71 ± 0.10a	1.84 ± 0.22a
C36:3 [PC(18:1/18:2)]	784.59	1.36 ± 0.07a	1.61 ± 0.23a
C36:2 [PC(18:0/18:2)]	786.60	3.61 ± 0.24a	5.15 ± 0.70b
C36:1 [PC(16:0/20:1) or (18:0/18:1)]	788.62	3.26 ± 0.31ab	4.29 ± 0.34a
C38:7 [PC(22:6/16:1)]	802.54 (−)	12.76 ± 0.38a	13.62 ± 3.09a
C38:6 [PC(22:6/16:0)]	804.55 (−)	22.51 ± 0.74a	16.52 ± 3.66a
C38:6 [PC(22:6/16:0)]	806.57	0.73 ± 0.03a	1.09 ± 0.15a
C38:5 [PC(18:2/20:3)]	808.59	1.14 ± 0.26a	1.15 ± 0.25a
C38:4 [PC(18:0/20:4)]	810.60	2.02 ± 0.07ab	2.40 ± 0.29a
C38:3 [PC(18:0/18:0)]	812.62	0.56 ± 0.04a	0.64 ± 0.11a
C40:5 [PC(20:4/20:1)]	836.62	0.61 ± 0.16a	0.58 ± 0.01a
C40:7 [PC(22:6/18:1)]	830.57 (−)	5.62 ± 0.33a	6.35 ± 1.11a
C40:6 [PC(22:6/18:0)]	832.59 (−)	4.98 ± 0.58a	4.4 ± 0.71a
C38:1 [PC(20:1/18:0)]	838.63	0.11 ± 0.03b	0.22 ± 0.02a
TAG lipid species	m/z	control yolk	CLA yolk
C48:0 (16:0/16:0/16:0)	824.77	0.32 ± 0.07b	0.55 ± 0.09a
C50:3 (14:0/18:1/18:2) or (16:0/18:3/16:0)	846.75	1.59 ± 0.12a	0.95 ± 0.05b
C50:2 (18:1/14:0/18:1)	848.77	3.42 ± 0.17a	2.73 ± 0.25a
C50:1 (16:0/16:0/18:1)	850.78	3.30 ± 0.07a	2.61 ± 0.39ab
C50:0 (16:0/16:0/18:0)	852.80	0.67 ± 0.08b	0.98 ± 0.09a
C52:5	870.75	0.31 ± 0.08b (14/18:1/20:4)	1.0 ± 0.04a (18:2/16:0/18:3)
C52:4	872.77	2.63 ± 0.30b (16:0/18:3/18:1)	5.05 ± 0.35a (18:2/16:0/18:2)
C52:3 (16:1/18:1/18:1)	874.78	13.62 ± 0.70b	13.15 ± 1.54b
C52:2 (16:0/18:1/18:1)	876.80	17.44 ± 0.34a	12.52 ± 1.35b
C52:1 (18:0/18:1/16:0)	878.82	5.70 ± 0.40a	5.41 ± 0.89a
C52:0 (18:0/16:0/18:0)	880.83	0.96 ± 0.10ab	1.49 ± 0.29a
C54:5 (18:3/18:1/18:1)	898.78	0.30 ± 0.07b (18:3/18:1/18:1)	0.90 ± 0.14a (18:2/18:2/18:1)
C54:4 (18:1/18:2/18:1)	900.80	1.10 ± 0.14c	1.60 ± 0.04b
C54:3 (18:1/18:1/18:1)	902.82	2.48 ± 0.12b	2.26 ± 0.15b
C54:2 (18:1/18:1/18:0)	904.83	3.74 ± 0.25a	2.25 ± 0.31b
C54:1 (18:1/18:0/18:0)	906.85	2.15 ± 0.23a	1.36 ± 0.03b
C54:0 (18:0/18:0/18:0)	908.86	0.55 ± 0.07b	0.83 ± 0.04a
PE lipid species	m/z	control yolk	CLA yolk
C34:2 [PE(18:2/16:0)]	714.51 (−)	3.25 ± 0.40a	3.4 ± 0.61a
C34:1 [PE(18:1/16:0)]	716.52 (−)	7.72 ± 0.12a	5.12 ± 1.05a
C36:4 [PE(18:3/18:1)]	738.51 (−)	3.14 ± 0.05a	2.7 ± 0.41a
C36:3 [PE(18:2/18:1)]	740.53 (−)	1.94 ± 0.06a	1.35 ± 0.25a
C36:2 [PE(18:1/18:1)]	742.54 (−)	5.73 ± 0.39a	6.15 ± 1.87a
C36:1 [PE(18:0/18:1)]	744.55 (−)	7.16 ± 0.49a	4.8 ± 1.02b
C38:6 [PE(22:6/16:0)]	762.51 (−)	2.57 ± 0.48ab	1.56 ± 0.32b
C38:5 [PE(18:1/20:4)]	764.52 (−)	3.48 ± 0.05a	1.84 ± 0.31b
C38:4 [PE(18:1/20:3)]	766.54 (−)	12.35 ± 0.4a	8.03 ± 1.97b

[a]Values in the same row with the same letter are not significantly different ($P = 0.05$). Lipid species with m/z (−) indicates species was detected in negative ion mode. Values in the same row with the same letter are not significantly different (α level = 0.05).

control eggs than for CLA eggs. CLA yolks contain a C52:5 TAG species that has a linoleic, linolenic, and palmitic acid chains, while control yolks have a species that has myristic, oleic, and arachidonic acid chains. It is likely that all three yolks have both isobaric mass species, and the database indicated the most probable species based on the FAMEs for each yolk type. The three fatty acids identified in C52:5 were all present at elevated levels in CLA yolks. The same rationale holds for the difference in C52:4 identifications for the three egg types. The C52:4 species contains two linoleic acid chains coupled with a palmitic chain. CLA-rich yolks contained the highest amount of this particular species, and it is a likely candidate for CLA incorporation. This species was also significantly higher in CLA-rich yolks, but this species more likely contains two linoleic acid chains and one oleic chain. The increased prevalence of this species in CLA-rich yolks also indicates a potential candidate for CLA incorporation. Other TAG species containing one, two, or three oleic chains were significantly lower in CLA-rich yolk lipids (C54:4, C54:3, C54:2, C54:1) compared to control yolks.

Phosphatidylethanolamine Species. All PE species were detected in the negative ion mode ESI-MS. CLA-rich yolks had significantly lower C36:1, C38:6, C38:5, and C38:4 compared to control commercial yolk PE. There were no significant difference in any of the PE species abundances between both commercial egg types.

In summary, the CLA rich eggs with 120 mg of CLA had significantly more SFAs and less MUFAs than did the control eggs. Comparable findings have been previously reported,[12−18] but this study provided a comprehensive overview of intact lipid species and determined differences among CLA and commercially available eggs. The separated TAG fatty acid compositions of all three yolk types were similar to their respective total fatty acid composition. In CLA-rich yolks, 50% of the CLA was in the TAG and located predominately in species C52:5 and C52:4. Other TAG species containing linoleic acid were not at elevated levels. The PL fatty acid composition was not significantly different among egg types. All PC species containing one or two linoleic acid chains were most abundant in CLA-rich yolks. CLA-rich yolks contained more LPC than did the controls. Although CLA and control yolks did not show differences in total PE, CLA did lower the amount of certain PE species relative to the control eggs.

The TAG and total PL fractions contain similar amounts of CLA. A previous study using a commercially available CLA source reported preferential CLA incorporation in the TAG

dx.doi.org/10.1021/jf501100y | J. Agric. Food Chem. 2014, 62, 6608−6615

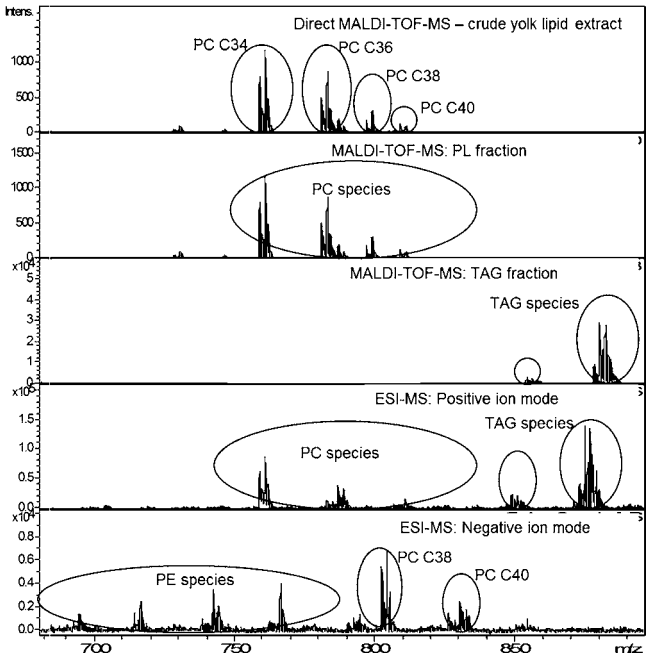

Figure 5. CLA-rich egg yolk lipid extract spectra resulting from different MS analysis. In direct MALDI-TOF-MS, the presence of PC suppressed TAG peaks. Fractionating the PL and TAG eliminated suppression. ESI-MS in positive ion mode allowed quantification of TAG and PC species, while negative ion mode allowed quantification of PE.

fraction versus PC and PE CLA content.[19] Their method of lipid species fractionation did not enable them to ensure complete separation without possible contamination. TLC allowed complete separation and collection of species without any overlap. TAG fractions contained more SFAs and less PUFAs than did the control egg yolks. CLA incorporation showed increased LPC concentration and modified the total PL composition. Although the yolk fatty acid composition is substantially different as a result of CLA incorporation, the relative composition of the lipid classes are maintained. Describing egg yolk lipids by both fatty acid analysis and molecular species analysis may help characterize the functional properties of different lipid species in egg nutrition studies.

Interest in egg yolk PC production for pharmaceutical applications has increased due to their high levels at 33% of total yolk lipids. This study illustrated that CLA-enriched PLs and TAGs are produced through feed modification and may be isolated for further nutraceutical uses. This extensive yolk lipid profiling described how CLA incorporation affected other lipid species in the yolk. Providing the most comprehensive egg lipid profile to date may offer insight in further physiological and nutritional studies on CLA-rich and other designer eggs.

AUTHOR INFORMATION

Corresponding Authors

*E-mail: seshinn@uark.edu.
*E-mail: rliyana@uark.edu.
*E-mail: jlay@uark.edu.
*E-mail: aproctor@uark.edu.

Notes

The authors declare no competing financial interest.

ACKNOWLEDGMENTS

The authors thank the University of Arkansas Poultry Science Department for their collaboration, advisement, and quality animal care.

REFERENCES

(1) Pariza, M. W. A beef-derived mutagenesis modulator inhibits initiation of mouse epidermal tumors by 7,13-dimethbenz[a]-anthracene. *Carcinogensis* **1985**, *6*, 591−593.
(2) McGuire, M. A.; McGuire, M. K. Conjugated linoleic acid (CLA): A ruminant fatty acid with beneficial effects on human health. *J. Anim. Sci.* **2000**, *77*, 1−8.
(3) Blankson, H.; Stakkestad, J. A.; Fagertun, H.; Thom, E.; Wadstein, J.; Gudmundsen, O. Conjugated linoleic acid reduces body fat mass in overweight and obese humans. *J. Nutr.* **2000**, *12*, 2943−2948.
(4) Risérus, U.; Berglund, L.; Vessby, B. Conjugated linoleic acid (CLA) reduced abdominal adipose tissue in obese middle-aged men with signs of the metabolic syndrome: A randomized controlled trail. *Int. J. Obes.* **2002**, *25*, 1129−35.
(5) Park, Y.; Storkson, J. M.; Albright, K. J.; Jiu, W.; Pariza, M. W. Evidence that the trans-10, cis-12 isomer of conjugated linoleic acid induces body composition changes in mice. *Lipids* **1999**, *34*, 235−241.
(6) Jain, V. P.; Proctor, A.; Lall, R. Pilot-scale production of conjugated linoleic acid-rich soy oil by photoirradiation. *J. Food Sci.* **2008**, *73*, 183−192.
(7) Shah, U.; Proctor, A.; Lay, J. O., Jr; Moon, K. Determination of CLA trans, trans positional isomerism in CLA-rich soy oil by GC−MS and silver ion HPLC. *J. Am. Oil Chem. Soc.* **2012**, *89*, 979−985.
(8) Gilbert, W.; Gadang, V.; Proctor, A.; Jain, V.; Devareddy, L. Trans, trans conjugated linoleic acid enriched soybean oil reduces fatty liver and lowers serum cholesterol in obese Zucker rats. *Lipids* **2011**, *46*, 961−968.
(9) Beppu, F.; Hosokawa, M.; Tanaka, L.; Kohno, H.; Tanaka, T.; Miyashita, K. Potent inhibitory effect of trans-9, trans-11 isomer of conjugated linoleic acid on the growth of human colon cancer cells. *J. Nutr. Biochem.* **2006**, *17*, 830−36.
(10) Islam, M.; Kim, Y.; Jang, W.; Lee, S.; Kim, H.; Kim, S.; Kim, J.; Ha, Y. A mixture of *trans, trans* conjugated linoleic acid induces apoptosis in MCF-7 human breast cancer cells with reciprocal expression of Bax and Bcl-2. *J. Agric. Food Chem.* **2008**, *56*, 5970−5976.
(11) Lee, Y.; Heuvel, J. Inhibition of macrophage adhesion activity by 9 trans,11 trans- conjugated linoleic acid. *J. Nutr. Biochem.* **2010**, *21*, 490−497.
(12) Chamruspollert, M.; Sell, J. L. Transfer of dietary conjugated linoleic acid to egg yolks of chicken hens. *Poult. Sci.* **1999**, *78*, 1138−1150.
(13) Meluzzi, N.; Tallarico, A.; Sirri, F.; Minelli, G.; Franchini, A. Dietary conjugated linoleic acid supplementation of laying hens: Effects on egg fatty acids composition and quality. *Ital. J. Anim. Sci.* **2003**, *1*, 456−458.
(14) Kim, J. H. Effect of dietary supplementation with conjugated linoleic acid, with oleic, linoleic, or linolenic acid, on egg quality characteristics and fat accumulation in the egg yolk. *Poult. Sci.* **2007**, *86* (6), 1180−1186.
(15) Raes, K.; Huyghebaert, D.; Smet, S.; Nollet, L.; Arnoutsm, S.; Demeyer, D. The deposition of conjugated linoleic acids in eggs of laying hens fed diets varying in fat level and fatty acid profile. *J. Nutr.* **2002**, *132*, 182−189.
(16) Schaefer, K. Incorporation of dietary linoleic and conjugated linoleic acids and related effects on eggs of laying hens. *Lipids* **2001**, *36* (11), 1217−1222.
(17) Yang, L. Differential incorporation of conjugated linoleic acid isomers into egg yolk lipids. *J. Agric. Food Chem.* **2002**, *50* (17), 4941−4946.

(18) Chamruspollert, M.; Sell, J. L. Transfer of dietary conjugated linoleic acid to egg yolks of chicken hens. *Poult. Sci.* **1999**, *78*, 1138−1150.
(19) Du, M.; Ahn, D. U.; Sell, J. L. Effect of dietary conjuagted linoleic acid on the composition of egg yolk lipids. *Poult. Sci.* **1999**, *78*, 1639−1645.
(20) Fuchs, B.; Suess, R.; Nimptsh, A.; Schiller, J. MALDI-TOF-MS directly combined with TLC: A review of the current state. *Chromatographia* **2009**, *69*, S95−S105.
(21) Johanson, R. A.; Buccafusca, R.; Quong, J. N.; Shaw, M. A.; Berry, G. T. Phosphatidylcholine removal from brain lipid extracts expands lipid detection and enhances phosphoinositide quantification by matrix-assisted laser desorption/ionization time-of-flight (MALDI-TOF) mass spectrometry. *Anal. Biochem.* **2007**, *362*, 155−167.
(22) Lou, X.; van Dongen, J. L. J.; Vekemans, A. J. M.; Meijer, E. W. Matrix suppression and analyte suppression effects of quaternary ammonium salts in matrix-assisted laser desorption/ionization time-of-flight mass spectrometry: An investigation of suppression mechanism. *Rapid Commun. Mass Spectrom.* **2009**, *23*, 3077−3082.
(23) Fuchs, B.; Schiller, J.; Suess, R.; Schuerenberg, M.; Suckau, D. A direct and simple method of coupling matrix-assisted laser desorption/ionization time-of-flight spectrometry (MALDI-TOF MS) to thin-layer chromatography (TLC) for the analysis of phospholipids from egg yolk. *Anal. Bioanal. Chem.* **2007**, *389*, 827−834.
(24) Emerson, B.; Gidden, J.; Lay, J. O.; Durham, B. A rapid separation technique for overcoming suppression of triacylglycerols by phosphatidylcholine using MALDI-TOF MS. *J. Lipid Res.* **2010**, *51*, 2428−2434.
(25) Fhaner, C. J.; Sichang, L.; Hong, J.; Simpson, R. J.; Reid, G. E. Comprehensive lipidome profiling of isogenic primary and metastatic colon adenocarcinoma cell lines. *Anal. Chem.* **2012**, *84* (21), 8917−8926.
(26) Shinn, S. E.; Proctor, A. Rapid lipid extraction from egg yolks. *J. Am. Oil Chem. Soc.* **2012**, *90*, 367−369.
(27) Lall, R. K.; Proctor, A.; Jain, V. P. A rapid, micro FAME preparation method for vegetable oil fatty acid analysis by gas chromatography. *J. Am. Oil Chem. Soc.* **2009**, *86*, 309−314.
(28) White, T.; Bursten, S.; Federighi, D.; Lewis, R. A.; Nudelman, E. High-resolution separation and quantification of neutral lipid and phospholipid species in mammalian cells and sera by multi-one-dimensional thin-layer chromatography. *Anal. Biochem.* **1998**, *258*, 109−117.
(29) Marc, A. Composition and structure of hen egg yolk. In *Bioactive Egg Compounds*; Huopalahti, R., Lopez-Fandino, R., Anton, M., Schade, R., Eds.; Springer: New Delhi, India, 2007.

of winter wheat grain due to an enriched atmospheric CO_2 concentration.

Therefore, the aim of the present study was to get more detailed information on the structural composition of the protein fractions prolamin and glutelin of winter wheat, winter barley and maize grains cultivated using the FACE technique. Osborne fractionation was performed to isolate the single protein fractions followed by proving the purity by SDS-PAGE. To characterize prolamins and glutelins in detail a size exclusion high performance liquid chromatography (SE-HPLC) method was developed. In addition, kernels were observed by scanning electron microscopy (SEM) to study differences in protein-starch bodies. These investigations should also explain the observed variations in digestibility of crude protein. The study intended to assess the potential impact of a future atmospheric CO_2 concentration expected by 2050 on the protein composition and quality of these important animal feedstuffs.

MATERIAL AND METHODS

Materials. The experiment with winter wheat and barley was conducted on a 22 ha experimental field site and the investigation on maize was performed on a 10 ha field site located at the experimental station of the Friedrich Loeffler Institute (FLI), Federal Research Institute for Animal Health, Braunschweig, Germany. A FACE system engineered by Brookhaven National Laboratory and previously described by Weigel and Manderscheid[7] with experimental rings of 20 m in diameter was used to study CO_2 enrichment effects on maize cv. Romario (silage maize), winter wheat cv. Batis (one of most frequently cultivated bread wheat varieties in Germany) and barley cv. Theresa (one of most frequently cultivated barley varieties in Germany) as well as the influence of N fertilization of winter wheat and barley. Therefore, two (barley and wheat) or three (maize) of the FACE rings were treated with blowers with air of ambient CO_2 concentration (AMBI, 380 ppm atmospheric CO_2) and the other two (barley and wheat) or three (maize) with blowers with CO_2 enriched air (FACE, 550 ppm atmospheric CO_2). The FACE rings were placed exactly at the same position in each growing season.

For winter wheat and barley, two different N fertilization levels were applied in each half of the rings to study interactions between CO_2 enrichment and N supply. One was an adequate N fertilization (N100) for each crop species and one was a reduced fertilization with 50% (N50) of the adequate N treatment as it was described by Weigel and Manderscheid.[22] For both crops the space between the two fertilization levels was set to approximately 1 m.

Varieties of all three cereals were chosen because of their general reliable yield forecasts. For analytical use, kernels of winter wheat and winter barley of the two cultivation seasons and kernels of maize cultivar were predried, milled at 1 mm and stored at −20 °C.

Protein Extraction. A modified Osborne fractionation according to Wieser et al.[23] was performed to separate the protein fractions of all three cultivars. 0.5 g milled (1 mm) flour was extracted two times with 0.5 mol L^{-1} sodium chloride (NaCl, ≥ 99%, Ph.Eur., USP, Carl Roth GmbH Co., Karlsruhe, Germany) for 10 min at room temperature (RT ∼ 23 °C).

Supernatant (albumins/globulins) was dialyzed (ZelluTrans, regenerated Cellulose Tubular Membrane, 6000−8000 Da, 1.67 mL/cm, Carl Roth GmbH Co., Karlsruhe, Germany) against water to separate both protein fractions in water - soluble albumins and water insoluble globulins.

Precipitate (prolamins/glutelins) was extracted twice with 70% ethanol (EtOH, Rotipuran, ≥ 99.8%, p.a., Carl Roth GmbH Co., Karlsruhe, Germany) for 30 min at RT. The supernatant consisted of EtOH-soluble prolamins. Precipitate was extracted twice with a solvent of 50% 1-propanol containing 1% dithiothreitol (DTT), 0.05 M tris-HCl, and 2 M urea (all chemicals at least ≥99%, p.a. quality, Carl Roth GmbH Co., Karlsruhe, Germany) for 20 min at 60 °C.

Each extraction step was initiated by vortexing until complete mixing and continued by vortexing at 600 rpm (MS1 minishaker, JKA Works Ic., Wilmington, NC, U.S.A.). All separations of supernatants and precipitates were performed by centrifugation for 10 min at 3000 rpm (Varifuge 3.OR, Heraus Sepatech, Osterode, Germany). All supernatants were dried to constant mass at 60 °C by centrifugal evaporator (Christ RVC 2-18HCL, Osterode, Germany).

SDS-PAGE. Isolated protein fractions were treated with 7 mM SDS (>99%, Carl Roth GmbH Co., Karlsruhe, Germany) and 200 mM DTT prior to separation in 4−20% Mini-PROTEAN TGX gels (Bio−Rad, Hercules, CA, U.S.A.) using a modified method of Laemmli.[24] Proteins were completely dissociated by boiling the samples at 95 °C for 5 min. Electrophoresis was carried out at 50 V for 30 min followed by 200 V for 1 h until the tracking dye, bromophenol blue (ACS, Carl Roth GmbH Co., Karlsruhe, Germany), had reached the bottom of the gel. Molecular weight markers were Roti-Mark 10−150 and Roti-Mark PRESTAINED (Carl Roth GmbH Co., Karlsruhe, Germany) to identify the individual protein groups on the gel. After electrophoresis, gels were stained in a Coomassie brilliant blue G-250 (Carl Roth GmbH Co., Karlsruhe, Germany) solution overnight and destained in water−methanol−pure acetic acid (40/10/50, v/v/v).

SE-HPLC. SE-HPLC was performed by using a Shimadzu instrument (liquid chromatograph, LC-20AT; autosampler, SIL-20AC; column oven, CTO-10ASvp; diode array detector, SPD-M20A) and a Yarra 3 μ SEC-2000 column (300 × 7.8 mm, Phenomenex; Torrance, CA) with guard cartridges (Phenomenex; Torrance, CA). Data was collected and analyzed using the CLASS-VP-6.14 SP2A software (Shimadzu). Mobile phases (50 mM phosphate buffer containing 0.1% SDS) were prepared by mixing a 50 mM disodium hydrogen phosphate dihydrate solution and a 50 mM sodium dihydrogen phosphate monohydrate solution according to Henderson−Hasselbalch equation for required pH values of 6.60 (A) and 6.94 (B).

Gliadin (from wheat, Sigma, Steinheim, Germany) and glutenin standards (Osborne fractionation of gluten, from wheat, Sigma, Steinheim, Germany) as well as grain protein samples (concentration: 2−35 mg mL^{-1}) were weighed and dissolved in mobile phase B by using an ultrasonic bath (FB15051, Fischer Scientific, Singen, Germany). Standards and samples were filtered (syringe filters, 0.45 μm, PVDF, anchor GmbH) before injection (50 μL). The measurements were performed at 25 °C with a flow rate of 0.7 mL/min and a gradient of mobile phase (0 min 100% B, 16 min 0% B, 22 min 100% B for re-equilibration). The monitoring wavelength was 214 nm with a run time of 30 min. Calibration and evaluation of logarithm scale with the standard proteins bovine serum albumin, ovalbumin, myoglobin, and cytochrome c were carried out to determine the sizes of the single protein subfractions.

SEM. For scanning electron micrographs of milled kernels of all three cultivars, an environmental SEM (EVO LS25, Carl Zeiss SMT GmbH, Oberkochen, Germany) was used. The voltage of the electron beam was 8.0 kV and a secondary electron detector was used. In preparation, kernels were fractured at ambient temperature at 1 mm.

Statistics. Data were evaluated by analysis of variance (ANOVA) after testing for normal distribution and variance homogeneity using the Kolmogorov−Smirnov test and the Bartlett-χ-square test, respectively. A complete 3-factorial design of ANOVA was used to evaluate the results for wheat and barley with the cultivation year (2000 and 2003), the CO_2 level (AMBI and FACE), the N-fertilization level (50 and 100% of adequate N-supply) and the corresponding interactions being the fixed factors. For evaluating the maize results the CO_2 level was the only fixed factor. Significance was assumed at $p < 0.05$ and STATISTICA for Windows Operating System (Version 10.0., StatSoft, Inc., 2011) was used for statistical evaluations.[25]

RESULTS

Protein Extraction and SDS-PAGE. The relative amounts of the single protein fractions were obtained by gravimetric analysis after Osborne fractionation. Tables 1−3 summarizes the effect of different N fertilization, CO_2 treatment and crop growing year on the percentages of the four fractions of winter barley, wheat, and maize.

Table 1. Crude Protein Content [g/kg DM] and Relative Amounts of the Protein Fractions Albumins, Globulins, Hordeins, and Glutelins, Determined by Osborne Fractionation [% CP] and Its Subfractions, Determined by SE-HPLC [% Protein Fraction] as Influenced by N Fertilization (N50, Half of Average N Supply; N100, Average N Supply) and CO_2 Supply (AMBI, 380 ppm; FACE, 550 ppm) of Winter Barley, $n = 4$[a]

year	CO_2	N	CP	ALB	GLO	HOR	D[b]	C[b]	B[b]	γ[b]	GLU	HMW[c]	LMW[c]
2000	AMBI	100	121	2.72 ± 1.07	18.91 ± 1.93	56.97 ± 5.08	16.25 ± 6.94	32.50 ± 2.65	38.22 ± 2.65	5.42 ± 2.14	19.68 ± 1.24	60.76 ± 0.04	39.24 ± 0.04
		50	99	2.28 ± 0.87	19.51 ± 3.96	58.97 ± 2.97	13.71 ± 2.28	25.50 ± 4.76	57.61 ± 6.79	3.18 ± 1.03	22.09 ± 2.83	60.56 ± 0.09	39.44 ± 0.92
	FACE	100	101	4.85 ± 1.87	23.76 ± 0.07	58.21 ± 9.43	18.78 ± 3.03	29.60 ± 1.77	43.25 ± 1.77	8.37 ± 1.63	23.03 ± 4.37	59.50 ± 1.47	40.50 ± 1.74
		50	81.4	2.96 ± 3.55	23.14 ± 4.60	63.00 ± 7.90	12.84 ± 1.58	24.78 ± 2.29	58.63 ± 2.29	3.75 ± 0.50	22.18 ± 7.33	56.96 ± 2.41	43.04 ± 2.04
2003	AMBI	100	110	4.50 ± 2.17	15.08 ± 4.03	58.43 ± 2.34	10.46 ± 1.90	30.22 ± 4.12	54.17 ± 4.12	5.15 ± 0.79	19.99 ± 1.16	76.77 ± 1.41	23.52 ± 1.00
		50	92.4	6.33 ± 0.54	11.63 ± 3.30	58.70 ± 6.92	6.24 ± 0.74	27.48 ± 0.87	61.55 ± 1.02	4.73 ± 0.12	21.93 ± 0.06	78.07 ± 0.76	21.93 ± 0.77
	FACE	100	97.3	6.05 ± 5.78	15.43 ± 2.12	52.71 ± 11.62	8.08 ± 2.66	22.30 ± 7.65	65.87 ± 7.65	3.76 ± 1.09	17.62 ± 3.08	75.70 ± 0.53	24.30 ± 0.53
		50	82.4	4.37 ± 5.95	19.72 ± 4.83	58.89 ± 2.92	5.68 ± 1.43	24.75 ± 2.22	63.73 ± 2.22	5.85 ± 0.76	18.66 ± 0.48	74.16 ± 6.05	25.84 ± 5.95
							ANOVA (p-values)						
year			0.083	0.246	0.005	0.492	<0.001	0.028	<0.001	0.231	0.296	<0.001	<0.001
CO_2			<0.001	0.696	0.020	0.983	0.152	0.065	0.006	0.188	0.270	0.147	0.166
N			<0.001	0.674	0.576	0.452	<0.001	0.185	<0.001	0.015	0.358	0.033	0.034
CO_2 × year			0.220	0.784	0.650	0.381	0.301	0.849	0.445	0.236	0.090	0.515	0.579
N × year			0.390	0.702	0.743	0.763	0.012	0.040	<0.001	<0.001	0.416	0.189	0.160
CO_2 × N			0.641	0.484	0.200	0.305	0.275	0.511	0.127	0.864	0.452	0.142	0.113
CO_2 × N × year			0.928	0.767	0.437	0.943	0.337	0.968	0.491	0.262	0.985	0.884	0.821

[a]ALB, albumins; GLO, globulins; HOR, hordeins; GLU, glutelins; HMW, high molecular weight; LMW, low molecular weight. [b]Percentage of hordein fraction. [c]Percentage of glutelin fraction.

Table 2. Crude Protein Content [g/kg DM] and Relative Amounts of the Protein Fractions Albumins, Globulins, Gliadins, and Glutenins Determined by Osborne Fractionation [% CP] and Its Subfractions, Determined by SE-HPLC [% Protein Fraction] As Influenced by N Fertilization (N50, Half of Average N Supply; N100, Average N Supply) and CO_2 Supply (AMBI, 380 ppm; FACE, 550 ppm) of Winter Wheat, $n = 4$[a]

year	CO_2	N	CP	ALB	GLO	GLI	$\omega5$[b]	$\omega1,2$[b]	α/β[b]	γ[b]	GLU	x-HMW[c]	y-HMW[c]	LMW[c]
2002	AMBI	100	149	28.12 ± 2.04	9.63 ± 1.85	46.50 ± 3.88	9.45 ± 1.10	8.90 ± 5.22	60.07 ± 12.14	21.58 ± 7.77	18.96 ± 4.40	25.86 ± 2.82	53.20 ± 1.22	19.09 ± 1.61
		50	133	20.97 ± 2.50	12.56 ± 0.24	51.00 ± 6.00	15.87 ± 0.59	7.64 ± 0.37	55.46 ± 0.87	20.73 ± 0.62	22.44 ± 9.48	25.43 ± 0.90	35.02 ± 8.22	39.55 ± 0.14
	FACE	100	141	30.55 ± 2.90	12.25 ± 1.09	46.98 ± 6.99	12.39 ± 4.17	6.57 ± 2.74	57.44 ± 3.49	18.07 ± 5.32	17.09 ± 5.64	20.85 ± 2.46	55.09 ± 1.34	24.05 ± 3.57
		50	118	12.90 ± 2.66	14.28 ± 1.70	52.55 ± 3.44	15.95 ± 1.59	8.02 ± 2.49	55.29 ± 2.68	20.73 ± 1.71	16.89 ± 7.36	29.63 ± 3.57	32.86 ± 2.66	37.51 ± 1.39
2005	AMBI	100	126	37.79 ± 4.21	7.71 ± 1.25	43.73 ± 2.63	12.10 ± 1.63	11.32 ± 1.88	47.02 ± 4.50	29.56 ± 4.08	10.34 ± 1.41	19.76 ± 9.89	47.11 ± 0.89	24.65 ± 1.49
		50	101	38.13 ± 7.63	11.47 ± 1.87	39.81 ± 1.41	14.27 ± 1.22	10.30 ± 0.59	47.15 ± 1.20	28.28 ± 0.77	11.64 ± 4.24	25.85 ± 0.74	40.19 ± 0.65	33.97 ± 5.66
	FACE	100	109	40.31 ± 11.94	9.16 ± 2.86	38.16 ± 7.35	13.97 ± 1.47	11.58 ± 0.47	46.60 ± 1.79	27.00 ± 2.32	11.07 ± 2.02	26.76 ± 2.32	41.25 ± 4.13	31.99 ± 6.36
		50	118	42.14 ± 5.89	10.81 ± 1.84	37.67 ± 4.14	14.04 ± 0.92	11.86 ± 0.47	45.62 ± 0.87	28.48 ± 1.52	13.79 ± 1.31	19.27 ± 4.59	38.91 ± 7.43	41.83 ± 3.13
								ANOVA (p-values)						
year			<0.001	0.001	<0.001	<0.001	0.965	0.007	0.002	<0.001	<0.001	0.066	0.671	0.135
CO_2			0.001	0.940	0.618	0.568	0.145	0.515	0.527	0.138	0.328	0.016	0.599	0.042
N			<0.001	0.084	0.011	0.052	0.002	0.400	0.577	0.624	0.581	0.068	0.002	<0.001
CO_2 × year			0.480	0.520	0.663	0.166	0.995	0.412	0.716	0.913	0.536	0.481	0.068	0.134
N × year			0.416	0.048	0.363	0.166	0.173	0.749	0.398	0.614	0.302	0.153	0.092	0.077
CO_2 × N			0.704	0.449	0.374	0.358	0.071	0.109	0.343	0.107	0.577	0.048	0.240	0.459
CO_2 × N × year			0.451	0.531	0.142	0.819	0.822	0.806	0.938	0.886	0.572	0.004	0.048	0.387

[a]ALB, albumins; GLO, globulins; GLI, gliadins; GLU, glutenins; HMW, high molecular weight; LMW, low molecular weight. [b]Percentage of gliadin fraction. [c]Percentage of glutenin fraction.

dx.doi.org/10.1021/jf501958a | J. Agric. Food Chem. 2014, 62, 6616−6625

Table 3. Crude Protein Content [g/kg DM] and Relative Amounts of the Protein Fractions Albumins, Globulins, Zeins and Glutelins (Determined by Osborne Fractionation [% CP] and Its Subfractions, Determined by SE-HPLC [% Protein Fraction] As Influenced by CO_2 Supply (AMBI, 380 ppm; FACE, 550 ppm) of Maize, $n = 6$[a]

year	CO_2	CP	ALB	GLO	ZEIN	γ^b	β^b	α^b	δ^b	GLU	HMW[c]	LMW[c]
2008	AMBI	83.1	12.48 ± 2.26	12.53 ± 2.57	48.68 ± 2.05	21.47 ± 1.81	27.06 ± 1.92	32.41 ± 2.05	19.05 ± 0.31	26.61 ± 5.84	63.92 ± 8.33	36.08 ± 8.17
	FACE	84.4	8.01 ± 3.52	4.79 ± 2.90	55.53 ± 5.56	23.53 ± 1.99	19.74 ± 8.63	15.95 ± 3.68	27.29 ± 8.60	33.46 ± 2.73	75.55 ± 1.72	24.77 ± 1.73
ANOVA (p-values)												
	CO_2	0.59	0.616	<0.001	0.006	0.150	0.197	<0.001	0.006	0.019	0.004	0.004

[a]ALB, albumins; GLO, globulins; GLU, glutelins; HMW, high molecular weight; LMW, low molecular weight. [b]Percentage of zein fraction. [c]Percentage of glutelin fraction.

Albumins, total glutelins and hordeins, the prolamin fraction of winter barley (Table 1) did not show any variations in contrast to globulins which increased significantly from about 19 to 24% in 2000 and from about 12 to 20% in 2003 under elevated CO_2. Additionally, the crop growing conditions of the different years also led to varied globulin contents.

Significant influences of the crop growing year for all four fractions of winter wheat could be demonstrated (Table 2). The relative amount of albumins and globulins increased significantly from approximately 12−30% and 10−14% in 2002 to about 38−42% and 38−44% in 2005, whereas the percentages of gliadins, the prolamin fraction of wheat, and glutenins, wheat glutelin fraction, decreased strongly by 5−10% within these years. Moreover, globulins were significantly reduced by about 2 or 3% at a higher N supply.

Table 3 and Figure 1 summarize the effects of an atmospheric CO_2 enrichment on maize. All fractions, except albumins showed significant changes. The content of globulins decreased significantly from 12 to 5% under elevated atmospheric CO_2 concentration. Zein, the prolamin fraction of maize, and glutelins were strongly increased due to a higher CO_2 supply. Both fractions rose by 14 and 18%, respectively.

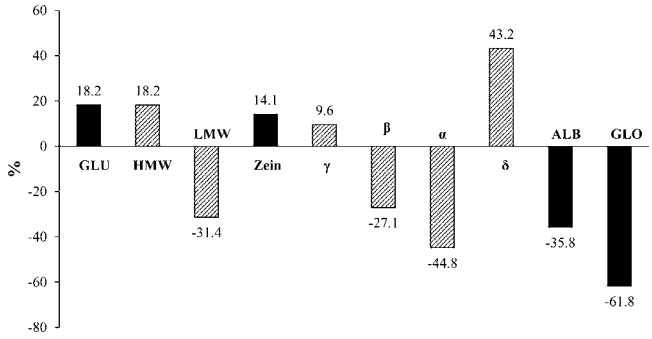

Figure 1. Relative percentage changes of the amounts of protein fractions and subfractions of maize grains by elevated CO_2 (FACE) compared with ambient CO_2 (AMBI), abbreviations see Table 3.

After Osborne fractionation, SDS-PAGE was done to prove the purity of the isolated protein fractions. All four fractions showed their typical lanes in the gel. For example, wheat grain prolamins were recognized at a molecular weight of 27 000−35 000 (α-, β-, and γ-gliadins) and at 37 000−52 000 (ω1,2- and ω5-gliadins). Glutelin subfractions were analyzed at a molecular weight of 32000−35000 (LMW subunits), at 60000−88000 (x-type HMW subunits) and at 96 000 to 120 000 (y-type HMW subunits).

SE-HPLC. Validation of the developed SE-HPLC method resulted in a relative standard deviation (RSD) of not more than 4.1% for repeatability and 13.9% for day-to-day precision of standard glutenin. The limit of quantitation (LOQ) with a signal-to-noise ratio (S/N) of 10 amounted to 308 μg/mL. Standard gliadin showed a RSD of maximum 6.4% for repeatability and 14.8% for day-to-day precision. LOQ was 164 μg/mL.

Prolamin and glutelin fractions of all three analyzed cultivars could be separated with the same developed method. Chromatograms of winter wheat gliadin and glutenin are shown exemplary in Figure 2 and 3. The main subfractions could be clearly separated. The relative amounts and the statistical results of these subfractions are also summarized in Tables 1−3 for the respective cultivar.

dx.doi.org/10.1021/jf501958a | J. Agric. Food Chem. 2014, 62, 6616−6625

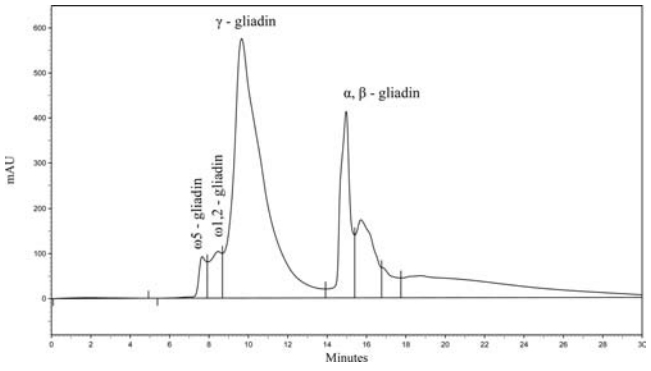

Figure 2. SE-HPLC chromatogram of the prolamin fraction of winter wheat.

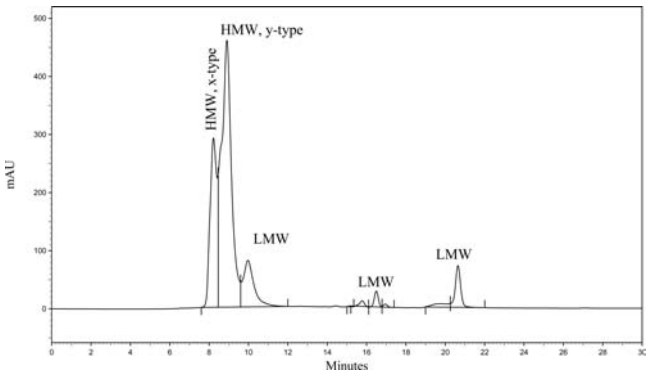

Figure 3. SE-HPLC chromatogram of the glutelin fraction of winter wheat.

Different crop growing years had a strong influence on the content of all winter barley hordein and glutelin polymers, except for γ-hordein (Table 1). A significant decrease of D- and C-hordein and LMW polymer as well as a strong increase of B-hordein and HMW polymer from 2000 to 2003 is stated. An enriched atmospheric CO_2 concentration induced a considerable increase of B-hordein in a range from 1 to 11%. Comparing the different N fertilization levels, the relative amounts of D-hordein, γ-hordein, and HMW polymers rose strongly and B-hordein and LMW polymers declined significantly from N50 to N100.

Table 2 summarizes the relative amounts of gliadin and glutenin subfractions of winter wheat. Comparing the growing years 2002 and 2005, the content of ω1,2- and α/β-gliadins increased by about 3 and 10%. In contrast, the relative amount of γ-gliadin decreased strongly by approximately 8% from 2002 to 2005. A higher N fertilization indicated a significant decline of ω5-gliadin and LMW subunits and a significant increase of y-HMW subunits. Depending on the growing year, N supply and CO_2 treatment, the content of y-HMW subunits rose from AMBI to FACE by about 2% at N100 in 2002 and by 6% in 2005. Furthermore, an increase from FACE to AMBI by 3% at N50 in 2002 and by 2 in 2005 was observed. A comparable effect of year, N supply and CO_2 interaction was observed in x-HMW subunits. For example, their amount was increased by 30% from FACE, N100 to FACE, N50 in 2002.

The percentages and the changes of zein and glutelin subfractions of maize are given in Table 3 and Figure 1. Both, HMW and LMW polymers as well as α- and δ-zeins were strongly affected by atmospheric CO_2 concentration. The contents of HMW polymers and δ-zein were significantly enhanced from 64 to 76% and from 19 to 27% under elevated CO_2 supply. In contrast, LMW polymers and α-zein were considerably reduced by more than 30%.

Protein−Starch Bodies Observed by SEM. Scanning electron micrographs of barley, wheat, and maize grown under different CO_2 treatments showed some marked differences. Barley grown under AMBI conditions (Figure 4a) showed some small agglomerates of proteins at starch granules. Starch granules of barley treated with elevated CO_2 were more intensively covered with this protein matrix (Figure 4b, note smaller scale compared to part a). In Figure 5, the starch bodies of winter wheat kernels of both CO_2 treatments are adjacent to densely packed protein bodies and no obvious differences between both treatments could be observed. The most pronounced differences were found for maize. Starch granules of AMBI maize kernels were relatively free of adherent protein material and only some granules were tightly covered with this (described by arrows in the figure), whereas protein bodies of FACE maize grains were densely wrapped with starch (Figure 6).

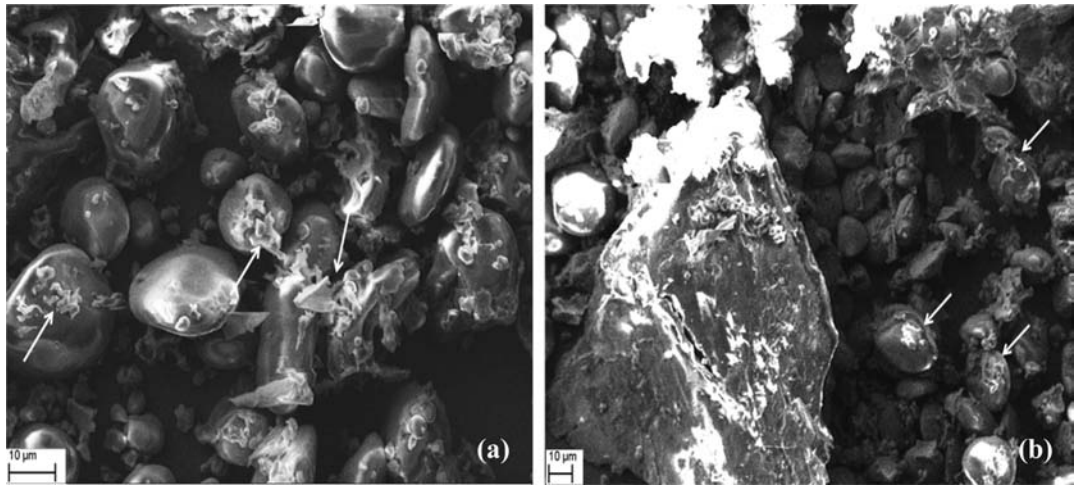

Figure 4. Scanning electron micrographs of winter barley grain cultivated under ambient (a) and elevated (b) atmospheric CO_2 concentration, some typical protein bodies are arrowed.

dx.doi.org/10.1021/jf501958a | J. Agric. Food Chem. 2014, 62, 6616−6625

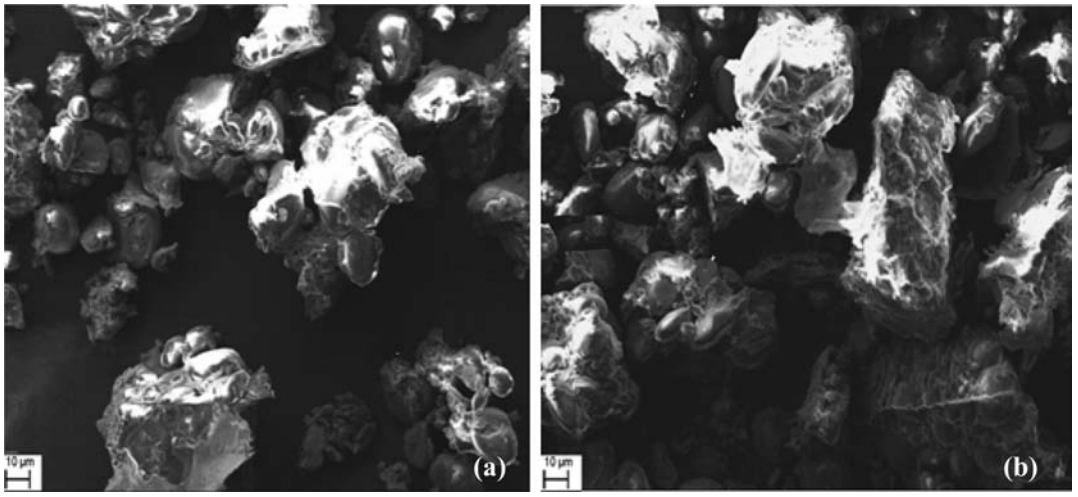

Figure 5. Scanning electron micrographs of winter wheat grain cultivated under ambient (a) and elevated (b) atmospheric CO_2 concentration.

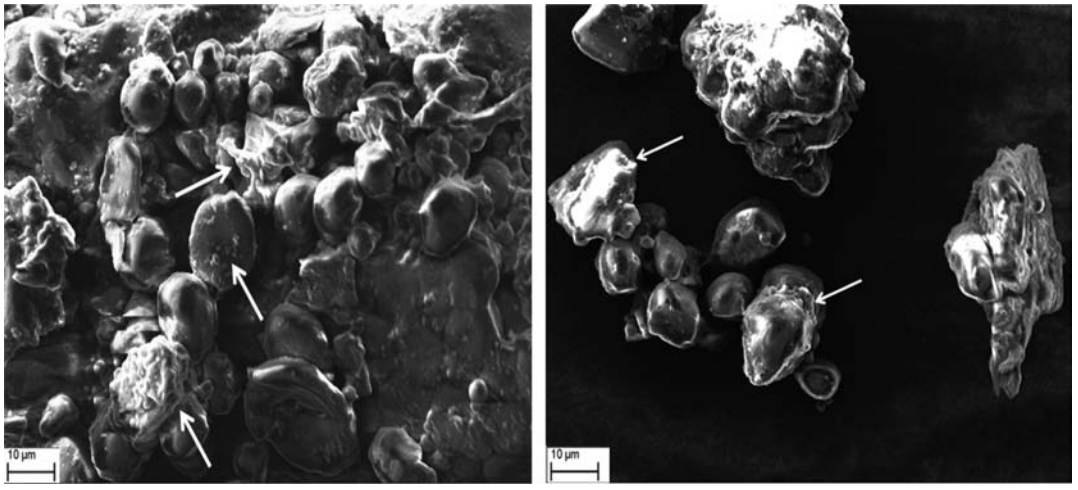

Figure 6. Scanning electron micrographs of maize grain cultivated under ambient (a) and elevated (b) atmospheric CO_2 concentration, some typical protein bodies are arrowed.

DISCUSSION

The present study investigated the effects of different CO_2 and N treatment on the content and composition of proteins in winter wheat and barley of two different crop growing years. Furthermore, influences of elevated CO_2 concentration were studied on maize proteins.

The effect of N fertilization on wheat crude protein and albumin content is in agreement with previous studies,[15,21,26,27] showing an increase of crude protein due to a higher N supply and a small influence on albumins. Investigations of Wieser and Seilmeier[28] and Wieser et al.[21] on the relative amounts of all wheat gluten subfractions indicated an increase at a higher N supply. Furthermore, Shewry et al.[17] found that the protein composition in barley grains was influenced by the N level in soil. A higher N fertilization increased the total gluten protein content in barley grains. The present results partly support these observations. The subfractions of wheat glutenin were significantly influenced, except for x-HMW glutenin subunits. The LMW glutenin subunits showed a significant decrease, and y-HMW glutenin subunits are strongly increased under a higher N fertilization level (Table 2). In general, LMW glutenin subunits within the total glutenin fraction are low and the proportion of HMW subunits is high. Total glutenin consists predominately of LMW glutenin subunits and HMW glutenin subunits belong to the minor components of the gluten proteins.[19] Wieser[15] found in his studies approximately twice as many LMW subunits as HMW subunits. In contrast, a contrary result of both subfractions was described in the present study. Possibly, there was not a clear separation of HMW and LMW glutenin subunits in the SE-HPLC analysis or some high molecular weight gliadins could be as a residue in glutenin Osborne fraction. The gliadin subfractions were not significantly affected by a higher N supply, only ω5-gliadin decreased (Table 2). The total gluten content in barley was not affected by N fertilization in the present study, but most of its subfractions were influenced significantly (Table 1). In contrast to the already mentioned literature, Wang et al.[29] described only small differences in the content of all protein main fractions, which is in agreement with the results of this study. Consequently, differences in percentage composition of the protein fractions seem to depend on the cultivar itself and on the N supply level.[30,31] Moreover, it is stated that the response of single protein fractions to agronomic factors such as sowing date and application time varied with the type of protein fraction and with genotype.[29] The quality of grains is often affected by the crop growing year and the cultivars itself, where the growing season significantly influences wet gluten content and rheological properties and different cultivars

dx.doi.org/10.1021/jf501958a | J. Agric. Food Chem. 2014, 62, 6616−6625

showed variations in quality parameters. These differences were based on genetic specificity according to expression of quality characteristics and cultivar reaction to environmental factors. Especially the quality parameters and environmental factors have impacts on prolamins and glutelins from ripening to maturity.[31] Therefore, methods for mass spectrometry and 2-D electrophoreses were developed to identify the gluten proteins in detail and to construct databases including cultivar specific gluten protein sequences. On this basis, several authors[32−34] documented changes of individual proteins of different cultivars by proteome maps resulting from applications of mineral nutrients or/and different air temperatures. Hurkman et al.[32] described an alteration of individual gliadin and glutenin accumulation profiles of wheat cv. Butte 86 during grain development due to higher temperature and a variation in the fertilizer regime. They found that both high temperature and fertilizer will increase the proportions of most HMW subunits and ω-gliadins and some of the α-gliadins while the proportions of LMW subunits and few γ-gliadins will decrease. In addition, Altenbach et al.[33] analyzed an increase in the ratio of HMW to LMW subunits and of gliadins to glutenins in experiments with a postanthesis fertilizer in wheat cv. Butte 86. According to the results of the present study, the ratio of gliadins/glutenins of winter wheat did not show any significant influences of N fertilization level, CO_2 enrichment, or environment. All ratios were in the same range whereas the ratio of HMW/LMW subunits significantly rose with an increased N supply in the present study. Additionally, an environmental effect was observed in winter barley, where the HMW/LMW polymer ratio differed significantly due to the crop growing year and different N fertilizer level. Both zein to glutelin and HMW to LMW polymer ratios were strongly affected by the different atmospheric CO_2 concentrations of maize. The zein/glutelin ratio decreased from 1.83 to 0.60 and the HMW/LMW polymer ratio increased from 1.77 to 3.05 in the present study.

Environmental conditions, such as precipitation or global radiation can also influence the proportion and amount of proteins in the developing kernel. The decrease in crude protein, albumins, globulins, and glutelins and the increase of prolamins in winter wheat and barley within the two growing years may be related to a diversity in climate conditions, for example higher precipitation in 2002 or a stronger global radiation in 2005.[22] Dupont et al.[34] also described the influence of variations in air temperature on the protein composition of wheat cv. Butte 86. The study was done under controlled environments, a moderate regime (24 °C at day/17 °C at night) and a high temperature regime (37 °C at day/28 °C at night) in combination with postanthesis mineral supply. They analyzed increased protein content under moderate temperatures with mineral supply. Increases in the content of ω-gliadins and HMW glutenin subunits and a decrease in LMW glutenin subunits were analyzed. In contrast, the high temperature regime had only little effects on the protein composition due to mineral supply. Several other authors[27,35,36] stated that kernel growth is directly influenced by soil N and air temperature. Therefore, it can be summed up that N supply could directly increase grain protein content especially monomeric gliadins, but this effect may differ between cultivars. Moreover, heat or drought could increase the protein content in combination with a reducing yield because of their effects on starch production.[34] As there are no relevant changes of the grain weight of wheat[37] (e.g., in 2002: AMBI/N100, 40.6 mg; AMBI/N50, 40.7 mg; FACE/N100, 42.7 mg; FACE/N50, 42.4 mg) and barley[38] (e.g., in 2000: AMBI/N100, 44.4 mg; AMBI/N50, 42.3 mg; FACE/N100, 45.8 mg; FACE/N50, 43.2 mg) no dilution effects caused by an enhanced starch production are expected. However, the grain weight of maize was significantly increased from 255 mg to 273 mg due to an elevated atmospheric CO_2 concentration.[35] Therefore, differences between zein and α-zein were not significantly influenced with increased CO_2. However, all other protein fractions and subfractions showed strong variations. A dilution caused by increased starch content could be denied.

The elevated atmospheric CO_2 concentration resulted in a decrease of crude protein content of barley (Table 1) and wheat grain (Table 2), but in a constant concentration in maize grain (Table 3), which correlates with several previous studies.[26,39−41] Moreover, the results of the present study revealed changes in the proportion of the different protein fractions and subfractions of barley and maize grain caused by CO_2 enrichment. Prolamins of barley are rich in proline and glutamine.[18] Wroblewitz et al.[40] showed a decrease of the relative amounts of proline and glutamine of barley which could explain the reduced C-hordein fraction, which consists of approximately 40% glutamine.[42] Hence, a direct correlation between the CO_2 effect on specific protein fractions and their glutamine content might be deduced.

Assessing the observed effects, an impact on the nutritional value may be possible. Akin et al.[43] investigated effects of an elevated atmospheric CO_2 concentration on the digestibility of nutrients. They found that the in vitro digestibility of young leaf blades of wheat grown under elevated CO_2 concentration tended to be higher than of plants cultivated under ambient CO_2. This was accompanied by a loss of crude protein and an increase of fiber fractions under elevated CO_2. An influence on the digestibility and degradability of maize grain, cultivated at different atmospheric CO_2 concentrations was also studied by Wroblewitz et al.[20] They observed an increased crude protein digestibility in broiler chicken trails and a lowered degradability of FACE maize grain proteins in in sacco studies. The decreased degradability could be caused by differences in the protein fractions albumin, globulin, zein, glutelin, and their subfractions. Also, differences in the stage of maturity could affect the structure and consequently the degradability of proteins.[44] During maturation the percentage of zein rose from about 5 to 35% and the distribution of albumin and globulin changed.[45] Therefore, analyses regarding the composition and amounts of globulins, albumins, zein, and glutelin could help to interpret variations in protein digestibility and ruminal degradability.

In addition, a change in amino acid composition of winter wheat and barley as described by Wroblewitz et al.[40] could also hint at a shift in the protein fractions and subfractions, as suggested by the present results, with consequences for digestibility and degradability. For evaluating the nutritional value, a look on the limiting amino acids lysine, methionine, threonine and tryptophan is necessary. A decrease of them could result in malnutrition of monogastric livestock when not counterbalanced.[10] The sulfur-containing amino acids such as methionine and other essential amino acids, especially lysine, are mostly represented in the metabolic proteins, albumins, and globulins. Storage proteins (prolamins and glutelins), which are primarily responsible for many aspects of grain quality[46] are rich in glutamine and proline. Hence, a higher digestibility and better nutritional value could be expected with enhanced globulin content as it was found in the present study for barley.

Moreover, structural differences of protein-starch bodies could affect the digestibility and degradability of cereal grain due to physicochemical constellations hampering the accessibility of digestive enzymes. McAllister et al.[47] described a

relationship between kernel hardness and affinity between starch and protein. Increased kernel hardness was correlated with a higher degree of association between both components.[48] In addition, a high correlation of protein-starch bodies and digestive properties in the rumen was stated. By increasing hardness the concentrations of zein increase and glutelin decrease. Zein limits the accessibility of the starch granules to ruminal microbes.[44] The structure of the protein-starch body seems to be responsible for differences in ruminal degradability of maize grains.[47] The present study could show differences in the starch−protein structure of barely and maize, which could be caused by the variation of protein fractions and subfractions. Hence, an impact on digestibility and degradability parameters is possible. As it is shown in the study of Wroblewitz et al.,[20] the crude protein degradability of FACE maize grain is significantly reduced. This could be affected by an increased kernel hardness and consequently by a shift in zein and glutelin fractions which was confirmed by the present SE-HPLC analysis. However, the changes in the starch−protein structure and, as a result, in kernel hardness were not distinct enough to influence starch degradability.

The reported changes in protein composition and quality of cereal grains under elevated CO_2 concentration could result in a necessity of dietary counterbalancing with other protein compounds and/or pure amino acids to meet the required nutrients for an adequate human and animal nutrition.

Beside influences on digestibility and degradability, differences in the protein composition could also affect bread making quality and malt quality. The rheological behavior of dough depends on the amounts and proportions of gluten protein fractions and subfractions, which are responsible for crumb structure and bread volume.[21] One of the most important characteristics for baking quality is the bread volume, which has been shown to be strongly correlated with crude protein content, total gluten proteins and glutenin macropolymers.[11] Numerous studies have shown that differences in amounts and proportions of gluten protein fractions and subfractions have significant effects on dough properties.[21,49] All of these parameters were significantly reduced by CO_2 enrichment in the present investigation. The present study also examined variations in the proportion of gliadins and glutenin subfractions due to crop growing year, N supply and significantly reduced crude protein content. Thus, a decrease in bread volume and a negative effect on wheat grain quality could be expected. However, only a single wheat cultivar was examined in one site. To get a more knowledge of expected reductions in relevant grain proteins, it is necessary to perform studies at diverse sites and with more cultivars.

Barley is used for malting and subsequently for the production of beer. According to Wang et al.[29] the protein concentration in barley grains is negatively correlated with malt extract and viscosity and malt quality is influenced by different N applications. Several authors[29,50,51] described a great effect of N fertilization level on the protein content and the protein fractions. Howard et al.[50] compared the hordein composition and the malt quality of three barley cultivars grown at five N regimes in each of two years. They determined a great variation in grain protein contents, malt extract values and in the proportions of the B-, C- and D-hordeins, whereas D-hordein partly varied over a 10-fold range. Moreover, they stated that the total protein displayed a strong, negative correlation with malt extract. D-hordein showed the most negative correlation with malt extract, which was independent of cultivar. Therefore, they declared that the measurement of D-hordein offers an option for the prediction of malting quality over a wide range of environmental conditions and cultivars. Molina-Cano et al.[51] showed that regional trends affect the negative correlation between malt extract yield and barley protein content from different varieties. In general, a trend decreasing malt extract yield with rising protein content was observed. In the present study, a wide variation of the hordein subfractions, especially D-hordein, and crude protein content due to environmental differences, such as the N supply, was observed. These results indicate the importance of adopting suitable N supply regimes that are specific for individual malting barley varieties to improve resulting malt quality. Furthermore, these observations could also indicate an influence of CO_2 supply on malt quality.

The current investigation demonstrated clearly that an elevated atmospheric CO_2 concentration and reduced N supply will alter the protein composition and hence the grain quality and nutritional value of wheat, barley, and maize. The protein fractions globulins and B-hordeins of barley were significantly enhanced due to an elevated atmospheric CO_2 concentration. Under same CO_2 enrichment, the protein fractions zein, δ-zein, maize glutenin, and its HMW polymers were also significantly increased, whereas globulins, α-zein, and maize LMW polymers were extensively decreased. A reduced N fertilization level affected mostly the prolamin subfractions of winter barley and wheat. D- and γ-hordein of barley significantly declined and B-hordein increased at a reduced N fertilizer level. In wheat, ω5-gliadin was significantly enhanced at reduced N supply. An influence of other crop growing conditions could be proved by analyzing barley and wheat grains of two different growing years. The present study shows that the developed SE-HPLC method is a quite rapid and cheap tool to characterize proteins and changes in protein composition. It could help to draw conclusions on variations in the composition of amino acids, on the protein quality and consequently on the nutritional value. Supplementations of proteins or amino acids on feedstuff would need a respective adjustment in the future. The present study only investigated one cultivar of each cereal. To get more information on the reaction of different cultivars on the factors such as crop growing year, N fertilization, and atmospheric CO_2 concentration, additional investigations would be interesting. This method builds a basis for further studies to explain whether other genotypes as well as high quality grain will react in the same way. Whether additional N supply to the soil may compensate the CO_2 effects and reshift the equilibrium of C- and N-providing resources remains open and is critical for economic as well as ecological reasons.

AUTHOR INFORMATION

Corresponding Author

*Tel.: +49 0 531 596 3128. Fax: +49 0 531 5963199. Email: liane.huether@fli.bund.de.

Notes

The authors declare no competing financial interest.

ACKNOWLEDGMENTS

The study was supported by the Federal Ministry of Food, Agriculture and Consumer Protection (BMELV) via the Federal Office for Agriculture and Food (BLE) within the network GrainUp−a collaborative research project: Innovation characterization and improvement of the feeding value of cereal grains. Brookhaven National Laboratory engineered the FACE apparatus and we are grateful to Dr. George Hendrey,

Mr. Keith Lewin, and Dr. John Nagy for their support. The FACE project with maize was supported by the German Federal Ministry of Education and Research (BMBF). Support by Prof. Dr. Stephan Scholl and Simone Schulze from the Institute for Chemical and Thermal Process Engineering of the Technical University Braunschweig for allocating the SEM is acknowledged.

■ ABBREVIATIONS USED

ALB	albumins
AMBI	ambient conditions
CO_2	carbon dioxide
DTT	dithiothreitol
FACE	Free Air Carbon Dioxide Enrichment
GLI	gliadins
GLO	globulins
GLU	glutelins/glutenins
HMW	high molecular weight
LMW	low molecular weight
HOR	hordeins
LOQ	limit of quantitation
N	nitrogen
ppm	parts per million
RSD	relative standard deviation
S/N	signal-to-noise
SDS	sodium dodecyl sulfate
SDS-PAGE	sodium dodecyl sulfate polyacrylamide gel electrophoresis
SE-HPLC	size exclusion high performance liquid chromatography

■ REFERENCES

(1) Dlugokencky, E.; Tans, P. *Trends in Atmospheric Carbon Dioxide*; NOAA: Washington, DC; www.esrl.noaa.gov/gmd/ccgg/trends/ (accessed April 16, 2014)

(2) IPCC *Climate Change 2007: The Physical Science Basis. Contribution of Working Group I to the Fourth Assessment Report of the Intergovernmental Panel on Climate Change*; Cambridge University Press, Cambridge, U.K., 2007.

(3) Högy, P.; Fangmeier, A. Effects of elevated atmospheric CO_2 on grain quality of wheat. *J. Cereal Sci.* **2008**, *48*, 580−591.

(4) Hendrey, G. R.; Kimball, B. A. The FACE program. *Agric. For. Meteorol.* **1994**, *70*, 3−14.

(5) Ghannoum, O. C4 photosynthesis and water stress. *Ann. Bot.* **2009**, *103*, 635−644.

(6) Wu, D.-X.; Wang, G.-X.; Bai, Y.-F.; Liao, J.-X. Effects of elevated CO_2 concentration on growth, water use, yield and grain quality of wheat under two soil water levels. *Agric. Ecosyst. Environ.* **2004**, *104*, 493−507.

(7) Weigel, H. J.; Manderscheid, R. CO_2 enrichment effects on forage and grain nitrogen content of pasture and cereal plants. *J. Crop. Improv.* **2005**, *13*, 73−89.

(8) Loladze, I. Rising atmospheric CO_2 and human nutrition: Toward globally imbalanced plant stoichiometry? *Trends Ecol. Evol.* **2002**, *17*, 457−461.

(9) Taub, D. R.; Wang, X. Why are nitrogen concentrations in plant tissues lower under elevated CO_2? A critical examination of the hypotheses. *J. Integr. Plant Biol.* **2008**, *50*, 1365−1374.

(10) Friedman, M. Nutritional value of proteins from different food sources. A review. *J. Agric. Food Chem.* **1996**, *44*, 6−29.

(11) Weegels, P. L.; Hamer, R. J.; Schofield, J. D. Functional properties of wheat glutenin. *J. Cereal Sci.* **1996**, *23*, 1−17.

(12) Shewry, P. R.; Halford, N. G. Cereal seed storage proteins: Structures, properties, and role in grain utilization. *J. Exp. Bot.* **2002**, *53*, 947−958.

(13) Huang, S.; Adams, W. R.; Zhou, Q.; Malloy, K. P.; Voyles, D. A.; Anthony, J.; Kriz, A. L.; Luethy, M. H., Improving nutritional quality of maize proteins by expressing sense and antisense zein genes. *J. Agric. Food Chem.* **2004**, *52*.

(14) Osborne, T. B. *The Proteins of the Wheat Kernel*; Carnegie Institution: Washingtong, DC, 1907.

(15) Wieser, H. Comparative investigations of gluten proteins from different wheat species. I. Qualitative and quantitative composition of gluten protein types. *Eur. Food Res. Technol.* **2000**, *211*, 262−268.

(16) Wilson, C. M.; Shewry, P. R.; Faulks, A. J.; Miflin, B. J. Extraction and separation of barley glutelins and their relationship to other endosperm proteins. *J. Exp. Bot.* **1981**, *32*, 1287−1293.

(17) Shewry, P.; Tatham, A.; Halford, N. Nutritional control of storage protein synthesis in developing grain of wheat and barley. *Plant Growth Regul.* **2001**, *34*, 105−111.

(18) Mickowska, B.; Socha, P.; Urminska, D.; Cieslik, E. The comparison of prolamins extracted from different varieties of wheat, barley, rye, and triticale species: Amino acid compostion, electrophoresis, and immunodetection. *J. Microb. Biotechnol. Food Sci.* **2012**, *1*, 742−752.

(19) Wieser, H. Chemistry of gluten proteins. *Food Microbiol.* **2007**, *24*, 115−119.

(20) Wroblewitz, S.; Hüther, L.; Berk, A.; Lebzien, P.; Kluth, H.; Manderscheid, R.; Erbs, M.; Weigel, H.-J.; Wätzig, H.; Dänicke, S. The impact of free air carbon dioxide enrichment (FACE) on nutrient digestibility of maize grains in pigs and broiler chickens and on ruminal in sacco degradability. *Anim. Feed Sci. Technol.* **2014**, DOI: 10.1016/j.anifeedsci.2014.06.018.

(21) Wieser, H.; Manderscheid, R.; Erbs, M.; Weigel, H.-J. Effects of elevated atmospheric CO_2 concentrations on the quantitative protein composition of wheat grain. *J. Agric. Food Chem.* **2008**, *56*, 6531−6535.

(22) Weigel, H.-J.; Manderscheid, R. Crop growth responses to free air CO_2 enrichment and nitrogen fertilization: Rotating barley, ryegrass, sugar beet, and wheat. *Eur. J. Agron.* **2012**, *43*, 97−107.

(23) Wieser, H.; Antes, S.; Seilmeier, W. Quantitative determination of gluten protein types in wheat flour by reversed-phase high-performance liquid chromatography. *Cereal Chem.* **1998**, *75*, 644−650.

(24) Laemmli, U. K. Cleavage of structural proteins during the assembly of the head of bacteriophage T4. *Nature* **1970**, *227*, 680−685.

(25) *STATISTICA* for Windows Operating System, Version 10.0.; Statsoft Inc.: Tulsa, OK, 2011.

(26) Erbs, M.; Manderscheid, R.; Jansen, G.; Seddig, S.; Pacholski, A.; Weigel, H.-J. Effects of free-air CO_2 enrichment and nitrogen supply on grain quality parameters and elemental composition of wheat and barley grown in a crop rotation. *Agric. Ecosyst. Environ.* **2010**, *136*, 59−68.

(27) Godfrey, D.; Hawkesford, M.; Powers, S. J.; Millar, S.; Shewry, P. R. Effects of crop nutrion and wheat grain composition and end use quality. *J. Agr. Food Chem.* **2010**, *58*, 3012−3021.

(28) Wieser, H.; Seilmeier, W. The influence of nitrogen fertilization on quantities and proportions of different protein types in wheat flour. *J. Sci. Food Agric.* **1998**, *76*, 49−55.

(29) Wang, J.; Chen, J.; Dai, F.; Wu, F.; Yang, J.; Zhang, G. Protein fractions in barley grains as affected by some agronomic factors and their relationships to malt quality. *Cereal Res. Commun.* **2007**, *35*, 129−140.

(30) Linina, A.; Ruza, A. Cultivar and nitrogen fertiliser effects on fresh and stored winter wheat grain quality indices. *Proc. Latv. Acad. Sci. B Nat. Exact. Appl. Sci.* **2012**, *66*, 177−184.

(31) Zecevic, V.; Boskovic, J.; Knezevic, D.; Micanovic, D.; Milenkovic, S. Influence of cultivar and growing season on quality properties of winter wheat (*Triticum aestivum* L.). *Afr. J. Agric. Res.* **2013**, *8*, 2545−2550.

(32) Hurkman, W. J.; Tanaka, C. K.; Vensel, W. H.; Thilmony, R.; Altenbach, S. B. Comparative proteomic analysis of the effect of temperature and fertilizer on gliadin and glutenin accumulation in the developing endosperm and flour from *Triticum aestivum* L. cv. Butte 86. *Proteome Sci.* **2013**, *11*, DOI: 10.1186/1477-5956-11-8.

(33) Altenbach, S.; Tanaka, C.; Hurkman, W.; Whitehand, L.; Vensel, W.; Dupont, F. Differential effects of a post-anthesis fertilizer regimen on the wheat flour proteome determined by quantitative 2-DE. *Proteome Sci.* **2011**, *9*, 46.
(34) Dupont, F. M.; Hurkman, W. J.; Vensel, W. H.; Tanaka, C.; Kothari, K. M.; Chung, O. K.; Altenbach, S. B. Protein accumulation and composition in wheat grains: Effects of mineral nutrients and high temperature. *Eur. J. Agron.* **2006**, *25*, 96−107.
(35) Manderscheid, R.; Erbs, M.; Weigel, H. J. Interactive effects of free-air CO_2 enrichment and drought stress on maize growth. *Europ. J. Agron.* **2014**, *52*, 11−21.
(36) Fowler, D. B. Crop nitrogen demand and grain protein concentration of spring and winter wheat. *Agron. J.* **2003**, *95*, 260−265.
(37) Manderscheid, R.; Frühauf, C.; Pacholski, A.; Weigel, H. J. Wirkung von freiland-CO_2-anreicherung (FACE) in kombination mit unterschiedlicher stickstoffversorgung auf die ertragskomponenten und das kornwachstum von wintergetreide. *Mitt. Ges. Pflanzenbauwiss.* **2004**, *16*, 97−98.
(38) Manderscheid, R.; Pacholski, A.; Frühauf, C.; Weigel, H.-J. Effects of free air carbon dioxide enrichment and nitrogen supply on growth and yield of winter barley cultivated in a crop rotation. *Field Crops Res.* **2009**, *110*, 185−196.
(39) Blumenthal, C.; Rawson, H. M.; McKenzie, E.; Gras, P. W.; Barlow, E. W. R.; Wrigley, C. W. Changes in wheat grain quality due to doubling the level of atmospheric CO_2. *Cereal Chem.* **1996**, *73*, 762−766.
(40) Wroblewitz, S.; Hüther, L.; Manderscheid, R.; Weigel, H.-J.; Wätzig, H.; Dänicke, S. The effect of free air carbon dioxide enrichment and nitrogen fertilisation on the chemical composition and nutritional value of wheat and barley grain. *Arch. Anim. Nutr.* **2013**, *67*, 263−278.
(41) Meibaum, B.; Riede, S.; Schröder, B.; Manderscheid, R.; Weigel, H.-J.; Breves, G. Elevated CO_2 and drought stress effects on the chemical composition of maize plants, their ruminal fermentation and microbial diversity in vitro. *Arch. Anim. Nutr.* **2012**, *66*, 473−489.
(42) Tatham, A. S.; Drake, A. F.; Shewry, P. R. A conformational study of a glutamine- and proline-rich cereal seed protein, C hordein. *Biochem. J.* **1985**, *226*, 557−62.
(43) Akin, D. E.; Kimball, B. A.; Windham, W. R.; Pinter, P. J., Jr; Wall, G. W.; Garcia, R. L.; LaMorte, R. L.; Morrison Iii, W. H. Effect of free-air CO_2 enrichment (FACE) on forage quality of wheat. *Anim. Feed Sci. Technol.* **1995**, *53*, 29−43.
(44) Mlyneková, Z.; Čerešňáková, Z. Degradation of starch and crude protein in dent and dent × flint maize hybrids in different stages of maturity. *Slovak J. Anim. Sci.* **2013**, *46*, 61−67.
(45) Ortega, E. I.; Villegas, E.; Bjarnason, M.; Short, K. Changes in dry matter and protein fractions during kernel development of quality protein maize. *Cereal Chem.* **1991**, *68*, 482−486.
(46) Högy, P.; Wieser, H.; Köhler, P.; Schwadorf, K.; Breuer, J.; Erbs, M.; Weber, S.; Fangmeier, A. Does elevated atmospheric CO_2 allow for sufficient wheat grain quality in the future? *J. Appl. Bot. Food Qual.* **2009**, *82*, 114−121.
(47) McAllister, T. A.; Phillippe, R. C.; Rode, L. M.; Cheng, K. J. Effect of the protein matrix on the digestion of cereal grains by ruminal microorganisms. *J. Anim. Sci.* **1993**, *71*, 205−12.
(48) Dombrink-Kurtzman, M. A.; Bietz, J. A. Zein composition in hard and soft endosperm of maize. *Cereal Chem.* **1993**, *70*, 105−108.
(49) Cornish, G. B.; Békés, F.; Eagles, H. A.; Payne, P. I. Prediction of dough properties for bread wheats. In *Gliadin and Glutenin: The Unique Balance of Wheat Quality*; AACC International, Inc.: St. Paul, MN, 2006; Chapter 8, pp 243−280.
(50) Howard, K. A.; Gayler, K. R.; Eagles, H. A.; Halloran, G. M. The relationship between D hordein and malting quality in barley. *J. Cereal Sci.* **1996**, *24*, 47−53.
(51) Molina-Cano, J. L.; Rubió, A.; Igartua, E.; Gracia, P.; Montoya, J. L. Mechanisms of malt extract development in barleys from different european regions: I. Effect of environment and grain protein content on malt extract yield. *J. Inst. Brew.* **2000**, *106*, 111−116.

Instrumentation. An Agilent 1260 HPLC (Santa Clara, CA) was used for all chromatographic analyses. The HPLC system consisted of a model G1311B pump and degasser, G1329B autosampler, G1315C DAD/UV−vis detector, G1316A column heater, and a system controller. Data were processed using ChemStation for LC 3D systems, version B.04.03.

Samples and Sample Preparation. Tannins from grape (pre-veraison Cabernet Sauvignon berry skin tissue) as well as wine (2010 and 2012 Cabernet Sauvignon) were used for standard additions and thermodynamic standards. Extraction, purification, and separation into different molecular mass fractions were accomplished using a previously described procedure.[26] The resultant tannin fractions used in the current study have been previously characterized.[9] Whenever powdered tannin standards were dissolved in solution, solutions were subsequently allowed to equilibrate for at least 24 h before use. This allowed for stable thermodynamic measurements to be obtained.

Wines used for analysis were sourced from either various wineries within California or a wine merchant in the case of the Bordeaux. Wines were sterile-filtered with 13 mm, 0.45 μm polytetrafluoroethylene (PTFE) filters (Grace Davison Discovery Sciences, Waukegan, IL) before injection. For 2012 and 2013 wines, analyses took place approximately 4 months after pressing. For all other wines, only vintage information was available.

Phloroglucinolysis for the Mean Degree of Polymerization (mDP) Determination. Phloroglucinolysis, according to the method by Kennedy and Jones,[27] using a modified HPLC method,[26] was used to determine mDP of isolated tannins.

Serial Dilutions. To determine the impact of tannin concentration on tannin stickiness, high and low average molecular mass wine tannin fractions (mDP of 15.4 and 2.9, respectively), previously shown to vary in their retention thermodynamics (ΔH = −12 088 and −2328 J/mol, respectively[9]), were dissolved (10 g/L) in an aqueous buffer solution (pH 4.6) containing methanol (15%, v/v), 40 mM sodium acetate, and 20 mM HCl and were serially diluted with this buffer, to 0.31 g/L. Solutions were analyzed using the optimized HPLC method. In addition to serially diluted tannin samples, a wine (2012 California north coast Cabernet Sauvignon press wine) was serially diluted 5 times with the same aqueous buffer solution prior to analysis (experiment conducted 10 months after pressing).

Standard Additions. Purified wine tannin fractions varying in enthalpy of interaction were added to a 2012 California north coast Petit Verdot wine to examine their impact on wine stickiness. Low-molecular-weight (mDP = 2.9) and high-molecular-weight (mDP = 22.7) tannins were added in half, equivalent, and double the experimentally measured tannin concentration of the wine.

Gelatin Fining. Fining experiments were carried out using Inocolle Extra N1 gelatin (15 000 MM, Scott Laboratories, Petaluma, CA). Gelatin (20 mg) was rehydrated in water (500 mg/L) according to manufacturer guidelines. A total of 2 mg of wine tannin (mDP = 15.4) was rehydrated in an aqueous solution (pH 4.6, 2395 mg/L) containing methanol (15%, v/v), 40 mM sodium acetate, and 20 mM HCl and allowed to equilibrate for 48 h before analysis. After 48 h, the gelatin solution was serially diluted with water from its initial concentration to a minimum concentration of 7.8 mg/L. Gelatin-containing solutions were then mixed with the tannin solution in a 1:1 ratio in microcentrifuge tubes. After mixing, samples were centrifuged at 735*g* for 2 min in an Eppendorf 5415 C centrifuge (Hamburg, Germany) and the supernatant was then analyzed.

Optimized HPLC Method. The optimized HPLC method for measuring tannin stickiness used a polystyrene divinylbenzene reversed-phase column (PLRP-S, 2.1 × 50 mm, 100 Å, 3 μm, Agilent Technologies, Santa Clara, CA) protected with a guard column (PRP-1, 3 × 8 mm, Hamilton Company, Reno, NV).

The mobile phases consisted of 1.5% (w/w) 85% H_3PO_4 in water (153 mM, mobile phase A) and 20% (v/v) mobile phase A in acetonitrile (B) with a flow rate of 0.30 mL/min. The linear gradient was as follows: time in min (% B), 0 (14%), 10.0 (34%), 10.0−13.5 (34%), 15.3 (70%), 15.3−17.0 (70%), and 17.0−20.0 (14%). This method was modified from previously published methods,[9,28] with modifications designed to reduce run time.

To determine tannin stickiness, samples were run at four column temperatures (25−40 °C, in 5 °C increments). A blank sample (water) was run at all temperatures and was subtracted from sample signals to eliminate background absorbance. All temperatures were converted into kelvin to calculate thermodynamic parameters in SI units. Tannin elution was monitored at 280 nm.

Calculations. Chromatograms were integrated as described previously, with minor modifications.[9] Briefly and following baseline subtraction of a water blank, a baseline at 0 mAU across the sample peak area was performed. Following this, the resulting peak area was split at 16.8 min, corresponding to the elution of tannin_P. The tannin eluting prior to 16.8 min was separated from overlapping resolved material by tangent skimming.

From integration results, the alternative retention factor was calculated as follows:

$$k_{alt} = \frac{\text{tannin}_T}{\text{tannin}_T - \text{tannin}_P} \quad (1)$$

where, as previously described,[9] tannin_T is the total tannin peak area and tannin_P is the partial tannin peak area.

The alternative retention factor is related to thermodynamics of interaction according to the following equation:

$$\ln k_{alt} = -\frac{\Delta H^\circ}{RT} + \frac{\Delta S^\circ}{R} + \ln \text{Ø} \quad (2)$$

where ΔH° and ΔS° are the specific enthalpy and entropy of interaction, respectively, R is the gas constant, T is temperature, and Ø is the mobile phase ratio. The specific enthalpy was calculated by plotting the natural logarithm (ln) of k_{alt} versus the reciprocal of the column temperature in kelvin at each of the four temperatures (i.e., van't Hoff plot in Figure 1). The specific enthalpy of interaction (tannin stickiness) was calculated from the slope of the best fit line (slope equivalent to $-\Delta H^\circ/R$).

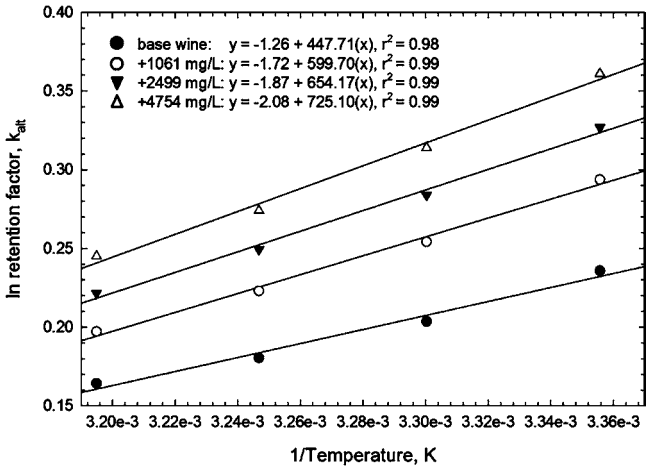

Figure 1. van't Hoff plot of the alternative retention factor (k_{alt}) versus the reciprocal temperature (in K) for the retention of red wine tannins on polystyrene divinylbenzene, following the standard addition of a tannins (mDP = 15.4), with best fit equations shown.

The concentration of tannin (on the basis of tannin_T) was reported in (−)-epicatechin equivalents using an (−)-epicatechin standard and was determined at 303 K (30 °C). In addition to (−)-epicatechin, a grape skin or wine tannin standard (mDP = 39.0 and 15.4, respectively) served as a stickiness standard. Stickiness standards were prepared by dissolving grape skin or wine tannins in an aqueous solution containing methanol (15%, v/v), 40 mM sodium acetate, and 20 mM HCl. Stickiness standards did not vary by more than 10% across all experiments. Given that the variation in experimental results

dx.doi.org/10.1021/jf501666z | J. Agric. Food Chem. 2014, 62, 6626−6631

was less than 5% suggests that the stickiness standards changed over time.

RESULTS AND DISCUSSION

The mouthfeel quality of red wine is an important management consideration, and tannins, which contribute astringency, are central to it. In addition to tannin, the matrix of red wine (e.g., ethanol, residual sugar, and polysaccharides) is known to have an impact on astringency perception. With regard to tannins and in addition to concentration, its composition (e.g., subunit composition, size distribution, pigment incorporation, and oxidation) is considered to affect tannin activity or its stickiness. Stickiness is defined as the observed variation in the enthalpy of interaction between tannin and a hydrophobic surface. In this case, the hydrophobic surface is polystyrene divinylbenzene, and previous studies have found that stickiness variation with the tannin structure is similar to variations observed when using ITC to monitor the tannin interaction with poly-L-proline.[8,9] In contrast to analytical methodology available for measuring the tannin concentration, methodology for the measurement of stickiness is lacking. Stickiness measurements based on the thermodynamics of the tannin interaction with a hydrophobic surface suggest that this analytical approach has utility. The current study was initiated to develop a method for measuring tannin stickiness in red wine by reversed-phase HPLC following direct injection.

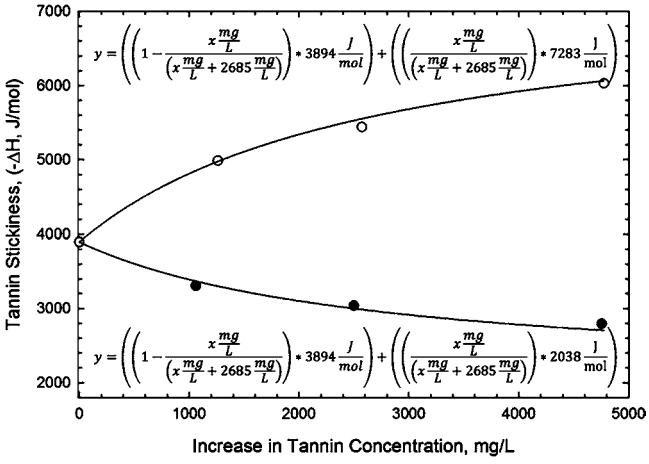

Figure 2. Effect of the standard addition of (●) low-mDP and (○) high-mDP tannins to a base wine, with theoretical equations representing the fractional contribution of base wine tannin as well as added tannin shown.

Table 1. Effect of Gelatin Addition on the Tannin Concentration and Stickiness

	tannin			
added gelatin (mg/L)	concentration (mg/L)	percentage remaining (%)	stickiness (−ΔH, J/mol)	percentage remaining (%)
0	1198[a]	100.0	11927	100.0
3.9	1158	96.7	11517	96.6
7.8	1107	92.4	11054	92.7
15.6	1067	89.1	10894	91.3
31.3	963	80.4	10104	84.7
62.5	807	67.4	8336	69.9
125.0	566	47.3	5417	45.4
250.0	286	23.9	1997	16.7

[a]The initial concentration was adjusted 50% to adjust for 1:1 dilution.

The analytical method that forms the basis of this method has been described previously.[9] In that study, a modified analytical method was used to measure the stickiness of various grape and wine tannins. In the present study, alterations to the HPLC method were made to increase throughput and remove potential baseline interference. To increase throughput, the flow rate was increased to 0.3 mL/min and the number of temperatures monitored was reduced to four. The binary mobile phase gradient remained identical to the previous method but with alterations made to compensate for the increased flow rate. With regard to a reduction in the number of temperature points, the elimination of higher temperatures resulted in a linear van't Hoff plot. Following baseline subtraction, integration, and k_{alt} determination, van't Hoff plots from data collected at 298−313 K had good correlation (Figure 1; r^2 = 0.99). The slope of the line from this relation was used to determine the enthalpy of interaction as described previously.[29] The enthalpy of interaction is referred to as tannin stickiness.

Tannin Stickiness Is an Intensive Property. Unlike the tannin concentration and wine matrix components that change with dilution, compositional variation should not be affected by dilution. Therefore, tannin stickiness, if related to composition/conformation, should be an intensive thermodynamic property. To explore this, solutions of tannin (in wine and wine-like systems) were serially diluted. In addition, a wine was subjected to a standard addition of tannins with varying degrees of stickiness.

With regard to serial dilutions, the stickiness of serially diluted solutions containing high-molecular-weight (mDP = 15.4) and low-molecular-weight (mDP = 2.9) wine tannin fractions was determined. Tannin concentrations in the six serially diluted solutions varied from 10 to 0.31 g/L. The stickiness for the high-molecular-weight samples was −11 928 ± 257 J/mol (±standard deviation, 2.16% error). Similarly, the stickiness for low-molecular-weight tannin solutions was −2261 ± 93 J/mol (±standard deviation, 4.11% error). A 2012 Cabernet Sauvignon press wine, which was serially diluted 5 times, had a stickiness value of −4905 ± 152 J/mol (±standard deviation, 3.10% error).

To provide additional evidence that the value for stickiness was a feature of tannin contained in the sample and not related to the concentration, a 2012 Petit Verdot wine was subjected to the standard addition of two wine tannins varying in stickiness (Figure 2). To the base wine (stickiness = −3894 J/mol) was added two tannins (either −2038 or −7283 J/mol). As expected from the results obtained from serially diluted systems, the experimental results were consistent with calculated results and were a function of the fractional contribution of the base wine tannin and the added tannin. In so far as tannin stickiness is sensorially relevant to wine, these results suggest that the addition of exogenous tannins will modify tannin perception beyond concentration alone. Furthermore, the results from standard addition and serial dilution collectively indicate that the analytical method provided good reproducibility and confirmed that stickiness is an intensive property.

Effect of Wine Production Practice: The Case of Gelatin Fining. The results above indicate that stickiness is a property of tannin and is concentration-independent, and thus, stickiness can be distinguished from the concentration. This

dx.doi.org/10.1021/jf501666z | J. Agric. Food Chem. 2014, 62, 6626−6631

Table 2. Concentration and Stickiness of Tannins in Bordeaux Varietal Red Wines and Across Multiple Vintages

			tannin[a]		ranking[b]		percentage of the maximum value (%)[c]	
vintage	region[d]	variety	concentration (mg/L)	stickiness ($-\Delta H$, J/mol)	concentration	stickiness	concentration	stickiness
2013	north coast, CA	Cabernet Franc	4099	2648	25	28	79	64
		Cabernet Sauvignon	4636	3327	9	12	90	80
		Cabernet Sauvignon	5179	3447	1	9	100	83
		Cabernet Sauvignon	4349	2718	18	26	84	65
		Cabernet Sauvignon	4030	2361	27	33	78	57
		Cabernet Sauvignon	4311	2333	21	34	83	56
		Cabernet Sauvignon	4326	2759	19	25	84	66
		Cabernet Sauvignon	4555	2673	11	27	88	64
		Merlot	4415	2311	16	36	85	55
		Petit Verdot	4641	2164	8	37	90	52
2012	central coast, CA	Cabernet Sauvignon	3181	2782	35	23	61	67
		Cabernet Sauvignon	3160	2122	36	39	61	51
		Cabernet Sauvignon	2533	2921	43	19	49	70
		Cabernet Sauvignon	2850	2322	40	35	55	56
		Cabernet Sauvignon	2930	1896	38	43	57	45
		Merlot	3088	2025	37	40	60	49
2011	central coast, CA	Cabernet Sauvignon	2871	1896	39	42	55	45
2010	central coast, CA	blend	4357	2384	17	31	84	57
		blend	2760	2993	41	17	53	72
		Cabernet Sauvignon	4130	2379	24	32	80	57
		Cabernet Sauvignon	4083	2396	26	30	79	57
		Cabernet Sauvignon	3372	2774	33	24	65	67
		Cabernet Sauvignon	2582	2792	42	22	50	67
		Cabernet Sauvignon	4289	1838	22	44	83	44
		Cabernet Sauvignon	1326	2010	44	41	26	48
		Cabernet Sauvignon	3741	2423	31	29	72	58
		Merlot	3634	2941	32	18	70	71
		Merlot	4013	2860	28	20	77	69
		Merlot	3294	3020	34	16	64	72
2009	central coast, CA	Cabernet Sauvignon	4322	2139	20	38	83	51
		Cabernet Sauvignon	4010	3823	29	2	77	92
		Cabernet Sauvignon	4182	4170	23	1	81	100
	Bordeaux, France	blend	4719	3497	7	8	91	84
		blend	5033	3514	2	6	97	84
		blend	4881	3292	5	14	94	79
		blend	4521	3382	13	11	87	81
		blend	3977	3029	30	15	77	73
		blend	4524	3302	12	13	87	79
		blend	4606	3397	10	10	89	81
		blend	4422	3570	15	4	85	86
		blend	4893	3552	4	5	94	85
		blend	4432	2792	14	21	86	67
		blend	4827	3507	6	7	93	84
		blend	4954	3631	3	3	96	87

[a]Tannin concentration and stickiness, with stickiness equivalent to the negative enthalpy of interaction. [b]Ranking of the tannin concentration and stickiness, with lower numbers ranked higher in concentration and stickiness. [c]Percent of the highest tannin concentration and stickiness. [d]Region where fruit was produced (CA = California).

method can therefore be used to explore the role of grape and wine production practices on stickiness. Previous studies indicate that tannin size, plant tissue origin (seed versus skin), and wine age will affect stickiness.[8,9] The effects of a myriad of additional factors on stickiness are intriguing candidates for study (e.g., fruit maturity, vine water status, wine microoxygenation, and pigment incorporation). To provide an example of utility, the effect of gelatin fining on the wine tannin concentration and stickiness was explored.

The protein interaction with tannin is considered the basis of astringency and is used for the removal of excess tannin in wine. From previous studies on the interaction of tannins with macromolecules,[30−34] it would be expected that gelatin should preferentially remove larger molecular mass tannins and with potential effects on composition. It would be predicted therefore that as the concentration of tannin declined with gelatin addition, so too would tannin stickiness. To explore this, solutions of serially diluted gelatin were combined with a prepared wine tannin solution (initial stickiness of −11 927 J/

dx.doi.org/10.1021/jf501666z | J. Agric. Food Chem. 2014, 62, 6626−6631

mol). As expected, the results indicated that, as the concentration of tannin declined, so too did its stickiness (Table 1). Previous research has shown that gelatin additions to wines decrease the tannin concentration,[32] but the current result suggests that the strength of the hydrophobic tannin−protein interaction plays an important role in perceived astringency in gelatin-fined wines as well.

Analysis of Wines. To provide some insight into stickiness variation, a set of commercial wines was analyzed. The wines presented in Table 2 were Bordeaux varietals and were sourced from commercial vineyards or a wine shop. Wines varied in age and region. The concentration of tannin and stickiness for the wines varied considerably. A linear regression across the set of wines analyzed yielded a line with a positive slope (e.g., an observed increase in stickiness with the concentration) although with a low correlation (r^2 = 0.24). It is particularly interesting to note that a range of stickiness values is possible at any given tannin concentration. A ranking of wines in order of increasing concentration and stickiness confirmed that varied concentration−stickiness relationships existed. There was a greater variation in the tannin concentration in this set of wines, where the lowest concentration observed was at 26% of the maximum. This is in contrast to the least sticky wine being 44% of the maximum stickiness. It is evident that a much larger data set needs to be gathered, with associated sensory analysis, to understand the extent to which stickiness varies and is relevant to wine production, management, and appreciation.

Implications. Historically, tannin structure−activity relationships in red wine have been limited by our understanding of the tannin structure. Considerable effort has been invested into red wine tannin structure elucidation,[35−37] yet paradoxically, our knowledge as a proportion of material presence remains limited. Added to this, understanding the role that various grape and wine production practices have on sensory properties is often thought to be limited by our understanding of how process affects structure. Finally, understanding activity of tannins has been dependent upon sensory studies. In addition to the complexity of using humans as analytical instruments, wine matrix and tannin concentration often confound sensory evaluation.[38,39] The development of an objective method for measuring tannin activity provides a new avenue for exploring the effect of various processes on activity without first understanding structure and, therefore, has increased our ability to explore process−activity relationships. In addition, this method provides researchers with a method for measuring the effect of known structure variation on activity without the use of human subjects.

To fully understand the new information provided by this analytical method, the relationship between tannin stickiness and sensory perception needs to be investigated. Although data to date are consistent with tannin stickiness being related to anecdotal differences in astringency quality between grape and wine tannins, direct relationships between stickiness and perception need to be explored.

AUTHOR INFORMATION

Corresponding Author

*Telephone: +1-559-278-7179. Fax: +1-559-278-4795. E-mail: jakennedy@csufresno.edu.

Funding

We thank the American Vineyard Foundation for project funding.

Notes

The authors declare no competing financial interest.

REFERENCES

(1) Haslam, E. *Practical Polyphenolics: From Structure to Molecular Recognition and Physiological Action*; Cambridge University Press: New York, 1998; p 422.

(2) Kennedy, J. A.; Matthews, M. A.; Waterhouse, A. L. Changes in grape seed polyphenols during fruit ripening. *Phytochemistry* **2000**, *55*, 77−85.

(3) Kennedy, J. A.; Hayasaka, Y.; Vidal, S.; Waters, E. J.; Jones, G. P. Composition of grape skin proanthocyanidins at different stages of berry development. *J. Agric. Food Chem.* **2001**, *49*, 5348−5355.

(4) Cerpa-Calderon, F. K.; Kennedy, J. A. Berry integrity and extraction of skin and seed proanthocyanidins during red wine fermentation. *J. Agric. Food Chem.* **2008**, *56*, 9006−9014.

(5) Aron, P. M.; Kennedy, J. A. Compositional investigation of phenolic polymers isolated from *Vitis vinifera* L. cv. Pinot noir during fermentation. *J. Agric. Food Chem.* **2007**, *55*, 5670−5680.

(6) McRae, J. M.; Kennedy, J. A. Wine and grape tannin interactions with salivary proteins and their impact on astringency: A review of current research. *Molecules* **2011**, *16*, 2348−2364.

(7) Gawel, R.; Oberholster, A.; Francis, I. L. A 'mouth-feel wheel': Terminology for communicating the mouth-feel characteristics of red wine. *Aust. J. Grape Wine Res.* **2000**, *6*, 203−207.

(8) McRae, J. M.; Falconer, R. J.; Kennedy, J. A. Thermodynamics of grape and wine tannin interaction with polyproline: Implications for red wine astringency. *J. Agric. Food Chem.* **2010**, *58*, 12510−12518.

(9) Barak, J. A.; Kennedy, J. A. HPLC retention thermodynamics of grape and wine tannins. *J. Agric. Food Chem.* **2013**, *61*, 4270−4277.

(10) Nicholls, A.; Sharp, K. A.; Honig, B. Protein folding and association: Insights from the interfacial and thermodynamic properties of hydrocarbons. *Proteins* **1991**, *11*, 281−296.

(11) Mahler, H.-C.; Friess, W.; Grauschopf, U.; Kiese, S. Protein aggregation: Pathways, induction factors and analysis. *J. Pharm. Sci.* **2009**, *98*, 2909−2934.

(12) Rosenberg, M.; Kjelleberg, S. Hydrophobic interactions: Role in bacterial adhesion. *Adv. Microb. Ecol.* **1986**, *9*, 353−393.

(13) McManus, J. P.; Davis, K. G.; Beart, J. E.; Gaffney, S. H.; Lilley, T. H.; Haslam, E. Polyphenol interactions. Part 1. Introduction; some observations on the reversible complexation of polyphenols with proteins and polysaccharides. *J. Chem. Soc., Perkin Trans. 2* **1985**, 1429−1438.

(14) Frechet, J. M. Functional polymers and dendrimers: Reactivity, molecular architecture, and interfacial energy. *Science* **1994**, *263*, 1710−1715.

(15) Autumn, K.; Liang, Y. A.; Hsieh, S. T.; Zesch, W.; Chan, W. P.; Kenney, T. W.; Fearing, R.; Fuyll, R. J. Adhesive force of a single gecko foot-hair. *Nature* **2000**, *405*, 681−685.

(16) Siebert, K. J. Effects of protein−polyphenol interactions on beverage haze, stabilization, and analysis. *J. Agric. Food Chem.* **1999**, *47*, 353−362.

(17) Bindon, K. A.; Smith, P. A.; Holt, H.; Kennedy, J. A. Interaction between grape-derived proanthocyanidins and cell wall material. 2. Implications for vinification. *J. Agric. Food Chem.* **2010**, *58*, 10736−10746.

(18) Frazier, R. A.; Deaville, E. R.; Green, R. J.; Stringano, E.; Willoughby, I.; Plant, J.; Mueller-Harvey, I. Interactions of tea tannin and condensed tannins with proteins. *J. Biopharm. Biomed. Anal.* **2010**, *51*, 490−495.

(19) Vidal, S.; Francis, L.; Noble, A.; Kwiatkowski, M.; Cheynier, V.; Waters, E. Taste and mouth-feel properties of different types of tannin-like polyphenolic compounds and anthocyanins in wine. *Anal. Chim. Acta* **2004**, *513*, 57−65.

(20) Vidal, S.; Francis, L.; Guyot, S.; Marnet, N.; Kwiatkowski, M.; Gawel, R.; Cheynier, V.; Waters, E. J. The mouth-feel properties of grape and apple proanthicyanidins in a wine-like medium. *J. Sci. Food Agric.* **2003**, *83*, 564−573.

(21) Brás, N. F.; Gonçalves, R.; Mateus, N.; Fernandes, P. A.; Ramos, M. J.; de Freitas, V. Inhibition of pancreatic elastase by polyphenolic compounds. *J. Agric. Food Chem.* **2010**, *58*, 10668−10676.
(22) Poncet-Legrand, C.; Gautier, C.; Cheynier, V.; Imberty, A. Interactions between flavan-3-ols and poly(L-proline) studied by isothermal titration calorimetry: Effect of the tannin structure. *J. Agric. Food Chem.* **2007**, *55*, 9235−9240.
(23) Singleton, V. L.; Orthofer, R.; Lamuela-Raventós, R. M. Analysis of total phenols and other oxidation substrates and antioxidants by means of Folin−Ciocalteu reagent. *Methods Enzymol.* **1999**, *299*, 152−178.
(24) Mercurio, M. D.; Dambergs, R. G.; Herderich, M. J.; Smith, P. A. High throughput analysis of red wine and grape phenolics—Adaptation and validation of methyl cellulose precipitable tannin assay and modified somers color assay to a rapid 96 well plate format. *J. Agric. Food Chem.* **2007**, *55*, 4651−4657.
(25) Harbertson, J. F.; Kennedy, J. A.; Adams, D. O. Tannin in skins and seeds of Cabernet Sauvignon, Syrah, and Pinot noir berries during ripening. *Am. J. Enol. Vitic.* **2002**, *53*, 54−59.
(26) Kennedy, J. A.; Taylor, A. W. Analysis of proanthocyanidins by high-performance gel permeation chromatography. *J. Chromatogr. A* **2003**, *995*, 99−107.
(27) Kennedy, J. A.; Jones, G. P. Analysis of proanthocyanidin cleavage products following acid-catalysis in the presence of excess phloroglucinol. *J. Agric. Food Chem.* **2001**, *49*, 1740−1746.
(28) Peng, Z.; Iland, P. G.; Oberholster, A.; Sefton, M. A.; Waters, E. J. Analysis of pigmented polymers in red wine by reverse phase HPLC. *Aust. J. Grape Wine Res.* **2002**, *8*, 70−75.
(29) Cole, L.; Dorsey, J. Temperature dependence of retention in reversed-phase liquid chromatography. 1. Stationary-phase considerations. *J. Anal. Chem.* **1992**, *64*, 1317−1323.
(30) Bindon, K. A.; Smith, P. A.; Kennedy, J. A. Interaction between grape-derived proanthocyanidins and cell wall material. 1. Effect on proanthocyanidin composition and molecular mass. *J. Agric. Food Chem.* **2010**, *58*, 2520−2528.
(31) Bindon, K. A.; Kennedy, J. A. Ripening-induced changes in grape skin proanthocyanidins modify their interaction with cell walls. *J. Agric. Food Chem.* **2011**, *59*, 2696−2707.
(32) Maury, C.; Sarni-Manchado, P.; Lefebvre, S.; Cheynier, V.; Moutounet, M. Influence of fining with different molecular weight gelatins on proanthocyanidin composition and perception of wines. *Am. J. Enol. Vitic.* **2001**, *52*, 140−145.
(33) Prigent, S. V. E.; Voragen, A. G. J.; van Koningsveld, G. A.; Baron, A.; Renard, C. M. G. C.; Gruppen, H. Interactions between globular proteins and procyanidins of different degrees of polymerization. *J. Dairy Sci.* **2009**, *92*, 5843−5853.
(34) Poncet-Legrand, C.; Gautier, C.; Cheynier, V.; Imberty, A. Interactions between flavan-3-ols and poly(L-proline) studied by isothermal titration calorimetry: Effect of the tannin structure. *J. Agric. Food Chem.* **2007**, *55*, 9235−9240.
(35) Cheynier, V.; Dueñas-Paton, M.; Salas, E.; Maury, C.; Souquet, J.-M.; Sarni-Manchado, P.; Fulcrand, H. Structure and properties of wine pigments and tannins. *Am. J. Enol. Vitic.* **2006**, *57*, 298−305.
(36) Monagas, M.; Bartolomé, B.; Gómez-Cordovés, C. Updated knowledge about the presence of phenolic compounds in wine. *Crit. Rev. Food Sci. Nutr.* **2005**, *45*, 85−118.
(37) Monagas, M.; Bartolomé, B.; Gómez-Cordovés, C. Evolution of polyphenols in red wines from *Vitis vinifera* L. during aging in the bottle. *Eur. Food Res. Technol.* **2005**, *220*, 331−340.
(38) Fontoin, H.; Saucier, C.; Teissedre, P. L.; Glories, Y. Effect of pH, ethanol and acidity on astringency and bitterness of grape seed oligomers in model wine solutions. *Food Qual. Pref.* **2008**, *19*, 286−291.
(39) Lesschaeve, I.; Noble, A. C. Polyphenols: Factors influencing their sensory properties and their effects on food and beverage preferences. *Am. J. Clin. Nutr.* **2005**, *81*, 330S−335S.

ingredients obtained from natural sources, which can often fully replace potentially dangerous synthetic additives.

MATERIALS AND METHODS

Chemicals. The constituents of plant EOs studied included eugenol (Eug; 4-allyl-2-methoxyphenol), carvacrol (Ca; 5-isopropyl-2-methylphenol), thymol (T; 2-isopropyl-5-methylphenol), borneol (B; endo-(1*S*)-1,7,7-trimethylbicyclo[2.2.1]heptan-2-ol), and eucalyptol (Euc; 1,8-cineole; 1,3,3-trimethyl-2-oxabicyclo[2.2.2]octane). The DNA-damaging agent used was hydrogen peroxide (H_2O_2). Positive controls included gallic acid (GA), ascorbic acid (AA), butylated hydroxytoluene (BHT), quercetin, and ethylenediaminetetraacetic acid disodium salt dihydrate ($Na_2EDTA{\cdot}2H_2O$), and reagents 1,1-diphenyl-2-picrylhydrazyl radical (DPPH), dimethyl sulfoxide (DMSO), cremophor EL, ethidium bromide (EtBr) were obtained from Fluka or Sigma, Sigma-Aldrich Co. (Steinheim, Germany, or St. Louis, MO, USA). *R. officinalis* essential oil (Ph. Eur. 4) was purchased from Calendula Inc., Nova Lubovna, Slovakia (lot 5-014-009-12-06, containing approximately 25% 1,8-cineole, 19% α-pinene, 19% camphor, 17% *p*-cymene, 9% camphene, 5% β-pinene, 2% borneol, and 4% unidentified compounds as specified by the manufacturer). All plant volatiles were kept at room temperature and diluted in appropriate reaction mixtures just before the experiments. William's medium was purchased from PAN-Biotech GmbH (Aidenbach, Germany), fetal bovine serum (FBS) and antibiotics were purchased from GIBCO BRL (Paisley, UK), and phosphate-buffered saline (PBS; Ca^{2+}- and Mg^{2+}-free) was purchased from Oxoid Limited (Basingstoke, UK). All other reagents and chemicals used were of analytical grade.

Reducing Power Assay. The reducing capacities of the plant volatiles were determined according to the method of Zhao et al.[6] In this assay, the yellow color of the test solution is changed to various shades of green and blue, depending on the reducing power of each compound. The presence of reducing agents (i.e., antioxidants) induces the conversion of the Fe^{3+}/ferricyanide complex into the ferrous forms. In brief, different concentrations of selected essential oil components, intact RO, and GA, used as a positive control, were mixed in 1 mL of methanol with 2.5 mL of phosphate buffer (0.2 M, pH 6.6) and 2.5 mL of potassium ferricyanide $[K_3Fe(CN)_6]$ (1%). The mixtures were incubated at 50 °C for 20 min. Trichloroacetic acid (2.5 mL, 10%) was added to each mixture and centrifuged at 3000 rpm for 10 min. Finally, the upper layer of supernatants (2.5 mL) was mixed with 2.5 mL of distilled water and 0.5 mL of $FeCl_3$ (0.1%), and the absorbances were recorded at 700 nm (GENESYS 10 Bio, Spectronic). The higher absorbance of the reaction mixture indicates the higher reducing power.

1,1-Diphenyl-2-picrylhydrazyl Radical Scavenging Activity. Selected plant volatiles were investigated for their radical scavenging activity using a modified DPPH assay.[7] DPPH is a stable free radical. The methanolic solution of this compound is dark purple (absorbs light at a wavelength of 517 nm) at the radical state. When DPPH reacts with an antioxidant, by providing hydrogen atoms or by electron donation, it is reduced to the molecular form, which is yellow. In brief, methanol (100 μL) solution of DPPH radical at the concentration of 0.05 mg/mL was added to 50 μL of various concentrations of plant volatiles or AA, used as a positive control. The experiments were carried out at room temperature. The decrease in absorbance at 500 nm was measured at 0, 15, 30, and 60 min using a spectrophotometer (Multiscanreader RC, Labsystems, Vantaa, Finland), and the DPPH$^{\bullet}$ scavenging activities of plant volatiles were then expressed as percentage of DPPH$^{\bullet}$ scavenging activity using the formula

$$\text{scavenging of DPPH radicals (\%)} = [(A_{\text{control}} - A_{\text{sample}})/A_{\text{control}}] \times 100$$

where A_{control} is the absorbance of the control reaction, containing all reagents except the tested compounds, and A_{sample} is the absorbance of tested compounds. Methanol was used as a blank.

Hydroxyl Radical ($^{\bullet}$OH) Scavenging Activity. For the determination of $^{\bullet}$OH scavenging activity, hydroxyl radicals ($^{\bullet}$OH) were generated in an L-ascorbic acid/$CuSO_4$ system. The assay is based on quantification of cytochrome *c* oxidation.[8] In this experiment, OH radicals were generated in 1 mL of 0.15 mM sodium phosphate buffer (pH 7.4) containing 100 μM L-ascorbic acid, 100 μM $CuSO_4$, 12 μM cytochrome *c*, and the samples of plant volatiles to be tested at different concentrations. The mixture was incubated at 25 °C for 90 min. The change in transmittance caused by the color change of cytochrome *c* was measured at 550 nm using a spectrophotometer (GENESYS 10 Bio, Spectronic). The inhibition of $^{\bullet}$OH generation by 500 μg/mL thiourea was taken as 100%. BHT was used as a positive control. The inhibition ratio was calculated using the formula

$$\text{scavenging of OH radicals (\%)} = [(T - T_2)/(T - T_1)] \times 100$$

where T is the transmittance of the $^{\bullet}$OH generation system and T_1 and T_2 are the transmittances of the control (no $^{\bullet}$OH generation) and test systems, respectively.

DNA Topology Assay. The method of electrophoretically monitored DNA-damaging activity and DNA protectivity was described in detail by Cipak et al.[9] In brief, the reaction mixture (final volume of 10 mL) contained 200 ng of plasmid DNA in buffer and either Fe^{2+} alone, tested compounds alone, or combinations of tested compounds with Fe^{2+}. Specific details of agent concentrations are given in the caption of Figure 6. Single- (ss) and double-strand (ds) DNA breaks were assayed by measuring the conversion of supercoiled DNA, form I, to relaxed forms (II + III, Figure 1).

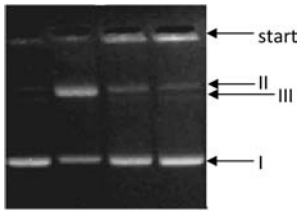

Figure 1. Electrophoretic changes induced in the plasmid DNA by the influence of Fe^{2+} (form I = supercoiled DNA, form II = ssDNA breaks, form III = dsDNA breaks).

Topological changes of DNA molecules correspond with the electrophoretical mobility of DNA topoisomers. Analysis of DNA modifications was made by agarose gel electrophoresis (1.5% agarose, 60 min, 60 V). The DNA was visualized by staining with EtBr (1 mg/mL) and UV illumination (UV Transilluminator MiniBISPro, DNR Bio Imaging Systems Ltd.).

Fe^{2+}-Chelating Activity Assay. Some results obtained by the above-mentioned techniques were verified by Fe^{2+}-chelating activity assay, as one of the mechanisms of antioxidant action is a chelation of transition metals, which prevents decomposition of hydroperoxide and Fenton-type reactions. Fe^{2+}-chelating assay uses an iron reagent, ferrozine, which forms complexes with Fe^{2+}. In the presence of chelating agents, the complex formation is disrupted with the result of color reduction. The chelating activity of borneol and two positive controls (quercetin and $Na_2EDTA{\cdot}2H_2O$) toward ferrous ions was studied by using the method described by Rajic et al.[10]

HepG2 Cell Line and Treatment of Cells. Malignant human hepatoma HepG2 cell line was obtained from Prof. A. R. Collins (University of Oslo, Norway) and cultured in William's medium, supplemented with 10% FBS and antibiotics (penicillin, 200 U/mL; streptomycin and kanamycin, 100 μg/mL). Cells were cultured on plastic Petri dishes at 37 °C in a humidified atmosphere of 5% CO_2.

Eugenol, carvacrol, and eucalyptol were dissolved immediately before use in complete culture medium to final concentrations of 0.05−0.6 (Eug), 0.025−0.2 (Ca), and 0.5−5 (Euc) mM, respectively. Thymol (T) was disolved in DMSO and diluted to final concentrations of 0.1−0.5 mM in complete culture medium. RO was dissolved in cremophor EL and 70 °C William's medium to 1.25%

dx.doi.org/10.1021/jf501006y | J. Agric. Food Chem. 2014, 62, 6632−6639

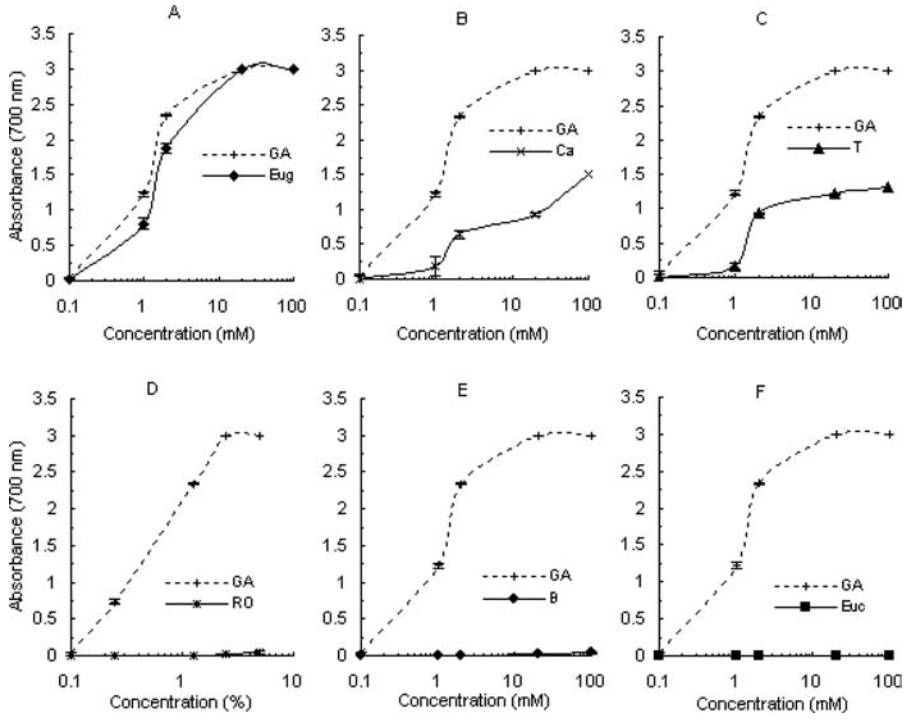

Figure 2. Reducing power of eugenol (A), carvacrol (B), thymol (C), *Rosmarinus officinalis* oil (D), borneol (E), and eucalyptol (F). Gallic acid (GA) is shown as a positive control.

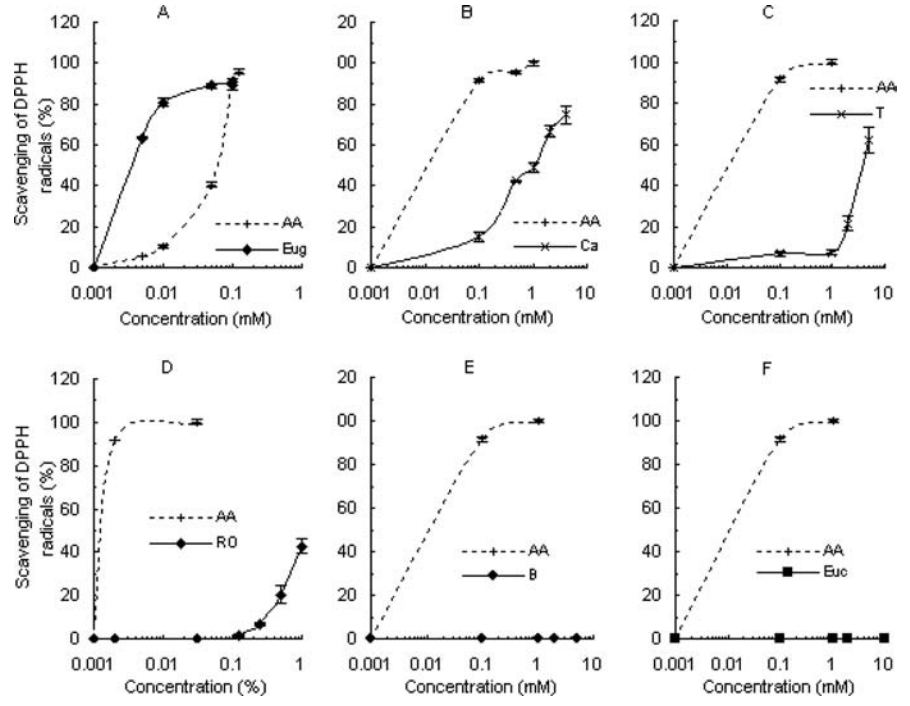

Figure 3. DPPH radical scavenging activity of eugenol (A), carvacrol (B), thymol (C), *Rosmarinus officinalis* oil (D), borneol (E), and eucalyptol (F). Ascorbic acid (AA) is shown as a positive control.

stock solution and further diluted to final concentrations of 0.00625−0.0625‰ in complete culture medium. Borneol (B) was disolved in ethyl alcohol (500 mM) and diluted to final concentrations of 0.5−3 mM in complete culture medium. Appropriate control cells were kept in complete William's medium with or without the addition of solvents. HepG2 cells were treated for 24 h.

Single-Cell Gel Electrophoresis (SCGE; Comet Assay). Assessment of DNA damage in HepG2 cells was performed by the use of the SCGE (comet assay), which represents a sensitive method for measuring DNA damage at the level of single cells. The method of SCGE according to Singh et al.[11] was followed with minor modifications made by Gabelova et al.[12] In brief, appropriate controls and HepG2 cells preincubated with volatiles for 24 h were trypsinized, centrifuged, and resuspended in 0.75% low melting point agarose in PBS. A volume of 85 μL of the cell suspension (approximately (2−2.5) $\times$ 10^4 cells) was spread on a base layer (100 μL of 1% normal melting point agarose in PBS) on a microscopic slide. When the agarose had solidified, half of the samples (slides) was submerged for 5 min in 250

dx.doi.org/10.1021/jf501006y | J. Agric. Food Chem. 2014, 62, 6632−6639

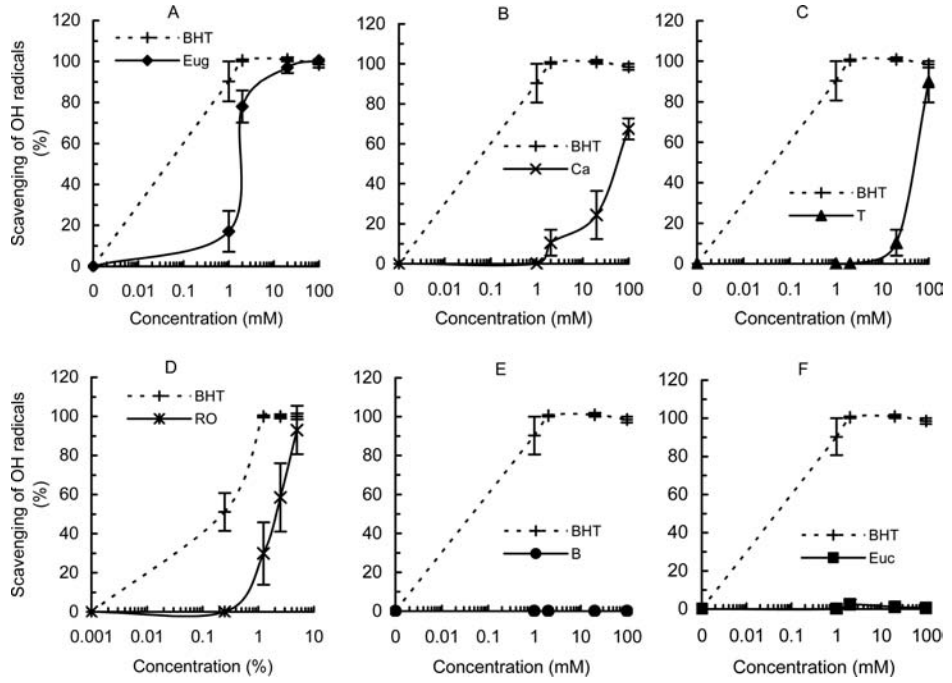

Figure 4. Hydroxyl radicals scavenging activity of eugenol (A), carvacrol (B), thymol (C), *Rosmarinus officinalis* oil (D), borneol (E), and eucalyptol (F). Butylated hydroxytoluene (BHT) is shown as a positive control.

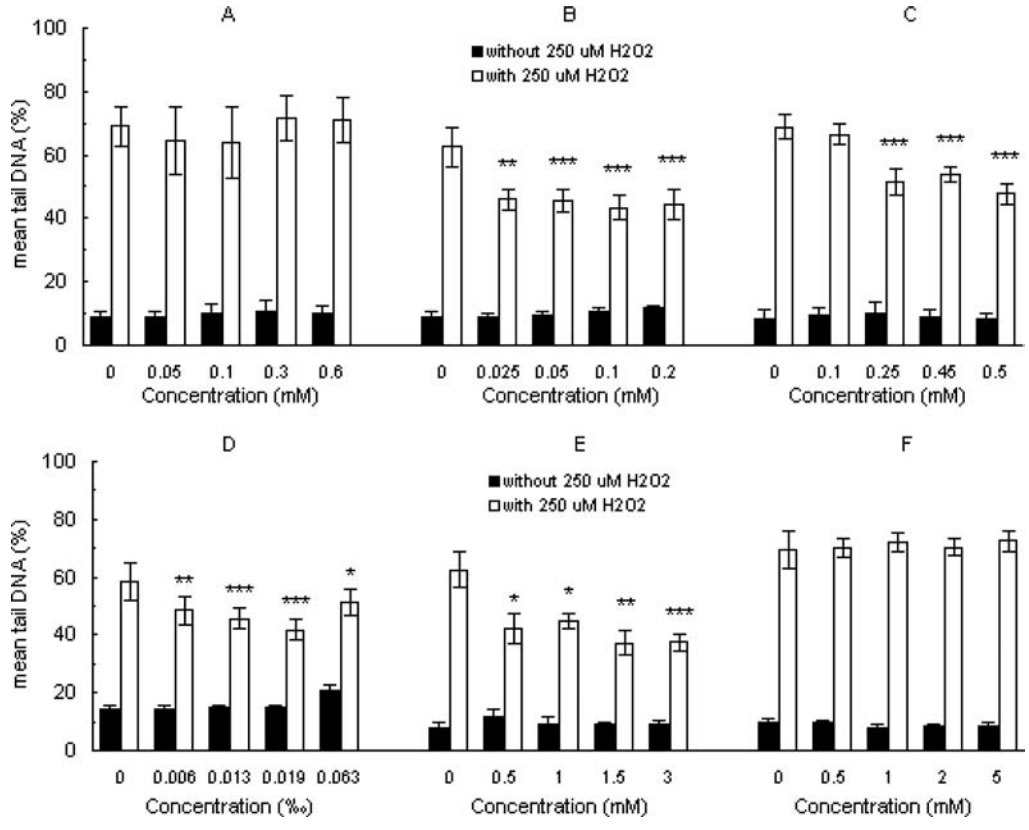

Figure 5. Effects of 24 h of pretreatment of HepG2 cells with eugenol (A), carvacrol (B), thymol (C), *Rosmarinus officinalis* oil (D), borneol (E), and eucalyptol (F) on DNA damage induced by 250 μM H_2O_2. Black columns represent the level of DNA strand breaks induced by 24 h of treatment with EOs or RO; white columns represent the level of DNA strand breaks induced by H_2O_2 alone (0) or after pretreatment with different concentrations of the EOs or RO studied and then with H_2O_2. (*) $p < 0.05$, (**) $p < 0.01$, and (***) $p < 0.001$ indicate significant differences between HepG2 cell cultures treated with H_2O_2 alone and cultures pretreated with volatiles and then exposed to H_2O_2.

μM H_2O_2 in PBS on ice for induction of DNA damage and then placed in a lysis mixture (2.5 M NaCl, 0.1 M Na_2EDTA, 10 mM Tris-HCl, pH 10.0, 1% Triton X-100) for 1 h at 4 °C to remove cellular proteins. The second part of the samples was placed in a lysis mixture

dx.doi.org/10.1021/jf501006y | J. Agric. Food Chem. 2014, 62, 6632−6639

immediately after 5 min in cold PBS. After lysis, the slides were transferred to an electrophoresis buffer (0.3 M NaOH, 1 mM Na_2EDTA, pH >13.0) for unwinding (40 min at 4 °C). A current of 25 V (0.3 A) was then applied for 30 min. The slides were neutralized with 0.4 M Tris-HCl (pH 7.5) and stained with EtBr (5 μg/mL). For each sample, 100 EtBr-stained nucleoids were evaluated and scored with an Olympus fluorescent microscope and computerized image analysis (Komet 5.5, Kinetic Imaging, Liverpool, UK) for determination of the percentage of DNA in the tail.

Statistical Analysis. The results are expressed as means ± standard deviations (SD) from at least three independent experiments carried out in triplicates. Student's *t* test was performed to determine the significance of differences between HepG2 cell cultures treated with H_2O_2 and cultures pretreated with volatiles and then exposed to H_2O_2 in the comet assay. Differences with p values <0.05 were considered to be statistically significant.

RESULTS AND DISCUSSION

Although reactive oxygen species (ROS) are unavoidable byproducts of cellular oxygen metabolism,[13] damage to cellular macromolecules such as lipids, proteins, and DNA may occur if production of ROS overcomes the antioxidant capacity of cells. It is thought that such a state of "oxidative stress" contributes to the pathogenesis of a number of human diseases.[13,14] Reducing power assays can show that the tested compounds are electron donors. They can reduce the oxidized intermediates of lipid peroxidation.[15] The synthetic nitrogen-centered DPPH radical and also the •OH radical are often used in testing of scavenging activity (antioxidant capacity) of compounds. •OH radical is one of the extremely potent ROS in biological systems. It can rapidly react with and degrade susceptible biologically relevant substrates.[16] In the DPPH assay the polar phase of radical scavenging is measured; at scavenging of •OH radicals the oxidation of cytochrome *c* is assayed.[8,15]

Antioxidant Effects of Eug, Ca, T, RO, B, and Euc. With the help of the reducing power assay we measured antioxidative activities (the presence of reducers) in the substances tested (Figure 2). Reducing power capacity was compared with that of GA, which is known to be a strong reducing agent. Eugenol was the most active among the samples, followed by carvacrol and thymol. RO, borneol, and eucalyptol did not manifest any reducing power in comparison to the positive control used.

Figures 3 and 4 show that the volatiles tested are capable of different degrees of DPPH and OH radical scavenging. In the DPPH assay the highest activity was shown by eugenol. Lower activities were observed for carvacrol, thymol, and *R. officinalis* oil. These four volatiles were also able to scavenge •OH radicals at a significant level. Borneol and eucalyptol were not active in any of these tests. The results obtained suggest that some of EO components tested could prevent reactive radical species from reaching biomolecules such as lipoproteins, polyunsaturated fatty acids, DNA, amino acids, proteins, and sugars.

DNA-Protective Effects of Eug, Ca, T, RO, B, and Euc. For the evaluation of EOs from the point of view of DNA damage or DNA protection, we used the single-cell gel electrophoresis assay (comet assay). At the given concentration ranges (IC ≤ 50) EO components and intact RO did not induce DNA damage in HepG2 cells. H_2O_2, a strong oxidant, induces in HepG2 cells a significant increase of DNA damage. This compound represents a useful oxidant not only for investigating the mechanism of oxidative cell injury but also for the study of protective effects of different natural compounds.

Figure 5 represents the percentage of DNA strand breaks induced in human hepatoma HepG2 cells after 24 h of treatment with different concentrations of the compounds tested, as well as the DNA-protective effect of 24 h of preincubation of HepG2 cells in the presence of the above-mentioned compounds.

As shown in Figure 5A, preincubation of HepG2 cells in the presence of a strong antioxidative compound (eugenol) did not reduce DNA lesions induced by H_2O_2. Similar results were obtained in mammalian cells of different origin (HepG2, Caco-2, and VH10 cells) in our previous study.[17] Thompson et al.[18] described hepatotoxicity of eugenol manifested by different phenomena: suppression of gap junction-mediated intercellular communication, depletion of glutathione, membrane depolarization of mitochondria, rise of intracellular Ca^{2+}, and depolarization of plasma membrane as well as acidification of cytoplasm. On the other hand, various authors discovered numerous useful effects of eugenol. This compound manifests DNA-protective and anti-inflammatory properties against liver injury in rats influenced by thioacemide,[19] protects murine peritoneal macrophages in vitro against toxicity of nicotine,[20] reduces chemically induced skin cancer in mice,[21] protects rat kidney against nephrotoxicity induced by gentamicine,[22] protects rats against acute cardiotoxicity induced by doxorubicin,[23] reduces gastric damage in vivo,[24] attenuates pulmonary damage induced by exhaust particles,[25] etc.

Panels B and C of Figure 5 show statistically significant DNA-protective effects of antioxidants carvacrol and thymol. Ozkan and Erdogan[26] proved that carvacrol and thymol were able to protect human lung H1299 cells against H_2O_2-induced cytotoxicity as well as against membrane and DNA damage. It was also found that carvacrol protects primary rat hepatocytes against exogenous oxidative DNA damage induced by H_2O_2.[27] Beneficial effects of carvacrol and thymol were investigated many times also in tests on experimental mice and rats. Carvacrol and thymol improved H_2O_2-induced injury on isolated rat pancreas cells,[28] suppressed inflammatory marker gene D-galactosamine expression in rats,[29] and ameliorated hepatotoxicity induced by thioacemide in the liver of Wistar rats.[30] Carvacrol also protects rat livers against defects caused by ischemia and reperfusion.[31] Lower, nontoxic concentrations of carvacrol and thymol significantly reduced 2-amino-3-methylimidazo[4,5-*f*]-quinoline (IQ)- and mitomycin C (MMC)-induced DNA damage.[32] Thymol moreover protects Chinese hamster lung fibroblasts[33,34] as well as Swiss albino mice and Sprague–Dawley rats[35] against oxidative stress induced by radiation or aflatoxin.

Figure 5D shows that although the antioxidative effect of RO is not unambiguous (panel D in Figures 2–4), this compound manifests a significant DNA-protective effect against H_2O_2-induced DNA lesions in HepG2 cells. Zegura et al.[36] proved that extract of rosemary reduces mutations in *Salmonella typhimurium* TA98 and provides DNA protection against oxidative agents in HepG2 cells. In our previous study we found that the administration of RO to rats efficiently and significantly decreased the level of DNA damage in primary hepatocytes, which were influenced by H_2O_2 and other oxidative agents.[37] The protective effects of RO toward the status of antioxidant enzymes in older rats proved the findings of Posadas et al.,[38] Ngo et al.[39] highlighted the importance of RO in cancer prevention.

As previously mentioned, borneol and eucalyptol did not manifest any antioxidant activity (panels E and F in Figures 2–4). These results correspond with observations of Sokmen et al.,[40] who did not determine any antioxidant activity of borneol

and eucalyptol in DPPH assay, on thin layer chromatography (TLC), at inhibition of superoxide radicals, in TBARS assay, and at inhibition of lipid peroxide formation. It is therefore interesting that pre-H_2O_2-treatment of HepG2 cells in the presence of borneol, a compound that has no antioxidant activity, significantly reduced the level of H_2O_2-induced DNA lesions and manifested a significant protective effect (Figure 5E). Borneol is also active ex vivo because if it was added to the drinking water of male Sprague–Dawley rats, the level of oxidant-induced DNA lesions in isolated hepatocytes was reduced.[41] Eucalyptol, the last tested compound, shows neither antioxidative nor DNA-protective effects. It is noteworthy that eucalyptol, which represents one of the main components of rosemary oil, has a much lower antioxidant activity than rosemary oil alone.[42] Although unable to protect DNA of HepG2 cells against H_2O_2, eucalyptol was able to protect DNA of HepG2 and B lymphoid NC-NC cells against *tert*-butyl hydroperoxide.[43]

Chelation Ability of Eug, Ca, T, RO, B, and Euc. It is known that the main cause of flavonoid-mediated DNA protection against effects of H_2O_2 represents chelation of iron ions.[44] We therefore tried to ascertain the chelation ability of the substances tested. DNA topology assay, which responds sensitively to the occurrence of metals and generation of free radicals in a reaction medium, was used with this aim. The assay is based on electrophoretic detection of topological changes induced in plasmid DNA.[45] As in DNA topology assay, both chelating and antioxidative activities can be detected. We used the Fe^{2+}-chelating activity assay for estimation of chelation activity of borneol. The method is based on the measurement of ferrozine complexes with Fe^{2+}. In the presence of chelating agents the complex formation is disrupted and can be detected spectrophotometrically.[15]

Figure 6 shows the electrophoretic monitoring of changes induced in the structure of plasmid DNA by the influence of Fe^{2+} and changes of DNA topology after application of EOs or RO. These changes could indicate a creation of DNA lesions or DNA repair. Whereas Fe^{2+} treatment of plasmid generated ssDNA breaks (Figure 6, lanes 2), treatment with EOs and RO did not induce any ssDNA breaks (Figure 6, lanes 3–6). DNA-protective effect was assessed by measuring the degree of protection against Fe^{2+}-induced DNA breaks (Figure 6, lanes 7–10). As is evident from Figure 6, carvacrol (Figure 6B, lanes 7–10), RO (Figure 6D, lanes 7–10), and eucalyptol (Figure 6F, lanes 7–10) showed no protective effect in DNA topology assay. Eugenol and thymol were able to preserve plasmid DNA only at the higher concentrations (Figure 6A,C, lanes 7 and 8). The most effective DNA-protective capacity was manifested by borneol; it preserved plasmid DNA against Fe^{2+}-induced damage at all concentrations tested (Figure 6E, lanes 7–10).

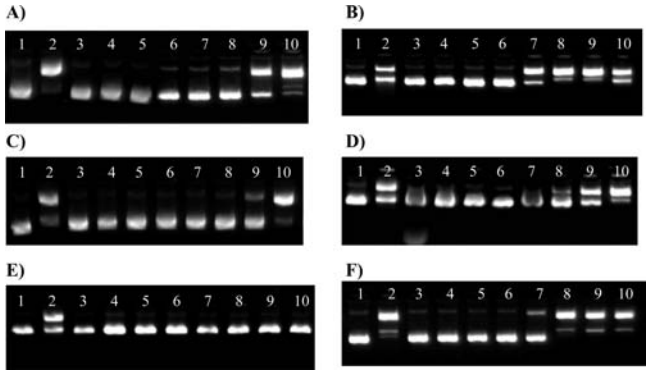

Figure 6. Electrophoretic monitoring of changes induced in the structure of plasmid DNA by the influence of Fe^{2+} and changes of DNA topology after application of EOs or RO (eugenol (A), carvacrol (B), thymol (C), *Rosmarinus officinalis* oil (D), borneol (E), eucalyptol (F)). Lanes (A–F): 1, pBR; 2, pBR + Fe^{2+}; 3, pBR + 10 mM EOs; 4, pBR + 1 mM EOs; 5, pBR + 0.1 mM EOs; 6, pBR + 0.01 mM EOs; 7, pBR + 10 mM EOs + Fe^{2+}; 8, pBR + 1 mM EOs + Fe^{2+}; 9, pBR + 0.1 mM EOs + Fe^{2+}; 10, pBR + 0.01 mM EOs + Fe^{2+}.

Antioxidative and Chelation Effects of Natural Compounds. Different authors had interest in this topic. Ogata et al.[46] proved that eugenol and dieugenol have different mechanisms of antioxidant effect. It was also found that eugenol suppresses the creation of the superoxide anion in the system xanthine–xanthine oxidase and prevents the oxidation of Fe^{2+} in Fenton reaction, which generates $^{\bullet}OH$.[47] Investigation of the structure–activity relationship in isoeugenol and eugenol showed that the lipid peroxidation and autoxidation of Fe^{2+} ions were inhibited by the influence of isoeugenol and less effectively by eugenol. These observations suggest that side-chain structure in addition to the phenolic ring had an important role in the antioxidant function of eugenol.[48] Carvacrol and thymol decreased peroxidation of phospholipid liposomes in the presence of Fe^{3+} and ascorbate. They are good scavengers of peroxyl radicals,[49] and their antioxidant effects are manifested in β-carotene bleaching (BCB) test and in DPPH and TBARS assays.[50] Bounatirou et al.[51] found that carvacrol, a monohydroxylated compound, was not able to form the complex with Fe^{2+}. The findings of these authors correspond with results of DNA topology assay. We assume that observed differences between activity of carvacrol (Figure 6B) and its isomer thymol (Figure 6C) correlate with a better stabilization of radicals in the chemical structure of thymol.

R. officinalis oil shows certain $DPPH^{\bullet}$ and $^{\bullet}OH$ scavenging activities (Figures 3D and 4D), but it has no reducing power and is not able to protect plasmid DNA against Fe^{2+}-induced damage. The antioxidative activity of RO confirmed the results of Viuda-Martos et al.,[52] which were obtained using various techniques. Similar to eucalyptol, borneol showed no reducing power or radical-scavenging activity. It is therefore very interesting that in the DNA topology assay borneol manifested a strong protective effect against DNA damage caused by Fe^{2+} ions (Figure 6E, lanes 7–10). It is not inconceivable that borneol protects plasmid DNA by a mechanism independent of its antioxidant properties, which are very weak or nonexistent (as was proved in reducing power and $DPPH^{\bullet}$ and $^{\bullet}OH$ radical scavenging assays). The DNA-protective mechanism of borneol can be explained only partially by its Fe^{2+}-chelating ability, which was relatively weak (10%, $ChEC_{50}$ = 48.73 mM) compared to, for example, $Na_2EDTA{\cdot}2H_2O$ (97%, $ChEC_{50}$ = 0.515 mM) and quercetin (85%, $ChEC_{50}$ = 2.92 mM) used as positive controls. Borneol, a secondary alcohol, possesses high lipophilic properties resulting from its large bicyclic terpenoid skeleton besides some hydrophilic properties based on its relatively small alcoholic functional group. We proposed that in the DNA topology assay borneol molecules can protect DNA by hydrogen bond interactions with DNA. This reaction could proceed on the polar phosphates in the DNA backbone via van der Waals interactions between neighboring big borneol hydrocarbon skeletons, forming a protective lipophilic shield around plasmid DNA. To support this explanation of borneol protective properties, other experiments with basic lipophilic

dx.doi.org/10.1021/jf501006y | J. Agric. Food Chem. 2014, 62, 6632–6639

semibulky *tert*-butyl and isobutyl alcohols were set up. The results corresponded to those obtained for borneol; for example, plasmid DNA was protected against the damaging effect of Fe^{2+} (data not shown).

On the basis of six independent techniques used in this paper we can conclude that the components of EOs (Eug, Ca, T, B, Euc) and intact RO showed various degrees of reducing power, radical scavenging, chelating, and DNA-protective capacity. It is remarkable that a high antioxidative activity of eugenol had no DNA-protective effect toward H_2O_2. On the other hand, borneol, which lacks antioxidant activity, was able to protect DNA of HepG2 cells against H_2O_2 as well as plasmid DNA against Fe^{2+}-induced damage. We expect that the protective effect of borneol against the DNA-damaging effects of H_2O_2 and Fe^{2+} ions may be evoked mainly by its lipophilic chemical character. The comparison of the antioxidative activities of the studied phytochemicals with their DNA-protective effects did not confirm direct relationships between observed characteristics. Different causes of protective effects of natural compounds have been considered and discussed by various scientists (in addition to antioxidative activity and metal chelation ability, also induction of antioxidative enzymes, modulation of gene expression, and interactions with signal transduction pathways). We think that the DNA-protective effects of various natural compounds represent an extensive complex of known and hitherto unknown molecular mechanisms and need further detailed investigations.

AUTHOR INFORMATION

Corresponding Author

*(E.H.) Phone: +421 2 59327 113. Fax: +421 2 59327 506. E-mail: Eva.Horvathova@savba.sk.

Funding

This study was supported by the Scientific Grant Agency of the Ministry of Education of Slovak Republic and Academy of Sciences (VEGA) Grants 1/0025/11, 2/0012/12, 1/0053/14 and Slovak Research and Development Agency Grant APVV-0040-10.

Notes

The authors declare no competing financial interest.

ACKNOWLEDGMENTS

We thank Associate Professor Andrej Bohac, Ph.D. (Department of Organic Chemistry, Faculty of Natural Sciences, Comenius University in Bratislava) for chemical expertise and elucidation of our results. We are also thankful to Alzbeta Vokalikova, Anna Moravkova, and Viera Dytrichova for excellent technical assistance.

REFERENCES

(1) Burt, S. Essential oils: their antibacterial properties and potential applications in foods − a review. *Int. J. Food Microbiol.* **2004**, *94*, 223−253.

(2) Ait-Ouazzou, A.; Cherrat, L.; Espina, L.; Loran, S.; Rota, C.; Pagan, R. The antimicrobial activity of hydrophobic essential oil constituents acting alone or in combined processes of food preservation. *Innovative Food Sci. Emerging Technol.* **2011**, *12*, 320−329.

(3) Slamenova, D.; Horvathova, E. Cytotoxic, anti-carcinogenic and antioxidant properties of the most frequent plant volatiles − minireview. *Neoplasma* **2013**, *60*, 343−354.

(4) Ruberto, G.; Baratta, M. T. Antioxidant activity of selected essential oil components in two lipid model systems. *Food Chem.* **2000**, *69*, 167−174.

(5) Yildirim, A.; Mavi, A.; Kara, A. A. Determination of antioxidant and antimicrobial activities of *Rumex crispus* L. extracts. *J. Agric. Food Chem.* **2001**, *49*, 4083−4089.

(6) Zhao, J.; Liu, T.; Ma, L.; Yan, M.; Gu, Z.; Huang, Y.; Xu, F.; Zhao, Y. Antioxidant and preventive effects of extract from *Nymphaea candida* flower on *in vitro* immunological liver injury of rat primary hepatocyte cultures. *Evidence-Based Complement. Alternat. Med.* **2011**, 497673, DOI: 10.1093/ecam/nep003, 8 pp.

(7) Buricova, L.; Reblova, Z. Czech medicinal plants as possible sources of antioxidants. *Czech J. Food Sci.* **2008**, *26*, 132−138.

(8) Cipak, L.; Grausova, L.; Miadokova, E.; Novotny, L.; Rauko, P. Dual activity of triterpenoids: apoptotic versus antidifferentiation effects. *Arch. Toxicol.* **2006**, *80*, 429−435.

(9) Cipak, L.; Miadokova, E.; Dingova, L.; Kogan, G.; Novotny, L.; Rauko, P. Comparative DNA protectivity and antimutagenicity studies using DNA-topology and Ames assays. *Toxicol. in Vitro* **2001**, *15*, 677−681.

(10) Rajic, Z.; Koncic, M. Z.; Miloloza, K.; Perkovic, I.; Butula, I.; Bucar, F.; Zorc, B. Primaquine-NSAID twin drugs: synthesis, radical scavenging, antioxidant and Fe^{2+} chelating activity. *Acta Pharm.* **2010**, *60*, 325−337.

(11) Singh, N. P.; McCoy, M. T.; Tice, R. R.; Schneider, E. L. A simple technique for quantitation of low levels of DNA damage in individual cells. *Exp. Cell. Res.* **1988**, *175*, 184−191.

(12) Gabelova, A.; Slamenova, D.; Ruzekova, L.; Farkasova, T.; Horvathova, E. Measurement of DNA strand breakage and DNA repair induced with hydrogen peroxide using single cell gel electrophoresis, alkaline DNA unwinding and alkaline elution of DNA. *Neoplasma* **1997**, *44*, 380−388.

(13) McCord, J. M. The evolution of free radicals and oxidative stress. *Am. J. Med.* **2000**, *108*, 652−659.

(14) Thannickal, V. J.; Fanburg, B. L. Reactive oxygen species in cell signaling. *Am. J. Physiol. Lung Cell Mol. Physiol.* **2000**, *279*, 1005−1028.

(15) Chanda, S.; Dave, R. *In vitro* models for antioxidant activity evaluation and some medicinal plants possessing antioxidant properties − an overview. *Afr. J. Microbiol. Res.* **2009**, *3*, 981−996.

(16) Halliwell, B.; Aeschbach, R.; Loliger, J.; Aruoma, O. I. The characterization of antioxidants. *Food Chem. Toxicol.* **1995**, *33*, 601−617.

(17) Slamenova, D.; Horvathova, E.; Wsolova, L.; Sramkova, M.; Navarova, J. Investigation of anti-oxidative, cytotoxic, DNA-damaging and DNA-protective effects of plant volatiles eugenol and borneol in human-derived HepG2, Caco-2 and VH10 cell lines. *Mutat. Res.* **2009**, *677*, 46−52.

(18) Thompson, D. C.; Barhoumi, R.; Burghardt, R. C. Comparative toxicity of eugenol and its quinone methide metabolite in cultured liver cells using kinetic fluorescence bioassays. *Toxicol. Appl. Pharmacol.* **1998**, *149*, 55−63.

(19) Yogalakshmi, B.; Viswanathan, P.; Anuradha, C. V. Investigation of antioxidant, anti-inflammatory and DNA-protective properties of eugenol in thioacetamide-induced liver injury in rats. *Toxicology* **2010**, *268*, 204−212.

(20) Kar Mahapatra, S.; Chakraborty, S. P.; Majumdar, S.; Bag, B. G.; Roy, S. Eugenol protects nicotine-induced superoxide mediated oxidative damage in murine peritoneal macrophages *in vitro*. *Eur. J. Pharmacol.* **2009**, *623*, 132−140.

(21) Kaur, G.; Athar, M.; Alam, M. S. Eugenol precludes cutaneous chemical carcinogenesis in mouse by preventing oxidative stress and inflammation and by inducing apoptosis. *Mol. Carcinog.* **2010**, *49*, 290−301.

(22) Said, M. M. The protective effect of eugenol against gentamicin-induced nephrotoxicity and oxidative damage in rat kidney. *Fundam. Clin. Pharmacol.* **2011**, *25*, 708−716.

(23) Fouad, A. A.; Yacoubi, M. T. Mechanisms underlying the protective effect of eugenol in rats with acute doxorubicin cardiotoxicity. *Arch. Pharm. Res.* **2011**, *34*, 821−828.

(24) Jung, J.; Lee, J. H.; Bae, K. H.; Jeong, C. S. Anti-gastric actions of eugenol and cinnamic acid isolated from *Cinnamomi ramulus*. *Yakugaku Zasshi* **2011**, *131*, 1103−1110.
(25) Zin, W. A.; Silva, A. G.; Magalhaes, C. B.; Carvalho, G. M.; Riva, D. R.; Lima, C. C.; Leal-Cardoso, J. H.; Takiya, C. M.; Valenca, S. S.; Saldiva, P. H.; Faffe, D. S. Eugenol attenuates pulmonary damage induced by diesel exhaust particles. *J. Appl. Physiol.* **2012**, *112*, 911−917.
(26) Ozkan, A.; Erdogan, A. A comparative study of the antioxidant/prooxidant effects of carvacrol and thymol at various concentrations on membrane and DNA of parental and drug resistant H1299 cells. *Nat. Prod. Commun.* **2012**, *7*, 1557−1560.
(27) Slamenova, D.; Horvathova, E.; Marsalkova, L.; Wsolova, L. Carvacrol given to rats in drinking water reduces the level of DNA lesions induced in freshly isolated hepatocytes and testicular cells by H_2O_2. *Neoplasma* **2008**, *55*, 394−399.
(28) Dagli Gul, A. S.; Fadillioglu, E.; Karabulut, I.; Yesilyurt, A.; Delibasi, T. The effects of oral carvacrol treatment against H_2O_2-induced injury on isolated pancreas islet cells of rats. *Islets* **2013**, *5*, 149−155.
(29) Aristatile, B.; Al-Assaf, A. H.; Pugalendi, K. V. Carvacrol suppresses the expression of inflammatory marker genes in D-galactosamine-hepatotoxic rats. *Asian−Pac. J. Trop. Med.* **2013**, *6*, 205−211.
(30) Nafees, S.; Ahmad, S.; Arjumand, W.; Rashid, S.; Ali, N.; Sultana, S. Carvacrol ameliorates thioacetamide-induced hepatotoxicity by abrogation of oxidative stress, inflammation, and apoptosis in liver of Wistar rats. *Hum. Exp. Toxicol.* **2013**, *32*, 1292−1304.
(31) Canbek, M.; Uyanoglu, M.; Bayramoglu, G.; Senturk, H.; Erkasap, N.; Koken, T.; Uslu, S.; Demirustu, C.; Aral, E.; Husnu Can Baser, K. Effects of carvacrol on defects of ischemia-reperfusion in the rat liver. *Phytomedicine* **2008**, *15*, 447−452.
(32) Aydin, S.; Basaran, A. A.; Basaran, N. The effects of thyme volatiles on the induction of DNA damage by the heterocyclic amine IQ and mitomycin C. *Mutat. Res.* **2005**, *581*, 43−53.
(33) Archana, P. R.; Nageshwar Rao, B.; Ballal, M.; Satish Rao, B. S. Thymol, a naturally occurring monocyclic dietary phenolic compound protects Chinese hamster lung fibroblasts from radiation-induced cytotoxicity. *Mutat. Res.* **2009**, *680*, 70−77.
(34) Archana, P. R.; Nageshwar Rao, B.; Satish Rao, B. S. Modulation of gamma ray-induced genotoxic effect by thymol, a monoterpene phenol derivative of cymene. *Integr. Cancer Ther.* **2011**, *10*, 374−383.
(35) Archana, P. R.; Nageshwar Rao, B.; Satish Rao, B. S. *In vivo* radioprotective potential of thymol, a monoterpene phenol derivative of cymene. *Mutat. Res.* **2011**, *726*, 136−145.
(36) Zegura, B.; Dobnik, D.; Niderl, M. H.; Filipic, M. Antioxidant and antigenotoxic effects of rosemary (*Rosmarinus officinalis* L.) extracts in *Salmonella typhimurium* TA98 and HepG2 cells. *Environ. Toxicol. Pharmacol.* **2011**, *32*, 296−305.
(37) Horvathova, E.; Slamenova, D.; Navarova, J. Administration of rosemary essential oil enhances resistance of rat hepatocytes against DNA-damaging oxidative agents. *Food Chem.* **2010**, *123*, 151−156.
(38) Posadas, S. J.; Caz, V.; Largo, C.; De la Gandara, B.; Matallanas, B.; Reglero, G.; De Miguel, E. Protective effect of supercritical fluid rosemary extract, *Rosmarinus officinalis*, on antioxidants of major organs of aged rats. *Exp. Gerontol.* **2009**, *44*, 383−389.
(39) Ngo, S. N.; Williams, D. B.; Head, R. J. Rosemary and cancer prevention: preclinical perspectives. *Crit. Rev. Food Sci. Nutr.* **2011**, *51*, 946−954.
(40) Sokmen, A.; Sokmen, M.; Daferera, D.; Polissiou, M.; Candan, F.; Unlu, M.; Akpulat, H. A. The *in vitro* antioxidant and antimicrobial activities of the essential oil and methanol extracts of *Achillea biebersteini* Afan. (Asteraceae). *Phytother. Res.* **2004**, *18*, 451−456.
(41) Horvathova, E.; Kozics, K.; Srancikova, A.; Hunakova, L.; Galova, E.; Sevcovicova, A.; Slamenova, D. Borneol administration protects primary rat hepatocytes against exogenous oxidative DNA damage. *Mutagenesis* **2012**, *27*, 581−588.
(42) Wang, W.; Wu, N.; Zu, Y. G.; Fu, Y. J. Antioxidative activity of *Rosmarinus officinalis* L. essential oil compared to its main components. *Food Chem.* **2008**, *108*, 1019−1022.
(43) Mitic-Culafic, D.; Zegura, B.; Nikolic, B.; Vukovic-Gacic, B.; Knezevic-Vukcevic, J.; Filipic, M. Protective effect of linalool, myrcene and eucalyptol against *t*-butyl hydroperoxide induced genotoxicity in bacteria and cultured human cells. *Food Chem. Toxicol.* **2009**, *47*, 260−266.
(44) Melidou, M.; Riganakos, K.; Galaris, D. Protection against nuclear DNA damage offered by flavonoids in cells exposed to hydrogen peroxide: the role of iron chelatation. *Free Radical Biol. Med.* **2005**, *39*, 1591−1600.
(45) Rauko, P.; Romanova, D.; Miadokova, E.; Macakova, K.; Novotny, L.; Elford, H. L.; Szekeres, T. DNA-protective activity of new ribonucleotide reductase inhibitors. *Anticancer Res.* **1997**, *17*, 3437−3440.
(46) Ogata, M.; Hoshi, M.; Urano, S.; Endo, T. Antioxidant activity of eugenol and related monomeric and dimeric compounds. *Chem. Pharm. Bull.* **2000**, *48*, 1467−1469.
(47) Reddy, A. C.; Lokesh, B. R. Studies on the inhibitory effects of curcumin and eugenol on the formation of reactive oxygen species and the oxidation of ferrous iron. *Mol. Cell. Biochem.* **1994**, *137*, 1−8.
(48) Ito, M.; Murakami, K.; Yoshino, M. Antioxidant action of eugenol compounds: role of metal ion in the inhibition of lipid peroxidation. *Food Chem. Toxicol.* **2005**, *43*, 461−466.
(49) Aeschbach, R.; Loliger, J.; Scott, B. C.; Murcia, A.; Butler, J.; Halliwell, B.; Aruoma, O. I. Antioxidant action of thymol, carvacrol, 6-gingerol, zingerone and hydroxytyrosol. *Food Chem. Toxicol.* **1994**, *32*, 31−36.
(50) Kulisic, T.; Radonic, A.; Katalinic, V.; Milos, M. Use of different methods for testing antioxidative activity of oregano essential oil. *Food Chem.* **2004**, *85*, 633−640.
(51) Bounatirou, S.; Smiti, S.; Miguel, M. G.; Faleiro, L.; Rejeb, M. N.; Neffati, M.; Costa, M. M.; Figueiredo, A. C.; Barroso, J. G.; Pedro, L. G. Chemical composition, antioxidant and antibacterial activities of the essential oils isolated from Tunisian *Thymus capitatus* Hoff. et Link. *Food Chem.* **2007**, *105*, 146−155.
(52) Viuda-Martos, M.; Navajas, Y. R.; Zapata, E. S.; Fernandez-Lopez, J.; Perez-Alvarez, J. A. Antioxidant activity of essential oils of five spice plants widely used in a Mediterranean diet. *Flavour Fragrance J.* **2010**, *25*, 13−19.

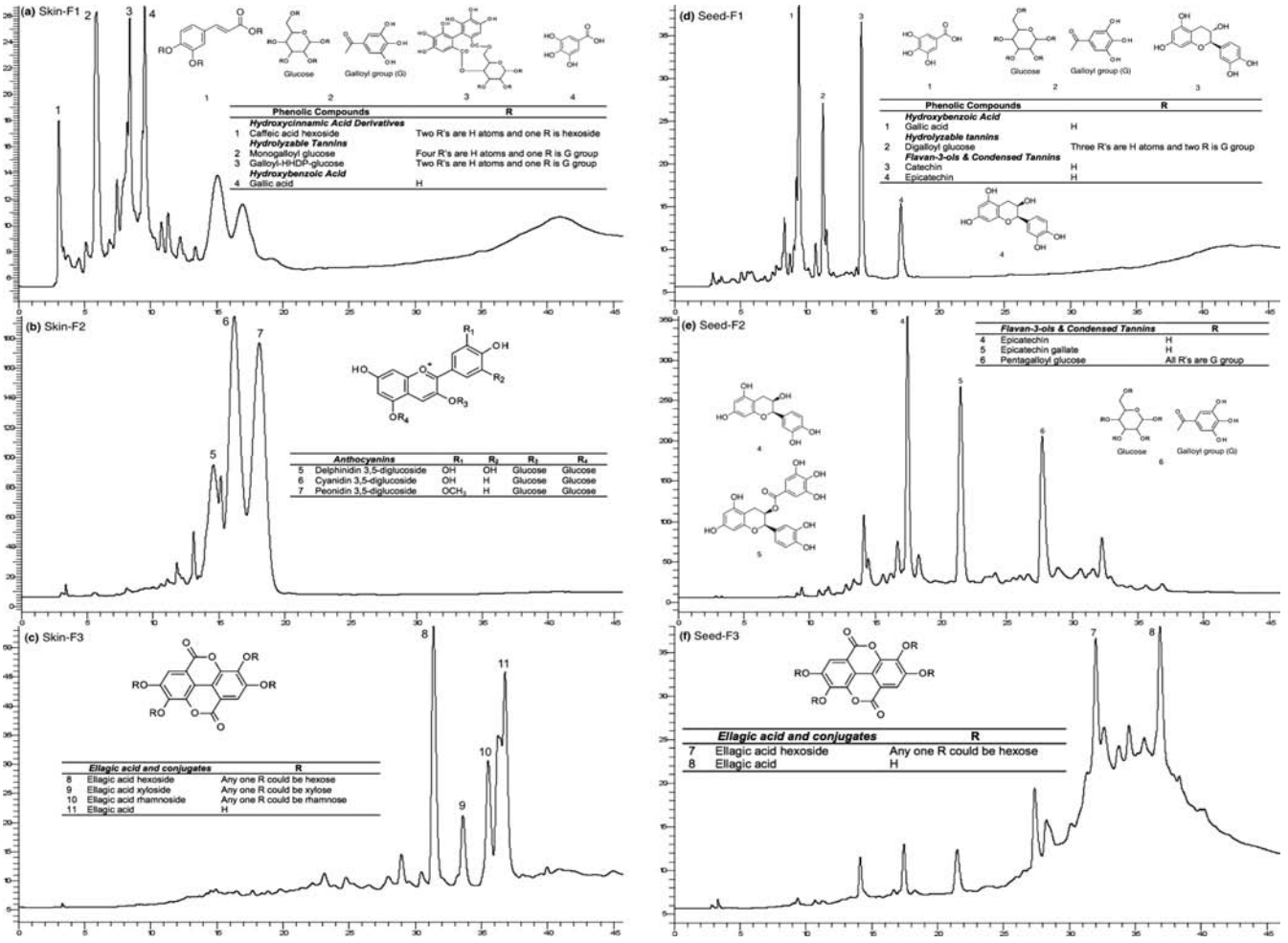

Figure 1. Phenolic compounds and their structures found in muscadine grape skin and seeds: (a, b, and c) Noble skin fractions 1, 2, and 3, respectively; (d, e, and f) Noble seed fractions 1, 2, and 3, respectively.

O157:H7 (204P) strains were obtained from Dr. Tung-shi Huang's laboratory at Auburn University, Auburn, AL, USA.

Antibiotics and Chemicals. Ampicillin and streptomycin were purchased from Fisher Scientific (Fair Lawn, NJ, USA). Nalidixic acid was purchased from Sigma-Aldrich (St. Louis, MO, USA). Plant-derived phenolic standards, including gallic acid, caffeic acid, catechin, ellagic acid, and quercetin, were purchased from Sigma-Aldrich. All of the above commercially purchased chemicals were dissolved in sterile distilled water to a concentration of 5000 mg/L. Folin and Ciocalteu's phenol reagent (2 N), 2,2-diphenyl-1-picrylhydrazyl (DPPH), and 6-hydroxy-2,5,7,8-tetramethylchroman-2-carboxylic acid (Trolox) were purchased from Sigma-Aldrich. Sodium carbonate and HPLC grade organic solvents were purchased from Fisher Scientific Co. (Pittsburgh, PA, USA).

Grape Materials and Extraction, Separation, and Identification of Grape Phenolic Compounds. Fully ripened muscadine grape (*Vitis rotundifolia* Michx.) cv. Noble (red) and cv. Carlos (bronze) were harvested from the Center for Viticulture and Small Fruit Research (latitude 30.65 N, longitude 84.60 W) at Florida A&M University on August 24, 2012. Harvested samples were shipped to the University of Florida on the same day and stored under refrigeration (4 °C). Grape skin and seeds were separated manually from berries and freeze-dried in a freeze-dryer (Advantage, The Virtis Co., Gardiner, NY, USA) within the following 3 days. The freeze-dried samples were stored in vacuum-packaged polyethylene pouches at −20 °C until analyzed.

Plant-extracted phenolic compounds (Figure 1) were prepared in-house at the Food and Environmental Toxicology Laboratory from muscadine grape skin and seeds. Phenolic compounds from grape were extracted and isolated according to a method adapted from a previous study.[16] Freeze-dried grape skin and seeds (defatted) were ground sufficiently with a stainless steel grinder (Omni-Mixer 17105, OCI Instruments, Waterbury, CT, USA) to a fine powder (≤0.25 mm). Powder (5 g) from each sample was extracted with 30 mL of 70% methanol. The extraction flasks were vortexed for 30 s, sonicated for 10 min, kept at room temperature (22 °C) for 60 min, and sonicated for an additional 5 min. The extracts were transferred to tubes and centrifuged at 2820*g* and 0 °C for 10 min (J-LITEJLA-16.250, Beckman Coulter Inc., Brea, CA, USA), and the supernatant was collected in separate glass tubes. Residue was re-extracted with the same procedure. The collected supernatant (60 mL) was evaporated in a rotary evaporator (Büchi, Labortechnik AG, Flawil, Switzerland) under reduced pressure at 40 °C to remove solvent. The concentrates obtained after evaporation were redissolved in 5 mL of distilled water and sonicated for 5 min.

A solid-phase extraction technique adapted from a previous study[17] was used to separate fractions of phenolic compounds. Briefly, two C18 Sep-Pak cartridges (Whatman Chromatography, ODS-5) were connected and preconditioned by sequentially passing 12 mL of ethyl acetate, 12 mL of absolute methanol, and 12 mL of 0.01 N aqueous hydrogen chloride (HCl) through the cartridges. The prepared redissolved extract (0.5 mL) was loaded onto cartridges. Each cartridge was rinsed separately with 12 mL of 0.01 N aqueous HCl (fraction 1, F1), 12 mL of 10% methanol (F2), and 12 mL of 30% methanol (F3) for Carlos skin extract; for Noble skin extract, the cartridges were rinsed with 4 mL of 0.01 N aqueous HCl (F1), 15 mL of 10% methanol (with 0.1% HCl) (F2), and 12 mL of methanol (with 0.1% HCl) (F3); and finally for Carlos and Noble seed extracts, the

dx.doi.org/10.1021/jf501073q | J. Agric. Food Chem. 2014, 62, 6640−6649

cartridges were rinsed with 12 mL of 0.01 N aqueous HCl (F1), 12 mL of 30% methanol (F2), and 12 mL of 50% methanol (F3). To obtain a sufficient volume for subsequent study, four individual separations of each extract were performed and then combined. The collected fractions were evaporated in a rotary evaporator under reduced pressure at 40 °C to remove the solvent. The concentrates obtained after evaporation were dissolved in distilled water and stored at 4 °C until analyzed.

The above-described extracts and their fractions were subjected to chromatographic analyses by HPLC (Hitachi, L-7000 series, Japan) with an analytical SB-C18 column (Zorbax Stablebond, 4.6 mm × 250 mm, 5 μm, Agilent Technologies). Mobile phase was 0.5% formic acid in water (solvent A) and 0.5% formic acid in 60% methanol (solvent B) under the following gradient: 0−3 min, 5% B; 3−8 min, 30% B; 8−25 min, 50% B; 25−30 min, 70% B; 30−35 min, 80% B; 35−47 min, 100% B; 47−51 min, 5% B. The flow rate was 0.9 mL/min. Injection volume was 20 μL. Detection was accomplished with a UV detector (Hitachi, L-7400, Japan) set at an absorbance wavelength of 280 nm. The retention times for each eluted component in the analyzed samples were compared to those of the following standards: gallic acid, caffeic acid, catechin, epicatechin, epicatechin gallate, *trans*-resveratrol, ellagic acid, quercetin, and cyanidin-3,5-diglucoside.

Standards for caffeic acid hexoside, mono-, di-, and pentagalloyl glucose, ellagic acid hexoside, xyloside, rhamnoside, delphinidin-3,5-diglucoside, and peonidin-3,5-diglucoside were not available. Thus, a second HPLC system was employed to confirm their identification by ESI-MS detection in the selective reaction monitoring (SRM) mode. The LC-MS analyses were performed on a Thermo-Finnigan Surveyor HPLC system (Thermo-Finnigan, San Jose, CA, USA) equipped with a TSQuantum controlled by XCalibur data analysis software (version 1.3, Thermo-Finnigan). The column and mobile phase used were the same as described above for the HPLC analysis. The MS acquisition was with ESI interface in negative ionization mode at the following conditions: sheath gas (N_2) pressure, 42 arb; auxiliary gas (N_2) pressure, 20 arb; spray voltage 3.96 kV; capillary temperature, 414 °C; collision gas pressure, 1.5 mTorr; collision energy, 22 V. These compounds were identified on the basis of their mass fragmentation data compared with and identical to those reported by the literature.[18]

Phenolic Content and Antioxidant Activity Assay. Total phenolic content of each extract or fraction was determined by the Folin−Ciocalteu colorimetric method[19] with an ultraviolet−visible Beckman Coulter DU-640 spectrophotometer (Beckman Instruments, Fullerton, CA, USA) and expressed as milligrams of gallic acid equivalents per gram of dry matter. The unitary antioxidant activity of each extract or fraction was evaluated using the DPPH radical scavenging capacity assay[20] and expressed as moles of Trolox equivalents per gram of polyphenols.

Antibacterial Activity Assay. Antibacterial activities of the phenolics (experimental compounds) were determined by agar disc diffusion method,[21] and pathogenic bacteria for the test were listed above. Isolated colonies of test bacterial strains grown overnight on tryptic soy agar plates (TSA; Difco, Becton Dickson, Sparks, MD, USA) were cultured in Mueller−Hinton broth (MHB; Difco, Becton Dickinson) at 37 °C for 18 h. The turbidity of bacterial suspensions was adjusted to approximately 2.0 × 10^8 CFU/mL (optical density at 600 nm = 0.2). Bacterial suspensions were evenly swab-inoculated on surfaces of Mueller−Hinton agar (MHA; Difco, Becton Dickinson). Then each sterile blank disc (6 mm in diameter, Difco, Becton Dickinson) was placed on the surface of the test MHA plates, impregnated with 20 μL of experimental compounds (Table 2, in triplicate per compound), and incubated at 37 °C for 24 h. Commercial antibiotics (ampicillin, nalidixic acid, and streptomycin at 10 μg/disc) and distilled water prepared in the same manner as the experimental compounds were used as positive and negative controls, respectively. The size of the zone of inhibition was measured, and the antibacterial activity was expressed in terms of the average diameter of the zone of inhibition in millimeters. The absence of a zone of inhibition (≤6 mm) was interpreted as the absence of antibacterial activity.

The MIC was determined using an Alamar blue assay adapted from a previous study.[21] Briefly, serial dilutions of experimental compounds in MHB (100 μL) with test bacteria at a density of 5 × 10^6 CFU/mL were incubated in flat-bottom, polystyrene, non-tissue-culture-treated 96-well microtiter plates at 37 °C without shaking for 20 h. After 20 h, 10 μL of Alamar blue (AB; Invitrogen, Life Technologies, Carlsbad, CA, USA) was added to the wells and the plates were shaken gently and incubated for 1 h at 37 °C. Plates were gently shaken again, and absorbances at 570 and 600 nm were obtained in a microplate reader (ELX808 Universal, Bio-Tek Instruments, Winooski, VT, USA). Controls included medium alone (blank), diluted medium plus experimental compounds plus AB (negative), and medium plus cells plus AB (positive). Percent reduction of AB was calculated using the manufacturer's formula (absorbance difference between 570 and 600 nm for each experimental well divided by the difference in positive control). Assays were performed in triplicate, and the average percent reduction was used to determine MIC. The AB MIC was defined as the lowest concentration of the experimental compound resulting in ≤50% reduction of AB and a purplish well 60 min after the addition of AB.[22]

To investigate the correlation of Alamar blue reduction to colony-forming units per milliliter (CFU/mL), CFU/mL was obtained from the same wells used to obtain AB absorbances. Before AB was added to all treated wells, 10 μL of the well culture was removed and serially diluted (10-fold) in 0.1% peptone water followed by plating (20 μL of the dilution) on TSA. Colonies were counted after incubation at 37 °C for 24 h and recorded as CFU/mL. Pearson's two-tailed correlations were calculated between Alamar blue reduction and CFU/mL.

Time−Kill and Synergy Assay. Time−kill assays were performed using a method adapted from a previous study.[23] Briefly, bacteria were cultured to exponential phase (1.0 × 10^8 CFU/mL, OD_{600} = 0.15) in MHB and challenged with antibiotics or experimental compounds at 4 × MIC or 500 mg/L. Synergy between antibiotics and phenolic compounds was tested at 0.9 × MIC. Bacterial viability was monitored every hour (0−6 h) by plating cultures onto TSA and counting colonies after incubation at 37 °C for 24 h as described previously. To detect bacterial lysis following the challenge with antibacterial agents, the culture turbidity of early exponential phase cultures was monitored every hour (0−6 h) and finally at 24 h by absorbance measurements at 600 nm at 37 °C. Synergy between antibiotics and phenolic compounds was defined as follows, using $\log_{10}$ CFU/mL at 24 h: synergy was >2 $\log_{10}$ kill, additivity was >1−2 $\log_{10}$ kill, indifference was 1 $\log_{10}$ kill to 2 $\log_{10}$ growth, and antagonism was >2 $\log_{10}$ growth compared to the most active drug alone. Bactericidal activity was defined as a ≥3 $\log_{10}$ CFU/mL kill at 24 h from baseline.[24]

Antibiofilm Activity Assay. The planktonic cell susceptibility to polyphenols and polyphenols inhibiting biofilm formation were determined using the Alamar blue assay adapted from a previous study.[21] Briefly, serial dilutions of experimental compounds in MHB (100 μL, with diluted 2500 to 5 mg/L) with bacteria at a density of 5 × 10^6 CFU/mL were incubated in round-bottom, polystyrene, non-tissue-culture-treated 96-well microtiter plates at 37 °C without shaking for 20 h. After 20 h, visual MICs were identified by the dot at the bottom of the well (the well before dots appear is defined as the MIC point); then, the content of each well was aspirated and transferred to a new flat-bottom plate; 10 μL of Alamar blue was subsequently added to the new plate wells and analyzed as the previous procedure to determine the MICs of planktonic cells. After this, the original round-bottom plate wells (after transferring) were gently washed twice with 250 μL sterile physiological saline to remove nonadherent bacteria; 100 μL of sterile distilled water was added to these wells followed by 10 μL of Alamar blue and analyzed as the previous procedure to determine the minimum biofilm inhibitory concentration (MBIC).

To determine the reduction capability of polyphenols on preformed biofilm, assays were performed in flat-bottom plates with bacteria incubated at a density of 5 × 10^6 CFU/mL in 100 μL of MHB. First, plates were incubated at 37 °C without shaking for 24 h to allow biofilm formation. Then, 2-fold dilutions (diluted 2500 to 5 mg/L) of experimental compounds in MHB were prepared external to the

plates. After 24 h of incubation, well contents were aspirated from all experimental and control wells, wells were gently washed twice with 250 μL of sterile physiological saline, and 100 μL of the appropriate diluted compounds was added. Preformed biofilms were exposed to compounds for 20 h at 37 °C without shaking. After 20 h, 10 μL of Alamar blue was added to the wells and analyzed as previously described.

Statistical Analysis. Experimental results were expressed as means ± standard error (SE) of three independent replicates. Data were subjected to ANOVA, and significant differences were tested by post hoc comparison test (Student−Newman−Keuls) at $P < 0.05$. Microsoft Excel 2008 and SPSS 20.0 for Windows were used for this analysis and for calculating Pearson's correlation coefficients.

RESULTS

Muscadine Grape Phenolic Compounds and Antioxidant Activity. Phenolic compounds from muscadine grape (Noble and Carlos) skins and seeds were separated into three fractions, respectively, and chromatograms of identified phenolics from Noble skin and seed fractions are presented in Figure 1. Caffeic acid hexoside, hydrolyzable tannins, and gallic acid were the major phenolics in fraction 1 of Noble skin polyphenols (Figure 1a). Anthocyanins were the major phenolics in the corresponding fraction 2 (Figure 1b), and ellagic acid and its conjugates were in fraction 3 (Figure 1c). Polyphenol fractions from Carlos skin were different from those from Noble skin, with richer ellagic acid and conjugates in fraction 3, but almost no anthocyanins in fraction 2 (data not shown). However, polyphenol fractions from Noble and Carlos seeds showed similar profiles, with hydroxybenzoic acid, hydrolyzable tannins, and little flavan-3-ols distributed in fraction 1 (Figure 1d), major flavan-3-ols and condensed tannins distributed in fraction 2 (Figure 1e), and ellagic acid and its conjugates distributed in fraction 3 (Figure 1f). Overall, anthocyanins (fraction 2, 22.6 mg/g) were the major phenolics for Noble skin, whereas it was ellagic acid and its conjugates (fraction 3, 20.5 mg/g) for Carlos skin; flavan-3-ols and condensed tannins (fraction 2, 38.8, and 40.8 mg/g, respectively) were the major phenolics for Noble and Carlos seeds (Table 1).

Antioxidant activity of phenolic compounds varied greatly among tested samples (Table 1). For the polyphenol standards, gallic acid showed the strongest antioxidant activity per unit and ranked in order as gallic acid > ellagic acid > quercetin > catechin > caffeic acid. For the polyphenol extracts, fraction 3 showed the strongest antioxidant activity per unit and ranked in order as fraction 3 (ellagic acid and conjugates) > fraction 1 (hydroxybenzoic acid and hydrolyzable tannins) > fraction 2 (anthocyanins or flavan-3-ols and condensed tannins). As expected, antioxidant activity for the nonseparated grape skin or seed extracts varied among their corresponding activities of the fractions.

Antibacterial Activity of Phenolic Compounds. Antibacterial activity of phenolic compounds was initially screened by the standard agar disc diffusion method and then subjected to the MIC test. Table 2 showed that the inhibition of bacterial growth was quite drug and species dependent. Muscadine grape skin and seed polyphenol extracts exhibited a broad spectrum of antibacterial activity against Gram-positive bacteria (*S. aureus*), but exhibited little to no antibacterial efficacy against Gram-negative bacteria (*Salmonella enterica* ser. Typhimurium, *S. sonnei* ATCC 25931, and *E. coli* O157:H7 204P). Inhibition by seed polyphenols (Carlos seed vs Noble seed) against *S. aureus* was positively dependent on concentration, whereas skin polyphenols (Carlos skin vs Noble skin) were negatively dependent. Although Carlos skin was used at higher polyphenol concentration than Carlos seed, its inhibition was significantly weaker than that of the later. These findings indicated that the antibacterial activity of muscadine grape phenolic compounds was not only concentration dependent but also phenolic specific dependent. Gallic acid exhibited good antibacterial activity on tested *S. aureus* strains, whereas ellagic acid showed slightly less inhibition at 100 μg/disc. Caffeic acid, catechin, and quercetin exhibited little to no antibacterial efficacy against *S. aureus* at this concentration. None of these polyphenol standards was found to show inhibition on Gram-negative bacteria in this study. The susceptibility of all tested bacteria to the three antibiotics (positive control, 10 μg/disc) varied significantly with zones of inhibition ranging from 0 to 43.8 mm. In general, ampicillin and streptomycin showed stronger inhibition than nalidixic acid in this study.

Muscadine grape polyphenols were further demonstrated to have good antibacterial activity against Gram-positive bacteria (*S. aureus*) as shown by an MIC of 74−367 mg/L for skin polyphenols and 67−173 mg/L for seed polyphenols (Table 3). Inhibition for different phenolic fractions was significantly

Table 1. Phenolic Content and Antioxidant Activity of Experimental Compounds[a]

exptl compd	phenolic content[b] (mg/g)	antioxidant activity per unit[c] (mmol/g)
polyphenol standards		
gallic acid		11.1 ± 0.2a
caffeic acid		5.1 ± 0.2e
catechin		5.3 ± 0.3e
ellagic acid		9.8 ± 0.6ab
quercetin		9.4 ± 0.4b
polyphenol extracts[d]		
Carlos skin (CK) polyphenols	39.0 ± 2.1c	6.3 ± 0.5d
CK-F1	9.1 ± 0.8f	7.4 ± 0.3cd
CK-F2	8.7 ± 0.7f	5.9 ± 0.2de
CK-F3	20.5 ± 1.4e	8.7 ± 0.6bc
Noble skin (NK) polyphenols	35.9 ± 2.5d	5.3 ± 0.3e
NK-F1	5.5 ± 0.3h	7.9 ± 0.5c
NK-F2	22.6 ± 1.8e	5.0 ± 0.4e
NK-F3	7.5 ± 0.3g	8.9 ± 0.8bc
Carlos seed (CS) polyphenols	50.8 ± 3.4b	10.1 ± 0.4ab
CS-F1	5.1 ± 0.2h	8.4 ± 0.2bc
CS-F2	38.8 ± 1.2c	7.4 ± 0.3cd
CS-F3	7.1 ± 0.4g	10.8 ± 0.5a
Noble seed (NS) polyphenols	58.2 ± 3.5a	9.2 ± 0.3b
NS-F1	7.6 ± 0.6g	8.6 ± 0.2bc
NS-F2	40.8 ± 3.1c	6.9 ± 0.1d
NS-F3	8.9 ± 0.6f	11.1 ± 0.5a

[a]Results are expressed as means of triplicate determinations ± SE; different letters within columns indicate significant difference ($P < 0.05$). [b]Phenolic content of extracts is expressed as milligrams gallic acid equivalents per gram dry matter. [c]Antioxidant activity was determined by DPPH assay and expressed as millimoles Trolox equivalents per gram polyphenols. [d]Fractions 1−3 for Carlos and Noble skins and seeds were eluted from tandem C18 Sep-Pak cartridges with different solvents: skins, F1, 0.01 N HCl; F2, 10% MeOH; F3, 30% MeOH; and seeds, F1, 0.01 N HCl; F2, 30% MeOH; F3, 50% MeOH.

dx.doi.org/10.1021/jf501073q | J. Agric. Food Chem. 2014, 62, 6640−6649

Table 2. Antibacterial Activity of Experimental Compounds against Selected Foodborne Pathogens Using the Disc Diffusion Method

	zone of inhibition[a] (mm) on MHA					
	Gram-positive bacteria			Gram-negative bacteria		
exptl compd	*S. aureus* ATCC-35 548	*S. aureus* ATCC 12600-U	*S. aureus* ATCC 29247	*S. enterica* ser. Typhimurium	*S. sonnei* ATCC 25931	*E. coli* O157:H7 204P
antibiotic controls						
ampicillin (10 μg/disc)	0	43.8 ± 1.2a,A	13.5 ± 0.5b,D	24.2 ± 0.8a,B	19.0 ± 0.5a,C	9.2 ± 0.1b,E
nalidixic acid (10 μg/disc)	0	0	0	0	19.7 ± 0.3a	0
streptomycin (10 μg/disc)	15.2 ± 0.3a,C	14.0 ± 0.2b,D	0	19.8 ± 0.6b,A	14.0 ± 0.2b,D	17.6 ± 0.4a,B
polyphenol standards						
gallic acid (100 μg/disc)	14.7 ± 0.5a,B	11.3 ± 0.3c,C	17.7 ± 0.6a,A	0	0	0
caffeic acid (100 μg/disc)	0	0	8.2 ± 0.3ef	0	0	0
catechin (100 μg/disc)	0	0	0	0	0	0
ellagic acid (100 μg/disc)	12.7 ± 0.3[b]	12.3 ± 0.5[b]	14.0 ± 0.2[b]	0	0	0
quercetin (100 μg/disc)	0	0	8.8 ± 0.2e	0	0	0
polyphenol extracts						
Carlos skin (390 μg/disc)	9.0 ± 0.3e,A	8.2 ± 0.1e,B	7.8 ± 0.3f,B	0	0	0
Noble skin (290 μg/disc)	10.6 ± 0.2d,A	10.1 ± 0.2d,A	10.7 ± 0.2d,A	0	0	0
Carlos seed (340 μg/disc)	12.4 ± 0.2c,A	11.4 ± 0.3c,AB	12.0 ± 0.1c,A	0	7.2 ± 0.3c,C	0
Noble seed (450 μg/disc)	14.1 ± 0.1b,A	13.5 ± 0.2b,AB	14.0 ± 0.5b,A	0	7.7 ± 0.2c,C	0

[a]Results are expressed as means of triplicate determinations ± SE; results with different lower case letters in columns and different upper case letters in rows are significantly different ($P < 0.05$); results >6 mm were considered effective against bacteria, ≤6 mm were considered noneffective and recorded as 0. [b]Partial inhibition within a zone and not included in the statistical analysis.

different. In general, the nonseparated skin and seed polyphenols exhibited comparable or even better inhibition than some of their corresponding fractions. This indicated there might be a synergistic effect between different phenolics in inhibiting bacteria growth. Muscadine grape polyphenols also showed good antibacterial activity against Gram-negative bacteria (*S. sonnei* ATCC 25931) with an MIC of 112−735 mg/L while exhibiting fair antibacterial efficacy against *S. enterica* ser. Typhimurium and *E. coli* O157:H7 204P with MICs of 224−1976 and 304−1540 mg/L, respectively. The phenolic concentration required to inhibit Gram-negative bacteria ranged from 1 to 16 times higher than that required for Gram-positive bacteria. Unexpectedly, almost no inhibition (≥2500 mg/L) was found for the commercial polyphenol standards on all tested bacterial strains. The inhibition of antibiotic controls on all study strains, even though within the same species, varied greatly and were either very strong (≤20 mg/L) or almost none (≥1250 mg/L). By contrast, muscadine grape polyphenols displayed consistent antibacterial activity within one species, such as *S. aureus* (Table 3) and *Salmonella enterica* ser. Typhimurium (data not completely shown). This indicated that muscadine grape polyphenols had a broad spectrum of antibacterial activity and possibly could be used to treat these antibiotic-resistant strains.

Evaluation of Bacterial Killing and Synergistic Effect by Phenolic Compounds. To further evaluate the bactericidal activity of phenolic compounds, the killing kinetics of these compounds were assessed against *S. aureus* ATCC 35548 alongside established antibiotics. At 4 × MIC, Noble skin and seed polyphenols caused reductions in cell viability of 4.7 and 4.9 $\log_{10}$ CFU/mL after 6 h in MHB, respectively, whereas streptomycin caused a reduction of 6.1 $\log_{10}$ CFU/mL (Figure 2a). Gallic acid and ellagic acid caused only a slight bacteriostatic effect at 500 mg/L. Significant synergism between antibiotics and polyphenols at sub-MIC were observed. Ampicillin (150 mg/L), with a high MIC of 2500 mg/L, when added with gallic acid (500 mg/L), ellagic acid (500 mg/L), Noble skin (0.9 × MIC), and Noble seed (0.9 × MIC) caused reductions in cell viability of 0.5, 3.9, 5.1, and 4.8 $\log_{10}$ CFU/mL, respectively (Figure 2b), whereas the addition of streptomycin with gallic acid, ellagic acid, Noble skin, and Noble seed caused reductions in cell viability of 1.6, 4.0, 5.0, and 6.2 $\log_{10}$ CFU/mL, respectively (Figure 2c). Although both gallic acid and ellagic acid had little effect on bacterial viability individually, when combined with antibiotics, ellagic acid showed considerably stronger bactericidal activity than gallic acid, especially after 2 h. Synergy of streptomycin and Noble seed (at 0.9 × MIC) was better than streptomycin or Noble seed (at 4 × MIC) alone and was the strongest bactericidal activity among all of the treatments. These indicated that combining grape polyphenols with antibiotics could maximize the bactericidal activity while reducing the usage of antibiotics.

Bacterial lysis showed that, at 4 × MIC, Noble skin and seed polyphenols caused a reduction in culture turbidity over a 6 h period, whereas streptomycin exhibited an increase (Figure 2d). This indicated Noble skin and seed polyphenols were bactericidal and killed bacteria with concomitant cell lysis, whereas streptomycin was nonlytic but bactericidal. Antibiotics combined with Noble seed polyphenols exhibited stronger bacterial lysis ability than skin polyphenols (Figure 2e,f). Overall, there was a positive correlation ($r = 0.84$) between bacterial number ($\log_{10}$ CFU/mL) and culture turbidity (OD_{600}) at 6 h. After 24 h, as the turbidity of the control continued to increase, all treatments except gallic acid caused a reduction in culture turbidity. This suggests that with plenty of time, phenolic compounds promoted a loss of culture turbidity as well as a loss of bacterial viability.

Antibiofilm Activity of Phenolic Compounds. To investigate the resistance of biofilm versus planktonic-grown strains, Alamar blue MICs of nalidixic acid against a variety of

Table 3. Minimum Inhibitory Concentration (MIC) of Experimental Compounds against Human Pathogenic Bacteria

	mean MIC (mg/L) value[a]					
	Gram-positive bacteria			Gram-negative bacteria		
exptl compd	*S. aureus* ATCC 35548	*S. aureus* ATCC 12600-U	*S. aureus* ATCC 29247	*S. enterica* ser. Typhimurium	*S. sonnei* ATCC 25931	*E. coli* O157:H7 204P
antibiotic controls						
ampicillin	2500a,A	<5i,D	1250b,B	<5g,D	<5h,D	10e,C
nalidixic acid	20g,C	156e,B	20i,C	2500a,A	<5h,D	1250b,A
streptomycin	20g,B	20h,B	>2500A	10f,C	10g,C	10e,C
polyphenol standards						
gallic acid	2500a	2500a	>2500	2500a	2500a	>2500
caffeic acid	2500a	2500a	2500a	>2500	>2500	2500a
catechin	>2500	2500a	>2500	>2500	>2500	>2500
ellagic acid	>2500	>2500	>2500	>2500	>2500	>2500
quercetin	>2500	>2500	>2500	>2500	>2500	>2500
polyphenol extracts[b]						
Carlos skin (CK) polyphenols	152c,C	304c,B	152e,C	608c,A	304d,B	304d,B
CK-F1	119d,C	238d,B	119f,C	476d,A	119f,B	476c,A
CK-F2	183b,D	367b,C	367c,C	1470b,A	735b,B	1470b,A
CK-F3	149c,D	149e,D	298d,C	1191b,A	595b,B	1191b,A
Noble skin (NK) polyphenols	113d,C	226d,B	113f,C	903c,A	226e,B	903bc,A
NK-F1	112d,C	112ef,C	112f,C	224e,B	112f,C	448c,A
NK-F2	145c,C	290c,C	145e,C	1159b,A	579b,B	1.159b,A
NK-F3	74f,D	148e,C	74gh,D	297e,B	148f,C	593c,A
Carlos seed (CS) polyphenols	67f,C	67g,C	67h,C	1069b,A	268e,B	1069b,A
CS-F1	87ef,C	173e,C	173e,C	1386b,A	348d,B	1386b,A
CS-F2	148c,B	74g,C	74gh,C	1181b,A	148f,B	1181b,A
CS-F3	78e,C	156e,B	78gh,C	624c,A	156f,B	624c,A
Noble seed (NS) polyphenols	88ef,C	88fg,C	88g,C	1403b,A	352d,B	1403b,A
NS-F1	123d,D	123ef,D	123f,D	1976a,A	492c,C	988bc,B
NS-F2	69f,D	138e,C	69h,D	1107b,A	276e,B	1107b,A
NS-F3	97e,C	97f,C	97g,C	1540b,A	193ef,B	1540b,A

[a]MICs were determined by the Alamar blue assay. MIC is defined as the lowest experimental compound concentration resulting in ≤50% reduction of AB (average of three experiments) and a purplish well 60 min after addition of AB. Results with different lower case letters in columns and different upper case letters in rows are significantly different ($P < 0.05$). MIC values >2500 mg/L were not included in the statistical analysis. Test strains were inoculated at 5×10^6 CFU/mL in each well. [b]Fractions 1−3 for Carlos and Noble skins and seeds were eluted from tandem C18 Sep-Pak cartridges with different solvents: skins, F1, 0.01 N HCl; F2, 10% MeOH; F3, 30% MeOH; and seeds, F1, 0.01 N HCl; F2, 30% MeOH; F3, 50% MeOH.

pathogenic bacteria and MBICs against their preformed biofilm were studied (Table 4). Alamar blue MBICs increased at least 4-fold relative to planktonic MICs. These data are consistent with previous reports of many-fold increases in drug resistance of biofilm versus planktonic-grown strains.[22,25]

A variety of antibiotics and phenolic compounds with different mechanisms were further studied on planktonically grown *S. aureus* susceptibility, inhibition of biofilm formation, and resistance of preformed biofilm (Table 5). Visual and Alamar blue MICs for planktonically grown strains were identical, with ellagic acid as an exception. Thus, MICs can be generally determined visually or spectrophotometrically. MBICs for inhibiting biofilm formation were within 2-fold dilutions lower than MICs, whereas MBICs of preformed biofilm were at least 16-fold higher than MICs. For example, the MIC of Carlos seed polyphenols against planktonic-grown *S. aureus* ATCC 35548 was 40 mg/L, that against biofilm formation was 20 mg/L, and that against preformed biofilm was as high as 641 mg/L. These findings indicated that grape polyphenols were able to inhibit bacteria biofilm formation at a sub-MIC concentration without killing the bacteria; however, to eradicate the preformed biofilm, a high concentration of phenolic compounds is needed.

DISCUSSION

This study demonstrated that muscadine grape skin and seed polyphenols had potent bactericidal activity against planktonic cells and biofilm formation of Gram-positive bacteria *S. aureus*. The fact that polyphenols acted to cause cell lysis and therefore compromise the integrity of the bacterial membrane may explain why these compounds have the ability to eradicate *S. aureus* biofilms; potent antibiofilm activity is a property that is often associated with membrane-perturbing agents.[26] The limited activity of grape polyphenols against Gram-negative bacteria was probably because of the limited ingress across the outer membrane.[27] However, another intrinsic mechanism that has been insufficiently studied is efflux, and multidrug efflux pumps have been shown to be associated with the insusceptibility of *E. coli* to various biocidal agents.[28]

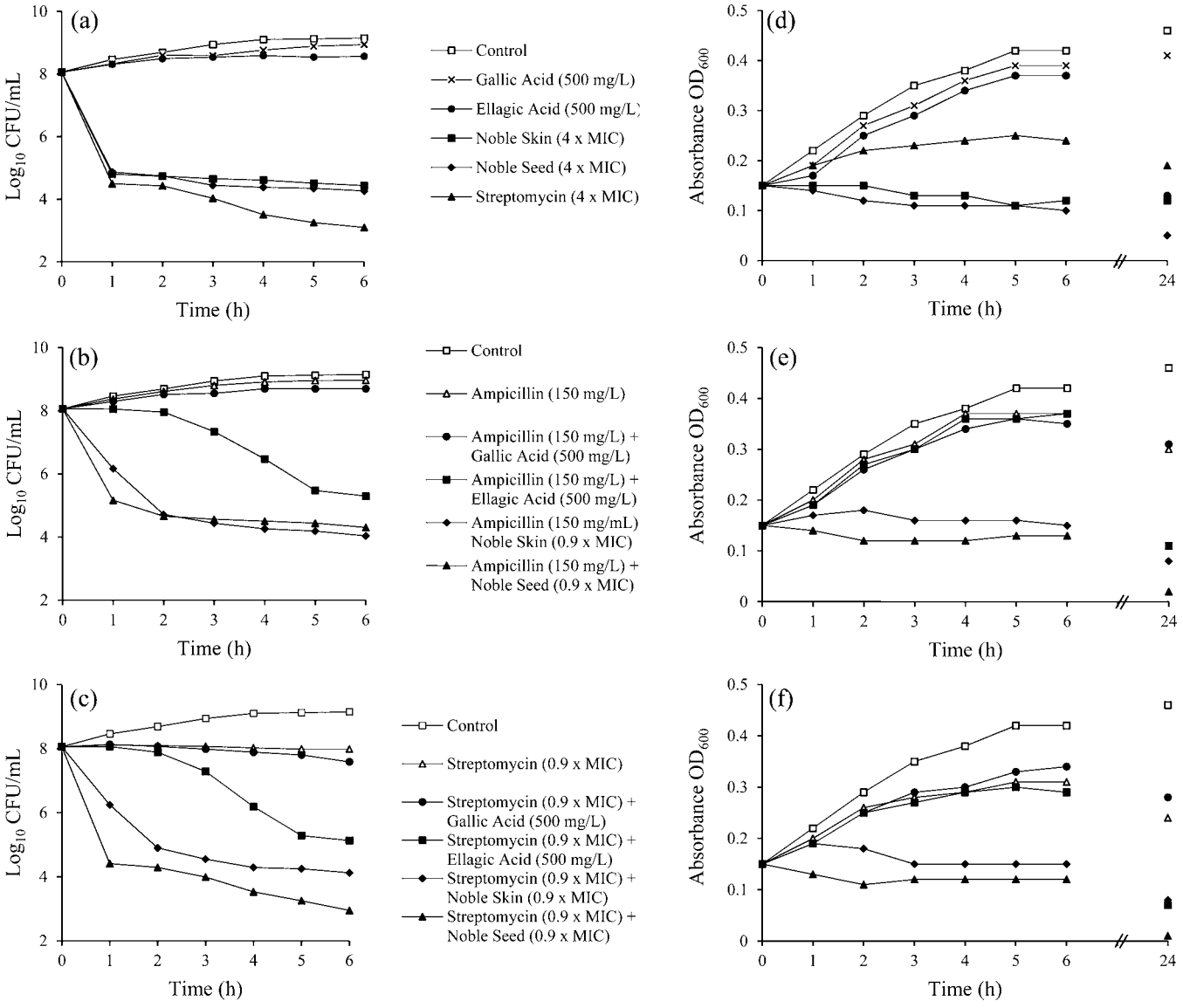

Figure 2. Evaluation of killing (a–c) and lytic (d–f) action of experimental compounds and their synergism with antibiotics against *S. aureus* ATCC 35548 in MHB (means of three independent replicates). MICs of Noble skin, Noble seeds, and streptomycin were 113, 88, and 20 mg/L, respectively.

A positive correlation (r = 0.72) between antioxidant (Table 1) and antibacterial (Table 2) activities of polyphenol standards against *S. aureus* on agar medium was found. Also, a weak positive correlation (r = 0.53) between antioxidant (Table 1) and antibacterial (Table 3) activities of muscadine polyphenols against *S. aureus* was observed. These findings suggested that the stronger the antioxidant activity per unit polyphenols, the better the antibacterial activity against *S. aureus*. However, strong antibacterial activity against *S. aureus* does not necessarily mean strong antioxidant activity because no antioxidant activity was demonstrated for antibiotics (ampicillin, nalidix acid, and streptomycin) (data not shown). Similar to a previous finding,[29] there was a positive correlation (r = 0.77) between total polyphenol content and total antioxidant activity for these grape extracts and fractions. Nonetheless, higher phenolic levels do not necessarily correlate with increased inhibition against *S. aureus* but rather the type and concentration of compounds present in these extracts.

Interestingly, compared to grape phenolic extracts, commercial phenolic standards gallic acid and ellagic acid exhibited stronger antioxidant activity per unit, 11.1 and 9.8 mmol/g, respectively (Table 1), and also showed good antibacterial activity on tested *S. aureus* strains using the disc diffusion method (Table 2). However, further Alamar blue MIC tests (Table 3) and time-killing study (Figure 2) suggested that gallic acid and ellagic acid possess negligible antibacterial efficacy against *S. aureus*. This contradictory finding indicated the very different antibacterial mechanism of gallic acid and ellagic acid on a solid surface versus in a liquid. Other phenolic standards, caffeic acid, catechin, and quercetin, exhibited little to no inhibition on the tested strains in all assays. Therefore, it seems that antibacterial activities of commercial phenolic standards were weaker compared to the muscadine grape phenolic extracts. One possible reason was that the antibacterial activities of these phenolics were lost during their processing or these phenolics existed as ineffective isomer forms. Another possible reason was that synergism between multiple phenolics

dx.doi.org/10.1021/jf501073q | J. Agric. Food Chem. 2014, 62, 6640–6649

Table 4. Minimum Inhibitory Concentration (MIC) of Nalidixic Acid against Pathogenic Bacteria and Minimum Biofilm Inhibitory Concentration (MBIC) against Their Preformed Biofilm Reduction

pathogenic bacteria	MIC[a] (mg/L)	MBIC[ab] (mg/L)
Gram-positive bacteria		
Staphylococcus aureus ATCC 35548	20	1250*
S. aureus ATCC 12600-U	156	625*,#
S. aureus ATCC 29247	20	1250*
Gram-negative bacteria		
Salmonella enterica ser. Typhimurium	2500	>2500
Shigella sonnei ATCC 25931	<5	1250*
E. coli O157:H7 204P	1250	>2500*

[a]MIC or MBIC defined as the lowest nalidixic acid concentration resulting in ≤50% reduction of AB (average of three experiments) and a purplish well 60 min after addition of AB. [b]*, significant differences between MICs of nalidixic acid versus MBICs ($P < 0.05$); #, significant differences between MBICs of nalidixic acid against biofilms within the same *S. aureus* species ($P < 0.05$).

Table 5. Minimum Inhibitory Concentration (MIC) of Experimental Compounds against *S. aureus* ATCC 35548 and Minimum Biofilm Inhibitory Concentration (MBIC) against Its Biofilm Formation and Preformed Biofilm Reduction

exptl compd	MIC[a] (mg/L) (visual)	MIC[b,c] (mg/L) (planktonic cell)	MBIC[b,c] (mg/L) (biofilm formation)	MBIC[b,c] (mg/L) (biofilm reduction)
ampicillin	2500	2500	1250*	>2500#
nalidixic acid	20	20	5*	1250*,#
streptomycin	20	20	5*	625*,#,
gallic acid	>2500	>2500	>2500	>2500
ellagic acid	312	>2500	2500	>2500
Carlos skin phenolics	122	122	61*	1950*,#
Noble skin phenolics	113	113	57*	1808*,#
Carlos seed phenolics	40	40	20*	641*,#
Noble seed phenolics	51	51	25*	801*,#

[a]Visual MIC was identified by the dot at the bottom of the well. The well before dots appear was defined as MIC point. [b]Planktonic cell MIC or MBIC defined as the lowest experimental compound concentration resulting in ≤50% reduction of AB (average of three experiments) and a purplish well 60 min after addition of AB. [c]*, significant differences between MICs (visual and planktonic cell) of experimental compounds versus MBICs (biofilm formation and reduction) ($P < 0.05$); #, significant differences between MBICs of experimental compounds against biofilm formation versus preformed biofilm reduction ($P < 0.05$).

increased their antibacterial activities. These findings can be further supported by other authors' reports that pure catechin and epicatechin possess negligible antibacterial activity against Gram-positive and Gram-negative bacteria,[30] whereas plant-extracted whole polyphenols exhibited good antibacterial activity against several foodborne pathogenic bacteria.[31] For instance, the mean MICs against *S. aureus* ranged from 98 to 389 mg/L and those against *E. coli* ranged from 450 to 1519 mg/L. Also, in this study, whole extracted skin and seed polyphenols exhibited comparable or even better inhibition than their corresponding fractions. Therefore, whole extracted polyphenols were used in the following studies.

This study also investigated the correlation between Alamar blue (AB) percent reduction by bacteria metabolic activity,[22] and the existing bacteria number per well on Carlos seed polyphenols and ellagic acid at various concentrations. Results showed that percent reduction of AB had a significant correlation (r = 0.94 and 0.92, respectively) with existing bacteria number (Figure 3). Carlos seed polyphenols at 40 mg/L inhibited the bacteria number at the initial level (6 $\log_{10}$ CFU/mL) with a 24.9% reduction of AB after 20 h of incubation, whereas at 160 mg/L (4 × MIC) bacteria were killed with no reduction of AB. Ellagic acid at 2500 mg/L reduced bacteria number by 1.4 $\log_{10}$ CFU/mL with a 39.2% reduction of AB after 20 h of incubation. These confirmed that the colorimetric AB assay is a reliable, reproducible means of determining bacteria antibiotic susceptibility. A previous study also showed that the AB assay was a good means of determining biofilm antibiotic susceptibility and had good to

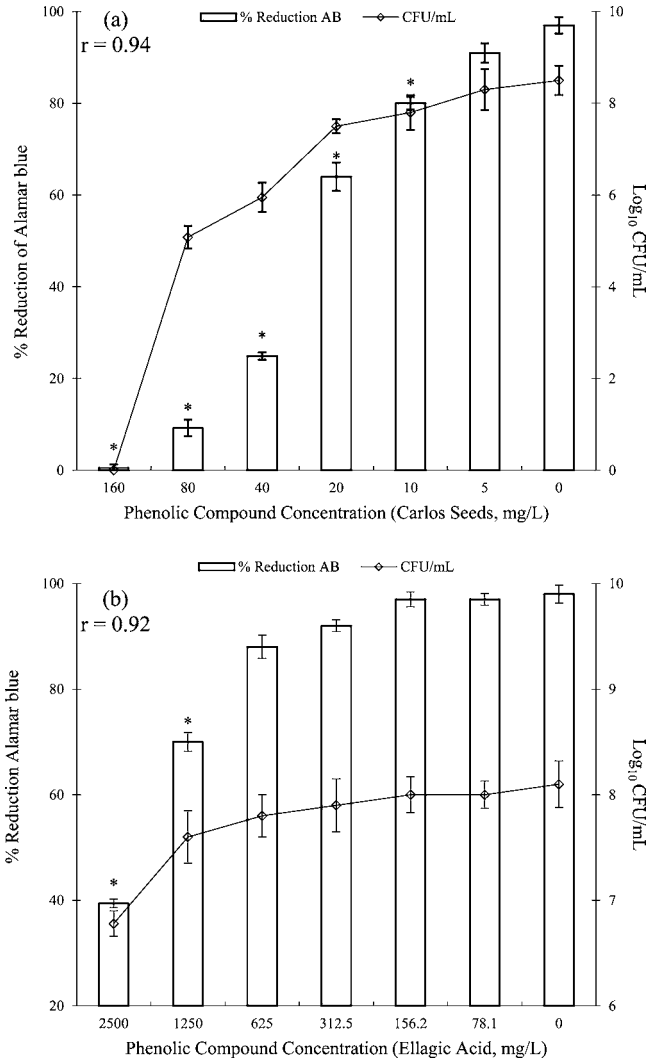

Figure 3. Percent reduction of Alamar blue (bars) and $\log_{10}$ CFU/mL (◇—◇) for phenolic compounds on *S. aureus* ATCC 35548: means of three independent replicates. Test strains were inoculated at 5×10^6 CFU/mL in each well. (*) Values differ significantly ($P < 0.05$) from values without phenolic compounds.

dx.doi.org/10.1021/jf501073q | J. Agric. Food Chem. 2014, 62, 6640−6649

excellent correlation with two other biofilm susceptibility methods, XTT reduction and viable counts.[22]

The antibacterial mechanisms of phenolics are attracting more and more research in recent years. The membrane interaction of phenolics is a prevailing theory.[30] Phenolics are partially hydrophobic; this character may allow them to interact with the lipid bilayer of bacterial cytoplasmic membrane and lipopolysaccharide interfaces more effectively by decreasing membrane stability.[32] For example, epicatechin gallate could rapidly enter the cytoplasmic membrane, causing an immediate reduction in bilayer fluidity.[33] The cytoplasmic membrane constitutes the selective barrier controlling cellular ingress and egress of materials and houses many of the enzymes involved in bioenergetic functions, cell wall synthesis, and macromolecule secretion. Penetration of phenolics into this phospholipid bilayer will have a profound outcome on a wide range of essential cell functions. Intercalation of these chemical structures could induce membrane disruption that permits solute equilibration across the bilayer, resulting in cell death, but more subtle interactions at subinhibitory concentrations induce reorganization of membrane architecture with implications for the capacity of the target bacteria to cause disease in the susceptible host.[32] Phenolics also were found to prevent the formation of biofilms in this study (Table 5) as well as others' report.[34,35] This may further support the membrane-interactive mechanism because potent antibiofilm activity is a property that is often associated with membrane-perturbing agents.[26] Thus, phenolics exhibit at least two biological activities: inhibition of bacterial growth at high concentrations and/or induction of bacteria membrane disruption and prevention of biofilm formation at lower concentrations. In view of these activities, phenolics may be useful in a synergistic approach with conventional antibiotics against antibiotic-resistant forms of pathogens (e.g., multidrug-resistant clinical isolates, MRSA) in clinical medicine. Our time−killing study (Figure 2) indicated that muscadine Noble seed phenolics combined with ampicillin or streptomycin at subinhibitory concentrations greatly reduced *S. aureus* ATCC 35548 (MRSA) cell viability by 4.8 or 6.2 $\log_{10}$ CFU/mL, respectively.

Naturally occurring molecules, predominantly secondary metabolites, are the source of the majority of drugs in clinical use today, and they continue to be an important basis of new therapeutics for bacterial infectious diseases.[36] Phenolics are secondary metabolites in muscadine grapes and play important roles in the strong resistant character of this species to pests and diseases, including Pierce's disease.[37] Evidence is emerging that phenolics may be useful in the control of common oral infections, such as dental caries and periodontal disease.[38,39] In this case, phenolics can be incorporated into rinse and toothpaste formulations. Muscadine phenolics also have been proven to possess strong anticancer activities, such as inhibiting proliferation of colon[8] and prostate[9] cancer cells by inducing apoptosis. Importantly, phenolics are widely distributed in edible grapes,[40] and they have minimal toxicity.[41] Therefore, even though outstanding bactericidal properties cannot be achieved because of a relatively high concentration required in this study and the partial metabolism of these by intestinal bacteria,[42] phenolic agents still have promise as supplements for nutraceutical value and conventional antibacterial chemotherapies by inhibiting the growth of foodborne pathogens in the body. The broad ability of muscadine phenolics to have strong antibacterial activity, to inhibit biofilm formation, and to synergistically work with antibiotics may stimulate a muscadine byproduct market as natural food preservatives, potential antibiotic replacements, and/or natural sanitizers for processing equipment where foodborne pathogens reside.

AUTHOR INFORMATION

Corresponding Author

*(M.R.M.) Mail: University of Florida, Food and Environmental Toxicology Lab, 1642 S.W. 23rd Dr., Bldg. 685, P.O. Box 110720, Gainesville, FL 32611-0720, USA. Phone: (352) 392-1978, ext. 405. Fax: (352) 392-1988. E-mail: martym@ufl.edu.

Notes

The authors declare no competing financial interest.

ACKNOWLEDGMENTS

We are grateful to the Center for Viticulture and Small Fruit Research at Florida A&M University for providing muscadine grape materials and to USDA/IR4 Lab at University of Florida for assisting in HPLC-MS/MS analysis.

REFERENCES

(1) Centers for Disease Control and Prevention (CDC). CDC Data and Statistics, 2011; http://www.cdc.gov/foodborneburden/PDFs/FACTSHEET_A_FINDINGS_updated4-13.pdf.

(2) Jones, T. F.; Kellum, M. E.; Porter, S. S.; Bell, M.; Schaffner, W. An outbreak of community-acquired foodborne illness caused by methicillin-resistant *Staphylococcus aureus*. *Emerging Infect. Dis.* **2002**, *8*, 82−84.

(3) Ethelberg, S.; Sorensen, G.; Kristensen, B.; Christensen, K.; Krusell, L.; Hempel-Jorgensen, A.; Perge, A.; Nielsen, E. M. Outbreak with multi-resistant *Salmonella typhimurium* DT104 linked to carpaccio, Denmark. *Epidemiol. Infect.* **2005**, *135*, 900−907.

(4) Stafford, R.; Kirk, M.; Selvey, C.; Staines, D.; Smith, H.; Towner, C.; Salter, M. An outbreak of multi-resistant *Shigella sonnei* in Australia: possible link to the outbreak of shigellosis in Denmark associated with imported baby corn from Thailand. *Eur. Surveillance* **2007**, *12*, 272−272.

(5) Manges, A. R.; Johnson, J. R.; Foxman, B.; O'Bryan, T. T.; Fullerton, K. E.; Riley, L. W. Widespread distribution of urinary tract infections caused by a multidrug-resistant *Escherichia coli* clonal group. *N. Engl. J. Med.* **2001**, *345*, 1007−1013.

(6) Todd, J. K. *Staphylococcal* infections. *Pediatr. Rev.* **2005**, *26*, 444−450.

(7) Harro, J. M.; Peters, B. M.; O'May, G. A.; Archer, N.; Kerns, P.; Prabhakara, R.; Shirtliff, M. E. Vaccine development in *Staphylococcus aureus*: taking the biofilm phenotype into consideration. *FEMS Immunol. Med. Microbiol.* **2010**, *59*, 306−323.

(8) Mertens-Talcott, S. U.; Lee, J. H.; Percival, S. S.; Talcott, S. T. Induction of cell death in Caco-2 human colon carcinoma cells by ellagic acid rich fractions from muscadine grapes (*Vitis rotundifolia*). *J. Agric. Food Chem.* **2006**, *54*, 5336−5343.

(9) Hudson, T. S.; Hartle, D. K.; Hursting, S. D.; Nunez, N. P.; Wang, T. T.; Young, H. A.; Arany, P.; Green, J. E. Inhibition of prostate cancer growth by muscadine grape skin extract and resveratrol through distinct mechanisms. *Cancer Res.* **2007**, *67*, 8396−8405.

(10) Mellen, P. B.; Daniel, K. R.; Brosnihan, K. B.; Hansen, K. J.; Herrington, D. M. Effect of muscadine grape seed supplementation on vascular function in subjects with or at risk for cardiovascular disease: a randomized crossover trial. *J. Am. Coll. Nutr.* **2010**, *29*, 469−75.

(11) Kim, T. J.; Weng, W. L.; Stojanovic, J.; Lu, Y.; Jung, Y. S.; Silva, J. L. Antimicrobial effect of muscadine seed extracts on *E. coli* O157: H7. *J. Food Prot.* **2008**, *71*, 1465−1468.

(12) Kim, T. J.; Silva, J. L.; Jung, Y. S. Antibacterial activity of fresh and processed red muscadine juice and the role of their polar compounds on *Escherichia coli* O157: H7. *J. Appl. Microbiol.* **2009**, *107*, 533−539.

(13) Just, J. R.; Daeschel, M. A. Antimicrobial effects of wine on *Escherichia coli* O157:H7 and *Salmonella Typhimurium* in a model stomach system. *J. Food Sci.* **2003**, *68*, 285−290.
(14) Fernandes, J.; Comes, F.; Couto, J. A.; Hogg, T. The antimicrobial effect of wine on *Listeria innocua* in a model stomach system. *Food Control* **2007**, *18*, 1477−1483.
(15) Daglia, M.; Papetti, A.; Grisoli, P.; Aceti, C.; Dacarro, C.; Gazzani, G. Antibacterial activity of red and white wine against oral *streptococci*. *J. Agric. Food Chem.* **2007**, *55*, 5038−5042.
(16) Xu, C.; Zhang, Y.; Wang, J.; Lu, J. Extraction, distribution and characterisation of phenolic compounds and oil in grape seeds. *Food Chem.* **2010**, *122*, 688−694.
(17) Dae-Ok Kim, D.; Lee, C. Y. *Curr. Protocols Food Anal. Chem.* **2002**, I1.2.1−I1.2.12.
(18) Sandhu, A. K.; Gu, L. Antioxidant capacity, phenolic content, and profiling of phenolic compounds in the seeds, skin, and pulp of *Vitis rotundifolia* (Muscadine grapes) as determined by HPLC-DAD-ESI-MS^n. *J. Agric. Food Chem.* **2010**, *58*, 4681−4692.
(19) Singleton, V. L.; Rossi, J. A. Colorimetry of total phenolics with phosphomolybdic-phosphotungstic acid reagents. *Am. J. Enol. Vitic.* **1965**, *16*, 144−158.
(20) Brand-Williams, W.; Cuvelier, M. E.; Berset, C. Use of a free-radical method to evaluate antioxidant activity. *LWT−Food Sci. Technol.* **1995**, *28*, 25−30.
(21) Bauer, A. W.; Kirby, W. M.; Sherris, J. C.; Turck, M. Antibiotic susceptibility testing by standardized single disc method. *Am. J. Clin. Pathol.* **1966**, *45*, 493−496.
(22) Pettit, R. K.; Christine, A. W.; Melissa, J. K.; Hoffmann, H.; Pettit, G. R.; Tan, R.; Franks, K. S.; Horton, M. L. Microplate Alamar blue assay for *Staphylococcus epidermidis* biofilm susceptibility testing. *Antimicrob. Agents Chemother.* **2005**, *7*, 2612−2617.
(23) Oliva, B.; Miller, K.; Caggiano, N.; O'Neill, A. J.; Cuny, G. D.; Hoemann, M. Z.; Hauske, J. R.; Chopra, I. Biological properties of novel antistaphylococcal quinoline-indole agents. *Antimicrob. Agents Chemother.* **2003**, *47*, 458−466.
(24) Pillai, S. K.; Moellering, R. C.; Eliopolous, G. M. Antimicrobial combinations. In *Antibiotics in Laboratory Medicine*, 5th ed.; Lorian, V., Ed.; Lippincott Williams & Wilkins: Philadelphia, PA, USA, 2005; pp 365−438.
(25) Donlan, R. M.; Costerton, J. W. Biofilms: survival mechanisms of clinically relevant microorganisms. *Clin. Microbiol. Rev.* **2002**, *15*, 167−193.
(26) Hurdle, J. G.; O'Neill, A. J.; Chopra, I.; Lee, R. E. Targeting bacterial membrane function: an underexploited mechanism for treating persistent infections. *Nat. Rev. Microbiol.* **2011**, *9*, 62−75.
(27) Ooi, N.; Chopra, I.; Eady, A.; Cove, J.; Bojar, R.; O'Neill, A. J. Antibacterial activity and mode of action of *tert*-butylhydroquinone (TBHQ) and its oxidation product, tert-butylbenzoquinone (TBBQ). *J. Antimicrob. Chemother.* **2013**, *68*, 1297−1304.
(28) Tenover, F. C. Mechanisms of antimicrobial resistance in bacteria. *Am. J. Med.* **2006**, *119*, 3−10.
(29) Xu, C.; Zhang, Y.; Cao, L.; Lu, J. Phenolic compounds and antioxidant properties of different grape cultivars grown in China. *Food Chem.* **2010**, *119*, 1557−1565.
(30) Taylor, P. W.; Hamilton-Miller, J. M. T.; Stapleton, P. D. Antimicrobial properties of green tea catechins. *Food Sci. Technol. Bull.* **2005**, *2*, 71−81.
(31) Taguri, T.; Tanaka, T.; Kouno, I. Antimicrobial activity of 10 different plant polyphenols against bacteria causing food-borne disease. *Biol. Pharm. Bull.* **2004**, *27*, 1965−1969.
(32) Taylor, P. W. Alternative natural sources for a new generation of antibacterial agents. *Int. J. Antimicrob. Agents.* **2013**, *42*, 195−201.
(33) Anderson, J. C.; McCarthy, R. A.; Paulin, S.; Taylor, P. W. Anti-staphylococcal activity and antibiotic resistance attenuating capacity of structural analogues of (−)-epicatechin gallate. *Bioorg. Med. Chem. Lett.* **2011**, *21*, 6996−7000.
(34) Blanco, A. R.; Sudano-Roccaro, A.; Spoto, G. C.; Nostro, A.; Rusciano, D. Epigallocatechin gallate inhibits biofilm formation by ocular *staphylococcal* isolates. *Antimicrob. Agents Chemother.* **2005**, *49*, 4339−4343.
(35) Stapleton, P. D.; Shah, S.; Ehlert, K.; Hara, Y.; Taylor, P. W. The lactam-resistance modifier (−)-epicatechin gallate alters the architecture of the cell wall of *Staphylococcus aureus*. *Microbiology* **2007**, *153*, 2093−2103.
(36) Newman, D. J.; Cragg, G. M. Natural products as sources of new drugs over the last 25 years. *J. Nat. Prod.* **2007**, *70*, 461−477.
(37) Clayton, C. N. *N. C. Agric. Exp. Stn. Bull.* **1995**, *No. 451*, 37.
(38) Hirasawa, M.; Takada, K.; Makimura, M.; Otake, S. Improvement of periodontal status by green tea catechins using a local delivery system: a clinical pilot study. *J. Period. Res.* **2002**, *37*, 433−438.
(39) Sakanaka, S.; Okada, Y. Inhibitory effects of green tea polyphenols on the production of a virulence factor of the periodontal-disease-causing anaerobic bacterium *Porphyromonas gingivalis*. *J. Agric. Food Chem.* **2004**, *52*, 1688−1692.
(40) Xu, C.; Zhang, Y.; Zhu, L.; Huang, Y.; Lu, J. Influence of growing season on phenolic compounds and antioxidant properties of grape berries from vines grown in subtropical climate. *J. Agric. Food Chem.* **2011**, *59*, 1078−1086.
(41) da Silva, C. R.; de Andrade Neto, J. B.; de Sousa Campos, R.; Figueiredo, N. S.; Sampaio, L. S.; Magalhães, H. I. F.; Cavalcanti, B. C.; Gaspar, D. M.; de Andrade, G. M.; Lima, I. S. P.; de Barros Viana, G. S.; de Moraes, M. O.; Lobo, M. D. P.; Grangeiro, T. B.; Júnior, H. V. N. Synergistic effect of the flavonoids catechin, quercetin and epigallocatechin gallate with fluconazole induce apoptosis in *Candida tropicalis* resistant to fluconazole. *Antimicrob. Agents Chemother.* **2014**, *58*, 1468−1478.
(42) Kohri, T.; Matsumoto, N.; Yamakawa, M.; Suzuki, M.; Nanjo, F.; Hara, Y.; Oku, N. Metabolic fate of (−)-epigallocatechin gallate in rats after oral administration. *J. Agric. Food Chem.* **2001**, *49*, 4102−4112.

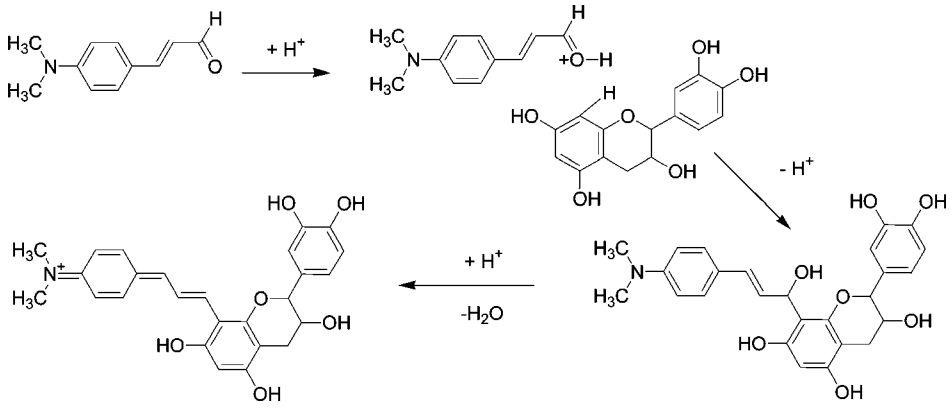

Figure 1. Putative reaction mechanism of DMACA with flavanols in an acidic medium (according Delcour and De Varebeke[4] by analogy with the reaction of vanillin).

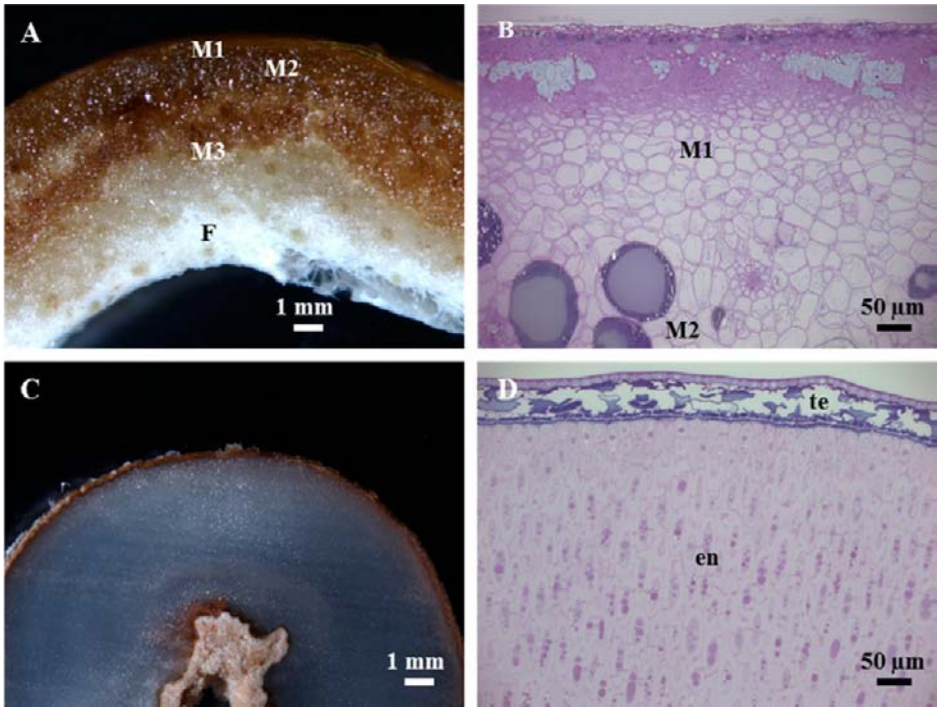

Figure 2. Light micrographs of Deglet Nour dates pericarp and stone cross sections: (A,B) pericarp, (C,D) stone, (A,C) binocular observation of thick sections, (B,D) semithin sections stained with toluidine blue. M1, external zone of the pericarp including the epicarp; M2, mesocarp zone 2; M3, mesocarp zone 3; F, fibrous zone; en, endosperm; te, testa.

tannins in chlorophyllous tissues of several tracheophyta species was investigated,[11] showing that tannins are polymerized in a new chloroplast-derived organelle, named the tannosome. More specifically concerning date tissues, ultrathin sections of frozen pericarp were observed by transmission electron microscopy by Shomer et al. (1998).[12] These authors suggested that tannins were specifically located in the cells of the epicarp. However, only TEM observation cannot clearly make the difference between tannins and other polyphenolic classes such as flavonols which are also present in date epidermis tissues.[1] Indeed, both flavonols and tannins are molecules containing C═C conjugated double-bond systems. Therefore, after the treatment of tissues with osmium tetroxide, both flavonols and tannins containing zones would appear as highly electron-dense on the TEM pictures.

Thus, the localization of tannins in dates tissues is still badly known with accuracy. By coupling light microscopy after specific staining and TEM, the purpose of this study is to give more accurate evidence of condensed tannin localization in edible tissues of dates. Their localization in the stones is also considered because these compounds were recently characterized and quantified in this part of the fruits.

MATERIALS AND METHODS

Solvents, Reagents, and Phenolic Standards. Ethanol and hydrochloric acid were from Merck (Allemagne). 4-Dimethylamino cinnamaldehyde (DMACA) and uranyl acetate were purchased from Sigma-Aldrich (France), and glutaraldehyde and LRwhite resin were purchased from Agar Scientific (UK). Water was purified using a Milli-Q system from Millipore (France).

Plant Materials. Ripe Deglet Nour dates (*Phoenix dactylifera* L.) were harvested during the 2009 season in the region of Kebili, Tunisia.

Microscopy. *Sample Preparation.* For light and electron microscopy observations, the fruit was thawed out and blocks of tissue (1 mm^3) were cut from the pericarp (including the epicarp and

dx.doi.org/10.1021/jf5013715 | J. Agric. Food Chem. 2014, 62, 6650−6654

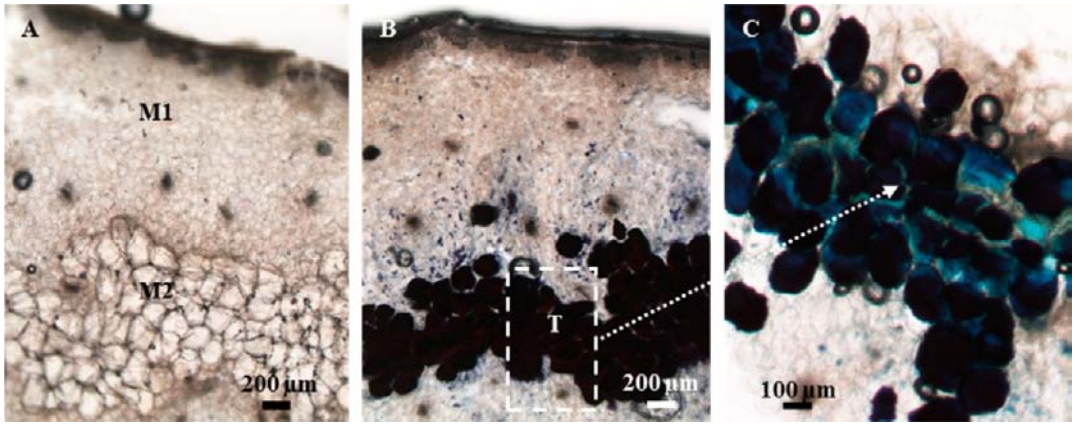

Figure 3. Tannins localization with DMACA staining. Light micrographs of Deglet Nour dates pericarp cross sections M1 + M2 (thick sections): (A) witness pericarp, (B) pericarp stained with DMACA, and (C) pericarp stained with DMACA at higher magnification. T, tannins; M1, external zone of the pericarp; M2, mesocarp zone.

mesocarp) and the stone were fixed with 3% glutaraldehyde in a 0.1 M phosphate buffer at pH 7.4 for 24 h at 4 °C, rinsed several times with 0.1 M phosphate buffer at pH 7.4, and then postfixed with 1% osmium tetroxide (OsO_4) in deionized water.

After being postfixed, tissues were rinsed 5 times with deionized water, followed by dehydration through a graded aqueous ethanol series (30, 50, 70, 85, 95, and 100%). The samples were then progressively infiltrated with London Resin White acrylic (LRW) according to the following schedule: 20, 40, 60, and 80% LRW/ethanol and overnight in pure LRW. The infiltrated samples were finally embedded by LRW resin and polymerized for 48 h at 55 °C.

For light microscopy, semithin sections (1 μm) were obtained using an ultramicrotome (UC7, Leica), mounted on glass slides, and stained with a solution of toluidine blue 1% in Na_2CO_3 2.5% for histology. The observation was carried out using an inverted epifluorescence microscope (Axiovert 135M, Carl Zeiss). The images are taken with the objectives ×10 and ×40. The software acquisition used is "Archimed". Observations were taken using a color camera (Retiga 2000R, Microvision).

For transmission electron microscopy, ultrathin sections (80 nm) contrasted with uranyl acetate 2% in aqueous solution were examined with a JEM-1230 (Jeol) with an accelerating voltage of 80 kV. The images were obtained with a camera (ES500W, Gatan) associated with software acquisition "Digital Micrograph."

Tannins Localization by Light Microscopy in Combination with DMACA Staining. Thick sections of the pericarp (150 μm) were obtained with a vibratome (HM 650 V, Microm). The operation consists of placing a drop of reagent DMACA (0.3% w/v) in a mixture of DMACA methanol/6 N HCl (1/1: v/v) on sections and has been incubated for 20 min at 4 °C. Rinsing is carried out several times in deionized water. The observation was made directly by light microscopy in bright field.[5]

RESULTS AND DISCUSSION

Cellular Organization of the Date Tissues. On the basis of images obtained with a binocular stereo zoom microscope and light microscope, Figure 2 describes the morphology of the soft tissues corresponding to the pericarp (edible part of the fruit) (Figure 2A,B) and the hard tissues corresponding to the stone (Figure 2C,D), respectively. Soft tissues were divided into four zones. Regarding the edible tissues, the most external zone (M1) included the epidermis (epicarp) and some subepidermal layers. The second zone (M2) corresponded to mesocarp tissues containing some large cells as observed on the lower part of Figure 2B. The M3 zone including the main part of the mesocarp and the most inner part of the soft tissues (F) revealed a fibrous zone corresponding to unstructured cells which encompasses the stone.

Obviously, the cellular architecture of the stone is very different from that of the pericarp. Two main different tissue zones are clearly observable: the testa, corresponding to the peripheral zone, is approximately 100 μm thickness which surrounds the endosperm that corresponds to the inner part (Figure 2D).

The testa shows several well-defined layers of cells. The most external is composed of small cells showing rectangular form and whose cell wall is very thick and sclerotized as can be deduced from the intense coloration by toluidine blue (Figure 2D). Then the most inner part of the testa is composed of two internal and parallel layers of well-organized cells situated approximately at 80 μm from the surface of the stone (Figure 2D). The most external layer appears more deeply stained by toluidine blue than the most internal one, suggesting that these two types of cells do not have the same composition. It is interesting to see that the testa shows this very particular tissue organization showing cells with different cell wall thickness, sizes, and orientations. This may confer to the testa very specific physical properties acting as a protective barrier. Below this external layer, an unstructured and inhomogeneous zone of around 50 μm thickness containing large free cells with very variable forms is observable (Figure 2D). Concerning the endosperm zone (Figure 2D) which corresponds to storage tissues, it is composed of large-sized cells only weakly colored by toluidine blue and orientated perpendicularly to the cells of the testa. This tissue likely contains proteins and oils the latter taking the form of globules of darker color clearly visible in the cells (Figure 2D).

Localization of Tannins in the Pericarp. *Tannins Localization by Light Microscopy in Combination with DMACA Staining.* In our recent study, condensed tannins were characterized in date tissues by phloroglucinolysis associated with HPLC-UV and mass spectrometry.[1]

We showed that these compounds were oligomers and polymers of (−)-epicatechin highly concentrated both in the edible parts and the stones.

The DMACA staining of condensed tannins allowed us to localize these compounds in the edible tissues of the date (Figure 3). Interestingly, the staining was not distributed in the whole tissues but was very specifically located in the external part of the mesocarp approximately at 1500 μm inside the

dx.doi.org/10.1021/jf5013715 | J. Agric. Food Chem. 2014, 62, 6650−6654

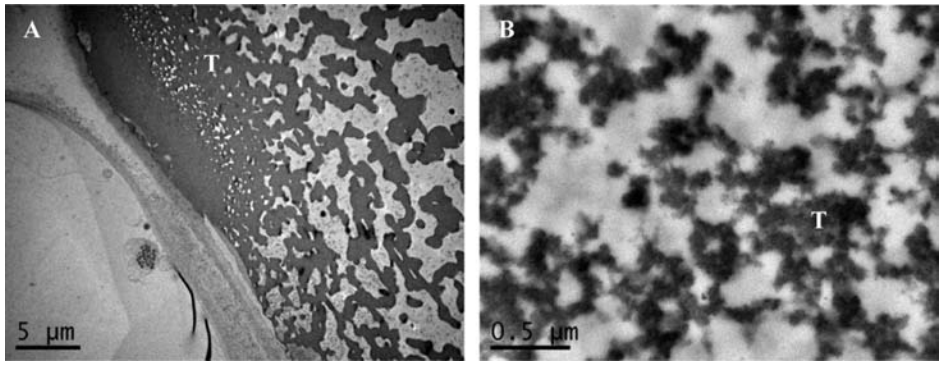

Figure 4. Transmission electron micrographs of the mesocarp in the transition zone between M1 and M2. (A) tannins free cell (on the left) and tannins containing cell (on the right). (B) Observation at higher magnification. T, tannins (T).

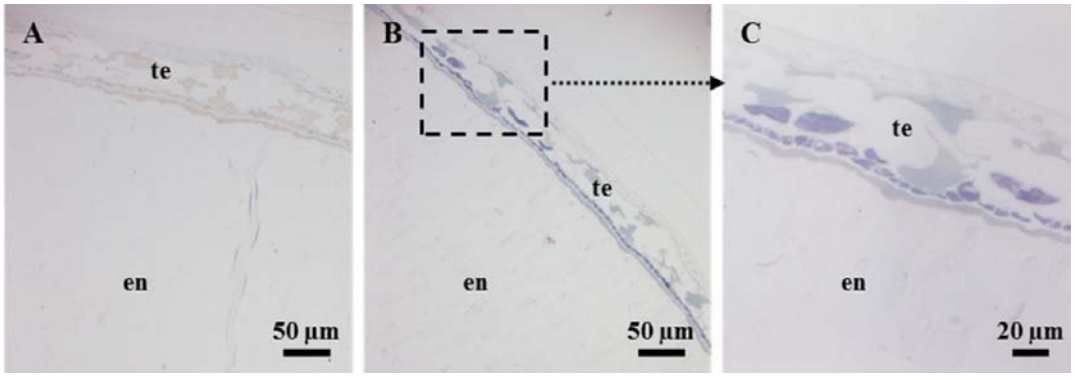

Figure 5. Light micrographs of cross sections (semithin sections) of the stone of Deglet Nour dates: (A) witness stone, (B) stained with DMACA, (C) stained with DMACA at higher magnification. en, endosperm; te, testa.

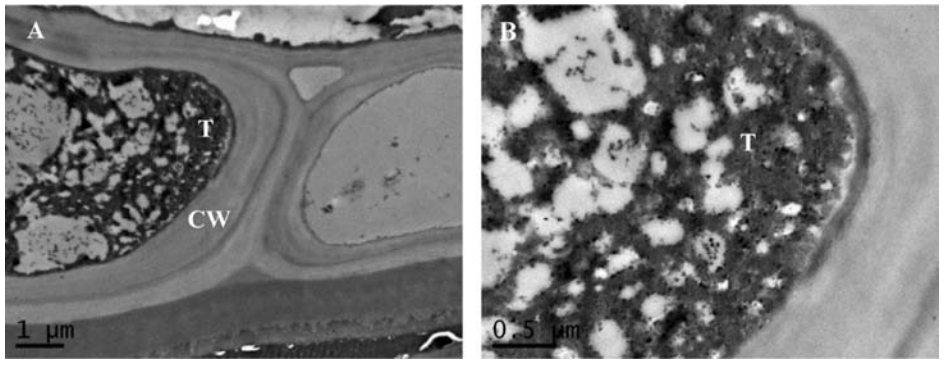

Figure 6. Transmission electron micrographs in the stone: (A) form of a continuous deposit extremely dense to the electrons, (B) form of granular units, observation at higher magnification. CW, cell wall; T, tannins.

pericarp and with a thickness close to 1000 μm (Figure 3B). Higher magnification (Figure 3C) revealed that the tannins are located in 3−5 layers of very large spherical cells reaching 200 μm diameter and having thin cell walls. The intense blue coloration seems to fill almost completely the intracellular area suggesting the massive presence of these flavanols in the vacuoles. Although DMACA staining does not permit to distinguish between flavanol monomers (i.e., catechins) and condensed tannins (i.e., proanthocyanidins), it is likely that those flavanols mainly correspond to highly polymerized procyanidins as it was shown in our previous study.[1]

Localization of Tannins by Transmission Electron Microscopy (TEM). Polyphenols and particularly those containing *o*-diphenol groups in their structure are highly osmiophilic agents.[13] Therefore, when they are present in the tissues, condensed tannins are responsible for high electron density creating contrasted zones in TEM images.

In a previously published work conducted on dates using TEM observation, Shomer et al. (1998)[12] proposed that tannins were probably located in the subepidermal zone (M1) of the epicarp on the basis of high density areas of this tissue zone. This hypothesis was invalidated by our observations in light microscopy after specific staining of flavanols structures with DMACA. Tannins are specifically located in the mesocarp (M2) in large-sized cells situated at 1500 μm from the epicarp cells.

Electron-dense precipitates are visible in the vacuoles of the mesocarp cells after the treatment of samples by osmium tetroxide (Figure 4A). These precipitates are in the form of granules of different sizes. The size of the granules is up to 0.2

dx.doi.org/10.1021/jf5013715 | J. Agric. Food Chem. 2014, 62, 6650−6654

μm in diameter (Figure 4B). The precipitates sometimes form clusters fused to tonoplast.

Tannins Localization in the Dates Stone. *Tannins Localization by Light Microscopy.* The DMACA staining of cross sections of the stone allowed us to observe the organization of tannins (Figure 5B,C). Tannins are specifically located in a single cell layer situated approximately at 50 μm from the surface of the testa (Figure 5B). In addition, close to this layer, some very large cells containing tannins are observed in the unstructured zone of the testa. Interestingly, knowing that tannins are antimicrobial and antifungal agents,[14] this organization makes us think that they are located in a specific cell layer, forming a defensive barrier that likely protects the stone against pathogen attacks.

The flavonoid accumulation pattern was examined in young seedlings and mature tissues of wild-type *Arabidopsis*. Flavonoid accumulation in mature plants was localized in cauline leaves, pollen, stigmata, floral primordia and in the stems of young actively growing inflorescences.[15]

Tannins Localization by TEM. The tannins of these cells are characterized by a continuous deposit extremely dense to the electrons. It consists of similar elements and expressing the same characters. This layer is formed by rectangular cells stacked to one another. The observations by transmission electron microscopy allow us to have some information on the dimensions of the cells tannins whose sizes range from 20 to 40 μm (Figure 6A). One also notices that these cells are characterized by the plasmic membranes surrounded by a thick rigid cell wall.

These tannins are present in cells of different forms. They mainly occur in the form of a continuous deposit extremely dense to the electrons (Figure 6A) and sometimes in the form of granular units (Figure 6B). Generally speaking, we did not detect the tannins localized in the cell wall as in the case of the grape proved by Amrani Joutei et al. (1994).[9]

To conclude, the observation of pericarp tissues by light and transmission electron microscopy revealed that tannins are located in the vacuoles of very large mesocarp cells. These cells are in turn located at 1500 μm from the surface. The microscopic approach has allowed us, for the first time, to locate the tannins in the stone. Those tannins are located in a specific cell layer located at 50 μm from the surface.

From this work, we can conclude on the high specificity of tannins organization in the pericarp and the stone of the date. This very specific organization may be related to the physiological role of tannins as active components able to protect the fruit and the seed against pathogen attacks. Interestingly, tannins in the stones may be also involved in the germination mechanisms.[16] As perspectives to this work, we would like to observe different stages of ripening fruits in order to have a better understanding of the building of the tannin pool in the fruit (i.e., structure and location) during growing and maturation.

AUTHOR INFORMATION

Corresponding Author

*E-mail: hedi.hammouda@yahoo.fr.

Funding

This work was supported by the Tunisian Ministry of Higher Education and Scientific Research and by the Doctoral School "Vie Agro Santé" in France.

Notes

The authors declare no competing financial interest.

ABBREVIATIONS USED

DMACA, 4-dimethylaminocinnamaldehyde

REFERENCES

(1) Hammouda, H.; Chérif, J. K.; Trabelsi-Ayadi, M.; Baron, A.; Guyot, S. Detailed polyphenol and specially tannin composition and its variability in Tunisian dates (*Phoenix dactylifera L.*) at different maturity stages. *J. Agric. Food Chem.* **2013**, *61*, 3252−3263.

(2) Halloin, J. M. Localisation and changes in catechin and tannins during development and ripening of cottonseed. *New Phytol.* **1982**, *90*, 651−657.

(3) Felker, F. C.; Peterson, D. M.; Nelson, O. E. Development of tannin vacuoles in chalaza and seed coat of barley in relation to early chalazal necrosis in the seg 1 mutant. *Planta* **1984**, *161*, 540−549.

(4) Delcour, J. A.; De Varebeke, D. J. A new colourimetric assay for flavanoids in pilsner beers. *J. Inst. Brewing* **1985**, *91*, 37−40.

(5) Li, Y. G.; Tanner, G.; Larkin, P. The DMACA-HCl protocol and the threshold proanthocyanidin content for bloat safety in forage legumes. *J. Sci. Food Agric.* **1996**, *70*, 89−101.

(6) Feucht, W.; Treutter, D.; Polster, J. Flavanol binding of nuclei from tree species. *Plant Cell Rep.* **2004**, *22*, 430−436.

(7) Cadot, Y.; Minana Castello, M. T.; Chevalier, M. Flavan-3-ol compositional changes in grape berries (*Vitis vinifera* L. cv Cabernet Franc) before veraison, using two complementary analytical approaches, HPLC reversed phase and histochemistry. *Anal. Chim. Acta* **2006**, *563*, 65−75.

(8) Auger, B.; Marnet, N.; Gautier, V.; Maia-Grondard, A.; Leprince, F.; Renard, M.; Guyot, S.; Nesi, N.; Routaboul, J.-M. A Detailed Survey of Seed Coat Flavonoids in Developing Seeds of *Brassica napus* L. *J. Agric. Food Chem.* **2010**, *58*, 6246−6256.

(9) Amrani Joutei, K.; Glories, Y.; Mercier, M. Localisation des tannins dans la pellicule de baie de raisin. *Vitis* **1994**, *33*, 133−138.

(10) Lees, G. L.; Wall, K. M.; Beveridge, T. H.; Suttill, N. H. Localization of condensed tannins in apple fruit peel, pulp and seeds. *Can. J. Bot.* **1995**, *73*, 1897−1904.

(11) Brillouet, J. M.; Romieu, C.; Schoefs, B.; Solymosi, K.; Cheynier, V.; Fulcrand, H.; Verdeil, J. L.; Conejero, G. The tannosome is an organelle forming condensed tannins in the chlorophyllous organs of Tracheophyta. *Ann. Bot. (London)* **2013**, *112*, 1003−1014.

(12) Shomer, I.; Borochov-Neori, H.; Luzki, B.; Merin, U. Morphological, structural and membrane changes in frozen tissues of Madjhoul date (*Phoenix dactylifera* L.) fruits. *Postharvest Biol. Technol.* **1998**, *14*, 207−215.

(13) Nielson, A. J.; Griffith, W. P. Tissue fixation and staining with osmium tetroxide: the role of phenolic compounds. *J. Histochem. Cytochem.* **1978**, *26*, 138−140.

(14) Sannomiya, M.; Montoro, P.; Piacente, S.; Pizza, C.; Brito, A.; Vilegas, W. Application of liquid chromatography/electrospray ionization tandem mass spectrometry to the analysis of polyphenolic compounds from an infusion of *Byrsonima crassa* Niedenzu. *Rapid Commun. Mass Spectrom.* **2005**, *19*, 2244−2250.

(15) Peer, W. A.; Brown, D. E.; Tague, B. W.; Muday, G. K.; Taiz, L.; Murphy, A. S. Flavonoid accumulation patterns of transparent testa mutants of Arabidopsis. *Plant Physiol.* **2001**, *126*, 536−548.

(16) Jia, L. G.; Wu, Q. Y.; Ye, N. H.; Liu, R.; Shi, L.; Xu, W. F.; Zhi, H.; Bin Rahman, A.; Xia, Y. J.; Zhang, J. H. Proanthocyanidins Inhibit Seed Germination by Maintaining a High Level of Abscisic Acid in *Arabidopsis thaliana*. *J. Integr. Plant Biol.* **2012**, *54*, 663−673.

been shown to be a major contributor for vasodialatory mechanism,[27] and actives modulating NO production in endothelial cells have been classically used to screen molecules for vascular health benefits.[28] Additionally, there are also reports of some of the small molecular weight polyphenols being bioavailable[29] without any biotransformation.

A global database on the polyphenol levels of various black tea has been published.[21] The data suggest that there is a huge variation in polyphenol levels among the black teas grown across the globe.[21] There has been no attempt made to date to understand how these variations in the levels and composition of flavonoids correlate with their bioefficacy for vascular function. Also, it is not clear if bioefficacy of tea polyphenols is linked to their amount in general, or whether it is driven by specific composition of polyphenol in tea.[30]

In the present study, we investigated representative teas from select geographies for their influence on in vitro markers of endothelial function. Tea infusions were quantified for their polyphenolic content, and their biological functions were evaluated as free radical scavenging, intracellular antioxidant property, and NO production in endothelial cells. Further, the composition of all of these tea infusions were analyzed and correlated with investigated biological markers using the Pearson correlation. This study provides knowledge on the variability in polyphenolic content of WoBTs and their correlation to biological functions such as antioxidant property and NO enhancement properties implicated in endothelial function in vitro and therefore eventually might influence the in vivo cardiovascular benefits of tea.

MATERIALS AND METHODS

Materials. 4-Amino-5-methylamino-2′,7′-difluororescein diacetate (DAF FM-DA) and 5-(and -6)-chloromethyl-2′,7′-dichloro-dihydro-fluorescein diacetate acetyl ester (CM-H2DCFDA) were purchased from Invitrogen (OR). DMEM, 2,2-diphenyl-1-picrylhydrazyl free radical (DPPH), α-tocopherol, *N*-acetyl-L-cysteine (NAC) hydrogen peroxide (H_2O_2), Folin−Ciocalteu's phenol (FC) reagent, and water (HPLC grade) were purchased from Sigma Chemical Co. (MO). Unless specified, all other reagents were procured from Sigma Chemical Co. (MO). Black tea samples were procured from Unilever R&D, Colworth.

Preparation of Black Tea Infusion. Tea infusions were prepared as mentioned elsewhere.[21] Briefly, black tea was finely ground with mortar and pestle and passed through 0.5 mm sieve to remove tea fibers. 100 mL of boiling water (HPLC grade) was poured unto 2 g of ground powder and stirred. The content was allowed to stand for 2 min, followed by a stir. The content was filtered through 0.4 μm Whattman filter placed under vacuum. The infusion was immediately frozen in liquid nitrogen to prevent further oxidation or degradation. This process was employed to reduce variability during the extraction process as factors like particle size, fibers, and temperature play a very crucial role in the extraction process. The extraction process was standardized to maximize the yield of flavonoids and its batch to batch reproducibility.

Quantification of Polyphenol in the Infusion Using the Folin−Ciocalteu (FC) Method. The total polyphenol content of the infusion was determined colorimetrically using Folin−Ciocalteu (FC) phenol reagent[21] as per ISO 14502-1. Briefly, 20 μL of 1:20 diluted tea infusion was mixed with 40 μL of Na_2CO_3 in a 96-well microtiter plate. 50 μL of FC reagent was added after 5 min and incubated in the dark for 1 h. Reaction product was measured at 765 nm using TECAN-2000. Different concentrations of gallic acid were used as standard, and polyphenols were quantified as gallic acid equivalents.

Quantification of Catechin, Theobromine, and Gallic Acid by HPLC. Catechins, caffeine, theobromine (TB), and gallic acid (GA) were analyzed by ISO 14502-2:2005(E) method.[31] For HPLC analysis, a Phenomenx phenyl-hexyl, 5 μm, 4.6 × 250 mm HPLC column was used. The mobile phase A was 9% (volume fraction) acetonitrile, 2% (volume fraction) acetic acid with 20 μg/mL EDTA, and mobile phase B was 80% (volume fraction) acetonitrile, 2% (volume fraction) acetic acid with 20 μg/mL EDTA. Separation was carried out at 1 mL/min flow rate at 35 °C and detection at 278 nm using Agilent HPLC (1100 Series). HPLC analysis was carried out using a gradient elution. Binary gradient conditions: 0% mobile phase B for 10 min, then over 15 min, a linear gradient to 32% mobile phase B, and hold at this composition for 10 min; then reset to 0% mobile phase B to equilibrate for 10 min before next injection. Standard compounds were used to generate calibration curves.

Quantification of Theaflavins (TFs) by HPLC. Theaflavins were analyzed by using the HPLC method.[32] Nova-Pak C-18, 60A, 4 μm, 3.9 × 150 mm HPLC column was used. Mobile phase A was 2% (volume fraction) acetic acid, and mobile phase B was acetonitrile. Separation was carried out at 1 mL/min flow rate at 40 °C and detection at 380 nm using Shimadzu LC-10A HPLC. Standard theaflavins were used to generate calibration curves.

UPLC Fingerprinting of Thearubigins. The UPLC analysis of tea infusions was done using the method developed in house. For UPLC analysis, a Phenomenex Kinetex C18, 100 × 2.1 mm, 1.7u, 100A column was used. Mobile phase A was 0.5% (volume fraction) acetic acid in water, and mobile phase B was 100% acetonitrile. Separation was carried out at 0.2 mL/min flow rate at 35 °C and detection at 350 nm using the Agilent 1290 series system. UPLC analysis was carried out using a gradient elution. Binary gradient conditions: 0% mobile phase B for 5 min, then over 50 min, a linear gradient to 25% mobile phase B, 30% mobile phase B until 55 min and coming back to 0% mobile phase B at 56 min and then to equilibrate for 4 min before next injection. The known compounds like catechins, theaflavins, chlorogenic acid, caffeine, theogalline, gallic acid, theobromine, and flavonol glycosides were identified by injecting their standards, and all of the remaining peaks that were not identified were considered as thearubigin peaks. Because thearubigins are complex compounds and their standards are not commercially available, the method was validated for repeatability of retention time (RT) and recovery of known compounds by UPLC.

Determination of Free Radical Scavenging Property Using DPPH Assay. The radical scavenging capacities of black tea infusions were determined using the DPPH radical method.[22] Briefly, 1 mL of 1:20 diluted infusion was added to 1 mL of 2 mM ethanolic DPPH solution in a cuvette. The mixture was shaken vigorously, and the absorbance was measured at 517 nm at 0 and 30 min. α-Tocopherol (200 μM) served as a positive control. All of the tests were performed in triplicate, and the inhibition rate was calculated according to the formula of Yen and Duh.[33]

Cell Culture. The human endothelial cell line (EA.hy926) was procured from American Type Culture Collection (ATCC; VA). Cells were cultured in DMEM (Sigma) supplemented with 2 mM L-glutamine, 100 U/mL penicillin, 100 μg/mL streptomycin, and 10% vol/vol FBS (Gibco, Invitrogen). Human umbilical vein endothelial cells (HUVECs) were purchased from Lonza. HUVECs were cultured in M199 supplemented with endothelial growth factor, 0.001% heparin sulfate, 10% fetal bovine serum (FBS) (v/v), 1% penicillin (w/v), and streptomycin (w/v). Cells were incubated at 37 °C in 95% humidified air and 5% CO_2. After 70−80% confluence was attained, the cells were subcultured by trypsinization.

Determination of Antioxidant Property of Black Tea Infusion. Tea infusion-induced antioxidant property was determined as described previously.[34] Briefly, EA.hy926 (2.5×10^4) cells were seeded onto 96-well flat bottom tissue culture plates for 6 h. After adherence, cells were treated with black tea infusion for 24 h, followed by wash to remove adhered polyphenols. The cells were then loaded with DCF-DA (1 μM) for 30 min followed by a wash with serum free medium. Subsequently, cells were treated with 100 μM H_2O_2 for 5 min. The antioxidant capacity of cell is determined by its ability to quench H_2O_2 entering inside the cellular compartment. The free intracellular H_2O_2 was determined by its reaction with DCF dye. The fluorescence intensity was measured at excitation/emission maxima of

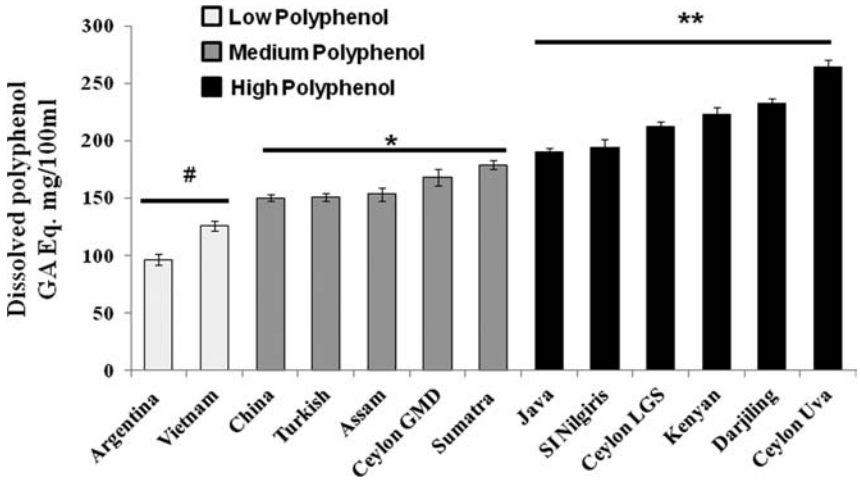

Figure 1. Dissolved polyphenol levels in the prepared tea infusion for the global black teas (WoTs). The samples were prepared and the polyphenol were quantified by Folin−Ciocalteu (FC) phenol method using gallic acid as standard. Data are presented as mean ± SD. Statistical comparisons were made using Student *t* test. "*" and "**" values were statistically significant (*$p < 0.05$; **$p < 0.01$) with respect to teas with low polyphenols (#).

495/515 nm, respectively, using TECAN 2000. Cells treated with the infusion but without H_2O_2 served as normalization control. NAC (25 μg/mL) was used as positive control.

Measurement of Intracellular Nitric Oxide (NO) in Endothelial Cells Using Flow Cytometry. Intracellular NO production was measured using flow cytometry.[35] EA.hy926 (1×10^5) cells were seeded in 24-well tissue culture plates. Cells were starved for 12−14 h after adherence to reduce basal NO levels. Cells were loaded with DAF FM-DA (1 μM) for 30 min and washed twice. Subsequently, cells were stimulated with black tea infusion for 30 min, in the presence or absence of L-NAME (10 mM; 30 min preincubation). The stimulated cells were trypsinized and fixed with 2% PFA for 15 min. A population of 10 000 cells were gated and segregated on the basis of their relative fluorescence intensities using FACS Calibur (Becton Dickenson; San Diego, CA). The mean fluorescence yield was measured and compared to the respective population in untreated cells.

Statistical Analyses. Data are presented as mean ± SD of at least three independent experiments ($n = 3$) in triplicate. Variances of mean values were statistically analyzed by the Student's *t* test. $p \leq 0.01$ was considered significant. Pearson correlation was carried out using Sigma stat software to observe the correlation between NO production and antioxidant property versus various ingredients in tea infusion.

RESULTS AND DISCUSSION

On the basis of the extent of fermentation, tea is classified into three major types: black (maximum oxidized), green (minimum oxidized), and oolong (partially oxidized) tea. The compositional profile of flavonoids also varies with the extent of oxidation reactions;[25] however, the amounts of total polyphenols in tea remain comparable, if made from the same leaf source.[34] Because the water extractability of flavonoid species differs, infusions of these teas also vary in terms of their end-cup composition.[34] Also, composition of flavonoids differs, based on the process of tea making (orthodox (rolling tea leaves) or CTC (cut, tear, curl)),[36] nature of tea variety,[34] and region in which it is grown.[21] This intrinsic variation of flavonoids within teas can affect both end-cup delivery of flavonoids and their composition. Considering flavonoids are the main efficacious species in tea, such variations are likely to cause differences in the extent of benefits delivered by various teas. In this Article, we investigated the polyphenol extractability of various black teas and evaluated their antioxidant property and NO enhancement ability in endothelial cells.

Polyphenol Content in Black Tea Across Geographies. Black teas originating from various geographies (Supporting Information Figure 1) were used in the study, and the tea infusions were prepared (as mentioned in M&M) and analyzed for their total polyphenol levels using Folin−Ciocalteu reagent[21] and expressed as gallic acid equivalents. The data are represented in Figure 1. There was a significant variation in the extractability of polyphenols under normally used conditions for brewing tea (data not shown). These findings are similar to those reported previously.[37,38] Variability of polyphenols in end cup may be the result of the inherent variation in polyphenol levels present in the tea leaves or due to their extractability.[38] The major reason for variation in extractability in turn arises due to the difference in the particle size and the nature of infusion protocol. We ensured minimum variability in extraction by standardizing the protocol for infusion preparation by maintaining uniformity in granule size (0.2−0.4 mm), infusion time (3 min), cycles of stirring (8 cycles), and filtration time (1 min), so as to get reproducible polyphenol extraction.

When analyzed for polyphenols levels in various tea infusions (Figure 1), Ceylon Uva (name associated with Uva province), Darjeeling, Kenya, Ceylon LGS (Ceylon, low grown semi-shaded), SI (South Indian) Nilgiries and Java teas contained high polyphenol levels (above 200 mg equiv GA/100 mL), while teas from Vietnam and Argentina contained the least amounts (∼100 mg equiv GA/100 mL). Chinese, Turkish, Assam, Ceylon GMD (Ceylon, good medium dust), and Sumatra teas contained intermediate polyphenols levels (125−175 mg equiv GA/100 mL). Our data suggest that the variation in the levels of polyphenol exists in black teas (ranging from ∼100−250 mg equiv GA/100 mL/2g black tea) across geographies (WoBTs). Such variations in polyphenol levels in teas from various geographies have previously been reported.[21] The difference in the polyphenol levels has been shown to be associated with the altitude in which these teas have been grown.[39,40] In these studies, they demonstrated that amounts of all of the catechins increased significantly with increasing altitude. Although higher levels of polyphenols would exhibit

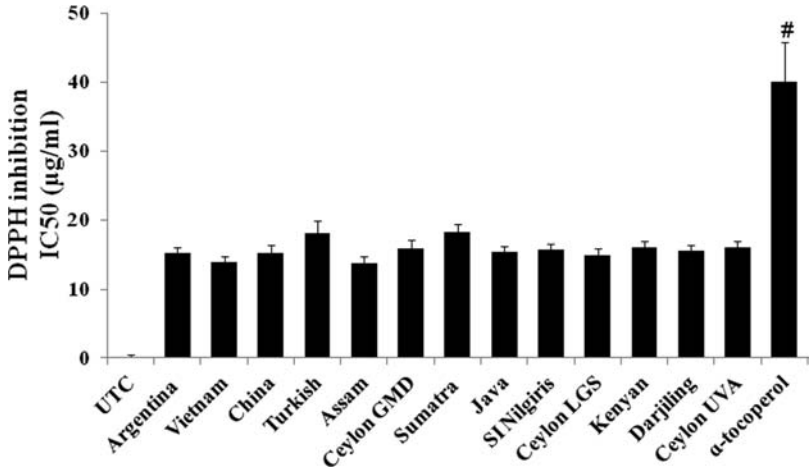

Figure 2. DPPH (1,1-diphenyl-2-picrylhydrazyl) free radical scavenging property of different black tea infusions normalized to polyphenol levels. The tea infusions were normalized to 25 μg/mL gallic acid equivalents. DPPH free radical scavenging property was determined as mentioned in M&M. Data represented as IC50 ± SD (μg/mL). α-tocopherol (200 μM) was used as positive control. Statistical comparisons were made using Student t test. The "#" values were statistically significant ($p < 0.01$) with respect to untreated control (UTC) and various tea samples. Free radical scavenging properties amongst WoT samples were not significantly different.

higher biological activities, to understand the influence of composition of polyphenol on biological activity, we equalized the polyphenol levels of different teas (WoBTs) and evaluated their biological functions.

Free Radical Scavenging Property of Different Black Teas. Oxidation of lipids and protein has been implicated in various diseases etiologies,[41] especially in vascular pathophysiology.[42,43] Mechanistically, increase in the levels of reactive species in the plasma leads to generation of oxidized lipid and proteins, which are electrophilic in nature.[44] These reactive molecules (reactive lipid/protein species) interact with cellular nucleophiles such as the amino acids cysteine, lysine, and histidine, which are components of cell surface receptors. Binding of electrophilic molecules changes the conformation or activation status of receptor, resulting in altered signaling pathways[44] or generation of intracellular ROS species. Also, increased levels of superoxides and peroxides react with NO produced in endothelial cells, resulting in reduced bioavailability of NO[12,13,45] for its function.

Consumption of phyto-chemicals rich in flavonoids is reported to increase oxygen radical absorbance capacity (ORAC), Trolox equivalent antioxidant capacity (TEAC), and total radical trapping parameter (TRAP) levels in plasma, which are physiological measures of free radical scavenging property in vivo.[46] On the basis of this hypothesis, we used the 1,1-diphenyl-2-picrylhydrazyl radical (DPPH)-based in vitro scavenging assay to test the ability of components to act as free radical scavengers or hydrogen donors and to evaluate the free radical scavenging property of tea phyto-chemicals.

The free radical scavenging properties of different teas were evaluated. The IC_{50} is represented in Figure 2. All of the tested tea infusions showed good DPPH scavenging property (Supporting Information Figure 2), but at equivalent polyphenol concentrations, their efficacies were not significantly different from each other (Figure 2). Similar correlation was deduced by Anesini et al.,[47] for Argentinean commercial teas. In general, the radical-scavenging property of flavonoids depends on the molecular structure and the substitution pattern of hydroxyl groups, that is, on the availability of phenolic hydrogen and on the possibility of stabilization of the resulting phenoxyl radicals via hydrogen bonding or by expanded electron delocalization.[48] However, in addition to free radical scavenging property, the intracellular antioxidant elements such as GSH and free radical reducing enzymes (SOD, catalase and peroxidase) play a crucial role in determining redox properties of cells. Such intracellular antioxidant systems prevent the uncontrolled generation of free radicals and activated oxygen species, or inhibit their reactions with biological materials, thereby preventing protein malfunction. eNOS uncoupling is one of such pathophysiological alterations observed in endothelial dysfunction.[9,49]

Ideally, vasodilatation measured as flow-mediated dilation (FMD) with tea intervention should be the basis of evaluation of VF in humans,[6] but such measurements are resource intensive and practically not viable for investigating multiple samples.[50] Therefore, physiologically relevant biomarkers such as antioxidant activity (AOX) and eNOS activity measured as increases in NO levels were chosen as representative surrogate in vitro measures of vascular function.[9,49]

Alteration in the in Vitro Redox Property by Various Black Teas. Cardiovascular risk factors such as hypertension, hypercholesterolemia, diabetes mellitus, or chronic smoking stimulate the generation of reactive oxygen species in the endothelium.[9] This increase in intracellular ROS species plays an important role in vascular damage and progression of various vascular diseases, including atherosclerosis, ischemic heart disease, hypertension, and congestive heart failure.[2,9,28] Cellular mechanisms of ROS production involve sources such as the mitochondrial respiratory chain family of NADPH oxidases, xanthine oxido-reductase, or uncoupled nitric oxide synthase. All of these enzyme levels are found to be up-regulated and activated in animal models of hypertension, diabetes, and in patients with sedentary lifestyle and cardiovascular risk.[9,51] On the other hand, an accelerated degradation of NO (by its reaction with $O_2^{\cdot-}$) is likely to occur in vascular disease, which in turn leads to eNOS uncoupling and enzyme dysfunction.[52] Generation of ROS is counteracted by its destruction through antioxidant systems like super oxide dismutase, catalase, glutathione redox cycle, and ROS scavengers.[12]

The antioxidant benefit of tea is largely due to its ability to increase antioxidant enzymes[2,3] and enhance intracellular ROS

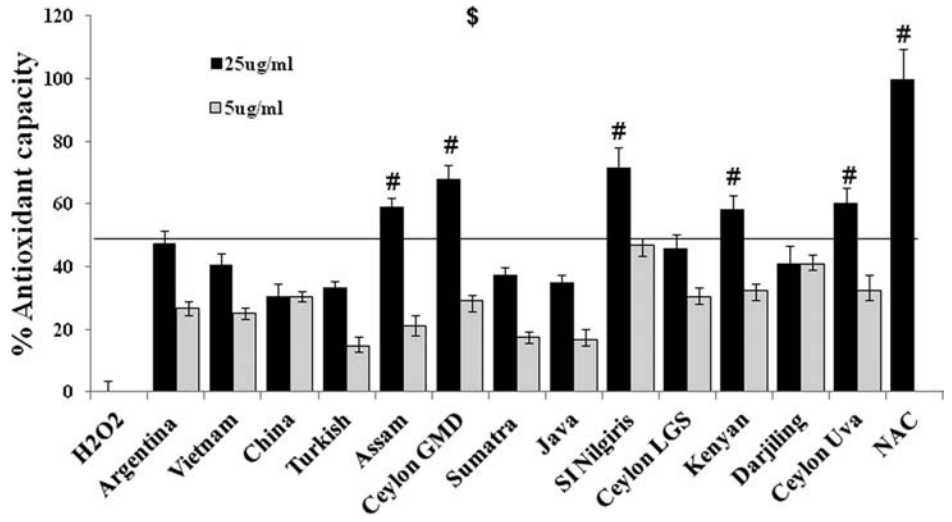

Figure 3. Antioxidant property of different black tea infusions at equivalent polyphenol levels in endothelial cells. EA.Hy926 cells were treated with different concentrations of tea infusions (5−25 μg/mL) for 24 h. *N*-Acetyl cystiene (NAC) was used as positive control (100% H_2O_2 scavenging). Cells treated with H_2O_2 served as negative control (0% H_2O_2 scavenging). Data represented for 25 μg/mL (■) and 5 μg/mL (□) with mean ± SD (n = 3). Statistical comparisons were made using the Student t test. Values were considered statistically significant ($^{\#}p < 0.01$) if % antioxidant capacity is above 50%. The antioxidant capacity of all WoTs was statistically significant ($^{\$}p$) to negative control ($H_2O_2$).

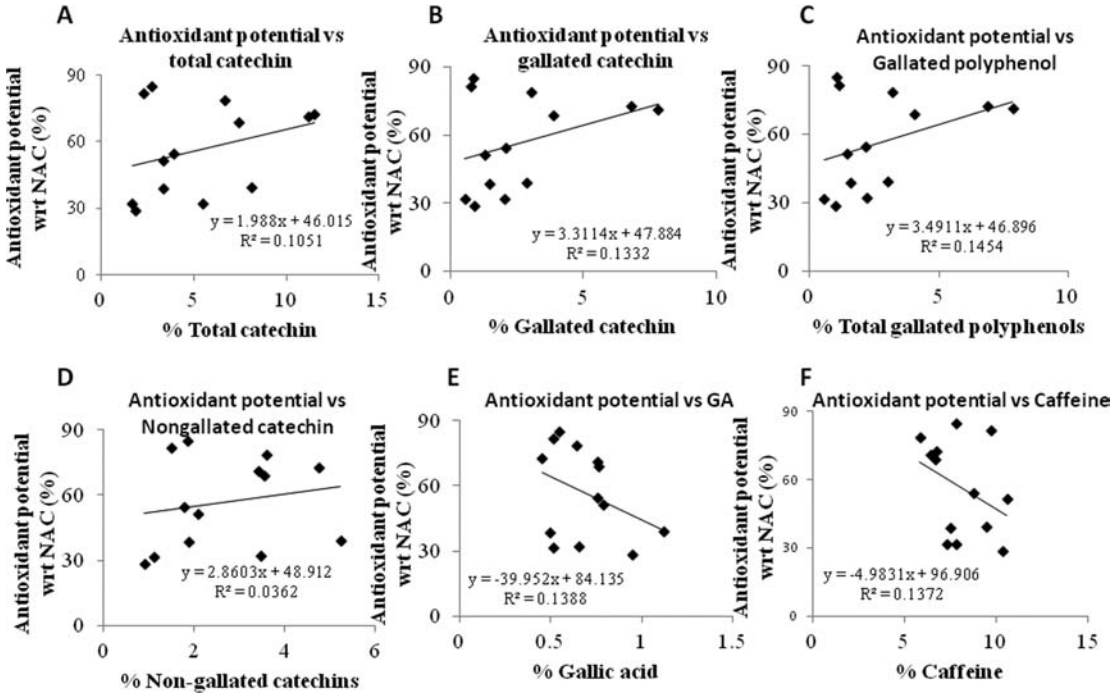

Figure 4. Pearson-correlation analysis between antioxidant property (AOX) and various components in tea infusion. (A) AOX versus total catechins; (B) AOX versus gallated catechin (EGCG+ECG+CG); (C) AOX versus total gallated polyphenols (EGCG+ECG+CG+TF4); (D) AOX versus nongallated catechins (EC+EGC+GC); (E) AOX versus gallic acid; and (F) AOX versus caffeine. The correlation graph was derived with 25 μg/mL PP of tea infusion.

scavengers such as GSH,[2,9] which prevents deleterious effects of intracellular ROS. Thus, this mechanism presumes to play a major role in mediating the cardio-protective effect of tea.[2,3,9,28] To evaluate the antioxidant property of these teas under cellular conditions, cells were pretreated with tea, followed by oxidant trigger, H_2O_2. *N*-Acetyl-L-cysteine (NAC) was used as positive control. The data are represented in Figure 3. The assays were performed at equated polyphenol levels to capture any effects due to compositional variations of tea infusions.

Among the tested black teas, infusions from Ceylon GMD, Nilgiries, Kenya, Assam, and Ceylon Uva showed higher antioxidant property (>50% H_2O_2 scavenging) (Figure 3) as compared to other teas. Because teas were tested at equated polyphenol levels, the data indicate that the chemical composition of tea infusion rather than polyphenol amount contributes to the observed antioxidant (AOX) benefit. Although we did not analyze the type of cellular antioxidant components like GSH, SOD, catalase, and other free radical scavenging enzymes, the results represent the total intracellular

dx.doi.org/10.1021/jf501611w | J. Agric. Food Chem. 2014, 62, 6655−6668

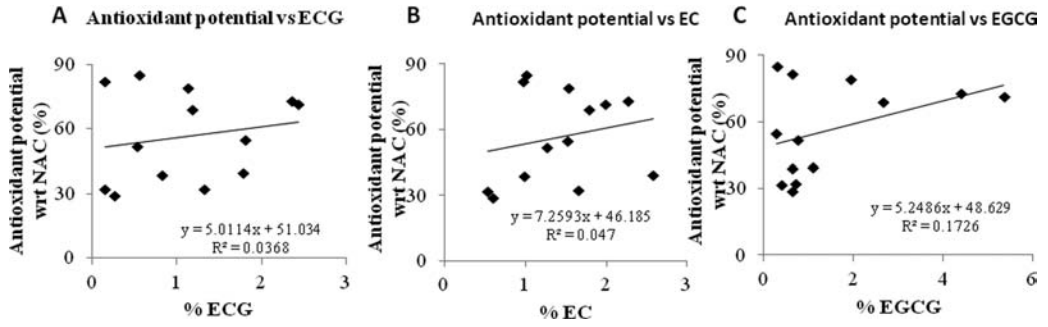

Figure 5. Pearson-correlation analysis between antioxidant property and specific catechins in tea infusion. (A) AOX versus ECG; (B) AOX versus EC; (C) AOX versus EGCG. The correlation graph was derived with 25 μg/mL PP of tea infusion.

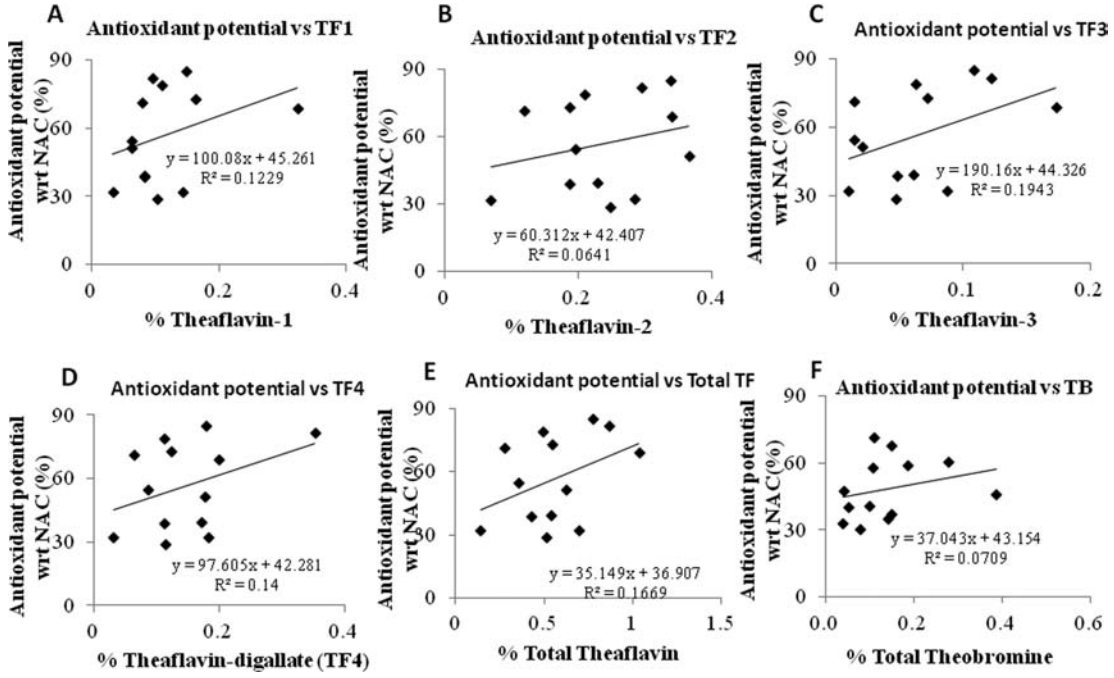

Figure 6. Pearson-correlation analysis between antioxidant property and specific theaflavins (TFs) and phenoli acids in tea infusion. (A) AOX versus TF1; (B) AOX versus TF2; (C) AOX versus TF3; (D) AOX versus TF4; (E) AOX versus total TFs; and (F) AOX versus theobromine (TB). The correlation graph was derived with 25 μg/mL PP of tea infusion.

scavenging capacity generated after pretreatment with tea infusion, which does represent the net effect of all of these protective enzymes.

There was no significant correlation between AOX property and various tea actives (Figures 4–7). However, there was nonsignificant positive association with total catechins, gallated catechins, and gallated polyphenols, while nongallated catechins showed neutral effect (Figure 4A–D). Specifically, epicatechin-gallate (ECG) and epicatechin (EC) showed neutral correlation, while epigallocatechin-gallate (EGCG) showed nonsignificant positive correlation (Figure 5A–C). Among theaflavins (Figure 6A–E), TF1 (r^2 = 0.12), TF3 (r^2 = 0.19), and TF4 (r^2 = 0.14) showed nonsignificant positive correlation, while TF3 showed neutral effect (r^2 = 0.06). However, nonflavonoid polyphenol was also evaluated for their function. Gallic acid (r^2 = 0.13) and caffeine (r^2 = 0.13) showed nonsignificant negative correlation (Figure 4E,F), while theobromine (r^2 = 0.07) showed neutral effect (Figure 6F).

A large proportion of polyphenols in black tea exists as oligomeric species termed as thearubigins (TRs); however, the complete chemical characterization of these TRs is still under investigation. Nicholai and others have reported extensive studies on SII TRs.[53−55] By employing advanced analytical techniques such as electronspin transform ion cyclotron resonance mass spectroscopy (ESI-FTICR), they[53] showed that TRs are comprised of several thousands of compounds, with a molecular weight ranging between 1 and 1.5KDa.[18,55] They also observed a typical Gaussian hump in caffeine precipitated SII TRs,[18] containing majorly trimers and tetramers of flavan-3-ols.[18] Spectroscopic studies showed that TRs have basic catechin structure with benzotropolone and *ortho*-quinone moieties.[53] The group has also investigated the possible mechanism on how these molecules are formed using MALDI-TOF studies of SII TRs. They suggest the formation of polyhydroxylated species, which are formed via oxidation and nuclieophilic addition of water and hydrogen peroxide to catechin dimer and oligomers. All of these extensive reports provide information that thearubigins have flavonoid backbone structure.[53,55]

Among flavonoids, flavan-3-ols (catechins) have absorption maxima at 278 nm, flavonols and chlorogenic acids at 350 nm, and oligomeric flavonoids (theaflavins) at 380 and 460 nm.[56]

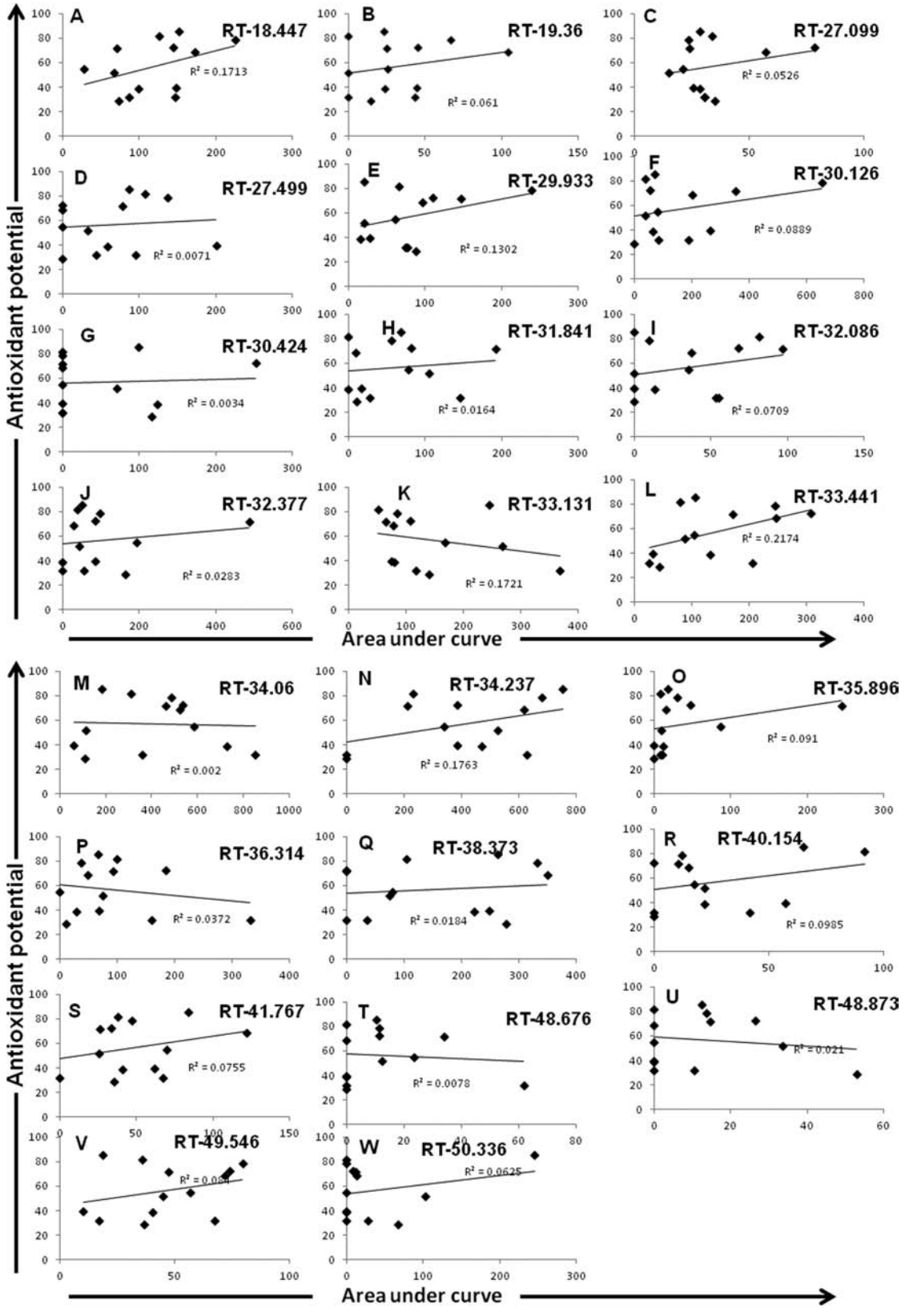

Figure 7. Pearson-correlation analysis between antioxidant property and various TRs (A–W) with specified retention time (RT) in tea infusion. The correlation graph was derived with 25 μg/mL PP of tea infusion.

During fermentation of tea, oxidation of monomeric flavonoids leads to formation of TRs. Such transformation involves oxidation followed by coupling and ring condensation reaction. These reactions would result in products with increased conjugation and absorption at longer wavelengths. Hence, oxidized catechins or TRs should have absorption maxima also at ~380 nm, which has been used to relatively quantify their amounts.[56] The known phenolic acids, flavonol glycosides, and

dx.doi.org/10.1021/jf501611w | J. Agric. Food Chem. 2014, 62, 6655–6668

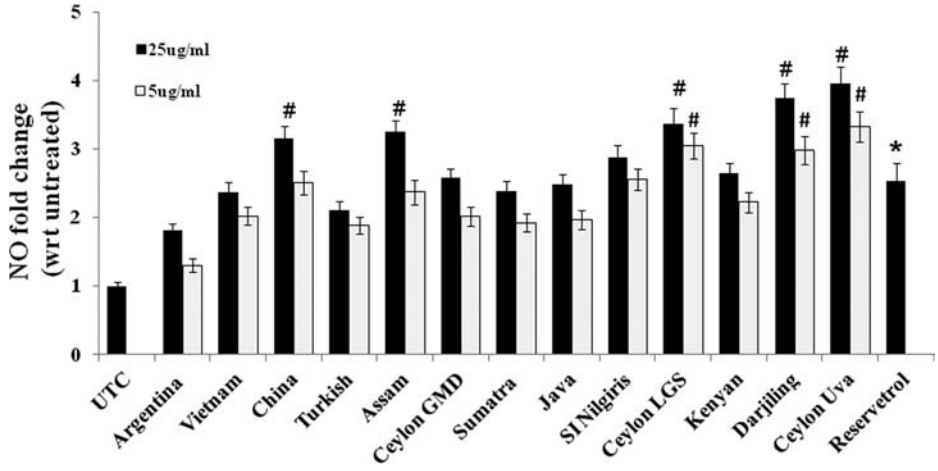

Figure 8. Nitric oxide stimulating potential of different black tea infusions at equivalent polyphenol levels in endothelial cells. The infusions were evaluated for NO enhancement in EAHy926 cells. The cells were treated with different concentrations of tea infusions (25 μg/mL (■) and 5 μg/mL (□)) for 30 min. Data are presented as mean ± SD (n = 5). Reservetrol (10 μM) was used as positive control. Statistical comparisons were made using Student t test. "#" and "*" values were statistically significant ($p < 0.01$) with respect to untreated control (UTC) and Argentinean tea sample (lowest in NO enhancement).

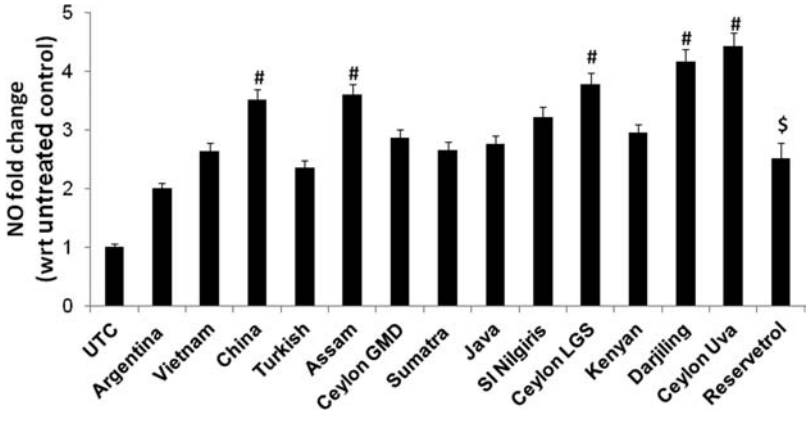

Figure 9. Nitric oxide stimulating potential of different black tea infusions at equivalent polyphenol levels in HUVEC. The data represent NO levels in primary HUVEC at 25 μg/mL concentration of tea infusion for 30 min. The "#" values were statistically significant ($p < 0.01$) with respect to reservetrol ($).

TFs that absorb at this wavelength were not considered for TR analysis.

We observed several peaks in the UPLC chromatogram (Supporting Information Figure 3A−C) after elimination of known components of black tea such as catechins, TFs, phenolic acids, and flavonol glycosides. The peaks that showed absorption at 380 nm and had retention time above 18 min were considered as thearubigin (TR) peaks. For correlation purpose, we only considered 29 major peaks that were consistently present in majority of the tea (Figure 7). The TR peaks having retention time of 18.447, 29.933, 33.441, and 34.237 (Figure 7A, E, L, and N) showed nonsignificant positive correlation with antioxidant potential, while TR peaks having retention time of 33.131 showed nonsignificant negative correlation (Figure 7K).

Among the tested black teas, infusions from Ceylon GMD, Nilgiries, Kenya, Assam, and Ceylon Uva showed higher antioxidant property. This may be due to the presence of a higher amount of theobromine and gallated catechins, which are previously reported to increase expression of antioxidant enzymes.[57,58] Our data suggest that none of the other actives analyzed showed significant correlation with antioxidant property of tea. However, these actives in tea showed nonsignificant positive correlation, indicating that positive species such as catechins, TFs, and some TRs might cumulatively be responsible for the observed AOX benefit of black tea. Further work is required to evaluate the mechanisms involved in the induction of cellular antioxidant property by specific flavonoids/phenolic acids.

In Vitro Efficacy of Teas To Promote Endothelial NO Production. Endothelial dysfunction (ED) significantly contributes to pathogenesis and clinical manifestation of CVD.[6,9] ED is characterized by decreased endothelial NO production in endothelial cell.[6,27] Black tea is reported to activate eNOS and thus enhance NO production in endothelial cells.[9,28] We analyzed 13 black teas, with distinct polyphenol amounts and composition, for their NO potentiating effect after normalizing for their polyphenol concentration. The results are represented in Figure 8. Variable response to agonist stimulation has been reported in different endothelial cell-types.[59] We evaluated NO production in response to various tea infusions (25 μg/mL) in primary HUVEC (Figure 9). The stimulatory response for the tested tea infusion behaved in a similar manner in both EA.hy926 (Figure 8) and HUVEC

dx.doi.org/10.1021/jf501611w | J. Agric. Food Chem. 2014, 62, 6655−6668

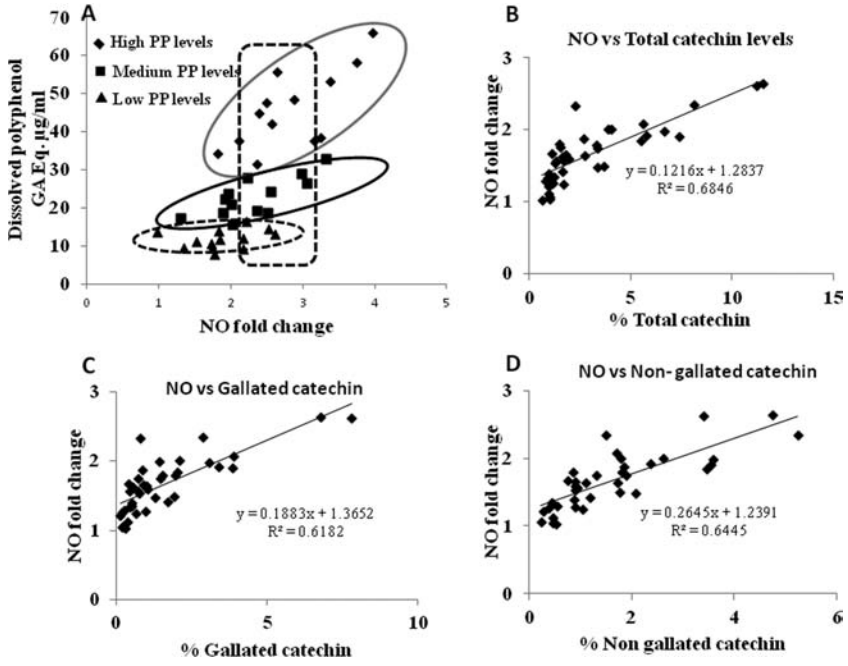

Figure 10. Pearson-correlation analysis between nitric oxide (NO) levels and various components in tea infusion. (A) NO versus total polyphenols (PP); the circled clusters indicate quantitative correlations of PP (gray circles (rhomboid) indicate PP range from 30 to 65 μg/mL GA equiv; black circles (square) indicate PP range from 15 to 30 μg/mL GA equiv, and black dotted circles (triangle) indicate PP range from 5 to 15 μg/mL GA equiv) with NO levels. The data indicate that NO potentiating effect increases with increasing concentration of PP. The dotted box represents qualitative correlation of PP with NO level. The data indicate that some teas are efficient enough to produce NO levels (2−3-fold) at very low PP concentration. (B) NO versus total catechins. (C) NO versus gallated catechin (EGCG+ECG+CG). (D) NO versus nongallated catechin (EC+EGC +GC). The correlation graph was derived with 25 μg/mL PP of tea infusion.

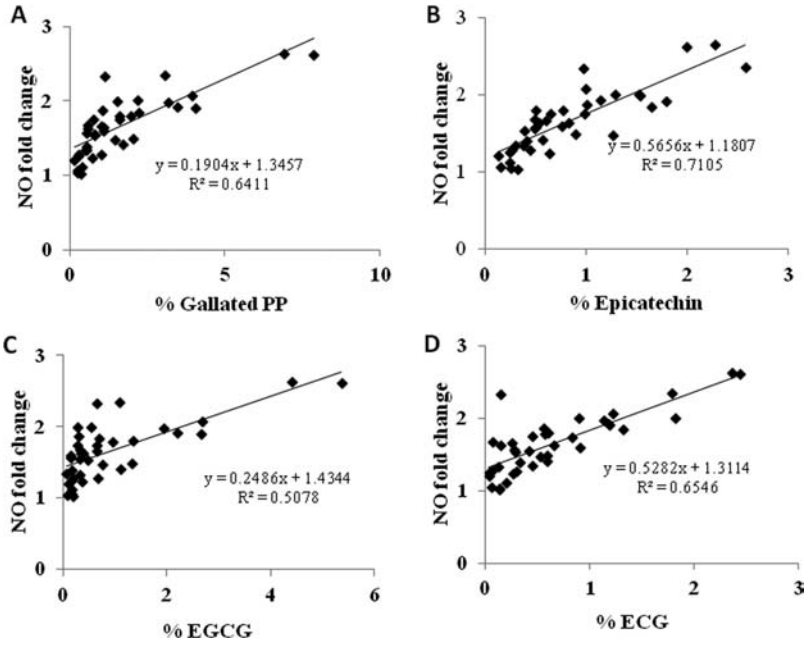

Figure 11. Pearson-correlation analysis between nitric oxide levels and specific flavonoids in tea infusion. (A) NO versus gallated PP (EGCG+ECG +CG+TF4); (B) NO versus EC; (C) NO versus EGCG; (D) NO versus ECG. The correlation graph was derived with 25 μg/mL PP of tea infusion.

(Figure 9). Although, in general, higher polyphenol levels resulted in higher NO levels (Figure 10A), the NO potentiating effect of WoBTs did not always correlate with the polyphenol levels (Figure 10A). Tea infusions from Assam, Darjeeling, and Ceylon (UVA), which had higher polyphenols as compared to other teas, showed higher NO enhancement as compared to other teas. Darjeeling teas, while being comparable in polyphenol levels to Kenyan teas, showed the highest NO enhancement (Figure 9).

The data suggest the possibility that composition of polyphenols, besides quantity, plays a significant role in eNOS activation by various geographical teas. Several functional species in tea are reported to stimulate eNOS enzyme and enhance NO production in endothelial cells. These include

dx.doi.org/10.1021/jf501611w | J. Agric. Food Chem. 2014, 62, 6655−6668

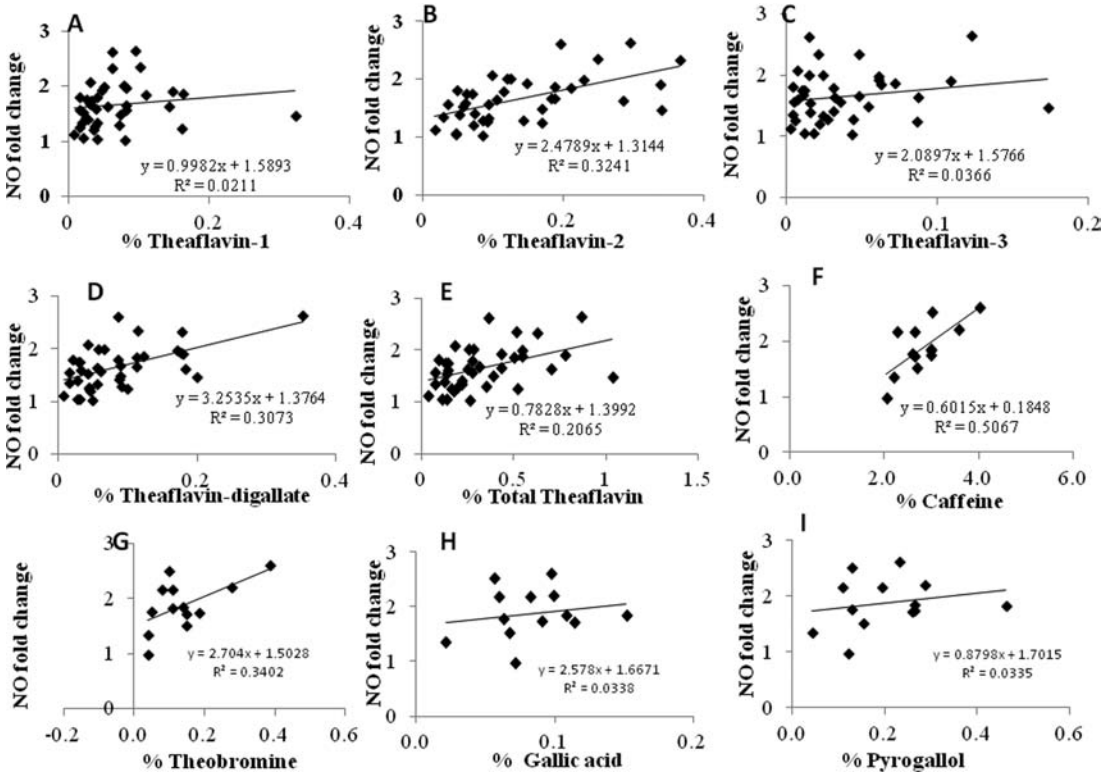

Figure 12. Pearson-correlation analysis between nitric oxide levels and specific theaflavins (TFs) and phenolic acids in tea infusion. (A) NO versus TF1; (B) NO versus TF2; (C) NO versus TF3; (D) NO versus TF4; (E) NO versus total TFs; (F) NO versus caffeine; (G) NO versus theobromine; (H) NO versus gallic acid; (I) NO versus pyrogallol. The correlation graph was derived with 25 μg/mL PP of tea infusion.

catechins,[5] theaflavins,[5,9,25] and flavones like quercetin, kaempferol, and rutin[3,24,26] and thearubigins.[5] Nonflavonoid components in tea like L-theanine,[60] theobromine,[61,62] and caffeine[63] are also reported to contribute to this function.

When analyzed for the correlation between NO production and different flavonoid components, total catechin showed significant correlation (Figure 10B; r^2 = 0.68). In general, the levels of catechins in black tea varied from 0.9% to 11.5%. There was a good correlation with gallated catechins (Figure 10C; r^2 = 0.61), nongallated catechins (Figure 10D; r^2 = 0.64), and gallated polyphenols (Figure 11A; r^2 = 0.64). This indicates that, in addition to gallated catechin, gallated polyphenols, which include gallated TFs and gallated TRs, would contribute to improve NO enhancement. There was no significant difference, however, between gallated and nongallated catechins (Figure 10C and D). Among the catechins, EC (Figure 11B; r^2 = 0.71), EGCG (Figure 11C; r^2 = 0.50), and ECG (Figure 11D; r^2 = 0.0.65) showed significant positive correlation.

We also analyzed the correlation for various TF species (Figure 12A–E). Total TFs showed mild positive correlation (r^2 = 0.20), although strong positive correlation was observed for gallated TFs like TF2 (r^2 = 0.32) and TF4 (TF4, r^2 = 0.30), while nongallated TFs like TF1 (r^2 = 0.02) and TF3 (r^2 = 0.03) showed neutral effects. The amounts of such TF species are very low; hence, their contribution toward NO stimulatory effect might be negligible. We also analyzed for some of the major phenolic acids in black tea such as caffeine, theobromine, gallic acid, and pyrogallol. Caffeine (r^2 = 0.50) and theobromine (r^2 = 0.34) (Figure 12F,G) showed significant positive correlation, while other phenolic acids failed to show any correlation (Figure 12H,I).

A large proportion (70%) of flavonoids in the black tea are present as TRs.[17] The TRs fractions are reported to show NO enhancement in endothelial cells and dilation of mesenteric arteries.[5] We evaluated the correlation between NO production and different TR peaks obtained by UPLC chromatogram. We could not find any significant positive correlation with the majority of the TR peaks (Figure 13). However, TR peak having retention time of 32.37 and 35.89 (Figure 13J and O) showed positive correlation with NO enhancement, while TR peak corresponding to retention time of 33.13 showed negative correlation (Figure 13K). From our data, it is evident that, among polyphenol, catechins (EC, EGCG, and ECG) are maximally active, while contribution by theaflavins remains miniscule. However, two of the investigated UPLC-based TR peaks showed positive correlation, while one TR peak showed negative correlation. This suggests that black tea has diverse pharmacological species, which strongly influence the NO potentiating effect in endothelial cells. Moreover, isolation, characterization, and screening of TRs would be an open area of investigation.

Among the tested tea infusion, Ceylon Uva, Darjeeling, Ceylon LGS, Assam, and China tea showed significant NO potentiating effect. We observed a higher amount of gallated catechin, TFs (TF2 and TF4), and some of the positive TR species to be present in these teas, which may alone or in combination explain enhanced NO production by these teas.

We also tried to understand the correlation between tea/tea ingredient-mediated increase in NO enhancement and antioxidant capacity of the cell. We observed no correlation between NO production in endothelial cell with enhanced intracellular free radical scavenging property (Figure 14; r^2 = 0.01). It is reported that increased levels of ROS would

dx.doi.org/10.1021/jf501611w | J. Agric. Food Chem. 2014, 62, 6655–6668

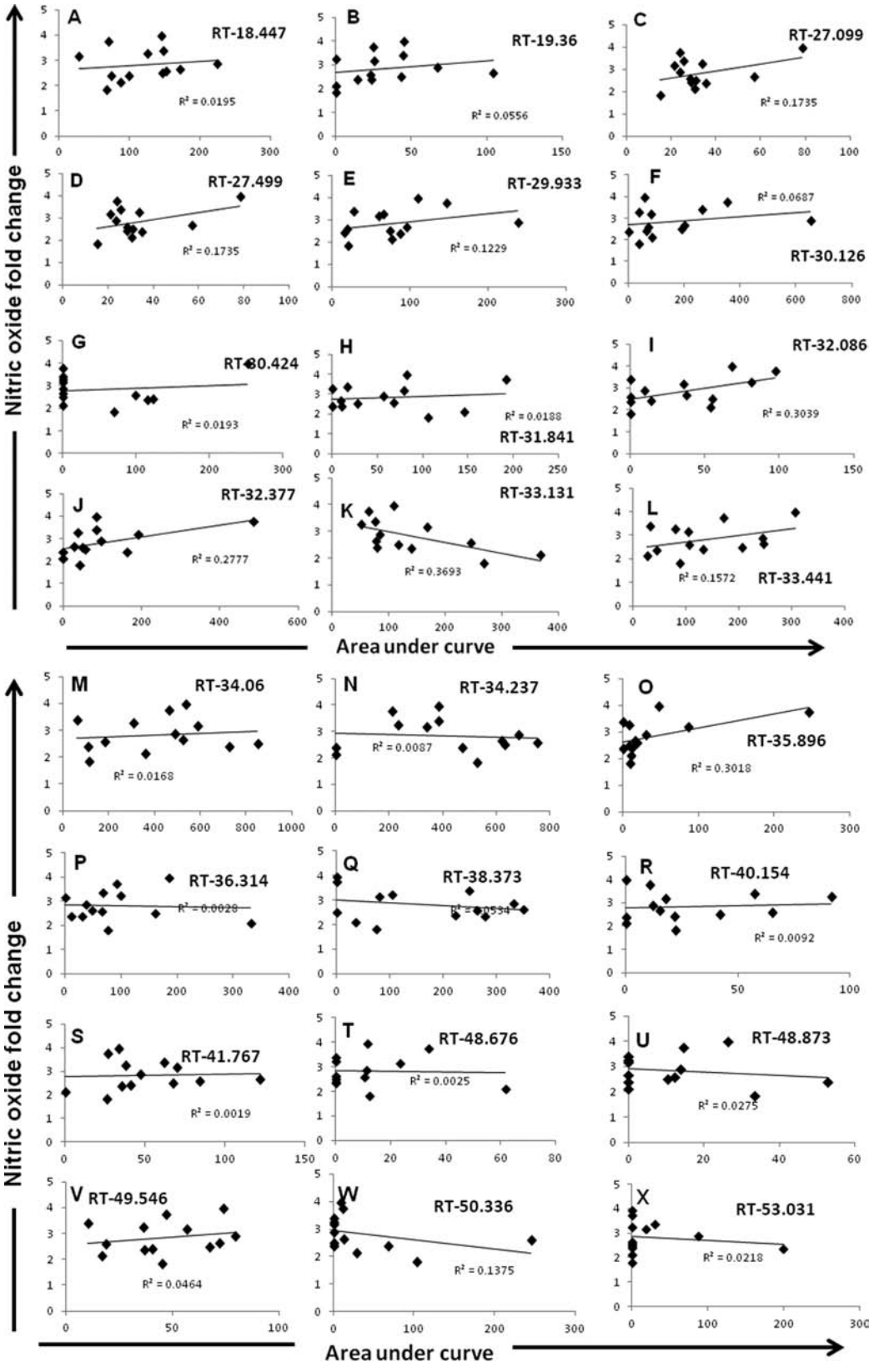

Figure 13. Pearson-correlation analysis between NO levels and various TRs (A–X) with specified retention time (RT) in tea infusion. The correlation graph was derived with 25 μg/mL PP of tea infusion.

dissipate NO levels and contribute toward ED. However, it needs to be further evaluated how the antioxidant activity of tea could potentiate NO bioavailability under stress conditions that would normally prevail in the in vivo situation, and both the antioxidant and the eNOS activity of tea synergistically could contribute to the vascular benefit efficacy of specific teas.

Further, spatial distribution of NO and ROS can also be crucial in NO dissipation under physiological stress. Under

dx.doi.org/10.1021/jf501611w | J. Agric. Food Chem. 2014, 62, 6655–6668

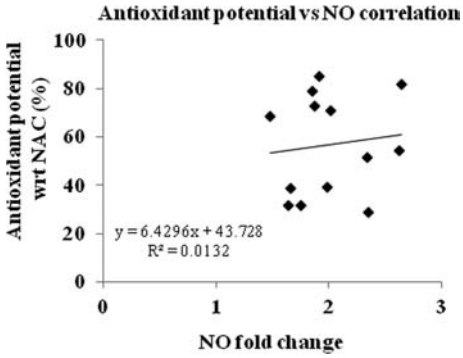

Figure 14. Pearson-correlation analysis between nitric oxide levels and antioxidant property of various tea infusions. The correlation graph was derived with 25 μg/mL PP of tea infusion.

condition of stress, ROS is generated from the mitochondria and has been shown to play a major role in NO dissipation.[9,49] In our experiments, we used H_2O_2 as the source of ROS (external species), which could be different from the ROS generated under physiological condition. Further experimentation would be needed to dissect their specific effects.

In summary, we used 13 black teas (WoBTs) representative of varied geographies, to address the contribution of quantity and composition of tea flavonoids on antioxidant and NO enhancement properties. Even though the endothelial cells were treated with tea infusions containing equated amounts of polyphenols, they induced different levels of cellular antioxidant activity and NO levels, suggesting that the composition of polyphenols in tea infusions determines the response. Statistical analysis using Pearson correlation indicated that the majority of ingredients in black tea such as catechins, TFs, TRs, and phenolic acids moderately influence antioxidant potential in endothelial cells, while its NO potentiating effect is mainly regulated by catechins in tea. Our data also suggest that the net effect of black tea on VF benefit may be due to a multitude of ingredients, majorly influencing NO enhancement, while also mildly contributed by its antioxidant benefit. Most interestingly, we also found that gallic acid and caffeine negatively affect antioxidant property, while caffeine and theobromine positively affect NO levels in endothelial cell.

One of the limitations in our study was the absence of characterization of specific TRs and evaluation of their efficacy on biological function. The study was also limited to in vitro investigation using cell free and cellular systems, as these systems do not adequately address issues of bioavailability and metabolic transformation. These would be the areas in which further investigations need to be undertaken.

■ ASSOCIATED CONTENT

Supporting Information

Figures showing illustration of geographical teas, DPPH (1,1-diphenyl-2-picrylhydrazyl) free radical scavenging property of different black tea infusions in end cup, and UPLC fingerprinting for thearubigins. This material is available free of charge via the Internet at http://pubs.acs.org.

■ AUTHOR INFORMATION

Corresponding Authors

*Tel.: +91 80-39831217. Fax: +91 80-28453086. E-mail: paul.dias@unilever.com.

*Tel.: +91 80-39831068. Fax: +91 80-28453086. E-mail: anita.damodaran@unilever.com.

Notes

The authors declare no competing financial interest.

■ ACKNOWLEDGMENTS

We acknowledge Vikas Pawar, Unilever R&D, Mumbai for his technical help and for the critical review of data by Dr. Gurmeet Singh, Unilever R&D, Colworth and Dr. Sujatha Jayaraman, Unilever R&D, Bangalore.

■ ABBREVIATIONS

EC, epicatechin; ECG, epicatechingallate; EGCG, (−)-epigallocatechin-3-gallate; TF-2, theaflavin-3-gallate; TF-3, theaflavin-3′-gallate; TF-4, theaflavin-3,3′-digallate; WoBTs, world of black teas; ED, endothelial dysfunction; AOX, antioxidant property; CTC, cut tear curl

■ REFERENCES

(1) Peterson, J.; Dwyer, J.; Bhagwat, S.; et al. Major flavonoids in dry tea. *J. Food Compos. Anal.* **2005**, *18*, 487−501.

(2) Butt, M. S.; Imran, A.; Sharif, M. K.; et al. Black tea polyphenols: A mechanistic treatise. *Crit. Rev. Food Sci. Nutr.* **2014**, *54*, 1002−11.

(3) Kay, C. D.; Hooper, L.; Kroon, P. A.; Rimm, E. B.; Cassidy, An. Relative impact of flavonoid composition, dose and structure on vascular function: A systematic review of randomised controlled trials of flavonoid rich food products. *Mol. Nutr. Food Res.* **2012**, *56*, 1605−16.

(4) Arab, L.; Khan, F.; Lam, H. Tea consumption and cardiovascular disease risk. *Am. J. Clin. Nutr.* **2013**, *98*, 1651S−9S.

(5) Lorenz, M.; Urban, J.; Engelhardt, U.; Baumann, G.; Stangl, K.; Stangl, V. Green and black tea are equally potent stimuli of NO production and vasodilation: new insights into tea ingredients involved. *Basic Res. Cardiol.* **2009**, *104*, 100−10.

(6) Ras, R. T.; Streppel, M. T.; Draijer, R.; Zock, P. L. Flow-mediated dilation and cardiovascular risk prediction: A systematic review with meta-analysis. *Int. J. Cardiol.* **2012**, *168*, 344−51.

(7) Franzini, L.; Ardigo, D.; Valtuena, S.; et al. Food selection based on high total antioxidant capacity improves endothelial function in a low cardiovascular risk population. *Nutr., Metab. Cardiovasc. Dis.* **2012**, *22*, 50−7.

(8) Uto-Kondo, H.; Ayaori, M.; Kishimoto, Y.; et al. Consumption of polyphenol-rich juar tea increases endothelium-bound extracellular superoxide dismutase levels in men with metabolic syndrome: link with LDL oxidizability. *Int. J. Food Sci. Nutr.* **2013**, *64*, 407−14.

(9) Dias, P. M.; Joshi, M. K. Endothelial dysfunction as a risk factor for cardiovascular disease; its modulation by phyto-ingredients and implication in better cardiovascular health. *Oxid. Antioxid. Med. Sci.* **2012**, *1*, 75−85.

(10) Anter, E.; Chen, K.; Shapira, O. M.; Karas, R. H.; Keaney, J. F. p38 mitogen-activated protein kinase activates eNOS in endothelial cells by an estrogen receptor dependent pathway in response to black tea polyphenols. *Circ. Res.* **2005**, *96*, 1072−8.

(11) Joy, S.; Siow, R. C.; Rowlands, D. J.; et al. The isoflavone equol mediates rapid vascular relaxation Ca2+- independent activation of endothelial nitric-oxide synthase/Hsp90 involving Erk1/2 and Akt phosporylation in human endothelial cell. *J. Biol. Chem.* **2006**, *281*, 27335−45.

(12) Higdon, J. V.; Frei, B. Tea catechins and polyphenols: health effects, metabolism, and antioxidant functions. *Crit. Rev. Food Sci. Nutr.* **2003**, *43*, 89−143.

(13) Frei, B.; Higdon, J. V. Antioxidant activity of tea polyphenols in vivo: evidence from animal studies. *J. Nutr.* **2003**, *133*, 3275−84.

(14) Luczaj, W.; Skrzydlewska, E. Antioxidative properties of black tea. *Prev. Med.* **2005**, *40*, 910−8.

(15) Niki, E.; Yoshida, Y.; Saito, Y.; Noguchi, N. Lipid peroxidation: mechanisms, inhibition, and biological effects. *Biochem. Biophys. Res. Commun.* **2005**, *338*, 668−76.
(16) Montezano, A. C.; Touyz, R. M. Reactive oxygen species and endothelial function - Role of nitric oxide synthase uncoupling and nox family nicotinamide adenine dinucleotide phosphate oxidases. *Basic Clin. Pharmacol. Toxicol.* **2012**, *110*, 87−94.
(17) Lorenz, M. Cellular targets for the beneficial actions of tea polyphenols. *Am. J. Clin. Nutr.* **2013**, *98*, 1642S−50S.
(18) Drynan, J. W.; Clifford, M. N.; Obuchowicz, J.; Kuhnert, N. The chemistry of low molecular weight black tea polyphenols. *Nat. Prod. Rep.* **2010**, *27*, 417−62.
(19) Han, X.; Shen, T.; Lou, H. Dietary polyphenols and their biological significance. *Int. J. Mol. Sci.* **2007**, *8*, 950−88.
(20) Balentine, D. A.; Wiseman, S. A.; Bouwens, L. C. The chemistry of tea flavonoids. *Crit. Rev. Food Sci. Nutr.* **1997**, *37*, 693−704.
(21) Obuchowicz, J.; Engelhardt, U. H.; Donnelly, K. Flavanol database for green and black teas utilising ISO 14502−1 and ISO 14502−2 as analytical tools. *J. Food Compos. Anal.* **2011**, *24*, 411−7.
(22) Roy, M. K.; Koide, M.; Rao, T. P.; Okubo, T.; Ogasawara, Y.; Juneja, L. R. ORAC and DPPH assay comparison to assess antioxidant capacity of tea infusions: relationship between total polyphenol and individual catechin content. *Int. J. Food Sci. Nutr.* **2010**, *61*, 109−24.
(23) Deanfield, J.; Donald, A.; Ferri, C.; et al. Endothelial function and dysfunction. Part I: Methodological issues for assessment in the different vascular beds: a statement by the Working Group on Endothelin and Endothelial Factors of the European Society of Hypertension. *J. Hypertens.* **2005**, *23*, 7−17.
(24) Williamson, G.; Manach, C. Bioavailability and bioefficacy of polyphenols in humans. II. Review of 93 intervention studies. *Am. J. Clin. Nutr.* **2005**, *81*, 243−55.
(25) Lambert, J. D.; Sang, S.; Yang, C. S. Biotransformation of green tea polyphenols and the biological activities of those metabolites. *Mol. Pharmaceutics* **2007**, *4*, 819−25.
(26) Perez-Vizcaino, F.; Duarte, J.; Santos-Buelga, C. The flavonoid paradox: conjugation and deconjugation as key steps for the biological activity of flavonoids. *J. Sci. Food Agric.* **2012**, *92*, 1822−5.
(27) Trinity, J. D.; Groot, H. J.; Layec, G.; et al. Nitric oxide and passive limb movement: a new approach to assess vascular function. *J. Physiol.* **2012**, *590*, 1413−25.
(28) Schmitt, C. A.; Dirsch, V. M. Modulation of endothelial nitric oxide by plant-derived products. *Nitric Oxide* **2009**, *21*, 77−91.
(29) Del Rio, D.; Calani, L.; Scazzina, F.; Jechiu, L.; Cordero, C.; Brighenti, F. Bioavailability of catechins from ready-to-drink tea. *Nutrition* **2010**, *26*, 528−33.
(30) Vinson, J. A.; Mandarano, M.; Hirst, M.; Trevithick, J. R.; Bose, P. Phenol antioxidant quantity and quality in foods: beers and the effect of two types of beer on an animal model of atherosclerosis. *J. Agric. Food Chem.* **2003**, *51*, 5528−33.
(31) Wei, K.; Wang, L. Y.; Zhou, J.; et al. Comparison of catechins and purine alkaloids in albino and normal green tea cultivars (Camellia sinensis) by HPLC. *Food Chem.* **2012**, *130*, 720−4.
(32) Xu, Y.; Jin, Y.; Wu, Y.; Tu, Y. Isolation and purification of four individual theaflavins using semi-preparative high performance liquid chromatography. *J. Liq. Chromatogr. Relat. Technol.* **2010**, *33*, 1791−801.
(33) Yen, G. C.; Duh, P. D. Scavenging effect of methanolic extracts of peanut hulls on free-radical and active-oxygen species. *J. Agric. Food Chem.* **1994**, *42*, 629−32.
(34) Carloni, P.; Tiano, L.; Padella, L.; et al. Antioxidant activity of white, green and black tea obtained from the same tea cultivar. *Food Res. Int.* **2012**, *53*, 900−8.
(35) Paul, D. M.; Vilas, S. P.; Kumar, J. M. A flow-cytometry assisted segregation of responding and non-responding population of endothelial cells for enhanced detection of intracellular nitric oxide production. *Nitric Oxide* **2011**, *25*, 31−40.
(36) Shinde, A.; Das, S.; Datta, A. K. Quality improvement of orthodox and CTC tea and performance enhancement by hybrid hot air-radio frequency (RF) dryer. *J. Food Eng.* **2012**, *116*, 444−9.
(37) Li, S.; Lo, C. Y.; Pan, M. H.; Lai, C. S.; Ho, C. T. Black tea: chemical analysis and stability. *Food Funct.* **2013**, *4*, 10−8.
(38) Bhuyan, L. P.; Sabhapondit, S.; Baruah, B. D.; Bordoloi, C.; Gogoi, R.; Bhattacharyya, P. Polyphenolic compounds and antioxidant activity of CTC black tea of North-East India. *Food Chem.* **2013**, *141*, 3744−51.
(39) Ohno, A.; Oka, K.; Sakuma, C.; Okuda, H.; Fukuhara, K. Characterization of tea cultivated at four different altitudes using 1H NMR analysis coupled with multivariate statistics. *J. Agric. Food Chem.* **2011**, *59*, 5181−7.
(40) Chen, Y.; Jiang, Y.; Duan, J.; Shi, J.; Xue, S.; Kakuda, Y. Variation in catechin contents in relation to quality of Huang Zhi Xiang Oolong tea (Camellia sinensis) at various growing altitudes and seasons. *Food Chem.* **2010**, *119*, 648−52.
(41) Bergamini, C. M.; Gambetti, S.; Dondi, A.; Cervellati, C. Oxygen, reactive oxygen species and tissue damage. *Curr. Pharm. Des.* **2004**, *10*, 1611−26.
(42) Montezano, A. C.; Touyz, R. M. Molecular mechanisms of hypertension - reactive oxygen species and antioxidants: a basic science update for the clinician. *Can. J. Cardiol.* **2012**, *28*, 288−95.
(43) Montezano, A. C.; Touyz, R. M. Reactive oxygen species, vascular noxs, and hypertension: Focus on translational and clinical research. *Antioxid. Redox Signaling* **2014**, *20*, 164−82.
(44) Ashlee, H.; Anne, R.; Joo, Y. O.; Aimee, L.; Victor, M. Cell signalling by reactive lipid species: new concepts and molecular mechanisms. *Biochem. J.* **2012**, *442*, 453−64.
(45) Carr, A. C.; McCall, M. R.; Frei, B. Oxidation of LDL by myeloperoxidase and reactive nitrogen species: Reaction pathways and antioxidant protection. *Arterioscler., Thromb., Vasc. Biol.* **2000**, *20*, 1716−23.
(46) Prior, R. L.; Cao, G. In vivo total antioxidant capacity: comparison of different analytical methods1. *Free Radical Biol. Med.* **1999**, *27*, 1173−81.
(47) Anesini, C.; Ferraro, G. E.; Filip, R. Total polyphenol content and antioxidant capacity of commercially available tea (Camellia sinensis) in Argentina. *J. Agric. Food Chem.* **2008**, *56*, 9225−9.
(48) Amic, D.; Amic, D. D.; Beslo, D.; Trinajstic, N. Structure-radical scavenging activity relationships of flavonoids. *Croat. Chem. Acta* **2003**, *76*, 55−61.
(49) Wray, D. W.; Nishiyama, S. K.; Harris, R. A.; et al. Response to antioxidants and endothelial dysfunction in young and elderly people: Is flow-mediated dilation useful to assess acute effects? *Hypertension* **2012**, *60*, e6−e7.
(50) Lekakis, J.; Abraham, P.; Balbarini, A.; et al. Methods for evaluating endothelial function: a position statement from the European Society of Cardiology Working Group on Peripheral Circulation. *Eur. J. Cardiovasc. Prev. Rehabil.* **2011**, *18*, 775−89.
(51) Schulz, E.; Gori, T.; Münzel, T. Oxidative stress and endothelial dysfunction in hypertension. *Hypertens. Res.* **2011**, *34*, 665−73.
(52) Forstermann, U.; Sessa, W. C. Nitric oxide synthases: regulation and function. *Eur. Heart J.* **2012**, *33*, 829−37.
(53) Kuhnert, N. Unraveling the structure of the black tea thearubigins. *Arch. Biochem. Biophys.* **2010**, *501*, 37−51.
(54) Kuhnert, N.; Drynan, J. W.; Obuchowicz, J.; Clifford, M. N.; Witt, M. Mass spectrometric characterization of black tea thearubigins leading to an oxidative cascade hypothesis for thearubigin formation. *Rapid Commun. Mass Spectrom.* **2010**, *24*, 3387−404.
(55) Drynan, J. W.; Clifford, M. N.; Obuchowicz, J.; Kuhnert, N. MALDI-TOF mass spectrometry: avoidance of artifacts and analysis of caffeine-precipitated SII thearubigins from 15 commercial black teas. *J. Agric. Food Chem.* **2012**, *60*, 4514−25.
(56) Bailey, R. G.; Nursten, H. E.; McDowell, I. Comparative study of the reversed-phase high-performance liquid chromatography of black tea liquors with special reference to the thearubigins. *J. Chromatogr., A* **1991**, *542*, 115−28.
(57) Higdon, J. V.; Frei, B. Tea catechins and polyphenols: health effects, metabolism, and antioxidant functions. *Crit. Rev. Food Sci. Nutr.* **2003**, *43*, 89−143.

(58) Na, H. K.; Kim, E. H.; Jung, J. H.; Lee, H. H.; Hyun, J. W.; Surh, Y. J. (−)-Epigallocatechin gallate induces Nrf2-mediated antioxidant enzyme expression via activation of PI3K and ERK in human mammary epithelial cells. *Arch. Biochem. Biophys.* **2008**, *476*, 171−7.
(59) Di, X.; Yan, J.; Zhao, Y.; et al. L-Theanine protects the APP (Swedish mutation) transgenic SH-SY5Y cell against glutamate-induced excitotoxicity via inhibition of the NMDA receptor pathway. *Neuroscience* **2010**, *168*, 778−86.
(60) Siamwala, J. H.; Dias, P. M.; Majumder, S.; et al. l-Theanine promotes nitric oxide production in endothelial cells through eNOS phosphorylation. *J. Nutr. Biochem.* **2012**, *24*, 595−605.
(61) Corti, R.; Flammer, A. J.; Hollenberg, N. K.; Luscher, T. F. Cocoa and cardiovascular health. *Circulation* **2009**, *119*, 1433−41.
(62) Ried, K.; Sullivan, T. R.; Fakler, P.; Frank, O. R.; Stocks, N. P. Effect of cocoa on blood pressure. *Cochrane Database Syst. Rev.* **2012**, *8*, CD008893.
(63) Shechter, M.; Shalmon, G.; Scheinowitz, M.; et al. Impact of acute caffeine ingestion on endothelial function in subjects with and without coronary artery disease. *Am. J. Cardiol.* **2011**, *107*, 1255−61.

Table 1. ^{1}H NMR Spectroscopic Data (400 MHz, $CDCl_3$) of Compounds 1−5[a]

	1	2	3	4	5
position	δ_H mult (J in Hz)	δ_H mult (J in Hz)	δ_H mult (J in Hz)	δ_H mult (J in Hz)	δ_H mult (J in Hz)
1	4.61 d (3.6)	5.57 d (4.0)	5.35 d (3.5)	5.98 s	6.01 s
2	5.34 m	4.47 m	4.57 m		
3	2.39 m	2.40−2.44 m	2.40−2.44 m	3.40 dd (12.8, 7.4)	3.42 dd (12.8, 7.4)
	1.87 dd (15.1, 1.4)	1.90 m	1.92 m	2.31 dd (12.8, 1.4)	2.28 dd (12.8, 1.4)
4	2.51 m	2.49−2.60 m	2.52 m	3.02 m	3.02 m
6	5.66 s	5.67 s	6.26 s	6.24 s	5.62 s
7	2.39 m	2.40−2.44 m	2.64 d (3.4)	2.69 d (3.2)	2.49 t (2.9)
8	2.61 ddd (16.1, 7.0, 3.3)	2.49−2.60 m	4.45 m		2.57 ddd (16.3, 7.3, 3.4)
	2.28 dd (16.4, 3.1)	2.23 dd (16.4, 2.9)		4.45 t (3.2)	2.35 dd (16.3, 2.9)
9	5.08 d (6.8)	5.04 d (6.8)	4.97 s	4.93 s	5.07 d (6.8)
12	1.21 d (7.6)	1.31 d (7.6)	1.23 d (7.6)	1.41 d (7.5)	1.01 d (7.5)
13	1.42 s	1.60 s	1.57 s	1.46 s	1.34 s
14	1.53 s	1.45 s	1.43 s	1.48 s	1.54 s
15	1.49 s	1.44 s	1.49 s	1.58 s	1.54 s
Ac	2.05 s	1.73 s	2.06 s	1.72 s	1.73 s
6-Bz					
2′/6′	8.06 d (7.5)	8.07 d (7.5)	8.06 d (7.5)	8.02 d (7.5)	8.06 dd (7.5, 2.5)
3′/5′	7.47 t (7.5)	7.45 t (7.5)	7.49 t (7.5)	7.42 t (7.5)	7.45 t (7.5)
4′	7.58 t (7.5)	7.57 t (7.5)	7.59 t (7.5)	7.60 t (7.5)	7.57 t (7.5)
9-Bz					
2′/6′	8.09 d (7.5)	8.09 d (7.5)	8.08 d (7.5)	8.06 d (7.5)	8.04 dd (7.5, 2.5)
3′/5′	7.50 t (7.5)	7.49 t (7.5)	7.50 t (7.5)	7.50 t (7.5)	7.50 t (7.5)
4′	7.62 t (7.5)	7.61 t (7.5)	7.63 t (7.5)	7.63 t (7.5)	7.63 t (7.5)

[a]Assignments were performed by one-dimensional (1D) and two-dimensional (2D) [correlation spectroscopy (COSY), heteronuclear single-quantum coherence (HSQC), and heteronuclear multiple-bond correlation (HMBC)] NMR experiments.

temperature (each for 12 h). The extracts were combined and evaporated in vacuum. The resulting crude extract (9.52 g) was sequentially dispersed in water and extracted by petroleum ether (PE), EtOAc, and *n*-BuOH. The EtOAc extract (9.5 g) was dissolved in MeOH/tetrahydrofuran (THF) (50:50) and subjected to preparative HPLC on a column (50 × 250 mm, 10 μm) of 10 μm Agela Vennsil XBP C_{18}, at a flow rate of 100 mL/min and detection wavelength of 214/254 nm, using a CH_3CN−10 mM NH_4HCO_3 gradient as the eluant (0−15 min, 45−85% CH_3CN; 15−20 min, 95% CH_3CN; 20−24 min, 45% CH_3CN) to give six fractions (fractions 1−6). Fraction 4 eluting at 12.0−15.0 min was collected and further separated by Gilson-281 preparative HPLC on a Shimadzu C_{18} (21.2 × 250 mm, 15 μm) column, at a flow rate of 30 mL/min and detection wavelength of 214/254 nm, using a CH_3CN−0.1% HCO_2H−H_2O gradient as the eluant (0−20 min, 54−64% CH_3CN; 20−25 min, 95% CH_3CN) to afford six subfractions. Each subfraction was further purified repeatedly on a Gilson-215 preparative HPLC on an Agela Durashell C_{18} (21.2 × 50 mm, 5 μm) column, at a flow rate of 20 mL/min and detection wavelength of 214/254 nm, using a CH_3CN−10 mM NH_4HCO_3−H_2O gradient as the eluant (0−8 min, 65% CH_3CN; 8−11 min, 95% CH_3CN) to yield pure compounds **6** (3.8 mg), **3** (3.7 mg), **4** (110 mg), and **2** (10 mg). The PE extract (36.4 g) was chromatographed on Gilson-281 preparative HPLC on a Shimadzu C_{18} column (21.2 × 250 mm, 15 μm), eluting with a mixture of CH_3CN−0.1% FA−water gradient (0−16 min, 45−75% CH_3CN; 16−21 min, 95% CH_3CN; 21−25 min, 45% CH_3CN) to afford four fractions (CP-1−CP-4). CP-2 and CP-3 were further purified by the same chromatographic conditions to yield compounds **1** (29.6 mg), **5** (1.5 mg), and **7** (1.5 mg).

*Wightianine A (**1**).* Amorphous white powder; $[\alpha]_D^{28.6}$ +17.3 (*c* 0.33, MeOH); UV (MeOH) λ_{max} (log ε), 201 (4.62), 234 (4.20), 263 (4.37), 300 (3.72) nm; CD λ (MeOH) nm ($\Delta\varepsilon$), 220 (+4.65), 247 (+6.85), 236 (−2.14), 280 (−4.27); IR (KBr) ν, 3506, 1718, 1602, 1452, 1387, 1276, 1107, 1025 cm^{-1}; ^{1}H and ^{13}C NMR ($CDCl_3$), see Tables 1 and 2, respectively; HRMS (ESI) *m*/*z* calcd for $[C_{31}H_{36}O_8 + Na]^+$, 559.2302 $[M + Na]^+$; found, 559.2321.

*Wightianine B (**2**).* Amorphous white powder; $[\alpha]_D^{25.2}$ +42.4° (*c* 0.69, $CHCl_3$); UV (MeOH) λ_{max} (log ε), 204 (4.28), 232 (4.42), 275 (3.30), 282 (3.22) nm; IR (KBr) ν_{max}, 3448, 1718, 1276, 1108, 1027 cm^{-1}; ^{1}H and ^{13}C NMR ($CDCl_3$), see Tables 1 and 2, respectively; MS (ESI) *m*/*z*, 559.79 $[M + Na]^+$; HRMS (ESI) *m*/*z* calcd for $[C_{31}H_{36}O_8 + Na]^+$, 559.2302 $[M + Na]^+$; found, 559.2305.

*Wightianine C (**3**).* Amorphous white powder; UV (MeOH) λ_{max} (log ε), 212 (4.62), 232 (4.20), 263 (4.37), 289 (3.72) nm; IR (KBr) ν_{max}, 3438, 1725, 1108, 1021 cm^{-1}; ^{1}H and ^{13}C NMR ($CDCl_3$), see Tables 1 and 2, respectively; MS (ESI) *m*/*z*, 575.31 $[M + Na]^+$; HRMS (ESI) *m*/*z* calcd for $[C_{31}H_{36}O_9 + Na]^+$, 575.2252 $[M + Na]^+$; found, 575.2242.

*Wightianine D (**4**).* Amorphous white powder; $[\alpha]_D^{15.4}$ +0.86 (*c* 0.21, acetone); UV (MeOH) λ_{max} (log ε), 210 (4.62), 234 (4.21), 266 (4.37); CD λ (MeOH) ($\Delta\varepsilon$), 249 (+12.0), 291 (−29.7); IR (KBr) ν, 3471, 1753, 1725, 1601, 1452, 1370, 1315, 1272, 1231, 1178, 1107 cm^{-1}; ^{1}H and ^{13}C NMR ($CDCl_3$), see Tables 1 and 2, respectively; HRMS (ESI) *m*/*z* calcd for $[C_{31}H_{34}O_9 + Na]^+$, 573.2095 $[M + Na]^+$; found, 573.2115.

*Wightianine E (**5**).* Amorphous white powder; IR (KBr) ν_{max}, 3435, 1744, 1718, 1109 cm^{-1}; ^{1}H and ^{13}C NMR ($CDCl_3$), see Tables 1 and 2, respectively; MS (ESI) *m*/*z*, 557.82 $[M + Na]^+$; HRMS (ESI) *m*/*z* calcd for $[C_{31}H_{34}O_8 + Na]^+$, 557.2146 $[M + Na]^+$; found, 557.2154.

*Compound **6**.* Amorphous white powder; ^{1}H and ^{13}C NMR were in agreement with published values;[8] MS (ESI) *m*/*z*, 649.2 $[M + H]^+$; HRMS (ESI) *m*/*z* calcd for $[C_{32}H_{40}O_{14} + Na]^+$, 671.2211 $[M + Na]^+$; found, 671.2215.

*Compound **7** (Ejap-4).* Amorphous white powder; ^{1}H and ^{13}C NMR were in agreement with published values;[9] MS (ESI) *m*/*z*, 633.3 $[M + H]^+$; HRMS (ESI) *m*/*z* calcd for $[C_{32}H_{41}O_{13} + H]^+$, 633.3119 $[M + H]^+$; found, 633.3114.

Computation. Merck molecular force field (MMFF) and density functional theory (DFT) calculations were run with Spartan'10 (Wave Function, Inc., Irvine, CA), with standard parameters and convergence criteria. Time-dependent density functional theory (TDDFT) calculations were run with Gaussian'09,[10] with default grids and convergence criteria. Conformational searches were run with the

Table 2. ^{13}C NMR Spectroscopic Data (100 MHz, $CDCl_3$) of Compounds 1−5[a]

	1	2	3	4	5
position	δ_C	δ_C	δ_C	δ_C	δ_C
1	68.9, CH	74.1, CH	68.8, CH	77.6, CH	77.5, CH
2	73.8, CH	69.1, CH	73.8, CH	204.5, C	204.9, C
3	31.2, CH_2	32.7, CH_2	31.3, CH_2	44.0, CH_2	43.9, CH_2
4	34.1, CH	34.3, CH	33.9, CH	38.8, CH	38.9, CH
5	90.0, C	90.3, C	90.7, C	89.8, C	89.0, C
6	80.2, CH	80.0, CH	76.3, CH	76.0, CH	80.0, CH
7	49.1, CH	49.0, CH	55.7, CH	55.7, CH	49.0, CH
8	31.6, CH_2	31.8, CH_2	74.8, CH_2	74.7, CH_2	32.5, CH_2
9	73.3, CH	73.5, CH	80.4, CH	80.6, CH	73.3, CH
10	51.5, C	50.1, C	50.7, C	54.7, C	55.9, C
11	82.8, C	82.7, C	81.7, C	82.6, C	83.7, C
12	18.8, CH_3	19.2, CH_3	18.7, CH_3	18.1, CH_3	18.2, CH_3
13	19.2, CH_3	21.4, CH_3	19.5, CH_3	20.7, CH_3	20.0, CH_3
14	26.1, CH_3	26.1, CH_3	25.7, CH_3	25.6, CH_3	26.0, CH_3
15	30.9, CH_3	30.6, CH_3	31.3, CH_3	31.2, CH_3	30.7, CH_3
Ac					
CO	171.5, C	169.8, C	171.5, C	169.4, C	169.4, C
CH_3	21.4, CH_3	20.7, CH_3	21.5, CH_3	20.0, CH_3	20.0, CH_3
6-Bz					
CO	165.6, C	165.7, C	165.7, C	165.4, C	165.6, C
1′	129.7, C	130.1, C	130.0, C	129.7, C	129.6, C
2′/6′	129.6, CH	129.7, CH	129.7, CH	129.6, CH	129.5, CH
3′/5′	128.5, CH	128.6, CH	128.7, CH	128.8, CH	128.5, CH
4′	133.4, CH	133.3, CH	133.3, CH	133.6, CH	133.5, CH
9-Bz					
CO	165.7, C	165.7, C	165.7, C	165.4, C	165.7, C
1′	128.7, C	130.1, C	130.0, C	128.7, C	129.2, C
2′/6′	129.6, CH	129.7, CH	129.7, CH	129.9, CH	129.8, CH
3′/5′	128.7, CH	128.6, CH	128.7, CH	128.6, CH	128.8, CH
4′	133.3, CH	133.3, CH	133.3, CH	133.8, CH	133.6, CH

[a]Assignments were made by a combination of 1D and 2D (COSY, HSQC, and HMBC) NMR experiments.

Monte Carlo algorithm implemented in Spartan'10 using MMFF. All structures thus obtained were optimized with the DFT method using B3LYP functional and 6-31G(d) basis set.[10] The most stable B3LYP/6-31G(d) structures within 2 kcal/mol were re-optimized using B3LYP functional and 6-311+G(d,p) basis set.[10]

Preliminary TDDFT calculations were run using B3LYP and CAM-B3LYP functionals and Ahlrichs' SVP and TZVP basis sets.[11] The B3LYP/SVP combination was then employed for the final calculations, including 60 excited states (roots). CD spectra were generated using SpecDis[12] by applying a Gaussian band shape with 0.3 eV exponential half-width, from dipole-length rotational strengths. The difference with dipole velocity values was checked to be minimal for all relevant transitions.

Antifungal Bioassay. The test phytopathogenic fungi used in this study were *Fusarium solani*, *Fusarium oxysporum* f. sp. *vasinfectum*, *Cytospora* sp., and *Fusarium graminearum*. All of the fungi were isolated from infected plant organs at the Northwest A&F University.

Antifungal activity was examined by the microbroth dilution method in 96-well culture plates using a potato dextrose (PD) medium.[13,14] The test compounds was made up to 2 mg/mL in dimethyl sulfoxide (DMSO). Two commercial fungicides, carbendazim and hymexazol (Aladdin Chemistry Co., Ltd.), were used as a positive control, and the solution of equal concentration of DMSO was used as a negative control. The tested fungi were incubated in the PD medium for 18 h at 28 ± 0.5 °C at 150 rpm, and the spores of different microorganism concentrations were diluted to approximately 1×10^6 colony forming units (CFU)/mL with PD medium. Test compounds (10 μL) were added to 96-well microplates, and 90 μL of PD medium was added. Serial dilutions were made in the 96-well round-bottom sterile plates in triplicate in 50 μL of PD medium, and then 50 μL of the fungal suspension was added. After incubation for 48 h at 28 ± 0.5 °C, minimum inhibitory concentration (MIC) was taken as the lowest concentration of the test compounds in the wells of the 96-well plate, in which no microbial growth could be observed.

Insecticidal Assay. An insecticidal assay was performed by the method previously reported,[15] in which *Mythimna separata* was used as the test target. All samples for the insecticidal test were dissolved in acetone.

RESULTS AND DISCUSSION

Structural Elucidation. A 95% ethanolic extract of the dried whole plant of *P. wightiana* was successively partitioned between PE, EtOAc, *n*-BuOH, and water. The PE- and EtOAc-soluble extracts were separated and purified repeatedly by preparative reversed-phase HPLC to afford five new sesquiterpene compounds, wightianines A−E (**1**−**5**), along with two known compounds (**6** and **7**) (Scheme 1). Structural elucidation of the compounds was achieved by spectroscopic analysis and comparison to closely related compounds.

Compound **1** was obtained as an amorphous white powder with the molecular formula $C_{31}H_{36}O_8$, which was deduced from the HR-ESI−MS molecular ion at m/z 559.2321 ($[M + Na]^+$, calcd 559.2302). The IR spectrum shows the presence of hydroxyl (3506 cm^{-1}) and carbonyl (1718 cm^{-1}) groups, and the UV spectrum reveals the presence of an aromatic moiety (234 and 263 nm). The ^1H and ^{13}C NMR spectroscopic data of compound **1** (Tables 1 and 2) suggest that it belongs to a class

dx.doi.org/10.1021/jf501767s | J. Agric. Food Chem. 2014, 62, 6669−6676

Scheme 1. Structures of Compounds 1−7

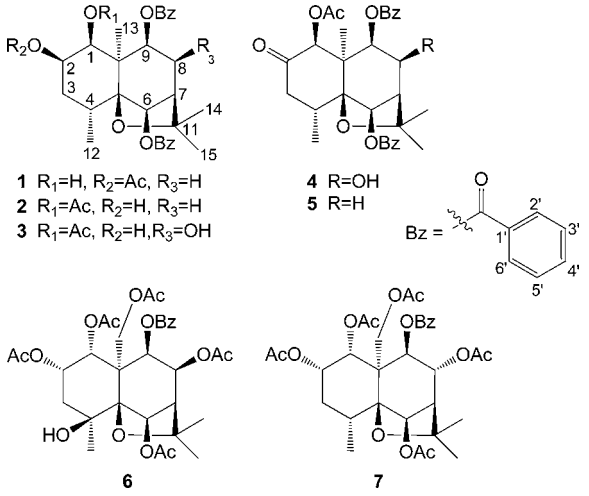

of sesquiterpene polyol esters with a dihydro-β-agarofuran skeleton found in the Celastraceae plants.[16,17] The ^{1}H NMR spectrum (Table 1) shows the presence of one acetyl group (δ_H 2.05), two benzoate groups between δ_H 7.47 and 8.09, four methyl groups, including three tertiary methyl groups (δ_H 1.49, 1.53, and 1.42) and a secondary methyl group [δ_H 1.21 (d, J = 7.6 Hz)], two sets of methylene protons [δ_H 2.39 (1H, m), 1.87 (1H, dd, J = 15.1 and 1.4 Hz); 2.61 (1H, ddd, J = 16.1, 7.0, and 3.3 Hz), 2.28 (1H, dd, J = 16.4 and 3.1 Hz)], and six methine protons (δ_H 5.66, 4.61, 5.08, 5.34, 2.61, and 2.39), including one bearing an acetoxy group at δ_H 5.34 (m, H-2). The ^{13}C NMR and distortionless enhancement by polarization transfer (DEPT) spectra (Table 2) in combination with HSQC data indicate that compound **1** has an agarofuran skeleton[16] with 15 carbons, including four methyl carbons at δ_C 18.8 ppm (C-12), 19.2 (C-13), 26.1 (C-14), and 30.9 (C-15), two methylene carbons at δ 31.2 (C-3) and 31.6 (C-8), six methine carbons at δ_C 68.9 (C-1), 73.8 (C-2), 34.1 (C-4), 80.2 (C-6), 49.1 (C-7), and 73.3 (C-9), and three quaternary carbons at δ_C 90.0 (C-5), 51.5 (C-10), and 82.8 (C-11). The ^{13}C NMR quaternary signals at δ 90.0 (C-5) and 82.8 (C-11) are characteristic of dihydro-β-agarofuran.[8] All of these data indicate that compound **1** is a polyester sesquiterpene with a 1,2,6,9-tetrasubstituted dihydro-β-agarofuran skeleton.

The substitution pattern of compound **1** was established by a HMBC experiment (Figure 1). Correlations were found of H-1 (δ_H 4.61) with C-2, C-10, and C-13, H-2 (δ_H 5.34) with the carbonyl signal (δ_C 171.5) of the acetate group, and H-6 (δ_H 5.66) and H-9 (δ_H 5.08) with the carbonyls (δ_C 165.6 and 165.7) of the two benzoate moieties, respectively. The relative stereochemistry was established on the basis of the coupling constants and confirmed by a nuclear Overhauser effect spectrometry (NOESY) experiment. In this class of dihydro-β-agarofuran sesquiterpenes, the stereochemistry of the ring junctions is generally *trans* and H-6 is axial,[18−20] which is corroborated by the NOESY cross-peaks observed between H-1 (δ_H 4.61) and H-13 (δ_H 1.42) and between H-13 and H-9 (Figure 2). Furthermore, in the COSY experiment, the vicinal coupling constant of H-1/H-2 ($J_{1,2}$ = 3.6 Hz) indicates a *cis* relationship between H-1 and H-2. This evidence proves that the relative configuration of the substituents is 1β, 2β, 6β, and 9β.

Because compounds **1**−**5** contain two benzoate moieties each, their absolute configuration could be in principle assigned

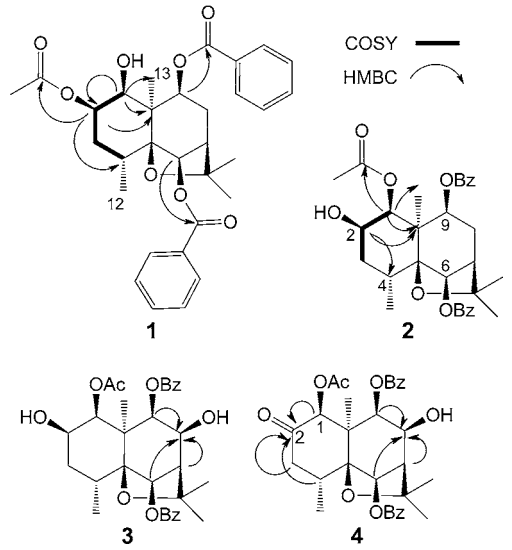

Figure 1. Key COSY and HMBC correlations of compounds **1**−**4**.

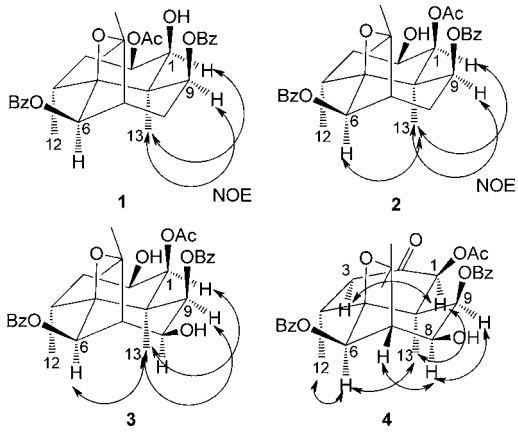

Figure 2. Key nuclear Overhauser effects (NOEs) of compounds **1**−**4**.

using the dibenzoate chirality method, the most common extension of the electronic CD exciton chirality protocol.[21] The exciton-coupled CD (ECCD) protocol is based on the sign of the bisignate CD bands (exciton couplet) observed in the major absorption region of the benzoates (π−π^* ^1L_a transition around 235 nm). The sign of the couplet is generally related to the absolute sense of twist between the electric transition dipole moments, which are oriented respectively along the long axes of the benzoate chromophores (C-1′/C-4′ direction). In compounds **1**−**5**, however, the dibenzoate 1,4-arrangement makes their π−π^* transition dipoles oriented almost parallel to each other. For exactly parallel arrangement, the predicted exciton coupling is zero. For slight deviations from the parallel, ECCD couplets are usually weak and difficult to predict.[21,22] Therefore, to assign the absolute configuration of compounds **1** and **4**, we preferred to apply quantum mechanic full CD calculations. This treatment, described in the next section, allowed us to establish compound **1** as (1*S*,2*R*,4*R*,5*S*,6*R*,7*R*,9*S*,10*S*)-2β-acetoxy-6β,9β-dibenzoyloxy-1β-hydroxydihydro-β-agarofuran and named wightianine A.

Compound **2** was also obtained as an amorphous white powder with the same molecular formula $C_{31}H_{36}O_8$ as compound **1**. The HR-ESI−MS molecular ion is at m/z 559.2305 [M + Na]$^+$ (calcd for $C_{31}H_{36}NaO_8$, 559.2302). Its IR

dx.doi.org/10.1021/jf501767s | J. Agric. Food Chem. 2014, 62, 6669−6676

spectrum shows absorption bands for hydroxyl (3448 cm^{-1}) and ester carbonyl (1718 cm^{-1}) groups, and the UV spectrum reveals the presence of an aromatic moiety (232 and 275 nm).

The ^1H NMR spectrum (Table 1) shows the presence of one acetyl group (δ_H 1.73), two benzoate groups between δ_H 7.45 and 8.09, four methyl groups, including three tertiary methyl groups (δ_H 1.44, 1.45, and 1.60) and a secondary methyl group [δ_H 1.31 (d, J = 7.6 Hz)], two sets of methylene protons [δ_H 2.40−2.44 (1H, m), 1.90 (1H, m); 2.49−2.60 (1H, m), 2.23 (1H, dd, J = 16.4 and 2.9 Hz)], and six methine protons (δ_H 5.67, 5.57, 5.04, 4.47, 2.49−2.60, and 2.40−2.44), including one bearing an acetoxy group at δ_H 4.47 (m, H-2). The ^1H and ^{13}C NMR spectra of compound **2** (Tables 1 and 2) closely resemble those of compound **1**, suggesting that compound **2** should be an isomer of compound **1**. A comparison of the similar ^1H and ^{13}C NMR spectra of compounds **1** and **2** reveals the presence of an acetyl group at C-1 (δ_C 74.1) in compound **2** because of the shifts of the signals of the H-1 proton from δ_H 4.61 in compound **1** to δ_H 5.57 in compound **2**. Thus, it is concluded that compound **2** was a 1-acetyl-2-deacetyl derivative of compound **1**. This is further confirmed by the HMBC correlations of H-1 (δ_H 5.57) with C-10 (δ_C 50.1), C-13 (δ_C 21.4), and the carbonyl signal (δ_C 169.8) of the acetate group (Figure 1). Unambigous assignments of the ^1H and ^{13}C NMR data and the relative configuration are deduced from the COSY, HMBC, and NOESY experiments (Figures 1 and 2). Its absolute configuration can be assigned from the biosynthetic point of view. Therefore, compound **2** is identified as (1*S*,2*R*,4*R*,5*S*,6*R*,7*R*,9*S*,10*R*)-1*β*-acetoxy-6*β*,9*β*-dibenzoyloxy-2*β*-hydroxydihydro-*β*-agarofuran and named wightianine B.

Compound **3** was isolated as an amorphous white powder with the molecular formula $C_{31}H_{36}O_9$, as evidenced by the HR-ESI−MS molecular ion at m/z 575.2242 ($[M + Na]^+$, calcd 575.2252). The molecular formula indicates that compound **3** contains one more oxygen atom than compound **2**. The IR spectrum shows the presence of hydroxyl (3438 cm^{-1}) and carbonyl (1725 cm^{-1}) groups, while the NMR spectra show one acetyl group (δ_H 2.06, s; δ_C 171.5, s, and 21.5, q) and two benzoyl groups (δ_H 7.49−8.08; δ_C 165.7, s, and 128.7−133.3). Further comparison of the ^1H and ^{13}C NMR spectroscopic data of compound **3** (Tables 1 and 2) to those of compound **2** reveals that compound **3** contains one less methylene group and one more methine bearing a hydroxyl group. The position of the hydroxyl group was determined to be at C-8 (δ_C 74.8) by the evidence of downfield shifts of the carbon signals from δ_C 49.0 (C-7) and δ_C 73.5 (C-9) in compound **2** to δ_C 55.7 (C-7) and δ_C 80.4 (C-9) in compound **3**, respectively. This conclusion is further supported by the HMBC correlations of H-6, H-7, and H-9 with C-8 (Figure 1). Analysis of the coupling constants for H-1/H-2 ($J_{1/2}$ = 3.5 Hz) and H-7/H-8 ($J_{7/8}$ = 3.4 Hz) reveals their *cis* configuration. Therefore, the hydroxyl and ester groups are located on the β face, as confirmed by the NOESY correlations shown in Figure 2. The locations and relative configurations of the esters and hydroxyl groups in compound **3** were deduced from analysis of its COSY, HMBC, and NOESY spectra (Figures 1 and 2). Similarly, its absolute configuration was assigned from the biosynthetic point of view. Thus, compound **3** is identified as (1*S*,2*R*,4*R*,5*S*,6*R*,7*R*,8*S*,9*R*,10*S*)-2*β*-acetoxy-6*β*,9*β*-dibenzoyloxy-1*β*,8*β*-dihydroxydihydro-*β*-agarofuran and named wightianine C.

Compound **4** gives the molecular formula $C_{31}H_{34}O_9$ based on the HR-ESI−MS molecular ion at m/z 573.2115 $[M + Na]^+$ (calcd for $C_{31}H_{34}NaO_9$, 573.2095), indicating that compound **4** contains two less hydrogens than compound **3**. The IR spectrum shows the presence of hydroxyl (3471 cm^{-1}) and carbonyl (1753 and 1725 cm^{-1}) groups. The NMR spectra prove the presence of one acetyl group (δ_H 1.72, s; δ_C 169.4, s, and 20.0, q) and two benzoyl groups (δ_H 7.42−8.06; δ_C 165.4 and 128.6−133.8). Further comparison of the NMR data of compound **4** (Tables 1 and 2) to those of compound **3** reveals that they are very similar, except for the presence of one ketonic carbonyl at δ_C 204.5 (s, C-2) in compound **4**, instead of one hydroxyl methine [δ_C 73.8 (d, C-2); δ_H 4.57 (m)] in compound **3**. The position of the ketone group was determined to be at C-2, as evidenced by the downfield shifts of the carbon signals from δ_C 68.8 (C-1), 31.3 (C-3), and 33.9 (C-4) in compound **3** to δ_C 77.6 (C-1), 44.0 (C-3), and 38.8 (C-4) in compound **4**, respectively. This is further supported by the HMBC correlations of H-1, H-3, and H-4 with C-2 (δ_C 204.5) (Figure 1). The coupling constant ($J_{7,8}$ = 3.2 Hz) for H-7 and H-8 indicates their *cis* relationship. This suggests that the hydroxyl group at C-8 is β-orientated. The locations and relative configurations of the ester groups in compound **4** were further assigned from its COSY, HMBC, and NOESY spectra (Figures 1 and 2). In addition, the absolute configuration of compound **4** was determined by quantum mechanic CD calculations (see the next section). Therefore, compound **4** is identified as (1*S*,4*R*,5*S*,6*R*,7*R*,8*S*,9*R*,10*S*)-1*β*-acetoxy-6*β*,9*β*-dibenzoyloxy- 8*β*-hydroxy-2-oxo-dihydro-*β*-agarofuran and named wightianine D.

Compound **5** gives the molecular formula $C_{31}H_{34}O_8$, as evidenced by the HR-ESI−MS molecular ion at m/z 557.2154 ($[M + Na]^+$, calcd 557.2146). The molecular formula indicates that compound **5** contains one less oxygen than compound **4**. Further comparison of the NMR data of compound **5** (Tables 1 and 2) to those of compound **4** reveals that they are very similar, except for the presence of a methylene [δ_C 32.5 (t, C-8); δ_H 2.57 (ddd, J = 16.3, 7.3, and 3.4 Hz, H-8*α*), 2.35 (dd, J = 16.3 and 2.9 Hz, H-8*β*)] in compound **5**, instead of one hydroxyl methine [δ_C 74.7 (d, C-8); δ_H 4.45 (t, J = 3.2 Hz)] in compound **4**. The locations and relative configurations of the esters in compound **5** were assigned on the basis of its HMBC and NOESY spectra (Figures 1 and 2). From the prospective of biosynthesis, its absolute configuration can be proposed. Thus, the structure of compound **5** is elucidated as (1*S*,4*R*,5*S*,6*R*,7*R*,9*S*,10*R*)-1*β*-acetoxy-6*β*,9*β*-dibenzoyloxy-2-oxo-dihydro-*β*-agarofuran and named wightianine E.

When their physical and spectral data were compared to those reported in the literature, two known dihydro-*β*-agarofurans **6** and **7** were identified as 1*α*,2*α*,6*β*,8*β*,13-pentaacetoxy-9*β*-benzoyloxy-4*β*-hydroxy-*β*-dihydroagarofuran,[8] isolated from *Celastrus angulatus* and Ejap-4 from *Euonymus japonicus*,[9] respectively.

To date, 462 dihydro-*β*-agarofuran sesquiterpenes have been reported from the Celastraceae plants.[23] These metabolites have usually been described as the primary characteristic constituents of the family. Interestingly, 2-oxo-dihydro-*β*-agarofuran-type sesquiterpenes are very rare natural products, as examplied by triptogelin A-4, which had been described previously in *Tripterygium wilfordii* var. Regelii.[24] To our knowledge, the present study is the second report of the sesquiterpenoids of this class from the alternative family Saxifragaceae. Importantly, the sesquiterpenes with a dihydro-*β*-agarofuran scaffold as "privileged structures" have attracted considerable attention from synthetic chemists and pharmacol-

ogists because of their complex structures and biological activities, such as immunosuppressive,[25,26] cytotoxic,[17,18] anti-HIV,[25,27] antiherpetic,[28] reversing multi-drug-resistance (MDR) phenotype,[29,30] antitumor,[31,32] and insecticidal[8] activities.

Conformational Analysis and Absolute Configuration Assignment. Compounds **1** and **4** were selected as representatives of the two classes of wightianines (with 2-hydroxy/2-acetoxy and 2-oxo substituents, respectively) to assign their absolute configuration by quantum mechanic CD calculations.[33] First, the conformation of compounds **1** and **4** was studied by means of a well-established protocol based on a preliminary conformational analysis based on molecular mechanics, followed by geometry optimizations with DFT.[22] Starting from a structure of compounds **1** and **4** with arbitrary (1*S*,2*R*,4*R*,5*S*,6*R*,7*R*,9*S*,10*S*)-**1** and (1*S*,4*R*,5*S*,6*R*,7*R*,8*S*,9*R*,10*S*)-**4** configurations, respectively, the conformational analysis was run using a Monte Carlo algorithm and the MMFF. All MMFF minima within 10 kcal/mol were optimized with DFT at the B3LYP/6-31G(d) level. Finally, the relevant DFT minima (within 2 kcal/mol) were re-optimized at the B3LYP/6-311G+(d,p) level. For compound **1**, four low-energy conformers were obtained with relative internal energies within 2 kcal/mol; they differed in the conformation of 9-benzoate and 2-acetate groups (Figure 3). For compound **4**, only two low-energy

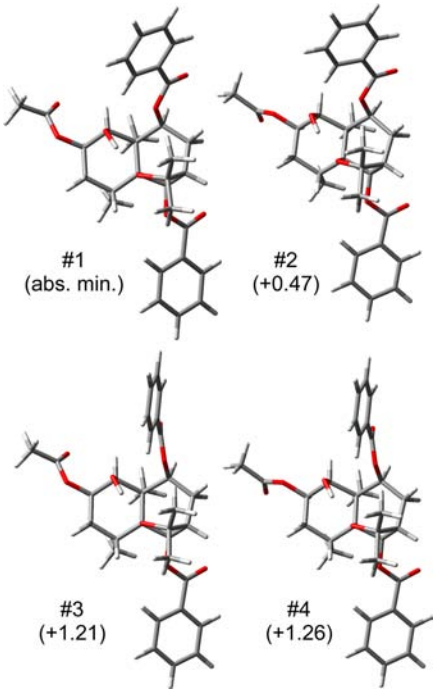

Figure 3. DFT-optimized [B3LYP/6-31G(d) level] low-energy structures for (+)-(1*S*,2*R*,4*R*,5*S*,6*R*,7*R*,9*S*,10*S*)-**1** and relative internal energies.

conformations were obtained, differing in the conformation of the 6-benzoate group (Figure 4). Both of them have the cyclohexanone ring in a twist conformation, probably to relieve the steric hindrance between 1β-acetate and 9β-benzoate groups, with the latter hydrogen-bonding to 8-OH. This conformation is confirmed by the strong NOE between H-1α and H-3α (see Figure 2).

The CD spectra of compounds (+)-**1** and (+)-**4** were recorded in methanol (Figures 5 and 6). They show several

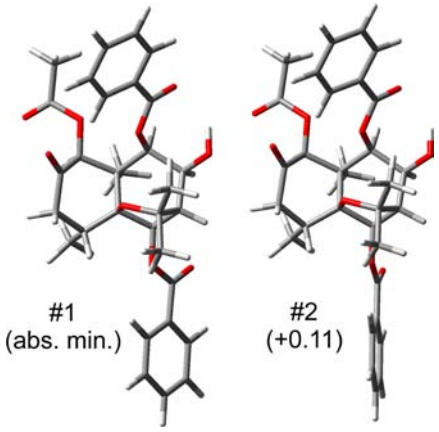

Figure 4. DFT-optimized [B3LYP/6-31G(d) level] low-energy structures for (+)-(1*S*,4*R*,5*S*,6*R*,7*R*,8*S*,9*R*,10*S*)-**4** and relative internal energies.

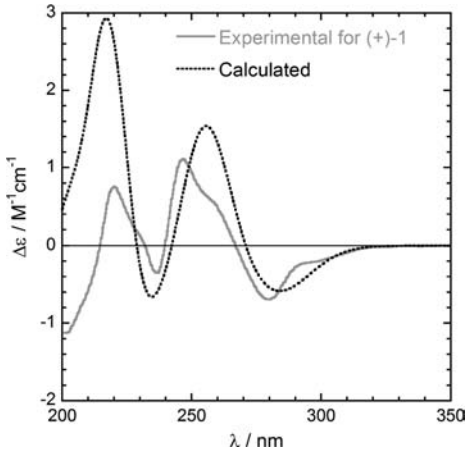

Figure 5. CD spectra of (+)-(1*S*,2*R*,4*R*,5*S*,6*R*,7*R*,9*S*,10*S*)-**1** recorded in methanol (1.9 mM, 0.1 cm cell, solid line) and calculated with TDDFT (B3LYP/SVP level, dotted line) as the Boltzmann average at 300 K for the four structures shown in Figure 3. The calculated spectrum was obtained as the sum of Gaussians with 0.3 eV bandwidth, and it is scaled and red-shifted by 30 nm for comparison.

bands between 200 and 350 nm, because of the benzoate and (for compound **4**) carbonyl chromophore. In both cases, the spectra are quite weak and there is no clear-cut exciton couplet with crossover (zero value) around 235 nm, where the benzoate $\pi-\pi^*$ ^1L_a transition occurs. This demonstrates that the ECCD protocol (see the previous section) cannot be applied directly.[21,22] Rather, we calculated the CD spectra of compounds **1** and **4** with TDDFT[33] using DFT-optimizing structures as input geometries and averaging the calculated spectra for the various low-energy conformations with the respective Boltzmann factors at 300 K (using internal energies). The calculated averages with B3LYP/SVP, shown in Figures 5 and 6, reproduce well the experimental CD profiles. Therefore, the absolute configurations of compounds **1** and **4** are established as (+)-(1*S*,2*R*,4*R*,5*S*,6*R*,7*R*,9*S*,10*S*)-**1** and (+)-(1*S*,4*R*,5*S*,6*R*,7*R*,8*S*,9*R*,10*S*)-**4**.

Biological Activity. Five compounds selected (because of a limited quantity of samples) were examined for their antifungal activity toward phytopathogenic fungi (*F. solani*, *F. oxysporum* f. sp. *vasinfectum*, *Cytospora* sp., and *F. graminearum*) *in vitro* using a mycelial growth inhibitory rate method.[13,14] As shown in

dx.doi.org/10.1021/jf501767s | J. Agric. Food Chem. 2014, 62, 6669−6676

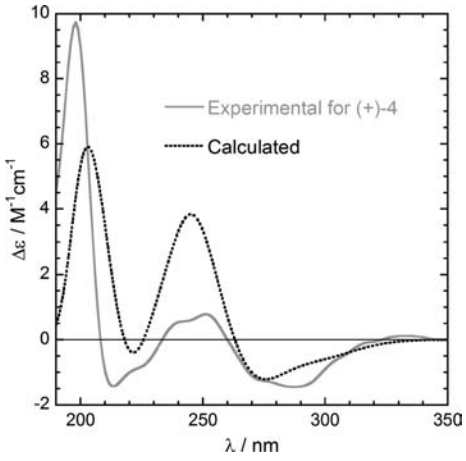

Figure 6. CD spectra of (+)-(1*S*,4*R*,5*S*,6*R*,7*R*,8*S*,9*R*,10*S*)-**4** recorded in methanol (1.5 mM, 0.02 cm cell, solid line) and calculated with TDDFT (B3LYP/SVP level, dotted line) as the Boltzmann average at 300 K for the two structures shown in Figure 4. The calculated spectrum was obtained as the sum of Gaussians with 0.3 eV bandwidth, and it is scaled and red-shifted by 20 nm for comparison.

Table 3, of these isolated compounds tested, only compounds **2** and **7** both inhibited mycelial growth of *Cytospora* sp. with minimum inhibitory concentration (MIC) values of 0.78 μg/mL, which are the same as the two positive controls hymexazol and carbendazim, demonstrating that these compounds were good fungicides. Additionally, compound **2** also showed marked antifungal effects on *F. graminearum* and *F. oxysporum* with their respective MIC data of 12.5 and 50 μg/mL. In contrast, the other compounds were almost inactive at 100 μg/mL of MIC data. A preliminary structure−antifungal activity relationship of these test compounds is given as follows. When a hydroxyl group attached to C-2 instead of an acetoxy group at C-2 of compound **1**, as seen in compound **2**, the antifungal activity against *F. graminearum* and *Cytospora* sp. was largely increased, as compared to that of compound **1**. However, conversion of OH at C-2 to a ketone group can lead to a loss of activity (compound **1** versus compound **4**). When theree is one H at C-4 instead of a tertiary OH at C-4 of compound **6**, as seen in compound **7**, the activity against *Cytospora* sp. was highly increased, as compared to that of compound **6**. From this evidence (Table 3), it can be concluded that the presence of the number, nature, and position of substituent groups of these test compounds could influence antifungal activity to the phytopathogens tested in this study.

Insecticidal activity of compounds **1**−**7** was tested against the fourth instar larvae of *M. separata*. However, in the present study, none of these tested compounds was found to display insecticidal activity to *M. separata*.

In conclusion, seven sesquiterpene esters (**1**−**7**) were isolated from the whole plant of *P. wightiana*, and their structures were elucidated by spectroscopic analyses and electronic CD studies. Compounds **2** and **7** were both found to display high antifungal property against the plant pathogen *Cytospora* sp.

■ ASSOCIATED CONTENT

Ⓢ Supporting Information

1D and 2D NMR and HR-ESI−MS spectra of compounds **1**−**5** (Figures S1−S30). This material is available free of charge via the Internet at http://pubs.acs.org.

■ AUTHOR INFORMATION

Corresponding Author

*Telephone: +86-29-87092515. E-mail: jinminggao@nwsuaf.edu.cn.

Author Contributions

‖D.M.W. and C.C.Z. contributed equally to this work.

Funding

This work was financially supported by the Forestry Research Foundation for the Public Service Industry of China (200904004) and the Program for Youth Barebone Talents of Northwest A&F University (Z111020902).

Notes

The authors declare no competing financial interest.

■ REFERENCES

(1) Fu, L. Q.; Lang, K. Y. *Higher Flora of China*; Qingdao Publishing Group: Qingdao, China, 2003; Vol. *6*, pp 430−441.

(2) Bruce, A. B.; Donevan, L. S.; Bhat, U. G. Flavonoids of some species of *Bergenia*, *Francoa*, *Parnassia* and *Lepuropetalon*. *Biochem. Syst. Ecol.* **1986**, *14*, 75−77.

(3) Wen, X.-B.; Miao, F.; Zhou, L.; Zhang, M.; He, Q.-L. *In vitro* antioxidant activity of *Parnassia wightiana* W. extracts. *Chin. J. Nat. Med.* **2012**, *10*, 190−195.

(4) Tang, J.-J.; Zhang, F.-Y.; Wang, D.-M.; Tian, J.-M.; Dong, S.; Gao, J.-M. Semisynthesis and antifeedant activity of new derivatives of a dihydro-β-agarofuran from *Parnassia wightiana*. *Int. J. Mol. Sci.* **2013**, *14*, 19484−19493.

(5) Liu, H. W.; Yu, X. Z.; Padula, D.; Pescitelli, G.; Lin, Z. W.; Wang, F.; Ding, K.; Lei, M.; Gao, J. M. Lignans from *Schisandra sphenanthera* Rehd. et Wils. and semisynthetic schisantherin A analogues: Absolute configuration, and their estrogenic and anti-proliferative activity. *Eur. J. Med. Chem.* **2013**, *59*, 265−273.

(6) Wei, S.; Gao, J.; Wu, W.; Ji, Z.; Zhang, J. Simultaneous identification of multiple celangulins from the root bark of *Celastrus angulatus* using high-performance liquid chromatography−diode array detector−electrospray ionisation−tandem mass spectrometry. *Phytochem. Anal.* **2012**, *23*, 23−33.

Table 3. Antifungal Data of Some Compounds against Four Plant Pathogens *in Vitro*[a]

compound	*F. solani* CFCC86805	*F. oxysporum* ACCC30026	*F. graminearum* ACCC36249	*Cytospora* sp. ACCC30052
1	>100	100	>100	100
2	>100	50	12.5	0.78
4	>100	100	>100	100
6	>100	>100	>100	>100
7	>100	>100	>100	0.78
hymexazol	100	50	3.12	0.78
carbendazim	0.78	100	1.57	0.78

[a]Results are expressed as MIC values in μg/mL.

(7) Zhang, C. L.; Gao, J. M.; Zhu, W. Steroidal saponins from the rhizomes and roots of *Smilax scobinicaulis*. *Phytochem. Lett.* **2012**, *5*, 49−52.
(8) Wu, W.; Wang, M.; Zhu, J.; Zhou, W.; Hu, Z.; Ji, Z. Five new insecticidal sesquiterpenoids from *Celastrus angulatus*. *J. Nat. Prod.* **2001**, *64*, 364−367.
(9) Rozsa, Z.; Perjesi, A.; Pelczer, I.; Argay, G.; Kalman, A. New sesquiterpene esters and alkaloids from *Euonymus japonicus*: The 'Ejap' series. X-ray molecular structures of Ejap-2, -3, -4, -5, -6, and -10. *J. Chem. Soc., Perkin Trans. 1* **1989**, 1079−1087.
(10) Frisch, M. J.; Trucks, G. W.; Schlegel, H. B.; Scuseria, G. E.; Robb, M. A.; Cheeseman, J. R.; Scalmani, G.; Barone, V.; Mennucci, B.; et al. *Gaussian 09, Revision a.02*; Gaussian, Inc.: Wallingford, CT, 2009.
(11) All references about DFT functionals and basis sets can be found in the on-line documentation for Gaussian'09 at http://www.gaussian.com/g_tech/g_ur/g09help.htm.
(12) Bruhn, T.; Schaumlöffel, A.; Hemberger, Y.; Bringmann, G. SpecDis: Quantifying the comparison of calculated and experimental electronic circular dichroism spectra. *Chirality* **2013**, *25*, 243−249.
(13) Li, X. J.; Zhang, Q.; Zhang, A. L.; Gao, J. M. Metabolites from *Aspergillus fumigatus*, an endophytic fungus associated with *Melia azedarach*, and their antifungal, antifeedant, and toxic activities. *J. Agric. Food Chem.* **2012**, *60*, 3424−3431.
(14) Li, X. J.; Tang, H. Y.; Duan, J. L.; Gao, J. M.; Xue, Q. H. Bioactive alkaloids produced by *Pseudomonas brassicacearum* subsp. *neoaurantiaca*, an endophytic bacterium from *Salvia miltiorrhiza*. *Nat. Prod. Res.* **2013**, *27*, 496−499.
(15) Wei, S. P.; Ji, Z. Q.; Zhang, H. X.; Zhang, J. W.; Wang, Y. H.; Wu, W. J. Isolation, biological evaluation and 3D-QSAR studies of insecticidal/narcotic sesquiterpene polyol esters. *J. Mol. Model.* **2011**, *17*, 681−693.
(16) Furukawa, M.; Makino, M.; Uchiyama, T.; Ishimi, K.; Ichinohe, Y.; Fujimoto, Y. Sesquiterpene pyridine alkaloids from *Hippocratea excelsa*. *Phytochemistry* **2002**, *59*, 767−777.
(17) Kuo, Y.-H.; Chen, C.-H.; King, M.-L.; Wu, T.-S.; Lee, K.-H. Sesquiterpene pyridine alkaloids from *Maytenus emarginata*: Emarginatine-C and -D and cytotoxic emarginatine-E and emarginatinine. *Phytochemistry* **1994**, *35*, 803−807.
(18) Chang, F. R.; Hayashi, K.; Chen, I. H.; Liaw, C. C.; Bastow, K. F.; Nakanishi, Y.; Nozaki, H.; Cragg, G. M.; Wu, Y. C.; Lee, K. H. Antitumor agents. 228. Five new agarofurans, reissantins A−E, and cytotoxic principles from *Reissantia buchananii*. *J. Nat. Prod.* **2003**, *66*, 1416−1420.
(19) Kim, S. E.; Kim, Y. H.; Lee, J. J. A new sesquiterpene ester from *Celastrus orbiculatus* reversing multidrug resistance in cancer cells. *J. Nat. Prod.* **1998**, *61*, 108−111.
(20) Kim, S. E.; Kim, H. S.; Hong, Y. S.; Kim, Y. C.; Lee, J. J. Sesquiterpene esters from *Celastrus orbiculatus* and their structure−activity relationship on the modulation of multidrug resistance. *J. Nat. Prod.* **1999**, *62*, 697−700.
(21) Harada, N.; Nakanishi, K. *Circular Dichroic Spectroscopy. Exciton Coupling in Organic Stereochemistry*; University Science Books: Mill Valley, CA, 1983.
(22) Pescitelli, G.; Di Bari, L.; Berova, N. Conformational aspects in the studies of organic compounds by electronic circular dichroism. *Chem. Soc. Rev.* **2011**, *40*, 4603−4625.
(23) Gao, J. M.; Wu, W. J.; Zhang, J. W.; Konishi, Y. The dihydro-β-agarofuran sesquiterpenoids. *Nat. Prod. Rep.* **2007**, *24*, 1153−1189.
(24) Takaishi, Y.; Noguchi, H.; Murakami, K.; Nakano, K.; Tomimatsu, T. Sesquiterpene esters, triptogelin A-1−A-4, from *Tripterygium wilfordii* var. regelii. *Phytochemistry* **1990**, *29*, 3869−3873.
(25) Duan, H.; Takaishi, Y.; Bando, M.; Kido, M.; Imakura, Y.; KuoHsiung Lee, K. H. Novel sesquiterpene esters with alkaloid and monoterpene and related compounds from *Tripterygium hypoglaucum*: A new class of potent anti-HIV agents. *Tetrahedron Lett.* **1999**, *40*, 2969−2972.
(26) Zhang, Y. L.; Xu, Y.; Lin, J. F. Immunosuppresive effects of wifortrine and euonine. Immunosuppresive effects of wifortrine and euonine. *Acta Pharm. Sin.* **1989**, *24*, 568−572.
(27) González, A. G.; Andrés, L. S.; Ravelo, A. G.; Luis, J. G.; Jiménez, I. A.; Domínguez, X. A. Minor constituents from *Orthosphenia mexicana*. *J. Nat. Prod.* **1989**, *52*, 1338−1341.
(28) Luo, Y.; Zhou, M.; Ye, Q.; Pu, Q.; Zhang, G. Dihydroagarofuran derivatives from the dried roots of *Tripterygium wilfordii*. *J. Nat. Prod.* **2012**, *75*, 98−102.
(29) Cortes-Selva, F.; Jimenez, I. A.; Munoz-Martinez, F.; Campillo, M.; Bazzocchi, I. L.; Pardo, L.; Ravelo, A. G.; Castanys, S.; Gamarro, F. Dihydro-β-agarofuran sesquiterpenes: A new class of reversal agents of the multidrug resistance phenotype mediated by P-glycoprotein in the protozoan parasite *Leishmania*. *Curr. Pharm. Des.* **2005**, *11*, 3125−3139.
(30) Perestelo, N. R.; Sánchez-Cañete, M. P.; Gamarro, F.; Jiménez, I. A.; Castanys, S.; Bazzocchi, I. L. Overcoming human P-glycoprotein-dependent multidrug resistance with novel dihydro-β-agarofuran sesquiterpenes. *Eur. J. Med. Chem.* **2011**, *46*, 4915−4923.
(31) Takaishi, Y.; Ohshima, S.; Nakano, K.; Tomimatsu, T.; Tokuda, H.; Nishino, H.; Iwashima, A. Structures of sesquiterpene polyol esters from *Celastrus stephanotiifolius* with potential tumor promotion inhibitory activity. *J. Nat. Prod.* **1993**, *56*, 815−824.
(32) Ujita, K.; Takaishi, Y.; Tokuda, H.; Nishino, H.; Iwashima, A.; Fujita, T. Inhibitory effects of triptogelin A-1 on 12-*O*-tetradecanoylphorbol-13-acetate-induced skin tumor promotion. *Cancer Lett.* **1993**, *68*, 129−133.
(33) Autschbach, J.; Nitsch-Velasquez, L.; Rudolph, M. Time-dependent density functional response theory for electronic chiroptical properties of chiral molecules. *Top. Curr. Chem.* **2011**, *298*, 1−98.

Maranhao, and Minas Gerais have demonstrated both acceptable yields and consumer acceptance of the biofortified varieties.[17−19] These preliminary results have provided the impetus to continue breeding for further enrichment of βC content in cassava. Comparative studies on the impact of genotype and traditional style of cooking on retention of the provitamin A carotenoid and its bioaccessibility are needed.

Brazilians include cassava in many different food recipes. Boiled and fried cassava, as well as cassava flour, are the most common sources of this staple food. Previous studies have shown the preparation of cassava flour can markedly decrease the content of βC.[20] Research regarding the bioaccessibility of βC from different varieties of biofortified cassava grown in Brazil has been limited. Insights regarding the interactions among carotenoid content, home cooking styles, and the bioaccessibility of βC are needed to help direct the efforts of breeders, food scientists, and nutrition educators to strategically develop and implement programs aimed at increasing the vitamin A status of populations at risk of suboptimal vitamin A nutrition.

The primary objective of the present study was to investigate the effects of genotype and styles of traditional Brazilian preparation on the content, retention, and bioaccessibility of provitamin A in biofortified cassava developed and grown in Brazil.

MATERIALS AND METHODS

Reagents. Chromatographic grade solvents, fetal bovine serum (FBS), fungizone, penicillin−streptomycin, L-glutamine, and nonessential amino acids were purchased from Life Technologies Corp. (Grand Island, NY, USA). Dulbecco's modified minimum essential medium (DMEM) with 25 mmol/L glucose, Hepes buffer, bile extract, and bile extract and digestive enzymes were purchased from Sigma-Aldrich (St. Louis, MO, USA). All other reagents and supplies were purchased from ThermoFisher Scientific (Pittsburgh, PA, USA) unless otherwise indicated.

Varieties of Cassava. Cassava roots from two lineages were provided by the Biofortication program of the Brazilian Research Agriculture Corporation (Embrapa) and by the Nutritional Breeding program from the Agronomic Institute of Campinas (IAC) (Table 1). All varieties are considered "sweet" cassava because they have low cyanide content (<100 ppm) and are advantageous for small-scale production and domestic consumption. The six varieties provided by Embrapa were grown in the northeastern (NE) region at Cruz das Almas, Bahia, Brazil, and the roots were harvested at 14 months, that is, prior to senescence. One variety of white cassava was included as a control as it is commonly grown in NE Brazil. Three varieties from IAC were grown in the southeastern (SE) region at Santa Maria da Serra, São Paulo, Brazil, and harvested at 9 months, which is optimal for these lineages. Cassava roots were harvested in March 2013. Three separate plants from each of the nine varieties were randomly harvested. Roots were cleaned and immediately waxed for transport to Piracicaba, São Paulo, Brazil.

Table 1. Varieties of Cassava Investigated

variety	type	source
lineage 1[a]		
Saracura	control (Con)	Embrapa
Dourada	parental (PA)	Embrapa
Gema de Ovo	parental (PA)	Embrapa
Jari	progeny (PR)	Embrapa
clone 14-11	progeny (PR)	Embrapa
clone 03-15	progeny (PR)	Embrapa
lineage 2[b]		
576-70	parental (PA)	IAC
265-97	progeny (PR)	IAC
06-01	progeny (PR)	IAC

[a]Lineage 1. Saracura is a white cassava normally grown in NE Brazil. Dourada and Gema de Ovo were selected from a germplasm bank in 2001. Progeny were bred for high βC content and yield in 2003. [b]Lineage 2. Variety 576-70 was bred for acceptable agronomic and organoleptic characteristics in 1970. Varieties 265-97 and 06-01 were bred for high yield and increased βC content in 1997 and 2001, respectively.

Cooking of Cassava. Waxed roots were processed 24−48 h after harvest. Roots were washed, peeled, and cut in a room that excluded direct artificial or natural light to limit degradation of carotenoids. Initially, small cubes (3 cm^3) were used to determine average boiling times (see below). Afterward, roots from each plant were cut longitudinally into 10 cm fourths. Fourths from each root were either boiled or boiled and fried as described below. Raw and cooked cassava were stored at −80 °C in vacuum-sealed bags. Small cubes (3 cm^3) initially were used to determine average boiling times due to differences in moisture content and food matrix (see below). Three replicate samples of each were processed independently as follows.

Boiled Cassava. Twelve cubes (3 cm^3) of each variety were immersed in 7 L of distilled water and boiled at 100 °C. A stainless steel Mattson apparatus with 12 pins calibrated with 90 g weight was used according to the method of Oliveira et al.[21] to determine appropriate boiling time for each variety to standardize tenderness as generally done when cassava is cooked at home. Mean boiling time was defined as that required for penetration of 7 of the 12 pins into the cubes. Determined boiling times for each variety are listed in Table 2. Root fourths of 10 cm lengths from each genotype were then boiled in 7 L of water to determine carotenoid retention and for simulated digestion.

Fried Cassava. Two boiled fourths of 10 cm length from opposite sides of the root were randomly selected and placed in a stainless steel basket. The basket was immersed in soybean oil at 180 °C for 5 min in an electric deep fryer (Tedesco, FE-101). Samples remained suspended in the basket at room temperature until excess oil was drained.

Raw, boiled, and fried cassava were wrapped in aluminum foil to avoid exposure to light and packed under vacuum using nylon−polyethylene bags with low permeability to oxygen. Packages were frozen at −80 °C and shipped to The Ohio State University in Styrofoam containers with gelled ice. Samples arrived frozen and were immediately placed in a −80 °C freezer. Samples were stored frozen for a maximum of 4 months and thawed in a cold room overnight without light before homogenization in a food processor (Cuisinart Smart Stick Hand Blender) for analysis and further testing.

Moisture and Fat Contents. Moisture was determined according to an AOAC method.[22] Samples of each variety were weighed and maintained overnight at 65 °C with circulating air to constant weight. Lipids from raw and boiled cassava were first extracted into petroleum ether from three varieties. Results were similar to previous literature, that is, ≤0.3%.[23] Consequently, lipids were extracted only from fried samples for all varieties according to the method of Folch et al.[24] Samples of fried cassava (1.5 g) were homogenized with 3 mL of phosphate buffer saline (PBS) using a Polytron homogenizer, mixed with 4 mL of methanol, and vortexed for 2 min. After the addition of chloroform (8 mL), the mixture was vortexed for 2 min, centrifuged at 1000*g* for 15 min at 4 °C, and left overnight in a dark cold room. The lower phase was collected in weighed glass tubes, solvent was evaporated, and the difference in weight of the tube before use and after evaporation of solvent represented lipid content.

In Vitro Digestion. Oral, gastric, and small intestinal phases of simulated digestion were performed as described by Thakkar et al.[25] with slight modification. The quantity of fried cassava digested was 0.3−1.5 g, so that there was <0.075 g of adsorbed oil per reaction to ensure complete digestion of triglyceride. Because the bioaccessibility of hydrocarbon carotenoids requires the presence of lipid digestion products as well as bile salts,[26] soybean oil (2.5 wt %/wt) was added to boiled cassava (2.0−2.5 g per reaction) before digestion. As the concentration of βC in soybean oil was 1.1 μg/mL, it contributed

Table 2. Mean Boiling Time and Moisture, Lipid, and βC Contents of Nine Varieties of Raw and Cooked Cassava[a]

variety[b]	boiling time[c] (min)	moisture (% FW)			lipids (% FW)		total βC (μg/g FW)		
		raw	boiled	fried	fried	raw	boiled	fried
lineage 1								
Saracura (Con)	38.3	66.7 ± 4.4bcA	68.5 ± 3.0dA	55.5 ± 5.0bcB	4.8 ± 0.49d	0.45 ± 0.06fA	0.41 ± 0.11fA	0.34 ± 0.03eA
Dourada (PA)	41.3	69.4 ± 2.8bA	70.6 ± 2.0cdA	60.8 ± 2.6bB	2.6 ± 0.17f	2.4 ± 0.16eA	2.4 ± 0.26eA	2.2 ± 0.36dA
Gema de Ovo (PA)	35.2	65.9 ± 3.3bcA	64.2 ± 2.3dA	57.1 ± 1.5bB	2.0 ± 0.01g	4.0 ± 0.26dA	2.9 ± 0.44deB	3.1 ± 0.21dAB
clone 14-11 (PR)	25.4	79.3 ± 3.9aA	77.6 ± 1.5bcAB	72.3 ± 2.3aB	3.2 ± 0.08e	5.3 ± 0.34dA	4.0 ± 0.43cdB	5.0 ± 0.33cAB
Jari (PR)	33.5	83.0 ± 1.2aA	86.9 ± 2.5aA	76.2 ± 3.2aB	2.1 ± 0.14g	8.1 ± 0.47bcB	6.4 ± 0.48abC	9.1 ± 0.49aA
clone 03-15 (PR)	22.6	79.7 ± 0.7aAB	80.2 ± 2.1abA	74.3 ± 3.2aB	2.1 ± 0.04g	10.3 ± 1.69aA	7.2 ± 1.14aB	7.8 ± 0.56bB
lineage 2								
576-70 (PA)	16.4	60.2 ± 2.1cB	67.0 ± 0.3dA	48.1 ± 2.9cdC	8.4 ± 0.25b	2.6 ± 0.32eA	2.0 ± 0.20eA	2.5 ± 0.56dA
265-97 (PR)	12.4	63.3 ± 2.0bcA	65.0 ± 0.6dA	44.6 ± 5.6dB	6.7 ± 0.13c	7.3 ± 0.55cA	5.3 ± 0.48bcB	5.2 ± 1.32cB
06-01 (PR)	28.1	63.3 ± 2.1bcB	71.3 ± 3.4cdA	45.1 ± 1.7dC	13.7 ± 0.37a	8.7 ± 0.23bA	7.1 ± 1.34aB	5.9 ± 1.77cC

[a]Data for moisture and lipids are means ± SD, $n = 3$. Different lower case letters within columns for moisture, lipids, and total βC indicate that means for varieties differ significantly ($p < 0.05$). Different upper case letters within rows for moisture and total βC indicate that means for raw, boiled, and fried samples differ significantly ($p < 0.05$). [b]From Table 1: Con, control variety; PA, parental variety; PR, progeny (biofortified) variety. [c]Average boiling time was determined as time until 7 of 12 pins (90 g each) penetrated root sections.

55 ng of the carotenoid per digestion of boiled cassava. Assuming the concentration of βC in oil used for frying was similar, the amount of βC in adsorbed oil ranged from 2.0 to 13.7% of the wet weight (see Table 2) and was not accounted for in the presented results. Briefly, each cooked sample was digested in triplicate, and digestions were repeated at least once for a total of $n \geq 6$. Samples were homogenized with basal salts solution (120 mol/L NaCl, 6 mmol/L $CaCl_2$, and 5 mmol/L KCl) using a Polytron homogenizer. The same basal salts solution was used to properly adjust the volumes in each step. Synthetic saliva (6 mL) containing 106.6 units/mL α-amylase was added to cassava samples to initiate oral digestion in a shaking (85 rpm) water bath at 37 °C for 10 min. Samples were subsequently subjected to simulated gastric and small intestinal digestion with shaking (85 rpm) at 37 °C using the enzyme activities and bile extract content previously used in our laboratory for the coupled in vitro digestion/Caco-2 cell model.[27] These are (final concentrations) 1.7 units porcine pepsin/mL, 0.4 mg/mL porcine pancreatin, 8.3 units porcine pancreatic lipase/mL, and 2.4 mg bile extract/mL. After conclusion of the small intestinal phase of digestion, chyme was centrifuged at 5000*g* for 45 min at 4 °C to separate the aqueous fraction and nondigested materials. A portion of the aqueous fraction was collected and filtered (0.22 μm pores) to prepare the micelle fraction. Aliquots of chyme and micelle fraction were stored under nitrogen gas at −80 °C for a maximum of 1 week before extraction and analysis. Carotene contents of digested cassava (i.e., chyme) and the filtered aqueous fraction (i.e., mixed micelle fraction) are indicative of the stability of carotenoids in cooked cassava during digestion and the efficiency of micellarization (EM) during the small intestinal phase of digestion, respectively. Standard procedures were taken to minimize exposure to light and air during each stage of digestion.

Uptake of *all-trans*-βC by Caco-2 Cells. Human intestinal colonic carcinoma Caco-2 cells were purchased from American Type Culture Collection (ATCCHTB37). Details for the maintenance of the cultures have been described previously.[27] Briefly, T75 flasks were seeded with (0.4−0.6) × 10^6 cells and maintained in high-glucose DMEM supplemented with 4 mmol/L L-glutamine, 1% nonessential amino acids, 15 mmol/L HEPES buffer, antibiotics, and 15% (v/v) heat-inactivated FBS, pH 7.4, until the monolayer was confluent. FBS content of medium was reduced to 7.5% for postconfluent cultures, and fresh medium was added every 2 days. Cultures were incubated in a humidified atmosphere of 95% air/5% CO_2 at 37 °C. Monolayers from passages 22−31 were used for experiments when cultures were 10−14 days postconfluent, that is, once well differentiated. Cellular uptake of βC in micelles generated during digestion of boiled and fried cassava was performed for four varieties containing the highest concentrations of βC. Analysis was limited to *all-trans*-βC because accurate quantification of the relatively low amounts of *cis* isomers of βC in the cells was not possible. To initiate experiments, monolayers were washed once with basal DMEM before addition of 12.5 mL of DMEM (pH 6.5) containing 25% (v/v) mixed micelle fraction generated during the simulated digestion. The integrity of the monolayer was assessed by phase contrast microscopy after 0, 1, 2, and 4 h. No changes in gross morphology of the monolayer or cells were noted for any treatment. Test medium was removed after 4 h, and monolayers were washed once with ice-cold PBS containing 2 g/L bovine serum albumin and twice with ice-cold PBS to remove extracellular carotenoids. Ice-cold PBS (6 mL) was added to flasks, and cells were collected using a plastic scraper. The cell suspension was centrifuged at 400*g* for 5 min at 4 °C. Supernatant was discarded, and cell pellets were stored under nitrogen gas at −20 °C for a maximum of 1 week before extraction and analysis of carotenoids. Protein content per flask was determined by bicinchoninic acid assay (BCA) analyses with bovine serum albumin as standard. Average protein content per flask was 12.1 ± 0.8 mg/T75 flask.

Carotenoid Extraction and Analysis. Carotenoids were extracted according to the method of Kimura et al.[28] with slight modifications. Homogenized samples (3 g) of raw, boiled, and fried cassava were extracted to determine the profile and quantity of carotenoids. Samples were ground with cold acetone (50 mL) and Celite (~3 g) using a mortar and pestle. Extraction was repeated until the residue

dx.doi.org/10.1021/jf5018302 | J. Agric. Food Chem. 2014, 62, 6677−6686

was colorless. Combined extracts were mixed with petroleum ether in a separatory funnel, and the petroleum ether fraction was collected and filtered with aliquots transferred to vials for evaporation of the solvent. Thawed cell pellets were suspended in 5 mL of PBS and sonicated (5 s with tube in ice bath) to determine cell accumulation of carotenoids. Carotenoids in chyme and micelle fraction (aliquots of 5−7 mL) and cell pellets suspended in 5 mL of PBS were extracted into 10 mL of tetrahydrofuran/methanol (1:1, v/v) before the addition of 10 mL of hexane and mixing. Tubes were centrifuged at 3000*g* for 10 min at 4 °C. The upper layer was collected, and solvent was evaporated under a stream of nitrogen gas at 30−35 °C. Dried extracts were solubilized in appropriate volumes of methanol and MTBE (1:1, v/v), filtered (0.22 μm pores; Millipore), and analyzed. β-Apo-8′-carotenal (10 μg/mL in methanol) was used as internal standard to estimate the efficiency of recovery of carotenoids during extraction. Recoveries of β-apo-8′-carotenal when added to homogenates containing raw, boiled, and fried cassava were 97.5 ± 7, 96.9 ± 9, and 94.5 ± 10%, respectively. Recoveries of internal standard from chyme and aqueous fractions after digestions were 99.7 ± 3 and 95.7 ± 3%, respectively, for boiled cassava and 97.8 ± 4 and 90.9 ± 12%, respectively, for samples from fried cassava. β-Apo-8′-carotenal recoveries from sonicated samples of Caco-2 cells were 93.4 ± 6 and 91.9 ± 7% for experiments initiated with boiled cassava and fried cassava, respectively.

The HPLC system consisted of a Waters 2695 separation system with a 2996 photodiode array detector. An analytical polymeric YMC C_{30} column (4.6 mm × 150 mm, 5 μm; Waters, Milford, MA, USA) was protected by a C_{18} guard (4.6 mm × 50 mm) column containing the same material.[27] *all-trans* and *cis* isomers of βC were identified by comparison of retention times and spectra with pure standard for the former (>98% purity) and characteristics from the literature for the latter. βC was monitored at 450 nm. The area under the curve for *all-trans*-βC was compared to that for a six-point standard curve generated with pure βC and the concentration calculated using the absorption coefficient ($A^{1\%,\ 1cm}$) of 2592 for *all-trans*-βC.[29] *Cis* isomers of βC were identified by their UV−vis spectrum[29] and retention times as reported in the literature. The amounts of *cis* isomers of βC were estimated using area under the curve against the standard curve and absorption coefficient of *all-trans*-βC.

Data Analysis. Data were analyzed for significant differences using ANOVA for effects of genotype, cooking style, and interactions between genotype and cooking styles. The interactions analysis had a factorial model of 9 varieties × 3 cooking styles and were considered significant at 1% ($p < 0.01$). Means were compared using the Tukey test and significant at 5% ($p < 0.05$). Pearson's test of correlation was used and significant differences defined at 1% ($p < 0.01$). Software used for the ANOVA and Tukey tests was the Statistical Analysis System (SAS Inc., Cary, NC, USA), and correlation tests were performed using Statistical Assistance software Assistant 7.7 beta (UFCG, Campo Grande, PB, Brazil).

RESULTS

Effects of Variety and Style of Cooking on the βC Content in Cassava. Moisture content of raw cassava root for varieties in lineage 1 ranged from 60 to 83% and was greater than those in lineage 2 (Table 2; $p < 0.05$). The differences in moisture contents of these two lineages are likely due to differences in climate, cultivation conditions, and perhaps age at harvest in the two geographic locations. Cassava roots received from IAC were grown in southeastern Brazil for 9 months in a tropical climate, whereas roots received from Embrapa were grown in northeastern Brazil for 14 months in a semiarid climate. Moisture was minimally altered for seven of the nine varieties after boiling. There was approximately a 10% increase in moisture content of varieties 576-70 and 06-01 ($p < 0.05$) after boiling. Frying the boiled cassava resulted in significantly decreased moisture content of root flesh in all nine varieties, although the extent of loss differed across varieties. During frying, roots from lineage 2 varieties lost significantly more water than those from lineage 1. Accordingly, there was a significant interaction between variety and cooking styles as factors for moisture content ($p < 0.01$). Lipid content of the six fried varieties of cassava from lineage 1 ranged from 2.0 to 4.8% FW, whereas lipid content of the three fried varieties from lineage 2 was significantly greater (6.7−13.7% FW). The greater amounts of dry matter in cassava roots from lineage 2 than in roots from lineage 1 was positively correlated with increased capacity to adsorb oil during frying ($p < 0.001$, $r = 0.7546$).

βC was the only carotenoid detected in all tested genotypes of cassava, although its content varied markedly across the varieties (Figure 1). Roots from Saracura and clone 03-15

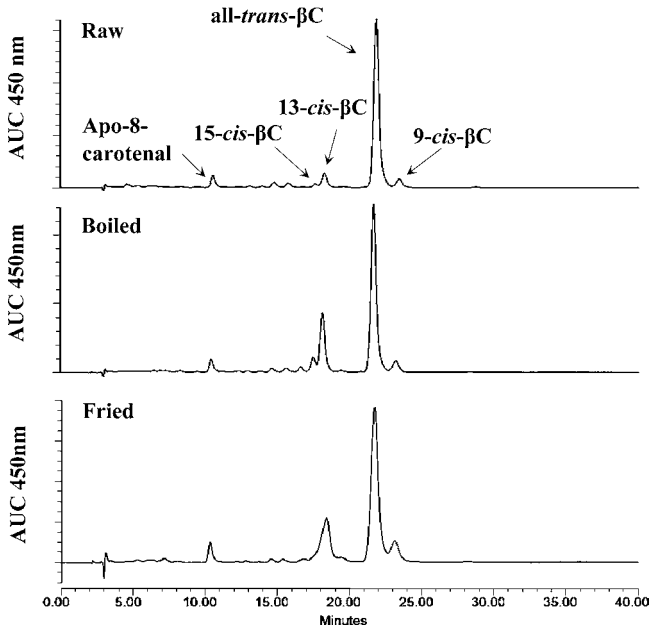

Figure 1. Representative chromatograms of raw, boiled, and fried cassava (Jari variety).

varieties had the lowest and highest concentrations of βC, respectively (Table 2). Varieties generated for the purpose of increasing provitamin A content contained at least 10−22-fold more βC per gram FW than the Saracura variety that is commonly grown and consumed in northeastern Brazil. With the exception of clone 14-11, the four other crossed varieties had significantly higher total βC per gram FW than the parental varieties. There was a significant interaction between variety and cooking styles for total βC per gram FW ($p < 0.01$). Boiling was associated with a decline in total βC content per gram FW for six of the nine varieties of cassava. With the exception of variety 06-01, total βC concentration was not further decreased ($p > 0.05$) when boiled cassava was briefly fried. Fried Jari contained the highest amounts of total βC among the ready-to-eat cassavas.

The quantities of *all-trans*- and *cis*-isomers of βC in raw and cooked varieties were determined (Table 3), because *all-trans*-βC has greater vitamin A equivalence than *cis* isomers.[3] Varieties with greater concentrations of total βC (Table 2) also contained higher amounts of *all-trans*-βC (Table 3). The four varieties with the highest total βC content had the greatest percentages of *all-trans*-βC (83−87%), whereas the four genotypes with lowest estimated amounts of total βC content contained 50−70% *all-trans*-βC (Table 3). These data indicate that breeding

dx.doi.org/10.1021/jf5018302 | J. Agric. Food Chem. 2014, 62, 6677−6686

Table 3. *all-trans-βC*, Total *cis-βC*, Potential Retinol Equivalents (RE), and Recommended Daily Intake (RDI) Provided by Nine Varieties of Raw and Cooked Cassava[a]

variety[b]	*all-trans-βC*[c] (μg/g FW)		total *cis-βC*[c] (μg/g FW)		potential RE[c] (μg/100 g FW)		% RNI[d]	
	raw	boiled	fried	raw	boiled	fried	boiled	fried	boiled	fried
lineage 1										
Saracura (Con)	0.23 ± 0.04fA	0.20 ± 0.07eA	0.20 ± 0.02fA	0.22 ± 0.03dA	0.17 ± 0.05dA	0.15 ± 0.02fA	4.7 ± 1.5eA	4.4 ± 0.5dA	1.0	1.0
Dourada (PA)	1.70 ± 0.17eA	1.42 ± 0.07dA	1.24 ± 0.40eA	0.73 ± 0.05cA	1.02 ± 0.28cA	1.00 ± 0.37eA	32.2 ± 2.2dA	29.1 ± 5.6cA	7.1	6.5
Gema de Ovo (PA)	2.07 ± 0.15eA	1.46 ± 0.14dA	1.59 ± 0.10eA	1.96 ± 0.12aA	1.42 ± 0.31bB	1.48 ± 0.12dB	36.2 ± 4.8cdA	38.9 ± 2.6cA	8.0	8.6
clone 14-11 (PR)	3.78 ± 0.21dA	2.27 ± 0.36cB	2.61 ± 0.14dB	1.51 ± 0.19bB	1.75 ± 0.18bB	2.37 ± 0.21bA	52.6 ± 6.5cA	63.5 ± 3.9bA	11.7	14.1
Jari (PR)	7.01 ± 0.59bA	4.28 ± 0.33bC	6.03 ± 0.34aB	1.13 ± 0.15bC	2.08 ± 0.20aB	3.10 ± 0.19aA	89.0 ± 6.7abB	127.0 ± 6.9aA	19.8	28.2
clone 03-15 (PR)	8.99 ± 1.56aA	5.09 ± 0.85aB	5.45 ± 0.40bB	1.30 ± 0.18bB	2.13 ± 0.31aA	2.30 ± 0.19bA	103.0 ± 16.6aA	110.0 ± 8.0aA	22.9	24.4
lineage 2										
576-70 (PA)	1.64 ± 0.24eA	1.11 ± 0.11dA	1.34 ± 0.32eA	0.98 ± 0.20cA	0.87 ± 0.10cA	1.11 ± 0.25eA	25.8 ± 2.5dA	31.7 ± 7.4cA	5.7	7.0
265-97 (PR)	6.06 ± 0.44cA	3.78 ± 0.27bB	3.40 ± 0.90cB	1.25 ± 0.16bB	1.48 ± 0.39bB	1.82 ± 0.43cA	75.6 ± 5.7bA	72.0 ± 18.6bA	16.8	16.0
06-01 (PR)	7.22 ± 0.16bA	4.74 ± 0.87aB	3.93 ± 1.11cC	1.44 ± 0.09bC	2.33 ± 0.49aA	1.99 ± 0.66cB	98.8 ± 18.5aA	82.2 ± 24.1bB	22.0	18.3

[a]Data are means ± SD, $n = 6$. Different lower case letters within columns indicate that means of varieties differ significantly ($p < 0.05$). Different upper case letters within rows indicate that means of raw, boiled and fried samples differ significantly ($p < 0.05$). [b]From Table 1: Con, control variety; PA, parental variety; PR, progeny (biofortified variety). [c]RE, retinol equivalents. Calculated according to FAO[33] assuming approximately 33% of *βC* is available for absorption and conversion to vitamin A is 50% for *all-trans-βC* and 25% for *cis-βC*.[33] [d]Calculated as percent of Recommended Nutrient Intake (RNI) of 450 μg/day RE for children 4–6 years of age provided by consuming 100 g of cooked cassava.

for high *β*C was associated with selective enrichment of *all-trans-β*C. *all-trans-β*C content in cooked cassava was lower than in raw cassava, although the decrease was significant ($p < 0.05$) for only five of the nine varieties (i.e., clone 14-11, Jari, clone 03-15, 265-97, and 06-01). Both boiling and frying increased total *cis-β*C in varieties containing high amounts of total *β*C, suggesting at least partial isomerization of *all-trans-β*C. Several processes can affect the quantity and isomeric profile of carotenoids in cassava root during cooking. These include heat-induced oxidation, degradation, and isomerization, as well as mass interchanges with boiling water or heated oil.[30,31] The latter can mask the effects of carotenoid degradation and lead to errors in calculating retention.[31] Therefore, the retention of *all-trans-β*C (Figure 2) also was calculated on the basis of dry weight (DW). The general impact of cooking on the concentration of *all-trans-β*C per gram DW was similar to that when expressed on the basis of fresh weight. That is, boiling decreased the amount of *all-trans-β*C per gram DW to a greater extent in varieties containing relatively high concentrations of the carotenoid (Figure 2a), and frying significantly decreased the amounts of total *β*C (data not shown) and *all-trans-β*C per gram DW (Figure 2b) while increasing total *cis-β*C content per gram DW (data not shown) for all varieties. There was no significant correlation between retention of *all-trans-β*C and either boiling time or moisture content of raw cassava. 9-*cis*- and 13-*cis-β*C, along with lesser amounts of 15-*cis-β*C, were detected in all varieties of raw and cooked cassava. As expected with increasing temperature,[31] the 13-*cis* isomer of *β*C was preferentially increased during cooking (data not shown). For example, the estimated mean concentrations of 13-*cis-β*C were 3.1 and 9.4 μg/g DW in raw and fried cassava, respectively.

Potential retinol equivalents (RE) considers the amounts of *all-trans-β*C and *cis-β*C in ready-to-eat cassava.[33,34] Except for control and parental lines, the concentration of *all-trans-β*C in all progeny varieties significantly decreased as a result of cooking raw cassava. Nevertheless, the biofortified varieties of cooked cassava contained significantly more RE than their respective parental varieties (Table 3). *all-trans-β*C content per gram FW was not significantly different in boiled and fried cassava, except for the Jari and 06-01 varieties, for which the fried cassava had significantly higher and lower concentrations of the isomer, respectively. A 100 g portion of fried Jari cassava contained 28% of recommended nutrient intake (RNI) for 4–6-year-old children, which is 28 times greater than that provided by an equivalent consumption of the Saracura variety of fried white cassava.

Effects of Variety and Style of Cooking on the Bioaccessibility of *β*C in Cassava. As previously reported for cooked cassava,[25,32] recovery of *β*C in chyme following completion of the small intestinal phase of digestion exceeded 70% for boiled and fried Saracura and Jari varieties from lineage 1 and the three varieties in lineage 2 (data not shown). However, recoveries of *β*C in chyme for boiled and fried clones 14-11 and 03-15 and for boiled Dourada and Gema de Ovo varieties were only 40–60%. The losses were primarily associated with greater losses of *cis-β*C as recovery of *all-trans-β*C generally exceeded 80% (Figure 3a). *β*C released from the food matrix must be incorporated into mixed micelles during the small intestinal phase of digestion to be accessible for uptake by absorptive epithelial cells in the gut, possible cleavage to retinoids, and absorption of the carotenoid and its metabolites for delivery to peripheral tissues. The percentage of the carotenoid in the predigested sample that partitions in mixed

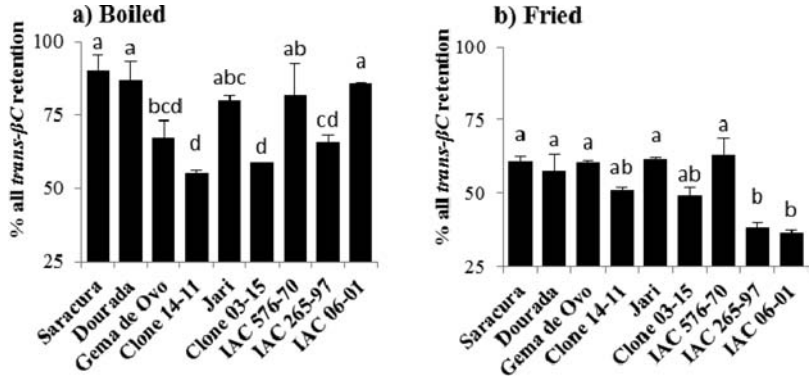

Figure 2. Relative retention of *all-trans-βC* per gram dry weight after boiling (a) and frying (b) cassava root. Data are the mean ± SD, $n = 6$. Different letters within each panel indicate means are significantly different ($p < 0.05$).

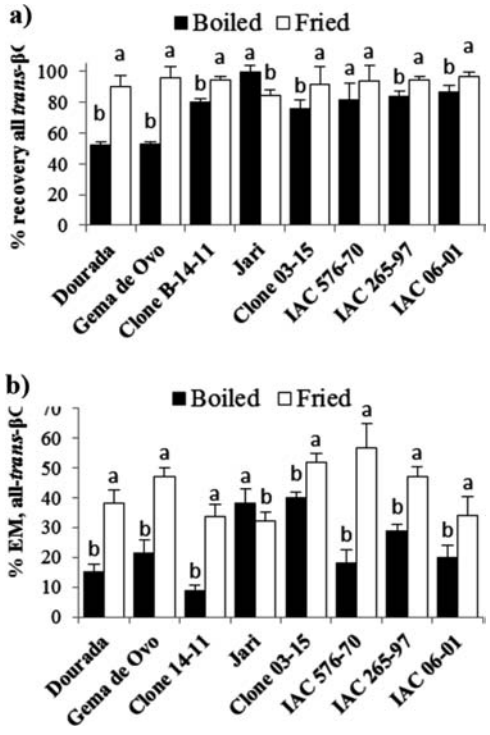

Figure 3. Recovery of *all-trans-βC* after simulated digestion of cooked cassava (a) and efficiency of micellarization (EM) of the carotenoid isomer (b). Recovery indicates the percentage of *all-trans-βC* in the cooked root that was detected in chyme at the end of the small intestinal phase of digestion. EM is the percentage of *all-trans-βC* in the cooked digestion before simulated digestion that partitioned in the filtered aqueous, that is, mixed micelle fraction of chyme. Data are the mean ± SD, $n = 6$. Different letters above error bars for each variety within a panel indicate that means for boiled and fried cassava of the variety differ significantly ($p < 0.05$).

micelles during the small intestinal phase of digestion is referred to as the efficiency of micellarization. The efficiency of micellarization of *all-trans-βC* in digested boiled cassava ranged from 9 to 40% (Figure 3b). There was a significant interaction ($p < 0.01$) between variety and cooking style. Frying cassava increased the efficiency of micellarization of *all-trans-βC* for seven of eight varieties. The efficiency of micellarization of *cis-βC* during digestion of varieties of boiled and fried cassava ranged from 8 to 25% and from 19 to 40%, respectively, and was significantly less than that of *all-trans-βC* for each respective variety cooked in the same manner (data not shown).

With the exception of clone 14-11, the estimated amount of bioaccessible, that is, micellarized, provitamin A after digestion of ready-to-eat biofortified varieties exceeded that of their respective parental varieties ($p < 0.05$, Table 4). The quantities of both *all-trans-βC* and *cis-βC* in mixed micelles after simulated digestion of fried cassava were significantly greater than that in micelles after digestion of boiled cassava. There was a robust correlation ($p < 0.01$) between the amounts of total *βC* and *all-trans-βC* in cassava root and the quantity incorporated into mixed micelles during simulated digestion (Figure 4). The trend for fried cassava exceeded that for boiled cassava because frying enhanced the efficiency of micellarization ($p < 0.05$).

Monolayers of differentiated Caco-2 cells were used to verify that *all-trans-βC* in the mixed micelles generated during digestion of cooked cassava for the four varieties with the highest concentrations was available for uptake across the brush border membrane. The quantity of *all-trans-βC* accumulated by Caco-2 cells was greater when monolayers were exposed to micelles generated during digestion of fried compared to boiled cassava (Table 5). Also, cellular accumulation of *all-trans-βC* from apical medium during exposure to the micelle fraction generated during digestion of fried variety 265-97 exceeded that in cells incubated with the micelle fractions after digestion of fried cassava for the other three varieties. The amount of *all-trans-βC* in the micelle fraction of fried and digested variety 265-97 was less than that in the micelle fractions for digested and fried Jari and clone 03-15 (Table 4). This suggests that other components in the micelle fraction may have influenced the transfer of *βC* from micelles across the apical membrane of the Caco-2 cells.

DISCUSSION

Biofortification represents a sustainable approach to reduce micronutrient and protein deficiencies in rural areas of developing countries.[35,36] It is important to ensure that biofortified staple food crops contain adequate concentrations of micronutrients to improve the nutritional status of populations at risk. To do so requires information about the impact of postharvest processing and styles of cooking on the amounts of nutrients of interest delivered to the plate, their bioacessibility, and consumer acceptance of the new varieties. We examined the influences of variety and two common domestic styles of cooking on the retention and bioaccessibility of *βC* in biofortified cassava. We chose to include white cassava (low *βC* content) in addition to several varieties from two parental lineages and their progeny containing elevated amounts of *βC* in the investigation

dx.doi.org/10.1021/jf5018302 | J. Agric. Food Chem. 2014, 62, 6677−6686

Table 4. Estimated Bioaccessible βC per 100 g FW of Cooked and Digested Cassava[a]

	bioaccessible βC (μg/100 g FW)											
	total βC				*all-trans*-βC				total *cis*-βC			
variety	boiled		fried		boiled		fried		boiled		fried	
lineage 1												
Dourada	30 ±	2.8fB	73 ±	4.3fA	21 ±	3.3dB	48 ±	1.6fA	9 ±	2.3dB	25 ±	2.9fA
Gema de Ovo	56 ±	1.3eB	132 ±	5.3eA	30 ±	1.9dB	75 ±	5.2eA	26 ±	1.4cB	57 ±	1.4cdA
clone 14−11	35 ±	4.8fB	138 ±	2.6eA	21 ±	4.2dB	86 ±	1.4eA	14 ±	1.7dB	52 ±	1.2dA
Jari	216 ±	21.7bB	255 ±	12.9bA	163 ±	29.8bB	195 ±	18.3bA	52 ±	6.2aB	60 ±	4.3bcA
clone 03-15	258 ±	3.5aB	352 ±	19.8aA	206 ±	4.0aB	278 ±	21.1aA	53 ±	1.6aB	74 ±	5.4aA
lineage 2												
576-70	32 ±	1.6fB	122 ±	8.2eA	20 ±	3.3dB	78 ±	7.0eA	12 ±	2.3dB	44 ±	1.7eA
265-97	140 ±	16.7cB	225 ±	5.7cA	106 ±	13.1cB	162 ±	5.6cA	34 ±	5.9bB	64 ±	1.7bA
06-01	118 ±	6.2dB	195 ±	5.0dA	93 ±	6.9cB	137 ±	25.4dA	25 ±	2.3cB	58 ±	13.5bcA

[a]Data are means ± SD, $n = 6$. Different lower case letters within columns indicate that the estimated amount of bioaccessible βC is significantly affected by style of cooking ($p < 0.05$). Different upper case letters within a row indicate that style of cooking significantly influences the amount of bioaccessible isomers of βC ($p < 0.05$).

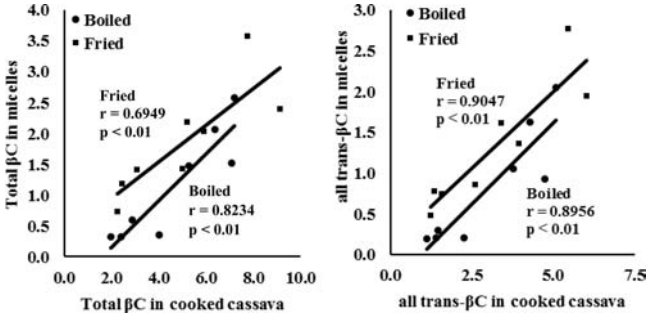

Figure 4. Total βC (a) and *all-trans*-βC (b) content in mixed micelles of digested boiled and fried cassava are highly correlated with βC content of cooked cassava. Data were analyzed by Pearson's correlation test for eight varieties of cassava that were either boiled or fried after boiling.

Table 5. Caco-2 Cell Uptake of *all-trans*-βC from Apical Medium Containing Mixed Micelles Generated by in Vitro Digestion of Cooked Cassava[a]

	all-trans-βC accumulation[b] (ng/mg cell protein)			
variety	boiled		fried	
lineage 1				
Jari	95 ±	2.3aB	107 ±	2.4cA
clone 03−15	92 ±	1.2aB	125 ±	2.1bA
lineage 2				
265-97	70 ±	5.3bB	158 ±	13.6aA
06-01	48 ±	3.6cB	86 ±	10.2dA

[a]Differentiated cultures of Caco-2 cells were incubated with mixed micelles generated during digestion of indicated varieties of cooked cassava for 4 h. Data are means ± SD, $n = 7$. Different lower case letters within columns indicate that means of varieties differ significantly ($p < 0.05$). Different upper case letters within rows indicate that means for cooking style differ significantly ($p < 0.05$). [b]Results were standardized per 1 g of fresh weight cassava.

because white cassava is widely consumed in NE Brazil. The basic differences in these two lineages of cassava were genotypic inheritance and geographical location of production (Table 1). Boiling cassava to acceptable texture and frying the boiled cassava in soybean oil were selected as common household styles of preparing cassava for investigation. Established methods were used to simulate the digestion of the cooked roots.[25,37,38] The predictive reliability of in vitro digestion of foods rich in carotenoids was reported by Reboul and colleagues,[37] who found that the percentage of carotenoids in foods recovered in micelles during in vitro digestion and in vivo during digestion by healthy humans were highly correlated ($r = 0.90$), as was the relative extent of micellarization during simulated digestion and relative bioavailability from meals with the same vegetables in human studies ($r = 0.98$). Among the key outcomes of the study are the following. Conventional breeding methods in Brazil produced progeny containing as high as 22-fold more βC on fresh weight basis than commonly consumed white cassava (Table 2) and the majority of the additional amount of the carotenoid was the *all-trans* isomer (Table 3). Cassava roots from lineage 2 grown in a tropical region had lower moisture content and greater capacity to adsorb oil during frying (Table 2). Also, frying boiled cassava generally did not induce additional significant reductions in cassava root compared to only boiling (Table 2). The amount of bioaccessible βC after simulated digestion of fried cassava exceeded that in boiled cassava due to increased efficiency of partitioning of the carotenoid in the former from the matrix to mixed micelles (Table 4; Figure 3b).

New varieties of cassava containing higher concentrations of βC have been generated by taking advantage of the biodiversity of cassava in Brazil. The Jari, 265-97, 06-01, and clone 03-15 varieties containing 7−10 μg/g FW of total βC are currently among the highest reported concentrations of total βC in biofortified cassava. Concentrations of total βC as high as 7 μg/g FW in cultivars of cassava in the Harvest Plus program of Nigeria were previously used to investigate the effects of genotype and cooking styles on the bioaccessibility of the provitamin.[25,38] Genetically modified cassava with roots containing as much as 6 μg βC/g FW[32] were similarly investigated. Ceballos et al.[39] reported that the use of a rapid cycling recurrent selection model for cross-breeding cassava in Colombia increased βC content in progenies to 10 μg/g FW. It is important to note that βC concentration is not the sole characteristic for selecting potential varieties for widespread planting as agronomic traits and economic viability also are important factors. Early efforts in Brazil produced the 576-70 variety of cassava that is characterized by its high yield, resistance to disease, increased content of βC, and favorable organoleptic properties.[40,41] This variety subsequently was crossed with SRT-797

dx.doi.org/10.1021/jf5018302 | J. Agric. Food Chem. 2014, 62, 6677−6686

Ouro do Vale variety to produce the 265-97and 06-01 varieties. Investments from Harvest Plus beginning in 2004 intensified breeding efforts with cassava that have generated new varieties including Jari and clones 03-15 and 14-11. Despite success with the biofortification of cassava with βC using conventional breeding,[25,39−43] further advances are needed to generate varieties with acceptable agroeconomic and organoleptic properties that will deliver adequate βC to the plate to meet up to 50% of the daily requirements for vitamin A.

The present study adds to recent reports that conventional breeding is useful for generating varieties of cassava that contain relatively high amounts of βC and possess other desirable agroeconomic characteristics.[14,39,43] There is a diverse germplasm from the Amazon region containing as high as 25 μg βC/g fresh weight in roots that can be used for crossing with varieties possessing other favorable characteristics.[43,44] To reduce VAD, both a relatively high content of βC and an abundance of *all-trans*-βC isomer are important because the *all-trans* isomer is cleaved into two molecules of retinal, whereas *cis* isomers produce only a single molecule of retinal when cleaved.[45] Retention of *all-trans*-βC in fried cassava (36−63%) was less than that after boiling, and there was preferential partial isomerization of *all-trans*-βC to 13-*cis*-βC as reported by others for fried yellow-fleshed cassava.[25,32,38,42,46,47] It is well established that heat induces isomerization of carotenoids prior to degradation and preferentially isomerizes *all-trans*-βC to 13-*cis*-βC because the activation energy for isomerization about the central double bound is lower than that for the other double bonds in the carotenoid.[30,31,48] Our findings suggest that a 100 g portion of ready-to-eat biofortified cooked cassava can provide as much as 28% of the recommended nutrient intake for 4−6-year-old children[33] depending on the variety, the content of βC in the root, and the style of cooking (Table 3). Similar results were obtained when we used the dietary reference intake values established by the Institute of Medicine as a reference.[49] As much as 55 μg/day of vitamin A expressed as retinol activity equivalent (RAE) is provided by 100 g of ready-to-eat biofortified cooked cassava for an additional 20% of the estimated average requirement (EAR) for children 4−6 years old (Supporting Information Table 1).

The bioacessibility of βC refers to the amount that is released from the food matrix and solubilized in mixed micelles for delivery to absorptive epithelial cells.[50] The three-phase (oral, gastric and intestinal) in vitro digestion method has been used to investigate the digestive stability and micellarization of provitamin A carotenoids from several high-starch foods including cassava, sweet potato, and grains.[25,32,51,52] Recovery of total βC after in vitro digestion of the majority of the biofortified varieties of cassava in the present study generally exceeded 70%, and simulated digestion of the cassava minimally affected the relative amounts of *all-trans*- and *cis*-isomers of the carotenoid as previously reported for other conventionally bred and transgenic biofortified varieties of cassava.[25,32,38] We noted a greater range in the efficiency of micellarization of βC during digestion of the different varieties of boiled cassava in this study, that is, 9−40%, than in boiled roots from conventionally bred cassava (25−30%) grown in Nigeria[38] and in transgenic cassava grown in Puerto Rico (30−45%).[31] With the exception of the cooked Jari variety, micellarization of βC during simulated digestion of fried cassava exceeded that for boiled roots. The greater adsorption of oil to fried cassava roots from lineage 2 than for fried roots from lineage 1 was associated with more efficient micellarization of βC during digestion. This observation is not surprising as dietary fat facilitates the solubilization and micellarization of carotenoids.[26,53] In contrast to our observation with the Jari variety, Gomes et al.[42] reported that micellarization of βC during digestion of fried Jari cassava was twice as great as that following digestion of boiled cassava. This difference may have been due to the greater fat content of the fried Jari root in the former study (11%/g FW) after boiling under pressure for 30 min before frying for 8 min as opposed to only 2% fat/g FW in our study in which cassava was boiled for 33 min at 1 atm and fried for 5 min. This suggests that the specific conditions of the boiling process and the moisture content of the root can affect the adsorption of oil during frying.

In agreement with our previous study with biofortified varieties developed in Nigeria,[25] the quantity of βC micellarized during simulated digestion of cooked cassava varieties was directly proportional to βC in the ready-to-eat cassava (Figure 4). Uptake of *all-trans*-βC by Caco-2 cells confirmed that micellarized βC was available to the enterocyte-like cells (Table 5). Together, these results suggest that breeders should continue to select for higher βC concentrations and palatability in high-yield varieties of cassava. Among the varieties investigated in the present study, fried biofortified cassavas from lineage 2 appear to be most beneficial from a nutritional perspective because of their relatively short boiling time, greater capacity to adsorb oil during the frying process, and relatively efficiency of micellarization of βC during digestion. The results from the present study further support the hypothesis that biofortification of cassava root with βC is a useful strategy for reducing VAD in vulnerable populations without requiring major changes in local and ethnic styles of home cooking.

■ ASSOCIATED CONTENT

Supporting Information

Additional table. This material is available free of charge via the Internet at http://pubs.acs.org.

■ AUTHOR INFORMATION

Corresponding Author

*(M.L.F.) Phone: (614) 560-9401. Fax: (61)4 292-4339. E-mail: failla.3@osu.edu.

Funding

Funding for this study was provided by Harvest Plus and the Ohio Agricultural Research and Development Center. Funds for travel and living expenses of P.B. at The Ohio State University were provided by FAPESP.

Notes

The authors declare no competing financial interest.

■ ACKNOWLEDGMENTS

We thank Drs. Marilia Nutti and Teresa L. Valle for providing cassava roots from EMBRAPA and IAC, respectively.

■ REFERENCES

(1) Food and Agriculture Organization (FAO) of the United Nations. *Synthesis of Guiding Principles on Agriculture Programing for Nutrition*; FAO: Rome, Italy, 2013; pp 1−83.

(2) World Health Organization (WHO). *Global Prevalence of Vitamin A Deficiency in Populations at Risk 1995−2005; WHO Global Database on Vitamin A Deficiency*; WHO: Geneva, Switzerland, 2009; pp 1−49.

(3) Kohlmeier, M. *Nutrient Metabolism: Structures, Functions, and Genetics*; Academic Press: London, UK, 2003; pp 464−478.

(4) Ramalho, R. A.; Hypovitaminosis, A. In *Nutrition in Public Health*; Taddei, J. A., Lang, R. M. F., Silva, G. L., Tolo, M. H. A., Eds.; Ed.a Rubio: Rio de Janeiro, Brazil, 2011; pp 211−221.
(5) Fernández-García, E.; Carvajal-Lérida, I.; Jarén-Galán, M.; Garrido-Fernández, J.; Pérez-Gálvez, A.; Hornero-Méndez, D. Carotenoids bioavailability from foods: from plant pigments to efficient biological activities. *Food Res. Int.* **2012**, *46*, 438−450.
(6) Ambrósio, C. L. B.; Campos, F. A. C. S.; Faro, Z. P. Carotenoids as an alternative against hypovitaminosis. *Annu. Rev. Nutr.* **2006**, *19*, 233−243.
(7) Weber, D.; Grune, T. The contribution of β-carotene to vitamin A supply of humans. *Mol. Nutr. Food Res.* **2012**, *56*, 251−258.
(8) Food Agriculture Organization (FAO) of the United Nations. *The State of Food and Agriculture; Food System for Better Healthy*; FAO: Rome, Italy, 2013; pp 3−67.
(9) Sayre, R.; Beeching, J. R.; Cahoon, E. B.; Egesi, C.; Fauquet, C.; Fellman, J.; Fregene, M.; Gruissem, W.; Mallowa, S.; Manary, M.; Maziya-Dixon, B.; Mbanaso, A.; Schachtman, D. P.; Siritunga, D.; Taylor, N.; Vanderschuren, H.; Zhang, P. The BioCassava Plus Program: biofortification of cassava for Sub-Saharan Africa. *Annu. Rev. Plant Biol.* **2011**, *62*, 251−272.
(10) Hirschi, K. D. Nutrient biofortification of food crops. *Annu. Rev. Nutr.* **2009**, *29*, 401−421.
(11) Saltzman, A.; Birol, E.; Bouis, H. E.; Boy, E.; De Moura, F. F.; Islam, Y.; Pfeiffer, W. H. Biofortification: progress toward a more nourishing future. *Global Food Security* **2012**, *2*, 9−17.
(12) Welch, R. M.; Graham, R. D. Breeding crops for enhanced micronutrient content. *Plant Soil* **2002**, *245*, 205−214.
(13) Gegios, A.; Amthor, R.; Maziya-Dixon, B.; Egesi, C.; Mallowa, S.; Nungo, R.; Gichuki, S.; Mbanaso, A.; Manary, M. J. Children consuming cassava as a staple food are at risk for inadequate zinc, iron and vitamin A intake. *Plant Foods Hum. Nutr.* **2010**, *65*, 64−70.
(14) Mezette, T. F.; Carvalho, C. R. L.; Morgano, M. A.; Silva, M. G.; Parra, E. S. B.; Galera, J. M. V.; Valle, T. L. Selection of sweet cassava elite-clones for agronomical, technological and chemical characteristics. *Bragantia* **2009**, *68*, 601−609.
(15) Consultative Group on International Agricultural Research (CGIAR). *A4NH 2012 Annual Report: On the Path to Better Nutrition & Health*; International Food Policy Research Institute: Washington, DC, USA, 2012; pp 8−22.
(16) Mezette, T. F.; Blumer, C. G.; Veasey, E. A. Morphological and molecular diversity among cassava genotypes. *Pesq. Agropec. Bras.* **2013**, *48*, 510−518.
(17) Netto, R. S. M.; Curado, F. F.; Costa, D.; Vieira, D. A. S.; Costa, J. O.; Morais, R. S. Food intake of students to Pacatuba's rural area, Sergipe. 3rd Annual Biofortification Meeting in Brazil. 2009, Aracaju, Brazil; htpp://www.biofort.com.br (accessed Nov 20, 2013).
(18) Silva, M. D. R.; Nascimento, S.T. J. R. M.; Oliveira, B. A.; Lima, J. X. P. T.; Aureliano, M. T. M.; Sousa, D. C. B.; Ribeiro, E. C. B.; Bringel, J. G.; Silva, L. A.; Araújo, M. J.; Oliveira, F. D.; Pereira, G. P.; Silva, K. D.; Costa, K. M.; Braúna, L. F. G.; Araújo, L. T. S.; Silva, A. P.; Barbosa, G. V.; Costa, J. M. A.; Chaves, T. M.; Lucena, T. D.; Lima, T. D. S. Potential evaluation of food utilizations with more high levels of iron and zinc and in the school meals of São Luis − Maranhao. 3rd Annual Biofortification Meeting in Brazil, 2009, Aracaju, Brazil; htpp://www.biofort.com.br (accessed Nov 20, 2013).
(19) Curado, F. F.; Queiroz, V. A. V.; Dias, A. C. P.; Silva, M. D. R.; Netto, R. S. M. Evaluation of the potential use of biofortified foods in school diets in municipalities of Maranhao, Sergipe and Minas Gerais, Brazil. 3rd Annual Biofortification Meeting in Brazil, 2009, Aracaju, Brazil; htpp://www.biofort.com.br (accessed Nov 20, 2013).
(20) Oliveira, R. G. A.; Carvalho, M. J. L.; Nutti, M. R.; Carvalho, L. V. J.; Fukuda, W. G. Assessment and degradation study of total carotenoid and β-carotene in bitter yellow cassava (*Manihot esculenta* Crantz) varieties. *Afr. J. Food Sci.* **2010**, *4*, 148−155.
(21) Oliveira, M. A.; Leonel, M.; Cabello, C.; Cereda, M. P.; Janes, D. A. Methodology for cooking and technologies analyses in different cassava varieties. *Cienc. Agrotec.* **2005**, *29*, 126−133.
(22) Association of Official Analytical Chemists (AOAC) International. Official Method 926.08: moisture content. In *Official Methods of Analysis*, 16th ed.; AOAC International: Arlington, VA, USA, 1995; p 58.
(23) *Brazilian Table of Food Composition Table (TACO-Project)*, 4th ed.; Brazilian Ministry of Health and NEPA-UNICAMP; Center of Studies and Research in Food, University of Campinas: Campinas, Brazil, 2011; p 116.
(24) Folch, J.; Lees, M.; Stanley, G. H. S. A simple method for the isolation and purification of total lipids from animal tissues. *J. Biol. Chem.* **1957**, *226*, 497−509.
(25) Thakkar, S. K.; Maziya-Dixon, B.; Dixon, A. G. O.; Failla, M. L. β-Carotene micellarization during in vitro digestion and uptake by Caco-2 cells is directly proportional to β-carotene content in different genotypes of cassava. *J. Nutr.* **2007**, *137*, 2229−2233.
(26) Yonekura, L.; Nagao, A. Intestinal absorption of dietary carotenoids. *Mol. Nutr. Food Res.* **2007**, *51*, 107−115.
(27) Chitchumroonchokchai, C.; Schwartz, S. J.; Failla, M. L. Assessment of lutein bioavailability from meals and a supplement using simulated digestion and Caco-2 human intestinal cells. *J. Nutr.* **2004**, *134*, 2280−2286.
(28) Kimura, M.; Kobori, C. N.; Rodriguez-Amaya, D. B.; Nestel, P. Screening and HPLC methods for carotenoids in sweet-potato, cassava and maize for plant breeding trials. *Food Chem.* **2007**, *100*, 1734−1746.
(29) Britton, G. UV/visible spectroscopy. In *Carotenoids*; Britton, G., Jensen, S. L., Pfander, H., Eds.; Birkhauser: Basel, Switzerland, 2011; pp 13−62.
(30) Mercadante, A. Z. Carotenoids in foods: sources and stability during processing and storage. In *Food Colorants: Chemical and Functional Properties*; Socaciu, S., Ed.; CRC Press: Boca Raton, FL, USA, 2007; pp 213−235.
(31) Rodriguez-Amaya, D. B.; Kimura, M. *Handbook for Carotenoid Analysis*; Harvest Plus Technical Monograph Series 2; Harvest Plus: Washington, DC, USA, and Cali, Colombia, 2004; pp1−51.
(32) Failla, M. L.; Chitchumroonchokchai, C.; Siritunga, D.; Moura, F. F.; Fregene, M.; Sayre, R. T. Retention during processing and bioaccessibility of β-carotene in high β-carotene transgenic cassava root. *J. Agric. Food Chem.* **2012**, *60*, 3861−3866.
(33) Food Agriculture Organization/World Health Organization (FAO/WHO). *Human Vitamin and Mineral Requirements*; Report 7th Joint FAO/WHO Expert Consultation, Bangkok, Thailand; FAO: Rome, Italy, 2001; pp 7−25.
(34) Scott, K. J.; Rodriguez-Amaya, D. Pro-vitamin A carotenoid conversion factors: retinol equivalents, fact or fiction? *Food Chem.* **2000**, *69*, 125−127.
(35) Miller, D. D.; Welch, R. M. Food system strategies for preventing micronutrient malnutrition. *Food Policy* **2013**, *42*, 115−128.
(36) Hotz, C.; McClafferty, B. From harvest to health: challenges for developing biofortified staple foods and determining their impact on micronutrient status. *Food Nutr. Bull.* **2007**, *28*, S271−S279.
(37) Reboul, E.; Richelle, M.; Perrot, E.; Desmoulins-Malezet, C.; Pirisi, V.; Borel, P. Bioaccessibility of carotenoids and vitamin E from their main dietary sources. *J. Agric. Food Chem.* **2006**, *54*, 8749−8755.
(38) Thakkar, S. K.; Huo, T.; Maziya-Dixon, B.; Failla, M. L. Impact of style of processing on retention and bioaccessibility of β-carotene in cassava (*Manihot esculenta* Crantz). *J. Agric. Food Chem.* **2009**, *57*, 1344−1348.
(39) Ceballos, H.; Morante, N.; Sánchez, T.; Ortiz, D.; Aragón, I.; Chávez, A. L.; Pizarro, M.; Calle, F.; Dufour, D. Rapid cycling recurrent selection for increased carotenoids content in cassava roots. *Crop Sci.* **2013**, *53*, 1−10.
(40) Villela, O. V.; Pereira, A. S.; Lorenzi, J. O.; Valle, T. L.; Monteiro, D. A.; Ramos, M. T. B.; Schmidt, N. C. Competition among cassava clones selected for table and industry. *Bragantia* **1985**, *44*, 559−568.
(41) Ceballos, H.; Luna, J.; Escobar, A. F.; Ortiz, D.; Pérez, J. C.; Sánchez, T.; Pachón, H.; Dufour, D. Spatial distribution of dry matter

in yellow fleshed cassava roots and its influence on carotenoid retention upon boiling. *Food Res. Int.* **2012**, *45*, 52−59.
(42) Gomes, S.; Torres, A. G.; Godoy, R.; Pacheco, S.; Carvalho, J.; Nutti, M. Effects of boiling and frying on the bioaccessibility of β-carotene in yellow-fleshed cassava roots (*Manihot esculenta* Crantz cv. BRS Jari). *Food Nutr. Bull.* **2013**, *34*, 65−74.
(43) Njoku, D. N.; Vernon, G.; Egesi, C. N.; Asante, I.; Offei, S. K.; Okogbenin, E.; Kulakow, P.; Eke-okoro, O. N.; Ceballos, H. Breeding for enhanced β-carotene content in cassava: constraints and accomplishments. *J. Crop Improv.* **2011**, *25*, 560−571.
(44) Iglesias, C.; Mayer, J.; Chavez, L.; Calle, F. Genetic potential and stability of carotene content in cassava roots. *Euphytica* **1997**, *94*, 367−373.
(45) Harrison, E. H. Mechanisms involved in the intestinal absorption of dietary vitamin A and provitamin A carotenoids. *Biochim. Biophys. Acta* **2012**, *1821*, 70−77.
(46) Vimala, B.; Thushara, R.; Nambisan, B.; Sreekumar, J. Effect of processing on the retention of carotenoids in yellow-fleshed cassava (*Manihot esculenta* Crantz) roots. *Int. J. Food Sci. Technol.* **2011**, *46*, 166−169.
(47) Carvalho, L. M. J.; Oliveira, A. R. G.; Godoy, R. L. O.; Pacheco, S.; Nutti, M.; Carvalho, J. L. V.; Pereira, E. J.; Fukuda, W. G. Retention of total carotenoid and β-carotene in yellow sweet cassava (*Manihot esculenta* Crantz) after domestic cooking. *Food Nutr. Res.* **2012**, *56*, http://dx.doi.org/10.3402/fnv:v56iO.15788.
(48) Zechmeister, L. Cis-trans isomerization and stereochemistry of carotenoids and diphenylpolyenes. *Chem. Rev.* **1944**, *34*, 267−344.
(49) Food and Nutrition Board, Institute of Medicine. *Dietary Reference Intakes: Vitamin A, Vitamin K, Arsenic, Boron, Chromium, Copper, Iodine, Iron, Manganese, Molybdenum, Nickel, Silicon, Vanadium and Zinc*; National Academy Press: Washington, DC, USA, 2001; pp 65−126.
(50) Failla, M. L.; Chitchumroonchokchai, C. *In Vitro Models As Tools for Screening the Relative Bioavailabilities of Provitamin A Carotenoids in Foods*; HarvestPlus Technical Monograph Series 3; HarvestPlus: Washington, DC, USA, and Cali, Colombia, 2005; pp 1−32.
(51) Failla, M. L.; Thakkar, S. K.; Kim, J. Y. In vitro bioaccessibility of β-carotene in orange fleshed sweet-potato (*Ipomoea batatas* Lam). *J. Agric. Food Chem.* **2009**, *57*, 10922−10927.
(52) Kean, E. G.; Hamaker, B. R.; Ferruzzi, M. G. Carotenoid bioaccessibility from whole grain and degermed maize meal products. *J. Agric. Food Chem.* **2008**, *56*, 9918−9926.
(53) Failla, M. L.; Chitchumroonchokchai, C.; Ferruzzi, M. L.; Goltz, S. R.; Campbell, W. W. Unsaturated fatty acids promote bioaccessibility and basolateral secretion of carotenoids and α-tocopherol. *Food Funct.* **2014**, *5*, 1101−1112.

Table 1. Compounds Identified in MSX and Their UV Absorbance

peak	compd	UV (nm)
S1	(6*R*)-6-hydroxy-3-(hydroxymethyl)-2-cyclohexenone	238
S2	3,4-dihydro-5-(hydroxymethyl)pyran-2-one	228, 284
S3	4,4′-dihydroxy-3,3′,5,5′-tetramethoxystilbene	222, 331
S4	4,4′-dihydroxy-3,3′,5′-trimethoxystilbene	222, 331
S5	4-hydroxy-2-(hydroxymethyl)-5-methyl-3(2*H*)- furanone	271
S6	benzenemethanol	229, 284
S7	5-(hydroxymethyl)furfural	229, 284
S8	4-methyl-1,2-venzenediol	210, 288
S9	4-(hydroxymethyl)-1,2-benzenediol	228, 276, 308
1	2-hydroxy-3,4-dihydroxyacetophenone	229, 276, 307
2	catechol	210, 276
3	C-veratroylglycol	231, 280, 310
4	*threo*,*threo*-1-[4-(2-hydroxy-2-(4-hydroxy-3-methoxyphenyl)-1-(hydroxymethyl)ethoxy)-3-methoxyphenyl]-1,2,3-propanetriol	230, 279
5	2,3-dihydroxy-1-(4-hydroxy-3,5-dimethoxyphenyl)-1-propanone	216, 306
6	4-acetylcatechol	231, 280, 312
7	tyrosol	231, 280, 312
8	catechaldehyde	231, 280, 312
9	1,2-diguaiacyl-1,3-propanediol	210, 226(s),[a] 280
10	3′,5′-dimethoxy-4′-hydroxy-2-hydroxyacetophenone	228, 300
11	leptolepisol D	210, 229(s),[a] 280
12	3,4-dihydroxy-2-methylbenzadehyde	233, 285
13	vanillin	229, 280, 309
14	fraxetin	229, 338
15	syringaldehyde	216, 307
16	syringenin	224, 273
17	scopoletin	229, 345
18	*threo*-guaiacylglycerol-*β*-*O*-4′-dihydroconiferyl alcohol	228, 279
19	*erythro*-guaiacylglycerol-*β*-*O*-4′-dihydroconiferyl alcohol	229, 279
20	3-[[4-[(6-deoxy-*α*-L-mannopyranosyl)oxy]-3-methoxyphenyl]methyl]-5-(3,4-dimethoxyphenyl)dihydro-3-hydroxy-4-(hydroxymethyl)-2(3*H*)-furanone	231, 278
21	5-(3″,4″-dimethoxyphenyl)-3-hydroxy-3-(4′-hydroxy-3′-methoxybenzyl)-4-(hydroxymethyl)dihydrofuran-2-one	232, 280
22	1-(2,3,4-trihydroxy-5-methylphenyl)ethanone	230, 295
23	*erythro*-1-(4-hydroxy-3-methoxyphenyl)-2-[4-(3-hydroxypropyl)-2,6-dimethoxyphenoxy]-1,3-propanediol	228, 279
24	icariside E_4	225, 280
25	3′,4′,5′-trihydroxyacetophenone	231, 284
26	dehydroconiferyl alcohol	211, 230(s),[a] 282
27	sakuraresinol	210, 236(s),[a] 280
28	secoisolariciresinol	231, 281
29	acernikol	210, 231, 280
30	(1*S*,2*R*)-2-[2,6-dimethoxy-4-[(1*S*,3a*R*,4*S*,6a*R*)-tetrahydro-4-(4-hydroxy- 3,5-dimethoxyphenyl)-1*H*,3*H*-furo[3,4-*c*]furan-1-yl]phenoxy]-1-(4-hydroxy-3-methoxyphenyl)-1,3-propanediol	210, 232(s),[a] 280
31	buddlenol E	210, 229(s),[a] 280
32	2-[4-[2,3-dihydro-3-(hydroxymethyl)-5-(3-hydroxypropyl)-7-methoxy-2-benzofuranyl]-2,6-dimethoxyphenoxy]-1-(4-hydroxy-3-methoxyphenyl)-1,3-propanediol	211, 232(s),[a] 281
33	(*E*)-3,3′-dimethoxy-4,4′-dihydroxystilbene	222, 331

[a] "s" indicates a shoulder peak.

(arginine, threonine, proline, etc.), vitamins (riboflavin, niacin, thiamine, etc.), and organic acids (fumaric acid, malic acid, etc.) in maple materials.[7] Therefore, given our ongoing research interest in maple products, the primary objective of this project was to investigate the nutraceutical potential of a novel maple syrup derived extract (named MSX) produced under food-grade conditions starting from declassified maple syrup generated by the industry. Here we report (1) chemical compositional (quantification of sugars, minerals, amino acids, organic acids, vitamins, fiber, and ash), (2) phytochemical identification (by HPLC-DAD methods as well as by isolation and subsequent structure elucidation by NMR), (3) in vitro biological (antioxidant, anti-inflammatory, and glucose consumption bioassays), and (4) in vivo safety (acute animal toxicity) studies on MSX. This is the first chemical and biological study of a food-grade extract derived from maple syrup.

2. MATERIALS AND METHODS

2.1. General Experimental Procedures. All 1D nuclear magnetic resonance (^{1}H and ^{13}C NMR) and 2D NMR [^{1}H−^{1}H correlation

spectroscopy (COSY), heteronuclear single-quantum coherence (HSQC), heteronuclear multiple-bond coherence (HMBC)] experiments were acquired either on a Bruker 300 MHz or a Varian 500 MHz instrument. Unless otherwise stated, deuterated methanol (CD_3OD) was used as the solvent for all of the NMR experiments. HR-ESIMS data were acquired using a Waters SYNAPT G2-S QTOFMS system. High-performance liquid chromatography (HPLC) was performed on a Hitachi Elite LaChrom system (Pleasanton, CA) consisting of an L-2130 pump, L-2200 autosampler with L-2455 diode array detector (DAD), and L-2490 refractive index (RI) and L-2485 fluorescence (FL) detectors, all operated by EZChrom Elite software. Medium-pressure liquid chromatography (MPLC) was carried out on prepacked C18 columns. Optical rotation was performed on an AutoPol III automatic polarimeter (Rudolph Research, Flanders, NJ) with samples dissolved in methanol at room temperature. CD spectra were recorded on a JASCO J-810 spectropolarimeter.

2.2. Chemicals and Reagents. All solvents were either ACS or HPLC grade and were obtained from Pharmco-AAPER through Wilkem Scientific (Pawcatuck, RI). Sephadex LH-20, XAD-16 Amberlite resin, 2,2-diphenyl-1-picrylhydrazyl (DPPH), the Folin–Ciocalteau reagent, and all of the cell culture supplies were purchased from Sigma-Aldrich (St. Louis, MO). Standards of compounds used to aid in the phytochemical characterization of MSX were previously isolated and identified (by NMR) from maple syrup and maple sap by our laboratory.[4−7]

2.3. Production of MSX. In collaboration with the Federation of Maple Syrup Producers of Quebec (FPAQ), our laboratory has previously investigated the chemical constituents present in maple sap and syrup[4−7] and maple plant parts,[15−18] which has resulted in the isolation and identification (by NMR) of more than 100 compounds. Maple syrup is classified into different grades (light to dark) on the basis of light transmission. Notably, maple syrup with light transmission of <26.9% is classified as no. 3 dark (Canadian classification), and these products are not used for normal table consumption but rather as commercial ingredients. For the current project, we used two "declassified" grades of maple syrup samples named T_{15} and T_{21} (provided by FPAQ; T_{15} and T_{21} represent the degree of light transmission) which are also not suitable for normal table maple syrup consumption. With the ultimate goal of developing a food-grade maple syrup extract that would be suitable for human consumption, we initially developed laboratory-scale methods using an FDA food-grade approved resin, Amberlite XAD-16, and food-grade solvents (water and denatured ethanol) according to previously published methods.[19] Briefly, each of the maple syrup (T_{15} and T_{21}) starting materials were separately adsorbed onto the XAD-16 resin column and eluted with copious amounts of water to predominantly remove sugars. The adsorbed extract was subsequently eluted from the resin with denatured ethanol to yield MSX-1 (from T_{15}) and MSX-2 (from T_{21}) as dark brown free-flowing powders after solvent removal in vacuo. This small-scale laboratory method was then scaled-up to the pilot level (by SiliCycle Inc., Quebec City, Canada) using a glass column (height 6 feet, diameter 6 in.) filled with XAD-16 resin (ca. 6.7 kg of dry mass). The resin column was prewashed with deionized water (2 × 10 L) and then loaded with a 5 L portion of the declassified maple syrup sample diluted with 2.1 L of deionized water. Once the mixture was adsorbed, a second 5 L portion of the maple syrup sample (in 2.1 L of deionized water) was adsorbed onto the resin column, and sugars were eluted from the column with six consecutive 15 L portions of deionized water. Afterward, the adsorbed extract was eluted with three consecutive 15 L portions of denatured ethanol. The combined ethanol fractions were dried in vacuo on a rotary evaporator (temperature of the water bath <40 °C) to afford dark brown free-flowing solids of the MSX samples with yields of ca. 1.53−1.55 g/kg of the respective starting maple syrup sample. The XAD-16 resin column was then reconditioned with two 10 L portions of deionized water, and the process was repeated with fresh declassified maple syrup samples to yield additional samples of MSX-1 and MSX-2, ca. 300 g each. A portion of each of the MSX-1 and MSX-2 samples (ca. 100 g each) was shipped frozen to our laboratory and immediately stored at −20 °C on receipt.

2.4. Identification of Compounds 1−33 (by HPLC-DAD) in MSX. We have established HPLC-DAD methods to identify compounds (on the basis of comparison of retention times and UV spectra) in a variety of maple-derived materials using authentic standards previously isolated from maple sap and maple syrup by our group.[4−7] Therefore, on the basis of comparison of the HPLC-DAD profiles to that of pure maple syrup (chromatogram shown in Figure 2A), we were able to identify 33 compounds (**1−33**; compound identities shown in Table 1 and chemical structures shown in Figure 1) in phenolic-enriched extracts of each of the MSX samples (see Figure 2B,C). To accomplish this, phenolic-enriched extracts of the MSX samples (1.5 g each) were prepared as previously reported for pure maple syrup by liquid−liquid partitioning with ethyl acetate (40 mL × 3).[5,7] The combined ethyl acetate extracts were dried under reduced pressure in vacuo (water bath kept at 40 °C), and accurate masses were obtained as follows: 282 mg (for MSX-1) and 310 mg (for MSX-2). All samples were dissolved in dimethyl sulfoxide (DMSO), standardized to solid content (50 mg/mL), and then subjected to HPLC-DAD analyses using an Alltima C18 column (250 × 4.6 mm i.d., 5 μM; Alltech) with a flow rate of 0.75 mL/min and an injection volume of 20 μL. A linear gradient solvent system consisting of solvent A (0.1% aqueous trifluoroacetic acid) and solvent B (methanol) at room temperature was used as follows: 0−30 min, from 5% to 33.4% B; 30−80 min, from 33.4% to 71% B; 80−85 min, from 71% to 100% B; 85−86 min, from 100% to 5% B; 86−94 min, 5% B.

2.5. Isolation and Identification (by NMR) of Compounds S1−S9 from MSX. We pursued the isolation and structure elucidation (by NMR) of nine compounds (**S1−S9**; see Table 2) from the MSX samples which, despite their presence in pure maple syrup as evident from the HPLC-DAD profile (see Figure 2), were not obtained from our previous isolation studies.[4−6] Given the similarities in the HPLC-DAD profiles of the MSX-1 and MSX-2 samples (see parts B and C, respectively, of Figure 2), we sought to increase the quantity of initial starting material for our planned isolation studies by combining the MSX samples (1:1, w/w; total of 140.0 g). The combined MSX sample was subjected to liquid−liquid partitioning with ethyl acetate (700 mL × 3) to yield a dried MSX ethyl acetate extract (MSX−EtOAc; 29.0 g) after solvent removal in vacuo. The MSX−EtOAc (29.0 g) extract was subjected to C18 MPLC eluting with a gradient system of MeOH/H_2O (5:95 to 100:0, v/v) to afford eight major fractions (A1−A8). Fraction A1 (1.2 g) was chromatographed over a Sephadex LH-20 column (4 × 65 cm) with MeOH/H_2O (1:1, v/v) and was further purified by reversed-phase semipreparative HPLC with MeOH/0.1% TFA in water (0.8:99.2, v/v) to afford compound **S1** (9.2 mg, t_R = 19.5 min). Fraction A2 (1.5 g) was chromatographed over a Sephadex LH-20 column (4 × 65 cm) with MeOH/H_2O (1:1, v/v) and was further purified by reversed-phase semipreparative HPLC with MeOH/0.1% TFA in water (4:96, v/v) to afford compounds **S2** (2 mg, t_R = 29.8 min) and **S5** (10.1 mg, t_R = 19.4 min) and then with MeOH/0.1% TFA in water (2.6:97.4, v/v) to afford compound **S7** (9.8 mg, t_R = 37.1 min). Fraction A3 (0.5 g) was chromatographed over a Sephadex LH-20 column (4 × 65 cm) with MeOH/H_2O (1:1, v/v) and was then further purified by reversed-phase semipreparative HPLC with MeOH/0.1% TFA in water (10:90, v/v) to afford compounds **S6** (4 mg, t_R = 43.0 min) and **S8** (3.8 mg, t_R = 26.8 min) and with MeOH/0.1% TFA in water (5:95, v/v) to afford compound **S9** (5.1 mg, t_R = 34.7 min). Similarly, fraction A7 (0.9 g) was chromatographed over a Sephadex LH-20 column (4 × 65 cm) with MeOH/H_2O (1:1, v/v) and was then further purified by reversed-phase semipreparative HPLC with MeOH/0.1% TFA in water (41:59, v/v) to afford compounds **S3** (3 mg, t_R = 75.3 min) and **S4** (12.6 mg, t_R = 80.2 min).

*2.5.1. Data for (6R)-6-hydroxy-3-(hydroxymethyl)-2-cyclohexenone (**S1**):* yellow oil; $[\alpha]_D^{20}$ +27.8 (*c* 0.9, MeOH); CD (MeOH) 232 (Δε −4.62), 247 (Δε −10.49), 323 (Δε −0.39) nm; HR-ESIMS *m*/*z* 141.0557 $[M - H]^-$ (calcd for $C_7H_9O_3$, 141.0552); ^1H and ^{13}C NMR data shown in Table 3.

*2.5.2. Data for 3,4-dihydro-5-(hydroxymethyl)pyran-2-one (**S2**):* white amorphous powder; HR-ESIMS *m*/*z* 127.0396 $[M - H]^-$ (calcd for $C_6H_7O_3$, 127.0395); ^1H and ^{13}C NMR data shown in Table 3.

dx.doi.org/10.1021/jf501924y | J. Agric. Food Chem. 2014, 62, 6687−6698

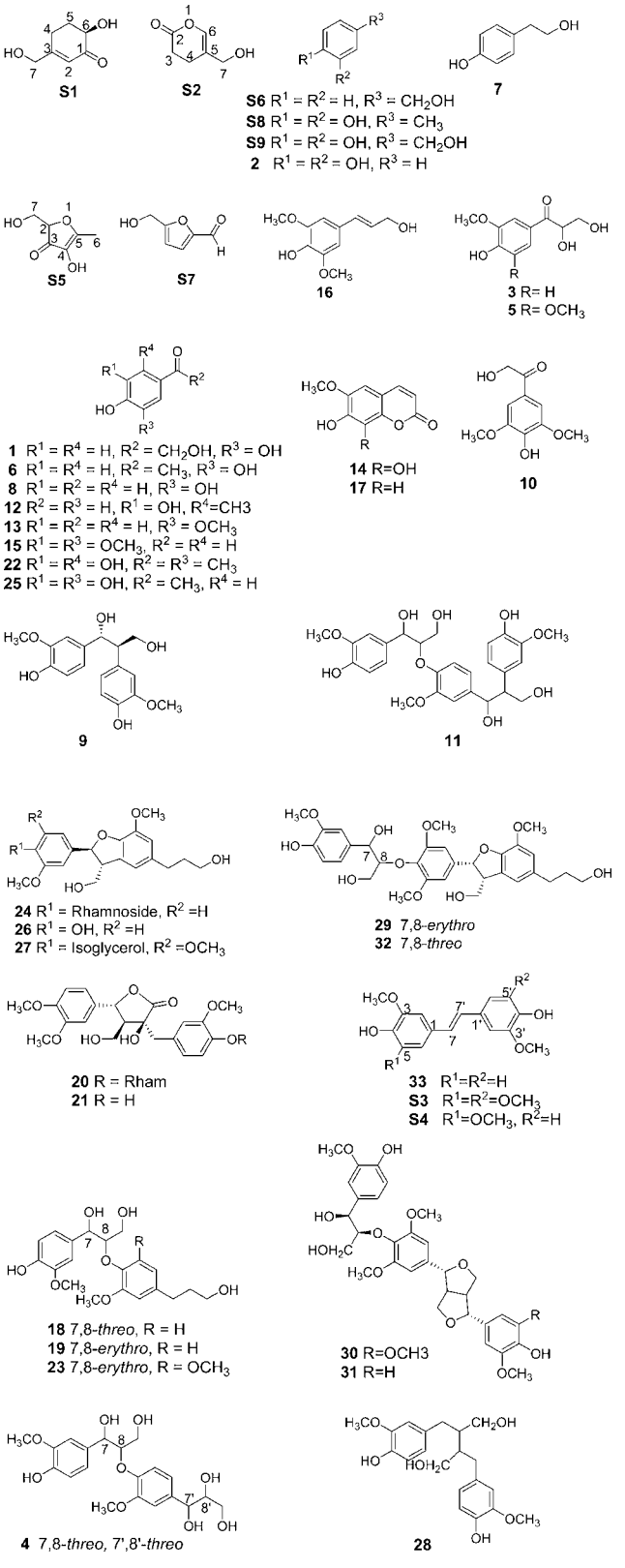

Figure 1. Chemical structures of compounds identified in MSX samples.

*2.5.3. Data for 4,4′-dihydroxy-3,3′,5,5′-tetramethoxystilbene (**S3**):* purple amorphous powder; (+)ESIMS m/z 355.1076 $[M + Na]^+$, calcd for molecular formula $C_{18}H_{20}O_6$; ^{1}H NMR (300 MHz, CD_3OD) δ 3.83 (12H, s, 3,3′,5,5′-OCH_3), 6.76 (4H, s, H-2,2′,4,4′), 6.88 (2H, s, H-7,7′). The NMR data are consistent with those in the previous literature report.[20]

*2.5.4. Data for 4,4′-dihydroxy-3,3′,5-trimethoxystilbene (**S4**):* yellow amorphous powder; (+)ESIMS m/z 325.0977 $[M + Na]^+$, calcd for molecular formula $C_{17}H_{18}O_5$; ^{1}H NMR (300 MHz, CD_3OD) δ 3.81 (6H, s, 3,5-OCH_3), 3.83 (3H, s, 3′-OCH_3), 6.71 (1H, d, J = 8.0 Hz, H-5′), 6.74 (2H, s, H-2,6), 6.86 (2H, s, H-7,7′), 6.91 (1H, d, J = 8.0 Hz, H-6′), 7.05 (1H, s, H-2′). The NMR data are consistent with those in the previous literature report.[20]

*2.5.5. Data for 4-hydroxy-2-(hydroxymethyl)-5-methyl-3(2H)-furanone (**S5**):* yellow oil; (+)ESIMS m/z 167.0240 $[M + Na]^+$, calcd for molecular formula $C_6H_8O_4$; ^{1}H NMR (300 MHz, CD_3OD) δ 3.97 (1H, dd, J = 10.5 Hz, H-2), 4.03 (1H, dd, J = 10.5 Hz, J = 4.3 Hz, $-CH_2$), 4.18 (1H, dd, J = 10.5 Hz, J = 4.3 Hz, $-CH_2$), 1.89 (3H, s, $-CH_3$); ^{13}C NMR (300 MHz, CD_3OD) δ 15.5 (C-6), 68.9 (C-7), 72.5 (C-2), 132.6 (C-5), 161.1 (C-4), 189.1 (C-3). The NMR data are consistent with those in the previous literature report.[21]

*2.5.6. Data for benzenemethanol (**S6**):* colorless oil; (+)ESIMS m/z 131.0392 $[M + Na]^+$, calcd for molecular formula C_7H_8O; ^{1}H NMR (300 MHz, $CDCl_3$) δ 7.36 (2H, d, J = 7.5 Hz, H-2,6), 7.31 (3H, m, H-3,4,5), 4.67 (2H, s, H-7). The NMR data are consistent with those in the previous literature report.[22]

*2.5.7. Data for 5-(hydroxymethyl)-2-furaldehyde, also known as 5-(hydroxymethyl)furfural (HMF; **S7**):* yellow oil; (+)ESIMS m/z 149.0132 $[M + Na]^+$, calcd for molecular formula $C_6H_6O_3$; ^{1}H NMR (300 MHz, CD_3OD) δ 9.48 (1H, s, −CHO), 7.33 (1H, d, J = 3.5 Hz, H-3), 6.53 (1H, d, J = 3.5 Hz, H-4), 4.56 (2H, s, $-CH_2$). The NMR data are consistent with those in the previous literature report.[23]

*2.5.8. Data for 4-methyl-1,2-benzenediol (**S8**):* colorless amorphous powder; (+)ESIMS m/z 147.0342 $[M + Na]^+$, calcd for molecular formula $C_7H_8O_2$; ^{1}H NMR (300 MHz, CD_3OD) δ 6.52 (1H, d, J = 8.4 Hz, H-5), 6.47 (1H, s, H-3), 6.39 (1H, d, J = 8.4 Hz, H-6), 2.06 (3H, s, $-CH_3$). The NMR data are consistent with those in the previous literature report.[24]

*2.5.9. Data for 4-(hydroxymethyl)-1,2-benzenediol (**S9**):* colorless amorphous powder; (+)ESIMS m/z 163.0290 $[M + Na]^+$, calcd for molecular formula $C_7H_8O_3$; ^{1}H NMR (300 MHz, CD_3OD) δ 7.33 (1H, s, H-3), 7.33 (1H, d, J = 8.1 Hz, H-6), 6.79 (1H, d, J = 8.1 Hz, H-5), 4.73 (2H, s, $-CH_2$). The NMR data are consistent with those of the previous literature report.[25]

2.6. Quantification of Compounds S5 and S7 in MSX Samples. Because compounds **S5** and **S7** appeared as major compounds in the MSX-2 sample (HPLC-DAD chromatogram shown in Figure 2C), the levels of these compounds were quantified in both MSX samples. HPLC-DAD analyses were conducted using an Alltima C18 column (250 × 4.6 mm i.d., 5 μM; Alltech) with a flow rate of 0.75 mL/min and an injection volume of 20 μL. A linear gradient solvent system consisting of solvent A (0.1% TFA in water) and solvent B (methanol) at room temperature was used as follows: 0−19 min, from 5% to 23% B; 20−21 min, from 23% to 100% B; 22−23 min, from 100% to 5% B; 23−41 min, 5% B. For quantification purposes, calibration curves were constructed for each of the pure compounds, **S5** and **S7**, as follows: **S5** [$y = (4 \times 10^8)x + 102305$ with $r^2 = 1$]; **S7** [$y = (4 \times 10^8)x + 3 \times 10^6$ with $r^2 = 0.9974$].

2.7. Quantification of the Total Phenolic Content of MSX Samples. The MSX samples were quantified for total phenolic content using the Folin−Ciocalteau method on the basis of gallic acid equivalents (GAEs) as previously reported.[26] Briefly, each MSX sample (3.1 mg) was dissolved in 10 mL of methanol/H_2O (1:1, v/v), and 200 μL of each sample was incubated with 3 mL of methanol/H_2O (1:1, v/v) and 200 μL of Folin−Ciocalteau reagent for 10 min at 25 °C. After this, 600 μL of a 20% sodium carbonate (Na_2CO_3) solution was added to each tube and the resulting solution vortexed. The tubes were then further incubated for an additional 20 min at 40 °C and then immediately cooled in an ice bath to room temperature. The samples and standard (gallic acid) were processed identically. The absorbance was determined at 755 nm, and the final results were calculated from the standard curve obtained from a Spectramax plate reader (Molecular Devices, Sunnyvale, CA).

2.8. Antioxidant Activity of MSX Samples. The antioxidant potentials of the MSX samples were determined by the DPPH free radical scavenging assay as previously reported.[27] The assay was conducted in a 96-well format using serial dilutions of 100 μL aliquots of

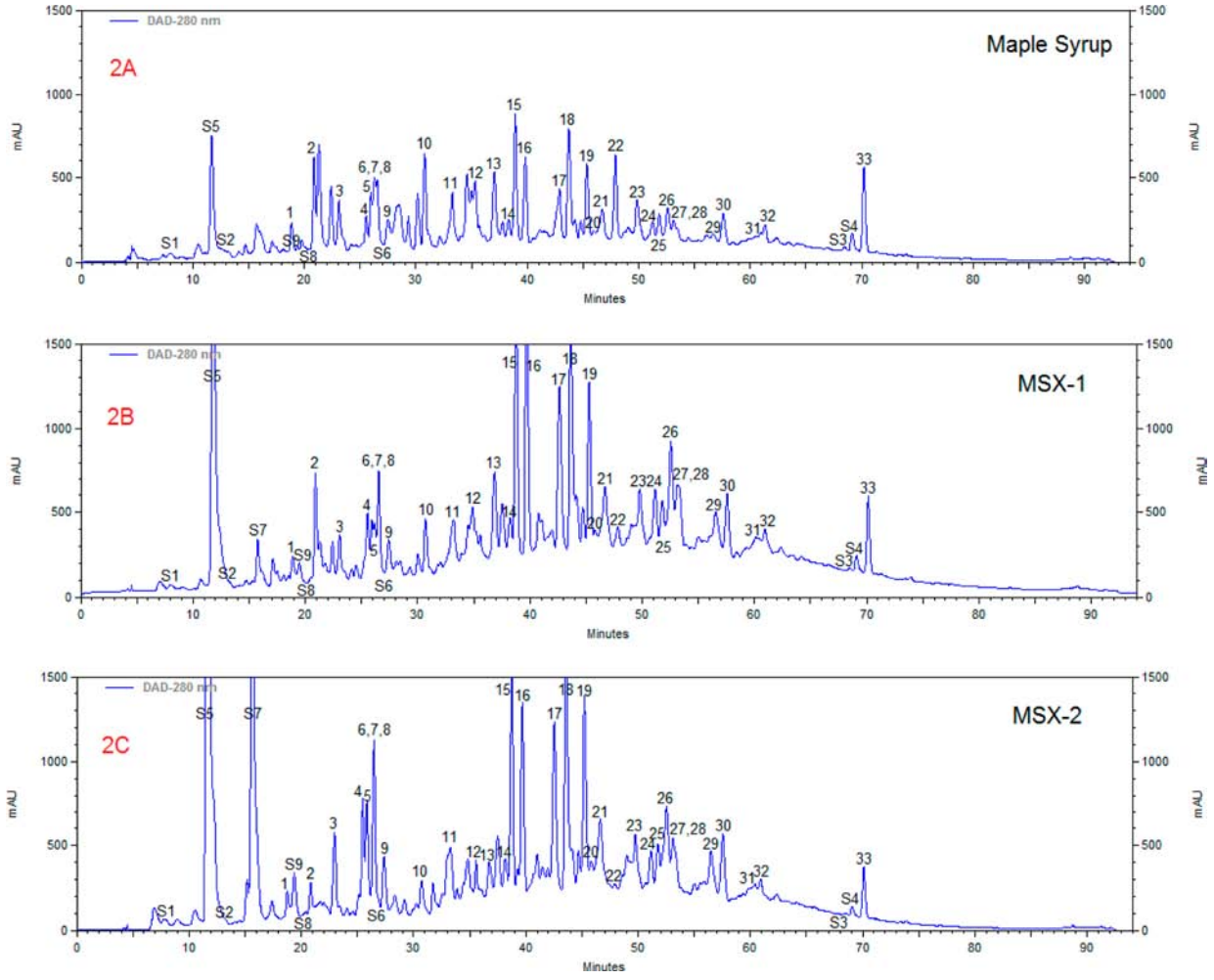

Figure 2. HPLC-DAD chromatograms of maple syrup (A), MSX-1 (B), and MSX-2 (C) at a detection wavelength of 280 nm. Peaks labeled **1**−**9** and **11**−**33** were identified by comparison to phenolic standards previously isolated from maple syrup.[4−6] Peak **10** was identified by comparison to phenolic standard previously isolated from maple sap.[7] Peaks S1−S9 were isolated and identified (by NMR) from MSX for the first time. The names of the compounds are listed in Table 1, and their chemical structures are shown in Figure 1

Table 2. Compounds S1−S9 Isolated from MSX and Identified by NMR

compd	identity	ref for NMR data
S1	(6*R*)-6-hydroxy-3-(hydroxymethyl)-2-cyclohexenone	
S2	3,4-dihydro-5-(hydroxymethyl)pyran-2-one	
S3	4,4′-dihydroxy-3,3′,5,5′-tetramethoxystilbene	20
S4	4,4′-dihydroxy-3,3′,5′-trimethoxystilbene	20
S5	4-hydroxy-2-(hydroxymethyl)-5-methyl-3(2*H*)-furanone	21
S6	benzenemethanol	22
S7	5-(hydroxymethyl)furfural	23
S8	4-methyl-1,2-benzenediol	24
S9	4-(hydroxymethyl)-1,2-benzenediol	25

test samples (ranging from 26 to 2500 μg/mL), and then DPPH (150 μL) was added to each well to yield a final DPPH concentration of 137 μM. The absorbance was determined after 30 min at 515 nm, and the scavenging capacity (SC) was calculated as SC (%) = $[(A_0 - A_1/A_0)] \times 100$, where A_0 is the absorbance of the reagent blank and A_1 is the absorbance of the test samples. The control contained all reagents except the compounds, and all tests were performed in triplicate. IC_{50} values denote the concentration (μg/mL) of sample required to scavenge 50% of the DPPH free radicals (Table 4).

Table 3. ^{1}H NMR and ^{13}C NMR Data for Compounds S1 and S2[a]

	S1		S2	
position	δ_C	δ_H	δ_C	δ_H
1	200.3			
2	120.0	6.00 s	176.5	
3	167.0		21.7	2.53 m
4	25.1	2.32 m	21.7	2.53 m
5	31.0	1.78 m	133.1	
		2.19 m		
6	72.3	4.05 m	148.3	7.33 s
7	63.3	4.07 br s	72.1	4.76 s

[a] ^{1}H NMR (500 MHz) and ^{13}C NMR (125 MHz) for **S1**; ^{1}H NMR (300 MHz) and ^{13}C NMR (75 MHz) for **S2**.

2.9. Cell Culture. The RAW 264.7 mouse macrophage cells (ATCC, Manassas, VA) were cultured in Dulbecco's modified Eagle's medium (DMEM) supplemented with 10% fetal bovine serum (FBS), penicillin G (100 U/mL), and streptomycin (100 μg/mL) (Sigma-Aldrich) and maintained at 37 °C in 5% CO_2 humidified air. Lipopolysaccharide (LPS) was purchased from Sigma-Aldrich. The cultured human hepatoma HepG2 cell line (ATCC) was grown in DMEM (Lonza, Allendale, NJ) containing normal glucose (4.5 mmoL/L D-glucose)

dx.doi.org/10.1021/jf501924y | J. Agric. Food Chem. 2014, 62, 6687−6698

Table 4. Total Phenolic Contents of MSX Samples and Their DPPH Free Radical Scavenging Activities

sample	total phenolic content of MSX[a] (mg/100 g of gallic acid equivalents)	total phenolic content of MSX−EtOAc (mg/100 g of gallic acid equivalents)	DPPH free radical scavenging activity of MSX[a,b] (IC_{50}, μg/mL)
MSX-1	16648.15	26278.28	97.6 ± 4.73
MSX-2	16337.83	27441.33	102.4 ± 7.25

[a]Assay conducted with neat samples of original MSX samples. [b]Positive controls, ascorbic acid and BHT, have IC_{50} values of 40 and 3000 μM, respectively.[5]

supplemented with 10% FBS, 100 units/mL penicillin, and 100 μg/mL streptomycin. Cells were incubated in a humidified atmosphere of 5% CO_2 at 37 °C.

2.10. Assay for Nitrite Concentration. The nitrite concentration assay was conducted according to methods previously described by our group for an ethyl acetate extract of pure maple syrup (MS−EtOAc).[14] Briefly, RAW 264.7 macrophages were seeded (1×10^5 cells/100 μL) in 96-well plates. After 24 h of incubation, the RAW 264.7 cells were stimulated with 100 ng/mL LPS followed by treatment with ethyl acetate extracts of the MSX samples (50 and 100 μg/mL solubilized in DMSO) for 24 h. The final DMSO concentration in the cell culture medium was <0.1%. After 24 h of incubation, cell culture supernatants were collected for nitrite (NO) and prostaglandin E2 (PGE_2) measurements (further described below). Cell culture supernatants were incubated with an equal volume of modified Griess reagent (Sigma-Aldrich) for 20 min at room temperature. The optical densities were measured at 540 nm, and the nitrite levels were determined by comparison to a standard curve. The assay was performed using three individual wells for each sample.

2.11. Assay for PGE_2 Release. PGE_2 was determined using the above cell supernatants as previously described.[14] Briefly, PGE_2 levels were measured using an enzyme immunosorbent (EIA) kit (Cayman Chemical, Ann Arbor, MI) according to the manufacturer's protocol. The experiment was performed with three individual samples per treatment.

2.12. Glucose Assay. The glucose assay was performed as described previously[28] with some modifications. Briefly, HepG2 cells were cultured in complete medium with 10% FBS to ∼80% cell confluence in 96-well plates and subjected to the assays. After the cells were confluent, the medium was replaced with medium containing 1% FBS and low glucose (1 mmol/L). After overnight incubation, the cells were treated with the MSX samples dissolved in DMSO (each at 50 and 100 μg/mL concentrations) for 7 h. The cell supernatants were assayed for glucose concentration using a glucose assay kit (Eton Bioscience Inc., Charlestown, MA). The absorbance was measured at 490 nm. The experiment was performed in triplicate.

2.13. Amino Acid Contents of MSX Samples by HPLC-FL. The amino acid contents of the MSX samples were determined by using the AccQ Tag amino acid analysis assay from Waters Corp. (Milford, MA) as previously reported.[7] Briefly, this assay uses the Waters AccQ Fluor reagent to derivatize amino acids which are subsequently separated by reverse-phase HPLC and quantitated by fluorescence detection (FL) using a Waters AccQ Tag column. Peaks were identified by comparison of their retention times to amino acid reference standards.

2.14. Organic Acid Contents of MSX Samples by HPLC-DAD. The organic acid contents of the MSX samples were determined by HPLC-DAD analyses using an Allure organic acid column (150 × 4.6 mm) purchased from Restek Corp. (Bellefonte, PA) as reported.[7] Peaks were identified on the basis of comparison of their retention times to those of organic acid standards. Each sample was injected in triplicate.

2.15. Vitamin Contents of MSX Samples by HPLC-DAD. The vitamin contents of the MSX samples were determined by HPLC-DAD analyses using a Luna 5 μm C18 column (250 × 4.6 mm) purchased from Phenomenex (Torrance, CA) with a flow rate of 1.0 mL/min and column temperature of 25 °C. A linear gradient solvent system consisting of solvent A (0.1% TFA in water) and solvent B (acetonitrile) was used as follows: 0−5 min, 0% B; 5−11 min, from 0% to 25% B; 11−17 min, from 25% to 40% B; 17−18 min, from 40% to 60% B; 18−20 min, from 60% to 0% B; 20−28 min, 0% B. For quantification purposes, calibration curves were constructed for each vitamin standard as follows: riboflavin (B2) [$y = 143176x + 8066.6$ with $r^2 = 0.9981$]; niacin (B3) [$y = 56212x - 813.11$ with $r^2 = 0.9975$]. Aliquots of each MSX sample (a 10-fold dilution of a stock solution of 100 mg/mL) were centrifuged at 10 000 rpm for 5 min, and then the supernatant (30 μL aliquots) was injected directly for HPLC-DAD analyses. Peaks were identified on the basis of comparison of their retention times to those of vitamin standards. Each sample was injected in triplicate.

2.16. Sugar Contents of MSX Samples by HPLC-RI. The sugar contents of the MSX samples were determined by HPLC-RI analyses using a Waters Sugar-Pak I column (300 × 6.5 mm, 10 μm) purchased from Waters Corp. according to methods previously reported.[7] The isocratic solvent system consisted of ethylenediaminetetraacetic acid calcium disodium salt (EDTA; 50 mg/L) over 15 min. The standard for the complex sugars (6.0 mg) eluted before sucrose and was isolated as a single peak after repeated injections of pure maple syrup using the same HPLC conditions as previously reported[7] except that pure deionized (DI) water was substituted for EDTA. For quantification purposes, calibration curves were constructed for each sugar standard (dissolved in DI water) as follows: sucrose [$y = 527830x + 312928$ with $r^2 = 0.9999$]; glucose [$y = 572734x + 1703$ with $r^2 = 1$]; fructose [$y = 545540x + 5351.5$ with $r^2 = 1$]; complex sugars [$y = 511030x + 93196$ with $r^2 = 1$]. Peaks were identified on the basis of comparison of their retention times to that of each of the standards. Each sample was injected in triplicate.

2.17. Mineral Contents of MSX Samples by Inductively Coupled Plasma Mass Spectrometry (ICP-MS). The analyses of the mineral contents of the MSX samples were conducted by using ICP-MS on a Thermo Scientific iCAP Qa instrument coupled to an ASX-510 HS high-speed autosampler (Thermo Scientific, West Palm Beach, FL) as previously reported.[7] Calibration standards of the minerals Na, Mg, Al, K, Ca, Fe, Mn, Cu, Zn, As, Se, Mo, and Cd and the internal standard, Y, were purchased from Ultra Scientific (North Kingstown, RI). A MARS5Microwave digestion system and reaction vessels for digestion of MSX samples were purchased from CEM Corp. (Matthews, NC). Each MSX sample (10 mg) was combined with nitric acid (1 mL; ICP-MS grade) and digested in reaction vessels in the microwave. The digested solutions were transferred to 1.5 mL centrifuge tubes and centrifuged for 10 min at 10 000 rpm at 4 °C. An aliquot of each digested solution (200 μL) was further diluted to 10 mL with DI water and then submitted for ICP-MS analysis. Standard curves for each of the minerals were obtained on the day of the analysis, and the internal standard, Y, was added to every sample to ensure the accuracy of the method.

2.18. Animal Toxicity Studies on MSX Samples. The animal toxicity studies were conducted by ITR Laboratories Canada Inc. (Quebec City, Canada) under a contract with FPAQ. The study followed a well-established protocol of a 7 day oral toxicity study in Sprague−Dawley rats ($n = 10$ consisting of 5 males and 5 females per treatment group) to determine the toxicity of the MSX samples. The test samples and control/vehicle treatments were administered once daily by oral gavage (using a gavage needle attached to a syringe) for 7 consecutive days at doses of 100, 300, and 1000 mg/kg/day for each MSX sample. Therefore, animals of group 1 were administered the vehicle item (0.5% carboxymethyl cellulose) alone, animals of groups 2, 3, and 4 were administered MSX-1 (at doses of 100, 300, and 1000 mg/kg/day, respectively), and animals of groups 5, 6, and 7 were administered MSX-2 (at doses of 100, 300, and 1000 mg/kg/day, respectively). The dose volume was 10 mL/kg for all animals, and the actual volume administered to each rat was calculated and adjusted on the basis of the body mass of each animal. All animals were euthanized upon completion of the treatment period (day 8), and following an overnight period without food, the animals were anesthetized with

isoflurane to allow collection of blood samples for clinical pathology evaluation, followed by exsanguination. To avoid autolytic changes, the necropsy examination of the carcass was conducted as soon as possible on all animals. Gross pathology consisted of an external examination, including identification of all clinically recorded lesions, as well as a detailed internal examination. A staff pathologist was available for consultation during all necropsies. For animals euthanized at termination, organs identified in the tissue preservation section were dissected, trimmed free of fat, and weighed, and the body mass to relative organ masses were calculated. The study plan was reviewed and assessed by the Animal Care Committee (ACC) of ITR, and the ACC acceptance of the study plan was maintained on file at ITR. All animals used in the study were cared for in accordance with the principles outlined in the current *Guide to the Care and Use of Experimental Animals* as published by the Canadian Council on Animal Care and the *Guide for the Care and Use of Laboratory Animals*, an NIH publication.

2.19. Ash and Fiber Contents of MSX samples. The ash and fiber contents of the MSX samples were carried out by Covance Laboratories (Madison, WI) using approved standard operating procedures (SOPs) that followed the Official Methods of Analysis of AOAC International (for ash and fiber contents).

3. RESULTS AND DISCUSSION

3.1. Preparation of MSX. Maple syrup is a popular and widely consumed natural sweetener, but to date, there are no reported studies of any food-grade extracts derived from this sweetener. Many plant food industries have expanded and diversified their product portfolios with commercial botanical extracts, e.g., grape seed and cranberry extracts (derived from the squeezed fruit pulp and seeds after juicing), which are widely used as functional food and nutraceutical ingredients. Notably, many of these generally regarded as safe (GRAS) extracts have grown in consumer acceptance and are being increasingly studied in both academic and industrial research laboratories for their chemical compositional and biological effects. Therefore, all of the aforementioned factors, in addition to our group's ongoing interest in maple products, prompted the initiation of this project, which sought to develop a proprietary maple syrup extract (named MSX). For this project, two declassified maple syrup samples (see the Materials and Methods for details) were used to generate the MSX samples, named MSX-1 and MSX-2. The MSX samples were produced in a pilot-scale facility using adsorption chromatography with an FDA food-grade approved resin (Amberlite XAD-16) and food-grade solvents (water and denatured ethanol). MSX appears as a dark brown free-flowing dried powder after solvent removal.

3.2. Chemical Composition of MSX. *3.2.1. Phytochemicals.* A total of 42 phytochemicals (the compound structures are shown in Figure 1, and the identities are listed in Table 1) were identified in MSX using a combination of (1) HPLC-DAD methods (by comparison to chemical standards previously isolated by our laboratory from maple sap and syrup)[4−7] and (2) isolation (by various chromatographic methods) and structure elucidation (by NMR) of those compounds for which chemical standards were lacking. Therefore, among the 42 compounds, 33 (**1**−**33**) compounds were identified by HPLC-DAD and 9 (**S1**−**S9**) compounds were isolated and identified by NMR. Notably, among the nine isolates, two compounds (**S1** and **S2**) are new compounds, and a detailed description of their structure elucidation is being reported here for the first time. Details of the phytochemical characterization of MSX are provided below.

*3.2.1.1. Identification of Compounds **1**−**33** in MSX by HPLC-DAD.* Figure 2A shows the HPLC-DAD chromatogram of an ethyl acetate extract of pure maple syrup from which compounds **1**−**33** were identified on the basis of comparison of their HPLC-DAD retention times and UV spectra (see Table 1) to those of authentic standards previously isolated from maple sap and syrup by our laboratory.[4−7] The HPLC profiles of the MSX-1 and MSX-2 samples (see parts B and C, respectively, of Figure 2) showed close similarities to the HPLC profile of pure maple syrup (Figure 2A), allowing for the identification of compounds **1**−**33** therein. The striking similarities of the HPLC profile of the pure maple syrup sample to the HPLC profiles of the MSX samples suggest that phytochemicals present in pure maple syrup persist in these declassified maple syrup samples. While it was not possible to determine the levels of all of the individual phytochemicals present in the MSX sample given the complex overlapping peaks in the HPLC-DAD profiles, we conducted quantitative studies based on two major compounds, namely, **S5** and **S7** (further described below; see Table 5) present therein. In addition, we quantified the MSX samples to total polyphenol contents (further described below).

Table 5. Levels (%) of Compounds S5 and S7 in the MSX Samples

sample	compd **S5**	compd **S7**
MSX-1	0.095	0.004
MSX-2	0.132	0.049

*3.2.1.2. Identification of Compounds **S1**−**S9** in MSX Samples by Isolation and Structure Elucidation (by NMR).* In the current study, apart from the identification of compounds **1**−**33** (by HPLC-DAD methods), an additional nine compounds (compounds **S1**−**S9**; Table 2) were isolated and identified (using mass spectral and NMR data and by comparison to literature data when available). Notably, all of these nine compounds were originally present in pure maple syrup (peaks are apparent in the HPLC chromatogram shown in Figure 2A), but these compounds were not isolated in our previous phytochemical studies.[4−7] Among the nine isolates, two are new compounds, (6*R*)-6-hydroxy-3-(hydroxymethyl)-2-cyclohexenone (**S1**) and 3,4-dihydro-5-(hydroxymethyl)pyran-2-one (**S2**), two are stilbene derivatives, 4,4′-dihydroxy-3,3′,5,5′-tetramethoxystilbene (**S3**) and 4,4′-dihydroxy-3,3′,5′-trimethoxystilbene (**S4**), two are furan derivatives, 4-hydroxy-2-(hydroxymethyl)-5-methyl-3(2*H*)-furanone (**S5**) and 5-(hydroxymethyl)furfural (**S7**), and three are Ar−C1 derivatives (**S6**, **S8**, and **S9**). Among these nine isolates, only **S7**, a known product of the Maillard reaction, has previously been reported from maple syrup,[29] and thus, all of the other eight isolates are being reported from maple syrup herein for the first time. Also, the isolation and structure elucidation of two additional stilbenoids (compounds **S3** and **S4**) supports our previous report of the occurrence of the stilbene phenolic subclass in maple syrup [where (*E*)-3,3′-dimethoxy-4,4′-dihydroxystilbene was previously reported[4]]. The NMR data for all nine isolates (**S1**−**S9**) are provided herein (see the Materials and Methods), but only the detailed structure elucidation of the two new compounds (**S1** and **S2**) is discussed below.

*3.2.1.2.1. Elucidation of Compound **S1**.* Compound **S1** was obtained as a yellow oil with a molecular formula of $C_7H_{10}O_3$ as determined by the HR-ESIMS m/z 141.0557 $[M - H]^-$ (calcd for $C_7H_9O_3$, 141.0552) data with 3 degrees of unsaturation. The ^1H and ^{13}C NMR data (Table 3) of compound **S1** revealed the presence of an α,β-unsaturated ketone moiety [δ_C 120.0, 167.0 and 200.3; δ_H 6.00 (1H, s)], one oxygenated methine group [δ_C 72.3; δ_H 4.05 (1H, m)], and three methylene groups (δ_C 25.1,

dx.doi.org/10.1021/jf501924y | J. Agric. Food Chem. 2014, 62, 6687−6698

31.0, and 63.3). The aforementioned NMR data and the HMBC correlations (see Figure 3) from H-2 (δ_H 6.00) to C-6, C-7, and

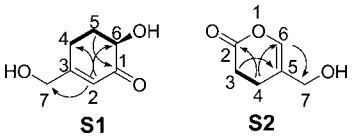

Figure 3. Key ^{1}H−^{1}H COSY (−) and HMBC (H → C) correlations of compounds **S1** and **S2**.

C-4, along with the C-4−C-5−C-6 spin system (from the ^{1}H−^{1}H COSY data) implied that the planar structure of compound **S1** was 6-hydroxy-3-(hydroxymethyl)-2-cyclohexenone. The only chiral center (C-6) in the structure of compound **S1** was assigned an *R* configuration on the basis of a negative Cotton effect at 323 nm ($\Delta\varepsilon$ −0.39, n → π^* transition of the α,β-unsaturated ketone) in the CD spectrum.[30] Notably, while this is the first reported occurrence of compound **S1**, its methoxylated derivative, 6-hydroxy-3-(methoxymethyl)-2-cyclohexenone, has been previously reported, but the latter compound was obtained by synthesis and not as an isolated natural product.[31]

*3.2.1.2.2. Elucidation of Compound **S2**.* Compound **S2** was isolated as an amorphous powder with a molecular formula of $C_6H_8O_3$ as established by the HR-ESIMS *m/z* 127.0396 [M − H]$^-$ (calcd for $C_6H_7O_3$, 127.0395) data with 3 degrees of unsaturation. The ^{13}C NMR data of compound **S2** showed resonance signals typical of an ester carbonyl group at δ_C 176.5, a single C−C double bond (δ_C 148.3 and 133.1), and three methylene groups (δ_C 21.7, 21.7 and 72.1). The linkage from C-2 to C-4 was determined by the ^{1}H−^{1}H COSY correlation of H-3/H-4 and the HMBC correlations (see Figure 3) from H-4 and H-3 to C-2. The HMBC correlation between H-4 and C-6 and between H-3 and C-5 and the carbon resonance signal of C-2 (δ_C 176.5) revealed the connection between C-2 and C-6 was via an oxygen. The HMBC correlations from H_2-7 (δ_H 4.76) to C-5 and C-6 indicated that an oxygenated methylene (CH_2-7) was attached to C-5. Therefore, the structure of **S2** was elucidated as that of the new compound 3,4-dihydro-5-(hydroxymethyl)-pyran-2-one.

3.2.1.3. Quantification Studies of MSX Based on Total Polyphenol Content. Given that maple syrup is known to contain phenolics,[4] the MSX-1 and MSX-2 samples were evaluated for total polyphenol content (see Table 4). As expected, because these are extracts, the polyphenol contents of the MSX samples were far greater than that of the original pure maple syrup (ca. 16% vs 0.04% GAEs). However, the polyphenol levels of MSX−EtOAc extracts (ca. 27% GAEs) were in a range similar to that of MS−EtOAc (ca. 30% GAEs) which we have recently reported shows anti-inflammatory effects in an LPS-stimulated RAW264.7 macrophage model[14] (further discussed below). However, the aforementioned MS−EtOAc extract was not produced under food-grade conditions, unlike the MSX samples which are being investigated in the current study for human consumption (i.e., for nutraceutical applications).

*3.2.1.4. Quantification Studies of MSX Based on the Levels of Compounds **S5** and **S7**.* Several furan derivatives, in particular, 5-(hydroxymethyl)furfural (HMF; compound S7), are well-known Maillard products formed during heat-processing of sugary foods, including the natural sweeteners honey and maple syrup.[28,32] Interestingly, HMF has been a subject of debate due to reports of its potential toxicity, although this is still a controversial issue as this compound has been shown to exert antioxidant, antitumor, and anti-inflammatory effects.[33,34] Thus, since the two furan derivatives isolated in this study, namely, compounds **S5** and **S7**, appeared as major peaks in the HPLC-DAD chromatogram of the MSX-2 sample (see Figure 2C), we sought to determine their levels in both of the MSX samples (see Table 5). Of the two MSX samples, MSX-2 contained higher levels of both compounds **S5** and **S7** (0.132% and 0.049%, respectively), and among the two compounds, **S5** was present in higher levels than **S7** in both of the MSX samples. We did not attempt to correlate the levels of any individual constituents present in the MSX samples to their overall biological activities (further discussed in section 3.4). However, given the occurrence of the furan derivatives therein, and the aforementioned controversial reports of the potential toxicity of HMF,[33,34] we also evaluated the MSX samples for toxicity using an animal model (further discussed in section 3.3). Moreover, animal toxicity studies are especially relevant if the MSX samples are to be utilized for future nutraceutical applications.

3.2.2. Sugars. The sugar contents (sucrose, glucose, fructose, and complex sugars) of the MSX samples were quantitated in this study (see Table 6). The MSX samples contained similar levels of total sugars (ca. 50%), and similar to pure maple syrup, sucrose was the most abundant sugar. Apart from sucrose, the MSX samples also contained complex sugars, glucose, and fructose. The detection of complex sugars in the MSX samples is not surprising considering that the presence of these constituents has been previously reported in pure maple syrup.[2] Complex polysaccharides are being increasingly used as functional food ingredients and have interesting biological effects,[35,36] and thus, their presence in MSX, beyond sucrose alone, is interesting from a human health perspective.

3.2.3. Amino Acids. The levels of amino acids, namely, arginine, threonine, proline, and histidine, in the MSX samples are shown in Table 7. Among these amino acids, proline was the most abundant, reaching levels of ca. 19 mg/100 g of the MSX samples.

3.2.4. Organic Acids. The levels of the organic acids, malic acid and fumaric acid in the MSX samples are shown in Table 7. Among the two organic acids, malic acid was the most abundant, reaching levels of ca. 781 and 341 mg/100 g in the MSX-1 and MSX-2 samples, respectively.

3.2.5. Minerals. The mineral contents of the MSX samples are shown in Table 8, and among the two samples, MSX-1 had greater mineral levels compared to the MSX-2 sample, which is in

Table 6. Average Sugar and Vitamin Contents of MSX Samples

	sugar content[a] (mg/100 g)				vitamin content[a] (mg/100 g)	
sample	sucrose	glucose	fructose	complex sugar	B2	B3
MSX-1	38635.18 ± 63.04	63.76 ± 9.25	6.99 ± 0.82	16231.72 ± 20.68	410.26 ± 0.43	7.13 ± 0.01
MSX-2	41136.41 ± 67.21	284.10 ± 11.16	233.65 ± 19.01	8927.52 ± 9.12	290.45 ± 0.06	9.83 ± 0.03

[a]Assay conducted with neat samples of original MSX samples.

Table 7. Average Amino Acid and Organic Acid Contents of MSX Samples

	amino acid content[a] (mg/100 g)			organic acid content[a] (mg/100 g)	
sample	arginine + threonine	proline	histidine	malic acid	fumaric acid
MSX-1	10.06 ± 0.18	19.13 ± 0.32	2.52 ± 0.05	780.99 ± 0.39	15.92 ± 0.02
MSX-2	9.93 ± 0.09	19.29 ± 0.28	0.80 ± 0.05	341.85 ± 0.17	7.51 ± 0.02

[a]Assay conducted with neat samples of original MSX samples.

Table 8. Average Mineral Contents of MSX Samples

	mineral content[a] (mg/100 g)							
sample	K	Ca	Mg	Na	Mn	Al	Zn	Fe
MSX-1	128.35 ± 6.66	380.48 ± 33.10	124.51 ± 9.54	4.86 ± 1.23	58.45 ± 4.06	0.32 ± 0.04	90.98 ± 8.08	0.70 ± 0.07
MSX-2	70.50 ± 7.68	212.78 ± 17.41	48.79 ± 3.94	3.52 ± 1.52	53.19 ± 4.43	0.46 ± 0.11	23.81 ± 2.59	0.44 ± 0.08

[a]Assay conducted with neat samples of original MSX samples.

agreement with the ash data for the two MSX samples (see Table 9, further described below). Among the minerals that were quantitated, magnesium, potassium, calcium, and zinc were the most abundant, reaching levels of ca. 124, 128, 380, and 90 mg/100 g in the MSX-1 sample.

3.2.6. Vitamins. Similar to pure maple syrup,[1] the MSX samples contained two major vitamins, namely, riboflavin (B2) and niacin (B3), and their levels are shown in Table 6. Among the two vitamins, riboflavin was the most abundant, reaching levels of 410 and 290 mg/100 g in the MSX-1 and MSX-2 samples, respectively.

3.2.7. Ash and Fiber. The ash and fiber contents of the MSX samples (assays conducted by Covance) are shown in Tables 9 and 10, respectively. The ash content of the MSX-1 sample was greater than that of the MSX-2 sample (ca. 2.2% vs 1.1%), which correlated with the higher mineral content of the MSX-1 sample compared to the MSX-2 sample (Table 8, discussed above). Interestingly, both of the MSX samples contained ca. 11% total dietary fiber, which was present primarily as soluble fiber (Table 10).

Table 9. Ash Contents of MSX Samples

sample	ash content[a] (%)
MSX-1	2.21
MSX-2	1.10

[a]Assay conducted with neat samples of original MSX samples.

Table 10. Fiber Contents of MSX Samples

	total dietary fiber content[a] (%)			
sample	insoluble dietary fiber	sum of measured fibers	high molecular weight soluble dietary fiber	low molecular weight soluble dietary fiber
MSX-1	<0.75	10.9	5.59	5.31
MSX-2	<0.75	10.9	5.59	5.31

[a]Assay conducted with neat samples of original MSX samples.

3.3. Animal Toxicity Studies in Sprague–Dawley Rat. Animal safety studies were conducted to determine the toxicity of the MSX-1 and MSX-2 samples following once daily oral gavage administration for 7 consecutive days to Sprague–Dawley rat. Parameters monitored during the study included mortality, clinical observations, body masses, and food consumption. In addition, hematology, coagulation, clinical chemistry, and urinalysis parameters were evaluated on day 8. At termination (day 8), all animals were euthanized and subjected to a gross necropsy examination and organ mass measurements. Subsequently, a complete list of tissues were retained and examined microscopically. There were no deaths, no clinical signs, and no changes in body masses, food consumption hematology, coagulation, clinical chemistry, urinalysis, or organ masses that could be attributed to the administration of either the MSX-1 or MSX-2 sample at doses of up to 1000 mg/kg/day. Similarly, there were no microscopic or macroscopic findings which could be attributed to the test samples. Thus, the daily oral administration of the MSX samples for 7 consecutive days to the Sprague–Dawley rat was well tolerated and did not result in any signs of overt toxicity.

3.4. In Vitro Biological Studies of MSX Samples. *3.4.1. MSX Samples Show DPPH Free Radical Scavenging Activity.* In the nutraceutical and functional food industry, many extracts which contain phenolic compounds are well-known to exhibit antioxidant activities. Moreover, published studies have shown that phenolic-enriched extracts of maple sap and maple syrup, as well as their purified phenolic constituents, show antioxidant effects.[4,5,13] Therefore, the MSX-1 and MSX-2 samples were evaluated for their antioxidant effects in the DDPH free radical scavenging assay, and they showed IC_{50} values of ca. 97 and 102 μg/mL, respectively (see Table 4), which were comparable to that of a phenolic-enriched ethyl acetate extract of pure maple syrup (further discussed below; IC_{50} = 75.5 μg/mL).[5] While these samples are all extracts and cannot be compared, on the basis of molar equivalents, to well-known antioxidants commonly used as positive controls, such as ascorbic acid (vitamin C) and butylated hydroxytoluene (BHT; a commercial synthetic antioxidant), we did evaluate the latter compounds in the DPPH assay, and they showed IC_{50} values of ca. 40 and 3000 μM, respectively.[5]

3.4.2. MSX Samples Lowered Nitrite and PGE_2 Concentrations in RAW 246.7 Cell Culture Media. Phenolic-enriched extracts of maple sap and maple syrup, derived by partitioning with ethyl acetate (EtOAc), have been reported to lower nitrite levels [measured as nitric oxide (NO) levels] in cell culture media in LPS-stimulated RAW 264.7 macrophages,[13] a bioassay which is widely used to evaluate the anti-inflammatory effects of natural products. Using the same RAW 264.7 macrophage model, our group has recently investigated the anti-inflammatory effects of an EtOAc extract of pure maple syrup (MS–EtOAc) which showed inhibition of both NO and PGE_2.[14] In that study, we also evaluated the anti-inflammatory effects of several

individual phenolic constituents present in the MS−EtOAc, and among these pure compounds, a stilbenoid, namely, 3,3′-dimethoxy-4,4′-dihydroxystilbene (compound **33**),[4] was the most active compound in the anti-inflammatory assay. However, overall, we observed that the anti-inflammatory effect of the total extract was greater than any of its single purified constituent alone. Notably, the MS−EtOAc extract that we studied in that previous project[14] is not suitable for human consumption (i.e., was not produced under food-grade conditions), unlike the MSX samples which are being studied here. Therefore, in the current study we additionally sought to evaluate the anti-inflammatory effects of phenolic-enriched MSX−EtOAc extracts (see Figure 4). As previously discussed, since we had found that a stilbene

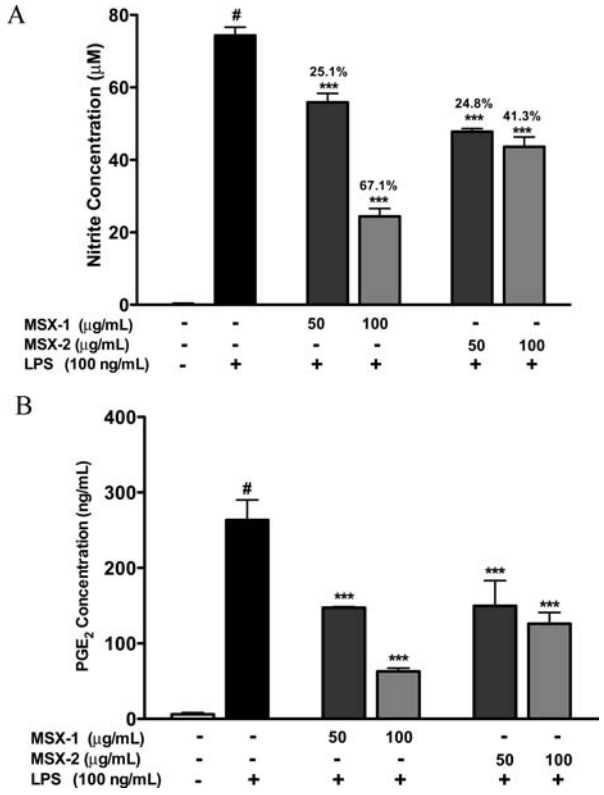

Figure 4. Effects of MSX ethyl acetate extracts on (A) nitrite and (B) PGE_2 production in LPS-stimulated RAW 264.7 cells. Cells were cotreated with LPS (100 ng/mL) and samples (50 and 100 μg/mL) for 24 h. MSX extracts inhibited NO and PGE_2 levels in LPS-stimulated macrophages in a concentration-dependent manner. The values are expressed as the means ± SD of three individual samples. Three asterisks indicate $P < 0.001$ as compared with the LPS-treated macrophages; significant differences between groups were determined using a one-way ANOVA test followed by Dunnett's multiple comparison test. A pound sign indicates $P < 0.001$ for the solvent control compared with the LPS-treated cells; the significant difference was determined using unpaired Student's t test.

(compound **33**) was the most active among the various subclasses of phenolic compounds in the anti-inflammatory assay,[14] and since we isolated two additional stilbene derivatives from the MSX samples reported herein, namely, 4,4′-dihydroxy-3,3′,5,5′-tetramethoxystilbene (**S3**) and 4,4′-dihydroxy-3,3′,5′-trimethoxystilbene (**S4**), we evaluated the two latter compounds for their ability to inhibit the NO level in the RAW 264.7 macrophages. Interestingly, while compound **S3** (at 25 and 50 μM concentrations) did not show any significant decrease in NO levels in the LPS-stimulated macrophages (approximately 2% inhibition), compound **S4** (at 25 and 50 μM concentrations) inhibited the NO levels by 38.8% ± 2.5% and 78.3% ± 2.8%, respectively. Similar to our previous report,[14] we confirmed that compound **33** significantly reduced the NO concentration in the LPS-treated macrophage media by almost 100% ± 1.3%. While it is difficult to make conclusive structure−activity-related (SAR) observations on the basis of data accumulated from only these three stilbenoids, it would appear that substitution of a methoxyl (OCH_3) group at position 5′ (i.e., the R^2 position as in compound **S3**) leads to a significant reduction in bioactivity in this assay.

Similar to our recent published data with MS−EtOAc, both of the MSX−EtOAc extracts significantly inhibited nitrite levels in cell media (Figure 4A). The MSX-1 ethyl acetate extract significantly reduced nitrite production by 25.1% (at 50 μg/mL) and 67.1% (at 100 μg/mL). Also, treatment with 50 and 100 μg/mL concentations of the MSX-2 ethyl acetate extract inhibited nitrite levels by 24.8% and 41.3%, respectively. Thus, the current results show that the MSX−EtOAc extracts lowered nitrite production in a concentration-dependent manner in LPS-stimulated RAW 264.7 cells similar to our previous report for MS−EtOAc.[14]

As a follow-up to the nitrite assay, we also evaluated the levels of PGE2 in cell media. As shown in Figure 4B, PGE_2 levels were elevated following LPS treatment (263.3 ± 26.5 ng/mL), whereas in the absence of LPS, the PGE_2 levels were close to baseline. The levels of PGE_2 were markedly reduced to 147.4 and 62.9 ng/mL by 50 and 100 μg/mL MSX-1 ethyl acetate extract treatment, respectively. Similarly, treatment with 50 and 100 μg/mL MSX-2 ethyl acetate extract lowered PGE_2 levels in LPS-stimulated macrophages to 149.7 and 126.1 ng/mL, respectively. Therefore, taken together, these results suggest that the MSX−EtOAc extracts were capable of reducing NO and PGE_2 in LPS-induced macrophages.

3.4.3. MSX Samples Decreased Glucose Levels in HepG2 Cell Media. Recent published data in a diabetic animal model have shown that pure maple syrup has the ability to reduce plasma glucose levels compared to sucrose solution alone.[11] It has been reported that plant extracts, such as rosemary extract, can regulate glucose and lipid metabolism in HepG2 liver hepatocytes.[27] Therefore, using this cell-culture model, we examined the potential of the MSX samples to regulate glucose consumption, along with the clinical drug metformin, a well-known AMP-dependent protein kinase (AMPK) activator. As shown in Figure 5, the MSX-1 and MSX-2 samples significantly

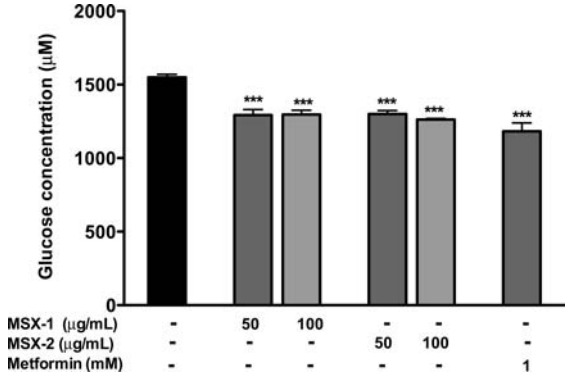

Figure 5. Effects of MSX samples on glucose consumption by HepG2 cells.

decreased glucose levels in the cell supernatants. The glucose levels in the media with 50 and 100 μg/mL MSX-1 treatment were lowered by almost 16% compared to that of the control group. Similarly, the MSX-2 treatment, at 50 and 100 μg/mL concentrations, reduced media glucose levels by about 16% and 18% respectively. Metformin, at 1 mM concentration, also dramatically decreased glucose levels by 23% as compared to that of the control in the HepG2 cell culture media. Therefore, our preliminary in vitro studies reported here lend support to the recent published in vivo study with maple syrup.[11]

In summary, in this project we have conducted chemical compositional, in vitro biological, and in vivo animal safety studies of a novel maple syrup derived extract for potential functional food and nutraceutical applications. To the best of our knowledge, this is the first reported study of a food-grade maple syrup extract.

AUTHOR INFORMATION

Corresponding Author

*Phone: 401-874-9367. Fax: 401-874-5787. E-mail: nseeram@uri.edu.

Funding

This project was supported by Agriculture and Agri-Food Canada (AAFC) through the AgriInnovation program under the Growing Forward policy framework. The animal toxicity study was conducted by ITR Canada and was funded by the Federation of Maple Syrup Producers of Quebec (FPAQ) and AAFC. The large-scale production of the MSX samples was conducted by Silicycle Inc. and was funded by FPAQ. The NMR data were acquired at a research facility at the University of Rhode Island supported in part by National Science Foundation EPSCoR Cooperative Agreement No. EPS-1004057. The ICP mass spectral data were acquired on an instrument located at the University of Rhode Island in the RI-INBRE core facility obtained with Grant No. P20RR016457 from the National Center for Research Resources (NCRR), a component of the National Institutes of Health (NIH).

Notes

The authors declare no competing financial interest.

REFERENCES

(1) Perkins, T. D.; van den Berg, A. K. Maple syrup-production, composition, chemistry, and sensory characteristics. *Adv. Food Nutr. Res.* **2009**, *56*, 101−143.

(2) Storz, G.; Darvill, A. G.; Albersheim, P. Characterization of polysaccharides isolated from maple syrup. *Phytochemistry* **1986**, *25*, 437−441.

(3) Ball, D. W. The chemical composition of maple syrup. *J. Chem. Educ.* **2007**, *84*, 1647−1650.

(4) Li, L.; Seeram, N. P. Maple syrup phytochemicals include lignans, coumarins, a stilbene and other previously unreported antioxidant phenolic compounds. *J. Agric. Food Chem.* **2010**, *58*, 11673−11679.

(5) Li, L.; Seeram, N. P. Further investigation into maple syrup yields three new lignans, a new phenylpropanoid, and twenty-six other phytochemicals. *J. Agric. Food Chem.* **2011**, *59*, 7708−7716.

(6) Li, L.; Seeram, N. P. Quebecol, a novel phenolic compound isolated from Canadian maple syrup. *J. Funct. Foods* **2011**, *3*, 125−128.

(7) Yuan, T.; Li, L.; Zhang, Y.; Seeram, N. P. Pasteurized and sterilized maple sap as functional beverages: Chemical composition and antioxidant activities. *J. Funct. Foods* **2013**, *5*, 1582−1590.

(8) Kermasha, S.; Goetghebeur, M.; Dumont, J. Determination of phenolic compound profiles in maple products by high performance liquid chromatography. *J. Agric. Food Chem.* **1995**, *43*, 708−716.

(9) Abou-Zaid, M. M.; Nozzolillo, C.; Tonon, A.; Coppens, M.; Lombardo, A. D. A. High performance liquid chromatography characterization and identification of antioxidant polyphenols in maple syrup. *Pharm. Biol.* **2008**, *46*, 117−125.

(10) Watanabe, Y.; Kamei, A.; Shinozaki, F.; Ishijima, T.; Iida, K.; Nakai, Y.; Arai, S.; Abe, K. Ingested maple syrup evokes a possible liver-protecting effect-physiologic and genomic investigations with rats. *Biosci., Biotechnol., Biochem.* **2011**, *75*, 2408−2410.

(11) Nagai, N.; Ito, Y.; Taga, A. Comparison of the enhancement of plasma glucose levels in type 2 diabetes Otsuka Long-Evans Tokushima fatty rats by oral administration of sucrose or maple syrup. *J. Oleo Sci.* **2013**, *62*, 737−743.

(12) González-Sarrías, A.; Li, L.; Seeram, N. P. Effects of maple (*Acer*) plant part extracts on proliferation, apoptosis and cell cycle arrest of human tumorigenic and non-tumorigenic colon cells. *Phytother. Res.* **2012**, *26*, 995−1002.

(13) Legault, J.; Girard-Lalancette, K.; Grenon, C.; Dussault, C.; Pichette, A. Antioxidant activity, inhibition of nitric oxide over-production, and in vitro antiproliferative effect of maple sap and syrup from *Acer saccharum*. *J. Med. Food* **2010**, *13*, 460−468.

(14) Nahar, P. P.; Driscoll, M. V.; Li, L.; Slitt, A. L.; Seeram, N. P. Phenolic mediated anti-inflammatory properties of a maple syrup extract in RAW 264.7 murine macrophages. *J. Funct. Foods* **2014**, *6*, 126−136.

(15) Yuan, T.; Wan, C.; Gonzalez-Sarrias, A.; Kandhi, V.; Cech, N. B.; Seeram, N. P. Phenolic glycosides from sugar maple (*Acer saccharum*) bark. *J. Nat. Prod.* **2011**, *74*, 2472−2476.

(16) Wan, C.; Yuan, T.; Xie, M.; Seeram, N. P. *Acer rubrum* phenolics include A-type procyanidins and a chalcone. *Biochem. Syst. Ecol.* **2012**, *44*, 1−3.

(17) Wan, C.; Yuan, T.; Li, L.; Kandhi, V.; Cech, N. B.; Xie, M.; Seeram, N. P. Maplexins, a-glucosidase inhibitors from red maple (*Acer rubrum*) stems. *Bioorg. Med. Chem. Lett.* **2012**, *22*, 597−600.

(18) Yuan, T.; Wan, C.; Liu, K.; Seeram, N. P. New maplexins F-I and phenolic glycosides from red maple (*Acer rubrum*) bark. *Tetrahedron* **2012**, *68*, 959−964.

(19) Seeram, N. P.; Lee, R.; Hardy, M. L.; Heber, D. Rapid large-scale purification of ellagitannins from pomegranate husk, a by-product of the commercial juice industry. *Sep. Purif. Technol.* **2005**, *41*, 49−55.

(20) Gierer, J.; Nilvebrant, N. Lignin chromophores. Part III. Syntheses of hydroxy- and alkoxystilbenes via aryl migration. *J. Wood Chem. Technol.* **1991**, *11*, 171−193.

(21) Ames, J. M.; Bailey, R. G.; Mann, J. Analysis of furanone, pyranone, and new heterocyclic colored compounds from sugar-glycine model Maillard systems. *J. Agric. Food Chem.* **1999**, *47*, 438−443.

(22) Hu, K.; Wu, X.; Shen, J.; Zhou, Y.; Jiang, Z.; Cheng, G. ^{1}H NMR spectrum simplification of phenyl compounds containing electro-negative groups by intermolecular interactions. *Tetrahedron Lett.* **2008**, *49*, 2324−2328.

(23) Li, G.; Chen, F.; Shen, L.; Shen, S.; Zhang, J.; Si, J. Chemical constituents from roots and rhizomes of *Acorus tatarinowii*. *Zhongcaoyao* **2013**, *44*, 808−811.

(24) Xie, S.; Li, G.; Zhang, K.; Wang, H.; Tan, Y.; Wang, J. Isolation and identification of chemical constituents from *Cynomorium songaricum*. *Shenyang Yaoke Daxue Xuebao* **2012**, *29*, 525−528.

(25) Du, X.; Zhao, B.; Zheng, Z.; Xu, Q.; Su, W. Study on the isolation identification and antitumor activity of a phenol derivative from mangrove fungus BYY-1. *Jimei Daxue Xuebao, Ziran Kexueban* **2011**, *16*, 424−428.

(26) Singleton, V. L.; Rossi, J. A. Colorimetry of total phenolics with phosphomolybdic-phosphotungstic acid reagents. *Am. J. Enol. Vitic.* **1965**, *16*, 144−158.

(27) Nanjo, F.; Goto, K.; Seto, R.; Suzuki, M.; Sakai, M.; Hara, Y. Scavenging effects of tea catechins and their derivatives on 1,1-diphenyl-2-picrylhydrazyl radical. *Free Radical Biol. Med.* **1996**, *21*, 895−902.

(28) Tu, Zh.; Moss-Pierce, T.; Ford, P.; Jiang, T. A. Rosemary (*Rosmarinus officinalis* L.) extract regulates glucose and lipid metabolism by activating AMPK and PPAR pathways in HepG2 cells. *J. Agric. Food Chem.* **2013**, *61*, 2803−2810.

(29) Filipic, V. J.; Underwood, J. C.; Dooley, C. J. Trace components of the flavor fraction of maple syrup. *J. Food Sci.* **1969**, *34*, 105−110.
(30) Snatzke, G. Circular dichroismus-IX: Modifizierung der octantenregel für α,β- ungesättigte ketone: Transoide enone. *Tetrahedron* **1965**, *21*, 421−438.
(31) Tamura, Y.; Yakura, T.; Terashi, H.; Haruta, J.; Kita, Y. Hypervalent iodine oxidation of α,β-unsaturated carbonyl compounds. *Chem. Pharm. Bull.* **1987**, *35*, 570−577.
(32) Hošťálková, A.; Klingelhöfer, I.; Morlock, G. E. Comparison of an HPTLC method with the reflectoquant assay for rapid determination of 5-hydroxymethylfurfural in honey. *Anal. Bioanal. Chem.* **2013**, *405*, 9207−9218.
(33) Zirbes, L.; Nguyen, B. K.; De Graaf, D. C.; De Meulenaer, B.; Reybroeck, W.; Haubruge, E.; Saegerman, C. Hydroxymethylfurfural: A possible emergent cause of honey bee mortality? *J. Agric. Food Chem.* **2013**, *61*, 11865−11870.
(34) Kim, H. K.; Choi, Y. W.; Lee, E. N.; Park, J. K.; Kim, S. G.; Park, D. J.; Kim, B. S.; Lim, Y. T.; Yoon, S. 5-Hydroxymethylfurfural from black garlic extract prevents TNFα-induced monocytic cell adhesion to HUVECs by suppression of vascular cell adhesion molecule-1 expression, reactive oxygen species generation and NF-κB activation. *Phytother. Res.* **2011**, *25*, 965−974.
(35) Zhang, L.; Koyyalamudi, S. R.; Jeong, S. C.; Reddy, N.; Bailey, T.; Longvah, T. Immunomodulatory activities of polysaccharides isolated from *Taxillus chinensis* and *Uncaria rhyncophylla*. *Carbohydr. Polym.* **2013**, *98*, 1458−1465.
(36) Giavasis, I. Bioactive fungal polysaccharides as potential functional ingredients in food and nutraceuticals. *Curr. Opin. Biotechnol.* **2014**, *26*, 162−173.

Barnyardgrass has also developed resistance to conventional synthetic herbicides.[22]

Brachiaria is also especially invasive in South America.[25] It is native to Africa, where it occurs in the savannas and is important in the diet of large herbivores from that continent. These plants were introduced to Brazil to serve as pasture but they have spread throughout the country.[26] They are very competitive to native plants, more tolerant to fire and they can markedly modify the environment in which they dominate.[27]

Our hypothesis is that allelochemicals from cardoon have phytotoxic potential and could inhibit the development of other invasive weeds such as barnyardgrass and brachiaria. The aim of the study described here was to bioprospect cardoon leaf extracts through the isolation and purification of secondary metabolites with phytotoxic activity. It was envisaged that the results could explain the invasive behavior and the compounds identified could be used as natural herbicide models in the future. As part of this study, we selected the most phytotoxic extract from the leaves of cardoon, as identified by etiolated wheat coleoptile and phytotoxicity bioassays. A bioassay-guided fractionation of this extract was carried out in order to isolate and identify the chemical constituents. Their bioactivity profiles were assayed on the standard target species lettuce, watercress, tomato, and onion, as well as the weeds barnyardgrass and brachiaria.

MATERIALS AND METHODS

General Experimental Procedures. Infrared (IR) spectra (KBr) were recorded on a Fourier transform infrared (FT-IR) Spectrum 1000 spectrometer (PerkinElmer, Waltham, MA, U.S.A.). Nuclear magnetic resonance (NMR) spectra were run on 500 and 400 MHz spectrometers (Agilent, Palo Alto, CA, U.S.A.). Chemical shifts are given in ppm with respect to residual ^{1}H signals of $CHCl_3$-d_1 (δ 7.25), and ^{13}C signals are referenced to the solvent signal (δ 77.00). Optical rotations were determined at room temperature on a polarimeter model 241 (PerkinElmer, Waltham, MA, U.S.A.) (on the sodium D line). HRMS were obtained on a Synapt G2 UPLC-QTOF ESI mass spectrometer (Waters, Milford, MA, U.S.A.). HPLC was carried out on a HPLC cromatographer (Merck-Hitachi, Tokio, Japan), with RI detection. Silica gel 0.060−0.200, 60A from Acros Organics (Geel, Belgium) and Lichroprep RP 18 (40−63 μm) from Merck (Darmstadt, Germany) were used for column chromatography. Thin layer chromatography were run on TLC Silica gel 60 F_{254} aluminum sheet and TLC Silica gel 60 RP-18 F_{254S} aluminum sheet from Merck (Darmstadt, Germany). HPLC columns used were a semipreparative column 250 mm × 10 mm i.d., 10 μm Lichrospher 100 RP-18 (Merck, Darmstadt, Germany) with a guard column LiChrospher RP-18 (Merck, Darmstadt, Germany) and an analytical column 250 mm × 4.5 mm i.d., 5 μm Gemini 110A RP-18 (Phenomenex, Torrance, CA, U.S.A.) with a guard column SecurityGuard Cartridges Gemini RP-18 (Phenomenex, Torrance, CA, U.S.A.).

Ultrasound extractions were performed in an ultrasonic bath (360 W, J.P. Selecta, Barcelona, Spain) in two series of 15 min.

Chemicals. Chloroform, *n*-hexane, methanol, dichloromethane, ethyl acetate. and acetone Hipersolv Chromanorm for HPLC were obtained from VWR Internacional (Radnor, PA, U.S.A.). MagniSolv Chloroform-D1 deuteration degree min. 99.8% for NMR spectroscopy from Merck (Darmstadt, Germany).

Isolation of Compounds. Aerial plant material was collected in Jerez de la Frontera (Cadiz, Spain) in the fifth growth stage (ripe fruits).[28] Leaves were dried in an oven for 72 h at 40 °C and powdered in an industrial mill. Dried material (472 g) with 4 L of *n*-hexane at room temperature (in portions of about 120 g of plant, 2 × 500 mL) using an ultrasonic bath in order to defat the material. The plant residue was re-extracted in two different steps.

In step one, dichloromethane, ethyl acetate, acetone, methanol, and water were used to extract defatted material (5 g each, 2 × 50 mL of solvent) using an ultrasonic bath and these extractions yielded, after removal of the solvent, 180 mg (dichloromethane), 305 mg (ethyl acetate), 449 mg (acetone), 490 mg (methanol), and 1643 mg (water). These extracts were bioassayed with etiolated wheat coleoptiles. The ethyl acetate extract was the most active.

In step two, the rest of the defatted material (418 g) was extracted with 6 L of ethyl acetate in portions of 70 g of plant with 2 × 500 mL each using an ultrasonic bath to yield 12.19 g of material. This extract was chromatographed in a column (250 mm × 60 mm i.d., 300 g of silica gel 60A) using hexane/acetone mixtures of increasing polarity from 0 to 100% in acetone increasing 10% each time and finishing with 100% methanol (500 mL of each polarity) to afford 11 fractions: A−L. These fractions were bioassayed with etiolated wheat coleoptiles and the most bioactive fractions were assayed for phytotoxicity on standard target species.

Fractions D, E, F, and G showed bioactivity in the wheat coleoptile bioassay and these were rechromatographed. Fraction D (hexane/acetone, 70:30 v/v, 512 mg) was subjected to chromatographic column (250 mm × 40 mm i.d., 175 gr of silica gel 60A) using hexane/acetone mixtures of increasing polarity from 20 to 100% in acetone, increasing 10% each time and finishing with 100% methanol (250 mL of each polarity) to afford 8 fractions (D1−D8). Fraction D4 (144 mg, 5 mg/injection) was purified by HPLC (RP-18 semipreparative column) using water/acetone (40:60 v/v, flow 3 mL/min) to yield **1** (23 mg, retention time 11 min). Fraction D5 (155 mg) was subjected to chromatographic column (200 mm × 30 mm i.d., 60 gr of silica gel 60A) using dichloromethane/acetone mixtures of increasing polarity from 30 to 100% in acetone increasing 10% each time and finishing with 100% methanol (150 mL of each polarity) to afford 4 fractions (D5.1−D5.4). Fraction D5.1 (55 mg, 5 mg/injection) was purified by HPLC (RP-18 semipreparative column) using water/acetone (45:55 v/v, flow 3 mL/min) to yield **2** (7.1 mg, retention time 6 min) and a second peak (retention time 7 min). This peak was further purified by HPLC using water/acetone (70:30 v/v, flow 1 mL/min, 0.5 mg/injection, RP-18 analytical column) to yield **3** (0.7 mg, retention time 19 min).Fraction E (hexane/acetone, 50:50 v/v, 301 mg) was subjected to chromatographic column (200 mm × 40 mm i.d., 140 g silica gel 60A) using dichloromethane/acetone mixtures of increasing polarity from 20 to 100% in acetone increasing 10% each time and finishing with 100% methanol (200 mL of each polarity) to afford 3 fractions (E1, E2, and E3). Fraction E1+E2 (146 mg) was subjected to a chromatographic column (60 × 95 mm i.d., 200 g of silica gel RP-18) using water/methanol mixtures from 10 to 100% in methanol increasing 10% each time (150 mL of each polarity) to afford four fractions (E1.1−E1.4). Fraction E1.1 (84 mg, 5 mg/injection) was purified by HPLC (RP-18 semipreparative column) using water/acetone (45:55 v/v, flow 3 mL/min) to yield **2** (10 mg, retention time 6 min) and a second peak (retention time 7.9 min). This peak was further purified by HPLC using water/acetone (75:25 v/v, flow 1 mL/min, 0,5 mg/injection, RP-18 analytical column) to yield **4** (1.5 mg, retention time 18.7 min). Fraction F was mainly composed of **5** (241 mg). Fraction G (hexane/acetone, 40:60 v/v, 352 mg) was subjected to chromatographic column (200 × 40 i.d., 140 g silica gel 60A) using dichloromethane/acetone mixtures of increasing polarity from 40 to 100% in acetone increasing 10% and finishing with 100% methanol (200 mL of each polarity) to afford 3 fractions (G1−G3). Fraction G2 (145 mg, 5 mg/injection) was purified by HPLC (RP-18 semi-preparative column) using water/acetone (40:60 v/v, flow 3 mL/min) to yield **6** (36 mg, retention time 9 min).

Coleoptile Bioassay. Wheat seeds (*Triticum aestivum* L. cv. Duro) were sown in 15 cm diameter Petri dishes moistened with water and grown in the dark at 25 ± 1 °C for 4 days.[29] The roots and caryopses were removed from the shoots. The latter were placed in a Van der Weij guillotine and the apical 2 mm were cut off and discarded. The next 4 mm of the coleoptiles were removed and used for bioassays. All manipulations were performed under a green safelight.[30] Crude extracts, fractions or pure compounds were predissolved in dimethyl sulfoxide (0.1%) and diluted in phosphate-citrate buffer containing 2% sucrose[30] at pH 5.6 to the final bioassay concentrations (0.8, 0.4, and

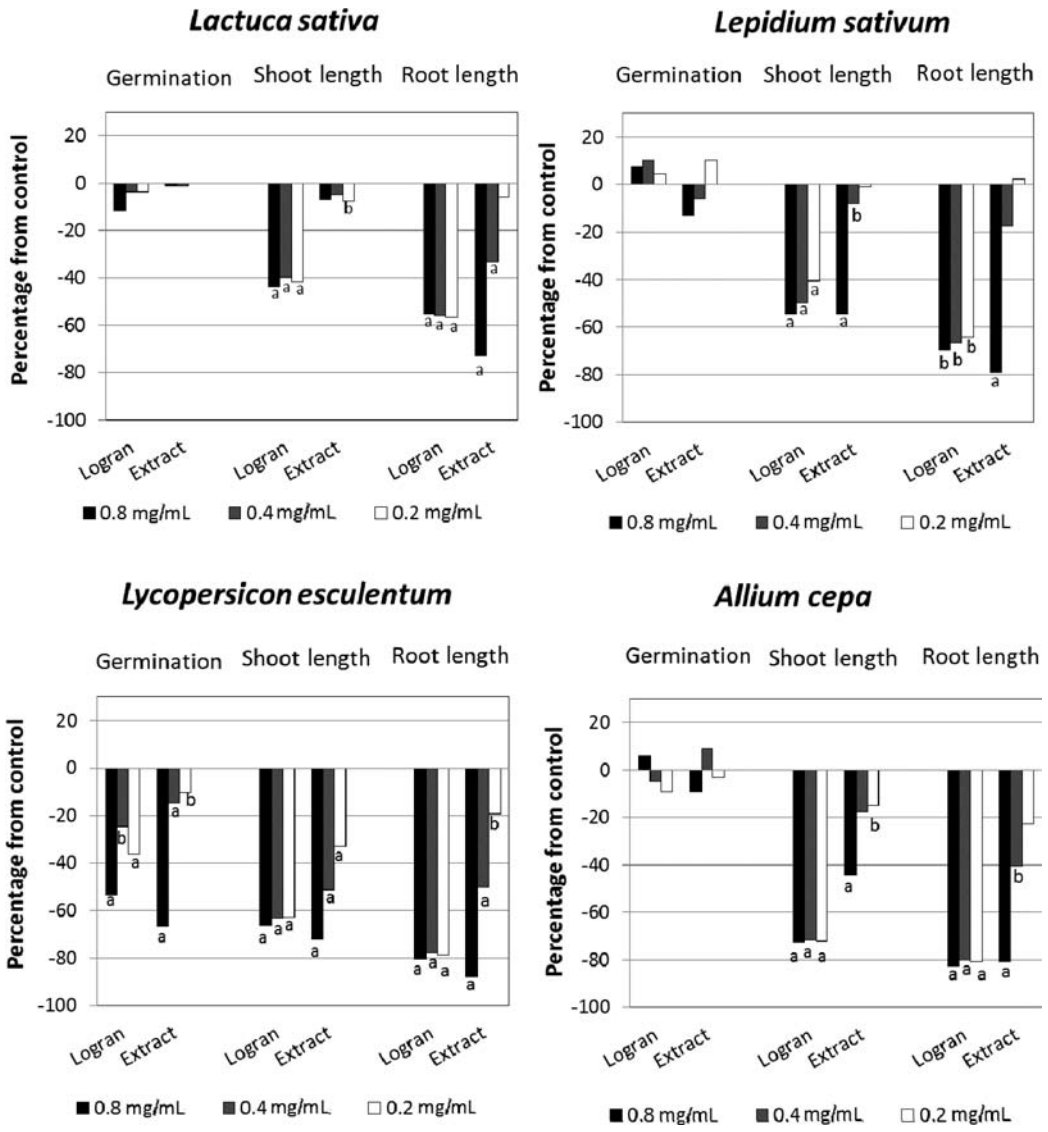

Figure 1. Effects of the herbicide Logran and ethyl acetate (EtOAc) leaf extract of cardoon (*Cynara cardunculus*) on standard target species growth. Values are expressed as percentage difference from control.

0.2 mg/mL for extracts and fractions, and 10^{-3}, 3×10^{-4}, 10^{-4}, 3×10^{-5}, and 10^{-5} M for compounds).

Parallel controls were also run. The commercial herbicide Logran, whose original formulation is a combination of N^2-*tert*-butyl-N^4-ethyl-6-(methylsulfanyl)-1,3,5-triazine-2,4-diamine (terbutryn, 59.4%) and 2-(2-chloroethoxy)-*N*-[(4-methoxy-6-methyl-1,3,5-triazin-2-yl)-carbamoyl]benzene-1-sulfonamide (triasulfuron, 0.6%), was used as positive control according to a comparison study reported previously.[31] This reference was used at the same concentrations and under the same conditions as reported previously. Control samples (buffered aqueous solutions with dimethyl sulfoxide and without any test compound) were used for all of the plant species assayed.

Each assay was carried out in duplicate. Five coleoptiles and 2 mL of solution were placed in each test tube (three tubes per dilution) and the tubes were rotated at 0.25 rpm in a roller tube apparatus for 24 h at 25 °C in the dark. The coleoptiles were measured by digitalization of their images. Data were statistically analyzed using Welch's test.[32] Data are presented as percentage differences from control. Thus, zero represents the control, positive values represent stimulation of the studied parameter, and negative values represent inhibition.

Phytotoxicity Bioassays. The selection of target plants was based on an optimization process carried out in our search for a standard phytotoxicity bioassay.[31] Several Standard Target Species were proposed, including the monocotyledon onion (*Allium cepa* L.) and the dicotyledons tomato (*Lycopersicon esculentum* Will.), cress (*Lepidium sativum* L.), and lettuce (*Lactuca sativa* L.), which were assayed for this study. In addition, two weed species were added as target plants in this bioassay: the monocotyledon barnyardgrass (*E. crus-galli* L.) and the dicotyledon brachiaria (*Urochloa decumbens* (Stapf) R.D. Webster).

Bioassays were conducted using Petri dishes (50 mm diameter) with one sheet of Whatman No. 1 filter paper as a support. Germination and growth were conducted in aqueous solutions at controlled pH by using 10^{-2} M 2-[*N*-morpholino]ethanesulfonic acid (MES) and 1 M NaOH (pH 6.0). The extracts, fractions or compounds to be assayed were dissolved in dimethyl sulfoxide and these solutions were diluted with buffer (5 μL dimethyl sulfoxide solution/mL buffer) so that test concentrations for each extract or fraction (0.8, 0.4, and 0.2 mg/mL) and compound (10^{-3}, 3×10^{-4}, 10^{-4}, 3×10^{-5}, and 10^{-5} M) were achieved. Parallel controls were also run as described before for coleoptile bioassays.

Four replicates were used for tomato, cress, onion, and lettuce, each containing 20 seeds. Treatment, control or internal reference solution (1 mL) was added to each Petri dish. After adding the seeds and aqueous solutions, Petri dishes were sealed with Parafilm to ensure

dx.doi.org/10.1021/jf501976h | J. Agric. Food Chem. 2014, 62, 6699−6706

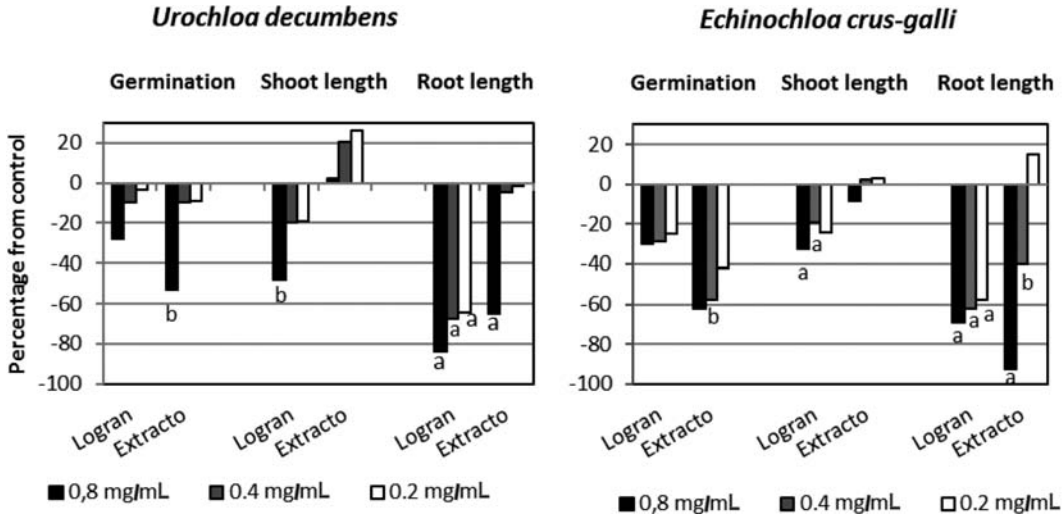

Figure 2. Effects of the herbicide Logran and ethyl acetate (EtOAc) leaf extract of cardoon (*Cynara cardunculus*) on weed growth. Values are expressed as percentage difference from control.

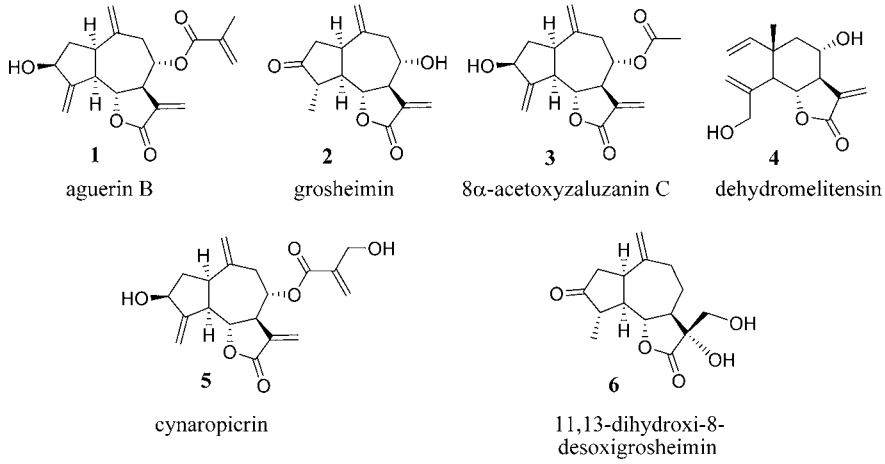

Figure 3. Compounds isolated from cardoon (*Cynara cardunculus*). Aguerin B, **1**, grosheimin, **2**, 8α-acetoxyzaluzanin C, **3**, and dehydromelitensin, **4**, cynaropicrin, **5**, and 11,13-dihydroxy-8-desoxygrosheimin, **6**.

closed-system models. Seeds were further incubated at 25 °C in a Memmert ICE 700 controlled environment growth chamber. The photoperiod was 24 h of dark for onion, tomato, cress, and lettuce, and 16/8 h light/dark for barnyardgrass and brachiaria. Bioassays took 4 days for cress, 5 days for tomato, 6 days for lettuce, 7 days for onion, and 8 days for barnyardgrass and brachiaria. After growth, plants were frozen at −10 °C for 24 h to avoid subsequent growth during the measurement process.

Evaluated parameters (germination rate, root length, and shoot length) were recorded using a Fitomed system,[33] which allowed automatic data acquisition and statistical analysis using its associated software. Data were analyzed statistically using Welch's test, with significance fixed at 0.01 and 0.05. Results are presented as percentage differences from the control. Zero represents control, positive values represent stimulation, and negative values represent inhibition.

RESULTS AND DISCUSSION

Dried leaves of cardoon (55 g) defatted with hexane were extracted with dichloromethane (dichloromethane, 0.33% yield), ethyl acetate (ethyl acetate, 0.55% yield), acetone (acetone, 0.82% yield), and methanol (methanol, 0.89% yield), and then with distilled water (water, 2.98% yield). The extracts were tested in the etiolated wheat coleoptile bioassay.[31] This is a rapid test that is sensitive to a wide range of bioactive substances[34] including plant growth regulators, herbicides, antimicrobials, mycotoxins, and assorted pharmaceuticals.

The extracts that showed the highest inhibition levels in the coleoptile bioassay were those extracted with dichloromethane, ethyl acetate, and acetone, which showed the highest inhibition values (around 90%) at 0.8 mg/mL. The methanol and water extracts showed lower inhibitory activity (77% and 58% at 0.8 mg/mL, respectively). The dichloromethane and ethyl acetate extracts retained high activity levels at lower concentrations. Thus, the inhibition of these extracts at 0.4 and 0.2 mg/mL were dichloromethane 90 and 75%, respectively, and ethyl acetate 87 and 69%, respectively.

Although dichloromethane and ethyl acetate extracts showed almost the same activity values, the ethyl acetate extract was selected for further study because the yield was higher. As a result, the ethyl acetate extract was evaluated in the phytotoxicity assay (Figures 1 and 2). The concentrations tested in this bioassay were identical to those described previously. The standard target species were lettuce, tomato, cress, and onion[31] (Figure 1) and the weed species were barnyardgrass and brachiaria (Figure 2).

The parameter that was most markedly affected by the extract was root length (Figures 1 and 2). The inhibition shown

by the extract was higher than or equal to that of Logran at 0.8 mg/mL on both standard target species and weeds roots, with values close to 80% inhibition in most species. The extract was also active on the germination of tomato, brachiaria, and barnyardgrass, and on the shoot length of cress, tomato, onion, and barnyardgrass.

These results clearly show that the extract obtained from cardoon has phytotoxic activity not only on standard target species plants but also on important weed species. Therefore, it was decided to isolate and identify the constituent compounds and study their bioactivity in an effort to understand the invasive behavior of the plant and to discover new tools for weed control.

The ethyl acetate extract was chromatographed on silica gel using hexane/acetone mixtures of increasing polarity to afford fractions A to L. These fractions were used in etiolated wheat coleoptile bioassays to biodirect the purification of the allelochemicals. The most active fractions were those with intermediate polarities, that is, fractions D, E, F, and G. In particular, fractions D, F and G presented inhibition values close to 100% at 0.8 mg/mL.

The chromatographic separation of fractions D, E, F, and G allowed us to isolate six sesquiterpene lactones. The isolated compounds were identified by their spectroscopic data (^{1}H NMR, ^{13}C NMR, HMQC, COSY, HMBC, IR, and MS) in comparison to those reported in the literature for aguerin B,[35] **1**, grosheimin,[36] **2**, 8α-acetoxyzaluzanin C,[35] **3** dehydromelitensin,[37] **4**, cynaropicrin,[35] **5** and 11,13-dihydroxy-8-deoxygrosheimin,[38] **6**. (Figure 3). Sesquiterpenic lactones are characteristic of Asteraceae.[39] Metabolites **2** and **5** have been reported recently from cardoon extracts[40] whereas compounds **1**, **3**, **4** and **6** are reported for the first time from this species.

The bioactivities of compounds **1**, **2**, **5**, and **6** were assessed in a wheat coleoptile bioassay from 10^{-3} M to 10^{-5} M. Compounds **3** and **4** were not tested because insufficient sample was available (less than 1 mg). Compounds **1**, **2**, and **5** showed high inhibitory activity on the coleoptile elongation, with almost 90% activity at 10^{-3} M (Figure 4). Compounds **1**, **2**, and **5** were also active at the second concentration (3.10^{-4} M) (70, 75 and 55% inhibition, respectively) and their activity decreased from a concentration of 10^{-4} M and below.

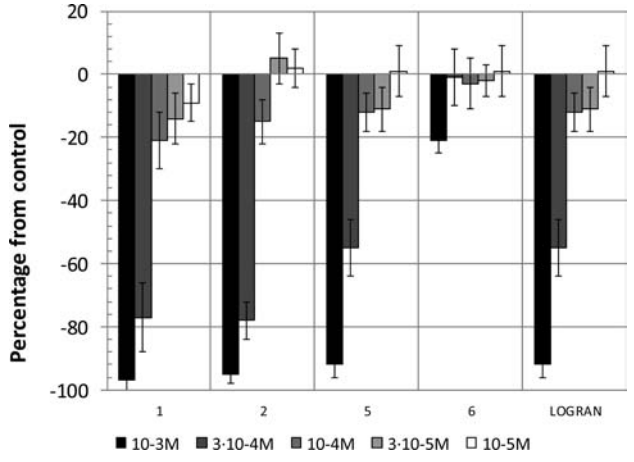

Figure 4. Effects of compounds aguerin B, **1**, grosheimin, **2**, cynaropicrin, **5**, and 11,13-dihydroxy-8-desoxygrosheimin, **6**, from cardoon (*Cynara cardunculus*) on the elongation of etiolated wheat coleoptiles.

Since compounds **1**, **2**, and **5** were very active in the coleoptile bioassay, their phytotoxicity was also tested on standard target species (Figure 5) development. Germination was the least affected parameter, although the compounds were much more active at 10^{-3} M on cress and tomato than the reference herbicide. Indeed, inhibition reached levels of almost 90% on tomato germination.

Shoot length was only affected by compounds at the highest concentration and, in most cases, the inhibition levels were higher than those of the reference herbicide, with values close to 70% in the cases of **5** on lettuce and **1** and **5** on cress and tomato (Figure 5).

Root length was the variable that was most affected by the allelochemicals, mainly at the first concentration (10^{-3} M) but also at the second one (3.10^{-4} M). As for other parameters, the compounds were more phytotoxic than the reference herbicide in most cases. Compounds **1**, **2**, and **5** were very active (from 70 to 90% inhibition) on root length of cress and tomato. Compounds **2** and **5** also showed activity on onion root length.

In view of the results described above, compounds **1**, **2**, and **5** were also tested on the weeds barnyardgrass and brachiaria with a photoperiod of 16/8 h light/dark (Figure 6). Germination was once again the parameter that was least affected and the compounds were more active at 10^{-3} M on brachiaria than the reference herbicide, with inhibition of 90% on brachiaria. Shoot length was not affected by any of the compounds with the exception of **2** on brachiaria at the highest concentration, which gave a value close to 80% inhibition.

As for the standard target species species, root length was the parameter that was most markedly affected by the allelochemicals, mainly at the first concentration (10^{-3} M). All compounds were more active than the reference herbicide (from 70 to 90%) on the root length of the two weeds barnyardgrass and brachiaria.

The extracts, fractions and compounds showed similar activity profiles in the wheat coleoptile and seedling bioassays (Figure 1, 2, 4, 5, and 6) and this indicates that the bioactivity of the extracts and fractions can be explained by the presence of the compounds identified.

The analysis of compounds **1**, **2**, **5**, and **6** enabled some observations to be made concerning the relationship between their structure and activity, considering the structures of the molecules and the differences between them. The absence of activity in **6** could be explained by the absence of an α-methylene group, which is present in the other compounds. Changes in the lateral chain or oxidation pattern at C-3 in **1**, **2**, and **5** seems to have little influence on the activity.

As observed in the phytotoxicity bioassay on the extracts (Figures 1 and 2), compounds **1**, **2**, and **5** were active not only on standard target species but also on the very important weeds (Figures 5 and 6). Other guaianolide sesquiterpene lactones have been reported to be cytotoxic,[41] fungicidal,[42] antiviral, and antimicrobial.[43] Allelopathic activity has also been described.[44−46] The amounts in which these compounds are biosynthesized and their wide spectrum of biological activity, including phytotoxicity, suggest that they may be involved in the defense mechanism of this species. This variety of biological activities supports the "economy of resources" principle, which states that a defense metabolite is cheaper in terms of resource investment if it can serve more than one purpose. Allelopathy, a general defense mechanism present in plants, can involve these metabolites.[47]

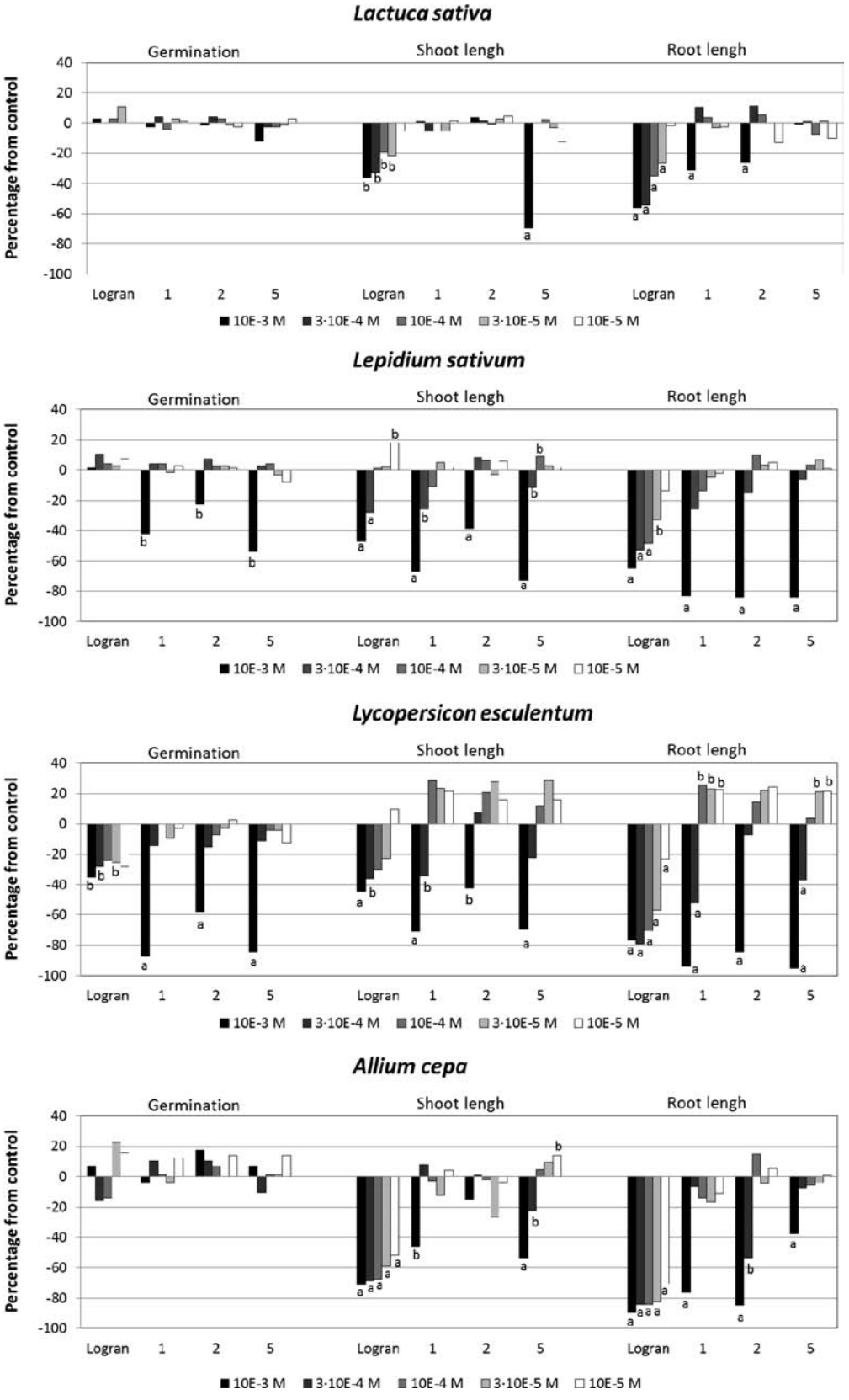

Figure 5. Effects of compounds aguerin B, **1**, grosheimin, **2**, and cynaropicrin, **5**, from cardoon (*Cynara cardunculus*) on standard target species growth. Values are expressed as percentage difference from control.

The strong phytotoxicity shown by the extracts and the pure major compounds aguerin B, **1**, grosheimin, **2**, and cynaropicrin, **5**, on the important weeds brachiaria and barnyardgrass demonstrates the strong potential of *C. cardunculus* for use in the biological control of weeds. This species could be used as a plant applied as a cover crop, as

dx.doi.org/10.1021/jf501976h | *J. Agric. Food Chem.* 2014, 62, 6699−6706

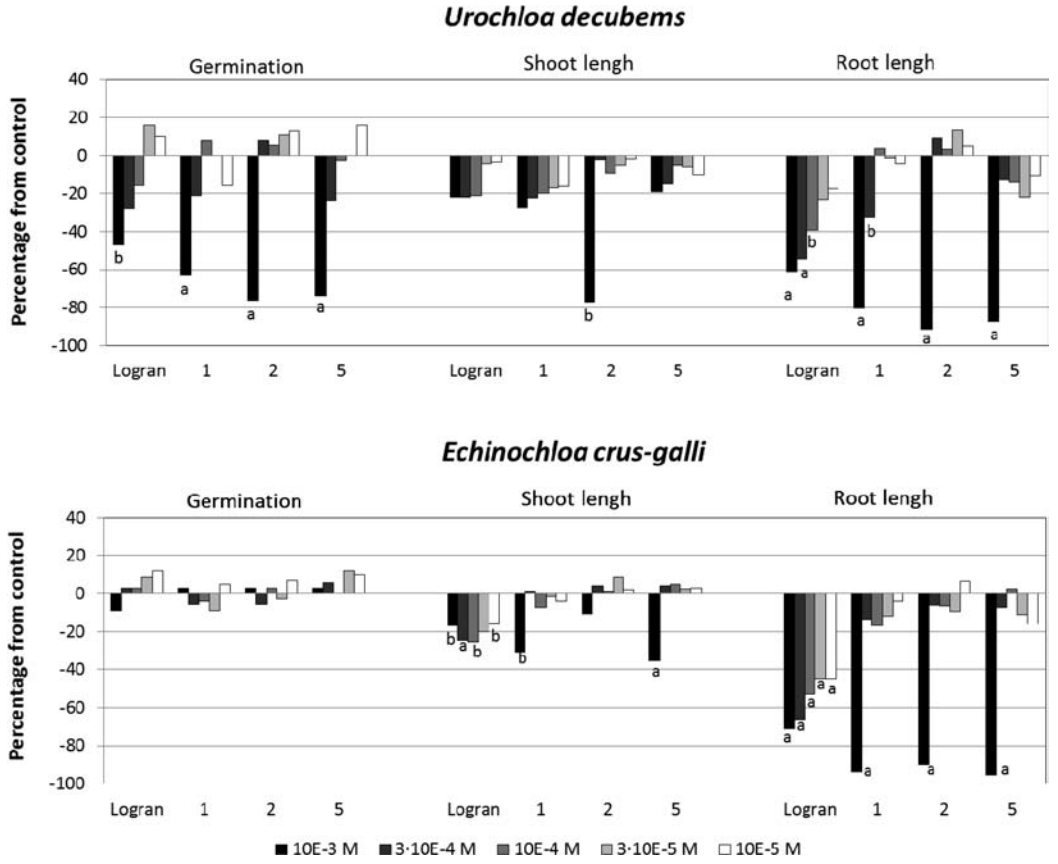

Figure 6. Effects of compounds aguerin B, **1**, grosheimin, **2**, cynaropicrin, **5**, from cardoon (*Cynara cardunculus*) on weed growth. Values are expressed as percentage difference from control.

mulching and plant extracts or as a source of natural herbicide models.

AUTHOR INFORMATION

Corresponding Author

*Tel: +34 956.012.770. Fax: +34 956.016.193. Email: famacias@uca.es.

Notes

The authors declare no competing financial interest.

ACKNOWLEDGMENTS

This research was supported by the CNPq (Conselho Nacional de Pesquisa), Brazil, the Ministerio de Educación y Ciencia (Project No. AGL2009-08864 (AGR), and Junta de Andalucía (PAI-III, AGR-5822), Seville, Spain.

REFERENCES

(1) Pimentel, D.; Zuniga, R.; Morrison, D. Update on the environmental and economic costs associated with alien-invasive species in the United States. *Ecol. Econ.* **2005**, *52*, 273−288.

(2) van Kleunen, M.; Weber, E.; Fischer, M. A meta-analysis of trait differences between invasive and non-invasive plant species. *Ecol. Lett.* **2010**, *13*, 235−245.

(3) Mack, R. N.; Simberloff, D.; Lonsdale, W. M.; Evans, H.; Clout, M.; Bazzaz, F. A. Biotic invasions: Causes, epidemiology, global consequences, and control. *Ecol. Appl.* **2000**, *10*, 689−710.

(4) Rice, E. L. *Allelopathy*; Academic Press: New York, NY, 1984.

(5) Chou, C. H. Roles of allelopathy in plant biodiversity and sustainable agriculture. *Crit. Rev. Plant Sci.* **1999**, *18*, 609−636.

(6) Hagan, D. L.; Jose, S.; Lin, C. H. Allelopathic exudates of cogongrass (*Imperata cylindrica*): Implications for the performance of native pine savanna plant species in the southeastern U.S. *J. Chem. Ecol.* **2013**, *39*, 312−322.

(7) Sardans, J.; Llusia, J.; Niinemets, U.; Owen, S.; Penuelas, J. Foliar mono- and sesquiterpene contents in relation to leaf economic spectrum in native and alien species in Oahu (Hawaii). *J. Chem. Ecol.* **2010**, *36*, 210−226.

(8) Weidenhamer, J. D.; Callaway, R. M. Direct and indirect effects of invasive plants on soil chemistry and ecosystem function. *J. Chem. Ecol.* **2010**, *36*, 59−69.

(9) Vyvyan, J. R. Allelochemicals as leads for new herbicides and agrochemicals. *Tetrahedron* **2002**, *58*, 1631−1646.

(10) Macías, F.; Oliveros-Bastidas, A.; Marín, D.; Carrera, C.; Chinchilla, N.; Molinillo, J. G. Plant biocommunicators: Their phytotoxicity, degradation studies, and potential use as herbicide models. *Phytochem. Rev.* **2008**, *7*, 179−194.

(11) Pignone, D.; Sonnante, G. Wild artichokes of south Italy: Did the story begin here? *Genet. Resour. Crop Ev.* **2004**, *51*, 577−580.

(12) White, V. A. Environmental physiology of an invasive weed, *Cynara cardunculus*. University of California Press, Riverside, CA, 2004.

(13) Marushia, R. G.; Holt, J. S. Reproductive strategy of an invasive thistle: Effects of adults on seedling survival. *Biol. Invasions* **2008**, *10*, 913−924.

(14) White, V. A.; Holt, J. S. Competition of artichoke thistle (*Cynara cardunculus*) with native and exotic grassland species. *Weed Sci.* **2005**, *53*, 826−833.

(15) Prados, F.; Pino, A.; Fernández-Salguero, J. Effect of a powdered vegetable coagulant from cardoon *Cynara cardunculus* in the accelerated ripening of Manchego cheese. *Int. J. Food Sci. Technol.* **2007**, *42*, 556−561.

(16) Valentao, P.; Fernandes, E.; Carvalho, F.; Andrade, P. B.; Seabra, R. M.; Bastos, M. L. Antioxidative properties of cardoon (*Cynara*

cardunculus L.) infusion against superoxide radical, hydroxyl radical, and hypochlorous acid. *J. Agric. Food Chem.* **2002**, *50*, 4989−4993.
(17) Velez, Z.; Campinho, M.; Guerra, Â.; García, L.; Ramos, P.; Guerreiro, O.; Felício, L.; Schmitt, F.; Duarte, M. Biological characterization of *Cynara cardunculus* L. methanolic extracts: Antioxidant, anti-proliferative, anti-migratory, and anti-angiogenic activities. *Agriculture* **2012**, *2*, 472−492.
(18) Kukic, J.; Popovic, V.; Petrovic, S.; Mucaji, P.; Ciric, A.; Stoikovic, D.; Sokovic, M. Antioxidant and antimicrobial activity of *Cynara cardunculus* extracts. *Food Chem.* **2008**, *107*, 861−868.
(19) Fratianni, F.; Tucci, M.; De Palma, M.; Pepe, R.; Nazzaro, F. Polyphenolic composition in different parts of some cultivars of globe artichoke (*Cynara cardunculus* L. var. *scolymus* (L.) Fiori). *Food Chem.* **2007**, *104*, 1282−1286.
(20) Slanina, J.; Paulova, H.; Humpa, O.; Bochorakova, H.; Taborska, E. 1,5-dicaffeoylquinic acid, an antioxidant component of *Cynara cardunculus* leaves. *Scr. Med. Fac. Med. Univ. Brun. Masaryk.* **1999**, *72*, 9−17.
(21) Mucaji, P.; Grancai, D.; Nagy, M.; Visnovská, Z.; Ubik, K. Apigenin-7-methylglucuronide from *Cynara cardunculus* L. *Ces. Slov Farm.* **2000**, *49*, 75−77.
(22) Talbert, R. E.; Burgos, N. R. History and management of herbicide-resistant barnyardgrass (*Echinochloa crus-galli*) in Arkansas rice. *Weed Technol.* **2007**, *21*, 324−331.
(23) Mitich, L. W. Index for "Intriguing world of weeds". *Weed Technol.* **1991**, *5*, 916−918.
(24) Holm, L. G.; Plucknett, D. L.; Pancho, J. V.; Herberger, J. P. *The World'S Worst Weeds: Distribution and Biology*; University Press of Hawaii: Honolulu, HI, 1977.
(25) Souza, L. S.; Losasso, P. H. L.; Oshiiwa, M.; Garcia, R. R.; Goes Filho, L. A. Effects of *Brachiaria decumbens* control bands on the initial development and productivity of *Coffea arabica*. *Planta Daninha* **2006**, *24*, 715−720.
(26) Williams, D.; Baruch, Z. African grass invasion in the Americas: Ecosystem consequences and the role of ecophysiology. *Biol. Invasions* **2000**, *2*, 123−140.
(27) D'Antonio, C. M.; Vitousek, P. M. Biological invasions by exotic grasses, the grass/fire cycle, and global change. *Annu. Rev. Ecol. Evol. Syst.* **1992**, *23*, 63−87.
(28) Raccuia, S. A.; Melilli, M. G. Seasonal dynamics of biomass, inulin, and watersoluble sugars in roots of *Cynara cardunculus* L. *Field Crop Res.* **2010**, *116*, 147−153.
(29) Hancock, C.; Barlow, H.; Lacey, H. The east malling coleoptile straight growth test method. *J. Exp. Bot.* **1964**, *15*, 166−176.
(30) Nitsch, J. P.; Nitsch, C. Studies on the growth of coleoptile and first internode sections. A new, sensitive, straight-growth test for auxins. *Plant Physiol.* **1956**, *31*, 94−111.
(31) Macias, F. A.; Castellano, D.; Molinillo, J. M. G. Search for a standard phytotoxic bioassay for allelochemicals. Selection of standard target species. *J. Agric. Food Chem.* **2000**, *48*, 2512−2521.
(32) Martín, A.; Luna, J. d. D. *Bioestadística para las ciencias de la salud*; Ediciones Norma: Madrid, Spain, 1990.
(33) Castellano, D. *Optimización de bioensayos alelopáticos. Aplicación en la búsqueda de herbicidas naturales*. PhD dissertation, Universidad de Cádiz, Spain, 2002.
(34) Cutler, S. J.; Hoagland, R. E.; Cutler, H. G. Evaluation of selected pharmaceuticals as potential herbicides: bridging the gap between agrochemicals and pharmaceuticals. In *Allelopathy in Ecological Agriculture and Forestry*; Narwal, S. S.; Hoagland, R. E.; Dilday, R. H.; Reigosa, R. M. J., Eds.; Springer: New York, 2000; pp 129−137.
(35) Ha, T. J.; Jang, D. S.; Lee, J. R.; Lee, K. D.; Lee, J.; Hwang, S. W.; Jung, H. J.; Nam, S. H.; Park, K. H.; Yang, M. S. Cytotoxic effects of sesquiterpene lactones from the flowers of *Hemisteptia lyrata* B. *Arch. Pharm. Res.* **2003**, *26*, 925−928.
(36) Chen, W.; Liu, Q.; Wang, J.; Zou, J.; Meng, D.; Zuo, J.; Zhu, X.; Zhao, W. New guaiane, megastigmane, and eudesmane-type sesquiterpenoids and anti-inflammatory constituents from *Youngia japonica*. *Planta Med.* **2006**, *72*, 143−150.
(37) Cardona, M. L.; Garcia, B.; Pedro, J. R.; Sinisterra, J. F. Sesquiterpene lactones and an elemane derivative from *Onopordon corymbosum*. *Phytochemistry* **1989**, *28*, 1264−1267.
(38) Medjroubi, K.; Benayachel, F.; Leon, F.; Bermejo, J. Complete assignement of the ^{13}C and ^{1}H NMR spectra of two known guayanolides isolated from *Centaurea*. *Rev. Colomb. Quím.* **2003**, *2*, 17−22.
(39) Seaman, F. C. Sesquiterpene lactones as taxonomic characters in the Asteraceae. *Bot. Rev.* **1982**, *48*, 121−595.
(40) Ramos, P. A. B.; Guerra, A. R.; Guerreiro, O.; Freire, C. S. R.; Silva, A. M. S.; Duarte, M. F.; Silvestre, A. J. D. Lipophilic extracts of *Cynara cardunculus* L. var. altilis (DC): A source of valuable bioactive terpenic compounds. *J. Agric. Food Chem.* **2013**, *61*, 8420−8429.
(41) Muhammad, I.; Takamatsu, S.; Mossa, J. S.; El-Feraly, F. S.; Walker, L. A.; Clark, A. M. Cytotoxic sesquiterpene lactones from *Centaurothamnus maximus* and *Vicoa pentanema*. *Phytother. Res.* **2003**, *17*, 168−173.
(42) Wedge, D. E.; Galindo, J. C. G.; Macias, F. A. Fungicidal activity of natural and synthetic sesquiterpene lactone analogs. *Phytochemistry* **2000**, *53*, 747−757.
(43) Özçelik, B.; Gürbüz, I.; Karaoglu, T.; Yeşilada, E. Antiviral and antimicrobial activities of three sesquiterpene lactones from *Centaurea solstitialis* L. ssp. *solstitialis*. *Microbiol. Res.* **2009**, *164*, 545−552.
(44) de Luque, A. P.; Galindo, J. C. G.; Macias, F. A.; Jorrin, J. Sunflower sesquiterpene lactone models induce *Orobanche cumana* seed germination. *Phytochemistry* **2000**, *53*, 45−50.
(45) Macias, F. A.; Galindo, J. C. G.; Molinillo, J. M. G.; Castellano, D. Dehydrozaluzanin C: A potent plant growth regulator with potential use as a natural herbicide template. *Phytochemistry* **2000**, *54*, 165−171.
(46) Macías, F. A.; Velasco, R. F.; Castellano, D.; Galindo, J. C. Application of Hansch's model to guaianolide ester derivatives: A quantitative structure-activity relationship study. *J. Agric. Food Chem.* **2005**, *53*, 3530−3539.
(47) Macías, F. A.; Molinillo, J. M. G.; Varela, R. M.; Galindo, J. C. G. Allelopathy—A natural alternative for weed control. *Pest Manage. Sci.* **2007**, *63*, 327−348.

Table 1. Selected Additives, Their Acronyms, Proposed Actions, and Literature Sources

type	additive	abbrev	proposed action	ref
base	NaOH	NaOH	promote protein−protein interactions	19−21
	NH_4OH	AH	promote protein−protein interactions	16 18
acid/base	citric acid/NaOH	CA/N	cross-linking	22, 23
acid	salicylic acid	SA	retard protein−protein interactions	21, 32
	citric acid	CA	cross-linking	33, 34
	ascorbic acid	AA	improve protein behavior	35
reactive	Jeffamine EDR 176	JF	provide reactive amine sites	36
	benzoyl peroxide	BP	thermally decomposing oxidant	30, 35, 37
denaturant	sodium dodecyl sulfate	SDS	allow protein rearrangement	26, 27
	urea	U	allow protein rearrangement	24, 28, 29
reductant	sodium bisulfite	SB	allow protein rearrangement	38, 39

MATERIALS AND METHODS

Materials. Oilseed meals of crambe (11.1 ± 0.02% db water) and carinata (10.1 ± 0.06% db water) were produced by the petroleum distillate method of Appelqvist[31] performed at room temperature to avoid protein thermal denaturation. Carinata seeds were graciously provided by Agriculture Canada (Saskatoon, Canada) and crambe seeds (with pod) supplied by the Plant Research Institute (Wageningen, The Netherlands). Monosodium phosphate (NaH_2PO_4), as monohydrate, was provided by Baker (Deventer, The Netherlands), and glycerol (99.5%) was graciously supplied by Karlshamns Tefac AB (Karlshamn, Sweden). Trifluoroacetic acid (TFA) and acetonitrile (ACN) (Merck) were of spectroscopy grade and isocratic chromatography grade, respectively. All water was purified on a Milli-Q system (Millipore Corp., Bedford, MA, USA).

Additives Used. Ten different chemical additives across five different types were selected on the basis of previous literature. The selected chemical additives, the reason for their selection, and reference(s) related to their previous use in protein based plastics are summarized in Table 1. Addition levels were selected from the references.

Methods. *Protein Content.* Nitrogen content of the deoiled meal was performed in duplicate with the Dumas method (Flash 2000 NC Analyzer, Thermo Scientific, USA), nitrogen to protein conversion factor N × 6.25, and protein content together with an example of other constituents are given in Table 2.

Table 2. Selected Industrial Oil Meal Components (Percent, Dry Basis)

component	carinata	crambe
protein[a]	43.7 ± 1.9	20.5 ± 1.2
ash	5.7[47]	7.4[62]
glucosinolates	5.6[47]	4.5−7[62]
phytic acid	3.4[47]	NR[b]
fiber	34.9[47]	22.1[62]
soluble sugars	6.2[47]	8.3[48]
polyphenols	0.3[47]	NR

[a]Current study. [b]NR, not reported.

Mixing Procedure. All samples contained the same amount of water, 5.25 parts per 70 parts oilseed meal, to match the water contained in the highest level of ammonium hydroxide (25% solution). Where the additive was hydrated, this was accounted for in the water addition. Additives, water (if necessary), and glycerol (30 parts per 70 parts oilseed meal by weight) were premixed before addition to the oilseed meals. In cases when the additives were not soluble under these conditions (NaOH 4.5 parts, SDS 4.5 parts, SA, BP), they were added as a dry powder to the meal before mixing. All additive doses are listed as parts additive per hundred parts combined oilseed meal and glycerol (70 parts and 30 parts, respectively).

Hot Compression Molding. The oilseed meal was mixed with the additive/glycerol/water blend by hand using a mortar and pestle until evenly mixed (3−5 min). The mixture was then formed in a heated hydraulic press (Polystat 400s, Servitech, Germany) between aluminum plates with polyethylene terephthalate release film using a 0.5 mm thick aluminum frame with a 100 mm × 100 mm central opening to control the size and thickness of the film. A molding temperature of 130 °C, a pressure of 10 MPa on the sample area, and a pressing time of 10 min were used on all samples on the basis of previous work.[6] After removal from the press, the sheets were cooled in the frame between room temperature aluminum sheets. The cooled oilseed meal sheets were removed from the frame using a scalpel.

This process produced a wide range of macroscopic morphologies, from well-formed free-standing films to sticky incoherent films that were impossible to remove from the release films whole. All samples were processed via HPLC and water immersion; only well-formed films proceeded to tensile testing.

SE-HPLC. The amount and size distribution of soluble protein in the films were determined by a three-step extraction procedure.[40] Samples of each film were hand cut to a maximum particle size of approximately 0.2 mm, and triplicate samples of 16.5 (±0.05) mg each were weighed into 1.5 mL centrifuge tubes. Protein extractions were carried out in 1.4 mL of extraction buffer, 0.5% (w/v) SDS, 0.05 M NaH_2PO_4, pH 6.9. Three extractions were carried out serially on each sample. The extractions were as follows; extraction 1, vortexing for 10 s followed by shaking 5 min at 2000 rpm; extraction 2, 30 s of ultrasonication at an amplitude of 5 μm (Sanyo Soniprep, Tamro, Sweden); extraction 3, 30 + 60 s of ultrasonication at 5 μm. After each extraction, the supernatant was recovered for further analysis, and the residuals were resuspended in extraction buffer for the next extraction.

Analysis was performed with a Waters 2690 separations module and a Waters 996 photodiode array detector at a flow of 0.2 mL/min (50% ACN, 0.1% TFA; 50% H_2O, 0.1% TFA). A 20 μL sample of supernatant was injected onto a column, Phenomenex Biosep-SEC-S 4000 (300 mm × 4.5 mm, Torrance, CA, USA) with a prefilter (Phenomenex SecurityGuard GFC 4000). Absorption spectra were collected in 3D for 30 min and analyzed with Empower Pro software (Waters, Empower 2). Chromatograms were extracted at 210 nm and integrated into two arbitrary fractions: high molecular weights (HMw) from 8 to 18.3 min and low molecular weights (LMw) from 18.3 to 30 min. The solubility is defined as the area of the elution intervals normalized to the total protein extracted from the raw oilseed meals and corrected for individual sample meal content (eq 1). Error bars reported in HPLC data indicate one standard deviation. Interference due to the absorption of salicylic acid at 210 nm was removed from the data by manual peak selection.

$$\%\ \text{solubility} = \frac{\text{integrated fraction area}}{\text{total integrated raw meal area}} \times \frac{\text{total sample mass}}{\text{sample meal mass}} \times 100 \quad (1)$$

Tensile Testing. Tensile specimens were cut with an ISO 37, type 3, sample cutter (Elastocon AB, Sweden) and conditioned for a

dx.doi.org/10.1021/jf5015928 | J. Agric. Food Chem. 2014, 62, 6707−6715

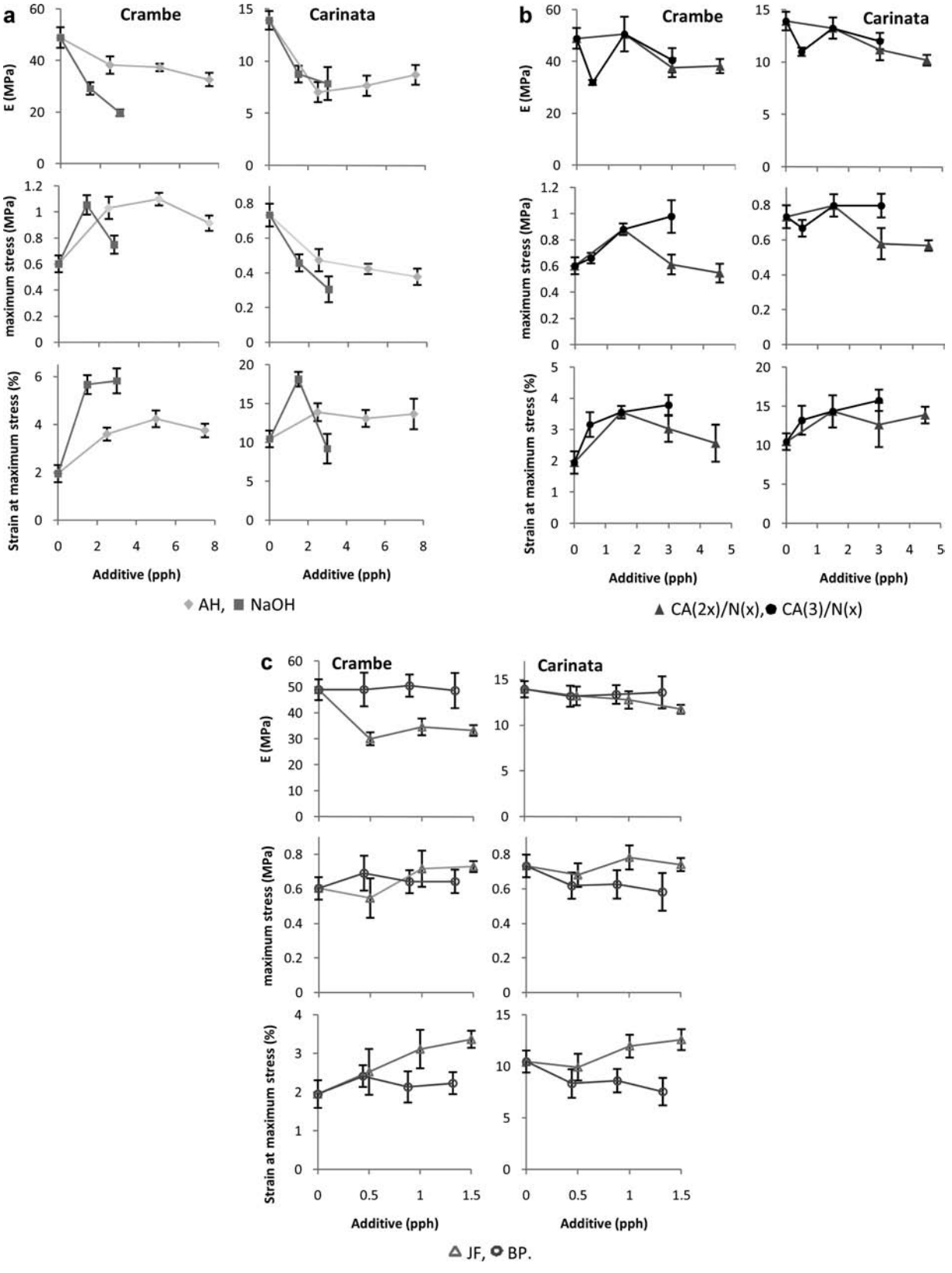

Figure 1. Tensile properties of compression-molded crambe and carinata oilseed meals. Error bars represent one standard deviation.

minimum of 48 h at 23 °C and 50% relative humidity prior to testing. The thickness was calculated as an average of five measurements, and the specimens were tested at 23 °C and 50% relative humidity using a crosshead speed of 10 mm/min and a 30 mm clamp separation (Instron 5566, Instron AB, Sweden).

The stress was calculated from the force divided by the cross-section area and the strain using the length of the reduced width section.[41] Strain at maximum stress was considered as the measurement for ductility as the failure mode was not consistent with slow tearing, making the determination of the strain at break inconsistent. Young's

dx.doi.org/10.1021/jf5015928 | J. Agric. Food Chem. 2014, 62, 6707−6715

modulus (E modulus) was calculated from the maximum slope after the initial toe correction.[41] A minimum of nine replicates were used; error bars in reported data indicate one standard deviation. Films excluded from tensile testing due to poor quality on pressing are listed as n/a in the Supporting Information.

Immersion Testing. Five replicate samples were removed from the oilseed meal films with a 5 mm diameter punch and weighed. Samples were lyophilized (Modulo, Edwards, UK) for a minimum of 48 h, weighed, and immersed in water for 24 h at 4 °C to prevent microbial growth. Following immersion, disks were removed from the water and held vertically for 10 s; the pendant drop was removed on fresh filter paper, and the disk was blotted between two dry pieces of filter paper (Munktell 1701, Falun, Sweden) under a 25 g weight, resulting in a pressure of 64.5 Pa for 10 s, then weighed. The disks were again lyophilized for a minimum of 48 h and weighed. The water absorption and mass loss during immersion were calculated on a dry basis. Error bars in reported data indicate one standard deviation. Films that lost coherence during immersion are listed as n/a in the Supporting Information.

RESULTS AND DISCUSSION

The present study on the effect of various additive types on tensile properties, protein solubility, protein molecular weight (Mw) distribution, and water uptake upon immersion produced a wide range of positive and negative results compared to a control with no additives. Here we have selected to present the results of those films with additives that contributed to interesting tensile properties. Those films with additives either having little effect or showing a negative

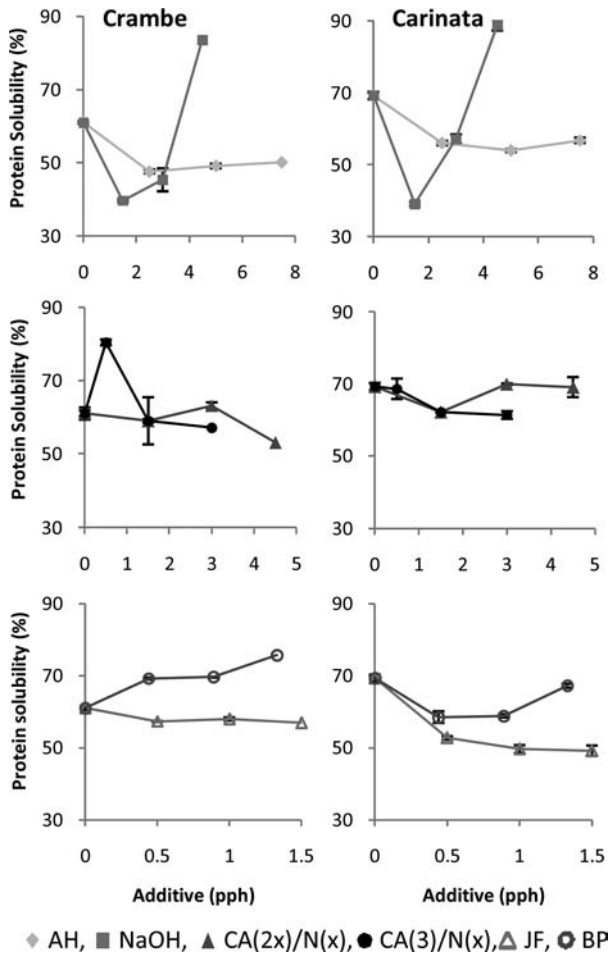

Figure 2. Total protein solubility of compression-molded crambe and carinata oilseed meals. Solubility is normalized to the total solubility of raw meal. Error bars represent one standard deviation.

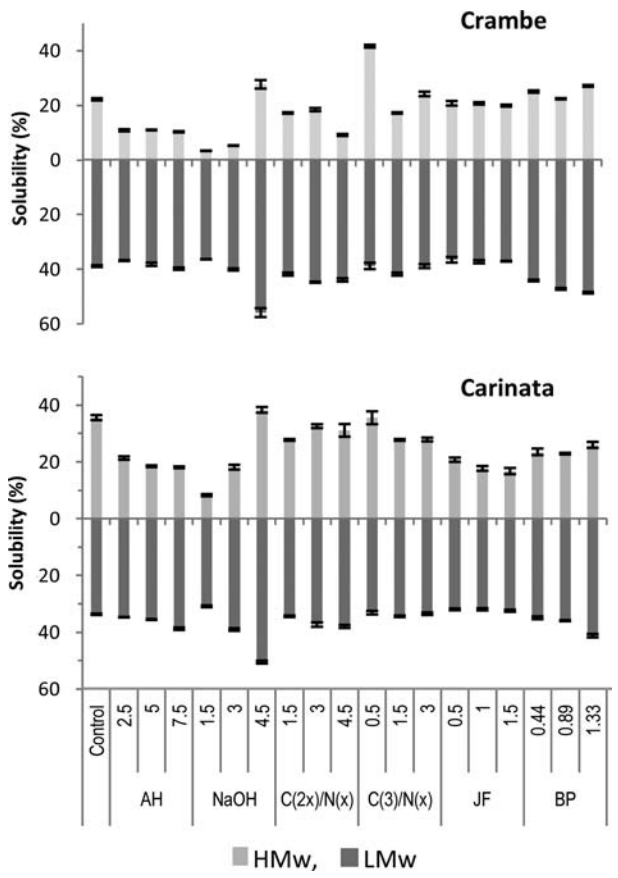

Figure 3. Protein solubility of compression-molded crambe and carinata oilseed meals divided into HMw and LMw fractions. Solubility is normalized to the total solubility of raw meal. Error bars represent one standard deviation.

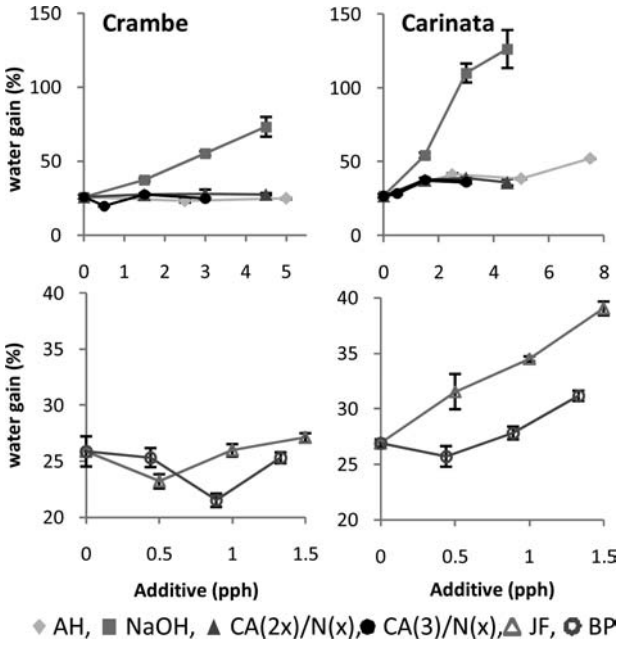

Figure 4. Water absorption of compression-molded crambe and carinata oilseed meals. Error bars represent one standard deviation.

dx.doi.org/10.1021/jf5015928 | J. Agric. Food Chem. 2014, 62, 6707−6715

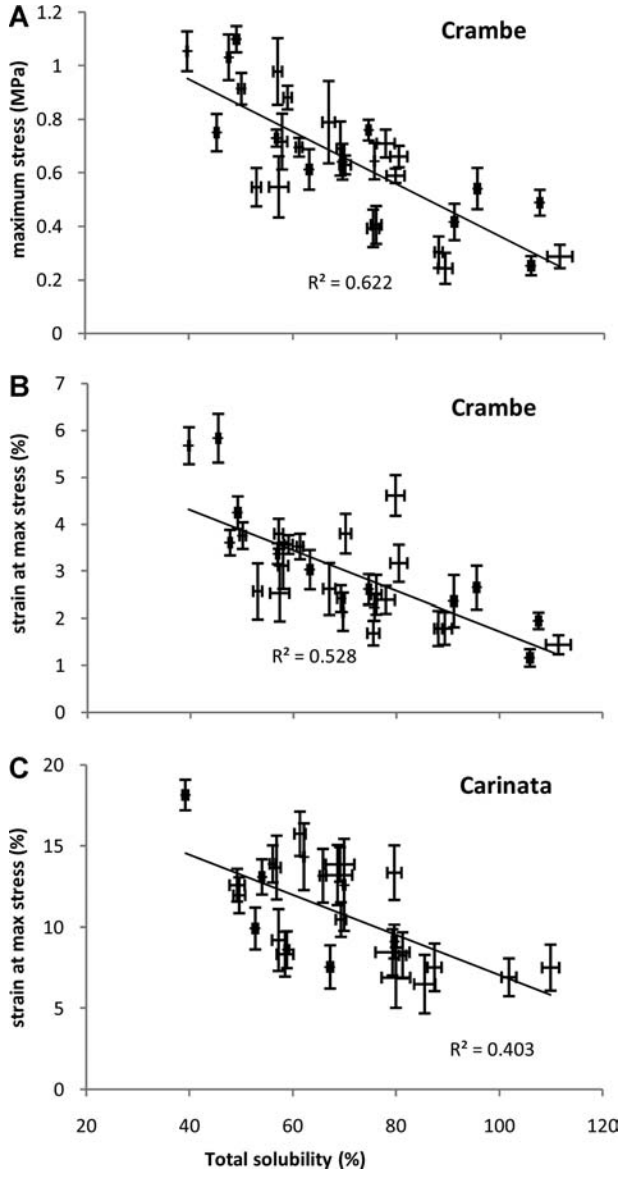

Figure 5. Selected tensile properties versus protein solubility of compression-molded crambe (A, B) and carinata (C) oilseed meals. Solubility is normalized to the total solubility of raw meal. Error bars represent one standard deviation.

influence on properties are treated to only a limited extent, although all results are included in the Supporting Information.

Effect of Additives with a Basic pH. Addition of NaOH (1.5) and AH (2.5) resulted in increased strain at maximum stress for both crambe and carinata (Figure 1a) as well as increased maximum stress in crambe (Figure 1a). Protein solubility decreased with additions of NaOH (1.5) and AH (all levels) (Figure 2). In particular, the extractability of the HMw fraction decreased compared to controls at the NaOH doses that resulted in increased tensile properties (Figure 3). Previous work on protein-based plastic materials has shown increased strength and decreased protein solubility, especially of HMw proteins, when AH was used as an additive. The increased strength and decreased protein solubility at increased pH have been attributed to reorganization and polymerization of the proteins.[42−44]

Thermal processing of proteins under basic conditions has been found to favor the formation of residue−residue reactions such as lanthionine and isopeptide cross-links[43,45,46] and, as sugars are present in both meals,[47,48] Maillard type cross-links.[49] Thus, building on previous results of increased protein polymerization by creating a basic environment in protein systems, in this study we propose that increases in protein aggregation have occurred in the present oil crop residue based plastics in a similar way, despite the low protein content.

Increasing the NaOH dose above 1.5 resulted in decreased mechanical properties (Figure 1a), whereas at these doses solubility increased markedly (Figure 2). Increased levels of AH did not induce further strength increases in crambe (Figure 1a), nor did the solubility decrease for either meal (Figure 2). These tensile-solubility relationships at higher levels of NaOH and AH may be the result of exhaustion of the available mechanisms for solubility reduction already occurring at the lowest additive level. A pH environment far from the isoelectric point is known to improve the properties of protein-based films.[19] Although the isoelectric points for the individual proteins in our meals are not specifically known, combined carinata proteins demonstrated solubility minima at pH 3.5 and 5,[47] whereas the minimum for crambe is approximately 5.5,[50] both from aqueous alkaline extracted seed meal. The most common storage proteins in brassica, cruciferin and napin, have isoelectric points of approximately 7.2 and ≤10, respectively, as measured in rapeseed.[51] An alternative explanation of the effect of NaOH and AH is that the properties vary related to the distance from the isoelectric points of the proteins.

The pH is also known to affect the interaction between proteins and other constituents of brassica oilseed meals. Although the bulk of the evidence in this area is from aqueous solutions, increased pH enhances many processes including interactions between proteins and phenolic compounds,[52] Maillard reactions with sugars,[53] and phytic acid as a protein complexing agent that depends on pH.[51] Indeed, phenolic acids have been added to purified plant proteins as cross-linking agents.[54]

E modulus was not positively affected by NaOH and AH in any case examined, despite changes in protein solubility. *E* modulus is a composite property resulting from deforming of all components, whereas maximum stress and strain at maximum stress are local phenomena. If the protein fraction is considered under the polymer entropic elasticity theory,[55] secondary structure such as α-helix and β-sheet have been shown to have an effect on the response of protein materials that is not accounted for in their increased molecular weight due to aggregation. In our case the proteins exhibit increased aggregation, but do not contribute to an increased *E* modulus. The analysis of VanKleef[55] suggests that changes in secondary structure, which do not contribute to the SE-HPLC response, may be responsible for a lowered stiffness of the protein fraction despite increased aggregation.

Water uptake varied greatly between NaOH and AH, with NaOH showing markedly higher water uptake (Figure 4). It has been shown that in protein-based materials made with AH there is no residual pH effect as the free ammonia evaporates.[16] For NaOH it is expected that there will be a residual pH effect that can continue to modify the protein environment during the water uptake test, possibly allowing more complete protein unfolding in water. Lower protein aggregation at higher NaOH levels coupled with the residual pH effect could result in a very loose and easily expanded protein network, allowing high water uptake levels.

Citric Acid−NaOH Blends. Addition of CA(3)/N(x) blends resulted in increased strain at maximum stress for both crambe and carinata while also increasing the maximum stress in crambe in a dose-dependent manner (Figure 1b). Protein solubility showed a slight decrease with increased NaOH, although the lowest NaOH level (3/0.5) in crambe demonstrated a pronounced increase in solubility due to the high acidity (Figure 2). This indicates low protein polymerization, similar to additions of CA alone (Supporting Information). CA is known to suppress lysinoalanine cross-linking in food protein systems,[45] one possible mechanism for the increased solubility in this case.

Solution pH is also known to be a determining factor in the interaction of secondary plant metabolites in oilseed meal with proteins. For example, maximum precipitation of phytates occurs at low pH values for both napin and cruciferin in rapeseed,[56] whereas phenolic compounds (sinapic acid) have been found to bind tightly to canola cruciferin at pH 4 and adversely affect heat-set gels. It should be noted that the cited works on phenolic and phytate interaction with brassica proteins are in solution or gels at <100 °C, where the lack of water and high temperatures in our case could result in quite different effects.

Maximum stress results for crambe and carinata and strain at maximum stress for crambe indicate a behavior of increased tensile properties due to increased protein polymerization with a decreasing ratio of CA to NaOH. Thus, the changes in behavior are most likely a result of pH changes, which may also be the background factor in property changes from additions of NaOH and AH. The molecular weight distribution (Figure 3) indicates similar behavior as in the addition of bases without CA, with no indication of carboxylic acid cross-linking.

For CA($2x$)/N(x) the acid/base ratio was held constant as the total dose was increased. When this additive blend was applied, the maximum stress and strain at maximum stress peaked at the lowest dose and decreased thereafter, with a more pronounced behavior in crambe than in carinata (Figure 1b). Total solubility changed only slightly until the highest dose (9/4.5), at which crambe solubility decreased (Figure 2). The balanced addition of CA and NaOH resulted in only small changes in the Mw profile with dose until the highest dose (9/4.5), at which a marked decrease was seen in HMw solubility for crambe (Figure 3). If carboxylic acid cross-linking was occurring in the CA($2x$)/N(x) case, a dose-dependent decrease in solubility would be expected as more citric acid is available. The changes seen in behavior with dose could be due to interference by carboxylic acid groups with amino groups[57] or hydroxyl groups,[22] reducing protein−protein interactions without forming cross-links, as the behavior could not be explained by a pH shift because the ratio of CA to NaOH is constant. Neither CA/N treatment showed an appreciable effect on water gain, suggesting that the treatments have little consequence for the protein network (Figure 4).

Reactive Additives. The addition of JF resulted in an increase in strain at maximum stress for both crambe and carinata with little change in maximum stress (Figure 1c). Protein solubility in crambe was unaffected by JF additions, whereas carinata solubility decreased with dose of JF (Figure 2), with the decreases coming from the HMw part of the protein Mw distribution (Figure 3). Thus, the behavior of the JF films does not clearly indicate significant protein interactions. The increase in strain at maximum stress is possibly due to a small plasticizer effect by the JF terminal amino groups interrupting protein−protein interactions. The decrease in E modulus of crambe may also be due to a plasticizing effect, which is made more pronounced by the low protein content compared to carinata, resulting in higher plasticizer level per unit of protein. Water uptake changed little in crambe with JF addition, whereas in carinata there was an increase with dose (Figure 4), reflecting the slight changes seen in the carinata network through HMw protein polymerization (Figure 3). Although JF contains two reactive amino groups, there seems to be little interaction with the proteins at the conditions of hot pressing in this study. Shifting the system to a higher pH may promote reactions with amino acids as seen between amino group containing residues.[45]

In contrast to the previously discussed additives, benzoyl peroxide caused changes in protein Mw distribution with an increase in soluble LMw proteins with dose (Figure 3). Total protein solubility in crambe showed a steady increase, whereas carinata demonstrated an initial decrease followed by a rise in solubility with BP addition (Figure 2). These subtle Mw and solubility changes did not have appreciable effects on tensile properties (Figure 1c). The active peroxides produced by decomposing BP are known to cause protein aggregation or fragmentation depending on the details of the situation.[58] In the present films, peroxide behavior is further complicated by the presence of antioxidant plant phenolics,[59] which can neutralize reactive species. The change in carinata solubility (Figure 2) and water uptake (Figure 4) after the first dose (0.44) may indicate that at the lowest dose the peroxides have a site to act upon, reducing solubility, whereas above that dose there is an excess of reactive species resulting in protein fragmentation. In crambe it is possible that this threshold is passed below the lowest dose studied. In other protein systems, peroxides have been shown to need catalysts or enzymes to produce effective cross-linking,[30,35] and these have not been added. In our system there seems to be little overall peroxide effect.

Denaturing and Reducing Agents. In previous work denaturing agents such as SDS[26,27] and U[24,28,29] and the reducing agent SB[38,39] have been shown to have positive effects on protein-based materials. In our case these additives have a universally detrimental effect (Supporting Information). SDS addition is expected to result in a disruption of weak protein−protein interactions, allowing protein rearrangement; in our case it would seem that the disruption resulted in a plasticizing effect, but no advantageous protein−protein interactions resulted, perhaps due to the interference of phenolics or phytates. At our pressing temperatures U is likely to partially degrade into cyanate and ammonium,[60] resulting in protein carbamylation and loss of reactive lysine residues, preventing reactions such as lysinoalanine cross-linking. In solution U has been shown to result in the dissociation of rapeseed cruciferin at high concentrations such as 4 M.[56]

In addition to its use as an additive to improve protein-based plastics and adhesives[38,39] SB has been used to avoid phenol oxidation and polyphenol attachment in brassica protein extraction and purification,[61] and the prevention of these activities may adversely affect protein aggregation in our case. The presence of SB can also result in disulfide bond reduction reducing aggregation. It is this activity that is suggested as allowing protein unfolding and reorganization, but in our case it appears that during hot pressing the conditions do not allow the formation of aggregated forms after reorganization.

Protein Solubility and Tensile Property Relationships. SE-HPLC data (Figures 2 and 3) indicate that changes in solubility occur primarily in the HMw fraction of the proteins with additive type, with the exception of NaOH, which showed changes in both Mw categories. Total solubility of proteins in extraction buffer correlated to changes in maximum stress and strain at maximum stress for crambe (R^2 0.62 and 0.53, respectively), whereas for carinata only a weak relationship was found in strain at maximum stress (R^2 0.40; Figure 5). This reduction in total solubility is due to the proteins reaching a high degree of aggregation under the process conditions, indicating protein−protein interactions that result in improved properties. These relationships included all tensile data, including those cases where the performance was degraded compared to the control. Thus, a general increase in protein aggregation resulting in increased tensile properties could be noted. Despite the low protein content in the present oilseed residual plastic films, protein aggregation seems to be key, as has been reported in previous works on crop-based plastics, although many are at higher protein contents.[14,19,21,42]

Of the additives tested, NaOH had the greatest positive effect on tensile properties, with increases of 105% in maximum stress and 200% in strain at maximum stress for crambe and a 70% increase in strain at maximum stress for carinata (Figure 1a). These changes were reflected in protein solubility and Mw distribution changes (Figures 2 and 3), with the best performance occurring at the lowest NaOH concentration. As the properties generally decrease with increases in NaOH above the lowest dose, it is possible that the optimum NaOH level is lower than the lowest level investigated herein for both meals. The fact that AH had positive effects on the mechanical properties in a similar manner to NaOH (Figure 1a) suggests that an increased pH has a generally beneficial effect up to the pH at which protein fragmentation occurs (Figure 3).

The high content of other constituents in the oilseed meals,[47,48,62] for example, sugars, phenolics, and fiber, undoubtedly plays a role by interacting with both proteins and additives. Despite this fact, substantial increases in mechanical properties were accomplished where additives contributed to protein aggregation, and elevated pH will be a key parameter in future work to improve protein polymerization and thereby the properties of seed residual based materials.

■ ASSOCIATED CONTENT

Supporting Information

Tables S1 and S2 containing tensile, protein solubility, and water uptake data for all additives, including those that had a detrimental effect on tensile performance. This material is available free of charge via the Internet at http://pubs.acs.org.

■ AUTHOR INFORMATION

Corresponding Author

*(W.R.N.) Phone: +46 40 415344. Fax: +46 40 415519. E-mail: bill.newson@slu.se.

Funding

We gratefully acknowledge VINNOVA, Formas, Bioraffinaderi Öresund, EC FP7 project ICON, and the Swedish strategic research program Trees and Crops for the Future (TC4F) for their support of this work.

Notes

The authors declare no competing financial interest.

■ ABBREVIATIONS USED

TFA, trifluoroacetic acid; ACN, acetonitrile; *E* modulus, Young's modulus; Mw, molecular weight; HMw, high molecular weight; LMw, low molecular weight; AH, ammonium hydroxide (NH_4OH); CA/N, citric acid/NaOH blends; SA, salicylic acid; CA, citric acid; AA, ascorbic acid; JF, Jeffamine EDR 176; BP, benzoyl peroxide; SDS, sodium dodecyl sulfate; U, urea; SB, sodium bisulfite

■ REFERENCES

(1) Carlsson, A. S.; Zhu, L.-H.; Andersson, M.; Hofvander, P. Platform crops amenable to genetic engineering−a requirement for successful production of bio-industrial oils through genetic engineering. *Biocatal. Agric. Technol.* **2014**, *3* (1), 58−64.

(2) Taylor, D.; Falk, K.; Palmer, C.; Hammerlindl, J.; Babic, V.; Mietkiewska, E.; Jadhav, A.; Marillia, E.; Francis, T.; Hoffman, T. *Brassica carinata* − a new molecular farming platform for delivering bio industrial oil feedstocks: case studies of genetic modifications to improve very long chain fatty acid and oil content in seeds. *Biofuels, Bioprod. Biorefin.* **2010**, *4* (5), 538−561.

(3) Rakow, G.; Getinet, A. In *Brassica carinata an Oilseed Crop for Canada*, Proceedings of the International Symposium on Brassicas 1997; Rennes, F. R., Thomas, G., Monteiro, A. A., Eds.; Acta Hortaculturae ISHS: Rennes, France, 1998; pp 419−428.

(4) Oplinger, E.; Oelke, E.; Kaminski, A.; Putnam, D.; Teynor, D.; Doll, J.; Kelling, K.; Durgan, B.; Noetzel, D. Crambe. In *Alternative Fields Crops Manual*; University of Wisconsin: Madison, WI, USA, July 1991.

(5) Li, X.; Fan, J.; Gruber, J.; Guan, R.; Frentzen, M.; Zhu, L.-H. Efficient selection and evaluation of transgenic lines of *Crambe abyssinica*. *Front. Plant Sci.* **2013**, *4*.

(6) Newson, W.; Kuktaite, R.; Hedenqvist, M.; Gällstedt, M.; Johansson, E. Oilseed meal based plastics from plasticized, hot pressed *Crambe abyssinica* and *Brassica carinata* residuals. *J. Am. Oil Chem. Soc.* **2013**, *90*, 1229−1237.

(7) Rouilly, A.; Orliac, O.; Silvestre, F.; Rigal, L. New natural injection-moldable composite material from sunflower oil cake. *Bioresour. Technol.* **2006**, *97* (4), 553−561.

(8) Baganz, K.; Lang, H.; Meißner, G. Industrial use of oilseed meal: a reasonable injection moulding compound. *Lipid−Fett* **1999**, *101* (8), 306−307.

(9) Rouilly, A.; Rigal, L. Agro-materials: a bibliographic review. *Polym. Rev.* **2002**, *42* (4), 441−479.

(10) Rasheed, F.; Newson, W. R.; Plivelic, T. S.; Kuktaite, R.; Hedenqvist, M. S.; Gällstedt, M.; Johansson, E. Structural architecture and solubility of native and modified gliadin and glutenin proteins: non-crystalline molecular and atomic organization. *RSC Adv.* **2014**, *4* (4), 2051−2060.

(11) Li, N.; Qi, G.; Sun, X. S.; Stamm, M. J.; Wang, D. Physicochemical properties and adhesion performance of canola protein modified with sodium bisulfite. *J. Am. Oil Chem. Soc.* **2012**, *89* (5), 897−908.

(12) Wäsche, A.; Wurst, S.; Borcherding, A.; Luck, T. Film forming properties of rape-seed protein after structural modification. *Nahrung/Food* **1998**, *42* (03−04), 269−271.

(13) Jang, S.; Lim, G. O.; Song, K. B. Preparation and mechanical properties of edible rapeseed protein films. *J. Food Sci.* **2011**, *76* (2), C218−C223.

(14) Johansson, E.; Spencer, G.; Bettini, E.; Cho, S.-W.; Marttila, S.; Kuktaite, R.; Gällstedt, M.; Hedenqvist, M. Biobased materials production from biodiesel residuals of rapeseed. *ISRN Mater. Sci.* **2012**, DOI: 10.5402/2012/193541.

(15) Zhang, H.; Mittal, G. Biodegradable protein based films from plant resources: a review. *Environ. Prog. Sustainable Energy* **2010**, *29* (2), 203−220.

(16) Marquie, C.; Aymard, C.; Cuq, J. L.; Guilbert, S. Biodegradable packaging made from cottonseed flour: formation and improvement

by chemical treatments with gossypol, formaldehyde, and glutaraldehyde. *J. Agric. Food Chem.* **1995**, *43* (10), 2762−2767.
(17) Álvarez-Chávez, C. R.; Edwards, S.; Moure-Eraso, R.; Geiser, K. Sustainability of bio-based plastics: general comparative analysis and recommendations for improvement. *J. Cleaner Prod.* **2012**, *23* (1), 47−56.
(18) Kuktaite, R.; Plivelic, T. S.; Cerenius, Y.; Hedenqvist, M. S.; Gällstedt, M.; Marttila, S.; Ignell, R.; Popineau, Y.; Tranquet, O.; Shewry, P. R.; Johansson, E. Structure and morphology of wheat gluten films: from polymeric protein aggregates toward superstructure arrangements. *Biomacromolecules* **2011**, *12* (5), 1438−1448.
(19) Olabarrieta, I.; Cho, S. W.; Gällstedt, M.; Sarasua, J. R.; Johansson, E.; Hedenqvist, M. S. Aging properties of films of plasticized vital wheat gluten cast from acidic and basic solutions. *Biomacromolecules* **2006**, *7* (5), 1657−1664.
(20) Gennadios, A.; Brandenburg, A. H.; Weller, C. L.; Testin, R. F. Effect of pH on properties of wheat gluten and soy protein isolate films. *J. Agric. Food Chem.* **1993**, *41* (11), 1835−1839.
(21) Ullsten, N. H.; Cho, S.-W.; Spencer, G.; Gällstedt, M.; Johansson, E.; Hedenqvist, M. S. Properties of extruded vital wheat gluten sheets with sodium hydroxide and salicylic acid. *Biomacromolecules* **2009**, *10* (3), 479−488.
(22) Reddy, N.; Li, Y.; Yang, Y. Alkali catalyzed low temperature wet crosslinking of plant proteins using carboxylic acids. *Biotechnol. Prog.* **2009**, *25* (1), 139−146.
(23) Reddy, N.; Jiang, Q.; Yang, Y. Preparation and properties of peanut protein films crosslinked with citric acid. *Ind. Crops Prod.* **2012**, *39*, 26−30.
(24) Türe, H.; Gällstedt, M.; Kuktaite, R.; Johansson, E.; Hedenqvist, M. S. Protein network structure and properties of wheat gluten extrudates using a novel solvent-free approach with urea as a combined denaturant and plasticiser. *Soft Matter* **2011**, *7* (19), 9416−9423.
(25) Manamperi, W. A.; Pryor, S. W. Properties of canola protein-based plastics and protein isolates modified using SDS and SDBS. *J. Am. Oil Chem. Soc.* **2012**, *89* (3), 541−549.
(26) Rhim, J. W.; Gennadios, A.; Weller, C. L.; Hanna, M. A. Sodium dodecyl sulfate treatment improves properties of cast films from soy protein isolate. *Ind. Crops Prod.* **2002**, *15* (3), 199−205.
(27) Mo, X.; Sun, X. Thermal and mechanical properties of plastics molded from sodium dodecyl sulfate-modified soy protein isolates. *J. Polym. Environ.* **2000**, *8* (4), 161−166.
(28) Mo, X.; Sun, X. Thermal and mechanical properties of plastics molded from urea-modified soy protein isolates. *J. Am. Oil Chem. Soc.* **2001**, *78* (8), 867−872.
(29) Kuktaite, R.; Plivelic, T. S.; Türe, H.; Hedenqvist, M. S.; Gällstedt, M.; Marttila, S.; Johansson, E. Changes in the hierarchical protein polymer structure: urea and temperature effects on wheat gluten films. *RSC Adv.* **2012**, *2* (31), 11908−11914.
(30) Qin, G.; Rivkin, A.; Lapidot, S.; Hu, X.; Preis, I.; Arinus, S. B.; Dgany, O.; Shoseyov, O.; Kaplan, D. L. Recombinant exon-encoded resilins for elastomeric biomaterials. *Biomaterials* **2011**, *32* (35), 9231−9243.
(31) Appelqvist, L.-Å. Further studies on a multisequential method for determination of oil content in oilseeds. *J. Am. Oil Chem. Soc.* **1967**, *44* (3), 209−214.
(32) Ullsten, N. H.; Gällstedt, M.; Johansson, E.; Gräslund, A.; Hedenqvist, M. S. Enlarged processing window of plasticized wheat gluten using salicylic acid. *Biomacromolecules* **2006**, *7* (3), 771−776.
(33) Chiou, B. S.; Jafri, H.; Cao, T.; Robertson, G. H.; Gregorski, K. S.; Imam, S. H.; Glenn, G. M.; Orts, W. J. Modification of wheat gluten with citric acid to produce superabsorbent materials. *J. Appl. Polym. Sci.* **2013**, *129* (6), 3192−3197.
(34) Selling, G.; Sessa, D. J. Multivalent carboxylic acids to modify the properties of zein. *Ind. Crops Prod.* **2007**, *25* (1), 63−69.
(35) Joye, I. J.; Lagrain, B.; Delcour, J. A. Use of chemical redox agents and exogenous enzymes to modify the protein network during breadmaking − a review. *J. Cereal Sci.* **2009**, *50* (1), 11−21.
(36) Wretfors, C.; Cho, S.-W.; Kuktaite, R.; Hedenqvist, M. S.; Marttila, S.; Nimmermark, S.; Johansson, E. Effects of fiber blending and diamines on wheat gluten materials reinforced with hemp fiber. *J. Mater. Sci.* **2010**, *45* (15), 4196−4205.
(37) AkzoNobel. Crosslinking elastomers and thermoplastics: organic peroxides and auxiliaries, 2011.
(38) Rouilly, A.; Mériaux, A.; Geneau, C.; Silvestre, F.; Rigal, L. Film extrusion of sunflower protein isolate. *Polym. Eng. Sci.* **2006**, *46* (11), 1635−1640.
(39) Min, Z.; Song, Y.; Zheng, Q. Influence of reducing agents on properties of thermo-molded wheat gluten bioplastics. *J. Cereal Sci.* **2008**, *48* (3), 794−799.
(40) Gällstedt, M.; Mattozzi, A.; Johansson, E.; Hedenqvist, M. S. Transport and tensile properties of compression-molded wheat gluten films. *Biomacromolecules* **2004**, *5* (5), 2020−2028.
(41) ASTM Standard D 638-86, standard test for tensile properties; American Society for testing and Materials: Philadelphia, PA, USA, 1986.
(42) Johansson, E.; Malik, A. H.; Hussain, A.; Rasheed, F.; Newson, W.; Plivelic, T. S.; Hedenqvist, M.; Gällstedt, M.; Kuktaite, R. Wheat gluten polymer structures: the impact of genotype, environment and processing on their functionality in various applications. *Cereal Chem.* **2013**, *90* (4), 367−376.
(43) Rombouts, I.; Lagrain, B.; Delcour, J. A.; Türe, H.; Hedenqvist, M. S.; Johansson, E.; Kuktaite, R. Crosslinks in wheat gluten films with hexagonal close-packed protein structures. *Ind. Crops Prod.* **2013**, *51*, 229−235.
(44) Ullsten, H. G. M.; Spencer, G.; Johansson, E.; Marttila, S.; Ignell, R.; Hedenqvist, M. S. Extruded high quality materials from wheat gluten. *Biopolym. Renewable Resour.* **2010**, *1*, 173−186.
(45) Friedman, M. Chemistry, biochemistry, nutrition, and microbiology of lysinoalanine, lanthionine, and histidinoalanine in food and other proteins. *J. Agric. Food Chem.* **1999**, *47* (4), 1295−1319.
(46) Rombouts, I.; Lagrain, B.; Brijs, K.; Delcour, J. A. β-Elimination reactions and formation of covalent cross-links in gliadin during heating at alkaline pH. *J. Cereal Sci.* **2010**, *52* (3), 362−367.
(47) Pedroche, J.; Yust, M.; Lqari, H.; Girón-Calle, J.; Alaiz, M.; Vioque, J.; Millán, F. *Brassica carinata* protein isolates: chemical composition, protein characterization and improvement of functional properties by protein hydrolysis. *Food Chem.* **2004**, *88* (3), 337−346.
(48) Steg, A.; Hindle, V.; Liu, Y.-G. By-products of some novel oil seeds for feeding: laboratory evaluation. *Anim. Feed Sci. Technol.* **1994**, *50* (1), 87−99.
(49) Singh, H. Modification of food proteins by covalent crosslinking. *Trends Food Sci. Technol.* **1991**, *2*, 196−200.
(50) Massoura, E.; Vereijken, J.; Kolster, P.; Derksen, J. T. P. Proteins from *Crambe abyssinica* oilseed. I. Isolation procedure. *J. Am. Oil Chem. Soc.* **1998**, *75* (3), 323−327.
(51) Wanasundara, J. P. D. Proteins of Brassicaceae oilseeds and their potential as a plant protein source. *Crit. Rev. Food Sci. Nutr.* **2011**, *51* (7), 635−677.
(52) Tan, S. H.; Mailer, R. J.; Blanchard, C. L.; Agboola, S. O. Canola proteins for human consumption: extraction, profile, and functional properties. *J. Food Sci.* **2011**, *76* (1), R16−R28.
(53) Ajandouz, E. H.; Desseaux, V.; Tazi, S.; Puigserver, A. Effects of temperature and pH on the kinetics of caramelisation, protein cross-linking and Maillard reactions in aqueous model systems. *Food Chem.* **2008**, *107* (3), 1244−1252.
(54) Neo, Y. P.; Perera, C. O.; Nieuwoudt, M. K.; Zujovic, Z.; Jin, J.; Ray, S.; Gizdavic-Nikolaidis, M. Influence of heat-curing on the structure and physicochemical properties of phenolic-acid loaded proteinaceous electrospun fibers. *J. Agric. Food Chem.* **2014**, *62* (22), 5163−5172.
(55) Van Kleef, F. Thermally induced protein gelation: gelation and rheological characterization of highly concentrated ovalbumin and soybean protein gels. *Biopolymers* **1986**, *25* (1), 31−59.
(56) Schwenke, K.; Mothes, R.; Marzilger, K.; Borowska, J.; Kozlowska, H. Rapeseed protein polyanion interactions − turbidimetric studies in systems with phosphate-containing polyanions: phytic acid and octametaphosphate. *Food/Nahrung* **1987**, *31* (10), 1001−1013.

(57) Reddy, N.; Li, Y.; Yang, Y. Wet cross-linking gliadin fibers with citric acid and a quantitative relationship between cross-linking conditions and mechanical properties. *J. Agric. Food Chem.* **2008**, *57* (1), 90−98.
(58) Davies, K. Protein damage and degradation by oxygen radicals. I. General aspects. *J. Biol. Chem.* **1987**, *262* (20), 9895−9901.
(59) Matthäus, B. Antioxidant activity of extracts obtained from residues of different oilseeds. *J. Agric. Food Chem.* **2002**, *50* (12), 3444−3452.
(60) Rombouts, I.; Lagrain, B.; Delcour, J. A.; Türe, H.; Hedenqvist, M. S.; Johansson, E.; Kuktaite, R. Crosslinks in wheat gluten films with hexagonal close-packed protein structures. *Ind. Crops Prod.* **2013**, *51*, 229−235.
(61) Berot, S.; Compoint, J.; Larre, C.; Malabat, C.; Gueguen, J. Large scale purification of rapeseed proteins (*Brassica napus* L.). *J. Chromatogr., B* **2005**, *818* (1), 35−42.
(62) Carlson, K.; Tookey, H. Crambe meal as a protein source for feeds. *J. Am. Oil Chem. Soc.* **1983**, *60* (12), 1979−1985.

Table 1. Primer Pairs Used for Real-Time Quantitative RT-PCR

gene name	gene annotation[a]	sequence for the forward and reverse primers	expected fragment size (bp)
VvF3′H	VIT_17s0000g07200	F 5′- ATTCGCCACCCTGAAATGAT-3′ R 5′-AGCCGTTGATCTCACAGCTC-3′	196
VvF3′5′H	VIT_06s0009g02810	F 5′-GAAGTTCGACTGGTTATTAACAAAGAT-3′ R 5′-AGGAGGAGTGCTTTAATGTTGGTA-3′	156
VvUFGT	VIT_16s0039g02230	F 5′-CATGTCTCAAACCACCACCAAC −3′ R 5′-TGGTGCTGAAGAAGGAGAAGAC −3′	137
VvAOMT1	VIT_01s0010g03510	F 5′-GGGACATTGGACTTTGCGATG-3′ R 5′-TAACCAACTTCAGCAGCAGC-3′	79
VvAOMT2	VIT_01s0010g03490	F 5′-CCATGTCCAGCTCAAGTCACAAGG-3′ R 5′-TTCAGCTGCTCATGCTCTCTTGGG-3′	90
VvAOMT3	VIT_01s0010g03470	F 5′-AGAGAGCATGAGCAGCTGAGAG-3′ R 5′-TCCTTCGTCAACAGGCACATTC-3′	90
VvABCC1	VIT_16s0050g02480	F 5′- AGGGTCTAGGCTCCATTGTTG-3′ R 5′-ACCAGTATCCGGCTTCTTCG-3′	106
VvAM1	VIT_16s0050g00930	F 5′-GTTCGGCTTTCAATTGCCTCG-3′ R 5′- CCTTCCCACCCATTAAAAGC-3′	146
VvAM2	VIT_16s0050g00910	F 5′- TGAATTTTAATGGGTGGGAGGC-3′ R 5′-TCATTGGAGACCCGAATGCTT-3′	73
VvAM3	VIT_16s0050g00900	F 5′- GGTTGGAGGTCGTGATGTTC-3′ R 5′-TTGGAGACCCGAATGCTCAC-3′	58
VvGST	VIT_04s0079g00690	F 5′- CCTGATTTCCTCCTTCGACAGC-3′ R 5′-GCCTGAAATCGCCATCTTCTACC-3′	64
VvMybA1	VIT_02s0033g00380	F 5′-AGGAAGCCATCATCCACTTCACC-3′ R 5′-TGCTCAGCTAACAGGCTTTCCC-3′	71
VvMyb5B	VIT_06s0004g00570	F 5′-AGTCCAGTCGTTCGGGTTC-3′ R 5′-GCAGGGTGTTGAAGCCAAAT-3′	157
VvACT1	VIT_04s0044g00580	F 5′-CTTGCATCCCTCAGCACCTT-3′ R 5′-TCCTGTGGACAATGGATGGA-3′	82

[a]According to CRIBI Grape Genome (http://genomes.cribi.unipd.it/grape/).

anthocyanins,[22] Francisco et al.[23] recently reported that an ATP binding cassette protein (ABCC1) transports anthocyanidin 3-*O*-glucosides, with a preferential transport for malvidin 3-*O*-glucoside.

In this work we demonstrated the existence of significant variation for the anthocyanin profiles among clones from the same cultivar and also identified the variation in the amount of a particular anthocyanin as the main distinguishing factor within those profiles, where genetic variation and differential gene expression of particular genes seem to be important factors to determine the clonal difference in anthocyanin profile.

MATERIALS AND METHODS

Berry Sampling. The assays were performed during the vintages 2010 and 2012, at the Bodegas Esmeralda (BESA) clone collection localized at La Pirámide vineyard (Catena Zapata Winery, Agrelo, Mendoza; 34°55′21″ S, 69°7′4″ E). The collection included 131 clones (116 from BESA, 12 from FCA-UNCuyo, and 3 from INTA). Clones were sorted in 34 rows with four clones per row with a plantation density of 4000 plants per hectare (1.25 m × 2.00 m). The vineyard was a homogeneous field without slope, and all of the plants were under artificial irrigation. Each experimental unit (clone) was represented by approximately 45 plants. Ripening state of the samples was determined on the basis of berry density as an indicator of accumulated sugar levels. Density was estimated by berry flotation in a range of NaCl solutions, each having a decrease in salinity of 20 g NaCl L^{-1} (from 160 to 80 g NaCl L^{-1}).[24]

Varietal Identity Testing of the Clones through Microsatellite Analysis. Young leaves were sampled from every clone and kept frozen at −80 °C. DNA was extracted using a DNeasyTM Plant Mini Kit (Qiagen, Valencia, CA, USA) according to the manufacturer's protocol. Nine nuclear microsatellite markers were studied (VVS2, VVMD5, VVMD27, VVMD28, ssrVrZAG29, ssrVrZAG62, ssrVrZAG67, ssrVrZAG83, and ssrVrZAG112), using a multiplex PCR, according to the method of Ibáñez et al.[25]

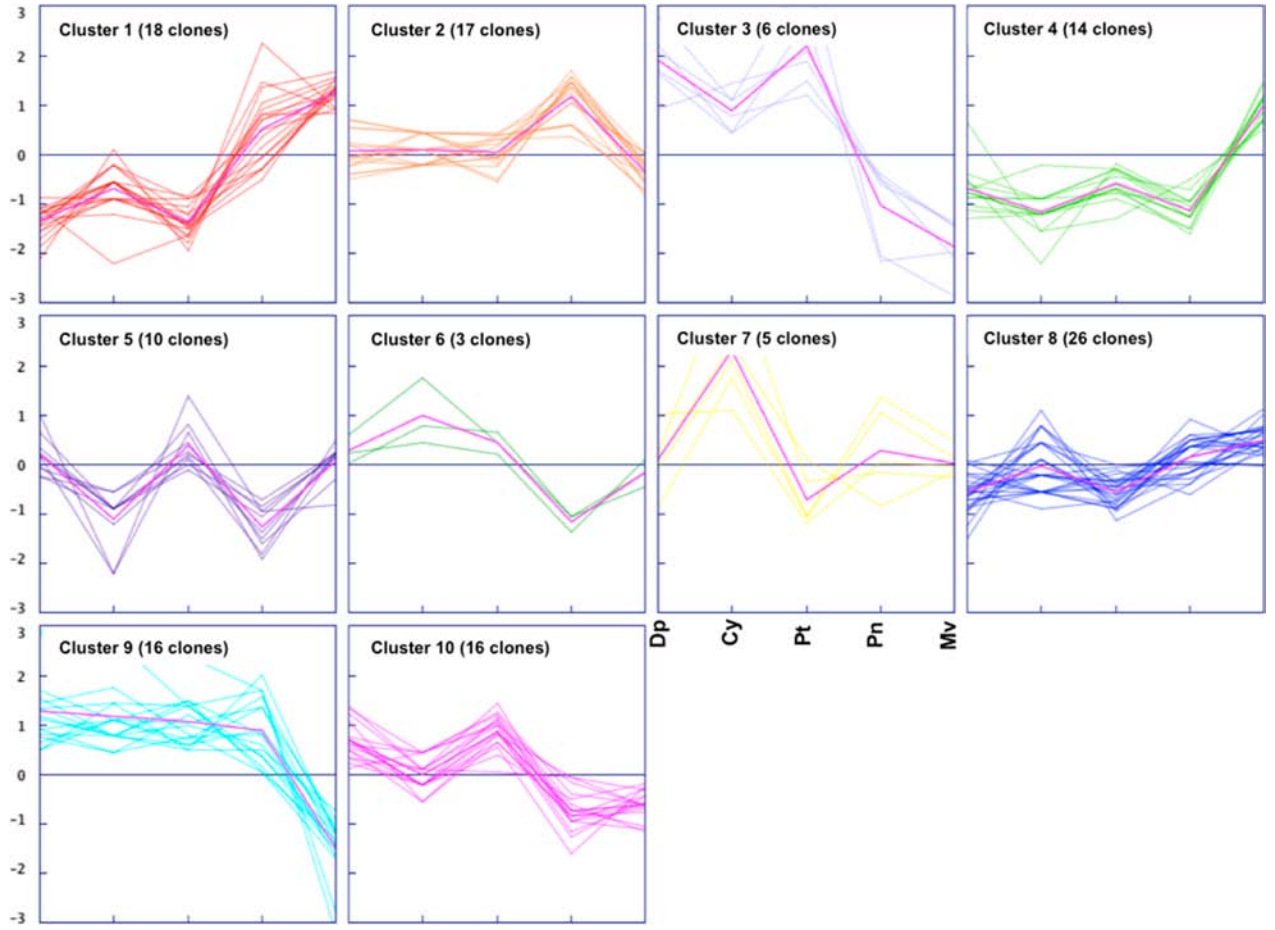

Figure 1. Clustering analysis of 131 Malbec clones according to their anthocyanin profiles using the *k*-means method. A five-point profile of each clone was obtained after adding up the glycosylated, acetylated, and coumaroylated forms for each anthocyanin: delphinidin (Dp), cyanidin (Cy), petunidin (Pt), peonidin (Pn), and malvidin (Mv). The number of clones per cluster is indicated in parentheses.

Extract Preparation from Skins. Three hundred berries per clone were randomly collected at a density of 140−160 g L^{-1} of NaCl (approximately 24 °Brix) in nylon bags from different positions within clusters from every plant. The samples were kept in ice to prevent dehydration and transported to the laboratory, where they were weighed, frozen, and conserved at −80 °C. Berry anthocyanins were extracted as previously described[3,26,27] with minor modifications. Briefly, skins and seeds were separated by hand from 50 berries, weighed, and ground with 30 mL of ultrapure water. Forty milliliters of hydroalcoholic solution (ethanol/water, 12:88, v/v) containing 5 g/L of tartaric acid was added to the ground material. The final weight of the suspension was adjusted to 100 g with ultrapure water. The pH of extracts was adjusted to 3.6 with NaOH or HCl. Extracts were macerated for 2 h at 25 °C using an orbital shaker at 200 rpm and then centrifuged for 15 min at 4000 rpm.

HPLC-DAD Analysis of Anthocyanins. Two milliliters of skin extracts per experimental unit were filtered through a 0.45 μm pore size nylon membrane, and then 100 μL was injected in the high-performance liquid chromatograph coupled to diode array detector (HPLC-DAD) system (PerkinElmer, Shelton, CT, USA). Separation was performed at 25 °C using a Chromolith Performance C18 column (100 mm × 4.6 mm i.d., 2 μm; Merck, Darmstadt, Germany) with a Chromolith guard cartridge (10 mm × 4.6 mm). A gradient consisting of solvent A (water/formic acid, 90:10, v/v) and solvent B (acetonitrile) was applied at a flow rate of 1.1 mL/min from 0 to 22 min and at flow rate of 1.5 mL/min from 22 to 35 min as follows: 96−85% A and 4−15% B from 0 to 12 min, 85−85% A and 15−15% B from 12 to 22 min, 85−70% A and 15−30% B from 22 to 35 min. This was followed by a final wash with 100% methanol and re-equilibration of the column. Photodiode array detection was performed from 210 to 600 nm, and the quantification was carried out by peak area measurements at 520 nm, according to the method of Fanzone et al.[28] Anthocyanin amount was expressed by using malvidin-3-glucoside chloride as standard (Extrasynthese, Lyon, France) for a calibration curve (R^2 = 0.98). Identification and confirmation of anthocyanic pigments were performed by HPLC-DAD/ESI-MS as described by Monagas et al.[29]

RNA Isolation, cDNA Synthesis, and Real-Time Quantitative PCR (qRT-PCR) Expression Analysis. For gene expression studies, post-véraison berries were harvested at a density of 100−120 g L^{-1} of NaCl, frozen, and conserved at −80 °C. Total RNA was extracted from berry skins according to the procedures described by Reid et al.[30] Final RNA purification and DNase digestion of contaminating DNA in the RNA samples were performed using the SV Total RNA Isolation System (Promega) following standard protocols. Reactions for cDNA synthesis and qRT-PCR were performed according to Lijavetzky et al.[31] using a StepOne Real-Time PCR System (Applied Biosystems, Life Technologies). Nontemplate controls were included for each primer pair, and each qRT-PCR reaction was completed in quadruplicate. Expression data were normalized against the grapevine *ACT1* gene (*VIT_04s0044g00580*). A normalization gene was chosen after the comparison of *ACT1*, *EFa1* (*VIT_06s0004g03220*) and *UBI* (*VIT_16s0098g01190*) genes using NormFinder software.[32] All three genes were previously tested for grapevine gene expression analysis.[30] Relative quantification was performed by means of the ΔΔCt method using StepOne software v2.2.2 (Applied Biosystems, Life Technologies). Gene-specific primers were designed using the QuantPrime web tool,[33] and the sequences are described in Table 1.

Statistical Methods. Clustering analysis of HPLC-DAD data was performed using the *k*-means method[34] implemented in Genesis

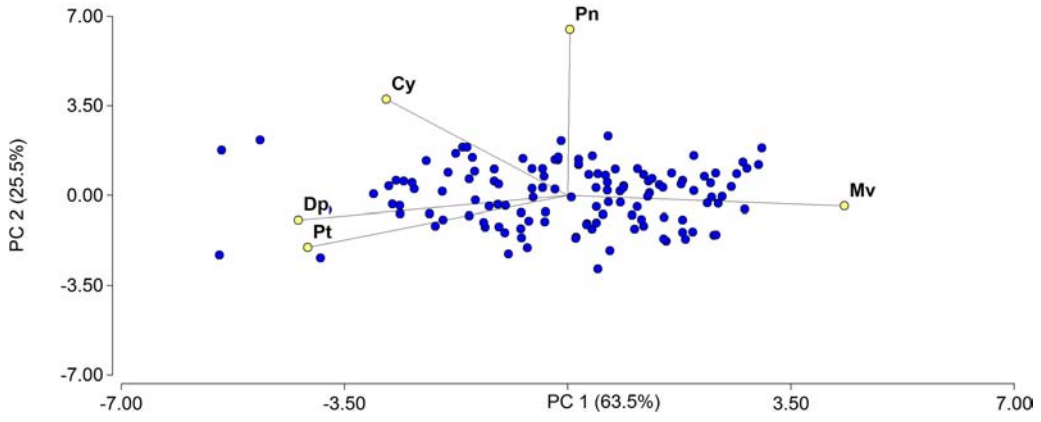

Figure 2. Principal component analysis (PCA) of the anthocyanin profile data of the 131 studied samples. The first (PC1) and second (PC2) principal components are represented. Each of the five points determining the profiles described in Figure 1 was treated as a variable (Dp, Cy, Pt, Pn, and Mv).

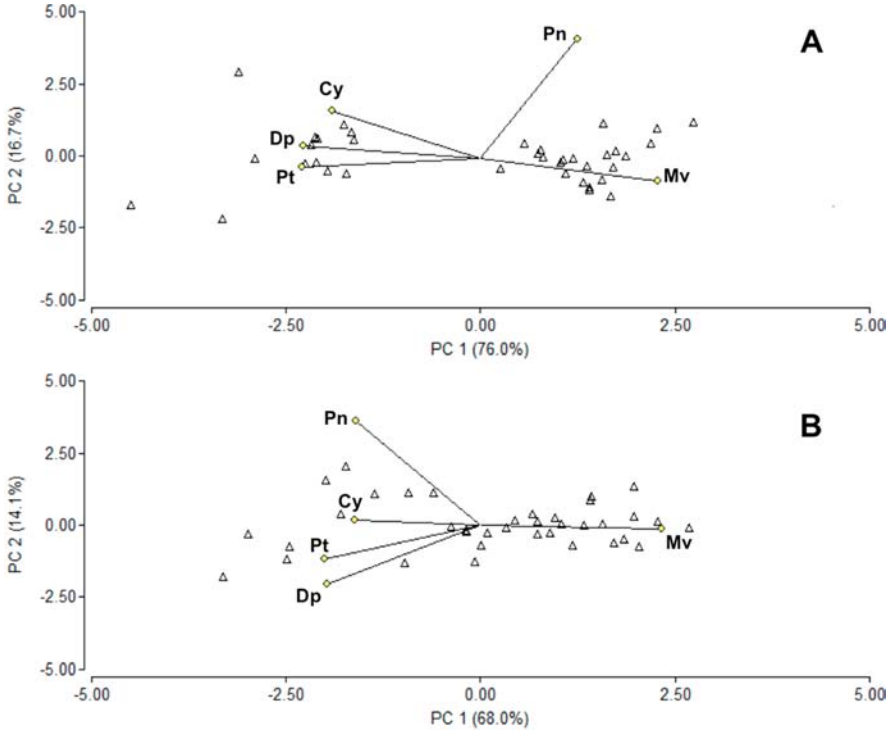

Figure 3. Principal component analysis (PCA) of the anthocyanin profile data of selected clones representing both extremes of the Mv content distribution described in Table S3 in the Supporting Information. Plots correspond to the data collected in 2010 (A) and 2012 (B). The first (PC1) and second (PC2) principal components are represented.

software v.1.7.6.[35] Principal component analysis[36] and linear regression analysis were carried out by means of InfoStat software.[37] Additional statistical calculations for the qRT-PCR analysis (group analysis: adjusted *p* values using Benjamini−Hochberg) were carried out with the help of DataAssist software v.3.01 (Applied Biosystems, Life Technologies).

RESULTS

All of the Clones Studied Belong to the Cultivar Malbec. Before performing any biochemical analysis, we first verified the cultivar identity of the 131 sampled clones by analyzing nine microsatellite markers. As shown in Table S1 in the Supporting Information, all of the samples presented the same genotype for the nine analyzed microsatellite markers. This genotype was compared with the ICVV database (www.icvv.es) and the European *Vitis* database (www.eu-vitis.de) and matched with Cot (prime name for Malbec at the *Vitis* International Variety Catalogue-VIVC, www.vivc.de). The total probability of identity found for this set of nine microsatellite markers was very low (6.93×10^{-12}),[25] and allows concluding that all of the studied samples belong to the cultivar Malbec.

Malbec Clones Can Be Discriminated by Their Anthocyanin Profiles. To evaluate the phenotypic variation for the anthocyanin profile of the 131 Malbec accessions of the studied collection, we performed a HPLC-DAD analysis.[3,26−28] For each Malbec clone 15 anthocyanins were considered: delphinidin (Dp), cyanidin (Cy), petunidin (Pt), peonidin (Pn), and malvidin (Mv) in their glycosylated, acetylated, and coumaroylated derivative forms (i.e., Dp3Gl, Cy3Gl, Pt3Gl, Pn3Gl, Mv3Gl, Dp3acGl, Cy3acGl, Pt3acGl, Pn3acGl,

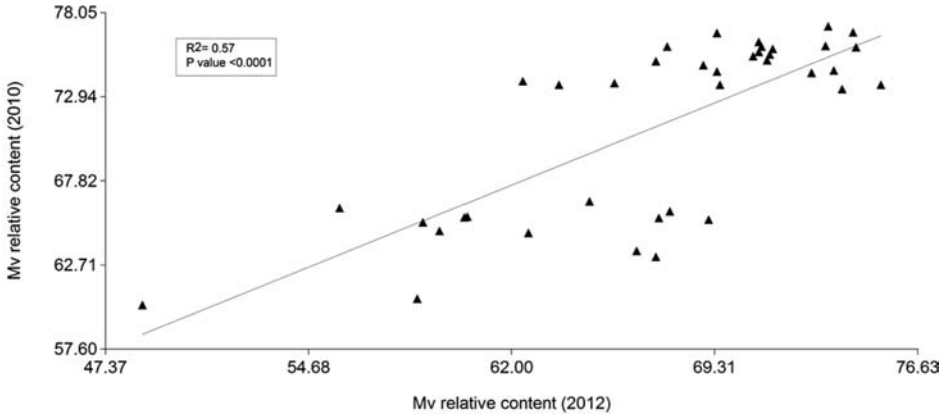

Figure 4. Correlation between malvidin (Mv) relative content of selected extreme clones during two different seasons (2010 and 2012).

Mv3acGl, Dp3cumGl, Cy3cumGl, Pt3cumGl, Pn3cumGl, and Mv3cumGl; Supporting Information Figure S1). The absolute and relative contents of those anthocyanins in samples of the clone collection are shown in Table S2 in the Supporting Information. Surprisingly, we obtained a broad spectrum of anthocyanin profiles among the clones. To have a comprehensive outlook of those different profiles, clones were grouped on the basis of their anthocyanin profiles using a *k*-means clustering analysis.[34] A five-point profile of each sample was obtained after adding the glycosylated, acetylated, and coumaroylated derivatives for each anthocyanin. As observed in Figure 1, the clones presenting similar profiles were clustered in 10 different profile groups. As expected, the larger cluster (cluster 8) included clones showing little variation with respect to the median profile. However, another five clusters grouped clones displaying high or low proportion of particular anthocyanins (clusters 1, 3, 4, 7, and 9).

Malbec Clones Are Mainly Separated by Variation in Mv Content. To further evaluate the variation observed within the Malbec clone collection, a principal component analysis (PCA) over the anthocyanin profile data of the 131 studied samples was performed (Figure 2). For this analysis each of the five points determining the profiles described in Figure 1 was treated as a variable (Dp, Cy, Pt, Pn, and Mv). First and second principal components (PC1 and PC2) explained together almost 90% of the variability for the anthocyanin profile (63.5 and 25.5%, respectively). PC1 pointed out the role of Mv content variation as the main discriminating factor within the clones. Dp and Pt contents were found negatively correlated with Mv, in agreement with both Dp and Pt being Mv precursors.[38] On the other hand, Pn content seems to be independent with respect to Mv, whereas Cy, a precursor of Pn, displayed an intermediate behavior (Figure 2).

Putative Genetic Effects on Mv Content and Anthocyanin Profiles Variation. After verifying the existence of different anthocyanin profiles within the clone collection and identifying the Mv content as the main variation source, we proceeded to evaluate the extent of conservation of the observed anthocyanin profiles in different years as an indication of the existence of an underlying genetic effect. For this purpose, we selected about 30% of clones representing both extremes of the Mv content distribution (Supporting Information Table S3). Data from the selected clones displayed similar PCA results as the complete collection, with an obvious increase of the PC1 (led by Mv) and a consequent decrease in the PC2 (Figure 3A). The same selected clones were further analyzed by HPLC-DAD in a second-year replication. The PCA performed on the selected clones during 2012 (Figure 3B) displayed again a large effect of Mv content on the evaluated phenotypic variation, as reflected in the PC1 value (68%). Besides the PCA results, this putative genetic effect could also be observed in Figure 4, where the linear regression analysis between the Mv content of the selected clones (2010 vs 2012) displayed highly statistically significant results with an $R^2 = 0.57$ (p value < 0.0001). Additionally, Dp and Pt presented also a highly significant correlation; Cy was just slightly correlated, whereas Pn showed no correlation (Table 2).

Table 2. Linear Regression Analysis between Individual Anthocyanin Contents Measured in 2010 and 2012

variable[a]	n	r^2	r^2 adj	p value
Mv	38	0.57	0.56	<0.0001
Dp	38	0.47	0.45	<0.0001
Pt	38	0.41	0.39	<0.0001
Cy	38	0.15	0.13	0.0168
Pn	38	0.04	0.01	0.2369

[a]Delphinidin (Dp), cyanidin (Cy), petunidin (Pt), peonidin (Pn), and malvidin (Mv) as the sum of their corresponding glycosylated, acetylated, and coumaroylated derivatives.

Variation in Mv Content Is Associated with Distinct Patterns of Gene Expression during Biosynthesis and Transport of Anthocyanins. We evaluated the putative influence of different genes related to biosynthesis and transport of anthocyanins on the variation in Mv contents (and the anthocyanin profiles) within the Malbec clone collection. To perform such analysis we designed qRT-PCR specific primers for 13 grapevine genes comprising 6 structural genes [(i) flavonoid 3′-hydroxylase (*F3′H*); (ii) flavonoid 3′,5′-hydroxylase (*F3′5′H*); (iii) UDP-glucose:flavonoid-3-*O*-glucosyltransferase (*UFGT*); (iv) *O*-methyltransferase 1 (*OMT1*); (v) *OMT2*; and (vi) *OMT3*],[17−19,39] 5 anthocyanin transporters [(i) glutathione-*S*-transferase (*GST*); (ii) ATP binding cassette C1 (*ABCC1*); (iii) anthoMATE1 (*AM1*); (iv) *AM2*; and (v) *AM3*;[18,22,23]], and 2 *MYB* transcription factors [(i) *MYBA1* and (ii) *MYB5b*].[14−16,18,40] Sequences for the forward and reverse primers as well as the PCR expected fragment size are detailed in Table 1. We measured the transcript accumulation of each gene in two groups of four clones corresponding to both Mv content extremes in the clone collection (Supporting Information Table S4). Clones selected

for each of the groups belong to (i) contrasting *k*-means clusters (Figure 1), (ii) opposite extremes at all PCAs (Figures 2 and 3), and (iii) opposite extremes of Mv content (Figure 5; Table S3 in the Supporting Information). Interestingly, although the anthocyanin profiles of both groups are clearly different (Figure 5b; Supporting Information Table S4), the total amount of anthocyanins is almost the same (Figure 5a). Consequently, with significant difference in Mv, the proportions of trisubstituted/disubstituted anthocyanins and methylated/unmethylated anthocyanins were higher in the high Mv content group (Supporting Information Table S4).

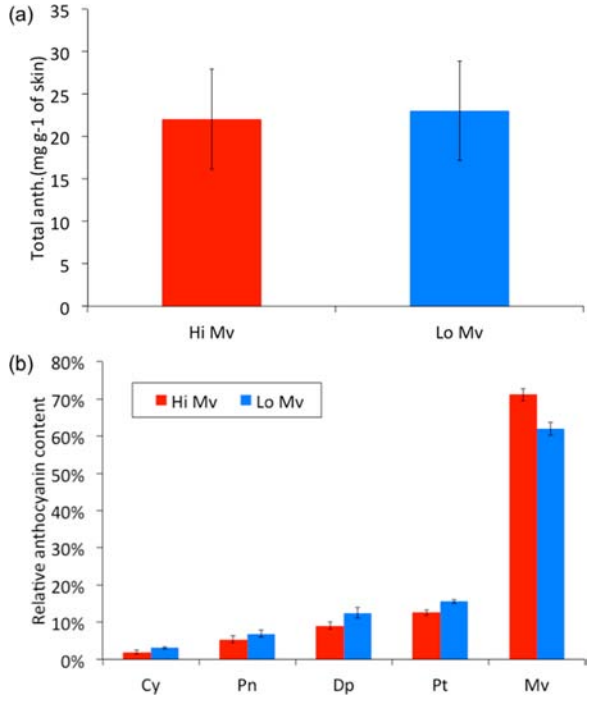

Figure 5. Anthocyanin content and metabolite profiles in berry skin of two groups of four Malbec clones corresponding to both Mv content extremes in the clone collection: (a) total anthocyanins expressed as mg g^{-1} of skin of malvidin equivalents; (b) anthocyanin profiles expressed as the relative concentration of cyanidin (Cy), peonidin (Pn), delphinidin (Dp), petunidin (Pt), and malvidin (Mv). High Mv content clones: MB25, FM5, FM4, and MB5. Low Mv content clones: MB81, MB30, MB77, and MB113.

As previously reported by Fournier-Level et al.[19] for other colored cultivars, no expression of *OMT3* was detected in grape skins of Malbec (data not shown). Unsurprisingly, most genes displayed slight difference between the two compared groups (Figure 6). Two of the structural genes showed significant variations, one related to anthocyanin hydroxylation (*F3′5′H*) and other involved in anthocyanin methoxylation (*OMT1*). The gene showing the more extreme differences was a putative anthocyanin transporter (*AM2*) with a fold change close to 2.9× and a *p* value of 0.0088. Finally, neither of the two *MYB* transcription factors analyzed (*MYBA1* and *MYB5b*) showed gene expression differences between the high and low Mv content groups (Figure 6).

DISCUSSION

Anthocyanin profiles, in combination with different statistical methods, have been efficiently employed as biochemical markers to discriminate grapevine varieties, hybrids, and wild accessions.[6,11,41,42] However, information about the use of those tools to depict intracultivar variation is very limited.[10] We tested the usefulness of anthocyanin profiles to identify variation among Malbec grapevine clones by analyzing a large collection comprising 131 accessions grown in the same vineyard. The amount of variation observed in the studied collection largely exceeded our expectations considering the close genetic relationship between the clones (Supporting Information Table S1). Accordingly, 10 different clone clusters were discriminated by means of *k*-means analysis. Even though this study shows a high proportion of clones with median-like profiles (Figure 1), about 41% of the clones are grouped in four clusters characterized by the predominance of high or low Mv relative contents (clusters 1, 3, 4, and 9). Moreover, the additional evaluation of the HPLC-DAD data by means of PCA (Figure 2) clearly indicates the key role of the Mv relative content variation for shaping the phenotypic distribution of the clones of the collection. As the value of PC1 indicates, Mv content explained 63.5% of the phenotypic variation for the anthocyanin profiles. The analysis of the anthocyanin profiles of six different Tempranillo clones was previously reported by Revilla et al.[10] The authors concluded that the analyzed clones were affected mostly by weather conditions despite slight differences in the profile of a particular clone. Conversely, the size of our collection and probably the diversity in the origin of the Malbec clones allowed in our case the detection of a broad variation spectrum (Supporting Information Table S2; Figure 1). These findings encouraged us to more deeply analyze the origins of the differences between the anthocyanin profiles among the Malbec clones.

The assessment of the genetic variation among clones of the same grapevine cultivar has been performed by means of different molecular marker techniques.[43−49] The aim of these works is looking for intravarietal variation at the DNA level of the studied cultivars. Some of the reports also describe the correlation between molecular markers and the geographical origin of the clones or with particular phenotypic traits.[43,47,49] Even though these reports clearly show the existence of intravarietal genetic variability at the DNA level, no information regarding the intravarietal analysis of genetic variation for particular quality traits has been presented so far. To contribute some information on this subject, we analyzed a large set of Malbec clones in two different seasons for their anthocyanin profiles. We particularly focused on the Mv relative content, the main source of phenotypic variation for that trait in our study (Figure 2). We selected two groups of clones from both extremes of phenotypic distribution after the 2010 experiment, and we tested them again during a subsequent season. Results from 2012 were similar to those of 2010, as observed in both the PCA and correlation analysis (Figures 3 and 4). These findings suggest a putative genetic effect on the regulation of the Mv content, because clones presenting low or high Mv content during 2010 performed correspondingly during 2012 season. Additionally, as a support of the conservation of the anthocyanin profiles, the two other trisubstituted anthocyanins (Dp and Pt) presented also a highly significant correlation. However, among the disubstituted anthocyanins, Cy was just slightly correlated, whereas Pn showed no correlation (Table 2). As expected, we also detected important environmental variation, which was presumably responsible for the more average-like behavior of some of the selected clones, that is, less extreme in 2012 than in 2010 (Figure 3). These results suggested that environmental effects seem to affect differentially

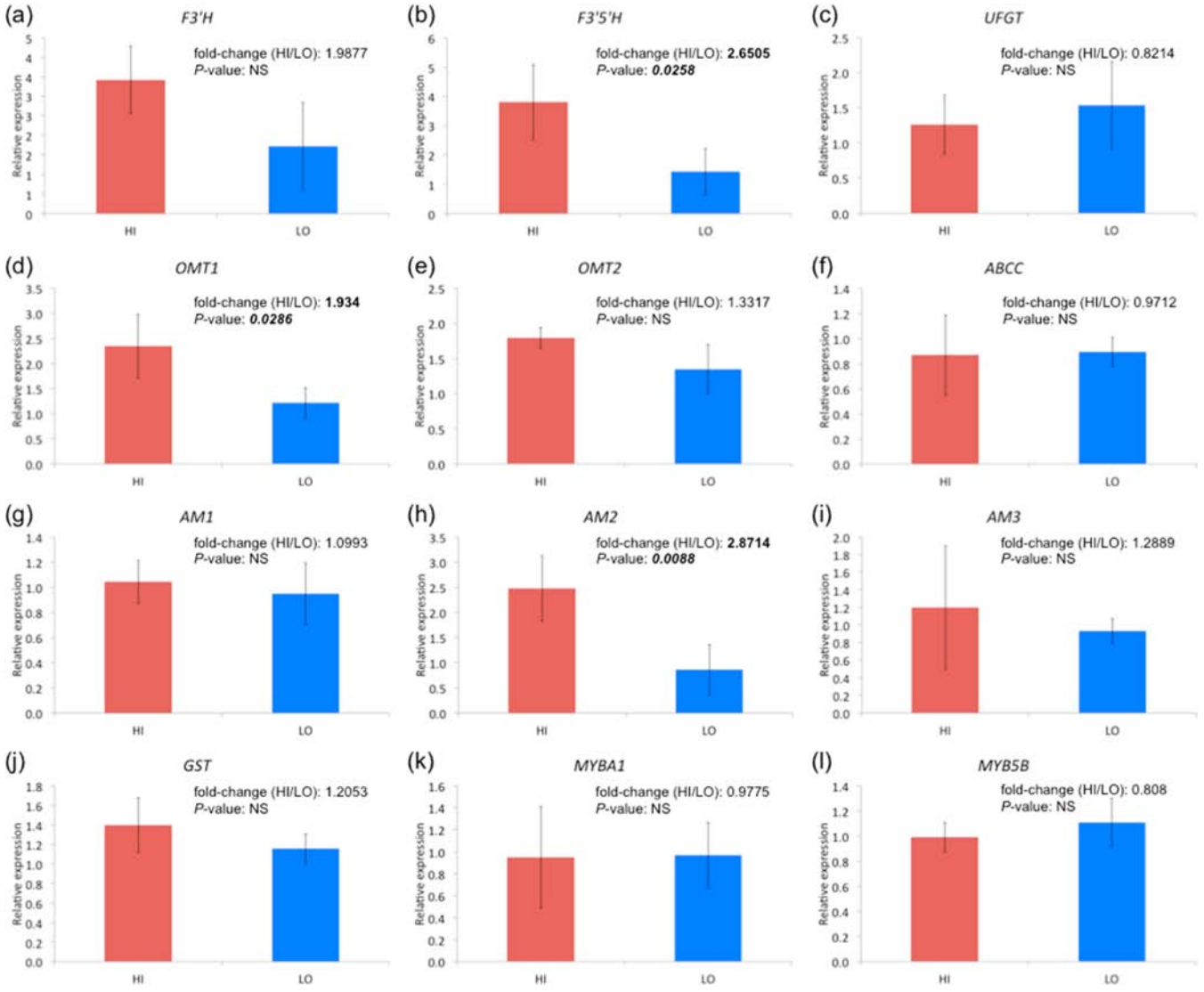

Figure 6. qRT-PCR amplification of 12 grapevine genes in berry skins of two groups of four Malbec clones corresponding to both Mv content extremes in the clone collection; comparison of the average relative expression (fold change) of high Mv content clones versus low Mv content clones: (a) F3′H; (b) F3′5′H; (c) UFGT; (d) OMT1; (e) OMT2; (f) ABCC; (g) AM1; (h) AM2; (i) AM3; (j) GST; (k) MYBA1; (l) MYB5b. NS indicates not significant Benjamini–Hochberg false discovery rate test.

the di- and trisubstituted anthocyanins, because Cy and Pn presented a higher environmental dependence than Dp, Pt, and Mv (Figure 4 and Table 2). We found little information on the analysis of genetic variation affecting anthocyanin profiles of clones of the same cultivar. In the paper on the Tempranillo cultivar mentioned above,[10] the authors concluded that the variation in the analyzed anthocyanin fingerprint depends mainly on agroclimatic factors and not on genetic differences among clones. Interestingly, the presented results showed that the only Tempranillo clone showing consistent differences was characterized by variations on the relative proportion of Mv during three different seasons. Despite the described variation indicating that the Tempranillo clones were affected mostly by weather conditions, genotypic effects seemed also to be present in that experiment.[10]

The huge natural variation for grape berry color is under the control of several genes and transcription factors that act at different points of the anthocyanin biosynthetic pathway.[50,51] Besides the master role of *UFGT* (and their main regulators, *MYBA1* and *MYBA2*) in determining the presence of anthocyanins in colored grapes,[13−16] the cultivar-specific function of other genes along the pathway is accepted to be involved in the regulation of the quantitative nature of grape skin color variation as well as of their different hues.[18,50] Whereas anthocyanin hydroxylases[18,39,52,53] participate in the modulation of anthocyanin composition upstream of *UFGT*, *O*-methyltransferases (*OMTs*)[19−21] and anthocyanin transporters[22,23] also play important roles downstream of *UFGT*. It is important to note that the molecular and biochemical studies mentioned above are mainly based on functional analyses of these significant genes by using different colored cultivars and usually by comparing white genotypes versus colored genotypes. In the present work we report for the first time the expression analysis of several of the genes involved in anthocyanin profile variation at an intravarietal level by evaluating a Malbec clone collection. We analyzed the expression of each gene in two groups of four clones corresponding to the extremes of the Mv content distribution (Supporting Information Table S4). Therefore, it is expected that differences in gene expression between the two groups

should be related to differences in the concentration of anthocyanins.

Several studies showed the correlation between the expression of *UFGT* and *GST* as well as those of the transcription factors *MYBA1* and *MYB5B* with the accumulation of total anthocyanins.[18,40,50,54] The expression of *UFGT*, *GST*, *MYBA1*, and *MYB5B* in our experiment showed no significant differences between the groups of high and low Mv (Figure 6c,j,k,l), in agreement with the total anthocyanin results displayed in Figure 5a, where both groups of clones presented similar mean values. We can infer from these results that profile differences between the groups of high and low Mv content are not due to variation in total amount of anthocyanins. As seen in Figure 5b and in Table S4 in the Supporting Information, the extreme value of Mv in the high Mv content group is compensated by a decrease in the other four anthocyanins.

Analysis of the transcriptional control of anthocyanin biosynthetic genes in different cultivars bearing extreme phenotypes for berry pigmentation showed that the predominance of trisubstituted anthocyanins (Dp, Pt, and Mv) was associated with higher ratios of *F3′5′H*/*F3′H* gene transcription.[18] Although our work was performed with clones of the same colored cultivar, we also observed a predominance of trisubstituted anthocyanins in the high Mv content group (Supporting Information Table S4; Figure 5b). Consistent with this result, the expression of *F3′5′H* showed a significant fold change (>2.65×; p value = 0.0258) between the contrasting Mv content groups (Figure 6b), whereas *F3′H* presented a lower and not significant fold change (Figure 6a). Accordingly, as mentioned above, in the comparison of 2010 and 2012 HPLC data, trisubstituted anthocyanins showed a putative higher genetic effect (Figure 4 and Table 2).

The positive correlation between the expression of different anthocyanin *OMTs* and the anthocyanin methylation level at ripening has been thoroughly studied.[18,19,51,55] Particularly, Fournier-Level et al.[19] showed that *OMT1* seems to be the fundamental gene for anthocyanin methylation, whereas *OMT2* may be responsible for fine and specific differences in the level of methylated anthocyanins. Additionally, the analysis of an OMT from Cabernet Sauvignon[20] showed that the highest specific activity of the enzyme was found for Dp, which is converted by this enzyme in two steps to Mv, the most abundant anthocyanin in most red grapes.[56] In agreement with these previous studies, we found a significant differential gene expression for *OMT1* (but not for *OMT2*) when comparing the high and low Mv content groups (Figure 6d,e). It is worth mentioning that the higher ratio of methylated/unmethylated anthocyanins reported for the high Mv content group in Table S4 in the Supporting Information is solely due to Mv, because the other methylated anthocyanins (Pn and Pt) presented lower percentages. We can infer that similarly to the observation reported by Lücker for Cabernet Sauvignon,[20] in the studied collection of Malbec clones, *OMT1* is involved in the conversion of Dp and Pt, which leads to the high contents of Mv of the extreme clones (Figures 2 and 3; Supporting Information Table S4).

Despite the increasingly deep understanding of anthocyanin biosynthesis and regulation, little is known about the molecular aspects of their transport.[22,23] In grapevine, different anthocyanin transporters have been characterized. Conn et al.[57] reported the involvement of *GST* in vacuolar accumulation of anthocyanins by exporting them to the tonoplast membrane. Two MATEs (*AM1* and *AM3*) have been described to specifically transport acylated anthocyanins, but not glucosylated ones.[22] More recently, a tonoplast-localized ABCC-type protein (ABCC1) was characterized with a preferential malvidin 3-*O*-glucoside transporter function.[23] As we mentioned above, *GST* showed no expression differences between the high and low Mv content groups (Figure 6j). Additionally, neither *AM1* and *AM3* nor *ABCC1* appeared to be involved in the variations in the profiles of Malbec clones in the collection (Figure 6f,g,i). Interestingly, the gene showing the highest expression differences between the extreme Mv content groups is a still uncharacterized anthoMATE (*AM2*).[22] As seen in Figure 6h, *AM2* presented a fold- change of 2.9× with a p value < 0.01, suggesting the putative involvement of this gene in the anthocyanin profile variation within the Malbec clones. As proposed by Gomez et al.,[22] the existence of other transport mechanisms has to be elucidated and characterized to have more evidence about a hypothetical relationship between the transport mechanisms and the final anthocyanin composition.

This work reveals the existence of variation for the anthocyanin profiles among clones from grapevine cultivar Malbec by using an appropriate sample size as well as suitable analytical and statistical tools. We also identified the variation in Mv derivative content as the main discriminating factor within the anthocyanin profiles, with a putative genetic variation involvement. We finally show that the increase in Mv content of the extreme clones is associated with a higher expression of different genes at distinct points of the anthocyanin biosynthesis pathway. Clones displaying relatively higher Mv content also presented elevated gene expression for anthocyanin hydroxylase (*F3′5′H*), an anthocyanin *O*-methyltransferase (*OMT1*), and a putative anthocyanin transporter (*AM2*). These results suggest focusing our attention on the gene expression variation at different steps of the anthocyanin biosynthesis pathway because modulation of the final anthocyanin profile seems to be fine-tuned by multiple genes performing different functions on the pathway.

■ ASSOCIATED CONTENT

Supporting Information

Tables S1−S4 and Figure S1. This material is available free of charge via the Internet at http://pubs.acs.org.

■ AUTHOR INFORMATION

Corresponding Author

*(D.L.) E-mail: dlijavetzky@conicet.gov.ar. Fax: +54 261 96046. Phone: +54 261 4135000, ext. 1307.

Author Contributions

‖A.P.-N. and D.L. share equal senior authorship.

Funding

This work was funded by ANPCyT (PICT-2008-00270 and PAE-PICT-2007-02360) and SECTyP-UNCuyo (A504A/11) grants to D.L. and MINCyT-MICINN (Argentine−Spain) bilateral collaboration grant to D.L. and J.M.M.-Z. (ES/09/07). We also received partial funding from Bodegas Esmeralda S.A.

Notes

The authors declare no competing financial interest.

■ ACKNOWLEDGMENTS

We kindly thank Silvia Hernaiz for her technical assistance and Martin Fanzone for his helpful support in the analytical assay discussion. We are very grateful to Bodegas Esmeralda (BESA)

for providing the clone collection localized at La Pirámide vineyard (Catena Zapata Winery).

REFERENCES

(1) Mazza, G. Anthocyanins in grapes and grape products. *Crit. Rev. Food Sci. Nutr.* **1995**, *35*, 341−371.
(2) Mattivi, F.; Guzzon, R.; Vrhovsek, U.; Stefanini, M.; Velasco, R. Metabolite profiling of grape: flavonols and anthocyanins. *J. Agric. Food Chem.* **2006**, *54*, 7692−7702.
(3) Peña-Neira, A.; Caceres, A.; Pastenes, C. Low molecular weight phenolic and anthocyanin composition of grape skins from cv. Syrah (*Vitis vinifera* L.) in the Maipo Valley (Chile): effect of clusters thinning and vineyard yield. *Food Sci. Technol. Int.* **2007**, *13*, 153−158.
(4) Gonzalez-San Jose, M. L.; Santa-Maria, G.; Diez, C. Anthocyanins as parameters for differentiating wines by grape variety, wine-growing region, and wine-making methods. *J. Food Compos. Anal.* **1990**, *3*, 54−66.
(5) Arozarena, I.; Ayestarán, B.; Cantalejo, M.; Navarro, M.; Vera, M.; Abril, I.; Casp, A. Anthocyanin composition of Tempranillo, Garnacha and Cabernet Sauvignon grapes from high- and low-quality vineyards over two years. *Eur. Food Res. Technol.* **2002**, *214*, 303−309.
(6) Ryan, J. M.; Revilla, E. Anthocyanin composition of Cabernet Sauvignon and Tempranillo grapes at different stages of ripening. *J. Agric. Food Chem.* **2003**, *51*, 3372−3378.
(7) Yamane, T.; Jeong, S. T.; Goto-Yamamoto, N.; Koshita, Y.; Kobayashi, S. Effects of temperature on anthocyanin biosynthesis in grape berry skins. *Am. J. Enol. Vitic.* **2006**, *57*, 54−59.
(8) Haselgrove, L.; Botting, D.; Heeswijck, R.; Høj, P. B.; Dry, P. R.; Ford, C.; Land, P. G. I. Canopy microclimate and berry composition: the effect of bunch exposure on the phenolic composition of *Vitis vinifera* L cv. Shiraz grape berries. *Aust. J. Grape Wine Res.* **2000**, *6*, 141−149.
(9) Esteban, M. A.; Villanueva, M. J.; Lissarrague, J. R. Effect of irrigation on changes in the anthocyanin composition of the skin of cv Tempranillo (*Vitis vinifera* L) grape berries during ripening. *J. Sci. Food Agric.* **2001**, *81*, 409−420.
(10) Revilla, E.; Garcia-Beneytez, E.; Cabello, F. Anthocyanin fingerprint of clones of Tempranillo grapes and wines made with them. *Aust. J. Grape Wine Res.* **2009**, *15*, 70−78.
(11) Ortega-Regules, A.; Romero-Cascales, I.; López-Roca, J. M.; Ros-García, J. M.; Gómez-Plaza, E. Anthocyanin fingerprint of grapes: environmental and genetic variations. *J. Sci. Food Agric.* **2006**, *86*, 1460−1467.
(12) Holbach, B.; Marx, R.; Zimmer, M. Bedeutung Der Shikimisäure Und Des Anthocyanspektrums Für Die Charakterisierungvon Rebsorten. *Lebensmittelchemie* **2001**, *55*, 32−34.
(13) Walker, A. R.; Lee, E.; Bogs, J.; McDavid, D. A. J.; Thomas, M. R.; Robinson, S. P. White grapes arose through the mutation of two similar and adjacent regulatory genes. *Plant J.* **2007**, *49*, 772−85.
(14) Kobayashi, S.; Goto-Yamamoto, N.; Hirochika, H. Retrotransposon-induced mutations in grape skin color. *Science* **2004**, *304*, 982.
(15) Lijavetzky, D.; Ruiz-Garcia, L.; Cabezas, J. A.; De Andres, M. T.; Bravo, G.; Ibanez, A.; Carreno, J.; Cabello, F.; Ibanez, J.; Martinez-Zapater, J. M. Molecular genetics of berry colour variation in table grape. *Mol. Genet Genomics* **2006**, *276*, 427−435.
(16) This, P.; Lacombe, T.; Cadle-Davidson, M.; Owens, C. L. Wine grape (*Vitis vinifera* L.) color associates with allelic variation in the domestication gene VvmybA1. *Theor. Appl. Genet.* **2007**, *114*, 723−730.
(17) Castellarin, S. D.; Di Gaspero, G.; Marconi, R.; Nonis, A.; Peterlunger, E.; Paillard, S.; Adam-Blondon, A. F.; Testolin, R. Colour variation in red grapevines (*Vitis vinifera* L.): genomic organisation, expression of flavonoid 3′-hydroxylase, flavonoid 3′,5′-hydroxylase genes and related metabolite profiling of red cyanidin-/blue delphinidin-based anthocyanins in berry skin. *BMC Genomics* **2006**, *7*, 12.
(18) Castellarin, S. D.; Di Gaspero, G. Transcriptional control of anthocyanin biosynthetic genes in extreme phenotypes for berry pigmentation of naturally occurring grapevines. *BMC Plant Biol.* **2007**, *7*, 46.
(19) Fournier-Level, A.; Hugueney, P.; Verries, C.; This, P.; Ageorges, A. Genetic mechanisms underlying the methylation level of anthocyanins in grape (*Vitis vinifera* L.). *BMC Plant Biol.* **2011**, *11*, 179.
(20) Lücker, J.; Martens, S.; Lund, S. T. Characterization of a *Vitis vinifera* cv. Cabernet Sauvignon 3′,5′-*O*-methyltransferase showing strong preference for anthocyanins and glycosylated flavonols. *Phytochemistry* **2010**, *71*, 1474−1484.
(21) Hugueney, P.; Provenzano, S.; Verries, C.; Ferrandino, A.; Meudec, E.; Batelli, G.; Merdinoglu, D.; Cheynier, V.; Schubert, A.; Ageorges, A. A novel cation-dependent *O*-methyltransferase involved in anthocyanin methylation in grapevine. *Plant Physiol.* **2009**, *12*, 12.
(22) Gomez, C.; Terrier, N.; Torregrosa, L.; Vialet, S.; Fournier-Level, A.; Verries, C.; Souquet, J. M.; Mazauric, J. P.; Klein, M.; Cheynier, V. Grapevine MATE-type proteins act as vacuolar H^+-dependent acylated anthocyanin transporters. *Plant Physiol.* **2009**, *150*, 402.
(23) Francisco, R. M.; Regalado, A.; Ageorges, A.; Burla, B. J.; Bassin, B.; Eisenach, C.; Zarrouk, O.; Vialet, S.; Marlin, T.; Chaves, M. M.; Martinoia, E.; Nagy, R. ABCC1, an ATP binding cassette protein from grape berry, transports anthocyanidin 3-*O*-glucosides. *Plant Cell* **2013**, *25*, 1840−1854.
(24) Carbonell-Bejerano, P.; Santa María, E.; Torres-Pérez, R.; Royo, C.; Lijavetzky, D.; Bravo, G.; Aguirreolea, J.; Sánchez-Díaz, M.; Antolín, M. C.; Martínez-Zapater, J. M. Thermotolerance responses in ripening berries of *Vitis vnifera* L. cv Muscat Hamburg. *Plant Cell Physiol.* **2013**, *54*, 1200−1216.
(25) Ibáñez, J.; Vargas, A. M.; Palancar, M.; Borrego, J.; de Andres, M. T. Genetic relationships among table-grape varieties. *Am. J. Enol. Vitic.* **2009**, *60*, 35−42.
(26) Fanzone, M. L.; Zamora, F.; Jofré, V.; Assof, M.; Pena-Neira, A. Phenolic composition of malbec grape skins and seeds from Valle de Uco (Mendoza, Argentina) during ripening. Effect of cluster thinning. *J. Agric. Food Chem.* **2011**, *59*, 6120−6136.
(27) Cáceres, A.; Peña-Neira, Á.; Galvez, A.; Obreque-Slier, E.; López-Solís, R.; Canals, J. M. Phenolic compositions of grapes and wines from cultivar Cabernet Sauvignon produced in Chile and their relationship to commercial value. *J. Agric. Food Chem.* **2012**, *60*, 8694−8702.
(28) Fanzone, M.; Peña-Neira, A.; Jofre, V.; Assof, M.; Zamora, F. Phenolic characterization of Malbec wines from Mendoza Province (Argentina). *J. Agric. Food Chem.* **2010**, *58*, 2388−2397.
(29) Monagas, M.; Núñez, V.; Bartolomé, B.; Gómez-Cordovés, C. Anthocyanin-derived pigments in Graciano, Tempranillo, and Cabernet Sauvignon wines produced in Spain. *Am. J. Enol. Vitic.* **2003**, *54*, 163−169.
(30) Reid, K. E.; Olsson, N.; Schlosser, J.; Peng, F.; Lund, S. T. An Optimized grapevine RNA isolation procedure and statistical determination of reference genes for real-time RT-PCR during berry development. *BMC Plant Biol.* **2006**, *6*, 27.
(31) Lijavetzky, D.; Almagro, L.; Belchi-Navarro, S.; Martinez-Zapater, J. M.; Bru, R.; Pedreno, M. A. Synergistic effect of methyljasmonate and cyclodextrin on stilbene biosynthesis pathway gene expression and resveratrol production in Monastrell grapevine cell cultures. *BMC Res. Notes* **2008**, *1*, 132.
(32) Andersen, C. L.; Jensen, J. L.; Ørntoft, T. F. Normalization of real-time quantitative reverse transcription-PCR data: a model-based variance estimation approach to identify genes suited for normalization, applied to bladder and colon cancer data sets. *Cancer Res.* **2004**, *64*, 5245−5250.
(33) Arvidsson, S.; Kwasniewski, M.; Riaño-Pachón, D. M.; Mueller-Roeber, B. QuantPrime − a flexible tool for reliable high-throughput primer design for quantitative PCR. *BMC Bioinformatics* **2008**, *9*, 465.
(34) Tavazoie, S.; Hughes, J. D.; Campbell, M. J.; Cho, R. J.; Church, G. M. Systematic determination of genetic network architecture. *Nat. Genet.* **1999**, *22*, 281−285.

(35) Sturn, A.; Quackenbush, J.; Trajanoski, Z. Genesis: cluster analysis of microarray data. *Bioinformatics* **2002**, *18*, 207−208.
(36) Raychaudhuri, S.; Stuart, J. M.; Altman, R. B. Principal components analysis to summarize microarray experiments: application to sporulation time series. *Pac. Symp. Biocomput.* **2000**, 455−466.
(37) Di Rienzo, J. A.; Casanoves, F.; Balzarini, M. G.; Gonzalez, L.; Tablada, M.; Robledo, C. W. InfoStat, version 2011, 2011.
(38) Holton, T. A.; Cornish, E. C. Genetics and biochemistry of anthocyanin biosynthesis. *Plant Cell* **1995**, *7*, 1071−1083.
(39) Bogs, J.; Ebadi, A.; McDavid, D.; Robinson, S. P. Identification of the flavonoid hydroxylases from grapevine and their regulation during fruit development. *Plant Physiol* **2006**, *140*, 279−291.
(40) Deluc, L.; Bogs, J.; Walker, A. R.; Ferrier, T.; Decendit, A.; Merillon, J. M.; Robinson, S. P.; Barrieu, F. The transcription factor VvMYB5b contributes to the regulation of anthocyanin and proanthocyanidin biosynthesis in developing grape berries. *Plant Physiol.* **2008**, *147*, 2041−2053.
(41) Revilla, E.; Carrasco, D.; Benito, A.; Arroyo-Garcia, R. Anthocyanin composition of several wild grape accessions. *Am. J. Enol. Vitic.* **2010**, *61*, 536−543.
(42) De Rosso, M.; Tonidandel, L.; Larcher, R.; Nicolini, G.; Ruggeri, V.; Dalla Vedova, A.; De Marchi, F.; Gardiman, M.; Flamini, R. Study of anthocyanic profiles of twenty-one hybrid grape varieties by liquid chromatography and precursor-ion mass spectrometry. *Anal. Chim. Acta* **2012**, *732*, 120−129.
(43) Moncada, X.; Pelsy, F.; Merdinoglu, D.; Hinrichsen, P. Genetic diversity and geographical dispersal in grapevine clones revealed by microsatellite markers. *Genome* **2006**, *49*, 1459−1472.
(44) Imazio, S.; Labra, M.; Grassi, F.; Winfield, M.; Bardini, M.; Scienza, A. Molecular tools for clone identification: the case of the grapevine cultivar "Traminer". *Plant Breed.* **2002**, *121*, 531−535.
(45) Blaich, R.; Konradi, J.; Ruhl, E.; Forneck, A. Assessing genetic variation among Pinot noir (*Vitis vinifera* L.) clones with AFLP markers. *Am. J. Enol. Vitic.* **2007**, *58*, 526−529.
(46) Wegscheider, E.; Benjak, A.; Forneck, A. Clonal variation in Pinot noir revealed by S-SAP involving universal retrotransposon-based sequences. *Am. J. Enol. Vitic.* **2009**, *60*, 104−109.
(47) Meneghetti, S.; Costacurta, A.; Morreale, G.; Calò, A. Study of intra-varietal genetic variability in grapevine cultivars by PCR-derived molecular markers and correlations with the geographic origins. *Mol. Biotechnol.* **2012**, *50*, 72−85.
(48) Resta, P.; Fanizza, G.; Ricciardi, L.; Chaabane, R. Analysis of a spontaneous mutant and selected clones of cv. Italia (*Vitis vinifera*) by AFLP markers. *Vitis* **2003**, *42*, 27−30.
(49) González Techera, A.; Jubany, S.; Ponce de León, I.; Boido, E.; Dellacassa, E.; Carrau, F.; Hinrichsen, P.; Gaggero, C. Molecular diversity within clones of cv. Tannat (*Vitis vinifera*). *Vitis* **2006**, *43*, 179−185.
(50) Cardoso, S.; Lau, W.; Eiras Dias, J.; Fevereiro, P.; Maniatis, N. A candidate-gene association study for berry colour and anthocyanin content in *Vitis vinifera* L. *PLoS One* **2012**, *7*, No. e46021.
(51) Ageorges, A.; Fernandez, L.; Vialet, S.; Merdinoglu, D.; Terrier, N.; Romieu, C. Four specific isogenes of the anthocyanin metabolic pathway are systematically co-expressed with the red colour of grape berries. *Plant Sci.* **2006**, *170*, 372−383.
(52) Jeong, S. T.; Goto-Yamamoto, N.; Hashizume, K.; Esaka, M. Expression of the flavonoid 3′-hydroxylase and flavonoid 3′,5′-hydroxylase genes and flavonoid composition in grape (*Vitis vinifera*). *Plant Sci.* **2006**, *170*, 61−69.
(53) Castellarin, S. D.; Di Gaspero, G.; Marconi, R.; Nonis, A.; Peterlunger, E.; Paillard, S.; Adam-Blondon, A.-F.; Testolin, R. Colour variation in red grapevines (*Vitis vinifera* L.): genomic organisation, expression of flavonoid 3′-hydroxylase, flavonoid 3′,5′-hydroxylase genes and related metabolite profiling of red cyanidin-/blue delphinidin-based anthocyanins in berry skin. *BMC Genomics* **2006**, *7*, 12.
(54) Cutanda-Perez, M.-C.; Ageorges, A.; Gomez, C.; Vialet, S.; Terrier, N.; Romieu, C.; Torregrosa, L. Ectopic expression of VlmybA1 in grapevine activates a narrow set of genes involved in anthocyanin synthesis and transport. *Plant Mol. Biol.* **2009**, *69*, 633−648.
(55) Matus, J. T.; Loyola, R.; Vega, A.; Peña-Neira, A.; Bordeu, E.; Arce-Johnson, P.; Alcalde, J. A. Post-veraison sunlight exposure induces MYB-mediated transcriptional regulation of anthocyanin and flavonol synthesis in berry skins of *Vitis vinifera*. *J. Exp. Bot.* **2009**, *60*, 853−867.
(56) Mori, K.; Goto-Yamamoto, N.; Kitayama, M.; Hashizume, K. Loss of anthocyanins in red-wine grape under high temperature. *J. Exp. Bot.* **2007**, *58*, 1935−1945.
(57) Conn, S.; Curtin, C.; Bézier, A.; Franco, C.; Zhang, W. Purification, molecular cloning, and characterization of glutathione S-transferases (GSTs) from pigmented *Vitis vinifera* L. cell suspension cultures as putative anthocyanin transport proteins. *J. Exp. Bot.* **2008**, *59*, 3621−3634.

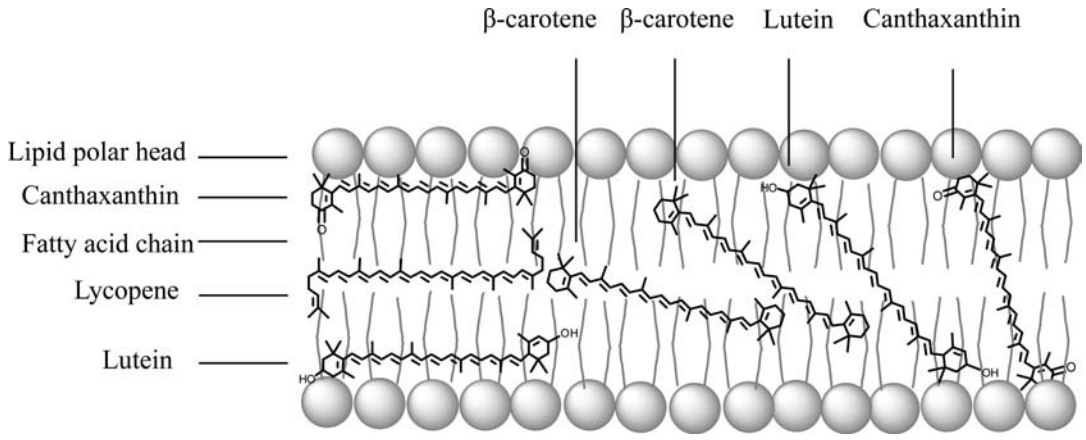

Figure 1. Schematic representation of the probable patterns of localization and orientation of carotenoid pigments in the egg yolk phosphatidylcholine (EYPC) membrane. The following carotenoids were used as examples: lycopene, β-carotene, lutein, and canthaxanthin.

biocompatible, biodegradable, and nontoxic. To our knowledge, there is a little consideration regarding the antioxidant activity of carotenoids in liposomes composed of mixed lipids including EYPC and nonionic surfactant Tween 80.

Moreover, it is noted that when liposome is utilized as a delivery system in nutraceuticals and functional food, one has to consider, primarily, the stability of liposomes during processing and storage. Therefore, encapsulated carotenoids should not only be able to exert antioxidant effects, but also maintain the physicochemical stability of the liposomes. However, carotenoids have contrasting effects on the membrane properties, owing to their various chemical structures. For instance, polar carotenoid incorporation can rigidify the lipid membranes and increase their stability, whereas the effects of apolar carotenoids are negligible or opposite.[18] Alternatively, the encapsulated concentration of carotenoids into liposomes may be much greater than that normally found in a natural membrane, since high loading contents are preferred for food applications. When exceeding a certain concentration, carotenoids probably display pro-oxidation properties. In turn, the liposomal membrane damaged by the lipid peroxidation would not effectively protect encapsulated carotenoids. Our recent study has also demonstrated the concentration-dependent capacity of lutein to adjust the penetration of oxygen into lipid bilayer and consequently, the liposomes stability.[19] Taking these factors into consideration, a compromise of carotenoids encapsulated concentration should be found in the design of carotenoid-loaded liposomal systems.

Further understanding of the influence of liposome encapsulation on the antioxidant activity of carotenoid will be crucial for the health benefits of encapsulated carotenoid. Herein, carotenes (lycopene and β-carotene) and xanthophylls (lutein and canthaxanthin) were studied that are known antioxidants commonly found in the human diet (Figure 1). The in vitro assays, including 2,2-diphenyl-1-picrylhydrazyl (DPPH) scavenging ability and ferric reducing antioxidant power (FRAP), were carried out to investigate the antioxidant activities of carotenoids; either after they were mixed with liposomes or after they were incorporated into liposomes. The lipid peroxidation inhibition capacity (LPIC) of these carotenoids during preparation, auto-oxidation, or induced by ferric iron/ascorbate was also evaluated by determining the lipids oxidation product, the thiobarbituric acid-reactive substance (TBARS). Meanwhile, the depletion of carotenoid after oxidation was determined. On the basis of the experimental data, the probable mechanism of LPIC as well as the self-protection of carotenoids were correlated to the effects of carotenoids on membrane properties (dynamic and structure).

MATERIALS AND METHODS

Materials. Egg yolk phosphatidylcholine (EYPC) was purchased from Chemical Reagent Plant of East China Normal University (Shanghai, China). Carotenoids, including lycopene, β-carotene, lutein, and canthaxanthin (all 98% purity), were a gift from Zhejiang Medicine Co., Ltd. (Zhejiang, China). Petroleum ether (30−60 °C) and polyoxyethylene sorbitan monooleate (Tween 80) were purchased from China Medicine (Group) Shanghai Chemical Reagent Co. (Shanghai, China). 2,2-Diphenyl-1-picrylhydrazyl (DPPH) was purchased from Sigma Chemical Co. (St. Louis, MO, U.S.A.). All other chemicals used were of analytical grade.

Preparation of Carotenoid-Loaded Liposomes. Liposomes loading carotenoids were prepared by the thin-film evaporation method according to our recent report.[20] Carotenoid was dissolved in 2 mL chloroform together with the lipids composed of EYPC and Tween 80 at the fixed mass ratio of 1:0.72. After dissolution, the liposomal system brought to dryness by the use of a rotary evaporator at 55 °C (organic solvent removal). The sample was further vacuum-dried in an oven (at 50 °C) to ensure complete removal of the solvent, followed by hydration with 40 mL of 0.01 M phosphate buffer solution, 150 mM NaCl, PBS, pH 7.4, under vortexing for 60 min at 55 °C. The liposomal suspension was then subjected to a probing sonication process in an ice bath for 10 min at 240 W with a sequence of 5 s of sonication and 5 s of rest using a sonicator (Sonics & Materials, Inc., 20 kHz). The final sample preparations were transferred in vials under nitrogen bed and stored in the refrigerator (at 4 °C in dark) until use.

Encapsulation Efficiency and Loading Content. The determination of encapsulation efficiency (EE) was performed by extraction according to our earlier method with a slight modification.[21] Briefly, aliquots of 0.5 mL carotenoid-loaded liposomes and 3 mL petroleum ether were mixed by being vortexed vigorously for 3 min at an ambient temperature. The mixed sample was centrifuged at 2000 r/min for 5 min, and the supernatant was collected. The above operation was repeated twice, and the collected supernatant was combined together in a tube, followed by dilution to 10 mL with petroleum ether. The free amount of carotenoids were quantified spectrophotometrically (UV-1600 spectrophotometer; Mapada Instruments Co., Ltd., China) at 470, 455, 440, and 460 nm for lycopene, β-carotene, lutein, and canthaxanthin, respectively, with petroleum ether as a blank. Each experiment was carried out in triplicate.

The total amount of carotenoid was expressed relative to the mass of lipids through the initial carotenoid concentration (IC = $m_{\text{carotenoid}}$/

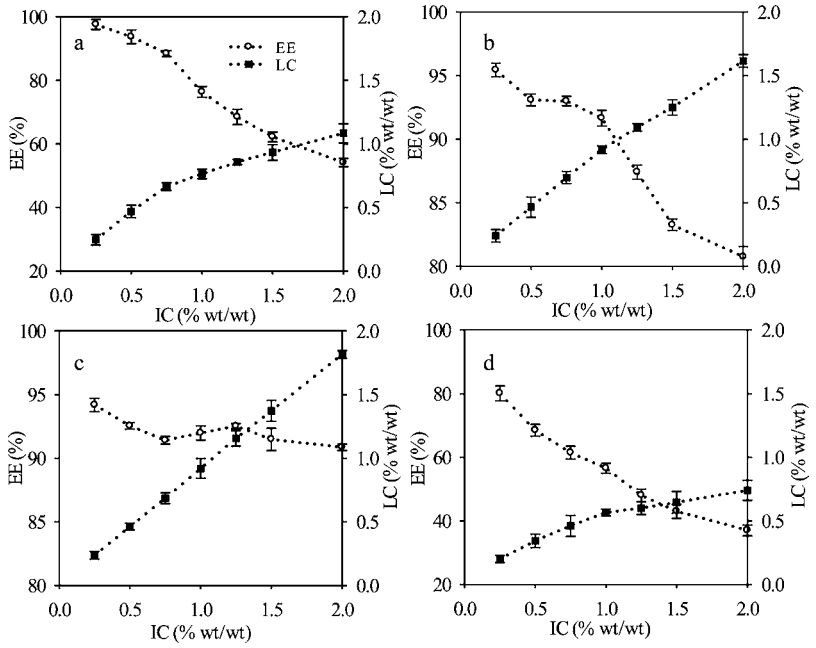

Figure 2. Encapsulation efficiency (EE) and loading content (LC) as a function of IC: lycopene (a); β-carotene (b); lutein (c); and canthaxanthin (d). Data were expressed as the mean value ± standard deviation (n = 3).

m_{lipids}, % wt/wt). The amount of carotenoid loaded into the liposomes was calculated as the difference between the total amount used to prepare loading liposomes and that recovered by extraction. The carotenoid encapsulation efficiency (EE, %) and loading content (LC, % wt/wt) was respectively calculated using the following equations:

$$\mathrm{EE} = \frac{\text{incorp. carotenoids}}{\text{total carotenoid}} \times 100$$

$$\mathrm{LC} = \frac{\text{incorp. carotenoids}}{\text{amount of lipid}} \times 100$$

where "incorp. carotenoids" is the incorporated amount of carotenoids and "total carotenoid" is the total amount of carotenoid.

DPPH Radical-Scavenging Activity. DPPH radical-scavenging activity of samples was measured according to the work published by our research group with a slight modification.[22] In the assay, 0.7 mL of carotenoid-loaded liposomes (or the direct mixture of carotenoid-DMSO solution and pure liposomes) was mixed with 0.2 mL of DPPH solution (0.4 mM in ethanol). The carotenoid in DMSO solution was adjusted to the same concentration as the carotenoid-loaded liposomes. Then, the solution was incubated at 37 °C in the dark for 40 min. Distilled water mixing with DPPH solution instead of the sample mixing served as a control. A sample blank was prepared by replacing the DPPH with ethanol. The absorbance of the sample after incubation was measured at 525 nm using a UV-1600 spectrophotometer (Meipuda Co., Shanghai, China). A low absorbance of the reaction mixture indicates a high free radical scavenging activity. The percentage of DPPH-scavenging ($\mathrm{DPPH_{scav}}$) activity was calculated as follows:

$$\mathrm{DPPH_{scav}}(\%) = \left(1 - \frac{A_{\text{sample}} - A_{\text{sample control}}}{A_{\text{blank}}}\right) \times 100$$

Ferric Reducing Antioxidant Power (FRAP) Assay. Either the carotenoid-loaded liposomes or mixture between carotenoid-DMSO solution and pure liposomes (1 mL) was mixed with 1 mL of potassium ferricyanide (2.5%, w/v) followed by incubation at 50 °C for 20 min. After incubation, 5 mL of trichloroacetic acid (10%, w/v) was added to the mixture, which was centrifuged at 5000 r/min for 2 min. The obtained supernatant (1 mL) was treated with 2 mL of distilled water and 0.5 mL of $FeCl_3$ (0.1%, w/v), followed by incubation for 10 min. The absorbance of the reaction mixture was measured at 700 nm with a UV-1600 spectrophotometer (Meipuda Co., Shanghai, China). The blank was the sample using water instead of potassium ferricyanide. The larger the absorbance, the higher the reducing power becomes.[7]

Lipid Peroxidation Analysis. The lipid peroxidation inhibition capacity (LPIC) was determined by thiobarbituric acid reactive substance (TBARS). The measurements were based on our recent study:[23] a solution containing thiobarbituric acid (15%, w/v) (TBA), trichloroacetic acid (0.37%, w/v) (TCA), and hydrochloric acid (1.8%, v/v) (HCl) was added to 1 mL of liposomal sample and mixed, followed by heating at 100 °C water bath for 30 min to promote the formation of a pink pigment resulting from the reaction with malondyaldehyde [$(MDA)_2$-TBA]. Afterward, the mixture was cooled rapidly with an ice bath, centrifuged for 5 min at 2000 r/min, and filtrated. The absorbance of the filtrate was measured by spectrophotometer at 535 nm (A_{535nm}). A_c and A_s were the absorbance at 535 nm of carotenoid-free liposomes and carotenoid-loaded liposomes, respectively. The inhibition activity of TBARS ($\mathrm{TBARS_{inhib}}$) during initial sample preparation procedure was calculated by following equation:

$$\mathrm{TBARS_{inhib}}(\%) = \frac{A_c - A_S}{A_c} \times 100$$

When evaluating the LPIC of carotenoid induced by Fe^{3+}/ascorbate, the liposomal samples were first mixed with $FeCl_3$ (1 mL, 400 μmol/L) and ascorbic acid (1 mL, 400 μmol/L). After incubation at 37 °C for 60 min, the TBA-TCA-HCl solution was added. When evaluating the auto-oxidation of liposomal membrane, all samples were incubated at 37 °C in an uncovered, shaking water bath. At proper time intervals, an aliquot (1 mL) of each sample was removed and combined with 5 mL TBA-TCA-HCl solution. The determination procedure of TBARS was the same as described above. The amount of retained carotenoid during oxidation treatment was measured by determining the total and free amount of carotenoid in the same way as the determination of EE as described above. The change in TBARS induced by Fe^{3+}/ascorbate or during auto-oxidation and retention rate (RR, %) were calculated, respectively, as follows:

$$\text{change in TBARS}(\%) = \frac{\text{TBARS ox} - \text{TBARS initial}}{\text{TBARS initial}} \times 100$$

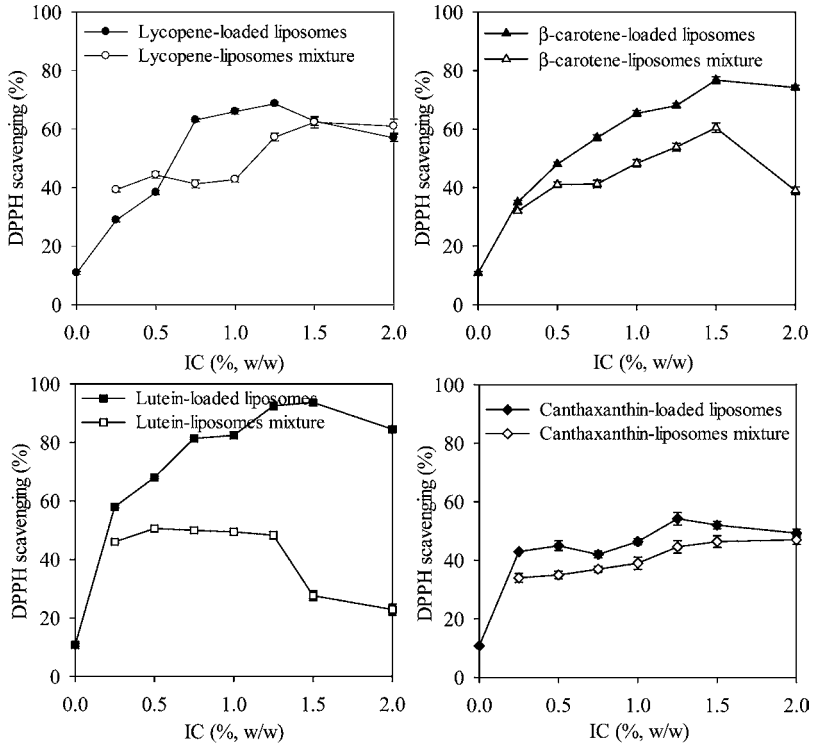

Figure 3. DPPH radical-scavenging activity of carotenoids when incorporated into liposomes or directly mixed with liposomes. Each point represents the mean value ± standard deviation (n = 3).

$$RR_{incorp.} = \frac{\text{incorp. carotenoids in liposomes after ox}}{\text{incorp. carotenoids initial}} \times 100$$

$$RR_{mixed} = \frac{\text{total carotenoid mixed susp ox}}{\text{total carotenoid initial}} \times 100$$

where "TBARS ox" is TBARS after predetermined oxidation time; "TBARS initial" is TBARS initially prepared; "incorp. carotenoids in liposomes after ox" is the inorporated amount of carotenoids in liposomes after oxidation treatment; "incorp. carotenoids initial" is the incorporated amount of carotenoid initially prepared; "total carotenoid mixed susp. after ox" is the total amount of carotenoid in mixed suspension after oxidation treatment; and "total carotenoid initial" is the total amount of carotenoid initially prepared.

Statistical Analysis. Data were presented as a mean value with its standard deviation indicated (mean ± SD). The experiments were done in triplicate. Statistical significance (P < 0.05) was determined using one-way analysis of variance (ANOVA) with SPSS 19.0 FOR Windows (SPSS Inc., Chicago, IL, U.S.A.).

RESULTS AND DISCUSSION

Carotenoids Loading. The carotenoid EE and LC in liposomal systems were analyzed separately by extraction and centrifugation. As shown in Figure 2a, the EE of lycopene exceeded 80% in the range of 0.25%−0.75%, whereas beyond this range the values greatly decreased. LC data also revealed that lycopene was incorporated only up to a very low concentration and membrane nearly reached saturation at 1.50%, corresponding to an LC value of around 0.95%. The poor incorporating ability can be explained by the strong lipophilicity of lycopene molecules, leading them positioned deeply in bilayer hydrophobic core.[24] EE of lutein and β-carotene were found at a high level; the values exceeded 90% and 80% respectively even though the concentration was increased to 2.00% (Figure 2b,c). Their LC values that were found to be very close to the initial concentration (IC), further indicated that the added carotenoids can be effectively incorporated into liposomal membranes within the studied concentration. β-carotene has been shown to have flexible location and orientation in liposomal membrane, owing to the presence of two-β ionone rings.[24] Lutein can orientate vertically to the membrane plane through hydrogen bonding between their polar end groups and membrane's polar region (as depicted in Figure 1). The vertical fashion contributed to the strong inserting ability because more molecules were able to be inserted across the bilayer besides their presence in the hydrophobic core. A similar conclusion has also been reported by an earlier study,[25] that liposomes containing lutein had the largest diameter compared with β-cryptoxanthin and zeaxanthin liposome. However, a great concentration-dependent decrease of EE was observed for canthaxanthin, where the value decreased to around 35% at the 2.00% concentration (Figure 2d). Lipid membrane nearly reached saturation by 1.00% canthaxanthin with the LC values of around 0.65%. Although polar canthaxanthin adopted similar orientation to lutein due to the presence of keto groups, its incorporating ability into liposomal membrane was very weak compared with other carotenoids. One probable explanation was that canthaxanthin molecules did not fit into the membrane architectures as well as did lutein, and they are not as lipid soluble as β-carotene and lycopene.[26]

DPPH Assay. The DPPH method, which is based on the reduction of DPPH· in alcoholic solution in the presence of a hydrogen-donating antioxidant, is the most frequently used one for in vitro antioxidant activity.[27] The DPPH scavenging activity of four kinds of carotenoids, either incorporated into liposomes or directly mixed with liposomes, is presented in Figure 3. In the mixture of carotenoids solution and liposomes, the addition of carotenoid increased the DPPH scavenging activity to some extent. When the concentration was <1.0%,

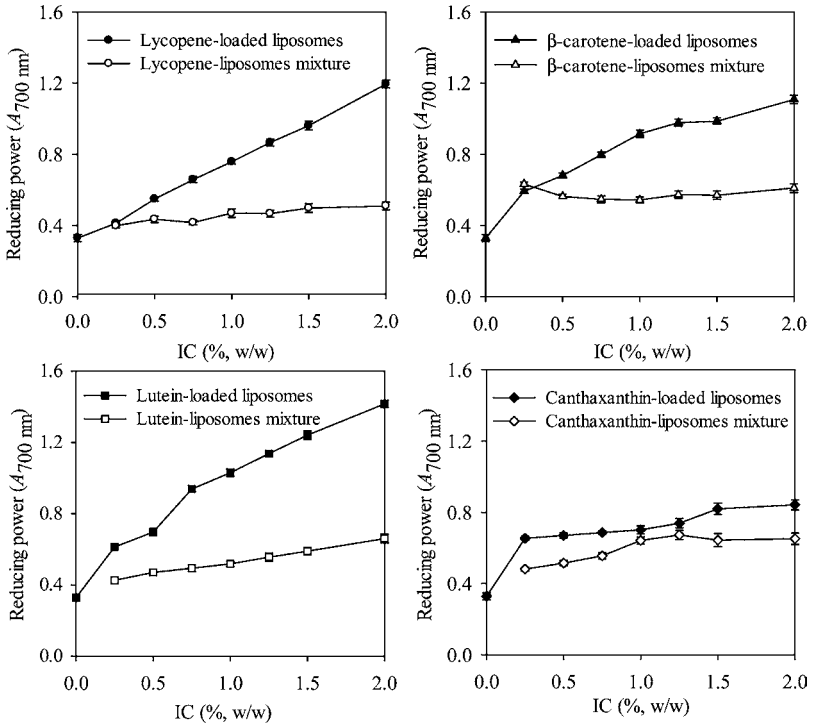

Figure 4. Reducing power of carotenoids when incorporated into liposomes or directly mixed with liposomes. Each point represents the mean value ± standard deviation (n = 3).

carotenoids displayed similar scavenging ability to each other and also showed concentration-dependency. Beyond 1.0%, lycopene displayed the highest DPPH scavenging activity, followed by β-carotene, canthaxanthin, and lutein. The scavenging ability to DPPH was mainly affected by the structural features in carotenoids, that is, the length of conjugated double bonds (CDB) and participation of chemical groups on the β-ionone ring. Owing to the fact that the orbital overlap in the chromophor is enough to form a stable carotenoid radical, acyclic carotenoid lycopene with 11 CDB has strong DPPH scavenging ability. Although β-carotene has 11 CDB, two double bonds in the cyclohexene rings are not planar with the rest of the molecular backbone.[28] For lutein and canthaxanthin, besides the low number of CDB (both 10), the presence of hydroxyl and keto functional groups on the terminal rings, respectively, considerably decreased their antioxidant efficiency for DPPH.[29]

When incorporated into liposomes, all carotenoids exhibited an increase in DPPH scavenging activity as compared to those directly mixed with liposomes. One probable reason was the enhanced water solubility and dispersion of carotenoids by liposome encapsulation. In the concentration range of 0.25%−1.25%, each carotenoid displayed a concentration-dependent increase of DPPH scavenging. Besides, the trend of antioxidant activity was modified, ranging from the strongest to the weakest: lutein > β-carotene > lycopene > canthaxanthin. Due to the vertical orientation in the opposite polar membrane zones, lutein and β-carotene are accessible to react with DPPH at the membrane surface. However, it is difficult for lycopene to trap DPPH because of its deep location in the bilayer hydrophobic core, far from the membrane surface (Figure 1). The poor scavenging ability of canthaxanthin was mainly due to the very low degrees of its incorporation into the lipid bilayer. It was interesting to find that the DPPH scavenging of each carotenoid decreased slightly when the concentration was >1.25%. It may be the consequence of the extent of carotenoid aggregation, causing the decrease of antioxidant efficiency.[4]

FRAP Assay. Some reducing substances in the sample could provide electrons to reduce Fe^{3+} to Fe^{2+}. The Fe^{2+} can be monitored by measuring the formation of Perl's Prussian blue at 700 nm. Figure 4 shows that when mixed with liposomes, lutein seemed to display relatively stronger FRAP activity than other carotenoids. FRAP activity was not only affected by the CDB number, but also by the steric hindrance between carotenoids and ferric *di*-TPTZ complex. Despite having 10 CDBs, the presence of hydroxyl functions in the 3(3,)-position at the ring system can reduce the steric hindrance, and consequently improve the FRAP activity of lutein.[29] However, the differences of FRAP activity between other carotenoids was not apparent and also no concentration-dependence was detected. This observation was a little different from the conclusion of a previous observation.[29] The contradiction might be due to the reaction conditions, such as reaction time, solvents, concentration, and wavelength used.[29,30] Another probable explanation was the inhomogeneous dispersion of carotenoids in their direct mixture with liposomes.

When incorporated into the lipid bilayer, the FRAP activity of each carotenoid was enhanced. It was probably due to the reduced steric hindrance of molecules after they were encapsulated. The highest FRAP activity was observed with lutein, followed by β-carotene, lycopene, and canthaxanthin. This trend was well in agreement with their activities to scavenge DPPH. However, ferricyanide is also an oxidizing agent impermeable through lipid bilayers and membrane, and therefore extensively used to assess the exposition of redox groups to the aqueous medium.[7] The vertical fashion made lutein and β-carotene favorable to react with ferric *di* -TPTZ complex at the membrane surface. Unexpectedly, although lycopene is located in the bilayer core, its FRAP activity showed highly concentration-dependent increase. It has been demon-

strated that the parallel fashion of lycopene could decrease the penetration barrier for small molecules to the liposomal membrane.[31] Thus, we speculated that the loosened membrane structure created more opportunities for lycopene to react with ferricyanide. For canthaxanthin, undoubtedly, the slight increase of FRAP activities and lower DPPH scavenging ability was the consequence of their poor incorporation ability.

Lipid Peroxidation Assay. Another mechanism of the antioxidant defense system is the lipid peroxidation inhibition capacity (LPIC). EYPC may undergo peroxidation due to the presence of polyunsaturated acyl chains in lipid molecules, leading to high membrane permeability.[32] Thus, the protection from lipid peroxidation owing to the carotenoids antioxidation may in turn retain the incorporated carotenoids more effectively. The product of peroxidation can be determined spectrophotometrically by the thiobarbituric acid reactive substances (TBARS), and the inhibition rate of TBARS after initial preparation of liposomes is shown in Figure 5. Within a certain concentration range, the lipid peroxidation during liposome preparation was inhibited by lycopene (0.25%−0.75%), β-carotene (0.25%−1.25%), lutein (0.25%−1.50%), and canthaxanthin (0.25%). In particular, the more lutein molecules incorporated (0.25% to 1.25%), the more significant the increase of TBARS inhibition rate became ($P < 0.05$). Beyond the above corresponding concentration ranges, the four kinds of carotenoids would display significant pro-oxidant properties in a concentration-dependent manner ($P < 0.05$). Meanwhile, it was noteworthy that the carotenoids having strong TBARS inhibition activity also had a high EE, but their EE decreased with the appearance of pro-oxidation phenomena. A previous study had revealed that there was a possibility of carotenoid oxidative degradation during the experimental procedures.[33] However, it was also indicated that there was a relationship between lipid peroxidation and carotenoid depletion, as discussed below.

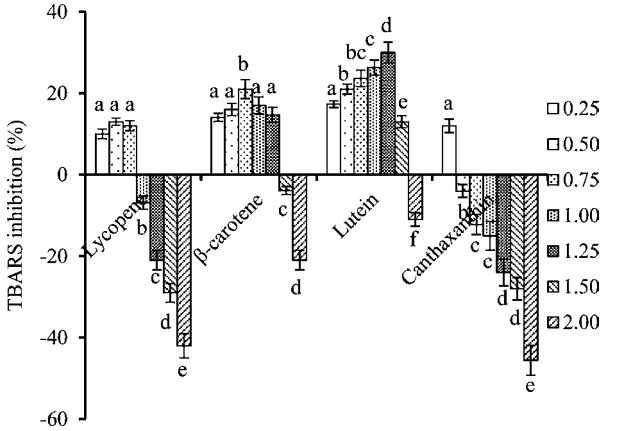

Figure 5. Effect of carotenoid incorporated in liposomes on the inhibition of thiobarbituric acid reactive substance (TBARS) formation in liposome system during preparation. Each point represents the mean value ± standard deviation ($n = 3$). Different letters represents a significant difference ($P < 0.05$).

Iron was used as an oxidizing agent on the consideration that it is present in human body and is involved in oxidative processes. Thus, it is necessary to investigate the lipid peroxidation inhibition capacity (LPIC) induced by Fe^{3+}/ascorbate mixture either after carotenoids were mixed with liposomes ($LPIC_{mixed}$) or after carotenoids were incorporated into liposomes ($LPIC_{inco}$). Without addition of carotenoids, serious lipid peroxidation was induced by iron, and the formation of TBARS was increased by around 120% (Figure 6). In the presence of carotenoids, the TBARS production was significantly reduced ($P < 0.05$) in both mixed and loaded liposomes, except for the liposomes loading canthaxanthin from 1.00% to 1.50%. Note that although lycopene (<1.00%) and canthaxanthin (0.25%) displayed significantly stronger $LPIC_{inco}$ than $LPIC_{mixed}$ ($P < 0.05$), at higher concentration, the effect was opposite. β-Carotene and lutein possessed stronger $LPIC_{inco}$, regardless of the concentration. At 1.25%, both β-carotene and lutein had the strongest $LPIC_{inco}$, with around 46% and 10% TBARS increase respectively, compared with $LPIC_{mixed}$ at around 80% and 75% in their direct mixture.

Table 1 shows that in the carotenoid−liposome mixture, the depletion of carotenoids did not show obvious concentration dependency. With the exception of lycopene at 2.00%, the retention rates of carotenoids in mixture (RR_{mixed}) were less than those in the liposomes (RR_{inco}). It was understandable because in mixed liposomal suspension, most of the carotenoids covered upon the membrane surface and directly reacted with pro-compounds. When incorporated into liposomes, the retaining ability of the lipid bilayer was highly affected by the type and concentration of the incorporated carotenoid. No significant differences in RR_{inco} for lycopene were found in the range of 0.25%−0.75% ($P > 0.05$), and the values were above 75%. Beyond this range, RR_{inco} decreased significantly ($P < 0.05$) which were even closer to RR_{mixed}. By contrast, liposomes strongly retained β-carotene and lutein in the wide concentration range of 0.25%−1.25% with RR_{inco} values above 70% and 80%, respectively. Note that the change tendency of RR_{inco} was consistent with $LPIC_{inco}$. Interestingly, the RR values of canthaxanthin still exceeded 70%, even though its $LPIC_{inco}$ was not pronounced.

The outcomes of the peroxidation assays are affected by the type and amount of initiator used in the system. The current study further employed the method which occurs under normal atmospheric oxygen conditions without addition of exogenous initiators, making the present model study more valid physiologically.[34] In addition, the method by monitoring the auto-oxidation of liposomes allowed us to observe the effects of carotenoids on the progress of peroxidation over a longer period of time compared with the conventional methods where membranes are exposed to higher concentration of free radicals over a shorter time period. Figures 7 and 8 show the change of TBARS in the carotenoid−liposome mixture and carotenoid-loaded liposomes during the auto-oxidation process, as well as the retention rate of the carotenoids. It was found that in the direct mixture, the addition of β-carotene, lutein, or canthaxanthin (especially at high concentrations) can retard and reduce the generation of TBARS, even though this $LPIC_{mixed}$ was not very pronounced (Figure 7). Meanwhile, the carotenoids were gradually depleted with prolonging the incubation time (Figure 8). Lycopene presented relatively effective $LPIC_{mixed}$ only at high concentration ranging from 1.00 to 2.00%. At lower concentrations, not only does the generated amount of TBARS product greatly increase, but also its RR_{mixed} decreases rapidly and greatly compared with the other carotenoids. Oxidation models initiated by peroxyl radicals also demonstrated that lycopene was destroyed most rapidly but was least effective as an antioxidant.[16] It was noted that both $LPIC_{mixed}$ and RR_{mixed} did not show obvious concen-

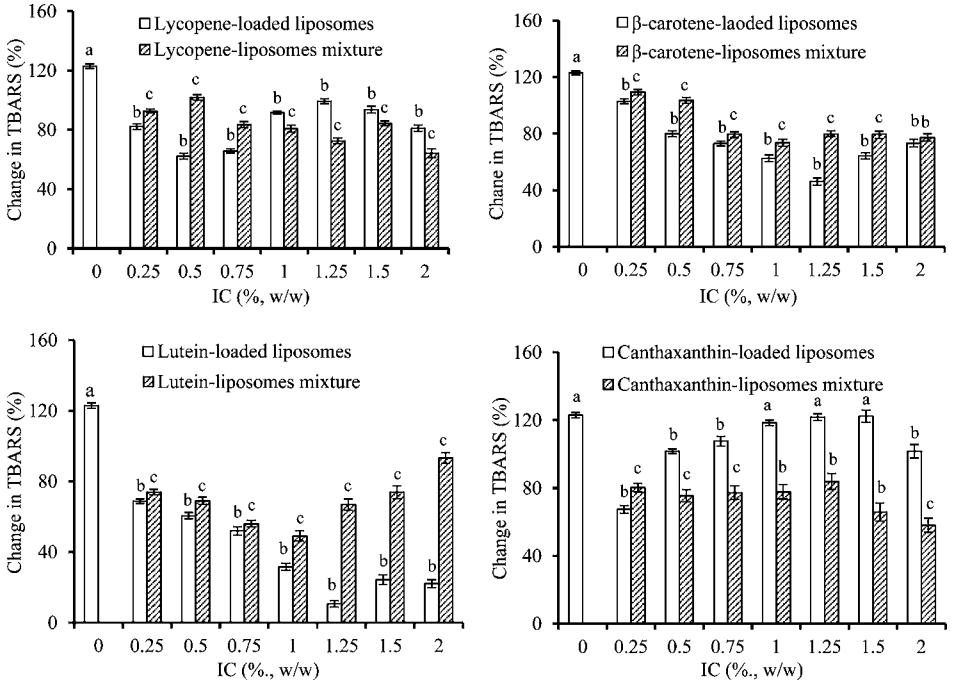

Figure 6. Effect of carotenoids either incorporated in liposomes or directly mixed with pure liposomes on the inhibition of thiobarbituric acid reactive substance (TBARS) formation in liposome system induced by Fe^{3+}/ascorbate. Each point represents the mean value ± standard deviation (n = 3). In each concentration, the increase of thiobarbituric acid reactive substance (TBARS) in pure liposomes, liposome-carotenoid direct mixture, and carotenoid-loaded liposome was compared with each other. Different letters represent a significant difference ($P < 0.05$).

Table 1. Retention Rates of Carotenoids in Liposomes (RR_{Inco}, %) and in Mixture (RR_{mixed}, %) as a Function of IC (%) after Lipid Peroxidation Induced by Fe^{3+}/Ascorbate Mixture[a]

	lycopene		β-carotene		lutein		canthaxanthin	
IC(%)	RR_{inco}	RR_{mixed}	RR_{inco}	RR_{mixed}	RR_{inco}	RR_{mixed}	RR_{inco}	RR_{mixed}
0.25	75.9 ± 1.2a	65.3 ± 1.3abc	73.1 ± 0.8a	69.3 ± 1.6a	80.2 ± 0.7a	72.3 ± 1.2ab	79.9 ± 0.5a	68.8 ± 1.4ab
0.50	76.1 ± 1.1a	67.4 ± 2.0ab	75.9 ± 0.5b	67.3 ± 2.4ab	82.9 ± 0.4b	71.6 ± 1.7abc	8.6 ± 0.9ab	70.3 ± 1.8ab
0.75	75.8 ± 0.7a	68.4 ± 1.7a	76.4 ± 0.5b	68.3 ± 2.0a	82.8 ± 0.8b	73.7 ± 1.8a	75.4 ± 1.2bc	69.5 ± 2.3ab
1.00	70.2 ± 0.6b	65.1 ± 1.9abc	76.6 ± 1.1b	70.2 ± 1.7a	83.1 ± 1.1b	68.4 ± 2.0cd	72.5 ± 1.6cd	70.8 ± 2.5a
1.25	66.6 ± 1.3c	64.8 ± 2.5abc	75.3 ± 0.9b	67.5 ± 2.5ab	82.4 ± 1.6b	69.8 ± 2.5bc	70.8 ± 2.1d	68.4 ± 3.0a
1.50	63.9 ± 1.8d	63.6 ± 2.7bc	72.5 ± 1.6a	63.2 ± 2.1c	81.1 ± 1.2ab	68.5 ± 2.2cd	71.1 ± 2.7d	67.9 ± 3.6ab
2.00	61.3 ± 2.1e	63.4 ± 2.0c	69.3 ± 1.3c	64.4 ± 1.9bc	76.4 ± 1.9c	65.6 ± 1.9d	70.3 ± 3.0d	65.3 ± 3.9b

[a]Results are expressed as mean value ± standard deviation (n = 3). Different letters represent a significant difference ($P < 0.05$).

tration-dependency, which may be due to the inhomogeneous dispersion of the system.

Lycopene (from 0.25 to 1.00%), when incorporated into liposomes, exhibited stronger $LPIC_{inco}$ than $LPIC_{mixed}$. The lipid peroxidation was retarded until 1 h, followed by a slight oxidation. Over a whole incubation period, the increase percentage of TBARS was kept below 30% (Figure 7). Furthermore, although their RR_{inco} gradually decreased, the values were maintained above 75% (Figure 8). At higher loading concentrations (>1.00%), however, liposomes began to be oxidized during the initial 0.5 h, even displaying a high degree of oxidation than pure liposomes. Additionally, the RR_{inco} of lycopene dramatically decreased, and after 2 h, the values were around 69% (1.25%), 65% (1.50%), and 62% (2.00%), respectively. By contrast, β-carotene and lutein exerted sustained and effective $LPIC_{inco}$ over the whole incubation period. In particular, in the range of 0.75%−1.25%, the generated TBARS amount as well as the depletion of carotenoids was almost leveled off after 1 h. β-Carotene and lutein displayed the strongest $LPIC_{inco}$ at 1.00% and 1.25%, respectively. The TBARS increase percentage was only 19% (β-carotene) and 13% (lutein), corresponding with the RR_{inco} values of around 85% and 90%, respectively. In the case of canthaxanthin, it seemed that its $LPIC_{inco}$ was strong only when incorporated at 0.25% and 0.50%. When the concentration increased further, the $LPIC_{inco}$ became less apparent, together with the appearance of a rapid oxidation process within 1 h. Besides, a highly concentration-dependent increase of depletion was observed. For liposomes with 2% canthaxanthin loading, their TBARS amount was increased by 44% at 2 h with around 30% depletion of incorporated canthaxanthin.

In addition to the direct reaction with pro-oxidant elements instead of lipids, the modulating effect of carotenoids on the physicochemical property of membrane could strongly control the $LPIC_{inco}$ of carotenoids. The effect of apolar carotenoid lycopene at low concentration, which guarantee a monomeric state of the pigment in the hydrophobic membrane core, may be negligible in the fluid state of the lipid phase.[35] Thus, the integrity of liposomal membrane was probably preserved, even though lycopene was incorporated into it. This conclusion can

dx.doi.org/10.1021/jf405622f | J. Agric. Food Chem. 2014, 62, 6726−6735

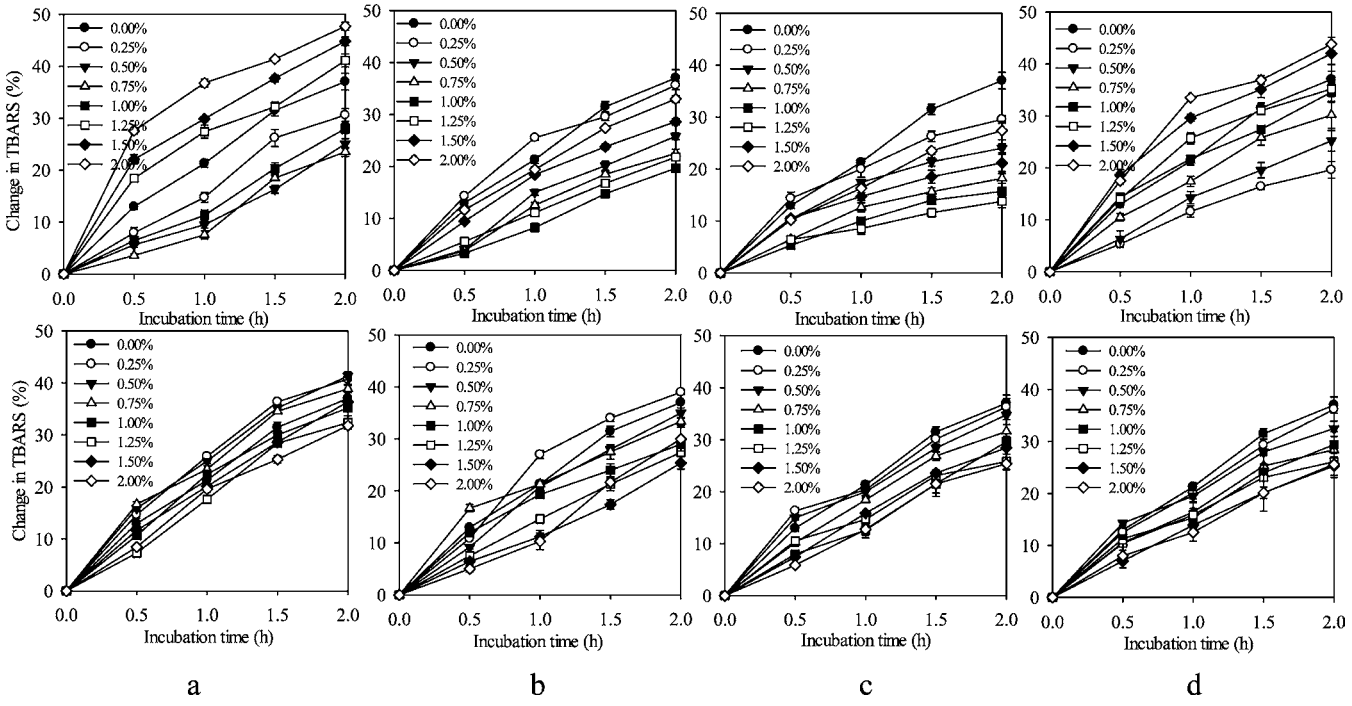

Figure 7. Effect of carotenoids either incorporated in liposomes (top image) or directly mixed with pure liposomes (bottom image) on the inhibition of thiobarbituric acid reactive substance (TBARS) formation in liposome system during 2 h incubation at 37 °C in an uncovered, shaking water bath. Lycopene (a), β-carotene (b), lutein (c), and canthaxanthin (d). Each point represents the mean value ± standard deviation (n = 3).

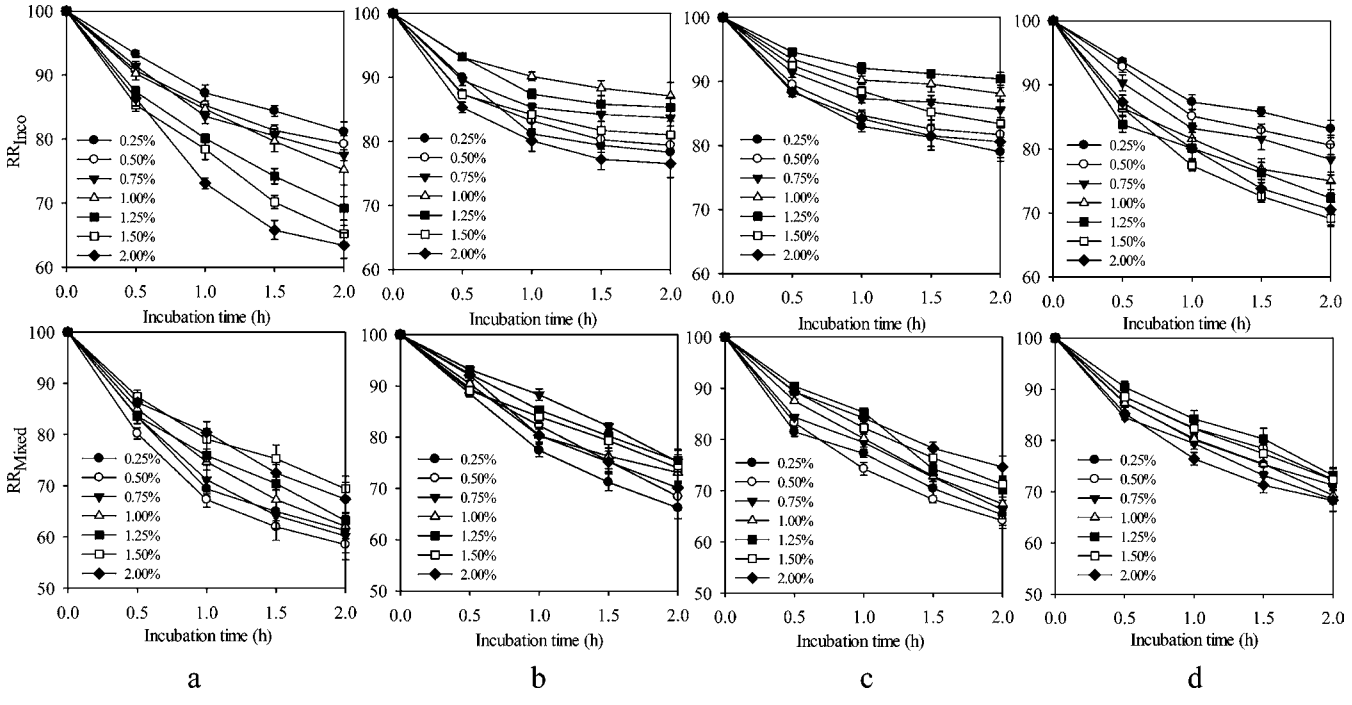

Figure 8. Retention rates of carotenoids in liposomes (RR_{inco}, %) and in mixture (RR_{mixed}, %) as a function of IC (%) during auto-oxidation of liposomes at 37 °C in an uncovered, shaking water bath. Lycopene (a), β-carotene (b), lutein (c), and canthaxanthin (d). Each point represents the mean value ± standard deviation (n = 3).

explain why lycopene (<1.00%) was not only effectively retained in hydrophobic core, but also displayed a certain antioxidation in each lipid peroxidation assay. However, with further increase in the concentration, lycopene probably disturbed the order of the lipid acyl chains and increased the motional freedom of lipids in the headgroup region, although the apolar carotenoid remained in the hydrophobic core, as supported by X-ray diffraction[34] and nuclear magnetic resonance.[31] Such a disturbing effect could decrease the penetration barrier for molecular oxygen and other small molecules to the liposomal membrane. As a consequence, lycopene was rapidly degraded by iron or oxygen, and the lipid was not effectively protected from peroxidation. Even lycopene displayed a pro-oxidation property during liposome preparation

dx.doi.org/10.1021/jf405622f | J. Agric. Food Chem. 2014, 62, 6726−6735

and autoperoxidation process. Our findings were consistent with those of Woodall et al.[16] that, in EYPC liposomes, the lycopene showed a high rate of destruction but poor protection against lipid peroxidation.

Owing to the vertical orientation, lutein can exert a rigidifying effect on the fluidity and order of the polar lipid heads and hydrophobic core.[36] Consequently, the liposomal membrane was less susceptible to the inversion of small molecules because lutein restricts not only the membrane permeation of polar molecules,[37] but also the depth of ion penetration into the bilayer.[38] This effect was also possible for β-carotene, in case it adopted a flexible orientation (Figure 1). In turn, the resultant compact membrane reduced the change of the direct reaction of carotenoids with an external pro-compound. Taking these points into consideration, it is understandable that the incorporation of lutein and β-carotene effectively inhibited the lipid peroxidation induced either by ferric iron or oxygen, while their own depletion was small. Furthermore, the $LPIC_{inco}$ of lutein was positively correlated with its incorporated concentration in the range of 0.25%−1.25%, as the more lutein incorporated, the more pronounced the rigidifying effect became. Nevertheless, it should be pointed out that at 1.50% and 2.00%, both lutein and β-carotene exhibited a decrease of antioxidant capacity to some extent. It was very likely due to the variation of location and orientation. In particular, in the case of lutein, parts of the molecules were probably horizontally oriented to the membrane plane owing to the terminal hydroxyl-containing ring having relative rotational freedom in structure (Figure 1).[39] As a result of this structural feature, lutein could produce a disturbing effect on the membrane structure and display similar antioxidation as apolar carotenoids do.[34]

Canthaxanthin tended to adopt vertical fashion as lutein did, concomitantly, exerting the rigidifying effects.[40] However, in each lipid peroxidation model, $LPIC_{inco}$ was pronounced only at 0.25%. Obviously, the incorporation tendency into the lipid bilayer limited its antioxidant efficiency. From 0.50%, canthaxanthin exerted very weak antioxidation or even pro-oxidation. There is a possibility that (in the case of lutein) a certain fraction of canthaxanthin adopts an horizontal orientation with respect to the plane of the lipid bilayer and links different polar lipid heads via hydrogen bonding.[40] The population of the horizontal fraction increases with the increase in the concentration of the pigment in the lipid phase. The resultant disturbing effect may explain, in part, the appearance of pro-oxidation. It was interesting to find that although canthaxanthin led to destabilization of liposomes, the depletion of its own was not considerable compared with lycopene. The proposed fact was that the electron withdrawing effect of the C═O groups in canthaxanthin resulted in low reactivity of the β-ring, which would be the first part encountered by aqueous radicals.[16]

CONCLUSIONS

This study investigated the influence of liposome encapsulation on the antioxidant activity of four kinds of dietary carotenoids. Through the antioxidant models, including DPPH, FRAP, and lipid peroxidation inhibition capacity, it has been demonstrated that carotenoid encapsulation in liposomes enhanced their antioxidant activity. Additionally, carotenoids exhibited various antioxidant activities in liposomes, ranging from the strongest to the weakest: lutein > β-carotene > lycopene > canthaxanthin. Furthermore, it was revealed that lutein and β-carotene incorporation not only inhibited the lipid peroxidation, but also protected them against pro-oxidation elements. By contrast, lycopene and canthaxanthin showed a high rate of destruction, but poor protection against lipid peroxidation. Conclusively, these findings were strongly correlated with the incorporation efficiencies of the aforementioned carotenoids into liposomal membrane and their modulating effects on the membrane dynamics and structural properties.

AUTHOR INFORMATION

Corresponding Author

*Phone: 86-510-85884496; fax: 86-510-85884496; e-mail: sqxia2006@hotmail.com.

Funding

This research was financially supported by the natural science foundation of Jiangsu Province (BK20141111), projects of the National Natural Science Foundation for Young Scholars of China (31000815), the National 125 Program of China (2012BAD33B05), SKLF-TS 200904, and 111 project-B07029.

Notes

The authors declare no competing financial interest.

REFERENCES

(1) Halliwell, B. Commentary Oxidative Stress, Nutrition and Health. Experimental Strategies for Optimization of Nutritional Antioxidant Intake in Humans. *Free. Radical. Res.* **1996**, *25*, 57−74.

(2) Davies, K. J. Oxidative stress: The paradox of aerobic life. *Biochem. Soc. Symp.* **1995**, *61*, 1−31.

(3) Nishino, H. Cancer prevention by carotenoids. *Mutat. Res.-Fundam. Mol. M* **1998**, *402*, 159−163.

(4) Cantrell, A.; McGarvey, D. J.; George Truscott, T.; Rancan, F.; Böhm, F. Singlet oxygen quenching by dietary carotenoids in a model membrane environment. *Arch. Biochem. Biophys.* **2003**, *412*, 47−54.

(5) Mortensen, A.; Skibsted, L. H.; Sampson, J.; Rice-Evans, C.; Everett, S. A. Comparative mechanisms and rates of free radical scavenging by carotenoid antioxidants. *FEBS Lett.* **1997**, *418*, 91−97.

(6) Edwards, K. A.; Baeumner, A. J. Analysis of liposomes. *Talanta* **2006**, *68*, 1432−1441.

(7) Xia, S.; Xu, S.; Zhang, X.; Zhong, F. Effect of Coenzyme Q10 Incorporation on the Characteristics of Nanoliposomes. *J. Phys. Chem. B* **2007**, *111*, 2200−2207.

(8) Were, L. M.; Bruce, B. D.; Davidson, P. M.; Weiss, J. Size, Stability, and Entrapment Efficiency of Phospholipid Nanocapsules Containing Polypeptide Antimicrobials. *J. Agric. Food Chem.* **2003**, *51*, 8073−8079.

(9) da Silva Malheiros, P.; Daroit, D. J.; Brandelli, A. Food applications of liposome-encapsulated antimicrobial peptides. *Trends Food Sci. Technol.* **2010**, *21*, 284−292.

(10) Marsanasco, M.; Márquez, A. L.; Wagner, J. R.; del V. Alonso, S.; Chiaramoni, N. S. Liposomes as vehicles for Vitamins E and C: An alternative to fortify orange juice and offer Vitamin C protection after heat treatment. *Food Res. Int.* **2011**, *44*, 3039−3046.

(11) Yokota, D.; Moraes, M.; Pinho, S. C. Characterization of lyophilized liposomes produced with non-purified soy lecithin: A case study of casein hydrolysate microencapsulation. *Braz. J. Chem. Eng.* **2012**, *29*, 325−335.

(12) Moraes, M.; Carvalho, J. M. P.; Silva, C. R.; Cho, S.; Sola, M. R.; Pinho, S. C. Liposomes encapsulating β-carotene produced by the proliposomes method: Characterization and shelf life of powders and phospholipid vesicles. *Int. J. Food Sci. Technol.* **2013**, *48*, 274−282.

(13) Xia, F.; Hu, D.; Jin, H.; Zhao, Y.; Liang, J. Preparation of lutein proliposomes by supercritical anti-solvent technique. *Food Hydrocolloid* **2012**, *26*, 456−463.

(14) Peng, C.-H.; Chang, C.-H.; Peng, R. Y.; Chyau, C.-C. Improved membrane transport of astaxanthine by liposomal encapsulation. *Eur. J. Pharm. Biopharm.* **2010**, *75*, 154−161.

(15) McClements, D. J. Design of Nano-Laminated Coatings to Control Bioavailability of Lipophilic Food Components. *J. Food Sci.* **2010**, *75*, R30−R42.
(16) Woodall, A. A.; Britton, G.; Jackson, M. J. Carotenoids and protection of phospholipids in solution or in liposomes against oxidation by peroxyl radicals: Relationship between carotenoid structure and protective ability. *Biochim. Biophys. Acta−Gen. Subjects* **1997**, *1336*, 575−586.
(17) Nara, E.; Miyashita, K.; Ota, T. Oxidative stability of liposomes prepared from soybean PC, chicken egg PC, and salmon egg PC. *Biosci. Biotechnol. Biochem.* **1997**, *61*, 1736−1738.
(18) Gruszecki, W. I.; Strzałka, K. Carotenoids as modulators of lipid membrane physical properties. *Biochim. Biophys. Acta−Mol. Basis Dis.* **2005**, *1740*, 108−115.
(19) Tan, C.; Xia, S.; Xue, J.; Xie, J.; Feng, B.; Zhang, X. Liposomes as Vehicles for Lutein: Preparation, Stability, Liposomal Membrane Dynamics, and Structure. *J. Agric. Food Chem.* **2013**, *61*, 8175−8184.
(20) Tan, C.; Xue, J.; Shabbar, A.; Feng, B.; Zhang, X. M.; Xia, Q. S. Liposomes as Delivery Systems for Carotenoids: Comparative Studies of Loading Ability, Storage Stability and in vitro Release. *Food Funct.* **2014**, DOI: 10.1039/c3fo60498e.
(21) Xia, S.; Xu, S.; Zhang, X. Optimization in the Preparation of Coenzyme Q10 Nanoliposomes. *J. Agric. Food Chem.* **2006**, *54*, 6358−6366.
(22) Song, N.; Tan, C.; Huang, M.; Liu, P.; Eric, K.; Zhang, X.; Xia, S.; Jia, C. Transglutaminase cross-linking effect on sensory characteristics and antioxidant activities of Maillard reaction products from soybean protein hydrolysates. *Food Chem.* **2013**, *136*, 144−151.
(23) Tan, C.; Xue, J.; Eric, K.; Feng, B.; Zhang, X.; Xia, S. Dual Effects of Chitosan Decoration on the Liposomal Membrane Physicochemical Properties As Affected by Chitosan Concentration and Molecular Conformation. *J. Agric. Food Chem.* **2013**, *61*, 6901−6910.
(24) van de Ven, M.; Kattenberg, M.; van Ginkel, G.; Levine, Y. K. Study of the orientational ordering of carotenoids in lipid bilayers by resonance-Raman spectroscopy. *Biophys. J.* **1984**, *45*, 1203−1209.
(25) Pintea, A.; Diehl, H. A.; Momeu, C.; Aberle, L.; Socaciu, C. Incorporation of carotenoid esters into liposomes. *Biophys. Chem.* **2005**, *118*, 7−14.
(26) Socaciu, C.; Lausch, C.; Diehl, H. A. Carotenoids in DPPC vesicles: Membrane dynamics. *Spectrochim. Acta, Part A* **1999**, *55*, 2289−2297.
(27) Shon, M.-Y.; Kim, T.-H.; Sung, N.-J. Antioxidants and free radical scavenging activity of *Phellinus baumii* (Phellinus of Hymenochaetaceae) extracts. *Food Chem.* **2003**, *82*, 593−597.
(28) Jiménez-Escrig, A.; Jiménez-Jiménez, I.; Sánchez-Moreno, C.; Saura-Calixto, F. Evaluation of free radical scavenging of dietary carotenoids by the stable radical 2,2-diphenyl-1-picrylhydrazyl. *J. Sci. Food Agric.* **2000**, *80*, 1686−1690.
(29) Müller, L.; Fröhlich, K.; Böhm, V. Comparative antioxidant activities of carotenoids measured by ferric reducing antioxidant power (FRAP), ABTS bleaching assay (αTEAC), DPPH assay and peroxyl radical scavenging assay. *Food Chem.* **2011**, *129*, 139−148.
(30) Liu, D.; Shi, J.; Colina Ibarra, A.; Kakuda, Y.; Jun Xue, S. The scavenging capacity and synergistic effects of lycopene, Vitamin E, Vitamin C, and β-carotene mixtures on the DPPH free radical. *LWT−Food Sci. Technol.* **2008**, *41*, 1344−1349.
(31) Jeżowska, I.; Wolak, A.; Gruszecki, W. I.; Strzałka, K. Effect of β-carotene on structural and dynamic properties of model phosphatidylcholine membranes. II. A 31P-NMR and 13C-NMR study. *Biochim. Biophys. Acta−Biomembr.* **1994**, *1194*, 143−148.
(32) Asayama, K.; Aramaki, Y.; Yoshida, T.; Tsuchiya, S. Permeability Changes by Peroxidation of Unsaturated Liposomes with Ascorbic Acid/Fe^{2+}. *J. Liposome Res.* **1992**, *2*, 275−287.
(33) Socaciu, C.; Jessel, R.; Diehl, H. A. Carotenoid incorporation into microsomes: Yields, stability and membrane dynamics. *Spectrochim. Acta, Part A* **2000**, *56*, 2799−2809.
(34) McNulty, H. P.; Byun, J.; Lockwood, S. F.; Jacob, R. F.; Mason, R. P. Differential effects of carotenoids on lipid peroxidation due to membrane interactions: X-ray diffraction analysis. *Biochim. Biophys. Acta−Biomembr.* **2007**, *1768*, 167−174.
(35) Strzałka, K.; Gruszecki, W. I. Effect of β-carotene on structural and dynamic properties of model phosphatidylcholine membranes. I. An EPR spin label study. *Biochim. Biophys. Acta−Biomembr.* **1994**, *1194*, 138−142.
(36) Gruszecki, W. Carotenoids in Membranes. In *The Photochemistry of Carotenoids*; Frank, H., Young, A., Britton, G., Cogdell, R., Eds.; Springer: Netherlands, 2004; Vol. *8*, pp 363−379.
(37) Walter, A.; Gutknecht, J. Permeability of small nonelectrolytes through lipid bilayer membranes. *J. Membr. Biol.* **1986**, *90*, 207−217.
(38) Snel, M. M. E.; Marsh, D. Accessibility of spin-labeled phospholipids in anionic and zwitterionic bilayer membranes to paramagnetic relaxation agents. Continuous wave power saturation EPR studies. *Biochim. Biophys. Acta−Biomembr.* **1993**, *1150*, 155−161.
(39) Frank, H. A.; Young, A. J.; Britton, G. *The Photochemistry of Carotenoids*; Kluwer: Dordrecht, 1999.
(40) Sujak, A.; Gabrielska, J.; Milanowska, J.; Mazurek, P.; Strzałka, K.; Gruszecki, W. I. Studies on canthaxanthin in lipid membranes. *Biochim. Biophys. Acta−Biomembr.* **2005**, *1712*, 17−28.

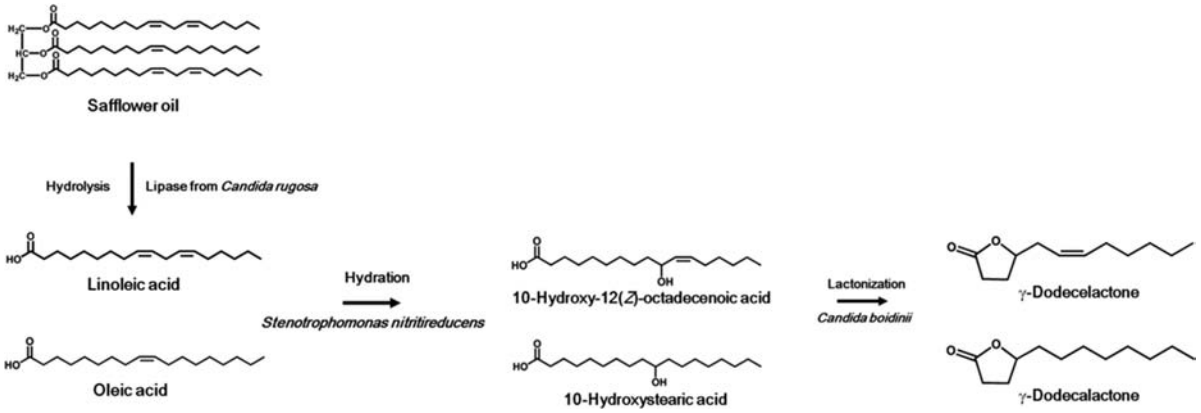

Figure 1. Production of γ-lactones from safflower oil by lipase and whole cells of *S. nitritireducens* and *C. boidinii* via fatty acids and hydroxy fatty acids.

MATERIALS AND METHODS

Materials. Safflower oil and γ-dodecelactone were purchased from Santa Cruz Biotechnology (Santa Cruz, CA, USA) and Penta International (West Caldwell, NJ, USA), respectively. γ-Dodecalactone, lipase from *Candida rugosa*, and fatty acids, including linoleic acid, oleic acid, and palmitic acid, were purchased from Sigma (St. Louis, MO, USA).

Preparation of Hydroxy Fatty Acids. 10-Hydroxystearic acid was produced by the reaction of whole recombinant *Escherichia coli* cells expressing oleate hydratase from *Stenotrophomonas maltophilia*.[21] The reaction was performed in 50 mM citrate/phosphate buffer (pH 6.5) containing 50 g/L oleic acid, 10 g/L of *E. coli* cells, and 0.05% (w/v) Tween 40 at 35 °C for 4 h. 10-Hydroxy-12(*Z*)-octadecenoic acid was produced by the reaction of whole *S. nitritireducens* cells.[22] The reaction was performed in 50 mM Tris-HCl buffer (pH 7.5) containing 20 g/L linoleic acid, 20 g/L of *S. nitritireducens* cells, and 0.02% (w/v) Tween 80 at 30 °C for 2 h. 10-Hydroxystearic acid and 10-hydroxy-12(*Z*)-octadecenoic acid were prepared from the obtained reaction products by the following low-temperature solvent fractional crystallization.[9] An equal volume of ethyl acetate was added to the reaction products, and the ethyl acetate from the reaction mixture was removed using a rotary evaporator. The extract was mixed with 30% acetonitrile and 70% acetone at room temperature. The solution obtained was incubated at −80 °C for 24 h in a deep freezer. The liquid fraction containing the unsaturated fatty acid was separated at room temperature, and the remaining solid fraction containing hydroxy fatty acid was obtained. The acetonitrile and acetone in the solid fraction were removed using a rotary evaporator. This fractionation procedure was repeated three times, and the obtained products of 10-hydroxystearic acid and 10-hydroxy-12(*Z*)-octadecenoic acid with high purity (>99%) were identified by GC and GC-MS.[21,23] The two hydroxy fatty acids were used as the standard compounds for product analysis, and 10-hydroxy-12(*Z*)-octadecenoic acid was also used as a substrate for γ-dodecelactone production.

Microorganisms. The isolated strain *S. nitritireducens*[22] was used for 10-hydroxy-12(*Z*)-octadecenoic acid production from linoleic acid. *E. coli* ER2566 expressing oleate hydratase from *S. maltophilia* KCTC 1773 was used for the production of 10-hydroxystearic acid from oleic acid. *C. boidinii* KTCT 17776, *Candida palmioleophila* KTCT 17452, *Candida tropicalis* KTCT 7221, *Citeromyces matritensis* KTCT 17714, *Cryprococcus curvatus* KTCT 7225, *Saccharomyces cerevisiae* KTCT 7704, *Schizosaccharomyces pombe* KTCT 7167, *Sporobolomyces odorus* KTCT 17242, *Starmerella bombicola* KTCT 17652, *Waltomyces lipofer* KTCT 17657, and *Y. lipolytica* KTCT 17170 were used for γ-dodecelactone production from 10-hydroxy-12(*Z*)-octadecenoic acid.

Media. *S. nitritireducens* was cultivated in nutrient broth containing 5 g/L peptone and 3 g/L beef extract. Recombinant *E. coli* cells were cultivated in Luria−Bertani (LB) agar. The growth medium was yeast malt (YM) broth containing 10 g/L glucose, 3 g/L malt extract, and 5 g/L peptone. The induction medium contained 5 g/L glucose, 7 g/L oleic acid, 0.1 g/L yeast extract, 2.1 g/L potassium phosphate monobasic, 4.51 g/L potassium phosphate dibasic, 0.1 g/L sodium chloride, 0.2 g/L magnesium sulfate, 9.14 mg/L iron sulfate heptahydrate, 0.5 mg/L zinc chloride, and 1.56 mg/L copper sulfate. The reaction medium contained 50 mM citrate/phosphate buffer (pH 5.5), 3.4 g/L yeast nitrogen base, 0.5 g/L 10-hydroxy-12(*Z*)-octadecenoic acid, and 0.05% (w/v) Tween 80.

Culture and Reaction Conditions. The cells were cultivated on the YM agar plate. After 1 day, a single colony in the plate was inoculated into 15 mL of the growth medium and cultivated at 30 °C with agitation at 200 rpm for 12 h. The seed culture was then transferred into a 2 L baffled flask containing 500 mL of the induction medium and was cultivated at 30 °C with agitation at 200 rpm for 15 h. The cells from the culture medium were harvested by centrifugation at 13000*g* for 20 min at 4 °C and then were washed twice with 50 mM citrate/phosphate buffer (pH 5.5). The harvest cells were used for γ-dodecelactone production from 10-hydroxy-12(*Z*)-octadecenoic acid. Unless otherwise stated, the biotransformation reaction was performed in a 500 mL-baffled flask containing 100 mL of the reaction medium at pH 5.5 and 25 °C with agitation of 200 rpm for 3 h. For lactonization, the pH of the reaction solution was adjusted to 2.0 by adding 6M HCl and then incubated at 100 °C for 30 min.[9,10,14]

Selection of Inducer and Determination of Induction Process. Fatty acids and hydroxy fatty acids, including lauric acid, stearic acid, oleic acid, erucic acid, linoleic acid, 10-hydroxydecanoic acid, and 10-hydroxystearic acid, were used as inducers for the β-oxidation pathway. To select inducer, *C. boidinii* cells were cultivated in the induction medium supplemented with 7 g/L inducer. The effect of inducer on γ-dodecelactone production from 10-hydroxy-12(*Z*)-octadecenoic acid was investigated using whole *C. boidinii* cells, and thus the best inducer oleic acid was selected. To determine the concentration of oleic acid for increased γ-dodecelactone production, the concentration of oleic acid was varied from 0 to 15 g/L in the induction medium containing 5 g/L glucose. To determine the optimal concentration of glucose, the concentration of glucose was varied from 1 to 15 g/L in the induction medium containing 7 g/L oleic acid. The cells were cultivated at 30 °C with agitation at 200 rpm for 15 h. To determine the induction time for the increased activity of β-oxidation, the cells were cultivated in the induction medium containing 5 g/L glucose and 7 g/L oleic acid at 30 °C with agitation at 200 rpm for 24 h. Samples were withdrawn at several intervals within 24 h. *C. boidinii* cells obtained from the cultures were harvested, and γ-dodecelactone production from 10-hydroxy-12(*Z*)-octadecenoic acid using the harvested cells was conducted at 30 °C and pH 5.5 for 3 h.

Effects of pH and Temperature on γ-Dodecelactone Production. The effect of pH on γ-dodecelactone production from 10-hydroxy-12(*Z*)-octadecenoic acid by whole *C. boidinii* cells was evaluated by varying the pH from 4.0 to 6.5 in 50 mM citrate/phosphate buffer while a constant temperature of 25 °C was maintained. To evaluate the effect of temperature, the temperature

dx.doi.org/10.1021/jf501081z | J. Agric. Food Chem. 2014, 62, 6736−6745

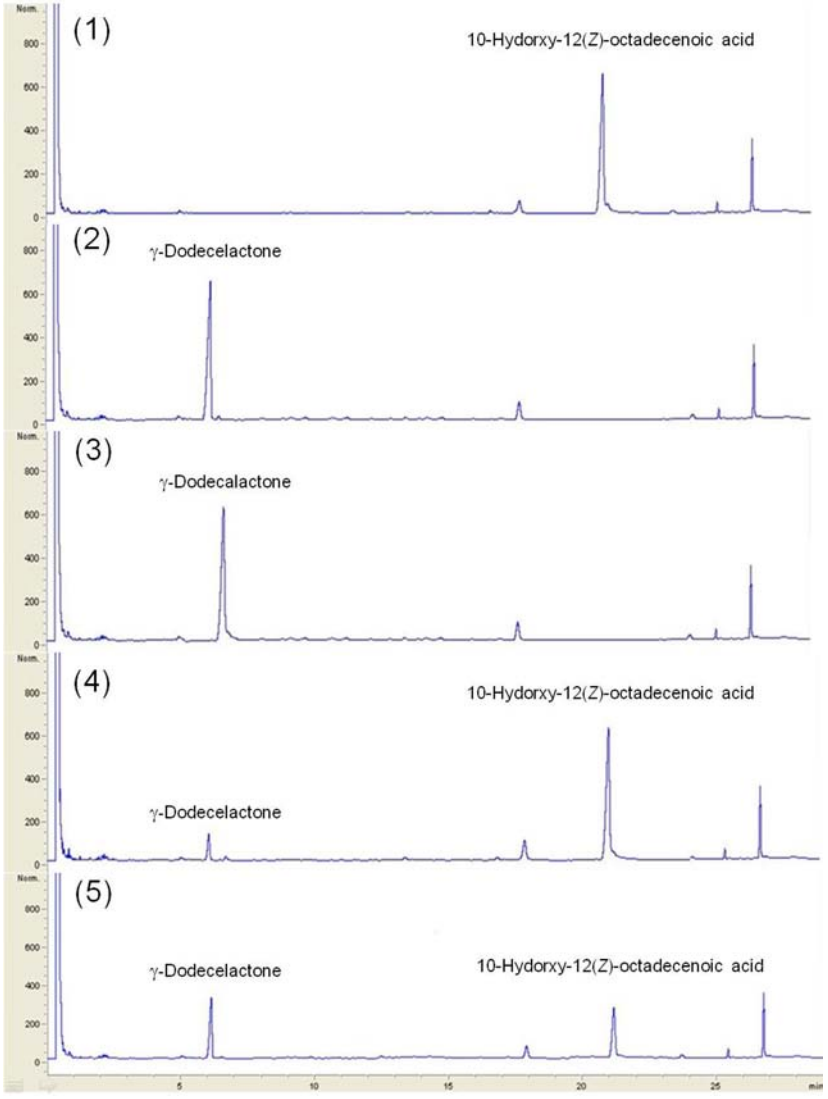

Figure 2. Gas chromatograms of 10-hydroxy-12(*Z*)-octadecenoic acid, γ-dodecelactone, and γ-dodecalactone. The reaction of whole *C. boidinii* cells was performed in 50 mM citrate/phosphate buffer (pH 5.5) containing 3.4 g/L yeast nitrogen base, 5 g/L 10-hydroxy-12(*Z*)-octadecenoic acid, 30 g/L cells, and 0.05% (w/v) Tween 80 at 25 °C with agitation of 200 rpm. (1) Gas chromatogram of 10-hydroxy-12(*Z*)-octadecenoic acid standard. The retention time of 10-hydroxy-12(*Z*)-octadecenoic acid was 21.1 min. (2) Gas chromatogram of γ-dodecelactone standard. The retention time of γ-dodecelactone was 6.1 min. (3) Gas chromatogram of γ-dodecalactone standard. The retention time of γ-dodecalactone was 6.7 min. (4) Gas chromatogram of the reaction solution at 3 h. (5) Gas chromatogram of the reaction solution at 6 h.

was varied from 15 to 35 °C while the pH was constantly maintained at 5.5. The reactions were performed under the above-described standard reaction conditions; only the pH and temperature were varied.

Effects of Cell and Substrate Concentrations on γ-Dodecelactone Production. The optimal concentrations of cells and substrate for the increased production of γ-dodecelactone from 10-hydroxy-12(*Z*)-octadecenoic acid by whole *C. boidinii* cells were determined by varying the cell concentration from 5 to 40 g/L at a constant 10-hydroxy-12(*Z*)-octadecenoic acid concentration of 5 g/L and by varying the substrate concentration from 2.5 to 15 g/L at a constant cell concentration of 30 g/L. The reactions were performed under the above-described standard reaction conditions; only the cell and substrate concentrations were varied.

Production of γ-Dodecelactone from 10-Hydroxy-12(*Z*)-octadecenoic Acid. γ-Dodecelactone production from 10-hydroxy-12(*Z*)-octadecenoic acids by whole *C. boidinii* cells was performed in 50 mM citrate/phosphate buffer (pH 5.5) containing 3.4 g/L yeast nitrogen base, 5 g/L 10-hydroxy-12(*Z*)-octadecenoic acid, 30 g/L cells, and 0.05% (w/v) Tween 80 at 25 °C for 8 h.

Production of γ-Lactones from Safflower Oil. The hydrolysis of fatty acids from safflower oil by lipase from *C. rugosa* was carried out in 50 mM Tris-HCl buffer (pH 7.5) containing 7.5 g/L safflower oil, 1 g/L lipase, and 0.02% (w/v) Tween 80 at 37 °C for 30 min. To inactivate the lipase and arrest the reaction, the reaction solution was boiled at 100 °C for 50 min.[24] The production of hydroxy fatty acids by whole cells of *S. nitritireducens* was conducted in 50 mM Tris-HCl buffer (pH 7.5) containing the hydrolysate obtained from 7.5 g/L safflower oil, 20 g/L cells, and 0.02% (w/v) Tween 80 at 30 °C with agitation at 200 rpm for 90 min, under anaerobic conditions.[22] An equal volume of ethyl acetate was added to the cell reaction solution, the ethyl acetate from the reaction mixture was removed using a rotary evaporator, and the concentration of 10-hydroxy-12(*Z*)-octadecenoic acid in the reaction solution was adjusted to 5.0 g/L by dissolving the residue for the production of γ-lactones. The time course reactions for the production of γ-lactones by whole *C. boidinii* cells were carried out in 50 mM citrate/phosphate buffer (pH 5.5) containing 3.4 g/L yeast nitrogen base, 5.0 g/L 10-hydroxy-12(*Z*)-octadecenoic acid, 0.85 g/L 10-hydroxystearic acid, 0.27 g/L linoleic acid, 0.07 g/L oleic acid, 0.31

g/L palmitic acid, 30 g/L cells, and 0.05% (w/v) Tween 80 at 25 °C for 7 h.

Analytical Methods. The cell mass was determined by calibrating the optical density at 600 nm to the dry cell weight. The concentration of glucose in the medium was analyzed using a glucose assay kit (Asan Pharm, Seoul, South Korea). Heptadecanoic acid at 50 mM was used as an internal standard. The silylation of linoleic acid, oleic acid, palmitic acid, 10-hydroxy-12(*Z*)-octadecenoic acid, and 10-hydroxystearic acid was conducted by mixing pyridine and *N*-methyl-*N*-(trimethylsilyl)trifluoroacetamide with a ratio of 3:1. Silylated fatty acids, silylated hydroxy fatty acids, and γ-lactones were analyzed by a gas chromatography (Agilent 7890 N, Santa Clara, CA, USA) with a flame ionization detector and a Supelco SPB-1 capillary column. The column temperature was increased from 100 to 220 °C at the rate of 5 °C/min for 24 min, and then it was maintained at 220 °C. The injector and detector temperatures were maintained at 260 and 250 °C, respectively. γ-Dodecelactone (ring form), γ-dodecalactone, γ-dodecelactone (open form), palmitic acid, linoleic acid, oleic acid, 10-hydroxy-12(*Z*)-octadecenoic acid, and 10-hydroxystearic acid were detected on the basis of their retention times of 6.1, 6.7, 10.8, 14.3, 17.3, 17.9, 21.1, and 21.8 min, respectively. The γ-lactones, fatty acids, and hydroxy fatty acids in the reaction samples after hydrolysis of safflower oil and γ-dodecelactone and 10-hydroxy-12(*Z*)-octadecenoic acid in the reaction samples of whole *C. boidinii* cells containing 5 g/L 10-hydroxy-12(*Z*)-octadecenoic acid were identified to have the same retention times as those of their corresponding standards. The amounts of the products were calculated by calibrating the peak areas to the concentrations of γ-lactones, fatty acids, and hydroxy fatty acid standards.

RESULTS AND DISCUSSION

Selection of an Efficient γ-Dodecelactone-Producing Strain. In the GC profiles, the peaks for the substrate and the product obtained from the reaction solutions of whole *C. boidinii* cells were detected at the same retention times as those of the 10-hydroxy-12(*Z*)-octadecenoic acid and γ-dodecelactone standards, respectively (Figure 2). The open and ring forms of γ-dodecelactone in the reaction solutions of whole *C. boidinii* cells before and after acidification were analyzed by the GC. The open and ring forms of γ-dodecelactone before acidification were detected (Supporting Information Figure S1A). The open and ring forms of γ-dodecelactone were distinguishable from each other, showing different retention times in the GC profile. However, after acidification, the open form of γ-dodecelactone was converted to the ring form, and then it disappeared (Supporting Information Figure S1B).

The yeast *Sporobolomyces odorus*[25] and the fungi *Fusarium poae*[5,26] and *P. roqueforti*[20] have been reported to produce γ-dodecelactone. However, the yield of γ-dodecelactone produced by these microorganisms was very low. To obtain an efficient γ-dodecelactone-producing strain, 11 yeast strains were screened for γ-dodecelactone production from 10-hydroxy-12(*Z*)-octadecenoic acid. Seven of the 11 yeast strains exhibited γ-dodecelactone-producing activity, and the efficiency of production was in the following order: *C. boidinii* > *C. curvatus* > *C. palmioleophila* > *S. bombicola* > *Y. lipolytica* > *S. odorus* > *S. cerevisiae*. However, *C. tropicalis*, *C. matritensis*, *S. pombe*, and *W. lipofer* did not produce γ-dodecelactone (Figure 3). The activity of *C. boidinii*, which was approximately 10-fold higher than that of the known γ-dodecelactone-producing stain *S. odorus*, was the highest among the 11 yeast strains. Thus, *C. boidinii* was selected as an efficient γ-dodecelactone-producing yeast and was used for γ-dodecelactone production. *C. boidinii* has been known to produce saturated lactones such as γ-dodecalactone and δ-dodecalactone.[27,28] However, the production of the monounsaturated lactone γ-dodecelactone by *C. boidinii* has not been reported yet.

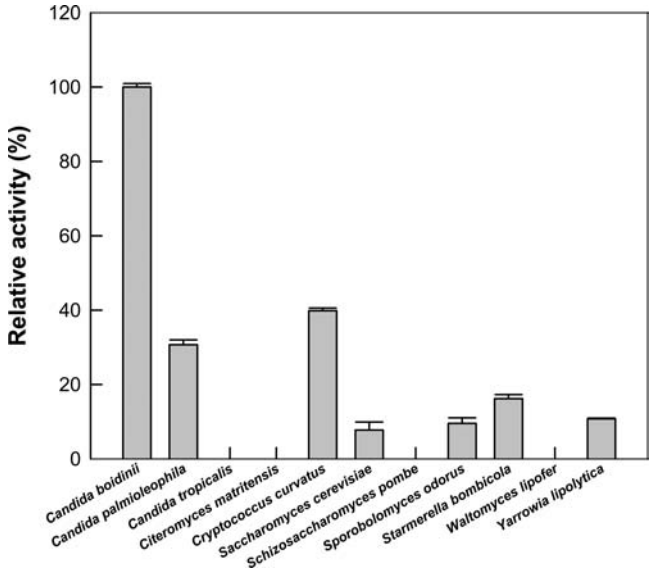

Figure 3. γ-Dodecelactone production from 10-hydroxy-12(*Z*)-octadecenoic acid by whole cells of the yeast strains. The reactions were performed in 50 mM citrate/phosphate buffer (pH 5.5) containing 3.4 g/L yeast nitrogen base, 5 g/L cells, 0.5 g/L 10-hydroxy-12(*Z*)-octadecenoic acid, and 0.05% (w/v) Tween 80 at 25 °C with agitation at 200 rpm for 3 h. The data represent the means of three separate experiments, and error bars represent the standard deviation.

Induction of *C. boidinii* Cells for the Increased Production of γ-Dodecelactone from 10-Hydroxy-12(*Z*)-octadecenoic Acid. *C. boidinii* was cultivated in the induction medium supplemented with 7 g/L inducer, and then the induced whole cells were used in the reactions for γ-dodecelactone production from 10-hydroxy-12(*Z*)-octadecenoic acid for 3 h. The inducers tested included lauric acid, stearic acid, oleic acid, linoleic acid, erucic acid, 10-hydroxydecanoic acid, and 10-hydroxystearic acid. The activity of *C. boidinii* cells for γ-dodecelactone production followed the order oleic acid > stearic acid > erucic acid > control (with no addition of inducer) > linoleic acid >10-hydroxystearic acid > 10-hydroxydecanoic acid (Figure 4A).

The maximum production of γ-lactones by *W. lipofer* was observed at 5 g/L oleic acid as an inducer.[9] Thus, the concentration of oleic acid was varied from 0 to 15 g/L for γ-dodecelactone production using *C. boidinii* cells. The γ-dodecelactone-producing activity was the highest when oleic acid was used as an inducer at a concentration of 7 g/L (Figure 4B). γ-Dodecelactone production by the cells induced with 7 g/L oleic acid was 2.2-fold higher than that by the noninduced cells. The concentration of glucose as an additional carbon source for the maximum production of γ-lactones by *W. lipofer* was 1 g/L,[9] and the growth medium of *C. boidinii*, which was yeast malt (YM) broth, contained 10 g/L glucose. Thus, glucose at various concentrations from 1 to 15 g/L was added to the induction medium containing 7 g/L oleic acid for increasing the activity for γ-dodecelactone production. The optimal concentration of glucose for γ-dodecelactone production was 5 g/L (Figure 4C). To decide the induction time, *C. boidinii* cells were cultivated in the induction medium for 24 h. A sample was withdrawn at regular time points, and γ-

dx.doi.org/10.1021/jf501081z | J. Agric. Food Chem. 2014, 62, 6736−6745

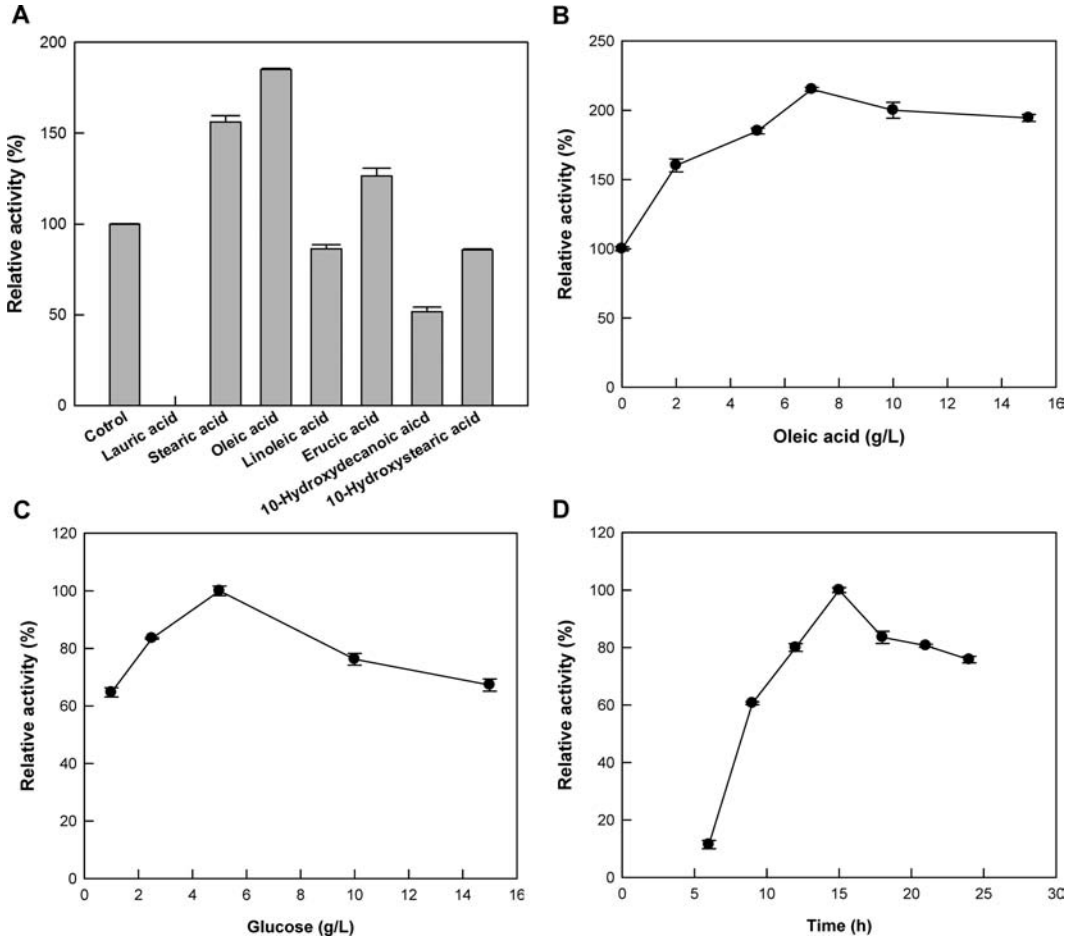

Figure 4. Induction of *C. boidinii* cells for increasing γ-dodecelactone production from 10-hydroxy-12(*Z*)-octadecenoic acid. After induction, the reactions were performed in 50 mM citrate/phosphate buffer (pH 5.5) containing 3.4 g/L yeast nitrogen base, 5 g/L cells, 0.5 g/L 10-hydroxy-12(*Z*)-octadecenoic acid, and 0.05% (w/v) Tween 80 at 25 °C with agitation at 200 rpm for 3 h. (A) Effect of inducer type. *C. boidinii* cells were grown on the induction medium containing 7 g/L inducer. The control reaction was γ-dodecelactone production by cells that were cultivated in the growth medium without the inducer. (B) Effect of oleic acid concentration. *C. boidinii* cells were cultivated in the induction medium by varying the concentration of oleic acid from 0 to 15 g/L. (C) Effect of glucose concentration. *C. boidinii* cells were cultivated in the induction medium by varying the concentration of glucose from 1 to 15 g/L. (D) Effect of induction time. *C. boidinii* cells were cultivated in the induction medium containing 7 g/L oleic acid and 5 g/L glucose for 24 h. Samples were withdrawn within 24 h at several intervals. The data represent the means of three separate experiments, and error bars represent the standard deviation.

dodecelactone-producing activity of *C. boidinii* was determined. The maximum γ-dodecelactone-producing activity was observed at 15 h of induction time (Figure 4D). Therefore, *C. boidinii* cells grown on the induction medium containing 7 g/L oleic acid and 5 g/L glucose for 15 h of induction time were used for γ-dodecelactone production. Under these induction conditions, γ-dodecelactone production by the induced cells was 14-fold higher than that by the noninduced cells.

Fatty acids have been used as inducers of the β-oxidation pathway.[29−31] Among the fatty acids, oleic acid has been determined to be the most effective inducer[9,32,33] of the enzymes related to the β-oxidation pathway of yeast.[34,35] High glucose concentrations repress the enzymes related to the β-oxidation pathway,[36,37] whereas low glucose concentrations stimulate the β-oxidation pathway.[9] When *W. lipoper* cells were induced, the induction time (12 h) in the medium containing oleic acid and glucose for the increased activity of β-oxidation was 4 h of progress time after glucose exhaustion (8 h).[9] In the induction of *C. boidinii* cells, glucose was exhausted at 12 h, and induction time for the increased activity of β-oxidation (15 h) was 3 h of progress time after glucose exhaustion. The activity of *C. boidinii* cells for γ-dodecelactone production appeared to be maximal at 3−4 h of progress time after glucose exhaustion.

Determination of the Reaction Conditions for the Increased Production of γ-Dodecelactone from 10-Hydroxy-12(*Z*)-octadecenoic Acid by Induced *C. boidinii* Cells. The reaction conditions for saturated γ-lactone production have been investigated.[9,14,38,39] However, to the best of our knowledge, the reaction conditions for unsaturated γ-lactone production have not been investigated. Therefore, the pH, temperature, and concentrations of cells and substrate for γ-dodecelactone production from 10-hydroxy-12(*Z*)-octadecenoic acid were investigated using induced whole *C. boidinii* cells. The maximal activity for γ-dodecelactone production from 10-hydroxy-12(*Z*)-octadecenoic acid was observed at pH 5.5 and 25 °C (Figure 5). γ-Lactone production was performed at pH 6.5 and 35 °C by *W. lipofer*[40] and at pH 7.0 and 25 °C by baker's yeast.[41]

The concentrations of whole *W. lipofer* cells for the maximum production of γ-dodecalactone[14] and γ-lactones[9] were 30 and 20 g/L, respectively. To determine the concentration of whole *C. boidinii* cells for the maximal

dx.doi.org/10.1021/jf501081z | J. Agric. Food Chem. 2014, 62, 6736−6745

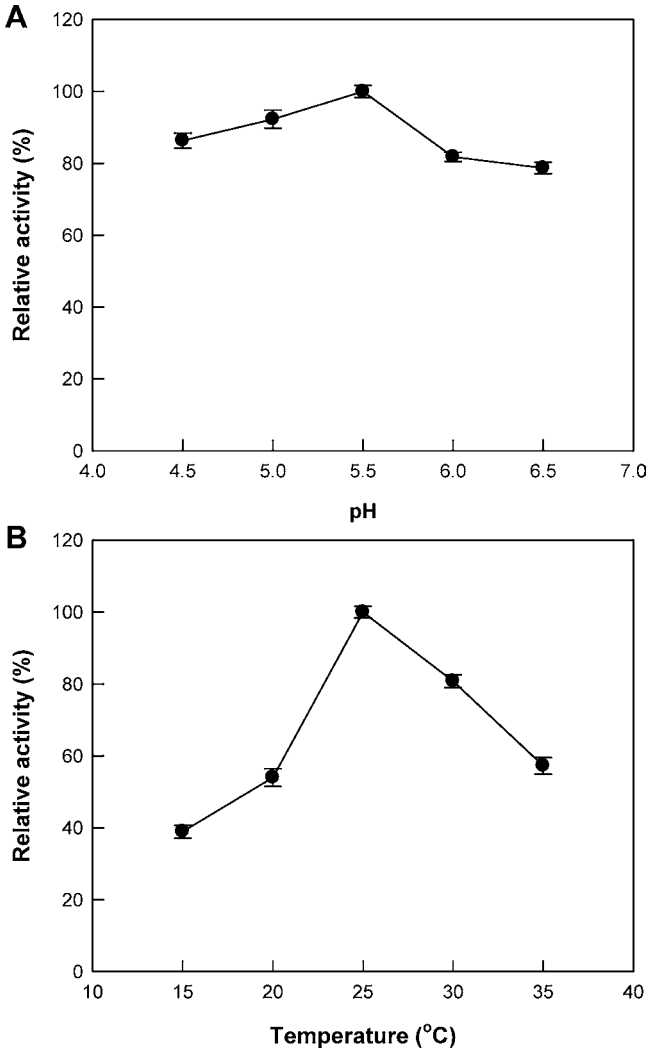

Figure 5. Effects of pH and temperature on the production of γ-dodecelactone from 10-hydroxy-12(*Z*)-octadecenoic acid by whole *C. boidinii* cells. The data represent the means of three separate experiments, and error bars represent the standard deviation. (A) Effect of pH. The reactions were performed by varying the pH from 4.0 to 6.5 in 50 mM citrate/phosphate buffer containing 3.4 g/L yeast nitrogen base, 5 g/L cells, 0.5 g/L 10-hydroxy-12(*Z*)-octadecenoic acid, and 0.05% (w/v) Tween 80 at 25 °C with agitation at 200 rpm for 3 h. (B) Effect of temperature. The reactions were performed by varying the temperature from 15 to 35 °C in 50 mM citrate/phosphate buffer (pH 5.5) containing 3.4 g/L yeast nitrogen base, 5 g/L cells, 0.5 g/L 10-hydroxy-12(*Z*)-octadecenoic acid, and 0.05% (w/v) Tween 80 with agitation at 200 rpm for 3 h.

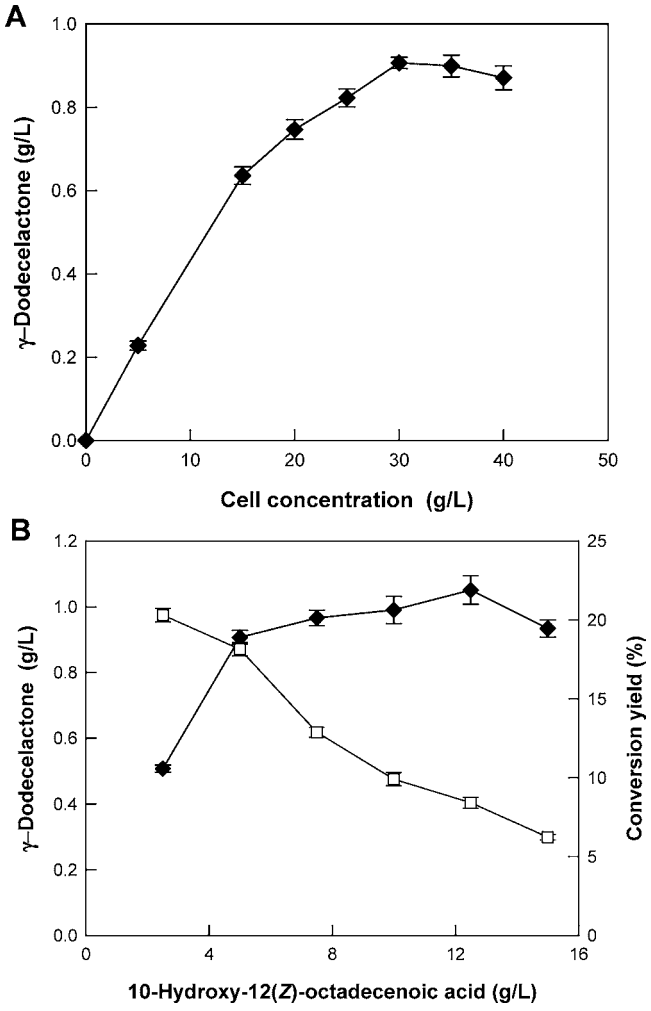

Figure 6. Effects of the concentrations of cells and substrate on the production of γ-dodecelactone from 10-hydroxy-12(*Z*)-octadecenoic acid. The data represent the means of three separate experiments, and error bars represent the standard deviation. (A) Effect of the concentration of cells. The reactions were performed by varying the cell concentration from 5 to 40 g/L in 50 mM citrate/phosphate buffer (pH 5.5) containing 3.4 g/L yeast nitrogen base, 5 g/L 10-hydroxy-12(*Z*)-octadecenoic acid, and 0.05% (w/v) Tween 80 at 25 °C with agitation at 200 rpm for 3 h. (B) Effect of substrate concentration: production (◆) and conversion yield (□) of γ-dodecelactone from 10-hydroxy-12(*Z*)-octadecenoic acid. The reactions were performed by varying the concentration of 10-hydroxy-12(*Z*)-octadecenoic acid from 2.5 to 15 g/L in 50 mM citrate/phosphate buffer (pH 5.5) containing 3.4 g/L yeast nitrogen base, 30 g/L cells, and 0.05% (w/v) Tween 80 at 25 °C with agitation at 200 rpm for 3 h.

production of γ-dodecelactone, the concentration of the induced cells was varied from 5 to 40 g/L using 5 g/L 10-hydroxy-12(*Z*)-octadecenoic acid as a substrate for 3 h (Figure 6A). Below 30 g/L cells, 10-hydroxy-12(*Z*)-octadecenoic acid production increased with increasing cell concentration; however, above 30 g/L, it reached a plateau. As the cell concentration was higher than 30 g/L, the high viscosity of the reaction solution interfered with mass transfer in the aqueous phase, resulting in the conversion rate decreased. These results indicated that the cell concentration for the maximal production of γ-dodecelactone was 30 g/L.

The concentration of saturated hydroxy fatty acids, including 10-hydroxystearic acid, 12-hydroxystearic acid, and 12-hydroxydodecanoic acid, for the maximum production of saturated lactones, including γ-dodecalactone, γ-decalactone, and γ-butyrolactone, respectively, was 60 g/L.[9,14] The antimicrobial activities of monounsaturated hydroxy fatty acids were significantly higher than those of saturated hydroxy fatty acids.[42] Thus, the production of the monounsaturated lactone γ-dodecelactone was investigated with the range of low concentrations for 10-hydroxy-12(*Z*)-octadecenoic acid as a substrate from 2.5 to 15 g/L using 30 g/L cells for 3 h (Figure 6B). At concentrations below 12 g/L 10-hydroxy-12(*Z*)-octadecenoic acid, γ-dodecelactone production increased with increasing concentration of 10-hydroxy-12(*Z*)-octadecenoic acid. However, the conversion yield decreased as the concentration of substrate increased. This may be due to the

dx.doi.org/10.1021/jf501081z | J. Agric. Food Chem. 2014, 62, 6736−6745

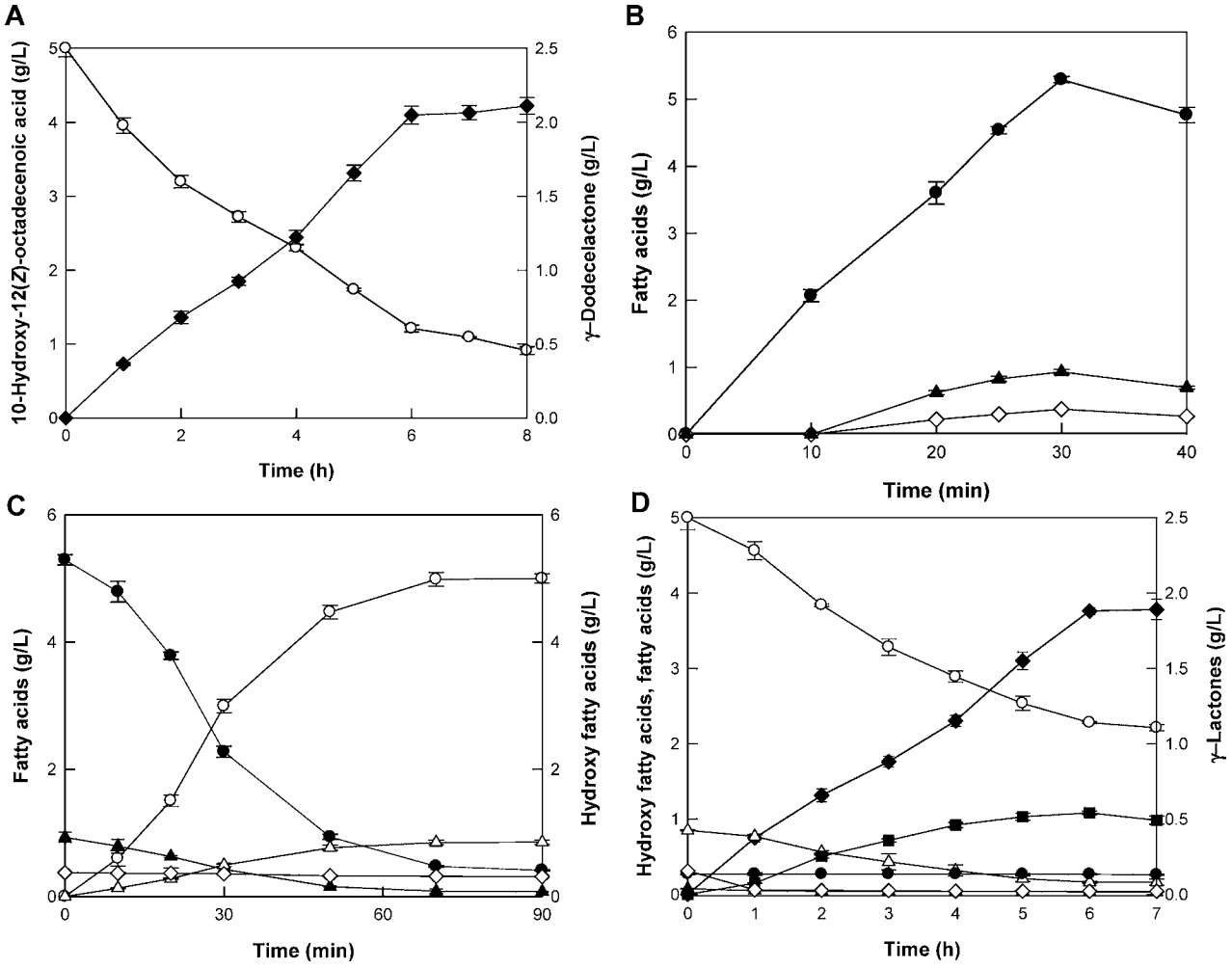

Figure 7. Time course reactions for the production of fatty acids, hydroxy fatty acids, and γ-lactones by lipase, *S. nitritireducens*, and *C. boidinii*, respectively. The data represent the means of three separate experiments, and error bars represent the standard deviation. (A) Production of γ-dodecelactone from 10-hydroxy-12(*Z*)-octadecenoic acid by whole *C. boidinii* cells. The reactions for the production of γ-dodecelactone (◆) were performed in 50 mM citrate/phosphate buffer (pH 5.5) containing 3.4 g/L yeast nitrogen base, 30 g/L cells, 5 g/L 10-hydroxy-12(*Z*)-octadecenoic acid (○), and 0.05% (w/v) Tween 80 at 25 °C with agitation at 200 rpm for 8 h. (B) Production of fatty acids from safflower oil by lipase from *C. rugosa*. Fatty acids were linoleic acid (●), oleic acid (▲), and palmitic acid (◇). The reactions were performed in 50 mM Tris-HCl buffer (pH 7.5) containing 1 g/L lipase, 7.5 g/L safflower oil, and 0.02% (w/v) Tween 80 at 37 °C with agitation at 200 rpm for 40 min. (C) Production of hydroxy fatty acids from fatty acids by whole *S. nitritireducens* cells. Linoleic acid (●) and oleic acid (▲) were converted to 10-hydroxy-12(*Z*)-octadecenoic acid (○) and 10-hydroxystearic acid (△), respectively, by whole *S. nitritireducens* cells. However, palmitic acid (◇) was not converted. The reactions were performed in 50 mM Tris-HCl buffer (pH 7.5) containing safflower oil hydrolysate, 20 g/L cells, and 0.02% (w/v) Tween 80 at 30 °C with agitation at 200 rpm for 90 min under anaerobic conditions. (D) Production of γ-lactones from hydroxy fatty acids by whole *C. boidinii* cells. The cells well-consumed oleic acid (▲) and linoleic acid (●); however, they poorly consumed palmitic acid (◇). The reactions for the production of γ-dodecelactone (◆) and γ-dodecalactone (■) were performed in 50 mM Tris-HCl buffer (pH 5.5) containing 3.4 g/L yeast nitrogen base, 30 g/L cells, 5 g/L 10-hydroxy-12(*Z*)-octadecenoic acid (○), 0.85 g/L 10-hydroxystearic acid (△), and 0.05% (w/v) Tween 80 at 25 °C with agitation at 200 rpm for 7 h.

antimicrobial activity of 10-hydroxy-12(*Z*)-octadecenoic acid to cells.[42] Therefore, a substrate concentration of 5 g/L 10-hydroxy-12(*Z*)-octadecenoic acid for γ-dodecelactone production was selected as a suitable concentration to improve the performance in terms of both conversion yield and product concentration.

Production of γ-Dodecelactone from 10-Hydroxy-12(*Z*)-octadecenoic Acid by Induced *C. boidinii* Cells. The reaction conditions for the increased production of γ-dodecelactone by whole *C. boidinii* cells were pH 5.5 and 25 °C with 30 g/L cells and 5 g/L 10-hydroxy-12(*Z*)-octadecenoic acid. Under these conditions, induced *C. boidinii* cells produced 2.1 g/L (10.7 mM) γ-dodecelactone from 5 g/L (16.7 mM) 10-hydroxy-12(*Z*)-octadecenoic acid after 6 h, with a molar conversion yield of 64% (corresponding to 42%, w/w) and a volumetric productivity of 350 mg/L/h (Figure 7A). After 8 h, the production of γ-dodecelactone was observed to decrease, because γ-dodecelactone was degraded by the cells.[43] Yeast cells consume γ-lactones as carbon source by extensive β-oxidation degradation,[43] and γ-lactones are thus converted to viable biomass for longer cell maintenance.[44,45]

Production of γ-Dodecelactone from Lipase-Treated Safflower Oil by Two-Step Whole-Cell Biotransformation. γ-Dodecelactone production from safflower oil as a substrate via 10-hydroxy-12(*Z*)-octadecenoic acid intermediate was performed by an enzymatic hydrolysis reaction and a two-

dx.doi.org/10.1021/jf501081z | J. Agric. Food Chem. 2014, 62, 6736−6745

Table 1. Biotransformation of Safflower Oil to γ-Lactones

step	substrate (g/L) [mM]	product (g/L) [mM]	productivity (g/L/h)	step yield (g/g) [mM/mM]	total yield (%, g/g)
hydrolysis (lipase from *Candida rugosa*)	safflower oil (7.50)	linoleic acid (5.30)	10.6 ± 0.09	0.71	0.71
		oleic acid (0.93)	1.86 ± 0.89	0.12	0.12
		palmitic acid (0.37)	0.740 ± 0.005	0.05	0.05
hydration (*Stenotrophomonas nitritireducens*)	linoleic acid (5.30) [18.90]	10-hydroxy-12-(*Z*)-octadecenoic acid (5.00) [16.78]	4.27 ± 0.09	0.94 [0.89]	0.67
	oleic acid (0.93) [3.20]	10-hydroxystearic acid (0.85) [2.82]	0.73 ± 0.03	0.91 [0.88]	0.12
lactonization (*Candida boidinii*)	10-hydroxy-12-(*Z*)-octadecenoic acid (5.00) [16.78]	γ-dodecelactone (1.88) [9.60]	0.310 ± 0.004	0.38 [0.57]	0.25
	10-hydroxystearic acid (0.85) [2.82]	γ-dodecalactone (0.54) [2.7]	0.090 ± 0.002	0.64 [0.96]	0.08

Table 2. Conversion Yield and Productivity of γ-Lactones from Oil

strain	method	substrate (g/L)	product (mg/L)	conversion yield (%)	productivity (mg/L/h)	ref
Yarrowia lipolytica	fermentation	castor oil (10)	γ-decalactone (610)	0.061	4	48
		castor oil (30)	γ-decalactone (1839)	0.0613	10	15
Geotrichum fragrans	fermentation	castor oil (50)	γ-decalactone (600)	0.012	6	16
Penicillium roqueforti	fermentation	soybean oil (5)	γ-dococelactone (1.84)	0.00036	0.025	20
		copra oil (5)	γ-dococelactone (1.5)	0.0003	0.0125	
Candida boidinii	enzymatic reaction and two-step whole cell biotransformation	safflower oil (7.5)	γ-dococelactone (1880)	25	235 (43[a])	this study

[a]Productivity included the preparation time of whole cells.

step whole-cell biotransformation process. The conversion yield and productivity at each step during the conversion reactions are presented in Table 1. Natural safflower oil was hydrolyzed by lipase from *C. rugosa* because *S. nitritireducens* could not perform the hydroxylation of safflower oil. The reactions for the oil hydrolysis were performed using 7.5 g/L safflower oil and 1 g/L lipase at pH 7.5, 35 °C, and 200 rpm for 40 min (Figure 7B). At 30 min, safflower oil hydrolysate contained 5.3 g/L linoleic acid, 0.93 g/L oleic acid, and 0.37 g/L palmitic acid. After 30 min, the contents of these fatty acids decreased with increasing reaction time because lipase could catalyze the reverse reaction.[46] Therefore, the reactions were terminated at 30 min.

The first cell biotransformation step for γ-dodecelactone production from lipase-treated safflower oil hydrolysate was the conversion of unsaturated fatty acids into hydroxy fatty acids by hydrating the double bond in the unsaturated fatty acids from water.[47] The maximum production of hydroxy fatty acid by whole *S. nitritireducens* cells was observed at pH 7.5, 30 °C, and 20 g/L cells, under anaerobic conditions.[22] Under these conditions, *S. nitritireducens* cells converted 5.3 g/L linoleic acid and 0.93 g/L oleic acid in the hydrolysate obtained from 7.5 g/L safflower oil into 5 g/L 10-hydroxy-12(*Z*)-octadecenoic acid and 0.85 g/L 10-hydroxystearic acid after 90 min, respectively (Figure 7C), with molar conversion yields of 89 and 86% and volumetric productivities of 3333 and 567 mg/L/h, respectively (Table 1).

The second cell biotransformation step was the conversion of hydroxy fatty acids into γ-lactones by the induced whole *C. boidinii* cells. Under the conditions of pH 5.5 and 25 °C with 30 g/L cells and 5 g/L 10- hydroxy-12(*Z*)-octadecenoic acid, the induced *C. boidinii* cells produced 1.88 g/L γ-dodecelactone and 0.54 g/L γ-dodecalactone from 5 g/L 10-hydroxy-12(*Z*)-octadecenoic acid and 0.85 g/L 10-hydroxystearic acid after 6 h, respectively (Figure 7D), with conversion yields of 57 and 96% (mol/mol) and volumetric productivities of 313 and 90 mg/L/h, respectively (Table 1). The cells well-consumed oleic acid and linoleic acid; however, they poorly consumed palmitic acid. The total concentration of the two γ-lactones produced from 7.5 g/L safflower oil by an enzymatic hydrolysis reaction and a two-step whole-cell biotransformation process was 2.42 g/L for 8 h of the reaction time, with a volumetric productivity of 303 mg/L/h and a conversion yield of 32% (w/w). Several rounds of biotransformation reusing whole *S. nitritireducens* and *C. boidinii* cells were performed (Supporting Information Figure S2). The activities of the cells were decreased with increasing number of reuse and then showed 11 and 24% after the fourth batch, respectively. Thus, the hydration activity of *S. nitritireducens* and the β-oxidation activity *C. boidinii* cells are unstable.

The conversion yield and productivity of γ-lactones from oil are summarized in Table 2. The reported volumetric productivities of γ-decalactone from castor oil were 4 mg/L/h,[48] 10 mg/L/h,[15] and 6 mg/L/h.[16] The conversion yield and productivity of γ-dodecelactone using soybean oil were 0.00036% (w/w) and 0.025 mg/L/h, respectively, and those using copra oil were 0.0003% (w/w) and 0.0125 mg/L/h, respectively.[20] These yields and productivities were very low. In the present study, 1.88 g/L γ-dodecelactone was produced from 7.5 g/L safflower oil for 8 h of reaction time, with a conversion

dx.doi.org/10.1021/jf501081z | J. Agric. Food Chem. 2014, 62, 6736−6745

yield of 25% (w/w) and a volumetric productivity of 235 mg/L/h. The time to prepare whole *S. nitritireducens* and *C. boidinii* cells was 21 and 15 h, respectively. Thus, the total time to produce γ-dodecelactone from safflower oil, including the preparation time of whole cells, was 44 h. The volumetric productivity calculated from the total time was 43 mg/L/h. These conversion yield and productivity values of γ-dodecelactone from oil were 69400- and 4.3-fold higher than the previously reported highest conversion yield and productivity, respectively. These results indicate that the two-step whole cell biotransformation process via hydroxy fatty acid intermediate is an efficient method for increasing γ-lactone production from oil. A process developed in this study for the production of γ-dodecelactone from safflower oil contained an enzymatic reaction plus two-step biotransformation. The first step was the hydrolysis of safflower oil, the second step was the hydration of fatty acid, and the third step was the lactonization of hydroxy fatty acid. In the second step, the reaction was performed using oil hydrolysate obtained from the first step by adding *S. nitritreducens* cells without additional extraction or purification. In the third step, the reaction was performed using the extracted solution after the reaction solution obtained from the first step by adding *C. boidinii* cells with extraction to adjust the concentration of hydroxy fatty acid and without purification. In the industrial and large-scale production, this extraction can be omitted. The process containing an enzymatic reaction plus two-step biotransformation can be performed without extraction and purification by only adding enzyme and cells. Therefore, the process is not too complex for industrial and large-scale production.

In conclusion, the production of the flavor γ-dodecelactone from safflower oil was demonstrated via an enzymatic hydrolysis reaction and a two-step whole cell biotransformation process. Lipase-treated safflower oil hydrolysate containing linoleic acid was converted into 10-hydroxy-12(*Z*)-octadecenoic acid by whole *S. nitritireducens* cells and was subsequently converted to γ-dodecelactone by induced whole *C. boidinii* cells. To the best of our knowledge, our bioprocess exhibits the highest productivity and yield of γ-lactone produced from a natural oil reported to date. Thus, the two-step whole cell biotransformation process via the intermediate hydroxy fatty acid may be useful in lactone production from oils.

■ ASSOCIATED CONTENT

Supporting Information

Figures S1 and S2. This material is available free of charge via the Internet at http://pubs.acs.org.

■ AUTHOR INFORMATION

Corresponding Author

*(D.-K.O.) Phone: (822) 454-3118. Fax: (822) 444-5518. E-mail: deokkun@konkuk.ac.kr.

Funding

This study was supported by a grant from the Bioindustry Technology Development Program, Ministry for Agriculture, Food and Rural Affairs (No. 112002-3), Republic of Korea.

Notes

The authors declare no competing financial interest.

■ REFERENCES

(1) Endrizzi, A.; Pagot, Y.; Le Clainche, A.; Nicaud, J. M.; Belin, J. M. Production of lactones and peroxisomal β-oxidation in yeasts. *Crit. Rev. Biotechnol.* **1996**, *16*, 301−329.

(2) Okamoto, K.; Chimori, M.; Iwanaga, F.; Hattori, T.; Yanase, H. Production of γ-lactones by the brown-rot basidiomycete *Piptoporus soloniensis*. *J. Biosci. Bioeng.* **2002**, *94*, 182−185.

(3) Longo, M. A.; Sanroman, M. A. Production of food aroma compounds: microbial and enzymatic methodologies. *Food Technol. Biotechnol.* **2006**, *44*, 335−353.

(4) Farbood, M. I.; Morris, J. A.; Mclean, L. B. Fermentation process for preparing 10-hydroxy-C18-carboxylic acid and γ-dodecalactone derivatives. EP patent 0578388, 1998.

(5) Guichard, E.; Mosandl, A.; Hollnagel, A.; Latrasse, A.; Henry, R. Chiral γ-lactones from *Fusarium poae*. *Z. Lebensm. Unters. Forsch.* **1991**, *193*, 26−31.

(6) Mariaca, R. G.; Imhof, M. I.; Bosset, J. O. Occurrence of volatile chiral compounds in dairy products, especially cheese − a review. *Eur. Food Res. Technol.* **2001**, *212*, 253−261.

(7) Massolo, A.; Dani, F. R.; Bella, N. Sexual and individual cues in the peri-anal gland secretum of crested porcupines (*Hystrix cristata*). *Mamm. Biol.* **2009**, *74*, 488−496.

(8) Ando, K.; Katahira, H.; Ochiai, K.; Ogata, N.; Ozawa, K.; Saitoh, C.; Tokunaga, C.; Yashiro, A.; Yokoi, A. Process for producing a bran pickles flavoring solution. U.S. patent 7037672, 2002.

(9) An, J. U.; Oh, D. K. Increased production of γ-lactones from hydroxy fatty acids by whole *Waltomyces lipofer* cells induced with oleic acid. *Appl. Microbiol. Biotechnol.* **2013**, *97*, 8265−8272.

(10) Feron, G.; Dufosse, L.; Pierard, E.; Bonnarme, P.; Quere, J. L.; Spinnler, H. E. Production, identification, and toxicity of γ-decalactone and 4-hydroxydecanoic acid from *Sporidiobolus* sp. *Appl. Environ. Microbiol.* **1996**, *62*, 2826−2831.

(11) Wache, Y.; Aguedo, M.; Nicaud, J. M.; Belin, J. M. Catabolism of hydroxyacids and biotechnological production of lactones by *Yarrowia lipolytica*. *Appl. Microbiol. Biotechnol.* **2003**, *61*, 393−404.

(12) Wache, Y.; Aguedo, M.; Choquet, A.; Gatfield, I. L.; Nicaud, J. M.; Belin, J. M. Role of β-oxidation enzymes in γ-decalactone production by the yeast *Yarrowia lipolytica*. *Appl. Environ. Microbiol.* **2001**, *67*, 5700−5704.

(13) Aguedo, M.; Gomes, N.; Garcia, E. E.; Wache, Y.; Mota, M.; Teixeira, J. A.; Belo, I. Decalactone production by *Yarrowia lipolytica* under increased O_2 transfer rates. *Biotechnol. Lett.* **2005**, *27*, 1617−1621.

(14) An, J. U.; Joo, Y. C.; Oh, D. K. New biotransformation process for production of the fragrant compound γ-dodecalactone from 10-hydroxystearate by permeabilized *Waltomyces lipofer* cells. *Appl. Environ. Microbiol.* **2013**, *79*, 2636−2641.

(15) Gomes, N.; Braga, A.; Teixeira, J. A.; Belo, I. Impact of lipase-mediated hydrolysis of castor oil on γ-decalactone production by *Yarrowia lipolytica*. *J. Am. Oil Chem. Soc.* **2013**, 1131−1137.

(16) Neto, R. S.; Pastore, G. M.; Macedo, G. A. Biocatalysis and biotransformation producing γ-decalactone. *J. Food Sci.* **2004**, *69*, C677−C680.

(17) Lee, S. L.; Chou, C. C. Effects of various fatty acid components of castor oil on the growth and production of γ-decalactone by *Sporobolomyces odorus*. *J. Ferment. Bioeng.* **1996**, *82*, 42−45.

(18) Piazza, G. J.; Farrell, H. M., Jr. Generation of ricinoleic acid from castor oil using the lipase from ground oat (*Avena sativa* L.) seeds as a catalyst. *Biotechnol. Lett.* **1991**, *13*, 179−184.

(19) Krzyczkowska, J. The use of castor oil in the production of γ-decalactone by *Yarrowia lipolytica* KKP 379. *Chem. Technol.* **2012**, *61*, 58−61.

(20) Chalier, P.; Crouzet, J. Production of lactones by *Penicillium roqueforti*. *Biotechnol. Lett.* **1992**, *14*, 275−280.

(21) Joo, Y. C.; Seo, E. S.; Kim, Y. S.; Kim, K. R.; Park, J. B.; Oh, D. K. Production of 10-hydroxystearic acid from oleic acid by whole cells of recombinant *Escherichia coli* containing oleate hydratase from *Stenotrophomonas maltophilia*. *J. Biotechnol.* **2012**, *158*, 17−23.

(22) Yu, I. S.; Kim, H. J.; Oh, D. K. Conversion of linoleic acid into 10-hydroxy-12(*Z*)-octadecenoic acid by whole cells of *Stenotrophomonas nitritireducens*. *Biotechnol. Prog.* **2008**, *24*, 182−186.
(23) Yu, I. S.; Yeom, S. J.; Kim, H. J.; Lee, J. K.; Kim, Y. H.; Oh, D. K. Substrate specificity of *Stenotrophomonas nitritireducens* in the hydroxylation of unsaturated fatty acid. *Appl. Microbiol. Biotechnol.* **2008**, *78*, 157−163.
(24) Gordillo, A.; Obradors, N.; Montesinos, J. L.; Valero, F.; Lafuente, F. J.; Salo, C. Stability studies and effect of the initial oleic acid concentration on lipase production by *Candida rugosa*. *Appl. Microbiol. Biotechnol.* **1995**, *43*, 38−41.
(25) Lee, S. L.; Chou, C. C. Growth and production of γ-decalactone and *cis*-6-dodecen-4-olide by *Sporobolomyces odorus* in the presence of fatty acids and oils. *J. Ferment. Bioeng.* **1994**, *78*, 114−116.
(26) Latrasse, A.; Guichard, E.; Piffaut, C.; Fournier, N.; Dufosse, L. Chirality of the γ-lactones formed by *Fusarium poae* INRA 45. *Chirality* **1993**, *5*, 379−384.
(27) Boog, A. L. G. M.; Peters, A. L. J.; Roos, R. Process for producing δ-lactones from 11-hydroxy fatty acids. U.S. patent 5215901, 1993.
(28) Boog, A. L. G. M.; van Grinsven, A. M.; Peters, A. L. J.; Roos, R.; Wieg, A. J. Process for producing γ-lactones. U.S. patent 5789212, 1998.
(29) Endrizzi, A.; Awade, A. C.; Belin, J. M. Presumptive involvement of methyl ricinoleate β-oxidation in the production of γ-decalactone by the yeast *Pichia guilliermondii*. *FEMS Microbiol. Lett.* **1993**, *114*, 153−159.
(30) Pagot, Y.; Le Clainche, A.; Nicaud, J. M.; Wache, Y.; Belin, J. M. Peroxisomal β-oxidation activities and γ-decalactone production by the yeast *Yarrowia lipolytica*. *Appl. Microbiol. Biotechnol.* **1998**, *49*, 295−300.
(31) Veenhuis, M.; Mateblowski, M.; Kunau, W. H.; Harder, W. Proliferation of microbodies in *Saccharomyces cerevisiae*. *Yeast* **1987**, *3*, 77−84.
(32) Dommes, P.; Dommes, V.; Kunau, W. H. β-Oxidation in *Candida tropicalis* partial purification and biological function of an inducible 2,4-dienoyl coenzyme a reductase. *J. Biol. Chem.* **1983**, *258*, 10846−10852.
(33) Valenciano, S.; Lucas, J. R. D.; Pedregosa, A.; Monistrol, I. F.; Laborda, F. Induction of β-oxidation enzymes and microbody proliferation in *Aspergillus nidulans*. *Arch. Microbiol.* **1996**, *166*, 336−341.
(34) Einerhand, A. W.; Kos, W.; Smart, W. C.; Kal, A. J.; Tabak, H. F.; Cooper, T. G. The upstream region of the *FOX3* gene encoding peroxisomal 3-oxoacyl-coenzyme A thiolase in *Saccharomyces cerevisiae* contains ABF1- and replication protein A binding sites that participate in its regulation by glucose repression. *Mol. Cell. Biol.* **1995**, *15*, 3405−3414.
(35) Dmochowska, A.; Dignard, D.; Maleszka, R.; Thomas, D. Y. Structure and transcriptional control of the *Saccharomyces cerevisiae POX1* gene encoding acylcoenzyme A oxidase. *Gene* **1990**, *88*, 247−252.
(36) Wilson, W. A.; Hawley, S. A.; Hardie, D. G. Glucose repression/derepression in budding yeast: SNF1 protein kinase is activated by phosphorylation under derepressing conditions, and this correlates with a high AMP:ATP ratio. *Curr. Biol.* **1996**, *6*, 1426−1434.
(37) Stanway, C. A.; Gibbs, J. M.; Berardi, E. Expression of the FOX1 gene of *Saccharomyces cerevisiae* is regulated by carbon source, but not by the known glucose repression genes. *Curr. Genet.* **1995**, *27*, 404−408.
(38) Gomes, N.; Aguedo, M.; Teixeira, J. A.; Belo, I. Oxygen mass transfer in a biphasic medium: Influence on the biotransformation of methyl ricinoleate into γ-decalactone by the yeast *Yarrowia lipolytica*. *Biochem. Eng. J.* **2007**, *35*, 380−386.
(39) Gomes, N.; Teixeira, J. A.; Belo, I. Empirical modelling as an experimental approach to optimize lactone production. *Catal. Sci. Technol.* **2010**, *1*, 86−92.
(40) An, J. U.; Joo, Y. C.; Oh, D. K. New biotransformation process for production of the fragrant compound γ-dodecalactone from 10-hydroxystearate by permeabilized *Waltomyces lipofer* cells. *Appl. Environ. Microbiol.* **2013**, *79*, 2636−2641.
(41) Gocho, S.; Tabogami, N.; Inagaki, M.; Kawabata, C.; Komai, T. Biotransformation of oleic acid to optically active γ-dodecalactone. *Biosci., Biotechnol., Biochem.* **1995**, *59*, 1571−1572.
(42) Black, B. A.; Zannini, E.; Curtis, J. M.; Ganzle, M. G. Antifungal hydroxy fatty acids produced during sourdough fermentation: microbial and enzymatic pathways, and antifungal activity in bread. *Appl. Environ. Microbiol.* **2013**, *79*, 1866−1873.
(43) Welsh, F. W.; Murray, W. D.; Williams, R. E. Microbiological and enzymatic production of flavor and fragrance chemicals. *Crit. Rev. Biotechnol.* **1989**, *9*, 105−169.
(44) Nago, H.; Matsumoto, M.; Nakai, S. 2-Deceno-δ-lactone-producing fungi, strains of *Fusarium solani*, isolated by using a medium containing decano-δ-lactone as the sole carbon source. *Biosci., Biotechnol., Biochem.* **1993**, *57*, 2107−2110.
(45) Spinnler, H. E.; Dufosse, L.; Souchon, I.; Latrasse, A.; Piffaut Juffard, C.; Voilley, A.; Delest, P. Production of γ-decalactone by bioconversion. FR patent 2705971, 1994.
(46) Rajendran, A.; Palanisamy, A.; Thangavelu, V. Lipase catalyzed ester synthesis for food processing industries. *Braz. Arch. Biol. Technol.* **2009**, *52*, 207−219.
(47) Koritala, S.; Hosie, L.; Hou, C. T.; Hesseltine, C. W.; Bagby, M. O. Microbial conversion of oleic acid to 10-hydroxystearic acid. *Appl. Microbiol. Biotechnol.* **1989**, *32*, 299−304.
(48) Farbood, M. I.; Willis, B. J. Production of γ-decalactone. WO patent 1983001072, 1983.

U.S. Food and Drug Administration (FDA). Sulfite-containing compounds including sodium sulfite (GRAS 182.3798), sodium bisulfite (GRAS 182.3739), and sodium metabisulfite (GRAS 182.3766) are on the FDA's GRAS list. Sulfites are multipurpose compounds commonly used as calcium, potassium, or sodium salts in the food and pharmaceutical industries as preservatives or antioxidants. They are also used to slow food oxidation and can sometimes affect the smell and taste of foods.[26] Sulfite-containing compounds occur naturally in foods, such as garlic, onions, cheeses, and eggs, and drinks, such as wine, beer, and some teas.

Although they are generally considered safe, sulfites can cause contact dermatitis and have been highlighted as a cause of cosmetic allergy.[27−29] However, allergies to preservatives such as sodium sulfite and its derivatives are considered rare.[30,31] The FDA requires labeling when sulfites are used as preservatives in a final product; however, when sulfites are used in food-processing steps, labeling is required only when the sulfite residual is ≥10 ppm.[32] The use of sulfite-containing compounds on fresh fruits and vegetables was banned in 1986 because of potential allergic reactions, and those suffering from asthma are at elevated risk of sulfite sensitivity.[33] Nevertheless, sodium metabisulfite is currently included as a preservative in therapeutic epinephrine,[34] and according to the prescription information for EpiPen, sodium metabisulfite is included as a preservative in the epinephrine shot used to counteract a severe food allergy reaction. Each 0.3 mL dose from an EpiPen autoinjector contains 0.5 mg of sodium metabisulfite. Individuals suffering from sulfide oxidase deficiency are also sulfite sensitive because of their inability to convert sulfites to sulfates.[35]

The development of new, cost-effective processing methods that can lower or eliminate the ability of tree nuts and peanuts to cause allergic reactions is important for the prevention of severe reactions. The reaction between sulfite and cysteine disulfides within proteins is reversible at alkaline pH and has been shown to disrupt disulfide bonds of several proteins.[36] Standard protocols using sodium sulfite to break disulfide bonds, referred to as sulfitolysis, can be used to introduce a negative charge on modified cysteines.[37] Here, using cashew extracts and purified Ana o 3, we evaluated the ability of sodium sulfite to target cashew allergens having structure and stability that are dependent upon cysteine disulfide bonds. We assessed the effect of sulfite addition on the structure of cashew allergens and their innate capacity to bind IgE from cashew allergic individuals.

EXPERIMENTAL PROCEDURES

Materials. "Ready to eat" cashews were purchased from Nuts Online (http://www.nuts.com, Cranford, NJ, USA). Roasted cashews were prepared by heating "ready to eat" cashews in an oven at 177 °C for 20 min. Sodium sulfite and dithiothreitol (DTT) were purchased from Sigma-Aldrich (St. Louis, MO, USA), spin columns from Millipore (Carrigtwohill, CO, USA), SDS-PAGE Any kD Mini-Protean TGX precast Tris-glycine gels from Bio-Rad (Hercules, CA, USA), and Novex 4−20% Tris−glycine gels from Life Technologies (Carlsbad, CA, USA). Sequencing-grade modified trypsin from Promega (Madison, WI, USA) was used for sample digestion prior to mass spectrometry. Biotinylated anti-human IgE antibody was purchased from Southern Biotech (Birmingham, AL, USA). IRdye-680-labeled streptavidin, IRdye-680, and IRdye-800 secondary antibodies were purchased from LI-COR (Lincoln, NE, USA). Nonsterile Maxisorp 96-well Nunc microtiter plates were purchased from Thermo Scientific (Rochester, NY, USA).

Cashew Extract Preparation. Raw and roasted cashews were ground with a coffee grinder and defatted with petroleum ether in a Soxhlet apparatus overnight. Defatted cashew flour (0.4 g) was placed in 10 mL of 0.2 M Tris, 0.2 M NaCl, pH 8.0, and vortexed for 30 s and then sonicated twice on ice for 15 s using a Sonic Dismembrator (Fisher Scientific Co., Orlando, FL, USA). Extract solutions were centrifuged for 30 min at 12000 rpm at 4 °C, and clarified cashew extracts were collected. Protein concentrations were determined using a NanoDrop (ThermoFisher, Pittsburgh, PA, USA), and samples were stored at −20 °C.

SDS-PAGE. Proteins were resolved by SDS-PAGE with either a Mini Protean system II (Bio-Rad) or a Novex Mini Cell gel rig (Life Technologies) and prestained Precision Plus molecular weight markers (Bio-Rad). Prior to electrophoresis, 4× NuPAGE LDS sample buffer (Life Technologies) was added to the protein samples using a 1:4 (v/v) ratio. Samples were heated at 65 °C for 15 min, and after electrophoresis, protein bands were visualized with Safe Stain (Invitrogen, Grand Island, NY, USA). Gel images were captured, and normalization of protein load in each lane was confirmed by quantifying the 680 nm channel signal on an Odyssey CLX infrared imaging system (LI-COR).

Cashew Extract Treatment. Cashew extract (125 μg) was incubated with various concentrations of sodium sulfite (0−100 mM) and at different temperatures (0−100 °C) for 15 min. Control samples were heated with or without added 5 mM DTT. Sample aliquots were removed and combined with SDS-PAGE sample buffer lacking reducing agent prior to analysis with SDS-PAGE or immunoblotting.

Rabbit Antibodies. Rabbit antibody production was performed by Pierce Biotechnology Inc. (Rockford, IL, USA). Briefly, prescreened rabbits were immunized with 1 mg of cashew extract made from "ready to eat" cashew nuts and then boosted at days 14, 28, and 42 with 0.5 mg of cashew extract at each injection. Test rabbits were phlebotomized, and sera were screened for antibodies against total cashew protein. Large-volume phlebotomies were collected from high-titer rabbits, and serum was stored at −80 °C for later use.

Human Sera. Clinically relevant sera from cashew-allergic patients (from >7 to 55 years of age) with a documented history of cashew allergy supported by in vivo (skin test) or in vitro (serum immunoassay) cashew-specific IgE were collected at Dallas-Allergy Immunology (Dallas, TX, USA). The study protocol was approved by the North Texas Institutional Review Board.

Immunoblotting. Cashew extract samples (25 μg) treated with DTT, water, or sodium sulfite were subjected to SDS-PAGE (with loading buffer lacking reducing agent) and transferred to a PVDF membrane for Western blot or spotted (5 μg) on to PVDF membrane for dot-blot. Blotted PVDF (Millipore, Billerica, MA, USA) was blocked for 1 h at room temperature in PBST with 2% (w/v) nonfat dry milk. Rabbit anti-cashew antibody was diluted 1:1000 in PBST and incubated overnight at 4 °C. The membranes were then washed three times for 5 min in PBST and incubated for 30 min with anti-rabbit IRdye-680 (1:10000 in PBST) at room temperature. The membranes were washed as above and visualized using an Odyssey CLx (LI-COR) infrared imaging system. Immunoblotting for IgE (Western blot and dot blot) was performed overnight using similar methods with sera pooled from six cashew allergic patients. Membranes were washed as above and incubated for 1 h at room temperature with biotinylated anti-IgE (1:1000 in PBST). Membranes were then washed and incubated for 30 min at room temperature with IRdye-680-labeled streptavidin (1:5000 in PBST) and visualized with an Odyssey CLx instrument.

Circular Dichroism (CD). Ana o 3 was purified as described in Mattison et al.[16] Purified native and chemically treated Ana o 3 samples were analyzed by far-UV CD (185−250 nm) on a Jasco-815 spectropolarimeter (JASCO, Oklahoma City, OK, USA) as described previously[16] with minor changes. Briefly, treated Ana o 3 samples were buffer exchanged into 5 mM sodium phosphate (pH 6.8) with a 3 kDa spin column and then diluted to a protein concentration of 0.1 mg/mL for analysis. CD spectra were acquired using a quartz cuvette with a 1 cm path length at 25 °C with a 2 nm bandwidth and a response time of 1 s. Three acquisitions were obtained for each sample, and background

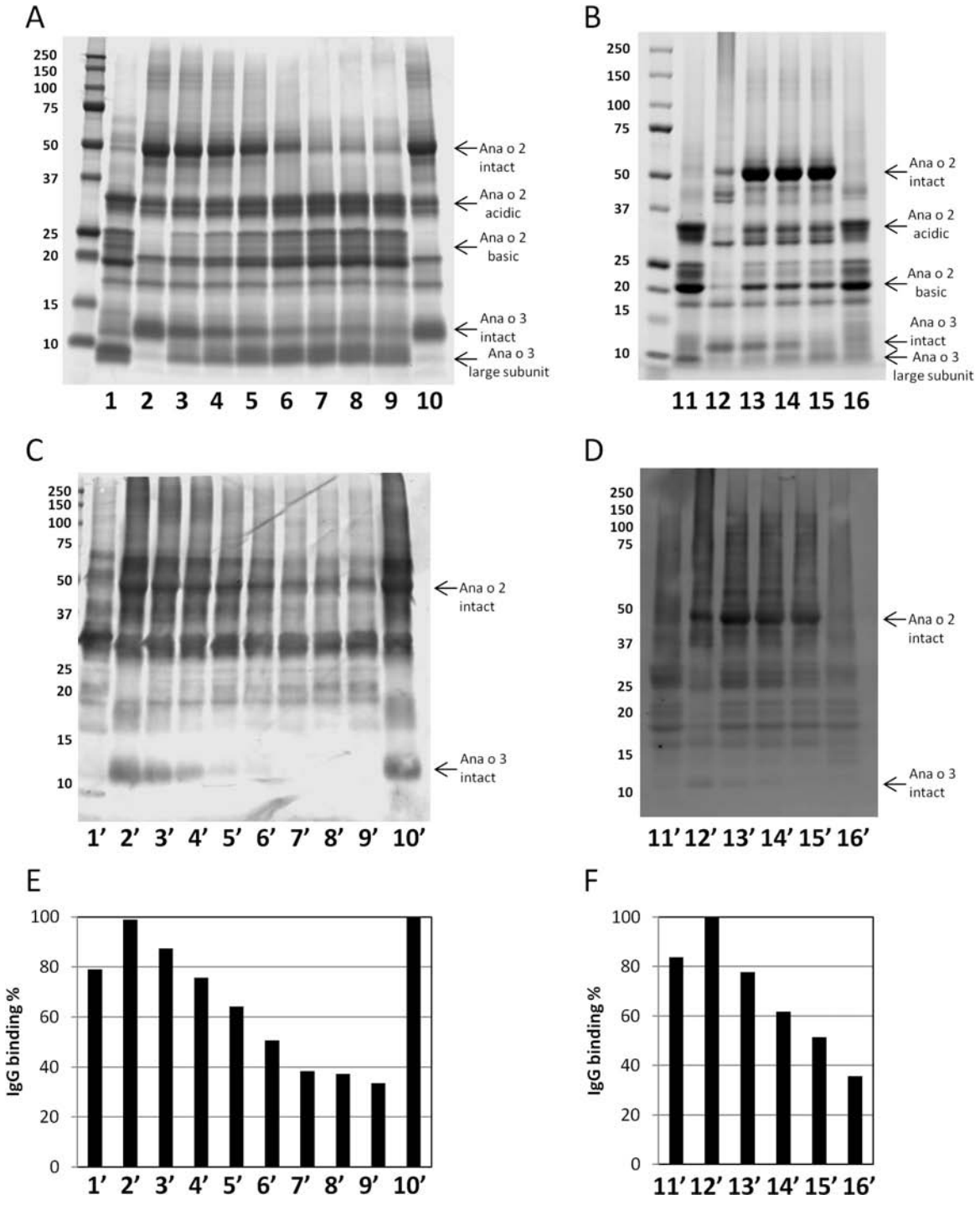

Figure 1. Sodium sulfite alters cashew protein migration and lowers antibody binding. Cashew nut extract (125 μg) subjected to treatment with various amounts of sodium sulfite and temperature was analyzed by nonreducing SDS-PAGE and rabbit anti-cashew antibodies. Cashew extract incubated for 15 min at 100 °C with sodium sulfite or 5 mM DTT was analyzed by SDS-PAGE (A) and immunoblot with rabbit anticashew antibodies (C). Lanes: (1, 1′) 5 mM DTT; (2, 2′, 10, 10′) buffer control, 100 °C; (3, 3′) 1 mM sodium sulfite; (4, 4′) 2.5 mM sodium sulfite; (5, 5′) 5 mM sodium sulfite; (6, 6′) 10 mM sodium sulfite; (7, 7′) 25 mM sodium sulfite; (8, 8′) 50 mM sodium sulfite; (9, 9′) 100 mM sodium sulfite. Sodium sulfite treatment of cashew extracts is temperature dependent. Cashew extract (125 μg) was subjected to treatment with 50 mM sodium sulfite at various temperatures and analyzed by SDS-PAGE (B) and immunoblot with rabbit anti-cashew antibodies (D). Lanes: (11, 11′) 5 mM DTT at 100 °C; (12, 12′) buffer control, 100 °C; (13, 13′) 50 mM sodium sulfite, 37 °C; (14, 14′) 50 mM sodium sulfite, 50 °C; (15, 15′) 50 mM sodium sulfite, 65 °C; (16, 16′) 50 mM sodium sulfite, 100 °C. Rabbit IgG binding was visualized with IRdye-680-labeled anti-rabbit IgG secondary antibody. Quantification of IgG antibody binding in each respective lane (C and D) is shown in panels E and F, and molecular weight markers are indicated on the left side of each gel or immunoblot.

measurements were subtracted. Mean residue ellipticity was calculated using a mean residue weight of 114.5 g/mol, and the K2D3 web server (http://www.ogic.ca/projects/k2d3/) was used to estimate secondary structure.[33]

dx.doi.org/10.1021/jf501117p | J. Agric. Food Chem. 2014, 62, 6746−6755

LC-MS/MS Mass Spectrometry. Following treatment with sodium sulfite, ammonium bicarbonate (100 mM) and calcium chloride (1 mM) were added to defatted cashew extracts made from "ready to eat" cashew nuts. Sequencing-grade modified trypsin (0.2 μg) was added, and samples were allowed to digest for 1 h at 37 °C with gentle mixing. Following acidification with formic acid, samples were analyzed via LC-MS/MS with an Agilent 1200 LC system, an Agilent Chip Cube interface, and an Agilent 6520 Q-TOF tandem mass spectrometer (Agilent Technologies, Santa Clara, CA, USA) as described previously.[16] Raw data files were extracted, sequenced, and searched against a custom food allergen database containing the Ana o 1, Ana o 2, and Ana o 3 sequences. Peptides were searched for sulfite (SO_3) cysteine modifications resulting in an 80 Da mass shift after incorporation of the corresponding mass change into the Spectrum Mill search algorithm.

Competetive ELISA. Microtiter plates were coated with 1 μg of raw cashew extract per well in coating buffer (15 mM Na_2CO_3, 35 mM $NaHCO_3$, pH 9.6) and incubated overnight at 4 °C. Cashew extract was discarded, and the plate was blocked with PBST containing 1% BSA (w/v) at room temperature for 1 h. Plates were washed three times with PBST following blocking and all experimental incubation steps to remove unbound proteins. Treated or untreated cashew extract was centrifuged with 3 kDa spin columns to remove unreacted sodium sulfite or DTT. Samples were then buffer exchanged in 100 mM Tris, pH 8.3, by 10-fold dilution and centrifugation four times using the spin columns to further dilute any remaining sodium sulfite or DTT. Samples were resuspended in 200 μL of buffer and serially diluted 10-fold with 100 mM Tris, pH 8.3. Competition samples, to evaluate IgE binding, were made using 12.5 μL of treated cashew sample, 12.5 μL of pooled sera, and 25 μL of 100 mM Tris, pH 8.3. Samples were added to the microtiter plates and incubated at 37 °C for 1 h. Plates were washed, and 50 μL of biotinylated anti-IgE (1:1000 in PBST) was added to each well and then incubated at 37 °C for 30 min. Plates were washed with PBST, and 50 μL of streptavidin-labeled IRdye-680 (1:5000 in PBST) was added to each well. Plates were incubated at 37 °C for 30 min, washed, and then imaged with the Odyssey CLx instrument. The data in the plot are presented as percent of IgE inhibition using the following formula: IR680 value of uninhibited control − IR680 value of inhibited sample/IR680 value of uninhibited control × 100.

RESULTS

Some nut allergens, including Ana o 2 and Ana o 3, contain disulfide bonds important for their structure; disruption of these bonds can result in lowered antibody binding. To determine if sulfite compounds could disrupt cashew nut IgE binding epitopes, we incubated cashew extracts with sodium sulfite. As shown in Figure 1A, addition of sodium sulfite and heating at 100 °C dissociated Ana o 2 and Ana o 3 and altered their SDS-PAGE migration patterns in cashew extracts. Concentrations as low as 1 mM sodium sulfite disrupted disulfide bonds and altered the migration pattern of at least a portion of the Ana o 2 and Ana o 3 proteins in the extract. Increasing the sodium sulfite concentration resulted in a gradient of dissociation and in the migration pattern of Ana o 2 and Ana o 3 proteins. Elevated sodium sulfite resulted in an increasing appearance of the Ana o 2 acidic (∼33 kDa) and basic (∼20−25 kDa) subunits and the large Ana o 3 subunit migrating just below the 10 kDa marker. At higher concentrations of sodium sulfite (25−100 mM), we observed a migration pattern very similar to that seen using 5 mM DTT (Figure 1A). Similar results were obtained when cashew extracts were incubated with 50 mM sodium bisulfite, sodium metabisulfite, and potassium sulfite, but not sodium thiosulfate (not shown).

Next, we altered the incubation temperature to determine if the dissociation and altered migration of the Ana o 2 and Ana o 3 allergens in cashew extracts treated with sodium sulfite were dependent upon temperature. Disruption of a small portion of Ana o 3 in the extract was observed at 37 °C in the presence of 50 mM sodium sulfite. More of the dissociated large subunit of Ana o 3 can be observed just below the 10 kDa marker as the temperature was increased to 50, 65, or 100 °C (Figure 1B). Extensive disruption of Ana o 2 and alteration in its migration pattern were not observed until the incubation temperature reached 100 °C (Figure 1B). These results indicated that Ana o 3 was more sensitive to sodium sulfite-induced disruption compared to Ana o 2 in the extracts. We did not observe a noticeable shift in the cashew extract protein migration pattern when samples were treated at temperatures below 37 °C in the presence of sodium sulfite.

To evaluate the immunological consequences of sodium sulfite treatment on cashew extracts, we raised antibodies against cashew proteins in rabbits. Western blots using these rabbit polyclonal antibodies indicated that there was a reduction in IgG binding to cashew proteins in sulfite-treated extracts (Figure 1C). We quantified the antibody binding signal and found that overall IgG binding was lowered by 60−70% at sodium sulfite concentrations of ≥25 mM and incubation at 100 °C (Figure 1E). In particular, we noticed a reduction in antibody binding to the slower migrating, higher molecular weight forms >75 kDa (Figure 1C,E). These forms have been associated with heating-induced cross-linking of peanut and other food allergens during processing and can alter IgE binding.[38−44] We also observed that binding to Ana o 3 was lowered at sodium sulfite concentrations as low as 1 mM and was undetectable at higher concentrations (Figure 1C,E). Similarly, antibody binding to Ana o 2 and other higher molecular weight proteins was lowered as sodium sulfite concentration increased. At ≥37 °C, we observed a reduction in antibody binding to cashew proteins treated with 50 mM sodium sulfite (Figure 1D,F). However, when extracts were incubated at 100 °C in the presence of 50 mM sodium sulfite, we observed the dissociation of Ana o 2 subunits and the largest reduction in overall binding to cashew proteins (Figure 1D,F).

Different food preparation methods have been shown to alter antibody binding, and nuts are commonly roasted before consumption. We next tested the effect of sodium sulfite on extracts made from roasted cashews. Extracts made from previously roasted cashews were treated with sodium sulfite, and we observed similar results. Figure 2A shows the disruption of Ana o 2 and Ana o 3 proteins into subunits from both the raw and roasted cashew samples after the sodium sulfite treatment. Whereas there was greater IgG binding to the roasted extracts, overall IgG binding was lowered in both raw and roasted sodium sulfite-treated extracts (Figure 2B). Although IgG binding to higher molecular weight cross-linked forms was lowered as it was to DTT-treated extracts, the reduction in IgG binding was not as great in the roasted extracts. We observed an approximate 50% reduction in binding to the extracts of roasted nuts after the IgG signal was normalized to the roasted nut control extract (Figure 2C). Notably, in each of our experiments, binding to the large subunit of Ana o 3 was markedly lowered in sodium sulfite-treated samples compared to control treated extracts.

Reducing agents have been shown to disrupt the structure of 2S albumins, including Ara h 2, Ber e 1, and Ana o 3, increasing their sensitivity to digestive proteases.[16,23,25] We compared the structure of purified Ana o 3 after treatment with water, DTT, or sodium sulfite using far-UV CD (Figure 3). The DTT-

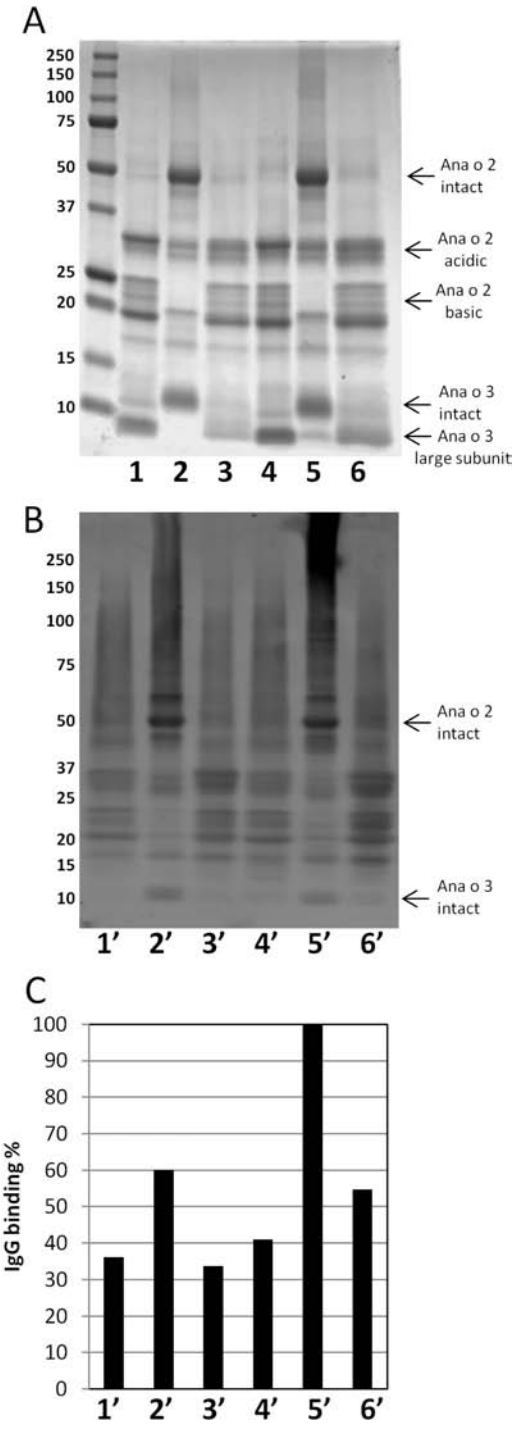

Figure 2. Sodium sulfite alters roasted cashew extract migration and lowers antibody binding. Raw or roasted cashew nut extract (125 μg), subjected to treatment with 5 mM DTT, buffer control, or 50 mM sodium sulfite at 100 °C, was analyzed by nonreducing SDS-PAGE (A) and rabbit anti-cashew antibodies (B). Lanes: (1, 1′) raw extract with 5 mM DTT; (2, 2′) raw extract buffer control; (3, 3′) raw extract 50 mM sodium sulfite; (4, 4′) roasted extract with 5 mM DTT; (5, 5′) roasted extract buffer control; (6, 6′) roasted extract 50 mM sodium sulfite. Rabbit IgG binding was visualized with IRdye-680-labeled anti-rabbit IgG secondary antibody (C). Quantification of rabbit anti-cashew IgG antibody binding in each respective lane is indicated in panel C, and molecular weight indicators are indicated on the side of each gel or immunoblot.

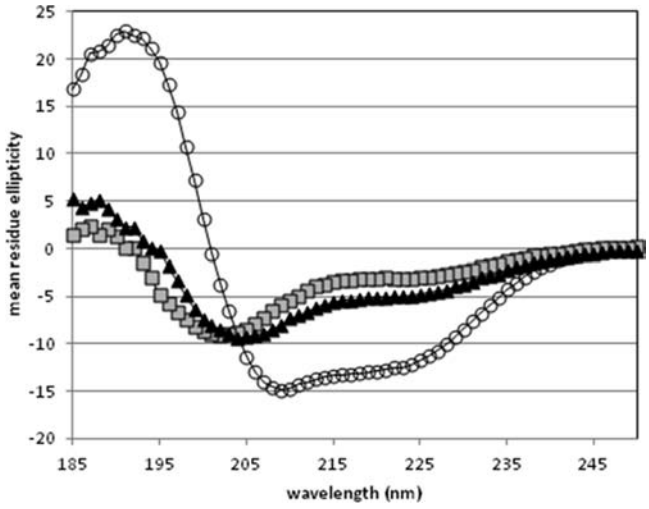

Figure 3. Ana o 3 protein structure is disrupted by sodium sulfite. Purified Ana o 3 was analyzed by circular dichroism from 185 to 250 nm in native form or after treatment with either DTT or sodium sulfite. Open circles represent native Ana o 3 after mock treatment at 65 °C, gray squares represent Ana o 3 after treatment with 5 mM DTT at 65 °C, and black triangles represent Ana o 3 after sodium sulfite treatment (50 mM) at 65 °C.

treated sample had an estimated 4% and the sodium sulfite-treated protein, 7%, α-helical content. The β-sheet content of the protein was also lowered slightly to 12% for DTT-treated and to 13% for sodium sulfite-treated extracts. Thus, sodium sulfite disrupts Ana o 3 structure to an extent similar to treatment of the protein with the reducing agent DTT.

Sodium sulfite is expected to attack the disulfide bond containing cysteine residues within the cashew allergens Ana o 2 and Ana o 3. To confirm that these bonds were targets of sodium sulfite, we digested treated extracts and analyzed the peptide mixture by mass spectrometry to find evidence of sulfite-modified cysteine-containing peptides. Indeed, tryptic peptide masses consistent with modification of Cys76 or Cys77 and Cys 89 in Ana o 3 were observed (Table 1). Peptides containing the expected modified cysteines were detected with an 80 Da shift, corresponding to the addition of sulfite ion (SO_3). These cysteine residues are expected to be part of the disulfide bond network important for Ana o 3 structure and stability. Importantly, the Cys76 and Cys77 residues in Ana o 3 lie within a previously mapped dominant IgE epitope.[14] We were unable to obtain confirmation of the precise location of the modified residue(s) within peptides because of the facile loss of the SO_3 modification prior to or during peptide fragmentation. A similar difficulty has been observed in attempts to specifically identify modified residues in insulin and BSA modified by sodium sulfite.[45] We also observed evidence of a SO_3 modification within several Ana o 2 cysteine-containing peptides (Table 1). The Cys25 and Cys101 SO_3 modified residues lie within or near previously mapped IgE epitopes that strongly react with Ana o 2.[13] Our mass spectrometry analysis further indicated that sodium sulfite disrupted cysteine disulfide bonds within Ana o 3 in cashew extracts.

It is evident from the analysis that sodium sulfite treatment can alter the structure of some cashew allergens, as well as the ability of rabbit IgG antibodies to bind these allergens. To determine if sodium sulfite treatment alters IgE binding to cashew allergens, we performed several IgE binding assays.

dx.doi.org/10.1021/jf501117p | J. Agric. Food Chem. 2014, 62, 6746−6755

Table 1. Potential Sites of Sulfite-Modified Cysteine Residues in Cashew Allergens Ana o 2 and Ana o 3

protein	Cys residue	peptide	m/z obs (Da)	z	MH^+ (Da)	calcd MH^+ (Da)	Δ mass (Da)
Ana o 2	25	(R)QEWQQQDECQIDRLDALEPDNRVEYEAGTVEAWDPNHEQFR(C)	1014.237	5	5067.1557	4987.225	79.9307
Ana o 2	58	(R)CAGVALVR(H)	434.7047	2	868.4016	788.445	79.9566
Ana o 2	101	(R) HTIQPNGLLLPQYSNAPQLIYVVQGEGMTGISYPGCPETYQAPQQGR(Q)	1039.708	5	5194.5102	5114.514	79.9962
Ana o 2	146	(R)FRRGDIIAIPAGVAHWCYNEGNSPVVTVTLLDVSNSQNQLDRTPR(K)	1012.709	5	5059.5147	4979.534	79.9807
Ana o 3	76, 77	(R)ECCQELQEVDR(R)	716.2723	2	1431.5368	1351.562	79.9748
Ana o 3	89	(R)CQNLEQMVR(Q)	600.7483	2	1200.4888	1120.524	79.9648

Figure 4 shows Western blot binding of IgE from a pool of six cashew-allergic patients' sera to sodium sulfite treated cashew extracts. Overall IgE binding to cashew proteins was lowered in both the DTT- and sodium sulfite-treated samples compared to the mock treated control. Quantification of the IgE signal indicated that binding to sodium sulfite- and DTT-treated extracts was lowered by 80−90% compared to mock treated extracts (Figure 4). In particular, reduction of Ana o 2 and Ana o 3 disulfide bonds with either DTT or sodium sulfite clearly lowered binding to both of these allergens. IgE binding to both of the faster migrating dissociated Ana o 2 subunits and the large subunit of Ana o 3 was markedly lowered (Figure 4).

Individual variation in IgE binding to nut allergens by allergy patients is well documented. We continued the IgE binding analysis by comparing IgE binding of individual cashew allergic sera to treated cashew extracts using dot-blots. Aliquots of treated or untreated cashew extract were spotted onto a PVDF membrane, allowed to dry, and extensively washed. We evaluated IgE binding to the bound material using six individual cashew-allergic patients' sera, and in every case IgE binding to the sodium sulfite-treated extract was lowered compared to the untreated control (Figure 5). When samples were incubated at 65 °C in the presence of sodium sulfite or DTT, the IgE signal was lowered to approximately half of the control sample with most of the sera samples we tested. Five of the six sodium sulfite-treated samples had IgE binding values ranging from 50 to 58% of the untreated control. The remaining sample was lowered to only 67% of the untreated control. IgE binding to the DTT-treated samples was also lowered to an extent equivalent to or greater than that of the sodium sulfite treatment for each of the sera. The DTT-treated samples had IgE binding values ranging from 16 to 53% of the untreated control. When extracts were incubated at 100 °C, the results were more dramatic. In both the sodium sulfite- and DTT-treated extracts, IgE binding was lowered to ≤10% of control treated extracts in five of six serum samples. In the remaining sample, IgE binding was lowered to 10% for sodium sulfite treatment and 16% for DTT. Our analysis of the cashew-allergic patients' serum samples indicated that treatment of cashew extracts with sodium sulfite could effectively lower IgE binding to cashew allergens.

To confirm these findings, IgE binding to the control and sodium sulfite-treated extracts was evaluated using competitive ELISA with the pooled cashew-allergic patients' sera. For these experiments, unreacted DTT or sodium sulfite was removed from extracts treated at 65 or 100 °C with centrifugation and buffer exchange over a course of 3 h using a 3 kDa cutoff spin filter to lower the remaining concentration to <0.01 mM following treatment. Representative plots from this analysis are shown in Figure 6, and both the DTT and sodium sulfite-treated extracts did not compete as well as control treated extract for IgE binding. Whereas the effect was more pronounced with DTT, sodium sulfite-treated extracts were a weaker competitor for IgE binding compared to untreated control extracts (Figure 6). Again, the reduction in IgE binding was greater when extracts were heated at 100 °C. Even at the highest protein concentration used, the sodium sulfite or DTT 100 °C treated extracts could not inhibit 50% of the IgE binding. These findings are consistent with the reduction of IgE binding we observed in the Western blot analysis (Figure 4).

DISCUSSION

Generation of hypoallergenic nuts via breeding, genetic engineering, or processing steps would provide a much-needed solution for those suffering from severe nut allergies. In addition, hypoallergenic nuts may be useful as immunotherapy reagents. Several studies have characterized the stability and allergenicity of cashew and other nut allergens to chemical, physical, mechanical, and enzymatic processing methods.[17,21,22,42,46−48] 2S albumins are common nut allergens, dependent upon cysteine disulfide bonds for their structure, and laboratory reducing agents have been used to decrease their potency as allergens. We hypothesized that there may be milder reducing agents that could have the same effect on these nut allergens. Our results with the GRAS compound sodium sulfite support our hypothesis. We observed clear changes in the migration pattern of redox-sensitive cashew allergens such as Ana o 2 and Ana o 3 following treatment of cashew extracts with sodium sulfite at elevated temperatures. This simple procedure was able to disrupt allergen structure and markedly lower in vitro IgE binding to cashew allergens in extracts.

The use of sulfating agents such as sodium sulfite could act at multiple levels to lower IgE binding to allergens. First, they target disulfide bonds and can destroy conformational IgE epitopes that require those bonds, thereby reducing IgE binding. This is supported by our SDS-PAGE and CD data showing that Ana o 2 and Ana o 3 structures were altered. Consistent with our results, experiments with purified peanut allergens Ara h 2 and Ara h 6 comparing reduced and native forms have demonstrated that conformational epitopes are of great significance for IgE binding to these 2S albumins.[46] Similar findings have been observed with soy protein,[49] and treatment of soy glycinin with sodium bisulfite has been shown to dissociate the acidic and basic subunits.[50,51] Second, sulfating agents covalently attach a large negatively charged sulfite ion to cysteine residues they have attacked,[37,45] and this charge is likely to repel IgE from linear epitopes harboring those residues, thereby reducing IgE binding. The decrease in IgE binding we observed in both immunoblot and ELISA assays supports our conclusion that both structural and linear epitopes are likely affected. Third, although not tested here, a sulfite attack of disulfide bonds and a loss of allergen structural integrity could lead to increased protease sensitivity in the stomach and a reduction in the amount of the protein available

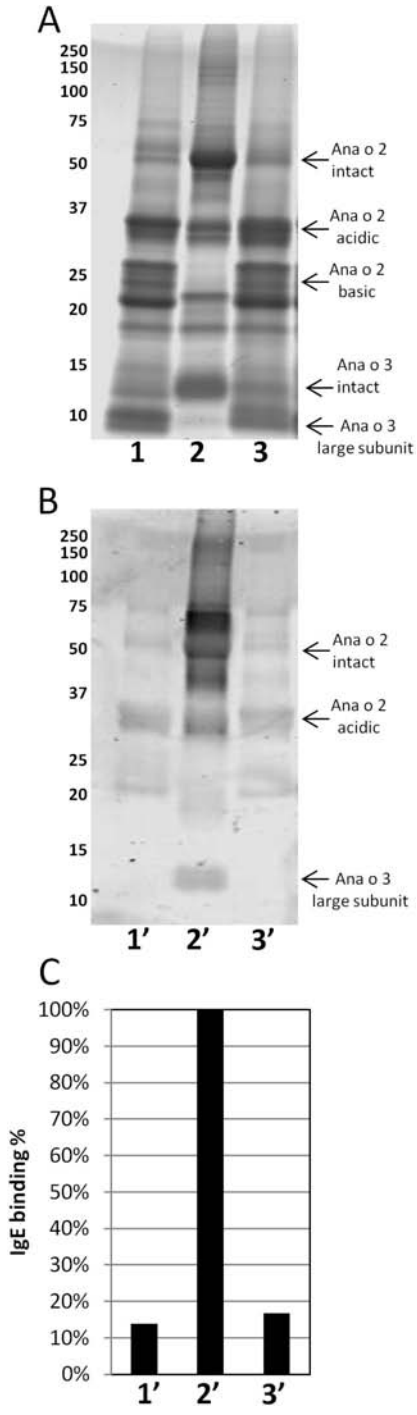

Figure 4. IgE binding to cashew extract is lowered following sodium sulfite treatment. Cashew extract (125 μg) was subjected to treatment with 5 mM DTT, buffer control, or 50 mM sodium sulfite at 100 °C and evaluated by SDS-PAGE (A) and IgE binding by Western blot (B). Lanes: (1, 1′) 5 mM DTT; (2, 2′) buffer control; (3, 3′) 50 mM sodium sulfite. Serum samples from a pool of six cashew-allergic patients were combined, diluted 1:10, and analyzed for IgE binding in control or sodium sulfite- or DTT-treated cashew extracts. IgE binding was visualized with IRdye-680-labeled streptavidin after incubation with biotinylated anti-human IgE secondary antibody. Quantification of IgE binding is shown in panel C, and molecular weight indicators are indicated.

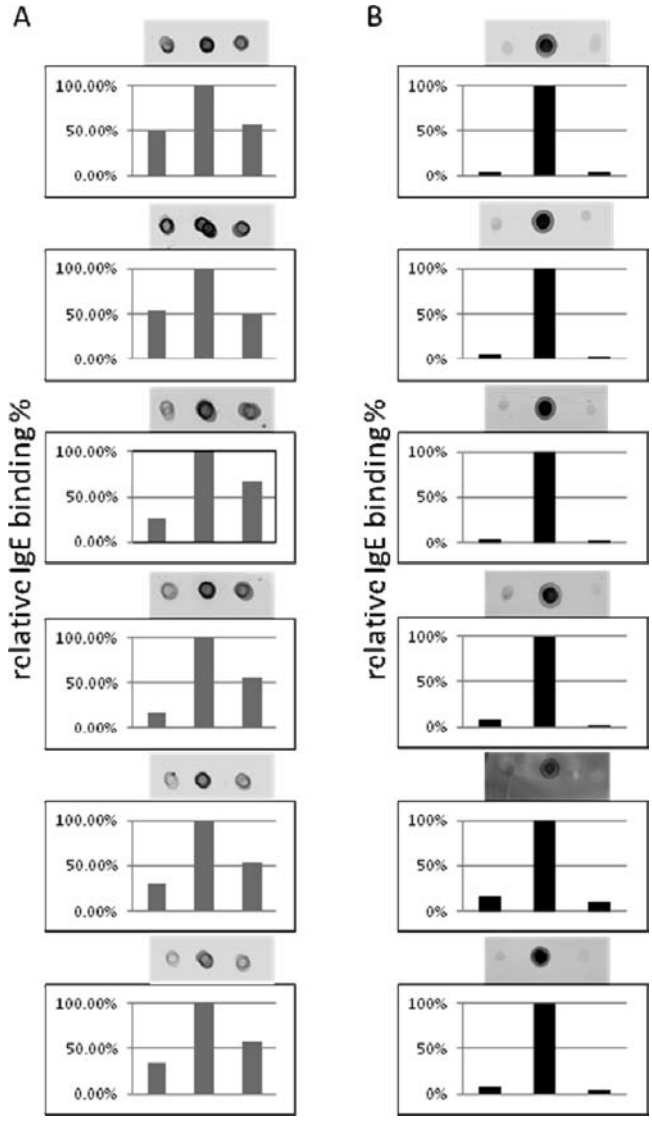

Figure 5. IgE binding to cashew extract is lowered following sodium sulfite treatment. Cashew extract (125 μg) was subjected to treatment with 50 mM sodium sulfite or 5 mM DTT at 65 °C (A) or 100 °C (B) and evaluated for IgE binding by dot-blot. For each panel the left column represents DTT treatment, the middle column the control, and the right column sodium sulfite treatment. Serum samples from individual cashew-allergic patients were diluted 1:5, and IgE binding was visualized with IRdye-680-labeled streptavidin after incubation with biotinylated anti-human IgE secondary antibody. Relative IRdye-680 units are indicated on the *y*-axis, and quantification of IgE binding is shown in the accompanying immunoblot.

for allergic response. Proteolyzed cashew extracts exhibit less IgE binding in vitro and a lowered allergenic response in mice.[16,47] Furthermore, proteolysis of sorghum protein can be increased by treatment with reducing agents including sodium sulfite compounds.[52,53] Finally, sulfite has been used to prevent browning, promote expenditure of reducing sugars and lysine in a reaction model, and act as an inhibitor of the Maillard reaction.[26,54] Studies have shown that Maillard reaction products can influence IgE binding to food allergens.[38−44] Our SDS-PAGE and immunoblot results also demonstrated that the addition of sodium sulfite to cashew nut extracts lowered the appearance of high molecular weight protein aggregates that are associated with Maillard reaction products in heated nut extracts.[43,48,55,56]

dx.doi.org/10.1021/jf501117p | J. Agric. Food Chem. 2014, 62, 6746−6755

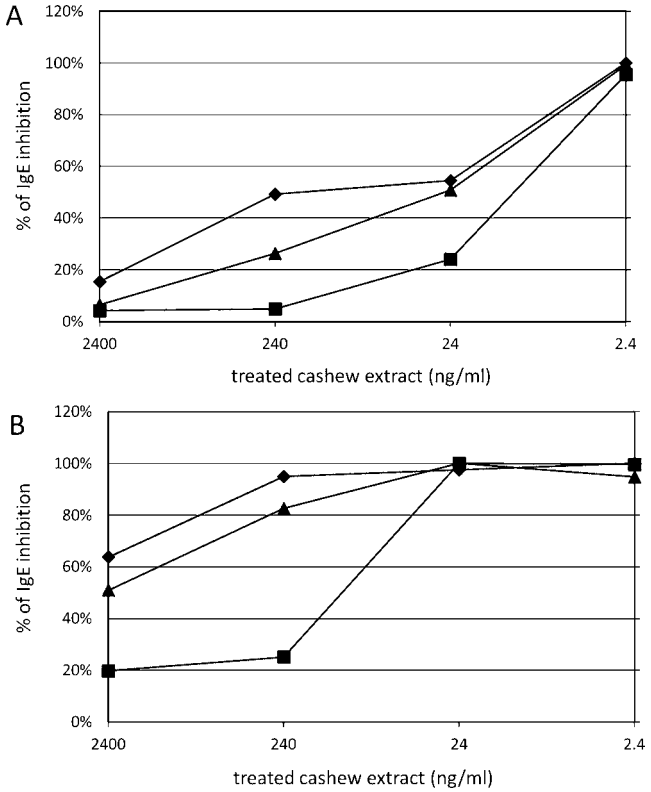

Figure 6. Sodium sulfite-treated cashew extract lowered IgE binding. Cashew extracts (squares) or cashew extracts pretreated with DTT (diamonds) or sodium sulfite (triangles) were evaluated for IgE binding in a competitive ELISA after incubation at 65 °C (A) or 100 °C (B). Cashew extract samples were serially diluted 10-fold, and IgE binding was evaluated in microtiter plates coated with 1 μg of cashew extract. Serum samples from a pool of six cashew-allergic patients were combined, diluted 1:4, and analyzed for IgE binding to sodium sulfite- or DTT-treated cashew extracts. Cashew extract concentration is indicated on the *x*-axis, and relative IgE binding in IRdye-680 units is indicated on the *y*-axis.

Our findings indicate that treatment of cashew extracts with sodium sulfite can be used to disrupt Ana o 3 structure and lower IgE binding. However, reductions in IgE binding do not always correlate with lowered basophil activation.[57] Basophil degranulation capacity has been shown to reside primarily with the 2S albumins of peanuts.[58−62] Several factors are likely to influence basophil degranulation by nut allergens, but if the same phenomenon is observed with cashew nut extracts, it would be expected that Ana o 3 may be the primary elicitor of basophil degranulation among cashew nut allergens. Further research that tests sulfite-treated cashew extracts in basophil activation assays or a mouse food allergy model or uses skin prick tests is necessary to determine the safety and efficacy of this method in attenuating cashew allergenicity.

Current FDA regulations require labeling at ≥10 ppm (10 mg/L) when sulfites are used in food processing. The current study used sodium sulfite at 50 mM or 6.302 g/L (6313 ppm) in the treatment step, which exceeds the labeling requirement. However, sulfite that has been incorporated into the nut proteins may no longer be biologically active, and any residual sulfite may be removed with additional steps. There are likely safe methods for removing or consuming residual sulfite or combining physical or mechanical steps with titrated amounts of sulfite during treatment. It may be that removal of excess sulfite in solution is easier using whole nuts compared to nut extracts, and sulfite absorbed into the nut may be expended if the treatment is performed early in the nut-processing procedure. Sulfite ions that have reacted with proteins, carbohydrates, or lipid components in foods may not be biologically active or accessible to cause allergy. The reversible nature and reactivity of sulfite adducts have been debated, and the current study did not address the long-term consequences to cashew allergen structure and IgE binding following removal of sulfite after treatment. We tested other sodium sulfite compounds and found that the addition of sodium bisulfite, sodium metabisulfite, or potassium sulfite also resulted in a similarly altered SDS-PAGE migration pattern of cashew proteins consistent with that observed with DTT. Further studies are necessary to extend these findings to whole nuts, as well as to determine the effects sulfite has on the sensory and quality characteristics of nuts.

AUTHOR INFORMATION

Corresponding Author

*(C.P.M.) Mail: Southern Regional Research Center, Agricultural Research Service, U.S. Department of Agriculture, 1100 Robert E. Lee Blvd., New Orleans, LA 70124, USA. Phone: (504) 286-4392. Fax: (504) 286-4419. E-mail: chris.mattison@ars.usda.gov.

Funding

This research was supported by funds from the U.S. Department of Agriculture−Agricultural Research Service and the Allergy/Immunology Research Center of North Texas. Mention of trade names, commercial products, or companies in this paper is solely for the purpose of providing specific information and does not imply recommendation or endorsement by the U.S. Department of Agriculture.

Notes

The authors declare no competing financial interest.

ACKNOWLEDGMENTS

We thank Si-Yin Chung, Jack Davis, Nathalie Plundrich, Tim Sanders, and Yvette Bren-Mattison for helpful discussion and critical evaluation of the material presented.

REFERENCES

(1) Gupta, R. S.; Springston, E. E.; Warrier, M. R.; Smith, B.; Kumar, R.; Pongracic, J.; Holl, J. L. The prevalence, severity, and distribution of childhood food allergy in the United States. *Pediatrics* **2011**, *128*, e9−e17.

(2) Sicherer, S. H.; Munoz-Furlong, A.; Godbold, J. H.; Sampson, H. A. US prevalence of self-reported peanut, tree nut, and sesame allergy: 11-year follow-up. *J. Allergy Clin. Immunol.* **2010**, *125*, 1322−1326.

(3) Herbert, L. J.; Dahlquist, L. M.; Bollinger, M. E. Maternal intolerance of uncertainty, anxiety, and adherence with food challenge referrals. *J. Health Psychol.* **2013**, *18*, 1209−1219.

(4) Herbert, L. J.; Dahlquist, L. M. Perceived history of anaphylaxis and parental overprotection, autonomy, anxiety, and depression in food allergic young adults. *J. Clin. Psychol. Med. Settings* **2008**, *15*, 261−269.

(5) Bollinger, M. E.; Dahlquist, L. M.; Mudd, K.; Sonntag, C.; Dillinger, L.; McKenna, K. The impact of food allergy on the daily activities of children and their families. *Ann. Allergy Asthma Immunol.* **2006**, *96*, 415−421.

(6) Gupta, R.; Holdford, D.; Bilaver, L.; Dyer, A.; Holl, J. L.; Meltzer, D. The economic impact of childhood food allergy in the United States. *JAMA Pediatr.* **2013**, *167*, 1026−1031.

(7) Fleischer, D. M. The natural history of peanut and tree nut allergy. *Curr. Allergy Asthma Rep.* **2007**, *7*, 175−181.
(8) Davoren, M.; Peake, J. Cashew nut allergy is associated with a high risk of anaphylaxis. *Arch. Dis. Child.* **2005**, *90*, 1084−1085.
(9) Clark, A. T.; Anagnostou, K.; Ewan, P. W. Cashew nut causes more severe reactions than peanut: case-matched comparison in 141 children. *Allergy* **2007**, *62*, 913−916.
(10) Radauer, C.; Breiteneder, H. Evolutionary biology of plant food allergens. *J. Allergy Clin. Immunol.* **2007**, *120*, 518−525.
(11) Moreno, F. J.; Clemente, A. 2S albumin storage proteins: what makes them food allergens? *Open Biochem. J.* **2008**, *2*, 16−28.
(12) Wang, F.; Robotham, J. M.; Teuber, S. S.; Tawde, P.; Sathe, S. K.; Roux, K. H. Ana o 1, a cashew (*Anacardium occidental*) allergen of the vicilin seed storage protein family. *J. Allergy Clin. Immunol.* **2002**, *110*, 160−166.
(13) Wang, F.; Robotham, J. M.; Teuber, S. S.; Sathe, S. K.; Roux, K. H. Ana o 2, a major cashew (*Anacardium occidentale* L.) nut allergen of the legumin family. *Int. Arch. Allergy Immunol.* **2003**, *132*, 27−39.
(14) Robotham, J. M.; Wang, F.; Seamon, V.; Teuber, S. S.; Sathe, S. K.; Sampson, H. A.; Beyer, K.; Seavy, M.; Roux, K. H. Ana o 3, an important cashew nut (*Anacardium occidentale* L.) allergen of the 2S albumin family. *J. Allergy Clin. Immunol.* **2005**, *115*, 1284−1290.
(15) Sathe, S. K.; Sze-Tao, K. W. C.; Wolf, W. J.; Hamaker, B. R. Biochemical characterization and in vitro digestibility of the major globulin in cashew nut (*Anacardium occidentale*). *J. Agric. Food Chem.* **1997**, *45*, 2854−2860.
(16) Mattison, C. P.; Grimm, C. C.; Wasserman, R. L. In vitro digestion of soluble cashew proteins and characterization of surviving IgE-reactive peptides. *Mol. Nutr. Food Res.* **2014**, *58*, 884−893.
(17) Venkatachalam, M.; Monaghan, E. K.; Kshirsagar, H. H.; Robotham, J. M.; O'Donnell, S. E.; Gerber, M. S.; Roux, K. H.; Sathe, S. K. Effects of processing on immunoreactivity of cashew nut (*Anacardium occidentale* L.) seed flour proteins. *J. Agric. Food Chem.* **2008**, *56*, 8998−9005.
(18) Su, M.; Venkatachalam, M.; Teuber, S. S.; Roux, K. H.; Sathe, S. K. Impact of γ-irradiation and thermal processing on the antigenicity of almond, cashew nut, and walnut proteins. *J. Sci. Food Agric.* **2004**, *84*, 1119−1125.
(19) Porterfield, H. S.; Murray, K. S.; Schlichting, D. G.; Chen, X.; Hansen, K. C.; Duncan, M. W.; Dreskin, S. C. Effector activity of peanut allergens: a critical role for Ara h 2, Ara h 6, and their variants. *Clin. Exp. Allergy* **2009**, *39*, 1099−1108.
(20) Shin, S.; Wong, J. H.; Kobrehel, K.; Buchanan, B. B. Reduction of castor-seed 2S albumin protein by thioredoxin. *Planta* **1993**, *189*, 557−560.
(21) Buchanan, B. B.; Adamidi, C.; Lozano, R. M.; Yee, B. C.; Momma, M.; Kobrehel, K.; Ermel, R.; Frick, O. L. Thioredoxin-linked mitigation of allergic responses to wheat. *Proc. Natl. Acad. Sci. U.S.A.* **1997**, *94*, 5372−5377.
(22) del Val, G.; Yee, B. C.; Lozano, R. M.; Buchanan, B. B.; Ermel, R. W.; Lee, Y. M.; Frick, O. L. Thioredoxin treatment increases digestibility and lowers allergenicity of milk. *J. Allergy Clin. Immunol.* **1999**, *103*, 690−697.
(23) Koppelman, S. J.; Nieuwenhuizen, W. F.; Gaspari, M.; Knippels, L. M.; Penninks, A. H.; Knol, E. F.; Hefle, S. L.; de Jongh, H. H. Reversible denaturation of Brazil nut 2S albumin (Ber e1) and implication of structural destabilization on digestion by pepsin. *J. Agric. Food Chem.* **2005**, *53*, 123−131.
(24) Hazebrouck, S.; Guillon, B.; Drumare, M. F.; Paty, E.; Wal, J. M.; Bernard, H. Trypsin resistance of the major peanut allergen Ara h 6 and allergenicity of the digestion products are abolished after selective disruption of disulfide bonds. *Mol. Nutr. Food Res.* **2012**, *56*, 548−557.
(25) Sen, M.; Kopper, R.; Pons, L.; Abraham, E. C.; Burks, A. W.; Bannon, G. A. Protein structure plays a critical role in peanut allergen stability and may determine immunodominant IgE-binding epitopes. *J. Immunol.* **2002**, *169*, 882−887.
(26) Taylor, S. L.; Higley, N. A.; Bush, R. K. Sulfites in foods: uses, analytical methods, residues, fate, exposure assessment, metabolism, toxicity, and hypersensitivity. *Adv. Food Res.* **1986**, *30*, 1−76.
(27) Oliphant, T.; Mitra, A.; Wilkinson, M. Contact allergy to sodium sulfite and its relationship to sodium metabisulfite. *Contact Dermatitis* **2012**, *66*, 128−130.
(28) Madan, V.; Walker, S. L.; Beck, M. H. Sodium metabisulfite allergy is common but is it relevant? *Contact Dermatitis* **2007**, *57*, 173−176.
(29) Malik, M. M.; Hegarty, M. A.; Bourke, J. F. Sodium metabisulfite − a marker for cosmetic allergy? *Contact Dermatitis* **2007**, *56*, 241−242.
(30) Boden, S. R.; Wesley Burks, A. Anaphylaxis: a history with emphasis on food allergy. *Immunol. Rev.* **2011**, *242*, 247−257.
(31) Chapman, J. A.; Bernstein, I. L.; Lee, R. E.; Oppenheimer, J.; Nicklas, R. S.; Portnoy, J. M.; Sicherer, S. H.; Schuller, D. E.; Spector, S. L.; Khan, D.; Lang, D.; Simon, R. A.; Tilles, S. A.; Blessing-Moore, J.; Wallace, D.; Teuber, S. S. Food allergy: a practice parameter. *Ann. Allergy Asthma Immunol.* **2006**, *96*, S1−S68.
(32) FDA. *Code Fed. Regul.* **2013**, *3*, 21CFR182.3798.
(33) Lester, M. R. Sulfite sensitivity: significance in human health. *J. Am. Coll. Nutr.* **1995**, *14*, 229−232.
(34) Roth, J. V.; Shields, A. A dilemma: how does one treat anaphylaxis in the sulfite allergic patient since epinephrine contains sodium metabisulfite? *Anesth. Analg.* **2004**, *98*, 1499 (author reply p 1500)..
(35) Vally, H.; Misso, N. L.; Madan, V. Clinical effects of sulphite additives. *Clin. Exp. Allergy* **2009**, *39*, 1643−1651.
(36) Cecil, R.; Wake, R. G. The reactions of inter- and intra-chain disulphide bonds in proteins with sulphite. *Biochem. J.* **1962**, *82*, 401−406.
(37) Crankshaw, M. W.; Grant, G. A. Modification of cysteine. *Curr. Protoc. Protein Sci.* **2001**, *Chapter 15*, Unit15 1.
(38) Nowak-Wegrzyn, A.; Fiocchi, A. Rare, medium, or well done? The effect of heating and food matrix on food protein allergenicity. *Curr. Opin. Allergy Clin. Immunol.* **2009**, *9*, 234−237.
(39) Mills, E. N.; Sancho, A. I.; Rigby, N. M.; Jenkins, J. A.; Mackie, A. R. Impact of food processing on the structural and allergenic properties of food allergens. *Mol. Nutr. Food Res.* **2009**, *53*, 963−969.
(40) Vissers, Y. M.; Blanc, F.; Skov, P. S.; Johnson, P. E.; Rigby, N. M.; Przybylski-Nicaise, L.; Bernard, H.; Wal, J. M.; Ballmer-Weber, B.; Zuidmeer-Jongejan, L.; Szepfalusi, Z.; Ruinemans-Koerts, J.; Jansen, A. P.; Savelkoul, H. F.; Wichers, H. J.; Mackie, A. R.; Mills, C. E.; Adel-Patient, K. Effect of heating and glycation on the allergenicity of 2S albumins (Ara h 2/6) from peanut. *PLoS One* **2011**, *6*, No. e23998.
(41) Vissers, Y. M.; Iwan, M.; Adel-Patient, K.; Stahl Skov, P.; Rigby, N. M.; Johnson, P. E.; Mandrup Muller, P.; Przybylski-Nicaise, L.; Schaap, M.; Ruinemans-Koerts, J.; Jansen, A. P.; Mills, E. N.; Savelkoul, H. F.; Wichers, H. J. Effect of roasting on the allergenicity of major peanut allergens Ara h 1 and Ara h 2/6: the necessity of degranulation assays. *Clin. Exp. Allergy* **2011**, *41*, 1631−1642.
(42) Blanc, F.; Vissers, Y. M.; Adel-Patient, K.; Rigby, N. M.; Mackie, A. R.; Gunning, A. P.; Wellner, N. K.; Skov, P. S.; Przybylski-Nicaise, L.; Ballmer-Weber, B.; Zuidmeer-Jongejan, L.; Szepfalusi, Z.; Ruinemans-Koerts, J.; Jansen, A. P.; Bernard, H.; Wal, J. M.; Savelkoul, H. F.; Wichers, H. J.; Mills, E. N. Boiling peanut Ara h 1 results in the formation of aggregates with reduced allergenicity. *Mol. Nutr. Food Res.* **2011**, *55*, 1887−1894.
(43) Maleki, S. J.; Chung, S. Y.; Champagne, E. T.; Raufman, J. P. The effects of roasting on the allergenic properties of peanut proteins. *J. Allergy Clin. Immunol.* **2000**, *106*, 763−768.
(44) Chung, S. Y.; Butts, C. L.; Maleki, S. J.; Champagne, E. T. Linking peanut allergenicity to the processes of maturation, curing, and roasting. *J. Agric. Food Chem.* **2003**, *51*, 4273−4277.
(45) Raftery, M. J. Selective detection of thiosulfate-containing peptides using tandem mass spectrometry. *Rapid Commun. Mass Spectrom.* **2005**, *19*, 674−682.
(46) Apostolovic, D.; Luykx, D.; Warmenhoven, H.; Verbart, D.; Stanic-Vucinic, D.; de Jong, G. A.; Velickovic, T. C.; Koppelman, S. J.

Reduction and alkylation of peanut allergen isoforms Ara h 2 and Ara h 6; characterization of intermediate- and end products. *Biochim. Biophys. Acta* **2013**, *1834*, 2832−2842.
(47) Kulis, M.; Macqueen, I.; Li, Y.; Guo, R.; Zhong, X. P.; Burks, A. W. Pepsinized cashew proteins are hypoallergenic and immunogenic and provide effective immunotherapy in mice with cashew allergy. *J. Allergy Clin. Immunol.* **2012**, *130*, 716−723.
(48) Chung, S. Y.; Maleki, S. J.; Champagne, E. T. Allergenic properties of roasted peanut allergens may be reduced by peroxidase. *J. Agric. Food Chem.* **2004**, *52*, 4541−4545.
(49) Petruccelli, S.; Anon, M. C. Partial reduction of soy protein isolate disulfide bonds. *J. Agric. Food Chem.* **1995**, *43*, 2001−2006.
(50) Zhang, L.; Sun, X. S. Effect of sodium bisulfite on properties of soybean glycinin. *J. Agric. Food Chem.* **2008**, *56*, 11192−11197.
(51) Kella, N. K.; Kang, Y. J.; Kinsella, J. E. Effect of oxidative sulfitolysis of disulfide bonds of bovine serum albumin on its structural properties: a physiochemical study. *J. Protein Chem.* **1988**, *7*, 535−548.
(52) Elkhalifa, A. E. O.; Chandrashekar, A.; Mohamed, B. E.; El Tinay, A. H. Effect of reducing agents on the in vitro protein and starch digestibilities of cooked sorghum. *Food Chem.* **1999**, *66*, 323−326.
(53) Hamaker, B. R.; Kirleis, A. W.; Butler, L. G.; Axtell, J. D.; Mertz, E. T. Improving the in vitro protein digestibility of sorghum with reducing agents. *Proc. Natl. Acad. Sci. U.S.A.* **1987**, *84*, 626−628.
(54) Xu, X. B.; Ma, F.; Yu, S. J.; Guan, Y. G. Simultaneous analysis of N^{ε}-(carboxymethyl)lysine, reducing sugars, and lysine during the dairy thermal process. *J. Dairy Sci.* **2013**, *96*, 5487−5493.
(55) Su, G.; Cui, C.; Ren, J.; Yang, B.; Zhao, M. Effect of xylose on the molecular and particle size distribution of peanut hydrolysate in Maillard reaction system. *J. Sci. Food Agric.* **2011**, *91*, 2457−2462.
(56) Chung, S. Y.; Champagne, E. T. Association of end-product adducts with increased IgE binding of roasted peanuts. *J. Agric. Food Chem.* **2001**, *49*, 3911−3916.
(57) Shi, X.; Guo, R.; White, B. L.; Yancey, A.; Sanders, T. H.; Davis, J. P.; Burks, A. W.; Kulis, M. Allergenic properties of enzymatically hydrolyzed peanut flour extracts. *Int. Arch. Allergy Immunol.* **2013**, *162*, 123−130.
(58) Koid, A. E.; Chapman, M. D.; Hamilton, R. G.; Van Ree, R.; Versteeg, S. A.; Dreskin, S. C.; Koppelman, S. J.; Wuenschmann, S. Ara h 6 complements Ara h 2 as an important marker for IgE reactivity to peanut. *J. Agric. Food Chem.* **2013**, *62*, 206−213.
(59) Zhuang, Y.; Dreskin, S. C. Redefining the major peanut allergens. *Immunol. Res.* **2013**, *55*, 125−134.
(60) Chen, X.; Wang, Q.; El-Mezayen, R.; Zhuang, Y.; Dreskin, S. C. Ara h 2 and Ara h 6 have similar allergenic activity and are substantially redundant. *Int. Arch. Allergy Immunol.* **2013**, *160*, 251−258.
(61) Zhuang, Y.; Durrani, S.; Hodges, B. D.; Dreskin, S. C.; Chen, X. Expression of recombinant Ara h 6 in *Pichia pastoris* but not in *Escherichia coli* preserves allergic effector function and allows assessment of specific mutations. *Mol. Nutr. Food Res.* **2012**, *56*, 986−995.
(62) Chen, X.; Zhuang, Y.; Wang, Q.; Moutsoglou, D.; Ruiz, G.; Yen, S. E.; Dreskin, S. C. Analysis of the effector activity of Ara h 2 and Ara h 6 by selective depletion from a crude peanut extract. *J. Immunol. Methods* **2011**, *372*, 65−70.

surface display, bacterial spore surface display systems have been widely used for their resistance to heat, radiation, and chemicals in a harsh environment.[21] Moreover, *Bacillus subtilis* is classified as generally recognized as safe (GRAS) by the U.S. Food and Drug Administration, and its genetic information, spore structure, and mature genetic manipulation techniques are established, thus making it an excellent strain for a food-grade surface display system.[22−24]

In the present study, a surface display system was constructed based on *B. subtilis* 168 for the production of D-tagatose using CotX as an anchoring protein. After active L-AI was successfully observed on the spore surface of *B. subtilis* 168 and a higher efficiency to catalyze D-galactose to produce D-tagatose was exhibited, the potential of using a food-grade expression system to produce D-tagatose was confirmed. To the best of our knowledge, this is the first report for D-tagatose production using anchored L-AI on the spore surface of *B. subtilis* 168.

MATERIALS AND METHODS

Chemicals. D-Tagatose (≥99% purity) and D-galactose (≥98% purity) were purchased from Aladdin Industry Co., Ltd. (Shanghai, China). Ex-Taq DNA polymerase, restriction enzymes, T4 DNA ligase, ampicillin, and erythromycin were supplied by Takara Biotechnology Co., Ltd. (Dalian, China). Trypsin and proteinase K were purchased from Sigma. All other chemicals were analytical grade.

Plasmid and Strain Construction. To display L-AI on the surface of *B. subtilis* 168 spores, we constructed a genetic fusion: *cotX-araA*. The DNA fragment with the *cotX* (GenBank Accession No. NP_389058) promoter and structure gene from the genome of *B. subtilis* 168 was amplified by primers P1 and P2 (Table 1), digested with *Xba* I and *Kpn*I, and ligated into pJS700a cloning vector to generate the plasmid pJS700a-*cotX*.[25] The *araA* gene (GenBank Accession No. HM150718) was amplified from the genome of *L. fermentum* CGMCC2921 using primers P3 and P4 (Table 1), digested with *Kpn*I and *EcoR* I, and cloned into the same restriction endonuclease sites of plasmid pJS700a-*cotX* to obtain the plasmid pJS700a-*cotX-araA*.

Table 1. Oligonucleotides Used In This Study

oligonucleotides (forward, 5′ to 3′)	name
GCTCTAGATTACTTTGTCTGCCGACGAGA (*Xba* I underlined)	P1
CCGGTACCGAGGACAAGAGTGATAACTAGGATG (*Kpn*I underlined)	P2
AGAGGTACCATGCGTAAGATGCAAGATTAC (*Kpn*I underlined)	P3
CCGGAATTCCTACTTGATGTTGATAAAGT (*EcoR* I underlined)	P4

The competent cells of *B. subtilis* 168 were prepared as previously described.[26] The cells transformed by chemical transformation methods were cultured in 3 mL of Luria−Bertani (LB) medium at 37 °C and spread onto LB plates containing 4 μg/mL of erythromycin (Em). Plates were incubated at 37 °C overnight, and Em-resistant (Em^r) clones were selected and identified using the amylase activity assay.[27] To verify the amylase activity of colonies, we stained the colonies cultivated on LB plates containing 0.1% starch with iodine potassium iodide solution.

Culture Conditions of the Bacterial Strains and the Purification of Spores. For the formation of spores, *B. subtilis* 168 was cultivated in Difco-sporulation media (DSM) as described elsewhere.[28] After cultivation in DSM at 37 °C for 24 h, the spores and sporangial cells of *B. subtilis* 168 with recombinant plasmids were harvested by centrifugation and resuspended in 0.1 M sodium phosphate buffer (pH 6.5). The suspension was treated with 0.5% lysozyme for 1 h and then centrifuged at 5000 rpm (4470*g*) for 15 min. After the sediments were washed with 1 M NaCl, 1 M KCl, and phosphate buffer, the washed spores were obtained and resuspended in phosphate buffer at 4 °C without the addition of phenylmethylsulfonyl fluoride (PMSF).[16] The *E. coli* DH5α strain, used for the plasmid amplification for nucleotide cloning and sequencing, was grown in LB medium at 37 °C.

Activity Assays of the Anchored L-AI. Activity of spore surface-displayed L-AI was determined at 70 °C, pH 6.5, in 1 mL of 36 g/L of D-galactose and the washed spore suspension. After a 30 min reaction, the system was transferred to ice to terminate the reaction.

The generated D-tagatose was first examined using the cysteine-carbazol-sulfuric acid method, and the absorbance was measured at 560 nm.[29] Then, both D-tagatose and D-galactose were analyzed by high-performance liquid chromatograph (HPLC), using a Rezex RCM-Monosaccharide Ca^{2+} column at 80 °C with distilled water as the mobile phase at an elution rate of 0.5 mL/min. The components were analyzed with a refractive index detector RI-101.[30] The HPLC and Rezex RCM-Monosaccharide Ca^{2+} column were purchased from Agilent (Wilmington, DE) and Phenomenex (Guangzhou, China).

The standard linear graph prepared with different D-tagatose concentrations was used to calibrate the generated D-tagatose concentration from the reaction. One unit of enzyme activity is defined as the amount of displayed L-AI required to catalyze the production of 1 μmol D-tagatose per min.[30] The number of spores was calculated by direct counting with a Burker chamber under an optical microscope.[16]

Examination for the Properties of the Anchored L-AI. To examine the properties of the anchored L-AI, 30 mL of reaction mixture in a 250 mL Erlenmeyer flask was used with variations as follows. The optimization of temperature and pH were conducted with 36 g/L of D-galactose and the washed spore suspension from 10 mL of spore fermentation broth (containing about 8.4×10^8 spores) for 30 min. The optimal temperature of the anchored L-AI was analyzed over the range of 55−90 °C. The effect of the pH on enzyme activity was determined using the standard assay conditions at 70 °C with sodium acetate (pH 4.0−6.0), phosphate (pH 6.0−8.0), and Tris-HCl (pH 8.0−9.0). In addition, the thermal stabilities of spore surface-displayed L-AI were determined by incubating the reaction mixtures at 70, 75, and 80 °C for 90 min at pH 6.5, and the residual activities were determined using the standard activity assays every 15 min.

Production of D-Tagatose Using the Anchored L-AI. The optimization of substrate concentration was conducted with D-galactose at 25, 50, 100, 150, and 200 g/L for 24 h using the washed spore suspension from 10 mL of spore fermentation broth. The optimal cell dosage was determined by using the washed spore suspension prepared from 5, 10, 20, 30, 40, 50, 60, and 70 mL of spore fermentation broth for 24 h. Sufficient shaking was performed each time before samples were obtained from the spore fermentation broth. Finally, 100 mL of reaction mixture (containing about 1.4×10^{10} spores) in a 500 mL Erlenmeyer flask was used to determine the reusability of the spore surface-displayed L-AI in the production of D-tagatose. The reusability experiments were conducted by recycling the anchored L-AI for several cycles. The concentrations of D-tagatose and D-galactose were measured by HPLC. After each biotransformation batch, the amount of spores was counted, and the activity of the anchored L-AI was assayed. Subsequently, reaction mixtures were centrifuged and the sediment was reused for another batch.

RESULTS

Gene Clone and Construction of Recombinant Plasmid. To construct the recombinant plasmid, the *cotX* gene of the outer coat protein CotX (18.6 kDa) and the *araA* gene from *L. fermentum* CGMCC2921 were amplified successfully. Then, the *cotX* and *araA* genes were ligated into pJS700a to construct the recombinant plasmid pJS700a-*cotX-araA* (Figure 1), which was verified by the digestion method. DNA sequencing results also demonstrated that a correct recombinant plasmid pJS700a-*cotX-araA* was obtained.

Transformation of the Plasmid pJS700a-*cotX-araA* and Activity Assays of the Anchored L-AI. The

dx.doi.org/10.1021/jf501937j | J. Agric. Food Chem. 2014, 62, 6756−6762

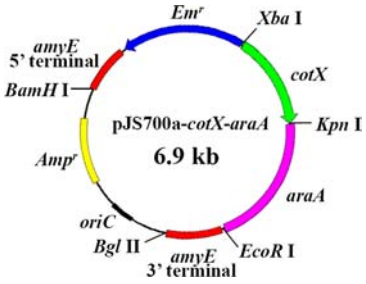

Figure 1. Construction of recombinant plasmid pJS700a-*cotX-araA*.

recombinant plasmid pJS700a-*cotX-araA* was transformed into *B. subtilis* 168, in which *cotX-araA* gene fusion was integrated into *B. subtilis*168 chromosome at *amyE* locus by double crossover events. As the integration of *cotX-araA* gene fusion at *amyE* locus disrupted the expression of amylase, colonies on starch-containing LB plate turned blue after staining by iodine potassium iodide solution, whereas *B. subtilis* 168 wild-type strain exhibited a distinctive yellow color due to the normal expression of amylase gene that resulted in hydrolysis of starch in the plate (Figure 2A).

A cotX-specific promoter was used in the surface display system to initiate expression of L-AI and sporulation of *B. subtilis* synchronously, whereas the outer coat protein CotX expressed at the coat of *B. subtilis* 168 was used as an anchoring motif for the display of L-AI. Assays of the surface-displayed L-AI revealed an activity value of 2.02×10^{-10} U/spore. The expression of L-AI on the external surface of *B. subtilis* 168 spores was verified by protease treatment. Purified spores of *B. subtilis* 168 (pJS700a-*cotX-araA*) were suspended in phosphate buffer containing 0.1% trypsin or 0.1% proteinase K for 1 h.[15] A control sample with the spores was also prepared in phosphate buffer without protease. As shown in Figure 2B, the activity of spores treated by protease was markedly lower than that of intact spores. This observation was due to the addition of protease to the outside environment of spores that cannot penetrate through the spore wall. This result indicated that the L-AI is located on the surface of spores.[31]

Properties of the Anchored L-AI. The optimal temperature and pH of the anchored L-AI were first examined in the present study. As shown in Figure 3, using D-galactose (36 g/L) as the substrate, the highest conversion efficiency of D-galactose was detected at 70 °C and pH 6.5. Enzyme stability is an important factor in the long-term commercial application of an enzymatic bioconversion.[32] In the temperature range of 65−80

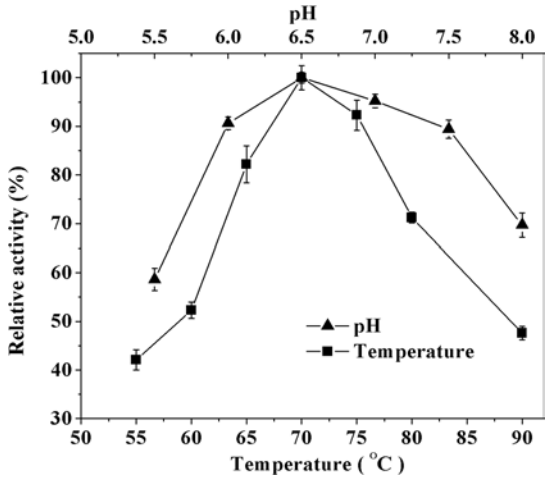

Figure 3. Effect of temperature (■) and pH (▲) on the displayed L-AI.

°C, the relative activity of the anchored L-AI remained >70% of the highest level, which suggested that the thermal stability was improved compared with the recombinant L-AI expressed in *E. coli*.[12] To verify this speculation, we examined the stability of the displayed L-AI treated at different temperatures. As shown in Figure 4, the activities of anchored L-AI incubated at 70 and

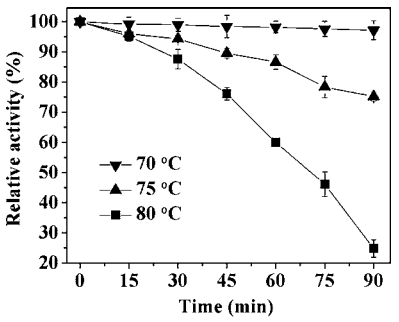

Figure 4. Thermostability of anchored L-AI incubated at (▼) 70 °C, (▲) 75 °C, and (■) 80 °C. The initial activity was defined as 100%.

75 °C for 30 min were not significantly decreased, and the relative activity even retained >75% of the highest level when incubated at 80 °C for 45 min. Moreover, within the pH range of 6.0−7.5, the relative activity of surface-displayed L-AI remained >90% of the highest level. These results indicated

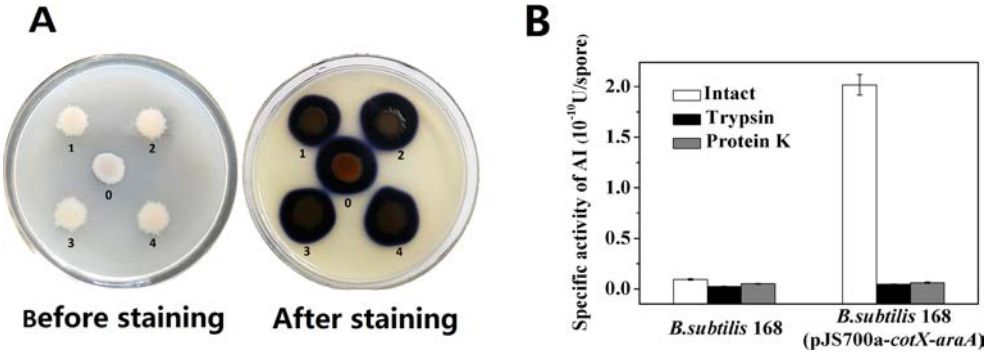

Figure 2. (A) Identification of recombinant strains by analysis of amylase activity. (0) *B. subtilis* 168 as a control; (1, 2, 3, and 4) recombinant strains with *amyE* disruption. (B) Activities of L-AI displayed on spore surface: (□) intact spores; (■) spores treated with 0.1% trypsin for 1 h; (gray bar) spores treated with 0.1% protein K for 1 h.

dx.doi.org/10.1021/jf501937j | J. Agric. Food Chem. 2014, 62, 6756−6762

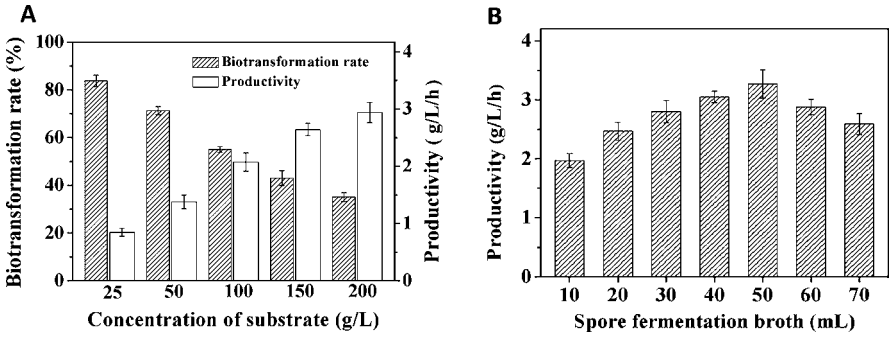

Figure 5. (A) Effect of the D-galactose concentration. (B) Effect of the recombinant spore dosage.

that the spore surface-displayed L-AI exhibited high biotransformation capability toward D-galactose over wide ranges of temperature and pH.

Biocatalytic Production of D-Tagatose Using the Anchored L-AI. To obtain the maximum D-tagatose yield and efficiently utilize the substrate at the same time, we studied the concentration of D-galactose in the efficient production of D-tagatose using the washed spore suspension from 10 mL of spore fermentation broth. As shown in Figure 5A, an increase in D-galactose concentrations resulted in a decrease in conversion rate and an increase in D-tagatose yield. Although the conversion rate was 84% at the reaction system with 25 g/L of D-galactose, the D-tagatose yield was 0.85 g/L/h. On the contrary, the D-tagatose yield was improved to 2.78 g/L/h at the reaction system with 200 g/L of D-galactose, but the conversion rate decreased markedly (35%), which may lead to the low production efficiency and the waste of raw materials. On the basis of the above analysis, 100 g/L of D-galactose, with which the conversion rate was 51% and the D-tagatose yield was 2.01 g/L/h at the reaction system, was chosen as the optimal concentration for D-tagatose production.

Then, we analyzed the effect of the dosage of spore fermentation broth on this biotransformation. The different dosages of spore fermentation broth were added into the reaction mixture containing 100 g/L of D-galactose as the substrate. After the biotransformation at 70 °C for 24 h, the optimum dosage of spore fermentation broth was confirmed to be 50 mL (Figure 5B), corresponding to an ~75% yield of D-tagatose.

In investigating the reusability of spore surface-displayed L-AI, the reactions were conducted under the optimal transformation conditions (Figure 6). After each reaction cycle, spores with anchored L-AI were isolated by centrifugation and then washed with 0.1 M phosphate sodium buffer (pH 6.5). The anchored L-AI maintained high specific activities (1.72×10^{-10} U/spore, 85% of the initial activity) toward D-galactose within 5 reaction cycles. The conversion rate was maintained at 56% at the third cycle. However, the amount of spores decreased significantly after three cycles and only 20% of the initial amount was retained at the end of the fifth cycle. The biotransformation rate of the anchored L-AI was also gradually decreased from 75% to 19% at the end of the fifth cycle.

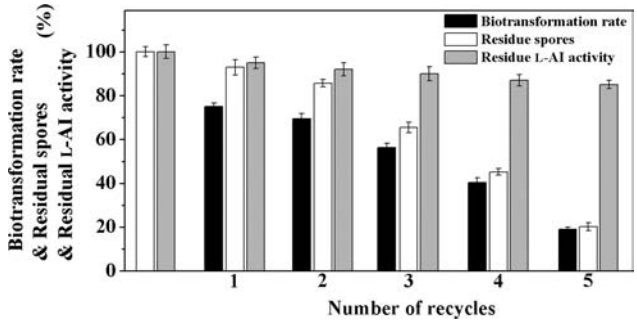

Figure 6. Recycling of spore surface-displayed L-AI for the production of D-tagatose. (■) Biotransformation rate of D-galactose; (□) residual amount of spores; (gray bar) residual activity of spore surface-displayed L-AI. The initial addition amount of spores and specific activity was defined as 100%.

■ DISCUSSION

Enzymatic synthesis of D-tagatose from D-galactose using L-AI has drawn wide attention. In previous studies, L-AI was always expressed in *E. coli* strains and used for D-tagatose production in the form of free enzyme or immobilized enzyme or contained in whole cells. However, the genetic background of *E. coli* remains controversial in application of the food industry, and the time-consuming purification processes restricted the use of an isolated enzyme. Therefore, it was important to explore the possibility of producing D-tagatose using L-AI carried by food-grade whole cells or a natural structure of cells, such as spores.

It is reported that bacterial spores may be good carriers of target proteins. Spores of *B. subtilis* are generally recognized as safe microbial resources and are used as additives in human and animal food. Moreover, *B. subtilis* draws considerable attention for its advantages of mature molecular genetic manipulation and detailed knowledge of its spore structure. All of these attributes make spores of *B. subtilis* an appealing medium for displaying heterogeneous proteins on its surface. In the present study, we introduced a novel system using the natural and robust spores of *B. subtilis* 168 with L-AI displayed on the surface for the enzymatic synthesis of D-tagatose.

The spores of *B. subtilis* are encased in a protective coat consisting of an inner and an outer layer, which are composed of >70 different proteins.[33] Most of the proteins successfully used in surface display were located in the outer layer, such as CotB, CotC, and CotG. Of these, CotB and CotC have always been used in the production of vaccines and antigens,[17,34] and CotG was reportedly used in biocatalysis with whole cells.[16,35] CotX, another outer spore coat protein, has not been documented in the application of displaying heterogeneous enzymes on the spore surface. CotX is synthesized inside the sporulating mother cells and deposited on the spore surface as spores emerge.[33] In the present study, we finally generated fusion protein CotX-AI, which was anchored on the spore surface of *B. subtilis* 168 successfully. According to the analysis of the biocatalytic reaction, the high conversion rate of the substrate and the stability during the recycling process

dx.doi.org/10.1021/jf501937j | J. Agric. Food Chem. 2014, 62, 6756−6762

demonstrate that this surface display system can be qualified for industry application. The confirmation of the availability of CotX also enriched the choice of spore coat proteins for use in surface display technology.

Existing L-AIs from wild or recombinant strains remain flawed in terms of being provided with appropriate biocatalytic temperature or pH for the industrial production of D-tagatose. For instance, L-AI from *Lactobacillus sakei* 23K was acid-tolerant, but the enzyme was rapidly inactivated at temperatures greater than 50 °C.[36] In another example, the optimal temperature of L-AI from *Geobacillus thermodenitrificans* was the expected result (70 °C), but its relative activity was markedly decreased at pH 7.0.[32] More examples are listed in Table 2. Conversely, Bacillus spores, which are formed in response to nutrient starvation, are robust and can withstand extreme heat, desiccation, and chemicals.[19] The thermal stability examined in the present study indicated that the incubation of the displayed L-AI at the temperature range of 65−80 °C within 30 min would not significantly decrease the relative activity of the enzyme. Moreover, the optimal catalytic temperature of anchored L-AI is 70 °C, whereas 92% activity was retained at 75 °C after 30 min. For the industrial production of D-tagatose from D-galactose, isomerization performed at the temperature range of 60−70 °C is the most suitable temperature condition, which is advantageous for the production, such as higher conversion yield, better sugar solubility, and lower risk of microbial contamination.[1,2] However, temperatures more than 75 °C also introduce undesirable consequences, such as browning and byproducts formation.[14] Furthermore, pH of 6.5, examined as the optimal pH of anchored L-AI, meet the industrial requirement for maintaining the pH within the range of 6.0−6.5. At this pH range, the browning changes can be controlled markedly,[14,39] and the production processes are simplified because the optimal pH of lactose hydrolase used for producing D-galactose from lactose is also in this range. Thus, the suitable temperature and pH make the anchored L-AI a desirable enzyme for the production of D-tagatose. The wide range of temperature available also offers elasticity during the industrial production.

Table 2. Optimal Temperature and pH of L-AI from Various Microorganisms for Industrial Production of D-Tagatose

organism	optimal temperature (°C)	optimal pH
Lactobacillus fermentum CGMCC2921(this work)	70	6.5
L. fermentum CGMCC2921[12]	65	6.5
Lactobacillus sakei 23K[36]	30−40	5.0−7.0
Bacillus licheniformis[37]	50	7.5
Alicyclobacillus acidocaldarius[38]	65	6.0−6.5
Thermoanaerobacter mathranii[2]	65	8.0
Geobacillus thermodenitrificans[31]	70	8.5
Thermotoga maritima[39]	90	7.0

After the optimization of the operating conditions, recombinant spores harboring the pJS700a-*cotX-araA* plasmid were able to catalyze 100 g/L of D-galactose into 75 g/L of D-tagatose in 24 h, and even yield 56 g/L of D-tagatose at the end of the third recycle. Compared with previous studies of L-AIs from various microorganisms with a different expression vector (Table 3), the conversion yield of the anchored L-AI is relatively higher. This result suggests that the anchored L-AI on the surface of the recombinant spores is a promising alternative for D-tagatose production. Moreover, it was expressed in a food-grade system and excludes the lengthy purification method. However, at the fifth batch, the conversion rate of D-galactose decreased to 25% of that of the first batch. It is worth noting that the amount of spores decreased to 41% of the first batch and the specific activity of anchored L-AI remained 86%, which indicates that the decrease in the conversion yield can be mostly attributed to the reduction of spore amount. Xu et al.[16] reported that the addition of nisin could inhibit the germination of *Bacillus* spores, which finally improved the conversion yield in the reaction by controlling the reduction of the spore amount. In addition, the reduction of spore amount may also be influenced by the environment with continuous vibrations and a high temperature solution, which is bound to damage the structure of spores to some extent. In our study, the reduction of spore amount could be mostly caused by the harsh environment. To overcome this difficulty, we are considering immobilized spores to adapt the mechanical strength during production.

The cost estimate is crucial to judge the significance of a new production method. In our study, the cost estimate mainly includes the medium for culturing bacteria and the substrate used in the catalytic reaction. For instance, cost comparison of different methods used to produce 10 kg of D-tagatose is shown in Table 4, and because the culture medium used for culturing spores in our study was poor nutrition, its cost saving reached 99.1%. However, the crucial factor of the cost saving was the higher conversion yield. To produce 10 kg of D-tagatose, the substrate (D-galactose) used in our study was much lower than the research conducted by Xu et al. Finally, the different culture medium and the lower amount of substrate made the cost savings achieve 45.4%.

To the best of our knowledge, this is the first report for the development of a food-grade spore surface display system for the production of D-tagatose from D-galactose by using recombinant spores. The reported system exhibited both a higher conversion yield rate and a cost-saving production

Table 3. Bioconversion of D-Galactose into D-Tagatose Using L-Arabinose Isomerases from Various Microorganisms with Different Expression Systems

source organism	expression system	conversion conditions	substrate (g/L)	conversion rate (%)	yield (g/L/h)
L. fermentum CGMCC2921(this work)	*B. subtilis* 168	70 °C, 24 h	100	75 ± 3.5	3.13 ± 0.15
L. fermentum CGMCC2921[12]	*E. coli* BL21	65 °C, 24 h	100	55	2.29
L. sakei 23K[36]	*E. coli* BL21	40 °C, 7 h	9	36	0.46
E. coli[10]	*E. coli* BL21	37 °C, 24 h	10	43	0.18
G. thermodenitrificans[32]	*E. coli* BL21	65 °C, 5 h	18	46	1.66
L. plantarum NC8[40]	*E. coli* HB101	60 °C, 6 h	9.9	30	0.50
B. longum[13]	*L. lactis*	35 °C, 144 h	300	36	0.75

dx.doi.org/10.1021/jf501937j | J. Agric. Food Chem. 2014, 62, 6756−6762

Table 4. Cost Comparison of Different Methods to Produce 10 kg of D-Tagatose[a]

			method 1[12]		method 2 (this study)		
materials		cost ($/t)	amount (kg)	cost ($)	amount (kg)	cost ($)	cost savings (%)
culture medium	tryptone	3 160	6.667	21.068	0.0258	0.0815	
	beef extract	1 200			0.0077	0.0092	
	yeast extract	3 300	3.333	10.999			
	inorganic salt[b]		6.667	6.107	0.4662	0.2523	
total-1[c]				38.174		0.343	99.1
substrate	D-galactose	20 000	33.333	666.667	19.231	384.615	42.3
total-2[c]				704.841		384.958	45.4

[a]The analysis of cost to produce 10 kg of D-tagatose was based on the best result in our study. [b]The inorganic salt of method 1 represents NaCl in LB culture medium, and the inorganic salt of method 2 represents NaCl, KCl, $MgSO_4 \cdot 7H_2O$, $Ca(NO_3)_2$, $MnCl_2$, and $FeSO_4$ in the DSM culture medium. [c]Total-1 represents the total cost of culture medium used in different methods, and total-2 represents the total cost of culture medium and the substrate.

method of D-tagatose. The value-added production process using surface-displayed enzymes could help meet the demand of the food industry and can generally be applicable to numerous biocatalytic reactions in other industries.

AUTHOR INFORMATION

Corresponding Author

*Associate Professor, Sha Li Nanjing University of Technology, State Key Laboratory of Materials-Oriented Chemical Engineering, College of Food Science and Light Industry, 30 Puzhu South Road, Nanjing 211816, People's Republic of China. Tel./Fax: +86-25-58139433. E-mail: lisha@njtech.edu.cn.

Funding

This work was supported by the National Basic Research Program of China (2013CB733603), the National High Technology Research and Development Program of China (2012AA021503), the National Nature Science Foundation of China (31371732), and the Program for Changjiang Scholars and Innovative Research Team in University (IRT1066).

Notes

The authors declare no competing financial interest.

REFERENCES

(1) Kim, P. Current studies on biological tagatose production using L-arabinose isomerase, a review and future perspective. *Appl. Microbiol. Biotechnol.* **2004**, *65*, 243−249.

(2) Jorgensen, F.; Hansen, O. C.; Stougaard, P. Enzymatic conversion of D-galactose to D-tagatose: Heterologous expression and characterisation of a thermostable L-arabinose isomerase from *Thermoanaerobacter mathranii*. *Appl. Microbiol. Biotechnol.* **2004**, *64*, 816−822.

(3) Buemann, B.; Toubro, S.; Raben, A.; Blundell, J.; Astrup, A. The acute effect of D-tagatose on food intake in human subjects. *Br. J. Nutr.* **2000**, *84*, 227−231.

(4) Zehener, L. R. D-Tagatose as a low-calorie carbohydrate sweetener and bulking agent. European Patent EP 0257626 B1, 1988.

(5) Marzur A. W. Functional sugar substitutes with reduced calories. European Patent EP 0341062 A3, 1989.

(6) Lu, Y.; Levin, G. V.; Donner, T. W. Tagatose, a new antidiabetic and obesity control drug. *Diabetes, Obes. Metab.* **2008**, *10*, 109−134.

(7) Troyono, E.; Martinez-Castro, I.; Olano, A. Kinetics of galactose and tagatose formation during heat-treatment of milk. *Food Chem.* **1992**, *45*, 41−43.

(8) Levin, G. V.; Zehner, L. R.; Saunders, J. P.; Beadle, J. R. Sugar substitutes: Their energy values, bulk characteristics, and potential health benefits. *Am. J. Clin. Nutr.* **1995**, *62*, 1161S−1168S.

(9) Oh, D. K. Tagatose: Properties, applications, and biotechnological processes. *Appl. Microbiol. Biotechnol.* **2007**, *76*, 1−8.

(10) Yoon, S. H.; Kim, P.; Oh, D. K. Properties of L-arabinose isomerase from *Escherichia coli* as biocatalyst for tagatose production. *World J. Microbiol. Biotechnol.* **2003**, *19*, 47−51.

(11) Kim, H. J.; Ryu, S. A.; Kim, P.; Oh, D. K. A feasible enzymatic process for D-tagatose production by an immobilized thermostable L-arabinose isomerase in a packed-bed bioreactor. *Biotechnol. Prog.* **2003**, *19*, 400−404.

(12) Xu, Z.; Qing, Y.; Li, S.; Feng, X.; Xu, H.; Ouyang, P. A novel L-arabinose isomerase from *Lactobacillus fermentum* CGMCC2921 for D-tagatose production: Gene cloning, purification and characterization. *J. Mol. Catal. B: Enzym.* **2011**, *70*, 1−7.

(13) Salonen, N.; Nyyssölä, A.; Salonen, K.; Turunen, O. *Bifidobacterium longum* L-arabinose isomerase—Overexpression in *Lactococcus lactis*, purification, and characterization. *Appl. Biochem. Biotechnol.* **2012**, *168*, 392−405.

(14) Rhimi, M.; Aghajari, N.; Juy, M.; Chouayekh, H.; Maguin, E.; Haser, R.; Bejar, S. Rational design of *Bacillus stearothermophilus* US100 L-arabinose isomerase: Potential applications for D-tagatose production. *Biochimie* **2009**, *91*, 650−653.

(15) Xu, Z.; Li, S.; Fu, F.; Li, G.; Feng, X.; Xu, H.; Ouyang, P. Production of D-tagatose, a functional sweetener, utilizing alginate immobilized *Lactobacillus fermentum* CGMCC2921 Cells. *Appl. Biochem. Biotechnol.* **2012**, *166*, 961−973.

(16) Xu, X.; Gao, C.; Zhang, X.; Che, B.; Ma, C.; Qiu, J.; Tao, F.; Xu, P. Production of *N*-acetyl-D-neuraminic acid by use of an efficient spore surface display system. *Appl. Environ. Microbiol.* **2011**, *77*, 3197−3201.

(17) Wang, X.; Chen, W.; Tian, Y.; Mao, Q.; Lv, X.; Shang, M.; Li, X.; Yu, X.; Huang, Y. Surface display of Clonorchis sinensis enolase on *Bacillus subtilis* spores potentializes an oral vaccine candidate. *Vaccine* **2014**, *32*, 1338−1345.

(18) Kim, J.; Schumann, W. Display of proteins on *Bacillus subtilis* endospores. *Cell. Mol. Life Sci.* **2009**, *66*, 3127−3136.

(19) Stahl, S.; Uhlen, M. Bacterial surface display: Trends and progress. *Trends Biotechnol.* **1997**, *15*, 185−192.

(20) Park, J. P.; Choi, M. J.; Kim, S. H.; Lee, S. H.; Lee, H. Preparation of sticky *Escherichia coli* through surface display of an adhesive catecholamine moiety. *Appl. Environ. Microbiol.* **2014**, *80*, 43−53.

(21) Nicholson, W. L.; Munakata, N.; Horneck, G.; Melosh, H. J.; Setlow, P. Resistance of *Bacillus* endospores to extreme terrestrial and extraterrestrial environments. *Microbiol. Mol. Biol. Rev.* **2000**, *64*, 548−572.

(22) Kunst, F. The complete genome sequence of the Gram-positive bacterium *Bacillus subtilis*. *Nature* **1997**, *390*, 249−256.

(23) Driks, A. The *Bacillus* spore coat. *Phytopathology* **2004**, *94*, 1249−1251.

(24) Setlow, P. Spores of *Bacillus subtilis*: Their resistance to and killing by radiation, heat and chemicals. *J. Appl. Microbiol.* **2006**, *101*, 514−525.

(25) Ning, D.; Leng, X.; Li, Q.; Xu, W. Surface-displayed VP28 on *Bacillus subtilis* spores induce protection against white spot syndrome

virus in crayfish by oral administration. *J. Appl. Microbiol.* **2011**, *111*, 1327−1336.
(26) Bron, S. Plasmids. In *Molecular biological methods for Bacillus*; Harwood, C., Cutting, S., Eds.; John Wiley and Sons: Chichester, U.K., 1990; pp 75−174.
(27) Li, G.; Tang, Q.; Chen, H.; Yao, Q.; Ning, D.; Chen, K. Display of *Bombyx mori* Nucleopolyhedrovirus GP64 on the *Bacillus subtilis* Spore Coat. *Curr. Microbiol.* **2011**, *62*, 1368−1373.
(28) Nicholson, W. L.; Setlow, P. Sporulation, germination and outgrowth. In *Molecular biological methods for Bacillus*; Harwood, C., Cutting, S., Eds.; John Wiley and Sons: Chichester, U.K., 1990; pp 391−450.
(29) Haider, T.; Husain, Q. Immobilization of *β*-D-galactosidase from *Aspergillus oryzae* via immunoaffinity support. *Biochem. Eng. J.* **2009**, *43*, 307−314.
(30) Zhan, Y.; Xu, Z.; Li, S.; Liu, X.; Xu, L.; Feng, X.; Xu, H. Coexpression of *β*-D-galactosidase and L-arabinose isomerase in the production of D-tagatose: A functional sweetener. *J. Agric. Food Chem.* **2014**, *62*, 2412−2417.
(31) Kim, J. H.; Lee, C. S.; Kim, B. G. Spore-displayed streptavidin: A live diagnostic tool in biotechnology. *Biochem. Biophys. Res. Commun.* **2005**, *331*, 210−214.
(32) Kim, H. J.; Oh, D. K. Purification and characterization of an L-arabinose isomerase from an isolated strain of *Geobacillus thermodenitrificans* producing D-tagatose. *J. Biotechnol.* **2005**, *120*, 162−173.
(33) Pan, J. G.; Kim, E. J.; Yun, C. H. *Bacillus* spore display. *Trends Biotechnol.* **2012**, *30*, 610−612.
(34) Isticato, R.; Cangiano, G.; Tran, H. T.; Ciabattini, A.; Medaglini, D.; Oggioni, M. R.; Felice, M. D.; Pozzi, G.; Rizza, E. Surface display of recombinant proteins on *Bacillus subtilis* spores. *J. . Bacteriol.* **2001**, *183* (21), 6294−6301.
(35) Qu, Y.; Wang, J.; Zhang, Z.; Shi, S.; Li, D.; Shen, W.; Shen, E.; Zhou, J. Catalytic transformation of HODAs using an efficient *meta*-cleavage product hydrolase-spore surface display system. *J. Mol. Catal. B: Enzym.* **2014**, *102*, 204−210.
(36) Rhimi, M.; Ilhammami, R.; Bajic, G.; Boudebbouze, S.; Maguin, E.; Haser, R.; Aghajari, N. The acid tolerant L-arabinose isomerase from the food grade *Lactobacillus sakei* 23K is an attractive D-tagatose producer. *Bioresour. Technol.* **2010**, *101*, 9171−9177.
(37) Prabhu, P.; Tiwari, M. K.; Jeya, M.; Gunasekaran, P.; Kim, I. W.; Lee, J. K. Cloning and characterization of a novel L-arabinose isomerase from *Bacillus licheniformis*. *Appl. Microbiol. Biotechnol.* **2008**, *81*, 283−290.
(38) Lee, S. J.; Lee, D. W.; Choe, E. A.; Hong, Y. H.; Kim, S. B.; Kim, B. C.; Pyun, Y. R. Characterization of a thermoacidophilic L-arabinose isomerase from *Alicyclobacillus acidocaldarius*: Role of Lys-269 in pH optimum. *Appl. Environ. Microbiol.* **2005**, *71*, 7888−7896.
(39) Lee, D. W.; Jang, H. J.; Choe, E. A.; Kim, B. C.; Lee, S. J.; Kim, S. B.; Hong, Y. H.; Pyun, Y. R. Characterization of a thermostable L-arabinose (D-galactose) isomerase from the hyperthermophilic eubacterium *Thermotoga maritima*. *Appl. Environ. Microbiol.* **2004**, *70*, 1397−1404.
(40) Chouayekh, H.; Bejar, W.; Rhimi, M.; Jelleli, K.; Mseddi, M.; Bejar, S. Characterization of an L-arabinose isomerase from the *Lactobacillus plantarum* NC8 strain showing pronounced stability at acidic pH. *FEMS Microbiol. Lett.* **2007**, *277*, 260−267.

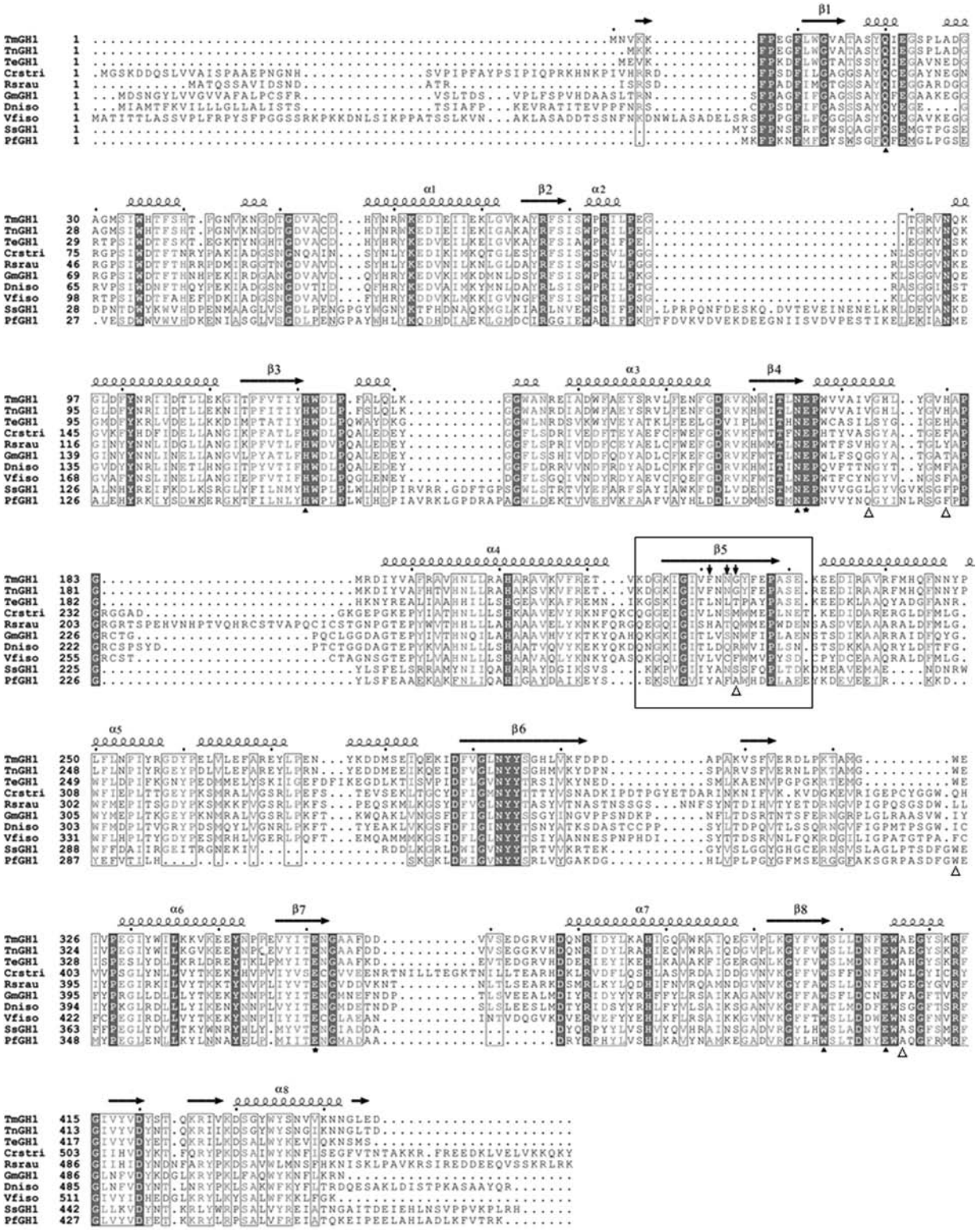

Figure 1. Multiple sequence alignment of GH1 representatives. A multiple sequence alignment of *β*-glucosidases and flavonoid glucosidases from GH1. TmGH1, *T. maritima* BglA (Q08638); TnGH1, *T. neapolitana* BglA (AF039487); TeGH1, *T. ethanolicus* (GU391423); Crstri, *Catharanthus roseus* strictosidine *β*-glucosidase (Q9M7N7); Rsrau, *Rauvolfia serpentina* raucaffricine *β*-glucosidase (Q9SPP9); GmGH1, *Glycine max* (soy) isoflavonoid glucosidase (AB259819); Dniso, *Dalbergia nigrescens* isoflavonoid glucosidase (AY766303); Vfiso, *Viburnum furcatum* isoflavonoid *β*-glucosidase (AB122081); SsGH1, *S. solfataricus* BglA (P22498); PfGH1, *P. furiosus* BglA (AAC25555). The alignment was generated with ClustalW, and the secondary structure elements of Tm-BglA were aligned at the top with the ESPript program. The regions of sequence identity are shown in gray. The region selected for mutagenesis is marked by a thin arrowhead above the sequence, stars indicate acid/base and nucleophilic catalytic residues, a black triangle below the sequence indicates residues forming subsite −1, and a white triangle below the sequence indicates residues forming subsite +1.

dx.doi.org/10.1021/jf501932v | J. Agric. Food Chem. 2014, 62, 6763−6770

Table 1. Mutagenic Primer Sequences[a]

primer	direction	mutants	primer sequence
1	forward	F221L	AGTG**CTC**AATAATGGATATTTCGAACCTGC
2	forward	N223L	AGTTTTCAAT**CTG**GGATATTTCGAACCTGCG
3	forward	G224T	AGTATTCAACAAC**ACC**TATTTCGAACCTGCGAGT
4	forward	F221L/N223L	AGTG**CTC**AAT**CTG**GGATATTTCGAA
5	forward	F221L/G224T	AGTA**CTC**AACAAC**ACC**TATTTCGAA
6	forward	N223L/G224T	AGTTTTCAAT**CTGACC**TATTTCGAACCTGCG
7	forward	F221L/N223L/G224T	AGTA**CTC**AAT**CTGACC**TATTTCGAACCTGCG
8	reverse		ATTCCGATCTTTCCATCTTTCACG

[a]Bold residues indicate the sites of mutation.

which may be formed by several subsites (+1,+2, +3, and so on).[15−18] The −1 subsite of various β-glycosidases have been studied,[16] and have shown that the glycone specificity is determined by a hydrogen network formed between glycone hydroxyls and amino acid residues of the subsite, and the amino acid residues close to the aglycone binding subsites +1 varied with various β-glucosidases in GH1 (Figure 1). Based on the sequence alignment of family 1 enzymes and analysis of the TmBglA structural model, three residues (F221, N223, and G224) in the active site pocket located on β-strand 5 close to sugar binding subsite +1 were selected for mutagenesis to investigate the influence on the enzyme kinetics (using the substrate *p*-nitrophenyl β-D-glucopyranoside (*p*NPG)), thermostability and pH profiles, and the hydrolysis of flavonoid glycosides (soy isoflavone glycosides and quercetin glucosides) in order to modulate the specificity of β-glucosidases that have valuable biotechnological applications.

MATERIALS AND METHODS

Strains, Plasmids, and Chemicals. The *p*-nitrophenyl (*p*NP) glycoside substrate *p*NPG as well as Isoflavone standards of daidzin (Din), daidzein, genistin (Gin), and genistein were purchased from Sigma Chemical Co. (St. Louis, MO, USA). High-performance liquid chromatography (HPLC) grade methanol and acetonitrile were purchased from Fisher Scientific (Hanover Park, IL, USA). Quercetin glucosides standards of quercetin-3,4′-*O*-glucose (Q3,4′), quercetin-3-*O*-glucose (Q3), quercetin-4′-*O*-glucose (Q4′), quercetin (Q) were purchased from Extrasynthese Chemical Co. (Genay, France). *Escherichia coli* (*E. coli*) JM109 (Promega, Madison, WI, USA) was used as host for the expression of β-glucosidase A gene from *T. maritima*, via plasmid pHsh.[19] DNA-modifying enzymes and polymerases were purchased from TAKARA (Dailian, China). All oligonucleotide primers were synthesized by Sangon (Shanghai, China). All other chemicals used were analytical grade reagents unless otherwise stated. Recombinant enzyme was induced by a temperature shift from 30 to 42 °C. *E. coli* was grown in Luria−Bertani (LB) supplemented with 100 μg of ampicillin mL^{-1}.

Sequence Alignment and Molecular Docking. The sequences of Tm-BglA and other GH1 β-glycosidases were aligned using ClustalW 2.0.12 and ESPript.[20] The structure of β-D-cellotetraose was docked into the active site of Tm-BglA (PDB code 2WC4) using AutoDock version 4.2.[21] The coordinate files of both protein and ligand required for docking calculation were prepared by AutoDockTools. The nonpolar hydrogens were deleted by the program, and the partial charges were merged to the carbon atoms. The sugar substrates were treated as rigid, and the rotatable bonds were set automatically by the program. The protein portion was set as flexible receptor by assigning the catalytic residues (E165 and E351) as flexible residues. AutoGrid was performed to precalculate the grid map of interaction energy prior to docking. The grid size was set at 60 × 60 × 60 with a grid point spacing of 0.258 Å at the center of protein. A Lamarckian genetic algorithm was used with a population size of 300, a maximum number of energy evaluations of 2500000, a maximum number of generations of 25000, and uniform crossover mode. Other parameters were set as default. The docked conformation was visualized using Accelrys DS Visualizer 3.0.[22]

Cloning and Site-Directed Mutagenesis. Plasmid constructions were carried out according to standard procedures.[23] The *T. maritima* β-glucosidase A gene, *Tm-bglA*, based upon that reported in Genbank entry X74163, was amplified with pET-20b-*Tm-bglA* as a template[7,8] and ligated at restriction sites XbaI and XhoI with pHsh;[19] the resulting recombinant plasmid was named as pHsh-*Tm-bglA*. Mutagenesis was performed in order to introduce the following designed changes F221L, N223L, G224T, F221L/N223L, F221L/G224T, N223L/G224T, and F221L/N223L/G224T, respectively. Eight oligonucleotides for each mutation were designed to contain the corresponding nucleotide changes (see Table 1). These oligonucleotides and pHsh-*Tm-bglA* as template were used to introduce mutations using polymerase chain reaction (PCR) under the following conditions: one cycle of denaturation at 95 °C for 5 min, 30 cycles of denaturation at 94 °C for 40 s, annealing at 55 °C for 40 s, extension at 72 °C for 4 min, and extra extension at 72 °C for 7 min. The PCR products were purified using the QIAquick PCR purification kit, phosphated with T4 polynucleotide kinase, and ligated into the expression vector pHsh,[19] resulting in the expression vectors containing exchange mutant Tm-BglA. The nucleotide changes were then sequenced by the Biological Services Unit of Shanghai.

Expression and Purification. To unambiguously characterize the activity of the mutational protein, the recombinant protein was purified to homogeneity as follows. *E. coli* JM109 containing pHsh-*Tm-bglA* and mutational plasmid were grown in LB media at 30 °C, pH 7.0 containing 100 μg of ampicillin mL^{-1} to an OD_{600} of 0.7−0.8, then transferred into a 42 °C shaking incubator, and grown for a further 9 h at 42 °C. The cells were harvested by centrifugation, washed twice with water, and then resuspended in binding buffer (5 mM imidazole, 0.5 M NaCl, and 20 mM Tris-HCl, pH 7.9). After sonication and centrifugation (30 min, 9600*g*, 4 °C), the supernatant was heated for 30 min at 70 °C to remove most of the host cell proteins by centrifugation. The resulting supernatants were purified by Ni-affinity chromatography (Novagen) to homogeneity as determined by the sodium dodecyl sulfate polyacrylamide gel electrophoresis (SDS-PAGE) using 12% polyacrylamide running gels with 4% polyacrylamide stacking gels. Protein concentration was determined by the Bradford method.[24]

Enzyme Assays. Enzyme activity was quantified by *p*NP release from *p*NPG. The reactions were performed in 50 mM potassium phthalate buffer (PPB, pH 6.2) containing 2 mM *p*NPG and 10 μL of suitably diluted enzyme for 5 min at 90 °C; the reaction was stopped by the addition of 600 μL of 1 M Na_2CO_3. The color that developed was read at 405 nm and translated to micromoles of *p*NP using a standard graph prepared under the same conditions. One unit was determined as the amount of enzyme producing 1 μmol of *p*NP/min under the preceding assay conditions. All reactions were done in triplicate.

Determiation of Kinetic Parameters. For determinations of the kinetic parameters (K_m, V_{max}, and k_{cat}/K_m) of *p*NPG, reaction was carried out at the optimum conditions using 0.2−2.0 mM *p*NPG. Kinetic parameters K_m and V_{max} were determined by the Lineweaver−Burk representation of the Michaelis−Menten model. Each experi-

dx.doi.org/10.1021/jf501932v | J. Agric. Food Chem. 2014, 62, 6763−6770

ment was done in duplicate, and measurements were made in triplicate. The standard error was recorded to be <2%.

The kinetic properties of the hydrolysis of Q4′ were determined by incubating the Q4′ at five concentrations in the range of 0.0215−0.215 mM. The standard reaction mixture (final volume, 50 μL) containing 5% dimethyl sulfoxide (DMSO) in 100 mM pH 5.0 PPB with 20 pmol of Tm-BglA and 10 pmol of G224T at 90 °C. The mixture without enzyme was preincubated at 90 °C for 5 min. After 5 min, the reactions were stopped by ice water cooling and freeze-dried and resuspended in 50 μL of methanol for HPLC analysis. The liberated Q was detected by measuring the absorbance at 260 nm; its amounts were calculated from standard curves of the Q peak areas over the 0.018−3.7 μmol range. The enzyme activity using Q4′ is expressed in units (U). A 1 U amount corresponds to the amount of enzyme required to release 1 μmol of Q/min under the described conditions. Each test was carried out with at least three replicates. The relative standard deviation was recorded to <2%. Obtained data were analyzed using graphpad prism 5.0, using a time range allowing the output of a Michaelis−Menten curve.

Hydrolysis of Isoflavone Glycosides and Quercetin Glucosides. First, onion extract from 10 g of onion skin was extracted for 40 min at 95 °C in 200 mL of 95% (w/v) ethanol, centrifuged (9600*g*, 4 °C, 30 min) and dried by speed vacuum, then resuspended in 25 mL of sterile double-distilled water (ddH_2O), and filtered through a 0.45 μm filter. To compare the hydrolysis of seven mutants toward flavone glycosides, 0.1 μmol of Din and 0.1 μmol of Gin were incubated with the purified Tm-BglA and mutant enzymes in 50 mM sodium phosphate buffer (SPB, pH 6.2) in a thermostatically controlled incubator at 90 °C, respectively. The flavone glycosides were where particular care was taken to ensure their complete solubility.[25,26] Equal molar concentrations of eight enzymes were assayed for their hydrolysis efficiencies toward the flavone glycosides. The reactions were stopped by ice water cooling before analysis, and 50 μL of methanol were then added to the hydrolyzed solutions. Aliquots of the methanol extract were spotted on thin layer chromatography plates using silica gel 60 F_{254} (Yantai Jiangyou Silica Gel Development Co., Ltd., China). The plate was developed with ethyl acetate/butanone/methanol/water (10:7:1:1, by vol) for the hydrolysis of daidzin and genistin, and with ethyl acetate/butanone/formic acid/water (5:3:1:1, by vol) and 2% aluminum trichloride methanol solution for quercetin glucosides; the products on the plate were visualized by absorbance under UV light at 254−365 nm.

Enzyme activity of the seven mutants and Tm-BglA for quercetin glucosides was determined using 20 μL of onion extracts, 20 pmol of enzymes, and 50 mM SPB (pH 6.2) in a 100 μL reaction volume at 90 °C for 10 min; then the hydrolyzed solutions were added into 300 μL of methanol. Samples of 20 μL were withdrawn and analyzed by HPLC to detect the hydrolysis of the quercetin glucosides. The analytical HPLC was carried out using the Agilent Zorbax SB-C18 column (4.6 × 250 mm, 5 μm). A gradient sequence using methanol (A) and 0.05% phosphoric acid solution (B) was utilized in the following proportions: 70% B (20 min), 30% B (5 min), 10% B (3 min), and 70% B (4 min) at a flow rate of 1 mL min^{-1}.

RESULTS

Structural Considerations and Mutation Strategy. The structure and the residues forming −1 subsite and the noncovalent interactions formed with the glycone of Tm-BglA have been reported; interacting residues included Gln20, His121, Asn165, Trp398, Glu405, and Trp406. In order to predict the interactions between Tm-BglA and the glycone substrate, cellotetraose was docked into the active site pocket of Tm-BglA to analyze putative interactions at the aglycone binding region. From the docked position of cellotetraose, 27 residues of Tm-BglA were predicted to be interacted with cellotetraose. Among these, the residues forming −1 subsite conforms to the report and the aglycone +1 subsite is formed by the residues V173, H180, N222, W324, and 407A (Figure 1). Inspection of residues surrounding the +1 subsite showed a nonconserved region at the "floor" of the active site, more precisely at the end of β-strand 5 (F221, N222, N223, G224, Y225, and F226). The nonconserved natures of these residues were shown by superimposition of known structures as well as analyzing a multiple sequence alignment. Superimposition of 3D structures of GH1 enzymes with diverse substrate specificities confirmed the variable area of β-strand 5 in the vicinity of the substrate pocket binding as well as variability in the loops. The variability at the end of β-strand 5 was also authenticated by the multiple sequence alignment of the Tm-BglA with other GH1 flavonoid-hydrolyzing enzymes (Figure 1). It was shown that the GH1 β-glucosidase (Te-BglA), from the *Th. ethanolicus* JW200, could more effectively hydrolyze isoflavone glucosides of soy flour to their aglycones than could Tm-BglA from *T. maritima*,[8] possibly due to the difference in amino acid residues around their glycone binding pockets. Therefore, the F221, N223, and G224 at the end of β-strand 5 were targeted for site-directed mutagenesis through replacement of the amino acid residues of Tm-BglA with the corresponding residues of Te-BglA, generating three single mutants, F221L, N223L, and G224T, as well as the corresponding three double mutants (F221L/N223L, F221L/G224T, and N223L/G224T) and one triple mutant (F221L/N223L/G224T).

Construction, Expression, and Purification of Mutant Enzymes. Seven expression vectors containing exchange mutant Tm-BglA were constructed as described in Materials and Methods. The nucleotide sequence of each mutant Tm-BglA was confirmed by DNA sequencing. These mutant and wild-type Tm-BglA (WT) were expressed in *E. coli*, purified by immobilized Ni-affinity chromatography after heat treatment and revealed by single bands on SDS-PAGE with apparent molecular masses of 52 kDa (Figure 2), which were in accordance with the theoretically calculated molecular mass.

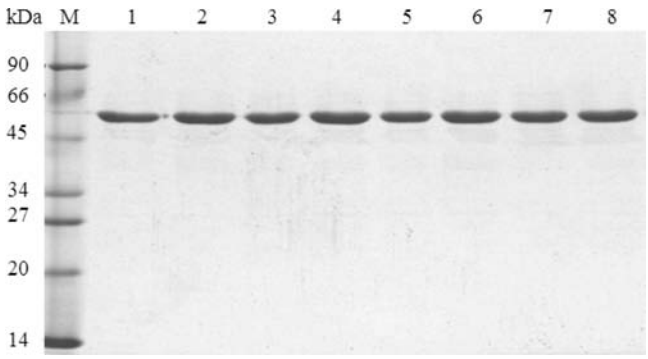

Figure 2. SDS-PAGE analysis of purified Tm-BglA and mutants: lane M, molecular mass standards; lane 1, Tm-BglA; lane 2, F221L; lane 3, N223L; lane 4, G224T; lane 5, F221/N223L; lane 6, F221L/G224T; lane 7, N223L/G224T; lane 8, F221L/N223L/G224T. Each lane except for the standards contained 2 μg of protein.

pH and Thermal Properties of Mutant and Wild-Type β-Glucosidases. The optimal temperatures and thermostabilities of seven variants were compared to those of WT in Figure 3A,B. All of the enzymes were optimally active at 90 °C except for G224T of which the optimal temperature was 95 °C. Nonetheless, the relative activity of seven mutants was lower than that of WT within the temperature range from 35 to 85

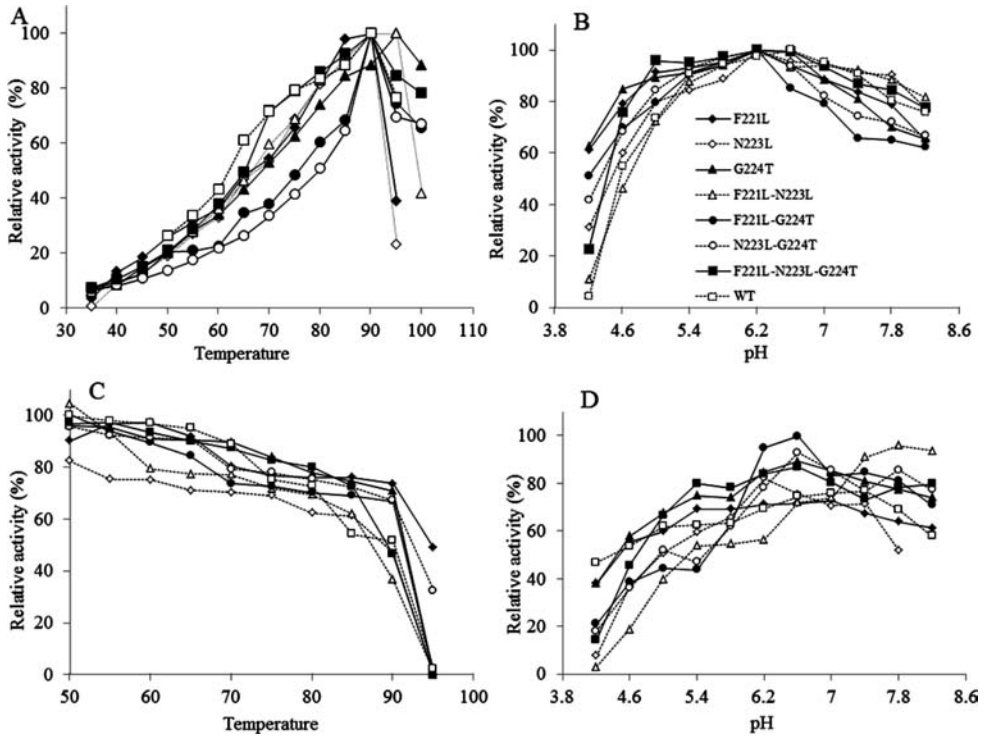

Figure 3. The optimal temperature (A), pH (B), heat stability (C), and pH stability (D) profiles of mutant and wild type β-glucosidases. Temperature dependence at pH 6.2 (A) and pH dependence at 90 °C (B) when a 5 min assay was used. The highest level of activity was defined as 100%. For heat stability (C), a 0.075 μg of purified enzyme in 50 mM PPB (pH 6.2) was perincubated for 1 h at a temperature range of 50−95 °C in the absence of substrate. For pH stability (D), 0.075 μg of purified enzyme in 50 mM PPB (pH 4.2 −8.2) was preincubated for 1 h at 37 °C in the absence of substrate. Full activity was determined at each pH value. The activity of the enzyme without preincubation was defined as 100%. Activity was determined at their optimal pH and temperature. Data are expressed as the means of three experiments, and the standard deviation for the mean was recorded to be <2%.

Table 2. Kinetic Parameters of the Tm-BglA and Seven Mutants[a]

enzyme	K_m (mM)	V_{max} (U·mg^{-1})	K_{cat} (s^{-1})	K_{cat}/K_m ($mM^{-1}·s^{-1}$)
		Hydrolysis of *p*NPG		
Tm-BglA	0.60 ± 0.01	299 ± 2	239 ± 4	398
F221L	0.80 ± 0.08	513 ± 22	448 ± 10	564
N223L	0.54 ± 0.04	257 ± 6	224 ± 5	414
G224T	0.87 ± 0.05	488 ± 12	426 ± 10	492
F221L/N223L	0.76 ± 0.03	415 ± 5	362 ± 4	474
F221L/G224T	0.72 ± 0.05	514 ± 13	448 ± 12	624
N223L/G224T	0.55 ± 0.03	467 ± 9	407 ± 8	740
F221L/N223L/G224T	0.78 ± 0.05	526 ± 9	459 ± 8	588
		Hydrolysis of Q4′		
Tm-BglA	0.066 ± 0.013	2.1 ± 0.29	17.6 ± 2.5	267
G224T	0.050 ± 0.002	3.5 ± 0.15	42.4 ± 1.8	848

[a]The kinetic parameters were determined at their optimal pH and temperature for the substrate concentrations ranging from 0.2 to 2.0 mM for *p*NPG and from 0.0215 to 0.215 mM for Q4′, using the standard assay as described in Materials and Methods.

°C. All seven mutants were stable up to 85 °C, which were the same as that of WT.

The pH properties of seven mutants and WT are shown in Figure 3C,D. The pH optima for the seven mutants were observed at pH 6.2 which are not altered from the pH optimum profile characteristic of WT. In contrast, seven mutants were found to decrease in stability within the pH below 5.0 compared to that of WT, whereas they displayed stability within the pH range from pH 6.5 to 8.3 and were even more stable than that of WT.

Kinetic Parameters of Mutant and Wild-Type Enzymes in pNPG Hydrolysis. The kinetic properties of WT and seven mutants for the hydrolysis of *p*NPG were determined at pH 6.2. The results are shown in Table 2. The K_m (mM) values of N223L and N223L/G224T calculated were 0.54 and 0.55, respectively, which were slightly lower than that for the WT (0.60), whereas the K_m (mM) for F221L, G224T, F221L/N223L, F221L/G224T, and F221L/N223L/G224T were 0.80, 0.87, 0.76, 0.72, and 0.78, respectively, which were slightly higher than that for the WT. Similarly, the k_{cat} (s^{-1}) value for N223L was 224, which was almost similar to the WT (239), whereas k_{cat} for F221L, G224T, F221L/N223L, F221L/G224T, N223L/G224T, and F221L/N223L/G224T were 448, 426, 362, 448, 407, and 459, respectively, which were increased

dx.doi.org/10.1021/jf501932v | J. Agric. Food Chem. 2014, 62, 6763−6770

about 1-fold compared to that of the WT. k_{cat}/K_m (s^{-1} mM^{-1}) values obtained for F221L, N223L, G224T, F221L/N223L, F221L/G224T, N223L/G224T, and F221L/N223L/G224T were 564, 414, 492, 474, 624, 740, and 588, respectively, and were obviously higher than that for the WT (398).

Hydrolysis of Isoflavone Glycosides and Quercetin Glucosides. The hydrolysis of isoflavonoid glycosides by WT and seven mutants were evaluated (Figure 4), and the hydrolysates were analyzed by thin-layer chromatography (TLC). The Gin were partially digested by the seven mutants and WT after 10 min reaction; the digested Gin by F221L, F221L/G224T, N223L/G224T, and F221L/N223L/G224T were less than that by the WT (Figure 4A). After 30 min of incubation, the hydrolysis of Gin by WT, N223L, and F221L/N223L were complete, but the reactions with other mutants (F221L, G224T, F223L/G224T, F221L/G224T, and F221L/N223L/G224T) retained a few Gin (Figure 4B). Meanwhile, Din were almost completely digested with WT after 10 min reaction, whereas after the reactions in the seven mutants some Din remained (Figure 4C). After 30 min of incubation, the Din was completely digested by G224T, N223L, F221L/G224T, and F221L/N223L/G224T; in the reactions with F221L, F221L/N223L, and N223L/G224T amounts of Din still remained (Figure 4D).

Subsequently, the hydrolysis of the quercetin glycosides and the free aglycones produced after reactions with or without enzyme were analyzed by TLC. As shown in Figure 4E, the Q4′ were almost completely digested by all of the variants carrying a mutation at position 224 (G224T, F221L/G224T, N223L/G224T, and F221L/N223L/G224T) after a 10 min reaction, whereas amounts of Q4′ remained in the reactions containing the WT and other mutants (F221L, N223L, and F221L/N223L). After 30 min of incubation, a little of Q4′ still remained in the reactions with N223L and F221L/N223L compared to almost complete digestion of the WT and F221L (Figure 4F). Therefore, the changes of components for hydrolyzing quercetin glucosides were further analyzed by HPLC (Figure 5). For the hydrolysis of Q3,4′, eight enzymes partially hydrolyzed the Q3,4′substrate to Q3 within the reaction time of 10 min except N223L and F221L/N223L (Figure 5A), which is consistent with that their increase of the component of Q3 (Figure 5B). The single, double, and triple mutants carrying a mutation at position 224 (G224T, F221L/G224T, N223L/G224T, and F221L/N223L/G224T) completely converted the Q4′ to Q after reactions for 10 min compared to the Q4′ that remained for the WT (Figure 5C) and had a higher yield of Q than WT (Figure 5D). The G224T resulted in a significant increase of 35.5% for conversion of Q4′ and 28.6% for conversion of Q3,4′ in accord with an increased turnover number (k_{cat}, 2.4×) and catalytic efficiency (k_{cat}/K_m,

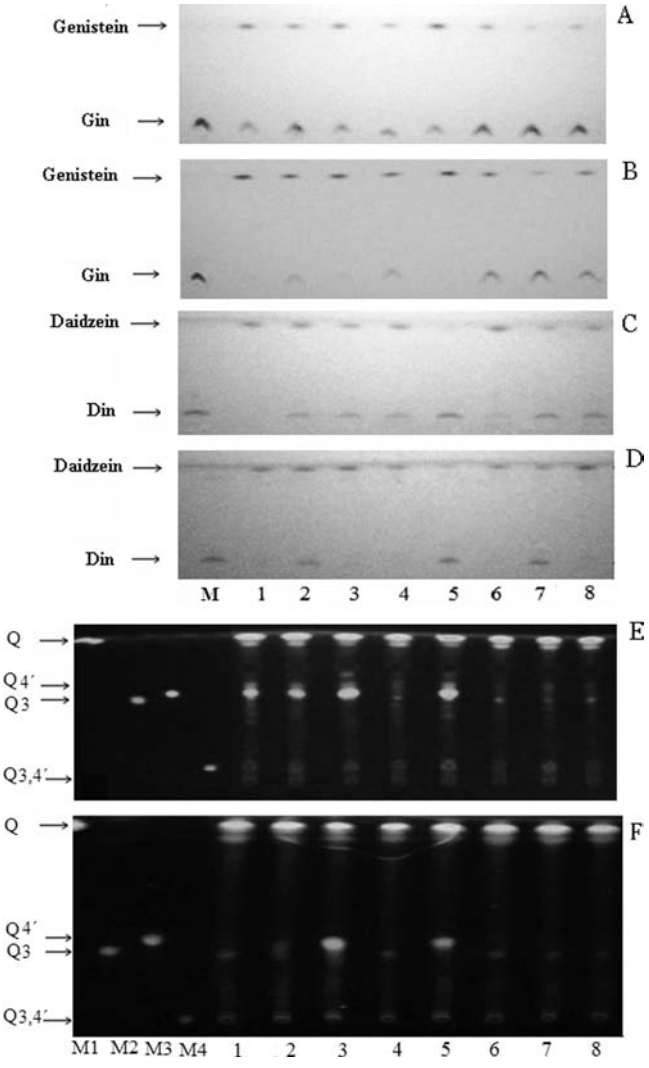

Figure 4. TLC analysis of the hydrolysis of isoflavonoid glycoside by mutants and WT. Hydrolysis of genistin (A and B), daidzin (C and D), and quercetin glycoside (E and F) in 50 mM SPB (pH 6.2) with mutants and WT for 10 min (A, C, and E) and 30 min (B, D, and F) at 70 °C. Lanes M, isoflavone glycosides (Din and Gin); lanes M1, quercetin; lanes M2, quercetin-3-*O*-glucose; lanes M3, quercetin-4′-*O*-glucose; lanes M4, quercetin-3,4′-*O*-glucose; lanes 1, reaction liquid with WT; lane 2, reaction liquid with F221L; lane 3, reaction liquid with N223L; lane 4, reaction liquid with G224T; lane 5, reaction liquid with F221/N223L; lane 6, reaction liquid with F221L/G224T; lane 7, reaction liquid with N223L/G224T; lane 8, reaction liquid with F221L/N223L/G224T.

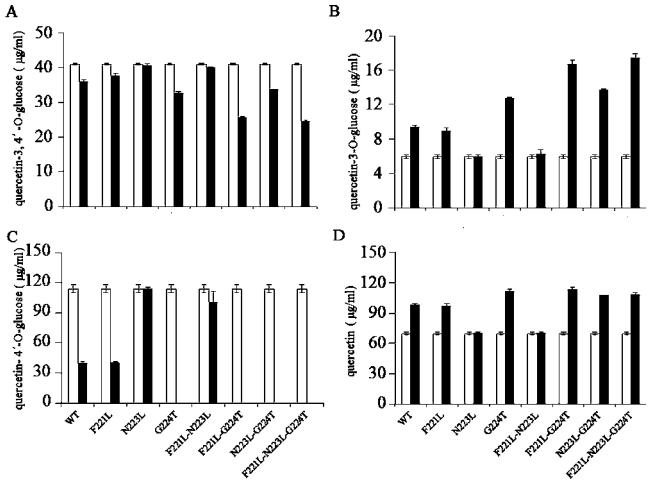

Figure 5. HPLC analysis of the hydrolysis of quercetin glycoside by mutant and wild type Tm-BglA (WT). Analysis of quercetin-3,4′-*O*-glucose (A), quercetin-3-*O*-glucose (B), quercetin-4′-*O*-glucose (C), and quercetin (D). White bars represent the quercetin glycoside concentration at time 0 min, and black bars are for the remaining quercetin glycoside concentration after 10 min incubation with the enzyme.

dx.doi.org/10.1021/jf501932v | J. Agric. Food Chem. 2014, 62, 6763−6770

3.2×) as indicated by a decrease of 24% in K_m for Q4′ (Table 2). However, 100% of Q4′, Q3, and Q3,4′ remained in the reactions containing N223L and F221L/N223L, indicating that the mutation at position 223 removed all hydrolytic activity on quercetin glucosides.

DISCUSSION

The *T. maritima* β-glucosidase A (Tm-BglA) effectively hydrolyzed isoflavone glucosides of soy flour to their aglycones and has demonstrated the great potential of a biocatalyst for food, medicine, and various agroindustrial processes. Pioneering studies suggested that GH 1 β-glucosidases have different capabilities of hydrolyzing flavone glycosides, reflecting that the amino acid residues located within the aglycone binding pocket varied with the enzymes. To investigate the role of the amino acid residues located within the aglycone binding pocket of Tm-BglA, the F221, N223, and G224 at the end of β-strand 5 were targeted for site-directed mutagenesis through replacement of the amino acid residues of Tm-BglA with the corresponding residues of Te-BglA from *T. ethanolicus* JW200. Seven mutants were constructed and expressed. All mutants prepared in this study were catalytically active, indicating that the selected amino acid residues were not an influence for active expression of Tm-BglA but resulted in slight shifts in optimum temperature and heat stability, and significant changes in hydrolysis activity of *p*NPG, isoflavone glycosides, and quercetin glucosides. All of the mutants showed pH-activity curves narrower on the basic side and wider on the acid side and had similar optimal pH and stability at pH 6.5−8.3 and were more stable up to 85 °C, but G224T displayed a higher optimal temperature (95 °C), indicating that the mutation at position G224 caused structural perturbation to change its thermal properties of Tm-BglA.

The enzyme kinetics (K_m, V_{max}, and k_{cat}/K_m) of Tm-BglA and the seven mutants for the hydrolysis of artificial substrate *p*NPG were studied in more detail. The seven mutants indicated an obvious increase in catalytic efficiency toward *p*NPG but an increase or no change in K_m, suggesting that F221, N223, and G224 were the key residues to determine *p*NPG binding of the substrate. All mutants did not have an increase in catalytic efficiency toward isoflavonoid glycosides. The F221L mutant showed a decrease in catalytic efficiency toward isoflavonoid glycosides whereas it did not affect the hydrolytic activity on quercetin-3,4′-*O*-glucose and quercetin-4′-*O*-glucose. In addition, the N223L mutation also decreased the catalytic efficiency on isoflavonoid glycosides but removed all hydrolytic activity of quercetin glucosides. These results indicate that the differences in catalytic efficiency between Tm-BglA and Te-BglA are not primarily due to differences in the residues that directly contact the substrate but rather drawn from differences in more remote residues in both aglycone and glycone binding pockets.[21] However, a mutation in the analogous position in *T. neapolita* TnBgl1 A, N221S, increased catalytic efficiency in both Q3 and Q4′ hydrolysis,[9] suggesting a preferred polar residue at this position toward quercetin glucosides hydrolysis.

Contrarily, the G224T mutant had a dramatic effect upon flavonoid-hydrolyzing activity, which decreased the catalytic efficiency in soy isoflavone glycosides, whereas G224T and corresponding double and triple mutants carrying G224T mutant increased the catalytic efficiency in Q3,4′ and Q4′. The G224 position has also shown significance in structural homologues of Tm-BglA. In this study, the k_{cat}/K_m (s^{-1} mM^{-1}) values obtained for G224T were obviously higher than that for the wild-type Tm-BglA, whereas G222F in TnBgl1A, corresponding to position G224, reduced catalytic efficiency (k_{cat}/K_m) for *p*NPG hydrolysis.[27] These results further support the influence of G224 on aglycone specificity. A close look at the binding interactions of G224 in the presence of Q4′ shows that the residue is interacting with residues in neighboring strands of the Tm-BglA (the backbone carbonyls of N222, N223, N246, and Y295; Figure 6), and G224 is

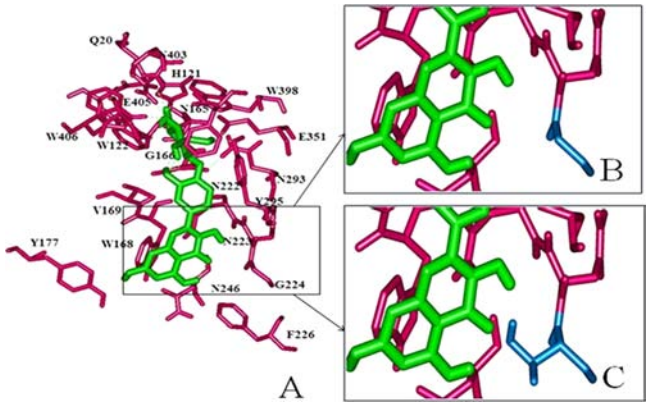

Figure 6. Model of Tm-BglA containing a docked structure of quercetin-4′-*O*-glucose. The quercetin-4′-*O*-glucose molecule is colored in green. In panel A, the residues of Tm-BglA interacted with quercetin-4′-*O*-glucose are labeled and depicted in red stick models. In panel B and panel C the amino acids at position 224 are colored by blue. The figure was drawn with Accelrys DS Visualizer 3.0.

located near the narrowest part of the active-site cleft, and previous finding suggest spatial hindrance is a mechanism for the reduced catalytic activity that occurs after insertion of a bulkier amino acid in this position.[12] In the present study, G224T increased the turnover number and catalytic efficiency for Q4′, and decreased the distance between the residue at position 224 and the C4 of the substrate Q4′ from 3.166 to 2.057 Å, likely because it is closer to the quercetin backbone of Q4′ to enhance the interaction between the enzyme and the substrate. Furthermore, the replacement G with T containing the OH side chain introduced structures similar to Q4′ (e.g., 5-OH and 3-OH on the quercetin backbone) accessible to an environment more suited for Q4′ in the aglycone binding pockets in accord with a decrease in K_m for Q4′.

In conclusion, F221, N223, and G224 at the end of β-strand 5 of Tm-BglA were selected for mutagenesis to investigate the influence on the kinetic properties and hydrolysis of glucosylated flavonoid. Our results suggest that three residues play an important role in determining the substrate specificity of Tm-BglA. G224T resulted in a dramatic increase conversion of Q4′ (35.5%) and Q3,4′ (28.6%) in accord with an increased turnover number (k_{cat}/K_m, 1.4×) and catalytic efficiency (k_{cat}/K_m, 2.2×) as well as a decrease in K_m (0.24) for Q4′, which we report herein have valuable biotechnological applications.

AUTHOR INFORMATION

Corresponding Author

*Phone: +86-25-85794123. Fax: +86-25-83598901. E-mail: xueyemin@njnu.edu.cn.

Funding

This work was supported by grants from Jiangsu Key Laboratory for Biomass-Based Energy and Enzyme Technology

(Huaiyin Normal University; JSBEET1301), grants from Jiangsu Provincial Engineering Laboratory for Biomass Conversion and Process Integration of China (JPELBCPL2012002), and grants from the Jiangsu Provincial Six Big Talent Peak Project (2013-NY-030).

Notes

The authors declare no competing financial interest.

REFERENCES

(1) Harborne, J. B. The flavonoids: Advances in research since 1986, Vol. 3: Chapman & Hall: London, U.K., 1994.

(2) Ho. C. T.; Lee, C. Y.; Huang, M. T. Phenolic Compounds in Food and Their Effects on Health I: Analysis, *Occurrence and Chemistry*, Vol. *605*; American Chemical Society: Washington, DC, USA, 1992.

(3) Rochfort, S. J.; Imsic, M.; Jones, R.; Trenerry, V. C.; Tomkins, B. Characterization of flavonol conjugates in immature leaves of pak choi [Brassica rapa L. Ssp. chinensis L. (Hanelt.)] by HPLC-DAD and LC-MS/MS. *J. Agric. Food Chem.* **2006**, *54* (13), 4855−4860.

(4) Izumi, T.; Piskula, M. K.; Osawa, S.; Obata, A.; Tobe, K.; Saito, M.; Kataoka, S.; Kubota, Y.; Kikuchi, M. Soy isoflavone aglycones are absorbed faster and in higher amounts than their glucosides in humans. *J. Nutr.* **2000**, *130* (7), 1695−1699.

(5) Kim, B. N.; Yeom, S. J.; Kim, Y. S.; Oh, D. K. Characterization of a β-glucosidase from *Sulfolobus solfataricus* for isoflavone glycosides. *Biotechnol. Lett.* **2012**, *34* (1), 125−129.

(6) Yeom, S. J.; Kim, B. N.; Kim, Y. S.; Oh, D. K. Hydrolysis of isoflavone glycosides by a thermostable β-glucosidase from *Pyrococcus furiosus*. *J. Agric. Food Chem.* **2012**, *60* (6), 1535−1541.

(7) Song, X.; Xue, Y.; Wang, Q.; Wu, X. Comparison of three thermostable β-glucosidases for application in the hydrolysis of soybean isoflavone glycosides. *J. Agric. Food Chem.* **2011**, *59* (5), 1954−1961.

(8) Xue, Y.; Yu, J.; Song, X. Hydrolysis of soy isoflavone glycosides by recombinant β-glucosidase from hyperthermophile Thermotoga maritima. *J. Ind. Microbiol. Biotechnol.* **2009**, *36* (11), 1401−1408.

(9) Khan, S.; Pozzo, T.; Megyeri, M.; Lindahl, S.; Sundin, A.; Turner, C.; Karlsson, E. N. Aglycone specificity of *Thermotoga neapolitana* β-glucosidase 1A modified by mutagenesis, leading to increased catalytic efficiency in quercetin-3-glucoside hydrolysis. *BMC Biochem.* **2011**, *12*, 11.

(10) Verdoucq, L.; Czjzek, M.; Moriniere, J.; Bevan, D. R.; Esen, A. Mutational and structural analysis of aglycone specificity in maize and sorghum beta-glucosidases. *J. Biol. Chem.* **2003**, *278*, 25055−25062.

(11) Berrin, J. G.; Czjzek, M.; Kroon, P. A.; McLauchlan, W. R.; Puigserver, A.; Williamson, G.; Juge, N. Substrate (aglycone) specificity of human cytosolic beta-glucosidase. *Biochem. J.* **2003**, *373*, 41−48.

(12) Zouhar, J.; Vevodova, J.; Marek, J.; Damborsky, J.; Su, X. D.; Brzobohaty, B. Insights into the functional architecture of the catalytic center of a maize beta-glucosidase Zm-p60.1. *Plant Physiol.* **2001**, *127*, 973−985.

(13) Henrissat, B.; Callebaut, I.; Fabrega, S.; Lehn, P.; Mornon, J.-P.; Davies, G. Conserved catalytic machinery and the prediction of a common fold for several families of glycosyl hydrolases. *Proc. Natl. Acad. Sci. U. S. A.* **1995**, *92* (15), 7090−7094.

(14) Jenkins, J.; Lo Leggio, L.; Harris, G.; Pickersgill, R. β-Glucosidase, β-galactosidase, family A cellulases, family F xylanases and two barley glycanases form a superfamily of enzymes wit 8-fold β/α architecture and with two conserved glutamates near the carboxy-terminal ends of β-strands four and seven. *FEBS Lett.* **1995**, *362* (3), 281−285.

(15) Davies, G.; Wilson, K.; Henrissat, B. Nomenclature for sugar-binding subsites in glycosyl hydrolases. *Biochem. J.* **1997**, *321* (Pt 2), 557.

(16) Marana, S. R. Molecular basis of substrate specificity in family 1 glycoside hydrolases. *IUBMB Life* **2006**, *58* (2), 63−73.

(17) Zechel, D. L.; Boraston, A. B.; Gloster, T.; Boraston, C. M.; Macdonald, J. M.; Tilbrook, D. M. G.; Stick, R. V.; Davies, G. J. Iminosugar glycosidase inhibitors: Structural and thermodynamic dissection of the binding of isofagomine and 1-deoxynojirimycin to β-glucosidases. *J. Am. Chem. Soc.* **2003**, *125* (47), 14313−14323.

(18) Gloster, T. M.; Meloncelli, P.; Stick, R. V.; Zechel, D.; Vasella, A.; Davies, G. J. Glycosidase inhibition: an assessment of the binding of 18 putative transition-state mimics. *J. Am. Chem. Soc.* **2007**, *129* (8), 2345−2354.

(19) Shao, W.; Wu, H.; Pei, J. A plasmid vector controlled by the Sygma 32 factor of Escherichia coli and its use for the expression of heterologous protein. International Patent PCT WO2006/002574A1, 2006.

(20) Gouet, P.; Robert, X.; Courcelle, E. ESPript/ENDscript: Extracting and rendering sequence and 3D information from atomic structures of proteins. *Nucleic Acids Res.* **2003**, *31* (13), 3320−3323.

(21) Ratananikom, K.; Choengpanya, K.; Tongtubtim, N.; Charoenrat, T.; Withers, S. G.; Kongsaeree, P. T. Mutational analysis in the glycone binding pocket of *Dalbergia cochinchinensis* β-glucosidase to increase catalytic efficiency towards mannosides. *Carbohydr. Res.* **2013**, *373*, 35−41.

(22) Basha, S. H.; Prasad, R. N. In-Silico screening of Pleconaril and its novel substituted derivatives with Neuraminidase of H1N1 Influenza strain. *BMC Res. Notes* **2012**, *5* (1), 105 DOI: 10.1186/1756-0500-5-105.

(23) Maniatis, T, Fritsch, E. F., Sambrook, J.: Molecular cloning: A laboratory manual, Vol. *545*; Cold Spring Harbor Laboratory : Cold Spring Harbor, NY, USA, 1982.

(24) Bradford, M. M. A rapid and sensitive method for the quantitation of microgram quantities of protein utilizing the principle of protein-dye binding. *Anal. Biochem.* **1976**, *72* (1), 248−254.

(25) Lambert, N.; Kroon, P. A.; Faulds, C. B.; Plumb, G. W.; McLauchlan, W. R.; Day, A. J.; Williamson, G. Purification of cytosolic β-glucosidase from pig liver and its reactivity. *Biochim. Biophys. Acta* **1999**, *1435* (1−2), 110−116.

(26) Chuankhayan, P.; Rimlumduan, T.; Svasti, J.; Cairns, J. R. K. Hydrolysis of soybean isoflavonoid glycosides by Dalbergia β-glucosidases. *J. Agric. Food Chem.* **2007**, *55* (6), 2407−2412.

(27) Lundemo, P.; Adlercreutz, P.; Karlsson, E. N. Improved transferase/hydrolase ratio through rational design of a family 1β-glucosidase from *Thermotoga neapolitana*. *Appl. Environ. Microbiol.* **2013**, *79* (11), 3400−3405.

amphipathic termini, and is expressed by *Escherichia coli* as an insoluble recombinant protein. The insoluble fusion protein was mixed with triacylglycerol and phospholipid and reconstituted as AOBs, in which the lipophilic portion of oleosin is embedded in the triacylglycerol core and the amphipathic arms, fused with the target enzyme, are protruding on the surface[13] As illustrated in previous studies, the target enzyme tends to refold itself naturally and present itself in a biologically functional form on the surface of the AOB.[12,14] Therefore, AOB-based immobilization is an efficient way to achieve purification and immobilization of the recombinant enzyme in one step.

In this study, the CC-DPEase gene was constructed to allow *E. coli* to reveal the oleosin-fused protein. The purification, refolding, and immobilization of CC-DPEase were simultaneously accomplished upon reconstitution of the AOBs. To examine the alterations of enzyme characteristics due to the immobilization, central composite design (CCD) combined with response surface modeling (RSM) was employed for the planned statistical optimization of enzyme activity. The reusability and thermal stability of the AOB-immobilized CC-DPEase were also determined.

MATERIALS AND METHODS

Construction of CC-DPEase Expression Plasmid. The DNA fragments encoding CC-DPEase (GenBank accession no. ACL75304) were amplified by polymerase chain reaction (PCR) from the plasmid pET-21a-CC-DPEase[15] using the forward primer (5′ AGATCTATGAAACATGGTATATAC 3′) and reverse primer (5′ GGTACCGGAGTGTTTATG 3′). These two primers were designed to place a *Bgl*II site at the 5′ end and a *Kpn*I site at the 3′ end of the PCR products, respectively. The PCR fragments encoding CC-DPEase were digested with restriction endonucleases *Bgl*II and *Kpn*I. The fragments were then ligated with the *Bgl*II–*Kpn*I-digested plasmid pET29Ole,[16] generating pET29-DPEase-Ole, which was then sequenced to ensure that no errors were introduced during PCR. The resultant plasmids were used to transform *E. coli* BL21 (DE3) (Novagene, Madison, WI, USA) by standard techniques.[17] The *E. coli* BL21 (DE3) transformants were selectively grown at 37 °C on Luria–Bertani (LB) agar plates (Difco Laboratories, Detroit, MI, USA) containing kanamycin (50 μg/mL) (Sigma-Aldrich Co., St. Louis, MO, USA).

Expression of Recombinant Proteins. The *E. coli* BL21 (DE3) transformants were cultured in LB broth at 37 °C with shaking at 250 rpm for overnight. The overnight culture was subsequently seeded at a 1:100 dilution into 50 mL of fresh LB broth. The cell cultures were maintained at 37 °C with shaking at 250 rpm, and the cell proliferation was measured turbidimetrically at 600 nm (OD600). Once the cells reached an OD600 of 0.5, the cells were induced to express the recombinant protein with 100 μM isopropyl-D-1-thiogalactopyranoside (IPTG; Sigma-Aldrich Co.). After 4 h of induction, the *E. coli* cells were harvested by centrifugation at 5000*g* for 10 min at 4 °C.

Immobilization of CC-DPEase on AOB. The preparation of AOBs was carried out according to the method described by Chiang et al.[18] The *E. coli* cell pellet was resuspended in 1 mL of 50 mM sodium phosphate buffer (pH 7.4), ultrasonicated (Misonix, Farmingdale, NY, USA) for 10 min, and then fractionated into supernatant and pellet by centrifugation at 13000*g* for 10 min at 4 °C. To reconstitute the AOBs, the pellet fraction of the *E. coli* cell lysate containing 550 μg of oleosin-fused recombinant proteins was resuspended in 1 mL of 50 mM sodium phosphate buffer (pH 7.4) and then mixed with 15 mg of olive oil (Sigma-Aldrich Co.) and 150 μg of phospholipid (Sigma-Aldrich Co.). The mixture was subjected to ultrasonication for 10 min. The reconstituted AOBs were collected after centrifugation at 13000*g* for 10 min at 4 °C and were washed with 50 mM sodium phosphate buffer solution (pH 7.4). The results of each step of AOB reconstitution were monitored using sodium dodecyl sulfate–polyacrylamide gel electrophoresis (SDS-PAGE).[19] Confocal microscopic observation of the AOB-immobilized CC-DPEase was performed using a Leica TCS SP5 II spectral confocal microscope mounted on a Leica DMI 6000B inverted microscope (Leica Microsystems, Heidelberg, Germany) with a HCX PLAPO CS 63×/1.4-0.6 oil immersion objective.

CC-DPEase Activity Analysis. The enzyme activity of the AOB-immobilized CC-DPEase was determined using D-fructose (50 g/L; Sigma-Aldrich Co.) as the substrate in a reaction mixture containing sodium phosphate buffer (50 mM, pH 7.0), Co^{2+} (0.1 mM), and enzyme (0.5 μM) at 72 °C for 10 min. The reaction was stopped by boiling for 10 min, and then the amount of D-psicose epimerized from D-fructose was determined by using a high-performance liquid chromatography (HPLC) method.[10] The concentrations of D-psicose and D-fructose in the samples were determined by HPLC performed on a Shimadzu (Kyoto, Japan) LC-20 AT delivery system equipped with an RID-10A refractive index detector (Shimadzu), a Sugar-Pak I column (Waters Corp., Milford, MA, USA; 300 × 5 mm i.d.), and a Rheodyne injector (Rheodyne Inc., Cotati, CA, USA). The column was eluted at 80 °C with deionized water and a flow rate of 0.4 mL/min. One unit of enzyme activity was defined as that producing 1 μmol of D-psicose per minute from D-fructose under the assay conditions, with specific activity expressed as units per milligram of protein. The protein concentration was determined using the Lowry assay against a standard curve of bovine serum albumin, fraction V (Sigma-Aldrich Co.).[20]

The bioconversion rate of D-fructose to D-psicose by the AOB-immobilized CC-DPEase was determined using D-fructose (50 g/L; Sigma-Aldrich Co.) as substrate in a reaction mixture containing sodium phosphate buffer (50 mM, pH 7.0), Co^{2+} (0.1 mM), and enzyme (0.5 μM) at 72 °C for 30 min.

Optimal pH and Temperature of the AOB-Immobilized CC-DPEase. The pH and temperature are the key factors affecting enzyme activity of CC-DPEase;[10] therefore, we chose pH (denoted X_1) and temperature (denoted X_2) as the factors and CC-DPEase activity (denoted Y) as the response in the statistical experimental design. The optimal pH and temperature for the AOB-immobilized CC-DPEase were determined by applying CCD experimental design combined with RSM and regression analyses. On the basis of the CCD, a set of 13 experiments including 4 factorial points, 4 axial points, and 5 central points were performed. The experimental index numbers, scaled values, and actual values are shown in Table 1. The scaled values were defined as follows: $X_1 = (\mathrm{pH} - 7)$; $X_2 = (T - 72.5)/7.5$. The statistical experimental design, data, and regression analyses were carried out

Table 1. Process Variables Used in the CCD and Treatment Combinations and Mean Experimental Responses for AOB-Immobilized CC-DPEase

	scaled values (X_1 = pH; X_2 = T)		actual values (X_1 = pH; X_2 = T)		
index no.	X_1	X_2	X_1	X_2	CC-DPEase activity[a] (U/mg of total protein)
1	−1	−1	6	65	77.94
2	0	−1.41	7	61.89	130.43
3	−1.41	0	5.59	72.5	0.26
4	0	0	7	72.5	160.92
5	1	1	8	80	72.83
6	0	0	7	72.5	165.96
7	0	0	7	72.5	161.91
8	1.41	0	8.41	72.5	12.94
9	0	0	7	72.5	165.87
10	1	−1	8	65	66.93
11	0	1.41	7	83.11	118.49
12	0	0	7	72.5	155.69
13	−1	1	6	80	73.37

[a]Results represent the mean of three experiments.

dx.doi.org/10.1021/jf502022w | J. Agric. Food Chem. 2014, 62, 6771−6776

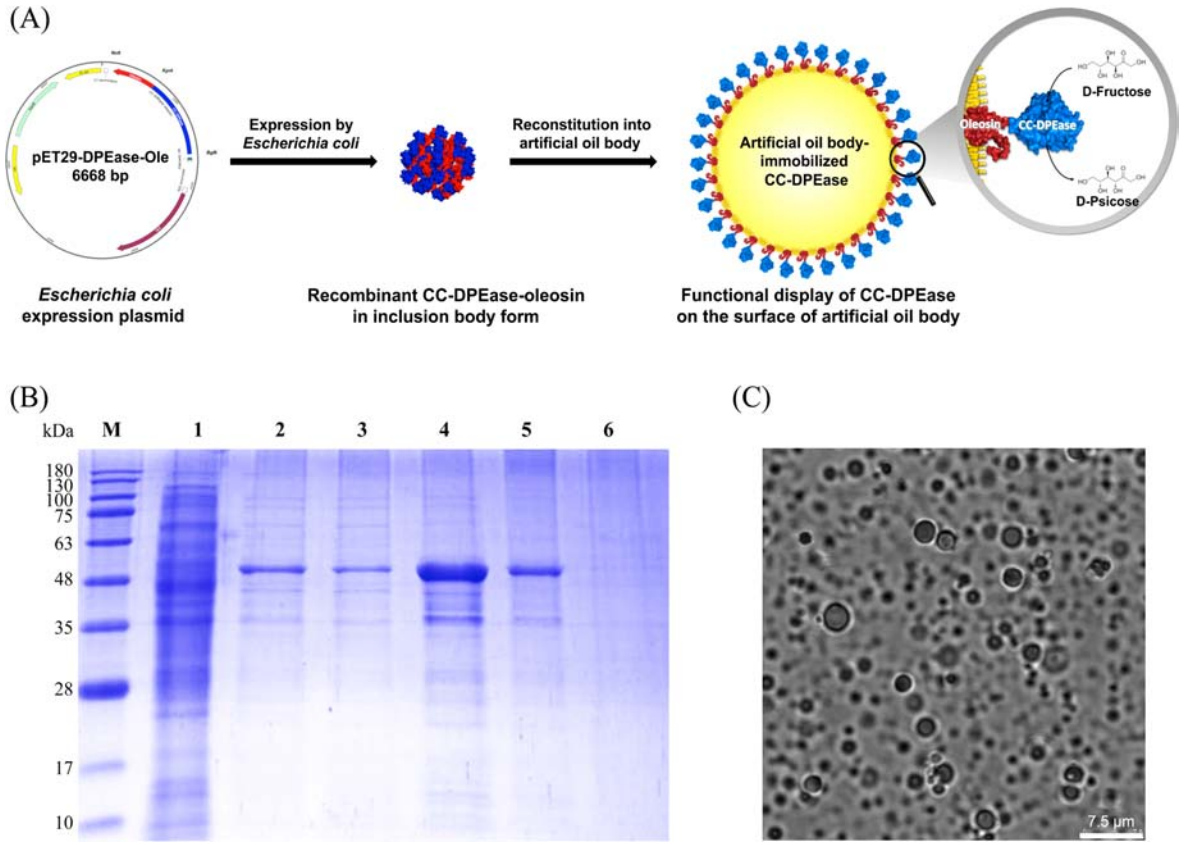

Figure 1. Immobilization of CC-DPEase on artificial oil bodies (AOBs): (A) scheme of production of AOB-immobilized CC-DPEase; (B) SDS-PAGE analysis of CC-DPEase immobilized on AOBs (lanes: M, molecular weight marker; 1, cell lysate of the recombinant *E. coli* before IPTG induction; 2, cell lysate of the recombinant *E. coli* after IPTG induction; 3, soluble fraction of the cell lysate after centrifugation; 4, insoluble fraction of the cell lysate after centrifugation; 5, AOBs; 6, remaining supernatant after AOB recovery); (C) confocal microscopic observation of AOB-immobilized CC-DPEase (bar = 7.5 μm).

using Design Expert software (version 8.0.6, Stat-Ease Inc., Minneapolis, MN, USA). Regression analysis of the experimental data yielded linear, quadratic, and cubic polynomial models. Model analyses, lack-of-fit tests, and *R*-squared analyses were performed to validate the reliability of these models. A model with a significant *P* value ($P < 0.05$) in the model analyses, insignificant *P* value ($P > 0.05$) in lack-of-fit tests, maximum *R*-squared value, and smallest predicted residual sum of the squares (PRESS) was selected. Analysis of variance (ANOVA) was employed to determine the significance of the optimized model.

After the optimal pH and temperature for the AOB-immobilized CC-DPEase were predicted, the actual activity of the AOB-immobilized CC-DPEase was determined at the optimal conditions to compare the predicted values and experimental data and check the reliability of the RSM. Student's *t* test was used to detect the differences between the predicted and actual values.[21]

Thermal Stability of AOB-Immobilized CC-DPEase. The thermal stability of AOB-immobilized CC-DPEase was determined by incubation of the enzyme at 55 or 72 °C in sodium phosphate buffer (50 mM, pH 7.0) containing 0.1 mM Co^{2+}. Aliquots were withdrawn at intervals of 0, 10, 30, 60, and 120 min, and the residual enzyme activities were measured as specified.

Reusability of AOB-Immobilized CC-DPEase. The reusability of AOB-immobilized CC-DPEase was determined by incubation of the enzyme at 72 °C for 10 min in sodium phosphate buffer (50 mM, pH 7.0) containing 0.1 mM Co^{2+} and D-fructose (50 g/L). At the end of the reaction, the immobilized enzyme was recovered by centrifugation, and the supernatant was removed for analysis of the amount of D-psicose epimerized from D-fructose. The reaction was restarted by administration of the recovered enzymes in a fresh substrate solution.

RESULTS AND DISCUSSION

Simultaneous Refolding, Purification, and Immobilization of CC-DPEase on AOBs. The scheme of production of AOB-immobilized CC-DPEase is shown in Figure 1A. The DNA fragments encoding CC-DPEase were fused to the oleosin gene and overexpressed in *E. coli*. After induction with IPTG at 37 °C, a band of about 51 kDa corresponding to the CC-DPEase−oleosin fusion proteins was observed in the induced recombinant *E. coli* (Figure 1B, lane 2). The CC-DPEase−oleosin fusion proteins were generally found in the insoluble fraction of the cell lysate after centrifugation (Figure 1B, lane 4). After reconstitution into AOBs, most of the CC-DPEase−oleosin fusion proteins were present in the oil body fraction after centrifugation, and almost none of the CC-DPEase−oleosin fusion protein was found in the supernatant fraction (Figure 1B, lanes 5 and 6). According to the confocal microscopic observation (Figure 1C), the sizes of the AOBs ranged from 0.5 to 3.5 μm, with a mean size of 2.0 μm. The CC-DPEase activities of proteins obtained from each step of the AOB reconstitution were determined by HPLC using D-fructose as the substrate. Detectable levels of CC-DPEase activity were observed in the reconstituted AOBs but not in the insoluble fraction of the cell lysate of the induced recombinant bacteria, indicating that CC-DPEase was immobilized on the AOB surface and folded into the active structure. From 1.0 g (wet weight) of *E. coli* cells, we obtained 17.33 mg of CC-DPEase−oleosin fusion proteins and reconstituted 1.65 mL of

dx.doi.org/10.1021/jf502022w | J. Agric. Food Chem. 2014, 62, 6771−6776

AOBs. The protein concentration of the reconstituted AOBs was 10.5 mg/mL.

Optimization of Reaction Conditions for the AOB-Immobilized CC-DPEase. Mu et al. indicated that environmental pH and temperature were the key factors affecting the activity of CC-DPEase.[10] Therefore, we chose these two factors and employed a CCD experimental design and RSM analysis to determine the reaction conditions for optimal enzyme activity of the AOB-immobilized CC-DPEase. On the basis of the CCD experimental design, a set of 13 experiments were performed. The scaled and actual values of pH and temperature performed in the experiments and the results for enzyme activities are shown in Table 1. Regression analysis of the experimental data yielded linear, quadratic, and cubic polynomial models. In the analysis of the mathematical models, the quadratic model appeared to be the most accurate ($P < 0.05$), with insignificant lack-of-fit ($P > 0.05$) and the smallest PRESS value (Supporting Information Table S1). These results suggested that the quadratic model was more reliable and accurate than the other models.

The quadratic regression equation obtained was

$$Y = -4956.10 + 1038.45 \times \mathrm{pH} + 41.11 \times T - 75.93 \times \mathrm{pH}^2 - 0.30 \times T^2 + 0.35 \times \mathrm{pH} \times T \quad (1)$$

where Y is the predicted response for a specific activity (U/mg of total protein) of the AOB-immobilized CC-DPEase and pH and T are the actual values for pH and temperature (see Table 1).

The three-dimensional plot as functions of pH and temperature on the specific activities of the AOB-immobilized CC-DPEase is shown in Figure 2. The model predicted that the maximum specific activity of the AOB-immobilized CC-DPEase (162.13 ± 6.83 U/mg) would be observed at 72 °C and pH 7.0. To confirm the applicability of the model, the specific activity of AOB-immobilized CC-DPEase was determined at the suggested optimum conditions. The experimental activity of 166.22 ± 0.53 U/mg confirmed the accuracy of the model.

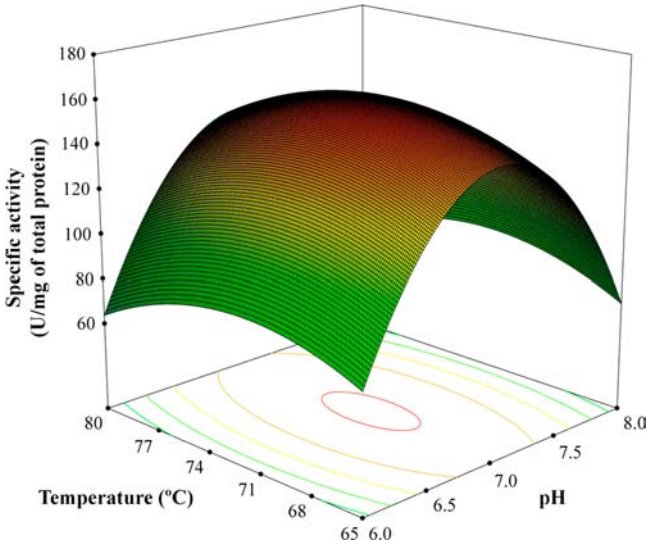

Figure 2. Response surface plot for the effects of pH and temperature on the specific activity of AOB-immobilized CC-DPEase.

Immobilization of enzymes can cause slight distortions in the enzyme structure, resulting in alterations in their activity, specificity, or stability.[22] Thus, we determined the optimal pH and temperature for the maximum enzyme activity of the AOB-immobilized CC-DPEase. We found that the maximum enzyme activity of the AOB-immobilized CC-DPEase occurred at pH 7.0 and 72 °C, which was different from that of the free-form CC-DPEase (pH 8.0 and 55 °C).[10] Therefore, we suggest that immobilization of CC-DPEase on AOB increased the optimal temperature but decreased the optimal pH of the enzyme activity. To compare the bioconversion rate of D-fructose to D-psicose by the AOB-immobilized CC-DPEase and by the free-form CC-DPEase, we performed epimerization reactions mediated by the AOB-immobilized CC-DPEase in the optimal reaction conditions for the free-form CC-DPEase (pH 8.0 and 55 °C) or for the AOB-immobilized CC-DPEase (pH 7.0 and 72 °C). The bioconversion rate of D-fructose to D-psicose by the AOB-immobilized CC-DPEase at pH 8.0 and 55 °C was 32.5%. This rate was similar to that of the free-form CC-DPEase reported by Mu et al.[10] In contrast, the bioconversion rate of D-fructose to D-psicose by the AOB-immobilized CC-DPEase at pH 7.0 and 72 °C was higher (45.8 vs 32.5%) than at the optimal reaction conditions for free-form CC-DPEase (pH 8.0 and 55 °C). In many cases, immobilization has an adverse effect upon enzyme activity because the interaction of the enzyme with carrier causes the distortion of the enzyme. To avoid degradation of enzyme properties, immobilization of the enzyme on a carrier via a linker is useful because the enzyme is flexible and reacts with the substrate more easily.[22] In this study, we introduced a linker polypeptide between the CC-DPEase and oleosin domains in the CC-DPEase−oleosin fusion protein. The AOB-immobilized CC-DPEase showed a bioconversion rate similar to that of the free-form enzyme, indicating that the CC-DPEase domain in the fusion protein was able to present its original conformation and maintain its functionality.

Thermal Stability of the AOB-Immobilized CC-DPEase. The thermal stability of AOB-immobilized CC-DPEase was evaluated by exposing the enzyme to 55 or 72 °C for 120 min. The residual activity of the AOB-immobilized CC-DPEase after incubation at 55 °C for 120 min was 85%, which was similar to that of the free-form CC-DPEase reported by Mu et al.[10] When the AOB-immobilized CC-DPEase was incubated at 72 °C for 120 min, the residual activity was 71% (Supporting Information Figure S1).

Thermal stability is an essential requirement for industrial enzymes because the reaction at higher temperatures can increase the bioconversion rate, reduce the reactants solubility, and reduce the risk of contamination during biocatalytic processes.[23] CC-DPEase has considerable potential in industrial practice because it possesses a remarkable thermal stability. Compared to *A. tumefaciens* DPEases, CC-DPEase has a similar bioconversion rate of 32%, but the half-life of CC-DPEase (9.5 h at 55 °C) is much longer than that of *A. tumefaciens* DPEase (8.9 min at 55 °C).[10,15] For the purpose of recovery and reuse, we immobilized CC-DPEases on AOBs and demonstrated that the bioconversion rate of D-fructose to D-psicose by the AOB-immobilized CC-DPEase was similar to that of the free-form enzyme. Thus, the AOB-immobilized CC-DPEase has potential application in the production of D-psicose at a lower cost than that of the free-form enzyme.

Reusability of the AOB-Immobilized CC-DPEase. To evaluate the feasibility of recovery and recycle of the AOB-immobilized CC-DPEase, the relative activity of the AOB-immobilized CC-DPEase was determined during five consec-

utive rounds of bioconversion of D-fructose to D-psicose at pH 7.0 and 72 °C. The AOB-immobilized CC-DPEase retained >50% of its initial activity after five cycles of enzyme use (Supporting Information Figure S2). Immobilized enzymes are preferred in biocatalytic processes for industrial applications because immobilized enzymes can be recycled and thus reduce the cost of production. AOB-immobilized enzymes can be easily and simply recovered from the surface of the reaction mixture by flotation centrifugation. Therefore, several enzymes, including D-hydantoinase, xylanase, and glucanase, have been immobilized on AOBs in previous studies.[12−14] Results in the previous and in our studies proved that, under optimal conditions, AOB-immobilized enzymes could be reused many times, thereby lowering the cost of enzymes for industrial application where the cost of enzymes is high.

In conclusion, the gene encoding CC-DPEase was cloned and expressed as an oleosin-fused protein in *E. coli*. Simultaneous refolding, purification, and immobilization of the active C-DPEase were accomplished as a result of reconstituting the AOBs. CCD experimental design combined with RSM and regression analyses were successfully applied to determine the optimal pH and temperature for the AOB-immobilized CC-DPEase. The optimum conditions for maximum enzyme activity of the AOB-immobilized CC-DPEase were observed at 72 °C and pH 7.0. Moreover, the AOB-immobilized CC-DPEase had a bioconversion rate and thermal stability similar to those of the free-form enzyme, but could be reused five times while retaining >50% of its activity. These results prove that the AOB-immobilized CC-DPEase has potential application in the production of D-psicose at a lower cost than the free-form enzyme does.

■ ASSOCIATED CONTENT

Supporting Information

Table S1 and Figurs S1 and S2. This material is available free of charge via the Internet at http://pubs.acs.org.

■ AUTHOR INFORMATION

Corresponding Authors

*(R.-T.G.) Phone: 86-22-84861999. Fax: 86-2-24828701. E-mail: guo_rt@tib.cas.cn.

*(J.-R.L.) Phone: 886-2-33666011. Fax: 886-2-33666001. E-mail: jrliu@ntu.edu.tw.

Author Contributions

[Δ]These authors contributed equally to this work.

Funding

This research was conducted using funds partially provided by Grant NSC 102-2628-B-002-007-MY2 from the National Science Council, Taiwan, Republic of China.

Notes

The authors declare no competing financial interest.

■ ABBREVIATIONS USED

AOB, artificial oil body; CCD, central composite design; DPEase, D-psicose 3-epimerase; DTEase, D-tagatose 3-epimerase; HPLC, high-performance liquid chromatography; IPTG, isopropyl-L-D-thiogalactopyranoside; RSM, response surface modeling; SDS-PAGE, sodium dodecyl sulfate−polyacrylamide gel electrophoresis

■ REFERENCES

(1) International Society of Rare Sugars. Definition of rare sugars. In *Proceedings of the 5th Symposium of International Society of Rare Sugars*, Kagawa, Japan, 2011.

(2) Tang, S.-Y. Rare sugars: applications and enzymatic production. *J. Biocatal. Biotransformation* **2012**, *01*, 2.

(3) Chung, M.-Y. M.; Oh, D.-K. D.; Lee, K. W. K. Hypoglycemic health benefits of D-psicose. *J. Agric. Food Chem.* **2012**, *60*, 863−869.

(4) Baek, S. H. S.; Park, S. J. S.; Lee, H. G. H. D-psicose, a sweet monosaccharide, ameliorate hyperglycemia, and dyslipidemia in C57BL/6J db/db mice. *J. Food Sci.* **2010**, *75*, H49−H53.

(5) Suna, S. S.; Yamaguchi, F. F.; Kimura, S. S.; Tokuda, M. M.; Jitsunari, F. F. Preventive effect of D-psicose, one of rare ketohexoses, on di-(2-ethylhexyl) phthalate (DEHP)-induced testicular injury in rat. *Toxicol. Lett.* **2007**, *173*, 107−117.

(6) Granström, T. B.; Takata, G.; Tokuda, M.; Izumori, K. Izumoring: a novel and complete strategy for bioproduction of rare sugars. *J. Biosci. Bioeng.* **2004**, *97*, 89−94.

(7) Itoh, H.; Okaya, H.; Khan, A. R.; Tajima, K.; Hayakawa, S.; Izumori, K. Purification and characterization of D-tagatose 3-epimerase from *Pseudomonas* Sp, St-24. *Biosci., Biotechnol., Biochem.* **1994**, *58*, 2168−2171.

(8) Zhang, L.; Mu, W.; Jiang, B.; Zhang, T. Characterization of D-tagatose-3-epimerase from *Rhodobacter sphaeroides* that converts D-fructose into D-psicose. *Biotechnol. Lett.* **2009**, *31*, 857−862.

(9) Kim, H. J.; Hyun, E. K.; Kim, Y. S.; Lee, Y. J.; Oh, D. K. Characterization of an *Agrobacterium tumefaciens* D-psicose 3-epimerase that converts D-fructose to D-psicose. *Appl. Environ. Microbiol.* **2006**, *72*, 981−985.

(10) Mu, W.; Chu, F.; Xing, Q.; Yu, S.; Zhou, L.; Jiang, B. Cloning, expression, and characterization of a D-psicose 3-epimerase from *Clostridium cellulolyticum* H10. *J. Agric. Food Chem.* **2011**, *59*, 7785−7792.

(11) Zhu, Y. Y.; Men, Y. Y.; Bai, W. W.; Li, X. X.; Zhang, L. L.; Sun, Y. Y.; Ma, Y. Y. Overexpression of D-psicose 3-epimerase from *Ruminococcus* sp. in *Escherichia coli* and its potential application in D-psicose production. *Biotechnol. Lett.* **2012**, *34*, 1901−1906.

(12) Hung, Y.-J. Y.; Peng, C.-C. C.; Tzen, J. T. C. J.; Chen, M.-J. M.; Liu, J.-R. J. Immobilization of *Neocallimastix patriciarum* xylanase on artificial oil bodies and statistical optimization of enzyme activity. *Bioresour. Technol.* **2008**, *99*, 8662−8666.

(13) Chiang, C.-J.; Chen, H.-C.; Kuo, H.-F.; Chao, Y.-P.; Tzen, J. T. C. A simple and effective method to prepare immobilized enzymes using artificial oil bodies. *Enzyme Microb. Technol.* **2006**, *39*, 1152−1158.

(14) Zeng, Y.-F.; Hung, Y.-J.; Chen, M.-J.; Peng, C.-C.; Tzen, J. T. C.; Liu, J.-R. Simultaneous refolding, purification, and immobilization of recombinant *Fibrobacter succinogenes* 1,3−1,4-β-D-glucanase on artificial oil bodies. *J. Chem. Technol. Biotechnol.* **2009**, *84*, 1480−1485.

(15) Chan, H.-C. H.; Zhu, Y. Y.; Hu, Y. Y.; Ko, T.-P. T.; Huang, C.-H. C.; Ren, F. F.; Chen, C.-C. C.; Ma, Y. Y.; Guo, R.-T. R.; Sun, Y. Y. Crystal structures of D-psicose 3-epimerase from *Clostridium cellulolyticum* H10 and its complex with ketohexose sugars. *Protein Cell* **2012**, *3*, 123−131.

(16) Peng, C.-C.; Shyu, D. J. H.; Chou, W.-M.; Chen, M.-J.; Tzen, J. T. C. Method for bacterial expression and purification of sesame cystatin via artificial oil bodies. *J. Agric. Food Chem.* **2004**, *52*, 3115−3119.

(17) Green, M. R.; Sambrook, J. *Molecular Cloning: A Laboratory Manual*, 4th ed.; Cold Spring Harbor Laboratory Press: Cold Spring Harbor, NY, USA, 2012.

(18) Chiang, C.-J.; Chen, H.-C.; Chao, Y.-P.; Tzen, J. T. C. Efficient system of artificial oil bodies for functional expression and purification of recombinant nattokinase in *Escherichia coli*. *J. Agric. Food Chem.* **2005**, *53*, 4799−4804.

(19) Laemmli, U. K. Cleavage of structural proteins during the assembly of the head of bacteriophage T4. *Nature* **1970**, *227*, 680−685.

(20) Lowry, O. H.; Rosebrough, N. J.; Farr, A. L.; Randall, R. J. Protein measurement with the Folin phenol reagent. *J. Biol. Chem.* **1951**, *193*, 265−275.
(21) Montgomery, D. C. *Design and Analysis of Experiments*, 8th ed.; Wiley: New York, 2012.
(22) Rodrigues, R. C.; Ortiz, C.; Berenguer-Murcia, Á.; Torres, R.; Fernández-Lafuente, R. Modifying enzyme activity and selectivity by immobilization. *Chem. Soc. Rev.* **2013**, *42*, 6290−6307.
(23) Ward, O. P.; Moo-Young, M. Thermostable enzymes. *Biotechnol. Adv.* **1988**, *6*, 39−69.

MATERIALS AND METHODS

Reagents and Solutions. Caffeine (CAS Registry No. 58-08-2), (+)-catechin (>99.0% (HPLC), CAS Registry No. 154-23-4) (C), (−)-epicatechin (>95.0% (HPLC), CAS Registry No. 490-46-0) (EC), (−)-epicatechin gallate (>98% (HPLC), CAS Registry No. 1257-08-5) (ECG), (−)-catechin gallate (>98% (HPLC), CAS Registry No. 130405-40-2) (CG), (−)-epigallocatechin (>95.0% (HPLC), CAS Registry No. 970-74-1) (EGC), (−)-gallocatechin (>98% (HPLC), CAS Registry No. 3371-27-5) (GC), (−)-gallocatechin gallate (>98% (HPLC), CAS Registry No. 4233-96-9) (GCG), (−)-epigallocatechin gallate (>95.0% (HPLC), CAS Registry No. 989-51-5) (EGCG), formic acid (>98%, CAS Registry No. 64-18-6), and acetic acid (>99%, CAS Registry No. 64-19-7) were all supplied by Sigma-Aldrich Química S.A. Methanol (high-performance liquid chromatography (HPLC) grade) CAS Registry No. 67-56-1 was provided by Scharlab (Mollet del Vallés, Spain). Ultrapure water was obtained from a Millipore Milli-Q_{PLUS} 185 system (Madrid, Spain).

An individual solution of each catechin and caffeine standard of 50 μg/g in methanol was used for the study. For building the calibration curve, a mixture of standards from caffeine and eight catechins with concentrations ranging between 1 ng/g and 75 μg/g in methanol was prepared. A 50 μg/g solution of green tea extract (GTE) was also prepared in methanol. The solution was filtered through a syringe filter of 0.22 μm pore size (KX Syringe Filter, 25 mm, 0.22 μm Nylon, Kinesis, UK) prior to injection.

Green Tea Extract and Polymeric Active Films. Green tea extract Sunphenon 90 MB (GTE) was supplied by TAIYO Europe (Filderstadt, Germany), and it contained around 75% total catechins (w/w), according to the HPLC determination provided by the supplier company.

The active packaging was manufactured and supplied by the Spanish company ARTIBAL S.A. (Sabiñánigo, Spain). It consisted of a solvent base coating layer (varnish) with a constant concentration of GTE (1% of green tea extract in the coating solution) applied on a plastic film of polyethylene terephthalate (PET). The system was under EU patent EP1477519-A1.[31] The coating varnish is approved for food contact. Active films contained the active substance expressed as percentage of active agent/weight active layer and the grammage of the material was 3.0 g/m^2. The PET film was 23 μm thick with a density of 18.73 ± 0.02 g/m^2. Coated films without GTE were used as blanks.

UPLC-MS/Q-TOF for the Analysis of Catechins and Caffeine Standards. Chromatography was carried out in an Acquity TM system using an Acquity UPLC BEH C18 column of 1.7 μm particle size (2.1 mm × 100 mm), both from Waters (Milford, MA, USA). Chromatography was carried out at 0.3 mL/min column flow, and the column temperature was 35 °C. The solvents used as mobile phase were water with 0.1% formic acid (eluent A) and methanol with 0.1% formic acid (eluent B). The gradient used was 0−6 min, 5% B; 6−8 min, 95% B; and 8−10 min, 5% B. The volume of sample injected was 5 μL.

Eluting compounds were detected by a time-of-flight mass spectrometer (TOF) LCT Premier XE from Waters with an electrospray probe in positive mode (ESI+) and in negative mode (ESI−) in W mode. Cone voltages were optimized between 20 and 50 V. Finally, 30 V was selected for the analysis because all catechin peaks were detected. Other MS parameters were as follows: desolvation gas flow, 600 L/h; desolvation gas temperature, 450 °C; source temperature, 120 °C. The MS range acquired was 50−1200 Da.

MassLynx (v. 4.1) software (Waters) was used to acquire and process the chromatographic and MS data.

UPLC-MS/TQ for the Analysis of GTE and for the Migration Tests. A system consisting of an Acquity Ultra Performance LC TQ detector (triple quadrupole; Waters) was used for the analysis. An ESI probe was used in positive (ESI+) and in negative (ESI−) mode as the ionization source, and MassLynx (v. 4.1) software (Waters) was used to acquire and process the chromatographic and MS data.

Chromatography was carried out in the Acquity system using an Acquity UPLC BEH C18 column of 1.7 μm particle size (100 mm × 2.1 mm) from Waters. Catechins and caffeine were separated under the following conditions: flow rate, 0.3 mL/min; injection volume, 10 μL; column temperature, 35 °C; solvents used as mobile phase were water with 0.1% formic acid (eluent A) and methanol with 0.1% formic acid (eluent B); and gradient used was 0−6 min, 5% B; 6−8 min, 95% B; and 8−10 min, 5% B.

Eluting compounds were detected and quantified by MS in both positive and negative modes under the following ionization conditions: capillary voltage, ±3.50 kV; source temperature, 120 °C; desolvation gas temperature, 450 °C; cone gas flow, 40 L/h; desolvation gas flow, 450 L/h. The cone voltage selected was 30 V. The compounds were detected in SIR mode, and the m/z ratios selected were 289.07 (C and EC, ESI−), 305.07 (EGC and GC, ESI−), 441.08 (ECG and CG, ESI−), 457.08 (EGCG and GCG, ESI−), and 195.08 (caffeine, ESI+).

Migration Tests. For migration experiments, a 6 cm × 12 cm piece of active plastic film was immersed in a 20 mL simulant solution. The simulants used for the migration test were Milli-Q water (simulant A from Directive 2002/72[32]) and 3% acetic acid in purified water (simulant B). The solutions were kept in an oven at 70 °C for 2 h. Finally, the solutions were analyzed by UPLC-MS/TQ using the same chromatographic method previously described. The concentration of GTE in the active plastic films was 1% in the coating solution. Plastic films without GTE were used as blanks. All of these samples were prepared in triplicate. The migration values were expressed as micrograms of compound per kilogram of food simulant. The migration values were corrected by taking into account the proportion of laminate/food simulant used in these experiments (72 cm^2 of laminate/20 mL of simulant) and those established in EU Regulation 10/2011 on plastic materials (6 dm^2 of laminate/1 kg of food simulant).[33]

Spectroscopic Analysis of Catechins and Caffeine Standards: The Continuous Variations Method (Job's Method). A 0.09 μM solution of catechin standard and 0.09 μM solution of epicatechin standard were prepared in methanol. A 0.13 μM solution of caffeine was also prepared in methanol. Five solutions were prepared and mixed to give solutions of mole fraction (X) of catechins solution varying from 0 to 1. Specifically, the different molar fraction solutions prepared were 0, 0.25, 0.5, 0.75, and 1. The measurements were carried out in a 1 cm quartz cell, and the volume of the final mixture was 3 mL. The absorbance of the mixtures was measured at 279 nm with a UV-1700 PharmaSpec UV−vis spectrophotometer (Shimadzu, Kyoto, Japan). All of the measurements were performed in triplicate.

Computer Simulation of Complexes between Caffeine and Catechins. Chem Draw and Chem 3D Pro 12.0 (Cambridge Soft Corp., Cambridge, MA, USA) were the softwares used to simulate the complexes between caffeine and catechins. These softwares are powerful tools for producing a nearly unlimited variety of biological and chemical drawings and can generate, operate, calculate, and predict realistic molecular structures and associated properties such as energies involved. Using Chem 3D Pro energy calculations with MM2 force field can be carried out.[34] MM2 methods include (1) "energy minimization" for locating stable conformation (global minimum), (2) "molecular dynamics" for studying molecular motion of atoms, and (3) "compute properties" for reporting the total steric energy (TSE) in a current conformation of a model.[35]

To optimize the model measurements, the minimum RMS gradient was fixed as 0.100, which was a reasonable compromise between accuracy and speed of calculations and afforded results close to a global minimum value of energy. The step interval, which determines the time between molecular dynamics steps, was fixed as 2 fs, and the frame interval value, which determines the interval at which frames and statistics are collected, was 10 fs. These values provided short periods of analysis. The heating/cooling rate was approximately 1.0 kcal/atom/ps because it minimally disturbed the trajectory of atoms. Finally, the target temperature was 300 K. The simulation is terminated when the target temperature is reached.

RESULTS AND DISCUSSION

Migration Test. Catechins and caffeine are the major ingredients in GTE. These compounds are known for their

antioxidant properties and can be incorporated into packaging materials to protect foodstuffs. In this work, active plastic films containing 1% green tea extract in the coating formula were evaluated. The migration values of catechins and caffeine were studied in two different food simulants. The most relevant analytical parameters for UPLC-MS/TQ are shown in Table 1.

Table 1. Analytical Features of the UPLC-MC/TQ Method

name	linear range (μg/kg)	LOD (μg/kg)	LOQ (μg/kg)	RSD (%, n = 3)
(+)-C	0.22−52.34	0.07	0.22	2.60
(−)-EC	0.09−52.34	0.03	0.09	3.37
(−)-GC	9.66−52.34	2.90	9.66	1.41
(−)-EGC	4.70−52.34	1.41	4.70	1.14
(−)-ECG	0.95−52.34	0.29	0.95	2.90
(−)-CG	0.44−52.34	0.13	0.44	1.25
(−)-EGCG	0.29−52.34	0.09	0.29	3.29
(−)-GCG	0.47−52.34	0.14	0.47	2.27
caffeine	0.07−24.56	0.02	0.07	1.05

Good results were obtained in terms of limit of detection (LOD), limit of quantification (LOQ), and reproducibility. The LOD values were between 0.02 μg/kg (caffeine) and 2.90 μg/kg (GC). In fact, the stereoisomers GC and EGC were the catechins with the lowest LODs. The RSD values were below 4%. The linear ranges obtained were calculated with at least five calibration points, and the results varied from 0.09 to 52.34 μg/kg for catechins. For caffeine, the linear range obtained was from 0.07 to 24.56 μg/kg.

Table 2 shows the migration values of catechins and caffeine found in the migration experiments for both simulants. The

Table 2. Migration Values of Catechins and Caffeine in Two Aqueous Simulants by UPLC-MS/TQ

name	simulant Milli-Q water (μg/kg)	simulant 3% acetic acid in water (μg/kg)
(+)-C	10.44 ± 0.76	22.52 ± 0.98
(−)-EC	18.76 ± 0.04	82.12 ± 0.87
(−)-GC	ND[a]	ND
(−)-EGC	ND	ND
(−)-ECG	15.46 ± 1.02	160.52 ± 4.51
(−)-CG	5.79 ± 0.45	13.30 ± 2.34
(−)-EGCG	4.20 ± 1.08	213.80 ± 6.76
(−)-GCG	3.94 ± 0.16	16.17 ± 0.43
caffeine	548.27 ± 4.33	1107.51 ± 5.65

[a]ND, not detected.

migration values were calculated for all catechins and caffeine except for GC and EGC, for which values were not detected in any simulant. Caffeine exhibited the highest migration value for simulants A and B, 548.27 ± 4.33 and 1107.51 ± 5.65 μg/kg, respectively. Approximately, the migration value of caffeine in simulant B was twice the migration value in simulant A. Catechins showed migration values from 3.94 ± 0.16 to 18.76 ± 0.04 μg/kg for simulant A and from 13.30 ± 2.34 to 213.80 ± 6.76 μg/kg for simulant B. It can be seen that the migration values for all green tea components took place in a major extension for simulant B. This fact can be related to the solubility of the catechins and caffeine in the different simulants. For simulant B, which was 3% acetic acid in purified water, the catechins and caffeine can be easily protonated, and therefore the solubility of these compounds from the plastic material is increased. However, for simulant A, which was Milli-Q water, the solubility was not so favorable, as the molecules are not protonated in water and therefore the migration values were lower than in simulant B.

On the other hand, the *cis* isomers (EC, ECG, and EGCG) exhibited higher migration values than the *trans* isomers (C, CG, and GCG). This fact can be related to the initial concentration of each catechin in the GTE (Table 3, column

Table 3. Concentration Values of Catechins and Caffeine of Green Tea Extract in the Absence (without H^+) and Presence (5% H^+) of Formic Acid

name	concn (μg/g), without H^+	%RSD (n = 3) without H^+	concn (μg/g), 5% H^+	%RSD (n = 3), 5% H^+	concn increase (%)
(+)-C	0.18	1.31	0.25	3.23	29.90
(−)-EC	3.13	0.95	3.95	1.23	20.75
(−)-GC	2.18	1.05	2.21	1.45	1.68
(−)-EGC	3.10	3.47	3.12	0.43	0.66
(−)-ECG	2.35	4.82	2.35	2.01	0.01
(−)-CG	0.98	1.47	1.01	0.23	2.39
(−)-EGCG	29.58	0.37	29.62	1.56	0.14
(−)-GCG	1.92	1.64	1.96	4.56	1.70
caffeine	4.10	4.74	4.88	4.87	15.95

2). For all *cis* isomers, the initial concentration was higher than the initial concentration of the *trans* isomers. As a consequence, the migration of the *cis* isomers such as EC, ECG, and EGCG from the material was higher than that for the *trans* isomers.

Migration values of catechins and caffeine were higher for the acidic food simulant (simulant B) than for water. To understand the behavior of green tea components, several experiments based on the influence of pH on the catechins and caffeine standards as well as on the green tea extract were investigated.

Influence of Acidic Media in Catechins and Caffeine Standards and in GTE. The high increase of caffeine is of concern, as this compound would be incorporated into the food. The migration tests showed a considerable influence of pH in the specific migration values of catechins and caffeine. To understand better the release of free caffeine and some catechins, an in-depth study was carried out. First, an acidic medium (formic acid) was added to several standard solutions of tea catechins and caffeine to evaluate the influence of the media in the tea components. Different stereoisomer mixtures of pure catechins were prepared, and caffeine was added to each catechin mixture. Specifically, the mixtures prepared in methanol were as follows: C, EC, and caffeine; GC, EGC, and caffeine; ECG, CG, and caffeine; EGCG, GCG, and caffeine. All of these mixtures were prepared in equimolecular concentrations of 50 μg/g each one (1:1:1). The samples were analyzed by UPLC-MS/Q-TOF in the absence of formic acid and after the addition of 5% formic acid. The area values were calculated in both cases, and the differences observed in the different mixtures were expressed as percent of area increase. Figure 1 shows the results obtained for these experiments. The combination of C, EC, and caffeine (1:1:1) was the mixture that showed the major change in the precent of area increase. After the addition of formic acid, the area of C increased 15.83%, the area of EC increased 13.41%, and the area of caffeine increased 14.45%. The proportions of C, EC, and caffeine increase were about the same, and it can be related to the concentration of each standard in the mixture. The percent

dx.doi.org/10.1021/jf5011287 | J. Agric. Food Chem. 2014, 62, 6777−6783

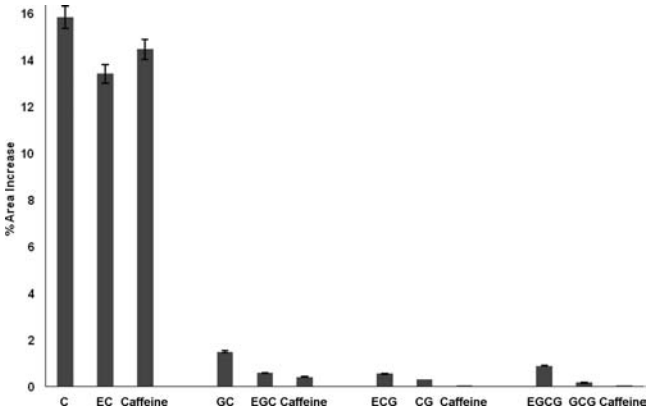

Figure 1. Percentage of area increase of different equimolecular mixtures of stereoisomers of catechins and caffeine (1:1:1) after addition of 5% formic acid.

area increase for the rest of the mixtures was almost unchanged. In fact, the percent area increase for the different mixtures was as follows: GC (1.89%), EGC (0.58%), and caffeine (0.41%); ECG (0.56%), CG (0.30%), and caffeine (0.06%); EGCG (0.89%), GCG (0.16)%, and caffeine (0.04%).

After the analysis of the different standard mixtures, the influence of the acidic media was evaluated in the GTE. GTE contains the eight catechins and caffeine previously studied as standards, but not as equimolecular proportions. A 50 μg/g solution of GTE in methanol was prepared in triplicate. The chromatographic analysis was carried out by UPLC-MS/TQ before and after the addition of 5% formic acid. This technique allowed us to quantify the variation of the different catechins and caffeine when formic acid was added. The results are shown in Table 3, where the second column lists the initial concentration of each green tea component before the addition of formic acid. Caffeine showed an initial concentration value of 4.10 μg/g. As can be seen, the proportion of catechins was not equimolecular, the *cis* isomers EC (3.13 μg/g), EGC (3.10 μg/g), ECG (2.35 μg/g), and EGCG (29.62 μg/g) being the most concentrated compounds in the GTE. The *trans* isomers showed initial concentration values below 2.18 μg/g (GC). The last column in Table 3 shows the concentration increase of the different catechins and caffeine after the addition of formic acid, expressed as percentage. Again, C (29.90%), EC (20.75%), and caffeine (44.93%) exhibited the major changes. The other catechins exhibited a variation below 2.39% (CG). In all cases the percentage of relative standard deviation was below 5%.

From the results obtained for the standards by UPLC-MS/Q-TOF and for GTE by UPLC-MS/TQ, it can be concluded that caffeine, C, and EC increased their concentration as a consequence of the addition of formic acid. According to the literature, C forms a 1:1 complex with caffeine by intermolecular hydrogen bonds[22] as well as EC, which forms also a 1:1 complex.[21] It is known that caffeine behaves as a very feeble base and reacts with acids. Experimental methods have explored the most stable protonated structure corresponding to the most basic site in the molecule, and the structure protonated from the N7 site (Figure 2), MH^+ (N7) was the most stable among the ions studied.[36] From this bibliography, it can be concluded that in the absence of formic acid, C and EC can exist as a C−caffeine complex anda an EC−caffeine complex, which present intermolecular interactions between molecules. However, in the presence of formic acid, the

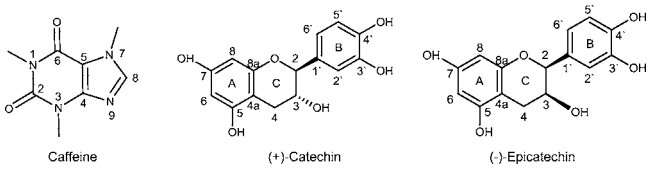

Figure 2. Structures of caffeine, (+)-catechin, and (−)-epicatechin.

molecules of caffeine can be protonated as quaternary ammonium salts and, consequently, the intermolecular interactions present in the complexes between C and caffeine and the complexes of EC and caffeine can be broken. As a result of this breakdown, molecules of C, EC, and caffeine can be released as individual free molecules and their concentrations increase. Furthermore, the sum of percent concentration increase for C and EC was approximately the same percentage value obtained for caffeine. These results suggest that for each molecule of caffeine liberated, one molecule of C or one molecule of EC will be liberated after the breakdown of the C−caffeine or EC−caffeine complex. This conclusion can be supported by the stoichiometry of the C−caffeine (1:1) or EC−caffeine (1:1) complexes proposed by Ishizu et al.[21,22] This fact is interesting and opens new ways to trap active compounds by chemical interaction with catechins.

Spectroscopic Analysis of Catechins and Caffeine Standards: The Continuous Variations Method (Job's Method). To confirm the formation of complexes between catechin and epicatechin with caffeine and their stoichiometry, a spectroscopic analysis based on the continuous variations method has been carried out. This method is often referred to as Job's method,[36] and it is an easy and common method for the determination of the reactant stoichiometry of chemical equilibrium. In this method, the measured concentration of the complex between catechin or epicatechin with caffeine (or a parameter that is proportional to its concentration such as its UV−vis maximum absorbance) is plotted against the mole fraction of the catechin or epicatechin solution reactant, whereas the sum of the reactant concentrations (catechin solution plus caffeine solution) is kept constant. This plot is referred to as Job's plot. Figure 3 shows the Job's plots of the C−caffeine system (dashed line) and the EC−caffeine system (continuous line). Five solutions of catechin derivate and caffeine were measured at different mole fractions, from 0 to 1, with a constant concentration of 0.03 μM. The maximum point of the curve, which corresponds to the maximum concentration

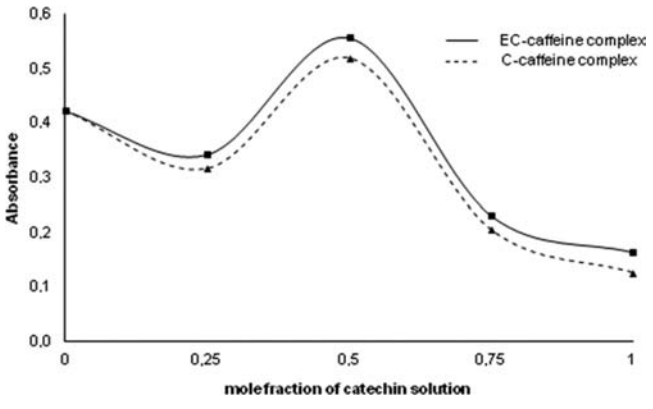

Figure 3. Job's plots of C−caffeine system (dashed line) and EC−caffeine system (continuous line).

dx.doi.org/10.1021/jf5011287 | J. Agric. Food Chem. 2014, 62, 6777−6783

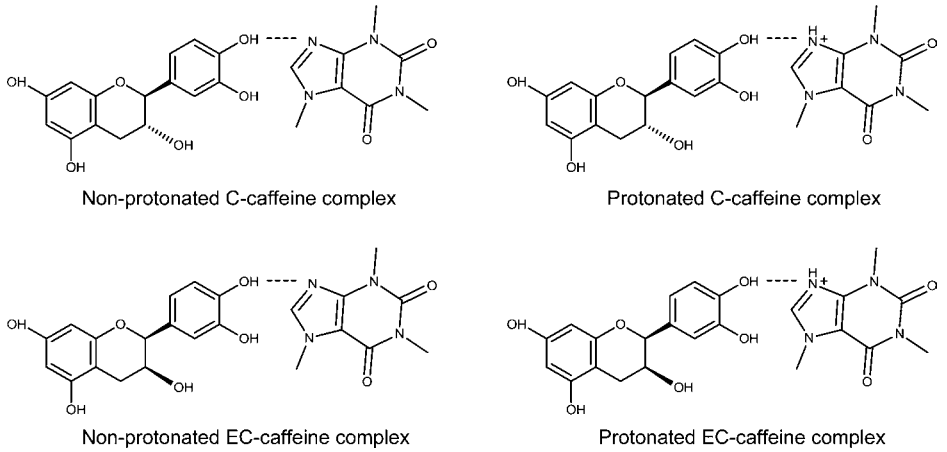

Figure 4. Structures of nonprotonated and protonated C−caffeine and EC−caffeine complexes.

of the catechin−caffeine complex, determined the stoichiometry of the equilibrium reaction. From this curve, the stoichiometry obtained for the C−caffeine complex was 1:1, and the absorbance value at this point was 0.518. In the case of the EC−caffeine complex, the stoichiometry of the complex was also 1:1 and the absorbance value was 0.556. Error bars show the relative standard deviation expressed as percentage (% RSD), and %RSD was below 2% for all measures.

The continuous variations method demonstrated that the complex between catechin and epicatechin with caffeine is formed in equimolecular proportions (1:1). These results confirm the conclusions given after the UPLC analysis of the green tea standards and the GTE. UPLC and spectrophotometric analyses confirm that catechin and epicatechin form complexes with caffeine by intermolecular interactions and these complexes are formed in 1:1 complex association.

An Approach: Simulation of Complexes of Tea Catechins with Caffeine. According to the results presented above, C and EC formed a complex with caffeine by intermolecular interactions, and this fact agrees with the previous bibliography.[21,22] Spectroscopic analysis also demonstrated that these complexes are formed in 1:1 complex association, catechin−caffeine complex and epicatechin−caffeine complex. The increase of the concentration value of free caffeine in the presence of formic acid means that caffeine was protonated as a quaternary ammonium salt. Consequently, the complexes between C and EC with caffeine can be broken and the different molecules can be liberated, thus increasing their concentrations. A molecular modeling approach was proposed to confirm the results experimentally obtained. Chem 3D Pro software was selected as the molecular modeling to perform this study.

The structures of C, EC, caffeine, protonated caffeine (Figure 2), and the complexes of C and EC with caffeine based on the structures determined by Ishazu et al.[21,22] (Figure 4) were drawn by Chem Draw. On the other hand, the protonated complexes of C and EC with caffeine were also drawn by Chem Draw software (Figure 4). The protonated site of caffeine was the N7 site according to the literature.[37] The hydrogen bond is represented by a dashed line in all structures (Figure 4).

Several dihedral angles of the catechin−caffeine complexes were calculated by Chem 3D Pro, and the values obtained are shown in Table 4. The dihedral angle values calculated for protonated and nonprotonated structures were the same. Therefore, Table 4 shows the dihedral angle values of nonprotonanted structures. The dihedral angle values obtained by the software were compared with the values determined by Ishazu et al.,[21,22] and they exhibited high similarity. Therefore, the results afforded by the software could be considered sufficiently reliable.

Table 4. Comparison of Chem 3D Pro Values and Ishazu et al.[21,22] Values of Several Dihedral Angles of the Complexes between C or EC and Caffeine

dihedral angle	Chem 3D Pro value	Ishazu et al. value
$H_2-C_2-C_3-H_3$ (C−caffeine)	173.1°	169.0°
$C_1'-C_2-C_3-O$ (C−caffeine)	52.4°	48.7°
$H_2-C_2-C_3-H_3$ (EC−caffeine)	66.1°	60.23°
$O_1-C_2-C_3-H_3$ (EC−caffeine)	176.0°	179.6°

Table 5 shows the computed properties of C, EC, caffeine, protonated caffeine, and the different complexes, nonprotonated and protonated, between C or EC and caffeine after the geometry optimization. For this, MM2 calculations were carried out by Chem 3D Pro software. The protocol of the procedure was as follows: (1) To calculate the computed properties of the structures proposed before the geometry optimization, different energy values were given such as stretch, bend, torsion, van der Waals, dipole−dipole, and charge−dipole. The energy values calculated for C, EC, caffeine, and protonated caffeine were the best energy values obtained after the MM2 job. However, the energy values obtained for all complexes were high TSE for the current conformation, and these results indicated that the geometry of these complexes was not optimized. The TSE values of complexes were approximately 2000 kcal/mol for all cases. (2) To obtain the geometry optimization, which corresponds to a minimum energy point, an energy minimization job was performed for each complex. For all structures evaluated, the TSE of the structures was much lower after geometry optimization. (3) A molecular dynamic job was performed to simulate the motion of the forces acting on the atoms. (4) Finally, a second computed properties job was performed after the energy minimization and molecular dynamic jobs. At this point, the total steric energy value was the best value obtained by running the MM2 methodology, which corresponded to the minimum energy value for the complex studied, and therefore the conformation that was more likely to exist.

These TSE values as well as the energy values of stretch, bend, torsion, van der Waals, dipole−dipole, and charge−dipole

dx.doi.org/10.1021/jf5011287 | J. Agric. Food Chem. 2014, 62, 6777−6783

Table 5. Energy Values of Several Parameters Calculated by Chem Pro 12.0 of Catechin, Epicatechin, Caffeine, Protonated Caffeine, and Nonprotonated and Protonated C−Caffeine and EC−Caffeine Complexes

energy (kcal/mol)	C	EC	caffeine	protonated caffeine	nonprotonated C−caffeine	protonated C−caffeine	nonprotonated EC−caffeine	protonated EC−caffeine
strech	1.0824	1.1529	0.8574	0.8763	2.2376	2.2405	2.2845	2.2357
bend	5.4820	6.6179	22.3571	21.5206	16.2340	29.4483	16.9875	29.8070
strech−bend	−0.0838	−0.0048	−0.0961	−0.0124	−0.0097	−0.0664	0.0271	−0.0321
torsion	−14.6109	−13.6778	1.9123	1.9651	−8.4744	−10.8780	−9.3759	−11.2062
non-1,4 VDW	−12.4550	−12.3518	0.3622	1.0650	−13.6243	−5.4612	−13.7413	−5.8387
1,4-VDW	12.6950	12.2932	9.2112	9.2406	25.3927	25.5631	25.2569	25.3394
charge−dipole				6.6489		−5.2226		−4.3414
dipole−dipole	0.0655	0.0616	−12.1210	−11.8936	−7.8468	−13.0465	−6.9793	−12.0958
total steric energy	−7.8248	−5.9089	22.4832	29.4105	13.9091	22.5772	14.4597	23.8679

are shown in Table 5 for the different structures. The aim of this simulation was to compare the main differences between nonprotonated and protonated complexes. For this purpose, the conclusions of this study were based on the total steric energy values. First, the sum of individual TSE values of C and caffeine (14.6584 kcal/mol) was compared to the TSE value of nonprotonated C−caffeine complex (13.9091 kcal/mol). Similarly, the sum of individual TSE values of EC and caffeine (16.5743 kcal/mol) was compared to the TSE value of the nonprotonated EC−caffeine complex (14.4597 kcal/mol). In both cases, the TSE values were lower for the C and EC complexes, and it was concluded that both C and EC were more likely to form caffeine complexes. With respect to the protonation of caffeine, the sum of the individual TSE values of C and protonated caffeine (21.5857 kcal/mol) was compared to the TSE value of protonated C−caffeine complex (22.5772 kcal/mol) and the sum of the individual TSE values of EC and protonated caffeine (23.5016 kcal/mol) was compared to the TSE value of protonated EC−caffeine complex (23.8679 kcal/mol). These differences showed that the protonated complexes of C and EC were less likely to exist than the molecules not arranged.

The differences of energy between nonprotonated and protonated complexes were also compared. The TSEs obtained for C−caffeine (13.9091 kcal/mol) and EC−caffeine (14.4597 kcal/mol) nonprotonated complexes were lower than the values obtained for C−caffeine (22.5772 kcal/mol) and EC−caffeine (23.8679 kcal/mol) protonated complexes. Once again, these results suggested that the nonprotonated complexes were more likely to exist compared to the protonated complexes.

The simulation data showed that protonated complexes were less stable than nonprotonated complexes, and these results consolidated the idea that the intermolecular hydrogen bond among catechins−caffeine complexes can be broken, giving individual molecules of C, EC, and the ammonium salt of caffeine, to establish the most stable conformation. Both the experimental work and the simulation studio concluded that C and EC form equimolecular complexes with caffeine in neutral media. However, the presence of an acidic media involves the breakdown of the intermolecular interactions between molecules, giving C, EC, and the ammonium salt of caffeine as free molecules.

This work recovers important information about the green tea components and their behavior depending on the pH of the media. The starting migration analysis of active packaging films containing GTE showed unexpected migration values for 3% acetic acid simulant. Specifically, the migration values in acidic simulant were more than double the migration values for aqueous simulant. To explain these results, a detailed UPLC analysis of green tea standards as well as green tea extract was performed. From the chromatographic results obtained and the previously reported literature, the formation of equimolecular complexes between catechins and caffeine through intermolecular interactions is proposed. The complexes can exist in neutral media but can be broken in acidic media as a consequence of the protonation of caffeine. A spectroscopic analysis based on the continuous variations method, also called Job's method, was carried out to verify the stoichiometry of the C-−affeine complex and EC−caffeine complex proposed. The results obtained for Job's method confirm that these complexes are formed in 1:1 complex association. Finally, a simulation studio based on the stabilization energies of the protonated and nonprotonated catechin complexes was performed to confirm

the conclusions achieved from the experimental work. The simulation showed that the total steric energies of the nonprotonated complexes are higher than the protonated complexes and therefore more stable and likely to exist. The conclusions reached from the simulation studio support the information given by the experimental analysis.

AUTHOR INFORMATION

Corresponding Author

*(C.N.) Phone: +34 976 761873. Fax: +34 976 2388. E-mail: cnerin@unizar.es.

Funding

This research has been financed by Project INNPACTO 2010/0486 from the MICINN, Ministerio de Ciencia e Innovación, Spain. We thank Project Gobierno de Aragón and European Social Funds for financing the research group GUIA-T-10.

Notes

The authors declare no competing financial interest.

REFERENCES

(1) Bose, M.; Lambert, J. D.; Ju, J.; Reuhl, K. R.; Shapses, S. A.; Yang, C. S. The major green tea polyphenol, (−)-epigallocatechin-3-gallate, inhibits obesity, metabolic syndrome, and fatty liver disease in high-fat-fed mice. *J. Nutr.* **2008**, *138*, 1677−1683.

(2) Murase, T.; Haramizu, S.; Shimotoyodome, A.; Tokimitsu, I. Reduction of diet-induced obesity by a combination of tea-catechin intake and regular swimming. *Int. J. Obes.* **2006**, *30*, 561−568.

(3) Sharma, A.; Gupta, S.; Sarethy, I. P.; Dang, S.; Gabrani, R. Green tea extract: possible mechanism and antibacterial activity on skin pathogens. *Food Chem.* **2012**, *135*, 672−675.

(4) Shiota, S.; Shimizu, M.; Mizushima, T.; Ito, H.; Hatano, T.; Yoshida, T.; Tsuchiya, T. Marked reduction in the minimum inhibitory concentration (MIC) of β-lactams in methicillin-resistant Staphylococcus aureus produced by epicatechin gallate, an ingredient of green tea (*Camellia sinensis*). *Biol. Pharm. Bull.* **1999**, *22*, 1388−1390.

(5) Frei, B.; Higdon, J. V. Antioxidant activity of tea polyphenols in vivo: evidence from animal studies. *J. Nutr.* **2003**, *133*, 3275−3284.

(6) Roy, M. K.; Koide, M.; Rao, T. P.; Okubo, T.; Ogasawara, Y.; Juneja, L. R. ORAC and DPPH assay comparison to assess antioxidant capacity of tea infusions: relationship between total polyphenol and individual catechin content. *Int. J. Food Sci. Nutr.* **2010**, *61*, 109−124.

(7) Chung, S. Y.; Xin, W. Green tea and cancer prevention. *Nutr. Cancer* **2010**, *62*, 931−937.

(8) Singh, B. N.; Shankar, S.; Srivastava, R. K. Green tea catechin, epigallocatechin-3-gallate (EGCG): mechanisms, perspectives and clinical applications. *Biochem. Pharmacol.* **2011**, *82*, 1807−1821.

(9) Yuan, J. M.; Sun, C.; Butler, L. M. Tea and cancer prevention: epidemiological studies. *Pharm. Res.* **2011**, *64*, 123−135.

(10) Nathanson, J. A. Caffeine and related methylxanthines − possible naturally-occurring pesticides. *Science* **1984**, *226*, 184−187.

(11) Glade, M. J. Caffeine − not just a stimulant. *Nutrition* **2010**, *26*, 932−938.

(12) Perva-Uzunalic, A.; Skerget, M.; Knez, Z.; Weinreich, B.; Otto, F.; Gruner, S. Extraction of active ingredients from green tea (*Camellia sinensis*): extraction efficiency of major catechins and caffeine. *Food Chem.* **2006**, *96*, 597−605.

(13) Gaffney, S. H.; Martin, R.; Lilley, T. H.; Haslam, E.; Magnolato, D. The association of polyphenols with caffeine and α-cyclodextrin and β-cyclodextrin in aqueous-media. *Chem. Commun.* **1986**, *2*, 107−109.

(14) Horman, I.; Viani, R. Nature and conformation of caffeine-chlorogenate complex of coffee. *J. Food Sci.* **1972**, *37*, 925−927.

(15) Martin, R.; Lilley, T. H.; Falshaw, C. P.; Haslam, E.; Begley, M. J.; Magnolato, D. The caffeine potassium chlorogenate molecular-complex. *Phytochemistry* **1987**, *26*, 273−279.

(16) Maruyama, N.; Suzuki, Y.; Sakata, K.; Yagi, A.; Ina, K.; Duke, C. C. NMR spectroscopic and computer-graphics studies on the creaming down of tea. *Int. Symp. Tea Sci.* **1991**, 145−149.

(17) Cai, Y.; Gaffney, S. H.; Lilley, T. H.; Magnolato, D.; Martin, R.; Spencer, C. M.; Haslam, E. Polyphenol interactions. 4. Model studies with caffeine and cyclodextrins. *J. Chem. Soc., Perkin Trans. 2* **1990**, *12*, 2197−2209.

(18) Hayashi, N.; Ujihara, T.; Kohata, K. Binding energy of tea catechin/caffeine complexes in water evaluated by titration experiments with H-1-NMR. *Biosci., Biotechnol., Biochem.* **2004**, *68*, 2512−2518.

(19) Ishizu, T.; Tsutsumi, H.; Sato, T. Interaction between gallocatechin gallate and caffeine in crystal structure of 1:2 and 2:2 complexes. *Tetrahedron Lett.* **2009**, *50*, 4121−4124.

(20) Ishizu, T.; Tsutsumi, H.; Sato, T.; Yamamoto, H.; Shiro, M. Crystal structure of complex of gallocatechin gallate and caffeine. *Chem. Lett.* **2009**, *38*, 230−231.

(21) Ishizu, T.; Sato, T.; Tsutsumi, H.; Yamamoto, H. Stereochemical structure determination of caffeine complexes with galloylated and non-galloylated catechins. *Chem. Lett.* **2010**, *39*, 607−609.

(22) Tsutsumi, H.; Kinoshita, Y.; Sato, T.; Ishizu, T. Configurational studies of complexes of various tea catechins and caffeine in crystal state. *Chem. Pharm. Bull.* **2011**, *59*, 1008−1015.

(23) Ishizu, T.; Kajitani, S.; Tsutsumi, H.; Sato, T.; Yamamoto, H.; Hirata, C. Configurational studies of complexes of tea catechins with caffeine and various cyclodextrins. *Planta Med.* **2011**, *77*, 1099−1109.

(24) De Dicastillo, C. L.; Nerin, C.; Alfaro, P.; Catala, R.; Gavara, R.; Hernandez-Munoz, P. Development of new antioxidant active packaging films based on ethylene vinyl alcohol copolymer (EVOH) and green tea extract. *J. Agric. Food Chem.* **2011**, *59*, 7832−7840.

(25) Shin, H. S.; Lee, Y. Antioxidant-impregnated food packaging materials for inhibition of lipid oxidation. *Food Sci. Biotechnol.* **2003**, *12*, 737−746.

(26) Vargas, M.; Pastor, C.; Chiralt, A.; McClements, D. J.; Gonzalez-Martinez, C. Recent advances in edible coatings for fresh and minimally processed fruits. *Crit. Rev. Food Sci. Nutr.* **2008**, *48*, 496−511.

(27) Colon, M.; Nerin, C. Role of Catechins in the antioxidant capacity of an active film containing green tea, green coffee, and grapefruit extracts. *J. Agric. Food Chem.* **2012**, *60*, 9842−9849.

(28) Peng, Y.; Wu, Y.; Li, Y. Development of tea extracts and chitosan composite films for active packaging materials. *Int. J. Biol. Macromol.* **2013**, *59*, 282−289.

(29) Silva-Weiss, A.; Ihl, M.; Sobral, P. J. A.; Gomez-Guillen, M. C.; Bifani, V. Natural additives in bioactive edible films and coating: funcionality and applications in foods. *Food Eng. Rev.* **2013**, *5*, 200−216.

(30) Aznar, M.; Rodriguez-Lafuente, A.; Alfaro, P.; Nerin, C. UPLC-Q-TOF-MS analysis of non-volatile migrants from new active packaging materials. *Anal. Bioanal. Chem.* **2012**, *404*, 1945−1957.

(31) Garces, O.; Nerin C.; Beltran, J. A.; Roncales, P. EU patent EP1477519-A1, 2004.

(32) Commission Directive (EU) No. 72/2002 of 6 August 2002 relating to plastic materials and articles intended to come into contact with foodstuffs.

(33) Commission Regulation (EU) No. 10/2011 of 14 January 2011 on plastic materials and article intended to come into contact with food.

(34) Stan, T. C. *An Introduction to Computational Biochemistry*; Wiley-Liss: New York, 2002; Vol. 14, pp 285−314.

(35) Office, C. *Chem 3D User's Manual*; Cambridge Soft Corp.: Cambridge, MA, USA, 2005.

(36) Job, P. Formation and stability of inorganic complexes in solution. *Ann. Chim.* **1928**, *9*, 113−203.

(37) Bahrami, H.; Tabrizchi, M.; Farrokhpour, H. Protonation of caffeine: a theoretical and experimental study. *Chem. Phys.* **2013**, *415*, 222−227.

is performed, and due to the complexity of the yeast metabolome, there is a loss of information because the focus is not on the overall system. An untargeted approach allows the visualization of the process and reveals new insights by detecting as many metabolites as possible in a single step.[17,19] In an attempt to get as close as possible to this holistic metabolic view of a complex biological process, the aim of the present work is to build a metabolic profiling pipeline able to identify metabolites from a perturbed data set and latter validate them in their biochemical context. This newly developed methodology reproduces in a micro scale (5 mL) the same metabolic events that are usually monitored in a larger scale enabling the high throughput analysis of samples. The 5 mL fermentations were monitored online and noninvasively through the continuous sampling of the volatile fraction by headspace—solid phase microextraction (HS-SPME) analyzed by gas chromatography coupled to a mass spectrometry detection system (GC-MS) in order to capture as much information regarding the fermentation process as possible.

In order to evaluate the proposed pipeline a commercial stain of *Saccharomyces cerevisiae* fermented synthetic grape must containing the same concentration (200 mg/L) of different sources (ammonium and amino acids) of yeast assimilable nitrogen. These 5 mL fermentations were analyzed and the pipeline was validated by comparing them to a second set of fermentations performed on a larger scale (500 mL). The metabolic information was subjected to preprocessing through algebraic normalization (Pareto) using MarkerLynx, both in one dimension (1D), where the total ion chromatogram per sample was used and in two dimensions (2D), where the integrity time vs m/z per sample was used. Multivariate variable analysis (MVA) was used to evaluate the potential of a high throughput pipeline. This type of approach needs validation with the study of real time perturbations in a time course of some chemical compounds (targeted approach).

MATERIALS AND METHODS

Chemicals. The highest purity chemicals were used throughout the experiments. All chemicals were from Sigma-Aldrich (Germany) or Merck (Germany) unless otherwise stated.

Strain, Media, and Culture Conditions. The yeast strain used in this study was *Saccharomyces cerevisiae* VIN13 (Anchor yeast, Cape Town, South Africa). The yeast preculture was grown in the fermentation medium described below and containing NH_4Cl (1g/L) as nitrogen source. The yeast, precultured to the logarithmic growth phase, was centrifuged and resuspended in saline solution. Fermentation vessels were inoculated with the preculture to an OD_{600} of 0.1 (final cell density of approximately 10^6 cells/mL).

Fermentations were carried out in grape juice medium adapted from Jiranek et al.[20] The synthetic media was prepared by the combination of two aqueous solutions prepared and sterilized separately. The first solution contained glucose (100 g/L), fructose (100 g/L), citric acid (0.2 g/L), malic acid (3 g/L), K_2HPO_4 (1.14 g/L), $MgSO_4{\cdot}7H_2O$ (1.23 g/L), $CaCl_2{\cdot}2H_2O$ (0.44 g/L), KH tartrate (2.5 g/L). All the compounds were dissolved in distilled water, and the pH was set to 3.3 with KOH 10 M. This solution was autoclaved for sterilization. The second solution contained NH_4Cl and/or amino acids as described in Table 1, trace elements stock (final concentration in the synthetic grape must: $MnCl_2{\cdot}4H_2O$ 200 μg/L, $ZnCl_2$ 135 μg/L, $FeSO_4$ 36 μg/L, $CuCl_2$ 15 μg/L, H_3BO_3 5 μg/L, $Co(NO_3)_2.6H_2O$ 30 μg/L, $NaMoO_4.2H_2O$ 25 μg/L, and KIO_3 10 μ/L) and vitamin stock (final concentration in the synthetic grape must: myo-inositol 100 mg/L, pyridoxine HCl 2 mg/L, nicotinic acid 2 mg/L, Ca pantothenate 1 mg/L, thiamine HCl 0.5 mg/L, K para-aminobenzoate 0.2 mg/L, riboflavin 0.2 mg/L, biotin 0.125 mg/L, and folic acid 0.2 mg/L).[20]

Table 1. Different Fermentation Media (M1−5)

media	description
M1	without amino acids just 200 mg N/L of NH_4Cl (50 mg/L) (control)
M2	NH_4Cl (50 mg/L) and cysteine, alanine, arginine, asparagine, aspartic acid, glutamine, glutamic acid, glycine, histidine, isoleucine, leucine, lysine, methionine, phenylalanine, proline, serine, threonine, tryptophan, tyrosine, and valine (150 mg/L)
M3	NH_4Cl (50 mg/L) and the preferred amino acids (arginine, asparagine, aspartic acid, glutamine, glutamic acid) (150 mg/L)
M4	NH_4Cl (50 mg/L) and the amino acids precursors of "aroma compounds" (isoleucine, leucine, phenylalanine, tyrosine, valine) (150 mg/L)
M5	NH_4Cl (50 mg/L) and S-containing amino acids (cysteine and methionine) (150 mg/L)

This second solution was filter sterilized and added to the first solution.

Experimental Data Set. The synthetic grape must for each treatment (M1−5) contained 200 mg/L of a nitrogen source which varied in its composition (Table 1). For the evaluation of the scale effect each fermentation treatment was performed in two volumes, 5 and 500 mL. Each 5 mL sample (M1−5 × 3 replicates) was sampled and analyzed directly after one another nine times (intervals of almost 45 min). The 500 mL samples (M1−5 × 3 replicates) were sampled daily for volatile fraction analysis.

In order to monitor and synchronize all the fermentations, two additional sets of the 5 mL fermentations were carried out. One set was frequently sampled for optical density (OD) measurements at 600 nm. The second set of the 5 mL fermentation replicates was used only for weight measurements. The 500 mL fermentations were monitored frequently for both OD and weight measurements. For logistical reasons, the 5 mL fermentations were only monitored for the first 150 h after inoculation. The 500 mL were monitored to the end in order to evaluate whether the yeast was able to complete the fermentation process under the conditions tested.

Growth Measurement. Cell proliferation was determined with a spectrophotometer (Powerwave$_x$, Bio-Tek Instruments, Bedfordshire, U.K.) by measuring the optical density (600 nm) over the experimental period.

Volatile Analysis. A small-scale fermentation setup (5 mL) was designed using the 15 mL SPME vials for the CombiPAL auto sampler (CTC Analytics AG, Zwingen, Switzerland). Fermentations were carried out on the 32-sample tray and were left to ferment at ambient temperature (20 °C ± 2). In order to avoid the influence of any additional stress, such as heating and agitation, sampling took place directly out of the tray. A SPME (CAR/DVB Carboxen) fiber (Supelco, Bellefonte, PA) was used to collect headspace volatiles every 24 h from each sample. Elevated pressure due to CO_2 production was avoided by inserting a small piece of fused silica GC column in the septum of the vial-cap.

An automated system for the online process monitoring was used thus allowing the monitoring of the fermentation evolution over time. The 5 mL samples taken daily from the 500 mL fermentation were placed in identical vials and analyzed through the same procedure as the 5 mL fermentations. Sampling took place from the headspace of the fermentation vials with an extraction time of 10 min at ambient temperature (20 ± 2 °C) directly from the sample tray. Afterward the SPME fiber was thermally desorbed in the injection port of the GC-MS instrument (Agilent Technologies, Little Falls, Wilmington, U.S.A.) for 1 min at 240 °C in splitless mode and left for a further 9 min in the split mode to clean the fiber. The carrier gas used was helium, the split flow was 50 mL·min^{-1}, and the flow through the column was 1.2 mL·min^{-1}. The column used was a J&W FFAP (Free Fatty Acid phase, Agilent Technologies) of 60 m length, 0.25 mm inner diameter, with a film thickness of 0.5 um. The GC oven temperature program was as follows: 40 °C held for 2 min and then ramped to 240 °C at 10 °C·min^{-1} and held for 2 min. The transferline to the MS was heated to 250 °C, and the ion source temperature and the quadrupole temperature was set to 240 and 150 °C, respectively.

dx.doi.org/10.1021/jf502082z | J. Agric. Food Chem. 2014, 62, 6784−6793

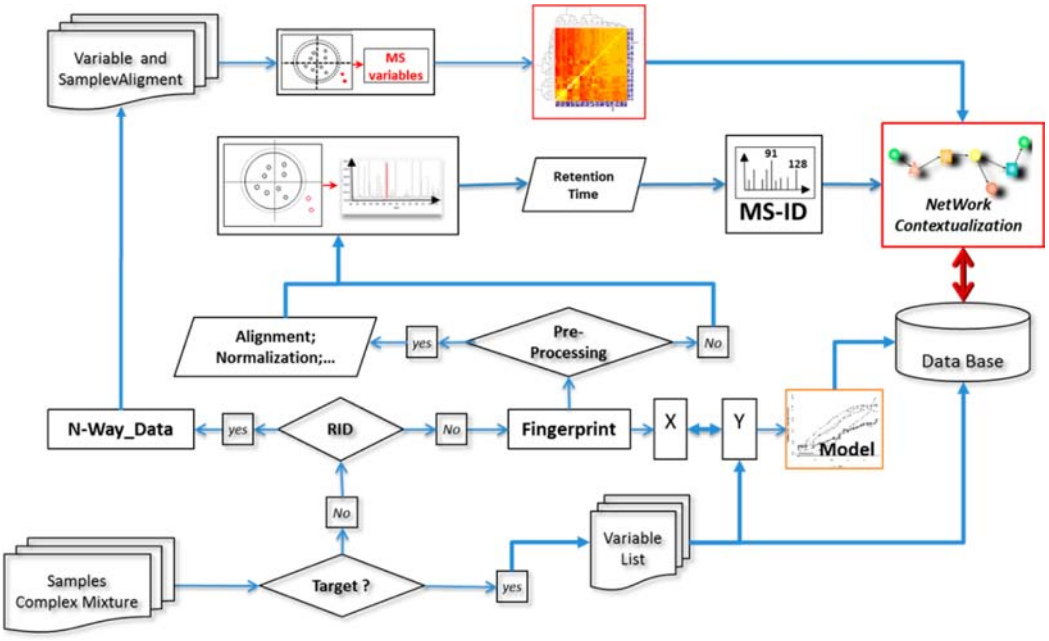

Figure 1. Metabolomic analysis pipeline.

The MS was operated in full-scan mode, scanning from 35 to 650 amu, with and ionization energy of 70 eV and an electron multiplier voltage of 1541 V.

Data Preprocessing. The ASCII file of chromatographic data obtained from each sample was extracted and a matrix created containing all the Total Ion Count features (TIC-Fingerprint). The normalized matrix was then imported into The UnscramblerX 10.1 (Camo, Norway) where baseline correction was performed and the first stage of the alignment of chromatograms done using correlation optimized warping. This algorithm aligns chromatograms by means of sectional linear stretching and compression, which shifts the peaks of one chromatogram to correlate with those of the other chromatograms in the data set.[21]

MarkerLynx XS (version 4.1, Waters, U.S.A.) was also used for peak deconvolution, peak integration (using apex track peak detection), and sample alignment. The peaks from different samples were aligned so that the same peaks (defined with retention time and m/z), most probably the same compound, are placed in the same row for all samples. The parameters used were XIC window 0.50 Da, peak width at 5% height 20 s, intensity threshold 1000 counts, mass window 0.45 Da, retention time window 0.10 min and noise elimination level 10. The list of features originated was then subjected to multivariate analysis. The matrix resulted from MarkerLynx underwent correlational analysis using Excel.

Normalization Methods. The fingerprint data (TIC) and the matrix generated in MarkerLynx were subjected to normalization: mean centering and Pareto normalization (dividing each feature by the square root of the standard deviation).

Statistical Analysis. The relative growth rates and CO_2 liberation in different volumes and different media were evaluated via two-way analysis of variance (ANOVA), using Microsoft Office Excel, version 2010.

Data was analyzed with PCA (principal component analysis), and OPLS-DA, using SIMCA-P+ (version 12.0.1, Umetrics, Sweden). Due to the large number of variables and few observations these methods highlight important information by correlating the variables.

PCA is an unsupervised technique that classifies samples according to their common spectral characteristics facilitating the observation of relationships between samples and highlighting the variables responsible for the variation (it projects the total variation on a plane, onto a smaller set of variables, called principal components (PCs), which are a linear combination of all the initial variables). The scores (the original data in the new system, a projection of the samples) and loadings (the weights applied, the original variables) plots may reveal clusters or outliers and the corresponding variables that have influence on the distribution of samples.

OPLS-DA is a modified version of PLS (partial least-squares), a supervised method, allowing the extraction of more information used for group classification/separation. The advantage is that the information about the discriminating classes is presented in its first component which makes easier to understand which variables are the responsible for this same separation due to the separation of systematic variation into a predictive and an orthogonal compound.[22] The sequence presented in this section is the metabolomics pipeline applied as represented in Figure 1.

RESULTS/DISCUSSION

Fermentation Kinetic Parameters. For logistical reasons, the 5 mL fermentations were only monitored for the first 150 h of the fermentation (Figure 2c, g). The 500 mL fermentations were monitored to the end in order to evaluate whether the yeast was able to complete the fermentation process under the nutrient conditions tested (Figure 2a, e). The percent weight loss (CO_2 production) was measured in order to evaluate the fermentation kinetics in both fermentation sets (Figure 2e, g). The relative rates of CO_2 production were calculated using the slope of CO_2 production vs time (Figure 2h). For the 500 mL fermentation, the slope was calculated for the 150 h period (Figure 2f). When the monitoring of the 5 mL fermentations cessed, they had lost 43% of the total CO_2 released by the 500 mL fermentations. Therefore, only this period is the focus of this study. A two-way analysis of variance (ANOVA) was applied to the relative rates of CO_2 production and the data showed that there were no significant differences between different media or different volumes ($p > 0.05$).

The yeast growth was also monitored for the entire fermentation process in 500 mL and until yeasts reached a quasi-stationary phase (OD of about 6) in 5 mL fermentations. The relative rates of cell growth were calculated using the slope of OD (600 nm) vs time in the exponential growth phase (Figure 2d). Once again for the 500 mL fermentations, only the data for the first 150 h was considered (Figure 2b). A two-way

dx.doi.org/10.1021/jf502082z | J. Agric. Food Chem. 2014, 62, 6784−6793

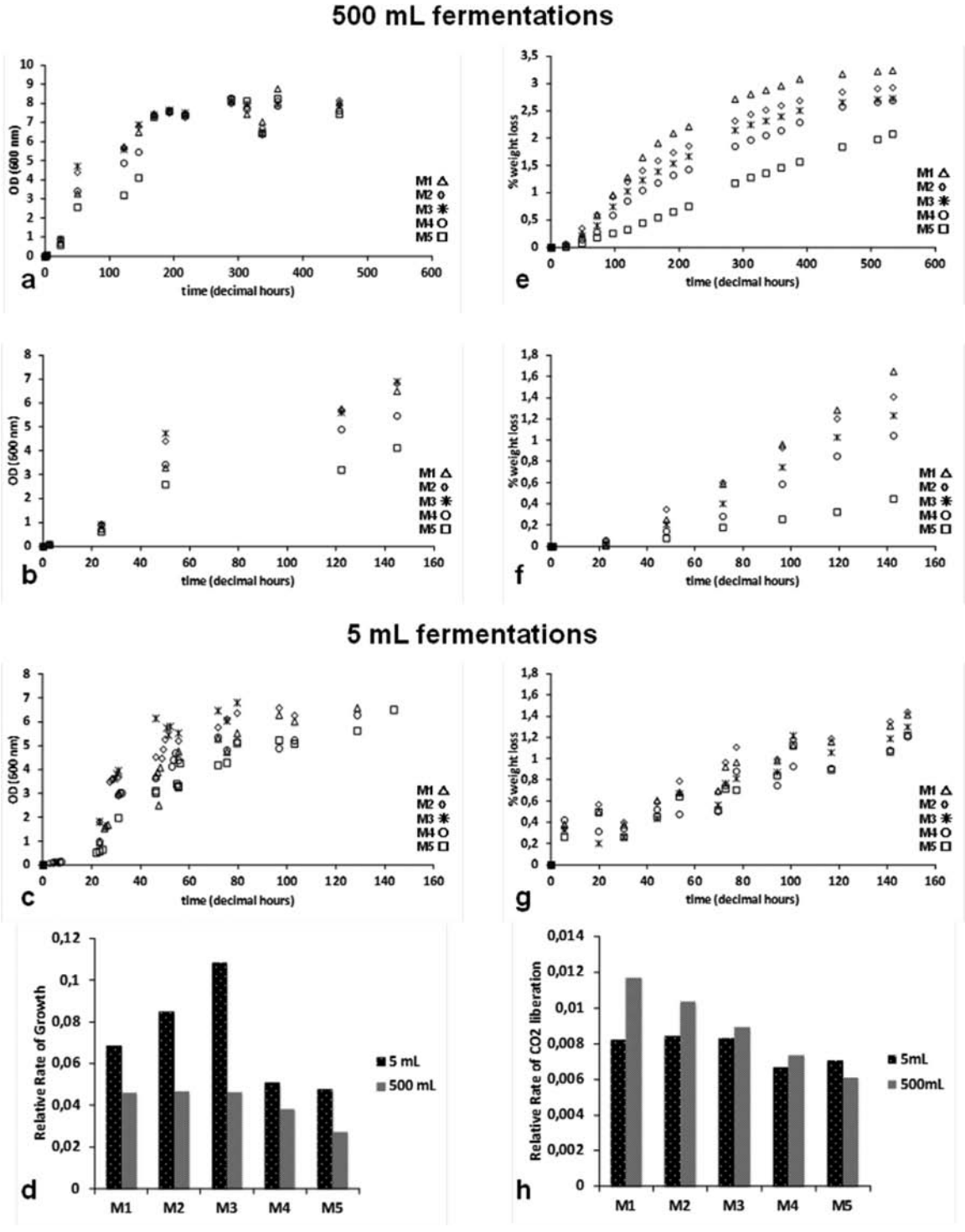

Figure 2. Profiles of yeast growth obtained through OD measurements at 600 nm in (a) 500 mL fermentations for the entire fermentation process and (b) for the first 150 h, (c) in 5 mL fermentations for 150 h and (d) relative rates of growth; % weight loss (CO_2 production) in 500 mL fermentations (e) for the entire fermentation process and (f) for the first 150 h (g) in 5 mL fermentations for 150 h and (h) relative rates of CO_2 production.

analysis of variance (ANOVA) was applied to this data, and it was concluded that although there were no significant differences between media ($p > 0.05$) there were significant differences between volumes ($p < 0.05$).

Data from the entire 500 mL fermentations process (Figure 2a, e) showed that despite the differences in the nitrogen composition of different media, *Saccharomyces cerevisiae* was able to perform the fermentation process in all media. In a media completely deficient in amino acids the yeast has the ability to use precursor metabolites, carbon skeletons originated from the central metabolic pathways, as starting substrates for the synthesis of amino acids. The tricarboxylic acid cycle is not functional during fermentation, so yeasts replace the cycle intermediates through anaplerotic reactions.[23,24]

Screening by TIC. Our initial goal with the fingerprint analysis (TIC) was to examine the intrinsic variation in both

dx.doi.org/10.1021/jf502082z | J. Agric. Food Chem. 2014, 62, 6784−6793

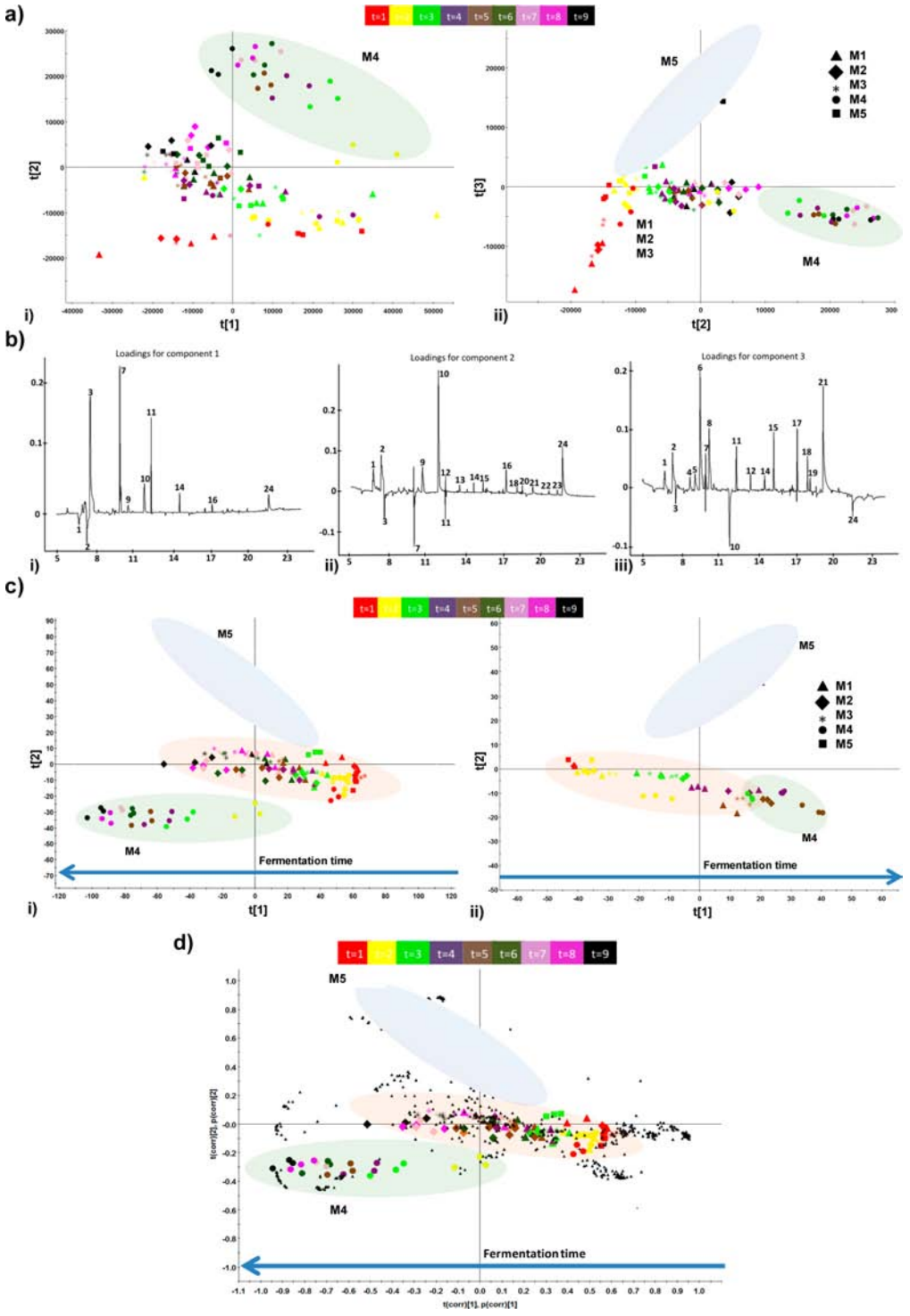

Figure 3. (a) PCA score plots of normalized raw data. (i) PC1 vs PC2; (ii) PC2 vs PC3. (b) PCA loading plots of normalized raw data for (i) PC1, (ii) PC2, (iii) PC3 for (1) ethyl acetate; (2) ethanol; (3) unknown 1; (4) isobutyl acetate; (5) ethyl butanoate; (6) methyl thiolacetate; (7) 2-methyl-1-propanol; (8) ethyl thiolacetate; (9) isoamyl acetate; (10) 3-methyl-1-butanol; (11) unknown 3; (12) ethyl hexanoate; (13) acetoin; (14) unknown 4; (15) ethyl octanoate; (16) benzaldehyde; (17) dihydro-2-methyl-3(2H)-thiophenone; (18) ethyl decanoate; (19) 3-methylsulfanylprop-1-ene; (20) unknown (74//60/41); (21) methionol; (22) phenylethyl acetate; (23) benzyl alcohol; (24) 2-phenylethanol. (c) PCA score plots of normalized data after preprocessing with MarkerLynx and normalization by Pareto (i) 5 mL, (ii) 500 mL. (d) Biplot of the two first PC after preprocessing with MarkerLynx and normalized by Pareto (5 mL fermentations).

data sets to determine if the volatile fraction of the samples followed similar trends and/or media clustering prior to feature extraction techniques.

The raw data was first evaluated by PCA using the non-normalized data (data not shown) to verify the samples, and to detect outliers or trends within the different media applied in the TIC-Fingerprint matrix. For the 5 mL data set, the first three principal components showed 97% of the total variation and it was possible to observe a cluster with samples related to M4 (branch chain and aromatic amino acids). However, it was

dx.doi.org/10.1021/jf502082z | J. Agric. Food Chem. 2014, 62, 6784−6793

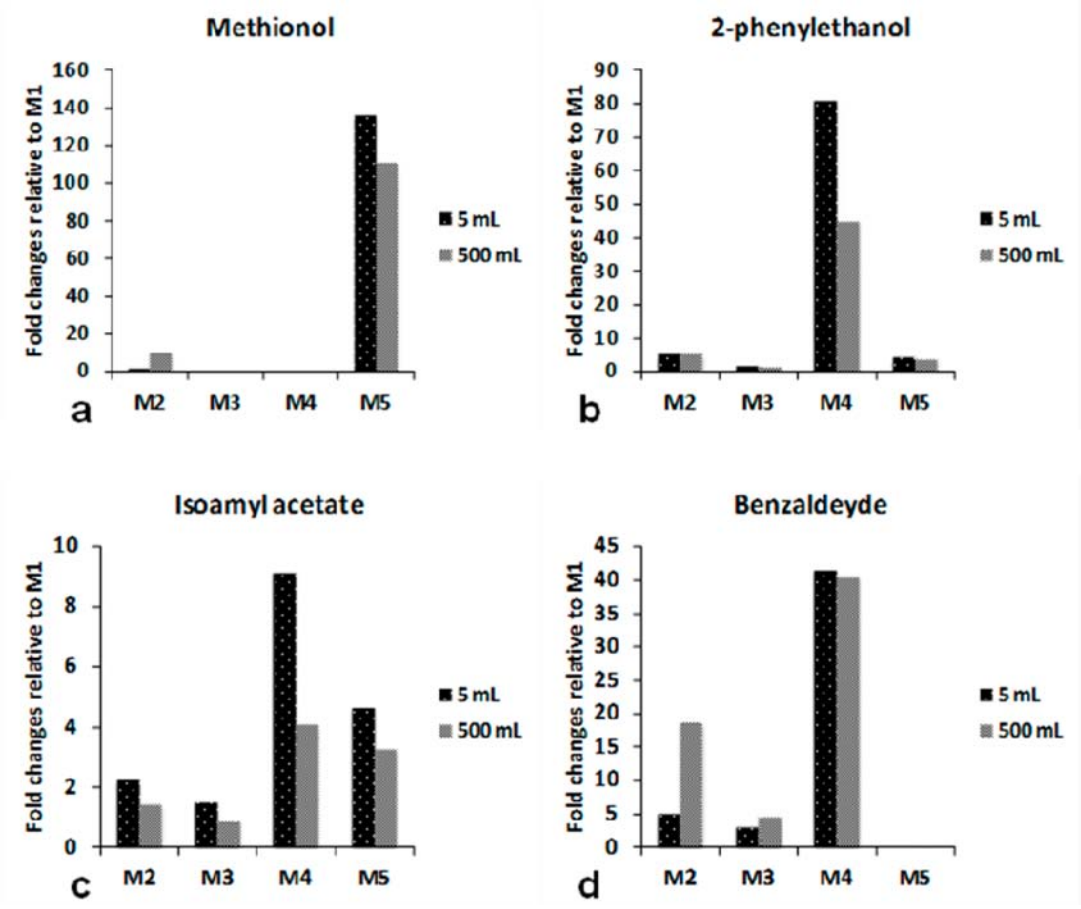

Figure 4. Fold changes relative to M1 (control) in 5 and 500 mL fermentations for (a) methionol, (b) 2- phenylethanol, (c) isoamyl acetate, and (d) benzaldehyde.

necessary to reach component 6 to visualize another cluster with the data of M5 (sulfur-containing amino acids) (just 0.37% of the variation was explained by this component). In the case of the 500 mL data set, the first three principal components showed 95% of the total variation, with M4 forming a cluster. To see another cluster it was necessary to reach component 4 (2% of variation explained). The second cluster found was for M5 as seen with the 5 mL fermentations. This suggests that metabolites, such as the volatile compounds produced in M4, may dominate and in so doing obscure others (such as the volatile compounds from S-containing amino acids medium). This may be overcome performing a mathematical normalization on data to minimize these differences. Pareto normalization is used to avoid problems such as baseline influence and variations in peak shapes, among others; the raw data was compared to this data set. The results confirmed that some metabolites hide others. The plots (Figure 3a, b) show that the second component separates the data from M4 and the third explains the medium containing sulfur amino acids (M5), while the first component is explained by fermentation products (with 79% and 88% (data not shown) of the total variation for the 5 and 500 mL samples, respectively).

2D "Landscape" Data Preprocessing. *Effect of Sample Discrimination.* In PCA, each chromatogram and all its information is compressed and projected onto a single point. Each point represents the entire exogenous volatile metabolome at a moment. PCA was performed to understand how samples cluster together (scores) (Figure 3c). These PCA score plots show that the metabolism of yeast is affected by the amino acids supplied in the media but not by the volume of media. In the case of the 5 mL data set, three principal components explained 67% of the total variation while in the 500 mL data set this explained 44%. For both fermentation volumes, the first component (x vector) describes the fermentations over time (kinetics). Indeed, at the beginning of fermentation (initial sampling point) there were no differences in the volatile metabolome, suggesting that the yeast is initiating metabolic pathways in response to the different fermentation media. In the second component, orthogonal to the first one, the result was, once again, similar for both 5 and 500 mL samples. It was possible to distinguish three clusters: M5 samples (cysteine and methionine), M4 samples (phenylalanine, tyrosine, valine, leucine, and isoleucine), and a cluster consisting of M1, M2, and M3. This suggests that it is possible to track the different metabolic pathways that yeast follows over time due to nutrient variation. When evaluating each medium (M) separately, a time dependent expression pattern emerged. For example, in the 5 mL fermentation score plot (Figure 3c(i)), medium M4 displays a time separation between sampling points 3, 4, and 5 whereas the last ones (6, 7, 8, and 9) are grouped in a shorter time range. These differences in volatile compound synthesis are potentially related to variations in gene expression between yeast subjected to different nutrient conditions. Differences in gene expression and consequent proteomic and metabolomic changes enable yeast to survive regardless the nutrient availability.[23,24]

dx.doi.org/10.1021/jf502082z | J. Agric. Food Chem. 2014, 62, 6784−6793

A biplot was constructed in order to understand and analyze how samples cluster together (scores) and identify which variables (metabolites) most contributed to their separation (loadings) (Figure 3d). This potentially allows metabolic discovery through the identification of possible biomarkers.[25] The biomarkers identified in each media were the same in both 5 and 500 mL samples. It was possible to identify ethyl acetate and ethanol for the cluster formed with M1, M2, and M3. Ethanol is one of main products of fermentation and ethyl acetate is formed from ethanol and acetyl-CoA by alcohol acyltransferase and is the most abundant ester produced during alcoholic fermentation.[13,26] This cluster contains media that placed fewer nutrient constraints on yeast growth as they contained glutamate and ammonia, which are the principal precursors for the synthesis of nitrogenous compounds.[24] This may somewhat contribute to the similarities in the volatile profiles detected. The compounds identified as being responsible for the clustering of M5 were sulfur containing compounds which originated from cysteine and methionine metabolism, such as methyl thioacetate, ethyl thiolacetate, dihydro-2-methyl-3(2H)-thiophenone, and methionol (a product of methionine degradation via Ehrlich pathway[27]) (Figure 4a). These may have a negative contribution to aroma due to the formation of thiols and sulfides.[28]

The clustering of M4 was due to the presence of some products resulting from the Ehrlich pathway, namely isoamyl alcohol and 2-phenylethanol (Figure 4b) together with hexanoic acid and benzyl alcohol. The higher alcohols isoamyl alcohol and 2-phenylethanol are formed by the decarboxylation and subsequent reduction of α-keto acids produced as intermediates of the amino acids leucine, isoleucine, and phenylalanine catabolism (Ehrlich pathway). Since their production from the corresponding amino acids is coupled to the oxidation of NADH, in anaerobic conditions yeasts use them as alternative electron acceptors.[29] These results are in agreement with literature.[30−32]

In order to gain more information and to contextualize each pathway in the global yeast metabolome an OPLS-DA between media was applied. The results generated with this approach corroborate the presence of the compounds identified in the PCA plots. Additionally, it was also possible to identify other compounds (with a correlation greater than 0.7) such as isoamyl acetate (Figure 4c), benzaldehyde (Figure 4d), and phenylethyl acetate in the case of M4 while for M5 was possible to observe isobutyl acetate and 3-methylsulfanylprop-1-ene. These were also confirmed by an OPLS with determined compounds (phenylethanol representing M4 and methionol representing M5) (data not shown). Phenylethyl acetate is the product of the esterification of phenylethanol and acetyl-CoA enzymatic by acetyltrasferase.[33,34] Isoamyl acetate is the enzymatic esterification product of acetyl-CoA with isoamyl alcohol. Isoamyl alcohol is produced from leucine, via the Ehrlich pathway or from α-ketoisocaproic acid through the anabolic pathway.[30,31] As expected, the production of both acetate esters increased dramatically in M4, as the amino acid precursors were present in great quantities.[35] The production of benzaldehyde (Figure 4e) by *Saccharomyces cerevisiae* was previously reported by Delfini et al.[36] Thereafter, several research groups have studied the mechanisms behind that process in different microorganisms and in vitro,[37] and several metabolic pathways have been proposed. While in some species this process is enzyme catalyzed,[37] in others it is also a chemical reaction involving metal ions and O_2.[38] Based on the fermentation conditions employed in this study (relatively low temperature, acidic pH, and anaerobic conditions), some of the possibilities referred in literature may be excluded; however, the data we possess does not allow the formation of a hypothesis regarding the mechanism behind benzaldehyde formation. However, the data shows that benzaldehyde production was favored in a medium containing phenylalanine (M4), which has been suggested as a possible precursor in several studies.[36−38] Further work should be done to confirm this observation. Benzaldehyde in turn can be reduced to benzyl alcohol, explaining its presence in the same medium.[38,39]

Isobutyl acetate results from the combination of acetyl-CoA with isobutyl alcohol produced from valine, via the Ehrlich pathway or from the anabolic pathway via α-ketoisovaleric acid.[40] This compound was significantly affected by sulfur containing amino acids, an effect that was also observed, although to a lesser extent, in isoamyl acetate. In M5 neither valine nor leucine was available, thus isobutyl and isoamyl alcohol were synthesized from the corresponding α-ketoacids generated through the de novo synthesis pathway from glucose.[23] According to the literature the production of acetate esters is more closely related to acetate than to higher alcohol production.[26] Therefore, the formation of high concentrations of acetates in media supplemented with sulfur containing amino acids may be due to the high production of acetyl-CoA from cysteine. Several pathways of cysteine degradation lead to pyruvate formation[41] that is converted to acetyl-CoA via cytosolic pyruvate dehydrogenase (PDH) bypass, which is an alternative route to the PDH reaction for the conversion of pyruvate to acetyl-CoA during fermentation.[29] Further work is needed to clarify this result. 3-methylsulfanylprop-1-ene is a sulfur compound resulting from the metabolism of cysteine or methionine, the only amino acids containing sulfur atoms. The compounds observed using a targeted strategy were the same ones described in the untargeted approach, which validates this untargeted approach. The results also show that although the fermentation performance is affected by the fermentation volume, there are no scale differences concerning the quality and formation kinetics of the volatile compounds identified using the applied workflow. It would be necessary to perform further work in order to validate its applicability in complex media. Additionally, the implications of these perturbations on a sensory level would need to be validated using greater volumes.

Since the scale effect seems not to affect the quality of the volatile fraction, this workflow may lead to the discovery of new compounds or the possible modification of known pathways and showing the systemic response to perturbations. To check this hypothesis, the correlation between the coexpression of metabolites were analyzed for the 5 mL data set in the matrix generated by MarkerLynx. In this study, these correlations did not identify the presence any new compounds. The highest correlations observed were between metabolically related volatile compounds, for example, ethyl hexanoate and ethyl octanoate (0.998), isobutyl acetate and ethyl octanoate (0.985), ethyl thiolacetate and ethyl octanoate (0.984). No negative correlations were found, which might be due to the duration of the period monitored. More alterations would have occurred over the time, changing the ultimate chemical profile.

Time Profile of Volatile Synthesis. The high throughput procedure presented in this study allowed the acquisition of snapshots of the biochemical events related to the fermentation process. The linking of the kinetic profile of each volatile

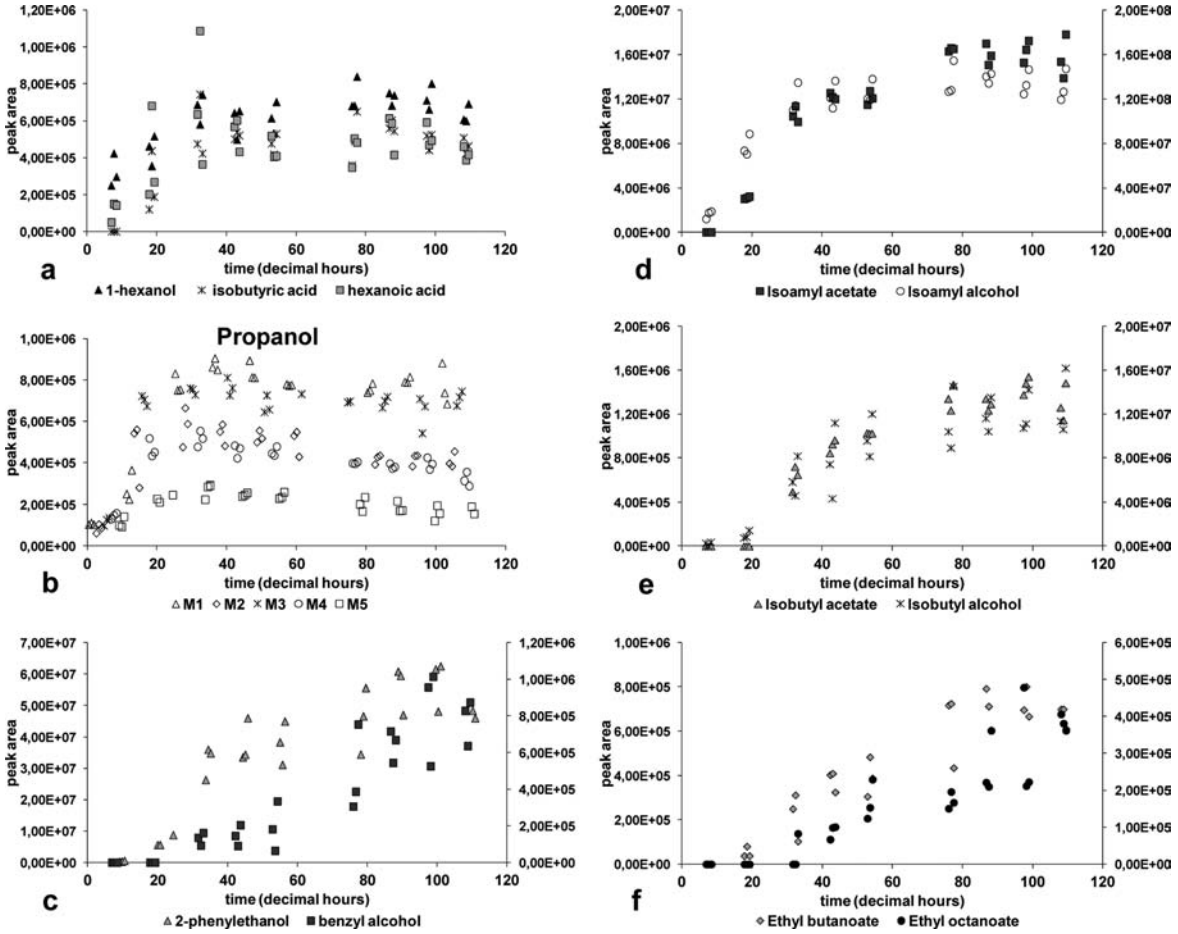

Figure 5. Kinetic profile of (a) 1-hexanol, isobutyric, and hexanoic acid in M4, (b) propanol in five media (M1−5), (c) 2-phenylethanol and benzyl alcohol in M4, (d) isoamyl acetate and isoamyl alcohol in M4, (e) isobutyl acetate and isobutyl alcohol in M4, (f) ethyl butanoate and ethyl octanoate in M4.

compound obtained in "real time" by GC-MS for 5 mL fermentations and the corresponding yeast growth curves obtained by OD measuring at 600 nm (Figure 2c) enabled the establishment of the metabolic time profile of the volatile fraction. A detailed description of the M4 data follows, but a similar approach could be done for each of the five media. During the first 20 h after the inoculation, during the lag phase, yeasts are adapting to the new media conditions, so there is no increase in the yeast population (OD remains unchanged). Although no growth occurs, yeast immediately begins to metabolize sugars and other nutrients present in media with consequent production of ethanol. There are several metabolites whose concentration start to increase during this phase namely hexanol, propanol, isobutyric, and hexanoic acids (Figure 5a). Hexanol is usually formed during the prefermentative stage of winemaking and is believed to be reductively formed by yeast from hexanal, which in turn is formed from linoleic acid.[42] Propanol reach maximum concentration few hours after inoculation and in agreement with the literature its increase was greater in the media without amino acids[43] and lower in the media containing only sulfur containing amino acids which may be related to the negative relationship between *n*-propanol production and H_2S formation from methionine and cysteine metabolism (Figure 5b).[44,45] After an adaptation period, yeast start growing. This exponential growth phase is influenced by several factors such as temperature, concentration of ammonia, amino acids, and other nutrients, and also by the oxygen level. During this phase yeasts use all the available nutrients to obtain energy and increase their population, which may reach 10^7−10^8 cells/mL. At the beginning of the exponential growth phase the concentration of higher alcohols and acids resulting either directly from sugars or from amino acid metabolism trough the Ehrlich pathway starts to increase or in some cases has already reached its maximum due to the yeast's high demand for new proteins needed for growth and reproduction. Isoamyl alcohol and isobutyric acid reached maximum concentrations about 24 h after inoculation and their concentrations remained constant (Figure 5a, d). The concentrations of isobutanol (Figure 5e), 2-phenylethanol, and benzyl alcohol (Figure 5c) started to increase at the beginning of this stage and their concentration continued increasing for the period monitored, indicating a possible continued increase in their production during the stationary phase.

During fermentation two groups of esters are synthesized: acetate esters and ethyl fatty acid esters. The synthesis of acetate esters isoamyl acetate and isobutyl acetate starts when their substrates, isoamyl alcohol, and isobutyl alcohol, are available in the media, and their time of expression is parallel to that of their precursor alcohols (Figures 5d, e).

The synthesis of ethyl fatty acid esters (ethyl hexanoate, ethyl octanoate, and ethyl decanoate) only started almost toward the end of the exponential growth phase (Figure 5f). According to literature the rate of ethyl ester formation is influenced by the

dx.doi.org/10.1021/jf502082z | J. Agric. Food Chem. 2014, 62, 6784−6793

concentrations of the two cosubstrates (acyl coenzyme A component and ethanol) and the activity of the enzymes involved in their synthesis and hydrolysis (e.g., acyl-CoA: ethanol *O*-acyltransferases, Eeb1 and Eht1). It has been suggested that the fatty acid precursor level rather than the activity of the biosynthetic enzymes is the major limiting factor for ethyl ester production.[46] Ethyl butanoate is formed from ethanol and propanoic acid derived from α-ketobutyrate,[47] an intermediate in the metabolism of several amino acids. Unlike other ethyl fatty acid esters, its concentration rises continuously from the beginning of the exponential growth period, probably due to the availability of both cosubstrates in the media since the beginning of the fermentation process (Figure 5f). After this period, yeast stops growing probably due to some nutrient deficiencies and the toxic effects of ethanol and other substances produced during alcoholic fermentation, resulting in a stationary phase. Finally yeast start dying and the population gradually decreases (decline phase).

The proposed methodology proved to be a useful tool capable of generating new insights concerning the implications of a given nutrient on the final product's volatile fraction. This knowledge can be quite useful for wine industry since it allows the possibility of modifying wine aroma by either increasing the desirable or eliminating the undesirable odors. This work culminates with the development a new metabolic profiling pipeline that relies on an unsupervised and untargeted approach applied to data acquired by a noninvasive methodology (HS-SPME/GC-MS) utilizing a small fermentation volume which allows the high throughput analyses that enables "real time" monitoring of the metabolic changes inherent to the biochemical dynamics of a perturbed complex biological system and the extraction of molecular candidates that are latter validated on its biochemical context. The pipeline proposed has several practical applications such as yeast phenotyping studies or exploring the impact of nutrient availability on yeast metabolism and subsequent volatile fraction quality. These results do require sensory validation on a larger scale.

AUTHOR INFORMATION

Corresponding Author

*Phone: +351 22 558 0001. Fax: +351 22 509 0351. Email: asferreira@porto.ucp.pt.

Notes

The authors declare no competing financial interest.

ACKNOWLEDGMENTS

This research was funded by the project "Wine Metrics: Revealing the Volatile Molecular Feature Responsible for the Wine Like Aroma a Critical Task Toward the Wine Quality Definition." (PTDC/AGR-ALI/121062/2010) and partially supported by ESB/UCP plurianual funds through the POS-Conhecimento Program that includes FEDER funds through the program COMPETE (Programa Operacional Factores de Competitividade) by national funds through FCT (Fundação para a Ciência e a Tecnologia) and Winetech, the Technology and Human Resources Programme and the South African National Science Foundation.

REFERENCES

(1) Martínez-Gil, A. M.; Garde-Cerdán, T.; Lorenzo, C.; Félix Lara, J.; Pardo, F.; Rosario Salinas, M. Volatile compounds formation in alcoholic fermentation from grapes collected at maturation stages: Influence of nitrogen compounds and grape variety. *J. Food Sci.* **2012**, *77* (1), C71−C79.

(2) Rodríguez, M. E.; Lopes, C. A.; Barbagelata, R. J.; Barda, N. B.; Caballero, A. C. Influence of *Candida pulcherrima* Patagonian strain on alcoholic fermentation behavior and wine aroma. *Int. J. Food Microbiol.* **2010**, *138* (1−2), 19−25.

(3) Winter, G.; Van der Westhuizen, T. J.; Higgins, V.; Curtin, C.; Ugliano, D. Contribution of cysteine and glutathione conjugates to the formation of the volatile thiols 3-mercaptohexan-1-ol (3MH) and 3-mercaptohexyl acetate (3MHA) during fermentation by *Saccharomyces cerevisiae*. *Aust. J. Grape Wine Res.* **2011**, *17* (2), 285−290.

(4) Howell, K. S.; Cozzolino, D.; Bartowsky, E. J.; Fleet, G. H.; Henschke, P. A. Metabolic profiling as a tool for revealing *Saccharomyces* interactions during wine fermentation. *FEMS Yeast Res.* **2006**, *6* (1), 91−101.

(5) Romano, P.; Fiore, C.; Paraggio, M.; Caruso, M.; Capece, A. Function of yeast species and strains in wine flavor. *Int. J. Food Microbiol.* **2003**, *86* (1−2), 169−180.

(6) Barrajón, N.; Capece, A.; Arévalo-Villena, M.; Briones, A.; Romano, P. Co-inoculation of different *Saccharomyces cerevisiae* strains and influence on volatile composition of wines. *Food Microbiol.* **2011**, *28* (5), 1080−1086.

(7) Fleet, G. Yeast interactions and wine flavor. *Int. J. Food Microbiol.* **2003**, *86* (1−2), 11−22.

(8) Hernández-Orte, P.; Cacho, J. F.; Ferreira, V. Relationship between varietal amino acid profile of grapes and wine aromatic composition. Experiments with model solutions and chemometric study. *J. Agric. Food Chem.* **2002**, *50* (10), 2891−2899.

(9) Hernández-Orte, P.; Ibarz, M. J.; Cacho, J.; Ferreira, V. Addition of amino acids to grape juice of the Merlot variety: Effect on amino acid uptake and aroma generation during alcoholic fermentation. *Food Chem.* **2006**, *98* (2), 300−310.

(10) Hernández-Orte, P.; Ibarz, M. J.; Cacho, J.; Ferreira, V. Effect of the addition of ammonium and amino acids to musts of Airen variety on aromatic composition and sensory properties of the obtained wine. *Food Chem.* **2005**, *89* (2), 163−174.

(11) Torija, M.; Beltran, G.; Novo, M.; Poblet, M.; Guillamón, J. M.; Mas, A.; Rozès, N. Effects of fermentation temperature and *Saccharomyces* species on the cell fatty acid composition and presence of volatile compounds in wine. *Int. J. Food Microbiol.* **2003**, *85* (1−2), 127−136.

(12) Bisson, L. Stuck and sluggish fermentations. *Am. J. Enol. Viticult.* **1999**, *50* (1), 107−119.

(13) Ugliano, M.; Travis, B.; Francis, I. L.; Henschke, P. A. Volatile composition and sensory properties of shiraz wines as affected by nitrogen supplementation and yeast species: Rationalizing nitrogen modulation of wine aroma. *J. Agric. Food Chem.* **2010**, *58* (23), 12417−12425.

(14) Vilanova, M.; Ugliano, M.; Varela, C.; Siebert, T.; Pretorius, I. S.; Henschke, P. A. Assimilable nitrogen utilisation and production of volatile and non-volatile compounds in chemically defined medium by *Saccharomyces cerevisiae* wine yeasts. *Appl. Microbiol. Biotechnol.* **2007**, *77* (1), 145−157.

(15) Bell, S. J.; Henschke, P. A. Implications of nitrogen nutrition for grapes, fermentation and wine. *Aust. J. Grape Wine Res.* **2005**, *11* (3), 242−295.

(16) Hall, R. D. Plant metabolomics: From holistic hope, to hype, to hot topic. *New Phytol.* **2006**, *169* (3), 453−468.

(17) Boccard, J.; Veuthey, J.-L.; Rudaz, S. Knowledge discovery in metabolomics: An overview of MS data handling. *J. Sep. Sci.* **2010**, *33* (3), 290−304.

(18) Verpoorte, R.; Choi, Y. H.; Kim, H. K. Metabolomics: What's new? *Flavour Fragr. J.* **2010**, *25* (3), 128−131.

(19) Griffiths, W. J.; Koal, T.; Wang, Y.; Kohl, M.; Enot, D. P.; Deigner, H. P. Targeted metabolomics for biomarker discovery. *Angew. Chem., Int. Ed. Engl.* **2010**, *49* (32), 5426−5445.

(20) Jiranek, V.; Langridge, P.; Henschke, P. A. Amino acid and ammonium utilization by *Saccharomyces cerevisiae* wine yeasts from a chemically defined medium. *Am. J. Enol. Vitic.* **1995**, *46*, 75−83.

(21) Gong, F.; Liang, Y.-Z.; Fung, Y.-S.; Chau, F.-T. Correction of retention time shifts for chromatographic fingerprints of herbal medicines. *J. Chromatogr. A* **2004**, *1029* (1−2), 173−183.
(22) Wiklund, S.; Johansson, E.; Sjostrom, L.; Mellerowicz, E. J.; Edlund, U.; Shockcor, J. P.; Gottfries, J.; Moritz, T.; Trygg, J. Visualization of GC/TOF-MS-Based Metabolomics data for identification of biochemically interesting compounds using OPLS class models. *Anal. Chem.* **2007**, *80* (1), 115−122.
(23) Maaheimo, H.; Fiaux, J.; Çakar, Z. P.; Bailey, J. E.; Sauer, U.; Szyperski, T. Central carbon metabolism of *Saccharomyces cerevisiae* explored by biosynthetic fractional ^{13}C labeling of common amino acids. *Eur. J. Biochem.* **2001**, *268*, 2464−2479.
(24) Ljungdahl, P. O.; Daignan-Fornier, B. Regulation of amino acid, nucleotide, and phosphate metabolism in *Saccharomyces cerevisiae*. *Genetics* **2012**, *190* (3), 885−929.
(25) Schlatzer, D. M.; Dazard, J. E.; Ewing, R. M.; Ilchenko, S.; Tomcheko, S. E.; Eid, S.; Ho, V.; Yanik, G.; Chance, M. R.; Cooke, K. R. Human biomarker discovery and predictive models for disease progression for idiopathic pneumonia syndrome following allogeneic stem cell transplantation. *Mol. Cell. Proteomics.* **2012**, *11* (6), M111.015479.
(26) Torrea, D.; Varela, C.; Ugliano, M.; Ancin-Azpilicueta, C.; Leigh Francis, I.; Henschke, P. A. Comparison of inorganic and organic nitrogen supplementation of grape juice—Effect on volatile composition and aroma profile of a Chardonnay wine fermented with *Saccharomyces cerevisiae* yeast. *Food Chem.* **2011**, *127* (3), 1072−1083.
(27) Perpète, P.; Duthoit, O.; De Maeyer, S.; Imray, L.; Lawton, A. I.; Stavropoulos, K. E.; Gitonga, V. W.; Hewlins, M. J. E.; Richard Dickinson, J. Methionine catabolism in *Saccharomyces cerevisiae*. *FEMS Yeast Research* **2006**, *6* (1), 48−56.
(28) Mestres, M.; Busto, O.; Guasch, J. Analysis of organic sulphur compounds in wine aroma. *J. Chromatogr., A* **2000**, *881* (1−2), 569−581.
(29) Remize, F.; Andrieu, E.; Dequin, S. Engineering of the pyruvate dehydrogenase bypass in *Saccharomyces cerevisiae*: Role of the cytosolic Mg(2+) and mitochondrial K(+) acetaldehyde dehydrogenases Ald6p and Ald4p in acetate formation during alcoholic fermentation. *Appl. Environ. Microb.* **2000**, *66* (8), 3151−3159.
(30) Dickinson, J. R.; Harrison, S. J.; Dickinson, J. A.; Hewlins, M. J. E. An Investigation of the Metabolism of Isoleucine to Active Amyl Alcohol in *Saccharomyces cerevisiae*. *J. Biol. Chem.* **2000**, *275* (15), 10937−10942.
(31) Dickinson, J. R.; Lanterman, M. M.; Danner, D. J.; Pearson, B. M.; Sanz, P.; Harrison, S. J.; Hewlins, M. J. E. A ^{13}C nuclear magnetic resonance investigation of the metabolism of leucine to isoamyl alcohol in *Saccharomyces cerevisiae*. *J. Biol. Chem.* **1997**, *272* (43), 26871−26878.
(32) Hazelwood, L. A.; Daran, J. M.; vanMaris, A. J.; Pronk, J. T.; Dickinson, J. R. The Ehrlich pathway for fusel alcohol production: A century of research on *Saccharomyces cerevisiae* metabolism. *Appl. Environ. Microb.* **2008**, *74* (8), 2259−2266.
(33) Verstrepen, K. J.; Van Laere, S. D. M.; Vanderhaegen, B. M. P.; Derdelinckx, G.; Dufour, J. P.; Pretorius, I. S.; Winderickx, J.; Thevelein, J. M.; Delvaux, F. R. Expression levels of the yeast alcohol acetyltransferase genes *ATF1*, Lg-*ATF1*, and *ATF2* control the formation of a broad range of volatile esters. *Appl. Environ. Microbiol.* **2003**, *69* (9), 5228−5237.
(34) Saerens, S. M. G.; Delvaux, F. R.; Verstrepen, K. J.; Thevelein, J. M. Production and biological function of volatile esters in *Saccharomyces cerevisiae*. *Microb. Biotechnol.* **2010**, *3* (2), 165−177.
(35) Yoshimoto, H.; Fukushige, T.; Yonezawa, T.; Sone, H. Genetic and physiological analysis of branched-chain alcohols and isoamyl acetate production in *Saccharomyces cerevisiae*. *Appl. Microbiol. Biotechnol.* **2002**, *59* (4−5), 501−508.
(36) Delfini, C.; Gaia, P.; Bardi, L.; Mariscalco, G.; Contiero, M.; Pagliara, A. Production of benzaldeyde, benzyl alcohol, and benzoic acid by yeast and *Botrytis cinerea* isolated from grape musts and wines. *Vitis* **1991**, *30*, 253−263.
(37) Okrasa, K.; Guibé-Jampel, E.; Plenkiewicz, J.; Therisod, M. In vitro bi-enzymatic synthesis of benzaldehyde from phenylalanine: practical and mechanistic studies. *J. Mol. Catal. B-Enzym.* **2004**, *31* (4−6), 97−101.
(38) Lapadatescu, C.; Giniès, C.; Quéré, J.; Bonnarme, P. Novel scheme for biosynthesis of aryl metabolites from L-phenylalanine in the fungus *Bjerkandera adusta*. *Appl. Environ. Microbiol.* **2000**, *66*, 1517−1522.
(39) Groot, M. N.; de Bont, J. A. Conversion of phenylalanine to benzaldehyde initiated by an aminotransferase in *Lactobacillus plantarum*. *Appl. Environ. Microbiol.* **1998**, *64*, 3009−3013.
(40) Dickinson, J. R.; Harrison, S. J.; Hewlins, M. J. E. An investigation of the metabolism of valine to isobutyl alcohol in *Saccharomyces cerevisiae*. *J. Biol. Chem.* **1998**, *273* (40), 25751−25756.
(41) Nelson, D. L.; Cox, M. M. *Lehninger Principles of Biochemistry*, 5th ed.; W.H. Freeman Company: New York, 2008; 687−703.
(42) Crouzet, J. Les enzymes et l'arôme des vins. *Rev. Fran. Enol.* **1986**, *102*, 42−49.
(43) Garde-Cerdán, T.; Ancín-Azpilicueta, C. Effect of the addition of different quantities of amino acids to nitrogen-deficient must on the formation of esters, alcohols, and acids during wine alcoholic fermentation. *LWT - Food Sci. Technol.* **2008**, *41* (3), 501−510.
(44) Giudici, P.; Zambonelli, C.; Kunkee, R. E. Increased production of *n*-propanol in wine by yeast strains having an impaired ability to form hydrogen sulfide. *Am. J. Enol. Viticult.* **1993**, *44* (1), 17−21.
(45) Linderholm, A. L.; Findleton, C. L.; Kumar, G.; Hong, Y.; Bisson, L. F. Identification of genes affecting hydrogen sulfide formation in *Saccharomyces cerevisiae*. *Appl. Environ. Microbiol.* **2008**, *74* (5), 1418−1427.
(46) Saerens, S. M.; Delvaux, F.; Verstrepen, K. J.; Van Dijck, P.; Thevelein, J. M.; Delvaux, F. R. Parameters affecting ethyl ester production by *Saccharomyces cerevisiae* during fermentation. *Appl. Environ. Microb.* **2008**, *74* (2), 454−61.
(47) Cordente, A. G.; Swiegers, J. H.; Hegardt, F. G.; Pretorius, I. S. Modulating aroma compounds during wine fermentation by manipulating carnitine acetyltransferases in *Saccharomyces cerevisiae*. *FEMS Microbiol. Lett.* **2007**, *267* (2), 159−166.

Table 1. Constituent Monosaccharide Composition of Chicory Root Pulp (CRP) and Ensiled Chicory Root Pulp (ECRP)[a]

	mol %								
	Rha	Ara	Xyl	Man	Gal	Glc	UA	total	carbohydrate yield (% w/w) [g in fraction per 100 g in CRP/ECRP]
CRP	1	15	4	4	7	31	38	64[b]	100
CRP soluble	1	27	1	13	6	19	33	50	12
CRP insoluble	1	12	4	2	7	33	40	68	87
ECRP	2	15	4	3	7	31	38	56	100
ECRP soluble	2	27	0	3	8	3	57	62	48
ECRP insoluble	1	5	7	3	5	56	21	55	55

[a]Rha, rhamnose; Ara, arabinose; Xyl, xylose; Man, mannose; Gal, galactose; Glc, glucose; UA, uronic acid. [b]Contains 6% w/w inulin.[11]

In Vitro Fermentation. The fermentation medium used in this study was modified standard ileal efflux medium (SIEM) according to that of Ladirat et al.[12] Tween 80 was omitted from the fermentation medium because it influenced the analysis of polysaccharide degradation products. All medium components were purchased from Tritium Microbiology (Veldhoven, The Netherlands). The pH of the buffered fermentation medium was adjusted to 5.8, simulating the pH in the proximal colon; during fermentation the pH was maintained between 5.8 and 6.3. The inoculum was a standardized pool of adult fecal inoculum according to the validated protocol described by Minekus et al.[13] and prepared from eight healthy European adults (25−45 years old) who did not receive antibiotics during 2 months before donation. The inoculum (6 mL) was incubated in the modified SIEM (54 mL) for activation.[12]

CRP and ECRP (100 mg) were added to 9 mL of the modified SIEM in 25 mL bottles for each time point (0, 2, 6, 8, 12, and 24 h). The activated inoculum (1 mL) was added to the fermentation medium and flushed with CO_2. The bottles were immediately closed with rubber stoppers and sealed with aluminum caps. Fermentations were performed in duplicate for each substrate at 37 °C and shaken at 300 rpm until 24 h. A blank with only microbiota was taken as a control.

Fermentation digests were inactivated at 100 °C for 5 min and split into two parts. One part was reserved for direct analysis, and the other part of the fermentation digest was freeze-dried for further characterization.

Part of the dried fermentation digest was suspended in Millipore water (10 mg/mL) and centrifuged (10 min, 9000*g*, 4 °C) to obtain soluble and insoluble fractions. The insoluble fraction was freeze-dried and used along with the original dried fermentation digest for analyzing constituent monosaccharide content and composition. Constituent monosaccharide content in the soluble fraction was calculated from the difference in individual monosaccharide contents between the dried fermentation digest and the dried insoluble fraction of the fermentation digest. All samples were analyzed in duplicate.

Analytical Methods. *Constituent Monosaccharide Composition.* The constituent monosaccharide content and composition were determined using a prehydrolysis step with 72 (w/w%) sulfuric acid at 30 °C for 1 h followed by hydrolysis with 1 M sulfuric acid at 100 °C for 3 h. The monosaccharides formed upon hydrolysis were derivatized to alditol acetates and analyzed by gas chromatography using inositol as an internal standard.[14] The colorimetric *m*-hydroxydiphenyl assay[15] was used to determine the total uronic acid (UA) content.

Molecular Weight Distribution. Fermentation digests were centrifuged (10 min, 18000*g*, 24 °C) to obtain the soluble fraction, which was analyzed for molecular weight distribution using high-performance size exclusion chromatography (HPSEC) on an Ultimate 3000 HPLC (Dionex, Sunnyvale, CA, USA) as described before.[11] Three TSK-Gel columns in series (4000−3000−2500 SuperAW; 150 × 6 mm) were used for the analysis. They were preceded by a TSK Super AW-L guard column (35 × 4.6 mm). All columns were from Tosoh Bioscience (Tokyo, Japan). The molecular weight was estimated on the basis of a standard curve of pullulan standards.

Oligosaccharide Profiling. High-performance anion exchange chromatography (HPAEC) was performed on an ICS5000 system (Dionex), equipped with a Dionex CarboPac PA-1 column (2 × 250 mm) in combination with a Carbopac PA-1 guard column (2 × 50 mm). A volume of 10 μL of the soluble fraction of the fermentation digests (diluted twice with Millipore water) was injected into the system using a Dionex ICS5000 autosampler. The system was equipped with pulsed amperometric detection. The flow rate was 0.3 mL/min, and the gradient used was as described elsewhere.[16] The software used was Chromeleon version 7 (Dionex). Oligomers of galacturonic acid (DP 1−DP 5) were used as standards to identify and quantify galacturonic acid oligomers in the elution profile.

Analysis of Short-Chain Fatty Acids and Organic Acids. SCFAs and organic acids (lactate and succinate) were analyzed as described elsewhere.[17]

Microbiota Composition. Samples from a twin batch fermentation of CRP were analyzed for microbiota composition. The microbiota compositions for two independent duplicates of a 9 h fermentation digest of CRP (Supporting Information Figure S1) were similar, indicating reproducibility for fermentations of the cell wall material. The microbiota composition for ECRP fermentation was not performed due to limitations in the sample amount.

The molecular techniques used in isolation and amplification of DNA sequences followed by sequence processing and sequence analyses are as described previously.[18] In short, DNA was isolated from the fermentation digests using the AGOWA mag Mini kit (DNA Isolation Kit; AGOWA, Berlin, Germany), and a polymerase chain reaction (PCR) amplicon library was obtained by amplification of the V5−V7 hypervariable region of the small subunit rDNA gene (16S rDNA). The library was sequenced unidirectionally in the forward direction (A adapter) in one run in the 454 GS-FLX titanium sequencer (Roche, Branford, CT, USA) by Keygene (Wageningen, The Netherlands). Sequences extracted were processed using modules in the Mothur version 1.20.0 software platform module and aligned using the "align.seqs" command and an adaptation of the Bacterial SILVA SEED database as a template (http://www.mothur.org/wiki/Alignment_database). Aligned sequences were clustered into operation taxonomic units (OTUs; defined by 97% similarity) and were calculated by the average linkage clustering commando method.

RESULTS AND DISCUSSION

Characteristics of Fibers in Chicory Root Pulp and Ensiled Chicory Root Pulp. Table 1 shows the constituent monosaccharide composition of CRP and ECRP .[11] CRP is abundant in carbohydrates (64% w/w), of which 58% w/w represents CWPs and 6% w/w represents minor levels of the storage polysaccharide inulin with an average DP of 18.[11] The CWPs calculated from the mole percent monosaccharide composition and total sugar content (w/w %) (Table 1) contain 62% pectin (uronic acid + rhamnose + arabinose + galactose), 27% cellulose (arising from glucose not present in xyloglucan), and 11% hemicellulose (xylose + mannose + fucose + glucose in xyloglucan) as characterized earlier.[11] The carbohydrates present in the total soluble fraction represent only 12% of the CRP carbohydrates. As determined earlier for the dialyzed soluble fraction,[11] half is arabinose-rich pectin and

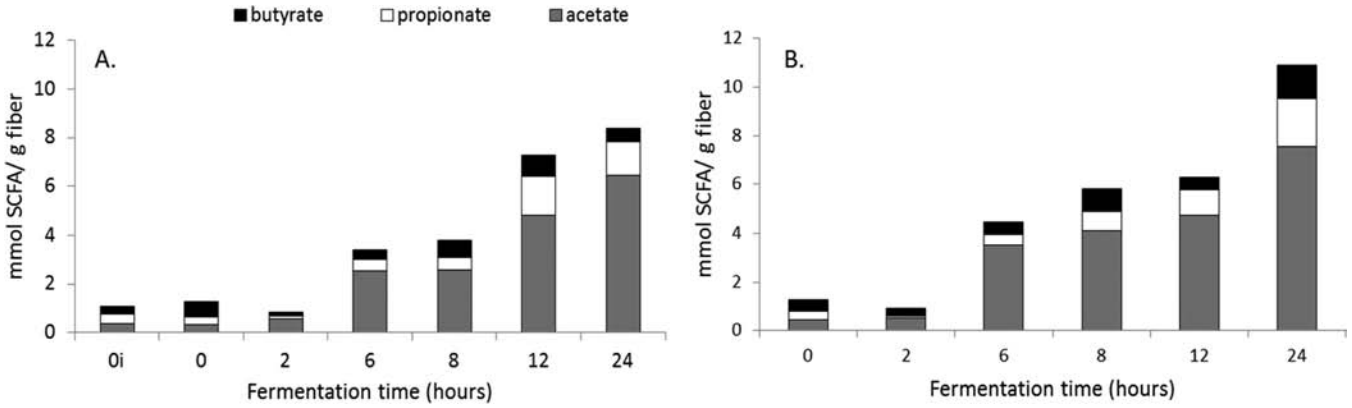

Figure 1. Short-chain fatty acid production during fermentation of (A) chicory root pulp (CRP) and (B) ensiled chicory root pulp (ECRP). Succinate and lactate levels are not shown due to low levels (<0.1 mmol/g fiber). 0i, inoculum + medium. Values present means of duplicate measurements. Values with corresponding standard deviations are presented in Table S1 of the Supporting Information.

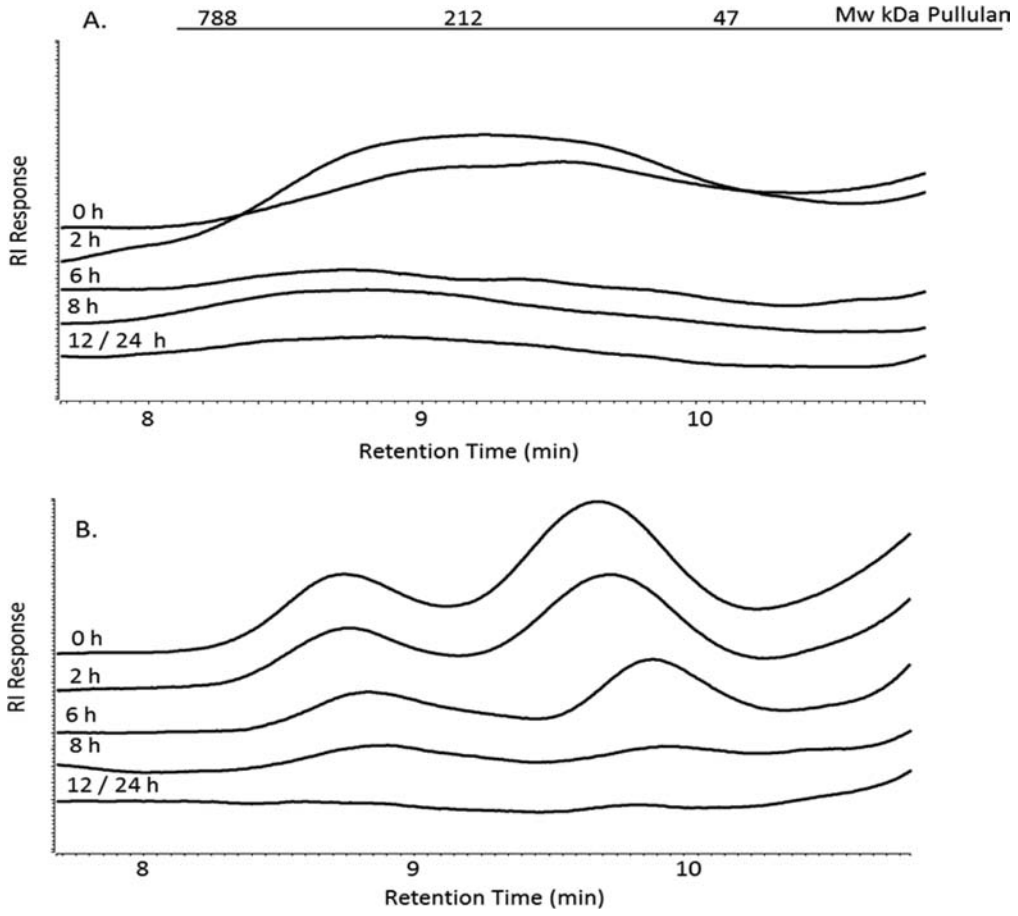

Figure 2. HPSEC elution patterns of fermentation digests during fermentation of (A) chicory root pulp (CRP) and (B) ensiled chicory root pulp (ECRP). Pullulan was used as a calibrant.

the other half is inulin, as is the case for the total soluble fraction. Almost 87% of the carbohydrates from CRP are insoluble and have a polysaccharide composition similar to that of the total CRP (Table 1).

The ECRP is rather similar in composition to CRP (Table 1), but contains no inulin.[11]

As indicated by the higher carbohydrate recovery (48%) in the soluble fraction from ECRP compared to that from CRP (12%) (Table 1), ECRP has more soluble fibers than CRP. Dominant among the sugars solubilized are the pectic sugars as seen from the sugar composition (Table 1). As determined from an earlier study for the dialyzed soluble fraction,[11] ECRP represents 4 times more pectic sugars than that from CRP as is the case for the total soluble fraction. The pectic sugars from the insoluble network of CRP are extractable only under severe conditions, such as chelating agents and alkali.[11] Apparently, they can be solubilized by ensiling. As a consequence, the insoluble fraction of ECRP represents a lower recovery of carbohydrates (55%) compared to CRP (87%) and is enriched in (hemi)cellulose (Table 1).

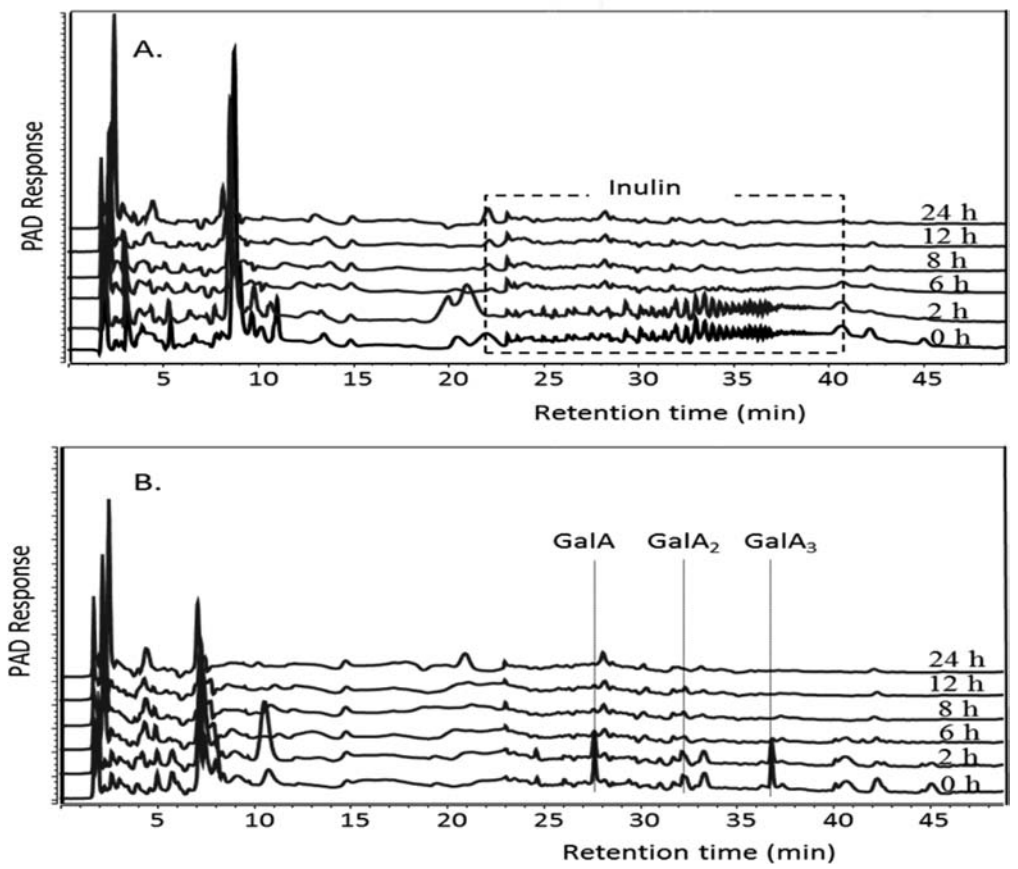

Figure 3. HPAEC elution profile of fermentation digests during fermentation of (A) chicory root pulp (CRP) and (B) ensiled chicory root pulp (ECRP). GalA, galacturonic acid; $GalA_2$, dimer of GalA.

Fermentation of CRP and ECRP: Short-Chain Fatty Acid Production. CRP and ECRP were well fermented as indicated by the increase in the levels of SCFAs produced (mmol/g substrate) in time (Figure 1) as well as from the decrease in CWP content discussed later in this study. The values including the corresponding standard deviation are presented in Supporting Information Table S1. The SCFA levels at the start of fermentation (0 h) for CRP and ECRP arose from the inoculum added to the medium as seen from similar levels between the inoculum blank (0i) and 0 h for CRP and ECRP fermentation. The initial SCFA levels (0 h) for both CRP and ECRP are higher than found for the digests after 2 h of fermentation, indicating utilization of SCFAs during the first 2 h. After 24 h of fermentation of CRP, 8.4 mmol SCFAs/g substrate was present.

Compared to CRP fermentation (Figure 1A), ECRP fermentation was quicker as high levels of SCFAs were produced within a short time period (6 h) of fermentation (Figure 1B). Besides a faster ECRP fermentation, a higher SCFA production (10.9 mmol/g after 24 h of ECRP fermentation) was seen compared to CRP fermentation (8.4 mmol/g). This indicated that the modified cell wall network of ECRP with a higher ratio of soluble/insoluble polysaccharides (0.8) (Table 3) compared to CRP (ratio 0.3) (Table 3) is more fermentable than that of CRP. The ratios of acetate/propionate/butyrate were similar between CRP (77:16:6) and ECRP (69:18:13) after 24 h of fermentation. Because the carbohydrate compositions of CRP and ECRP are similar, this suggested that fermentation of an open cell wall network has limited influence on utilization by the microbiota. This similarity in the SCFA ratio has also been observed for fermentations of sugar beet pulp and autoclaved beet pulp.[10]

Minor levels of intermediate fatty acids,[19] lactate and succinate (<0.1 mmol/g), were observed throughout the fermentation period. The fermentation of higher oligomers of inulin (discussed later) indeed resulted in very little butyrate and lactate formation. Fermentation of higher oligomers of inulin (DP >20) by the microbiota has been reported to more greatly hinder the production of butyrate and lactate than that of short oligomers of inulin (DP <10).[20,21]

Molecular Weight Distribution of Soluble Fibers. HPSEC elution profiles of solubles from CRP and ECRP fermentation digests are shown in Figure 2. For CRP fermentation, an increase in the amount of soluble material corresponding to high molecular weight (M_w) (8−10 min, 47−788 kDa) was seen after 2 h of inoculation. From 6 h onward, an almost complete disappearance in the high M_w fraction suggested degradation/utilization of the high M_w polysaccharide. This implies either rapid utilization of fibers solubilized during fermentation or direct utilization of insoluble fibers directly by the microbiota system.

Compared to the elution profile of CRP fermentation blank (0 h), the elution profile of the ECRP blank showed a 52% higher amount of high M_w material, as expected from the higher pectin solubility.[11] This material is present in two populations (8−9 min, 212−788 kDa; and 9−10 min, 47−212 kDa). After 6 h of fermentation, a decrease is seen in the intensity of both peaks, indicating degradation of both populations. These populations are almost completely utilized after 8 h of

dx.doi.org/10.1021/jf501254z | J. Agric. Food Chem. 2014, 62, 6794−6802

Table 2. Residual Carbohydrate Levels and Constituent Monosaccharide Composition of Digests Obtained from in Vitro Fermentation of Chicory Root Pulp (CRP) and Ensiled CRP (ECRP)[a]

		mol %							
fermentation time (h)	residual carbohydrate levels (mg from 90 mg of starting material)	Rha	Ara	Xyl	Man	Gal	Glc	UA	total (% w/w)
				CRP					
0 (blank)	56	2	14	4	5	8	35	32	7
		0.00	*0.69*	*0.25*	*0.67*	*0.10*	*0.36*	*0.19*	*0.00*
2	46	2	14	4	5	8	35	32	7
		0.03	*0.05*	*0.06*	*0.02*	*0.05*	*0.06*	*0.12*	*0.04*
12	42	2	14	5	3	8	35	34	7
		0.01	*0.00*	*0.02*	*0.02*	*0.01*	*0.11*	*0.29*	*0.44*
24	28	2	4	8	4	6	65	10	4
		0.15	*0.02*	*0.55*	*0.08*	*0.13*	*0.50*	*0.25*	*0.04*
				ECRP					
0 (blank)	55	2	14	4	3	8	35	34	7
		0.00	*0.06*	*0.01*	*0.03*	*0.01*	*0.32*	*0.03*	*0.32*
2	48	2	15	4	3	8	36	32	7
		0.20	*0.10*	*0.16*	*0.38*	*0.35*	*1.55*	*2.43*	*0.29*
12	35	2	6	6	4	7	53	22	5
		0.25	*0.69*	*0.50*	*0.36*	*1.17*	*0.02*	*1.43*	*0.71*
24	22	2	2	9	5	5	68	10	4
		0.43	*0.10*	*0.33*	*0.04*	*0.41*	*0.27*	*1.08*	*0.22*

[a]Rha, rhamnose; Fuc, fucose; Ara, arabinose; Xyl, xylose; Man, mannose; Gal, galactose; Glc, glucose; UA, uronic acid. The values presented are means of duplicate measurements, with standard deviations in italics.

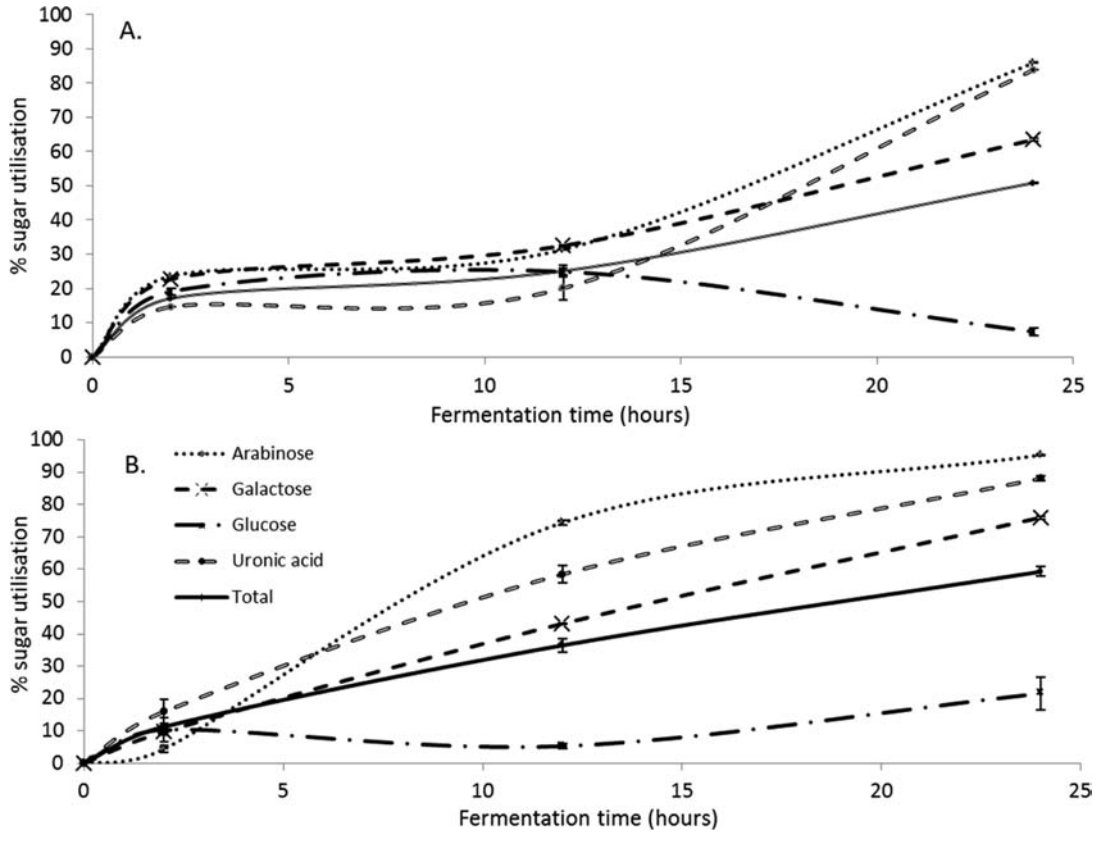

Figure 4. Utilization (%) of monosaccharides during in vitro fermentation originally present in (A) chicory root pulp (CRP) and (B) ensiled chicory root pulp (ECRP). Values presented are means of duplicate measurements, with standard errors of the means (vertical bars).

fermentation. As for CRP fermentation, almost no high M_w solubles could be seen after 12 and 24 h of ECRP fermentation.

Oligomer Utilization. To determine oligomers formed/utilized during CRP and ECRP fermentation, soluble fractions from fermentation digests were analyzed using HPAEC (Figure 3). Before the start of CRP fermentation (0 h), higher oligomers of inulin (average DP of 18)[11] were observed. Because short oligomers of inulin were removed by the

dx.doi.org/10.1021/jf501254z | J. Agric. Food Chem. 2014, 62, 6794−6802

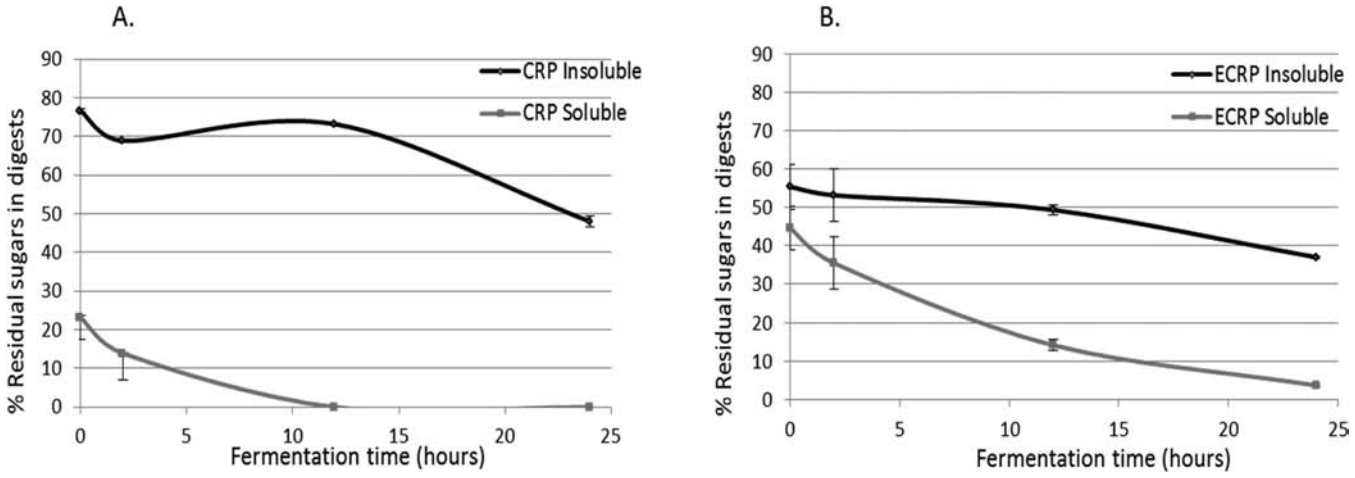

Figure 5. Total sugars in soluble and insoluble fractions of fermentation digests of percent original sugars during (A) chicory root pulp (CRP) fermentation and (B) ensiled chicory root pulp (ECRP) fermentation. Values are means of duplicate measurements with standard errors shown by vertical bars on the curves.

industrial extraction from the root, the pulp contains only higher oligomers of inulin. Within 6 h, inulin is almost completely utilized.[11]

During fermentation, CWPs are degraded to lower M_w material, and in a previous study using sources other than CRP for CWPs, intermediate oligosaccharides could be clearly recognized.[16] However, in this study, no oligomers formed from CWPs were observed during CRP fermentation. *Bacteroides* sp., becoming dominant during CRP fermentation, as discussed later, are known to be motile and to possess "specialized polysaccharide utilization systems" in which cell surface proteins are involved in binding to different polysaccharides and transporting the oligomers that are formed directly over the bacterial membrane.[22,23] Such systems likely prevent diffusion of oligomers. Another possibility for the absence of oligomers could arise from rapid cross feeding of oligomers by other fermenting bacteria.[24]

Before the start of ECRP fermentation (0 h), a number of peaks can be identified as oligomers of galacturonic acid (GalA) on the basis of standards of GalA oligomers used (Figure 3B). These oligomers represent approximately 14% of total ECRP GalA and arose from ECRP after the process of ensiling. These oligomers are shown to decrease within the first 6 h of ECRP fermentation, pointing to their utilization. Similar to the CRP fermentation, no new oligomers are formed.

Changes in CRP Fiber Composition during Fermentation. Direct utilization of CWPs during CRP fermentation can be revealed from the decrease in the total carbohydrate content as well as from the constituent monosaccharides during fermentation. The constituent monosaccharide compositions of CRP fermentation digests are shown in Table 3. Low concentrations (w/w%) of carbohydrates in all of the fermentation digests are due to the presence of high concentrations of other fermentation media components, such as proteins and salts.[12,13] The constituent monosaccharide composition of the CRP fermentation blank (0 h) (Table 2) is similar to that of CRP (Table 1), indicating that the carbohydrates present in the medium before fermentation do not contain carbohydrates other than from CRP fibers. After 24 h of fermentation, 51% of CRP total carbohydrates were utilized (Figure 4A). This is rather similar to the degradability of sugar beet fiber showing 60% carbohydrate utilization after 24 h of fermentation with human fecal inoculum.[25]

Until 12 h of fermentation, the constituent monosaccharide composition remained similar, although 25% of all carbohydrates were utilized. This indicated unspecific utilization of CWPs in the first 12 h of fermentation. This is also seen in Figure 4A from 0 to 12 h of fermentation. As the fermentation continued from 12 to 24 h, the carbohydrate content was further reduced by another 25% and the constituent monosaccharide composition changed considerably. This suggests a more specific utilization of CWPs from 12 h onward. The calculated decrease in arabinose (Ara), galactose (Gal), and GalA by 86, 63, and 84%, respectively, after 24 h (Figure 4A), indicated enhanced utilization of arabinan, galactan, and homogalacturonan (HG) from CRP, respectively. The unexpected decrease in glucose utilization from 12 to 24 h (Figure 4A) might arise from an increase in bacterial cell walls containing glucose.[26]

The enzyme machinery from the fermenting bacteria seemed to be so efficient in degrading arabinan that the 14% level of resistant arabinan after 24 h of fermentation is only half of the arabinan remaining in the cell wall matrix after severe extraction by strong alkali.[11] This indicated that even part of the heavily entangled arabinan was utilized during fermentation.

Changes in Ensiled CRP Fiber Composition during Fermentation. The presence of more soluble fibers in a more open cell wall network in ECRP compared to CRP was hypothesized to have an effect on the fiber utilization during fermentation of the cell wall network. The constituent monosaccharide compositions of the fermentation digests obtained during fermentation of ECRP are shown in Table 2.

After 24 h of fermentation, 59% of all carbohydrates are utilized from ECRP (Figure 4B). The 8% higher carbohydrate utilization compared to CRP indicates a slightly higher fermentability of ECRP over CRP as has been seen from the higher SCFA production as discussed earlier. Unexpectedly, the increase in SCFA production (30%) is much higher than the 8% higher carbohydrate utilization. ECRP fermentation was also quicker as was indicated from the high level of carbohydrate utilization (36%) within a short time period of 12 h compared to only 25% carbohydrate utilization for 12 h of CRP fermentation (Table 2).

dx.doi.org/10.1021/jf501254z | J. Agric. Food Chem. 2014, 62, 6794−6802

Table 3. Constituent Carbohydrates Present in Soluble and Insoluble Fractions of Pecent Original Carbohydrates in Fermentation Digests during in Vitro Fermentation of Chicory Root Pulp (CRP) and Ensiled CRP (ECRP)[a]

time (h)	Rha	Ara	Xyl	Man	Gal	Glc	UA	total
CRP Insoluble Fraction								
0 (blank)	62 ± 1.5	81 ± 0.4	84 ± 0.7	50 ± 0.7	72 ± 0.3	76 ± 0.5	80 ± 0.5	77 ± 0.5
2	52 ± 2.7	66 ± 0.0	70 ± 0.4	50 ± 1.6	58 ± 0.4	69 ± 0.4	75 ± 0.6	69 ± 0.3
12	91 ± 0.0	67 ± 1.7	68 ± 0.4	46 ± 2.2	65 ± 1.0	75 ± 0.2	79 ± 0.6	73 ± 0.3
24	43 ± 0.6	14 ± 0.0	88 ± 3.2	52 ± 0.3	35 ± 2.7	92 ± 0.8	14 ± 1.8	48 ± 1.3
CRP Soluble Fraction								
0 (blank)	38 ± 1.5	19 ± 0.4	16 ± 0.7	50 ± 0.7	28 ± 0.3	24 ± 0.5	20 ± 0.5	23 ± 0.5
2	37 ± 2.7	11 ± 0.0	26 ± 0.4	48 ± 1.6	20 ± 0.4	12 ± 0.4	10 ± 0.6	14 ± 0.3
12	9 ± 0.0	0 ± 1.7	12 ± 0.4	0 ± 2.2	0 ± 1.0	0 ± 0.2	0 ± 0.6	0 ± 0.3
24	15 ± 0.6	0 ± 0.0	0 ± 3.2	0 ± 0.3	1 ± 2.7	0 ± 0.8	2 ± 1.8	0 ± 1.3
ECRP Insoluble Fraction								
0 (blank)	47 ± 5	39 ± 2.2	100 ± 0.0	61 ± 6.0	55 ± 3.8	80 ± 8.1	33 ± 4.3	55 ± 5.8
2	45 ± 1.9	33 ± 2.2	96 ± 16.9	60 ± 10.3	47 ± 5.0	79 ± 13.1	31 ± 1.8	53 ± 6.9
12	37 ± 0.1	19 ± 0.1	93 ± 5.8	60 ± 1.8	41 ± 1.5	79 ± 2.6	28 ± 0.1	49 ± 1.3
24	26 ± 3.6	5 ± 0.0	86 ± 3.2	56 ± 0.6	16 ± 0.2	76 ± 0.7	9 ± 0.1	37 ± 0.3
ECRP Soluble Fraction								
0 (blank)	53 ± 5	61 ± 2.2	0 ± 0.0	39 ± 6.0	45 ± 3.8	20 ± 8.1	67 ± 4.3	45 ± 5.8
2	49 ± 1.9	62 ± 2.2	2 ± 16.9	31 ± 10.3	43 ± 5	10 ± 13.1	53 ± 1.8	35 ± 6.9
12	38 ± 0.1	7 ± 0.1	3 ± 5.8	24 ± 1.8	15 ± 1.5	16 ± 2.6	14 ± 0.1	14 ± 1.3
24	35 ± 3.6	0 ± 0.0	5 ± 3.2	8 ± 0.6	8 ± 0.2	3 ± 0.7	3 ± 0.1	4 ± 0.3

[a]Values are means of duplicate measurements with corresponding standard error. Rha, rhamnose; Fuc, fucose; Ara, arabinose; Xyl, xylose; Man, mannose; Gal, galactose; Glc, glucose; UA, uronic acid.

As for CRP fermentation, specific CWPs consisting of Ara, GalA, and Gal are favorably utilized the most during ECRP fermentation, but to a larger extent compared to CRP fermentation (Figure 4). As seen in Figure 4, the sugar utilization for ECRP is more pronounced than CRP fermentation after 12 h than after 24 h of fermentation. At 12 h, the sugar utilization was determined to be 31 and 74% Ara, 20 and 58% GalA, and 32 and 43% Gal for CRP and ECRP, respectively (Figure 4). This rapid increase in carbohydrate utilization coincides with the higher levels of soluble fibers composed of Ara, Gal, and GalA in ECRP. This indicated that processing of CRP, increasing the levels of soluble fibers and modifying the cell wall network, increased the degradability and the rate of fermentation of specific CWPs.

Utilization of Soluble/Insoluble Fibers from Cell Wall Materials during Fermentation. The presence of soluble fibers and/or more open CWP network of the remaining insoluble fibers in ECRP seems to enhance fermentation. To elaborate on this observation, carbohydrate levels in both soluble and insoluble fractions of digests from percent original carbohydrates are shown in Figure 5. Levels of individual carbohydrates in soluble and insoluble fractions of fermentation digests from percent original individual carbohydrates are shown in Table 3.

Utilization of Soluble/Insoluble Fibers from CRP. The insoluble fibers in CRP are utilized only after 12 h when all soluble fibers have been utilized. This is also in agreement with HPSEC in which no soluble fibers could be seen after 12 h of fermentation (Figure 2). Insoluble fibers are mostly utilized between 12 and 24 h of fermentation shown by the decrease from 73 to 48% of residual insoluble carbohydrates. Insoluble fiber utilization mostly involved pectic sugars of Ara, GalA, and Gal as indicated from Table 3. Only 18% of all insoluble pectin (GalA + Rha + Ara + Gal) (calculated from Table 3) remained unfermentable after 24 h, suggesting a high fermentability of insoluble pectin from the CRP plant cell wall.

For ECRP fermentation, utilization of soluble fibers can be seen from the decrease in the residual soluble carbohydrate levels from 45 to 4% from 0 to 24 h (Figure 5B). Utilization of insoluble fibers is slow and lower than found for the soluble fiber as shown by the decrease from 55 to 37% of residual insoluble carbohydrates (Figure 5B). Soluble fibers consisting of pectic sugars (Table 3) are thus preferentially utilized. This suggests that the increased rate and higher level (8%) of carbohydrate utilization in ECRP fermentation compared to CRP fermentation is due to fermentation of soluble pectin fibers that are present in high amounts in ECRP.

Compared to CRP, for ECRP, only 9% of all pectin (Rha + Gala + Ara + Gal) originally present remained unfermentable (calculated from Table 3). This suggested that pectin in the hypothesized more open structure of the ECRP cell wall was more degradable than the pectin in the CRP cell wall structure, contributing to an increased fermentability of ECRP. Other than pectin, the ECRP cell wall contained quite some cellulose + hemicellulose sugars (glucose + xylose + mannose) that were unfermentable (75%) (calculated from Table 3). This suggested that the fermentative degradation of the CWP network was selective for pectin fibers and preferably soluble pectin. This is in agreement with the limited degradation of (hemi)cellulose by the human gut microbiota in human subjects.[27]

Microbiota Composition during CRP Fermentation. The microbiota composition during the course of fermentation is expected to be modulated on the basis of the composition of the fiber added during fermentation.[28] The main genera present in the microbiota of the fermentation digest for CRP fermentation (Figure 6) are expressed as percent abundance of genera of the total microbiota in the fermentation digest. The highest increase was seen for *Bacteroides* sp. (8%), which remain the most dominant bacteria after 24 h of fermentation. In contrast, decreases were seen for *Dorea* sp. (1.5%), *Sutterella* sp. (5.7%), and *Clostridium* XIVa sp. (6%). The relative

dx.doi.org/10.1021/jf501254z | J. Agric. Food Chem. 2014, 62, 6794−6802

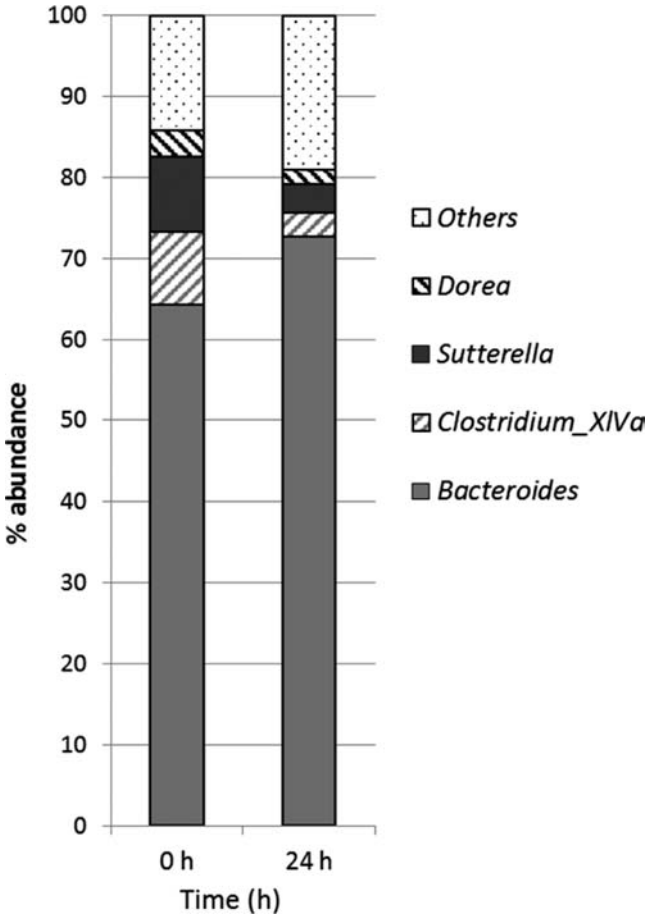

Figure 6. Microbiota composition during fermentation of chicory root pulp (CRP) expressed as percent abundance of genera of the total microbiota in the fermentation digest.

abundance of less dominant genera is presented in Table S2 in the Supporting Information.

The fermentation digest at 24 h of fermentation showed an increase in *Clostridium sensu stricto* sp. (1.34%) and *Lachnospiracea incertae sedis* sp. (1.21%) (Supporting Information Table S2).

Although *Lachnospiracea incertae sedis* sp. is a butyrate producer[29] and increased during fermentation, the observed lower butyrate/(acetate + propionate) ratio of 6:94 after 24 h compared to 50:50 at the start of fermentation (Figure 1) could be due to the decrease in butyrate producers,[30,31] such as *Clostridium* XIVa sp., *Faecalibacterium* sp. (0.94%), and *Butyricicoccus* sp. (0.57%) (Supporting Information Table S2).

Despite the presence of the bifidogenic inulin fraction,[32] no growth of *Bifidobacterium* sp. was seen after 24 h of fermentation, because inulin (6% of all CRP carbohydrates) was already utilized within 6 h of fermentation.

Although changes in the microbiota composition are seen during CRP fermentation, the significance of the change in the complex community of microbiota is hard to understand. Part of the significance may be understood when correlated to metabolite production, fiber degradation, and utilization. It is likely that *Bacteroides* sp., identified as the dominant bacteria in fermenting CRP, are responsible for the shown utilization of arabinan, galactan, and homogalacturonan and an increase in acetate and propionate. *B. thetaiotaomicron*, known to be highly abundant among *Bacteroides* sp.,[33] has been estimated to include 236 glycoside hydrolase genes.[34,35] Production of enzymes during the course of fermentation is up-regulated on the basis of the polysaccharides present during fermentation.[34]

Although it is not possible to include the microbiota composition for ECRP fermentation, measurements of different fiber degradations clearly point to differences in microbiota composition. As has been seen earlier,[36] differences in microbiota composition were found between soluble fibers (pullulan and soluble corn fiber) and insoluble fibers (resistant starch and cellulose). Because ECRP has more soluble fibers than CRP, it is probable that the soluble fiber degrading bacteria will be more dominant during ECRP fermentation than during CRP fermentation.

This study revealed that processing (ensiling) of chicory root pulp to open the cell wall network and solubilize pectin from the cell wall network will increase the fermentation rate of soluble pectin fibers as well as insoluble pectin fibers in the pulp. Processing an agricultural byproduct would thus be an option if an increased fermentation rate of cell wall polysaccharides is desired for the final dietary fiber product.

■ ASSOCIATED CONTENT

Supporting Information

Figure S1 and Tables S1 and S2. This material is available free of charge via the Internet at http://pubs.acs.org.

■ AUTHOR INFORMATION

Corresponding Author

*(H.G.) Phone: +31 317 483 211. Fax: +31 317 483 211. E-mail: harry.gruppen@wur.nl.

Funding

This project is jointly financed by the European Union, European Regional Development Fund, and The Ministry of Economic Affairs, Agriculture and Innovation, Peaks in the Delta, the Municipality of Groningen, and the Province of Groningen as well as the Dutch Carbohydrate Competence Center (CCC WP2a) and Royal Cosun. K.V. acknowledges the support of the European Science Foundation (ESF), within the framework of the Research Networking Programme, the European Network for Gastrointestinal Health Research.

Notes

The authors declare no competing financial interest.

■ ABBREVIATIONS USED

DF, dietary fiber; CRP, chicory root pulp; HG, homogalacturonan; RG, rhamnogalacturonan; ECRP, ensiled chicory root pulp; Ara, arabinose; Gal, galactose; Glc, glucose; Xyl, xylose; Man, mannose; Fuc, fucose; GalA/UA, galacturonic acid/uronic acid; Rha, rhamnose; CWP, cell wall polysaccharides; PS, polysaccharides

■ REFERENCES

(1) DeVries, J. W.; Camire, M. E.; Cho, S.; Craig, S.; Gordon, D.; Jones, J. M.; Li, B.; Lineback, D.; Prosky, L.; Tungland, B. C. The definition of dietary fiber. *Cereal Foods World* **2001**, *46*, 112−129.

(2) Parkar, S. G.; Redgate, E. L.; Wibisono, R.; Luo, X.; Koh, E. T. H.; Schröder, R. Gut health benefits of kiwifruit pectins: comparison with commercial functional polysaccharides. *J. Funct. Foods* **2010**, *2*, 210−218.

(3) Vince, A.; McNeil, N.; Wager, J.; Wrong, O. The effect of lactulose, pectin, arabinogalactan and cellulose on the production of organic acids and metabolism of ammonia by intestinal bacteria in a faecal incubation system. *Br. J. Nutr.* **1990**, *63*, 17−26.

(4) Fukunaga, T.; Sasaki, M.; Araki, Y.; Okamoto, T.; Yasuoka, T.; Tsujikawa, T.; Fujiyama, Y.; Bamba, T. Effects of the soluble fibre pectin on intestinal cell proliferation, fecal short chain fatty acid production and microbial population. *Digestion* **2003**, *67*, 42−49.
(5) Gibson, G. R.; Roberfroid, M. B. Dietary modulation of the human colonic microbiota: Introducing the concept of prebiotics. *J. Nutr.* **1995**, *125*, 1401−1412.
(6) Brown, R. Effect of lactulose and other laxatives on ileal and colonic pH as measured by a radiotelemetry device. *Gut* **1974**, *15*, 999−1004.
(7) Cummings, J. H.; Macfarlane, G. T. The control and consequences of bacterial fermentation in the human colon. *J. Appl. Microbiol.* **1991**, *70*, 443−459.
(8) Roediger, W. E. W. The colonic epithelium in ulcerative-colitis − an energy-deficiency disease. *Lancet* **1980**, *2*, 712−715.
(9) Bufill, J. A. Colorectal-cancer − evidence for distinct genetic categories based on proximal or distal tumor location. *Ann. Intern. Med.* **1990**, *113*, 779−788.
(10) Guillon, F.; Barry, J.-L.; Thibault, J.-F. Effect of autoclaving sugar-beet fibre on its physico-chemical properties and its *in vitro* degradation by human faecal bacteria. *J. Sci. Food Agric.* **1992**, *60*, 69−79.
(11) Ramasamy, U. S.; Gruppen, H.; Schols, H. A. Structural and water-holding characteristics of untreated and ensiled chicory root pulp. *J. Agric. Food Chem.* **2013**, *61*, 6077−6085.
(12) Ladirat, S. E.; Schols, H. A.; Nauta, A.; Schoterman, M. H. C.; Keijser, B. J. F.; Montijn, R. C.; Gruppen, H.; Schuren, F. H. J. High-throughput analysis of the impact of antibiotics on the human intestinal microbiota composition. *J. Microbiol. Methods* **2013**, *92*, 387−397.
(13) Minekus, M.; Smeets-Peeters, M.; Bernalier, A.; Marol-Bonnin, S.; Havenaar, R.; Marteau, P.; Alric, M.; Fonty, G.; Huis in't Veld, J. H. A computer-controlled system to simulate conditions of the large intestine with peristaltic mixing, water absorption and absorption of fermentation products. *Appl. Microbiol. Biotechnol.* **1999**, *53*, 108−114.
(14) Englyst, H. N.; Cummings, J. H. Simplified method for the measurement of total non-starch polysaccharides by gas-liquid chromatography of constituent sugars as alditol acetates. *Analyst* **1984**, *109*, 937−942.
(15) Ahmed, A. E. R.; Labavitch, J. M. A simplified method for accurate determination of cell wall uronide content. *J. Food Biochem.* **1978**, *1*, 361−365.
(16) Jonathan, M. C.; van den Borne, J. J. G. C.; van Wiechen, P.; Souza da Silva, C.; Schols, H. A.; Gruppen, H. *In vitro* fermentation of 12 dietary fibres by faecal inoculum from pigs and humans. *Food Chem.* **2012**, *133*, 889−897.
(17) Ladirat, S. E.; Schuren, F. H.; Schoterman, M. H.; Nauta, A.; Gruppen, H.; Schols, H. A. Impact of galacto-oligosaccharides on the gut microbiota composition and metabolic activity upon antibiotic treatment during *in vitro* fermentation. *FEMS Microbiol. Ecol.* **2014**, *87*, 41−51.
(18) Leijdekkers, A. G. M.; Aguirre, M.; Venema, K.; Bosch, G.; Gruppen, H.; Schols, H. A. In vitro fermentability of sugar beet pulp derived oligosaccharides using human and pig fecal inoculum. *J. Agric. Food Chem.* **2014**, *62*, 1079−1087.
(19) Cummings, J. H. Short chain fatty acids in the human colon. *Gut* **1981**, *22*, 763−779.
(20) Stewart, M. L.; Timm, D. A.; Slavin, J. L. Fructooligosaccharides exhibit more rapid fermentation than long-chain inulin in an *in vitro* fermentation system. *Nutr. Res. (N.Y.)* **2008**, *28*, 329−334.
(21) van Nuenen, M. H.; Diederick Meyer, P.; Venema, K. The effect of various inulins and *Clostridium difficile* on the metabolic activity of the human colonic microbiota in vitro. *Microb. Ecol. Health Dis.* **2003**, *15*, 137−144.
(22) Kuwahara, T.; Yamashita, A.; Hirakawa, H.; Nakayama, H.; Toh, H.; Okada, N.; Kuhara, S.; Hattori, M.; Hayashi, T.; Ohnishi, Y.; Mekalanos, J. J. Genomic analysis of *Bacteroides fragilis* reveals extensive DNA inversions regulating cell surface adaptation. *Proc. Natl. Acad. Sci. U.S.A.* **2004**, *101*, 14919−14924.
(23) McBride, M. J.; Xie, G.; Martens, E. C.; Lapidus, A.; Henrissat, B.; Rhodes, R. G.; Goltsman, E.; Wang, W.; Xu, J.; Hunnicutt, D. W.; Staroscik, A. M.; Hoover, T. R.; Cheng, Y.-Q.; Stein, J. L. Novel features of the polysaccharide-digesting gliding bacterium *Flavobacterium johnsoniae* as revealed by genome sequence analysis. *Appl. Environ. Microbiol.* **2009**, *75*, 6864−6875.
(24) Flint, H. J.; Duncan, S. H.; Scott, K. P.; Louis, P. Interactions and competition within the microbial community of the human colon: links between diet and health. *Environ. Microbiol.* **2007**, *9*, 1101−1111.
(25) Barry, J. L.; Hoebler, C.; Macfarlane, G. T.; Macfarlane, S.; Mathers, J. C.; Reed, K. A.; Mortensen, P. B.; Nordgaard, I.; Rowland, I. R.; Rumney, C. J. Estimation of the fermentability of dietary fibre *in vitro*: a European interlaboratory study. *Br. J. Nutr.* **1995**, *74*, 303−322.
(26) Osborn, M. Structure and biosynthesis of the bacterial cell wall. *Annu. Rev. Biochem.* **1969**, *38*, 501−538.
(27) Slavin, J. L.; Brauer, P. M.; Marlett, J. A. Neutral detergent fiber, hemicellulose and cellulose digestibility in human subjects. *J. Nutr.* **1981**, *111*, 287−297.
(28) Gibson, G. R.; Probert, H. M.; Loo, J. V.; Rastall, R. A.; Roberfroid, M. B. Dietary modulation of the human colonic microbiota: updating the concept of prebiotics. *Nutr. Res. Rev.* **2004**, *17*, 259−275.
(29) Salonen, A.; de Vos, W. M.; Palva, A. Gastrointestinal microbiota in irritable bowel syndrome: present state and perspectives. *Microbiology* **2010**, *156*, 3205−3215.
(30) Louis, P.; Flint, H. J. Diversity, metabolism and microbial ecology of butyrate-producing bacteria from the human large intestine. *FEMS Microbiol. Lett.* **2009**, *294*, 1−8.
(31) Van den Abeele, P.; Belzer, C.; Goossens, M.; Kleerebezem, M.; De Vos, W. M.; Thas, O.; De Weirdt, R.; Kerckhof, F. M.; Van de Wiele, T. Butyrate-producing *Clostridium* cluster XIVa species specifically colonize mucins in an *in vitro* gut model. *ISME J.* **2013**, *7*, 949−961.
(32) Meyer, D. Prebiotic dietary fibres and the immune system. *Agro Food Ind. Hi-Tech* **2008**, *19*, 12−15.
(33) Bjursell, M. K.; Martens, E. C.; Gordon, J. I. Functional genomic and metabolic studies of the adaptations of a prominent adult human gut symbiont, *Bacteroides thetaiotaomicron*, to the suckling period. *J. Biol. Chem.* **2006**, *281*, 36269−36279.
(34) Sonnenburg, J. L.; Xu, J.; Leip, D. D.; Chen, C.-H.; Westover, B. P.; Weatherford, J.; Buhler, J. D.; Gordon, J. I. Glycan foraging *in vivo* by an intestine-adapted bacterial symbiont. *Science* **2005**, *307*, 1955−1959.
(35) Flint, H. J.; Bayer, E. A.; Rincon, M. T.; Lamed, R.; White, B. A. Polysaccharide utilization by gut bacteria: potential for new insights from genomic analysis. *Nat. Rev. Microbiol.* **2008**, *6*, 121−131.
(36) Maathuis, A.; Hoffman, A.; Evans, A.; Sanders, L.; Venema, K. The effect of the undigested fraction of maize products on the activity and composition of the microbiota determined in a dynamic *in vitro* model of the human proximal large intestine. *J. Am. Coll. Nutr.* **2009**, *28*, 657−666.

of whether allergic reactions can be elicited in allergic patients by residues of fining agents in wine is still unanswered. Kirschner et al.[14] investigated the tolerability of casein-, ovalbumin-, and isinglass-fined wines in 14 allergic patients by skin prick tests (SPT), as well as by double-blind, placebo-controlled food challenge (DBPCFC) with fined and filtered wines. The highly concentrated fining agents were allergenic in the SPT, but no patient reacted adversely to the oral challenge of the fined and filtered wines. However, in another study by Rolland et al.[12] after DBPCFC with fined and unfined wines, unspecific subjective, but no objective, symptoms occurred, which does not allow a clear interpretation. Because of this situation, since July 2, 2012, the application of fining agents such as casein and milk-derived products during wine processing has to be labeled if the final product contains 0.25 mg/L or more allergenic protein, which is a threshold given by Organisation Internationale de la Vigne et du Vin (OIV, Paris, France) regulations. This is a legal threshold under Regulation (EU) No. 579/2012 in conjunction with Regulation (EU) No. 1234/2007.

The method recommended by OIV for the detection of potentially allergenic residues of fining agents proteins in wine is ELISA with a limit of detection (LOD) of ≤0.25 mg/L and a limit of quantification (LOQ) of ≤0.5 mg/L. For this purpose various sensitive ELISA methods are described in the literature detecting ovalbumin, casein, and casein-derived products as well as dried hen's egg white.[2,15−18] Drawbacks of ELISA methods in this case are interfering compounds in the matrix such as polyphenols in red wine, as described by Weber et al.[15] and Monaci et al.[19] In recent years also a number of MS-based methods have been reported for the detection of residual allergenic fining agents in red and white wines.[19−24] With MS techniques LODs and LOQs in the lower milligrams per liter range up to 51 mg/L of fining agent residues in wine are achieved. A big benefit of MS analysis compared to ELISA is the possibility for simultaneous detection of, for example, casein and ovalbumin. However, a drawback of MS methods is that it is a nonimmunological method and the antigenicity of the target protein(s) is not considered, which might be important for allergen analysis.

The aim of the study was to develop very sensitive ELISA methods with detection limits in the micrograms per liter region to investigate possible casein fining agent residues in wine. These methods could then be used for risk assessment related to residues of allergenic wine fining agents and may avoid unnecessary labeling, which may lead to uncertainty and decreased quality of life in allergic consumers.[15,25]

For this purpose it is necessary to study the heterogeneity of different casein fining agents and get information on the influence of different standard substances as calibration reference on the results of the assay.

The characterization of different casein wine fining agents was done by lithium dodecyl sulfate−polyacrylamide gel electrophoresis (LDS-PAGE) with silver staining and immunoblot. For the quantification of these described possible fining agent residues in wine an indirect ELISA as well as an indirect sandwich ELISA were developed. Therefore, polyclonal antibodies raised against a casein fining agent were used for immunoblotting and ELISA development to achieve a higher specifity by considering all residual allergenic milk proteins remaining from the fining procedure with a casein-derived product.

The LODs and lower limits of quantification (LLOQ) depend on the type of ELISA, the calibrating substance, and the dilution of the analyzed wine and show the complexity of the wine matrix, especially for red wine.

The developed ELISA methods were used to investigate wines after using certain technological treatments to remove wine fining agents.

MATERIALS AND METHODS

Casein Standard and Fining Agents. Casein of analytical grade from Merck KGa (Darmstadt, Germany) was used as casein standard.

For matrix calibration the fining agent KalCasin was used, which is described as a potassium milk caseinate. It was obtained directly from the manufacturer, Erbslöh Geisenheim AG (Geisenheim, Germany), and had a protein content of approximately 76% by the Kjeldahl method.

Investigated and characterized fining agents were 12 casein products of different commercial European producers (Agrovin, Begerow, Enartis, Erbslöh, Laffort, Spindal, Vason) organized in OENOPPIA (International Association of Oenology Industrials for Oenological Products and Practice, Paris, France).

Antibodies. The capture antibodies for the sandwich ELISA, which were also used as primary antibodies for the indirect ELISA as well as for immunoblotting, were polyclonal antibodies raised against one fining agent, which is described as potassium caseinate. Antibody production was done by Eurogentec (Seraing, Belgium). For this three rabbits were immunized against this fining agent four times in four week intervals. The serum samples were taken 10 days after the second, third, and fourth immunizations and purified using affinity chromatography. Affinity chromatography was performed at CNBr Sepharose, and the antibodies were eluted with 100 mM glycine (pH 2.5). The antibodies were conserved with 0.01% thimerosal in phosphate-buffered saline (PBS), and the purity was >85%, determined by SDS-PAGE. The concentration of the purified antibodies was 1.1 mg/mL.

The primary antibodies for the indirect sandwich ELISA were produced by Immunology Consultants Laboratory (Newberg, OR, USA) against bovine casein in sheep. The concentration of the antibodies was 1.0 mg/L.

The secondary antibodies, used for the indirect ELISA as well as for the immunoblot, were HRP-conjugated goat anti-rabbit antibodies, obtained from Dako (Dako GmbH, Glostrup, Denmark). The concentration of the antibodies was 0.25 mg/L.

The secondary antibodies for the indirect sandwich-ELISA were produced by Immunology Consultants Laboratory against sheep, conjugated with HRP. The concentration of the antibodies was 1.0 mg/L.

Wine. Method development and validation were done with well-known experimental wines, produced by the Wine Research Institute Geisenheim in the context of project AiF 16330N, "Reducing the concentration of allergenic fining agents in the final wine by technological treatment". An unfined white wine of the grape variety Mueller Thurgau (vintage 2009) and an unfined red wine of the grape variety Regent (vintage 2009) were used as matrix for method development of the ELISAs. These wines were produced according to common winegrowers practice and finally bottled through a filter layer into 0.75 L bottles. The musts were inoculated with yeast (*Saccharomyces cereviseae*) and fermented at 16−18 °C. No fining procedure was done before filling.

Within the project different wine fining procedures were investigated concerning their effectiveness in reducing the content of certain allergenic wine fining agents in the final product wine. For that the described red wine and the described white wine were fined with the maximal permitted dose of wine fining agent as well as with double the maximal dose to demonstrate a worst-case scenario. This is to protect allergic consumers also from an accidental overdosage by the winegrower. These wines were produced according to common winegrower practice and finally bottled through a filter layer into 0.75 L bottles.

Eight processes to remove the fining agent were performed in 120 L flasks to simulate a wine tank. The wine was fined with 40 (A) and 80 g (B) KalCasin/hL wine.

To investigate whether there is a decrease of potential allergenic wine fining agent residues during the production process and how efficiently the different fining procedures work, two different production steps of every produced wine were analyzed by ELISAs. These two investigated production steps were the first after removal of the fining agent with different techniques (I) and the second after sterile filtration into commercially available bottles (II), respectively. The investigated red and white wines are presented in Table 1.

Table 1. Investigated White (WW) and Red (RW) Wines

wine		technique
WW1	RW1	I. 0.45 μm filtration
		II. sterile filtration
WW2	RW2	I. addition of bentonite
		II. sterile filtration

The following two filtration techniques and enological procedures used for wine production are discussed in this publication: (1) 0.45 μm filtration, using a Type 419A, grade B (beverage version) SEITZ-MEMBRAcart cartridge with 0.45 μm pore size from Pall Corp. (Port Washington, NY, USA); and (2) addition of bentonite, using Aktivit bentonite from Erbslöh. Immediately after these treatments, sterilizing filtration was performed on all wines, using SEITZ-EK 200 × 200 mm depth filter sheets from Pall Corp., and the wines were bottled into 0.75 L bottles. For example, the term WW1AII describes the white wine fined with 40 g/hL KalCasin, treated with process 1 to remove the fining agent, at processing step II, after sterile filtration.

Lithium Dodecyl Sulfate−Polyacrylamide Gel Electrophoresis. For electrophoretical separation, the casein standard and different fining agents were prepared in 10−13 mg/50 mL solutions with 10 mM carbonate solution under shaking on a horizontal shaker for at least 30 min.

All chemicals were of analytical grade. The proteins were separated as described by Steinhoff et al.[26] Precast NuPAGE Bis-Tris 12% gels (Invitrogen GmbH, Karlsruhe, Germany) were performed under denaturing conditions at 200 V using NuPAGE 3-(*N*-morpholino)-propansulfonic acid (MOPS) SDS running buffer (Invitrogen). For electrophoresis the protein solutions were diluted 1:2 with LDS sample buffer, which contained dithiothreitol (DDT) for reduction. Every lane was loaded with 20 μL of sample solution. The unpicked proteins were further silver stained or blotted on a nitrocellulose membrane.

Silver Staining. Detection of the separated proteins was done by a silver staining procedure according to Heukeshoven et al.[27] as described by Steinhoff et al.[26] At first, the proteins were fixed in the gel by treatment with 30% ethanol and 10% acetic acid in water for 30 min. Afterward, an incubation with a solution containing 0.1% sodium thiosulfate, 30% ethanol, and 6.8% sodium acetate in water occurred for 30 min. This was followed by a washing step with water. Then the gel was incubated in a silver nitrate solution (0.2% silver nitrate and 0.02% formaldehyde in water) for 20 min. Finally, development occurred with 2.5% sodium carbonate and 0.01% formaldehyde in water. Stop solution was prepared with 1.8% ethylendiaminetetraacetate (EDTA) in water.

Immunoblotting. All chemicals were of analytical grade. Immunoblotting was performed according to the method of Steinhoff et al.[26] By LDS-PAGE separated proteins were electrophoretically transferred onto a nitrocellulose membrane (Whatman, Maidstone, UK) via semidry western blotting. The dried membranes first were blocked with blocking solution (0.5% polyethylene-sorbitan monolaurate (Tween20), 0.9% sodium chloride, and 0.6% tris(hydroxymethyl)-aminomethane (Tris)) to inhibit nonspecific binding to the membrane. The membrane was incubated with the primary antibody, anti-potassium caseinate antibody (1/10000), followed by incubation with the secondary HRP conjugates anti-rabbit antibody (1/20000) at room temperature. Finally, staining was performed with staining solution containing 0.06% 3,3′,5,5′-tetramethylbenzidine (TMB), 0.2% dioctylsodium sulfosuccinate (DONS), 25% ethanol, 0.7% citric acid, and 1% Na_2HPO_4 in water. The protein weight marker was stained by adding Ponceau red solution.

Quantitative Indirect Sandwich and Indirect ELISA. Fining agent and protein standard solutions were prepared by dissolving about 12.5 mg of the respective substance in 50 mL of 10 mM carbonate solution under shaking on a horizontal shaker for at least 30 min. Depending on the ELISA to be undertaken, the calibration solutions were prepared by dilution with carbonate buffer (indirect ELISA) or PBS−Tween20 buffer (indirect sandwich ELISA).

All chemicals were of analytical grade. Buffer preparation was done according to the method of Weber et al.[15] Coating buffer (carbonate buffer, pH 9.6) contained 75 mM Na_2CO_3 and 175 mM $NaHCO_3$ in bidistilled water. Blocking solution (Tris−Tween20 buffer, pH 9.6) contained 50 mM Tris, 150 mM NaCl, and 0.5% Tween20 in bidistilled water. Washing solution (PBS−Tween20 buffer, pH 7.4) contained 10 mM $NaH_2PO_4 \cdot H_2O$, 70 mM Na_2HPO_4, 150 mM NaCl, and 0.5% Tween20 in bidistilled water. Citric buffer (pH 4.0) contained 210 mM citric acid monohydrate and 300 mM KOH in bidistilled water. The substrate solution was freshly prepared with 5 mg of TMB, dissolved in 125 μL of acetone filled to 1 mL with methanol, 19 mL of citric buffer, and 200 μL of H_2O_2 (1%). The stop solution was made of 2 M H_2SO_4 in bidistilled water.

An indirect ELISA procedure was modified according to the method of Weber et al.[2] Two hundred microliters per well sample solution in coating buffer was coated to a polystyrene microtiter plate (MaxiSorp F96, Nunc, Roskilde, Denmark) overnight at 8−9 °C. The plate was washed three times with 300 μL/well blocking solution. Subsequently, free binding sites of the wells were blocked with 250 μL/well blocking solution for 2 h at room temperature by horizontal shaking to inhibit unspecific bindings of the antibodies. Afterward, the plate was washed three times with 300 μL/well washing solution and incubated with 200 μL/well primary antibody in PBS−Tween20 (1:10000) for 1 h by shaking at room temperature. Then the plate was washed three times with 300 μL/well washing solution. Finally, 200 μL/well secondary antibody in washing solution (1:2000) was added and incubated for 1 h by shaking at room temperature. The plate was then washed three times with washing solution and three times with citric buffer. The enzymatic colorimetric reaction was performed by adding 200 μL/well substrate solution (TMB). By the HRP-catalyzed oxidation of the TMB, a blue compound is generated. The reaction was stopped after 5 min by adding 100 μL/well stop solution, which leads to a color change to yellow. The measurement occurs at 450 nm with 630 nm as reference wavelength.

For method validation the measurement occurs in 1/10 diluted white wine and 1/20 diluted red wine.

For the indirect sandwich ELISA method, the assay protocol of Weber et al.[2] was also used as guideline. The procedure started by coating a polystyrene microtiter plate (MaxiSorp F96, Nunc) with 200 μL/well capture antibody in coating buffer (1/20000) overnight at 8−9 °C. Afterward, the plate was washed three times with 300 μL/well blocking solution. Subsequently, free binding sites of the wells were blocked with 250 μL/well blocking solution for 2 h at room temperature by horizontal shaking to inhibit unspecific bindings. Then the plate was washed three times with 300 μL/well washing solution again and incubated with 200 μL/well sample solution in PBS−Tween20 for 1 h by shaking at room temperature. After a reapplied washing step, 200 μL/well primary antibody in washing solution (1/20000) was added. Then the plate was washed three times with 300 μL/well washing solution again and incubated with 200 μL/well secondary antibody in washing solution (1/20000) for 1 h by shaking at room temperature. Finally, the plate was washed three times with washing solution and three times with citric buffer. The colorimetric reaction was performed by adding 200 μL/well substrate solution as described for the indirect ELISA. The measurement occurs at 450 nm with 630 nm as reference wavelength.

For method validation the measurement occurs in 1/10 diluted white wine and 1/10 diluted red wine.

Washing of the microwell plates was done using an eight-channel automatic microplate washer ELx50 (BioTek, Winooski, VT, USA). Optical density (OD) was read using a MRX microplate reader

(Dynex Technologies, Chantilly, VA, USA) using the software Revelation G 3.2 (Dynex Technologies). Analysis of the measured data was done with SoftMax Pro 5.4 software (Molecular Devices, Sunnyvale, CA, USA).

Evaluation. The evaluation of the ELISAs occurred on the basis of a logistic four-parameter regression using the software SoftMax Pro 5.4 (Molecular Devices). The four-parameter curve is one of the most reliable and most flexible evaluations for immunoassays. The equation of a four-parameter curve is $y = [(A - D)/(1 + (x/c)^B] + D$ with y = extinction, A = lower asymptote, B = raising in the central point, D = upper asymptote, and x = concentration (Figure 1).

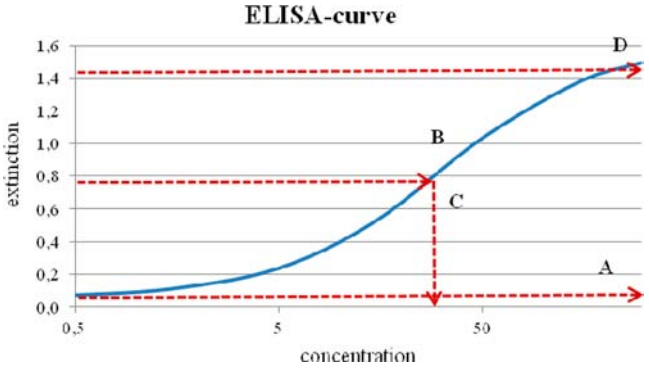

Figure 1. Sample diagram four-parameter regression.

The LOD was determined as the concentration of analyte for which the extinction of the blank value plus its standard deviation is lower than the extinction for the concentration of analyte minus its standard deviation. The LOD as well as the LLOQ are the most important statistical parameters for ELISA methods. A common practice is to use the signal-to-noise rate of the measured blank value for determination.[28,29] This is estimated as nonreliable because only the blank value is considered.

Additionally, a precision profile according to Ekins[30] was developed. This precision profile takes the variance of the nonconformance above the curve progression (heteroscedasticity) into account. In this way the relative nonconformance for every analyte concentration can be defined, and by incorporating a threshold for this relative nonconformance, the measurement range with LLOQ and upper limit of quantification (ULOQ) can be determined.[30−32] In this case the threshold for the relative nonconformance was defined with 20%.

Accuracy was checked by spiking unfined experimental wine samples with casein or KalCasin within the calibration range, respectively, and determining these recovery rates.

RESULTS AND DISCUSSION

Characterization of Different Casein Wine Fining Agents. A total of 12 commercially available casein wine fining agents of six European manufacturers were investigated by LDS-PAGE and silver staining as well as immunoblotting. These fining agents are denoted fining agents 1−12 in this publication, independent from their production and contained proteins.

The LDS-PAGE with silver staining (Figure 2) shows that every product contains not only casein (19−25 kDa) but also other milk allergens in different amounts, except for fining agent 7 (Figure 2, lane 7), which apparently mainly contains the whey proteins α-lactalbumin (ALA, 14.2 kDa) and β-lactoglobulin (BLG, 18.3 kDa). All other casein fining agents (Figure 2, lanes 1−6, 8−12) show similar protein band compositions, similar to the casein standard (Figure 2, lane Std), but with partially different band intensities. For electrophoresis, the fining agents, as well as the casein standard, were applied in concentrations from 200 to 250 mg/L. In two fining agents no bands were

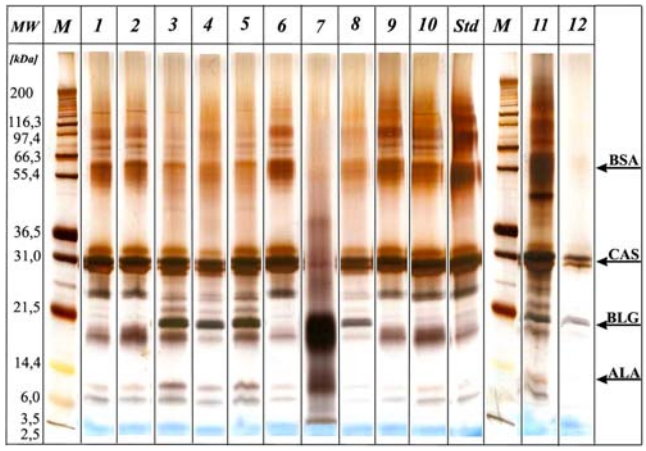

Figure 2. LDS-PAGE and silver-staining of the casein fining agents. MW, molecular weight (kDa); M, molecular weight marker; lanes 1−12, fining agents 1−12; Std, casein standard; BSA, bovine serum albumin (66.4 kDa); CAS, casein (19−25 kDa); BLG, β-lactoglobulin (18.3 kDa); ALA, α-lactalbumin (14.2 kDa).

detectable with this concentration; thus, the sample concentrations were increased to 2000 and 4000 mg/L. Degraded proteins were also detectable in the electropherogram of the casein products.

The described results of the unspecific silver staining are supported by specific immunochemical staining with an antibody raised against one commercially available fining agent. This antibody detects besides casein also the other milk proteins ALA, BLG, and bovine serum albumin (BSA, 66.4 kDa) as shown in Figure 3, whereas the antibody apparently has a low

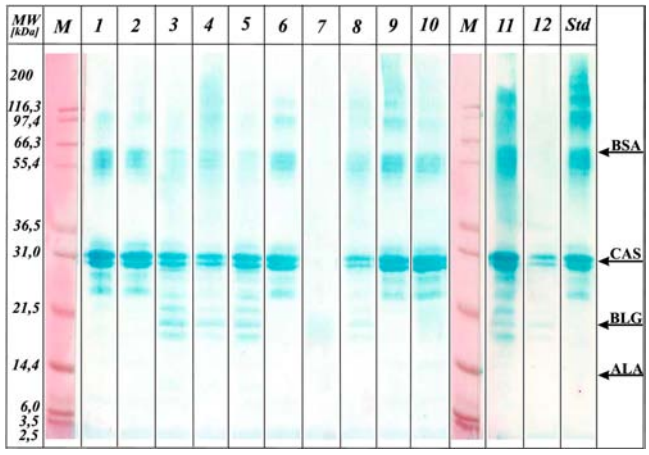

Figure 3. Immunoblot of the casein fining agents. MW, molecular weight (kDa); M, molecular weight marker; lanes 1−12, fining agents 1−12; Std, casein standard; BSA, bovine serum albumin (66.4 kDa); CAS, casein (19−25 kDa); BLG, β-lactoglobulin (18.3 kDa); ALA, α-lactalbumin (14.2 kDa).

affinity to the whey proteins ALA and BLG. Some of the degraded proteins are also detected with different intensity by the used antibody. With immunochemical staining the differences of the fining agents from one another as well as from the casein standard become more obvious. Most of the fining agents show more detectable protein bands than the casein standard (Figure 3, lane Std).

The demonstrated investigations of the different casein fining agents by LDS-PAGE and immunoblot show the necessity to

dx.doi.org/10.1021/jf5006098 | J. Agric. Food Chem. 2014, 62, 6803−6812

have analytical methods for determination of fining agent residues in wine, which are able to not only detect casein but also take into account the other milk allergens as well as the degraded proteins that are present in the fining agents and show detectable antigenicity as well.

ELISA Method Validation with a Casein Standard and a Casein Fining Agent. Validation of the developed ELISA methods was done in white wine as well as in red wine, although casein is mostly used for white wine, according to Lifrani et al.[17] Four calibration curves of four stock solutions with seven standard concentrations and a blank value were measured on one microtiter plate respectively (intra-assay validation). Every standard concentration for calibration was measured in triplicate on every plate. For testing the repeatability, every calibration was repeated on three different days. Thus, for every standard solution 36 measured data were acquired. Precision profiles according to Ekins[30] with percental normed data were determined for the different ELISAs. Furthermore, wine samples were spiked within the calibration range for measuring the recovery rates. Described validations were done with a casein standard (Merck), as well as a casein fining agent (KalCasin), to investigate the variance of the results depending on the used calibration standard and to get some information about the need for standardized calibration substances. This is particularly important if a threshold is given by law.

Casein has to be declared on a wine label if ≥0.25 mg/L allergenic protein remains in the final product, given by the OIV regulations. Furthermore, the OIV defines thresholds for LOD and LLOQ concerning ELISA methods developed for the analysis of wine. Thus, an accepted ELISA method for wine analysis needs to have a LOD of ≤0.25 mg/L casein or rather potentially allergenic residues of fining agent proteins, as well as a LLOQ of ≤0.5 mg/L casein or rather potentially allergenic residues of fining agent proteins. It is extremely important to have legally defined thresholds for potentially allergenic residues of wine fining agents in the final product to protect allergic consumers as well as to give research establishments, producers, and inspection agencies the possibility to control these potential residues. In this context it is necessary to give clear definitions concerning the potential residues. The threshold given by OIV is referred to "potentially allergenic residues of fining agent proteins in wine". It is problematic when an analytical method, for example, an ELISA, detects only caseins, although the fining agent contains beside caseins other milk proteins or degraded parts of the concerning proteins. This is also a problem for ovalbumin-specific ELISA methods and fining agents derived from hen's egg white.

The aim of this study was to develop methods for risk assessment of allergenic casein wine fining agent residues in wine to protect sensitive consumers. Thus, methods should be developed with as low as possible LOD and LLOQ by using calibration standards already taken in the processing of the wine samples and for production of antibodies.

Indirect ELISA versus Indirect Sandwich ELISA. At first, the indirect ELISA was developed for white wine. In agreement with previous publications[15,16] measuring casein in red wine by an indirect ELISA was unreliable. In unfined red wines, diluted 1/10 as the white wine, false-positive results were determined using the developed assay. Thus, an indirect sandwich ELISA was developed to investigate casein in red wine. Sandwich ELISA methods are supposed to be more specific because of the used capture antibody, which ideally binds only the target protein. Unfortunately, this assay also did not lead to satisfying results for red wine with regard to the LLOQ and recovery rates when used in 1/10 dilutions. Finally, the indirect ELISA could be identified as a reliable method for use when 1/20 diluted red wine was analyzed. However, both assays, indirect ELISA and indirect sandwich ELISA, are applicable for white wine. These investigations show that wine is a complex matrix and not easily handled. Some reasons for this are its low pH and the existence of much higher levels of phenolic compounds in red than in white wine.[15]

Statistical Data of the ELISA Methods. The precision profiles of the different calibrations including the mean calibration curve of all calibrations, respectively, are shown in Figures 4−11. The presented diagrams of the precision profiles show the standardized calibration curve of the three performed calibrations as a black continuous line. The tolerable failure was ascertained at 20% (gray line), and the curve of the precision profile is shown as a black dotted line. For validation LLOQ and ULOQ were determined, giving the measurement range of the ELISA, respectively, defined as intersections of the

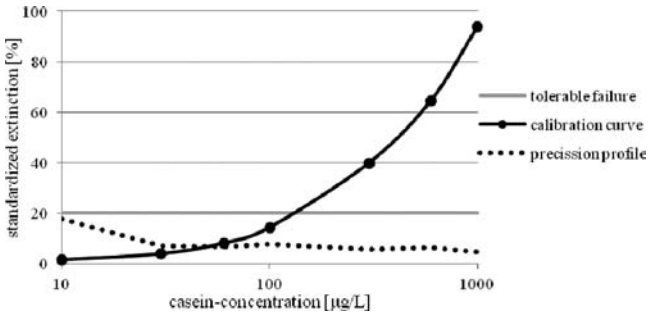

Figure 4. Precision profile of the indirect ELISA matrix calibration with casein in white wine.

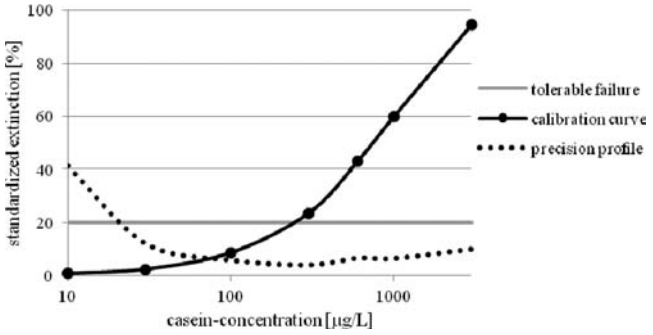

Figure 5. Precision profile of the indirect ELISA matrix calibration with casein in red wine.

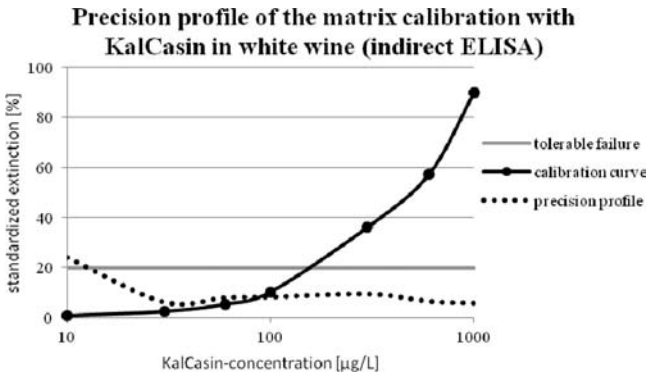

Figure 6. Precision profile of the indirect ELISA matrix calibration with KalCasin in white wine.

dx.doi.org/10.1021/jf5006098 | J. Agric. Food Chem. 2014, 62, 6803−6812

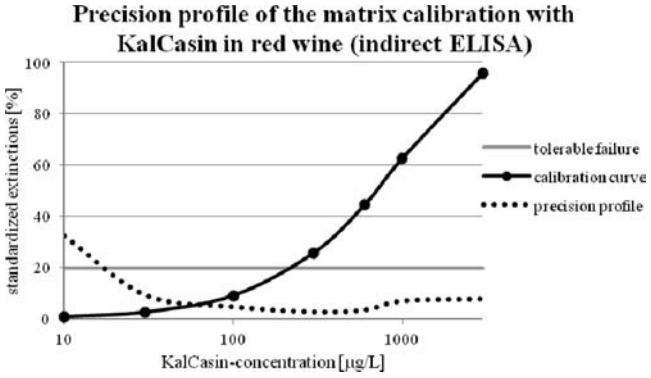

Figure 7. Precision profile of the indirect ELISA matrix calibration with KalCasin in red wine.

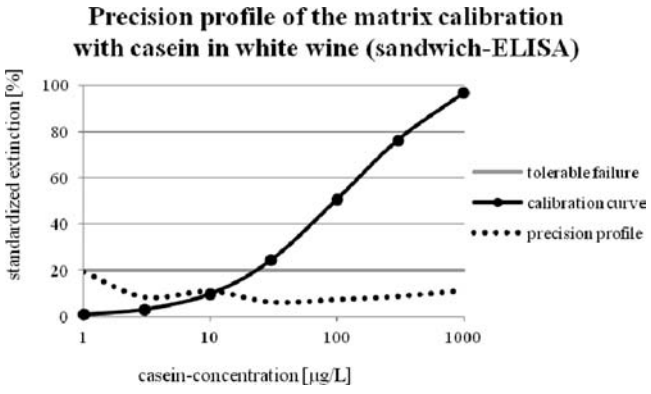

Figure 8. Precision profile of the sandwich ELISA matrix calibration with casein in white wine.

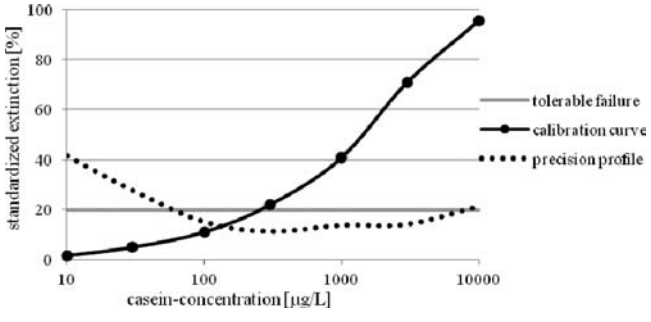

Figure 9. Precision profile of the sandwich ELISA matrix calibration with casein in red wine.

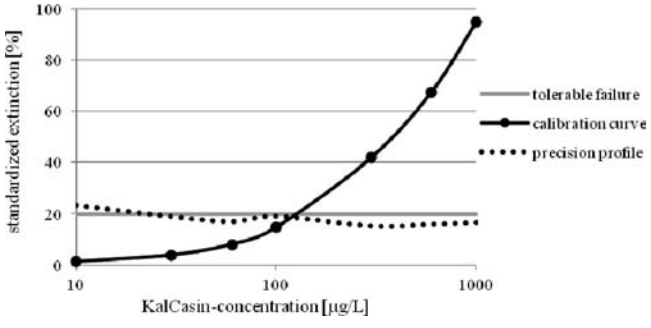

Figure 10. Precision profile of the sandwich ELISA matrix calibration with KalCasin in white wine.

precision profile curve with the tolerable failure line. All statistical data of the indirect and sandwich ELISA are mentioned in Tables 2−5.

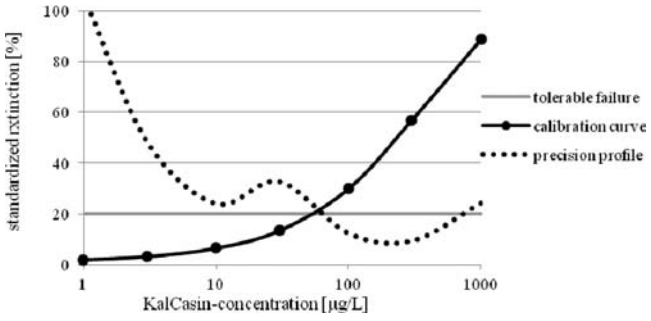

Figure 11. Precision profile of the sandwich ELISA matrix calibration with KalCasin in red wine.

In all developed assays, for white as well as red wine, the LOD of 0.25 mg/L (250 μg/L) accordingly requested by the OIV was reached for the detection of casein and the fining agent. The formerly described heteroskedasticity or the variance of the nonconformance is illustrated in the intra-assay coefficients of variation presented in Tables 2 − 5. The high data were determined for the standard solutions with the lower concentrations. For higher analyte concentration the intra-assay coefficients of variation are usually in the range of 10%. This discrepancy is caused through the sigmoidal curve progression. In the range of very low casein concentrations the curve reaches a plateau (see Figures 4−11). In this section small deviations in measured OD lead to comparatively huge deviations of the determined concentrations.

Accuracy was investigated by spiking the wine with casein and KalCasin at different amounts within the linear area of the calibration range and determining the recovery rates. Calibration curves were prepared with the same substance, which was used for wine spiking, respectively. For indirect ELISA the recovery rates ranged from 59 to 114% (casein) and from 64 to 84% (KalCasin) in white wine. Recovery rates determined with the indirect sandwich ELISA in white wine ranged between 66 and 78% for casein, whereas KalCasin showed no acceptable accuracy with recovery rates lower than 30%.

In red wine the recovery rates were achieved between 63 and 92% (casein) as well as 78 and 91% (KalCasin) for the indirect ELISA, determined in 1/20 diluted wine. In contrast, in 1/10 diluted red wine, for the indirect sandwich ELISA no satisfying recovery rates, <20% (casein) and <10% (KalCasin), could be achieved.

The concentration of casein in spiked wine with an OD significantly different from the blank value is defined as the LOD. For this, an unspiked and equally diluted wine was used for blank value. All presented assays were able to detect casein and KalCasin, respectively, according to the threshold of 250 μg/L allergenic protein, given by the OIV. For all developed ELISA methods the LODs are between 10 and 200 μg/L, usually just below the range of the first standard solution (Tables 2−5). The measurement range defined by the LLOQ and ULOQ can be determined from the precision profile (Figures 4−11). ELISA methods used for analysis of allergens in wine have to be able to quantify the allergen with a LLOQ of $\leq$500 μg/L. Looking at the statistical data, it can be seen that the indirect sandwich ELISA was not able to quantify casein as well as KalCasin in red wine under mentioned conditions with LLOQs around 730 μg/L. In contrast, the indirect ELISA is applicable for 1/20 diluted red wine with LLOQs of 491.20 μg/L (casein) and 414.56 μg/L (KalCasin). With both assays a quantification of casein and KalCasin in white wine is possible.

dx.doi.org/10.1021/jf5006098 | J. Agric. Food Chem. 2014, 62, 6803−6812

Table 2. Data of the Indirect ELISA Method Validation with 1/10 Diluted White Wine

	fining agent (KalCasin)	casein
standard curve		
calibration range (μg/L)	10−1000	10−1000
intraassay coefficients of variation (%)	3−80.7	3.2−68.7
recovery rate for spiked wine samples		
recovery rate (%)	64−84	59−114
statistical data		
LOD[a] in wine (μg/L) (blank + SD_{blank} < x − SD_x)[b]	100	100
measurement range in wine (μg/L) (LLOQ−ULOQ)[c]	146.26−10000	100−10000

[a]LOD, limit of detection [b]SD, standard deviation; x, value of solution x; SD_x, standard deviation of solution x. [c]LLOQ, lower limit of quantification; ULOQ, upper limit of quantification.

Table 3. Data of the Indirect ELISA Method Validation with 1/20 Diluted Red Wine

	fining agent (KalCasin)	casein
standard curve		
calibration range (μg/L)	10−3000	10−3000
intraassay coefficients of variation (%)	1.6−52.5	2.5−68.7
recovery rate for spiked wine samples		
recovery rate (%)	78−91	63−92
statistical data		
LOD[a] in wine (μg/L) (blank + SD_{blank} < x − SD_x)[b]	200	200
measurement range in wine (μg/L) (LLOQ−ULOQ)[c]	414.56−60000	491.24−60000

[a]LOD, limit of detection. [b]SD, standard deviation; x, value of solution x; SD_x, standard deviation of solution x. [c]LLOQ, lower limit of quantification; ULOQ, upper limit of quantification.

Table 4. Data of the Indirect Sandwich ELISA Method Validation with 1/10 Diluted White Wine

	fining agent (KalCasin)	casein
standard curve		
calibration range (μg/L)	10−1000	1−10000
intraassay coefficients of variation (%)	5.9−46.4	1.2−47.6
recovery rate for spiked wine samples		
recovery rate (%)	<30	66−78
statistical data		
LOD[a] in wine (μg/L) (blank + SD_{blank} < x − SD_x)[b]	100	10
measurement range in wine (μg/L) (LLOQ−ULOQ)[c]	254.63−10000	10−10000

[a]LOD, limit of detection. [b]SD, standard deviation; x, value of solution x; SD_x, standard deviation of solution x. [c]LLOQ, lower limit of quantification; ULOQ, upper limit of quantification.

Table 5. Data of the Indirect Sandwich ELISA Method Validation with 1/10 Diluted Red Wine

	fining agent (KalCasin)	casein
standard curve		
calibration range (μg/L)	10−10000	10−10000
intraassay coefficients of variation (%)	4.7−35.9	2.5−48.3
recovery rate for spiked wine samples		
recovery rate (%)	<10	<20
statistical data		
LOD[a] in wine (μg/L) (blank + SD_{blank} < x − SD_x)[b]	100	100
measurement range in wine (μg/L) (LLOQ−ULOQ)[c]	735.08−100000	732.58−100000

[a]LOD, limit of detection [b]SD, standard deviation; x, value of solution x; SD_x, standard deviation of solution x. [c]LLOQ, lower limit of quantification; ULOQ, upper limit of quantification.

With the LLOQ of 100 μg/L (indirect) and 10 μg/L (sandwich) quantification of casein are more sensitive than for KalCasin with LLOQs of 146.26 μg/L (indirect) and 254.63 μg/L (sandwich). Qualitative analysis of casein in white wine is more sensitive using the indirect sandwich ELISA with a LOD of 10 μg/L, whereas for KalCasin in the indirect sandwich ELISA and casein as well as KalCasin using the indirect ELISA a LOD of 100 μg/L is achieved. Qualitative red wine analysis is more sensitive using the indirect sandwich ELISA with a LOD of 100 μg/L for casein as well as KalCasin in contrast to the indirect ELISA with a LOD of 200 μg/L for casein as well as for the fining agent. However, as previously mentioned, the recovery rates for red wine analysis are <20% using the sandwich method.

Analysis of Fined Wines. The results of the investigated wines treated with two different processing steps are given in Table 6. The white wines, diluted 1/10, were investigated using

dx.doi.org/10.1021/jf5006098 | J. Agric. Food Chem. 2014, 62, 6803−6812

Table 6. Results of the Fined Red (RW) and White (WW) Wines Using the Developed ELISA Methods, Indirect ELISA for WW, and Indirect Sandwich ELISA for RW, with Casein and KalCasin as Calibration Substance (A:40g/hL KalCasin, B: 80g/hL KalCasin)

wine	processing step	allergen content[a] (μg/L)	below the value of 0.25 mg/L given by the OIV
allergen content determined as casein			
RW1AI	0.45 μm filtration	x < LOD	yes
RW1AII	sterilizing filtration	x < LOD	yes
RW1BI	0.45 μm filtration	x < LOD	yes
RW1BII	sterilizing filtration	x < LOD	yes
RW2AI	addition of bentonite	x < LOD	yes
RW2AII	sterilizing filtration	x < LOD	yes
RW2BI	addition of bentonite	x < LOD	yes
RW2BII	sterilizing filtration	x < LOD	yes
WW1AI	0.45 μm filtration	x < LOD	yes
WW1AII	sterilizing filtration	x < LOD	yes
WW1BI	0.45 μm-filtration	x < LOD	yes
WW1BII	sterilizing filtration	x < LOD	yes
WW2AI	addition of bentonite	x < LOD	yes
WW2AII	sterilizing filtration	x < LOD	yes
WW2BI	addition of bentonite	x < LOD	yes
WW2BII	sterilizing filtration	x < LOD	yes
allergen content determined as KalCasin			
RW1AI	0.45 μm filtration	x < LOD	yes
RW1AII	sterilizing filtration	x < LOD	yes
RW1BI	0.45 μm filtration	x < LOD	yes
RW1BII	sterilizing filtration	x < LOD	yes
RW2AI	addition of bentonite	x < LOD	yes
RW2AII	sterilizing filtration	x < LOD	yes
RW2BI	addition of bentonite	x < LOD	yes
RW2BII	sterilizing filtration	x < LOD	yes
WW1AI	0.45 μm filtration	x < LOD	yes
WW1AII	sterilizing filtration	x < LOD	yes
WW1BI	0.45 μm filtration	x < LOD	yes
WW1BII	sterilizing filtration	x < LOD	yes
WW2AI	addition of bentonite	x < LOD	yes
WW2AII	sterilizing filtration	x < LOD	yes
WW2BI	addition of bentonite	LOD < x < LLOQ	yes
WW2BII	sterilizing filtration	x < LOD	yes

[a]LOD, limit of detection; LLOQ, lower limit of quantification.

the developed indirect ELISA. The red wines, diluted 1/10, were investigated using the developed indirect sandwich ELISA. The LOD of 100 μg/L of these ELISA methods is lower than the required LOD of 250 μg/L given by OIV.

The determined data show no detectable allergen content after the second processing step (sterilizing filtration) of the red wine as well as in the white wine using the developed ELISA methods. Thus, the value of 0.25 mg/L, given by the OIV, is complied with and labeling of the final wine is not necessary. An allergen content also is not detectable in the first processing step of the red wines. For the first processing step of the white wine, only WW2BI, with 80 g/hL KalCasin fined white wine after the addition of bentonite, shows a detectable amount of allergen between LOD and LLOQ (100 and 146.26 μg/L) using KalCasin for calibration.

This indicates the higher sensitivity using the fining agent in contrast to casein for calibration, because using casein for calibration leads to no detectable residues of the fining agent.

Concluding Remarks. Some formerly published studies fulfill the requirements for ELISA methods detecting potentially allergenic residues of fining agent proteins in wine. Weber et al.[2] developed an indirect ELISA for the detection of total casein and casein-derived fining agents with LOD of 5 μg/L casein, whereas a method for the quantification of caseinates in wine developed by Restani et al.[17] with a LOD of 280 μg/L and a LOQ of 760 μg/L no longer conforms with the criteria established by the OIV, which were given in 2012. In addition to these immunological-based methods many MS-based methods for the detection of residual allergenic wine fining agents were recently published. Matarozzi et al.[23] investigated red wines treated with α-casein, β-casein, and ovalbumin by liquid chromatography−electrospray−tandem mass spectrometry. In this case for caseinate a LOD of 200 μg/L was calculated. In 2013 Monaci et al.[22] published a MS-based multiallergen quantification of fining-related egg and milk proteins in white wines. With this method LODs between 400 and 900 μg/L are achieved for the detection of casein fining agent. A method published by Cereda et al.[33] is described to have a LOD of 1 μg/L casein in white wine, and 3.8 μg/L fining agent in red wine is described by D'Amato et al.[23] Summing up, ELISA as well as MS-based methods are very sensitive and able to detect residual allergenic wine fining agents. For this purpose it is beneficial that ELISA as an immunological-based method considers the antigenicity of the target proteins.

The method validation illustrates again that wine, especially red wine, is a complex matrix. This supports former publications and their results concerning allergen detection in wine.[15,21] Here the validation of a method for a risk assessment consideration in a very low area of concentration (μg/L and not mg/L) demonstrates very impressively these interferences by a complex matrix. Furthermore, it can be seen that results differ according to the standard used for calibration. Having homogeneous standard substances is important for the comparison of results acquired with different assays and in different laboratories. As shown by LDS-PAGE and immunoblot different casein fining agents also contain other milk allergens in different amounts, which might also be a problem for allergic consumers and have to be measured. As food allergy is very individual, people who are allergic to "milk" can be allergic to different milk proteins with variable intensity of allergic reactions.[25,34] Thus, a method that takes into account all milk proteins is necessary to have a reliable method and to implement the legal request for thresholds as discussed previously. Furthermore, possible different processings of the fining agents might result in different affinities of the contained proteins to the used antibody, and consequently this also might yield altered allergenic potency for allergic people. With regard to the described results an underestimation of residual allergenic fining agents in the analyzed final wine is possible if common ELISA methods commercially available are used for the detection of for example casein.

In conclusion, ELISA methods for the sensitive quantification of casein fining agents in white and red wines were developed, also taking into account other possible milk allergens in the

casein fining agents by antibodies developed against a commercial casein fining agent. These methods enable a risk assessment for fining agent residues in casein-fined wines to protect allergic consumers. Within the research project "Reducing the concentration of allergenic fining agents in final wine by technological treatment" (AiF 16330N), the development of technological procedures that reduce the concentration of allergenic substances used in wine treatment was aimed for. For the evaluation of these reductions and the risk assessment of well-defined wines and well-known fining agents used in wine processing these developed highly sensitive ELISA methods were needed.

AUTHOR INFORMATION

Corresponding Author

*(A.P.-K.) E-mail: angelika.paschke@uni-hamburg.de.

Funding

The research project (AiF 16330 N) was funded under the program to promote Industrial Joint Research (IGF) of the Federal Ministry of Economics and Technology (via AiF) by the Research Association of the German Food Industry (FEI).

Notes

The authors declare no competing financial interest.

ACKNOWLEDGMENTS

We thank Bettina Jacobsen for technical support. We also thank Dr. Jürgen Meinl and Sigmar Görtges from Erbslöh (Geisenheim, Germany) as well as the other members of OENOPPIA for providing us the fining agents.

ABBREVIATIONS USED

ALA, alpha-lactalbumin; BLG, beta-lactoglobulin; BSA, bovine serum albumin; CAS, casein; CMA, cow's milk allergy; DBPCFC, double-blind, placebo-contolled food challenge; DONS, dioctylsodium sulfosuccinate; EDTA, ethylenediaminetetraacetate; ELISA, enzyme-linked immunosorbent assay; HRP, horseradish peroxidase; LDS-PAGE, lithium dodecyl sulfate−polyacrylamide gel electrophoresis; LLOQ, lower limit of quantification; LOD, limit of detection; M, molecular weight marker; MW, molecular weight; OD, optical density; OENOPPIA, International Association of Oenology Industrials for Oenological Products and Practice; OIV, Organisation Internationale de la Vigne et du Vin; PBS, phosphate-buffered saline; SDS, sodium dodecyl sulfate; SPT, skin prick test; TMB, 3,3′,5,5′-tetramethylbenzidine; Tris, tris(hydroxymethyl)-aminomethane; Tween20, polyethylene-sorbitan monolaurate; ULOQ, upper limit of quantification

REFERENCES

(1) Tschiersch, C.; Nikfardjam, M. P.; Schmidt, O.; Schwack, W. Degree of hydrolysis of some vegetable proteins used as fining agents and its influence on polyphenol removal from red wine. *Eur. Food Res. Technol.* **2010**, *231*, 65−74.

(2) Weber, P.; Steinhart, H.; Paschke, A. Determination of the bovine food allergen casein in white wines by quantitative indirect ELISA, SDS-PAGE, Western blot and immunostaining. *J. Agric. Food Chem.* **2009**, *57*, 8399−8405.

(3) Wal, J.-M. Bovine milk allergenicity. *Ann. Allergy Asthma Immunol.* **2004**, *93*, 2−11.

(4) Exl, B. M.; Fritsche, R. Cow's milk protein allergy and possible means for its prevention. *Nutrition* **2001**, *17*, 642−651.

(5) Skripak, J. M.; Matsui, E. C.; Mudd, K.; Wood, R. A. The natural history of IgE-mediated cow's milk allergy. *J. Allergy Clin. Immunol.* **2007**, *120*, 1172−1177.

(6) Lam, H.-Y.; van Hoffen, E.; Michelsen, A.; Guikers, K.; van der Tas, C. H. W.; Bruijnzeel-Koomen, C. A. F. M. Cow's milk allergy in adults is rare but severe: both casein and whey proteins are involved. *Clin. Exp. Allergy* **2008**, *38*, 995−1002.

(7) Sicherer, S. H.; Sampson, H. A. Food allergy. *J. Allergy Clin. Immunol.* **2010**, *125*, 116−125.

(8) Liu, A. H.; Jaramillo, R.; Sicherer, S. H.; Wood, R. A.; Bock, S. A.; Burks, A. W.; Massing, M.; Cohn, R. D.; Zeldin, D. C. National prevalence and risk factors for food allergy and relationship to asthma: results from the national Health and Nutrition Examination Survey 2005−2006. *J. Allergy Clin. Immunol.* **2010**, *126*, 798−806.

(9) Osterballe, M.; Mortz, C. G.; Hansen, T. K.; Andersen, K. E.; Bindslev-Jensen, C. The prevalence of food hypersensitivity in young adults. *Pediatr. Allergy Immunol.* **2009**, *20*, 686−692.

(10) Gupta, R. S.; Springston, E. E.; Warrier, M. R.; Smith, B.; Kumar, R.; Pongracic, J.; Holl, J. L. The prevalence, severity, and distribution of childhood food allergy in the United States. *Pediatrics* **2011**, *128* (1), e9−e17.

(11) Hochwallner, H.; Schulmeister, U.; Swoboda, I.; Spitzauer, S.; Valenta, R. Cow's milk allergy: from allergens to new forms of diagnosis, therapy and prevention. *Methods* **2014**, *66*, 22−33.

(12) Rolland, J. M.; Apostolou, E.; Deckert, K.; de Leon, M. P.; Douglass, J. A.; Glaspole, I. N.; Bailey, M.; Stockley, C. S.; O'Hehir, R. E. Potential food allergens in wine: double-blind, placebo-contolled trial and basophil activation analysis. *Nutrition* **2006**, *22*, 882−888.

(13) Mezdour, S.; Brule, G.; Korlczuk, J. Physicochemical analysis of casein solubility in water-ethanol solutions. *Lait* **2006**, *86*, 435−452.

(14) Kirschner, S.; Belloni, B.; Kugler, C.; Ring, J.; Brockow, K. Allergenicity of wine containing processing aids: a double-blind, placebo-controlled food challenge. *J. Invest. Allergol. Clin. Immunol.* **2009**, *19*, 210−217.

(15) Weber, P.; Steinhart, H.; Paschke, A. Investigation of allergenic potential of wines fined with various proteinogenic fining agents by ELISA. *J. Agric. Food Chem.* **2007**, *55*, 3127−3133.

(16) Rolland, J. M.; Apostoloum, E.; de Leon, M. P.; Stockley, C. S.; O'Hehir, R. E. Specific and sensitive enzyme-linked immunosorbent assays for analysis of residual allergenic food proteins in commercial bottled wine fined with egg white, milk, and non-grape-derived tannins. *J. Agric. Food Chem.* **2008**, *56*, 349−354.

(17) Lifrani, A.; Dos Santos, J.; Dubarry, M.; Rautureau, M.; Blachier, F.; Tome, D. Development of animal models and sandwich-ELISA tests to detect the allergenicity and antigenicity of fining agent residues in wines. *J. Agric. Food Chem.* **2009**, *57*, 525−534.

(18) Restani, P.; Uberti, F.; Danzi, R.; Ballabio, C.; Pavanllo, F.; Tarantion, C. Absence of allergenic residues in experimental and commercial wines fined with caseinates. *Food Chem.* **2012**, *134*, 1438−1445.

(19) Monaci, L.; Losito, I.; Palmisano, F.; Visconti, A. Identification of allergenic milk proteins markers in fined white wines by capillary liquid chromatography-electrospray ionization-tandem mass spectrometry. *J. Chromatogr.* **2010**, *1217*, 4300−4305.

(20) Monaci, L.; Losito, I.; Palmisano, F.; Godula, M.; Visconti, A. Towards the quantification of residual milk allergens in caseinate-fined white wines using HPLC coupled with single-stage Orbitrap mass spectrometry. *Food Addit. Contam., Part A* **2011**, *28*, 304−314.

(21) Tolin, S.; Pasini, G.; Curioni, A.; Arrigoni, G.; Masi, A.; Mainente, F.; Simonato, B. Mass spectrometry detection of egg proteins in red wines treated with egg white. *Food Conrol* **2012**, *23*, 87−94.

(22) Monaci, L.; Losito, I.; De Angelis, E.; Pilolli, R.; Visconti, A. Multi-allergen quantification of fining-related egg and milk proteins in white wines by high-resolution mass spectrometry. *Rapid Commun. Mass Spectrom.* **2013**, *27*, 2009−2018.

(23) D'Amato, A.; Kravchuk, A. V.; Bachi, A.; Righetti, P. G. Noah's nectar: the proteome content of a glass or red wine. *J. Proteomics* **2010**, *73*, 2370−2377.

(24) Mattarozzi, M.; Milioli, M.; Bignardi, C.; Elviri, L.; Corradini, C.; Carreri, M. Investigation of different sample pre-treatment routes for liquid chromatography-tandem mass spectrometry detection of caseins and ovalbumin in fortified red wine. *Food Control* **2014**, *38*, 82−87.
(25) Steinhart, H.; Paschke, A.; Zunker, K. When the immune system falsely reacts: food allergies − an individual risk. *Biol. Unserer Zeit.* **2001**, *31*, 398−407.
(26) Steinhoff, M.; Fischer, M.; Paschke-Kratzin, A. Comparison of extraction conditions for milk and hen's egg allergens. *Food Addit. Conta.m, Part A* **2011**, *28*, 373−383.
(27) Heukeshoven, J.; Dernick, R. Neue Ergebnisse zum Mechanismus der Silberfärbung. Presented at Electrophoresis Forum '86; Technical University Munich, 1986; pp 22−27.
(28) Kiening, M.; Niessner, R.; Drs, E.; Baumgartner, S.; Krska, R.; Bremer, M.; Tomkies, V.; Reece, P.; Danks, C.; Immer, U.; Weller, M. G. Sandwich immunoassay for the determination of peanut and hazelnut traces in foods. *J. Agric. Food Chem.* **2005**, *53*, 3321−3327.
(29) Morishita, N.; Kamiya, K.; Matsumoto, T.; Salaki, S.; Teshima, R.; Urisu, A.; Moriyama, T.; Ogawa, T.; Akiyama, H.; Morimatsu, F. Reliable enzyme-linked immunosorbent assay for the determination of soybean proteins in processed foods. *J. Agric. Food Chem.* **2008**, *56*, 6818−6824.
(30) Ekins, R. P. The "Precision profile": its use in RIA assessment and design. *Ligand Q.* **1981**, *4*, 33−44.
(31) Hintemann, T. Entwicklung, Optimierung, Validierung und Automatisierung eines Immunoassays zur sensitiven Detektion des endokrinen Disruptors 17 beta-Östradiol im Wasserkreislauf. Thesis, Institut für Nutzpflanzenwissenschaften und Ressourcenschutz, Fachbereich Pflanzenernährung, Univeryity Bonn, 2006.
(32) Holzhauser, T.; Vieths, S. Indirect competitive ELISA for determination of traces of peanut (*Arachis hypogaea* L.) protein in complex food matrixes. *J. Agric. Food Chem.* **1999**, *47*, 603−611.
(33) Cereda, A.; Kravchuk, A. V.; D'Amato, A.; Bachi, A.; Righetti, P. G. Proteomics of wine additives: mining for the invisible via combinatorial peptide ligand libraries. *J. Proteomics* **2010**, *73* (9), 1732−1739.
(34) Monaci, L.; Tregoat, V.; van Hengel, A. J.; Anklam, E. Milk allergens their characteristics and their detection in food: A review. *Eur. Food Res. Technol.* **2006**, *223* (2), 149−179.

fluorescence spectroscopy suitable for the study of HSA−keracyanin interaction. Besides, CD technique was utilized to quantitatively evaluate the secondary structure alterations of HSA upon binding to keracyanin chloride.

MATERIALS AND METHODS

Materials. HSA and keracyanin were purchased from Sigma-Aldrich Corp (St. Louis, MO). Mature mulberry fruits were bought from Nanjing, China, freeze-dried, and finally ground to powder. Organic solvents used for ESI-MS/MS and HPLC were chromatographic grade and were bought from Sinopharm Co., Ltd. (Beijing, China). All other chemicals (analytical grade) were bought from Sinopharm Co., Ltd. (Beijing, China). A 0.2 M stock solution of pH = 7.4 phosphate buffer was prepared by mixing NaH_2PO_4 and Na_2HPO_4 in ultrapure water. Ultrapure water was used throughout.

Methods. *Pigment Extraction Condition Screening and Identification.* In order to obtain the optimal extraction liquor, mulberry freeze-dried powder was weighed in the test tubes (0.05 g for each), and 10 mL of extraction solvent was added immediately to each tube. The ten extraction solvents were ethyl acetate, 1-butanol, acetone, alcohol, alcohol solution (70%), alcohol solution (50%), alcohol solution (30%), water, HCl solution (pH = 1), and alcohol (50%)−HCl mixture solution (pH = 3), respectively. The samples were processed using ultrasonic vibration with a water bath for 30 min to ensure a well mixed extraction. Then the supernatant was filtered through the filter paper and was diluted with water to a final volume of 50 mL. The absorbance spectrum of these solutions was recorded in the range of 200 to 800 nm. For extraction efficiency comparison, the method from Lee[13] was used to determinate the total anthocyanin content. We compared the extraction efficiencies of ten extraction solvents and chose the best one to do further analysis. We also weighed the dry residues of the extract using different liquors.

Mulberry freeze-dried powder (2 g) was added to 30 mL of petroleun ether (lipid-removal solvent). Then the mixture was stirred constantly with 60 °C water bath for half an hour. Supernatant was removed after centrifugation at 2000 rpm, and repeated extraction was done 5 times, after which the solvent was evaporated. The sample was then put into the optimal pigment extraction liquor (70% alcohol solution) and was processed using ultrasonic vibration with water bath for 30 min 4 times. All the extracts were transferred to a 300 mL round flask and evaporated by a rotary evaporator (30 rpm, 500 Pa, and 50 °C) to obtain solid substance (the crude mulberry anthocyanin extract). The pigment extract obtained here was utilized for separation and further analysis.

The TBE-300A HSCCC instrument was made by Shanghai Tongtian Co., Ltd. (Shanghai, China). For HSCCC experiment, a solvent system made up of methyl *tert*-butyl ether, 1-butanol, acetonitrile, water, and trifluoroacetic acid (10:30:10:50:0.05; %, v/v) was used. The two phases were separated and prepared for use after mixing of 1000 mL of solvent in a separating funnel. The instrument was then rotated at 850 rpm for equilibration of the solvent. 220 mg of anthocyanin mulberry extract was first dissolved in 5 mL of mobile phase, after which aqueous mobile phase was injected at 1.5 mL/min. The eluates at different time points were detected using a UV−vis detector at 280 nm.

HPLC analysis was performed on a Shimadzu LC-20AT liquid chromatography system (Shimadzu, Tokyo, Japan). The solvent system was composed of phase A (water:acetonitrile:formic acid = 96:3.3:0.55; %, v/v) and phase B (acetonitrile:water:formic acid = 55:44:0.55; %, v/v). Gradient conditions: 0−20 min, 6−20% A in B; 20−30 min, 20−40% A in B; 30−35 min, 40−60% A in B; 35−40 min 60−70% A in B. A reequilibration of 6 min was made afterward. The flow rate was 0.8 mL min^{-1}, and 20 μL aliquots were injected into the column. Diluted extracts were trasferred into the Kinetex PFP 100A column (Phenomenex Inc., Torrance, USA), and anthocyanins were detected at 280 nm. During the chromatography analysis UV−vis absorption spectra were recorded.

Samples separated from HSCCC were prepared for structural identification using a Thermo Fisher LCQ DecaXP MAX mass spectrometer (Thermo Fisher Scientific Inc., Waltham, MA). The MS/MS spectra were obtained using positive mode, and the ESI voltage was set at 5000 V. The sheath, aux, and sweep gas flow rates were adjusted at 9, 5, and 0 arb, respectively. All the spectra were collected within a scan range of 50−1200 m/z.

Spectroscopic Characterization of HSA−Keracyanin Interaction. Fluorescence experiments were carried out on a fluorimeter Hitachi F-4500 (Hitachi, Tokyo, Japan). Quartz cuvettes with a size of 1 × 1 × 4 cm were used in all the experiments. Voltage of the photomultiplier was set at 700 V. Excitation and emission slit widths were both set at 5 nm. All the spectra were recorded under the speed of 1200 nm min^{-1}.

The fluorescence spectra were corrected for the inner filter effects (IFEs) using the following formula:

$$F_{ideal}(\lambda_{ex}, \lambda_{em}) = F_{obs}(\lambda_{ex}, \lambda_{em})CF_p(\lambda_{ex})CF_s(\lambda_{em}) \approx F_{obs}(\lambda_{ex}, \lambda_{em})10^{(A_{em}+A_{ex})/2} \quad (1)$$

where CF_p and CF_s are the correction factors for excitation and emission light at λ_{ex} and λ_{em}, respectively. A_{ex} and A_{em} stand for the absorbance at λ_{ex} and λ_{em}, respectively. F_{obs} represents the observed fluorescence intensity.[14]

In quest of the fluorescence quenching mechanism, the well-known Stern−Volmer formula was applied to analyze and calculate the fluorescence data:

$$F_0/F = 1 + K_q\tau_0[Q] = 1 + K_{SV}[Q] \quad (2)$$

where F_0 and F represent the fluorescence intensities of a protein in the absence and presence of the ligand, and K_q and K_{SV} are the bimolecular quenching rate constant and the Stern−Volmer quenching constant, respectively. τ_0 is the average fluorescence lifetime of the fluorophore in the absence of quencher, and it is 10 ns for biomacromolecules. [Q] is the molar concentration of the quencher (keracyanin).

The binding information on the HSA−keracyanin system is determinated by the following formula:

$$\lg\frac{F_0 - F}{F} = \lg K_A + n \lg [Q] \quad (3)$$

K_A is the binding constant, and n is the average number of binding sites for one HSA molecule.

By utilizing the Van't Hoff equation, we calculated the corresponding thermodynamic parameters:

$$\ln\left(\frac{K_2}{K_1}\right) = \frac{\Delta H^\circ}{R}\left(\frac{1}{T_1} - \frac{1}{T_2}\right) \quad (3)$$

where K is the binding constant calculated from the above step, R is the universal gas constant with a value of 8.314 J·mol^{-1}·K^{-1}, ΔH° and ΔS° are the changes in enthalpy and entropy. Gibbs free energy change (ΔG°) associated with the interaction of HSA and keracyanin can be calculated from

$$\Delta G^\circ = \Delta H^\circ - T\Delta S^\circ = -RT \ln K^\circ \quad (4)$$

The energy transfer efficiency E is defined by the following equation:

$$E = 1 - \frac{F}{F_0} = \frac{R_0^6}{R_0^6 + r^6} \quad (4)$$

where R_0 is the Förster critical distance and r is the average distance between the donor and the acceptor. R_0 is usually calculated from the following equation:

$$R_0^6 = 8.8 \times 10^{-25}k^2N^{-4}\Phi J \quad (6)$$

where k^2 is the orientation factor, N is the refractive index, and Φ is the quantum yield of the donor. The spectral overlap integral between the donor fluorescence spectrum and the acceptor absorbance spectrum is represented by J, and it is expressed as

dx.doi.org/10.1021/jf500705s | J. Agric. Food Chem. 2014, 62, 6813−6819

$$J = \frac{\sum F(\lambda)\,\varepsilon(\lambda)\,\lambda^4\,\Delta\lambda}{\sum F(\lambda)\,\Delta\lambda} \quad (7)$$

where $F(\lambda)$ stands for fluorescence intensity of the donor at wavelength λ, and $\varepsilon(\lambda)$ is the molar absorption coefficient of the acceptor at wavelength λ.

For synchronous fluorescence analysis, the spectra were collected by setting the differences of excitation and emission wavelengths at 15 or 60 nm ($\Delta\lambda = \lambda_{ex} - \lambda_{em}$ = 15 or 60 nm). The rest of the experimental conditions are the same with the steady-state fluorescence measurements.

CD measurements were performed on a JASCO-815 CD spectropolarimeter (Jasco Co. Ltd., Tokyo, Japan). CD spectra of 2 × 10^{-7} M HSA with or without pigment were measured between 190 and 260 nm using a 1 × 1 × 4 cm quartz cuvette. All the samples were prepared in pH 7.4 phosphate buffer, and the spectra were recorded at 25 °C. The contents of secondary conformation of the protein were analyzed using online SELCON3 program.

All the absorption spectra in this study were collected using a Shimadzu UV-2450 (Shimadzu, Tokyo, Japan) spectrophotometer equipped with a 1 × 1 × 4 cm quartz cell.

RESULTS AND DISCUSSION

Optimization of the Extraction Liquor. Absorption spectra of the extraction obtained using different solvents are shown in Figure S1 (Supporting Information). There are two typical peaks for anthocyanins, one at around 280 nm (corresponding to its aromatic ring structures) and the other at around 530 nm. The extraction obtained by alcohol solution (70%) tested by the two ways results in the highest weight of solid extract, showing the best yield of anthocyanins (Table S1, Supporting Information).

HSCCC Separation. The mobile phase flow rate and the revolution speed were optimized prior to the separation of anthocyanins. The results indicate that fast flow rate resulted in poor separation, and the chromatogram peaks easily huddled. Besides, when the revolution speed was set in the range of 800−900 rpm, the separation was not apparently influenced. Based on these facts, 1.5 mL/min flow rate and 850 rpm revolution speed were chosen as the experimental conditions. Separation of natural products using HSCCC depends on the suitability of solvent systems to a great extent. Figure 1 shows the HSCCC chromatogram for 220 mg of mulberry crude extract separation with 1000 mL of a solvent system comprising methyl *tert*-butyl ether, 1-butanol, acetonitrile, water, and trifluoroacetic acid (10:30:10:50:0.05; %, v/v) according to the literature. The HSCCC run yields four peaks that correspond to fractions I−IV (27.9%, 25.7%, 41.3%, and 5.1%), respectively. The shaded part of the peaks was obtained and concentrated. This isolation gives more than 95% purity for fractions II−IV based on HPLC analysis.

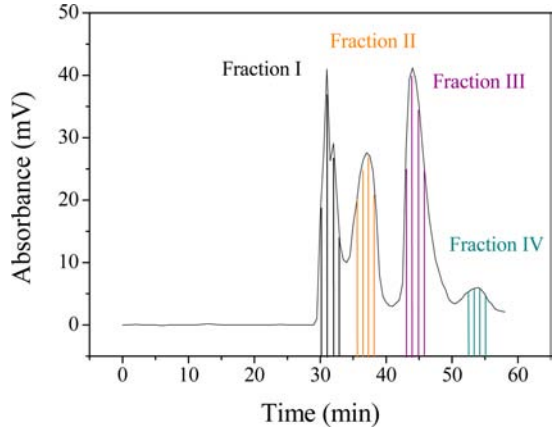

Figure 1. Chromatography of the crude ethanol solution extract of mulberry by preparative HSCCC using solvent system of methyl *tert*-butyl ether, 1-butanol, acetonitrile, water, and trifluoroacetic acid (10:30:10:50:0.05; %, v/v). Stationary phase: upper organic phase. Mobile phase: lower aqueous phase.

Solvent systems with high polarity are necessary for preparative separation of monomeric anthocyanin glycosides using HSCCC. For routine isolation, the aqueous solvent was usually employed as mobile phase, and 0.05% trifluoroacetic acid is required for stabilization of anthocyanins. In this way, the elution was in "head to tail" mode, and stable signals can be detected. Because anthocyanins are generally covalently bound with polymers and polysaccharides, the multiple peaks at the HPLC profile of fraction I are due to these complexes. Fraction I was also subjected to HPLC and represented a complicated mixture of components (Figure S2A, Supporting Information). Similar fractions were acquired from earlier isolation of anthocyanins using HSCCC in "head to tail" mode.[15−17]

Confirmation of Anthocyanin Structure. In order to elucidate the precise structure of the compounds, the fractions from HSCCC analysis were submitted to the ESI-MS/MS. Fraction II produced a molecular ion peak at *m*/*z* 595 (100) and MS^2 fragments with 287 (100) and 449 (37) U. The first fragment coincides with the cyanidin moiety, due to the loss of rutinose (308 U), and the second one at *m*/*z* 449 is due to the loss of the deoxyhexose (146 U) molecular fragment (Figure S3, Supporting Information). Fraction III reveals a molecular ion peak at *m*/*z* 595 (100) and fragment ions at *m*/*z* 287 (100) and 449 (26) U, indicating that it is a cyanidin derivative with similar structure of fraction II (Figure 2). Considering the elution order of the fractions from HSCCC, *m*/*z* values of the fragments, and previously published work,[18−20] fractions II and III should be identified as cyanidin 3-*O*-(6″-*O*-*α*-rhamnopyranosyl-*β*-glucopyranoside) and cyanidin 3-*O*-(6″-*O*-*α*-rhamnopyranosyl-*β*-galactopyranoside), respectively. Fraction IV shows a major molecular ion *m*/*z* 479 (100) confirmed probably as petunidin 3-*O*-*β*-glucopyranoside, however with other unknown ion peaks at *m*/*z* 385 (47), 499 (42), 249 (32) U, etc. as impurities (Figure S4, Supporting Information). HPLC analysis shows two major peaks for this fraction (Figure S2, Supporting Information). Comparisons were made for fractions II and III, both of which show fine purity.

HSA Fluorescence Quenching by Keracyanin and the Interaction Mechanism. HSA possesses three intrinsic fluorophores: Trp, Tyr, and Phe residues. However, most of the intrinsic fluorescence of HSA is contributed by Trp alone, taking up more than 95% of the fluorescence intensity.[21,22] Thus, alterations of HSA fluorescence intensity should be due to the change of Trp residue. Fluorescence measurements give information concerning the intermolecular distance, binding constants, binding sites, and binding mode for small molecule−protein interaction.[23−25] To elucidate the binding mechanism of keracyanin−HSA interaction, steady-state fluorescence spectra of HSA were recorded after addition of different amounts of keracyanin (Figure 3A). By exciting at 295 nm, the strong fluorescence emission band at 340 nm can be detected, which is due to the single Trp residue (No. 214 residue, shown in Figure S5, Supporting Information), which is located in the hydrophobic cavity.[26−28] The addition of keracyanin causes significant decrease in HSA fluorescence intensity, showing that

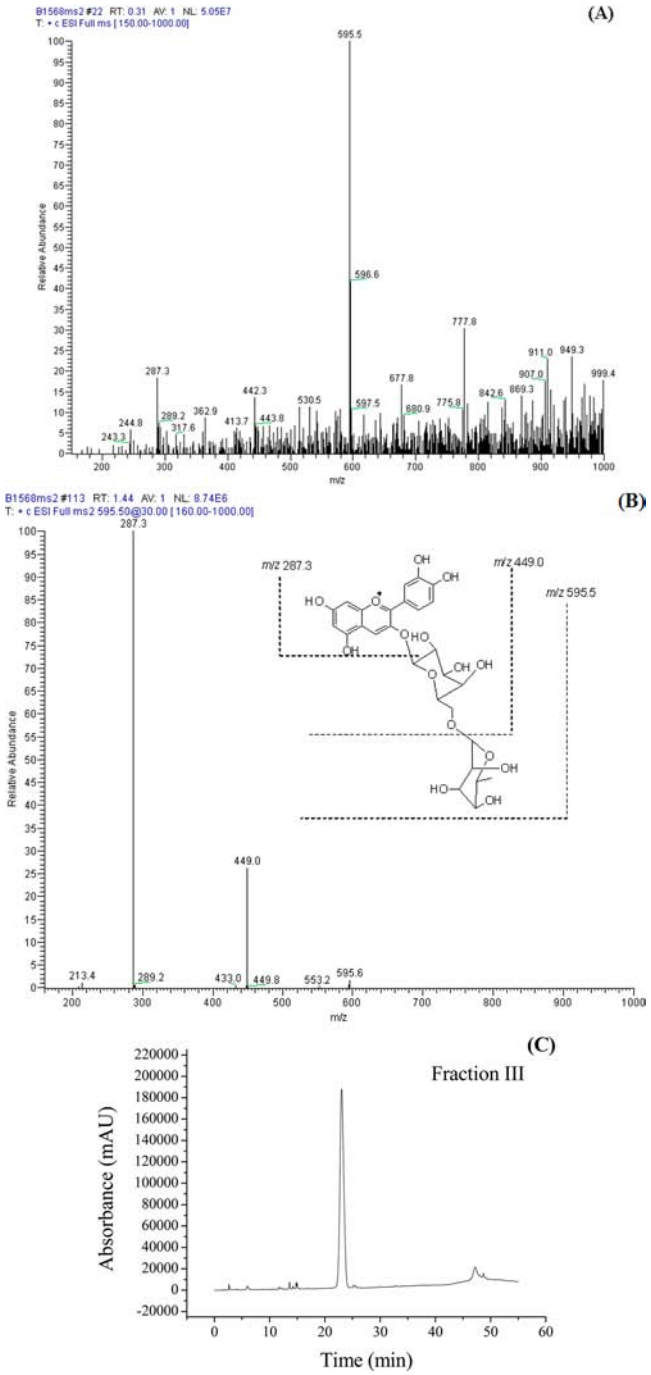

Figure 2. (A) MS and (B) MS/MS spectra of fraction III in mulberry separated from HSCCC. (C) HPLC chromatograms of fraction III separated from HSCCC (UV spectrum).

the intrinsic fluorescence of HSA was quenched upon keracyanin binding. It also implies that the microenvironment of Trp-214 was altered after interacting with keracyanin.

The quenching rate in the studied range shows good linearity after eliminating IFE (Figure 3B). In order to elucidate whether the quenching is dynamic or static, the Stern−Volmer quenching constant K_{SV} and the bimolecular quenching rate constant K_q were calculated. K_q was found to be larger than the maximum diffusion collision rate constant (2.0×10^{10} M^{-1} s^{-1}).[29] Besides, increment of the quenching constants is apparently observed with decreasing temperature, demonstrating that the fluorescence quenching of HSA was attributed to static mode in another way. Hence it can be safely considered that static quenching mechanism is dominant for HSA−keracyanin interaction.

Binding constants of HSA−keracyanin interaction were calculated using the fluorescence intensity at 340 nm. The results at different temperatures are shown in Table 1. Generally speaking, high binding constants for protein ligand interactions are within the range of 10^6−10^8 M^{-1}. The obtained binding constant of the HSA−keracyanin system is 2.49×10^4 M^{-1} at 298 K, which indicates a relatively weak interaction between keracyanin and HSA. The binding number for the interaction is about 1, suggesting that keracyanin binds the protein in 1 to 1 mode at 298 K. As lower (at 10^4 to 10^3 scales) binding constants and fewer binding sites are observed for high temperature, HSA may bind fewer keracyanin molecules at weaker forces at body temperature than room temperature, making keracyanin easier to be released from plasma protein to target organs.

In general, the binding forces between ligands and proteins involve electrostatic forces, H-bonding, van der Waals interaction, and hydrophobic forces. From the viewpoint of Ross,[30] if positive enthalpy change and entropy change implies hydrophobic interaction, then negative enthalpy change and positive entropy change suggests electrostatic force, and negative enthalpy change and entropy change reflects the van der Waals force or H-bonding. ΔS° can be treated as a constant since the temperature did not change too much, and the values of ΔH°, ΔS°, and ΔG° at 293 K, 298 K, and 303 K are listed in Table 1. ΔH° and ΔS° calculated in this work are all negative, suggesting that the dominating force is van der Waals force or hydrogen bonds.

Secondary Structure of HSA on Binding to Keracyanin. CD has been long used for evaluating conformational alterations of protein when binding ligands. The far-UV CD spectrum of HSA in the absence and presence of keracyanin was hence recorded for secondary structural evaluation. HSA was structurally dominated by α-helix, showing two negative peaks at 208 and 222 nm.[31,32] By adding keracyanin to HSA (Figure 4), the negative peaks decrease correspondingly, indicating decreased content of α-helix. However, the peak shape and position do not change with the ellipticity value, demonstrating that HSA managed to retain the overall structure. The decrease in β-sheet (from 7.4% to 6.7% to 5.9%) and α-helix (from 60.4% to 58.3% to 54.7%) contents and increase in random coil (from 23.4 to 24.5 to 25.6) structure are due to partial protein conformational changes in the HSA−keracyanin complexes. Loss of α-helical content also indicates destruction of H-bondings which maintain the special structure of α-helix. Combined with the fact that hydrogen bonds may form in the interaction, it can be concluded that keracyanin first perturbs the hydrogen bonds of HSA and then establishes new ones with the protein.

Energy Transfer from Trp of HSA to Keracyanin. Fluorescence resonance energy transfer (FRET) is a powerful and sensitive method to evaluate the possibility of energy trasfer from Trp residue of HSA to ligands and to estimate the binding distance between them. From Förster's nonradiative energy transfer theory, energy transfer occurs when the distance between the donor and the acceptor is less than 8 nm as calculated, and there is enough overlap area between the receptor's absorption spectrum and the fluorescence emission spectrum of donor.[33]

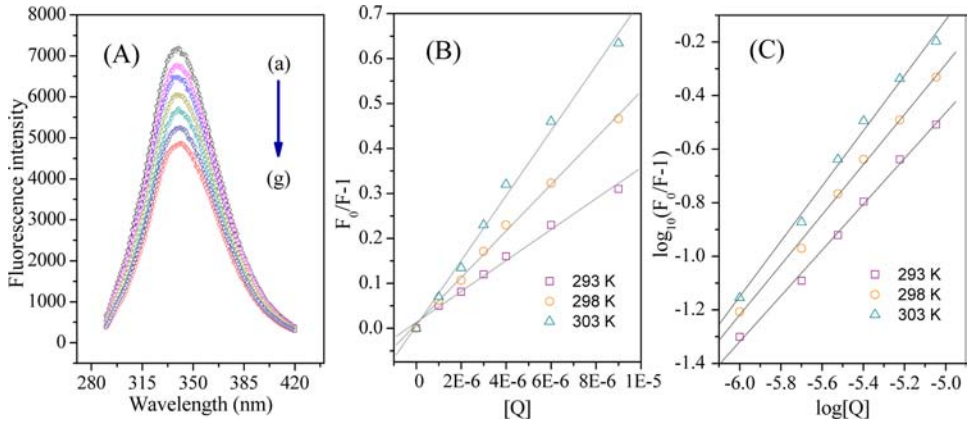

Figure 3. (A) Fluorescence emission spectra of HSA in the presence of keracyanin. C_{HSA}, 1×10^{-6} M; $C_{keracyanin}$ (a–g), 0, 1, 2, 3, 4, 6, and 9×10^{-6} M; pH 7.4, T = 298 K. (B) Stern–Volmer and (C) Hill plots of fluorescence data at different temperatures.

Table 1. Quenching, Binding, and Thermodynamic Parameters for HSA–Keracyanin System

	Stern–Volmer quenching constants			binding params			thermodynamic params		
T (K)	K_q (M^{-1} s^{-1})	K_{SV} (M^{-1})	R	K_A (M^{-1})	n	R	$\Delta G°$ (J·mol^{-1})	$\Delta S°$ (J·mol^{-1}·K^{-1})	$\Delta H°$ (J·mol^{-1})
293	7.23×10^{12}	7.23×10^{4}	0.9960	1.06×10^{5}	1.03	0.9969	-2.82×10^{4}	−621	
298	5.18×10^{12}	5.18×10^{4}	0.9986	2.49×10^{4}	0.936	0.9984	-2.51×10^{4}	−622	-2.10×10^{5}
303	3.44×10^{12}	3.44×10^{4}	0.9968	6.44×10^{3}	0.855	0.9981	-2.21×10^{4}	−621	

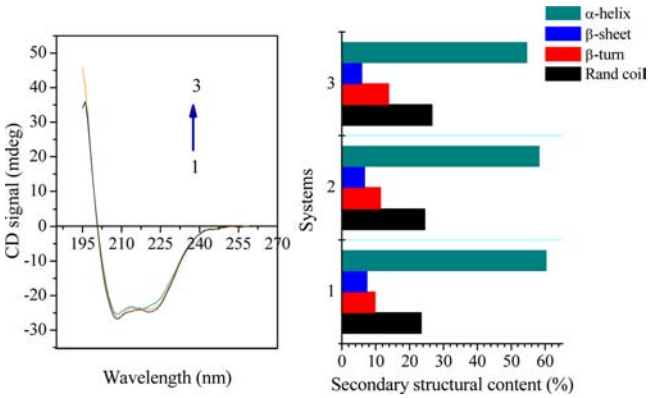

Figure 4. CD spectra of HSA–keracyanin system obtained at room temperature and pH 7.4 with secondary structural content shown. C_{HSA}: 2×10^{-7} M. $C_{keracyanin}$: 0, 5, and 10×10^{-7} M for 1–3.

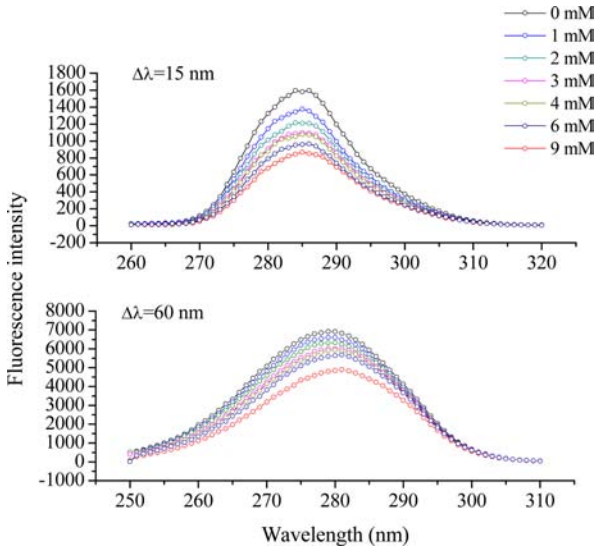

Figure 5. Synchronous fluorescence spectra of HSA in the presence of keracyanin at 298 K when $\Delta\lambda$ = 60 or 15 nm.

It has been reported for HSA that Φ = 0.118, N = 1.336, and k^2 = 2/3,[34,35] and J in eq 6 was the integration of the UV–vis absorption spectrum of keracyanin and the fluorescence emission spectrum of HSA, as shown in Figure S6 (Supporting Information). According to eqs 4–6, the values of J, E, r, and R_0 were calculated to be 2.43×10^{-15} cm^3 M^{-1}, 0.0967, 2.82, and 1.94 nm, respectively. These results show that the value for r is between 2 and 8 nm and is also on the $0.5R_0$–$1.5R_0$ scale, indicating the existence of energy transfer between HSA and keracyanin. Besides, 2.82 nm is near enough for microenvironmental alteration of Trp-214 by keracyanin.

Conformational Changes of HSA by Keracyanin. Characteristic information on the microenvironmental changes in the vicinity of fluorophores was investigated by synchronous fluorescence spectra. When $\Delta\lambda$ is set at 15 nm, the fluorescence spectra give information for Tyr, and 60 nm for Trp.[36] The synchronous fluorescence spectra of the HSA–keracyanin system are shown in Figure 5. While no obvious change is found when $\Delta\lambda$ is set at 15 nm, the emission maxima experienced a red shift from 279 to 281 nm when $\Delta\lambda$ = 60 nm. Thus, it can be concluded that the hydrophilicity around Trp-214 increases compared with that of Tyr. Water molecules are sufficient to perturb the vicinity of Trp-214 with the help of keracyanin binding, making the microenvironment from nonpolar to slightly polar.

The 3D fluorescence spectra for the HSA–keracyanin interaction system are presented in Figure 6 with peak information summarized in Table 2, where we can get the microenvironmental and conformational information on HSA upon keracyanin interaction. As we can seen in Figure 6, peak a results from the Rayleigh scattering of water (λ_{ex} = λ_{em}), whereas the strong peak b mainly reflects the characteristics of chromophores (mainly Trp residue) of HSA, and peak c is related to the polypeptide backbone structure of HSA.[37,38] As

dx.doi.org/10.1021/jf500705s | J. Agric. Food Chem. 2014, 62, 6813–6819

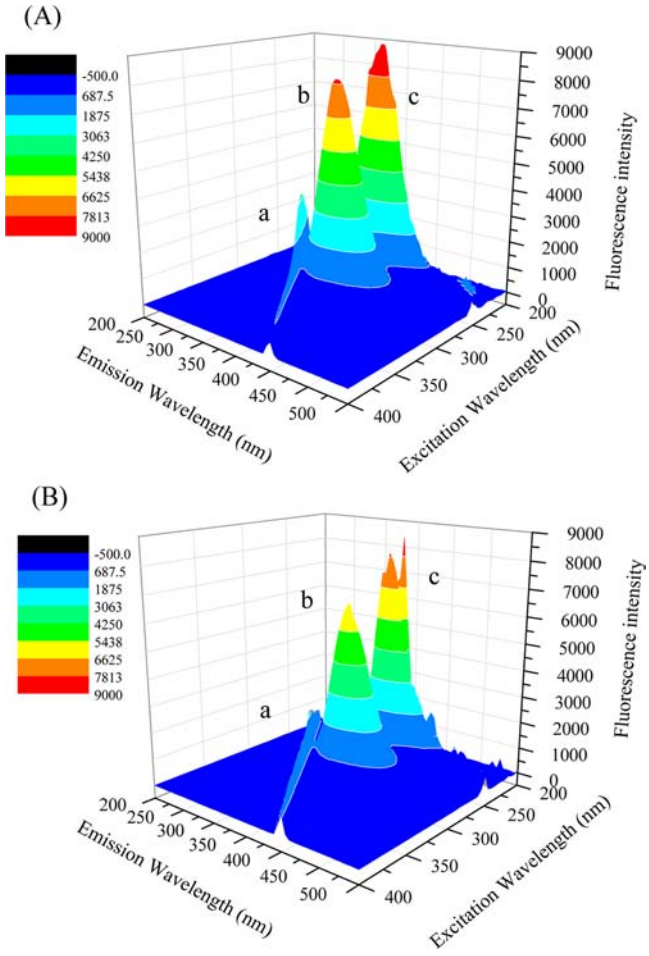

Figure 6. Three-dimensional fluorescence spectra of HSA without (A) and with keracyanin addition (B). C_{HSA}, 2×10^{-6} M; $C_{keracyanin}$, 5×10^{-6} M; pH 7.4, T = 298 K.

shown in Figure 6 and Table 2, with the addition of keracyanin the fluorescence of both peaks b and c is quenched and the fluorescence maximum of peak c red shifts slightly from 337 to 341 nm. These phenomena suggest that keracyanin perturbs the microenvironment of Trp-214 upon interaction with HSA, inducing slight unfolding or adaptive rearrangement of the polypeptide backbone of the protein.

Besides, the 3D structure of HSA is known to be composed of three homologous domains with two subdomains for each. The hydrophobic cavity, where Trp-214 locates, is in the center of the three domains. The binding site of keracyanin might be located in this pocket. The interaction of keracyanin causes changes of polarity of the hydrophobic microenvironment (also proved by synchronous fluorescence study), leading to protein conformational changes.

HSCCC technique makes it possible to separate anthocyanin-rich natural products and yield some pure anthocyanins on a semipreparative scale. Anthocyanins from mulberry most probably include cyanidin 3-*O*-(6″-*O*-*α*-rhamnopyranosyl-*β*-galactopyranoside) (keracyanin), cyanidin 3-*O*-(6″-*O*-*α*-rhamnopyranosyl-*β*-glucopyranoside), and petunidin 3-*O*-*β*-glucopyranoside. Details on the interaction between keracyanin and HSA were revealed using spectroscopy. Intrinsic fluorescence of HSA has been quenched by keracyanin following static mechanism, which is induced by the formation of a certain kind of new complex. The binding of keracyanin to HSA is moderate and equimolar. Thermodynamic parameters indicate that the reaction is spontaneous, with H-bonding and van der Waals forces playing the major role. Synchronous fluorescence spectroscopic results demonstrate that keracyanin gets close to Trp residues whereas the microenvironment around Tyr residues is almost unchanged. We have discovered and interpreted the structural changes of HSA by keracyanin complexation from CD and three-dimensional fluorescence analyses. Energy probably transfers from Trp to keracyanin in the binding process, and the binding distance between the two was estimated to be 2.82 nm at 298 K. The research results are expected to provide useful information for not only natural product separation and identification but the interactions of the carrier proteins with anthocyanin, which will be helpful for the development of food chemistry, clinical medicine, and life sciences.

■ ASSOCIATED CONTENT

Ⓢ Supporting Information

Absorption spectra of pigment extract, HPLC and MS spectral data of the fractions, structure of HSA, and spectral overlap of keracyanin-HSA. This material is available free of charge via the Internet at http://pubs.acs.org.

■ AUTHOR INFORMATION

Corresponding Author

*E-mail: pengxiali@126.com. Fax/tel: +86-025-84392062.

Author Contributions

‡Authors F.S., Y.W., and X.Z. contributed equally to this work.

Funding

This work was supported by Special Fund for National Forestry Scientific Research in the Public Interest (201204402-1) and Science & Technology Development Project of Shandong Province (2013GZX20109).

Notes

The authors declare no competing financial interest.

■ ACKNOWLEDGMENTS

Thanks are given to Research Center for Food Safety & Inspection Engineering of Shandong Province and Science & Technology Department of Shandong Province for their support.

Table 2. 3D Fluorescence Information of HSA−Keracyanin System

	HSA			HSA−keracyanin		
peaks	peak position $\lambda_{ex}/\lambda_{em}$ (nm/nm)	Stokes $\Delta\lambda$ (nm)	fluorescence intensity	peak position $\lambda_{ex}/\lambda_{em}$ (nm/nm)	Stokes $\Delta\lambda$ (nm)	fluorescence intensity
a	275/275	0	3290	285/285	0	1615
b	278/335	57	7973	280/337	57	5940
c	227/340	43	8790	230/341	71	7337

REFERENCES

(1) Bridle, P.; Timberlake, C. Anthocyanins as natural food colours—selected aspects. *Food Chem.* **1997**, *58*, 103−109.

(2) Fukumoto, L.; Mazza, G. Assessing antioxidant and prooxidant activities of phenolic compounds. *J. Agric. Food Chem.* **2000**, *48*, 3597−3604.

(3) Chen, P.-N.; Chu, S.-C.; Chiou, H.-L.; Kuo, W.-H.; Chiang, C.-L.; Hsieh, Y.-S. Mulberry anthocyanins, cyanidin 3-rutinoside and cyanidin 3-glucoside, exhibited an inhibitory effect on the migration and invasion of a human lung cancer cell line. *Cancer Lett.* **2006**, *235*, 248−259.

(4) Zafra-Stone, S.; Yasmin, T.; Bagchi, M.; Chatterjee, A.; Vinson, J. A.; Bagchi, D. Berry anthocyanins as novel antioxidants in human health and disease prevention. *Mol. Nutr. Food Res.* **2007**, *51*, 675−683.

(5) Zhao, X.; Sheng, F.; Zheng, J.; Liu, R. Composition and Stability of Anthocyanins from Purple Solanum tuberosum and Their Protective Influence on Cr(VI) Targeted to Bovine Serum Albumin. *J. Agric. Food Chem.* **2011**, *59*, 7902−7909.

(6) Papadopoulou, A.; Green, R. J.; Frazier, R. A. Interaction of flavonoids with bovine serum albumin: a fluorescence quenching study. *J. Agric. Food Chem.* **2005**, *53*, 158−163.

(7) Xiao, J.; Chen, T.; Cao, H.; Chen, L.; Yang, F. Molecular property−affinity relationship of flavanoids and flavonoids for HSA in vitro. *Mol. Nutr. Food Res.* **2011**, *55*, 310−317.

(8) Xiao, J.; Mao, F.; Yang, F.; Zhao, Y.; Zhang, C.; Yamamoto, K. Interaction of dietary polyphenols with bovine milk proteins: Molecular structure−affinity relationship and influencing bioactivity aspects. *Mol. Nutr. Food Res.* **2011**, *55*, 1637−1645.

(9) Cao, G.; Muccitelli, H. U.; Sánchez-Moreno, C.; Prior, R. L. Anthocyanins are absorbed in glycated forms in elderly women: a pharmacokinetic study. *Am. J. Clin. Nutr.* **2001**, *73*, 920−926.

(10) Cahyana, Y.; H Gordon, M. Interaction of anthocyanins with human serum albumin: influence of pH and chemical structure on binding. *Food Chem.* **2013**, *141* (3), 2278−2285.

(11) Edirisinghe, I.; Banaszewski, K.; Cappozzo, J.; McCarthy, D.; Burton-Freeman, B. M. Effect of black currant anthocyanins on the activation of endothelial nitric oxide synthase (eNOS) in vitro in human endothelial cells. *J. Agric. Food Chem.* **2011**, *59*, 8616−8624.

(12) Cao, G.; Prior, R. L. Anthocyanins are detected in human plasma after oral administration of an elderberry extract. *Clin. Chem.* **1999**, *45*, 574−576.

(13) Lee, J.; Durst, R. W.; Wrolstad, R. E. Determination of total monomeric anthocyanin pigment content of fruit juices, beverages, natural colorants, and wines by the pH differential method: Collaborative study. *J. AOAC Int.* **2005**, *88*, 1269−1278.

(14) Zhao, X. C.; Liu, R. T.; Chi, Z. X.; Teng, Y.; Qin, P. F. New Insights into the Behavior of Bovine Serum Albumin Adsorbed onto Carbon Nanotubes: Comprehensive Spectroscopic Studies. *J. Phys. Chem. B* **2010**, *114*, 5625−5631.

(15) Noguer, M.; Cerezo, A. B.; Rentzsch, M.; Winterhalter, P.; Troncoso, A. M.; García-Parrilla, M. C. Simulated digestion and antioxidant activity of red wine fractions separated by high speed countercurrent chromatography. *J. Agric. Food Chem.* **2008**, *56*, 8879−8884.

(16) Chen, L.; Xin, X.; Lan, R.; Yuan, Q.; Wang, X.; Li, Y. Isolation of cyanidin 3-glucoside from blue honeysuckle fruits by high-speed counter-current chromatography. *Food Chem.* **2014**, *152*, 386−390.

(17) Zanatta, C. F.; Cuevas, E.; Bobbio, F. O.; Winterhalter, P.; Mercadante, A. Z. Determination of anthocyanins from camu-camu (Myrciaria dubia) by HPLC-PDA, HPLC-MS, and NMR. *J. Agric. Food Chem.* **2005**, *53*, 9531−9535.

(18) Du, Q.; Zheng, J.; Xu, Y. Composition of anthocyanins in mulberry and their antioxidant activity. *J. Food Compos. Anal.* **2008**, *21*, 390−395.

(19) Wu, X.; Liang, L.; Zou, Y.; Zhao, T.; Zhao, J.; Li, F.; Yang, L. Aqueous two-phase extraction, identification and antioxidant activity of anthocyanins from mulberry (*Morus atropurpurea* Roxb.). *Food Chem.* **2011**, *129*, 443−453.

(20) Wu, X.; Prior, R. L. Systematic identification and characterization of anthocyanins by HPLC-ESI-MS/MS in common foods in the United States: fruits and berries. *J. Agric. Food Chem.* **2005**, *53*, 2589−2599.

(21) Shvedova, A. A.; Kisin, E.; Murray, A. R.; Johnson, V. J.; Gorelik, O.; Arepalli, S.; Hubbs, A. F.; Mercer, R. R.; Keohavong, P.; Sussman, N.; Jin, J.; Yin, J.; Stone, S.; Chen, B. T.; Deye, G.; Maynard, A.; Castranova, V.; Baron, P. A.; Kagan, V. E. Inhalation vs. aspiration of single-walled carbon nanotubes in C57BL/6 mice: inflammation, fibrosis, oxidative stress, and mutagenesis. *Am. J. Physiol.* **2008**, *295*, L552−L565.

(22) Beauchemin, R.; N'Soukpoe-Kossi, C. N.; Thomas, T. J.; Thomas, T.; Carpentier, R.; Tajmir-Riahi, H. A. Polyamine analogues bind human serum albumin. *Biomacromolecules* **2007**, *8*, 3177−3183.

(23) Charbonneau, D.; Beauregard, M.; Tajmir-Riahi, H. A. Structural Analysis of Human Serum Albumin Complexes with Cationic Lipids. *J. Phys. Chem. B* **2009**, *113*, 1777−1784.

(24) Bourassa, P.; Kanakis, C. D.; Tarantilis, P.; Pollissiou, M. G.; Tajmir-Riahi, H. A. Resveratrol, Genistein, and Curcumin Bind Bovine Serum Albumin. *J. Phys. Chem. B* **2010**, *114*, 3348−3354.

(25) Charbonneau, D. M.; Tajmir-Riahi, H. A. Study on the Interaction of Cationic Lipids with Bovine Serum Albumin. *J. Phys. Chem. B* **2010**, *114*, 1148−1155.

(26) Liu, A.; Sun, K.; Yang, J.; Zhao, D. Toxicological effects of multi-wall carbon nanotubes in rats. *J. Nanopart. Res.* **2008**, *10*, 1303−1307.

(27) Hu, Y. J.; Ou-Yang, Y.; Dai, C. M.; Liu, Y.; Xiao, X. H. Binding of berberine to bovine serum albumin: spectroscopic approach. *Mol. Biol. Rep.* **2010**, *37*, 3827−3832.

(28) Hu, Y. J.; Liu, Y.; Xiao, X. H. Investigation of the Interaction between Berberine and Human Serum Albumin. *Biomacromolecules* **2009**, *10*, 517−521.

(29) Zhao, X.; Liu, R.; Teng, Y.; Liu, X. The interaction between Ag(+) and bovine serum albumin: A spectroscopic investigation. *Sci. Total Environ.* **2011**, *409*, 892−897.

(30) Ross, P. D.; Subramanian, S. Thermodynamics of protein association reactions: forces contributing to stability. *Biochemistry* **1981**, *20*, 3096−3102.

(31) Bosca, F. Seeking to Shed Some Light on the Binding of Fluoroquinolones to Albumins. *J. Phys. Chem. B* **2012**, *116*, 3504−3511.

(32) Cheng, X. X.; Lui, Y.; Zhou, B.; Xiao, X. H.; Liu, Y. Probing the binding sites and the effect of berbamine on the structure of bovine serum albumin. *Spectrochim. Acta, Part A* **2009**, *72*, 922−928.

(33) Teng, Y.; Zhang, H.; Liu, R. Molecular interaction between 4-aminoantipyrine and catalase reveals a potentially toxic mechanism of the drug. *Mol. BioSyst.* **2011**, *7*, 3157−3163.

(34) Liu, W. P.; Yang, W. C.; Liu, H. J.; Tong, S. L.; Fang, Z. H. Interaction between triazine herbicide and catalase by fluorescence spectrum. *Spectrosc. Spectral Anal.* **2003**, *23*, 926−929.

(35) Polet, H.; Steinhardt, J. Binding-induced alterations in ultraviolet absorption of native serum albumin. *Biochemistry* **1968**, *7*, 1348−1356.

(36) Wu, Y. Study on the interaction between salicylic acid and catalase by spectroscopic methods. *J. Pharm. Biomed. Anal.* **2007**, *44*, 796−801.

(37) Xia, Z.; Jing, J. Binding analysis of pazufloxacin mesilate to catalase using spectroscopic methods. *J. Mol. Struct.* **2008**, *882*, 96−100.

(38) Francioli, P.; Etienne, J.; Hoigne, R.; Thys, J. P.; Gerber, A. Treatment of streptococcal endocarditis with a single daily dose of ceftriaxone sodium for 4 weeks. Efficacy and outpatient treatment feasibility. *JAMA: J. Am. Med. Assoc.* **1992**, *267*, 264−267.

Table 1. Volatile Composition of Wines, in Milligrams per Liter, Produced by Fermentations with Different Levels of [U-^{13}C]-Glucose Enrichment[a]

			atom percent excess of hexose (APE_{hex})			
compound	RT[b]	Q ion[c]	0	0.01	0.1	1.0
ethanol	na[d]	43	114848	112466	114059	118289
isobutyl acetate	10.591	43	0.14	0.11	0.09	0.08
ethyl butyrate	11.571	71	0.23	0.25	0.21	0.19
ethyl isovalerate	13.383	57	0.04	0.05	0.03	0.07
isobutyl alcohol	14.297	43	30.70	28.25	27.77	26.25
1-butanol	16.875	56	1.45	1.42	1.44	1.45
isoamyl acetate	18.744	43	3.41	2.98	2.46	2.55
isoamyl alcohol	20.300	55	74.07	102.70	84.88	81.49
ethyl hexanoate	21.413	88	0.34	0.35	0.27	0.28
hexyl acetate	23.332	43	0.15	0.17	0.18	0.15
ethyl lactate	26.774	43	5.65b	16.97a	13.84a	12.45a
1-hexanol	27.144	56	0.74	0.97	0.83	0.76
ethyl octanoate	30.802	88	0.21	0.38	0.23	0.24
ethyl 3-hydroxybutyrate	34.474	43	0.13	0.18	0.15	0.14
propanoic acid	35.567	74	3.73	4.32	3.36	3.00
isobutyric acid	36.723	43	2.11	2.29	1.82	1.51
butyric acid	39.111	60	0.30	0.15	0.13	0.16
ethyl decanoate	39.228	88	1.34a	1.98b	1.39a	1.16a
isovaleric acid	40.685	60	0.64	0.86	0.75	0.65
diethyl succinate	40.815	101	0.12	0.22	0.18	0.18
methionol	42.374	61	1.59	2.60	2.23	1.96
phenylethyl acetate	45.970	104	0.37	0.34	0.29	0.27
hexanoic acid	47.107	60	3.57	4.52	3.84	3.36
β-phenylethanol	49.401	91	15.88	22.19	18.82	18.92
octanoic acid	54.254	60	5.82	6.19	5.68	4.52
decanoic acid	60.752	60	2.78a	0.93b	1.09b	0.88b

[a]Letters within a row indicate significant difference using the Bonferroni family error rate $\alpha = 0.05$; if no letters are present, then no significant differences were observed for that compound. [b]RT = retention time in minutes. [c]Q ion = quantifier ion by GC-MS. [d]Measured using direct injection method.

used to study their formation in wine.[13] However, to yield detectable changes using a typical GC-MS system, stable isotope tracers must be added at a concentration of at least >0.5% (and generally higher) of the endogenous concentration,[14] which may be prohibitively expensive and, as mentioned above, create the risk of affecting fermentation physiology. Radioisotopes can be employed at lower concentrations due to their low natural abundance, with labeled compounds typically detected following off-line separation via a scintillation counter. In wine, [^{3}H]-malvidin glucoside has been used as a model to track the fate of anthocyanins before and after fermentation,[15] and [U-^{14}C]-glucose, -leucine, and -isoleucine have been used to follow volatile production in grain mash fermentations.[16] In practice, radioisotopes are rarely used as tracers in food chemistry studies because of associated hazards.

An alternative to conventional tracer experiments with GC-MS is high-precision isotope ratio measurement by gas chromatography combustion isotope ratio mass spectroscopy (GC-C-IRMS). In GC-C-IRMS, organic compounds are combusted to CO_2 following their elution from a GC, and the isotopomers of CO_2 (m/z 44, 45, 46) are measured by IRMS for each peak.[14] GC-C-IRMS has been used for natural abundance studies of wine, primarily for studies on authenticity and adulteration. For example, $^{13}C/^{12}C$ ratios can be used to detect illegal addition of cane sugar (derived from a C4 plant) to grape juice (derived from a C3 plant) prior to fermentation and, in combination with D/H and $^{18}O/^{16}O$ ratios, can serve as geographical fingerprints for wine provenance.[17] The major advantage of GC-C-IRMS for tracer studies is that it can achieve much higher precison than conventional GC-MS; in practice, ^{13}C enrichments as low as ~0.1 atom percent excess (APE) can be utilized for tracer studies.[18] GC-C-IRMS has been used for tracer studies in a number of disciplines where a sizable endogenous pool of a potential precursor exists and large degrees of enrichment are not possible for economic or other practical reasons.[14] For example, GC-C-IRMS has been used to monitor the fate and metabolism of dietary omega-3 fatty acids in animal studies.[19] GC-C-IRMS has also been used in conjunction with $^{13}CO_2$ labeling studies of chamber-grown grapevines to determine the timing of biosynthesis of glycoconjugate precursors,[20] but to our knowledge GC-C-IRMS has not been used for tracer studies of wine fermentations or in related areas of food processing.

In this work, we report the use of GC-C-IRMS as a novel approach to follow the path of a stable isotope tracer during the alcoholic fermentation of hexose. Uniformly labeled [U-^{13}C]-glucose was added to a grape must prior to fermentation at trace levels (0.01, 0.1, and 1 APE), and its contribution to a diverse range of fermentation volatiles (i.e., fusel alcohols, fatty acids, and their associated esters) was assessed. This technique can be used as a more general approach for studying the origin and fate of compounds in food systems while minimizing tracer concentration.

dx.doi.org/10.1021/jf500947x | J. Agric. Food Chem. 2014, 62, 6820−6827

MATERIALS AND METHODS

Fermentations. Fermentations were conducted using Riesling juice sourced from the Cornell research vineyards in Lansing, NY, USA, during the 2010 harvest. Fruit (450 kg) was received by the Cornell Vinification and Brewing Technology Laboratory, where it was crushed, destemmed, basket pressed, and settled overnight at ambient conditions. Approximately 30 L was siphoned into two 20 L Nalgene containers (Thermo Fisher Scientific, Waltham, MA, USA) and frozen at −20 °C. Before use, the juice was thawed in a 40 °C water bath for 1 h and mixed by inversion. Glucose, fructose, and yeast assimilable nitrogen (YAN) were quantified by enzymatic colorimetric methods using a Chemwell 2910 Multianalyzer (Unitech Scientific, Hawaiian Gardens, CA, USA). To supplement the initial juice YAN content of 40 mg N/L, diammonium hydrogen phosphate (674 mg/L) and Fermaid K (Lallemand, Santa Rosa, CA, USA) (250 mg/L) were added to yield a final YAN concentration of 214 mg N/L. Yeast (EC1118, Lallemand) was rehydrated in 40 °C spring water (Crystal Rock, Watertown, CT, USA) with 40 g/L GoFerm (Scott Laboratories, Petaluma, CA, USA), and the juice (5 L) was inoculated at a rate of 0.3 g/L. Aliquots of 541 g (500 mL) of inoculated must were then added to 1 L Pyrex media bottles (Corning Inc., Tewksbury, MA, USA). One treatment served as a control (no [U-^{13}C]-glucose added), and uniformly labeled [U-^{13}C]-glucose (Cambridge Isotope Laboratories, Andover, MA, USA) was added at one of three levels: 1.0 APE (1.0150 g/500 mL), 0.1 APE (0.1015 g/500 mL), or 0.01 APE (0.0102 g/500 mL). Fermentations were carried out in triplicate for each of the four treatments (three tracer levels + one control). The fermenters were topped with a three-piece airlock with a floating bubbler (Buon Vino Manufacturing, Cambridge, ON, Canada). Fermentations were conducted over a 10 day period at ambient temperatures in a dark cabinet and were measured for residual sugar after all fermenters had stopped producing CO_2. At completion, all fermentations had residual sugar (glucose, fructose) values of <0.5 g/L. The wine was stabilized by the addition of 50 mg/L of SO_2 and then frozen and stored at −20 °C until needed for further analysis.

Sample Preparation. Volatile components were extracted from wine using the method described by Ortega and others.[21] To a 15 mL screw-capped borosilicate glass centrifuge tube were added 4.5 g of $(NH_4)_2SO_4$, 3 mL of wine, 7 mL of water, and 0.2 mL of dichloromethane (DCM). For GC-MS quantification 15 μL of a 140 μg/mL solution of 2-octanol was added to the sample as in internal sample; this step was omitted for the GC-C-IRMS analysis. The samples were mixed for 1 h using a carousel rotating at 20 rpm to invert the tubes and then centrifuged at 2500*g* for 10 min. Approximately 1.5 mL of the emulsified bottom layer was recovered with a glass Pasteur pipet, transferred to a 2.2 mL microfuge tube, and centrifuged for 4 min at 14000*g*. Finally, 100 μL of the DCM layer was transferred to an Agilent GC autosampler vial with a 250 μL microvolume insert.

Quantification and Identification of Volatiles by GC-MS. Compounds in the DCM extracts were identified and quantified by gas chromatography−mass spectrometry (GC-MS). An HP 6890 GC with a split/splitless inlet (Agilent Technologies, Palo Alto, CA, USA) and autoinjector was coupled to an Agilent 5795 quadrupole mass selective detector (MSD). A 60 m × 0.32 mm × 0.25 μm Aglient HP-INNOWax column (polyethylene glycol) was used. The GC conditions were as follows: initial head pressure at 8.57 psi with a column flow of 1.6 mL/min in constant flow mode, inlet at 250 °C, 2 μL splitless injection, and total flow through the injector of 84.8 mL/min. The oven parameters were as follows: initial temperature 35 °C (held for 2 min) ramped to 40 °C at 5 °C/min (held 5 for min), ramped to 200 °C at 3 °C/min (held for 5 min), and ramped to 250 °C at 25 °C/min (held for 20 min). The MSD was operated with an ionization energy of 70 eV with the electron multiplier voltage of 1700 V. The MSD was scanned over the mass range of m/z 33−300. Chemstation MSD (Agilent Technologies) was used for data processing. Compound identification was performed by matching retention times and mass spectra of peaks to authentic standards, and peak areas were normalized to that of the 2-octanol internal standard. Calibration curves were generated from the analysis of known concentrations of pure standards spiked into a model wine. Calibration curves for all 26 compounds had an $r^2 > 0.99$. Quantifier ions and retention times for each compound are listed in Table 1.

Due to its coelution with the extraction solvent DCM, ethanol was quantified separately via a direct injection method.[22] Wine was filtered through a 0.25 μm filter and 100 μL diluted with 900 μL of water; 1 μL of this sample was then injected at a 50:1 split into a 250 °C inlet. The oven parameters were as follows: initial 35 °C (held for 2 min) ramped to 40 °C at 5 °C/min (held for 5 min), ramped to 70 °C at 5 °C/min (held for 5 min), and ramped to 250 °C at 25 °C/min (held for 7 min).

Carbon Isotope Ratio Analysis of Wine Volatiles by GC-C-IRMS. The design and operation of the GC-C-IRMS system are described in more detail elsewhere.[23] Briefly, the HP 6890 GC-MS described above was coupled to a Thermo MAT 253 IRMS (Bremen, Germany) via a specially designed combustion interface. The IRMS was tuned for high linearity with the conduction limit open three full turns and operated at a source pressure of 9.3×10^{-7} Torr and an accelerating potential of 9.5 kV. The measured absolute sensitivity was ∼1600 molecules/ion. Data were collected and analyzed using ISODAT 3.0 (Thermo Scientific). The GC column was connected to an online microcombustion reactor via a four-way rotary valve, which permitted solvent diversion to the MSD and sample introduction into IRMS. The microcombustion reactor was constructed from a continuous fused silica capillary (50 cm × 0.53 mm i.d.) hand packed with three 15 cm × 0.1 mm wires (one Cu, one Pt, and one Ni wire) in the center of the capillary. The capillary portion containing the wires was mechanically retained in a 30 cm × 0.8 mm i.d. alumina tube with metal fittings (Valco Instruments, Houston, TX, USA) on both ends. The exposed ends of the capillary were connected to the interface with press-tight fittings. The alumina tube was maintained at 950 °C using a 30 cm Thermcraft tube furnace (Winston-Salem, NC, USA), which had a 15 cm heated zone. Water generated due to combustion was removed from the system using a Nafion water trap (dimensions = 10 cm × 0.8 mm i.d.) immediately following the combustion reactor. The open-split consisted of the 0.6 m × 0.075 mm capillary connected to the IRMS inlet at one end, with the other end directly inserted into the postwater trap transfer line. For analysis of wine volatiles, excluding ethanol, a 60 m × 0.32 mm × 0.25 μm Agilent HP-INNOWax column described above was used. The GC conditions were as follows: initial head pressure at 8.57 psi with a column flow of 1.6 mL/min in constant flow mode, inlet at 250 °C, 2 μL splitless injection, and total flow through the injector of 84.8 mL/min. The oven parameters were as follows: initial 35 °C (held for 2 min) ramped to 40 °C at 5 °C/min (held for 5 min), ramped to 200 °C at 3 °C/min (held for 5 min), and ramped to 250 °C at 25 °C/min (held for 20 min).

Because of ethanol's coelution with the extraction solvent, DCM, it was characterized by GC-C-IRMS separately from the other measured compounds. Sample preparation, injection technique, and GC conditions were the same as described for GC-MS.

ISODAT 3.0 was used to calculate isotope ratios in delta notation; ^{17}O corrections were made using the Santrock and Hayes method.[24] Background was determined using the individual background determination with a 5 s moving linear regression, whereas peak detection was set to a slope of 0.5 mV/s for peak start and 0.4 mV/s for peak end. For calibration, CO_2 gas pulses were admitted directly to the IRMS source from a Conflo III device (Thermo Scientific). CO_2 was supplied by a pressurized tank during each GC-C-IRMS run for isotope ratio standardization, with three 30 s pulses at the beginning and three at the end of each chromatogram. The isotope ratio of the CO_2 standard gas was traceable to the international standard Vienna Pee Dee Belemnite (VPDB) (R_{VPDB} = 0.011180) by running calibration standards containing fatty acid methyl ester (FAME) 17:0 and FAME 21:0 with known isotope ratios determined by off-line dual-inlet IRMS.[25] This FAME standard was run at the beginning and end of each day's runs to determine the "apparent" isotope ratio of the CO_2 gas pulses, which in turn could be used to calculate the isotope ratios of wine components during analytical runs. This calibration

approach addresses fractionation in the GC-C-IRMS system because the FAME standards go through the same path as the wine components (i.e., GC, online combustion, water trap, open split, IRMS).[25] Isotope ratios are reported as $\delta^{13}C_{VPDB}$ in units of "per mil" (‰) and based on the International System of Units (SI), where $\delta^{13}C_{VPDB}$ is defined as

$$\delta^{13}C_{VPDB} = \frac{R_X - R_{VPDB}}{R_{VPDB}} \quad (1)$$

R_X and R_{VPDB} represent the $^{13}C/^{12}C$ isotope ratio of an analyte compound X and the VPDB standard, respectively.

Bulk Analysis of Grape Must Carbon Isotope Ratio by Elemental Analyzer-IRMS (EA-IRMS). A 2 mL aliquot of the frozen Riesling juice (no [U-^{13}C]-glucose added) was submitted to the Cornell Stable Isotope Laboratory (COIL) for EA-IRMS analysis. Five microliters of juice taken from a 2 mL frozen aliquot was used for bulk stable isotope analysis using a continuous flow system.[26] The sample was combusted at 900 °C in a Carlo Erba NC2500 elemental analyzer, and resultant CO_2 was transferred via a Conflo IV interface (Thermo Scientific) to a Delta V isotope ratio mass spectrometer (Thermo Scientific) for carbon isotope analysis. Isotope ratios are reported in delta notation, as described above.

Statistical Analysis. All linear regression analysis and ANOVA calculations were carried out using MiniTab (Minitab, Reading, MA, USA) statistical analysis software.

Isotope Addition and APE Calculations. APE is defined in eq 2

$$APE = 100(F_{HEXe} - F_{HEXn}) \quad (2)$$

where F_{HEXe} is the atom fraction of the enriched hexose and F_{HEXn} is the atom fraction of the native hexose pool. F_{HEXe} is calculated by the amount of [U-^{13}C]-glucose added to the system. The mass balance equation (eq 3) can be rearranged to eq 4, where F_{ULG} is the atom fraction of uniformly labeled glucose and m_{ULG} is the mass.

$$F_{HEXe}m_{HEXe} = F_{ULG}m_{ULG} + F_{HEXn}m_{HEXn} \quad (3)$$

$$F_{HEXe} = \frac{F_{ULG}m_{ULG}}{m_{HEXe}} + \frac{F_{HEXn}m_{HEXn}}{m_{HEXe}} \quad (4)$$

For tracer level additions of [U-^{13}C]-glucose, the atom fraction of uniformly labeled glucose (F_{ULG}) = 1, the mass fraction (m_{HEXn}/m_{HEXe}) will be ~1, and eq 4 simplifies to

$$F_{HEXe} = \frac{m_{ULG}}{m_{HEXe}} + F_{HEXn} \quad (5)$$

Combining eqs 2 and 5 yields eq 6 and provides a good approximation for the APE of the enriched hexose pool (APE_{HEX}) as a function of the amount of [U-^{13}C]-glucose added to the fermentation and the original hexose concentration.

$$APE_{HEX} = 100\left(\frac{m_{ULG}}{m_{HEXe}}\right) \quad (6)$$

Calculating the Percentage of Carbon Derived from Hexose in Volatile Compounds. The observed APE of each volatile (APE_{obsd}) was calculated from experimental data for each volatile in each tracer fermentation, where R_E is the $^{13}C/^{12}C$ ratio in the enriched sample and R_N is the mean $^{13}C/^{12}C$ ratio of the corresponding compound in the natural abundance fermentations:[14]

$$APE_{obsd} = \frac{R_E - R_N}{1 + (R_E - R_N)} \quad (7)$$

To determine the percent of each volatile compound that originated from hexose substrate, (APE_{obsd}) was assumed to be related to the APE of the hexose pool (APE_{hex}) by eq 8.

$$APE_{obsd} = \alpha\ (\%\ \text{from hexose}) \times (APE_{HEX}) \quad (8)$$

APE_{hex} is a factor of the tracer level (eq 6). The apparent fractionation factor, α, can arise from kinetic isotope effects and can potentially vary among compounds. However, in most biochemical processes, α is expected to range from between 0.98 and 1.02, and assuming $\alpha = 1$ will introduce negligible error. Equation 8 can be simplified and rearranged to solve for the percent of carbon in a given volatile derived from hexose sugars (eq 9).

$$\%\ \text{fom hexose} = \frac{APE_{obsd}}{APE_{HEX}} \quad (9)$$

RESULTS AND DISCUSSION

Volatile Composition of Fermentations. A summary of the average concentration of volatile compounds by level of enrichment is given in Table 1. Mean concentrations of each compound were within the range of values reported previously in the analysis of wine samples.[21] Individual ANOVAs were calculated for each of the 28 compounds by level of enrichment. To account for potential type 1 error due to the number of comparisons, the Bonferroni correction was applied using a family error rate of $\alpha = 0.05$. Whereas most compounds did not show significant differences, ethyl lactate, ethyl decanoate, and decanoic acid show significant differences between the control fermentation and the enriched fermentations. These differences may have arisen because the control fermentation was conducted at a different time from the enriched fermentations, rather than as an effect of enrichment treatment. In particular, production of midchain fatty acids such as decanoic acid and their corresponding ethyl esters is known to be affected by variation in oxygen status during fermentation.[27] However, for all other compounds, the lack of difference indicates that labeling does not perturb the system.

Native $^{13}C/^{12}C$ Ratios. Table 2 reports the native isotope ratios of 19 volatile compounds in the experimental Riesling wine, expressed as $\delta^{13}C$ values. Literature reports on compound-specific isotope ratios of wine volatiles other than ethanol are relatively rare,[28] and to our knowledge our work represents the largest number reported to date. Significant

Table 2. $\delta^{13}C$ Values in Natural Abundance Control Fermentations[a]

compound	n	$\delta^{13}C_{VPDB}$ (‰)	SD (‰)	group[b]
acetic acid	3	−13.48	2.25	A
isobutyric acid	3	−17.78	3.78	A, B
decanoic acid	3	−22.84	1.84	B, C
isoamyl alcohol	3	−24.12	1.69	B, C D
hexanoic acid	3	−24.24	1.29	B, C, D
isobutyl alcohol	3	−24.47	0.40	B, C, D
octanoic acid	3	−24.63	1.19	B, C, D
ethyl octanoate	3	−24.80	1.97	B, C, D
ethyl lactate	2	−25.84	0.46	B, C, D, E, F
1-butanol	3	−25.89	2.03	C, D, E
ethyl hexanoate	3	−25.94	1.88	C, D, E
ethyl 3-hydroxybutyrate	3	−27.02	2.74	C, D, E, F
ethanol	3	−27.47	0.10	C, D, E, F
isoamyl acetate	3	−28.58	2.15	C, D, E, F
hexyl acetate	3	−29.15	7.55	C, D, E, F
methionol	3	−29.40	0.59	C, D, E, F
β-phenylethanol	3	−31.29	0.86	D, E, F
phenylethyl acetate	3	−33.97	1.66	F
1-hexanol	2	−34.19	0.21	E, F

[a]Results are for means and standard deviations of fermentation replicates. [b]Compounds with different letters differ at $p < 0.05$ level (Tukey's test).

dx.doi.org/10.1021/jf500947x | J. Agric. Food Chem. 2014, 62, 6820−6827

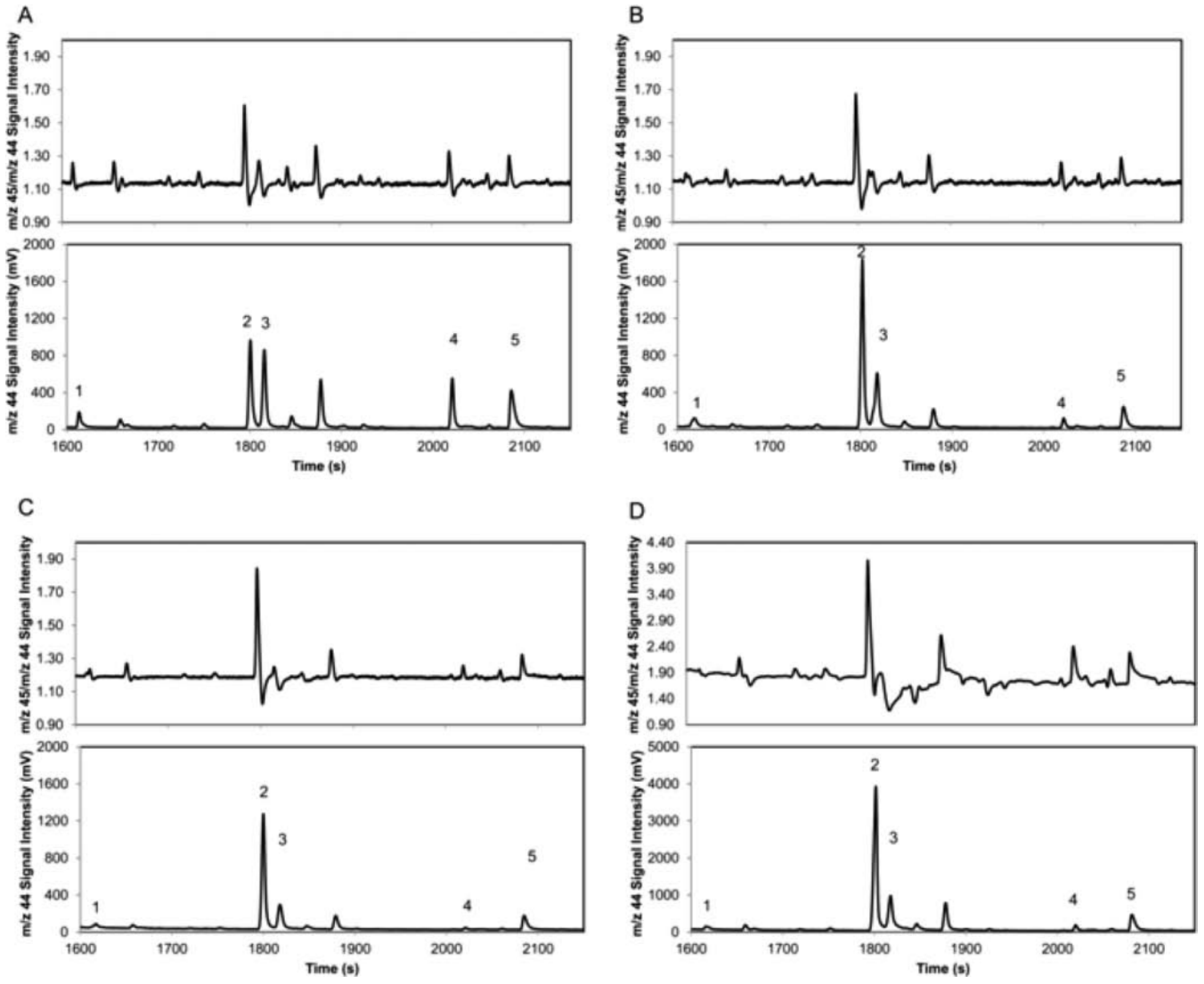

Figure 1. IRMS chromatograms of wine extract at different levels of ^{13}C enrichment: (A) control; (B) 0.01% [U-^{13}C]-glucose; (C) 0.1% [U-^{13}C]-glucose; (D) 1.0% [U-^{13}C]-glucose. The m/z 44 and 45 signals represent CO_2 ions containing ^{12}C and ^{13}C, respectively, from aroma compounds after separation and combustion. The top trace of each chromatogram depicts the 45/44 ratio. Peak identification: 1, hexyl acetate; 2, ethyl lactate; 3, hexanol; 4, ethyl octanoate; 5, acetic acid.

differences were observed in natural abundance isotope ratios among volatile compounds, and $\delta^{13}C$ values ranged from −13 to −35‰. Fewer compounds were characterized by GC-C-IRMS than were quantified by GC-MS because the combustion step of GC-C-IRMS converts all compounds to CO_2; thus, coeluting peaks cannot be resolved as they can be in GC-MS through use of a unique m/z ion to quantify each compound.[14] Precision, calculated as the standard deviation (SD) of $\delta^{13}C$ values (‰) from fermentation replicates, ranged from ±0.1‰ (ethanol) to ±7.5‰ (hexyl acetate), with a mean value of ±1.9‰. This precision is lower than that for benchmark values for high-precision GC-C-IRMS, SD ($\delta^{13}C$) < 0.4‰,[26] because it reflects biological variability among the fermentation replicates rather than analytical variability alone. We observed much better precision, SD ($\delta^{13}C$) < 1.4‰, for analytical replicates of the same fermentation samples. The higher precision observed for ethanol likely reflects the fact that it is the major fermentation product throughout alcoholic fermentation, and, thus, should be less prone to fractionation. Furthermore, the sample preparation did not require extraction. By comparison, many of the other volatiles in Table 2 account for <0.1% of the initial hexose substrate and thus may be more sensitive to changes in conditions among fermentation replicates.

The isotope ratio of ethanol ($\delta^{13}C$ = −27.47‰) was within the range typically observed for wine[29] and was depleted with respect to the isotope ratio for the bulk grape juice ($\delta^{13}C$ = −26.57‰). The depletion of ethanol and concurrent enrichment of CO_2 with respect to the sugar substrate has been previously reported and is believed to occur because ethanol is derived from the C-1, C-2, C-5, and C-6 positions of hexoses, which are depleted with respect to the C-3 and C-4 positions.[30] Several short- and mid-chain fatty acids (acetic, isobutyric, and decanoic) were enriched with respect to ethanol, as has been previously reported.[28] These volatile fatty acids are produced by yeast toward the end of fermentation.[31] Because lighter isotopes of sugars are metabolized preferentially during fermentation,[32] the observed effect may be due to enrichment of the hexose pool by the time the majority of these fatty acids are formed. However, as mentioned under Materials and

dx.doi.org/10.1021/jf500947x | J. Agric. Food Chem. 2014, 62, 6820−6827

Methods, this fractionation effect is small and constant and thus will not compromise results from labeling studies. Most other volatiles, including fusel alcohols, ethyl esters, and several acetate esters, did not differ significantly in isotope ratio from ethanol. The most depleted compound measured was 1-hexanol ($\delta^{13}C = -34.19‰$). As discussed in the next section, this is likely because hexanol is primarily derived from the ^{13}C-depleted grape lipid fraction[29] as opposed to being synthesized by yeast from sugars. Phenylethyl acetate was also significantly depleted with respect to ethanol, although the reason for this was unclear.

Determination of Hexose Contribution to Volatiles through Tracer Experiments. Typical chromatograms obtained at different levels of [U-^{13}C]-glucose enrichment are shown in Figure 1. With increasing enrichment of the hexose pool the m/z 45 trace increased relative to the m/z 44 trace for compounds such as ethyl lactate that derive most of their carbon from sugar. The 45/44 ratio for compounds that are derived primarily from grape compounds other than sugars, such as hexanol, did not change significantly. APE_{obsd} of volatile compounds in each fermentation experiment were calculated using eq 7, and the percent of carbon derived from the hexose pool was calculated by plotting APE_{obsd} versus APE_{hex} (eq 9). Representative plots are shown in Figure 2 for octanoic acid,

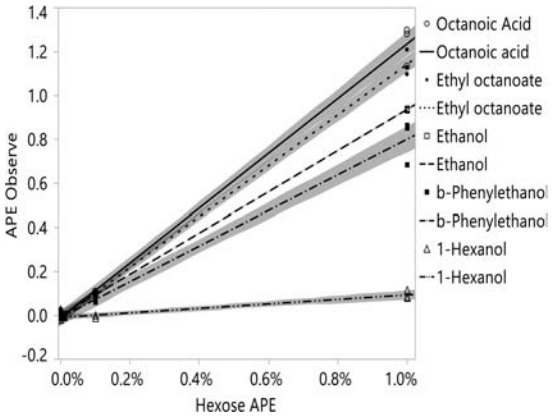

Figure 2. Linear regression of observed APE versus hexose APE. Shaded areas represent the 95% confidence interval.

ethyl octanoate, ethanol, β-phenylethanol, and 1-hexanol, where the slope represents the percent of carbon within a compound derived from the hexose pool. Figure 3 and Supplementary Table 1 in the Supporting Information report the fraction of carbon derived from hexose in each volatile compound. The error associated with measurements of percent hexose in individual compounds follows a similar pattern to what was observed in natural abundance studies.[16] The contribution of the hexose pool to ethanol, which is present in large quantities and represents a major fermentation product, can be determined with high confidence ($94 \pm 0.5\%$), whereas the error associated with low-concentration volatiles such as ethyl 3-hydroxybutyrate increases by an order of magnitude or greater.

The contribution of hexoses to ethanol (94%) was somewhat surprising, as it indicated that a small amount of non-hexose substrate contributed to ethanol formation. Excluding the possibility of impure standards or experimental error, one likely explanation is that fermentable sugars other than hexoses contributed to ethanol. In particular, sucrose is reported to be

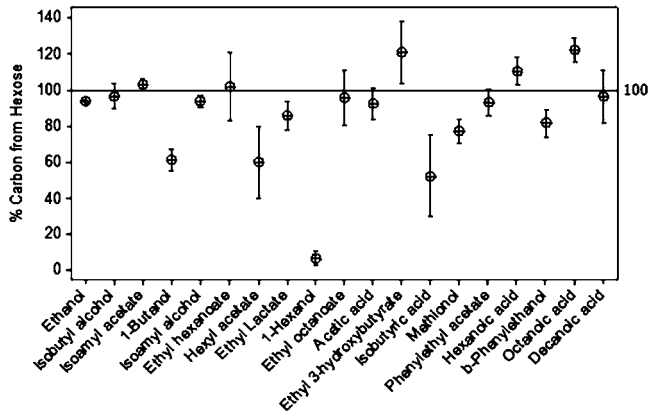

Figure 3. Contribution of hexose-derived carbon to each compound. The mean is indicated by the circles, and the error bars represent the 95% confidence interval.

present in musts at concentrations of 2−10 g/kg,[33] or up to 5% of the hexose concentration in our work. Unfortunately, sucrose was not measured, and it was not possible to evaluate this hypothesis.

Like ethanol, nearly all wine volatiles measured in our studies were derived primarily from hexoses (Figure 3 and Supporting Information Supplementary Table 1). Notably, fusel alcohols associated with amino acid metabolism (e.g., methionol, β-phenylethanol, isoamyl alcohol, isobutyl alcohol) were >75% hexose derived. The acetate esters (isoamyl acetate, phenylethyl acetate) are formed by acetylation of fusel alcohols and were also derived primarily from hexoses. This indicates that the major contributor to these fusel alcohols is the anabolic pathway, in which carbon skeletons are synthesized de novo from hexoses,[7] as opposed to catabolism of amino acids via the Ehrlich pathway.[8] A third potential source for β-phenylethanol is from juice in either a free or glycosylated form, although, based on data from a previous study, this could account for only 3% of the total β-phenylethanol observed.[34] To our knowledge, this is the first time that the relative contributions of different pathways to fusel alcohols in a wine fermentation have been evaluated. Whereas the values observed here are likely dependent on fermentation conditions such as yeast strain, our observation that the anabolic pathway is dominant is consistent with the amounts of fusel alcohols produced and the typical concentrations of amino acids in must available for Ehrlich degradation. For example, we observed ca. 100 mg/L of isoamyl alcohol in wine, whereas typical leucine concentrations in juice are reported to be <25 mg/L.[35] Although glucose labeling studies have not, to our knowledge, been previously performed on wine fermentations, [U-^{14}C]-glucose has been used to track production of fusel alcohols in grain mash fermentations.[16] In the earlier work, 25−45% of fusel alcohols were derived from glucose (no replicates), substantially less than in our current study. The discrepancy may be because the mash fermentation was performed at lower gravity, which would have decreased the relative importance of the anabolic pathway once amino acid sources were exhausted.

The high contribution (>90%) of the hexose pool to straight-chain fatty acids (hexanoic, octanoic, and decanoic) and their corresponding ethyl esters (ethyl hexanoate and ethyl octanoate) was as expected; these compounds are known to be produced by yeast fatty acid metabolism and, in the case of ethyl esters, through subsequent esterification with ethanol.[7]

Interestingly, two of the fatty acids (octanoic and hexanoic) and ethyl 3-hydroxybutyrate had apparent hexose contributions slightly but significantly greater than 100% (103−121%). Because these semipolar compounds demonstrated slight tailing and because GC-C-IRMS peak tails are ^{13}C depleted, hexose contributions of more than 100% may be an analytical artifact. Unlike the straight-chain fatty acids, only about half of the branched-chain isobutyric acid was derived from the hexose pool (Supporting Information Supplementary Table 1). Branched-chain fatty acids have been shown to decrease with supplementation of must with ammonia salts,[36] suggesting that they may arise from catabolism of amino acids.[37] This result may indicate that a significant portion of isobutyric acid arises from valine catabolism with the fermentation conditions employed.

Only one compound, 1-hexanol, was derived primarily from non-hexose sources. Although hexanol is generally present at concentrations of ≥1 mg/L in wine, alcoholic fermentation of juice-like media in the absence of non-sugar-grape derived compounds results in no detectable hexanol.[6] Hexanol is detectable in grape must and can also be produced during fermentation by the reduction of C_6 aldehydes and unsaturated C_6 alcohols.[38] These C_6 compounds are largely derived from enzymatic oxidation of unsaturated fatty acids during grape crushing.[39] Unsaturated fatty acids, along with other lipids, are known to be ^{13}C-depleted in plants,[40] a result which correlates with our previous observation that native hexanol is depleted as compared to other wine volatiles (Table 2). Hexyl acetate, formed by enzymatic esterification of hexanol,[41] is enriched to the level predicted by the mass balance of acetic acid and hexanol (Table 2).

Recommended Enrichment Levels for GC-C-IRMS Studies of Fermentations. The precision of GC-C-IRMS depends not only on the precision of the analytical instrumentation but also on the concentration of the compound of interest, the ^{13}C enrichment level, and the degree of biological variability. The fermentations were enriched with 0.01, 0.1, and 1.0% [U-^{13}C]-glucose, corresponding to roughly +11, +110, and +1100‰ maximal possible enrichments in volatiles, respectively. The average SD values for the three enrichment treatments were 1.7, 6.4, and 53.4‰ across increasing enrichment treatments. Defining the limit of detection as 3 times the noise, the smallest contribution of hexose to a volatile compound would be APE_{obsd} = 46, 17, and 15 for the 0.01, 0.1, and 1.0 APE treatments, although this will vary among compounds. Because of the marginal improvements associated with using 1.0 APE and the high costs of [U-^{13}C]-glucose, using 0.1 APE provides the best balance of cost and variability. For 500 mL fermentations containing 100 g of hexose per 500 mL of must, generating 0.1 APE requires 0.1 g of [U-^{13}C]-glucose, or $15 per fermentation at current prices of $150 per gram of [U-$^{13}C$]-glucose. Lower tracer levels may be possible, but will require limiting variability across replicates.

In conclusion, this study is the first evaluation of a method utilizing GC-C-IRMS to trace the origin of volatile compounds during the fermentation of grape juice into wine by enriching the hexose pool with ^{13}C. Under the conditions studied, the majority of fermentation volatiles studied, including most esters, fatty acids, and alcohols, derive at least 50% of their carbon from hexoses. Hexanol was the only compound observed to be majority (>90%) derived from grape compounds other than sugars. Using 0.1 APE of [U-^{13}C]-glucose provides the optimal balance between precision and cost. In future studies, the effects of varying physiological conditions, such as temperature, soluble solids concentration, and nutrient status, on the relative importance of different pathways could be quantified by this approach, assuming adequate analytical performance. This method could also be applied to other complex food systems, such as Maillard reactions, to clarify the contributions of different pathways while minimizing costs.

■ ASSOCIATED CONTENT

Ⓢ Supporting Information

Supplementary Table 1. This material is available free of charge via the Internet at http://pubs.acs.org.

■ AUTHOR INFORMATION

Corresponding Author

*(G.L.S.) E-mail: gls9@cornell.edu. Phone: (607) 592-1504.

Notes

The authors declare no competing financial interest.

■ REFERENCES

(1) Ferreira, V. Volatile aroma compounds and wine sensory attributes. In *Managing Wine Quality*; Reynolds, A. G., Ed.; Woodhead Publishing: Oxford, UK, 2010.

(2) Siebert, T. E.; Wood, C.; Elsey, G. M.; Pollnitz, A. P. Determination of rotundone, the pepper aroma impact compound, in grapes and wine. *J. Agric. Food Chem.* **2008**, *56*, 3745−3748.

(3) Nelson, R.; Acree, T.; Lee, C.; Butts, R. Methyl anthranilate as an aroma constituent of American wine. *J. Food Sci.* **1977**, *42*, 57−59.

(4) Baumes, R. Wine aroma precursors. In *Wine Chemistry and Biochemistry*; Moreno-Arribas, M. V., Polo, M. C., Eds.; Springer Science + Business Media: Berlin, Germany, 2009; p 251.

(5) Capone, D. L.; Van Leeuwen, K.; Taylor, D. K.; Jeffery, D. W.; Pardon, K. H.; Elsey, G. M.; Sefton, M. A. Evolution and occurrence of 1,8-cineole (eucalyptol) in Australian wine. *J. Agric. Food Chem.* **2011**, *59*, 953−959.

(6) Ugliano, M.; Bartowsky, E. J.; McCarthy, J.; Moio, L.; Henschke, P. A. Hydrolysis and transformation of grape glycosidically bound volatile compounds during fermentation with three *Saccharomyces* yeast strains. *J. Agric. Food Chem.* **2006**, *54*, 6322−6331.

(7) Ugliano, M.; Henschke, P. A. Yeasts and wine flavor. In *Wine Chemistry and Biochemistry*; Moreno-Arribas, M. V., Polo, M. C., Eds.; Springer Science + Business Media: Berlin, Germany, 2009; p 314.

(8) Hazelwood, L. A.; Daran, J. M.; van Maris, A. J. A.; Pronk, J. T.; Dickinson, J. R. The Ehrlich pathway for fusel alcohol production: a century of research on *Saccharomyces cerevisiae* metabolism. *Appl. Environ. Microbiol.* **2008**, *74*, 2259.

(9) Hernandez-Orte, P.; Ibarz, M.; Cacho, J.; Ferreira, V. Addition of amino acids to grape juice of the Merlot variety: effect on amino acid uptake and aroma generation during alcoholic fermentation. *Food Chem.* **2006**, *98*, 300−310.

(10) Hernández-Orte, P.; Ibarz, M.; Cacho, J.; Ferreira, V. Effect of the addition of ammonium and amino acids to musts of Airen variety on aromatic composition and sensory properties of the obtained wine. *Food Chem.* **2005**, *89*, 163−174.

(11) Garde-Cerdan, T.; Ancin-Azpilicueta, C. Effect of the addition of different quantities of amino acids to nitrogen-deficient must on the formation of esters, alcohols, and acids during wine alcoholic fermentation. *Lebensm.-Wiss. Technol.* **2008**, *41*, 501.

(12) Schieberle, P. The Carbon Module Labeling (CAMOLA) technique: a useful tool for identifying transient intermediates in the formation of Maillard-type target molecules. *Ann. N.Y. Acad. Sci.* **2005**, *1043*, 236−248.

(13) Diaz-Maroto, M. C.; Schneider, R.; Baumes, R. Formation pathways of ethyl esters of branched short-chain fatty acids during wine aging. *J. Agric. Food Chem.* **2005**, *53*, 3503−3509.

(14) Brenna, J. T. High-precision gas isotope ratio mass spectrometry: recent advances in instrumentation and biomedical applications. *Acc. Chem. Res.* **1994**, *27*, 340−346.
(15) Zimman, A.; Waterhouse, A. L. Incorporation of malvidin-3-glucoside into high molecular weight polyphenols during fermentation and wine aging. *Am. J. Enol. Vitic.* **2004**, *55*, 139−146.
(16) Reazin, G.; Scales, H.; Andreasen, A. Mechanism of major congener formation in alcoholic grain fermentations. *J. Agric. Food Chem.* **1970**, *18*, 585−589.
(17) Reid, L. M.; O'Donnell, C. P.; Downey, G. Recent technological advances for the determination of food authenticity. *Trends Food Sci. Technol.* **2006**, *17*, 344−353.
(18) Asche, S.; Michaud, A. L.; Brenna, J. T. Sourcing organic compounds based on natural isotopic variations measured by high precision isotope ratio mass spectrometry. *Curr. Org. Chem.* **2003**, *7*, 1527−1543.
(19) Goodman, K. J.; Brenna, J. T. High sensitivity tracer detection using high-precision gas chromatography-combustion isotope ratio mass spectrometry and highly enriched uniformly carbon-13 labeled precursors. *Anal. Chem.* **1992**, *64*, 1088−1095.
(20) Baumes, R.; Wirth, J.; Bureau, S.; Gunata, Y.; Razungles, A. Biogeneration of C13-norisoprenoid compounds: experiments supportive for an apo-carotenoid pathway in grapevines. *Anal. Chim. Acta* **2002**, *458*, 3−14.
(21) Ortega, C.; Lopez, R.; Cacho, J.; Ferreira, V. Fast analysis of important wine volatile compounds: development and validation of a new method based on gas chromatographic-flame ionisation detection analysis of dichloromethane microextracts. *J. Chromatogr., A* **2001**, *923*, 205−214.
(22) Wang, M.; Choong, Y.; Su, N.; Lee, M. A rapid method for determination of ethanol in alcoholic beverages using capillary gas chromatography. *J. Food Drug Anal.* **2003**, *11*, 133−140.
(23) Zhang, Y.; Tobias, H. J.; Brenna, J. T. Steroid isotopic standards for gas chromatography-combustion isotope ratio mass spectrometry (GCC-IRMS). *Steroids* **2009**, *74*, 369−378.
(24) Santrock, J.; Studley, S. A.; Hayes, J. Isotopic analyses based on the mass spectra of carbon dioxide. *Anal. Chem.* **1985**, *57*, 1444−1448.
(25) Caimi, R. J.; Houghton, L. A.; Brenna, J. T. Condensed-phase carbon isotopic standards for compound-specific isotope analysis. *Anal. Chem.* **1994**, *66*, 2989−2991.
(26) Brenna, J. T.; Corso, T. N.; Tobias, H. J.; Caimi, R. J. High-precision continuous-flow isotope ratio mass spectrometry. *Mass Spectrom. Rev.* **1997**, *16*, 227−258.
(27) Zamora, F. Biochemistry of alcoholic fermentation. In *Wine Chemistry and Biochemistry*; Moreno-Arribas, M. V., Polo, M. C., Eds.; Springer Science + Business Media: Berlin, Germany, 2009; p 3.
(28) Spitzke, M. E.; Fauhl-Hassek, C. Determination of the $^{13}C/^{12}C$ ratios of ethanol and higher alcohols in wine by GC-C-IRMS analysis. *Eur. Food Res. Technol.* **2010**, *231*, 247−257.
(29) Hobbie, E. A.; Werner, R. A. Intramolecular, compound-specific, and bulk carbon isotope patterns in C3 and C4 plants: a review and synthesis. *New Phytol.* **2004**, *161*, 371−385.
(30) Rossmann, A.; Butzenlechner, M.; Schmidt, H. Evidence for a nonstatistical carbon isotope distribution in natural glucose. *Plant Physiol.* **1991**, *96*, 609−614.
(31) Viegas, C. A.; Rosa, M. F.; Sá-Correia, I.; Novais, J. M. Inhibition of yeast growth by octanoic and decanoic acids produced during ethanolic fermentation. *Appl. Environ. Microbiol.* **1989**, *55*, 21−28.
(32) Hunkeler, D.; Andersen, N.; Aravena, R.; Bernasconi, S. M.; Butler, B. J. Hydrogen and carbon isotope fractionation during aerobic biodegradation of benzene. *Environ. Sci. Technol.* **2001**, *35*, 3462−3467.
(33) Margalit, Y. *Concepts in Wine Chemistry*; Crum, J. D., Ed.; Wine Appreciation Guild: San Francisco, CA, USA, 2004.
(34) Ugliano, M.; Moio, L. Free and hydrolytically released volatile compounds of *Vitis vinifera* L. cv. Fiano grapes as odour-active constituents of Fiano wine. *Anal. Chim. Acta* **2008**, *621*, 79−85.
(35) Ough, C.; Huang, Z.; An, D.; Stevens, D. Amino acid uptake by four commercial yeasts at two different temperatures of growth and fermentation: effects on urea excretion and reabsorption. *Am. J. Enol. Vitic.* **1991**, *42*, 26−40.
(36) Vilanova, M.; Ugliano, M.; Varela, C.; Siebert, T.; Pretorius, I. S.; Henschke, P. A. Assimilable nitrogen utilisation and production of volatile and non-volatile compounds in chemically defined medium by Saccharomyces cerevisiae wine yeasts. *Appl. Microbiol. Biotechnol.* **2007**, *77*, 145−157.
(37) Styger, G.; Prior, B.; Bauer, F. F. Wine flavor and aroma. *J. Ind. Microbiol. Biotechnol.* **2011**, *38*, 1145−1159.
(38) Herraiz, T.; Herraiz, M.; Reglero, G.; Martin-Alvarez, P. J.; Cabezudo, M. D. Changes in the composition of alcohols and aldehydes of C6 chain length during the alcoholic fermentation of grape must. *J. Agric. Food Chem.* **1990**, *38*, 969−972.
(39) Joslin, W.; Ough, C. Cause and fate of certain C6 compounds formed enzymatically in macerated grape leaves during harvest and wine fermentation. *Am. J. Enol. Vitic.* **1978**, *29*, 11−17.
(40) Chikaraishi, Y.; Naraoka, H.; Poulson, S. R. Hydrogen and carbon isotopic fractionations of lipid biosynthesis among terrestrial (C3, C4 and CAM) and aquatic plants. *Phytochemistry* **2004**, *65*, 1369−1381.
(41) Dennis, E. G.; Keyzers, R. A.; Kalua, C. M.; Maffei, S. M.; Nicholson, E. L.; Boss, P. K. Grape contribution to wine aroma: production of hexyl acetate, octyl acetate, and benzyl acetate during yeast fermentation is dependent upon precursors in the must. *J. Agric. Food Chem.* **2012**, *60*, 2638−2646.

Table 1. Chemical Structures of Flavanols in Extracts from GTL

Chemical structure		Flavanol	R1	R2	R3	Molecular Weight
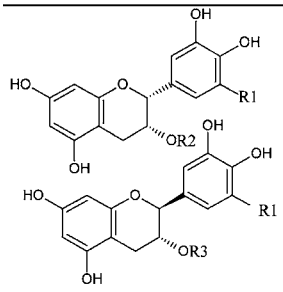	Epicatechins	Epicatechin (EC)	H	H		290.27
		Epicatechin gallate (ECG)	H	Gallate		442.37
		Epigallocatechin gallate (EGCG)	OH	Gallate		458.37
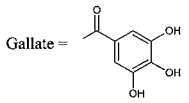	Epicatechin epimers	Catechin (Ct)	H		H	290.27
		Catechin gallate (CG)	H		Gallate	442.37
		Gallocatechin gallate (GCG)	OH		Gallate	458.37

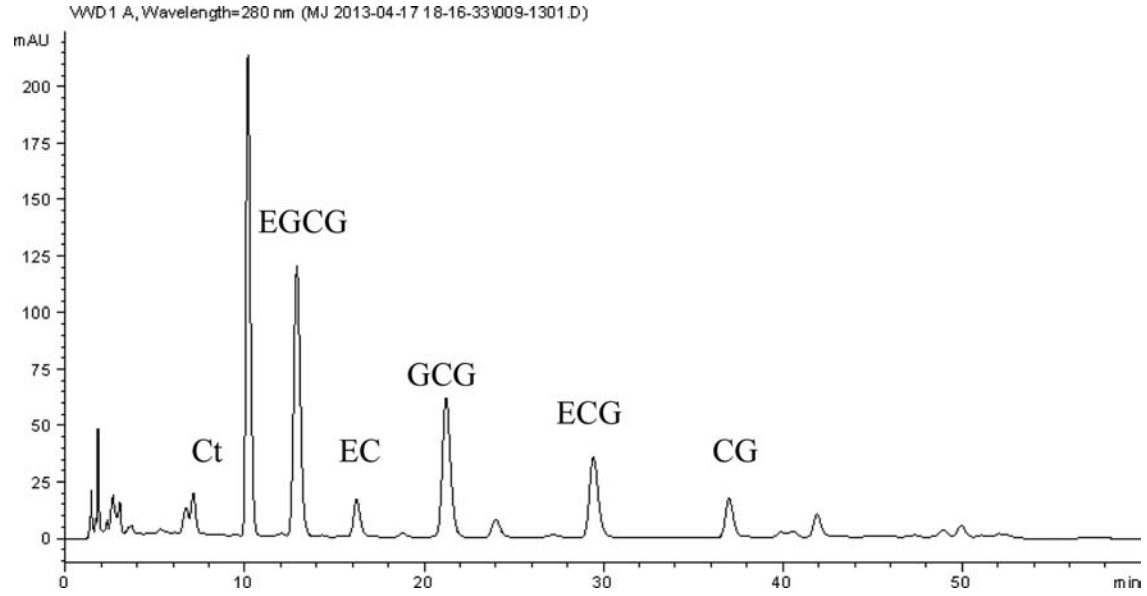

Figure 1. HPLC chromatograms of flavanols from GTL. Flavanol extracts: Ct, EGCG, EC, GCG, ECG, and CG.

the oven. The resultant extracts (about 30 mL) were collected into glass vials. All aqueous SWE extracts were dried with the aid of a freeze-dryer for 24 h (Ilshin, Gyeonggi-do, Korea). The solid content of the SWE extracts was typically 0.3−0.4 g/g GTL. The pressure was maintained at around 10 MPa during SWE. The extraction time and temperature conditions were varied in separate experiments using only purified water as follows: extraction temperatures of 110, 130, 150, 170, and 190 °C and extraction times of 5, 10, and 15 min. A factorial design therefore produced 15 conditions for GTL. The temperature and time conditions giving the maximum extraction efficiency were selected as optimum conditions for several plants.

For the conventional extractions, 98% ethanol (Samchun Pure Chemicals, Seoul, Korea) and 99.8% methanol (Duksan Pure Chemicals, Ansan, Korea) were used at 60 °C for 2 h with 22 mL of solvent and 1 g of GTL in the water bath (C-WB1, Changshin Scientific, Seoul, Korea).

High-Performance Liquid Chromatography. The extracts were simply pretreated and then qualitatively and quantitatively analyzed by high-performance liquid chromatography (HPLC; 1260 series, Agilent Technologies, Waldbronn, Germany) with a Zorbax C18 column (4.6 mm × 150 mm, 5 μm pore size; Agilent Technologies), using a modified version of the method described by Choung and Lee.[13] For analysis of the six kinds of flavanols studied herein, the samples were pretreated with 0.1 g of freeze-dried extract with 20 mL of a purified water/ethanol (Duksan Pure Chemicals)/phosphoric acid (Samchun Pure Chemicals, Pyeongtaek, Korea) solution (48:50:2, v/v). The samples were then mixed well in a vortex mixer for 10 min prior to HPLC analysis. The HPLC mobile phase used for analysis comprised 0.1% phosphoric acid in water (solvent A) and methanol (solvent B) at a flow rate of 1.0 mL/min, with an initial A:B ratio of 80:20%. The proportion of solvent A was subsequently changed as follows: to 75% for 25 min, then to 65% for 25 min, and finally to 75% for 10 min in the analysis. Ten-microliter aliquots were injected into the HPLC system, and detection was performed at 280 nm. The resulting extracts were filtered through a 0.45 μm polyvinylidene filter (Whatman) and then analyzed by HPLC.

Data Analysis. The extraction yield (expressed in units of mg/g dried plant material) was calculated from the calibration curves of the standard flavanols. All peak chromatograms of the extracts were identified qualitatively by spiking experiments. The optimum SWE

dx.doi.org/10.1021/jf5012006 | J. Agric. Food Chem. 2014, 62, 6828−6833

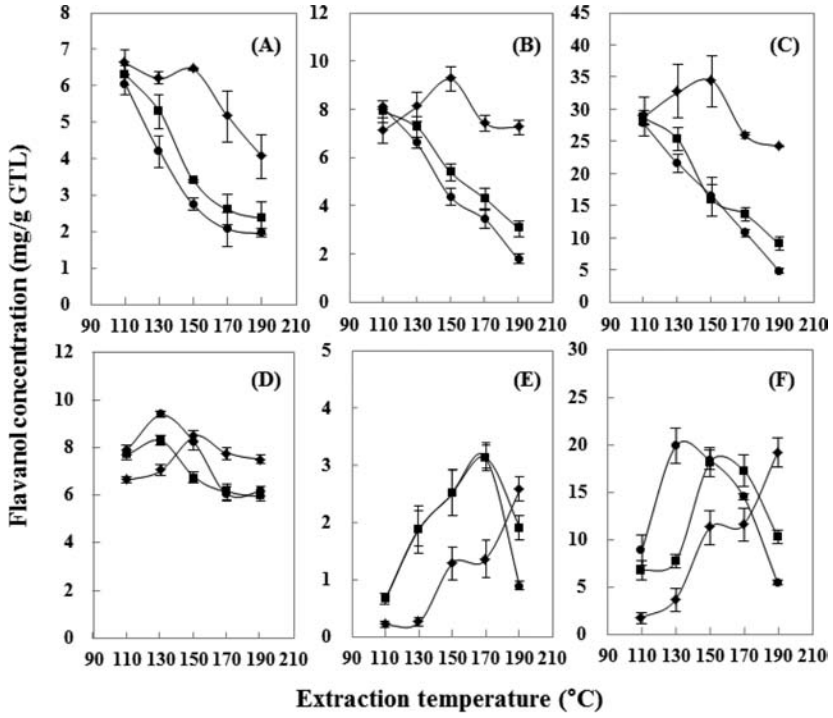

Figure 2. Effect of temperature on the SWE of the epicatechins EC (A), ECG (B), and EGCG (C) and the epimers Ct (D), CG (E), and GCG (F) for extraction times of 5 (◆), 10 (■), and 15 min (●). All of the experiments were conducted in triplicate. Data are the mean and SD values.

Table 2. Effect of Extraction Temperature and Time on the Yield of ECs and Epimers with Epimerization in Subcritical Water

			proportion of flavanol (%)				
compound		configuration	110 °C	130 °C	150 °C	170 °C	190 °C
			5 min				
epicatechin	EC	2*R*,3*R*	49.99	46.93	43.25	40.04	35.21
epimer	Ct	2*S*,3*R*	50.01	53.07	56.75	59.96	64.79
epicatechin	ECG	2*R*,3*R*	97.13	96.96	87.81	84.54	73.78
epimer	CG	2*S*,3*R*	2.87	3.04	12.19	15.46	26.22
epicatechin	EGCG	2*R*,3*R*	94.30	89.88	75.36	69.15	55.99
epimer	GCG	2*S*,3*R*	5.70	10.12	24.64	30.85	44.01
			10 min				
epicatechin	EC	2*R*,3*R*	44.96	38.96	33.66	29.87	28.47
epimer	Ct	2*S*,3*R*	55.04	61.04	66.34	70.13	71.53
epicatechin	ECG	2*R*,3*R*	92.33	79.43	68.30	57.67	61.80
epimer	CG	2*S*,3*R*	7.67	20.57	31.70	42.33	38.20
epicatechin	EGCG	2*R*,3*R*	81.02	76.76	46.90	44.24	47.14
epimer	GCG	2*S*,3*R*	18.98	23.24	53.10	55.76	52.86
			15 min				
epicatechin	EC	2*R*,3*R*	43.34	30.92	24.99	25.53	24.09
epimer	Ct	2*S*,3*R*	56.66	69.08	75.1	74.47	75.91
epicatechin	ECG	2*R*,3*R*	90.11	72.23	60.95	58.32	64.76
epimer	CG	2*S*,3*R*	9.89	27.77	39.05	41.68	35.24
epicatechin	EGCG	2*R*,3*R*	75.97	52.17	47.24	42.92	46.97
epimer	GCG	2*S*,3*R*	24.03	47.83	52.76	57.08	53.03

conditions, in terms of the extraction temperature and extraction time, for GTL were chosen on the basis of the highest flavanol contents.

RESULTS AND DISCUSSION

HPLC Analysis for Flavanols from GTL. The obtained extracts were analyzed qualitatively and quantitatively by HPLC. The calibration indicated a highly linear regression of the peak areas versus concentrations of each standard (R^2 value of 1 for EC, ECG, EGCG, Ct, and CG, and of 0.998 for GCG). Figure 1 shows the chromatograms of the six different flavanol extracts from GTL.

Optimization of SWE Conditions for Extraction of the Six Flavanols. SWE was performed at temperatures between 110 and 190 °C and for processing times of 5−15 min to

dx.doi.org/10.1021/jf5012006 | J. Agric. Food Chem. 2014, 62, 6828−6833

determine the optimum temperature and time for the extraction of the precursor epicatechins (EC, ECG, and EGCG) and the epicatehin epimers (Ct, CG, and GCG) from GTL. The results obtained for the flavanols are presented in Figure 2. The SWE yields of the epicatechins were clearly time-dependent, being unstable at extraction times >5 min, whereas those of the epimers were both time- and temperature-dependent. The optimum SWE temperature/time conditions for EC, ECG, EGCG, Ct, CG, and GCG were 110 °C/5 min, 150 °C/5 min, 150 °C/5 min, 130 °C/15 min, 170 °C/10 min, and 130 °C/15 min, respectively. The extraction of total flavanols was notably degraded at temperatures >150 °C. These results are analogous to those of Yang and Hildebrand,[14] who found that temperatures >190 °C resulted in degradation, oxidation, and odorous extracts of flavonoids such as flavanols.

The efficiency of flavanol extraction depends upon factors such as the type of solvent, extraction temperature, extraction time, ratio of solvent to solute, and sample particle size. In the present study, the effects of SWE temperature and processing time on flavonol yields from GTL were investigated. The major flavanols extracted from GTL were EGCG and GCG. As shown in Figure 2, the concentration of EGCG extracted decreased dramatically for longer extraction times. The SWE yield of the other epicatechins, EC and ECG, was also time-dependent. However, the concentration of GCG first increased and then decreased with a 15 min extraction time. The SWE yields of the epimers Ct and CG were dependent upon both processing temperature and time. These results are similar to those of Vuong et al.,[15] who found that the epicatechin structure was more unstable than the epimer structure at temperatures >80 °C.

Effect of Epimerization of Flavanols on Subcritical Water. The epicatechins (EC, ECG, and EGCG) and epimers (Ct, CG, and GCG) can in part be converted back to their isomers via a process of epimerization. An epimerization change is likely to occur in a high-temperature environment, such as when using SWE, because heating results in the conversions of EGCG to GCG, ECG to CG, and EC to Ct.[16−18]

Table 2 lists the effects of extraction time and temperature on the epimerization of flavanols in subcritical water. The proportion of flavanol was calculated as follows:

$$\text{proportion of flavanol (\%)} = \text{compound concentration}/(\text{compound concentration} + \text{their isomer concentration}) \times 100$$

The conversion of flavanols to their isomers is reversible, but flavanols are usually only epimerized from ECs (2*R*,3*R*) to epimers (2*S*,3*R*) under high-temperature and high-pressure conditions with a long extraction time. As indicated by the results in Table 2, epimerization was accelerated over a long extraction time, thus reducing the proportions of ECs but gradually increasing those of epimers. In addition, ECs were epimerized more rapidly at higher extraction temperatures, thus again reducing the proportions of ECs and increasing those of epimers. However, at temperatures >170 °C there was very little epimerization, so that any remaining flavanols were destroyed.

Figure 3 shows a typical phase diagram for the SWE of flavanol at different temperatures (110−190 °C). The extraction of flavanols can be divided into three phases (I, II, and III) on the basis of the predominating effect of extraction efficiency, epimerization, and destruction. In phase I there was a significant increase in epimer extraction efficiency by 150 °C. Furthermore,

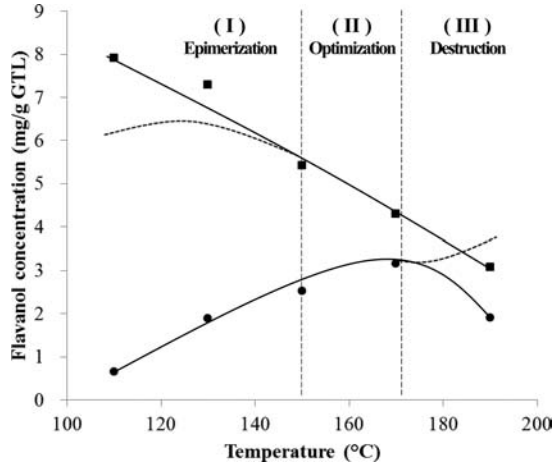

Figure 3. Typical phase diagram of ECs (■) and epimers (●) during SWE (solid line). The flavanol yield during a 5 min extraction time at various temperatures is shown (dotted-dashed line).

a few ECs were converted to epimers; in particular, the extraction efficiency of ECs for a short extraction time of 5 min (dotted-dashed line of phase I) was increased because the optimum extraction conditions had been reached and then subsequently decreased due to epimerization. In phase II there was an increase in the extraction efficiency of epimers continued to 170 °C, whereas that of ECs decreased. This means that most ECs were converted to epimers and the optimization of temperature for extracting epimers was attained, leading to some destruction at high temperature. In phase III, at extremely high temperatures the unstable flavanols, including both ECs and epimers, were destroyed. This is likely to have resulted in negligible epimerization of flavanols, with the exception of epimers at an extraction time of 5 min (dotted-dashed line of phase III), in which there was increased extraction due to epimerization of ECs. Therefore, extracting flavanols based on chemical structure is adequate for epimer structures such as Ct, CG, and GCG due to the epimerization of flavanols at high temperatures in subcritical water.

Comparison of Extraction Yields of Flavanols among Extraction Solvents. The adequacy of SWE relative to conventional extraction methods (using ethanol and methanol as solvents with extraction conditions of 60 °C and 2 h) was evaluated. As indicated in Figure 4, the maximum total yield of the six flavanols studied was 71.36 ± 4.23 mg/g GTL (mean ± SD) under extraction temperature/time conditions of 150 °C/5 min. The efficiency of SWE was slightly higher than that obtained using conventional extraction with either methanol (yield = 70.87 ± 0.57 mg/g GTL) or ethanol (yield = 60.43 ± 1.14 mg/g GTL).

The data presented in Figure 4 indicate that SWE is more effective at extracting epimers than epicatechins, which is due to the relatively high extraction temperature. The efficiency of SWE (yield = 21.69 ± 1.41 mg/g GTL) for epimers including Ct, CG, and GCG was higher than that of the conventional extraction solvents such as methanol (yield = 7.68 ± 0.09 mg/g GTL) and ethanol (yield = 6.98 ± 0.01 mg/g GTL). Therefore, the concentration of epimers greatly influences the efficiency of the total flavanols yield for optimize extraction conditions. GCG is an epimer of EGCG; an epimerization change is likely to occur in a high-temperature environment such as when using SWE, because heating results in the conversion of EGCG to GCG.[4] In the case of using organic solvents, small reductions were

dx.doi.org/10.1021/jf5012006 | J. Agric. Food Chem. 2014, 62, 6828−6833

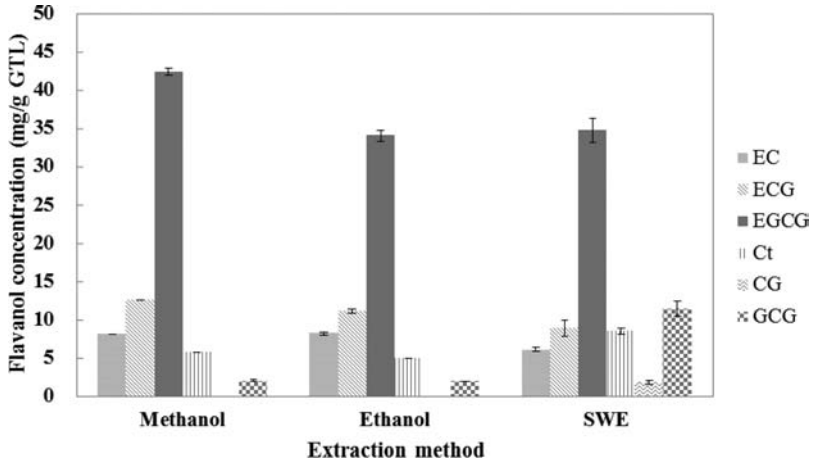

Figure 4. Comparison of yields of EC, ECG, EGCG, Ct, CG, and GCG obtained using conventional methanol and ethanol extraction methods (under temperature/time conditions of 60 °C/2 h) and SWE method (under temperature/time conditions of 150 °C/5 min). All experiments were conducted in triplicate. Data are the mean and SD values.

observed in the yield of unstable EGCG with long extraction times. The epimers Ct, CG, and GCG were poorly extracted with both methanol and ethanol. Because gallocatechin (GC) and epigallocatechin (EGC), which are known secondary major flavonols in green tea leaves, were very unstable at high operating temperatures (110−190 °C), the extraction yields by the SWE were not reproducible and those two compounds were excluded from consideration in this study. Wang and Helliwell[19] also reported that GC and EGC were taking place in other reactions such as oxidation or degradation for a given set of SWE conditions. Zhu et al.[20] and Yoshida et al.[5] demonstrated that flavanols in alkaline solutions were extremely unstable and degraded almost completely, whereas in acidic solutions they were stable. Although high extraction yields of other epicatechins could be obtained in SWE due to the relatively acidic character of subcritical water, GC and EGC were easily degraded at high temperature and the extraction yields of those two compounds did not influence the efficiency of the total flavanols yield.

Moreover, SWE has some excellent advantages: it is ecofriendly and nontoxic (using only purified water) and requires a shorter extraction time than conventional solvent-based methods, which make it an efficient recovery method.

Adequacy of Flavanol Extraction Based on Chemical Structure. The extraction of flavanols was affected by differences in physicochemical characteristics of the compounds, including their melting points and molecular weights. Flavanols have a lower melting point (at around 200 °C) than flavonoids.[16] Thus, EGCG, with the lowest melting point, has been considered too unstable to allow extraction.[21]

Flavanols including the gallates have large molecular weights and a stable structure. In addition, like gallate, gallic acid is soluble in alcohol, ether, acetone, and water (at 1.5 g/100 mL and 20 °C). Therefore, gallate catechins such as CG, GCG, ECG, and EGCG were extracted using subcritical water at higher optimum temperatures (i.e., >150 °C), indicating a relatively low dielectric constant.

The solubility in subcritical water is quantified by the solvent conditions and is influenced by the solute.[9] The polarity of the subcritical water solvent is determined by the dielectric constant (ε), which is lowered by increasing the temperature; less polar compounds can thus be extracted by subcritical water acting as an organic polar solvent.[22] Flavanols dissolve well in organic solvents such as ethanol;[23] however, flavanols with no oxygen molecule at position 4 were not adequate solutes at temperatures >170 °C in SWE. This finding is similar to that obtained with anthrone, whereby the presence of oxygen increases the solubility by 10 times over that of anthracene at SWE temperatures between 150 and 160 °C.[9] These results confirm that flavonols and flavanones that have an oxygen molecule at position 4 are more favorably extracted at higher temperatures than are flavanol catechins in SWE.[12] The yield of total flavanols from GTL was maximal under extraction temperature/time conditions of 150 °C/5 min. Pineiro et al.[24] also reported that the extraction of catechins and epicatechins from grape seeds was optimum under SWE conditions of 130 °C/10 min.

In addition, the chemical compositions and flavanols concentration of the extract obtained by SWE were compared with the initial composition of the original material. The proximate analysis including carbohydrates, protein, lipids, ash, fiber, catechins, and caffeine contents is presented in Table 3. These results indicate that approximately 86.26% of flavanols was recovered from the original GTL material. Especially, epicatechin epimers (Ct, CG, and GCG) of approximately 95.43% were extracted by using the SWE method from the initial GTL.

Table 3. Chemical Composition of the GTL Used in This Study and the Extracts Yielded by SWE[a]

component	/g GTL	/g freeze-dried SWE extracts
total carbohydrate (%)	36.67 ± 0.76	33.72 ± 2.23
crude protein (%)	15.03 ± 0.82	24.18 ± 0.52
crude lipids (%)	1.54 ± 0.14	1.54 ± 0.35
crude ash (%)	5.82 ± 0.07	17.59 ± 0.15
crude fiber (%)	35.93 ± 0.25	17.97 ± 2.22
EC (mg)	7.16 ± 0.21	6.05 ± 0.02
ECG (mg)	9.93 ± 0.37	8.89 ± 0.85
EGCG (mg)	42.90 ± 3.67	34.74 ± 3.52
Ct (mg)	9.02 ± 0.41	8.52 ± 0.19
CG (mg)	2.01 ± 0.02	1.76 ± 0.29
GCG (mg)	11.71 ± 0.93	11.42 ± 1.80
caffeine (mg)	24.23 ± 0.55	12.36 ± 0.56

[a]SWE was operated under optimum extraction temperature/time conditions of 150 °C/5 min. Data are the mean ± SD values of at least three measurements.

dx.doi.org/10.1021/jf5012006 | J. Agric. Food Chem. 2014, 62, 6828−6833

The ecofriendly SWE of flavanols is affected by both the subcritical-water solvent and the structure of the compounds. Flavanols lacking an oxygen molecule at position 4 are not adequate solutes at temperatures above 170 °C in SWE. However, the SWE was found to be slightly more efficient than extraction with two conventional solvents. SWE of the epicatechins EC, EGCG, and ECG was time-dependent, and SWE of the epimer catechins Ct, GCG, and CG was both temperature- and time-dependent. In addition, SWE appears to be a more effective solvent for extracting epimers compared to the precursor epicatechins. Thus, SWE appears to be an environmentally friendly, nontoxic, efficient, and selective extraction method that requires shorter extraction times than its conventional organic-solvent counterpart. SWE could have practical applications in the effective extraction of antioxidant polyphenolic compounds from various types of plant. Furthermore, this method can be easily implemented on an industrial scale.

AUTHOR INFORMATION

Corresponding Author

*(M.-S.C.) Phone: +82-2-32774508. Fax: +82-2-32774508. E-mail: mschung@ewha.ac.kr.

Funding

This research was supported by the Basic Science Research Program through the National Research Foundation of Korea (NRF) funded by the Ministry of Education (No. 2013R1A1A2A10060325).

Notes

The authors declare no competing financial interest.

ABBREVIATIONS USED

Ct, catechin; CG, catechin gallate; EC, epicatechin; ECG, epicatechin gallate; EGC, epigallocatechin; EGCG, epigallocatechin gallate; GC, gallocatechin; GCG, gallocatechin gallate; GTL, green tea leaves; HPLC, high-performance liquid chromatography; SWE, subcritical-water extraction

REFERENCES

(1) Fujiki, H. Two stages of cancer prevention with green tea. *J. Cancer Res. Clin.* **1999**, *125*, 589−597.

(2) Higdon, J.; Frei, B. Tea catechins and polyphenols: health effects, metabolism, and antioxidant functions. *Crit. Rev. Food Sci.* **2003**, *43*, 89−143.

(3) Anderson, O.; Markham, K. Chapter 4. Flavonoids in foods. *Flavonoids (Chemistry, Biochemistry, and Applications)*; CRC Press/Taylor and Francis Group: Boca Raton, FL, USA, 2006.

(4) Wang, R.; Zhou, W.; Jiang, X. Reaction kinetics of degradation and epimerization of epigallocatechin gallate in aqueous system over a wide temperature range. *J. Agric. Food Chem.* **2008**, *56*, 2694−2701.

(5) Yoshida, Y.; Kiso, M.; Goto, T. Efficiency of the extraction of catechins from green tea. *Food Chem.* **1999**, *67*, 429−433.

(6) Chang, C.; Chiu, K.; Chen, Y.; Chang, C. Separation of catechins from green tea using carbon dioxide extraction. *Food Chem.* **2000**, *68*, 109−113.

(7) Naczk, M.; Shahidi, F. Review: Extraction and analysis of phenolics in food. *J. Chromatogr., A* **2004**, *1054*, 95−111.

(8) Hu, J.; Zhou, D.; Chen, Y. Preparation and antioxidant activity of green tea extract enriched in epigallocatechin and epigallocatechin gallate. *J. Agric. Food Chem.* **2009**, *57*, 1349−1353.

(9) Carr, A.; Mammucari, R.; Foster, N. A review of subcritical water as a solvent and its utilisation for the processing of hydrophobic organic compounds. *Chem. Eng. J.* **2011**, *172*, 1−17.

(10) Ko, M.; Cheigh, C.; Cho, S.; Chung, M. Subcritical water extraction of flavonol quercetin from onion skin. *J. Food Eng.* **2011**, *102*, 327−333.

(11) Cheigh, C.; Chung, E.; Chung, M. Enhanced extraction of flavanones hesperidin and narirutin from *Citrus unshiu* peel using subcritical water. *J. Food Eng.* **2012**, *110*, 472−477.

(12) Ko, M.; Cheigh, C.; Chung, M. Relationship analysis between flavonoids structure and subcritical water extraction. *Food Chem.* **2014**, *143*, 147−155.

(13) Choung, M.; Lee, M. Optimal HPLC condition for simultaneous determination of catechins and caffeine in green tea extracts. *Korean J. Crop Sci.* **2008**, *53*, 224−232.

(14) Yang, Y.; Hildebrand, F. Phenanthrene degradation in subcritical water. *Anal. Chim. Acta* **2006**, *555*, 364−369.

(15) Vuong, Q.; Golding, J.; Nguyen, M.; Roach, P. Extraction and isolation of catechins from tea. *J. Sep. Sci.* **2010**, *33*, 3415−3428.

(16) Seto, R.; Nakamura, H.; Nanjo, F.; Hara, Y. Preparation of epimers of tea catechins by heat treatment. *Biosci., Biotechnol., Biochem.* **1997**, *61*, 1434−1439.

(17) Suzuki, M.; Sano, M.; Yoshida, R.; Degawa, M.; Miyase, T.; Maeda-Yamamoto, M. Epimerization of tea catechins and O-methylated derivatives of (−)-epigallocatechin-3-*O*-gallate: relationship between epimerization and chemical structure. *J. Agric. Food Chem.* **2003**, *51*, 510−514.

(18) Liang, H.; Liang, Y.; Dong, J.; Lu, J. Tea extraction methods in relation to control of epimerization of tea catechins. *J. Sci. Food Agric.* **2007**, *87*, 1748−1752.

(19) Wang, H.; Helliwell, K. Epimerisation of green tea infusions. *Food Chem.* **2000**, *70*, 337−344.

(20) Zhu, Q.; Zhang, A.; Tsang, D.; Huang, Y.; Chen, Z. Stability of green tea catechins. *J. Agric. Food Chem.* **1997**, *45*, 4624−4628.

(21) Labbé, D.; Têtu, B.; Trudel, D.; Bazinet, L. Catechin stability of EGC- and EGCG-enriched tea drinks produced by a two-step extraction procedure. *Food Chem.* **2008**, *111*, 139−143.

(22) Curren, M.; King, J. Solubility of triazine pesticides in pure and modified subcritical water. *Anal. Chem.* **2001**, *73*, 740−745.

(23) Kang, J.; Chung, S.; Row, K. Comparison of experimental and calculated solubilities of (+)-catechin in green tea. *J. Ind. Eng. Chem.* **2002**, *8*, 354−358.

(24) Pineiro, Z.; Palma, M.; Barroso, C. Determination of catechins by means of extraction with pressurized liquids. *J. Chromatogr., A* **2004**, *1026*, 19−23.

mixtures of proteins and a biosurfactant *Quillaja* Bark Saponin at the air−water and oil−water interfaces have also been described in detail by Wojciechowski and co-workers.[22−24]

Recently, we reported that natural sweetener stevioside (STE), the most abundant component of steviol glycosides, exhibited a notable surface activity and could also be developed into a new type of biosurfactant.[25] The emulsions prepared by the mixtures of soy protein isolate (SPI) and STE showed a remarkable physical stability with small oil droplet size of ∼220 nm.[25] STE is a diterpene ent-kaurene glycoside, which consists of a hydrophobic headgroup, called diterpenoid or steviol backbone, with hydrophilic glucosyl and sophorosyl residues. The amphiphilic structure of STE molecules is similar to that of triterpenoid saponins, thus determining their potential capability as biosurfactants. Moreover, STE also exhibits many nontrivial biological activities, such as antitumor progression and antihyperglycemic and immunomodulatory effects.[26] In another recent work,[27] we further found that the soy protein−STE mixtures displayed interesting competition adsorption behavior by their mutual interactions at the interface, which were positively reflected in the corresponding emulsions with the long-term stability. All these present works to a large extent support the capability of STE as a new biosurfactant and further research on the mixed protein−STE systems due to their potential practical applications as foam/emulsion formulations.

Considering the fact that the behavior of adsorbed layers at the air−water interface obviously differs from that at the oil−water interface due to their different degrees of polarity and hydrophobicity,[3,5,12] which can strongly influence the properties of respective foams and emulsions, it is therefore of interest to further study the adsorption of soy protein−STE mixtures at the air−water interface and their relation to the corresponding foaming characteristics. Moreover, to the best of our knowledge, no report about the interactions between protein and STE in the bulk and at the air−water interface has been found to date. Thus, in this work, we focus on the adsorption of soy protein−STE mixtures at the air−water interface by using a combination of dynamic surface tension and dilational rheological studies. The soy glycinin (11S), the major and pure globulin of soybeans, is employed in this study because of its structural and functional properties extensively studied. The bulk 11S−STE interactions are first investigated by fluorescence spectroscopy and isothermal titration calorimetry (ITC) measurements to helpfully understand surface behavior of the mixtures. Subsequently, the foamability and foam stability in mixed 11S−STE systems are determined, and a possible stabilization mechanism is finally proposed to clarify the correlation between surface behavior and the actual foaming properties.

MATERIALS AND METHODS

Materials. STE (purity >95%) was purchased from Jining Aoxing Stevia Products Co., Ltd., China. Pyrene was purchased from Sigma-Aldrich (St. Louis, MO). Defatted soy flour was provided by Shandong Yuwang Industrial and Commercial Co., Ltd., China. The protein content of soy flour was 55.10% (determined by micro-Kjeldahl method, $N \times 6.25$, dry basis). 11S globulin was prepared as described by Yuan et al.[28] Protein content of 11S globulin was 96.29%, determined by Dumas method ($N \times 6.25$) in a Rapid N Cube (Elementar France, Villeurbanne, France). All other chemicals used were of analytical grade.

Sample Preparation. All samples were prepared in 10 mM phosphate buffer solution (pH 7.0) using ultrapure water (18.2 MΩ·cm) at room temperature (25 °C). The absence of surface active contaminants in the phosphate buffer was checked by surface tension measurements before sample preparation. No aqueous solutions with a surface tension other than that accepted in the literature (72−73 mN/m at 25 °C) were used. The 11S globulin solution was prepared by dispersing the freeze-dried protein in 10 mM phosphate buffer (pH 7.0) for 2 h under mild magnetic stirring and then was left overnight at 4 °C to allow complete hydration. All measurements were made at constant 11S concentration (0.1 wt %) and varying STE concentration (0−2 wt %) at pH 7.0. The mixed 11S−STE systems were obtained by mixing the appropriate volume of each double concentrated 11S and STE solutions up to the required concentration and stirring for a further 30 min before any measurements.

Fluorescence Spectroscopy Measurements. To investigate the effect of STE addition on the intrinsic fluorescence of 11S, fluorescence spectra of solutions containing a fixed 11S concentration (1 mg/mL) and different STE concentrations in 10 mM phosphate buffer (pH 7.0) were recorded using an F7000 fluorescence spectrophotometer (Hitachi Co., Japan) at 25 °C. The excitation wavelength was set at 295 nm, and the emission spectra were collected from 310 to 500 nm. Both the excitation and emission slit widths were set at 5 nm. The reference sample consisting of the phosphate buffer and STE was checked for fluorescence signals. The data on the tryptophan (Trp) fluorescence quenching were analyzed according to the Stern−Volmer equation (eq 1):

$$F_0/F = 1 + k_q\tau_0[Q] = 1 + K_{SV}[Q]$$

In this equation F_0 and F are the fluorescence intensities in the absence and presence of a quencher, respectively, $[Q]$ is the quencher concentration, K_{SV} is the Stern−Volmer quenching constant, k_q is the bimolecular quenching rate constant, and τ_0 is the lifetime of fluorescence in absence of a quencher. Hence, K_{SV} was determined by linear regression of a plot of F_0/F versus $[Q]$ according to eq 1.

Pyrene was used as the fluorescence probe to determine the micropolarity of STE with and without 11S solution (1 mg/mL). Each spectrum was measured in the wavelength range 350−500 nm with the excitation wavelength being 335 nm. The excitation and emission slit widths were set at 5 and 2.5 nm, respectively. The intensity ratio of I_{373} to I_{385} of the pyrene fluorescence spectrum shows the micropolarity where the probe exists. The final concentration of pyrene in each sample was 6.0×10^{-7} M.

Isothermal Titration Calorimetry (ITC). The ITC measurements were performed in a Nano ITC Low Volume instrument (TA Instruments, Newcastle, DE) at 25 °C. In a typical experiment, 250 μL 11S solution (1 mg/mL) was inserted into the sample cell, and the syringe was filled with 50 μL of STE solution (50 mg/mL). All solutions were prepared in phosphate buffer (10 mM, pH 7.0) and were degassed before each titration. After reaching equilibrium, STE solution was titrated into the sample cell as a sequence of 25 injections of 2 μL aliquots. The time delay between successive injections was 350 s. The contents of the sample cell were stirred throughout the experiment at 250 rpm to ensure thorough mixing. Control experiments included the titration of STE into buffer, buffer into protein, and buffer into buffer. The last two controls resulted in small and equal enthalpy changes for each successive injection of buffer and, therefore, were not further considered in the data analysis. Corrected raw data refer to experimental data after subtraction of the STE into buffer control data. The corrected data obtained as a plot of heat flow (μcal s^{-1}) against time (min) were then integrated peak-by-peak and normalized to obtain a plot of observed enthalpy change per mole of STE (ΔH, kcal mol^{-1}) against the STE concentration (mM). The experimental data were further fitted to the one-site independent binding model using the TA Nano Analyzer software, providing the thermodynamic parameters K_a (binding constant), ΔH (enthalpy change), ΔS (entropy change), and n (number of STE molecules bound per mole of 11S).

Dynamic Surface Properties Measurements. The dynamic surface properties of 11S, STE, and 11S−STE mixtures at the air−

water interface were monitored by recording temporal evolution of surface pressure and surface dilatational parameters using an optical contact angle meter (OCA-20, DataPhysics Instruments GmbH, Germany) equipped with oscillating drop accessory (ODG-20), as described elsewhere.[30] All the experiments were carried out at 25 °C. The solutions were placed in the syringe and were allowed to equilibrate for 30 min to reach the desired constant temperature before the measurements. The drop of sample solution was formed in a rectangular glass cuvette. The cuvette was sealed with a Parafilm M laboratory film (Pechiney Plastic Packaging Company, U.S.A.) and partially filled with the solution under test to saturate the air surrounding the drop and reduce the water evaporation, which could decrease the drop volume and thus falsify the test.

Dynamic Surface Tension. A drop of sample solution (12 μL) was delivered and allowed to stand for 180 min to achieve adsorption at the air−water interface. An image of the drop was continuously recorded by a CCD camera and digitalized. The surface tension (γ) was calculated through the shape analysis of a pendant drop according to the Young−Laplace equation analysis. The surface pressure is $\pi = \gamma_0 - \gamma$, where γ_0 is the surface tension of phosphate buffer (10 mM, pH 7.0) and γ is the time-dependent surface tension of the tested solutions. The average standard accuracy of the surface tension for at least three measurements with different drops was roughly 0.5 mN/m.

Dilatational Rheological Properties. To obtain surface dilatational parameters, sinusoidal interfacial compression and expansion were performed by decreasing and increasing the drop volume at 10% of deformation amplitude ($\Delta A/A$) and 0.1 Hz of angular frequency (ω). The drop was subjected to repeated measurements of five sinusoidal oscillation cycles followed by a time corresponding to 50 cycles without any oscillation up to 180 min required to complete adsorption. Details of this experiment are given elsewhere.[31,32] The surface viscoelastic parameters, i.e., surface dilatational modulus, E, its elastic, E_d, and viscous, E_v, components were derived from the change in surface tension (γ) (dilatational stress) resulting from a small change in surface area (dilatational strain). The surface dilatational modulus (E) is a complex quantity and composed of real and imaginary parts ($E = E_d + iE_v$). The real part of the dilatational modulus or storage component is the dilatational elasticity (E_d). The imaginary part of the dilatational modulus or loss component is the surface dilatational viscosity (E_v).

Foam Formation and Stability Measurements. The foaming properties of pure STE and 11S−STE mixtures were characterized through their foam formation and stability measured in a Foam Tester R2000 instrument (SITA Messtechnik, GmbH, Germany) at 25 °C, as described elsewhere.[33] In all experiments, the used volume of the foaming solutions was 300 mL. The same 11S and STE concentrations were used as in the surface properties study. Every foam test consisted of two cycles, namely, the foam generation and foam decay. Foams were generated by stirring the solutions at 1000 rpm and stopping every 10 s to measure the foam volume by the sensor unit. After 15 such cycles, the foam generation stopped and the foam was left to decay. During decaying, the foam volume was measured for every 1 min. The height of the foam column (mL) in a generation period is taken as a measure of the foamability. The stability of the foam is estimated by measuring the half-life ($t_{1/2}$, min) of the foam, the time taken for the height to decay to half of the maximum.

Statistical Analysis. Unless specified otherwise, three independent trials were performed, each with a new batch of sample preparation. All measurements were carried out in triplicate, and an analysis of variance (ANOVA) of the data was performed using the SPSS 19.0 statistical analysis system. Duncan Test was used for comparison of mean values among three treatments using a level of significance of 5%.

RESULTS AND DISCUSSION

Interactions between 11S and STE in Bulk Solution. The interaction between proteins and LMW surfactants in bulk solution is usually believed to influence the properties of surface layers and thus the formation and stability of foams.[12,13] Herein, to helpfully understand the adsorption behavior of the mixtures, the bulk 11S−STE interactions were thus studied by fluorescence spectroscopy and ITC, as shown in Figures 1 and 2.

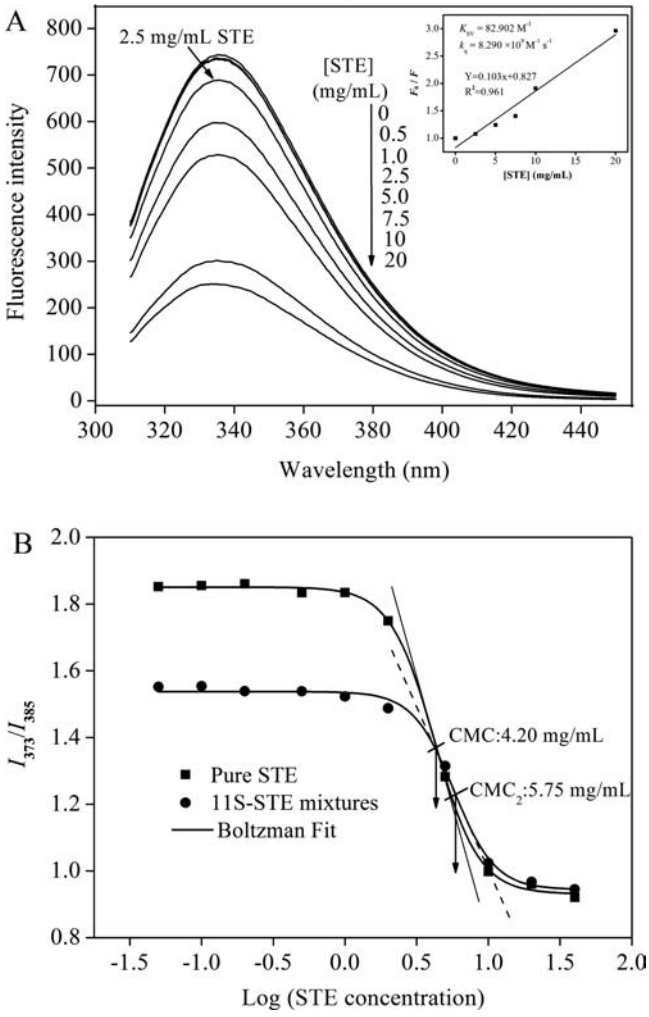

Figure 1. (A) Effect of STE on the intrinsic Trp fluorescence of 11S (1 mg/mL). The inset shows the Stern−Volmer plots describing fluorescence quenching of 11S in the presence of STE. (B) Pyrene fluorescence intensity ratios I_{373}/I_{385} in different STE concentrations with (CMC_2) and without (CMC) 11S. CMC: critical micelles concentration.

Effect of STE on Trp Intrinsic Fluorescence. Figure 1A shows the effect of STE on the Trp intrinsic fluorescence emission spectrum of 11S. The pure 11S exhibited an emission spectrum centered at around 335 nm. For STE concentrations below 1 mg/mL, there were no changes on the fluorescence intensity of 11S, indicating no obvious 11S−STE interactions. Addition of increasing STE concentrations from 2.5 mg/mL to 20 mg/mL gave rise to a progressive quenching of Trp fluorescence of 11S. Data fitting to eq 1 allowed determination of the Stern−Volmer quenching constant. As shown in the inset of Figure 1A, the value of k_q (8.29×10^9 M^{-1} s^{-1}) is much lower than the maximal dynamic quenching constant (2.0×10^{10} M^{-1} s^{-1}), indicating that the fluorescence quenching induced by STE is dynamic quenching.[29] This is in agreement with our previous study,[25] suggesting that STE cannot act as a direct Trp fluorescence quencher. Thus, this fluorescence attenuation should be the consequence of STE-induced protein

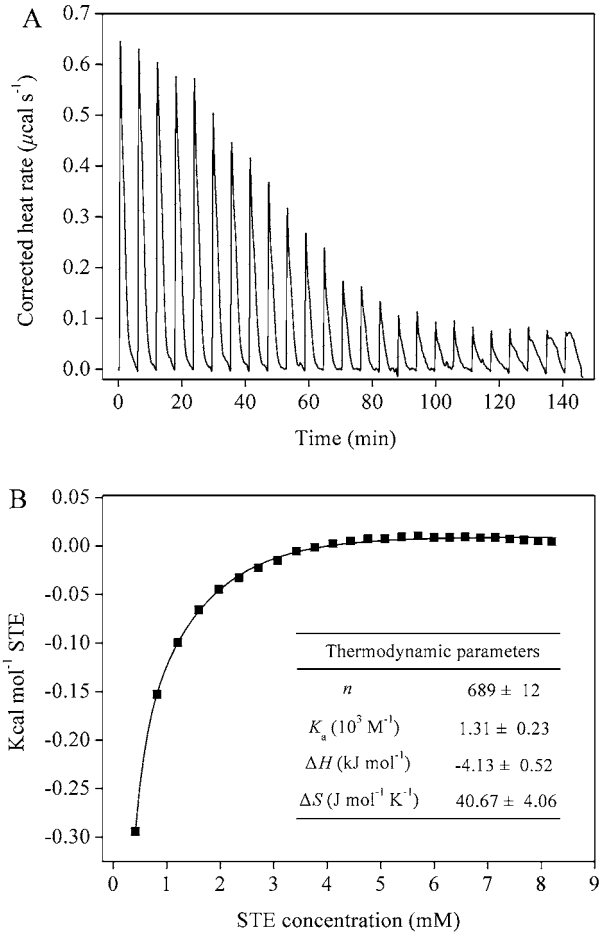

Figure 2. ITC determination of the binding of STE to 11S. (A) Heat flows recorded upon injection of STE solution (50 mg/mL) into 11S solution (1 mg/mL) at 25 °C. (B) Molar heat values obtained through integration of the individual heat flow signals as a function of the STE concentration. The solid line is the theoretical fit.

conformational changes. A similar behavior has been observed for the interaction of trehalose lipid biosurfactant with BSA.[34] In addition, as the concentration of STE was increasing from 7.5 mg/mL to 20 mg/mL (above the CMC of STE, see Figure 1B), the maximum emission wavelength underwent a moderate blue shift from 335 to 332 nm, revealing the movement of the Trp residues into a more hydrophobic environment, which was probably due to the interaction with hydrophobic portions of STE molecules (monomers and micelles).

Pyrene Fluorescence. The fluorescence emission of hydrophobic pyrene probe is sensitive to its microenvironmental polarity. A lower I_{373}/I_{385} value stands for higher hydrophobicity of the microenvironment. Upon micellization, pyrene partitions into or close to the hydrophobic interior of micelles, and consequently the intensity ratio I_{373}/I_{385} is changed.[35,36] The changes of the I_{373}/I_{385} values on the logarithm of STE concentrations with and without 11S were recorded and shown in Figure 1B. As can be seen, for STE concentrations below 1 mg/mL, compared to pure STE, 11S−STE mixtures showed lower I_{373}/I_{385} values, suggesting a higher hydrophobicity of the microenvironment, which was due to the hydrophobic domains in 11S. Moreover, no significant difference ($p > 0.05$) in the I_{373}/I_{385} values was observed when compared with that of pure 11S (1.54), indicating that there might be no obvious 11S−STE interactions when STE concentration was below 1 mg/mL. This result is in good agreement with the analysis of Trp intrinsic fluorescence (Figure 1A). The critical micelle concentration (CMC) of STE was determined from the threshold concentration, where the pyrene I_{373}/I_{385} begins to change markedly.[35,36] Therefore, the CMC values of STE in the absence and presence of 11S were determined as 4.20 mg/mL (CMC) and 5.75 mg/mL (CMC_2), respectively. The higher CMC value of STE in the presence of 11S revealed that there was interaction between 11S and STE, which sequestered STE molecules and reduced the concentration of free monomeric STE, thus increasing the STE concentration for formation of free micelles.[11] This result further supported previous analysis of Trp intrinsic fluorescence (Figure 1A).

ITC. The interaction between 11S and STE was further quantitatively studied by ITC, as shown in Figure 2. Upon injecting aliquots of STE solution (around 12 times above the CMC of STE) into 11S solution, the corrected heat trace peaks in Figure 2A demonstrated exothermic enthalpy released in the titration process, which should be caused by the binding of STE to 11S. On the basis of the fluorescence measurements (Figure 1), we can thus conclude that, upon the presence of STE micelles, STE could actually bind to the 11S cooperatively, forming the micelle-like clusters at the surface of 11S, thus resulting in the formation of exothermic peaks. Furthermore, with increasing STE addition, a decrease in exothermic peaks was observed (Figure 2A), suggesting the number of available binding sites on the 11S decreased. Once the protein became saturated with STE, the addition of more STE led to a plateau in the exothermic peaks (Figure 2A). The thermodynamic parameters were determined from the titration curve in Figure 2B. The binding ratio (n) was calculated to be 686 (±12), suggesting that 11S became saturated with 686 molecules of monomer STE bound per molecule of 11S. The binding ratio value was higher than those observed for the interactions between β-lactoglobulin and different types of LMW surfactants, such as SDS, alkyl trimethylammonium chlorides, or alkyl maltopyranosides.[11,37] This high binding ratio further supported the formation of STE clusters or micelles at the surface of 11S, in agreement with the Trp intrinsic fluorescence analysis (Figure 1A). Moreover, the larger molecular size of 11S (~360 kDa) could also provide a greater number of binding sites for STE. Interactions with binding constant $K_a > 10^4$ M^{-1} are considered to be of high affinity.[38] Thus, the binding constant ($K_a = 1.31 \times 10^3 \pm 0.23 \times 10^3$ M^{-1}) observed in this study indicated that binding of STE with 11S was much weaker, probably suggesting a nonspecific interaction.[34] In addition, the binding entropy was positive ($\Delta S = 40.67 \pm 4.06$ kJ mol^{-1} K^{-1}), indicating that the interaction was mostly driven by entropy. Since it is generally accepted that an entropy-driven reaction mainly involves hydrophobic interactions,[34,38] the present result suggested that STE binding to 11S should be mainly driven by interacting unspecifically with hydrophobic domains of 11S, which was again in line with the results of Trp intrinsic fluorescence (Figure 1A). Similar findings on the interaction of trehalose lipid biosurfactant with BSA were observed.[34]

Surface Behavior of 11S−STE Mixtures. *Dynamic Surface Tension.* The time evolution of surface tension (γ) for 11S−STE mixtures at the air−water interface is shown in Figure 3A. In all cases, the surface tension values gradually decreased with adsorption time, which can be associated with the surface-active substances adsorption at the interface. For pure 11S, it can be observed that the surface was already

dx.doi.org/10.1021/jf502027u | J. Agric. Food Chem. 2014, 62, 6834−6843

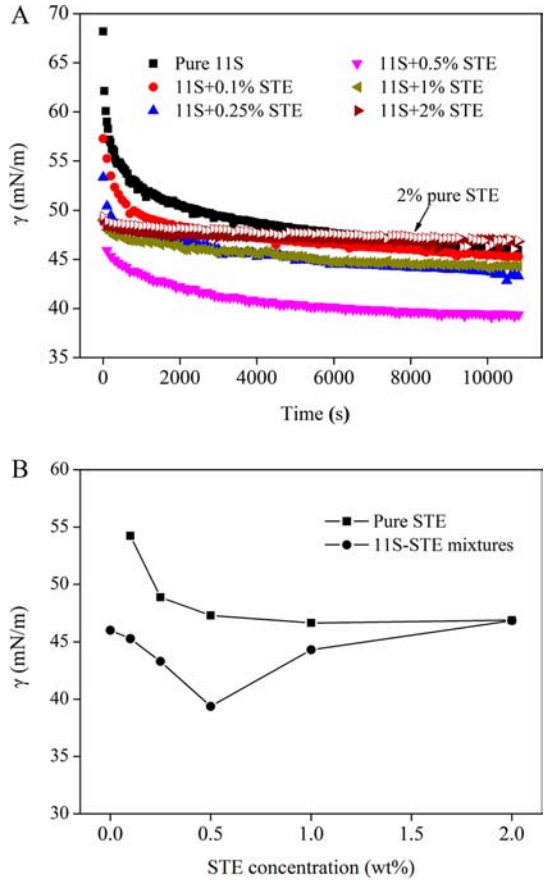

Figure 3. (A) Surface tension (γ) as a function of time for mixed solutions of 0.1% 11S with different STE concentrations (0–2%) at the air–water interface. (B) Surface tension versus the concentration of STE for solutions with and without 0.1% 11S. The values represent the surface tension after 180 min of adsorption.

saturated at the present bulk concentration (0.1%), in agreement with previous studies.[15,31,39] For 11S–STE mixtures, at low STE concentration (0.1%), the surface tension decay showed a very similar trend as compared to pure 11S, indicating that the surface layer was mainly dominated by 11S. However, with increasing STE concentrations to intermediate level (0.25 and 0.5%), especially at 0.5% STE, the surface tension decay curves started to differentiate markedly when compared to that of pure 11S, where a significant increase in the decay rate was observed. Upon the further increase of STE concentration (1 and 2%), an obvious slowing down of surface tension decay was found as compared with that of 0.5% STE. Moreover, the dynamic curve of the mixture (2%) started to resemble that for 2% pure STE (Figure 3A).

The surface tension after 180 min of adsorption from mixed 11S and STE systems is compared to the corresponding values for pure STE in Figure 3B. The surface tension value for pure 11S was 46.0 mN/m after 180 min, which is in consistent with previously reported results.[15,31] With increasing STE concentrations from 0.1% to 0.5%, an obvious decrease in surface tension values was found. Furthermore, it is noteworthy that the surface tension values of mixtures were always lower than those of pure 11S and STE, indicating mixed 11S–STE surface layers were formed. However, with increasing STE concentrations from 1% to 2%, the surface tension values of mixtures started to increase again, suggesting the decreased surface activity. Moreover, the surface tension value of the mixture (2%) coincided with that of pure 2% STE, which indicated that the interface was completely dominated by STE.

Surface Dilatational Rheology. The dynamic dilatational properties for pure and mixtures of 11S and STE are shown in Figure 4. The evolution of the dilatational modulus was

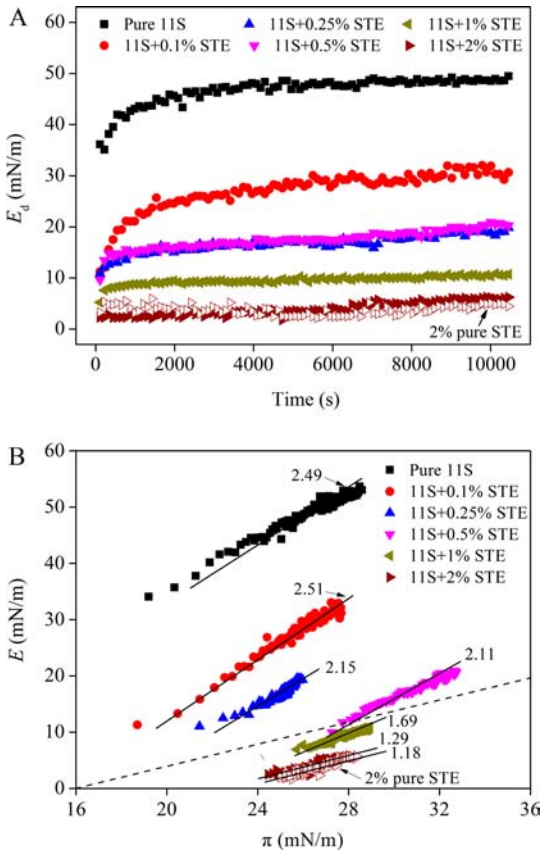

Figure 4. (A) Time-dependent dilatational elasticity (E_d) for adsorbed layers formed from mixed solutions of 0.1% 11S with various amounts of STE (0–2%) at the air–water interface. (B) Surface dilatational modulus (E) plotted as a function of surface pressure (π) for the above mixed solutions. Frequency: 0.1 Hz. Amplitude of deformation: 10%.

followed at the frequency of 0.1 Hz, which was tuned to give a good response for soy globulin, as it allows the collection of enough data points within the present adsorption time.[15,31,39] In all cases, it can be noticed that (data not shown) the values for surface dilatational modulus (E) were very similar to those for the dilatational elasticity (E_d), and the dilatational viscosity (E_v) values were low. Thus, from a rheological point of view, these results suggested the surface layers behaved as viscoelastic (primarily elastic) during the adsorption period studied here.[15]

Figure 4A presents the dynamic elastic modulus (E_d) of surface layers during the adsorption of 11S–STE mixtures. In all cases, the gradual increase in E_d with adsorption time should be associated with the adsorption of surface-active components at the interface. For pure 11S, the E_d increased gradually with time to reach 49.5 mN/m after 180 min, which is similar to those found by others,[15,31,39] implying that strong viscoelastic interfacial networks were formed mainly due to a combined effect of protein adsorption and development of strong intermolecular interactions and conformation changes at the interface.[1,15,31,40] With increasing amounts of STE in mixtures, even at low STE concentration (0.1%), the E_d clearly decreased as compared to that of pure 11S. This should be mainly due to

dx.doi.org/10.1021/jf502027u | J. Agric. Food Chem. 2014, 62, 6834–6843

the fact that the presence of STE could break down the protein intermolecular interactions, thus weakening the film and reducing the viscoelastic properties.[1,41] Similar findings were also reported for soy globulins/Tween 20 and hen egg-white lysozyme/C_{10}DMPO mixtures at the air−water interface.[14,15] Nevertheless, at intermediate STE concentrations (0.25 and 0.5%), it is very interesting to note that no marked difference in E_d values with increasing STE concentrations was observed. This result revealed that mixed 11S−STE surface layers showed a plateau in the elastic behavior within the STE concentration range. With the further increase in STE concentration (1 and 2%), the E_d values started to decrease again. At high STE concentration of 2%, the E_d value of the mixture was very close to that of 2% pure STE, which led to the conclusion that the interface was predominantly covered by STE. This result is in line with dynamic surface tension analysis (Figure 3). On the other hand, all pure STE samples (0.1−2%) showed very low E_d values (around 5.0−8.0 mN/m) (data not shown), indicating the interface stabilized by pure STE exhibited a low elasticity. Similar behaviors were also observed for many other LMW surfactants.[1,3,15,40]

The evolution of E with π in the surface layer for the adsorption of 11S−STE mixtures is shown in Figure 4B. The curve of E versus π generally reflects the surface equation of state of the adsorbed material at the interface, and if the E is only due to the amount of surface-active components adsorbed at the interface, all E data should be normalized in a single master curve of E versus π.[42] For pure 11S, it can be seen clearly that E increased almost immediately with increasing π value, and this dependence reflects the existence and the increase of interactions between the adsorbed protein residues. Moreover, E was higher at longer adsorption times, in line with the theory of Lucassen−Reynders.[43] The slope (2.49) of the $E-\pi$ plot was higher than 1 (represented by the dotted line in Figure 4B), which implied an important nonideal behavior for higher molecular interactions between the adsorbed proteins compared with those for an ideal behavior.[43] With increasing STE concentrations from 0.1% to 1%, all the slopes of $E-\pi$ plots were higher than 1, revealing an important nonideal behavior with higher molecular interactions between film-forming components. The low STE concentration (0.1%) showed a slope value of 2.51, which was similar to that of pure 11S (2.49), indicating that the interface was mainly dominated by 11S. This is consistent with the dynamic surface tension analysis (Figure 3). In addition, it is worth noting that, the mixtures with STE concentrations of 0.25% and 0.5% also exhibited high slope values of 2.15 and 2.11, respectively, which suggested the presence of high molecular interactions between the adsorbed 11S and STE at the interface. However, with further increasing STE concentrations (1 and 2%), the slope values started to decrease. At high STE concentration (2%), the $E-\pi$ plot partially overlapped with that of 2% pure STE, and the slope (1.29) was also very close to that of pure STE (1.18). These results indicated that the adsorption layer was formed mainly by STE, which again are in good agreement with previous analysis (Figures 3 and 4A). In addition, in all cases of pure STE (0.1−2%), the slope values of $E-\pi$ plots were around 1 (characteristic of the behavior of an ideal gas) (data not shown), thus revealing the E is only due to the amounts of STE adsorbed at the interface without apparent STE−STE interfacial interactions, in line with their behaviors at the oil−water interface.[27]

Foaming Properties of 11S−STE Mixtures. On the basis of the characterization of surface layers, we attempted to relate these findings to the properties of macroscopic foams formed from 11S−STE mixtures with the same compositions as used in the surface properties study. Thus, the foamability and foam stability of 11S−STE mixtures were measured, as shown in Figures 5 and 6, respectively.

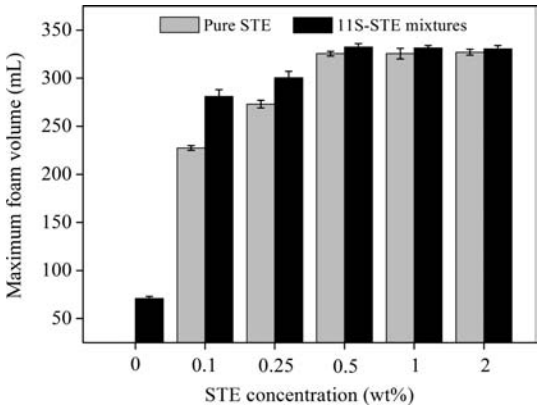

Figure 5. Maximum foam volume obtained from the solutions of pure STE (0.1−2%) and mixtures of 0.1% 11S with various amounts of STE (0−2%).

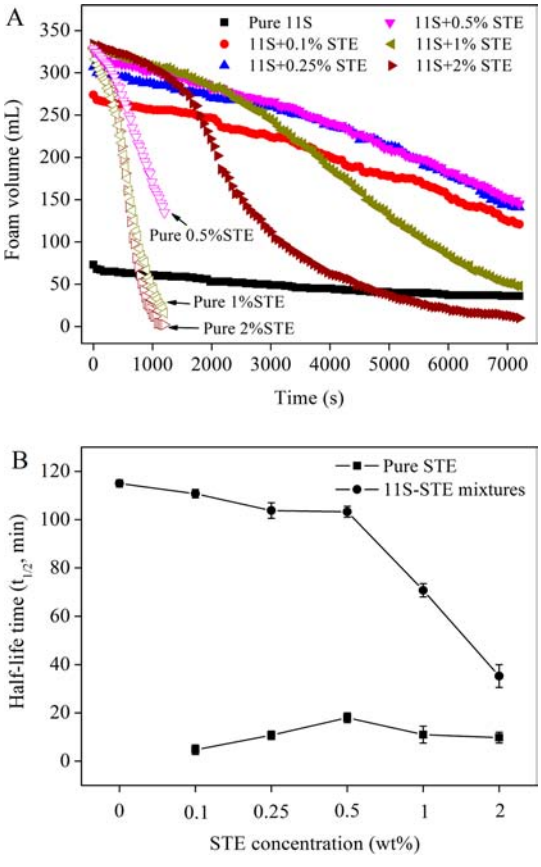

Figure 6. (A) Foam volume as a function of time for the solutions of pure STE (0.5−2%) and mixtures of 0.1% 11S with various amounts of STE (0−2%). (B) Half-life ($t_{1/2}$) of the foams formed by pure STE (0.1−2%) and the above mixed solutions.

dx.doi.org/10.1021/jf502027u | J. Agric. Food Chem. 2014, 62, 6834−6843

Foamability. Foam formation is influenced by the adsorption of foaming agents at the air−water interface and their ability to reduce surface tension.[3,9,44,45] The maximum foam volume for different systems was measured to assess their foamability (Figure 5). As shown in Figure 5, pure 11S exhibited a low foam volume, suggesting a very poor foaming capacity. This might be due to the large size and close-packed globular conformation of 11S,[46] which hindered its rapid adsorption at the interface during foaming, thus impairing the foaming capacity. The high initial surface tension value of 11S supported this analysis (Figure S, Supporting Information [SI]). This is in line with previous study,[46] which suggested that high 11S concentration (2% or more) was required to make good foams. Compared to that of pure 11S, even at the addition of low STE concentration (0.1%), the maximal foam volume was significantly increased. Moreover, with increasing STE concentration from 0.1% to 0.5%, a gradual increase in the maximal foam volume was observed, suggesting the improved foaming capacity. This improving effect should be due to the greater ability for the mixtures to lower surface tension (Figure 3), hence, facilitating the foaming process. In the presence of high STE concentrations (1 and 2%), no significant difference ($p > 0.05$) in the maximal foam volume was observed when compared to that of the mixture containing 0.5% STE. This result should be mainly attributed to their similar initial surface tension values (Figure S, SI). On the other hand, at the same concentration (0.1%), the foamability of pure STE was better than that of pure 11S (Figure 5), which should be due to the fast adsorption of STE at the interface and thus the lower initial surface tension (Figure S, SI), which could contribute to foamability. Meanwhile, under STE concentration range from 0.1% to 0.5%, the 11S−STE mixtures exhibited a higher foaming capacity as compared to pure STE. However, at high STE concentrations (1 and 2%), the foamability results for pure STE and the mixed systems were very similar. These results perfectly matched the general trends seen in initial surface tension data (Figure S, SI), suggesting a strong relationship between the foamability and the initial surface tension of foaming agents.

Foam Stability. Foams are thermodynamically unstable, and their relative stability is governed by factors such as liquid drainage, coarsening, and coalescence.[47] To evaluate the foam stability, the foam volume versus time after foam generation and the half-life time ($t_{1/2}$) of foams were measured, as presented in A and B of Figure 6, respectively. In all cases, it can be clearly seen that, despite the poor foaming capacity (Figure 5), the foam formed by pure 11S exhibited the lowest foam decay rate (Figure 6A) and the maximum value of $t_{1/2}$ at 115 min (Figure 6B), indicating pure 11S-stabilized foam was very stable against bubble coarsening and coalescence. With increasing STE concentration from 0.1% to 0.5%, compared to those of pure 11S, the rate of foam decay was slightly increased (Figure 6A), and the formed foams also had slightly lower $t_{1/2}$ values (Figure 6B). These results suggested that, under the STE concentration range (0.1−0.5%) used, the 11S−STE mixtures could still make relatively stable foams. Moreover, it is worth noting that, despite increasing STE concentrations from 0.25% to 0.5%, no significant difference ($p > 0.05$) was observed in foam decay rates and $t_{1/2}$ values. Also, the decay curve of 0.25% practically overlapped with that of 0.5% (Figure 6A). These results indicated that the foams formed by 11S−STE mixtures (0.25 and 0.5%) showed very similar stability. However, at high STE concentrations (1 and 2%), with increasing STE concentration, the dramatic increase in decay rates and decrease in $t_{1/2}$ values were observed, respectively. Moreover, the decay curve and $t_{1/2}$ value started to be close to those of pure STE. These results completely reproduced the general trends observed in the data from surface properties (Figures 3 and 4); therefore, it can be concluded that interfacial results might be correlated to foam stability. On the other hand, despite the good foaming capacity of pure STE (Figure 5), the foams formed by pure STE in the studied concentration range (0.1−2%) showed very poor stability, as evidenced by high foam decay rates and low $t_{1/2}$ values (Figure 6). Similar behavior was observed in foams stabilized by many other LMW surfactants.[1,15]

General Discussion. Here, the results obtained at different scales, from the molecular to the macroscopic point of view, are discussed to try to provide understanding of the mechanism underlying the foamability and foam stability for 11S−STE mixed systems. On the basis of the results of surface tension (Figure 3), it is thus reasonable to speculate that, at intermediate STE concentrations (0.25 and 0.5%), a strong synergy in reducing the surface tension was observed in 11S−STE mixtures, in agreement with the previous study where similar behavior was seen at the oil−water interface.[27] This effect could be explained by the formation of 11S−STE complex at the adsorbed layer, which might possess higher surface activity than that of the individual components (Figure 3B). This speculation is supported by the results of fluorescence spectroscopy and ITC (Figures 1 and 2), which indicated that the 11S−STE complex was formed already in the bulk prior to its adsorption at the interface. The obvious binding of STE with 11S in bulk occurred mainly by nonspecific hydrophobic interactions when STE concentration was above 1 mg/mL (Figures 1 and 2). The binding is rather weak, as evidenced by ITC analysis (Figure 2), but appears to be sufficiently intense to result in the conformational changes of 11S (Figure 1A). Therefore, we can conclude that the complexation with STE might promote the partial dissociation of protein and loosen its rigid structure, which would facilitate further unfolding of 11S upon reaching the interface, thus increasing the surface tension decay rate (Figure 3A). Similar phenomena were reported in the mixtures of β-lactoglobulin/β-casein and *Quillaja* Bark Saponin.[23,24] On the other hand, at low STE concentration (0.1%), complexation of a small amount of STE could not change the protein conformation markedly (Figures 1 and 2). Despite the low initial surface tension (Figure S, SI) due to the fast adsorption of STE, the overall adsorption behavior of 11S−STE mixtures would be similar to that of pure 11S, as evidenced by the surface tension decay of the mixture (0.1%) (Figure 3A). Furthermore, at high STE concentrations (1 and 2%, above the CMC of STE, see Figure 1B), large amounts of STE micelles would exist in the bulk. Meanwhile, with increasing binding of STE, the formation of STE clusters or micelles at the surface of 11S (Figures 1 and 2) might make the complex more hydrophilic, thus leading to the decrease in its surface activity. Considering the initial surface tension of 11S−STE mixture was very close to that of pure STE (Figure S, SI), therefore, we can speculate that the preferential adsorption of small STE molecules over 11S−STE complex at the interface occurred, thus leading to the conclusion that the interface is predominantly covered by STE (Figures 3 and 4). Similar behavior was reported for conventional surfactants, e.g., Tween 20 or SDS, which could also remove proteins completely from the interface.[3,17,41]

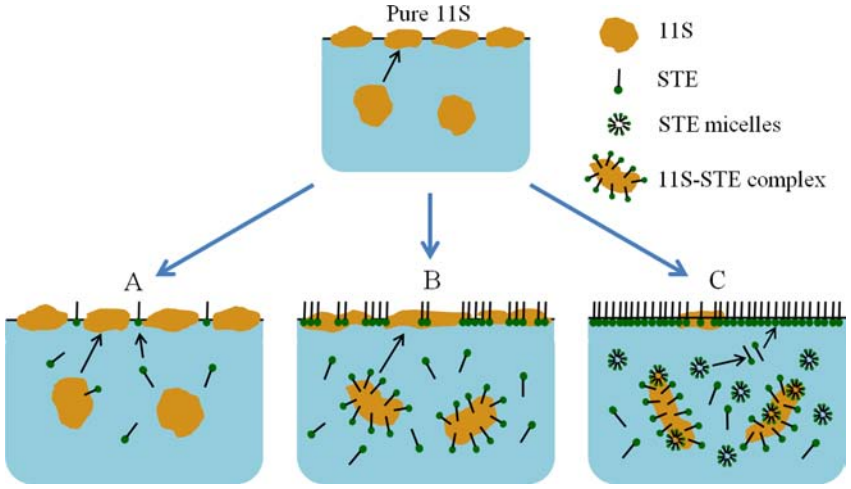

Figure 7. Schematic illustration of bulk behavior and adsorption at the air−water interface of 11S−STE mixtures with (A) low STE concentration (0.1%); (B) intermediate STE concentration (0.25−0.5%); (C) high STE concentration (1−2%).

The results of dynamic elastic modulus (E_d) and $E-\pi$ curves exhibited good correlation with each other (Figure 4). For 11S−STE mixtures, it is very interesting to note that, at intermediate STE concentrations (0.25 and 0.5%), a plateau in the elasticity for mixed surface layers was clearly seen (Figure 4A). This behavior could be explained with the partial dissociation and looseness of protein structure, induced by the binding of STE, which could promote further unfolding of 11S at the interface. The unfolding of 11S would facilitate enhancing protein−protein and protein−STE interactions at the surface layer, as evidenced by high slope values of $E-\pi$ plots (Figure 4B), thus increasing the E_d value.[15,41] This increase might offset the lost elastic modulus due to increasing STE concentration at the interface, and thus endowed the mixed surface layer with a plateau in the elasticity. These analyses were in line with surface tension analyses (Figure 3) and supported by fluorescence and ITC results (Figures 1 and 2).

On the basis of the above analysis, we can conclude that the synergy in surface tension decay and the plateau in surface elasticity appear to be crucial to the understanding of the dynamic surface properties for 11S−STE mixtures. Moreover, it is noteworthy to mention that no such behavior has been reported for protein/conventional surfactant mixtures. In general, for protein/nonionic surfactant mixtures, a monotonous decrease of the equilibrium surface tension and dilatational elasticity is observed, whereas for ionic surfactants, the surface tension exhibits a sharp decrease below the CMC, which is accompanied by a maximum of dilatational elasticity as the concentration of surfactant increases in the mixture.[3,12,14]

Considering the real foaming process, the link between surface characteristics and foaming properties is far from straightforward. However, in view of all of these present results, it could be speculated that there is a clear correlation between the surface behavior and the actual foaming properties for 11S−STE mixtures. As discussed previously, the foamability appeared to be affected strongly by the initial surface tension values of foaming agents (Figure 5 and Figure S in the SI). Furthermore, surface elasticity is generally believed to play an important role in foam stability.[1,3,40,47] Thus, despite poor foaming capacity of pure 11S (Figure 5), the formed foam remained very stable (Figure 6), which should be due to the formation of surface layers with high surface elasticity (Figure 4A) that protect the bubbles against coalescence.[1,3,7,40,47] Nevertheless, at intermediate STE concentrations (0.25 and 0.5%), surprisingly, although there was a dramatic decrease in surface elasticity (Figure 4A), no marked effect on the foam stability for the mixtures was observed (Figure 6). This suggested that the surface elasticity is not always the major factor influencing the stability of the mixed foams. Indeed, it is often stated and observed that protein−LMW surfactant mixtures could even give more stable foams than proteins alone.[1,45] The addition of the LMW surfactants will make the rather rigid protein layer more flexible and mobile, and the formed mixed surface layer might then be much better able to respond to deformations, which would prevent film rupture and thus have a positive effect on the foam stability.[1,45] This idea is consistent with the present observation on the stability of foams formed by 11S−STE mixtures (especially at 0.25 and 0.5%) (Figure 6) and is also supported by similar results on previous emulsion systems.[27] Accordingly, it might be speculated that the mixed surface layer stabilized by 11S and STE not only provided a relatively constant elasticity (Figure 4A) but also possessed a certain relaxation mechanism due to the existence of STE by the Gibbs−Marangoni effect,[1,3,4,6] thus endowing the foams with considerable stability (Figure 6). On the other hand, upon further increase of STE concentration (1 and 2%), the interface was gradually covered by STE (Figures 3 and 4) due to the preferential adsorption of STE molecules. Consequently the interface became weaker (low surface elasticity, see Figure 4A), and thus the resultant foams became less stable (Figure 6).

From these series of experiments and analysis, to better understand the correlation between the surface behavior and the actual foaming properties, a schematic illustration of bulk and surface behaviors of 11S−STE mixtures is proposed and shown in Figure 7. In the case of pure 11S, the slow adsorption at the interface impaired its foaming capacity (Figure 5 and Figure S in the SI); however, the formed surface layer with a high dilational elasticity (Figure 4) contributed to the generation of very stable foam (Figure 6). Upon the addition of low STE concentration (0.1%), the foamability of the mixture was obviously increased due to the fast adsorption of STE (Figure 5 and Figure S in the SI). Despite the marked effect on the surface dilational properties by STE, the interface was still mainly dominated by 11S (Figures 3 and 4). At intermediate STE concentrations (0.25 and 0.5%), the weak

dx.doi.org/10.1021/jf502027u | J. Agric. Food Chem. 2014, 62, 6834−6843

binding of STE with 11S in bulk occurred by nonspecific hydrophobic interactions (Figures 1 and 2). However, the binding was believed to be sufficiently intense to promote the partial dissociation and looseness of protein's rigid structure (Figure 1A). This would facilitate further unfolding of 11S upon adsorption and thus enhance the protein−protein and protein−STE interfacial interactions. These analyses were supported by the strong synergy in reducing surface tension and the plateau in surface elasticity for mixed layers (Figures 3 and 4), which endowed the corresponding foams with a fine foaming capacity, making the layer be better able to respond to applied stresses without rupturing and providing considerable foam stability against bubble coalescence (Figures 5 and 6). In addition, when high STE concentrations (1 and 2%) were added, large amounts of STE micelles formed in bulk. The preferential adsorption of STE molecules over the 11S−STE complex resulted in the formation of a surface layer covered mainly by STE (Figures 3 and 4), and thus the resultant foams became less stable due to low surface elasticity (Figures 4A and 6).

In conclusion, we have studied the adsorption of 11S−STE mixtures at the air−water interface by combining several approaches on different length scales. The obtained results showed clearly that the foaming properties of the mixtures were correlated with their surface behavior, which was found to be strongly influenced by 11S−STE interactions in the bulk. Compared to pure 11S, the surface dilational properties and foaming capacity were markedly affected even at low STE concentration (0.1%). When intermediate STE concentrations (0.25−0.5%) were added, the weak binding of STE with 11S in bulk occurred by nonspecific hydrophobic interactions, which appeared to be sufficiently intense to induce conformational changes of 11S, as evidenced by fluorescence and ITC. As a result, the strong synergy in reducing surface tension and the plateau in surface elasticity for mixed 11S−STE layers formed from the weakly interacting mixtures were clearly observed. This effect could be explained by the complexation with STE, which might facilitate the partial dissociation and further unfolding of 11S upon adsorption, thus enhancing the protein−protein and protein−STE interfacial interactions. These surface properties were positively reflected in foams produced by the weakly interacting system, which exhibited good foaming capacity and considerable stability probably due to better response to external deformations without film rupture. At high STE concentrations (1−2%, above its CMC), the preferential adsorption of STE molecules occurred, and thus the interface was predominantly covered by STE. Consequently, the resultant foams became less stable due to low surface elasticity.

Considering the conditions of practical foam formation and evolution, which mainly involve large deformation and high strain rates, the link between the present surface measurements and foaming properties is not straightforward. Further work is required on the study of the detailed microstructure and mechanical properties of adsorbed protein−STE layers under nonlinear conditions and large deformations using appropriate experimental techniques.[45,48] However, these results obtained in this work provide valuable information on the relation between the surface behavior and foaming properties of the 11S−STE mixtures. We expect that these findings would open up the potential of mixed protein−STE systems as foam/emulsion formulations in industrial applications.

■ ASSOCIATED CONTENT

Supporting Information

Figure of initial surface tension values versus the concentration of STE for solutions with and without 0.1% 11S. This material is available free of charge via the Internet at http://pubs.acs.org.

■ AUTHOR INFORMATION

Corresponding Author

*Tel: (086) 20-87114262. Fax: (086) 20-87114263. E-mail: fexqyang@scut.edu.cn.

Notes

The authors declare no competing financial interest.

■ ACKNOWLEDGMENTS

This research was supported by grants from the Chinese National Natural Science Foundation (Serial numbers: 31371744, 31301432, and 31130042), and the Fundamental Research Funds for the Central Universities (SCUT, 2013ZM0052).

■ REFERENCES

(1) Bos, M. A.; Van Vliet, T. Interfacial rheological properties of adsorbed protein layers and surfactants: a review. *Adv. Colloid Interface Sci.* **2001**, *91*, 437−471.

(2) Pugnaloni, L. A.; Dickinson, E.; Ettelaie, R.; Mackie, A. R.; Wilde, P. J. Competitive adsorption of proteins and low-molecular-weight surfactants: computer simulation and microscopic imaging. *Adv. Colloid Interface Sci.* **2004**, *107*, 27−49.

(3) Maldonado-Valderrama, J.; Rodríguez Patino, J. M. Interfacial rheology of protein−surfactant mixtures. *Curr. Opin. Colloid Interface Sci.* **2010**, *15*, 271−282.

(4) Miller, R.; Alahverdjieva, V. S.; Fainerman, V. B. Thermodynamics and rheology of mixed protein−surfactant adsorption layers. *Soft Matter* **2008**, *4*, 1141−1146.

(5) Damodaran, S. Protein stabilization of emulsions and foams. *J. Food Sci.* **2005**, *70*, R54−R66.

(6) Wilde, P.; Mackie, A.; Husband, F.; Gunning, P.; Morris, V. Proteins and emulsifiers at liquid interfaces. *Adv. Colloid Interface Sci.* **2004**, *108−109*, 63−71.

(7) Murray, B. S. Stabilization of bubbles and foams. *Curr. Opin. Colloid Interface Sci.* **2007**, *12*, 232−241.

(8) Kotsmar, Cs.; Grigoriev, D. O.; Xu, F.; Aksenenko, E. V.; Fainerman, V. B.; Leser, M. E.; Miller, R. Equilibrium of adsorption of mixed milk protein/surfactant solutions at the water/air interface. *Langmuir* **2008**, *24*, 13977−13984.

(9) Petkova, R.; Tcholakova, S.; Denkov, N. D. Foaming and foam stability for mixed polymer−surfactant solutions: Effects of surfactant type and polymer charge. *Langmuir* **2012**, *28*, 4996−5009.

(10) Taylor, D. J. F.; Thomas, R. K.; Penfold, J. Polymer/surfactant interactions at the air/water interface. *Adv. Colloid Interface Sci.* **2007**, *132*, 69−110.

(11) Otzen, D. Protein−surfactant interactions: A tale of many states. *Biochim. Biophys. Acta, Proteins Proteom.* **2011**, *1814*, 562−591.

(12) Kotsmar, C.; Pradines, V.; Alahverdjieva, V. S.; Aksenenko, E. V.; Fainerman, V. B.; Kovalchuk, V. I.; Krägel, J.; Leser, M. E.; Noskov, B. A.; Miller, R. Thermodynamics, adsorption kinetics and rheology of mixed protein−surfactant interfacial layers. *Adv. Colloid Interface Sci.* **2009**, *150*, 41−54.

(13) Krägel, J.; O'Neill, M.; Makievski, A. V.; Michel, M.; Leser, M. E.; Miller, R. Dynamics of mixed protein−surfactant layers adsorbed at the water/air and water/oil interface. *Colloids Surf., B* **2003**, *31*, 107−114.

(14) Alahverdjieva, V. S.; Grigoriev, D. O.; Fainerman, V. B.; Aksenenko, E. V.; Miller, R.; Möhwald, H. Competitive adsorption from mixed hen egg-white lysozyme/surfactant solutions at the air−

water interface studied by tensiometry, ellipsometry, and surface dilational rheology. *J. Phys. Chem. B* **2008**, *112*, 2136−2143.
(15) Ruíz-Henestrosa, V. P.; Carrera Sánchez, C.; Rodríguez Patino, J. M. Adsorption and foaming characteristics of soy globulins and Tween 20 mixed systems. *Ind. Eng. Chem. Res.* **2008**, *47*, 2876−2885.
(16) Dickinson, E. Proteins at interfaces and in emulsions. Stability, rheology and interactions. *J. Chem. Soc., Faraday Trans.* **1998**, *94*, 1657−1669.
(17) Chen, J.; Dickinson, E. Protein/surfactant interfacial interactions part 2. Electrophoretic mobility of mixed protein + surfactant systems. *Colloids Surf., A* **1995**, *100(C)*, 267−277.
(18) Güçlü-Üstündağ, Ö.; Mazza, G. Saponins: properties, applications and processing. *Crit. Rev. Food Sci. Nutr.* **2007**, *47*, 231−258.
(19) Stanimirova, R.; Marinova, K.; Tcholakova, S.; Denkov, N. D.; Stoyanov, S.; Pelan, E. Surface rheology of saponin adsorption layers. *Langmuir* **2011**, *27*, 12486−12498.
(20) Golemanov, K.; Tcholakova, S.; Denkov, N.; Pelan, E.; Stoyanov, S. D. Surface shear rheology of saponin adsorption layers. *Langmuir* **2012**, *28*, 12071−12084.
(21) Golemanov, K.; Tcholakova, S.; Denkov, N.; Pelan, E.; Stoyanov, S. D. Remarkably high surface visco-elasticity of adsorption layers of triterpenoid saponins. *Soft Matter* **2013**, *9*, 5738−5752.
(22) Wojciechowski, K.; Piotrowski, M.; Popielarz, W.; Sosnowski, T. R. Short- and mid-term adsorption behaviour of Quillaja Bark Saponin and its mixtures with lysozyme. *Food Hydrocolloids* **2011**, *25*, 687−693.
(23) Piotrowski, M.; Lewandowska, J.; Wojciechowski, K. Biosurfactant−protein mixtures: Quillaja bark saponin at water/air and water/oil interface in presence of β-lactoglobulin. *J. Phys. Chem. B* **2012**, *116*, 4843−4850.
(24) Wojciechowski, K.; Kezwon, A.; Lewandowska, J.; Marcinkowski, K. Effect of β-casein on surface activity of Quillaja bark saponin at fluid/fluid interfaces. *Food Hydrocolloids* **2014**, *34*, 208−216.
(25) Wan, Z. L.; Wang, J. M.; Wang, L. Y.; Yang, X. Q.; Yuan, Y. Enhanced physical and oxidative stabilities of soy protein-based emulsions by incorporation of a water-soluble stevioside−resveratrol complex. *J. Agric. Food Chem.* **2013**, *61*, 4433−4440.
(26) Bunprajun, T.; Yimlamai, T.; Soodvilai, S.; Muanprasat, C.; Chatsudthipong, V. Stevioside enhances satellite cell activation by inhibiting of NF-κB signaling pathway in regenerating muscle after cardiotoxin-induced injury. *J. Agric. Food Chem.* **2012**, *60*, 2844−2851.
(27) Wan, Z. L.; Wang, L. Y.; Wang, J. M.; Zhou, Q.; Yuan, Y.; Yang, X. Q. Synergistic interfacial properties of soy protein−stevioside mixtures: Relationship to emulsion stability. *Food Hydrocolloids* **2014**, *39*, 127−135.
(28) Yuan, Y.; Wan, Z. L.; Yin, S. W.; Teng, Z.; Yang, X. Q.; Qi, J. R.; Wang, X. Y. Formation and dynamic interfacial adsorption of glycinin/chitosan soluble complex at acidic pH: Relationship to mixed emulsion stability. *Food Hydrocolloids* **2013**, *31*, 85−93.
(29) Lakowicz, J. R. *Principles of Fluorescence Spectroscopy*, 3rd ed.; Springer Science + Business Media: New York, 2006.
(30) Tamm, F.; Sauer, G.; Scampicchio, M.; Drusch, S. Pendant drop tensiometry for the evaluation of the foaming properties of milk-derived proteins. *Food Hydrocolloids* **2012**, *27*, 371−377.
(31) Ruíz-Henestrosa, V. P.; Sánchez, C. C.; Rodríguez Patino, J. M. Effect of sucrose on functional properties of soy globulins: adsorption and foam characteristics. *J. Agric. Food Chem.* **2008**, *56*, 2512−2521.
(32) Wang, J. M.; Xia, N.; Yang, X. Q.; Yin, S. W.; Qi, J. R.; He, X. T.; Yuan, D. B.; Wang, L. J. Adsorption and dilatational rheology of heat-treated soy protein at the oil−water interface: relationship to structural properties. *J. Agric. Food Chem.* **2012**, *60*, 3302−3310.
(33) Karakashev, S. I.; Ozdemir, O.; Hampton, M. A.; Nguyen, A. V. Formation and stability of foams stabilized by fine particles with similar size, contact angle and different shapes. *Colloids Surf., A* **2011**, *382*, 132−138.
(34) Zaragoza, A.; Teruel, J. A.; Aranda, F. J.; Marqués, A.; Espuny, M. J.; Manresa, Á.; Ortiz, A. Interaction of a *Rhodococcus sp.* trehalose lipid biosurfactant with model proteins: Thermodynamic and structural changes. *Langmuir* **2012**, *28*, 1381−1390.
(35) Aguiar, J.; Carpena, P.; Molina-Bolívar, J. A.; Ruiz, C. C. On the determination of the critical micelle concentration by the pyrene 1:3 ratio method. *J. Colloid Interface Sci.* **2003**, *258*, 116−122.
(36) Bhattacharya, S.; Haldar, J. Thermodynamics of micellization of multiheaded single-chain cationic surfactants. *Langmuir* **2004**, *20*, 7940−7947.
(37) Hansted, J. G.; Wejse, P. L.; Bertelsen, H.; Otzen, D. E. Effect of protein−surfactant interactions on aggregation of β-lactoglobulin. *Biochim. Biophys. Acta, Proteins Proteom.* **2011**, *1814*, 713−723.
(38) Turnbull, W. B.; Daranas, A. H. On the value of *c*: Can low affinity systems be studied by isothermal titration calorimetry? *J. Am. Chem. Soc.* **2003**, *125*, 14859−14866.
(39) Ruíz-Henestrosa, V. P.; Sánchez, C. C.; Rodríguez Patino, J. M. Formulation engineering can improve the interfacial and foaming properties of soy globulins. *J. Agric. Food Chem.* **2007**, *55*, 6339−6348.
(40) Rouimi, S.; Schorsch, C.; Valentini, C.; Vaslin, S. Foam stability and interfacial properties of milk protein−surfactant systems. *Food Hydrocolloids* **2005**, *19*, 467−478.
(41) Mackie, A. R.; Wilde, P. The role of interactions in defining the structure of mixed protein−surfactant interfaces. *Adv. Colloid Interface Sci.* **2005**, *117*, 3−13.
(42) Rodríguez Patino, J. M.; Molina Ortiz, S. E.; Carrera Sánchez, C.; Rodríguez Niño, M. R.; Cristina Añón, M. Dynamic properties of soy globulin adsorbed films at the air−water interface. *J. Colloid Interface Sci.* **2003**, *268*, 50−57.
(43) Lucassen-Reynders, E. H.; Lucassen, J.; Garrett, P. R.; Giles, D.; Hollway, F. Dynamic surface measurements as a tool to obtain equation of state data for soluble monolayers. *Adv. Chem. Ser.* **1975**, *144*, 272−285.
(44) Rodríguez Patino, J. M.; Carrera Sánchez, C.; Rodríguez Niño, M. R. Implications of interfacial characteristics of food foaming agents in foam formulations. *Adv. Colloid Interface Sci.* **2008**, *140*, 95−113.
(45) Langevin, D. Aqueous foams: A field of investigation at the frontier between chemistry and physics. *ChemPhysChem* **2008**, *9*, 510−522.
(46) Martin, A. H.; Bos, M. A.; Van Vliet, T. Interfacial rheological properties and conformational aspects of soy glycinin at the air/water interface. *Food Hydrocolloids* **2002**, *16*, 63−71.
(47) Georgieva, D.; Cagna, A.; Langevin, D. Link between surface elasticity and foam stability. *Soft Matter* **2009**, *5*, 2063−2071.
(48) Sagis, L. M. C. Dynamic properties of interfaces in soft matter: Experiments and theory. *Rev. Mod. Phys.* **2011**, *83*, 1367−1403.

Wine volatiles are huge in number because they derive from three factors: the grapes, the fermentation by yeast, and the storage of wine.[20] Moreover, grape variety and its cultivation, oenological practice, and aging influence the specific aroma profile of a wine.[11] Thus, an enormous natural and process-related variation is achieved. Untargeted MS data of wines underpin this complexity. Hence, a clearly defined sample collection and sufficient number of samples are of particular relevance for classification. Further, the appropriate procedure for data treatment that follows data conversion is of special interest. For example, a large amount of irrelevant variables occurs in GC−MS data and could mislead interpretation of data.[21] The appropriate sampling and treatment strategy is particularly important for serving the current demand for the validation of the resultant classification models.[22−25]

To face such a challenge, the present fingerprinting study of volatiles was conducted and its suitability for German white wine varietal authentication was explored. The analysis was carried out with commercially available white wine samples, and it is therefore assumed that the natural diversity and a wide range of biological and oenological effects on the wine composition were covered. After the HS−SPME−GC−MS analysis, the raw data were converted applying an available metabolomics tool. Then, the appropriateness of the proposed method, including data treatment and processing, was shown by investigating reliability and relevance. Finally, a validated multi-class model was achieved. Additionally, details of the resultant classification model were shown by visualizing the classification performance.

MATERIALS AND METHODS

Samples. A total of 272 commercial German dry white wine samples, obtained in 2011, with a varietal purity of 100% according to the producers, were transferred to 50 mL amber glass bottles and stored at 4 °C in the dark until analysis. A total of 198 wine samples of the botanical origin Riesling (56 samples), Müller-Thurgau (34 samples), Silvaner (44 samples), Pinot Gris (30 samples), and Pinot Blanc (34 samples) formed the main data set 1. Further, 74 additional wine samples, including Riesling (40 samples), Pinot Gris (20 samples), and Pinot Blanc (14 samples) origin, formed data set 2. Samples were of vintage 2009 and 2010 and diverse origin regarding vineyard location in Germany. The German wine quality categories employed were (a) quality wine from specific wine-growing regions and (b) Kabinett, a quality wine with special attributes. The distribution of vintage in data set 2 was of 2009 with 40 samples (all Riesling) and 2010 with 34 samples (all Pinot).

Chemicals. All reagents used were of analytical quality. To form the internal standard mix, 3,7-dimethyl-3-octanol (purity > 98%) and 2-hexyl-1-decanol (purity > 97%), both purchased from Sigma-Aldrich (Schnelldorf, Germany), were solved in ethanol absolute per analysi (p.A.), Merck (Darmstadt, Germany). The solution contained on average 30.9 $\mu g\ g^{-1}$ of 3,7-dimethyl-3-octanol and 1.5 $\mu g\ g^{-1}$ of 2-hexyl-1-decanol. The mix was stored at −20 °C until analysis and renewed each 5−7 days. The compounds were chosen because of their general absence in wine. They demonstrated stability within the wine matrix and were used to control the mass feature alignment in the pre-processing step. The repeatability of their main fragment areas was tested by successive injections of 17 independent aliquots of a wine sample, each 10 mL mixed with 20 μL of internal standard mix. This resulted in 7 and 8% relative standard deviation of the peak area for tetrahydrolinalool and 2-hexyl-1-decanol, respectively. The internal standard mix was equally prepared and used for data set 2 sample preparation.

Furthermore, butylhydroxytoluene (BHT), purchased from Sigma-Aldrich, was used for identification of a non-wine compound causing sample outliers. The reference standards (*R*)-(+)-limonene (purity = 97%), γ-terpinene (purity > 97%), and 2-phenylethyl acetate (purity > 99%) were provided by Sigma-Aldrich. α-Terpineol (purity = 95%) was purchased from ABCR (Karlsruhe, Germany), and 1,1,6-trimethyl-1,2-dihydronaphthalene (TDN) (purity = 98%) was synthesized by VeZerf (Idar-Oberstein, Germany).

HS−SPME Sample Extraction and GC−MS Analysis. To extract samples, 10 mL of cooled wine (4 °C) and 20 μL of internal standard mix were filled in a 20 mL amber headspace vial, which was then immediately closed using headspace analysis screw caps with silicone/polytetrafluoroethylene (PTFE) septa of 1.3 mm thickness. Sample bottles were exclusively opened at the time of sample preparation. Samples of identical origin regarding grape variety were distributed equally across all sequences of measurement to ensure their comparability because of possibly biased analytical variation. For this purpose, the measurement order was chosen randomized along with a block design.

The HS−SPME of the wine volatiles was examined by full automation and online desorption of the analytes to the GC system using a MPS 2 device from Gerstel (Mülheim a. d. Ruhr, Germany). This ensured a steady throughput of samples and constant SPME parameters. The mono material fiber polydimethylsiloxane (PDMS), 100 μm thickness, 10 mm length (Supelco), purchased from Sigma-Aldrich, Germany, was chosen because of its low enrichment of ethanol, which avoided overload of the GC column. The extraction time for the PDMS fiber was 45 min at a temperature of 40 °C. The prior incubation time was 15 min at 40 °C, and the samples were agitated at 250 rpm during incubation and extraction. Immediately after the extraction, the desorption of analytes was carried out by hot injection at 260 °C, splitless for 2 min, in a narrow liner (0.75 mm internal diameter, Supelco). The split/splitless injector was equipped with a Merlin Microseal, Supelco, and, therefore, operated septumless. Bake-out of the SPME fiber was conducted for 10 min in a bake-out station at 250 °C immediately before every sample extraction. To check fiber intactness and detect possibly carry over of substances, fibers were desorbed without prior extraction twice a day and once every 10−15 samples (fiber blank). New SPME fibers and fibers not used for more than 1 day were conditioned at 250 °C for 30 min.

Analysis was carried out on an Agilent Technologies GC 6890 and MS detector 5973 inert (Böblingen, Germany). The desorbed sample analytes were separated on an Agilent J&W DB 1701 (30 m length, 0.25 μm film thickness, and 0.25 nm internal diameter). A helium flow of 1.1 mL min^{-1} was used. The initial oven temperature of 40 °C was held for 3 min and, after that, was first increased by 6 °C min^{-1} to 100 °C, with a hold time of 1 min, and second increased by 6 °C min^{-1} to 240 °C, with a hold time of 5 min. Finally, the temperature of 280 °C was held for 5 min to reduce contamination (total run time of 48 min). After transfer at 280 °C to the MS source with standard electron impact ionization at 230 °C, the quadrupole analysis (150 °C) was carried out in the range of mass/charge ratios of m/z 35−320, with 4.86 scans s^{-1}.

Another extraction device and GC−MS instrument was used for independent measurements; a different operator examined the similarly prepared samples of data set 2. The instrument used was of the same type and, therefore, identical in construction to the instrument described above. Identical analytical equipment, GC column type, and HS−SPME−GC−MS procedure were used.

Pre-processing and Data Treatment. The three-dimensional GC−MS raw data were converted to a matrix ($N \times M$) giving the intensity values for N samples of M extracted mass features or variables, which comprise the mass/charge ratio (m/z) per time unit (scan). On the basis of the original Agilent files, we performed this pre-processing step with the MetAlign software (http://www.wageningenur.nl, version 080311).[9,26,27] The result was stored as a CSV file.

After this, already extracted mass features, which could confound classification, were removed: (1) previously known and constant GC contaminants comprising cyclosiloxanes from SPME, siloxanes from sample vial septa (m/z 207, 281, etc.), and phthalates (m/z 149), (2) exceptionally disturbing mass features detected by exploratory data analysis with principal component analysis, and (3) mass features

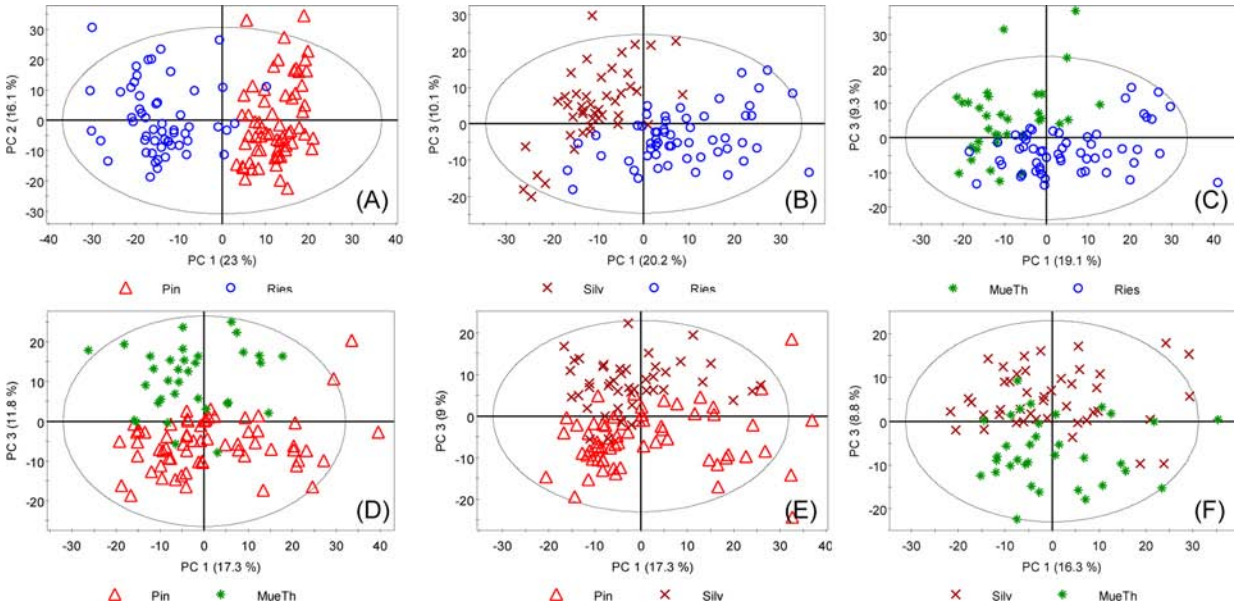

Figure 1. PCA score plots based on restricted numbers of white wine samples (data set 1): (A) Riesling and Pinot (N = 120), (B) Riesling and Silvaner (N = 100), (C) Riesling and Müller-Thurgau (N = 90), (D) Pinot and Müller-Thurgau (N = 98), (E) Pinot and Silvaner (N = 108), and (F) Müller-Thurgau and Silvaner (N = 78). Data set completely treated as proposed, $N \times M$ = 198 × 952. PC $n(x)$: n order number of PC and x explained variance in X [$R^2(X)$] regarding PC n. Ries (circles) = Riesling; Pin (triangles) = Pinot; Silv (crosses) = Silvaner; and MueTh (stars) = Müller-Thurgau.

associated with the internal standards after completion of controlling the alignment step of MetAlign.

Additional preliminary variable reduction to reduce noise[22] was carried out, so that the mass features with occurrence in less than 80% of samples in relation to each of the individual varietal classes used for modeling were removed. Thereby a mass feature with "no occurrence" in a sample was detectable by the constant low value set in the preprocessing step regarding intensities below the absolute threshold. A further step comprised the substitution of all retained mass feature intensities below the absolute threshold by zero to enhance usable signals of low signal-to-noise ratio.

Finally, three steps of common pretreatment methods were followed:[22,28,29] (1) square root transformation lowered heteroscedasticity typical for GC−MS data without changing the actual distribution (pseudo-scaling), (2) the row (sample-wise) scaling to constant total was used to compensate for the wide time range of measuring, and (3) directly prior to data analysis, the column scaling method autoscaling was used.

The variable reduction and pretreatment were examined using Excel (Microsoft Office, version 2010) and SIMCA-P+ (Umetrics, version 12.01.0).

Processing and Multivariate Data Analysis. Principal component analysis (PCA) was used for visualization of the analytical-derived connections among samples and between samples and mass features independent of the origin of samples (unsupervised analysis). It was performed for the purpose of exploratory data analysis. PLS-DA was used for the modeling of samples in relation to the settled classes Y (supervised analysis). A PLS-DA model was based on selected variables deriving from the variable importance in the projection (VIP) value of the variables of an orthogonal PLS-DA (OPLS-DA) model. VIP is the sum of all model dimensions of the contributions of variable influence. Variables with VIP values above 1 are supposed to be the most relevant for explaining Y in relation to the whole model[29] and were, therefore, exclusively used to build a PLS-DA model. OPLS-DA separates the modeled variation into the Y-predictive and Y-orthogonal (Y-unrelated) variation[30] and removes the latter from the model. This statistical technique was therefore most suitable to select the most contributing variables.

Four diagnostic parameters were considered to evaluate the performance of a classification model. First, the goodness of fit (R^2) of a model represents the explained variance used to extract the latent variables [principal components (PCs)] from the total data in relation to the class membership (Y). Second, the goodness of prediction of Y (Q^2) of a model gives an estimation of the result of internal cross-validation by leaving out $^1/_7$ of the data in turn.[29] Third, the classification power of classes was established by assigning test samples to a training model and revealing the percentage of accurately classified samples in relation to all predicted samples per class (% CC). Finally, the visual tool of receiver operating characteristic (ROC) curve analysis was employed, recently recommended to be used to evaluate the classification power of models.[22,24,25,31] A ROC curve is performed when plotting the proportion of true positives (TP) or the sensitivity against the proportion of false positives (FP)[22] or 1 minus the specificity under a varying decision threshold of classification. Thereby, the sensitivity is defined as TP/(TP + FN), and the specificity is defined as TN/(TN + FP), where FN values are false negatives and TN values are true negatives.

The optimization of each performed PLS-DA model was necessary, which means that the relevant number of PC was determined to avoid overoptimiztic modeling. This was carried out by considering (a) the gap between R^2 and Q^2, which should be as small as possible, and (b) Q^2, which should still be increasing.[29] Furthermore, for optimization, the results of a response permutation test, examined with 100 iterations and calculated by linear regression, in general, may not exceed 30% of the permuted R^2 of the random models; otherwise, overfitting of the original model was assumed.[29]

For the external validation of classification models, the OPLS-DA training models were made up of classes of equal size. At least 22 samples (two-class models) or 29 samples (four-class model) of each class were used to form representative training classes. To obtain these, the test samples were removed from the total set of class samples by a randomized selection per measuring block. This procedure was of advantage in comparison to a pure randomized selection because of the restricted number of possible iterations of the validation process. Thus, the chance of each sample to be a part of the test data was increased. At the same time, the analytical variation was considered. The variables were selected from an OPLS-DA training model to build a PLS-DA training model. The latter was optimized as described above, and the test samples were assigned to the PLS-DA training model, giving the prediction result % CC of each class. The

Table 1. Comparison of Two-Class PLS-DA Models Based on Independent Samples and Measurements (Selected Samples of Data Set 1 and Data Set 2)[a]

model	class	members (true class)	correct classification (%)	R^2 (%)	Q^2 (%)	RMSEP	selected variables (VIP > 1)	GC–MS peaks (VIP > 1)
1	Pinot	6	100	93	92	0.16	358	41
	Riesling	21	100					
2	Pinot	11	100	85	84	0.22	175	29
	Riesling	17	100					

[a]Classification of Pinot (Pinot Gris/Pinot Blanc) versus Riesling samples, with test data prediction to the training data (average of three iterations). Training set of model 1: 22 samples per class (N = 44). Training set of model 2: 23 samples per class (N = 46). RMSEP = root mean square error of prediction.

procedure was repeated 3 times (two-class models) or 10 times (four-class model).

Excel (Microsoft Office, version 2010) was used for data set splitting. PCA, PLS-DA, OPLS-DA, response permutation, and VIP/variable selection were examined using SIMCA-P+ (Umetrics, version 12.01.0). ROC curve analysis was carried out with SPSS for Windows (IBM, version 12.0.2) based on the Y prediction values of the test samples assigned to the PLS-DA training models. The determination of associated signals or compounds based on mass features detected in exploratory analysis was examined by consulting the total ion chromatograms (TICs) of samples and a database match of their mass spectra with the National Institute of Standards and Technology (NIST) standard reference database (NIST, version 08).

RESULTS AND DISCUSSION

Exploratory Data Analysis. An untargeted approach was pursued for the classification of wine varietals, so that no GC peaks or mass features were *a priori* selected. Instead, the full information on 7290 scans (data set 1) was pre-processed. The time window of 10–36 min was used, and a data matrix was obtained, comprising 198 observations and the intensities of 6911 mass features for m/z 50 to 320 ($N \times M$ = 198 × 6911).

During exploratory analysis using PCA, we identified and then removed disturbing mass features. These were detected causing strikingly outer-lying samples by comparison of score plots (samples) with loading plots (variables). The TIC of samples were subsequently considered and followed by the examination of MS database match. Non-wine-related mass features comprised additional siloxane signals (m/z 73, 147, 207, 281, etc.) and m/z 205 and 220 deriving from butylhydroxytoluene (BHT), identified by standard addition. All of these mass signals are known to be frequently detected in GC–MS because they derive from common non-wine compounds widely used in technical applications.[32] Furthermore, wine-related mass features causing outer lying of samples were observed, among them the main fragments of ethyl-octanoate and ethyldecanoate. The disturbance was caused by the extreme detector saturation and the oversized width of these peaks, which could not be correctly aligned in the pre-processing step. Thus, the complete set of mass features in relation to these compounds was removed. Other observed alignment errors could be corrected by adjusting the user-defined parameters in the pre-processing step. Finally, the cleared data matrix of data set 1 was of size $N \times M$ = 198 × 5638.

The clustering ability of the data was also revealed by PCA, and the varietal classes used for classification were determined. Pinot Gris and Pinot Blanc wine samples showed identical centering and distributing tendencies and, therefore, formed a joint group "Pinot". This might be due to the fact that, from a botanical view, the two Pinot varietals are related. The similarity has been confirmed by a two-class PLS-DA model of Pinot Gris versus Pinot Blanc wine, which resulted in a model of zero PC, revealing the non-existence of a difference in variation between the two groups. Finally, the four disjoint groups Riesling, Müller-Thurgau, Silvaner, and Pinot are examined. The data display the most distinct variation between Pinot and Riesling wines. Figure 1A shows their grouping mainly along the axis of

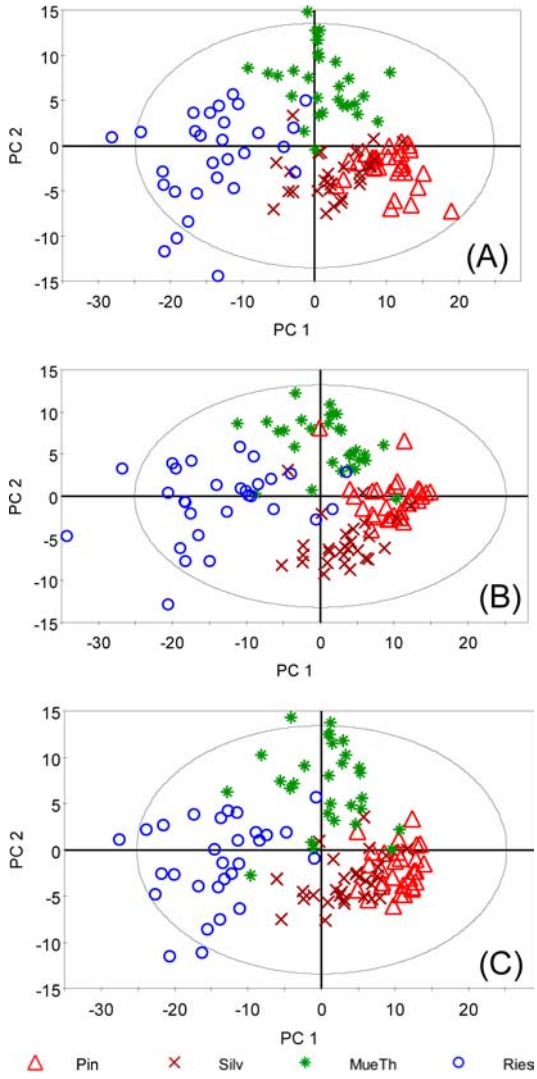

Figure 2. Score plots of example four-class PLS-DA training models (data set 1). Classification of Pinot (Pin, triangles; Pinot Gris and Pinot Blanc) versus Silvaner (Silv, crosses) versus Müller-Thurgau (MueTh, stars) versus Riesling (Ries, circles). A) Training model 2: $N \times M$ = 116 × 290, four PCs, 70.3% R^2; 65.3% Q^2. (B) Training model 7: $N \times M$ = 116 × 305, three PCs, 62.7% R^2; 57.7% Q^2. (C) Training model 10: $N \times M$ = 116 × 285, four PCs, 73.8% R^2; 66.6% Q^2.

dx.doi.org/10.1021/jf502042c | J. Agric. Food Chem. 2014, 62, 6844–6851

Table 2. Test Sample Predictions to Four-Class PLS-DA Training Models (Data Set 1)[a]

class	members (true class)	correct classification (%)	Pinot (predicted)	Silvaner (predicted)	MueTh (predicted)	Riesling (predicted)	AUC
Pinot	35	91	31.8	2	1	0.2	0.97
Silvaner	15	97	0.2	14.5	0.2	0.1	0.98
MueTh	5	80	0.6	0.1	4	0.3	0.96
Riesling	27	93	0	0.8	1.2	25	0.99

[a]Classification of Riesling versus Müller-Thurgau (MueTh) versus Silvaner versus Pinot (Pinot Gris and Pinot Blanc), with correct classification and confusion matrix of the average of 10 iterations. Training data: $N \times M = 116 \times 289$ (average). Test data: $N = 82$. AUC = area under the ROC curve (average).

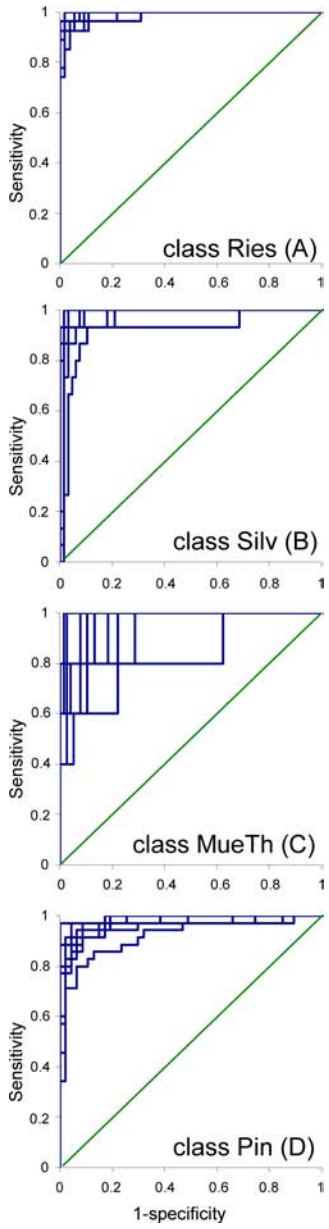

Figure 3. ROC curve analysis of four-class PLS-DA model (data set 1). Per class, all 10 ROC curves of test sample assignment to the training models are shown for classification of (A) Riesling (Ries) versus (B) Silvaner (Silv) versus (C) Müller-Thurgau (MueTh) versus (D) Pinot (Pin; Pinot Gris and Pinot Blanc).

the first PC with an explained variation of 23% $R^2(X)$. In contrast, more PCs are needed to achieve discrimination between other groups (panels B–F of Figure 1). Thus, these cases show sufficient but less variation regarding varietal differences.

Discrimination within the used sample set could not be demonstrated between the vintages 2009 and 2010, between the different quality categories, and between different German vineyard locations. A different study design might be necessary to prove any differences based on these factors. Accordingly, the found varietal classes appeared virtually homogeneous because no influence of the above factors could be detected. Therefore, multi-class varietal classification was examined on the basis of all samples. However, a few samples visually appeared slightly outside a varietal class. This was due to either natural variation or unknown reasons because no further information about samples was available.

Investigating Reliability of Classification. The two-class classification of Riesling versus Pinot using PLS-DA training models resulted in 100% CC for test samples of both classes. However, we could not be certain whether this excellent classification outcome is constant or varies depending upon other factors than the difference of the varietals. Thus, our objective was to conduct a simple approach to find out whether the classification ability was indeed of general validity.

Other factors of variation for a given method of analytics, data treatment, and statistical analysis are as follows: (a) the wine samples used, (b) the extraction by SPME, the GC separation, the MS ionization, and separation as well as detection, and finally, (c) the actual implementation of the given concept of feature extraction.

The present experiment was performed in varying all of these three factors. This comprised new samples (data set 2) measured on a second device. The obtained data were then pre-processed with newly established and appropriate parameters. Details on the MetAlign parameters applied are given with the Supporting Information. All equivalent samples of data set 1 were selected (71 samples). The proposed pre-processing and data treatment was equally applied to the two data sets (selected samples of data set 1 and data set 2). Then, PLS-DA training models based on selected variables were build. Model 1 was then related to the selected samples of data set 1, and model 2 was related to data set 2.

Table 1 shows the results of external validation for the two models. A 100% correct classification for Riesling and Pinot is always obtained, independent from the sample collection and the analytical device used. For modeling the classification question, in both cases, only one PC is necessary. The obtained difference between R^2 and Q^2 for each model was rather small, which demonstrates for both models their excellent prediction ability. However, the prediction of model 2 was based on a lower average percentage of explained variance (R^2). This could be due to a relatively higher degree of other variation sources constituting the data and the possible fact that the differences in relation to the varietals are less pronounced, respectively. Slight

differences in the data distribution of the two models could therefore be assumed. A difference in variable selections was shown in relation to the number resulting from the two data sets, which apply to a different number of peaks in the TIC. Nevertheless, both variable selections qualitatively provided a consistent prediction result. In contrast to the explained variance, the root-mean-square error of prediction (RMSEP) of the external validation is an absolute measure, with its use most suitable to compare models.[21] The average prediction error here was only slightly higher for model 2 and, on the whole, was fairly low pronounced.

Hence, such factors as samples, instrumental device, and feature extraction do not influence the classification result among Riesling and Pinot wine. The difference in the measuring results regarding the varietals was larger than the variation caused by the other factors. Therefore, a constant varietal prediction results from the proposed strategy. This suggests the applicability also to other laboratories. According to Esslinger et al., this kind of investigation is rare in the field of untargeted research but will be needed for future applications to meet control requirements.[4] When reliability is defined here as the frequency with which the classification results are within an allowable error, the experiment achieves 100% reliability for an example classification question. This is due to the fact that the two trials achieve identical results.

Multi-class Varietal Classification and Its Relevance. The present study focuses on the five most frequent German white wine varietals. These are cultivated in Germany on 77% of the white grape vineyard area (2012[33]). For classification, all samples of data set 1 were used, forming the four proposed classes. The PLS-DA training models on average were build with 289 selected variables. Three examples of score plots of the 10 training models are shown in panels A−C of Figure 2. Fairly good clustering of classes is observed. Four PCs on average were necessary to model the differences between the classes. All training models were on average explained by 70% of the variance (R^2). The goodness of prediction obtained was on average 64% (Q^2) which is a typical result achieved by metabolomics data.[29] Because the presented model additionally showed a low difference between R^2 and Q^2, its fairly good prediction ability is demonstrated.

In external validation, the test samples of Riesling, Silvaner, and Pinot classes achieved on average 91−97% CC (Table 2). We could not achieve such results for Müller-Thurgau samples. The small number of Müller-Thurgau test samples might be the reason for a less accurate classification.

Furthermore, we determined some of the substances here contributing to the classification among the four classes. This was examined considering the selected variables with occurrence in at least 8 of 10 PLS-DA training models. The concerned mass features were then related to peaks in the TIC of several example samples. Further, those were subjected to a MS database match. Identification was assumed for more than 90% compliance. It is to be noted that, from the results, no information was available on the absolute contribution of substances to the prediction because of the pretreatment applied. Further, the relation of compounds to a certain varietal class could not be revealed because of the complexity of the model. The monoterpenoids linalool, γ-terpinen*, α-terpineol*, and limonene*, the C_{13}-norisoprenoids 1,1,6-trimethyl-1,2-dihydronaphthalene (TDN)* and vitispirane, and the esters 2-phenylethyl acetate*, methyloctanoate, and methyldecanoate were reliably identified. The marked substances (*) were additionally verified by retention time and mass spectral accordance to reference standards. These findings revealed some varietal-related compounds of monoterpenoids and C_{13}-norisoprenoids[11,34−36] contributing to the white wine classification. These are typical white-wine-related odorants.[34] For example, TDN is typical for Riesling and has a kerosene like odor.[11] Additionally, esters as alcoholic-fermentation-derived aroma compounds contributed, presumably indirectly, as previously reported, for example, regarding the classification of South African wines.[37] All of the contributing compounds were favorably extracted by the used PDMS SPME fibers. Polar compound groups, such as the aliphatic alcohols and acids, were not considered for classification because these were hardly extracted. This shows the volatiles "editing" character of the SPME technique.[1]

In the present study, a validated German white wine prediction based on untargeted data of volatile compounds is established for the first time. The most important German varieties are presented on the basis of commercial samples from all over Germany, comprising two vintages and two quality categories. Therefore, a broad variation of samples is considered. Moreover, the contributing variables are related to important odorants. It should be noted here that the developed method of data treatment, in particular, underpins the consideration of mass features with low signal-to-noise intensity in GC−MS, such as, e.g., linalool. Therefore, also compounds of low sensory threshold are considered for classification. On the whole, the significant relevance of the analytical method and data treatment for white wine is shown. Because the method also shows its ability to achieve reliable results, it is therefore highly adequate for German white wine varietal classification. The untargeted HS−SPME−GC−MS approach might be therefore considered along with other methods, which are used for verifying the botanical origin of white wine varietals, such as the determination of shikimic acid concentration or the application of NMR, to discriminate among a higher number of varietals. Godelmann et al.[38] successfully classified German white wine according to the botanical origin using untargeted NMR data. However, the NMR study equally joined Pinot Gris and Pinot Blanc samples for varietal classification because of their similarity. Therefore, further research on Pinot Gris and Pinot Blanc wine discrimination is of interest. Moreover, the current study could be extended regarding the number of Müller-Thurgau samples. To additionally meet the requirements of the global market, the extension to internationally cultivated white wine varietals would be useful.

Performance of Classification. The correct classification rate (% CC) is widely used to express the results of a classification model. However, this depends upon not only the model but also the decision that a sample belong to a certain class and not to the other nearest or overlapping class. Thus, the % CC normally does not give the full information about a class. ROC curve analysis overcomes the predefinition of a decision rule and visualizes the full performance of a class under varying thresholds. The area under the ROC curve (AUC) additionally gives a value to assess the classification quality of a class. Very good classification performance is discussed to be achieved for an AUC value of above 0.9 and good performance for a value of at least 0.8.[24] An AUC value of 0.5 indicates a full lack of discriminative power.

Thus, the here obtained model achieves very good performance for all classes. The AUC of all classes was above

0.95 (Table 2). However, to observe the differences of the classes in detail, we assessed the performance of each class by the shape of the curves. In a class with a high prediction performance, the ROC curve first rises vertically from the point (0/0) and then abruptly changes direction and continues horizontally toward the point (1/1). In cases of a lower predictive ability, the curve is flattened toward the diagonal line. This line represents pure random prediction. To compare the class performance, ROC curves of the 10 PLS-DA test data predictions were displayed overlapped per class (panels A–D of Figure 3).

First, of all classes, the Riesling class (Figure 3A) shows the best classification performance because all curves are close to the top left corner. In contrast, some of the Müller-Thurgau class curves (Figure 3C) are mostly flattened against the diagonal line and, therefore, show the lowest overall classification performance. This again could be due to a low test sample number. It can be seen that the height of a step in a curve is in relation to the sample number of the class. Furthermore, the Pinot and Silvaner classes show more cases of curves that are lowered at the horizontal part (panels B and D of Figure 3), meaning observed high FP rates.

These results of ROC curve analysis give a comprehensive impression of a class. For example, when considering a possible low FP rate, the Riesling class turns out to be the least sensitive because the test samples showed the maximum of about 30% FP. In contrast, the Pinot class proves to be the most sensitive class because up to about 90% FP was observed. Additionally, this technique could be of interest for future investigations, adjusting a model, for example, in relation to the requirement of a low outcome of FP.

■ ASSOCIATED CONTENT

Ⓢ Supporting Information

Additional information on the established pre-processing and data treatment method, with the MetAlign process including the parameter choice (Table S1) and deviations from the MetAlign processing, formulas of the applied pretreatment (Table S2), impact of the proposed data treatment on the discrimination of white wines (Figure S1), and advantage of the applied variable selection strategy (Table S3 and Figure S2). This material is available free of charge via the Internet at http://pubs.acs.org.

■ AUTHOR INFORMATION

Corresponding Author

*Telephone: +49-30184123393. E-mail: carsten.fauhl-hassek@bfr.bund.de.

Notes

The authors declare no competing financial interest.

■ ACKNOWLEDGMENTS

The authors thank G. Scholten and H. Rudy from DLR Mosel, Germany, for providing the reference chemical 1,1,6-trimethyl-1,2-dihydronaphthalene (TDN).

■ REFERENCES

(1) Pico, Y. *Chemical Analysis of Food: Techniques and Applications*; Academic Press: Waltham, MA, 2012.

(2) Chabreyrie, D.; Chauvet, S.; Guyon, F.; Salagoïty, M.-H.; Antinelli, J. F.; Medina, B. Characterization and quantification of grape variety by means of shikimic acid concentration and protein fingerprint in still white wines. *J. Agric. Food Chem.* **2008**, *56*, 6785–6790.

(3) Koek, M. M.; Jellema, R. H.; van der Greef, J.; Tas, A. C.; Hankemeier, T. Quantitative metabolomics based on gas chromatography mass spectrometry: Status and perspectives. *Metabolomics* **2011**, *7*, 307–328.

(4) Esslinger, S.; Riedl, J.; Fauhl-Hassek, C. Potential and limitations of non-targeted fingerprinting for authentication of food in official control. *Food Res. Int.* **2014**, *60*, 189–204.

(5) Shepherd, L. V. T.; Fraser, P.; Stewart, D. Metabolomics: A second-generation platform for crop and food analysis. *Bioanalysis* **2011**, *3*, 1143–1159.

(6) Hall, R. D.; Hardy, N. W. Practical applications of metabolomics in plant biology. In *Plant Metabolomics. Methods and Protocol*; Hardy, N. W., Hall, R. D., Eds.; Humana Press (Springer): New York, 2012; pp 1–10.

(7) Checa, A.; Saurina, J. Metabolomics and PDO. In *Food Protected Designation of Origin Methodologies and Applications*; de la Guardia, M., Gonzálvez, A., Eds.; Elsevier: Oxford, U.K., 2013. Checa, A.; Saurina, J. Chapter 6—Metabolomics and PDO. *Compr. Anal. Chem.* **2013**, *60*, 123–143.

(8) Smith, C. A.; Want, E. J.; O'Maille, G.; Abagyan, R.; Siuzdak, G. XCMS: Processing mass spectrometry data for metabolite profiling using nonlinear peak alignment, matching, and identification. *Anal. Chem.* **2006**, *78*, 779–787.

(9) Lommen, A. Metalign: Interface-driven, versatile metabolomics tool for hyphenated full-scan mass spectrometry data preprocessing. *Anal. Chem.* **2009**, *81*, 3079–3086.

(10) Cajka, T.; Hajslova, J. Volatile compounds in food authenticity and traceability testing. In *Food Flavors: Chemical, Sensory and Technological Properties*; Jelen, H., Ed.; CRC Press: Boca Raton, FL, 2012; pp 355–411.

(11) Styger, G.; Prior, B.; Bauer, F. F. Wine flavor and aroma. *J. Ind. Microbiol. Biotechnol.* **2011**, *38*, 1145–1159.

(12) Cozzolino, D.; Smyth, H. Analytical and chemometric-based methods to monitor and evaluate wine protected designation. In *Food Protected Designation of Origin Methodologies and Applications*; de la Guardia, M., Gonzálvez, A., Eds.; Elsevier: Oxford, U.K., 2013. Cozzolino, D.; Smyth, H. Chapter 15—Analytical and chemometric-based methods to monitor and evaluate wine protected designation. *Compr. Anal. Chem.* **2013**, *60*, 385–408.

(13) Caligiani, A.; Cirlini, M.; Palla, G. Volatile compounds for the authentication of wine and derived products. In *Food Authentication Using Bioorganic Molecules*; Sforza, S., Ed.; DEStech Publications: Lancaster, PA, 2013; pp 327–360.

(14) Tikunov, Y.; Lommen, A.; De Vos, C. H. R.; Verhoeven, H. A.; Bino, R. J.; Hall, R. D.; Bovy, A. G. A novel approach for nontargeted data analysis for metabolomics. Large-scale profiling of tomato fruit volatiles. *Plant Physiol.* **2005**, *139*, 1125–1137.

(15) Guo, J.; Yue, T.; Yuan, Y. Feature selection and recognition from nonspecific volatile profiles for discrimination of apple juices according to variety and geographical origin. *J. Food Sci.* **2012**, *77*, C1090–C1096.

(16) Malheiro, R.; Guedes De Pinho, P.; Soares, S.; César da Silva Ferreira, A.; Baptista, P. Volatile biomarkers for wild mushrooms species discrimination. *Food Res. Int.* **2013**, *54*, 186–194.

(17) Rocha, S. M.; Coutinho, P.; Barros, A.; Delgadillo, I.; Coimbra, M. A. Rapid tool for distinction of wines based on the global volatile signature. *J. Chromatogr. A* **2006**, *1114*, 188–197.

(18) Marti, M. P.; Busto, O.; Guasch, J. Application of a headspace mass spectrometry system to the differentiation and classification of wines according to their origin, variety and ageing. *J. Chromatogr. A* **2004**, *1057*, 211–217.

(19) Boscaini, E.; Mikoviny, T.; Wisthaler, A.; Hartungen, E. V.; Märk, T. D. Characterization of wine with PTR–MS. *Int. J. Mass Spectrom.* **2004**, *239*, 215–219.

(20) Bakker, J.; Clarke, R. J. *Wine Flavour Chemistry*, 2nd ed.; Wiley-Blackwell: Chichester, U.K., 2012.

(21) Kjeldahl, K.; Bro, R. Some common misunderstandings in chemometrics. *J. Chemom.* **2010**, *24*, 558–564.

(22) Brereton, R. G. *Chemometrics for Pattern Recognition*; Wiley: Chichester, U.K., 2009.
(23) Brereton, R. G. Consequences of sample size, variable selection, and model validation and optimization, for predicting classification ability from analytical data. *Trends Anal. Chem.* **2006**, *25*, 1103−1111.
(24) Broadhurst, D. I.; Kell, D. B. Statistical strategies for avoiding false discoveries in metabolomics and related experiments. *Metabolomics* **2006**, *2*, 171−196.
(25) Oliveri, P.; Downey, G. Multivariate class modeling for the verification of food-authenticity claims. *Trends Anal. Chem.* **2012**, *35*, 74−86.
(26) Lommen, A. Data (pre-)processing of nominal and accurate mass LC−MS or GC−MS data using metalign. In *Plant Metabolomics. Methods and Protocol*; Hardy, N. W., Hall, R. D., Eds.; Humana Press (Springer): New York, 2012; pp 229−253.
(27) De Vos, R. C. H.; Moco, S.; Lommen, A.; Keurentjes, J. J. B.; Bino, R. J.; Hall, R. D. Untargeted large-scale plant metabolomics using liquid chromatography coupled to mass spectrometry. *Nat. Protoc.* **2007**, *2*, 778−791.
(28) van den Berg, R. A.; Hoefsloot, H. C. J.; Westerhuis, J. A.; Smilde, A. K.; van der Werf, M. J. Centering, scaling, and transformations: Improving the biological information content of metabolomics data. *BMC Genomics* **2006**, *7*, No. 142.
(29) Eriksson, L.; Johansson, E.; Kettaneh-Wold, N.; Trygg, J.; Wikström, C.; Wold, S. *Multi- and Megavariate Data Analysis. Part I Basic Principles and Applications*; Umetrics AB: Umeå, Sweden, 2006.
(30) Eriksson, L.; Johansson, E.; Kettaneh-Wold, N.; Trygg, J.; Wikström, C.; Wold, S. *Multi- and Megavariate Data Analysis. Part II Advanced Applications and Method Extensions*; Umetrics AB: Umeå, Sweden, 2006.
(31) Brown, C. D.; Davis, H. T. Receiver operating characteristics curves and related decision measures: A tutorial. *Chemom. Intell. Lab. Syst.* **2006**, *80*, 24−38.
(32) Hübschmann, J. *Handbook of GC/MS. Fundamentals and Applications*; Wiley-VCH: Weinheim, Germany, 2001.
(33) *Statistics on German Wine 2013−2014*; http://www.germanwines.de (press service/statistics, accessed April 2014).
(34) Fischer, U. Wine aroma. In *Flavours and Fragrances. Chemistry, Bioprocessing and Sustainability*; Berger, R. G., Ed.; Springer: Berlin, Germany, 2007; pp 241−267.
(35) Ebeler, S. E.; Thorngate, J. H. Wine chemistry and flavor: Looking into the crystal glass. *J. Agric. Food Chem.* **2009**, *57*, 8098−8108.
(36) Mendes-Pinto, M. M. Carotenoid breakdown products−the norisoprenoids−in wine aroma. *Arch. Biochem. Biophys.* **2009**, *483*, 236−245.
(37) Tredoux, A.; De Villiers, A.; Májek, P.; Lynen, F.; Crouch, A.; Sandra, P. Stir bar sorptive extraction combined with GC−MS analysis and chemometric methods for the classification of South African wines according to the volatile composition. *J. Agric. Food Chem.* **2008**, *56*, 4286−4296.
(38) Godelmann, R.; Fang, F.; Humpfer, E.; Schütz, B.; Bansbach, M.; Schäfer, H.; Spraul, M. Targeted and nontargeted wine analysis by ^{1}H NMR spectroscopy combined with multivariate statistical analysis. Differentiation of important parameters: Grape variety, geographical origin, year of vintage. *J. Agric. Food Chem.* **2013**, *61*, 5610−5619.

Table 1. Presence and Identity of pH 4.6 Soluble Peptides from α_{S1}-CN Formed by Plasmin in Directly Heated UHT Milk; Peptides with Q Values >1400 Are Potentially Bitter and Are Shown in Bold

		storage time				
peptide[a]	mass	day 1	4 weeks	8 weeks	14 weeks	Q value[b]
α_{S1}-CN f(1−7)	874.55		x	x	x	1777
α_{S1}-CN f(1−22)	2615.48		x	x	x	1297
α_{S1}-CN f(23−34)	1383.72		x	x	x	1833
α_{S1}-CN f(23−36)	1640.86			x	x	1718
α_{S1}-CN f(35−42)	945.51			x	x	1030
α_{S1}-CN f(80−90)	1336.67	x	x	x	x	1054
α_{S1}-CN f(80−100)	2585.37				x	1342
α_{S1}-CN f(80−102)	2826.54			x		1396
α_{S1}-CN f(91−100)	1266.70			x	x	1660
α_{S1}-CN f(91−102)	1507.88			x	x	1710
α_{S1}-CN f(91−103)	1635.97			x	x	1694
α_{S1}-CN f(91−105)	1927.14				x	1759
α_{S1}-CN f(100−105)	678.45			x	x	1753
α_{S1}-CN f(101−124) + P	2916.53				x	1358
α_{S1}-CN f(103−124) + P	2675.35		x	x	x	1304
α_{S1}-CN f(104−119) + P	1950.95				x	1339
α_{S1}-CN f(104−124) + P	2547.26		x	x	x	1294
α_{S1}-CN f(106−119) + P	1659.79			x	x	1218
α_{S1}-CN f(106−124) + P	2256.10		x	x	x	1201
α_{S1}-CN f(120−124)	614.32			x	x	1152
α_{S1}-CN f(125−132)	909.47				x	756
α_{S1}-CN f(194−199)	747.36		x	x	x	1703

[a]Phosphorylations are indicated after the peptide. [b]Q value was calculated according to Ney (1971) in cal mol^{-1}. Presence of peptides at different storage times is indicated by 'x'.

this time more than 90% of α- and β-CNs were hydrolyzed. The relatively low degree of β-lg denaturation in the UHT milk of 36.7 ± 3.2% indicated that the age gelation may be caused by a different mechanism than complexation of κ-CN with denatured β-lg. At this level of β-lg denaturation, only a very limited fraction of β-lg is associated with κ-CN.[22,23]

The aim of the present study was to analyze the peptide formation and specificity of PL in this UHT milk and to relate the peptides found with the previously observed bitter off-flavor and age gelation of the UHT milk during storage.

MATERIALS AND METHODS

Milk Processing. Three batches of 1 day old pasteurized (72 °C for 15 s) and homogenized milk (1.5% fat) were obtained from Arla Foods Stockholm Dairy (Sweden) during three consecutive weeks. The milk was preheat treated at 74 °C for 180 s in a tubular heat exchanger before being subjected to a direct steam infusion heat treatment at >150 °C for <0.2 s (UHT pilot plant, APV/SPX, Silkeborg, Denmark). After flash cooling to 67 °C, the milk was homogenized (pressure 160/40 bar), further cooled to 20 °C, and packed aseptically in 300 mL glass bottles. The UHT milk was stored in the dark at 20 °C in a climate chamber for 14 weeks. One bottle was used once every week of the storage period for analysis. The sterility of each batch of processed milk was tested according to ISO 4833.[24]

Sample Preparation. A volume of 15 mL of milk was taken from each bottle and adjusted to pH 4.6 with 1 M HCl followed by centrifugation at 11000*g* for 10 min at 4 °C. The clear supernatant was recovered and stored at −20 °C until further analysis. At the time of analysis, the samples were thawed for 60 min at room temperature. One mL of the sample was centrifuged at 13200*g* at 5 °C for 10 min and used for the analysis. Sample preparation was performed in duplicate.

Peptide Analysis. Ultra-high-performance liquid chromatography (uHPLC) was performed on an Agilent 1290 Infinity uHPLC (Agilent Technologies, Santa Clara, CA, USA) coupled to a quadrupole-time-of-flight mass spectrometer (Q-TOF MS, Agilent 6530 Accurate Mass Q-TOF LC/MS, Agilent Technologies) with a Jetstream interface.

Depending on the peptide concentration, 10 or 20 μL of the sample was injected to the uHPLC-Q-TOF-MS system. The column was an Xbridge BEH 300 (rp-C_{18}, 3.5 μm 2.1 mm × 250 mm) (Waters, Milford, MA, USA) operated at 45 °C. Buffer A was Milli-Q water with 0.05% trifluoroacetic acid (TFA) (v/v and buffer B acetonitrile with 0.1% (v/v) TFA. A linear gradient was applied with 100% buffer A from 3 min, 100% to 45% buffer A at 45 min at a flow rate of 0.3 mL min^{-1}. Peptides were monitored at 214 nm.

The Q-TOF MS was run in 4 GHz high resolution mode. The Jetstream interface added a sheath gas at 350 °C with a flow of 8 L min^{-1}. A nozzle voltage of 100 V was applied to improve the ionization. The drying gas temperature was set to 325 °C at a flow rate of 10 L min^{-1}. The capillary voltage was set to 2.5 kV in the first time segment (3.0−24.0 min) and to 4.0 kV in the second time segment (24.0−35.2 min) to achieve optimal ionization for both small and large peptides. Spectra in the mass range from 300 to 3200 m/z were recorded in positive mode with a resolution of 20000 in the Q-TOF. Tandem mass spectra of the two most abundant ions with a charge state of 1, 2, or 3 in each MS spectrum were obtained in collision-induced dissociation (CID) mode (collision gas nitrogen, isolation width 1.3 m/z (narrow) at 5 different fixed collision energies and flexible collision energies optimized for larger peptides. The fixed collision energies were 10, 20, 30, 50, and 100 V, and the flexible energy settings were based on charge state and m/z (singly charged: offset 18 V, slope 3 V m/z^{-1}; doubly charged: offset 2 V, slope 2.2 V m/z^{-1}; triply charged: offset 3.5 V, slope 1.5 V m/z^{-1}). Mass spectra and UV chromatograms were analyzed by MassHunter software (version B 6.01, Agilent Technologies).The MS spectra were investigated for potential peptides formed by plasmin, which were not identified by MS/MS, using the "Find by Formula" feature in MassHunter. Matching ions and isotopic patterns were further evaluated with regard to their retention time.

Database Search. The obtained tandem mass spectra were analyzed with Mascot v2.4 (Matrix Science, London, UK). Tandem mass spectra were searched against a custom database containing

known genetic and PTM (post translation modification) variants of major milk proteins. The following search parameters were applied: protease: unspecific; mass tolerance for precursor ions 15 ppm and 0.6 Da for product ions; variable modifications: phosphorylations serine, oxidation methionine. Only identified peptides (expect score <0.05) that were present in at least two of the three replicates were considered.

Relative Quantification of Identified Peptides. Peaks in the UV chromatogram were identified by their corresponding MS spectra and retention time of the identified peptides by MS/MS. The retention time shift between the UV and MS signal was approximately 0.25 min. Only peaks without or with only minor overlaps with other components in the MS spectra were considered. In order to compare the rate of peptide formation, the integrated UV peak area was divided by a calculated molar extinction coefficient (ε) for the peptide as described previously.[25] Phosphorylation of serine was not taken into account. Peak areas were further normalized for the initial casein distribution to correct for the differences in peptide concentration. The casein composition was based on the UV peak area corrected for the calculated ε (α_{S1}-CN: 30%, α_{S2}-CN: 13%, β-CN: 44%, κ-CN: 13%). Calculated ε in M^{-1} cm^{-1} were 346843 (α_{S1}-CN), 375032 (α_{S2}-CN), 331417 (β-CN) and 279859 (κ-CN).

Assessment of Bitterness. Bitterness of peptides was evaluated by applying Ney's Q-rule based on peptide hydrophobicity.[26] An average hydrophobicity Q of the peptide is calculated as the sum of the amino acids side chains hydrophobicity divided by the number of amino acid residues of the peptide. Peptides with a Q value >1400 cal/res^{-1} are considered bitter

RESULTS AND DISCUSSION

A total of 84 different casein-derived peptides were identified by the uHPLC-Q-TOF analysis (Tables 1−4). In the 1 day old milk (analyzed 1 day after processing), only 11 peptides could be identified by MS/MS. This number is small compared to other recent studies, which used more profound peptide extraction and concentration methods.[18,19] The main objective in this study, however, was to study the proteolysis and development of peptides during storage rather than the peptide profile of the milk used for the UHT treatment. The majority by number of the peptides identified were derived from α_{S2}-CN (36 peptides), followed by α_{S1}-CN (31) and β-CN (17). During the entire storage period, no peptides derived from κ-CN were detected, indicating that indigenous proteases other than PL, such as cathepsin D, were probably heat inactivated as could be expected due to their lower heat stability compared with PL and also that the raw material had not contained heat stable proteases from psychotrophic bacteria, which are known to be able to hydrolyze κ-CN.[27,28] More than 75% of the peptides (66 peptides out of 79) could be assigned to be the result of PL action solely (Table 4). In the remaining 18 identified peptides, PL was responsible for either the N- or C-terminal cleavage in 11 of the 18 identified peptides.

Identified Peptides Formed by Plasmin. Identified peptides derived from α_{S1}-CN and the storage time of their appearance is shown in Table 1. The position of the peptides within in the α_{S1}-CN sequence is shown in Figure 1. The only peptide present after 1 day of storage was α_{S1}-CN f(80−90), suggesting Lys_{79}-His_{80} and Arg_{90}-Tyr_{91} to be the initial sites cleaved by PL. After 4 weeks of storage, the peptides identified originated from the N-terminal region of α_{S1}-CN (Arg_{22}-Phe_{23} and Lys_7-His_8), from the central, lysine-rich region (Lys_{102}-Lys_{103}, Lys_{103}-Tyr_{104}, Lys_{105}-Val_{106}, and Lys_{124}-Glu_{125}) as well as the C-terminal end with cleavage at Lys_{193}-Thr_{194}. The peptides α_{S1}-CN f(91−102), α_{S1}-CN f(91−103), and α_{S1}-CN f(91−105) were not identified until after 8 or 14 weeks of storage,

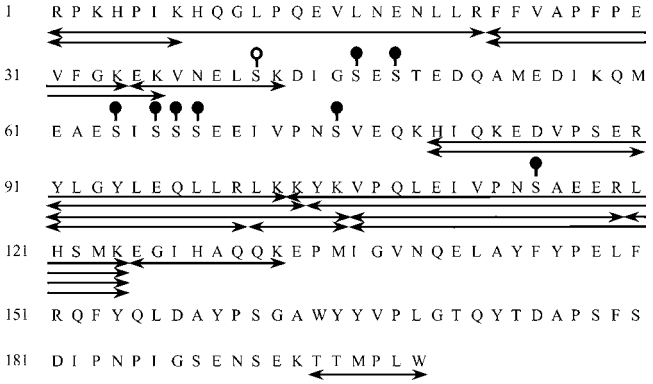

Figure 1. Primary structure of bovine α_{S1}-CN B-8P. Phosphoserine residues are indicated by circles. Open circle indicates a possible phosphorylation at Ser_{41}. Identified pH 4.6 soluble peptides formed by plasmin during storage at 20 °C are indicated by arrows.

indicating that Lys_{79}-His_{80} and Lys_{124}-Glu125 are the two major cleavage sites in the central region of α_{S1}-CN. The peptides α_{S1}-CN f(23−34), α_{S1}-CN f(23−36), and α_{S1}-CN f(35−42) appeared after 4−8 weeks of storage. This implies a sequential cleavage of the N-terminal region of α_{S1}-CN by PL beginning at Arg_{22}-Phe_{23} and subsequently Lys_{34}-Glu_{35} and Lys_{36}-Val_{37}. Peptides containing these cleavage sites Arg_{100}-Leu_{101}, Arg_{119}-Leu_{120}, and Lys_{132}-Glu_{133} occur only after 8 or 14 weeks of storage and seem not to be preferred by PL. The late or slow cleavage at these positions is most likely due to the preference of PL for cleaving after lysine rather than after arginine[29] and their close proximity to the major cleavage sites makes a further hydrolysis in the vicinity unlikely.

The identified cleavage sites of PL and the order of occurrence are in good agreement with previous studies using purified α_{S1}-CN[17,29] with the exception of the cleavage sites at Arg_{151}-Gln_{152}, a proposed major cleavage site by McSweeney et al.,[17] and at Lys_{58}-Gln_{59}. Relevant peptides and polypeptides containing the cleavage site Arg_{151}-Gln_{152} (α_{S1}-CN f(125−151), α_{S1}-CN f(133−151), α_{S1}-CN f(106−151), and α_{S1}-CN f(152−199)) were not detected. The cleavage site Arg_{151}-Gln_{152} is located in middle of the most hydrophobic region of α_{S1}-CN (Figure 4A), which has been identified as the main polymerization and interaction region of α_{S1}-CN via hydrophobic interactions.[30] In contrast to purified α_{S1}-CN, this region is likely to be inaccessible for PL and Arg_{151}-Gln_{152} and was also not hydrolyzed by trypsin in a micellar system.[31,32] The second not-present cleavage site, Lys_{58}-Gln_{59}, is placed between the two phosphoserine clusters of α_{S1}-CN (residues 41−51 and 61−70). The phosphoserine residues tightly bind to the calcium phosphate clusters in the casein micelle, which makes this region inaccessible for enzymatic hydrolysis.[31,33]

The largest numbers of peptides present as a result of PL activity derives from α_{S2}-CN (Table 2). After 1 day of storage, peptides originating from the N- and C-terminal region of α_{S2}-CN were present (Figure 2). The C-terminal region of α_{S2}-CN has previously been shown to be exposed and easily accessible for hydrolysis,[34] and the appearance of α_{S2}-CN f(182−188) and α_{S2}-CN f(174−181) after 4 weeks of storage suggests a sequential hydrolysis of the C-terminal region. Initial cleavage sites are Lys_{197}-Thr_{198} and Lys_{188}-Ala_{189}, followed by Lys_{181}-Thr_{182} and Lys_{173}-Phe_{174}. After the same storage time, peptides originating from the central region of α_{S2}-CN were formed by hydrolysis of Arg_{114}-Asn_{115}, Lys_{136}-Lys_{137}, Lys_{137}-Thr_{138}, Lys_{149}-

Table 2. Presence and Identity of pH 4.6 Soluble Peptides from α_{S2}-CN Formed by Plasmin in Directly Heated UHT Milk; Peptides with Q Values >1400 Are Potentially Bitter and Are Shown in Bold

		storage time				
peptide[a]	mass	day 1	4 weeks	8 weeks	14 weeks	Q value[b]
α_{S2}-CN f(1−21) + 4P	2745.99	x	x	x	x	880
α_{S2}-CNf(1−24)[c] + 4P	3131.19	x	x	x	x	851
α_{S2}-CN f(25−45)[d]	2380.15				x	1019
α_{S2}-CN f(71−80)	1245.64			x	x	1245
α_{S2}-CN f(115−125)	1194.67				x	1331
α_{S2}-CN f(115−136) + 2P	2587.16		x	x	x	939
α_{S2}-CN f(115−137) + 2 P	2715.25			x	x	963
α_{S2}-CN f(115−149) + 3 P	4162.85		x		x	971
α_{S2}-CN f(115−150) + 3 P[c]	4290.94		x	x	x	986
α_{S2}-CN f(137−149) + P	1593.70		x	x	x	1025
α_{S2}-CN f(137−150) + P	1721.80		x	x	x	1059
α_{S2}-CNf(138−149) + P	1465.61		x	x	x	986
α_{S2}-CN f(138−150) + P	1593.70		x	x	x	1025
α_{S2}-CN f(150−165)	1990.12			x	x	1215
α_{S2}-CN f(151−165)	1862.03			x	x	1177
α_{S2}-CN f(151−166)	1990.12			x	x	1197
α_{S2}-CN f(151−173)	2893.61			x	x	1177
α_{S2}-CN f(153−165)	2632.88				x	1208
α_{S2}-CN f(166−173)	1049.60			x	x	1176
α_{S2}-CN f(167−173)	921.50			x	x	1130
α_{S2}-CN f(171−181)	1397.77			x	x	1762
α_{S2}-CN f(174−181)	978.55		x	x	x	1846
α_{S2}-CN f(174−188)	1863.00			x	x	1463
α_{S2}-CN f(182−188)	902.46		x	x	x	971
α_{S2}-CN f(182−197)	1982.06		x	x	x	1434
α_{S2}-CN f(182−207)	3214.78		x		x	1644
α_{S2}-CN f(189−197)	1097.61		x	x	x	1793
α_{S2}-CN f(189−199)	1326.75			x	x	1644
α_{S2}-CNf(189−207)	2330.33	x	x	x	x	1892
α_{S2}-CNf(198−205)	974.59			x	x	1814
α_{S2}-CNf(198−207)	1250.74	x	x	x	x	1980
α_{S2}-CNf(200−207)	1021.60		x	x	x	2233

[a]Phosphorylations are indicated after the peptide. [b]Q value was calculated according to Ney (1971) in cal mol^{-1}. [c]Peptide was identified by MS only. [d]Intramolecular disulfide bond. Presence of peptides at different storage times is indicated by 'x'.

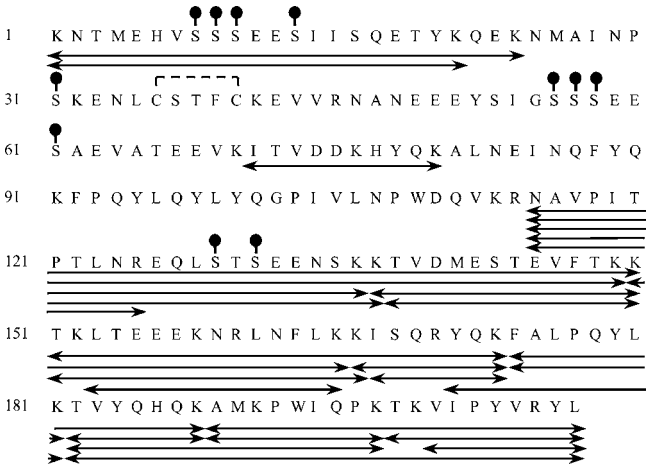

Figure 2. Primary structure of bovine α_{S2}-CN A-11P. Phosphoserine residues are indicated by circles. The dotted line between Cys_{36} and Cys_{40} indicates the intramolecular disulfide bridge. Identified pH 4.6 soluble peptides formed by plasmin during storage at 20 °C are indicated by arrows.

Lys_{150}, and Lys_{150}-Thr_{151}. Earlier studies suggest that the cleavage sites Lys_{149}-Lys_{150} and Lys_{150}-Thr_{151} are preferred over Arg_{114}-Asn115,[16] but the simultaneous appearance of α_{S2}-CN f(115−136), α_{S2}-CN f(137−149), and α_{S2}-CN f(138−150) indicate that PL readily hydrolyzed all of these cleavage sites. After 8 weeks of storage peptides originating from the region 151−173 in α_{S2}-CN were identified. The late appearance of these peptides indicates a sequential hydrolysis of this region from an N- and C-terminal direction after the preferred cleavage sites Lys_{150}-Thr_{151} and Lys_{173}-Phe_{174} are hydrolyzed. The least preferred cleavage sites in α_{S2}-CN seem to be Arg_{125}-Glu_{126} and Lys_{152}-Leu_{153}, which are either in close proximity to phosphoserine residues or to major cleavage sites (Figure 2). Although the region 25−114 contains eight potential cleavage sites for PL, only α_{S2}-CN f(71−80) and α_{S2}-CN f(25−45) could be identified. Masses corresponding to peptides including the cleavage site Lys_{91}-Phe_{92}, Lys_{32}-Glu_{33}, and Lys_{41}-Glu_{42} were not present in the milk. The not-present cleavage at Lys_{91}-Phe_{92} is located in a hydrophobic region of α_{S2}-CN (Figure 4B), which may be inaccessible for enzymatic hydrolysis.[35] Cleavage of this bond can be additionally hindered by Pro_{93} which induces a change in the secondary structure of α_{S2}-CN.[35] Lys_{32}-Glu_{33} and Lys_{41}-Glu_{42} are located in the proximity of the two

dx.doi.org/10.1021/jf502088u | J. Agric. Food Chem. 2014, 62, 6852−6860

Table 3. Presence and Identity of pH 4.6 Soluble Peptides from β-CN Formed by Plasmin in Directly Heated UHT Milk; Peptides with Q Values >1400 Are Potentially Bitter and Are Shown in Bold

		storage time				
peptide[a]	mass	day 1	4 weeks	8 weeks	14 weeks	Q value[b]
β-CN f(1−25) + 4P	3121.26			x	x	1006
β-CN f(1−28) + 4P	3476.48	x	x	x	x	1057
β-CN f(1−29) + 4P	3604.58	x	x	x	x	1072
β-CN f(29−48) + P	2559.13	x	x	x	x	818
β-CN f(33−48) + P	2060.82			x	x	614
β-CN f(98−105)	872.48		x	x	x	1328
β-CN f(98−107)	1137.63	x	x	x	x	1262
β-CN f(100−105)	645.32		x	x	x	1238
β-CN f(100−107)	910.47		x	x	x	1179
β-CN f(106−113)	1012.52		x	x	x	1655
β-CN f(108−113)	747.36		x	x	x	1873
β-CN f(170−176)	779.49		x	x	x	1777

[a]Phosphorylations are indicated after the peptide. [b]Q value was calculated according to Ney (1971) in cal mol^{-1}. Presence of peptides at different storage times is indicated by 'x'.

cysteine residues of α_{S2}-CN. The majority of the α_{S2}-CN molecules is present in a form with an intramolecular disulfide bond, which induces a tight loop in the protein[34,36] which may limit the accessibility of Lys_{41}-Glu_{42} and Lys_{32}-Glu_{33} for PL. To our knowledge, the cleavage of Arg_{45}-Asn_{46}, Lys_{70}-Ile_{71}, Lys_{80}-Ile_{81}, Arg_{125}-Glu_{126}, Lys_{166}-Ile_{167}, and Arg_{205}-Tyr_{206} has not been reported earlier for PL in either model studies or as part of the indigenous peptide profile in milk. This could be attributed to the low concentration of α_{S2}-CN in milk or a different conformation of α_{S2}-CN in model systems.[31,35]

In comparison to α_{S2}-CN, only a relatively small number of peptides was identified derived from β-CN (Table 3). The peptides β-CN f(1−28), β-CN f(1−29), β-CN f(29−48), and β-CN f(98−107) were present in the milk after 1 day of storage. After 4 weeks of storage, all the observed peptides except β-CN f(33−48) and β-CN f(1−25) were present. The identified peptides mainly derived from cleavage around the two major cleavage sites of PL in β-CN, Lys_{105}-His_{106}, and Lys_{107}-Glu_{108} (Figure 3). The peptide β-CN f(170−176) was the only identified peptide originating from the hydrophobic C-terminal part of β-CN and in contrast to earlier studies using trypsin,[31,37] no peptides were identified from hydrolysis of Arg_{183}-Asp_{184} and Arg_{202}-Gly_{203}.

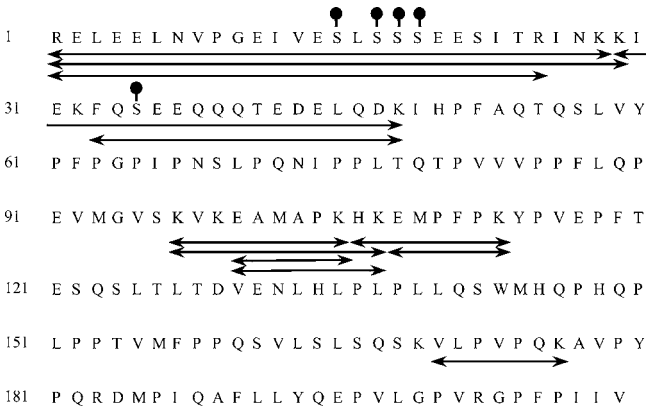

Figure 3. Primary structure of bovine β-CN A^2-5P. Phosphoserine residues are indicated by circles. Identified pH 4.6 soluble peptides formed by plasmin during storage at 20 °C are indicated by arrows.

Peptides Formed by Other Proteases. Peptides that were identified in the UHT milk samples and which cannot be assigned to be a result of PL activity alone are summarized in Table 4. Most peptides deriving from α_{S1}-CN or β-CN indicate activity of cathepsins alone or in combination with PL.[28,38,39] Peptides formed by cathepsins alone were identified after 1 day of storage or after 4 weeks of storage in the case of α_{S1}-CN f(1−14). Peptides formed by the combined activity of cathepsins and PL on the other hand appear after 4−8 weeks of storage. This indicates that cathepsins were active in the raw or pasteurized milk, but inactivated by the UHT treatment and that the polypeptides formed by cathepsins were further hydrolyzed by residual PL to smaller peptides. With the exception of cathepsin D, the heat stability of cathepsins is largely unknown. Although cathepsin D in its active form can partially survive HTST pasteurization,[40] it is unlikely that sufficient active cathepsins are present after the UHT treatment to significantly contribute to the observed proteolysis. The peptides deriving from α_{S2}-CN originate from the C-terminal of the protein. With the exception of α_{S2}-CN f(201−206), the peptides contained the PL cleavage site Lys_{197}-Thr_{198}. The apparently unspecific C-terminal cleavage site of the peptides suggests activity of carboxypeptidases in the raw milk or heat-induced hydrolysis.[41,42]

Peptide Development during Storage. The presence of identified peptides after different storage periods gives a good indication of preferred and uncleaved cleavage sites of PL in the UHT milk system, but only gives limited information on the actual concentration and development of the peptides. Semiquantitative analysis of the peptides using MS spectra was not possible because their response factors are unknown and their intensity might be affected by ion suppression of coeluting components. The UV chromatograms at 214 nm were therefore used for a relative quantification and comparison of the peptides. Due to substantial overlap of large areas in the chromatogram, only a limited number of peaks could be used for such relative quantification. Quantified peptides included α_{S1}-CN f(1−22), α_{S1}-CN f(106−124), α_{S2}-CN f(1−21), α_{S2}-CN f(1−24), α_{S2}-CN f(115−150), as well as β-CN f(1−28) and β-CN f(29−48). A comparison of the UV peaks and the extracted ion chromatograms are shown in the Supporting Information together with MS spectra of the peaks.

Table 4. Presence and Identity of pH 4.6 Soluble Casein Derived Peptides Formed by Other Proteases in Directly Heated UHT Milk; Peptides with Q Values >1400 Are Potentially Bitter and Are Shown in Bold

		storage time					protease[b]	
peptide	mass	day 1	4 weeks	8 weeks	14 weeks	Q value[a]	N-terminal	C-terminal
α_{S1}-CN f(1−8)	1011.62	x		x	x	1618	−	?
α_{S1}-CN f(1−14)	1663.93		x	x	x	1309	−	CB
α_{S1}-CN f(1−21)	2459.38	x	x	x	x	1324	−	CG
α_{S1}-CN f(1−24)	2909.61		x	x	x	1410	−	CB,CD
α_{S1}-CN f(3−7)	621.40				x	1598	CB	PL
α_{S1}-CN f(24−36)	1089.59			x	x	1646	CB,CD	PL
α_{S1}-CN f(25−36)	1236.66			x	x	1563	CB,CD	PL
α_{S1}-CN f(180−199)	2215.05	x	x	x	x	1232	CG	−
α_{S1}-CN f(185−199)	1688.81		x	x	x	1232	?	−
α_{S2}-CN f(198−202)	556.36		x	x	x	1844	PL	CP
α_{S2}-CN f(198−203)	719.42		x	x	x	2015	PL	CP
α_{S2}-CN f(198−204)	818.49		x	x		1969	PL	CP
α_{S2}-CN f(201−206)	809.44				x	2292	?	CP
β-CN f(96−105)	1087.61		x	x	x	1180	CD,CG	PL
β-CN f(96−107)	1352.76		x	x		1262	CD,CG	PL
β-CN f(106−125)	2390.16			x	x	1482	PL	CD
β-CN f(108−125)	2125.00			x	x	1535	PL	CD
β-CN f(163−169)	761.43				x	909	CB,CD	PL

[a]Q value was calculated according to Ney (1971) in cal mol^{-1}. [b]Possible responsible proteases for N- and C-terminal cleavage are indicated: CB, cathepsin B; CD, cathepsin D; CG, cathepsin G; PL, plasmin; CP, carboxypeptidase; −, no cleavage; ?, unknown protease. Presence of peptides at different storage times is indicated by 'x'.

A comparison of peptides originating from the N-terminus of their parent proteins is shown in Figure 5. The peptide β-CN f(1−28) had the highest formation rate. During the first 4−5 weeks of storage, the relative concentration increased exponentially, reflecting the previously described increase in PL activity and rate of peptide formation. From 5 weeks of storage and further on, the relative concentration of β-CN f(1−28) increased almost linearly and then leveled out after 12 weeks of storage. The decrease in the rate of formation could be linked to changes in the matrix induced by the starting gelation of the milk after 11 weeks of storage. Further degradation of β-CN f(1−28) to β-CN f(1−25) may also reduce the concentration. Since the proteose peptones β-CN f(1−105) and β-CN f(1−107) were still present after 14 weeks of storage (data not shown), substrate depletion can be excluded as a cause for the reduced rate of formation. The peptide α_{S2}-CN f(1−24) showed the same initial rate of formation as β-CN f(1−28) and leveled off after 6 weeks of storage. The peptide α_{S2}-CN f(1−21) exhibited a lower rate of formation than α_{S2}-CN f(1−24), but in contrast to α_{S2}-CN f(1−24), continued to increase after 6 weeks of storage. This indicates a hydrolysis of α_{S2}-CN f(1−24) to α_{S2}-CN f(1−21) that may be caused by substrate depletion of the cleavage site Lys_{24}-Asn_{25}. The development of α_{S1}-CN f(1−22) differed from the other N-terminal peptides. The initial lag phase was not observable for α_{S1}-CN f(1−22), and the overall concentration was significantly lower compared to that of the N-terminal peptides derived from α_{S2}- and β-CN. The cleavage sites for these peptides in α_{S2}- and β-CN are in very hydrophilic domains of the proteins (Figure 4 A−C), while the cleavage site Arg_{22}-Phe_{23} in α_{S1}-CN is in a hydrophobic domain involved in casein−casein interactions.[43]

Peptides being present as the result of two proteolytic cleavages are shown in Figure 6. They exhibited an extended lag phase compared to the N-terminal peptides, due to the time needed to form their precursors. As discussed above, α_{S2}-CN f(115−150) originates from two of the most preferred cleavage sites in α_{S2}-CN and showed the highest formation rate. The peptide α_{S1}-CN f(106−124) developed almost in the same manner as α_{S1}-CN f(1−22) within the first 6 weeks of storage but showed a higher rate of formation from 7 weeks of storage on. These findings further highlight the preference of PL for cleavage sites located in the hydrophilic regions of the caseins. Gagnaire et al. (1998) found that the proteose peptones β-CN f(1−105/7) were retained in the casein micelle, while β-CN f(29−105/7) was released into the serum phase.[31] This release limits further hydrolysis of these proteose peptones by the casein-associated PL, which explains why β-CN f(29−48) was only formed in very small amounts.

Destabilization of Casein Micelles by Proteolysis. PL enters the milk from the blood[44] and associates itself with the casein micelle.[45] Whether PL is able to enter the micellar structure or is located entirely on the surface of the casein micelle is unknown. It becomes obvious from Figure 3 that the majority of the major cleavage sites of PL within the caseins, similar to those of trypsin,[31,32] are located at the most hydrophilic and serum-exposed regions of the proteins. β-CN is mainly present in the interior of the casein micelle[46] and is proposed to stabilize water or serum channels within the casein micelle.[47,48] α_{S2}-CN is involved in the binding to calcium phosphate clusters, regions that are hypothesized to be surrounded by hydrophobic domains[11] and likely to be inaccessible for PL. The rapid cleavage, within 4 weeks of storage, of the N-terminal regions of β-CN and α_{S2}-CN implies that PL is able to penetrate the casein micelle. In relation to a destabilization of the casein micelle by proteolysis, it is notable that the minor cleavage sites, together with some of the major cleavage sites, are located at the boundary between hydrophilic, hydrophobic, or phosphorylated regions of the caseins (Figure 4A−C). Thus, PL hydrolyses around the regions essential for the internal integrity and stabilization of the casein micelle, i.e. hydrophobic interaction between caseins, interactions of

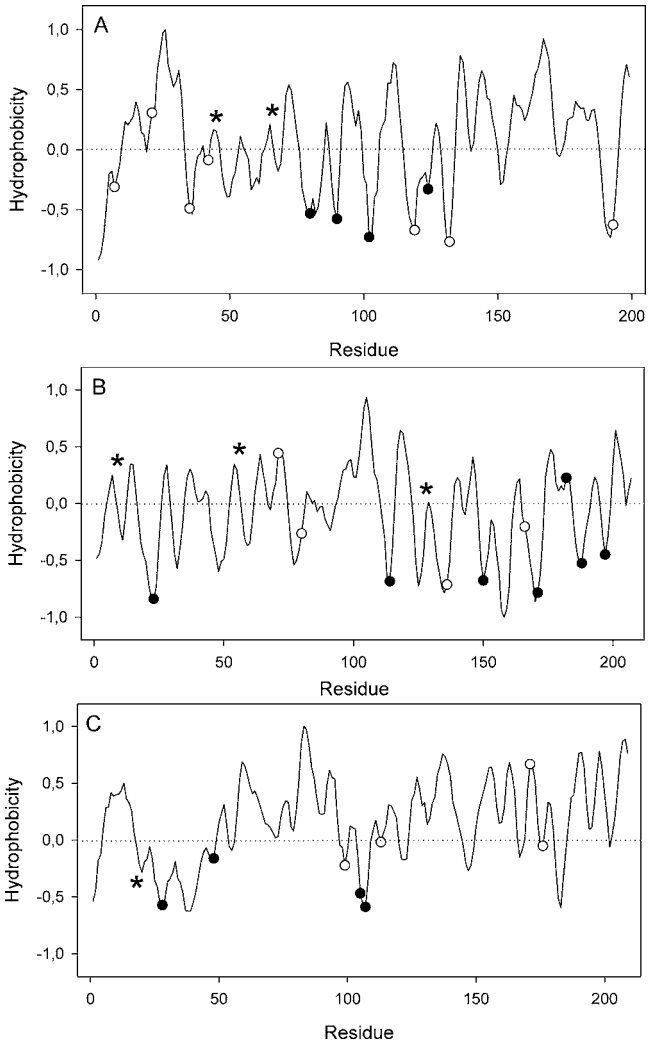

Figure 4. Hydrophobicity distribution in α_{S1}-CN (A), α_{S2}-CN (B), and β-CN (C) with major (●) and minor (○) cleavage sites of plasmin and phosphoserine clusters (*). Classification of major and minor cleavage sites is based on Tables 1−3. Hydrophobicity was calculated according to Tanford (1962) using an average of seven amino acids with a relative weight for the amino acid center being one and 0.75, 0.5, and 0.25 for the amino acids one, two, or three positions from the center amino acid. Positive values indicate hydrophobic and negative values, hydrophilic regions.

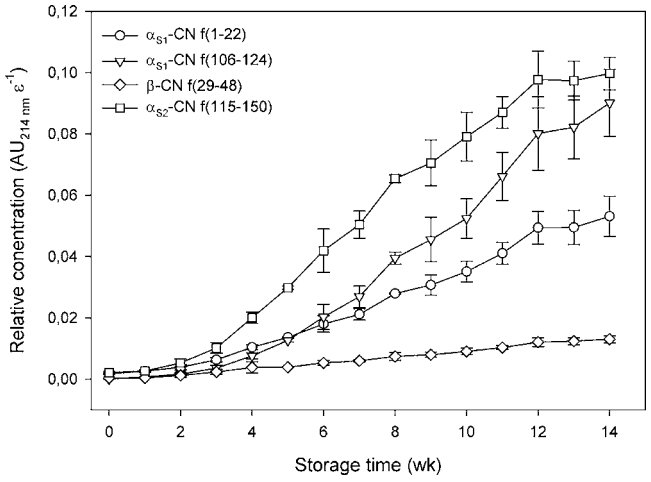

Figure 5. Development of casein-derived N-terminal peptides formed by plasmin in milk preheat treated at 72 °C for 180 s and subjected to direct steam infusion (>150 °C for <0.2 s) during storage at 20 °C. Relative concentration is based on peak area of UV absorbance at 214 nm corrected for the peptides theoretical molar extinction at 214 nm. Peptide concentration is normalized for α_{S2}-CN.

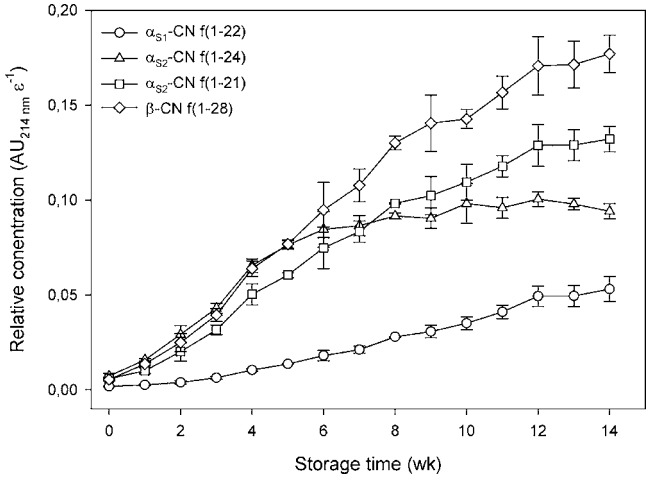

Figure 6. Development of casein-derived peptides formed by plasmin in milk preheat treated at 72 °C for 180 s and subjected to direct steam infusion (>150 °C for <0.2 s) during storage at 20 °C. Relative concentration is based on peak area of UV absorbance at 214 nm corrected for the peptides theoretical molar extinction at 214 nm. Peptide concentration is normalized for α_{S2}-CN.

caseins with calcium phosphate, and ionic or salt interactions between caseins. Cleavage of these regions in the casein micelle would lead to a loosening of the micelle structure, which correlates with the reported increase in micelle size after incubation with PL.[49] A looser structure is hypothesized to allow PL to reach previously inaccessible regions, which can explain the initial resistance of α_{S1}-CN to hydrolysis.

Age gelation of UHT milk has been proposed to be a two-stage process of proteolysis and physicochemical changes that lead to the gelation.[50] Proteolysis-induced age gelation of UHT milk by PL which does not involve the κ-CN−β-lg -complex, could occur after a critical number of the casein−casein and casein−calcium phosphate interaction sites have been hydrolyzed and the remaining interactions are not sufficient to maintain a micellar arrangement. While at the point of gelation, more than 95% of the α_S- and β-CN were hydrolyzed,[1] the peptide development showed that far from all cleavage sites were hydrolyzed completely. This indicates that a large number of amphiphilic and charged polypeptides were present in the milk system that could form and stabilize a gel network. While some proteolysis is needed for gelation, the extent of proteolysis has not yet been related with gelation. The lack of consistency in degree of proteolysis in relation to age gelation and PL activity described in previous studies could also be attributed to differences in processing conditions and levels of PL activity (direct or indirect UHT treatments, addition of PL to UHT milk).[2,50−53] Different processing conditions can greatly affect the protein matrix in milk, such as the degree of whey protein denaturation on casein micelles,[22] thereby influencing the substrate accessibility and the proteolytic pattern of PL in milk. A high PL activity could result in a fast breakdown of polypeptides to small peptides, which are unable to form a gel. Our results suggest that the proteolytic

pathway of caseins by PL is more important for the destabilization of the casein micelles than the overall decrease in the level of intact caseins.

Potential Bitter Peptides. Potential bitter peptides with a Q value >1400 cal mol^{-1} are highlighted in Table 1−4. Bitterness of peptides from β-CN was found in the γ-CN fraction after hydrolysis with PL,[3] and analysis of tryptic digests of β-CN have shown that β-CN f(203−209) is extremely bitter.[37] The potential bitter peptides found in the present study were β-CN f(108−113) and β-CN f(170−176), which have previously been described sensorially as tickling and burning.[37] The bitter peptide β-CN f(203−209) was not identified in the UHT milk or was only present in a very low concentration. Previously described bitter peptides deriving from α_{S1}-CN, that can be formed by PL, are α_{S1}-CN f(23−34) and α_{S1}-CN f(91−100).[54,55] Besides α_{S1}-CN f(91−100), all peptides from residue 91 to 100−105 found in the milk had Q values >1400, and were potentially bitter. The smaller peptides α_{S1}-CN f(1−7) and α_{S1}-CN f(194−199) were highly hydrophobic, and could have contributed to bitterness. The peptides α_{S2}-CN f(182−207), α_{S2}-CN f(189−207), and α_{S2}-CN f(198−207) have been correlated with bitterness and were also present early in the storage period in the UHT milk.[16] Besides α_{S2}-CN f(182−188), all peptides deriving from the C-terminal region of α_{S2}-CN from residue 171 and onward are potentially bitter. Cleavage of Arg_{205}-Tyr_{206} in α_{S2}-CN gives rise to the bitter dipeptide Tyr-Leu.[56] The identified potential bitter peptides indicate that the bitterness caused by PL might mainly be caused by hydrolysis of α_{S1}- and α_{S2}-CN, rather than β-CN as previously reported.[3] Several peptides formed by the combined action of PL and cathepsins were potentially bitter as well. Most of these peptides derive from the N-terminal region of α_{S1}-CN and the C-terminal region of α_{S2}-CN.

A bitter off-flavor was detected in the milk after 6 weeks of storage, which intensified rapidly within 1 week of storage.[1] The concentration and sensory thresholds of the potential bitter peptides in the UHT milk are unknown, and the bitterness cannot be attributed to a specific peptide. We suggest that either the overall concentration of bitter peptides reached the sensory threshold after 7 weeks of storage or that one or several bitter peptides with a lower sensory threshold were formed very rapidly in the storage period between 5 and 7 weeks. Similar to trypsin, PL has the capability to form a range of potential bitter peptides, but further studies are necessary to confirm the bitterness of these peptides and their sensory threshold.

In conclusion, the special UHT process used allowed the investigation of specificity and effect of PL in a sterile milk system, without causing substantial changes to the milk by the heat treatment. PL showed a different specificity in the milk system compared to previous model studies, and 6 new cleavage sites of PL in α_{S2}-CN could be identified. The relative quantification of peptides and time of their appearance allowed a direct comparison of formation rates of peptides to assess the affinity of plasmin to certain cleavage sites. We could show that PL is able to produce potentially bitter peptides and bitterness was most likely caused by peptides arising from α_{S1}- and α_{S2}-CN. The observed proteolytic pattern indicated that PL-mediated proteolysis can destabilize the casein micelle and explain proteolysis-induced age gelation of milk.

■ ASSOCIATED CONTENT

Supporting Information

Spectra of peptides used for relative quantification and proteins in Mascot database used for identification. This material is available free of charge via the Internet at http://pubs.acs.org.

■ AUTHOR INFORMATION

Corresponding Author

*(V.M.R.) Phone: +45 87 33 2783. Fax: +45 87 46 6688. E-mail: valentin.rauh@arlafoods.com.

Funding

The Danish Agency for Science, Technology and Innovation (DASTI) is thanked for financial support of the study.

Notes

The authors declare no competing financial interest.

■ ACKNOWLEDGMENTS

We thank laboratory technicians Vibeke Mortensen and Betina Hansen at the Arla Strategic Innovation Center for assistance with the analysis and helpful discussions.

■ REFERENCES

(1) Rauh, V. M.; Sundgren, A.; Bakman, M.; Ipsen, R.; Paulsson, M.; Larsen, L. B.; Hammershøj, M. Plasmin activity as a possible cause for age gelation in UHT milk produced by direct steam infusion. *Int. Dairy J.* **2014**, DOI: 10.1016/j.idairyj.2013.12.007.

(2) Kelly, A. L.; Foley, J. Proteolysis and storage stability of UHT milk as influenced by milk plasmin activity, plasmin/β-lactoglobulin complexation, plasminogen activation and somatic cell count. *Int. Dairy J.* **1997**, *7*, 411−420.

(3) Harwalkar, V. R.; Cholette, H.; McKellar, R. C.; Emmons, D. B. Relation Between Proteolysis and Astringent Off-Flavor in Milk. *J. Dairy Sci.* **1993**, *76*, 2521−2527.

(4) Bastian, E. D.; Lo, C. G.; David, K. M. M. Plasminogen Activation in Cheese Milk: Influence on Swiss Cheese Ripening. *J. Dairy Sci.* **1997**, *80*, 245−251.

(5) Crudden, A.; Patrick; Fox, F.; Kelly, A. L. Factors affecting the hydrolytic action of plasmin in milk. *Int. Dairy J.* **2005**, *15*, 305−313.

(6) Mara, O.; Roupie, C.; Duffy, A.; Kelly, A. L. The Curd-forming Properties of Milk as Affected by the Action of Plasmin. *Int. Dairy J.* **1998**, *8*, 807−812.

(7) Ismail, B.; Nielsen, S. S. Invited review: Plasmin protease in milk: current knowledge and relevance to dairy industry. *J. Dairy Sci.* **2010**, *93*, 4999−5009.

(8) Prado, B. M.; Sombers, S. E.; Ismail, B.; Hayes, K. D. Effect of heat treatment on the activity of inhibitors of plasmin and plasminogen activators in milk. *Int. Dairy J.* **2006**, *16*, 593−599.

(9) Prado, B. M.; Ismail, B.; Ramos, O.; Hayes, K. D. Thermal stability of plasminogen activators and plasminogen activation in heated milk. *Int. Dairy J.* **2007**, *17*, 1028−1033.

(10) Saint-Denis, T.; Humbert, G.; Gaillard, J. L. Heat inactivation of native plasmin, plasminogen and plasminogen activators in bovine milk: a revisited study. *Lait* **2001**, *81*, 715−729.

(11) McMahon, D. J.; Oommen, B. S. Casein Micelle Structure, Functions, and Interactions. In *Advanced Dairy Chemistry*; McSweeney, P. L. H., Fox, P. F., Eds.; Springer: New York, 2013; pp 185−209.

(12) White, J. H.; Zavizion, B.; O'Hare, K.; Gilmore, J.; Guo, M. R.; Kindstedt, P.; Politis, I. Distribution of plasminogen activator in different fractions of bovine milk. *J. Dairy Res.* **1995**, *62*, 115−122.

(13) Ismail, B.; Choi, L. H.; Were, L. M.; Nielsen, S. S. Activity and nature of plasminogen activators associated with the casein micelle. *J. Dairy Sci.* **2006**, *89*, 3285−3295.

(14) Eigel, W. N.; Butler, J. E.; Ernstrom, C. A.; Farrell, H. M.; Harwalkar, V. R.; Jenness, R.; Whitney, R. M. Nomenclature of Proteins of Cow's Milk: Fifth Revision. *J. Dairy Sci.* **1984**, *67*, 1599−1631.

(15) Eigel, W. N. Formation of γ1-A2, γ2-A2 and γ3-A caseins by in vitro proteolysis of β-CASEIN A2 with bovine plasmin. *Int. J. Biochem* **1977**, *8*, 187−192.
(16) Le Bars, D.; Gripon, J.-C. Specificity of plasmin towards bovine αs2-casein. *J. Dairy Res.* **1989**, *56*, 817−821.
(17) McSweeney, P. L. H.; Olson, N. F.; Fox, P. F.; Healy, A.; Højrup, P. Proteolytic specificity of plasmin on bovine α_{s1}-casein. *Food Biotechnol* **1993**, *7*, 143−158.
(18) Baum, F.; Fedorova, M.; Ebner, J.; Hoffmann, R.; Pischetsrieder, M. Analysis of the endogenous peptide profile of milk: identification of 248 mainly casein-derived peptides. *J. Proteome Res.* **2013**, *12*, 5447−5462.
(19) Dallas, D. C.; Guerrero, A.; Parker, E. A.; Garay, L. A.; Bhandari, A.; Lebrilla, C. B.; Barile, D.; German, J. B. Peptidomic profile of milk of holstein cows at peak lactation. *J. Agric. Food Chem.* **2013**, *62*, 58−65.
(20) McMahon, D. J., Age-gelation of UHT milk: Changes that occur during storage, their effect on shelf life and the mechanism by which age-gelation occurs. In *Heat Treatments and Alternative Methods*; International Dairy Federation: Brussels, Belgium, 1996; pp 315−325.
(21) Datta, N.; Deeth, H. C. Age Gelation of UHT Milk—A Review. *Food Bioprod. Process.* **2001**, *79*, 197−210.
(22) Crudden, A.; Oliveira, J. C.; Kelly, A. L. Kinetics of changes in plasmin activity and proteolysis on heating milk. *J. Dairy Res.* **2005**, *72*, 493−504.
(23) Anema, S. G.; Li, Y. Effect of pH on the Association of Denatured Whey Proteins with Casein Micelles in Heated Reconstituted Skim Milk. *J. Agric. Food Chem.* **2003**, *51*, 1640−1646.
(24) ISO, *Microbiology of food and animal feeding stuffs - horizontal method for the enumeration of microorganisms - Colony-count technique at 30 °C*. ISO 4833. International Standardisation Organisation: Geneva, Switzerland, 2003.
(25) Kuipers, B. J.; Gruppen, H. Prediction of molar extinction coefficients of proteins and peptides using UV absorption of the constituent amino acids at 214 nm to enable quantitative reverse phase high-performance liquid chromatography-mass spectrometry analysis. *J. Agric. Food Chem.* **2007**, *55*, 5445−5451.
(26) Ney, K. H. Voraussage der Bitterkeit von Peptiden aus deren Aminosäurezu-sammensetzung. *Z. Lebensm. Unters. Forsch.* **1971**, *147*, 64−68.
(27) Hachana, Y.; Kraiem, K.; Paape, M. J. Effect of plasmin, milk somatic cells and psychrotrophic bacteria on casein fractions of ultra high temperature treated milk. *Food Sci. Technol. Res.* **2010**, *16*, 79−86.
(28) Larsen, L. B.; Benfeldt, C.; Rasmussen, L. K.; Petersen, T. E. Bovine milk procathepsin D and cathepsin D: coagulation and milk protein degradation. *J. Dairy Res.* **1996**, *63*, 119−130.
(29) Le Bars, D.; Gripon, J. C. Hydrolysis of α_{s1}-casein by bovine plasmin. *Lait* **1993**, *73*, 337−344.
(30) Malin, E. L.; Brown, E. M.; Wickham, E. D.; Farrell, H. M. Contributions of terminal peptides to the associative behavior of α_{s1}-casein. *J. Dairy Sci.* **2005**, *88*, 2318−2328.
(31) Gagnaire, V.; Léonil, J. Preferential sites of tryptic cleavage on the major bovine caseins within the micelle. *Lait* **1998**, *78*, 471−489.
(32) Diaz, O.; Gouldsworthy, A. M.; Leaver, J. Identification of peptides released from casein micelles by limited trypsinolysis. *J. Agric. Food Chem.* **1996**, *44*, 2517−2522.
(33) Holt, C.; de Kruif, C. G.; Tuinier, R.; Timmins, P. A. Substructure of bovine casein micelles by small-angle X-ray and neutron scattering. *Colloids Surf., A* **2003**, *213*, 275−284.
(34) Farrell, H. M., Jr.; Malin, E. L.; Brown, E. M.; Mora-Gutierrez, A. Review of the chemistry of α_{S2}-casein and the generation of a homologous molecular model to explain its properties. *J. Dairy Sci.* **2009**, *92*, 1338−1353.
(35) Tauzin, J.; Miclo, L.; Roth, S.; Mollé, D.; Gaillard, J. L. Tryptic hydrolysis of bovine α_{S2}-casein: identification and release kinetics of peptides. *Int. Dairy J.* **2003**, *13*, 15−27.
(36) Rasmussen, L. K.; Højrup, P.; Petersen, T. E. Disulphide arrangement in bovine caseins: localization of intrachain disulphide bridges in monomers of κ- and α_{s2}-casein from bovine milk. *J. Dairy Res.* **1994**, *61*, 485−493.
(37) Bumberger, E.; Belitz, H. D. Bitter taste of enzymic hydrolysates of casein. I. Isolation, structural and sensorial analysis of peptides from tryptic hydrolysates of beta-casein. *Z. Lebensm. Unters. Forsch.* **1993**, *197*, 14−19.
(38) Considine, T.; Geary, S.; Kelly, A. L.; McSweeney, P. L. H. Proteolytic specificity of cathepsin G on bovine α_{s1}- and β-caseins. *Food Chem.* **2002**, *76*, 59−67.
(39) Considine, T.; Healy, Á.; Kelly, A. L.; McSweeney, P. L. H. Hydrolysis of bovine caseins by cathepsin B, a cysteine proteinase indigenous to milk. *Int. Dairy J.* **2004**, *14*, 117−124.
(40) Moatsou, G.; Bakopanos, C.; Katharios, D.; Katsaros, G.; Kandarakis, I.; Taoukis, P.; Politis, I. Effect of high-pressure treatment at various temperatures on indigenous proteolytic enzymes and whey protein denaturation in bovine milk. *J. Dairy Res.* **2008**, *75*, 262−269.
(41) Larsen, L. B.; Hinz, K.; Jorgensen, A. L.; Moller, H. S.; Wellnitz, O.; Bruckmaier, R. M.; Kelly, A. L. Proteomic and peptidomic study of proteolysis in quarter milk after infusion with lipoteichoic acid from *Staphylococcus aureus*. *J. Dairy Sci.* **2010**, *93*, 5613−5626.
(42) Gaucher, I.; Mollé, D.; Gagnaire, V.; Gaucheron, F. Effects of storage temperature on physico-chemical characteristics of semi-skimmed UHT milk. *Food Hydrocolloids* **2008**, *22*, 130−143.
(43) Farrell, H. M., Jr.; Brown, E. M.; Hoagland, P. D.; Malin, E. L. Higher Order Structures of the Caseins: A Paradox? In *Advanced Dairy Chemistry—1 Proteins*; Fox, P. F., McSweeney, P. L. H., Eds.; Springer: New York, 2003; pp 203−231.
(44) Berglund, L.; Andersen, M. D.; Petersen, T. E. Cloning and characterization of the bovine plasminogen cDNA. *Int. Dairy J.* **1995**, *5*, 593−603.
(45) Rollema, H. S.; Visser, S.; Poll, J. K. Spectrophotometric assay of plasmin and plasminogen in bovine milk. *Milchwissenschaft* **1983**, *38*, 214−217.
(46) Marchin, S.; Putaux, J. L.; Pignon, F.; Leonil, J. Effects of the environmental factors on the casein micelle structure studied by cryo transmission electron microscopy and small-angle X-ray scattering/ultrasmall-angle X-ray scattering. *J. Chem. Phys.* **2007**, *126*, 045101.
(47) Dalgleish, D. G. On the structural models of bovine casein micelles-review and possible improvements. *Soft Matter* **2011**, *7*, 2265−2272.
(48) Trejo, R.; Dokland, T.; Jurat-Fuentes, J.; Harte, F. Cryo-transmission electron tomography of native casein micelles from bovine milk. *J. Dairy Sci.* **2011**, *94*, 5770−5775.
(49) Crudden, A.; Afoufa-Bastien, D.; Fox, P. F.; Brisson, G.; Kelly, A. L. Effect of hydrolysis of casein by plasmin on the heat stability of milk. *Int. Dairy J.* **2005**, *15*, 1017−1025.
(50) Manji, B.; Kakuda, Y. The Role of Protein Denaturation, Extent of Proteolysis, and Storage Temperature on the Mechanism of Age Gelation in a Model System. *J. Dairy Sci.* **1988**, *71*, 1455−1463.
(51) Kohlmann, K. L.; Nielsen, S. S.; Ladisch, M. R. Effects of a Low Concentration of Added Plasmin on Ultra-High Temperature Processed Milk. *J. Dairy Sci.* **1991**, *74*, 1151−1156.
(52) Aroonkamonsri, J. The Role of Plasmin and Bacterial Proteinases on Age Gelation of UHT Milk (*Pseudomonas fluorescens*, *Pseudomonas fragi*, *Pseudomonas luteola*, *Vibrio fluvialis*). Ph.D. Thesis, University of Guelph, Canada, 1996.
(53) Newstead, D. F.; Paterson, G.; Anema, S. G.; Coker, C. J.; Wewala, A. R. Plasmin activity in direct-steam-injection UHT-processed reconstituted milk: Effects of preheat treatment. *Int. Dairy J.* **2006**, *16*, 573−579.
(54) Matoba, T.; Hayashi, R.; Hata, T. Isolation of bitter peptides from tryptic hydrolysate of casein and their chemical structure. *Agric. Biol. Chem.* **1970**, *34*, 1235−1243.
(55) Hill, R.; Van Leeuwen, H. Bitter peptides from hydrolysed casein coprecipitate. *Aust. J. Dairy Technol.* **1974**, *29*, 32−34.
(56) Kim, H. O.; Li-Chan, E. C. Quantitative structure-activity relationship study of bitter peptides. *J. Agric. Food Chem.* **2006**, *54*, 10102−10111.

those measurements, we propose a toxicokinetic model for the absorption, distribution, and excretion of seven PFAAs in pigs. The behavior of PFAAs in pigs is also of interest because pigs are touted a biomedical model[26] of human physiology. Additionally, understanding the toxicokinetics in domestic pigs may help relate the body burden of wild boars (a related subspecies) to the environmental ubiquity of PFAAs. Our main focus is understanding PFAA kinetics from feed to porcine livestock and food products for consumer risk assessment and protection.

MATERIALS AND METHODS

Chemicals. Native and ^{13}C-labeled PFAAs were purchased from Wellington Laboratories, Guelph, ON, Canada. Methanol absolute, acetonitrile, formic acid (99%), and ammonium acetate (all ULC-MS) were purchased from Biosolve, Valkenswaard, The Netherlands. Sodium acetate anhydrous (p.a.), potassium hydroxide (p.a.), ammonia (25% p.a.), and acetic acid (100% p.a.) were obtained from Merck, Darmstadt, Germany. Pepsine (from porcine gastric mucosa), Lipase Type VII (L 1754), and Protease Type XIV (P 5147) were purchased from Sigma-Aldrich, Steinheim, Germany. Glycerol (99%) was obtained from ACROS Organics, Geel, Belgium. Water was double distilled using distillation unit 2001/2 of the Gesellschaft für Lebensmittel-Forschung.

Animals, Housing, and Feeding. Three groups of fattening pigs (German Landrace breed) consisting of 10 gilts (female pigs), 10 barrows (castrated male pigs), and 10 young boars (uncastrated prepubescent male pigs) were purchased from a commercial breeding farm (Agrargenossenschaft Groß Machnow, Germany) and transported to the experimental station of the Federal Institute for Risk Assessment (BfR). The animal experiment was authorized by the Landesamt für Gesundheit and Soziales in Berlin with approval G0043/10, complying with the German Animal Welfare Act (Tierschutzgesetz) and supervised by the BfR institutional animal welfare officer. The fattening pigs with initial body weight (BW) of 83 ± 12 kg (mean ± sample standard deviation) were separately housed in pens of eight experimental animals and two control animals with free access to water and restrictive feeding (2 kg/day and animal). Room temperature was 21 °C, and humidity was kept constant at approximately 68% throughout the entire feeding study. Health status of the fattening pigs was checked daily. The BW of each animal was recorded once a week. Upon arrival, all fattening pigs received a commercial cereal-based nonpelleted feed for 14 days, which was gradually exchanged during the first 7 days for the pelleted control diet with approximately 17% hay (adaption period). After the adaption period, fattening pigs were fed either PFAA-contaminated feed (3 × 8 experimental animals) or PFAA-free feed (3 × 2 control animals) for 21 days. Discussions refer to experimental animals, except where control animals are explicitly mentioned.

Contaminated Feed Cultivation and Preparation. PFAA-contaminated hay and barley were cultivated and harvested from a PFAA-contaminated region in Lower Saxony, Germany. The agricultural patch was polluted from the use of a soil improver provided by a recycling company that laced it with industrial waste containing high concentrations of PFAS.[27] To counteract an uneven contaminant distribution in the soil, the final feed was homogenized. PFAA-contaminated barley and hay used for the PFAA feed were determined to be substantially equivalent to PFAA-free varieties of barley and hay with regard to nutritional value. The control feed and the PFAA feed fulfilled the recommendations for nutrient and energy requirements of fattening pigs of the Society of Nutrition Physiology (GfE).[28] Nutrition data are shown in the Supporting Information (Table S1).

Sampling of Feed, Tissues, and Excretions. For PFAA analysis in feed, pooled samples were taken to obtain five representative feed samples for each week (2 weeks of adaption, 3 weeks of experimental feeding). Samples of blood plasma were taken of each experimental animal toward the end of the adaption period (day −4), twice a week during PFAA feeding (days 4, 8, 11, 15, and 18), and at the day of slaughter (22). Blood from control animals was taken at the end of the adaption period as well as at the day of slaughter. The blood was collected by puncturing the *vena jugularis* in a lithium−heparin monovette and centrifuged to obtain the plasma, pipetted off, and stored frozen (−20 °C) until analysis in PFAA-free polypropylene vessels. Urine was collected with varying regularity during feeding, weighing, or blood sampling. After the 21 days of the feeding period, the pigs had an average BW of 103 ± 11 kg and were fasted for 20 h before being slaughtered at the BfR slaughterhouse according to approved methods. Pigs were immediately killed by blood removal after stunning. To prevent cross-contamination between control and experimental animals, controls were slaughtered first. Liver and kidneys were carefully removed, weighed, and individually frozen in PFAA-free bags at −20 °C. The bladder was removed, and the urine it contained was emptied into polypropylene vessels. Samples of muscle tissue from the *musculus longissimus dorsi* (further termed dorsal muscle tissue), *musculus obliquus externus/internus abdominalis*, and *transversus abdominis* (further termed ventral muscle tissue) and the fat tissue covering the dorsal muscle tissue were frozen at −20 °C. Subsequent sample preparation and analysis were performed by the Chemical and Veterinary Analytical Institute Münsterland-Emscher-Lippe (CVUA-MEL). To avoid interferences between PFAA and biomolecules, matrix-specific sample preparations were performed. Plasma and urine was treated with half-concentrated formic acid.[29] Feed samples were extracted with methanol, and an aliquot was diluted with water (VDLUFA-Method). Liver, kidney, and muscle tissue meat samples were hydrolyzed with pepsine.[30] Sample solutions were purified and concentrated with solid phase extraction on an OasisWAX column[31] (60 mg/3 mL).

Analytical Determination. A total of 12 compounds was analyzed using high-performance liquid chromatography coupled with tandem mass spectrometry (HPLC-MS/MS). These included the following seven PFCAs, perfluorohexanoic acid (PFHxA), perfluoroheptanoic acid (PFHpA), PFOA, PFNA, perfluorodecanoic acid (PFDA), perfluoroundecanoic acid (PFUnA), and perfluorododecanoic acid (PFDoA); and the following five PFSAs, perfluorobutanesulfonic acid (PFBS), perfluorohexanesulfonic acid (PFHxS), perfluoroheptanesulfonic acid (PFHpS), PFOS, and perfluorodecanesulfonic acid (PFDS). The limit of detection (LOD) was 0.2 μg/kg for solid samples and 0.2 μg/L for liquid samples for all PFAAs except PFDS, with an LOD of 0.5 μg/kg for solid samples and 0.5 μg/L for liquid samples. It was not possible to identify perfluorobutanoic acid (PFBA) and perfluoropentanoic acid (PFPA) unequivocally because both substances show only one mass transition in multiple reaction monitoring mode (MRM) during HPLC-MS/MS analysis. Due to this fact, the substances were withdrawn from the substance spectra. PFPS, PFNS, PFUnS, and PFDoS were also excluded because standard substances were not commercially available. See Table S2 in the Supporting Information for a complete list of relevant substances for this study.

Analytical Measurement. The purified solutions were measured using HPLC-MS/MS, run in negative ion MRM mode. The separation was performed on an Agilent 1200 SL HPLC system. MS/MS detection was performed with an Agilent 6460 triple-quadrupole mass spectrometer equipped with an electrospray interface (ESI) operating in the negative ion mode. The MRM settings are published elsewhere.[32] The relative standard deviations were around 20% for concentrations near the limit of quantification (LOQ) and 10−15% for higher concentrations.

Quantification and Isomer Separation. Quantification was performed with isotope-labeled standards and a seven-point calibration curve. The LOD was defined as the signal-to-noise ratio of 3:1 of the qualifier ion. The LOQ is defined as the concentration at which a substance is identified unequivocally and quantified with a relative standard deviation of 20% or lower. In the case of PFOS, it could be ensured that only the linear isomer was quantified. Due to the fact that standard substances of branched PFHxA, PFHpA, PFBS, PFHpS, and PFHxS were not commercially available, it was not possible to ascertain that all of the branched substances are separated completely

from the linear ones. Only peaks with the same retention time as the respective linear substances were integrated. The ratios of the two most intense MRM transitions of the integrated PFHpS and PFHxS are the same as in the linear standard substance. Due to the finding that the transitions of the branched isomers differ from the transitions of the linear substances in the case of PFOS, this is an indication that the uncertainty caused by the branched isomers is small for PFHpS and PFHxS. The PFCA concentrations in the analyzed matrices were very low, so that a differentiation between the linear and the branched substances was not possible. It is described in the literature that 78% of the PFOA manufactured by the 3M Co. using electrochemical fluorination is linear.[33] The ratios of the two most intense MRM transitions of the integrated PFCA were the same as in the linear standard substances. Thus, it can be assumed that also in the case of PFCAs, the potential uncertainty caused by the branched isomers is small. The analytical method is described in more detail in the Supporting Information and by Ehlers.[30]

Body Weight of Pigs as a Function of Time. The pigs were weighed two times during the 14 day adaptation period, three times during the 21 day PFAA-contaminated diet experiment, and once more before being slaughtered on day 22 for a total of six BW measurements $M_k^{\text{exptl}}(t)$ per pig. To interpolate between those measurements, the BW function

$$M_k(t) = \omega_{A,k} + \omega_{B,k}(t + \theta)^{\omega_{C,k}} \quad (1)$$

was fitted to the experimental weights $M_k^{\text{exptl}}(t)$ using the nonlinear least-squares Levenberg–Marquardt algorithm[34] with fitted constants ω. Equation 1 is the empirical Janoschek growth equation,[35,36] valid only for the short experimental period of 35 days. Note that other growth equations should be used for longer periods of fattening time. The offset $\theta = 14$ days represents the adaptation period, so that $t = 1$, 2, 3, .., 21 days represent the experimental period in which PFAA-contaminated feed was fed. See Figure S1 and Table S3 in the Supporting Information for the three fitted ω constants for each individual pig (k).

Estimation of the Mass of Tissues. Several sources of data[37−40] were compounded to provide a consistent picture of the weight of each part of the pig (blood, edible and inedible tissues). Blood was estimated as $p_B = 6.5\%$ of BW.[40] Hematocrit (proportion of red blood cells and other cells to plasma) was taken[40] as 39%. From these two values, we calculate the mass of blood plasma (P) as $m_{P,k}(t) = 0.03965 M_k(t)$. The carcass is composed of edible parts of a slaughtered pig excluding blood, kidney, liver, and others deemed unfit for human consumption in some cultures. The weight of the carcass of pig k is then estimated as $(1 - p_B)M_k(t) - m_{L,k} - m_{K,k}$, where $m_{L,k}$ is the measured weight of liver (L) and $m_{K,k}$ is the measured weight of kidney (K). The amount of muscle tissue and fat tissue is calculated as a fraction of the weight of the carcass. From Table 6.2 of ref 37 we use the estimates valid for a pig between 90 and 100 kg, which indicate 62.6% of carcass is muscle tissue and 18.9% of carcass is fat tissue (F). Because we separately analyzed the PFAA content for samples of dorsal and ventral muscle tissues, we further differentiate between them. From Figure 6.1 of ref 37 we assign 51.5% of muscles as dorsal muscle tissues (D: chop, filet, and ham) and 48.5% of muscles as ventral muscle tissues (V: belly, jowl, blade shoulder, blade, knuckle, and dewlap). The mass of each tissue is given by

$$m_{X,k}(t) = p_X[(1 - p_B)M_k - m_{L,k} - m_{K,k}], \text{ with } X = \text{F, D, V} \quad (2)$$

and constants $p_F = 0.189$, $p_D = 0.626 \times 0.515$, and $p_V = 0.626 \times 0.485$. Other parts of the carcass not analyzed in this study represent 18.6% of its weight (bones, tendons, and skin, Table 6.2 of ref 37). Other parts of the body excluded from the carcass, such as the head, are neglected.

Urine Output. A pig urinates[39] between 5 and 30 mL/kg BW. The total urine output as a function of time is between $m_{U,k}(t) = 0.005 \times M_k(t)$ and $0.030 \times M_k(t)$ in L/day. We are forced to estimate the urine output per pig because it was not practicable to quantify the liquid volume per day in the experiment. The urine concentration $C_{U,j,k}^{\text{exptl}}(t)$ of each PFAA substance j in pig k was however experimentally determined every few days.

Mathematical Model of Toxicokinetics. We propose a two-compartment, first-order toxicokinetic model of the pig for each of the seven PFAA substances. The blood plasma represents the model's central compartment (compartment 1). The edible tissues taken together represent compartment 2 (Figure 1). To simplify notation,

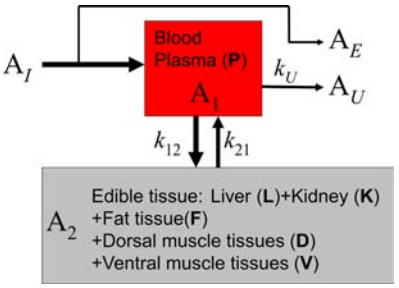

Figure 1. Graphical representation of the two-compartment model. The amount of PFAA in feed is designated as the intake A_I. The amount of PFAA in the central compartment is A_1, whereas the amount in edible tissue is designated A_2. The kinetic constants k_{12} and k_{21} quantify the speed of exchange. A_E is the amount found in feces, considered a fraction f_E of intake A_I, which bypasses A_1 unabsorbed. A_U is the amount excreted in urine, and k_U is the urinal elimination constant. Such a model is fitted independently for each substance and pig.

we will in most cases omit the subscripts for substance (j) and pig (k). The dynamic behavior of the amount of substance present A_1 and A_2 is described by two coupled ordinary differential equations:

$$\frac{dA_1(t)}{dt} = A_1(t) - A_E(t) - k_{12}A_1(t) + k_{21}A_2(t) - k_U A_1(t) \quad (3a)$$

$$\frac{dA_2(t)}{dt} = k_{12}A_1(t) - k_{21}A_2(t) \quad (3b)$$

The kinetic constants k_{12} and k_{21} quantify the speed of substance exchange between compartments 1 and 2, whereas k_u is the urinal excretion rate constant for each substance. These three kinetic constants are the fitted model parameters. $A_E(t)$ is the amount excreted in feces as a function of time t. $A_1(t)$ is the PFAA intake per unit of time or, in other words, the amount ingested by a pig, calculated from measurements

$$A_1(t) = C_I^{\text{exptl}}(t) m_I^{\text{exptl}}(t) \quad (4)$$

where $C_I^{\text{exptl}}(t)$ is the experimentally analyzed feed concentration of PFAA. The feed concentration was held nearly constant for each substance in the carry-over experiment. The second term, $m_I^{\text{exptl}}(t)$, is the average amount of feed intake per day for each pig. To provide estimates for the model parameters k_{12},k_{21}, and k_u, we integrate a form of eqs 3 to best fit the experimentally observed A_1^{exptl} and A_2^{exptl} as described under Numerical Method To Fit the Model to Experiment. Time series of seven data points were experimentally measured for the concentration of all seven PFAAs in blood plasma (P), from which we calculate the amount of each substance in compartment 1

$$A_1^{\text{exptl}}(t) = C_P^{\text{exptl}}(t) m_P(t) \quad (5)$$

where $C_P^{\text{exptl}}(t)$ is the experimental plasma concentration and $m_P(t)$ is the mass of the blood plasma. Because only one data point per pig and substance was measured after slaughter for each edible tissue, we group liver (L), kidney (K), fat (F), dorsal muscle tissues (D), and ventral muscle tissues (V) into the peripheral or edible tissue compartment (compartment 2). The total amount of PFAA in edible tissue compartment 2 at slaughter date $t_{\text{end}} = 22$ days is

dx.doi.org/10.1021/jf405827u | J. Agric. Food Chem. 2014, 62, 6861−6870

$$A_2^{\text{exptl}}(t_{\text{end}}) = \sum_{X=\text{L,K,F,D,V}} C_X^{\text{exptl}}(t_{\text{end}}) m_X(t_{\text{end}}) \quad (6)$$

The amount in edible tissues at the beginning of the experiment t_0 = 0 days is confirmed experimentally to be negligible, $A_2^{\text{exptl}}(t_0) = 0$. The amount excreted in feces is assumed proportional to the amount ingested, so $A_E(t) = f_E A_1(t)$, where the constant f_E for each substance is obtained from previously published experimental data for sheep[22] (Table 1). This simply means that the amount excreted in feces is estimated as an unabsorbed proportion (outer arrow A_E in Figure 1) of the ingested amount. The assumption was made that pigs behave like sheep just in this respect. The fractions in Table 1 are small, so they do not affect the mass balance greatly, but are used for completeness. Furthermore, the amount excreted in urine is a result of the model through the fitted k_U. We assume that there is no metabolic interaction between the substances, so that the models for each of the seven PFAAs are independent from each other. See Figure 1 for a graphical representation of the model.

Table 1. Fractions of Ingested PFAA Deemed Unabsorbed and Excreted in Feces of Sheep from Data in Reference 22 and Table 63 of Reference 30[a]

substance	fraction excreted in feces f_E (%)	substance	fraction excreted in feces f_E (%)
PFHpS	0.65	PFBS	4.30
PFHxS	1.35	PFHxA	4.35
PFHpA	3.20	PFOS	8.45
PFOA	3.95		

[a]These data were used to estimate the feces contribution in the mass balance for pigs of Figure 2.

Excretion in Urine. For each pig, the PFAA concentration of urine $C_U^{\text{exptl}}(t)$ was analyzed for up to four samples spread over the total 22 days. On average, 2.5 urine samples per pig were measured, plus 1 sample after slaughter (from bladder contents). These data were put on equal footing among pigs by performing a least-squares linear fit of the urinal PFAA concentration of the form $C_U^{\text{exptl}}(t) = \beta\, t$. This functional form was chosen by inspecting the apparent linear rise of the experimental blood plasma concentration $A_1^{\text{exptl}}(t)$ for most substances and pigs (Figure 3). Consistent with a linear rise in plasma concentration is a linear rise in urine concentration $C_U(t)$ for first-order kinetics, disregarding the variation in liquid amount. Using the linear fit for $C_U^{\text{exptl}}(t)$ above, the total cumulative urine excretion from experiment is integrated as

$$A_U^{\text{exptl, total}} = \int C_U^{\text{exptl}}(t) m_U(t)\, dt \quad (7)$$

Likewise, the cumulative amount excreted in urine for the model is obtained by integrating

$$A_U^{\text{total}} = \int k_U A_1(t)\, dt \quad (8)$$

Excretion via Feces. The PFAA amounts excreted in feces were not analyzed, because they were presumed to be relatively small with respect to the total cumulative PFAA dose. This assumption is confirmed by the mass balance, because most of the PFAA dose is accounted for by tissues and urine without resorting to the feces (Figure 2). It has been shown experimentally that anionic salts of PFOA and PFOS are secreted by the bile into the intestinal lumen.[41] It is hypothesized that PFOA and PFOS are recycled within enterohepatic circulation,[42] so that material already absorbed is not excreted into feces. Because we did not measure the PFAA content of feces but nevertheless wanted to have an estimate of the amounts excreted, we resorted to extrapolating the results obtained from measurements in sheep feces (ref 22 and Table 63 of ref 30). From the cumulative PFAA amounts that were ingested by sheep, we calculate the fractions of PFAA that remained unabsorbed and were excreted (Table 1).

Normalization of Mass Balance Equations. The mass balance performed using the pig physiological parameters, measured weights, and experimental PFAA concentration data is close to an average of 100% (Figure 2) of the cumulative ingested PFAA, calculated as the total amount of substance j ingested by pig k in the 22 days of the experiment. As suggested in ref 43, we opt for normalizing the data, so that the sum of accumulated and excreted PFAA mass becomes exactly

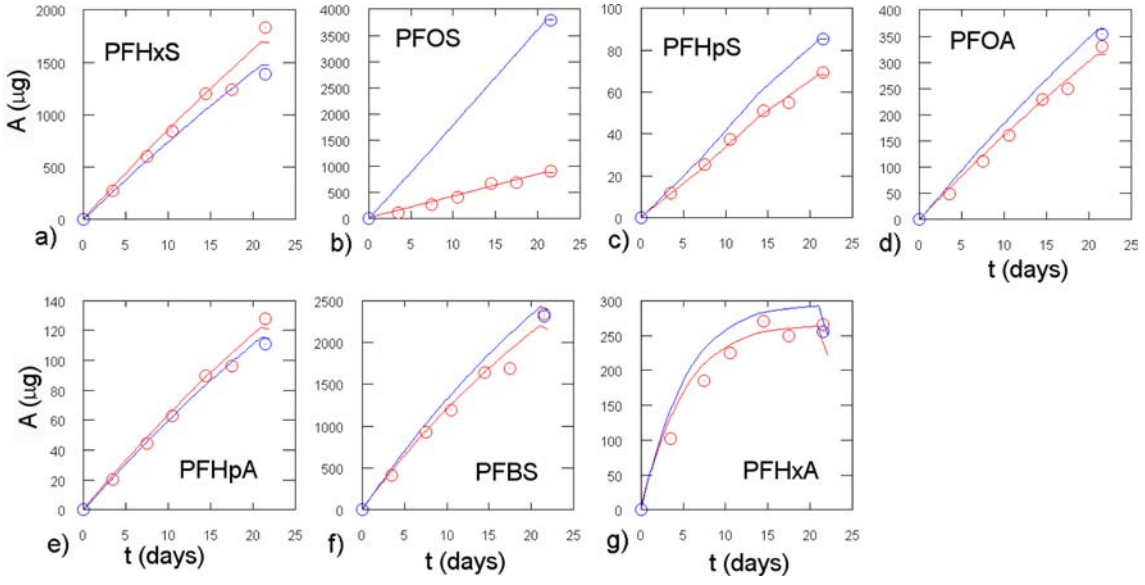

Figure 3. Dynamic behavior of the amount A of seven PFAA substances in an exemplary pig (gilt 8, one of 24 pigs, chosen for its similarity to the mean behavior). Circles correspond to experimental data (mediated by the pig physiological and growth estimates), and lines are the model solution of eq 10 using best-fit kinetic parameters. The substances are ordered from slowest (a) to fastest (g) urinary excretion k_U. The color red stands for the amount A_1 in blood plasma or central compartment. The color blue stands for the amount A_2 in the edible tissue compartment. Only the data for PFHxA suggest approach to steady state between days 1 and 21. Chart b stands out because most of the PFOS partitioned to edible tissue, in contrast to the rest of the PFAAs (panels a and c–g). On day 22, animals were fasted before slaughter (so the curves on that day show only excretion as a downward trend).

dx.doi.org/10.1021/jf405827u | J. Agric. Food Chem. 2014, 62, 6861–6870

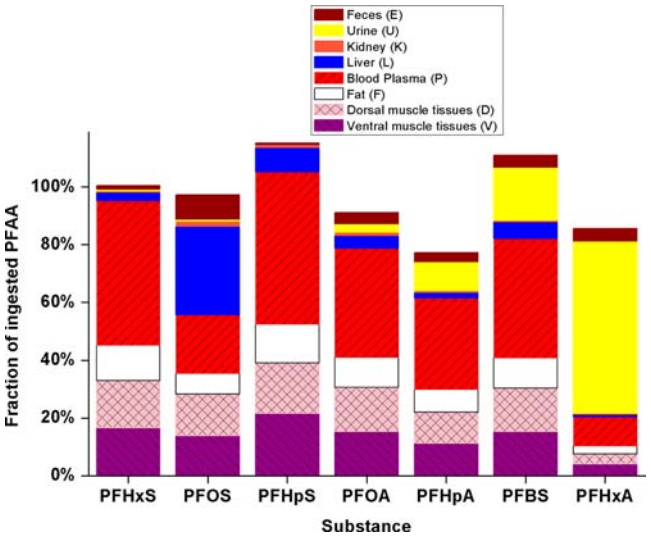

Figure 2. Mass balance for the seven PFAAs shows the ratio of substance in each tissue and excretion to the total cumulative PFAA ingested in feed. The substances are ordered from lowest percentage excreted (left) to highest percentage excreted in 21 days (right). By comparing the height of each bar, one gains insight into the relative affinity of each substance for the given matrices. The mass balance shown accounts on average for 97% of the PFAAs ingested and has not been normalized by eq 9.

equal to 100% of the total ingested and absorbed PFAA for each substance and each pig individually. The normalization factor for the mass balance equations is the ratio of PFAA found in tissues and excretions to PFAA ingested from feed, so that

$$\alpha = \frac{A_1^{\text{exptl}}(t_{\text{end}}) + A_2^{\text{exptl}}(t_{\text{end}}) + A_U^{\text{exptl, total}}}{\sum_{t=1}^{22} A_I^{\text{exptl}}}\left(\frac{1}{1-f_E}\right) \quad (9)$$

The normalization is performed by multiplying the first two terms of the right-hand side of eq 3a with the factor α in eq 9 and recognizing that $A_E(t) = f_E A_1(t)$. After rearranging, we obtain the set of differential equations

$$\frac{dA_1(t)}{dt} = \alpha(1-f_E)A_1(t) - k_{12}A_1(t) + k_{21}A_2(t) - k_U A_1(t) \quad (10a)$$

$$\frac{dA_2(t)}{dt} = k_{12}A_1(t) + k_{21}A_2(t) \quad (10b)$$

We thus fit the normalized model eqs 10 to self-consistent, mass-balanced data. Because of this normalization, the amount excreted in feces A_E (estimated from sheep data) is only relevant for the mass balance of Figure 2, but the terms A_E and f_E disappear from eqs 10 and do not have an effect on the fitted model constants k_{12}, k_{21}, and k_U for the pig. Physiologically this is due to the fact that A_E is an unabsorbed substance which bypasses distribution into the animal's tissues (Figure 1).

Numerical Method To Fit the Model to Experiment. To provide estimates for the model parameters k_{12},k_{21}, and k_u for each substance (j) and pig (k), we perform numerical integration of eqs 10 to best fit the experimentally observed A_1^{exptl} (7 data points, eq 5) and A_2^{exptl} (2 data points, eq 6). In some but not all cases, measurements for the PFAA concentrations in urine were available. In such cases, the best fit is performed as described before and simultaneously integrating eq 8 for the model A_U^{total} and fitting to $A_U^{\text{exptl, total}}$ (1 data point, eq 7). We are thus using 3 model fit parameters and a total of 9 (and in some cases 10) experimental data points. We have chosen to perform fixed effects modeling, meaning that we treat each pig and each substance separately. With this approach, we guarantee a best fit for each case and explore the intersubject variability a posteriori. An alternative approach not followed would have been to fit all pigs at the same time with one random effects model per substance, in a population pharmacokinetics fashion.[44] The MATLAB-compatible program code was written and run in the freely available GNU Octave 3.2.4 language. The dynamic behavior of the amount of substance in the compartments, eqs 10, is integrated using the explicit Runge–Kutta method of order (4,5) in Octave's ode45 algorithm. For the relevant cases, the cumulative amounts excreted in urine in experiment, eq 7, and in model, eq 8, are integrated using the trapezoidal rule. The feed intake $A_I(t)$ is calculated using eq 4. The best fit is performed by nonlinear least-squares minimization of the difference between model and experimental results using the Levenberg–Marquardt algorithm.[34]

Elimination Half-Life. From the fitted model constants, we may calculate the elimination half-life

$$\tau_{1/2} = \frac{\ln(2)}{k_U}(1 + k_{12}/k_{21}) \quad (11)$$

This equation is valid for a two-compartment model with fast equilibrium between compartments. The elimination half-life is thus valid for both compartments, blood plasma and edible tissue.

RESULTS AND DISCUSSION

Twelve PFAAs were analyzed[30] in every sample. Among those 12, 7 substances were detected well above the LOD of 0.2 μg/kg in feed and found in samples of most tissues, blood plasma, and urine: PFHxA, PFHpA, PFOA, PFBS, PFHxS, PFHpS, and PFOS. We present full results for these seven substances, as they were consistently found in amounts that allow for numerical analysis. A special case is PFNA, found in very small amounts in most plasma, liver, and kidney samples, but below the LOD of 0.2 μg/kg in feed and other tissues. Four further substances were below the LOD in all matrices except for the liver: PFDA, PFUnA, PFDoA (LOD = 0.2 μg/kg), and PFDS (LOD = 0.5 μg/kg).[30] The above five substances will not be further discussed, as the data preclude numerical analysis. See Table S2 in the Supporting Information for a complete list of relevant substances.

PFAA Concentration in Contaminated Feed. The mean concentration of each substance $\overline{C_I^{\text{exptl}}}$ in the PFAA-contaminated feed is listed in Table 2. The measured concentrations of PFAA varied slightly because of separate batch preparation for each of the three pig genders and for each of the 3 weeks (reflected as standard deviation in Table 2). These details are given in Table S4 of the Supporting

Table 2. Mean Concentration of Each PFAA $\overline{C_I^{\text{exptl}}}$ in Contaminated Intake (I) Feed on a Dry Basis (Arithmetic Mean ± Standard Deviation)[a]

substance	$\overline{C_I^{\text{exptl}}}$ (μg/kg)
PFOS	137 ± 13
PFBS	132 ± 11
PFHxS	91.3 ± 8.0
PFHxA	47.8 ± 4.4
PFOA	22.4 ± 2.6
PFHpA	10.2 ± 1.7
PFHpS	3.99 ± 0.50

[a]Averaging was performed for days 1–21 of the experiment and all 24 pigs. The LOD was 0.2 μg/kg. For the slightly variable individual measured values for each feed preparation by gender and week, see Table S4 in the Supporting Information.

dx.doi.org/10.1021/jf405827u | J. Agric. Food Chem. 2014, 62, 6861–6870

Inormation. The control feed was verified to have a PFAA concentration below the LOD.[30]

PFAA Partitioning to Blood and Edible Tissues. PFAAs distributed into all studied tissues of the pigs, blood plasma, muscle tissues, fat tissue, liver, and kidney (Figure 2), in line with the results in other species.[1] The mass balance of the PFAAs found in blood plasma and edible tissues accounts on average for 97% of the PFAA mass in the feed. The remaining 3% may be attributed to measurement errors and/or partitioning into tissues that were not measured, such as the brain and gastrointestinal tract. For most investigated substances (PFHxS, PFHpS, PFOA, PFHpA, PFBS, and PFHxA), blood plasma became the largest reservoir of unexcreted PFAAs by amount in the body of pigs. PFAAs are known to concentrate in the blood circulation of mammalian organisms, where they bind to proteins such as serum albumin.[45,46] The results show that PFAAs have an even higher affinity for blood plasma relative to other tissues in pigs than in cows and sheep.[21,22] PFAAs are not alone among persistent pollutants in their ability to bind to blood proteins. A study in pigs found that hydroxylated PCBs also accumulate in their blood.[47] This ability to strongly bind to blood proteins and the low clearance and slow excretion in the urine were recently proposed as the best predictors for a chemical's bioaccumulation potential and long half-life.[48] All three factors are present simultaneously in PFAAs, especially in long-chain PFSAs for pigs. After blood plasma, the next most important reservoirs for PFAAs were dorsal muscle, ventral muscle, and fat tissues. Considered together as meat, these three tissues account for between 40% (PFOS) and 49% (PFOA) of unexcreted, accumulated PFAAs. Note that the percentages in Figure 2 refer to both PFAA unexcreted and excreted during the time of the experiment. In contrast to exclusively lipophilic contaminants such as PCDD/Fs,[35] all seven PFAAs were found in similar amounts and concentrations in both fat as well as muscle tissues, in line with findings of PFAA in fat of mice[1] and rats.[49] This supports pooling of the results for muscle tissue and fat as "meat". Likewise, it contradicts the notion that PFAAs are always lipophobic and thus should be absent from fat tissue. This notion may stem from confusion between the (strongly lipophobic) perfluoroalkyl group, a protonated PFAA and its deprotonated version. A study using ion transfer cyclic voltammetry found deprotonated PFSAs and PFCAs to be around 100 times more lipophilic that their nonfluorinated alkyl counterparts,[50] for example, regular fatty acids. At physiological pH, PFSAs and PFCAs are predominantly deprotonated, lending credibility to our findings in fat tissue. Accumulated PFAA in the kidney accounted for under 2% of unexcreted substance. The liver accounted for under 7% of unexcreted PFAAs for all substances except PFOS. The substance PFOS showed a somewhat lower affinity for pig blood plasma and a markedly higher affinity for the liver (35% of unexcreted PFOS). This is likely related to specific protein binding. A study on the binding of several PFAS to human liver fatty acid binding protein (L-FABP)[51] showed that all studied PFAS bound to L-FABP but that PFOS had the strongest binding affinity. In this work, we have used a partitioning-type model, where the interaction with proteins is not an input of the model, as it was in ref 52. Our results may thus be compared a posteriori to in vitro protein binding affinities, because that information was not explicitly used in the model. Finally, because we were able to quantify all 12 PFAAs analyzed in liver samples, even the 5 PFAAs that we could not detect in other matrices, we support the use of liver samples in monitoring programs of farm animals and wild boars.

Baseline Levels of PFAAs in Control Pigs and Background Contamination. Even newborn animals may have body burdens, as maternal−fetal PFOA and PFOS transfer has been demonstrated in rats and humans.[17] Here, PFAA concentrations were found to be below LOD in the six control animals for all tissues and substances, except for PFOS in some liver samples. PFOS in the liver of control animals was always below 1 μg/kg BW, or >1000 times lower than in the experimental animals. PFAAs were also below LOD in drinking water and animal litter.[23]

Dynamic Behavior of PFAAs in Pigs. A very good fit was found for most pigs and substances between the dynamic model of eqs 10 and the experimental data. To exemplify the results, we chose gilt 8 for the plots in Figure 3, because this pig most closely resembles the average pig. The complete plots for all 24 pigs and the average pig are presented in the Supporting Information (Figures S2−S8) for all seven substances. The substances are ordered from slowest (PFHxS) to fastest (PFHxA) urinary excretion (Figure 3). On day 22, all curves display a slight to marked downward trend for both compartments. The curves do not mean a steady state was established, but rather reflect a short depuration period as the animals were fasted before slaughter. The numerical method to fit eqs 10 to experiment is not easily convergent when k_{12} and k_{21} (the rate of mass flow from compartment 1 to 2 and the rate between 2 and 1) are independently fitted. The physiological correlate for this lack of convergence is a fast equilibrium between the blood plasma and edible tissue compartments compared to the urinary excretion rate (so fast that it cannot be convergently calculated precisely). In mathematical language, this means that $k_{12} \gg k_U$ and $k_{21} \gg k_U$ simultaneously. Because we are not interested in the precise independent values of k_{12} and k_{21}, we opt for fitting only the partitioning ratio k_{21}/k_{12} with fast equilibrium between compartments 1 and 2. We thus reduce the number of fitted model constants to only two (k_{21}/k_{12} and k_U). In this way, the numerical method becomes convergent. Another validation of the model prediction of a fast equilibrium between blood plasma and edible tissue is the linear increase of the amount of PFAA in blood plasma for most substances. The red circles in Figure 3a−f display an increase that is almost linear with intercept zero (see also Figures S2−S8 in the Supporting Information). This experimental observation is only mediated by the pig growth functions and no further modeling. A linear increase in PFAA amounts can happen only if the excretion is very slow (compared to the 21 days of the experiment) and if k_{12} and k_{21} are large in comparison. PFHxA displayed nonlinear behavior approaching the steady state. However, the experimental red circles in Figure 3g also suggest a steady state curve shape consistent with fast equilibrium between compartments 1 and 2. We have de facto created a one-compartment model, not a priori, but as a result of the calculations. The Supporting Information section "Concise description of the toxicokinetic model and its constants" provides a compact implementation-ready overview.

Gender Differences in Elimination. This study with pigs found no statistically significant gender difference in elimination half-life between gilts, barrows, and young boars. The statistical insignificance result was obtained with the nonparametric Kruskal−Wallis test (p = 0.01) using the program SPSS 12.0.2G. This is in line with the lack of sex differences in renal elimination in many species, such as rabbits and mice,[53] and

differs from the marked testosterone-regulated difference in the renal elimination of PFCAs found in rats[49] and some fish.[54] The elimination half-life, eq 11, includes information from all model parameters. As no gender differences were found in pigs, averaging was performed using the results for all pigs.

Plasma Elimination Half-Life. From the fitted model constants, we may calculate the elimination half-life (Figure 4)

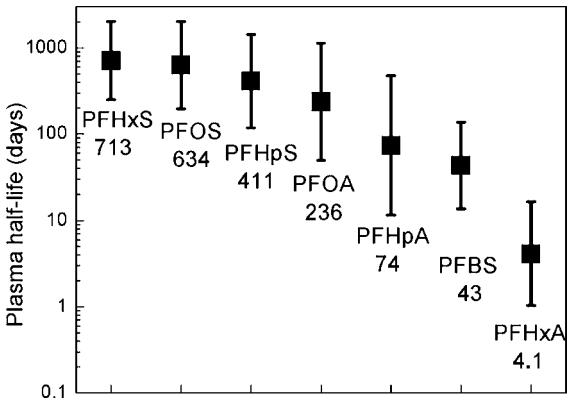

Figure 4. Elimination half-life $\tau_{1/2}$ of PFAAs in pigs. The squares denote the geometric average over up to 24 pigs, and the bars show 95% variability (Student's t statistics). These values reflect both the blood plasma and the edible tissue elimination half-lives, because plasma and edible tissue were found to be in fast equilibrium with each other.

from eq 11. The fast equilibrium between central (plasma) and peripheral (edible tissue) compartments is very advantageous for consumer risk management, because the values in Figure 4 are directly relevant to the elimination of PFAAs from edible tissues. The elimination half-life of PFAAs in pigs is mostly determined by the chemical end-group (sulfonic vs carboxylic acid); half-lives of PFSAs are much longer than for PFCAs. The chain length[10] plays a secondary role. The elimination half-lives are longer than those in trout,[55] rat,[1] Angus cattle,[56] mouse, and monkey[1] but shorter than those for humans.[1,14,17,25] PFHxS has a longer average half-life than PFOS, despite having a shorter chain, in agreement with results in humans.[1,14,17,25] Likewise, a study[14] in humans found a relatively large half-life variability using data from up to 66 individuals, similar to the large variability (vertical bars in Figure 4) in the current study with 24 pigs. It is impossible to separate the systematic from the stochastic variability, but these results may reflect an inherent variability in pig metabolism. Each PFAS may exist in several chain isomers (one linear and several branched). Other studies have found the half-life of each chain isomer to be different.[12,14] In this study, we were able to ensure that only linear PFOS was analytically quantified, without interference from branched isomers. By methodological analogy, although not with full certainty, the quantification of the rest of the substances was also only for the respective linear isomer. See Quantification and Isomer Separation for more details.

Biomagnification Factors. The biomagnification factor (BMF) (also called the bioconcentration factor) measures the ability of a substance to concentrate in an organism's living tissues in relation to the concentration in feed. The BMF is meaningful only in the steady state (ss) and is defined as

$$\mathrm{BMF}_X = \frac{C_X^{\mathrm{ss}}}{\overline{C_I^{\mathrm{exptl}}}} \tag{12}$$

for each substance, where X = plasma (P), liver (L), kidney (K), fat (F), dorsal muscle (D), ventral muscle (V), or whole pig. The concentration in feed $\overline{C_I^{\mathrm{exptl}}}$ is in Table 2. The steady state plasma concentration is obtained as $C_P^{ss} = A_1^{ss}/m_P$. To obtain the amount in blood plasma at steady state A_1^{ss}, one sets the differential eqs 3 to zero and algebraically solves for A_1. Likewise, we solve for the steady state total amount in edible tissue A_2^{ss}. If we assume fast equilibrium between edible tissues, we may use the experimental relative amounts in each tissue (cf. eq 8) to obtain

$$C_Y^{\mathrm{ss}} = \frac{A_Y^{\mathrm{exptl}}(t_{\mathrm{end}})}{A_2^{\mathrm{exptl}}(t_{\mathrm{end}})} \frac{A_2^{\mathrm{ss}}}{m_Y(t_{\mathrm{end}})} \tag{13}$$

where Y = liver (L), kidney (K), fat (F), dorsal muscle (D), ventral muscle (V), or whole pig, where $m_{\mathrm{whole}} = M(t)$, eq 1. Here we have presupposed that the tissues have reached their final weight at t_{end} = 22 days of the experiment. In this 3 week study, the steady state was only observed for PFHxA in some pigs (Figure 3g). The model predicts that the steady state is approached to 95% completion in $t_{95\%\mathrm{ss}} = 22 \pm 14$ days for PFHxA. We may use the model to numerically extrapolate and predict $t_{95\%\mathrm{ss}}$ for other substances. For PFBS, $t_{95\%\mathrm{ss}} = 217 \pm 120$ days and between 1 and 10 years for the rest of the compounds (Supporting Information Table S5). Both BMF and $t_{95\%\mathrm{ss}}$ depend only on the compound through the model constants and do not depend on $\overline{C_I^{\mathrm{exptl}}}$. The extrapolated steady state (eq 13) assumes a linear half-life behavior, which may be a flawed assumption if renal resorption saturation[57] is relevant for the concentrations considered (see section on Limitations). The computed BMF, eq 12, is listed in Table 3 by tissue groups, where meat is an average of D, V, and F.

Table 3. Biomagnification Factor, Dimensionless (Arithmetic Mean) from Equation 12[a]

substance	mean BMF whole pig	mean BMF meat	mean BMF liver
PFHxS	20.1	13.1	48
PFHpS	12.7	8.3	81
PFOS	17.9	9.7	503
PFOA	7.9	5.3	32.8
PFHpA	2.7	1.8	7.0
PFBS	1.2	0.8	6.
PFHxA	0.13	0.08	0.42

[a]Mean for all 24 pigs. For more detailed information on tissue-specific BMF, see Supporting Information Table S5.

Limitations. A drawback worth mentioning is the inability of this study to detect a possible interaction among substances regarding absorption, distribution, and excretion. Because we have chosen to study a mixture of PFAAs arising from a contaminated cultivation site, we cannot rule out that the specific pattern of substances (Table 2) results in a specific toxicokinetic profile. Likewise, we have not analyzed any PFAA precursors possibly present in the feed. The presence of precursors cannot be ruled out in the industrial waste that contaminated the soil.[27] The mass balance closes to 97% (Figure 2). Possible explanations for this good agreement in terms of PFAA precursors are (a) the feed did not contain precursors, (b) precursors were present, but the pigs' metabolic bioconversion is too slow to show up in 3 weeks, or (c) part of the PFAAs go into tissues not tested, such as the brain, whereas

the PFAAs from precursors balance this mechanism out. The two-compartment model includes no provision for saturation of binding,[52,57] but we know from experiments that blood proteins can bind much larger amounts than those observed here.[45,46] However, a mechanism known to be saturable in other organisms is renal PFAA resorption through organic anion transporters.[17] In our model, renal resorption is implicitly part of the renal excretion constant k_U and includes no saturable equations.[52,57] Saturable renal resorption may lead to nonlinear half-life, with faster elimination at higher plasma concentrations. The present experimental data are not designed for fitting renal resorption, so this caveat should be considered for half-life (Figure 4) and BMF (Table 3).

Consequences for Food Safety. The elimination half-lives are very long compared to the lifetime of a farm pig (~180 days) before slaughter, except for PFHxA. Even if contaminated animals are fed uncontaminated feed for weeks or months, it is not expected to see significant declines in PFAA levels. This has consequences for risk management. The EFSA has set a TDI limit of 0.15 μg/kg BW/day for PFOS and 1.5 μg/kg BW/day for PFOA.[8] No TDI is yet available for other PFAAs.[9] From the EFSA TDI and total exposure, including total diet studies, it is possible to derive exposure guidelines for pork. It is very important to produce consistent regulations for maximum content of PFAAs in animal feed and animal products, which is possible only when both a toxicokinetic model and a maximum exposure are available. This has been done for dioxins and other lipophilic pollutants in, for example, chicken feed/eggs.[58] Although lipophilic pollutants have different toxicokinetic properties from PFAAs, the general concepts needed to relate the maximum levels in feed and food are the same. The present toxicokinetic model enables such a quantitative connection between porcine feed and food product PFAA concentrations.

■ ASSOCIATED CONTENT

Ⓢ Supporting Information

More details, such as a compact description of the model and its constants. This material is available free of charge via the Internet at http://pubs.acs.org.

■ AUTHOR INFORMATION

Corresponding Author

*(J.N.) E-mail: jorge.numata@bfr.bund.de. Phone +49-30-18412-1942. Fax +49-30-18412-2961.

Funding

We gratefully acknowledge financial support from the INTERREG project SafeGuard.

Notes

The authors declare no competing financial interest.

■ ABBREVIATIONS USED

PFAAs	perfluoroalkyl acids
PFSAs	perfluoroalkyl sulfonic acids
PFCAs	perfluoroalkyl carboxylic acids
PFBS	perfluorobutanesulfonic acid
PFHxS	perfluorohexanesulfonic acid
PFHpS	perfluoroheptanesulfonic acid
PFOS	perfluorooctanesulfonic acid
PFDS	perfluorodecanesulfonic acid
PFBA	perfluorobutanoic acid
PFPA	perfluoropentanoic acid
PFHxA	perfluorohexanoic acid and
PFHpA	perfluoroheptanoic acid
PFOA	Perfluorooctanoic acid
PFNA	perfluorononanoic acid
PFDA	perfluorodecanoic acid
PFUnA	perfluoroundecanoic acid
PFDoA	perfluorododecanoic acid
DiPAPs	polyfluoroalkyl-diester phosphate surfactants
L-FABP	liver fatty acid binding protein
PBT	persistent bioaccumulative and toxic
TDI	tolerable daily intake
LOD	limit of detection
LOQ	limit of quantification
HPLC-MS/MS	high-performance liquid chromatography coupled with tandem mass spectrometry
MRM	multiple reaction monitoring
UCL-MS	ultraliquid chromatography−mass spectrometry
ESI	electrospray interface
BW	body weight
BMF	biomagnification factor
ss	steady state

■ REFERENCES

(1) Lau, C. Perfluorinated compounds. In *Molecular, Clinical and Environmental Toxicology Volume 3: Environmental Toxicology*; Luch, A., Ed.; Springer: Basel, Switzerland, 2012.

(2) Lindstrom, A. B.; Strynar, M. J.; Libelo, E. L. Polyfluorinated compounds: past, present, and future. *Environ. Sci. Technol.* **2011**, *45*, 7954−7961.

(3) Kissa, E. *Fluorinated Surfactants and Repellents*, 2nd ed.; Dekker: New York, 2001; Vol. 97.

(4) Martin, J. W.; Mabury, S. A.; Solomon, K. R.; Muir, D. C. G. Progress toward understanding the bioaccumulation of perfluorinated alkyl acids. *Environ. Toxicol. Chem.* **2013**, *32*, 2421−2423.

(5) Buhrke, T.; Kibellus, A.; Lampen, A. In vitro toxicological characterization of perfluorinated carboxylic acids with different carbon chain lengths. *Toxicol. Lett.* **2013**, *218*, 97−104.

(6) Grandjean, P.; Budtz-Jørgensen, E. Immunotoxicity of perfluorinated alkylates: calculation of benchmark doses based on serum concentrations in children. *Environ. Health* **2013**, *12*, 35.

(7) Fletcher, T.; Savitz, D.; Steenland, K. C8 Probable Link Reports, http://www.c8sciencepanel.org, 2012.

(8) European Food Safety Authority, Scientific opinion of the panel on contaminants in the food chain on perfluorooctane sulfonate (PFOS), perfluorooctanoic acid (PFOA) and their salts. *EFSA J.* **2008**, *653*, 1−131.

(9) European Food Safety Authority, Scientific report on perfluoroalkylated substances in food: occurrence and dietary exposure. *EFSA J.* **2012**, *10*, 2743.

(10) Buck, R. C.; Franklin, J.; Berger, U.; Conder, J. M.; Cousins, I. T.; de Voogt, P.; Jensen, A. A.; Kannan, K.; Mabury, S. A.; van Leeuwen, S. P. J. Perfluoroalkyl and polyfluoroalkyl substances in the environment: terminology, classification, and origins. *Integr. Environ. Assess. Manage.* **2011**, *7*, 513−541.

(11) D'eon, J. C.; Mabury, S. A. Production of perfluorinated carboxylic acids (PFCAs) from the biotransformation of polyfluoroalkyl phosphate surfactants (PAPS): exploring routes of human contamination. *Environ. Sci. Technol.* **2007**, *41*, 4799−4805.

(12) Ross, M. S.; Wong, C. S.; Martin, J. W. Isomer-specific biotransformation of perfluorooctane sulfonamide in Sprague-Dawley Rats. *Environ. Sci. Technol.* **2012**, *46*, 3196−3203.

(13) Trier, X.; Granby, K.; Christensen, J. H. Polyfluorinated surfactants (PFS) in paper and board coatings for food packaging. *Environ. Sci. Pollut. Res.* **2011**, *18*, 1108−1120.

(14) Zhang, Y.; Beesoon, S.; Zhu, L.; Martin, J. W. Biomonitoring of perfluoroalkyl acids in human urine and estimates of biological half-life. *Environ. Sci. Technol.* **2013**, *47*, 10619−10627.

(15) Vestergren, R.; Cousins, I. T. Tracking the pathways of human exposure to perfluorocarboxylates. *Environ. Sci. Technol.* **2009**, *43*, 5565−5575.
(16) Klenow, S.; Heinemeyer, G.; Brambilla, G.; Dellatte, E.; Herzke, D.; de Voogt, P. Dietary exposure to selected perfluoroalkyl acids (PFAAs) in four European regions. *Food Addit. Contam. A* **2013**, *30*, 2141−2151.
(17) Loccisano, A. E.; Longnecker, M. P.; Campbell, J. L., Jr.; Andersen, M. E.; Clewell, H. J., 3rd. Development of PBPK models for PFOA and PFOS for human pregnancy and lactation life stages. *J. Toxicol. Environ. Health A* **2013**, *76*, 25−57.
(18) Stahl, T.; Heyn, J.; Thiele, H.; Hüther, J.; Failing, K.; Georgii, S.; Brunn, H. Carryover of perfluorooctanoic acid (PFOA) and perfluorooctane sulfonate (PFOS) from soil to plants. *Arch. Environ. Contam. Toxicol.* **2009**, *57*, 289−298.
(19) Watanabe, M. X.; Kunisue, T.; Tao, L.; Kannan, K.; Subramanian, A.; Tanabe, S.; Iwata, H. Dioxin-like and perfluorinated compounds in pigs in an Indian open waste dumping site: toxicokinetics and effects on hepatic cytochrome P450 and blood plasma hormones. *Environ. Toxicol. Chem.* **2010**, *29*, 1551−1560.
(20) Norden, M.; Berger, U.; Engwall, M. High levels of perfluoroalkyl acids in eggs and embryo livers of great cormorant (*Phalacrocorax carbo sinensis*) and herring gull (*Larus argentatus*) from Lake Vanern, Sweden. *Environ. Sci. Pollut. Res. Int.* **2013**, *20*, 8021−8030.
(21) van Asselt, E. D.; Kowalczyk, J.; van Eijkeren, J. C.; Zeilmaker, M. J.; Ehlers, S.; Fürst, P.; Lahrssen-Wiederholt, M.; van der Fels-Klerx, H. J. Transfer of perfluorooctane sulfonic acid (PFOS) from contaminated feed to dairy milk. *Food Chem.* **2013**, *141*, 1489−1495.
(22) Kowalczyk, J.; Ehlers, S.; Fürst, P.; Schafft, H.; Lahrssen-Wiederholt, M. Transfer of perfluorooctanoic acid (PFOA) and perfluorooctane sulfonate (PFOS) from contaminated feed into milk and meat of sheep: pilot study. *Arch. Environ. Contam. Toxicol.* **2012**, *63*, 288−298.
(23) Kowalczyk, J.; Ehlers, S.; Oberhausen, A.; Tischer, M.; Fürst, P.; Schafft, H.; Lahrssen-Wiederholt, M. Absorption, distribution, and milk secretion of the perfluoroalkyl acids PFBS, PFHxS, PFOS, and PFOA by dairy cows fed naturally contaminated feed. *J. Agric. Food Chem.* **2013**, *61*, 2903−2912.
(24) Vestergren, R.; Orata, F.; Berger, U.; Cousins, I. T. Bioaccumulation of perfluoroalkyl acids in dairy cows in a naturally contaminated environment. *Environ. Sci. Pollut. Res.* **2013**, *20*, 7959−7969.
(25) Olsen, G. W.; Burris, J. M.; Ehresman, D. J.; Froehlich, J. W.; Seacat, A. M.; Butenhoff, J. L.; Zobel, L. R. Half-life of serum elimination of perfluorooctanesulfonate,perfluorohexanesulfonate, and perfluorooctanoate in retired fluorochemical production workers. *Environ. Health Perspect.* **2007**, *115*, 1298−1305.
(26) Groenen, M. A. M.; Archibald, A. L.; Uenishi, H.; Tuggle, C. K.; Takeuchi, Y.; Schook, L. B. Analyses of pig genomes provide insight into porcine demography and evolution. *Nature* **2012**, *491*, 393−398.
(27) Arenholz, U.; Bergmann, S.; Bosshammer, K.; Busch, D.; Dreher, K.; Eichler, W.; Geueke, K.-J.; Grubert, G.; Hähnle, J.; Harff, K.; Kraft, M.; Leisner-Saaber, J.; Oberdörfer, M.; Rauchfuss, K.; Respondek, R.; Reupert, R.; Rose-Luther, J.; Schroers, S.; Tiedt, M.; Just, P.; Poschner, A.; Susset, B. *LANUV − Fachbericht 34 Verbreitung von PFT in der Umwelt: Ursachen - Untersuchungsstrategie - Ergebnisse - Maßnahmen*; Landesamt für Natur, Umwelt und Verbraucherschutz Nordrhein-Westfalen: Germany, 2011.
(28) *Empfehlungen zur Energie und Nährstoffversorgung bei Schweinen*, Auflage 1/2006 ed.; DLG-Verlag: Frankfurt, Germany, 2006.
(29) Kärrman, A.; van Bavel, B.; Järnberg, U.; Hardell, L.; Lindström, G. Development of a solid-phase extraction-HPLC/single quadrupole MS method for quantification of perfluorochemicals in whole blood. *Anal. Chem.* **2005**, *77*, 864−870.
(30) Ehlers, S. *Analytik von Perfluoralkylsäuren in verschiedenen Matrices zur Klärung der Toxikokinetik in Tierarten, die der Lebensmittelgewinnung dienen*. Westfälische Wilhelms-Universität Münster, 2012.
(31) Taniyasu, S.; Kannan, K.; So, M. K.; Gulkowska, A.; Sinclair, E.; Okazawa, T.; Yamashita, N. Analysis of fluorotelomer alcohols, fluorotelomer acids, and short- and long-chain perfluorinated acids in water and biota. *J. Chromatogr., A* **2005**, *1093*, 89−97.
(32) Bernsmann, T.; Fürst, P. Determination of perfluorinated compounds in human milk. *Organohalog. Compd.* **2008**, *70*, 718−721.
(33) Benskin, J. P.; De Silva, A. O.; Martin, L. J.; Arsenault, G.; McCrindle, R.; Riddell, N.; Mabury, S. A.; Martin, J. W. Disposition of perfluorinated acid isomers in Sprague-Dawley rats. Part 2: Subchronic dose. *Environ. Toxicol. Chem.* **2009**, *28*, 555−567.
(34) Marquardt, D. D. An algorithm for least-squares estimation of non-linear parameters. *J. Soc. Ind. Appl. Math.* **1963**, *11*, 431−441.
(35) Adolphs, J.; Kleinjung, F.; Numata, J.; Mielke, H.; Abraham, K.; Schafft, H.; Müller-Graf, C.; Greiner, M. A probabilistic model for the carry-over of PCDD/Fs from feed to growing pigs. *Chemosphere* **2013**, *93*, 474−479.
(36) Pfeiffer, H.; Lengerken, G. v.; Gebhardt, G. *Wachstum und Schlachtkörperqualität*; VEB Deutscher Landwirtschaftsverlag: Berlin, Germany, 1984.
(37) Branscheid, W.; Honikel, K.-O.; Lengerken, G. v. *Qualität von Fleisch und Fleischwaren: Band 1. 2. überarbeitete und erweiterte*, Auflage ed.; Deutscher Fachverlag: Frankfurt, Germany, 2007.
(38) Elsner, F. L. Messung der Nierenperfusion mittels DCE-MRI am narkotisierten Schwein. Freie Universität, Berlin, Germany, 2012.
(39) Aiello, S. E.; Moses, M. A. *The Merck Veterinary Manual Online*, 2011.
(40) *Empfehlung zur Blutentnahme bei Versuchstieren, insbesondere kleinen Versuchstieren*; GV-SOLAS: Marburg, Germany, 2009.
(41) Johnson, J. D.; Gibson, S. J.; Ober, R. E. Cholestyramine-enhanced fecal elimination of carbon-14 in rats after administration of ammonium [^{14}C]perfluorooctanoate or potassium [^{14}C]-perfluorooctanesulfonate. *Fundam. Appl. Toxicol.* **1984**, *4*, 972−976.
(42) Fricke, M.; Lahl, U. Risikobewertung von Perfluortensiden als Beitrag zur aktuellen Diskussion zum REACH-Dossier der EU-Kommission. *UWSF* **2005**, *17*, 36−49.
(43) Chiu, W. A.; Barton, H. A.; DeWoskin, R. S.; Schlosser, P.; Thompson, C. M.; Sonawane, B.; Lipscomb, J. C.; Krishnan, K. Evaluation of physiologically based pharmacokinetic models for use in risk assessment. *J. Appl. Toxicol.* **2007**, *27*, 218−237.
(44) Urien, S.; Lokiec, F. Population pharmacokinetics of total and unbound plasma cisplatin in adult patients. *Br. J. Clin. Pharmacol.* **2004**, *57*, 756−763.
(45) Bischel, H. N.; MacManus-Spencer, L. A.; Zhang, C.; Luthy, R. G. Strong associations of short-chain perfluoroalkyl acids with serum albumin and investigation of binding mechanisms. *Environ. Toxicol. Chem.* **2011**, *30*, 2423−2430.
(46) Luo, Z.; Shi, X.; Hu, Q.; Zhao, B.; Huang, M. Structural evidence of perfluorooctane sulfonate transport by human serum albumin. *Chem. Res. Toxicol.* **2012**, *25*, 990−992.
(47) Mizukawa, H.; Nomiyama, K.; Kunisue, T.; Watanabe, M. X.; Subramanian, A.; Takahashi, S.; Tanabe, S. Accumulation features of hydroxylated-PCBs (OH-PCBs) in the blood of pigs collected from a dumping site for municipal wastes in India. In *Interdisciplinary Studies on Environmental Chemistry — Environmental Specimen Bank*; Isobe, T., Nomiyama, K., Subramanian, A., Tanabe, S., Eds.; Global COE Ehime University: Japan, 2010; pp 175−181.
(48) Tonnelier, A.; Coecke, S.; Zaldívar, J.-M. Screening of chemicals for human bioaccumulative potential with a physiologically based toxicokinetic model. *Arch. Toxicol.* **2012**, *86*, 393−403.
(49) Vanden Heuvel, J. P.; Kuslikis, B. I.; Van Rafelghem, M. J.; Peterson, R. E. Tissue distribution, metabolism, and elimination of perfluorooctanoic acid in male and female rats. *J. Biochem. Toxicol.* **1991**, *6*, 83−92.
(50) Jing, P.; Rodgers, P. J.; Amemiya, S. High lipophilicity of perfluoroalkyl carboxylate and sulfonate: implications for their membrane permeability. *J. Am. Chem. Soc.* **2009**, *131*, 2290−2296.
(51) Zhang, L.; Ren, X.-M.; Guo, L.-H. Structure-based investigation on the interaction of perfluorinated compounds with human liver fatty acid binding protein. *Environ. Sci. Technol.* **2013**, *47*, 11293−11301.

(52) Ng, C. A.; Hungerbühler, K. Bioconcentration of perfluorinated alkyl acids: how important is specific binding? *Environ. Sci. Technol.* **2013**, *47*, 7214−7223.
(53) Hundley, S. G.; Sarrif, A. M.; Kennedy, G. L. Absorption, distribution, and excretion of ammonium perfluorooctanoate (APFO) after oral administration to various species. *Drug Chem. Toxicol.* **2006**, *29*, 137−145.
(54) Lee, J. J.; Schultz, I. R. Sex differences in the uptake and disposition of perfluorooctanoic acid in fathead minnows after oral dosing. *Environ. Sci. Technol.* **2010**, *44*, 491−496.
(55) De Silva, A. O.; Tseng, P. J.; Mabury, S. A. Toxicokinetics of perfluorocarboxylate isomers in rainbow trout. *Environ. Toxicol. Chem.* **2009**, *28*, 330−337.
(56) Lupton, S. J.; Huwe, J. K.; Smith, D. J.; Dearfield, K. L.; Johnston, J. J. Absorption and excretion of ^{14}C-perfluorooctanoic acid (PFOA) in Angus cattle (*Bos taurus*). *J. Agric. Food Chem.* **2012**, *60*, 1128−1134.
(57) Loccisano, A. E.; Campbell, J. L., Jr.; Butenhoff, J. L.; Andersen, M. E.; Clewell, H. J., 3rd. Comparison and evaluation of pharmacokinetics of PFOA and PFOS in the adult rat using a physiologically based pharmacokinetic model. *Reprod. Toxicol.* **2012**, *33*, 452−467.
(58) Van Eijkeren, J. C. H.; Zeilmaker, M. J.; Kan, C. A.; Traag, W. A.; Hoogenboom, L. A. A toxicokinetic model for the carry-over of dioxins and PCBs from feed and soil to eggs. *Food Addit. Contam.* **2006**, *23*, 509−517.

Table 1. Real-Time PCR Primer Pairs. PCR Primers Used in the Gene Expression Analysis

gene name	description	primer sequence	primer size (bp)
Refer-actin	mactin-F	5′-GAGACCTTCAACACCCCAGC-3′	
	mactin-R	5′-ATGTCACGCACGATTTCCC-3′	263
IL-4	mIL-4-F	5′-TGTAGGGCTTCCAAGGTGCT-3′	
	mIL-4-R	5′-TGATGCTCTTTAGGCTTTCCAG-3′	199
IL-5	mIL-5-F	5′-GTGAAAGAGACCTTGACACAGCTG-3′	
	mIL-5-R	5′-CACACCAAGGAACTCTTGCAGGTA-3′	290
IL-12	mIL-12-F	5′-ACTCGGCTCCTCATGGACAT-3′	
	mIL-12-R	5′-TGCAACAGTCAGGCTCTT-3′	278
IFN-γ	mIFN-γ-F	5′-TGAAAGACAATCAGGCCATCA-3′	
	mIFN-γ-R	5′-CTGGACCTGTGGGTTGTTGA-3′	140
GATA3	mGATA3-F	5′-CCACGGGAGCCAGGTATG-3′	
	mGATA3-R	5′-CGGAGGGTAAACGGACAGAG-3′	169
GATA4	mGata4-F	5′-CCTGGAAGACACCCCAATCT-3′	
	mGata4-R	5′-GGTAGTGTCCCGTCCCATCT-3′	115
T-bet	mT-bet-F	5′-TGGACCCAACTGTCAACTGC-3′	
	mT-bet-R	5′-CTCGGAACTCCGCTTCATAAC-3′	173
STAT1	mSTAT1-F	5′-ACGCTGCCTATGATGTCTCG-3′	
	mSTAT1-R	5′-ACGGGATCTTCTTGGAAGTTATC-3′	163
STAt3	mSTAT3-F	5′-TGACCAATAACCCCAAGAACG-3′	
	mSTAT3-R	5′-TGACACCCTGAGTAGTTCACACC-3′	181
STAT6	mSTAT6-F	5′-AGCATCTTGCCGCACATCA-3′	
	mSTAT6-R	5′-GGCAGGTGGCGGAACTCT-3′	128
eotaxin	mEotaxin-F	5′-TGCTCACGGTCACTTCCTTC-3′	
	mEotaxin-R	5′-GGTGCTTTGTGGCATCCTG-3′	231
MCP-1	mMCP-1-F	5′-GCTGACCCCAAGAAGGAATG-3′	
	mMCP-1-R	5′-TTGAGGTGGTTGTGGAAAAGG-3′	184
MIP-2	mMIP-2F	5′-CACCAACCACCAGGCTACAG-3′	
	mMIP-2R	5′-GCTTCAGGGTCAAGGCAAAC-3′	189

TiO_2 is considered to be an inert and poorly soluble matter. As a common additive in many foods, TiO_2 is used for whitening and brightening foods, particularly for confectionaries, white sauces and dressings, and certain powdered foods.[28] It has been estimated that in the UK the dietary intake of TiO_2 is 5 mg per person per day.[29] The quantity of TiO_2 cannot exceed 1% by weight of the food according to the federal regulations of the U.S. government. In 1969, WHO reported that the LD_{50} of TiO_2 for rats is greater than 12 g kg^{-1} BW after an oral administration. Therefore, a potential exposure route for the general population is oral ingestion. The studies of both longer exposure duration and the lower dose of TiO_2 are of interest for risk assessors. In view of the above, therefore, the aim of the present study was stated to be the investigation of whether the liver inflammation observed in the earlier studies is mediated by Th2 factors in mice for longer exposure duration and the lower dose.

MATERIALS AND METHODS

Chemicals. The preparation and characteristics of TiO_2 NPs particles including the anatase structure, size, surface area, mean hydrodynamic diameter, and ζ potential have been described in our previously work.[30,31] X-ray-diffraction (XRD) was used to detect the anatase structure and size with a charge-coupled device (CCD) diffractometer (Mercury 3 Versatile CCD detector; Rigaku Corporation, Tokyo, Japan) using Ni-filtered Cu Kα radiation. The NP size was determined using a TecnaiG220 transmission electron microscope (TEM) (FEI Co., USA). The surface area of NPs was determined by Brunauer−Emmett−Teller (BET) adsorption measurements on a Micromeritics ASCORBIC ACIDP 2020M+C instrument (Micromeritics Co., USA). The average aggregate or agglomerate size and ζ potential of NPs were measured by dynamic light scattering (DLS) using a Zeta PALS + BI-90 Plus (Brookhaven Instruments Corp., USA). XRD measurements suggested that TiO_2 NPs showed an anatase structure. The average particle size of powdered TiO_2 NPs suspended in 0.5% w/v HPMC solvent after 24 h (5 mg/mL) incubation ranged from 5 to 6 nm, and the surface area was 174.8 m^2/g. The mean hydrodynamic diameter of TiO_2 NPs in HPMC solvent (5 mg/mL) ranged from 208 to 330 nm (mainly 294 nm), and the ζ potential after 24 h incubation was 9.28 mV.[31] The anatase structure, size, surface area, mean hydrodynamic diameter, and ζ potential have been described in the Supporting Information.

Animals and Treatment. 160 CD-1 (ICR) male mice (20 ± 2 g body weight) were purchased from the Animal Center of Soochow University (China). All mice were housed in stainless steel cages in a ventilated animal room. Room temperature of the housing facility was maintained at 24 ± 2 °C with a relative humidity of 60 ± 10% and a 12 h light/dark cycle. Distilled water and sterilized food were available for mice *ad libitum*. Prior to dosing, the mice were acclimated to this environment for 5 days. All procedures used in animal experiments conformed to the U.S. National Institutes of Health Guide for the Care and Use of Laboratory Animals.

TiO_2 NP powder was dispersed onto the surface of 0.5% w/v HPMC, and the suspension containing TiO_2 NPs was treated ultrasonically for 30 min and mechanically vibrated for 5 min. The mice were randomly divided into four groups (n = 30 each), including a control group treated with 0.5% w/v HPMC and three experimental groups treated with 2.5, 5, or 10 mg/kg body weight (BW) TiO_2 NPs. The mice were weighed, the volume of TiO_2 NP suspensions was calculated for each mouse, and the fresh TiO_2 NP suspensions were gavaged to the mice by a gavage needle every day for six months. Any symptoms, growth state (weighing all animals every day), eating and drinking (quantitatively measuring food and water consumption every day), activity, and/or mortality were observed and recorded carefully daily during the six months.

Liver Indices. After six months, mice were weighed and then sacrificed after ether anesthesia. Blood samples were collected from the

eye vein by rapidly removing the eyeball, and serum was collected by centrifuging the blood samples at 1200*g* for 10 min. The livers of all animals were quickly removed and placed on ice. After weighing the body and livers, the liver indices were calculated as the ratio of liver (wet weight, mg) to body weight (g).

Titanium Content Analysis. The frozen liver tissues (n = 5 each) were thawed, and approximately 0.3 g samples were weighed, digested, and analyzed for titanium content. Prior to elemental analysis, the liver tissues were digested overnight with nitric acid (ultrapure grade), combined with 0.5 mL of H_2O_2, and incubated at 160 °C in high-pressure reaction containers in an oven until the samples were completely digested. The solutions were incubated at 120 °C to remove any remaining nitric acid until the solutions were clear. Finally, the remaining solutions were diluted to 3 mL with 2% nitric acid. Inductively coupled plasma-mass spectrometry (ICP-MS; Thermo Elemental X7; Thermo Electron Co., Waltham, MA, USA) was used to determine the titanium concentration in the samples. Indium (20 ng/mL) was chosen as an internal standard element. Elemental titanium (isotopes ^{48}Ti or ^{49}Ti) was quantified using ICP-MS against titanium standards, which also contained the internal standard.

Biochemical Analysis of Liver Functions. Serum biochemical functions including alanine aminotransferase (ALT), aspartate aminotransferase (AST), alkaline phosphatase (ALP), and lactate dehydrogenase (LDH) concentrations (n = 5 each) were determined by ELISA (R&D Systems, Minneapolis, MN, USA). All biochemical assays were performed using a clinical automatic chemistry analyzer (type 7170A, Hitachi, Japan).

Histopathological Examination of the Liver. All histopathological examinations were performed using standard laboratory procedures. Five sets of liver tissues from each dose group were embedded in paraffin blocks, sliced to 5 μm thickness, and placed on separate glass slides (five slices from each kidney). After hematoxylin−eosin staining, the sections were evaluated by a histopathologist unaware of the treatments, using an optical microscope (U−III Multipoint Sensor System; Nikon, Tokyo, Japan).

Observation of Hepatocyte Ultrastructure. Livers (n = 5 each) were fixed in a fresh solution of 0.1 M sodium cacodylate buffer containing 2.5% glutaraldehyde and 2% formaldehyde followed by a 2 h fixation period at 4 °C with 1% osmium tetroxide in 50 mM sodium cacodylate (pH 7.2−7.4). Staining was performed overnight with 0.5% aqueous uranyl acetate. The specimens were dehydrated in a graded series of ethanol (75, 85, 95, and 100%) and embedded in Epon 812. Ultrathin sections were obtained, contrasted with uranyl acetate and lead citrate, and observed with a Hitachi H600 TEM (Hitachi Co., Japan). Liver apoptosis was determined based on the changes in nuclear morphology (e.g., chromatin condensation and fragmentation).

Assay of Cytokine Expression. The levels of mRNA expression of *IL-4*, *IL-5*, *IL-12*, *FN-γ*, *GATA3*, *GATA 4*, *T-bet*, *STAT1*, *STAt3*, *STAT6*, *eotaxin*, *MCP-1*, and *MIP-2* in the livers (n = 5 each) were determined using real-time quantitative (q)RT-PCR, as described previously.[32] Synthesized cDNA was generated by qRT-PCR with primers designed with Primer Express Software (Applied Biosystems, Foster City, CA, USA) according to the manufacturer's guidelines, and the sequences are listed in Table 1. The right livers from mice with or without TiO_2 NP treatment were homogenized using QIAzol lysis reagent with a TissueRuptor (Roche, USA). Total RNA from the homogenates was isolated using Tripure isolation reagent (Roche, USA) according to the manufacturer's instructions. The RT reagent (Shinegene, China) of 30 μL was prepared by mixing 15 μL of 2× RT buffer, 1 μL of random primer in a concentration of 100 pmol·μL^{-1}, 1 μL of RTase, 5 μL of RNA, and 8 μL of DEPC water together. The reaction condition was 25 °C for 10 min, 40 °C for 60 min, and 70 °C for 10 min. The internal reference gene was actin3. qRT-PCR was performed using the 7500 real-time PCR system (ABI) with SYBR Premix Ex Taq (Takara) according to the manufacturer's instructions. The gene expression analysis and experimental system evaluation were performed according to the standard curve and quantitation reports.

To determine IL-4, IL-5, IL-12, IFN-γ, GATA3, GATA4, T-bet, STAT1, STAt3, STAT6, eotaxin, MCP-1, and MIP-2 levels in the mouse liver tissues, ELISAs were performed using commercial kits specific for each protein (R&D Systems, Minneapolis, MN, USA), following the manufacturer's instructions. The absorbance was measured on a microplate reader at 450 nm (Varioskan Flash; Thermo Electron, Finland), and the concentrations of IL-4, IL-5, IL-12, IFN-γ, GATA3, GATA4, T-bet, STAT1, STAt3, STAT6, eotaxin, MCP-1, and MIP-2 were calculated from a standard curve for each sample.

Statistical Analysis. All results are expressed as means ± standard error (SE). One-way analysis of variance (ANOVA) was carried out to compare the differences of means among the multigroup data using SPSS 19 software (SPSS, Inc., Chicago, IL, USA). Dunnett's test was performed when each data set was compared with the solvent control data. Statistical significance for all tests was judged with a probability level of 0.05 (p < 0.05).

RESULTS

Body Weight, Liver Indices, and Titanium Accumulation. During the treatment, all mice were all at growth state. The daily behaviors such as food consumption, drinking, and activity in TiO_2 NP-treated groups were not significantly different from those of the control group. Figure 1 shows the net increase in body weight, liver weight, and liver indices caused by TiO_2 NP exposure. TiO_2 NP exposure resulted in significant reductions in the net increase of body weight and increases in liver indices as compared with the controls (p < 0.05), but liver weight did not exhibit differences among the four groups (p > 0.05). Furthermore, there was significant titanium accumulation with increased TiO_2 NP dose (Figure 2, p < 0.001). The decreased body weight and increased liver indices caused by TiO_2 NP exposure may be related to liver dysfunction and tissue injury, which were confirmed by the biochemical assays and histopathological observations of mouse livers.

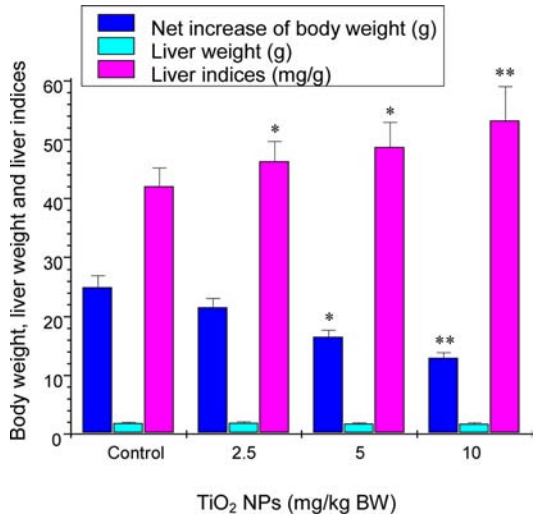

Figure 1. Net increase of body weight, liver weight, and liver indices of male mice after gavage administration of TiO_2 NPs for six consecutive months. *p < 0.05, and **p < 0.01. Values represent means ± SE (n = 40).

Histopathological Evaluation. The histological changes in the liver specimens are shown in Figure 3. Unexposed liver samples exhibited normal architecture including intact hepatic lobule and normal blood sinusoid opening (Figure 3), while those from five mice of each group exposed to increasing TiO_2 NP concentrations exhibited severe pathological changes,

dx.doi.org/10.1021/jf501428w | J. Agric. Food Chem. 2014, 62, 6871−6878

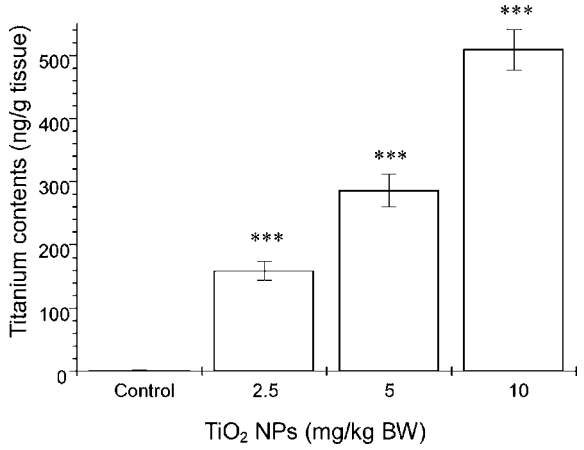

Figure 2. Titanium contents in mouse livers after gavage administration of TiO_2 NPs for six consecutive months. ***p < 0.001. Values represent means ± SE (n = 5).

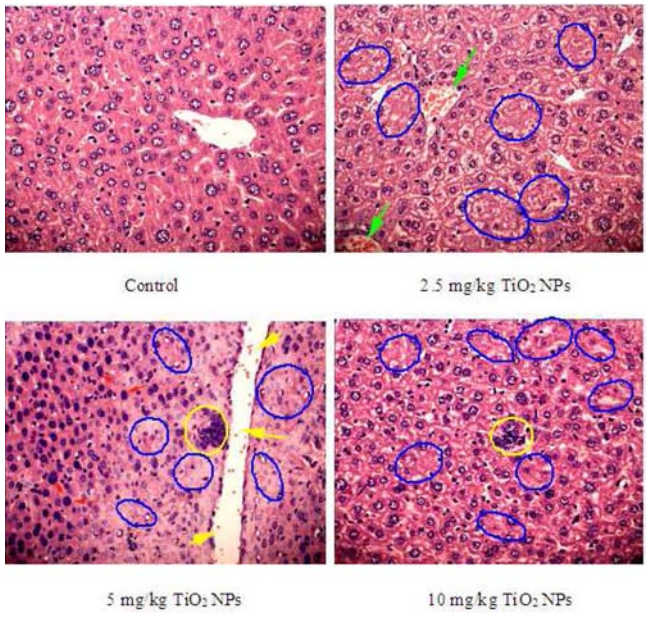

Figure 3. Histopathological observation of livers after gavage administration of TiO_2 NPs for six consecutive months (n = 5). The control group (unexposed mice) showed intact hepatic lobule and normal blood sinusoid opening (400×). The 2.5 mg/kg TiO_2 NP group presented with vein congestion (green arrows), angiectasis and hyperemia (white arrows), and neorobiosis of hepatocytes (blue circles) (400×). The 5 mg/kg TiO_2 NP group presented with inflammatory cell infiltration (yellow circle), macrophages (red arrows)), hepatic tissue crevice (yellow arrows), and neorobiosis of hepatocytes (blue circles) (400×). The 10 mg/kg TiO_2 NP group presented with inflammatory cell infiltration (yellow circle) and neorobiosis of hepatocytes (blue circles) (400×).

including angiectasis and hyperemia, infiltration of inflammatory cells, macrophage aggregation, hepatic tissue crevice, and hepatocyte necrosis (Figure 3). The results suggested that chronic exposure to TiO_2 NPs resulted in significant pathological changes in the livers, which may be related to cytokine expression.

Observation of Hepatocyte Ultrastructure. Changes to hepatocyte ultrastructure in the mouse liver samples are presented in Figure 4. As shown, hepatocytes of the control group contained elliptical nuclei with homogeneous chromatin

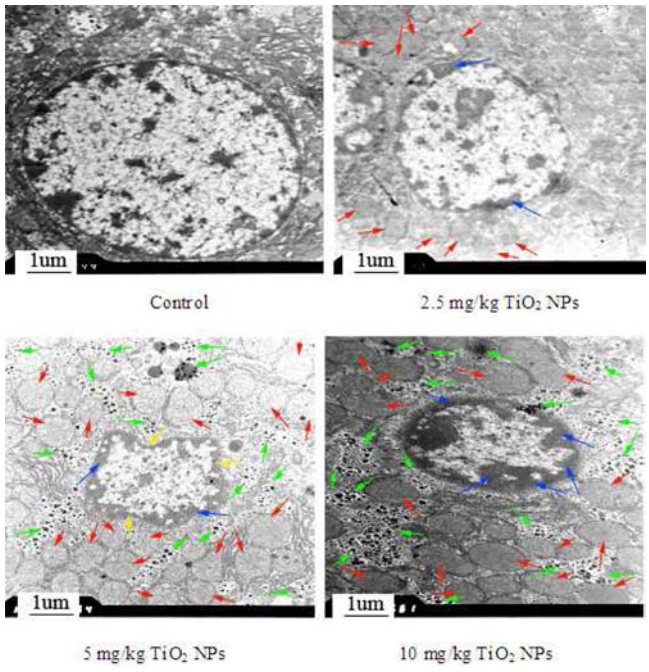

Figure 4. Ultrastructure observation of hepatocytes in mouse liver after gavage administration of TiO_2 NPs for six consecutive months (n = 5). The control showed elliptical nuclei with homogeneous chromatin (10,000×). The 2.5 mg/kg TiO_2 NP exposure group exhibited light mitochondrial swelling (red arrows) and chromatin marginalization (blue arrows) (10,000×). The 5 mg/kg TiO_2 NP exposure group exhibited mitochondrial swelling (red arrows), nuclear membrane collapse (yellow arrows), chromatin marginalization (blue arrows), and TiO_2 NP deposition in the cytoplasm (green arrows) and/or mitochondria (green arrows) (10,000×). (d) The 10 mg/kg TiO_2 NP exposure group exhibited severe mitochondrial swelling (red arrows), chromatin marginalization (blue arrows), and significant TiO_2 NP deposition in the cytoplasm and/or on nuclear membrane (green arrows) (10,000×).

(Figure 4); however, ultrastructure of hepatocytes in the liver treated with TiO_2 NPs indicated a typical apoptosis, including significant mitochondrial swelling, nuclear membrane collapse, and chromatin marginalization (Figure 4). In addition, we also significantly observed black particle agglomerates in the cytoplasm, in mitochondria, and/or on nuclear membranes in the TiO_2 NP-exposed hepatocytes (Figure 4), further confirming that TiO_2 NPs were deposited in the mouse liver.

Liver Function. The changes in the serum biochemical parameters induced by TiO_2 NP exposure are presented in Table 2. With increased TiO_2 NP dose, the levels of ALT, AST, ALP, and LDH were gradually increased, respectively (p < 0.05 or 0.01), suggesting that chronic exposure to TiO_2 NPs resulted in hepatic dysfunction.

Th2 Factor Expression. Mice with TiO_2 NP-induced hepatopathy presented with a significant, dose-dependent increase in Th2-type cytokines IL-4 and IL-5 and Th1-type cytokine IL-12 expression in the liver tissue (Tables 3, 4) (p < 0.05). This was associated with marked up-regulation of the measured IL-4 and IL-12 target genes, including IFN-γ, GATA3, GATA4, T-bet, STAt3, STAT6, eotaxin, MCP-1, and MIP-2, and significant down-regulation of STAT1 expression in the mouse liver under conditions of TiO_2 NP-induced hepatopathy (Tables 3, 4) (p < 0.05). These findings pointed to the promoted activation of the IL-4-mediated pathway in mice following exposure to TiO_2 NPs.

Table 2. Changes of Biochemical Parameters in the Blood Serum of Mice after Gavage Administration of TiO_2 NPs for Six Consecutive Months

	TiO_2 NPs (mg/kg BW)			
index	control	2.5	5	10
ALT (U/L)	27.44 ± 1.58	28.61 ± 1.63	38.95 ± 2.04[a]	41.43 ± 2.27[a]
AST (U/L)	103.26 ± 5.56	110.75 ± 5.78	142.81 ± 7.69[a]	175.96 ± 9.06[b]
ALP (U/L)	125.48 ± 6.48	132.78 ± 6.89	161.27 ± 8.36[a]	176.78 ± 9.18[b]
LDH (U/L)	876.74 ± 45.84	903.08 ± 46.25	1272.91 ± 65.68[a]	1352.65 ± 68.66[b]
T-Bil (μmol/L)	1.75 ± 0.11	1.68 ± 0.11	1.25 ± 0.08[a]	1.31 ± 0.07[b]
TChol (mmol/L)	2.65 ± 0.23	2.98 ± 0.29	3.64 ± 0.32[b]	4.08 ± 0.41[b]
TG (mmol/L)	2.01 ± 0.21	2.53 ± 0.25[a]	3.49 ± 0.31[b]	4.14 ± 0.46[c]

[a]$p < 0.05$. [b]$p < 0.01$. [c]$p < 0.001$. Values represent means ± SE ($n = 5$).

Table 3. qRT-PCR Assay of mRNA Expression in Mouse Livers after Gavage Administration of TiO_2 NPs for Six Consecutive Months

	TiO_2 NPs (mg/kg BW)			
ratio of gene/actin	control	2.5	5	10
IL-4	0.65 ± 0.12	1.09 ± 0.12[a]	1.88 ± 0.16[b]	2.42 ± 0.21[c]
IL-5	2.48 ± 0.21	2.74 ± 0.22	3.01 ± 0.25[a]	4.18 ± 0.32[b]
IL-12	1.56 ± 0.13	1.68 ± 0.12	2.07 ± 0.18[a]	2.86 ± 0.25[b]
IFN-γ	2.61 ± 0.23	3.06 ± 0.23	3.27 ± 0.35[a]	4.89 ± 0.45[b]
GATA3	1.56 ± 0.12	1.64 ± 0.11	2.74 ± 0.24[a]	3.04 ± 0.35[b]
GATA 4	0.89 ± 0.11	0.93 ± 0.15	1.39 ± 0.12[a]	1.48 ± 0.12[a]
T-bet	1.19 ± 0.15	1.55 ± 0.14[a]	1.62 ± 0.17[a]	2.66 ± 0.22[b]
RORγt	2.21 ± 0.18	2.91 ± 0.22[a]	3.36 ± 0.37[b]	5.91 ± 0.41[c]
STAT1	6.62 ± 0.53	5.57 ± 0.45	4.33 ± 0.32[a]	3.66 ± 0.28[b]
STAt3	0.76 ± 0.08	0.88 ± 0.10	1.59 ± 0.13[b]	2.76 ± 0.25[c]
STAT6	2.45 ± 0.16	2.94 ± 0.19[a]	3.87 ± 0.26[b]	3.99 ± 0.29[c]
eotaxin	0.89 ± 0.06	1.36 ± 0.09[a]	1.51 ± 0.10[a]	2.27 ± 0.18[b]
MCP-1	1.32 ± 0.16	1.98 ± 0.18[a]	2.25 ± 0.20[a]	2.33 ± 0.22[a]
MIP-2	2.15 ± 0.21	2.74 ± 0.27[a]	3.03 ± 0.31[a]	3.57 ± 0.35[b]

[a]$p < 0.05$. [b]$p < 0.01$. [c]$p < 0.001$. Values represent means ± SE ($n = 5$).

Table 4. ELISA Assay of Protein Expression in Mouse Livers after Gavage Administration of TiO_2 NPs for Six Consecutive Months

	TiO_2 NPs (mg/kg BW)			
protein expression (ng/g tissue)	control	2.5	5	10
IL-4	176.15 ± 9.81	295.39 ± 15.67[a]	529.48 ± 27.45[b]	555.82 ± 28.89[b]
IL-5	672.08 ± 34.56	742.54 ± 39.55[a]	1115.71 ± 53.61[b]	1148.78 ± 57.66[b]
IL-12	422.76 ± 23.28	555.28 ± 29.67[a]	570.97 ± 31.62[a]	798.06 ± 45.32[b]
IFN-γ	707.31 ± 38.72	879.26 ± 46.73[a]	896.17 ± 48.99[a]	1341.19 ± 63.81[b]
GATA3	429.98 ± 23.53	648.46 ± 35.66[b]	752.54 ± 39.65[b]	993.82 ± 55.97[c]
GATA4	241.19 ± 13.42	352.03 ± 18.58[a]	396.69 ± 21.29[a]	465.11 ± 25.52[b]
T-bet	322.49 ± 18.22	420.05 ± 24.06[a]	439.02 ± 22.37[a]	630.86 ± 33.71[b]
RORγt	598.91 ± 32.86	788.61 ± 45.28[a]	1520.56 ± 79.31[b]	1611.61 ± 86.95[b]
STAT1	1794.02 ± 96.28	1709.47 ± 89.67	1283.43 ± 66.56[b]	991.86 ± 53.01[b]
STAt3	205.96 ± 13.32	218.48 ± 14.06	435.89 ± 23.42[b]	657.96 ± 35.18[c]
STAT6	663.95 ± 35.57	696.74 ± 37.11	1058.77 ± 55.02	1091.29 ± 56.09
eotaxin	247.39 ± 13.69	368.56 ± 19.55[a]	419.21 ± 23.76[a]	625.17 ± 32.09[b]
MCP-1	357.72 ± 18.87	536.58 ± 28.16[b]	619.75 ± 34.62[b]	631.43 ± 35.75[b]
MIP-2	582.65 ± 33.01	792.54 ± 42.51[a]	831.13 ± 45.73[a]	999.47 ± 53.35[b]

[a]$p < 0.05$. [b]$p < 0.01$. [c]$p < 0.001$. Values represent means ± SE ($n = 5$).

DISCUSSION

The results of the present study indicate that gavage administration of 2.5, 5, or 10 mg/kg of TiO_2 NPs for six consecutive months led to body weight reduction, increased liver indices (Figure 1), and titanium accumulation (Figure 2). This resulted in an inflammatory response, macrophage aggregation, and hepatocyte necrosis in the livers (Figure 3) and ultrastructure damages of hepatocytes (Figure 4). Our previous studies observed that TiO_2 NP exposures with 10–250 mg/kg BW for 14, 60, or 90 consecutive days led to liver histopathological changes, including congestion of vascellum, wide-bound basophilia, focal ischemia,[2] large overall fatty

degeneration, inflammatory cell infiltration, necrosis,[3] congestion of interstitial vessels,[4] focal inflammatory cell infiltration and edema,[5] and apoptosis.[33] ALT, AST, ALP, and LDH are cellular enzymes that indicate the presence of injury in the liver. Under healthy circumstances, ALT, AST, ALP, and LDH are contained within the cell. When cellular injury occurs, the enzymes are released from the cytoplasm into the bloodstream, suggesting liver damage.[34] In the current study, TiO_2 NP exposure significantly elevated the serum ALT, AST, ALP, and LDH levels (Table 2), which is consistent with previous reports in our laboratory experiments[2−4] and may be cellular injury in the mouse liver (Figure 4). The liver injury and dysfunction caused by exposure to TiO_2 NPs may be involved in the impairment of immune-mediated function in mice, such as alteration in Th2-mediated gene expression in the liver.

Our previous studies had demonstrated that TiO_2 NP-induced hepatic inflammation was associated with overexpression of nucleic factor (NF)-κB, IκB kinase, NF-κBP52, NF-κBP65, NF-κB-inducible kinase (NIK), Toll-like receptor (TLR)-2 and -4, and proinflammatory cytokines including macrophage migration inhibitory factor, tumor necrosis factor-α, IL-6, IL-1β, cross-reaction protein, IL-4, IL-10, and IL-2 expression in mice.[2,3] In this study, however, a relationship between TiO_2 NP-induced liver injury and immunological factors was demonstrated (Tables 3 and 4). Elevated IL-4 has been reported in human liver diseases such as chronic hepatitis C[35] and primary biliary cirrhosis.[36] In the current study, increased IL-4 expression was also demonstrated to be involved in the TiO_2 NP-induced liver injury for longer exposure duration and lower dose. The administration of 2.5, 5, or 10 mg/kg of TiO_2 NPs for six consecutive months significantly increased the expression of hepatic IL-5, IL-12, STAT3, STAT6, and eotaxin-1, whereas TiO_2 NPs decreased STAT1 expression (Tables 3 and 4). These results suggested that Th2-mediated factors could be involved in the TiO_2 NP-induced liver injury for longer exposure duration and lower dose. It has been reported that IL-4 activates STAT6, which induces IL-5 and eotaxins-1,[25] and induces SOCS1 and SOCS3, which inhibit the STAT1 activity.[37] STAT3 is a transcription factor that participates in many biological processes, especially those of cell survival and proliferation.[38,39] IL-12 induces the tyrosine phosphorylation and DNA binding of STAT3 and STAT4.[40] Serine phosphorylation has been noted to increase transcriptional activation of STAT proteins.[41] On the other hand, STAT6 is necessary for the normal development of Th2 cells.[24] Therefore, the increased expression in the STAT3 and STAT6 due to exposure to TiO_2 NPs may indicate the protection of lymphocytes against apoptosis induction and development of Th2 cells.

T-bet and GATA play early roles in Th cell development to regulate IFN-γ and IL-4/IL-5 gene expression, respectively. The cytokines IL-12 and IL-4/IL-5 secondarily act via STATs to promote cell growth and extinguish expression of either GATA or T-bet.[42] GATA transcription factors belong to the family of zinc finger DNA-binding proteins and play critical roles in cell growth and differentiation.[43] Studies have shown that GATA1, GATA2, and GATA3 are involved in hematopoietic cell differentiation, whereas GATA4, GATA5, and GATA6 control specification and differentiation of mesoderm- and endoderm-derived cell types.[44,45] Our data demonstrated that TiO_2 NP exposure significantly up-regulated T-bet, IFN-γ, GATA3, and GATA4 expression in the liver (Tables 3 and 4), implying that these Th2-related factors may be associated with the TiO_2 NP-induced liver injury due to its hematogenic function for longer exposure duration and the lower dose.

A number of chemokines are responsible for the recruitment of inflammatory cells into the liver during the development of injury. MCP-1 is a CCL-type chemokine responsible for the recruitment of monocytes to sites of inflammation.[46] MIP-2 belongs to the CXC-type chemokine family and acts on CXC receptor 2. The chemokine is synthesized by activated tissue macrophages. MIP-2 performs similar functions to increase neutrophil egress from the bone marrow and mediate transmigration of these cells into the peripheral tissues.[47,48] Eotaxin-1/CCL11 is a chemokine belonging to the CC family and has been shown to be a potent chemoattractant for eosinophils both *in vitro* and *in vivo*.[49] Increased production of eotaxin-1 has been associated with allergic diseases.[50−52] It has also been shown that eotaxin-1 neutralization in mice substantially reduced eosinophil recruitment after Ag challenge. IL-5 is thought to be infiltrating T cells or eosinophils, and its overexpression exacerbates Th2 immune responses.[53] Kay also suggested that eotaxin-1 and IL-5 are involved in inflammation.[20] Therefore, the present study showed that the overexpression of MCP-1, MIP-2, eotaxin-1, and IL-5 (Tables 3 and 4) may be involved in the TiO_2 NP-induced hepatic inflammation such as infiltration of inflammatory cells and macrophage aggregation (Figure 3). However, possible direct evidence that Th2 factor expression is involved in the control of hepatic inflammation induced by chronic TiO_2 NP toxicity should be further confirmed in future experiments.

In conclusion, hepatotoxicity is closely associated with increased expression of IL-4, IL-5, IL-12, IFN-γ, GATA3, GATA4, T-bet, STAt3, STAT6, eotaxin, MCP-1, and MIP-2 and decreased STAT1 expression due to TiO_2 NP exposure in the mouse liver. Therefore, TiO_2 NP-induced liver injury may be via alteration of Th2 cytokine expression and/or a possible IL-4-mediated pathway in mice. The present study provides new insights into the mechanisms of TiO_2 NP-induced liver injury.

■ ASSOCIATED CONTENT

Supporting Information

This material is available free of charge via the Internet at http://pubs.acs.org.

■ AUTHOR INFORMATION

Corresponding Author

*Tel: 86-0512-61117563. Fax: 86-0512- 65880103. E-mail: Hongfsh_cn@sina.com.

Author Contributions

‡J. Hong, L. Wang, X. Zhao, and X. Yu contributed equally to this work.

Funding

This work was supported by National Natural Science Foundation of China (grant no. 81273036, 30901218), a Project Funded by the Priority Academic Program Development of Jiangsu Higher Education Institutions, and National New Ideas Foundation of Student of China (grant no. 111028534).

Notes

The authors declare no competing financial interest.

REFERENCES

(1) Iavicoli, I.; Leso, V.; Bergamaschi, A. Toxicological effects of titanium dioxide nanoparticles: a review of in vivo studies. *J. Nanomater.* **2012**, 1−36.

(2) Ma, L. L.; Zhao, J. F.; Wang, J.; Liu, J.; Duan, Y. M.; Liu, H. T.; Li, N.; Yan, J. Y.; Ruan, J.; Wang, H.; Hong, F. S. The acute liver injury in mice caused by nano-anatase TiO_2. *Nanoscale Res. Lett.* **2009**, *4*, 1275−1285.

(3) Cui, Y. L.; Liu, H. T.; Zhou, M.; Duan, Y. M.; Li, N.; Gong, X. L.; Hu, R. P.; Hong, M. M.; Hong, F. S. Signaling pathway of inflammatory responses in the mouse liver caused by TiO_2 nanoparticles. *J. Biomed. Mater. Res. Part A* **2011**, *96A*, 221−229.

(4) Duan, Y. M.; Liu, J.; Ma, L. L.; Li, N.; Liu, H. T.; Wang, J.; Zheng, L.; Liu, C.; Wang, X. F.; Zhang, X. G.; Yan, J. Y.; Wang, H.; Hong, F. S. Toxicological characteristics of nanoparticulate anatase titanium dioxide in mice. *Biomaterials* **2010**, *31*, 894−899.

(5) Cui, Y. L.; Liu, H. T.; Ze, Y. G.; Zhang, Z. L.; Hu, Y. Y.; Cheng, Z.; Hu, R. P.; Gao, G. D.; Cheng, J.; Gui, S. X.; Sang, X. Z.; Sun, Q. Q.; Wang, L.; Tang, M.; Hong, F. S. Gene expression in liver injury caused by long-term exposure to titanium dioxide nanoparticles in mice. *Toxicol. Sci.* **2012**, *128* (1), 171−185.

(6) Gui, S. X.; Zhang, Z. L.; Zheng, L.; Sun, Q. Q.; Sang, X. Z.; Liu, X. R.; Gao, G. D.; Cui, Y. L.; Cheng, Z.; Cheng, J.; Tang, M.; Hong, F. S. The molecular mechanism of kidney injury of mice caused by exposure to titanium dioxide nanoparticles. *J. Hazard. Mater.* **2011**, *195*, 365−370.

(7) Sang, X. Z.; Zheng, L.; Sun, Q. Q.; Li, N.; Cui, Y. L.; Hu, R. P.; Gao, G. D.; Cheng, Z.; Cheng, J.; Gui, S. X.; Liu, H. T.; Zhang, Z. L.; Hong, F. S. The chronic spleen injury of mice following long-term exposure to titanium dioxide nanoparticles. *J. Biomed. Mater. Res. Part A* **2012**, *100A* (4), 894−902.

(8) Sang, X. Z.; Li, B.; Ze, Y. G.; Hong, J.; Ze, X.; Gui, S. X.; Sun, Q. Q.; Liu, H. T.; Zhao, X. Y.; Sheng, L.; Liu, D.; Yu, X. H.; Hong, F. S. Toxicological effects of nanosized titanium dioxide-induced spleen injury in mice. *J. Agric. Food Chem.* **2013**, *61* (23), 5590−5599.

(9) Sun, Q. Q.; Tan, D. L.; Ze, Y. G.; Sang, X. Z.; Liu, X. R.; Gui, S. X.; Cheng, Z.; Cheng, J.; Hu, R. P.; Gao, G. D.; Liu, G.; Zhu, M.; Zhao, X. Y.; Sheng, L.; Wang, L.; Tang, M.; Hong, F. S. Pulmotoxicological effects caused by long-term titanium dioxide nanoparticles exposure in mice. *J. Hazard. Mater.* **2012**, *235*−*236*, 47−53.

(10) Sun, Q. Q.; Tan, D. L.; Zhou, Q. P.; Liu, X. R.; Cheng, Z.; Liu, G.; Zhu, M.; Sang, X. Z.; Gui, S. X.; Cheng, J.; Hu, R. P.; Tang, M.; Hong, F. S. Oxidative damage of lung and its protective mechanism in mice caused by long-term exposure to titanium dioxide nanoparticles. *J. Biomed. Mater. Res. Part A* **2012**, *100A* (10), 2554−2562.

(11) Wang, J. X.; Zhou, G. Q.; Chen, C. Y.; Yu, H. W.; Wang, T. C.; Ma, Y. M.; Jia, G.; Gao, Y. X.; Li, B.; Sun, J.; Li, Y. F.; Jiao, F.; Zhao, Y. L.; Chai, Z. F. Acute toxicity and biodistribution of different sized titanium dioxide particles in mice after oral administration. *Toxicol. Lett.* **2007**, *168*, 176−185.

(12) Liu, H. T.; Ma, L. L.; Zhao, J. F.; Liu, J.; Yan, J. Y.; Ruan, J.; Hong, F. S. Biochemical toxicity of nano-anatase TiO_2 particles in mice. *Biol. Trace Elem. Res.* **2009**, *129*, 170−180.

(13) Gui, S. X.; Sang, X. Z.; Zheng, L.; Ze, Y. G.; Zhao, X. Y.; Sheng, L.; Sun, Q. Q.; Cheng, Z.; Cheng, J.; Hu, R. P.; Wang, L.; Hong, F. S.; Tang, M. Intragastric exposure to titanium dioxide nanoparticles induced nephrotoxicity in mice, assessed by physiological and gene expression modifications. *Part. Fibre Toxicol.* **2013**, *10*, 4.

(14) Gui, S. X.; Li, B. Y.; Zhao, X. Y.; Sheng, L.; Hong, J.; Yu, X. H.; Sang, X. Z.; Sun, Q. Q.; Ze, Y. G.; Wang, L.; Hong, F. S. Renal injury and Nrf2 modulation in mouse kidney following exposure to titanium dioxide nanoparticles. *J. Agric. Food Chem.* **2013**, *61*, 8959−8968.

(15) Li, B.; Ze, Y. G.; Sun, Q. Q.; Zhang, T.; Sang, X. Z.; Cui, Y. L.; Wang, X. C.; Gui, S. X.; Tan, D. L.; Zhu, M.; Zhao, X. Y.; Sheng, L.; Wang, L.; Hong, F. S.; Tang, M. Molecular mechanisms of nanosized titanium dioxide-induced pulmonary injury in mice. *PLoS One* **2013**, *8* (2), e55563.

(16) Ma, L. L.; Liu, J.; Li, N.; Wang, J.; Duan, Y. M.; Yan, J. Y.; Liu, H. T.; Wang, H.; Hong, F. S. Oxidative stress in the brain of mice caused by translocated nanoparticulate TiO_2 delivered to the abdominal cavity. *Biomaterials* **2010**, *31*, 99−105.

(17) Ze, Y. G.; Zheng, L.; Zhao, X. Y.; Gui, S. X.; Sang, X. Z.; Su, J. J.; Guan, N.; Zhu, L. Y.; Sheng, L.; Hu, R. P.; Cheng, J.; Cheng, Z.; Sun, Q. Q.; Wang, L.; Hong, F. S. Molecular mechanism of titanium dioxide nanoparticles-induced oxidative injury in the brain of mice. *Chemosphere* **2013**, *92*, 1183−1189.

(18) Ze, Y. G.; Hu, R. P.; Wang, X. C.; Sang, X. Z.; Ze, X.; Li, B.; Su, J. J.; Wang, Y.; Guan, N.; Zhao, X. Y.; Gui, S. X.; Zhu, L. Y.; Cheng, Z.; Cheng, J.; Sheng, L.; Sun, Q. Q.; Wang, L.; Hong, F. S. Neurotoxicity and gene-expressed profile in brain-injured micecaused by exposure to titanium dioxide nanoparticles. *J. Biomed. Mater. Res. Part A* **2014**, *102A* (2), 470−478.

(19) Ze, Y. G.; Sheng, L.; Zhao, X. Y.; Hong, J.; Ze, X.; Yu, X. H.; Pan, X. Y.; Lin, A. A.; Zhao, Y.; Zhang, C.; Zhou, Q. P.; Wang, L.; Hong, F. S. TiO_2 Nanoparticles induced hippocampal neuroinflammation in mice. *PLoS One* **2014**, *9* (3), e92230.

(20) Kay, A. B. Allergy and allergic diseases. *N. Engl. J. Med.* **2001**, *344*, 30−37.

(21) Heneghan, M. A.; McFarlane, I. G. Current and novel immunosuppressive therapy for autoimmune hepatitis. *Hepatology* **2002**, *35*, 7−13.

(22) Holt, M. P.; Ju, C. Mechanisms of drug-induced liver injury. *AAPS J.* **2006**, *8*, 48−54.

(23) Leonard, W. J.; O'Shea, J. J. Jaks and STATs: biological implications. *Annu. Rev. Immunol.* **1998**, *16*, 293−322.

(24) Nelms, K.; Keegan, A. D.; Zamorano, J.; Ryan, J. J.; Paul, W. E. The IL-4 receptor signaling mechanisms biologic functions. *Annu. Rev. Immunol.* **1999**, *17*, 701−738.

(25) Jaruga, B.; Hong, F.; Sun, R.; Radaeva, S.; Gao, B. Crucial role of IL-4/STAT6 in T cell-mediated hepatitis: up-regulating eotaxins and IL-5 and recruiting leukocytes. *J. Immunol.* **2003**, *171*, 3233−3244.

(26) Kidd, P. Th1/Th2 balance: the hypothesis, its limitations, and implications for health and disease. *Altern. Med. Rev.* **2003**, *8*, 223−246.

(27) Steinman, L. A brief history of Th17, the first major revision in the Th1/Th2 hypothesis if T cell-mediated tissue damage. *Nat. Rev. Med.* **2007**, *13*, 139−145.

(28) Powell, J. J.; Faria, N.; Thomas-McKay, E.; Pele, L. C. Origin and fate of dietary nanoparticles and microparticles in the gastrointestinal tract. *J. Autoimmun.* **2010**, *34*, J226−J233.

(29) Lomer, M. C. E.; Hutchinson, C.; Volkert, S.; Greenfield, S. M.; Catterall, A.; Thompson, R. P. H.; Powell, J. J. Dietary sources of inorganic microparticles and their intake in healthy subjects and patients with Crohn's disease. *Br. J. Nutr.* **2004**, *92*, 947−955.

(30) Yang, P.; Lu, C.; Hua, N.; Du, Y. Titanium dioxide nanoparticles co-doped with Fe^{3+} and Eu^{3+} ions for photocatalysis. *Mater. Lett.* **2002**, *57*, 794−801.

(31) Hu, R. P.; Zheng, L.; Zhang, T.; Cui, Y. L.; Gao, G. D.; Cheng, Z.; Chen, J.; Tang, M.; Hong, F. S. Molecular mechanism of hippocampal apoptosis of mice following exposure to titanium dioxide nanoparticles. *J. Hazard. Mater.* **2011**, *191*, 32−40.

(32) Liu, W. H.; Saint, D. A. Validation of a quantitative method for real time PCR kinetics. *Biochem. Biophys. Res. Commun.* **2002**, *294*, 347−353.

(33) Cui, Y. L.; Gong, X. L.; Duan, Y. M.; Li, N.; Hu, R. P.; Liu, H. T.; Hong, M. M.; Zhou, M.; Wang, L.; Wang, H.; Hong, F. S. Hepatocyte apoptosis and its molecular mechanisms in mice caused by titanium dioxide nanoparticles. *J. Hazard. Mater.* **2010**, *183*, 874−880.

(34) Ozer, J.; Ratner, M.; Shaw, M.; Bailey, W.; Schomaker, S. The current state of serum biomarkers of hepatotoxicity. *Toxicology* **2008**, *245*, 194−205.

(35) Spanakis, N. E.; Garinis, G. A.; Alexopoulos, E. C.; Patrinos, G. P.; Menounos, P. G.; Sklavounou, A.; Manolis, N. E.; Gorgoulis, V. G.; Valis, D. Cytokines serum levels in patients with chronic HCV infection. *J. Clin. Lab. Anal.* **2002**, *16*, 40−46.

(36) Harada, K.; Water, J. V.; Leung, P. S. C.; Coppel, R. L.; Ansari, A.; Nakanuma, Y.; Gershwin, M. E. In situ nucleic acid hybridization of cytokines in primary biliary cirrhosis: predominance of the Th1 subset. *Hepatology* **1997**, *25*, 791−796.
(37) Palmer, C. D.; Restifo, P. N. Suppressors of cytokine signaling (SOCS) in T cell differentiation, maturation, and function. *Trends Immunol.* **2009**, *30*, 592−602.
(38) Battle, T. E.; Frank, D. A. The role of STATs in apoptosis. *Curr. Mol. Med.* **2002**, *2*, 381−392.
(39) Nagy, Z. S.; Rui, H.; Stepkowski, S. M.; Karras, J.; Kirken, R. A. A preferential role for STAT5, not constitutively active STAT3, in promoting survival of a human lymphoid tumor. *J. Immunol.* **2006**, *177*, 5032−5040.
(40) Cho, S. S.; Bacon, C. M.; Sudarshan, C.; Rees, R. C.; Finbloom, D.; Pine, R.; O'Shea, J. J. Activation of STAT4 by IL-12 and IFN-γ. *J. Immunol.* **1996**, *157*, 4781−4789.
(41) Nelms, K.; Keegan, A. D.; Zamorano, J.; Ryan, J. J.; Paul, W. E. The IL-4 receptor: signaling mechanisms and biological functions. *Annu. Rev. Immunol.* **1999**, *17*, 701−738.
(42) Murphy, K. M.; Reiner, S. L. The lineage decisions of helper T cells. *Nat. Rev. Immunol.* **2002**, *2*, 933−944.
(43) Patient, R. K.; McGhee, J. D. The GATA family (vertebrates and invertebrates). *Curr. Opin. Genet. Dev.* **2002**, *12* (4), 416−422.
(44) Molkentin, J. D. The zinc finger-containing transcription factors GATA-4, -5, and -6. Ubiquitously expressed regulators of tissue-specific gene expression. *J. Biol. Chem.* **2000**, *275* (50), 38949−38952.
(45) Bresnick, E. H.; Lee, H. Y.; Fujiwara, T.; Johnson, K. D.; Keles, S. GATA switches as developmental drivers. *J. Biol. Chem.* **2010**, *285* (41), 31087−31093.
(46) Zimmermann, H. W.; Trautwein, C.; Tacke, F. Functional role of monocytes and macrophages for the inflammatory response in acute liver injury. *Front. Physiol.* **2012**, *3*, 56.
(47) De Filippo, K.; Henderson, R. B.; Laschinger, M.; Hogg, N. Neutrophil chemokines KC and macrophage;inflammatory protein;2 are newly synthesized by tissue macrophages using distinct TLR signaling pathways. *J. Immunol.* **2008**, *180*, 4308−4315.
(48) Sadik, C. D.; Kim, N. D.; Luster, A. D. Neutrophils cascading their way to inflammation. *Trends Immunol.* **2011**, *32* (10), 452−460.
(49) Zimmermann, N.; Hershey, G. K.; Foster, P. S.; Rothenberg, M. E. Chemokines in asthma: cooperative interaction between chemokines and IL-13. J. *Allergy Clin. Immunol.* **2003**, *111*, 227−243.
(50) Nakamura, H.; Weiss, S. T.; Israel, E.; Luster, A. D.; Drazen, J. M.; Lilly, C. M. Eotaxin and impaired lung function in asthma. *Am. J. Respir. Crit. Care Med.* **1999**, *160*, 1952−1956.
(51) Greiff, L.; Petersen, H.; Mattsson, E.; Andersson, M.; Erjefalt, J. S.; Linden, M.; Svensson, C.; Persson, C. G. Mucosal output of eotaxin in allergic rhinitis and its attenuation by topical glucocorticosteroid treatment. *Clin. Exp. Allergy* **2001**, *31*, 1321−1327.
(52) Yawalkar, N.; Uguccioni, M.; Scharer, J.; Braunwalder, J.; Karlen, S.; Dewald, B.; Braathen, L. R.; Baggiolini, M. Enhanced expression of eotaxin and CCR3 in atopic dermatitis. *J. Invest. Dermatol.* **1999**, *113*, 43−48.
(53) Masterson, J. C.; McNamee, E. N.; Hosford, L.; Capocelli, K. E.; Ruybal, J.; Fillon, S. A.; Doyle, A. D.; Eltzschig, H. K.; Rustgi, A. K.; Protheroe, C. A.; Lee, N. A.; Lee, J. J.; Furuta, G. T. Local hypersensitivity reaction in transgenic mice with squamous epithelial IL-5 overexpression provides a novel model of eosinophilic oesophagitis. *Gut* **2014**, *63*, 43−53.

structural characterization after tedious compound isolation. Since its introduction for anthocyanin analysis,[10] HPLC has become the technique of choice for their qualitative and quantitative analysis. Further development in the mid-1980s of improved reversed-phase columns and coupling to photodiode array detectors represented a great advance, as a single analysis allowed separation and information for structural identification to be obtained on the basis of chromatographic retention and UV−vis spectra, which notably provides more clues for compound identification. Mass spectrometry atmospheric pressure ionization (API) interfaces, and especially electrospray ionization (ESI) and atmospheric pressure chemical ionization (APCI) interfaces, led in the 1990s to hyphenation of HPLC and MS. This facilitated the identification of a plethora of compounds, including new anthocyanin families, such as pyranoanthocyanins, flavone/flavanol-linked anthocyanins or dimeric anthocyanins, as well as other related anthocyanin-like pigments such as oaklins resulting from the condensation of catechins and hydroxycinnamic acids.[11] Many of these new pigments were first identified in red wines to be further reported in plant tissues. According to Andersen and Jordheim,[12] by 2013 the number of anthocyanins identified in nature was 702, with about 200 additional structures proposed as tentative.

Nowadays the introduction of a new generation of HPLC as favored by the development of new column supports and smaller particle sizes has allowed further decreasing the analysis time and increasing peak capacity and sensitivity. Also, high-resolution mass spectrometers (HR-MS), such as time-of-flight (TOF), Fourier transform ion cyclotron resonance (FTICR-MS), and Orbitrap equipment, able to provide accurate masses have been developed, making possible the distinction between compounds differing in mass by around 20 mDa. The enhanced selectivity of these new instruments reduces interfering background ions, increasing sensitivity compared with triple-quadrupole and ion trap systems. Another advantage of these instruments is that compound signals may be used directly for compound tentative identification. Indeed, the combination of these high-resolution spectrometers coupled to the new high-capacity separation techniques and enhanced software platforms opens improved prospectives for qualitative (nontargeted compound identification) and quantitative analyses using single runs. Also, developments in mass spectrometry imaging (MSI) should be expected to help in visualizing the spatial distribution of compounds by their molecular masses, which should have an impact in determining tissue distributions and establishing biological targets of metabolites.

An interesting feature of LC-MS is that it provides another separation dimension to HPLC, through the use of selective detection modes, such as monitoring single ions, extracting particular ions, or recording characteristic transitions in the fragmentation of compounds. Selective detection increases sensitivity and the possibility of detecting and quantifying metabolites in biological samples, allowing important progress in understanding the processes of anthocyanin absorption and biotransformation in the human organism.

Hyphenation of liquid chromatography to NMR spectroscopy is another promising tool for the separation and structural elucidation of unknown compounds in mixtures. Even though it emerged in the mid-1990s this technique has not yet become popular, among others due to the existence of technical drawbacks that hamper its application. The technique is mostly restricted to H NMR, as low abundance of ^{13}C isotopes limits obtaining C NMR spectra to peaks of high concentration. In the particular case of anthocyanins, problems may also arise from their existence as different forms in equilibrium. Recent advances have been made concerning the improvement in NMR flow probe technology, introduction of new techniques for solvent suppression, or coupling to an online solid-phase extraction unit for concentrating the eluted peaks prior to spectra recording so as to increase the sensitivity (LC-SPE-NMR). This has contributed to improve the sensitivity, so that an increase in its applications should be expected in coming years, also favored by the introduction of cheaper equipment making the technique available to more laboratories.[13]

UNCOVERING FLOWER COLOR

It is well-known that anthocyanins are structurally dependent on the conditions and composition of the media where they are dissolved and suffer interactions among them and with other compounds that influence their chemical equilibria and modify their color. Kinetic and thermodynamic equilibria between colored and colorless anthocyanin forms as a function of the pH and temperature have been well established since the works performed by Brouillard and co-workers in the 1970s.[7,8] Anthocyanins are usually represented as their red flavylium cation, but in aqueous media this form undergoes rapid proton transfer reactions, leading to blue quinoidal bases, and hydration, generating colorless hemiketals in equilibrium with chalcone structures. The highly colored flavylium forms predominate only in very acidic solutions, whereas in weakly acidic aqueous media, even if they are kept in conditions (temperature, pH, light, oxygen) similar to those found in plant vacuoles, anthocyanins mostly occur as colorless species and tend further to degrade by irreversible cleavage of their molecules. Nevertheless, in their natural media, anthocyanins are able to express intense red, blue, or violet colors even at weakly acidic pH values, and, furthermore, the same anthocyanin can be found in different flowers providing distinct colorations.[14] This apparent paradox is explained by the existence of stabilizing mechanisms, among which the processes of copigmentation and metal complexation are prominent.[9,15] Nevertheless, although basic mechanisms involved in flower pigmentation have been clarified to a considerable extent, many unresolved questions remain. Further research has still to be undertaken to extend our understanding about the molecular and biological bases that control color expression and stability. Physicochemical studies are required to identify the most promising chromophores and to establish the influence of structural differences on the formation of metalloanthocyanins and the atomic structure of intra- and intermolecular stacking. Also, a better understanding is needed about charge transfer effects implicated in spectral shifts, mechanisms of metal and pigment transport into vacuoles, or the identification of transcriptional factors and the regulatory network controlling anthocyanin biosynthesis.[15] Expected advances in these fields in the coming years should offer plant breeders new options to produce flowers with the desired coloration.

ENHANCING ANTHOCYANIN PRODUCTION

Anthocyanins are produced by a branch of the flavonoid pathway (i.e., shikimate/phenylpropanoid pathway), and their synthesis constitutes the most studied secondary metabolic pathway in plants. Actually, most of the knowledge about transcriptional regulation in plants has initially come from studies of the regulation of anthocyanin biosynthesis in the monocot maize, further extended to dicots, with *Arabidopsis* as a paradigm.[1]

The identification of transcription factors and a better understanding of the regulatory network controlling anthocyanin biosynthesis in plants are crucial prerequisites for the development of plants with enhanced or improved anthocyanin composition. By 1990, all of the enzymes involved in the early specific part of anthocyanin biosynthesis (from chalcone to anthocyanidin) had been solved, and cloning of the anthocyanin synthetic genes was nearly completed. Since that time, several genes coding for glycosyltransferases and acyltransferases in flower petals have been cloned, and several transcriptional factors regulating anthocyanin biosynthesis have been described.[15] Available findings indicate that transcription factors regulating anthocyanins share a great conservation of functional domains and that functional diversification in a species and among closely related species generally resides more in regulatory sequences than in coding regions. This high conservation may help in selecting the proper heterologous regulators to obtain anthocyanin-rich varieties through metabolic engineering.

The transcription factors controlling anthocyanin biosynthesis have been characterized for many species and an "MBW" regulatory complex consisting of a ternary complex of R2R3MYB, bHLH, and WD-Repeat proteins.[16] Thus, manipulating the anthocyanin pathway has often involved the overexpression of heterologous MYB and bHLH genes.[1] Various transgenic approaches have been taken to increase flavonoid levels in tomato fruit by overexpressing either the structural or regulatory genes involved in the biosynthetic pathway. Most of these attempts have exploited heterologous genes, and in only one case was an endogenous tomato regulatory gene (ANT1) overexpressed in tomato plants. Although a significant increase in the final content of some flavonoids (flavonols, in particular) was obtained, in tomato, the overexpression by activation tagging of the MYB ANT1 gene realized only a partial enhancement of anthocyanins,[1] which either were expressed in only the vegetative tissues of the plant or induced only a partial, spotted pigmentation, mostly limited to the peel of the fruit, which could be explained by the low availability of flavonoid biosynthetic precursors or the absence of other limiting regulatory factors (e.g., bHLH).[17] These constraints were overcome by Butelli et al.,[18] who produced a tomato highly enriched with anthocyanins throughout the fruit tissues, averaging ∼3 mg/g fresh weight, by the ectopic expression of two selected transcription factors (Del, a bHLH-type TF, and Ros1, an R2R3MYB-type TF) from the ornamental flower snapdragon (*Antirrhinum majus* L.). Interestingly, the high production of anthocyanins in these "purple" tomatoes was not obtained at the expense of other major classes of tomato fruit pigments, and the antioxidant activity attributable to the carotenoid fraction remained unchanged.[17]

Similar developments could be anticipated for the development of other anthocyanin-rich crops or ornamental plants. Furthermore, given that the biological properties of different anthocyanin compounds and of the other classes of flavonoids are often molecule-specific, a major objective of metabolic engineering approaches might be not only increasing but also optimizing their levels and composition in crops so that they could eventually be promoted as functional foods. Additionally, researchers could exploit natural genetic resources, either as an alternative to genetic engineering approaches or to strengthen them.[17]

■ ANTHOCYANINS IN FOOD

For years the main focus on anthocyanins in food has been put on their influence in color. In intact plant tissues (i.e., unprocessed fruits and vegetables), anthocyanins remain relatively stable. Nonetheless, tissue disruption during food processing affects anthocyanin extractability and stability. It has been suggested that anthocyanin extraction from berries into juice could be limited by their interaction with macromolecules from disrupted cell walls such as polysaccharides, tannins, and proteins. However, the factors that govern those interactions are still not well-defined and remain a promising research area. On the other hand, storage may also affect anthocyanin stability, leading to color changes. In food systems, in addition to be subjected to the equilibria among structural forms, anthocyanins can be involved in chemical and enzymatic reactions that may degrade them to colorless products or transform them into new structures. Indeed, the search for improved processing and storage methods to better control anthocyanin losses or to address anthocyanin reactions in the "right" direction to obtain more stable and desired colors constitutes a major challenge for the food industry.

Anthocyanin stability and reactions have been particularly studied in red wine, in which a variety of anthocyanin-derived products have been identified over the past two decades, such as pyranoanthocyanins and anthocyanin-flavanol condensed pigments, either directly linked or involving aldehydes, anthocyanin dimers, or xanthylium pigments.[11] Similar products have further been found in fruits and vegetables[19−22] and other plant-derived food.[23,24] Some of these compounds possess interesting chromatic properties, displaying a variety of colors from orange to blue and being more resistant to color bleaching by water or sulfur dioxide attack, so that they show more color capacity at weakly acidic and neutral pH values than original anthocyanins.[11] Anthocyanins are authorized as food additives both in the European Union (E-163) and the United States, where the Food and Drug Administration (FDA) includes them as natural "Colorants Exempt from Certification".[12] However, the applications of anthocyanins as food colorants are seriously limited due to their problems of stability. In these circumstances, the improved color properties that exhibit some anthocyanin-derived pigments make them potential candidates for their use as natural food colorants, which is particularly relevant taking into account the current concerns and restrictions for the use of synthetic dyes.

Owing to the current interest in the potential associations between anthocyanin consumption and health promotion, the estimation of the dietary intake of anthocyanins has also become a point of interest, so that adequate relationships with the incidence of chronic diseases can be established. It is, however, difficult to properly calculate anthocyanin consumption.[12] Accurate data on the qualitative and quantitative anthocyanin composition in foods and beverages are neither always available nor easy to obtain due to the structural diversity of anthocyanins and their stability problems. Anthocyanin contents can vary tremendously within a certain type of food depending on varietal, agronomic, and environmental conditions and, furthermore, both degradation and formation of derived products have great influence in the anthocyanin contents and profiles in processed foods and beverages. Indeed, stability is a very important (and challenging) element when considering the impact of dietary anthocyanins on the human organism. The common anthocyanins show instability toward a variety of chemical and physical parameters, including oxygen, high temperatures, light, pH

values, enzymes, and reactions with compounds in the food or body systems, which may vary anthocyanin properties.[12]

Estimations made by different researchers varied within a wide range, oscillating from 3 to 150 mg/day, depending on the country and nutrition habits. In a rough calculation, average adult intake of anthocyanins in Europe and the United States has been estimated on the scale of 10 mg/day.[12] Further studies are, nevertheless, required to increase our knowledge on anthocyanin composition in most consumed foods over different countries, taking into account that not only total intake is important but also qualitative profiles should have an influence on their putative health-promoting effects. Moreover, attention will also have to be paid to the increasing popularity of food supplements and the developing market for functional foods, as they may contribute substantially to a rise in the dietary intake levels.

BIOAVAILABILITY AND HEALTH ISSUES

Dietary anthocyanins have been related with health promotion, namely, relief of oxidative stress and protection against coronary heart disease, and also with antimicrobial anti-inflammatory and anticarcinogenic activities, control of obesity and diabetes, or improvement of vision.[2] The biological effects of anthocyanins have been classically associated with their antioxidant capacity, although the actual mechanisms involved at the physiological level are yet to be established, and a recent emerging view is that modulatory effects affecting signaling pathways in cells should also be important.[17]

For understanding of the exact impact of dietary anthocyanins on health and their underlying mechanisms, further knowledge is required about their bioavailability. Aspects such as absorption and biotransformation, the exact nature and amount of circulating metabolites, and their activity, tissue distribution, and accumulation or the forms able to reach particular cellular or molecular targets are still largely unknown. In these circumstances, the ability to detect, identify, and determine the metabolites at physiological concentrations is crucial. Furthermore, pure metabolites are required to be used in activity and mechanistic studies but are not always available as commercial standards. In this matter, chemical or enzymatic syntheses constitute different promising strategies to obtain some in vivo occurring anthocyanin metabolites.[25]

A fraction of anthocyanins could be absorbed both in the stomach and in the small intestine. The pH changes considerably in the human body from the stomach (1.5) to the intestine surface (5.3), urine (5.75), liver (7.0), and blood (7.40), and, therefore, anthocyanins will thus most probably under physiological conditions occur on different structural forms similar to those described in model systems.[12] Anthocyanin structure (e.g., type of aglycone, number and type of glycosyl and acyl moieties) would influence form distribution and stability, thus affecting their bioavailability, metabolism, or degradation mechanisms. Furthermore, a part of the anthocyanins in processed foods, and also in intact plants, may occur in the form of more complex structures (e.g., derived pigments), the equilibrium schemes, stability, and reactivity characteristics of which are not well elucidated and should differ from those of the simple anthocyanins.[12] Finally, the relevance of the food matrix and the interactions between anthocyanins and other food components, both macronutrients and bioactives, must also be considered. At present, most of this knowledge is to a large extent lacking.

Existing data indicate that the proportion of absorbed anthocyanins including their metabolized derivatives is very low. Actually, anthocyanins have been reported to have one of the lowest bioavailabilities of all of the dietary flavonoid subclasses,[26] with typical urinary excretion of the total amount of anthocyanins and their derivatives well below 1% of the ingested amount. Nevertheless, recent studies using ^{13}C-labeled anthocyanins carried out in humans by Czank et al.[27] have concluded that these compounds could be more bioavailable than previously reported. Thus, on the basis of the recovered ^{13}C dose, cyanidin-3-*O*-glucoside (Cy3G) was established to have a relative bioavailability in humans of 12.38 ± 1.38% on average, from which 0.18 ± 0.11% of the ^{13}C dose was recovered from blood, 5.37 ± 0.67% from urine, and 6.91 ± 1.59% from breath, whereas 32.13 ± 6.13% of the ^{13}C was found in feces. The fate of the remaining ingested ^{13}C remains unknown, although there was considerable interindividual variability in the recovery of the ^{13}C tracer that ranged from 15.1 to 99.3%, probably as a result of a high variation in gastric and intestinal transit times, composition, and catabolic activity of colonic flora and the ability to take up and excrete catabolites and metabolites.

The accumulation of multiple phenolic metabolites might ultimately be responsible for the reported bioactivity of anthocyanins, with the gut microflora apparently playing an important role in the biotransformation process. Although phase II conjugates of Cy3G and cyanidin (cyanidin-glucuronide, methyl cyanidin-glucuronide, and methyl Cy3G-glucuronide) were detected, the most important metabolites corresponded to products from the anthocyanin degradation (i.e., benzoic, phenylacetic and phenylpropenoic acids, phenolic aldehydes, and hippuric acid) and their phase II conjugates, which were found at 60- and 45-fold higher concentrations than their parent compounds in urine and plasma, respectively.[27] An interesting observation was the rapid appearance of Cy3G degradation products and their phase II conjugates within the serum, which suggested that some degradation likely occurred in the small intestine (either pre- or postabsorption) and, therefore, anthocyanin C-ring cleavage may not require the action of colonic microflora. Estimates made by Czank et al.[27] of the half-lives of elimination for ^{13}C-labeled metabolites were between 12.44 ± 4.22 and 51.62 ± 22.55 h, which suggested a relatively slow urinary clearance of some metabolites. Long elimination half-lives may be the result of a combination of hepatic recycling, enterohepatic circulation, and prolonged colonic production and absorption. All in all, these data suggested that anthocyanins would be as bioavailable as other flavonoid subclasses, such as flavan-3-ols and flavones, which have relative bioavailabilities between 2.5% and 18.5%.[26]

Further intervention studies using different anthocyanins and food matrices are, nevertheless, required to confirm these preliminary conclusions on anthocyanin absorption and bioavailability, as well as to establish their putative effects on human health. It is expected that the advances in analytical methodologies enabling the identification and quantification of metabolites, both in food and in body fluids and tissues, together with bioinformatic strategies should allow the characterization of changes produced in the human metabolome as a consequence of anthocyanin intake, so that possible biomarkers of consumption and effects can be identified and adequate relationships with the incidence of diseases established.

THE SEVENTH INTERNATIONAL WORKSHOP ON ANTHOCYANINS (IWA 2013)

Advances in anthocyanin research are revised every two years in the International Workshop on Anthocyanins (IWA), the last edition of which took place in the beautiful city of Porto (Portugal). The IWA is the only world congress that focuses exclusively on anthocyanins and represents an essential meeting point for all people working in these amazing molecules. Since the first IWA took place in Melbourne (Australia) back in 2000, five more IWA meetings have been held in Australia (Adelaide 2002 and Sydney 2004), New Zealand (Rotorua 2006), Japan (Nagoya 2009), and the United States (Charlotte, NC, 2011). In September 2013, the IWA came for the first time to Europe, with the goal of bringing together scientists from universities, institutes, and industries, from different research areas but with the common ground of working on anthocyanins and attracting European researchers who did not have the opportunity to join the previous workshops. The meeting was divided into six topics: (1) biosynthesis, trafficking, and functionality; (2) genetic and metabolic engineering; (3) horticultural and ornamental plants; (4) phytochemistry and analysis; (5) anthocyanin in health and nutrition; and (6) anthocyanins in foods and industry. Around 130 participants from 21 different countries attended the IWA 2013, presenting 16 invited lectures (6 plenary lectures and 10 invited keynotes), 21 regular oral communications, and 80 posters. In relation to previous IWAs, which were more focused on plant anthocyanins (physiological roles, biosynthesis, metabolic engineering, etc.), the Porto meeting was enlarged upon food anthocyanins, as related to sensory properties and health.

This highlights issue presents a selection of papers from IWA 2013 dealing with anthocyanin accumulation in plants, relationship with color expression and stability in plants and food, copigmentation effects, stability during food processing and storage, chemical applications, bioavailability and effects in model systems, properties of anthocyanin-related pigments, microbial degradation, or influence on allergenic properties of food components. Now the countdown to the 8th International Workshop on Anthocyanins, which will take place in Montpellier (France) in 2015 organized by Dr. Véronique Cheynier, is on.

We thank the Editor-in-Chief, Prof. Jim Seiber, and the *JAFC* editorial office for the opportunity to publish this special issue, as well as to all submitting authors and reviewers for their invaluable contributions.

Celestino Santos-Buelga[*,†]
Nuno Mateus[§]
Victor De Freitas[§]

[†]Grupo de Investigacion en Polifenoles, Facultad de Farmacia, Universidad de Salamanca, Campus Miguel de Unamuno, 37007 Salamanca, Spain

[§]Chemistry Investigation Centre (CIQ), Department of Chemistry, Faculty of Sciences, University of Porto, 4169-007 Porto, Portugal

AUTHOR INFORMATION

Corresponding Author

*(C.S.-B.) Phone: +34 923 294 537. Fax: +34 923 294 515. E-mail: csb@usal.es.

Notes

The authors declare no competing financial interest.

REFERENCES

(1) Petroni, K.; Tonelli, C. Recent advances on the regulation of anthocyanin synthesis in reproductive organs. *Plant Sci.* **2011**, *181*, 219−229.

(2) He, J. A.; Giusti, M. Anthocyanins: natural colorants with health-promoting properties. *Annu. Rev. Food Sci. Technol.* **2010**, *1*, 163−187.

(3) Willstatter, B.; Everest, A. E. Ueber den Farbstoff der Kornblume. *Liebigs Ann. Chem.* **1913**, *401*, 189−209.

(4) Wheldale, M. Our present knowledge of the chemistry of the mendelian factors for flower-colour. *J. Genet.* **1914**, *4*, 109−129.

(5) Robinson, G. M.; Robinson, R. A survey on anthocyanins I. *Biochem. J.* **1931**, *25*, 1687−1705.

(6) Asen, S.; Stewart, R. N.; Norris, K. H. Co-pigmentation of anthocyanins in plant tissues and its effect on colour. *Phytochemistry* **1972**, *11*, 1139−1144.

(7) Brouillard, R.; Delaporte, B.; Dubois, J. E. Chemistry of anthocyanins pigments 2. Kinetic and thermodinamic study of proton transfer, hydration, and tautomeric reactions of malvidin-3-glucoside. *J. Am. Chem. Soc.* **1977**, *99*, 8461−8468.

(8) Brouillard, R.; Dubois, J. E. Mechanism of the structural transformations of anthocyanins in acidic media. *J. Am. Chem. Soc.* **1977**, *99*, 1359−1364.

(9) Goto, T.; Kondo, T. Structure and molecular stacking of anthocyanins-flower color variation. *Ang. Chem. Int. Eng. Ed.* **1991**, *30*, 17−33.

(10) Wulf, L. W.; Nagel, C. W. Analysis of phenolic acids and flavonoids by high-pressure liquid chromatography. *J. Chromatogr.* **1976**, *116*, 271−279.

(11) de Freitas, V. A. P.; Mateus, N. Updating wine pigments. In *Recent Advances in Polyphenol Research. Vol. 2*; Santos-Buelga, C., Escribano-Bailon, M. T., Lattanzio, V., Eds.; Wiley-Blackwell: Chichester, UK, 2010; pp 59−80.

(12) Andersen, Ø. M.; Jordheim, M. Basic anthocyanin chemistry and dietary sources. In *Anthocyanins in Health and Disease*; Wallace, T. C., Giusti, M., Eds.; CRC Press: Boca Raton, FL, USA, 2013; pp 13−90.

(13) Timmers, M.; Urban, S. On-line (HPLC-NMR) and off-line phytochemical profiling of the Australian plant *Lasiopetalum macrophyllum*. *Nat. Prod. Commun.* **2012**, *7*, 551−560.

(14) Brouillard, R.; Chassaign, S.; Isorez, G.; Kueny-Stotz, M.; Figueiredo, P. The visible anthocyanins: from research to applications. In *Recent Advances in Polyphenol Research. Vol. 2*; Santos-Buelga, C., Escribano-Bailon, M. T., Lattanzio, V., Eds.; Wiley-Blackwell: Chichester, UK, 2010; pp 1−22.

(15) Yoshida, K.; Mori, M.; Kondo, T. Blue flower color development by anthocyanins: from chemical structure to cell physiology. *Nat. Prod. Rep.* **2009**, *26*, 884−915.

(16) Davies, K. M.; Albert, N. W.; Schwinn, K. E. From landing lights to mimicry: the molecular regulation of flower colouration and mechanisms for pigmentation patterning. *Funct. Plant Biol.* **2012**, *39*, 619−638.

(17) Gonzali, S.; Mazzucato, A.; Perata, P. Purple as a tomato: towards high anthocyanin tomatoes. *Trends Plant Sci.* **2009**, *14*, 237−24.

(18) Butelli, E.; Titta, L.; Giorgio, M.; Mock, H. P.; Matros, A.; Peterek, S.; Schijlen, E. G. W. M.; Hall, R. D.; Bovy, A. G.; Luo, J.; Martin, C. Enrichment of tomato fruit with health-promoting anthocyanins by expression of select transcription factors. *Nat. Biotechnol.* **2008**, *26*, 1301−1308.

(19) Fossen, T.; Rayyan, S.; Andersen, Ø. M. Dimeric anthocyanins from strawberry (*Fragaria ananassa*) consisting of pelargonidin 3-glucoside covalently linked to four flavan-3-ols. *Phytochemistry* **2004**, *65*, 1421−1428.

(20) Gonzalez-Paramas, A. M.; Lopes, F.; Martin, P.; Macz, G.; Gonzalez-Manzano, S.; Alcalde, C.; Perez, J.; Escribano-Bailon, M. T.; Rivas-Gonzalo, J. C.; Santos-Buelga, C. Flavanol-anthocyanin condensed pigments in plant extracts. *Food Chem.* **2006**, *94*, 428−436.

(21) Fossen, T.; Andersen, Ø. M. Anthocyanins from red onion, *Allium cepa*, with novel aglycone. *Phytochemistry* **2003**, *62*, 1217−1220.

(22) Vidal, S.; Meudec, E.; Cheynier, V.; Skouroumounis, G.; Hayasaka, Y. Mass spectrometric evidence for the existence of

oligomeric anthocyanins in grape skin. *J. Agric. Food Chem.* **2004**, *52*, 7144−7151.
(23) Tarascou, I.; Mazauric, J.-P.; Meudec, E.; Souquet, J.-M.; Cunningham, D.; Nojeim, S.; Cheynier, V.; Fulcrand, H. Characterisation of genuine and derived cranberry proanthocyanidins by LC-ESI-MS. *Food Chem.* **2011**, *128*, 802−810.
(24) McDougall, G. J.; Gordon, S.; Brennan, R.; Stewart, D. Anthocyanin-flavanol condensation products from black currant (*Ribes nigrum* L.). *J. Agric. Food Chem.* **2005**, *53*, 7878−7885.
(25) Fernandes, I.; Azevedo, J.; Faria, A.; Calhau, C.; de Freitas, V.; Mateus, N. Enzymatic hemisynthesis of metabolites and conjugates of anthocyanins. *J. Agric. Food Chem.* **2009**, *57*, 735−745.
(26) Manach, C.; Williamson, G.; Morand, C.; Scalbert, A.; Remesy, C. Bioavailability and bioefficacy of polyphenols in humans. I. Review of 97 bioavailability studies. *Am. J. Clin. Nutr.* **2005**, *81*, 230S−242S.
(27) Czank, C.; Cassidy, A.; Zhang, Q.; Morrison, J.; Preston, T.; Kroon, P. A.; Botting, N. P.; Kay, C. D. Human metabolism and elimination of the anthocyanin, cyanidin-3-glucoside: a ^{13}C-tracer study. *Am. J. Clin. Nutr.* **2013**, *97*, 995−1003.

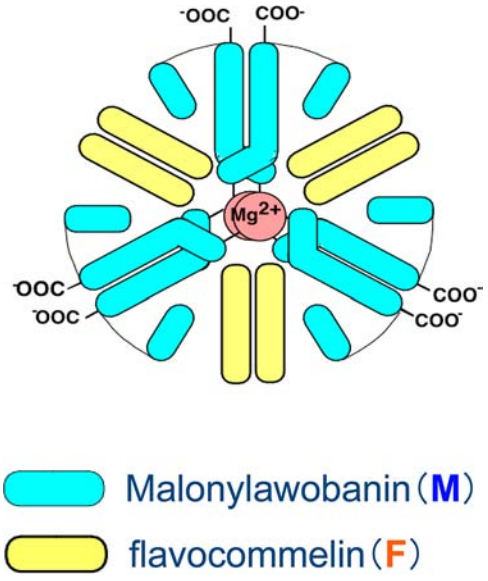

Figure 2. Self-assembly of malonylawobanin and flavocommelin (courtesy from Prof. Kumi Yoshida).

compound 4′,7-dihydroxyflavylium found in the Dragon's blood resins.[8]

The flavylium cation (AH^+) is stable only at very acidic pH values because the two reactions in which it is involved, deprotonation to give the quinoidal base (A), eq 1, and hydration leading to the hemiketal (B), eq 2, are pH dependent.

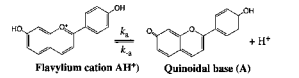

$K_a = k_a/k_{-a}$ (deprotonation) (1)

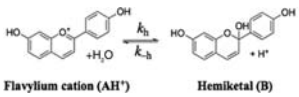

$K_h = k_h/k_{-h}$ (hydration) (2)

These two parallel reactions are in competition and occur on different scales of time: proton transfer in microseconds and hydration in minutes to subseconds, depending on pH. As a consequence upon a pH jump from very acid solutions (where AH^+ is the dominant species) to higher pH values, hereafter designated direct pH jump, A appears as a kinetic product that usually fades with time, because it is not the most stable species at the equilibrium. The hemiketal (chromene) is involved in a tautomeric process that leads to ring opening with the formation of a *cis*-chalcone form, eq 3. This reaction usually occurs on the subsecond time scale.

Finally, the *cis*-chalcone isomerizes and gives the *trans*-chalcone, eq 4, on the time scale of seconds or many days depending on the flavylium substitution pattern.

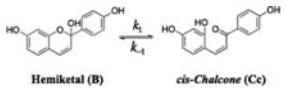

$K_t = k_t/k_{-t}$ (tautomerization) (3)

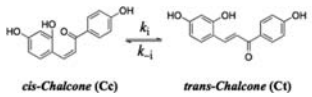

$K_i = k_i/k_{-i}$ (isomerization) (4)

The colored species of the network are the flavylium cation and the quinoidal base, the last one red-shifted in comparison with the former.

The analysis of the thermodynamic equilibria of the flavylium compounds becomes easier if eq 5 is considered.[9,10] Equation 5 is equivalent to a single acid−base equilibrium between flavylium cation and a conjugate base, CB, defined as the sum of the concentrations of the other species in the network, [CB] = [A] + [B] + [*Cc*] + [Ct]

$$AH^+ + H_2O \rightleftharpoons CB + H_3O^+$$

$$K'_a = K_a + K_h + K_hK_t + K_hK_tK_i \quad (5)$$

From the set of eqs 1−5 it is easy to obtain the pH-dependent mole fraction distribution of the network species.

$$\chi_{AH^+} = \frac{[H^+]}{[H^+] + K'_a}; \quad \chi_A = \frac{K_a}{[H^+] + K'_a};$$

$$\chi_B = \frac{K_h}{[H^+] + K'_a}; \quad \chi_{Cc} = \frac{K_hK_t}{[H^+] + K'_a};$$

$$\chi_{Ct} = \frac{K_hK_tK_i}{[H^+] + K'_a} \quad (6)$$

When a relatively high *cis*−*trans* isomerization barrier is present as in anthocyanins, it is very useful to define a pseudoequilibrium attained before formation of significant amounts of Ct.

$$AH^+ + H_2O \rightleftharpoons CB^\wedge + H_3O^+$$

$$K^\wedge_a = K_a + K_h + K_hK_t \quad (7)$$

$$[CB^\wedge] = [A] + [B] + [Cc]$$

The mole fraction distribution of the species at the pseudoequilibrium, AH^+, A, B, and Cc, can be obtained from the expressions of eq 6 by substituting K'_a by $K^\wedge_a$.

Equation 5 refers to the thermodynamic equilibrium and thus can be used for all of the systems independently of whether have a high or low *cis*−*trans* isomerization barrier. In Figure 4A the absorption spectra regarding the compound 4′,7-dihydroxyflavylium at the equilibrium are shown. Inspection of this figure identifies from the shape and position of the absorption spectra the flavylium cation at lower pH values and at higher pH values the quinoidal base (absorbing around 490 nm) and *trans*-

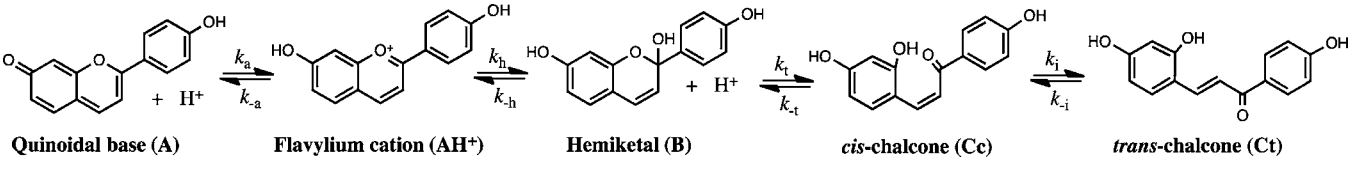

Figure 3. Network of chemical reactions of the natural compound 4′,7-dihydroxyflavylium. The equilibrium constants are defined as $K_n = k_n/k_{-n}$ (n = a, h, t, i).

dx.doi.org/10.1021/jf404869m | J. Agric. Food Chem. 2014, 62, 6885−6897

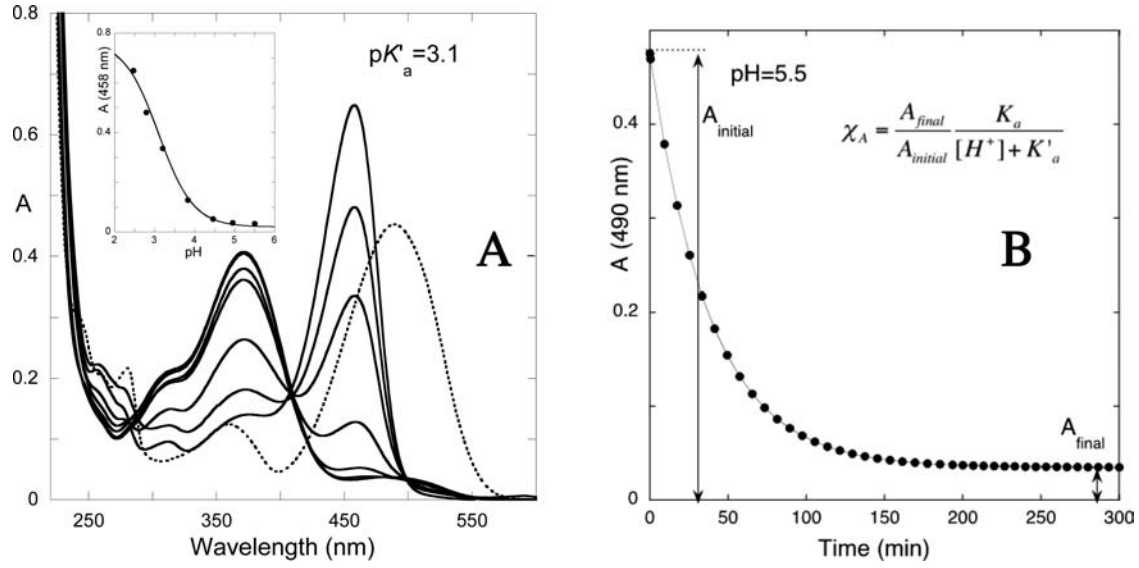

Figure 4. (A) Absorption spectra of equilibrated solutions of the compound 4′,7-dihydroxyflavylium (2.7×10^{-5} M) as a function of pH. Fitting was achieved through eq 5; for comparison purposes the absorption spectrum obtained immediately after the pH jump to 5.5 is shown (pointed line). Reprinted with permission from ref 19. (B) Trace of a direct pH jump from pH 1.0 to 5.5.

chalcone (absorbing around 360 nm), respectively minor and major products. In Figure 4B the trace corresponding to a pH jump from pH 1.0 to 5.5 taken at 490 nm is represented. The initial absorbance is due to the conversion of practically all flavylium cation into quinoidal base (absorption due to the total concentration C_0, see the respective absorption spectra Figure 4A, pointed line); at the equilibrium the absorbance corresponds to the remaining quinoidal base. The ratio $A_{final}/A_{initial}$ is equal to the mole fraction of quinoidal base at the equilibrium given by eq 6, permitting the calculation of the constant K_a from the previously known value of K'_a (Figure 4A).

One important breakthrough for the comprehension of the flavylium chemistry was the discovery of Brouillard and Dubois[9] that in acidic to neutral medium hemiketal is formed only through the hydration of flavylium cation and not from the quinoidal base.

The comprehension of the flavylium network of chemical reactions gains from the drawing of an energy level diagram easily achieved if the equilibrium constants of eqs 1−4 are known. The energy level diagram where all of the network species are positioned[11] is easily obtained from the relationship $\Delta G^0 = -RT \ln K$, where ΔG° is the standard Gibbs energy, R the gas constant, T the absolute temperature, and K the equilibrium constant for each process of the network.

The next discussion concerns flavylium networks exhibiting high *cis*−*trans* isomerization barriers, the paradigm of anthocyanins.

The relative position of each network species is very dependent on the substitution pattern of the flavylium core. The example of Figure 5 is representative of anthocyanins. In the case of a direct pH jump, for example, from pH 1.0, where the flavylium cation is the dominant species, to pH = pK_a, half of the flavylium cation is transformed in quinoidal base in a short time (less than the mixing time of a stopped-flow apparatus), according to eq 8:

$$k_1 = k_a + k_{-a}[H^+] \quad (8)$$

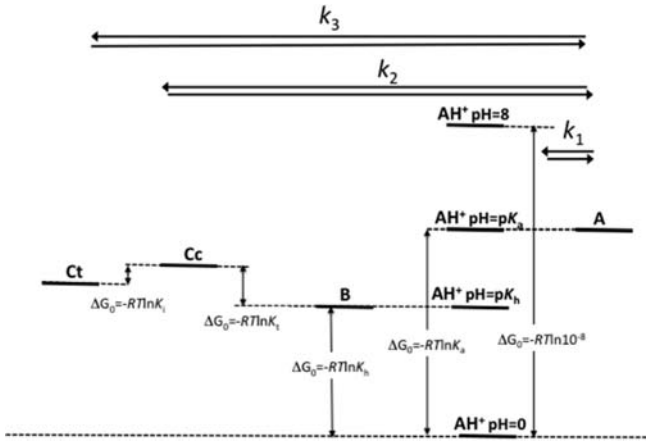

Figure 5. Energy level diagram of the flavylium network of chemical reactions, exhibiting a pattern representative of anthocyanins.

The base does not react in acidic to neutral pH values, and as a consequence the hydration of the flavylium cation (much slower than proton transfer in eq 1) is the next rate observed by stopped flow or in a common spectrophotometer (if it is slow enough). In the example of this pH jump, equal amounts of flavylium cation and quinoidal base disappear to give the more stable species. It must be emphasized that the interconversion between B and Cc is also very fast, and "once B is formed from the hydration of the flavylim cation" immediately it equilibrates with Cc. The last step (k_3, see below) is the formation of Ct, which is much slower. The second process with observed rate constant k_2 (eq 9) can thus be equivalent to a reversible first-order equilibrium involving two species: by one side AH^+ in fast equilibrium with A and by the other B in fast equilibrium with Cc. Without entering into a discussion of complex mathematical deductions,[12] the meaning of eq 9 can be extracted by considering that this observed rate constant is the sum of the direct process and the reverse one. The direct process is given by the rate constant k_h, which should be multiplied by the fraction of flavylium available to react $[H^+]/([H^+] + K_a)$ due to the discovery of Brouillard and Dubois that

dx.doi.org/10.1021/jf404869m | J. Agric. Food Chem. 2014, 62, 6885−6897

B in acidic medium is formed only through the reaction of AH^+. The reverse reaction is the formation of AH^+ from B accounted for by the term $k_{-h}[H^+]$. However, not all B is available to react, and thus the respective rate constant should be multiplied by its mole fraction resulting from the fast equilibrium between B and Cc, that is, $(1)/(1 + K_t)$.

$$k_2 = \frac{[H^+]}{[H^+] + K_a} k_h + \frac{1}{1 + K_t} k_{-h}[H^+] \quad (9)$$

At this stage of the kinetics, AH^+, A, B, and Cc are in pseudoequilibrium, $K^{\wedge}_a$.

The equilibrium is reached when Ct is formed; by a similar reasoning eq 10 can be written

$$k_3 = \frac{K_h K_t}{[H^+] + K^{\wedge}_a} k_i + k_{-i} = \frac{K_h K_t}{[H^+] + K_a + K_h + K_h K_t} k_i + k_{-i} \quad (10)$$

The first term corresponds to the formation of Ct from Cc given by k_i multiplied by the fraction of Cc available to give Ct (due to the formation of the pseudoequilibrium eq 7) plus the reverse isomerization reaction k_{-i}. Representation of this last process (in the case of the high *cis*−*trans* isomerization barrier) is shown in Figure 6.

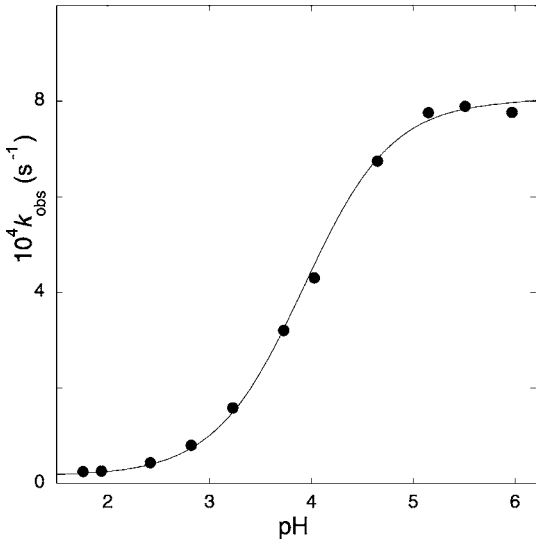

Figure 6. pH dependence of the rate constant of the slowest process upon a direct pH jump from solutions of 3′,4′-dihydroxy-7-*O*-*β*-D-glucopyranosyloxyflavylium at pH 1.0 to higher pH values: fitting was achieved with eq 10. Reprinted with permission from ref 18. Copyright 2013 Royal Society of Chemistry.

In the scheme shown in Figure 5, the data regarding the different kinetic process can be added, and in this way both thermodynamic and kinetic information of the system can be visualized.

In many other flavylium networks the *cis*−*trans* isomerization barrier is very small and the pseudoequilibrium is not formed; steps 2 and 3 above-described are transformed into one step.[13] Assuming that the equilibrium between AH^+ and A as well between B and Cc is reached during the kinetic process, the following equation can be deduced, again from simple reasoning without the use of more complex mathematical deductions.

$$A \underset{H^+}{\overset{K_a}{\rightleftharpoons}} AH^+ \underset{k_{-h}H^+}{\overset{k_h}{\rightleftharpoons}} B \overset{K_t}{\rightleftharpoons} Cc \underset{k_{-i}}{\overset{k_i}{\rightleftharpoons}} Ct \quad (11)$$

(equilibrium, equilibrium)

This is equivalent to the equilibrium

$$X \underset{k_{-1}}{\overset{k_1}{\rightleftharpoons}} Y \underset{k_{-2}}{\overset{k_2}{\rightleftharpoons}} Z \quad (12)$$

where the equilibrium between AH^+ and A is assigned to X, and the equilibrium between B and Cc to Y and Ct to Z.

Assuming the steady state for Y, the observed rate constant is given by eq 13

$$k_{obs} = \eta_{Y(direct)} k_2 + \eta_{Y(reverse)} k_{-1} \quad (13)$$

where $\eta_{Y(direct)} = (k_1)/(k_{-1} + k_2)$ is the formation efficiency of Y during the direct process and k_2 the rate of Z formation during the same process, $\eta_{Y(reverse)} = (k_{-2})/(k_{-1} + k_2)$ is the formation efficiency of Y in the reverse process, and k_{-1} is the rate of X formation in this last process.

In the scheme shown in eq 12 k_1 is equal to $([H^+])/([H^+] + K_a) \times k_h$ because k_h should be multiplied by the mole fraction of AH^+ available due to its equilibrium with A; k_2 is equal to $(K_t)/(1 + K_t)k_i$ due to the equilibrium between B and Cc. With regard to the reverse processes, k_{-2} is identified as k_{-i} and k_{-1} as $k_{-h}[H^+](1)/(1 + K_t)$, the last term also due to the equilibrium between B and Cc.

Substituting these constants in eq 13

$$k_4 = \frac{\frac{[H^+]}{[H^+] + K_a} k_h k_i \frac{K_t}{1 + K_t} + k_{-i} k_{-h}[H^+] \frac{1}{1 + K_t}}{\frac{k_{-h}[H^+]}{1 + K_t} + k_i \frac{K_t}{1 + K_t}} = \frac{\frac{[H^+]}{[H^+] + K_a} k_h k_i K_t + k_{-i} k_{-h}[H^+]}{k_{-h}[H^+] + k_i k_t} \quad (14)$$

dividing by k_{-h} gives the expression usually reported in the literature:

$$k_4 = \frac{\frac{[H^+]}{[H^+] + K_a} K_h K_t k_i + k_{-i}[H^+]}{[H^+] + k_i \frac{K_t}{k_{-h}}} \quad (15)$$

Now we have the kinetic equations to deal with flavylium derivatives exhibiting high or low *cis*−*trans* isomerization barriers.

In Figure 7, the bell-shaped curve is represented for the compound 3′,4′,7-trihydroxyflavylium (black circles).[14]

The same curve is obtained in the presence of *β*-cyclodextrin (see below the respective discussion).

The fitting of the bell-shaped curve permits us to obtain the following parameters that should be confirmed by other independent relationships based on different experimental data (see below):

$$K_a;\ K_h K_t k_i;\ k_{-i};\ \frac{k_i K_t}{k_{-h}}$$

Determination of the Rate and Equilibrium Constants of the Network. Two different strategies to calculate the rate and equilibrium constants of the network of flavylium compounds are used, depending on the existence or not of a thermal *cis*−*trans* isomerization barrier. In both cases, however, it is necessary the use of the so-called reverse pH jumps, which consist of the acidification of equilibrated or pseudoequilibrated

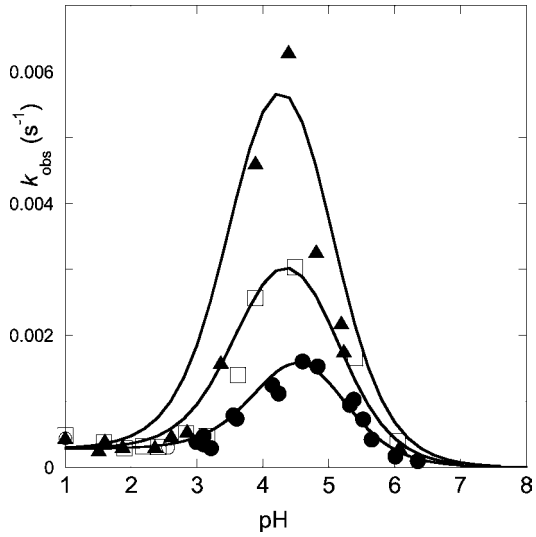

Figure 7. Representation of the rate constants regarding the formation of *trans*-chalcone upon a pH jump from equilibrated solutions of the compound 3′,4′,7-trihydroxyflavylium at pH 1.0 to higher pH values: (●) no *β*-cyclodextrin; (□) 4.8 mM; (▲) 8.3 mM. Fitting was achieved with eq 15. Reprinted with permission from ref 14. Copyright 2013 Royal Society of Chemistry.

solutions at moderate pH values. An example of a reverse pH jump is given in Figure 8.[15]

The ratio between the amplitude of the two exponentials Cc/B gives the equilibrium constant K_t. In the case of anthocyanins the mole fraction of Cc (and Ct) is very small, and thus this measurement should be repeated several times to find a value with statistical meaning.

In the case of the existence of a high *cis*−*trans* isomerization barrier as in anthocyanins, a step-by-step procedure to carry out this calculation was previously reported.[16] The constant K'_a is obtained from the fitting of the data as reported in Figure 4A. The constant K_a is obtained as shown in Figure 4B. Moreover, the fitting of k_2 (eq 9) allows us to determine k_h and k_{-h} and thus K_h, because the other constants are already known. The calculation of the hydration constant, K_h, should be coherent with the kinetic data of the reverse pH jumps as those represented in Figure 4B. The first process to be observed in the reverse pH jumps is the hydration reaction from all B present at the equilibrium (or even pseudoequilibrium). Taking into account that the final pH is very acidic, there is a change of regime in the sense that the hydration becomes faster than tautomerization. On this basis it can be considered that all B reacts to give AH^+ before significant changes in the Cc concentration take place. In other words, there is no equilibrium between B and Cc to consider and eq 16 is different from eq 9. (This difference is small if the constant K_t is small.)

$$k_5 = \frac{[H^+]}{[H^+] + K_a} k_h + k_{-h}[H^+] \tag{16}$$

$$k_6 = k_{-t} \tag{17}$$

A last much slower process leads to flavylium cation from Ct (not shown in Figure 4B). Due to the fact that no B is accumulated, the back reaction from B to Cc is not significant, and eq 17 can be used and k_{-t} obtained.

As shown above, once K_t, K_a, and K_h have been calculated and from the value of K'_a, the remaining equilibrium constant K_i is also found. With regard to the rate constants, $k_t = K_t k_{-t}$, k_i, and k_{-i} are achieved from the kinetics of the slowest process (eq 10) and the equilibrium constant K_i.

Summarizing the step-by-step procedure permits us to obtain all of the rate and equilibrium constants and, for example, to draw an energy level diagram such as the one reported in the scheme reported in Figure 5.

When the *cis*−*trans* isomerization barrier is small and the bell-shaped curve is followed, the strategy should be different, because the data acquired from the bell-shaped curve (eq 15) are not adequate to calculate all of the constants of the system.

Photochemistry: A Powerful Tool. As shown above, when the system possesses a high *cis*−*trans* isomerization barrier, it is possible to access all of the equilibrium and rate constants. However, when the barrier is very small, the species B and Cc are more or less elusive, and the only reliable data are

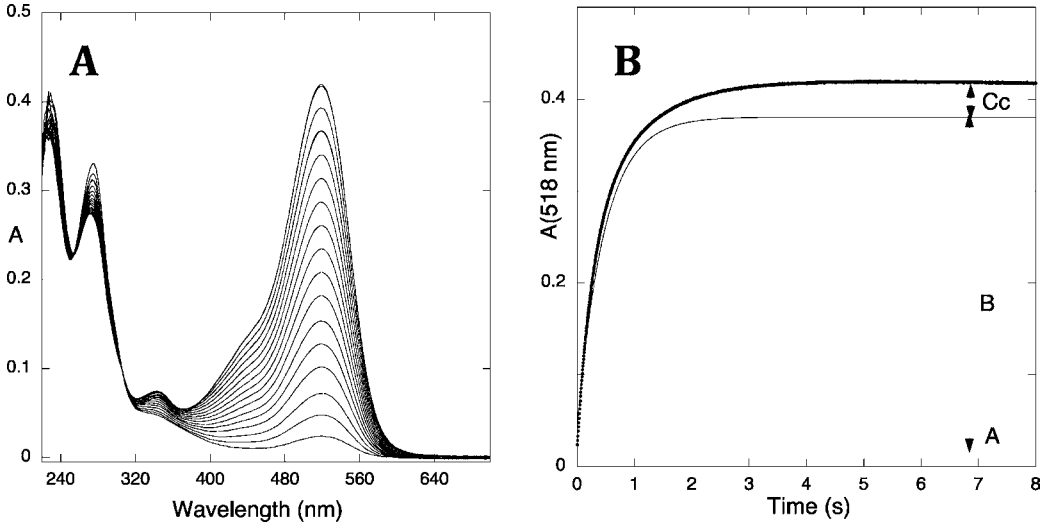

Figure 8. (A) Spectral variations upon a reverse pH jump from an equilibrated solution of oenin (2×10^{-5} M) at pH 5.2 to pH 1.1. (B) Kinetic trace at 518 nm, fitted with a biexponential law with k_{obs1} = 2.1 s^{-1} and k_{obs2} = 0.5 s^{-1}. Bold line, experimental data; thin line, fast process (monoexponential). Reprinted with permission from ref 15. Copyright 2012 Elsevier.

dx.doi.org/10.1021/jf404869m | J. Agric. Food Chem. 2014, 62, 6885−6897

taken from the bell-shaped curve. Moreover, according to our experience there are multiple solutions of the bell-shaped curve, and as a consequence other relationships between equilibrium and rate constants should be achieved. When the compounds show photochemistry, the problem is easily solved.

Photochromism occurs in many flavylium derivatives including deoxyanthocyanins. A necessary requirement to observe this phenomenon is the existence of significant amounts of Ct at the equilibrium.

The photochromism arises from the formation of the flavylium cation (or quinoidal base) upon irradiation of the *trans*-chalcone (Figure 9).

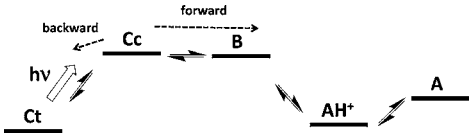

Figure 9. Photochromism in the flavylium network.

The irradiation of the *trans*-chalcone leads to the appearance of the *cis*-chalcone in a very fast process that takes 16 ns in the case of 4′,7-dihydroxyflavylium (not shown).[17] As presented in Figure 9 the *cis*-chalcone has two alternatives to react (because it is not thermodynamically stable): (i) backward to recover *trans*-chalcone and (ii) forward to give flavylium cation/quinoidal base. The last kinetic process is pH dependent, increasing with increasing proton concentration, and thus the photochromism can be modulated by the pH. One important aspect is the change of regime that takes place only at more acidic pH values (not assessed by direct pH jumps). At these pH values the hydration is faster than tautomerization and, as a consequence, the last one becomes the rate-determining step (see below).

The photochromism of flavylium compounds is a general phenomenon. In Figure 10 the spectral variations taking place upon steady state irradiation of the bioinspired compound 3′,4′-dihydroxy-7-*O*-*β*-D-glucopyranosyloxyflavylium (Figure 11) are shown.[18]

Flash photolysis is a powerful technique that can give further information regarding the flavylium-based photochromic systems. This technique was used, for example, to study the photochromism of the compound 4′,7-dihydroxyflavylium inside *β*-cyclodextrin, but it is a rather general technique (Figure 12).[19] When the absorption is followed at 371 nm, the bleaching immediately after the flash occurs because the *cis*-chalcone absorbs less than the *trans*-chalcone. The partial recovery corresponding to the first kinetic step is due to the backward reaction restoring part of the initial *trans*-chalcone. When the absorption is followed at the flavylium cation/quinoidal base (459 nm), the appearance of these species is observed (the relative fraction depending on the pH). The rate constants at both wavelengths follow a first-order kinetics and are equal within experimental error as expected from two parallel reactions. In a longer time scale the system reverts totally to the initial *trans*-chalcone, defining in this way a photochromic system.

Representation of the rate constants of Figure 12 as a function of pH (see Figure 13) is accounted for by eqs 9 and 18.

At higher pH jumps the rate-determining step is the hydration reaction and eq 9 ($(k_2 = ([H^+])/([H^+] + K_a)k_h +$

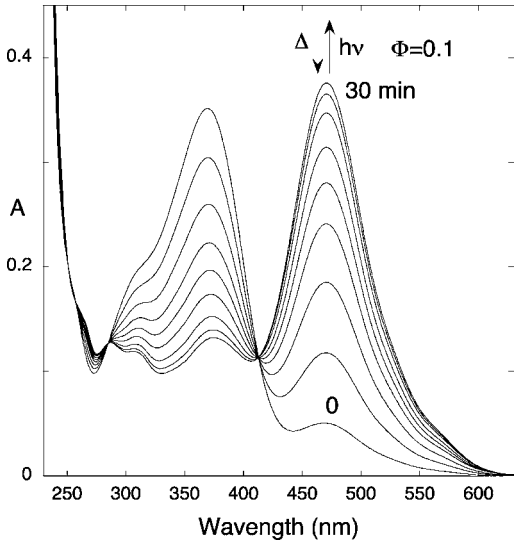

Figure 10. Spectral modifications as a function of irradiation time at 365 nm, pH 3.7, of the compound 3′,4′-dihydroxy-7-*O*-*β*-D-glucopyranosyloxyflavylium. Reprinted with permission from ref 18. Copyright 2013 Royal Society of Chemistry.

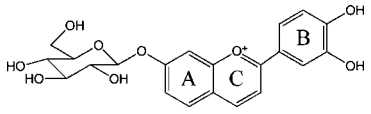

Figure 11. 3′,4′-Dihydroxy-7-*O*-*β*-D-glucopyranosyloxyflavylium.

$(1)/(1 + K_t)k_{-h}[H^+]))$ is followed. At lower pH values the hydration becomes faster than tautomerization (it is directly proportional to $[H^+]$) and eq 18 should be used.

$$k_7 = k_{-t} + k^H[H^+] + k^{OH}[OH^-] \quad (18)$$

In eq 18 the basic and acid catalysis of the tautomerization reaction as reported by McClelland and co-workers was considered.[20]

The reaction quantum yield is another source of kinetic information (Figure 14). When the hydration is the rate-determining step, the equilibrium between B and Cc is established, and the forward and backward reactions are respectively given by eqs 19 and 20:

$$k_{forward} = \frac{k_{-h}[H^+]}{1 + K_t} \quad (19)$$

$$k_{backward} = \frac{K_t}{1 + K_t}k_i \quad (20)$$

Neglecting the contribution of k_{-i} as well as $k_h[H^+]/([H^+] + K_a)$ (k_{-i} is relatively very small; on the other hand, the hydration is the rate-determining step at moderately acidic pH values, and this term has a negligible contribution), the pH dependence of the quantum yield is thus given by eq 21:

$$\Phi = \Phi_0 \frac{k_{forward}}{k_{forward} + k_{backward}} = \frac{[H^+]}{[H^+] + \frac{K_t k_i}{k_{-h}}} \quad (21)$$

The fitting from eq 21 should be coherent with the same parameter taken from the bell-shaped curve of eq 15.

dx.doi.org/10.1021/jf404869m | J. Agric. Food Chem. 2014, 62, 6885−6897

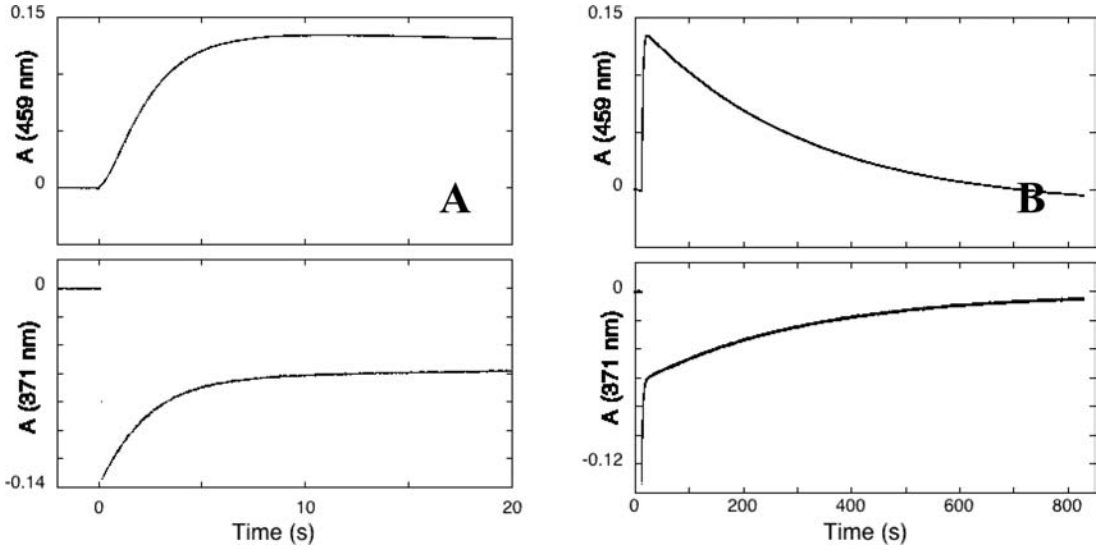

Figure 12. (A) Flash photolysis of the compound 4′,7-dihydroxyflavylium (2.7×10^{-5} M) in the presence of β-cyclodextrin (9 mM) at pH 3.6. The trace at 459 nm corresponds to the flavylium cation absorption, whereas that at 371 nm corresponds to the *trans*-chalcone. (B) The same observed in a larger time scale to evidence the reversibility of the photochromic system. Reprinted with permission from ref 18. Copyright 2013 Royal Society of Chemistry.

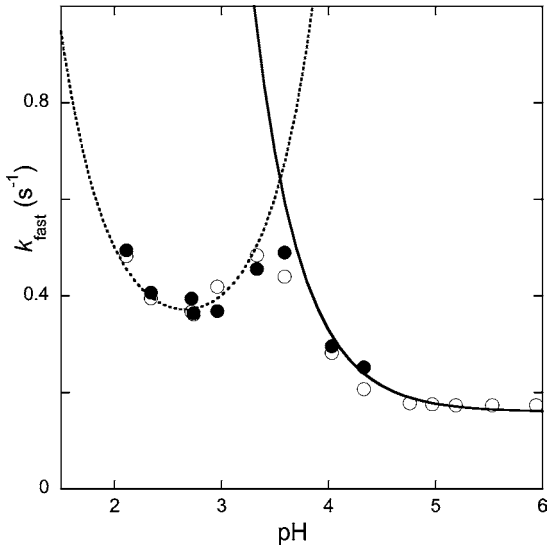

Figure 13. Typical dependence of the flash photolysis rate constants (faster process) as a function of pH: (●) monitored at the flavylium absorption maximum; (○) monitored at the *trans*-chalcone maximum. Full line fitting was achieved with eq 9 $k_{-h}/(1 + K_t) = 1700\ s^{-1}\ M^{-1}$; $k_i K_t//(1 + K_t) = 0.16\ s^{-1}$. Traced line fitting was achieved with eq 18 $k_{-t} = 0.28\ s^{-1}$; $k^H = 21\ s^{-1}\ M^{-1}$; $k^{OH} = 8 \times 10^9\ s^{-1}\ M^{-1}$. The experimental points correspond to the compound 3′,4′,7-trihydroxyflavylium in the presence of 4.8 mM β-cyclodextrin.

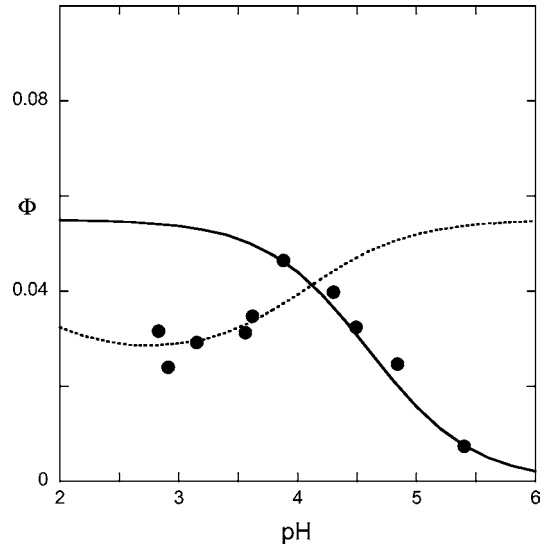

Figure 14. Quantum yields as a function of pH, fitted using eqs 21 and 22 for $K_t/k_i/k_{-h} = 2.5 \times 10^{-5}\ M^{-1}$; $k_{-t} = 0.45\ s^{-1}$; $k^H = 26\ M^{-1}\ s^{-1}$; $k^{OH} = 8 \times 10^9\ M^{-1}\ s^{-1}$; $k_i = 0.5\ s^{-1}$; $\Phi_0 = 0.055$. The experimental points correspond to the quantum yields of the compound 3′,4′,7-trihydroxyflavylium in the presence of 4.8 mM β-cyclodextrin.

When the rate-determining step is the tautomerization reaction, as observed in Figure 5 (change of regime), the pH dependence of the quantum yield follows eq 22:

$$\Phi = \Phi_0 \frac{k_{-t} + k^H[H^+] + k^{OH}[OH]^-}{k_{-t} + k^H[H^+] + k^{OH}[OH]^- + k_i} \quad (22)$$

To calculate all of the rate and equilibrium constants of the system, the more practical way is to carry out a global fitting of the bell-shaped curve (eq 15 together with eqs 9, 18, 21, and 22). In particular, eq 21 should be coherent with the values obtained from the bell-shaped curve. The procedure above-reported allows us to draw an energy level diagram also observed for the compound lacking a high *cis*−*trans* isomerization barrier. Such an example is reported in the scheme shown in Figure 15. Comparing the schemes shown in Figures 5 and 15 (respectively for compounds with and without the *cis*−*trans* isomerization barrier), the most interesting feature is the high energy level of species B and Cc, confirming our observation that they are more or less elusive species.

BIOINSPIRED APPLICATIONS

Flavylium Network in Confined Medium. Bioinspired application within the framework of flavylium chemistry includes compounds made by synthesis possessing some features of the anthocyanins and other natural related

dx.doi.org/10.1021/jf404869m | J. Agric. Food Chem. 2014, 62, 6885−6897

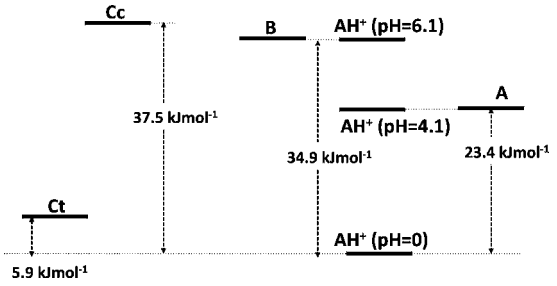

Figure 15. Energy level diagram of the compound 3′,4′,7-trihydroxyflavylium.

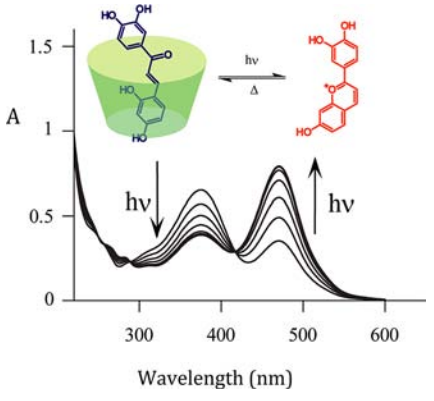

Figure 16. Representation of the compound 3′,4′,7-trihydroxyflavylium inside the cavity of the β-cyclodextrin according to the NMR data (ROESY). Irradiation at 365 nm gives rise to the formation of flavylium cation that migrates to the bulk solutions.

compounds, in particular following the same network of chemical reactions.

One question that can be posed is how the flavylium network behaves in different matrices. Recently the compounds 3′,4′,7-trihydroxyflavylium and 4′,7-dihydroxyflavylium were studied in the presence of β-cyclodextrin.[14,19] The main conclusion is that the *trans*-chalcone is preferentially stabilized by the β-cyclodextrin and that its interaction with flavylium cation is practically negligible (association constant ≈ 0). This is an interesting example of the so-called anticopigmentation effect,[21−23] because in the presence of β-cyclodextrin the rate to reach the equilibrium increases, favoring the colorless species (see Figure 7). According to the NMR data (ROESY) the position of the Ct inside the β-cyclodextrin can be determined (Figure 16). In addition, upon irradiation the formation of flavylium cation can be observed, and because this form does not interact with the host, it should migrate to the bulk solution, emptying in this way the cavity.

Figure 17. Flavylium cation of dracoflavylium and respective quinoidal base.

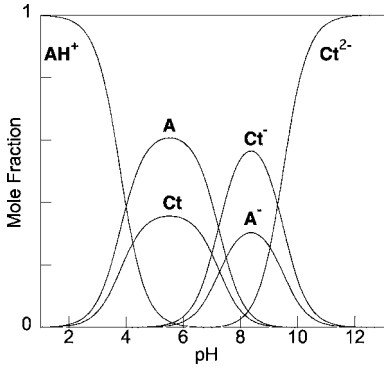

Figure 18. Mole fraction distribution of dracoflavylium. Reprinted with permission from ref 27. Copyright 2007 Wiley.

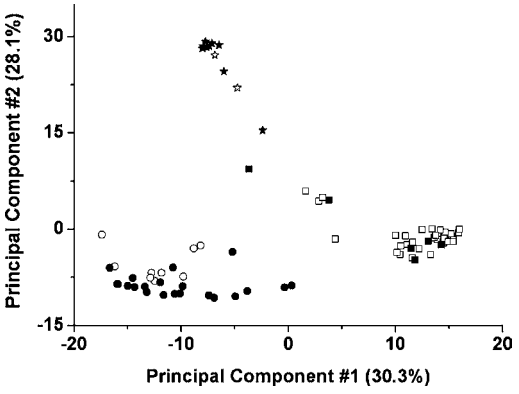

Figure 19. Principal component analysis scores for reference samples of *Dracaena draco* (squares), *Dracaena cinnabari* (circles), and *Daemonorops draco* (stars) representing 58.4% of total data variance. The model was obtained from mean-centered HPLC chromatograms acquired at 462 nm between 15.3 and 28.9 min. Reprinted with permission from ref 8. Copyright 2008 Elsevier.

Table 1. Dyes Giving the Characteristic Color to Dragon's Blood and the Year Reported

dracorhodin	nordracorhodin	dracorubin	*dracoflavylium*
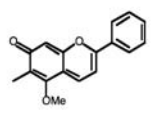	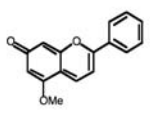	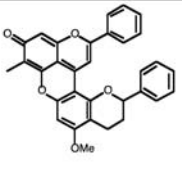	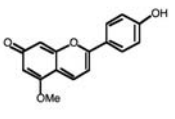
1943, 1950	*1971*	*1936; 1976*[d]	2006

dx.doi.org/10.1021/jf404869m | *J. Agric. Food Chem.* 2014, 62, 6885−6897

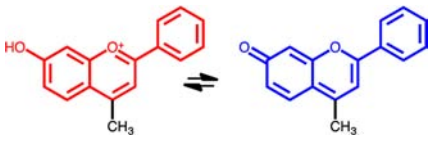

Figure 20. Chemical structure of 7-hydroxy-4-methylflavylium.

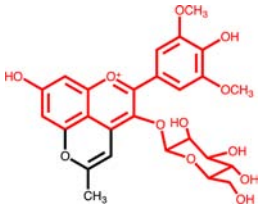

Figure 21. Chemical structure of methylpyranomalvidin-3-*O*-glucoside.

This example is in contrast with the behavior of 4′,7-dihydroxyflavylium in the presence of molecular clips as hosts. In that case the flavylium cation is stabilized to complexation with the host, whereas the *trans*-chalcone is poorly stabilized.[24]

Dragon's Blood. An Example of How Chemical Information Can Be Lost. Dragon's blood is a natural resin, presenting a rich deep red color, obtained from various trees, namely, *Dracaena draco* and *Dracaena cinnabaris* belonging to the Liliacae family. It is known that it appears in injured areas of the tree.[25] Dragon's blood has been used for centuries for medical and artistic purposes.[26] Despite the characterization of many compounds from Dragon's blood resins, with precise geographic origins and plant species, none could be responsible for the red color of the resins, except those reported in Table 1.[27]

Researchers familiar with the flavylium network of chemical reactions immediately recognized in these structures the quinoidal bases. However, the information that the red color of the resin named Dragon's blood is related to natural flavylium compounds has been misleading during the past decades, up to the description of dracofavylium.[27] Figure 17 shows a picture of the quinoidal base and flavylium cation colors.

More recently, the compound 4′,7-dihydroxyflavylium was also identified as one of the colorants of Dragon's blood.[8]

One interesting feature of dracoflavylium is its pH-dependent mole fraction distribution, which is very different from that of anthocyanins as well as from most of the synthetic flavylium compounds reported.[1] In dracoflavylium the more stable species at moderately acidic pH values is the quinoidal base (Figure 18). The color of Dragon's blood is given by the quinoidal base, which in these compounds is the major species at these pH values.

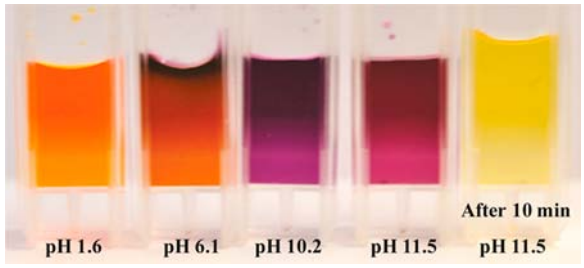

Figure 23. Formation of quinoidal base and ionized quinoidal bases from the flavylium cation of methylpyranomalvidin-3-*O*-glucoside and respective colors. Reprinted with permission from ref 29.

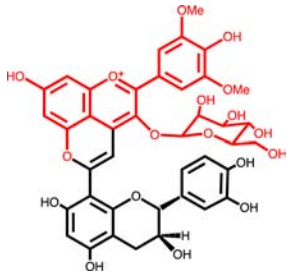

Figure 24. Chemical structure of pyranomalvidin-3-*O*-coumaroylglucoside-(+)-catechin.

Profit can be taken from the fact that these dyes belong to the family of flavylium network chemical reactions.[8] A simple and rapid liquid chromatographic method with diode array UV−vis spectrophotometric detection has been developed for the authentication of Dragon's blood resins from *Dracaena* and *Daemonorops* trees. The method uses an extract at pH 1.0 to have the flavylium cation of the different dyes. Using this method it was discovered that the flavylium chromophores differ among the species and could be used as markers to differentiate them. A study of parameters, such as time of extraction, proportion of methanol, and pH, was undertaken to optimize the extraction of the flavylium compounds. This method was then used to make extracts from samples of Dragon's blood resin obtained from material of known botanical origin. From the samples analyzed, 7-dihydroxy-5-methoxy-6-methylflavylium (dracorhodin), 4′,7-dihydroxy-5-methoxyflavylium (dracoflavylium), and 4′,7-dihydroxyflavylium were selected as species markers for *Daemonorops* spp., *Dracaena draco*, and *Dracaena cinnabari*, respectively. The chromatograms from these samples were used to build an HPLC-DAD database. The ability to discriminate among species of Dragon's blood using the single marker compounds was compared with a principal component analysis of the chromatograms in the HPLC-DAD database. The results from the HPLC-DAD method based on the presence of these flavylium markers was unequivocal. The HPLC-DAD method

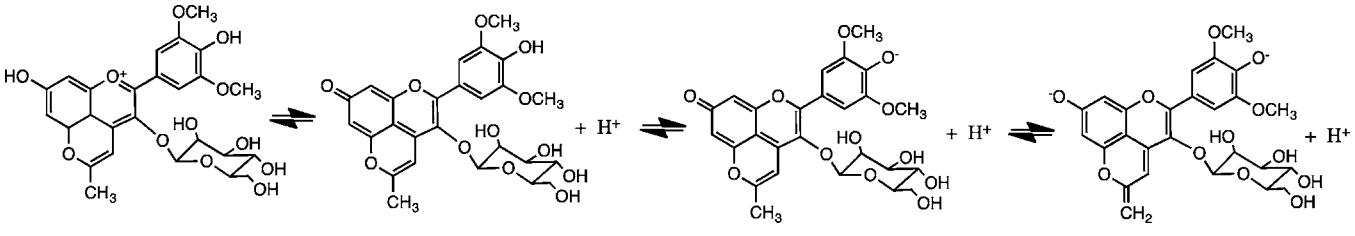

Figure 22. Formation of quinoidal base and ionized quinoidal bases from the flavylium cation in methylpyranomalvidin-3-*O*-glucoside.

dx.doi.org/10.1021/jf404869m | *J. Agric. Food Chem.* 2014, 62, 6885−6897

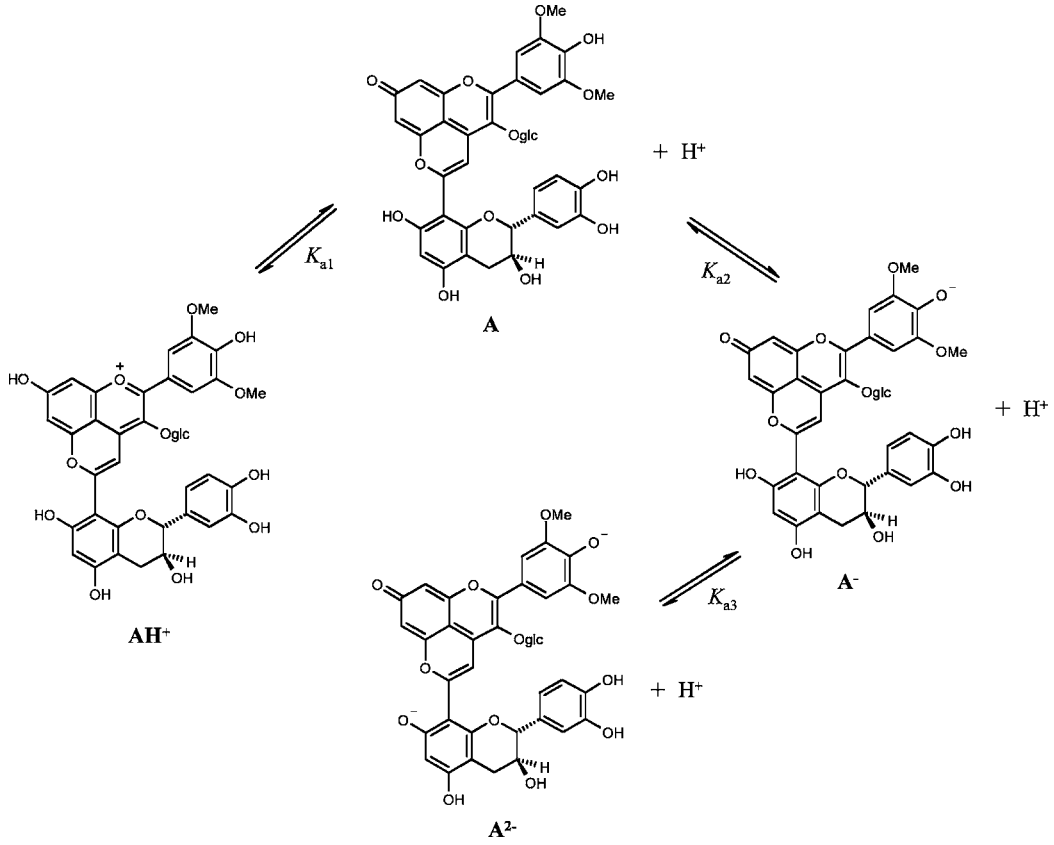

Figure 25. Acid–base equilibria involving pyranomalvidin-3-*O*-coumaroylglucoside-(+)-catechin.

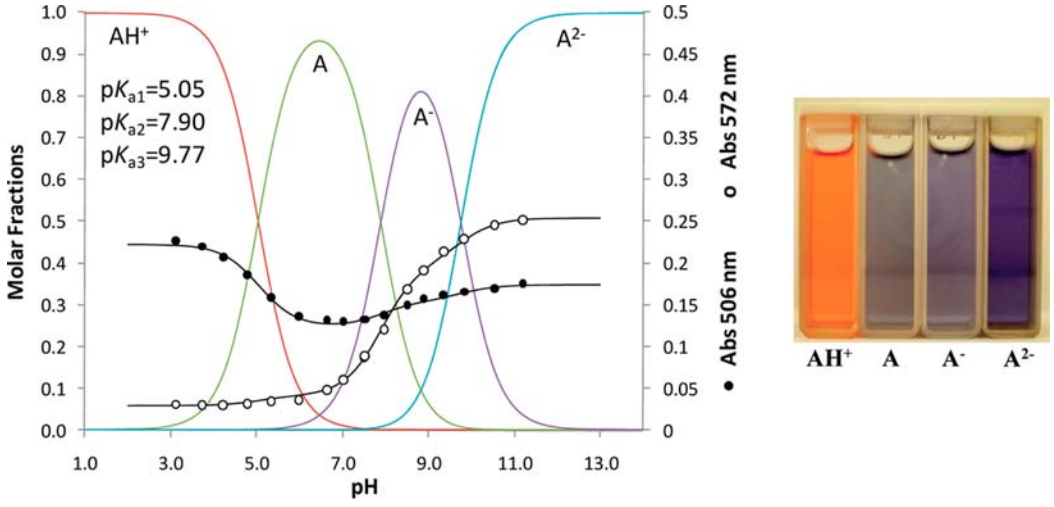

Figure 26. Mole fraction distribution of the flavylium cation and quinoidal bases of pyranomalvidin-3-*O*-coumaroylglucoside-(+)-catechin. Reprinted with permission from ref 30.

was subsequently applied to 37 samples of Dragon's blood resins from the historical samples in the Economic Botany Collection, Royal Botanic Gardens, Kew, UK (Figure 19). The method identified anomalies in how samples in this collection had been labeled. It is clear that the method can be used to evaluate the provenance of samples used in different areas of cultural heritage. It also could be used to monitor the trade of endangered species of Dragon's blood and the species being used in complex formulations of traditional Chinese medicine.

Strategies To Avoid Hydration. The fact that 4-substituted flavylium compounds do not hydrate was previously described for the compound 7-hydroxy-4-methylflavylium (Figure 20).[28]

One family of compounds related to 4-methyl-7-hydroxyflavylium is pyranoanthocyanins. The pyranoanthocyanins are anthocyanin-derived pigments with a common structural feature: the presence of an additional pyranic ring between C-4 and the 5-hydroxyl group of anthocyanins. Different pyranoanthocyanin pigments have been identified in red wines over the years. Methylpyranomalvidin-3-*O*-glucoside (Figure 21) was obtained through the reaction of malvidin-3-glucoside with acetoacetic acid lithium salt.[29]

dx.doi.org/10.1021/jf404869m | *J. Agric. Food Chem.* 2014, 62, 6885–6897

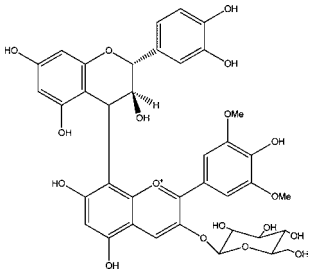

Figure 27. Chemical structure of catechin-(4,8)-malvidin-3-*O*-glucoside. The chiral carbons of catechin are 2*R*(+),3*S*(−), and from epicatechin both 2*R*,3*R* are (−).

As in the previous example the compound is very stable and the main reactions result from the deprotonation of flavylium cation at higher pH values to form the quinoidal base and the respective ionized quinoidal bases (Figure 22). These reactions are very fast, and only at very basic pH values does the last form take a few minutes to be formed (Figure 23). Another example concerns the compound pyranomalvidin-3-*O*-coumaroylglucoside-(+)-catechin (Figure 24).[30]

As in the previous example the equilibrium is established between flavylium cation and quinoidal base and respective ionized quinoidal bases (Figures 25 and 26).

Different is the behavior of the compound malvidin-3-*O*-glucoside-catechin-(4,8) (Figure 27).[31] This compound behaves like common anthocyanins (Figure 28). Figure 28 is given as an example of how all of the thermodynamic and kinetic information regarding a flavylium-derived network can be presented. At the left side the mole fraction distribution of the network species was calculated by means of eq 6, clearly indicating that at moderately acidic pH values the most stable species is the hemiketal. In the right part of Figure 28 an overview of the relative stability is given, together with the rates of interconversion between the different network species. The catechin in position 8 does not affect significantly the behavior of the anthocyanin malvidin-3-*O*-glucoside (oenin).

In conclusion, the substitution at position 4 seems to be a sufficient requirement to confer stability toward hydration. A possible explanation for this behavior is that the hydration starts from the attack at position 4 followed by a migration. This question is now under study.

Dye-Sensitized Solar Cells. Solar energy conversion is one of the most relevant questions of modern society. In particular,

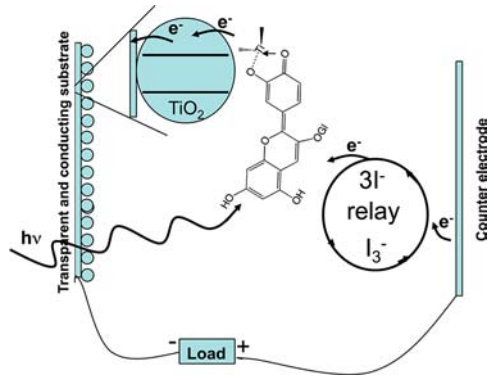

Figure 29. Scheme of a DSSC based on cyanidin. Reprinted with permission from ref 32.

dye-sensitized solar cells (DSSCs) are a very attractive solution because they are easy to fabricate, low in cost, and flexible in color, shape, and transparency.[32,33] The most efficient DSSCs are based on ruthenium and osmium complexes. These metals are toxic and expensive and, as a consequence, alternatives are needed. A very promising one is based on natural dyes. Grätzel[32] reported the first DSSC based on cyanidin (Figure 29). It is worth noting the fact that the flavylium species attached to the titanium dioxide is the quinoidal base. Light excitation of the quinoidal base leads to the injection of an electron into the titanium dioxide (radical cation). As a consequence, the quinoidal base becomes positively charged. The titanium dioxide is deposited into a conductive glass, and thus the electron is conducted through the device to the counter electrode (producing the electric current). In the counter electrode the electron is transferred to a relay, in this case I_3^-, which by itself transfers the electron to the oxidized form of the quinoidal base, closing the cycle. As mentioned in the Introduction, the base in moderately acidic conditions does not hydrate (the hydration takes place from the flavylium cation) and thus, in principle, could confer stability to the device. More recently, Calogero[34] used dyes of eggplant, arriving at a conversion of 0.7% that compares with 0.57% from the initial cyanidin-based Grätzel DSSC.

The DSCC can profit from the concept of bioinspiration.[35] Whereas the anthocyanins available are more or less reduced to six most common structures, there are many possibilities to synthesize new flavylium derivatives designed to obtain better

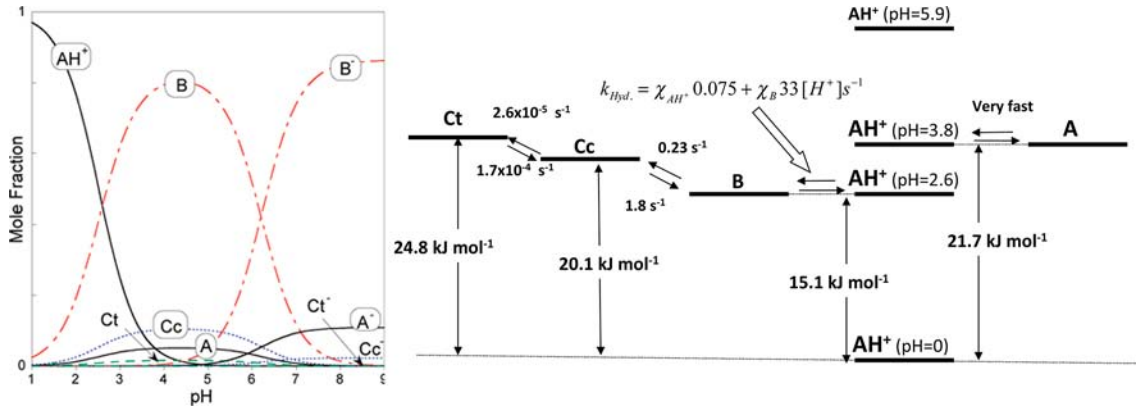

Figure 28. Complete characterization of the compound catechin-(4,8)-malvidin-3-*O*-glucoside, showing the respective mole fraction distribution, energy level of the species at the equilibriumm and rates of interconversion between the different networks of chemical reactions species.

dx.doi.org/10.1021/jf404869m | J. Agric. Food Chem. 2014, 62, 6885−6897

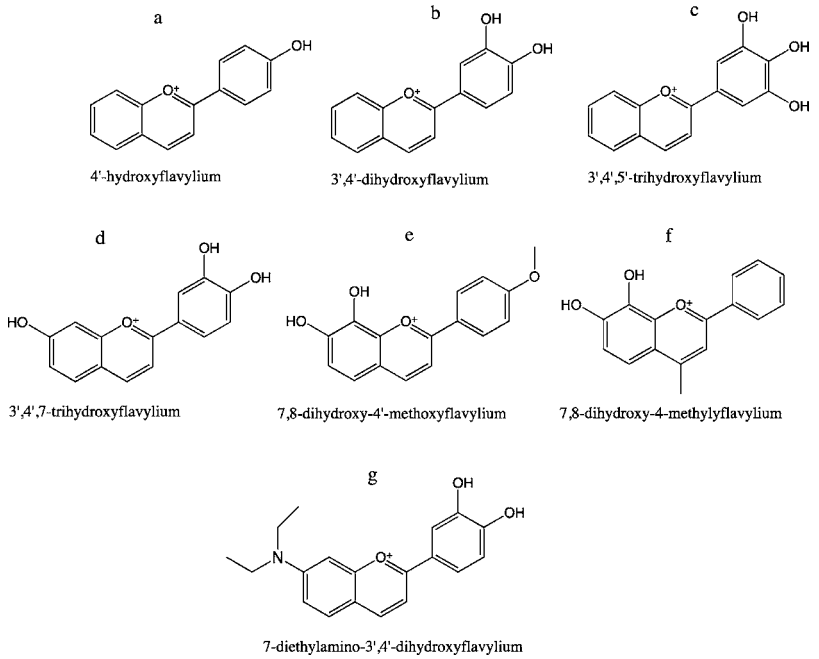

Figure 30. Bioinspired compounds used in DSSCs. Reprinted with permission from ref 35. Copyright 2013 Royal Society of Chemistry.

performances of DSSC. For this purpose we have prepared the compounds reported in Figure 30.

The most efficient synthetic flavylium compounds are **d** and in particular **g**. In both cases there are donors in positions 7 and 4′. In the case of compound **g**, the reported efficiency was 2.1%, but recently a value of 3.5% was obtained (unpublished data).

Through this work we demonstrated that there are big advantages in looking at natural flavylium compounds and synthetic ones as components of the same reality, due to the existence of a common network of chemical reactions. Knowledge of the physical−chemical behavior of flavylium derivatives is indispensable in the study of the properties of these compounds. As an example, flavylium cation is stable only in very acidic media, which is not the most common situation in biological systems except in the stomach during part of the digestion. On the other hand, natural flavylium compounds are a source of inspiration for the synthesis of new (synthetic) flavylium compounds. With regard to the applications of the latter, it is not proved that they can substitute for the natural ones, for example, as food additives or antioxidants, but this is a possible field for future research. What seems to be unquestionable is the application of bioinspired flavylium compounds as interesting photochromic systems or light absorbers in dye-sensitized solar cells.

AUTHOR INFORMATION

Corresponding Author

*E-mail: fp@fct.unl.pt. Phone: +351212948355. Fax: +3512948550.

Funding

This work has been supported by Fundacão para a Ciência e Tecnologia (FCT) and REQUIMTE through Grant PEst-C/EQB/LA0006/2011 and Project PTDC/QUI-QUI/117996/2010.

Notes

The authors declare no competing financial interest.

REFERENCES

(1) Pina, F.; Melo, M. J.; Laia, C. A. T.; Parola, A. J.; Lima, J. C. Chemistry and applications of flavylium compounds: a handful of colors. *Chem. Soc. Rev.* **2012**, *41*, 869−908.

(2) Zafra-Stone, S.; Yasmin, T.; Bagchi, M.; Chatterjee, A.; Vinson, J. A.; Bagchi, D. Berry anthocyanins as novel antioxidants in human health and disease prevention. *Mol. Nutr. Food Res.* **2007**, *51*, 675−683.

(3) Büllow, C.; Wagner, H. Derivatives of 1,4-benzopyranol, the mother substance of a new class of pigments. II. *Ber. Dtsch. Chem. Ges.* **1901**, *34*, 1782−1804.

(4) Willstätter, R. Nobel Lecture, 1915 (available at http://www.nobelprize.org/).

(5) Goto, T.; Kondo, T. Structure and molecular stacking of anthocyanins-flower color variation. *Angew. Chem., Int. Ed.* **1991**, *30*, 17−33.

(6) Yoshida, K.; Mori, M.; Kondo, T.; Tamura, H.; Goto, T. *Nature* **1992**, *358*, 515−518.

(7) Yoshida, K.; Mori, M.; Kondo, T. Blue flower color development by anthocyanins: from chemical structure to cell physyology. *Nat. Prod. Rep.* **2009**, *26*, 884−915.

(8) Sousa, M. M.; Melo, M. J.; Parola, A. J.; Seixas de Melo, J. S.; Catarino, F.; Pina, F.; Cook, E. M.; Simmonds, M. S. J.; Lopes, J. A. Flavylium chromophores as species markers for dragon's blood resins from *Dracaena* and *Daemonorops* trees. *J. Chromatogr., A* **2008**, *1209*, 153−161.

(9) Brouillard, R.; Dubois, J.-E. Mechanism of structural transformations of anthocyanins in acidic media. *J. Am. Chem. Soc.* **1977**, *99*, 1359−1364.

(10) Brouillard, R.; Lang, J. The hemicetal cis-chalcone equilibrium of malvin, a natural anthocyanin. *Can. J. Chem.* **1990**, 68755−68761.

(11) Pina, F.; Melo, M. J.; Maestri, M.; Ballardini, R.; Balzani, V. Photochromism of 4′-methoxyflavylium perchorate. A "write-lock-read-unlock-erase" molecular switching device. *J. Am. Chem. Soc.* **1997**, *119*, 5556−5561.

(12) Petrov, V.; Pina, F. Complete resolution of the reaction rates of flavylium networks. The role played by 2-phenyl-2*H*-chromen-4-ol and the hydroxyl attack to the quinoidal base. *J. Math. Chem.* **2010**, *47*, 1005−1026.

(13) Pina, F.; Petrov, V.; Laia, C. A. T. Photochromism of flavylium systems. An overview of a versatile multistate system. *Dyes Pigm.* **2012**, *92*, 877−889; Corrigendum: **2013**, *99*, 256.

(14) Basílio, N.; Fernandes, A.; de Freitas, V.; Gago, S.; Pina, F. Effect of β-cyclodextrin on the chemistry of 3′,4′,7- trihydroxyflavylium. *New J. Chem.* **2013**, *37*, 3166−3173.
(15) Leydet, Y.; Gavara, R.; Petrov, V.; Diniz, A. M.; Parola, A. J.; Lima, J. C.; Pina, F. The effect of self-aggregation on the determination of the kinetic and thermodynamic constants of the network of chemical reactions in 3-glucoside anthocyanins. *Phytochemistry* **2012**, *83*, 125−135.
(16) Pina, F. Chapter 1. Thermodynamic and kinetic processes of anthocyanins and related compounds and their bio-inspired applications. *Recent Advances in Polyphenols Research*; Wiley-Blackwell: Chichester, UK, 2014; Vol. 4, in press.
(17) Leydet, Y.; Batat, P.; Jonusauskas, G.; Denisov, S.; Lima, J. C.; Parola, A. J.; McClenaghan, N. D.; Pina, F. Impact of water on the cis-trans photoisomerization of hydroxychalcones. *J. Phys. Chem.* **2013**, *117*, 4167−4173.
(18) Petrov, V.; Gavara, R.; Dangles, O.; Al Bittar, S.; Mora-Soumille, N.; Pina, F. Flash photolysis and stopped-flow UV-visible spectroscopy study of 3′,4′-dihydroxy-7-*O*-β-D-glucopyranosyloxyflavylium chloride, an anthocyanin analogue exhibiting efficient photochromic properties. *Photochem. Photobiol. Sci.* **2013**, *12*, 576−581.
(19) Petrov, V.; Stanimirov, S.; Petrov, I. K.; Fernandes, A.; de Freitas, .V.; Pina, F. Emptying the β-cyclodextrin cavity by light. Photochemical removal of the *trans*-chalcone of 4′,7-dihydroxyflavylium. *J. Phys. Chem. A* **2013**, *117*, 10692−10701.
(20) McClelland, R. A.; Gedge, S. Hydration of the flavylium ion. *J. Am. Chem. Soc.* **1980**, *102*, 5838−5848.
(21) Dangles, O.; Stoeckel, C.; Wigand, M. C.; Brouillard, R. Two very distinct types of anthocyanin complexation: copigmentation and inclusion. *Tetrahedron Lett.* **1992**, *33*, 5227−5230.
(22) Dangles, O.; Wigand, M. C.; Brouillard, R. Anthocyanin anti-copigment effect. *Phytochemistry* **1992**, *31*, 3811−3812.
(23) Fernandes, A.; Sousa, A.; Azevedo, J.; Mateus, N.; Freitas, V. Effect of cyclodextrins on the thermodynamic and kinetic properties of cyanidin-3-*O*-glucoside. *Food Res. Int.* **2013**, *51*, 748−755.
(24) Gomes, R.; Parola, A. J.; Bastkowski, F.; Polkowska, J.; Klaerner, F.-G. Host-guest interactions between molecular clips and multistate systems based on flavylium salts. *J. Am. Chem. Soc.* **2009**, *131*, 8922−8938.
(25) Adolt, R.; Pavlis, J. Age structure and growth of *Dracaena cinnabari* populations on Socotra. *Trees* **2004**, *18*, 43−53.
(26) Cennino Cennini. *Il libbro dell'Arte*; Brunello, F., Ed.; Neri Pozza Ed.e: Vicenza, Italy, 1982; p 44 (Chapter XLIII).
(27) Melo, M. J.; Sousa, M.; Parola, A. J.; de Melo, J. S; Catarino, F.; Marçalo, J.; Pina, F. Identification of 7,4′-dihydroxy-5-methoxyflavylium in "dragon's blood". To be or not to be an anthocyanin. *Chem.−Eur. J.* **2007**, *13*, 1417−1422.
(28) Pina, F.; Melo, M. J.; Santos, H.; Lima, J. C.; Abreu, I.; Ballardini, R.; Maestri, M. Excited state proton transfer in synthetic flavylium salts. 4-Methyl-7-hydroxyflavylium and 4′,7-dihydroxyflavylium. Example of a four level molecular device to invert the population of the excited state. *New J. Chem.* **1998**, 1093−1098.
(29) Oliveira, J.; Petrov, V.; Parola, A. J.; Pina, F.; Azevedo, J.; Teixeira, N.; Bras, N. F.; Fernandes, P. A.; Ramos, M. J.; de Freitas, V. Chemical behavior of methylpyranomalvidin-3-*O*-glucoside in aqueous solution studied by NMR and UV-visible spectroscopy. *J. Phys. Chem. B* **2011**, *115*, 1538−1545.
(30) Cruz, L.; Petrov, V.; Teixeira, N.; Mateus, N.; Pina, F.; de Freitas, V. Establishment of the chemical equilibria of different types of pyranoanthocyanins in aqueous solutions. Evidence for the formation of aggregation in pyranomalvidin-3-*O*-coumaroylglucoside-(+)-catechin. *J. Phys. Chem. B* **2010**, *114*, 13232−13240.
(31) Nave, F.; Petrov, V.; Pina, F.; Teixeira, N.; Mateus, N.; de Freitas, V. Thermodynamic and kinetic properties of a red wine pigment: catechin-(4,8)-malvidin-3-*O*-glucoside. *J. Phys. Chem. B* **2010**, *114*, 13487−13496.
(32) Cherepy, N. J.; Smestad, G. P.; Gratzel, M.; Zhang, J. Z. Ultrafast electron injection: implications for a photoelectrochemical cell utilizing an anthocyanin dye-sensitized TiO_2 nanocrystalline electrode. *J. Phys. Chem. B* **1997**, *101*, 9342−9351.
(33) Tennakone, K.; Kumara, G. R. R. A.; Kumarasinghe, A. R.; Wijayantha, K. G. U.; Sirimanne, P. M. A dye-sensitized nano-porous solid-state photovoltaic cell. *Semicond. Sci. Technol.* **1995**, *10*, 1689−1693.
(34) Calogero, G.; Di Marco, G. Red Sicilian orange and purple eggplant fruits as natural sensitizers for dye-sensitized solar cells. *Sol. Energy Mater. Sol. Cells* **2008**, *92*, 1341−1346.
(35) Calogero, G.; Sinopoli, A.; Citro, I.; Di Marco, G.; Petrov, V.; Diniz, A. M.; Parola, A. J.; Pina, F. Synthetic analogues of anthocyanins as sensitizers for dye-sensitized solar cells. *Photochem. Photobiol. Sci.* **2013**, *12*, 883−894.

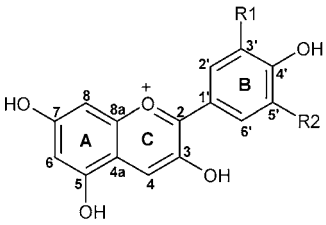

Anthocyanidins	R1	R2
Pelargonidin	H	H
Cyanidin	OH	H
Delphinidin	OH	OH
Peonidin	OCH_3	H
Petunidin	OCH_3	OH
Malvidin	OCH_3	OCH_3

Figure 1. General structure of anthocyanidins (flavylium form).

they are biotransformed into their metabolites, which are absorbed. In the intestinal microbiota, anthocyanins are extensively metabolized, especially by genera and species with enzymes necessary to catalyze these reactions. Dietary polyphenols are substrates for several enzymes located in the small intestine and colon and in the liver (hydrolyzing and conjugating enzymes, phase I and phase II, respectively).[12−15] Therefore, the colon is being considered as an active site for metabolism rather than a simple excretion route and has been receiving much attention from the scientific community.[16] This conversion is often essential for absorption and modulates the biological activity of these dietary compounds, not only due to the direct bioactivity of the products of microbiota metabolism, which is different from that of the parent compounds, but also because of their prebiotic activity in modulating the microbiota composition.[17,18]

PRODUCTS OF COLONIC METABOLISM OF ANTHOCYANINS

Microbiota catabolism results in the production of new phenolic compounds, which may be absorbed and exhibit different bioactivity from that of the parents, and plays an important role in systemic and local health effects.[19] Information regarding the colonic metabolism of anthocyanins is scarce and diffuse, especially because the metabolism of the microbiota is often studied after an intervention with a whole food or beverage, which contains not only anthocyanins but also other phenolic compounds. In addition, animal and human studies comprise an underlying interindividual variability that can hardly be overcome.

Early in vitro studies on the metabolism of anthocyanins by gut microflora have concluded that bacterial metabolism involved the cleavage of glycosidic linkages and breakdown of anthocyanidin heterocycle.[20] Protocatechuic acid was indicated as the major metabolite of gut microflora, but the techniques employed did not allow the identification of other metabolites.[20] This phenolic acid was also the major human metabolite detected in feces after blood orange juice consumption as a cyanidin-3-glucoside source.[21] Keppler et al.[22] have also confirmed the cleavage of the 3-glycosidic linkage and the instability of the anthocyanidin, which is rapidly converted to phenolic acids. Furthermore, O-demethylation of phenolic acids was also shown.[22]

In vitro incubation of phenolic compounds with human gut fecal matter has been a first approach to determine the anthocyanin metabolites formed by microbiota catabolism. Incubation of a red wine extract with a batch of human fecal microbiota resulted in a rapid decline of malvidin-3-glucoside and its acylated forms, but complete degradation of anthocyanins was observed only after 30 h of incubation.[23] The fast catabolism of anthocyanins was attributed to the presence of β-glucosidase activity of the microbiota.[20] The acylation forms of anthocyanins also seem to be degraded easily.[23]

The breaking of the heterocyclic C-ring of anthocyanins and degradation into phloroglucinol derivatives (from A-ring) and benzoic acids (from B-ring) are usually the result of bacterial metabolism.[22] In Sanchez-Patan et al., phloroglucinol was not detected, but instead, the dihydroxylated benzene catechol/pyrocatechol were progressively formed with incubation time. Unlike other studies,[24,25] in the model used by Sanchez-Patan et al.,[23] only an increase in syringic acid was observed, but no changes in protocatechuic and vanillic acids. However, an increase in benzoic acid was observed, which could be indicative of O-demethylation metabolites being extensively dehydroxylated, giving rise to benzoic acid as the final degradation product.

Two phenolic acids and one aldehyde (3-*O*-methylgallic acid, syringic acid, and 2,4,6-trihydroxybenzaldehyde) have also been noted as colonic metabolites of anthocyanins from grapes.[26] The primary phenolic degradation product detected in the incubation of human gut microflora with malvidin-3-glucoside was syringic acid and transitorily gallic acid and pyrogallol.[27] Once again, syringic acid demethylation of the B-ring is proposed to account for gallic acid formation.[27] When other anthocyanins are incubated, the main metabolites found are gallic, syringic, and *p*-coumaric acids.[27]

Moreover, the supplementation of human volunteers with raspberry anthocyanins resulted in the increase of catechol, resorcinol, pyrogallol, 4-hydroxybenzoic acid, 3,4-dihydroxybenzoic acid (protocatechuic acid), tyrosol, 3-(3′-hydroxyphenyl)propionic acid, and 3-(3′,4′-dihydroxyphenyl)-propionic acid.[25] In this study, an in vivo approach was used, and as in other in vivo studies, with the advantage of being closer to what happens in regular human consumption of anthocyanins, but it also has the disadvantage of increasing the confounding factors that may affect and influence anthocyanin metabolism by colonic microflora.

An intervention study performed with red wine, which is a very good source of anthocyanins, revealed significant changes in eight metabolites: 3,5-dihydroxybenzoic acid, 3-*O*-methylgallic acid, *p*-coumaric acid, phenylpropionic acid, protocatechuic acid, vanillic acid, syringic acid, and 4-hydroxy-5-(phenyl)valeric acid.[28] It is important to highlight that red wine has several other phenolic compounds, other than anthocyanins, that can give rise to these products, but the *O*-methyl benzoic acids such as syringic and vanillic acids could arise from methoxylated anthocyanin catabolism[19,20] and protocatechuic acid from cyanidin. *p*-Coumaric acid may also be a product from *p*-coumaroyl-acylated anthocyanins.[29] In addition, alcohol does not seem to affect the performance of the microbial catabolism as there were no changes with red wine and dealcoholized red wine interventions.[28]

A recent paper described the metabolism of cyanidin-3-glucoside in human microbiota-associated rats and determined protocatechuic acid, 2,4,6-trihydroxybenzaldehyde, and 2,4,6-trihydroxybenzoic acid (gallic acid) as the main colonic metabolites.[24] Nevertheless, other metabolites were found but not identified.

In a very recent study that makes use of isotopically labeled cyanidin-3-glucoside (6,8,10,3′,5′-$^{13}C_5$-C3G), the human metabolism and pharmacokinetics of this anthocyanin were studied after an ingestion of 500 mg.[30] It is very interesting

dx.doi.org/10.1021/jf501808a | J. Agric. Food Chem. 2014, 62, 6898−6902

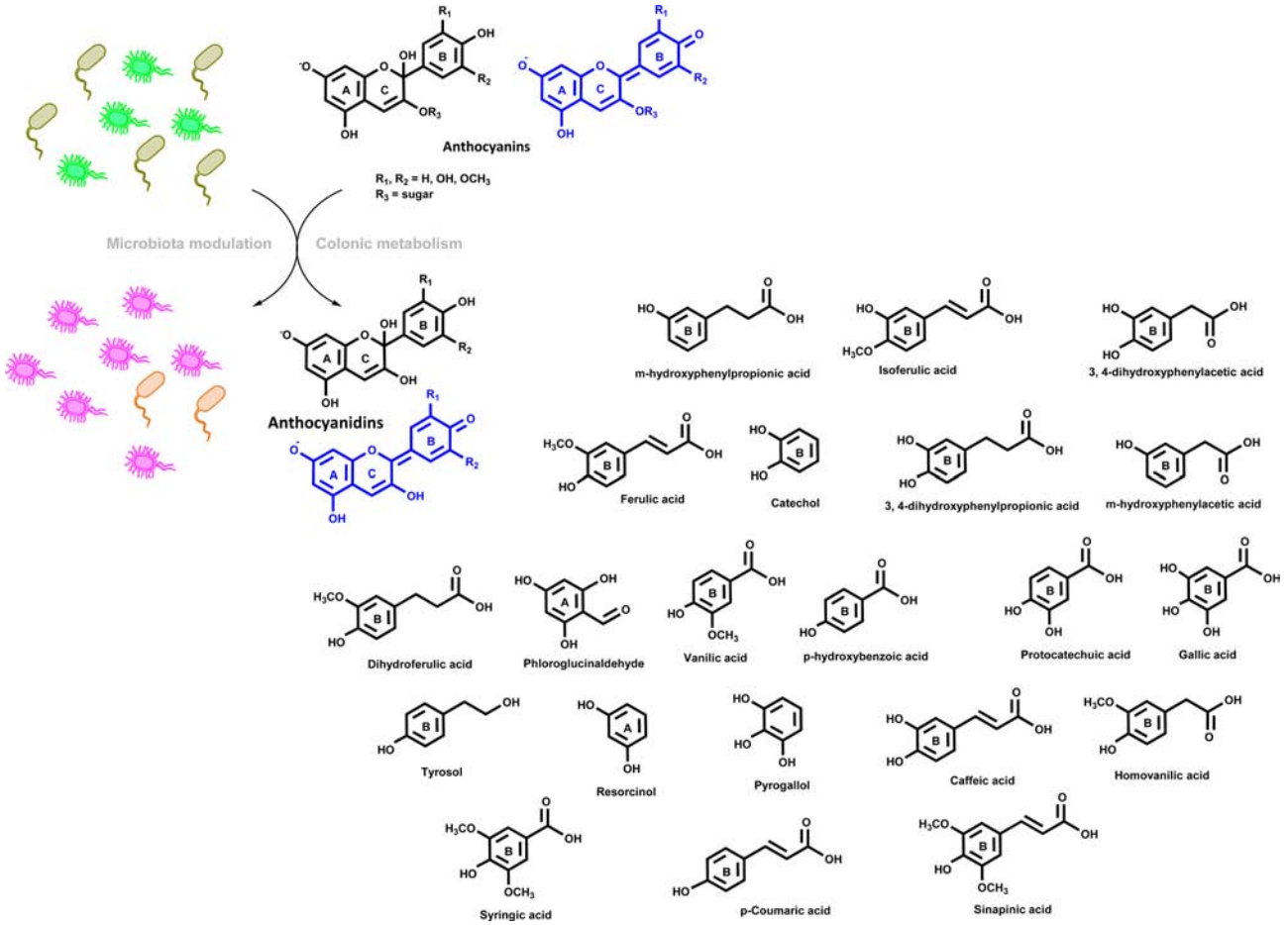

Figure 2. Schematic representation of anthocyanin microbiota modulation and most common detected colonic metabolites. On the one hand, interaction between the microbiota and anthocyanins results in a change of the abundance of certain bacterial groups (prebiotic activity), and, on the other hand, the microbiota is responsible for anthocyanin metabolization giving rise to anthocyanidins and a wide variety of simple phenolics. Anthocyanins are represented, according to the intestine pH range, in their carbinol anionic pseudobase and quinoidal anionic forms.

to observe that the higher ^{13}C-dose recovery was in feces and that the maximal concentration of total metabolites in feces was reached 24 h postconsumption,[30] highlighting the importance of colonic metabolization and degradation on the bioavailability and bioactivity of anthocyanins. A thorough analysis of these metabolites showed that B-ring derived ferulic acid was present at the highest concentrations within the feces, followed by the A-ring derived ferulic acid and protocatechuic acid.[31] Phase II metabolites of protocatechuic acid were also identified in feces by the presence of methyl-3,4-dihydroxybenzoate and methyl vanillate, suggesting that dimethylation is a product of microbial metabolism.[31] The detection of caffeic acid and its methyl metabolite, ferulic acid, within the feces supports the assumption that phenylpropenoic acids arise from cyanidin-3-glucoside as a result of bacterial cleavage of the C-ring in the colon,[31] as has already been proposed.[25,26]

It is worth noting that several factors differ within studies such as the microbiota origin species, the amount of anthocyanins tested in vitro and in vivo, the source of the anthocyanins, or the accuracy and sensitivity of the techniques used to identify the metabolites. Nevertheless, there is an interesting set of studies indicating that anthocyanins are metabolized in the colonic microflora, initially by deglycosylation and in a second phase by degradation into simple phenolic acids. Some of these acids appear to be consistent across studies, such as protocatechuic, vanillic, syringic, gallic, and *p*-coumaric, the latter as a product of acylated anthocyanins (Figure 2). These acidic metabolites are probably absorbed through monocarboxylic acids transporters (MCTs) by the epithelial cells.

■ ANTHOCYANIN MODULATION OF MICROBIOTA

No systematic reviews have been undertaken to assess the role of xenobiotic biotransformation in the colon, in particular with regard to anthocyanins. As described earlier, on the one hand, anthocyanins are subjected to metabolism by microbiota, and, on the other hand, they and/or their metabolites may modulate growth of specific bacteria from the microbiota (Figure 2).

There is evidence that the composition of the human intestinal microbiota has an influence on health and the incidence of disease and that gut health is largely determined by the complex interaction between host and gastrointestinal microbiota.[32]

Putatively beneficial bacteria such as *Bifidobaterium* spp. and *Lactobacillus* spp. are genera which include bacteria that have been observed to contribute to human health at different levels. They have been shown to enhance the gut barrier function, stimulate the host immune system, prevent diarrhea or allergies, participate in the activation of provitamins, and modulate lipid metabolism.[33,34] However, there are other bacterial species associated with negative implications, such as *Clostridium*

dx.doi.org/10.1021/jf501808a | J. Agric. Food Chem. 2014, 62, 6898−6902

difficile, which has been associated with inflammatory bowel disease.[35]

In vitro incubation of malvidin-3-glucoside with fecal slurry enhanced the growth of total bacteria including *Bifidobaterium* spp. and *Lactobacillus* spp.[27] with no effect observed on *Bacteroides* spp. growth. Interestingly, malvidin-3-glucoside mixed with other anthocyanins yielded a synergistic effect regarding the enhancement of growth of the beneficial bacterial group.[27] Gallic acid, one of the microbiota anthocyanin metabolites, was shown to reduce a group of potentially harmful bacteria such as *Clostridium histolyticum*, without negative effect on beneficial bacteria.[27] In addition, it significantly reduced *Bacteroides* spp. growth and enhanced total bacterial number and *Atopobium* spp.[27] Sanchez-Patan et al. also found decreased growth in the *C. histolyticum* group when incubating a red wine extract with human fecal bacteria, but no other changes were found. A similar result in the *C. histolyticum* group has also been described in human volunteers after red wine consumption.[36] It is noteworthy that red wine is a very complex polyphenolic mixture, so it is not possible to attribute these effects directly or solely to anthocyanins.[23]

Supplementation of mice with regular apples and genetically engineered apples for high biosynthesis of anthocyanins resulted in changes in the overall population of bacteria and in the number of some individual species.[37] Animals fed any of the apple-supplemented diet showed a greater number of bacteria than control mice. Moreover, a significant increase in *Bifidobaterium* spp. was observed.[37] Accordingly, a 6 week consumption of a blueberry drink by human volunteers significantly increased *Bifidobaterium* spp.[18]

The microbiota was also studied after an intervention in human volunteers with red wine and dealcoholized red wine. The distribution ratio of different genera within Bacteroidetes and Firmicutes phyla was different between baseline and intake periods,[36] with increased Firmicutes concentration after red wine consumption. At baseline, Bacteroides and Prevotellaceae frequencies were lower than those after the polyphenol intake periods, whereas the *Clostridium* frequency was similar. After the dealcoholized red wine and red wine periods, the Bacteroides, *Clostridium*, and Prevotellaceae frequencies were similar when analyzed by denaturing gradient gel electrophoresis (DGGE).[36]

Major groups of intestinal bacteria possess β-glucosidase activity, including *Bifidobaterium* spp. and *Lactobacillus* spp. They possess the ability to metabolize phenolic compounds during growth, supplying energy to cells and enriching the medium for bacterial growth with the release of glucose. These bacterial groups are associated with beneficial effects in the large intestine including the antimicrobial effect of pathogenic microorganisms by production of short-chain fatty acids, as well as by competition for growth substrate and adhesion sites.[38]

In vitro, animal and human intervention studies with the purpose of studying anthocyanin effect on gut microbiota are few and, due to the diversity of techniques to study microbiota, the different sources of anthocyanins, and the study designs, it is very difficult to relate them and reach a conclusion. In addition, whether anthocyanins exert a direct or indirect effect (mediated by their microbiota biotransformation products) on bacteria growth remains to be clarified. Nevertheless, there is broad agreement that polyphenols, and in particular anthocyanins, have the ability to modulate colonic bacteria growth.[7]

Several data from experimental models and human subjects support the fact that changing the gut microbiota by means of prebiotics and/or probiotics may participate in the control of several parameters involved in the development of metabolic diseases associated with obesity.[1] Further research is required to consolidate the prebiotic effects associated with the consumption of anthocyanin and to understand the mechanisms by which the gut microbiota interact with the host to provide new bases for putative dietary intervention.

The bioactivity of anthocyanins is significantly mediated through their several cellular pathways. With regard to all of the described bioactivities it must be assumed that they are absorbed (are bioavailable) and/or that they affect the microbiota, exerting in these ways their biological effects (as microbiota modulators). It is crucial to emphasize the benefits for bioavailability and/or bioactivity from anthocyanin metabolites that are synthesized by the colonic microbiota.

Finally, the present evidence supports the biotechnology applications of anthocyanins in the human diet and the interest of clinical trials to further assess their biokinetics.

AUTHOR INFORMATION

Corresponding Author

*(C.C.) E-mail: ccalhau@med.up.pt. Phone/fax: +351 22 551 36 24.

Funding

Financial support from Fundação para a Ciência e Tecnologia (FCT) − Fundo Social Europeu, Programa Operacional Potencial Humano da EU (POPH), PTDC/AGR-TEC/2227/2012, SFRH/BPD/75294/2010 and SFRH/BPD/86173/2012, is gratefully acknowledged.

Notes

The authors declare no competing financial interest.

REFERENCES

(1) Cani, P. D.; Delzenne, N. M. The role of the gut microbiota in energy metabolism and metabolic disease. *Curr. Pharm. Des.* **2009**, *15*, 1546−1558.

(2) Armougom, F.; Henry, M.; Vialettes, B.; Raccah, D.; Raoult, D. Monitoring bacterial community of human gut microbiota reveals an increase in *Lactobacillus* in obese patients and Methanogens in anorexic patients. *PLoS One* **2009**, *4*, No. e7125.

(3) Ley, R. E.; Turnbaugh, P. J.; Klein, S.; Gordon, J. I. Microbial ecology: human gut microbes associated with obesity. *Nature* **2006**, *444*, 1022−1023.

(4) Moreira, A. P.; Texeira, T. F.; Ferreira, A. B.; Peluzio, M. C.; Alfenas, R. C. Influence of a high-fat diet on gut microbiota, intestinal permeability and metabolic endotoxaemia. *Br. J. Nutr.* **2012**, *108*, 801−809.

(5) Cani, P. D.; Amar, J.; Iglesias, M. A.; Poggi, M.; Knauf, C.; Bastelica, D.; Neyrinck, A. M.; Fava, F.; Tuohy, K. M.; Chabo, C.; Waget, A.; Delmee, E.; Cousin, B.; Sulpice, T.; Chamontin, B.; Ferrieres, J.; Tanti, J. F.; Gibson, G. R.; Casteilla, L.; Delzenne, N. M.; Alessi, M. C.; Burcelin, R. Metabolic endotoxemia initiates obesity and insulin resistance. *Diabetes* **2007**, *56*, 1761−1772.

(6) Selma, M. V.; Espin, J. C.; Tomas-Barberan, F. A. Interaction between phenolics and gut microbiota: role in human health. *J. Agric. Food Chem.* **2009**, *57*, 6485−6501.

(7) Parkar, S. G.; Trower, T. M.; Stevenson, D. E. Fecal microbial metabolism of polyphenols and its effects on human gut microbiota. *Anaerobe* **2013**, *23*, 12−19.

(8) Rastmanesh, R. High polyphenol, low probiotic diet for weight loss because of intestinal microbiota interaction. *Chem.−-Biol. Interact.* **2011**, *189*, 1−8.

(9) Mazza, G.; Miniati, E. *Anthocyanins in Fruits, Vegetables, and Grains*; CRC Press: Boca Raton, FL, USA, 1993; Chapter 1, pp 6−23.

(10) Francis, F. J. Food colorants: anthocyanins. *Crit. Rev. Food Sci. Nutr.* **1989**, *28*, 273−314.
(11) Andersen, Ø.; Jordheim, M. Basic anthocyanin chemistry and dietary sources. In *Anthocyanins in Health and Disease*, 1st ed.; Wallace, T., Giusti, M., Eds.; CRC Press: New York, 2014; Vol. 1, pp 13−89.
(12) Rice-Evans, C. Flavonoid antioxidants. *Curr. Med. Chem.* **2001**, *8*, 797−807.
(13) Tapiero, H.; Tew, K. D.; Ba, G. N.; Mathe, G. Polyphenols: do they play a role in the prevention of human pathologies? *Biomed. Pharmacother.* **2002**, *56*, 200−207.
(14) Rechner, A. R.; Kuhnle, G.; Bremner, P.; Hubbard, G. P.; Moore, K. P.; Rice-Evans, C. A. The metabolic fate of dietary polyphenols in humans. *Free Radical Biol. Med.* **2002**, *33*, 220−235.
(15) Kay, C. D. Aspects of anthocyanin absorption, metabolism and pharmacokinetics in humans. *Nutr. Res. Rev.* **2006**, *19*, 137−146.
(16) Aura, A.-M. Microbial metabolism of dietary phenolic compounds in the colon. *Phytochem. Rev.* **2008**, *7*, 407−429.
(17) Landete, J. M. Updated knowledge about polyphenols: functions, bioavailability, metabolism, and health. *Crit. Rev. Food Sci. Nutr.* **2012**, *52*, 936−948.
(18) Vendrame, S.; Guglielmetti, S.; Riso, P.; Arioli, S.; Klimis-Zacas, D.; Porrini, M. Six-week consumption of a wild blueberry powder drink increases bifidobacteria in the human gut. *J. Agric. Food Chem.* **2011**, *59*, 12815−12820.
(19) Williamson, G.; Clifford, M. N. Colonic metabolites of berry polyphenols: the missing link to biological activity? *Br. J. Nutr.* **2010**, *104* (Suppl. 3), S48−S66.
(20) Aura, A. M.; Martin-Lopez, P.; O'Leary, K. A.; Williamson, G.; Oksman-Caldentey, K. M.; Poutanen, K.; Santos-Buelga, C. In vitro metabolism of anthocyanins by human gut microflora. *Eur. J. Nutr.* **2005**, *44*, 133−142.
(21) Vitaglione, P.; Donnarumma, G.; Napolitano, A.; Galvano, F.; Gallo, A.; Scalfi, L.; Fogliano, V. Protocatechuic acid is the major human metabolite of cyanidin-glucosides. *J. Nutr.* **2007**, *137*, 2043−2048.
(22) Keppler, K.; Humpf, H. U. Metabolism of anthocyanins and their phenolic degradation products by the intestinal microflora. *Bioorg. Med. Chem.* **2005**, *13*, 5195−5205.
(23) Sanchez-Patan, F.; Cueva, C.; Monagas, M.; Walton, G. E.; Gibson, G. R.; Quintanilla-Lopez, J. E.; Lebron-Aguilar, R.; Martin-Alvarez, P. J.; Moreno-Arribas, M. V.; Bartolome, B. In vitro fermentation of a red wine extract by human gut microbiota: changes in microbial groups and formation of phenolic metabolites. *J. Agric. Food Chem.* **2012**, *60*, 2136−2147.
(24) Hanske, L.; Engst, W.; Loh, G.; Sczesny, S.; Blaut, M.; Braune, A. Contribution of gut bacteria to the metabolism of cyanidin 3-glucoside in human microbiota-associated rats. *Br. J. Nutr.* **2013**, *109*, 1433−1441.
(25) Gonzalez-Barrio, R.; Edwards, C. A.; Crozier, A. Colonic catabolism of ellagitannins, ellagic acid, and raspberry anthocyanins: in vivo and in vitro studies. *Drug Metab. Dispos.* **2011**, *39*, 1680−1688.
(26) Forester, S. C.; Waterhouse, A. L. Identification of Cabernet Sauvignon anthocyanin gut microflora metabolites. *J. Agric. Food Chem.* **2008**, *56*, 9299−9304.
(27) Hidalgo, M.; Oruna-Concha, M. J.; Kolida, S.; Walton, G. E.; Kallithraka, S.; Spencer, J. P.; de Pascual-Teresa, S. Metabolism of anthocyanins by human gut microflora and their influence on gut bacterial growth. *J. Agric. Food Chem.* **2012**, *60*, 3882−3890.
(28) Jimenez-Giron, A.; Queipo-Ortuno, M. I.; Boto-Ordonez, M.; Munoz-Gonzalez, I.; Sanchez-Patan, F.; Monagas, M.; Martin-Alvarez, P. J.; Murri, M.; Tinahones, F. J.; Andres-Lacueva, C.; Bartolome, B.; Moreno-Arribas, M. V. Comparative study of microbial-derived phenolic metabolites in human feces after intake of gin, red wine, and dealcoholized red wine. *J. Agric. Food Chem.* **2013**, *61*, 3909−3915.
(29) Monagas, M.; Bartolome, B.; Gomez-Cordoves, C. Updated knowledge about the presence of phenolic compounds in wine. *Crit. Rev. Food Sci. Nutr.* **2005**, *45*, 85−118.
(30) Czank, C.; Cassidy, A.; Zhang, Q.; Morrison, D. J.; Preston, T.; Kroon, P. A.; Botting, N. P.; Kay, C. D. Human metabolism and elimination of the anthocyanin, cyanidin-3-glucoside: a (13)C-tracer study. *Am. J. Clin. Nutr.* **2013**, *97*, 995−1003.
(31) de Ferrars, R. M.; Czank, C.; Zhang, Q.; Botting, N. P.; Kroon, P. A.; Cassidy, A.; Kay, C. D. The pharmacokinetics of anthocyanins and their metabolites in humans. *Br. J. Pharmacol.* **2014**, DOI: 10.1111/bph.12676.
(32) Sekirov, I.; Russell, S. L.; Antunes, L. C.; Finlay, B. B. Gut microbiota in health and disease. *Physiol. Rev.* **2010**, *90*, 859−904.
(33) Gibson, G. R. Prebiotics as gut microflora management tools. *J. Clin. Gastroenterol.* **2008**, *42* (Suppl. 2), S75−S79.
(34) Burcelin, R.; Garidou, L.; Pomie, C. Immuno-microbiota cross and talk: the new paradigm of metabolic diseases. *Semin. Immunol.* **2012**, *24*, 67−74.
(35) Rastall, R. A.; Gibson, G. R.; Gill, H. S.; Guarner, F.; Klaenhammer, T. R.; Pot, B.; Reid, G.; Rowland, I. R.; Sanders, M. E. Modulation of the microbial ecology of the human colon by probiotics, prebiotics and synbiotics to enhance human health: an overview of enabling science and potential applications. *FEMS Microbiol. Ecol.* **2005**, *52*, 145−152.
(36) Queipo-Ortuno, M. I.; Boto-Ordonez, M.; Murri, M.; Gomez-Zumaquero, J. M.; Clemente-Postigo, M.; Estruch, R.; Cardona Diaz, F.; Andres-Lacueva, C.; Tinahones, F. J. Influence of red wine polyphenols and ethanol on the gut microbiota ecology and biochemical biomarkers. *Am. J. Clin. Nutr.* **2012**, *95*, 1323−1334.
(37) Espley, R. V.; Butts, C. A.; Laing, W. A.; Martell, S.; Smith, H.; McGhie, T. K.; Zhang, J.; Paturi, G.; Hedderley, D.; Bovy, A.; Schouten, H. J.; Putterill, J.; Allan, A. C.; Hellens, R. P. Dietary flavonoids from modified apple reduce inflammation markers and modulate gut microbiota in mice. *J. Nutr.* **2014**, *144*, 146−154.
(38) Gibson, G. R.; Wang, X. Regulatory effects of bifidobacteria on the growth of other colonic bacteria. *J. Appl. Bacteriol.* **1994**, *77*, 412−420.

clarified juice. Concentrated chokeberry juice was a gift from Artemis International (Fort Wayne, IN, USA). Concentration of ACN in chokeberry juice was normalized to 60 nmol Cy-3-glu equiv/mL by diluting with deionized (DI) water prior to storage in 20 mL aliquots at −20 °C until chemical analysis and use in the human trial. The qualitative and quantitative profile of ACNs was not altered during storage at −20 °C for 1 month.

Characterization of Juices. Content of monomeric anthocyanins of each juice was measured by pH differential method.[18] The total polyphenolic content of each juice was analyzed by using the Folin−Ciocalteu assay and reported as gallic acid equivalents.[19] Soluble sugar and pH were measured by portable refractometer (Fisher Scientific, 13-946-21, 0−32 °Brix) and by pH meter (Accument XL15, Fisher Scientific), respectively. The ACN profile of each juice was analyzed by HPLC as described below.

Experimental Design. The human study protocol was approved by the Institutional Review Board of The Ohio State University (IRB#20090058). Thirteen systemically and dentally healthy subjects (as evidenced by clinical attachment levels ≤2 mm and probing depths ≤3 mm and a low DMF (decayed, missing, filled teeth) index) over the age of 20 were recruited for the study. Subjects who had antibiotic therapy or professional cleaning within the previous 3 months, used immunosuppressant medications, bisphosphonates, or steroids, reported pregnancy, or a history of diabetes or HIV were excluded from this study to minimize variations in salivary secretion and oral bacterial profiles.[20,21]

A crossover study design with washout was used to investigate the role of oral microbiota on the metabolism of ACNs in the oral cavity. Subjects were instructed to refrain from consumption of ACN-containing foods, coffee, and tea for 24 h prior to the study. On the day of study, subjects brushed their teeth after awakening, avoided use of antibacterial mouthwash, and did not consume breakfast until arrival at the clinic. Control buccal cells were collected by brushing the left buccal mucosa 10 times with a toothbrush, followed by rinsing with 20 mL of phosphate-buffered saline (PBS), and used to determine baseline ACNs. Subsequently, chokeberry juice (20 mL in preweighed polypropylene tube) was retained and swished around the mouth for 5 min. Samples were not smelled to minimize the effects of smell on salivary production. Chokeberry juice remaining in the tube was measured gravimetrically. The retentate was expectorated and collected along with subsequent oral rinse (20 mL deionized water) in preweighed tubes to determine total amount of juice and saliva expectorated. A new toothbrush was used to collect buccal cells from the right buccal mucosal surface followed by saline rinse as for collection of control buccal cells. Tubes were reweighed to estimate the amount of saliva in retained juice and oral rinse. After a 1 week wash-out period, subjects were asked to follow the same procedures prior to arrival at the clinic, where they received professional oral cleaning to remove the oral bacterial biofilms, followed by rinsing with 15 mL of 0.12% chlorhexidine gluconate (Colgate-Palmolive, New York, NY, USA) for 1 min and followed by a 5 min wash-out period. Subjects retained chokeberry juice in their mouth using the same protocol of the previous week. Control buccal scrapings, retained chokeberry juice, and postjuice buccal scrapings were collected and processed using the same procedures as described above.

To determine the effect of ACN structure on stability and delivery to buccal tissue, juices from chokeberry and grape were assigned to subjects in a randomized crossover design with a 1 week wash-out period between juice treatments. Human subjects (n = 12) were instructed to abstain from consuming ACN-containing foods and beverages after 10 p.m. on the evening before testing. On the day of study, subjects brushed their teeth and consumed breakfast before arrival at clinic. Each subject served as their own internal control. Control buccal cells were collected prior to retention of juice, followed by postretention collection of buccal cells from the opposite cheek as described above. Data from one subject who reported accidental swallowing of a portion of the chokeberry juice were excluded.

Sample Processing. Retained juices and aqueous oral rinse were separately weighed and acidified with 88% formic acid (final concentration = 5% by adding 1.2:20 v/w) within 30 min after sample collection. Both solutions were combined, filtered (0.22 μm pore size), and stored at −20 °C until analysis. Buccal scrapings were centrifuged (130g, 5 min, 4 °C) to separate soluble mucus from buccal cells. Cell pellets were washed three times with 10 mL of cold sodium phosphate buffer (0.1 M, pH 6.0) and centrifuged to separate extracellular ACNs and mucin from buccal cells.[22] Washed cell pellets were resuspended in sodium phosphate buffer and stored at −20 °C. Pooled supernatant containing mucus from each subject also was stored at −20 °C), lyophilized to dryness, resolubilized in 15 mL of 1:1 (v/v) methanol/water for quantification of mucin, and filtered (0.22 μm pore size) for HPLC analysis of ACNs.

ACN Extraction from Buccal Epithelial Cells. Preliminary studies were performed to determine the efficiency of extraction of ACNs from buccal cell pellets. Extraction solvents tested were methanol, acetronitrile, acetone, and 70% acetone. All solvents were acidified with formic acid (5% final concentration) to stabilize ACNs. ACN-rich extracts (15 nmol of Cy-3-glu equivalents in 25 μL of 0.01% HCl solution) from chokeberry and red grape were added to 0.25 mL suspensions of control washed buccal cells isolated from two subjects. Suspensions were sonicated (30 s, ice−water bath) before addition of 0.75 mL of test solvents and frozen (−20 °C) overnight. Samples were thawed, sonicated for 20 min in an ice−water bath, and centrifuged (20800g, 5 min). Supernatant was collected, and the pellet was re-extracted twice. Supernatants for the three extractions were transferred to a preweighed tube, concentrated by evaporation under N_2 (30 min, 37 °C), weighed, and filtered (0.22 μm pore size) prior to HPLC analysis. Recovery was calculated as (amount ACNs extracted/amount ACNs added) × 100%. Recovery using 70% acetone solvent exceeded 84% for all ACNs in chokeberry and red grape juices (data not shown), which was considerably greater than recovery after extraction into the other solvents tested (i.e., 36−51%). The extent of recovery of each ACN was not significantly affected by type of monosaccharide. Therefore, ACNs in all test samples were extracted into acidified 70% acetone for analysis.

HPLC Analysis. The content of ACNs in juices, retentate, mucus, and cell extracts was analyzed by HPLC-PDA-ESI-MS according to previously published methods[17] and reported as Cy-3-glu equivalents. Identification of ACNs was based on retention time (t_R) and $\lambda_{max\text{-}vis}$ and matched molecular weights of parent compounds and daughter fragments with those of available anthocyanin standards, isolated chokeberry anthocyanins, and reported elution profiles for chokeberry[23,24] and red grape.[25−27] The cellular content of ACNs was normalized by DNA content in isolated cell pellets (Quantification of DNA in Buccal Cells). The quantity of ACNs in the mucus layer was normalized per milligram of mucin (Quantification of Mucin).

Separation, identification, and quantification of reported phenolic metabolites were performed using a HPLC-PDA-ESI-MS system[17] with the mobile phase consisting of (A) 0.1% formic acid in water and (B) 0.1% formic acid in acetonitrile. The gradient for the mobile phase was 0−30 min, 0−30% B; 30−31 min, 30−100% B; 31−32 min, 100−0% B; 32−37 min, 0% B. Partial flow from PDA detector was negatively ionized by the mass spectrometer with previously published parameters.[17] Mass spectra were obtained using scan mode (from m/z 50−800 with scan speed of 1000 amu/s) and selective ion monitoring (SIM) mode for PCA, PGA, gallic acid, syringic acid, vanillic acid, and 4-hydroxybenzoic acid at m/z 153, 153, 169, 197, 167, and 137, respectively.

Quantification of DNA in Buccal Cells. DNA in buccal cell aliquots was determined by diphenylamine (DPA) assay. The purpose of this test was to provide a basis for normalizing ACNs per unit buccal cells and allow for comparisons among the samples given that the number of cells collected for each buccal scrapping varies.

Briefly, 1 volume of cold acetaldehyde (0.16% in DI water) was mixed with 5 volumes of perchloric acid (20% v/v in DI water) to prepare the reagent. Cell suspensions were sonicated (20 min in ice bath) and aliquoted (40 μL) into a 96-well plate before addition of 60 μL of acetaldehyde solution. After mixing, 100 μL of DPA (4% in glacial acetic acid) was added to wells and the plate was incubated at 37 °C for 24 h. Absorbance was measured at 595 nm (corrected by subtraction of absorbance at a reference wavelength of 700 nm).

Corrected absorbance was compared to a five-point curve using DNA from herring sperm as standard.

Quantification of Mucin. Mucin concentrations in buccal washings were determined by using a modification of the previously described[29] Alcian Blue assay.[30] Aliquots of supernatant were incubated for 30 min in a 1:1 (v/v) of 1% solution of Alcian Blue in 50 mM sodium acetate buffer containing 25 mM $MgCl_2$, pH 5.8, under constant agitation at room temperature. Samples were centrifuged (705*g*, 20 min), and supernatant was discarded. The pellets were washed twice with 1 mL of 40% (v/v) ethanol in 50 mM sodium acetate buffer containing 25 mM $MgCl_2$, pH 5.8, briefly vortexed, and incubated for 5 min before centrifugation (705*g*, 20 min); supernatant was discarded. Mucin−dye complexes were dissociated by the addition of 1 mL of dioctyl sulfosuccinate solution (1:90 w/v in DI water) followed by brief mixing and ultrasonication at 40 W for 10 s with a VibraCellTM (Sonics & Materials, Danbury, CT, USA). Samples were centrifuged (705*g*, 1 min) to eliminate the foam generated during sonication. The absorbance of the dye was determined spectrophotometrically at 605 nm and compared to a five-point standard curve using known concentrations of mucin from bovine submaxillary glands as standard. This method does not distinguish larger (MG1) and smaller (MG2) mucins.

Statistical Analysis. Each sample (retained juices, oral washes, and washed buccal cells) collected and prepared from each subject was aliquoted for a minimum of three independent analyses. Statistical analysis was performed using SPSS release 19.0 for Windows (SPSS Inc., Chicago, IL, USA). Mixed-model analysis of ACN structure (fixed factor) and subject (random factor) with Bonferoni's adjustment of mean comparison was used. Pearson's product moment correlation analysis was used to determine correlation between salivary secretion and extent of degradation of ACNs. Repeated-measures ANOVA was used to evaluate the effect of inhibition of oral microbiota on reduction of ACN loss in the oral cavity. Independent-samples *t* test was used to compare (1) extent of ACN association with mucus and buccal cells between chokeberry and red grape juices and (2) abundance (%) of each ACN between samples, that is, juice, retained juice, mucus-bound, and buccal cell-associated fractions. Differences were considered significant at $P < 0.05$ unless indicated otherwise.

RESULTS

Characterization of Chokeberry and Red Grape Juices. Red grape and chokeberry were chosen because of their distinctive anthocyanin profiles, which were confirmed and monitored by HPLC-PDA-ESI-MS. Characteristics of each juice are listed in Table 1. Chokeberry juice contained four ACNs differing in the type of monosaccharides conjugated to the C3 position of the Cy aglycone. This material was chosen to allow for comparisons of anthocyanin structures with the same aglycone but different sugar substitutions. Red grape juice contained different anthocyanidins with each conjugated at the C3 position to glucose. This material was chosen to allow for evaluation of the impact of the type of aglycone, as it provides different aglycone structures, all with the same glycosylation pattern (just one glucose). ACN concentration in red grape juice was slightly less than that in chokeberry. Although the content of phenolic compounds and the pH for the two juices were comparable, red grape juice contained higher sugar content than chokeberry juice.

Metabolism of ACN in the Oral Cavity. Thirteen subjects (9 females, 4 males; ages 32.8 ± 9.5 years, range = 24−50 years; and body mass index (BMI) = 22.3 ± 3.1) were recruited for oral retention of chokeberry and red grape juices. Mean losses of total ACNs during the 5 min retention in the mouth were 12.5 ± 1.6% (range = 6.1−25.2%) and 15.3 ± 1.8% (range = 7.9−30.5%) for chokeberry and red grape juices, respectively. The loss of Cy-3-xyl was significantly ($P < 0.05$) greater than that of Cy-3-gal and Cy-3-arabinose in chokeberry juice (Figure 1A). Losses of Dp- and Pt-glucosides exceeded those of Cy-, Pn-, and Mv-glucosides during oral retention of red grape, although only the loss of Dp-3-glu was significantly greater than that of the other anthocyanidins ($P < 0.05$) (Figure 1B).

Table 1. Characteristics of Chokeberry and Red Grape Juices[a]

	chokeberry juice	red grape juice
monomeric ACN (nmol Cy-3-glu equiv/mL)	64.1 ± 1.4	52.9 ± 2.2
ACN composition (% of total ACN)	Cy-3-gal, 58.1 ± 1.1	Dp-3-glu, 9.3 ± 0.9
	Cy-3-glu, 3.8 ± 0.2	Cy-3-glu, 12.5 ± 0.1
	Cy-3-arab, 26.7 ± 0.2	Pt-3-glu, 8.0 ± 0.1
	Cy-3-xyl, 11.3 ± 1.0	Pn-3-glu, 42.2 ± 0.8
		Mv-3-glu, 28.1 ± 0.1
phenolic compounds (mg gallic acid equiv/mL)	272.4 ± 17.4	279.5 ± 7.8
pH	3.75	3.89
sugar (°Brix)	0.4 ± 0.2	19.6 ± 0.2

[a]Data are the mean ± SD of three independent analyses.

Microbial-Mediated Metabolism of ACN. Loss of ACNs during oral retention decreased in 8 of 10 individuals following treatment to reduce bacterial load (matched-pair analysis; Figure 2). The antimicrobial treatment also significantly decreased the mean loss of total ACNs in chokeberry juice from 9.57 ± 0.64 to 8.11 ± 0.77% ($P = 0.036$), supporting the likelihood that the observed loss was in part contributed by microbial activity during the 5 min retention. The extent of loss of ACNs was dependent on structure, with Cy-3-Glu and Cy-3-Gal demonstrating significantly greater loss in the presence of bacteria ($P < 0.01$, repeated-measured ANOVA, Figure 3).

Delivery of ACN to Mucus and Buccal Epithelium. Buccal scrapings were fractionated into mucus and epithelial cells to determine the relative distribution of ACNs delivered to the surface of this oral tissue. Greater than 97% of chokeberry ACNs in the buccal scraping were associated with mucus. The relative amounts of Cy-3-glu and Cy-3-arab in the mucus layer were significantly ($P < 0.01$) greater than that of Cy-3-xyl (Figure 4A). The relative amount of Cy-3-glu in washed buccal epithelial cells was significantly ($P < 0.05$) greater than those of the other Cy-3-monosaccharides (Figure 4B). The amount of red grape ACN associated with buccal mucus fraction was >98% of total scraping ACN after oral retention of the juice for 5 min. ACNs associated with mucus were significantly ($P < 0.001$) affected by anthocyanidin structure. Dp-3-glu was not detected in the mucus fraction, and the relative amount of Pt-3-glu was lower ($P < 0.05$) than those of Cy-, Pn-, and Mv-3-glucosides (Figure 5A). Dp- and Pt-3-glu were detected in the washed buccal cell fraction, although the relative amounts were lower than those of Cy-, Pn-, and Mv-3-glucosides ($P = 0.09$) (Figure 5B).

The amount of mucus-associated ACNs from red grape juice (Figure 5) was significantly less than that from chokeberry (Figure 4) (50.6 ± 11.1 vs 139.4 ± 18.5 μg ACN (mg mucin)$^{-1}$ (mg specific ACN intake)$^{-1}$, respectively; $P = 0.001$). Similarly, the total amount of ACNs from red grape juice that was present

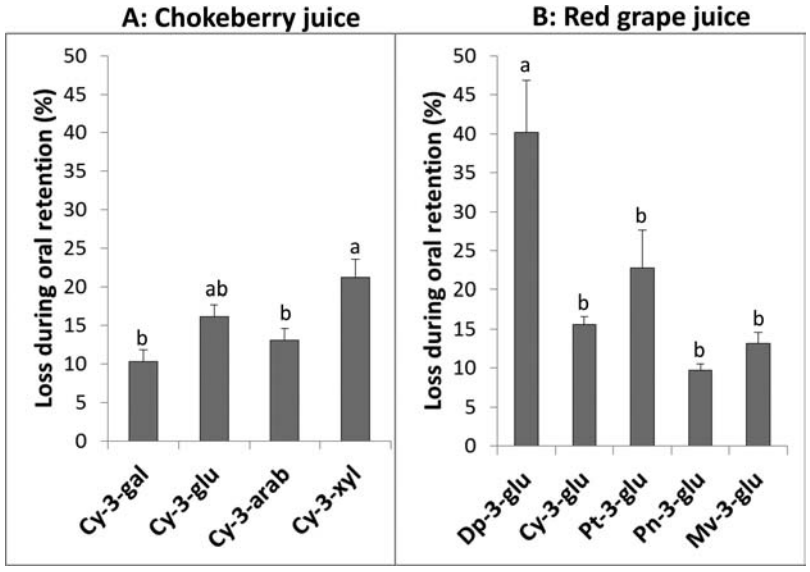

Figure 1. Loss of ACN during 5 min of retention of chokeberry (A) and red grape (B) juices in the oral cavity. Data are the mean ± SEM for 12 and 13 participants for chokeberry juice and red grape juice, respectively. Columns with different letters are significantly different ($P < 0.05$, two-sample t test).

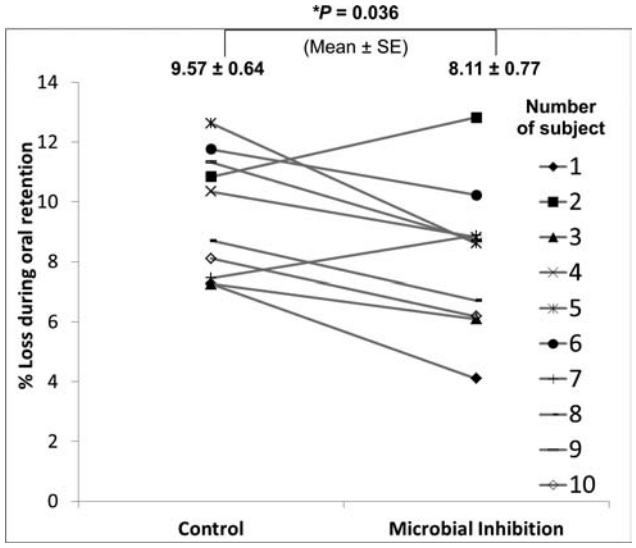

Figure 2. Extent of loss of total ACN in chokeberry juice during retention in the oral cavity was significantly decreased after removal of plaque and rinsing with antibacterial mouthwash. Matched-pair analysis and lines represent change in total chokeberry ACN in the oral cavity before and after removal of bacterial biofilms. The asterisk (∗) denotes significant ($P < 0.05$) difference between microbe-rich and microbe-depleted environments of 10 subjects.

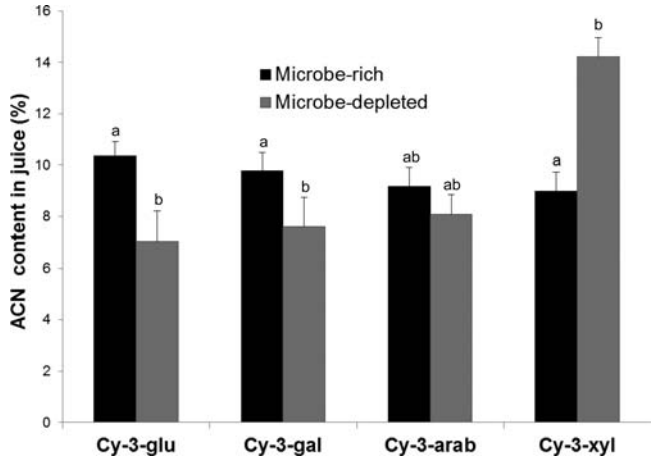

Figure 3. Degradation of ACN following treatment to reduce oral bacterial load. Data are the mean ± SEM for 10 subjects. Different letters above bars indicate that means differ significantly ($P < 0.05$).

in washed buccal cells was less than that after retention of chokeberry juice in the mouth for 5 min (2.16 ± 0.64 vs 13.5 ± 2.3 μg ACN (mg DNA)$^{-1}$ (mg specific ACN intake)$^{-1}$, respectively ($P = 0.001$). Moreover, comparison within the same subjects showed lesser relative amounts of red grape ACN in both mucus-associated and cellular fractions ($n = 5$ and 9, respectively).

To assess changes in the ACN profile of chokeberry and red grape juices during oral retention and delivery to the buccal surface, relative abundances of each ACN (i.e., percent area under curve at 520 nm) in juice, after retention in the mouth, and associated with buccal mucus and epithelium are compared in Figure 6. Notably, increases of relative abundance of Cy-3-arab (by 70%, $P < 0.001$) and Cy-3-glu (by 330%, $P < 0.001$), as well as decreases in Cy-3-gal (by 30%, $P < 0.001$) and Cy-3-xyl (by50%, $P < 0.005$), were observed in buccal cells compared to intact chokeberry juice (Figure 6A). Decreased relative amounts of Dp-3-glu (by 80%, $P < 0.001$) and Pt-3-glu (by 63%, $P < 0.005$) were coupled with increased relative amounts of Pn-3-glu (by 30%, $P < 0.001$) in buccal cells compared to red grape juice (Figure 6B).

Because protocatechuic acid (PCA) and cyanidin aglycone were recently reported to be present in the saliva of several subjects after oral retention of black raspberry juice for 3 min,[31] we examined the juice and cell extracts for the presence of possible metabolites before and after oral retention. HPLC chromatograms (250−600 nm) of juices and cell extract before and after retention were compared. Phloroglucinal aldehyde (PGA) was not found in any samples, which may be due to instability of aldehyde. PCA could not be quantified in retained chokeberry juice due to coelution with other compounds.

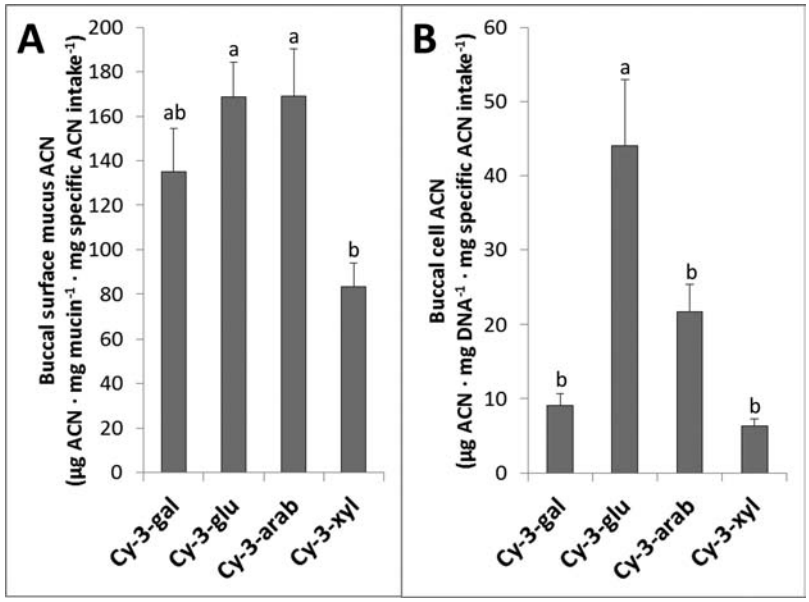

Figure 4. Adherence of chokeberry cyanidins to buccal surface mucus (A) and delivery to buccal epithelial cells (B). Data are the mean ± SEM for 8 subjects (A) and 12 subjects (B), respectively. Different letters above bars indicate that means differ significantly ($P < 0.05$).

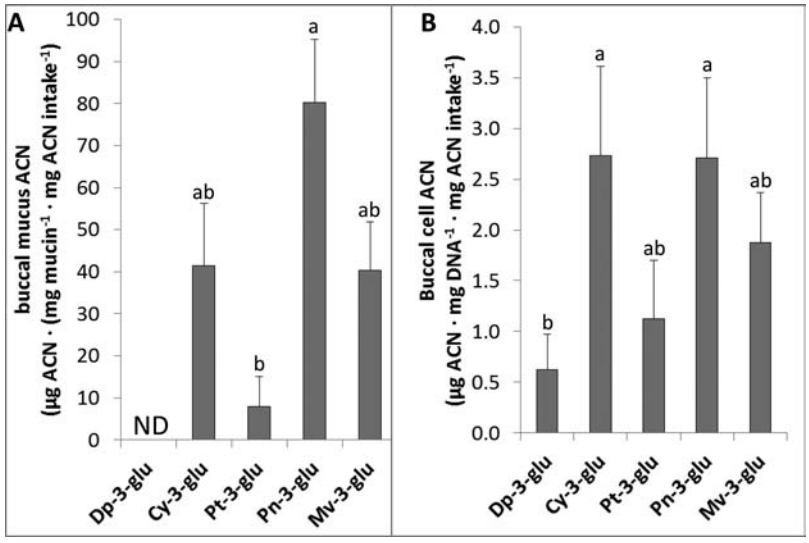

Figure 5. Adherence of ACN to buccal mucus (A) and delivery to epithelium (B) during retention of red grape juice in the oral cavity. Data are the means ± SEM for 8 subjects (A) and 12 subjects (B). Different letters above error bars indicate that means are significantly different ($P < 0.05$, A; $P = 0.09$, B). ND, not detected.

Cyanidin aglycone and PCA also were not detected in buccal cell extracts collected from 11 subjects after retention of chokeberry juice rinse (limits of detection for cyanidin aglycone and PCA are 2.0 and 3.6 ng/mL, respectively). Similarly, there was no detectable gallic acid, PCA, vanillic acid, or syringic acid, compounds that have been reported as products of cleaved B-ring of Dp, Cy, Pn, and Mv, respectively,[28,32−34,35] in either postrinse red grape juice or buccal cell extracts (limits of detection for gallic acid, vanillic acid, and syringic acid were 2.0, 2.5, and 3.3 ng/mL, respectively).

DISCUSSION

ACN-rich fruits and extracts have been shown to possess chemopreventive and chemotherapeutic activities in oral cell lines,[11,32] hamster buccal tissue,[10] rat esophagous,[36] and the human oral cavity.[13,14] This efficacy of ACN has been reported to be dependent on chemical structure.[37,38] It is also known that ACNs are degraded in the gastrointestinal (GI) tract[32,39,40] and the oral cavity.[17,31] An understanding on the effect of ACN structure on its relative stability, types of metabolites produced in the oral cavity, and availability to oral tissues is expected to provide insights for dietary recommendations and the strategic formulation of ACN-containing foods, beverages, confectionaries, and muco-adhesive gels for the promotion of oral health. We recently showed that the extent of biological and chemical degradation of ACNs in saliva is dependent in part on their chemical structure.[17] More specifically, Dp- and Pt-glycosides were degraded to a greater extent than Cy-, Pn-, and Mv-glycosides during ex vivo incubation in saliva. In the present study, we investigated the in vivo stability of ACN in the oral cavity and the levels of these compounds in buccal mucus and epithelial cells in the same human subjects who participated in

dx.doi.org/10.1021/jf405180k | J. Agric. Food Chem. 2014, 62, 6903−6910

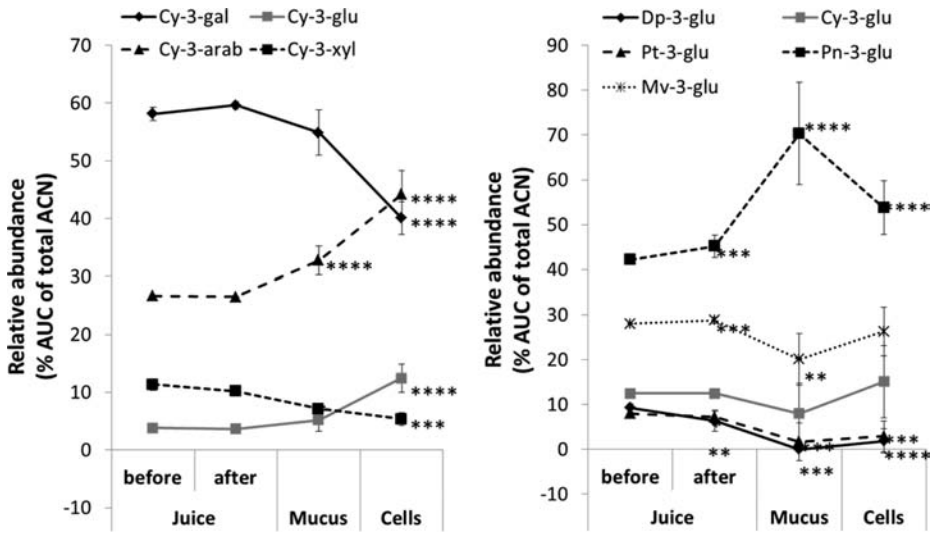

Figure 6. Change of ACN profile of ACN in chokeberry (A) and red grape (B) juices during oral retention and delivery to the buccal surface. Data are the mean ± SD for ≥8 subjects. Asterisks denote statistical difference compared to juice before retention at $P < 0.05$ (*), < 0.01 (**), < 0.005 (***), and <0.001 (****).

the earlier ex vivo study.[17] Loss of endogenous ACN from juice during brief retention in the oral cavity was used as a surrogate for metabolism in the present study. Because this loss may be attributable to spontaneous degradation, metabolism by oral microbiota,[17] adsorption to teeth and mucus,[41] and uptake by epithelial tissues,[31] the effect of each of these parameters was measured.

The extent of in vivo loss of chokeberry and red grape ACNs was affected by their structures (Figure 1B). The relative amount of Cy-3-xyl in chokeberry juice decreased during oral retention (Figure 1A), and this loss could not be attributable to selective binding to mucus (Figure 4A), metabolism by bacteria (Figure 3), or uptake by buccal epithelium (Figure 4B). Bermudez-Soto et al. reported that Cy-3-xyloside was less stable than the other Cy-3-glycosides during in vitro digestion of chokeberry juice.[42] Loss of Cy-3-gal, on the other hand, appeared to be due to microbial degradation and binding to mucus.

The preferential loss of Dp-3-glu from red grape juice during oral retention was similar to that during ex vivo incubation in saliva.[17] Our results are also in agreement with the report that glycosides of Dp, but not those of Pt, Cy, Pn, or Mv, in Concord grape juice were preferentially lost from the mouth to the ileum of ileostomy subjects.[43] However, the extent of loss could not be attributable to mucus binding (Figure 5A) or epithelial cell uptake (Figure 5B), leading us to speculate that microbial degradation or other causes may be responsible for this observation. The amount of saliva secreted during oral retention of red grape juice significantly exceeded that from subjects during retention of chokeberry juice (data not shown). We suspect that this was due to the higher concentration of simple sugars in the red grape juice (Table 1). Losses of Dp-3-glu and Pt-3-glu during 5 min of retention of red grape juice in the oral cavity were significantly ($P < 0.05$) correlated with amount of secreted saliva (data not shown). Enhanced salivary flow is associated with increased concentrations of sodium and bicarbonate ions in saliva.[44] We have shown that the presence of inorganic constituents, including bicarbonate, in artificial saliva resulted in the preferential degradation of Dp and Pt.[17]

We recently reported that microbial activity was a major contributor of ex vivo degradation of ACNs in saliva at 37 °C.[17] To evaluate whether oral microbiota contribute to the in vivo metabolism of ACNs in the oral cavity during a 5 min oral retention of chokeberry juice, the extent of loss of ACNs was compared in individual subjects before and after extensive oral disinfection (dental prophylaxis and antibacterial mouth rinse). This method has been shown to reduce the total bacterial load in the oral cavity significantly.[3] Because oral bacteria exhibit significant interindividual variability, a crossover study design was used to examine the effects of bacteria on loss of ACN during retention of juice in the oral cavity. The intervention resulted in a notable inhibition (ca. 15%) of ACN loss during the brief period of retention of juice in the oral cavity (Figure 3), suggesting that oral bacteria play a vital role in the metabolism of ACNs and may be a source of increasing availability of bioactive compounds to the host tissues.

We investigated whether there was preferential delivery of specific ACNs to buccal cells, because squamous cell carcinomas originate in this anatomical location[45] and because ACNs from black raspberries have been shown to inhibit oral cancer in hamsters[12] and human buccal lesions.[13,14] Chokeberry juice was used to investigate the effect of the type of conjugated monosaccharide on delivery of ACNs to the buccal epithelium. Strikingly, Cy-3-glu was preferentially enriched in the buccal epithelium (Figures 4B and 6A), suggesting preferential binding or uptake. When suspensions of buccal epithelial cells from two subjects were spiked with ACN-rich extract from chokeberry and incubated at 0 °C for 5 min, the relative amounts of the four Cy-glycosides were not significantly altered. This suggests that the increased bioavailability of Cy-3-glu compared to that of the other Cy-3-glycosides in chokeberry juice was temperature dependent and likely to be enzyme mediated. It has been reported that transport of Cy-3-glu by Caco-2 human intestinal cells exceeds that of Cy-3-gal.[46] The authors suggested that this difference was mediated by the specificity of the sodium-dependent glucose cotransporter-1 (SGLT1).[31] SGLT1 has also been detected in primary human buccal epithelial cells.[31,47] The possibility that Cy-3-glu is preferentially bound or taken up into

buccal epithelium during the brief retention of chokeberry juice in the oral cavity by SGLT1 and/or other unidentified transporters warrants further investigation.

Red grape juice allowed us to assess the effect of anthocyanidin structure on the bioavailability of ACNs to the buccal epithelium as it contains five distinct anthocyanidin-3-glucose compounds. Preferential loss of Dp-3-glu and Pt-3-glu in expectorated juice (Figure 1B) was coupled with lesser amounts of these ACN associated with both buccal mucus and buccal cells (Figure 5). These data suggest that the instability of Dp and Pt in the oral cavity lessens their accessibility to the buccal epithelial cells. Similarly, Stalmach et al. reported that loss of Dp-glycosides in Concord grape juice was greater than that of Pt-, Cy-, Pn-, and Mv-glycosides during passage from the mouth to the ileum of human ileostomists.[43] Delivery of ACNs to the washed buccal cell fraction during retention of red grape juice in the oral cavity was less than that for chokeberry juice (Figures 4 and 5). This difference appears to be due to the lower amount of ACN in the red grape juice (Table 1) and the greater instability of Dp-3-glu and Pt-3-glu.

Genistin (genistein-7-*O*-glucoside) is taken up by the SSC-9 human oral epithelial cell line and hydrolyzed to genistein aglycone.[48] It is possible that once ACNs are taken up by buccal epithelial cells, they are metabolized to anthocyanin aglycones that spontaneously degrade to phenolic compounds. Other investigators have reported that the degradation product PCA was detected in saliva from 2 of 10 subjects 4 h after an oral rinse with black raspberry for 3 min.[31] We did not detect ACN aglycone, PCA, PGA, or other phenolic products of ACN B-ring in the buccal cell extracts from 11 subjects immediately after the 5 min retention of chokeberry or red grape juices in the oral cavity. It appears that the generation of bioactive metabolites of ACNs may require increased duration of ACNs in the oral cavity. The possibility that there is time-dependent release of ACNs from mucin with some of the compounds becoming available to the buccal epithelium for uptake and metabolism merits investigation.

In summary, the present study provides novel insights on the effect of ACN structure on oral stability and delivery to the buccal mucosa. The results demonstrate that ACNs can be degraded in the human oral cavity and that the loss is partially due to microbial activity. These results also suggest that the structure of ACNs can affect oral stability and delivery to the buccal surface. Cy-3-glu appeared to be preferentially transferred to the buccal epithelium compared to other Cy-3-glycosides. Instability of Dp-3-glu and Pt-3-glu in the oral cavity resulted in association of lesser amounts of the ACNs with the buccal epithelium. The instability appeared to be associated with the amount of salivary secretion. These in vivo results with ACNs in a food matrix generally largely agree with the ex vivo stability and metabolism of ACNs in saliva.[17] The source of ACNs merits consideration for development of ACN-containing products for promoting oral health. The relationship between oral metabolism of ACNs and efficacy, for example, anti-inflammatory activity, as well as the role of metabolites of ACNs, warrants further investigation.

AUTHOR INFORMATION

Corresponding Author

*(M.M.G.) Phone: (614) 247-8016. Fax: (614) 292-0218. E-mail: giusti.6@osu.edu.

Funding

This research was supported by the Ohio Agricultural Research and Development Center (OARDC).

Notes

The authors declare no competing financial interest.

ACKNOWLEDGMENTS

We appreciate help from Maria Moreno-Cruz on clinical screening of subjects. We thank Enzyme Development Corp. (New York, NY, USA) for donation of food-grade pectinase and Artemis International (Fort Wayne, IN, USA) for the gift of concentrated chokeberry juice.

ABBREVIATIONS USED

ACN, anthocyanin/anthocyanidin; CDC, Centers for Disease Control and Prevention; Cy, cyanidin; DMF, decayed, missing, filled teeth; Dp, delphinidin; DPA, diphenylamine assay; GI, gastrointestinal; Mv, malvidin; PCA, protocatechuic acid; PGA, phloroglucinal acid; Pn, peonidin; Pt, petunidin; SGLT1, sodium-dependent glucose cotransporter-1; WHO, World Health Organization

REFERENCES

(1) Jemal, A.; Siegel, R.; Xu, J.; Ward, E. Cancer statistics, 2010. *CA Cancer J. Clin.* **2010**, *60*, 277−300.

(2) Petersen, P. E.; Bourgeois, D.; Ogawa, H.; Estupinan-Day, S.; Ndiaye, C. The global burden of oral diseases and risks to oral health. *Bull. World Health Organ.* **2005**, *83*, 661−669.

(3) Sischo, L.; Broder, H. L. Oral health-related quality of life: what, why, how, and future implications. *J. Dent. Res.* **2011**, *90*, 1264−1270.

(4) Eke, P. I.; Dye, B. A.; Wei, L.; Thornton-Evans, G. O.; Genco, R. J. Prevalence of periodontitis in adults in the United States: 2009 and 2010. *J. Dent. Res.* **2012**, *91*, 914−920.

(5) Tomar, S. L.; Cohen, L. K. Attributes of an ideal oral health care system. *J. Public Health Dent.* **2010**, *70* (Suppl. 1), S6−14.

(6) Sakagami, H.; Oi, T.; Satoh, K. Prevention of oral diseases by polyphenols (review). *In Vivo* **1999**, *13*, 155−171.

(7) Block, G.; Patterson, B.; Subar, A. Fruit, vegetables, and cancer prevention: a review of the epidemiological evidence. *Nutr. Cancer.* **1992**, *18* (1), 1−29.

(8) Saman, D. M. A review of the epidemiology of oral and pharyngeal carcinoma: update. *Head Neck Oncol.* **2012**, *4*, 1−7.

(9) Petti, S.; Scully, C. Polyphenols, oral health and disease: a review. *J. Dent.* **2009**, *37*, 413−423.

(10) Zhang, Y.; Seeram, N.; Lee, R.; Feng, L.; Heber, D. Isolation and identification of strawberry phenolics with antioxidant and human cancer cell antiproliferative properties. *J. Agric. Food Chem.* **2008**, *56*, 670−675.

(11) Seeram, N. P.; Adams, L. S.; Zhang, Y.; Lee, R.; Sand, D.; Scheuller, H. S.; Heber, D. Blackberry, black raspberry, blueberry, cranberry, red raspberry, and strawberry extracts inhibit growth and stimulate apoptosis of human cancer cells in vitro. *J. Agric. Food Chem.* **2006**, *54*, 9329−9339.

(12) Casto, B. C.; Kresty, L. A.; Kraly, C. L.; Pearl, D. K.; Knobloch, T. J.; Schut, H. A.; Stoner, G. D.; Mallery, S. R.; Weghorst, C. M. Chemoprevention of oral cancer by black raspberries. *Anticancer Res.* **2002**, *22*, 4005−4015.

(13) Shumway, B. S.; Kresty, L. A.; Larsen, P. E.; Zwick, J. C.; Lu, B.; Fields, H. W.; Mumper, R. J.; Stoner, G. D.; Mallery, S. R. Effects of a topically applied bioadhesive berry gel on loss of heterozygosity indices in premalignant oral lesions. *Clin. Cancer Res.* **2008**, *14*, 2421−2430.

(14) Mallery, S. R.; Zwick, J. C.; Pei, P.; Tong, M.; Larsen, P. E.; Shumway, B. S.; Lu, B.; Fields, H. W.; Mumper, R. J.; Stoner, G. D. Topical application of a bioadhesive black raspberry gel modulates

gene expression and reduces cyclooxygenase 2 protein in human premalignant oral lesions. *Cancer Res.* **2008**, *68*, 4945−4957.
(15) Song, J.; Li, X.; Zeng, L.; Liu, H.; Xie, M. Determination of cyanidin-3-glucoside (red kernel food colour) in beverages by high performance liquid chromatography and a study of its degradation by quadruple time-of-flight mass spectrometry. *Food Addit. Contam.* **2011**, *28*, 1645−1656.
(16) Andersen, Ø.M.; Jordheim, M. Basic anthocyanin chemistry and dietary sources. Chapter 2. In *Anthocyanins in Health and Disease*; Wallace, T. C., Giusti, M. M., Eds.; Taylor and Francis Group, CRC Press: Boca Raton, FL, USA, 2014; pp 13−90.
(17) Kamonpatana, K.; Giusti, M. M.; Chitchumroonchokchai, C.; MorenoCruz, M.; Riedl, K. M.; Kumar, P.; Failla, M. L. Susceptibility of anthocyanins to ex vivo degradation in human saliva. *Food Chem.* **2012**, *135*, 738−747.
(18) Giusti, M. M.; Wrolstad, R. E. Characterization and measurement of anthocyanins by UV-vis spectroscopy. In *Current Protocols in Food Analytical Chemistry*; Wrolstad, R. E., Acree, T. E., An, H., Decker, E. A., Penner, M. H., Reid, D. S., Schwartz, S. J., Shoemaker, C. F., Sporns, P., Eds.; Wiley: Hoboken, NJ, USA, 2001; Vol. 1, pp F1.2.1−1.2.13.
(19) Waterhouse, A. L. Determination of total phenolics. In *Handbook of Food Analytical Chemistry*, 1st ed.; Wrolstad, R. E., Acree, T. E., Decker, E. A., Penner, M. H., Reid, D. S., Schwartz, S. J., Shoemaker, C. F., Smith, D. M., Sporns, P., Eds.; Wiley: Hoboken, NJ, USA, 2005; pp I1.1.1−I1.1.8.
(20) Socransky, S. S.; Haffajee, A. D. Periodontal microbial ecology. *Periodontol. 2000* **2005**, *38*, 135−187.
(21) Dawes, C. Physiological factors affecting salivary flow rate, oral sugar clearance, and the sensation of dry mouth in man. *J. Dent. Res.* **1987**, *66*, 648−653.
(22) Sakanaka, S.; Aizawa, M.; Kim, M.; Yamamoto, T. Inhibitory effects of green tea polyphenols on growth and cellular adherence of an oral bacterium, *Porphyromonas gingivalis*. *Biosci., Biotechnol., Biochem.* **1996**, *60*, 745−749.
(23) Wu, X.; Gu, L.; Prior, R. L.; McKay, S. Characterization of anthocyanins and proanthocyanidins in some cultivars of *Ribes*, *Aronia*, and *Sambucus* and their antioxidant capacity. *J. Agric. Food Chem.* **2004**, *52*, 7846−7856.
(24) Zheng, W.; Wang, S. Y. Oxygen radical absorbing capacity of phenolics in blueberries, cranberries, chokeberries, and lingonberries. *J. Agric. Food Chem.* **2003**, *51*, 502−509.
(25) Cai, H.; Marczylo, T. H.; Teller, N.; Brown, K.; Steward, W. P.; Marko, D.; Gescher, A. J. Anthocyanin-rich red grape extract impedes adenoma development in the apc(min) mouse: pharmacodynamic changes and anthocyanin levels in the murine biophase. *Eur. J. Cancer* **2010**, *46*, 811−817.
(26) Frank, T.; Netzel, M.; Strass, G.; Bitsch, R.; Bitsch, I. Bioavailability of anthocyanidin-3-glucosides following consumption of red wine and red grape juice. *Can. J. Physiol.* **2003**, *81*, 423−435.
(27) Castillo-Munoz, N.; Fernandez-Gonzalez, M.; Gomez-Alonso, S.; Garcia-Romero, E.; Hermosin-Gutierrez, I. Red-color related phenolic composition of Garnacha Tintorera (*Vitis vinifera* L.) grapes and red wines. *J. Agric. Food Chem.* **2009**, *57*, 7883−7891.
(28) Forester, S. C.; Waterhouse, A. L. Identification of cabernet sauvignon anthocyanin gut microflora metabolites. *J. Agric. Food Chem.* **2008**, *56*, 9299−9304.
(29) Sarosiek, J.; Rourk, R. M.; Piascik, R.; Namiot, Z.; Hetzel, D. P.; McCallum, R. W. The effect of esophageal mechanical and chemical stimuli on salivary mucin secretion in healthy individuals. *Am. J. Med. Sci.* **1994**, *308*, 23−31.
(30) Hall, R. L.; Miller, R. J.; Peatfield, A. C.; Richardson, P. S.; Williams, I.; Lampert, I. A colorimetric assay for mucous glycoproteins using alcian blue. *Biochem. Soc. Trans.* **1980**, *8*, 72.
(31) Mallery, S. R.; Budendorf, D. E.; Larsen, M. P.; Pei, P.; Tong, M.; Holpuch, A. S.; Larsen, P. E.; Stoner, G. D.; Fields, H. W.; Chan, K. K.; Ling, Y.; Liu, Z. Effects of human oral mucosal tissue, saliva, and oral microflora on intraoral metabolism and bioactivation of black raspberry anthocyanins. *Cancer Prev. Res.* **2011**, *4*, 1209−1221.
(32) Zdarilová, A.; Rajnochová Svobodová, A.; Chytilová, K.; Simánek, V.; Ulrichová, J. Polyphenolic fraction of *Lonicera caerulea* L. fruits reduces oxidative stress and inflammatory markers induced by lipopolysaccharide in gingival fibroblasts. *Food Chem. Toxicol.* **2010**, *48*, 1555−1561.
(33) Keppler, K.; Humpf, H. U. Metabolism of anthocyanins and their phenolic degradation products by the intestinal microflora. *Bioorg. Med. Chem.* **2005**, *13*, 5195−5205.
(34) Fleschhut, J.; Kratzer, F.; Rechkemmer, G.; Kulling, S. E. Stability and biotransformation of various dietary anthocyanins in vitro. *Eur. J. Nutr.* **2006**, *45*, 7−18.
(35) Woodward, G.; Kroon, P.; Cassidy, A.; Kay, C. Anthocyanin stability and recovery: implications for the analysis of clinical and experimental samples. *J. Agric. Food Chem.* **2009**, *57*, 5271−5278.
(36) Stoner, G. D.; Wang, L. S.; Seguin, C.; Rocha, C.; Stoner, K.; Chiu, S.; Kinghorn, A. D. Multiple berry types prevent *N*-nitrosomethylbenzylamine-induced esophageal cancer in rats. *Pharm. Res.* **2010**, *27*, 1138−1145.
(37) Jing, P.; Bomser, J. A.; Schwartz, S. J.; He, J.; Magnuson, B. A.; Giusti, M. M. Structure−function relationships of anthocyanins from various anthocyanin-rich extracts on the inhibition of colon cancer cell growth. *J. Agric. Food Chem.* **2008**, *56*, 9391−9398.
(38) Marko, D.; Puppel, N.; Tjaden, Z.; Jakobs, S.; Pahlke, G. The substitution pattern of anthocyanidins affects different cellular signaling cascades regulating cell proliferation. *Mol. Nutr. Food Res.* **2004**, *48*, 318−325.
(39) He, J.; Wallace, T. C.; Keatley, K. E.; Failla, M. L.; Giusti, M. M. Stability of black raspberry anthocyanins in the digestive tract lumen and transport efficiency into gastric and small intestinal tissues in the rat. *J. Agric. Food Chem.* **2009**, *57*, 3141−3148.
(40) He, J.; Magnuson, B. A.; Giusti, M. M. Analysis of anthocyanins in rat intestinal contents − impact of anthocyanin chemical structure on fecal excretion. *J. Agric. Food Chem.* **2005**, *53*, 2859−2866.
(41) Proctor, G. B.; Pramanik, R.; Carpenter, G.; Rees, G. D. Salivary proteins interact with dietary constituents to modulate tooth staining. *J. Dent. Res.* **2005**, *84*, 73−78.
(42) Bermudez-Soto, M.; Tomas-Barberan, F.; Garcia-Conesa, M. Stability of polyphenols in chokeberry (*Aronia melanocarpa*) subjected to in vitro gastric and pancreatic digestion. *Food Chem.* **2007**, *102*, 865−874.
(43) Stalmach, A.; Edwards, C. A.; Wightman, J. D.; Crozier, A. Gastrointestinal stability and bioavailability of (poly)phenolic compounds following ingestion of Concord grape juice by humans. *Mol. Nutr. Food Res.* **2012**, *56*, 497−509.
(44) Dawes, C. Rhythms in salivary flow rate and composition. *Int. J. Chronobiol.* **1974**, *2*, 253−279.
(45) Casiglia, J.; Woo, S. B. A comprehensive review of oral cancer. *Gen. Dent.* **2001**, *49*, 72−82.
(46) Yi, W.; Akoh, C. C.; Fischer, J.; Krewer, G. Absorption of anthocyanins from blueberry extracts by Caco-2 human intestinal cell monolayers. *J. Agric. Food Chem.* **2006**, *54*, 5651−5658.
(47) Oyama, Y.; Yamano, H.; Ohkuma, A.; Ogawara, K.; Higaki, K.; Kimura, T. Carrier-mediated transport systems for glucose in mucosal cells of the human oral cavity. *J. Pharm. Sci.* **1999**, *88*, 830−834.
(48) Browning, A. M.; Walle, U. K.; Walle, T. Flavonoid glycosides inhibit oral cancer cell proliferation − role of cellular uptake and hydrolysis to the aglycones. *J. Pharm. Pharmacol.* **2005**, *57*, 1037−1041.

During ontogeny, plants live through different phases with distinct morphological and physiological features.[13] Although crop plants are often harvested before they have transitioned to the generative phase or completed reproduction, their development can be divided into growth stages with pronounced differences regarding morphology and physiology. The concentration of flavonoids and phenolic acids, for instance, is subject to variation throughout plant development.[14,15] Because it is commonly consumed as a leaf vegetable, lettuce is harvested before it enters generative growth. Nonetheless, there are distinguishable growth stages related to head formation as described by Krug et al.:[16] The process of head formation is based on reorientation of leaves from their primary horizontal rosette state toward an upright position, progressively bending inward to form a head, which will grow and become larger and denser with an increasing number of leaves. Obviously, this affects at least the distribution of radiation within the plant. In red leaf lettuce, young leaves have a lower quercetin aglycone concentration than older ones,[10] and the overall concentration of flavonol glycosides and caffeic acid derivatives of whole heads is higher in lettuce plants in early growth stages than in later growth stages.[12]

Although the light dependency of flavonoid biosynthesis in general is well-known, Kubasek et al.[17] additionally found the developmental stage to influence the induction of pivotal flavonoid biosynthesis genes in *Arabidopsis thaliana* (Brassicaceae) seedlings. When it comes to studying development-dependent effects of radiation on plants, many studies have focused on UV radiation.[10,17,18] Interestingly, Reifenrath and Müller[18] detected an interaction between UV radiation and leaf age regarding their effect on flavonol concentration in *Nasturtium officinale* (Brassicaceae). This indicates that the same elicitor could lead to a different response from the same plant, depending on the plant's growth stage. Indeed, flavonoid aglycones in red leaf lettuce display a development-dependent response to UV radiation.[10]

In the presented experiment, we studied the relationship between the concentration of several flavonoid glycosides as well as caffeic acid derivatives and low-level PPFD in three growth stages of two red leaf lettuce cultivars in a climate-controlled greenhouse. We wanted to examine the following hypotheses: (I) The concentrations of the major phenolic compounds of red leaf lettuce respond to PPFD levels below 225 μmol m^{-2} s^{-1}, as are common in Central European greenhouses in cool seasons. (II) Flavonoid glycosides and caffeic acid derivatives respond in a structure-dependent manner. (III) Their PPFD response is development-dependent.

MATERIALS AND METHODS

Plant Cultivation. We conducted the experiment in Grossbeeren (52°20′ N, 13°18′ E), Germany, in March−April 2012. The mean temperature in the greenhouse was 16.3 °C (minimum, 11.7 °C; maximum, 23.6 °C). Red oak leaf and red lollo lettuce (*Lactuca sativa* L. var. *crispa* L. cv. Eventai RZ and *L. sativa* L. var. *crispa* L. cv. Satine, respectively; RijkZwaan, De Lier, The Netherlands) was sown in rockwool cubes, kept at ca. 10 °C for 2 days for germination, and subsequently grown in a conventional greenhouse until the experiment started. When plants had developed four true leaves and a mean aboveground mass of 0.9 g 5 weeks after sowing, they were transferred into the experimental setting, where they were grown hydroponically, using nutrient film technique. The nutrient solution was prepared according to the method of Sonneveld and Straver[19] and checked for macronutrient concentration every week. The greenhouse area was divided into four blocks, according to differences in radiation intensity due to greenhouse construction elements. Additionally, half of each block was covered with a shading net, reducing the photosynthetic photon flux (PPFD) by 45%. This way, we obtained data on flavonoid glycoside and caffeic acid derivative concentrations in two cultivars of red leaf lettuce related to eight PPFD levels, ranging from 43 to 230 μmol m^{-2} s^{-1}. We followed the natural light cycle; no additional lighting was supplied. The PPFD was monitored permanently in each block with light meters LI 190SA Quantum (LI-COR Inc., Lincoln, NE, USA) and recorded by a data logger (DATATAKER, Victoria, Australia). Greenhouse glass has a very good transmissibility for visible and near-infrared wavebands but allows only 64% of UV-A and <1% of UV-B and UV-C radiation, respectively, to pass. Of the UV wavebands, UV-B is generally considered to be most bioactive.[10] We harvested the aboveground organs at three dates, obtaining data on different growth stages within the horticulturally interesting vegetative growth phase: Harvest 1 took place 12 days after planting (DAP), before head formation started. Harvest 2 took place shortly after head formation started (21 DAP), and at harvest 3, mature heads were formed (35 DAP). Harvest dates were set on the basis of experience gained in previous experiments.

Plant Growth Characteristics. At all harvest dates, the mean head weight of three plants per PPFD level and cultivar was used to obtain the mean head mass (n = 8). Values for head mass are given in grams of fresh matter (FM). To obtain dry matter (DM) content, weight before and after lyophilization was compared. Values for DM content are given as percent of FM.

Additionally, we counted the number of leaves (minimum length = 1.5 cm) and measured the maximum diameter of three lettuce heads for each PPFD level and cultivar (n = 8).

Light use efficiency was calculated for plants before and after the onset of head formation. This value displays how much dry matter plants accumulated per intercepted mole of PPFD. For each block and cultivar the intercepted PPFD was calculated separately, based on the measured head diameter. The PPFD absorbing surface area (m^2) was approximated by a circle. This area was multiplied with the PPFD integral (mol m^{-2}) for the intervals between the first and second and the second and third harvest dates, respectively. Light use efficiency (g mol^{-1}) was obtained as the ratio of the plants' dry matter gain (g) between the respective harvest dates and the corresponding intercepted PPFD.

Sample Preparation. A mixed sample from three plants was prepared for each cultivar, treatment, and replication. Only limp or deteriorated outer leaves were removed. Within 30 min after harvesting, the plants were cut in smaller pieces, mixed, frozen at −20 °C until lyophilized (Christ Beta 1-16, Osterode, Germany), and ground with an ultracentrifuge mill (hole size = 0.25 mm; ZM 200, Retsch, Haan, Germany).

Analyses of Phenolic Compounds. Flavonol and flavone glycosides as well as caffeic acid derivatives were analyzed via HPLC-DAD-ESI-MS according to the method of Becker, Kläring, Kroh, and Krumbein.[12] In short, 0.5 g of lyophilized, pulverized lettuce powder was extracted with 25 mL of aqueous methanol (50% MeOH) for 90 min at room temperature. The extract was centrifuged, and the supernatant was cleaned with PTFE filters and analyzed via HPLC-DAD-ESI-MS^2. The anthocyanin method was similar, except for a slightly different composition of the extraction agent and a shorter extraction time: The extraction agent was acidified aqueous methanol (40% MeOH, 10% acetic acid). Extraction of anthocyanin glycosides took 15 min.

The system used for analysis consists of an Agilent HPLC series 1100 Ion Trap (Agilent, Waldbronn, Germany). The compounds were separated on a Prodigy column (ODS 3, 150 × 3 mm, 5 μm, 100 Å; Phenomenex, Aschaffenburg, Germany) with a security guard C18 (ODS 3, 4 × 3 mm, 5 μm, 100 Å) at 30 °C using a water/acetonitrile gradient. DAD wavelength for quantification was 330 nm for caffeic acid derivatives, 350 nm for flavonol and flavone glycosides, and 520 nm for anthocyanidin glycosides.

Statistical Analyses. To study the effect of plant ontogeny, radiation intensity, cultivar, and their interactions on flavonoid glycosides and caffeic acid derivatives, multiple regression analysis

was performed. Representing plant growth stage, DAP was included to study the influence of ontogeny. Radiation intensity is included as PPFD (given in μmol m^{-2} s^{-1}). On the basis of previous experience[12] we considered the mean PPFD during the last 12 days before harvest to be an important factor influencing flavonoid biosynthesis. The two cultivars entered the analysis as cultivar 1 (red oak leaf) and cultivar 2 (lollo rosso), respectively. The resulting equations presented in this study contain only terms having an influence on the investigated variable that significantly differs from zero. A significance level of α = 0.01 was applied.

Growth characteristics were evaluated via two-way ANOVA (Fisher's F test).

Calculations were performed using STATISTICA (version 10, Statsoft Inc., Tulsa, OK, USA).

RESULTS AND DISCUSSION

Influence of Cultivar. Throughout ontogeny, red oak leaf lettuce had a higher number of leaves and greater diameter and head mass than lollo rosso (Table 1). The concentration of phenolic compounds in lettuce can be greatly influenced by genotype,[20] but lollo rosso and red oak leaf lettuce showed only quantitative and no qualitative differences. Concentrations were mostly higher in red lollo rosso, which is largely in line with results by DuPont et al.[21] Multiple regression analysis listed the cultivar as an influential factor on quercetin-3-*O*-(6″-*O*-malonyl)-glucoside, quercetin-3-*O*-glucoside, quercetin-3-*O*-glucuronide/luteolin-7-*O*-glucuronide, and chicoric acid concentrations (Table 2).

Table 1. Plant Growth Characteristics of Two Red Leaf Lettuce Cultivars, Grown in Low Mean Daytime PPFD (43−230 μmol m^{-2} s^{-1}) for 12, 21, and 35 Days after Planting (DAP), Respectively: Number of Leaves, Diameter, and Head Mass in Fresh Matter (FM) (Mean ± SD of the Eight PPFD Levels, n = 8)

DAP	cultivar	no. of leaves	diameter (cm)	head mass (g FM)
12	red oak leaf	10.3 ± 0.2	28.8 ± 2.8	9.2 ± 1.5
21	red oak leaf	18.6 ± 2.5	37.7 ± 3.7	52.6 ± 24.3
35	red oak leaf	30.7 ± 5.0	41.3 ± 2.1	199.7 ± 66.5
12	lollo rosso	7.3 ± 0.5	16.6 ± 1.2	7.5 ± 2.1
21	lollo rosso	11.5 ± 2.1	26.7 ± 0.3	33.8 ± 13.1
35	lollo rosso	21.0 ± 5.1	32.9 ± 0.6	137.0 ± 65.5

Plant Growth Characteristics. Table 1 presents the head mass, number of leaves, and head diameter per cultivar at the three harvest dates. As intended, the plants were in three distinct growth stages. Twelve days after planting, head mass and number of leaves of both cultivars were still low. The leaves formed an open rosette in which all leaves were exposed to radiation. From 12 to 21 DAP, head mass increased only moderately while there was a remarkable increase in diameter. The rosette was much denser at the second harvest date with leaves partly overlapping. From 21 to 35 DAP, there was a marked increase in head mass but not so much in diameter. Independent of cultivar, there was a significantly higher increase in head mass from 21 to 35 DAP compared to the earlier period, whereas the increase in diameter was higher from 12 to 21 DAP compared to the later period.

These results corroborate our visual assessment that plants had not yet developed a head 12 DAP, but that this process had begun at 21 DAP and continued until 35 DAP and is in agreement with the literature.[16] In the following, we named the three studied growth stages accordingly: preheading (harvest 12 DAP) and heading stages (harvest 21 DAP) and mature heads (harvest 35 DAP), respectively.

Table 2. Results of Multiple Regression Analysis: Equations Present the Significantly Influential Factors on the Single Phenolic Compounds of Red Leaf Lettuce (n = 48, α = 0.01)[a]

compound	equation	R^2
Cy3MG	= 1.075774 − 0.148608 × DAP + 0.019459 × PPFD − 0.000028 × PPFD^2 + 0.003040 × DAP^2 − 0.000077 × PPFD × DAP	0.88
Q3G	= 0.061983 − 0.012242 × DAP + 0.033398 × cultivar + 0.001004 × PPFD − 0.000002 × PPFD^2 + 0.000215 × DAP^2	0.69
Q3MG	= 6.472664 − 0.765445 × DAP + 2.181619 × cultivar + 0.020639 × PPFD + 0.013099 × DAP^2	0.77
Q3Gc/L7Gc	= 0.761703 − 0.107507 × DAP + 0.236988 × cultivar + 0.007146 × PPFD − 0.000015 × PPFD^2 + 0.001859 × DAP^2	0.82
chicoric acid	= 1.003199 − 0.108660 × DAP + 0.893134 × cultivar + 0.002311 × DAP^2 − 0.021650 × cultivar × DAP	0.75
chlorogenic acid	= 0.932527 − 0.019782 × DAP	0.45
caffeoylmalic acid	= 0.170214 − 0.001731× DAP	0.17

[a]DAP, days after planting; PPFD, photosynthetic photon flux density in μmol m^{-2} s^{-1}; cultivar, red oak leaf (1) and lollo rosso (2); Cy3MG, cyanidin-3-*O*-(6″-*O*-malonyl)-glucoside; Q3G, quercetin-3-*O*-glucoside; Q3MG, quercetin-3-*O*-(6″-*O*-malonyl)-glucoside; Q3Gc/L7Gc, quercetin-3-*O*-glucuronide/luteolin-7-*O*-glucuronide. The value of R^2 displays the coefficient of determination.

The light use efficiency between the first and second harvests was significantly lower than that between the second and third harvest dates (0.3 and 0.7 g mol^{-1}, respectively). No significant differences between the cultivars were detected. This indicates that the photosynthetic capacity in the first interval was lower than in the second, as plants accumulated less biomass per intercepted mole of PPFD.

Phenolic Compounds. In our HPLC-DAD-ESI-MS^3 analyses of flavonol, flavone, and anthocyanidin glycosides as well as caffeic acid derivatives in red leaf lettuce, we identified three quercetin glycosides, one luteolin glycoside, one cyanidin glycoside, and several caffeic acid derivatives. The main phenolic compound was chicoric acid (di-*O*-caffeoyltartaric acid), followed by quercetin-3-*O*-(6″-*O*-malonyl)-glucoside, cyanidin-3-*O*-(6″-*O*-malonyl)-glucoside, quercetin-3-*O*-glucuronide, luteolin-7-*O*-glucuronide, chlorogenic acid (5-*O*-caffeoylquinic acid), caffeoylmalic acid, and quercetin-3-*O*-glucoside. These compounds were previously reported for red leaf lettuce.[8,21] Quercetin-3-*O*-glucuronide and luteolin-7-*O*-glucuronide coeluted and were quantified as sum. Mass spectrometric data suggested they on average contributed equal shares to the peak evaluated via DAD, which is in line with data obtained by DuPont, Mondin, Williamson, and Price.[21]

Flavonoid Glycosides. The results for flavonoid glycosides are presented in Figure 1 and Table 2. Generally, all flavonoid glycosides were present in higher concentrations in plants in earlier growth stages than in later ones, with the larger difference between preheading stage and heading stage than between heading stage and mature heads. Remarkably, the concentrations of all flavonoid glycosides increased with PPFD even in the very low levels studied. The response depended on structure and growth stage.

dx.doi.org/10.1021/jf404782n | J. Agric. Food Chem. 2014, 62, 6911−6917

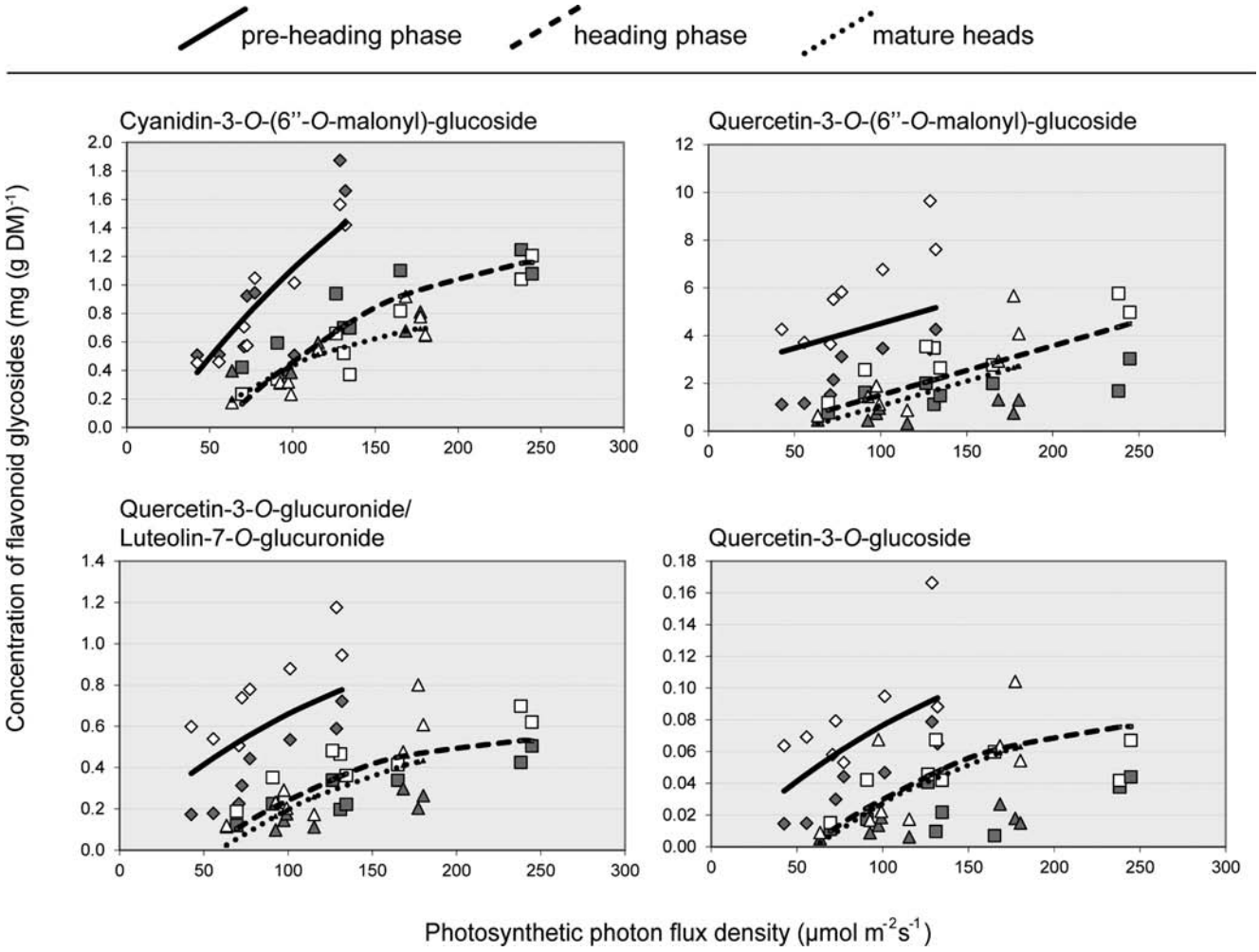

Figure 1. Concentration of flavonoid glycosides per gram dry matter (DM) of red leaf lettuce in three different growth stages in relation to photosynthetic photon flux density (in μmol m^{-2} s^{-1}). The relationship was evaluated via multiple regression analysis. Gray symbols represent values of red oak leaf lettuce; white symbols represent lollo rosso values. Diamonds represent values of preheading phase, squares represent values of heading phase, and triangles represent values of mature heads. The solid line is based on the values of preheading stage, the broken line is based on values of heading stage, and the dotted line is based on values of mature heads.

In detail, with regard to cyanidin-3-*O*-(6″-*O*-malonyl)-glucoside, the lettuce plants' response to radiation varied between the growth stages considered. Multiple regression analysis revealed an interaction between PPFD and plant age: Increasing PPFD had a stronger influence on smaller plants than larger ones. Furthermore, the increase of cyanidin-3-*O*-(6″-*O*-malonyl)-glucoside concentration with rising PPFD was becoming slower with rising PPFD (due to the negative influence of the square term of PPFD), suggesting the approach of a saturation level in PPFD ranges higher than those studied here. Due to the positive influence of the square term of DAP, the differences of cyanidin-3-*O*-(6″-*O*-malonyl)-glucoside concentration between growth stages were more pronounced between preheading and heading phases than between heading and mature heads.

The interaction between PPFD and plant age is most interesting and has not been reported this clearly before. With regard to UV radiation, Behn, Schurr, Ulbrich, and Noga[10] detected a similar age-dependent response when comparing leaves of different age. They cultivated red leaf lettuce for 21 days under UV-B exclusion and subsequently transferred the plants to an environment with ambient UV-B intensity for 2 days. Following this short-term exposure to UV-B radiation, the cyanidin concentration increased only in inner (= young) leaves of lettuce heads. Because responsiveness generally decreased with increasing leaf and plant age, they concluded that younger leaves have an increased requirement for cyanidin as photoprotectant as they have a lower capacity to utilize radiation energy compared to older ones. The light use efficiency of young lettuce was indeed much lower than that of older plants: Per intercepted mole of PPFD, older plants accumulated more than double the dry matter younger ones did. This increase during ontogeny is in line with the literature.[22] Concordantly, the PPFD required for maximum photosynthesis of lettuce plants increases with plant age.[23] This implies an imbalance between captured light energy and its utilization in carbon fixation in early growth stages as has been suggested for juvenile tree leaves by Hughes et al.[24] The surplus energy poses an oxidative threat to plant cells. This suggests that young plants were protecting themselves by anthocyanin accumulation and may explain the higher responsiveness of young plants, even to such low radiation intensities as we studied.

Although the role of anthocyanins in planta is to some degree still subject to discussion, their protective role against photoinhibition and photooxidation in leaves is widely accepted:[25] They absorb light in the green and yellow

dx.doi.org/10.1021/jf404782n | J. Agric. Food Chem. 2014, 62, 6911−6917

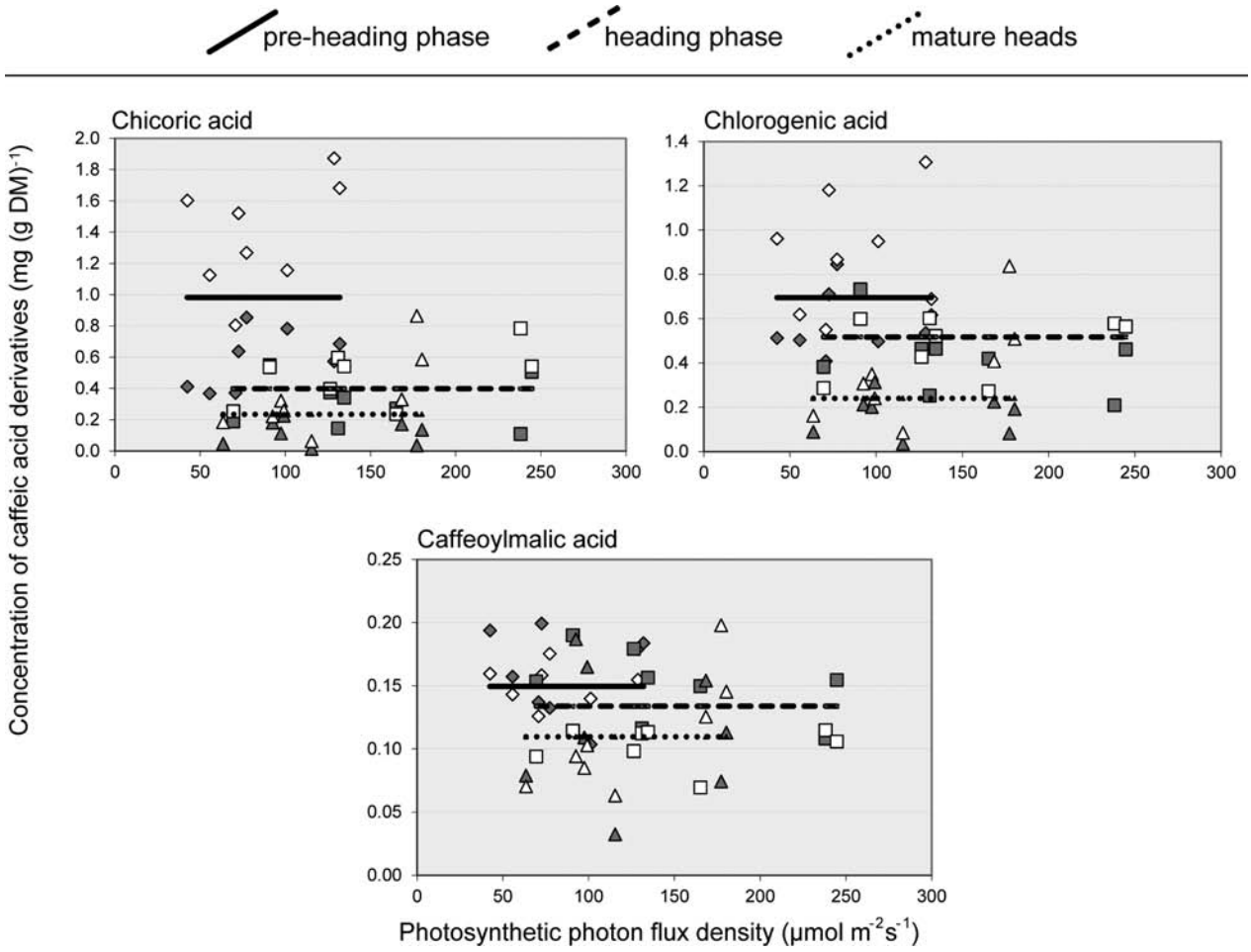

Figure 2. Concentration of caffeic acid derivatives per gram dry matter (DM) of red leaf lettuce in three different growth stages in relation to photosynthetic photon flux density (in μmol m^{-2} s^{-1}). The relationship was evaluated via multiple regression analysis. Gray symbols represent values of red oak leaf lettuce; white symbols represent lollo rosso values. Diamonds represent values of preheading phase, squares represent values of heading phase, and triangles represent values of mature heads. The solid line is based on the values of preheading stage, the broken line is based on values of heading stage, and the dotted line is based on values of mature heads.

wavebands (500−600 nm) and can, therefore, shield the photosynthetic apparatus against surplus radiation, which cannot be used for carbon assimilation and may therefore lead to oxidative damage of photosynthetic tissue.[26] On the other hand, they have a high antioxidant capacity[27] and can counteract reactive oxygen species formed, for example, by photochemistry.[28] Especially during light-sensitive ontogenetic stages, for example, in juvenile leaves in which the photosynthetic apparatus is not yet fully functional, these qualities become obvious.[24] Young leaves are more valuable to plants than old leaves and should, hence, be very effectively protected against harmful impacts.[18]

The concentrations of quercetin-3-*O*-(6″-*O*-malonyl)-glucoside, quercetin-3-*O*-glucoside, and quercetin-3-*O*-glucuronide/luteolin-7-*O*-glucuronide also increased with rising PPFD and decreased with plant age. Between preheading and heading plants the difference regarding concentration was very pronounced. Between heading plants and mature heads, on the other hand, there is hardly any detectable difference. The general increase of the concentration of quercetin glycosides with radiation is in line with previous results.[9,10] Yet, it has not been demonstrated before with regard to such low PPFD levels. Other than for cyanidin glycosides, we did not detect an interaction between PPFD and plant age with regard to quercetin glycoside concentration. Accordingly, Behn, Schurr, Ulbrich, and Noga[10] also found the UV-B response of cyanidin to be more strongly influenced by leaf age than the response of quercetin: Quercetin concentration increased in all of the studied leaf ages.

The effects we detected were clearly structure dependent. On the one hand, they were related to the aglycone: Cyanidin glycosides responded plant age-dependently, whereas quercetin glycosides did not. On the other hand, the glycosidic moiety appears to play a role, too. Otherwise, the three quercetin glycosides would have shown the same response. Yet, in the radiation levels we studied, quercetin-3-*O*-(6″-*O*-malonyl)-glucoside concentration increased linearly with PPFD ,whereas the quercetin-3-*O*-glucoside and quercetin-3-*O*-glucuronide/luteolin-7-*O*-glucuronide concentrations were negatively influenced by the square term of PPFD. Hence, the increase of their concentration was not linear but abated with rising PPFD. This implies that the latter compounds approached a saturation level at higher PPFD than we studied.

All of the presented results were related to dry matter. Yet, for consumers, the concentration-related fresh matter is also interesting. In our experiment dry matter content was not influenced by PPFD but decreased with increasing plant age (data not shown). Therefore, considering the concentration per

dx.doi.org/10.1021/jf404782n | J. Agric. Food Chem. 2014, 62, 6911−6917

100 g of fresh matter, the influence of PPFD corresponds to the results obtained for data related to dry matter, whereas the influence of plant age was even more pronounced.

All studied flavonoid glycosides displayed a remarkable, unexpectedly strong response to changes in PPFD level between approximately 50 and 150 μmol m^{-2} s^{-1}, which was independent of plant age. This demonstrates an impressive PAR sensitivity of the regulative mechanisms.

As mentioned earlier (Introduction and Influence of Cultivar), one major aspect of progressing plant age in the vegetative growth phase of lettuce is the increasing number of leaves accompanied by a change in plant architecture: the formation of a more or less dense head. As a result, the distribution of radiation within the plant is changed. With more leaves shading each other, less biomass per head is directly exposed to radiation. The light-dependent flavonoid biosynthesis, however, will only take place in the exposed tissue.[29] The relative decrease of light-exposed, flavonoid-synthesizing tissue per plant may explain the decrease of flavonoid glycosides we measured with progressing head formation.

Yet, according to Kubasek, Ausubel, and Shirley,[17] flavonoid biosynthesis regulation is influenced by environmental as well as developmental factors. When studying the mRNA level of four flavonoid biosynthesis genes in *Arabidopsis thaliana* seedlings, they found that mRNA levels were higher in 3-day-old than in 7-day-old seedlings, although plants were exposed to identical radiation conditions. They concluded that the gene expression potential was related to plant age. Despite obvious differences between the plants studied by Kubasek, Ausubel, and Shirley[17] and our experiment (different radiation conditions and different plant species), these results may at least be partly transferrable to lettuce in more advanced growth stages: The interaction between plant age and PPFD regarding cyanidin glycoside allows for the speculation that the decreasing concentration with plant age may not only be due to the mentioned dilution effect but also be influenced by growth-stage-dependent variation in the induction capacity of genes involved in biosynthesis. As we detected an interaction only between plant age and radiation concerning cyanidin glycosides, we suppose that the decrease of quercetin glycosides with plant age is due to the relative decrease of radiation-exposed tissue in more developed heads, whereas the decrease in cyanidin glycoside concentration is (additionally) mediated by decreasing biosynthetic capacity with increasing leaf age.

In further studies, it would therefore be interesting to take a closer look and compare the induction of genes at the junction leading to quercetin or cyanidin biosynthesis, for instance, the mRNA levels of flavonol synthase and dihydroflavonol 4-reductase, respectively.[15] Yet, considering the high number of levels at which regulatory processes can take place following transcription (stability of mRNA, translator effectivity, enzyme activation, and more), it might be additionally interesting to study the quantity and activity of the respective enzymes.

Caffeic Acid Derivatives. The results for caffeic acid derivatives are presented in Figure 2 and Table 2. Independent of growth stage, PPFD had no significant influence on the concentration of any of the caffeic acid derivatives. Unlike PPFD, progressing ontogeny had an influence on the concentrations of all three caffeic acid derivatives: They decreased with plant age, however to various degrees.

The decrease of chicoric acid concentration was counteracted by the positive influence of the square term of DAP. Hence, it was markedly higher in the preheading than in the heading stage, whereas the latter did not differ as much from the mature heads' concentration. We observed a significant influence of the cultivar on chicoric acid concentration. Chlorogenic and caffeoylmalic acid were only significantly influenced by DAP, that is, plant age.

The result that none of the three studied caffeic acid derivatives was influenced by PPFD is not in line with Oh, Carey, and Rajashekar,[9] who found an increase of caffeic acid derivatives with increased radiation. However, they exposed their small lettuce plants to 800 μmol m^{-2} s^{-1} for 1 day; this is much higher than the PPFD incident in our experiment (50–250 μmol m^{-2} s^{-1}). According to Fu et al.,[30] lettuce suffers no stress under 100–400 μmol m^{-2} s^{-1} but serious stress under 800 μmol m^{-2} s^{-1}. Furthermore, greenhouse glass absorbs UV radiation to a large degree and phenolic acids are discussed as UV protectants in red leaf lettuce.[31] Hence, incident radiation in this experiment may have lacked the intensity and UV wavelengths needed to trigger caffeic acid derivative biosynthesis.

In conclusion, we could partly confirm our first hypothesis: Quercetin and cyanidin glycosides responded to PPFD at low levels, whereas caffeic acid derivatives did not. Consequently, the measured responses were structure-dependent and the second hypothesis could be fully confirmed. The third hypothesis that the PPFD response is development dependent could be confirmed only for cyanidin-3-*O*-(6″-*O*-malonyl)-glucoside, which responded differently to increasing levels of PPFD depending on the plant's growth stage. Our results highlight how important it is to consider the plant's developmental stage when its physiology is studied.

For lettuce cultivation in greenhouses and the application of energy-saving screens, this implies that screen application during red leaf lettuce production is possible without reducing the concentration of chicoric, chlorogenic, or caffeoylmalic acid, no matter in which growth stage plants are shaded by the screen. Unfortunately, this is not true for cyanidin and quercetin glycosides. Yet, in mature heads losses due to reduced radiation were smaller than with younger plants with regard to three of four flavonoid glycosides.

The high concentration of polyphenols in preheading leaf lettuce and their response to shading may be especially interesting for producers of baby leaf lettuce. Furthermore, the selection of cultivars that are less sensitive to shading and maintain higher concentrations of phytonutrients under these conditions may represent interesting prospects for future studies.

AUTHOR INFORMATION

Corresponding Author

*(C.B.) E-mail: becker@igzev.de. Phone: +49 (0) 33701 78362.

Funding

This research was supported by the German Federal Ministry for Environment, Nature Conservation and Nuclear Safety and the Rentenbank managed by the Federal Ministry of Food, Agriculture and Consumer Protection with the assistance of the Federal Agency for Agriculture and Food.

Notes

The authors declare no competing financial interest.

■ ACKNOWLEDGMENTS

We thank Kersten Maikath, Uwe Kunert, Ingrid Rathenow, Angela Schmidt, Anna Hahn, Juliane Hepting, Susanne Neugart, and Elke Büsch very much for their valuable help and support.

■ ABBREVIATIONS USED

Q3G, quercetin-3-*O*-glucoside; Q3MG, quercetin-3-*O*-(6″-*O*-malonyl)-glucoside; Q3Gc, quercetin-3-*O*-glucuronide; L7Gc, luteolin-3-*O*-glucuronide; Cy3MG, cyanidin-3-*O*-(6″-*O*-malonyl)-glucoside; PPFD, photosynthetic photon flux density; PAR, photosynthetically active radiation; UV, ultraviolet (radiation); mRNA, messenger ribonucleic acid; SD, standard deviation; DAP, days after planting; FM, fresh matter; DM, dry matter; ACN, acetonitrile; MeOH, methanol; HPLC-DAD-ESI-MS, high-performance liquid chromatograph with diode array detector coupled via electrospray ionization interface to mass spectrometer

■ REFERENCES

(1) Meyer, J. Extremely insulated greenhouse concept with non-fossil fuel heating system. *Acta Hortic.* **2011**, 201−208.

(2) Bakker, J. C.; Adams, S. R.; Boulard, T.; Montero, J. L. Innovative technologies for an efficient use of energy. *Acta Hortic.* **2007**, *801*, 49−62.

(3) Frangi, P.; Piatti, R.; Amoroso, G. Evaluation of different screens for energy saving in the greenhouse. *Acta Horict.* **2011**, 275−279.

(4) Klaering, H.-P.; Krumbein, A. The effect of constraining the intensity of solar radiation on the photosynthesis, growth, yield and product quality of tomato. *J. Agron. Crop Sci.* **2013**, DOI: 10.1111/jac.12018.

(5) Leyva, A.; Jarillo, J. A.; Salinas, J.; Martinezzapater, J. M. Low temperature induces the accumulation of phenylalanine ammonia lyase and chalcone synthase messenger RNAs of *Arabidopsis thaliana* in a light dependant manner. *Plant Physiol.* **1995**, *108*, 39−46.

(6) Boudet, A. M. Evolution and current status of research in phenolic compounds. *Phytochemistry* **2007**, *68*, 2722−2735.

(7) Mulabagal, V.; Ngouajio, M.; Nair, A.; Zhang, Y.; Gottumukkala, A. L.; Nair, M. G. *In vitro* evaluation of red and green lettuce (*Lactuca sativa*) for functional food properties. *Food Chem.* **2010**, *118*, 300−306.

(8) Llorach, R.; Martínez-Sánchez, A.; Tomás-Barberán, F. A.; Gil, M. I.; Ferreres, F. Characterisation of polyphenols and antioxidant properties of five lettuce varieties and escarole. *Food Chem.* **2008**, *108*, 1028−1038.

(9) Oh, M.-M.; Carey, E. E.; Rajashekar, C. B. Environmental stresses induce health-promoting phytochemicals in lettuce. *Plant Physiol. Biochem.* **2009**, *47*, 578−583.

(10) Behn, H.; Schurr, U.; Ulbrich, A.; Noga, G. Development-dependent UV-B responses in red oak leaf lettuce (*Lactuca sativa* L.): physiological mechanisms and significance for hardening. *Eur. J. Hortic. Sci.* **2011**, *76*, 33−40.

(11) Tsormpatsidis, E.; Henbest, R. G. C.; Battey, N. H.; Hadley, P. The influence of ultraviolet radiation on growth, photosynthesis and phenolic levels of green and red lettuce: potential for exploiting effects of ultraviolet radiation in a production system. *Ann. Appl. Biol.* **2010**, *156*, 357−366.

(12) Becker, C.; Kläring, H.-P.; Kroh, L. W.; Krumbein, A. Temporary reduction of radiation does not permanently reduce flavonoid glycosides and phenolic acids in red lettuce. *Plant Physiol. Biochem.* **2013**, *72*, 154−160.

(13) Hackett, W. P. Differential expression and functional significance of anthocyanins in relation to phasic development in *Hedera helix* L. *Adv. Bot. Res.* **2002**, *37*, 95−102.

(14) Krumbein, A.; Saeger-Fink, H.; Schonhof, I. Changes in quercetin and kaempferol concentrations during broccoli head ontogeny in the three broccoli cultivars. *J. Appl. Bot. Food Qual.* **2007**, *81*, 136−139.

(15) Treutter, D. Managing phenol contents in crop plants by phytochemical farming and breeding − visions and constraints. *Int. J. Mol. Sci.* **2010**, *11*, 807−857.

(16) Krug, H.; Liebig, H.-P.; Stützel, H. *Gemüseproduktion*; Eugen Ulmer GmbH: Stuttgart, Germany, 2002.

(17) Kubasek, W. L.; Ausubel, F. M.; Shirley, B. W. A light-independent developmental mechanism potentiates flavonoid gene expression in *Arabidopsis* seedlings. *Plant Mol. Biol.* **1998**, *37*, 217−223.

(18) Reifenrath, K.; Müller, C. Species-specific and leaf-age dependent effects of ultraviolet radiation on two Brassicaceae. *Phytochemistry* **2007**, *68*, 875−885.

(19) Sonneveld, C.; Straver, N. *Nutrient Solutions for Vegetables and Flowers Grown in Water or Substrates*; Glasshouse Crops Research Station: Naaldwijk, The Netherlands, 1988; Vol. 7, p 16.

(20) Gazula, A.; Kleinhenz, M. D.; Streeter, J. G.; Miller, A. R. Temperature and cultivar effects on anthocyanin and chlorophyll b concentrations in three related Lollo Rosso lettuce. *Hortscience* **2005**, *40*, 1731−1733.

(21) DuPont, S. M.; Mondin, Z.; Williamson, G.; Price, K. R. Effect of variety, processing and storage on the flavonoid glycoside content and composition of lettuce and endive. *J. Agric. Food Chem.* **2000**, *48*, 3957−3964.

(22) Wheeler, T. R.; Hadley, P.; Ellis, R. H.; Morison, J. I. L. Changes in growth and radiation use by lettuce crops in relation to temperature and ontogeny. *Agric. For. Meteorol.* **1993**, *66*, 173−186.

(23) Sanchez, C. A.; Allen, R. J.; Schaffer, B. Growth and yield of crisphead lettuce under various shade conditions. *J. Am. Soc. Hortic. Sci.* **1989**, *114*, 884−890.

(24) Hughes, N. M.; Morley, C. B.; Smith, W. K. Coordination of anthocyanin decline and photosynthetic maturation in juvenile leaves of three deciduous tree species. *New Phytol.* **2007**, *175*, 675−685.

(25) Hatier, J.-H. B.; Gould, K. S. Anthocyanin function in vegetative organs. In *Anthocyanins*; Gould, K., Davies, K., Winefield, C., Eds.; Springer Science + Business Media: New York, 2009.

(26) Gould, K. S. Nature's Swiss army knife: the diverse protective roles of anthocyanins in leaves. *J. Biomed. Biotechnol.* **2004**, *5*, 314−320.

(27) Rice-Evans, C.; Miller, N.; Paganga, G. Antioxidant properties of phenolic compounds. *Trends Plant Sci.* **1997**, *2*, 152−159.

(28) Neill, S. O.; Gould, K. S. Anthocyanins in leaves: light attenuators or antioxidants? *Funct. Plant Biol.* **2003**, *30*, 865−873.

(29) Hohl, U.; Neubert, B.; Pforte, H.; Schonhof, I.; Böhm, H. Flavonoid concentrations in the inner leaves of head lettuce genotypes. *Eur. Food Res. Technol.* **2001**, *213*, 205−211.

(30) Fu, W.; Li, P.; Wu, Y. Effects of different light intensities on chlorophyll fluorescence characteristics and yield in lettuce. *Sci. Hortic.* **2012**, *135*, 45−51.

(31) García-Macías, P.; Ordidge, M.; Vysini, E.; Waroophan, S.; Battey, N. H.; Gordon, M. H.; Hadley, P.; John, P.; Lovegrove, J. A.; Wagstaffe, A. Changes in the flavonoid and phenolic acid contents and antioxidant activity of red leaf lettuce (Lollo Rosso) due to cultivation under plastic films varying in ultraviolet transparency. *J. Agric. Food Chem.* **2007**, *55*, 10168−10172.

calafate was delphinidin-3-glucoside, followed by petunidin-3-glucoside and malvidin-3-glucoside, with a total of 18 anthocyanins being detected.[12] Among them, five dihexoside derivatives, from delphinidin, cyanidin, petunidin, peonidin, and malvidin aglycones, were detected, characterized by two independent neutral losses of 162 amu in their respective MS/MS spectra. However, the identity and position of these sugars could not be determined by HPLC-DAD-MS/MS.[12]

On the other hand, identification and quantitation of hydroxycinnamic acid derivatives in calafate were recently determined. Twenty hydroxycinnamic acid derivatives were identified showing very high levels of these compounds, with a mean concentration of 4.19 μmol/g (n = 54), which is up to 1.5 times higher than those of other widely consumed berries.[15] Among these hydroxycinnamic acid derivatives, four isomeric caffeoyl-hexaric acids characterized by a neutral loss of 162 amu in their respective ESI-MS/MS spectra were detected. However, the identity of the hexaric acid moiety could not be established. These caffeoyl-hexaric acids accounted for a total proportion of 49.6 ± 10.9% among total hydroxycinnamic acid derivatives found in calafate berries, thus highlighting the importance of the contribution of these derivatives to the pool of hydroxycinnamic acids in calafate.

The high levels of anthocyanins and hydroxycinnamic acid derivatives in calafate berries made the unequivocal identification of each compound in the fruit relevant to demonstrate the nutraceutical value of this interesting fruit. In this context, the main aim of this research is the structural elucidation of anthocyanidin dihexosides and caffeoyl-hexaric acids in calafate berries. With this purpose, the isolation of these compounds using a combination of countercurrent chromatography (fast centrifugal partition chromatography, FCPC), solid phase extraction, and semipreparative HPLC was used, followed by structural elucidation by spectroscopic techniques, including online UV−vis, ESI-MS/MS, and ^{1}H and ^{13}C NMR.

MATERIALS AND METHODS

Chemicals. Ethyl acetate and hydrochloric acid of analytical grade were obtained from Fisher Scientific (Leicestershire, UK). 1-Butanol, trifluoroacetic acid (TFA) of synthesis grade, and methanol of HPLC grade were provided by Scharlab SL (Barcelona, Spain). Ammonia 20% of PRS grade, acetonitrile of HPLC grade, and formic acid 98% of PRS grade were purchased from Panreac Química SLU (Castellar del Vallès, Spain), and water was of Milli-Q quality. D-Saccharic acid potassium salt (standard for D-glucaric acid) and mucic acid (standard for D-galactaric acid) came from Sigma-Aldrich Química SL (Madrid, Spain). Malvidin-3,5-diglucoside and caffeoyl-tartaric acid used for optimization of MS working conditions were obtained from Phytolab (Vestenbergsgreuth, Germany).

Calafate Berry Samples. Mature calafate berries (*B. microphylla* G. Forst) were collected from the Magallanes and Aysén regions of the Chilean Patagonia, 42 samples in year 2011 and 26 samples in year 2012. A taxonomical identification, by comparison of the species with those from the University of Concepción Herbarium, was carried out to ensure the identity of the samples. Aliquots of 10 g of each berry sample were used for the analysis of the total content and distribution of hydroxycinnamic acid derivatives following a previously reported method.[15] A mix of all the samples from year 2012 was used for the isolation of anthocyanidin dihexosides and caffeoyl-hexaric acids.

Extraction Procedures. *Crude Calafate Extract.* Two kilograms of fresh calafate was extracted with 1000 mL of methanol/water (93:7). The extract was treated for 45 s with the ultrasonic bar, followed by 16 h of mechanical shaking under darkness. After centrifugation, the separated supernatant was transferred and the residual solid washed three times with the same solvent, using a total of 2000 mL, by mechanical shaking for 15 min. After elimination of excess methanol by rotatory evaporation at 35 °C, the extract was freeze-dried and stored at −20 °C until use for liquid−liquid extraction.

Liquid−Liquid Extraction. In a separation funnel, 100 mL of solvents A and B (A, ethyl acetate/1-butanol/water (77:15:8) + 0.1% TFA; B, ethyl acetate/1-butanol/water (40:46:14) + 0.1% TFA) were mixed together with approximately 1 g of whole calafate extract. After shaking, the two phases were separated: the aqueous phase contained the anthocyanidin dihexosides, whereas the organic phase held hydroxycinnamic acid derivatives and anthocyanidin 3-glucosides. The aqueous phase was concentrated by rotatory evaporation at 35 °C for further fractionation by FCPC, whereas the hydroxycinnamic acid derivatives in the organic phase were purified by SPE.

Isolation of Anthocyanidin Dihexosides. *Fast Centrifugal Partition Chromatography (FCPC).* To obtain a fraction enriched in anthocyanidin dihexosides, countercurrent chromatography was carried out using an FCPC system, model FCPC-200 (Kromatron, Sainte-Gemmes-sur-Loire, France), with a total rotor volume of 198 mL and 840 partition cells. The FCPC system was connected to a semipreparative ternary pump, model BETA-50 (ECOM, Czech Republic), a UV−vis detector, model Flash 06S DAD 600 (ECOM, Czech Republic), and a fraction collector. Samples were manually injected from a 10 mL loop through a 3725i valve (Rheodyne, Rohnert Park, CA, USA). The stationary phase was a mixture of ethyl acetate/1-butanol/water (4:5:91) with 0.1% TFA. Two mobile phases were required: A, ethyl acetate/1-butanol/water (77:15:8) with 0.1% TFA; and B, ethyl acetate/1-butanol/water (40:46:14) + 0.1% TFA. The separation was carried out by an elution−extrusion system, in ascending mode in the first case and in descending mode in the extrusion. The injection volume was 8 mL of aqueous calafate liquid−liquid extraction phase, previously freeze-dried and redissolved in 10 mL of a mixture of stationary phase and mobile phase A (50:50). The flow of the mobile phase was 5 mL/min with a linear gradient in ascending mode as follows: at 0 min, 75% mobile phase A and 25% B; at 65 min, 100% mobile phase B; at 122 min, 100% mobile phase B; from 122.001 to 142 min change to descending mode with 100% of stationary phase. Fraction collection was every 2 min from 22 to 142 min, and detection was performed at 520 nm.

Semipreparative HPLC. The FCPC fractions enriched in anthocyanidin dihexosides were purified by semipreparative chromatography using an HPLC system consisting of a U6K injector, a 510 pump, and a 996 DAD detector (Waters, Milford, MA, USA). The semipreparative column was a 250 × 10 mm i.d., 5 μm, Kromasil C18 (Análisis Vínicos, Tomelloso, Spain). The mobile phases and the elution gradient were based on the method described by the International Organization of Vine and Wine (OIV) for anthocyanin separation with modifications.[16] Acetonitrile was changed to methanol to reduce the analysis cost and the generation of toxic residues, whereas the formic acid proportions were modified to adapt to this change. Two solvent mixtures were used for the mobile phase: water/methanol/formic acid (92:3:5) (A) and water/methanol/formic acid (45:50:5) (B). The optimized gradient was as follows: at 0 min using 1 mL/min, 75% mobile phase A; at 2 min using 2 mL/min, 75% A; at 30 min, 75% A; at 40 min, 60% A; at 41 min, 0% A; at 44 min, 0% A; at 46 min, 75% A; at 50 min, 75% A; and at 52 min, 75% A and change to 1 mL/min. The injection volume was 250 μL, and detection was at 520 nm. After separation, the eluates were dried by rotatory evaporation at 35 °C, and they were redissolved in methanolic 0.1 M HCl to obtain the hydrochloride form of anthocyanins. A preconcentration by rotatory evaporation at 35 °C, followed by redissolution in water and freeze-drying, was required before NMR analysis.

Repurification of Malvidin Dihexoside by SPE. An additional purification step was necessary in the case of malvidin dihexoside because the semipreparative HPLC eluate contained nonanthocyanin compounds. SPE was carried out in 500 mg, 6 mL, Bond Elut Plexa PCX cartridges (Agilent, Waldbronn, Germany), which combine cationic exchange and reversed phase as retention mechanisms.[17] The process began with a preconditioning step using 5 mL of methanol and 5 mL of water. The malvidin dihexoside eluate was dried and

redissolved in 0.1 M HCl, then was loaded into the PCX cartridge, and cleaned up with 3 × 5 mL of methanol to remove nonanthocyanin compounds. After that, the malvidin dihexoside was eluted with 2% ammonia in 80% methanol until disappearance of blue-colored material from the cartridge, followed by neutralization with enough drops of 4 M HCl to restore the red-colored flavylium cationic form of the anthocyanin. This eluate was dried by rotatory evaporation at 35 °C, redissolved in 0.1 M HCl, and then loaded into an 820 mg, Sep-Pak Plus C18, SPE cartridge (Waters, Milford, MA, USA), which had been previously conditioned with 5 mL of methanol and 5 mL of water. After a cleanup step (6 × 5 mL of 0.1 M HCl) to remove excess ammonium chloride, the purified malvidin dihexoside was eluted with 3 × 5 mL of methanolic 0.1 M HCl, dried by rotatory evaporation at 35 °C, redissolved in water, frozen, and freeze-dried in the dark.

Isolation of Caffeoyl-hexaric Acids. *SPE.* A column filled with 10 g of PCX resin, recovered from PCX cartridges, was used for removing anthocyanins contained in the organic phase separated after liquid−liquid partition of calafate extracts, thus allowing a partial purification and enrichment of hydroxycinnamic acid derivatives. The process began with a preconditioning step using methanol and water (30 mL of each). The organic phase containing hydroxycinnamic acid derivatives was dried by rotatory evaporation at 35 °C, redissolved in 0.1 M HCl (20 mL), and loaded into the column followed by a cleanup step using 0.1 M HCl (2 × 30 mL) and, finally, the hydroxycinnamic acid derivatives were eluted using methanol (3 × 30 mL), the anthocyanins being retained by the stationary phase. The eluates were dried by rotatory evaporation at 35 °C and redissolved in 20 mL of phase A used for semipreparative HPLC and were ready for injection in the next step.

Semipreparative HPLC. The enriched fraction in hydroxycinnamic acid derivatives obtained by SPE was separated by using the semipreparative HPLC equipment described above. The separation conditions were based on a method previously described for hydroxycinnamic acid derivatives determination in calafate but with modification,[15] consisting of the substitution of acetonitrile with methanol. The mobile phases were 0.1% formic acid (A) and 100% methanol (B). The optimized gradient was as follows: at 0 min, using 1 mL/min, 85% mobile phase A; at 2 min, using 2 mL/min, 85% A; at 14 min, 75% A; at 25 min, 75% A; 26 min, 0% A; 35 min, 0% A; 36 min, 85% A; 45 min, 85% A; and at 46 min, 85% mobile phase A and change to 1 mL/min. The injection volume was 250 μL, and detection was performed at 320 nm. The isolated compounds were frozen and freeze-dried before NMR analysis.

Analysis by HPLC-DAD-ESI-MS/MS of Intermediate FCPC and Semipreparative HPLC Fractions and Isolated Compounds. The HPLC-DAD-ESI-MS/MS system was an Agilent 1100 series system coupled with a DAD, model G1315B, and an LC-MSD Trap VL, model G2445C VL, with electrospray ionization (ESI-MS/MS) detectors (Agilent, Waldbronn, Germany). Control and data analyses were carried out by an Agilent ChemStation (version B.01.03) data-processing station and Agilent LC-MS Trap software (version 5.3). The chromatographic separation was carried out in a 2.1 × 150 mm i.d., 3.5 μm, Zorbax Eclipse XDB-C18 (Agilent) column with a flow of 0.190 mL/min at 40 °C, and the injection volume was 10 μL. The mobile phases were: A, formic acid/acetonitrile/water (8.5:3:88.5); B, formic acid/acetonitrile/water (8.5:50:41.5); and C, formic acid/methanol/water (8.5:90:1.5). Anthocyanin analysis was carried out using a binary linear gradient between only solvents A and B as follows: at 0 min, 6% B; 10 min, 30% B; 30 min, 50% B; 34 min, 100% B; 36 min, 100% B; and 42 min, 6% B. The monitoring was at 520 nm, and the MS/MS conditions were positive ionization mode and ionization and fragmentation parameters optimized by direct infusion of a solution of malvidin-3,5-diglucoside in phase A. In the case of hydroxycinnamic acid derivatives, the linear gradient was as follows: at 0 min, 2% B and 0% C; 8 min, 4% B and 0% C; 37 min, 17% B and 13% C; 51 min, 30% B and 20% C; 51.5 min, 40% B and 30% C; 56 min, 50% B and 50% C; 57 min, 50% B and 50% C; and 64 min, 0% B and 0% C. In this case, the monitoring was at 320 nm and the MS/MS conditions were negative ionization mode and ionization and fragmentation parameters optimized by direct infusion of a solution of caffeoyltartaric acid in phase A.

Hydrolysis of Caffeoyl-hexaric Acids. Two of the caffeoyl-hexaric acids isolated in high purity were subjected to alkaline hydrolysis to release the hexaric acid moiety that was further compared to available standards of hexaric acids (D-glucaric and D-galactaric acids) by ^{1}H NMR. We followed a previously described hydrolysis method[18] that was combined with a further purification method by SPE. One milligram of caffeoyl-hexaric acid was dissolved in a 0.1 M solution of K_2CO_3 (8 mg) in D_2O (0.6 mL) and heated at 80 °C for 60 min in the oven. The ^{1}H NMR spectrum of this reaction mixture was very complex, and the identification of signals attributable to hexaric acid was not clear. Thus, a further cleanup step was carried out. Strongly acidic ion-exchange resin (Panreac Química S.L.U., Castellar del Vallès, Spain) was added (10 mg) to the hydrolysis mixture to remove excess carbonate ions by acidification of the medium. Then, the released hexaric acid was separated following an SPE method inspired by previous work on flavonol glycosides separation based on their acidity.[19] The acidified hydrolysis solution was loaded in a 500 mg, 6 mL, Oasis MAX SPE cartridge, filled with a stationary phase that combines reversed-phase and anionic exchange materials (Waters, Milford, MA, USA), previously conditioned with 5 mL of methanol and 5 mL of water. After washing with water (5 mL), the released hexaric acid was eluted by adding methanol (2 × 5 mL), and the retained compounds, including the released caffeic acid and other degradation products, were removed with 2% HCl in methanol (2 × 5 mL). After drying by rotatory evaporation at 35 °C, the eluate containing the hexaric acid was dissolved in D_2O (0.6 mL) and its ^{1}H NMR spectrum was recorded.

Structure Elucidation by Nuclear Magnetic Resonance (NMR) Spectroscopy. The NMR analyses were recorded in a Varian Inova NMR spectrometer (Agilent, Palo Alto, CA, USA), operating at 500 MHz for ^{1}H and at 125 MHz for ^{13}C. The samples of anthocyanins were dissolved in an acidic mixture of CD_3OD/CF_3COOD (95:5) to maintain the flavylium cation, whereas hydroxycinnamic acid derivatives were dissolved in CD_3OD. The identification of proton signals of hexoses was assisted by one-dimensional (1D)-TOCSY spectra. Two-dimensional (2D) spectra were recorded to help peak identification: gCOSY, gHMBC, gHSQC, and NOESY spectra in the case of anthocyanins and gCOSY, gHMBC, and gHSQC spectra for hydroxycinnamic acid derivatives. The spectrometer was equipped with a gradient amplifier and a four-nucleus 5 mm ^{1}H{^{15}N−^{31}P}PFG high-field indirect detection probe. All 1D and 2D experiments were performed at 298 K using standard pulse sequences from the Varian library.

RESULTS AND DISCUSSION

Isolation of Anthocyanidin Dihexosides and Caffeoyl-hexaric Acids from Calafate Berries. The liquid−liquid extraction of the whole calafate extract allowed the partition of main classes of occurring phenolic compounds into two phases.[12,15] The aqueous phase contained a mixture of calafate anthocyanins, mainly dihexosides, 3-rutinosides, and 3-glucosides. In contrast, the organic phase contained hydroxycinnamic acid derivatives and some anthocyanins, mainly 3-glucosides.

The aqueous phase was subjected to countercurrent chromatography by FCPC and resulted in the elution of anthocyanidin 3-glucosides (peak at 46−60 min) and anthocyanidin 3-rutinosides (peak at 70−82 min) following the order of increasing polarity. The more polar anthocyanidin dihexosides were retained by the stationary phase and did not elute after 125 min. Therefore, they were recovered in the further extrusion step (peak at 126−132 min). The extruded fraction mainly contained the dihexosides of B-ring trisubstituted anthocyanidins, namely, delphinidin, petunidin, and malvidin, together with minor amounts of the corresponding dihexosides of the B-ring disubstituted anthocyanidins, namely,

cyanidin and peonidin (Figure 1). All of these compounds exhibited MS and MS/MS spectra with signals at the expected

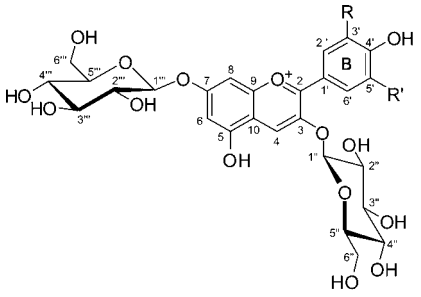

1: R = R' = OH (delphinidin-3,7-β-*O*-diglucoside)
2: R = H; R' = OH (cyanidin-3,7-β-*O*-diglucoside)
3: R = OH; R' = OCH_3 (petunidin-3,7-β-*O*-diglucoside)
4: R = H; R' = OCH_3 (peonidin-3,7-β-*O*-diglucoside)
5: R = R' = OCH_3 (malvidin-3,7-β-*O*-diglucoside)

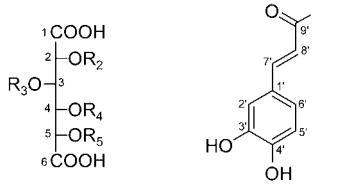

glucaric acid moiety *trans*-caffeoyl moiety

6: R_2 = R_4 = R_5 = H; R_3 = *trans*-caffeoyl
7: R_2 = R_3 = R_5 = H; R_4 = *trans*-caffeoyl
8: R_3 = R_4 = H; R_2 = H and R_5 = *trans*-caffeoyl (or reverse)

Figure 1. Structures of anthocyanidin dihexosides and caffeoyl-hexaric acids identified in calafate berries.

m/z values for their suggested structures.[12,20] The MS spectra showed molecular ions at 627, 611, 641, 625, and 655 for the respective dihexosides of delphinidin, cyanidin, petunidin, peonidin, and malvidin. The MS/MS spectra showed two fragment ions from each molecular ion, generated by independent and successive losses of two hexose units. The signal corresponding to the first hexose loss (m/z values of 465, 449, 479, 463 and 493, respectively) was always a little bit more intense than the second one, thus suggesting that both hexose units were linked separately to the anthocyanidin core.[20] The loss of the two hexose units led to their corresponding anthocyanidin aglycones at the expected m/z values of 303, 287, 317, 301, and 331, respectively. The further separation by semipreparative HPLC allowed the isolation of sufficient amounts of high-purity compounds for an NMR study, showing single peaks in their DAD chromatograms at 520 nm and no other signal in their MS spectra than that attributable to the expected molecular ions, in the cases of the major dihexoside anthocyanidins, consisting of delphinidin (5.9 mg), petunidin (12.5 mg), and malvidin (4.4 mg). Malvidin dihexoside coeluted with a nonanthocyanin compound, showing MS and MS/MS signals at m/z values of 490 and 328, respectively, and an extra purification step was necessary. The impurity was effectively removed by selective retention and further elution of the malvidin dihexoside in the SPE cartridge (PCX) filled with a stationary phase that combines reverse phase and cationic exchange materials.[17] The other two minor compounds were isolated in low amounts and were not pure enough to perform a complete NMR study. Hence, the dihexoside of peonidin (0.6 mg) was determined on the basis of its retention time and UV−vis, MS/MS, and ^{1}H NMR data, which matched those previously reported for this compound when isolated from Garnacha Tintorera grapes.[21] Finally, the occurrence of cyanidin dihexoside (1.6 mg) was suggested only on the basis of its congruent UV−vis and MS/MS data.

Caffeoyl-hexaric acids were first concentrated by SPE on C18 cartridges from the organic phase obtained by liquid−liquid extraction of whole calafate extract and then subjected to semipreparative HPLC. Three isomeric caffeoyl-hexaric acids were isolated showing common MS and MS/MS spectra, with signals at m/z values of 371 assigned to the pseudomolecular and fragment ions appearing at m/z values of 209 and 191.[15] Two of those isomers, eluting at 2.6 and 2.9 min, were stable and could be isolated in amounts of 2.3 and 4.1 mg, respectively, which were sufficient for further NMR study. In contrast, the third isomer, eluting at 3.2 min, was unstable and was partially degraded to a new chromatographic peak at 3.4 min, showing pseudomolecular and fragment ions at m/z values of 353 and 191, respectively, during the subsequent process of concentration of the HPLC fractions in which it was collected. The degradation product could likely be a δ-lactone, as has previously been reported for this kind of compound.[22]

Structure Elucidation of Anthocyanidin Dihexosides and Caffeoyl-hexaric Acids from Calafate Berries. In addition to matching of UV−vis and MS/MS data with those previously reported,[12,15] the structure elucidation of anthocyanidin dihexosides and caffeoyl-hexaric acids isolated from calafate was completed by NMR spectroscopy.

In the case of anthocyanidin dihexosides, the assignment of the anthocyanidin structures of delphinidin, petunidin, and malvidin was based on the agreement of ^{1}H and ^{13}C chemical shifts (Table 1) with those widely described in the literature[23] and was assisted by gHMBC and gHSQC 2D heteronuclear experiments. With regard to hexoses, two doublets assignable to sugar anomeric protons were always found in the ^{1}H NMR spectra: one of them resonated within the range of 5.38−5.43 ppm and the other within the range of 5.21−5.23 ppm, in accordance with previously reported data for the similar peonidin derivative.[21] The two sugars were determined as glucose on the basis of 1D-TOCSY experiments, because all homonuclear coupling constants between successive proton couples (J_{HH} from H-2″ to H-5″ and also from H-2‴ to H-5‴) ranged within 8−11 Hz, thus indicating their axial disposition in the cyclic sugar structure as expected for glucose. Moreover, the coupling constant between H-1 and H-2 for each glucose unit had values of 7−8 Hz, thus indicating a β-anomeric linkage between the sugar and the anthocyanidin core in all cases. The linkage position of the glucose units to the anthocyanidin core was achieved in two ways (Figure 2): long-range ^{1}H−^{13}C heteronuclear coupling between each anomeric proton and its respective carbon position of linkage in the anthocyanidin structure by gHMBC correlation experiments, and the nuclear Overhauser effect between each anomeric proton and the protons situated close to the respective linkage position by 2D-NOESY experiments. Thus, the glucose showing the resonance of the anomeric proton H-1″ at 5.38−5.43 ppm was linked to the C-3 position of the anthocyanidin because H-1″ correlated with C-3 (gHMBC) and also with H-4 (NOESY), and the glucose with the anomeric proton H-1‴ resonating at 5.21−

dx.doi.org/10.1021/jf5012825 | J. Agric. Food Chem. 2014, 62, 6918−6925

Table 1. NMR Spectroscopic Data Recorded in CD_3OD/CF_3COOD (95:5) for Anthocyanidin 3,7-β-*O*-Diglucosides 1, 3, 4, and 5

	1		3		4	5	
position	^1H (J_{HH}) (ppm; Hz)	^{13}C (ppm)	^1H (J_{HH}) (ppm; Hz)	^{13}C (ppm)	^1H (J_{HH}) (ppm; Hz)	^1H (J_{HH}) (ppm; Hz)	^{13}C (ppm)
benzopyran ring							
2		164.4		163.2			164.4
3		146.0		145.6			145.8
4	8.92 s	133.0	8.80 s	133.3	9.07	9.04 s	134.2
5		157.2		157.0			157.2
6	6.82 (2)	102.5	6.80 bs	103.0	6.83 bs	6.86 (2)	102.9
7		165.9		166.2			166.1
8	7.20 (2)	94.4	7.18 bs	94.8	7.54 bs	7.41 bs	94.8
4[a]		112.4		112.6			113.1
8[a]		155.4		155.0			155.9
flavonoid B-ring							
1′		118.4		118.4			118.9
2′	7.79 s	111.8	7.82 (2)	108.7	8.30 (2)	8.07 s	110.2
3′		146.4		148.3			148.7
4′		144.7		145.7			146.3
5′		146.4		146.4	7.08 (9)		148.7
6′	7.79 s	111.8	7.71 (2)	113.3	8.40 (9; 2)	8.07 s	110.2
OCH_3			3.89 s	56.2	4.03	4.02 s	56.1
sugar moiety at C-3							
1″	5.39 (8)	102.1	5.39 (8)	102.1	5.38 (8)	5.43 (8)	102.4
2″	3.75 (9)	73.2	3.69 (8; 9)	73.6		3.68 (11; 8)	73.6
3″	3.60 (9)	76.5	3.62 (8; 9)	77.0		3.58 (9)	76.8
4″	3.48 (10)	70.0	3.48 (9)	69.9		3.44 (11)	69.9
5″	3.62 m	77.5	3.67 m	77.5[a]		3.63 m	77.6
6″a	3.76 (13; 8)	61.0	3.76 (12; 5)	61.1		3.72 (13; 7)	61.1
6″b	3.94 (12; 2)		3.97 (13)			3.95 (13)	
sugar moiety at C-7							
1‴	5.21 (8)	100.4	5.23 (8)	100.5	5.21 (7)	5.22 (7)	100.8
2‴	3.56 m	73.1	3.57 m	73.4		3.57 (9)	73.4
3‴	3.56 m	76.5	3.57 m	76.6		3.53 (9)	76.6
4‴	3.42 m	70.0	3.41 m	70.1		3.40 (9)	69.9
5‴	3.64 m	77.5	3.68 m	77.7[a]		3.64 (9; 4)	77.6
6‴a	3.75 (11; 4)	61.1	3.74 (12; 5)	61.4		3.72 (11; 4)	61.3
6‴b	3.99 (12; 2)		4.01 (12)			3.98 (12)	

[a]Signals could be interchanged.

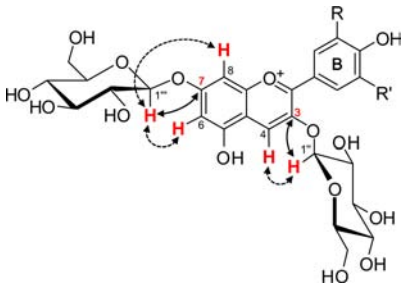

Figure 2. 2D homonuclear (NOESY, dotted arrows) and heteronuclear (gHMBC, solid arrows) correlations found in the NMR experiments of anthocyanidin 3,7-β-*O*-diglucosides that helped assignment of the glucose linkage positions (compound **1**, delphinidin 3,7-β-*O*-diglucoside, R = R′ = OH; compound **3**, petunidin 3,7-β-*O*-diglucoside, R = OH, R′ = OCH_3; compound **5**, malvidin 3,7-β-*O*-diglucoside, R = R′ = OCH_3).

5.23 ppm was linked to the C-7 position of the anthocyanidin, as H-1‴ correlated with C-7 (gHMBC) and protons H-6 and H-8 (NOESY). Therefore, the dihexosides of delphinidin, petunidin, and malvidin were unambiguously identified as delphinidin-3,7-β-*O*-diglucoside (**1**), petunidin-3,7-β-*O*-diglucoside (**3**), and malvidin-3,7-β-*O*-diglucoside (**5**), respectively. For peonidin dihexoside, it was not possible to record the ^{13}C NMR spectrum or to perform 2D-NMR experiments for the assignment of the type of hexoses and their linkage positions because of the low amount isolated. However, the matching of the retention time and the UV−vis, MS, MS/MS, and ^1H NMR spectroscopic data obtained for this peonidin dihexoside with those reported[21] for peonidin-3,7-β-*O*-diglucoside (**4**) provided strong evidence to suggest it would have the same structure. Finally, the NMR study was not possible for the cyanidin dihexoside because it was not pure and the purification attempts were unsuccessful. In this case, we can only suggest a tentative classification as cyanidin-3,7-β-*O*-diglucoside (**2**) that could complete the series of these kinds of derivatives in calafate, having also been found for 3-glucosides and 3-rutinosides derivatives.[12] This suggestion was supported by the following data: the congruent elution order for the series of anthocyanidin glycosides in reversed-phase C18 columns (e.g., anthocyanidin 3-glucosides and anthocyanidin 3,5-diglucosides elute in the order delphinidin < cyanidin < petunidin < peonidin < malvidin), because cyanidin dihexoside eluted

dx.doi.org/10.1021/jf5012825 | J. Agric. Food Chem. 2014, 62, 6918−6925

between delphinidin-3,7-β-*O*-diglucoside (**1**) and petunidin-3,7-β-*O*-diglucoside (**3**); the similarity of its UV−vis spectra, namely, wavelength of maximum absorbance and shape of the visible absorption band, when compared to that of the other B-ring disubstituted derivative, peonidin-3,7-β-*O*-diglucoside (**4**); and the *m*/*z* value of its molecular ion and the finding of the expected MS/MS fragmentation pattern.

Compounds **1**−**5** belong to a rare glycosylation substitution pattern that is seldom found among anthocyanins. Whereas 3,5-diglucosides are widely found in plant materials, 3,7-diglucosides have a more restrictive substitution pattern.[24] As far as we know, 3,7-diglucosides have been identified only in some flowers but not in fruits and berries, and they include the following structures: the nonacylated 3,7-diglucosides of cyanidin, delphinidin, and petunidin, and the (poly)acylated 3,7-diglucosides and 3,7-diglycosides of pelargonidin, cyanidin, delphinidin, petunidin, and malvidin.[24−32] Our group recently demonstrated the occurrence of peonidin 3,7-diglucoside as a very minor anthocyanin in Garnacha Tintorera grape and wine samples.[21] Therefore, compound **5** (malvidin 3,7-diglucoside) was never reported in plant materials. Moreover, the structure elucidation of compounds **1** and **3**, reported previously,[28,29] was based only on ^{1}H NMR and 2D homonuclear correlation (nuclear Overhauser effect) data. We are now reporting additional data on ^{13}C NMR and 2D heteronuclerar correlations (gHSQC and gHMBC) that reinforce the assignments of the 3,7-diglucosides of delphinidin and petunidin. Finally, we can conclude that a remarkable result of this work is that the complete series of five anthocyanidin 3,7-diglucosides has been found for the first time in a fruit, specifically a berry.

The unambiguous elucidation of the structures of caffeoyl-hexaric acids is a difficult challenge to overcome. The hexaric acid moiety exists in open form and has up to four possible linkage positions of the caffeoyl residue depending on the symmetry of the hexaric acid. Hence, we have to first determine the kind of hexaric acid involved in our compounds. The proposed strategies imply the hydrolysis of the ester and further analysis of the released hexaric acid moiety by GC after derivatization or directly by ^{1}H NMR.[8,18,22] After hydrolysis of the two pure caffeoyl-hexaric acids isolated from calafate, we isolated the released hexaric acid moiety by SPE, and its ^{1}H NMR spectrum matched that of a standard of D-glucaric acid (Figure 3). Each hexaric acid gives rise to characteristic and differentiated ^{1}H NMR spectra.[18] The identification of the linkage position of the caffeoyl residue to the hexaric acids is an additional challenge, as the pseudo symmetry of some of them (e.g., glucaric acid) does not allow for distinction between linkage positions 2 and 5, nor between 3 and 4, by NMR spectroscopy,[33] even when 2D homo- and heteronuclear correlation experiments (gCOSY, gHSQC, and gHMBC) are used.[18,34] The linkage of the caffeoyl residue causes an increase in the chemical shift of the corresponding attached proton[18,33] and helps the identification of the linkage position. Further analysis of the multiplicity of the poorly resolved proton signal of the linkage position allows distinguishing between "inner" (3 or 4; broad double doublet or triplet) or "outer" (2 or 5; broad doublet) positions (Table 2). On the basis of the aforementioned arguments, and in agreement with previously reported data for similar compounds,[8,18,33] the two analyzed caffeoyl-hexaric acid isomers were identified as 3-*trans*-caffeoyl-glucaric acid (**6**) and 4-*trans*-caffeoyl-glucaric acid (**7**), but it was not possible to determine which of the two positional

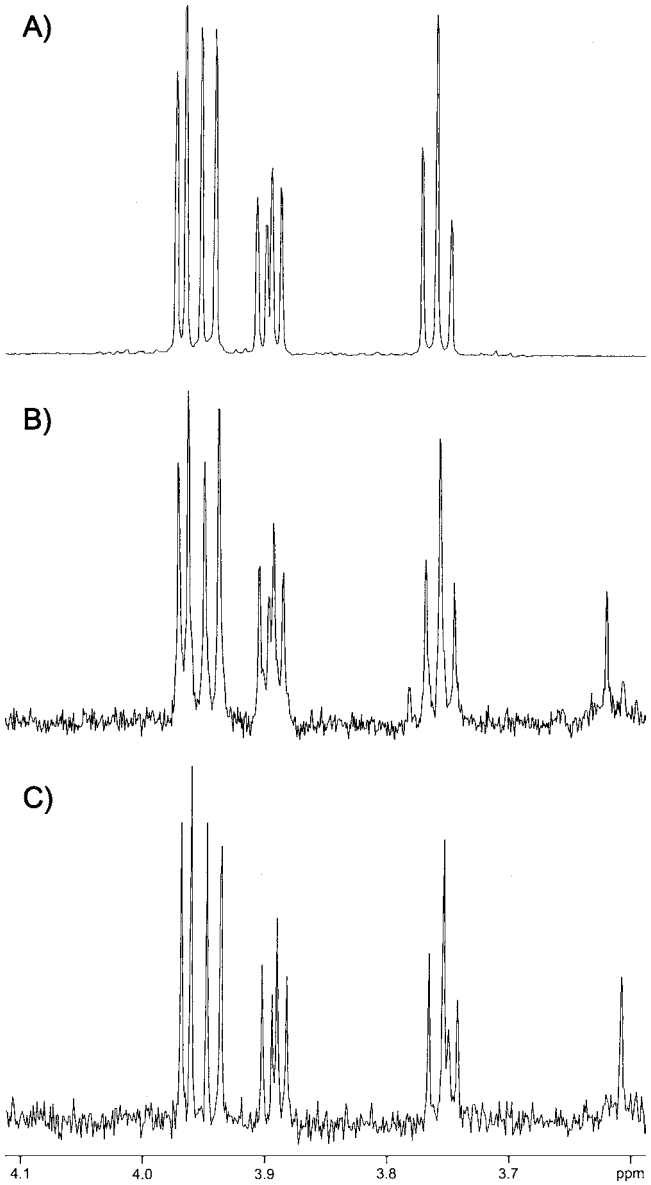

Figure 3. ^{1}H NMR spectra (500 MHz in D_2O) of the fractions containing the released hexaric acids in the hydrolysis experiments of isomeric caffeoyl hexaric acids isolated from calafate: (A) D-glucaric acid standard; (B) glucaric acid released from the first isomer; (C) glucaric acid released from the second isomer.

isomers corresponded to each compound. For one of these isomers, that eluting at 2.9 min, it was possible to record the ^{13}C NMR spectra (Table 2), and the results were in agreement with previously reported data.[22,34] The third detected isomer was degraded during the isolation process, and its structure was tentatively suggested to be 2- or 5-*trans*-caffeoyl-glucaric acid (**8**) on the basis of only UV−vis and MS/MS data.

The levels of caffeoyl-glucaric acids in 68 samples collected in years 2011 and 2012 were analyzed, showing high concentrations (Table 3) that corroborate previously reported data.[15] In addition, the total sum of caffeoyl-glucaric acid concentrations accounted for 42−43% of total hydroxycinnamic acid derivatives found in calafate berries, which reinforce the importance of these compounds within the pool of hydroxycinnamic acid derivatives of this Patagonian wild berry, in agreement with previous findings.[15]

dx.doi.org/10.1021/jf5012825 | J. Agric. Food Chem. 2014, 62, 6918−6925

Table 2. NMR Spectroscopic Data Recorded in CD_3OD of *trans*-Caffeoyl-glucaric Acid Isomers 6 and 7

	6	7	
position	^1H (J_{HH}) (ppm; Hz)	^1H (J_{HH}) (ppm; Hz)	^{13}C (ppm)
caffeoyl moiety			
1′			126.88
2′	7.04 (2)	7.05 bs	114.01
3′			145.58
4′			148.22
5′	6.76 (8)	6.77 (8)	115.30
6′	6.93 (8; 2)	6.93 (8)	121.73
7′	7.58 (16)	7.58 (16)	145.70
8′	6.32 (16)	6.31 (16)	114.65
9′			167.93
glucaric acid moiety[a]			
1			177.31 e
2	3.96 bd a	4.27 (2) c	72.11 f
3	4.08 bt b	5.46 (7; 2) d	76.19 g
4	5.59 bt b	4.36 bd (6) d	72.34 g
5	4.34 bd a	4.17 bs b	71.61 f
6			176.35 e

[a]Signals followed by the same letter could be interchanged.

Table 3. Concentrations (Total Range and Mean Value for Each Year) of Different Caffeoyl-hexaric Acid Isomers and Total Hydroxycinnamic Acid Derivatives (HCAs) Found in Samples of Calafate Berries Collected in South Patagonia over Two Successive Years

compound	range (μmol/g)	year 2011 (n = 42) (μmol/g)	year 2012 (n = 26) (μmol/g)
caffeoyl-hexaric acid (isomer 1)[a]	0.02−1.07	0.35	0.24
caffeoyl-hexaric acid (isomer 2)[a]	0.05−2.34	0.81	0.63
caffeoyl-hexaric acid (isomer 3)[b]	0.02−1.25	0.45	0.24
caffeoyl-hexaric acid (isomer 4)[c]	0.01−0.42	0.13	0.07
total HCAs	1.18−6.28	4.11	2.65

[a]Differentiation between 3-*trans*-caffeoyl-glucaric acid (**6**) and 4-*trans*-caffeoyl-glucaric acid (**7**) is not possible. [b]2- or 5-*trans*-caffeoyl-glucaric acid (**8**). [c]Unidentified isomer.

In summary, the calafate berry contains unusual anthocyanins identified as the complete series of 3,7-β-*O*-diglucosides of the five anthocyanidins usually found in calafate, namely, delphinidin, cyanidin, petunidin, peonidin, and malvidin. Following separation and purification steps, it was possible to isolate the three major anthocyanins of this kind, and their structures were unambiguously determined as delphinidin-3,7-β-*O*-diglucoside (**1**), petunidin-3,7-β-*O*-diglucoside (**3**), and malvidin-3,7-β-*O*-diglucoside (**5**). Additionally, strong evidence suggested that peonidin-3,7-β-*O*-diglucoside (**4**) was another of these anthocyanins, whereas cyanidin-3,7-β-*O*-diglucoside (**2**) could be tentatively identified as the fifth anthocyanin completing the series of anthocyanidin 3,7-diglucosides of calafate, as found for other anthocyanin series of this berry, such as those of 3-glucosides and 3-rutinosides. Calafate also accounts for a high content of hydroxycinnamic acid derivatives with caffeoyl-hexaric acid isomers being important compounds. After isolation, two of these compounds were classified as 3- and 4-*trans*-caffeoyl-glucaric acids (**6** and **7**), although it was not possible to determine the linkage position for each isomer. A third isomer was also isolated, but it easily degraded; it is thought to be the 2- or 5-*trans*-caffeoyl-glucaric (**8**) acid, and more research needs to be developed to confirm this tentative determination.

■ ASSOCIATED CONTENT

Supporting Information

Tables S1, S2, and S3. This material is available free of charge via the Internet at http://pubs.acs.org.

■ AUTHOR INFORMATION

Corresponding Author

*(I.H.-G.) Phone:++34-926-295253. Fax: ++34-926-295351. E-mail: isidro.hermosin@uclm.es.

Funding

A.R., C.M., C.V., and D.v.B. are grateful for FONDECYT Grant 1100944 (CONICYT, Chile) and doctoral fellowships of A.R. (Becas Chile, CONICYT, Chile). S.G.-A. and M.V. G. thank the Fondo Social Europeo and Junta de Comunidades de Castilla-La Mancha for cofunding of their contracts through the INCRECYT program.

Notes

The authors declare no competing financial interest.

■ REFERENCES

(1) Clifford, M. N. Anthocyanins — nature, occurrence and dietary burden. *J. Sci. Food Agric.* **2000**, *80*, 1063−1072.

(2) Pojer, E.; Mattivi, F.; Johnson, D.; Stockley, C. The case for anthocyanins consumption to promote human health: a review. *Compr. Rev. Food Sci. Food Saf.* **2013**, *12*, 483−508.

(3) Huang, H. P.; Shih, Y. W.; Chang, Y. C.; Hung, C. N.; Wang, C. J. Chemoinhibitory effect of mulberry anthocyanins on melanoma metastasis involved in the Ras/PI3K pathway. *J. Agric. Food Chem.* **2008**, *56*, 9286−9293.

(4) Bishayee, A.; Mbimba, T.; Thoppil, R.; Haznagy-Radnay, E.; Sipos, P.; Darvesh, A.; Folkesson, H.; Hohmann, J. Anthocyanin-rich black currant (*Ribes nigrum* L.) extract affords chemoprevention against diethylnitrosamine-induced hepatocellular carcinogenesis in rats. *J. Nutr. Biochem.* **2011**, *22*, 1035−1046.

(5) Moze, S.; Polak, T.; Gasperlin, L.; Koron, D.; Vanzo, A.; Ulrih, N.; Abram, V. Phenolics in Slovenian bilberries (*Vaccinium myrtillus* L.) and blueberries (*Vaccinium corymbosum* L.). *J. Agric. Food Chem.* **2011**, *59*, 6998−7004.

(6) Paredes-López, O.; Cervantes-Ceja, M.; Vigna-Pérez, M.; Hernández-Pérez, T. Berries: improving human health and healthy aging, and promoting quality life — a review. *Plant Foods Hum. Nutr.* **2010**, *65*, 299−308.

(7) Pandino, G.; Lombardo, S.; Mauromicale, G.; Williamson, G. Phenolic acids and flavonoids in leaf and floral stem of cultivated and wild *Cynara cardunculus* L. genotypes. *Food Chem.* **2011**, *126*, 417−422.

(8) Elliger, C. A.; Lundin, R. E.; Haddon, W. F. Caffeyl esters of glucaric acid in *Lycopersicon esculentum* leaves. *Phytochemistry* **1981**, *20*, 1133−1134.

(9) Kim, D.; Lee, D.; Lee, S.; Seong, A.; Gin, D.; Hwang, J.; Park, J. Chlorogenic acid suppresses pulmonary eosinophilia, IgE production, and Th2-type cytokine production in an ovalbumin-induced allergic asthma: activation of STAT-6 and JNK is inhibited by chlorogenic acid. *Int. Immunopharmacol.* **2010**, *10*, 1242−1248.

(10) Lee, S.; Lee, H.; Nam, T.; Eom, S.; Heo, H.; Lee, C.; Kim, D. Neuroprotective effect of caffeoylquinic acids from *Artemisia princeps* Pampanini against oxidative stress-induced toxicity in PC-12 cells. *J. Food Sci.* **2011**, *76*, C250−C256.

(11) Martincorena, C.; Rodríguez, R. *Berberidaceae-Betulaceae. Flora de Chile*, 1st ed.; Universidad de Concepción: Concepción, Chile, 2003; Vol. 2 (2), pp 1−23.
(12) Ruiz, A.; Hermosín-Gutiérrez, I.; Mardones, C.; Vergara, C.; Herlitz, E.; Vega, M.; Dorau, C.; Winterhalter, P.; von Baer, D. Polyphenols and antioxidant activity of calafate (*Berberis microphylla*) fruits and other native berries from south Chile. *J. Agric. Food Chem.* **2010**, *58*, 6081−6089.
(13) Speisky, H.; López Alarcón, C.; Gómez, M.; Fuentes, J.; Sandoval Acuña, C. First web-based database on total phenolics and oxygen radical absorbance capacity (ORAC) of fruits produced and consumed within the South Andes Region of South America. *J. Agric. Food Chem.* **2012**, *60*, 8851−8859.
(14) Ruiz, A.; Hermosín-Gutiérrez, I.; Vergara, C.; von Baer, D.; Zapata, M.; Hitschfeld, A.; Obando, L.; Mardones, C. Anthocyanin profiles in south Patagonian wild berries by HPLC-DAD-ESI-MS/MS. *Food Res. Int.* **2013**, *51*, 706−713.
(15) Ruiz, A.; Mardones, C.; Vergara, C.; Hermosín-Gutiérrez, I.; von Baer, D.; Hinrichsen, P.; Rodríguez, R.; Arribillaga, D.; Dominguez, E. Analysis of hydroxycinnamic acids derivatives in calafate (*Berberis microphylla* G. Forst) berries by liquid chromatography with photodiode array and mass spectrometry detection. *J. Chromatogr., A* **2013**, *1281*, 38−45.
(16) OIV (Office International de la Vigne et du Vin). Resolution OENO 22/2003, Paris, France, 2003.
(17) Castillo-Muñoz, N.; Gómez-Alonso, S.; García-Romero, E.; Hermosín-Gutiérrez, I. Flavonol profiles of *Vitis vinifera* red grapes and their single-cultivar wines. *J. Agric. Food Chem.* **2007**, *55*, 992−1002.
(18) Takenaka, M.; Yan, X.; Ono, H.; Yoshida, M.; Nagata, T.; Nakanishi, T. Caffeic acid derivatives in the roots of yacon (*Smallanthus sonchifolius*). *J. Agric. Food Chem.* **2003**, *51*, 793−796.
(19) Castillo-Muñoz, N.; Gómez-Alonso, S.; García-Romero, E.; Gómez, M. V.; Velders, A. H.; Hermosín-Gutiérrez, I. Flavonol 3-*O*-glycosides series of *Vitis vinifera* cv. Petit Verdot red wine grapes. *J. Agric. Food Chem.* **2009**, *57*, 209−219.
(20) Castillo-Muñoz, N.; Fernández-González, M.; Gómez-Alonso, S.; García-Romero, E.; Hermosín-Gutiérrez, I. Red-color related phenolic composition of Garnacha Tintorera (*Vitis vinifera* L.) grapes and red wines. *J. Agric. Food Chem.* **2009**, *57*, 7883−7891.
(21) Castillo-Muñoz, N.; Winterhalter, P.; Weber, F.; Gómez, M. V.; Gómez-Alonso, S.; García-Romero, E.; Hermosín-Gutiérrez, I. Structure elucidation of peonidin 3,7-*O*-*β*-diglucoside isolated from Garnacha Tintorera (*Vitis vinifera* L.) grapes. *J. Agric. Food Chem.* **2010**, *58*, 11105−11111.
(22) Nagels, L.; Van Dongen, W.; Parmentier, F. Cestric acid, a caffeic acid ester from *Cestrum euanthes*. *Phytochemistry* **1982**, *21*, 743−746.
(23) Fossen, T.; Andersen, Ø. M. Spectroscopic techniques applied to flavonoids. In *Flavonoids. Chemistry, Biochemistry and Applications*; Andersen, Ø. M., Markham, K. R., Eds.; CRC Press, Taylor & Francis Group: Boca Raton, FL, USA, 2006; pp 53−68.
(24) Strack, D.; Busch, E.; Klein, E. Anthocyanin patterns in european orchids and their taxonomic and phylogenetic relevance. *Phytochemistry* **1989**, *28*, 2127−2139.
(25) Toki, K.; Saito, N.; Kuwano, H.; Shigihara, A.; Honda, T. Acylated pelargonidin 3,7-glycosides from pink flowers of *Senecio cruentus*. *Phytochemistry* **1995**, *38*, 1509−1512.
(26) Saito, N.; Toki, K.; Özden, S.; Honda, T. Acylated delphinidin glycosides in the blue-violet flowers of *Consolida armeniaca*. *Phytochemistry* **1996**, *41*, 1599−1601.
(27) Saito, N.; Toki, K.; Suga, A.; Honda, T. Acylated pelargonidin 3,7-glycosides from red flowers of *Delphinium hybridum*. *Phytochemistry* **1998**, *49*, 881−886.
(28) Nørbæk, R.; Kondo, T. Anthocyanins from flowers of *Crocus* (Iridaceae). *Phytochemistry* **1998**, *47*, 861−864.
(29) Nørbæk, R.; Kondo, T. Further anthocyanins from flowers of *Crocus antalyensis* (Iridaceae). *Phytochemistry* **1999**, *50*, 325−328.
(30) Saito, N.; Tatsuzawa, F.; Yazaki, Y.; Shigihara, A.; Honda, T. 7-Polyacylated delphinidin 3,7-diglucosides from the blue flowers of *Leschenaultia* cv. Violet Lena. *Phytochemistry* **2007**, *68*, 673−679.
(31) Tatsuzawa, F.; Saito, N.; Shigihara, A.; Honda, T.; Toki, K.; Shinoda, K.; Yukawa, T.; Miyoshi, K. An acylated cyanidin 3,7-diglucoside in the bluish flowers of *Bletilla striata* 'Murasaki Shikibu' (Orchidaceae). *J. Jpn. Soc. Hortic. Sci.* **2010**, *79*, 215−220.
(32) Tatsuzawa, F.; Saito, N.; Yukawa, T.; Honda, T.; Shinoda, K.; Kato, K.; Miyoshi, K. Acylated cyanidin 3,7-diglucosides in the red-purple flowers of *Sophronitis wittigiana* (Orchidaceae). *J. Jpn. Soc. Hortic. Sci.* **2014**, *83*, 64−71.
(33) Strack, D.; Gross, W.; Wray, V.; Grotjahn, L. Enzymic synthesis of caffeoylglucaric acid from chlorogenic acid and glucaric acid by a protein preparation from tomato cotyledons. *Plant Physiol.* **1987**, *83*, 475−478.
(34) Maas, M.; Petereit, F.; Hensel, A. Caffeic acid derivatives from *Eupatorium perfoliatum* L. *Molecules* **2009**, *14*, 36−45.

Table 1. Identification of Phenolic Compounds in Blackberry Fruits in Positive and Negative Ionization with HPLC-MS, MS^2, and MS^3

phenolic group	peak	t_R [a]	M^+ or $[M-H]^-$ (m/z) [b]	MS^2 (m/z)	MS^3 (m/z)	tentative identification	expressed in
anthocyanins	1	11.88	449	287		cyanidin-3-*O*-glucoside	cyanidin-3-*O*-galactoside
	2	12.49	595	449	287	cyanidin-3-*O*-rutinoside	cyanidin-3-*O*-galactoside
	2	12.49	419	287		cyanidin-3-*O*-arabinoside	cyanidin-3-*O*-galactoside
	3	13.12	433	271		pelargonidin-3-*O*-glucoside	pelargonidin-3-*O*-glucoside
	4	14.61	419	287		cyanidin-3-*O*-xyloside	cyanidin-3-*O*-galactoside
	5	16.41	535	449	287	cyanidin-3-*O*-(6″-malonylglucoside)	cyanidin-3-*O*-galactoside
	5	16.41	593	287		cyanidin-3-*O*-(6″-dioxalylglucoside)	cyanidin-3-*O*-galactoside
hydroxycinnamic acids and their derivatives	6	11.24	353	191, 179		3-caffeoylquinic acid (neochlorogenic acid)	3-caffeoylquinic acid
	7	14.60	325	163		*p*-coumaric acid hexoside	*p*-coumaric acid
flavanols	8	14.62	289	245		catechin	catechin
	9, 10	15.73, 16.02	577	451, 425, 407, 289		procyanidin dimer 1−2	procyanidin B_1
	11	17.27	289	245		epicatechin	epicatechin
	12	18.48	865	577, 695, 451, 425, 407, 289		procyanidin trimer	procyanidin B_1
ellagic acid derivatives	13, 14	19.69, 20.08	935	633, 301		galloyl bis HHDP glucose isomer 1−2	ellagic acid
	15, 16	21.24, 21.93	433	301	257, 229, 185	ellagic acid pentoside 1−2	ellagic acid
	17, 18	24.42, 24.65	447	315	301	methylellagic acid pentoside 1−2	ellagic acid
flavonols	19	22.08	609	301		quercetin-3-*O*-rutinoside	quercetin-3-*O*-rutinoside
	20	22.90	463	301		quercetin-3-*O*-galactoside	quercetin-3-*O*-galactoside
	21	23.10	491	315		isorhamnetin-3-*O*-glucuronide	isorhamnetin-3-*O*-glucoside
	22	23.10	463	301		quercetin-3-*O*-glucoside	quercetin-3-*O*-glucoside
	23	23.22	593	285		kaempferol-3-*O*-(6″-coumaroylglucoside)	kaempferol-3-*O*-glucoside
	24	23.76	593	285		kaempferol-3-*O*-rutinoside	kaempferol-3-*O*-glucoside
	25	23.89	607	463	301	quercetin-3-*O*-(6″-(hydroxyl-3-methylglutaroyl)-galactoside	qauercetin-3-*O*-galactoside
	26	23.92	433	301		quercetin-3-*O*-pentoside	quercetin-3-*O*-arabinofuranoside
	27	24.11	477	301		quercetin-3-*O*-glucuronide	quercetin-3-*O*-galactoside
	28	24.25	433	301		quercetin-3-*O*-arabinofuranoside	quercetin-3-*O*-arabinofuranoside
	29	24.53	447	285		kaempferol-3-*O*-galactoside	kaempferol-3-*O*-glucoside
	30	24.63	433	301		quercetin-3-*O*-xyloside	quercetin-3-*O*-xyloside
	31	24.63	447	285		kaempferol-3-*O*-glucoside	kaempferol-3-*O*-glucoside
	32	24.76	505	463	301	quercetin-3-*O*-(6″-acetylgalactoside)	quercetin-3-*O*-galactoside
	33	25.08	505	463	301	quercetin-3-*O*-(6″-acetylglucoside)	quercetin-3-*O*-galactoside
	34	25.40	461	315		isorhamnetin-3-*O*-rhamnoside	isorhamnetin-3-*O*-glucoside
	35	27.19	489	285		kaempferol-3-*O*-(6″-acetylglucoside)	kaempferol-3-*O*-glucoside

[a] t_R, retention time. [b] M^+ (m/z) anthocyanins were obtained in the positive ion mode, other phenolics in the negative ion mode.

seasonal period of harvest, cultivar (early ripening cultivars were less affected by processing), and duration of long-term frozen storage (1 year). Late-ripening cultivars were characterized by a significant decrease in total anthocyanin content and particularly cyanidin 3-glucoside, which was most easily degraded during processing and the storage period.

In the available literature the impact of processing and storage on blackberry fruit metabolites (with emphasis on anthocyanins) was mostly studied on juice, puree, and canned fruit. Studies on freezing and frozen storage of fresh fruit are rare and limited to only a few compounds or total content levels of phenolic groups. Therefore, to increase the understanding of what is happening with nutraceuticals during prolonged storage in frozen blackberry fruit, more comprehensive studies are required. The objective of this study was to investigate the effect of slow and fast freezing of blackberry fruits followed by frozen storage of the fruit for 7 months on the composition of individual anthocyanins and other phenolics as well as sugars and organic acids in six blackberry cultivars.

MATERIALS AND METHODS

Plant Material and Juice Color and pH Analyses. Fully ripe blackberry fruits of 'Black Satin', 'Chester Thornless', 'Cacanska Bestrna', 'Thornless Evergreen', 'Loch Ness', and 'Thornfree' cultivars were harvested in the orchard of the Agricultural Institute (central Slovenia; latitude, 46°10′ N; longitude, 14°41′ E) from July 27 until August 6. After harvest, the blackberry fruits were immediately transferred into the laboratory on ice. The berries were randomly divided into three treatments: 1, harvest treatment, fresh fruits were immediately analyzed; 2, liquid N treatment, fruits were shock frozen in liquid nitrogen for 5 min and then stored in a deep freezer at −20

dx.doi.org/10.1021/jf405143w | J. Agric. Food Chem. 2014, 62, 6926−6935

Table 2. pH Values and Color Parameters (Mean and Standard Error (SE)) of Juice Extracted from Different Blackberry Cultivars at Harvest and after 7 Months of Frozen Storage at −20 °C[a]

		pH			color intensity			% yellow			% red			% blue			tonality		
cultivar	treatment	mean	SE	sig[b]	mean	SE	sig	mean	SE	sig	mean	SE	sig	mean	SE	sig	mean	SE	sig
'Black Satin'	harvest	3.06	0.03	cd	25.83	0.82	cd	25.82	0.30	bc	72.16	0.73	gh	2.04	0.44	bc	0.358	0.008	bc
	liq N	3.17	0.03	ef	32.39	0.41	fg	28.98	0.35	g	67.20	0.80	b	3.80	0.44	fg	0.432	0.010	hi
	−20	3.20	0.04	ef	28.29	0.82	de	30.86	0.36	h	63.76	0.72	a	5.40	0.39	h	0.484	0.011	j
'Cacanska Bestrna'	harvest	3.26	0.04	fg	16.4	0.41	a	27.94	0.10	f	70.02	0.18	de	2.02	0.10	bc	0.399	0.003	efg
	liq N	3.23	0.02	ef	22.55	0.82	b	28.04	0.32	f	68.98	0.68	cd	2.98	0.38	def	0.407	0.009	fg
	−20	3.13	0.02	de	27.47	1.23	de	27.68	0.37	ef	69.92	0.70	de	2.38	0.35	cde	0.396	0.009	efg
'Chester Thornless'	harvest	2.88	0.04	ab	29.52	0.82	e	25.38	0.06	ab	72.80	0.14	h	1.82	0.12	bc	0.348	0.001	b
	liq N	3.02	0.03	c	42.23	1.23	j	27.08	0.20	de	70.82	0.34	efg	2.12	0.16	bcd	0.382	0.005	de
	−20	3.16	0.02	ef	34.44	0.82	g	26.66	0.16	d	72.98	0.27	h	0.36	0.10	a	0.365	0.003	bcd
'Thornless Evergreen'	harvest	2.83	0.03	a	24.19	1.23	bc	24.70	0.24	a	76.25	0.18	i	1.73	0.09	bc	0.327	0.006	a
	liq N	3.06	0.03	cd	38.54	1.23	i	27.70	0.16	ef	69.00	0.42	cd	3.26	0.27	efg	0.401	0.005	efg
	−20	3.04	0.01	cd	35.67	0.82	gh	28.10	0.23	f	67.82	0.60	bc	4.06	0.40	g	0.415	0.007	gh
'Loch Ness'	harvest	2.85	0.02	a	34.03	0.82	g	26.66	0.22	d	72.02	0.33	fgh	1.32	0.12	b	0.370	0.005	cd
	liq N	3.04	0.02	cd	44.69	1.64	j	27.43	0.23	ef	70.23	0.49	de	2.50	0.23	cde	0.391	0.006	ef
	−20	2.97	0.05	bc	37.31	1.64	hi	27.75	0.21	ef	69.73	0.27	de	2.48	0.10	cde	0.398	0.004	efg
'Thornfree'	harvest	3.20	0.02	ef	32.8	0.82	fg	26.36	0.08	cd	72.02	0.20	fgh	1.64	0.19	bc	0.366	0.002	bcd
	liq N	3.33	0.05	g	33.21	0.82	fg	27.72	0.27	ef	70.48	0.66	def	1.78	0.40	bc	0.394	0.008	efg
	−20	3.13	0.04	de	30.34	1.23	ef	29.50	0.27	g	67.06	0.52	b	3.42	0.30	fg	0.440	0.007	i
harvest		3.01	0.03	A	27.13	0.82	A	26.14	0.17	A	72.54	0.29	C	1.76	0.18	A	0.361	0.004	A
liq N		3.14	0.03	C	35.60	1.03	C	27.83	0.26	B	69.45	0.57	B	2.74	0.31	B	0.401	0.007	B
−20		3.10	0.03	B	32.25	1.09	B	28.43	0.27	C	68.54	0.51	A	3.02	0.27	B	0.416	0.007	C
p treatment		0.0000			0.0000			0.0000			0.0000			0.0000			0.0000		
p cultivar		0.0000			0.0000			0.0000			0.0000			0.0000			0.0000		
p INT		0.0000			0.0000			0.0000			0.0000			0.0000			0.0000		

[a]Liq N, fast freezing method with liquid nitrogen prior to frozen storage; −20, slow freezing method in freezer with no initial fast freezing applied. [b]Letters a−j in columns denote significant differences (Duncan's test, $p < 0.05$) between interaction (INT) cultivar × treatment; letters A−C in columns denote significant differences (LSD test, $p < 0.05$) between different treatments.

dx.doi.org/10.1021/jf405143w | J. Agric. Food Chem. 2014, 62, 6926−6935

°C; and 3, −20 treatment, fruits were stored in the freezer at −20 °C with no pretreatment of liquid nitrogen (slow freezing). Fruits were kept in the freezer for 7 months and immediately analyzed afterward. For each treatment six repetitions were performed, each repetition containing 100 g of blackberry fruit.

The fruits were crushed with a pestle and mortar, and the extracted blackberry juice was used for pH measurements (S20 SevenEasy pH meter, Mettler Toledo, Columbus, OH, USA) and spectrophotometric determination (Perkin-Elmer, UV−vis Lambda Bio 20 spectrophotometer, Waltham, MA, USA) of chromatic parameters. The chromatic parameters used to describe the color of blackberry juice were measured as color intensity (CI) and tonality (To) according to the method of Fragoso et al.[16] Color intensity represents the total amount of color and was calculated as the sum of the absorbances at 420, 520, and 620 nm measured in a 10 mm optical path quartz cuvette. Tonality indicates the relationship of the yellow-orange pigments (420 nm) over the red ones (520 nm):

$$\mathrm{CI} = A_{420} + A_{520} + A_{620}$$

$$\mathrm{To} = A_{420}/A_{520}$$

$$\%\ \mathrm{yellow} = (A_{420}/\mathrm{CI}) \times 100$$

$$\%\ \mathrm{red} = (A_{520}/\mathrm{CI}) \times 100$$

$$\%\ \mathrm{blue} = (A_{620}/\mathrm{CI}) \times 100$$

Extraction and Analysis of Individual Phenolics. Extraction was carried out as described by Mikulic-Petkovsek et al.[17] Fresh berries were ground to a fine paste in a mortar chilled with liquid nitrogen, and 5 g was extracted with 10 mL of methanol containing 3% (v/v) formic acid and 1% (w/v) 2,6-di-*tert*-butyl-4-methylphenol (BHT) in a cooled ultrasonic bath for 1 h. BHT was added to the samples to prevent oxidation during the extraction and formic acid for anthocyanin stabilization to the extraction solution. After extraction, samples were centrifuged at 12800*g* for 5 min at 4 °C, and the supernatants were filtered through Chromafil A0-20/25 polyamide filters (Macherey-Nagel, Düren, Germany). Frozen berries were extracted according to the same procedure as fresh blackberries. When taken out of the freezer, the frozen berries were left at room temperature for 20 min to thaw prior to extraction.

The HPLC analysis was performed on a Surveyor HPLC system with a PDA detector (Thermo Finnigan, San Jose, CA, USA). The column was a Gemini C18 (150 × 4.6 mm, 3 μm; Phenomenex, Torrance, CA, USA) operated at 25 °C. The elution solvents were aqueous 0.1% formic acid in double-distilled water (A) and 0.1% formic acid in acetonitrile (B). Samples were eluted using a linear gradient from 5 to 20% B in the first 15 min, followed by a linear gradient from 20 to 30% B for 5 min, then an isocratic mixture for 5 min, followed by a linear gradient from 30 to 90% B for 5 min, and then an isocratic mixture for 15 min before returning to the initial conditions[18] with some modifications, with an injection amount of 20 μL and a flow rate of 0.6 mL min^{-1}. Anthocyanins were detected and quantified at 530 nm, hydroxycinnamic acids at 310 nm, flavanols at 280 nm, and flavonols and ellagic acid derivatives 350 nm.

Phenolic compounds were identified on a Thermo Electron LCQ Deca XP MAX (Thermo Finnigan) mass spectrometer with electrospray ionization (ESI) operating in a positive (anthocyanins) or negative (all the other phenolics) ionization mode. Analyses were carried out using full scan, data-dependent MS^n scanning from m/z 100 to 1000. The MS data are presented in Table 1. The capillary temperature was 250 °C, the sheath gas and auxiliary gas were 60 and 15 units, respectively, and the source voltage was 3 kV for negative and 4 kV for positive ionization. The identification of compounds was confirmed by comparing retention times and their spectra as well as by adding the standard solution to the sample and by fragmentation and comparison to literature data. The concentrations of phenolics were calculated from peak areas of samples and corresponding standards. Concentrations were expressed in milligrams per kilogram FW (fresh weight). For compounds lacking standards, quantification was carried out using similar compounds as standards.

Sugar and Organic Acid Extraction and Analysis. Five grams of blackberry fruits was homogenized in 25 mL of double-distilled water using an Ultra-Turrax T-25 (Ika-Labortechnik, Staufen, Germany) and left for 30 min at room temperature as reported by Mikulic-Petkovsek et al.[17] The extracts for evaluation of vitamin C content were stabilized at low pH level with 3% metaphosphoric acid. After the extraction, the homogenate was centrifuged at 12800*g* for 7 min at 10 °C. The supernatant was filtered through a 0.20 μm cellulose ester filter (Macherey-Nagel) and transferred into a vial, and 20 μL of the sample was used for the analysis. The analysis of primary metabolites was carried out using a Surveyor HPLC system with a refractive index (RI) detector (Thermo Finnigan). The separation of sugars was carried out using a Rezex RCM-monosaccharide column from Phenomenex operated at 65 °C. The mobile phase was double-distilled water, and the flow rate was 0.6 mL/min; the run time was 30 min. Organic acids were analyzed with the same HPLC system, equipped with a UV detector set at 210 and 245 nm for ascorbic acid, using a Rezex ROA column from Phenomenex, as described by Mikulic-Petkovsek et al.[17] The column temperature was set at 65 °C. The elution solvent was 4 mM sulfuric acid at a flow rate of 0.6 mL min^{-1}. The duration of the analysis was 30 min. The concentration of an individual metabolite was calculated according to a calibration curve of corresponding standard solutions. The concentrations of sugars and organic acids were expressed as grams per kilogram or milligrams per kilogram FW.

Chemicals. The following standards were used for the determination of sugars and organic acids: sucrose, fructose, and glucose; ascorbic, citric, malic, and fumaric acid from Fluka Chemie (Buchs, Switzerland); tartaric and shikimic acid from Sigma-Aldrich Chemie GmbH (Steinheim, Germany). The following standards were used for the quantification of phenolic compounds: 3-caffeoylquinic acid, ellagic acid, rutin (quercetin-3-*O*-rutinoside), and pelargonidin-3-glucoside from Sigma-Aldrich Chemie GmbH; (−)-epicatechin, quercetin-3-galactoside, quercetin-3-glucoside, *p*-coumaric acid, procyanidin B1, cyanidin-3-galactoside, and kaempferol-3-glucoside from Fluka Chemie GmbH; quercetin-3-*O*-arabinofuranoside and quercetin-3-*O*-xyloside from Apin Chemicals (Abingdon, UK); isorhamnetin-3-*O*-glucoside from Extrasynthese (Genay Cedex, France); and (+)-catechin from Roth (Karlsruhe, Germany). Methanol for extraction of phenolics was acquired from Sigma. The chemicals for the mobile phases were HPLC-MS grade acetonitrile and formic acid from Fluka Chemie GmbH. Water for the mobile phase was twice distilled and purified with the Milli-Q system (Millipore, Bedford, MA, USA).

Statistical Analysis. The data were analyzed with the Statgraphics Plus 4.0 program (Manugistics Inc., Rockville, MD, USA) using two-way analysis of variance (ANOVA). Factorial analysis described the differences among treatments and cultivars and, additionally, their interaction. The differences between cultivars and cultivar × treatment interaction were tested using the Duncan test at a 0.05 significance level, whereas differences between treatments were tested using the LSD test at a 0.05 significance level. Means and standard errors of the parameters were calculated from six replicates ($n = 6$).

RESULTS AND DISCUSSION

Blackberry quality parameters and metabolic composition were evaluated and quantified at harvest and after 7 months of frozen storage at −20 °C. The storage treatments differed in the initial freezing of the berries; these were either shock frozen with liquid nitrogen or transferred to the freezer where the fruits were slowly frozen.

pH Value and Color Parameters. The average pH value of fruit juice at harvest was 3.01 and increased after 7 months of frozen storage to average values of 3.1 and 3.14 in liquid N pretreated fruit and slow freezing treatments, respectively (Table 2). The cultivars with the highest pH value were 'Thornfree' and 'Cacanska Bestrna' with pH 3.2. On the other

dx.doi.org/10.1021/jf405143w | J. Agric. Food Chem. 2014, 62, 6926−6935

Table 3. Total Sugars and Organic Acids, Their Ratio, and Vitamin C Content (Mean and Standard Error (SE)) in Different Blackberry Cultivars at Harvest and after 7 Months of Frozen Storage at −20 °C[a]

		total organic acids (g kg^{-1} FW)			total sugars (g kg^{-1} FW)			sugars/organic acids ratio			vitamin C (mg kg^{-1} FW)		
cultivar	treatment	mean	SE	sig[b]	mean	SE	sig	mean	SE	sig	mean	SE	sig
'Black Satin'	harvest	6.25	0.79	a	34.02	1.71	a	5.64	0.46	ef	78.70	5.40	g
	liq N	14.16	0.32	def	63.32	1.59	ef	4.50	0.19	cd	21.84	1.45	abc
	−20	13.55	1.09	def	70.11	1.72	f	5.32	0.50	def	37.20	2.81	de
'Cacanska Bestrna'	harvest	17.17	1.18	gh	58.08	2.09	e	3.46	0.36	b	86.26	5.13	g
	liq N	18.71	0.90	h	51.03	0.67	cd	2.76	0.18	ab	15.00	2.77	a
	−20	21.61	1.35	i	42.78	4.45	b	2.00	0.17	a	27.00	3.72	bcd
'Chester Thornless'	harvest	7.01	0.26	a	32.67	2.41	a	4.64	0.24	cde	62.66	2.81	f
	liq N	12.28	0.73	cd	66.13	2.09	f	5.46	0.41	def	12.48	2.22	a
	−20	12.04	0.63	cd	63.20	0.91	ef	5.32	0.37	def	16.80	2.23	ab
'Thornless Evergreen'	harvest	8.21	0.47	ab	50.48	2.41	c	6.22	0.39	fg	65.50	2.59	f
	liq N	12.31	0.56	cd	86.12	0.51	h	7.06	0.37	g	39.22	3.84	e
	−20	14.17	0.30	def	77.81	1.12	g	5.50	0.14	def	34.30	4.19	de
'Loch Ness'	harvest	12.76	0.22	cde	69.33	3.25	f	5.53	0.28	def	38.52	4.57	e
	liq N	13.11	0.24	cde	67.50	2.93	f	5.14	0.29	def	16.86	1.31	ab
	−20	16.03	1.53	fg	57.41	4.22	de	3.74	0.48	bc	29.20	4.11	cde
'Thornfree'	harvest	15.35	1.49	efg	47.12	1.16	bc	3.18	0.33	b	22.12	4.86	abc
	Liq N	14.49	0.94	def	46.46	1.52	bc	3.26	0.28	b	19.46	4.85	abc
	−20	10.45	0.69	bc	49.04	1.64	bc	4.78	0.37	cde	15.78	1.71	ab
harvest		11.13	0.74	A	48.62	2.17	A	4.78	0.34	A	58.97	4.23	C
liq N		14.18	0.62	B	63.43	1.55	C	4.70	0.29	A	20.82	2.75	A
−20		14.64	0.93	B	60.06	2.34	B	4.44	0.34	A	26.72	3.13	B
p treatment		0.0000			0.0000			0.2147			0.0000		
p cultivar		0.0000			0.0000			0.0000			0.0000		
p INT		0.0000			0.0000			0.0000			0.0000		

[a]Liq N, fast freezing method with liquid nitrogen prior to frozen storage; −20, slow freezing method in freezer with no initial fast freezing applied. [b]Letters a−i in columns denote significant differences (Duncan's test, $p < 0.05$) between interaction (INT) cultivar × treatment; letters A−C in columns denote significant differences (LSD test, $p < 0.05$) between different treatments.

hand, the pH value of the juice extracted from fresh fruit of 'Loch Ness' cultivar was only 2.9. Blackberries are characterized by low pH values of the juice extracted from fresh fruit, and Wu et al.[10] measured pH values of two blackberry cultivars in the ranges of 3.2 and 4.3. Refrigerated storage at 2 °C caused an increase of fruit pH value, which could be associated with a lower content of titratable acidity. In their study during long-term frozen storage, the pH value remained rather constant.

Attractive color is one of the main visual features of fruit and berry products,[19] and blackberries are well-known for their intense dark color. Color intensity represents the total amount of color, and color composition indicates the contribution of blue, red, and yellow color to the overall color appearance (Table 2). Color intensity of blackberry fruit increased from harvest until the end of frozen storage in both freezing treatments. Similarly, frozen storage also altered the composition of red, yellow, and blue hues. The percent of red color decreased and the percent of yellow and blue hues increased during storage. It is well-known that anthocyanin properties (including their effect on color) are highly influenced by anthocyanin structure and the pH[20] value of cell sap. Therefore, the changes in monitored color parameters after 7 months of frozen storage could partly be explained with higher pH values of the juice of most analyzed cultivars. Anthocyanins are extremely pH sensitive, which results in different color expression depending on various pH values. Lower pH values stabilize their structure and lead to a darker appearance of the fruit. However, isolated anthocyanins and color hues remain quite stable during frozen storage if kept in low-pH solvents (pH values between 1.1 and 3). Higher pH values caused a shift to orange hues after frozen storage.[20] A similar trend has been detected for the tonality parameter, which indicates the relationship between yellow orange and red pigments and increased from harvest until the end of storage in both treatments.

Sugars, Organic Acids, and Vitamin C. The composition and the amounts of sugars and organic acids as well as their relationship are a crucial quality index for blackberries,[1] determining their taste.

The principal sugars in blackberry fruits were glucose, fructose, and sucrose. Their content levels and proportions varied among cultivars, which is in accordance with previous results.[1,21] Generally, freezing conditions and long-term frozen storage resulted in better extraction of individual and total

Table 4. Content of Different Phenolic Groups (Mean and Standard Error (SE) in mg kg^{-1} FW) in Different Blackberry Cultivars at Harvest and after 7 Months of Frozen Storage at −20 °C[a]

		hydroxycinnamic acids			flavanols			flavonols			ellagic acid derivatives			anthocyanins		
cultivar	treatment	mean	SE	sig[b]	mean	SE	sig	mean	SE	sig	mean	SE	sig	mean	SE	sig
'Black Satin'	harvest	17.06	0.39	d	83.36	2.95	ab	14.62	1.07	ab	39.52	3.16	d	545.68	18.96	a
	liq N	16.36	1.22	d	83.36	8.19	ab	25.65	1.50	def	31.30	5.47	cd	539.74	34.22	a
	−20	22.18	0.35	e	147.35	21.67	c	32.35	2.96	fg	107.67	2.51	f	839.44	24.16	cd
'Cacanska Bestrna'	harvest	9.96	1.03	ab	60.88	7.55	a	12.62	2.13	a	14.30	1.82	ab	481.34	64.19	a
	liq N	11.48	0.50	bc	66.36	5.93	a	19.76	1.31	abcd	12.22	0.93	ab	582.86	42.43	ab
	−20	13.58	0.44	c	76.96	5.50	ab	28.72	1.54	efg	16.78	2.02	ab	820.24	56.22	cd
'Chester Thornless'	harvest	20.38	0.83	e	70.58	8.25	ab	24.35	1.24	cdef	12.60	1.75	ab	1007.98	47.95	e
	liq N	19.94	1.21	e	71.40	6.09	ab	36.14	3.45	g	13.50	1.12	ab	996.72	85.25	e
	−20	19.72	0.72	e	72.74	2.96	ab	36.69	2.62	g	13.74	0.61	ab	971.14	75.15	de
'Thornless Evergreen'	harvest	46.20	1.44	j	317.60	20.13	f	68.04	4.42	h	69.65	8.66	e	531.42	32.12	a
	liq N	43.30	1.90	i	299.06	17.69	f	65.69	5.90	h	74.30	8.47	e	598.14	31.54	ab
	−20	36.12	1.33	h	253.86	11.36	e	67.02	3.52	h	70.07	5.87	e	461.24	29.24	a
'Loch Ness'	harvest	8.60	0.22	a	200.08	12.32	d	26.75	2.32	def	21.04	4.65	abc	1228.14	40.64	f
	liq N	7.54	0.31	a	151.88	15.65	c	24.32	2.66	cdef	8.32	1.35	a	956.93	49.06	de
	−20	8.48	0.29	a	192.30	3.35	d	27.98	2.38	def	25.60	7.29	bc	1184.19	75.90	f
'Thornfree'	harvest	20.42	0.22	e	80.50	7.83	ab	16.98	1.80	abc	14.93	1.42	ab	713.50	31.27	bc
	liq N	26.40	0.92	f	101.78	9.76	b	22.50	1.57	bcde	13.06	1.02	ab	833.00	45.81	cd
	−20	30.95	0.93	g	60.48	5.49	a	24.93	1.64	cdef	11.96	1.04	a	1096.3	39.96	ef
harvest		20.47	0.69	A	135.50	9.84	A	27.23	2.16	A	28.67	3.58	A	751.34	39.19	A
liq N		20.84	1.01	AB	128.97	10.55	A	32.34	2.73	B	25.45	3.06	A	751.23	48.05	A
−20		21.84	0.68	B	133.95	8.34	A	36.28	2.44	C	40.97	3.22	B	895.43	50.11	B
p treatment		0.0287			0.5294			0.0000			0.0000			0.0000		
p cultivar		0.0000			0.0000			0.0000			0.0000			0.0000		
p INT		0.0000			0.0000			0.0094			0.0000			0.0000		

[a]Liq N, fast freezing method with liquid nitrogen prior to frozen storage; −20, slow freezing method in freezer with no initial fast freezing applied. [b]Letters a−j in columns denote significant differences (Duncan's test, $p < 0.05$) between interaction (INT) cultivar × treatment; letters A−C in columns denote significant differences (LSD test, $p < 0.05$) among different treatments.

sugars (Table 3). This could be due to cell wall degradation as well as disruption of different membranes during freezing, resulting in better extraction.[22] Similar results were recorded for blueberry in a study by Wu et al.,[10] where total soluble solids remained stable or even increased by 20% in specific cultivars during 6 months of frozen storage. Cultivar-specific response was also determined in our experiment. As shown by Kopjar et al.,[13] specific sugars such as glucose can have a positive effect on anthocyanin content in blackberry juice by preventing their degradation during storage.

The main organic acids detected in blackberry fruit were citric, malic, and tartaric acid. Citric and malic acids were the predominant organic acids,[1,23] depending on the cultivar analyzed. Several minor organic acids were identified in blackberry fruit such as fumaric and shikimic acid; however, their contribution to total organic acid content is not significant. Similar to total sugars, higher extraction of total organic acids was achieved after frozen storage compared to harvest treatment (Table 3). Wu et al.,[10] on the other hand, report stable or decreased levels in titratable acidity depending on analyzed cultivar after 6 months of frozen storage. Despite better extraction of total analyzed sugars and organic acids after frozen storage, their relationship remained constant and did not change among treatments. Consequently, blackberry fruits preserve their characteristic sour-sweet taste even after long-term frozen storage regardless of the initial freezing method or conditions. The relationship between sugars and organic acids was highest in the fruit of cultivar 'Thornless Evergreen'.

Another important organic acid, not counted in total organic acid content levels, is ascorbic acid (vitamin C). As expected, vitamin C content decreased during storage in both frozen treatments (Table 3). This has previously been determined for raspberry, blackberry, and blueberry fruits after long-term storage.[22,24] The reduction of vitamin C in our experiment was more pronounced in fast-frozen fruits compared to fruit subjected to slow freezing. The cultivars with low amounts of vitamin C at harvest such as 'Loch Ness' and 'Thornfree' lost about 50% or less during frozen storage. On the other hand, cultivars with initially higher content of vitamin C were characterized by an even higher loss (up to 80%).

Phenolics. Derivatives of hydroxycinnamic acids were not present in high amounts in blackberries (Table 4). Only two

dx.doi.org/10.1021/jf405143w | J. Agric. Food Chem. 2014, 62, 6926−6935

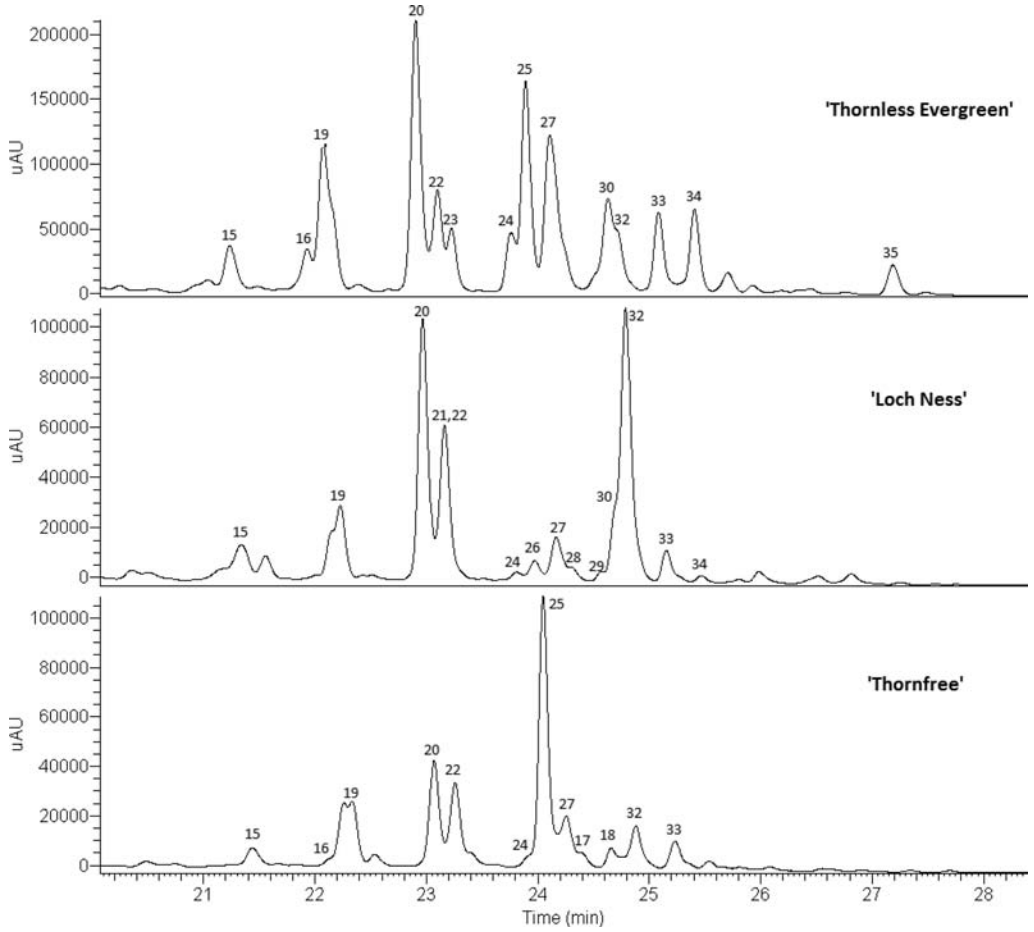

Figure 1. Flavonol profile of fresh blackberry fruit of 'Thornless Evergreen', 'Loch Ness', and 'Thornfree' cultivars. Peak numbers correspond to the compounds listed in Table 1

hydroxycinnamic acids were confirmed by MS analysis, namely, neochlorogenic acid in all cultivars and *p*-coumaric acid hexoside (not detected in 'Loch Ness' and 'Thornless Evergreen' cultivars). The 'Thornless Evergreen' cultivar contained the highest levels of neochlorogenic acid among the analyzed cultivars. Fast freezing followed by frozen storage did not affect the content of hydroxycinnamic acids in blackberry fruit; meanwhile, slow freezing resulted in higher extraction of this phenolic group compared to the harvest treatment. As shown by the study of Kopjar et al.,[13] hydroxycinnamic acids can be efficiently used as copigments stabilizing anthocyanins during storage of blackberry juice and preventing their degradation. This has also been described by Howard et al.,[8] who determined that anthocyanin acylation with cinnamic and organic acids greatly improves their stability and also the color of plant tissue and juice.

A great variety of flavonol glycosides has been determined in blackberry fruit. Three aglycones prevailed, namely, quercetin, kaempferol, and isorhamnetin, and details on their spectra and MS^n data of individual flavonol compounds are presented in Table 1. Quercetin glycosides were most abundant in fresh and frozen blackberry fruits as previously described by Mikulic Petkovsek et al.[3] Similar to the group of hydroxycinnamic acids, the extraction of flavonols was increased after long-term frozen storage, especially when slow freezing was applied levels Similarly, Türkben et al.[14] also measured higher levels of quercetin glycosides after long-term storage of the 'Chester Thornless' cultivar, whereas an opposite effect has been recorded in other blackberry cultivars analyzed. As mentioned previously, a better extraction of flavonols could be related to tissue damage by freezing, especially in the slow-freezing conditions. The effect of freezing damage can best be observed at thawing when a loss of turgor due to damaged cell walls and cell membranes results in permanent transfer of intracellular sap to the extracellular fluid, which cannot be reversed after thawing.[11] This can potentially be linked with a better extraction of various compounds compared to the harvest treatment when the cells are still intact. However, no significant differences have been recorded among treatments in 'Loch Ness' and 'Thornless Evergreen' cultivars. The latter was characterized by the highest content of total flavonols and a great abundance of individual flavonols compared to other cultivars analyzed (Figure 1).

Flavanols were the only group of phenolics that did not express any differences in the extracted amounts among different treatments (Table 4). Again, the highest total flavanol content was measured in 'Thornless Evergreen' and 'Loch Ness' cultivars. In fruit of both cultivars quantifiable amounts of catechin have be detected as opposed to other analyzed blackberry cultivars in which only epicatechin and different procyanidin units have been identified. Together with ellagic acid derivatives, flavanols present the tannin pool of blackberry fruits and, interestingly, cultivars with high flavanol content also contained high levels of ellagic acid derivatives (Table 4). The only exception was the 'Loch Ness' cultivar characterized by moderately high levels of flavanols and low contents of ellagic

Table 5. Content of Individual Anthocyanins (Mean and Standard Error (SE) in mg kg^{-1} FW) in Different Blackberry Cultivars at Harvest and after 7 Months of Frozen Storage at −20 °C[a]

		Cy 3-arabinoside			Cy 3-glucoside			Cy 3- (6″-dioxalylglucoside)			Cy 3-(6″-malonylglucoside)			Cy 3-xyloside			Cy 3-rutinoside			Pel 3-glucoside		
cultivar	treatment	mean	SE	sig[b]	mean	SE	.sig	mean	SE	sig	mean	SE	sig	mean	SE	sig	mean	SE	sig	mean	SE	sig
'Black Satin'	harvest	17.12	0.62	d	404.38	16.89	ab	96.34	2.87	ef	9.36	0.28	a	15.54	0.25	cd	ND	ND		2.94	0.09	abc
	liq N	14.40	0.63	c	403.64	26.57	ab	95.62	6.35	ef	9.28	0.61	a	14.30	0.72	c	ND	ND		2.50	0.11	ab
	−20	20.52	0.60	f	623.06	20.07	de	155.22	5.68	h	15.06	0.56	bc	21.66	0.58	ef	ND	ND		3.92	0.27	cde
'Cacanska Bestrna'	harvest	ND	ND		398.58	56.16	ab	47.60	4.98	cd	25.26	2.64	ef	5.04	0.23	a	ND	ND		4.86	0.37	ef
	liq N	ND	ND		488.92	36.02	bc	54.68	3.90	d	28.96	2.07	f	4.98	0.51	a	ND	ND		5.32	0.60	f
	−20	ND	ND		681.18	50.35	ef	80.76	6.17	e	42.80	3.28	g	8.72	1.12	ab	ND	ND		6.78	0.52	g
'Chester Thornless'	harvest	ND	ND		790.23	42.91	fg	111.92	3.36	fg	24.68	0.49	ef	62.80	2.36	h	ND	ND		15.48	0.40	h
	liq N	ND	ND		793.62	69.2	fg	103.66	8.16	f	22.28	1.76	de	63.46	4.42	h	ND	ND		17.13	0.84	i
	−20	ND	ND		783.86	52.75	fg	99.86	5.47	f	21.48	1.18	de	63.43	3.64	h	ND	ND		19.00	0.86	j
'Thornless Evergreen'	harvest	5.84	0.29	b	405.10	30.70	ab	34.22	2.33	bc	48.10	3.37	h	15.58	0.82	cd	29.26	1.43	b	2.94	0.10	abc
	liq N	5.96	0.28	b	460.40	25.53	abc	33.52	1.40	bc	49.30	2.05	h	16.20	0.83	cd	29.84	1.43	b	2.92	0.15	abc
	−20	4.56	0.15	b	351.62	22.75	a	27.24	2.01	b	40.06	2.95	g	12.62	0.54	bc	22.88	0.75	a	2.26	0.22	a
'Loch Ness'	harvest	1.84	0.05	a	1137.97	38.27	h	0.40	0.02	a	18.04	0.91	cd	15.44	0.65	cd	51.83	0.77	d	3.74	0.17	bcde
	liq N	1.38	0.10	a	881.80	46.14	g	0.31	0.03	a	14.16	1.16	abc	10.96	0.77	bc	43.63	2.44	c	2.82	0.16	abc
	−20	1.74	0.08	a	1095.22	71.14	h	0.38	0.02	a	17.32	0.90	cd	13.48	1.12	bc	49.62	2.42	d	3.46	0.34	abcd
'Thornfree'	harvest	18.80	0.77	e	552.60	22.64	cd	108.76	9.18	fg	10.46	0.87	ab	19.50	0.64	de	ND	ND		3.38	0.21	abcd
	liq N	25.37	1.49	g	683.08	25.93	ef	111.08	10.27	fg	10.68	0.98	ab	25.43	1.16	f	ND	ND		4.38	0.64	def
	−20	29.00	0.95	h	910.95	32.73	g	121.00	6.40	g	11.62	0.62	ab	32.90	1.82	g	ND	ND		5.32	0.43	f
harvest		10.90	0.43	A	614.81	34.60	A	66.54	3.79	A	22.65	1.43	A	22.33	0.83	A	40.54	1.10	B	5.56	0.22	A
liq N		11.78	0.62	B	618.58	38.23	A	66.48	5.02	A	22.44	1.43	A	22.56	1.40	A	36.74	1.94	A	5.84	0.42	A
−20		13.96	0.45	C	740.98	41.63	B	80.74	4.29	B	24.72	1.58	B	25.47	1.47	B	36.25	1.56	A	6.79	0.44	B
p treatment		0.0000			0.0000			0.0000			0.0482			0.0015			0.0368			0.0000		
p cultivar		0.0000			0.0000			0.0000			0.0000			0.0000			0.0000			0.0000		
p INT		0.0000			0.0000			0.0000			0.0000			0.0001			0.0028			0.0002		

[a]Liq N, fast freezing method with liquid nitrogen prior to frozen storage; −20, slow freezing method in freezer with no initial fast freezing applied; Cy, cyanidin; Pel, pelargonidin; ND, not detected. [b]Letters a–j in columns denote significant differences (Duncan's test, $p < 0.05$) between interaction (INT) cultivar × treatment; letters A–C in columns denote significant differences (LSD test, $p < 0.05$) among different treatments.

dx.doi.org/10.1021/jf405143w | J. Agric. Food Chem. 2014, 62, 6926−6935

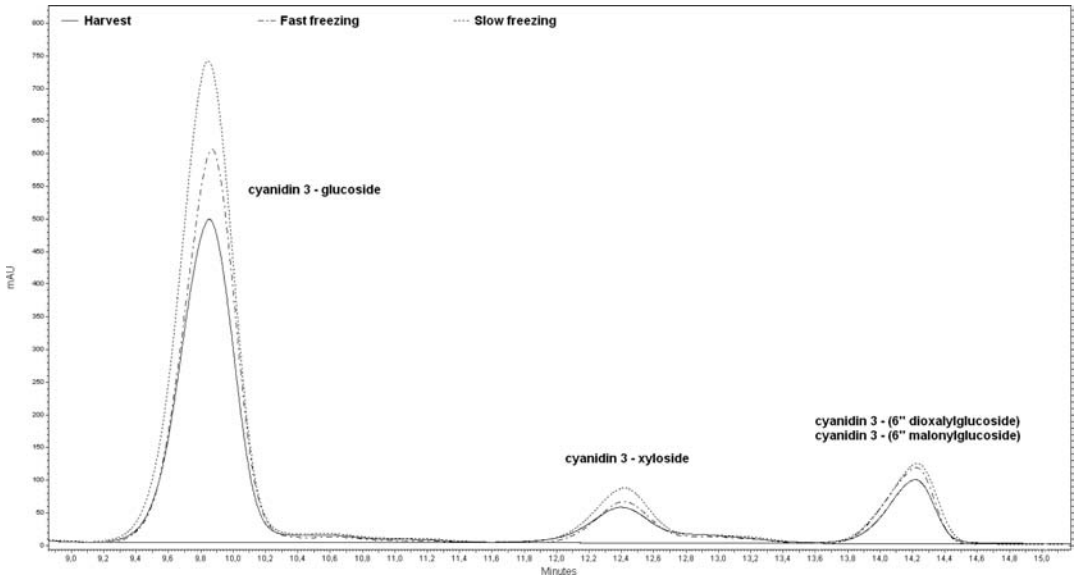

Figure 2. Anthocyanin profile of 'Thornfree' cultivar after dilution of the sample with methanol 1:3. Higher anthocyanin content was characteristic for fruit subjected to freezing treatments and 7 months of storage compared to the harvest sampling.

acid derivatives. Most of these derivatives were better extracted after slow freezing and frozen storage. On the other hand, fast freezing and long-term frozen storage did not exhibit a similar effect. Considering that ellagic acid is a phenolic compound strongly linked to the cell walls,[14,25] damage due to slow freezing could result in better extraction of this specific compound. Blackberry ellagitannins were also reportedly stable during different processing procedures.[8] Contrary to our results, de Ancos et al.[25] reported a 14−21% decrease of extracted ellagic acid after acid hydrolysis in raspberry fruits stored for 12 months. The authors associated this with higher polyphenol oxidase activity linked to the cell wall.

In blackberries, the following anthocyanins yielding the aglycone cyanidin with glycosylation on the 3-position of the C ring have been identified: cyanidin 3-galactoside, cyanidin 3-glucoside, cyanidin 3-arabinoside, cyanidin 3-xyloside, cyanidin 3-(6″-malonylglucoside), and cyanidin 3-(6″-dioxalylglucoside). Additionally, an anthocyanin yielding pelargonidin aglycone and glucose has been confirmed with MS^n analysis in all cultivars, but the amount was rather small (Table 5). All of the quantified anthocyanins have previously been reported in fruita of different blackberry cultivars.[1] 'Loch Ness' and 'Thornless Evergreen' cultivars were the only cultivars in which cyanidin 3-rutinoside has been detected in small amounts, although this anthocyanin is reported as the major anthocyanin of Andean blackberry (*Rubus glaucus*) wines.[26] An additional minor anthocyanin, namely, cyanidin 3-arabinoside, could not be determined in 'Cacanska Bestrna' and 'Chester Thornless' cultivars. Cyanidin 3-glucoside was the prevalent anthocyanin in all analyzed cultivars, ranging from 74.3% of total analyzed blackberry anthocyanins in fruit of the 'Black Satin' cultivar to 92.3% in the 'Loch Ness' cultivar. Cyanidin 3-glucoside was most susceptible to degradation reactions occurring during processing and frozen storage of raspberries.[15] On the contrary, in our study cyanidin 3-glucoside remained relatively stable during blackberry long-term frozen storage or even increased if slow freezing was applied. An example is shown in Figure 2 for cultivar 'Thornfree'.

The amounts of total analyzed anthocyanins differed significantly among analyzed blackberry cultivars; 'Loch Ness' contained the highest and 'Thornless Evergreen' the lowest total anthocyanins levels (Table 4). In combination with a low juice pH value and high anthocyanin content, the juice of the 'Loch Ness' cultivar was characterized by the highest color intensity. Fast freezing with liquid nitrogen and long-term frozen storage did not influence the composition of anthocyanins. All compounds identified in berries at harvest were also present after 7 months of frozen storage. The slow-freezing treatment resulted in higher content of anthocyanins probably due to a better extraction of phenolics compared to the harvest treatment. Conversely, fast freezing did not exhibit an important influence on anthocyanin content. Poiana et al.[22] spectophotometrically analyzed total anthocyanin levels in blueberries and raspberries and reported decreases of 9% after 10 months and 3% after 6 months of storage compared to fresh fruit content. Similarly, Hager et al.[9] determined that quick freezing and frozen storage of intact blackberry fruits did not result in a loss of total analyzed anthocyanins or their polymerization. A cultivar-specific constant or moderately increased content of spectrophotometrically quantified total anthocyanins has been reported in a study of Wu et al.[10] after 6 months of blackberry storage. This is in accordance with our results suggesting that blackberry anthocyanins are protected from degradation when frozen and can be frozen-stored up to no less than 7 months. Ioannou et al.[27] determined that the flavonoid environment is important for understanding flavonoid behavior during food processing and storage. Positive or negative synergies can occur between flavonoids and other compounds in the food matrix, and therefore predictions are difficult to make.

The present study indicates that deep freezing (either fast or slow) is an appropriate way of preserving plant metabolites in blackberry fruits for at least 7 months of frozen storage. The fruit content of most compounds (such as individual anthocyanins) remained constant or even increased due to ice crystal damage of cell structures and better extraction, especially when slow freezing has been applied. The treatment is similar to the conditions consumers generate at home when deep freezing the fruit. However, a loss of vitamin C cannot be prevented during storage, and a fast use of thawed fruits is

necessary. Cultivar-specific composition and content of metabolites have also been demonstrated in the present study and may present an important factor in the choice of healthy fruit. Additional research should be conducted to predict ideal harvest maturity because high anthocyanin content levels cause the fruits to turn black before they are optimally ripe, and long-term experience is needed to select an appropriate picking time, especially because the fruits ripen subsequently.

For further research it is essential to know the composition of fresh fruit and the effect of deep freezing as one of the easiest methods for storing blackberries for off-season use. Therefore, our results can be useful for further studies on food processing and human metabolomic research.

AUTHOR INFORMATION

Corresponding Author

*(R.V.) E-mail: robert.veberic@bf.uni-lj.si. Fax: +386 1 423 10 88. Phone: +386 1 320 31 41.

Funding

This research is part of program Horticulture P4-0013-0481, funded by the Slovenian Research Agency.

Notes

The authors declare no competing financial interest.

REFERENCES

(1) Kaume, L.; Howard, L. R.; Devareddy, L. The blackberry fruit: a review on its composition and chemistry, metabolism and bioavailability, and health benefits. *J. Agric. Food Chem.* **2012**, *60*, 5716−5727.

(2) Schmidl, A.; Oeggl, K. Subsistence strategies of two Bronze Age hill-top settlements in the eastern Alps-Friaga/Bartholomaberg (Vorarlberg, Austria) and Ganglegg/Schluderns (South Tyrol, Italy). *Veg. Hist. Archaeobot.* **2005**, *14*, 303−312.

(3) Mikulic-Petkovsek, M.; Slatnar, A.; Stampar, F.; Veberic, R. HPLC-MSn identification and quantification of flavonol glycosides in 28 wild and cultivated berry species. *Food Chem.* **2012**, *135*, 2138−2146.

(4) Slatnar, A.; Jakopic, J.; Stampar, F.; Veberic, R.; Jamnik, P. The effect of bioactive compounds on in vitro and in vivo antioxidant activity of different berry juices. *PLoS One* **2012**, *7*, DOI: 10.1371/journal.pone.0047880.

(5) Veberic, R.; Trobec, M.; Herbinger, K.; Hofer, M.; Grill, D.; Stampar, F. Phenolic compounds in some apple (*Malus domestica* Borkh) cultivars of organic and integrated production. *J. Sci. Food Agric.* **2005**, *85*, 1687−1694.

(6) Schmitzer, V.; Slatnar, A.; Mikulic-Petkovsek, M.; Veberic, R.; Krska, B.; Stampar, F. Comparative study of primary and secondary metabolites in apricot (*Prunus armeniaca* L.) cultivars. *J. Sci. Food Agric.* **2011**, *91*, 860−866.

(7) Milivojevic, J.; Slatnar, A.; Mikulic-Petkovsek, M.; Stampar, F.; Nikolic, M.; Veberic, R. The influence of early yield on the accumulation of major taste and health-related compounds in black and red currant cultivars (*Ribes* spp.). *J. Agric. Food Chem.* **2012**, *60*, 2682−2691.

(8) Howard, L. R.; Prior, R. L.; Liyanage, R.; Lay, J. O. Processing and storage effect on berry polyphenols: challenges and implications for bioactive properties. *J. Agric. Food Chem.* **2012**, *60*, 6678−6693.

(9) Hager, T. J.; Howard, L. R.; Prior, R. L. Processing and storage effects on monomeric anthocyanins, percent polymeric color, and antioxidant capacity of processed blackberry products. *J. Agric. Food Chem.* **2008**, *56*, 689−695.

(10) Wu, R. Y.; Frei, B.; Kennedy, J. A.; Zhao, Y. Y. Effects of refrigerated storage and processing technologies on the bioactive compounds and antioxidant capacities of 'Marion' and 'Evergreen' blackberries. *LWT−Food Sci. Technol.* **2010**, *43*, 1253−1264.

(11) Petzold, G.; Aguilera, J. M. Ice morphology: fundamentals and technological applications in foods. *Food Biophys.* **2009**, *4*, 378−396.

(12) Brownmiller, C.; Howard, L. R.; Prior, R. L. Processing and storage effects on monomeric anthocyanins, percent polymeric color, and antioxidant capacity of processed blueberry products. *J. Food Sci.* **2008**, *73*, H72−H79.

(13) Kopjar, M.; Jaksic, K.; Pilizota, V. Influence of sugars and chlorogenic acid addition on anthocyanin content, antioxidant activity and color of blackberry juice during storage. *J. Food Process. Preserv.* **2012**, *36*, 545−552.

(14) Turkben, C.; Sariburun, E.; Demir, C.; Uylaser, V. Effect of freezing and frozen storage on phenolic compounds of raspberry and blackberry cultivars. *Food Anal. Methods* **2010**, *3*, 144−153.

(15) de Ancos, B.; Ibanez, E.; Reglero, G.; Cano, M. P. Frozen storage effects on anthocyanins and volatile compounds of raspberry fruit. *J. Agric. Food Chem.* **2000**, *48*, 873−879.

(16) Fragoso, S.; Guasch, J.; Acena, L.; Mestres, M.; Busto, O. Prediction of red wine colour and phenolic parameters from the analysis of its grape extract. *Int. J. Food Sci. Technol.* **2011**, *46*, 2569−2575.

(17) Mikulic-Petkovsek, M.; Slatnar, A.; Schmitzer, V.; Stampar, F.; Veberic, R.; Koron, D. Chemical profile of black currant fruit modified by different degree of infection with black currant leaf spot. *Sci. Hortic.−Amsterdam* **2013**, *150*, 399−409.

(18) Wang, S. Y.; Zheng, W.; Galletta, G. J. Cultural system affects fruit quality and antioxidant capacity in strawberries. *J. Agric. Food Chem.* **2002**, *50*, 6534−6542.

(19) Rein, M. J.; Heinonen, M. Stability and enhancement of berry juice color. *J. Agric. Food Chem.* **2004**, *52*, 3106−3114.

(20) Torskangerpoll, K.; Andersen, O. M. Colour stability of anthocyanins in aqueous solutions at various pH values. *Food Chem.* **2005**, *89*, 427−440.

(21) Milivojevic, J.; Maksimovic, V.; Nikolic, M.; Bogdanovic, J.; Maletic, R.; Milatovic, D. Chemical and antioxidant properties of cultivated and wild *Fragaria* and *Rubus* berries. *J. Food Qual.* **2011**, *34*, 1−9.

(22) Poiana, M. A.; Moigradean, D.; Raba, D.; Alda, L. M.; Popa, M. The effect of long-term frozen storage on the nutraceutical compounds, antioxidant properties and color indices of different kinds of berries. *J. Food Agric. Environ.* **2010**, *8*, 54−58.

(23) Kafkas, E.; Kosar, M.; Turemis, N.; Baser, K. H. C. Analysis of sugars, organic acids and vitamin C contents of blackberry genotypes from Turkey. *Food Chem.* **2006**, *97*, 732−736.

(24) Sousa, M. B.; Canet, W.; Alvarez, M. D.; Tortosa, M. E. The effect of the pre-treatments and the long and short-term frozen storage on the quality of raspberry (cv. Heritage). *Eur. Food Res. Technol.* **2005**, *221*, 132−144.

(25) de Ancos, B.; Gonzalez, E. M.; Cano, M. P. Ellagic acid, vitamin C, and total phenolic contents and radical scavenging capacity affected by freezing and frozen storage in raspberry fruit. *J. Agric. Food Chem.* **2000**, *48*, 4565−4570.

(26) Arozarena, I.; Ortiz, J.; Hermosin-Gutierrez, I.; Urretavizcaya, I.; Salvatierra, S.; Cordova, I.; Marin-Arroyo, M. R.; Noriega, M. J.; Navarro, M. Color, ellagitannins, anthocyanins, and antioxidant activity of Andean blackberry (*Rubus glaucus* Benth.) wines. *J. Agric. Food Chem.* **2012**, *60*, 7463−7473.

(27) Ioannou, I.; Hafsa, I.; Hamdi, S.; Charbonnel, C.; Ghoul, M. Review of the effects of food processing and formulation on flavonol and anthocyanin behaviour. *J. Food Eng.* **2012**, *111*, 208−217.

MATERIALS AND METHODS

Chemicals and Reagents. Ascorbic acid, dehydroascorbic acid, and cetrimide (cetyltrimethylammonium bromide) were purchased from Sigma-Aldrich (Steinheim, Germany); formic acid, methanol, potassium dihydrogen phosphate, and sodium benzoate, all of analytical grade, were from Panreac Química S.A. (Barcelona, Spain). 1,2-Phenylenediamine dihydrochloride (OPDA) was from Fluka Chemika (Neu-Ulm, Germany). Cyanidin 3-glucoside was from Polyphenols (Sandnes, Norway). Milli-Q water used was produced using an Elix3Millipore water purification system coupled to a Milli-Q module (model Adventage10) (Molsheim, France).

Experimental Design. Pomegranate fruits from cv. Mollar de Elche (M) and cv. Wonderful (W), harvested in the Alicante region (southeastern Spain), were provided by "Cambayas Coop. V." (Elche, Alicante, Spain). Pomegranates were cut in halves, and the juices of each cultivar were obtained by pressure with a laboratory pilot press (Zumonat C-40; Somatic AMD, Valencia, Spain).[11,14]

Pomegranate varietal juices were mixed in different proportions: 75% M + 25% W, 50% M + 50% W, and 25% M + 75% W, keeping also two control juices of 100% 'Mollar de Elche' (100% M) and 100% 'Wonderful' (100% W), respectively. Homogenized blended and pure juices were centrifuged (3 min at 2754*g*), and sodium benzoate (200 mg/L) was added to prevent spoilage.[12] Juices were placed in screw-capped vials (10 mL) and stored in the dark at both 5 and 25 °C for 70 days. Triplicate solutions were prepared for each juice, and the mean values were reported in each case. Analyses were carried out at days 0, 6, 13, 20, 28, 42, 56, and 70.

Quality Parameters of Juices. pH, titratable acidity (TA), and total soluble solids (TSS) were evaluated as quality indices.[18] The pH values were measured using a pH-meter (GLP 21, Crison Ltd., Barcelona, Spain). The TA was determined by titrating 2 mL of juice (raised to a 20 mL final volume with Milli-Q water) with 0.1 N NaOH (pH 8.1). Results were expressed as grams of anhydrous citric acid per 100 mL. TSS contents were recorded in a hand refractometer (Atago N1, Atago, Tokyo, Japan) at 20 °C with values being expressed as °Brix. Measurements were repeated twice for each replicate. Ratio, also known as maturity index (MI), was calculated as the relationship between TSS and TA.

Identification and Quantification of Anthocyanins. The anthocyanin profile of pomegranate juices was assessed by liquid chromatography coupled to mass spectrophotometry (HPLC-ESI-MS^n), according to the method of Gironés-Vilaplana.[19] HPLC analyses for anthocyanin quantification were performed on a Merck-Hitachi liquid chromatograph (Tokyo, Japan), equipped with a diode array detector UV−vis L-7455, an autosampler L-7200, a pump L-7100, and an interface D-7000. Chromatograms were recorded and processed on a Merck-Hitachi D-7000 HSM PC-based chromatography data system. A 20 μL sample was analyzed on a Luna C_{18} column (25 cm × 0.46 cm, 5 μm particle size; Phenomenex, Macclesfield, UK) with a security guard C18-ODS (4.0 × 3.0 mm) cartridge system (Phenomenex), using a mobile phase of water/formic acid (95:5, v/v) (solvent A) and HPLC grade methanol (solvent B). Elution was performed at a flow rate of 1 mL/min. The linear gradient started with 1% B, remaining at isocratic conditions during 5 min, reaching 20% B at 20 min, 40% B at 30 min, 95% B at 35 min, and 1% B after 41 min. UV chromatograms were recorded at 520 nm. Anthocyanins were quantified by the absorbance of their corresponding peaks as cyanidin 3-glucoside.

Prior to injection, samples were centrifuged during 5 min at 10480*g* (model EBA 21, Hettich Zentrifugen, Tuttlingen, Germany) at room temperature. The supernatant was filtered through a 0.45 μm nylon membrane (Simplepure; Membrane Solutions, Plano, TX, USA) before HPLC analysis.

Extraction and Analysis of Vitamin C. Ascorbic acid (AA) and dehydroascorbic acid (DHAA) contents were determined by HPLC-UV as described elsewhere and fully detailed in González-Molina et al.[20] The vitamin C content was calculated by the addition of ascorbic acid and dehydroascorbic acid contents, and results were expressed as milligrams per 100 mL.

Color Measurement. Color measurement was determined as in Pérez-Vicente et al.[11] Samples were measured in glass cells of 2 mm path length (CT-A22) at 520 nm using a Minolta CM-508i tristimulus color spectrophotometer (Osaka, Japan) coupled with a CM-A760 transmittance adaptor, illuminant D65, and 10° observer according to the CIELAB 76 convention. Data (CIE L^*, CIE a^*, CIE b^*, chroma, and hue angle) were processed using the Minolta Software Chromacontrol S, PC-based colorimetric data system.

Statistical Analyses and Kinetics of Phytochemical Degradation. Analysis of variance (ANOVA) and multiple-range tests (Scheffé's test) were carried out using the IBM SPSS Statistics 19 software package (SPSS Inc., Chicago, IL, USA). Pearson correlation analyses were also performed.

The degradation kinetics of most phytochemicals follows the first-order eq 1 reaction[21,22]

$$C_t = C_0 \exp(\pm kt) \quad (1)$$

where C_t and C_0 are the concentration of bioactive compounds (anthocyanins and vitamin C) (mg/100 mL) at time t and t_0, respectively, k is the rate constant, and t is the storage time (days). Moreover, the half-life value ($t_{1/2}$) was calculated as $t_{1/2} = ((\ln 2)/k)$. D value (time required for 90% degradation of bioactive) was also calculated as $D = (1/k)$.

RESULTS AND DISCUSSION

Quality Parameters of Juices. No significant differences ($p > 0.05$) in the quality parameters (pH, TSS, TA, and MI) assayed during storage were noted and, hence, results are presented as mean values for all of the experiments (Table 1).

Table 1. Quality Parameters of Pure and Blended Varietal Pomegranate Juices through the Storage Period

juice	pH	TSS[a]	TA[b]	MI[c]
100% M	3.58 a[d]	16.75 e	0.27 e	63.2 a
75% M + 25% W	3.11 b	17.10 d	0.64 d	26.9 b
50% M + 50% W	2.92 c	17.50 c	1.09 c	16.1 c
25% M + 75% W	2.81d	17.85 b	1.39 b	12.9 cd
100% W	2.76 e	18.20 a	1.78 a	10.3 d
LSD[e]	0.01***	0.04***	0.01***	0.86***

[a]TSS, total soluble solids. [b]TA, titratable acidity (g citric acid/100 mL). [c]MI, maturity index (TSS/TA). Statistical treatment notes. [d]Means (n = 3) within a column followed by different letters are significantly different at $P < 0.05$ according to the Scheffé multiple range test. [e]LSD, least significant difference. Significant at (*) $P < 0.05$, (**) $P < 0.01$, and (***) $P < 0.001$.

The pH values in the juices decreased with the percentage of 'Wonderful' juice added, varying from ∼3.60 to ∼2.70 for 100% M and 100% W, respectively. TSS ranged between ∼16.7 for 100% M and ∼18.2 for 100% W, which cannot be considered an important difference despite its statistical significance. Otherwise, TA displayed severe differences among juices, oscillating between ∼0.30 and ∼1.80 g/100 mL for 100% M and 100% W, respectively. Acidity was augmented with increasing percentage of 'Wonderful' juice added in a dose−response effect, as expected. Consequently, the maturity index (MI), which is mainly influenced by TA for pomegranate juices,[14] was depleted as the 'Wonderful' juice proportion was increased in the blended juices.

The pomegranate cultivars chosen to develop the blended juices were widely distinct. 'Wonderful' is a worldwide variety rich in phytochemicals, with a deep red color, but too much acid. On the other hand, the Spanish 'Mollar de Elche' exhibits interesting organoleptical properties (high lightness and

elevated sweetness/sourness balance), although it is prone to suffer browning during processing and storage.[14] Both varietal juices might serve as complementary ones because the addition of 'Wonderful' to 'Mollar de Elche' juices could ameliorate the visual appearance of browning[10] as well as 'Mollar de Elche' addition to 'Wonderful' juices could improve their sensory properties by smoothing their high acidity. Moreover, a point worth mentioning is that pomegranate juices mixed at different percentages of each variety presented intermediate values of pH (Table 1). This fact turned these mixtures into valuable samples to study the degradation of anthocyanins at different pH conditions within a similar complex matrix, avoiding the oversimplification of common model systems.[23,24]

Evolution of Anthocyanins in Blended Varietal Pomegranate Juices. The anthocyanin profile of pomegranate juices was characterized by delphinidin, cyanidin, and pelargonidin 3-glucosides and 3,5-diglucosides (Table 2; Figures 1 and 2), in accordance with previous papers.[2,25] The amounts of these colored flavonoids were largely affected by the cultivar group, and total anthocyanin concentrations ranged from 23 to 171 mg/100 mL for 100% M and 100% W, respectively, in good agreement with those previously reported by Mena et al.[14] Varietal blends exhibited intermediate values according the proportion of varietal juices used, as expected. Major individual anthocyanins for all juices were cyanidin 3-glucoside, accounting for 31% of the total anthocyanin amount; delphinidin glycosides, both 3,5-diglucoside and 3-glucoside, 23% each one; and cyanidin 3,5-diglucoside, 20%. Pelargonidin glycosides accounted for only 3% of the total anthocyanins.

Table 2. Identification of Anthocyanins in Pomegranate Juice by HPLC-ESI-MS^n (Positive Mode)

ID	compound	RT (min)	$[M]^+$ (m/z)	MS^2 ion fragments (m/z)[a]	MS^3 ion fragments (m/z)
1	delphinidin 3,5-diglucoside	25.1	627	**465**,[b] 303	303
2	cyanidin 3,5-diglucoside	26.6	611	**449**, 287	287
3	pelargonidin 3,5-diglucoside	28.1	595	**433**, 271	271
4	delphinidin 3-glucoside	29.5	465	**303**	
5	cyanidin 3-glucoside	31.2	449	**287**	
6	pelargonidin 3-glucoside	32.7	433	**271**	

[a]Fragment ions are listed in order of relative abundances. [b]MS^2 ions in bold were those subjected to MS^3 fragmentation.

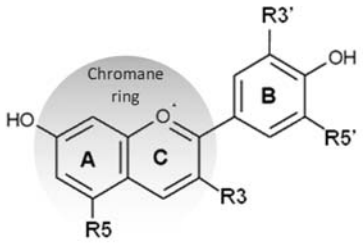

Anthocyanin	R3'	R5'	R3	R5
Pelargonidin 3-glucoside	H	H	Glc	OH
Pelargonidin 3,5-diglucoside	H	H	Glc	Glc
Cyanidin 3-glucoside	OH	H	Glc	OH
Cyanidin 3,5-diglucoside	OH	H	Glc	Glc
Delphinidin 3-glucoside	OH	OH	Glc	OH
Delphinidin 3,5-diglucoside	OH	OH	Glc	Glc

Figure 1. Chemical structures of the anthocyanins found in pomegranate juices. Glc, glucose.

The loss of anthocyanins during storage (Figure 3) fitted well to exponential curves for the two selected temperatures (Table 3). These results indicated that pigment degradation at isothermal conditions followed first-order reaction kinetics, as usually reported for red juices.[4,10,21,22] The rate constant (k) increased at higher storage temperature, pointing out the notable influence of temperature on accelerated anthocyanin degradation.[8,22] Half-life values ($t_{1/2}$) ranged from 98 to 374 days at 5 °C and between 28 and 87 for 25 °C. D values pointing out the time required for the degradation of 90% of anthocyanins ranged between 141 and 539 days for juices stored at 5 °C and between 40 and 125 days at 25 °C. These differences of pigment shelf life between storage temperatures showed the role of the storage conditions in the preservation of the phytochemical composition of pomegranate juices. A point worth mentioning is that the shelf life values herein reported were considerably higher than those reported for thermally pasteurized pomegranate juices.[8−10] This fact emphasizes the need for developing novel approaches avoiding thermal treatments and limiting microbial load at fresh juice to preserve as much as possible the anthocyanin content of commercial pomegranate juices.

Kinetic parameters (Table 3) revealed a significant cultivar effect on the evolution of anthocyanins during storage at both 5 and 25 °C. The rate constant was clearly higher as the proportion of ;Mollar de Elche; juice was increased, the highest rate constants being recorded for 100% M. One hundred percent W juice registered rate constants 3.7- and 3.1-fold lower than those found for 100% M at 5 and 25 °C, respectively.

The blended juices used in the present work could be regarded as suitable samples to shed light on the factors behind the so-called cultivar effect. They displayed intermediate k values proving that drops in anthocyanins were diminished in the mixtures proportionally to the percentage of 'Wonderful' juice added (Table 3). Then, the blend containing merely 25% of 'Wonderful' juice (75% M + 25% W) could not only increase the anthocyanin content of 'Mollar de Elche'-based pomegranate juices but also preserve to a great extent the pigment composition through storage. In this sense, data herein obtained have shown that the higher pigment concentration, the lower degradation rate (Table 3). This phenomenon linking superior preservation to high anthocyanin concentrations could be attributed mainly to the formation of self-association complexes of copigmentation (the aggregation of different anthocyanin monomers in relatively concentrated matrixes).[26] Similarly, other complexes, adducts between flavan-3-ols and anthocyanins, have been found in fresh pomegranate juices.[27]

Another explanation behind the cultivar effect observed and the higher preservation of anthocyanins in those juices containing a higher percentage of 'Wonderful' varietal juice could be related to the effect of pH. Actually, a higher stability of anthocyanins is linked to lower pH values.[6] Differences of pH recorded for 50% M + 50% W, 25% M + 75% W, and 100% W (between 2.92 and 2.76, Table 1) were not so dramatic as the differences observed for anthocyanin shelf life in these same juices (Table 3). However, the stability of anthocyanins could be severely compromised at this restricted pH range

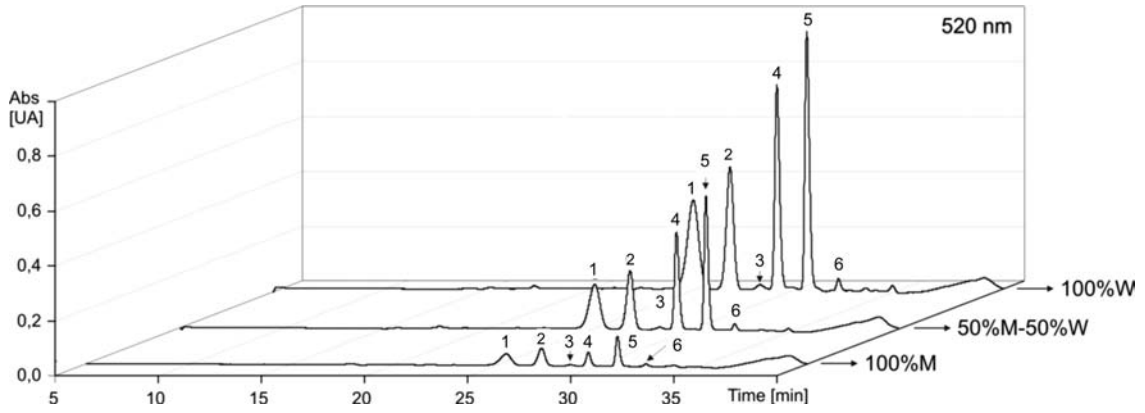

Figure 2. Chromatographic profile at 520 nm of anthocyanins registered in pomegranate juices. Peaks: (1) delphinidin 3,5-diglucoside; (2) cyanidin 3,5-diglucoside; (3) pelargonidin 3,5-diglucoside; (4) delphinidin 3-glucoside; (5) cyanidin 3-glucoside; (6) pelargonidin 3-glucoside.

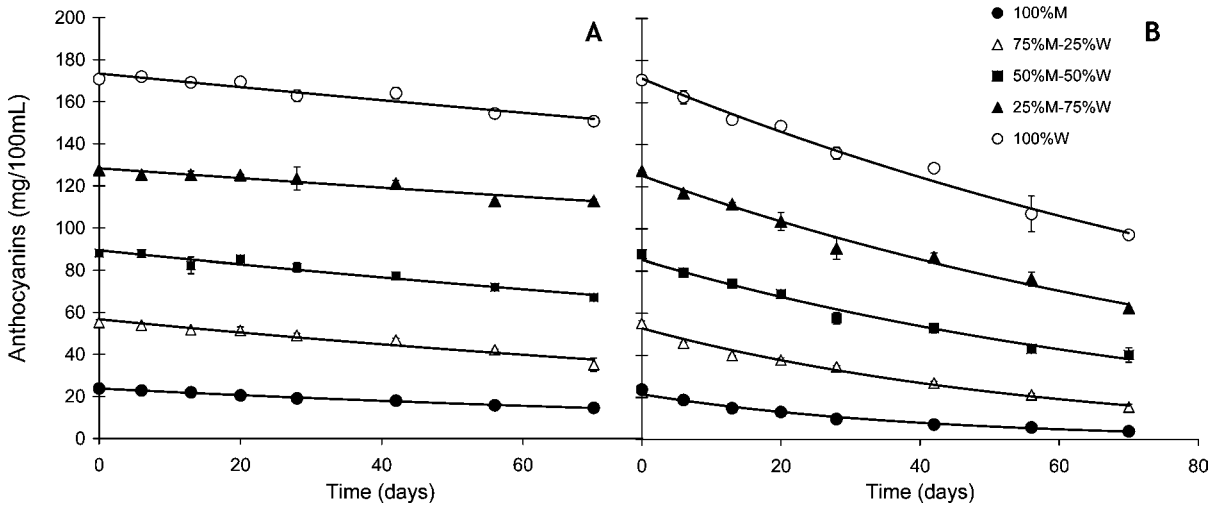

Figure 3. Total anthocyanin content of pomegranate juices and their first-order degradation kinetics under different storage temperatures: (A) 5 °C; (B) 25 °C. Error bars are presented as standard error of the mean (SEM). For corresponding kinetic parameters cf. Table 3.

Table 3. Kinetic Parameters of Anthocyanin Degradation in Pomegranate Juices during Storage at Different Temperatures

storage temp (°C)	juice	variation kinetics (concentration in mg/100 mL)	R^2	$-k \times 10^3$ (day^{-1})	$t_{1/2}$ (days)	D value (days)
5	100% M	$y = 23.8\ \exp(-0.00707x)$	0.984	7.1	98.1	141.5
	75% M + 25% W	$y = 56.7\ \exp(-0.00588x)$	0.931	5.9	117.8	169.9
	50% M + 50% W	$y = 89.4\ \exp(-0.00384x)$	0.954	3.8	180.3	260.1
	25% M + 75% W	$y = 128.4\ \exp(-0.00186x)$	0.907	1.9	373.6	539.0
	100%	$y = 173.4\ \exp(-0.00190x)$	0.922	1.9	365.6	527.5
25	100% M	$y = 21.5\ \exp(-0.02476x)$	0.988	24.8	28.0	40.4
	75% M + 25% W	$y = 52.9\ \exp(-0.01689x)$	0.988	16.9	41.0	59.2
	50% M + 50% W	$y = 85.3\ \exp(-0.01147x)$	0.981	11.5	60.4	87.2
	25% M + 75% W	$y = 125.3\ \exp(-0.00955x)$	0.983	9.5	72.6	104.8
	100% W	$y = 171.5\ \exp(-0.00799x)$	0.986	8.0	86.8	125.2

considering how pH affects the equilibrium of anthocyanin structures (quinoidal base/flavylium cation) and pigment stability.[6] On the basis of these results, both pigment concentration and pH should be regarded as factors affecting anthocyanin stability and contributing to the cultivar effect. Finally, the superior content in citric acid of 'Wonderful' juice compared to 'Mollar de Elche'[14] may also contribute to the definition of the cultivar effect observed on anthocyanin stability.

Concerning structure stability, it could be pointed out that diglucosides were more stable than monoglucosides in those samples stored at 5 °C (5 and 24% of loss, respectively), as it is usually described attending to anthocyanin stability.[6,9,11,13,18] However, juices stored at 25 °C showed a different trend, and monoglucosides were revealed as the most stable anthocyanins (48% of loss for monoglucosides and 56% for diglucosides).

On the whole, decreases in the anthocyanin amounts could be explained attending to several processes taking part during storage: (1) polymerization reactions involving the condensa-

dx.doi.org/10.1021/jf405129q | J. Agric. Food Chem. 2014, 62, 6936−6943

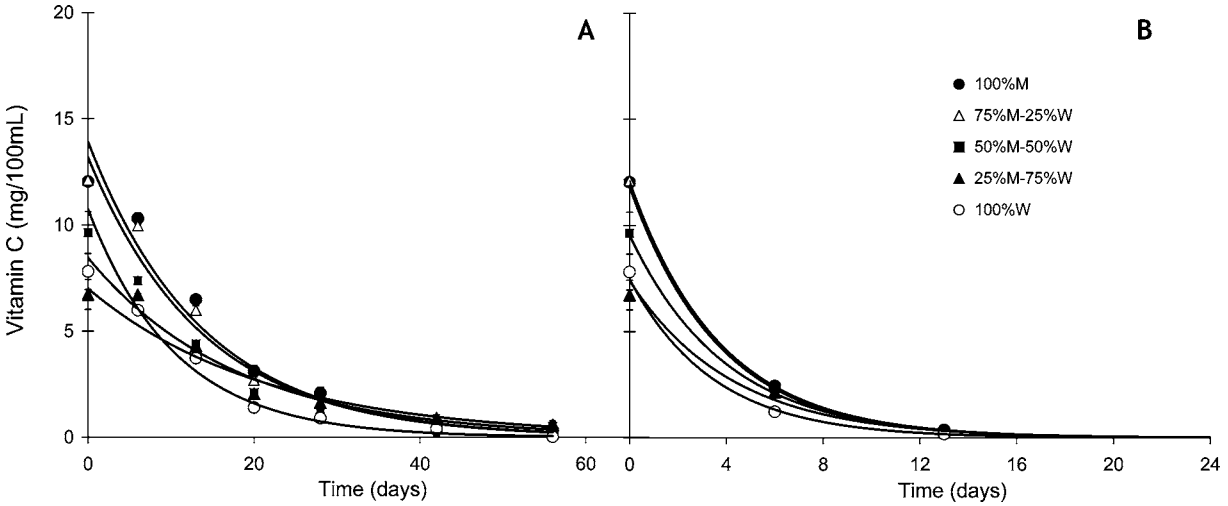

Figure 4. Vitamin C content of pomegranate juices and their first-order degradation kinetics under different storage temperatures: (A) 5 °C; (B) 25 °C. Error bars are presented as SEM. For corresponding kinetic parameters cf. Table 4.

Table 4. Kinetic Parameters of Vitamin C Degradation in Pomegranate Juices during Storage at Different Temperatures

storage temp (°C)	juice	variation kinetics (concentration in mg/100 mL)	R^2	$-k \times 10^3$ (day^{-1})	$t_{1/2}$ (day)	D value (day)
5	100% M	$y = 13.9\ \exp(-0.07254x)$	0.957	72.5	9.6	13.8
	75% M + 25% W	$y = 13.2\ \exp(-0.07216x)$	0.991	72.2	9.6	13.9
	50% M + 50% W	$y = 8.4\ \exp(-0.05609x)$	0.951	56.1	12.4	17.8
	25% M + 75% W	$y = 7.0\ \exp(-0.04719x)$	0.963	47.2	14.7	21.2
	100% W	$y = 10.7\ \exp(-0.09525x)$	0.952	95.3	7.3	10.5
25	100% M	$y = 12.1\ \exp(-0.26761x)$	0.999	267.6	2.6	3.7
	75% M + 25% W	$y = 11.8\exp(-0.27190x)$	0.999	271.9	2.5	3.7
	50% M + 50% W	$y = 9.5\ \exp(-0.25262x)$	0.999	252.6	2.7	4.0
	25% M + 75% W	$y = 7.4\ \exp(-0.23705x)$	0.990	237.1	2.9	4.2
	100% W	$y = 7.5\ \exp(-0.28721x)$	0.999	287.2	2.4	3.5

tion of anthocyanins with byproducts from the degradation of monosaccharides and organic acids, yielding furfurals and aldehyde compounds; (2) the occurrence of enzymes degrading anthocyanins; and (3) direct oxidation of anthocyanin with oxygen.[6,28,29]

Vitamin C Degradation and Its Relationship with Anthocyanins. Although pomegranate juice is not distinguished by possessing high vitamin C concentrations, it may play an important role in browning processes and anthocyanin degradation.[12]

Vitamin C was detected only in its oxidized form (dehydroascorbic acid). Its initial concentrations were 12.0 and 7.8 mg/100 mL for 100% M and 100% W, respectively. Vitamin C decreased following a first-order reaction kinetic at both selected temperatures through storage (Figure 4; Table 4). The rate constant (k) increased at higher storage temperature, the rate constant at 25 °C being up to 4-fold the rate constant recorded for the samples stored at 5 °C. This fact had a remarkable effect on the shelf life of vitamin C. Actually, whereas the half-life value ($t_{1/2}$) of juices stored at 5 °C ranged from 7 until 15 days, samples stored at 25 °C solely exhibited half-life values of 2.5 days. D values varied between 10 and 21 days for storage at 5 °C and were about 4 days at 25 °C. The degradation of vitamin C was not related to a certain cultivar pattern (Figure 4; Table 4).

The fast reduction in vitamin C content of pomegranate juices with added ascorbic acid has been attributed to pH and the presence of anthocyanins.[12] However, vitamin C has been preserved in juices combining lemon and pomegranate juices at different rates, where the influence of pH seemed to be negligible and, hence, this hypothesis should be ruled out.[18] On the other hand, whereas anthocyanins seem to play an essential role in vitamin C degradation,[7] decreases in vitamin C content were observed among all samples regardless of the kind of juice (Figure 4) and, thus, regardless of the anthocyanin content in the sample. Consequently, it is possible that endogenous vitamin C of pomegranate juices decreases without attending any contribution of external factors and due exclusively to its natural oxidative deterioration.

Color Parameters and the Role of Anthocyanins in Color Changes. Juice color varied significantly among varietal juices through storage (Figure 5). Lightness of pomegranate juices, represented as CIEL^* values, was in accordance with a previous study.[14] One hundred percent M showed the highest lightness, whereas 100% W displayed the lowest one. Significant differences were noted among varietal juices by the end of the storage period ($p < 0.001$) (Figure 5A,B). Whereas lightness of blended juices (75% M + 25% W, 50% M + 50% W, and 25% M + 75% W) and 100% W increased only slightly from day 42, a reduction was registered for 100% M for the first 42 days, prior to the final augment recorded (Figure 5A,B). General increases of lightness were in agreement with the trend followed by other unpasteurized pomegranate juices.[6,9,11,13,18]

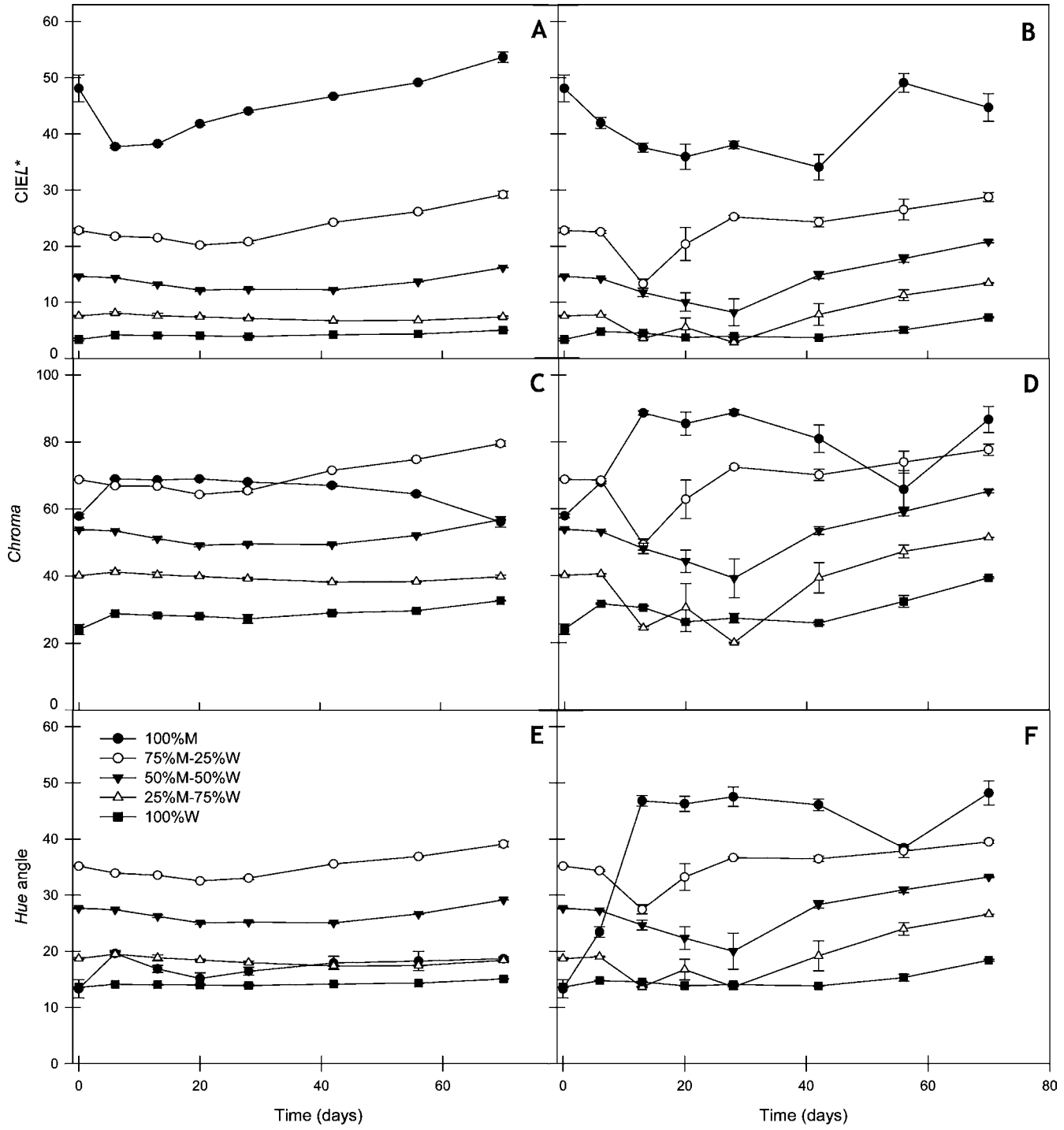

Figure 5. Evolution of color parameters in pure and blended varietal pomegranate juices through storage: CIE*L** in samples stored at (A) 5 °C and (B) 25 °C; chroma at (C) 5 °C and (D) 25 °C (D); hue angle at (E) 5 °C and (F) 25 °C. Error bars are presented as SEM.

Initial chroma values of blended juices were not the sum of their parts, and a different trend occurred among juices attending to their composition (Figure 5C,D). One hundred percent W and blended juices decreased and, then, increased during storage. On the contrary, 100% M was augmented and then decreased. These results stressed the significance of cultivar effect on the evolution of color intensity just as its influence on mixtures of different varietal juices. Similarly, a notable varietal effect was observed for hue angle (Figure 5E,F), especially in those samples stored at room temperature. Hue values of 100% W juice were preserved during storage at both temperatures, and they increased only slightly in blended juices. On the other hand, hue of 100% M juice was significantly increased during the first days, especially at 25 °C (Figure 5F), and then remained constant for the rest of the experiment. These color changes were consistent with the general increase of brownish hues reported for pomegranate juices.[9,11,12,18]

Changes oin CIE*L** and chroma values could be attributed to anthocyanins as a strong significant correlation was found among them ($r = -0.86$, $r = -0.89$, respectively; $p < 0.01$). However, anthocyanin degradation cannot fully account for the variations in hue angle values ($r = -0.66$; $p < 0.01$), so other

dx.doi.org/10.1021/jf405129q | J. Agric. Food Chem. 2014, 62, 6936−6943

compounds such as those formed as a consequence of browning processes (e.g., ascorbic acid degradation) or anthocyanin polymerization may contribute to hue variations.[8,12]

Color parameters as well as anthocyanin load in blended varietal pomegranate juices was mainly influenced by 'Wonderful' cultivar and not by 'Mollar de Elche'. In fact, despite the significant color variations in 100% M, a high stability of color parameters was observed in the blended juices, even for that juice containing merely 25% of 'Wonderful' juice (75% M + 25%W). This blend may also exhibit a great organoleptic potential as it preserves the genuine sensorial characteristics of the cultivar 'Mollar de Elche' (data not shown).[14] Consequently, blending different pomegranate juices could be regarded as an easy way to preserve juice color characteristics and pigment concentration of those varieties prone to color alterations such as 'Mollar de Elche'. These protective effects on the anthocyanin composition and color attributes of some of these blends could remain after realistic pasteurization treatments.[10] Therefore, the results herein presented may have direct implications for the pomegranate juice industry to solve browning problems during juice storage. Blending varietal pomegranate juices was useful not only to preserve the genuine characteristics of fresh juices but also to study different factors affecting anthocyanin stability while maintaining to the utmost the matrix studied. The role of anthocyanin concentration, pH, and the presence of ascorbic acid in pigment integrity was discussed, and it could contribute to the definition of cultivar effect in pomegranate juices. Finally, the present data could help to tackle anthocyanin degradation in other food matrices.

AUTHOR INFORMATION

Corresponding Author

*(C.G.-V.) CEBAS-CSIC Phytochemistry Lab, Research Group on Quality, Safety and Bioactivity of Plant Foods Food Science and Technology Department, P.O. Box 164, E-30100 Espinardo, Murcia, Spain. Phone: +34 968 396304. Fax: +34 968 396213. E-mail: cgviguera@cebas.csic.es.

Funding

We thank Fundación Agroalimed for financial support of this work (Project "Producción de Zumo de Caqui e Industrialización de Granada"). We are grateful to the Consolider-Ingenio 2010 Fun-C-Food project (CSD2007-00063) and "Grupo de Excelencia de la Región de Murcia" (04486/GERM/06). P.M. was funded by a grant of the FPU Fellowship Program from the Spanish Ministry of Education.

Notes

The authors declare no competing financial interest.

ACKNOWLEDGMENTS

We thank Dr. Raúl Domínguez-Perles for technical support with the graphic design.

REFERENCES

(1) Mena, P.; Gironés-Vilaplana, A.; Moreno, D. A.; García-Viguera, C. Pomegranate fruit for health promotion: myths and realities *Funct. Plant Sci. Biotechnol.* **2011**, *5*, 33−42.

(2) Gil, M. I.; García-Viguera, C.; Artés, F.; Tomás-Barberán, F. A. Changes in pomegranate juice pigmentation during ripening. *J. Sci. Food Agric.* **1995**, *68*, 77−81.

(3) Fischer, U. A.; Carle, R.; Kammerer, D. R. Identification and quantification of phenolic compounds from pomegranate (*Punica granatum* L.) peel, mesocarp, aril and differently produced juices by HPLC-DAD-ESI/MS^n. *Food Chem.* **2011**, *127*, 807−821.

(4) Maskan, M. Production of pomegranate (*Punica granatum* L.) juice concentrate by various heating methods: colour degradation and kinetics. *J. Food Eng.* **2006**, *72*, 218−224.

(5) Timberlake, C. F. Anthocyanins − occurrence, extraction and chemistry. *Food Chem.* **1980**, *5*, 69−80.

(6) Castañeda-Ovando, A.; Pacheco-Hernández, M. d. L.; Páez-Hernández, M. E.; Rodríguez, J. A.; Galán-Vidal, C. A. Chemical studies of anthocyanins: a review. *Food Chem.* **2009**, *113*, 859−871.

(7) Jurd, L. Some advances in the chemistry of anthocyanin-type plant pigments. *Chem. Plant Pigments* **1972**, 123−142.

(8) Alighourchi, H.; Barzegar, M. Some physicochemical characteristics and degradation kinetic of anthocyanin of reconstituted pomegranate juice during storage. *J. Food Eng.* **2009**, *90*, 179−185.

(9) Fischer, U. A.; Dettmann, J. S.; Carle, R.; Kammerer, D. R. Impact of processing and storage on the phenolic profiles and contents of pomegranate (*Punica granatum* L.) juices. *Eur. Food Res. Technol.* **2011**, *233*, 797−816.

(10) Mena, P.; Martí, N.; Saura, D.; Valero, M.; García-Viguera, C. Combinatory effect of thermal treatment and blending on the quality of pomegranate juices. *Food Bioprocess Technol.* **2013**, *6*, 3186−3199.

(11) Pérez-Vicente, A.; Serrano, P.; Abellán, P.; García-Viguera, C. Influence of packaging material on pomegranate juice colour and bioactive compounds, during storage. *J. Sci. Food Agric.* **2004**, *84*, 639−644.

(12) Martí, N.; Pérez-Vicente, A.; García-Viguera, C. Influence of storage temperature and ascorbic acid addition on pomegranate juice. *J. Sci. Food Agric.* **2002**, *82*, 217−221.

(13) Alighourchi, H.; Barzegar, M.; Abbasi, S. Anthocyanins characterization of 15 Iranian pomegranate (*Punica granatum* L.) varieties and their variation after cold storage and pasteurization. *Eur. Food Res. Technol.* **2008**, *227*, 881−887.

(14) Mena, P.; García-Viguera, C.; Navarro-Rico, J.; Moreno, D. A.; Bartual, J.; Saura, D.; Martí, N. Phytochemical characterisation for industrial use of pomegranate (*Punica granatum* L.) cultivars grown in Spain. *J. Sci. Food Agric.* **2011**, *91*, 1893−1906.

(15) Mena, P.; Vegara, S.; Martí, N.; García-Viguera, C.; Saura, D.; Valero, M. Changes on indigenous microbiota, colour, bioactive compounds and antioxidant activity of pasteurised pomegranate juice. *Food Chem.* **2013**, *141*, 2122−2129.

(16) Vegara, S.; Martí, N.; Mena, P.; Saura, D.; Valero, M. Effect of pasteurization process and storage on color and shelf-life of pomegranate juices. *LWT−Food Sci. Technol.* **2013**, *54*, 592−596.

(17) Vegara, S.; Mena, P.; Martí, N.; Saura, D.; Valero, M. Approaches to understanding the contribution of anthocyanins to the antioxidant capacity of pasteurized pomegranate juices. *Food Chem.* **2013**, *141*, 1630−1636.

(18) González-Molina, E.; Moreno, D. A.; García-Viguera, C. A new drink rich in healthy bioactives combining lemon and pomegranate juices. *Food Chem.* **2009**, *115*, 1364−1372.

(19) Gironés-Vilaplana, A.; Valentão, P.; Moreno, D. A.; Ferreres, F.; García-Viguera, C.; Andrade, P. B. New beverages of lemon juice enriched with the exotic berries maqui, açaí, and blackthorn: bioactive components and in vitro biological properties. *J. Agric. Food Chem.* **2012**, *60*, 6571−6580.

(20) González-Molina, E.; Moreno, D. A.; García-Viguera, C. Genotype and harvest time influence the phytochemical quality of fino lemon juice (*Citrus limon* (L.) Burm. F.) for industrial use. *J. Agric. Food Chem.* **2008**, *56*, 1669−1675.

(21) Garzón, G. A.; Wrolstad, R. E. Comparison of the stability of pelargonidin-based anthocyanins in strawberry juice and concentrate. *J. Food Sci.* **2002**, *67*, 1288−1299.

(22) Kirca, A.; Özkan, M.; Cemeroğlu, B. Storage stability of strawberry jam color enhanced with black carrot juice concentrate. *J. Food Process. Preserv.* **2007**, *31*, 531−545.

(23) Hernández-Herrero, J. A.; Frutos, M. J. Degradation kinetics of pigment, colour and stability of the antioxidant capacity in juice model

systems from six anthocyanin sources. *Int. J. Food Sci. Technol.* **2011**, *46*, 2550−2557.
(24) Sadilova, E.; Stintzing, F. C.; Kammerer, D. R.; Carle, R. Matrix dependent impact of sugar and ascorbic acid addition on color and anthocyanin stability of black carrot, elderberry and strawberry single strength and from concentrate juices upon thermal treatment. *Food Res. Int.* **2009**, *42*, 1023−1033.
(25) Mena, P.; Calani, L.; Dall'Asta, C.; Galaverna, G.; García-Viguera, C.; Bruni, R.; Crozier, A.; Del Rio, D. Rapid and comprehensive evaluation of (poly)phenolic compounds in pomegranate (*Punica granatum* L.) juice by UHPLC-MS^n. *Molecules* **2012**, *17*, 14821−14840.
(26) Boulton, R. The copigmentation of anthocyanins and its role in the color of red wine: a critical review. *Am. J. Enol. Vitic.* **2001**, *52*, 67−87.
(27) Sentandreu, E.; Navarro, J. L.; Sendra, J. M. LC-DAD-ESI/MS^n determination of direct condensation flavanol-anthocyanin adducts in pressure extracted pomegranate (*Punica granatum* L.) juice. *J. Agric. Food Chem.* **2010**, *58*, 10560−10567.
(28) Ochoa, M. R.; Kesseler, A. G.; Vullioud, M. B.; Lozano, J. E. Physical and chemical characteristics of raspberry pulp: storage effect on composition and color. *LWT−Food Sci. Technol.* **1999**, *32*, 149−153.
(29) Eiro, M. J.; Heinonen, M. Anthocyanin color behavior and stability during storage: effect of intermolecular copigmentation. *J. Agric. Food Chem.* **2002**, *50*, 7461−7466.

mercaptan.[12] In those conditions, interflavan linkages are disrupted and the flavanol units corresponding to extension and upper units of condensed tannins are liberated in the medium as flavanyl carbocations immediately converted into stable monomeric derivatives after trapping by the nucleophilic agent. At the same time, terminal flavanol units of condensed tannins are liberated as such in the reaction medium. Then, all of these reaction products can be easily separated and quantified by reversed phase HPLC.[13]

Apple flavonols are a series of quercetin (Q) glycosides namely: galactoside (hyperoside, generally the most concentrated), Q-3-*O*-glucoside (isoquercitrin), Q-3-*O*-rhamnoside (quercitrin), Q-3-*O*-rutinoside (rutin), Q-3-*O*-xyloside (reynoutrin), and Q-3-*O*-arabinoside (avicularin). Flavonols are yellow compounds mainly located in the peel of fruits and are poorly extractable. Therefore, juices and ciders are usually almost deprived of these components.[14] Among usually consumed fruits and fruit-derived foods, dihydrochalcones are the only group of flavonoids that can be considered specific for apples, although they can be present in low concentration in other species. One well-known compound of this class, namely, phloridzin (phloretin-2-glucoside), is present in apple tissues and apple juices and was also studied for its potential phytoestrogen activity.[15] In addition, phloridzin is considered as a feature compound for the adulteration of beverages with apple juice and hence used for quality control.[16] Phloridzin is also widely applied in the food, cosmetic, and pharmaceutical industries.[17]

Different from popular apple species, red-fleshed ones are characterized by high amounts of anthocyanins.[18,19] According to Sadilova et al.,[18] anthocyanins of the red-fleshed 'Weirouge' apples were mainly located in the peel at a concentration about 2.5 times higher than in the flesh. In both studies concerning 'Weirouge'[18] or 'Niedzwiedzkyana'[19] varieties, the anthocyanin class is mainly represented by cyanidin-3-*O*-galactoside (namely, ideain), although other cyanidin glycosides such as xyloside, arabinoside, rhamnoside, and glucoside have been also detected and quantified.[18] Interestingly, juices from red-fleshed varieties containing high levels of cyanidin-3-*O*-galactoside were generally the ones showing also a high antioxidant capacity.[19]

The fact that anthocyanins exist as several forms in equilibrium depending on the pH is well documented.[20,21] At low pH (~3), the colored flavylium cation form of anthocyanins is significantly present and is more stable. As the pH increases, colorless species (i.e., carbinol pseudobase and chalcones) may significantly contribute to this equilibrium.

Apple varieties strongly differ in quantitative content of each polyphenol.[7,9,22] The same was observed by comparing apples and juices made of them. According to Guyot et al.,[23] the extraction rates of hydroxycinnamic acids, dihydrochalcones, and flavanols during juice production differ according to variety. However, in general, apples with higher content of polyphenols gave juices with higher polyphenol concentrations in comparison to low-polyphenol-containing varieties. Interestingly, solid parts of the fruits act as selective barriers influencing the transfer of polyphenols from the fruits to the juices.[23] In particular, flavanol oligomers and polymers (i.e., condensed tannins) and especially those having a high degree of polymerization are largely adsorbed and retained on the apple pomace.

In the apple juice and cidermaking industries, enzymatic and nonenzymatic oxidations of polyphenols are important phenomena that contribute to the juice and cider quality.[3] Those reactions are responsible for the yellow-orange color of apple juices and ciders. After cell wall and cell membrane disruption, which occur when fruits are crushed and pressed, chlorogenic acid and, to a lower extent, catechins that contain a catechol group in their structure are enzymatically converted by the enzyme PPO into their corresponding *o*-quinones.[7] The quinones produced are very reactive species leading to the formation of neoformed polyphenolic structures involving most of the native polyphenols. As far as we know, there is no direct influence on anthocyanins, which are not considered as PPO substrates.[24] However, in a red wine model solution, it was found that anthocyanins can be indirectly involved by coupled oxidation reduction reaction with hydroxycinnamic acid *o*-quinones.[24] Furthermore, during juice or cider aging, there are series of nonenzymatic reactions involving polyphenol that potentially change the color. They may be favored at higher pH and in the presence of metal ions such as iron or copper.[18]

Among the different ways of inhibition or controlling of oxidation processes, the use of reducing agents is well documented. For instance, sulfites are highly effective and have been used in many products since antiquity.[7] In food technology, sulfite reagent doses are limited and banned for use in fresh fruits and vegetables because of their adverse effects on health.[25]

In the fermented beverages industry, concentrations of residual sulfites are generally not authorized above 350 and 200 mg/L for wines and ciders, respectively.[26,27] Ascorbic acid is also a widespread reducing agent. However, when it comes from the apple itself, it is rapidly consumed during crushing, as a consequence of cell wall disruption and oxidation reduction reaction with enzymatically produced *o*-quinones leading to the formation of dehydroascorbic acid. Then, dehydroascorbic acid may be degraded into a variety of products (aldehydes, ketones, carboxylic acids). A noticeable advantage of ascorbic acid is that there are fewer limitations for its use in food products (usually 50−150 mg/L in wines).

Food chemistry of anthocyanins[28] and in particular their sensitivity to oxidation have been well studied in the red wine model.[27] Then, pyranoanthocyanins appear as a class of very diverse anthocyanin derivatives that are largely involved in the evolution of wine color during aging.[29] In addition, anthocyanins and probably also their derivatives are known for their high antioxidant activity.

In this study, the qualitative and quantitative analyses of polyphenols of a red-fleshed apple cultivar and its clear and cloudy juices are presented. The transfer of polyphenols from fruits to juices, especially for anthocyanins responsible for red color, was measured. In a second part of the experiment, attention was paid to the stability of juice color depending on different parameters including oxygen presence, pH values, and addition of ascorbic acid, sulfites, and copper salt.

MATERIALS AND METHODS

Chemicals and Phenolic Standards. HPLC gradient grade methanol and acetonitrile were obtained from Carlo Erba reagents (Val de Reuil, France). Formic acid was purchased from NORMAPUR (VWR Prolabo, France). Ultrapure water was prepared with a Milli-Q water purification system (Millipore S.A., Molsheim, France). Ascorbic acid was from Fisher Scientific (Loughborough, UK). Copper(II) sulfate pentahydrate was from VWR (Fontenay Ss Bois, France). Sodium metabisulfite was from Merck (Darmstadt, Germany). Standards of (+)-catechin, (−)-epicatechin, 5-*O*-caffeoylquinic acid, *p*-coumaric acid, phloridzin, and avicularin (quercetin-3-*O*-arabinoside) were obtained from Sigma-Aldrich (Lyon, France). Hyperoside

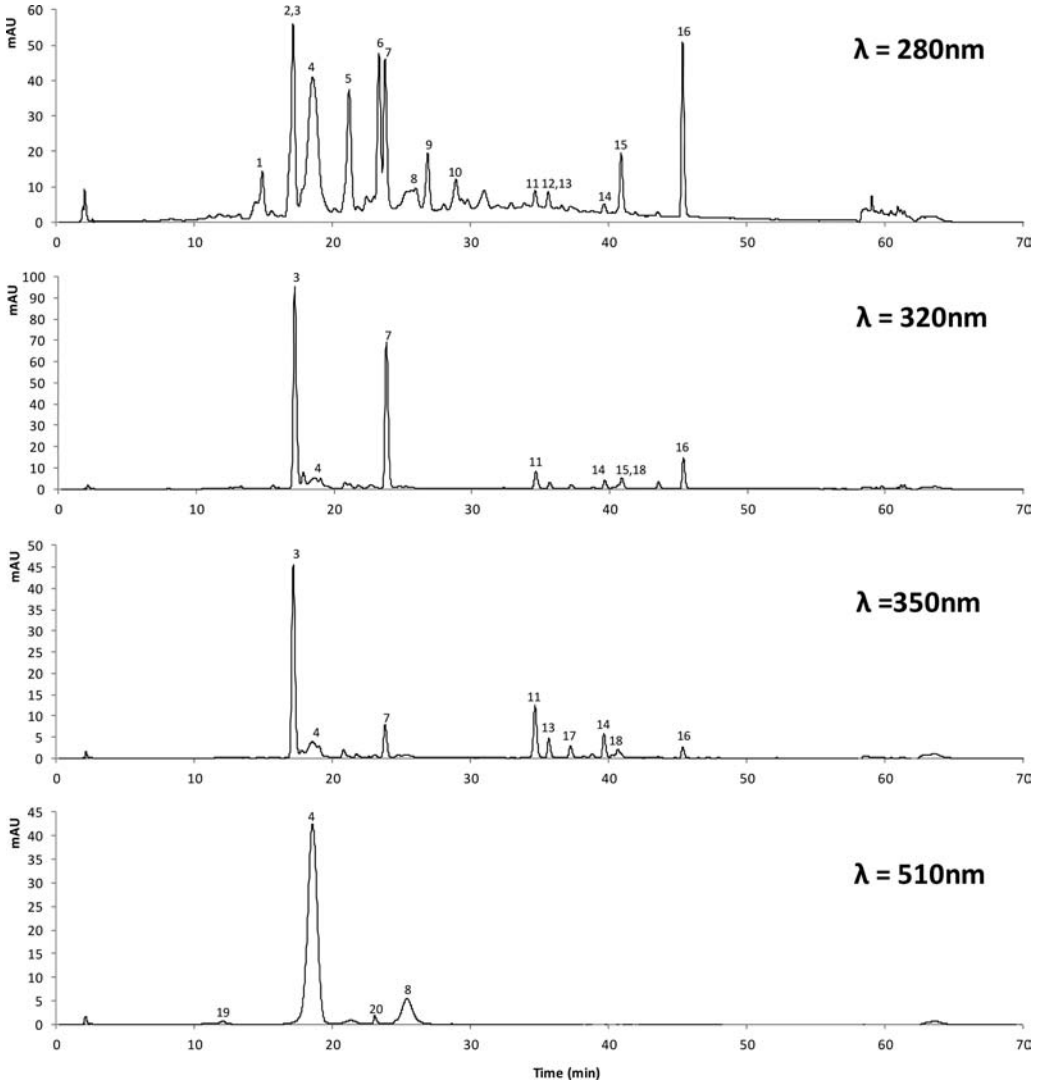

Figure 1. Reversed phase UV−visible chromatograms of the acidified methanol extract of the red-fleshed apple powder. Different wavelengths are used to optimize the detection of the phenolic compounds: (A) 280 nm, all phenolics are detected; (B) 320 nm, more specific for hydroxycinnamic; (C) 350 nm, more specific for flavonols; (D) 510 nm, more specific for anthocyanins.

(quercetin-3-*O*-galactoside), ideain chloride (cyanidin-3-*O*-galactoside chloride), procyanidin B1, and procyanidin B2 standards were purchased from Extrasynthese (Genay, France). (−)-Epicatechin-phloroglucinol, phloretin xyloglucoside, 4-*p*-coumaroylquinic acid, and procyanidin B5 were available standards purified in the laboratory from apple material by HPLC at the semipreparative scale.

Plant Material. A red-fleshed apple hybrid cultivar was selected at INRA Angers (code X4876). It was a cross between F2 parent *Malus pumila* varieties 'Jonathan' and 'Niedzwetzkyana'. Twenty kilograms of apples was harvested in late September 2012 at maturity stage "Starch 7"[30] in the experimental orchard of INRA Angers, Domaine de Beaucouzé.

Sample Preparation. *Fruit Sample Preparation.* Apples were sampled into three batches of 10 fruits. For each batch, fruits were mechanically cut and fruit pieces were randomly selected according to a systematic procedure.[42] This fresh material was immediately frozen in liquid nitrogen and freeze-dried. This dried material was crushed into a fine and homogeneous powder (Electrical Crusher Retsch, model YGG, Bioblock Scientific), which was stored at −30 °C until analysis.

Apple Juice Preparation. Apple juice was prepared in accordance with the internal procedure. Milling and pressing of the apples were performed in the same extraction instrument based on a modified hydropress 90 (Spiedel, Germany) modified by Demoisy (Baune, France). This instrument was specifically designed to limit oxidation during apple milling and pressing (3 bar) by keeping the atmosphere inert using carbon dioxide. The processed batch was approximately 15 kg of apples. A part of the juice was prevented from enzymatic oxidation by adding sodium fluoride (inhibitor of PPO, 0.2 g/L). The rest was left as nonprevented product. Juices were frozen and stored at −30 °C until use. Prevented juice was used for chromatographic characterization of the polyphenol profile, whereas nonprevented juice was used for the experimental design aiming to evaluate the stability of the color. Before analysis, the prevented apple juice was divided into two parts. The first part was centrifuged for 15 min at 3000 rpm on Beckman J2-21 floor model centrifuge. The supernatant, corresponding to "clear" juice, was recovered, whereas the second part was kept cloudy without any change and named "cloudy juice". Aliquots (0.5 mL) of both juices were freeze-dried overnight in 5 mL hemolysis tubes using a Lyovac GT2 freeze-drier (Leybold Vacuum, France). Freeze-dried samples were kept stored in a desiccator under vacuum at room temperature until analysis.

Analytical Procedures. *Determination of Simple Polyphenol Compounds in Fruits and Preserved Juice.* Simple polyphenols (i.e., hydroxycinnamic acids, monomeric flavanols, flavonols, dihydrochalcones, and anthocyanins) were extracted from freeze-dried apple powders using acidified methanol. About 50 mg of powder was precisely weighed in 5 mL hemolysis tubes and extracted using 1.2 mL

Table 1. LC-UV−Visible/MS Identification and Quantification[a] of the Main Phenolic Compounds in Red-Fleshed Apple Fruit and the Corresponding Clear Apple Juices

peak	Rt (min)	λ_{max}	$[M-H]^-$	MS/MS[b]	identified compound	in apple fruit (mg/100 g FW)	in clear juice[c] (mg/100 g FW)
1	14.7	279	577	425 (100); 451 (32); 407 (18); 289 (16)	procyanidin B1[d]	7.9 ± 0.2	11.7 ± 0.6
2	16.0	279	289	289 (100); 245 (22)	(+)-catechin[d]	11.6 ± 0.2	8.4 ± 0.4
3	17.0	325	353	191 (100); 179 (6)	5-caffeoylquinic acid[d]	16.6 ± 1.0	16.7 ± 0.8
4	18.4	512	447	285 (100)	cyanidin-3-galactoside[d]	37.2 ± 1.3	10.0 ± 0.5
5	21.0	279	577	425 (100); 451 (32); 407 (18); 289 (16)	procyanidin B2[d]	34.6 ± 1.1	21.3 ± 1.0
6	23.2	279	289	289 (100); 245 (51); 205 (9); 179 (6)	(−)-epicatechin[d]	23.3 ± 0.5	16 ± 0.9
7	23.6	312	337	173 (100); 163 (15)	4-*p*-coumaroylquinic acid[10,23]	14.1 ± 0.6	12.9 ± 0.6
8	25.2	512	417	285 (100)	cyanidin pentoside[19]	5.7 ± 0.2	1.2 ± 0.1
9	26.3	280	865	739 (100); 695 (79)	flavanol trimer	13.3 ± 0.7	7.5 ± 0.3
10	29.0	280	1153	1135 (100); 739 (42); 863 (36); 575 (19)	flavanol tetramer	6.7 ± 0.4	3.6 ± 0.1
11	34.5	350	463	301 (100); 300 (68)	quercetin 3-*O*-galactoside[d]	3.0 ± 0.7	0.5 ± 0.0
12	35.4	280	577	425 (100); 451 (32); 407 (18); 289 (16)	procyanidin B5	2.8 ± 0.4	0.5 ± 0.0
13	35.4	350	463	301 (100); 300 (53)	quercetin 3-*O*-glucoside[d]	0.9 ± 0.3	nd
14	39.4	350	433	433 (100); 271 (61); 365 (27)	quercetin 3-*O*-arabinoside	1.3 ± 0.2	0.1 ± 0.0
15	40.7	284	567	273 (100); 167 (6)	phloretin-2-xyloglucoside[10,23]	5.9 ± 0.5	4.6 ± 0.2
16	45.1	284	435	285 (100); 241 (13)	phloridzin[d]	12.7 ± 0.7	2.7 ± 0.1
17	37.0	350	433	301 (100); 300 (41)	quercetin 3-*O*-xyloside[d]	0.7 ± 0.1	0.1 ± 0.0
18	40.6	350	447	301 (100); 300 (51)	quercetin 3-*O*-rhamnoside[d]	0.1 ± 0.0	0.2 ± 0.0
19	12.0	524	737[e]	575 (100); 423 (7)	anthocyanin and flavanol adduct	0.3 ± 0.1	0.2 ± 0.0
20	23.1	495	517[e]	355 (100)	5-carboxy-pyranocyanidin-glucoside[19]	0.4 ± 0.0	0.4 ± 0.0

[a]Mean ± standard deviation, $n = 3$. [b]Energy of collision = 35%. [c]Expressed according to 100 g of fresh juice. nd, not detected. [d]Identified according to a commercial standard. [e]Detected in MS positive mode $[M]^+$.

of pure methanol containing 5% v/v formic acid for 15 min in an ultrasonic bath containing ice (Brasson 2200, USA). Then, samples were filtered on 0.45 μm PTFE filters (Uptidisc, Interchim, France), and the filtrates were ready for HPLC analysis. This procedure was performed in triplicate.

For the cloudy and clear preserved juices, freeze-dried samples were extracted by 1.2 mL of acidic methanol in the ultrasonic bath according to the same procedure. This procedure was performed in triplicate.

Depolymerization of Procyanidins by Acidolysis in the Presence of the Phloroglucinol. The procedure was adapted from that of Kennedy and Jones.[31] Phloroglucinolysis reaction gives access to the subunit composition of procyanidins. The interflavan linkages of procyanidins can be easily disrupted by acidolysis in organic acid medium, leading to the formation of flavanyl carbocations corresponding to the extension units of the procyanidin structure, whereas the terminal units are released in the medium as catechin molecules. Flavanyl carbocations are immediately trapped by nucleophilic phloroglucinol in excess, leading to flavanyl-phloroglucinol adducts. In the case of apple procyanidins, phloroglucinolysis releases (+)-catechin and (−)-epicatechin from the terminal subunits and a (−)-epicatechin−phloroglucinol adduct from the extension subunits. Then, the HPLC analysis of the phloroglucinolysis media gives access to the concentration of each type of terminal and extension catechin unit that initially composed the procyanidin fraction. Therefore, it is possible to estimate the average degree of polymerization (DPn), the average distribution of the catechin units, and the total concentration of procyanidins in the fruit or juice samples.[32]

Apple powder samples (50 mg in 5 mL hemolysis tubes) or freeze-dried cloudy and clear preserved apple juices were dispersed in 0.8 mL of methanol containing phloroglucinol (75 g/L) and ascorbic acid (15 g/L). Then, the reaction was started by adding 0.4 mL of HCl (0.3 N in methanol), and media were immediately incubated at 50 °C for 30 min. The reaction was stopped by placing the tubes in an ice bath and by adding 1.2 mL of 0.2 M aqueous sodium acetate. Samples were filtered on 0.45 μm PTFE filters (Uptidisc, Interchim). The filtrates were ready for HPLC analysis. All phloroglucinolyses were performed in triplicate.

HPLC-UV−Vis and Mass Spectrometry Analysis. Analysis was carried out using a system composed of a thermostated autosampler (model Surveyor, Thermo Finnigan, San Jose, CA, USA), a binary high-pressure pump (model 1100, Agilent Technologies, Palo Alto, CA, USA), a UV−vis diode array detector (model UV6000 LP, Thermo Finnigan), and an ion trap mass spectrometer equipped with an electrospray source (model LCQ Deca, Thermo Finnigan). The column was a ZORBAX Eclipse XDB-C18 column (Agilent Technologies, 2.1 × 150 mm; 3.5 μm) equipped with a precolumn (2.1 × 12.5 mm) of the same material and thermostated at 30 °C. Solvents were (A) acidified pure water (0.1% formic acid) and (B) acidified acetonitrile (0.1% formic acid), both degassed by flushing with helium. The flow rate was 0.2 mL/min and the gradient was as follows: initial, 3% B; 0−40 min, 20% B, linear; 40−55 min, 35% B, linear followed by washing and equilibrating the column. The UV−vis detection was performed in the 240−600 nm range. The ESI source was used in the negative mode with the following parameters: spray voltage (−5 kV), capillary voltage (−70 V), sheath gas (67 arbitrary units), auxiliary gas (4 arbitrary units), and capillary temperature (240 °C). The MS detection was carried out with the following parameters: MS spectra were acquired in full scan negative ionization mode in the m/z 50−2000 range to obtain the signals corresponding to the deprotonated $[M-H]^-$ molecular ions. The method also included the MS/MS dependent scan mode, which was used to obtain the product ion spectrum of the main molecular ions detected on the chromatogram in the full scan mode. The collision energy was optimized in the range of 25−35% (arbitrary units) to clearly observe the production of both parent and main daughter ions. Data were collected and processed by XCalibur software (version 1.2, Thermo

Finnigan). By comparison with available standards, the retention times, UV−vis spectra, full MS spectra, and MS/MS spectra were used for complete identification. When the standard was not available, those criteria were used for only a partial identification. Quantifications were carried out by integration of the peaks on UV−vis chromatograms at 280 nm for flavanols and dihydrochalcones, at 320 nm for hydroxycinnamates, at 350 nm for flavonols, and at 510 nm for anthocyanins (Figure 1). (+)-Catechin, (−)-epicatechin, procyanidin B2, caffeoylquinic acid, phloridzin, hyperoside, and ideain were quantified according to their own calibration curves, whereas other compounds were quantified "as equivalent" according to a reference compound belonging to the same polyphenol class and showing a very similar UV−vis spectrum (see Table 1).

Experimental Design for Color Stability Evaluation. In addition to oxygen, four factors, namely, the pH of the juice (pH), ascorbic acid concentration (AA), sulfite concentration (SO_2), and cupric ion concentration (Cu), were considered as they were suspected to have an effect (main and quadratic) on color evolution with potential interactions between them. To evaluate these effects, a central composite design (fixed to be rotable and orthogonal) was chosen with factors pH, AA, SO_2, and Cu at five levels for each. The design matrix was defined using the tutorial of Stagraphics software: the factor levels were encoded −2, −1, 0, 1, and 2, and the center value was replicated 12-fold, giving 36 total experiments. The range of the factors was chosen to correspond to those encountered in cider and dessert apple juices (from pH 3.0 to 4.4) or usually added in apple juice or cider processing (from 0 to 200 mg/L for ascorbic acid and from 0 to 80 mg/L for SO_2) or measured in the juices and ciders (from 0 to 400 μg/L for copper). This design was applied to both conditions, with oxygen (under air saturation at the starting of the experiment) and without oxygen (under argon for the duration of the experiment), so that oxygen was considered as a two-level factor.

The crude juice (ca. 600 mL) was first thawed at 10 °C in the presence of CO_2 to prevent it from oxidation. Then, the juice was clarified by the addition of 80 μL/L of pectinase (Rapidase C80 Max, DSM, The Netherlands) to hydrolyze pectins and protect the juice from undesirable residues during experiment. After a whole night, the juice was centrifuged for 20 min (Beckman J2-21 floor model centrifuge), and the clear juice corresponding to the supernatant was used for the experimental design.

The initial pH of the juice was 3.4 (model 827 pH Lab pHmeter, Metrohm, France). The juice was divided into five equal volumes for which the acidity was modified by addition of malic acid or potassium hydroxide. Then, the juice was distributed into 10 mL aliquots in glass flasks and mixed with different doses of ascorbic acid (0, 50, 100, 150, or 200 mg/L final), sodium metabisulfite $Na_2S_2O_5$ (0, 20, 60, 40, and 80 mg/L in SO_2 equivalent), and $CuSO_4$ (0, 100, 200, 300, or 400 μg/L in Cu equivalent) according to the design matrix (Table 2). Finally, 36 flasks were placed under argon atmosphere, and another 36 flasks were prepared under air-saturated atmosphere. Preparation of those samples was carried out with appropriate microbiological conditions to maintain low contamination risk: Vessels were sterilized in steam (120 °C, 20 min), laboratory tools were kept in alcohol, and the additions were done in sterile conditions. All flasks were capped hermetically with inert caps.

The storage experiment was carried out for 2 weeks. Samples were stored in the absence of light for 10 days at 35 °C and for 4 days at 50 °C. Samples under air and argon atmospheres were analyzed by HPLC-coupled to UV−vis and mass spectrometry detection on the first and last days of the experiment.

Spectrophotometric Measurements of the Juices and Data Conversion. The native clear juice and the clear juices from the experimental design were analyzed using a spectrophotometer to collect the data necessary for the calculation of the colorimetric parameters. Aliquots (200 μL) of the juices stored under air atmosphere were taken daily from each flask to measure the absorbance corresponding to the visible spectrum in the 400−700 nm region at room temperature using a microplate spectrophotometer (model SPECTRAmax PLUS 384, Molecular Devices). Samples with argon were analyzed only at the last day of storage. Mathematical processing of the visible spectra was used to convert the absorbance data into colorimetric CIE *L*, *a*, and *b* parameters. Then, colorimetrical values including lightness (*L*), saturation (*C**), and hue (*h*) were used for color characterization. The correctness of conversion was checked before by comparison of data from colorimetrical measurement and spectrophotometric data conversion of the same samples.

Table 2. Doses of Additives in the Solutions Used in the Experimental Design

pH of juice	ascorbic acid (mg/L)	SO_2 (mg/L)	Cu (μg/L)	no. of samples
3	100	40	200	1
3.35	150	20	300	1
3.35	150	20	100	1
3.35	150	60	300	1
3.35	150	60	100	1
3.35	50	20	300	1
3.35	50	20	100	1
3.35	50	60	300	1
3.35	50	60	100	1
3.7	0	40	200	1
3.7	100	0	200	1
3.7	100	40	0	1
3.7	100	40	200	12
3.7	100	40	400	1
3.7	100	80	200	1
3.7	200	40	200	1
4.05	150	20	300	1
4.05	150	20	100	1
4.05	150	60	300	1
4.05	150	60	100	1
4.05	50	20	300	1
4.05	50	20	100	1
4.05	50	60	300	1
4.05	50	60	100	
4.4	100	40	200	1

Statistical Analysis. Statistical analyses were done by Statistical Analysis and Data Visualization software, Statgraphic (Sigma Plus, France). The experimental design was analyzed by the general linear model.

RESULTS AND DISCUSSION

Phenolic Compounds in the Red-Fleshed Apple Fruits. The polyphenol profile of the fruit and the juice of the red-fleshed apple variety 'Jonathan' × 'Niedzwetzkyana' were characterized by reversed phase HPLC coupled to UV−vis and MS detection. Figure 1 shows the chromatograms of the fruit methanol extract at four different wavelengths to have a better observation of the different polyphenol classes: all polyphenols including more or less polymerized procyanidins are detected at 280 nm. For this reason, the chromatogram appears very crowded with significant baseline deviation corresponding to coelution of several compounds. Hydroxycinnamates were more selectively detected at 320 nm, and flavonols are clearly observable at 350 nm between 34 and 42 min. Finally, the wavelength 520 nm was suitable for the specific detection of anthocyanins. Most of the compounds were numbered and unambiguously identified on the basis of their chromatographic (RT) and spectrometric (UV−vis, MS/

dx.doi.org/10.1021/jf500336v | J. Agric. Food Chem. 2014, 62, 6944−6954

Table 3. Concentration of Phenolic Compounds Present in Apple Fruits and Apple Juices from Red-Fleshed Apples and Juice Extraction Rate[a,b]

	total flavanols	total HA	total flavonols	total anthocyanins	total DHC	total polyphenols
apple fruit (mg/100 g of FW)	392.1 ± 23.1	30.7 ± 1.7	5.0 ± 1.3	43.6 ± 1.6	18.6 ± 1.2	490.0 ± 28.9
cloudy juice (mg/100 mL)	165.1 ± 7.5	29.4 ± 5.2	1.0 ± 0.2	11.7 ± 2.0	7.3 ± 1.3	214.5 ± 16.2
clear juice (mg/100 mL)	164.4 ± 5.6	30.8 ± 1.3	0.9 ± 0.0	12.3 ± 0.6	7.6 ± 0.3	216.0 ± 7.8
extraction rate (%)	42	100	16	26	40	40

[a]Mean ± standard deviation, n = 3. [b]PCA, procyanidins; HA, hydroxycinnamic acids; DHC, dihydrochalcones.

Table 4. Concentrations[a] of Flavanols and Percentage of Terminal and Extension Procyanidin Subunits in Apple Fruits and Apple Juices

						procyanidins		
	(+)-catechin	(−)-epicatechin	total procyanidins	total flavanols	DPn[b] of flavanols	(+)-catechin t.su[c] (%)	(−)-epicatechin t.su[c] (%)	(−)-epicatechin e.su[d] (%)
apple fruit (mg/100 g of FW of the whole fruit)	11.6 ± 0.2	23.3 ± 0.5	357.1 ± 16.0	392.0 ± 16.7	3.6 ± 0.1	6.8	14	79.2
cloudy juice (mg/100 mL of juice)	8.1 ± 1.4	15.1 ± 2.7	135.7 ± 4.0	158.9 ± 8.1	2.49 ± 0.1	13	16.8	70.2
clear juice (mg/100 mL of juice)	8.4 ± 0.4	16 ± 0.9	133.6 ± 2.9	158.0 ± 4.2	2.47 ± 0.0	13.2	16.5	70.3

[a]Mean ± standard deviation, n = 3. [b]DPn, average degree of polymerization. [c]t.su, terminal subunits. [d]e.su, extension subunits.

Table 5. Literature Data for Concentrations of Phenolic Compounds in Apples and Apple Juices

type and no. of apple varieties		ref	total polyphenols	total PCA[a]	5-CQA[b]
red-fleshed X4876 apple	fruit (mg/100 g of FW)	present study	490 ± 29	283 ± 16	16.6 ± 1.0
	juice (mg/100 mL)		214−216	134	16−17
67 varieties from Poland	fruit (mg/100 g of FW)	23	104−544	47−468	0.3−59
19 English cider apples	fruit (mg/100 g of FW)	38	55−631		3−116
14 French cider apples	fruit (mg/100 g of FW)	10	104−699	51−473	15−119
31 Basque cider apples	juice (mg/100 mL)	45	66−1360	35−351	17−110
7 German cider apples	juice (mg/100 mL)	37	26−97		8−49
2 Polish dessert apples	juice (mg/100 mL)	15	25−104	6−76	8−13

[a]Procyanidins. [b]5-Caffeoylquinic acid.

MS) features by comparison with authentic standards when they were available. In other cases, they were only partially identified on the basis of their UV−vis and MS/MS spectra and by comparison with previously published data.

Thus, considering the phenolic compounds usually found in common apple fruits, seven flavanols: ((+)-catechin (2), (−)-epicatechin (6), procyanidins B1 (1), B2 (5), and B5 (12), one trimer (9), and one tetramer (10)), five flavonols (avicularin (14), hyperoside (11), isoquercitrin (13), quercitrin (18), and reynoutrin (17)), two hydroxycinnamic acids (5-caffeoylquinic acid (3) and 4-*p*-coumaroylquinic acid (7)), and two dihydrochalcones (phloridzin (16) and phloretin-2-xyloglucoside (15)) were detected and identified in the fruit (Figure 1).

For the particular class of anthocyanins that are responsible for the red color, four peaks were clearly observable on chromatograms at 510 nm (Figure 1D). The main peak (4) was unambiguously identified as ideain (i.e., cyanidin-3-*O*-galactoside), and peak 8 was identified as cyanidin pentoside, likely corresponding to cyanidin-3-*O*-xyloside, already described as the second most concentrated anthocyanins after ideain in red-fleshed apples.[33] Two red-colored compounds corresponding to peaks 19 and 20 were also detected. Referring to a previously mentioned publication, compound **20** with $[M]^+$ ion at m/z 517 and a main product ion at m/z 355 could be 5-carboxy-pyrano-cyanidin-galactoside, but the information was not confirmed.[18] According to its MS and MS/MS spectra, compound corresponding to peak 19 ($[M]^+$ = 737, Table 1) likely corresponded to an (epi)catechin-cyanidin-hexoside.

Phloroglucinolysis reaction directly applied on apple powder followed by HPLC analysis was used to define the total content of procyanidins and the average degree of polymerization of flavanols.

The total concentration of polyphenols in fruits assayed by HPLC amounted to 490 mg/100 g of fresh weight (Table 3).

In accordance with previously published data for which thiolysis or phloroglucinolysis reaction was used to quantify condensed tannins in apple fruits also considering their polymerized forms,[34,35] major constituents present in samples were flavanols, with >70% content of procyanidins in apples. Among them, procyanidin B2 was the most abundant molecular form, whereas within monomers, (−)-epicatechin prevailed. As generally observed for apple condensed tannins, procyanidin extension subunits were only (−)-epicatechin, whereas (+)-catechin was found as a small proportion of the terminal units. The average degree of polymerization (DPn) of the flavanol class in the apples equaled about 3.6 (Table 4).

The second dominant group in apples was anthocyanins, with 9% of average total polyphenol content (Table 3). The major anthocyanin was ideain, namely, the cyanidin-3-*O*-galactoside (Figure 1D, peak 4) with a concentration close to 37 mg/100 g FW (Table 1) accounting for 85% of total anthocyanins in the fruit. This can be compared to other studies on red-fleshed apples. For instance, this concentration

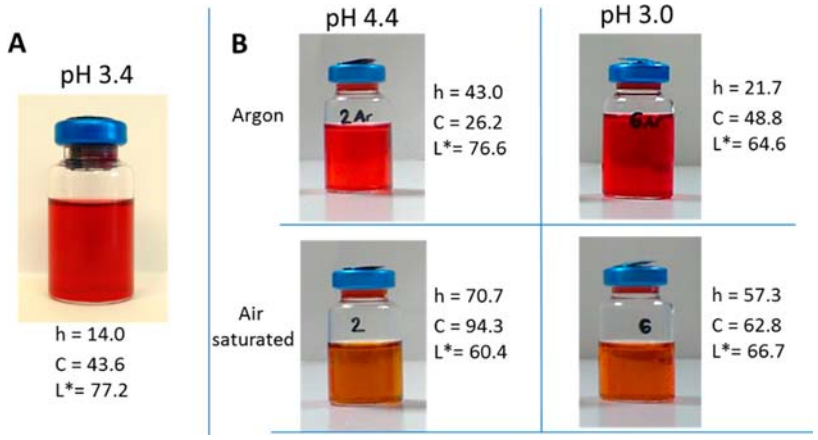

Figure 2. Pictures and colorimetric data of (A) the native clear red-fleshed apple juice without any additives and (B) four selected juices at the end (+14 days) of the color stability experiment: on the right, corrected pH 4.4; on the left, corrected pH 3.0; upper pictures, juices under argon atmosphere; lower pictures, juices under air-saturated atmosphere. All juices were diluted 4 times before spectrophotometric measurements.

of ideain in studied fruits was about 3 times higher than in 'Weirouge' apples studied by Sadilova et al., about 9.3 mg/100 g in unpeeled fruits.

Hydroxycinnamic acids, namely, 5-*O*-caffeoylquinic and 4-*p*-coumaroylquinic acid, represented >6% of total phenolic compounds (Table 3). These two compounds were present approximately at the same concentration, close to 15 mg/100 g FW (Table 1). Interestingly, in comparison to other apple varieties (Table 5), the red-fleshed cultivar was from 2 to 6 times less concentrated in 5-caffeoylquinic acid. Because this compound is the preferential substrate of PPO,[7] its presence at a very low concentration could be linked to a weak sensitivity of this apple variety to enzymatic oxidation.

Dihydrochalcones represented by phloridzin and phloretin-2-xyloglucoside accounted for only 3.8% of total phenolic compounds (Table 3), with phloridzin predominating at a concentration close to 13 mg/100 g FW, which is about 2 times higher than the level of phloretin-2-xyloglucoside (5.9 mg/100 g FW) (Table 1).

Flavonols accounted only for 1% of total phenolic compounds (Table 3), which represented 5.0 mg/100 g FW. They were represented by quercetin 3-*O*-galactoside (3.0 mg/100 g of fresh weight) and quercetin 3-*O*-arabinoside (1.3 mg/100 g of fresh weight). Other flavonols (quercetin glucoside, xyloside, and rhamnoside) were quantified in the range from 0.1 to 0.9 mg/100 g FW (Table 1). Quercetin 3-*O*-rutinoside (i.e., rutin), which is usually present in most apple varieties, was detected as only traces by mass spectrometry. Thus, it was not considered for UV–vis quantification in the present study.

The studied red-fleshed apples were rich in polyphenols. In comparison to other apple varieties, their phenolic quantity is included in the upper level (Table 5). They are characterized by a high concentration of procyanidins and a low amount of 5-caffeoylquinic acid. Red-colored apple juices are also rich in polyphenols but with a relatively low concentration of 5-CQA (Table 5).

Phenolic Compounds in the Juice and Their Extractability from the Fruits. The fruits for which polyphenol composition was described in the preceding paragraphs were used to produce a red-colored juice according to a standardized procedure. Distinction was made between the crude cloudy juice directly obtained after pressing and the clear juice obtained after centrifugation of the cloudy juice. Most of the simple phenolics found in the fruit were also found in the juice (Table 3). However, contrarily to what has been observed in some previous work,[14] no significant difference concerning the polyphenol composition was observed between the cloudy and centrifuged juices. For this reason, the following discussion will concern only the centrifuged clear juice.

Total polyphenol content in juice equaled 216 mg/100 mL (Table 3), which corresponds to an extraction rate of about 40%. This extraction rate was calculated by the ratio between the amount of polyphenol in the juice and the amount in the fruits that was processed to obtain this juice. As the juice yield has a high impact on this rate, we will use it only to compare the different phenols in a juice.

Total anthocyanins content was 12.3 mg/100 mL (Table 3), which corresponded to about 6% of the total polyphenol content and an extractability rate close to 26%. Logically, the main compound found in this class was cyanidin-3-*O*-galactoside, the one that is predominant in fruit flesh. Its extraction rate was close to 26%. Cyanidin pentoside was extractable in about 19%, whereas compound **19** (Table 1) corresponding to a putative anthocyanin–flavanol adduct and compound **20** corresponding to the tentatively identified 5-carboxy-pyrano-cyanidin-glucoside were both almost completely extracted in the juice.

As previously observed for apple juice when thiolysis or phloroglucinolysis coupled to HPLC was used for procyanidin oligomer and polymer characterization and quantification,[14,23] the main polyphenols found in red-fleshed apple juices were flavanols. Procyanidins were predominating with a concentration close to 135 mg/100 mL (Table 4). The extractability of flavanols in the juice was close to 42%, and their average degree of polymerization was close to 2.5.

Total content of hydroxycinnamic acids equaled 30.8 mg/100 mL in the clear juice. Interestingly, this value is very low in comparison to previously published data concerning apple juices. This fact can be mainly imputed to the very low concentration of 5-caffeoylquinic acid, which is almost at the same level of concentration as 4-*p*-coumaroylquinic acid (Table 1). Considering that 5-caffeoylquinic acid is the preferential substrate for PPO, this red-fleshed variety should not be sensitive to enzymatic oxidation and browning. Nevertheless, we noted that hydroxycinnamic acids were the most extractable polyphenol group with an extraction rate close to 100%.

Dihydrochalcones represented 3.5% of the phenolic content (Table 3) with an extraction rate close to 40%. Total dihydrochalcones were close to 7 mg/100 mL of juices (Table 3), with a predominance of phloretin-2-xyloglucoside compared to phloridzin (Table 1).

Flavonols were the least concentrated phenolic compounds in juices, with 0.4% of the total phenolic content (Table 3) and an extraction rate close to 16%. Quercetin 3-*O*-galactoside was the most concentrated flavanol, whereas the least abundant one was quercetin 3-*O*-arabinoside. Quercetin 3 -*O*-glucoside was not detected in the juices (Table 1).

Color of the Pure Juice. Figure 2A presents the picture of the pure, centrifuged juice at room temperature, directly before starting experimental design. Color was described in the CIE *Lab* scale by three orthogonal parameters, L^*, which represent the lightness, and a^* and b^*, which are related to redness and yellowness, respectively. It can be more convenient to express the two-dimensional coordinate system defined by a^* and b^* by the polar coordinates that are easier to understand in terms of color: the angle (h) in degrees representing the hue (0° for red and 90° for yellow) and the distance (C^*) from the center giving the saturation of the color (0° for gray, i.e., black to white depending on L^* and >60° for an intense color).

Figure 3 is used to indicate the hue position of different fruit juices or ciders in the CIE *Lab* representation. In comparison to

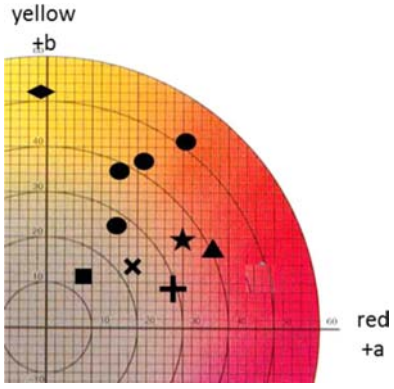

Figure 3. Position of different fruit juices in the CIE *Lab* color space: (▲) the studied red-fleshed apple juice; (●) four dessert apple juices;[37] (★) cranberry juice;[38] (×) raspberry juice;[38] (■) strawberry juice,[38] (+) grape juice;[39] (◆) French ciders.[36]

French ciders[36] or classical clear apple juices[37] made from dessert varieties, the studied red-fleshed juice was very different, characterized by a much higher a^* value (redness) and a lower b^* value (yellowness). Strawberry,[38] raspberry,[38] and grape[39] juices were slightly lower on the yellow scale, but showed about 2 times lower a^* values, giving a much paler red color than the red-fleshed apple juice. The closest juice on a color basis was cranberry juice[38] (Figure 3). When the juices were compared by using h and C^* values, the red-fleshed apple juice had the lowest hue (tend to pure red) and one of the highest saturation values, close to cranberry juice.[38]

Experimental Design Approach to Color Stability. Statistical analysis of the colorimetric data of 36 samples on the first day of the experiment ("start") and 72 samples on the last day ("finish") was performed to evaluate the stability of the juice color. The influences of oxygen (presence or absence of air in the flask), pH (3.0, 3.35, 3.7, 4.05, 4.4), ascorbic acid (from 0 to 200 mg/L), SO_2 (from 0 to 100 mg/L), and copper (from 0 to 400 μg/L) were tested for their effect (main and quadratic effects) on the color parameters: saturation (C^*), hue (h), and lightness (L^*). Furthermore, the effects of combinations of all these factors (interaction effect) were also estimated. For oxygen, only the main effect and interaction are available as only two modalities were used. Data were treated using the general linear model in Statgraphics software.

Figure 2B presents pictures of the samples under argon or air atmosphere at two different pH values (3.0 and 4.4) at the last day of the experimental design. For both pH values, oxygen-protected juices were redder and brighter. Samples that contained oxygen became brown-orange and less bright than those kept under argon atmosphere.

Figure 4 shows the value of the coefficients of the statistical model corresponding to the factors and interactions between factors that have a significant influence on the juice color parameters h, C, and L^*. A negative coefficient indicates a decreasing effect, whereas a positive one corresponds to an increasing effect. As all of the factors were coded from −2 to +2 corresponding to the range of encountered conditions, this

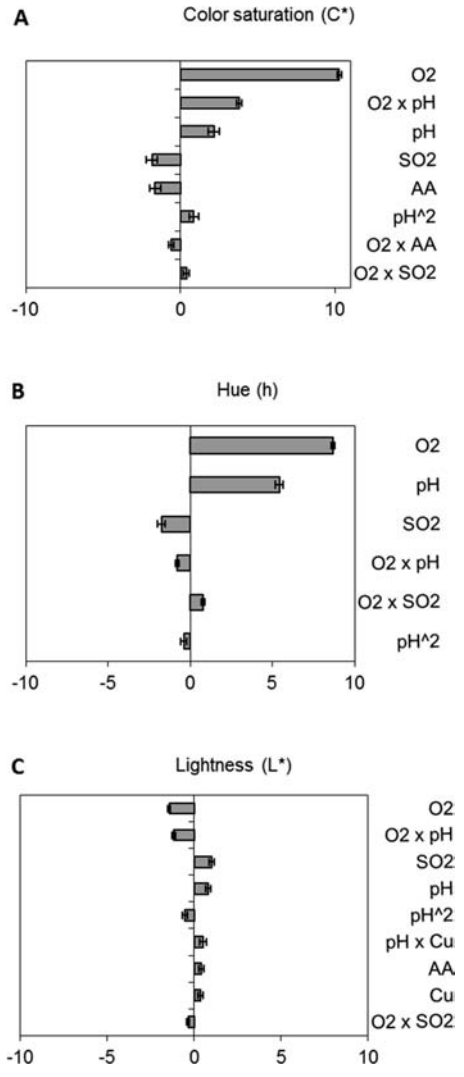

Figure 4. Coefficients of the statistical model describing the effect of the studied parameters (i.e., oxygen (O_2), pH, sulfites (SO_2), ascorbic acid (AA), and copper ions (Cu)) and their main interactions on the color saturation (A), hue (B), and lightness (C) of the clear red-fleshed apple juice.

dx.doi.org/10.1021/jf500336v | J. Agric. Food Chem. 2014, 62, 6944−6954

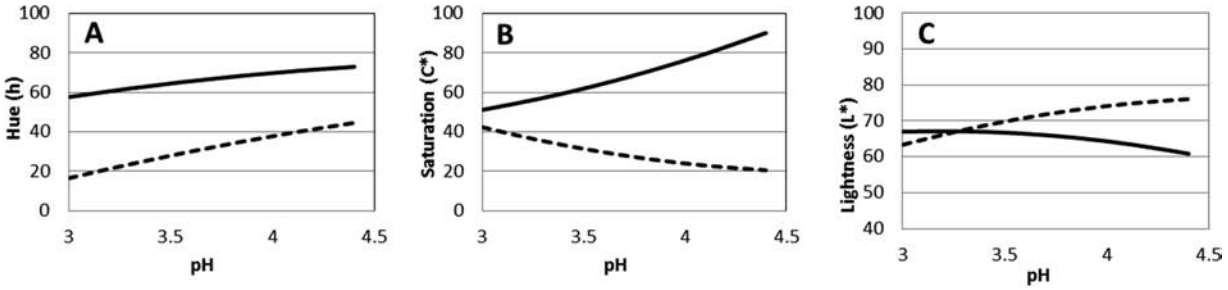

Figure 5. Effect of pH on the hue (A), saturation (B), and lightness (C) of the red-fleshed apple juice at the end of the storage period under air (solid line) or argon (dotted line) atmosphere.

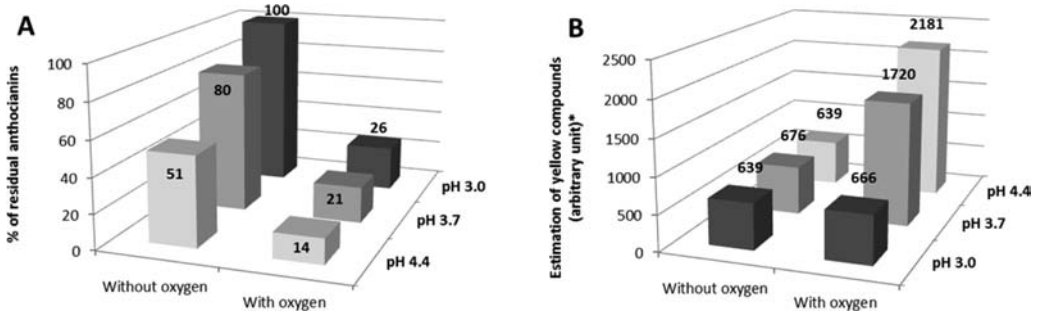

Figure 6. Impact of pH and oxygen on percentage of residual anthocyanins (A) and on formation of yellow compounds (B). * Corresponding to the total area of the chromatogram in the 400−460 nm region.

figure allows a comparison of the effects within the usual apple juice conditions. In general, the highest values of the coefficients were observed for saturation and hue, and only small values were observed for lightness. This indicated that lightness of the juice was not greatly modified during storage. In contrast, hue and saturation were strongly changed during the storage, and highest values were observed for the factors oxygen and pH, underlying the great impact of these factors on color change. Figure 5 gives a more detailed illustration of the effects of these two factors on the three color parameters. The presence of oxygen and the higher pH values always increased the hue angle (Figure 5A): when extreme conditions are accumulated (high pH in the presence of oxygen), the color of the initial juice changed from red (h = 20) to orange-yellow (h = 70), and the interaction that was observed between these factors was not high enough to change the sign of the global effect of each factor. These evolutions of the hue went together with changes of saturation and lightness. However, for these parameters, there were strong interactions between oxygen and pH so that the resulting effects of pH on saturation and lightness were inverted when oxygen was present (Figure 5B,C): in the oxygen-containing juices, an increase of pH from 3 to 4.4 led to an increase of saturation and a decrease of lightness. On the contrary, when the juice was under argon, an increase of pH reduced the saturation and enhanced the lightness. In addition, a quadratic effect of pH was observed for these three parameters, showing that the effect of pH is not linear. However, within the pH range that was tested, the quadratic effect was not high enough to give rise to a maximum or a minimum in the parameters.

The other factors also had significant effects on the color parameters, but their coefficients were lower: the effects of ascorbic acid and sulfites were in opposition to those of oxygen so that, as expected, these factors partially tend to prevent the evolution due to oxidation. A low effect of copper was observed on lightness (main effect P = 0.0296, interaction with pH P = 0.0120) but not on hue and saturation.

The high effect of oxygen on hue was not surprising because oxidation of anthocyanin is known to modify the color from pink/red toward yellow/orange, thus increasing the hue (Figures 4B and 5A). The concomitant increase of the saturation suggests that the new pigments that were produced by oxidation significantly contributed to the color saturation and, to a lesser extent, slightly reduced the lightness. The effect of pH was more complex due to the strong interactions with oxygen mainly observed for saturation (Figure 4A). However, those results were consistent with known mechanisms: On the one hand, a high pH favored autoxidation of anthocyanins that may produce new colored compounds such as pyranoanthocyanins[27] as already observed in wine models. Note that those neoformed colored compounds are not necessarily oxidation products of anthocyanins. For instance, they may result from nonenzymatic oxidation of flavanols leading to the formation of yellow compounds as previously observed in model solutions.[40,41] However, this oxidation occurs only when oxygen was present, which explains the interaction between the two factors pH and oxygen. On the other hand, a low pH is known to enhance red color due to a highest content of stable and red-colored flavylium cation forms of anthocyanins.[21] This effect reinforced the interaction (pH × oxygen) on saturation and lightness resulting in this inversion of the effect of pH depending of oxygen (Figure 5B,C). An effect of sulfites and ascorbic acid was expected, as these reagents are well-known reducing agents used in food industries. Their effect was actually in conflict with those of oxygen, which was consistent with their properties, but the reduction of the oxidation was rather low. This can be due to the small quantities of juice compared to an equivalent volume of air and also to the high diffusion rate of gases in such a small vial. The protective effect was probably limited by excessive oxygen availability in these

conditions. An effect of copper was also expected, but the results showed that, at the tested concentrations, the role of copper can be neglected compared to the other factors.

Taking advantage of the diode array UV−vis detection, HPLC analysis of selected juices at the end of the storage experiment allowed us to complete the information concerning color stability of the red-fleshed apple juice. As seen in Figure 6A, total anthocyanin content strongly changed during the storage. As observed for color stability, oxygen was the most important factor influencing the "red" compounds, so those two evolutions seem to be highly related. The level of decrease was clearly higher in oxygen-containing juices (from 75 to 86%), whereas under argon no more than 50% of the anthocyanins were degraded. The second factor influencing the stability of anthocyanins was the pH. The lowest amounts of anthocyanins were observed at pH 4.4 both at the beginning and at the end of the experiment, whereas at pH 3.0, more "red" compounds were detected on chromatograms. The decrease of anthocyanins in highly acidic conditions was around 74.5%, whereas at pH 4.4 it was up to 85.6%. This indicated that the level of decrease was highly related to the pH of the juice (Figure 6A).

The concentration of yellow compounds in the juices at the end of the storage period was estimated by measuring the global area between 5 and 45 min on the average chromatogram in the 400−460 nm range that reveals the absorbance due to yellow-orange (Figure 6B). For all pH values tested, the juices kept under argon atmosphere did not contain high amounts of yellow-orange compounds. In contrast, larger concentrations of yellow-orange compounds were found in the samples containing oxygen, and this concentration was much higher (close to 3.5 times more) for the juices at pH 4.4. Comparison with the 400−460 nm chromatograms of the juices at the beginning of the experiment (data not shown) revealed that most of the yellow-orange compounds found in the juices at the end of the storage period were not present in the fresh juices. These compounds likely corresponded to polyphenol oxidation products as already discussed, and further work is needed to characterize these neoformed yellow-orange compounds.

To conclude, the INRA red-fleshed X4876 apple cultivar was shown to be a raw fruit material producing an attractive red-colored clear apple juice. Interestingly, for several reasons, biochemical characteristics and in particular the polyphenol composition and distribution are favorable to red juice production with limitation of browning reactions during processing: (i) anthocyanins that are located in the flesh and responsible for the red color are highly extractable in the juice during pressing; (ii) compared to many other varieties, the juice is relatively acidic, which allows limiting the PPO activity and subsequent browning reactions; and (iii) the low concentration of chlorogenic acid, which is the preferential substrate of PPO, may also contribute to its low sensitivity to browning.

The study of the stability of the color revealed that the presence of oxygen in the juice was the main factor highly detrimental to color preservation, and this instability is enhanced when the pH increases. In those conditions, the juice turns orange-brown and HPLC analysis revealed as a consequence both anthocyanin degradation and the formation of yellow compounds likely corresponding to PPO products. In the conditions tested, the use of reducing compounds was only weakly effective for limiting the color degradation. In contrast, the reduction of oxygen level in the juice by using argon was highly effective. Further works would aim to identify those neoformed products responsible for color degradation. The present study was more particularly devoted to the color that happens during juice storage. However, it would also be essential to study the color degradation potentially occurring during fruit crushing and pressing when maximum PPO activity is available and also during apple juice fermentation for a particular use of this red juice in the cider industry.

■ ASSOCIATED CONTENT

Ⓢ Supporting Information

ANOVA tables for the colorimetric parameters C^*, h, and L^* and statistical prediction models for the three parameters C^*, h, and L^* describing the color of the red-fleshed juices after storage. This material is available free of charge via the Internet at http://pubs.acs.org.

■ AUTHOR INFORMATION

Corresponding Author

*(S.G.) E-mail: sylvain.guyot@rennes.inra.fr.

Notes

The authors declare no competing financial interest.

■ ACKNOWLEDGMENTS

We thank Bernard Petit from INRA, IRHS, Beaucouzé, France, for providing the apple fruits. We also thank Sylvain Hingant from IFPC and Gildas Le Bail from INRA for their contribution to the apple fruit sampling and juicemaking.

■ REFERENCES

(1) FAO. FAOSTAT WebSite, http://faostat3.fao.org/faostat-gateway/go/to/download/Q/QC/E (accessed Jan 2014).

(2) Clydesdale, F. M. Color as a factor in food choice. *Crit. Rev. Food Sci. Nutr.* **1993**, *33*, 83−101.

(3) Lea, A. G. H.; Drilleau, J.-F. Cidermaking. In *Fermented Beverage Production*, 2nd ed.; Lea, A. G. H., Piggott, J. R., Eds.; Kluwer Academic/Plenum Publishers: Dordrecht, The Netherlands, 2003; pp 59−87.

(4) Boyer, J.; Liu, R. H. Apple phytochemicals and their health benefits. *Nutr. J.* **2004**, *3*, 1−15.

(5) Fleuriet, A.; Macheix, J. J. Ciders and apple juice. In *Fruit Phenolics*; CRC Press: Boca Raton, FL, USA, 1990; pp 332−336.

(6) Guyot, S.; Marnet, N.; Laraba, D.; Sanoner, P.; Drilleau, J. F. Reversed-phase HPLC following thiolysis for quantitative estimation and characterization of the four main classes of phenolic compounds in different tissue zones of a French cider apple variety (*Malus domestica* var. Kermerrien). *J. Agric. Food Chem.* **1998**, *46*, 1698−1705.

(7) Nicolas, J. J.; Richard-Forget, F. C.; Goupy, P. M.; Amiot, M. J.; Aubert, S. Y. Enzymatic browning reactions in apple and apple products. *Crit. Rev. Food Sci. Nutr.* **1994**, *34*, 109−157.

(8) Guyot, S.; Le Bourvellec, C.; Marnet, N.; Drilleau, J.-F. Procyanidins are the most abundant polyphenols in dessert apples at maturity. *Lebensm. Wiss. Technol.* **2002**, *35*, 289−291.

(9) Sanoner, P.; Guyot, S.; Marnet, N.; Mollé, D.; Drilleau, J. F. Polyphenol profiles of french cider apple varieties (*Malus domestica* sp.). *J. Agric. Food Chem.* **1999**, *47*, 4847−4853.

(10) Lea, A. G.; Arnold, G. M. The phenolics of ciders: bitterness and astringency. *J. Sci. Food Agric.* **1978**, *29*, 478−483.

(11) Matsuo, T.; Tamaru, K.; Saburo, I. Chemical degradation of condensed tanin with phloroglucinol in acidic solvant. *Agric. Biol. Chem.* **1984**, *48*, 1199−1204.

(12) Thompson, R. S.; Jacques, D.; Haslam, E.; Tanner, R. J. N. Plant proanthocyanidins. Part I. Introduction; the isolation, structure, and distribution in nature of plant procyanidins. *J. Chem. Soc., Perkins* **1972**, 1387−1399.

(13) Rigaud, J.; Perez-Ilzarbe, J.; Ricardo Da Silva, J. M.; Cheynier, V. Micro method for the identification of proanthocyanidin using

thiolysis monitored by high-performance liquid chromatography. *J. Chromatogr., A* **1991**, *540*, 401−405.
(14) Oszmianski, J.; Wolniak, M.; Wojdylo, A.; Wawer, I. Comparative study of polyphenolic content and antiradical activity of cloudy and clear apple juices. *J. Sci. Food Agric.* **2007**, *87*, 573−579.
(15) Olson, M. L.; Kargacin, M. E.; Ward, C. A.; Kargacin, G. J. Effects of phloretin and phloridzin on Ca^{2+} handling, the action potential, and ion currents in rat ventricular myocytes. *J. Pharmacol. Exp. Ther.* **2007**, *321*, 921−929.
(16) Marchev, A.; Ivanov, I.; Vrancheva, R.; Pavlov, A. Solid phase extraction and HPLC determination of phloridzin in natural products. *Bulg. J. Agric. Sci.* **2013**, *19*, 201−203.
(17) Gosch, C.; Halbwirth, H.; Stich, K. Phloridzin: biosynthesis, distribution and physiological relevance in plants. *Phytochemistry* **2010**, *71*, 838−843.
(18) Sadilova, E.; Stintzing, F. C.; Carle, R. Chemical quality parameters and anthocyanin pattern of red-fleshed Weirouge apples. *J. Appl. Bot. Food Qual.* **2006**, *80*, 82−87.
(19) Rupasinghe, H. P. V.; Huber, G. M.; Embree, C.; Forsline, P. L. Red-fleshed apple as a source for functional beverages. *Can. J. Plant Sci.* **2010**, *90*, 95−100.
(20) Brouillard, R. Flavonoid and flower colour. In *The Flavonoids, Advances in Research since 1980*; Harborne, J., Ed.; Chapman and Hall: London, UK, 1988; pp 525−538.
(21) Brouillard, R.; Chassaing, S.; Isorez, G.; Kueny-Stotz, M.; Figueiredo, P. The visible flavonoids or anthocyanins: from research to applications. In *Recent Advances in Polyphenol Research*; Santos-Buelga, C., Escribano-Bailon, M. T., Lattanzio, V., Eds.; Wiley-Blackwell:Oxford, UK, 2010; Vol. 2, pp 1−22.
(22) Wojdylo, A.; Oszmianski, J.; Laskowski, P. Polyphenolic compounds and antioxidant activity of new and old apple varieties. *J. Agric. Food Chem.* **2008**, *56*, 6520−6530.
(23) Guyot, S.; Marnet, N.; Sanoner, P.; Drilleau, J.-F. Variability of the polyphenolic composition of cider apple (*Malus domestica*) fruits and juices. *J. Agric. Food Chem.* **2003**, *51*, 6240−6247.
(24) Sarni, P.; Fulcrand, H.; Souillol, V.; Souquet, J. M.; Cheynier, V. Mechanisms of anthocyanins degradation in grape must-like model solution. *J. Sci. Food Agric.* **1995**, *69*, 385−391.
(25) Lester, M. R. Sulfite sensitivity − significance in human health. *J. Am. Coll. Nutr.* **1995**, *14*, 229−232.
(26) Codex Alimentarius, GSFA Online, Food Additive Group Details, Sulfites; http://www.codexalimentarius.net/gsfaonline/groups/details.html?id=161 (accessed January 2014).
(27) Oliveira, C. M.; Ferreira, A. C. S.; De Freitas, V.; Silva, A. M. S. Oxidation mechanisms occurring in wines. *Food Res. Int.* **2011**, *44*, 1115−1126.
(28) Castaneda-Ovando, A.; Pacheco-Hernandez, M. D.; Paez-Hernandez, M. E.; Rodriguez, J. A.; Galan-Vidal, C. A. Chemical studies of anthocyanins: a review. *Food Chem.* **2009**, *113*, 859−871.
(29) de Freitas, V.; Mateus, N. Formation of pyranoanthocyanins in red wines: a new and diverse class of anthocyanin derivatives. *Anal. Bioanal. Chem.* **2011**, *401*, 1463−1473.
(30) Vaysse, P.; Landry, P. *Pomme-Poire, De la récolte au Conditionnement: Outils Pratiques*; CTIFL: Paris, France, 2004; p 124.
(31) Kennedy, J. A.; Jones, G. P. Analysis of proanthocyanidin cleavage products following acid-catalysis in the presence of excess phloroglucinol. *J. Agric. Food Chem.* **2001**, *49*, 1740−1746.
(32) Guyot, S.; Marnet, N.; Sanoner, P.; Drilleau, J. F. Direct thiolysis on crude apple materials for high-performance liquid chromatography characterization and quantification of polyphenols in cider apple tissues and juices. In *Methods in Enzymology − Flavonoids and Other Polyphenols*; Packer, L., Ed.; Academic Press: New York, 2001; Vol. 335, pp 57−70.
(33) Galvano, F.; La Fauci, L.; Lazzarino, G.; Fogliano, V.; Ritieni, A.; Ciappellano, S.; Battistini, N. C.; Tavazzi, B.; Galvano, G. Cyanidins: metabolism and biological properties. *J. Nutr. Biochem.* **2004**, *15*, 2−11.
(34) Kahle, K.; Kraus, M.; Richling, E. Polyphenol profiles of apple juices. *Mol. Nutr. Food Res.* **2005**, *49*, 797−806.
(35) Marks, S. C.; Mullen, W.; Crozier, A. Flavonoid and chlorogenic acid profiles of English cider apples. *J. Sci. Food Agric.* **2007**, *87*, 719−728.
(36) Alonso-Salces, R. M.; Guyot, S.; Herrero, C.; Berrueta, L. A.; Drilleau, J.-F.; Gallo, B.; Vicente, F. Chemometric classification of Basque and French ciders based on their total polyphenol contents and CIELab parameters. *Food Chem.* **2005**, *91*, 91−98.
(37) Falguera, V.; Gatius, F.; Ibarz, A.; Barbosa-Canovas, G. V. Changes on colour parameters caused by high-pressure processing of apple juice made from six different varieties. *Int. J. Food Sci. Technol.* **2012**, *47*, 2158−2164.
(38) Rein, M. J.; Heinonen, M. Stability and enhancement of berry juice color. *J. Agric. Food Chem.* **2004**, *52*, 3106−3114.
(39) Kim, J. S.; Yook, C. Color and flavor changes of grape juices stored in a cool and dark place for long-term preservation. *Food Sci. Biotechnol.* **2003**, *12*, 439−444.
(40) Oszmianski, J.; Cheynier, V.; Moutounet, M. Iron-catalyzed oxidation of (+)-catechin in model systems. *J. Agric. Food Chem.* **1996**, *44*, 1712−1715.
(41) Es-Safi, N. E.; Le Guerneve, C.; Fulcrand, H.; Cheynier, V.; Moutounet, M. Xanthylium salts formation involved in wine colour changes. *Int. J. Food Sci. Technol.* **2000**, *35*, 63−74.
(42) Renard, C. M. G. C. Variability in cell wall preparations: quantification and comparison of common methods. *Carbohydr. Polym.* **2005**, *60*, 515−522.

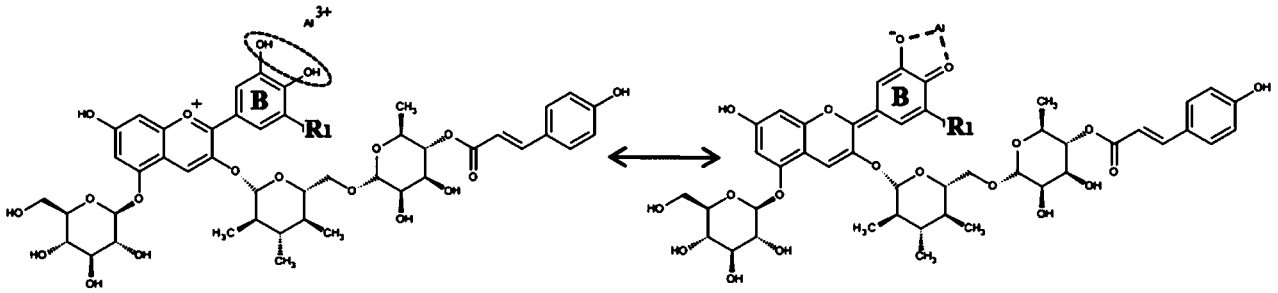

Figure 1. Al^{3+} chelation by cyanidin (B ring exhibiting catechol moiety) or delphinidin-3-*p*-coumaroyl-rutinoside-5-glucoside (B ring exhibiting pyrogallol moiety), where R_1 is H or R_1 is OH, respectively.

all being multivalent.[7] Al^{3+} anthocyanin complexes in ethanol have been reported to be relatively stable at pH 2−5 in reactions with delphinidin.[6] Cyanidin and delphinidin glucosides from berries had previously been found to develop blue-like hues with tin chelation, whereas iron chelates were more brown.[8] More recent publications emphasized the effects of B ring structure, acidic range pH, and buffer selection in anthocyanin complexation with trivalent metal ions (Fe^{3+} and Al^{3+}) in pectin and pectic fractions.[4] Unlike previous findings, ferric ion treated delphinidin-3-glucoside showed blue hues and farther bathochromic shifts than cyanidin and petunidin glucosides. These samples also showed highest stability over time.[4] The environment also can affect the stability of anthocyanin−metal chelates. In citrate and phosphate buffers, color shifts were not found to occur; however, metal chelation by anthocyanins seemed relatively unhindered in other buffers such as acetate and succinic acid.[4]

Aluminum has traditionally been considered innocuous to humans, but controversy has risen with links to neurotoxicity, dialysis encephalopathy, microcytic anemia, osteomalacia, and Alzheimer's disease.[9,10] However, no reports of dietary aluminum toxicity were found in the literature in healthy individuals.[11] The FDA considers aluminum sulfate as generally recognized as safe (GRAS) as a food additive with no usage limit, and aluminum salts may comprise 2% of the final product in synthetic lake type dyes.[12,13] Absorption from anthocyanin−aluminum colorants is likely low, based on anthocyanin chelating effects and aluminum's low bioavailability in water (0.3%).[9,11,14]

With still limited knowledge about the conditions supporting anthocyanin−metal chelation, the aim of this study was to explore factors conducive to blue color formation in acidic conditions typical of food products. This is one of the first known studies to evaluate the effects of food source anthocyanin structures, including acylated and nonacylated counterparts of delphinidin and cyanidin, with chelation of aluminum in varied conditions. The effects of differing anthocyanin concentrations and increasing concentrations of aluminum salt were evaluated to determine ideal conditions for complexation leading to most intense bathochromic and hyperchromic shifts in absorbance. These conditions were also carried out in the pH range 3−6 to better understand the role of pH in anthocyanin−metal chelation. Color stability was monitored by a 28 day study of delphinidin and acylated cyanidin chelates in different storage conditions.

MATERIALS AND METHODS

Materials. American eggplant (*Solanum melongena* L), Japanese eggplant (*Solanum melongena* L), red raspberry (*Rubus idaeus*), and red cabbage (*Brassica oleracea* var. *capitata* f. *rubra*) were purchased from a local grocery store in Columbus, OH, USA. Frozen whole black currants (*Ribes nigrum*) were purchased from CropPharms LLC (Staatsburg, NY, USA). A commercial black carrot (*Daucus carota* spp. *sativus*) anthocyanin powder was provided from D. D. Williamson (Louisville, KY, USA), and chokeberry (*Aronia melanocarpa*) juice concentrate was obtained from Artemis International (Fort Wayne, IN, USA). Aluminum chloride hexahydrate, USP 97.0−101.0% grade, was purchased and obtained from Sigma-Aldrich Co. (St. Louis, MO, USA). ACS grade sodium acetate anhydrous, 6 N hydrochloric acid (certified 5.95−6.05), trifluoroacetic acid, and sodium hydroxide N/10 (0.0995−0.1005) were purchased from Fisher Scientific (Fair Lawn, NJ, USA) as were all other standard ACS and HPLC grade reagents. For comparative purposes, powdered forms of brilliant blue or FD&C Blue No. 1 (certification no. AL9925) and indigotine or FD&C Blue No. 2 (certification no. AL2889), each having a color purity of 92%, were obtained from Noveon Hilton Davis, Inc. (Cincinnati, OH, USA). FD&C Blue No. 1 was diluted to 2.14×10^{-4} M with distilled water, whereas FD&C Blue No. 2 was diluted to 6.35×10^{-4} M.

Methods. *Extraction and Purification of Anthocyanins.* Extraction of anthocyanins from plant materials followed procedures described by Rodriguez-Saona and Wrolstad.[15] Whole plant samples (only peels from eggplant samples) were powdered with liquid nitrogen and treated with 0.01% HCl acidified 70% aqueous acetone before filtration, with repetition until plant material was discolored. Eggplant peels were instead treated with 3.0% trifluoroacetic acid acidified 70% aqueous acetone to reduce the brown discoloration, likely due to polyphenol oxidase, that occurred during extraction. After the filtrate was mixed with 1−2 volumes of chloroform, phase separation occurred overnight at 4 °C, except eggplant samples being limited to 4 h. The chloroform layer containing lipophilic compounds was appropriately discarded because chloroform is a mild carcinogen. Care should be taken to avoid introduction of bases to chloroform waste to avoid undue explosions. Aqueous layers were dried in a rotary evaporator at ∼37 °C under vacuum.

Anthocyanin Purification: Solid Phase Extraction. Crude anthocyanin extracts were purified by loading activated Waters Sep-pak C_{18} cartridges with samples. Loaded cartridges were washed with water acidified to 0.01% HCl to remove organic sugars and acids and then with ethyl acetate to remove phenolics. Anthocyanin pigments were recovered with 0.01% HCl acidulated methanol, which was removed in a rotary evaporator at 37 °C under vacuum. Pigments were stored in acidified water until further analysis.

Monomeric Anthocyanin Quantitation. Monomeric anthocyanins were quantitated by the pH differential method, described by Giusti and Wrolstad.[16] Briefly, anthocyanins were quantified by measuring the absorbance at 520 and 700 nm at pH 1 and 4.5 for each sample. On the basis of the difference of these absorbances, the concentration of monomeric anthocyanins of the solutions was determined. This information was then used to make dilution to known concentrations.

Monomeric anthocyanin pigments were quantitated using the formula ACN (mg/L) = $(A \times MW \times DF \times 1000)/(\varepsilon \times 1)$, with 1 cm path length. A was the absorbance, based on $(A_{\lambda 520} - A_{\lambda 700})_{pH\ 1} - (A_{\lambda 520} - A_{\lambda 700})_{pH\ 4.5}$. MW was the molecular weight of the sample's predominant anthocyanin, DF was the dilution factor used, and ε was

the molar absorptivity. Table 1 shows the values used for each sample's quantitation.

Table 1. Display of Anthocyanin, Associated Molecular Weight, and Molar Absorptivity Used for Monomeric Quantitation of Anthocyanins in Food Samples Evaluated

sample	anthocyanin	MW	molar absorptivity
American eggplant	delphinidin-3-rutinoside	647.0	26900[a]
Japanese eggplant	delphinidin-3-(*p*-coumaroylrutinoside)-5-glucoside	955.26	26900[a]
black currant	cyanidin-3-glucoside	484.8	26900[a]
red raspberry	cyanidin-3-glucorutinoside	757.0	26900[a]
chokeberry	cyanidin-3-glucoside	484.8	26900[a]
red cabbage	cyanidin-3- diglucoside-5-glucoside	773.0	30175
black carrot	cyanidin-3-xylosyl(feruloylglucosyl) galactoside	919.25	26900[a]

[a]Molar absorptivity of cyanidin-3-glucoside, used for monomeric quantitation.[16]

High-Pressure Liquid Chromatography (HPLC) Evaluation of Anthocyanins. Reverse phase HPLC was utilized to identify anthocyanins, with comparison to the literature. Samples were analyzed using a HPLC (Shimadzu, Columbia, MD, USA) system equipped with LC-20AD pumps and an SIL-20AC autosampler coupled to an LCMS-2010 mass spectrometer (Shimadzu) and an SPD-M20A photodiode array (PDA; Shimadzu) detector. LCMS Solution software (version 3, Shimadzu) was used to view results. Separation of anthocyanins was achieved on a reverse-phase Symmetry C_{18} column with 5 μm particle size and 4.6 × 150 mm column size (Waters Corp., Taunton, MA, USA), and a 4.6 × 22 mm Symmetry 2 micro guard column (Waters Corp., Bedford, MA, USA) was used. Samples were filtered through Phenomenex Phenex RC 0.2 μm, 15 mm membrane syringe filter (Torrance, CA, USA). The flow rate was set to 0.8 mL/min with a run time of 70 min, and PDA detection for 55 min. The solvents were phase A, 4.5% formic acid in LC-MS grade water, and phase B, LC-MS acetonitrile (Fisher Scientific Inc.). A binary gradient was used for solvent B: 0−35 min for 0−25% B, 35−40 min for 25−50% B, 40−45 min for 50−100% B, and returning B to 0% 50−55 min and maintained until 70 min. Spectral data were obtained from 250 to 700 nm, and elution of anthocyanins was monitored at 520 nm.

About 0.2 mL/min flow was diverted to a single-quadrupole ion-tunnel mass spectrometer equipped with an electrospray ionization (ESI) interface (Shimadzu). Mass spectrometry was performed under positive ion mode. Data were monitored using total ion scan (SCAN) (from m/z 200−1200) and selected ion monitoring at m/z 287 (cyanidin) and m/z 303 (delphinidin).

Formation of Complexes with Aluminum and Metal Salts in Acidulated Aqueous Solutions. (a) Evaluating Anthocyanin Structures, Concentrations, and Salt Ratios in Al^{3+} Complex Formation. To solutions of acidified water at pH 3 were added anthocyanin samples at three concentrations, based on monomeric quantitation: 25, 50, and 100 μM. Anthocyanin sources for this phase included American eggplant, black currant, red raspberry, chokeberry, red cabbage, and black carrot. $AlCl_3$ aqueous solutions were prepared to 0.057, 0.2288, and 0.4576 M. Salt solutions were added to anthocyanin solutions beginning at equal molar concentrations, then in factors of 10× to 100× molarity of anthocyanin content, then 500× and 1000×. Control samples for each concentration were maintained without salt addition for comparison. Three replicates were evaluated for each sample.

(b) Evaluating Color Stability over Time of Al^{3+} Complexed Anthocyanins. Anthocyanins from American eggplant and red cabbage were diluted in acidified water at pH 3 to 50 μM concentration. $AlCl_3$ salt solutions were added to anthocyanin solutions in factorial excesses of 0×, 1×, 100×, 500×, 1000×, and 2000× anthocyanin concentrations. Three replicates were evaluated for each sample in each storage condition, representing different product storages. Samples were stored for 28 days in each condition: dark storage at refrigeration temperatures (2−4 °C), dark storage at ambient temperatures (18−25 °C), and full light exposure from natural daylight ∼8 h and fluorescent lamps from above at ambient temperatures (18−25 °C).

(c) Evaluating the Effect of pH on Al^{3+} Complex Formation. Sodium acetate was used to prepare 1 M buffered solutions at pH 3, 4, 5, and 6. Anthocyanin samples from American eggplant, Japanese eggplant, chokeberry, and red cabbage were diluted to 50 μM solutions in each buffer. $AlCl_3$ solutions were added to achieve factorial excesses of 0×, 1×, 100×, 500×, 1000×, and 2000× over anthocyanin concentration. The pH of these and all samples was measured using a Mettler Toledo International Inc. S220 SevenCompact pH/ion meter (Schwerzenbach, Switzerland).

Spectrophotometry of Solutions with UV−Visible Transmission. Each sample from each phase of study was subjected to visible spectrophotometry and colorimetry. After 15 min of equilibration after salt addition, each sample was evaluated by visible transmittance (400−700 nm) spectrophotometry using 1 cm plastic cuvettes in a Shimadzu UV-2450 UV−visible spectrophotometer. Spectrograms were generated using UV Probe software, version 2.21 (Shimadzu) associated with this spectrophotometer model.

CIE-Lab Color of Solutions by Transmission. Samples were transferred to 2 mm path length plastic cells and read for CIE-*Lab*, chroma, and hue angle using a Hunter ColorQuest XE (Hunter Laboratories, Reston, VA, USA). The equipment was set for total transmittance, illuminant D65, and a 10° observer angle for all liquid samples.

Statistical Evaluation of Data. The mean and standard deviation of data replicates were calculated using Microsoft Office Excel 2010 (Office 14.0, Microsoft, Redmond, WA, USA). Data from evaluation of anthocyanin structures, concentrations, and salt ratios in Al^{3+} complex formation were conducted by one-way analysis of variance (ANOVA) (two-tailed, $\alpha = 0.05$) and Student's paired t test (two-tailed, $\alpha = 0.05$) of λ_{max} and associated absorbance comparing different anthocyanin concentration and increasing $AlCl_3$ concentration (0−1000× anthocyanin concentration) using Microsoft Office Excel 2010.

Stability over time of American eggplant and red cabbage anthocyanin−aluminum chelates was evaluated by the same testing on the λ_{max} and associated hue from the different salt treatments in differing storage conditions. Finally, the pH decreases likely caused by Al^{3+} chelation were also evaluated by one-way ANOVA (two-tailed, $\alpha = 0.05$). All other figures were also generated using this software.

RESULTS AND DISCUSSION

Evaluating Results from Reverse Phase HPLC-MS. Food samples used in this study represented two anthocyanin aglycone structures: delphinidin and cyanidin. American eggplant and black currant were chosen to represent glycosylated delphinidin. HPLC chromatograms are presented in Figure 2. The American eggplant showed delphinidin-3-rutinoside as the primary anthocyanin as indicated from its HPLC chromatogram and mass spectrometry and in agreement with previous literature.[17] Black currant chromatograms showed profiles similar to previous findings: delphinidin-3-rutinoside and cyanidin-3-rutinoside, each representing ∼40% of the anthocyanin profile.[18] Japanese and non-Japanese type eggplants share delphinidin as the primary anthocyanidin; however, the primary Japanese eggplant anthocyanin was acylated, delphinidin-3-(*p*-coumaroylrutinoside)-5-glucoside (or nasunin) (Figure 2).[17]

Sources and structures were more varied for cyanidin derivatives, being more prevalent in edible produce. Red raspberry and chokeberry were used as sources for glycosylated cyanidin. The main pigment in chokeberry was found to be

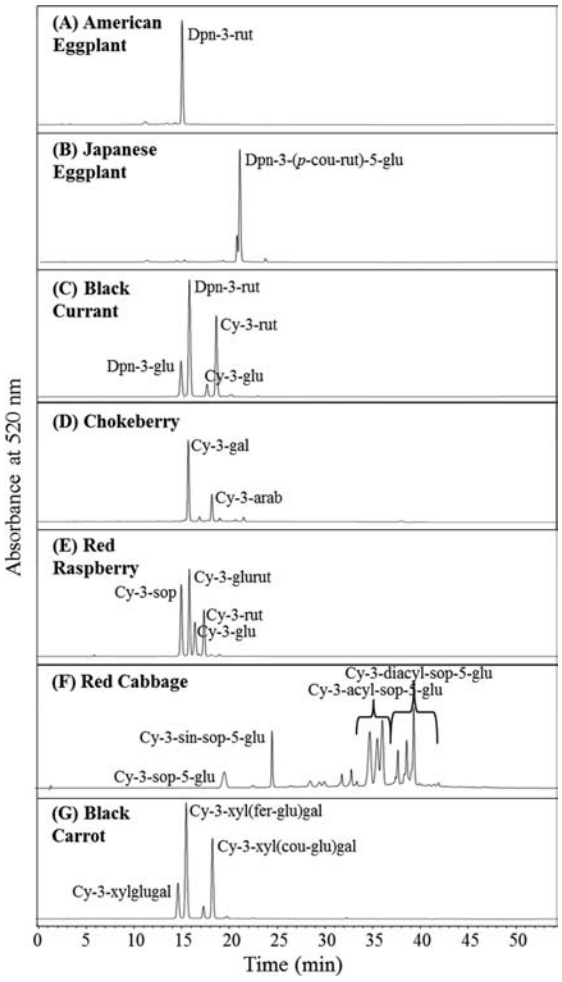

Figure 2. Reverse phase HPLC chromatograms of food sample anthocyanins: (A) American eggplant; (B) Japanese eggplant; (C) black currant; (D) chokeberry; (E) red raspberry; (F) red cabbage; (G) black carrot, with detection at 520 nm showing the main pigments identified.

cyanidin-3-galactoside, representing ~65% of the anthocyanin profile.[19] The chromatogram of red raspberries of this study showed four major pigments; most prevalent were cyanidin-3-sopohoroside and cyanidin-3-glucorutinoside.[20] Two sources of acylated cyanidin were also included in this study: red cabbage and black carrot. Several peaks for red cabbage were found, primarily various types and amounts of acylated of cyanidin-3-sopohoroside-5-glucoside.[21] Black carrot chromatograms showed five major peaks, resembling the profile of the 'Deep Purple' variety.[22] The major pigment of this variety was cyanidin-3-xylosyl(feruloylglucosyl)galactoside, agreeing with the literature.[22]

Evaluating Anthocyanin Structure, Concentrations, and Salt Ratios in Al^{3+} Complex Formation. In this portion of the study, samples were limited to sources of glycosylated delphinidin (American eggplant and black currant), glycosylated cyanidin (red raspberry and chokeberry), and acylated cyanidin (red cabbage and black carrot). This was intended to determine what role anthocyanin structure, concentration, and salt ratio played in metal complexation to induce bathochromic shifts toward blue colors.

All tested anthocyanins showed complexation to occur with aluminum, regardless of aglycon structure, type of glycosylation, or acylation. Each anthocyanin demonstrated both bathochromic and hyperchromic shifts when exposed to the metal ion. By comparison of B ring core structures, delphinidin-containing samples showed the farthest bathochromic shifts and become most blue-like at pH 3 (Table 2). Glycosylated delphinidin showed λ_{max} bathochromic shifts of 50 and 55 nm for American eggplant and black currant, respectively. Cyanidin samples showed lower bathochromic shifts ranging from 26 to 39 nm. These data indicate that increasing the number of free hydroxyl groups on the aglycone core structure leads to farther bathochromic shifts, agreeing with previous studies comparing petunidin, cyanidin, and delphinidin.[3]

Amount and type of common glycosylation do not seem to affect anthocyanin ability to chelate with metal ions but may mildly affect final solution color. When the two glycosylated cyanidin samples were compared, red raspberry anthocyanins demonstrated lower λ_{max} than chokeberry anthocyanins until high levels of Al^{3+} were achieved; Table 2 shows λ_{max} values of red raspberry anthocyanins to be about 10 nm less than those of chokeberry anthocyanins with $AlCl_3$ 100× anthocyanin content. However, both samples showed λ_{max} of 551−553 nm with $AlCl_3$ 500× anthocyanin content, with the exception of the chokeberry anthocyanins in 100 μM concentrations, which shifted to 567 nm but with constant final hue across all three anthocyanin concentrations. This occurrence did not follow the trend of other anthocyanin samples or concentrations. Perhaps due to the high anthocyanin content and high proportion of monoglycosylated cyanidin, additional intermolecular copigmentation could have occurred, leading to the shift in λ_{max}. This postulate does not explain why other anthocyanin samples did not exhibit the same trend, unless their individual complexes had already formed or were hindered related to additional structural components.

With acylation, cyanidin samples continued showing intense bathochromic and hyperchromic shifts in absorbance. The acylated samples did not seem to show larger hyperchromic shifts than nonacylated counterparts but did exhibit more intense chroma. The overall higher absorbances could be due to the proposed molecular stacking mechanisms of acylated anthocyanins, in which the acid groups are overlaid the anthocyanins.[23] This would increase the amount of electron density in that area, leading to intensification of signals found in spectrophotometry. Although the Al^{3+} complex colors of the two acylated cyanidin samples followed similar trends of absorbance increases, acylated cyanidin samples from red cabbage showed larger absorbance increases than acylated cyanidin pigments from black carrot (Table 2). Red cabbage anthocyanins also exhibited more blue-like colors, having a hue angle around ~298, whereas black carrot anthocyanin Al^{3+} chelates exhibited hue angles at ~316. These data suggest that the long sugar chain of black carrot anthocyanins may interfere with the molecular stacking arrangement, resulting in lower λ_{max} and fewer and less intense blue hues, as compared to red cabbage chelates.

Regardless of anthocyanin concentration (25−100 μM), all samples chelated Al^{3+}, showing bathochromic and hyperchromic shifts. However, the effects of increasing salt concentration (0−1000×) were less in lower anthocyanin concentration samples. At lower concentrations with the same factorial excesses of salt, samples demonstrated lesser bathochromic and hyperchromic shifts in absorbance compared to higher anthocyanin concentrations (Figures 3 and 4), until reaching optimum salt ratios where the same λ_{max} and hue angle

Table 2. Effects of Anthocyanin Concentration at pH 3 on Color Shifts, with λ_{max} and CIE-*Lab* Color Characteristics of Anthocyanins Complexed with $AlCl_3$ 100× Anthocyanin Concentration[a]

		color characteristics					
sample	[ACN] (μM)	*L*	*a**	*b**	chroma	hue	Δ hue
American eggplant	25	89.3 (1.2)	2.7 (0.4)	−5.8 (0.5)	6.3 (0.7)	295.2 (1.5)	279
	50	86.1 (0.8)	3.6 (1.2)	−10.1 (3.2)	10.7 (3.4)	289.4 (0.5)	284
	100	80.3 (1.5)	4.4 (1.6)	−10.6 (2.1)	11.5 (2.5)	291.9 (4.0)	264
black currant	25	89.9 (1.5)	5.0 (0.7)	−5.0 (0.9)	7.1 (0.8)	314.7 (7.0)	299
	50	81.1 (1.7)	11.1 (1.4)	−13.3 (3.1)	17.4 (3.2)	310.2 (4.1)	293
	100	71.7 (1.0)	17.3 (0.9)	−19.3 (1.0)	25.9 (1.5)	311.9 (0.0)	293
red raspberry	25	89.8 (0.1)	7.9 (1.0)	−5.0 (0.3)	9.2 (1.2)	329.1 (0.9)	320
	50	84.6 (2.6)	14.1 (2.4)	−9.7 (1.9)	17.1 (3.1)	325.6 (1.2)	317
	100	74.3 (0.8)	27.0 (1.6)	−16.1 (1.7)	31.3 (2.2)	329.3 (1.1)	318
chokeberry	25	88.1 (1.0)	9.0 (0.6)	−4.6 (0.7)	10.2 (0.8)	332.8 (2.8)	318
	50	83.3 (1.4)	13.2 (1.0)	−8.6 (1.5)	15.8 (1.7)	327.1 (2.5)	311
	100	73.5 (0.3)	22.7 (0.9)	−15.2 (0.5)	25.6 (1.4)	325.8 (0.1)	310
red cabbage	25	89.1 (0.9)	4.8 (0.9)	−7.7 (0.8)	9.1 (0.9)	301.6 (4.7)	−44
	50	81.0 (0.6)	9.0 (1.9)	−16.9 (1.2)	19.2 (1.9)	297.8 (3.4)	−47
	100	70.1 (3.6)	15.1 (3.5)	−28.2 (4.0)	30.4 (5.4)	297.9 (2.1)	−48
purple carrot	25	90.2 (0.8)	6.8 (0.2)	−5.0 (0.6)	8.4 (0.3)	323.6 (4.0)	−36
	50	83.7 (0.8)	12.5 (0.1)	−11.9 (1.0)	17.3 (0.7)	316.4 (2.6)	−42
	100	72.8 (0.3)	22.6 (0.9)	−22.4 (0.9)	29.0 (0.4)	315.2 (2.1)	−45

[a]In parentheses are the standard deviations, $n = 3$.

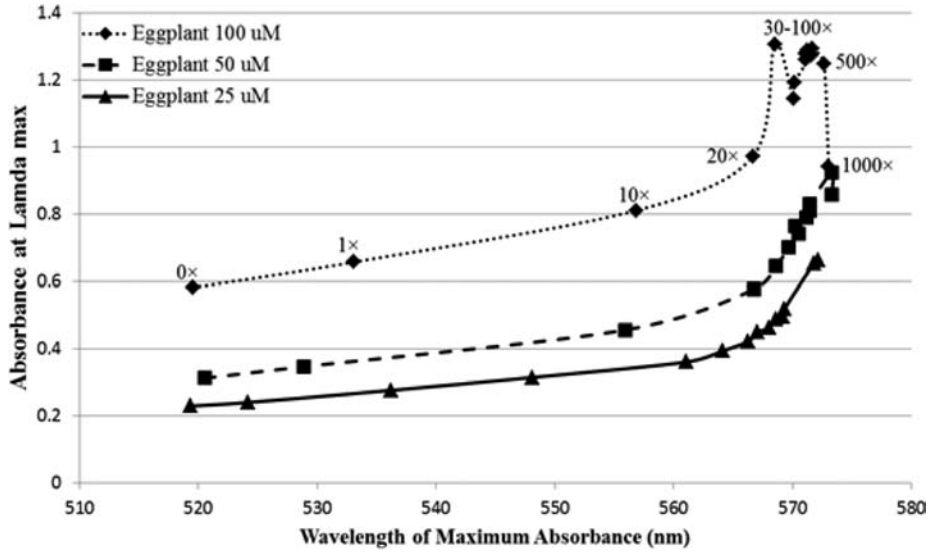

Figure 3. Visible absorbance (400−700 nm) of 25, 50, and 100 μM concentrations of American eggplant anthocyanins treated with factorial increases of $AlCl_3$ (0−1000×) over anthocyanin concentration at pH 3.

occurred. From the same anthocyanin source, the λ_{max} means resulting from each combination of salt treatment (0−1000×) and anthocyanin concentration were compared. *p* values of 6.64×10^{-8} or less were obtained from one-way ANOVA, indicating mean λ_{max} from each $AlCl_3$ treatment to be different from anthocyanins from the same sample.

Similar results were obtained from one-way ANOVA on absorbance of the same samples, giving *p* values of 1.82×10^{-6} or less, with the exception of 25 μM red raspberry anthocyanins. ANOVA resulted in *p* value of 0.05, for which the null hypothesis was still rejectable at 90% confidence. Typically, the increase in absorbance continued to rise with increasing anthocyanin content. Largest absorbance increases were found to occur with anthocyanins from black currants, which are roughly equal ratios of glycosylated delphinidin and cyanidin.[18] The hue reflects this anthocyanin profile, falling between the complex hues of either primarily delphinidin or cyanidin. With regard to the atypically high absorbance increases of black currant anthocyanins, responsibility could be attributed to intermolecular copigmentation between the

dx.doi.org/10.1021/jf405145r | J. Agric. Food Chem. 2014, 62, 6955−6965

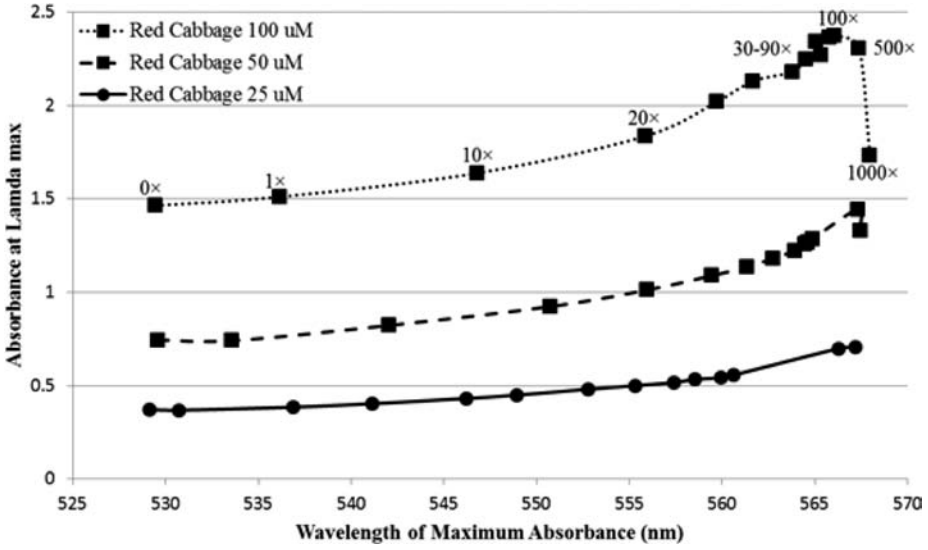

Figure 4. Visible absorbance (400−700 nm) of 25, 50, and 100 μM concentrations of red cabbage anthocyanins treated with factorial increases of $AlCl_3$ (0−1000×) over anthocyanin concentration at pH 3.

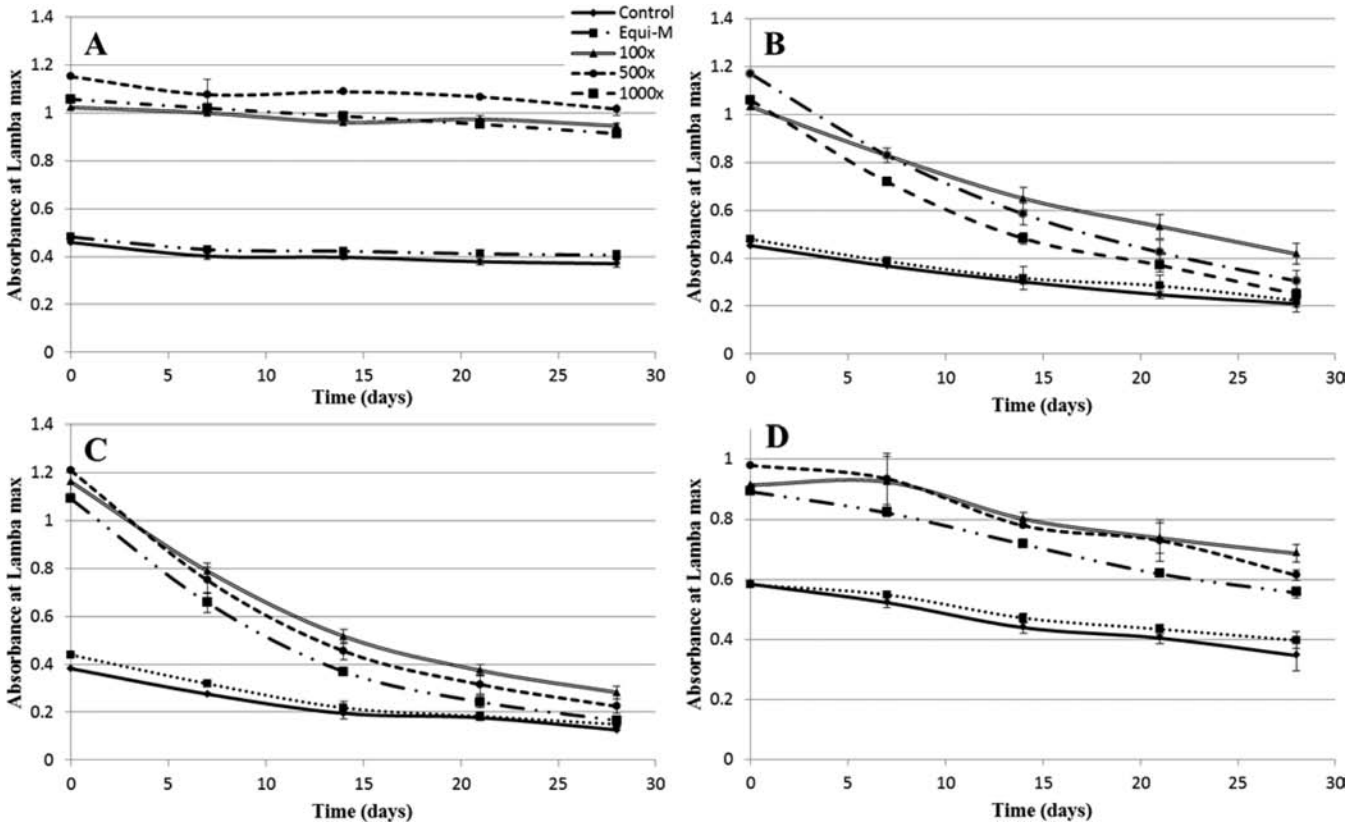

Figure 5. Changes in absorbance at λ_{max} of 50 μM anthocyanin solutions at pH 3 over 28 days of $AlCl_3$ (0−1000×) treated (A) delphinidin (American eggplant anthocyanins) with dark storage at 4 °C, (B) delphinidin with dark storage at ambient temperatures (19−25 °C), (C) delphinidin with light storage at ambient temperatures (19−25 °C), and (D) acylated cyanidin (red cabbage anthocyanins) with light storage at ambient temperatures (19−25 °C).

roughly equal ratios of cyanidin and delphinidin not found in other samples.

In addition to anthocyanin structure and concentration, $AlCl_3$ salt ratios were investigated to determine optimal ratios for preferred color development. Anthocyanin chelation with Al^{3+} was apparent essentially immediately with ion introduction to the system, causing visible color changes. Ideal $AlCl_3$ salt concentrations were found to be between 100× and 500× anthocyanin concentration, at which treated anthocyanins showed the highest intensity of absorbance and reached the farthest bathochromic shift (Figures 3 and 4). Comparing the λ_{max} means from $AlCl_3$ concentrations 100× and 500× anthocyanin content of 25 μM by Student's paired t test, p values of 0.02−0.09 were obtained. The λ_{max} values for these

dx.doi.org/10.1021/jf405145r | J. Agric. Food Chem. 2014, 62, 6955−6965

two salt concentration ratios on American eggplant, black currant, and red cabbage anthocyanins were found not to differ, having p values >0.06. The other samples were found not to differ with $AlCl_3$ concentrations 500× and 1000× anthocyanin content. The same results from t tests were obtained for 50 μM anthocyanin samples. For 100 μM anthocyanin samples, only chokeberry and red cabbage anthocyanin samples were similar with $AlCl_3$ concentrations 100−500×, and the remainder was similar with $AlCl_3$ concentrations 500−1000×.

In addition to λ_{max}, absorbance was evaluated by ANOVA and Student's paired t test for optimal salt ratios. A large excess of salt seemed to initiate some reversion of the color intensification achieved at lower ratios (Figures 3 and 4); a decrease in complex intensity can be noted at salt 1000× anthocyanin concentration in all anthocyanin concentrations (25−100 μM). This could be due to metal-induced pigment degradation or complex formation hindrance caused by the high salt concentration. By ANOVA, the absorbances of all anthocyanin concentrations with salt treatment were found different with p values of ≤0.005, except 25 μM red raspberry anthocyanin samples, which were still the same at 90%. From Student's t test, p values of ≤0.03 were found for all 50 and 100 μM anthocyanin samples with $AlCl_3$ concentrations 500× and 1000× anthocyanin content, except 100 μM chokeberry (p value = 0.09), supporting the observation that absorbance was decreasing with high $AlCl_3$ excesses of 1000×. Some slight decreases in absorbance were noted in 100 μM anthocyanins from American eggplant in the salt range of 30−90×, which did not follow general trends shown by other concentrations. On the basis of the largest absorbance and λ_{max} observed in these samples, optimal $AlCl_3$ concentration was found to be 100−500× anthocyanin concentration.

Evaluating Color Stability over Time (28 Days) of Al^{3+}-Complexed Anthocyanins. The mechanism for thermal degradation of anthocyanins has not been fully elucidated and therefore is still not understood (Schwartz and others, 2008). However, all three of the proposed pathways involve transformation of the flavylium cation to other forms more prevalent in higher pH, which then decompose into degradation products.[24] It has been proposed that chelation of metals by anthocyanins stabilizes the quinonoidal base form as well as protects it from nucleophilic attack by complexation coordination.[3,5] Metal chelation by anthocyanins has been shown to increase stability during storage as well as with thermal treatment.[3,25] Ferric chelates of cyanidin-3-glucoside showed improved stability to thermal treatment of 60 °C over 80 min, with intensity retention of ∼70%.[25] All chelates exhibited first-order kinetics of degradation, but those with delphinidin-3-glucoside in sugar beet pectin showed highest stability compared to glucosides of cyanidin and petunidin when stored at 20 ± 2 °C for 18−66 days.[3]

This study compared the stability of aluminum chelates of delphinidin-3-rutinoside (American eggplant) to that of acylated cyanidin glycosides (red cabbage), as the literature is limited about the stability of acylated anthocyanin−metal chelates. Highest stability for both samples was found in cold, dark storage as expected on the basis of ideal conditions for anthocyanin stability. For delphinidin chelates absorbance decreases were limited to ∼0.1 over 28 days, whereas almost no change was noted for acylated cyanidin samples (Figure 5). Much larger decreases in absorbance were noted for samples stored in ambient temperatures. Although those samples receiving light treatment showed slightly larger decreases, they did not differ significantly from dark storage samples, having p values of 0.1 and 0.5 from Student's paired t test for $AlCl_3$ levels 100× and 500× anthocyanin content. This indicates anthocyanin−metal complexes are more liable to heat treatment rather than light exposure. Degradation of delphinidin−Al chelates seems related to concentration with rate decreasing with time, in agreement with previous studies.[3] Acylated cyanidin chelates showed more linear degradation patterns (Figure 5). These samples also showed improved color stability, exhibiting lower changes in absorbance over time, likely resulting from the proposed molecular folding and stacking acylated anthocyanins can undergo protecting the chromophore.

Having used different ratios of salt to anthocyanin, it was possible to estimate concentrations for optimal anthocyanin chelate stability. Similarly to the decrease of absorbance noted with high excesses of $AlCl_3$, a large amount of salt also was found to diminish stability. From one-way ANOVA, all chelated sample means for λ_{max} were found to be different after 28 days, giving p values of ≤0.002 for each storage treatment. With salt 100−500× anthocyanin content, highest stability was noted on the basis of absorbance and hue angle. Those samples that received light and heat abuse showed $AlCl_3$ 100× to be slightly more stable than 500× based on hues, which differed by p value ≤0.02 from Student's paired t test. At this anthocyanin salt ratio (100×) perhaps the largest number of stabilized and protected complexes occurs.

Evaluating Effects of pH in Al^{3+} Complex Formation. Four samples were used in this phase of the study, American eggplant (glycosylated delphinidin), Japanese eggplant (acylated delphinidin), chokeberry (glycosylated cyanidin), and red cabbage (acylated cyanidin), to understand the effects of starting pH on final exhibited color. Decreases of overall solution pH were found to occur likely due to the release of hydrogen ions when anthocyanins chelate metals. At each of the starting pH levels tested (pH 3−6), all anthocyanins exhibited roughly equal decreases in pH in 1 M acetate buffer solutions (Figure 6). By one-way ANOVA, the pH decreases across each sample at starting pH levels were found not to differ by p values ≥0.23. These equivalent decreases in pH indicate the same concentration of H^+ ions being released from both aglycones. It is suggested that acidic pH may not limit the ability of these anthocyanins to chelate metals, despite the form

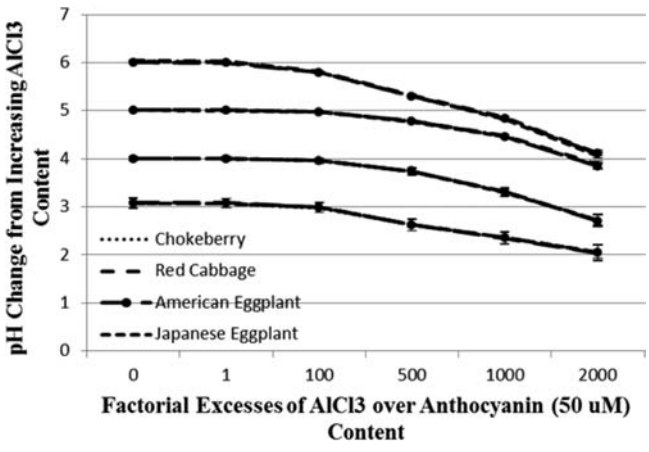

Figure 6. pH change of 50 μM anthocyanin sample solutions initiated by treatment with $AlCl_3$ (0−2000×) in 1 M sodium acetate buffers, pH 3, 4, 5, and 6.

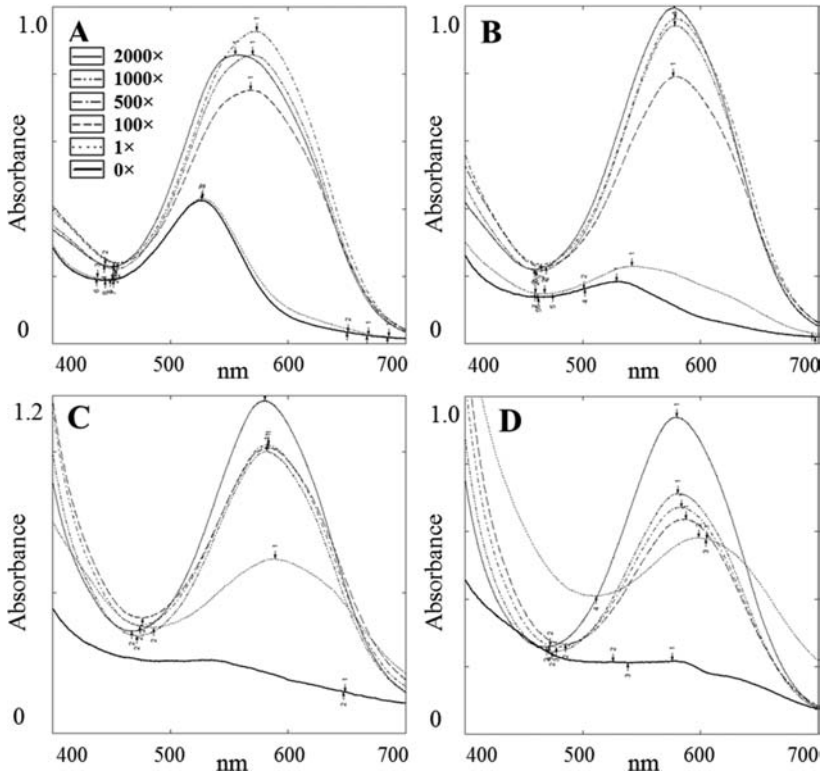

Figure 7. Visible (400−700 nm) absorbance of 50 μM acylated delphinidin (Japanese eggplant anthocyanins) treated with $AlCl_3$ 0−2000× anthocyanin concentration at (A) pH 3, (B) pH 4, (C) pH 5, and (D) pH 6.

equilibrium shifts. Addition of $AlCl_3$ to aqueous solutions can also cause pH decreases due to its ability to hydrolyze in water; however, using high-molarity buffer solutions helped to reduce these effects. In 1 M acetate buffers, pH decreases were minimized until after $AlCl_3$ salt concentrations exceeded 100× anthocyanin content (Figure 6), so color observations were due to complexation rather pH changes.

Even at more neutral pH, where anthocyanins tend to exhibit minimal color intensity, all Al^{3+}-treated samples showed bathochromic and hyperchromic shifts in visible spectrophotometry, becoming bluer than respective untreated anthocyanins. In agreement with previous studies, it was concluded that the predominant anthocyanin structure at said pH acts as the foundation against which the color of the anthocyanin complexes competes.[3] At low pH, where anthocyanins tend to appear in mostly red flavylium structures, those blue anthocyanin−metal complexes compete, giving the final solution a purple color. Conversely, at more neutral pH, where anthocyanins appear in colorless carbinol or yellow chalcone forms, the ultimate solution color is blue or blue-green with metal complex competition.

All samples, pH 3−6, followed the same general trend for Al^{3+} chelation depicted (Figure 7) for acylated delphindin (Japanese eggplant samples), showing hyperchromic shifts. In higher pH solutions, the absorbance of complexed solutions was not as intense as their respective counterparts in lower pH. Samples experienced only bathochromic shifts at low pH, until high levels of $AlCl_3$ 2000× anthocyanin concentration. The reverse was noted when the starting point was pH 6. With low salt concentrations (equimolar conditions), bathochromic shifts were first observed but became hypsochromic with increasing salt content. Across the tested pH range, the final λ_{max} terminated at similar wavelengths, within 10 nm, for pH 4−6 but were generally lower for samples starting at pH 3. Delphinidin samples showed greatest increases in λ_{max} versus cyanidin anthocyanins; interestingly, acylated anthocyanins tended to display lower increases in λ_{max} than nonacylated counterparts (Table 3). Despite similar λ_{max} values of Al^{3+} complexed anthocyanins, hue angles differed with changes in pH, as shown in Tab1e 3.

Starting at pH 3, no samples tested showed vivid blue hues. Acylated delphinidin (Japanese eggplant) demonstrated most blue-like hues, having a hue angle of 293 (Table 3). Other samples showed more purple-pink hues. Despite delphinidin having the pyrogallol moiety and exhibiting farthest bathochromic shifts upon Al^{3+} complexation, competition of H^+ ions from the acidic pH likely inhibited formation of pure blue colors. With inclusion of acylation on the molecule, the bathochromic shift was found to be no greater; however, there was a higher initial and terminating λ_{max} with metal chelation. Glycosylated cyanidin samples appeared much pinker than acylated counterparts upon complexation with Al^{3+}, which visually resembled delphinidin samples, although hue angles differed by about 10.

When increase in the starting pH to 4, anthocyanin−metal chelates began to approach blue hues. Results followed the same general trend for lower pH. Salt-treated glycosylated cyanidin samples were mostly pink, whereas acylated cyanidin from red cabbage exhibited similar hues to those of delphinidin. Both exhibited more blue-like color than at pH 3 with hues around 280−285; acylated cyanidin exhibited higher, more purple hue. Most interestingly, delphinidin acylated with coumaric acid (Japanese eggplant) showed pure blue color upon complexing with Al^{3+}. Hue of this sample treated with $AlCl_3$ 100× anthocyanin concentration was 265 and remained constant until reaching $AlCl_3$ 1000× and 2000×, becoming 269

Table 3. Effects of Acidic pH Change on Color Shifts, with λ_{max} and CIE-*Lab* Color Characteristics of 50 μM Anthocyanins (0×) and 50 μM Anthocyanins Complexed with $AlCl_3$ 100× Anthocyanin Concentration[a]

	pH		λ_{max} (nm)		*L*		*a**		*b**		chroma		hue	
sample	0×	100×	0×	100×	0×	100×	0×	100×	0×	100×	0×	100×	0×	100×
American eggplant	3.08 (0.11)	2.99 (0.10)	523 (0)	568 (1)	92.5 (0.1)	88.0 (0.3)	6.5 (0.4)	4.6 (0.3)	0.9 (0.1)	−7.1 (0.8)	6.6 (0.4)	8.5 (0.8)	7.9 (1.1)	302.8 (1.6)
	4.00 (0.04)	3.96 (0.05)	523 (4)	575 (1)	94.1 (0.2)	87.7 (0.1)	2.4 (0.0)	1.7 (0.0)	1.2 (0.1)	−8.2 (0.5)	2.7 (0.1)	8.3 (0.5)	25.7 (1.9)	281.7 (0.6)
	5.01 (0.01)	4.97 (0.02)	509[b]	578 (2)	94.5 (0.4)	88.2 (0.1)	0.9 (0.1)	0.2 (0.1)	1.2 (0.2)	−6.2 (0.2)	1.6 (0.2)	6.2 (0.2)	52.7 (1.6)	272.0 (0.6)
	6.00 (0.03)	5.79 (0.02)	509[b]	579 (3)	93.9 (0.6)	90.0 (0.8)	0.4 (0.6)	−0.2 (0.1)	1.2 (0.2)	−2.2 (0.7)	1.3 (0.4)	2.2 (0.7)	73.2 (2.5)	263.9 (6.5)
Japanese eggplant	3.07 (0.10)	2.98 (0.10)	527 (0)	569 (1)	92.7 (0.1)	87.6 (0.4)	6.5 (0.6)	3.5 (0.2)	−0.7 (0.4)	−8.3 (1.0)	6.5 (0.6)	9.0 (1.0)	353.6 (2.5)	292.7 (1.1)
	4.01 (0.05)	3.97 (0.05)	529 (1)	578 (1)	93.9 (0.3)	87.2 (0.3)	2.0 (0.1)	−0.7 (0.1)	0.5 (0.2)	−7.9 (0.5)	2.1 (0.1)	8.0 (0.5)	8.1 (16.4)	264.8 (0.6)
	5.01 (0.03)	4.97 (0.03)	534[b]	581 (2)	94.2 (0.3)	87.5 (1.0)	0.5 (0.1)	−2.6 (0.3)	1.1 (0.1)	−6.3 (0.9)	1.2 (0.1)	6.8 (1.0)	63.5 (2.5)	247.2 (1.1)
	6.03 (0.02)	5.80 (0.01)	540[b]	587 (1)	93.2 (0.6)	88.3 (1.2)	−0.6 (0.2)	−2.9 (0.5)	1.4 (0.3)	−2.2 (1.0)	1.6 (0.2)	3.6 (0.9)	115.3 (10.6)	216.2 (9.8)
chokeberry	3.07 (0.09)	2.98 (0.10)	513 (1)	534 (0)	92.1 (0.6)	89.0 (1.0)	8.3 (1.0)	9.3 (1.1)	1.8 (0.3)	−3.4 (0.4)	8.5 (1.0)	9.9 (1.2)	12.6 (0.5)	339.9 (1.0)
	4.01 (0.05)	3.97 (0.05)	511 (2)	558 (1)	93.8 (0.3)	88.6 (0.2)	3.6 (0.0)	5.9 (0.1)	1.1 (0.1)	−6.0 (0.2)	3.8 (0.0)	8.4 (0.2)	17.6 (1.3)	314.3 (0.7)
	5.01 (0.02)	4.97 (0.03)	508[b]	564 (1)	94.3 (0.2)	88.9 (0.2)	1.8 (0.0)	3.3 (0.0)	0.8 (0.2)	−4.7 (0.1)	2.0 (0.1)	5.7 (1.0)	25.1 (4.8)	305.6 (0.5)
	6.04 (0.02)	5.81 (0.02)	528[b]	568 (1)	93.8 (0.2)	89.6 (0.3)	1.0 (0.1)	1.4 (0.1)	0.5 (0.2)	−2.1 (0.2)	1.1 (0.2)	2.5 (0.3)	25.9 (7.2)	302.9 (1.4)
red cabbage	3.07 (0.10)	2.98 (0.10)	532 (1)	551 (0)	90.7 (0.4)	87.7 (0.3)	11.6 (0.3)	7.6 (0.3)	−3.3 (0.1)	−8.8 (0.1)	12.1 (0.3)	11.6 (0.1)	344.0 (0.4)	310.9 (1.2)
	4.01 (0.05)	3.97 (0.05)	539 (1)	572 (0)	91.7 (0.2)	87.1 (0.2)	7.0 (0.0)	2.8 (0.0)	−3.3 (0.1)	−10.6 (0.2)	7.8 (0.0)	10.9 (0.2)	334.5 (1.0)	284.6 (0.5)
	5.01 (0.03)	4.97 (0.03)	549 (2)	579 (1)	92.5 (0.2)	87.5 (0.0)	3.2 (0.1)	0.5 (0.0)	−3.0 (0.2)	−9.9 (0.3)	4.4 (0.1)	9.9 (0.3)	317.2 (2.4)	272.7 (0.1)
	6.04 (0.02)	5.81 (0.02)	555 (2)	589 (2)	92.3 (0.5)	88.4 (0.2)	0.1 (0.0)	−1.3 (0.0)	−3.3 (0.3)	−8.3 (0.2)	3.3 (0.3)	8.4 (0.2)	271.8 (0.7)	260.9 (0.2)

[a]In parentheses are the standard deviations, $n = 3$. [b]Values had to be estimated from spectrum due to low absorbance of untreated anthocyanins.

dx.doi.org/10.1021/jf405145r | J. Agric. Food Chem. 2014, 62, 6955−6965

and 274, respectively. As noted before, these high salt concentrations were also correlated with decreases in pH and increased H^+ competition against metal ions for the hydroxyl groups of the B ring.

Beginning at pH 5, more samples began to exhibit visibly blue colors. Delphinidin anthocyanins from American eggplant and acylated cyanidin from red cabbage showed hues of 272 with $AlCl_3$ concentrations 100× anthocyanin concentration. This hue was maintained until reaching $AlCl_3$ 2000×, where color reverted to higher hues. Salt-treated cyanidin samples formed unique purple-pink hues of 305−308, with hue increasing as salt concentration increased. Acylated delphinidin samples exhibited a wider range of hues than other samples from 230 to 263. The optimal pH for delphinidin-3-glucoside−ferric chelates was found to be 4.5 on the basis of formation and stabilization of the chelates.[3] Generally, absorbance of complexed solutions decreased as pH increased, except by comparing pH 3 and 4, where absorbance increased by about 0.1 except chokeberry anthocyanins, which were lower. Decreases in absorbance were highest by comparing pH 5 and 6, ranging from 0.9 to 0.25. From color and intensity evaluation, the ideal pH for blue color formation of anthocyanin−Al chelates likely lies in pH 4−5 range.

Similar trends were noted with starting pH 6; the highest amount of blue hues was exhibited from the most number of samples tested. Delphinidin and acylated cyanidin showed hues around 260, becoming more blue with the increasing pH. Cyanidin from chokeberry still did not exhibit blue colors at this pH, having hues around 300. It seems cyanidin, without acylation, lacks the necessary electron density and resonance to form blue colors in acidic pH with Al^{3+}. Acylated delphinidin exhibited a range of hues upon chelation with Al^{3+}, 216−260, depending on salt concentration and pH. These hues were found to be the most similar to the synthetic dyes FD&C Blue No. 1 and FD&C Blue No. 2, which were found to exhibit hues of 224.3 and 241.5, respectively. The colorant FD&C Blue No. 1 expressed a λ_{max} of 630, whereas Blue No. 2 showed λ_{max} of 610 nm, each of which easily correlated to their observed blue colors, in agreement with previous findings.[26] Despite the fact that these metalloanthocyanin complexes had much lower λ_{max} values, some were able to produce similar blue hues.

Unlike the findings from previous studies of anthocyanin−ferric chelates, precipitation of metalloanthocyanins was not observed until neutral or basic pH had been reached.[3] At pH 5, ferric anthocyanins were found to precipitate within 2 h of ion introduction, leaving the supernatant colorless after 24 h.[3] Data were not included, but anthocyanins were found to chelate to Al^{3+} in basic pH testing. However, when exposed to pH ≥7, the complexes almost immediately precipitated, leaving the supernatant mildly colored or colorless depending on salt concentration. Precipitates showed colors similar to their respective solution colors at pH 6.

Experiments revealed anthocyanins were able to interact with metals in wide concentration ranges, but salt ratio and pH determined final color and strength. Highest stability and color expression were found when catechol- or pyrogallol-bearing anthocyanins were mixed with $AlCl_3$ at ratios of 100−500× anthocyanin concentration. Anthocyanin color stability was also found to improve with metal chelation, exhibiting intense color for increased time. Three free hydroxyl groups on B rings of anthocyanins and acylation were found to further λ_{max} and blue color formation. Acylation proved critical to blue color development at low pH; acylated delphinidin exhibited blue hues at pH ≥2.5 when complexation occurred at pH 4. Nonacylated delphinidin−Al chelates did not express blue color until pH 5, and the same was noted for acylated cyanidin, in that red cabbage anthocyanins expressed blue hues at pH 5. Without acylation, cyanidin did not develop blue colors. This observation may be due to an effect of molecular folding occurring with acylated anthocyanins that increases electron density and resonance. With optimal anthocyanin−salt ratios, blue colors developed from metal−anthocyanins could be viable alternatives for synthetic blue colorants in food systems.

AUTHOR INFORMATION

Corresponding Author

*(M.M.G.) Phone: (614) 247-8016. Fax: (614) 292-0218. E-mail: Giusti.6@osu.edu.

Notes

The authors declare no competing financial interest.

ABBREVIATIONS USED

EU, European Union; FDA, U.S. Food and Drug Administration; GRAS, generally recognized as safe; HPLC-MS, high-pressure liquid chromatography−mass spectrometry; ESI, electrospray ionization; ANOVA, analysis of variance; ACN, anthocyanin; A, absorbance; MW, molecular weight; DF, dilution factor; Dpn, delphinidin; Cy, cyanidin; rut, rutinoside; *p*-cou, *para*-coumaric acid; gal, galactoside; arab, arabinoside; sop, sophoroside; acyl, acylated (could include sinapic, ferulic, coumaric, or caffeic acids); glurut, glucosyl-rutinoside; xyl, xyloside; fer, ferulic acid

REFERENCES

(1) Potera, C. The artificial food dye blues. *Environ. Health Concerns* **2010**, *118*, 428.

(2) U.S. Food and Drug Administration; Center for Food Safety and Applied Nutrition. Background Document for the Food Advisory Committee: Certified Color additives in Food and Possible Association with Attention Deficit Hyperactivity Disorder in Children, 2011; http://www.fda.gov/downloads/AdvisoryCommittees/CommitteesMeetingMaterials/FoodAdvisoryCommittee/UCM248549.pdf 2011 (accessed Oct 1, 2013).

(3) U.S. Food and Drug Administration. Listing of color additives exempt from certification; Spirulina extract. *Fed. Regist.* **2013**, *78* (156), 49117−49120.

(4) Buchweitz, M.; Carle, R.; Kammerer, D. R. Bathochromic and stabilizing effects of sugar beet pectin and an isolated pectic fraction on anthocyanins exhibiting pyrogallol and catechol moieties. *J. Food Chem.* **2012**, *135*, 3010−3019.

(5) Yoshida, K.; Mihoko, M.; Kondo, T. Blue flower color development by anthocyanins: from chemical structure to cell physiology. *Nat. Prod. Rep.* **2009**, *26*, 857−964.

(6) Schreiber, H. D.; Swink, A. M.; Godsey, T. D. The chemical mechanism for Al^{3+} complexing with delphinidin: a model for the bluing of hydrangea sepals. *J. Inorg. Biochem.* **2010**, *104*, 732−739.

(7) Bayer, E.; Egeter, H.; Fink, A.; Nether, K.; Wegman, K. Complex formation and flower color. *Angew. Chem., Int. Ed. Engl.* **1966**, *5*, 797−798.

(8) Pyysalo, H.; Kuusi, T. The role of iron and tin in discoloration of berry and red beet juices. *Z. Lebensm. Unters. Forsch.* **1973**, *153*, 224−233.

(9) Nayak, P. Aluminum: impacts and disease. *Environ. Res.* **2002**, *89*, 101−115.

(10) Becaria, A.; Campbell, A.; Bondy, S. C. Aluminum as a toxicant. *Toxicol. Ind. Health* **2002**, *18*, 309−320.

(11) Soni, M. G.; White, S. M.; Flamm, W. G.; Burdock, G. A. Safety evaluation of dietary aluminum. *Reg. Toxicol. Pharmacol.* **2001**, *33*, 66−79.
(12) Listing of Certified Provisionally Listed Colors and Specifications, Lakes (FD&C). *Code Fed. Regul.* **2013**, Subpart B, Section 51, Part 82, Title 21.
(13) Substances Generally Recognized as Safe, Multiple Purpose GRAS Food Substances. *Code Fed. Regul.* **2013**, Subchapter B, Part 182, Title 21.
(14) *Toxicological Profile for Aluminum*; Agency for Toxic Substances and Disease Registry, U.S. Department of Health and Human Services; Public Health Service: Atlanta, GA, USA, 2008.
(15) Rodriguez-Saona, L. E.; Wrolstad, R. E. Extraction, isolation, and purification of anthocyanins. In *Current Protocols in Food Analytical Chemistry*; Wrolstad, R. E., Acree, T. E., An, H., Decker, E. A., Penner, M. H., Reid, D. S., Schwartz, S. J., Shoemaker, C. F., Sporns, P., Eds.; Wiley: Hoboken, NJ, USA, 2001; Vol. 1, pp F1.1.1−F1.1.11.
(16) Giusti, M. M.; Wrolstad, R. E. Characterization and measurement of anthocyanins by UV-vis spectroscopy. In *Current Protocols in Food Analytical Chemistry*; Wrolstad, R. E., Acree, T. E., An, H., Decker, E. A., Penner, M. H., Reid, D. S., Schwartz, S. J., Shoemaker, C. F., Sporns, P., Eds.; Wiley: Hoboken, NJ, USA, 2001; Vol. 1, pp F1.2.1− 1.2.13.
(17) Azuma, K.; Ohyama, A.; Ippoushi, K.; Ichiyanagi, T.; Takeuchi, A.; Saito, T.; Fukuoka, H. Structures and antioxidant activity of anthocyanins in many accessions of eggplant and its related species. *J. Agric. Food Chem.* **2008**, *56*, 10154−10159.
(18) Slimestad, R.; Solheim, H. Anthocyanins from black currants (*Ribes nigrum* L). *J. Agric. Food Chem.* **2002**, *50*, 3228−3231.
(19) Oszmianski, J.; Sapis, J. C. Anthocyanins in fruit of *Aronia melanocarpa* (chokeberry). *J. Food Sci.* **1988**, *53*, 1241−1242.
(20) Boyles, M. J.; Wrolstad, R. E. Anthocyanin composition of red raspberry juice: influences of cultivar, processing, and environmental factors. *J. Food Sci.* **1993**, *58*, 1135−1141.
(21) McDougall, G. J.; Fyffe, S.; Dobson, P.; Stewart, D. Anthocyanins from red cabbage − stability to simulated gastrointestinal digestion. *Phytochemistry* **2007**, *68*, 1285−1294.
(22) Montilla, E. C.; Arzaba, M. R.; Hillebrand, S.; Winterhalter, P.. Anthocyanin compostition of black carrot (*Daucus carota* spp. *sativus* var. *atrorubens* Alef.) cultivars Antonina, Beta Sweet, Deep Purple, and Purple Haze. *J. Agric. Food Chem.* **2011**, *59*, 3385−3390.
(23) Giusti, M. M.; Wrolstad, R. E. Acylated anthocyanins from edible sources and their applications in food systems. *Biochem. Eng. J.* **2003**, *14*, 217−225.
(24) Schwartz, S. J.; von Elbe, J. H.; Giusti, M. M. Minor food components: colorants. In *Fennema's Food Chemistry*, 4th ed.; Damodaran, S., Parkin, K. L., Fennema, O. R., Eds.; Taylor & Francis Group: Boca Raton, FL, USA, 2008; Vol. 1, pp 571−638.
(25) Tachibana, N.; Kimura, Y.; Ohno, T. Examination of molecular mechanism for the enhanced stability of anthocyanins by metal cations and polysaccharides. *J. Food Chem.* **2014**, *143*, 452−458.
(26) Ahmadiani, N. *Anthocyanin Based Blue Colorants*. M.S. Thesis, The Ohio State University, Columbus, OH, USA, 2012.

markedly relevant from ornamental and phytochemical perspectives.

Surprisingly, few studies have been carried out on ornamental pot plants, and little has been published regarding the response of these plants to saline fertirrigation, probably because they have been generally irrigated with high-quality water. Those studies that have appeared reported that the saline fertirrigation had a negative effect on yield and decreased the flower quality.[11,12] However, the positive or negative effects of salt stress will depend on the degree of tolerance of plants and stress saline conditions, so the mechanisms of salt stress action are not yet completely clear, especially the impact on the pigment composition and color expression of the flower organ.

Thus, the aim of this study was to assess the effect of salt stress on various physiological characteristics (flower biomass production, abscisic acid (ABA) content, ion leakage, and leaf photochemical efficiency) of *H. rosa-sinensis*, which has been described as a moderately salt-tolerant specie.[13] More importantly, the anthocyanin composition and content of *Hibiscus* petals were also studied to evaluate the influence of stress saline conditions on the color expression of the flower organ, objectively measured by digital image analysis.

Recent advances in image acquisition technology offer the possibility of using technically sophisticated apparatus available at relatively low cost and the ability to evaluate areas in terms of millions of pixels. In this way, more detailed evaluations of objects with heterogeneous color such as plant tissues are possible, because every different color present in the image can be accounted for one or more pixels. Thus, image analysis arises as a good option for satisfying the need of measuring color in this kind of sample. In addition, possible color−anthocyanin composition relationships were studied by applying multivariate statistical analysis.

MATERIALS AND METHODS

Chemicals and Standards. Folin−Ciocalteu reagent, gallic acid, and quercetin standards were purchased from Sigma (St. Louis, MO, USA). Cyanidin-3-glucoside was purchased from Extrasynthese (Genay, France). The solvents used in chromatography were of HPLC grade and purchased from Merck (Darmstadt, Germany). All other chemicals were of analytical grade and supplied by Panreac Química (Barcelona, Spain).

Plant Material, Growing Technique, and Treatments. *H. rosa-sinensis* L. (cv. Porto) plants were grown in a greenhouse located in Pisa, Italy (latitude, 43°43′ N; longitude, 10°23′ E), under natural environmental conditions (22−26 °C). The plants were grown in pots containing a soil/pumice mixture (3:1, v/v) and were irrigated twice a day with drip irrigation. Drip irrigation was carried out using a standard nutrient solution (120 g per plant) with an electrical conductivity (EC) of 2.6 dS m^{-1} and pH 6.5. The composition of the standard nutrient solution was as follows (concentrations are expressed in mol m^{-3}): 11 N-NO_3 h, 1.3 P-PO, 6.2 K^+, 3.1 Ca^{2+}, 1.2 Mg^{2+}, 9 Na^+, and 1.7 S-SO_4^{2-}. Micronutrients were added at Hoagland's concentration (in mmol m^{-3}: B 25, 88 Fe, 1 Cu, 5 Zn, and 10 Mn).

When the experiment started, 40 plants were subjected to salt-stress fertirrigation with NaCl at 200 mM, and another 40 to standard fertirrigation (as control plants). This saline condition was selected to achieve a clearly marked discoloration of the petals to be related with the qualitative and quantitative modification of flower pigments. Plants were daily irrigated during 28 days. Fresh leaf and flower samples with no apparent physical, insect, or microbial damage were collected from control and treated *Hibiscus* plants, during or at the end of the experiment, and carefully transported to the laboratory for the downstream analysis.

Flower Fresh Weight. Ten fresh flowers per treatment were collected to determine the fresh weight biomass production, expressed in grams per flower. Flowers were sampled from different *Hibiscus* plants just at the end of the experiment (after 28 days) and directly analyzed.

Abscisic Acid Content Determination, Electrolyte Leakage, and Chlorophyll *a* Fluorescence Measurements. Leaves, petals, style-stigma plus stamens, and ovary samples (100 mg fresh weight, FW) were collected, weighed, frozen in liquid nitrogen, and then stored at −80 °C until analysis. ABA was measured after extraction in distilled water (water/tissue ratio = 10:1 v/w) overnight at 4 °C. Then ABA was determined by an indirect enzyme-linked immunosorbent assay (ELISA) based on the use of DBPA1 monoclonal antibody, raised against S(+)-ABA[14] as described previously.[15]

For electrolyte leakage, the leaves were sampled every 7 days until the end of the experiment. Ten leaf disks were incubated by shaking in 5 mL of distilled water for 4 h at room temperature. After the incubation, the conductivity in the solution was determined by using an HI8733 conductivity meter (Hanna Instruments). Then, the samples were autoclaved and cooled, and the conductivity was read again in the solutions. Ion leakage was expressed as a percentage of the total conductivity after autoclaving.[16] Chlorophyll *a* fluorescence transients were determined on dark-adapted leaves kept for 30 min at room temperature, using a portable Handy PEA (Hansatech, UK). Leaf fluorescence detection was measured by fast-response PIN photodiode with RG9 long-pass filter and an excitation light intensity (ultrabright red LEDs with a peak at 650 nm) of 3000 μmol m^{-2} s^{-1} (600 W m^{-2}) (Hansatech, technical manual). The parameters measured were F_o, F_m, and F_v/F_m. JIP analysis was performed to determine the performance index (PI).

The chlorophyll fluorescence in plants adapted under ambient light conditions was measured using an FMS2 portable chlorophyll fluorometer (Hansatech, UK). The light was measured using a PAR sensor, and the parameters measured were the efficiency of the photosystem II (FPSII), maximum fluorescence under light conditions (F_m'), electron transport rate (ETR).

Anthocyanin Extracts from *Hibiscus* Petals. Anthocyanin extracts were obtained from red petals of *Hibiscus* flowers. Nine petals per treatment were carefully taken from fresh flowers just at the end of the experiment (after 28 days), and samples were frozen at −20 °C until the analysis.

The extraction of anthocyanin compounds was carried out as follows. Petals were manually divided in two pieces: the base (narrow basal portion) and the limb (cup-shaped upper portion). Each part was individually analyzed (petal bases n = 18; petal limbs n = 18). Samples were freeze-dried for 24 h (lyophilizer CRYODOS -80, Telstar Varian DS 102). The total amount of each homogeneous lyophilized powder obtained was separately extracted with methanol containing 5% of concentrated hydrochloric acid, for 12 h, with occasional agitation and sonication, in darkness at room temperature (18−20 °C). Then, supernatants were centrifuged (4190*g*, 10 min), and all of the methanolic extracts were evaporated to dryness in a rotary evaporator at temperatures below 30 °C. The residues were dissolved in 500−1000 μL of distilled water and centrifuged at 4190*g* for 3 min.

A total of 36 anthocyanin extracts were obtained for their identification and quantification by spectrophotometric and chromatographic (HPLC-DAD-MS) analysis. They corresponded to nine replicates per two treatments and two petal zones, as follows: nine petal bases from control plants; nine petal limbs from control plants; nine petal bases from salt-stress plants, and nine petal limbs from salt-stress plants. Moreover, each sample was analyzed in triplicate.

Total Anthocyanin, Flavonol, and Phenolic Contents. The spectrophotometric determinations of total anthocyanin, flavonol, and phenolic contents were performed with a Hewlett-Packard UV−vis HP8452 spectrophotometer (Palo Alto, CA, USA), using 10 mm path length glass cells and distilled water as reference.

Total anthocyanin content was determined according to the pH differential method.[17] Samples were diluted with aqueous pH 1.0 and 4.5 buffers (potassium chloride solution, 0.025 M, pH 1; sodium acetate buffer, 0.4 M, pH 4.5) and left standing for 10 min, after which

the absorbance measurements were taken at 520 and 700 nm. The method assumes that anthocyanin pigments show zero absorbance at pH 4.5. The molar extinction coefficient of cyanidin-3-glucoside was 26900, and its molecular weight was 449.2 Da. Results were expressed in milligrams of anthocyanins (as cyanidin-3-glucoside equivalent) per 100 g of petal dry weight (DW).

Total flavonol content was determined using a modification of the Glories method,[18,19] originally for wine phenols. Samples were diluted 1:10 with 10% ethanol. The method consisted of placing 0.25 mL of sample or standard in a test tube and adding 0.25 mL of 0.1% HCl in 95% ethanol and 4.55 mL of 2% HCl. The solution was mixed and allowed to sit for approximately 15 min before the absorbance was read at 360 nm. The standard used was quercetin in 95% ethanol, and the results were expressed as milligrams of flavonols (expressed as quercetin equivalents) per 100 g of petal DW.

Total phenolic content (TPC) was determined using a modification of the Folin−Ciocalteu method.[20] Absorbance was measured at 765 nm, and the results were expressed as milligrams of polyphenol (expressed as gallic acid equivalents) per 100 g of petal DW.

HPLC-DAD-ESI/MS Analysis. HPLC-DAD analysis was performed in a Hewlett-Packard 1200 series liquid chromatograph equipped with a quaternary pump, column heater, UV−vis diode array detector, automatic injector, and ChemStation software. A Zorbax SB C18 column (4.6 mm × 250 mm, 4.6 μm particle size) thermostated at 35 °C was used. All analyses were made in triplicate by direct injection of the samples, previously filtered through a 0.45 μm nylon filter (E0034, Analisis Vinicos, Spain).

Chromatographic analysis was carried out following a modification of the method described in Quijada-Morin et al.[21] The solvents used were (A) an aqueous solution (0.1%) of trifluoroacetic acid (TFA) and (B) 100% HPLC grade acetonitrile.

The elution profile was as follows: isocratic 10% B for 3.25 min, from 10 to 15% B for 12.37 min, isocratic 15% B for 5.21 min, from 15 to 18% B for 5.21 min, from 18 to 30% B for 20.84 min, and from 30 to 35% B for 5.20 min. The flow rate was 0.8 mL min^{-1}, and the injection volume was 50 μL. The UV−vis spectra were recorded from 220 to 600 nm with a bandwidth of 2.0 nm. Detection was carried out at 520 nm as the preferred wavelength.

For the anthocyanin identification, the mass spectrometer was connected to the HPLC system via the DAD cell outlet. MS detection was performed in an API 3200 Qtrap (Applied Biosystems, Darmstadt, Germany) equipped with an ESI source and a triple-quadrupole ion trap mass analyzer that was controlled by Analyst 5.1 software. Zero grade air served as nebulizer gas (GS1) and turbo gas (GS2) for solvent drying. Nitrogen served as curtain (CUR) and collision gas (CAD). MS analysis was carried out in positive mode (ESI+). The setting used was optimized by direct infusion of a malvidin 3-*O*-glucoside solution: declustering potential (DP), 41 V; entrance potential (EP), 7.5 V; ion spray voltage (IS), 5000 V; GS1, 40 psi; GS2, 50 psi (600 °C); CUR, 20 psi; and CAD, set as "high". Both quadrupoles were set at unit resolution. Mass method consisted of three mass experiments: full mass analysis (EMS mode, collision energy (CE) 10 V), MS2 analysis (EPI mode, CE 25 V), and MS3 analysis (CE 30 V, excitation energy (AF2) 50 V). Spectra were recorded between m/z 150 and 1100.

Anthocyanin compounds were identified by comparison of their retention time, UV−vis spectra, and mass spectra features with data reported in the literature. Quantification of anthocyanins was calculated from the peak areas recorded at 520 nm using a calibration curve purchase standard of cyanidin-3-glucoside. Results were expressed as milligrams per 100 g of petal DW.

Color Analysis of *Hibiscus* Petals by Digital Image Analysis. Prior to the frozen treatment, the same fresh petals considered for the anthocyanin determination (n = 9 per treatment) were used to analyze the color of *Hibiscus* flowers by digital image analysis.

The image acquisition was performed with a DigiEye imaging system[22] consisting of a calibrated digital camera connected to a controlled illumination cabinet and a computer with appropriate software (DigiPix). The digital camera used for image acquisition was a 10.2-megapixel Nikon D80 with Nikkor 35 mm f/2D objective. It was connected via USB to a computer with a Pentium IV processor at 3.00 GHz. The cabinet (VeriVide DigiEye, Leicester, UK) was equipped with two fluorescent tubes that emulate the standard illuminant D65 and offer stable lighting conditions. Lamps were switched on at least 10 min before being used, according to the manufacturer's indications, to stabilize them. The camera was calibrated with the Gretag Macbeth Color Checker DC Chart to characterize its response by relating the RGB signals to CIE specifications under the fixed lighting conditions in the cabinet. For the color measurements, fresh petal samples were appropriately placed into the cabinet using a white background that ensures an adequate segmentation of sample image.

For each image, a 625 × 625 pixel fixed area was taken and CIELAB color parameter data (L^*, a^*, b^*, C^*_{ab}, and h_{ab}) were estimated according to the method of Rodríguez-Pulido et al.,[23] with the software Matlab.[24] The color data obtained were averages of three measurements. In addition, the Euclidean distance between two points in the three-dimensional space define by L^*, a^*, and b^* was used to calculate the color difference between control and saline samples as follows: $\Delta E^*_{ab} = [(\Delta L^*)^2 + (\Delta a^*)^2 + (\Delta b^*)^2]^{1/2}$.

Statistical Analysis. All statistical analyses were performed using Statistica v.8.0 software.[25] Univariate analysis of variance (ANOVA) was applied, using the general linear model procedure (GLM), to establish whether mean values of the phenological and physicochemical data obtained differed significantly as a function of the salinity treatment applied. The means values were compared by t test, Bonferroni test, or Tukey test at a significance level of $p < 0.05$. Correlations between color parameters and anthocyanin content were studied by forward stepwise multiple regression at a significance level of $p < 0.05$.

RESULTS AND DISCUSSION

Effect of Salt Stress on Abscisic Acid Content, Ion Leakage, and Photochemical Efficiency. The application of salt stress for a prolonged period influenced the morphology and physiology of *H. rosa-sinensis* plants.

In our conditions, the saline irrigation caused a significant decrease in flower fresh mass, which was about 60% after 28 days of treatment. The biomass reduction due to salt stress may be determined either by the decreased availability of water or by the NaCl toxicity.[26] Previous research on other ornamental flowers showed that quality parameters such as flower weight were unfavorably affected by salinity.[27] In fact, plants subjected to saline irrigation require additional energy in plant cells. This extra metabolic energy is likely to be consumed in processes related to osmotic adjustment within the cells, and hence less carbon is available for growth.[28] This is particularly relevant for plant visual quality, because the most decorative elements for ornamental plants are usually the flowers.

As reviewed by Ashraf and Harris,[29] salt-sensitive species showed an increase in electrolyte leakage in the leaves under saline conditions. Electrolyte leakage is an indicator for the extent of membrane damage under salt stress and was determined in the fully expanded leaves of salt-stressed *H. rosa-sinensis*. Low values of electrolyte leakage were recorded in the controls (0 mM). The presence of NaCl in the rooting medium induced a significant increase in electrolyte leakage in the leaves (Figure 1) and was greater as exposure time to saline treatment increased, reaching maximum values after 28 days.

The hormone ABA is well-known as a mediator in plant responses for both biotic and abiotic stresses. Endogenous ABA concentrations fluctuate in response to environmental conditions,[30] allowing plants to survive under adverse conditions, such as salt stress. In *H. rosa-sinensis* plants, salinity increased ABA content in leaves (Figure 2). This is consistent with other plant species that increase ABA production in response to salinity.[31] Moreover, ABA levels varied among the flower tissues

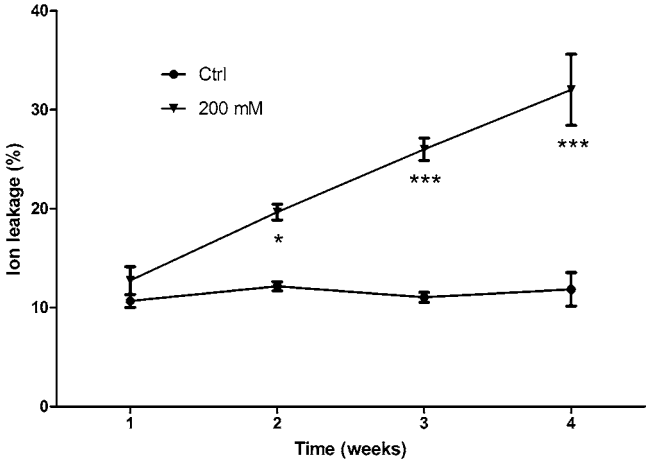

Figure 1. Cell damage trend over 28 days in *H. rosa-sinensis* leaves (means ± SD, $n = 3$). Asterisks indicate significant differences (Bonferroni post-test, $p < 0.05$) of ion leakage (%) after saline irrigation (related to the control).

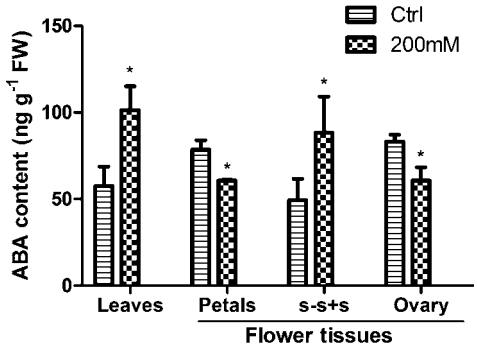

Figure 2. Effect of 200 mm NaCl on ABA content of *H. rosa-sinensis* tissues after 28 days of saline irrigation (means ± SD, $n = 4$). Asterisks indicate statistical differences (t test, $p < 0.05$) within the same tissue: s-s+s, style-stigma plus stamen.

examined, and as shown in Figure 2, its content enhanced in the style-stigma plus stamens, whereas in petals and ovary tissues it decreased. A possible relationship among the differential tissue rate of growth under salinity could explain the divergent trend of ABA levels in floral organs and needs to be further explored.

To better characterize the physiology of *Hibiscus*, the chlorophyll *a* fluorescence was measured. In dark-adapted leaves the PI declined drastically after 28 days of saline treatment, being 8.4 units in the control leaves, whereas in the treated plants it was 3.9 units. PI is an overall index that combines different fluorescence parameters and has been frequently employed to understand the responses of the photosynthetic apparatus to different physiological and environmental conditions.[10,32] Our results confirmed PI as a sensitive indicator of salt stress. Also, the chlorophyll *a* fluorescence measured from light-adapted leaves subjected to saline irrigation revealed a statistically relevant reduction in the relative quantum yield of PSII (0.7 in the control plants versus 0.4 under saline treatment), and these results are in agreement with the literature.[33]

To summarize, salinity promoted several physiological and biochemical changes in *Hibiscus* plant tissues including reduction of flower biomass and parameters associated with the functioning of the photosynthetic apparatus as well as fluctuation of ABA levels and increase in electrolyte leakage.

Effect of Salt Stress on Anthocyanin Composition and Color. Considering the heterogeneous color pattern of *H. rosa-sinensis* flowers with two red zones visually discernible, the base and the limb of petals were analyzed as separate groups to determine possible differences regarding their anthocyanin composition and content as well as to evaluate the influence of salt stress in each zone.

Results showed that the base and limb of flowers presented the same anthocyanin profile. The chromatographic analysis of the extracts, registered at 520 nm, shows the presence of five anthocyanins (Figure 3a), all of them identified as cyanidin derivatives according to their chromatographic and spectrometric features obtained in the HPLC-DAD-MS analysis (Table 1).

The major anthocyanin found in *H. rosa-sinensis* flowers was identified as cyanidin-3-sophoroside (peak 1), which accounted for 80% of total peak area. The mass spectrum of peak 1 (Figure 3b) obtained in the ESI positive mode exhibited an ion at m/z 611. MS/MS fragmentation of m/z 611 produced a daughter ion at m/z 287, which was indicative of the cyanidin moiety, as previously found in the literature.[34]

Peak 2 was identified as cyanidin-3-sambubidoside on the basis of its characteristic molecular ion at m/z 581 and a major fragment in MS^2 at m/z 287, which has been described as one of the most common anthocyanins in diverse *Hisbiscus* spp.[1] However, in our *H. rosa-sinensis* extracts, it was detected only in trace levels.

Peak 3 represented the second predominant anthocyanin in the analyzed extracts accounting for nearly 12% of total anthocyanins. Its fragmentation pattern showed a molecular ion at m/z 639, which produced two MS^2 daughter ions at m/z 449 ($M^+ - 190$), which corresponds to a cyanidin-hexose moiety, and m/z ratio at 287 ($M^+ - 190 - 162$), which corresponds to a cyanidin-aglycone moiety (Figure 3c). Although the MS^2 fragmentation pattern could not be confirmed with reported data, it indicated the sequential losses of an unidentified substituent (190 amu) and one hexose residue (162 amu, i.e., glucose as abundant sugar in plants) from aglycone. According to the literature, the glycoside moieties of anthocyanins are usually esterified with different organic or phenolic acids. Among them, the hibiscus acid has been described as a common compound of *Hibiscus* species showing a characteristic loss of 190 amu[35] when it appears as an esterification substituent. Moreover, the acylated nature of this compound is consistent with the relative retention time in the HPLC analysis, eluting before the corresponding 3-glycosides derivatives. Thus, peak 3 would tentatively correspond to a cyanidin-3-glucoside esterified by a hibiscus acid moiety.

In addition to the above-mentioned compounds, another two minor pigments were also detected (peaks 4 and 5), although their absorption or mass spectra were insufficient to allow speculation about their identity. Their structures still need to be elucidated by comparison of MS data with reference standards or using other spectroscopic techniques such as NMR.

The concentrations of the different anthocyanins detected by HPLC-DAD-MS together with the total content of anthocyanins, flavonols, and polyphenols assessed by rapid spectrophotometric methods are shown in Table 2, where the effect of saline fertirrigation can be observed.

Although there were five anthocyanins detected, quantitative differences for all of the individual compounds were observed

dx.doi.org/10.1021/jf502444u | J. Agric. Food Chem. 2014, 62, 6966−6974

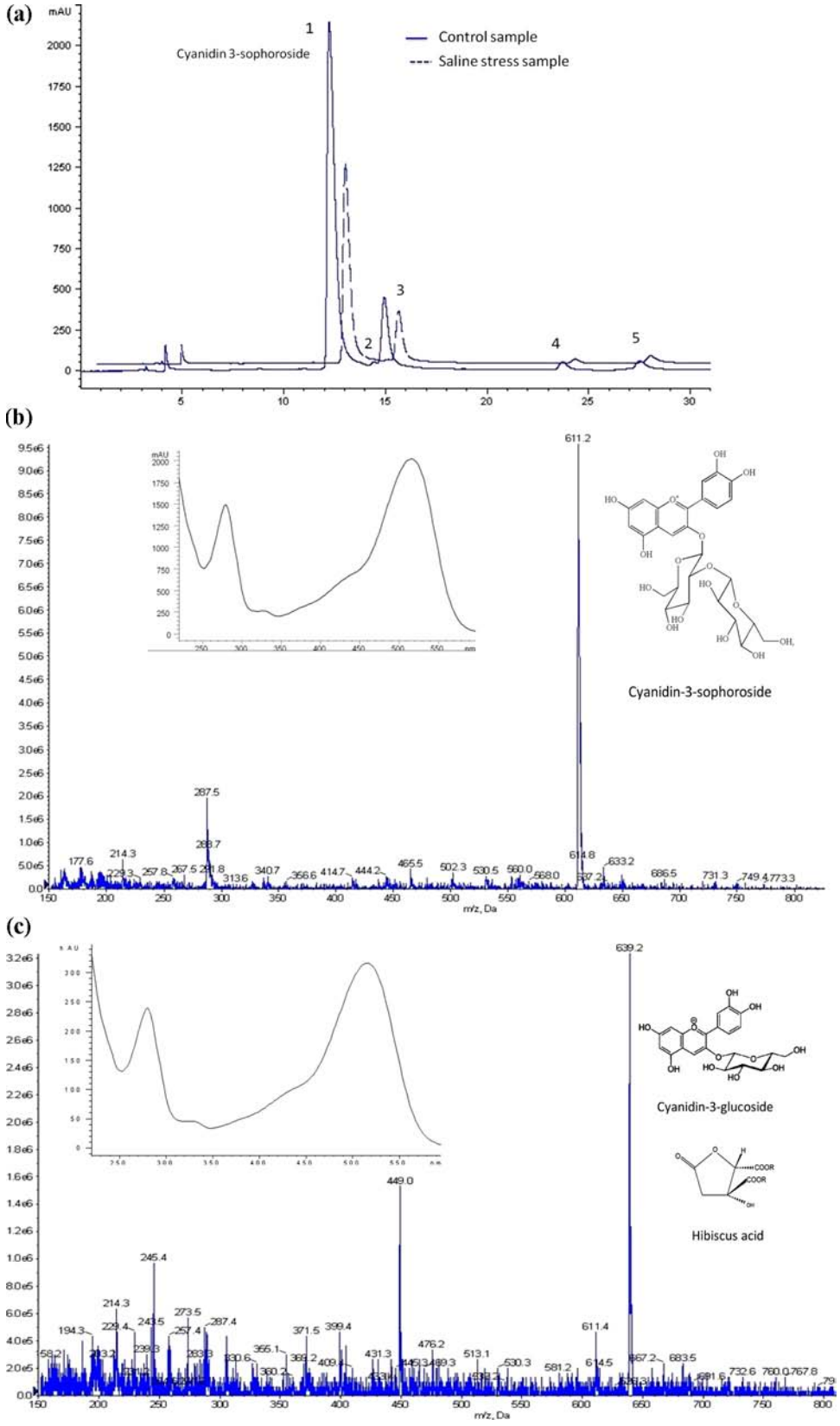

Figure 3. (a) HPLC chromatogram recorded at 520 nm showing the anthocyanin profile of an extract of *H. rosa-sinensis* flower under control and saline stress fertirrigation. The proposed identities of compounds associated with the peaks shown are given in Table 1. (b, c) Molecular ion, MS^2 fragment, and UV−vis spectra of the two major anthocyanins found in *H. rosa-sinensis* flower, associated with peak 1 (m/z 611; MS^2 287) and peak 3 (m/z 639.2; MS^2 449/287) in Table 1.

dx.doi.org/10.1021/jf502444u | J. Agric. Food Chem. 2014, 62, 6966−6974

Table 1. Retention Times, Mass Spectra Details, and Chromatographic UV−Vis Spectrum Data of Anthocyanins Found in *H. rosa-sinensis* Flower (Base and Limb, Control Sample)

peak	t_R (min)	MS^+ (m/z)	MS^2 frag	λ_{max} (nm)	compound	petal[a] base	petal[a] limb
1	12.2	611.2	287.5	516	cyanidin-3-sophoroside	*	*
2	14.4	581.0	287	516	cyanidin-3-sambubidoside	*	*
3	14.9	639.2	449/287	516	cyanidin-3-glc-hibiscus acid	*	*
4	23.7	639.1	287	518	cyanidin dv 1	*	*
5	27.4	566	287	518	cyanidin dv 2	tr	*

[a]tr, traces.

among the two distinct areas of the petals. Generally, the petal limb contained more anthocyanins and other phenolics than the base, which supports the heterogeneous color pattern exhibited by *H. rosa-sinensis* flowers. For the control sample, the average values of total anthocyanins, flavonols, and polyphenolic contents in the petal limb were found to be 821.5 ± 37.3, 23.0 ± 0.9, and 2252.4 ± 129.4 mg/100 g DW, whereas the global levels in the petal base were 228.0 ± 48.9, 12.9 ± 1.2, and 1077.9 ± 98.5 mg/100 g DW, respectively.

As can be observed, the saline treatment significantly ($p < 0.05$) affected the anthocyanin composition of *Hibiscus* flowers reducing its content (Figure 3a), but the magnitude of the effect was different in each zone of the petal (Table 2). The increase in the salinity of the nutrient solution was accompanied by a stronger decrease of the total anthocyanin content in the base than in the limb (30 vs 20%, approximately), which is mainly due to the cyanidin-3-sophoroside reduction in both cases. In particular, some of the individual anthocyanin compounds present in the limb were not affected by the saline treatment, which could explain the lower loss of pigments in this zone of the flower. As reported by other authors,[3] differences between the glycosyl units and acyl groups attached to the aglycone, and the site of their bonding, have a significant influence on the stability and reactivity of the anthocyanin molecule.

Furthermore, the saline fertirrigation caused a negative impact in the accumulation of other phenolic compounds because their total content was lower in flowers from plants grown with salinity stress conditions (25 and 15% lower for total flavonols and 29 and 10% lower for total polyphenols in the base and limb, respectively). There is considerable controversy in the literature concerning the positive and negative effects of salt stress on the phenolic composition of many plant species. Some authors have shown that the application of moderate salt stress stimulates anthocyanin synthesis.[7] However, our results are in agreement with those reported by Li et al.,[36] who observed that the anthocyanin content in grapes was negatively affected by high saline conditions (100−150 mM NaCl).

With regard to the color characteristics of *H. rosa-sinensis* flowers, Figure 4 shows the three-dimensional colorimetric representation of a petal sample (control plant) obtained by digital image analysis. It presents the L^*, C^*_{ab}, and h_{ab} CIELAB values assigned to each pixel of the petal image grouped with regard to the petal zone (base and limb; n = 100 pixels/petal zone), which provides a full characterization of the color variability of samples.[37] As can be seen, the color of the base

Table 2. Individual and Total Anthocyanin Content (Expressed as Cyanidin-3-glucoside Equivalents), Total Polyphenolic Content (as Gallic Acid Equivalents), and CIELAB Color Parameters of *H. rosa-sinensis* Flower (Base and Limb) for Control and Saline Treatments (Mean Values ± SD; Chemical Data, n = 18 Samples/Treatment; Color Data, n = 900 Pixels/Treatment)[a]

	H. rosa-sinensis petal			
	base		limb	
	control	saline	control	saline
compounds (mg/100 g DW)				
cyanidin-3-sophoroside	251.8 ± 16.6 a	152.5 ± 25.1 b	980.6 ± 62.8 a	668.0 ± 83.3 b
cyanidin-3-sambubidoside	tr	tr	tr	tr
cyanidin-3-glc-hibiscus acid	35.9 ± 7.5	33.0 ± 6.7	143.3 ± 23.2	166.2 ± 26.0
cyanidin dv 2	10.9 ± 1.1	10.6 ± 1.0	28.4 ± 1.2	25.2 ± 3.2
cyanidin dv 3	tr	tr	38.1 ± 7.8 a	43.0 ± 5.5 b
sum of anthocyanidins[b]	298.3 ± 25.4 a	196.4 ± 27.7 b	1190.1 ± 30.2 a	912.4 ± 35.8 b
total anthocyanins[c]	228.0 ± 48.9 a	158.9 ± 47.8 b	821.5 ± 37.3	689.9 ± 55.6
total flavonols[d]	12.9 ± 1.2 a	9.6 ± 0.1 b	23.0 ± 0.9 b	19.6 ± 1.7 b
total polyphenols[e]	1077.9 ± 98.51 a	764.5 ± 66.2 b	2252.5 ± 129.4	2019.3 ± 119.1
CIELAB color parameters				
L^*	26.9 ± 3.4 a	34.2 ± 4.3 b	30.9 ± 4.9 a	34.6 ± 5.0 b
a^*	23.2 ± 1.4	21.1 ± 2.7	30.4 ± 2.7 a	28.6 ± 2.5 b
b^*	15.6 ± 1.9 a	21.4 ± 2.9 b	24.1 ± 3.6 a	24.3 ± 3.9 b
C^*_{ab}	31.7 ± 1.7 a	27.9 ± 2.9 b	39.0 ± 3.0 a	37.8 ± 2.8 b
h_{ab}	33.9 ± 3.2 a	42.6 ± 5.0 b	38.3 ± 4.9 a	40.2 ± 5.7 b
ΔE^*_{ab}	9.6		4.1	

[a]Different letters in the same row indicate significant differences (Tukey test, $p < 0.05$) between control and saline treatment, for each petal zone. tr, traces. [b]Sum of all compounds identified by HPLC-DAD-MS. [c]As pH differential method. [d]As Glories method. [e]As Folin−Ciocalteu method.

dx.doi.org/10.1021/jf502444u | J. Agric. Food Chem. 2014, 62, 6966−6974

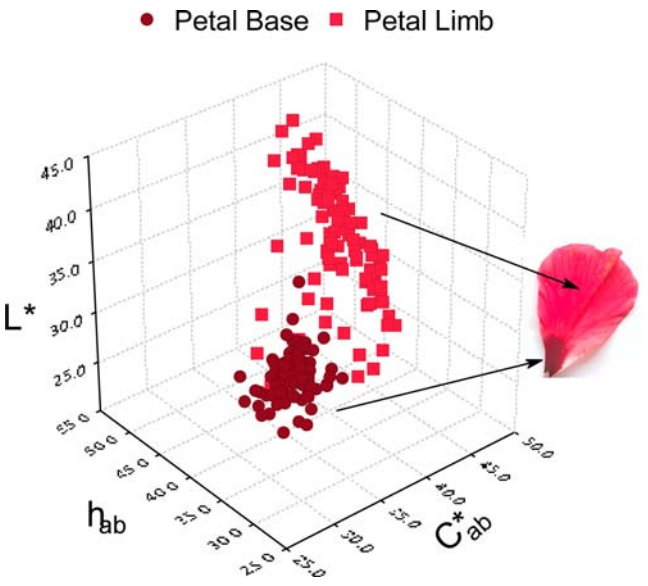

Figure 4. Tridimensional colorimetric representation (L^*, C^*_{ab}, h_{ab} CIELAB parameters) for a *H. rosa-sinensis* petal (base and limb; n = 100 pixels/flower zone) analyzed by digital image analysis.

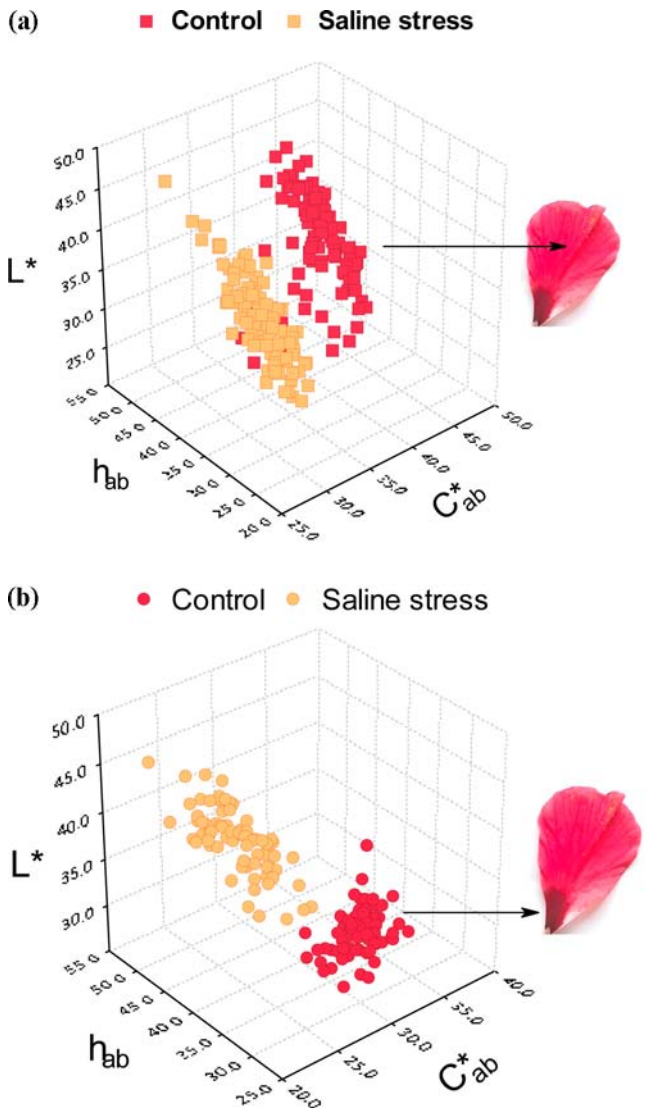

Figure 5. Changes in lightness (L^*), chroma (C^*_{ab}), and hue (h_{ab}) of an *H. rosa-sinensis* petal as a function of the fertirrigation treatment (control and 200 mM NaCl): (a) petal limb; (b) petal base (n = 100 pixels/flower zone, by digital images analysis).

could be easily distinguishable from the limb. Color points corresponding to the limb area appeared more disperse than those of the base and showed higher values of lightness (L^* ranging from 23 to 42 vs from 26 to 37 CIELAB units, respectively), chroma (C^*_{ab} ranging from 31 to 47 vs from 29 to 35 CIELAB units), and hue (h_{ab} ranging from 35° to 53° vs from 30° to 41°). This meant that the petal limb exhibits more vivid color with red-orange hues, which is consistent with the higher accumulation of red-orange forms of anthocyanins (cyanidin derivatives) in this flower zone.[38] On the contrary, the base of the petal corresponds to a more homogeneous redness area with darker and less saturated color, due to its lower concentration in cyanidin derivative pigments. Apart from the different amounts in pigments, the differences observed for the total content of flavonols and polyphenols in each petal zone (Table 2) may also account for the natural color variability of *Hibiscus* flowers because colorless phenolics are usually implied in the color expression of anthocyanins by means of copigmentation reactions contributing to color changes.[39]

For the whole set of samples, the mean color values for each petal zone regarding the fertirrigation treatment are summarized in Table 2, where p values for comparison among control and saline samples are shown. Results indicate that the color of *Hibiscus* flowers was significantly ($p < 0.05$) affected by salt treatment, which was in accordance with the effect induced in the pigment composition. The addition of 200 mM NaCl into nutrient solution resulted in quantitative (L^* and C^*_{ab}) and qualitative (h_{ab}) color variations both in the base and in the the limb of *Hibiscus* petals (Figure 5). Specifically, salt stress resulted in a general loss of color, as can be seen in Table 2. In each zone, L^* and h_{ab} values increased, whereas C^*_{ab} values decreased (L^* by 21 and 11%, h_{ab} by 20 and 5%, and C^*_{ab} by 12 and 3% in the base and limb, respectively), so *Hibiscus* flowers exhibited clearer and less vivid red color when they were fertirrigated under salt stress conditions, the effect being more marked in the base of the petals.

These results were also confirmed through the quantitative mean color difference (ΔE^*_{ab}) calculated among control and saline samples in each petal zone, which were 4.1 and 9.6 CIELAB units for the petal limb and base, respectively. Taking into account that ΔE^*_{ab} of up to 3 CIELAB units indicates color differences appreciable to the human eye,[40] it was confirmed that more important and hence more easily perceptible color loss was caused in the base of the *Hibiscus* petal, which is consistent with the higher reduction of the pigment concentration in this flower zone.

Apart from the assessment of color itself, the objective measurement of color can be harnessed for the rapid determination of pigments. In this regard, color measurements offer a series of advantages for this purpose, such as rapidity, nondestructiveness, and simplicity, among others. A forward stepwise multiple regression was performed for predicting the total anthocyanin content (mg/100 g DW) from the colorimetric data obtained by image analysis. In this respect, not only were conventional colorimetric coordinates (CIELAB) considered, but also other parameters related to heterogeneity of color that image analysis allows to be measured were evaluated. To quantify the heterogeneity of each sample, the

dx.doi.org/10.1021/jf502444u | J. Agric. Food Chem. 2014, 62, 6966−6974

point cloud produced when the color of all the pixels belonging to a sample was considered. These point clouds were fitted into an ellipsoid, and then the shape and orientation of these ellipsoids were included in the data set of the continuous predictors into the multiple regression. A deeper explanation of these parameters as well as the construction of ellipsoids can be found in Rodríguez-Pulido et al.[23] When both salt stress and control samples were used, the model included sequentially the variables chroma (C^*_{ab}), hue (h_{ab}), and the width of the ellipsoid that the pixels made up, and an $R^2 = 0.80$ was reached. However, the model improved when salt stress and control samples were used individually. For salt stress samples ($R^2 = 0.85$), the model included sequentially chroma (C^*_{ab}), hue (h_{ab}), and the orientation angle of the fitting ellipsoid. For control samples ($R^2 = 0.90$), the model included sequentially the length of the fitting ellipsoid, hue (h_{ab}), the orientation angle, and the mean color difference from the mean (MCDM).

As a summary, it was concluded that salt stress influences several physiological and biochemical changes in *Hibiscus* plant tissues including reduction of flower biomass and parameters associated with the functioning of the photosynthetic apparatus as well as fluctuation of ABA levels and increased electrolyte leakage. Results showed a higher preferential accumulation of pigments and other phenolics in the limb than in the base, which supports the heterogeneous color pattern exhibited by *H. rosa-sinensis* flowers. The increase in salinity was also accompanied by a decrease of the levels of most of the individual anthocyanin compounds present in *H. rosa-sinensis* flower, as well as of its total anthocyanin and phenolic contents, which was reflected in an important loss of color. Changes in the color as a result of salt stress occurred in different ways depending on the zone of the petal, being more marked at the basal portion of petals.

Due to the shape and heterogeneity of these samples, image analysis arises as a good alternative to measure their color as well as other features related to the appearance. Moreover, the anthocyanin content of petals could be estimated from their colorimetric data by applying multivariate statistical techniques. Although image analysis is not yet a substitute for conventional chemical analysis, it could be an attractive alternative due to its simplicity, versatility, and low cost, and thus it could become a useful way to assess the chemical characteristics and quality of biological samples of *Hibiscus* crops by controlling the variables.

AUTHOR INFORMATION

Corresponding Author

*(F.J.H.) Phone: +34 954556495. Fax: +34 954556110. E-mail: heredia@us.es.

Funding

This research was financially supported by the MIUR, PRIN 2009-201 (Italian government), and the Consejería de Economía, Innovación, Ciencia y Empleo, Junta de Andalucía (PE11-AGR7843 project and PE07-AGR02893 postdoctoral grant).

Notes

The authors declare no competing financial interest.

ACKNOWLEDGMENTS

We are indebted to the staff of Biology Service (SGI, Universidad de Sevilla) for technical assistance.

REFERENCES

(1) Gomes Maganha, E.; Da Costa Halmenschlager, R.; Moreira Rosa, R.; Pegas Henriques, J. A.; De Paula Ramos, A. L. L.; Saffi, J. Pharmacological evidences for the extracts and secondary metabolites from plants of the genus *Hibiscus*. *Food Chem.* **2010**, *118* (1), 1−10.

(2) Wong, S. K.; Lim, Y. Y.; Chan, E. W. C. Antioxidant properties of hibiscus: species variation, altitudinal change, coastal influence and floral colour change. *J. Trop. For. Sci.* **2009**, *21*, 307−315.

(3) Cisse, M.; Vaillant, F.; Acosta, O.; Claudie, D. M.; Dornier, M. Thermal degradation kinetics of anthocyanins from blood orange, blackberry, and roselle using the Arrhenius, Eyring, and Ball models. *J. Agric. Food Chem.* **2009**, *57*, 6285−6291.

(4) Tsai, T. C.; Huang, H. P.; Chang, Y. C.; Wang, C. J. Anthocyanin-rich extract from hibiscus sabdariffa linnaeus inhibits *N*-nitrosome hylurea-induced leukemia in rats. *J. Agric. Food Chem.* **2014**, *62*, 1572−1580.

(5) Rosa, R. M.; Melecchi, M. I.; da Costa Halmenschlager, R.; Abad, F. C.; Simoni, C. R.; Caramao, E. B. Antioxidant and antimutagenic properties of *Hibiscus tiliaceus* L. methanolic extract. *J. Agric. Food Chem.* **2006**, *54*, 7324−7330.

(6) Chen, C. C.; Hsu, J. D.; Wang, S. F.; Chiang, H. C.; Yang, M. Y.; Kao, E. S.; Ho, Y. C.; Wang, C. J. *Hibiscus sabdariffa* extract inhibits the development of atherosclerosis in cholesterol-fed rabbits. *J. Agric. Food Chem.* **2003**, *51*, 5465−5472.

(7) Borghesi, E.; González-Miret, M. L.; Escudero-Gilete, M. L.; Malorgio, F.; Heredia, F. J.; Meléndez-Martínez, A. J. Effects of salinity stress on carotenoids, anthocyanins, and color of diverse tomato genotypes. *J. Agric. Food Chem.* **2011**, *21*, 11676−11682.

(8) Lag-Brotons, A. J.; Soriano-Disla, J. M.; Gómez, I.; Navarro-Pedreño, J. Saline irrigation effects on *Cynara cardunculus* L. plants grown in Mediterranean soils. *Hort. Sci.* **2013**, *48*, 762−767.

(9) Sgherri, C.; Navari-Izzo, F.; Pardossi, A.; Soressi, G. P.; Izzo, R. The influence of diluted sea water and ripening stage on the content of antioxidants in fruits of different tomato genotypes. *J. Agric. Food Chem.* **2007**, *55*, 2452−2458.

(10) Ferrante, A.; Trivellini, A.; Malorgio, F.; Carmassi, G.; Vernieri, P.; Serra, G. Effect of seawater aerosol on leaves of six plant species potentially useful for ornamental purposes in coastal areas. *Sci. Hortic.* **2011**, *128*, 332−341.

(11) Wang, Y. T. Impact of salinity and media on growth and flowering of an hybrid *Phalaenopsis* orchid. *Hortic. Sci.* **1998**, *33*, 247−250.

(12) Wahome, P. K.; Jesch, H. H.; Grittner, I. Effect of NaCl on the vegetative growth and flower quality of roses. *J. Appl. Bot.* **2000**, *74*, 38−41.

(13) Curtis, P. S.; Lauchli, A. The effect of moderate salt stress on leaf anatomy in *Hibiscus cannabinus* (Kenaf) and its relation to leaf area. *Am. J. Bot.* **1987**, *74*, 538−542.

(14) Vernieri, P.; Paradossi, A.; Tognoni, F. Influence of chilling and drought on water relations and abscisic-acid accumulation in bean. *Aust. J. Plant Physiol.* **1991**, *18*, 25−35.

(15) Trivellini, A.; Ferrante, A.; Vernieri, P.; Serra, G. Effects of abscisic acid on ethylene biosynthesis and perception in *Hibiscus rosa-sinensis* L. flower development. *J. Exp. Bot.* **2011**, *62*, 5437−5452.

(16) Scotti Campos, P.; Thu Pham Thi, A. Effect of abscisic acid pretreatment on membrane leakage and lipid composition of *Vigna unguiculata* leaf discs subjected to osmotic stress. *Plant Sci.* **1997**, *130*, 11−18.

(17) Giusti, M.; Wrolstad, R. E. Characterization and measurement of anthocyanins by UV-visible spectroscopy. *Curr. Protoc. Food Analyt. Chem.* **2001**, F1.2.1−F1.2.13.

(18) Glories, Y. Reserches sur la matiere colorante des vins rouges. *Bull. Chim.* **1979**, *9*, 2649−2655.

(19) Mazza, G.; Fukumoto, L.; Delaquis, P.; Girard, B.; Ewert, B. Anthocyanins, phenolics, and color of Cabernet Franc, Merlot, and Pinot Noir wines from British Columbia. *J. Agric. Food Chem.* **1999**, *47*, 4009−4017.

(20) Singlenton, V. L.; Rossi, J. A. Colorimetry of total phenolics with phosphomolybdic-phosphotungstic acid reagents. *Am. J. Enol. Vitic.* **1965**, *16*, 144−158.
(21) Quijada-Morín, N.; Dangles, O.; Rivas-Gonzalo, J. C.; Escribano-Bailón, M. T. Physico-chemical and chromatic characterization of malvidin 3-glucoside-vinylcatechol and malvidin 3-glucoside-vinylguaiacol wine pigments. *J. Agric. Food Chem.* **2010**, *58*, 9744−9752.
(22) Luo, M. R.; Cui, C. G.; Li, C. Entitled apparatus and method for measuring colour (DigiEye System). British Patent Application 0124683.4, 2001.
(23) Rodríguez-Pulido, F. J.; Gordillo, B.; González-Miret, M. L.; Heredia, F. J. Analysis of food appearance properties by computer vision applying ellipsoids to colour data. *Comput. Elect. Agric.* **2013**, *99*, 108−115.
(24) The Mathworks Inc. *MATLAB* (version R2009b); Natick, MA, USA, 2009.
(25) StatSoft Inc. *STATISTICA* (data analysis software system, version 8); Tulsa, OK, USA, 2007; www.statsoft.com.
(26) Munns, R. Comparative physiology of salt and water stress. *Plant Cell Environ.* **2003**, *2*, 239−250.
(27) Veatch-Blohm, M. E.; Malinowski, M.; Keefer, D. Leaf water status, osmotic adjustment and carbon assimilation in colored calla lilies in response to saline irrigation. *Sci. Hortic.* **2012**, *144*, 65−73.
(28) Cheesman, J. M. Mechanisms of salinity tolerance in plants. *J. Plant Physiol.* **1988**, *87*, 547−550.
(29) Ashraf, M.; Harris, P. J. C. Potential biochemical indicators of salinity tolerance in plants. *Plant Sci.* **2004**, *166*, 3−16.
(30) Umezawa, T.; Hirayama, T.; Kuromori, T.; Shinozaki, K. The regulatory networks of plant responses to abscisic acid. In *Advances in Botanical Research: Plant Responses to Drought and Salinity Stress*, 1st ed.; Kader, J., Delseny, M., Eds.; Elsevier: London, UK, 2011; Vol. 57, pp 201−248.
(31) Wang, J.; Mopper, S.; Hasenstein, K. H. Effect of salinity on endogenous ABA, IAA, JA and SA in *Iris exagoga*. *J. Chem. Ecol.* **2001**, *2*, 327−342.
(32) Ferrante, A.; Maggiore, T. Chlorophyll a fluorescence measurements to evaluate storage time and temperature of *Valeriana* leafy vegetables. *Postharvest Biol. Technol.* **2007**, *45*, 73−80.
(33) Tezara, W.; Martínez, D.; Rengifo, E.; Herrera, A. Photosynthetic responses of the tropical spiny shrub *Lycium nodosum* (Solanaceae) to drought, soil salinity and saline spray. *Ann. Bot.* **2003**, *92*, 757−765.
(34) Vankar, P. S.; Shukla, D. Natural dyeing with anthocyanins from *Hibiscus rosa-sinensis* flowers. *J. Appl. Polym. Sci.* **2011**, *122*, 3361−3368.
(35) Fernández-Arroyo, S.; Rodríguez-Medina, I. C.; Beltrán-Debón, R.; Pasini, F.; Joven, J.; Micol, V.; Segura-Carretero, A.; Fernández-Gutiérrez, A. Quantification of the polyphenolic fraction and in vitro antioxidant and in vivo anti-hyperlipemic activities of *Hibiscus sabdariffa* aqueous extract. *Food Res. Int.* **2001**, *44*, 1490−1495.
(36) Li, X. L.; Wang, C. R.; Li, X. Y.; Yao, Y. X.; Hao, Y. J. Modifications of Kyoho grape berry quality under long-term NaCl treatment. *Food Chem.* **2013**, *139*, 931−937.
(37) González-Miret, M. L.; Ji, W.; Luo, R.; Hutchings, J.; Heredia, F. J. Measuring colour appearance of red wines. *Food Qual. Pref.* **2007**, *18*, 862−871.
(38) Heredia, F. J.; Francia-Aricha, E. M.; Rivas-Gonzalo, J. C.; Vicario, I. M.; Santos-Buelga, C. Chromatic characterization of anthocyanins from red grapes. I. pH effect. *Food Chem.* **1998**, *63*, 491−498.
(39) Gómez-Míguez, M.; González-Manzano, S.; Escribano-Bailón, M. T.; Heredia, F. J.; Santos-Buelga, C. Influence of different phenolic copigments on the color of malvidin 3-glucoside. *J. Agric. Food Chem.* **2006**, *54*, 5422−5429.
(40) Martínez, J. A.; Melgosa, M.; Pérez, M. M.; Hita, E.; Negueruela, A. I. Visual and instrumental color evaluation in red wines. *Food Sci. Technol. Int.* **2001**, *7*, 439−444.

oxidation. In fact, it has been recently reported that the addition of dehydrated waste grape skins during winemaking increased the concentration of some flavonoids in wines, preventing color loss during storage.[17,18]

Despite their potential use in enology, winemaking byproducts have received little attention in comparison to other wine additives (wood chips, enzymes, enological tannins, etc.), probably due to the difficulties related to the technical and legal concerns of its application. However, their application as natural wine additives could represent a sustainable alternative to maximize the exploitation of this valuable agricultural waste as well as to improve the quality of wines, making them more competitive. In this sense, further investigations are needed to advance the knowledge of the contribution of these agricultural byproducts to wine color and color stability.

Therefore, the main objective of this study was to compare the potential of different white winemaking byproducts (pomace, seeds, skins, and stems) as natural sources of antioxidants and copigments, in a model solution. The information reported in this work could be useful for high production winemaking areas.

MATERIALS AND METHODS

Standards and Reagents. Gallic acid, protocatechuic, caffeic, and caftaric acids, (+)-catechin (C), (−)-epicatechin (EC), quercetin, kaempferol, myricetin, sodium carbonate, potassium persulfate, and tartaric acid were purchased from Sigma-Aldrich (Madrid, Spain), and malvidin-3-glucoside was from Extrasynthese (Genay, France). Procyanidin dimer B1 standard was isolated in the laboratory by semipreparative HPLC.[19]

2,2-Azinobis(3-ethylbenzothiazoline-6-sulfonic acid) diammonium salt (ABTS) and 6-hydroxy-2,5,7,8-tetramethylchroman-2-carboxylic acid (Trolox) were purchased from Fluka (Madrid, Spain), and HPLC grade acetonitrile was from Carlo Erba (Rodano, Italy). Folin reagent, ethanol, and formic acid were obtained from Panreac (Barcelona, Spain).

Winemaking Byproducts and Sample Preparation. White winemaking byproducts from Zalema grapes (*Vitis vinifera* sp.) used in this study were pomace (PM), skins (SK), seeds (SD), and stems (ST). They were obtained from a winery located in Condado de Huelva Designation of Origin (southwestern Spain). The Zalema cultivar was selected because it is a high production variety rich in phenolic compounds that represents the main and more extensively white grape cultivated in the zone.

Pomace is the main organic winemaking byproduct generated from grape vinification, which is constituted by a mixture of skins and pulp rests, seeds, and stems. Three kilograms of pomace was collected the day of harvest after Zalema grapes were pressed for winemaking.

To be also individually used in the experiments, particles of stems, seeds, and skins were manually separated from the pomace. All winemaking byproducts were stored at −20 °C and further freeze-dried (lyophilizer Cryodos-80, Telstar Varian DS 102) until extracted. The moisture contents of byproducts were PM, 50%; ST, 40%; SD, 30%; and SK, 70% SK.

The extraction of the nonanthocyanin phenolic compounds from each winemaking byproduct was carried out in a wine-like medium containing 5 g/L tartaric acid in 12% ethanol, buffered with 1 M NaOH to pH 3.6, and ionic strength adjusted to 0.2 M by the addition of NaCl. For this purpose, 2 g of the homogeneous lyophilized powder of samples (PM, SD, SK, and ST) was individually macerated in 15 mL of wine-like medium for 12 h at room temperature (18−20 °C), with occasional agitation and sonication. The supernatants were centrifuged (4190*g*, 10 min) to separate out the liquid fraction containing the phenolic compounds extracted, which was filtered through 0.45 μm Millipore-AP20 filters (Bedford, MA, USA).

The crude phenolic solution obtained from each winemaking byproduct was analyzed for its phenolic composition (spectrophotometric and chromatographic analysis) and antioxidant activity. Also, they were used as a crude mixture of colorless phenolics (copigments) of wine anthocyanins in copigmentation experiments.

Total Phenolic Content. The spectrophotometric determination of the total phenolic content was performed with a Hewlett-Packard UV−vis HP8453 spectrophotometer (Palo Alto, CA, USA), using 10 mm path length glass cells and distilled water as reference.

The total phenolic content of the samples was determined using the Folin−Ciocalteu method.[20] Briefly, 0.25 mL of sample, 1.25 mL of Folin−Ciocalteu reagent, and 3.75 mL of a solution of sodium carbonate at 20% were mixed, and distilled water was added to make up a total volume of 25 mL. The solution was homogenized and left to stand for 120 min for the reaction to take place and stabilize. Absorbance was measured at 765 nm. Gallic acid was employed as a calibration standard, and results were expressed as gallic acid equivalents (mg GAE/L).

Phenolic Composition Analysis. Rapid-resolution liquid chromatography (RRLC) was performed on an Agilent 1260 system equipped with a diode array detector. Samples were filtered through a 0.45 μm pore size membrane filter, and 30 μL of sample was injected in a C18 Poroshell 120 column (2.7 μm particle size, 5 cm × 4.6 mm; Agilent, Palo Alto, CA, USA) maintained at 25 °C. Water/formic acid (99:1, v/v) as solvent A and acetonitrile as solvent B were used, setting the flow rate at 1.5 mL/min. The linear gradient elution was 0 min, 100% A; 5 min, 95% A and 5% B; 20 min, 50% A and 50% B; 22 min, 100% A; 25 min, 100% A. The wavelengths of detection were 280 nm (flavanols and benzoic acids), 320 nm (hydroxycinnamic acids and their tartaric esters), and 370 nm (flavonols).

Phenolic compounds were identified by their retention time, UV−vis spectra, and mass spectra data in an API 3200 Qtrap (Applied Biosystems, Darmstadt, Germany) equipped with an ESI source and a triple-quadrupole ion trap mass analyzer, as described by Jara-Palacios et al.[21] The identification of phenolic compounds was achieved by comparison of the retention times and mass spectra with those of the available pure standards and our data library.

The external calibration method was used for quantification by comparing the areas with standards of gallic, protocatechuic, caffeic, and *p*-coumaric acids, catechin, epicatechin, procyanidin B1, quercetin, and kaempferol. Caftaric and coutaric acids were quantified using the calibration curves of caffeic and *p*-coumaric acids, respectively. Procyanidin dimers B2, B3, and B4, procyanidin B2−3-*O*-gallate, trimers, and tetramer were quantified with the calibration curve of procyanidin B1. Quercetin and isorhamnetin derivatives were quantified as quercetin and kaempferol drivatives as kaempferol.

Total phenolic acids, total flavanols, total flavanol oligomers, and total flavonols were also calculated by the sum of individual phenolic acids, flavanols, flavanol oligomers, and flavonols identified, respectively. The samples were analyzed in triplicate and the results expressed as milligrams per liter.

Antioxidant Activity. The antioxidant activity was measured in vitro on the basis of the ability to scavenge the $ABTS^{\bullet+}$ radical.[22] The $ABTS^{\bullet+}$ radical was produced by the oxidation of 7 mM ABTS with potassium persulfate (2.45 mM) in water. The mixture was kept in the dark at room temperature for 16 h before using it, and then the $ABTS^{\bullet+}$ solution was diluted with phosphate-buffered saline (PBS) at pH 7.4 to give an absorbance of 0.70 ± 0.02 at 734 nm. Then, 50 μL of each sample was mixed with 2 mL of the $ABTS^{\bullet+}$ diluted solution and vortexed for 10 s, and the absorbance was measured at 734 nm after 4 min of reaction at 30 °C. Results were obtained by interpolating the absorbance of samples on a calibration curve obtained with Trolox (30−1000 μM). Three independent experiments in triplicate were performed for each sample, and the results were expressed as Trolox equivalent antioxidant activity (TEAC; μmol of Trolox equivalent (TE) with the same antioxidant activity of 1 L of sample).

Copigmentation Experiments. Copigmentation experiments were carried out in a wine-like medium using a crude anthocyanin solution prepared from Syrah red grapes and different crude phenolic solutions (colorless copigments) obtained from white winemaking byproducts.

The crude anthocyanin solution was obtained by macerating 1 g of homogeneous lyophilized powder of Syrah skins in 20 mL of wine-like medium (the same as previously described) for 12 h with occasional

Table 1. Mean Values and Standard Deviations (n = 3) of the Phenolic Composition, Total Phenolic Content, and Antioxidant Activity for the Crude Phenolic Solution from Winemaking Byproducts[a]

	pomace	skins	seeds	stems
total phenolic content[b] (mg/L)	1138.42 ± 0.19a	1049.01 ± 3.78b	2575.21 ± 5.59c	1000.56 ± 6.72b
total phenolic acids[c] (mg GAE/L)	45.93 ± 0.43a	28.16 ± 0.46b	30.56 ± 0.55c	31.34 ± 0.10d
total flavanols[c]	92.32 ± 1.23a	50.79 ± 2.65b	141.13 ± 0.76c	50.54 ± 0.07b
total oligomers[c]	77.26 ± 0.37a	40.91 ± 2.57b	98.97 ± 0.53c	37.89 ± 0.11b
total flavonols[c]	3.31 ± 0.00a	5.61 ± 0.01b	0.56 ± 0.01c	1.46 ± 0.07d
antioxidant activity (μmol TE/L)	463.29 ± 41.78a	297.53 ± 15.87b	888.73 ± 21.78c	305.57 ± 15.42b
benzoic acids				
gallic acid	36.13 ± 0.35a	22.33 ± 0.39b	30.18 ± 0.04c	20.12 ± 0.07d
protocatechuic acid	0.98 ± 0.19a	0.41 ± 0.03b	nd[d]	0.15 ± 0.01c
hydroxycinnamic acids				
caftaric acid	6.40 ± 0.01a	3.44 ± 0.06b	nd	8.67 ± 0.01c
caffeic acid	1.46 ± 0.01a	1.32 ± 0.01b	nd	1.92 ± 0.02c
cis-coutaric acid	0.26 ± 0.02a	0.28 ± 0.01a	0.15 ± 0.01b	0.17 ± 0.02b
trans-coutaric acid	0.70 ± 0.01a	0.38 ± 0.02b	0.23 ± 0.02c	0.31 ± 0.01d
flavanols				
(+)-catechin (C)	7.86 ± 0.98a	6.32 ± 0.04b	22.03 ± 0.07c	8.90 ± 0.03d
(−)-epicatechin (EC)	7.20 ± 0.25a	3.55 ± 0.04b	20.10 ± 0.37c	3.74 ± 0.01d
procyanidin B1	25.03 ± 0.07a	17.37 ± 1.20b	20.51 ± 0.03c	17.43 ± 0.03d
procyanidin B2	4.94 ± 0.81a	4.08 ± 0.03a	7.08 ± 0.07b	1.46 ± 0.02c
procyanidin B3	5.22 ± 0.07a	3.27 ± 0.5b	4.68 ± 0.05a	2.52 ± 0.04b
procyanidin B4	8.05 ± 0.33a	4.52 ± 0.03b	11.17 ± 0.07c	4.16 ± 0.02d
trimer C−C−EC	4.72 ± 0.53a	2.72 ± 0.05b	5.43 ± 0.05c	5.50 ± 0.02c
trimer C1	4.77 ± 0.50a	1.66 ± 0.03b	10.80 ± 0.04c	0.98 ± 0.03d
tetramer	5.80 ± 0.59a	3.52 ± 0.29b	9.08 ± 0.06c	1.33 ± 0.02d
procyanidin B2−3-*O*-gallate	18.73 ± 0.24a	3.78 ± 0.95b	30.22 ± 0.26c	4.52 ± 0.09d
flavonols				
quercetin 3-*O*-rutinoside	0.17 ± 0.01a	0.19 ± 0.01a	0.17 ± 0.02a	0.21 ± 0.07a
quercetin 3-*O*-glucuronide	0.38 ± 0.01a	0.57 ± 0.01b	0.15 ± 0.01c	0.20 ± 0.01d
quercetin 3-*O*-glucoside	2.07 ± 0.03a	3.48 ± 0.01b	0.24 ± 0.04c	0.86 ± 0.01d
kaempferol hexoside	0.20 ± 0.01a	0.27 ± 0.01a	nd	tr[e]
kaempferol 3-*O*-glucoside	0.18 ± 0.03a	0.65 ± 0.01b	nd	0.19 ± 0.01a
isorhamnetin 3-*O*-glucoside	0.15 ± 0.01a	0.19 ± 0.01a	nd	nd
quercetin	0.16 ± 0.01a	0.26 ± 0.02b	nd	tr
kaempferol	nd	tr	nd	tr

[a]Different letters in the same row indicate significant differences ($p < 0.05$) by Tukey test. [b]As Folin−Ciocalteu method. [c]Sum of individual phenolic acids, flavanols, oligomers, and flavonols identified, respectively. [d]Not detected. [e]Traces.

agitation and sonication. Then, it was centrifuged (4190g, 10 min) and the supernatant filtered through 0.45 μm Millipore-AP20 filters (Bedford, MA, USA). The phenolic composition (anthocyanin pigments and other colorless monomeric phenols) of the crude anthocynin solution was analyzed by HPLC following the method described in Gordillo et al.[23]

Copigmented solutions were prepared by adding separately each crude phenolic solution from winemaking byproducts (PM, ST, SD, and SK) to the crude anthocyanin solution at seven levels (50, 100, 200, 300, 400, 500, and 600 mg/L). The final anthocyanin concentration was the same in all cases (200 mg/L). All of the solutions (2 mL) were prepared in triplicate and equilibrated to reach equilibrium for 2 h and stored closed in darkness at 25 °C, after which their absorption spectra were recorded.

Colorimetric Measurement. The absorption spectra (380−770 nm) of all solutions were recorded at constant intervals ($\Delta\lambda$ = 2 nm) with a Hewlett-Packard UV−vis HP8453 spectrophotometer (Palo Alto, CA, USA), using 2 mm path length glass cells and distilled water as a reference.

The CIELAB parameters (L^*, a^*, b^*, C^*_{ab}, and h_{ab}) were calculated from the absorption spectra by using the original software CromaLab,[24] following the recommendations of the Commission International de L'Eclariage:[25] the 10° Standard Observer and Standard Illuminant D65.

Color difference (ΔE^*_{ab}) was determined by applying the CIE76 color difference formula. It was calculated as the Euclidean distance between two points in the three-dimensional CIELAB space defined by L^*, a^*, and b^*: $\Delta E^*_{ab} = [(\Delta L^*)^2 + (\Delta a^*)^2 + (\Delta b^*)^2]^{1/2}$. It is assumed that color differences (ΔE^*_{ab}) >3−5 units can be perceived by an average observer.[26]

Copigmentation Measurements. The spectrophotometric determination of the magnitude of the copigmentation was made by comparing the absorbance at 520 nm of the crude anthocyanin solution (A_0) and the absorbance at 520 nm of the same solution containing different crude phenolic mixtures from white winemaking byproducts (A_c), at each concentration level and expressed as the percentage $[(A_c - A_0)/A_0] \times 100$.[27]

The color variation due to copigmentation was also evaluated by tristimulus colorimetry according to the methodology described in Gordillo et al.,[16] which offers an objective measurement of color because

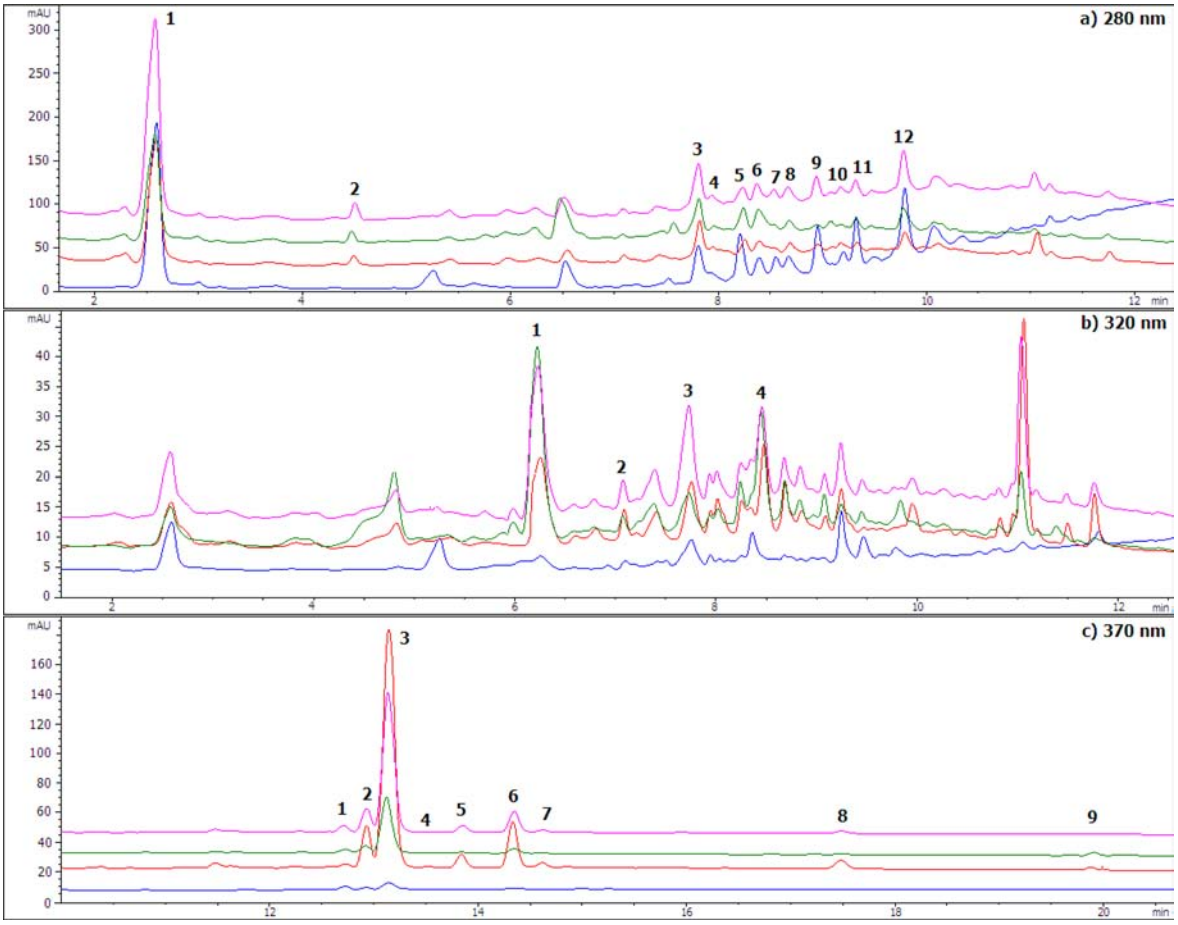

Figure 1. RRLC chromatograms recorded at 280, 320, and 370 nm of crude phenolic solution from seeds (blue), skins (red), stems (green), and pomace (magenta). Peaks: (a) 1, gallic acid; 2, protocatechuic acid; 3, procyanidin B1; 4, procyanidin B3; 5, catechin; 6, trimer C−C−EC; 7, tetramer; 8, procyanidin B4; 9, trimer C1; 10, procyanidin B2; 11, epicatechin; 12, procyanidin B2-*O*-gallate; (b) 1, caftaric acid; 2, *cis*-coutaric acid; 3, *trans*-coutaric acid; 4, caffeic acid; (c) 1, quercetin 3-*O*-rutinoside; 2, quercetin 3-*O*-glucuronide; 3, quercetin 3-*O*-glucoside; 4, quercetin pentose; 5, kaempferol hexoside; 6, kaempferol 3-*O*-glucoside; 7, isorhamnetin 3-*O*-glucoside; 8, quercetin; 9, kaempferol.

it is based on the consideration of the whole visible spectrum and allows the real assessment of color to be obtained. Following this methodology, diverse color difference formulas were applied in the CIELAB color space by using the scalar (L^*, a^*, b^*) and cylindrical (L^*, C^*_{ab}, h_{ab}) CIELAB color coordinates of samples. This provides a better evaluation of the quantitative and qualitative color implications of the copigmentation and their incidence on visual perception. The new colorimetric variables were determined as follows.

The total color of each sample was assessed as the CIELAB color difference (ΔE^*_{ab}) applied between its color (L^*, a^*, and b^*) with respect to distilled water ($L^* = 100$, $a^* = 0$, $b^* = 0$), as shown in eq 1. It represents a quantitative color attribute.

$$\text{total color: } \Delta E^*_{ab} = [(L^* - 0)^2 + (a^* - 0)^2 + (b^* - 0)^2]^{1/2} \quad (1)$$

The total color difference induced by copigmentation was assessed as the CIELAB color difference (ΔE^*_{ab}) applied between the color of the crude anthocyanin solution (L^*_0, a^*_0, and b^*_0) and the color of the same solution copigmented with each crude phenolic mixture from white winemaking byproducts (L^*_c, a^*_c, and b^*_c), as shown in eq 2:

$$\text{total color difference: } \Delta E^*_{ab(c-0)} = [(L^*_c - L^*_0)^2 + (a^*_c - a^*_0)^2 + (b^*_c - b^*_0)^2]^{1/2} \quad (2)$$

The relative contribution (%) of lightness, chroma, and hue to each total color difference induced by copigmentation was calculated by means of the color formulas shown in eqs 3, 4, and 5. They represent the weight of the three color attributes that make up the total color difference.

$$\text{relative contribution (\%) of lightness: } \%\Delta L = [(\Delta L_{c-0})^2/(\Delta E^*_{ab(c-0)})^2] \times 100 \quad (3)$$

$$\text{relative contribution (\%) of chroma: } \%\Delta C = [(\Delta C_{c-0})^2/(\Delta E^*_{ab(c-0)})^2] \times 100 \quad (4)$$

$$\text{relative contribution (\%) of hue: } \%\Delta h = [(\Delta h_{c-0})^2/(\Delta E^*_{ab(c-0)})^2] \times 100 \quad (5)$$

Δh_{c-0} being deduced as follows:

$$\Delta h_{c-0} = [(\Delta E^*_{ab(c-0)})^2 - ((\Delta L_{c-0})^2 + (\Delta C_{c-0}))^2]^{1/2}$$

Statistical Analysis. All statistical analyses were performed using Statistica v.8.0 software.[28] Univariate analysis of variance (Tukey test) was applied to establish differences for the phenolic composition, antioxidant activity, and copigmentation effects among the crude phenolic solutions from winemaking byproducts (GP, SD, SK, and ST). Moreover, correlations between the phenolic composition (main phenolic groups or individual phenolic compounds), and the antioxidant activity was studied by linear and multiple regressions. In all cases (differences or correlations), the statistically significant level was considered at $p < 0.05$.

RESULTS AND DISCUSSION

Phenolic Composition. A total of 24 phenolic compounds were identified and quantified in the crude phenolic solutions from winemaking byproducts by using the methodology and chromatographic conditions previously described. The phenolic profile of samples showed the presence of several types of monomeric and oligomeric colorless phenols belonging to diverse phenolic families. The benzoic acids, hydroxycinnamic acids, flavanols, and flavonols identified were the expected, well-known, compounds usually present in grapes. It included six phenolic acids (gallic, protocatechuic, caftaric, caffeic, *cis*-coutaric, and *trans*-coutaric acids); two monomeric flavanols (catechin and epicatechin), eight oligomeric flavanols (procyanidins B1, B2, B3, B4, and B2−3-*O*-gallate, two trimers, and one tetramer); and eight flavonols (quercetin and kaempferol aglycones, and 3-glycoside conjugated forms of quercetin, kaempferol, and isorhamnetin).

Table 2. Concentration and Distribution of Individual Phenolic Compounds Identified by HPLC in the Crude Anthocyanin Solution Prepared from Syrah Grape Skins

	concentration (mg/L ± SD, n = 3)	relative proportion (%)
total anthocyanins[a]	222.65 ± 10.03	95.8
total phenolic acids[a]	1.97 ± 0.02	0.9
total flavanols[a]	7.63 ± 0.97	3.3
anthocyanins		
delphinidin-3-glucoside	3.12 ± 0.09	4.2
cyanidin-3-glucoside	3.12 ± 0.14	1.3
petunidin-3-glucoside	12.42 ± 1.25	5.3
peonidin-3-glucoside	11.79 ± 1.62	5.1
malvidin-3-glucoside	98.32 ± 2.49	42.3
petunidin-3-acetyl-glucoside	5.35 ± 0.71	2.3
peonidin-3-acetyl-glucoside	8.09 ± 1.13	3.6
malvidin-3-acetyl-glucoside	39.47 ± 1.90	16.9
petunidin-3-*p*-coumaroyl-glucoside	2.9 ± 0.21	1.3
peonidin-3-*p*-coumaroyl-glucoside	6.34 ± 0.36	2.7
malvidin-3-*p*-coumaroyl-glucoside	25.13 ± 2.1	10.8
hydroxycinnamic acids		
caftaric acid	0.25 ± 0.01	0.1
cis-coutaric acid	0.76 ± 0.01	0.4
trans-coutaric acid	0.93 ± 2.1	0.4
flavanols	tr	
flavonols		
myricetin-3-*O*-glucuronide	0.96 ± 0.01	0.4
myricetin-3-*O*-glucoside	0.89 ± 0.01	0.4
quercetin-3-*O*-glucuronide	0.97 ± 0.03	0.4
quercetin-3-*O*-glucoside	2.95 ± 0.02	1.3
laricitrin-3-*O*-glucoside	0.18 ± 0.01	<0.1
kaempferol-3-*O*-glucoside	0.14 ± 0.01	<0.1
isorhamnetin-3-*O*-glucoside	0.92 ± 0.01	0.4
syringetin-3-*O*-glucoside	0.59 ± 0.01	0.3

[a]Sum of individual anthocyanins, phenolic acids, or flavonols identified, respectively.

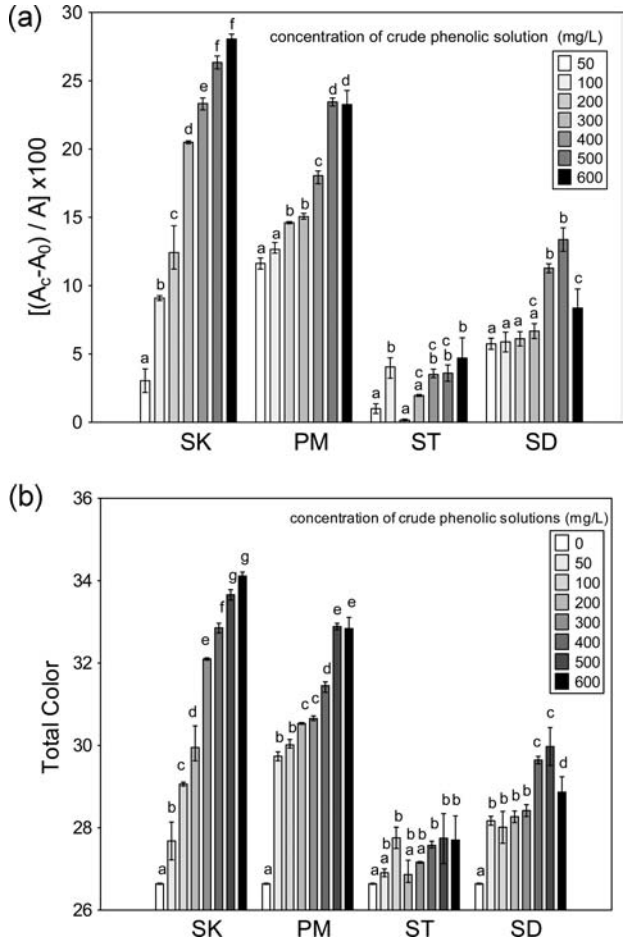

Figure 2. (a) Magnitude of copigmentation and (b) total color of the crude anthocyanin solution containing increasing concentrations of crude phenolic solutions from Zalema winemaking byproducts (SK, skins, PM, pomace; ST, stems; SD, seeds); mean ± SD, n = 3. Different letters in the same byproduct indicate significant differences (p < 0.05).

Table 1 summarizes the concentration for the mentioned phenolic compounds (mg/L) and the total phenolic content (mg GAE/L) of samples, showing the statistical differences found among them. In general terms, all samples presented important contents of total phenolics indicating that considerable amounts of bioactive compounds can be recovered from Zalema winemaking byproducts. As white wines are commonly elaborated by applying a shorter maceration time than used for red wines, the pomace obtained from white vinification is not as exhausted as that from red vinification, which increases its industrial value as a richer agricultural byproduct.[18] Nevertheless, significant differences (p < 0.05) were found for the total phenolic content among samples depending on the type of winemaking byproduct. The crude phenolic solution from SD showed the highest total phenolic content (around 2-fold the concentration of the other samples), which is consistent with previous studies.[29] The higher accumulation of phenolic compounds in seeds[30] but the lower extractability due to the solid cellular structure[31] could explain the greater phenolic potential of SD as winemaking byproduct. On the contrary, significantly (p < 0.05) lower contents of total phenolics were found in the crude phenolic solutions from SK and ST, indicating that they are comparatively poorer sources of phenolics.

The chromatographic analysis showed that crude phenolic solutions from PM, SK, SD, and ST had different qualitative and

dx.doi.org/10.1021/jf500978n | J. Agric. Food Chem. 2014, 62, 6975−6983

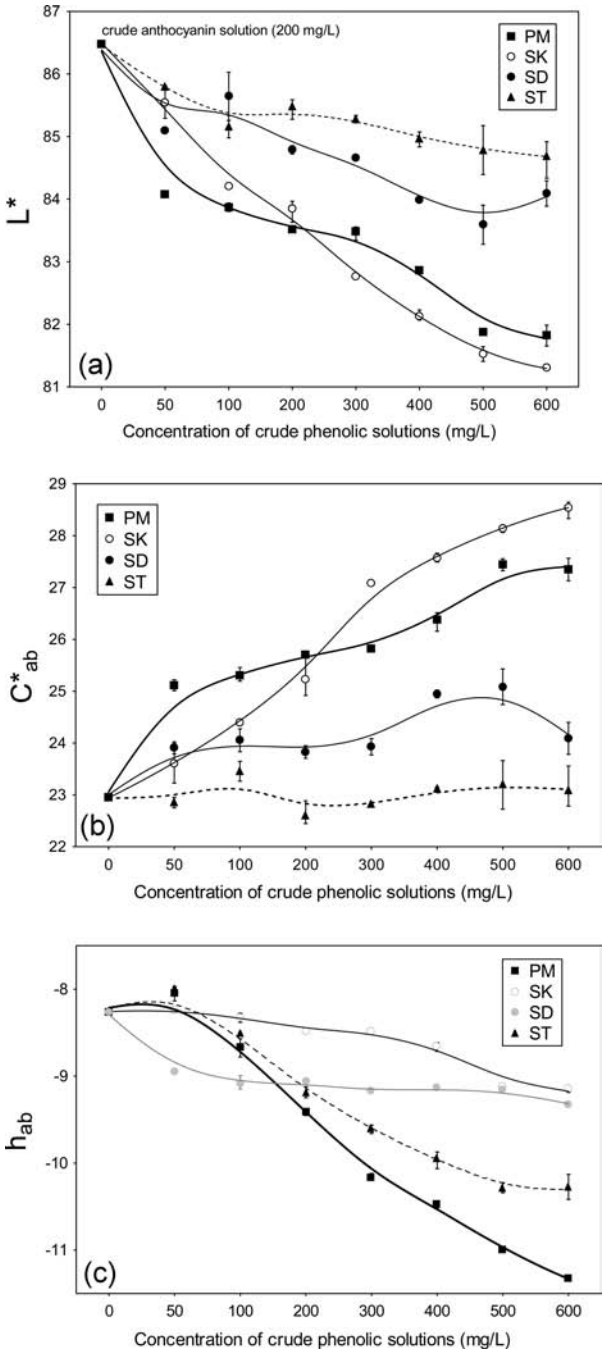

Figure 3. Changes in (a) lightness (L^*), (b) chroma (C^*_{ab}), and (c) hue (h_{ab}) of the crude anthocyanin solution after addition of increasing concentrations of crude phenolic solutions from Zalema winemaking byproducts (SK, skins; PM, pomace; ST, stems; SD, seeds); mean ± SD, $n = 3$.

quantitative phenolic profile (Figure 1), the differences being significant ($p < 0.05$) for most of the individual compounds identified (Table 1). These differences were also observed when compounds were grouped by phenolic families (phenolic acids, flavanols, and flavonols). Significantly higher contents of flavanols were found in the crude phenolic solutions from SD, which is in accordance with other studies.[8,32] The global level of flavanols was 35% higher than those found in the samples from PM and 64% higher than those from SK and ST. On the other hand, PM was the major source of phenolic acids, contributing to the crude phenolic solution at 34% higher than ST and SD and at 38% higher than SK. With regard to the flavonol contribution, SK represented the significantly richest source of these compounds in comparison with all other winemaking byproducts studied, as expected.

As far as individual compounds are concerned, great variability has been described in the literature about the distribution of phenolic acids in different types of winemaking byproducts, which is attributable to the influence of several factors such as grape variety, cultivation and climatic conditions, or the enological processes applied during winemaking.[33−35] However, the qualitative profile of phenolic acids did not differ much among samples. In particular, gallic acid was the main phenolic acid found in the samples being transferred in significantly ($p < 0.05$) higher quantity by PM. Caftaric acid was the second most abundant phenolic acid, ST and PM being the better sources.

In contrast, the group of flavonoids (flavanols and flavonols) varied considerably among samples. In the case of flavanols, significantly higher levels of monomeric compounds were obtained from SD, mainly due to a more important contribution in catechin and epicatechin. Nevertheless, Zalema winemaking byproducts contributed with greater quantities of oligomers than monomers to the total flavanol content (PM, 84%; SK, 80%; ST, 75%; and SD, 70%). Among them, procyanidins B1, B4, and B2−3-*O*-gallate were the most representative oligomers in all samples. Specifically, SD and PM were the significantly richest sources in oligomeric flavanols (98.9 and 77.3 mg/L in samples, respectively), contributing to the crude phenolic solution about 2.5-fold higher than SK and ST. With regard to flavonols, quercetin-3-glucoside was the predominant compound in all samples. The crude phenolic solution from SK was noteworthy for having significantly higher levels of all flavonols compared to those from PM, ST, and SD (6.6% of the total phenolic contribution versus 2.3, 1.7, and 0.3%, respectively).

The individual phenolic compounds present in the crude phenolic solution have critical importance because each compound can have different antiradical and copigmentation powers.[36,37] Thus, on the basis of the results obtained, differences on the antioxidant and copigmentation properties of samples were expected as well, because different heterogeneous phenolic mixtures coexisting in competing equilibria might result in additive or suppressive effects.[8,15]

Antioxidant Activity. Results showed that the antioxidant activity was in accordance with the total phenolic content of each sample (Table 1). Thus, the crude phenolic solution from SD, with the highest phenolic content, showed the greatest antioxidant activity (888.7 μmol TE/L) followed in decreasing order by those from GP, ST, and SK (463.3, 305.6, and 297.5 μmol TE/L, respectively).

Univariate linear regression was applied to these data to explore relationships between the total phenolic content and the antioxidant activity, and very strong and significant correlations ($R^2 = 0.98$, $p < 0.05$) were found, which indicate that Zalema winemaking byproducts represent good sources of natural antioxidants with high added value.

Also, a multiple regression analysis was performed to check the more influential phenolic groups (independent variables: total phenolic acids, total flavanols, and total flavonols) on the antioxidant activity (dependent variable). High multiple correlation coefficient ($R^2 = 0.99$) and significant correlation ($p < 0.05$) were obtained for the total flavanols ($\beta = 0.98$) followed by the total phenolic acids ($\beta = -0.18$).

On the other hand, two multiple regression analyses were carried out to determine the relative importance of individual

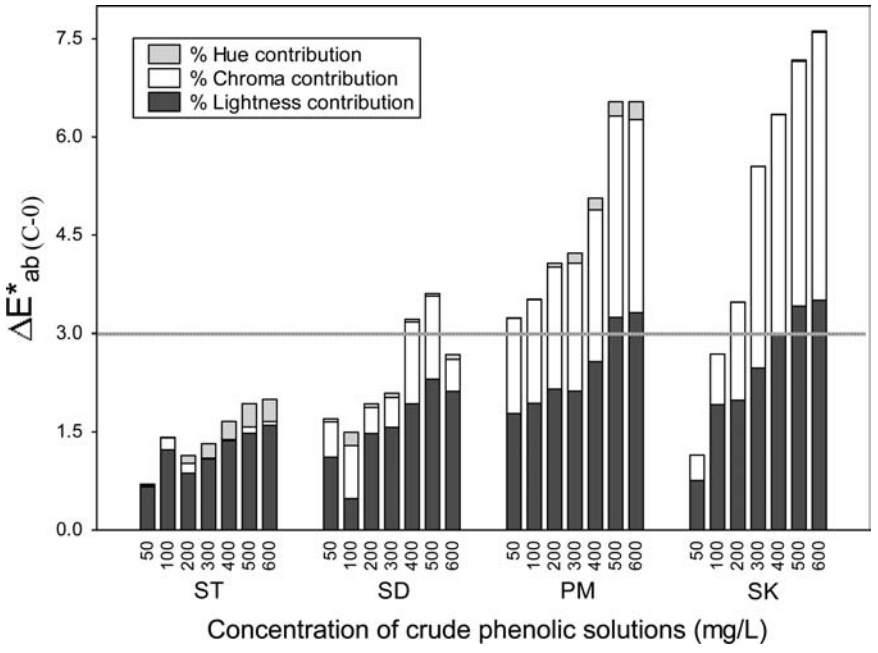

Figure 4. Total color difference induced by copigmentation ($\Delta E^*_{ab(c-0)}$) with the relative contribution of lightness, chroma, and hue (%ΔL, %ΔC, %Δh), calculated between the color of the crude anthocyanin solution and after addition of increasing concentrations of the crude phenolic solution from Zalema winemaking byproducts (SK, skins; PM, pomace; ST, stems; SD, seeds).

phenolic compounds on the antioxidant activity. First, a regression analysis between antioxidant activity (dependent variable) and individual flavanols (independent variables) was performed to assess the influence of these phenolic compounds. Results indicated good correlation ($R^2 = 0.98$) having catechin ($\beta = 0.83$), epicatechin ($\beta = 1.01$), trimer C1 ($\beta = 1.28$), and procyanidins B2 ($\beta = 0.54$) and B4 ($\beta = 0.68$) with significant influence ($p < 0.05$). Multiple regression analysis considering phenolic acids showed also a high multiple correlation coefficient ($R^2 = 0.99$) having caffeic acid ($\beta = -2.20$), caftaric acid ($\beta = 1.33$), *trans*-coutaric acid ($\beta = -1.20$), and gallic acid ($\beta = 1.22$) more influential than *cis*-coutaric and protocatechuic acids.

Copigmentation Effect. The crude anthocyanin solution obtained from Syrah skins was analyzed for its phenolic composition. Eleven anthocyans including nonacylated, acetylated, and *p*-coumaroylated forms of the five expected anthocyanidins (delphinidin, cyanidin, petunidin, peonidin, and malvidin) were identified by HPLC, which accounted for 95.8% of the total phenolic content. Also, the presence of other minor nonanthocyanin phenolic compounds was confirmed. They were mainly flavonols and phenolic acids, which accounted for <5% of the total phenolic compounds identified. The relative proportion of each identified compound is presented in Table 2.

Figure 2 shows the magnitude of copigmentation (a) and the total color (b) of the crude anthocyanin solution containing increasing concentrations of crude phenolic solutions from Zalema winemaking byproducts (PM, SK, SD, and SK). Immediate intermolecular copigmentation was observed in the mixtures, which are evidenced by the hyperchromic shift of the λ_{max} of the crude anthocyanin solution (520 nm) and also by an increase of its initial total color (26.6 CIELAB u). As observed, the magnitude of copigmentation differed depending on the type of winemaking byproduct and the phenolic concentration applied. Stronger copigmentation effects were produced by the crude phenolic solutions from SK and PM, which induced the highest hyperchromic shifts (from 2 to 28% and from 11 to 24%, respectively) and increases of the total color (from 26.6 to 34.4 and 32.5 CIELAB u, respectively). The effect was significantly ($p < 0.05$) more pronounced with increasing copigment concentration. In contrast, SD and ST appeared as the less effective sources of copigments because the addition of the crude phenolics solutions at increasing levels did not always result in progressive increases of the magnitude of copigmentation in the total color.

Our results indicate that the quantitative and qualitative profile of phenolic mixtures used as colorless copigments determined distinctive effects on the extent of multiple copigmentations, as previously reported by Gonzalez-Manzano et al.[15] Higher relative proportions of more effective copigments as flavonols (mainly quercetin derivatives), oligomeric flavanols (mainly B-type procyanidins), or some phenolic acids in SK and PM samples could explain their greater copigmentation effect observed.[36]

Also, it was confirmed that the color of the crude anthocyanin solution was improved by the crude phenolic solution from winemaking byproducts, which was manifested through positive changes in the CIELAB parameters (L^*, C^*_{ab}, and h_{ab}), shown in Figure 3). The progressive enrichment in colorless copigments resulted in decreasing lightness and hue values (L^* and h_{ab}) and increasing chroma (C^*_{ab}), which means a progressively darker and more saturated bluish color. However, important differences existed for the quantitative and qualitative color effects induced depending on the type of winemaking byproduct. In this sense, crude phenolic solutions from PM and SK decrease the initial values of lightness approximately by 6% (from 86.5 to 81.3 and 81.8 CIELAB u, respectively) and increase the chroma value by 24 and 19% (from 22.9 to 28.5 and 27.4 CIELAB u). For the qualitative attribute of color (h_{ab}), the effect was more important with crude phenolic solution from PM and ST, which decreases the initial hue value approximately in three grades (from −8.26° to −11.33° and −10.29°)

The total color differences, $\Delta E^*_{ab(c-0)}$ between the crude anthocyanin solution and those containing crude phenolic solution from winemaking byproducts at increasing concentration were calculated (Figure 4), which provide relevant color information related to visual perception. Moreover, the relative contribution of lightness (%ΔL), chroma (%ΔC), and hue (%Δh) to each color difference calculated permits us an objective comparison of the colorimetric effect among the samples. Results showed that the color changes were visually perceptible ($\Delta E^*_{ab} > 3$, according to Martínez et al.[26]) for the crude phenolic solution from PM at all the assayed concentrations, as well as for most of those from SK. In contrast, samples from SD and ST resulted in color differences of <3 CIELAB u (not clearly perceptible). This fact confirms again their poorer efficiency as copigments sources, which is consistent with the results obtained for the magnitude of copigmentation and total color.

With regard to winemanking byproducts causing perceptible color changes (SK and PM), it can be observed that both samples induced similar effects independent of the concentration tested. In general, the weight of the lightness and chroma modifications were more marked than in hue (%ΔL = 54 and 52%; %ΔC = 45 and 45.5; %Δh = 0.1 and 2%, as mean values, respectively, in SK and PM). This meant that for the same concentration of the SK and PM crude phenolic solutions, comparable darkening and greater quantity of color were induced without substantially modifying the original hue.

In summary, white winemaking byproducts from Zalema grape are rich sources of phenolic compounds consisting of mainly flavanoids and phenolic acids. The antioxidant activity of these compounds is related to the total phenolic content and particularly to the flavanol and phenolic acid contents. The copigmentation effects in model solution indicate that white winemaking byproducts could improve the anthocyanin color quality depending on the type of byproduct used as copigment source (PM, SK, SD, and ST) and the phenolic concentration applied, causing perceptible color changes. Therefore, the exploitation for their potential reuse in the wine industry could be of great interest, considering either the Zalema pomace or its individual components (seeds, stems, and skins).

AUTHOR INFORMATION

Corresponding Author

*(F.J.H.) Mail: Food Colour and Quality Lab., Dept. Nutrition and Food Science, Facultad de Farmacia, Universidad de Sevilla, 41012 Sevilla, Spain. Phone: +34 954556495. Fax: +34 954556110. E-mail: heredia@us.es.

Funding

This work was supported by Ministerio de Ciencia e Innovación (AGL2011-30254-C02-02), Ministerio de Educación (FPU predoctoral grant) and Consejería de Economía, Innovación, Ciencia y Empleo, Junta de Andalucía (P10-AGR-6331/AGR02893 posdoctoral grant).

Notes

The authors declare no competing financial interest.

ACKNOWLEDGMENTS

We are indebted to Vinícola del Condado winery (Condado de Huelva D.O.) for supplying samples and to Dr. Modesto J. Carballo (Biology Service, CITIUS, Universidad de Sevilla) for technical assistance.

REFERENCES

(1) Boye, J. I.; Arcand, Y. Current trends in green technologies in food production and processing. *Food Eng. Rev.* **2013**, *5*, 1−17.

(2) Ruggieri, L.; Cadena, E.; Martínez-Blanco, J.; Gasol, C. M.; Rieradevall, J.; Gabarrell, X.; Gea, T.; Sort, X.; Sánchez, A. Recovery of organic wastes in the Spanish wine industry. Technical, economic and environmental analyses of the composting process. *J. Clean. Prod.* **2009**, *17*, 830−838.

(3) Casazza, A. A.; Aliakbarian, B.; De Faveri, D.; Fiori, L.; Perego, P. Antioxidants from winemaking wastes: a study on extraction parameters using response surface methodology. *J. Food Biochem.* **2012**, *36*, 28−37.

(4) Devesa-Rey, R.; Vecino, X.; Varela-Alende, J. L.; Barral, M. T.; Cruz, J. M.; Moldes, A. B. Valorization of winery waste vs. the costs of not recycling. *Waste Manage.* **2011**, *31*, 2327−2335.

(5) Pedroza, M. A.; Carmona, M.; Pardo, F.; Salinas, M. R.; Zalacain, A. Waste grape skins thermal dehydration: potential release of colour, phenolic and aroma compounds into wine. *CYTA−J. Food* **2012**, *10*, 225−234.

(6) Chouchouli, V.; Kalogeropoulos, N.; Konteles, S. J.; Karvela, E.; Makris, D. P.; Karathanos, V. T. Fortification of yoghurts with grape (*Vitis vinifera*) seed extracts. *LWT−Food Sci. Technol.* **2013**, *53*, 522−529.

(7) Lavelli, V.; Sri Harsha, P. S. C.; Torri, L.; Zeppa, G. Use of winemaking by-products as an ingredient for tomato puree: the effect of particle size on product quality. *Food Chem.* **2014**, *152*, 162−168.

(8) Makris, D. P.; Boskou, G.; Andrikopoulos, N. K. Polyphenolic content and in vitro antioxidant characteristics of wine industry and other agri-food solid waste extracts. *J. Food Compos. Anal.* **2007**, *20*, 125−132.

(9) Parrado, J.; Escudero-Gilete, M. L.; Friaza, V.; García-Martínez, A.; González-Miret, M. L.; Bautista, J. D.; Heredia, F. J. Enzymatic vegetable extract with bioactive components: influence of fertiliser on the colour and anthocyanins of red grapes. *J. Sci. Food Agric.* **2007**, *87*, 2310−2318.

(10) Xia, E. Q.; Deng, G. F.; Guo, Y. J.; Li, H. B. Biological activities of polyphenols from grapes. *Int. J. Mol. Sci.* **2010**, *11*, 622−646.

(11) Rodriguez-Rodriguez, R.; Justo, M. L.; Claro, C. M.; Vila, E.; Parrado, J.; Herrera, M. D.; Alvarez de Sotomayor, M. Endothelium-dependent vasodilator and antioxidant properties of a novel enzymatic extract of grape pomace from wine industrial waste. *Food Chem.* **2012**, *135*, 1044−1051.

(12) Mendoza, L.; Yañez, K.; Vivanco, M.; Melo, R.; Cotoras, M. Characterization of extracts from winery by-products with antifungal activity against *Botrytis cinerea*. *Ind. Crops Prod.* **2013**, *43*, 360−364.

(13) Monagas, M.; Bartolomé, B.; Gómez-Cordovés, C. Updated knowledge about the presence of phenolic compounds in wine. *CRC Crit. Rev. Food Sci.* **2005**, *45*, 85−118.

(14) Boulton, R. The copigmentation of anthocyanins and its role in the color of red wine: a critical review. *Am. J. Enol. Vitic.* **2001**, *52*, 67−87.

(15) González-Manzano, S.; Dueñas, M.; Rivas-Gonzalo, J. C.; Escribano-Bailón, M. T.; Santos-Buelga, C. Studies on the copigmentation between anthocyanins and flavan-3-ols and their influence in the colour expression of red wine. *Food Chem.* **2009**, *114*, 649−656.

(16) Gordillo, B.; Rodríguez-Pulido, F. J.; Escudero-Gilete, M. L.; González Miret, M. L.; Heredia, F. J. Comprehensive colorimetric study of anthocyanic copigmentation in model solutions. Effects of pH and molar ratio. *J. Agric. Food Chem.* **2012**, *60*, 2896−2905.

(17) Pedroza, M. A.; Carmona, M.; Salinas, M. R.; Zalacain, A. Use of dehydrated waste grape skins as a natural additive for producing rosé wines: study of extraction conditions and evolution. *J. Agric. Food Chem.* **2011**, *59*, 10976−10986.

(18) Pedroza, M. A.; Carmona, M.; Alonso, G. L.; Salinas, M. R.; Zalacain, A. Pre-bottling use of dehydrated waste grape skins to improve colour, phenolic and aroma composition of red wines. *Food Chem.* **2013**, *136*, 224−236.

(19) González-Manzano, S.; Santos-Buelga, C.; Pérez-Alonso, J. J.; Rivas-Gonzalo, J. C.; Escribano-Bailón, M. T. Characterization of the mean degree polymerization of proanthocyanidins in red wines using liquid chromatography-mass spectrometry (LC-MS). *J. Agric. Food Chem.* **2006**, *54*, 4326−4332.

(20) Singlenton, V. L.; Rossi, J. A., Jr. Colorimetry of total phenolics with phosphomolybdic-phosphotungstic acid reagents. *Am. J. Enol. Vitic.* **1965**, *16*, 144−158.
(21) Jara-Palacios, M. J.; González-Manzano, S.; Escudero-Gilete, M. L.; Hernanz, D.; Dueñas, M.; González-Paramás, A. M.; Heredia, F. J.; Santos-Buelga, C. Study of Zalema grape pomace: phenolic composition and biological effects in *Caenorhabditis elegans*. *J. Agric. Food Chem.* **2013**, *61*, 5114−5121.
(22) Re, R.; Pellegrini, N.; Proteggente, A.; Pannala, A.; Yang, M.; Rice-Evans, C. Antioxidant activity applying an improved ABTS radical cation decolorization assay. *Free Radical Biol. Med.* **1999**, *26*, 1231−1237.
(23) Gordillo, B.; Cejudo-Bastasnte, M. J.; Rodríguez-Pulido, F. J.; González-Miret, M. L.; Heredia, F. J. Application of the differential colorimetry and polyphenolic profile to the evaluation of the chromatic quality of Tempranillo red wines elaborated in warm climate. Influence of the presence of oak wood chips during fermentation. *Food Chem.* **2013**, *141*, 2184−2190.
(24) Heredia, F. J.; Álvarez, C.; González-Miret, M. L.; Ramírez, A. *CromaLab, Análisis de Color*; Registro General de la Propiedad Intelectual, 2004.
(25) CIE. *Technical Report Colorimetry*; Commission Internationale de l'Eclairage Central Bureau: Vienna, Austria, 2004.
(26) Martínez, J. A.; Melgosa, M.; Pérez, M. M.; Hita, E.; Negueruela, A. I. Visual and instrumental color evaluation in red wines. *Food Sci. Technol. Int.* **2001**, *7*, 439−444.
(27) Boulton, R. B. A method for the assessment of copigmentation in red wines. Presented at the 47th Annual Meeting of the American Society for Enology and Viticulture, Reno, NV, USA, June 1996.
(28) StatSoft Inc. *STATISTICA (Data Analysis Software System)*, v 8; StatSoft Inc.: Tulsa, OK, USA, 2007.
(29) Pastrana-Bonilla, E.; Akoh, C. C.; Sellappan, S.; Krewer, G. Phenolic content and antioxidant capacity of muscadine grapes. *J. Agric. Food Chem.* **2003**, *51*, 5497−4503.
(30) Rustioni, L.; Bedgood, D. R., Jr.; Failla, O.; Prenzler, P. D.; Robards, K. Copigmentation and anti-copigmentation in grape extracts studied by spectrophotometry and post-column-reaction HPLC. *Food Chem.* **2012**, *132*, 2194−2201.
(31) Jensen, J. S.; Blachez, B.; Egebo, M.; Meyer, A. S. Rapid extraction of polyphenols from red grapes. *Am. J. Enol. Vitic.* **2007**, *58*, 451−460.
(32) Poudel, P. R.; Tamura, H.; Kataoka, I.; Mochioka, R. Phenolic compounds and antioxidantactivities of skins and seeds of five wild grapes and two hybrids native to Japan. *J. Food Compos. Anal.* **2008**, *21*, 622−625.
(33) Alonso, A. M.; Guillén, D. A.; Barroso, C.; Puertas, B.; García, A. Determination of antioxidant activity of wine by products and its correlation whit polyphenolic content. *J. Agric. Food Chem.* **2002**, *50*, 5832−5836.
(34) Kammerer, D.; Claus, A.; Carle, R.; Schieber, A. Polyphenol screening of pomace from red and white grape varieties (*Vitis vinifera* L.) by HPLC-DAD-MS/MS. *J. Agric. Food Chem.* **2004**, *52*, 4360−4367.
(35) Anastasiadi, M.; Pratsinis, H.; Kletsas, D.; Skaltsounis, A.; Haroutounian, S. Grape stem extracts: polyphenolic content and assessment of their in vitro antioxidant properties. *LWT−Food Sci. Technol.* **2012**, *48*, 316−322.
(36) Gómez-Míguez, M.; González-Manzano, S.; Escribano-Bailón, M. T.; Heredia, F. J.; Santos-Buelga, C. Influence of different phenolic copigments on the color of malvidin 3-glucoside. *J. Agric. Food Chem.* **2006**, *54*, 5422−5429.
(37) Anastasiadi, M.; Pratsinis, H.; Kletsas, D.; Skaltsounis, A.; Haroutounian, S. Bioactive non-coloured polyphenols content of grapes, wines and vinification by products: evaluation of the antioxidant activities of their extracts. *Food Res. Int.* **2010**, *43*, 805−813.

stabilize wines. This technique causes the precipitation of tartrates and unstable colloidal substances and aims at avoiding further undesirable precipitations and wine turbidity.[3] Nevertheless, cold can also precipitate coloring matter either by adsorption on the tartrate crystals or by the instability of colloidal coloring matter. The role of wine polysaccharides in preventing those phenomena has been proposed. The mannoproteins are considered to be protective colloids that can hinder tartrate crystallization,[3] avoiding the growth of the crystals. Furthermore, they play an important part in protein haze stabilization.[19] They are glycoproteins of the *Saccharomyces cerevisiae* cell wall that can be excreted to the wine during alcoholic fermentation or be released to the wine during yeast autolysis.[20] Although the compositions of these two types of mannoproteins are quite similar, only the mannoproteins released from cell walls seem to exert the stabilizing effects.[21] Recently, it has been reported that mannoproteins can also influence tannin aggregation by adsorption of the mannoproteins on the tannin molecule, preventing the growth of the tannin particles.[22,23] Nevertheless, Poncet-Legrand and co-workers[24] showed that the tannin-stabilizing effect depends on the molecular weight of the mannoprotein and also on other factors such as ethanol content or ionic strength. The results of that study confirmed that mannoproteins seem to act as steric stabilizers. Taking into account that mannoproteins were able to stabilize tannins, it was hypothesized that they might also act as stabilizers of the colloidal coloring matter. In fact, different mannoprotein-rich commercial preparations are now available,[25] and among the benefits claimed by manufacturers is the increase of color stabilization. However, studies on the effects of mannoproteins on wine color and pigment composition are scarce. Escot and co-workers[26] reported that the presence of mannoproteins released by yeast to the wine during alcoholic fermentation improved color stability. Guadalupe and co-workers, on the contrary, reported that the mannoproteins released by mannoprotein-overproducing yeasts affected neither wine color nor monomeric anthocyanin content,[27] whereas the addition of commercial mannoproteins during the prefermentation stage even caused a loss of stable wine color.[27,28] These differences in the behavior of mannoproteins might be related to differences in their composition. Fernández and co-workers[29] observed greater color intensity and a slight tendency to red tones when the wine was treated with lysated lees obtained by acidification and enzymatic treatment instead of those obtained only by acidification. Nevertheless, none of these works study the influence that mannoproteins can exert on the colloidal stability of anthocyanin-derived pigments, the influence of which on wine color cannot be neglected in aged wines. Furthermore, the usefulness of these products on preventing color loss by cold treatment has to be studied.

The objective of the present study was to assess the chemical and colloidal stabilization of wine color and pigment composition as a consequence of the addition during alcoholic fermentation of either an enological tannin containing hydrolyzable and condensed tannins or a mannoprotein obtained from yeast by enzymatic treatment. The effect of these two enological products on preventing the loss of coloring matter has also been studied after wines had been submitted to cold stabilization treatment. Samples were analyzed after malolactic fermentation and 10 weeks later to verify if the effects were maintained over time. CIELAB parameters were used to evaluate color modifications, whereas changes in pigment composition were assessed by HPLC-DAD-MS^n analysis.

MATERIALS AND METHODS

Samples. Three different wines (100 L of each) were made from *Vitis vinifera* L. cv. Tempranillo grapes. The first wine served as control (C), whereas the second and third wines were treated with an enological tannin and with a mannoprotein (product M), respectively (wines T and M). All of the wines were made in duplicate. Following the manufacturer's advice these enological products (100% soluble in wine) were added in equal amounts during alcoholic fermentation at densities 1100, 1060, and 1020 g/L, reaching a final concentration of 35 g/hL (dose recommended by manufacturer). Further details of these enological products are given below. Maceration−alcoholic fermentation lasted 12 days. Then, the wines were inoculated with *Oenococcus oeni* and malolactic fermentation (MLF) took place, lasting 20 days. After MLF, two aliquots of 10 L from each wine were separated from the rest of the sample. One aliquot was cold-treated, whereas the other was not subjected to this treatment. Cold treatment consisted in cooling samples at 4 °C during 48 h followed by centrifugation during 10 min at 3000 rpm. Both aliquots were filtered (2 μm) and then bottled (bottles of 750 mL). Furthermore, the precipitate was recovered and dissolved in model wine solution (5 g/L of tartaric acid in 12% aqueous ethanol adjusted to pH 3.6). The CIELAB color parameters and the pigment composition of the wines not subjected to cold treatment (C1, T1, and M1) and of those cold-treated (C1*, T1*, and M1*) as well as of the redissolved precipitates (C1p, T1p, and M1p) were then determined. Another bottle of each fraction (subjected and not subjected to cold) was kept in the dark and at 15 °C and analyzed 10 weeks after the first analysis (wines C2, T2, M2, C2*, T2*, and M2*).

Enological Tannin. The enological tannin (Tanin VR Color) was supplied by Laffort España (Rentería, Spain) and consisted of an extract from natural sources mainly constituted by catechins and proanthocyanidins (58.8%), oak ellagitannins (11.2%), and hydroxybenzoic acids (7.5%). The composition of the enological tannin was determined in our laboratory by means of HPLC-DAD-MS employing the conditions described by Ferrer-Gallego and co-workers[30] for the analysis of catechins and proanthocyanidins.

Yeast Mannoproteins (Product M). In a preliminary study two commercial mannoproteins and four different mannoproteins obtained by Laffort from *S. cerevisiae* by either enzymatic or thermal treatments were tested to evaluate their potential protective effect on the colloidal unstable coloring matter of the wines. Among all of the tested mannoproteins only one (product M, obtained by enzymatic treatment) showed a statistically significant protective effect, and for this reason it was selected for the present study. Other tested mannoproteins, on the contrary, even provoked additional precipitation, which is in accordance with the results of previous studies that did not find a protective effect of mannoproteins on coloring matter.[27,28] Gel permeation chromatography revealed that all of the tested mannoproteins contained three main peaks that were present in different percentages. In relation to the other mannoproteins, product M showed a higher percentage (50%) of the heaviest peak (70 kDa).

Colorimetric Measurements. Because wine color is dependent on pH, it was standardized in all of the samples to 3.6 with 0.1 N HCl (Panreac, Castellar del Vallès, Spain) prior to the spectrophotometric measurements. Absorption spectra (190−1100 nm) were recorded in a Hewlett-Packard UV−vis HP 8453 (Agilent Technologies, Waldbronn, Germany) spectrophotometer in 2 mm path length quartz cells. The analysis of color was made only from the visible spectra (380−770 nm) data, using the CIE 1964 standard observer (10° visual field) and the CIE standard illuminant D65 as references. CIELAB color parameters (L^*, a^*, b^*, C_{ab}^*, and h_{ab}) were calculated using the software CromaLab.[31] Color differences between different wine samples were determined by means of the CIELAB color difference formula:

$$\Delta E_{ab}^* = ((\Delta L^*)^2 + (\Delta a^*)^2 + (\Delta b^*)^2)^{1/2}$$

dx.doi.org/10.1021/jf4055825 | J. Agric. Food Chem. 2014, 62, 6984−6994

Table 1. CIELAB Parameters (Mean Values, $n = 2$) of the Different Samples (C, Control; T, Tannin-Treated; M, Mannoprotein-Treated) at the Different Sampling Points (1, after Malolactic Fermentation; 2, 10 Weeks after Malolactic Fermentation) and in Non-Cold-Treated and Cold-Treated (*) Samples[a]

Sampling Point 1					
	L^*	a^*	b^*	C_{ab}^*	h_{ab}
C1	59.04 a α,β	42.89 a α,β	0.34 a α,β	42.89 a α	0.44 a α,β
T1	51.38 a α,β	48.53 a α,β,χ	2.93 b β,χ	48.62 a α,β	3.44 b β
M1	48.91 a α	50.72 a χ	3.43 b χ	50.84 a β	3.87 b β
C1*	73.12 b 2	24.86 b 1	3.61 b 1	25.12 b 1	8.26 c 2
T1*	54.63 a 1	46.71 a 2	2.12 a,b 1	46.76 a 2	2.58 a,b 1,2
M1*	51.67 a 1	48.42 a 2	3.00 b 1	48.52 a 2	3.55 b 1,2
Sampling Point 2					
	L^*	a^*	b^*	C_{ab}^*	h_{ab}
C2	59.70 β	42.36 α	−1.30 α	42.39 α	−1.75 α
T2	52.10 α,β	47.63 α,β,χ	0.84 α,β,χ	47.65 α,β	0.99 α,β
M2	49.54 α,β	49.88 β,χ	1.16 α,β,χ	49.89 α,β	1.32 α,β
C2*	73.05 2	25.73 1	3.10 1	25.92 1	6.93 1,2
T2*	54.71 1	46.19 2	0.12 1	46.19 2	0.15 1
M2*	49.98 1	46.19 2	2.65 1	46.31 2	3.30 1,2
Differences Due to the Addition of Enological Products					
	ΔL^*	Δa^*	Δb^*	ΔC_{ab}^*	Δh_{ab}	ΔE_{ab}^*
T1−C1	−7.66	5.64	2.59	5.73	3.00	9.86
M1−C1	−10.13	7.84	3.09	7.95	3.44	13.17
Differences Due to Cold Treatment						
	ΔL^*	Δa^*	Δb^*	ΔC_{ab}^*	Δh_{ab}	ΔE_{ab}^*
C1*−C1	14.08 b	−18.03 b	3.27 a	−17.77 b	7.82 b	23.11 b
T1*−T1	3.25 a	−1.83 a	−0.81 a	−1.87 a	−0.86 a	3.82 a
M1*−M1	2.77 a	−2.30 a	−0.43 a	−2.32 a	−0.32 a	3.62 a
Differences Due to Time						
	ΔL^*	Δa^*	Δb^*	ΔC_{ab}^*	Δh_{ab}	ΔE_{ab}^*
C2−C1	0.66	−0.53	−1.64	−0.51	−2.19	1.85
T2−T1	0.72	−0.90	−2.09	−0.98	−2.45	2.39
M2−M1	0.63	−0.85	−2.28	−0.95	−2.55	2.51
C2*−C1*	−0.07	0.87	−0.51	0.80	−1.33	1.01
T2*−T1*	0.08	−0.52	−2.00	−0.57	−2.43	2.07
M2*−M1*	−1.70	−2.24	−0.35	−2.21	−0.25	2.83
T2−C1	−6.93	4.74	0.50	4.75	0.55	8.42
M2−C1	−9.50	6.98	0.81	7.00	0.88	11.82

[a]Differences due to the addition of the enological products, to cold treatment and time are also shown. Letters a−c following entries show the significance of the differences among the samples of the first sampling point (C1, T1, M1, C1*, T1*, and M1*). Letters α, β, and χ following entries show the significance of the differences due to time in non-cold-treated samples (C1, T1, M1, C2, T2, and M2). Numbers 1−3 following entries show the significance of the differences due to time in cold-treated samples (C1*, T1*, M1*, C2*, T2*, and M2*). $p < 0.05$ in all cases.

HPLC-DAD-ESI/MS^n Analyses. The anthocyanins and derivative pigments were analyzed by HPLC-DAD-MS^n in all of the wine samples (cold-treated and non-cold-treated) as well as in the precipitates of the cold-treated samples. Wine samples were diluted (1/5) with acidified water (pH 1.3, HCl) and filtered through a 0.45 μm Millex syringe-driven filter unit (Millipore Corp., Bedford, MA, USA) before HPLC-DAD-MS analysis. The precipitates that had been redissolved in model wine solution were also acidified (0.25 mL acidified water/mL sample) and filtered prior to the HPLC-DAD-MS analysis. Analyses were performed in a Hewlett-Packard 1100 series liquid chromatograph (Agilent Technologies, Waldbronn, Germany). An AQUA C18 reversed-phase, 5 μm, 150 mm × 4.6 mm column (Phenomenex, Torrance, CA, USA) thermostated at 35 °C was used. The HPLC-DAD conditions have been previously employed with satisfactory results in our laboratory in the analysis of wine samples.[32] Detection was carried out at 520 nm as the preferred wavelength. Spectra were recorded from 220 to 600 nm. The mass spectrometer was connected to the HPLC system via the DAD cell outlet. MS detection was performed in an API 3200 Qtrap (Applied Biosystems, Darmstadt, Germany) equipped with an ESI source and a triple-quadrupole ion trap mass analyzer that was controlled by Analyst 5.1 software. MS analysis was carried out in positive mode (ESI$^+$). Zero grade air served as nebulizer gas (GS1) and turbo gas (GS2) for solvent drying. Nitrogen served as curtain (CUR) and collision gas (CAD). Settings used were optimized by direct infusion of a malvidin 3-*O*-glucoside solution: declustering potential (DP), 41 V; entrance potential (EP), 7.5 V; ion spray voltage (IS), 5000 V; GS1, 40 psi; GS2, 50 psi (600 °C); CUR, 20 psi; and CAD, set as "high". Both quadrupoles were set at unit resolution. Mass method consisted of three mass experiments: full mass analysis (EMS mode, collision energy (CE) 10 V), MS^2 analysis (EPI mode, CE 25 V), and MS^3 analysis (CE 30 V, excitation energy (AF2) 50 V). Spectra were recorded between m/z 150 and 1300.

Compounds were identified from the data supplied by the HPLC-DAD-MS^n analyses of the samples (retention time, UV−vis spectra, m/z ratio, and fragmentation patterns) and by comparison to the data previously obtained in our laboratory for wine samples analyzed in the same conditions.[32] Thirty-one anthocyanins and derivative pigments were determined: 5 anthocyanin 3-*O*-glucosides, 5 anthocyanin 3-*O*-acetylglucosides, 8 anthocyanin 3-*O*-coumaroylglucosides (5 *trans*

dx.doi.org/10.1021/jf4055825 | J. Agric. Food Chem. 2014, 62, 6984−6994

isomers and 3 *cis* isomers), 2 anthocyanin 3-*O*-caffeoylglucosides, 7 flavanol–anthocyanin direct condensation products (F-A^+ dimers), 2 A-type vitisins, a B-type vitisin of malvidin 3-*O*-glucoside, and the vinylphenol–malvidin 3-*O*-glucoside pyranoanthocyanin. All of these compounds were considered for the quantitative analysis. As it usually happens in the analysis of wine samples by HPLC, an elevation of the baseline was observed at the end of the chromatogram corresponding to difficult resolution pigments, such as dimeric anthocyanins.[33] Although it is difficult to know the exact composition of these unresolved peaks, it is important to know their percentage over the total coloring matter because they show absorbance at 520 nm and can, therefore, contribute to the final color of the wine. Their contribution was assessed as the absorbance of the "hump" formed above the theoretical baseline. Because the final color of a wine depends both on the total pigment content and on the proportions of the different types of pigments, the percentage of each compound over the total area was calculated.

Total pigment content of each sample was also calculated and expressed as malvidin 3-*O*-glucoside (Extrasynthèse, Genay, France).

Statistical Analysis. The CIELAB parameters, the percentages of the different pigments, and their modifications with cold treatment and with time were analyzed by means of one-way analysis of variance (ANOVA) and Tukey's honestly significant difference test to assess the significance of the differences observed among samples ($p < 0.05$). An unsupervised pattern recognition method, principal components analysis (PCA), was used for data analysis. PCA was applied from the correlation matrix of the original variables (mean percentages of the 31 identified pigments and that of the difficult resolution pigments).

Student's *t* test was employed to evaluate the statistical significance between pairs of samples (95% confidence levels). The IBM-SPSS Statistics 21 for Windows software package (IBM, Armonk, NY, USA) was used to carry out the statistical analysis.

RESULTS AND DISCUSSION

Chromatic Analysis. It is relevant to first analyze the color modifications that are a direct consequence of the addition of these two enological products to the wine. It has been observed that the addition of either the enological tannin or product M causes a decrease in lightness (L^*) and an increase in a^* and b^* coordinates and consequently an increase in chroma (C_{ab}^*) and in hue (h_{ab}) in relation to those observed in nontreated samples (Table 1). Nevertheless, only the changes in b^* coordinate and in hue were statistically significant. Although the changes were more noticeable in the samples to which product M was added than in those treated with enological tannin, the differences among tannin and M-treated samples were not statistically significant (Table 1). Color differences between control and tannin- or M-treated wines were assessed by ΔE_{ab}^*. In both cases ΔE_{ab}^* was >3, which means that the color modifications induced by the treatments are visible to the human eye.[34] Previous studies on mannoproteins and their influence on wine color[27,28] reported that in the tested conditions the mannoproteins did not modify wine color in relation to control samples, and they even observed the precipitation of stable color when the mannoprotein was added to the wine as an extract but not when mannoprotein-overproducing yeast strains were used. This was not observed in the present study. Differences might be related to the type of mannoprotein employed. As previously indicated, the molecular weight, the source from which they are obtained, or the methodology employed to obtain them[21,24,29] can modify the effect of the mannoproteins. Nevertheless, as in our study, Guadalupe and co-workers[27] observed an increase in the b^* coordinate in wines fermented with a mannoprotein-overproducing yeast strain either in the absence or in the presence of a commercial mannoprotein.

Thus, from these first results it can be concluded that the addition of the enological tannin or product M to the wines modifies the values of the CIELAB color parameters observed in control wines.

Modification of the CIELAB Parameters after Cold Treatment. In relation to lightness, it was observed that the samples that underwent cold stabilization increased their L^* value in relation to those not subjected to cold treatment (see "Sampling Point 1" and "Differences Due to Cold Treatment" in Table 1). This fact can be related to the precipitation of compounds after cold treatment, either directly due to their own instability or indirectly by adsorption to compounds such as tartrates, which easily precipitate with cold. Differences have been observed among the different samples. In control samples L^* increased ca. 14 units after cold treatment. However, in the cases of either tannin- or M-treated wines the values of L^* determined in the samples not subjected to cold treatment (T1 and M1) and in those subjected to cold treatment (T1* and M1*, respectively) were not statistically different. Furthermore, ΔL^* due to cold treatment was not statistically different in tannin- or M-treated wines. This is indicative of a stabilizing effect of both types of compounds against cold precipitation.

As can be observed in Table 1 (see "Sampling Point 1" and "Differences Due to Cold Treatment"), cold treatment caused a significant increase in the b^* coordinate only in the case of control wines. On the contrary, the a^* coordinate decreased in all samples, although it was only statistically significant in the case of control wines. This might be pointing to a color stabilization effect toward cold treatment caused by the addition of these two enological products. From these two parameters (a^* and b^*), chroma (C_{ab}^*) and hue (h_{ab}) parameters can be calculated. Although chroma decreased in all of the samples after cold treatment, only the changes observed in control wines were significant. Thus, wines treated with the enological tannin or with product M were able to better maintain their own quantity of color after cold treatment. With respect to hue, after cold treatment, it significantly increased in control wines, shifting color toward more orange hues. On the contrary, hue remained quite stable after cold stabilization in tannin- or M-treated wines (Table 1).

From these results it seems that the addition of these two products to the wine allows a stabilization of the coloring matter against cold treatment. In fact, whereas cold treatment caused a color difference (ΔE_{ab}^*) of 23 units in control samples, in treated samples it hardly exceeded the human eye threshold of 3 units. The main initial drawback might be the slight shift of the wine color toward red-orange hues observed after the addition of these two enological products. However, after cold treatment, the color in the wines treated with these two products (T1* and M1*) is redder than that of cold-treated control wines (C1*) and darker and with higher chroma than that of control wines even before cold treatment (C1).

Modification of the CIELAB Parameters over Time. The color parameters of these samples were studied 10 weeks after cold treatment to determine if the effect of the addition of either the enological tannin or product M is maintained over time.

In all samples, the modification in lightness (ΔL^*) caused by time (between sampling points 2 and 1) is much lower than that caused by cold treatment (Table 1). This might indicate that there has not been an important quantitative change in pigment composition such as additional pigment precipitation.

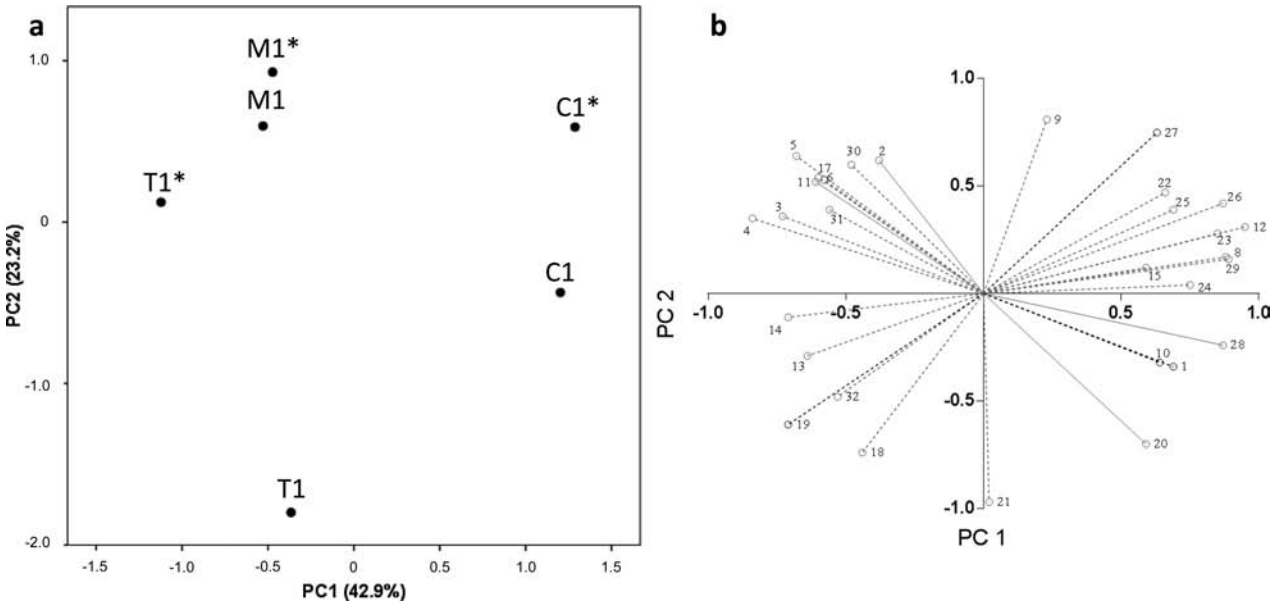

Figure 1. (a) Projection of the wine samples on the plane defined by the first and second principal components (PC2 vs PC1). These samples correspond to all wines (control, tannin- and M-treated wines) in the first sampling point either subjected to cold treatment (samples C1*, T1*, and M1*) or not (samples C1, T1, and M1). (b) Loading plot of the PCA. The identities of the original variables are indicated in Table 2.

Furthermore, the modifications in L^* (ΔL^*) produced by time were not significantly different among the different kinds of samples (control, tannin- or M-treated samples).

With respect to a^* and b^* parameters and their modification over time (Δa^* and Δb^* between sampling points 2 and 1, Table 1, "Differences Due to Time"), it can be seen that, in most cases, time produced a decrease in both parameters. In addition, no significant differences can be observed in the values of Δa^* and Δb^* among samples, which indicates that time affects a^* and b^* in a similar way in all of the samples, independently of the initial treatment. Because chroma and hue depend on a^* and b^* parameters, they also decreased over time in most of the samples (see ΔC_{ab}^* and Δh_{ab} in Table 1). As in the case of Δa^* and Δb^*, no significant differences were observed in the evolution of chroma and hue (ΔC_{ab}^* and Δh_{ab}) over time among the different treatments either in the samples not subjected to cold treatment or in the samples cold-treated (compare C2−C1, T2−T1, M2−M1, C2*−C1*, T2*−T1*, and M2*−M2). It has to kept in mind that, on the contrary, cold treatment did affect differently the samples treated either with the enological tannin or with product M, observing significant differences in the values of ΔL^*, ΔC_{ab}^*, and Δh_{ab} between control samples and the samples treated with any of these enological products. As indicated in the previous section, their addition has been proven to produce a stabilization of the initial color of the samples against cold treatment in relation to the samples to which these products were not added (compare C1*−C1 to T1*−T1 and M1−M1* in Table 1). This might indicate that the addition of these two types of enological products might be useful to prevent color loss due to cold but not to prevent changes in color due to age. Cold treatment mainly affects pigment composition by precipitation (reflected in the changes in L^* and C_{ab}^*, above all), whereas pigment evolution over time involves chemical modifications of the pigments initially present (reflected in the changes in h_{ab}), which can be accompanied or not by precipitation. Nevertheless, the time range between sampling points 1 and 2 is too low (10 weeks) to draw conclusions about the possible long-term effect in pigment composition. In fact, slight differences in the behavior of the color parameters over time have been observed among the different types of cold-treated samples. Although not statistically significant, they might be pointing out differences in the mechanisms of both types of products. Furthermore, although the magnitude of the modifications over time in chroma and hue (ΔC_{ab}^* and Δh_{ab}) has been the same in all types of samples, the final colors of the tannin- or M-treated samples not subjected to cold after 10 weeks show a hue similar to that of control wine before cold treatment at point 1 (compare T2−C1 and M2−C1, Table 1). This means that although these products have not been able to avoid the decrease in hue observed from point 1 to point 2, the initial increase caused in this parameter by their addition has made up for this decrease. In other words, they have also "stabilized" the hue of the nontreated wine. Furthermore, treated wines (T2 and M2) were darker and possessed higher chroma than control wine at the first sampling point (C1).

Pigment Analysis. Because the addition of the enological tannin or product M to the wine modified the initial color of the samples, it seems interesting to first analyze the modification induced in the pigment composition by these additions (compare C1, T1, and M1). In relation to total pigment content, the samples to which the enological tannin was added (T1) showed the highest pigment content (630.3 mg/L) followed by those treated with product M (M1, 582.6 mg/L). Control samples (C1) showed the lowest total content (541.3 mg/L). This lower pigment content explains the higher L^* value of control samples in relation to treated samples. The higher total pigment content observed in T1 samples might be related to a higher extraction of native grape pigments favored by the addition of the enological tannin as previously observed in our laboratory.[18] T1 samples also showed the highest contents for each group of pigments in relation to the other types of samples. For this reason, the differences among types of wines were lower when the percentages of the different groups of pigments were considered. To evaluate the relevance of the different wine pigments on the differences observed

dx.doi.org/10.1021/jf4055825 | J. Agric. Food Chem. 2014, 62, 6984−6994

Table 2. Individual Percentages of Pigments in Samples before Cold Treatment (C1, T1, and M1) and in Precipitates Obtained after Cold Treatment (C1p, T1p, and M1p) (Mean Values, $n = 2$)

		samples[a]					
peak/variable	compound[b]	C1	T1	M1	C1p	T1p	M1p
1	F-A$^+$ GC-Dp-3-glc	0.12 a	0.11 a	0.11 a	nd	nd	nd
2	F-A$^+$ GC-Pt-3-glc	0.22 a	0.21 a	0.22 a	nd	nd	nd
3	F-A$^+$ GC-Mv-3-glc	0.50 a	0.52 a	0.52 a	0.41 a	0.50 a	0.40 a
4	F-A$^+$ C-Cy-3-glc	0.20 a	0.21 a	0.22 a	nd	nd	nd
5	F-A$^+$ C−Pt-3-glc	0.30 a	0.34 a	0.40 a	nd	nd	nd
6	F-A$^+$ C-Pn-3-glc	0.42 a	0.43 a	0.43 a	0.28 a	0.38 a	0.30 a
7	F-A$^+$ C-Mv-3-glc	0.57 a	0.59 a	0.59 a	0.47 a	0.56 a	0.45 a
8	Dp-3-glc	10.09 c	9.61 c	9.63 c	8.74 a,b	8.15 a	9.34 b,c
9	Cy-3-glc	1.22 c	1.18 b,c	1.28 c	0.89 a	1.08 a,b,c	1.00 a,b
10	Pt-3-glc	10.99 b	11.01 b	10.83 b	9.30 a	9.07 a	10.37 b
11	Vit A Pt-3-glc	0.30 a	0.27 a	0.34 a,b	0.54 c	0.46 b,c	0.45 b,c
12	Pn-3-glc	3.37 a	3.08 a	3.18 a	3.30 a	3.05 a	3.30 a
13	Mv-3-glc	44.48 a	45.33 a	44.83 a	40.06 a	38.40 a	45.60 a
14	Vit A Mv-3-glc	0.53 a	0.55 a	0.59 a	1.44 c	1.13 b,c	0.96 a,b
15	Dp-3-acetylglc	0.46 a	0.46 a	0.44 a	0.41 a	0.42 a	0.41 a
16	Vit B Mv-3-glc	0.08 a	0.10 a	0.08 a	0.15 a	0.15 a	0.15 a
17	Cy-3-acetylglc	0.21 a	0.20 a	0.21 a	0.18 a	0.24 a	0.20 a
18	Pt-3-acetylglc	0.76 b	0.78 b	0.74 a,b	0.62 a	0.70 a,b	0.64 a,b
19	Dp-3-*p*coumglc (*cis*)	0.10 a	0.11 a,b	0.10 a	0.18 c	0.20 c	0.16 b,c
20	Pn-3-acetylglc	0.25 a	0.25 a	0.23 a	0.25 a	0.22 a	0.20 a
21	Mv-3-acetylglc	1.87 b	1.95 b	1.78 b	1.39 a	1.27 a	1.46 a
22	Dp-3-*p*coumglc (*trans*)	1.26 a	1.16 a	1.23 a	1.97 b	1.99 b	1.27 a
23	Pt-3-*p*coumglc (*cis*)	0.05 a,b	0.04 a	0.04 a	0.09 c	0.09 c	0.07 b,c
24	Pn-3-cafglc	0.07 a,b	0.05 a	0.05 a	0.12 c	0.09 b	0.07 a,b
25	Mv-3-cafglc	0.23 a	0.20 a	0.22 a	0.31 b	0.25 a	0.24 a
26	Cy-3-*p*cumglc (*trans*)	0.19 a	0.16 a	0.17 a	0.30 b	0.24 a	0.19 a
27	Pt-3-*p*cumglc (*trans*)	0.81 a	0.78 a	0.81 a	1.26 b	1.12 b	0.90 a
28	Mv 3-*p*coumglc (*cis*)	0.23 a	0.21 a	0.19 a	0.29 a	0.23 a	0.19 a
29	Pn 3-*p*coumglc (*trans*)	0.45 a	0.42 a	0.44 a	0.77 c	0.66 b,c	0.50 a,b
30	Mv 3-*p*coumglc (*trans*)	2.49 a	2.44 a	2.81 a	4.40 c	4.30 b,c	3.77 b
31	Vit VF Mv-3-glc	0.10 a	0.11 a	0.12 a	0.11 a	0.10 a	0.07 a
32	DRP	17.08 a	17.13 a	17.18 a	21.77 a	24.98 a	17.32 a

[a]Different letters in the same row indicate significant differences ($p < 0.05$). [b]F-A$^+$, flavanol−anthocyanin direct condensation products; GC, gallocatechin; C, catechin; Dp, delphinidin; Cy, cyanidin; Pt, petunidin; Pn, peonidin; Mv, malvidin; glc, glucoside; pcoum, *p*-coumaroyl; caf, caffeoy; Vit A, A-type vitisin; Vit B, B-type vitisin; Vit VF, vinylphenol pyranoanthocyanin; DRP, difficult resolution pigments.

among samples, a principal component analysis (PCA) was performed from the percentages of the individual pigments over the total pigment content. The three first principal components (PC1, PC2, and PC3) explained 85% of the total system variability. Figure 1a shows the projection of the wine samples on the plane defined by the first and second principal components (PC2 vs PC1). In the PCA plot the samples treated with any of these products (T1 or M1) are well separated from control samples (C1) along the PC1 factor. In fact, control samples have a positive value, whereas the two others are negative. Taking into account the loadings (Figure 1b and Table 2, for the identity of the variables), positive values are mainly correlated with grape native anthocyanins and negative values with F-A$^+$ derivative pigments and with A-type vitisins. This means that these types of derivative pigments are more represented in the samples treated with enological tannin or with product M than in control wines, whereas the weight of native anthocyanins is higher in control wines than in treated ones. In previous studies carried out in our laboratory not only in model solutions (data not shown) but also in wines,[18] it has been observed that the synthesis of these types of derivative pigments is favored by the presence of the enological tannin. With respect to the synthesis of A-type vitisins, it has been demonstrated that it requires the presence not only of anthocyanins and pyruvic acid but also of oxidants to complete the last step of the synthesis.[35] Ellagitannins, which are present in the enological tannin employed in the present study, can promote the conversion of oxygen into reactive oxygen species which, in turn, might take part in the last step of the A-type vitisin synthesis. On the other hand, the enological tannin employed in this study also contained oligomeric proanthocyanidins having interflavanic linkages that can be cleaved at the pH of the wine, releasing carbocations which, in turn, can react with anthocyanins and originate F-A$^+$ dimers.[32] Furthermore, this condensation reaction may be favored by the ellagitannins present in the enological tannin.[32,36]

With regard to wines treated with product M, no evidence supporting the higher formation of anthocyanin-derived pigments was clearly found. In a recent work, Andújar-Ortiz and co-workers[37] reported higher levels of vitisin B and of one isomer of malvidin 3-glucoside-ethyl-epicatechin in wines treated with glutathione-enriched inactive dry yeast (G-IDY) preparations than in control wines. Although no explanation is given, the higher contents of these two types of anthocyanin-

dx.doi.org/10.1021/jf4055825 | J. Agric. Food Chem. 2014, 62, 6984−6994

Table 3. Percentages of Different Pigment Groups in Samples before Cold Treatment (C1, T1, and M1) and in Precipitates Obtained after Cold Treatment (C1p, T1p, and M1p) (Mean Values, n = 2)

	samples[a]					
pigment group[b]	C1	T1	M1	C1p	T1p	M1p
F-A$^+$	2.34 a,b	2.40 a,b	2.50 b	1.15 a	1.43 a,b	1.15 a
monoglucosides	70.15 a	70.21 a	69.75 a	62.30 a	59.74 a	69.63 a
acetylglucosides	3.55 a	3.64 a	3.40 a,b	2.85 b	2.85 b	2.91 b
coumaroylglucosides	5.58 a	5.32 a	5.78 a	9.26 c	8.83 b,c	7.06 a,b
caffeoylglucosides	0.30 a,b	0.26 a	0.27 a,b	0.43 c	0.35 b,c	0.31 a,b
A-type vitisins	0.83 a	0.83 a	0.93 a,b	1.98 c	1.59 c	1.41 b,c
B-type vitisins	0.08 a	0.10 a	0.08 a	0.15 a	0.15 a	0.15 a
Vit VF Mv-3-glc	0.10 a	0.11 a	0.12 a	0.11 a	0.10 a	0.07 a
DRP	17.08 a	17.13 a	17.18 a	21.77 a	24.98 a	17.32 a

[a]Different letters in the same row indicate significant differences ($p < 0.05$). [b]F-A$^+$, flavanol-anthocyanin direct condensation products; Mv, malvidin; glc, glucoside; Vit VF, vinylphenol pyranoanthocyanin; DRP, difficult elution compounds.

derived pigments might be related to a higher availability of acetaldehyde in the G-IDY wines, which can be, in turn, related to the glutathione content. Thus, in that study, the addition of the G-IDY preparations caused a chemical transformation of the grape native anthocyanins into derivative pigments in which formation acetaldehyde is involved. This was not the case in the present work, and the higher percentages of A-type vitisins and F-A$^+$ derivative pigments in M-treated samples may be related to a colloidal stabilization of the coloring matter. In fact, some polysaccharides are traditionally considered as "protective" colloids, macromolecular colloids that coat other colloids present in the wine, thus preventing their agglomeration.[3] Riou and co-workers[22] demonstrated the different ability of different wine polysaccharides to prevent the aggregation of tannin colloids. Among them and at their usual concentration in wines, only mannoproteins were able to prevent the growth of tannin particles and, therefore, their flocculation and precipitation. These authors proposed that this protective effect was due to the adsorption of the mannoprotein on the particles formed by tannins. Further studies carried out by the same research group[24] confirmed that the mechanism involved was steric stabilization and that the molecular weight of the polysaccharide conditioned the activity of the mannoprotein. Medium (∼62 kDa) and low (∼51 kDa) molecular weight polymers were more efficient than high molecular weight polymers (∼337 kDa). Because F-A$^+$ dimers are originated from the direct condensation of a flavanol and an anthocyanin, a similar protective mechanism can be proposed for them. Product M, containing medium and low molecular weight polymers, might have prevented the aggregation of F-A$^+$ dimers or even the aggregation of these colored dimers with other proanthocyanidins that probably occurred in control samples.

The higher percentages of A-type vitisins found in M-treated samples might be also related to their colloidal stabilization. The additional pyran ring confers hydrophobicity to the molecules, making them less polar and less soluble in hydroalcoholic solutions (wine) than the original anthocyanins from which they are synthesized. Furthermore, unlike anthocyanins, the main species of which at wine pH is the colorless hemiketal form, the main species of the A-type vitisins is the orange quinonoidal base,[38] which can also be responsible for the lower solubility of these anthocyanin derivatives. The lower solubility might favor interactions (hydrophobic and/or $\pi-\pi$ interactions) between molecules that might induce their aggregation and cause their precipitation. Mannoproteins might have acted as steric stabilizers, being adsorbed on the pigment and thus lowering the possibility of aggregation.

Although along PC1 the samples treated with product M (M1) and those treated with the enological tannin (T1) showed similar values, they were well separated along PC2. In general, the positive values of PC2 correlate with most of the F-A$^+$ dimers and with all of the *trans*-isomers of the anthocyanin coumaroylglucosides, and the negative values correlate above all with acetylglucosides and with the *cis*-isomers of the coumaroylglucosides. M-treated samples showed positive values and tannin-treated samples showed negative values. In fact, although the percentages of coumaroyl derivatives were quite similar in both types of samples, the percentage represented by the *cis*-isomers was higher in the case of tannin-treated wines than in M-treated samples. This was also the case for acetyl derivatives, which represented higher percentages in the former than in the latter ones. On the contrary, the *trans*-isomers of the coumaroyl derivatives and the A-type vitisins were more represented in M-treated samples. Control wines showed percentages of *cis*-coumaroyl derivatives that were similar to those of tannin-treated wines and percentages of acetyl derivatives between those of treated wines. As a result, control wines showed a negative value of PC2.

Thus, the addition of either the enological tannin or product M to the wines causes some modifications in the pigment composition. The main composition differences between control and treated wines shown by PCA are the higher proportion of anthocyanin-derived pigments (A-type vitisins and F-A$^+$ dimers, above all) in treated samples in relation to control wines and between treated wines, the different proportions of *cis*- and *trans*-isomers of the coumaroyl derivatives, the different percentages of acetyl derivatives, and the different proportions of A-type vitisins. The changes in the color parameters observed in the treated wines (M1 and T1) in relation to control (C1) wine can be, therefore, explained by these changes in the composition. The decrease in lightness might be due to the higher pigment content observed in both types of treated samples in relation to control ones. In the case of tannin-treated wines, the decrease in L^* might be also due to other phenolic compounds supplied by the enological tannin such as proanthocyanidins. In the case of M-treated wines, L^* might partly decrease as a consequence of the polysaccharidic nature of the enological product tested. The increase in the hue observed in the treated samples in relation to control wines might be due to the increase in the percentage of the derivative

pigments that are redder or more orange (above all, A-type vitisins and F-A$^+$ dimers) at wine pH.

Modification of the Pigment Composition after Cold Treatment. Figure 1a also shows the location of the samples along PC1 and PC2 after cold treatment (C1*, T1*, and M1*). Cold treatment barely modified PC1 in control and M-treated wines, whereas it caused a decrease in PC1 in the samples to which enological tannin was added. This decrease correlates with an increase in the percentage represented by some anthocyanin derivatives (F-A$^+$ dimers and A-type vitisins) and with a decrease in the percentage of native grape anthocyanins. On the contrary, all types of samples increased the values of PC2 in relation to those of the samples not subjected to cold treatment. Taking into account the loadings of this PCA (Figure 1b), an increase in PC2 correlates with a decrease in acetyl and *cis*-coumaroyl derivatives and with an increase of the percentages of F-A$^+$ dimers, *trans*-coumaroyl derivatives, and some A-type vitisins. It has to be noted that M-treated samples showed the lowest change along PC2 after cold treatment. Thus, taking into account that these samples barely changed along PC1, the addition of product M to the samples seems to stabilize the pigment composition against cold treatment. To determine the compound groups that are mostly benefited by these enological practices, the percentages of the main pigments in the sample before cold treatment were compared to those determined in the precipitates (see Table 2 for the percentages of the individual compounds and Table 3 for the percentages of the main groups of pigments). It was first observed that in all types of wine the total percentage of the F-A$^+$ dimers was lower in the precipitates than in the sample not subjected to cold treatment. This means that independent of the addition of one or other enological product F-A$^+$ dimers are quite unaffected by cold treatment. In fact, some of these dimers that were present in the samples not subjected to cold treatment were not detected in the precipitates (Table 2). Although for most of the F-A$^+$ dimers the lowest percentages were found in the precipitates of the M-treated samples, differences among treatments were not significant. On the contrary, the difficult resolution pigments responsible for the hump observed at the last part of the chromatogram were more represented in the precipitates than in the samples before being cooled. This is indicative of certain instability of this type of pigment against cold treatment. The lowest increase in the percentages was found in M-treated wines, pointing to a stabilizing effect of this product in this type of compound. Although the exact nature of these difficult resolution pigments is not well established, they are supposed to be polymeric pigments, and, in fact, dimeric anthocyanins have been reported to be a part of this group of pigments.[33] Product M probably caused their colloidal stabilization. The enological tannin employed in this study, on the contrary, caused a higher precipitation of these compounds, which is probably related to the higher content (data not shown) detected in this type of sample. However, from a statistical point of view, the percentages of this group of compounds in the precipitates were not statistically different in the different wines. In all of the samples, the percentage of anthocyanin monoglucosides decreased in the precipitates in relation to the samples before cold treatment. However, M-treated samples were those for which the percentages changed less. With respect to acyl derivatives, it was observed that, in general, the percentages of the acetylglucosides were lower in the precipitates than in the samples not subjected to cold treatment, whereas coumaroyl and caffeoyl glucosides increased their percentages in the precipitates (Tables 2 and 3). This is indicative of a higher instability of coumaroyl and caffeoyl glucosides toward cold in relation to acetyl derivatives. However, differences were observed among treatments. In the case of the coumaroylglucosides, the percentages found in the precipitates of control and tannin-treated samples were statistically higher than those determined in the samples not subjected to cold treatment. In the case of the samples treated with product M, the percentages of most of the coumaroylglucosides were not statistically different from those determined in the sample before cold treatment (Table 2). This fact points to a protective effect of product M toward the precipitation of this group of compounds caused by cold treatment. Gonçalves and co-workers[39] reported higher retention of malvidin 3-*O*-*p*-coumaroylglucoside by wine polymeric material in relation to other acetylated and nonacylated anthocyanins, which was attributed to the higher hydrophobicity of the coumaroylglucosides, which can increase the hydrophobic interactions between them and the polymeric material. The studies of Morata and co-workers[40,41] on the adsorption of anthocyanins on yeast cell walls also demonstrated that coumaroyl derivatives were the most adsorbed compounds, even in different yeast strains. Taking into account that the structure of the mannoproteins present in the cell wall of *S. cerevisiae* is similar to that of the mannoproteins released by the yeast to the wines and that they can represent up to 50% of the cell wall[20] and 80% of the exocellular polysaccharides released by yeast to the wines,[3] it can be assumed that coumaroyl derivatives are more retained by product M than other anthocyanins, thus being protected from precipitation by cold treatment. In the case of caffeoyl derivatives, the increase of the percentage in the precipitate was significant only in control samples, thus indicating differences between control samples and tannin- or M-treated samples. The percentage of the A-type vitisins also increased in the precipitates of all types of samples, but again, M-treated samples were those that changed less (Tables 2 and 3). Cold treatment reduces the solubility of the pigments and, as previously indicated, the solubility of A-type vitisins seems to be lower than that of the anthocyanins from which they are synthesized. For this reason, A-type vitisins were more affected by cold treatment than anthocyanins and their percentages increased in the precipitates in relation to those found in non-cold-treated samples. Cold might have favored the hydrophobic interactions between molecules and caused their precipitation. The addition of product M might have reduced this precipitation by adsorption of the mannoprotein on the pigment molecule, hindering the hydrophobic interactions. The malvidin 3-*O*-glucoside vinylphenol pyranoanthocyanin seemed to be quite stable against cold treatment because its percentage in the precipitates was similar to that detected in the samples before cold treatment (Tables 2 and 3). Although differences between treatments were not significant, the precipitates from M-treated samples were those that showed the lowest percentages in relation to the initial percentages, which might be indicative of the possible protective effect of product M against the precipitation of this pyranoanthocyanin by cold. Thus, it can be seen that the most relevant changes in the percentages of the pigments between control samples and their precipitates (decrease of anthocyanin monoglucosides and their acetyl derivatives, increase of A-type vitisins and coumaroyl derivatives) were lowered with the use of product M. The addition of the enological tannin also

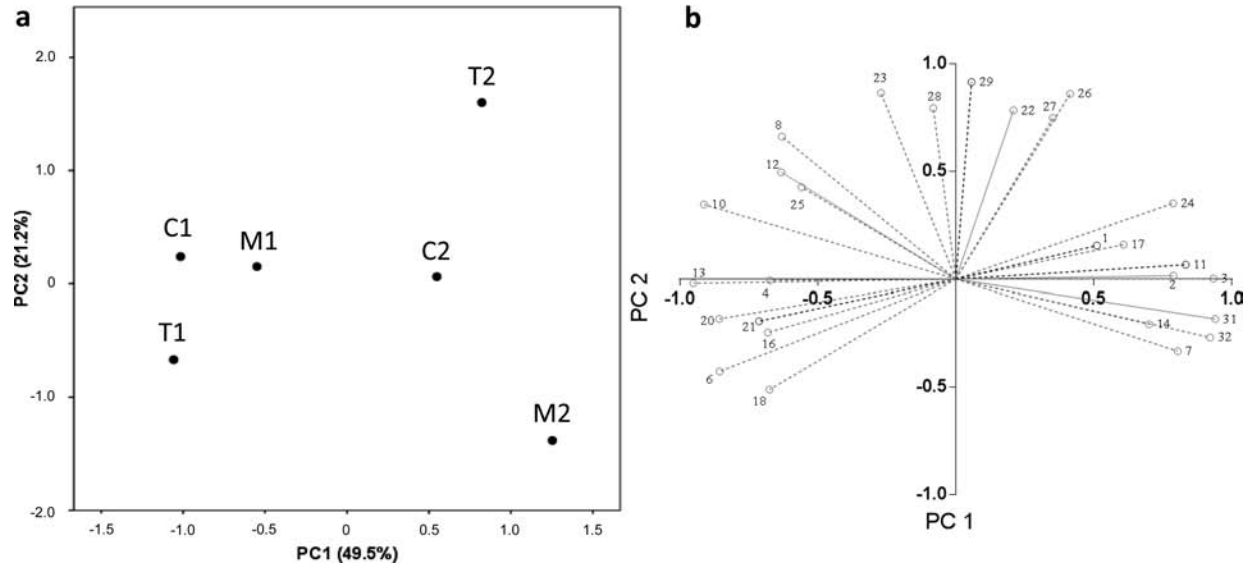

Figure 2. (a) Projection of the wine samples on the plane defined by the first and second principal components (PC2 vs PC1). These samples correspond to all wines (control, tannin- and M-treated wines) not subjected to cold in the first (samples C1, T1, or M1) and second sampling points (samples C2, T2, or M2). (b) Loadings of the original variables. The identities of the original variables are indicated in Table 2.

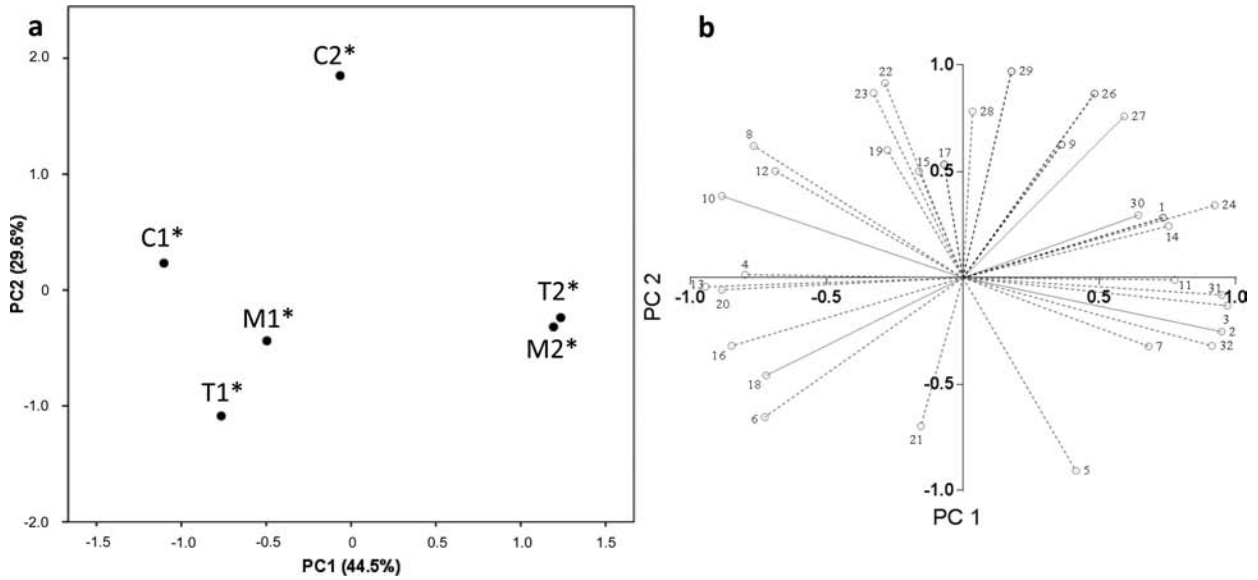

Figure 3. (a) Projection of the wine samples on the plane defined by the first and second principal components (PC2 vs PC1). These samples correspond to all wines (control, tannin- and M-treated wines) subjected to cold in the first (samples C1*, T1*, or M1*) and second sampling points (samples C2*, T2*, or M2*). (b) Loadings of the original variables. The identities of the original variables are indicated in Table 2.

preserved the samples from some of these changes, but the effect was lower than in M-treated samples.

Modification of the Pigment Composition over Time. Figures 2 and 3 show the score plots for the samples not subjected to cold treatment in both sampling points (C1, T1, M1, C2, T2, and M2, Figure 2) and for the samples subjected to cold treatment (C1*, T1*, M1*, C2*, T2*, and M2*, Figure 3). In both cases it can be seen that all of the samples are separated along PC1 according to sampling point, with the younger samples showing negative scores and the older ones, positive. According to the loadings (Figure 2b and 3b), this change from negative to positive scores with age is related to a decrease in anthocyanin monoglucosides, acetylglucosides, and B-type vitisin and to an increase in derivative pigments (F-A^+ dimers, A-type vitisins, malvidin 3-*O*-glucoside vinylphenol pyranoanthocyanin, and difficult resolution pigments). This is in accordance with what might be expected because as wine ages native anthocyanins react with other wine constituents, giving rise to anthocyanin-derived pigments. Nevertheless, some differences could be observed among treatments in both sample series (subjected and not subjected to cold treatment). In general, in sampling point 2, control samples were those that showed the lowest positive values of PC1. Tannin- or M-treated samples, on the contrary, showed the highest positive values. This means that independent of being cold-treated or not, tannin and M-treated wines still show higher percentages of derivative pigments than control wines after 10 weeks. In the series of wines not subjected to cold treatment (C2, T2, and M2), tannin- and M-treated samples were further separated along PC2, mainly due to higher percentages of derivative

dx.doi.org/10.1021/jf4055825 | J. Agric. Food Chem. 2014, 62, 6984−6994

pigments in M-treated samples and higher percentages of anthocyanin coumaroylglucosides in tannin-treated samples. However, these changes in the composition hardly cause differences in the CIELAB parameters because differences between T2 and M2 were not significant (Table 1). In the series of samples subjected to cold treatment (C2*, T2*, and M2*), there were no differences along PC2 between T2* and M2*. However, important differences along PC1 and PC2 could be observed between C2* and the treated samples (T2* and M2*) that were higher than in the case of the samples not subjected to cold. C2* shows a PC1 value next to zero and a PC2 positive value distant from the PC2 value of treated samples. This is related in both coordinates to lower percentages of derivative pigments. It has to be borne in mind that C2* samples come from C1*, control samples subjected to cold, that had already lost a part of the anthocyanin derivatives due to cold treatment. For this reason, differences between control and treated wines were higher in the cold-treated series than in the non-cold-treated ones. As previously indicated, C2* samples showed significantly higher values of lightness and lower values of chroma than treated wines (T2* and M2*). This means that even after 10 weeks from cold treatment, wines treated either with the enological tannin or with product M still show higher percentages of derivative pigments in relation to control wines.

In conclusion, the usefulness of the addition of either an enological tannin containing condensed and hydrolyzable tannins or a mannoprotein with medium−low molecular weight (product M) in stabilizing wine color against cold treatment has been demonstrated. Both enological treatments have been proven to slightly increase the hue of the wines to which they are added and to better maintain the color (L^*, C_{ab}^*, h_{ab}) of those samples after cold treatment than control samples. Furthermore, although time affected similarly all types of samples, after 10 weeks from malolactic fermentation (sampling point 2) tannin- and M-treated samples, either subjected to cold or not, still showed CIELAB color parameters more similar to those shown by control wines before cold treatment than those shown by control wines at sampling point 2. The pigment analysis has revealed that both enological treatments increased the percentages of anthocyanin-derived pigments in relation to control wines not only in wines not subjected to cold treatment but above all in cold-treated wines. In the case of the enological tannin, the higher percentages observed for these derivatives is probably due to a higher synthesis because the addition of the enological tannin can favor the extraction of anthocyanins from grapes during the maceration/alcoholic fermentation step and supplies substrates and/or oxidants to complete the synthesis reactions. Thus, the addition of the enological tannin leads to a chemical stabilization of the coloring matter of the wines, because grape native anthocyanins are transformed into anthocyanin-derived pigments that are chemically more resistant than anthocyanins toward hydration and/or SO_2 bleaching. In the case of the mannoprotein, it seems that the stabilization of the coloring matter consists of a colloidal stabilization. Cold treatment forced the precipitation of unstable coloring matter, revealing the unexpected colloidal instability of some chemically stable anthocyanin-derived pigments, such as A-type vitisins. However, the mannoprotein employed in the present study has been able to reduce the cold-induced precipitation of A-type vitisins and other derivative pigments and the spontaneous precipitation of these compounds in non-cold-treated samples. To our knowledge, this is the first report on the stabilizing effect of mannoproteins on anthocyanin derivative pigments. Further studies aim at evaluating the effect of the addition of both enological products to the same wine to attain a chemical and colloidal stability of the coloring matter.

AUTHOR INFORMATION

Corresponding Author

*(M.T.E.-B.) Phone: +34 923 294537. Fax: +34 923 294515. E-mail: escriban@usal.es.

Funding

Thanks are due to the Spanish MICINN (Project ref AGL2011-30254-C02-01) and to Project DEMETER program CENIT for financial support. I.G.-E. thanks the Spanish Ministerio de Educación for the F.P.U. predoctoral scholarship.

Notes

The authors declare no competing financial interest.

ACKNOWLEDGMENTS

We thank R. Boube for the preliminary studies from which the mannoprotein employed in the present study (product M) was selected.

REFERENCES

(1) Morrot, G.; Brochet, F.; Dubourdieu, D. The color of odors. *Brain Language* **2001**, *79*, 309−320.

(2) Österbauer, R. A.; Matthews, P. M.; Jenkinson, M.; Beckmann, C. F.; Hansen, P. C.; Calvert, G. A. Color of scents: chromatic stimuli modulate odor responses in the human brain. *J. Neurophysiol.* **2005**, *93*, 3434−3441.

(3) Ribéreau-Gayon, P.; Glories, Y.; Maujean, A.; Dubourdieu, D. *Handbook of Enology. Vol. 2. The Chemistry of Wine Stabilization and Treatments*, 2nd ed.; Wiley: Chichester, UK, 2003; 404 pp.

(4) Rentzsch, M.; Schwarz, M.; Winterhalter, P. Pyranoanthocyanins − an overview on structures, occurrence, and pathways of formation. *Trends Food Sci. Technol.* **2007**, *18*, 526−534.

(5) Sarni-Manchado, P.; Fulcrand, H.; Souquet, J.-M.; Cheynier, V.; Moutounet, M. Stability and color of unreported wine anthocyanin-derived pigments. *J. Food Sci.* **1996**, *61*, 938−941.

(6) Bakker, J.; Timberlake, C. F. Isolation, identification, and characterization of new color-stable anthocyanins occurring in some red wines. *J. Agric. Food Chem.* **1997**, *45*, 35−43.

(7) Asenstorfer, R. E.; Lee, D. F.; Jones, G. P. Influence of structure on the ionization constants of anthocyanin and anthocyanin-like wine pigments. *Anal. Chim. Acta* **2006**, *563*, 10−14.

(8) Quijada-Morín, N.; Dangles, O.; Rivas-Gonzalo, J. C.; Escribano-Bailón, M. T. Physico-chemical and chromatic characterization of malvidin 3-glucoside-vinylcatechol and malvidin 3-glucoside-vinyl-guaiacol wine pigments. *J. Agric. Food Chem.* **2010**, *58*, 9744−9752.

(9) Dueñas, M.; Salas, E.; Cheynier, V.; Dangles, O.; Fulcrand, H. UV-visible spectroscopic investigation of the 8,8-methylmethine catechin-malvidin 3-glucoside pigments in aqueous solution: structural transformations and molecular complexation with chlorogenic acid. *J. Agric. Food Chem.* **2006**, *54*, 189−196.

(10) Escribano-Bailón, M. T.; Álvarez-García, M.; Rivas-Gonzalo, J. C.; Heredia, F. J.; Santos-Buelga, C. Color and stability of pigments derived from the acetaldehyde-mediated condensation between malvidin 3-*O*-glucoside and (+)-catechin. *J. Agric. Food Chem.* **2001**, *49*, 1213−1217.

(11) Salas, E.; Le Guernevé, C.; Fulcrand, H.; Poncet-Legrand, C.; Cheynier, V. Structure determination and colour properties of a new directly linked flavanol-anthocyanin dimer. *Tetrahedron Lett.* **2004**, *45*, 8725−8729.

(12) Darias-Martín, J.; Carrillo, M.; Díaz, E.; Boulton, R. B. Enhancement of red wine colour by pre-fermentation addition of copigments. *Food Chem.* **2001**, *73*, 217−220.

(13) González-Manzano, S.; Dueñas, M.; Rivas-Gonzalo, J. C.; Escribano-Bailón, M. T.; Santos-Buelga, C. Studies on the copigmentation between anthocyanins and flavan-3-ols and their influence in the colour expression of red wine. *Food Chem.* **2009**, *114*, 649−656.
(14) Harbertson, J. F.; Parpinello, G. P.; Heymann, H.; Downey, M. O. Impact of exogenous tannin additions on wine chemistry and wine sensory character. *Food Chem.* **2012**, *131*, 999−1008.
(15) Bautista-Ortín, A. B.; Fernández-Fernández, J. I.; López-Roca, J. M.; Gómez-Plaza, E. The effects of enological practices in anthocyanins, phenolic compounds and wine colour and their dependence on grape characteristics. *J. Food Compos. Anal.* **2007**, *20*, 546−552.
(16) Parker, M.; Smith, P. A.; Birse, M.; Francis, I. L.; Kwiatkowski, M. J.; Lattey, K. A.; Liebich, B.; Herderich, M. J. The effect of pre- and post-ferment additions of grape derived tannin on Shiraz wine sensory properties and phenolic composition. *Aust. J. Grape Wine Res.* **2007**, *13*, 30−37.
(17) Pérez-Lamela, C.; García-Falcón, M. S.; Simal-Gándara, J.; Orriols-Fernández, I. Influence of grape variety, vine system and enological treatments on the colour stability of young red wines. *Food Chem.* **2007**, *101*, 601−606.
(18) Alcalde-Eon, C.; García-Estévez, I.; Ferreras-Charro, R.; Rivas-Gonzalo, J. C.; Ferrer-Gallego, R.; Escribano-Bailón, M. T. Adding oenological tannin vs. overripe grapes: effect on the phenolic composition of red wines. *J. Food Compos. Anal.* **2014**, DOI: 10.1016/j.jfca.2014.01.004.
(19) Dupin, I. V. S.; Stockdale, V. J.; Williams, P. J.; Jones, G. P.; Markides, A. J.; Waters, E. J. *Saccharomyces cerevisiae* mannoproteins that protect wine from protein haze: evaluation of extraction methods and immunolocalization. *J. Agric. Food Chem.* **2000**, *48*, 1086−1095.
(20) Ribéreau-Gayon, P.; Dubourdieu, D.; Donèche, B.; Lonvaud, A. *Handbook of Enology. Vol. 1. The Microbiology of Wine and Vinifications*, 1st ed.; Wiley: Chichester, UK, 2000; 454 pp.
(21) Pellerin, P.; Cabanis, J. C. Los glúcidos. In *Enología: Fundamentos Científicos y Tecnológicos*, 2nd ed.; Flanzy, C., Ed.; AMV Ediciones, Ediciones Mundi-Prensa: Madrid, Spain, 2003; 797 pp.
(22) Riou, V.; Vernhet, A.; Doco, T.; Moutounet, M. Aggregation of grape seed tannins in model wine-effect of wine polysaccharides. *Food Hydrocolloids* **2002**, *16*, 17−23.
(23) Rodrigues, A.; Ricardo-Da-Silva, J. M.; Lucas, C.; Laureano, O. Effect of commercial mannoproteins on wine colour and tannins stability. *Food Chem.* **2012**, *131*, 907−914.
(24) Poncet-Legrand, C.; Doco, T.; Williams, P.; Vernhet, A. Inhibition of grape seed tannin aggregation by wine mannoproteins: effect of polysaccharide molecular weight. *Am. J. Enol. Vitic.* **2007**, *58*, 87−91.
(25) Pozo-Bayón, M. A.; Andújar-Ortiz, M.; Moreno-Arribas, M. V. Scientific evidences beyond the application of inactive dry yeast preparations in winemaking. *Food Res. Int.* **2009**, *42*, 754−761.
(26) Escot, S.; Feuillat, M.; Dulau, L.; Charpentier, C. Release of polysaccharides by yeasts and the influence of released polysaccharides on colour stability and wine astringency. *Aust. J. Grape Wine Res.* **2001**, *7*, 153−159.
(27) Guadalupe, Z.; Martínez, L.; Ayestarán, B. Yeast mannoproteins in red winemaking: effect on polysaccharide, polyphenolic, and color composition. *Am. J. Enol. Vitic.* **2010**, *61*, 191−200.
(28) Guadalupe, Z.; Ayestarán, B. Effect of commercial mannoprotein addition on polysaccharide, polyphenolic, and color composition in red wines. *J. Agric. Food Chem.* **2008**, *5*, 9022−9029.
(29) Fernández, O.; Martínez, O.; Hernández, Z.; Guadalupe, Z.; Ayestarán, B. Effect of the presence of lysated lees on polysaccharides, color and main phenolic compounds of red wine during barrel ageing. *Food Res. Int.* **2011**, *44*, 84−91.
(30) Ferrer-Gallego, R.; García-Marino, M.; Hernández-Hierro, J. M.; Rivas-Gonzalo, J. C.; Escribano-Bailón, M. T. Statistical correlation between flavanolic composition, colour and sensorial parameters in grape seed during ripening. *Anal. Chim. Acta* **2010**, *660*, 22−28.
(31) Heredia, F. J.; Álvarez, C.; González-Miret, M. L.; Ramírez, A. *CromaLab Análisis de Color*; Registro General de la Propiedad Intelectual: Sevilla, Spain, 2004; SE-1052-04.
(32) Alcalde-Eon, C.; Escribano-Bailón, M. T.; Santos-Buelga, C.; Rivas-Gonzalo, J. C. Changes in the detailed pigment composition of red wine during maturity and ageing. A comprehensive study. *Anal. Chim. Acta* **2006**, *563*, 238−254.
(33) Alcalde-Eon, C.; Escribano-Bailón, M. T.; Santos-Buelga, C.; Rivas-Gonzalo, J. C. Identification of dimeric anthocyanins and new oligomeric pigments in red wine by means of HPLC-DAD-ESI/MS^n. *J. Mass Spectrom.* **2007**, *42*, 735−748.
(34) Martínez, J. A.; Melgosa, M.; Pérez, M. M.; Hita, E.; Negueruela, A. I. Visual and instrumental color evaluation in red wines. *Food Sci. Technol. Int.* **2001**, *7*, 439−444.
(35) Asenstorfer, R. E.; Markides, A. J.; Iland, P. G.; Jones, G. Formation of vitisin A during red wine fermentation and maturation. *Aust. J. Grape Wine Res.* **2003**, *9*, 40−46.
(36) Vivas, N.; Glories, Y. Role of oak wood ellagitannins in the oxidation process of red wines during aging. *Am. J. Enol. Vitic.* **1996**, *47*, 103−107.
(37) Andújar-Ortiz, I.; Pozo-Bayón, M. A.; Garrido, I.; Martín-Álvarez, P. J.; Bartolomé, B.; Moreno-Arribas, M. V. Effect of using glutathione-enriched inactive dry yeast preparations on the phenolic composition of rosé Grenache wines during winemaking. *J. Int. Sci. Vigne Vin* **2012**, *46*, 241−251.
(38) Asenstorfer, R. E.; Jones, G. P. Charge equilibria and p*K* values of 5-carboxypyranomalvidin-3-glucoside (vitisin A) by electrophoresis and absorption spectroscopy. *Tetrahedron* **2007**, *63*, 4788−4792.
(39) Gonçalves, F. J.; Rocha, S. M.; Coimbra, A. Study of the retention capacity of anthocyanins by wine polymeric material. *Food Chem.* **2012**, *134*, 957−963.
(40) Morata, A.; Gómez-Cordovés, M. C.; Suberviola, J.; Bartolomé, B.; Colomo, B.; Suárez, J. A. Adsorption of anthocyanins by yeast cell walls during the fermentation of red wines. *J. Agric. Food Chem.* **2003**, *51*, 4084−4088.
(41) Morata, A.; Gómez-Cordovés, M. C.; Colomo, B.; Suárez, J. A. Cell wall anthocyanin adsorption by different *Saccharomyces* strains during the fermentation of *Vitis vinifera* L. cv Graciano grapes. *Eur. Food Res. Technol.* **2005**, *220*, 341−346.

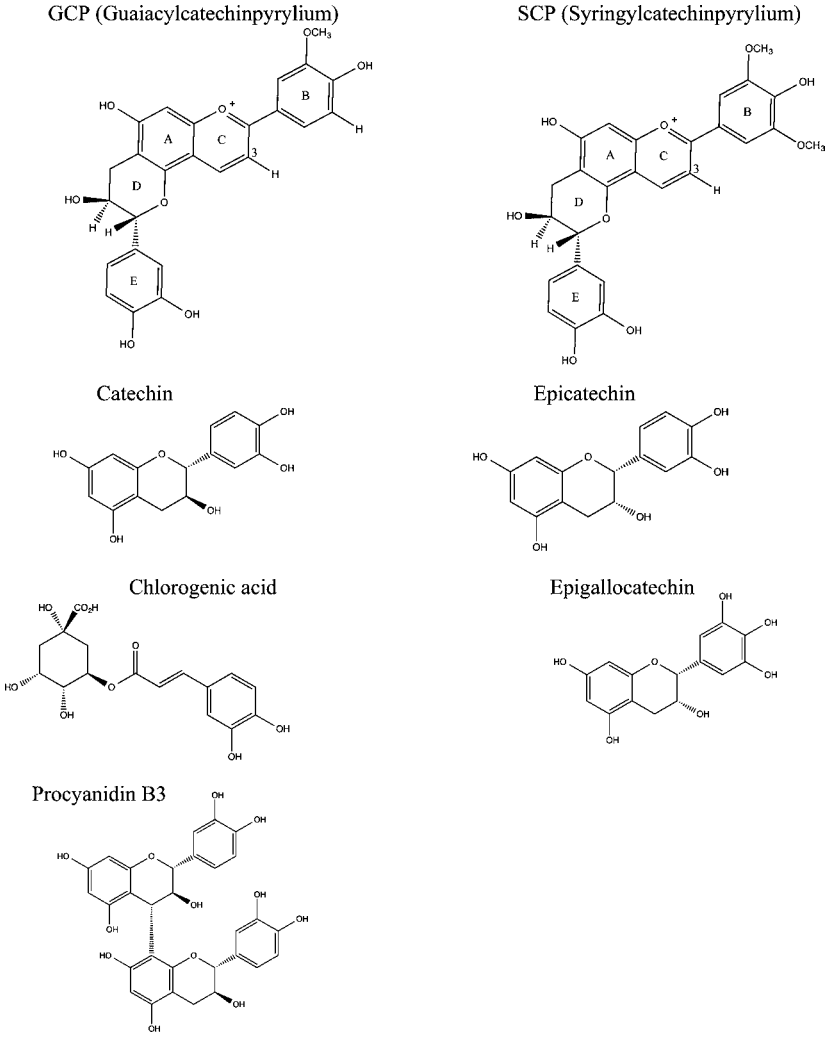

Figure 1. Chemical structures of the deoxyanthocyanidin derivatives, oaklins (GCP and SCP), and the copigments investigated in this work.

pigment/copigment solution was prepared by mixing a volume of pigment (10^{-4} M) solution with an aliquot of copigment solution to give the required pigment/copigment molar ratios of 1:0, 1:1, 1:5, 1:10, 1:20, 1:30, and 1:40. Each experiment was performed in triplicate. All of the solutions were left to equilibrate for 30 min before spectroscopic measurements. For GCP with the copigment epigallocatechin, the absorbance values were collected at the wavelength (λ_{max} 498 nm) of the isosbestic point of the flavylium cation (10^{-4} M) and its copigmentation complex (GCP/copigment molar ratio = 1:40). This parameter was determined in strongly acidic solutions (1 M aqueous HCl, pH ≈0) in which the flavylium ion is the sole anthocyanin form. However, for the rest of the copigments and for the pigment SCP, an isosbestic point was not observed; hence, the absorbance values were collected at the maximum absorption wavelength of free pigment (GCP/SCP) at pH 3.5 (λ_{max} 485 nm for GCP and 500 nm for SCP).

UV−Visible Spectroscopy. UV−visible spectra were recorded on a Bio-Tek Power Wave XS spectrophotometer at a constant temperature of 25 °C from 360 to 830 nm (1 nm sampling interval) using a 1 cm path length cell.

Data Analysis. The curve fittings were carried out using the software program MicroMath (Salt Lake City, UT, USA). Curve fittings were achieved through a least-squares regression method. Statistical analysis reported standard deviations and correlation coefficients.

Molecular Dynamic Simulations. The initial geometries of the pigments (GCP and SCP) and copigments (catechin, epicatechin, epigallocatechin, B3, and chlorogenic acid) molecules were built with GaussView software.[14] To calculate the optimized geometries and electronic properties for the subsequent parametrization of these compounds, the Gaussian 09 suite of programs[15] was used to perform restricted Hartree−Fock calculations (RHF), with the 6-31G(d) basis set. Atomic charges were further recalculated using the RESP algorithm.[16] This methodology was chosen for its consistency with that adopted in the parametrization process of the AMBER 10.0 simulation package.[17] Molecular dynamics (MD) simulations were performed with generalized Amber force field for small organic molecules (GAFF)[18] and the TIP3P model for the solute and water, respectively. Explicit solvation was included as a rectangular box with a 12 Å distance between the box faces and any atom of the compounds. One counterion (Cl^-) was employed to neutralize the positive charge of each system, which has a size of approximately 5700 atoms. All complex geometries were minimized in two stages: first, the solute was kept fixed and only the position of the counterion and water molecules was minimized (500 steps using the steepest descent algorithm and 1500 steps carried out using conjugate gradient); second, the full system was minimized (1000 steps using the steepest descent algorithm and 2000 steps carried out using conjugate gradient). Subsequently, an MD simulation of 100 ps at constant volume and temperature, and considering periodic boundaries conditions, was run, followed by 30 ns MD simulation with the NPT ensemble, in which Langevin dynamics was used (collision frequency of 1.0 ps^{-1}) to control the temperature at 303.15 K.[19] All simulations were carried out using the PMEMD module, implemented in the AMBER 10.0 simulation package.[17] Bond lengths involving a hydrogen atom were constrained using the SHAKE algorithm, and the equations of motion were integrated with a 2 fs time step using the Verlet leapfrog algorithm.[20] The particle-mesh Ewald (PME) method[21] was used to include the long-range interactions,

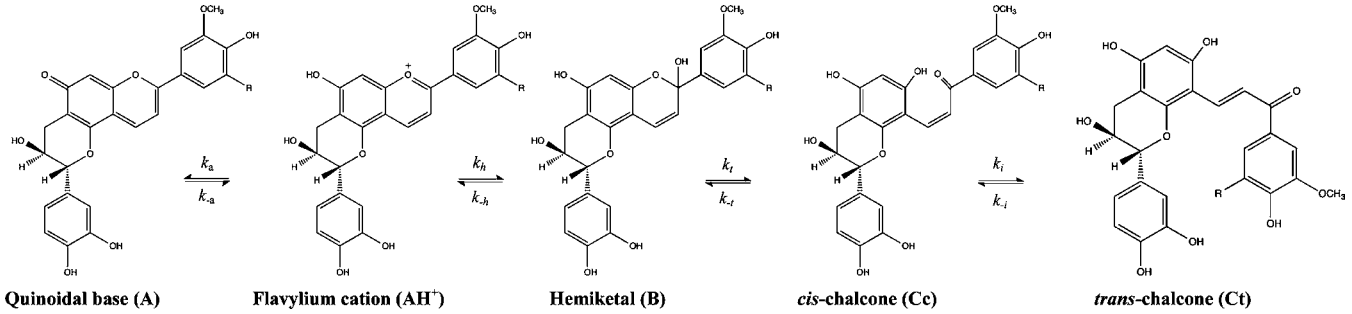

Figure 2. Network of chemical reactions of oaklins (R = OCH_3, SCP; R = H, GCP).

and the nonbonded interactions were truncated with a 10 Å cutoff. The MD trajectory was saved every 2 ps, and the MD results were analyzed with the PTRAJ module of AMBER 10.0.[17]

Calculation of Relative Binding Free Energies ($\Delta\Delta G_{binding}$). The molecular mechanics–Poisson–Boltzmann surface area (MM-PBSA) script[22−24] as implemented in the AMBER 10.0 simulations package[17] was used to calculate the binding free energies ($\Delta G_{binding}$) for all complexes. A series of 150 geometries was extracted every 100 steps of each simulation. The internal energy (bond, angle, and dihedral) and the electrostatic and van der Waals interactions were calculated using the Cornell et al. force field[25] with no cutoffs. The electrostatic solvation free energy was calculated by solving the Poisson–Boltzmann equation with the PBSA program. The nonpolar contribution to the solvation free energy due to van der Waals interactions between the solute and the solvent and cavity formation was modeled as a term that is dependent on the solvent-accessible surface area of the molecule. As these compounds possess similar structures and binding modes, the relative binding energies ($\Delta\Delta G_{binding}$) were calculated with respect to the most stable complex.

RESULTS AND DISCUSSION

The association of the oaklins GCP (guaiacylcatechin-pyrylium) and SCP (syringylcatechin-pyrylium) with the copigments selected (Figure 1) was quantitatively evaluated through the determination of the copigmentation binding constants (K_{CP}) for each pigment–copigment pair.

To minimize self-association effects in the intermolecular copigmentation studies, a low concentration of pigment (1×10^{-4} M) was used. Although ethanol largely reduces the copigmentation effect,[26] its inclusion in the experimental conditions was crucial to prevent precipitation during the spectroscopic analysis of the pigment and copigment compounds due to their low solubility in water.

Copigmentation Interactions Occurring in Oaklins. In a very acidic medium, only the flavylium cation is present, and the visible absorbance is

$$A_0 = \varepsilon_{AH^+} C$$

where C is the total pigment concentration and can be approximated to $C = [AH^+]$.

In contrast to anthocyanins, in which the contribution of quinonoidal bases (A) is negligible in mildly acidic medium (pH 3.5) and the hemiketal is the predominant species, in deoxyanthocyanidins, particularly oaklins, the equilibrium plateau occurs between the flavylium cation, the neutral quinoidal base, and the *trans*-chalcone, with the hemiketal and the *cis*-chalcone being transient species.[7] Copigmentation of the quinoidal bases could make a contribution, as those forms are also prone to stacking interactions with copigments. However, as the quinoidal bases and their copigmentation complexes absorb the visible light at higher wavelengths than their flavylium counterparts, no specific contribution is expected in the measured wavelength range (480–500 nm).[27] Copigmentation of quinoidal bases also promotes a high bathochromic shift (which is not observed in our case), especially with purine copigments such as caffeine and theophylline.[28]

With this in mind, the total concentration of the pigment for deoxyanthocyanidins at mildly acidic solutions can be represented by[11,29]

$$C = [AH^+] + [A] + [B] + [C_c] + [C_t]$$
$$= [AH^+] + [A] + [B']$$

where B′ is the pool of colorless forms in equilibrium.

The *apparent* thermodynamic constant for the overall reactions (Figure 2) taking place is thus given by

$$K'_a = K_a + K_h + K_h K_t + K_h K_t K_i$$

Being so, one can also write

$$C = \frac{[AH^+]}{1 + \frac{K'_a}{[H_3O^+]}}$$

In contrast to common anthocyanins in which $A_0 = ((\varepsilon_{AH^+}[AH^+])/(1 + (K_h/([H_3O^+]))))$, from the equations above and in the absence of the copigment one easily obtains

$$A_0 = \frac{\varepsilon_{AH^+} C}{1 + \frac{K'_a}{[H_3O^+]}} \quad (1)$$

In the presence of the copigment, and assuming a 1:1 stoichiometry for the complex, the visible absorbance at pH 3.5 becomes

$$A = \varepsilon_{AH^+} C + \varepsilon_{AHCP^+}[AHCP^+]$$

We thus have

$$A = \frac{\varepsilon_{AH^+} C(1 + rK_{CP}[CP])}{1 + \frac{K'_a}{[H_3O^+]} + K_{CP}[CP]} \quad (2)$$

with $r = (\varepsilon_{AHCP^+}/\varepsilon_{AH^+})$.

By combining eqs 1 and 2, A can also be expressed as[13,30]

$$A = \frac{\varepsilon_{AH^+} C(1 + rK_{CP}[CP])}{\frac{a}{r-a} + \frac{1}{(r-a)K_{CP}} \times \frac{1}{[CP]}} + A_0 \quad (3)$$

where $[CP]$ is the total concentration of the pigment, $a = (1/(1 + (K'_a/10^{-pH})))$, A and A_0 represent the visible absorbance of the pigment in the presence and absence of copigment, respectively, and r is the ratio of the molar absorption coefficient of the complex to that of the free flavylium ion. Because r is the ratio

dx.doi.org/10.1021/jf404640m | J. Agric. Food Chem. 2014, 62, 6995−7001

Table 1. Absorbance Values for the GCP/Copigment Complexes

pigment/copigment molar ratio	r = 1.06 catechin (λ_{max} 485 nm)	r = 1.01 epicatechin (λ_{max} 485 nm)	r = 1.01 chlorogenic acid (λ_{max} 485 nm)	r = 1.00 epigallocatechin (λ_{max} 498 nm)	r = 1.09 procyanidin B3 (λ_{max} 485 nm)
1:0 (A_0)	0.149	0.168	0.180	0.132	0.138
1:5	0.154	0.182	0.189	0.141	0.147
1:10	0.161	0.192	0.194	0.147	0.155
1:20	0.170	0.208	0.208	0.160	0.168
1:30	0.184	0.227	0.226	0.174	0.178
1:40	0.192	0.241	0.242	0.188	0.188

Table 2. Absorbance Values for the SCP/Copigment Complexes at the Maximum Wavelength (λ_{max} 500 nm)

pigment/copigment molar ratio	r = 1.23 catechin	r = 1.30 epicatechin	r = 1.28 chlorogenic acid	r = 1.38 epigallocatechin	r = 1.15 procyanidin B3
1:0 (A_0)	0.152	0.180	0.179	0.154	0.153
1:5	0.157	0.196	0.184	0.166	0.161
1:10	0.163	0.207	0.193	0.180	0.171
1:20	0.174	0.236	0.207	0.201	0.182
1:30	0.189	0.253	0.223	0.215	0.191
1:40	0.200	0.272	0.233	0.237	0.202

between the molar absorption coefficient of the copigmentation complex and the free flavylium ion, r = 1 by definition at the isosbestic point (determined at pH ≈0 to ensure total conversion of the pigment into the flavylium form). Surprisingly, it was only possible to determine the isosbestic point with the pair GCP/epigallocatechin. Indeed, for the rest of the compounds, at pH ≈0, an unexpected hyperchromic effect of the pigment−copigment complex was observed instead of a bathochromic shift, which is typical of copigmentation interactions. In these cases, the maximum absorption wavelength of the complex was selected for the calculations and parameter r was estimated to be the ratio between the absorbance of the copigmentation complex and the free flavylium form at this wavelength (Tables 1 and 2).

An absorbance increase with the copigment concentration is observed, which reflects a preferential association of the copigment to the flavylium cation and the subsequent shift of the hydration toward the colored forms.

For each copigment, a plot of absorbance as a function of wavelength was presented, and the typical behavior of copigmentation phenomena was perceived: increase of absorbance (hyperchromic effect) and a slight bathochromatic shift of λ_{max} as the copigment concentration increased. Figure 3 presents the absorption spectra of free GCP and GCP/epigallocatechin complex obtained at several molar ratios (Figure 3A) and the corresponding mathematical treatment to determine K_{CP} according to eq 3 (Figure 3B).

Equation 3 was used for the curve fitting of the experimental data $A = f([CP])$ to achieve the optimized values for K_{CP} as the sole adjustable parameter. Statistical analysis gave good correlation coefficients and standard deviations for the copigmentation constants (K_{CP}) (Table 3).

The highest copigmentation binding constants were observed for the complexes with the copigment epicatechin with both pigments (GCP and SCP). The two pigments also followed a similar copigmentation pattern, with the following highest copigmentation constants observed in decreasing order for epigallocatechin and procyanidin B3. For GCP, the lowest two were observed in decreasing order for chlorogenic acid and catechin, whereas for SCP the decreasing order was catechin and chlorogenic acid.

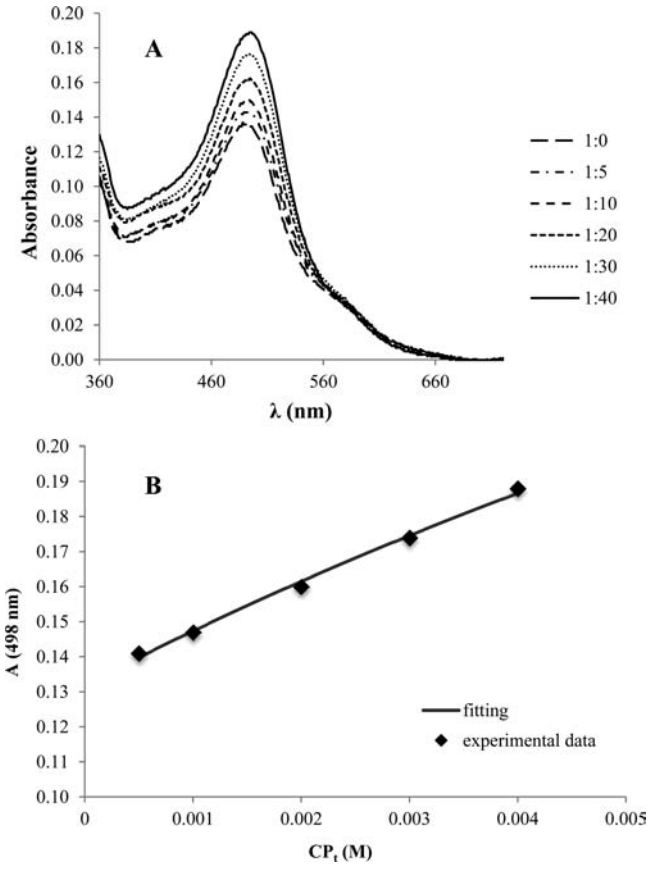

Figure 3. (A) Absorption spectra of GCP (0.1 mM) in the presence of epigallocatechin in a pH 3.5 phosphate buffer with 10% ethanol at 25 °C. Pigment/copigment molar ratios: 1:0, 1:5, 1:10, 1:20, 1:30, 1:40. (B) Plot of the visible absorbance at 498 nm as a function of copigment concentration; experimental points (◆) and theoretical curve (−) from a curve fitting according to eq 3 (pK'_a set at 3.05).

When comparing the copigmentation constants obtained for these deoxyanthocyanidin derivatives with the ones reported for anthocyanins, we observed similar results regarding their order of

dx.doi.org/10.1021/jf404640m | J. Agric. Food Chem. 2014, 62, 6995−7001

Table 3. Copigmentation Constants for the Oaklin/Copigment Complexes

	GCP		SCP		oenin	malvin
copigment	K_{CP}	R^2	K_{CP}	R^2	K_{CP}	K_{CP}
catechin	101 (±2)	0.997	96 (±3)	0.998	136 (±4)[13]	
epicatechin	176 (±5)	0.999	165 (±4)	0.998	99 (±2)[13]	
chlorogenic acid	125 (±4)	0.995	90 (±2)	0.998		350[32]
epigallocatechin	165 (±3)	0.998	152 (±4)	0.995	177 (±7)[13]	
procyanidin B3	130 (±4)	0.998	117 (±5)	0.996	48 (±2)[13]	

magnitude. However, we found some interesting results for some copigments, such as epicatechin and procyanidin B3, which presented higher binding constants than what was expected for anthocyanins.[13,31,32]

Computational Studies of Pigment−Copigment Complexes. To better characterize the copigmentation behavior of each complex, computational studies were performed on copigment molecules (catechin, epicatechin, epigallocatechin, B3, and chlorogenic acid) complexed with both GCP and SCP pigments. Molecular dynamics simulations of 30 ns were carried out for these 10 distinct complexes, which allowed the respective conformational space to be sampled to identify several conformations for each copigmentation complex studied. A similar protocol was used in previous studies in the literature.[5,13,33] The relative binding free energies obtained by the MM-PBSA approach[22−24] are in total agreement with the experimental results (Table 4), which suggests that the MD simulations provide an accurate portrait for conformational analysis. Although the theoretical $\Delta\Delta G_{binding}$ values fit qualitatively with the experimental values, the quantitative differences are 10 times higher, which could be due to some approximations within the computational method. These results suggest that both GCP and SCP pigments have the ability to interact with the copigment compounds tested. Considering the copigmentation group with the GCP as pigment, the $\Delta G_{binding}$ energy of the GCP−epicatechin complex is the most negative value, followed by GCP−epigallocatechin, GCP−B3, GCP−cholorogenic acid, and GCP−catechin. In relation to the group with the SCP as pigment, the ranking obtained for the binding free energies is SCP−epicatechin > SCP−epigallocatechin > SCP−B3 > SCP−catechin > SCP−cholorogenic acid. In fact, these data indicate that the GCP/SCP−epicatechin and GCP/SCP−epigallocatechin complexes display higher stability and their formation is thermodynamically favored when compared to the other complexes. However, the maximum experimental and theoretical $\Delta\Delta G$ binding values (0.36 and 2.73 kcal/mol, respectively) reveal a higher stability for all copigmentation complexes.

Table 4. Relative Binding Free Energies of the Copigmentation Complexes

		$\Delta\Delta G_{binding}$ (kcal/mol)	
pigment	copigment	theor	exptl[a]
GCP	epicatechin	0.00	0.00
	epigallocatechin	0.65	0.04
	procyanidin B3	1.39	0.18
	chlorogenic acid	1.77	0.20
	catechin	3.19	0.33
SCP	epicatechin	0.00	0.00
	epigallocatechin	0.36	0.05
	procyanidin B3	1.10	0.20
	catechin	1.77	0.32
	chlorogenic acid	2.73	0.36

[a]Experimental values calculated from Table 2 using $\Delta\Delta G = RT \ln(K_{pigment:epicatechin}/K_{pigment:X})$.

Figure 4 shows the closest geometries to the average structures for the 10 GCP−copigment and SCP−copigment complexes. As expected, the formation and stabilization of each complex is ensured by the establishment of hydrophobic interactions between the polyphenolic rings, as well as hydrogen bonds with the hydrophilic hydroxyl polar groups of both compounds. According to the literature, the formation of copigmentation complexes is driven by van der Waals interactions between the large planar surfaces of the pigment and copigment and the concomitant release of high-energy water molecules from the solvation shells (hydrophobic effect). Although the copigmentation systems studied here have large numbers of degrees of

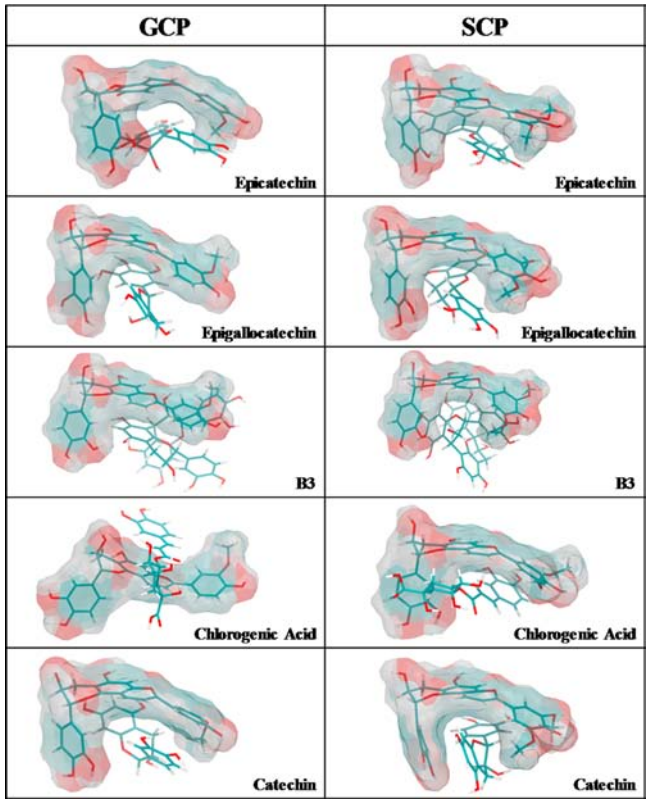

Figure 4. Closest geometries to the average structures of the GCP/SCP−epicatechin, GCP/SCP−epigallocatechin, GCP/SCP−procyanidin B3, GCP/SCP−cholorogenic acid, and GCP/SCP−catechin complexes. Carbon, oxygen, and hydrogen atoms are colored blue, red, and white, respectively. The charged pigment is depicted in a surface representation.

dx.doi.org/10.1021/jf404640m | J. Agric. Food Chem. 2014, 62, 6995−7001

freedom, the geometries displayed in Figure 4 show several optimized π-stacking arrangements. Hence, the proximity between aromatic planar surfaces of the pigment and copigment molecules should reflect the stability of each complex. The interplanar distances between the CAD nucleus, B and E rings of GCP/SCP, and the aromatic and benzopyrylium rings of each copigment were calculated along each MD simulation. Table 5

Table 5. Average Minimal Distances between Approximately Planar Surfaces of the GCP/SCP Pigments and Copigment Molecules in Each Copigmentation Complex

		average minimal distance (Å)		
pigment	copigment	CAD	B	E
GCP	epicatechin	4.95 (AC)	4.82 (B)	7.11 (AC)
	epigallocatechin	5.77 (AC)	5.97 (AC)	7.94 (B)
	procyanidin B3	5.81 (AC′)	5.52 (B′)	8.35 (AC′)
	chlorogenic acid	4.65 (B)	6.11 (B)	9.21 (B)
	catechin	5.31 (B)	6.56 (B)	8.44 (B)
SCP	epicatechin	5.28 (B)	6.37 (B)	6.60 (AC)
	epigallocatechin	5.65 (AC)	5.71 (AC)	7.18 (B)
	procyanidin B3	5.37 (AC)	4.87 (B)	6.83 (AC)
	catechin	5.48 (AC)	5.69 (B)	5.84 (AC)
	chlorogenic acid	5.78 (B)	5.11 (B)	7.59 (A)

shows the minimal distances obtained. The results show that the benzopyrylium and B rings of epicatechin and cholorogenic acid molecules are the closest planes to the CAD nucleous of GCP (4.95 and 4.65 Å, respectively). In addition, epicatechin is the copigment that has the nearest planes to the B and E rings of GCP (4.82 and 7.11 Å, respectively). Relative to the copigmentation complexes with SCP, epicatechin, B3, and catechin show minimal distances to the CAD, B, and E planes of this pigment (5.48, 4.87, and 5.84 Å, respectively). Because intermolecular distances of about 4 Å are consistent with van der Waals contacts, these data reveal that the shortest copigment−pigment distances were obtained for the complexes with the epicatechin copigment, which agrees with their highest stability constants (K).

According to the structures of the 10 complexes shown in Figure 4, it was observed that in both complexes (with GCP and SCP), the copigment epicatechin has its planar surfaces (AC and B) in an optimized position to establish a direct $\pi-\pi$ stacking and strong van der Waals contacts with CAD and B pigment planes. In both GCP and SCP complexes with epigallocatechin, the benzopyrylium provides a huge roughly planar polarizable surface that is strategically positioned in the middle of the pigment structure, establishing an accessible face and a closer contact with the B and E planes of both pigments. These facts contribute to a great association of epicatechin and epigallocatechin molecules to GCP/SCP pigments and thus to the also higher K values obtained for their complexes. For GCP/SCP-B3, it was observed that the AC′ nucleus of the copigment is located perpendicularly to the CAD plane of both pigments, which hampers the establishment of nonpolar contacts between both molecules. In relation to GCP/SCP−chlorogenic acid and GCP/SCP−catechin complexes, it was noted that there are several aromatic planes of these copigments facing solvent molecules, which prevents a simultaneous interaction of both moieties (A and B in chlorogenic acid; AC and B in catechin) with the CAD, B, and E nucleus of each pigment. Subsequently, because the hydrophobic contacts with the aromatic nucleus of oaklins are the major contributions to the copigmentation driving force, it is expected that chlorogenic acid and catechin have the smallest copigmentation binding contants. All of these structural data show that epicatechin and epigallocatechin copigments are closer to GCP and SCP pigments than B3, chlorogenic acid, and catechin molecules, which is in accordance with the first two copigments having the highest copigmentation binding constants for both pigments.

Furthermore, the copigmentation process could also be strengthened by H bonds involving the numerous hydroxyl groups from phenolic units. Table 6 shows the most important

Table 6. Most Important Hydrogen Bonds Established between Both Pigments (GCP and SCP) and Several Copigments during the MD Simulation of Each Complex

interaction	H bond	% of occurrence
OH-E ring (GCP)−OH-AC nucleus (epicatechin)	2.8 ± 0.1	5.8
OH-E ring (GCP)−OH-AC nucleus (epigallocatechin)	2.7 ± 0.1	5.8
OH-CAD nucleus (GCP)−OH-AC nucleus (procyanidin B3)	2.7 ± 0.1	12.7
OH-CAD nucleus (GCP)−OH-B ring (chlorogenic acid)	2.8 ± 0.1	14.0
OH-E ring (SCP)−OH-AC nucleus (epicatechin)	2.7 ± 0.1	5.3
OH-E ring (SCP)−OH-AC nucleus (epigallocatechin)	2.7 ± 0.1	5.1
OH-E ring (SCP)−OH-AC nucleus (procyanidin B3)	2.7 ± 0.1	22.7
OH-CAD nucleus (SCP)−OH-A ring (chlorogenic acid)	2.7 ± 0.1	14.0

hydrogen bond (H bond) interactions established within each copigmentation complex studied. As seen, with the exception of catechin, all copigments make one important H bond with each pigment, which contributes to the copigmentation complex formation.

The deoxyanthocyanidin derivatives studied (oaklins) presented intermolecular copigmentation interactions. Despite the loss of color in solution being already greatly diminished in oaklin compounds when compared to anthocyanins, not only because the pK'_a is greater but also because the mole fraction of the base is substantially higher at higher pH values, they also demonstrated that they were capable of presenting copigmentation interactions with some wine copigments that further stabilize the flavylium cation in hydroalcoholic solutions, with higher binding constants than the ones reported for anthocyanins in some cases.

Due to their higher stability in aqueous solutions and copigment interactions, oaklins continue to be regarded as potential food colorants. Further studies are still required to test their chromatic properties at different conditions (temperature, sulfites, etc.) as well as their antioxidant capabilities.

AUTHOR INFORMATION

Corresponding Author

*(V.d.F.) Phone: +351 226 082 858. Fax: +351 226 082 959. E-mail: vfreitas@fc.up.pt.

Funding

L.C. gratefully acknowledges a postdoctoral grant from Fundação para a Ciência e Tecnologia (FCT) (SFRH/BPD/72652/2010).

Notes

The authors declare no competing financial interest.

REFERENCES

(1) Freitas, V.; Sousa, C.; Silva, A. M. S.; Santos-Buelga, C.; Mateus, N. Synthesis of a new catechin-pyrylium derived pigment. *Tetrahedron Lett.* **2004**, *45*, 9349−9352.

(2) Sousa, C.; Mateus, N.; Perez-Alonso, J.; Santos-Buelga, C.; Freitas, V. Preliminary study of oaklins, a new class of brick-red catechinpyrylium pigments resulting from the reaction between catechin and wood aldehydes. *J. Agric. Food Chem.* **2005**, *53*, 9249−9256.

(3) Galland, S.; Mora, N.; Abert-Vian, M.; Rakotomanomana, N.; Dangles, O. Chemical synthesis of hydroxycinnamic acid glucosides and evaluation of their ability to stabilize natural colors via anthocyanin copigmentation. *J. Agric. Food Chem.* **2007**, *55*, 7573−7579.

(4) Yoshida, K.; Mori, M.; Kondo, T. *Nat. Prod. Rep.* **2009**, *26*, 884−915.

(5) Cruz, L.; Bras, N. F.; Teixeira, N.; Mateus, N.; Ramos, M. J.; Dangles, O.; De Freitas, V. Vinylcatechin dimers are much better copigments for anthocyanins than catechin dimer procyanidin B3. *J. Agric. Food Chem.* **2010**, *58*, 3159−3166.

(6) Gonzalez-Manzano, S.; Duenas, M.; Rivas-Gonzalo, J. C.; Escribano-Bailon, M. T.; Santos-Buelga, C. *Food Chem.* **2009**, *114*, 649−656.

(7) Sousa, A.; Petrov, V.; Araújo, P.; Mateus, N.; Pina, F.; Freitas, V. Thermodynamics, kinetics, and photochromism of oaklins: a recent family of deoxyanthocyanidins. *J. Phys. Chem. B* **2013**, *117*, 1901−1910.

(8) Mazza, G.; Brouillard, R. The mechanism of co-pigmentation of anthocyanins in aqueous solutions. *Phytochemistry* **1990**, *29*, 1097−1102.

(9) Asen, S.; Stewart, R. N.; Norris, K. H. Co-pigmentation effect of quercetin glycosides on absorption characateristics of cyanidin glycosides and color of red wing azalea. *Phytochemistry* **1971**, *10*, 171−175.

(10) Asen, S.; Stewart, R. N.; Norris, K. H. Copigmentation of aurone and flavone from petals of *Antirrhinum-majus*. *Phytochemistry* **1972**, *11*, 2739−2741.

(11) Awika, J. Behavior of 3-deoxyanthocyanidins in the presence of phenolic copigments. *Food Res. Int.* **2008**, *41*, 532−538.

(12) Dvorakova, M.; Moreira, M. M.; Dostalek, P.; Skulilova, Z.; Guido, L. F.; Barros, A. A. Characterization of monomeric and oligomeric flavan-3-ols from barley and malt by liquid chromatography-ultraviolet detection-electrospray ionization mass spectrometry. *J. Chromatogr., A* **2008**, *1189*, 398−405.

(13) Teixeira, N.; Cruz, L.; Brás, N. F.; Mateus, N.; Ramos, M. J.; Freitas, V. Structural features of copigmentation of oenin with different polyphenol copigments. *J. Agric. Food Chem.* **2013**, *61*, 6942−6948.

(14) Gaussian Inc., C.O.P., Bldg. 6, Pittsburgh, PA 15106, USA.

(15) Frisch, M. J.; Trucks, G. W.; Schlegel, H. B.; Scuseria, G. E.; Robb, M. A.; Cheeseman, J. R.; Scalmani, G.; Barone, V.; Mennucci, B.; Petersson, G. A.; Nakatsuji, H.; Caricato, M.; Li, X.; Hratchian, H. P.; Izmaylov, A. F.; Bloino, J.; Zheng, G.; Sonnenberg, J. L.; Hada, M.; Ehara, M.; Toyota, K.; Fukuda, R.; Hasegawa, J.; Ishida, M.; Nakajima, T.; Honda, Y.; Kitao, O.; Nakai, H.; Vreven, T.; Montgomery, J. A., Jr.; Peralta, J. E.; Ogliaro, F.; Bearpark, M.; Heyd, J. J.; Brothers, E.; Kudin, K. N.; Staroverov, V. N.; Kobayashi, R.; Normand, J.; Raghavachari, K.; Rendell, A.; Burant, J. C.; Iyengar, S. S.; Tomasi, J.; Cossi, M.; Rega, N.; Millam, N. J.; Klene, M.; Knox, J. E.; Cross, J. B.; Bakken, V.; Adamo, C.; Jaramillo, J.; Gomperts, R.; Stratmann, R. E.; Yazyev, O.; Austin, A. J.; Cammi, R.; Pomelli, C.; Ochterski, J. W.; Martin, R. L.; Morokuma, K.; Zakrzewski, V. G.; Voth, G. A.; Salvador, P.; Dannenberg, J. J.; Dapprich, S.; Daniels, A. D.; Farkas, Ö.; Foresman, J. B.; Ortiz, J. V.; Cioslowski, J.; Fox, D. J. *Gaussian 09*; Gaussian, Inc.: Wallingford, CT, USA, 2009.

(16) Bayly, C. I.; Cieplak, P.; Cornell, W.; Kollman, P. A. A well-behaved electrostatic potential based method using charge restraints for deriving atomic charges: the RESP model. *J. Phys. Chem.* **1993**, *97*, 10269−10280.

(17) Case, D. A.; Darden, T. A.; Cheatham, T. E., III; Simmerling, C. L.; Wang, J.; Duke, R. E.; Luo, R.; Crowley, M.; Walker, R. C. ; Zhang, W.; Merz, K. M.; Wang, B.; Hayik, S.; Roitberg, A.; Seabra, G.; Kolossváry, I.; Wong, K. F.; Paesani, F.; Vanicek, J.; Wu, X.; Brozell, S. R.; Steinbrecher; T.; Gohlke, H.; Yang, L.; Tan, C.; Mongan, J.; Hornak, V.; Cui, G.; Mathews, D. H.; Seetin, M. G.; Sagui, C.; Babin, V.; Kollman, P. A. *AMBER 10*; University of California: San Francisco, CA, USA, 2008.

(18) Wang, J. M.; Wolf, R. M.; Caldwell, J. W.; Kollman, P. A.; Case, D. A. Development and testing of a general amber force field. *J. Comput. Chem.* **2004**, *25*, 1157−1174.

(19) Izaguirre, J. A.; Catarello, D. P.; Wozniak, J. M.; Skeel, R. D. Langevin stabilization of molecular dynamics. *J. Chem. Phys.* **2001**, *114*, 2090−2098.

(20) Ryckaert, J. P.; Ciccotti, G.; Berendsen, H. J. C. Numerical-integration of Cartesian equations of motion of a system with constraints − molecular-dynamics of *n*-alkanes. *J. Comput. Phys.* **1977**, *23*, 327−341.

(21) Essmann, U.; Perera, L.; Berkowitz, M. L.; Darden, T.; Lee, H.; Pedersen, L. G. A smooth particle mesh Ewald method. *J. Chem. Phys.* **1995**, *103*, 8577−8593.

(22) Huo, S.; Massova, I.; Kollman, P. A. Computational alanine scanning of the 1:1 human growth hormone-receptor complex. *J. Comput. Chem.* **2002**, *23*, 15−27.

(23) Kollman, P. A.; Massova, I.; Reyes, C.; Kuhn, B.; Huo, S. H.; Chong, L.; Lee, M.; Lee, T.; Duan, Y.; Wang, W.; Donini, O.; Cieplak, P.; Srinivasan, J.; Case, D. A.; Cheatham, T. E. Calculating structures and free energies of complex molecules: combining molecular mechanics and continuum models. *Acc. Chem. Res.* **2000**, *33*, 889−897.

(24) Massova, I.; Kollman, P. A. Combined molecular mechanical and continuum solvent approach (MM-PBSA/GBSA) to predict ligand binding. *Perspect. Drug Discov.* **2000**, *18*, 113−135.

(25) Cornell, W. D.; Cieplak, P.; Bayly, C. I.; Gould, I. R.; Merz, K. M.; Ferguson, D. M.; Spellmeyer, D. C.; Fox, T.; Caldwell, J. W.; Kollman, P. A. A 2nd generation force-field for the simulation of proteins, nucleic-acids, and organic-molecules. *J. Am. Chem. Soc.* **1995**, *117*, 5179−5197.

(26) Dangles, O.; Brouillard, R. Polyphenol interactions − the copigmentation case − thermodynamic data from temperature variation and relaxation kinetics medium effect. *Can. J. Chem.* **1992**, *70*, 2174−2189.

(27) Pina, F. J. *Photochem. Photobiol. A* **1998**, *117*, 51−59.

(28) Haslam, E. *Practical Polyphenolics: From Structure to Molecular Recognition and Physiological Action*; Cambridge University Press: Cambridge, UK, 1998.

(29) Pina, F.; Melo, M. J.; Laia, C. A. T.; Parola, A. J.; Lima, J. C. *Chem. Soc. Rev.* **2012**, *41*, 869−908.

(30) Malien-Aubert, C.; Dangles, O.; Amiot, M. J. Influence of procyanidins on the color stability of oenin solutions. *J. Agric. Food Chem.* **2002**, *50*, 3299−3305.

(31) Berké, B.; Freitas, V. Influence of procyanidin structures on their ability to complex with oenin. *Food Chem.* **2005**, *3*, 453−460.

(32) Brouillard, R.; Wigand, M. C.; Dangles, O.; Cheminat, A. pH and solvent effects on the copigmentation reaction of malvin with polyphenols, purine and pyrimidine derivatives. *J. Chem. Soc.* **1991**, *2*, 1235−1241.

(33) Nave, F.; Bras, N. F.; Cruz, L.; Teixeira, N.; Mateus, N.; Ramos, M. J.; Di Meo, F.; Trouillas, P.; Dangles, O.; De Freitas, V. Influence of a flavan-3-ol substituent on the affinity of anthocyanins (pigments) toward vinylcatechin dimers and proanthocyanidins (copigments). *J. Phys. Chem. B* **2012**, *116*, 14089−14099.

anthocyanin-derived pigments. The molecular basis for the antioxidant properties mainly occurs by two different pathways: a hydrogen atom transfer or a single-electron transfer. These two mechanisms are described by eqs 1 and 2, respectively:[22−25]

$$ArOH + R^{\bullet} \rightarrow ArO^{\bullet} + RH \quad (1)$$

$$ArOH + R^{\bullet} \rightarrow ArOH^{\bullet+} + R^{-} \quad (2)$$

Previous computational studies have been performed on flavonoids and pyranoanthocyanins,[22−29] in which the bond dissociation energy (BDE) of their hydroxyl groups and the ionization potential (IP) were determined as the better representative descriptors for the radical scavenging ability. Lower BDE and IP values favor both H abstraction and the electron-transfer reactions and, in general, the gas phase computed values of BDE and IP for flavonoids fall in the ranges of 70−90 and 160−190 kcal/mol, respectively.[25]

In this paper, the geometrical features and the BDE and IP thermodynamic parameters of one anthocyanin and seven pyranoanthocyanins from aged wine have been computed to corroborate the experimentally determined antioxidant capability of these compounds.

MATERIALS AND METHODS

Chemicals. Dimethyl sulfoxide (DMSO) was purchased from Euriso-top; Trolox, 2,2-diphenyl-1-picrylhydrazyl, 2,2′-azobis[2-methylpropionamidine] dihydrochloride (AAPH), Hepes, NaCl, soybean L-α-phosphatidylcholine, iron(III) chloride ($FeCl_3$), and 2,4,6-tripyridyl-*s*-triazine (TPTZ) were purchased from Sigma-Aldrich.

TSK Toyopearl gel HW-40(S)-Tosoh (Tokyo, Japan), polyamide resin (100−120 mesh, SINOPEC, Hunan, China), acetonitrile (HPLC grade), and ethanol (absolute) were purchased from Carlo Erba (France); formic acid (98%, PA-ACS) and methanol (99.5%) were purchased from Panreac Química Sau (Spain); hydrochloridric acid (37% v/v), sodium hydroxide, and ethyl acetate were purchased from José M. Vaz Pereira, S.A. (Portugal).

Extraction of Anthocyanins. Anthocyanins were extracted from *Vitis vinifera* red grapes of Touriga Nacional variety by the addition of an acidulated solution of methanol/water (50% v/v) as described elsewhere.[30] The obtained anthocyanin extract was concentrated using a nanofiltration system (membrane Desal 5 model DK 150−300 Da). Methanol was evaporated by rotary evaporation under vacuum at 30 °C, and the solution was frozen in water and freeze-dried.

The anthocyanin extract, dissolved in water, was purified by column chromatography using a polyamide resin. The fraction recovered with a solution of 10% (v/v) aqueous methanol was analyzed by HPLC and found to contain anthocyanin-3-glucosides; another fraction recovered with a solution of water/methanol 40% (v/v) was shown to contain acylated anthocyanins. The fractions were concentrated in a rotary evaporator under vacuum and frozen in water for later lyophilization.[31] The pigments were purified by preparative HPLC (Knauer K-1001) fitted with a Purospher C-18 reversed-phase column, 250 mm × 25 mm i.d., at 520 nm using a UV−vis L-2420 Elite LaChrom detector. The injection volume was 2 mL. The solvents were (A) H_2O/HCOOH (9:1) and (B) HCOOH/MeOH/H_2O (1:5:4). The gradient consisted of a linear gradient from 60 to 0% A in 70 min at a flow rate of 5 mL/min for the isolation of malvidin-3-coumaroylglucoside and from 65 to 15% A in 70 min at a flow rate of 10 mL/min for the isolation of malvidin-3-glucoside. The column was washed with 100% B during 20 min and then stabilized at the initial conditions for another 20 min. The isolated compounds were frozen in water and freeze-dried. The purity of the compounds was confirmed by HPLC/DAD-ESI/MS and NMR.

Hemisynthesis and Purification of Pyranoanthocyanins. Oxovitisin (**9**) and the coumaroyl derivative of oxovitisin (**10**) were synthesized and purified according to the procedure described elsewhere;[32] vitisin B (**7**) and the coumaroyl derivative of vitisin B (**8**) were synthesized from the reaction of malvidin-3-glucoside and malvidin-3-coumaroylglucoside, respectively, with vinyloxytrimethylsilane as previously reported;[33] vitisin A (**6**) was obtained from the reaction of malvidin-3-glucoside with pyruvic acid in water at pH 2.6 and at 35 °C with a molar ratio 50:1 (pyruvic acid/malvidin-3-glucoside) over 5 days as previously reported;[32,34] methylpyranomalvidin-3-glucoside (MethylPyMv3gluc) (**11**) was synthesized and purified according to the literature;[7] PyMv3gluc-(+)-catechin (**4**), PyMv3coumgluc-(+)-catechin (**5**), PyMv3gluc-catechol (**2**), and PyMv3coumgluc-catechol (**3**) pigments were obtained according the procedures described elsewhere.[11,35,36] Briefly, solutions containing Mv3glc or Mv3coumglc (2.5 mM) were incubated with 8-vinyl-(+)-catechin, 8-vinyl-(−)-epicatechin, or 4-vinylcatechol (2−3 equiv) in 5−10% ethanol/water at pH 3.5 (adjusted with dilute HCl or NaOH) at 30 °C.

Purity Evaluation of the Compounds. The purity of all pigments obtained was confirmed by MS and NMR analysis by using a ^{1}H NMR (600.13 MHz) and ^{13}C NMR (150.90 MHz) in DMSO/TFA (9:1) on a Bruker Avance III 600 spectrometer with a TCI CryoProbe at 293 K using TMS as internal standard.

Radical Scavenging Assay (DPPH). The tested compound reacts with DPPH (2,2-diphenyl-1-picrylhydrazyl) and induces a decrease of the absorbance measured at 515 nm, which indicates the scavenging potential of the compounds. Because all tested pigments also absorb at 515 nm, their initial absorbance ($t = 0$) was subtracted. The reaction for scavenging DPPH radicals was performed in a microplate reader of 96-well plates (Biotek Powerwave XS with software KC4). The reaction was carried out on the plate wells with a temperature of 25 °C. A solution of 60 μM DPPH was prepared in methanol, and 297 μL of this latter solution was added in each well together with 3 μL of antioxidant. The compounds to be tested were previously dissolved in methanol and used in a final concentration of 10 μM. The decrease in absorbance was measured at 515 nm, at $t = 0$ and every 10 min, during 30 min. For the final results, the 0−20 min reaction time window was used. Antiradical activity was expressed as micromolar Trolox equivalents. The antiradical activity was calculated from the equation determined from linear regression after plotting standard solutions of Trolox with different concentrations.

Lipid Peroxidation Assay. Liposomes were prepared as described elsewhere.[19] Lipid peroxidation of L-α-phosphatidylcholine soybean lipid unilamellar vesicles (LUVs) was induced by peroxyl radicals generated at a constant rate, by thermal degradation of the azo compound AAPH in the presence or absence of antioxidants, and followed by measuring the oxygen consumption.

The rate of oxygen consumption was measured continuously with a Clark-type oxygen electrode (Hansatech) provided with an automatic recording apparatus. The reaction mixture containing 1220 μL of Hepes buffer (pH 7.4), 256 μL of liposomes (340 μM final concentration), and 2 μL of the antioxidant (1 mM initial concentration) tested, dissolved in methanol, was left in a 37 °C thermostated bath for 1 h. This mixture was introduced in a closed glass vessel, protected from light, thermostated at 37 °C, and provided with a stirrer, and the reaction was started by the addition of 22 μL of AAPH (10 mM final concentration).[37] The induction periods (Ti) in the presence of antioxidants were determined graphically from the profiles of oxygen consumption by the coordinates of the interception of tangents to the inhibited and uninhibited rates of oxidation.[19] In addition to the analysis of the anthocyanin-derived pigments, the antioxidant activity of Trolox (water-soluble analogue of vitamin E) was evaluated. The results were expressed in terms of ratio between these pigments and Trolox antioxidant capacities.

Theoretical and Computational Studies. The energies of all geometries of anthocyanin-derived pigments and their respective radicals were calculated in vacuum with the density functional theory (DFT) approach, at the unrestricted B3LYP[38−40] hybrid density functional level (Becke−Slater−HF exchange with Lee−Yang−Parr correlation functional) using the 6-311+G(d) basis set as implemented in the Gaussian 09 package.[41] The inclusion of polarization functions correctly takes into account intramolecular H bonds. The optimized structures were confirmed as true minima by vibrational analysis performed at the same level of theory. A temperature of 298.15 K and a pressure of 1 atm were used for vibrational frequency and thermal energy correction calculations. Single-point energy calculations using

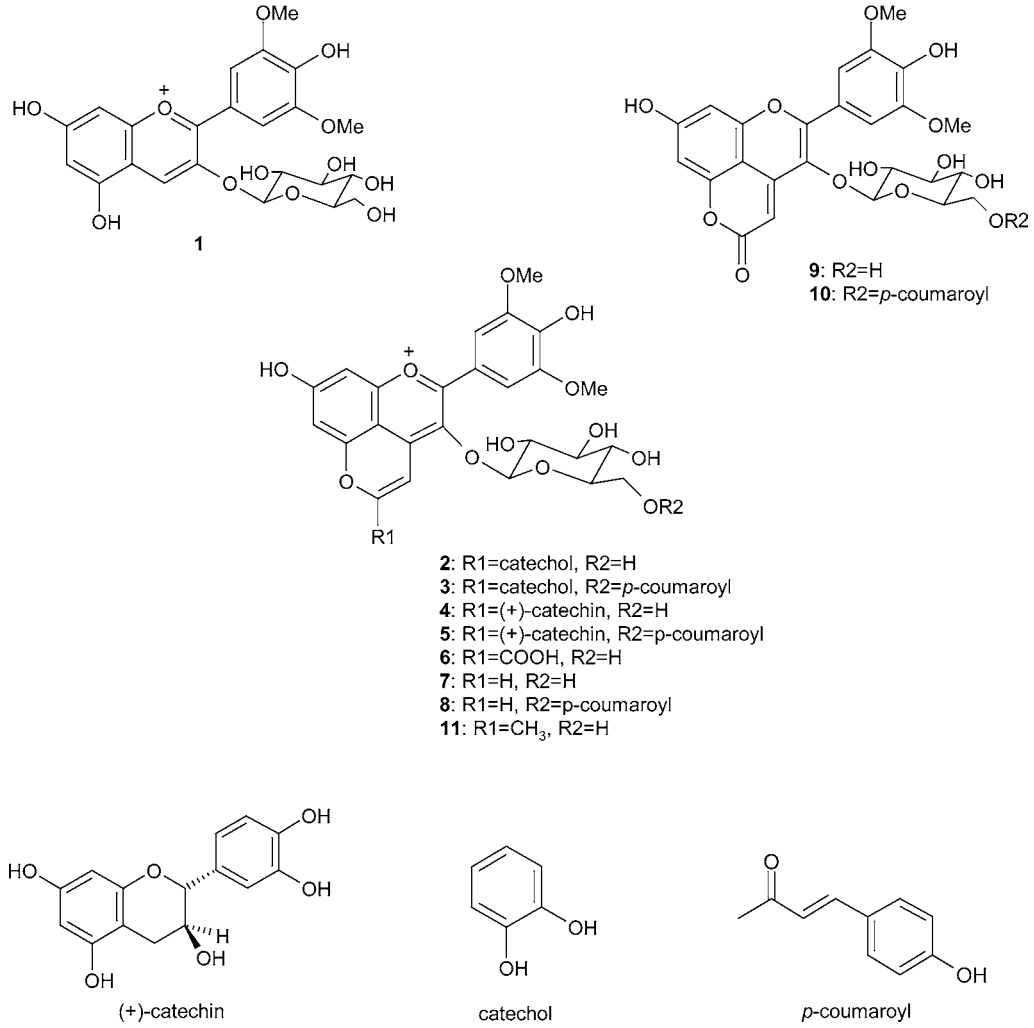

Figure 1. Structures of the pigments studied: malvidin-3-glucoside (**1**), PyMv3gluc-catechol (**2**), PyMv3coumgluc-catechol (**3**), PyMv3gluc-(+)-catechin (**4**), PyMv3coumgluc-(+)-catechin (**5**), vitisin A (**6**), vitisin B (**7**), coumaroyl derivative of vitisin B (**8**), oxovitisin (**9**), coumaroyl derivative of oxovitisin (**10**), and MethylpyMv3gluc (**11**).

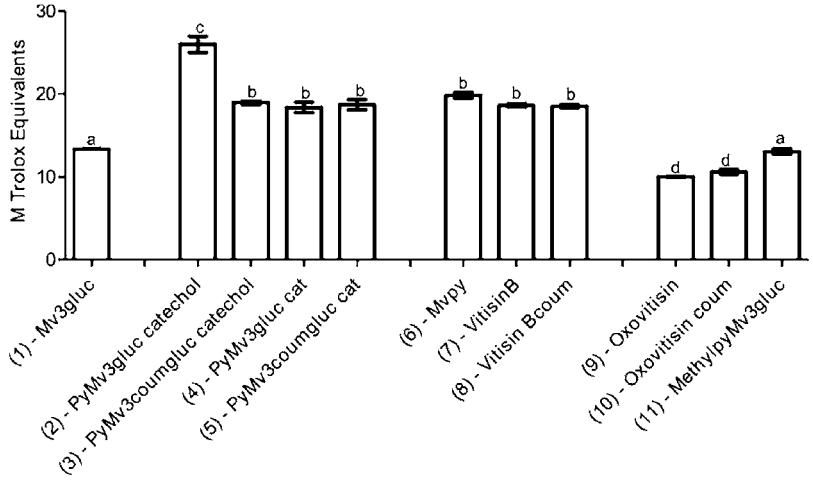

Figure 2. Radical scavenging activity assessed by the DPPH method. Columns represent mean ± standard deviation (SD), $p < 0.05$. Columns with the same letter do not differ statistically.

the 6-311++G(d,p) basis set were performed at the B3LYP level of theory. This basis set was specifically used because it provided very reliable results in other studies performed for polyphenolic antioxidants.[22,23,27,29] The unrestricted open-shell approach was used for radical species. No spin contamination was found for radicals; values were 0.750 in all cases. To evaluate the effect of the solvent environment, the energy of all optimized geometries (using a dielectric constant (ε) of 78.35 to mimic the water solution) was recalculated. Solvation energies

dx.doi.org/10.1021/jf404735j | J. Agric. Food Chem. 2014, 62, 7002−7009

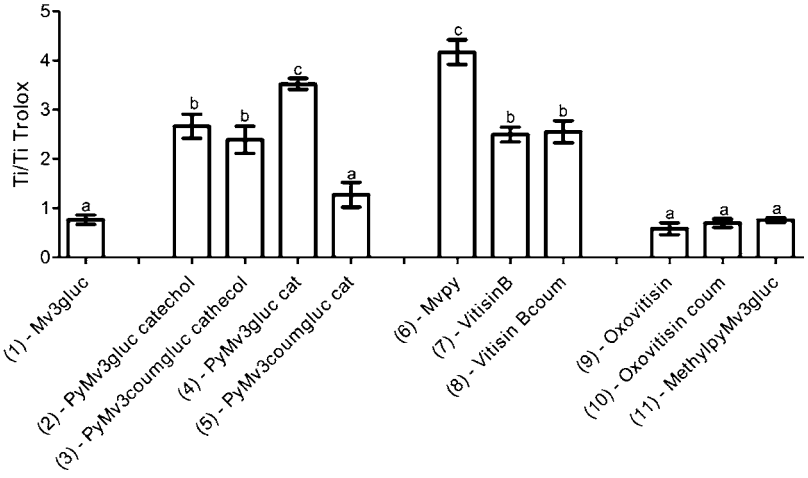

Figure 3. Inhibition of AAPH-initiated oxidation of soybean PC liposome by a 1.25 μM concentration of compound by monitoring oxygen consumption. Results are inhibition times in ratio to Trolox. Columns represent mean ± standard deviation (SD) $p < 0.05$. Columns with the same letter do not differ statistically.

were computed with the polarizable continuum method (PCM) using a polarizable conductor calculation model.[42] Gas-phase corrections were employed to calculate enthalpy values in the aqueous and alcoholic phases, as thermal corrections are expected to be similar in both gas and solvated phases.

Both BDE and IP values were computed at 298.15 K. The former is the sum of the enthalpy of the radical resulting from the hydrogen atom abstraction and that of the hydrogen atom minus the enthalpy of the parent molecule, whereas the latter is the enthalpy difference between the radical cation and the parent molecule.

Statistical Analysis. All tests were conducted at least in triplicate. Values are expressed as means ± standard deviation. Statistical significance was evaluated by one-way ANOVA, followed by the Bonferroni test. Differences were considered significant when $p < 0.05$. Columns with the same letter in the figures are not statistically different.

RESULTS AND DISCUSSION

This work aimed at studying some antioxidant features of pigments derived from malvidin-3-glucoside (the major anthocyanin present in *Vitis vinifera* red grapes). For this, 10 malvidin-3-glucoside derivatives belonging to different classes of pyranoanthocyanins were obtained by hemisynthesis (Figure 1). All of these pigments have already been detected in red wines, especially Port red wines, although in very low amounts.

The antioxidant features of these compounds were tested by assessing their antiradical potential (using the DPPH method) and their capacity to prevent lipid peroxidation using soybean L-α-phosphatidylcholine (PC) LUVs as lipid substrate. The protection against lipid peroxidation was assayed by monitoring oxygen consumption during oxidation of soybean PC liposomes. The antioxidant features of all the pyranoanthocyanins tested were compared to that of malvidin-3-glucoside.

DPPH. Following the method described in the literature[43] with some modifications, radical activities were determined by using DPPH as a free radical. Overall, the results indicate that all classes of pyranoanthocyanins tested displayed antiradical properties, as seen from Figure 2. The structural transformations of malvidin-3-glucoside into new pigments did not compromise its antiradical capacity, having even increased it in certain cases. Indeed, the three vitisin-like pigments tested were found to display a higher antiradical capacity. On the other hand, the oxovitisins tested and methylpyranomalvidin-3-glucoside were found to maintain an antiradical capacity similar to that of malvidin-3-glucoside (Figure 2). As to the pyranoanthocyanin-catechols and pyranoanthocyanin-catechins, the results are similar to those obtained with the vitisin-like pigments except for PyMv3gluc-catechol (also known as pinotin A) that displayed a 2-fold higher antiradical capacity than malvidin-3-glucoside (Figure 2). This outcome is likely to be related to the presence of an additional *o*-dihydroxyl group in its structure (catechol) combined with the extended conjugation of π electrons that could readily stabilize the radical scavenged. This structural feature is often associated with a higher radical scavenging capacity.[15,16,44,45] However, this outcome was not obtained in the case of the two pyranoanthocyanin-catechins tested (PyMv3-gluc-catechin and PyMv3coumgluc-catechin). Other structural features such as steric hindrances may partly impair the antiradical capacity of the compounds.

Altogether, the general tendency of the antiradical capacity observed in this study agrees with some data already reported in the literature, although only a marginal effect of the catechol moiety was observed in another work using a different lipid substrate.[46]

Monitoring Oxygen Consumption during the Oxidation of Liposomes. The protection afforded by these malvidin derivatives toward lipid peroxidation was assayed by monitoring oxygen consumption during oxidation of soybean PC liposomes (Figure 3). Liposomes were used as they are usually employed to mimic biological targets (e.g., cellular membranes). The evaluation of the antioxidant capacity of the anthocyanin pigments, against oxidation of soybean PC liposomes, was performed using AAPH as a peroxidation initiator, as commonly used in this kind of study. The generation of peroxyl radicals from AAPH induces a significant oxidation of phosphatidylcholine, because they are able to remove hydrogen atoms from polyunsaturated acyl chains, yielding radicals that lead to the propagation chain.[47] The data yielded from the oxygen consumption assays showed that all of the anthocyanin pigments scavenged efficiently the peroxyl radicals generated in the aqueous phase compared to the control assay (without any compound) (data not shown).

The results are presented in the form of a ratio between the induction time (Ti) of the compound tested and that of Trolox. This induction time is representative of the delayed time of oxygen consumption, which remains practically constant prior to the initiation of lipid peroxidation.[37]

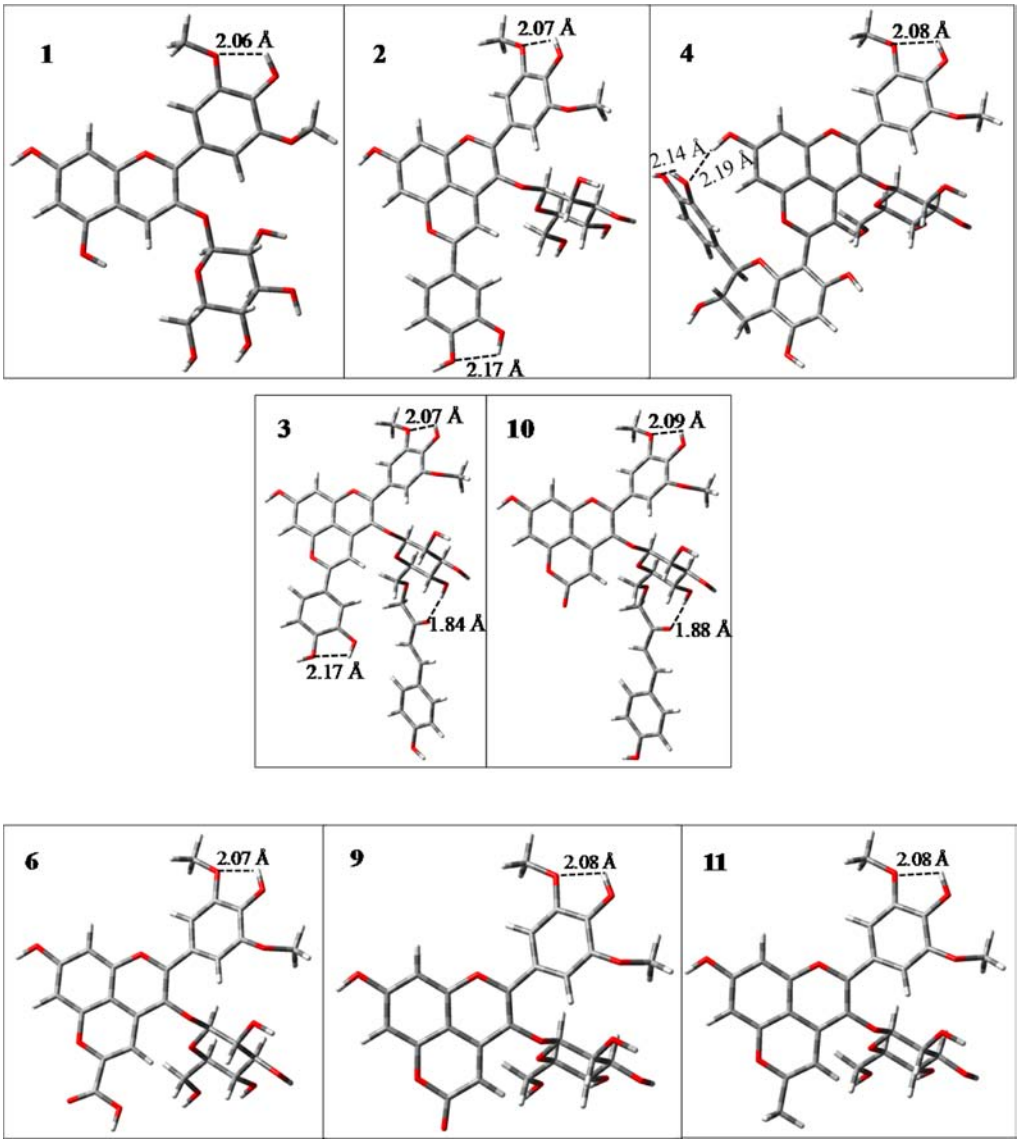

Figure 4. Optimized geometry of pigments **1**, **2**, **3**, **4**, **6**, **9**, **10**, and **11**. Oxygen, carbon, and hydrogen atoms are colored in red, gray, and white, respectively.

In the presence of any antioxidant, lipid peroxidation is delayed during a certain period of time that varies with the antioxidant capacity of the tested compound. The anthocyanin pigments are thought to trap AAPH-derived peroxyl radicals, inhibiting the initiation of lipid peroxidation. On the other hand, if located at the surface of the liposome, they may also quench liposome-derived peroxyl radicals, inhibiting the chain propagation.[48]

Bearing in mind the results obtained from the DPPH assay, one could assume that a similar trend was expected for the lipid peroxidation assay. However, some slight differences were observed.

The oxovitisins tested and methylpyranomalvidin-3-glucoside were found to maintain an antioxidant potential similar to that of malvidin-3-glucoside (Figure 3), as also observed in the DPPH assay (Figure 2). Furthermore, the vitisin-like pigments, the pyranoanthocyanin-catechols and pyranoanthocyanin-catechins, were found to delay the peroxidation of the PC liposomes more than malvidin-3-glucoside (Figure 3). These results also agree with those yielded from the DPPH assay. The only differences are related to PyMv3gluc-catechin and the pyruvic adduct of malvidin-3-glucoside Mv-py, also known as vitisin A. These two latter pigments were shown to be the most effective in delaying lipid peroxidation. The available data allow only speculation that this feature may be due to the proximity/affinity of the molecules toward the lipid layer, thereby promoting a higher protection through a more efficient radical scavenging capacity. This feature is closely related to the polarity of part of or the whole molecule.

Theoretical and Computational Studies. The pigments studied here were **1**, **2**, **3**, **4**, **6**, **9**, **10**, and **11**. and their optimized geometries are shown in Figure 4. All pyranoanthocyanins possess an intense π electron delocalization and conjugation that involve the rigid core composed by A−C−D rings and a less rigid B ring. In pigments **2** and **3**, the presence of the E ring draws electron flow that enhances the possibility of delocalization and conjugation in this part of the molecule. A similar behavior was observed in compound **4** that possesses a catechin group and allows a major delocalization and conjugation in this moiety.

Furthermore, all minimum energy structures are specially arranged to maximize the number of intramolecular H bonds

dx.doi.org/10.1021/jf404735j | J. Agric. Food Chem. 2014, 62, 7002−7009

Table 1. Relative Energies (Kilocalories per Mole) of All Anthocyanin/Pyranoanthocyanin Radical Species

	radical								
pigment	HO-4′	HO-5′	HO-7′	HO-2″	HO-3″	HO-4″	HO-5″	HO-7″	HO-4‴
1	0.0	4.4	12.7						
2	10.5		19.9		16.6	0.0			
3	2.1		11.7		9.4	0.0			6.1
4	3.1		13.7	24.4	3.9	0.0	8.9	4.9	
6	0.0		10.6						
9	0.0		5.9						
10	0.0	5.9							4.6
11	0.0		9.9						

within the B, E, and sugar rings. It was observed that in all molecules, the HO-4′ establishes a H bond to the adjacent 3′-OCH_3 group, whereas an additional H bond is established between the 3′-OH and 4′-OH groups of pigments **2** and **3**. Pigments **3** and **10** possess another H bridge established between the carbonyl group of the *p*-coumaroyl moiety and the 4-OH of glucose unit. Compound **4** shows two more specific H bonds, one within the catechin unit and another between an OH group of the catechin B ring and the OH group of the pyranoanthocyanin A ring. Furthermore, there are several H bonds established between the various hydroxyl groups of the pyranoanthocyanin sugar ring. However, they should not influence the reactivity of the polyphenol molecules, although these energetic H bonds can stabilize the whole systems.

Radicals from Hydrogen Abstraction. By abstracting an H atom from every HO group present on the eight molecules studied, two (for **6**, **9**, and **11**), three (for **1** and **10**), four (for **2**), five (for **3**), and seven (for **4**) radical species are obtained. The relative energies of all radicals are presented in Table 1, and the optimized geometries of all radicals are given in Figure SI-1 in the Supporting Information (SI). As observed, the HO-4′ radicals of pigments **1**, **6**, **9**, **10**, and **11** are the most stable, probably due to resonance effects around the radical center. For pigments **2**, **3**, and **4**, the absolute minimum of radical species is the HO-4″. Radical species **2** and **3** are particularly stabilized by the presence of the previously mentioned intramolecular H bond within the OH groups of catechol moiety, whereas the radical of compound **4** is also stabilized by the intermolecular H bond in the B ring of its catechin group.

Figure SI-1 also shows the highest values (colored in green) of atomic spin density distribution of the most stable radicals of all eight pigments. As seen, radical species of pigments **1**, **6**, **9**, **10**, and **11** have the spin density distribution more concentrated at O-4′, suggesting that the unpaired electron remains on the radical oxygen atom and that there is some involvement of the adjacent $-OCH_3$ groups and atoms of pyranoanthocyanin B ring due to the possibility of resonance effects. Similarly, the atomic spin density of pigments **2** and **3** shows that the unpaired electrons are located mostly on the O4″ atoms at E rings, as well as the unpaired electron of radical 4-O4″ is mainly placed on the O4″ atom. It was also observed that a certain delocalization around all atoms of the B ring of catechin group exists.

Radicals from Electron Abstraction. The optimized geometries of the eight radical cations are shown in Figure SI-2 in the SI. All cation radical species retain the intermolecular H bonds established in the parent stable molecule. Figure SI-2 also indicates that the atomic spin density of all cation radicals is mainly found at the pyranoanthocyanin B ring. Both cation radicals of **9** and **10** have a high atomic spin density concentrated at the oxygen atom of ring D, due to the high capacity of the carbonyl group to retain the unpaired electron.

Bond Dissociation Energy (BDE) and Ionization Potential (IP) Values. Table 2 shows the BDE and IP computed values for the eight pigments in the gas and aqueous media. The BDE gas phase values ranged between 64.6 and 73.3 kcal/mol, which slightly decrease in a water environment. Pigment **2** shows the lowest value of BDE in both vacuum and condensed phases. This pigment possesses two hydroxyl groups at rings B and E, and the high electron delocalization involving both aromatic rings causes a stabilization of radicals formed upon H abstraction, which affects and decreases the BDE value. In addition, the presence of two *O*-methyl groups around the OH group at the B ring favors the radical formation and allows low BDE values. Compared with pigments **2** and **3**, the addition of the bulky cathechin and *p*-coumaroyl groups increases the BDE value by approximately 4 and 6 kcal/mol (BDE values of 68.8 and 71.2 kcal/mol in vacuum, as well as 67.0 and 70.0 kcal/mol in water, respectively). Although pigments **6**, **9**, and **11** differ in the substituent group at C12 (COOH, CO, and CH_3 groups, respectively), their BDE values are very similar, which indicates the absence of specificity of this carbon position to BDE values. The addition of an extra *p*-coumaroyl group in pigment **10** increases the BDE value by approximately 2 kcal/mol, in relation to pigment **9**. According to the IP values computed for the eight anthocyanin/pyranoanthocyanins studied, the condensed media also decrease the energy required to extract a single electron. However, the drop in condensed IP values is more highlighted due to the occurrence of electrostatic interactions with the double-charged radicals. The lowest IP values (159 and 147 kcal/mol in the gas phase; 131 and 123 kcal/mol in water) exhibited by pigments **9** and **10**, respectively, indicate that they are better in donating a single electron to oxidant molecules in solution. These pigments are followed by pigments **2**, **4**, and **3**, in which their extra E rings/B catechin ring contribute to the lowering of

Table 2. Bond Dissociation Energies (BDE) and Ionization Potentials (IP) in the Gas Phase and Water Environment

	BDE		IP	
pigment	gas phase	water	gas phase	water
1	73.3	70.5	228	142
2	64.6	62.7	210	134
3	71.2	70.0	204	139
4	68.8	67.0	208	138
6	72.9	70.3	226	142
9	68.9	67.6	159	131
10	72.9	69.6	147	123
11	72.9	69.8	222	140

dx.doi.org/10.1021/jf404735j | J. Agric. Food Chem. 2014, 62, 7002−7009

the IP values because it allows a better distribution of the unpaired electron. The Mv-3-gluc molecule has the highest BDE and IP values in both gas and condensed phases, revealing a lesser ability of this molecule to act as a good antioxidant. Therefore, all of these results are in agreement with previous computational studies that suggested that the presence of D and E rings in pyranoanthocyanins contributes to the lowering of BDE values compared to anthocyanin molecules. In addition, an extended delocalization and conjugation of the π-electrons and the resonance phenomena greatly contributes to the mechanism of the electron transfer, decreasing the IP values.[23] Gas phase BDE values of the HO-4′ group in malvidin (96.0 kcal/mol)[49] and malvidin-3-*O*-β-glucoside (88.9 kcal/mol)[50] were computed at B3LYP/6-31G(d,p) and B3LYP/6-31G(d)//6-311G(2d,2p) levels. More recently, the gas and condensed phase BDE values of pigments **2** (78.5 and 89.9 kcal/mol), **6** (81.7 and 94.2 kcal/mol), and **9** (78.2 and 94.5 kcal/mol) were also computed at the B3LYP/6-311+G(d)//6-311++G(d,p) level.[26−29] The BDE values for these three molecules presented in this work are not exactly equal to the previous computational studies because the latter have substituted the glucose unit by a methyl group to reduce the computational effort. However, the ranking of the relative BDE and IP values of these molecules is similar, validating all of the other values.

In conclusion, the present experimental and computational data suggest that all classes of pyranoanthocyanins displayed antiradical properties, in particular the pigments **2**, **9**, **3**, **6**, and **11**. The only exceptions are the higher antiradical potential and antioxidant ability observed computationally for pigments **9**, **10**, and **11** when compared with experimental values. This unexpected result may be due to some approximations within the DFT method to describe BDE and IP values of uncharged molecules or some experimental conditions such as solubility problems associated with these specific molecules that can influence their antiradical potential. The antioxidant potential of anthocyanin derivatives, especially pigments derived from Mv-3-gluc, maintains the same level or is even increased. It was verified that the inclusion of a catechol or catechin moiety increases the antioxidant potential of the anthocyanin derivatives, which agrees with the key role of catechol proposed previously for the antioxidant capacity.[28,50]

■ ASSOCIATED CONTENT

Supporting Information

Figures SI-1 and SI-2 show the optimized geometries of radicals from H abstraction and cation radicals, respectively, of compounds **1**, **2**, **3**, **4**, **6**, **9**, **10**, and **11**; atomic spin density values of some atoms are also shown. This material is available free of charge via the Internet at http://pubs.acs.org.

■ AUTHOR INFORMATION

Corresponding Author

*(N.M.) E-mail: nbmateus@fc.up.pt. Fax: +351.220402562. Phone: +351.220402659.

Funding

We thank FCT (Fundação para a Ciência e Tecnologia) (POCI, FEDER, Programa Comunitário de Apoio) for two postdoctoral grants (SFRH/BPD/72652/2010 and SFRH/BPD/65400/2009), a Ph.D. grant (SFRH/BD/70053/2010), and a project grant (PTDC/AGR-TEC/2227/2012.

Notes

The authors declare no competing financial interest.

■ REFERENCES

(1) Rentzsch, M.; Weber, F.; Durner, D.; Fischer, U.; Winterhalter, P. Variation of pyranoanthocyanins in red wines of different varieties and vintages and the impact of pinotin A addition on their color parameters. *Eur. Food Res. Technol.* **2009**, *229*, 689−696.

(2) Brouillard, R.; Chassaing, S.; Fougerousse, A. Why are grape/fresh wine anthocyanins so simple and why is it that red wine color lasts so long? *Phytochemistry* **2003**, *64*, 1179−1186.

(3) Bakker, J.; Timberlake, C. F. Isolation, identification, and characterization of new color-stable anthocyanins occurring in some red wines. *J. Agric. Food Chem.* **1997**, *45*, 35−43.

(4) Fulcrand, H.; Benabdeljalil, C.; Rigaud, J.; Cheynier, V.; Moutounet, M. A new class of wine pigments generated by reaction between pyruvic acid and grape anthocyanins. *Phytochemistry* **1998**, *47*, 1401−1407.

(5) Mateus, N.; Pascual-Teresa, S. D.; Rivas-Gonzalo, J. C.; Santos-Buelga, C.; de Freitas, V. Structural diversity of anthocyanin-derived pigments in port wines. *Food Chem.* **2002**, *76*, 335−342.

(6) Mateus, N.; Silva, A. M. S.; Rivas-Gonzalo, J. C.; Santos-Buelga, C.; de Freitas, V. A new class of blue anthocyanin-derived pigments isolated from red wines. *J. Agric. Food Chem.* **2003**, *51*, 1919−1923.

(7) He, J.; Santos-Buelga, C.; Silva, A. M. S.; Mateus, N.; de Freitas, V. Isolation and structural characterization of new anthocyanin-derived yellow pigments in aged red wines. *J. Agric. Food Chem.* **2006**, *54*, 9598−9603.

(8) Fulcrand, H.; dos Santos, P.-J. C.; Sarni-Manchado, P.; Cheynier, V.; Favre-Bonvin, J. Structure of new anthocyanin-derived wine pigments. *J. Chem. Soc., Perkin Trans. 1* **1996**, *7*, 735−739.

(9) Hayasaka, Y.; Asenstorfer, R. E. Screening for potential pigments derived from anthocyanins in red wine using nanoelectrospray tandem mass spectrometry. *J. Agric. Food Chem.* **2002**, *50*, 756−761.

(10) Schwarz, M.; Jerz, G.; Winterhalter, P. Isolation and structure of pinotin A, a new anthocyanin derivative from Pinotage wine. *Vitis* **2003**, *42*, 105−106.

(11) Cruz, L.; Teixeira, N. R.; Silva, A. M. S.; Mateus, N.; Borges, J.; de Freitas, V. Role of vinylcatechin in the formation of pyranomalvidin-3-glucoside−(+)-catechin. *J. Agric. Food Chem.* **2008**, *56*, 10980−10987.

(12) Van Acker, S. A. B. E.; Van Den Berg, D.-j.; Tromp, M. N. J. L.; Griffioen, D. H.; Van Bennekom, W. P.; Van Der Vijgh, W. J. F.; Bast, A. Structural aspects of antioxidant activity of flavonoids. *Free Radical Biol. Med.* **1996**, *20*, 331−342.

(13) Tsuda, T.; Shiga, K.; Ohshima, K.; Kawakishi, S.; Osawa, T. Inhibition of lipid peroxidation and the active oxygen radical scavenging effect of anthocyanin pigments isolated from *Phaseolus vulgaris* L. *Biochem. Pharmacol.* **1996**, *52*, 1033−1039.

(14) Garcia-Alonso, M.; Rimbach, G.; Sasai, M.; Nakahara, M.; Matsugo, S.; Uchida, Y.; Rivas-Gonzalo, J. C.; Pascual-Teresa, S. D. Electron spin resonance spectroscopy studies on the free radical scavenging activity of wine anthocyanins and pyranoanthocyanins. *Mol. Nutr. Food Res.* **2005**, *49*, 1112−1119.

(15) Kahkonen, M. P.; Heinonen, M. Antioxidant activity of anthocyanins and their aglycons. *J. Agric. Food Chem.* **2003**, *51*, 628−633.

(16) Wang, H.; Cao, G.; Prior, R. L. Oxygen radical absorbing capacity of anthocyanins. *J. Agric. Food Chem.* **1997**, *45*, 304−309.

(17) Azevedo, J.; Fernandes, I.; Faria, A.; Oliveira, J.; Fernandes, A.; de Freitas, V.; Mateus, N. Antioxidant properties of anthocyanidins, anthocyanidin-3-glucosides and respective portisins. *Food Chem.* **2010**, *119*, 518−523.

(18) Fernandes, I.; Faria, A.; Azevedo, J.; Soares, S.; Calhau, C.; De Freitas, V.; Mateus, N. Influence of anthocyanins, derivative pigments and other catechol and pyrogallol-type phenolics on breast cancer cell proliferation. *J. Agric. Food Chem.* **2010**, *58*, 3785−3792.

(19) Faria, A.; Oliveira, J.; Neves, P.; Gameiro, P.; Santos-Buelga, C.; de Freitas, V.; Mateus, N. Antioxidant properties of prepared blueberry (*Vaccinium myrtillus*) extracts. *J. Agric. Food Chem.* **2005**, *53*, 6896−6902.

(20) Kong, J. M.; Chia, L. S.; Goh, N. K.; Chia, T. F.; Brouillard, R. Analysis and biological activities of anthocyanins. *Phytochemistry* **2003**, *64*, 923−933.
(21) Muselík, J.; García-Alonso, M.; Martín-López, M.; Žemlička, M.; Rivas-Gonzalo, J. Measurement of antioxidant activity of wine catechins, procyanidins, anthocyanins and pyranoanthocyanins. *Int. J. Mol. Sci.* **2007**, *8*, 797−809.
(22) Leopoldini, M.; Marino, T.; Russo, N.; Toscano, M. Density functional computations of the energetic and spectroscopic parameters of quercetin and its radicals in the gas phase and in solvent. *Theor. Chem. Acc.* **2004**, *111*, 210−216.
(23) Leopoldini, M.; Marino, T.; Russo, N.; Toscano, M. Antioxidant properties of phenolic compounds: H-atom versus electron transfer mechanism. *J. Phys. Chem. A* **2004**, *108*, 4916−4922.
(24) Leopoldini, M.; Pitarch, I. P.; Russo, N.; Toscano, M. Structure, conformation, and electronic properties of apigenin, luteolin, and taxifolin antioxidants. A first principle theoretical study. *J. Phys. Chem. A* **2004**, *108*, 92−96.
(25) Wright, J. S.; Johnson, E. R.; DiLabio, G. A. Predicting the activity of phenolic antioxidants: theoretical method, analysis of substituent effects, and application to major families of antioxidants. *J. Am. Chem. Soc.* **2001**, *123*, 1173−1183.
(26) Alcaro, S.; Chiodo, S. G.; Leopoldini, M.; Ortuso, F. Antioxidant efficiency of oxovitisin, a new class of red wine pyranoanthocyanins, revealed through quantum mechanical investigations. *J. Chem. Inf. Model.* **2013**, *53*, 66−75.
(27) Leopoldini, M.; Chiodo, S. G.; Russo, N.; Toscano, M. Detailed investigation of the OH radical quenching by natural antioxidant caffeic acid studied by quantum mechanical models. *J. Chem. Theory Comput.* **2011**, *7*, 4218−4233.
(28) Leopoldini, M.; Rondinelli, F.; Russo, N.; Toscano, M. Pyranoanthocyanins: a theoretical investigation on their antioxidant activity. *J. Agric. Food Chem.* **2010**, *58*, 8862−8871.
(29) Leopoldini, M.; Russo, N.; Toscano, M. The molecular basis of working mechanism of natural polyphenolic antioxidants. *Food Chem.* **2011**, *125*, 288−306.
(30) Oliveira, J.; Santos-Buelga, C.; Silva, A. M. S.; de Freitas, V.; Mateus, N. Chromatic and structural features of blue anthocyanin-derived pigments present in Port wine. *Anal. Chim. Acta* **2006**, *563*, 2−9.
(31) Mateus, N.; Silva, A. M. S.; Vercauteren, J.; de Freitas, V. Occurrence of anthocyanin-derived pigments in red wines. *J. Agric. Food Chem.* **2001**, *49*, 4836−4840.
(32) He, J. R.; Oliveira, J.; Silva, A. M. S.; Mateus, N.; De Freitas, V. Oxovitisins: a new class of neutral pyranone-anthocyanin derivatives in red wines. *J. Agric. Food Chem.* **2010**, *58*, 8814−8819.
(33) Oliveira, J.; de Freitas, V.; Mateus, N. A novel synthetic pathway to vitisin B compounds. *Tetrahedron Lett.* **2009**, *50*, 3933−3935.
(34) Oliveira, J.; Fernandes, V.; Miranda, C.; Santos-Buelga, C.; Silva, A.; de Freitas, V.; Mateus, N. Color properties of four cyanidin−pyruvic acid adducts. *J. Agric. Food Chem.* **2006**, *54*, 6894−6903.
(35) Cruz, L.; Borges, E.; Silva, A. M. S.; Mateus, N.; de Freitas, V. Synthesis of a new (+)-catechin-derived compound: 8-vinylcatechin. *Lett. Org. Chem.* **2008**, *5*, 530−536.
(36) Hakansson, A. E.; Pardon, K.; Hayasaka, Y.; de Sa, M.; Herderich, M. Structures and colour properties of new red wine pigments. *Tetrahedron Lett.* **2003**, *44*, 4887−4891.
(37) da Silva Porto, P. A.; Laranjinha, J. A.; de Freitas, V. A. Antioxidant protection of low density lipoprotein by procyanidins: structure/activity relationships. *Biochem. Pharmacol.* **2003**, *66*, 947−954.
(38) Becke, A. D. Density-functional exchange-energy approximation with correct asymptotic-behavior. *Phys. Rev. A* **1988**, *38*, 3098−3100.
(39) Becke, A. D. Density-functional thermochemistry. 4. A new dynamical correlation functional and implications for exact-exchange mixing. *J. Chem. Phys.* **1996**, *104*, 1040−1046.
(40) Lee, C. T.; Yang, W. T.; Parr, R. G. Development of the Colle-Salvetti correlation-energy formula into a functional of the electron-density. *Phys. Rev. B* **1988**, *37*, 785−789.
(41) Frisch, M. J.; Trucks, G. W.; Schlegel, H. B.; Scuseria, G. E.; Robb, M. A.; Cheeseman, J. R.; Scalmani, G.; Barone, V.; Mennucci, B.; Petersson, G. A.; Nakatsuji, H.; Caricato, M.; Li, X.; Hratchian, H. P.; Izmaylov, A. F.; Bloino, J.; Zheng, G.; Sonnenberg, J. L.; Hada, M.; Ehara, M.; Toyota, K.; Fukuda, R.; Hasegawa, J.; Ishida, M.; Nakajima, T.; Honda, Y.; Kitao, O.; Nakai, H.; Vreven, T.; Montgomery, J. A., Jr.; Peralta, J. E.; Ogliaro, F.; Bearpark, M.; Heyd, J. J.; Brothers, E.; Kudin, K. N.; Staroverov, V. N.; Kobayashi, R.; Normand, J.; Raghavachari, K.; Rendell, A.; Burant, J. C.; Iyengar, S. S.; Tomasi, J.; Cossi, M.; Rega, N.; Millam, N. J.; Klene, M.; Knox, J. E.; Cross, J. B.; Bakken, V.; Adamo, C.; Jaramillo, J.; Gomperts, R.; Stratmann, R. E.; Yazyev, O.; Austin, A. J.; Cammi, R.; Pomelli, C.; Ochterski, J. W.; Martin, R. L.; Morokuma, K.; Zakrzewski, V. G.; Voth, G. A.; Salvador, P.; Dannenberg, J. J.; Dapprich, S.; Daniels, A. D.; Farkas, Ö.; Foresman, J. B.; Ortiz, J. V.; Cioslowski, J.; Fox, D. J. *Gaussian 09*; Gaussian, Inc.: Wallingford CT, USA, 2009.
(42) Tomasi, J.; Mennucci, B.; Cammi, R. Quantum mechanical continuum solvation models. *Chem. Rev.* **2005**, *105*, 2999−3093.
(43) Bondet, V.; Brand-Williams, W.; Berset, C. Kinetics and mechanisms of antioxidant activity using the DPPH• free radical method. *Lebensm. Wiss. Technol.* **1997**, *30*, 609−615.
(44) Bors, W.; Heller, W.; Michel, C.; Saran, M. [36] Flavonoids as antioxidants: determination of radical-scavenging efficiencies. In *Methods in Enzymology*; Lester, P., Alexander, N. G., Eds.; Academic Press: New York, 1990; pp 343−355.
(45) Rice-Evans, C. A.; Miller, N. J.; Paganga, G. Structure-antioxidant activity relationships of flavonoids and phenolic acids. *Free Radical Biol. Med.* **1996**, *20*, 933−956.
(46) Goupy, P.; Bautista-Ortin, A. B.; Fulcrand, H.; Dangles, O. Antioxidant activity of wine pigments derived from anthocyanins: hydrogen transfer reactions to the DPPH radical and inhibition of the heme-induced peroxidation of linoleic acid. *J. Agric. Food Chem.* **2009**, *57*, 5762−5770.
(47) Esterbauer, H.; Gebicki, J.; Puhl, H.; Jürgens, G. The role of lipid peroxidation and antioxidants in oxidative modification of LDL. *Free Radical Biol. Med.* **1992**, *13*, 341−390.
(48) Niki, E.; Saito, T.; Kawakami, A.; Kamiya, Y. Inhibition of oxidation of methyl linoleate in solution by vitamin E and vitamin C. *J. Biol. Chem.* **1984**, *259*, 4177−4182.
(49) Estevez, L.; Mosquera, R. A. Conformational and substitution effects on the electron distribution in a series of anthocyanidins. *J. Phys. Chem. A* **2009**, *113*, 9908−9919.
(50) Borkowski, T.; Szymusiak, H.; Gliszczynska-Swiglo, A.; Rietjens, I.; Tyrakowska, B. Radical scavenging capacity of wine anthocyanins is strongly pH-dependent. *J. Agric. Food Chem.* **2005**, *53*, 5526−5534.

cell functions in an allergic immune response, leading to an alleviation of allergy symptoms.[15] Polyphenols are also known to have significant binding affinity for proteins, which can lead to the formation of soluble and insoluble (precipitated) protein−polyphenol complexes.[16] Protein−polyphenol interactions can either be through hydrogen bonding or hydrophobic interactions, or polyphenols may cross-link between proteins.[17,18] Several studies were conducted in which phenolic acids such as caffeic, chlorogenic, ferulic, gallic, and recently tannic acid were bound to peanut proteins to form insoluble complexes, which rendered the remaining soluble portion of peanut and peanut butter extracts less allergenic.[19−22] However, a practical means for efficient modification of allergenic peanut proteins with natural plant-derived polyphenols to form a hypoallergenic peanut ingredient suitable for OIT has not previously been accomplished.

Recently, we described a novel tactic for stably binding plant polyphenols to high-protein flours or protein isolates (soy, hemp, peanut, or pea) to create low-calorie, dry, health-protective matrices (granular or powdered ingredients) with improved bioavailability, efficacy, and shelf stability of the fruit-derived components.[23−27] In the present work, we describe a novel approach to bind selected polyphenols to peanut flour, the current active ingredient for OIT, with the goal of masking IgE binding epitopes and attenuating allergenicity. A series of fruit juices and plant extracts with different characteristic polyphenol profiles were stably complexed with peanut flour, and the modified peanut protein−polyphenol chimeric matrices were screened for qualitative changes in IgE binding capacity, secondary protein structure, basophil activation capability (ex vivo), and mast cell degranulation (in vivo), to gauge the potential for various polyphenol moieties to modulate allergenicity. The ultimate goal of this research is to create dry, edible peanut matrices (peanut flour stably complexed with polyphenols) with reduced allergic potential and associated side effects that retain properties integral for modulating the allergic response of patients as a highly controlled, hypoallergenic edible OIT ingredient.

MATERIALS AND METHODS

Materials and Reagents. Lipophilic Sephadex LH-20, Amberlite XAD-7, Folin−Ciocalteu reagent (FCR), 4-(dimethylamino)-cinnamaldehyde (DMAC), catechin, epicatechin, gallic acid, and pepsin from porcine gastric mucosa (3802 U mg^{-1} protein, 92% purity) were purchased from Sigma-Aldrich (St. Louis, MO, USA). Procyanidin A2 and procyanidin B1 were obtained from Chromadex (Irvine, CA, USA). Procyanidin trimer [epi-(4β → 6, 2β → O→7)-epi-(4β → 8, 2β → O→7)-cat] and tetramer [epi-(4β → 8, 2β → O→7)-epi-(4α → 6)-epi-(4β → 8, 2β → O→7)-cat] were obtained from Planta Analytica (Danbury, CT, USA). NuPAGE LDS sample buffer (4×) and Tris/glycine/SDS running buffer were purchased from Invitrogen (Carlsbad, CA, USA). Novex 16% Tricine gel, Novex Tricine SDS running buffer (10×), Novex Tricine SDS sample buffer (2×), NuPAGE reducing agent (10×), SeeBlue Plus2 prestained protein standard, MagicMark XP Western protein standard, SimplyBlue SafeStain, and bovine serum albumin (BSA) were purchased from Life Technologies (Grand Island, NY, USA). Criterion Precast Tris-HCl gel (10−20% polyacrylamide), Laemmli sample buffer, Bio-Safe Coomassie G-250 stain, and Precision Plus Protein Unstained standard were obtained from Bio-Rad (Hercules, CA, USA). Biotinylated goat IgG−anti-human-IgE was obtained from Kirkegaard & Perry Laboratory, Inc. (Gaithersburg, MD, USA). NeutrAvidin HRP (horseradish peroxidase), Super Signal West Pico Chemiluminescent Substrate, and Pierce BCA protein assay kit were purchased from Thermo Scientific (Rockford, IL, USA). Fluorescence-activated cell sorting (FACS) lysing solution was obtained from BD Biosciences (San Jose, CA, USA). Ethylenediaminetetraacetic acid (EDTA) and Roswell Park Memorial Institute medium (RPMI) were purchased from Cellgro (Manassas, VA, USA). Human rIL-3 was obtained from Miltenyi Biotec (Auburn, CA, USA). Cholera toxin was purchased from List Biologicals Laboratories, Inc. (Campbell, CA, USA).

Plant Materials. A series of fruit juice concentrates and plant extracts, representing different characteristic phytochemical profiles, was chosen to evaluate the relative efficacy of different polyphenolic groups to modulate the allergenicity of peanut flour. Elderberry (*Sambuccus nigra* L.) and aronia (*Aronia melanocarpa*) juice concentrates (65 °Brix) were provided by Artemis International (Fort Wayne, IN, USA). Muscadine grape (*Vitis rotundifolia*) juice concentrate from the Noble variety (65 °Brix) was obtained from Muscadine Products Corp. (Wray, GA, USA), and black currant (*Ribes nigrum*) juice concentrate (65 °Brix) was provided by The New Zealand Blackcurrant Co-operative Ltd. (Nelson, New Zealand). Cranberry (*Vaccinium macrocarpon* Ait.) juice concentrate (50 °Brix) was obtained from Urban Processing LLC (Wisconsin Rapids, WI, USA). Cinnamon powder (*Cinnamomum burmannii*, A grade, 3% oil) was purchased from Frontier Co-op (Norway, IA, USA), and organic green tea leaves (*Camellia sinensis*) from Sri Lanka were provided by QTrade Teas & Herbs (Cerritos, CA, USA). Light roast 12% fat peanut (PN) flour (*Arachis hypogaea* L.) was obtained from Golden Peanut Co. LLC (Alpharetta, GA, USA).

Preparation of Juices and Extracts. Dried green tea leaves were ground into a fine powder prior to extraction. Cinnamon or green tea powders were extracted with 50% ethanol (1:5; w/v). The mixtures were heated in a water bath at 60 °C for 1 h. Because the cinnamon powder extract was very viscous, it was subsequently diluted 1:1 (v/v) with 50% ethanol to obtain a final 1:10 (v/v) dilution. The solutions were centrifuged at 7000 rpm for 20 min (Sorvall RC-5B refrigerated centrifuge, DuPont Instruments, Wilmington, DE, USA) and filtered, and the ethanol was evaporated. The extracts were then reconstituted with water to original volume. Any precipitated material was separated by centrifugation, and the supernatant was filtered before treatment with PN flour. Juice concentrates required dilution prior to mixing with the PN flour because high viscosity otherwise interfered with effective mixing and separation of the flours. Aronia, Noble muscadine grape, and elderberry juice concentrates were diluted 2 times (1:1; v/v) with water. Black currant juice concentrate was diluted 4 times with water (1:3; v/v). Cranberry juice concentrate was diluted to both 2 times (1:1; v/v) and 4 times (1:3; v/v) with water. Degrees Brix was determined by measuring refractive index using an Abbemat 550 refractometer to estimate total sugar content (Anton Paar, Ashland, VA, USA).

Quantification of Polyphenols. Polyphenols were quantified in the original juices and extracts (Table 1). Total phenolics (TP) were determined using the Folin−Ciocalteu assay according to the method of Herald et al.[28] Results were expressed as milligrams per milliliter gallic acid equivalents (GAE) based on a gallic acid standard curve. Total proanthocyanidins (PAC) were determined using the 4-(dimethylamino)cinnamaldehyde (DMAC) assay with modifications.[29] Briefly, samples were diluted in 80% ethanol (v/v) when necessary. Fifty microliters of diluted or undiluted sample, blank (80% ethanol), or standard (procyanidin A2) was added to a 96-well plate. Subsequently, 150 μL of a 0.1% DMAC solution dissolved in acidified ethanol (ethanol, water, HCl; 75:12.5:12.5; v/v/v) was added to the plate and mixed using a multichannel pipet. Absorbance was measured using a Tecan Safire^2 plate reader (Tecan Group Ltd., Männedorf, Switzerland) at 640 nm for 30 min in 1 min intervals at 25 °C. Quantification of total PAC was performed from the maximum absorbance observed and expressed as micrograms per milliliter procyanidin A2 equivalents.

HPLC analysis of total monomeric anthocyanins (ANC) was performed using an Agilent Technologies 1200 series HPLC (Santa Clara, CA, USA) with a photodiode array (PDA) detector.[30] Samples were filtered through 0.2 μm cellulose syringe filters, and 5 μL was injected onto a Supelcosil-LC-18 column (250 mm × 4.6 mm × 5 μm,

Table 1. Total Phenolics (TP), Total Proanthocyanidins (PAC), and Total Monomeric Anthocyanins (ANC) Concentrations and °Brix Values in Juices and Extracts[a]

source	TP[b] (mg mL^{-1})	PAC[c] (mg mL^{-1})	ANC[d] (mg mL^{-1})	°Brix
cranberry juice 1:1 dilution	5.0 e	1.6	1.1	27.5 d
cranberry juice 1:3 dilution	2.1 de	0.7	0.5	14.1 f
cinnamon powder extract	0.9 f	0.4	NA[e]	2.5 h
green tea leaves extract	31.7 ab	59.5	NA	6.5 g
aronia juice	15.3 b	2.9	3.7	37.0 c
muscadine juice	8.8 d	0.4	3.3	39.6 a
black currant juice	12.9 c	2.0	2.5	19.9 e
elderberry juice	39.9 a	1.9	22.5	37.1 b

[a]Values within each column with different letters are significantly different at $p < 0.05$. [b]Determined by Folin−Ciocalteu assay and expressed as mg mL^{-1} gallic acid equiv. [c]Determined by DMAC assay as mg mL^{-1} procyanidin A2 equiv. [d]Determined by HPLC as mg mL^{-1} cyanidin-3-*O*-glucoside equiv. [e]NA, not applicable.

Supelco, Bellefonte, PA, USA) column, which was maintained at 30 °C. The mobile phase consisted of 5% formic acid in distilled H_2O (A) and 100% MeOH (B). Flow rate was set at 1 mL min^{-1} with a gradient as follows: 0−5 min, 10% B; 5−15 min, 15% B; 15−20 min, 20% B; 20−25 min, 25% B; 25−45 min, 30% B; 45−47 min, 60% B; 47−60 min, 10% B. Cyanidin-3-*O*-glucoside (0.25−1.0 mg mL^{-1}) was used as an external standard. ANC were detected at 520 nm and expressed as cyanidin-3-*O*-glycoside equivalents.

Preparation of Polyphenol-Fortified PN Matrices. PN flour was combined with diluted juice concentrates or extracts (30 g L^{-1}), mixed for 15 min at room temperature to allow sorption of polyphenols to PN proteins, and centrifuged for 20 min at 4000 rpm. A blank treatment (PN flour mixed with water only) was also prepared. The supernatant was decanted and filtered prior to analysis. The pellet was freeze-dried to afford the polyphenol-fortified PN matrix or blank (treated with water only) PN matrix. Polyphenols that were bound to PN matrices were extracted using the method described by Grace et al.[26] and quantified as described above in terms of milligrams of polyphenol per gram of polyphenol-fortified PN matrix.

Characterization of Polyphenol-Fortified or Blank PN Matrices and PN Flour. Moisture (percent) was determined gravimetrically by drying polyphenol-fortified PN matrices or unmodified PN flour in an oven for 6 h at 130 °C.[31] Percent fat was estimated using a Bruker minispec Plus mq$_{one}$ seed analyzer (Billerica, MA, USA). Water activity (a_w) was measured using an Aqua Lab 4TE device (DecagonDevices, Pullman, WA, USA). To determine protein solubility, 10% dispersions of polyphenol-fortified PN matrices or unmodified PN flour in phosphate-buffered saline (PBS, pH 7.5) were prepared. Total nitrogen content of the soluble fractions was determined using a 2400 CHN Elemental Analyzer (PerkinElmer, Norwalk, CT, USA).

PN Protein Distribution and PN-Specific IgE Binding. SDS-PAGE was used to observe protein distribution in polyphenol-fortified PN matrices and unmodified PN flour. PBS soluble fractions (from 10% dispersions; w/v) were added 1:1 to Laemmli buffer containing 5% mercaptoethanol. Samples were also solubilized in NuPAGE LDS sample buffer (10%; w/v) and centrifuged. Resulting LDS soluble fractions were added 1:1 to Laemmli buffer containing 5% mercaptoethanol. All samples were heated for 5 min at 95 °C. For PBS soluble fractions, equivalent protein (5.4 μg) was loaded per lane, whereas for LDS soluble fractions, equivalent volume (10 μL) was loaded per lane. Loaded samples were subjected to SDS-PAGE (55 min, 200 V) and stained with Bio-Safe Coomassie G-250 stain.

For the detection of PN-specific IgE binding by PN proteins, Western blotting was performed with pooled plasma from two PN-allergic individuals obtained from PlasmaLab (Everett, WA, USA). Both individuals had PN-specific IgE > 100 kU/L as determined via ImmunoCAP (Phadia, Uppsula, Sweden). SDS-PAGE resolved proteins were transferred to a polyvinylidene fluoride (PVDF) membrane (iBlot, Invitrogen, Carlsbad, CA, USA). The membrane was allowed to dry (30 min), rehydrated in MeOH (10−15 s), and washed with PBS containing 0.5% Tween20 (PBST, 1×) for 5 min. The membrane was then blocked in PBST containing 2% BSA for 1−2 h at room temperature. The membrane was incubated overnight with a 1:40 dilution (v/v) of pooled human plasma in PBST containing 2% BSA (primary antibody), then washed in PBST four times for 5−10 min, and subsequently incubated with biotinylated goat IgG−anti-human IgE (secondary antibody, 1:4000; v/v in PBST with 2% BSA) for 1 h. The membrane was again washed four times for 5−10 min and incubated with NeutrAvidin−horseradish peroxidase (HRP) conjugate (NA-HRP, 1:10000; v/v in PBST with 2% BSA) for 30 min. Finally, the membrane was washed for 5−10 min, incubated with Super Signal West Pico Chemiluminescent Substrate for 8 min, and developed on a ChemiDoc MP system (Bio-Rad).

Attenuated Total Reflectance−Fourier Transform Infrared Spectroscopy (ATR-FTIR). ATR-FTIR spectra of polyphenol-fortified PN matrices and unmodified PN flour were recorded using an IRPrestige-21 FTIR spectrometer (Shimadzu, Norcross, GA, USA) equipped with a MIRacle ATR accessory (Pike Technologies, Madison, WI, USA). Samples were pressed onto the surface of a ZnSe crystal using a micrometer pressure clamp. Spectra were collected in triplicate between the wavenumbers 600 and 4000 cm^{-1} and displayed between 1475 and 1800 cm^{-1}.

PN-Specific IgE Binding Capacity of PAC or ANC-Fortified PN Matrices. An Amberlite XAD-7 resin and acidified water (0.3% TFA; v/v) were used to remove free sugars, pectins, and organic acids from the cranberry juice concentrate to ultimately obtain a polyphenol-rich fraction. The fraction was freeze-dried, and the sugar-free polyphenol-rich extract was applied to a Sephadex LH-20 column (20 × 2 cm) and eluted with acidified (0.3% TFA) 80% MeOH (v/v) to collect the ANC-rich fraction. The column was then washed with 70% acetone (v/v) to elute the PAC-rich fraction. Organic solvents were evaporated and aqueous fractions were freeze-dried. The ANC or PAC fractions were dissolved in water and used to prepare ANC- or PAC-fortified PN matrices. IgE binding capacity of water-soluble or insoluble fractions of fortified PN matrices was evaluated by Western blotting as described above.

Specific Binding Capacity of Cranberry PAC to PN Flour. To investigate the specific binding capacity of individual PAC, HPLC analysis of cranberry juice before and after treatments with PN flour was performed. Prior to analysis, a cleanup step using Sephadex LH-20 was conducted to eliminate interfering compounds according to the method of Gu et al.[32] The PAC fraction was collected, and solvent was evaporated using a rotary evaporator system (Büchi, Flawil, Switzerland) and a SpeedVac concentrator (Thermo Fisher Scientific, Waltham, MA, USA). The dried residue was then resuspended in 2 mL of acetone/water/acetic acid (AWA, 70:29.5:0.5; v/v/v) and subsequently filtered through a 0.2 μm cellulose filter prior to HPLC analysis.

PAC were analyzed with a Dionex Summit HPLC system (Sunnyvale, CA, USA) consisting of a model P680 quaternary pump, an ASI-100 autosampler, a TCC-100 column oven, and an RF2000 fluorescence detector according to the method of Hammerstone et al.[33] with modifications described by Constanza et al.[34] Compounds were separated on a 5 μm, 250 × 4.6 mm, Luna silica column (Phenomenex, Torrence, CA, USA). The binary gradient consisted of dichloromethane, MeOH, water, and acetic acid (A, 82:14:2:2; v/v/v/v) and MeOH, water, and acetic acid (B, 96:2:2; v/v/v). The flow rate was set at 1 mL min^{-1} with a gradient as follows: 0−20 min, 0−11.7% B; 20−50 min, 11.7−25.6% B; 50−55 min, 25.6−87.7% B; 55−65 min, 87.7% B, isocratic; 65−70 min, 87.7−0% B. The peaks were monitored by fluorescence detection with excitation at 276 nm and emission at 316 nm. Quantification of compounds was performed by means of external calibration curves using monomer

(DP1) through tetramer (DP4) commercial standards. PAC with DP ≥5 including polymers were expressed as DP4 equivalents.

Basophil Degranulation Assay. Because the PN protein polyphenol-fortified matrices were largely insoluble, an existing basophil activation assay was modified to evaluate solid-phase PN flours.[35] For this assay, 1 mg of cranberry polyphenol-fortified PN matrix (prepared with 1:1 and 1:3 dilutions of cranberry juice concentrate) or unmodified PN flour was added to 200 μL of basophil media (RPMI-10 plus 2 ng mL^{-1} human rIL-3) and subsequently added to 200 μL of whole blood from PN-allergic children (PN-allergic subjects were enrolled in an IRB-approved protocol at UNC-Chapel Hill). Antigen and whole blood were mixed by pipetting up and down several times, and then samples were placed in a 37 °C humidified CO_2 incubator for 30 min. Reactions were stopped by addition of 50 μL of PBS plus 2 mM EDTA. Cells were stained for expression of CD123, CD203c, and CD63 at 4 °C in the dark for 30 min and then washed with staining buffer (PBS plus 0.5% BSA plus 2 mM EDTA). Red blood cells were lysed and white blood cells fixed with 4 mL of FACS lysing solution for 15 min at room temperature. Samples were centrifuged and pellets resuspended in staining buffer for flow cytometry. Samples were analyzed on a Canto II flow cytometer (BD, San Jose, CA, USA) with data processing on FlowJo software (TreeStar, Ashland, OR, USA). Basophils were identified as $CD123^+$ $CD203c^+$ lymphocytes, and degranulation was monitored by CD63 expression. Results are expressed as the percentage of basophils that were $CD63^+$.

Simulated Gastric Digestion Assay and IgE Binding Capacity of Digestive Products. To investigate the stability of PN proteins within unmodified PN flour or cranberry polyphenol-fortified PN matrix to pepsin digestion, a simulated gastric digestion assay was used. Simulated gastric fluid (SGF) was prepared as reported in the United States Pharmacopeia with minor changes.[36] A 0.2% solution of NaCl in water (w/v) was prepared and adjusted to a pH of 2.0 using 6 N or 1 N HCl. A 10 mL dispersion of either unmodified PN flour or cranberry polyphenol-fortified PN matrix was prepared in SGF (1.1%; w/v) and stirred on a stir plate for 5 min, the pH was subsequently adjusted with a few microliters of 1 N HCl (because adding PN flour or cranberry polyphenol-fortified PN matrix to SGF results in a slight pH increase), and the dispersions were completed to equal volume in two separate 15 mL centrifuge tubes using SGF. A 1 mL aliquot from each of the well-mixed dispersions was taken and added to two separate 2 mL centrifuge tubes (controls, no pepsin added). Dispersions, in tubes, were subsequently placed into a 37 °C water bath and prewarmed for 15 min while a 0.2 mg mL^{-1} pepsin solution in SGF (w/v) was prepared and also prewarmed (for only 5−10 min to prevent a possible loss of enzyme activity due to autodigestion). One milliliter of pepsin solution was subsequently added to each tube containing the dispersions (resulting in a total volume of 10 mL and a 1% dispersion per tube). One milliliter digestive aliquots were taken after 0.5, 2, 8, and 30 min, added to separate 2 mL centrifuge tubes, and immediately subjected to a 90 °C water bath for 15 min to inactivate pepsin. Each control (a 1 mL aliquot of each dispersion without pepsin) underwent the same heat treatment. Throughout the digestion period samples were inverted several times to secure proper mixing of dispersion and enzyme. Pepsin-inactivated digestive samples and control samples were subsequently centrifuged, and resulting supernatants were used for further analysis. SDS-PAGE and Western blotting were used to evaluate digestive samples and their respective controls for protein distribution and IgE binding capacity. For SDS-PAGE 40 μL of undiluted sample was added to 50 μL of Novex Tricine SDS sample buffer (2×) and 10 μL of NuPAGE reducing agent (10×), resulting in a final volume of 100 μL (according to the manufacturer's instructions). Samples were heated for 2 min at 85 °C. Ten microliters of each sample was loaded onto the gel, subsequently subjected to SDS-PAGE (90 min, 125 V), and stained with SimplyBlue SafeStain. Western blotting was performed as stated earlier in this paper.

Oral Challenges in PN Allergic Mice. Three-week-old C3H/HeJ female mice were purchased from Jackson Laboratories (Bar Harbor, ME, USA). Mice were allowed to acclimate to their new environment for 2 weeks before being used in protocols. Mice were housed under pathogen-free conditions with free access to water and food while being kept on a PN-free diet the entire study. All studies were approved by the IACUC at UNC Chapel Hill. To sensitize mice to PN, a PN extract from unmodified PN flour was prepared using PBS with NaCl. Briefly, unmodified PN flour was mixed with PBS (1:4; w/v) and stirred for 1 h while a constant pH of ∼8.5 was maintained using 12 M NaOH. The mixture was subsequently centrifuged at 30000*g* at 4 °C for 30 min and the resulting supernatant (PN extract) filtered using 0.8 and 0.2 μm membranes. The protein concentration in the PN extract was determined (Pierce BCA protein assay) and diluted to 10 mg mL^{-1} in PBS (v/v). The protein solution was stored frozen until needed. Mice were sensitized to PN proteins by oral gavage using PN extract plus cholera toxin as an adjuvant.[37] On days 1, 8, and 15 mice received 2 mg of PN proteins plus 10 μg of cholera toxin and on day 22 received 5 mg of PN proteins plus 10 μg of cholera toxin. Mice were challenged on day 36 with either unmodified PN flour (50 mg) or polyphenol-fortified PN matrix made with 1:1 dilution of cranberry juice (50 mg) suspended in PBS. Mice were bled 45 min after challenge by submandibular bleeding using a 4 mm lancet, and serum was subsequently assayed for mouse mast cell protease-1 (MMCP-1) as a marker of intestinal mucosal mast cell degranulation. MMCP-1 was quantified by ELISA according to the manufacturer's instructions (eBiosciences, San Diego, CA, USA). UNC IACUC approval number was 12-176.

Statistical Analysis. All flours and polyphenol-fortified PN matrices were prepared in triplicate, and analysis of variance was performed using JMP 10.0 (SAS, Cary, NC, USA). When significant ($p < 0.05$), means were separated using Student's t test. Basophil data were analyzed on GraphPad version 5 (La Jolla, CA, USA), and the data were compared by the Wilcoxon test, and the MMCP-1 data were compared by the Mann−Whitney test (one-tailed).

RESULTS AND DISCUSSION

Characterization of Polyphenol Sources. Although the polyphenolic sources chosen for this study have some overlapping chemical characteristics, we divided them into three main groups. Cranberry and cinnamon contain high levels of A-type PAC.[38,39] B-type PAC, on the other hand, can be found in aronia and green tea with the latter being also a rich source of PAC monomers such as catechin, epicatechin, or epigallocatechin gallate.[40,41] Noble muscadine grape, black currant, and elderberry feature high ANC concentrations and different characteristic ANC profiles.[42−44] Concentrations of total phenolics (TP), total proanthocyanidins (PAC), total monomeric anthocyanins (ANC), and °Brix values of the diluted juices and extracts before complexing with PN flour are provided in Table 1. TP concentration ranged from 0.9 mg mL^{-1} (cinnamon powder extract) to 39.9 mg mL^{-1} (elderberry juice). Green tea leaves extract showed the highest concentration of PAC (59.5 mg mL^{-1}), whereas the PAC content of cinnamon powder extract and muscadine juice was low (0.4 mg mL^{-1} for each). It should be noted that the DMAC assay has limitations when estimating total PAC levels, as the DMAC reagent reacts only with the terminal monomer of the PAC molecule, regardless of the size of the oligomer or polymer.[45] Therefore, plant sources rich in oligomeric/polymeric proanthocyanidins, such as cinnamon and aronia,[46] are usually underestimated when assayed with the DMAC reagent compared to those rich in monomeric proanthocyanidins such as green tea. The highest amount of ANC was observed in elderberry juice (22.5 mg mL^{-1}). Degrees Brix ranged from 2.5 (cinnamon powder extract) to 39.6 (Noble muscadine grape juice).

Characterization of Polyphenol-Fortified Matrices. Moisture (%), fat (%), water activity (a_w), and soluble nitrogen

(SN) are shown in Table 2. Degrees Brix (soluble sugar) values of juices and extracts were positively correlated with the

Table 2. Moisture, Fat, Water Activity (a_w), and Soluble Nitrogen (SN) of Unmodified Commercial Light Roast 12% Fat Peanut (PN) Flour and Polyphenol-Fortified PN Matrices[a]

source	moisture (%)	fat (%)	a_w	SN[b] (g L^{-1})
PN flour	2.0 i	11.7 b	0.3	0.59 a
blank[c]	3.4 h	13.9 a	0.3	0.16 d
cranberry juice 1:1 dilution	16.9 b	6.9 g	0.2	0.05 f
cranberry juice 1:3 dilution	10.4 e	10.9 d	0.1	0.06 f
cinnamon powder extract	5.0 g	11.2 c	0.3	0.11 e
green tea leaves extract	6.5 f	8.4 f	0.4	0.20 d
aronia juice	15.9 b	6.0 i	0.3	0.10 ef
muscadine juice	21.1 a	6.4 h	0.3	0.17 d
black currant juice	11.7 d	8.8 e	0.1	0.26 c
elderberry juice	13.2 c	5.9 i	0.2	0.45 b

[a]Values within each column with different letters are significantly different at $p < 0.05$. [b]SN concentrations were determined by preparing 10% (w/v) phosphate-buffered saline (PBS) solutions. [c]PN flour modified with water only.

moisture content of the prepared PN matrices ($r^2 = 0.82$). This is attributed to the hygroscopicity of residual sugar in the matrices prepared with juices with high sugar content. Additionally, fat content, which ranged from 5.9% (elderberry juice polyphenol-fortified PN matrix) to 13.9% (blank, flour modified with water only), was negatively correlated with moisture content ($r^2 = 0.71$). The a_w of all polyphenol-fortified PN matrices was ≤0.4, which is well below the limit for microbial growth. SN concentrations ranged from 0.1 g L^{-1} (both 1:1 and 1:3 dilutions of cranberry polyphenol-fortified PN matrices, cinnamon polyphenol-fortified PN matrix, and aronia polyphenol-fortified PN matrix) to 0.6 g L^{-1} (unmodified PN flour) (Table 2). Protein solubility decreased in all polyphenol-fortified PN matrices compared with unmodified flour, suggesting that polyphenols bound to PN proteins, rendering them less soluble. Whereas polyphenols in general have exhibited significant binding affinity for proteins, which can lead to the formation of soluble and insoluble protein−polyphenol complexes,[16] in particular, PAC are known to have a strong affinity for proteins, which likely explains the low SN of cranberry-, cinnamon-, and aronia-modified matrices.[47]

The concentrations of TP, total PAC, and total monomeric ANC bound to PN flours after complexation with the various diluted juices and extracts are shown in Table 3. The highest amount of total PAC was captured from green tea leaves extract (429.7 mg g^{-1}), whereas the lowest concentration of total PAC was observed in aronia polyphenol-fortified PN matrix (0.7 mg g^{-1}). As noted previously, the DMAC assay tends to underestimate total PAC for plants such as aronia, which feature oligomeric and polymeric PAC. Elderberry, which has inherently high ANC content (Table 1), resulted in the highest concentration of total ANC when complexed in the PN protein−polyphenol matrix (44.9 mg g^{-1}).

PN Protein Distribution and PN-Specific IgE Binding. To understand the potential for IgE binding modification, polyphenol-fortified PN matrices were screened using SDS-PAGE and subsequent Western blots using PN-specific IgE.

Table 3. Total Phenolics (TP), Total Proanthocyanidins (PAC), and Total Monomeric Anthocyanins (ANC) Concentrations Sorbed onto Commercial Light Roast 12% Fat Peanut (PN) Flour after Complexation with Different Juices and Extracts[a]

source	TP[b] (mg g^{-1})	PAC[c] (mg g^{-1})	ANC[d] (mg g^{-1})
cranberry juice 1:1 dilution	14.5	10.4 c	3.4 e
cranberry juice 1:3 dilution	14.6	7.4 cd	2.8 f
cinnamon powder extract	5.6	3.5 cd	NA
green tea leaves extract	18.3	429.7 a	NA
aronia juice	23.6	0.7 d	14.1 c
muscadine juice	19.8	1.8 d	6.0 d
black currant juice	24.0	55.3 b	21.9 b
elderberry juice	21.9	4.0 cd	44.9 a

[a]Values within each column with different letters are significantly different at $p < 0.05$. [b]Determined by Folin−Ciocalteu assay as mg g^{-1} gallic acid equiv. [c]Determined by DMAC assay as mg g^{-1} procyanidin A2 equiv. [d]Determined by HPLC as mg g^{-1} cyanidin-3-*O*-glucoside equiv.

For this approach, samples must first be solubilized, and two buffers were chosen for this purpose. LDS sample buffer, which is an anionic detergent that can disrupt hydrophobic and electrostatic interactions among macromolecular complexes, led to greater solubilization of PN proteins and resolution by SDS-PAGE than PBS, which is an isotonic buffer solution (Figure 1A,C). The major PN seed storage proteins and allergens, Ara h 1, Ara h 2, Ara h 3, and Ara h 6, were observed in the SDS-PAGE from LDS samples; however, Ara h 1 was not detected in the SDS-PAGE from PBS samples at these concentrations. Of the major seed storage proteins, Ara h 1 solubility is most affected by thermal processing (roasting), whereas Ara h 2 solubility is less affected.[48,49]

Although equal amounts of protein were loaded (5.4 μg), for several samples solubilized in PBS, no protein was resolved by SDS-PAGE, and this corresponded to reduced IgE binding on the Western blot (Figure 1A,B). This may be due to bound polyphenols interfering with protein staining and IgE binding or protein−polyphenol complexes, if present, being too large to be resolved on the gel. All major PN allergens from polyphenol-fortified PN matrices were more soluble in LDS than compared with PBS (Figure 1C). Whereas IgE binding was generally enhanced by solubilizing in LDS compared to PBS, IgE binding to several PN proteins in select LDS-solubilized samples, notably cranberry (1:1 dilution) and green tea, was reduced (Figure 1D). Whereas several LDS-solubilized samples showed reduced IgE binding in the middle and lower part of the membrane (medium to small molecular weight region), some, such as cranberry, green tea, or aronia, showed increased IgE binding in the upper part of the membrane (high molecular weight region). Changes in IgE binding behavior and pattern compared to untreated PN flour could be attributed to polyphenol interference with PN-specific IgE binding. In terms of hypoallergenicity, reduction of allergic potential of Ara h 1, Ara h 2, and Ara h 6 in particular is highly sought. Initially it was thought that Ara h 1 was the major PN allergen of concern;[50] however, studies have shown that Ara h 2 and Ara h 6 have a far more pronounced ability to release histamine from human basophils containing PN-specific IgE and have a higher reactivity in skin tests in PN-sensitive individuals compared to Ara h 1.[51−55] Thus, preventing IgE binding to

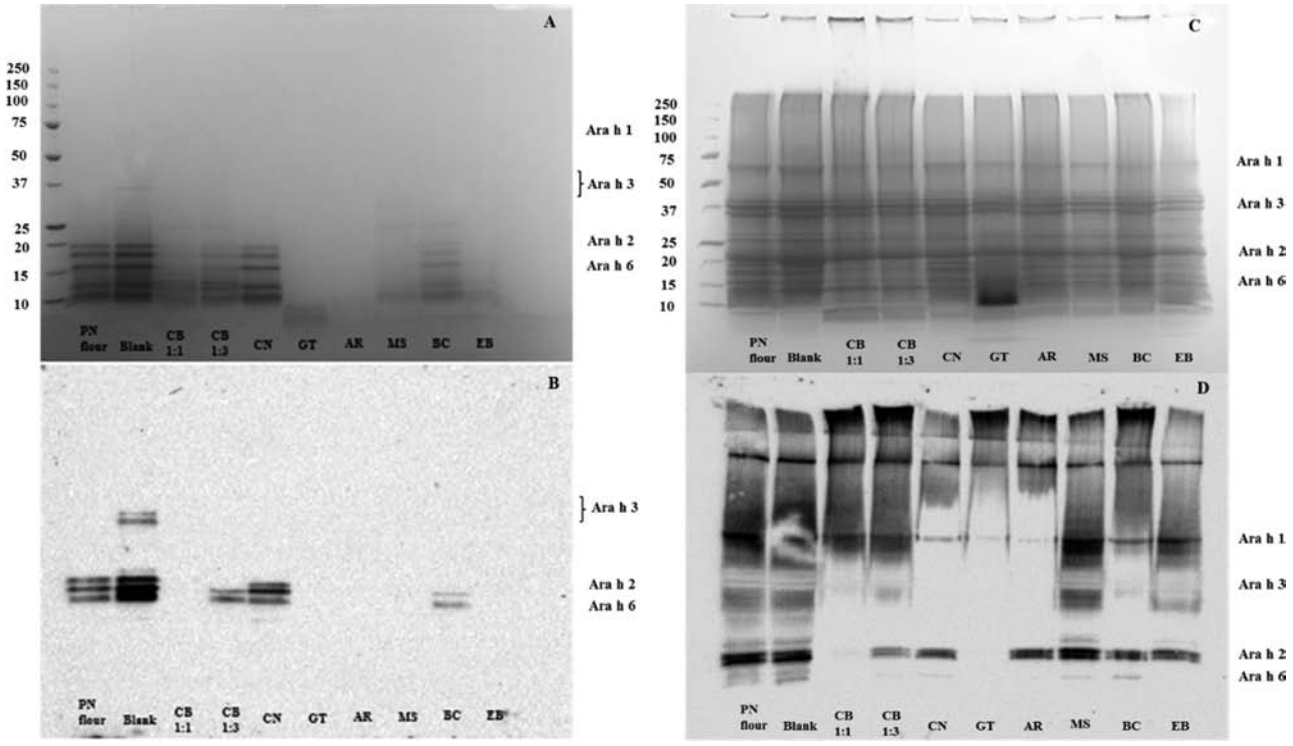

Figure 1. SDS-PAGE (A, C) and corresponding Western blot (B, D) of unmodified light roast 12% fat peanut (PN) flour and polyphenol-fortified peanut matrices (blank, peanut flour modified with water only; CB, cranberry juice (1:1 and 1:3 dilutions); CN, cinnamon powder extract; GT, green tea leaves extract; AR, aronia juice; MS, Noble muscadine grape juice; BC, black currant juice; EB, elderberry juice) solubilized in either PBS (A, B) or LDS (C, D), respectively. An equal amount of protein was loaded (5.4 μg) for PBS samples and an equal volume (10 μL) was loaded for LDS samples. Approximate locations for peanut allergens are shown. Gray scale was used for SDS-PAGE and contrast was optimized for both SDS-PAGE and Western blot.

Ara h 2 and Ara h 6, as observed in cranberry and green tea samples, may significantly reduce allergenicity.

In general, reduced IgE binding to one or more PN proteins in LDS extracts was observed particularly in the PAC-rich samples (cranberry, cinnamon, green tea, and aronia) and also in the ANC-rich black currant sample. In a separate experiment, PN flours were treated with fractions enriched in ANC and PAC (originally isolated and purified from cranberry juice concentrate) and tested for their polyphenol-class specific contributions to PN-specific IgE binding. Western blotting demonstrated that the PAC-rich fraction was more effective in reducing IgE binding than the ANC-rich fraction in both the soluble and insoluble fractions, but both reduced IgE binding compared to the blank, water-treated PN flour (Figure 2). This supports what we observed in the polyphenol-fortified PN matrices and is likely attributable to the natural affinity of PAC to proteins.[47] Additional experiments are needed to understand the mechanism of reduced IgE binding observed here; however, data suggest that some polyphenol-fortified PN matrices, particularly those prepared with cranberry juice and green tea extract, may potentially be hypoallergenic. Whereas proteins are denatured and bound to a PVDF membrane in this approach (i.e., conformational epitopes are disrupted), SDS-PAGE and Western blots were shown to be a reproducible screen for IgE binding modifications.

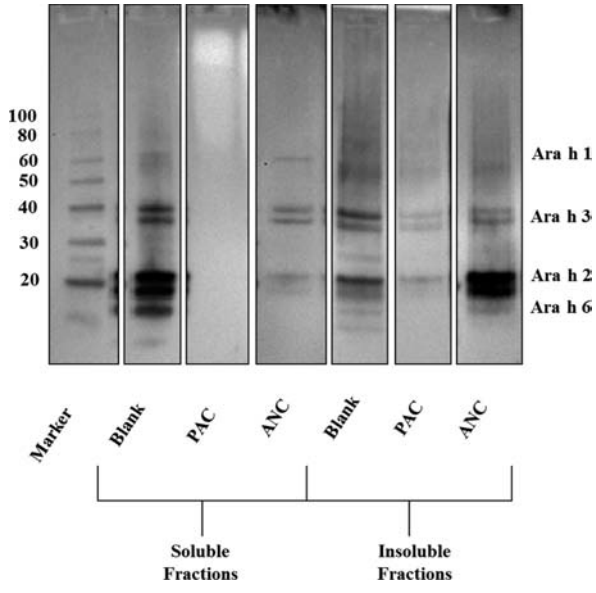

Figure 2. Western blots demonstrating peanut-specific IgE binding in protein extracted from peanut flour modified with water (blank), cranberry proanthocyanidin-fortified (PAC) peanut matrix, or cranberry anthocyanin-fortified (ANC) peanut matrix. Western blot individual lanes were combined from two separately conducted blots under the same conditions. Approximate locations for peanut allergens are shown.

ATR-FTIR Spectra. ATR-FTIR spectra of the polyphenol-fortified PN matrices were recorded to evaluate modification to protein secondary structure. This technique allows for evaluation of the modified flours in their natural insoluble powdered state. The most prominent bands were the amide I (1600−1700 cm^{-1}) and amide II (1480−1575 cm^{-1}) bands, which result from vibrations of the protein backbones (Figure

dx.doi.org/10.1021/jf405773b | J. Agric. Food Chem. 2014, 62, 7010−7021

3). Because a mixture of crude proteins was examined as opposed to a single purified PN protein, only qualitative

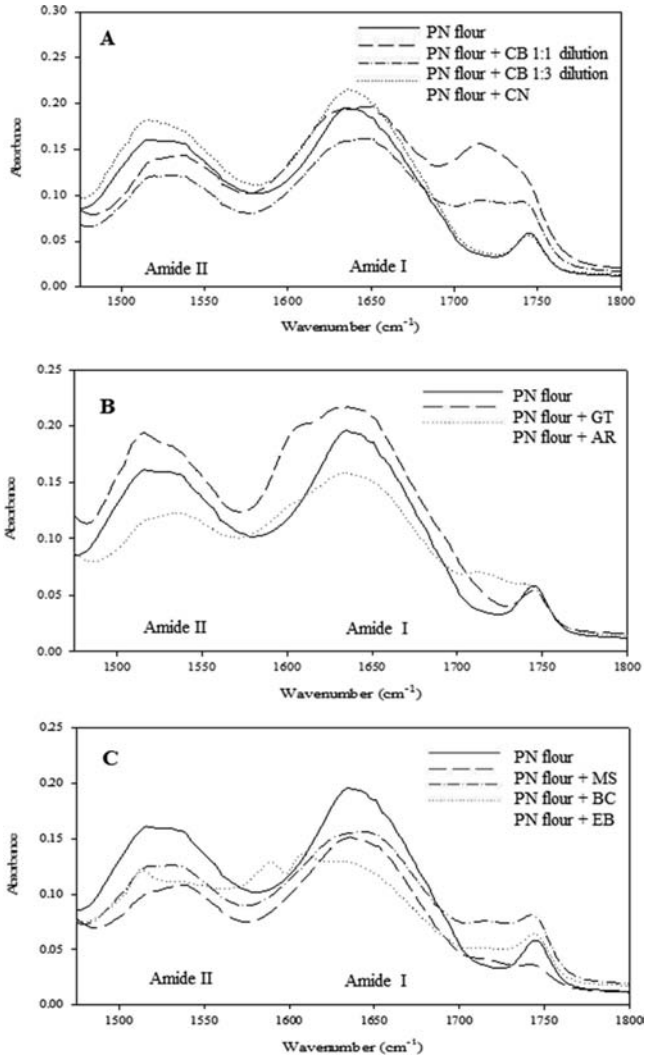

Figure 3. ATR-FTIR spectra (amide I and II bands) of unmodified light roast 12% fat peanut (PN) flour and peanut matrix modified with (A) proanthocyanidin A-type, (B) proanthocyanidin B-type, and (C) predominately anthocyanin-rich juices and extracts. CB, cranberry juice (1:1 and 1:3 dilutions); CN, cinnamon powder extract; GT, green tea leaves extract; AR, aronia juice, MS, Noble muscadine grape juice; BC, black currant juice; EB, elderberry juice.

indications of conformational changes in PN proteins were gained. Amide I and amide II bands were altered to some extent in all polyphenol-fortified PN matrices compared to unmodified PN flour. Generally, polyphenol-fortified PN matrices that displayed significantly altered IgE binding, including cranberry, aronia, elderberry, and green tea, also displayed altered FTIR profiles in the form of increased or decreased band intensities, band shifting or width changes, and/or appearance of additional peaks compared to the unmodified PN flour. Band shifting can indicate that hydrogen bonds were affected.[56] Because some of the polyphenol-fortified peanut matrices had a relatively high moisture content (up to 21.1% for muscadine modified matrix), it should be taken into account that water absorbs within the amide I region (1645 cm^{-1}, H−O−H bending vibration) and could, besides protein-bound polyphenols, contribute to observed spectrum changes.[57] Width changes are linked to the conformational freedom of a structure. Molecules that bind to proteins can lead to conformational restriction, thus reducing bandwidth.[56] These findings suggest that the decreased IgE binding observed in polyphenol-fortified PN matrices may be partly due to changes in protein secondary structure. However, because modified matrices were screened on a qualitative level, a water reference spectrum as well as further IR spectral data analysis methods would be needed to evaluate water interference and to break down and analyze overlapping bands in amide regions in a more qualitative and quantitative manner, respectively.

Characterization of Cranberry PAC Bound to PN Matrices. On the basis of decreased IgE binding specifically to Ara h 2 and Ara h 6 (Figure 1) and significantly altered FTIR spectra (Figure 3), the cranberry polyphenol-fortified PN matrix (rich in A-type PAC) was selected for further experiments. PAC isolated from cranberry juice (1:1 dilution) and from supernatants (spent juice) obtained after complexation with PN flour were analyzed to evaluate the capacity of individual PAC to bind to PN flour. HPLC chromatograms of PAC in the cranberry juice before (A) and after (B) treatment with PN flour are shown in Figure 4. PAC that were more highly polymerized showed a higher level of binding to PN flour (Figure 4B). Table 4 shows the amount of individual PAC bound to PN flour (mg g^{-1}). Polymerized PAC have a stronger binding capacity to proteins than PAC monomers or oligomers. Because noncovalent interactions between proteins and monomeric phenolic compounds such as catechins require relatively high molecular ratios of phenolic compounds to proteins (>100) to affect the functional properties of proteins, it is more likely that PAC and particularly polymerized PAC interacted with PN proteins.[47,58,59] Further experiments must investigate the binding nature of polyphenols to PN proteins.

Basophil Degranulation Assay. A modified basophil assay provided an ex vivo assessment of the ability of antigens to trigger degranulation of human basophils found in peripheral blood and allowed for testing the nonsoluble matrices in a whole blood basophil assay. The basophil activation test augments the IgE binding and FTIR data described above, as it allows for a functional assessment of the polyphenol-fortified PN matrices' capacity to cross-link IgE on basophils, leading to degranulation. PN protein−polyphenol matrices created with cranberry juice triggered significantly less basophil degranulation (median = 37.2% and range = 5.2−70.5% for the 1:1 dilution; median = 45.5% and range = 8.0−78.4% for the 1:3 dilution) than the unmodified PN flour (median = 66.1%, range = 15.5−94.0%) in the seven PN-allergic subjects studied with the basophil assay (Figure 5). Statistically significant reduction in activation level was found by comparing the cranberry polyphenol-fortified PN matrices to the unmodified PN flour (p = 0.015). Although basophil activation was not completely abrogated by cranberry modification of PN flour, the significant decrease in IgE cross-linking suggested enhanced hypoallergenicity.

The basophil assay results indicate that PN proteins complexed with cranberry phytochemicals have a decreased capacity to cross-link IgE, although there are important limitations to this finding. For example, the assay is conducted using edible PN matrices that are not exposed to acidic pH or digestive enzymes, which would be encountered following oral ingestion. Exposure to a low pH, such as that found in the stomach, as well as exposure to various digestive enzymes such as pepsin (stomach) may disrupt the PN protein−polyphenol

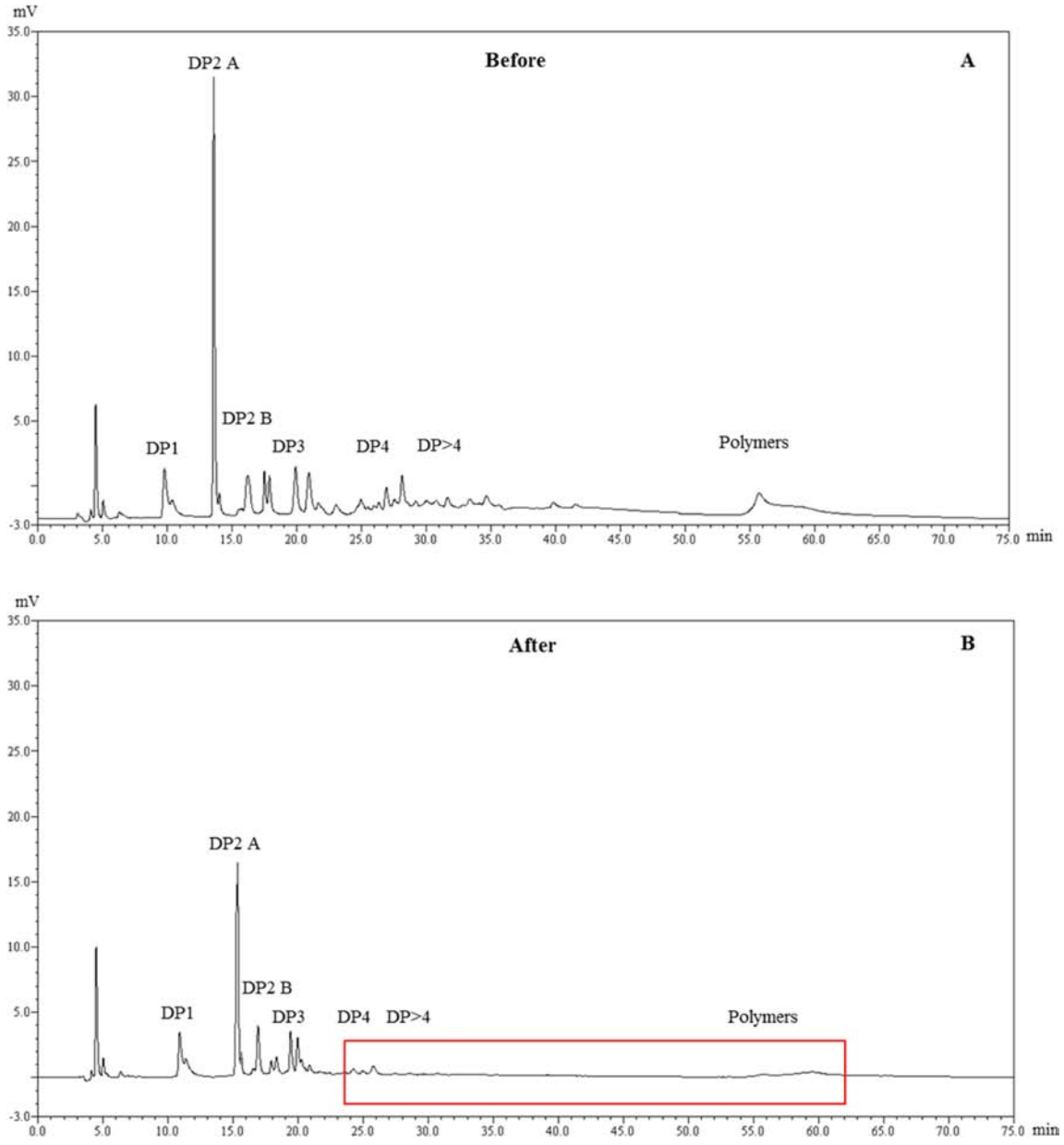

Figure 4. HPLC chromatogram of proanthocyanidin monomers and oligomers in cranberry (A) untreated 1:1 diluted juice (before) and (B) after complexation with commercial light roast 12% fat peanut (PN) flour (supernatant) with fluorescence excitation and emission wavelengths 276 and 316 nm. Box highlights proanthocyanidins that are highly complexed to peanut flour. DP, degree of polymerization; DP1, monomers; DP2 A, dimer type A; DP2 B, dimer type B; DP3, trimers; DP4, tetramers; DP>4, oligomers.

interactions and lead to the release of allergens that can cause reactions.

Simulated Gastric Digestion Assay. An in vitro digestion method was used to mimic the gastric digestion of unmodified PN flour or cranberry polyphenol-fortified PN matrix by pepsin in an acidic environment at a physiological temperature. This assay was used to evaluate and mimic protein stability and digestibility under harsh conditions such as those present in the stomach. Pepsin was obtained with the highest specific enzyme activity commercially available (3802 U mg^{-1} protein), whereas enzyme concentration (0.2 mg mL^{-1}) was optimized for a more gradual digestion of proteins. The digestibility of proteins can be evaluated by keeping track of the disappearance of intact protein bands on SDS-PAGE. PN proteins in unmodified PN flour as well as in cranberry polyphenol-fortified PN matrix were rapidly digested into smaller molecular weight digestive fragments (Figure 6A). In particular, Ara h 1 and Ara h 3 (acidic subunits) as indicated in the figure were significantly digested by pepsin in both unmodified PN flour and cranberry polyphenol-fortified PN matrix after 0.5 min. However, as expected, Ara h 2 and Ara h 6 in both unmodified PN flour and cranberry polyphenol-fortified PN matrix were highly resistant to enzymatic proteolysis. In addition, digestive fragments at ~10 and ~4 kDa were observed that likely correspond to pepsin-resistant fragments of Ara h 2 and Ara h 6 as previously observed in studies working with purified individual peanut allergens.[60,61] In fact, similar findings for Ara h 2 and Ara h 6 are not surprising, because both, although independent allergens, belong to the 2S albumin family and are 59% homologous with respect to their amino acid sequence.[62] Even

dx.doi.org/10.1021/jf405773b | J. Agric. Food Chem. 2014, 62, 7010−7021

Table 4. Amount of Individual Proanthocyanidins Sorbed onto Commercial Light Roast 12% Fat Peanut Flour after Complexation with Cranberry Juice (1:1 Dilution)

proanthocyanidin[a]	concentration[b] (mg g^{-1})	%[c]
DP1	0.2	11.7
DP2 A	5.2	40.6
DP2 B	1.4	29.7
DP3	6.8	52.4
DP4	5.3	63.0
DP>4	8.0	80.1
polymers	5.2	79.1

[a]DP, degree of polymerization; DP1, monomers; DP2 A, dimer type A; DP2 B, dimer type B; DP3, trimers; DP4, tetramers; DP>4, oligomers. [b]Estimated by external standard curves as mg proanthocyanidin sorbed to 1 g of matrix. [c]Calculated as percent proanthocyanidin of untreated juice complexed with peanut flour.

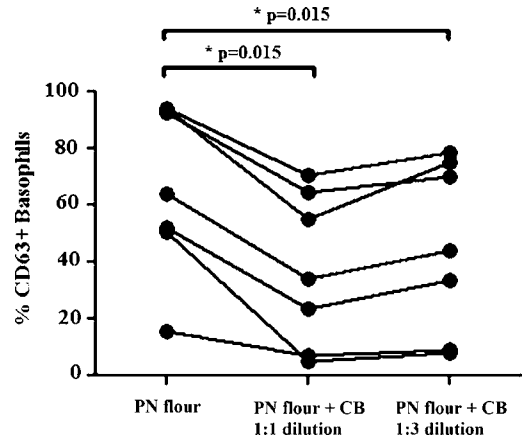

Figure 5. Basophil activation assay of unmodified light roast 12% fat peanut (PN) flour and polyphenol-fortified peanut matrices modified with 1:1 and 1:3 dilutions of cranberry juice (CB). Data shown are percentage of basophils that are degranulated on the basis of CD63$^+$ expression from seven peanut allergic subjects. Individual data are shown with significant differences indicated.

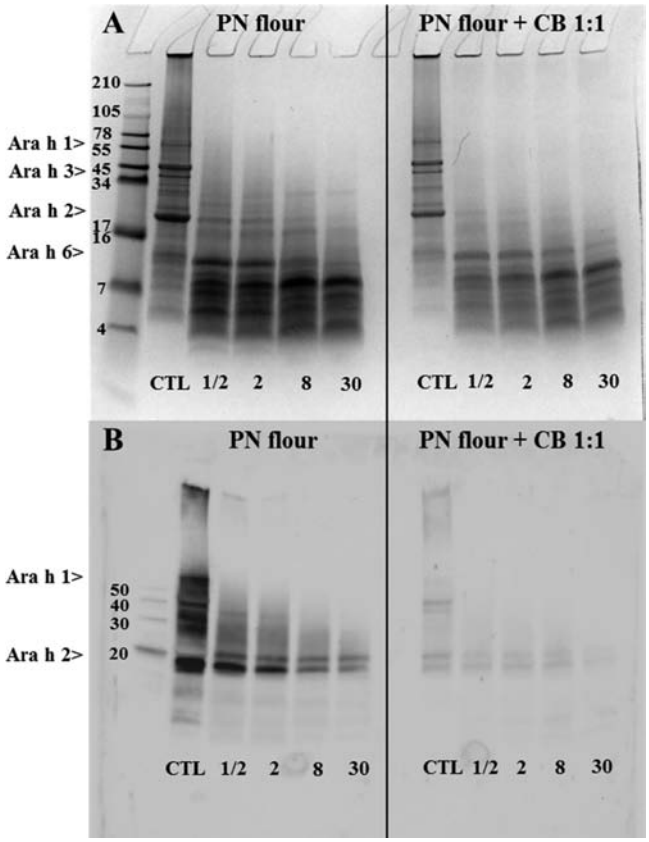

Figure 6. Pepsin simulated gastric digestion of unmodified light roast 12% fat peanut (PN) flour, cranberry polyphenol-fortified peanut matrix (PN flour + CB 1:1 dilution), and their respective controls (CTL; unmodified peanut flour or cranberry peanut matrix in simulated gastric fluid at pH 2 and no pepsin added) at time points 0.5, 2, 8, and 30 min: (A) SDS-PAGE under reducing conditions; (B) associated Western blot. Approximate locations for peanut allergens are shown.

though our findings were observed in both unmodified PN flour and cranberry modified PN matrix, more conclusive interpretations of resulting digestive fragments cannot be made on the basis of a mixture of various allergenic and nonallergenic peanut proteins present in our samples. Whereas digestion of PN proteins resulted in digestive fragments with various molecular weights, not all showed IgE binding on the respective Western blots (Figure 6B). Pepsin-resistant allergens Ara h 2 and Ara h 6 (see Figure 6A) both retained their IgE-binding capacity over the digestion period when unmodified PN flour was used, however, Ara h 6 to a much lesser extent. Ara h 2 remained immunoreactive throughout the digestion of cranberry polyphenol-fortified PN matrix, whereas IgE binding to Ara h 6 could barely be observed. Other studies also have shown that extensive digestion of peanut allergens by gastrointestinal enzymes can result in the survival or formation of peptide fragments that remain immunoreactive (intact and accessible IgE binding epitopes).[60,63,64] SDS-PAGE provided us with general information about how or to what extent PN proteins present in unmodified PN flour or cranberry polyphenol-fortified peanut matrix were broken down by pepsin, but only limited data could be obtained as to which digestive fragment (band) belongs to which intact allergenic or nonallergenic PN protein. Additionally, results gained from Western blots do not determine if digestive fragments remain or do not remain immunoreactive in vivo. Pepsin, trypsin, and chymotrypsin are all important enzymes that could influence the allergenicity of these cranberry–PN complexes in vivo. Thus, we next investigated the cranberry polyphenol-fortified PN matrix's allergenicity in an oral challenge in PN-allergic mice.

Oral Challenges in PN-Allergic Mice. To further evaluate the allergenic potential of the cranberry-fortified PN matrix in vivo, C3H/HeJ mice (n = 4 per group) were made allergic to PN proteins and challenged orally with either unmodified PN flour (control) or polyphenol-fortified PN matrix modified with 1:1 dilution of cranberry juice. No difference was observed in groups of mice for PN-specific IgE levels prior to oral challenge (data not shown). Levels of MMCP-1 were measured in sera of mice to gauge the ability of the cranberry polyphenol-fortified PN matrix to attenuate intestinal mucosal mast cell degranulation. Results showed that mice challenged with cranberry polyphenol-fortified PN matrix had significantly lower levels (using the Mann–Whitney test (one-tailed), we find a p value = 0.041) of MMCP-1 in their sera than mice challenged with unmodified PN flour (Figure 7). These results demonstrate that the cranberry–PN complexes are hypoallergenic in vivo because mast cells are degranulated to a lesser

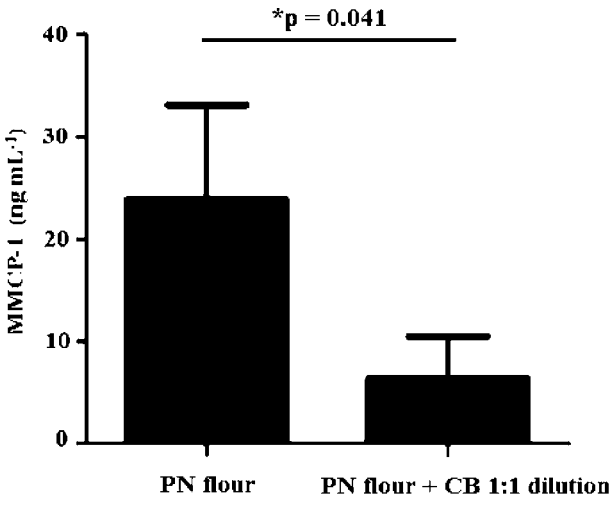

Figure 7. MMCP-1 levels in serum 45 min following oral challenge with unmodified light roast 12% fat peanut (PN) flour or polyphenol-fortified peanut matrix modified with 1:1 dilution of cranberry juice (CB) in peanut-allergic mice (n = 4 per group). Data shown are means plus standard deviation and showed significant difference when using the Mann−Whitney test (one-tailed) at p = 0.041.

extent than in mice challenged with the unmodified PN flour. Together, our data showing decreased IgE binding to the major PN allergens, decreased capacity to degranulate human basophils, and decreased allergic response in vivo in a mouse model led us to conclude that the cranberry polyphenol-fortified PN matrix is hypoallergenic.

To our knowledge, no other modified PN materials have been assessed for allergenicity in an oral challenge mouse model. However, similar assays were utilized to study egg allergens and the effects of heat-induced modifications.[65] The authors found that heating egg allergens caused reduced IgE binding and reduced responses in basophil assays, as well as reduced allergic symptoms following an oral challenge. The research suggests that structural modifications following heating may eliminate conformational IgE-binding epitopes. It is interesting that in our work, we also observed structural changes in proteins upon complexation of PN flour with cranberry polyphenols, without heating, as evidenced by ATR-FTIR.

Collectively, these results suggest that the cranberry polyphenol-fortified PN matrix is hypoallergenic and may have potential to serve as a safer second-generation ingredient for oral immunotherapy trials. Future trials with the other promising polyphenol sources are warranted to validate their efficacy as well. Although other technologies for producing hypoallergenic PN proteins have been described, including genetic engineering,[66] high-pressure processing,[67] enzymatic hydrolysis,[68] and controlled Maillard type modifications,[69] among others, there are challenging regulatory barriers, costs, and negative public perceptions associated with many of these approaches. In contrast, the technology we describe here is of food grade, is economical, and could be readily adapted to produce sufficient quantities of polyphenol-fortified PN matrices necessary for clinical applications. Importantly, this technology has also been demonstrated for a range of food grade plant and animal proteins, suggesting it could be readily adapted to treat other food allergies.

AUTHOR INFORMATION

Corresponding Author

*(M.A.L.) Mail: 600 Laureate Way, North Carolina Research Campus, Kannapolis, NC 28081, USA. E-mail: mlila@ncsu.edu. Phone: (704) 250-5400. Fax: (704) 250-5409.

Funding

This study was funded through the Everett W. Byrd Endowment and NC State appropriations for North Carolina State University at Kannapolis.

Notes

The authors declare no competing financial interest.

ACKNOWLEDGMENTS

We gratefully acknowledge the kind assistance of Kristin M. Price with Western blotting. We thank the Muscadine Products Corp. (Wray, GA, USA), The Super Grape (Magnolia, NC, USA), the New Zealand Blackcurrant Co-operative Ltd. (Nelson, New Zealand), Artemis International (Fort Wayne, IN, USA), and QTrade Teas & Herbs (Cerritos, CA, USA) for providing plant material. We also thank the Golden Peanut Co. LLC (Alpharetta, GA, USA) for providing the light roast 12% fat PN flour.

ABBREVIATIONS USED

PN, peanut; PN flour, light roast 12% fat peanut flour; ATR-FTIR, attenuated total reflectance−Fourier transform infrared spectroscopy; OIT, oral immunotherapy; a_w, water activity; SN, soluble nitrogen; LDS, lithium dodecyl sulfate; TP, total phenolics; GAE, gallic acid equivalents; PAC, proanthocyanidin; DMAC, 4-(dimethylamino)cinnamaldehyde; ANC, anthocyanin; DP, degree of polymerization; SGF, simulated gastric fluid

REFERENCES

(1) Decker, W. W.; Campbell, R. L.; Manivannan, V.; Luke, A.; St. Sauver, J. L.; Weaver, A.; Bellolio, M. F.; Bergstralh, E. J.; Stead, L. G.; Li, J. T. C. The etiology and incidence of anaphylaxis in Rochester, Minnesota: a report from the Rochester Epidemiology Project. *J. Allergy Clin. Immunol.* **2008**, *122*, 1161−1165.

(2) Ross, M. P.; Ferguson, M.; Street, D.; Klontz, K.; Schroeder, T.; Luccioli, S. Analysis of food-allergic and anaphylactic events in the National Electronic Injury Surveillance System. *J. Allergy Clin. Immunol.* **2008**, *121*, 166−171.

(3) Boyce, J. A.; Assa'ad, A.; Burks, A. W.; Jones, S. M.; Sampson, H. A.; Wood, R. A.; Plaut, M.; Cooper, S. F.; Fenton, M. J.; Arshad, S. H.; Bahna, S. L.; Beck, L. A.; Byrd-Bredbenner, C.; Camargo, C. A. J.; Eichenfield, L.; Furuta, G. T.; Hanifin, J. M.; Jones, C.; Kraft, M.; Levy, B. D.; Lieberman, P.; Luccioli, S.; McCall, K. M.; Schneider, L. C.; Simon, R. A.; Simons, F. E.; Teach, S. J.; Yawn, B. P.; Schwaninger, J. M. Guidelines for the diagnosis and management of food allergy in the United States: report of the NIAID-sponsored expert panel. *J. Allergy Clin. Immunol.* **2010**, *126*, S1−S58.

(4) Hefle, S. L.; Nordlee, J. A.; Taylor, S. L. Allergenic foods. *Crit Rev. Food Sci.* **1996**, *36*, S69−S89.

(5) Bock, S. A.; Muñoz-Furlong, A.; Sampson, H. A. Further fatalities caused by anaphylactic reactions to food, 2001−2006. *J. Allergy Clin. Immunol.* **2007**, *119*, 1016−1018.

(6) Skolnick, H. S.; Conover-Walker, M. K.; Koerner, B. C.; Sampson, H. A.; Burks, A. W.; Wood, R. A. The natural history of peanut allergy. *J. Allergy Clin. Immunol.* **2001**, *107*, 367−374.

(7) Burks, A. W. Peanut allergy. *Lancet* **2008**, *371*, 1538−1546.

(8) Sicherer, S. H.; Sampson, H. A. Food allergy. *J. Allergy Clin. Immunol.* **2010**, *125*, S116−S125.

(9) Sicherer, S. H.; Muñoz-Furlong, A.; Godbold, J. H.; Sampson, H. A. US prevalence of self-reported peanut, tree nut, and sesame allergy: 11-year follow-up. *J. Allergy Clin. Immunol.* **2010**, *125*, 1322−1326.
(10) Varshney, P.; Jones, S. M.; Scurlock, A. M.; Perry, T. T.; Kemper, A.; Steele, P.; Hiegel, A.; Kamilaris, J.; Carlisle, S.; Yue, X.; Kulis, M.; Pons, L.; Vickery, B.; Burks, A. W. A randomized controlled study of peanut oral immunotherapy: clinical desensitization and modulation of the allergic response. *J. Allergy Clin. Immunol.* **2011**, *127*, 654−660.
(11) Hofmann, A. M.; Scurlock, A. M.; Jones, S. M.; Palmer, K. P.; Lokhnygina, Y.; Steele, P. H.; Kamilaris, J.; Burks, A. W. Safety of a peanut oral immunotherapy protocol in children with peanut allergy. *J. Allergy Clin. Immunol.* **2009**, *124*, 286−291.
(12) Longo, G.; Barbi, E.; Berti, I.; Meneghetti, R.; Pittalis, A.; Ronfani, L.; Ventura, A. Specific oral tolerance induction in children with very severe cow's milk-induced reactions. *J. Allergy Clin. Immunol.* **2008**, *121*, 343−347.
(13) Labuckas, D. O.; Maestri, D. M.; Perelló, M.; Martínez, M. L.; Lamarque, A. L. Phenolics from walnut (*Juglans regia* L.) kernels: antioxidant activity and interactions with proteins. *Food Chem.* **2008**, *107*, 607−612.
(14) Majo, D. D.; La Guardia, M.; Giammanco, S.; La Neve, L.; Giammanco, M. The antioxidant capacity of red wine in relationship with its polyphenolic constituents. *Food Chem.* **2008**, *111*, 45−49.
(15) Singh, A.; Holvoet, S.; Mercenier, A. Dietary polyphenols in the prevention and treatment of allergic diseases. *Clin. Exp. Allergy* **2011**, *41*, 1346−1359.
(16) Papadopoulou, A.; Frazier, R. A. Characterization of protein−polyphenol interactions. *Trends Food Sci. Technol.* **2004**, *15*, 186−190.
(17) Charlton, A. J.; Baxter, N. J.; Khan, M. L.; Moir, A. J. G.; Haslam, E.; Davies, A. P.; Williamson, M. P. Polyphenol/peptide binding and precipitation. *J. Agric. Food Chem.* **2002**, *50*, 1593−1601.
(18) Siebert, K. J. Effects of protein−polyphenol interactions on beverage haze, stabilization, and analysis. *J. Agric. Food Chem.* **1999**, *47*, 353−362.
(19) Chung, S. Y.; Kato, Y.; Champagne, E. T. Polyphenol oxidase/caffeic acid may reduce the allergenic properties of peanut allergens. *J. Sci. Food Agric* **2005**, *85*, 2631−2637.
(20) Chung, S. Y.; Champagne, E. T. Effects of phytic acid on peanut allergens and allergenic properties of extracts. *J. Agric. Food Chem.* **2007**, *55*, 9054−9058.
(21) Chung, S. Y.; Champagne, E. T. Using phenolic compounds to reduce the allergenic properties of peanut extracts and peanut butter slurries. *J. Allergy Clin. Immunol.* **2008**, *121*, S249.
(22) Chung, S. Y.; Reed, S. Removing peanut allergens by tannic acid. *Food Chem.* **2012**, *134*, 1468−1473.
(23) Cheng, D. M.; Kuhn, P.; Poulev, A.; Rojo, L. E.; Lila, M. A.; Raskin, I. *In vivo* and *in vitro* antidiabetic effects of aqueous cinnamon extract and cinnamon polyphenol-enhanced food matrix. *Food Chem.* **2012**, *135*, 2994−3002.
(24) Plundrich, N.; Grace, M. H.; Raskin, I.; Lila, M. A. Bioactive polyphenols from muscadine grape and blackcurrant stably concentrated onto protein-rich matrices for topical applications. *Int. J. Cosmetic Sci.* **2013**, *35*, 394−401.
(25) Roopchand, D. E.; Kuhn, P.; Poulev, A.; Oren, A.; Lila, M. A.; Raskin, I. Biochemical analysis and in vivo hypoglycemic activity of grape polyphenol-soybean flour complex. *J. Agric. Food Chem.* **2012**, *60*, 8860−8865.
(26) Grace, M. H.; Guzman, I.; Roopchand, D. E.; Moskal, K.; Cheng, D. M.; Pogrebnyak, N.; Raskin, I.; Howell, A.; Lila, M. A. Enrichment of alternative food matrices with cranberry bioflavonoids creates unique and versatile functional food ingredients. *J. Agric. Food Chem.* **2013**, *61*, 6856−6864.
(27) Roopchand, D. E.; Grace, M. H.; Kuhn, P.; Cheng, D. M.; Plundrich, N.; Poulev, A.; Howell, A.; Fridlender, B.; Lila, M. A.; Raskin, I. Efficient sorption of polyphenols in soybean flour enables natural fortification of foods. *Food Chem.* **2012**, *131*, 1193−1200.
(28) Herald, T. J.; Gadgil, P.; Tilley, M. High-throughput micro plate assays for screening flavonoid content and DPPH-scavenging activity in sorghum bran and flour. *J. Sci. Food Agric.* **2012**, *92*, 2326−2331.
(29) Wallace, T. C.; Giusti, M. M. Evaluation of parameters that affect the 4-dimethylaminocinnamaldehyde assay for flavanols and proanthocyanidins. *J. Food Sci.* **2010**, *75*, C619−C625.
(30) Grace, M. H.; Ribnicky, D. M.; Kuhn, P.; Poulev, A.; Logendra, S.; Yousef, G. G.; Raskin, I.; Lila, M. A. Hypoglycemic activity of a novel anthocyanin-rich formulation from lowbush blueberry, *Vaccinium angustifolium* Aiton. *Phytomedicine* **2009**, *16*, 406−415.
(31) Young, J. H.; Whitaker, T. B.; Blankenship, P. D.; Brusewitz, G. H.; Troeger, J. M.; Steele, J. L.; Person, N. R., Jr. Effect of oven drying time on peanut moisture determination. *Trans. ASAE* **1982**, *25*, 491−496.
(32) Gu, L.; Kelm, M.; Hammerstone, J. F.; Beecher, G.; Cunningham, D.; Vannozzi, S.; Prior, R. L. Fractionation of polymeric procyanidins from lowbush blueberry and quantification of procyanidins in selected foods with an optimized normal-phase HPLC-MS fluorescent detection method. *J. Agric. Food Chem.* **2002**, *50*, 4852−4860.
(33) Hammerstone, J. F.; Lazarus, S. A.; Mitchell, A. E.; Rucker, R.; Schmitz, H. H. Identification of procyanidins in cocoa (*Theobroma cacao*) and chocolate using high-performance liquid chromatography/mass spectrometry. *J. Agric. Food Chem.* **1999**, *47*, 490−496.
(34) Constanza, K. E.; White, B. L.; Davis, J. P.; Sanders, T. H.; Dean, L. L. Value-added processing of peanut skins: antioxidant capacity, total phenolics, and procyanidin content of spray-dried extracts. *J. Agric. Food Chem.* **2012**, *60*, 10776−10783.
(35) Thyagarajan, A.; Jones, S. M.; Calatroni, A.; Pons, L.; Kulis, M.; Woo, C. S.; Kamalakannan, M.; Vickery, B. P.; Scurlock, A. M.; Burks, A. W.; Shreffler, W. G. Evidence of pathway-specific basophil anergy induced by peanut oral immunotherapy in peanut-allergic children. *Clin. Exp. Allergy* **2012**, *42*, 1197−1205.
(36) *U.S. Pharmacopeia 23*, Simulated gastric fluid and simulated intestinal fluid, The National Formulary 18; U.S. Pharmacopeial Convention: Rockville, MD, USA, 2006; 3171 pp.
(37) Li, X. M.; Serebrisky, D.; Lee, S. Y.; Huang, C. K.; Bardina, L.; Schofield, B. H.; Stanley, J. S.; Burks, A. W.; Bannon, G. A.; Sampson, H. A. A murine model of peanut anaphylaxis: T- and B-cell responses to a major peanut allergen mimic human responses. *J. Allergy Clin. Immunol.* **2000**, *106*, 150−158.
(38) Shan, B.; Cai, Y. Z.; Brooks, J. D.; Corke, H. Antibacterial properties and major bioactive components of cinnamon stick (*Cinnamomum burmannii*): activity against foodborne pathogenic bacteria. *J. Agric. Food Chem.* **2007**, *55*, 5484−5490.
(39) Neto, C. C. Cranberry and blueberry: evidence for protective effects against cancer and vascular diseases. *Mol. Nutr. Food Res.* **2007**, *51*, 652−664.
(40) Hou, D. X.; Masuzaki, S.; Hashimoto, F.; Uto, T.; Tanigawa, S.; Fujii, M.; Sakata, Y. Green tea proanthocyanidins inhibit cyclooxygenase-2 expression in LPS-activated mouse macrophages: molecular mechanisms and structure-activity relationship. *Arch. Biochem. Biophys.* **2007**, *460*, 67−74.
(41) Oszmianski, J.; Wojdylo, A. *Aronia melanocarpa* phenolics and their antioxidant activity. *Eur. Food Res. Technol.* **2005**, *221*, 809−813.
(42) Koeppen, B. H.; Herrmann, K. Flavonoid glycosides and hydroxycinnamic acid esters of blackcurrants (*Ribes nigrum*). Phenolics of fruits 9. *Z. Lebensm. Unters. Forsch.* **1977**, *164*, 263−268.
(43) Pastrana-Bonilla, E.; Akoh, C. C.; Sellappan, S.; Krewer, G. Phenolic content and antioxidant capacity of muscadine grapes. *J. Agric. Food Chem.* **2003**, *51*, 5497−5503.
(44) Wu, X.; Gu, L.; Prior, R. L.; McKay, S. Characterization of anthocyanins and proanthocyanidins in some cultivars of *Ribes*, *Aronia*, and *Sambucus* and their antioxidant capacity. *J. Agric. Food Chem.* **2004**, *52*, 7846−7856.
(45) Cunningham, D. G.; Vannozzi, S.; O'Shea, E.; Turk, R. Analysis and standardization of cranberry products. *ACS Symp. Ser.* **2002**, *No. 803*, 151−166.

(46) Gu, L.; Kelm, M. A.; Hammerstone, J. F.; Beecher, G.; Holden, J.; Haytowitz, D.; Gebhardt, S.; Prior, R. L. Concentrations of proanthocyanidins in common foods and estimations of normal consumption. *J. Nutr.* **2003**, *134*, 613−617.
(47) Haslam, E. Natural polyphenols (vegetable tannins) as drugs: possible modes of action. *J. Nat. Prod.* **1996**, *59*, 205−215.
(48) Lemon-Mulé, H.; Sampson, H. A.; Sicherer, S. H.; Shreffler, W. G.; Noone, S.; Nowak-Wegrzyn, A. Immunologic changes in children with egg allergy ingesting extensively heated egg. *J. Allergy Clin. Immunol.* **2008**, *122*, 977−983.
(49) Sathe, S. K.; Sharma, G. M. Effects of food processing on food allergens. *Mol. Nutr. Food Res.* **2009**, *53*, 970−978.
(50) Burks, A. W.; Williams, L. W.; Helm, R. M.; Connaughton, C.; Cockrell, G.; O'Brien, T. Identification of a major peanut allergen, Ara h I, in patients with atopic dermatitis and positive peanut challenges. *J. Allergy Clin. Immunol.* **1991**, *88*, 172−179.
(51) Koppelman, S. J.; Wensing, M.; Ertmann, M.; Knulst, A. C.; Knol, E. F. Relevance of Ara h1, Ara h2 and Ara h3 in peanut-allergic patients, as determined by immunoglobulin E Western blotting, basophil−histamine release and intracutaneous testing: Ara h2 is the most important peanut allergen. *Clin. Exp. Allergy* **2004**, *34*, 583−590.
(52) Koppelman, S. J.; de Jong, G. A.; Laaper-Ertmann, M.; Peeters, K. A.; Knulst, A. C.; Hefle, S. L.; Knol, E. F. Purification and immunoglobulin E-binding properties of peanut allergen Ara h 6: evidence for cross-reactivity with Ara h 2. *Clin. Exp. Allergy* **2005**, *35*, 490−497.
(53) McDermott, R. A.; Porterfield, H. S.; El Mezayen, R.; Burks, A. W.; Pons, L.; Schlichting, D. G.; Solomon, B.; Redzic, J. S.; Harbeck, R. J.; Duncan, M. W.; Hansen, K. C.; Dreskin, S. C. Contribution of Ara h 2 to peanut-specific, immunoglobulin E-mediated, cell activation. *Clin. Exp. Allergy* **2007**, *37*, 752−763.
(54) Palmer, G. W.; Dibbern, D. A., Jr.; Burks, A. W.; Bannon, G. A.; Bock, S. A.; Porterfield, H. S.; McDermott, R. A.; Dreskin, S. C. Comparative potency of Ara h 1 and Ara h 2 in immunochemical and functional assays of allergenicity. *Clin. Immmunol.* **2005**, *115*, 302−312.
(55) Porterfield, H. S.; Murray, K. S.; Schlichting, D. G.; Chen, X.; Hansen, K. C.; Duncan, M. W.; Dreskin, S. C. Effector activity of peanut allergens: a critical role for Ara h 2, Ara h 6, and their variants. *Clin. Exp. Allergy* **2009**, *39*, 1099−1108.
(56) Barth, A. Infrared spectroscopy of proteins. *Biochim. Biophys. Acta* **2007**, *1767*, 1073−1101.
(57) Kong, J.; Yu, S. Fourier transform infrared spectroscopic analysis of protein secondary structures. *Acta Biochim. Biophys. Sinica* **2007**, *39*, 549−559.
(58) Prigent, S. V. E.; Gruppen, H.; Visser, A.; van Koningsveld, G. A.; de Jong, G. A. H.; Voragen, A. G. J. Effects of non-covalent interactions with 5-*O*-caffeoylquinic acid (chlorogenic acid) on the heat denaturation and solubility of globular proteins. *J. Agric. Food Chem.* **2003**, *51*, 5088−5095.
(59) Porter, L. J.; Woodruffe, J. Haemanalysis: the relative astringency of proanthocyanidin polymers. *Phytochemistry* **1984**, *23*, 1255−1256.
(60) Koppelman, S. J.; Hefle, S. L.; Taylor, S. L.; de Jong, G. A. H. Digestion of peanut allergens Ara h 1, Ara h 2, Ara h 3, and Ara h 6: a comparative *in vitro* study and partial characterization of digestion-resistent peptides. *Mol. Nutr. Food Res.* **2010**, *54*, 1711−1721.
(61) Sen, M.; Kopper, R.; Pons, L.; Abraham, E. C.; Burks, A. W.; Bannon, G. A. Protein structure plays a critical role in peanut allergen stability and may determine immunodominant IgE-binding epitopes. *J. Immunol.* **2002**, *169*, 882−887.
(62) Lehmann, K.; Schweimer, K.; Reese, G.; Randow, S.; Suhr, M.; Becker, W. M.; Vieths, S.; Rosch, P. Structure and stability of 2S albumin-type peanut allergens: implications for the severity of peanut allergic reactions. *Biochem. J.* **2006**, *395*, 463−472.
(63) Maleki, S. J.; Kopper, R. A.; Shin, D. S.; Park, C. W.; Compadre, C. M.; Sampson, H.; Bannon, G. A. Structure of the major peanut allergen Ara h 1 may protect IgE-binding epitopes from degradation. *J. Immunol.* **2000**, *164*, 5844−5849.
(64) Sen, M.; Kopper, R.; Pons, L.; Abraham, E. C.; Burks, A. W.; Bannon, G. A. Protein structure plays a critical role in peanut allergen stability and may determine immunodominant IgE-binding epitopes. *J. Immunol.* **2002**, *169*, 882−887.
(65) Martos, G.; Lopez-Exposito, I.; Bencharitiwong, R.; Berin, M. C.; Nowak-Wegrzyn, A. Mechanisms underlying differential food allergy response to heated egg. *J. Allergy Clin. Immunol.* **2011**, *127*, 990−997.
(66) Li, X. M.; Srivastava, K.; Grishin, A.; Huang, C. K.; Schofield, B.; Burks, W.; Sampson, H. A. Persistent protective effect of heat-killed *Escherichia coli* producing "engineered", recombinant peanut proteins in a murine model of peanut allergy. *J. Allergy Clin. Immunol.* **2003**, *112*, 159−167.
(67) Johnson, P. E.; Van der Plancken, I.; Balasa, A.; Husband, F. A.; Grauwet, T.; Hendrickx, M.; Knorr, D.; Mills, E. N. C.; Mackie, A. R. High pressure, thermal and pulsed electric-field-induced structural changes in selected food allergens. *Mol. Nutr. Food Res.* **2010**, *54*, 1701−1710.
(68) Shi, X.; Guo, R.; White, B. L.; Yancey, A.; Sanders, T. H.; Davis, J. P.; Burks, A. W.; Kulis, M. Allergenic properties of enzymatically hydrolyzed peanut flour extracts. *Int. Arch Allergy Immunol.* **2013**, *162*, 123−130.
(69) Taheri-Kafrani, A.; Gaudin, J. C.; Rabesona, H.; Nioi, C.; Agarwal, D.; Drouet, M.; Chobert, J. M.; Bordbar, A. K.; Haertle, T. Effects of heating and glycation of β-lactoglobulin on its recognition by IgE of sera from cow milk allergy patients. *J. Agric. Food Chem.* **2009**, *57*, 4974−4982.

Table 1. Concentrations of Anthocyanins, Proanthocyanidins, and Chlorogenic Acid in Wild Blueberry Crude Extract and Semipurified Fractions

blueberry sample	anthocyanins,[a] mg/g	proanthocyanidins,[b] mg/g	chlorogenic acid,[c] mg/g (mmol/g)
crude extract (CE)	28.20 ± 0.9	10.44 ± 0.7	6.18 ± 0.2 (0.02)
polyphenol-rich (PPR)	424.37 ± 5.7	78.05 ± 3.1	35.6 ± 1.4 (0.10)
anthocyanin-rich (ANC)	830.18 ± 26.7	2.76 ± 0.2	25.84 ± 0.6 (0.07)
proanthocyanidin-rich (PAC)	10.09 ± 0.4	299.17 ± 10.6	5.04 ± 0.2 (0.01)
ethyl acetate (EA)	18.70 ± 0.6	15.13 ± 0.5	82.26 ± 1.6 (0.23)

[a]Anthocyanins were quantified by RP-HPLC as cyanidin-3-glucoside equivalents. [b]Proanthocyanidins were quantified by NP-HPLC as procyandin A-2 dimer. [c]Chlorogenic acid was quantified by RP-HPLC using a reference standard.

Maine. The composite was made in the fall of 2011, frozen by Cherryfield Foods at −15 °C (Cherryfield, ME, USA), and subsequently stored at −80 °C until extraction.

Extraction and Preparation of the Polyphenol-Rich Extract. The whole frozen blueberry fruits (100 g) were blended (Waring, Torrington, CT, USA) with methanol, acidified with 0.3% TFA (200 mL), and filtered first through multiple layers of muslin sheets and then on Whatman's filter paper no. 4 (Florham Park, NJ, USA) with the aid of suction. The collected hydroalcoholic extract was evaporated to about 50 mL using a rotary evaporator at a temperature not exceeding 40 °C. The obtained aqueous concentrated extract was partitioned against ethyl acetate (4 × 50 mL), and the organic solvent was evaporated to afford the ethyl acetate (EA) extract (0.25 g). The aqueous layer was loaded onto an Amberlite XAD-7 column (15 × 10 cm), preconditioned with acidified water (0.3% TFA). The resin was washed thoroughly with acidified water (0.3% TFA, ∼1 L) to remove free sugars, pectins, and organic acids. The polyphenol-rich mixture was then eluted with 0.5 L of methanol. The eluate was evaporated to remove the organic solvent and freeze-dried to yield 0.75 g of polyphenol-rich (PPR) extract.

Fractionation of the Polyphenol-Rich Extract. The PPR extract (0.5 g), obtained from the Amberlite XAD-7 column, was applied to a column packed with Sephadex LH-20 (20 × 2 cm) and preconditioned with H_2O/MeOH 80:20 (0.3% TFA), with an isocratic elution using the same solvent ratio. Four fractions (1−4), each of 80 mL, were collected starting when the colored material began to elute from the column. The column was then washed with 70% acetone (fraction 5) to elute oligomeric and polymeric proanthocyanidins. Solvents were evaporated (<40 °C) and immediately freeze-dried to afford 0.21, 0.06, 0.02, 0.1, and 0.18 g, respectively. Fraction 1 contained the highest anthocyanin concentration; thus, it was designated the anthocyanin-rich (ANC) fraction. Fraction 5 contained the oligomeric and polymeric proanthocyandins; thus, it was designated the proanthocyanidin-rich (PAC) fraction. Three samples from each extract/fraction were run for HPLC analysis.

HPLC-PDA Analysis. The HPLC analyses were conducted using an Agilent 1200 HPLC (Agilent Technologies, Santa Clara, CA, USA) with a photodiode array (PDA) detector and an autosampler with Chemstation software as a controller and for data processing.

Anthocyanin separation was performed using a reversed phase Supelcosil-LC-18 column, 25 mm × 4.6 mm × 5 μm (Supelco, Bellefonte, PA, USA). The mobile phase consisted of 5% formic acid in H_2O (A) and 100% methanol (B). The flow rate was constant during HPLC analysis at 1 mL/min with a step gradient of 10, 15, 20, 25, 30, 60, 10, and 10% of solvent B at 0, 5, 15, 20, 25, 45, 47, and 60 min, respectively. Samples were prepared by dissolving 5 mg in 1 mL of methanol and filtering through 0.2 μm nylon filters (Fisher Scientific, Pittsburgh, PA, USA) before 15 μL was injected onto the HPLC column with a constant temperature of 30 °C. Three concentrations of cyanidin-3-*O*-glucoside were prepared at 1.0, 0.5, and 0.25 μg/mL, where 15 μL was injected as an external standard. Quantification of anthocyanins was performed from the peak areas recorded at 520 nm with reference to the calibration curve obtained with cyanidin-3-*O*-glycoside. Blueberry extracts were analyzed in triplicate.

HPLC for chlorogenic acid was performed using a Synergi 4 μm Hydro-RP 80A column (250 mm × 4.6 mm × 5 μm, Phenomenex, Torrance, CA, USA). The mobile phase consisted of 2% acetic acid in distilled H_2O (solvent A) and 0.5% acetic acid in 50% acetonitrile in water (solvent B). The flow rate was set at 1 mL/min with a step gradient of 10, 15, 25, 55, 100, and 10% of solvent B at 0, 13, 20, 50, 54, and 60 min, respectively. Quantification was performed from the peak areas recorded at 280 nm to the calibration curve obtained with reference standards.

PAC separation was performed according to the method of Wallace and Giusti[16] using a normal phase Develosil Diol column, 250 mm × 4.6 mm × 5 μm (Phenomenex). The binary mobile phase consisted of (A) acetonitrile/acetic acid (98:2, v/v) and (B) methanol/water/acetic acid (95:3:2, v/v/v). Separation was accomplished using a linear gradient at 35 °C with 0.8 mL/min flow rate as follows: 0−35 min, 0−40% B; 35−40 min, 40−100% B; isocratic 100% B, 45 min; 100−0% B, 50 min; and 0% B to 55 min. The column was re-equilibrated for 5 min between samples. Eluate was monitored by fluorescence detection with excitation at 230 nm and emission at 321 nm as well as at 280 nm with the DAD detector. Proanthocyanidins were identified by comparison with available standards, reported in the literature,[16] and LC-ESI-MS.

Macrophage Cell Culture. The mouse macrophage cell line RAW 264.7 (ATCC TIB-71, obtained from American Type Culture Collection, Livingstone, MT, USA) was maintained in Dulbecco's modified Eagle's medium (DMEM, Life Technologies, NY, USA), supplemented with 100 IU/mL penicillin/100 μg/mL streptomycin (Fisher) and 10% fetal bovine serum (Life Technologies) at a density not exceeding 5×10^5 cells/mL and maintained at 37 °C in a humidified incubator with 5% CO_2. Unless otherwise specified, extracts and pure compounds for cell culture use were prepared in DMSO as 1000× stocks and stored at −20 °C until use.

Cell Viability Assay and Dose Range Determination Studies. RAW 264.7 cells were seeded in a 96-well plate (5×10^4 cells/well) for the viability assay. Cell viability was measured after 24 h of exposure by the 3-(4,5-dimethylthiazol-2-yl)-2,5-diphenyltetrazolium bromide (MTT) assay in triplicate and quantified spectrophotometrically at 550 nm[17] using a Synergy H1 microplate reader (BioTek). The concentrations of test reagents that showed no changes in cell viability compared with that vehicle (DMSO at a final concentration of 0.1%) were selected for further studies.

Anti-inflammatory in Vitro Assay. Cells were seeded in 24-well plates (5×10^5 cells/well) 24 h prior to treatment. The cells were pretreated for 1 h with blueberry extracts and fractions at 50, 100, or 150 μg/mL, or pure bioactive components malvidin-3-glucoside, epicatechin, and chlorogenic acid at 1 μM, the upper range of physiologically available doses reported for malvidin in portal circulation.[18] Cells were then elicited with lipopolysaccharide (LPS) at 1 μg/mL for an additional 6 h. For every experiment, one positive control (dexamethasone at 10 μM) and one negative control (DMSO at a final concentration of 0.1%) were included. Three replicates were made for both the treatments and the controls.

Total RNA Extraction, Purification, and cDNA Synthesis. The total RNA was isolated from RAW macrophages using TRIzol reagent (Life Technologies) following the manufacturer's instructions. RNA was quantified using the Synergy H1/Take 3 spectrophotometer (BioTek, Winooski, VT, USA). The cDNAs were synthesized using 2 μg of RNA for each sample using a commercially available high-capacity cDNA Reverse Transcription kit (Life Technologies), following

dx.doi.org/10.1021/jf4051599 | J. Agric. Food Chem. 2014, 62, 7022−7028

the manufacturer's protocol on an ABI GeneAMP 9700 (Life Technologies).

Quantitative PCR Analysis. The resulting cDNA was amplified in duplicate by real-time quantitative PCR using SYBR green PCR Master Mix (Life Technologies). To avoid interference due to genomic DNA contamination, only intron-overlapping primers were selected using Primer Express version 2.0 software (Applied Biosystems, Foster City, CA, USA) as follows: β-actin, forward primer 5′-AAC CGT GAA AAG ATG ACC CAG AT-3′, reverse primer 5′-CAC AGC CTG GAT GGC TAC GT-3′; COX2, forward primer 5′-TGG TGC CTG GTC TGA TGA TG-3′, reverse primer 5′-GTG GTA ACC GCT CAG GTG TTG-3′; iNOS, forward primer 5′-CCC TCC TGA TCT TGT GTT GGA-3′, reverse primer 5′-TCA ACC CGA GCT CCT GGA A-3′; IL6, forward primer 5′-TAG TCC TTC CTA CCC CAA TTT CC-3′, reverse primer 5′-TTG GTC CTT AGC CAC TCC TTC-3′; IL1β, forward primer 5′-CAA CCA ACA AGT GAT ATT CTC CAT G-3′, reverse primer 5′-GAT CCA CAC TCT CCA GCT GCA-3′; and Mcp1, forward primer 5′-CTT CTG GGC CTG CTG TTC A-3′, reverse primer 5′-GCA GCC TAC TCA TTG GGA TCA-3′. Quantitative PCR (qPCR) amplifications were performed on an ABI 7500 Fast real-time PCR (Life Technologies) using 1 cycle at 50 °C for 2 min and 1 cycle of 95 °C for 10 min, followed by 40 cycles of 15 s at 95 °C and 1 min at 60 °C. The dissociation curve was completed with 1 cycle of 1 min at 95 °C, 30 s at 55 °C, and 30 s at 95 °C. mRNA expression was analyzed using the ΔΔCT method and normalized with respect to the expression of the β-actin housekeeping genes using 7500 Fast System SDS software v1.3.0 (Life Technologies). A value of <1 indicates transcriptional down-regulation (inhibition of gene expression) compared with LPS, which shows maximum genetic induction. Values >1 imply overexpression of the particular gene in excess of LPS stimulation. Amplification of specific transcripts was further confirmed by obtaining melting curve profiles.

Statistical Analysis. Statistical analyses were performed using Prism 4.0 (GraphPad Software, San Diego, CA, USA). Data were analyzed by one-way ANOVA with treatment as a factor. Post hoc analyses of differences between individual experimental groups were made using Dunnett's multiple-comparison tests. Significance was set at $p < 0.05$. Values are reported as means ± SEM.

RESULTS AND DISCUSSION

Phenolic Compounds. Crude methanolic extract (CE) of wild lowbush blueberries contained anthocyanins (28.20 ± 0.9 mg/g extract), proanthocyanidins (16.85 ± 0.7 mg/g), and chlorogenic acid (6.18 ±0.2 mg/g) as major phenolic components (Table 1). In close agreement with previously published data,[19] anthocyanins comprised the highest content of total phenolic compounds, whereas chlorogenic acid was the major hydroxycinnamic acid found in blueberries (Figure 1). Polyphenol enrichment procedure over Amberlite resin resulted in 15- and 10-fold increases in anthocyanins and proanthocyanidins, respectively, in the polyphenol-rich (PRR) extract (Table 1). Partition of CE with ethyl acetate resulted in a phenolic acid-enriched fraction (EA) (Table 1; Figure 1C). Furthermore, Sephadex fractionation of the PRR extract afforded two semi-purified fractions: an anthocyanin-rich fraction (ANC) containing 830.18 ± 26.7 mg/g anthocyanins (Figure 1A) and a proanthocyanidin-rich fraction (PAC) containing 299.17 ± 10.6 mg/g oligomeric and polymeric proanthocyanidins (Figure 1B), a 30-fold increase over polyphenolic content of the original CE extract.

Malvidin glycosides were the most abundant anthocyainins present in the ANC fraction (324 mg/g), followed closely by delphinidin glycosides (250.5 mg/g), for a combined total of 67% (w/w) of the fraction (Table 2). Therefore, anthocyanin composition of blueberries was dominated by malvidin glycosides similar to that of grapes[20] but different from delphinidin- and cyanidin-dominated black currants[21] and bilberries,[22] cyanidin-dominated blackberries[23] and cranberries,[24] or pelargonidin-dominated strawberries.[25]

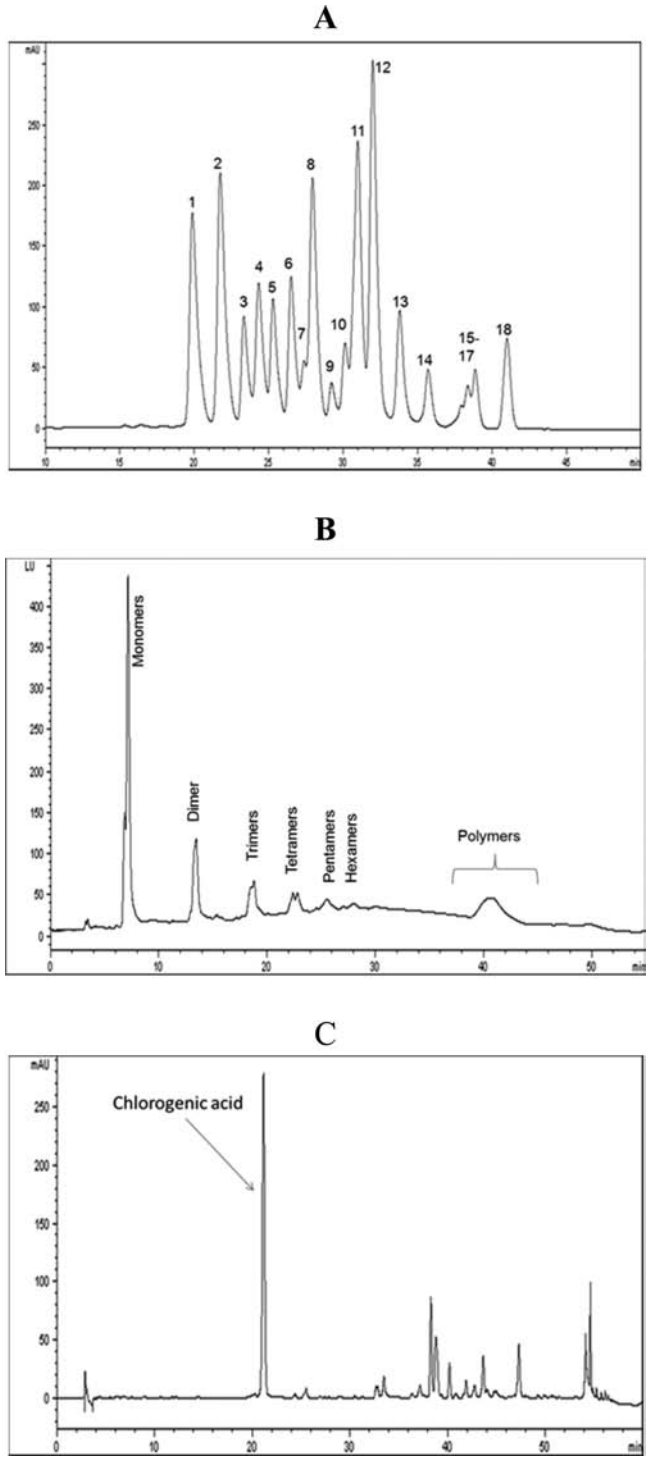

Figure 1. Analytical profiles of wild blueberry (*V. angustifolium*) fractions: (A) reversed phase HPLC-UV chromatograms for anthocyanins (A_{520}) in the anthocyanin-rich fraction (ANC) (refer to Table 2 for anthocyanin identification); (B) normal phase HPLC-FLD chromatogram for proanthocyanidins in the proanthocyanidin-rich fraction (PAC); (C) RP-HPLC-DAD chromatogram for the ethyl acetate fraction (EA) (280 nm).

Procyanidin monomers (catechin and epicatechin) represented 32% of the PAC fraction. Both of these flavanols have already been detected in blueberries in previous studies.[26]

dx.doi.org/10.1021/jf4051599 | J. Agric. Food Chem. 2014, 62, 7022−7028

Table 2. Concentrations of Individual Anthocyanin in the Anthocyanin-Rich (ANC) Fraction of Wild Blueberry

peak[a]	anthocyanins	mg/g[b]	mmol/g
1	delphinidin-3-galactoside	83.37 ± 1.2	0.18
2	delphinidin-3-glucoside	94.81 ± 1.5	0.20
3	cyanidin-3-galactoside	35.31 ± 1.2	0.08
4	delphinidin-3-arabinoside	50.93 ± 2.9	0.12
5	cyanidin-3-glucoside	43.06 ± 3.5	0.10
6	petunidin-3-galactoside	49.47 ± 1.8	0.10
7	cyanidin-3-arabinoside	14.61 ± 0.9	0.03
8	petunidin-3-glucoside	88.63 ± 1.4	0.19
9	peonidin-3-galactoside	14.83 ± 0.3	0.03
10	petunidin-3-arabinoside	23.76 ± 0.4	0.05
11	malvidin-3-galactoside	107.65 ± 1.8	0.22
12	malvidin-3-glucoside	125.10 ± 5.9	0.25
13	malvidin-3-arabinoside	42.71 ± 2.3	0.09
14	delphinidin-3-(6″-acetoyl)-glucoside	21.42 ± 1.1	0.04
15	cyanidin-3-(6″-acetoyl)-glucoside	6.81 ± 0.2	0.01
16	malvidin-3-(6″-acetoyl)-galactoside	11.30 ± 0.3	0.02
17	petunidin-3-(6″-acetoyl)-glucoside	16.40 ± 0.5	0.03
18	malvidin-3-(6″-acetoyl)-glucoside	28.93 ± 1.8	0.05

[a]For peak number, refer to the chromatogram in Figure 1. [b]Concentrations were measured by HPLC and calculated as cyanidin-3-glucoside.

Table 3. Proanthocyanidin Content of the Proanthocyanidin-Rich (PAC) Fraction of Wild Blueberry

proanthocyanidin	mg/g[a]	mmol/g
monomers	96.23 ± 3.8	0.33
dimers	43.74 ± 1.2	0.07
trimers	35.34 ± 0.6	0.04
tetramers	36.45 ± 1.3	0.03
pentamers	28.45 ± 1.7	0.02
hexamers	8.96 ± 0.5	0.01
polymers	49.98 ± 1.8	NA

[a]Concentrations were measured by HPLC and calculated as procyanidin A2.

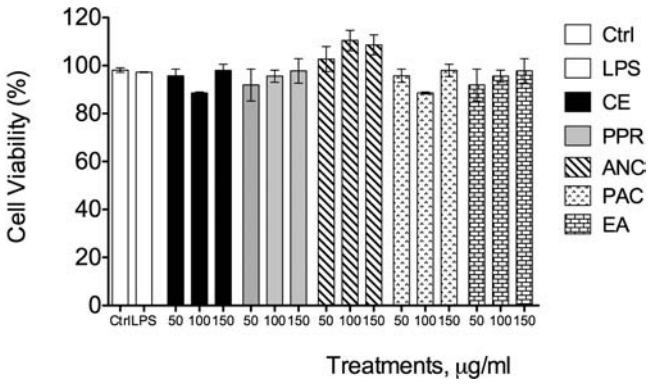

Figure 2. Effects of crude wild blueberry extract and its fractions on cell viability of murine RAW 264.7 macrophages. Cells were treated with crude extract (CE), polyphenol-rich (PPR), anthocyanin-rich (ANC), proanthocyanidin-rich (PAC), and ethyl acetate (EA) fractions for 24 h and cell viability was quantified spectrophotometrically by the MTT assay. Cell viability is reported as the mean ± SEM for three independent experiments.

The rest of the fraction contained proanthocyanidins with various degrees of polymerization (Table 3; Figure 1B). The predominant phenolic acid in blueberries was chlorogenic acid, and it was the predominant component of the EA fraction (82.26 ± 1.6 μg/mg, Figure 1C). The presence of chlorogenic acid in many berries including blueberries has been reported in a number of previous studies.[26,27] Which phenolic compound, either alone or interactively with others, contributes the most to biological effects of blueberries is still an open question.

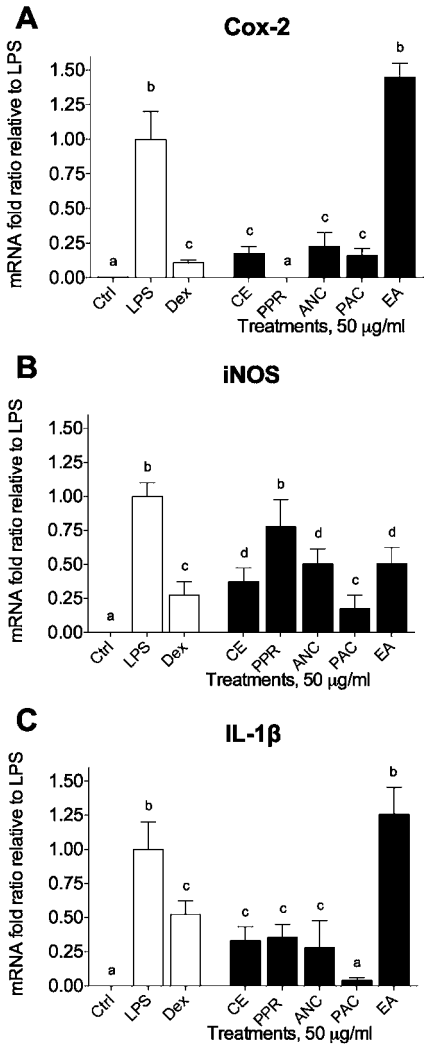

Figure 3. Effects of crude wild blueberry extract and its fractions on pro-inflammatory gene expression profiles associated with acute inflammatory response: (A) cyclooxygenase-2; (B) inducible nitric oxide synthase (iNOS); (C) cytokine IL-1β. Macrophages were pretreated with crude extract (CE), polyphenol-rich (PPR), anthocyanin-rich (ANC), proanthocyanidin-rich (PAC) and ethyl acetate (EA) fractions, and inflammatory response was induced with 1 μg/mL LPS for 6 h. Dexamethasone at 10 μM was used as a positive control. Fold changes in gene expression are reported as the mean ± SEM relative to LPS controls. Means not sharing the same letter are significantly different (one-way ANOVA, Tukey's post hoc test, $p < 0.05$ was considered significant).

Effect of Phenolic Fractions on Cell Viability. The cytotoxic effects of the phenolic fraction were evaluated by measuring RAW 264.7 macrophage viability by the MTT assay after 24 h of exposure (Figure 2). PPR, ANC, and EA fractions did not affect cell viability in the 50−150 μg/mL dose range used in the subsequent studies. CE and PAC fraction at 100 μg/mL reduced cell viability to 90%, but this result did not reach statistical significance and was not observed at a higher dose.

dx.doi.org/10.1021/jf4051599 | J. Agric. Food Chem. 2014, 62, 7022−7028

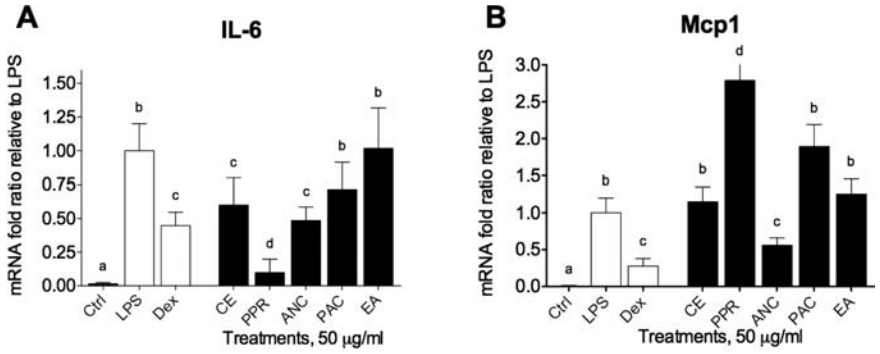

Figure 4. Effects of crude wild blueberry extract and its fractions on pro-inflammatory gene expression profiles associated with chronic inflammatory response: (A) cytokine IL-6; (B) monocyte chemotactic protein 1 (Mcp1/CCL2). Macrophages were pretreated with crude extract (CE), polyphenol-rich (PPR), anthocyanin-rich (ANC), proanthocyanidin-rich (PAC), and ethyl acetate (EA) fractions, and inflammatory response was induced with 1 μg/mL LPS for 6 h. Dexamethasone at 10 μM was used as a positive control. Fold changes in gene expression are reported as the mean ± SEM relative to LPS controls. Means not sharing the same letter are significantly different (one-way ANOVA, Tukey's post hoc test, $p < 0.05$ was considered significant).

Effect of Phenolic Fractions on Inflammatory Markers. Cell viability assays showed that none of the blueberry fractions were cytotoxic to RAW 264.7 macrophages at 50 μg/mL, an amount that is easily achievable in the gastrointestinal tract after consumption of berries or juices.[28] We then investigated the ability of blueberry phenolic fractions to modulate gene expression profiles for acute and chronic inflammation in the LPS-stimulated RAW 264.7 macrophages. For each assay, a negative control (vehicle alone), an induction control (1 μg/mL LPS), and a positive control (1 μg/mL LPS and 10 μM dexamethasone) were used to establish a reference baseline, maximum induction of marker genes, and assay effectiveness, respectively. The use of LPS as a systemic inducer of inflammatory response is warranted by its dual role in inducing both acute inflammatory response and endothelial cell injury[29] as well as low-level chronic inflammation associated with gastrointestinal dysfunction and increased flux of endotoxins.[30]

All blueberry fractions suppressed at least one biomarker of inflammation (Figures 3 and 4). Cox-2 expression was most strongly affected by all treatments with the exception of the EA fraction, which showed no activity ($p < 0.05$). Whereas the PAC fraction was most effective at suppressing the expression of acute pro-inflammatory genes iNOS and IL-1β ($p < 0.01$), it showed no significant effect for attenuation of the LPS-induced IL-6 or Mcp1 expression (Figure 4). On the contrary, ANC was the only fraction that showed borderline inhibition of both IL-6 and Mcp1 markers at 50 μg/mL ($p = 0.08$) and significant inhibition of Cox-2, iNOS, and IL-1β markers of acute inflammatory response ($p < 0.05$). The effect of ANC on IL-6 or Mcp1 markers may be potentiated in the presence of PAC components (Figure 4), as the PPR fraction that contains both ANC and PAC was the most effective at suppressing IL-6 expression ($p < 0.01$). Similar ANC and PAC fractions from blueberry–blackberry fermented beverages inhibited nitric oxide production, iNOS expression, and NF-κB activation as reported earlier.[7]

Comparative Effects of Major Phenolic Constituents. Treatment with three major phenolic compounds found in blueberries showed various levels of activity, ranging from no inhibition to substantial inhibition of expression (Figure 5). All pure compounds were tested at the concentration of 1 μM, the upper range of physiologically available doses reported for malvidin in portal circulation.[18] This concentration, however, is unlikely to be achieved in plasma following phase II liver metabolism, as studies performed in healthy volunteers receiving red wine[31] or grape juice[32] anthocyanins showed low detectable quantities of both 3-*O*-glucoside and *O*-glucuronide conjugates with C_{max} values in the 10 nmol/L range. Low systemic availability of anthocyanins may therefore suggest that their anti-inflammatory effects will be more pronounced in the gastrointestinal and mesenteric adipose tissues exposed to portal circulation.[30] These in vitro observations may not also be directly transferable to a postprandial in vivo situation in humans as shown for antioxidant effects of black currant anthocyanins.[33]

Malvidin-3-glucoside showed the highest anti-inflammatory activity ($p < 0.05$), whereas epicatechin and chlorogenic acid were largely ineffective at reducing mRNA expression of pro-inflammatory genes at this concentration with the exception of iNOS (Figure 5). A trend to inhibit iNOS expression was evident when macrophages were pretreated with chlorogenic acid. Other studies using higher concentrations of chlorogenic acid (>5 μM) reported reduction in nitric oxide production and iNOS and Cox-2 expression in RAW 264.7 macrophages and BV2 microglial cells treated with LPS.[34] Epicatechin at 1 μM also significantly reduced iNOS expression (Figure 5B). Similar effects were reported for epicatechin and related compounds at doses exceeding 8–20 μM.[35] Previous studies have also noted anti-inflammatory effects of malvidin glycosides in vitro, at supraphysiological concentrations that exceeded 10 μM in macrophages[36] and 25 μM in bovine aortic endothelial cells.[37] iNOS was the only marker showing some responsiveness to the three pure compounds when tested separately (Figure 5), but not when grouped together in the PPR fraction (Figure 3B). It is possible that the biological effects will depend on specific concentrations and molar ratios of bioactive compounds in a particular plant extract or fraction or the yet unknown interactions among the dietary bioactive compounds and the extract matrix itself.

It is also interesting to note that only anthocyanins and not other polyphenolic compounds used in this study (Figures 4 and 5) showed a profound inhibitory effect against monocyte chemoattractant protein (Mcp1) production in macrophages. A similar protective effect of red wine anthocyanins in primary human endothelial cells was reported previously.[38]

In summary, the anti-inflammatory activity of the blueberry extract was most prominent in the ANC fraction. The obtained results demonstrate that malvidin-3-glucoside, at concentrations that are attainable in the gastrointestinal tract and portal

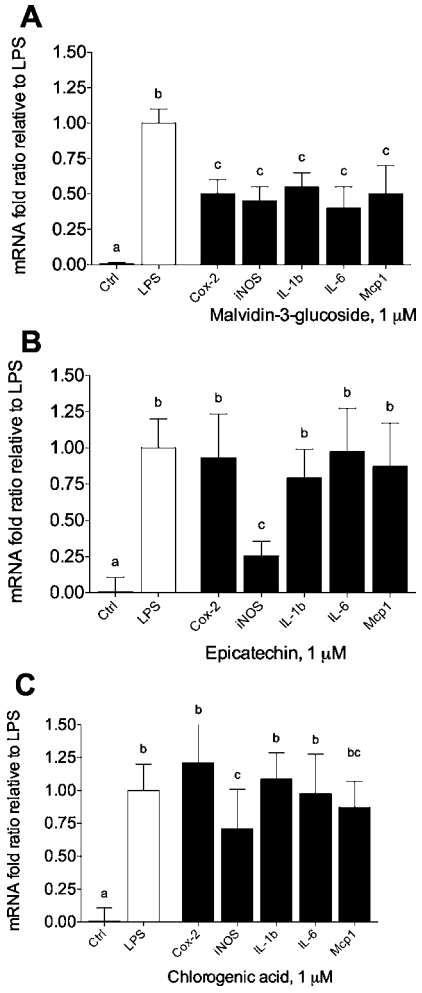

Figure 5. Effects of major phenolic constituents from wild blueberry extract on pro-inflammatory gene expression profiles: (A) malvidin-3-glucoside; (B) epicatechin; (C) chlorogenic acid. Macrophages were pretreated with 1 μM levels of individual compounds as specified, and inflammatory response was induced with 1 μg/mL LPS for 6 h. Dexamethasone at 10 μM was used as a positive control. Fold changes in gene expression are reported as the mean ± SEM relative to LPS controls. Means not sharing the same letter are significantly different (one-way ANOVA, Tukey's post hoc test, $p < 0.05$ was considered significant).

circulation, suppressed activation of key pro-inflammatory genes triggered by an inflammatory stimulus. These genes are central to the regulation of, among others, transcriptional regulation and cytokine-mediated acute and chronic inflammation. Thus, the obtained results suggest that malvidin-3-glucoside-containing diets could improve outcomes from immune and metabolic disorders linked to sustained inflammation.

AUTHOR INFORMATION

Corresponding Author

*(M.A.L.) Phone: (704) 250-5407. Fax: (704) 250-5409. E-mail: mlila@ncsu.edu.

Funding

This work was funded in part by NCSU Research and Innovation Grant 2012-2246 (MAL, SK) and an IFT Feeding Tomorrow scholarship to A.C.

Notes

The authors declare no competing financial interest.

REFERENCES

(1) Francis, F. J. Food colorants: anthocyanins. *Crit. Rev. Food Sci. Nutr.* **1989**, *28*, 273−314.

(2) Prior, R. L.; Cao, G.; Martin, A.; Sofic, E.; McEwan, J.; O'Brein, C.; Lischner, N.; Ehlenfeldt, M.; Kalt, W.; Krewer, G.; Mainland, C. M. Antioxidant capacity as influenced by total phenolic and anthocyanin content, maturity and variety of *Vaccinium* species. *J. Agric. Food Chem.* **1998**, *46*, 2686−2693.

(3) DeFuria, J.; Bennett, G.; Strissel, K. J.; Perfield, J. W., 2nd; Milbury, P. E.; Greenberg, A. S.; Obin, M. S. Dietary blueberry attenuates whole-body insulin resistance in high fat-fed mice by reducing adipocyte death and its inflammatory sequelae. *J. Nutr.* **2009**, *139*, 1510−1516.

(4) Schreckinger, M. E.; Wang, J.; Yousef, G.; Lila, M. A.; Gonzalez de Mejia, E. Antioxidant capacity and in vitro inhibition of adipogenesis and inflammation by phenolic extracts of *Vaccinium floribundum* and *Aristotelia chilensis*. *J. Agric. Food Chem.* **2010**, *58*, 8966−8976.

(5) Karlsen, A.; Retterstol, L.; Laake, P.; Paur, I.; Bohn, S. K.; Sandvik, L.; Blomhoff, R. Anthocyanins inhibit nuclear factor-kappaB activation in monocytes and reduce plasma concentrations of pro-inflammatory mediators in healthy adults. *J. Nutr.* **2007**, *137*, 1951−1954.

(6) Hou, D. X.; Masuzaki, S.; Hashimoto, F.; Uto, T.; Tanigawa, S.; Fujii, M.; Sakata, Y. Green tea proanthocyanidins inhibit cyclo-oxygenase-2 expression in LPS-activated mouse macrophages: molecular mechanisms and structure-activity relationship. *Arch. Biochem. Biophys.* **2007**, *460*, 67−74.

(7) Johnson, M. H.; de Mejia, E. G.; Fan, J.; Lila, M. A.; Yousef, G. G. Anthocyanins and proanthocyanidins from blueberry-blackberry fermented beverages inhibit markers of inflammation in macrophages and carbohydrate-utilizing enzymes in vitro. *Mol. Nutr. Food Res.* **2013**, *57*, 1182−1197.

(8) Hidalgo, M.; Martin-Santamaria, S.; Recio, I.; Sanchez-Moreno, C.; de Pascual-Teresa, B.; Rimbach, G.; de Pascual-Teresa, S. Potential anti-inflammatory, anti-adhesive, anti/estrogenic, and angiotensin-converting enzyme inhibitory activities of anthocyanins and their gut metabolites. *Genes Nutr.* **2012**, *7*, 295−306.

(9) Yousef, G. G.; Brown, A. F.; Funakoshi, Y.; Mbeunkui, F.; Grace, M. H.; Ballington, J. R.; Loraine, A.; Lila, M. A. Efficient quantification of the health-relevant anthocyanin and phenolic acid profiles in commercial cultivars and breeding selections of blueberries (*Vaccinium* spp.). *J. Agric. Food Chem.* **2013**, *61*, 4806−4815.

(10) Kimura, H.; Ogawa, S.; Akihiro, T.; Yokota, K. Structural analysis of A-type or B-type highly polymeric proanthocyanidins by thiolytic degradation and the implication in their inhibitory effects on pancreatic lipase. *J. Chromatogr., A* **2011**, *1218*, 7704−7712.

(11) Ingersoll, M. A.; Platt, A. M.; Potteaux, S.; Randolph, G. J. Monocyte trafficking in acute and chronic inflammation. *Trends Immunol.* **2011**, *32*, 470−477.

(12) Shi, C.; Pamer, E. G. Monocyte recruitment during infection and inflammation. *Nat. Rev. Immunol.* **2011**, *11*, 762−774.

(13) Crowe, S. M.; Westhorpe, C. L.; Mukhamedova, N.; Jaworowski, A.; Sviridov, D.; Bukrinsky, M. The macrophage: the intersection between HIV infection and atherosclerosis. *J. Leukocyte Biol.* **2010**, *87*, 589−598.

(14) Conductier, G.; Blondeau, N.; Guyon, A.; Nahon, J. L.; Rovere, C. The role of monocyte chemoattractant protein MCP1/CCL2 in neuroinflammatory diseases. *J. Neuroimmunol.* **2010**, *224*, 93−100.

(15) Kizelsztein, P.; Komarnytsky, S.; Raskin, I. Oral administration of triptolide ameliorates the clinical signs of experimental autoimmune encephalomyelitis (EAE) by induction of HSP70 and stabilization of NF-kappaB/IkappaBalpha transcriptional complex. *J. Neuroimmunol.* **2009**, *217*, 28−37.

(16) Wallace, T. C.; Giusti, M. M. Extraction and normal-phase HPLC-fluorescence-electrospray MS characterization and quantification of procyanidins in cranberry extracts. *J. Food Sci.* **2010**, *75*, C690−C696.

(17) Esposito, D.; Rathinasabapathy, T.; Schmidt, B.; Shakarjian, M. P.; Komarnytsky, S.; Raskin, I. Acceleration of cutaneous wound healing by brassinosteroids. *Wound Repair Regen.* **2013**, *21*, 688−696.
(18) Passamonti, S.; Vrhovsek, U.; Vanzo, A.; Mattivi, F. The stomach as a site for anthocyanins absorption from food. *FEBS Lett.* **2003**, *544*, 210−213.
(19) Gavrilova, V.; Kajdzanoska, M.; Gjamovski, V.; Stefova, M. Separation, characterization and quantification of phenolic compounds in blueberries and red and black currants by HPLC-DAD-ESI-MS^n. *J. Agric. Food Chem.* **2011**, *59*, 4009−4018.
(20) Bakker, J.; Timberlake, C. F. The distribution of anthocyanins in grape skin extracts of port wine cultivars as determined by high performance liquid chromatography. *J. Sci. Food Agric.* **1985**, *36*, 1315−1324.
(21) Slimestad, R.; Solheim, H. Anthocyanins from black currants (*Ribes nigrum* L.). *J. Agric. Food Chem.* **2002**, *50*, 3228−3231.
(22) Latti, A. K.; Riihinen, K. R.; Kainulainen, P. S. Analysis of anthocyanin variation in wild populations of bilberry (*Vaccinium myrtillus* L.) in Finland. *J. Agric. Food Chem.* **2008**, *56*, 190−196.
(23) Cuevas-Rodriguez, E. O.; Yousef, G. G.; Garcia-Saucedo, P. A.; Lopez-Medina, J.; Paredes-Lopez, O.; Lila, M. A. Characterization of anthocyanins and proanthocyanidins in wild and domesticated Mexican blackberries (*Rubus* spp.). *J. Agric. Food Chem.* **2010**, *58*, 7458−7464.
(24) Brown, P. N.; Shipley, P. R. Determination of anthocyanins in cranberry fruit and cranberry fruit products by high-performance liquid chromatography with ultraviolet detection: single-laboratory validation. *J. AOAC Int.* **2011**, *94*, 459−966.
(25) Aaby, K.; Skrede, G.; Wrolstad, R. E. Phenolic composition and antioxidant activities in flesh and achenes of strawberries (*Fragaria ananassa*). *J. Agric. Food Chem.* **2005**, *53*, 4032−4040.
(26) Moze, S.; Polak, T.; Gasperlin, L.; Koron, D.; Vanzo, A.; Poklar Ulrih, N.; Abram, V. Phenolics in Slovenian bilberries (*Vaccinium myrtillus* L.) and blueberries (*Vaccinium corymbosum* L.). *J. Agric. Food Chem.* **2011**, *59*, 6998−7004.
(27) Ehala, S.; Vaher, M.; Kaljurand, M. Characterization of phenolic profiles of northern European berries by capillary electrophoresis and determination of their antioxidant activity. *J. Agric. Food Chem.* **2005**, *53*, 6484−6490.
(28) Kahle, K.; Kraus, M.; Scheppach, W.; Ackermann, M.; Ridder, F.; Richling, E. Studies on apple and blueberry fruit constituents: do the polyphenols reach the colon after ingestion? *Mol. Nutr. Food Res.* **2006**, *50*, 418−423.
(29) Bannerman, D. D.; Goldblum, S. E. Mechanisms of bacterial lipopolysaccharide-induced endothelial apoptosis. *Am. J. Physiol.: Lung Cell. Mol. Physiol.* **2003**, *284*, L899−L914.
(30) Lam, Y. Y.; Mitchell, A. J.; Holmes, A. J.; Denyer, G. S.; Gummesson, A.; Caterson, I. D.; Hunt, N. H.; Storlien, L. H. Role of the gut in visceral fat inflammation and metabolic disorders. *Obesity* **2011**, *19*, 2113−2120.
(31) Garcia-Alonso, M.; Minihane, A. M.; Rimbach, G.; Rivas-Gonzalo, J. C.; de Pascual-Teresa, S. Red wine anthocyanins are rapidly absorbed in humans and affect monocyte chemoattractant protein 1 levels and antioxidant capacity of plasma. *J. Nutr. Biochem.* **2009**, *20*, 521−529.
(32) Stalmach, A.; Edwards, C. A.; Wightman, J. D.; Crozier, A. Gastrointestinal stability and bioavailability of (poly)phenolic compounds following ingestion of Concord grape juice by humans. *Mol. Nutr. Food Res.* **2012**, *56*, 497−509.
(33) Huebbe, P.; Giller, K.; de Pascual-Teresa, S.; Arkenau, A.; Adolphi, B.; Portius, S.; Arkenau, C. N.; Rimbach, G. Effects of blackcurrant-based juice on atherosclerosis-related biomarkers in cultured macrophages and in human subjects after consumption of a high-energy meal. *Br. J. Nutr.* **2012**, *108*, 234−244.
(34) Hwang, S. J.; Kim, Y. W.; Park, Y.; Lee, H. J.; Kim, K. W. Anti-inflammatory effects of chlorogenic acid in lipopolysaccharide-stimulated RAW 264.7 cells. *Inflamm. Res.* **2013**, *63*, 81−90.
(35) Mackenzie, G. G.; Carrasquedo, F.; Delfino, J. M.; Keen, C. L.; Fraga, C. G.; Oteiza, P. I. Epicatechin, catechin, and dimeric procyanidins inhibit PMA-induced NF-kappaB activation at multiple steps in Jurkat T cells. *FASEB J.* **2004**, *18*, 167−169.
(36) Bognar, E.; Sarszegi, Z.; Szabo, A.; Debreceni, B.; Kalman, N.; Tucsek, Z.; Sumegi, B.; Gallyas, F., Jr. Antioxidant and anti-inflammatory effects in RAW264.7 macrophages of malvidin, a major red wine polyphenol. *PLoS One* **2013**, *8*, e65355.
(37) Paixao, J.; Dinis, T. C.; Almeida, L. M. Malvidin-3-glucoside protects endothelial cells up-regulating endothelial NO synthase and inhibiting peroxynitrite-induced NF-kB activation. *Chem.−Biol. Interact.* **2012**, *199*, 192−200.
(38) Garcia-Alonso, M.; Rimbach, G.; Rivas-Gonzalo, J. C.; De Pascual-Teresa, S. Antioxidant and cellular activities of anthocyanins and their corresponding vitisins A − studies in platelets, monocytes, and human endothelial cells. *J. Agric. Food Chem.* **2004**, *52*, 3378−3384.

anatomical components the starchy endosperm, germ, and bran are present in the same relative proportions as they exist in the intact caryopsis". In April 2013, the AACCI further characterized a whole-grain product as being one that must contain 8 g or more of whole grain per 30 g of product.[27] The U.S. Food and Drug Administration (FDA) adopted the AACCI definition of whole grain; however, to qualify for the FDA whole-grain health claim at least 51% of the total weight of the product must be whole grain. The main whole-grain cereals consumed across the world are wheat, rice, and corn, followed by oats, rye, barley, triticale, millet, and sorghum.[18]

Carbohydrates. Starch is the main storage polysaccharide of cereal grains and is an important source of energy in the human diet. The endosperm of cereal grains contains mostly starch. In wheat, for example, starch comprises approximately 80−85% of the grain.[18] Starch is composed of amylose, a linear glucan with few branches, and amylopectin, which is a larger and more highly branched molecule. The ratios and molecular weights of the starch polymers vary widely among the cereals and help account for wide variations in functionality. Amylose comprises approximately 15−30% of total starch, and its content varies from one cereal to another.[28]

Dietary fiber includes macromolecules that resist digestion by human endogenous enzymes and is essentially composed of plant cell wall components.[19] These macromolecules are nonstarch polysaccharides, or structural carbohydrates.[29] Dietary fiber as defined by the AACCI is the edible part of plants and analogous carbohydrates that is resistant to digestion and absorption in the human small intestine with complete or partial fermentation in the large intestine. Dietary fiber includes polysaccharides, oligosaccharides, lignin, and associated plant substances.[27] Thus, the AACCI definition also includes resistant starch, which is starch that resists digestion in the small intestine, but is later fermented by the colonic microflora. There are several definitions of dietary fiber; some include resistant starch, whereas others do not include starch polysaccharides.[30] For labeling, dietary fiber is defined by a number of analytical methods that are accepted by the Association of Official Analytical Chemists International (AOAC). Thus, labeling and defining dietary fiber in the United States rely on analytical methods rather than an accurate definition that includes its role in health.[31]

Dietary fiber may be soluble or insoluble on the basis of its solubility in water and buffer solutions. Soluble fibers are easily fermented by the microflora of the large intestine. They consist of pectins, gums, inulin-type fructans, and some hemicelluloses. Insoluble fiber is poorly fermented, but it contributes to fecal bulk, thereby promoting laxation, and includes cellulose, some hemicelluloses, lignin, and arabinoxylan.[19]

Whole grains are an abundant source of dietary fiber and other bioactive components, with the bran and germ fractions containing higher proportions than the endosperm. For example, approximately 63% of the fiber component of wheat is found in the bran and germ.[18] During the refining process the bran and germ fractions are removed. Thus, most refined cereal products have lost the protective components.[18] Whole grains contain approximately 80% more dietary fiber than refined cereal products.[32] A product that contains the original components of a whole grain recombined to deliver the relative proportion that naturally occurs in the grain kernel is referred to as a reconstituted whole-grain product. The bulk of the whole-grain food products available on store shelves would be considered reconstituted whole-grain products.[32] In the United States, approximately 90% of the whole grains consumed are provided by ready-to-eat-cereals (28.7%), yeast breads (25.3%), hot cereals (13.75%), popcorn (12.4%), and crackers (6.4%).[33]

In a summary of the American Society for Nutrition Symposium on the health benefits of whole grains, Jonalagadda et al. determined that observational studies have consistently shown an association between whole-grain consumption and disease risk reduction; however, the evidence from interventional studies offered less support.[32] In an evaluation of studies using foods that conformed to the AACCI definition of whole grains, no effect of whole-grain consumption on cardiovascular disease (CVD) risk reduction was found. When the analysis was expanded to studies that included bran, germ, and fiber along with whole grains, the results of 14 observational studies suggested a protective effect of whole-grain consumption on CVD risk. In the expanded analysis, intervention studies for the most part supported a beneficial effect.[26] Similar associations have been determined for cereal fiber and whole grains on risk factors for obesity, diabetes, and CVD,[34] suggesting that the fiber component of whole grain may be the determining factor in the physiological responses. However, the mechanisms involved in eliciting the positive effect have not been clearly elucidated. The possibility of the synergistic actions of the other bioactive components cannot be excluded.[18]

It has been suggested that dietary fiber may be protective against colorectal cancer on the basis of the finding of a low incidence of colorectal cancer in rural, black Africans, whose diet contained large amounts of unprocessed food plants, especially cereals.[35] However, incontrovertible evidence from human studies of a protective role for dietary fiber in colorectal cancer is unavailable at this time. Large randomized controlled trials found no effect of supplementation of wheat bran[36] or dietary fiber[37] on the recurrence of colorectal adenomas.

In the large multicenter European Prospective Investigation into Cancer and Nutrition (EPIC) observational study, dietary fiber from foods was inversely related to incidence of large bowel cancer.[38] However, another large-scale epidemiological study showed no correlation between fiber intake and the risk of colorectal cancer.[39] Furthermore, in a pooled analysis of 13 prospective cohort studies it was found that high dietary fiber intake was not associated with a reduced risk of colorectal cancer when adjusted for other risk factors, but the study did find an increased risk among people with a low intake of dietary fiber (<10 g/day).[40] In a large prospective cohort of men and women in the NIH-AARP Diet and Health Study[41] that assessed dietary intake through self-administered food frequency questionnaires, although no association was found between fiber intake and colorectal cancer, a statistically significant inverse association between whole-grain consumption and colorectal cancer was observed. The authors suggested that whole-grain components other than fiber such as vitamins, minerals, phenols, and phytoestrogens may have an effect on colorectal carcinogenesis.

Starch is generally considered to be completely digestible; however, starches can contain significant amounts of resistant starch depending on the nature of the starch and the processing. The digestibility of starch and thereby the resistant starch content are influenced by several factors that affect its accessibility to enzymes such as the structure of the starch granule and whether it is disrupted or intact. Greater hydrolysis is achieved with hydration and heat treatments that cause gelatinization. The polymers in starches with high amylose

content can reassociate on cooling in a process called retrogradation, which is then poorly digested by amylases. Interactions with other food components such as the formation of lipid complexes may also reduce the rate of amylosis.[42]

In addition, grains also contain significant amounts of oligosaccharides such as oligofructose and inulin. These carbohydrates, which have a low level of polymerization, are nonviscous but have some effects similar to those of soluble fiber in the gastrointestinal tract.[43] Further dietary fiber, oligosaccharides, and resistant starch entering the large bowel can alter the gut microbiome and confer protective effects on health. The fiber and resistant starches are fermented to short-chain fatty acids (SCFAs), which may play an important role in the prevention and treatment of chronic disease. The molecular mechanisms by which SCFAs induce their effects are being actively investigated. Nevertheless, they have been shown to play an important role in the prevention and treatment of the metabolic syndrome, bowel disorders, and certain cancers.[44]

Proteins. A large proportion of the world supply of dietary protein, approximately 65%, is met by plant proteins with cereal grains (47%) and pulses, nuts, and oil seeds (8%) accounting for most of it.[45] In Western diets, protein from plant sources constitutes a lower proportion of protein intake compared to developing nations. The digestibility, amino acid composition, and presence of factors that influence digestibility are the major differences between plant and animal protein sources. However, contrary to popular belief, protein from plant sources can meet human protein needs. Whole grains are rich sources of protein, albeit low in the amino acid lysine. Diets that comprise plant sources of protein abundant in lysine such as pulses can complement whole-grain components. A lower protein to energy ratio may be the outcome compared to diets high in animal protein and more closely resembles the recommended intakes for protein.[46] Moreover, high intakes of animal protein are associated with obesity.[47] Plant sources of protein being lower in fat provide less energy.

Vitamins and Minerals. Whole-grain cereals are significant sources of the B-vitamins thiamin, niacin, pantothenic acid, and biotin. Wheat germ is rich in pyridoxine. However, whole-grain cereal products are not a particularly good source of folate. Moreover, the bioavailability in whole grains varies greatly and is far less than 100%. Of the B-vitamins, thiamin and pyridoxine have the greatest bioavailability.[18] Thiamin diphosphate functions as a coenzyme necessary for the oxidative decarboxylation of pyruvate, α-ketoglutarate, and the branched-chain amino acids. These reactions are necessary for generating energy. As a coenzyme it is involved in the synthesis of pentoses and NADPH. In addition, thiamin has a non-coenzyme role in membrane and nerve conduction.[48] Pyridoxal phosphate, the coenzyme form of vitamin B_6, is necessary for amino acid, lipid, and homocysteine metabolism as well as the synthesis of heme. It plays a role in the synthesis of serotonin from tryptophan and other neurotransmitters. A pyridoxine-dependent enzyme is also involved in homocysteine metabolism.[48]

Vitamin E functions as an antioxidant protecting the integrity of cellular membranes by preventing the oxidation of polyunsaturated lipids by free radicals.[49] In vivo studies among animals[50] and in human aortic endothelial cells[51] have shown that vitamin E prevents oxidative stress. The vitamin E content of whole-grain cereals is variable. Corn and rye are the richest sources, whereas wheat, barley, and oats have lesser amounts.[49] Vitamin E may also function to maintain selenium in the reduced state. Selenium is a cofactor for gluthathione peroxidase, an enzyme that protects against oxidative damage to tissues; however, the selenium content of cereals depends upon the soil in which the grain is grown.[52]

Whole grains and pulses are among the richest sources of magnesium, which may in part explain their favorable effects on insulin sensitivity and diabetes. In cardiac and vascular smooth muscle, magnesium has a role in the regulation of contractile proteins and sarcoplasmic reticular membrane transport of calcium ions (Ca^{2+}). It is a cofactor in ATPase activities and is involved in the metabolic regulation of energy-dependent cytoplasmic and mitochondrial pathways. Magnesium is found associated with calcium and phosphate in hydroxyapatite, the major component of bone. Additionally, magnesium is found on the surface of bone in an amorphous form that is thought to maintain serum levels through an exchangeable pool.[48] Intracellular magnesium concentration has also been shown to be effective in increasing insulin secretion and the rate at which glucose is cleared from the blood. It offsets calcium-related excitation−contraction coupling and decreases smooth cell responsiveness to depolarizing stimuli. Thus, magnesium may play a key role in modulating insulin-mediated glucose uptake and vascular tone.[53] However, calcium from whole-grain cereals may not contribute significantly to bone health because the calcium to potassium ratio in cereals is below the recommendation for effective calcium use by the body. More than 85% of the potassium content of cereals is supplied by phytic acid, which has a high affinity for hydroxyapatite. Thus, grain consumption may have a role in dental health through the cariostatic effect of phytic acid.[18]

Other minerals such as iron, zinc, copper, and manganese are cofactors of antioxidant enzymes and have other regulatory and metabolic functions. The physiological functions of zinc include bone formation, skin integrity, carbohydrate metabolism, and taste acuity.[48,54] Iron has an important role in respiration and energy metabolism, immune function, and cognitive development. Plant foods are primarily sources of nonheme iron. The absorption of nonheme iron is approximately 2−3%, which can be enhanced to 8% if it is ingested along with a source of vitamin C and meat, fish, or poultry.[48] Furthermore, whole grains have a high concentration of phytic acid, and chelation of minerals may reduce their bioavailability.

Phytonutrients. Phytochemicals are non-nutrient bioactive compounds in fruits, vegetables, grains, and other plant foods that may reduce the risk of chronic disease.[55] Phenolics are phytochemicals that form part of the plant defense mechanism and include phenolic acid, which contributes approximately two-thirds of the phenolics in our diets, the remaining being supplied by flavonoids.[55] The phenolic compounds in grains include derivatives of benzoic and cinnamic acids, anthocyanidins, quinones, flavonols, chalones, amino phenolic compounds, tocotrienols, tocopherols, and carotenoids.[56] Whole grains are a major source of phenolic acids such as ferulic, vanillic, caffeic, syringic, sinapic, and *p*-coumaric acids.[49] Whole grains have been associated with antioxidant activity, which may be attributed to their phytochemical content.

Phenolic acids are mostly found esterified or bound to plant cell wall polymers. These complexes can evade digestion to reach the colon intact, where they may be digested by organisms in the microbiome, thereby releasing the bound phenolic compounds to exert their physiological effects. Thus, unlike fruits and vegetables where the antioxidant polyphenols are either free or in the form of soluble conjugates and available

in the small intestine, in whole grains their site of action may be the colon.[49] This may in part be the reason why whole grains have been associated with reduced risk of colon cancer.

The antioxidant capacity of breads, ready-to-eat breakfast cereals, and uncooked cereals ranges from 13.18 to 24.79 Trolox equivalents (TE)/g, which is higher than that of most vegetables but far less than that of dry beans, which ranges from 80.4 to 149.21/g.[57] In vivo, the antioxidant potential may be higher than that derived from in vitro assays because fiber-associated compounds are generally not included.[49] The bound fractions make a significant contribution and are generally much higher than the free and soluble fractions.[58,59]

Carotenoids are a group of pigments synthesized by plants and select species of algae and fungi.[60] Approximately 90% of the carotenoids in the human diet consist of β-carotene, α-carotene, lycopene, cryptoxanthin, and lutein.[61] One of the characteristic features of carotenoids is a long series of alternating double and single bonds. Carotenoids scavenge free radicals and become free radicals themselves, but they can remain stable compounds because the free radical can be delocalized among the alternating single and double bonds. Thus, carotenoids make good antioxidants.[62] Despite a vast amount of research, a disease-preventing role is hard to ascribe to carotenoids,[60,63] which may be because the experimental designs have used an all or none approach more conducive to trials of drug efficacy, whereas the populations may not have been completely naïve to carotenoids. Carotenoids are ubiquitous components of food and may have small effects that aggregate over decades, working in synergy with other dietary components and lifestyle factors.[60]

Phytic acid present in whole grains chelates minerals such as zinc, iron, calcium, and magnesium, which reduces their bioavailability. On the positive side, phytic acid has been shown to reduce oxidative damage by suppressing iron-catalyzed oxidative reactions.[18] Phytic acid may also reduce oxidative damage to the intestinal epithelium associated with oxygen radicals produced by colonic bacteria.[52] However, the antioxidant effect of phytic acid from whole grains has not been evaluated.

Lignins are components of whole-grain cereals that may comprise 3−7% of the bran fraction. Structurally, lignins are related to lignans but differ from them by their polymeric nature and distribution in plants. Lignans are phytoestrogens present in whole grains such as corn, oats, wheat, and rye. Rats can metabolize lignins and lignans from cereal sources to mammalian lignans.[64] Lignans and their metabolites, the mammalian lignans enterodiol and enterolactone, have antioxidant potential due to their polyphenolic structure.[49] Lignins, because of their polymeric nature and their embedding in the cell wall, are usually considered inert in the digestive tract.[64] Lignans have been shown to be protective against certain cancers;[65] hence, if lignins are metabolized to lignans in humans as they are in rats, whole-grain cereal consumption might confer added anticancer effects.[18]

Plant sterols and stanols are found in grains, as well as pulses. These compounds are structurally similar to cholesterol. The mechanisms by which they are clinically beneficial include reduction in cholesterol absorption and transintestinal cholesterol synthesis, both of which result in increased fecal neutral sterol excretion to explain the low-density lipoprotein (LDL) cholesterol lowering effect of plant sterols and stanols.[66] The vast amount of evidence to support a cholesterol-lowering effect led to the recommendation for the inclusion of plant sterols and stanols in the diet because humans are unable to synthesize these compounds. However, the recommended level of 2 g/day is difficult to meet and the average consumption in the Western diet ranges from 0.2 to 0.4 g/day.[67] Thus, whole-grain consumption may help to meet the recommendation and potentially confer a cardioprotective effect.

COMPOSITION OF PULSES

Legumes are plants belonging to the Leguminosae family. They are second to cereals in providing food crops for the world.[68] Legumes include alfalfa, clover, lupin, green beans and peas, peanuts, soybeans, dry beans, broad beans, dry peas, chickpeas, and lentils. Pulses are annual leguminous crops yielding from 1 to 12 grains or seeds within a pod. The Food and Agriculture Organization (FAO) limits its definition of pulses to crops harvested solely for dry grain, thereby excluding crops harvested green for food such as green peas and green beans, and classifies these as vegetable crops. Also excluded are those crops used mainly for oil extraction, such as soybean and peanuts, and leguminous crops such as seeds of clover and alfalfa that are used exclusively for sowing purposes. Pulses contain approximately 55−65% of their total weight as carbohydrates, mainly starches.[69] The protein content of pulses ranges from about 20% (dry weight) in peas and beans to 38−40% in lupin.[68] A serving of pulses (half cup of cooked dried pulses) contains 2−4 g of fiber and 7−8 g of protein. Most beans are very low in fat, generally containing <5% of energy as fat except for chickpeas, lupin seeds, and soybeans, which contain from <15 to 47% fat.[70] Pulses contain substantial amounts of the B-vitamins and minerals important for human health, such as iron, calcium, and potassium, as well as phytochemicals: bioactive compounds, including enzyme inhibitors, lectins, oligosaccharides, and phenolic compounds.[71]

Carbohydrates. Starch digestibility affects the glycemic response and compared to cereal foods such as whole-grain breads, spaghetti, rice, breakfast cereals, and oatmeal, legumes elicit the lowest postprandial glucose responses.[72,73] The digestibility of starch from legumes is much lower than that ofcereal starch.[74−77] The rate at which legume starches are digested is approximately 45% lower than that of cereal starches.[75] Starch digestion is slowed in the small intestine if access to pancreatic amylase is hindered by the presence of other plant materials. Pulses have a rigid cell wall, which inhibits swelling and dispersion of the starch. Moreover, the crystallinity of starch in pulses as determined by the ordered arrangements of adjacent double-helix amylopectin is the B and C type, which is more resistant to digestion than the A type found in cereals.[19] Pulses contain 30−40% of amylose starch, which is 5−10% more amylose starch than cereals.[78] Higher amylose than amylopectin starch content correlates with higher resistant starch content.[19] Although it is difficult to quantify resistant starch because of a lack of standardized methods of analysis,[79] cooked pulses are prone to retrograde more quickly than cereals, which slows the process of digestion. Moreover, pulses are high in protein, and protein−starch interactions further hinder digestibility. Additionally, the presence of high amounts of dietary fiber in pulses may greatly lower the rate and extent of starch digestibility.[19]

Pulses are high in fiber even without including the resistant starch fraction, ranging from 4 to 19 g and averaging approximately 13 g per cup of mature dry seeds, cooked (boiled without salt).[80] Along with cereals, pulses are a primary source of phytates in the human diet. Phytates may reduce the

rate of starch digestion and delay the postprandial glycemic response.[81] Furthermore, α-amylase inhibitors found in pulses, particularly dry beans, in amounts ranging from 2 to 4 g/kg may also reduce starch availability.[82] Bean extracts containing α-amylase inhibitors have been shown to reduce starch digestion in vitro and cause weight loss in humans,[83] but the lack of consistent results[83−86] and the fact that residual phytohemagglutinin present in beans may cause adverse gastrointestinal events[87] warrant further investigation. Thus, pulses are known as slow-release carbohydrates because of their reduced digestibility.

The oligosaccharides raffinose, stachyose, and verbascose are present in pulses in amounts ranging from 1 to 12% of the dry weight of pulses. Humans lack α-galactosidases in the upper regions of the gastrointestinal tract; hence, the oligosaccharides enter the lower gut, where they are fermented by bacteria to produce carbon dioxide and hydrogen.[88] The flatulence and bloating associated with pulse consumption has been attributed to these nondigestible but rapidly fermentable oligosaccharides. The discomfort of possible gastrointestinal disturbances may deter pulse consumption,[89] although evidence suggests that flatulence or other gastrointestinal symptoms associated with the consumption of pulses may progress into tolerance.[90,91]

The amount and type of dietary fiber have major influences on the composition of intestinal microbiota and thereby the production of SCFAs.[44] However, it is likely that the diet-induced effects depend on pre-existent gut microbial composition, in interaction with the host phenotype. Changes in the diet such as increased nondigestible food ingredients can also result in shifts in microbiota distribution.[92] Nevertheless, the high oligosaccharide and resistant starch components of pulses are potentially good sources of substrates for SCFA production.

Humans share a mutual relationship with their gut microbiota marked by symbiosis, wherein one partner benefits without harming the other, or commensalism, wherein partners coexist without detriment but without any noticeable benefit.[93] The mucosal immune system selectively and actively tolerates the gut microbiota during steady-state conditions and will mount an inflammatory response once there is a threat of disease or infection. Once microbiota are under immune attack, a more pathogenic profile will emerge and the peaceful coexistence will cease. Commensal bacteria maintain a stable environment by inducing and modulating host innate immunity.[94] Thus, manipulations of the gut microbiome through the diet are therapeutic interventions that are not unthinkable; however, it is only long-term diets that appear to effect the desired changes.[95] Because α-galactosides, more commonly known as oligosaccharides, comprise 25−65% of the sugar fraction of legumes,[96] their prebiotic potential is worthy of exploration.

Proteins. Pulses accumulate large amounts of proteins during their development and are among the richest sources of dietary proteins. The proteins in pulses are largely storage proteins with globulins forming the largest component. Pulse storage proteins are relatively low in sulfur-containing amino acids, methionine and cysteine, as well as the aromatic amino acid tryptophan. However, they contain significant amounts of lysine, which is the limiting amino acid in cereals, making the two plant sources of proteins nutritionally complementary. The degree of complementation may also depend on the content of the second limiting amino acid, namely, threonine in cereals and tryptophan in pulses.[68] Meat consumption in the United States averages 212 g/day. High meat consumption is associated with higher intakes of energy and fat compared to lower meat intake and a greater likelihood of obesity.[47] High red meat intake is associated with less desirable levels of the biomarkers of inflammation and glucose metabolism (C-reactive protein, fasting insulin, and HbA1C), and a high body mass index (BMI) accounts for a significant proportion of this association.[97] Therefore, although protein needs in the United States are largely met by meat consumption, substitution with plant proteins provides a healthier option.

Pulse seeds contain several comparatively minor proteins called antinutrients, including enzymes, enzyme inhibitors, and lectins. The inhibition of various digestive enzymes, including trypsin, chymotrypsin, and amylase, reduces the bioavailability of nutrients, but their effect is usually manifest only if the seed or the flour is consumed uncooked, because cooking normally denatures the antinutrients.[68] The term antinutrient appears to be a misnomer as their extracts have beneficial effects on human health and the nutraceutical potential is worth noting.

Lectins account for 2.4−5% of the protein content of kidney beans. They directly inhibit HIV reverse transcriptase, an enzyme critical for replication of the human immunodeficiency virus, and β-glucosidase, which is required for processing of viral proteins.[82] Thus, lectins from kidney beans form an important component of antiretroviral therapy. Including raw kidney beans in the diet of obese rats reduces lipid accumulation, which may be due to reduced insulin levels caused by lectins.[98] Lectins can resist gastric digestion, yet they can be absorbed into the bloodstream while remaining biologically active, and these properties may contribute to their antitumor effects. Lectins may bind to cell membranes or receptors to cause cytotoxicity, apoptosis, and inhibition of tumor growth. They may also penetrate the cell to cause agglutination of cancer cells.[99] Lectins may have a role in weight management by increasing the shedding of brush border membranes to interfere with gastric secretion and nutrient absorption, but reports of lectin toxicity are conflicting.[100] Thus, further research on a safe and effective dose is needed before its therapeutic role in the treatment of obesity is promoted.

Protease inhibitors of the Bowman−Birk inhibitor family, from peas, have been shown to have antiproliferative effects in human colon cancer cells. These inhibitors also inhibit protease-mediated inflammation. However, the beneficial effects require the protein to be in the biologically active form. Although cooking deactivates these proteins, denaturation may not always be complete; thus, regular consumption may contribute to the beneficial effect.[68] Angiotensin-1 converting enzyme (ACE) raises blood pressure when it converts angiotensin-1 to a potent vasoconstrictor angiotensin-2, and ACE inhibitor drugs are used to treat hypertension. Chickpeas and peas contain ACE inhibitor peptides. In vitro digestion studies indicate that pea protein and red lentil isolates have antihypertensive activity.[101,102] Therefore, pulses and their extracts may possess the potential for anticarcinogenic, anti-inflammatory, and antihypertensive effects, but further research is needed.

Vitamins and Minerals. Pulses are also a good source of B-vitamins, namely, riboflavin, thiamin, niacin, pyridoxine, and folic acid. These vitamins have important functions in energy metabolism and fatty acid metabolic pathways. Niacin is a coenzyme in energy metabolism and fatty acid metabolic pathways. It is involved in the modification of chromosomal

Table 1. Energy, Macronutrient, and Fiber Contents of Common Legumes and Cereals[a]

	serving size	energy (kcal)	carbohydrate (g)	protein (g)	fat (g)	fiber[b] (g)
legumes						
pinto beans	1/2 cup	122	22.42	7.70	0.56	7.7
great northern beans	1/2 cup	104	18.66	7.37	0.40	6.2
navy beans	1/2 cup	127	23.71	7.49	0.56	9.6
black beans	1/2 cup	114	20.39	7.62	0.46	7.5
cowpeas (blackeyes, crowder, southern)	1/2 cup	99	17.75	6.61	0.45	5.6
kidney beans	1/2 cup	112	20.18	7.67	0.44	5.7
chickpeas	1/2 cup	134	22.48	7.27	2.12	6.2
split peas	1/2 cup	116	20.68	8.17	0.38	8.1
lentils	1/2 cup	115	19.93	8.93	0.38	7.8
lupin	1/2 cup	99	8.20	12.92	2.42	2.3
whole-grain products						
bread, whole wheat	1 slice	81	13.67	3.98	1.12	1.9
English muffin, whole wheat	1/2 muffin	67	13.33	2.90	0.69	2.2
bread pita, whole wheat	1, 4 in. diameter	74	15.40	2.74	0.73	2.1
crackers, whole wheat	6 crackers	118	19.20	2.92	3.90	2.8
oats, regular or quick, cooked with water	1/2 cup	83	14.04	2.97	1.78	2.0
ready-to-eat cereal, All Bran	1/2 cup	81	23.01	4.07	1.52	9.1
rice, brown, medium grain, cooked	1/2 cup	109	22.92	2.26	0.81	1.8
spaghetti, whole wheat, cooked	1/2 cup	87	18.58	3.73	0.38	3.2
popcorn, air popped	3.5 cups	108	21.78	3.62	1.29	4.1
refined grain products						
bread, white	1 slice	74	13.74	2.56	0.89	0.8
bread, rye	1 slice	83	15.46	2.72	1.06	1.9
barley, pearled, cooked	1/2 cup	97	22.15	1.77	0.35	3.0
pseudocereals						
amaranth, cooked	1/2 cup	125	22.99	4.67	1.94	2.60
quinoa, cooked	1/2 cup	111	19.70	4.07	1.78	2.60
buckwheat, cooked	1/2 cup	77	16.75	2.84	0.52	2.30

[a]Values are for one serving of mature dry legume seeds, cooked (boiled without salt), and one serving of cereals. Source: U.S. Department of Agriculture (USDA), Agricultural Research Service, 2012. USDA National nutrient database for Standard Reference26. Nutrient Data Laboratory Home Page, http://www.ars.usda.gov/ba/bhnrc/ndl. [b]Does not include all of the resistant starch fraction.

proteins that function in the nucleus in DNA repair and regulation as well as cell differentiation. Niacin is also required for mobilization of calcium from intracellular stores.[48] In societies where the chief dietary staple consists of cereals such as corn or sorghum, niacin deficiency is likely to occur because it is covalently bound to complex carbohydrates, although chemical treatment with bases such as limewater can improve availability.[48]

Beans are an excellent source of folate, and two or more servings of some pulses can provide approximately 400 μg, which represents 100% of the daily requirements.[71] Global DNA hypomethylation and targeted hypermethylation are considered deviant patterns of DNA methylation found in many human diseases, such as cancer, imprinting disorders, and developmental disabilities.[103−105] Reductions in global DNA methylation may be precipitated by a low folate status.[106]

Minerals are essential micronutrients in human health. Iron is essential for respiration and energy metabolism. Zinc is a component of numerous metalloenzymes having catalytic activity or structural integrity that are zinc-dependent.[48] Although the bioavailability of iron from pulses is relatively low, approximately 20−25% of zinc is bioavailable.[107] Zinc deficiency has been associated with cardiovascular and renal diseases.[108] Calcium is an important component of the structure of bones and teeth. It is involved in blood clotting, enzyme regulation, nerve transmission, and muscle contraction.[48] Calcium bioavailability from pulses is half that of milk; nevertheless, approximately 20% of the calcium content of beans is bioavailable.[109]

Pulses are high in potassium and low in sodium. The effects of potassium on blood pressure are intertwined with sodium. The kidneys are genetically predisposed to conserve sodium and excrete potassium. This adaptation is linked to prehistoric humans who consumed a diet rich in potassium and low in sodium. The linkage of modern diets rich in sodium and low in potassium to the pathogenesis of hypertension is supported very strongly by reductions in blood pressure with diets that reverse this cationic composition.[110,111]

Retained sodium not only replaces potassium, which is then excreted in the urine, but it is also stored extracellularly in skin, cartilage, and bone. It is readily mobilized to increase its level in body fluids. Thus, in the absence of conservation, a low-potassium diet leads to a potassium deficit in the body. Sodium retention and potassium depletion have direct effects on arterial wall endothelium and nitric oxide synthesis to promote vasoconstriction. Sodium restriction and a high-potassium diet reverse these effects.[111] Moreover, potassium deficiency is associated with glucose intolerance and impaired insulin secretion, whereas potassium infusion increases insulin secretion. Membrane depolarization induced by potassium may be the trigger for insulin secretion by pancreatic β cells.[112,113]

Phytonutrients. The major phenolic compounds in pulses are tannins, phenolic acids, and flavonoids. Phenolics have at

Table 2. Vitamin Contents of Common Legumes and Cereals[a]

	serving size	thiamin (mg)	riboflavin (mg)	niacin (mg)	pantothenic acid (mg)	pyridoxine (mg)	folate (μg)	vitamin E (α-tocopherol, mg)
legumes								
pinto beans	1/2 cup	0.165	0.053	0.272	0.180	0.196	147	0.800
great northern beans	1/2 cup	0.140	0.052	0.603	0.235	0.104	90	
navy beans	1/2 cup	0.216	0.060	0.591	0.242	0.126	127	0.010
black beans	1/2 cup	0.21	0.051	0.434	0.208	0.059	128	
cowpeas	1/2 cup	0.173	0.047	0.423	0.351	0.086	178	0.240
kidney beans	1/2 cup	0.142	0.051	0.512	0.195	0.106	115	0.030
chickpeas	1/2 cup	0.095	0.052	0.431	0.235	0.114	141	0.290
split peas	1/2 cup	0.186	0.055	0.872	0.583	0.047	64	0.030
lentils	1/2 cup	0.167	0.072	1.049	0.632	0.176	179	0.110
lupin	1/2 cup	0.111	0.044	0.411	0.156	0.007	49	
whole-grain products								
bread, whole wheat	1 slice	0.126	0.053	1.420	0.207	0.069	13	0.850
English muffin, whole	1/2 muffin	0.099	0.046	1.125	0.229	0.054	16	0.140
bread pita, whole wheat	1, 4 in. diameter	0.095	0.022	0.795	0.233	0.074	10	0.170
crackers, whole wheat	6 crackers	0.050	0.006	1.278	0.230	0.051	8	0.390
oats, regular or quick, cooked with water	1/2 cup	0.089	0.019	0.262	0.363	0.006	7	0.090
ready-to-eat cereal, All Bran	1/2 cup	0.704	0.840	4.588	0.329	3.720	406	0.380
rice, brown, medium grain, cooked	1/2 cup	0.099	0.012	1.297	0.382	0.145	4	-
spaghetti, whole wheat, cooked	1/2 cup	0.076	0.032	0.495	0.293	0.055	4	0.210
popcorn, air popped	3.5 cups	0.029	0.023	0.646	0.143	0.044	9	0.080
refined grain products								
bread, white	1 slice	0.149	0.068	1.338	0.150	0.024	31	0.060
bread, rye	1 slice	0.139	0.107	1.218	0.141	0.024	35	0.11
barley, pearled, cooked	1/2 cup	0.065	0.049	1.619	0.106	0.090	13	0.01
pseudocereals								
amaranth, cooked	1/2 cup	0.018	0.027	0.289	[b]	0.139	27	0.230
quinoa, cooked	1/2 cup	0.099	0.102	0.381	[b]	0.114	39	0.580
buckwheat, cooked	1/2 cup	0.034	0.033	0.790	0.302	0.065	12	0.080

[a]Values are for one serving of mature dry legume seeds, cooked (boiled without salt), and one serving of cereals. Source: U.S. Department of Agriculture (USDA), Agricultural Research Service, 2012. USDA National nutrient database for Standard Reference26. Nutrient Data Laboratory Home Page, http://www.ars.usda.gov/ba/bhnrc/ndl. [b]Value unavailable at source.

least one aromatic ring with one or more hydroxyl groups. They can transfer electrons to remove free radicals, chelate metal catalysts, activate enzymes, and inhibit oxidases.[114] These compounds are known to have antioxidant, anti-inflammatory, and antimicrobial properties[115] that protect body tissues against oxidative stress.[116] Flavonoids limit free radicals, free radical mediated cellular signaling, and inflammation.[117] They improve endothelial dysfunction and platelet aggregation.[118] Enhanced reactive oxygen species release from the vascular wall can affect the platelet activity cascade by scavenging nitric oxide and thereby decreasing the antiplatelet activity of the endothelium.[119]

Polyphenols reduce the expression of NADPH oxidase, an enzyme that generates superoxide anions in arterial cells, and increase the expression of antioxidant enzymes such as catalase and superoxide dismutase. Their antioxidant effects extend to inflammation-related proteins such as nuclear factor κB and cyclooxygenase-2. Thus, polyphenols reduce vasoconstriction and pro-inflammatory responses and promote vascular health by reducing oxidative stress induced degradation of nitric oxide.[120,121] Anthocyanins are present in pulses such as black beans,[82] red kidney beans, and pinto beans.[116] They have been shown to increase phase II antioxidant and detoxifying enzymes in human gastric adenocarcinoma cells[122] and breast epithelial cell lines exposed to a carcinogen.[123] Phenolic compounds have the potential to prevent tumor development. Lentils have the highest phenolic content, followed by red kidney beans and black beans.[82] The high pigmentation in dark-colored beans such as red kidney beans and black beans appears to increase their phenolic content.

Pulses contain other minor constituents such as phytic acid and saponins that promote human health. Phytic acid induces differentiation and maturation of malignant cells, often reverting cells to the normal phenotype. It can regulate the cell cycle to impede uncontrolled cell division, forcing malignant cells to either differentiate or go into apoptosis.[124] Saponins suppress the metastatic potential of tumors by regulation of enzymes involved in the apoptosis pathway, leading to programmed cell death.[82] Saponins form an insoluble complex with cholesterol to inhibit its intestinal absorption. By increasing the excretion of bile acids some saponins indirectly decrease cholesterol.[71,125] The energy, macronutrient, and fiber composition of select pulses and cereal products are presented in Table 1. The vitamin and mineral components are presented in Tables 2 and 3, respectively.

HEALTH BENEFITS OF WHOLE GRAINS

The evidence for an association between whole-grain consumption and health is largely supported by observational

dx.doi.org/10.1021/jf500932z | J. Agric. Food Chem. 2014, 62, 7029−7049

Table 3. Mineral Contents of Common Legumes and Cereals[a]

	serving size	Ca (mg)	Fe (mg)	Mg (mg)	P (mg)	K (mg)	Na (mg)	Zn (mg)	Cu (mg)	Mn (mg)	Se (mg)
legumes											
pinto beans	1/2 cup	39	1.79	43	126	373	1	0.84	0.187	0.387	5.3
great northern beans	1/2 cup	60	1.89	44	146	346	2	0.78	0.219	0.458	3.6
navy beans	1/2 cup	63	2.15	48	131	354	0	0.94	0.191	0.480	2.6
black beans	1/2 cup	23	1.81	60	120	305	1	0.96	0.180	0.382	1.0
cowpeas	1/2 cup	21	2.15	45	133	238	3	1.10	0.229	0.406	2.1
kidney beans	1/2 cup	31	1.96	37	122	358	1	0.88	0.191	0.381	1.0
chickpeas	1/2 cup	40	2.37	39	138	239	6	1.25	0.289	0.845	3.0
split peas	1/2 cup	14	1.26	35	97	355	2	0.98	0.177	0.388	0.6
lentils	1/2 cup	19	3.30	36	178	365	2	1.26	0.248	0.489	2.8
lupin	1/2 cup	42	1.00	45	106	203	3	1.15	0.192	0.561	2.2
whole-grain products											
bread, whole wheat	1 slice	52	0.79	24	68	81	146	0.57	0.073	0.696	8.2
wheat	1/2 muffin	87	0.81	23	93	69	120	0.53	0.070	0.591	13.3
bread pita, whole wheat	1, 4 in. diameter	r4	0.86	19	50	48	124	0.43	0.081	0.487	12.3
crackers, whole wheat	6 crackers	10	0.92	30	91	95	194	0.73	0.016	0.594	2.8
oats, regular or quick, cooked with water	1/2 cup	11	1.05	32	90	82	5	1.17	0.087	0.679	6.3
ready-to-eat cereal, All Bran	1/2 cup	121	5.46	112	356	316	80	3.84	0.322	2.297	2.9
rice, brown, medium grain cooked	1/2 cup	10	0.52	43	75	77	1	0.6	0.079	1.070	*b*
spaghetti, whole wheat, cooked	1/2 cup	10	0.74	21	62	31	2	0.57	0.117	0.965	18.1
popcorn, air popped	3.5 cups	2	0.89	40	100	92	2	0.86	0.073	0.312	0
refined grain products											
bread, white	1 slice	73	1.01	7	29	32	137	0.24	0.035	0.166	6.2
bread, rye	1 slice	23	0.91	13	40	53	193	0.36	0.060	0.264	9.9
barley, pearled, cooked	1/2 cup	9	1.04	17	42	73	2	0.64	0.082	0.203	6.8
pseudocereals											
amaranth, cooked	1/2 cup	58	2.58	80	182	166	7.00	1.06	0.183	1.050	6.8
quinoa, cooked	1/2 cup	16	1.38	59	141	159	6.00	1.01	0.178	0.584	2.6
buckwheat, cooked	1/2 cup	6	0.67	43	59	74	3.00	0.51	0.123	0.339	1.8

[a]Values are for one serving of mature dry legume seeds, cooked (boiled without salt) and one serving of cereals. Source: U.S. Department of Agriculture (USDA), Agricultural Research Service, 2012. USDA National nutrient database for Standard Reference26. Nutrient Data Laboratory Home Page, http://www.ars.usda.gov/ba/bhnrc/ndl. [b]Value unavailable at source.

studies, which precludes the establishment of causality.[126] Epidemiological data collected among a predominantly Caucasian population suggest that the consumption of three or more servings (3 oz equivalents) of whole grains is associated with a positive impact on body mass index (BMI), abdominal obesity, CVD risk reduction, and glucose homeostasis.[32] A comprehensive meta-analysis showed that compared with those who rarely or never consume whole grains, 48−80 g of whole grains or three to five servings of whole grains per day reduces the risk for type 2 diabetes and CVD by 26 and 21%, respectively. An inverse association between whole-grain intake and weight gain was also observed.[127]

Observational studies that reported an inverse association between whole grains and chronic disease investigated mixtures of whole grains and ≥25% of bran rather than whole grains alone.[128] However, there is a paucity of randomized controlled trials (RCTs) assessing the health effects of whole-grain consumption. Moreover, they are of short duration (≤1 year), measured biomarkers rather than end points of disease, and used a specific fiber, whole grain, or bran in doses that do not represent daily consumption. The existing evidence from RCTs suggests that whole grains alone are insufficient to exert a beneficial effect on disease risk reduction.[128,129]

Cardiovascular Disease. There is fairly consistent evidence to support an association between whole-grain consumption and a reduction in blood pressure.[130,131] Four or more servings of whole grains are associated with a 23% lower risk of hypertension.[130] The evidence from RCTs is less consistent. In one study substitution of three servings of refined cereals foods with whole-grain foods (100−120 g of whole-wheat foods or whole-wheat foods and oats) for 12 weeks lowered blood pressure.[132] In another study among 14 normal-weight healthy individuals, 48 g/day of whole-grain consumption for 3 weeks reduced blood pressure.[133] Replacement of 20% of the energy content of the Step 1 diet of the American Heart Association with whole grains reduced blood pressure in mildly hypercholesterolemic individuals.[134] However, 3 months of high-fiber cereal foods did not improve blood pressure in 23 diabetic individuals.[135]

A positive association between whole-grain consumption and improvements in coronary artery intima media thickness has been observed,[136,137] but the effect of whole-grain consumption on blood lipids is not clear. The effect of β-glucan, a soluble fiber found in oats and barley, on reducing low-density lipoprotein cholesterol is well documented,[138−142] but, apart from the quantity, other properties such as the molecular weight and solubility of β-glucan influence its physiological effects.[143] These properties, which determine the cholesterol-lowering effects, may be altered during processing. Thus, it is difficult to draw any definite conclusions as to the effects of these extracts compared to consumption of the whole grain. Furthermore, the effect of whole-grain foods prepared from

other cereal grains in lowering blood lipids is not consistent.[144−146]

Whole-grain consumption has been shown to decrease C-reactive protein, a marker of inflammation, in overweight adults with the metabolic syndrome consuming a hypocaloric diet for 4 weeks.[147] However, in the WHOLEheart study the addition of up to 120 g of whole grains to the diet over 8 and 16 weeks did not significantly improve markers of CVD risk, including C-reactive protein, among 316 overweight individuals.[144] A majority of the studies evaluating the effect of whole-grain consumption on cardiovascular risk included the fiber-rich bran and the germ as well as the whole grain in the definition of whole grain. When only studies that meet the FDA definition of whole grain are analyzed, it appears that there is insufficient evidence to support a claim that whole grains reduce the risk of CVD, suggesting that the fiber content of whole grains may to a large extent mediate its cardiovascular effects.[26] On conducting a systematic review of the scientific evidence including controlled clinical trials and prospective cohort studies in healthy individuals, Health Canada concluded that the current evidence may not be sufficient to support a health claim about whole grains and coronary heart disease.[148]

Diabetes and the Metabolic Syndrome. Epidemiological evidence indicates an inverse association between whole-grain consumption and type 2 diabetes.[10,149] A meta-analysis showed that a two serving per day increase in whole-grain consumption is associated with a 21% reduction in the risk for type 2 diabetes.[10] In a randomized crossover trial among 30 overweight individuals, markers of insulin sensitivity and inflammation were not significantly affected by the inclusion of whole grains in the diet for 6 weeks compared to refined grains intake. Insulin sensitivity was measured using the euglycemic hyperinsulinemic glucose clamp, which is considered the gold standard for measurement of insulin sensitivity.[150] However, in a smaller randomized crossover study among 11 overweight or obese hyperinsulinemic individuals, consumption of whole grains for 6 weeks improved insulin sensitivity measured using the glucose clamp.[151] Whole-grain consumption for 12 weeks had no effect on insulin sensitivity, compared to consumption of refined cereals assessed by the frequently sampled intravenous glucose tolerance test.[152] In other studies, consumption of high-fiber cereal foods for 3 months did not improve markers of glycemic control or risk factors for coronary heart disease in 23 subjects with type 2 diabetes.[135] However, in 61 subjects with the metabolic syndrome, a 12 week diet based on whole grains reduced postprandial insulin and triglyceride responses compared to a diet based on refined grains.[153] In a review of studies evaluating the effects of oat and barley products on blood glucose, it was determined that at least 4 g of β-glucan is needed to lower the glycemic response.[154] The FDA concurred with The 2010 Dietary Guidelines Advisory Committee and concluded that there is limited evidence for an association between whole-grain intake and reduced risk of type 2 diabetes.[155] The Grains for Health Foundation Summit 2012 arrived at a similar conclusion[156]

Obesity. Whole-grain products from rye, oats, barley, and wheat have been shown to increase satiety. Whole-grain rye is a good source of soluble and insoluble dietary fiber.[157] Arabinoxylan is the dominant fiber, and the water extractable component of arabinoxylan is highly viscous when dispersed in water.[158] Similarly, oats and barley contain the soluble fiber β-glucan in significant amounts, which exhibits a high viscosity at relatively low concentrations.[159] Viscous soluble dietary fiber delays gastric emptying and slows intestinal transit to reduce the absorption rate of nutrients, thereby increasing the possibility of interaction between nutrients and the cells that release satiety hormones.[160]

Whole-grain rye products have consistently been shown to increase satiety, compared to wheat bread.[161−168] The results of studies investigating the effect of β-glucan from oats and barley on satiety are inconsistent. Using β-glucan in doses ranging from 2.2 to 9 g, several studies found that satiety or satiety hormones increased,[143,169−174] whereas others found no effect of β-glucan on satiety.[175−177] The insoluble fiber found in breakfast cereals made with whole-grain wheat in amounts ranging from 26 to 33 g/meal also increased satiety compared to cornflakes of equal weight,[178] or equal energy content,[179] as well as compared with a breakfast of bacon and eggs.[180] However, subjective satiety and food intake following consumption of whole-grain bread providing 10.5 g of fiber per day for 3 weeks was not significantly different compared to refined grain bread providing 5.8 g of fiber per day.[133] Thus, the fiber component of whole grains through its effects on bulking and viscosity may help to keep consumers full for a prolonged period.

Observational studies have consistently shown that whole-grain consumption of approximately three servings (≥3 oz equivalents of whole-grain foods) per day is associated with lower BMI compared to refined grain intake.[11,181,182] Reductions in weight gain and abdominal obesity have also been observed with whole-grain consumption.[34,183] In the Health Professionals follow-up study, a prospective study assessing 8 year weight gain among health professionals, a 40 g per day increase in whole-grain intake from all foods reduced body weight by 0.49 kg. The addition of bran was found to further reduce the risk of weight gain. Every 20 g per day increase in bran intake reduced weight gain by 0.36 kg.[183]

The results of intervention trials have been less consistent. In studies evaluating the effect of whole-grain consumption over 4−12 weeks, no differences in weight loss were found when compared with control diets,[146,147,184−186] although one study found a reduction in fat mass[146] and another found a decrease in waist circumference[186] compared to refined grain consumption. In a meta-analysis including 21 RCTs, whole-grain intake reduced weight gain compared to control diets. However, heterogeneity among the studies, short intervention periods, and relatively small sample sizes limit the results of this analysis.[127]

More recently, a meta-analysis[187] evaluating the evidence from 26 RCTs investigating the effect of whole-grain consumption on body weight and body composition compared to non-whole-grain and refined-grain controls found no effect on body weight but a small beneficial effect on body fat. The average duration of the studies included in this analysis was 4−6 weeks, and to compensate for the short duration, the doses used in the studies represented whole-grain consumption that exceeded the highest level of intake among population groups that consume whole grains. Nevertheless, a meta-regression showed no dose−response relationship between whole-grain intake and differences in body weight.

Observational studies show reductions in weight gain of approximately 0.5 kg,[187] rather than weight loss, between consumers and nonconsumers of whole grains, which raises the possibility that the differences are a marker of a healthy lifestyle rather than the effect of whole grain intake per se. These subtle differences may be difficult to capture in relatively short-term

intervention trials, but longer-term trials may be fraught with the possibility of nonadherence to the diet. Thus, although there is some evidence to indicate that whole-grain consumption may lead to a reduction in fat mass, weight loss that is clinically significant remains to be established.

HEALTH BENEFITS OF PULSES

Cardiovascular Disease. Epidemiological evidence shows a 22% reduction in coronary heart disease and an 11% reduction in cardiovascular disease with consumption of legumes four times or more per week compared with once a week.[15] Intake of one serving of beans per day is associated with a reduced risk of myocardial infarction by 38% compared to no or less than one serving per day, after adjustment for factors such as smoking, diabetes, hypertension, abdominal obesity, and physical activity.[188] The evidence is not as strong as the evidence for a similar association from whole grain consumption; however, intervention trials, which permit the establishment of causality, show fairly consistently that legume consumption lowers total cholesterol and LDL-C, which is the most atherogenic lipoprotein.[71] Total cholesterol LDL-C levels were significantly improved by a high-pulse diet, compared to a high-protein diet, a fatty fish diet, and a control diet.[189] In hypercholesterolemic individuals, consumption of half a cup of baked beans per day as part of the usual diet for 8 weeks reduced total cholesterol by 5.6% and LDL-C by 5.4% compared to a control treatment consisting of half a cup of carrots.[190] Among individuals 50 years or older a pulse-based diet for 2 months reduced total cholesterol and LDL-C.[191] In other studies, chickpea supplementation significantly reduced total cholesterol and LDL-C.[192−194]

In the Legume Inflammation Feeding Experiment, a legume-rich, high-fermentable fiber diet designed to include foods that have a low glycemic index (GI), 21 g fiber/1000 kcal with a GI = 38 led, to greater reductions in total cholesterol and LDL-C compared to an American diet (9 g fiber/1000 kcal having a GI = 69, no legumes).[195] In diabetic participants, a pulse-rich low-GI diet consumed for 3 months lowered total cholesterol and triglycerides.[196] Meta-analyses of RCTs assessing the effect of pulses on blood lipids have shown that legume consumption lowers total and LDL-C levels.[197,198]

The hypocholesterolemic effects of pulses appear to be related to their soluble fiber component, which binds bile acid and decreases the reabsorption of bile acids. Furthermore, fermentation of soluble fiber in the colon and the production of SCFAs contribute to decreased hepatic cholesterol synthesis.[198] Pulse proteins containing the 7S globulin fraction also appear to lower plasma cholesterol and triglyceride levels.[199] Moreover, diets containing vegetable sources of fat and protein may reduce the risk factors for CVD.[200] Other components such as phospholipids and saponins may also contribute to the cholesterol-lowering effects.[198]

Consistent results from RCTs suggest that diets containing pulses may positively affect blood pressure. Consumption of four servings of pulses per week for 8 weeks within an energy-restricted diet reduced total cholesterol, LDL-C, and systolic blood pressure compared to an energy-restricted control diet without pulses.[201] In patients without diabetes, the consumption of pulses as part of energy-restricted diets reduced blood pressure.[189,201−203] A low-GI diet containing pulses reduced blood pressure and heart rate among diabetic individuals, compared to a high wheat fiber diet.[196] Isocalorically replacing foods with pulses significantly lowered the systolic and mean arterial blood pressure in individuals with and without hypertension.[204]

The reduction in cardiometabolic risk factors associated with pulse consumption may also be attributed to their antioxidant components. Besides, pulses have other components such as folic acid that reduce homocysteine levels to reduce the risk of stroke.[205] Markers of systemic inflammation such as interleukin-6 and tumor necrosis factor-α receptor-2,[206] as well as C-reactive protein[207] are inversely associated with intake of dietary fiber, which may contribute to the beneficial effect of pulse consumption on risk factors for cardiometabolic disease. Four servings of pulses per week within an energy-restricted diet reduced pro-inflammatory markers and markers of oxidative stress, after adjustment for weight loss, compared to an energy-restricted control diet without pulses.[201]

Diabetes and the Metabolic Syndrome. Besides being high in protein, pulses are a low-GI food. In a comparison of 24 common foods including grains, cereals and pasta, breakfast cereals, biscuits, and tuberous vegetables, legumes lowered the glycemic response by 45% when eaten by healthy individuals.[74] Compared to eight cereal foods, legumes have been shown to release 56% less sugars and oligosaccharides over a period of 5 h in healthy individuals.[208] When compared to isoenergetic meals containing potato flakes and meat, meals containing bean flakes and meat produced a significantly lower glycemic response.[209,210] In a meta-analysis of 20 randomized controlled trials, it was concluded that low-carbohydrate, low-GI, Mediterranean, and high-protein diets lead to greater improvements in glycemic control compared to control diets.[211]

Epidemiological as well as randomized controlled trials have demonstrated a beneficial effect of pulse consumption on the prevention and management of diabetes as well as the metabolic syndrome. Among middle-aged Chinese women, followed for approximately 5 years, a high intake of legumes, particularly soybeans, was associated with a decreased risk for diabetes.[212] In short-term experimental studies pulse consumption lowered blood glucose and insulin responses[74,213,214] and increased insulin sensitivity[214] when compared with white bread or pasta. A meta-analysis of RCTs evaluating the effects of pulse consumption on markers of glycemic control showed that pulses alone, or as part of a low-GI or high-fiber diet, improved glycosylated hemoglobin (HbA_{1c}) and fructosamine, both markers of glycemic control.[215] A low-GI pulse diet consumed by 121 diabetic individuals for 3 months, led to a fall in levels of HbA_{1c} by a mean of 0.5% compared to the wheat fiber diet. Participants were encouraged to increase pulse intake by 1 cup of cooked pulses/day or to increase insoluble fiber by consumption of whole-wheat products.[196] In subjects with diabetes, pinto, dark red kidney, and black beans each served with rice lowered the glycemic load (product of the GI and the available carbohydrate) of the meal and attenuated the blood glucose response compared to white rice alone.[216]

Pulses have also been shown to have a second-meal effect, whereby postprandial blood glucose response to a meal eaten a period of time after consumption of a particular food is lowered. Chickpeas and lentils have been shown to have a second-meal effect.[217−220] Although yellow peas did not have a second-meal effect,[217] 20 g of isolated yellow pea protein served in a tomato soup manifested a first-meal as well as a second-meal effect to lower the postprandial blood glucose response on both occasions.[221]

Central to the metabolic syndrome is insulin resistance and a cluster of associated cardiovascular risk factors such as

abdominal obesity, elevated blood pressure, and dyslipidemia. A significant association between legume intake and decreases in mean systolic blood pressure, fasting blood glucose, and increase in high-density lipoprotein cholesterol (HDL-C) levels was observed in 80 subjects diagnosed with the metabolic syndrome.[222] Consumption of 5 cups per week of pulses (yellow peas, chickpeas, navy beans, and lentils) over 8 weeks in an ad libitum diet reduced the risk factors of the metabolic syndrome, and these effects were equivalent to, or greater than, those precipitated by an energy-restricted diet.[17]

Obesity. Lentils have been shown to increase satiation (termination of a meal) compared to a meal consisting of pasta and sauce, but showed no effect on energy intake at a subsequent pizza meal served 4 h later.[213] Lentils as well as yellow peas reduced appetite and energy intake at a subsequent meal compared to a meal consisting of macaroni and cheese.[217] In other studies, daily energy intake decreased by 380 kcal in the subjects consuming 5 cups of pulses per week, which was similar to the reduction in intake of subjects placed on an energy-restricted diet.[17] A meal containing bean purée increased satiety over 4 h compared to the same meal substituted with potato purée.[209] The acute effect of chickpea breakfasts on satiety and energy intake was not significantly different,[223] but chickpea supplementation of approximately 104 g/day for 12 weeks increased satiety.[224] Bread in which 40% of wheat flour was replaced with lupin kernel produced greater satiety and lower energy intake at lunch compared to white bread.[225] Furthermore, a lupin-kernel fiber-enriched sausage patty produced greater effects on satiety than a conventional patty and an inulin fiber-enriched patty.[226] However, in another study consumption of bread produced by replacing of 10% of wheat flour with lupin flour had no effect on satiety or energy intake.[227] Thus, pulse consumption may have an effect on satiety, which can help consumers overcome environmental cues to eat or help them to adhere to calorie restriction.[71]

Epidemiological evidence shows an inverse association between bean consumption and body weight.[14] In intervention trials, rice and bean meals consumed twice daily increased weight loss at 1 month compared to meals consisting of lean meat; however, the effects did not persist over 2 months, possibly as a result of subjects dropping out of the study.[228] In a comparison of a high-pulse diet, a high-protein diet, a fatty fish diet, and a control diet excluding pulses and fish, for 8 weeks, the high-protein and high-pulse diets produced similar effects on weight loss. Furthermore, both diets increased weight loss compared to the control diet.[189] Four servings of pulses per week for 8 weeks within a 30% energy-restricted diet produced greater weight loss than an energy-restricted control diet that excluded pulses.[201]

A diet high in legumes including beans and peas for 3 weeks had no significant effect on body weight, but this duration may have been too short to assess weight change.[229] A high-pulse–low-GI diet reduced body weight after 3 months.[196] However, subjects provided pulses and whole grains for incorporation into their diets did not show significantly different weight loss after 6 or 18 months, compared to a control group provided refined cereals and high glycemic index foods, although waist circumference reduced at 18 months in subjects on the high-legume diet.[230] The endosperm of lupin seeds is used to produce flour that contains 40–45% protein and 25–30% fiber with negligible amounts of sugar and starch.[225] Although bread made with lupin flour has been shown to increase satiety,[225,231] it had no effect on weight loss, weight maintenance, or body composition in studies lasting for 12 months.[202,232] Thus, the consumption of pulses and other legumes may enhance weight loss, but its effects on long-term weight management have yet to be convincingly demonstrated.

WHOLE GRAINS AND PULSES

Dietary recommendations emphasize increasing intakes of foods that are nutrient dense and contain fiber while achieving and maintaining a healthy body weight.[22] The challenge lies in meeting these goals, especially, because grains, which are a major component of most diets, provide a substantial amount of energy. Whole grains provide approximately 2.4 g of fiber per serving (1 oz equivalent), whereas refined grains provide 0.7 g per serving.[233] According to the National Health Interview Survey 2000,[234] the average American consumes only half the intakes of dietary fiber (25–38 g/day) recommended by the Institute of Medicine.[235] A shift from low-fiber refined grains to whole-grain foods will help to meet dietary recommendations while lowering the metabolizable energy. Three servings of whole grains would provide approximately 7.5 g of fiber or one-fourth of the recommendation. Moreover, essential vitamins, minerals, and phytonutrients are lost in the milling process, making whole grains nutritionally dense compared to refined grains.[62,236]

Epidemiological data provide consistent evidence for the health benefits of whole-grain consumption; however, the same cannot be said for the results from RCTs. Part of the reason for the inconsistent results may be the grain structure. An intact botanical structure may delay or preclude starch absorption. Milling of wheat, for instance, separates the bran, germ, and endosperm. Reconstitution of the separated parts produces wholemeal flour, which elicits the same glycemic response as refined flour when incorporated into bread.[237] Nevertheless, the nutritional benefits of whole-grain foods are without doubt, and their consumption can make a fairly significant contribution to meeting dietary fiber recommendations, the health benefits of which have long been appreciated.[238] The consumption of cereal fiber, or mixtures of whole grains and bran, is modestly associated with reducing the risk of chronic disease including obesity, type 2 diabetes, and cardiovascular disease.[128]

Pulses are a rich source of protein, slow-release carbohydrates, dietary fiber, micronutrients, and other bioactive components associated with health benefits.[19] One serving of pulses contains approximately 7.6 g of fiber.[239] Unlike the evidence for whole-grain cereal foods, both epidemiological and experimental results provide substantial evidence for a protective effect against chronic disease. A diet that includes pulses meets the recommendations of the Dietary Guidelines for Americans 2010[22] and could contribute to increasing the fiber and lowering the energy density of a diet. Diets high in pulses may be recommended in the prevention and management of obesity and chronic diseases including diabetes, cancer, and cardiovascular disease. Vegetables, fruits, lean meats, and whole grains are among the other recommendations of the Dietary Guidelines. However, some of these products are expensive sources of energy,[240] which may in part explain their substitution with less expensive, energy-dense, nutrient-poor foods. Legumes, dried beans and peas in particular are relatively less costly than animal sources of protein, which can help to overcome the cost constraints of nutritious diets while providing a host of benefits in terms of improving the

Table 4. Impact of Whole Grain Intake on Obesity and Related Co-morbidities Based on Experimental Trials Reviewed

whole grain type	impact on disease		
	obesity	cardiovascular disease	metabolic syndrome/eiabetes
whole grains/ wheat bran	reduced cumulative energy intake (from breakfast and lunch);[178] reduced appetite and energy intake[179,180]	reduced blood pressure;[132−134] decreased C-reactive protein;[147] benefcial effect on total cholesterol and LDL-C[146]	improved insulin sensitivity;[151,185] reduced postprandial insulin and triglyceride responses;[153] improved postprandial glucose response[178,179]
	no effect on subjective satiety and/or energy intake[174,176]	no effect on blood pressure;[135] no effect on cardiometabolic risk factors;[144] no effect on total cholesterol and LDL-C[147]	no effect on postprandial blood glucose;[176] no effect on markers of insulin sensitivity and inflammation[150,152,135]
	no effect on body weight[146,147,184,185] but fat mass[146] and abdominal obesity reduced[147]		
barley and oats/ β-glucan	increased subjective satiety and reduced energy intake;[169,170,173] increased subjective satiety but no effect on energy intake[174]	reduced total cholesterol and/or LDL-C[138−142,186]	decreased insulin response response;[173] reduced postprandial glucose response;[175] at least 4 g of β-glucan needed to reduce postprandial glucose response[154]
	positively affected satiety hormones[169,172,173]		no effect on postprandial blood glucose[176]
	no effect on subjective satiety[175,177]		
	no effect on body weight but waist circumference reduced[186]		
rye	increased subjective satiety;[161,163,165,166,168] increased colonic fermentation and reduced energy intake at a subsequent meal but no effect on subjective satiety[167]	not assessed as a single component of the diet	improved glycemic/insulinemic response[161]
	no effect on energy intake[165,166]		

nutritional quality of the diets, lowering the energy density, and aiding in the prevention and management of chronic disease.

The emphasis on increasing intakes of whole grains has been consistent since the first Dietary Guidelines for Americans was released in 1980, yet, according to the NHANES 1999−2004, daily consumption of whole-grain servings was less than one-third of the recommended intakes.[20] In the absence of a universal definition of whole grains, part of the reason for the limited consumption of whole grains may be that consumers are confused as to what constitutes a whole-grain product.[129] Furthermore, in foods that are partially whole grain the relative proportions of whole-grain ingredients is unknown. Hence, a product that does not have whole grains as the first ingredient listed on the product package may contain anywhere from 1 to 49% whole-grain ingredients.[32] Ironically, among the USDA's top 20 food sources of fiber, whole-wheat bread, the most commonly consumed whole-grain component of the U.S. diet, is not present. On the other hand, 12 varieties of pulses are among the top 20 fiber sources.[239]

All refined grains are not completely devoid of nutrition. The enrichment process returns to the grains the nutrients lost in processing. Enriched grain products are required to have iron, thiamin, riboflavin, niacin, and folic acid added at specified minimum and maximum levels, according to the U.S. Code of Federal Regulations.[241] Nationwide fortification of enriched uncooked cereal grains with folic acid became mandatory in the United States in 1998.[242] Refined grain foods remain a major component of the diet in the United States, the United Kingdom, and Australia, which may be due to traditional preferences for refined grain products or unfamiliarity with cooking techniques. However, consumption of half the recommended grain intakes as refined grains is not associated with an increase in disease risk.[243] The inclusion of pulses in a meal containing refined grains provides a means of lowering the energy density of the meal and the postprandial glycemic response while helping to substantially meet dietary fiber recommendations. A meal containing pinto beans, dark red kidney beans, or black beans served with approximately half a cup of white rice has been shown to reduce the glycemic response compared to a meal containing only white rice.[216]

Pulses and whole grains contain a host of macronutrients, micronutrients, and other bioactive components essential for health, some of which are greater in one food group compared to the other. For instance, 1 cup (two servings) of beans and peas contains 15.2 g of fiber compared to 5 g contained in two servings of whole grains.[233] Pulses provide approximately 230 μg of folate per cup of cooked dried pulses (two servings) compared to 26 μg in two slices (two servings) of whole-wheat bread. Bread made with enriched flour has 90 μg of folate in two servings. Magnesium intake is often below the recommendations, and whole grains are a good source of magnesium.[244] However, the bran component has a higher content at 89 mg per one-fourth cup of wheat bran compared to 86 mg per cup of cooked brown rice. The content of magnesium in a cup of cooked pinto beans is 86 mg. The vitamin E content of two servings of whole-wheat bread is 1.70 mg, whereas in 1 cup of pulses it is 0.58 mg.[80]

Together, pulses and grains provide all of the indispensable amino acids to meet human requirements for growth and health. They are a rich source of nondigestible carbohydrates, which may strategically alter the balance of gut microbiota to promote health.[44] In a study among Korean adults, a dietary pattern consisting of whole grains and legumes was found to be

Table 5. Impact of Legume Intake on Obesity and Related Co-morbidities Based on Experimental Trials Reviewed[a]

legume type	impact on disease		
	obesity	cardiovascular disease	metabolic syndrome/diabetes
legumes	increased mitochondrial oxidation[189] reduced appetite and/or energy intake;[17,217] reduced body weight over 4−8 weeks[189,201,228] and over 3 months[196] no effect on body weight but waist circumference reduced at 18 months[230]	reduced total cholesterol[196] and LDL-C[189,195,201] but reduced HDL-C[189,195,201] reduced blood pressure[189,196,201]	reduced risk factors for metabolic syndrome;[17] reduced HbA1C[196] and blood glucose[74,213,216]
chickpeas	increased satiation[224] no effect on satiety and energy intake[223]	lowered total cholesterol and LDL-C[192−194]	lowered blood glucose;[74,213] reduced single-meal blood glucose but no effect over 6 weeks;[214] produced second-meal effect on blood glucose[217]
lentils	reduced appetite and/or energy intake[17,213,217]	not assessed as a single component of diet	lowered blood glucose;[74,213] produced second-meal effect on blood glucose;[217] produced first- and second-meal effects on blood glucose[218,219]
navy beans	no effect on appetite or energy intake compared to control	reduced total cholesterol and LDL-C[190]	lowered blood glucose[213]
yellow split peas	reduced appetite and energy intake[217]	not assessed as a single component of diet	lowered blood glucose[213]
lupin seeds	increased satiety and/or reduced energy intake[225,226,231] no effect on satiety or energy intake;[227] no effect on body weight[202,232]	reduced blood pressure;[202,203] no effect on blood lipids[232]	inconsistent effects on blood glucose[202,225,231,232]
Swedish brown beans	reduced hunger and positively affected satiety hormones following a subsequent meal[220]	lowered inflammatory markers and increased short-chain fatty acid concentrations following a second meal[220]	produced a second-meal effect on blood glucose and insulin responses[220]

[a]Adapted from Rebello et al., *Obesity Reviews* **2014**, *15*, 392−407.

dx.doi.org/10.1021/jf500932z | J. Agric. Food Chem. 2014, 62, 7029−7049

inversely associated with insulin resistance.[245] In a cross-sectional study among subjects participating in the Tehran Lipid and Glucose study, an inverse association was found between intake of fiber from cereal and legume sources and risk for the metabolic syndrome.[246] In participants with coronary artery disease, the replacement of refined grains at breakfast with a whole-grain and legume powder for 16 weeks had a positive impact on glucose, insulin, and homocysteine concentrations as well as lipid peroxidation.[247] The inclusion of whole-grain barley and legumes in a diet reduced cardiometabolic risk factors in 46 overweight women compared to a diet with a similar nutrient composition but lacking whole-grain barley and legumes.[248] Thus, a synergistic effect of legumes and whole grains on promoting human health is not entirely unfounded and bears further investigation. The impacts of whole-grain and legume consumption on obesity, cardiovascular disease, and diabetes, based on the experimental trials reviewed, are presented in Tables 4 and 5 respectively.

In conclusion, plant-based diets that include pulses and cereals, although associated with lower socioeconomic status[249] and fraught with difficulty in incorporating into the diet due to a bland taste, lack of knowledge of cooking techniques, and perceptions of flatulence from pulse consumption, can be a dietary strategy with significant implications on health. The evidence for the health benefits of pulse consumption is fairly robust from observational as well experimental studies. Whether the incorporation of pulses in the diet can be sustained in the long term is an important consideration that warrants investigation. Nevertheless, there is a need to establish more convenient delivery systems for pulses in familiar food forms to lower the energy density of these foods and provide health benefits. Federally mandated funding to promote consumption of pulses and the incorporation of pulse foods into the National School Lunch Program, which is presently being considered, will help to increase consumption.

Despite strong evidence from epidemiological studies assessing the health effects of whole-grain consumption, causality is difficult to establish mainly due to the dearth of RCTs. The assessment of biomarkers rather than disease end-points, variability in the definition of whole grains, and, especially, differences in grain structure are some of the factors associated with the lack of consistency in the results from RCTs. Although this should not undermine the potential health benefits of whole grains, it may be worthwhile to promote incorporating pulses into the diet along with traditionally preferred enriched grains to derive some of the benefits of whole-grain consumption. Finally, the host of nutrients and bioactive components contained in whole grains and pulses suggests the potential for a synergistic effect that could provide significant health benefits when these food groups are included in the diet.

AUTHOR INFORMATION

Corresponding Author

*(C.J.R.) Pennington Biomedical Research Center, 6400 Perkins Road, Baton Rouge, LA 70808, USA. Phone: (225) 763-2576. Fax: (225) 763-3022. E-mail: Candida.Rebello@pbrc.edu.

Notes

The authors declare no competing financial interest.

REFERENCES

(1) McNaughton, S. A.; Bates, C. J.; Mishra, G. D. Diet quality is associated with all-cause mortality in adults aged 65 years and older. *J. Nutr.* **2012**, *142*, 320−325.

(2) Samieri, C.; Sun, Q.; Townsend, M. K.; Chiuve, S. E.; Okereke, O. I.; Willett, W. C.; Stampfer, M.; Grodstein, F. The association between dietary patterns at midlife and health in aging: an observational study. *Ann. Int. Med.* **2013**, *159*, 584−591.

(3) Authors/Task Force Members: Ryden, L.; Grant, P. J.; Anker, S. D.; Berne, C.; Cosentino, F.; Danchin, N.; Deaton, C.; Escaned, J.; Hammes, H. P.; Huikuri, H.; Marre, M.; Marx, N.; Mellbin, L.; Ostergren, J.; Patrono, C.; Seferovic, P.; Uva, M. S.; Taskinen, M. R.; Tendera, M.; Tuomilehto, J.; Valensi, P.; Zamorano, J. L. ESC Committee for Practice Guidelines (CPG): Zamorano, J. L.; Achenbach, S.; Baumgartner, H.; Bax, J. J.; Bueno, H.; Dean, V.; Deaton, C.; Erol, C.; Fagard, R.; Ferrari, R.; Hasdai, D.; Hoes, A. W.; Kirchhof, P.; Knuuti, J.; Kolh, P.; Lancellotti, P.; Linhart, A.; Nihoyannopoulos, P.; Piepoli, M. F.; Ponikowski, P.; Sirnes, P. A.; Tamargo, J. L.; Tendera, M.; Torbicki, A.; Wijns, W.; Windecker, S. Document Reviewers: De Backer, G.; Sirnes, P. A.; Ezquerra, E. A.; Avogaro, A.; Badimon, L.; Baranova, E.; Baumgartner, H.; Betteridge, J.; Ceriello, A.; Fagard, R.; Funck-Brentano, C.; Gulba, D. C.; Hasdai, D.; Hoes, A. W.; Kjekshus, J. K.; Knuuti, J.; Kolh, P.; Lev, E.; Mueller, C.; Neyses, L.; Nilsson, P. M.; Perk, J.; Ponikowski, P.; Reiner, Z.; Sattar, N.; Schachinger, V.; Scheen, A.; Schirmer, H.; Stromberg, A.; Sudzhaeva, S.; Tamargo, J. L.; Viigimaa, M.; Vlachopoulos, C.; Xuereb, R. G. ESC Guidelines on diabetes, pre-diabetes, and cardiovascular diseases developed in collaboration with the EASD: The Task Force on diabetes, pre-diabetes, and cardiovascular diseases of the European Society of Cardiology (ESC) and developed in collaboration with the European Association for the Study of Diabetes (EASD). *Eur. Heart J.* **2013** *34*, 3035−3087

(4) Sofi, F.; Abbate, R.; Gensini, G. F.; Casini, A. Accruing evidence on benefits of adherence to the Mediterranean diet on health: an updated systematic review and meta-analysis. *Am. J. Clin. Nutr.* **2010**, *92*, 1189−1196.

(5) Trichopoulou, A.; Costacou, T.; Bamia, C.; Trichopoulos, D. Adherence to a Mediterranean diet and survival in a Greek population. *N. Engl. J. Med.* **2003**, *348*, 2599−2608.

(6) Lopez-Garcia, E.; Rodriguez-Artalejo, F.; Li, T. Y.; Fung, T. T.; Li, S.; Willett, W. C.; Rimm, E. B.; Hu, F. B. The Mediterranean-style diet pattern and mortality among men and women with cardiovascular disease. *Am. J. Clin. Nutr.* **2014**, *99*, 172−180.

(7) Boccardi, V.; Herbig, U. Telomerase gene therapy: a novel approach to combat aging. *EMBO Mol. Med.* **2012**, *4*, 685−687.

(8) Schroder, H. Protective mechanisms of the Mediterranean diet in obesity and type 2 diabetes. *J. Nutr. Biochem.* **2007**, *18*, 149−160.

(9) He, M.; van Dam, R. M.; Rimm, E.; Hu, F. B.; Qi, L. Whole-grain, cereal fiber, bran, and germ intake and the risks of all-cause and cardiovascular disease-specific mortality among women with type 2 diabetes mellitus. *Circulation* **2010**, *121*, 2162−2168.

(10) de Munter, J. S.; Hu, F. B.; Spiegelman, D.; Franz, M.; van Dam, R. M. Whole grain, bran, and germ intake and risk of type 2 diabetes: a prospective cohort study and systematic review. *PLoS Med.* **2007**, *4*, No. e261.

(11) Sahyoun, N. R.; Jacques, P. F.; Zhang, X. L.; Juan, W.; McKeown, N. M. Whole-grain intake is inversely associated with the metabolic syndrome and mortality in older adults. *Am. J. Clin. Nutr.* **2006**, *83*, 124−131.

(12) Jacobs, D. R., Jr.; Marquart, L.; Slavin, J.; Kushi, L. H. Whole-grain intake and cancer: an expanded review and meta-analysis. *Nutr. Cancer* **1998**, *30*, 85−96.

(13) Koh-Banerjee, P.; Rimm, E. B. Whole grain consumption and weight gain: a review of the epidemiological evidence, potential mechanisms and opportunities for future research. *Proc. Nutr. Soc.* **2003**, *62*, 25−29.

(14) Papanikolaou, Y.; Fulgoni, V. L., 3rd. Bean consumption is associated with greater nutrient intake, reduced systolic blood pressure, lower body weight, and a smaller waist circumference in

adults: results from the National Health and Nutrition Examination Survey 1999−2002. *J. Am. Coll. Nutr.* **2008**, *27*, 569−576.
(15) Bazzano, L. A.; He, J.; Ogden, L. G.; Loria, C.; Vupputuri, S.; Myers, L.; Whelton, P. K. Legume consumption and risk of coronary heart disease in US men and women: NHANES I Epidemiologic Follow-up Study. *Arch. Intern. Med.* **2001**, *161*, 2573−2578.
(16) Jenkins, D. J.; Kendall, C. W.; Augustin, L. S.; Mitchell, S.; Sahye-Pudaruth, S.; Blanco Mejia, S.; Chiavaroli, L.; Mirrahimi, A.; Ireland, C.; Bashyam, B.; Vidgen, E.; de Souza, R. J.; Sievenpiper, J. L.; Coveney, J.; Leiter, L. A.; Josse, R. G. Effect of legumes as part of a low glycemic index diet on glycemic control and cardiovascular risk factors in type 2 diabetes mellitus: a randomized controlled trial. *Arch. Intern. Med.* **2012**, *172*, 1653−1660.
(17) Mollard, R. C.; Luhovyy, B. L.; Panahi, S.; Nunez, M.; Hanley, A.; Anderson, G. H. Regular consumption of pulses for 8 weeks reduces metabolic syndrome risk factors in overweight and obese adults. *Br. J. Nutr.* **2012**, *108* (Suppl. 1), S111−S122.
(18) Fardet, A. New hypotheses for the health-protective mechanisms of whole-grain cereals: what is beyond fibre? *Nutr. Res. Rev.* **2010**, *23*, 65−134.
(19) Tharanathan, R. N.; Mahadevamma, S. Grain legumes − a boon to human nutrition. *Trends Food Sci. Technol.* **2003**, *14*, 507−518.
(20) O'Neil, C. E.; Nicklas, T. A.; Zanovec, M.; Cho, S. Whole-grain consumption is associated with diet quality and nutrient intake in adults: the National Health and Nutrition Examination Survey, 1999−2004. *J. Am. Diet. Assoc.* **2010**, *110*, 1461−1468.
(21) Lin, B.; Ye, S. The U.S. Grain Consumption Landscape: Who Eats Grain, in What Form, Where, and How Much? http://www.ers.usda.gov/publications/err-economic-research-report/err50.aspx#.UvULtvldU1Y (accessed Feb 7, 2014).
(22) USDA-DHHS. Dietary Guidelines for Americans in 2010. http://health.gov/dietaryguidelines/dga2010/DietaryGuidelines2010.pdf (accessed Dec 10, 2013).
(23) What Is the DASH Eating Plan? http://www.nhlbi.nih.gov/health/health-topics/topics/dash/ (accessed Dec 10, 2013).
(24) Willett, W. C.; Sacks, F.; Trichopoulou, A.; Drescher, G.; Ferro-Luzzi, A.; Helsing, E.; Trichopoulos, D. Mediterranean diet pyramid: a cultural model for healthy eating. *Am. J. Clin. Nutr.* **1995**, *61*, 1402S−1406S.
(25) Harris, K. A.; Kris-Etherton, P. M. Effects of whole grains on coronary heart disease risk. *Curr. Atheroscler. Rep.* **2010**, *12*, 368−376.
(26) De Moura, F. F.; Lewis, K. D.; Falk, M. C. Applying the FDA definition of whole grains to the evidence for cardiovascular disease health claims. *J. Nutr.* **2009**, *139*, 2220S−2226S.
(27) AACC International. Whole Grains. http://www.aaccnet.org/initiatives/definitions/Pages/WholeGrain.aspx (accessed Nov 15, 2013).
(28) Tharanathan, R. N. Food-derived carbohydrates − structural complexity and functional diversity. *Crit. Rev. Biotechnol* **2002**, *22*, 65−84.
(29) Lattimer, J. M.; Haub, M. D. Effects of dietary fiber and its components on metabolic health. *Nutrients* **2010**, *2*, 1266−1289.
(30) Tiwari, B. K.; Gowen, A.; McKenna, B. M. *Pulse Foods: Processing, Quality and Nutraceutical Applications*, 1st ed.; Academic Press: Amsterdam, The Netherlands, 2011; p *viii*, 475 pp.
(31) *Dietary Reference Intakes: Proposed Definition of Dietary Fiber*; National Academies Press: Washington, DC, USA, 2001.
(32) Jonnalagadda, S. S.; Harnack, L.; Liu, R. H.; McKeown, N.; Seal, C.; Liu, S.; Fahey, G. C. Putting the whole grain puzzle together: health benefits associated with whole grains − summary of American Society for Nutrition 2010 Satellite Symposium. *J. Nutr.* **2011**, *141*, 1011S−1022S.
(33) Bachman, J. L.; Reedy, J.; Subar, A. F.; Krebs-Smith, S. M. Sources of food group intakes among the US population, 2001−2002. *J. Am. Diet. Assoc.* **2008**, *108*, 804−814.
(34) Newby, P. K.; Maras, J.; Bakun, P.; Muller, D.; Ferrucci, L.; Tucker, K. L. Intake of whole grains, refined grains, and cereal fiber measured with 7-d diet records and associations with risk factors for chronic disease. *Am. J. Clin. Nutr.* **2007**, *86*, 1745−1753.
(35) Burkitt, D. P. Epidemiology of cancer of the colon and rectum. *Cancer* **1971**, *28*, 3−13.
(36) Alberts, D. S.; Martinez, M. E.; Roe, D. J.; Guillen-Rodriguez, J. M.; Marshall, J. R.; van Leeuwen, J. B.; Reid, M. E.; Ritenbaugh, C.; Vargas, P. A.; Bhattacharyya, A. B.; Earnest, D. L.; Sampliner, R. E. Lack of effect of a high-fiber cereal supplement on the recurrence of colorectal adenomas. Phoenix Colon Cancer Prevention Physicians' Network. *N. Engl. J. Med.* **2000**, *342*, 1156−1162.
(37) Lanza, E.; Yu, B.; Murphy, G.; Albert, P. S.; Caan, B.; Marshall, J. R.; Lance, P.; Paskett, E. D.; Weissfeld, J.; Slattery, M.; Burt, R.; Iber, F.; Shike, M.; Kikendall, J. W.; Brewer, B. K.; Schatzkin, A. The polyp prevention trial continued follow-up study: no effect of a low-fat, high-fiber, high-fruit, and -vegetable diet on adenoma recurrence eight years after randomization. *Cancer Epidemiol. Biomarkers Prev.* **2007**, *16*, 1745−1752.
(38) Bingham, S. A.; Day, N. E.; Luben, R.; Ferrari, P.; Slimani, N.; Norat, T.; Clavel-Chapelon, F.; Kesse, E.; Nieters, A.; Boeing, H.; Tjonneland, A.; Overvad, K.; Martinez, C.; Dorronsoro, M.; Gonzalez, C. A.; Key, T. J.; Trichopoulou, A.; Naska, A.; Vineis, P.; Tumino, R.; Krogh, V.; Bueno-de-Mesquita, H. B.; Peeters, P. H.; Berglund, G.; Hallmans, G.; Lund, E.; Skeie, G.; Kaaks, R.; Riboli, E. Dietary fibre in food and protection against colorectal cancer in the European Prospective Investigation into Cancer and Nutrition (EPIC): an observational study. *Lancet* **2003**, *361*, 1496−1501.
(39) Fuchs, C. S.; Giovannucci, E. L.; Colditz, G. A.; Hunter, D. J.; Stampfer, M. J.; Rosner, B.; Speizer, F. E.; Willett, W. C. Dietary fiber and the risk of colorectal cancer and adenoma in women. *N. Engl. J. Med.* **1999**, *340*, 169−176.
(40) Park, Y.; Hunter, D. J.; Spiegelman, D.; Bergkvist, L.; Berrino, F.; van den Brandt, P. A.; Buring, J. E.; Colditz, G. A.; Freudenheim, J. L.; Fuchs, C. S.; Giovannucci, E.; Goldbohm, R. A.; Graham, S.; Harnack, L.; Hartman, A. M.; Jacobs, D. R., Jr.; Kato, I.; Krogh, V.; Leitzmann, M. F.; McCullough, M. L.; Miller, A. B.; Pietinen, P.; Rohan, T. E.; Schatzkin, A.; Willett, W. C.; Wolk, A.; Zeleniuch-Jacquotte, A.; Zhang, S. M.; Smith-Warner, S. A. Dietary fiber intake and risk of colorectal cancer: a pooled analysis of prospective cohort studies. *JAMA, J. Am. Med. Assoc.* **2005**, *294*, 2849−2857.
(41) Schatzkin, A.; Mouw, T.; Park, Y.; Subar, A. F.; Kipnis, V.; Hollenbeck, A.; Leitzmann, M. F.; Thompson, F. E. Dietary fiber and whole-grain consumption in relation to colorectal cancer in the NIH-AARP Diet and Health Study. *Am. J. Clin. Nutr.* **2007**, *85*, 1353−1360.
(42) Bjorck, I.; Granfeldt, Y.; Liljeberg, H.; Tovar, J.; Asp, N. G. Food properties affecting the digestion and absorption of carbohydrates. *Am. J. Clin. Nutr.* **1994**, *59*, 699S−705S.
(43) Slavin, J. Why whole grains are protective: biological mechanisms. *Proc. Nutr. Soc.* **2003**, *62*, 129−134.
(44) den Besten, G.; van Eunen, K.; Groen, A. K.; Venema, K.; Reijngoud, D. J.; Bakker, B. M. The role of short-chain fatty acids in the interplay between diet, gut microbiota, and host energy metabolism. *J. Lipid Res.* **2013**, *54*, 2325−2340.
(45) Young, V. R.; Pellett, P. L. Plant proteins in relation to human protein and amino acid nutrition. *Am. J. Clin. Nutr.* **1994**, *59*, 1203S−1212S.
(46) Millward, D. J. The nutritional value of plant-based diets in relation to human amino acid and protein requirements. *Proc. Nutr. Soc.* **1999**, *58*, 249−260.
(47) Wang, Y.; Beydoun, M. A. Meat consumption is associated with obesity and central obesity among US adults. *Int. J. Obes. (London)* **2009**, *33*, 621−628.
(48) Gropper, S. S.; Smith, J. L.; Groff, J. L. *Advanced Nutrition and Human Metabolism*, 5th ed.; Wadsworth, Cengage Learning: Belmont, CA, USA, 2009; pp 323−532.
(49) Fardet, A.; Rock, E.; Remesy, C. Is the in vitro antioxidant potential of whole-grain cereals and cereal products well reflected in vivo? *J. Cereal Sci.* **2008**, *48*, 258−276.
(50) Golestani, A.; Rastegar, R.; Shariftabrizi, A.; Khaghani, S.; Payabvash, S. M.; Salmasi, A. H.; Dehpour, A. R.; Pasalar, P. Paradoxical dose- and time-dependent regulation of superoxide

dismutase and antioxidant capacity by vitamin E in rat. *Clin. Chim. Acta* **2006**, *365*, 153−159.
(51) Martin, A.; Wu, D.; Baur, W.; Meydani, S. N.; Blumberg, J. B.; Meydani, M. Effect of vitamin E on human aortic endothelial cell responses to oxidative injury. *Free Radical Biol. Med.* **1996**, *21*, 505−511.
(52) Slavin, J. Whole grains and human health. *Nutr Res. Rev.* **2004**, *17*, 99−110.
(53) Barbagallo, M.; Dominguez, L. J.; Galioto, A.; Ferlisi, A.; Cani, C.; Malfa, L.; Pineo, A.; Busardo, A.; Paolisso, G. Role of magnesium in insulin action, diabetes and cardio-metabolic syndrome X. *Mol. Aspects Med.* **2003**, *24*, 39−52.
(54) Oregon State University, Linus Pauling Institute. Micronutrient Research for Optimum Health. http://lpi.oregonstate.edu/infocenter/ (accessed Dec 12, 2013).
(55) Liu, R. H. Potential synergy of phytochemicals in cancer prevention: mechanism of action. *J. Nutr.* **2004**, *134*, 3479S−3485S.
(56) Adom, K. K.; Sorrells, M. E.; Liu, R. H. Phytochemicals and antioxidant activity of milled fractions of different wheat varieties. *J. Agric. Food Chem.* **2005**, *53*, 2297−2306.
(57) Wu, X.; Beecher, G. R.; Holden, J. M.; Haytowitz, D. B.; Gebhardt, S. E.; Prior, R. L. Lipophilic and hydrophilic antioxidant capacities of common foods in the United States. *J. Agric. Food Chem.* **2004**, *52*, 4026−4037.
(58) Pellegrini, N.; Serafini, M.; Salvatore, S.; Del Rio, D.; Bianchi, M.; Brighenti, F. Total antioxidant capacity of spices, dried fruits, nuts, pulses, cereals and sweets consumed in Italy assessed by three different in vitro assays. *Mol. Nutr. Food Res.* **2006**, *50*, 1030−1038.
(59) Liyana-Pathirana, C. M.; Shahidi, F. Importance of insoluble-bound phenolics to antioxidant properties of wheat. *J. Agric. Food Chem.* **2006**, *54*, 1256−1264.
(60) Hammond, B. R., Jr.; Renzi, L. M. Carotenoids. *Adv. Nutr.* **2013**, *4*, 474−476.
(61) Agarwal, S.; Rao, A. V. Carotenoids and chronic diseases. *Drug Metab. Drug Interact.* **2000**, *17*, 189−210.
(62) Okarter, N.; Liu, R. H. Health benefits of whole grain phytochemicals. *Crit. Rev. Food Sci. Nutr* **2010**, *50*, 193−208.
(63) Cooper, D. A. Carotenoids in health and disease: recent scientific evaluations, research recommendations and the consumer. *J. Nutr.* **2004**, *134*, 221S−224S.
(64) Begum, A. N.; Nicolle, C.; Mila, I.; Lapierre, C.; Nagano, K.; Fukushima, K.; Heinonen, S. M.; Adlercreutz, H.; Remesy, C.; Scalbert, A. Dietary lignins are precursors of mammalian lignans in rats. *J. Nutr.* **2004**, *134*, 120−127.
(65) Adlercreutz, H. Phyto-oestrogens and cancer. *Lancet Oncol.* **2002**, *3*, 364−373.
(66) De Smet, E.; Mensink, R. P.; Plat, J. Effects of plant sterols and stanols on intestinal cholesterol metabolism: suggested mechanisms from past to present. *Mol. Nutr. Food Res.* **2012**, *56*, 1058−1072.
(67) Plat, J.; Mackay, D.; Baumgartner, S.; Clifton, P. M.; Gylling, H.; Jones, P. J. Progress and prospective of plant sterol and plant stanol research: report of the Maastricht meeting. *Atherosclerosis* **2012**, *225*, 521−533.
(68) Duranti, M. Grain legume proteins and nutraceutical properties. *Fitoterapia* **2006**, *77*, 67−82.
(69) FAO. Pulses and derived products. http://www.fao.org/waicent/faoinfo/economic/faodef/fdef04e.htm (accessed Dec 15, 2013).
(70) Messina, M. J. Legumes and soybeans: overview of their nutritional profiles and health effects. *Am. J. Clin. Nutr.* **1999**, *70*, 439S−450S.
(71) Rebello, C. J.; Greenway, F. L.; Finley, J. W. A review of the nutritional value of legumes and their effects on obesity and its related co-morbidities. *Obes. Rev.* **2014**, *15*, 392−407.
(72) Jenkins, D. J.; Wolever, T. M.; Taylor, R. H.; Barker, H.; Fielden, H.; Baldwin, J. M.; Bowling, A. C.; Newman, H. C.; Jenkins, A. L.; Goff, D. V. Glycemic index of foods: a physiological basis for carbohydrate exchange. *Am. J. Clin. Nutr.* **1981**, *34*, 362−366.
(73) Jenkins, D. J.; Wolever, T. M.; Jenkins, A. L.; Thorne, M. J.; Lee, R.; Kalmusky, J.; Reichert, R.; Wong, G. S. The glycaemic index of foods tested in diabetic patients: a new basis for carbohydrate exchange favouring the use of legumes. *Diabetologia* **1983**, *24*, 257−264.
(74) Jenkins, D. J.; Wolever, T. M.; Taylor, R. H.; Barker, H. M.; Fielden, H. Exceptionally low blood glucose response to dried beans: comparison with other carbohydrate foods. *Br. Med. J.* **1980**, *281*, 578−580.
(75) Madhusudhan, B.; Tharanathan, R. N. Enzyme debranching studies on green gram (*Phaseolus aureus*) starch fractions. *Carbohydr. Polym.* **1996**, *29*, 41−44.
(76) Madhusudhan, B.; Tharanathan, R. N. Legume and cereal starches − why differences in digestibility? 2. Isolation and characterization of starches from rice (*O. sativa*) and ragi (finger millet, *E. coracana*). *Carbohydr. Polym.* **1995**, *28*, 153−158.
(77) Mahadevamma; Tharanathan, R. N. Resistant starch in wheat-based products: isolation and characterisation (2001, vol. 34, p 73). *J. Cereal Sci.* **2002**, *35*, 117−117.
(78) Thorne, M. J.; Thompson, L. U.; Jenkins, D. J. Factors affecting starch digestibility and the glycemic response with special reference to legumes. *Am. J. Clin. Nutr.* **1983**, *38*, 481−488.
(79) Costa, G. E. D.; Queiroz-Monici, K. D. S.; Reis, S. M. P. M.; de Oliveira, A. C. Chemical composition, dietary fibre and resistant starch contents of raw and cooked pea, common bean, chickpea and lentil legumes. *Food Chem.* **2006**, *94*, 327−330.
(80) USDA. Welcome to the US National Nutrient Database for Standard Reference. http://ndb.nal.usda.gov/ (accessed Dec 15, 2013).
(81) Thompson, L. U.; Button, C. L.; Jenkins, D. J. Phytic acid and calcium affect the in vitro rate of navy bean starch digestion and blood glucose response in humans. *Am. J. Clin. Nutr.* **1987**, *46*, 467−473.
(82) Campos-Vega, R.; Loarca-Pina, G.; Oomah, B. D. Minor components of pulses and their potential impact on human health. *Food Res. Int.* **2010**, *43*, 461−482.
(83) Celleno, L.; Tolaini, M. V.; D'Amore, A.; Perricone, N. V.; Preuss, H. G. A dietary supplement containing standardized *Phaseolus vulgaris* extract influences body composition of overweight men and women. *Int. J. Med. Sci.* **2007**, *4*, 45−52.
(84) Thom, E. A randomized, double-blind, placebo-controlled trial of a new weight-reducing agent of natural origin. *J. Int. Med. Res.* **2000**, *28*, 229−233.
(85) Udani, J.; Hardy, M.; Madsen, D. C. Blocking carbohydrate absorption and weight loss: a clinical trial using Phase 2 brand proprietary fractionated white bean extract. *Altern. Med. Rev.* **2004**, *9*, 63−69.
(86) Udani, J.; Singh, B. B. Blocking carbohydrate absorption and weight loss: a clinical trial using a proprietary fractionated white bean extract. *Altern. Ther. Health Med.* **2007**, *13*, 32−37.
(87) Nasi, A.; Picariello, G.; Ferranti, P. Proteomic approaches to study structure, functions and toxicity of legume seeds lectins. Perspectives for the assessment of food quality and safety. *J. Proteomics* **2009**, *72*, 527−538.
(88) Rochfort, S.; Panozzo, J. Phytochemicals for health, the role of pulses. *J. Agric. Food Chem.* **2007**, *55*, 7981−7994.
(89) Schneider, A. V. Overview of the market and consumption of pulses in Europe. *Br. J. Nutr.* **2002**, *88* (Suppl. 3), S243−S250.
(90) Winham, D. M.; Hutchins, A. M. Perceptions of flatulence from bean consumption among adults in 3 feeding studies. *Nutr. J.* **2011**, *10*, 128.
(91) Veenstra, J. M.; Duncan, A. M.; Cryne, C. N.; Deschambault, B. R.; Boye, J. I.; Benali, M.; Marcotte, M.; Tosh, S. M.; Farnworth, E. R.; Wright, A. J. Effect of pulse consumption on perceived flatulence and gastrointestinal function in healthy males. *Food Res. Int.* **2010**, *43*, 553−559.
(92) Diamant, M.; Blaak, E. E.; de Vos, W. M. Do nutrient-gut-microbiota interactions play a role in human obesity, insulin resistance and type 2 diabetes? *Obes. Rev.* **2011**, *12*, 272−281.

(93) Hooper, L. V.; Gordon, J. I. Commensal host-bacterial relationships in the gut. *Science* **2001**, *292*, 1115−1118.
(94) Chow, J.; Lee, S. M.; Shen, Y.; Khosravi, A.; Mazmanian, S. K. Host-bacterial symbiosis in health and disease. *Adv. Immunol.* **2010**, *107*, 243−274.
(95) Wu, G. D.; Chen, J.; Hoffmann, C.; Bittinger, K.; Chen, Y. Y.; Keilbaugh, S. A.; Bewtra, M.; Knights, D.; Walters, W. A.; Knight, R.; Sinha, R.; Gilroy, E.; Gupta, K.; Baldassano, R.; Nessel, L.; Li, H.; Bushman, F. D.; Lewis, J. D. Linking long-term dietary patterns with gut microbial enterotypes. *Science* **2011**, *334*, 105−108.
(96) Sanchez-Mata, M. C.; Penuela-Teruel, M. J.; Camara Hurtado, M.; Diez Marques, C.; Torija Isasa, M. E. Determination of mono-, di, and oligosaccharides in legumes by high performance liquid chromatography using an amino-bonded silica column. *J. Agric. Food Chem.* **1998**, *46*, 3648−3652.
(97) Ley, S. H.; Sun, Q.; Willett, W. C.; Eliassen, A. H.; Wu, K.; Pan, A.; Grodstein, F.; Hu, F. B. Associations between red meat intake and biomarkers of inflammation and glucose metabolism in women. *Am. J. Clin. Nutr.* **2013**, DOI: 10.3945/ajcn.113.075663.
(98) Pusztai, A.; Grant, G.; Buchan, W. C.; Bardocz, S.; de Carvalho, A. F.; Ewen, S. W. Lipid accumulation in obese Zucker rats is reduced by inclusion of raw kidney bean (*Phaseolus vulgaris*) in the diet. *Br. J. Nutr.* **1998**, *79*, 213−221.
(99) De Mejia, E. G.; Prisecaru, V. I. Lectins as bioactive plant proteins: a potential in cancer treatment. *Crit. Rev. Food Sci. Nutr.* **2005**, *45*, 425−445.
(100) Roy, F.; Boye, J. I.; Simpson, B. K. Bioactive proteins and peptides in pulse crops: pea, chickpea and lentil. *Food Res. Int.* **2010**, *43*, 432−442.
(101) Vermeirssen, V.; Augustijns, P.; Morel, N.; Van Camp, J.; Opsomer, A.; Verstraete, W. In vitro intestinal transport and antihypertensive activity of ACE inhibitory pea and whey digests. *Int. J. Food Sci. Nutr.* **2005**, *56*, 415−430.
(102) Boye, J. I.; Roufik, S.; Pesta, N.; Barbana, C. Angiotensin I-converting enzyme inhibitory properties and SDS-PAGE of red lentil protein hydrolysates. *LWT−Food Sci. Technol.* **2010**, *43*, 987−991.
(103) Cedar, H.; Bergman, Y. Programming of DNA methylation patterns. *Annu. Rev. Biochem.* **2012**, *81*, 97−117.
(104) Kulis, M.; Esteller, M. DNA methylation and cancer. *Adv. Genet.* **2010**, *70*, 27−56.
(105) Robertson, K. D. DNA methylation and human disease. *Nat. Rev. Genet.* **2005**, *6*, 597−610.
(106) Crider, K. S.; Yang, T. P.; Berry, R. J.; Bailey, L. B. Folate and DNA methylation: a review of molecular mechanisms and the evidence for folate's role. *Adv. Nutr.* **2012**, *3*, 21−38.
(107) Sandstrom, B.; Almgren, A.; Kivisto, B.; Cederblad, A. Effect of protein level and protein source on zinc absorption in humans. *J. Nutr.* **1989**, *119*, 48−53.
(108) Tomat, A. L.; Costa Mde, L.; Arranz, C. T. Zinc restriction during different periods of life: influence in renal and cardiovascular diseases. *Nutrition* **2011**, *27*, 392−398.
(109) Weaver, C. M.; Heaney, R. P.; Proulx, W. R.; Hinders, S. M.; Packard, T. Absorbability of calcium from beans. *J. Food Sci.* **1993**, *58*, 1401−1403.
(110) Adrogue, H. J.; Madias, N. E. Sodium and potassium in the pathogenesis of hypertension. *N. Engl. J. Med.* **2007**, *356*, 1966−1978.
(111) Adrogue, H. J.; Madias, N. E. Sodium surfeit and potassium deficit: keys to the pathogenesis of hypertension. *J. Am. Soc. Hypertens.* **2014**, *8*, 203−213.
(112) Rowe, J. W.; Tobin, J. D.; Rosa, R. M.; Andres, R. Effect of experimental potassium deficiency on glucose and insulin metabolism. *Metabolism* **1980**, *29*, 498−502.
(113) Dluhy, R. G.; Axelrod, L.; Williams, G. H. Serum immunoreactive insulin and growth hormone response to potassium infusion in normal man. *J. Appl. Physiol.* **1972**, *33*, 22−26.
(114) Heim, K. E.; Tagliaferro, A. R.; Bobilya, D. J. Flavonoid antioxidants: chemistry, metabolism and structure-activity relationships. *J. Nutr. Biochem.* **2002**, *13*, 572−584.
(115) Kalogeropoulos, N.; Chiou, A.; Ioannou, M.; Karathanos, V. T.; Hassapidou, M.; Andrikopoulos, N. K. Nutritional evaluation and bioactive microconstituents (phytosterols, tocopherols, polyphenols, triterpenic acids) in cooked dry legumes usually consumed in the Mediterranean countries. *Food Chem.* **2010**, *121*, 682−690.
(116) Crozier, A.; Jaganath, I. B.; Clifford, M. N. Dietary phenolics: chemistry, bioavailability and effects on health. *Nat. Prod. Rep.* **2009**, *26*, 1001−1043.
(117) Bouchenak, M.; Lamri-Senhadji, M. Nutritional quality of legumes, and their role in cardiometabolic risk prevention: a review. *J. Med. Food* **2013**, *16*, 185−198.
(118) Vita, J. A. Polyphenols and cardiovascular disease: effects on endothelial and platelet function. *Am. J. Clin. Nutr.* **2005**, *81*, 292S−297S.
(119) Ferroni, P.; Vazzana, N.; Riondino, S.; Cuccurullo, C.; Guadagni, F.; Davi, G. Platelet function in health and disease: from molecular mechanisms, redox considerations to novel therapeutic opportunities. *Antioxid. Redox Signal.* **2012**, *17*, 1447−1485.
(120) Andriantsitohaina, R.; Auger, C.; Chataigneau, T.; Etienne-Selloum, N.; Li, H.; Martinez, M. C.; Schini-Kerth, V. B.; Laher, I. Molecular mechanisms of the cardiovascular protective effects of polyphenols. *Br. J. Nutr.* **2012**, *108*, 1532−1549.
(121) Wang, S.; Melnyk, J. P.; Tsao, R.; Marcone, M. F. How natural dietary antioxidants in fruits, vegetables and legumes promote vascular health. *Food Res. Int.* **2011**, *44*, 14−22.
(122) Shih, P. H.; Yeh, C. T.; Yen, G. C. Effects of anthocyanidin on the inhibition of proliferation and induction of apoptosis in human gastric adenocarcinoma cells. *Food Chem. Toxicol.* **2005**, *43*, 1557−1566.
(123) Singletary, K. W.; Jung, K. J.; Giusti, M. Anthocyanin-rich grape extract blocks breast cell DNA damage. *J. Med. Food* **2007**, *10*, 244−251.
(124) Vucenik, I.; Shamsuddin, A. M. Protection against cancer by dietary IP6 and inositol. *Nutr. Cancer* **2006**, *55*, 109−125.
(125) Sidhu, G. S.; Oakenfull, D. G. A mechanism for the hypocholesterolaemic activity of saponins. *Br. J. Nutr.* **1986**, *55*, 643−649.
(126) Seal, C. J.; Brownlee, I. A. Whole grains and health, evidence from observational and intervention studies. *Cereal Chem.* **2010**, *87*, 167−174.
(127) Ye, E. Q.; Chacko, S. A.; Chou, E. L.; Kugizaki, M.; Liu, S. Greater whole-grain intake is associated with lower risk of type 2 diabetes, cardiovascular disease, and weight gain. *J. Nutr.* **2012**, *142*, 1304−1313.
(128) Cho, S. S.; Qi, L.; Fahey, G. C., Jr.; Klurfeld, D. M. Consumption of cereal fiber, mixtures of whole grains and bran, and whole grains and risk reduction in type 2 diabetes, obesity, and cardiovascular disease. *Am. J. Clin. Nutr.* **2013**, *98*, 594−619.
(129) Mobley, A. R.; Slavin, J. L.; Hornick, B. A. The future of recommendations on grain foods in dietary guidance. *J. Nutr.* **2013**, *143*, 1527S−1532S.
(130) Wang, L.; Gaziano, J. M.; Liu, S.; Manson, J. E.; Buring, J. E.; Sesso, H. D. Whole- and refined-grain intakes and the risk of hypertension in women. *Am. J. Clin. Nutr.* **2007**, *86*, 472−479.
(131) Flint, A. J.; Hu, F. B.; Glynn, R. J.; Jensen, M. K.; Franz, M.; Sampson, L.; Rimm, E. B. Whole grains and incident hypertension in men. *Am. J. Clin. Nutr.* **2009**, *90*, 493−498.
(132) Tighe, P.; Duthie, G.; Vaughan, N.; Brittenden, J.; Simpson, W. G.; Duthie, S.; Mutch, W.; Wahle, K.; Horgan, G.; Thies, F. Effect of increased consumption of whole-grain foods on blood pressure and other cardiovascular risk markers in healthy middle-aged persons: a randomized controlled trial. *Am. J. Clin. Nutr.* **2010**, *92*, 733−740.
(133) Bodinham, C. L.; Hitchen, K. L.; Youngman, P. J.; Frost, G. S.; Robertson, M. D. Short-term effects of whole-grain wheat on appetite and food intake in healthy adults: a pilot study. *Br. J. Nutr.* **2011**, *106*, 327−330.
(134) Behall, K. M.; Scholfield, D. J.; Hallfrisch, J. Whole-grain diets reduce blood pressure in mildly hypercholesterolemic men and women. *J. Am. Diet. Assoc.* **2006**, *106*, 1445−1449.

(135) Jenkins, D. J.; Kendall, C. W.; Augustin, L. S.; Martini, M. C.; Axelsen, M.; Faulkner, D.; Vidgen, E.; Parker, T.; Lau, H.; Connelly, P. W.; Teitel, J.; Singer, W.; Vandenbroucke, A. C.; Leiter, L. A.; Josse, R. G. Effect of wheat bran on glycemic control and risk factors for cardiovascular disease in type 2 diabetes. *Diabetes Care* **2002**, *25*, 1522−1528.

(136) Mellen, P. B.; Liese, A. D.; Tooze, J. A.; Vitolins, M. Z.; Wagenknecht, L. E.; Herrington, D. M. Whole-grain intake and carotid artery atherosclerosis in a multiethnic cohort: the Insulin Resistance Atherosclerosis Study. *Am. J. Clin. Nutr.* **2007**, *85*, 1495−1502.

(137) Erkkila, A. T.; Herrington, D. M.; Mozaffarian, D.; Lichtenstein, A. H. Cereal fiber and whole-grain intake are associated with reduced progression of coronary-artery atherosclerosis in postmenopausal women with coronary artery disease. *Am. Heart J.* **2005**, *150*, 94−101.

(138) Wolever, T. M.; Tosh, S. M.; Gibbs, A. L.; Brand-Miller, J.; Duncan, A. M.; Hart, V.; Lamarche, B.; Thomson, B. A.; Duss, R.; Wood, P. J. Physicochemical properties of oat β-glucan influence its ability to reduce serum LDL cholesterol in humans: a randomized clinical trial. *Am. J. Clin. Nutr.* **2010**, *92*, 723−732.

(139) Keenan, J. M.; Goulson, M.; Shamliyan, T.; Knutson, N.; Kolberg, L.; Curry, L. The effects of concentrated barley beta-glucan on blood lipids in a population of hypercholesterolaemic men and women. *Br. J. Nutr.* **2007**, *97*, 1162−1168.

(140) Naumann, E.; van Rees, A. B.; Onning, G.; Oste, R.; Wydra, M.; Mensink, R. P. β-Glucan incorporated into a fruit drink effectively lowers serum LDL-cholesterol concentrations. *Am. J. Clin. Nutr.* **2006**, *83*, 601−605.

(141) Behall, K. M.; Scholfield, D. J.; Hallfrisch, J. Diets containing barley significantly reduce lipids in mildly hypercholesterolemic men and women. *Am. J. Clin. Nutr.* **2004**, *80*, 1185−1193.

(142) Behall, K. M.; Scholfield, D. J.; Hallfrisch, J. Lipids significantly reduced by diets containing barley in moderately hypercholesterolemic men. *J. Am. Coll. Nutr.* **2004**, *23*, 55−62.

(143) Rebello, C. J.; Johnson, W. D.; Martin, C. K.; Xie, W.; O'Shea, M.; Kurilich, A.; Bordenave, N.; Andler, S.; van Klinken, B. J.; Chu, Y. F.; Greenway, F. L. Acute effect of oatmeal on subjective measures of appetite and satiety compared to a ready-to-eat breakfast cereal: a randomized crossover trial. *J. Am. Coll. Nutr.* **2013**, *32*, 272−279.

(144) Brownlee, I. A.; Moore, C.; Chatfield, M.; Richardson, D. P.; Ashby, P.; Kuznesof, S. A.; Jebb, S. A.; Seal, C. J. Markers of cardiovascular risk are not changed by increased whole-grain intake: the WHOLEheart study, a randomised, controlled dietary intervention. *Br. J. Nutr.* **2010**, *104*, 125−134.

(145) Giacco, R.; Clemente, G.; Cipriano, D.; Luongo, D.; Viscovo, D.; Patti, L.; Di Marino, L.; Giacco, A.; Naviglio, D.; Bianchi, M. A.; Ciati, R.; Brighenti, F.; Rivellese, A. A.; Riccardi, G. Effects of the regular consumption of wholemeal wheat foods on cardiovascular risk factors in healthy people. *Nutr. Metab. Cardiovasc. Dis.* **2010**, *20*, 186−194.

(146) Kristensen, M.; Toubro, S.; Jensen, M. G.; Ross, A. B.; Riboldi, G.; Petronio, M.; Bugel, S.; Tetens, I.; Astrup, A. Whole grain compared with refined wheat decreases the percentage of body fat following a 12-week, energy-restricted dietary intervention in postmenopausal women. *J. Nutr.* **2012**, *142*, 710−716.

(147) Katcher, H. I.; Legro, R. S.; Kunselman, A. R.; Gillies, P. J.; Demers, L. M.; Bagshaw, D. M.; Kris-Etherton, P. M. The effects of a whole grain-enriched hypocaloric diet on cardiovascular disease risk factors in men and women with metabolic syndrome. *Am. J. Clin. Nutr.* **2008**, *87*, 79−90.

(148) Summary of Health Canada's Assessment of a Health Claim about Whole Grains and Coronary Heart Disease. http://www.hc-sc.gc.ca/fn-an/label-etiquet/claims-reclam/assess-evalu/grains-heart-coeur-eng.php (accessed Dec 26, 2013).

(149) Liu, S. Intake of refined carbohydrates and whole grain foods in relation to risk of type 2 diabetes mellitus and coronary heart disease. *J. Am. Coll. Nutr.* **2002**, *21*, 298−306.

(150) Andersson, A.; Tengblad, S.; Karlstrom, B.; Kamal-Eldin, A.; Landberg, R.; Basu, S.; Aman, P.; Vessby, B. Whole-grain foods do not affect insulin sensitivity or markers of lipid peroxidation and inflammation in healthy, moderately overweight subjects. *J. Nutr.* **2007**, *137*, 1401−1407.

(151) Pereira, M. A.; Jacobs, D. R., Jr.; Pins, J. J.; Raatz, S. K.; Gross, M. D.; Slavin, J. L.; Seaquist, E. R. Effect of whole grains on insulin sensitivity in overweight hyperinsulinemic adults. *Am. J. Clin. Nutr.* **2002**, *75*, 848−855.

(152) Giacco, R.; Lappi, J.; Costabile, G.; Kolehmainen, M.; Schwab, U.; Landberg, R.; Uusitupa, M.; Poutanen, K.; Pacini, G.; Rivellese, A. A.; Riccardi, G.; Mykkanen, H. Effects of rye and whole wheat versus refined cereal foods on metabolic risk factors: a randomised controlled two-centre intervention study. *Clin. Nutr.* **2013**, *32*, 941−949.

(153) Giacco, R.; Costabile, G.; Della Pepa, G.; Anniballi, G.; Griffo, E.; Mangione, A.; Cipriano, P.; Viscovo, D.; Clemente, G.; Landberg, R.; Pacini, G.; Rivellese, A. A.; Riccardi, G. A whole-grain cereal-based diet lowers postprandial plasma insulin and triglyceride levels in individuals with metabolic syndrome. *Nutr. Metab. Cardiovasc. Dis.* **2014**, DOI: 10.1016/j.numecd.2014.01.007.

(154) Tosh, S. M. Review of human studies investigating the post-prandial blood-glucose lowering ability of oat and barley food products. *Eur. J. Clin. Nutr.* **2013**, *67*, 310−317.

(155) FDA. FDA approves tenuous health claim for whole grains and type 2 diabetes. http://www.ift.org/food-technology/daily-news/2013/october/02/fda-approves-tenuous-health-claim-for-whole-grains-and-type-2-diabetes.aspx (accessed Dec 23, 2013).

(156) McKeown, N. M.; Jacques, P. F.; Seal, C. J.; de Vries, J.; Jonnalagadda, S. S.; Clemens, R.; Webb, D.; Murphy, L. A.; van Klinken, J. W.; Topping, D.; Murray, R.; Degeneffe, D.; Marquart, L. F. Whole grains and health: from theory to practice − highlights of The Grains for Health Foundation's Whole Grains Summit 2012. *J. Nutr.* **2013**, *143*, 744S−758S.

(157) Andersson, R.; Fransson, G.; Tietjen, M.; Aman, P. Content and molecular-weight distribution of dietary fiber components in whole-grain rye flour and bread. *J. Agric. Food Chem.* **2009**, *57*, 2004−2008.

(158) Ragaee, S. M.; Campbell, G. L.; Scoles, G. J.; McLeod, J. G.; Tyler, R. T. Studies on rye (*Secale cereale* L.) lines exhibiting a range of extract viscosities. 1. Composition, molecular weight distribution of water extracts, and biochemical characteristics of purified water-extractable arabinoxylan. *J. Agric. Food Chem.* **2001**, *49*, 2437−2445.

(159) Sadiq Butt, M.; Tahir-Nadeem, M.; Khan, M. K.; Shabir, R.; Butt, M. S. Oat: unique among the cereals. *Eur. J. Nutr.* **2008**, *47*, 68−79.

(160) Kristensen, M.; Jensen, M. G. Dietary fibres in the regulation of appetite and food intake. Importance of viscosity. *Appetite* **2011**, *56*, 65−70.

(161) Rosen, L. A.; Ostman, E. M.; Bjorck, I. M. Postprandial glycemia, insulinemia, and satiety responses in healthy subjects after whole grain rye bread made from different rye varieties. 2. *J. Agric. Food Chem.* **2011**, *59*, 12149−12154.

(162) Rosen, L. A.; Ostman, E. M.; Bjorck, I. M. Effects of cereal breakfasts on postprandial glucose, appetite regulation and voluntary energy intake at a subsequent standardized lunch; focusing on rye products. *Nutr. J.* **2011**, *10*, 7.

(163) Isaksson, H.; Fredriksson, H.; Andersson, R.; Olsson, J.; Aman, P. Effect of rye bread breakfasts on subjective hunger and satiety: a randomized controlled trial. *Nutr. J.* **2009**, *8*, 39.

(164) Rosen, L. A.; Silva, L. O.; Andersson, U. K.; Holm, C.; Ostman, E. M.; Bjorck, I. M. Endosperm and whole grain rye breads are characterized by low post-prandial insulin response and a beneficial blood glucose profile. *Nutr. J.* **2009**, *8*, 42.

(165) Isaksson, H.; Sundberg, B.; Aman, P.; Fredriksson, H.; Olsson, J. Whole grain rye porridge breakfast improves satiety compared to refined wheat bread breakfast. *Food Nutr. Res.* **2008**, *52*, DOI: 10.3402/fnr/v52i0.1809.

(166) Isaksson, H.; Tillander, I.; Andersson, R.; Olsson, J.; Fredriksson, H.; Webb, D. L.; Aman, P. Whole grain rye breakfast - sustained satiety during three weeks of regular consumption. *Physiol. Behav.* **2012**, *105*, 877−884.

(167) Ibrugger, S.; Vigsnaes, L. K.; Blennow, A.; Skuflic, D.; Raben, A.; Lauritzen, L.; Kristensen, M. Second meal effect on appetite and fermentation of wholegrain rye foods. *Appetite* **2014**, *80*, 248−256.
(168) Isaksson, H.; Rakha, A.; Andersson, R.; Fredriksson, H.; Olsson, J.; Aman, P. Rye kernel breakfast increases satiety in the afternoon − an effect of food structure. *Nutr. J.* **2011**, *10*, 31.
(169) Vitaglione, P.; Lumaga, R. B.; Stanzione, A.; Scalfi, L.; Fogliano, V. β-Glucan-enriched bread reduces energy intake and modifies plasma ghrelin and peptide YY concentrations in the short term. *Appetite* **2009**, *53*, 338−344.
(170) Vitaglione, P.; Lumaga, R. B.; Montagnese, C.; Messia, M. C.; Marconi, E.; Scalfi, L. Satiating effect of a barley β-glucan-enriched snack. *J. Am. Coll. Nutr.* **2010**, *29*, 113−121.
(171) Lyly, M.; Liukkonen, K. H.; Salmenkallio-Marttila, M.; Karhunen, L.; Poutanen, K.; Lahteenmaki, L. Fibre in beverages can enhance perceived satiety. *Eur. J. Nutr.* **2009**, *48*, 251−258.
(172) Beck, E. J.; Tapsell, L. C.; Batterham, M. J.; Tosh, S. M.; Huang, X. F. Increases in peptide Y-Y levels following oat β-glucan ingestion are dose-dependent in overweight adults. *Nutr. Res. (N.Y.)* **2009**, *29*, 705−709.
(173) Beck, E. J.; Tosh, S. M.; Batterham, M. J.; Tapsell, L. C.; Huang, X. F. Oat β-glucan increases postprandial cholecystokinin levels, decreases insulin response and extends subjective satiety in overweight subjects. *Mol. Nutr. Food Res.* **2009**, *53*, 1343−1351.
(174) Schroeder, N.; Gallaher, D. D.; Arndt, E. A.; Marquart, L. Influence of whole grain barley, whole grain wheat, and refined rice-based foods on short-term satiety and energy intake. *Appetite* **2009**, *53*, 363−369.
(175) Hlebowicz, J.; Darwiche, G.; Bjorgell, O.; Almer, L. O. Effect of muesli with 4 g oat β-glucan on postprandial blood glucose, gastric emptying and satiety in healthy subjects: a randomized crossover trial. *J. Am. Coll. Nutr.* **2008**, *27*, 470−475.
(176) Hlebowicz, J.; Wickenberg, J.; Fahlstrom, R.; Bjorgell, O.; Almer, L. O.; Darwiche, G. Effect of commercial breakfast fibre cereals compared with corn flakes on postprandial blood glucose, gastric emptying and satiety in healthy subjects: a randomized blinded crossover trial. *Nutr. J.* **2007**, *6*, 22.
(177) Kim, H.; Behall, K. M.; Vinyard, B.; Conway, J. M. Short-term satiety and glycemic response after consumption of whole grains with various amounts of β-glucan. *Cereal Foods World* **2006**, *51*, 29−33.
(178) Hamedani, A.; Akhavan, T.; Abou Samra, R.; Anderson, G. H. Reduced energy intake at breakfast is not compensated for at lunch if a high-insoluble-fiber cereal replaces a low-fiber cereal. *Am. J. Clin. Nutr.* **2009**, *89*, 1343−1349.
(179) Samra, R. A.; Anderson, G. H. Insoluble cereal fiber reduces appetite and short-term food intake and glycemic response to food consumed 75 min later by healthy men. *Am. J. Clin. Nutr.* **2007**, *86*, 972−979.
(180) Holt, S. H.; Delargy, H. J.; Lawton, C. L.; Blundell, J. E. The effects of high-carbohydrate vs high-fat breakfasts on feelings of fullness and alertness, and subsequent food intake. *Int. J. Food Sci. Nutr* **1999**, *50*, 13−28.
(181) Liu, S.; Willett, W. C.; Manson, J. E.; Hu, F. B.; Rosner, B.; Colditz, G. Relation between changes in intakes of dietary fiber and grain products and changes in weight and development of obesity among middle-aged women. *Am. J. Clin. Nutr.* **2003**, *78*, 920−927.
(182) McKeown, N. M.; Troy, L. M.; Jacques, P. F.; Hoffmann, U.; O'Donnell, C. J.; Fox, C. S. Whole- and refined-grain intakes are differentially associated with abdominal visceral and subcutaneous adiposity in healthy adults: the Framingham Heart Study. *Am. J. Clin. Nutr.* **2010**, *92*, 1165−1171.
(183) Koh-Banerjee, P.; Franz, M.; Sampson, L.; Liu, S.; Jacobs, D. R., Jr.; Spiegelman, D.; Willett, W.; Rimm, E. Changes in whole-grain, bran, and cereal fiber consumption in relation to 8-y weight gain among men. *Am. J. Clin. Nutr.* **2004**, *80*, 1237−1245.
(184) Melanson, K. J.; Angelopoulos, T. J.; Nguyen, V. T.; Martini, M.; Zukley, L.; Lowndes, J.; Dube, T. J.; Fiutem, J. J.; Yount, B. W.; Rippe, J. M. Consumption of whole-grain cereals during weight loss: effects on dietary quality, dietary fiber, magnesium, vitamin B-6, and obesity. *J. Am. Diet Assoc* **2006**, *106*, 1380−1388 (quiz 1389−1390).
(185) Rave, K.; Roggen, K.; Dellweg, S.; Heise, T.; tom Dieck, H. Improvement of insulin resistance after diet with a whole-grain based dietary product: results of a randomized, controlled cross-over study in obese subjects with elevated fasting blood glucose. *Br. J. Nutr.* **2007**, *98*, 929−936.
(186) Maki, K. C.; Beiseigel, J. M.; Jonnalagadda, S. S.; Gugger, C. K.; Reeves, M. S.; Farmer, M. V.; Kaden, V. N.; Rains, T. M. Whole-grain ready-to-eat oat cereal, as part of a dietary program for weight loss, reduces low-density lipoprotein cholesterol in adults with overweight and obesity more than a dietary program including low-fiber control foods. *J. Am. Diet. Assoc.* **2010**, *110*, 205−214.
(187) Pol, K.; Christensen, R.; Bartels, E. M.; Raben, A.; Tetens, I.; Kristensen, M. Whole grain and body weight changes in apparently healthy adults: a systematic review and meta-analysis of randomized controlled studies. *Am. J. Clin. Nutr.* **2013**, *98*, 872−884.
(188) Kabagambe, E. K.; Baylin, A.; Ruiz-Narvarez, E.; Siles, X.; Campos, H. Decreased consumption of dried mature beans is positively associated with urbanization and nonfatal acute myocardial infarction. *J. Nutr.* **2005**, *135*, 1770−1775.
(189) Abete, I.; Parra, D.; Martinez, J. A. Legume-, fish-, or high-protein-based hypocaloric diets: effects on weight loss and mitochondrial oxidation in obese men. *J. Med. Food* **2009**, *12*, 100−108.
(190) Winham, D. M.; Hutchins, A. M. Baked bean consumption reduces serum cholesterol in hypercholesterolemic adults. *Nutr. Res. (N.Y.)* **2007**, *27*, 380−386.
(191) Abeysekara, S.; Chilibeck, P. D.; Vatanparast, H.; Zello, G. A. A pulse-based diet is effective for reducing total and LDL-cholesterol in older adults. *Br. J. Nutr.* **2012**, *108* (Suppl. 1), S103−S110.
(192) Pittaway, J. K.; Ahuja, K. D.; Cehun, M.; Chronopoulos, A.; Robertson, I. K.; Nestel, P. J.; Ball, M. J. Dietary supplementation with chickpeas for at least 5 weeks results in small but significant reductions in serum total and low-density lipoprotein cholesterols in adult women and men. *Ann. Nutr. Metab.* **2006**, *50*, 512−518.
(193) Pittaway, J. K.; Ahuja, K. D.; Robertson, I. K.; Ball, M. J. Effects of a controlled diet supplemented with chickpeas on serum lipids, glucose tolerance, satiety and bowel function. *J. Am. Coll. Nutr.* **2007**, *26*, 334−340.
(194) Pittaway, J. K.; Robertson, I. K.; Ball, M. J. Chickpeas may influence fatty acid and fiber intake in an ad libitum diet, leading to small improvements in serum lipid profile and glycemic control. *J. Am. Diet. Assoc.* **2008**, *108*, 1009−1013.
(195) Zhang, Z.; Lanza, E.; Kris-Etherton, P. M.; Colburn, N. H.; Bagshaw, D.; Rovine, M. J.; Ulbrecht, J. S.; Bobe, G.; Chapkin, R. S.; Hartman, T. J. A high legume low glycemic index diet improves serum lipid profiles in men. *Lipids* **2010**, *45*, 765−775.
(196) Jenkins, D. J.; Kendall, C. W.; Augustin, L. S.; Mitchell, S.; Sahye-Pudaruth, S.; Blanco Mejia, S.; Chiavaroli, L.; Mirrahimi, A.; Ireland, C.; Bashyam, B.; Vidgen, E.; de Souza, R. J.; Sievenpiper, J. L.; Coveney, J.; Leiter, L. A.; Josse, R. G. Effect of legumes as part of a low glycemic index diet on glycemic control and cardiovascular risk factors in type 2 diabetes mellitus: a randomized controlled trial. *Arch. Intern. Med.* **2012**, *172*, 1653−1660.
(197) Bazzano, L. A.; Thompson, A. M.; Tees, M. T.; Nguyen, C. H.; Winham, D. M. Non-soy legume consumption lowers cholesterol levels: a meta-analysis of randomized controlled trials. *Nutr. Metab. Cardiovasc.* **2011**, *21*, 94−103.
(198) Anderson, J. W.; Major, A. W. Pulses and lipaemia, short- and long-term effect: potential in the prevention of cardiovascular disease. *Br. J. Nutr.* **2002**, *88* (Suppl. 3), S263−S271.
(199) Duranti, M.; Lovati, M. R.; Dani, V.; Barbiroli, A.; Scarafoni, A.; Castiglioni, S.; Ponzone, C.; Morazzoni, P. The α′ subunit from soybean 7S globulin lowers plasma lipids and upregulates liver β-VLDL receptors in rats fed a hypercholesterolemic diet. *J. Nutr.* **2004**, *134*, 1334−1339.
(200) Halton, T. L.; Willett, W. C.; Liu, S.; Manson, J. E.; Albert, C. M.; Rexrode, K.; Hu, F. B. Low-carbohydrate-diet score and the risk of

coronary heart disease in women. *N. Engl. J. Med.* **2006**, *355*, 1991−2002.
(201) Hermsdorff, H. H.; Zulet, M. A.; Abete, I.; Martinez, J. A. A legume-based hypocaloric diet reduces proinflammatory status and improves metabolic features in overweight/obese subjects. *Eur. J. Nutr.* **2011**, *50*, 61−69.
(202) Belski, R.; Mori, T. A.; Puddey, I. B.; Sipsas, S.; Woodman, R. J.; Ackland, T. R.; Beilin, L. J.; Dove, E. R.; Carlyon, N. B.; Jayaseena, V.; Hodgson, J. M. Effects of lupin-enriched foods on body composition and cardiovascular disease risk factors: a 12-month randomized controlled weight loss trial. *Int. J. Obes. (London)* **2011**, *35*, 810−819.
(203) Lee, Y. P.; Mori, T. A.; Puddey, I. B.; Sipsas, S.; Ackland, T. R.; Beilin, L. J.; Hodgson, J. M. Effects of lupin kernel flour-enriched bread on blood pressure: a controlled intervention study. *Am. J. Clin. Nutr.* **2009**, *89*, 766−772.
(204) Jayalath, V. H.; de Souza, R. J.; Sievenpiper, J. L.; Ha, V.; Chiavaroli, L.; Mirrahimi, A.; Di Buono, M.; Bernstein, A. M.; Leiter, L. A.; Kris-Etherton, P. M.; Vuksan, V.; Beyene, J.; Kendall, C. W.; Jenkins, D. J. Effect of dietary pulses on blood pressure: a systematic review and meta-analysis of controlled feeding trials. *Am. J. Hypertens.* **2013**, *27*, 56−64.
(205) Wang, X.; Qin, X.; Demirtas, H.; Li, J.; Mao, G.; Huo, Y.; Sun, N.; Liu, L.; Xu, X. Efficacy of folic acid supplementation in stroke prevention: a meta-analysis. *Lancet* **2007**, *369*, 1876−1882.
(206) Ma, Y.; Hebert, J. R.; Li, W.; Bertone-Johnson, E. R.; Olendzki, B.; Pagoto, S. L.; Tinker, L.; Rosal, M. C.; Ockene, I. S.; Ockene, J. K.; Griffith, J. A.; Liu, S. Association between dietary fiber and markers of systemic inflammation in the Women's Health Initiative Observational Study. *Nutrition* **2008**, *24*, 941−949.
(207) North, C. J.; Venter, C. S.; Jerling, J. C. The effects of dietary fibre on C-reactive protein, an inflammation marker predicting cardiovascular disease. *Eur. J. Clin. Nutr.* **2009**, *63*, 921−933.
(208) Jenkins, D. J.; Ghafari, H.; Wolever, T. M.; Taylor, R. H.; Jenkins, A. L.; Barker, H. M.; Fielden, H.; Bowling, A. C. Relationship between rate of digestion of foods and post-prandial glycaemia. *Diabetologia* **1982**, *22*, 450−455.
(209) Leathwood, P.; Pollet, P. Effects of slow release carbohydrates in the form of bean flakes on the evolution of hunger and satiety in man. *Appetite* **1988**, *10*, 1−11.
(210) Torsdottir, I.; Alpsten, M.; Andersson, H.; Schweizer, T. F.; Tolli, J.; Wursch, P. Gastric emptying and glycemic response after ingestion of mashed bean or potato flakes in composite meals. *Am. J. Clin. Nutr.* **1989**, *50*, 1415−1419.
(211) Ajala, O.; English, P.; Pinkney, J. Systematic review and meta-analysis of different dietary approaches to the management of type 2 diabetes. *Am. J. Clin. Nutr.* **2013**, *97*, 505−516.
(212) Villegas, R.; Gao, Y. T.; Yang, G.; Li, H. L.; Elasy, T. A.; Zheng, W.; Shu, X. O. Legume and soy food intake and the incidence of type 2 diabetes in the Shanghai Women's Health Study. *Am. J. Clin. Nutr.* **2008**, *87*, 162−167.
(213) Mollard, R. C.; Zykus, A.; Luhovyy, B. L.; Nunez, M. F.; Wong, C. L.; Anderson, G. H. The acute effects of a pulse-containing meal on glycaemic responses and measures of satiety and satiation within and at a later meal. *Br. J. Nutr.* **2011**, 1−9.
(214) Nestel, P.; Cehun, M.; Chronopoulos, A. Effects of long-term consumption and single meals of chickpeas on plasma glucose, insulin, and triacylglycerol concentrations. *Am. J. Clin. Nutr.* **2004**, *79*, 390−395.
(215) Sievenpiper, J. L.; Kendall, C. W.; Esfahani, A.; Wong, J. M.; Carleton, A. J.; Jiang, H. Y.; Bazinet, R. P.; Vidgen, E.; Jenkins, D. J. Effect of non-oil-seed pulses on glycaemic control: a systematic review and meta-analysis of randomised controlled experimental trials in people with and without diabetes. *Diabetologia* **2009**, *52*, 1479−1495.
(216) Thompson, S. V.; Winham, D. M.; Hutchins, A. M. Bean and rice meals reduce postprandial glycemic response in adults with type 2 diabetes: a cross-over study. *Nutr. J.* **2012**, *11*, 23.
(217) Mollard, R. C.; Wong, C. L.; Luhovyy, B. L.; Anderson, G. H. First and second meal effects of pulses on blood glucose, appetite, and food intake at a later meal. *Appl. Physiol. Nutr. Metab.* **2011**, *36*, 634−642.
(218) Jenkins, D. J.; Wolever, T. M.; Taylor, R. H.; Griffiths, C.; Krzeminska, K.; Lawrie, J. A.; Bennett, C. M.; Goff, D. V.; Sarson, D. L.; Bloom, S. R. Slow release dietary carbohydrate improves second meal tolerance. *Am. J. Clin. Nutr.* **1982**, *35*, 1339−1346.
(219) Wolever, T. M.; Jenkins, D. J.; Ocana, A. M.; Rao, V. A.; Collier, G. R. Second-meal effect: low-glycemic-index foods eaten at dinner improve subsequent breakfast glycemic response. *Am. J. Clin. Nutr.* **1988**, *48*, 1041−1047.
(220) Nilsson, A.; Johansson, E.; Ekstrom, L.; Bjorck, I. Effects of a brown beans evening meal on metabolic risk markers and appetite regulating hormones at a subsequent standardized breakfast: a randomized cross-over study. *PLoS One* **2013**, *8*, No. e59985.
(221) Smith, C. E.; Mollard, R. C.; Luhovyy, B. L.; Anderson, G. H. The effect of yellow pea protein and fibre on short-term food intake, subjective appetite and glycaemic response in healthy young men. *Br. J. Nutr.* **2012**, *108* (Suppl. 1), S74−S80.
(222) Hosseinpour-Niazi, S.; Mirmiran, P.; Amiri, Z.; Hosseini-Esfahani, F.; Shakeri, N.; Azizi, F. Legume intake is inversely associated with metabolic syndrome in adults. *Arch. Iran. Med.* **2012**, *15*, 538−544.
(223) Johnson, S. K.; Thomas, S. J.; Hall, R. S. Palatability and glucose, insulin and satiety responses of chickpea flour and extruded chickpea flour bread eaten as part of a breakfast. *Eur. J. Clin. Nutr.* **2005**, *59*, 169−176.
(224) Murty, C. M.; Pittaway, J. K.; Ball, M. J. Chickpea supplementation in an Australian diet affects food choice, satiety and bowel health. *Appetite* **2010**, *54*, 282−288.
(225) Lee, Y. P.; Mori, T. A.; Sipsas, S.; Barden, A.; Puddey, I. B.; Burke, V.; Hall, R. S.; Hodgson, J. M. Lupin-enriched bread increases satiety and reduces energy intake acutely. *Am. J. Clin. Nutr.* **2006**, *84*, 975−980.
(226) Archer, B. J.; Johnson, S. K.; Devereux, H. M.; Baxter, A. L. Effect of fat replacement by inulin or lupin-kernel fibre on sausage patty acceptability, post-meal perceptions of satiety and food intake in men. *Br. J. Nutr.* **2004**, *91*, 591−599.
(227) Hall, R. S.; Thomas, S. J.; Johnson, S. K. Australian sweet lupin flour addition reduces the glycaemic index of a white bread breakfast without affecting palatability in healthy human volunteers. *Asia Pac. J. Clin. Nutr.* **2005**, *14*, 91−97.
(228) Sichieri, R.; Condo, A. N.; Saura, S. K. I.; Albino, C. C. Weight reduction diet with low fat based on rice and beans. *Arq. Bras. Endocrinol. Metab.* **1993**, *37*, 135−138.
(229) Karlstrom, B.; Vessby, B.; Asp, N. G.; Boberg, M.; Lithell, H.; Berne, C. Effects of leguminous seeds in a mixed diet in non-insulin-dependent diabetic patients. *Diabetes Res.* **1987**, *5*, 199−205.
(230) Venn, B. J.; Perry, T.; Green, T. J.; Skeaff, C. M.; Aitken, W.; Moore, N. J.; Mann, J. I.; Wallace, A. J.; Monro, J.; Bradshaw, A.; Brown, R. C.; Skidmore, P. M.; Doel, K.; O'Brien, K.; Frampton, C.; Williams, S. The effect of increasing consumption of pulses and wholegrains in obese people: a randomized controlled trial. *J. Am. Coll. Nutr.* **2010**, *29*, 365−372.
(231) Keogh, J.; Atkinson, F.; Eisenhauer, B.; Inamdar, A.; Brand-Miller, J. Food intake, postprandial glucose, insulin and subjective satiety responses to three different bread-based test meals. *Appetite* **2011**, *57*, 707−710.
(232) Hodgson, J. M.; Lee, Y. P.; Puddey, I. B.; Sipsas, S.; Ackland, T. R.; Beilin, L. J.; Belski, R.; Mori, T. A. Effects of increasing dietary protein and fibre intake with lupin on body weight and composition and blood lipids in overweight men and women. *Int. J. Obes. (London)* **2010**, *34*, 1086−1094.
(233) USDA. Nutrient profiles for food groups and subgroups. http://www.cnpp.usda.gov/Publications/USDAFoodPatterns/NutrientProfilesforAllFoodGroupsandSubgroups.pdf (accessed Jan 19, 2014).
(234) Thompson, F. E.; Midthune, D.; Subar, A. F.; McNeel, T.; Berrigan, D.; Kipnis, V. Dietary intake estimates in the National Health

Interview Survey, 2000: methodology, results, and interpretation. *J. Am. Diet. Assoc.* **2005**, *105*, 352−363 (quiz 487).
(235) IOM. Dietary Reference Intakes for Energy, Carbohydrate, Fiber, Fat, Fatty Acids, Cholesterol, Protein, and Amino Acids, 2002.
(236) USDA. What foods are in the grains group? http://www.choosemyplate.gov/food-groups/grains.html (accessed Jan 19, 2014).
(237) Venn, B. J.; Mann, J. I. Cereal grains, legumes and diabetes. *Eur. J. Clin. Nutr.* **2004**, *58*, 1443−1461.
(238) Slavin, J. Fiber and prebiotics: mechanisms and health benefits. *Nutrients* **2013**, *5*, 1417−1435.
(239) USDA. Food Sources of Selected Nutrients. http://www.health.gov/dietaryguidelines/dga2005/document/html/appendixB.htm (accessed Jan 19, 2014).
(240) Steinberg, D. Thematic review series: the pathogenesis of atherosclerosis. An interpretive history of the cholesterol controversy, part V: the discovery of the statins and the end of the controversy. *J. Lipid Res.* **2006**, *47*, 1339−1351.
(241) USDA. Comparison of analytical values for enrichment nutrients in selected grain products to federal enrichment standards. http://www.ars.usda.gov/research/publications/publications.htm?SEQ_NO_115=204192 (accessed Jan 20, 2014).
(242) USDA. A Temporal Association between Folic Acid Fortification and a Rise in Colorectal Cancer Rates May be Illuminating Important Biological Principles: a Hypothesis. http://www.ars.usda.gov/research/publications/publications.htm?seq_no_115=213919 (accessed Jan 20, 2014).
(243) Williams, P. G. Evaluation of the evidence between consumption of refined grains and health outcomes. *Nutr. Rev.* **2012**, *70*, 80−99.
(244) Volpe, S. L. Magnesium in disease prevention and overall health. *Adv. Nutr.* **2013**, *4*, 378S−383S.
(245) Song, S.; Paik, H. Y.; Song, Y. High intake of whole grains and beans pattern is inversely associated with insulin resistance in healthy Korean adult population. *Diabetes Res. Clin. Pract.* **2012**, *98*, e28−e31.
(246) Hosseinpour-Niazi, S.; Mirmiran, P.; Sohrab, G.; Hosseini-Esfahani, F.; Azizi, F. Inverse association between fruit, legume, and cereal fiber and the risk of metabolic syndrome: Tehran Lipid and Glucose Study. *Diabetes Res. Clin. Pract.* **2011**, *94*, 276−283.
(247) Jang, Y.; Lee, J. H.; Kim, O. Y.; Park, H. Y.; Lee, S. Y. Consumption of whole grain and legume powder reduces insulin demand, lipid peroxidation, and plasma homocysteine concentrations in patients with coronary artery disease: randomized controlled clinical trial. *Arterioscler. Thromb. Vasc. Biol.* **2001**, *21*, 2065−2071.
(248) Tovar, J.; Nilsson, A.; Johansson, M.; Bjorck, I. Combining functional features of whole-grain barley and legumes for dietary reduction of cardiometabolic risk: a randomised cross-over intervention in mature women. *Br. J. Nutr.* **2014**, *111*, 706−714.
(249) Newby, P. K. Plant foods and plant-based diets: protective against childhood obesity? *Am. J. Clin. Nutr.* **2009**, *89*, 1572S−1587S.

Table 1. Analytical Results for Metal in Oysters and Standard Reference Material (n = 3)

	standard oyster (NCSZC85007)			oyster		
	certified values (μg/g)	average results (μg/g)	RSD (%)	found (μg/g)	added (μg/g)	recovery (%)
Fe	370.9	360.2 ± 6.3	3.0	1310 ± 80	1300	105.2
Cu	139.7	131.2 ± 1.3	6.5	388.24 ± 2.1	388.00	106.1
As	6.67	6.1 ± 0.34	9.3	17.48 ± 0.72	17.00	101.2
Cd	4.56	4.24 ± 0.20	7.5	6.39 ± 0.32	6.00	99.3
Pb	0.84	0.78 ± 0.08	7.7	2.46 ± 0.11	2.50	99.8

Table 2. Total Phosphorus and Nitrate Nitrogen of Seawater in Gangwei, Zhao'an, Jiuzhen, and Fotan (mg/L, Mean ± SD; n = 3)

	GW	ZA	JZ	FT
total phosphorus	0.015 ± 0.004	0.035 ± 0.006	0.034 ± 0.008	0.043 ± 0.010
nitrate nitrogen	0.164 ± 0.032	0.182 ± 0.040	0.280 ± 0.042	0.419 ± 0.046

Young small size oysters were transplanted to these four bays (FT, JZ, GW, and ZA) and a 4-month experiment was conducted from last December, 2012 to March, 2013. A batch of oysters (30 individuals) about 5 cm were collected and brought to the laboratory immediately and thoroughly cleaned again to eliminate organic materials and appendiculate sediments. The soft tissues were isolated from the shell, dried, and ground as a powder by an agate mortar.

Preparation of Digestive Juices and Incubation of Gut Microbiota. The preparation of digestive juice and the incubation of gut microbiota were based on the reference.[15] According to human physiology, the process and time of digestion were designed.[16] The gastrointestinal inorganics, organics, bioenzyme, and gut microbiota were added to prepare the digestive juices.

Oyster (1.0 g) powder was digested successively in the bionic mouth, stomach, and intestine at 37 °C on a gentle oscillation as follows. The bionic gastrointestinal digestion process was initiated with the addition of 5 mL of saliva and oscillated for 5 min to simulate chewing. Then, 30 mL of gastric juice was added to the above sample and incubated for 3 h to simulate bionic gastric digestion. After gastric digestion, the pH value of the chyme was adjusted to 7.8 ± 0.2 with 1 mol/L NaOH, and then the chyme was mixed with 30 mL of duodenal juice, 15 mL of bile, and 15 mL of gut microbiota, and incubated on a gently rocking shaker for 7 h to simulate for intestinal digestion. All chymes were filtered with a 0.45 μm membrane.

Egg-derived (0.1 g) lecithin was dissolved in chloroform and then transferred into a rotatory evaporator to evaporate chloroform. Chyme (25 mL) was mixed with liposome to form a homogeneous liposome suspension, frozen at −71 °C in a super low freezer for 30 min, and then thawed at 37 °C. Such a freeze−thaw process was repeated 5 times to promote the metal speciation distribution in a liposome−water system. Affinity-liposome metals could be separated from water-soluble metals by 0.22 μm membrane.

Determination of Metal Concentration in Seawater, Oysters, and Affinity-Liposome Metal in the Chyme. Oysters (0.1 g, powder) were added to concentrated HNO_3 (4.0 mL) and Milli-Q water (4.0 mL), heated in a water bath at 80 °C until no smoke arose. Then, they were digested by concentrated HNO_3 (2.0 mL) and H_2O_2 (1.0 mL, 30%) in closed Teflon tubes for 10 min, using a microwave technique. Seawater which has been filtered by a 0.22 μm membrane, all of the affinity-liposome metal, or water-soluble metal was directly decomposed by concentrated HNO_3 (2.0 mL) and H_2O_2 (1.0 mL, 30%) in a microwave oven at the same conditions. After digestion, a dilution by water to 50 mL was carried out for metal determination by ICP-MS.

Statistical Analysis. SPSS 19.0 was used for the statistical analysis. Possible relationships between trophic status (nitrate N or total P) and metal content (or metal BAF or metal OBA) were examined by partial correlation analysis and quantified by the coefficient of determination, r. A significance level of $p < 0.05$ was adopted for all comparisons. The regressions were quantified by the coefficient of determination, R^2. The plots and regression lines were drawn in SigmaPlot for Windows, version 10.0.

Accuracy of the Method. The validity of the proposed method was checked by analyzing standard reference materials, and the results are shown in Table 1. The recoveries were reasonable for the analysis of Fe, Cu, As, Cd, and Pb in oysters, ranging from 99.3.−105.2%. Metal values were in good agreement with certified concentrations in both standard reference materials. The RSD was within 9.3%. Therefore, the described method can be applicable to the determination of low levels (mg/kg or mg/L) of metals (Fe, Cu, As, Cd, and Pb) in oysters, affinity-liposome metals, and those that are water-soluble in chyme.

RESULT

Trophic Status of Four Bays. Total phosphorus and nitrate nitrogen as trophic indicators of the bays in GW, ZA, JZ, and FT were determined and shown in Table 2. The bays of GW, ZA, JZ, and FT were semiclosed, the field experiment was done in winter (from December, 2012 to March, 2013), the seawater exchange rates were poor, and the concentration of N and P in the seawater was stable during our field experiment. These results were similar to those in the database from the Department of Ocean and Fisheries in Zhangzhou City, Fujian Province, China. Similar results were also reported for other semienclosed bays.[17,18] Total phosphorus and nitrate nitrogen in these four bays were varied from 0.016 to 0.043 mg/L and from 0.164 to 0.419 mg/L, respectively. On the basis of the seawater quality standard of China, except for GW, the trophic status of the other three bays was eutrophication in some ways.

Metal Bioaccumulation in Oysters and the Correlation of BAF and Trophic Status in Four Bays. Metal bioaccumulation in oysters under different trophic status is shown in Table 3. In seawater, the concentrations of these trace metals, except for Fe, were in the range of 0.11−6.53 μg/L; however, Fe content was from 0.26 to 2.11 mg/L. All metal contents in the seawater met the standard of clean bays. Fe contents in oysters ranged from 1.22 mg/g to 2.54 mg/g, and the other metals (Cu, As, Cd, and Pb) in oysters were enriched at the level of microgram per gram. Trace metals (Fe, Cu, As, Cd, and Pb) were largely bioaccumulated in oysters. BAF was used to evaluate metal bioaccumulation in oysters, which was significantly different ($p < 0.001$). Compared to the clean bay of GW, BAF in oysters was largely increased by 5.5 and 7.3 times for Fe in the trophic bays of JZ and FT, deceased by 0.5 times for Fe in trophic ZA, and 0.5−0.9 times for Cu in trophic ZA, JZ, and FT. However, the BAF of As was irregularly fluctuant, which did not relate to trophic status in seawater. The

dx.doi.org/10.1021/jf5001953 | J. Agric. Food Chem. 2014, 62, 7050−7056

Table 3. Metal Concentration of Seawater in Oysters in JZ, FT, ZA, and GW and BAF (n = 3)[a]

	GW			ZA			JZ			FT		
	C_s (μg/L)	C_o (μg/g)	BAF	C_s (μg/L)	conc. of oyster (μg/g)	BAF	conc. of seawater (μg/L)	conc. of oyster (μg/g)	BAF	conc. of seawater (μg/L)	conc. of oyster (μg/g)	BAF
Fe × 10^{-3}	1.14 ± 0.16	1.31 ± 0.08	1120	2.11 ± 0.20	1.22 ± 0.09	565	0.34 ± 0.08	2.54 ± 0.11	7299	0.26 ± 0.06	2.52 ± 0.13	9333
Cu	2.95 ± 0.25	388.24 ± 2.1	128556	6.53 ± 0.40	75.63 ± 0.8	11305	2.65 ± 0.21	109.24 ± 1.1	40162	2.40 ± 0.22	155.81 ± 1.3	63337
As	4.05 ± 0.44	17.48 ± 0.72	4212	4.52 ± 0.41	16.71 ± 0.66	3609	1.47 ± 0.45	9.50 ± 0.35	6291	1.29 ± 0.33	5.79 ± 0.28	4386
Cd	0.13 ± 0.03	6.39 ± 0.32	49535	0.28 ± 0.05	2.34 ± 0.21	7996	0.14 ± 0.03	3.39 ± 0.26	24926	0.11 ± 0.03	3.00 ± 0.24	27778
Pb	4.03 ± 0.21	2.46 ± 0.11	596	6.13 ± 0.33	2.21 ± 0.09	352	5.00 ± 0.30	3.09 ± 0.16	602	3.82 ± 0.20	2.42 ± 0.10	617

[a]Note: the density of seawater (ρ_w) was 1.025 g·cm^{-3}. Metal bioaccumulation factor (BAF) was estimated by proportion of the oysters' and water's mass concentration. BAF = $Conc_o \times (Conc_w \times \rho_w)^{-1}$; $Conc_o$ and $Conc_w$ stand for the concentrations of seawater and oyster, respectively.

BAF of Pb did not vary significantly. Compared with the clean GW bay, the BAF of Cd in trophic bays (ZA, JZ, and FT) was decreased by 0.4−0.8 times. Furthermore, the BAF of Cd was increased as the trophic status, and the effect of trophic status on metal bioaccumulation could be discussed by partial correlation.

Partial correlation between BAF of Cd and total P (or nitrate N) was highly significant (r = 0.999, p = 0.024 for total P; and r = 0.998, p = 0.035 for nitrate N). The BAFs of Cu and Pb in oysters were not significantly correlated (p > 0.05) with total P (r = −0.98, r = −0.93) or nitrate N (r = 0.96, r = 0.95). The BAF of Fe in oysters was not significantly correlated with nitrate N (r = 0.90, p > 0.05) and show no correlation with total P (r = −0.277). The bioaccumulation in oysters in four bays was significantly different (P < 0.01), but it was not correlated with total P or nitrate N.

Relationship between Trophic Status of Seawater and Metal Oral Bioavailability. Only metal bioaccumulation in oysters could not fully reflect the potential toxicity or nutrition of metals in oysters. Therefore, metal oral bioavailability in oysters was studied by bionic digestion and liposome extraction. After bionic digestion, metal complexes in oysters could be released and entered into the gastrointestinal tract, transformed into their final coordinated complexes by the functions of bioemzymes and gut microbiota. The affinity-liposome metals in the chyme were available for gastrointestinal absorption. Correlations of metal oral bioavailability in oysters and total P (or nitrate N) are shown in Figures 1 and 2, respectively. Oral bioavailability of trace metals (Fe, Cu, As, Cd, and Pb) in oysters was all below 24%, i.e., metal species distribution in the chyme of oysters was mainly water-soluble metals. Metal OBA in oysters was not beyond 3.9% for Cu, 8.0%−17.4% for Fe, and 7.7%−18.6% for Cd. Only a small fraction of Cu in oysters was absorbed by the bionic membrane. OBA of As in oysters under different trophic status ranged from 2.5% to 23.5%. OBA of Pb in oysters were ranged from 12.1% to 14.0%, which was not significant variation (two way analysis of variance, p = 0.15).

With the aggravation of eutrophication, As OBA in oysters was largely increased. The OBA of As was significantly positively correlated to nitrate N (R^2 = 0.973, P = 0.007) and total P (R^2 = 0.904, P = 0.049). The OBA of Fe was negative correlated to nitrate N (R^2 = 0.882, p = 0.061). However, the OBA of other metals did not show any correlation with total P or nitrate N (correlation significant at P > 0.05).

Safety Assessment of Oysters for Consumption Based on Metal Oral Bioavailability. Deficiency of essential metals or metal overload is harmful for human health. Oysters are a kind of widespread seafood. Hence, safe dosage and maximum consumption of oysters are important for people. The impact of coastal trophic status on the metal safety of oysters should be assessed. Maximum consumption value for oysters was calculated by the ratio of tolerable upper intake levels (or maximum level of daily intake)[19,20] to affinity-liposome metal content, and the results are shown in Table 4. The result demonstrated that the maximum level of daily intake of oysters was mainly controlled by affinity-metal content of As. The oyster's maximum levels of daily intake ranged from 132.3 g/d to 197.4 g/d. As the N and P content increased, the maximum consumption of oysters was significantly decreased. Metal safety assessment of oysters demonstrated that an oyster's quality was significantly influenced by coastal trophic status. Consequently, the contents of N, P, and metals in the coastal

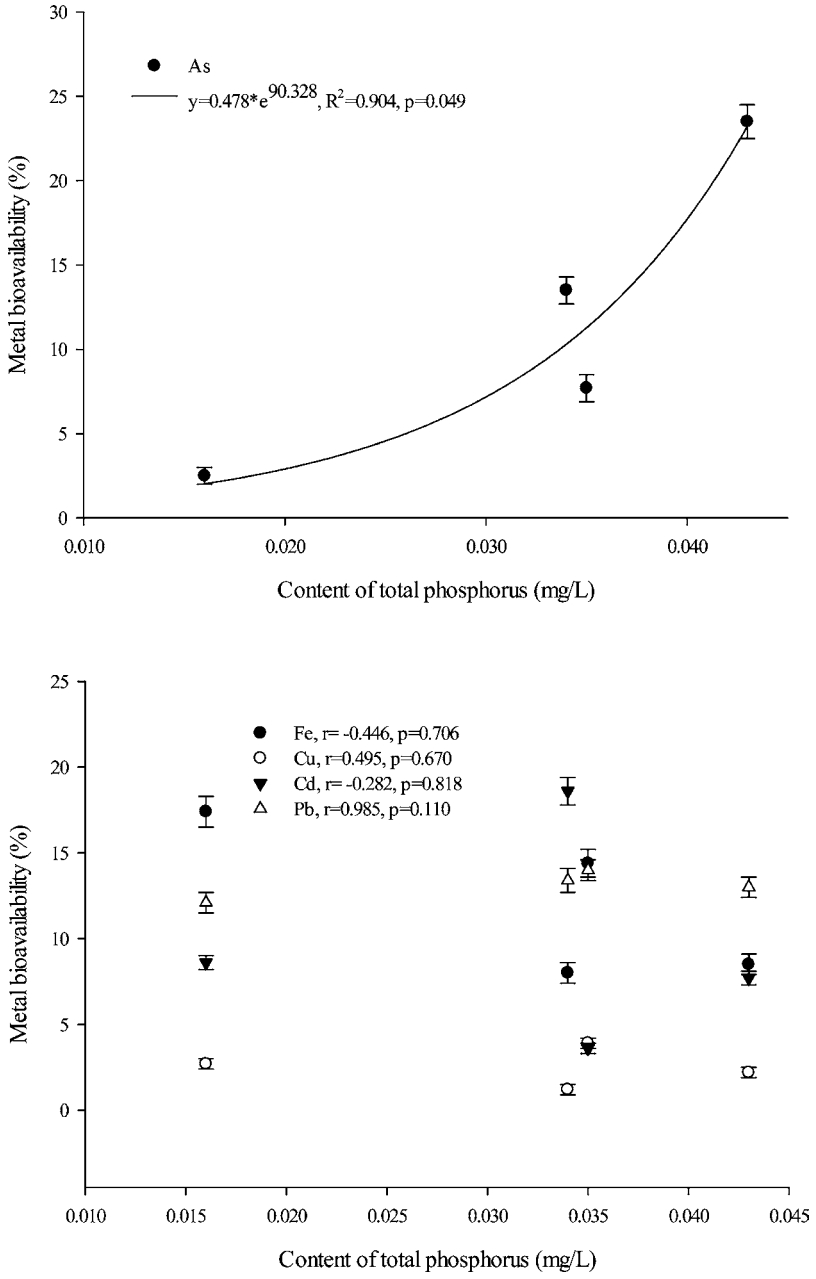

Figure 1. Relationship between the content of total phosphorus in seawater and metal oral bioavailability in oysters (two-tailed, partial correlation, $n = 3$).

seawater should be monitored simultaneously to avoid metal toxicity in oysters for consumption.

DISCUSSION

In coastal ecosystems, eutrophication has become a serious environmental problem.[21,22] The effect of trophic status on the metal bioaccumulation of an aquatic organism, such as crayfish[23] and fish,[24,25] has been reported. The input of macronutrients can not only change the concentration and ratio of marine nutrients but also affect algal structure (including species composition and abundance),[26] growth, cell shape, surface basic function groups, and biochemical compositions.[4] Coastal eutrophication also affected metal uptake and assimilation by marine algae and metal transfer in coastal food webs.[3,27] Oysters, as suspension-feeding bivalves, could assimilate metals from two sources, food particulates (e.g., algae and their debris) and dissolved metals in seawater.[28,29] The increase of N and P concentration was associated with increasing algal abundance and debris.[27] Because the bioconcentration factors of metals by marine algae were different for different metal species and nutrient regimes,[4] the influence of trophic status on metal BAF in oysters was also different with metal species. Increase of algal biomass or metal sedimentation in the debris in trophic bays may promote the ingestion of marine alga and debris. In our study, a significant positive effect of the trophic status of the seawater on the concentration of Cd in oysters (i.e., BAF) was observed. Consequently, the dominating assimilation pathway for Cd in oysters may be particulate ingestion.

After gastrointestinal digestion and gut metabolism of oysters, the affinity-liposome metals in the chyme were bioaccessible to the gastrointestinal tract, so they could be

dx.doi.org/10.1021/jf5001953 | J. Agric. Food Chem. 2014, 62, 7050−7056

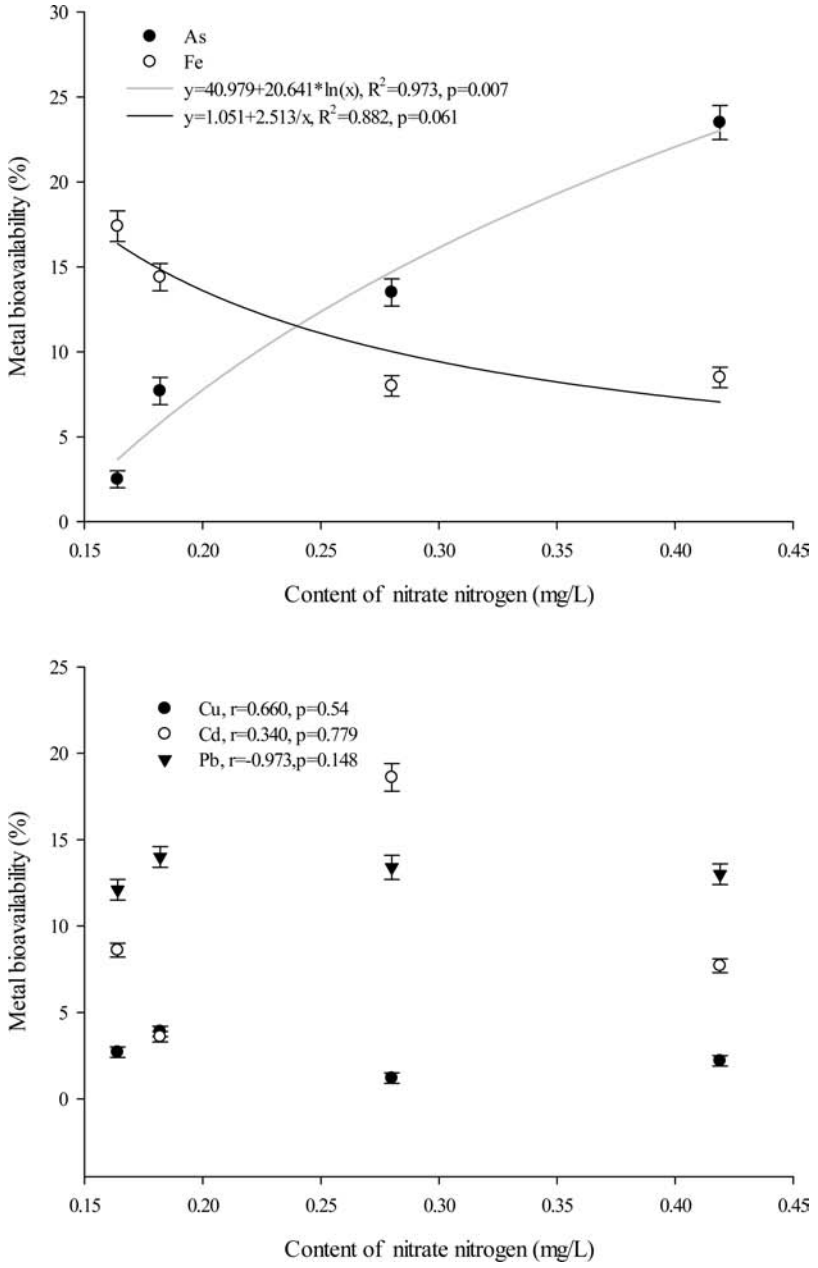

Figure 2. Relationship between the content of nitrate nitrogen in seawater and metal oral bioavailability in oysters (two-tailed, partial correlation, n = 3).

Table 4. Maximum Level of Daily Intake for Oysters[a]

		maximum consumption of oysters			
	Uls/ML value (mg/d)	GW (g/d)	ZA (g/d)	JZ (g/d)	FT (g/d)
Fe	45	197.4	256.1	221.5	210.1
Cu	10	954.0	3390.3	7628.5	2917.3
As	0.18[b]	411.9	139.9	140.4	132.3
Cd	0.3	545.9	3561.3	475.8	1298.7
Pb	0.3	1007.9	969.6	724.5	953.6

[a]Note: Uls, tolerable upper intake levels; ML, maximum level of daily intake without detriment to health. [b]UIs of inorganic arsenic BMDL was computed to be 0.18 mg/d for 60 kg weight people (3.0 μg/kg body weight per day) by WHO.

refined as the metals which were orally bioavailable to humans. Metal oral bioavailability was controlled by organic ligands.[30] Furthermore, the interaction of nitrogen and the food web may influence the metal speciation in organisms. In natural waters, the biosynthesis of organoarsenicals was enhanced by eutrophication, and arsenic speciation would be influenced by the balance of biological processes.[31] Metal ligands were closely related to metal oral bioavailability.[32] As and Fe were mainly distributed in heat-stable protein and granules, respectively, in marine molluscs (including oysters).[33] Subcellular distribution (including heat-stable protein and granules) of metal in marine oysters could be affected by the trophic status of seawater.[34] In our experience, the OBA of As was positively related to the trophic status of seawater, i.e., the OBA of As in oyster was increased as the aggravation of eutrophication in seawater and the OBA of Fe in oyster was negatively correlated to nitrate N. Metal bioaccumulation and oral bioavailability in oysters were significantly different. Through the Pearson correlation analysis,

dx.doi.org/10.1021/jf5001953 | J. Agric. Food Chem. 2014, 62, 7050−7056

only BAF of Fe was not significantly negative correlated to oral bioavailability (r = −0.992, P = 0.078). Consequently, this study suggested that As OBA in oysters could be used as a predictor of eutrophication in seawater and the potential toxicity of oysters for consumption.

In previous studies, metal bioaccessibility was indicated as the metal fraction of seafood which was released from seafood into the digestive tracts. Only the fraction of bioaccessible metals which could be absorbed by the biomembrane of the gastrointestinal tract was oral bioavailable metals. The concentration of bioaccessible metal was more than that of oral bioavailable metal and metal exposure via the consumption of seafood could be overestimated by this difference.

AUTHOR INFORMATION

Corresponding Author

*Tel: +86 596 2591395. Fax: +86 596 2591395. E-mail: lishunxing@mnnu.edu.cn; shunxing_li@aliyun.com.

Funding

This work is supported by the National Natural Science Foundation of China (41206096, 20775067, and 21175115), the Program for New Century Excellent Talents in University (NCET-110904), Outstanding Youth Science Foundation of Fujian Province, China (2010J06005), and the Science & Technology Committee of Fujian Province, China (2012Y0065).

Notes

The authors declare no competing financial interest.

ABBREVIATIONS USED

BAF, bioaccumulation factor; OBA, oral bioavailability; FT, Fotan; JZ, Jiuzhen; GW, Gangwei; ZA, Zhao'an

REFERENCES

(1) Cai, W. J.; Hu, X. P.; Huang, W. J.; Murrell, M. C.; Lehrter, J. C.; Lohrenz, S. E.; Chou, W. C.; Zhai, W. D.; Hollibaugh, J. T.; Wang, Y. Acidification of subsurface coastal waters enhanced by eutrophication. *Nat. Geosci.* **2011**, *4*, 766−770.

(2) Li, S. X.; Hong, H. S.; Zheng, F. Y.; Deng, N. S. Effects of metal pollution and macronutrient enrichment on the photoproduction of hydroxyl radicals in seawater by the alga *Dunaliella salina*. *Mar. Chem.* **2008**, *108*, 207−214.

(3) Li, S. X.; Zheng, F. Y. Effect of macronutrient enrichment on the size distribution, sorption, and bioconcentration factor of iron by coastal phytoplanktonic diatoms. *Mar. Environ. Res.* **2011**, *72*, 89−95.

(4) Li, S. X.; Hong, H. S.; Zheng, F. Y.; Deng, N. S.; Lin, F. Influence of nitrate on metal sorption and bioaccumulation in marine phytoplankton, *Dunaliella salina*. *Environ. Toxicol.* **2007**, *22*, 582−586.

(5) Wang, W. X.; Dei, R. C. Metal uptake in a coastal diatom influenced by major nutrients (N, P, and Si). *Water Res.* **2001**, *35*, 315−321.

(6) Silva, C. A. R.; Rainbow, P. S.; Smith, B. D.; Santos, Z. L. Biomonitoring of trace metal contamination in the Potengi estuary, Natal (Brazil), using the oyster Crassostrea Rhizophorae, a local food source. *Water Res.* **2001**, *35*, 4072−4078.

(7) Quiniou, F.; Damiens, G.; Gnassia-Barelli, M.; Geffard, A.; Mouneyrac, C.; Budzinski, H.; Roméo, M. Marine water quality assessment using transplanted oyster larvae. *Environ. Int.* **2007**, *33*, 27−33.

(8) Thiyagarajan, V.; Ko, G. W. K. Larval growth response of the Portuguese oyster (*Crassostrea angulata*) to multiple climate change stressors. *Aquaculture* **2012**, *370*−*371*, 90−95.

(9) Funes, V.; Alhama, J.; Navas, J.; López-Barea, J.; Peinado, J. Ecotoxicological effects of metal pollution in two mollusc species from the Spanish South Atlantic littoral. *Environ. Pollut.* **2006**, *139*, 214−223.

(10) Lannig, G.; Cherkasov, A. S.; Sokolova, I. M. Temperature-dependent effects of cadmium on mitochondrial and whole-organism bioenergetics of oysters (*Crassostrea virginica*). *Mar. Environ. Res.* **2006**, *62* (Suppl 1), S79−S82.

(11) Luoma, S. N.; Rainbow, P. S. Why is metal bioaccumulation so variable? Biodynamics as a unifying concept. *Environ. Sci. Technol.* **2005**, *39*, 1921−1931.

(12) Guo, L.; Hunt, B. J.; Santschi, P. H.; Ray, S. M. Effect of dissolved organic matter on the uptake of trace metals by American oysters. *Environ. Sci. Technol.* **2001**, *35*, 885−893.

(13) Alongi, D. M.; Boyle, S. G.; Tirendi, F.; Payn, C. Composition and behaviour of trace metals in post-oxic sediments of the Gulf of Papua, Papua New Guinea. *Estuarine, Coastal Shelf Sci.* **1996**, *42*, 197−211.

(14) Owens, R. E.; Balls, P. W. Dissolved trace metals in the Tay estuary. *Estuarine, Coastal Shelf Sci.* **1997**, *44*, 421−434.

(15) Li, S. X.; Chen, L. H.; Zheng, F. Y.; Li, Y. C. Effect of the cp4-epsps gene on metal bioavailability in maize and soybean using bionic gastrointestinal tracts and ICP-MS determination. *J. Agric. Food Chem.* **2013**, *61*, 1579−1584.

(16) Versantvoort, C. H. M.; Oomen, A. G.; Van de Kamp, E.; Rompelberg, C. J. M.; Sips, A. J. A. M. Applicability of an in vitro digestion model in assessing the bioaccessibility of mycotoxins from food. *Food Chem. Toxicol.* **2005**, *43*, 31−40.

(17) Hong, H. K.; Takahashi, S.; Min, B. Y.; Tanabe, S. Butyltin residues in blue mussels (*Mytilus edulis*) and arkshells (*Scapharca broughtonii*) collected from Korean coastal waters. *Environ. Pollut.* **2002**, *117*, 475−486.

(18) Lee, J. H.; Harrison, P. J.; Kuang, C.; Yin, K., Eutrophication Dynamics in Hong Kong Coastal Waters: Physical and Biological Interactions. In *The Environment in Asia Pacific Harbours*; Wolanski, E. Ed.; Springer: Netherlands, 2006; pp 187−206.

(19) Trumbo, P.; Yates, A. A.; Schlicker, S.; Poos, M. Dietary reference intakes: vitamin A, vitamin K, arsenic, boron, chromium, copper, iodine, iron, manganese, molybdenum, nickel, silicon, vanadium, and zinc. *J. Am. Diet. Assoc.* **2001**, *101*, 294−301.

(20) WHO Expert Committee on Food Additives. Seventy-second Meeting, Rome, 16−25 Feb 2010: Summary and Conclusions; Joint FAO/WHO Expert Committee on Food Additives: Rome, Italy, 2010; p 16; JECFA/72/SC: 2010.

(21) Syvitski, J. P. M.; Vörösmarty, C. J.; Kettner, A. J.; Green, P. Impact of humans on the flux of terrestrial sediment to the global coastal ocean. *Science* **2005**, *308*, 376−380.

(22) Halpern, B. S.; Walbridge, S.; Selkoe, K. A.; Kappel, C. V.; Micheli, F.; D'Agrosa, C.; Bruno, J. F.; Casey, K. S.; Ebert, C.; Fox, H. E.; Fujita, R.; Heinemann, D.; Lenihan, H. S.; Madin, E. M. P.; Perry, M. T.; Selig, E. R.; Spalding, M.; Steneck, R.; Watson, R. A global map of human impact on marine ecosystems. *Science* **2008**, *319*, 948−952.

(23) Larsson, P.; Holmqvist, N.; Stenroth, P.; Berglund, O.; Nyström, P.; Granéli, W. Heavy metals and stable isotopes in a benthic omnivore in a trophic gradient of lakes. *Environ. Sci. Technol.* **2007**, *41*, 5973−5979.

(24) Lithner, G.; Borg, H.; Ek, J.; Fröberg, E.; Holm, K.; Johansson, A.-M.; Kärrhage, P.; Rosén, G.; Söderström, M. The turnover of metals in a eutrophic and an oligotrophic lake in Sweden. *Ambio* **2000**, *29*, 217−229.

(25) Chen, C. Y.; Folt, C. L. High plankton densities reduce mercury biomagnification. *Environ. Sci. Technol.* **2005**, *39*, 115−121.

(26) Tyrrell, T. The relative influences of nitrogen and phosphorus on oceanic primary production. *Nature* **1999**, *400*, 525−531.

(27) Li, S. X.; Liu, F. J.; Zheng, F. Y.; Zuo, Y. G.; Huang, X. G. Effects of nitrate addition and iron speciation on trace element transfer in coastal food webs under phosphate and iron enrichment. *Chemosphere* **2013**, *91*, 1486−1494.

(28) Wang, W. X.; Fisher, N. S.; Luoma, S. N. Assimilation of trace elements ingested by the mussel Mytilus edulis: effects of algal food abundance. *Mar. Ecol.: Prog. Ser.* **1995**, *129*, 165−176.

(29) Ke, C. H.; Wang, W. X. Bioaccumulation of Cd, Se, and Zn in an estuarine oyster (*Crassostrea rivularis*) and a coastal oyster (*Saccostrea glomerata*). *Aquat. Toxicol.* **2001**, *56*, 33−51.
(30) Wells, M. L.; Trick, C. G. Controlling iron availability to phytoplankton in iron-replete coastal waters. *Mar. Chem.* **2004**, *86*, 1−13.
(31) Hasegawa, H.; Rahman, M. A.; Matsuda, T.; Kitahara, T.; Maki, T.; Ueda, K. Effect of eutrophication on the distribution of arsenic species in eutrophic and mesotrophic lakes. *Sci. Total Environ.* **2009**, *407*, 1418−1425.
(32) Li, S. X.; Lin, L. X.; Zheng, F. Y.; Wang, Q. X. Metal bioavailability and risk assessment from edible brown alga Laminaria japonica, using biomimetic digestion and absorption system and determination by ICP-MS. *J. Agric. Food Chem.* **2011**, *59*, 822−828.
(33) He, M.; Wang, W. X. Bioaccessibility of 12 trace elements in marine molluscs. *Food Chem. Toxicol.* **2013**, *55*, 627−636.
(34) Miao, A. J.; Wang, W. X. Cadmium toxicity to two marine phytoplankton under different nutrient conditions. *Aquat. Toxicol.* **2006**, *78*, 114−126.

Table 1. Descriptors of the Five Hot Pepper Cultivars Used in This Experiment

cultivar	*Capsicum* species	pungency category[a]	leaf characteristics	fruit characteristics	growth habit[b]	source
Yuyi	*annuum*	low	big leaf, ovate shape	bell, campanulate, blunt end	annual	Japan
Keenoo-Pama	*annuum*	medium	small leaf, lanceolate shape	short, slim, elongated, pointed end	perennial	Myanmar
Huay-Siiton	*annuum*	medium	small leaf, lanceolate shape	Thai chilli, elongated, pointed end	perennial	KKU, Thailand
BGH 1719	*chinense*	high	small leaf, deltoid shape	short, slim, elongated, pointed end	perennial	USDA, Brazil
Perennial	*annuum*	high	small leaf, deltoid shape	short, slim, campanulate, blunt end	perennial	USDA, Mexico

[a]High = >100,000 Scoville heat units (SHU); medium = 50,000−100,000 SHU; low = <50,000 SHU. [b]All cultivars were grown and harvested within one season. (Plant growth habits of these cultivars are typically perennial type, but actually grown and harvested as annual type.).

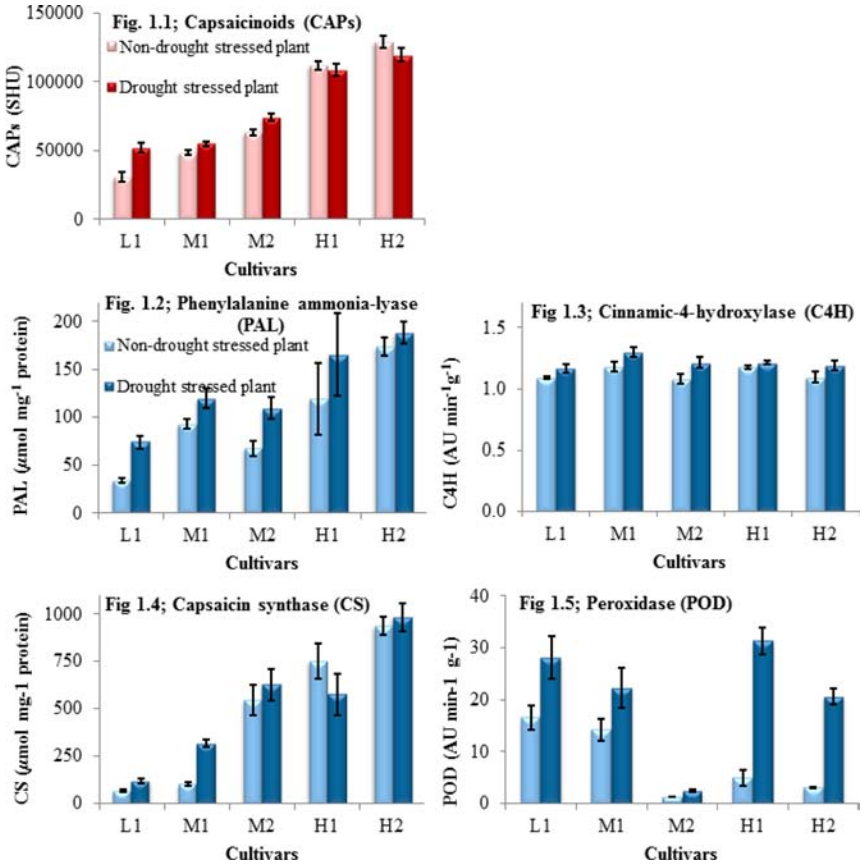

Figure 1. Sum of capsaicin and dihydrocapsaicin (CAPs) (redrawn from Phimchan et al.[7] (with permission from *HortScience*)) and activities of PAL, C4H, CS, and POD between non-drought-stressed and drought-stressed plants in the fruits of five hot pepper cultivars: one low pungent cultivar (L1, Yuyi), two medium pungent cultivars (M1, Huay-Siiton; M2, Keenoo-Pama), and two high pungent cultivars (H1, BGH 1719; H2, Perennial).

Phenylalanine Ammonia-lyase Activity. PAL activity was measured following the method of Koç et al.[11] with some modification from Ochoa-Alejo and Gómez-Peralta.[12] In this procedure, 0.5 g of fresh frozen fruit tissue was ground under 4 °C with 1.5 mL of 50 mM Tris-HCl buffer (pH 8.8) containing 1 mM EDTA, 15 mM β-mercaptoethanol, and 50 mM ascorbic acid. Then the mixture was centrifuged at 15,000 rpm for 30 min by using a Hettich Zentrifugen Universal 30RF model (Hettich GmbH & Co. KG, Kirchlengern, Germany), and after that, the supernatant was collected. The amount of protein was calculated by comparing the sample to the calibration curve obtained with bovine serum albumin (BSA) following the method of Bradford.[13] The absorbance at 595 nm was determined with a spectrophotometer using a Spectro SC-model (LaboMed, Inc., Los Angeles, CA, USA).

The assay mixture contained 0.1 mL of the enzyme extract, 1 mL of 100 mM Tris-HCl buffer (pH 8.8), 0.5 mL of 10 mM L-phenylalanine, and 0.4 mL of deionized water. The mixture was incubated for 1 h at 37 °C, and the reaction was terminated by adding 0.5 mL of 6 M HCl. Then the sample absorbance was measured at 290 nm with a spectrophotometer by using a GENESYS 10S UV−vis model (Thermo Scientific, Waltham, MA, USA). The calibration curve was constructed using cinnamic acid. The blank had the same constituent mixture as the sample.

Cinnamic-4-hydroxylase Activity. C4H activity was measured according to the method of Ochoa-Alejo and Gómez-Peralta[12] with some modification. One gram of fresh frozen fruit tissue was ground under 4 °C with 6 mL of 100 mM Tris-HCl buffer (pH 7.5). The extract was centrifuged at 15,000 rpm for 30 min at 4 °C, and the supernatant was collected as the enzyme extract.

The reaction mixture consisted of 1.5 mL of 100 mM Tris-HCl buffer (pH 7.5), 0.05 mL each of 20 mM glucose-6-phosphate, 12 mM β-mercaptoethanol, 8 mM cinnamic acid, and 8 mM NADP, 1000 units per 12.5 mL of G6P dehydrogenase, and 1 mL of the extract solution. The absorbance of the extracted solution at 340 nm was measured for 5 min by using an Agilent 8453 UV−visible model (Agilent Technologies, Inc., Santa Clara, CA, USA) with the time course method.

Capsaicin Synthase Activity. The procedure for the measurement of CS activity followed that of Ochoa-Alejo and Gómez-Peralta[12] with some modification. The extract was prepared by grinding 0.5 g of

dx.doi.org/10.1021/jf4051717 | J. Agric. Food Chem. 2014, 62, 7057−7062

Table 2. Phenylalanine Ammonia-lyase (PAL), Cinnamic-4-hydroxylase (C4H), Capsaicin Synthase (CS), and Peroxidase (POD) Activities under Control (C) and Drought Stress (D) Treatments

	PAL (μmol mg^{-1} protein)						C4H (AU min^{-1} g^{-1})					
	C[a]		D[a,b]				C[a]		D[a,b]			
cultivar	mean	SD	mean	SD	*t* test	% increase[c]	mean	SD	mean	SD	*t* test	% increase[c]
Yuyi	33.99 d	2.73	74.02 e	6.49	**	117.75	1.092 b	0.012	1.167 c	0.036	*	6.90
Huay-Siiton	92.59 bc	5.03	135.59 b	10.21	*	28.44	1.181 a	0.042	1.298 a	0.040	*	9.90
Keenoo-Pama	67.68 c	7.69	109.16 bc	11.12	*	61.26	1.084 b	0.040	1.215 b	0.047	*	12.02
BGH 1719	148.91 b	37.85	165.23 ab	43.51	ns	38.95	1.177 a	0.013	1.214 b	0.018	*	3.20
Perennial	173.54 a	9.54	188.32 a	11.79	ns	8.52	1.093 b	0.043	1.191 b	0.043	*	9.00
F test	**		**				*		**			
CV (%)	11.65		10.46				12.92		11.72			
	CS (μmol mg^{-1} protein)						POD (AU min^{-1} g^{-1})					
	C[a]		D[a,b]				C[a]		D[a,b]			
cultivar	mean	SD	mean	SD	*t* test	% increase[c]	mean	SD	mean	SD	*t* test	% increase[c]
Yuyi	67.60 f	5.34	119.60 g	11.23	*	76.90	16.50 a	2.310	28.13 ab	4.157	*	70.48
Huay-Siiton	104.90 ef	10.78	316.70 de	19.39	**	201.96	14.25 ab	2.116	22.26 bc	3.924	*	56.21
Keenoo-Pama	546.80 c	81.77	628.50 bc	83.85	ns	14.96	1.26 f	0.051	2.46 g	0.214	**	95.24
BGH 1719	752.40 ab	92.14	578.30 c	109.48	ns	−23.14	5.06 d	1.524	31.31 a	2.504	**	518.77
Perennial	936.40 a	47.09	982.70 a	76.22	ns	4.94	3.13 de	0.115	20.63 c	1.504	**	559.11
F test	**		**				**		**			
CV (%)	13.64		15.00				19.78		12.72			

[a]Means followed by different letters in the same column are significantly different ($P < 0.01$). [b]ns, *, ** nonsignificant, significant difference between control and drought within cultivar at $P < 0.05$ and 0.01 probability levels by *t* test, respectively. [c]Percentage increase was calculated with the equation [(drought − control)/control] × 100.

fresh fruit tissue with 6 mL of 100 mM Tris-HCl buffer (pH 6.8). The homogenate was centrifuged at 15,000 rpm for 30 min at 4 °C and the supernatant collected for enzyme source.

The reaction mixture contained 0.1 mL of 0.4 M Tris-HCl (pH 6.8), 10 μL of 0.2 M vanillylamine, 5 μL each of 40 mM ATP, 40 mM $MgCl_2$, and 40 mM 8-methyl-6-nonenoic acid, and 0.3 mL of extracted enzyme. The reaction was performed at 37 °C for 1 h and terminated with 0.1 mL of 1 M HCl. The assay mixture was extracted with 0.5 mL of chloroform and evaporated to dryness at 50 °C in vacuo. Then, 1 mL of acetone was added, and the mixture was placed on a shaker for 1 h. The mixture was filtered with 0.45 μm PVDF Millipore; 10 μL of filtered solution was used for each HPLC assay using a Shimadzu VP series model (Shimadzu Co., Kyoto, Japan).

Peroxidase Activity. POD activity was measured through adaptation of the method of Arnnok et al.[14] All steps of enzyme extraction were carried out at 4 °C. A total of 1 g of homogenized hot pepper tissue was extracted with 0.1 M phosphate buffer (pH 7) containing 5 g of polyvinylpyrolidone using a magnetic stirrer for 15 min. The homogenate was filtered through Whatman no. 41 filter paper and then centrifuged at 2500 rpm for 20 min. The supernatant was filtered through Whatman no. 42 filter paper and collected as an enzyme extract. The activity of POD was assayed at 470 nm. The reaction mixture contained 0.15 mL of 40% (v/v) guaiacol, 0.15 mL of 1% (v/v) H_2O_2, 2.66 mL of 0.1 M phosphate buffer (pH 7), and 40 μL of the enzyme extract. The blank sample contained the same mixture solution without the enzyme extract.

Statistical Analyses. Statistical analyses were conducted following the procedure of Gomez and Gomez.[15] Analysis of variances (ANOVA) in a randomized complete block design was used with LSD to compare the significant differences among cultivars within treatment, and a *t* test compared the significant differences between control and drought stress treatments within a cultivar. A percentage increase of enzyme activities was calculated by using the equation [(drought − control)/control] × 100. In addition, the sum of capsaicin and dihydrocapsaicin (CAPs) of the five hot peppers cultivars used in this experiment was redrawn from a previous experiment[7] to estimate the relationship between the responses of enzyme activities and capsaicinoid content to drought stress (Figure 1).

RESULTS

All enzyme activities, PAL, C4H, CS, and POD, differed significantly among cultivars within a treatment (Table 2). The cultivars grown under the control treatment gave enzyme activities significantly lower than those under drought stress, except for PAL within cv. BGH 1719 and Perennial and CS within cv. Keenoo-Pama, BGH 1719, and Perennial.

Phenylalanine Ammonia-lyase Activity. For both control and drought-stressed plants, the activities of PAL differed significantly among cultivars (Table 2). As expected, the values of PAL activity under both treatments of the high-pungent cultivars were high, followed by medium-pungent ones, and PAL activity was low in the low-pungent cultivar. The high-pungent cv. Perennial exhibited the highest value of PAL activity under drought stress and control treatments (188.32 and 173.54 μmol mg^{-1} protein, respectively). Even though the PAL activity of cv. BGH 1719 under control treatment (148.91 μmol mg^{-1} protein) was significantly lower than that of cv. Perennial, its value under drought stress (165.23 μmol mg^{-1} protein) was not significantly different from that of cv. Perennial. The PAL activities of the medium-pungent cv. Huay-Siiton under control and drought stress treatments (92.59 and 135.59 μmol mg^{-1} protein, respectively) were not significantly different from those of cv. Keenoo-Pama (67.68 and 109.16 μmol mg^{-1} protein, respectively) within treatment. Yuyi, the low-pungent cultivar, showed the lowest values of PAL activities under control and drought stress treatments (33.99 and 74.02 μmol mg^{-1} protein, respectively). Moreover, the increase percentages of this enzyme activity in the drought-stressed plants related to control ones were large and highly significant for the low-pungent cv. Yuyi (117.75%), followed by those of the medium-pungent cv. Keenoo-Pama (61.26%) and Huay-Siiton (28.44%). However, they were small and not significantly different for the high-pungent cv. BGH 1719 (39.0%) and Perennial (8.52%).

dx.doi.org/10.1021/jf4051717 | J. Agric. Food Chem. 2014, 62, 7057−7062

Cinnamic-4-hydroxylase Activity. Under control and drought stress treatments, the activities of C4H differed significantly among cultivars (Table 2). The significant difference of this enzyme's activity between the control and the treatment were found in all cultivars studied. For the control treatment, the value of medium-pungent cv. Huay-Siiton and the high-pungent cv. BGH 1719 exhibited high values of 1.181 and 1.177 AU min^{-1} g^{-1}, respectively. Under drought stress treatment, cv. Huay-Siiton presented the highest C4H value (1.298 AU min^{-1} g^{-1}), which was significantly higher than those of the other cultivars (1.167−1.215 AU min^{-1} g^{-1}). The low-pungent cv. Yuyi gave a low C4H value. Although the increase percentages of the drought-stressed plants related to the controls were not as large as those of PAL activities, a significant difference between control and drought-stressed plants was observed in all cultivars studied.

Capsaicin Synthase Activity. The activity of the CS enzyme was significantly different among cultivars under both the control and drought stress treatments (Table 2). Similarly to PAL activity, the responses of CS activities in cultivars with different pungency levels were elevated in the high-pungent cultivars, followed by medium-pungent, and lowest in the low-pungent cultivars under both treatments. However, the responses among cultivars were different within a treatment. The high-pungent cv. Perennial presented the highest values of CS under control and drought stress treatments (936.4 and 982.7 μmol mg^{-1} protein, respectively). The value of CS activity in the other high-pungent cultivar, cv. BGH 1719, in the control treatment (752.4 μmol mg^{-1} protein) was not significantly lower than that in cv. Perennial. However, its value in stress conditions (578.3 μmol mg^{-1} protein) was not as high as that of cv. Perennial. Of the medium-pungent cultivars, cv. Keenoo-Pama gave higher CS values under control and stress treatments (546.8 and 628.5 μmol mg^{-1} protein, respectively) compared to cv. Huay-Siiton (104.9 and 316.7 μmol mg^{-1} protein, respectively). As expected, the low-pungent cv. Yuyi had the lowest values of CS activities under control and drought stress treatments (67.6 and 119.6 μmol mg^{-1} protein, respectively). In addition, the increase in this enzyme's activity in the drought-stressed plants related to the control was large (201.96%). In addition, it was significantly different in the medium-pungent cv. Huay-Siiton and the low-pungent cv. Yuyi (76.90%), whereas it was not different for the other cultivars.

Peroxidase Activity. POD activities in all cultivars studied under drought stress treatment were significantly different among cultivars within a treatment and higher than those under the control treatment. The POD activity in the control treatment was contradictory to the other three enzyme activities (Table 2 and Figure 1). The POD enzyme activities were low in both of the high-pungent cultivars, BGH 1719 and Perennial, under control treatment (5.06 and 3.13 AU min^{-1} g^{-1}, respectively), but they were high under drought stress treatment (31.31 and 20.63 AU min^{-1} g^{-1}, respectively) and highly significantly different from those of the controls. For the medium-pungent cultivars, their POD activities in both treatments were not consistent. For example, cv. Huay-Siiton gave high values of POD activity under both control and drought stress treatments (14.25 and 22.26 AU min^{-1} g^{-1}, respectively), which were significantly higher than those of cv. Keenoo-Pama (1.26 and 2.46 AU min^{-1} g^{-1}, respectively). Moreover, the low-pungent cv. Yuyi gave high POD activity (16.50 and 28.13 AU min^{-1} g^{-1}, respectively); however, these values were not significantly different from those of cv. Huay-Siiton within a treatment. The increase of this enzyme's activity in the drought-stressed plants related to the control plants was large and highly significantly different for the high-pungent cv. BGH 1719 and Perennial (518.8 and 559.1%, respectively). A small increase of this enzyme activity was observed for the medium-pungent cv. Huay-Siiton and Keenoo-Pama and for the low-pungent cv. Yuyi (56.21, 95.24, and 70.48%, respectively), but they were all significantly different.

Relationship between Enzyme Activities and Capsaicinoid Responses to Drought Stress. The low- and medium-pungent cultivars under drought stress produced significantly higher amounts of capsaicin and dihydrocapsaicin (CAPs) than the control plants. The high-pungent cultivars did not significantly differ in capsaicinoid amount when subjected to drought stress conditions (Figure 1.1). The responses of PAL activity showed a trend similar to the responses of the capsaicinoid amounts under both treatments, with the values for PAL activities and capsaicinoid content low in the low- and medium-pungent cultivars and high in the high-pungent cultivars under both treatments (Figure 1.2). Moreover, the significant increase of PAL values in the low- and medium-pungent cultivars and the nonsignificant increase in the high-pungent cultivars were exactly the same responses of CAPs of those cultivars with different pungency levels under drought stress. The enzyme C4H activities did not show any association with the capsaicinoid responses, where C4H values in all cultivars with different pungency levels were all significantly increased compared to their control ones (Figure 1.3). The responses of CS activities and capsaicinoid amount in the low- and high-pungent cultivars showed a similar trend under drought stress; that is, both traits were increased for the low-pungent cultivar and not increased for the high-pungent ones (Figure 1.4). However, those values of both traits in the medium-pungent cultivars were inconsistent and not associated with capsaicinoid responses. Meanwhile, values of both traits in cv. Huay-Siiton were increased, but they were not for cv. Keenoo-Pama. In contrast to the other enzyme activities, POD values showed a negative trend for capsaicinoid amount under control treatment, where POD value was high in the low-pungent cultivar and low in the high-pungent cultivars (Figure 1.5). Nevertheless, these enzyme activities in all cultivars with different pungency levels were all significantly increased compared to their control plants.

DISCUSSION

PAL, C4H, CS, and POD are reported as the important enzymes in capsaicinoid biosynthesis.[9,16] In addition, they are the key enzymes involved for capsaicinoid changes under drought stress.[6] In this study, PAL activity showed an obvious trend associated with the capsaicinoids among hot pepper cultivars with different pungency levels. The three other enzyme activities, C4H, CS, and POD, had an inconsistent relationship to capsaicinoid content.

The different levels of enzyme activity among cultivars within a treatment and between treatments within a cultivar illustrated the significant interaction of the environments on the enzymes. These observations confirm previous studies that different pepper cultivars vary in their enzymatic responses.[10,14,18] Hot pepper cultivars with high capsaicinoid levels were less sensitive to drought stress as compared to the low- and medium-pungent cultivars. This indicates the stability of high-pungent cultivars under stress conditions to produce capsaicinoids. Our results concur with the finding by Gurung et al.[19] that capsaicinoid

amounts in high-pungent cultivars do not fluctuate as compared to low-pungent cultivars in the different environmental conditions. On the other hand, genotype by environment interaction does affect capsaicinoid production;[3] however, a genotype is the major factor compared to the environmental effect.[19]

It has been reported that capsaicinoid content increases under drought stress,[4] and the increase is related to four key enzymes of the capsaicinoid biosynthesis pathway.[6] The changes of these enzyme activities under drought imply that these enzymes were strongly influenced by the drought stress effects.[7] The enzymatic activities in the phenylpropanoid pathway starting from lignin and free phenolic compounds,[20] which are the products of the shikimate pathway, were increased by stress. Subsequently, they resulted in the increase of phenylalanine, the precursor of the capsaicinoid.[21] Thereafter, phenylalanine enters and converts to cinnamic acid, thus increasing this precursor under drought stress, which affects further enzyme activity in the capsaicinoid synsthesis pathway, including C4H, CS, and POD.[16] Our results showed increases of activity for the four enzymes for all of the cultivars under drought stress. Among these four enzymes, PAL changes under drought stress showed a complete association with capsaicinoids, in all five hot pepper cultivars examined. The changes of PAL and CAPs between the control and drought-stressed plants in the low- and medium-pungent cultivars were all significantly different, but they were not for the high-pungent cultivars. Moreover, the responses of PAL in the five cultivars concur with the results of Estrada et al.,[4] in which the PAL activities increased with water stress.

It is important to note that the C4H activities were significantly increased under drought stress, but those changes were not associated with an increase of capsaicinoids among the cultivars. CS activities showed a similar trend to PAL in that there was an unchanging amount in the stressed plants of high-pungent cultivars. PAL activity between the two medium-pungent cultivars was not associated with the capsaicinoid responses. The increase of CS activity was found in cv. Huay-Siiton and was not found in cv. Keenoo-Pama, whereas capsaicinoids in these two cultivars did increase. Furthermore, POD activity had a negative association with capsaicinoid amounts, which is similar to the observations reported by Contreras-Padilla and Yahia[22] and Di et al.[23] This adverse relationship might be attributed to the fact that POD activity is closely related to the oxidization of the capsaicinoid metabolism,[17] resulting in a decrease in POD activity, with an increase in the capsaicinoid amount. The significant increase in POD activity under drought stress observed for all cultivars studied was not associated with their capsaicinoid content. The increase in POD activity under drought stress in all cultivars studied clearly indicated a negative relationship between the evolution of capsaicinoids and POD activities due to its involvement in capsaicinoid degradation.[22,23] The increase in POD activity in our results contradicted the results of Sung et al.,[6] who found a decrease in POD activity under drought stress. The difference could be attributed to the fact that our stressed plants received a level of stress to alter the physiological metabolism,[24] for example, capsaicinoid biosynthesis, and resulted in an increase of this enzyme under the stress.

In conclusion, PAL, C4H, CS, and POD activities were found to differ due to drought stress induction. Under drought stress, the activities of the enzymes increased as compared to the optimum water application treatment. A novel discovery was that under drought stress the PAL enzyme was the only one to affect the capsaicinoid biosynthesis.

AUTHOR INFORMATION

Corresponding Author

*(S.T.) Phone/fax: +663203055. E-mail: suctec@kku.ac.th.

Funding

We are grateful to the Royal Golden Jubilee, Thailand Research Fund; National Science of Thailand and Development Association, Higher Education Research Promotion and National Research University Project of Thailand, Office of the Higher Education Commission, through the Food and Functional Food Research Cluster of Khon Kaen University, and Plant Breeding Research Center for Sustainable Agriculture, Khon Kaen University, Thailand; and New Mexico State University.

Notes

The authors declare no competing financial interest.

REFERENCES

(1) Suzuki, T.; Fujiwake, H.; Iwai, K. Intracellular localization of capsaicin and its analogues in *Capsicum* fruit. I. Microscopic investigation of the structure of the placenta of *Capsicum annuum* var. *annuum* cv. Karayatsubusa. *Plant Cell Physiol.* **1980**, *21*, 839−853.

(2) Harvell, K. P.; Bosland, P. W. The environment produces a significant effect on pungency of chiles (chillies). *HortScience* **1997**, *32* (7), 1292.

(3) Zewdie, Y.; Bosland, P. W. Evaluation of genotype, environment, and genotype-by-environment interaction for capsaicinoid in *Capsicum annuum*. *Euphytica* **2000**, *111*, 185−190.

(4) Estrada, B.; Pomar, F.; Diaz, J.; Merino, F.; Bernal, M. A. Pungency levels in fruits of the 'Padron' pepper with different water supply. *Sci. Hortic.* **1999**, *81*, 385−396.

(5) Bosland, P. W.; Votava, E. J. Chemical composition. In *Pepper: Vegetable and Spice Capsicums*, 2nd ed.; Bosland, P. W., Votava, E. J., Eds.; CABI: Wallingford, UK, 2012; Vol. 22, pp 83−98.

(6) Sung, Y.; Chang, Y. Y.; Ting, N. L. Capsaicin biosynthesis in water-stressed hot pepper fruits. *Bot. Bull. Acad. Sin.* **2005**, *46*, 35−42.

(7) Phimchan, P.; Techawongstien, S.; Chanthai, S.; Bosland, P. W. Impact of drought stress on the accumulation of capsaicinoids in *Capsicum* cultivars with different initial capsaicinoid levels. *HortScience* **2012**, *47*, 1204−1209.

(8) Fujiwake, H.; Suzuki, T.; Iwai, K. Capsaicinoid formation in the protoplast from the placenta of *Capsicum annuum* var. *annuum* cultivar Karayatsubusa fruits. *Agric. Biol. Chem.* **1982**, *46*, 2591−2592.

(9) Blum, E.; Mazourek, M.; O'Connell, M. A.; Curry, J.; Thorup, T.; Liu, K.; Jahn, M. M.; Paran, I. Molecular mapping of capsaicinoid biosynthesis genes and quantitative trait loci analysis for capsaicinoid content in *Capsicum*. *Theor. Appl. Genet.* **2003**, *108*, 79−86.

(10) Bernal, M. A.; Ros Barceló, A.; Merino, F. Histochemical localization of peroxidase in *Capsicum* fruits. *LWT−Food Sci. Technol.* **1994**, *27*, 197−198.

(11) Koç, E.; Üstün, A. S.; Íslek, C.; Arici, Y. K. Defence responses in leaves of resistant and susceptible pepper (*Capsicum annuum* L.) cultivars infected with different inoculum concentrations of *Phytophthora capsici* Leon. *Sci. Hortic.* **2011**, *128* (4), 434−442.

(12) Ochoa-Alejo, N.; Gomez-Peralta, J. E. Activity of enzymes involved in capsaicin biosynthesis in callus tissue and fruits of chili pepper (*Capsicum annuum* L.). *J. Plant Physiol.* **1993**, *141* (2), 147−152.

(13) Bradford, M. M. A rapid and sensitive method for the quantitation of microgram quantities of protein utilizing the principle of protein-dye binding. *Anal. Biochem.* **1976**, *72*, 248−254.

(14) Arnnok, P.; Ruangviriyachai, C.; Mahachai, R.; Techawongstien, S.; Chanthai, S. Opitimization and determination of polyphenol

oxidase and peroxidase activities in hot pepper (*Capsicum annuum* L.) pericarb. *Int. Food Res. J.* **2010**, *17*, 385−392.
(15) Gomez, K. A.; Gomez, A. A. *Statistical Procedures for Agricultural Research*, 2nd ed.; Wiley-Interscience: New York, 1976.
(16) Curry, J.; Aluru, M.; Mendoza, M.; Nevarez, J.; Melendrez, M.; O'Connell, M. A. Transcripts for possible capsaicinoid biosynthetic genes are differentially accumulated in pungent and non-pungent *Capsicum* spp. *Plant Sci.* **1999**, *148*, 47−57.
(17) Zapata, J. M.; Calderón, A. A.; Muñoz, R.; Ros Barceló, A. Oxidation of natural hydroxybenzoic acids by grapevine peroxidases: kinetics characteristics and substrate specificity. *Am. J. Enol. Vitic.* **1992**, *43*, 134−138.
(18) Perucka, I.; Materska, M. Phenylalanine ammonia-lyase and antioxidant activities of lipophillic fraction of fresh pepper fruits *Capsicum annuum* L. *Innovative Food Sci. Emerging Technol.* **2001**, *2* (3), 189−192.
(19) Gurung, T.; Techawongstien, S.; Suriharn, B.; Techawongstien, S. Impact of environments on the accumulation of capsaicinoids in *Capsicum* spp. *HortScience* **2011**, *46*, 1576−1581.
(20) Díaz, J.; Pormar, F.; Bernal, A.; Merino, F. Peroxidase and the metabolism of capsaicin in *Capsicum annuum* L. *Phytochem. Rev.* **2004**, *3*, 141−157.
(21) Estrada, B.; Bernal, M. A.; Díaz, J.; Pomar, F.; Merino, F. Fruit development in *Capsicum annuum*: changes in capsaicin, lignin, free phenolics, and peroxidase patterns. *J. Agric. Food Chem.* **2000**, *48*, 6234−6239.
(22) Contreras-Padilla, M.; Yahia, E. M. Changes in capsaicinoids during development maturation and senescence of chile pepper and relation with peroxidase activity. *J. Agric. Food Chem.* **1998**, *46* (6), 2075−2079.
(23) Di, Y.; Jiang, J. J.; Shih, J. C. The recent research of metabolism physiology in capsaicinoid. *China Veg.* **2000**, *3*, 48−50.
(24) Kramer, P. J. Water deficit and plant growth. In *Water Relations of Plants*; Academic Press: New York, 1983; pp 342−389.

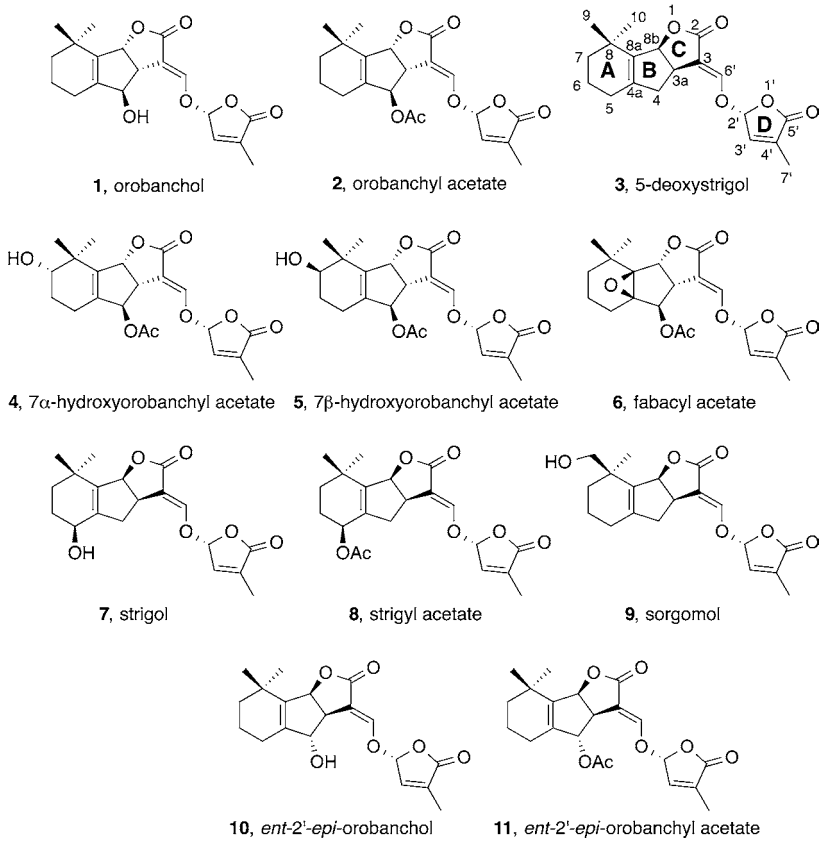

Figure 1. Structures of strigolactones used in this work: orobanchol (**1**), orobanchyl acetate (**2**), 5-deoxystrigol (**3**), 7α-hydroxyorobanchyl acetate (**4**), 7β-hydroxyorobanchyl acetate (**5**), fabacyl acetate (**6**), strigol (**7**), strigyl acetate (**8**), sorgomol (**9**), ent-2′-epi-orobanchol (**10**), and ent-2′-epi-orobanchyl acetate (**11**).

The parasitic plant species used were *O. crenata* (population collected on faba bean in Spain), *O. foetida* (collected on faba bean in Tunisia), and *P. aegyptiaca* (collected on faba bean in Israel). Parasitic seeds were collected from dry inflorescences using a 0.6 mm mesh-size sieve (Filtra, Barcelona, Spain) and stored dry in the dark at 4 °C until use.

Faba Bean Root Exudate Collection. Faba bean seeds were surface sterilized with 4% sodium hypochlorite containing 0.02% Tween 20. Then, they were rinsed three times with sterile distilled water and placed on moistened filter paper inside Petri dishes to allow imbibition and germination. Four days after imbibition, germinated faba been seeds (radicle from 0.5 to 3 cm long) were transferred to pots filled with sterile Perlite in a growth chamber (22 °C, 12/12 h d/night regime and 200 μmol/m^2/s irradiance). Plants were always watered with tap water and therefore suffering from nutrient starvation. Seven days after imbibition faba bean plant epicotyls emerged from Perlite, and 12 d after imbibition the first two leaves were expanded. Two, three, and four weeks after imbibition, faba bean plants were removed from the perlite and the roots were carefully washed with sterile distilled water. Faba bean plants were individually placed in tubes by immersing the roots for 24 h in sterile distilled water, allowing them to release the root exudates. The root solutions containing the faba bean root exudate were collected, and the total faba bean root contained in each tube was weighed. As exudation might vary accordingly with the amount of faba bean roots in each tube, which varied with faba bean plants and harvesting times, root solution per each individual plant was adjusted with sterile distilled water to achieve equivalent concentration of faba bean fresh root weight/mL of root solution across treatments. Three final concentrations were tested for all treatments in broomrape germination: 0.02 g of faba bean root (fresh weight)/mL of hydroponic media (root solution) and, in order to be sure that broomrape seeds could recognize any germination factor present in the root exudates from the resistant cultivars, we used two additional highly concentrated root exudate solutions: 0.04 and 0.1 g/mL. Those concentrations are higher than those normally used for faba bean—broomrape seed germination bioassays.[36]

Parasitic Seed Surface Sterilization and Conditioning. *Orobanche* and *Phelipanche* seeds were surface sterilized with 0.2% (w/v) formaldehyde containing 0.02% (v/v) Tween 20, rinsed with sterile distilled water, and dried for 60 min in a laminar airflow cabinet. Approximately 100 seeds of each broomrape species were placed separately on glass fiber filter paper (GFFP) discs of 1.5 cm diameter moistened with 120 μL of sterile distilled water and conditioned in a 10 cm sterile Petri dish in the dark at 20 °C for 10 d.

Root Exudate Bioassay on Broomrape Germination. GFFP discs containing 10 d-conditioned seeds of each species as described above were transferred onto a sterile sheet of paper to remove the excess of water used during seed conditioning and dry discs transferred to new 10 cm sterile Petri dishes. Differences in the ability displayed by each faba bean accession to induce broomrape germination was studied by applying triplicated aliquots of 100 μL of root exudate collected from each faba bean plant (four plants per faba bean line) at each harvesting time. Sterile distilled water was used as negative control. GR24 (10^{-6} M) was used as a second positive control in addition to the susceptible cultivar Prothabon. Distilled water and GR24 were applied on three additional discs of each *Orobanche* and *Phelipanche* species. Seeds were stored in the dark at 20 °C for 7 d to allow germination. The germination was scored for each disc by determining the number of germinated seeds on 100 seeds using a stereoscopic microscope. Seeds were considered germinated when radicle was visible through the seed coat.

Strigolactone Analysis and Quantitation. *Root Exudate Collection and Purification Using Ethyl Acetate.* Root exudates were collected as described previously.[40] Faba bean lines used were Prothabon as susceptible line and Navio and Quijote as resistant lines. Faba bean seeds were surface-sterilized in 70% ethanol and then with 1% NaClO. After being thoroughly rinsed with sterile distilled water, seeds were imbibed in water to allow germination for 2 d. Five seedlings were

dx.doi.org/10.1021/jf5027235 | J. Agric. Food Chem. 2014, 62, 7063−7071

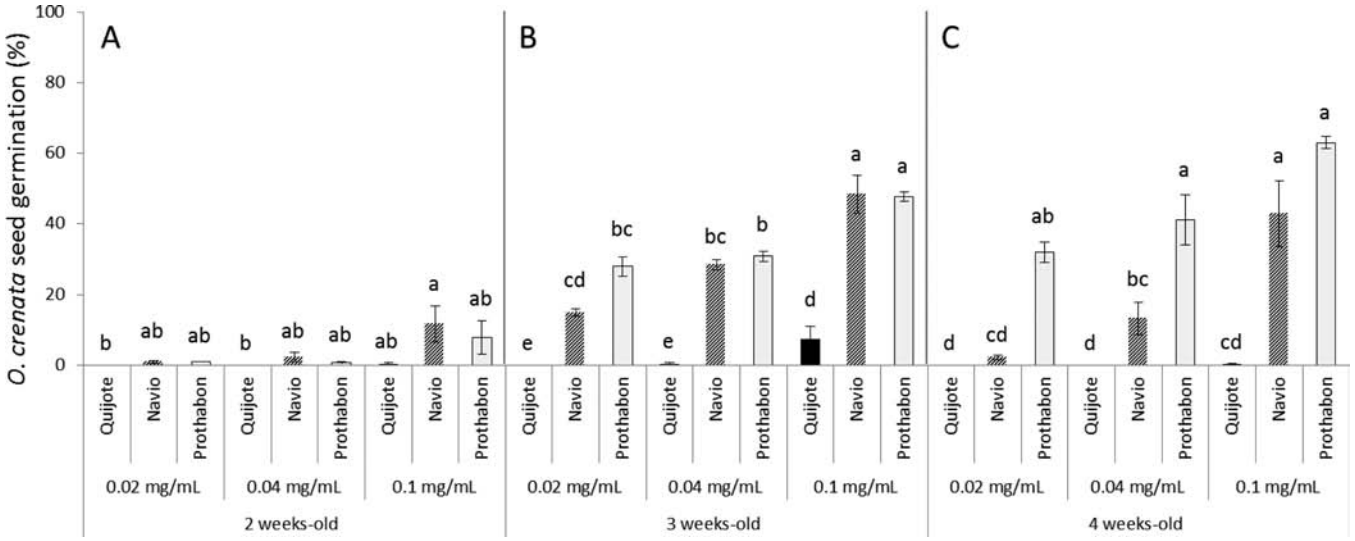

Figure 2. Effect of plant age, accession, and concentration of root exudates on germination of seeds of *Orobanche crenata*. Vertical bars represent standard error for $n = 4$. Analysis of variance was applied to transformed replicate data. For each plant age, bars with different letters are significantly different according to the Tukey test ($p = 0.05$). Negative control (distilled water) = 0%. Positive control (GR24, 10^{-6} M) = 61%.

transferred to a plastic cup (9 cm in diameter at top, 7.5 cm in diameter at the bottom, 8 cm deep, with 7 mm diameter holes on the bottom) placed in a larger plastic cup (8 cm in diameter at top, bottom 5.7 cm in diameter at the bottom, 13.5 cm deep, approximately 500 mL in volume) containing 400 mL of tap water as the culture medium. The culture medium (tap water) was frequently refreshed to allow aeration. The plants were grown in a growth chamber with a 14/10 h photoperiod at 23 °C. At 1, 2, 4, 6, 8, and 10 weeks after seed imbibition, the culture medium (tap water) was refreshed, allowing faba bean plants to release their root exudates in fresh tap water for 24 h before collection. One plastic cup was used for each faba bean line and stage of development. The tap water root exudates were extracted twice with ethyl acetate. Ethyl acetate solutions were combined, washed with 0.2 M K_2HPO_4 (pH 8.3), dried over anhydrous $MgSO_4$, and concentrated in vacuo.

Root Exudate Collection and Purification Using C18 SEPAK Cartridge. Faba bean seeds from cultivars Prothabon, Navio, and Quijote were surface sterilized and placed on sterile moistened filter paper inside Petri dishes to promote germination. Four-days-old faba been seedlings were individually transferred from the Petri dish to pots filled with sterile perlite in a growth chamber with a 14/10 h photoperiod at 23 °C. Plants were watered with tap water. After 2 weeks of cultivation in the pots, faba bean plants were removed from the Perlite and roots carefully washed with tap water. Faba bean plants were individually placed in 50 mL flasks containing sterile distilled water. Faba bean plants released in the tap water their root exudates during 24 h. Individually collected root exudate of four replicated plants per cultivar was individually loaded and purified in pre-equilibrated C18 SEPAK cartridges according with previous protocols.[36]

Strigolactone Analysis and Quantitation Using Liquid Chromatography−Tandem Mass Spectrometry. Identification of strigolactones was performed using a tandem mass spectrometer (Quattro LC Mass Spectrometer, Micromass, Manchester, U.K.) equipped with an electrospray ionization (ESI) source and coupled to a UPLC system (HITACHI Lachrom Ultra HPLC system, Hitachi, Japan). Chromatographic separation was achieved on a 2.1 mm × 50 mm, 2.0 μm, L-Column2 ODS column (CERI, Japan) by applying a methanol−water (MeOH-H_2O) gradient as follows: 0−3 min, 30−45% methanol; 3−8 min, 45−50% methanol; 8−12 min, 50−70% methanol; 12−15 min, 70−100% methanol, maintained for 3 min, then returning to 30% methanol over 1 min. Finally, the column was re-equilibrated under these conditions for 3 min, prior to the next run. The column was operated at 40 °C with a flow rate of 0.2 mL/min. The drying and nebulizing gas was nitrogen generated from pressurized air in an N2G nitrogen generator (Parker-Hanifin Japan, Tokyo, Japan). The nebulizer gas flow was set to approximately 100 L/h and the desolvation gas flow to 500 L/h. The interface temperature was set to 400 °C and the source temperature to 150 °C. The capillary and cone voltages were adjusted to orobanchol (**1**) and to the positive ionization mode. MS/MS experiments were conducted using argon as the collision gas, and the collision energy was set to 16 eV. The collision gas pressure was 0.15 Pa. The mass spectrometer was operated in positive ESI mode. Sample injection volume was 5 μL. Multiple reaction monitoring (MRM) was used for identification of strigolactones in root exudates and extracts by comparing retention times with 10 synthetic and natural strigolactone standards at 1 μM solution: orobanchol (**1**), orobanchyl acetate (**2**), 5-deoxystrigol (**3**), 7α-hydroxyorobanchyl acetate (**4**), 7β-hydroxyorobanhyl acetate (**5**), fabacyl acetate (**6**), strigol (**7**), strigyl acetate (**8**), sorgomol (**9**), *ent*-2′-epi-orobanchol (**10**), and *ent*-2′-epi-orobanchyl acetate (**11**) (Figure 1).[40,41]

Strigolactone Assays on Broomrape Germination. The effects of three major strigolactones in legume crops were tested on germination of broomrape species. The strigolactones detected in root exudates of faba bean lines Prothabon, Quijote, and Navio (i.e., orobanchol (**1**) and orobanchyl acetate (**2**)) were used in germination assays of seeds of *O. crenata*, *O. foetida*, and *P. aegyptiaca*. Although not detected in faba bean in the present work, 5-deoxystrigol (**3**) was also studied as it is known as a major strigolactonein Fabaceae.[40] These three strigolactones were tested at 10^{-6}, 10^{-7}, and 10^{-8} M on GFFP discs containing 10-d conditioned seeds of each parasitic species. GFFP discs containing the parasitic seeds conditioned as described above were transferred into a sterile sheet of paper to remove the excess of water and transferred to new 10 cm sterile Petri dishes. Each strigolactone was dissolved in acetone and diluted with sterile Milli-Q water to a final concentration of 0.7% of acetone. Aliquots of 100 μL of orobanchol (**1**), orobanchyl acetate (**2**), or 5-deoxystrigol (**3**) at each concentration were applied to triplicated GFFP discs containing parasitic seeds. This was done for each broomrape species separately. Petri dishes were sealed with Parafilm and incubated in the dark at 20 °C for 7 d. Milli-Q water containing 0.7% acetone was used as negative control. The germination was scored as described above.

Statistical Analysis. Experiments were performed using a completely randomized design. Percentage data were approximated to normal frequency distribution by means of angular transformation (180/Π × arcsine (sqrt[%/100])) and subjected to analysis of variance (ANOVA) using SPSS software for Windows, version 21.0 (SPSS Inc., Chicago, Illinois, USA). The significance of mean differences among treatments was evaluated by Tukey HSD test. Null hypothesis was rejected at the level of 0.05.

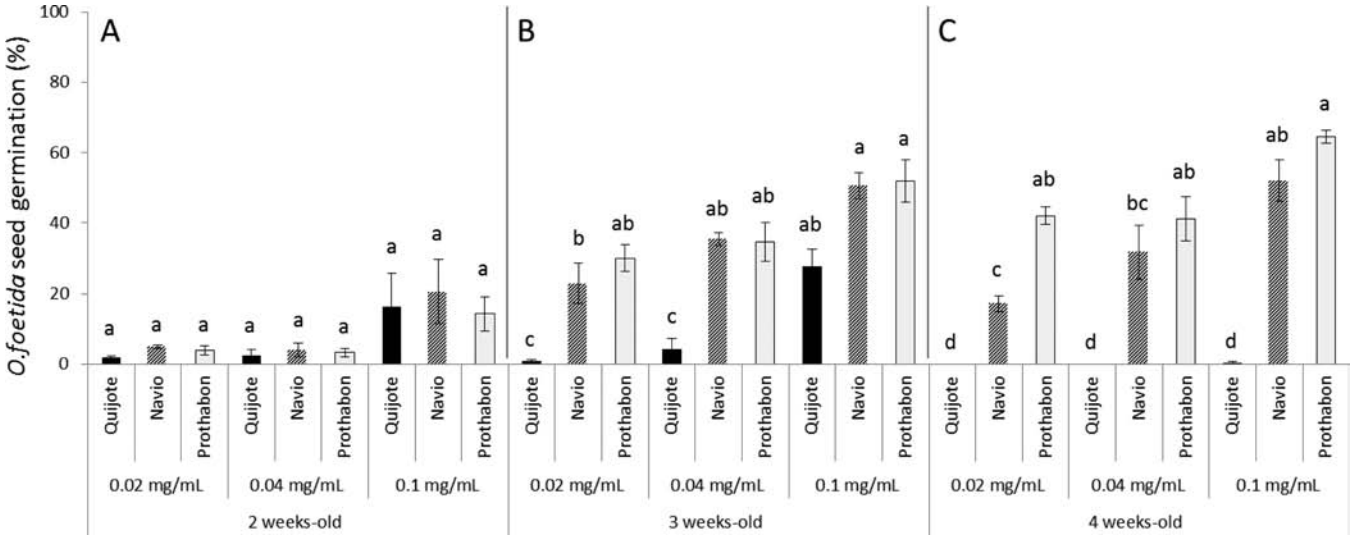

Figure 3. Effect of plant age, accession, and concentration of root exudates on germination of seeds of *Orobanche foetida*. Vertical bars represent standard error for $n = 4$. Analysis of variance was applied to transformed replicate data. For each plant age, bars with different letters are significantly different according to the Tukey test ($p = 0.05$). Negative control (distilled water) = 0%. Positive control (GR24, 10^{-6} M) = 0%.

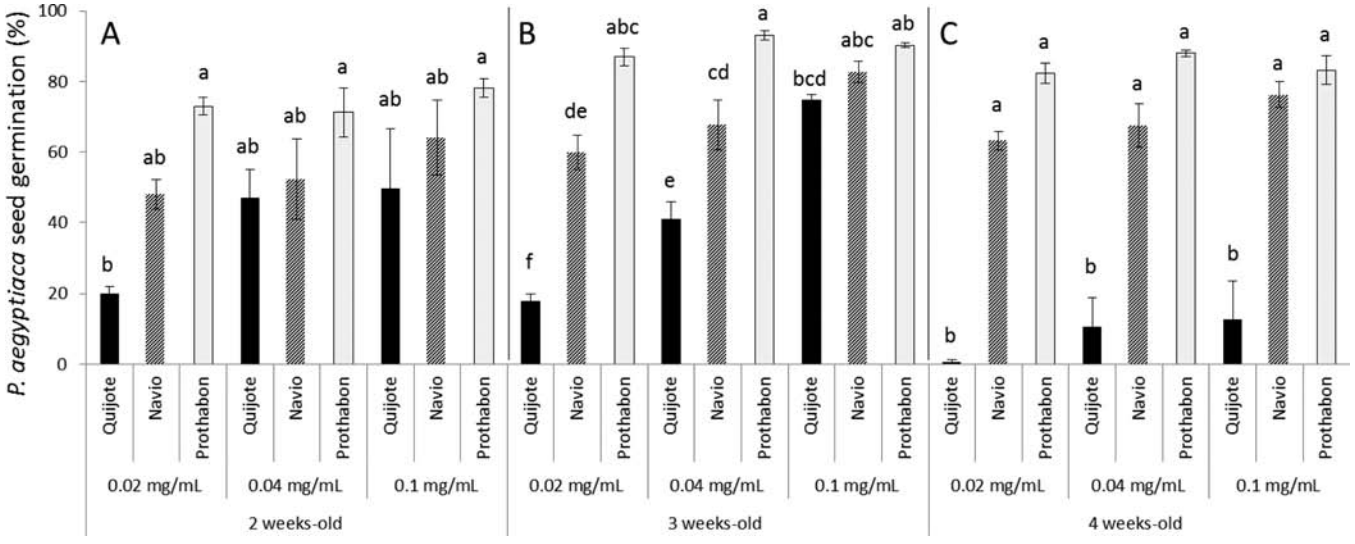

Figure 4. Effect of plant age, accession and concentration of root exudates on germination of seeds of *Phelipanche aegyptiaca*. Vertical bars represent standard error for $n = 4$. Analysis of variance was applied to transformed replicate data. For each plant age, bars with different letters are significantly different according to the Tukey test ($p = 0.05$). Negative control (distilled water) = 0%. Positive control (GR24, 10^{-6} M) = 91%.

RESULTS AND DISCUSSION

Time Course Analysis on Stimulatory Effect of Faba Bean Root Exudates on *Orobanche* and *Phelipanche* Seed Germination. The effects of faba bean cultivar (resistant cultivars: Quijote and Navio; and susceptible cultivar: Prothabon), plant age (2, 3 and 4 weeks old), and root exudate concentration (0.02, 0.04, and 0.1 g of faba bean root/mL of root solution) on germination of seeds of *O. crenata*, *O. foetida*, and *P. aegyptiaca* are shown in Figures 2, 3 and 4, respectively. In all cases, null germination was observed when broomrape seeds were treated with negative control (distilled water).

Significant effect in broomrape germination was observed for cultivar, (ANOVA, $p < 0.001$). Root exudates of the highly resistant cultivar Quijote induced the lowest levels of parasitic germination on all the broomrape species tested at all harvesting times (11.3% ± 2.1) followed by the moderately resistant cultivar Navio (35% ± 2.5). The susceptible cultivar Prothabon used as a positive control showed the highest stimulatory activity on germination of broomrape species (48% ± 3.1).

Significant effects in broomrape germination were observed both for plant age and the interaction plant age × cultivar (ANOVA, $p < 0.001$, $p < 0.001$ respectively). The effect of plant age was different in the different faba bean cultivars tested. The induction potential of parasitic germination by Quijote root exudate was not significantly different across life stages; however, root exudates collected from older Navio and Prothabon plants induced higher germination levels on *O. crenata* and *O. foetida* seeds.

Significant effect in broomrape germination was observed for broomrape species (ANOVA, $p < 0.001$). *P. aegyptiaca* was the parasitic species more responsive when exposed to faba bean root exudates. The germination average induced to *P. aegyptiaca* seeds by all faba bean cultivars at all harvesting times and root exudate concentrations was 59.4% ± 2.8, being significantly higher than

dx.doi.org/10.1021/jf5027235 | J. Agric. Food Chem. 2014, 62, 7063−7071

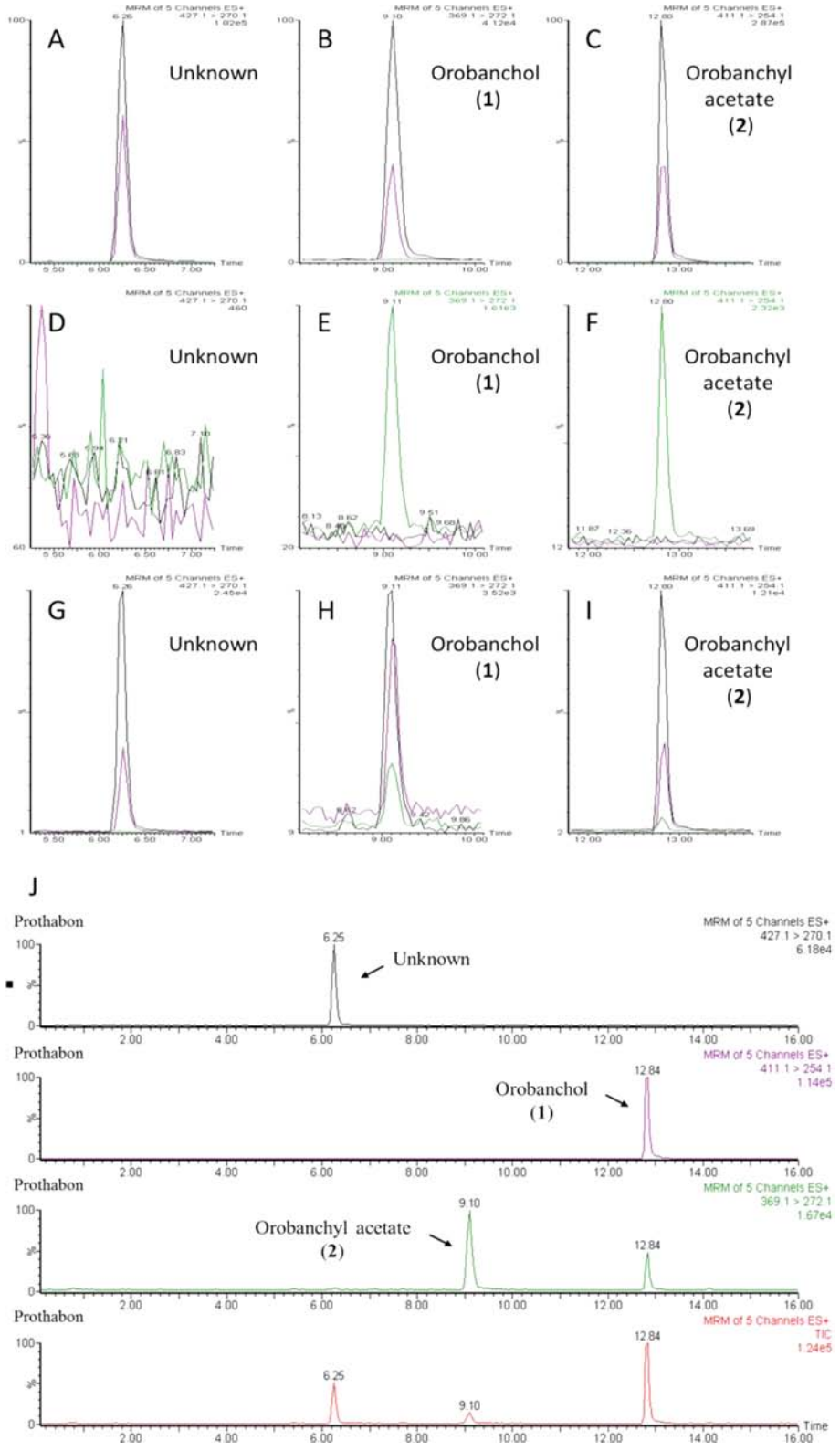

Figure 5. Liquid chromatography tandem mass spectrometry analysis of (A, B, C) faba bean susceptible line (Prothabon), (D, E, F) faba bean moderately resistant line (Navio), and (G, H, I) faba bean resistant line (Quijote). Root exudates were analyzed on 2-week-old faba bean plants (green line), 4-week-old faba bean plants (purple line), and 8-week-old faba bean plants (black line). (J) Representative UPLC chromatogram from a 4-week-old Prothabon root exudate sample.

the average induced to *O. crenata* (15.4% ± 2.0) and to *O. foetida* (22.2% ± 2.1).

For each broomrape species tested, significant effects in germination were observed for root exudate concentration (ANOVA, $p < 0.001$). Germination of broomrape species was not significantly affected by the interaction concentration × cultivar. Thus, we rule out the hypothesis that the resistance to broomrape in cultivars Quijote and Navio based on low levels of

dx.doi.org/10.1021/jf5027235 | J. Agric. Food Chem. 2014, 62, 7063−7071

Table 1. Quantitation (According to the Peak Area) of the Strigolactones Orobanchol (1) and Orobanchyl Acetate (2) in the Root Exudates of Resistant Cultivars Quijote and Navio and Susceptible Cultivar Prothabon[a]

	amount of strigolactones and unknown germination stimulant (peak area)								
	2-week-old			4-week-old			8-week-old		
	Quijote	Navio	Prothabon	Quijote	Navio	Prothabon	Quijote	Navio	Prothabon
orobanchol (1)	26.0	32.2	0.0	65.8	0.0	407.6	97.2	0.0	1200.6
orobanchyl acetate (2)	12.6	39.0	0.0	84.2	0.0	2467.0	221.8	0.0	5280.8
unknown	0.0	0.0	0.0	170.6	0.0	1264.6	566.6	0.0	2352.8

[a] Quantitation was also performed on the unknown germination stimulant.

broomrape seed germination is due to presence of germination inhibitors at the concentrations tested in this work.

Root exudates of the resistant faba bean cultivar Quijote induced negligible levels of seed germination of *O. crenata* at all concentrations and harvesting times tested. They showed also a negligible activity on germination of *O. foetida* at 0.02 g/mL (1.0% ± 0.3) and at 0.04 g/mL (2.0% ± 1.2) at all harvesting times tested. Only at the highest root exudate concentration (0.1 g/mL), Quijote root exudates stimulated some *O. foetida* germination, that although low was significant at 3 weeks (27.7% ± 6.7) but not at 2 and 4 weeks of plant cultivation. *P. aegyptiaca* germination was induced by 2- and 3-week-old Quijote plants (39.1% ± 6.9 and 38.1% ± 8.8), but this activity significantly decreased at 4-week-old to 7.4% ± 4.4. Quijote root exudate concentration had significant effect on *P. aegyptiaca* germination only when seeds were exposed to root exudates collected from 3-week-old Quijote plants.

As described before, root exudates of Navio induced higher germination than Quijote although still much lower than Prothabon. Root exudates of Navio plants showed activity on the three tested species, but this was higher on *P. aegyptiaca* seeds (64.1% ± 2.7) than on *O. crenata* (18.3% ± 3.1) and *O. foetida* (26.7% ± 3.1) seeds.

Prothabon root exudates induced germination of the three parasitic species tested. The average germination at all harvesting times and root exudate concentration for *P. aegyptiaca*, *O. crenata*, and *O. foetida* was 81.9% ± 1.5; 25.9% ± 3.7; and 32.3% ± 3.8, respectively. The Prothabon stimulation of broomrape seeds increased with harvesting time reaching maximum levels of germination for each broomrape species when Prothabon plants were 4 weeks old.

LC-MS/MS Analysis for Strigolactone Identification and Quantitation in Faba Bean Root Exudate. Root exudates collected from each faba bean cultivar were screened for the presence of strigolactones by LC-MS/MS. This analysis was repeated across faba bean development, 6 times at 1, 2, 4, 6, 8, and 10 weeks of cultivation. Strigolactone profiles of root exudates from 1- and 2-week-old plants were similar for each faba bean cultivar. Strigolactone profiles for 6-, 8-, and 10-week-old plants were similar for each faba bean cultivar.

LC-MS/MS analysis indicated that the same strigolactones were present in root exudates of all faba bean cultivars studied (Figure 5, Table 1). However, there were differences between cultivars in the pattern of strigolactone exudation. We observed a link between the low amounts of strigolactones exuded by Quijote and Navio, the low level of broomrape germination observed in vitro in this work and in previous reports,[36] and the high level of broomrape resistance observed in the field in these resistant cultivars.[36] For all faba bean cultivars the LC-MS/MS chromatograms showed two peaks at retention times 9.10 and 12.84 min, and they were identified as orobanchol (1) and orobanchyl acetate (2), using comparisons with 11 strigolactone standards (Figure 1). In addition, a peak at retention time 6.25 was collected and proved for germination stimulatory activity. This peak corresponds to an unknown germination stimulant and is currently under characterization. The susceptible cultivar Prothabon was the cultivar that exuded relatively larger amounts of strigolactones followed by Navio. The highly resistant cultivar Quijote was the cultivar whose root exudates contained the lowest amount of strigolactones.

There were also differences between cultivars in the timing of strigolactone detection along the faba bean development. Table 1 shows the pattern of strigolactone exudation at 2, 4, and 8 weeks. At early growth stages (1 and 2 weeks old), none or negligible amounts of strigolactones were detected in root exudates of any of the faba bean lines tested. These contents remained low as time increased in Navio but increased markedly in Prothabon. Strigolactones levels in Quijote were under detection limits in young plants. As Quijote plants grew, orobanchol (1) and orobanchyl acetate (2) were detected in their root exudates but their levels were very low across all life stages studied. Quijote plants exuded 83.8% less orobanchol (1), 96.6% less orobanchyl acetate (2), and 86.6% less of the unknown germination stimulant than Prothabon plants when compared at 4 weeks old and 91.9% less orobanchol (1), 95.8% less orobanchyl acetate (2), and 75.9% less unknown germination stimulant than Prothabon plants when compared at 8 weeks old.

In order to further confirm low exudation of strigolactones in Quijote plants, we analyzed by LC-MS/MS the root exudates individually collected from four replicated plants of Quijote, Navio, and Prothabon growing in 50 mL tubes. Previous to root exudate purification and LC-MS/MS analysis, aliquots of root exudate (at concentration 0.02 g/mL) of each plant and cultivar were tested on *P. aegyptiaca* and *O. crenata* germination. Differences in activity of the root exudates between susceptible control and resistant cultivars were confirmed, Prothabon root exudates being highly active on broomrape germination and Navio showing low activity, and very low or negligible levels of broomrape germination were induced by Quijote (data not shown). Our LC-MS/MS analysis showed that strigolactone levels, if any, were under detection limits for Quijote samples, while a peak corresponding to orobanchyl acetate (2) was detected in all Navio samples. In all Prothabon samples the peak corresponding to the unknown germination stimulant was always observed. This peak was collected and probed actively for germination stimulatory activity. This novel germination stimulant is currently under characterization.

Differential Effect of Pure Strigolactones on *Orobanche* and *Phelipanche* Seed Germination. Figure 6 shows the effects of strigolactone (orobanchol (1), orobanchyl acetate (2), and 5-deoxystrigol (3)) and strigolactone concentration (10^{-6} M, 10^{-7} M, and 10^{-8} M) on germination of seeds of

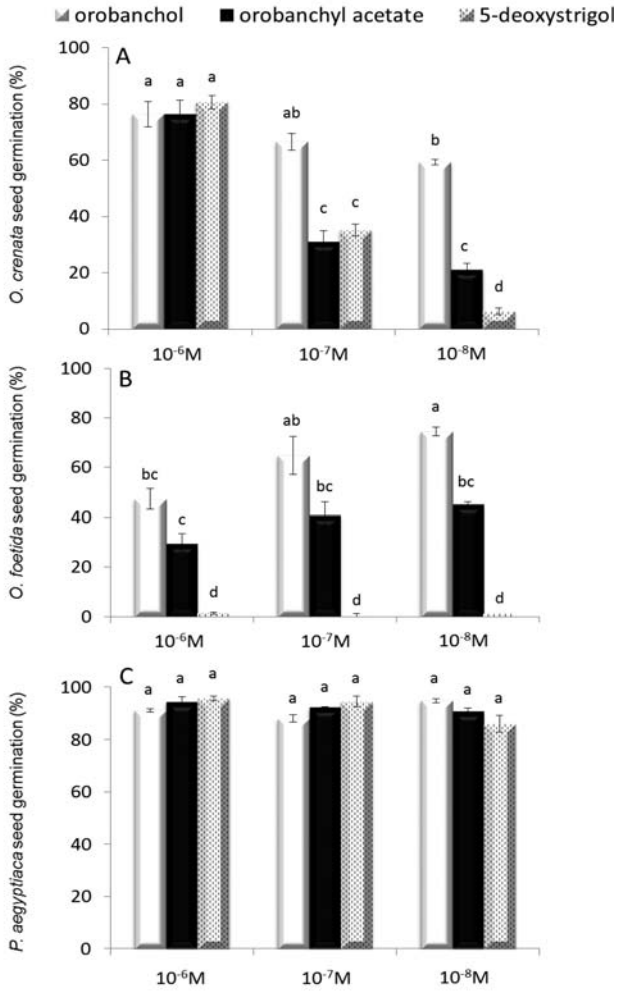

Figure 6. Effects of orobanchol (**1**), orobanchyl acetate (**2**), and 5-deoxystrigol (**3**) at decreasing concentrations on seed germination of *O. crenata* (A), *O. foetida* (B), and *P. aegyptiaca* (C). Vertical bars represent standard error for $n = 3$. The same letter per broomrape species indicates that differences are not statistically significant between SL and SL concentrations (Tukey test, $p < 0.05$). Negative controls (distilled water) = 0%, for *O. crenata*, *O. foetida*, and *P. aegyptiaca*.

O. crenata, *O. foetida*, and *P. aegyptiaca*. In all cases, null germination was observed when broomrape seeds were treated with distilled water (negative control). We observed significant differences in parasitic seed germination depending on the strigolactone tested ($p < 0.001$), the concentration applied ($p < 0.001$), the parasitic species tested ($p < 0.001$), and their interactions ($p < 0.001$).

Seeds belonging to *O. crenata* and *O. foetida* were more sensitive to orobanchol (**1**) and orobanchyl acetate (**2**) than to 5-deoxystrigol (**3**). The effect of strigolactone and strigolactone concentration was highly significant (ANOVA, $p < 0.001$ and $p < 0.001$ respectively for *O. crenata* seeds and $p < 0.001$ and $p = 0.007$ respectively for *O. foetida* seeds). Germination of *P. aegyptiaca* seeds was very sensitive to all strigolactones and strigolactone concentrations tested. The effect of strigolactone and strigolactone concentration was not significant (ANOVA, $p = 0.543$ and $p = 0.077$ respectively) showing a germination rate close to 90% in all cases.

The interaction between broomrape species × strigolactone × strigolactone concentration was highly significant (ANOVA, $p < 0.001$). The stimulatory effects of strigolactones on *O. crenata* seed germination increased at increased concentrations, being maximum (77.7% ± 2.2) at 10^{-6} M. This decrease was more marked for 5-deoxystrigol (**3**), which induced 6.3% ± 1.3% of *O. crenata* germination at 10^{-8} M, and moderate for orobanchyl acetate (**2**) (21.3% ± 2.2). On the contrary orobanchol (**1**) and orobanchyl acetate (**2**) effects on *O. foetida* germination increased as the strigolactone concentration decreases, showing a maximum germination rate of 74.5% ± 1.8 at 10^{-8} M. Remarkably, 5-deoxystrigol (**3**) was not effective inducing the germination of *O. foetida* seeds at the concentrations tested. High germination rates were observed on *P. aegyptiaca* seeds with all strigolactones and strigolactone concentrations.

Several measures are available for broomrape management; however, they are not fully applicable in a low input crop such as faba bean.[37,42] Therefore, development of resistant cultivars is the most desirable strategy.[42] Resistance in faba bean against broomrape has been based on mechanisms hampering the parasitic penetration and development in the host.[39] Only recently, resistance due to reduced parasitic seed germination has been discovered in faba bean against *O. crenata*, *O. foetida*, and *P. aegyptiaca*.[36,43] In the later study we have shown that the reduced susceptibility observed in the field by the cultivar Quijote was correlated with reduced stimulatory activity of broomrape in the *in vitro* germination test, but the underlying mechanisms were not determined.

Our LC-MS/MS analysis of root exudates from three faba bean cultivars has detected orobanchol (**1**) and orobanchyl acetate (**2**) both in susceptible and resistant cultivars. We have not detected 5-deoxystrigol (**3**), in spite that this strigolactone is common in the Fabaceae, as well as orobanchol (**1**) and orobanchyl acetate (**2**).[40] In addition to these known strigolactones, a third unknown germination stimulant was found.

A time course quantitation of strigolactone according to the peak area in LC-MS/MS[44] showed that the pattern of strigolactone exudation differs within faba bean cultivars and directly related with low levels of broomrape germination observed in vitro. As the roots of the susceptible cultivar Prothabon developed, strigolactone exudation increased greatly, this fact being in agreement with previous findings that production and exudation of strigolactones vary significantly with plant growth conditions and growth stages.[1] On the contrary, the resistant faba bean lines Quijote and Navio exuded low or undetected levels of strigolactones at all plant ages studied. Reduced broomrape infestation in the resistant lines might depend on a combination of low concentration of strigolactones in root exudate and their exudation pattern along the life stages that could avoid the correct timed encounter between parasites and host.

According with the results of strigolactone quantitation by LC-MS/MS, the germination tests carried out on seeds of three broomrape species showed that parasitic germination increased with the age of Prothabon plants from which root exudates were collected. Small differences between LC-MS/MS and the germination test were observed for the resistant varieties. As described before, LC-MS/MS analysis detected low or undetected amount of strigolactones in root exudates of Quijote and Navio at all life stages but their relative quantitation across the life cycle showed a small increase with age in Quijote but a small decrease in Navio plants. However, broomrape seed germination increased as Navio plants grew older and in Quijote plants the broomrape germination decreased when exposed to 4-

dx.doi.org/10.1021/jf5027235 | J. Agric. Food Chem. 2014, 62, 7063−7071

week-old plants. It is important to remark that Quijote root exudates induced low germination of *P. aegyptiaca*, a broomrape species highly sensitive to strigolactones. Also, they induced germination of *O. crenata* and *O. foetida* seeds only observed when applied at the highest concentrations, which was much higher than those commonly used in germination tests until now. Several factors may determine the observation of low but still significant broomrape germination when low or negligible levels of strigolactones were detected by LC-MS/MS. First, plant growth and root exudate collection for germination bioassays and strigolactone quantitation were carried out in independent laboratories. Activity of root exudates may change from experiment to experiment as production and exudation of strigolactones vary significantly with different environmental conditions.[1] These variations may be more remarkable when the production of germination stimulants is low as is the case for Quijote and Navio cultivars. Second, germination tests when carried out on seeds of the highly strigolactone-sensitive broomrape species such as *P. aegyptiaca* and *O. minor* are considered more sensitive for strigolactone detection than LC-MS/MS analysis. Third, LC-MS/MS analysis only detects major strigolactones from the myriad of compounds exuded by plant roots. Non-strigolactone-like molecules of unknown nature present in host root exudate can induce germination of the broomrape species tested in this work.[45,46] And last, faba bean samples analyzed by LC-MS/MS were obtained by ethyl acetate extraction washed with 0.2 M K_2HPO_4 to remove acidic substances. This procedure was done in order to facilitate direct comparisons between crude samples from different plants and cultivars by removing interference of acidic substances with electrospray ionization of strigolactones. This procedure may lead to removal of additional substances other than strigolactones in the faba bean root exudates with potential for broomrape germination.[45,46]

We have studied the effect of three major strigolactones typically found in legumes (orobanchol (**1**), orobanchyl acetate (**2**), and 5-deoxystrigol (**3**)), on three broomrape species that parasitize legumes but differ in their host ranges. *P. aegyptiaca* seeds highly germinated when exposed to all strigolactones, at all concentrations tested, confirming the sensitive nature of this broomrape species to strigolactones that correlates with the broad host range of this species.[47] Intriguing results were found for the more host-specific species *O. crenata* and *O. foetida*. First, in both broomrape species, orobanchol (**1**) induced much higher germination than orobanchyl acetate (**2**). Orobanchyl acetate (**2**) with less activity on *O. foetida* and *O. crenata* was found to be more abundant in root exudates of faba bean. This fact could point to a germination tuning between parasitic and host species through strigolactone concentration. In addition, 5-deoxystrigol (**3**) was not found in the faba bean root exudate tested in this work and was not active in inducing germination of *O. fetida,* a broomrape species with a very narrow host range for few legumes.[47] However, 5-deoxystrigol (**3**) was active inducing germination of *O. crenata*, a species that, although still being rather host-specific, expands its host range to other host families with different strigolactone exudation profiles, confirming previous observations.[48]

Results presented here show that low strigolactone exudation does exist within faba bean germplasm, contributing to resistance to broomrape. Therefore, selection for this trait is feasible in a breeding program. Inheritance of this trait should be studied, and it seems feasible that it might be simple inheritance, as was the case for low induction of *Striga* germination in sorghum.[49,50] This would be a great advantage as the resistances available before were of complex inheritance and, therefore, more difficult to breed for.[37] The use of molecular markers tightly linked to specific resistance mechanisms will allow their tracking in segregating populations, facilitating their pyramiding with other genes. The remarkable fact that low induction of germination is similarly operative against *O. crenata*, *O. foetida*, and *P. aegyptiaca* reinforces the value of this resistance.

AUTHOR INFORMATION

Corresponding Author

*Tel.: + 34 957499215. Fax: + 34 957499252. E-mail: monica.fernandez@ias.csic.es.

Funding

This work was supported by the Program for Promotion of Basic and Applied Researches for Innovation in Bio-oriented Industry to K.Y., T.K., and X.X. and to projects FP7-LEGATO and AGL2011-22524, cofinanced by FEDER funds to D.R. M.F.-A. has received the support of the European Union, in the framework of the International Outgoing European Marie Curie Postdoctoral Fellowship Programme (PIOF-GA-2009-252538), and from the Japan Society for the Promotion of Science Postdoctoral Fellowship ID noP 13390.

Notes

The authors declare no competing financial interest.

REFERENCES

(1) Xie, X.; Yoneyama, K.; Yoneyama, K. The strigolactone story. *Annu. Rev. Phytopathol.* **2010**, *48*, 93−117.

(2) Yan, H.; Saika, H.; Maekawa, M.; Takamure, I.; Tsutsumi, N.; Kyozuka, J.; Nakazono, M. Rice tillering dwarf mutant dwarf3 has increased leaf longevity during darkness-induced senescence or hydrogen peroxide-induced cell death. *Genes Genet. Syst.* **2007**, *82*, 361−366.

(3) Gomez-Roldan, V.; Fermas, S.; Brewer, P. B.; Puech-Pagès, V.; Dun, E. A.; Pillot, J. P.; Letisse, F.; Matusova, R.; Danoun, S.; Portais, J. C.; Bouwmeester, H.; Bécard, G.; Beveridge, C. A.; Rameau, C.; Rochange, S.F. Strigolactone inhibition of shoot branching. *Nature* **2008**, *455*, 189−194.

(4) Umehara, M.; Hanada, A.; Yoshida, S.; Akiyama, K.; Arite, T.; Takeda-Kamiya, N.; Magome, H.; Kamiya, Y.; Shirasu, K.; Yoneyama, K.; Kyozuka, J.; Yamaguchi, S. Inhibition of shoot branching by new terpenoid plant hormones. *Nature* **2008**, *455*, 195−200.

(5) Hu, Z.; Yan, H.; Yang, J.; Yamaguchi, S.; Maekawa, M.; Takamure, I.; Tsutsum, N.; Kyozuka, J.; Nakazono, M. Strigolactones negatively regulate mesocotyl elongation in rice during germination and growth in darkness. *Plant Cell Physiol.* **2010**, *51*, 1136−1142.

(6) Tsuchiya, Y.; Vidaurre, D.; Toh, S.; Hanada, A.; Nambara, E.; Kamiya, Y.; Yamaguchi, S.; McCourt, P. A small-molecule screen identifies new functions for the plant hormone strigolactone. *Nat. Chem. Biol.* **2010**, *6*, 741−749.

(7) Koltai, H. Strigolactones are regulators of root development. *New Phytol.* **2011**, *190*, 545−549.

(8) Toh, S.; Kamiya, Y.; Kawakami, N.; Nambara, E.; McCourt, P.; Tsuchiya, Y. Thermoinhibition uncovers a role for strigolactones in *Arabidopsis* seed germination. *Plant Cell Physiol.* **2012**, *53*, 107−117.

(9) Yoshida, S.; Shirasu, K. Plants that attack plants: molecular elucidation of plant parasitism. *Curr. Opin. Plant Biol.* **2012**, *15*, 708−713.

(10) Yoneyama, K.; Xie, X.; Kusumoto, D.; Sekimoto, H.; Sugimoto, Y.; Takeuchi, Y.; Yoneyama, K. Nitrogen deficiency as well as phosphorus deficiency in sorghum promotes the production and exudation of 5-deoxystrigol, the host recognition signal for arbuscular mycorrhizal fungi and root parasites. *Planta* **2007**, *227*, 125−32.

(11) Yoneyama, K.; Yoneyama, K.; Takeuchi, Y.; Sekimoto, H. Phosphorus deficiency in red clover promotes exudation of orobanchol,

the signal for mycorrhizal symbionts and germination stimulant for root parasites. *Planta* **2007**, *225*, 1031−1038.
(12) Umehara, M. Strigolactone, a key regulator of nutrient allocation in plants. *Plant Biotechnol.* **2011**, *28*, 429−437.
(13) Akiyama, K.; Matsuzaki, K.; Hayashi, H. Plant sesquiterpenes induce hyphal branching in arbuscular mycorrhizal fungi. *Nature* **2005**, *435*, 824−827.
(14) Jung, S. C.; Martinez-Medina, A.; Lopez-Raez, J. A.; Pozo, M. J. Mycorrhiza-induced resistance and priming of plant defenses. *J. Chem. Ecol.* **2012**, *38*, 651−664.
(15) Smith, S. E.; Read, D. J. *Mycorrhizal symbiosis*, 3rd ed.; Academic Press: New York, 2008.
(16) Smith, S. E.; Jakobsen, I.; Grønlund, M.; Smith, F. A. Roles of arbuscular mycorrhizas in plant phosphorus nutrition: interactions between pathways of phosphorus uptake in arbuscular mycorrhizal roots have important implications for understanding and manipulating plant phosphorus acquisition. *Plant Physiol.* **2011**, *156*, 1050−1057.
(17) Hirsch, A. M.; Bauer, W. D.; Bird, D. M.; Cullimore, J.; Tyler, B.; Yoder, J. I. Molecular signals and receptors − controlling rhizosphere interactions between plants and other organisms. *Ecology* **2003**, *84*, 858−868.
(18) Bouwmeester, H. J.; Roux, C.; Lopez-Raez, J. A.; Bécard, G. Rhizosphere communication of plants, parasitic plants and AM fungi. *Trends Plant Sci.* **2007**, *12*, 224−230.
(19) Yoder, J. I.; Scholes, J. D. Host plant resistance to parasitic weeds; recent progress and bottlenecks. *Curr. Opin. Plant Biol.* **2010**, *13*, 478−484.
(20) Rubiales, D.; Fernández-Aparicio, M.; Pérez-de-Luque, A.; Prats, E.; Castillejo, M. A.; Sillero, J.; Rispail, N.; Fondevilla, S. Breeding approaches for crenate broomrape (*Orobanche crenata* Forsk.) management in pea (*Pisum sativum* L.). *Pest Manage. Sci.* **2009**, *65*, 553−559.
(21) Fernández-Aparicio, M.; Westwood, J. H.; Rubiales, D. Agronomic, breeding, and biotechnological approaches to parasitic plant management through manipulation of germination stimulant levels in agricultural soils. *Botany* **2011**, *89*, 813−826.
(22) Pérez-de-Luque, A.; Jorrín, J.; Cubero, J. I.; Rubiales, D. Resistance and avoidance against *Orobanche crenata* in pea (*Pisum* spp.) operate at different developmental stages of the parasite. *Weed Res.* **2005**, *45*, 379−387.
(23) Rubiales, D.; Pérez-de-Luque, A.; Joel, D. M.; Alcántara, C.; Sillero, J. C. Characterization of resistance in chickpea to crenate broomrape (*Orobanche crenata*). *Weed Sci.* **2003**, *51*, 702−707.
(24) Rubiales, D.; Alcántara, C.; Pérez-de-Luque, A.; Gil, J.; Sillero, J. C. Infection of chickpea (*Cicer arietinum*) by crenate broomrape (*Orobanche crenata*) as influenced by sowing date and weather conditions. *Agronomie* **2003**, *23*, 359−362.
(25) Sillero, J. C.; Cubero, J. I.; Fernández-Aparicio, M.; Rubiales, D. Search for resistance to crenate broomrape (*Orobanche crenata*) in *Lathyrus*. *Lathyrus Lathyrism Newsl.* **2005**, *4*, 7−9.
(26) Sillero, J. C.; Moreno, M. T.; Rubiales, D. Sources of resistance to crenate broomrape in *Vicia* species. *Plant Dis.* **2005**, *89*, 22−27.
(27) Abbes, Z.; Kharrat, M.; Pouvreau, J. B.; Delavault, P.; Chaibi, W.; Simier, P. The dynamics of faba bean (*Vicia faba* L.) parasitism by *Orobanche foetida*. *Phytopathol. Mediterr.* **2010**, *49*, 239−248.
(28) Jorrín, J.; Pérez-de-Luque, A.; Serghini, K. How plants defend themselves against root parasitic angiosperms: molecular studies with *Orobanche* spp. In *Resistance to Orobanche: the State of the Art*; Cubero, J. I., Moreno, M. T, Rubiales, D., Sillero, J. C., Eds.; Publ. Junta de Andalucía: Sevilla, Spain, 1999; pp 9−15.
(29) Labrousse, P.; Arnaud, M. C.; Seryes, H.; Berville, A.; Thalouarn, P. Several mechanisms are involved in resistance of *Helianthus* to *Orobanche cumana* Wallr. *Ann. Bot.* **2001**, *88*, 859−868.
(30) Labrousse, P.; Arnaud, M. C.; Griveau, Y.; Fer, A.; Thalouran, P. Analysis of resistance criteria of sunflower recombined inbred lines against *Orobanche cumana* Wallr. *Crop Prot.* **2004**, *23*, 407−413.
(31) Dor, E.; Alperin, B.; Wininger, S.; Ben-Dor, B.; Somvanshi, V. S.; Koltai, H.; Kapulnik, Y.; Hershenhorn, J. Characterization of a novel tomato mutant resistant to *Orobanche* and *Phelipanche* spp. weedy parasites. *Euphytica* **2010**, *171*, 371−380.
(32) Ejeta, G. Breeding for *Striga* resistance in sorghum: Exploitation of an intricate host-parasite biology. *Crop Sci.* **2007**, *47*, 216−227.
(33) Pierce, S.; Mbwaga, A. M.; Press, M. C.; Scholes, J. D. Xenognosin production and tolerance to *Striga asiatica* infection of high-yielding maize cultivars. *Weed Res.* **2003**, *43*, 139−145.
(34) Duc, G.; Bao, S.; Baum, M.; Redden, B.; Sadiki, M.; Suso, M. J.; Vishniakova, M.; Zong, X. Diversity maintenance and use of *Vicia faba* L. genetic resources. *Field Crops Res.* **2010**, *115*, 270−278.
(35) Rubiales, D. Faba beans in sustainable agriculture. *Field Crops Res.* **2010**, *115*, 201−202.
(36) Fernández-Aparicio, M.; Moral, A.; Kharrat, M.; Rubiales, D. Resistance against broomrapes (*Orobanche* and *Phelipanche* spp.) in faba bean (*Vicia faba*) based in low induction of broomrape seed germination. *Euphytica* **2012**, *186*, 897−905.
(37) Pérez-de-Luque, A.; Eizenberg, H.; Grenz, J. H.; Sillero, J. C.; Avila, C. M.; Sauerborn, J.; Rubiales, D. Broomrape management in faba bean. *Field Crops Res.* **2010**, *115*, 319−328.
(38) Maalouf, F.; Khalil, S.; Ahmed, S.; Akintunde, A. N.; Kharrat, M.; El Shama'a, K.; Hajjar, S.; Malhotra, R. S. Yield stability of faba bean lines under diverse broomrape prone production environments. *Field Crops Res.* **2011**, *124*, 288−294.
(39) Pérez-de-Luque, A.; Lozano, M. D.; Moreno, M. T.; Testillano, P. S.; Rubiales, D. Resistance to broomrape (*Orobanche crenata*) in faba bean (*Vicia faba*): cell wall changes associated with pre-haustorial defensive mechanisms. *Ann. Appl. Biol.* **2007**, *151*, 89−98.
(40) Yoneyama, K.; Xie, X.; Sekimoto, H.; Takeuchi, Y.; Ogasawara, S.; Akiyama, K.; Hayashi, H.; Yoneyama, K. Strigolactones, host recognition signals for root parasitic plants and arbuscular mycorrhizal fungi, from Fabaceae plants. *New Phytol.* **2008**, *179*, 484−494.
(41) Kisugi, T.; Xie, X.; Kim, H. I.; Yoneyama, K.; Sado, A.; Akiyama, K.; Hayashi, H.; Uchida, K.; Yokota, T.; Nomura, T.; Yoneyama, K. Strigone, isolation and identification as a natural strigolactone from *Houttuynia cordata*. *Phytochemistry* **2013**, *87*, 60−64.
(42) Rubiales, D.; Fernández-Aparicio, M.; Wegmann, K.; Joel, D. Revisiting strategies for reducing the seedbank of *Orobanche* and *Phelipanche* spp. *Weed Res.* **2009b**, *49*, 23−33.
(43) Abbes, Z.; Kharrat, M.; Delavault, P.; Chaïbi, W.; Simier, P. Nitrogen and carbon relationships between the parasitic weed *Orobanche foetida* and susceptible and tolerant faba bean lines. *Plant Physiol. Biochem.* **2009**, *47*, 153−159.
(44) López-Ráez, J. A.; Charnikhova, T.; Mulder, P.; Kohlen, W.; Bino, R.; Levin, I.; Bouwmeester, H. Susceptibility of the tomato mutant high pigment-2dg (hp-2dg) to *Orobanche* spp. infection. *J. Agric. Food Chem.* **2008**, *56*, 6326−6332.
(45) Evidente, A.; Cimmino, A.; Fernández-Aparicio, M.; Andolfi, A.; Rubiales, D.; Motta, A. Polyphenols, including the new peapolyphenols A-C, from pea root exudates stimulate *Orobanche foetida* seed germination. *J. Agric. Food Chem.* **2010**, *58*, 2902−2907.
(46) Evidente, A.; Cimmino, A.; Fernández-Aparicio, M.; Rubiales, D.; Andolfi, A.; Melck, D. Soyasapogenol B and trans-22-dehydrocampesterol from common vetch (*Vicia sativa* L.) root exudates stimulate broomrape seed germination. *Pest Manage. Sci.* **2011**, *67*, 1015−1022.
(47) Fernández-Aparicio, M.; Yoneyama, K.; Rubiales, D. The role of strigolactones in host specificity of *Orobanche* and *Phelipanche* seed germination. *Seed Sci. Res.* **2011**, *21*, 55−61.
(48) Sugimoto, Y.; Ueyama, T. Production of (+)-5-deoxystrigol by *Lotus japonicus* root culture. *Phytochemistry* **2008**, *69*, 212−217.
(49) Ramaiah, K. V.; Chidley, V. L.; House, L. R. Inheritance of *Striga* seed-germination stimulant in sorghum. *Euphytica* **1990**, *45*, 33−38.
(50) Vogler, R. K.; Ejeta, G.; Butler, L. G. Inheritance of low production of *Striga* germination stimulant in sorghum. *Crop Sci.* **1996**, *36*, 1185.

To the best of our knowledge, there is no study reporting the exposure and risk assessment of chlorpyrifos in a maize field under different heights of maize. Although pesticide exposure assessments should be considered before and after the spraying process, the major objective of this study was to compare the potential dermal exposure (PDE) and internal dermal exposure (IDE) of various parts of the body and analyze potential inhalation exposure (PIE) with lever-operated knapsacks during spraying processes in a maize field at different maize plant heights. The margin of safety (MOS) was also calculated using the data obtained from the exposure evaluation to help estimate the status of the chlorpyrifos exposure of the applicators during the spraying process in maize fields year round.

MATERIALS AND METHODS

Chemicals and Reagents. The test item used in this study was a commercial insecticide, chlorpyrifos (EC, 48% w/v, Dow AgroSciences LLC, USA). Analytical standard chlorpyrifos was purchased from Sigma (St. Louis, MO, USA). Ethyl acetate, acetonitrile, and acetone were of analytical grade.

Study Site. Applicator exposure experiments were conducted in a maize (Sweet Jane169) field located in the city of ShaoXing, Zhejiang province, China, between May and June 2012. The maize field chosen was 100 m long and 100 m wide. The planting density of the maize field was 0.4 m × 0.2 m. The chosen field was divided into 10 plots. Each area of the plot was 8.0 m × 100 m with 20 rows of maize. Two rows of maize between two plots served as a neutral buffer zone, which was not treated with chlorpyrifos. Three types of pesticide exposure spraying environments (different growth or height of the maize field) were designed to analyze the potential exposure of chlorpyrifos during the application, namely, an average of 61.8 cm (A1), 108 cm (A2), or 212 cm (A3) height of the maize. Temperature, humidity, and wind speed were recorded before field trials were conducted. All exposure experiments were conducted under temperatures ranging between 29 and 33 °C, relative humidity of 56−79%, and a wind speed between 0.2 and 2.9 m s^{-1} (Supporting Information Table S1). Near the field, a warehouse was set for the pesticides and application equipment storage.

Workforce and Application Process. Four groups of personnel were divided in this study: (1) Two engineers who had been engaged in pesticide toxicology research for >5 years were in charge of the pesticides and spray equipment storage, and they also supervised the whole application process. (2) Five laboratory technicians mixed/loaded test pesticides, and they also collected samples from applicators after each field trial. (3) Eight farmers who had experience planting maize for more than 3 years, and they participated in the field application process. (4) Two agricultural technicians who had been engaged in agriculture for >5 years and had previously participated in other similar field trials also participated in the field application process. According to the "basic healthy check-up project directory"[17] issued by China Health Ministry, application personnel (totally 10 people) performed ordinary routine physical examination, and they were all healthy and disease-free. The height of applicators was 165−175 cm and their weights were 57.4−69.2 kg, with an average of 63.1 kg (Supporting Information Table S1).

All applicators used lever-operated knapsacks (SX-LK16 ShiXia; single-cone nozzle), which were calibrated at the beginning of the field study by the two engineers. According to the recommended dose of chlorpyrifos, the laboratory technician prepared a concentration of 960 ai mg L^{-1} chlorpyrifos liquid without any additives. The total spray volume for each applicator was 45 L. Because the capacity of each spray tank was only 15 L, laboratory technicians were responsible for refilling each applicator's tank three times (Supporting Information Table S1), but the time spent on the refilling was not included in the application time. All applicators followed their usual technique (right-hand operation, moving forward while spraying) without further instructions during the spraying process.

Dermal Exposure and Inhalation Exposure Assessments. According to OECD/GD (97) guidelines,[18] dermal exposure is measured by using the whole body dosimetry technique to collect samples from the applicators.[19] To measure the PDE and the IDE, each applicator wore 100% cotton inner (Hongdou underwear, Hongdou Home Apparel Co.) and outer protective garments (Xtep Sportswear, Xtep (China) Co., Ltd.), an inner hat wound with eight layers of gauze (20 cm × 40 cm), a hat with a brim, two layers of cotton gloves, and single-layer knee-high socks (Supporting Information Figure S1). The application personnel also wore 30 cm high rubber boots and protective masks.

PIE was measured using a personal air monitor equipped with an air pump (BUCK Libra plus LP-5) and solid sorbent (ORBO TM 609 Amberlite XAD-2 400/200 mg, Supelco), which traps pesticides in the air. The flow rate was 2 L min^{-1} during the application process.

Sample Collection. After each field trail was done, five laboratory technicians collected samples on site. The tubes with XAD-2 resins inside were cut and capped at both ends. Hats, gloves, and socks were carefully removed. The face, the surface of the protective mask, and the neck were wiped with eight layers of gauze (10 cm × 10 cm) containing 5 mL of 0.01% aerosol OT (Sinopharm Chemical Reagent Co., Ltd., China). Bare hands were washed with 0.01% aerosol OT for the mass balance. The inner and outer protective garments were cut into different sections as indicated in Figure 1. Clean sets of gloves were exchanged during the cutting of different sections of the protective garments. All samples were put into individual polyvinyl chloride bags, and they were transported to the laboratory within 6 h after the sampling, where they kept in refrigerators at −20 °C for later analysis.

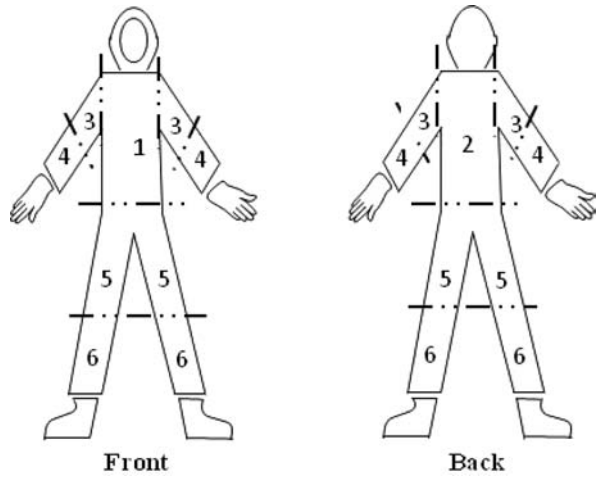

Figure 1. Protective garment segmentation maps (front and back).

Sample Analysis. Different sections of the inner and outer cotton protective garments and hats were all cut into pieces (less than 1 cm × 1 cm) by laboratory technicians with clean disposable gloves. The above treated samples were individually put into customized bottles, ethyl acetate (2 cm above the level of samples) was added, and then bottles were sealed and oscillated at 200 rpm for 1 h. Selection of extraction vessels and volume of extract added depended on sample types, such as a chest part placed in a 1000 mL bottle with a diameter of 12 cm, and then 800 mL of extraction reagent was added; a glove was placed in a 500 mL bottle with a diameter of 10 cm, and then 150 mL of extraction reagent was added; the gauze was placed in a 100 mL bottle, and then 50 mL of extraction reagent was added; XAD-2 resins were placed in a 50 mL bottle, and then 10 mL of extraction reagent was added. In addition, 100 mL of aerosol OT liquid (0.01%) for hand washing was accurately pipetted into a 500 mL bottle, 250 mL of acetonitrile was added, and then the above sample was shaken for 1 h. All extracts were concentrated to dryness and made to 2 mL volume with acetone. Finally, aliquots (2 mL) were passed through a 0.22 μm

Table 1. Potential Dermal Exposure (PDE; Milliliters per Hour) and Internal Dermal Exposure (IDE; Milliliters per Hour) for Applicators in a Maize Field at Different Plant Heights (Mean ± SD)

	A1		A2		A3	
body part	PDE	IDE	PDE	IDE	PDE	IDE
head	0.21 ± 0.06	0.10 ± 0.14	0.93 ± 3.22	0.20 ± 0.72	3.84 ± 2.12	2.57 ± 1.29
face	0.01 ± 0.02	0.01 ± 0.02	0.02 ± 0.03	0.02 ± 0.03	0.25 ± 0.31	0.25 ± 0.31
neck	0.02 ± 0.04	0.02 ± 0.04	0.01 ± 0.04	0.01 ± 0.04	0.17 ± 0.05	0.17 ± 0.05
back	0.24 ± 0.16	0.12 ± 0.13	3.44 ± 2.21	0.15 ± 0.11	34.26 ± 4.28	1.84 ± 1.37
chest	1.49 ± 3.89	0.14 ± 0.36	9.08 ± 13.1	0.28 ± 0.13	65.38 ± 12.0	0.86 ± 1.34
left upper arm	0.11 ± 0.14	0.02 ± 0.06	4.08 ± 1.81	0.08 ± 0.18	38.18 ± 21.9	1.10 ± 1.43
right upper arm	0.44 ± 0.51	0.20 ± 0.45	4.73 ± 1.89	0.58 ± 1.89	51.64 ± 44.1	1.72 ± 1.09
left forearm	0.13 ± 0.25	0.04 ± 0.07	4.51 ± 2.40	0.10 ± 0.24	29.24 ± 15.3	0.44 ± 0.11
right forearm	0.24 ± 0.76	0.05 ± 0.11	5.26 ± 2.90	0.12 ± 0.29	39.18 ± 30.7	0.40 ± 0.77
left hand	0.40 ± 1.20	0.30 ± 0.25	10.7 ± 14.5	0.72 ± 1.14	59.89 ± 19.2	1.13 ± 2.70
right hand	0.76 ± 1.66	0.75 ± 1.75	18.4 ± 20.1	0.22 ± 0.25	66.64 ± 19.8	2.05 ± 2.66
handwash		0.0025 ± 0.003		0.01 ± 0.017		0.10 ± 0.18
left thigh	6.05 ± 14.9	0.40 ± 0.58	8.43 ± 17.6	0.65 ± 1.18	11.57 ± 11.2	1.06 ± 0.43
right thigh	7.38 ± 22.3	0.57 ± 1.75	9.70 ± 10.2	0.58 ± 1.04	17.39 ± 11.4	1.72 ± 1.48
left lower leg	4.24 ± 10.4	0.26 ± 0.85	4.71 ± 10.2	0.22 ± 0.31	19.92 ± 12.8	2.29 ± 2.07
right lower leg	5.89 ± 7.59	0.40 ± 1.04	6.39 ± 13.8	0.34 ± 0.85	16.14 ± 18.7	0.63 ± 1.04
feet	0.23 ± 0.22		0.23 ± 0.43		8.41 ± 2.43	
total	27.81	3.37	90.59	4.28	462.12	18.32

filter (nylon filter, Target) and analyzed with a gas chromatograph. All samples were extracted and analyzed within 20 days after sampling.

Previously, analytical method validation verified the reliability of the above sample analysis methods. Chlorpyrifos was found stable within exposure matrices (e.g., cotton cloth, gloves, socks, XAD-2 resins, and gauze containing 5 mL of 0.01% aerosols OT and 0.01% aerosol OT), and it also showed stabilization during −20 °C refrigeration for 20 days of storage (Supporting Information Tables S1 and S2).

Analytical Conditions. All chromatographic analyses were performed on a Thermo Finnigan Trace (Thermo Electron Corp., USA) gas chromatograph equipped with a flame photometric detector (FPD) and a fused silica capillary column (DB-17, 30 m × 320 μm × 0.25 μm). The GC-FPD operating conditions for sample analysis were as follows: injector temperature, 250 °C; FPD temperature, 150 °C; oven temperature programmed from 220 °C (1 min isothermal) to 260 °C (held for 3 min at final temperature) at 20 °C min^{-1}; injection volume, 1 μL; carrier gas, N_2, flow rate, 2.0 mL min^{-1}; H_2, 90 mL min^{-1}; air; 115 mL min^{-1}.

Calculation of PDE, IDE, and PIE. Concentrations of the pesticide in each extract and the extraction reagent volume were used to calculate the amount of pesticide deposited on each coverall part. Then the PDE or IDE was calculated either with the amount of pesticide deposited and the derma exposure time (application time) (in mg h^{-1}) or with the amount of pesticide deposited, the concentration of pesticide formulation, and the derma exposure time (in mL h^{-1}).

XAD-2 resin pesticide adsorption amount (mg) was calculated with the XAD-2 resin pesticide extraction volume, the respiration rate (light work, 1740 L h^{-1}),[20] and the flow rate of the air pump, and then the PIE was calculated either with the amount of XAD-2 resin for pesticide adsorption and the dermal exposure time (in mg h^{-1}) or with the amount of XAD-2 resins for pesticide adsorption, the concentration of pesticide formulation, and the dermal exposure time (in mL h^{-1}).

Risk Assessment. PDE values by themselves do not define whether pesticide applications result in levels of exposure that could be considered to be safe or unsafe. Therefore, the margin of safety (MOS) was used to evaluate the safety of applicators' exposure to pesticides because it allows comparisons under very different field situations, such as different application techniques or different plant heights.[21]

When an MOS value was ≥1, it would mean safe working conditions for the operators. Conversely, it would mean unsafe working conditions if the MOS value was <1.[19] In this study, MOS was calculated to consider any risk in the spraying process. The MOS is defined as

$$\mathrm{MOS} = \mathrm{AE}/(\mathrm{DE} \times \mathrm{AF} \times \mathrm{SF})$$

where AE = acceptable exposure, DE = dermal exposure, AF = absorption factor, and SF = safety factor. The values considered in the present experiments are shown here. AE values are calculated on the basis of appropriate toxicological end-points according to the following expression: AE = AOEL × average body weight, as for chlorpyrifos, AOEL (acceptable operator exposure level) = 0.01 mg kg^{-1} day^{-1});[22] and an average body weight of 61.26 kg.

DE = (PDE or IDE + PIE) × EWT (exposure work time, 4 h day^{-1}) (as mg day^{-1} chlorpyrifos).[15,23]

AF = 0.11, considering an effective dermal absorption of 10%,[24] with an additional 1% added to include the inhaled fraction.[25]

SF = 1 as by definition the AOEL includes a safety factor.

Thus, the actual formula used was

$$\mathrm{MOS} = 5.569/\mathrm{DE}$$

RESULTS AND DISCUSSION

Dermal Exposure and Inhalation Exposure Assessments. The PDE and IDE results for applicators during the application of chlorpyrifos in the maize field are presented in Table 1. PDE refers to the potential dermal exposure under no personal protective equipment (PPE) circumstance; IDE refers to the internal dermal exposure under single -layer garment and gloves protection circumstance. Three spraying environments (A1, A2, and A3) were designed for this study: A1, the average maize height (61.8 cm) was below the applicators' waist; A2, the average maize height (108 cm) was close to the applicators' chest; and A3, the average maize height (212 cm) was above the applicators' head. As shown in Table 1, the total PDE values were 27.8, 90.6, and 462.1 mL h^{-1} for the applicators under A1, A2, and A3 spraying environments, respectively. In similar studies, Hughes et al.[19,26] reported that the total PDE value for applicators was 78.2 mL h^{-1} in a chard field with 40−50 cm plant height; in broccoli fields with an average 40−70 cm broccoli height, the total PDE value was 140 mL h^{-1}, and Choi

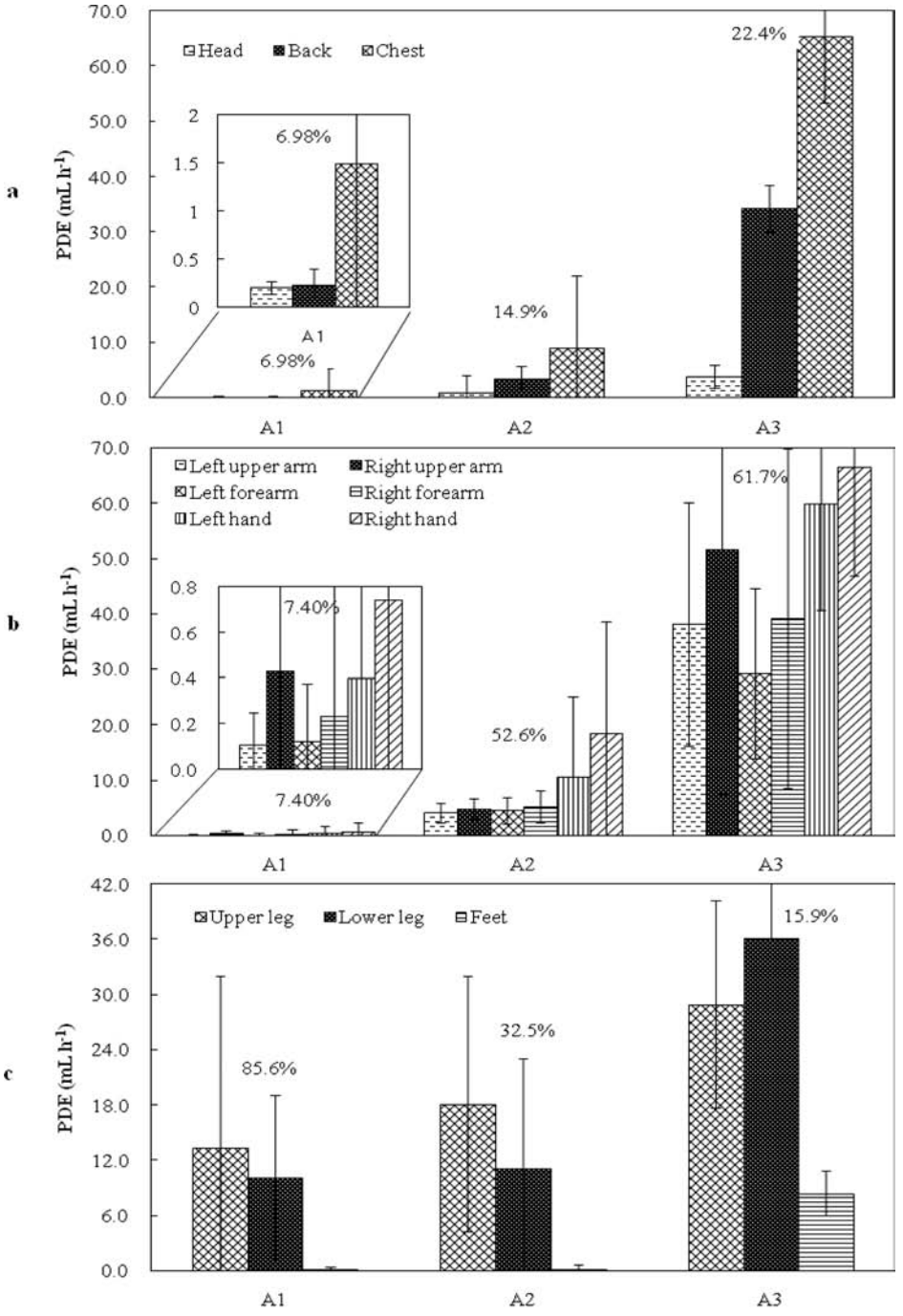

Figure 2. Potential dermal exposure (PDE) distribution on the head, back, and chest (a), the arms, forearms, and hands (b), and the legs and feet (c) in three spraying environments.

et al.[15] reported that the PDE measured reached 550−1180 mL h^{-1} in mandarin fields. Under experimental conditions similar to those of A3, Hughes et al.[27] reported that the total PDE value was 258 mL h^{-1} in a maize field with a maize planting density of 0.4 m × 0.8 m, which was slightly different from the results obtained in our study. The above difference of the PDE values could be related to maize planting density because the maize planting density was 0.4 m × 0.2 m in our present study, which was denser than that used in Hughes et al.[27] Generally, applicators would have more contact with plants if plant cultivation density was high in fields. Therefore, the degree of direct contact with plants could directly affect human pesticide exposure level.[28]

Evaluating pesticide exposure to applicators also considers clothing/protective garment penetration rate. In this study, the applicators wore double protective garments (100% cotton). The internal dermal exposure (IDE) was 3.37 mL h^{-1} for A1, 4.28 mL h^{-1} for A2, and 18.32 mL h^{-1} for A3, which accounted for 12.1, 4.7, and 4.0% of the total PDE under A1, A2, and A3 spraying environments, respectively (Table 1). Ten percent clothing penetration was assumed by many studies.[15,29,30] An average of 6.9% clothing penetration was obtained in our present study. The growth stage of crops and crop density could also affect the clothing penetration rate.[31] In addition, the clothing penetration rate is affected by many other factors, such as fabric thickness, yarn twist and wicking, the viscosity of

dx.doi.org/10.1021/jf501027s | J. Agric. Food Chem. 2014, 62, 7072−7077

pesticide mixtures, and the surface tension of pesticide mixtures.

PIE below the LOD was observed under A1 and A2 spraying conditions, respectively, but the PIE detected for A3 was 0.0121 mL h^{-1}, which accounted for 2.6×10^{-3}% of the total PDE and 3.6×10^{-5}% of the total spray volume in the study. Choi et al.[15] reported that the potential inhalation exposure for applicators was not observed in the mandarin fields; Kim et al.[29] observed the minimal amount of inhalation exposure for applicators in the paddy fields, accounting for 1.96×10^{-6}% of the total amount of pesticide applied. The results of our present study were similar to the results mentioned for the above research studies.

A characteristic distribution pattern of exposure was found on the applicators' bodies during spraying process, indicating nonuniformity of dermal exposure as suggested by previous studies.[14,23,32] As shown in Figure 2a, for the upper body (head, back, and chest), the exposure accounted for 6.98, 14.9, and 22.4% of the total PDE under A1, A2, and A3 spraying environments, respectively. It is noted that the chest under A2 and A3 spraying environments demonstrated relatively higher exposure than the head and back, which could be explained by the fact that the chests of the applicators had easy direct contact with the maize plants while moving forward during the application.

As shown in Figure 2b, the exposure of the arms and hands accounted for 7.4, 52.6, and 61.7% of the total PDE under A1, A2, and A3, respectively. The high exposure of pesticide under A2 and A3 could result from the spraying manner of the applicators. With an increase in the maize plant height, the applicators had to spray upward and downward; in addition, the upper leaves of the maize plants were denser than the lower parts of the maize plants. Therefore, the applicators' arms and hands were subsequently more exposed to the spray cloud or pesticide drift. It must be noted that there was far greater exposure on the hands than the section of the arms. Additionally, the right hand showed more exposure than the left hand (Figure 2b) in the three spraying environments. This difference could be explained by applicators using the right-hand to hold the spray lance during the application and the fact that large and fine spray droplets were more likely formed on the right hand. Hands can come into contact with many parts during the application, such as the spray instrument, clothes, or plants. Therefore, it is important to put great protection on hands during the application[33,34] to strengthen self-protection.

As shown in Figure 2c, the exposure of legs and feet accounted for 85.6% of the total PDE under A1 spraying environment. Under A1, the maize plant height was about 60 cm, so the lower half of the body of the applicators had higher PDE resulting from more contact with spray droplets during application. However, similar studies reported that legs and feet were usually the highest exposed body pars because of easy contact with spray droplets.[19,21,35,36] In the present study, the exposure of legs and feet only accounted for 32.5 and 15.9% of the total PDE under A2 (maize height = 108 cm) and A3 (maize height = 212 cm), respectively.

Risk Assessment. The PDE value provides quantitative information on a chemical substance loaded on uncovered body regions and clothing worn by pesticide applicators, but it cannot define whether the exposure level of pesticides to applicators is safe or not.[28,37] As shown in Table 2, under no PPE circumstance, the estimated MOS value for applicators ranged from 0.003 to 0.052 under the three exposure environments, which were ≪1. Under single-layer garment and gloves protection circumstance, the MOS value was also <1. By assuming A 10% clothing penetration rate, with double protective garments and double gloves protection circumstance, the MOS value reached only 0.8 under the A3 spraying environment, which still implied a risky spraying environment for the applicators. On the basis of the above results, we could conclude that the selected spraying environments were unsafe for the applicators under the present study conditions.

Table 2. Estimates of Dermal Exposure (DE), Margin of Safety (MOS), Exposure Control Need (ECN), and Safe Work Time (SWT) for Applicators at Different Plant Heights[a]

protective measures	application[b]	DE (mg day^{-1})	MOS	ECN (%)	SWT (h)
none	A1	106.8[c]	0.052	94.8	0.209
	A2	347.9[c]	0.016	98.6	0.064
	A3	1774.6[c]	0.003	99.7	0.013
single-layer garment and gloves	A1	12.9[d]	0.43	57.0	1.7
	A2	16.4[d]	0.34	66.0	1.4
	A3	70.4[d]	0.08	92.1	0.3
double-layer garment and gloves	A1	1.3[e]	4.3		
	A2	1.6[e]	3.4		
	A3	7.0[e]	0.8	45.7	3.2

[a]PDE (potential dermal exposure), IDE(internal dermal exposure) and PIE (potential inhalation exposures) unit as mg h^{-1}. [b]A1, average maize height of 62 cm; A2, average maize height of 108 cm; A3, average maize height of 212 cm. [c]DE = (PDE + PIE) × 4 h day^{-1}. [d]DE = (IDE + PIE) × 4 h day^{-1}. [e]DE = (IDE + PIE + feet PDE + PIE) × 10% of penetration through clothes ×4 h day^{-1}.

When an MOS value is <1, Machado-Neto[25] proposed to calculate ECN (exposure control need) value and SWT (safe work time) value to inform operators when to strengthen their personal protection and how long to continue the spraying process. The ECN value is calculated as follows: ECN = (1 − MOS) × 100.[25] The SWT value was calculated on the basis of the following formula: SWT = MOS × EWT (4 h day^{-1}).[15,24] In the present study, the ECN values calculated under no PPE were extremely high, and the SWT was only 0.013−0.209 h. Even with single-layer garment and gloves protection, the ECN values were still relatively high, and the SWT was not more than 2 h. Even if wearing double protective garments and double gloves in the A3 spraying environment, applicators should not work for more than 3.2 h.

To estimate the risk associated with similar pesticides used in maize fields, an interesting extrapolation was made. It was hypothesized that 10% imidacloprid diluted to 2000-fold (AOEL = 0.08 mg kg^{-1} day^{-1})[22] was applied in the present study condition, and the same PDE as measured for chlorpyrifos was assumed. The MOS values calculated would be >1 under A1 and A2 spraying environments without PPE circumstance. However, with single-layer garment and gloves protection circumstance, the MOS value was 8.3 for the A3 spraying environment, which was <1 under no PPE circumstance. Therefore, the risk associated with the pesticide application is also affected by the type of pesticide used and the concentration applied.

■ ASSOCIATED CONTENT

Supporting Information

Additional experimental details. This material is available free of charge via the Internet at http://pubs.acs.org.

■ AUTHOR INFORMATION

Corresponding Author

*(L.C.) Phone: +86-571-86409163. E-mail: caileiming2009@gmail.com.

Funding

This study was supported by the Twelve Five-Year National Scientific and Technological Project 2011BAE06B09.

Notes

The authors declare no competing financial interest.

■ REFERENCES

(1) Ghimire, N.; Woodward, R. T. Under- and over-use of pesticides: an international analysis. *Ecol. Econ.* **2013**, *89*, 73−81.

(2) Dharmani, C.; Jaga, K. Epidemiology of acute organophosphate poisoning in hospital emergency room patients. *Rev. Environ. Health* **2005**, *20*, 215−32.

(3) Litchfield, M. H. Estimates of acute pesticide poisoning in agricultural workers in less developed countries. *Toxicol. Rev.* **2005**, *24*, 271−278.

(4) Recena, M. C.; Pires, D. X.; Caldas, E. D. Acute poisoning with pesticides in the state of Mato Grosso do Sul, Brazil. *Sci. Total Environ.* **2006**, *357*, 88−95.

(5) Rodriguez, T.; Younglove, L.; Lu, C.; Funez, A.; Weppner, S.; Barr, D. B.; Fenske, R. A. Biological monitoring of pesticide exposures among applicators and their children in Nicaragua. *Int. J. Occup. Environ. Health* **2006**, *12*, 312−320

(6) Farahat, T. M.; Abdelrasoul, G. M.; Shebl, M. M.; Faratat, F. M.; Anger, W. K. Neurobehavioural effects among workers occupationally exposed to organophosphorus pesticides. *Occup. Environ. Med.* **2003**, *60*, 279−364.

(7) Rohlman, D.; Lasarev, M.; Anger, W.; Scherer, J.; Stupfel, J.; McCauley, L. Neurobehavioral performance of adult and adolescent agricultural workers. *Neurotoxicology* **2007**, *28*, 374−453.

(8) Rothlein, J.; Rohlman, D.; Lasarev, M.; Phillips, J.; Muniz, J.; McCauley, L. Organophosphate pesticide exposure and neurobehavioral performance in agricultural and nonagricultural Hispanic workers. *Environ. Health Perspect.* **2006**, *114*, 691−696.

(9) Steenland, K.; Dick, R. B.; Howell, R. J.; Chrislip, D. W.; Jines, C. J.; Reid, T. M.; Lehman, E.; Laber, P.; Krieq, E. F.; Knott, C. Neurologic functioning among termiticide applicators exposed to chlorpyifos. *Environ. Health Perspect.* **2000**, *108*, 293−300.

(10) Oliver, G. R.; Bolles, H. G.; Shuedut, B. A. Chlorpyrifos: probabilistic assessment of exposure and risk. *Neurotoxicology* **2000**, *21*, 203−208.

(11) Wang, C. T.; Li, S. K.; Han, B. T. Approaches to high-yielding and yield potential exploration in corn. *Sci. Technol. Rev.* **2006**, *24*, 8−11 (in Chinese with English abstract).

(12) Yu, Y.; Shi, D.; Shi, C.; Chen, J. Survey on farmer behaviors of applying pesticides and relevant suggestions in Zhejiang province. *China Plant Prot.* **2007**, *27*, 8−10 (in Chinese with English abstract).

(13) Li, M.; Zhang, G.; Tao, C. Approach of pesticide occupational risk assessment. *Chin. J. Pestic. Sci.* **2010**, *12*, 249−254 (in Chinese with English abstract).

(14) Machera, K.; Kapetanakis, E.; Charistou, A.; Goumenaki, E.; Glass, R. C. Evaluation of potential dermal exposure of pesticide spray operators in greenhouses by use of visible tracers. *J. Environ. Sci. Health B* **2002**, *37*, 113−121.

(15) Choi, H.; Moon, J. K.; Liu, K. H.; Park, H. W.; Ihm, Y. B.; Park, B. S.; Kim, J. H. Risk assessment of human exposure to cypermethrin during treatment of mandarin fields. *Arch. Environ. Contam. Toxicol.* **2006**, *50*, 437−442.

(16) Bjugstad, N.; Torgrimsen, T. Operator safety and plant deposits when using pesticides in greenhouses. *J. Agric. Eng. Res.* **1996**, *65*, 205−212.

(17) Zhang, H.; Yang, H.; Wang, T.; Li, J. Quality control of health examination in China: present situations and prospects. *Hosp. Admin. J. Chin. PLA* **2013**, *20*, 628−644 (in Chinese with English abstract).

(18) OECD. *Guidance Document for the Conduct of Studies of Occupational Exposure to Pesticides during Agricultural Application*; Environmental health and safety publications series on testing and assessment no. 9, OCDE/GD(97)148y; Paris, France, 1997.

(19) Hughes, E. A.; Zalts, A.; Ojeda, J. J.; Flores, A. P.; Glass, R. C.; Montserrat, J. M. Analytical method for assessing potential dermal exposure to captan, using whole body dosimetry, in small vegetable production units in Argentina. *Pest Manag. Sci.* **2006**, *62*, 811−818.

(20) U.S. EPA. *Occupational and Residential Exposure Test Guidelines, OPPTS 875*; 1000, EPA 712-C-96-261; Washington, DC, USA, 1996.

(21) Ramos, L. M.; Querejeta, G. A.; Flores, A. P.; Hughes, E. A.; Zalts, A.; Montserrat, J. M. Potential dermal exposure in greenhouses for manual sprayers: analysis of the mix/load, application and re-entry stages. *Sci. Total Environ.* **2010**, *408*, 4062−4068.

(22) UK-CDR Advisory Committee on pesticides. Comparison of AOEL, ADI, and ARfD values (ACP9/5), June 30, 2009; http://cot.food.gov.uk/pdfs/tox200928annex6.pdf.

(23) Fenske, R. A. Nonuniform dermal deposition patterns during occupational exposure to pesticides. *Arch. Environ. Contam. Toxicol.* **1990**, *19*, 332−337.

(24) UK-PSD Pesticides Safety Directorate. Glossary, 2006; http://www.pesticides.gov.uk/appendices.asp?id=744.

(25) Machado-Neto, J. G. Determinatiion of safe work time and exposure control need for pesticide applicators. *Bull. Environ. Contam. Toxicol.* **2001**, *67*, 20−26.

(26) Hughes, E.; Zalts, A.; Ojeda, J.; Montserrat, J.; Glass, R. Potential pesticide exposure of small scale vegetable growers in Moreno district. *Aspects Appl. Biol.* **2004**, *71*, 399−404.

(27) Hughes, E. A.; Flores, A. P.; Ramos, L. M.; Zalts, A.; Glass, C. R.; Montserrat, J. M. Potential dermal exposure to deltamethrin and risk assessment for manual sprayers: influence of crop type. *Sci. Total Environ.* **2008**, *391*, 34−40.

(28) Franklin, C. A.; Worgan, J. P. *Occupational and Residential Exposure Assessment for Pesticides*; Wiley: Chichester, UK, 2005.

(29) Kim, E.; Lee, H.; Hong, S.; Park, K. H.; An, X. H.; Kim, J. H. Comparative exposure of operators to fenthion during treatment in paddy field. *J. Korean Soc.* **2012**, *55*, 827−830 (in Korean).

(30) Garrod, A. N. I.; Rimmer, D. A.; Robertshaw, L.; Jons, T. Occupational exposure through spraying remedial pesticides. *J. Agric. Food Chem.* **1998**, *42*, 159−165.

(31) Lee, S.; Obendorf, S. K. Statistical model of pesticide penetration through woven work clothing fabrics. *Arch. Environ. Contam. Toxicol.* **2005**, *49*, 266−273.

(32) Van Hemmen, J. J.; Brouwer, D. H. Exposure assessment for pesticides: operators and harvesters risk evaluation and risk management. *Meded. Fac. Landbouwwet. Univ. Gent* **1997**, *62*, 113−130.

(33) Grover, R.; Cessna, A. J.; Muir, N. I.; Riedel, D.; Franklin, C. A. Factors affecting the exposure of ground-rig applicators to 2,4-D dimethyl-amine salt. *Arch. Environ. Contam. Toxicol.* **1986**, *15*, 677−686.

(34) Cessna, A. J.; Grover, R. Exposure of ground-rig applicators to the herbicide bromoxynil applied as a 1:1 mixture of butyrate and octanoate. *Arch. Environ. Contam. Toxicol.* **2002**, *42*, 36−382.

(35) Vidal, J. L. M.; Gonzalez, F. J. E.; Frenich, A. G.; Galera, M. M.; Aguilera, P. A.; Carrique, E. L. Assessment of relevant factors and relationships concerning human dermal exposure to pesticides in greenhouse applications. *Pest Manag. Sci.* **2002**, *58*, 784−790.

(36) Stamper, J. H.; Nigg, H. N.; Mahon, W. D.; Nielsen, A.; Royer, M. Pesticide exposure to greenhouse foggers. *Chemosphere* **1988**, *17*, 1007−1023.

(37) UK Predictive operator exposure model (POEM). *A Users Guide, Pesticides Safety Directorate*; York, UK, 1992.

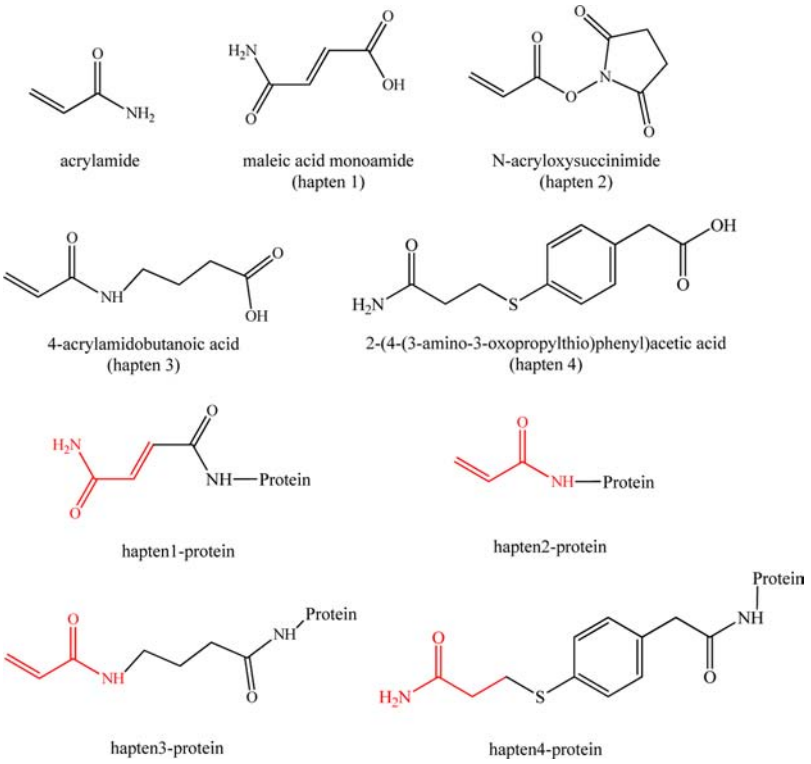

Figure 1. Chemical structures of acrylamide, its haptens, and the hapten−protein conjugates.

cakes.[14] These two methods have been reported to detect acrylamide directly; however, repeatability of these assays has been very poor because attempts using the same strategy to produce specific acrylamide antibodies have failed twice in our group. Preston et al. have designed a novel hapten by derivatizing acrylamide with 3-mercaptobenzoic acid and obtained a polyclonal antibody with high binding affinity for acrylamide derivative.[15] They proposed a competitive indirect enzyme-linked immunosorbent assay (ciELISA) for the indirect detection of acrylamide, necessitating a derivatization of extracted acrylamide with 3-mercaptobenzoic acid. This strategy appears helpful for the rapid determination of acrylamide, but its sensitivity is insufficient, with a LOD of 65.7 μg/kg.

In this study, several haptens against acrylamide were designed in attempts to obtain a specific acrylamide-affinity antibody. Although no antibodies with binding ability to free acrylamide were obtained, a polyclonal antibody was produced against 4-mercaptophenylacetic acid (4-MPA)-derivatized acrylamide (acrylamide-4-MPA) that showed high binding affinity to the derivative. A ciELISA for acrylamide via preanalysis derivatization was then developed, as acrylamide easily reacted at high yield with 4-MPA. The assay conditions were then optimized, and the assay was applied to detect acrylamide in several food samples.

MATERIALS AND METHODS

Materials and Reagents. Acrylamide (99%), methacrylamide, methyl acrylate, acrylic acid, acrolein, maleic acid monoamide, *N*-acryloxysuccinimide (NAS), and aminobutyric acid were purchased from J&K Scientific (Beijing, China). 4-MPA was obtained from Meryer Chemical Technology Co., Ltd. (Shanghai, China). Horseradish peroxidase (HRP)-conjugated goat anti-rabbit IgG was obtained from Boster Biotech Co., Ltd. (Wuhan, China). Keyhole limpet hemocyanin (KLH), dicyclohexyl carbodiimide (DCC), ovalbumin (OVA), *N*-hydroxysuccinimide (NHS), 3,3′,5,5′-tetramethylbenzidine (TMB), and complete and incomplete Freund's adjuvants were purchased from Sigma (St. Louis, MO, USA). Chromatographically pure methanol and acetonitrile were purchased from Guangzhou FanHong Trade Co., Ltd. Polystyrene ELISA plates were from Guangzhou Jiete Biotech Co. All other reagents were of analytical grade and obtained from a local chemical supplier (Yunhui Trade Co., Ltd., Guangzhou, China). Strata-X-C cartridge solid phase extraction cartridges were purchased from Phenomenex Science Apparatus Co. (Guangzhou, China).

Instruments. Plates were washed in a Multiskan MK2 microplate washer (Thermo Scientific, Hudson, NH, USA). ELISA values were read with a Multiskan MK3 microplate reader (Thermo Scientific). Ultraviolet−visible (UV−vis) spectra were recorded on a UV-160A Shimadzu spectrophotometer (Kyoto, Japan). Nuclear magnetic resonance (NMR) spectra were obtained with both DRX-400 and DRX-600 NMR spectrometers (Bruker, Rheinstetten, Germany). HPLC-MS/MS analysis was carried out by using the 1200 series HPLC system (Agilent Technologies, Santa Clara, CA, USA) equipped with the Triple Quad 5500 HPLC-MS/MS System (AB SCIEX, Framningham, MA, USA). HPLC-ECD analysis was carried out on the SPD-20A HPLC system (Shimadzu, Kyoto, Japan).

Buffers. The following buffers were used in this study: (1) 0.1 mol/L phosphate-buffered saline (PBS, pH 7.4) containing 0.05% Tween-20 for antibody dilution; (2) 0.05 mmol/L carbonate-buffered solution (pH 9.6) for coating; (3) 0.01 mmol/L PBS containing 0.05% Tween-20 (PBST, pH 7.4) for washing; (4) 0.1 mol/L citrate and sodium phosphate for substrate buffer (pH 5.5); (5) 10 mL of substrate buffer, 150 μL of 1% (w/v) solution of TMB in DMF, and 2.5 μL of 6% (w/v) H_2O_2 mixed for substrate solution; (6) 2.0 mol/L H_2SO_4 used for stopping reagent.

Synthesis and Characterization of Haptens. Haptens were synthesized as follows (Figure 1).

Hapten 1. Maleic acid monoamide was used directly as hapten 1.

Hapten 2, NAS was used directly as hapten 2.

Hapten 3. A 1 mL volume of acrylic acid was added to 1 mL of thionyl chloride and the mixture stirred at 50 °C for 3 h and then filtered to yield solution A. A 500 mg quantity of aminobutyric acid

dx.doi.org/10.1021/jf5015395 | J. Agric. Food Chem. 2014, 62, 7078−7084

Table 1. Characterization of Antiserum against Free Acrylamide Using Homologous and Heterologous Coating Antigens

	antiserum 1		antiserum 2		antiserum 3		antiserum 4	
coating antigen	titer[a] ($\times 10^3$)	inhibition[b] (%)	titer ($\times 10^3$)	inhibition (%)	titer ($\times 10^3$)	inhibition (%)	titer ($\times 10^3$)	inibition (%)
H1-OVA	256	2.0	1	−3.0	0	0	16	−4.0
H2-OVA	8	0	4	8.0	0	0	32	−1.3
H3-OVA	128	6.0	4	0.2	2	0	32	0
H4-OVA	1024	6.6	0	0	4	0	1024	0

[a]Antiserum dilution considered suitable while $A_{490\ nm}$ value approximately 1.0 at coating concentration of 1.0 mg/L. [b]Percentage inhibition calculated by following equation: inhibition (%) = $(A_{ck} - A_{analyte})/A_{ck}$. A_{ck} is the $A_{490\ nm}$ in the absence of analyte and $A_{analyte}$ is the $A_{490\ nm}$ in the presence of analyte (100 mg/L acrylamide).

was added to 2 mL of double-distilled H_2O, followed by the addition of 500 μL of 2 M NaOH and 2 mL of butylene oxide to obtain solution B. Next, solution A was slowly introduced dropwise into solution B and stirred overnight at room temperature. The mixture was then extracted with ethyl acetate and evaporated to obtain 4-acrylamidobutanoic acid (hapten 3). ESI-MS analysis (negative) m/z 156 $[M - H]^-$; ^1H NMR ($CDCl_3$, TMS, 300 MHz) δ 11.0 (s, 1H), 8.03 (brs, 1H), 6.48 (d, J = 10.2 Hz, 1H), 6.04−5.98 (m, 1H), 5.52−5.48 (m, 1H), 3.20−3.13 (m, 2H), 2.33−2.28 (m, 2H), and 1.94−1.89 (m, 2H).

Hapten 4. With stirring, 1.0 mmol of 4-MPA in 1.6 mL of methanol was added to a solution of 5 mmol of acrylamide in 0.8 mL of coating buffer. The mixture was left to stand at 37 °C in darkness for 1 h. Subsequent precipitation of the product was enhanced by the addition of 2 mL of deionized water and then dried under light vacuum in darkness for 0.5 h to obtain 2-(4-(3-amino-3-oxopropylthio)phenyl)-acetic acid (hapten 4). ESI-MS analysis (negative) m/z 238 $[M - H]^-$; ^1H NMR (CD_3OD, 400 MHz) δ 7.335−7.349 (d, J = 5.6 Hz, 2H), 7.233−7.247 (d, J = 5.6 Hz, 2H), 3.579 (s, 2H), 3.144−3.168 (m, 2H), and 2.488−2.513 (m, 2H).

Preparation of Hapten−Protein Conjugates. All four haptens were coupled to KLH for immunogens and to OVA for coating antigens. Haptens 1, 3, and 4 were conjugated to carrier proteins by the active ester method, as described by Sheng et al.[16] Hapten 2 was coupled to carrier proteins according to the method of Zhou et al.[13] The hapten−protein conjugates were then dialyzed against 0.01 M PBS at 4 °C for 24 h with six changes of PBS. UV−vis spectral data were used to confirm the structures of the final conjugates and the ratios of hapten to carrier protein determined using the 2,4,6-trinitrobenzenesulfonic acid method.[17]

Preparation of Polyclonal Antibodies. For each immunogen, intramuscular injections were given to two New Zealand white rabbits and a total of eight rabbits used to raise antibodies. The prepared immunogen (0.5 mg of coupled protein in 1 mL of PBS) was emulsified with 1 mL of Freund's complete adjuvant (1:1, v/v) for the first injection into a New Zealand rabbit weighing 1.2−2.2 kg, provided by Guangdong Medical Laboratory Animal Center. Then, Freund's incomplete adjuvant was used as the booster muscle injection, at intervals of 4 weeks. Bleed samples were collected 10 days after the fourth immunization, and the obtained antiserum was purified by the caprylic acid−ammonium sulfate method and separated into 1 mL aliquots held at −20 °C until use. Negative (control) serum was obtained from an unimmunized rabbit. All animal experiments were performed in compliance with the relevant protective and administrative laws for laboratory animals of China and conducted with the approval of the Institutional Authority for Laboratory Animal Care.

Competitive Indirect ELISA. Serum samples were screened for antibodies specific to the analyte (acrylamide or its derivative acrylamide-4-MPA) via a ciELISA. The 96-well plates were coated with coating antigens (1 mg/L, 100 μL/well) in carbonate buffer at 4 °C overnight. The wells were next washed two times with PBS Tween-20 (PBST) and blocked with 120 μL/well of 5% skimmed milk in PBST at 37 °C for 3 h, and the plates were dried at 37 °C for 1 h. The wells were then incubated with 50 μL of diluted acrylamide or its derivative standards in PBS, and 50 μL of diluted antibody in PBST was added. After 40 min in a water bath at 37 °C, the wells were washed five times with PBST and HRP-conjugated goat anti-rabbit IgG (diluted 1:5000) added with 100 μL/well. Finally, TMB solution (400 μL of 0.6% TMB−dimethyl sulfoxide and 100 μL of 1% H_2O_2 diluted with 25 mL of citrate−acetate buffer, pH 5.5) was added to the wells and incubated for 10 min. The reaction was quenched by the addition of 50 μL of 2 M H_2SO_4 and the absorbance recorded at 450 nm.

Optimization of Immunoassay. Experimental parameters, such as coating concentration, antibody dilution, and working buffer, were optimized to improve the optimal sensitivity of this immunoassay. The criteria used to evaluate immunoassay performance were maximal absorbance (A_{max}) and IC_{50} (50% inhibition of antibody binding) values, with the A_{max}/IC_{50} ratio being a convenient estimate of an influence on ELISA sensitivity and higher ratios indicating higher sensitivity.[18] Competitive curves were created in working buffer containing a concentration series of PO_4^{3-} (from 0.1 to 0.4 M), Tween-20 (from 0.08 to 0.5 M), or methanol (from 0 to 15%, v/v) to evaluate the effects of ELISA conditions on assay sensitivity.

Cross-Reactivity (CR). CR was studied using the standard acrylamide solution or its derivative and some of its analogues. CR values were calculated as follows: CR% = (IC_{50} of analyte/IC_{50} of analogue) × 100.

Data Analysis. Competitive curves were obtained by plotting absorbance against the logarithm of the analyte concentration. Sigmoid curves were generated using OriginPro 7.5 software (OriginLab Corp., Northampton, MA, USA): $Y = (A - D)/[1 + (x/C)^B] + D$, where A and D are the maximal and minimal Abs (A_{max} and A_{min}, respectively), B is the slope of the sigmoidal curve, and C is the concentration of acrylamide or its derivative that causes IC_{50}. The LOD was defined as the standard concentration of acrylamide or its derivative that inhibited 10% of antibody binding, and the detectable concentration range was defined as the standard concentration that inhibited 20−80% of acrylamide's or its derivative's standard antibody binding.[19]

Preparation of Samples. Samples of potato chips, cookies, and coffee were bought from a local supermarket. Samples of 4.0 g and 20.0 mL of water were placed in 50 mL centrifuge tubes and subjected to ultrasound for 1 min, followed by a defatting step using 20 mL of *n*-hexane and then centrifugation at 8200*g* at 15 °C for 10 min. The 10 mL supernatant was cleaned by solid phase extraction on a strata-X-C cartridge (Phenomenex Inc., Torrance, CA, USA). The eluate was subjected to HPLC-MS/MS analysis and derivatized to obtain acrylamide-4-MPA for ciELISA analysis. For derivatization, 1 mL of eluate was adjusted to pH 10 by adding aqueous NaOH and then 10 μg of 4-MPA. This reaction mixture was stirred in darkness at 70 °C for 30 min and then acidified to pH 2.0 with HCl. The resulting mixture was then extracted using ethyl acetate and the organic phase blown dry under a nitrogen stream. Finally, the residue was dissolved in 1 mL of PBS and diluted at least 4-fold with optimized working buffer to remove matrix effects prior to ciELISA analysis.

HPLC Conditions. The yield of acrylamide-4-MPA was characterized by HPLC-ECD. A 20 μL portion of sample was resolved at a 0.8 mL/min flow rate and 40 °C using an acetonitrile/acetic acid (plus 1 g of H_2O/L) gradient. A linear gradient was programmed over 15 min using 30−60% (acetonitrile content, by vol). The initial acetonitrile proportion (30%) was then pumped for 5 min before

the next injection was applied. The ECD quantitation channel was selected at 254 nm.

HPLC-MS/MS was used for acrylamide detection, with the spectra recorded by a mass spectrometer (AB SCIEX Triple Quad 5500, AB SCIEX) coupled to a spectra series HPLC (Shimadzu-20A) equipped with a SunFire HPLC column (250 × 4.6 mm, 5 μm; Waters Corp., Milford, MA, USA). A 20 μL portion of sample was separated at a 1.0 mL/min flow rate using an isocratic eluent (methanol/diluted acetic acid, 10:90, v/v, plus 1 g of H_2O/L). Analytes were determined using the above mass spectrometer equipped with a turbo-spray ion source. Quantitation was performed in multiple reaction monitoring (MRM) analysis mode. The respective MS parameters were as follows: curtain gas at 40 psi; collision gas at 6 psi; ion spray voltage at 5500 V; temperature at 650 °C for both; ion source gases 1 and 2 both at 55 psi; declustering potential at 57 V; and entrance potential at 12 V. The analyte indentities were confirmed with product/precursor ions as well as on the basis of the peak retention times corresponding to the standard. The $[M + H]^+$ (m/z 72.0) was selected as the parent acrylamide ion. Qualitative ions were selected at m/z 43 and quantitative ions at m/z 55. The mass spectrometer was controlled and quantitation performed using Analyst 1.5.1 software from AB SCIEX.

RESULTS AND DISCUSSION

Hapten Design and Antibody Production. The key step during the production of an immunoassay is to consider the design and synthesis of an optimal immunizing hapten. In the beginning, the goal was to produce an antibody with specificity against acrylamide, and for this purpose three haptens were designed. Maleic acid monoamide shares the common structure of acrylamide as well as a carboxyl group, which can be directly attached to carrier protein; therefore, it was first selected as a hapten (H1, Figure 1). After coupling to protein, the acrylamide amino linkage could be exposed. NAS (H2) was also employed as a hapten because it has been reported to be able to produce antibodies specific to free acrylamide.[13] After reaction with protein, the conjugate preserved the intact acrylamide structure, and the double bond could be exposed. However, the H2 spacer arm might have been too short, which might have resulted in embedding the hapten in the protein surface. Therefore, another hapten, 4-acrylamidobutanoic acid (H3), was synthesized through the reaction of acrylic acid and aminobutyric acid. These haptens were coupled to KLH and used to immunize rabbits, but the resulting antisera against the three haptens proved not to contain antibodies specific for free acrylamide (Table 1). The inability of the above immunogens to stimulate antibody production possessing the desired specificity for acrylamide was probably because of their diminutive mass of 71.08 Da and the lack of sufficient epitope for virgin B or T helper cell binding.

The double bond of acrylamide can easily react with sulfhydryl groups by Michael addition. Preston et al. have designed a hapten by reacting acrylamide with 3-mercaptobenzoic acid (3-MBA).[15] The corresponding antiserum showed specific binding to acrylamide-3-MBA in a ciELISA; however, the sensitivity of this ciELISA was unsatisfactory. In that study, immunogens were generated by coupling the hapten to carrier proteins via a carboxylic acid spacer. However, in relation to hapten design for small molecular weight compounds, a suitable spacer length between the hapten and the carrier protein should be beneficial for producing desired antibodies.[20] A previous study has indicated that hapten conformation can be altered when too short a spacer is employed for its conjugation

Table 2. Characterization of Antiserum 4 against Acrylamide-4-MPA Using Homologous and Heterologous Coating Antigens[a]

	antiserum 4	
coating antigen	titer ($\times 10^3$)	inhibition (%)
H1-OVA	16	0
H2-OVA	32	0
H3-OVA	32	0
H4-OVA	1024	86

[a]Analyte, 1 mg/L acrylamide-4-MPA.

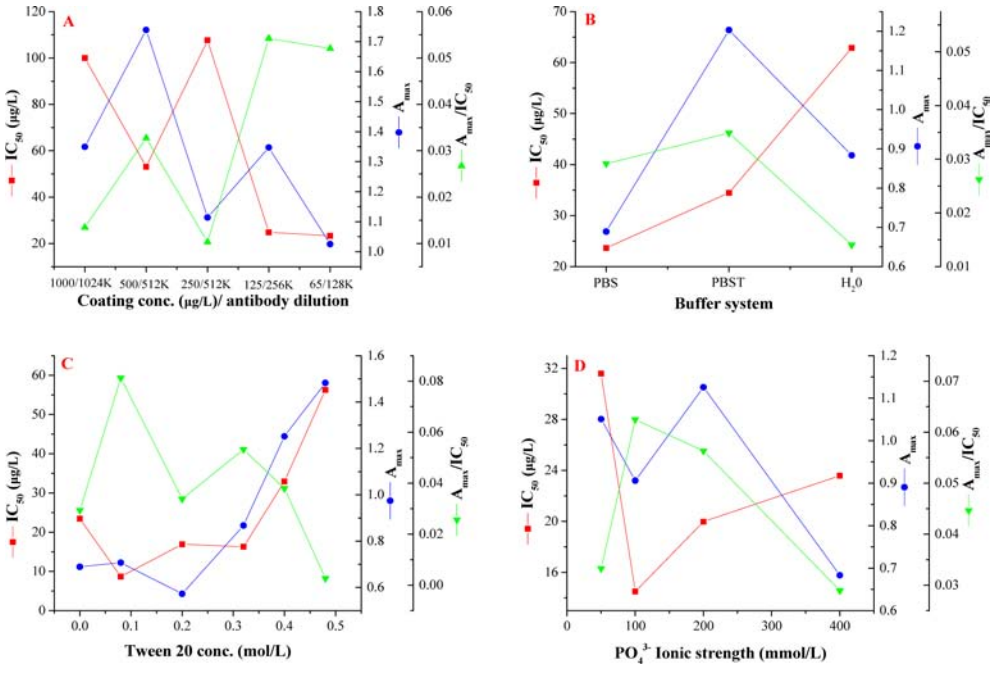

Figure 2. Effect of physicochemical parameters on ELISA performances (n = 3).

dx.doi.org/10.1021/jf5015395 | J. Agric. Food Chem. 2014, 62, 7078−7084

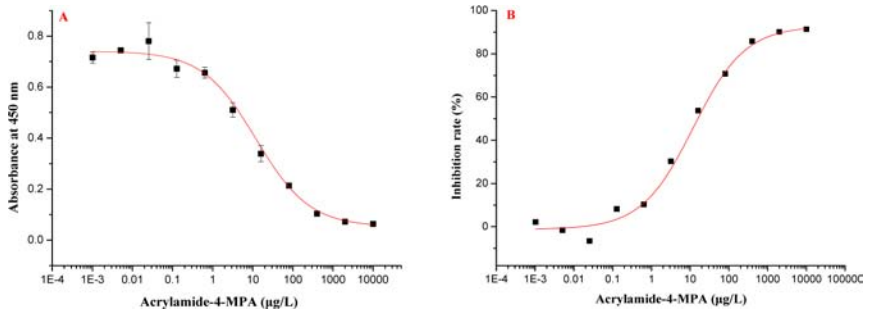

Figure 3. Standard curve (A) and inhibition curve (B) of acrylamide-4-MPA assessed by ciELISA.

Table 3. Cross-Reactivity of Obtained Antibody with Acrylamide-4-MPA and Its Analogues

Compound	Structure	CR%
acrylamide-4-MPA	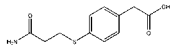	100
4-MPA	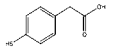	0.03
acrylamide		0.01
methacrylamide		0.09
methyl acrylate		0.01
acrylic acid		0.04
acrolein		0.01
maleic acid monoamide		0.05
N-acryloxysuccinimide (NAS)		0.01
4-acrylamidobutanoic acid	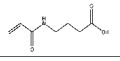	0.03

Table 4. Analysis of $L_9(3)^4$ Test Results

no.	(*A*) temperature (°C)	(*B*) reaction rime (min)	(*C*) pH	(*D*) molar ratio of 4-MPA/ acrylamide	yield of acrylamide-4-MPA (%)
1	37	15	8	2	32.1
2	37	30	9	5	64.2
3	37	50	10	10	32.9
4	50	15	9	10	21.6
5	50	30	10	2	91.2
6	50	50	8	5	93.2
7	70	15	10	5	79.7
8	70	30	9	10	68.1
9	70	50	8	2	83.6
K_1[a]	129.2	133.4	193.4	206.9	ΣY = 566.6
K_2[a]	206	223.5	169.4	237.1	
K_3[a]	231.4	209.7	203.8	122.6	
R^a[b]	102.2	76.3	34.4	114.5	

[a] K_i = Σ amount of target compounds at concentration *i*. [b] Refers to result of extreme analysis. $R^a = \max(K_i) - \min(K_i)$.

to carrier protein.[21] Therefore, in this study, 4-MPA instead of 3-MBA was reacted with acrylamide to obtain a novel hapten, which was then coupled to KLH to form an immunogen.

Table 5. Recoveries of Acrylamide from Spiked Food Samples by HPLC-MS/MS and Recoveries of Acrylamide Derivative from Spiked Food Samples by ciELISA

			recovery ± SD (%)	
food sample	HPLC concn (μg/kg)	spiked level (μg/kg)	ciELISA	HPLC-MS/MS
cookies	300	50.0	90.4 ± 19.2	96.1 ± 12.1
		200.0	107.7 ± 3.6	80.7 ± 9.2
		1000.0	81.9 ± 6.4	96.5 ± 5.2
potato chips	1368	50.0	104.9 ± 9.2	80.4 ± 11.4
		200.0	88.7 ± 7.9	90.0 ± 6.8
		1000.0	90.5 ± 8.8	95.0 ± 9.2
coffee	113	50.0	89.6 ± 8.1	74.5 ± 14.8
		200.0	73.7 ± 4.9	81.0 ± 7.3
		1000.0	112.3 ± 7.2	78.1 ± 6.6

Although the corresponding antiserum produced here showed no binding affinity for acrylamide (Table 1), it demonstrated significant binding to acrylamide-4-MPA (Table 2). As acrylamide can easily react with 4-MPA to yield acrylamide-4-MPA, an ELISA based on antiserum 4 could be developed to detect acrylamide by including a rapid preanalysis derivatization.

Development and Optimization of ciELISA. Antiserum 4 and hapten 4-OVA were used to develop a ciELISA for acrylamide-4-MPA. Several physicochemical parameters, including coating concentration, antibody dilution, ionic strength, and Tween-20 concentration, which are important in assay performance, were evaluated to improve ELISA performance. For each condition, standard curves for acrylamide-4-MPA were established (n = 3), and the maximum value of the inhibition curve (A_{max}) as well as the analyte concentration that produced 50% decreased inhibition in A_{max} (IC_{50}) was obtained from these curves. The results of these physicochemical parameter effects on ELISA performance are summarized in Figure 2.

For coating concentration and antibody dilution, a preliminary checkerboard titration was applied to choose several combinations of coating concentration and antibody dilution, under which the A_{450} was ∼1.0. The results indicated that the combination of coating concentration and antibody dilution at 125 μg/L and 1:256000, respectively, were optimal for the highest sensitivity (Figure 2A). For the working system, three solutions (PBST, PBS, 100 mmol/L, pH 7.4, and H_2O) were examined, and it was found that the A_{max}/IC_{50} ratio was highest with PBST (Figure 2B). Further study of Tween-20 concentration and ionic strength effects indicated that the

dx.doi.org/10.1021/jf5015395 | J. Agric. Food Chem. 2014, 62, 7078−7084

Table 6. Acrylamide Content in Different Food Samples

food sample	typical concn[4] (μg/kg)	mean concn[23] (μg/kg)	food sample name	HPLC-MS/MS concn (μg/kg)	ciELISA concn (μg/kg)
cookies	50−700	350	Chinese cookie	213	186.3
			compressed cookie	302	263.7
			hard cookie	574	655.8
			fermented cookies	113	81.4
potato chips	330−2300	752	Chinese potato chip	705	851.7
			French potato chip	626	743.7
			American potato chip	752	913.3
			potato crisp	1000	1161.4
			baked potato	1130	1427.5
coffee	100−668	220	coffee milk tea	179	151.2
			cappuccino instant coffee	595	558.3
			cafe latte	651	854.6
			instant coffee	113	129.7

optimal Tween-20 concentration and ionic strength were 0.08 and 0.1 mol/L, respectively (Figure 2C,D).

Sensitivity and Specificity. Using the optimized reaction conditions, dose−response and inhibition curves for acrylamide-4-MPA in assay buffer were constructed (Figure 3, panels A and B, respectively). The method exhibited an IC_{50} of 9.61 μg/kg and an LOD of 0.12 μg/kg for acrylamide-4-MPA (239 Da), whereas the detection linear range was 0.85−81.2 μg/kg, which was equivalent for acrylamide (71.08 Da) to an IC_{50} of 2.86 μg/kg, an LOD of 0.036 μg/kg, and a linear range of 0.25−24.15 μg/kg. The sensitivity of this assay was significantly improved compared to that of Preston et al.,[15] which might be attributed to the introduction of a suitable length spacer arm between the hapten and carrier protein. A similar conclusion, that the introduction of longer spacer arm rather than a monocarboxylic acid on benzene ring could led to antibody production with higher affinity to analyte, was also obtained by our group in antibody production and ELISA development for furaltadone metabolite 3-amino-5-morpholinomethyl-2-oxazolidinone.[22]

The selectivity of the present antibody and its applicability in actual acrylamide screening were investigated by examining the CRs of the antibody to a series of structural analogues and their derivatives. Acrylamide-4-MPA, 4-MPA, acrylamide, methacrylamide, methyl acrylate, acrylic acid, acrolein, maleic acid monoamide, NAS, and 4-acrylamidobutanoic acid were tested, and the results are summarized in Table 3. No CR was observed to any of the test compounds except acrylamide-4-MPA, suggesting that the antibody possessed high specificity for acrylamide-4MPA. As no CR to 4-MPA was detected, there was no need to remove unreacted 4-MPA after the derivatization step.

Optimization of Acrylamide-4-MPA Derivatization. The derivatization yield of acrylamide-4-MPA was improved by studying several derivatization conditions, such as the reaction's molar ratio of acrylamide/4-MPA, temperature, pH, and time, with the acrylamide-4-MPA content determined by HPLC-ECD. An $L_9(3^4)$ orthogonal experiment was performed after a series of preliminary single-factor experiments. As seen in Table 4, the influences on the mean compound extraction yields by these factors were found to decrease in the order molar ratio of acrylamide/4-MPA (D) > temperature (A) > time (B) > pH (C), according to the related R^a values. The reaction temperature was found to be an important yield determinant. The highest acrylamide-4-MPA derivatization yield was $A_3B_2C_3D_2$ (70 °C reaction temperature, 30 min reaction time, pH 10, 1:5 acrylamide/4-MPA molar ratio). Under the best conditions, the acrylamide-4-MPA derivatization yield was 93.2%.

Sample Preparation and Recovery Test. A standard HPLC-MS/MS method was developed here for acrylamide analysis. The acrylamide limit of detection by HPLC-MS/MS was 0.2 μg/L, and good linearity was observed over the acrylamide range of 0.9−1000 μg/L in each calibration, with a correlation coefficient of 0.9995.

Potato chips, cookies, and coffee samples were first analyzed for their acrylamide content by HPLC-MS/MS and then spiked with three different concentrations (50, 200, and 1000 μg/kg) of acrylamide standards. The samples were extracted by water and then derivatized with 4-MPA to form acrylamide-4-MPA. Next, the acrylamide-4-MPA content was analyzed using the optimized ciELISA procedure. Recoveries were tested from 81.9 to 107.7% for cookies, from 88.7 to 104.9% for potato chips, and from 73.7 to 112.3% for coffee (Table 5). Good correlations were observed between the results from ciELISA and standard HPLC-MS/MS (Table 5).

As a 20-fold dilution of the three samples was performed and good recoveries were observed from ciELISA, the IC_{50} of the proposed ciELISA for acrylamide in cookie, potato, and coffee samples was concluded to be 57.2 μg/L. The LOD and linear range here were 0.7 and 5.0−483 μg/kg for acrylamide, respectively, and the sensitivity almost the same as that of HPLC-MS/MS.

ciELISA Screening and HPLC-MS/MS Analysis of Blind Samples. Four different kinds of cookie samples, five potato chip samples, and four coffee samples were obtained from a local supermarket. The content of acrylamide in these samples was then determined by both ciELISA and HPLC-MS/MS; the results are shown in Table 6. A correlation coefficient of 0.9828 was obtained between the results of ciELISA and HPLC-MS/MS, indicating good reliability and accuracy for the proposed ciELISA. In acrylamide content, higher average concentrations were observed in potato samples. The results were equal to the typical concentration[4] and mean concentration[23] of acrylamide in these foods.

In conclusion, a ciELISA was developed for acrylamide detection via the determination of 4-MPA-derivatized acrylamide. For acrylamide, the IC_{50} was 2.86 μg/kg, the LOD 0.036

μg/kg, and the linear range 0.25−24.15 μg/kg in the chosen assay buffer. The recoveries from acrylamide-spiked potato chips, cookies, and coffee samples were tested from 73.7 to 112.3%, and good correlations were obtained between the results of ciELISA and standard HPLC-MS/MS. Although the sample pretreatment was not simple enough, it was more inexpensive than HPLC-MS/MS analysis. Additionally, the ciELISA was easy to apply with professorial training and suitable for routine acrylamide screening in a large number of food samples.

AUTHOR INFORMATION

Corresponding Authors

*(Y.-M. Sun) Mail: College of Food Science, South China Agricultural University, 483 Wushan Road, Tianhe District, Guangzhou 510642, China. Phone: +86 2085283925. Fax: +86 2085280270. E-mail: ymsun@scau.edu.cn.

*(Z.-L. Xu) E-mail: jallent@163.com.

Funding

This work was supported by the National Basic Research Program of China (973 Program, 2012CB720803) and the Science and Technology Innovation Project of Department of Education of Guangdong Province (2013KJCX0027).

Notes

The authors declare no competing financial interest.

REFERENCES

(1) Zhang, Y.; Yi, P. R.; Zhang, Y. New research developments on acrylamide: analytical chemistry, formation mechanism, and mitigation recipes. *Chem. Rev.* **2009**, *109*, 4375−4397.

(2) Heinz, F.; Aurelie, M. Dietary acrylamide intake of adults in the European Prospective Investigation into Cancer and Nutrition differs greatly according to geographical region. *Eur. J. Nutr.* **2013**, *52*, 1369−1380.

(3) International Agency for Research on Cancer,Lyon, France, 1994; pp 270.

(4) Ioannis, S. A.; Niki, D. Acrylamide: formation, occurrence in food products, detection methods, and legislation. *Crit. Rev. Food Sci.* **2014**, *54*, 708−733.

(5) Evrim, S.; Tekkeli, K.; Önal, C.; Önal, K. A review of current methods for the determination of acrylamide in food products. *Food Anal. Methods* **2012**, *5*, 29−39.

(6) International Food Safety Authorities Network (INFOSAN). *Acrylamide in Food Is a Potential Health Harzard*; Geneva, Switzerland, 2005; Vol. 3, p 1.

(7) Hoenicke, K.; Gatermann, R.; Harder, W.; Hartig, L. Analysis of acrylamide in different foodstuffs using liquid chromatography−tandem mass spectrometry and gas chromatography−tandem mass spectrometry. *Anal. Chim. Acta* **2004**, *520*, 207−215.

(8) Zhang, Y.; Dong, Y.; Ren, Y.-P.; Zhang, Y. Rapid determination of acrylamide contaminant in conventional fried foods by gas chromatography with electron capture detector. *J. Chromatogr., A* **2004**, *1116*, 209−216.

(9) Elisabet, B.; Oscar, N.; Luis, P.; Maria, T. G. Analysis of acrylamide in food products by in-line preconcentration capillary zone electrophoresis. *J. Chromatogr., A* **2006**, *1129*, 129−134.

(10) Philippe, P.; Lindinger, C. Y.; Imre, B. Proton transfer reaction mass spectrometry, a tool for on-line monitoring of acrylamide formation in the headspace of Maillard reaction systems and processed food. *Anal. Chem.* **2003**, *75*, 5488−5494.

(11) Nelson, A. F.; Silva, M. J.; Matos, A. K.; Maria, M. R. An electrochemical biosensor for acrylamide determination: merits and limitations. *Port. Electrochim. Acta* **2011**, *29*, 361−373.

(12) Chang, N. B.; Mani, S. Pesticide impact assessment via using enzyme-linked immunosorbent assay (ELISA) technique in the Lower Rio Grande River Basin, Texas. *Water Qual. Expo. Health* **2009**, *1*, 145−158.

(13) Zhou, S.; Zhang, C.; Wang, D.; Zhao, M. P. Antigen synthetic strategy and immunoassay development for detection of acrylamide in foods. *Analyst* **2008**, *133*, 903−909.

(14) Quan, Y.; Chen, M. L. Development of an enhanced chemiluminescence ELISA for the rapid detection of acrylamide in food products. *J. Agric. Food Chem.* **2011**, *59*, 6895−6899.

(15) Preston, A.; Fodey, T.; Elliott, C. Development of a high-throughput enzyme-linked immunosorbent assay for the routine detection of the carcinogen acrylamide in food, via rapid derivatization pre-analysis. *Anal. Chim. Acta* **2008**, *608*, 178−185.

(16) Sheng, W.; Li, Y.; Wang, S. Development of an enzyme-linked immunosorbent assay for the detection of gentamycin residues in animal-derived foods. *LWT−Food Sci. Technol.* **2013**, *50*, 204−209.

(17) Tinashe, B. R.; Victor, J. J.; Paul, D. S. Production, characterization and utility of a panel of monoclonal antibodies for the detection of toluene diisocyanate haptenated proteins. *J. Immunol. Methods* **2011**, *373*, 127−135.

(18) Li, M.; Wang, M. H. Development of immunoassays for detecting clothianidin residue in agricultural products. *J. Agric. Food. Chem.* **2013**, *61*, 3619−3623.

(19) Mika, K.; Hiroshi, Y.; Mikiko, U.; Takeshi, K.; Toshihide, T.; Masahiro, F.; Machiko, S.; Seiji, I.; Shigekazu, I.; Shiro, M. Development of an enzyme-linked immunosorbent assay for residue analysis of the insecticide emamectin benzoate in agricultural products. *J. Agric. Food Chem.* **2009**, *57*, 359−364.

(20) Ruud, M. T.; Chris, R.; Barbara, D.; Tomlinson, I. M. Antibody arrays for high-throughput screening of antibody−antigen interactions. *Nat. Biotechnol.* **2000**, *18*, 989−994.

(21) Xu, Z. L.; Wang, H.; Shen, Y. D. Â.; Mikaela, N.; Lei, H. T.; Beier, R. C.; Zheng, W. X.; Yang, J. Y.; She, Z. G.; Sun, Y. M. Conformational changes of hapten-protein conjugates resulting in improved broad-specificity and sensitivity of an ELISA for organophosphorus pesticides. *Analyst* **2011**, *136*, 2512−2520.

(22) Xu, Z. L.; Shen, Y. D.; Sun, Y. M.; Katrina, C.; Tian, Y. X.; Zhang, S. W.; Lei, H. T.; Jiang, Y. M. Novel hapten synthesis for antibody production and development of an enzyme-linked immunosorbent assay for determination of furaltadone metabolite 3-amino-5-morpholinomethyl-2-oxazolidinone (AMOZ). *Talanta* **2013**, *103*, 306−313.

(23) Javad, K.; Alain, L. B. Acrylamide in foods: chemistry and analysis. A review. *Food Bioprocess Technol.* **2011**, *4*, 340−363.

To perform complete analyses of both OP and pyrethoid insecticide degradation, methods for the extraction and analysis of both parent insecticide compounds and their degradates are required. A suitable method for the extraction of insecticides from foods and the subsequent analysis of these analytes by gas chromatography (GC) with electron capture detection has previously been developed.[20] However, few methods have been developed to analyze insecticide degradates in food.[9,12,14,21] None of the previously reported extraction methods combine analysis of pyrethroid and OP insecticide degradation products. Because both classes of insecticides may be used on a single crop, it is possible for degradates of both classes to be present in food.

As recognized in the Food Quality Protection Act of 1996,[22] risk factors unique to children make understanding their insecticide exposure particularly important. Children's physiological traits put them at higher risk for long-term damage from insecticide exposure.[9] For example, their high metabolic rate causes them to eat more food per kilogram of body weight than adults, and their lower detoxifying enzymatic activity and immature neurological system make this potentially heightened pesticide exposure even more hazardous.[9,23] Their behavioral tendencies, such as preference for foods that tend to contain higher amounts of insecticides and greater tendency to place fingers and objects in their mouths, also put them at risk for higher insecticide exposure.[9,24] Assuming insecticide degradates are present in food and other environmental matrices such as dust, the same risk factors that make children more likely to be exposed to insecticides also make them likely to be exposed to degradates. Hence, it is particularly important to understand children's exposure to insecticide degradates, especially in the case when measurement of such compounds as biomarkers of exposure is anticipated.

There are currently few data on the adsorption, further metabolism, and potential toxicity of many insecticide degradates.[9,12] Consequently, it is difficult to separate the health effects of insecticide degradates from those of the parent compounds. The ability to extract these compounds from food would allow research separating the health effects of the parent and degradate compounds.

For these reasons, a method for the extraction of insecticide degradates in baby food was developed. Degradates analyzed include malathion dicarboxylic acid (MDA), a hydrolysis degradation product of the OP insecticide malathion; 3,5,6-trichloro-2-pyridinol (TCPy), a hydrolysis degradate of the OP insecticides chlorpyrifos and chlorpyrifos-methyl; *cis*/*trans*-2,2-(dichloro)-2-dimethylvinylcyclopropane carboxylic acid (DCCA), a hydrolysis product of several pyrethroid insecticides; and 3-phenoxybenzoic acid (3-PBA), a nonspecific hydrolysis/oxidation product of several pyrethroid insecticides resulting from the hydrolysis of the insecticide and then subsequent oxidation of the degradate.

MATERIALS AND METHODS

Reagents and Materials. Methanol (HPLC grade), acetonitrile (HPLC grade), and glacial acetic acid were purchased from Sigma-Aldrich, Inc. (St. Louis, MO, USA). Water was purified in-house to 18.2 MΩ·cm with a Milli-Q water system (Millipore, Billerica, MA, USA). Oasis HLB mixed phase extraction sorbent extraction cartridges (200 mg, 6 mL) were purchased from Waters Corp. (Milford, MA, USA). Bond Elut reservoir cartridges were purchased from Agilent Technologies (Santa Clara, CA, USA).

Standards. MDA was purchased from Crescent Chemical Co. (Islandia, NY, USA). TCPy was purchased from Sigma-Aldrich (St. Louis, MO, USA). DCCA was purchased from Cambridge Isotope Laboratories (Tewksbury, MA, USA), and 3-PBA was purchased from Acros Organics (Pittsburgh, PA, USA). All standard purities were >95%. A stock solution containing 10 μg/g MDA, TCPy, DCCA, and 3-PBA in acetonitrile (ACN) was used to create standard dilutions from 5 to 2000 ng/mL. These dilutions were used to create matrix-based calibration curves ranging from 0.25 to 100 ng/g of matrix. This range was based on amounts of insecticide degradation products found previously in foods and juices.[9,12]

Isotopically labeled standards (MDA-D_6, DCCA-$^{13}C_3$, and 3-PBA-$^{13}C_6$) were purchased from Cambridge Isotope Laboratories. These standards were diluted to 1000 ng/mL made in ACN and used as internal standards (ISTDs).

Baby Foods. We have elected to use baby food in this work to avoid the typical heterogeneity associated with standard food samples. Numerous methods can be found in the literature to produce homogeneous food samples. The use of baby food, which has been processed into a uniform consistency, eliminates most of the heterogeneity associated with processing raw samples.

Baby foods were purchased from local grocery stores in Atlanta, GA, USA. Green beans, carrots, peas, apples, bananas, and pears were chosen on the basis of the vegetable and fruit baby foods most frequently purchased in the United States.[25] Two popular conventional brands of each were chosen, as well as an organic version of one of these conventional brands. Only organic baby food was used for method validation to minimize degradate contamination from the food itself.

Sample Preparation. The method developed here was based on an extraction of urinary insecticide metabolites previously reported but with substantial modification.[11,26] One gram (1.0 g) of baby food, 50 μL of labeled ISTD, and 2 mL of water were added to a trace-cleaned conical centrifuge tube. The tube was vortex mixed for 4 min at 1000 rpm and centrifuged for 7 min at 150*g*. An Oasis HLB cartridge was placed on a vacuum manifold and preconditioned with 3 mL of methanol (MeOH) and 3 mL of 1% acetic acid in water. The water extract (supernatant) was filtered through a Bond Elut Reservoir cartridge and then loaded onto the OASIS cartridge. After the cartridge was loaded, it was washed twice with 2 mL of 1:5:94 (v/v/v) acetic acid/MeOH/water. The cartridge was then dried under vacuum. A test tube was placed under the cartridge in the vacuum manifold, and the sample was eluted twice with 2.5 mL of methanol. Because the cartridge had been dried completely, vacuum was required to start the elution process. Once the eluate began to flow through the cartridge, the vacuum was broken and the eluate was allowed to flow out using gravity only. The eluate was evaporated to dryness using a Turbovap LV evaporator (Zymark Corp., Hopkinton, MA, USA) under air at 15 psi and 45 °C and was then reconstituted with 100 μL of 30:70 (v/v) MeOH/water. The sample was then vortex mixed briefly and centrifuged for 3 min before being transferred to an HPLC vial for analysis. Any residual particulate matter was left behind.

Analysis by LC-MS/MS. An Agilent 6460 triple-quadrupole HPLC-MS/MS (Agilent, Santa Clara, CA, USA) equipped with a negative mode electrospray ionization (ESI) interface was used to analyze samples. A Zorbax Eclipse Plus Phenyl-hexyl column (3.0 × 100 mm, 3.5 μm particle size, Agilent) was used for separation and kept at 45 °C. Solvent A was water with 1% acetic acid, and solvent B was MeOH with 1% acetic acid. The following parameters were used: the source temperature was 250 °C, the vaporizer gas flow (N_2) was 5 L/min, the nebulizer gas flow pressure was set to 35 psi, and the corona voltage was 3500 V. Each metabolite was matched to its own isotopically labeled internal standard with the exception of TCPy, for which no isotopically labeled standard was available. The best results were found when isotopically labeled DCCA was used as an internal standard for TCPy. Ions were analyzed in selected reaction monitoring (SRM) mode; their optimized precursor and product ions along with their optimized fragmentation and collision energies are shown in Table 1. Mass Hunter Quantitative software (Agilent Technologies) and Microsoft Excel (Redmond, WA, USA) were used for data analysis.

Table 1. Instrument Parameters for Optimized Quantification and Confirmation Ions of Insecticide Degradation Products with Fragmention Energies (FE), Collision Energies (CE), and Retention Times (RT)[a]

compound	precursor ion	product ion	FE (V)	CE (V)	RT (min)
MDA-ISTD	280	147	80	1	3.3
MDA	273	141	80	1	3.9
MDA	273	157	80	12	3.9
TCPy	198	198	96	0	7.3
TCPy	196	196	96	0	7.3
DCCA-ISTD	210	210	90	0	6.7
DCCA	207	207	90	0	8.2
DCCA	209	209	90	0	8.2
3-PBA-ISTD	219	99	98	20	7.4
3-PBA	213	93	122	16	9.0
3-PBA	213	169	122	8	9.0

[a]ISTD, internal standard; MDA, malathion dicarboxylic acid; TCPy, 3,5,6-trichloro-2-pyridinol; DCCA, *cis/trans*-3-(2,2-dichlorovinyl)-2,2-dimethylcyclopropane-1-carboxylic acid; 3-PBA, 3-phenoxybenzoic acid.

During compound identification and optimization, by infusing the solution containing standard chemicals into the LC-MS/MS system, a number of precursor/product ion pairs were identified for each analyte according to their fragmentation patterns. A multiple time segment containing a specific multiple reaction monitoring (MRM) experiment was created and used during MS/MS acquisition. We selected both the quantification and confirmation ions by monitoring the intensity, peak shape, background level, and potential interferences in different urine samples. The same procedure was also applied to the isotopically labeled internal standard.

Method Validation. *Limits of Detection (LODs).* LODs were calculated using replicates of blanks and low-spike (10 ng/g) samples as the lowest analyte concentration at which reliable detection was feasible. If analyte was detected in the blank samples, the following procedure was used to determine the LOD. Ten replicate samples were injected, and the mean blank concentration was determined. The standard deviation (SD_{blank}) of the blank concentrations was also determined. The LOD, defined here as the lowest concentration acceptable as a measured quantity, was defined by the equation

$$LOD = mean_{blank} + 3(SD_{blank})$$

If no analyte was detected in the sample, a different procedure was used to determine the LOD. MassHunter software afforded an estimate of the signal-to-noise ratio (S/N) for each sample taken. The reported LOD was determined by noting when S/N drops below 3 among the standards. If the S/N for the lowest standard was >3, we reported the LOD as the concentration that would have produced S/N = 3 based on extrapolation. If the extrapolated LOD falls below the lowest standard, the lowest standard was used as the LOD instead.

Accuracy and Precision. Method accuracy and precision were determined by measurements of spiked samples at two concentrations (10 and 25 ng/g). For each matrix, 1.0 g of each type of food was fortified with either parent or metabolite compounds to either 10 or 25 ng/g. These quality control (QC) samples were then extracted and analyzed alongside other samples. Percent spiked recovery (relative recovery; Table 2) was calculated on the basis of the percentage of observed concentrations of the nominal spiked concentrations. Within-run precision, presented as relative standard deviation (RSD), was also calculated for fruits and vegetables on the basis of these fortified samples.

Test for Analytic Degradation. To test for analytic degradation in baby food fruits and vegetables, six samples of 1.0 g of carrots and six samples of 1.0 g of apples were obtained. For each matrix, three of the samples were fortified with 25 ng/g parent insecticide (malathion, permethrin, and chlorpyrifos) per sample, and all samples were fortified with degradate ISTD at a final concentration of 50 ng/g. The samples were then immediately extracted and analyzed according to the insecticide metabolite procedure. To test for analytic degradation, we examined the concentration of analytes from fortified and unfortified samples. A two-tailed t test ($p = 0.05$) was used as the test criterion to ascertain that the degradate concentrations were identical regardless of parent insecticide spiking.

Table 2. Relative Recoveries for Degradation Products in Baby Food Expressed as Percentages[a]

	MDA	TCPy	DCCA	3-PBA
green beans				
QCL	85.8	119.5	100.0	94.5
QCH	93.1	95.4	93.4	97.8
peas				
QCL	109.8	93.0	104.6	91.0
QCH	106.8	84.5	110.2	94.1
carrots				
QCL	79.6	116.6	104.1	92.9
QCH	80.2	108.2	97.7	88.1
apples				
QCL	76.6	133.1	103.1	114.5
QCH	86.1	123.7	102.3	112.6
banana				
QCL	107.3	109.3	109.7	98.3
QCH	127.1	110.2	106.0	93.3
pears				
QCL	92.0	123.5	93.2	98.9
QCH	109.1	132.3	100.5	101.5

[a]QCL, low (10 ng/(g) quality control sample; QCH, high (25 ng/(g) quality control sample; MDA, malathion dicarboxylic acid; TCPy, 3,5,6-trichloro-2-pyridinol; DCCA, *cis/trans*-3-(2,2-dichlorovinyl)-2,2-dimethylcyclopropane-1-carboxylic acid; 3-PBA, 3-phenoxybenzoic acid. $N = 1$ in all cases.

Matrix Effects. Matrix effects were accounted for by developing calibration curves in a surrogate matrix. The surrogate matrices included one for vegetables and one for fruits consisting of an equal contribution of each individual food for the two classes.

Method Implementation. The method was used to measure pesticide degradates in several baby food samples on the basis of the most frequently purchased baby foods in the United States: green beans, carrots, peas, apples, bananas, and pears.[25] For each food, there were three samples: two different conventional brands and one organic brand.

RESULTS

Method Performance. The extraction and cleanup method produced mass chromatograms free of interfering peaks. A typical QC mass chromatogram is shown in Figure 1. Two sets of matrix-based calibration curves were created, one in vegetables and one in fruits. Calibration curves were linear and resulted in $R^2 > 0.98$ for all compounds. A typical matrix calibration plot is shown in Figure 2. Calibration curves for the other analytes can be found in the Supporting Information.

As shown in Table 3, relative recoveries were between 80 and 120% for all analyte/matrix combinations except TCPy in fruit. Table 3 summarizes method performance by showing average relative recovery, RSD, and LODs stratified by fruits and vegetables. All RSDs were under 15% with the exception of MDA.

Test for Analytic Degradation. Using a two-tailed t test ($p = 0.05$), we determined that there was no significant difference between insecticide degradate concentrations between identical food samples regardless of parent compound

dx.doi.org/10.1021/jf500779a | J. Agric. Food Chem. 2014, 62, 7085−7091

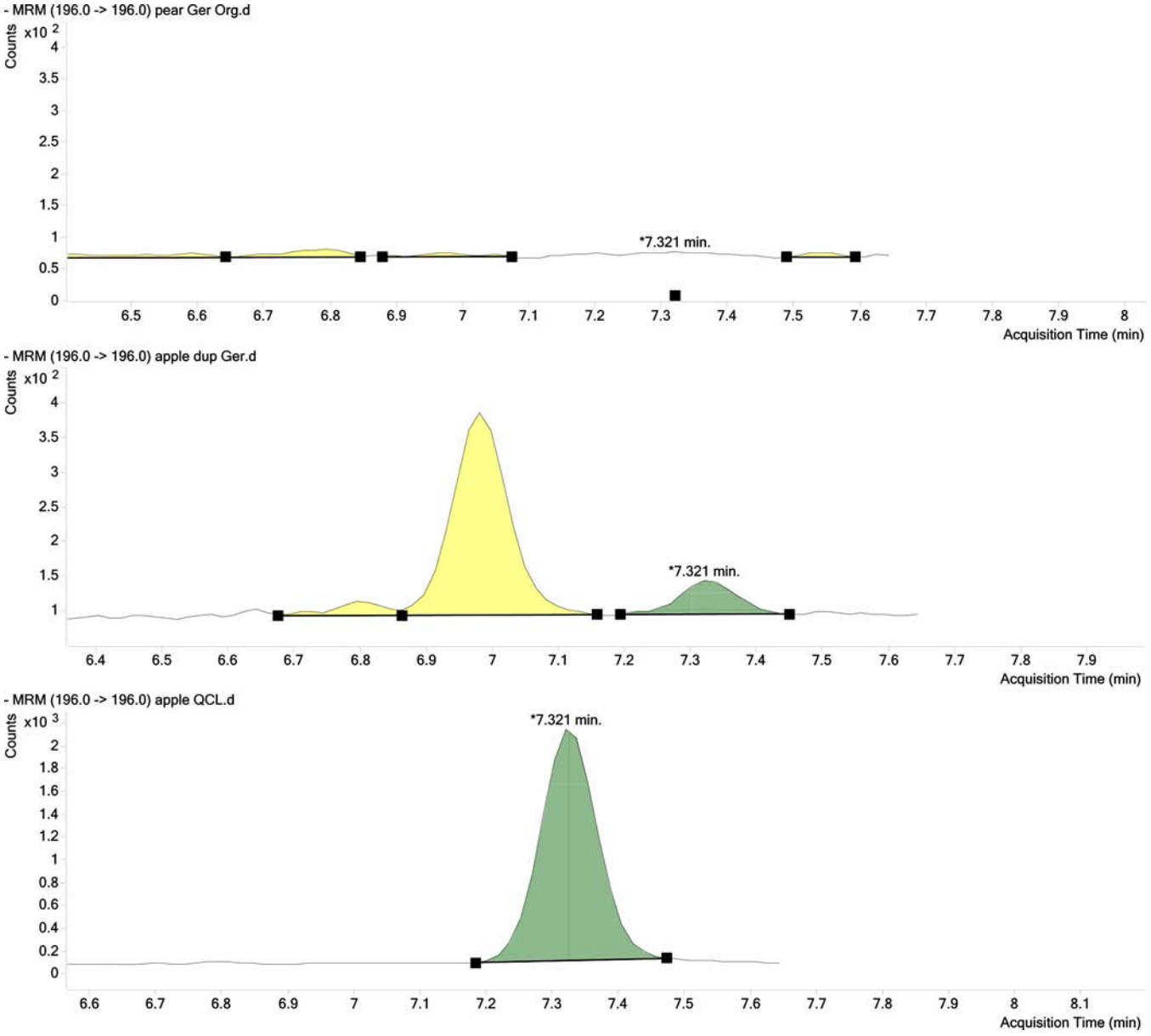

Figure 1. Comparison of chromatographic peaks for chromatogram of TCPy: (top) sample with no detection; (middle) peak detected at 7.321 min in an apple juice sample with a concentration below the LOQ (scale identical to top); (bottom) spiked quality control materials at 10 ng/g equivalent (note factor of 10 change in scale).

fortification. Table 4 presents average concentrations and standard deviations for spiked and nonspiked samples.

Method Implementation. Degradates were found in three samples. One conventional sample of pears contained TCPy at a concentration of 1.81 ng/g, the organic banana sample contained DCCA at a concentration of 1.64 ng/g, and the organic pea sample contained MDA at 3.63 ng/g. 3-PBA was not detected in any samples.

DISCUSSION

Method Performance. All degradate recoveries were between 80 and 120% except TCPy in fruit (122%), which is likely the result of the lack of an isotopically labeled analogue for TCPy. If DCCA, the labeled standard used as a surrogate standard for TCPy, was preferentially adsorbed by proteins or other matrix surfaces or interacted differently with the matrix from TCPy, falsely high recoveries (from calculations) could have resulted. Ion abundances in the mass spectrometer may have changed because of solvent and eluted matrix component composition changes resulting from retention time shifts. Such changes that are not matched by ISTD may also have led to less accurate recoveries.

Blanks were developed from matrix-matched samples with no detectable concentration of degradate under most circumstances. Each type of sample had numerous "blank" values associated with it. For example, blank "vegetable" samples included a measure of organic peas that displayed no measurable concentration of degradate. We choose foods labeled "organic" for our blank samples under the supposition that they would likely contain lower levels of any parent pesticide or degradate. This supposition was borne out as measurable concentrations of degradate in such systems were <LOD. For a small number of cases, we detected the presence of degradate in these "blank" samples. Under such a scenario,

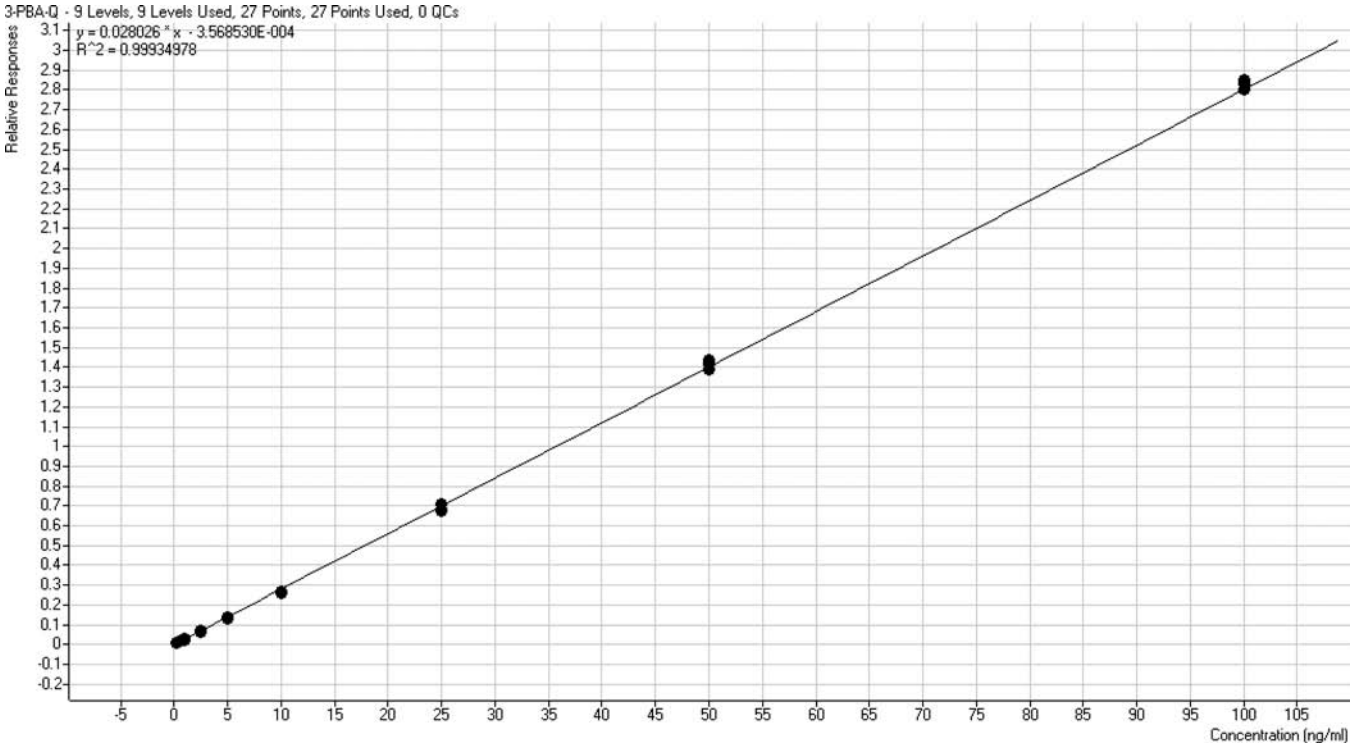

Figure 2. Calibration curve for 3-phenoxybenzoic acid, a degradate of many pyrethroid insecticides, in vegetables. All calibration points were injected in triplicate, and all points are present on the graph.

Table 3. Results for Recovery of Degradates from Fruits and Vegetables[a]

	QCL	QCH	LOD (ng/g)
vegetables			
MDA	91.7 ± 15.9	93.4 ± 13.3	2.3
TCPy	109.7 ± 14.5	96.0 ± 11.9	2.7
DCCA	102.9 ± 2.6	100.4 ± 8.7	0.87
3-PBA	92.8 ± 1.7	93.3 ± 4.9	0.25
fruits			
MDA	92.0 ± 15.4	107.5 ± 20.6	0.18
TCPy	122.0 ± 12.0	122.1 ± 11.1	0.76
DCCA	102.0 ± 8.3	102.0 ± 8.3	0.87
3-PBA	103.9 ± 9.2	102.5 ± 9.7	0.25

[a]Relative recoveries (±SDs) and limits of detection (LODs) are presented. QCL, low quality control material fortified to 10 ng/g; QCH, high quality control material fortified to 25 ng/g; MDA, malathion dicarboxylic acid; TCPy, 3,5,6-trichloro-2-pyridinol; DCCA, *cis/trans*-3-(2,2-dichlorovinyl)-2,2-dimethylcyclopropane-1-carboxylic acid; 3-PBA, 3-phenoxybenzoic acid. $N = 3$ in all cases.

Table 4. Test for Analytic Degradation in Vegetables and Fruits[a]

	spiked samples	nonspiked samples
carrots		
MDA	1.44 ± 0.01	1.43 ± 0.02
TCPy	0.26 ± 0.38	0.31 ± 0.12
DCCA	0.22 ± 0.38	nd
3-PBA	0.09 ± 0.01	0.08 ± 0.01
apples		
MDA	nd	nd
TCPy	nd	nd
DCCA	1.05 ± 0.26	0.46 ± 0.42
3-PBA	0.14 ± 0.01	0.13 ± 0.01

[a]Spiked samples were fortified with 25 ng/g malathion, chlorpyrifos, and permethrin, precursors to the four analytes. There was no significant difference found between sample concentrations using a two-tailed *t* test ($p = 0.05$). MDA, malathion dicarboxylic acid; TCPy, 3,5,6-trichloro-2-pyridinol; DCCA, *cis/trans*-3-(2,2-dichlorovinyl)-2,2-dimethylcyclopropane-1-carboxylic acid; 3-PBA, 3-phenoxybenzoic acid; nd, not detected. $N = 3$ in all cases.

the reported concentration after spiking had to be greater than the mean blank value plus 3 times the standard deviation of the blank value (mean + 3σ(blank)) to be considered as >LOD.

RSDs were <15% for all analytes except MDA. RSDs under 15% are preferred for analytical analyses.[27] MDA may have had less precise results because a deuterated MDA was used for an ISTD. Deuterium may have been exchanged much more easily during solvent interactions than ^{13}C or other isotopes, causing greater imprecision. Alternatively, the fact that MDA has two ionizable groups, thereby causing the possibility of four forms to be present at a given time, may contribute to its high RSD.

During compound optimization, no fragmentation was observed for both TCPY and DCCA. Although we could induce the "loss of chlorine" and use m/z of 35 as a product ion, it could come with higher background noises due to its low mass value. We thus decided to employ pseudotransitions for these compounds, which means the same m/z was detected in both Q1 and Q3 of the mass spectrometer.

Analytic Degradation. High concentrations of insecticides that could degrade into the target analytes were spiked into baby foods before extraction of degradates to test for analytic degradation. Even when using as much as 25 ng insecticide/g matrix, which is 100 times the lowest degradate calibration point used, statistically significant amounts of degradation products were not produced. This observation suggests that the use of this method to analyze the degradation of insecticides in

dx.doi.org/10.1021/jf500779a | J. Agric. Food Chem. 2014, 62, 7085−7091

food without creating false-positive detection of insecticide degradate is acceptable.

Although not statistically significant, there was a larger difference in DCCA concentrations in spiked versus unspiked samples of apples than of carrots. There is the potential that the lower pH of apples (pH 3.0−4.0) versus carrots (pH 4.5−6.0) contributes to the degradation of permethrin, the parent of DCCA, during extraction, thereby causing the larger analyte difference in spiked versus unspiked samples.[28]

Matrix Effects. Matrix effects are common in analyses of food samples and should be accounted for. In principle, there may well be a different matrix effect for each food analyzed. For single food analyses, this presents only minor problems as a matrix calibration curve can easily be constructed. However, for more complex samples, such as a duplicate diet sample, establishing separate calibration curves for each food is not practical. We made the compromise in our analysis to construct calibration curves separately for vegetables and fruits. These two food groups are likely to have different matrix characteristics with, for example, fruits being more acidic. We have included all foods of these two classes for which we performed analysis into two matrices and developed curves using these mixtures. All vegetable samples were analyzed using the curve developed using the vegetable mixture with similar protocols followed for fruit samples. We offer this as a compromise solution to the likely matrix effects problem.

Method Implementation. MDA, TCPy, and DCCA were all found in baby food, including some organic foods. 3-PBA was not found in any baby food. It is not certain whether 3-PBA, 3-phenoxybenzyl alcohol (3-PBAlc), or both compounds would be produced from the degradation of pyrethroids. Hydrolysis of these compounds should lead to 3-PBAlc, not 3-PBA. However, in the mammalian body, the alcohol moiety is transformed to the acid by an oxidase.[29] This oxidation may not happen in fruits and vegetables. Previous studies have demonstrated that the presence of antioxidants, such as those found in fruits and fruit juices, suppresses the production of pesticide oxidation degradates, so perhaps oxidation of 3-PBAlc to 3-PBA is suppressed by these compounds.[16,17]

Although the detection frequency of these three compounds may not seem very high (17% for MDA, TCPy, and DCCA) compared to insecticide degradate concentrations found in other studies, there are a few possible explanations. First of all, other studies in which pesticide degradate concentrations were found in food observed DAPs,[12,14,15] which are nonspecific degradates formed from 75% of the EPA-registered OP insecticides.[30] However, MDA is formed from only malathion, TCPy is formed from only chlorpyrifos and chlorpyrifos-methyl, and DCCA is formed from the three pyrethroids permethrin, cypermethrin, and cyfluthrin.[31] Because DAPs are formed by so many more insecticides than these three compounds, it makes sense that their detection frequency was higher than that of MDA, TCPy, and DCCA. Furthermore, two of the studies cited analyzed for DAPs and/or 3-PBA only in produce already known to contain the parent insecticide.[14,15] This sample preselection likely led to a larger degradate detection frequency than would happen if produce was analyzed regardless of parent insecticide content. Although 3-PBA, which is also a broad-range insecticide degradate, was not found in any of our baby food samples, this is possibly due to suppression of 3-PBAlc oxidation.

One may inquire as to the optimization of the final elution program of the SPE by comparing our work with normal-phase SPE or ion exchange SPE. However, in the case of a reversed phase SPE, a generic method provided by the manufacturer can be followed with minimum optimization process, as long as the isotopic analogues are used as internal standards and the target analytes are polar compounds. Our analytes are quite polar, and on the basis of their Log *P* values they can be dissolved in polar solvents such as acetonitrile, methanol, ethyl acetate, and acetone. We chose not to use acetonitrile to reduce the laboratory cost, and acetone is not recommended for use due to high chemical backgrounds. Using the same elution solvent, Olsson et al.[26] reported their extraction recoveries of >80% for all analytes except MDA. Although we are satisfied with our method LODs for most of the compound measured, we do recommend further optimization to increase the LOD of MDA if such analysis is deemed critical for a given study.

This method could be expanded to analyze produce or other foods for insecticide degradation products. If other foods were analyzed, prehomogenization using a blender, food processor, or other homogenization system before the extraction step would be required to ensure a true understanding of analyte content in the sample.

This method is suitable for the analysis of insecticide degradates in baby food. The presence of degradates in baby food discovered during method implementation supports the need for this method. Furthermore, the widespread measurement of these urinary metabolites for exposure assessment purposes highlights the need for a better understanding of the contribution of preformed environmental metabolites to urinary concentrations. Use of this method in food samples will allow a more complete understanding of insecticide degradation product concentrations in such samples, and this knowledge in turn will allow more accurate estimation of human insecticide exposure.

■ ASSOCIATED CONTENT

Ⓢ Supporting Information

Structures, calibration curves, and matrix effects. This material is available free of charge via the Internet at http://pubs.acs.org.

■ AUTHOR INFORMATION

Corresponding Author

*(P.B.R.) Mail: Analytical Exposure Science and Environmental Health Laboratory, Department of Environmental Health, Rollins School of Public Health, Emory University, Room 2041, 1518 Clifton Road, Atlanta, GA 30322, USA. Phone: (404) 727-3826. Fax: (404) 727-8744. E-mail: bryan@emory.edu.

Funding

This work was partially supported by NIH Grant 5RC1ES01829902 under the American Recovery and Reinvestment Act of 2009 and the National Children's Study under Contract HHSN267200700007C. S.A.R. was supported by Graduate and Postdoctoral Training in Toxicology Grant T32 ES012870. This paper is a contribution from the Analytical Exposure Science and Environmental Health Laboratory, Department of Environmental Health, Rollins School of Public Health, Emory University.

Notes

The authors declare no competing financial interest.

REFERENCES

(1) Bravo, R.; Caltabiano, L. M.; Weerasekera, G.; Whitehead, R. D.; Fernandez, C.; Needham, L. L.; Bradman, A.; Barr, D. B. Measurement of dialkyl phosphate metabolites of organophosphorus pesticides in human urine using lyophilization with gas chromatography-tandem mass spectrometry and isotope dilution quantification. *J. Exposure Anal. Environ. Epidemiol.* **2004**, *14*, 249−259.

(2) Kamel, F.; Engel, L. S.; Gladen, B. C.; Hoppin, J. A.; Alavanja, M. C.; Sandler, D. P. Neurologic symptoms in licensed private pesticide applicators in the agricultural health study. *Environ. Health Perspect.* **2005**, *113*, 877−882.

(3) Grube, A.; Donaldson, D.; Kiely, T.; Wu, L. In *Pesticides Industry Sales and Usage: 2006 and 2007 Market Estimates*; Office of Chemical Safety and Pollution Prevention, U.S. Environmental Protection Agency: Washington, DC, USA, 2011.

(4) Lu, C.; Barr, D. B.; Pearson, M.; Bartell, S.; Bravo, R. A longitudinal approach to assessing urban and suburban children's exposure to pyrethroid pesticides. *Environ. Health Perspect.* **2006**, *114*, 1419−1423.

(5) Barr, D. B. Biomonitoring of exposure to pesticides. *J. Chem. Health Saf.* **2008**, *231*, 1−10.

(6) Bradman, A.; Whitaker, D.; Quiros, L.; Castorina, R.; Claus Henn, B.; Nishioka, M.; Morgan, J.; Barr, D. B.; Harnly, M.; Brisbin, J. A.; Sheldon, L. S.; McKone, T. E.; Eskenazi, B. Pesticides and their metabolites in the homes and urine of farmworker children living in the Salinas Valley, CA. *J. Exposure Anal. Environ. Epidemiol.* **2007**, *17*, 331−349.

(7) Fenske, R.; Leffinwell, J. T. Method for the determination of dialkyl phosphate metabolites in urine for studies of human exposure to malathion. *J. Agric. Food Chem.* **1989**, *37*, 995−998.

(8) Lu, C.; Toepel, K.; Irish, R.; Fenske, R. A.; Barr, D. B.; Bravo, R. Organic diets significantly lower children's dietary exposure to organophosphorus pesticides. *Environ. Health Perspect.* **2006**, *114*, 260−326.

(9) Morgan, M. K.; Sheldon, L. S.; Croghan, C. W.; Jones, P. A.; Robertson, G. L.; Chuang, J. C.; Wilson, N. K.; Lyu, C. W. Exposures of preschool children to chlorpyrifos and its degradation product 3,5,6-trichloro-2-pyridinol in their everyday environments. *J. Exposure Anal. Environ. Epidemiol.* **2005**, *15*, 297−309.

(10) Naeher, L. P.; Tulve, N. S.; Egeghy, P. P.; Barr, D. B.; Adetona, O.; Fortmann, R. C.; Needham, L. L.; Bozeman, E.; Hilliard, A.; Sheldon, L. S. Organophosphorus and pyrethroid insecticide urinary metabolite concentrations in young children living in a southeastern United States city. *Sci. Total Environ.* **2010**, *408*, 1145−1153.

(11) Panuwet, P.; Prapamontol, T.; Chantara, S.; Barr, D. B. Urinary pesticide metabolites in school students from northern Thailand. *Int. J. Hyg. Environ. Health* **2009**, *212*, 288−297.

(12) Lu, C.; Bravo, R.; Caltabiano, L. M.; Irish, R. M.; Weerasekera, G.; Barr, D. B. The presence of dialkylphosphates in fresh fruit juices: implication for organophosphorus pesticide exposure and risk assessments. *J. Toxicol. Environ. Health Part A* **2005**, *68*, 209−227.

(13) ATSDR, Agency for Toxic Substances and Disease Registry. *Toxicological Profile for Malathion*; ATSDR: Atlanta, GA, USA, 2003.

(14) Zhang, X.; Driver, J. H.; Li, Y.; Ross, J. H.; Krieger, R. I. Dialkylphosphates (DAPs) in fruits and vegetables may confound biomonitoring in organophosphorus insecticide exposure and risk assessment. *J. Agric. Food Chem.* **2008**, *56*, 10638−10645.

(15) Chen, L.; Zhao, T.; Pan, C.; Ross, J. H.; Krieger, R. I. Preformed biomarkers including dialkylphosphates (DAPs) in produce may confound biomonitoring in pesticide exposure and risk assessment. *J. Agric. Food Chem.* **2012**, *60*, 9342−9351.

(16) Morgan, M. K.; Sheldon, L. S.; Jones, P. A.; Croghan, C. W.; Chuang, J. C.; Wilson, N. K. The reliability of using urinary biomarkers to estimate children's exposures to chlorpyrifos and diazinon. *J. Exposure Anal. Environ. Epidemiol.* **2011**, *21*, 280−290.

(17) Pico, Y.; Kozmutza, C. Evaluation of pesticide residue in grape juices and the effect of natural antioxidants on their degradation rate. *Anal. Bioanal. Chem.* **2007**, *389*, 1805−1814.

(18) Uygun, U.; Senoz, B.; Koksel, H. Dissipation of organophosphorus pesticides in wheat during pasta processing. *Food Chem.* **2008**, *109*, 355−360.

(19) Galera, M. M.; Garcia, M. D. G.; Lallena, J. A. R.; Lopez, T. L.; Vial, J. L. M. Dissipation of pyrethroid residues in peppers, zucchinis, and green beans exposed to field treatments in greenhouses: evaluation by decline curves. *J. Agric. Food Chem.* **2003**, *51*, 5745−5751.

(20) Hunter, R. E., Jr.; Riederer, A. M.; Ryan, P. B. Method for the determination of organophosphorus and pyrethroid pesticides in food via gas chromatography with electron-capture detection. *J. Agric. Food Chem.* **2010**, *58*, 1396−1402.

(21) Weerasekera, G.; Smith, K. D.; Quiros-Alcala, L.; Fernandez, C.; Bradman, A.; Eskenazi, B.; Needham, L. L.; Barr, D. B. A mass spectrometry-based method to measure dialkylphosphate degradation products of organophosphorous insecticides in dust and orange juice. *J. Environ. Monit.* **2009**, *11*, 1345−1351.

(22) FQPA, Food Quality Protection Act of 1996. Public Law 104-170, 1996.

(23) Bouchard, M. F.; Chevrier, J.; Harley, K. G.; Kogut, K.; Vedar, M.; Calderon, N.; Trujillo, C.; Johnson, C.; Bradman, A.; Barr, D. B.; Eskenazi, B. Prenatal exposure to organophosphate pesticides and IQ in 7-year-old children. *Environ. Health Perspect.* **2011**, *119*, 1189−1195.

(24) Todd, D. G.; Wohlers, D.; Citra, M. In *Toxicological Profile for Pyrethrins and Pyrethroids*; Agency for Toxic Substances and Disease Registry: Atlanta, GA, USA, 2003.

(25) Fox, M. K.; Pac, S.; Devaney, B.; Jankowski, L. Feeding infants and toddlers study: what foods are infants and toddlers eating? *J. Am. Diet. Assoc.* **2004**, *104*, s22−s30.

(26) Olsson, A. O.; Baker, S. E.; Nguyen, J. V.; Romanoff, L. C.; Udunka, S. O.; Walker, R. D.; Flemmen, K. L.; Barr, D. B. A liquid chromatography−tandem mass spectrometry multiresidue method for quantification of specific metabolites of organophosphorus pesticides, synthetic pyrethroids, selected herbicides, and deet in human urine. *Anal. Chem.* **2004**, *76*, 2453−2461.

(27) *Guidance for Industry: Bioanalytical Method Validation*; U.S. Food and Drug Administration: Washington, DC, USA, 2001.

(28) *Approximate pH of Foods and Food Products*; Center for Food Safety and Applied Nutrition, U.S. Food and Drug Administration: Washington, DC, USA, 2007.

(29) Todd, D. G.; Harper, C.; Burgess, P. In *Toxicological Profile for Diazinon*; Agency for Toxic Substances and Disease Registry: Atlanta, GA, USA, 2008.

(30) Barr, D. B.; Wong, L. Y.; Bravo, R.; Weerasekera, G.; Odetokun, M.; Restrepo, P.; Kim, D. G.; Fernandez, C.; Whitehead, R. D., Jr.; Perez, J.; Gallegos, M.; Williams, B. L.; Needham, L. L. Urinary concentrations of dialkylphosphate metabolites of organophosphorus pesticides: National Health and Nutrition Examination Survey 1999−2004. *Int. J. Environ. Res. Public Health* **2011**, *8*, 3063−3098.

(31) Barr, D. B.; Olsson, A. O.; Wong, L. Y.; Udunka, S.; Baker, S. E.; Whitehead, R. D.; Magsumbol, M. S.; Williams, B. L.; Needham, L. L. Urinary concentrations of metabolites of pyrethroid insecticides in the general U.S. population: National Health and Nutrition Examination Survey 1999−2002. *Environ. Health Perspect.* **2010**, *118*, 742−748.

Table 1. GC-NCI-MS and GC-MS/MS Parameters for OCPs and PYs

				GC-NCI-MS				GC-MS/MS			
no.	pesticide	mol wt (M_w)	retention time (min)	quantitation ion (mau)	qualitative ions (mau)			parent ion (mau)	daughter ions (mau)		collision energy (eV)
1	pentachlorobenzene	250.3	6.71	249.9	251.9	247.9	253.8				
2	pentachlorobenzene ($^{13}C_6$)	256.3	6.77	255.9	257.9	254	259.9				
3	α-BHC	290.8	9.076	254.9	256.9	253	71.6				
4	α-BHC ($^{13}C_6$)	296.8	9.076	260.9	259	262.9	187.1				
5	hexachlorobenzene	284.8	9.164	283.9	285.9	249.9	287.8				
6	hexachlorobenzene ($^{13}C_6$)	290.8	9.164	289.9	291.8	293.9	287.9				
7	empenthrin	274.4	9.33	167.3	168.4	169.5	121.4	167.3	165.5	163	35
8	β-BHC	290.8	9.776	254.9	256.9	71.6	70.6				
9	β-BHC ($^{13}C_6$)	296.8	9.776	261	263	259.1	187.1				
10	lindane	290.8	10.055	254.9	256.9	71.6	73.2				
11	lindane ($^{13}C_6$)	296.8	10.055	261	262.9	187.2	259				
12	tefluthrin	418.7	10.79	241.1	243	205.2	244.4	241.1	204.9	204.8	45
13	δ-BHC	290.8	10.92	254.9	256.9	71.6	73.2				
14	δ-BHC ($^{13}C_6$)	296.8	10.92	261	259	263	189.1				
15	vinclozolin	286.1	12.07	241.2	243.1	244.9	246.4	241.1	204.9	240.2	25
16	transfluthrin	371.2	12.35	207.1	209.1	137.3	210.9	207.1	205.5	204	45
17	heptachlor	373.3	12.459	299.8	236.8	265.9	301.9				
18	heptachlor ($^{13}C_{10}$)	383.3	12.459	309.9	307.9	311.9	276				
19	*o′,p*-dicofol	370.5	13.17	214.2	216	250.1	252	214.1	211.6	35.3	25
20	aldrin	364.9	13.998	236.9	329.9	234.9	331.9				
21	aldrin ($^{13}C_{12}$)	376.9	13.998	342	242	239.9	244				
22	dicofol	370.5	14.71	250.1	252	253.8	216.3	250.1	35.5	233.8	25
23	fenson	268.5	14.99	141.2	142.4	143.4	127.4	141.3	77.2	140.2	25
24	oxychlordane	423.8	16.105	236.1	349.9	351.9	423.9				
25	oxychlordane ($^{13}C_{10}$)	433.8	16.105	431.9	361.8	359.9	242				
26	*cis*-heptachlorepoxide	389.3	16.105	316.1	351.7	281.8					
27	*cis*-heptachlorepoxide ($^{13}C_{10}$)	399.3	16.105	399.8	327.9	290	325.9				
28	*trans*-heptachlorepoxide	389.3	16.331	236.9	353.8	281.8	234.9				
29	*trans*-chlordane	409.8	17.353	409.7	265.9	301.8	238.9				
30	*trans*-chlordane ($^{13}C_{10}$)	419.8	17.353	419.8	417.8	385.9	276				
31	allethrin	301.4	16.680, 16.753	167.3	168.5	134.4	169.6	167.3	165.9	164.7	35
32	prallethrin	300.4	17.207, 17.436	167.3	132.4	168.5	133.5	167.3	165.6	163.9	35
33	2,4′-DDE	318	17.565	246.2	318	248	212				
34	2,4′-DDE ($^{13}C_{12}$)	330	17.565	330	328	260	258.1				
35	*cis*-chlordane	409.8	17.841	266	264	236.9	409.8				
36	endosulfan I	406.9	17.959	407.7	241.9	373.7	301.8				
37	endosulfan I ($^{13}C_9$)	415.9	17.969	414.7	250	380.8	242				
38	*trans*-nonachor	444.2	18.092	443.6	299.9	236.9	335.8				
39	*trans*-nonachor($^{13}C_{10}$)	454.2	18.092	453.8	309.9	451.9	455.9				
40	chlorfenson	303.2	18.625	176.5	175.1	177.8	191.3	175.1	111	173.1	15
41	dieldrin	380.9	19.146	345.8	236.9	238.9	379.7				
42	dieldrin ($^{13}C_{12}$)	392.9	19.146	391.7	395.8	358	241.9				
43	4,4′-DDE	318	19.057	319.7	262	315.9	317.9				
44	4,4′-DDE ($^{13}C_{12}$)	330	19.057	329.9	322	326.2					
45	2,4′-DDD	320	19.301	248.1	212.4	246.1	73.5				
46	2,4′-DDD ($^{13}C_{12}$)	332	19.301	260.2	262.1	258	264.2				
47	endosulfan II	406.9	20.398	405.7	241.9	335.8	369.7				
48	endosulfan II ($^{13}C_9$)	415.9	20.408	414.7	344.8	378.8	250				
49	*cis*-nonachor	444.2	20.55	443.6	333.8	299.9	236.9				
50	*cis*-nonachor ($^{13}C_{10}$)	454.2	20.55	453.8	451.8	455.8	343.9				
51	4,4′-DDD	320	20.678	248.1	71.5	250	251.8				
52	4,4′-DDD ($^{13}C_{12}$)	332	20.678	260.1	262.1						
53	2,4′-DDT	354.5	20.733	246.1	212.1	71.5	281.1				
54	2,4′-DDT ($^{13}C_{12}$)	355.6	20.733	295.8	293.9	238.2					
55	endrin	380.9	20.932	272	236.1	306	381.8				
56	endrin ($^{13}C_{12}$)	392.9	20.932	282	284	358	392				
57	endosulfan sulfate	422.9	21.799	385.7	351.7	97.5	185.2				
58	endosulfan sulfate ($^{13}C_9$)	431.9	21.786	394.8	360.7	97.5	250				

dx.doi.org/10.1021/jf5012424 | J. Agric. Food Chem. 2014, 62, 7092−7100

Table 1. continued

				GC-NCI-MS				GC-MS/MS			
no.	pesticide	mol wt (M_w)	retention time (min)	quantitation ion (mau)	qualitative ions (mau)			parent ion (mau)	daughter ions (mau)		collision energy (eV)
59	4,4′-DDT	354.5	22.008	248.1	262.1	71.6	282.8				
60	4,4′-DDT ($^{13}C_{12}$)	355.6	22.008	274	275.8	73.5					
61	tetramethrin	331.4	23.659, 23.993	165.3	331.2	167.3	133.5	331.2	167.2	163.1	5
62	bifenthrin	422.9	23.69	205.2	386.1	241.1	243	386.2	205.4	204.3	45
63	d_5-bifenthrin	427.9	23.65	391.3	241.1	205.2	242.9				
64	fenpropathrin	349.4	24.19	141.4	142.6	221.3	322.2	141.4	139.5	137.9	35
65	phenothrin	350.4	24.701, 24.940	167.3	168.5	169.5	181.3	167.3	165.3	162.9	15
66	λ-cyhalothrin	449.9	25.403, 25.738	205.2	241.1	243	206.4	241.1	240.4	204.6	45
67	acrinathrin	541.4	26.15	333.1	167.2	305.1	334.5	333.1	166.8	164.7	25
68	cyphenothrin	375.5	26.511, 26.686, 26.744	167.3	168.5	348.2	169.5	167.3	165.8	168.6	35
69	permethrin	391.3	27.226, 27.472	207.2	209.1	171.2	354.1	207.1	205.9	203.7	25
70	d_6-*cis*-permethrin	397.3	27.4	213.2	215	217	179.2				
71	cyfluthrin	434.3	28.258, 28.462, 28.557, 28.647	207.2	209.1	171.2	173.1	207.1	206	204	25
72	cypermethrin	416.3	28.868, 29.082, 29.186, 29.257	207.2	209.1	171.3	173.2	207.1	205.8	201.6	25
73	d_6-*cis*-cypermethrin	422.6	29.021, 29.210	213.1	215.1	177.2	179.2				
74	flucythrinate	451.4	29.186, 29.593	243.2	244.3	199.3	245.3	243.2	198.8	196.7	25
75	τ-fluvalinate	502.9	30.782, 30.930	294.1	295.9	258.2	502	294.1	293	144.9	25
76	fenvalerate	419.9	30.533, 30.930	211.2	213	167.4	214.3	211.2	166.8	164.8	5
77	deltamethrin	505.2	32.06	81.5	79.5	137.4	296.9	296.9	79.2	81.4	5

In this study, a rapid, efficient, and sensitive method for the simultaneous determination of 31 OCPs and 19 PYs in Chinese teas by GC-NCI-MS and GC-MS/MS were developed. The established methods were validated according to the criteria by EU Commission Decision 2002/657/EC,[20] and a survey of 101 tea samples was conducted by the established method.

MATERIALS AND METHODS

Materials and Reagents. The Florisil cartridges (2 mg, 12 mL) were purchased from Agilent (Santa Clara, CA, USA); primary−secondary amine (PSA) powder with the size of 40−60 μm was also obtained from Agilent.

Acetone, hexane, and ethyl acetate (P.R. grade) were purchased from J. T. Baker (Deventer, The Netherlands); anhydrous sodium sulfate (P.R. grade) purchased from Sigma Co. (Beijing, China) was heated at 250 °C for 4 h and kept in a desiccator; sodium chloride (analytical reagent grade) was purchased from Beijing Chemical Industry (Beijing, China); deionized water was obtained from a Milli-Q water purification system (Millipore, Bedford, MA, USA).

Analytical Standards. Analytical reference standards of PYs and OCPs (listed in Table 1), d_6-*trans*-cypermethrin, d_6-*trans*-permethrin, d_5-bifenthrin, and 24 ^{13}C-labeled OCPs were all purchased from Dr. Ehrenstorfer GmbH (Augsburg, Germany), with purity of not less than 96.0%.

Standard Solution. The stock solution for all of the standards and the internal standards (IS) were prepared by accurately weighing a certain amount of the standard powder and then quantitatively dissolving by ethyl acetate at the concentration of 1000 mg/L, respectively. The mixed intermediate standard and internal standard solution were quantitatively diluted from the stock standard solutions with hexane, and the final concentrations of all the individual standards and the internal standards were 2 and 1 mg/L, respectively. All of the standard solutions were stored at −20 °C in amber glass bottles.

Tea Samples and Pretreatment. All 101 tea samples were purchased from local supermarkets (Beijing, China) in 2013, including green tea (n = 44), scented tea (n = 23), dark tea (n = 8), black tea (n = 13), and oolong tea (n = 13). The tea samples were ground by a homogenizer and filtered through a 40 mesh sieve. The grinding program was conducted as follows: ground for 3 s and halted for 5 s; 5−10 cycles were enough for each sample.

A negative green tea sample was selected as the blank for the recovery studies.

Sample Extraction. 2.0 g of ground tea powder was weighed by a balance with the precision of 1 mg; 40 μL of the mixed IS solution (1 mg/L) was spiked, and then the mixture was soaked by 10 mL of hot water (90−100 °C) for 30 min. 20 mL of acetone was added, and the mixture was vortexed for 1 min and then ultrasonicated for 30 min, and then centrifugation was performed at 7000 rpm for 5 min at 4 °C. The extracted solution was transferred and partitioned by 20 mL of hexane with the addition of 1.0 g of NaCl. Two partitions were performed, and the organic solutions were combined and evaporated to near dryness at 30 °C by rotary evaporation. The residues were redissolved with 3 mL of hexane.

Sample Cleanup. The Florisil cartridge (2 mg, 12 mL) with a layer (ca. 1 cm) of PSA on the sieve plate was prepared and preconditioned with 5.0 mL of acetone/hexane (1:9, v/v) and 5.0 mL of hexane. The extract was applied to the conditioned cartridge and eluted with 10 mL of acetone/hexane (1:9, v/v). The loading and eluting fluid were both collected and evaporated to dryness by a gentle nitrogen stream in a water bath at 30 °C. The residue was redissolved with 200 μL of hexane and filtered through a 0.22 μm PTFE filter for GC-NCI-MS analysis.

GC-NCI-MS Analysis. The analysis of the target analytes was performed on a DB-5 ms column (30 m × 0.25 mm i.d. × 0.25 μm) by Bruker 450 GC and 320 MS (triple-quadrupole mass spectrometry, MS workstation version 7.0 software) with the 8400 autosampler (Bruker, USA), operated under NCI for screening. Helium with a purity of not less than 99.999% was used as carrier gas at a constant flow of 1 mL/min. Methane gas was used as the reaction gas for NCI analysis, and the filament current was set to the default value. The GC oven temperature program was as follows: 80 °C kept for 1 min, raised to 200 °C at a rate of 20 °C/min, then raised to 240 °C at a rate of 15 °C/min, then raised to 286 °C at a rate of 5 °C/min, held for 5 min, and finally raised to 300 °C at a rate of 20 °C/min and held for 5 min. The temperature of the injection port and transform line were 250 °C. The splitless injection volume was 1 μL with a solvent delay time of 5 min.

The ion source temperature of 230 °C, MS quadrupole temperature of 40 °C, electron multiplier voltage of 1400 V, and ion source energy of 70 eV were used. Analysis was performed in the selected ion monitoring

Table 2. Linearity Curves, Limits of Detection (LODs), and Limits of Quantitation (LOQs) of 50 Standard Pesticides in Blank Tea Matrix

					GC-MS		GC-MS/MS
no.	pesticide	IS	RRF	r	LOD (μg/kg)	LOQ (μg/kg)	LOD (μg/kg)
1	pentachlorobenzene	pentachlorobenzene ($^{13}C_6$)		0.9975	0.03	0.1	
2	α-BHC	α-BHC ($^{13}C_6$)	0.92	0.9999	0.5	1.7	
3	hexachlorobenzene	hexachlorobenzene ($^{13}C_6$)	1	0.9982	0.03	0.1	
4	empenthrin	d_5-bifenthrin		0.9971	0.03	0.1	0.3
5	β-BHC	β-BHC ($^{13}C_6$)	0.85	0.9959	0.3	0.9	
6	lindane	lindane ($^{13}C_6$)	0.93	0.9975	0.1	0.4	
7	tefluthrin	d_5-bifenthrin		0.9985	0.03	0.08	0.2
8	δ-BHC	δ-BHC ($^{13}C_6$)	0.94	0.9969	1.1	3.6	
9	vinclozolin	endosulfan I ($^{13}C_9$)		0.9982	0.04	0.1	0.3
10	transfluthrin	d_5-bifenthrin		0.9986	0.03	0.09	0.3
11	heptachlor	heptachlor ($^{13}C_{10}$)	1	0.9970	3	10	
12	o',p-dicofol	endosulfan I ($^{13}C_9$)		0.9987	0.07	0.3	0.4
13	aldrin	aldrin ($^{13}C_{12}$)	0.95	0.9978	1.2	4.2	
14	dicofol	endosulfan I ($^{13}C_9$)		0.9968	0.07	0.3	0.4
15	fenson	endosulfan I ($^{13}C_9$)		0.9983	0.01	0.02	0.1
16	Oxychlordane	Oxychlordane($^{13}C_{10}$)	0.95	0.9959	0.2	0.6	
17	*cis*-heptachlorepoxide	*cis*-heptachlorepoxide ($^{13}C_{10}$)	1	0.9997	0.2	0.6	
18	*trans*-heptachlorepoxide	*cis*-heptachlorepoxide ($^{13}C_{10}$)	1.4	0.9969	0.4	1.4	
19	*trans*-chlordane	*trans*-chlordane ($^{13}C_{10}$)	0.99	0.9993	0.5	1.8	
20	allethrin	d_5-bifenthrin		0.9981	0.01	0.02	4.0
21	prallethrin	d_5-bifenthrin		0.9977	0.4	1.4	2.1
22	2,4′-DDE	2,4′-DDE ($^{13}C_{12}$)	0.97	0.9983	1.7	5.6	
23	*cis*-chlordane	endosulfan I ($^{13}C_9$)	0.89	0.9985	0.2	0.7	
24	endosulfan I	endosulfan I ($^{13}C_9$)		0.9977	0.2	0.7	
25	*trans*-nonachor	*trans*-nonachor ($^{13}C_{10}$)	1.12	0.9993	2.1	7.1	
26	chlorfenson	endosulfan I ($^{13}C_9$)		0.9959	0.05	0.2	0.4
27	dieldrin	dieldrin ($^{13}C_{12}$)	1.18	0.9992	1.8	5.9	
28	4,4′-DDE	4,4′-DDE ($^{13}C_{12}$)	1.03	0.9989	4.5	15	
29	2,4′-DDD	2,4′-DDD ($^{13}C_{12}$)	1.04	0.9993	3	10	
30	endosulfan II	endosulfan II ($^{13}C_9$)		0.9998	0.1	0.3	
31	*cis*-nonachor	*cis*-nonachor ($^{13}C_{10}$)	0.94	0.9998	0.3	0.9	
32	4,4′-DDD	4,4′-DDD ($^{13}C_{12}$)	1	0.9961	4.1	13.6	
33	2,4′-DDT	2,4′-DDT ($^{13}C_{12}$)	1.19	0.9926	4.1	13.6	
34	endrin	endrin ($^{13}C_{12}$)	0.92	0.9982	3.2	10.7	
35	endosulfan sulfate	endosulfan sulfate ($^{13}C_9$)		0.9981	0.03	0.08	
36	4,4′-DDT	4,4′-DDT ($^{13}C_{12}$)	1.1	0.9663	0.6	2	
37	tetramethrin (I, II)	d_5-bifenthrin		0.9973	0.3	0.9	2.1
38	bifenthrin	d_5-bifenthrin		0.9974	0.1	0.3	0.7
39	fenpropathrin	d_5-bifenthrin		0.9979	0.06	0.2	0.4
40	phenothrin (I, II)	d_5-bifenthrin		0.9969	0.7	2.3	4.0
41	λ-cyhalothrin (I, II)	d_5-bifenthrin		0.9967	0.02	0.06	0.2
42	acrinathrin	d_5-bifenthrin		0.9981	0.05	0.2	0.5
43	cyphenothrin (I, II, III)	d_6-*cis*-permethrin		0.9996	0.1	0.4	0.6
44	permethrin (I, II)	d_6-*cis*-permethrin		0.9968	0.7	2.4	5.0
45	cyfluthrin (I, II, III, IV)	d_6-*cis*-cypermethrin		0.9981	0.08	0.3	0.6
46	cypermethrin (I, II, III, IV)	d_6-*cis*-cypermethrin		0.9974	0.06	0.2	0.5
47	flucythrinate (I, II)	d_6-*cis*-cypermethrin		0.9946	0.03	0.1	0.3
48	τ-fluvalinate (I, II)	d_6-*cis*-cypermethrin		0.9993	0.04	0.1	0.3
49	fenvalerate (I, II)	d_6-*cis*-cypermethrin		0.9991	0.02	0.08	0.3
50	deltamethrin	d_6-*cis*-cypermethrin		0.9954	0.02	0.05	0.2

mode (SIM). Pesticides were identified according to retention times, the quantitative ions and three qualitative ions (Table 1), and the chromatogram is shown in the Supporting Information. Four ions were selected following the EU regulation (EEC657/2002). Pesticides were monitored in different time segments, and the dwell time for each ion was fixed by the instrument.

Calibration and Quantification. Three deuterium PYs and 24 ^{13}C-labled OCPs were used as IS as shown in Table 1. For the quantification of the OCPs, quantitative values were calculated using isotope dilution technique through a relative response factor (RRF) calculation.

GC-NCI-MS/MS Identification. GC-MS/MS identification was also conducted on a 450GC-320MS under NCI mode. The other parameters were the same as for the GC-NCI-MS method except for the ion source energy. With the ion source energy of 20 eV, ions with larger mass were more easily acquired, which is helpful for MS/MS detection. The mass

dx.doi.org/10.1021/jf5012424 | J. Agric. Food Chem. 2014, 62, 7092−7100

Table 3. Experimental Results of Accuracy and Precision in Blank Tea Matrix (n = 6)

		average recoveries (%)								
		low spiked level, 0.010 mg/kg			middle spiked level, 0.020 mg/kg			high spiked level, 0.100 mg/kg		
no.	pesticide	recovery	RSD[a]	RSD[b]	recovery	RSD[a]	RSD[b]	recovery	RSD[a]	RSD[b]
1	pentachlorobenzene	94.9	2.4	7.5	103.7	12.1	8.8	90.8	0.9	5.9
2	α-BHC	121.7	3.2	10.7	111.8	22.3	14.2	104.0	3.5	3.3
3	hexachlorobenzene	120.6	1.5	1.5	114.9	8.8	14.8	109.7	5.5	8.3
4	empenthrin	85.2	1.3	1.3	91.6	1.2	16.9	71.4	3.0	3.0
5	β-BHC	98.0	2.0	4.0	107.0	10.0	12.0	79.0	3.1	10.0
6	lindane	99.4	2.7	26.1	110.1	10.7	23.2	84.7	2.0	16.7
7	tefluthrin	87.1	1.3	1.3	92.3	1.7	15.3	95.2	1.3	3.0
8	δ-BHC	115.8	2.9	17.6	113.0	13.7	19.3	105.1	7.9	27.3
9	vinclozolin	88.1	2.7	14.0	101.4	17.2	9.0	95.0	5.8	20.8
10	transfluthrin	92.6	2.2	2.2	89.9	2.0	13.8	101.0	2.2	12.1
11	heptachlor	94.4	4.9	17.3	114.1	10.8	23.5	87.2	2.1	15.6
12	o',p-dicofol	94.9	2.4	14.0	101.4	17.2	9.0	95.0	5.8	20.8
13	aldrin	66.7	3.5	24.3	78.1	10.0	9.6	67.2	4.1	6.3
14	dicofol	85.9	3.7	5.5	102.2	10.4	14.3	80.6	10.3	18.9
15	fenson	98.1	4.1	4.1	77.0	20.3	11.4	76.0	1.6	9.2
16	oxychlordane	77.4	1.8	10.4	97.5	10.5	7.1	87.7	1.8	10.6
17	*cis*-heptachlorepoxide	76.6	3.7	7.5	99.9	15.9	12.6	91.5	2.1	7.8
18	*trans*-heptachlorepoxide	77.7	0.7	7.8	82.3	3.5	10.0	72.3	3.4	2.6
19	*trans*-chlordane	98.7	3.6	9.5	103.3	19.9	14.3	97.0	4.2	6.8
20	allethrin	105.3	1.6	3.6	93.6	1.9	9.7	116.6	0.7	9.3
21	prallethrin	100.1	1.5	19.2	93.5	2.6	8.5	114.5	0.7	20.0
22	2,4′-DDE	91.2	4.2	2.7	79.5	5.9	9.3	93.5	4.9	12.8
23	*cis*-chlordane	68.1	1.7	15.2	95.3	14.5	8.9	96.2	2.9	8.4
24	endosulfan I	80.0	2.5	13.2	98.8	21.9	12.4	101.4	4.2	8.6
25	*trans*-nonachor	89.1	2.9	19.7	90.6	14.9	13.4	88.9	2.6	7.6
26	chlorfenson	92.8	4.0	18.1	91.7	18.7	18.4	71.3	1.4	2.3
27	dieldrin	63.6	1.0	5.6	87.9	12.4	10.1	84.6	2.4	6.5
28	4,4′-DDE	90.2	11.1	22.9	80.3	10.9	10.1	103.1	7.7	5.7
29	2,4′-DDD	95.2	3.2	12.0	97.9	8.9	9.6	104.4	2.1	4.2
30	endosulfan II	88.1	0.5	6.8	95.3	13.8	7.8	95.2	2.3	6.6
31	*cis*-nonachor	68.3	2.1	3.1	76.8	11.6	9.7	74.9	1.7	2.5
32	4,4′-DDD	87.5	1.3	1.2	83.5	0.0	12.2	94.3	9.2	7.4
33	2,4′-DDT	62.5	3.1	10.4	60.1	2.6	3.6	68.7	2.1	2.1
34	endrin	78.2	8.2	8.2	97.4	7.9	21.6	80.4	0.6	9.3
35	endosulfan sulfate	88.1	2.2	4.9	86.7	10.0	8.3	90.6	1.5	2.9
36	4,4′-DDT	87.3	3.1	4.4	81.4	2.1	3.0	86.7	2.6	4.9
37	tetramethrin (I, II)	85.4	4.2	6.2	81.8	4.2	5.5	102.1	5.9	7.2
38	bifenthrin	107.3	1.5	8.9	100.3	2.1	1.3	96.8	0.8	1.3
39	fenpropathrin	113.7	7.8	15.1	96.1	2.4	14.5	103.1	8.8	1.3
40	phenothrin (I, II)	115.4	2.9	12.0	77.4	1.7	13.8	114.5	0.7	16.2
41	λ-cyhalothrin (I, II)	82.9	2.8	6.3	102.0	4.2	18.8	106.9	3.9	3.9
42	acrinathrin	93.2	7.4	13.1	78.6	11.7	17.1	85.3	1.8	11.0
43	cyphenothrin (I, II, III)	111.0	4.8	4.9	87.9	0.9	14.8	119.9	2.7	9.5
44	permethrin (I, II)	86.9	2.8	3.1	79.7	4.0	7.9	76.4	14.6	9.1
45	cyfluthrin (I, II, III, IV)	76.0	1.9	3.1	78.0	4.2	9.7	86.2	5.7	3.9
46	cypermethrin (I, II, III, IV)	92.4	10.4	18.5	80.7	10.5	9.1	96.4	6.1	7.9
47	flucythrinate (I, II)	70.4	3.3	20.6	95.5	8.9	13.6	90.9	17.6	10.6
48	τ-fluvalinate (I, II)	71.4	0.9	2.9	77.1	7.0	7.5	71.5	4.8	7.7
49	fenvalerate (I, II)	105.5	3.7	18.7	83.6	6.7	6.8	101.8	5.3	14.7
50	deltamethrin	103.0	3.6	15.9	92.1	8.0	17.6	87.1	6.7	5.8

[a]Interday recovery RSDs. [b]Intraday recovery RSDs.

parameters are provided in Table 1. The positive samples of pyrethroids were verified by the established GC-NCI-MS/MS method for the limited isotope-labeled IS. For OCPs, one-to-one IS were used leading to more reliable quantitation and qualitative analysis by GC-NCI-MS. Identification of the target compounds in the tea matrix was based on criteria set by Commission Decision 2002/657/EC.[20]

Quality Control. A positive sample containing bifenthrin and cypermethrin and a positive sample with 4,4′-DDE and dicfol were chosen as quality control samples. The quality control samples were both tested and quantified in every batch. A procedural blank, a matrix blank, and QC samples must be run in each batch to check for contamination, peak identification, and accurate quantification.

Table 4. Results for OCPs and PYs in Chinese Tea Samples

		MRL (mg/kg)		total				green tea				scented tea			
no.	compound	EU	China	concn	median	DR%	ER%	concn	median	DR%	ER%	conn	median	DR%	ER%
1	HCHs	0.02	0.20	ND−0.377	0.02	24.8	1.0	ND−0.002	0.00	39.5	0.0	ND−0.377	0.02	8.3	4.2
2	heptachlor			ND−0.100	0.05	15.8	0.0	ND−0.322	0.01	16.3	0.0	ND−0.099	0.01	8.3	0.0
3	dicfol	20		ND−2.624	1.10	46.5	0.0	ND−1.872	0.21	39.5	0.0	ND−2.381	0.15	62.5	0.0
4	endosulfan	30	10	ND−1.802	0.45	63.4	0.0	ND−0.888	0.16	52.1	0.0	ND−1.073	0.14	79.2	0.0
5	DDTs	0.02	0.20	ND−0.411	0.10	56.4	4.0	ND−0.159	0.04	46.5	0.0	ND−0.411	0.10	37.5	8.3
6	bifenthrin	5	30	ND−3.848	1.00	63.4	0.0	ND−3.848	0.19	50.0	0.0	ND−2.671	0.18	54.2	0.0
7	fenpropathrin	0.02	2	ND−0.070	0.00	7.9	0.0	ND−0.070	0.00	11.4	0.0	ND−0.021	0.00	4.2	0.0
8	phenothrin	0.1		ND−0.139	0.01	17.8	1.0	ND−0.006	0.01	9.1	0.0	ND−0.139	0.01	37.5	4.2
9	λ-cyhalothrin	15	3	ND−3.244	0.11	55.4	1.0	ND−0.492	0.08	34.1	0.0	ND−3.244	0.06	70.8	4.2
10	cyfluthrin			ND−0.055	0.00	6.9	0.0	ND−0.025	0.00	2.3	0.0	ND−0.055	0.00	12.5	0.0
11	cypermethrin	0.5	20	ND−0.499	0.14	46.5	0.0	ND−0.496	0.04	20.5	0.0	ND−0.499	0.03	58.3	0.0
12	τ-fluvalinate			ND−0.887	0.00	8.9	0.0	ND−0.040	0.00	0.0	0.0	ND−0.887	0.00	8.3	0.0
13	fenvalerate	0.05	2	ND−0.217	0.00	24.8	3.0	ND	0.00	27.3	2.3	ND−0.217	0.00	33.3	8.3
14	deltamethrin	5	5	ND−0.045	0.00	6.9	0.0	ND−0.045	0.00	0.0	0.0	ND−0.010	0.00	12.5	0.0

Table 5. Results for Multiple Pesticides in Different Tea Samples

		MRL (mg/kg)		dark tea				oolong tea				black tea			
no.	compound	EU	China	concn	median	DR%	ER%	concn	median	DR%	ER%	concn	median	DR%	ER%
1	HCHs[a]	0.02	0.20	ND−0.002	0.00	50.0	0.0	ND−0.037	0.00	7.7	0.0	ND−0.010	0.00	7.7	0.0
2	heptachlor			ND	0.00	0.0	0.0	ND−0.294	0.05	46.2	0.0	ND−0.054	0.00	7.1	0.0
3	dicfol	20		ND−0.035	0.02	50.0	0.0	ND−2.624	1.10	69.2	0.0	ND−0.113	0.01	15.4	0.0
4	endosulfan	30	10	ND−0.017	0.01	12.5	0.0	ND−1.802	0.45	84.6	0.0	ND−0.279	0.09	61.5	0.0
5	DDTs	0.02	0.20	ND−0.072	0.05	100.0	0.0	ND−0.202	0.09	100.0	7.7	ND−0.023	0.02	53.8	0.0
6	bifenthrin	5	30	ND−0.154	0.09	75.0	0.0	ND−3.848	1.00	100.0	0.0	ND−0.828	0.05	71.4	0.0
7	fenpropathrin	0.02	2	ND−0.007	0.00	0.0	0.0	ND−0.070	0.00	15.4	0.0	ND−0.004	0.00	0.0	0.0
8	phenothrin	0.1		ND	0.00	0.0	0.0	ND−0.006	0.00	30.8	0.0	ND−0.006	0.00	7.1	0.0
9	λ-cyhalothrin[b]	15	3	ND−0.068	0.02	37.5	0.0	ND−0.492	0.11	100.0	0.0	ND−0.200	0.05	57.1	0.0
10	cyfluthrin			ND−0.003	0.00	0.0	0.0	ND−0.025	0.00	7.7	0.0	ND−0.006	0.00	14.3	0.0
11	cypermethrin	0.5	20	ND−0.037	0.02	50.0	0.0	ND−0.496	0.14	84.6	0.0	ND−0.089	0.04	64.3	0.0
12	τ-fluvalinate			ND−0.020	0.00	37.5	0.0	ND−0.040	0.00	30.8	0.0	ND	0.00	0.0	0.0
13	fenvalerate	0.05	2	ND	0.00	0.0	0.0	ND	0.00	0.0	0.0	ND−0.038	0.00	35.7	0.0
14	deltamethrin	5	5	ND	0.00	0.0	0.0	ND−0.045	0.00	30.8	0.0	ND	0.00	0.0	0.0

[a]The BHCs (including α-BHC, β-BHC, γ-BHC (lindane), δ-BHC), heptachlors (heptachlor, *cis*-heptachlorepoxide, *trans*-heptachlorepoxide), chlordanes (oxychlordane, *trans*-chlordane, *cis*-chlordane), DDTs (2,4′-DDE, 4,4′-DDE, 2,4′-DDD, 4,4′-DDD, 2,4′-DDT, 4,4′-DDT), and endosulfans (α-endosulfan, β-endosulfan, endosulfan sulfate), were calculated individually and then added for the total amounts. [b]The concentrations of the two or more than two enantiomers of allethrin, prallethrin, tetramethrin, phenothrin, λ-cyhalothrin, cyphenothrin, permetrin, cyfulthrin, cypermethrin, flucythrinate, τ-fluvalinate, and fenvalerate were calculated together.

dx.doi.org/10.1021/jf5012424 | J. Agric. Food Chem. 2014, 62, 7092−7100

Table 6. Occurrence of OCPs and PYs in Chinese Tea Samples

		DR%					MRL		VR%			
compound	concn (mg/kg)	green tea	scented tea	dark tea	oolong tea	black tea	GB2763	EU	GB	EU	year	ref
HCHs	ND−0.377	39.5	8.3	50.0	7.7	7.7	0.02	0.20	24.8	1.0	2013	this research
	ND−0.385								2.9		2012	26
DDTs	ND−0.411	46.5	37.5	100.0	100.0	53.8	0.02	0.20		4.0	2013	this research
	ND−0.011										2007	1
	ND−0.044										2012	25
	ND−0.189								0	0	2012	26
endosulfan	ND−1.802	52.1	79.2	12.5	84.6	61.5	30	10	0	0	2013	this research
	ND−0.115									0	2012	25
dicfol	ND−2.624	39.5	62.5	50.0	69.2	15.4		20		0	2013	this research
	ND−0.992										2007	1
bifenthrin	ND−3.848	50.0	54.2	75.0	100.0	71.4	30	5	0	0	2013	this research
	ND−0.203										2007	1
	0.020−7.020										2006−2008	24
cyhalothrin	ND−3.244	34.1	70.8	37.5	100.0	57.1	3	15	1.0	0	2013	this research
	0.010−0.490										2006−2008	24
cypermethrin	ND−0.499	20.5	58.3	50.0	84.6	64.3	20	0.5	0	1.0	2013	this research
	0.020−1.370										2006−2008	24
	0.010−0.050										2007	23
	ND−0.106											25
fenvalerate	ND−0.217	27.3	33.3	0.0	0.0	35.7	2	0.05	0	3.0	2013	this research
	ND−0.317										2007	1
	0.010−2.320										2006−2008	24
	0.050−0.250		52.3		73.4					3.0	2007	23

RESULTS AND DISCUSSION

Sample Preparation. In this research, tea samples were soaked in hot water for 30 min and then extracted with acetone and hexane, which can effectively extract the target compounds and remove water-soluble impurities such as caffeine and tea polyphenols.[18] Considering the nonpolar or semipolar properties of OCPs and PYs, cartridges of Florisil, Carb-NH_2, diatomite, and neutral aluminum oxide were used to check the cleanup effect for tea extracts. The results showed that most of the pesticides could not be eluted from the neutral aluminum oxide cartridge, and the recoveries of some pesticides were not satisfied with the diatomite column. The Florisil and Carb-NH_2 cartridges were much more preferred. Considering the low cleanup ability to the lutein in tea matrix and the lower recoveries for *o,p′*-DDT (62.1%) and acrinathrin (65.8%) with Carb-NH_2 cartridge, the Florisil cartridge was selected. To sufficiently remove the pigments and other impurities such as fatty acids, organic acids, sugars,[11,21,22] and extra water from the matrix, the mixture of 150 mg of PSA powder and 500 mg of anhydrous sodium sulfate was placed on the sieve plate of the Florisil cartridge for better cleanup.

GC-NCI-MS and GC-NCI-MS/MS Detection. Although GC-MS provides qualitative and quantitative information on pesticide residues in foods, there were still some potential difficulties for the accurate qualitation because of the complicated matrix effect. For more accurate qualitation and higher sensitivity, a GC-MS/MS method under NCI mode for PYs analysis in tea samples was established for the first time. All of the positive samples were verified by the GC-MS/MS method.

Method Validation. Validation parameters for quantification of 31 OCPs and 19 PYs were obtained under the optimal conditions. Good linearity regression for all of the pesticides were in the range of 0.05−1.00 mg/L with correlation coefficients (r) of not less than 0.995 as shown in Table 2.

The LOD and LOQ are determined, following IUPAC recommendation, as the minimum detectable amount of analytes from blank sample spiked extract with signal-to-noise ratios (S/N) of 3:1 and 10:1, respectively. The LODs and LOQs were 0.02−4.5 and 0.1−15 μg/kg for GC-NCI-MS determination, respectively (Table 2). The LODs for GC-MS/MS determination ranged from 0.1 to 5.0 μg/kg.

The accuracy and precision of the method were examined by the interday and intraday reproducibility of the spiked blank tea samples at levels of 10, 20, and 100 μg/kg. The recoveries, as shown in Table 3, ranged from 61.4 to 119.9% with relative standard deviations (RSDs) of 0.5−17.7% for interday recovery and 1.2−18.8% for intraday recovery.

To evaluate the matrix effect, six-point (0.05, 0.1, 0.2, 0.4, 0.8, and 1.0 μg/mL with IS 0.2 μg/mL for each) neat solution calibration curves and matrix-matched calibration curves were constructed. The responses of most pesticides were slightly enhanced compared with that in the solvent; however, with the internal standards calibration, the matrix enhancement did not have much influence on the quantitation results.

Therefore, considering easy performance, the calibration curve by solvent was preferred.

Quality Control Results. The results of the quality control samples were relatively stable with the RSD of less than 3% for 12 batch analysis, indicating the reliable analysis results of all tea samples.

Contamination Levels of PYs in Chinese Tea. As shown in Tables 4 and 5, the most frequently detected PY in Chinese tea was bifenthrin, with the detection rate (DR) of 63.4% at concentrations of ND−3.848 mg/kg, followed by λ-cyhalothrin (55.4%, ND−3.244 mg/kg), cypermethrin (46.5%, ND−0.499 mg/kg), and fenvalerate (24.8%, ND−0.217 mg/kg). It was reported (Table 6) that the residues of bifenthrin, cyhalothrin, cypermethrin, and fenvalerate in Chinese tea during the years of 2006−2008 were 0.020−7.020 mg/kg (543 samples), 0.010−0.490 mg/kg (423 samples), 0.020−1.370 mg/kg (2321 samples), and 0.010−2.320 mg/kg (7095 samples), respectively.[23,24] It was obvious that PYs were still the major pesticides commonly used in tea plantations in China.

Interestingly, residues of PYs in teas differed with tea type. For example, fenvalerate, a pesticide restricted on tea plantation in China from 1999, was detected only in green tea samples and scented tea samples with a violation rate (VR) of 3.0%. A study in 2007[23] reported that the concentration of fenvalerate in Chinese tea samples was in the range of 0.050−0.250 mg/kg, with VR of 73.4% in oolong tea and 52.3% in scented tea. It could be inferred that the usage of fenvalerate on tea plantation was decreased after strict management by the government. In addition, there were two scented tea samples containing phenothrin and λ-cyhalothrin with the VR of 1.0%.

Contamination Levels of OCPs in Chinese Tea. Although the use of most OCPs has been banned or restricted in China, some OCPs were still detected in Chinese tea, such as endosulfan with a DR of 63.4% and the concentration range of ND−1.802 mg/kg, DDTs (56.4%, ND−0.411 mg/kg), HCHs (24.8%, ND−0.377 mg/kg), and heptachlor (15.8%, ND−0.102 mg/kg). Only three scented tea samples with concentrations of 0.411, 0.390, and 0.260 mg/kg, respectively, exceeded the MRL for DDTs (0.20 mg/kg). The major DDT residues in Chinese tea were 2,4′-DDD and 2,4′-DDE. As OCPs have been banned for decades in China, it was presumed that the DDTs were mainly from the soil or water through the ecological cycle. Moreover, DDTs were used as intermediates in the production of the pesticides dicofol and may occur as a major impurity in the final products.

In all, most of the OCPs and PYs were in compliance with the MRLs established in China and Europe, and thus Chinese tea was safe enough for human consumption and exportation in terms of OCP and PY residues.

■ ASSOCIATED CONTENT

Supporting Information

Figure 1. This material is available free of charge via the Internet at http://pubs.acs.org.

■ AUTHOR INFORMATION

Corresponding Authors

*(H.M.) Phone: +86-010-67770158. E-mail: miaoh@cfsa.net.cn.
*(Y.-N.W.) Phone: +86-010-67779118. E-mail: wuyongning@cfsa.net.cn

Funding

The research presented and the preparation of the manuscript were supported financially by the National Nature Science Foundation of China (No. 30700664) and the National Science and Technology Support Program of China (No. 2011BAK10B06).

Notes

The authors declare no competing financial interest.

■ ABBREVIATIONS USED

SPE, solid phase extraction; GC-MS, gas chromatography−mass spectrometry; OCPs, organochlorine pesticides; GC-MS/MS, gas chromatography−tandem mass spectrometry; NCI, negative chemical ionization; MRLs, maximum residue levels; IS, internal standard; LODs, limits of detection; LOQs, limits of quantification; RSDs, relative standard deviations; SIM, selective ion monitoring; EI, electron impact; HCHs, hexachlorocyclohexanes; DDTs, dichlorodiphenyltrichloroethanes

■ REFERENCES

(1) Ji, J.; Deng, C.; Zhang, H.; Wu, Y.; Zhang, X. Microwave-assisted steam distillation for the determination of organochlorine pesticides and pyrethroids in Chinese teas. *Talanta* **2007**, *71* (3), 1068−1074.

(2) Tanabe, S.; Iwata, H.; Tatsukawa, R. Global contamination by persistent organochlorines and their ecotoxicological impact on marine mammals. *Sci. Total Environ.* **1994**, *154* (2), 163−177.

(3) Wania, F.; Mackay, D. Peer reviewed: tracking the distribution of persistent organic pollutants. *Environ. Sci. Technol.* **1996**, *30* (9), 390−396.

(4) Zhou, Q.; Xiao, J.; Wang, W.; Liu, G.; Shi, Q.; Wang, J. Determination of atrazine and simazine in environmental water samples using multiwalled carbon nanotubes as the adsorbents for preconcentration prior to high performance liquid chromatography with diode array detector. *Talanta* **2006**, *68* (4), 1309−1315.

(5) Porazzi, E.; Pardo Martinez, M.; Fanelli, R.; Benfenati, E. GC-MS analysis of dichlobenil and its metabolites in groundwater. *Talanta* **2005**, *68* (1), 146−154.

(6) United Nations Environment Programme (UNEP). Stockholm Convention on Persistent Organic Pollutans; available online at http://www.pops.int/documents/convtext/convtext_en.pdf (verified on Nov 16, 2001).

(7) Rissato, S. R.; Galhiane, M. S.; Ximenes, V. F.; de Andrade, R.; Talamoni, J. L. B.; Libânio, M.; De Almeida, M. V.; Apon, B. M.; Cavalari, A. A. Organochlorine pesticides and polychlorinated biphenyls in soil and water samples in the northeastern part of São Paulo State, Brazil. *Chemosphere* **2006**, *65* (11), 1949−1958.

(8) Yang, C. S.; Chung, J. Y.; Yang, G.; Chhabra, S. K.; Lee, M. J. Tea and tea polyphenols in cancer prevention. *J. Nutr.* **2000**, *130* (2), 472S−478S.

(9) Jian, L.; Xie, L. P.; Lee, A. H.; Binns, C. W. Protective effect of green tea against prostate cancer: a case-control study in southeast China. *Int. J. Cancer* **2003**, *108* (1), 130−135.

(10) Hu, B.; Song, W.; Xie, L.; Shao, T. Determination of 33 pesticides in tea using accelerated solvent extraction/gel permeation chromatography and solid phase extraction/gas chromatography-mass spectrometry. *Chin. J. Chromatogr.* **2008**, *26* (1), 22−28.

(11) Chen, G.; Cao, P.; Liu, R. A multi-residue method for fast determination of pesticides in tea by ultra performance liquid chromatography−electrospray tandem mass spectrometry combined with modified QuEChERS sample preparation procedure. *Food Chem.* **2011**, *125* (4), 1406−1411.

(12) Jansson, C.; Pihlström, T.; Österdahl, B. G.; Markides, K. E. A new multi-residue method for analysis of pesticide residues in fruit and vegetables using liquid chromatography with tandem mass spectrometric detection. *J. Chromatogr., A* **2004**, *1023* (1), 93−104.

(13) Štajnbaher, D.; Zupančič-Kralj, L. Multiresidue method for determination of 90 pesticides in fresh fruits and vegetables using

solid-phase extraction and gas chromatography-mass spectrometry. *J. Chromatogr., A* **2003**, *1015* (1), 185−198.
(14) Zambonin, C. G.; Quinto, M.; De Vietro, N.; Palmisano, F. Solid-phase microextraction−gas chromatography mass spectrometry: a fast and simple screening method for the assessment of organophosphorus pesticides residues in wine and fruit juices. *Food Chem.* **2004**, *86* (2), 269−274.
(15) Perret, D.; Gentili, A.; Marchese, S.; Sergi, M.; D'Ascenzo, G. Validation of a method for the determination of multiclass pesticide residues in fruit juices by liquid chromatography/tandem mass spectrometry after extraction by matrix solid-phase dispersion. *J. AOAC Int.* **2002**, *85* (3), 724−730.
(16) Gonçalves, C.; Alpendurada, M. Multiresidue method for the simultaneous determination of four groups of pesticides in ground and drinking waters, using solid-phase microextraction-gas chromatography with electron-capture and thermionic specific detection. *J. Chromatogr., A* **2002**, *968* (1), 177−190.
(17) Huang, S. P.; Huang, S. D. Dynamic hollow fiber protected liquid phase microextraction and quantification using gas chromatography combined with electron capture detection of organochlorine pesticides in green tea leaves and ready-to-drink tea. *J. Chromatogr., A* **2006**, *1135* (1), 6−11.
(18) Rui, S. Y.; Hu, Q.; Cai, L. S.; Chen, Y. W. Elimination of caffeine disturbance to GC determination of pesticides residues in tea. *Food Sci.* **2009**, *12*, 043.
(19) Wong, J. W.; Zhang, K.; Tech, K.; Hayward, D. G.; Krynitsky, A. J.; Cassias, I.; Schenck, F. J.; Banerjee, K.; Dasgupta, S.; Brown, D. Multiresidue pesticide analysis of ginseng powders using acetonitrile-or acetone-based extraction, solid-phase extraction cleanup, and gas chromatography-mass spectrometry/selective ion monitoring (GC-MS/SIM) or -tandem mass spectrometry (GC-MS/MS). *J. Agric. Food Chem.* **2010**, *58* (10), 5884−5896.
(20) Commission Decision 2002/657/EC of 12 August 2002 implementing Council Directive 96/23/EC concerning the performance of analytical methods and the interpretation of results, as amended by Decision 2003/181/EC (4). *Off. J. Eur. Communities* **2002**, 8−36.
(21) Ministry of Health, Labour and Welfare. Analytical methods for residual compositional substances of agricultural chemicals, feed additives, and veterinary drugs in food; http://www.mhlw.go.jp/english/topics/foodsafety/positivelist060228/dl/060526-1a.pdf, 2005.
(22) Shimelis, O.; Yang, Y.; Stenerson, K.; Kaneko, T.; Ye, M. Evaluation of a solid-phase extraction dual-layer carbon/primary secondary amine for clean-up of fatty acid matrix components from food extracts in multiresidue pesticide analysis. *J. Chromatogr., A* **2007**, *1165* (1), 18−25.
(23) Huang, Z.; Li, Y.; Chen, B.; Yao, S. Simultaneous determination of 102 pesticide residues in Chinese teas by gas chromatography-mass spectrometry. *J. Chromatogr., B* **2007**, *853* (1), 154−162.
(24) Ding, H. Y.; Xie, W.; Jiang, X. Y.; Li, B.; Huang, L. F. Determination of 16 pyrethroids residues in tae samples by gel permeation chromatography-solid phase extraction. *Chin. J. Anal. Lab.* **2009**, *28* (S1), 14−19.
(25) Feng, J.; Tang, H.; Chen, D. Z.; Wang, G. N.; Li, L. Determination of pesticides in tea by isotope dilution gas chromatography-mass spectrometry coupled with solid-phase microextraction. *Anal. Methods* **2012**, *4*, 4198−4203.
(26) Guo, H.; Yang, Y. Z. Analysis on organochlorine pesticide residues and heavy metal contaminates of tea in Tongzhou district of Beijing. *Chin. J. Food Hyg.* **2012**, *22* (6), 551−553.

nidin-rich extracts were degraded under acidic conditions. These formed carbocations (upper units) react in the presence of flavan-3-ols as nucleophile agents to dimeric proanthocyanidins.

In a previous study, 57 samples with regard to the occurrence of dimeric procyanidins B1−B8 were analyzed.[14] In this context, dimeric procyanidins B1−B4, B6, and B7 in hazelnut skins were detected in low amounts.[14] According to Gu et al.,[2] hazelnut polymers are composed of 41.9% (−)-epicatechin, 39.5% (+)-catechin, 10.8% (epi)gallocatechin, and 0.5% epicatechin-3-*O*-gallate in their extension units. The conditions are appropriate for the use of semisynthesis to produce all eight dimeric procyanidins B1−B8 in higher amounts. Therefore, the aim of the present study is the isolation of B-type dimeric procyanidins in high amounts (i.e., 500 mg) after semisynthesis of hazelnut skins for the first time. Furthermore, the proanthocyanidin composition of hazelnut skins is not well-characterized in the literature until now. Here, we characterize for the first time various proanthocyanidins, that is, flavan-3-ol (epi)afzelechin, B-type dimeric propelargonidins, and different A- and B-type dimeric prodelphinidins, which occur naturally in hazelnut skins by LC-MS/MS and/or NMR spectroscopy.

MATERIALS AND METHODS

Chemicals. Water (deionized, Nanopure, Werner, Leverkusen, Germany), acetonitrile of HPLC quality (Fisher Scientific, Loughborough, UK), *tert*-butyl methyl ether (distilled, industrial quality), methanol (distilled, industrial quality), *n*-hexane (distilled, industrial quality), *n*-butanol, p.a. (Fisher Scientific), ethyl acetate, p.a. (Fisher Scientific), 2-propanol, p.a. (Sigma, Steinheim, Germany), (+)-catechin hydrate, ≥98% (Sigma), (−)-epicatechin, p.a. (Sigma), hydrochloric acid, 37% (Riedel-de-Haën, Seelze, Germany), ethanol, p.a. (Riedel-de-Haën), sodium hydrogen carbonate, p.a. (Merck, Darmstadt, Germany), and acetone-d_6 (Deutero GmbH, Kastellaun, Germany) were used.

High-Performance Liquid Chromatography Photodiode Array (HPLC-PDA) and HPLC−Electrospray Ionization Multiple Mass Spectrometry (HPLC-ESI-MS^n) Analysis. HPLC-PDA and HPLC-ESI-MS^n conditions were the same as described earlier.[12]

Optimization of the Reaction Conditions for Semisynthesis of Dimeric Procyanidins. The reaction conditions, such as ratio of substrates, reaction time, and reaction temperature, were described in Esatbeyoglu and Winterhalter.[12]

Sample Preparation for High-Speed (HSCCC) and Low-Speed Rotary Countercurrent Chromatography (LSRCCC) Separation. Hazelnut skin precipitate was obtained from 70% aqueous acetone extract of hazelnut skins after ethanol/*n*-hexane (5:13, v/v) precipitation as described earlier.[15] The precipitate, received after filtration, was used for semisynthesis.

For HSCCC. Amounts of 1 g of (+)-catechin or (−)-epicatechin and 500 mg of hazelnut skin precipitate were dissolved in 50 mL of 0.1 N methanolic HCl and kept at 40 °C for 30 min in a water bath. The reaction mixture was neutralized with about 10 mL of 0.5 N sodium hydrogen carbonate solution and evaporated, and the residue was lyophilized. About 1 g of the reaction mixture was applied for HSCCC separation.

For LSRCCC. For semisynthesis of dimeric procyanidins B1, B3, B6, and B7, 10 g of (+)-catechin and 10 g of hazelnut skin precipitate were used, and 10 g of (−)-epicatechin and 10 g of hazelnut skin precipitate were applied to semisynthesize dimeric procyanidins B2, B4, B5, and B8. Further conditions for sample preparation are given in Esatbeyoglu et al.[15] About 10 g of the reaction mixture was used for LSRCCC separation.

HSCCC. A high-speed countercurrent chromatograph model CCC-1000 (Pharma-Tech Research Corp., Baltimore, MD, USA) was equipped with three preparative coils of PTFE tubing, connected in series (total volume, 800 mL; 2.6 mm i.d.; 160 m length). A Biotronik HPLC pump BT 3020 pumped the two-phase solvent systems. The aqueous lower phase was used as mobile phase (elution mode, head to tail). All samples were dissolved in 10 mL upper and 10 mL lower phases and loaded into the system by loop injection. The amount of loaded sample, revolution speed of the apparatus, flow rate, and solvent systems are given in the discussions for the respective runs. The HSCCC separation was monitored at λ = 280 nm with a Knauer UV−vis detector (Berlin, Germany) and recorded on a plotter (BBC Goerz SE 120, Vienna, Austria; 3 cm/h). Fractions of 12 mL were collected using a Super Frac fraction collector (Pharmacia LKB, Bromma, Sweden).

LSRCCC. LSRCCC separation of dimeric procyanidins B1, B3, B6, and B7 was carried out according to the method of Esatbeyoglu et al.[15] For the LSRCCC separation (single coil, total volume, 5500 mL; 8.2 mm i.d.) of dimeric procyanidins B2, B4, B5, and B8, 12.4 g of the lyophilized filtrate of the semisynthetic process with (−)-epicatechin was dissolved in 100 mL upper and 100 mL lower phases and was loaded into the system via a sample loop. *tert*-Butyl methyl ether/*n*-butanol/water (4.5:0.5:5, v/v/v) was used as the two-phase solvent system. The flow rate was set at 4 mL/min, and the revolution speed at 50 rpm. The upper organic phase represented the mobile phase. LSRCCC separation was carried out in the "head-to-tail" elution mode. After an elution time of 39 h, the elution mode was switched to extrusion. In this case, the aqueous lower phase was pumped into the LSRCCC column. UV absorbance of the effluent was monitored at λ = 280 nm with a Knauer UV−vis detector. The elution was recorded on a Servogor 120 plotter (BBC Goerz Metrawatt SE 120, Vienna, Austria). About 50 mL fractions were collected by a fraction collector (Pharmacia LKB Super Frac).

Semipreparative HPLC. CCC fractions were purified on a preparative HPLC system from Knauer (Smartline 1000 HPLC pump, Smartline Manager 5000 solvent organizer and degasser, Wellchrom K-2600 UV detector). A Hypersil ODS C-18, 5 μm, 250 × 16 mm i.d. (M&W Chromatographietechnik GmbH, Berlin, Germany) semipreparative HPLC column was used for the isolation of proanthocyanidins. Water (solvent A) and acetonitrile (solvent B) were used as solvent systems. The flow rate was 6 mL/min. The following gradients were used for the isolation of proanthocyanidins: Gradient 1 for dimeric procyanidins B1 and B3 and dimeric prodelphinidin B2, 0 min, 8% B; 40 min, 25% B; 42 min, 100% B; 47 min, 100% B; 49 min, 8% B; 54 min, 8% B. Gradient 2 for dimeric procyanidins B2, B4, B5, and B7, 0 min, 10% B; 30 min, 30% B; 32 min, 100% B; 37 min, 100% B; 39 min, 10% B; 44 min, 10% B. Gradient 3 for dimeric procyanidin B6 and trimeric procyanidin C1, 0 min, 10% B; 40 min, 30% B; 42 min, 100% B; 47 min, 100% B; 49 min, 10%; 54 min, 10% B. Gradient 4 for dimeric procyanidin B8, 0 min, 10% B; 50 min, 35% B; 52 min, 100% B; 57 min, 100% B; 59 min, 10%; 64 min, 10% B. Gradient 5 for dimeric prodelphinidin B1, 0 min, 6% B; 50 min, 27% B; 52 min, 100% B; 57 min, 100% B; 59 min, 6% B; 65 min, 6% B. Gradient 6 for dimeric prodelphinidin B3, 0 min, 6% B; 40 min, 15% B; 42 min, 100% B; 47 min, 100% B; 49 min, 6% B; 54 min, 6% B. The fractions were monitored at λ = 280 nm. The purity of all compounds was confirmed by HPLC-PDA (>95%) at λ = 280 nm.

Phloroglucinolysis. Analysis was carried out according to the methods of Esatbeyoglu et al.[13] and Kennedy and Jones.[16] Phloroglucinol adducts (+)-catechin-(4α → 2)-phloroglucinol and (−)-epicatechin-(4β → 2)-phloroglucinol as reference compounds were obtained by HSCCC according to the method of Köhler and Winterhalter.[17]

Circular Dichroism. CD spectra were measured according to the method of Esatbeyoglu et al.[15]

Nuclear Magnetic Resonance (NMR) Spectroscopy. ^{1}H and ^{13}C NMR, ^{1}H−^{1}H correlated spectroscopy (COSY), ^{1}H−^{1}H phase-sensitive nuclear Overhauser enhancement spectroscopy (NOESY), heteronuclear single-quantum coherence (HSQC), and heteronuclear multiple-bond correlation (HMBC) experiments were performed at 300 or 240 K on a Bruker Avance ARX 400 NMR spectrometer equipped with a variable-temperature unit B VT-2000 (Rheinstetten, Germany). Samples were dissolved in acetone-d_6. Chemical shifts were

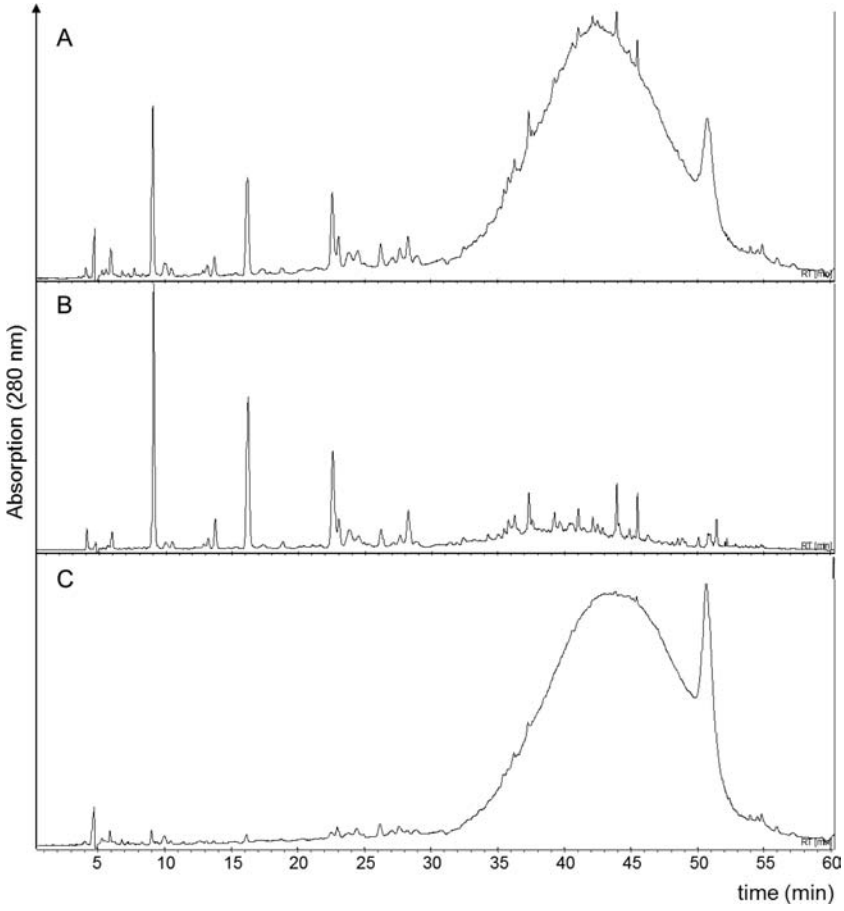

Figure 1. HPLC-PDA chromatograms at λ = 280 nm of the 70% acetone extract of hazelnut skins before (A) and after ethanol/*n*-hexane precipitation (B, filtrate; C, precipitate). Modified from Esatbeyoglu.[38]

referenced to the residual solvent signals and are reported in parts per million and coupling constants in hertz.

(−)-Epigallocatechin-4β → 8-(+)-catechin (dimeric prodelphinidin B1): amorphous white powder; λ_{max} = 228 and 276 nm; ESI-MS/MS *m/z* 593 $[M - H]^-$; MS/MS fragments *m/z* 575, 467, 425, 407, 303, 289, 245; CD (0.17 mmol/L in methanol) $[\theta]_{207}$ −84791, $[\theta]_{218}$ 84795, $[\theta]_{235}$ 35278, $[\theta]_{281}$ −5207.

^{1}H NMR (400 MHz, acetone-d_6, 240 K) δ 2.57 (dd, 1H, *J* = 6.8 Hz, *J* = 16.9 Hz, H4B*t*), 2.63 (dd, 1H, *J* = 5.5 Hz, *J* = 17.0 Hz, H4A*t*), 3.89 (m, 1H, H3*u*), 4.02 (1OH, OH3*u*), 4.06 (m, 1H, H3*t*), 4.52 (1OH, OH3*t*), 4.69 (sbr, 1H, H4*u*), 4.87 (d, 1H, *J* = 6.0 Hz, H2*t*), 5.03 (sbr, 1H, H2*u*), 5.89 (s, 1H, H6*t*), 5.92 (d, 1H, *J* = 1.9 Hz, H8*u*), 5.99 (d, 1H, *J* = 1.9 Hz, H6*u*), 6.45 (s, 2H, H2′*u*, H6′*u*), 6.68 (d, 1H, *J* = 8.1 Hz, H5′*t*), 6.86 (dd, 1H, *J* = 2.1 Hz, *J* = 8.1 Hz, H6′*t*), 6.88 (d, 1H, *J* = 2.1 Hz, H2′*t*).

Assignment of aromatic hydroxyl groups: 7.00 (OH7*t*), 7.70[a] (OH4′*u*), 8.27 (OH3′*u*, OH5′*u*), 8.41[a] (OH3′*t*), 8.62[b] (OH7*u*), 8.63[b] (OH5*t*), 8.72a,[c] (OH5*u*, OH4′*t*), 8.75[a, c] (OH5*u*). ([a, b, c] shifts are interchangeable.)

(−)-Epigallocatechin-4β → 8-(−)-epicatechin (dimeric prodelphinidin B2): amorphous white powder; λ_{max} = 228 and 276 nm; ESI-MS/MS *m/z* 593 $[M - H]^-$; MS/MS fragments *m/z* 575, 467, 425, 407, 303, 289, 245; CD (0.15 mmol/L in methanol) $[\theta]_{205}$ −84507, $[\theta]_{221}$ 63392, $[\theta]_{240}$ 38165, $[\theta]_{273}$ −10694, $[\theta]_{287}$ −452.

^{1}H NMR (400 MHz, acetone-d_6, 240 K), 90% major rotamer, δ 2.67 (dd, 1H, *J* = <1 Hz, *J* = 17.0 Hz, H4B*t*), 2.88 (dd, 1H, *J* = 4.5 Hz, *J* = 16.5 Hz, H4A*t*), 3.98 (m, 1H, H3*u*), 4.16 (1OH, OH3*u*), 4.31 (m, 1H, H3*t*), 4.31 (1OH, OH3*t*), 4.71 (d, 1H, *J* = 2.4 Hz, H4*u*), 4.97 (d, 1H, *J* = 2.2 Hz, H2*u*), 5.02 (sbr, 1H, H2*t*), 5.91 (s, 1H, H6*t*), 5.95[a] (d, 1H, *J* = ∼1.5 Hz, H8*u*), 5.99[a] (d, 1H, *J* = ∼1.5 Hz, H6*u*), 6.41 (s, 2H, H2′*u*, H6′*u*), 6.69 (d, 1H, *J* = 8.2 Hz, H5′*t*), 6.89 (dd, 1H, *J* = 1.8 Hz, *J* = 8.2 Hz, H6′*t*), 6.98 (1OH, OH7*t*), 7.14 (d, 1H, *J* = 1.8 Hz, H2′*t*). ([a] shifts are interchangeable.)

(+)-Gallocatechin-4α → 8-(+)-catechin (dimeric prodelphinidin B3): amorphous white powder; λ_{max} = 228 and 276 nm; ESI-MS/MS *m/z* 593 $[M - H]^-$; MS/MS fragments *m/z* 575, 467, 425, 407, 303, 289, 245; CD (0.17 mmol/L in methanol) $[\theta]_{204}$ 106643, $[\theta]_{215}$ −328118, $[\theta]_{240}$ −73079, $[\theta]_{271}$ 3371, $[\theta]_{284}$ −6290.

^{1}H NMR (400 MHz, aceton-d_6, 300 K), two rotamers A and B in a ratio of 55:45, δ 2.53* (dd, 1H, *J* = 7.9 Hz, *J* = 16.2 Hz, H4B*t*), 2.61 (dd, 1H, *J* = 8.1 Hz, *J* = 16.2 Hz, H4B*t*), 2.76* (dd, 1H, *J* = 5.4 Hz, *J* = 16.3 Hz, H4A*t*), 2.89 (dd, 1H, *J* = 5.3 Hz, *J* = 15.9 Hz, H4A*t*), 3.81* (m, 1H, H3*t*), 4.06 (m, 1H, H3*t*), 4.23* (d, 1H, *J* = 9.6 Hz, H2*u*), 4.28 (d, 1H, *J* = 9.1 Hz, H2*u*), 4.35* (ddd, 1H, *J* = 1.3 Hz, *J* = 8.1 Hz, *J* = 8.1 Hz, H3*u*), 4.45* (d, 1H, *J* = 7.9 Hz, H4*u*), 4.50 (t, 1H, *J* = 8.0 Hz, *J* = 9.0 Hz, H3*u*), 4.54 (d, 1H, *J* = 7.9 Hz, H4*u*), 4.62* (d, 1H, *J* = 7.1 Hz, H2*t*), 4.73 (d, 1H, *J* = 7.5 Hz, H2*t*), 5.78*[a] (d, 1H, *J* = 2.4 Hz, H8*u*), 5.84*[a] (d, 1H, *J* = 2.4 Hz, H6*u*), 5.85[a] (d, 1H, *J* = 2.4 Hz, H6*u*), 5.93[a] (d, 1H, *J* = 2.4 Hz, H8*u*), 6.04[b] (s, 1H, H6*t*), 6.17[b] (s, 1H, H6*t*), 6.19* (dd, 1H, *J* = 2.0 Hz, *J* = 8.2 Hz, H6′*t*), 6.37* (s, 2H, H2′*u*, H6′*u*), 6.55 (s, 2H, H2′*u*, H6′*u*), 6.59* (d, 1H, *J* = 2.0 Hz, H2′*t*), 6.65* (d, 1H, *J* = 8.2 Hz, H5′*t*), 6.77 (d, 1H, *J* = 8.1 Hz, H5′*t*), 6.88 (dd, 1H, *J* = 2.0 Hz, *J* = 8.1 Hz, H6′*t*), 7.02 (d, 1H, *J* = 2.0 Hz, H2′*t*). (* rotamer B; [a, b] shifts are interchangeable.)

^{13}C NMR (100 MHz, acetone-d_6, 300 K) δ 28.4* (C4*t*), 28.7 (C4*t*), 37.9* (C4*u*), 38.2 (C4*u*), 68.1* (C3*t*), 68.1 (C3*t*), 73.1* (C3*u*), 73.1 (C3*u*), 82.0* (C2*t*), 83.0 (C2*t*), 83.9* (C2*u*), 84.0 (C2*u*), 96.0 (C6*t*), 96.1[a] (C6*u*), 96.8[a] (C6*u*), 97.0[a] (C8*u*), 97.2[a] (C8*u*), 97.4* (C6*t*), 100.6 (C4a*t*), 101.9* (C4a*t*), 106.1* (C4a*u*), 106.4 (C4a*u*), 107.7* (C8*t*), 107.5 (C8*t*), 108.0* (C2′*u*, C6′*u*), 108.0 (C2′*u*, C6′*u*), 115.0 (C2′*t*), 115.1* (C2′*t*), 115.6 (C5′*t*), 115.8* (C5′*t*), 119.5* (C6′*t*), 120.0 (C6′*t*), 131.6[b] (C1′*u*), 131.7[b] (C1′*u*), 131.7[b] (C1′*t*), 131.9[b] (C1′*t*), 133.2 (C4′*u*), 133.3* (C4′*u*), 144.7*[c] (C3′*t*), 145.1*[c] (C4′*t*),

dx.doi.org/10.1021/jf501312a | J. Agric. Food Chem. 2014, 62, 7101−7110

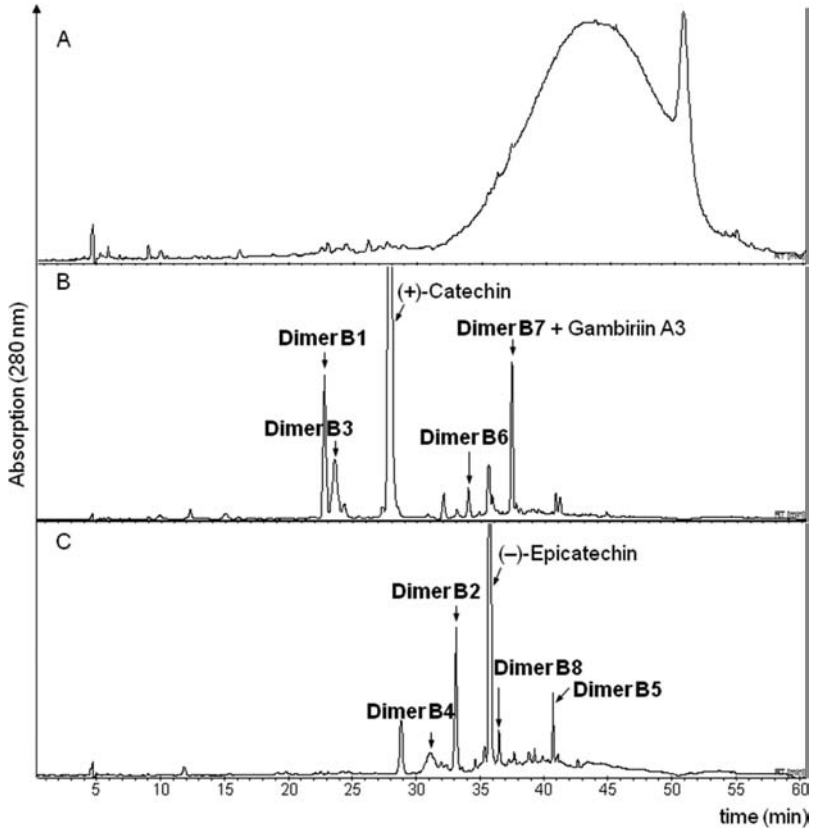

Figure 2. HPLC-PDA chromatograms at λ = 280 nm of the precipitate of hazelnut skins before (A) and after semisynthesis with (+)-catechin (B) and (−)-epicatechin (C). Modified from Esatbeyoglu.[38]

145.6[d] (C3′*t*), 145.7[d] (C4′*t*), 145.8* (C3′*u*, C5′*u*), 146.0 (C3′*u*, C5′*u*), 154.7 (C8a*t*), 154.7* (C8a*t*), 155.1[e] (C5*t*), 155.3[e] (C5*t*), 155.4[e] (C7*t*), 155.5[e] (C7*t*), 157.0[f] (C5*u*), 157.1[f] (C5*u*), 157.2[f] (C7*u*), 157.4[f] (C7*u*), 158.4 (C8a*u*), 158.6* (C8a*u*). (* rotamer B; [a, b, e, f] shifts and rotamers are interchangeable; [c, d] shifts are interchangeable.)

■ RESULTS AND DISCUSSION

Initially, the defatted 70% acetone extract of hazelnut skins was precipitated with ethanol and *n*-hexane in a ratio of 5:13 (v/v). This allows an enrichment of higher oligomeric and polymeric proanthocyanidins in the precipitate and an enrichment of lower oligomeric proanthocyanidins in the filtrate. Figure 1 shows the HPLC-PDA chromatograms of 70% acetone extract of hazelnut skins before and after precipitation. The proportion of flavan-3-ol constituents in the upper and terminal units of the hazelnut skin precipitate was determined by phloroglucinolysis, as published earlier.[4,14] The analysis showed that 30.7 ± 0.55% (+)-catechin-(4α → 2)-phloroglucinol and 62.9 ± 1.45% (−)-epicatechin-(4β → 2)-phloroglucinol are present in the upper units of the polymeric proanthocyanidin fraction of hazelnut skins. Also, 3.67 ± 0.15% (−)-epigallocatechin and 2.97 ± 0.11% (+)-gallocatechin as part of the upper unit were detected.

To find the optimal reaction conditions for semisynthesis of dimeric procyanidins, the influence of the reaction time, temperature, and ratio of reagents such as nucleophile agent, that is, (+)-catechin and (−)-epicatechin, as well as the polymeric procyanidin fraction (hazelnut precipitate) was determined (data not shown). The optimal reaction conditions for semisynthetic studies were 30 min at 40 °C with a ratio of substrates of 1:2 (hazelnut precipitate and nucleophile agent). For LSRCCC separation a ratio of 1:1, because of the cost of (−)-epicatechin as nucleophile agent, was chosen. Under these conditions a maximum formation of dimeric procyanidins and a minimum formation of byproducts, that is, gambiriins (chalcan-flavan-3-ol derivatives) are observed. It is possible to semisynthesize all eight dimeric procyanidins B1−B8 (Figure 2). This is due to the flavan-3-ol compositions of the polymeric procyanidin fraction of the hazelnut skin precipitate, which is composed of 30.7% (+)-catechin and 62.9% (−)-epicatechin. After reaction with (+)-catechin, the amount of dimeric procyanidins B1, B3, B6, and B7 increased. With (−)-epicatechin as nucleophile agent dimeric procyanidins B2, B4, B5, and B8 are formed.

Fractionation of the Semisynthetic Reaction Mixture by HSCCC. The fractionation of the semisynthetic reaction mixture, carried out with (+)-catechin as a nucleophile agent, was performed by HSCCC using the solvent system ethyl acetate/*n*-butanol/water (14:1:15, v/v/v).[11] Figure 3A shows the results of the HSCCC separation. Fraction I contained mainly A-type dimeric prodelphinidin (−)-EGC-(2β → O7, 4β → 8)-(+)-C[15] and an unknown B-type dimeric prodelphinidin. Further unknown A- and B-type dimeric prodelphinidins were found in fraction II. About 50 mg of B1 (purity = 95.5%) was obtained from fraction III. Fraction IV was composed of two B-type trimeric procyanidins EC-4β → 8-EC-4β → 8-C and EC-4β → 6-EC-4β → 8-C.[13] Dimeric procyanidin B3 was enriched in fraction V (37.1 mg; 87.6%). For compounds with partition coefficients (*K* values) >2, which remained on the CCC coil, the more apolar two-phase solvent system was used for fractionation. The chromatogram of the CCC separation acquired at 280 nm is shown in Figure 3B. Fraction I did not

dx.doi.org/10.1021/jf501312a | J. Agric. Food Chem. 2014, 62, 7101−7110

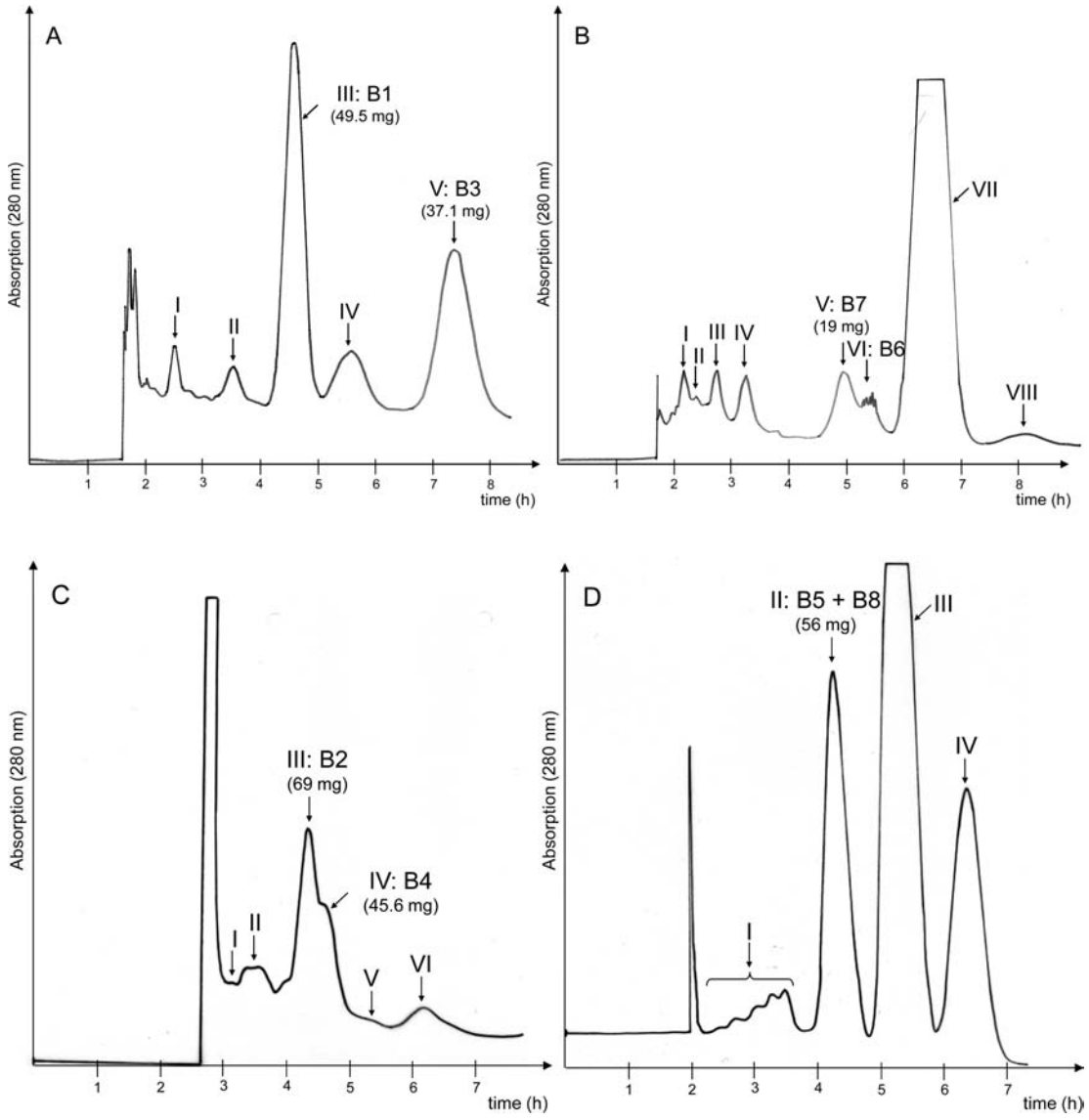

Figure 3. (A) HSCCC chromatogram of the reaction mixture of hazelnut skin precipitate and (+)-catechin. Sample load, 928 mg; solvent system, ethyl acetate/*n*-butanol/water (14:1:15, v/v/v); flow rate, 2.7 mL/min; revolution speed, 900 rpm. (B) HSCCC chromatogram of the coil (A). Sample load, 550 mg; solvent system, *n*-hexane/ethyl acetate/methanol/water (1:10:1:10, v/v/v/v); flow rate, 3 mL/min; revolution speed, 1000 rpm. (C) HSCCC chromatogram of the reaction mixture of hazelnut skin precipitate and (−)-epicatechin. Sample load, 1000 mg; solvent system, ethyl acetate/isopropanol/water (20:1:20, v/v/v); flow rate, 3 mL/min; revolution speed, 1000 rpm. (D) HSCCC chromatogram of the coil (C). Sample load, 395 mg; solvent system, *n*-hexane/ethyl acetate/methanol/water (1.2:10:1.2:10, v/v/v/v); flow rate, 2.7 mL/min; revolution speed, 1000 rpm. Modified from Esatbeyoglu.[38]

contain any relevant compounds. Fraction II contained mainly trimeric procyanidin C1. In fraction III unknown compounds, that is, galloylated dimeric procyanidins (m/z 729 $[M - H]^-$),[8] A-type trimeric procyanidin (m/z 863 $[M - H]^-$), B-type dimeric propelargonidin (m/z 561 $[M - H]^-$), and an A-type dimeric prodelphinidin (m/z 591 $[M - H]^-$) were enriched. The byproduct gambiriin A1 was found in fraction IV. Fraction V consisted of dimeric procyanidin B7 (18.8 mg, purity = 82.6%). B6 was enriched in fraction VI (10.8 mg, purity = 26.1%). Unreacted (+)-catechin was obtained from fraction VII (purity = 99.0%). The last fraction contained the second byproduct gambiriin A3.

To isolate dimeric procyanidins B2, B4, B5, and B8 the reaction mixture of the semisynthesis carried out with (−)-epicatechin was separated with the solvent system ethyl acetate/isopropanol/water (20:1:20, v/v/v) (Figure 3C). Fraction I contained several compounds, that is, B-type trimeric procyanidin, two B-type dimeric prodelphinidins, and two A-type dimeric prodelphinidins. One dimeric prodelphinidin was identified as EGC-4β → 8-EC (see below) and one A-type dimeric prodelphinidin as EGC-(2β → O5, 4β → 6)-C.[15] Fraction II contained compounds similar to those of fraction I. Two B-type trimeric procyanidins were identified as EC-4β → 6-EC-4β → 8-EC and trimer C1 (EC-4β → 8-EC-4β → 8-EC).[13] B2 was enriched (69 mg; purity = 88.7%) in fraction III and B4 in fraction IV (45.6 mg, purity = 70.5%). Fraction V consisted of A- and B-type dimeric prodelphinidins, an A-type dimeric procyanidin, and a trimeric procyanidin. A galloylated dimeric procyanidin (m/z 729 $[M - H]^-$)[8] was enriched in fraction VI. This CCC separation was repeated twice. Coil fractions of two CCC separations were divided into five fractions, and fraction II and III were combined to isolate B5

dx.doi.org/10.1021/jf501312a | J. Agric. Food Chem. 2014, 62, 7101−7110

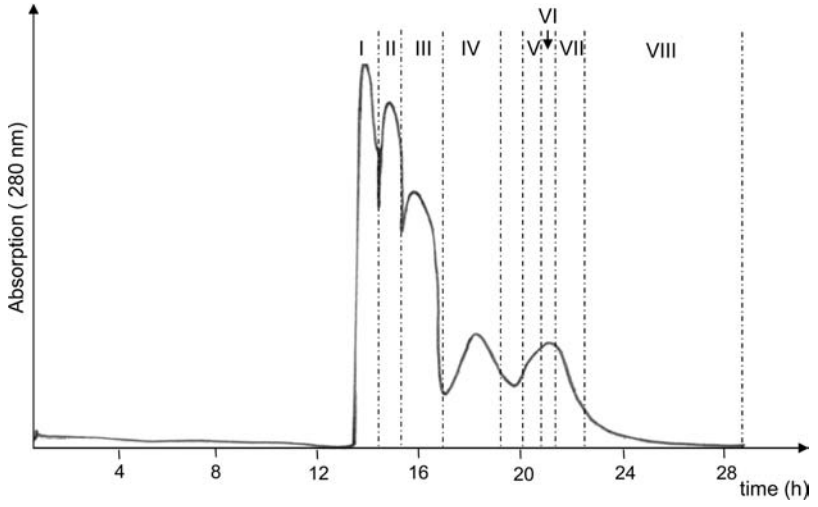

Figure 4. LSRCCC chromatogram of the filtrate of the reaction mixture of hazelnut skin precipitate and (+)-catechin after ethanol/*n*-hexane precipitation (5:13, v/v) (LSRCCC-1). Sample load, 9.58 g; solvent system, *tert*-butyl methyl ether/*n*-butanol/water (4.3:0.7:5, v/v/v); flow rate, 5 mL/min; revolution speed, 50 rpm; elution mode, U−H (upper organic phase as mobile phase; head to tail). Modified from Esatbeyoglu.[38]

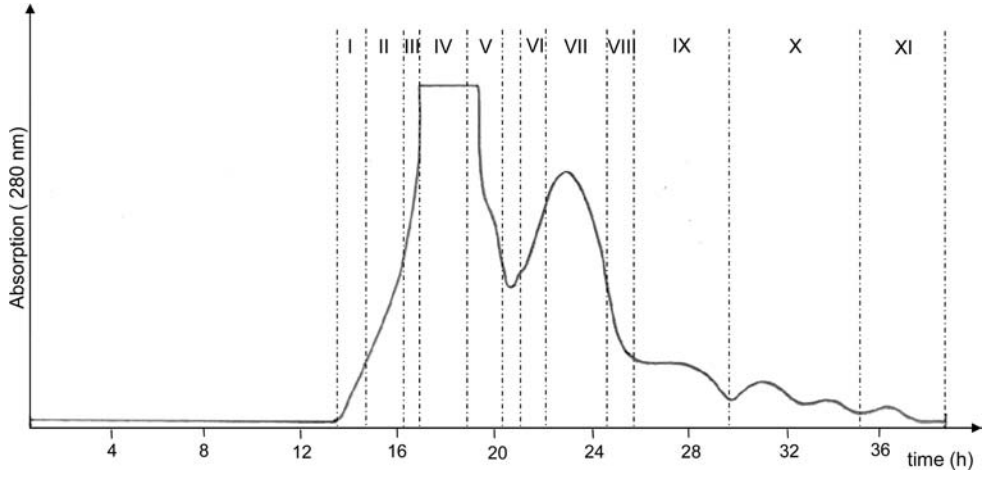

Figure 5. LSRCCC chromatogram of the reaction mixture of hazelnut skin precipitate and (−)-epicatechin (LSRCCC-2). Sample load, 12.4 g; solvent system, *tert*-butyl methyl ether/*n*-butanol/water (4.5:0.5:5, v/v/v); flow rate, 4 mL/min; revolution speed, 50 rpm; elution mode, U−H (upper organic phase as mobile phase; head to tail). Modified from Esatbeyoglu.[38]

and B8 (Figure 3D). The solvent system *n*-hexane/ethyl acetate/methanol/water (1.2:10:1.2:10, v/v/v/v) was selected for this separation. Fraction I was composed of polymeric procyanidins. Dimeric procyanidins B5 and B8 were found in fraction II (56 mg). High-purity (−)-epicatechin (98.4%) was recovered from fraction III, whereas fraction IV contained (+)-catechin (purity = 93.9%).

In summary, hazelnut skins are suitable substrates for semisynthesis of all eight B-type dimeric procyanidins B1−B8. To achieve a higher yield of dimeric procyanidins and enrichment of minor compounds, the separation of semisynthetic reaction mixture was carried out on a large scale by LSRCCC.

Fractionation of the Semisynthetic Reaction Mixture by LSRCCC. The reaction mixture, after semisynthesis with (+)-catechin, was precipitated with ethanol/*n*-hexane in a ratio of 5:13 (v/v). After filtration of this solution, the resulting filtrate (9.58 g) after evaporation and lyophilization was fractionated with the solvent system *tert*-butyl methyl ether/*n*-butanol/water (4.3:0.7:5, v/v/v) by LSRCCC. The first LSRCCC separation of procyanidins, from a semisynthetic reaction mixture of a commercial grape seed extract with (+)-catechin, has been described by Köhler.[18] In the current study, the isolation of proanthocyanidins from hazelnut skins after semisynthetic preparation was described for the first time. Figure 4 shows the LSRCCC separation of the filtrate of the reaction mixture of hazelnut skin precipitate and (+)-catechin after ethanol/*n*-hexane precipitation. The collected fractions were analyzed by HPLC-PDA at λ = 280 nm and combined to eight fractions. The coil fraction, which was obtained by extrusion, was divided into three fractions. Figure S1 in the Supporting Information shows the composition of some selected LSRCCC fractions. Due to the similar *K* values of dimeric procyanidins B6 and B7, (+)-catechin, and (−)-epicatechin, all compounds eluted in fractions I−III. Fraction I was composed of various proanthocyanidins, that is, 65.7% (+)-catechin, 7.6% (−)-epicatechingallate, 7.1% dimeric procyanidin B7 (coelution with gambiriin A3), and 2.0% dimeric procyanidin B6. Smaller amounts of A-type dimeric prodelphinidins, A-type trimeric proanthocyanidins (*m*/*z* 879 $[M - H]^-$ (Epi)C-(Epi)C-(Epi)GC, tentatively), B-type dimeric propelargonidins, and prodelphinidins [(Epi)GC-

dx.doi.org/10.1021/jf501312a | J. Agric. Food Chem. 2014, 62, 7101−7110

(Epi)GC (m/z 609 [M − H]$^-$)] as well as galloylated dimeric procyanidins (m/z 729 [M − H]$^-$) were found. From this fraction EGC-(2β → O5, 4β → 6)-C[15] and dimeric procyanidin B6 were isolated with the solvent system *n*-hexane/ethyl acetate/methanol/water (1.4:10:1.4:10, v/v/v/v) by HSCCC (data not shown). Fraction II was composed of 88.8% (+)-catechin, 4.2% dimeric procyanidin B7, 1.4% (−)-epicatechin, and 1.1% dimeric procyanidin B6. About 90% (+)-catechin, 3.9% (−)-epicatechin, and 2.0% dimeric procyanidin B7 were enriched in fraction III. Fraction IV contained dimeric procyanidin B3 (560 mg; purity = 76.9%). Fraction V consisted of 67.0% dimeric procyanidin B1 (168 mg) and the trimeric procyanidins EC-4β → 8-EC-4β → 8-C and EC-4β → 6-EC-4β → 8-C.[13] About 600 mg of dimeric procyanidin B1 was obtained from fractions VI and VII (purity = 81.1 and 90.1%, respectively). In fraction VIII dimeric procyanidin B1, A- and B-type dimeric prodelphinidins, B-type trimeric procyanidin, and a further A-type trimeric proanthocyanidin (m/z 879 [M − H]$^-$ (Epi)C-(Epi)C-(Epi)GC) were enriched. GC-4α → 8-C was isolated from this fraction by preparative HPLC. EGC-4β → 8-C and EGC-(2β → O7, 4β → 8)-C were obtained from coil fractions I and II. The structures of these B-type dimeric prodelphinidins are elucidated by NMR spectroscopy (see below). Trimeric procyanidin EC-4β → 8-C-4α → 8-C was enriched (276 mg; purity = 62.0%) in coil fraction III.[13]

Dimeric procyanidins B2, B4, B5, and B8 were isolated from the reaction mixture of the semisynthesis carried out with (−)-epicatechin and hazelnut skin precipitate by LSRCCC. To eliminate the polymeric compounds, the reaction mixture was treated with ethanol/*n*-hexane (5:13, v/v). This solution was filtered, and the obtained filtrate after evaporation and lyophilization was fractionated with the solvent system *tert*-butyl methyl ether/*n*-butanol/water (4.5:0.5:5, v/v/v). The LSRCCC separation is shown in Figure 5. After separation by elution as well as extrusion and analysis of selected samples by HPLC-PDA, 11 fractions from the elution and five coil fractions from the extrusion were obtained. Selected fractions are depicted in Figure S2 in the Supporting Information. Fraction I contained the more apolar compounds gambiriin A5, (−)-epicatechingallate, galloylated dimeric procyanidin, and (epi)afzelechin. (Epi)afzelechin is until now unknown for hazelnut skins.[2,8,9,19] Besides the compounds found in fraction I, fraction II contained dimeric procyanidins B5 and B8, (+)-catechin, and (−)-epicatechin. Fraction III was composed mainly of (−)-epicatechin (37.5%), (+)-catechin (28.1%), dimeric procyanidins B5 (13.0%), and B8 (3.7%). Besides these dimeric procyanidins, 83.4% (−)-epicatechin was obtained from fraction IV. Compounds in fractions I− IV show similar *K* values. For further isolation of compounds in fractions I−IV, separation was performed with HSCCC (data not shown). The main compound in fraction V was (−)-epicatechin (82.5%), and one B-type galloylated dimeric procyanidin was detected in minor amounts, as well. Fraction VI consisted of target compounds B2 (23.5%) and B4 (33.6%) as well as EC-4β → 8-EC-4β → 6-EC (5.1%).[13] Fraction VII contained dimeric procyanidins B2 and B4 in large amounts of 740 and 350 mg, respectively (calculated at λ = 280 nm by HPLC-PDA). Fraction VIII was composed of 44.3% dimeric procyanidin B2 and 10.9% B-type trimeric procyanidin C1, whereas fraction IX contained about 70% trimeric procyanidin C1. Up to 110 mg of procyanidin trimer C1 was isolated from this fraction. One B-type galloylated dimeric prodelphinidin (m/z 745 [M − H]$^-$) was also detected in smaller amounts. The main compound in fraction X was EC-4β → 6-EC-4β → 8-EC,[13] together with dimeric procyanidin B1 and A-type trimeric proanthocyanidin (m/z 879 [M − H]$^-$ (Epi)C-(Epi)C-(Epi)GC). The last fraction was composed of A- and B-type dimeric prodelphinidins as well as two B-type trimeric proanthocyanidins (m/z 881 [M − H]$^-$, according to ref 2 tentatively (Epi)GC-(Epi)C-(Epi)C). B-type dimeric prodelphinidin (−)-EGC-4β → 8-(−)-EC was isolated from coil fraction I, and its structure was elucidated by NMR spectroscopy (see below). This minor compound occurred naturally in hazelnut skins, confirmed by LC-MS/MS, and is described for the first time in this study. Smaller amounts of A- and B-type dimeric prodelphinidins (with (epi)gallocatechin as upper unit), trimeric proanthocyanidins, and trimeric proanthocyanidins (Epi)GC-(Epi)C-(Epi)C and (Epi)C-(Epi)GC-(Epi)C were identified by LC-MS/MS. Similar compounds were found in coil fractions II−IV. The last coil fraction contained EC-4β → 8-C-4α → 8-EC[13] and small amounts of a B-type trimeric proanthocyanidin (m/z 897 [M − H]$^-$, according to ref 20 tentatively (Epi)GC-(Epi)GC-(Epi)C).

C4 → C8 linked dimeric procyanidins B1 and B3 (about 600 mg; purity = 76.9−90.1%) as well as dimeric procyanidins B2 and B4 (740 and 350 mg) were isolated in large amounts for the first time. Dimeric procyanidins B5−B8 are formed in lower amounts because of steric hindrance.[21−23] Moreover, the semisynthesis of different B-type trimeric procyanidins (EC-4β → 8-EC-4β → 8-C, EC-4β → 6-EC-4β → 8-C, EC-4β → 6-EC-4β → 8-EC, trimer C1 (EC-4β → 8-EC-4β → 8-EC), EC-4β → 8-C-4α → 8-C, EC-4β → 8-EC-4β → 6-EC and EC-4β → 8-C-4α → 8-EC) was shown.

The structure of the minor compounds such as A- and B-type dimeric prodelphinidins EGC-4β → 8-EC, EGC-4β → 8-C, GC-4α → 8-C, EGC-(2β → O7, 4β → 8)-C, and EGC-(2β → O5, 4β → 6)-C are elucidated by NMR spectroscopy[13,15] and were described in hazelnut skins for the first time as well as dimeric prodelphinidins composed of (Epi)GC-(Epi)GC (m/z 609 [M − H]$^-$). Further unknown A- and B-type dimeric prodelphinidins (m/z 591 and 593 [M − H]$^-$) and B-type galloylated dimeric prodelphinidins (m/z 745 [M − H]$^-$) were detected. To date, the occurrence of prodelphinidins in hazelnuts was known, but not their exact structures and their galloylated forms.[2,4,8] The detection of the flavan-3-ol (epi)-afzelechin, B-type dimeric propelargonidins (m/z 561 [M − H]$^-$) and A-type dimeric procyanidin (m/z 575 [M − H]$^-$) were detected for the first time in hazelnut skins. Recently, the occurrence of A- and B-type trimeric proanthocyanidins consisting of (epi)catechin, (epi)gallocatechin, and (epi)-catechingallate units was described in roasted hazelnut skins.[8,9] In the present study, different types of proanthocyanidins such as an A-type trimeric procyanidin (m/z 863 [M − H]$^-$), A-type trimeric proanthocyanidins (m/z 879 [M − H]$^-$ tentatively (Epi)C-(Epi)C-(Epi)GC), and B-type trimeric proanthocyanidins (m/z 881 [M − H]$^-$ tentatively (Epi)GC-(Epi)C-(Epi)C and (Epi)C-(Epi)GC-(Epi)C; m/z 897 [M − H]$^-$ tentatively (Epi)GC-(Epi)GC-(Epi)C) were identified in hazelnut skins. The natural occurrence of these compounds in hazelnut skins was confirmed by LC-MS/MS by analyzing the hazelnut skin filtrate, which was obtained after precipitation of the 70% acetone extract.

Structure Elucidation of B-Type Dimeric Prodelphinidins. B-type dimeric prodelphinidins (−)-EGC-4β → 8-(+)-C, (−)-EGC-4β → 8-(−)-EC, and (+)-GC-4α → 8-(+)-C were

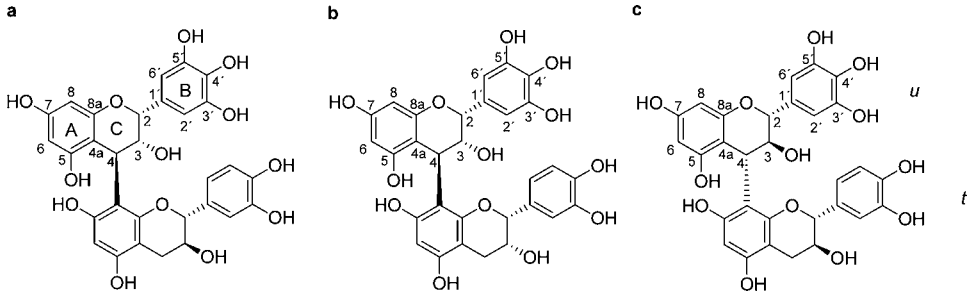

Figure 6. Chemical structures of the dimeric prodelphinidins B1 (a), B2 (b), and B3 (c). *u*, upper; *t*, terminal.

isolated as white amorphous solids from coil fraction I (LSRCCC-1 and LSRCCC-2) and fraction VIII (LSRCCC-1) of the LSRCCC separation after purification by preparative HPLC. Their chemical structures are shown in Figure 6. The structure of these compounds was determined on the basis of electrospray ionization mass spectrometry as well as by 1D and 2D ^{1}H NMR spectroscopic analysis that included COSY and NOESY. 1D and 2D ^{13}C NMR spectroscopy (HSQC, HMBC) were used for structure determination of (+)-GC-4α → 8-(+)-C, as well. All ^{1}H NMR spectra for (−)-EGC-4β → 8-(+)-C and (−)-EGC-4β → 8-(−)-EC were recorded at 240 K (400 MHz, acetone-d_6), and all ^{1}H and ^{13}C NMR spectra (400 and 100 MHz, respectively) of (+)-GC-4α → 8-(+)-C were recorded in acetone-d_6 at 300 K. Chemical shifts and coupling constants are given under Materials and Methods.

LC-MS/MS analysis yielded a molecular ion of $[M - H]^-$ m/z 593 with fragment ions m/z 575, 467, 425, 407, 303, 289, and 245, which indicated the presence of a B-type prodelphinidin (Supporting Information Figure S3). On the basis of the fragment ions m/z 425 and 289 derived from the quinone-methide cleavage and absence of m/z 305, it was concluded that (epi)gallocatechin was the upper unit and (epi)catechin the terminal unit.[2,20,24]

NMR spectra of dimeric prodelphinidins are similar to those of dimeric procyanidins.[25,26] Structure elucidation was performed as in refs 13 and 15, and only relevant data are shown here.

The relative configuration of both units was determined from the magnitude of the coupling constants $J_{2,3}$ and $J_{3,4}$ of the heterocyclic protons (C-ring).[27−32] EGC-4β → 8-C showed a 2,3-*cis*-3,4-*trans*- and 2,3-*trans*-configuration, EGC-4β → 8-EC a 2,3-*cis*-3,4-*trans*- and 2,3-*cis*-configuration, and GC-4α → 8-C a 2,3-*trans*-3,4-*trans*- and 2,3-*trans*-configuration.

Proton singlets at about δ 6.41, 6.45, and 6.55 (H2′ and H6′ are chemically equivalent) are evidence of trihydroxylated B-rings (pyrogallol ring: 3′,4′,5′-substitution) of the upper unit. All C-ring protons were assigned from inspection of COSY spectra. Long-range correlations between H2′ and H6′ (B-ring) as well as H2 (C-ring) allowed the identification of B- and C-rings of both units. Only one proton for H4 of the upper unit was determined. This observation confirmed (epi)gallocatechin as the upper unit.

NOE correlations of H2′ and H6′ of the terminal unit with H4 of the upper unit were characteristic of a 4 → 8 interflavanoid linkage. All compounds are linked C4 → C8. Due to the absence of NOE correlations between H2 and H4, the terminal unit is bound quasi-axially in EGC-4β → 8-EC and EGC-4β → 8-C. Detection of NOE correlations between H2 and H4 indicated that the terminal unit of GC-4α → 8-C is bound quasi-equatorially.

Compound EGC-4β → 8-EC showed a major rotamer (90%) and a minor rotamer (10%), whereas no rotamers were detected for EGC-4β → 8-C. The presence of (+)-gallocatechin in the upper unit leads to hindered rotation around the interflavanoid linkage, producing two major rotational isomers in a ratio of about 1:1 (55 to 45%). This leads to signal duplication in ^{1}H and ^{13}C NMR spectra at 300 K. In addition to EGC-4β → 8-EC and EGC-4β → 8-C, one- and two-dimensional ^{13}C NMR spectra were recorded for GC-4α → 8-C. H2′ and H6′ protons of the trihydroxylated B-ring C atoms ((epi)gallocatechin) showed a signal at about δ_C 108.0. Inspection of the region δ_C 115−120 show the signals of H2′, H5′, and H6′ of the dihydroxylated B-ring C atoms ((epi)catechins).[33−35] Signals at δ_C 83.0 and 84.0 suggested the 2,3-*trans* configuration of both units.[27] The observed data were in accordance with literature data.[34] The presence of two rotamers (25 °C, 500 MHz, acetone-d_6) was described later by Karonen et al.[26]

Structure Elucidation by Phloroglucinolysis and CD. The flavan-3-ol units and the interflavanoid bond of these compounds were confirmed by phloroglucinolysis. Degradation of >70% indicated a 4 → 8 interflavanoid linkage of these B-type dimeric prodelphinidins. Mild degradation yielded for compound EGC-4β → 8-EC 20.1% EGC-phloroglucinol for the upper unit and 54% EC for the terminal unit. EGC-4β → 8-C gave 18.2% EGC-phloroglucinol and 53.9% C and GC-4α → 8-C, 26.0% GC-phloroglucinol and 64.9% C. Moreover, these results indicated that 4 → 8-linked B-type dimeric prodelphinidins with (+)-gallocatechin in the upper unit were cleaved more quickly than those with (−)-epigallocatechin in the upper unit.

The absolute configuration at positions C2 and C4 was determined by CD spectra. All compounds ((−)-EGC-4β → 8-(+)-C, (−)-EGC-4β → 8-(−)-EC, (+)-GC-4α → 8-(+)-C) with 2*R* absolute stereochemistry showed a negative Cotton effect at 280 nm. Compounds (−)-EGC-4β → 8-(+)-C and (−)-EGC-4β → 8-(−)-EC showed a positive Cotton effect at 220−240 nm, indicating the 2β-4β-orientation (4*R* configuration).[36] However, the 2α−4α orientation (4*S* configuration) in (+)-GC-4α → 8-(+)-C was confirmed by the negative Cotton effect at 220−240 nm.

To date, the structure elucidation of these three dimeric prodelphinidins was done by ^{13}C NMR spectroscopy and acid-catalyzed degradation or ^{1}H NMR spectroscopy after derivatization (i.e., peracetylation), whereas Malik et al.[37] elucidated only the structure of EGC-4β → 8-EC by ^{1}H NMR spectroscopy without derivatization or degradation. Here, we describe to the best of our knowledge the NMR and assignment of the interflavanoid bond from ROESY spectra of B-type dimeric prodelphinidins for the first time in detail.

Structure elucidation was performed without the necessity of derivatization and degradation (i.e., phloroglucinolysis), ^{1}H NMR spectroscopy was sufficient.

■ ASSOCIATED CONTENT

Supporting Information

Figures S1−S3. This material is available free of charge via the Internet at http://pubs.acs.org.

■ AUTHOR INFORMATION

Corresponding Author

*(P.W.) Phone: +49-531-391-7200. Fax: +49-531-391-7230. E-mail: p.winterhalter@tu-bs.de.

Funding

This project was supported by a grant of the German Federal Ministry of Education and Research (BMBF − Bundesministerium für Bildung und Forschung, Grant 0313828C).

Notes

The authors declare no competing financial interest.

■ ACKNOWLEDGMENTS

We are grateful to B. Jaschok-Kentner and C. Kakoschke (Helmholtz Centre for Infection Research, Braunschweig, Germany) for NMR measurements and Wild Flavors GmbH & Co. KG (Berlin, Germany) for providing roasted hazelnut skins (*Corylus avellana* L.).

■ ABBREVIATIONS USED

HSCCC, high-speed countercurrent chromatography; LSRCCC, low-speed rotary countercurrent chromatography; EC, (−)-epicatechin; C, (+)-catechin; EGC, (−)-epigallocatechin; GC, (+)-gallocatechin; (Epi)C, (+)-catechin or (−)-epicatechin; (Epi)GC, (+)-gallocatechin or (−)-epigallocatechin

■ REFERENCES

(1) Manach, C.; Scalbert, A.; Morand, C.; Remesy, C.; Jimenez, L. Polyphenols: food sources and bioavailability. *Am. J. Clin. Nutr.* **2004**, *79*, 727−747.

(2) Gu, L.; Kelm, M. A.; Hammerstone, J. F.; Beecher, G.; Holden, J.; Haytowitz, D.; Prior, R. L. Screening of foods containing proanthocyanidins and their structural characterization using LC-MS/MS and thiolytic degradation. *J. Agric. Food Chem.* **2003**, *51*, 7513−7521.

(3) De Pascual-Teresa, S.; Santos-Buelga, C.; Rivas-Gonzalo, J. C. Quantitative analysis of flavan-3-ols in Spanish foodstuffs and beverages. *J. Agric. Food Chem.* **2000**, *48*, 5331−5337.

(4) Gu, L.; Kelm, M. A.; Hammerstone, J. F.; Beecher, G.; Holden, J.; Haytowitz, D.; Gebhardt, S.; Prior, R. L. Concentrations of proanthocyanidins in common foods and estimations of normal consumption. *J. Nutr.* **2004**, *134*, 613−617.

(5) Cos, P.; De Bruyne, T.; Hermans, N.; Apers, S.; Berghe, D. V.; Vlietinck, A. J. Proanthocyanidins in health care: current and new trends. *Curr. Med. Chem.* **2004**, *11*, 1345−1359.

(6) Pelvan, E.; Alasalvar, C.; Uzman, S. Effects of roasting on the antioxidant status and phenolic profiles of commercial Turkish hazelnut varieties (*Corylus avellana* L.). *J. Agric. Food Chem.* **2012**, *60*, 1218−1223.

(7) Food and Agriculture Organization of the United Nations. *FAO Statistical Yearbook 2012*; http://faostat3.fao.org/home/index.html#DOWNLOAD (accessed Dec 28, 2013).

(8) Del Rio, D.; Calani, L.; Dall'Asta, M.; Brighenti, F. Polyphenolic composition of hazelnut skin. *J. Agric. Food Chem.* **2011**, *59*, 9935−9941.

(9) Monagas, M.; Garrido, I.; Lebrón-Aguilar, R.; Gómez-Cordovés, M. C.; Rybarczyk, A.; Amarowicz, R.; Bartolomé, B. Comparative flavan-3-ol profile and antioxidant capacity of roasted peanut, hazelnut, and almond skins. *J. Agric. Food Chem.* **2009**, *57*, 10590−10599.

(10) Schmitzer, V.; Slatnar, A.; Veberic, R.; Stampar, F.; Solar, A. Roasting affects phenolic composition and antioxidative activity of hazelnuts (*Corylus avellana* L.). *J. Food Sci.* **2011**, *76*, S14−S19.

(11) Köhler, N.; Wray, V.; Winterhalter, P. New approach for the synthesis and isolation of dimeric procyanidins. *J. Agric. Food Chem.* **2008**, *56*, 5374−5385.

(12) Esatbeyoglu, T.; Winterhalter, P. Preparation of dimeric procyanidins B1, B2, B5, and B7 from a polymeric procyanidin fraction of black chokeberry (*Aronia melanocarpa*). *J. Agric. Food Chem.* **2010**, *58*, 5147−5153.

(13) Esatbeyoglu, T.; Jaschok-Kentner, B.; Wray, V.; Winterhalter, P. Structure elucidation of procyanidin oligomers by low temperature ^{1}H NMR spectroscopy. *J. Agric. Food Chem.* **2011**, *59*, 62−69.

(14) Esatbeyoglu, T.; Wray, V.; Winterhalter, P. Dimeric procyanidins: screening for B1 to B8 and semisynthetic preparation of B3, B4, B6, and B8 from a polymeric procyanidin fraction of white willow bark (*Salix alba*). *J. Agric. Food Chem.* **2010**, *58*, 7820−7830.

(15) Esatbeyoglu, T.; Wray, V.; Winterhalter, P. Identification of two novel prodelphinidin A-type dimers from roasted hazelnut skins (*Corylus avellana* L.). *J. Agric. Food Chem.* **2013**, *61*, 12640−12645.

(16) Kennedy, J. A.; Jones, G. P. Analysis of proanthocyanidin cleavage products following acid-catalysis in the presence of excess phloroglucinol. *J. Agric. Food Chem.* **2001**, *49*, 1740−1746.

(17) Köhler, N.; Winterhalter, P. Large-scale isolation of flavan-3-ol phloroglucinol adducts by high-speed counter-current chromatography. *J. Chromatogr., A* **2005**, *1072*, 217−222.

(18) Köhler, N. *Entwicklung und Anwendung leistungsfähiger präparativer gegenstromverteilungschromatographischer Trenntechniken*; Cuvillier Verlag: Göttingen, Germany, 2006 (Ph.D. thesis, in German).

(19) Phenol-Explorer 3.0: database on polyphenol contents in foods; http://www.phenol-explorer.eu/contents/food/716 (accessed Jan 24, 2014).

(20) Friedrich, W.; Eberhardt, A.; Galensa, R. Investigation of proanthocyanidins by HPLC with electrospray ionization mass spectrometry. *Eur. Food Res. Technol.* **2000**, *211*, 56−64.

(21) Hemingway, R. W.; Foo, L. Y.; Porter, L. J. Linkage isomerism in trimeric and polymeric 2,3-*cis*-procyanidins. *J. Chem. Soc., Perkin Trans. 1* **1982**, *5*, 1209−1216.

(22) Viviers, P. M.; Kolodziej, H.; Young, D. A.; Ferreira, D.; Roux, D. G. Synthesis of condensed tannins. Part 11. Intramolecular enantiomerism of the constituent units of tannins from the Anacardiaceae: stoichiometric control in direct synthesis: derivation of ^{1}H nuclear magnetic resonance parameters applicable to higher oligomers. *J. Chem. Soc., Perkin Trans. 1* **1983**, *10*, 2555−2562.

(23) Baldé, A. M.; Pieters, L. A.; Wray, V.; Kolodziej, H.; Vanden Berghe, D. A.; Claeys, M.; Vlietinck, A. J. Dimeric and trimeric proanthocyanidins possessing a doubly linked structure from *Pavetta owariensis*. *Phytochemistry* **1991**, *30*, 4129−4135.

(24) Monagas, M.; Garrido, I.; Lebrón-Aguilar, R.; Bartolomé, B.; Gómez-Cordovés, C. Almond (*Prunus dulcis* (Mill.) D.A. Webb) skins as a potential source of bioactive polyphenols. *J. Agric. Food Chem.* **2007**, *55*, 8498−8507.

(25) Danne, A.; Petereit, F.; Nahrstedt, A. Proanthocyanidins from *Cistus incanus*. *Phytochemistry* **1993**, *34*, 1129−1133.

(26) Karonen, M.; Leikas, A.; Loponen, J.; Sinkkonen, J.; Ossipov, V.; Pihlaja, K. Reversed-phase HPLC-ESI/MS analysis of birch leaf proanthocyanidins after their acidic degradation in the presence of nucleophiles. *Phytochem. Anal.* **2007**, *18*, 378−386.

(27) Fletcher, A. C.; Porter, L. J.; Haslam, E.; Gupta, R. K. Plant proanthocyanidins. Part 3. Conformational and configurational studies of natural procyanidins. *J. Chem. Soc., Perkin Trans. 1* **1977**, *14*, 1628−1637.

(28) Botha, J. J.; Young, D. A.; Ferreira, D.; Roux, D. G. Synthesis of condensed tannins. Part 1. Stereoselective and stereospecific syntheses of optically pure 4-arylflavan-3-ols, and assessment of their absolute

stereochemistry at C-4 by means of circular dichroism. *J. Chem. Soc., Perkin Trans. 1* **1981**, *4*, 1213−1219.
(29) Van der Westhuizen, J. H.; Ferreira, D.; Roux, D. G. Synthesis of condensed tannins. Part 2. Synthesis by photolytic rearrangement, stereochemistry, and circular dichroism of the first 2,3-*cis*-3,4-*cis*-4-arylflavan-3-ols. *J. Chem. Soc., Perkin Trans. 1* **1981**, *4*, 1220−1226.
(30) Delcour, J. A.; Ferreira, D.; Roux, D. G. Synthesis of condensed tannins. Part 9. The condensation sequence of leucocyanidin with (+)-catechin and with the resultant procyanidins. *J. Chem. Soc., Perkin Trans. 1* **1983**, *8*, 1711−1717.
(31) Kolodziej, H. ^{1}H NMR spectral studies of procyanidin derivatives: diagnostic ^{1}H NMR parameters applicable to the structural elucidation of oligomeric procyanidins. In *Plant Polyphenols: Synthesis, Properties, Significance*; Hemingway, R. W., Laks, P. E., Eds.; Plenum Press: New York, 1992; pp 295−319.
(32) Weinges, K.; Schick, H.; Rominger, F. X-Ray structure analysis of procyanidin B1. *Tetrahedron* **2001**, *57*, 2327−2330.
(33) Czochanska, Z.; Foo, L. Y.; Newman, R. H.; Porter, L. J. Polymeric proanthocyanidins. Stereochemistry, structural units, and molecular weight. *J. Chem. Soc., Perkin Trans. 1* **1980**, *10*, 2278−2286.
(34) Sun, D.; Wong, H.; Foo, L. Y. Proanthocyanidin dimers and polymers from *Quercus dentata*. *Phytochemistry* **1987**, *26*, 1825−1829.
(35) Porter, L. J. Tannins. In *Methods in Plant Biochemistry, I: Plant Phenolics*; Harborne, J. B., Ed.; Academic Press: London, UK, 1989; pp 389−419.
(36) Barrett, M. W.; Klyne, W.; Scopes, P. M.; Fletcher, A. C.; Porter, L. J.; Haslam, E. Plant proanthocyanidins. Part 6. Chiroptical studies. Part 95. Circular dichroism of procyanidins. *J. Chem. Soc., Perkin Trans. 1* **1979**, *10*, 2375−2377.
(37) Malik, A.; Kuliev, Z. A.; Akhmedov, U. A.; Vdovin, A. D.; Abdullaev, N. D. Catechins and proanthocyanidins of *Alhagi sparsifolia*. I. *Chem. Nat. Compd.* **1997**, *33*, 174−178.
(38) Esatbeyoglu, T. *Analyse wertgebender Inhaltsstoffe von Aronia melanocarpa sowie Charakterisierung und Isolierung von Proanthocyanidinen*; Cuvillier Verlag: Göttingen, Germany, 2011 (Ph.D. thesis, in German).

oxidation of phenolic hydroxyls leading to the formation of *O*-quinone via semiquinone form. Therefore, it may be argued whether these four easily oxidized phenolic acids are true representatives of "total phenolic acids" having diverse oxidation potentials.

There is very limited study about the usage of GC electrodes as electrochemical TAC sensors. Milardović et al. developed an amperometric antioxidant activity method, based on the reduction of 2,2′-diphenyl-1-picrylhydrazyl radical ($DPPH^{\bullet}$) at the GC electrode; because the cyclic voltammograms of a number of water- and ethanol-soluble common antioxidants gave either irreversible or undefined oxidation peaks, electrochemical reduction of $DPPH^{\bullet}$ was conducted in the presence and absence of antioxidants, but potential selection was critical due to the electrochemical interferences of caffeic acid and trolox.[9] The electrochemical $ABTS^{\bullet+}$ assay is based on measuring catalytic voltammetric currents caused by antioxidants acting as reductant toward the electrochemically generated $ABTS^{2+}$ (thereby enabling reoxidation of $ABTS^{\bullet+}$ on the electrode) in edible oils; this method produced rather high blank values in the trolox calibration curve, and trolox addition to sunflower oil matrices did not yield perfectly linear responses.[10]

It may be argued that novel electrochemical TAC methods should be based on indirect determinations, that is, on the redox behavior of a single electroactive species capable of reacting with antioxidants with a definite stoichiometry and kinetics, because, otherwise, irreversible or undefined peaks of phenolics oxidation may emerge within a range of potentials, making an evaluation of the results obtained with complex samples very difficult and sometimes inaccurate. Although an electrochemical CUPRAC method (based on CV and chronoamperometry) of antioxidant analysis has very recently been published,[11] it does not cover a wide range of antioxidant compounds, and there is no DPV method in the literature for the determination of cupric reducing antioxidant capacity of complex samples. Therefore, the aims of this study are to develop a new electrochemical technique using DPV–CUPRAC methodology for pure phenolic antioxidants, ascorbic acid, and their complex matrices such as herbal teas and to compare the results obtained by the proposed assay with those obtained by spectrophotometric CUPRAC assay. Compared to other chromogenic reagents of similar properties (i.e., $DPPH^{\bullet}$ and $ABTS^{\bullet+}$), the CUPRAC reagent has been shown to be much less dependent on phenolic lipophilicity, steric effects of accessibility, solvent composition, pH, dissolved oxygen, and daylight.[12]

MATERIALS AND METHODS

Chemicals. The following chemicals of analytical reagent grade were supplied from the corresponding sources: copper(II) chloride, ammonium acetate, hydrochloric acid, sodium hydroxide, potassium chloride, ascorbic acid, and syringic acid were purchased from Merck Chemicals (Darmstadt, Germany); gallic acid, neocuproine, chlorogenic acid, (−)epicatechin, *p*-coumaric acid, quercetin, ferulic acid, vanillic acid, trolox, acetic acid, nitric acid, methanol, and absolute ethanol were supplied from Sigma-Aldrich Chemicals (Steinheim, Germany); (−)-catechin and kaempferol were obtained from Fluka (Buchs, Switzerland).

Samples and Standards. The herbal tea samples (green tea, marjoram, sage, and alchemilla) were obtained from local markets (Istanbul, Turkey). The fine dried herbal tea samples were extracted with the aid of a microwave-assisted extraction (MAE) system (Milestone ETHOS ONE, Shelton, CT, USA). MAE was utilized in 12 Teflon closed vessels with an automatic fiber optic temperature control system; dried sample (0.5 g) was extracted with 10 mL of $EtOH/H_2O$ (4:1, v/v) mixtures at 80 °C for 3 min after 3 min of temperature balancing time, and the microwave power (0−1500 W) was adjusted automatically according to temperature (5 min). The obtained ethanolic extracts were filtered through a filter paper, then through 0.45 μm PTFE syringe filters (Whatman), and kept at 4 °C until use. All standard solutions of antioxidant polyphenols were initially prepared in absolute EtOH at a concentration of 10 mM and diluted (to 1 mM) using bidistilled water (Millipore Synergy UV, Molsheim, France). Thus, the polyphenol working solutions were finally in 10% EtOH medium, except quercetin, which was finally prepared in 50% EtOH due to the aqueous solubility limitation. All standard solutions were stored at −20 °C prior to analysis. For spectrophotometric measurements, $CuCl_2$ solution (10 mM) and ammonium acetate buffer solution (1 M, pH 7.0) were prepared in bidistilled water, and neocuproine solution (7.5 mM) was prepared in EtOH. For electrochemical measurements, $CuCl_2$ solution (2 mM) and acetic acid/acetate buffer solution (supporting electrolyte, 0.1 M, pH 4.76) were prepared in bidistilled water, and neocuproine solution (4 mM) was prepared in EtOH.

DPV–CUPRAC Assay (Proposed Method). DPV was performed using a potentiostat model Reference 600 (Potentiostat/Galvanostat/ZRA, Gamry) in a three-electrode configuration, employing a GC electrode (Gamry, 3 mm disk, 7 mM OD) as the working electrode, platinum wire as the counter electrode, and Ag/AgCl (∼5 mol/L KCl) as the reference electrode. The GC electrode was polished before electrochemical measurements; that is, the electrode surface was manually polished with an alumina suspension (Baikowski Int. Corp.; 0.05 μm) on polishing cloth for 2 min and rinsed with distilled water; then, the electrode was immersed in $EtOH/H_2O$ (1:1, v/v) mixture, transferred to an ultrasonication bath for 3−4 min, and rinsed with ultrapure water. Finally, the electrode was immersed in distilled water and ultrasonication was repeated.

The required volume of antioxidant standards and samples (herbal tea extracts) was added by micropipet into a mixture solution of the supporting electrolyte and Cu(II)−Nc chelate in the electrochemical cell. The reaction mixture was left to react for ∼1 min on a stirrer at room temperature. The voltammograms were recorded immediately to minimize adsorption of polyphenols (or other electroactive species) onto the GC electrode surface. DPV conditions were as follows: scan range, from +0.6 to −0.25 V; pulse size, 50 mV; step size, 4 mV; pulse time, 0.1 s; and sample period, 0.5 s. The cyclic voltammograms were recorded on a freshly polished GC electrode by scanning the potential from +0.8 to −0.2 V at a scanning rate of 40 mV/s.

The TAC values of herbal teas were determined by DPV experiments, and the results were expressed as millimoles of trolox equivalents per gram of tea (mmol TE/g tea). The standard calibration curves of trolox and other phenolics were obtained by measuring the currents (I_p) at the cathodic reduction peak potential of the $Cu(Nc)_2^{2+}/Cu(Nc)_2^{+}$ redox couple before and after reaction with antioxidants, taking the difference (ΔI_p), and plotting this difference versus concentration of antioxidant standard.

Spectrophotometric CUPRAC Assay. The spectrophotometric CUPRAC method described by Apak et al. is based on the reduction of a cupric neocuproine complex (Cu(II)−Nc) by antioxidants to the highly colored cuprous form (Cu(I)−Nc).[12] One milliliter of $CuCl_2$, 1 mL of Nc solution, and 1 mL of NH_4Ac solution were added to x mL of the analyte, followed by $(1.1-x)$ mL of H_2O. The absorbance of the final solution (of 4.1 mL total volume) at 450 nm was read against a reagent blank after 30 min of standing at room temperature. The absorption measurements were recorded in matched quartz cuvettes using a Varian CARY Bio 100 UV−vis spectrophotometer (Mulgrave, Victoria, Australia) having a spectral resolution of ≈1 nm. The calibration curves (absorbance versus concentration graphs) of each antioxidant were constructed under the described conditions, and their TEAC coefficients, found as the ratio of the molar absorptivity of the concerned compound to that of trolox in the CUPRAC assay, were calculated. All spectrophotometric analyses were carried out in triplicate and performed at room temperature.

Statistical Analysis. Statistical analyses were realized using Excel software (Microsoft Office 2002) for calculating the means and the standard errors of the means. Results were expressed within 95% confidence interval as mean ± ($t_{0.05}s/n^{1/2}$), where $t_{0.05}$ is the Student's table t value for 4 degrees of freedom and s is the standard deviation of n = 5 measurements. Using SPSS software for Windows (version 13), the data were interpreted by two-way analysis of variance (ANOVA).[13]

RESULTS AND DISCUSSION

Electrochemical Behavior of $Cu(Nc)_2^{2+}$ Reagent. The cyclic voltammogram of $Cu(Nc)_2^{2+}$ reagent (prepared in 1:2 molar ratio of metal to ligand, i.e., 2 mL of 2 mM Cu(II) + 2 mL of 4 mM Nc) in 6 mL of 0.1 M acetic acid/acetate buffer solution (supporting electrolyte, pH 4.76) at a glassy carbon electrode shows the existence of $Cu(Nc)_2^{2+}/Cu(Nc)_2^{+}$ redox couple (Figure 1). An oxidation (anodic) peak appeared at

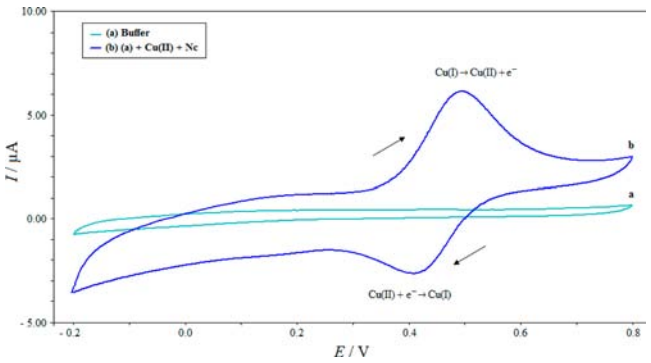

Figure 1. Cyclic voltammogram of $Cu(Nc)_2^{2+}$ reagent (scan rate = 40 mV/s): (a) acetic acid/acetate buffer solution (0.1 M, pH 4.76) (supporting electrolyte); (b) acetic acid/acetate buffer solution + 0.4 mM Cu(II) + 0.8 mM Nc. CV scan was made negatively from +0.8 to −0.2 V (one cycle) and at a rate of 40 mV/s.

approximately 0.5 V and a reduction (cathodic) peak at approximately 0.41 V. Compared to the electrochemical CUPRAC method of Cárdenas et al. carried out in pH 7 ammonium acetate buffer,[11] it can be clearly seen from the voltammogram in Figure 1 that pH 4.76 acetate buffer produced better electrochemical reversibility.

Figure 2 shows the DPVs of copper(II), cupric−neocuproine complex, and trolox in acetic acid/acetate buffer medium and under identical conditions. It is apparent from this figure that the presence of 2 equiv of neocuproine per 1 equiv of copper(II) leads to a substantial change (of about 0.43 V) in the potential of the Cu(II)/Cu(I) redox couple due to the selective stabilization of tetrahedral cuprous state by neocuproine (i.e., the logarithmic stability constants of the concerned copper chelates, $Cu(Nc)_2^{2+}$ and $Cu(Nc)_2^{+}$, have been reported as 12 and 19, respectively).[14] The reduction potential of the cupric−neocuproine complex was found at approximately 0.41 V with DPV. The peak current of cupric−neocuproine (Figure 2d) decreased as a result of reaction with trolox (Figure 2e) without a significant shift in reduction potential.

Electrochemistry of $Cu(Nc)_2^{2+}$ Reagent in the Presence of Trolox. Concentrations of trolox >0.001 mM led to a corresponding decrease of the cathodic peak currents (see Figure 3A,B). When trolox is added in the electrochemical cell containing $Cu(Nc)_2^{2+}$, it is easily oxidized to the quinone form, whereas Cu(II)−Nc is reduced to the highly colored Cu(I)−Nc chelate. As the concentration of trolox increases, the

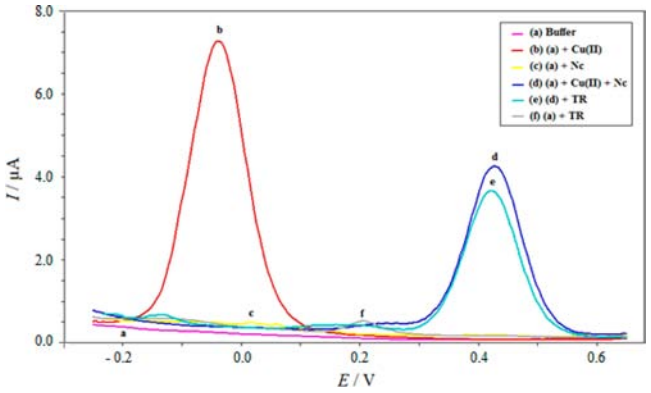

Figure 2. Differential pulse voltammograms of (a) acetic acid/acetate buffer solution (0.1 M, pH 4.76) (supporting electrolyte), (b) acetic acid/acetate buffer solution + 0.4 mM Cu(II), (c) acetic acid/acetate buffer solution + 0.8 mM Nc, (d) acetic acid/acetate buffer solution + Cu(II) + Nc, (e) acetic acid/acetate buffer solution + Cu(II) + Nc + 0.08 mM TR, and (f) acetic acid/acetate buffer solution + 0.08 mM TR. Scans range from +0.7 to −0.25 V; pulse size, 50 mV; step size, 4 mV; pulse time, 0.1 s, and sample period, 0.5 s.

cathodic voltammetric currents decrease further, because the $Cu(Nc)_2^{2+}$ complex in the media is reduced to the $Cu(Nc)_2^{+}$ form in proportion to trolox. Thus, the initial amount of $Cu(Nc)_2^{2+}$ cannot be maintained upon trolox addition, causing a pronounced decrease in cathodic currents (Figure 3A,B). On the other hand, with increasing trolox concentrations, more $Cu(Nc)_2^{+}$ will be produced, and its electrochemical oxidation (anodic peak) currents at approximately 0.5 V show a slight increase (Figure 3A). The decrease in cathodic peak current upon trolox addition is taken as a measure of trolox concentration (Figure 3C). The dependence of ΔI_p on trolox concentration (C_{TR}) is presented in Figure 3C, where ΔI_p is defined as the difference between the measured DPV peak currents in the absence of trolox ($I_{p,0}$) and in the presence of corresponding trolox concentrations ($I_{p,x}$), that is, $\Delta I_p = I_{p,0} - I_{p,x}$. The calibration equation corresponding to the regression line as ΔI_p versus C_{trolox} using the DPV method was $\Delta I_p/\mu A = 46.66 C_{TR}/\text{mmol L}^{-1} + 0.019$. This equation was also used for TAC determination of herbal teas, reported as trolox equivalents.

The linear concentration range for trolox in the proposed method was 0.001−0.005 mM (correlation coefficient r = 0.9995, N = 5), within which the relative standard deviation (RSD) was 3.1%. The limit of detection (LOD) and the limit of quantification (LOQ) were calculated using the equations LOD = $3s_{bl}/m$ and LOQ = $10s_{bl}/m$, respectively, where s_{bl} is the standard deviation of a blank and m is the slope of the calibration line. The LOD and LOQ for trolox were found as 0.18 and 0.61 μM, respectively.

Determination of Polyphenols by Voltammetric and Spectrophotometric Methods. The chromogenic oxidizing reagent of the spectrophotometric CUPRAC method, that is, (Cu(II)−Nc) chelate, reacts with n-electron reductant antioxidants (AO) in the following reaction:[12,15]

$$n\text{Cu(Nc)}_2^{2+} + n\text{-electron reductant (AO)} \rightarrow n\text{Cu(Nc)}_2^{+} + n\text{-electron oxidized product} + n\text{H}^{+} \quad (1)$$

In this reaction, the reactive Ar−OH groups of polyphenolic antioxidants are oxidized to the corresponding quinones (e.g.,

dx.doi.org/10.1021/jf5017797 | J. Agric. Food Chem. 2014, 62, 7111−7117

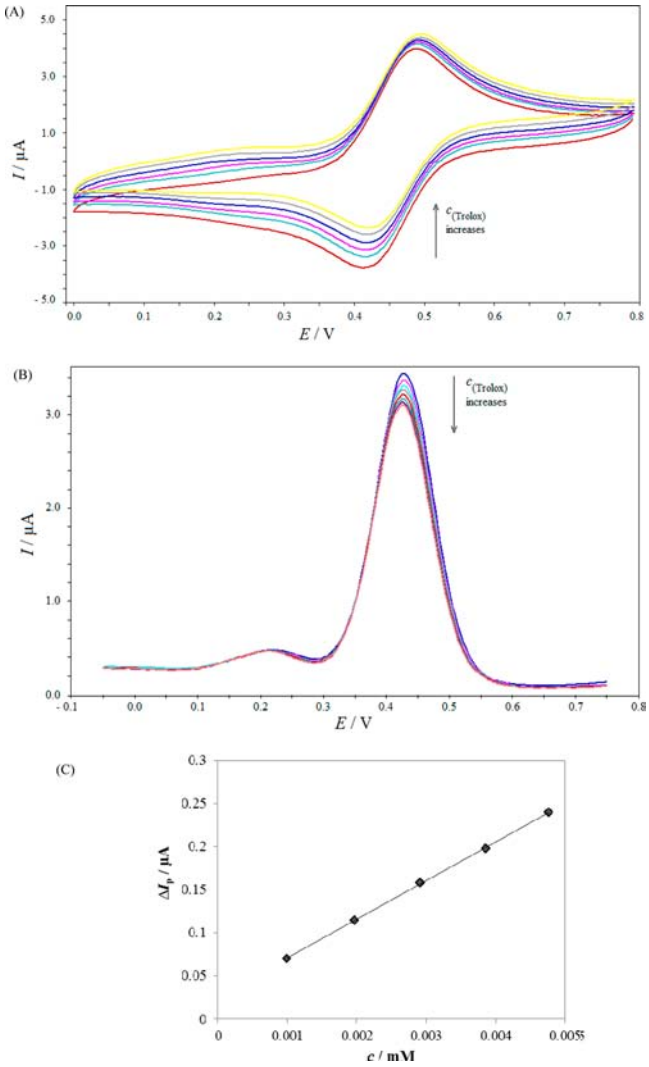

Figure 3. Cyclic (A) and differential pulse (B) voltammograms of $Cu(Nc)_2^{2+}$ reagent, showing the effect of increasing trolox concentration in the range of 0.001−0.005 mM; (C) dependence of ΔI_p on trolox concentration. ΔI_p is defined as the difference between the measured DPV peak currents in the absence of trolox ($I_{p,0}$) and in the presence of corresponding trolox concentrations ($I_{p,x}$), that is, $\Delta I_p = I_{p,0} - I_{p,x}$. Supporting electrolyte was acetic acid/acetate buffer solution (0.1 M, pH 4.76), and other conditions were the same as in Figure 2.

ascorbic acid is 2e-oxidized to dehydroascorbic acid, and trolox is 2e-oxidized to the corresponding quinone), whereas Cu(II)−Nc is reduced to the highly colored Cu(I)−Nc chelate showing maximum absorption at 450 nm. Spectrophotometric CUPRAC is a relatively fast assay, where most of the tested antioxidants reach ≥80% of their maximal molar absorptivities within ≥1 min and do not show a distinct capacity change within 30 min. However, slow-reacting antioxidants (i.e., naringenin, hesperetin) may show a dramatic capacity change within 30 min.[12,16] Therefore, the relatively short measurement time of the electrochemical CUPRAC method does not pose major problems in electron-transfer kinetics of most antioxidants.

The recommended voltammetric method for TAC assay is based on the electrochemical reduction of $Cu(Nc)_2^{2+}$ at the GC electrode polarized at a potential lower than the reduction potential of $Cu^{II,I}(Nc)_2$ redox couple (which is about 0.6 V). Antioxidant capacities of 12 antioxidant compounds, namely, hydroxybenzoic acids (vanillic acid, gallic acid, syringic acid), hydroxycinnamic acids (*p*-coumaric acid, ferulic acid, chlorogenic acid), flavonols (kaempferol and quercetin), flavon-3-ols (epicatechin and catechin), and others (trolox and ascorbic acid), were electrochemically determined.

Table 1 summarizes the related linear equations, correlation coefficients, linear ranges, and LOD and LOQ values of the antioxidant compounds tested by the DPV−CUPRAC method (for comparison, the corresponding values found by the conventional spectrophotometric−CUPRAC method are also listed in Table 1). The electrochemical determination of the antioxidant capacity of these phenolic groups (except for *p*-coumaric and ferulic acids) was performed under the same experimental conditions used for quantifying trolox (Table 1). A linear response of the peak current as a function of concentration was observed for phenolic compounds over the concentration ranges studied.

The LOD values of the phenolics found with the DPV−CUPRAC method were lower than those found with spectrophotometric−CUPRAC. The LOD (0.18 μM) found by the recommended DPV method was much lower than that of the electrochemical CUPRAC method of Cárdenas et al.[11] It is also noteworthy that the LOD values for CT and CGA found with the proposed DPV procedure (0.15 and 0.24 μM, respectively) are lower than the corresponding LODs of 1.03 and 0.28 μM, reported by Blasco et al., who used a flow injection system with a glassy carbon electrode.[17]

The voltammetric trolox equivalent antioxidant capacity ($TEAC_{voltammetric}$, defined as mM trolox equivalents of 1.0 mM antioxidant solution under investigation) was simply calculated by dividing the slope of the linear calibration equations of phenolics under investigation by that of trolox under corresponding conditions (i.e., the slope of trolox was 46.66 μA/mM) using eq 2.

$$TEAC_{voltammetric} = \frac{slope_{AO}}{slope_{TR}} \text{ (AO, antioxidant; TR, trolox)} \quad (2)$$

The spectrophotometric trolox equivalent antioxidant capacity ($TEAC_{spectrophotometric}$) values of the phenolics in 10% ethanol were likewise calculated by dividing the molar absorptivity (ε) of each antioxidant by the molar absorptivity of trolox (ε_{trolox} was 15.36 L $mmol^{-1}$ cm^{-1} under the specified conditions) using eq 3.

$$TEAC_{spectrophotometric} = \frac{\varepsilon_{AO}}{\varepsilon_{TR}} \quad (3)$$

The $TEAC_{voltammetric}$ and $TEAC_{spectrophotometric}$ values were compared (Table 2) to yield compatible results. For the tested phenolic antioxidants, the voltammetric method correlated linearly with spectrophotometric method (r = 0.9791, N = 5) (Figure 4). A similar investigation on the interrelationship of spectrophotometric and DPV[10] modification of ABTS/persulfate assay gave slightly different results for the TEAC coefficients of gallic and ascorbic acids (unreported data), naturally requiring more measurements on antioxidant varieties to reach any conclusion. It should be remembered here that spectrophotometric−CUPRAC measures the absorbance of the $Cu(Nc)_2^{+}$ formed at pH 7.0, whereas voltammetric−CUPRAC measures the reduction current of the remaining $Cu(Nc)_2^{2+}$ at pH 4.76, after reaction with antioxidants; therefore, this

dx.doi.org/10.1021/jf5017797 | J. Agric. Food Chem. 2014, 62, 7111−7117

Table 1. Analytical Performance of Various Antioxidant Compounds Calculated with Respect to the Voltammetric (DPV) and Spectrophotometric (Conventional CUPRAC) Methods

polyphenol		linear range (mM)	linear calibration eq (10% EtOH)	r	LOD (μM)	LOQ (μM)
Voltammetric Method						
hydroxybenzoic acids	vanillic acid (VA)	$(0.99-4.76) \times 10^{-3}$	$y = 62.69c + 0.032$	0.9995	0.23	0.76
	gallic acid (GA)	$(0.49-2.38) \times 10^{-3}$	$y = 141.41c + 0.037$	0.9998	0.12	0.39
	syringic acid (SA)	$(0.99-4.76) \times 10^{-3}$	$y = 69.44c + 0.036$	0.9994	0.23	0.78
hydroxycinnamic acids	*p*-coumaric acid (CMA)	$(0.99-4.76) \times 10^{-3}$	$y = 60.77c + 0.084$	0.9998	0.62	2.07
	ferulic acid (FRA)	$(0.99-4.76) \times 10^{-3}$	$y = 54.23c + 0.006$	0.9943	0.05	0.16
	chlorogenic acid (CGA)	$(0.49-2.38) \times 10^{-3}$	$y = 126.68c + 0.068$	0.9988	0.24	0.80
flavonols	kaempferol (KAM)	$(0.99-4.76) \times 10^{-3}$	$y = 74.11c + 0.024$	0.9992	0.15	0.48
	quercetin (QR)	$(0.49-2.38) \times 10^{-3}$	$y = 193.77c + 0.051$	0.9995	0.12	0.39
flavon-3-ols	epicatechin (EC)	$(0.49-2.38) \times 10^{-3}$	$y = 145.93c - 0.039$	0.9992	0.12	0.40
	catechin (CT)	$(0.49-2.38) \times 10^{-3}$	$y = 134.71c + 0.045$	0.9953	0.15	0.50
others	trolox (TR)	$(0.99-4.76) \times 10^{-3}$	$y = 46.66c + 0.019$	0.9995	0.18	0.61
	L-ascorbic acid (AA)	$(0.99-4.76) \times 10^{-3}$	$y = 51.32c - 0.035$	0.9990	0.31	1.02
Spectrophotometric Method						
hydroxybenzoic acids	vanillic acid (VA)	$(4.88-24.40) \times 10^{-3}$	$y = 23.05c + 0.021$	0.9996	0.41	1.36
	gallic acid (GA)	$(2.44-12.20) \times 10^{-3}$	$y = 54.42c + 0.034$	0.9999	0.28	0.94
	syringic acid (SA)	$(4.88-14.64) \times 10^{-3}$	$y = 24.83c + 0.013$	0.9999	0.24	0.80
hydroxycinnamic acids	*p*-coumaric acid (CMA)	$(12.20-61.00) \times 10^{-3}$	$y = 12.59c + 0.051$	0.9989	1.82	6.07
	ferulic acid (FRA)	$(4.88-24.40) \times 10^{-3}$	$y = 23.39c + 0.007$	0.9993	0.13	0.45
	chlorogenic acid (CGA)	$(4.88-24.40) \times 10^{-3}$	$y = 47.21c + 0.024$	0.9995	0.38	1.27
flavonols	kaempferol (KAM)	$(4.88-24.40) \times 10^{-3}$	$y = 34.15c + 0.034$	0.9995	0.45	1.49
	quercetin (QR)	$(2.44-12.20) \times 10^{-3}$	$y = 84.51c + 0.028$	0.9992	0.15	0.50
flavon-3-ols	epicatechin (EC)	$(2.44-12.20) \times 10^{-3}$	$y = 60.38c + 0.017$	0.9994	0.13	0.42
	catechin (CT)	$(4.88-24.40) \times 10^{-3}$	$y = 51.67c + 0.041$	0.9993	0.36	1.19
others	trolox (TR)	$(6.10-30.48) \times 10^{-3}$	$y = 15.36c - 0.010$	0.9993	0.29	0.98
	L-ascorbic acid (AA)	$(6.10-30.48) \times 10^{-3}$	$y = 16.96c - 0.022$	0.9996	0.58	1.94

Table 2. Trolox Equivalent Antioxidant Capacities (TEAC) of Various Antioxidant Compounds Determined According to DPV and Spectrophotometric (CUPRAC) Methods[a]

polyphenol	$TEAC_{voltammetric}$	$TEAC_{spectrophotometric}$
trolox (TR)	1.00	1.00
hydroxybenzoic acids		
vanillic acid (VA)	1.34 ± 0.01	1.50 ± 0.08
gallic acid (GA)	3.03 ± 0.23	3.54 ± 0.05
syringic acid (SA)	1.49 ± 0.08	1.61 ± 0.25
hydroxycinnamic acids		
p-coumaric acid (CMA)	1.30 ± 0.08	0.82 ± 0.04
ferulic acid (FRA)	1.16 ± 0.11	1.52 ± 0.09
chlorogenic acid (CGA)	2.72 ± 0.19	3.07 ± 0.12
flavonols		
kaempferol (KAM)	1.59 ± 0.12	2.22 ± 0.15
quercetin (QR)	4.15 ± 0.19	5.50 ± 0.45
flavon-3-ols		
epicatechin (EC)	3.13 ± 0.25	3.93 ± 0.17
catechin (CT)	2.89 ± 0.03	3.36 ± 0.12
others		
L-ascorbic acid (AA)	1.10 ± 0.07	1.10 ± 0.03

[a]Data presented as mean ± ($t_{0.05}s/n^{1/2}$), $N = 5$.

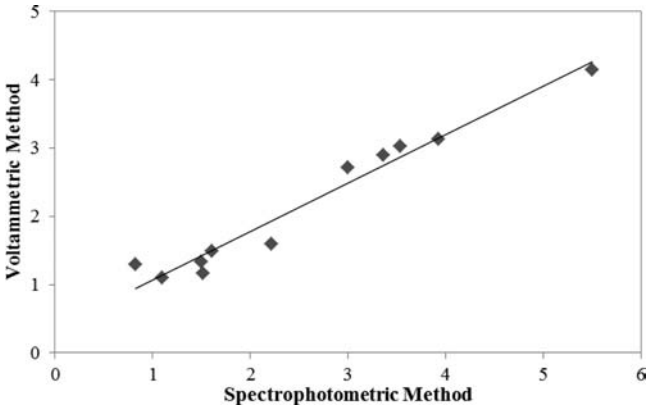

Figure 4. Correlation between spectrophotometric and voltammetric CUPRAC assays ($r = 0.9791$, $N = 5$) for found TEAC values of antioxidant standards.

correlation is highly satisfactory. The slight discrepancies of the spectrophotometric TEAC values obtained by the CUPRAC method shown in Table 2 from those available in the literature[15] may have arisen from the differences in solvent composition (i.e., measurements in this work were performed in 10% EtOH-containing aqueous media).

TAC Measurements of Herbal Teas. Addition of certain amounts of herbal tea extracts to the electrochemical cell containing $Cu(Nc)_2^{2+}$ reagent caused a successive decrease of the DPV peak currents (Figure 5A). Apparently, the antioxidants present in herbal teas exerted an electrochemical effect similar to that of trolox, as represented by eq 1. The decrease in DPV current intensities of $Cu(Nc)_2^{2+}$ reagent as a result of increasing herbal tea extract volume ratio ($V_{herbal\ teas}/V_{total}$, %) is shown for the tested herbal tea extracts in Figure 5B. The good linearity between these two parameters confirms that the voltammetric–CUPRAC method can be used for the determination of TAC of herbal teas and similar complex antioxidant samples. The TAC values of herbal teas were calculated with the use of eq 4, where ΔI_p is the difference in current intensity, m is the mass of dry herbal tea sample, V is volume, and DF is dilution factor.

dx.doi.org/10.1021/jf5017797 | J. Agric. Food Chem. 2014, 62, 7111–7117

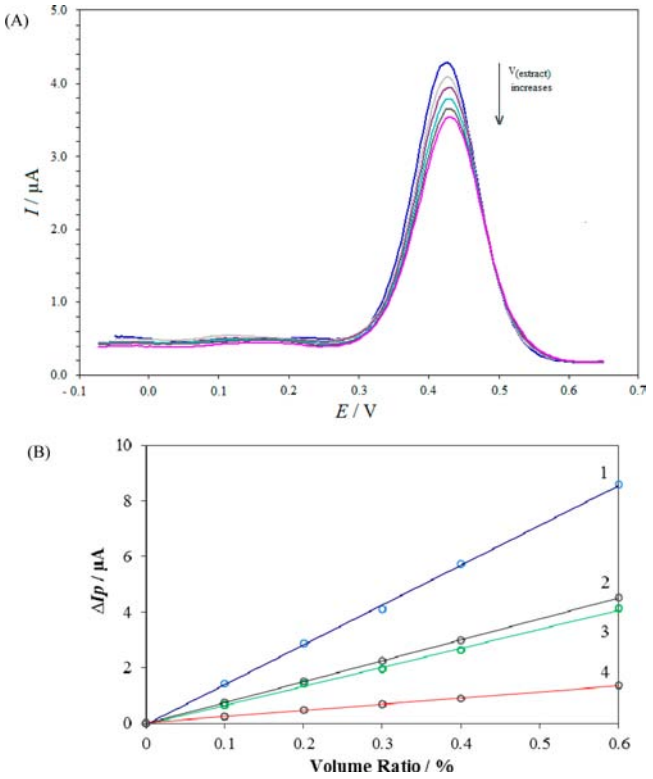

Figure 5. (A) Differential pulse voltammograms of $Cu(Nc)_2^{2+}$ reagent showing the effect of increasing herbal tea extract volume parts; (B) dependence of ΔI_p on the volume ratio ($V_{herbal\ teas}/V_{total}$, %) of green tea (1), marjoram (2), sage (3), and alchemilla (4) herbal teas. The calibration lines were found $y = 14.276x - 0.022$ $r = 0.9997$; $y = 7.512x - 0.002$, $r = 0.9999$; $y = 6.825x + 0.023$, $r = 0.9990$; and $y = 2.231x + 0.018$, $r = 0.9995$, respectively ($N = 5$). Supporting electrolyte was acetic acid/acetate buffer solution (0.1 M, pH 4.76), and other conditions were the same as in Figure 2.

$$\mathrm{TAC_{voltammetric}\ (mmol/g)} = \frac{\Delta I_p \pm \text{intercept}}{(\Delta I_p/c)_{TR}} \times \frac{V_{total}}{V_{sample}} \times \frac{V_{extract}\ (mL)}{m\ (g)} \times DF \times 10^{-3} \quad (4)$$

The analytical results for total antioxidant capacity (expressed in mmol trolox equivalents per g of dry herbal tea sample) by voltammetric method were found to be 1.23 ± 0.06, 0.80 ± 0.11, 0.68 ± 0.02, and 0.40 ± 0.03 mmol/g for green tea, sage, marjoram, and alchemilla, respectively. The corresponding spectrophotometric findings with the conventional CUPRAC method were 1.19 ± 0.11, 0.70 ± 0.02, 0.66 ± 0.01, and 0.38 ± 0.02 mmol/g for green tea, marjoram, sage, and alchemilla, respectively.

The TAC values of tested herbal tea samples measured by the developed voltammetric method were in good agreement with those of spectrophotometric–CUPRAC (Figure 6). The two-way analysis of variance (ANOVA) comparison by the aid of F test of the mean-squares of "between treatments" and of residuals[13] for a number of real samples (herbal teas) enabled the conclusion that there was no significant difference between the population means for a given sample. In other words, calculated total antioxidant contents were alike at a 95% confidence level ($F_{exptl} = 1.875$, $F_{crit(table)} = 6.608$, $F_{exptl} < F_{crit(table)}$ at $P = 0.05$). Thus, the proposed methodology was

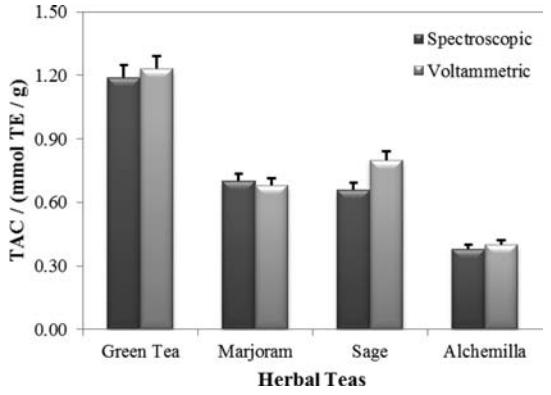

Figure 6. Total antioxidant capacities (mmol TE/g) of herbal teas (green tea, marjoram, sage, and alchemilla) determined by differential pulse voltammetric and spectrophotometric CUPRAC methods. Data are presented as mean ± ($t_{0.05}s/n^{1/2}$), $N = 5$. ($P = 0.05$, F_{exptl} =1.875, $F_{crit(table)} = 6.608$, $F_{exptl} < F_{crit(table)}$.)

validated. The proposed voltammetric method correlated linearly with the spectrophotometric method ($r = 0.9803$, $N = 5$), and the TAC values found with the two methods for herbal teas were compatible by ±3.2%.

Performance and Prospects of the DPV–CUPRAC Method. The developed DPV–CUPRAC method has been demonstrated for a variety of antioxidant compounds and validated against the well-documented spectrophotometric–CUPRAC procedure and can be an interesting alternative to spectrophotometric methods for determining the TAC of phenolic compounds in some herbal teas. The voltammetric method may be potentially useful for turbid and colored samples in which plant pigments may obscure the color of cuprous–neocuproine chromophore in spectrophotometry. The proposed method is easy and fast and showed better sensitivity (lower detection limits) than similar electrochemical assays. The electrochemical results showed that TACs of herbal teas were in the order green tea > sage > marjoram > alchemilla, in compliance with the results of the spectrophotometric–CUPRAC assay.

A separate turbidity investigation was undertaken in which TACs of filtered and unfiltered orange and peach nectars were assayed by DPV–and spectrophotometric–CUPRAC methods. The DPV–CUPRAC assay results (for both filtered and unfiltered samples) were close or comparable to those (for filtered sample) found by the spectrophotometric–CUPRAC method (Table 3). However, the unfiltered nectars gave high CUPRAC absorbances and therefore yielded positive errors in spectrophotometry. All spectrophotometric measurements, by nature, require the elimination of particulate matter (by filtration) before absorbance measurement. As a result, the proposed electrochemical assay proved to be efficient for turbid

Table 3. TACs of Some Nectars As Assayed by DPV – and Spectrophotometric– CUPRAC Methods[a]

sample	$TAC_{DPV-CUPRAC}$ (mmol trolox equiv/L nectar)	$TAC_{spect-CUPRAC}$ (mmol trolox equiv/L nectar)
orange nectar	1.96 ± 0.03 (2.04 ± 0.09)	1.82 ± 0.01 (4.5 ± 0.21)
peach nectar	1.57 ± 0.08 (1.53 ± 0.08)	1.51 ± 0.03 (3.5 ± 0.17)

[a]Data presented as mean ± ($t_{0.05}s/n^{1/2}$), $N = 5$. TAC values in parentheses represent turbid sample results.

dx.doi.org/10.1021/jf5017797 | J. Agric. Food Chem. 2014, 62, 7111–7117

samples for which the widely used spectrophotometric TAC assays are not accurately responsive.

AUTHOR INFORMATION

Corresponding Author

*(R.A.) Phone: +90 212 4737070. Fax: +90 212 473 7180. E-mail: rapak@istanbul.edu.tr.

Funding

S.B. thanks Istanbul University Research Fund, Bilimsel Arastirma Projeleri (BAP) Yurutucu Sekreterligi, for the support given to his Ph.D. Thesis Project 29746 and to Istanbul University, Institute of Pure and Applied Sciences (I.U. Fen Bilimleri Enstitüsü), for the support given to his Ph.D. thesis work with the title "Development of a Novel Electrochemical Method for Determining the Total Antioxidant Capacity of Foodstuff". We expresss our gratitude to T.R. Ministry of Development for the Advanced Research Project of Istanbul University (2011K120320).

Notes

The authors declare no competing financial interest.

REFERENCES

(1) Çelik, S. E.; Özyürek, M.; Güçlü, K.; Apak, R. Solvent effects on the antioxidant capacity of lipophilic and hydrophilic antioxidants measured by CUPRAC, ABTS/persulphate and FRAP methods. *Talanta* **2010**, *81*, 1300−1309.

(2) Ames, B. N. Dietary carcinogens and anti-carcinogens (oxygen radicals and degenerative diseases). *Science* **1983**, *221*, 1256−1264.

(3) Block, G.; Patterson, B.; Subar, A. Fruit, vegetables and cancer prevention: a review of the epidemiologic evidence. *Nutr. Cancer* **1992**, *18*, 1−29.

(4) Magarelli, G.; da Silva, J. G.; de Sousa Filho, I. A.; Lopes, I. S. D.; de Souza, J. R.; Hoffmann, L. V.; de Castro, C. S. P. Development and validation of a voltammetric method for determination of total phenolic acids in cotton cultivars. *Microchem. J.* **2013**, *109*, 23−28.

(5) Novak, I.; Šeruga, M.; Komorsky-Lovrić, Š. Electrochemical characterization of epigallocatechin gallate using square-wave voltammetry. *Electroanalysis* **2009**, *21*, 1019−1025.

(6) Korotkova, E. I.; Karbainov, Y. A.; Shevchuk, A. V. Study of antioxidant properties by voltammetry. *J. Electroanal. Chem.* **2002**, *518*, 56−60.

(7) Kilmartin, P. A.; Zou, H.; Waterhouse, A. L. A cyclic voltammetry method suitable for characterizing antioxidant properties of wine and wine phenolics. *J. Agric. Food Chem.* **2001**, *49*, 1957−1965.

(8) Campanella, L.; Bonanni, A.; Bellantoni, D.; Favero, G.; Tomassetti, M. Comparison of fluorimetric, voltammetric and biosensor methods for the determination of total antioxidant capacity of drug products containing acetylsalicylic acid. *J. Pharm. Biomed. Anal.* **2004**, *36*, 91−99.

(9) Milardović, S.; Ivekovic, D.; Grabarić, B. S. A novel amperometric method for antioxidant activity determination using DPPH free radical. *Bioelectrochemistry* **2006**, *68*, 175−180.

(10) Gulaboski, R.; Mirčeski, V.; Mitrev, S. Development of a rapid and simple voltammetric method to determine total antioxidative capacity of edible oils. *Food Chem.* **2013**, *138*, 116−121.

(11) Cárdenas, A.; Gómez, M.; Frontana, C. Development of an electrochemical cupric reducing antioxidant capacity method (CUPRAC) for antioxidant analysis. *Electrochim. Acta* **2014**, *128*, 113−118.

(12) Apak, R.; Güçlü, K.; Özyürek, M.; Karademir, S. E. Novel total antioxidant capacity index for dietary polyphenols and vitamins C and E, using their cupric ion reducing capability in the presence of neocuproine: CUPRAC method. *J. Agric. Food Chem.* **2004**, *52*, 7970−7981.

(13) Miller, J. C.; Miller, J. N. *Statistics for Analytical Chemists*, 3rd ed.; Ellis Horwood, Prentice Hall: New York, London, 1993.

(14) Tütem, E.; Apak, R. Spectrophotometric determination of trace amounts of copper(I) and reducing agents with neocuproine in the presence of copper(II). *Analyst* **1991**, *116*, 89−94.

(15) Apak, R.; Güçlü, K.; Özyürek, M.; Çelik, S. E. Mechanism of antioxidant capacity assays and the CUPRAC (cupric ion reducing antioxidant capacity) assay. *Microchim. Acta* **2008**, *160*, 413−419.

(16) Çelik, S. E.; Özyürek, M.; Güçlü, K.; Apak, R. Determination of antioxidants by a novel on-line HPLC-cupric reducing antioxidant capacity (CUPRAC) assay with post-column detection. *Anal. Chim. Acta* **2010**, *674*, 79−88.

(17) Blasco, A. J.; Rogerio, M. C.; González, M. C.; Escarpa, A. Electrochemical index as a screening method to determine "total polyphenolics" in foods: a proposal. *Anal. Chim. Acta* **2005**, *539*, 237−244.

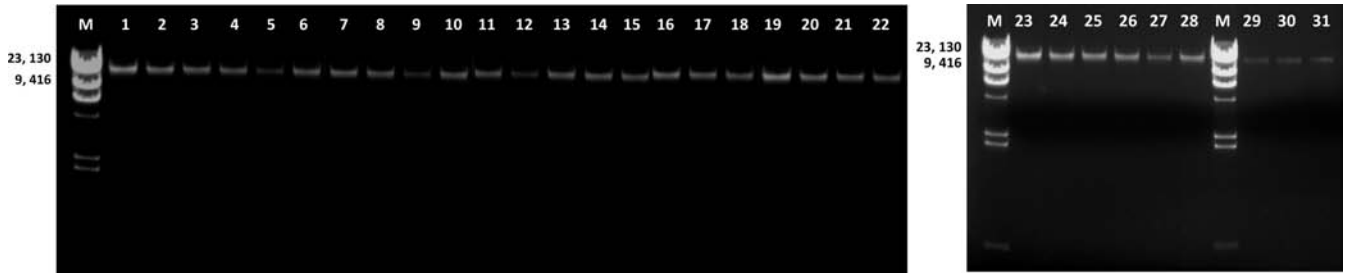

Figure 1. Electrophoretic pattern of purified high molecular weight genomic DNA of test samples used for specificity studies. Lane M, Lambda DNA/*Hind*III marker; lanes 1−6, wild type samples of maize, cotton, rice, eggplant, soybean, potato; lanes 7−18, *Bt*11, *Bt*176, GA21, NK603, MIR162, MIR604, MON810, MON863, MON89034, TC1507, 3272, 59122; lanes 19−26, MON531, MON15985, Event1, GFM-*cry1A*, MLS-9124, MON1445, MON88913, Widestrike; lane 27, LL Rice; lane 28, *Bt* eggplant event EE1; lane 29, GTS-40-3-2 event of soybean; lane 30, GM wheat event MON71800; lane 31, GM potato with *AmA1* gene.

	1	2	3	4	5	6	7	8	9	10	11	12
A	*Adh1*	GA21	3272	LL Rice	*cry1Ac*	*P-35S*	*Adh1*	GA21	3272	LL Rice	*cry1Ac*	*P-35S*
B	*Sad1*	NK603	59122	EE1	*cry1Ab*	*P-nos*	*Sad1*	NK603	59122	EE1	*cry1Ab*	*P-nos*
C	*sps*	MIR162	MON531	GTS 40-3-2	*cry1Ab/Ac*	*T-nos*	*sps*	MIR162	MON531	GTS 40-3-2	*cry1Ab/Ac*	*T-nos*
D	*β-fructosidase*	MIR604	MON15985	*P35S - cry1Ac*	*cry2Ab*	*T-35S*	*β-fructosidase*	MIR604	MON15985	*P35S - cry1Ac*	*cry2Ab*	*T-35S*
E	*Lectin*	MON810	MON1445	*P35S-cry1C*	*cry3A*	*nptII*	*Lectin*	MON810	MON1445	*P35S-cry1C*	*cry3A*	*nptII*
F	*UGPase*	MON863	MON88913	*P35S-uidA*	*cry1C*	*pat*	*UGPase*	MON863	MON88913	*P35S-uidA*	*cry1C*	*pat*
G	Bt11	MON89034	Event281	*ctp2-cry2Ab*	*epsps*	*bar*	Bt11	MON89034	Event281	*ctp2-cry2Ab*	*epsps*	*bar*
H	Bt176	TC1507	Event3006	*ctp2-cp4epsps*	*AmA1*	control	Bt176	TC1507	Event3006	*ctp2-cp4epsps*	*AmA1*	control

events	construct regions	genes	control elements	endogenous genes
*Bt*11	*P35S-cry1AC*	*cry1Ac*	*P-35S*	*Adh1*
*Bt*176	*P35S-cry1C*	*cry1Ab*	*P-nos*	*Sad1*
GA21	*P35S-uidA*	*cry1Ab/Ac*	*T-nos*	*sps*
NK603	*ctp2-cry2Ab*	*cry2Ab*	*T-35S*	*β-fructosidase*
MIR162	*ctp2-epsps*	*cry3A*		*lectin*
MIR604		*cry1C*		*UGPase*
MON810		*epsps*		
MON863		*AmA1*		
MON89034		*nptII*		
TC1507		*pat*		
3272		*bar*		
59122				
MON531				
MON15985				
MON1445				
MON88913				
281-24-236 (Event 281)				
3006-210-23 (Event 3006)				
LL Rice				
EE1				
GTS 40-3-2				

Figure 2. Multitarget prespotted plate layout for screening and detection of GM crops/events: 21 event-, 5 construct-, 15 transgenic element-specific assays, and 6 taxon-specific assays.

dx.doi.org/10.1021/jf502190e | *J. Agric. Food Chem.* 2014, 62, 7118−7130

Table 1. Primers and Probes Employed in this Study

target	primer sequence (5′-3′)	probe sequence (5′-3′)	ref
Adh1	Adh1F: CCAGCCTCATGGCCAAAG	CTTAGGGGCAGACTCCCGTGTTCCCT	(20) http://gmo-crl.jrc.ec.europa.eu/gmomethods/docs/GA21_Validation_Report+Protocol[1].pdf
	Adh1R: CCTTCTTGGCGGCTTATCTG		
Sad1	Sad11F: GGTAGATCGAAGTGCTACAAAGAC	CCCACGAAGCCCAATACACAAC	21
	Sad11R: GATTTAACTGTCCAACTTGCATCAC		
sps	sps_12-L: TTGCGCCTGAACGGATAT	GACGCACGGACGGCTCGGA	22
	sps_12-R: CGGTTGATCTTTTCGGGATG		
B-fructosidase	PomtomF: CTGCCTCCGTCAAGATTTGGTCACT	TAATTCATCCAACCATATCT	23
	PomtomR: CTCTTCCCTTTCTTGATGG		
Lectin	KVM164: CTTTCTCGCACCAATTGACA	CCACAAACACATGCAGGTTATCTT	http://gmo-crl.jrc.ec.europa.eu/summaries/EURL-VL-04-10%20VP.pdf
	KVM165: TCAAACTCAACAGCGACGAC		
UGPase	UGP_15-L: CTCTCCATACTCTCTGCTCCTCG	TCACAATCTTCTTCTCTGCTATGGTCACTGCT	24
	UGP_15-R: CGGCATCAGCAGGAGAAAG		
Bt 11	F: TGTGTGGCCATTTATCATCGA	TTCCATGACCAAAATCCCTTAACGTGAGT	25
	R: CGCTCAGTGGAACGAAAACTC		
*Bt*176	*Bt*176F: GGCCGTGAACGAGCTGTT	AGCAACCAGATCGGCCGACACC	(26) http://gmo-crl.jrc.ec.europa.eu/summaries/Bt176_CRLVL1804_validated_Method.pdf
	*Bt*176R: GGGAAGAAGCCTACATGTTTTCTAA		
GA21	F: CGTTATGCTATTTGCAACTTTAGAACA	TTTCTCAACAGCAGGTGGGTCCGGGT	(20) http://gmo-crl.jrc.ec.europa.eu/gmomethods/docs/GA21_Validation_Report+Protocol[1].pdf
	R: GCGATCCTCCTCGCGTT		
NK603	NK603F:ATGAATGACCTCGAGTAAGCTTGTTAA	TGGTACCACGCGACACACTTCCACTC-	(27) http://gmo-crl.jrc.ec.europa.eu/summaries/NK603-WEB-Protocol%20Validation.pdf
	NK603R: AAGAGATAACAGGATCCACTCAAACACT		
MIR162	MIR162-f1: GCGCGGTGTCATCTATGTTACTAG	TCTAGACAATTCAGTACATTAAAAACGTCCGCCA	(28) http://gmo-crl.jrc.ec.europa.eu/summaries/MIR162_validated_Method.pdf
	MIR162-r1: TGCCTTATCTGTTGCCTTCAGA		
MIR604	MIR604F: GCGCACGCAATTCAACAG	AGGCGGGAAACGACAATCTGATCATG	(29) http://gmo-crl.jrc.ec.europa.eu/summaries/MIR604_validated_Method_correctedversion1.pdf
	MIR604R: GGTCATAACGTGACTCCCTTAATTCT		
MON810	F: TCGAAGGACGAAGGACTCTAACGT	AACATCCTTTGCCATTGCCCAGC	30
	R: GCCACCTTCCTTTTCCACTATCTT		
MON863	MON863F: GTAGGATCGGAAAGCTTGGTAC	TGAACACCCATCCGAACAAGTAGGGTCA	(31) http://gmo-crl.jrc.ec.europa.eu/summaries/MON863-WEB-Protocol-Validation.pdf
	MON863R: TGTTACGGCCTAAATGCTGAACT		
MON89034	MON89034-1: TTCTCCATATTGACCATCATACTCATT	ATCCCCGGAAATTATGTT	(32) http://gmo-crl.jrc.ec.europa.eu/summaries/MON89034_validated_Method.pdf)
	MON89034-2: CGGTATCTATAATACCGTGGTTTTTAAA		
TC1507	MaiY-F1: TAGTCTTCGGCCAGAATGG	TAACTCAAGGCCCTCACTCCG	33
	MaiY-R3: CTTTGCCAAGATCAAGCG-		
3272	ES3272-F: TCATCAGACCAGATTCTCTTTTATGG	ACTGCTGACGCGGCCAAACACTG	(34) http://gmo-crl.jrc.ec.europa.eu/gmomethods/docs/jrc48922_event3272_validation_report_and_protocol.pdf
	ES3272-R: CGTTTCCCGCCTTCAGTTTA		
59122	DAS-59122-7-rbf1:GGGATAAGCAAGTAAAAGCGCTC	TTTAAACTGAAGGCGGGAAACGACAA	35

dx.doi.org/10.1021/jf502190e | J. Agric. Food Chem. 2014, 62, 7118−7130

Table 1. continued

target	primer sequence (5′-3′)	probe sequence (5′-3′)	ref
	DAS-59122-7-rbr1:5′-CCTTAATTCTCCGCTCATGATCAG-3′		
MON531	MON531-F: TCCCATTCGAGTTTCTCACGT MON531-R: AACCAATGCCACCCCACTGA	TTGTCCCTCCACTTCTTCTC	36
MON15985	MON15985-F: GTTACTAGATCGGGGATATCC MON15985-R: AAGGTTGCTAAATGGATGGGA	CCGCTCTAGAACTAGTGGATCTGCACTGAA	37
MON1445	MON1445-F: GGAGTAAGACGATTCAGATCAAACAC MON1445-R: ATCGACCTGCAGCCCAAGCT	ATCAGATTGTCGTTTCCCGCCTTCAGTTT	38
MON88913	F: GGCTTTGGCTACCTTAAGAGAGTC R: CAAATTACCCATTAAGTAGCCAAATTAC	AACTATCAGTGTTTGACTACAT	39
Event 281	F: CTCATTGCTGATCCATGTAGATTTC R: GGACAATGCTGGGCTTTGTG	TTGGGTTAATAAAGTCAGATTAGAGGGAGACAA	40
Event 3006	F: AAATATTAACAATGCATTGAGTATGATG R: 5′-ACTCTTTCTTTTTCTCCATATTGACC-3′	TACTCATTGCTGATCCATGTAGATTTCCCG	40
LL Rice	MDB616: AGCTGGCGTAATAGCGAAGAGG MDB694: TGCTAACGGGTGCATCGTCTA	CGCACCGATTATTTATACTTTTAGTCCACCT	41
EE1	EE1-F: GCTGGGATCAGATAGTCG EE1-R: ATGCGGTGATAATTGAATGC	TGTTACCAAAAGTGCTGTCAATAAACACT	8
GTS 40-3-2	40-3-2AF-TTCATTCAAAATAAGATCATACATACAGGTT 40-3-2AR-GGCATTTGTAGGAGCCACCTT	CCTTTTCCATTTGGG	42
P35S-cry1Ac	35S-cry1Ac-F: CTTCGCAAGACCCTTCCTCTAT 35S-cry1Ac-R: GAACTCTTCGATCCTCTGGTTG	ACATCAACGAATGCATTCCA	17
P35S-cry1C	35S-cry1C-F: GGTCCGTCCTGTAGAAACCA 35S-cry1C-R: TCCGTTCTCCATCCAAAAGT	GGAAAATAATCAAAATCAATGCA	present study
P35S-uidA	35S-uidA-F: TGGTCCGTCCTGTAGAAACC 35S-uidA-R: AATATCTGCATCGGCGAACT	GATCGCGAAAACTGTGGAAT	17
ctp2-cry2Ab2	CTCR-F: ATTGAAAGAAAGAGTGGGATGACGTTA CTCR-R: GACCAGAGTTCAGGACGGAGTT	CGGCGTGCATGCTTGCCATG	43
ctp2-cp4EPSPS	GT73-TmF: GGGATGACGTTAATTGGCTCTG GT73-TmR: GGCTGCTTGCACCGTGAAG	CACGCCGTGGAAACAGAAGACATGACC	44
cry1Ac	Cry1Ac-F: TTGCCTGAGTTGTCCGTGATC Cry1Ac-R: GACGGAACGCTGATTGTTCTGT	CGGTGACTTCAACAATGGCCTCA	15
cry1Ab	CRY1-F: CCCATCGACATCAGCCTGAGC CRY1-R: CAGGAAGGCGTCCCACTGG	ATGTCCACCAGGCCCAGCACG	http://gmdd.shgmo.org/primer/view/genespecific/13
cry1Ab/Ac	*Bt*-F1(mod): GAGGAAATGCGTATTCAATTCAAC *Bt*-R1: TTCTGGACTGCGAACAATGG	ACATGAACAGCGCCTTGACCACAGC	http://www.bvl.bund.de
cry2Ab	Cry2Ab-F: GAGTCCTTCGAGACCACCC Cry2Ab-R: TCCTCTCGTCGTCCGCAA	TCCGCCGTCCACTGCACTACAAC	16
cry3A	Cry3A-F: GCTACGAGAGCTGGGTGAAC Cry3A-R: TCTCGATGTTGCTGAAGGTG	GAGGTGAAGACCGAGCTGAC	present study
cry1C	Cry1C-F: TAGTTGGCCCTTCTCAATGG Cry1C-R: CGAAGGAATGTCCCTTTCAA	CAGCAACCAGGACCAGAGTA	present study

dx.doi.org/10.1021/jf502190e | J. Agric. Food Chem. 2014, 62, 7118−7130

Table 1. continued

target	primer sequence (5′-3′)	probe sequence (5′-3′)	ref
epsps	Sttmf3a: GCAAATCCTCTGGCCTTTCC	TTCATGTTCGGCGGTCTCGCG	45
	Sttmr2a: CTTGCCCGTATTGATGACGTC		
AmA1	AmA-F: CCATTGAACCAGATGAAAATAAAAGC	AATTGGACGTGCAAAAGTCGAACCT	present study
	AmA-R: TTTAGAGCCGGTATCAATTTGACTTG		
P-53S	P35S1-5: ATTGATGTGATATCTCCACTGACGT	CCCACTATCCTTCGCAAGACCCTTCCT	46
	P35S1-3: CCTCTCCAAATGAAATGAACTTCCT		
P-nos	Pnos-F: ACCATTATTGCGCGTTCAAA	CTGACGTTCCATAAATTCCCCTCGG	47
	Pnos-R: GATTGAGAGTGAATATGAGACTCTAATTG		
T-nos	Tnos-F: CATGTAATGCATGACGTTATTTATG	TGGGTTTTTATGATTAGAGTCCCGCAAT	47
	Tnos-R: GCTATATTTTGTTTTCTATCGCGTAT		
T-35S	T35SM-F: CCCTTAGTATGTATTTGTATTTGTAAAATACTTC	TATCAATAAAATTTCTAATTC	47
	T35SM-R: GGATTTTAGTACTGGATTTTGGTTTTAG		
nptII	nptII_7-L: AAGATGGATTGCACGCAGGTT	CCAGTCATAGCCGAATAGCCTCTCCACC	48
	nptII_7-R: AGAGCAGCCGATTGTCTGTTG		
pat	KVM-5: TTGAGGGTGTTGTGGCTGGTA	CTTCCAGGGCCCAGCGTAAGCA	49
	KVM-6: TGTCCAATCGTAAGCGTTCCT		
bar	RapB-F1: ACAAGCACGGTCAACTTCC	TACCGAGCCGCAGGAACC	44
	RapB-R1: GAGGTCGTCCGTCCACTC		

dx.doi.org/10.1021/jf502190e | J. Agric. Food Chem. 2014, 62, 7118−7130

Table 2. Verification of Results for Specificity of Targets on Prespotted Plate[a]

| | test samples | targets | | |

DNA Extraction. Genomic DNA was isolated from 100 to 200 mg of homogenized seed powder or planting material using DNeasy Plant Mini kit (Qiagen Gmbh, Hilden, Germany), as per manufacturer's instructions. The integrity and purity of genomic DNA were determined by agarose gel electrophoresis. Intact DNA of high molecular weight was obtained (Figure 1). DNA samples were quantified by measuring UV absorption at 260 nm, while DNA purity was evaluated on the basis of the UV absorption ratio at 260 nm/280 nm ranging from 1.6 to 1.9 using a Quawell UV−vis spectrophotometer Q5000 (Quawell, CA, USA). DNA samples were diluted to a concentration of 25 ng/μL for specificity experiments and tested for the absence of PCR inhibitors.[14] To determine limit of detection (LOD) of the targets, working solutions with 1.0, 0.1, 0.05, 0.025, 0.01, and 0.005% GM content were prepared by mixing the DNA samples of particular GM events positive for specific targets with the corresponding non-GM counterpart.

Selection of Targets and Methods. The multitarget RTi-PCR based screening system developed in the present study aims to detect 21 GM events of five crops, namely, maize (12 events), cotton (6 events), one GM event each of eggplant, rice and soybean, 5 construct regions (junction regions of two transgenic elements), 15 commonly employed transgenic elements (11 transgenes, 2 promoters and 2 terminators) along with 6 taxon-specific targets as shown in Figure 2. Taxon-specific assays for six crops (cotton, eggplant, maize, potato, rice, and soybean) were included as internal control for corresponding GM event-specific/element-specific assays. TaqMan probes and primers for *cry1C*, modified *cry3A*, *AmA1*, *P35S-cry1C* were designed using the primer design software Primer3 (version 0.4.0) (http://bioinfo.ut.ee/primer3-0.4.0/). Primers and probes for event-specific detection of *Bt* eggplant event EE1, for *cry1Ac* and *cry2Ab* transgenes, *P35S-cry1Ac* and *P35S-uidA* construct regions were previously reported by our laboratory.[8,15−17] Details of other oligonucleotides used are listed in Table 1. Prior to development of prespotted plates, primers and probes were tested and verified using respective RTi-PCR assays.

The RTi-PCR plate includes 47 targets along with a negative amplification control in duplicate, allowing the simultaneous analysis of two test samples per plate (Figure 2). Primers and probes were prespotted in each well in lyophilized format at a final concentration of 900 nM primers/250 nM probes. Primer and probe synthesis and automatic spotting were outsourced (Applied Biosystems, Foster City, CA, USA). All probes were labeled with 6-carboxyfluorescein (FAM) and 6-carboxytetramethylrhodamin (TAMRA) at the 5′ and 3′ ends, respectively.

Real-Time PCR Assay. RTi-PCR assays were performed using 96-well prespotted plates on a 7500 Real-Time PCR system (Applied Biosystems, Foster City, CA, USA) in 25 μL reactions containing 100 ng of template DNA, 1× TaqMan Universal PCR Master Mix (Applied Biosystems). Thermal profile used was 30 °C for 5 min for allowing the dissolution of lyophilized primers and probes, 95 °C for 1 min, followed by 45 cycles of 95 °C for 15 s and 60 °C for 60 s.

Experimental Design. The specificity of each method spotted on the plate was tested against the DNA samples obtained from wild-type plant species and most of the GM events/crops, as shown in Table 2. The expected results for each target have been compiled in Table 2, based on the information from publicly available databases, namely, http://www.igmoris.nic.in, http://www.cera-gmc.org, http://www.gmo-compass.org, http://gmdd.shgmo.org/, http://www.envfor.nic.in/divisions/csurv/geac/geac_home.html, and from *in silico* analysis (http://gmo-crl.jrc.ec.europa.eu/jrcgmomatrix/). Prior to conducting specificity experiments, one of the plates was tested with test samples positive for each target in one set I of the plate (1−48 wells), and the second set II (49−96 wells) with water (nontemplate control) as negative control was run simultaneously, to check the false positive results.

To test sensitivity of all 47 target-specific assays included in the multitarget system, LOD was determined by testing each DNA test sample for GM content up to 1.0, 0.1, 0.05, 0.025, 0.01, and 0.005%, in 16 PCR replicates, for each target. Sensitivity of the system in terms of copy number (LOD_{copies}) was also calculated using the 1C value corresponding to the weight in picograms per haploid host plant genome.[18]

Repeatability and intermediate-repeatability of developed multitarget system was confirmed by single-laboratory experiments performed by four operators. Each operator ran two plates in duplicate, accounting for a total of four replications per operator, hence 16 replications per assay.

For assessing the practical utility and applicability of developed system:

(i) A sample of stacked GM cotton event MON15985 × MON88913 was tested. DNA of stacked GM cotton event was loaded in each well of the plate to check for the presence or absence of specific targets, and hence analyzed in duplicate (Sets S1 and S2 of the plate).

(ii) Two powdered samples, labeled as A and B, unknown to the operators, were also tested. Sample A comprised of homogenized seed powder of non-GM wheat, whereas sample B comprised homogenized seed powder from reference material of GM event TC1507.

(iii) Samples of the Proficiency Program organized by the United States Department of Agriculture and the Grain Inspection, Packers and Stockyards Administration (USDA-GIPSA) in 2013 were tested for specific GM maize events and corresponding transgenic elements, included in the prespotted plate.

RESULTS AND DISCUSSION

In the present "RTi-PCR-based multitarget screening system", element-, construct-, and event-specific assays have been combined so as to facilitate preliminary screening of an unknown sample for its GM status. The 47 targets included in the system may facilitate event-specific detection of 21 GM events and further screening of more than 140 GM events under field trials in India.[13]

Specificity and Sensitivity of Developed Multitarget System. The present work describes multitarget TaqMan RTi-PCR-based screening system consisting of a 96-well plate coated with lyophilized primers and probes, in which a sample can be tested in duplicate for 47 targets. Five *Bt* cotton events, i.e., MON531, MON15985, GFM-*cry1A*, Event 1, and MLS-9124 are authorized for commercial cultivation in India. These events can be efficiently detected on developed multitarget system using event-specific assays for MON531 and MON15985 and construct-specific assays, i.e., *P35S-cry1Ac*, *P35S-uidA*, *P35S-cry1C*, and *ctp2-cry2Ab*. The outcomes of the applicability of event- and construct-specific assays included in the system to detect commercially authorized Indian GM events may be interpreted as follows: (i) If sample contains MON531 event, then MON531 event- and *P35S-cry1Ac* construct-specific targets would amplify; (ii) If sample contains MON15985 event, then MON531 and MON15985 event-specific along with *P35S-cry1Ac*, *P35S-uidA*, *ctp2-cry2Ab* construct-specific targets would amplify; (iii) If sample contains Event1, then only *P35S-cry1Ac* construct-specific target would amplify; (iv) If sample contains GFM-*cry1A* event, then both the *P35S-cry1Ac* and *P35S-uidA* specific targets would amplify; and (v) If sample contains MLS-9124 event, then only *P35S-cry1C* specific target would amplify.

The *ctp2-epsps* construct-specific assay detects the imported wheat GM event MON71800 for herbicide tolerance. As the adventitious presence of this event was reported in the Oregon fields in the United States in June 2013 (http://westernfarmpress.com/blog/oregon-gmo-mystery-wheat-whodunit), so we used the DNA of imported sample of the same event (imported for research purposes) just to check whether the developed system is capable of tracing this event, and further confirmation can be done with the respective event-

Table 3. Performance of Each Target-Specific RTi-PCR Expressed as Ct ± Standard Deviation, LOD (% GM content) and LOD (copies)

well	target	sample tested for LOD experiments[a]	mean Ct ± SD[b]	LOD (%)	LOD (copies)
A1, A7	*Adh1*	maize	29.38 ± 1.25	0.01	4
B1, B7	*Sad1*	cotton	32.05 ± 1.14	0.05	18
C1, C7	*SPS*	rice	28.21 ± 0.58	0.1	222
D1, D7	*β-fructosidase*	eggplant	26.25 ± 0.17	0.1	102
E1, E7	*Lectin*	soy	30.55 ± 0.21	0.1	88
F1, F7	*UGPase*	potato	24.35 ± 0.87	0.1	55
G1, G7	*Bt*11	*Bt*11	36.83 ± 0.39	0.01	4
H1, H7	*Bt*176	*Bt*176	38.01 ± 0.13	0.1	36
A2, A8	GA21	GA21	37.34 ± 1.00	0.1	36
B2, B8	NK603	NK603	35.47 ± 1.02	0.025	9
C2, C8	MIR162	MIR162	37.54 ± 1.34	0.1	36
D2, D8	MIR604	MIR604	34.07 ± 1.24	0.01	4
E2, E8	MON810	MON810	37.35 ± 0.67	0.05	18
F2, F8	MON863	MON863	36.34 ± 1.47	0.1	36
G2, G8	MON89034	MON89034	31.29 ± 0.11	0.1	36
H2, H8	TC1507	TC1507	36.58 ± 0.64	0.1	36
A3, A9	3272	3272	35.95 ± 0.87	0.01	4
B3, B9	59122	59122	33.01 ± 0.08	0.01	4
C3, C9	MON531	MON531	34.96 ± 0.68	0.01	4
D3, D9	MON15985	MON15985	31.92 ± 0.04	0.1	42
E3, E9	MON1445	MON1445	32.78 ± 1.36	0.1	42
F3, F9	MON88913	MON88913	31.49 ± 0.32	0.1	42
G3, G9	281-24-236	Widestrike	29.23 ± 0.08	0.05	21
H3, H9	3006-210-23	Widestrike	28.54 ± 0.52	0.01	4
A4, A10	LLRice	LLRice	34.68 ± 0.73	0.1	222
B4, B10	EE1	EE1	27.01 ± 0.36	0.05	51
C4, C10	GTS 40-3-2	GTS 40-3-2	34.49 ± 0.08	0.1	88
D4, D10	*P35S-cry1Ac*	MON15985	35.05 ± 0.05	0.025	10
E4, E10	*P35S-cry1C*	MLS-9124	32.68 ± 0.42	0.1	42
F4, F10	*P35S-uidA*	MON15985	33.78 ± 0.44	0.1	42
G4, G10	*ctp2-cry2Ab2*	MON15985	33.22 ± 0.09	0.1	42
H4, H10	*ctp2-epsps*	MON71800	28.93 ± 0.11	0.1	6
A5, A11	*cry1Ac*	MON15985	32.45 ± 2.82	0.1	42
B5, B11	*cry1Ab*	*Bt*176	34.56 ± 0.40	0.01	4
C5, C11	*cry1Ab-Ac*	GFM-*cry1A*	27.95 ± 0.06	0.1	42
D5, D11	*cry2Ab*	MON15985	36.41 ± 0.69	0.1	42
E5, E11	*cry3A*	MIR604	32.17 ± 0.54	0.1	36
F5, F11	*cry1C*	MLS9124	38.07 ± 0.28	0.1	42
G5, G11	*epsps*	GTS 40-3-2	28.36 ± 0.18	0.1	88
H5, H11	*AmA1*	Potato_AmA1	25.92 ± 0.09	0.01	5
A6, A12	*P-35S*	MON15985	31.09 ± 2.13	0.1	42
B6, B12	*P-nos*	MLS9124	30.48 ± 0.60	0.1	42
C6, C12	*T-nos*	MON15985	30.80 ± 1.56	0.01	4.2
D6, D12	*T-35S*	*Bt*176	30.16 ± 1.16	0.1	36
E6, E12	*nptII*	MON15985	33.01 ± 1.38	0.1	42
F6, F12	*pat*	59122	32.40 ± 0.41	0.01	4
G6, G12	*bar*	*Bt*176	38.12 ± 0.40	0.05	7

[a]Number of replications per assays was 16 (as indicated in ISO 5725-3-1994, estimates of repeatability should be obtained on sufficient number of test results, at least 15 replicates[50]). [b]Positive amplification was considered below Ct value of 40.

specific assay. Other selected targets include 11 transgenes, 2 promoters (*P-35S*, *P-nos*), and 2 terminators (*T-35S*, *T-nos*) (Figure 2), facilitating further screening of more than 140 GM events under field trials which were indigenously developed or imported for research purposes.[13]

Prior to conducting specificity experiments, one of the plates was tested with test samples positive for each target in one set I of the plate, and the second set II with water (nontemplate control) was run simultaneously. All the targets were amplified in set I, whereas no amplification was observed in set II as expected, thus eliminating the possibility of false positives in the reactions. Specificity of each method was assessed and further confirmed by testing with wild-type plant species and most of the GM events/crops, against the whole set of methods. All 47 assays successfully amplified the targets (event-, construct-, element-specific) only in the corresponding GM events/crops (Table 3), and taxon-specific targets in the corresponding plant

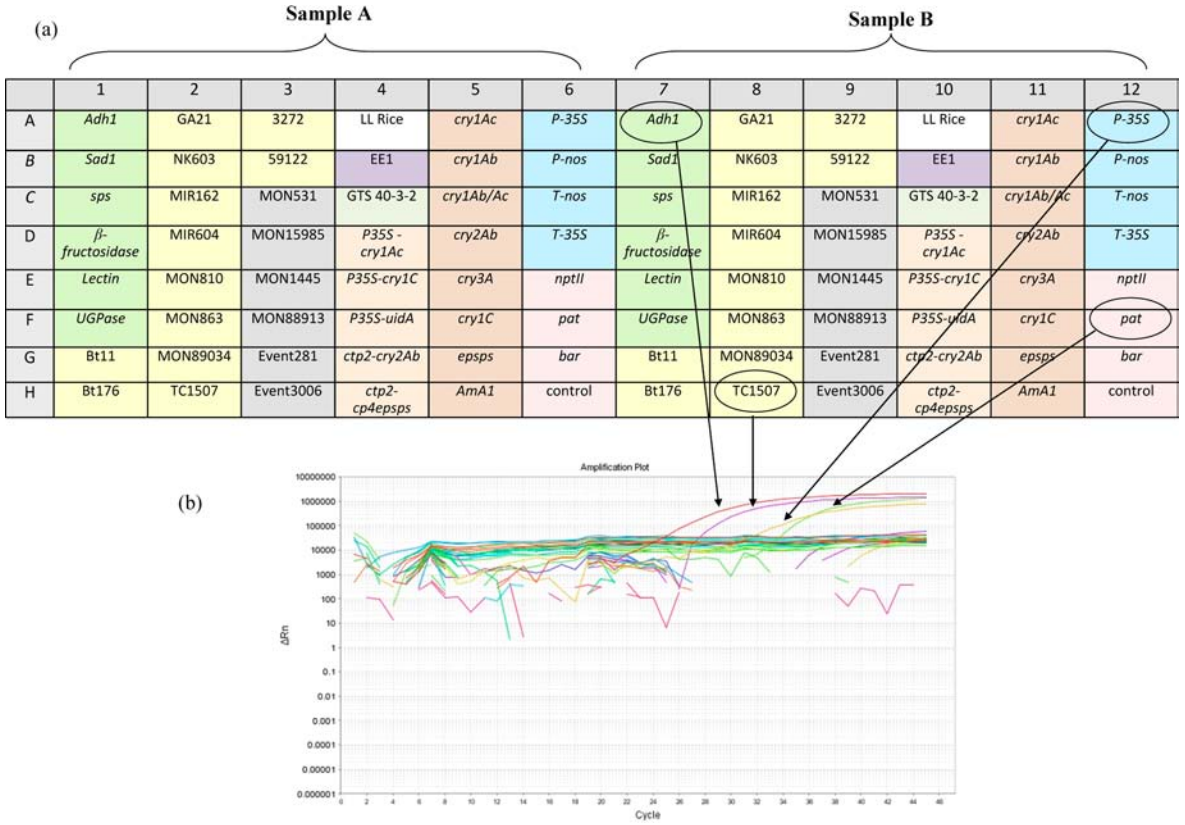

	1	2	3	4	5	6	7	8	9	10	11	12
A	*Adh1*	GA21	3272	LL Rice	*cry1Ac*	*P-35S*	*Adh1*	GA21	3272	LL Rice	*cry1Ac*	*P-35S*
B	*Sad1*	NK603	59122	EE1	*cry1Ab*	*P-nos*	*Sad1*	NK603	59122	EE1	*cry1Ab*	*P-nos*
C	*sps*	MIR162	MON531	GTS 40-3-2	*cry1Ab/Ac*	*T-nos*	*sps*	MIR162	MON531	GTS 40-3-2	*cry1Ab/Ac*	*T-nos*
D	*β-fructosidase*	MIR604	MON15985	*P35S - cry1Ac*	*cry2Ab*	*T-35S*	*β-fructosidase*	MIR604	MON15985	*P35S - cry1Ac*	*cry2Ab*	*T-35S*
E	*Lectin*	MON810	MON1445	*P35S-cry1C*	*cry3A*	*nptII*	*Lectin*	MON810	MON1445	*P35S-cry1C*	*cry3A*	*nptII*
F	*UGPase*	MON863	MON88913	*P35S-uidA*	*cry1C*	*pat*	*UGPase*	MON863	MON88913	*P35S-uidA*	*cry1C*	*pat*
G	Bt11	MON89034	Event281	*ctp2-cry2Ab*	*epsps*	*bar*	Bt11	MON89034	Event281	*ctp2-cry2Ab*	*epsps*	*bar*
H	Bt176	TC1507	Event3006	*ctp2-cp4epsps*	*AmA1*	control	Bt176	TC1507	Event3006	*ctp2-cp4epsps*	*AmA1*	control

Figure 3. Practical applicability of developed multitarget screening system for simultaneous analysis of two unknown samples (Samples A and B) per plate; (a) targets amplified in the system are encircled; (b) amplification profile of the targets amplified in the test samples. Details of samples unknown to the operators: Sample A: Homogenized seed powder of non-GM wheat. Sample B: Homogenized seed powder of GM maize event TC1507.

species. The amplification results were in line with the information from theoretical data, as shown in Table 2.

Plate performance was determined by the Ct values of each target from the amplification data of 16 replications. Mean Ct values for the targets ranged from 24.35 ± 0.87 to 38.12 ± 0.40 as shown in Table 3. Results were consistent in terms of Ct values, and the mean standard deviation ranged from 0.05 to 2.82.

To determine LOD of different RTi-PCR assays, DNA dilutions with GM content of 1.0, 0.1, 0.05, 0.025, 0.01, and 0.005% were analyzed. LOD is the lowest amount or concentration of analyte in a sample, which can be reliably detected, but not necessarily quantified, as demonstrated by single-laboratory validation. Since the analytical method should detect the presence of the analyte at least 95% of the times at the LOD, ensuring ≤5% false negative results (Codex Alimentarious Commission CAC-GL 74-2010,[19] http://gmo-crl.jrc.ec.europa.eu/doc/Min_Perf_Requirements_Analytical_methods.pdf), 16 replicates were tested for each target. Most of the assays detected the target sequence in respective DNA samples up to 0.1% of GM target; however, assays for detection of NK603 event and *P35S-cry1Ac* construct region detected up to 0.025%. LOD of GM events, namely, 3272, 59122, MON531, MIR604, *Bt*11, Event 3006 and genes *Adh1*, *cry1Ab*, *T-nos*, *pat*, *AmA1* was found to be 0.01% (Table 3, Figure S1 of the Supporting Information). Sensitivity in terms of LOD_{copies} was also estimated, and the results are in agreement with different genome sizes[18] of the individual plant species selected for testing of respective targets. Each assay was found sensitive enough to detect the respective target, with the LOD_{copies} ranging from 4 to 222. Fourteen of the targets, namely, *Adh1*, *Bt*11, NK603, MIR604, 3272, 59122, MON531, Event 3006, *P35S-cry1Ac*, *ctp2-epsps*, *cry1Ab*, *AmA1*, *bar*, *pat* demonstrated LOD_{copies} up to 10 copies, and the sensitivity of most of these targets in the multitarget system was also in line with that of EU-validated protocols.

Overall LOD of present multitarget system was established up to 0.1%, revealing that it can efficiently detect samples with GM content as low as 0.1% of each of the 47 targets in a single run. However, the developed system can be efficiently used for qualitative testing for checking the presence/absence of 47 targets in an unknown sample, if 0.1% content of particular target is present (for some targets, detection limit was up to 0.01%, as mentioned earlier). Twenty-one GM events can be efficiently checked for their presence in an unknown sample using this system. In the case of presence of particular GM event(s) in the sample, further quantification can be done to determine the content of a particular event by running separate RTi-PCR using the reference materials to generate the standard curve.

Applicability of the Multitarget System. Practical applicability of developed system was tested using DNA sample of stacked GM cotton event, MON15985 × MON88913. RTi-PCR analysis was performed in duplicate for each target. Detection of a stacked GM event is based on the use of event-specific detection assays developed for the parental GM events contributing the stack. In both the replicates S1 and S2, amplification signal was detected only for specific targets

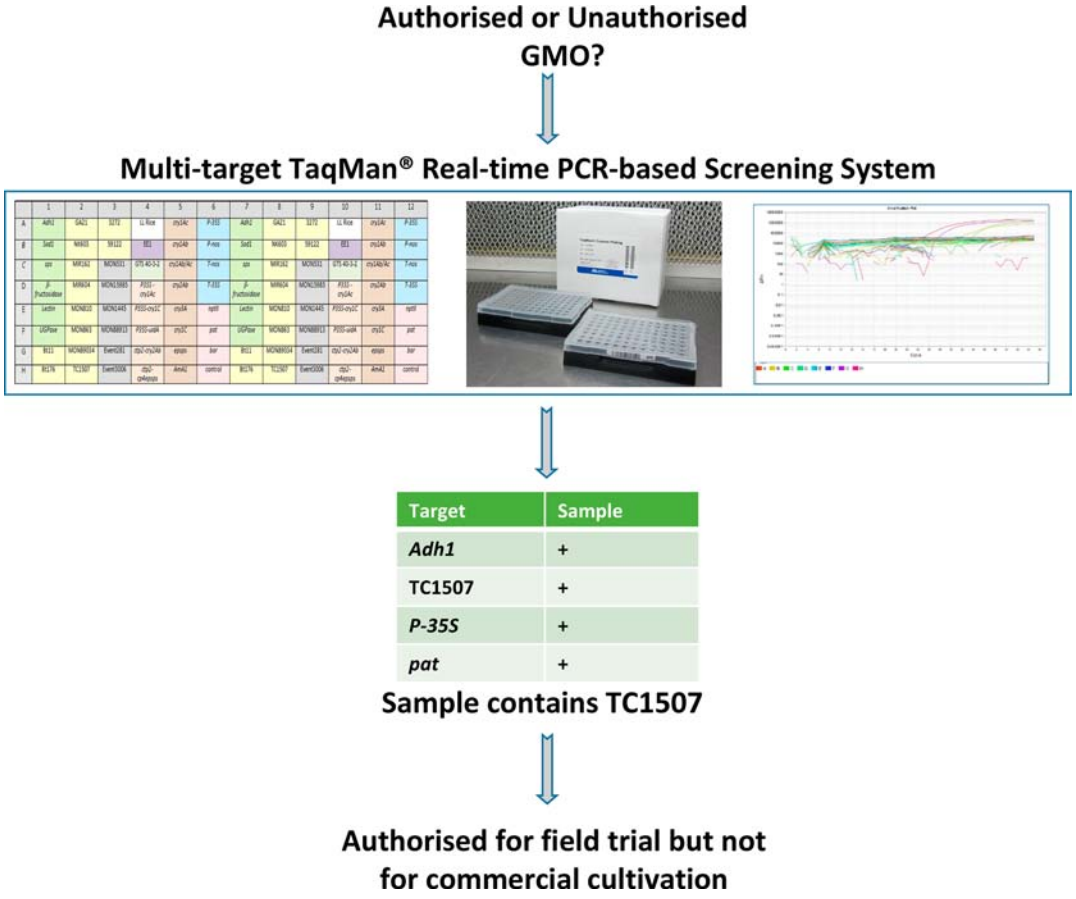

Figure 4. Workflow of developed multitarget RTi-PCR-based screening system to check for unauthorized GM events.

Table 4. Screening Pattern obtained on Pre-spotted Plate using Maize Samples of Proficiency Testing[a]

| test samples | targets | | |

tested for specific GM maize events and their respective transgenic elements. The results obtained were as expected; for example, in the Sample 1, five of the GM maize events, namely, MON810, *Bt*176, *Bt*11, NK603, Event 3272 along with the respective transgenic elements were detected, as shown in Table 4. The results of proficiency test samples were satisfactory and in agreement with the final results of the USDA-GIPSA Proficiency Program-2013.

With only a few simple steps involved, the present multitarget GMO screening tool offers efficient and rapid testing of GM status of a sample while significantly reducing both workload and chances of contamination. The approximate cost of the prespotted plate for testing a DNA sample for presence/absence of 47 targets would be INR 20000 to 26000. This multitarget approach is user-friendly and flexible which may facilitate detection of all the commercialized GM events of India and screening of more than 140 GM events that were under field trials (2006-2012), the scope of which may further be enhanced by including more transgenic elements of upcoming authorized GM events in Indian context, as per the availability of RTi-PCR methods.

■ ASSOCIATED CONTENT

Supporting Information

Bar diagrams showing limit of detection (LOD) of the 47 target-specific multitarget screening system in terms of (a) % GM content and (b) copies (Figure S1); verification of practical utility of developed multitarget screening system using stacked GM cotton event, MON15985 × MON88913 in two replicates, S1 and S2; (a) targets amplified in the system are encircled; (b) amplification profile of the targets amplified in the sample of selected stacked event (Figure S2). This material is available free of charge via the Internet at http://pubs.acs.org.

■ AUTHOR INFORMATION

Corresponding Author

*E-mail: gurinder.randhawa@rediffmail.com or gjr@nbpgr.ernet.in. Phone: +91-9811974396.

Funding

The authors duly acknowledge the grant provided by the Department of Biotechnology, Ministry of Science and Technology, Government of India, for funding the project entitled "Multi-target System for GM Detection and Quantification in GM Food Crops". The research grant provided to P.S. and R.K.B. as Senior Research Fellowship, by Department of Biotechnology is duly acknowledged.

Notes

The authors declare no competing financial interest.

■ ACKNOWLEDGMENTS

Thanks are due to the Director, National Bureau of Plant Genetic Resources, for providing necessary facilities. Our special thanks to Dr. Maddalena Querci, Dr. Francesco Gatto and Dr. Sabrina Rosa, Institute for Health and Consumer Protection, Molecular Biology and Genomics Unit, European Commission-Joint Research Centre, Ispra, Italy, for continuous technical guidance and critical review of the manuscript.

■ ABBREVIATIONS USED

Adh1, alcohol dehydrogenase 1; *AmA1*, amaranth seed albumin from *Amaranthus hypochondriacus*; *bar*, *Streptomyces hygroscopicus* phosphinothricin *N*-acetyltransferase; *ctp2*, chloroplast transit peptide 2; *epsps*, 5-enol-pyruvylshikimate-3-phosphate synthase; GM, genetically modified; GMO, genetically modified organism; LOD, limit of detection; *nptII*, *neomycin phosphotransferase II*; PCR, polymerase chain reaction; *P-35S*, *Cauliflower Mosaic Virus* 35S promoter; *P-nos*, nopaline synthase promoter; *pat*, *Streptomyces viridochromogenes* phosphinotricin acetyltransferase; RTi-PCR, real-time PCR; *Sad1*, stearoyl-ACP desaturase; *SPS*, sucrose phosphate synthase; *T-35S*, *Cauliflower Mosaic Virus* 35S terminator; *T-nos*, nopaline synthase terminator; *UGPase*, UDP-glucose pyrophosphorylase; *uidA*, *β*-glucuronidase

■ REFERENCES

(1) James, C. *Global Status of Commercialized Biotech/GM Crops 2013*; The International Service for the Acquisition of Agri-biotech Applications (ISAAA): Ithaca, NY, 2013; Vol. *46*.

(2) Randhawa, G. J.; Singh, M.; Bansal, K. C. *DNA-based G. M. Detection, Identification & Quantfication*; Technical Bulletin, National Bureau of Plant Gentic Resources: New Delhi, 2014, 6p.

(3) Randhawa, G. J.; Singh, M.; Morisset, D.; Sood, P.; Žel, J. Loop-mediated isothermal amplification: Rapid visual and real-time methods for detection of genetically modified crops. *J. Agric. Food Chem.* **2013**, *61* (47), 11338−11346.

(4) Viljoen, C. D. Detection of living modified organisms (LMOs) and the need for capacity building. *Asian Biotechnol. Dev. Rev.* **2005**, *7*, 55−69.

(5) Holst-Jensen, A.; Rønning, S. B.; Løvseth, A.; Berdal, K. G. PCR technology for screening and quantification of genetically modified organisms (GMOs). *Anal. Bioanal. Chem.* **2003**, *375*, 985−993.

(6) Querci, M.; Foti, N.; Bogni, A.; Kluga, L.; Broll, H.; Van den Eede, G. Real-time PCR-based ready-to-use multi-target analytical system for GMO detection. *Food Anal. Methods* **2009**, *2*, 325−336.

(7) Piednoir, E. B.; Lievens, A.; Vandermassen, E.; Guillaume, E.; Mbella, M.; Casi, A. L.; Roosens, N.; Sneyers, M.; Van den Bulcke, M. Four new SYBR_Green qPCR screening methods for the detection of Roundup Ready, LibertyLink, and *cry1Ab* traits in genetically modified products. *Eur. Food Res. Technol.* **2012**, *234*, 13−23.

(8) Randhawa, G. J.; Sharma, R.; Singh, M. Qualitative and event-specific real-time PCR detection methods for *Bt* brinjal event EE-1. *J. AOAC Int.* **2012**, *95* (6), 1933−1739.

(9) Huber, I. C.; Block, A.; Sebah, D.; Debode, F.; Morisset, D.; Grohmann, L.; Berben, G.; Štebih, D.; Milavec, M.; Žel, J.; Busch, U. Development and validation of duplex, triplex and pentaplex real-time PCR screening assays for the detection of genetically modified organisms in food and feed. *J. Agric. Food Chem.* **2013**, *61* (43), 10293−10301.

(10) Dinon, A. Z.; Prins, T. W.; Kok, E. J. Development and validation of real-time PCR screening methods for detection of *cry1A.105* and *cry2Ab2* genes in genetically modified organisms. *Anal. Bioanal. Chem.* **2011**, *400* (5), 1433−1442.

(11) Kluga, L.; Folloni, S.; Van den Bulcke, M.; Van den Eede, G.; Querci, M. Applicability of the real-time PCR-based ready-to-use multi-target analytical systems for GMO detection in processed maize matrices. *Eur. Food Res. Technol.* **2012**, *234*, 109−118.

(12) Cottenet, G.; Blancpain, C.; Sonnard, V.; Chuah, P. F. Development and validation of a multiplex real-time PCR method to simultaneously detect 47 targets for the identification of genetically modified organisms. *Anal. Bioanal. Chem.* **2013**, *405* (21), 6831−6844.

(13) Randhawa, G. J.; Morisset, D.; Singh, M.; Žel, J. GMO matrix: A cost-effective approach for screening unauthorized genetically modified events in India. *Food Control* **2014**, *38*, 124−129.

(14) Žel, J.; Mazzara, M.; Savini, C.; Cordeil, S.; Camloh, M.; Štebih, D.; Cankar, K.; Gruden, K.; Morisset, D.; Van den Eede, G. Method validation and quality management in the flexible scope of accreditation: An example of laboratories testing for genetically modified organisms. *Food Anal. Methods* **2008**, *1* (2), 61−72.

(15) Randhawa, G. J.; Singh, M. Multiplex, construct-specific and real-time PCR-based analytical methods for *Bt* rice with *cry1Ac* gene. *J. AOAC Int.* **2012**, *95* (1), 186−194.
(16) Randhawa, G. J.; Chhabra, R.; Singh, M. Decaplex and real-time PCR based detection of MON531 and MON15985 *Bt* cotton events. *J. Agric. Food Chem.* **2010**, *58* (18), 9875−9881.
(17) Chhabra, R.; Randhawa, G. J.; Bhoge, R. K.; Singh, M. Qualitative and quantitative PCR-based detection methods for authorized genetically modified cotton events in India. *J. AOAC Int.* **2014**, in press.
(18) Arumuganathan, K.; Earle, E. Nuclear DNA content of some important plant species. *Plant Mol. Biol. Rep.* **1991**, *9* (3), 208−218.
(19) Codex Committee On Methods Of Analysis And Sampling Guidelines On Performance Criteria And Validation Of Methods For Detection, Identification And Quantification Of Specific DNA Sequences And Specific Proteins In Foods; CAC/GL 74−2010; Codex alimentarius commission; WHO: Rome, 2010.
(20) Delobel, C.; Larcher, S.; Savini, C.; Mazzara, M.; Van Den Eede, G. Event-specific method for the quantification of maize line GA21 using real-time PCR - Validation report and protocol - Report on the verification of performance of a DNA extraction method for maize grains; EURL-GMFF Online Publication, 2007, DOI: 10.2788/62889.
(21) Guan, Q.; Wang, X.; Teng, D.; Yang, Y.; Tian, F.; Yin, Q.; Wang, J. Construction of a standard reference plasmid for detecting GM cotton seed meal. *Appl. Biochem. Biotechnol.* **2011**, *165* (1), 24−34.
(22) Jiang, L.; Yang, L.; Zhang, H.; Guo, J.; Mazzara, M.; Van den Eede, G.; Zhang, D. International collaborative study of the endogenous reference gene, sucrose phosphate synthase (*SPS*), used for qualitative and quantitative analysis of genetically modified rice. *J. Agric. Food Chem.* **2009**, *57* (9), 3525−3532.
(23) Chaouachi, M.; Malki, R. L.; Berard, A.; Romaniuk, M.; Laval, V.; Brunel, D.; Yves Bertheau, Y. Development of a real-time PCR method for the differential detection and quantification of four *Solanaceae* in GMO analysis: Potato (*Solanum tuberosum*), tomato (*Solanum lycopersicum*), eggplant (*Solanum melongena*), and pepper (*Capsicum annuum*). *J. Agric. Food Chem.* **2008**, *56* (6), 1818−1828.
(24) Rho, J. K.; Lee, T.; Jung, S. I.; Kim, T. S.; Park, Y. H.; Kim, Y. M. Qualitative and quantitative PCR methods for detection of three lines of genetically modified potatoes. *J. Agric. Food Chem.* **2004**, *52* (11), 3269−3274.
(25) Delobel, C.; Larcher, S.; Mazzara, M.; Van Den Eede, G. Event-specific method for the quantification of maize event *Bt*11 using real-time PCR - Validation report and protocol. Online Publication, 2008, DOI: 10.2788/4370.
(26) Savini, C. In-house validation of an event-specific method for the quantification of maize *Bt*176 using real-time PCR - Validation report and protocol. EURL-GMFF Online Publication, 2011.
(27) Mazzara, M.; Paoletti, C.; Puumalainen, J. Event-specific method for the quantitation of maize line NK603 using real-time PCR. EURL-GMFF Online Publication, 2005.
(28) Delobel, C.; Bonfini, L.; Querci, M.; Mazzara, M.; Cordeil, S.; Van Den Eede, G. Event-specific method for the quantification of maize MIR162 using real-time PCR - Validation report and protocol. EURL-GMFF Online Publication, 2011.
(29) Mazzara, M.; Munaro, B.; Foti, N.; Savini, C.; Van Den Eede, G. Event-specific method for the quantification of maize line MIR604 using real-time PCR - Validation report and protocol - Maize seeds sampling and DNA extraction. EURL-GMFF Online Publication, 2007, DOI 10.2788/30596.
(30) Mazzara, M.; Van den Eede, G.; Savini, C.; Grazioli, E. Report on the verification of the performance of a MON810 event-specific method on maize line MON810 using real-time PCR. EURL-GMFF Online Publication, 2009.
(31) Mazzara, M.; Foti, N.; Price, S. Event-specific method for the quantitation of maize line MON863 using real-time PCR. EURL-GMFF Online Publication, 2005.
(32) Savini, C.; Bogni, A.; Grazioli, E. Event-specific method for the quantification of maize line MON89034 using real-time PCR. EURL-GMFF Online Publication, 2008, DOI: 10.2788/68713.
(33) Mazzara, M.; Foti, N.; Price, S.; Paoletti, C.; Van den Eede, G. Event-specific method for the quantitation of maize line TC1507 using real-time PCR - Validation report and protocol -Sampling and DNA extraction of maize TC1507. EURL-GMFF Online Publication, 2005.
(34) Delobel, C.; Foti, N.; Mazzara, M. Event-specific method for the quantification of maize event 3272 using real-time PCR. EURL-GMFF Online Publication, 2008.
(35) Mazzara, M.; Grazioli, E.; Larcher, S.; Savini, C.; Van den Eede, G. Event-specific method for the quantitation of maize line DAS-59122−7 using real-time PCR - Validation report and protocol. EURL-GMFF Online Publication, 2006.
(36) Mazzara, M., Bogni, A., Foti, N. and Van Den Eede, G. Event-specific method for the quantification of cotton line MON531 using real-time PCR - Validation report and protocol. EURL-GMFF Online Publication, 2008, DOI: 10.2788/43936.
(37) Savini, C.; Mazzara, M.; Munaro, B.; Van den Eede, G. Event-specific method for the quantification of cotton line MON15985 using real-time PCR - Validation report and protocol. EURL-GMFF Online Publication, 2008, DOI 10.2788/4378.
(38) Mazzara, M.; Bogni, A.; Van den Eede, G. Event-specific method for the quantification of cotton line MON1445 using real-time PCR. EURL-GMFF Online Publication, 2008, DOI: 10.2788/4455.
(39) Delobel, C.; Luque Perez, E.; Pinski, G.; Bogni, A.; Mazzara, M.; Van den Eede, G. Event-specific method for the quantification of cotton MON88913 using real-time PCR - Validation report and protocol. EURL-GMFF Online Publication, 2009, DOI: 10.2788/58818.
(40) Mazzara, M.; Larcher, S.; Savini, C.; Charles Delobel, C.; Van den Eede, G. Event-specific methods for the quantitation of the hybrid cotton line 281−24−236/3006−210−23 using real-time PCR - Validation report and protocol - Sampling and DNA extraction of cotton seeds″ EURL-GMFF Online Publication, 2006.
(41) Mazzara, M.; Grazioli, E.; Savini, C.; Van den Eede, G. Event-specific method for the quantitation of rice line LLRICE62 using real-time PCR - Validation report and protocol - Sampling and DNA extraction of rice. EURL-GMFF Online Publication, 2006, DOI 10.2788/31940.
(42) Mazzara, M.; Munaro, B.; Larcher, S.; Grazioli, E.; Delobel, C.; Savini, C.; Van den Eede, G.; Event-specific method for the quantification of soybean line 40−3-2 using real-time PCR - Validation report and protocol - Report on the validation of a DNA extraction m,ethod for soybean seeds. EURL-GMFF Online Publication, 2007, DOI: 10.2788/61824.
(43) Lee, S. H.; Kim, J. K.; Yi, B. Y. Detection methods for biotech cotton MON15985 and MON88913 by PCR. *J. Agric. Food Chem.* **2007**, *55* (9), 3351−3357.
(44) Grohmann, L.; Brunen-Nieweler, C.; Nemeth, A.; Waiblinger, H. U. Collaborative trial validation studies of real-time PCR-based GMO screening methods for detection of the *bar* gene and the *ctp2-cp4epsps* construct. *J. Agric. Food Chem.* **2009**, *57*, 8913−8920.
(45) Terry, C. F.; Shanahan, D. J.; Ballam, L. D.; Harris, N.; McDowell, D. G.; Parkes, H. C. Real-time detection of genetically modified soya using Lightcycler and ABI 7700 platforms with TaqMan, Scorpion, and SYBR Green I chemistries. *J. AOAC Int.* **2002**, *85* (4), 938−944.
(46) Kuribara, H.; Shindo, Y.; Matsuoka, T.; Takubo, K.; Futo, S.; Aoki, N.; Hirao, T.; Akiyama, H.; Goda, Y.; Toyada, M.; Hino, A. Novel reference molecules for quantitation of genetically modified maize and soybean. *J. AOAC Int.* **2002**, *85* (5), 1077−1089.
(47) Pansiot, J.; Chaouachi, M.; Cavellini, L.; Romaniuk, M.; Ayadi, M.; Bertheau, Y.; Laval, V. Development of two screening duplex PCR assays for genetically modified organism quantification using multiplex real-time PCR master mixes. *Eur. Food Res. Technol.* **2011**, *232*, 327−334.
(48) Weng, H.; Pan, A.; Yang, L.; Zhang, C.; Liu, Z.; Zhang, D. Estimating number of transgene copies in transgenic rapeseed by real-time PCR assay with *HMG I/Y* as an endogenous reference gene. *Plant. Mol. Biol. Rep.* **2004**, *22* (3), 289−300.

(49) Weighardt, F.; Barbati, C.; Paoletti, C.; Querci, M.; Kay, S.; de Beuckeleer, M.; Van den Eede, G. Real-time polymerase chain reaction-based approach for quantification of the *pat* gene in the T25 *Zea mays* event. *J. AOAC Int.* **2004**, *87*, 1342−1355.
(50) ISO 5725-3-1994. Accuracy (Trueness and Precision of Measurement Methods and Results − Part 3: Intermediate Measures of the Precision of a Standard measurement Method. International Organisation for Standardisation, Geneva, Switzerland.

were approved by the Committee on Animal Research at Ajou Medical Center, Ajou University.

Experimental Treatment. For in vitro experiments, AITC and ASA were dissolved in 70% PEG−saline. The final concentration of 70% PEG−saline never exceeded 0.1%. For ex vivo and in vivo experiments, AITC and ASA were dissolved in 70% PEG−saline. Seventy percent PEG−saline solution did not influence platelet aggregation. All agents were prepared just before use.

Preparation of Platelet-Rich Plasma (PRP) from Rat and Human Blood. PRP from rat blood was prepared as described previously.[15,16] Briefly, SD rats weighing 200−240 g were lightly anesthetized with diethyl ether. A volume of 8−10 mL of blood was collected from the abdominal aorta into a syringe containing 3.8% sodium citrate. The ratio of blood to 3.8% sodium citrate was adjusted to 1:9 v/v. After centrifugation at 150*g* for 10 min at room temperature, supernatants (PRP) were used for the aggregation study. To prepare washed platelets (WP), blood was collected into a syringe containing acid citrate dextrose (ACD; 2.5% trisodium citrate, 2% dextrose, and 1.5% citric acid) and adjusted to a ratio of 1:9 v/v. After centrifugation at 150*g* for 10 min at room temperature, the platelets were isolated and then centrifuged again at 150*g* for 10 min in washing buffer (Tyrode's solution containing 10% ACD buffer and 0.3% BSA). Platelets were diluted with Tyrode's solution (11.9 mM NaCl, 2.7 mM KCl, 2.1 mM $MgCl_2$, 0.4 mM NaH_2PO_4, 11.9 mM $NaHCO_3$, 11.1 mM glucose, and 3.5 mg/mL bovine serum albumin, pH 7.2). To make platelet-poor plasma (PPP) from rat blood, PRP was centrifuged at 1200*g* for 10 min at room temperature, and supernatants were obtained as PPP. For PRP from human blood, human platelet suspensions were supplied from the Red Cross (Suwon, Korea). Human blood was collected from healthy human volunteers who had not taken medicine as indicated by the Red Cross guide.

In Vitro Platelet Aggregation and Shape Change in Rat PRP. The platelet aggregation study was performed as previously described.[17,18] Briefly, PRP was diluted with Tyrode's solution containing 0.3% BSA and adjusted to about 2×10^8 platelets/mL. PRP was stimulated to aggregate by using different aggregating agents at the following final concentrations: collagen, 2 μg/mL; thrombin, 0.2 U/mL; ADP, 2.5 μM; AA, 100 μM; and U46619, 1 μM. We decided the concentrations of agonists on the basis of the results from preliminary experiments (data not shown). Platelet aggregation was recorded for 5 min after stimulation by using whole blood/optical Lumi-Aggregometer (Chrono-Log). Aggregations were measured and expressed as percent changes in light transmission with respect to PPP. Data of light transmission assay were calculated to percent change by using Chrono-Log software. In the in vitro study, PRP was preincubated with AITC or ASA at 37 °C for 3 min before being stimulated with the aggregating agents. To monitor shape change, a platelet shape change study was performed as previously described.[19] Platelets (2×10^8 platelets/mL) were preincubated with apyrase (2 U/mL), indomethacin (10 μM), and EGTA (1 mM) before the addition of collagen.

Determination of Cytotoxicity in Rat PRP. To determine the cytotoxicity of AITC, lactate dehydrogenase (LDH) release from platelets was measured as previously described.[20] After incubation of PRP (2×10^8 platelets/mL) with 70% PEG−saline or different concentrations of AITC for 3 min at 37 °C, PRP was centrifuged at room temperature at 10000*g* for 1 min. A 25 μL aliquot of the supernatant was mixed with 100 μL of NADH solution (0.03% β-NAD, reduced form of the disodium salt in phosphate buffer) and 25 μL of pyruvate solution (22.7 mM pyruvic acid in phosphate buffer) at room temperature. Reductions in absorbance at 340 nm because of conversion of NADH to NAD^+ were measured to determine LDH activity in supernatants. LDH release is expressed as the percentage of the total enzyme activity in platelets completely lysed with 0.2% Triton X-100.

Measurement of TXA_2 Production and ATP Release in Rat and Human PRP. Measurement of TXA_2 production was conducted using a TXB_2 EIA kit (Cayman Chemical Co, Ann Arbor, MI, USA) as previously described.[21] PRP (2×10^8 platelets/mL) was incubated for 3 min in the presence or absence of samples, and then collagen (2 μg/mL) was added and PRP was incubated at 37 °C for 5 min with stirring. EDTA (10 mM) was added to stop TXA_2 production. After centrifugation at 12000*g* for 3 min, the amount of TXB_2 was measured according to the manufacturer's instructions.

Detection of ATP release was determined as previously described.[22] PRP (2×10^8 platelets/mL) was incubated at 37 °C with stirring at 1200 rpm. After addition of the luciferin−luciferase reagent, collagen (2 μg/mL) was added to initiate the reaction. PRP was incubated with AITC (30, 100, or 300 μM) for 3 min before the addition of luciferin−luciferase reagent.

Determining the $[Ca^{2+}]_i$ in Rat PRP. The intracellular Ca^{2+} was determined with Fura-2/AM as described previously.[23] Briefly, the PRP was incubated with 6 μM Fura-2/AM for 60 min at 37 °C. The Fura-2-loaded washed platelets (10^8 mL^{-1}) were then preincubated with AITC for 3 min with 1 mM $CaCl_2$. Next, WPs were stimulated with collagen (2 μg/mL) for 5 min. Fura-2 fluorescence was measured in a spectrofluorometer with an excitation wavelength that ranged from 340 to 380 nm, changing every 0.5 s, and an emission wavelength of 510 nm. The $[Ca^{2+}]_i$ was calculated as[24]

$$[Ca^{2+}]_i \text{ in cytosol} = 224 \text{ nM} \times (F - F_{min})/(F_{max} - F)$$

where 224 nM is the dissociation constant of the Fura-2−Ca^{2+} complex and F_{min} and F_{max} represent the fluorescence intensity levels at very low and very high Ca^{2+} concentrations, respectively. F_{min} is the fluorescence intensity of the Fura-2−Ca^{2+} complex at 510 nm, after the platelet suspension containing 20 mM Tris/10 mM EGTA had been solubilized by 0.1% Triton X-100. F_{max} is the fluorescence intensity of the Fura-2−Ca^{2+} complex at 510 nm, after the platelet suspension containing 1 mM $CaCl_2$ had been solubilized by 0.1% Triton X-100. F indicates the fluorescence intensity of the Fura-2 complex at 510 nm after WPs were stimulated by collagen, with 1 mM $CaCl_2$ and AITC or vehicle.

Western Blotting. The immunoassay was performed as previously described.[4] The WPs (2×10^8 platelets/mL) were stimulated by collagen (2 μg/mL) in the presence or absence of AITC (300 μM). Reactions were terminated by adding 10 mM EDTA and centrifuged at 12000*g* for 3 min. After the addition of ice-cold platelet lysis buffer (1% NP40, 15 mM HEPES, 75 mM NaCl, 1 mM EDTA, 1 mM phenylmethanesulfonyl fluoride (PMSF), 1 mM sodium fluoride (NAF), 1 mM Na_3VO_4, 1 μg/mL leupeptin, and 1 μg/mL aprotinin; pH 7.4), lysates were centrifuged at 13000*g* for 10 min at 4 °C. The supernatants were collected, and protein concentration was determined using a BCA protein assay (Thermo Scientific, Vernon Hills IL, USA). Equal volumes of protein were resolved using SDS-PAGE (10%) and transferred to PVDF membranes. The PVDF membranes were blocked with 5% nonfat dry milk in TBS and incubated with the primary antibody diluted in TBS buffer (1:1000 ratio, 4 °C overnight). Immunoblots were then incubated again with a horseradish peroxidase (HRP)-conjugated secondary antibody, and then the immune-reactive bands were visualized with a LAS 4000 (Fuji, Honshu, Japan) using a Western blot detection system (WestZol, Intron, Seoul, Korea).

Ex Vivo Platelet Aggregation Study in Rat. Two hours before experiments, SD rats were orally administered 70% PEG−saline, AITC (0.3, 1, 3 mg/kg), or ASA (50 mg/kg). Rat blood samples were collected, and the platelet aggregation study was performed as described above.

In Vivo Acute Pulmonary Thromboembolism Study in Mouse. Acute pulmonary thromboembolism model was performed as previously described.[25] Male ICR mice weighing 35−40 g were fasted for 6 h before experiments. AITC and ASA were dissolved in 70% PEG−saline. Mice were orally administered AITC or ASA 2 h before experiments were performed. Collagen (500 μg/kg) plus epinephrine (25 μg/mL) was injected to the tail vein to induce thrombosis. Each mouse was watched for 15 min to determine whether the mouse was paralyzed, dead, or recovered from the acute thrombotic challenge.

In Vivo Mouse Tail Bleeding Time Assay. Mouse tail bleeding times were recorded as previously described.[26,27] Male ICR mice

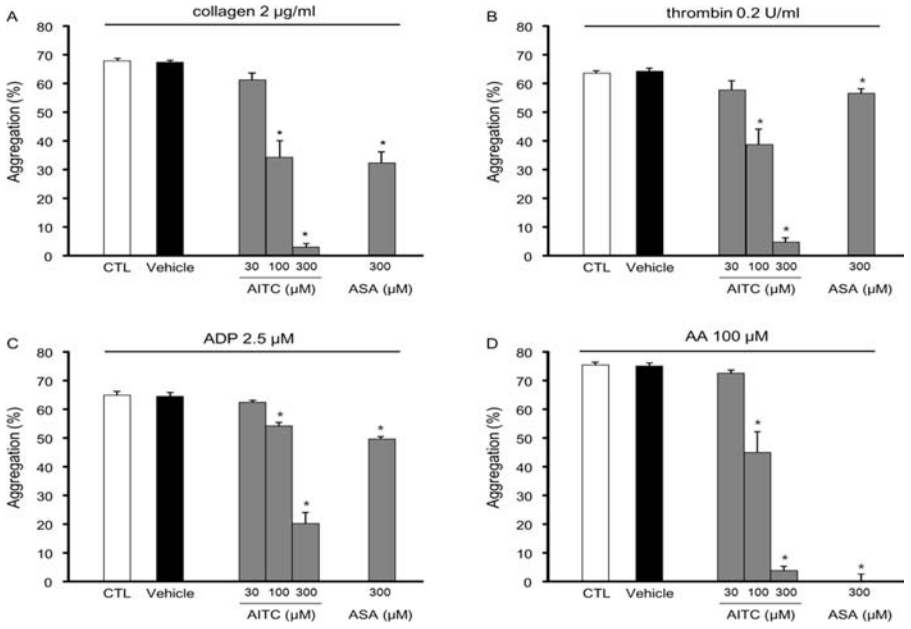

Figure 1. Concentration-dependent inhibitory effect of AITC on in vitro platelet aggregation. Platelets were preincubated with 70% PEG−saline (vehicle group), ASA (300 μM), or AITC (30, 100, or 300 μM) or not (control group) for 3 min at 37 °C. After preincubation, platelets were stimulated by the following agonists: collagen, 2 μg/mL (A); thrombin, 0.2 U/mL (B); ADP, 2.5 μM (C); or arachidonic acid (AA), 100 μM (D). Data are expressed as means ± SEMs (n = 5). (*) P < 0.05 versus vehicle.

weighing 35−40 g were fasted for 16 h before experiments. Two hours after the oral administration of AITC (0.3, 1, or 3 mg/kg) or ASA (50 mg/kg), the mice were anesthetized with ketamine (100 mg/kg) and xylazine (10 mg/kg). Thereafter, the mice were individually placed on a hot plate to control body temperature, and tails were transected 3 mm from the tips by using a razor blade. The tail was then immersed in a 15 mL clear conical tube containing warmed saline (37 °C). The time until the cessation of blood flow was then measured. Bleeding time was defined as the time taken for bleeding to stop for 15 s.

Statistical Analysis. In the thromboembolism experiment, the chi-square test was used to determine significant differences between the vehicle and treated groups. Statistical significance was considered at P < 0.05. In other experiments, data were expressed as means ± SEMs of at least three experiments. One-way ANOVA followed by Dunnett's test or the paired t test by using Sigma Stat statistical software (San Rafael, CA, USA) was used for the analysis. Significance was accepted for P values of <0.05.

RESULTS AND DISCUSSION

Effect of AITC on Rat Platelet Aggregation in Vitro. To evaluate the antiplatelet effect of AITC, we first examined its effect on rat platelet aggregation induced by various agonists. During pathological thrombogenesis, platelets are activated after binding to collagen on a vascular lesion. Activated platelets initiate intrinsic pathways, such as arachidonic acid (AA) liberation, to release secondary agonists including ADP, which in turn activate other platelets.[28] Thrombin initiates platelet activation through cleavage of the N-terminal exodomain of the protease-activated receptor.[29] Thrombus formation is induced by multiple physiological ligands and, thus, an antiplatelet agent that affects only one type of ligand-platelet interaction is likely to have a limited preventive effect against thrombogenesis.[27] Therefore, an antiplatelet agent that acts on multiple platelet activation pathways has been suggested to be a more effective compound for treating platelet-involved cardiovascular disease. Indeed, dual antiplatelet therapy, such as a combination of clopidogrel and ASA, has been shown to be more effective in inhibiting pathogenic thrombi.[30] ASA inhibits platelet aggregation through inhibition of cyclooxygenase, and clopidogrel inhibits platelet activation through irreversible binding to the $P2Y_{12}$ ADP receptor on platelet membrane.

In this study, PRP was stimulated by collagen (2 μg/mL), thrombin (0.2 U/mL), ADP (2.5 μM), or AA (100 μM) to induce platelet aggregation. The platelet aggregations induced by collagen, thrombin, ADP, and AA (68, 64, 62, and 74%, respectively) were significantly inhibited by either 100 or 300 μM AITC (6, 8, 18, and 5%, respectively) (Figure 1). In addition, AITC showed lower IC_{50} values than ASA in collagen, thrombin or ADP-induced platelet aggregation (Table 1). Taken together, these results indicate that AITC inhibits platelet aggregations induced by multiple agonists, and thus it may have beneficial potential for the prevention of platelet-related disorders.

Table 1. IC_{50} of AITC and ASA for Platelet Aggregation in Vitro[a]

agonist[b]	AITC IC_{50} (μM)	ASA IC_{50} (μM)
collagen	112.8 ± 16.3	312.7 ± 30.6
thrombin	100.6 ± 10.7	1314.7 ± 76.4
ADP	149.7 ± 17.7	1422.6 ± 129.1
AA	167.2 ± 22.6	27.3 ± 0.9

[a]Results are expressed as means ± SDs. [b]Concentration of agonists were as follows: collagen (2 μg/mL), thrombin (0.2 U/mL), ADP (2.5 μM), and AA (100 μM).

Effect of AITC on Platelet Cytotoxicity. To examine the cytotoxicity of AITC, LDH release from platelets was measured. LDH release is used as an index of cellular injury, including injury to platelets.[31] There was no significant LDH release from platelets treated with either vehicle (70% PEG−saline) or AITC (30, 100, or 300 μM) (Table 2). These findings suggest that the antiplatelet effect of AITC was not the result of cytotoxic effects, such as platelet membrane disruption.

dx.doi.org/10.1021/jf4041518 | J. Agric. Food Chem. 2014, 62, 7131−7139

Table 2. Effect of AITC on LDH Release by Platelets[a]

treatment	LDH release[b]
CTL	11.2 ± 1.6
vehicle	13.1 ± 1.7
AITC 300 μM	11.5 ± 1.6
AITC 100 μM	11.8 ± 2.2
AITC 30 μM	10.1 ± 2.0

[a]Data are expressed as means ± SEMs (n = 5). [b]LDH release was measured after rat platelet-rich plasma was treated with either vehicle or AITC (30, 100, or 300 μM) for 3 min. P < 0.05 versus vehicle.

Effects of AITC on TXA_2 Production, ATP Release, and Ca^{2+} Increase in Rat PRP. Platelets are activated by various agonists including collagen. Activated platelets recruit other platelets to form aggregation. To recruit other platelets, activated platelets secrete TXA_2 and granules containing ATP and ADP, which act as paracrine activators.[22,32] Through interaction with the T_P receptor on the platelet membrane, TXA_2 plays a key role in platelet shape change and fibrinogen receptor (GPIIb/IIIa) activation, subsequently leading to platelet aggregation.[33,34] A parallel process involves release of ATP and ADP, which then bind to $P2X_1$ and $P2Y_1/P2Y_{12}$ receptors, respectively, leading to Ca^{2+} entry and amplification of platelet activation and shape change.[35]

Because TXA_2 production and ATP release follow platelet activation, they are well-known indicators of platelet activation.[36] To evaluate the mechanism of the antiplatelet effect of AITC, TXA_2 production and ATP release were examined in this study. Because TXA_2 is unstable and quickly converted to its stable form, TXB_2, the production of TXB_2 was measured instead. Collagen-induced TXB_2 production (4022 pg/mL) was significantly inhibited by AITC at a concentration of 300 μM (1320 pg/mL), but not by 100 μM (3812 pg/mL) (Figure 2A). Consistently, AITC significantly inhibited platelet aggregation induced by U46619 (77%), a thromboxane A_2 receptor agonist, only at the concentration of 300 μM (11%) (Supporting Information file 1). These findings suggest that the antiplatelet effect of 100 μM AITC (Figure 1) may be attributed to a mechanism other than the TXA_2 inhibition pathway. To investigate the mechanism underlying the effect of 100 μM AITC, the effect of AITC on granule secretion was examined by measuring ATP release, which reflects the release of ADP, because ATP/ADP release from granules is known to be activated independently of TXA_2 pathway.[22,37] AITC, at the concentrations of both 100 and 300 μM, significantly inhibited collagen-induced ATP release by 48 and 84%, respectively (Figure 2B). From these results, it is suggested that the antiplatelet effect of AITC at 100 μM is likely to be attributed to inhibition of ATP/ADP release rather than TXA_2 inhibition, whereas the antiplatelet effect of 300 μM AITC is attributed to inhibition of both ATP/ADP release and TXA_2.

Another biomarker of platelet activation is intracellular Ca^{2+} increase. After collagen binds platelet membrane receptor, intracellular Ca^{2+} increases and plays a key role in TXA_2, ATP/ADP secretion, and shape change.[38] In addition, increasing

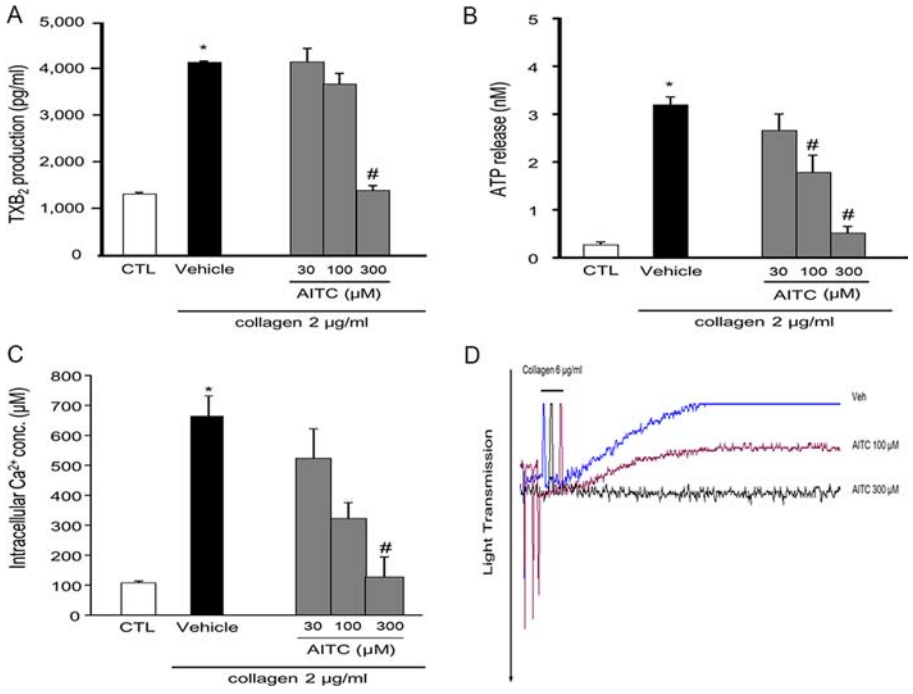

Figure 2. Inhibitory effect of AITC on collagen-induced TXA_2 production (A), ATP release (B), intracellular Ca^{2+} increase (C), and platelet shape change (D). For the TXA_2 assay, platelets were preincubated with AITC (30, 100, or 300 μM) for 3 min, and then platelets were stimulated with collagen (2 μg/mL) for 6 min. The amount of TXA_2 was determined by measuring TXB_2 concentrations using an EIA kit (n = 8). For ATP measurement, platelets were preincubated with AITC (30, 100, or 300 μM) for 3 min before the addition of a luciferin−luciferase reagent. After the luciferin−luciferase reagent was added, platelets were stimulated with collagen (2 μg/mL) for 6 min. ATP release was measured using a lumi-aggregometer (n = 8). For measurement of intracellular Ca^{2+} increase, platelets were loaded with Fura-2/AM. The platelets were preincubated with or without AITC (30, 100, or 300 μM) for 3 min and stimulated with collagen 2 μg/mL (n = 5). For measurement of platelet shape change, platelets were preincubated with apyrase (2 U/mL), indomethacin (10 μM), EGTA (1 mM), and with or without AITC (30, 100, or 300 μM) for 3 min followed by stimulation with collagen (6 μg/mL) and traces recorded. Data are expressed as means ± SEMs (n = 5). (*) P < 0.05 versus control. (#) P < 0.05 versus vehicle.

dx.doi.org/10.1021/jf4041518 | J. Agric. Food Chem. 2014, 62, 7131−7139

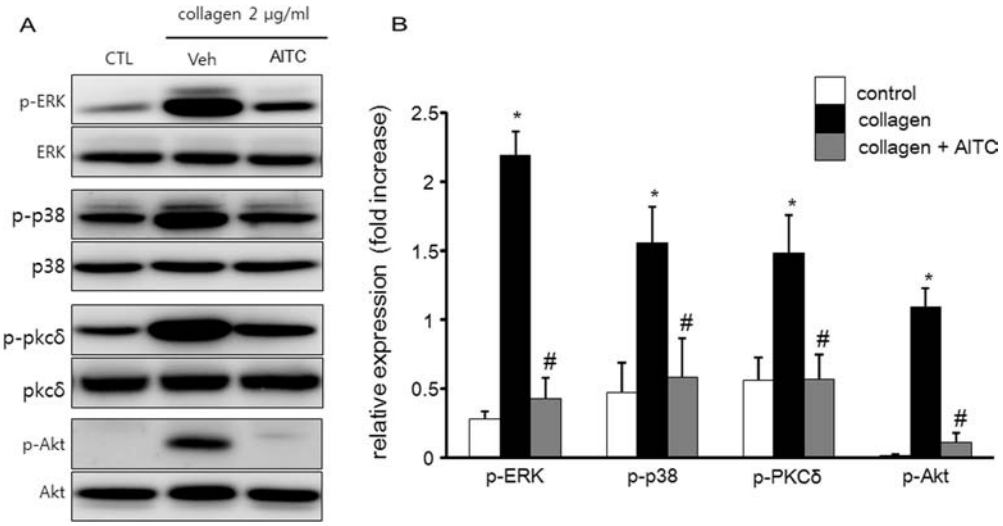

Figure 3. Effect of AITC on protein phosphorylation. (A) AITC attenuated collagen-activated platelet Akt, PKCδ, ERK, and p38 phosphorylation. Washed platelets were preincubated with either vehicle or AITC (300 μM) for 3 min with stirring. After preincubation, washed platelets were stimulated with collagen (2 μg/mL) for 5 min. Platelet lysates were analyzed by a Western blot immunoassay. (B) Relative expression was compared between total expression and phosphorylated expression. Values in bar graphs are means ± SEMs (n = 4). (∗)P < 0.05 versus control. (#) P < 0.05 versus vehicle.

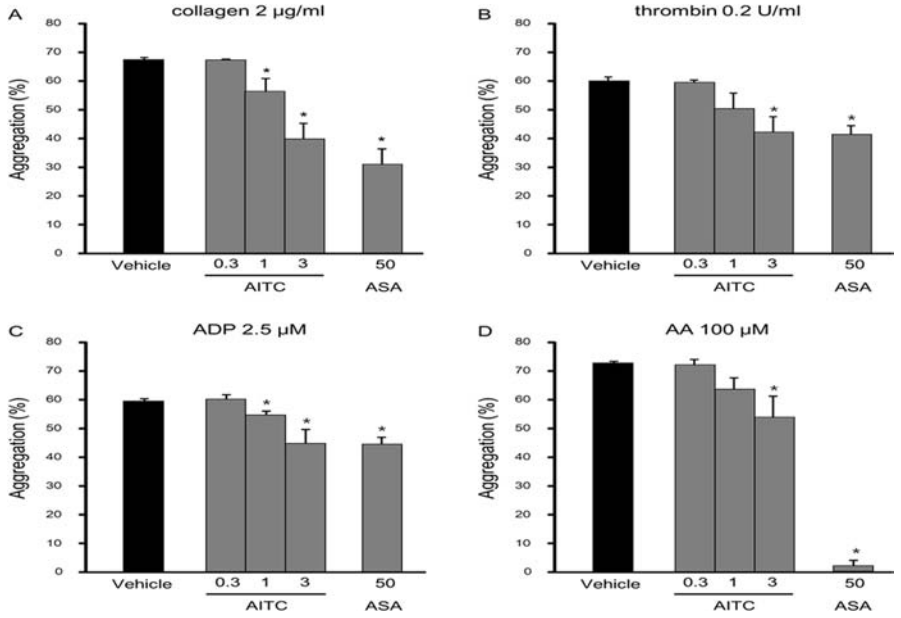

Figure 4. AITC inhibits ex vivo platelet aggregation after oral administration in a dose-dependent manner. AITC (0.3, 1, or 3 mg/kg) or ASA (50 mg/kg) was administered 2 h before blood collection. Platelet aggregation was induced by the following agonists: collagen, 2 μg/mL (A); thrombin, 0.2 U/mL (B); ADP, 2.5 μM (C); AA, 100 μM (D). Data are expressed as means ± SEMs (n = 6). (∗) P < 0.05 versus vehicle.

Ca^{2+} contributes to platelet aggregation through transformation of fibrinogen binding receptor GPIIb/IIIa. Transformed GPIIb/IIIa has high affinity with fibrinogen to aggregate platelets through fibrinogen binding. Furthermore, high intracellular Ca^{2+} contributes to platelet shape change through dissociation of actin−profilin complexes.[39] In this study, the effects of AITC on intracellular Ca^{2+} increase and shape change were examined to elicit its inhibitory mechanism on platelet aggregation. Collagen-induced intracellular Ca^{2+} increase (612 μM) was significantly inhibited by AITC at 100 and 300 μM (350 and 181 μM, respectively) (Figure 2C). In addition, collagen-induced platelet shape change was also inhibited by 100 and 300 μM AITC. These results suggest that the antiplatelet mechanisms of AITC at 100 and 300 μM may involve its inhibition of intracellular Ca^{2+} increase and shape change.

Effects of AITC on Phosphorylation of PLCγ, p38, ERK, PKCδ, and Akt. At the sites of atherosclerotic lesion, collagen is the most important thrombogenic component of the subendothelial matrix. Collagen binds to receptors on the platelet membrane, including the glycoprotein VI (GPVI) receptor, which has recently been considered as a new therapeutic target to prevent platelet aggregation with fewer side effects.[40,41] Recent studies have shown that inhibition of GPVI contributes to protection from thrombi with mild side effects, such as minor bleeding.[42,43] In the process of platelet

dx.doi.org/10.1021/jf4041518 | J. Agric. Food Chem. 2014, 62, 7131−7139

aggregation, collagen binding to GPVI receptor triggers activation of PLCγ/protein kinase C delta (PKCδ)/extracellular signal-regulated kinases (ERK) and/or p38 mitogen-activated protein kinases (p38) signaling pathway and phosphoinositide 3-kinase (PI3K)/protein kinase B (Akt) signaling.[44] PLCγ is a specific signaling molecule for the collagen-induced platelet activation pathway, whereas Akt, PKCδ, ERK, and p38 are common molecules for all of the collagen-, thrombin- and ADP-induced signaling pathways for platelet activation.[45,46] The phosphorylation of Akt, PKCδ, ERK, and p38 is known to contribute to platelet activation, which can lead to thrombogenesis.[44,46−48] In this context, phosphorylation of proteins in the collagen-activated pathway was examined in this study to investigate the underlying action of signaling pathway mechanism of AITC. AITC was shown to markedly inhibit the phosphorylation of Akt, PKCδ, ERK, and p38 induced by collagen (2 μg/mL) (Figure 3), but not PLCγ phosphorylation (Supporting Information file 2). From these results, it is suggested that the inhibitory effect of AITC on collagen-induced platelet aggregation is, at least partially, mediated through Akt, PKCδ, ERK, and p38 inhibition rather than PLCγ suppression.

Effect of AITC on ex Vivo Platelet Aggregation in Rat. To investigate the ex vivo effect of AITC in rat, AITC was orally administered at 0.1, 0.3, 1, 3, or 10 mg/kg. Compared to vehicle treatment, AITC at 3 mg/kg po significantly inhibited platelet aggregation induced by collagen (2 μg/mL), thrombin (0.2 U/mL), ADP (2.5 μM), and AA (100 μM) (Figure 4).

Table 3. ID_{50} of AITC and ASA for Platelet Aggregation ex Vivo[a]

agonist[b]	AITC ID_{50} (mg/kg)	ASA ID_{50} (mg/kg)
collagen	6.2 ± 0.6	84.0 ± 8.9
thrombin	13.3 ± 0.9	837.0 ± 28.3
ADP	27.9 ± 0.7	450.0 ± 14.1
AA	24.1 ± 1.3	27.3 ± 5.5

[a]Results are expressed as means ± SDs. [b]Concentration of agonists were as follows: collagen (2 μg/mL), thrombin (0.2 U/mL), ADP (2.5 μM), and AA (100 μM).

Also, IC_{50} values of AITC and ASA were suggested at Table 3. ASA at 50 mg/kg was used as positive control. There was no antiplatelet effect of AITC at 0.1 and 0.3 mg/kg, and there was no significant difference in antiplatelet effect between 3 and 10 mg/kg AITC (data not shown). These results indicate that per orally treated AITC has a significant antiplatelet effect in rat, although further information such as pharmacokinetic data may be needed to link in vitro concentrations to in vivo doses of AITC.

Protective Effect of AITC on Pulmonary Thromboembolism Attack in Mouse. The goal of antiplatelet agents is prevention of thrombosis such as venous thromboembolism, which is the third most common vascular disease after heart attack and stroke.[49] The acute pulmonary thromboembolism mouse model, widely used to investigate antithrombotic therapeutic compounds, was evaluated to determine the protective effect of AITC against thromboembolism attack.[50] In the present study, oral administration of 3 mg/kg AITC had a protective effect against mortality (63%) caused by pulmonary thromboembolism (Table 4). This means that the antiplatelet effect of AITC is maintained in vivo.

Table 4. Effect of AITC on Acute Pulmonary Thromboembolism in Mice[a]

treatment	paralyzed or dead animals/total	protection (%)
CTL	8/8	0
vehicle	14/15	7
AITC		
0.3 mg/kg	11/13	15[b]
1 mg/kg	9/15	40[b]
3 mg/kg	6/16	63[b]
ASA		
50 mg/kg	3/15	80[b]

[a]The chi-square test used to examine the difference between the vehicle and treated group. [b]$P < 0.05$ versus vehicle.

Effect of AITC on Mouse Tail Bleeding Times. We investigated whether AITC has a prolonging effect on mouse tail bleeding time. Because the bleeding time reflects normal platelet function during physiologic hemostasis,[26] a prolongation effect of bleeding time has been used as an indicator for the side effect.[20] Because 3 mg/kg AITC and 50 mg/kg ASA showed similar inhibitory effects on collagen-induced platelet aggregation, we estimated bleeding time at those concentrations (3 mg/kg AITC and 50 mg/kg ASA). As shown in Figure 5, the prolonged bleeding time by 3 mg/kg AITC was

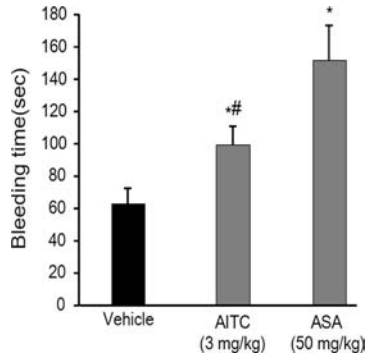

Figure 5. Effect of AITC on mouse tail bleeding time. AITC (3 mg/kg) or ASA (50 mg/kg) was given orally to mice 2 h before experiments. Data are expressed as means ± SEMs ($n = 10$). (*) $P < 0.05$ versus vehicle. (#) $P < 0.05$ versus ASA.

significantly less (40% less) than that by 50 mg/kg ASA, even though AITC still induced prolongation ($P < 0.05$). These results imply that AITC elicits an antiplatelet effect with less bleeding adverse effect.

Antiplatelet Effect of AITC in PRP from Human Blood. To investigate the effect of AITC on human blood, a platelet aggregation experiment was performed with PRP from human blood. Similar to the inhibitory effect of AITC on rat PRP, 100 and 300 μM AITC significantly inhibited platelet aggregation of human PRP induced by collagen, thrombin, ADP, and AA (Figure 6). AITC also inhibited TXB_2 production and ATP release in human platelets.

In conclusion, the present study is the first to demonstrate the antiplatelet activity of AITC in vitro, ex vivo, and in vivo. These effects of AITC seem to be mediated, at least partially, through inhibition of TXA_2 production, ATP/ADP release, and intracellular Ca^{2+} increase. AITC also showed protective effect against thromboembolism attack. These findings suggest that AITC may have therapeutic potential for the prevention of

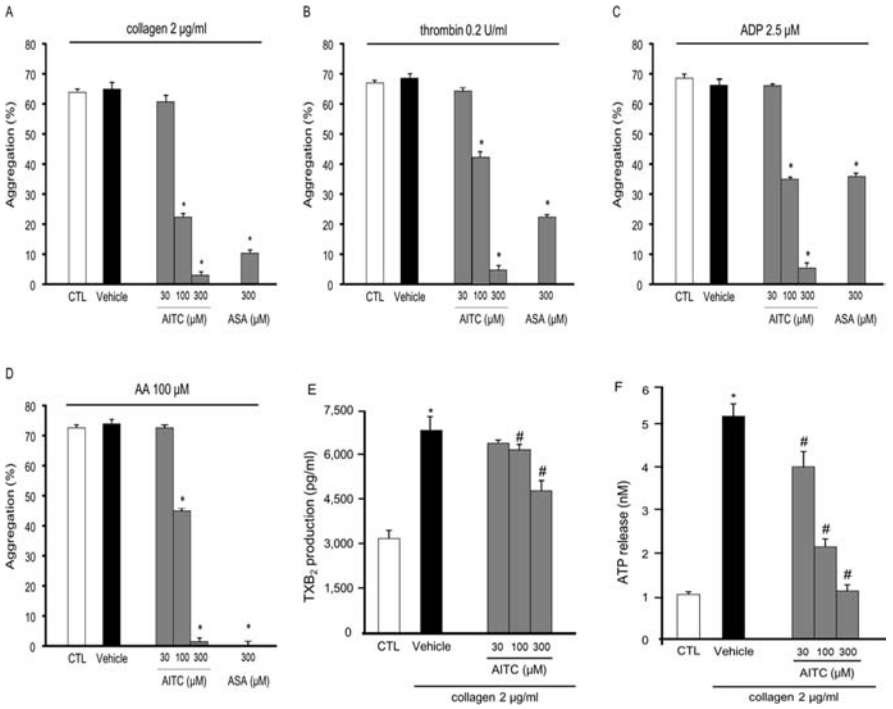

Figure 6. Effect of AITC on human platelet. Platelets were preincubated with 70% PEG−saline (vehicle group), ASA (300 μM), or AITC (30, 100, or 300 μM) or not (control group) for 3 min at 37 °C. After preincubation, platelets were stimulated by the following agonists: collagen, 2 μg/mL (A); thrombin, 0.2 U/mL (B); ADP, 2.5 μM (C); or arachidonic acid (AA), 100 μM (D) (n = 5). For the TXA_2 assay (E), platelets were preincubated with AITC (30, 100, or 300 μM) for 3 min, and then platelets were stimulated with collagen (2 μg/mL) for 6 min. The amount of TXA_2 was determined by measuring TXB_2 concentrations using an EIA kit (n = 4). For ATP measurement (F), platelets were preincubated with AITC (30, 100, or 300 μM) for 3 min before the addition of a luciferin−luciferase reagent. After the luciferin−luciferase reagent was added, platelets were stimulated with collagen (2 μg/mL) for 6 min. ATP release was measured using a lumi-aggregometer (n = 4). Data are expressed as means ± SEMs (n = 6). (*) $P < 0.05$ versus vehicle.

aberrant platelet activation, although further study remains to be performed for the potential of clinical application.

■ ASSOCIATED CONTENT

Supporting Information

File 1. Platelets were preincubated with 70% PEG−saline (vehicle group), ASA (300 μM), or AITC (30, 100, or 300 μM) or not (control group) for 3 min at 37 °C. After preincubation, platelets were stimulated by the U46619 (1 μM). Data are expressed as means ± SEM (n = 5). (*) $P < 0.05$ versus vehicle. File 2. Effect of AITC on PLCγ phosphorylation. Washed platelets were preincubated with either vehicle or AITC (300 μM) for 3 min with stirring. After preincubation, washed platelets were stimulated with collagen (2 μg/mL) for 5 min. Platelet lysates were analyzed by a Western blot immunoassay. This material is available free of charge via the Internet at http://pubs.acs.org.

■ AUTHOR INFORMATION

Corresponding Author

*(Y.-S.J.) Mail: College of Pharmacy, Ajou University, San 5, Woncheon-dong, Youngtong-gu, Suwon 443-749, Republic of Korea. Phone: +82-31-219-3444. Fax: +82-31-219-3435. E-mail: yisjung@ajou.ac.kr.

Funding

This research was supported by Bioindustry Technology Development Program (111093-3), Ministry for Food, Agriculture, Forestry and Fisheries, Republic of Korea, and by a grant from the Next-Generation BioGreen 21 Program (No. PJ009074), Rural Development Administration, Republic of Korea.

Notes

The authors declare no competing financial interest.

■ ABBREVIATIONS USED

AA, arachidonic acid; ADP, adenosine diphosphate; AITC, allyl isothiocyanate; Akt, protein kinase B; ASA, acetylsalicylic acid; ATP, adenosine triphosphate; ERK, extracellular signal-regulated kinases; GPVI, glycoprotein VI; p38, p38 mitogen-activated protein kinases; PI3K, phosphoinositide 3-kinase; PKCδ, protein kinase C delta; PPP, platelet-poor plasma; PRP, platelet-rich plasma; $TXA(B)_2$, thromboxane $A(B)_2$; WP, washed platelet

■ REFERENCES

(1) Furie, B.; Furie, B. C. Mechanisms of thrombus formation. *N. Engl. J. Med.* **2008**, *359*, 938−949.

(2) Warkentin, T. E. Aspirin for dual prevention of venous and arterial thrombosis. *N. Engl. J. Med.* **2012**, *367*, 2039−2041.

(3) Ryu, K. H.; Han, H. Y.; Lee, S. Y.; Jeon, S. D.; Im, G. J.; Lee, B. Y.; Kim, K.; Lim, K. M.; Chung, J. H. *Ginkgo biloba* extract enhances antiplatelet and antithrombotic effects of cilostazol without prolongation of bleeding time. *Thromb. Res.* **2009**, *124*, 328−334.

(4) Endale, M.; Lee, W. M.; Kamruzzaman, S. M.; Kim, S. D.; Park, J. Y.; Park, M. H.; Park, T. Y.; Park, H. J.; Cho, J. Y.; Rhee, M. H. Ginsenoside-Rp1 inhibits platelet activation and thrombus formation via impaired glycoprotein VI signalling pathway, tyrosine phosphorylation and MAPK activation. *Br. J. Pharmacol.* **2012**, *167*, 109−127.

(5) Zhang, Y. Allyl isothiocyanate as a cancer chemopreventive phytochemical. *Mol. Nutr. Food Res.* **2010**, *54*, 127−135.

(6) Yang, R.; Zhou, Q.; Wen, C.; Hu, J.; Li, H.; Zhao, M.; Zhao, H. Mustard seed (*Sinapis alba* Linn) attenuates imiquimod-induced psoriasiform inflammation of BALB/c mice. *J. Dermatol.* **2013**, *40*, 543−552.
(7) Dwivedi, C.; Muller, L. A.; Goetz-Parten, D. E.; Kasperson, K.; Mistry, V. V. Chemopreventive effects of dietary mustard oil on colon tumor development. *Cancer Lett.* **2003**, *196*, 29−34.
(8) Sengupta, A.; Ghosh, M. Modulation of platelet aggregation, haematological and histological parameters by structured lipids on hypercholesterolaemic rats. *Lipids* **2010**, *45*, 393−400.
(9) Allyl isothiocyanate. *IARC Monogr. Eval. Carcinog. Risks Hum.* **1999**, *73*, 37−48.
(10) Son, M. H.; Lee, J. Y. Standardization of processing conditions of mustard powder and mustard oil for quality improvement. *Korean J. Food Cookery Sci.* **2006**, *12*, 131−139.
(11) Sharma, H. K.; Ingle, S.; Singh, C.; Sarkar, B. C.; Upadhyay, A. Effect of various process treatment conditions on the allyl isothiocyanate extraction rate from mustard meal. *J. Food Sci. Technol.* **2012**, *49*, 368−372.
(12) Wagner, A. E.; Boesch-Saadatmandi, C.; Dose, J.; Schultheiss, G.; Rimbach, G. Anti-inflammatory potential of allyl-isothiocyanate − role of Nrf2, NF-(kappa) B and microRNA-155. *J. Cell Mol. Med.* **2012**, *16*, 836−843.
(13) Mori, N.; Kurata, M.; Yamazaki, H.; Hosokawa, H.; Nadamoto, T.; Inoue, K.; Fushiki, T. Intragastric administration of allyl isothiocyanate reduces hyperglycemia in intraperitoneal glucose tolerance test (IPGTT) by enhancing blood glucose consumption in mice. *J. Nutr Sci. Vitaminol. (Tokyo)* **2013**, *59*, 56−63.
(14) Bhattacharya, A.; Li, Y.; Geng, F.; Munday, R.; Zhang, Y. The principal urinary metabolite of allyl isothiocyanate, *N*-acetyl-*S*-(*N*-allylthiocarbamoyl)cysteine, inhibits the growth and muscle invasion of bladder cancer. *Carcinogenesis* **2012**, *33*, 394−398.
(15) Kim, H.; Oh, S. J.; Liu, Y.; Lee, M. Y. A comparative study of the anti-platelet effects of *cis*- and *trans*-resveratrol. *Biomol. Ther.* **2011**, *19*, 201−205.
(16) Pyo, M. K.; Lee, Y.; Yun-Choi, H. S. Anti-platelet effect of the constituents isolated from the barks and fruits of *Magnolia obovata*. *Arch. Pharmacal Res.* **2002**, *25*, 325−328.
(17) Lee, W.; Ku, S. K.; Bae, J. S. Antiplatelet, anticoagulant, and profibrinolytic activities of baicalin. *Arch. Pharmacal Res.* **2014**, DOI: 10.1007/s12272-014-0410-9.
(18) Eskandariyan, Z.; Esfahani Zadeh, M.; Haj Mohammad Ebrahim Tehrani, K.; Mashayekhi, V.; Kobarfard, F. Synthesis of thioether derivatives of quinazoline-4-one-2-thione and evaluation of their antiplatelet aggregation activity. *Arch. Pharmacal Res.* **2014**, *37*, 332−339.
(19) Wraith, K. S.; Magwenzi, S.; Aburima, A.; Wen, Y.; Leake, D.; Naseem, K. M. Oxidized low-density lipoproteins induce rapid platelet activation and shape change through tyrosine kinase and Rho kinase-signaling pathways. *Blood* **2013**, *122*, 580−589.
(20) Seo, E. J.; Lee, D. U.; Kwak, J. H.; Lee, S. M.; Kim, Y. S.; Jung, Y. S. Antiplatelet effects of *Cyperus rotundus* and its component (+)-nootkatone. *J. Ethnopharmacol.* **2011**, *135*, 48−54.
(21) Seo, E. J.; Lee, S. Y.; Kang, S. S.; Jung, Y. S. *Zizyphus jujuba* and its active component jujuboside B inhibit platelet aggregation. *Phytother. Res.* **2013**, *27*, 829−834.
(22) Flevaris, P.; Li, Z.; Zhang, G.; Zheng, Y.; Liu, J.; Du, X. Two distinct roles of mitogen-activated protein kinases in platelets and a novel Rac1-MAPK-dependent integrin outside-in retractile signaling pathway. *Blood* **2009**, *113*, 893−901.
(23) Kamruzzaman, S. M.; Endale, M.; Oh, W. J.; Park, S. C.; Kim, K. S.; Hong, J. H.; Kwak, Y. S.; Yun, B. S.; Rhee, M. H. Inhibitory effects of *Bulnesia sarmienti* aqueous extract on agonist-induced platelet activation and thrombus formation involves mitogen-activated protein kinases. *J. Ethnopharmacol.* **2010**, *130*, 614−620.
(24) Schaeffer, J.; Blaustein, M. P. Platelet free calcium concentrations measured with fura-2 are influenced by the transmembrane sodium gradient. *Cell Calcium* **1989**, *10*, 101−113.
(25) Mekhfi, H.; Belmekki, F.; Ziyyat, A.; Legssyer, A.; Bnouham, M.; Aziz, M. Antithrombotic activity of argan oil: an in vivo experimental study. *Nutrition* **2012**, *28*, 937−941.
(26) Cho, J.; Furie, B. C.; Coughlin, S. R.; Furie, B. A critical role for extracellular protein disulfide isomerase during thrombus formation in mice. *J. Clin. Invest.* **2008**, *118*, 1123−1131.
(27) Yu, H. Y.; Park, S. W.; Chung, I. M.; Jung, Y. S. Anti-platelet effects of yuzu extract and its component. *Food Chem. Toxicol.* **2011**, *49*, 3018−3024.
(28) Wagner, D. D.; Burger, P. C. Platelets in inflammation and thrombosis. *Arterioscler. Thromb. Vasc. Biol.* **2003**, *23*, 2131−2137.
(29) De Candia, E. Mechanisms of platelet activation by thrombin: a short history. *Thromb. Res.* **2012**, *129*, 250−256.
(30) Chen, Z. M.; Jiang, L. X.; Chen, Y. P.; Xie, J. X.; Pan, H. C.; Peto, R.; Collins, R.; Liu, L. S.; et al. Addition of clopidogrel to aspirin in 45,852 patients with acute myocardial infarction: randomised placebo-controlled trial. *Lancet* **2005**, *366*, 1607−1621.
(31) Moon, C. H.; Jung, Y. S.; Kim, M. H.; Lee, S. H.; Baik, E. J.; Park, S. W. Mechanism for antiplatelet effect of onion: AA release inhibition, thromboxane A(2)synthase inhibition and TXA(2)/PGH(2)receptor blockade. *Prostaglandins, Leukotrienes Essent. Fatty Acids* **2000**, *62*, 277−283.
(32) Jennings, L. K. Mechanisms of platelet activation: need for new strategies to protect against platelet-mediated atherothrombosis. *Thromb. Haemostasis* **2009**, *102*, 248−257.
(33) Mangin, P.; Ohlmann, P.; Eckly, A.; Cazenave, J. P.; Lanza, F.; Gachet, C. The P2Y1 receptor plays an essential role in the platelet shape change induced by collagen when TxA2 formation is prevented. *J. Thromb. Haemostasis* **2004**, *2*, 969−977.
(34) Lee, D. H.; Kim, Y. J.; Kim, H. H.; Cho, H. J.; Ryu, J. H.; Rhee, M. H.; Park, H. J. Inhibitory effects of epigallocatechin-3-gallate on microsomal cyclooxygenase-1 activity in platelets. *Biomol. Ther.* **2013**, *21*, 54−59.
(35) Gachet, C. ADP receptors of platelets and their inhibition. *Thromb. Haemostasis* **2001**, *86*, 222−232.
(36) Offermanns, S. Activation of platelet function through G protein-coupled receptors. *Circ. Res.* **2006**, *99*, 1293−1304.
(37) Reimers, H. J.; Packham, M. A.; Mustard, J. F. Labeling of the releasable adenine nucleotides of washed human platelets. *Blood* **1977**, *49*, 89−99.
(38) Jackson, S. P. Arterial thrombosis − insidious, unpredictable and deadly. *Nat. Med.* **2011**, *17*, 1423−1436.
(39) Jin, J.; Daniel, J. L.; Kunapuli, S. P. Molecular basis for ADP-induced platelet activation. II. The P2Y1 receptor mediates ADP-induced intracellular calcium mobilization and shape change in platelets. *J. Biol. Chem.* **1998**, *273*, 2030−2034.
(40) Mangin, P. H.; Tang, C.; Bourdon, C.; Loyau, S.; Freund, M.; Hechler, B.; Gachet, C.; Jandrot-Perrus, M. A humanized glycoprotein VI (GPVI) mouse model to assess the antithrombotic efficacies of anti-GPVI agents. *J. Pharmacol. Exp. Ther.* **2012**, *341*, 156−163.
(41) Cimmino, G.; Golino, P. Platelet biology and receptor pathways. *J. Cardiovasc. Transl. Res.* **2013**, *6*, 299−309.
(42) Nieswandt, B.; Schulte, V.; Bergmeier, W.; Mokhtari-Nejad, R.; Rackebrandt, K.; Cazenave, J. P.; Ohlmann, P.; Gachet, C.; Zirngibl, H. Long-term antithrombotic protection by in vivo depletion of platelet glycoprotein VI in mice. *J. Exp Med.* **2001**, *193*, 459−469.
(43) Li, H.; Lockyer, S.; Concepcion, A.; Gong, X.; Takizawa, H.; Guertin, M.; Matsumoto, Y.; Kambayashi, J.; Tandon, N. N.; Liu, Y. The Fab fragment of a novel anti-GPVI monoclonal antibody, OM4, reduces in vivo thrombosis without bleeding risk in rats. *Arterioscler. Thromb. Vasc. Biol.* **2007**, *27*, 1199−1205.
(44) Liou, J. T.; Mao, C. C.; Liu, F. C.; Lin, H. T.; Hung, L. M.; Liao, C. H.; Day, Y. J. Levobupivacaine differentially suppresses platelet aggregation by modulating calcium release in a dose-dependent manner. *Acta Anaesthesiol. Taiwan* **2012**, *50*, 112−121.
(45) O'Brien, K. A.; Stojanovic-Terpo, A.; Hay, N.; Du, X. An important role for Akt3 in platelet activation and thrombosis. *Blood* **2011**, *118*, 4215−4223.

(46) Yacoub, D.; Theoret, J. F.; Villeneuve, L.; Abou-Saleh, H.; Mourad, W.; Allen, B. G.; Merhi, Y. Essential role of protein kinase C delta in platelet signaling, alpha IIb beta 3 activation, and thromboxane A2 release. *J. Biol. Chem.* **2006**, *281*, 30024−30035.
(47) Roger, S.; Pawlowski, M.; Habib, A.; Jandrot-Perrus, M.; Rosa, J. P.; Bryckaert, M. Costimulation of the Gi-coupled ADP receptor and the Gq-coupled TXA2 receptor is required for ERK2 activation in collagen-induced platelet aggregation. *FEBS Lett.* **2004**, *556*, 227−235.
(48) Kuliopulos, A.; Mohanlal, R.; Covic, L. Effect of selective inhibition of the p38 MAP kinase pathway on platelet aggregation. *Thromb. Haemostasis* **2004**, *92*, 1387−1393.
(49) Coombes, R. Venous thromboembolism caused 25,000 deaths a year, say MPs. *BMJ* **2005**, *330*, 559.
(50) DiMinno, G.; Silver, M. J. Mouse antithrombotic assay: a simple method for the evaluation of antithrombotic agents in vivo. Potentiation of antithrombotic activity by ethyl alcohol. *J. Pharmacol. Exp. Ther.* **1983**, *225*, 57−60.

of the livers in relation to their phenotypes and allows us to better understand the biological mechanisms underlying the variations of foie gras technological quality. This could in turn suggest new and more adapted farming practices aimed at reducing variability.

MATERIALS AND METHODS

Experimental procedures were performed in accordance with French National Guidelines for the care and use of animals for research purposes (Certificate of Authorization to Experiment on Living Animals no. 7740, Ministry of Agriculture and Fish Products).

Animal Design. The animals studied here are male mule ducks, produced within the framework of a QTL detection experiment based on a grandson design,[9] in which they are measured to estimate the value of their common duck (*Anas platyrhynchos*) mothers. Two common duck parental lines were crossed: the heavy Pekin INRA37 and the Kaiya INRA444 to produce 7 F1 males, of which 3 were mated to 20 INRA444 female common ducks to produce 98 backcross (BC) female common ducks in 3 F1 half-sib families. These BC ducks were then crossed with 23 Muscovy (*Cairina moschata*) drakes to produce a total of 294 mule ducks in two hatching batches. The mule ducks were bred from 0 to 12 weeks of age in growing batches of 50 animals.[11] At 12 weeks of age, ducks were overfed in two successive series for a period of 12 days. Each overfeeding series was performed by two different crammers (one for the morning and one for the evening and a total of three crammers for all batches). Animals were slaughtered at the end of the overfeeding period. Livers were sampled at 20 min post-mortem by a small slit in the animal abdomen and frozen in liquid nitrogen for biochemical analyzes. Carcasses were refrigerated for 24 h at 4 °C. Then, they were eviscerated and livers collected for foie gras preparation.

Data Recording. *Liver Quality Traits.* Phenotypic measures were collected on mule ducks. Liver weights (LW) were collected just after evisceration at 24 h post-mortem. The liver melting rate (MR), corresponding to fat loss during cooking, is measured by sterilizing 60 g of refrigerated liver for 50 min at 105 °C. It is expressed as a percentage of the liver quantity before cooking. Protein contents were estimated using a near-infrared spectrophotometer (FOSS NIRSystem) on ground liver.[12] The results are expressed as a percentage of fresh liver weight (crude liver protein content, LprotCc, %) or as a percentage of dry liver weight (dry liver protein content, LprotDc, %) to limit the impact of liver lipid contents on the trait.

Analyses of Soluble Proteins by Bidimensional Electrophoresis. The bidimensional electrophoresis method for foie gras analyses was described by Theron et al.[8] and was performed here on the foie gras samples of all 294 mule ducks taken at 20 min post-mortem.

For protein extraction, the fatty liver samples, stored frozen at −80 °C, were ground in liquid nitrogen to obtain a fine powder. Three hundred micrograms of this powder was then homogenized in a low ionic strength buffer (LIS), 40 mM Tris-HCl (pH 8), at 4 °C in a ratio of 1:4 (w/v) using a glass bead agitator MM400 (Retsch, Haan, Germany). The homogenate was centrifuged at 4 °C for 10 min at 10000g, and the fat cake supernatant was removed before a second homogenization was performed. After the second centrifugation, the supernatant containing the soluble protein fraction was collected and stored at −80 °C. The protein concentration was determined by using the Bradford[13] assay (Bio-Rad).

To perform bidimensional electrophoresis, 500 μg of proteins was incorporated in a buffer composed of 7 M urea, 2 M thiourea, 2% CHAPS (w/v), 0.4% carrier ampholyte (v/v), 1% DTT (w/v), and bromophenol blue. For the first dimension, samples were loaded onto immobilized pH gradient strips (pH 5−8, 17 cm, Bio-Rad), and isoelectric focusing (IEF) was performed using a Protean IEF cell system (Bio-Rad). Strips were first passively rehydrated for 16 h, after which a rapid voltage ramping was applied until a total of 86 kVh was reached. IEF was followed by successive incubation in an equilibration buffer containing 1% DTT and another containing 2.5% iodoacetamide and bromophenol blue. These buffers were both composed of 6 M urea, 30% glycerol, 2% SDS, and 50 mM Tris-HCl, pH 8.8. Equilibrated strips were loaded for the second dimension for a 12% sodium dodecyl sulfate−polyacrylamide gel electrophoresis (SDS-PAGE) using a Protean II XL system (Bio-Rad). After migration, gels were rinsed three times in permuted water and stained overnight with Coomassie Blue (Fermentas Page Blue). IEF was performed on 30 series of 12 samples and for each IEF series, SDS-PAGE was performed on 2 series of 6 samples, according to the capacities of our IEF and SDS-PAGE devices. Some damaged or unreadable gels were redone and a total of 360 gels made.

Two hundred and ninety-four stained gels were scanned using an Image Master 2D Platinum (GE Healthcare, Uppsala, Sweden), and the spots quantifications were done with Samespots software (TotalLab Ltd., Newcastle-upon-Tyne, UK). As the general aspect of a gel has an impact on the quality of the image analyses, problems concerning the aspect of the gels were recorded by annotating them in three categories: clear (no problem with the gel), blurred, and broken. Spot matching was performed across all 294 gels. Artifacts and spots detected by the software but not visible to the naked eye were removed from the analyses. The software calculated the intensity of each of the 326 remaining spots for each of the 294 samples.

Differentially expressed spots were manually excised from the gels using pipet tips and sent to the proteomics platform in Clermont-Ferrand (PFEMcp, INRA, Clermont-Ferrand Theix, France) for identification.

Spot Identification. *Protein Digestion.* The spots were destained with 100 μL of 25 mM NH_4HCO_3 with acetonitrile 95:5 (v/v) for 30 min and then washed twice in 100 μL of 25 mM NH_4HCO_3 with acetonitrile 50:50 (v/v) before dehydratation in 100% acetonitrile. Gel spots were completely dried using a Speed Vac, and trypsin digestion was performed at 37 °C over 5 h with 12 μL of trypsin (12.5 ng/μL; V5111, Promega) in 25 mM NH_4HCO_3. Peptide extraction was optimized by adding 9.6 μL of acetronitrile 100%, followed by 10 min of sonication. Then tryptic digests were concentrated for 5 min in a SpeedVac to eliminate acetronitrile and transferred to HPLC tubes, before LC-MS/MS analysis.

Nano-LC-MS/MS Analysis. For nano-LC-MS/MS analysis, peptide mixtures were analyzed by online nanoflow liquid chromatography using an Ultimate 3000 RSLC (Dionex, Voisins le Bretonneux, France). Eight microliters of peptide mixture was first preconcentrated at a flow rate of 20 μL/mn with a nano trap column of 5 cm length × 100 μm i.d., (Acclaim PepMap 100 C18, 5 μm, 100A nanoViper) equilibrated with trifluoroacetic acid 0.05% in water and then analyzed according to its hydrophobicity with a nanocapillary column of 15 cm length × 75 μm i.d., 2 μm, 100 Å (Acclaim PepMap 100 C18, Dionex) equilibrated with 0.5% formic acid in water. The solvent gradient increased linearly from 4 to 50% acetonitrile in 0.5% formic acid at a flow rate of 300 nL/mn for 45 mn. Identifications were attempted using an LTQ VELOS mass spectrometer (ThermoFisher Scientific, Courtaboeuf, France). The eluate was electrosprayed in positive-ion mode at 2.7 kV through a nanoelectrospray ion source that was operated in a CID top 10 mode (i.e., 1 full scan MS and the 10 major peaks in the full scan were selected for MS/MS). Full-enhanced-scan MS spectra were acquired with 1 microscan (m/z 400−1400), and dynamic exclusion was used with 2 repeat counts, 20 s repeat duration, and 120 s exclusion duration. For MS/MS, the isolation width for ion precursor was fixed at 1 m/z and single charged species were rejected; fragmentation used 35% normalized collision energy as the default activation of 0.25.

Database Search and Protein Identification. For raw data processing, Thermo Proteome Discoverer 1.4 (v: 1.4.0.288) was used with MASCOT (v 2.3) for database search (http://www.matrixscience.com). UniP_tax_Aves (150722 sequences) was used as database for protein identification, and the following parameters were considered for the searches: peptide mass tolerance was set to 1.5 Da, fragment mass tolerance was set to 0.5 Da, and a maximum of 2 missed cleavages was allowed. Moreover, variable modifications were methionine oxidation (M) and carbamidomethylation (C) of cysteine. Protein identifications were considered as valid if at least two peptides with a statistically significant Mascot score >48 were assigned. Ion score is $-10\log(P)$, where P is the probability that the observed match

is a random event. Individual ion scores >48 indicate identity or extensive homology at $p < 0.05$.

Identifications with only two unique peptides were manually validated with criteria of match fragment ions (occurrence of uninterrupted y- or b-ion series of at least three consecutive amino acids, preferred cleavages N-terminal to proline bonds, and mass occuracy).

The identification method was not able to annotate all of the analyzed spots of our set. For these spots, a manual annotation was performed on the basis of the peptide sequences given by the mass spectrometer. Alignments of the peptide sequences were done using BLASTP (http://blast.ncbi.nlm.nih.gov) on the nonredundant protein sequences database using all of the species. For each spot, alignment was done for the three longer peptides, and the validation of the spot annotation depended on three criteria. The e value had to be $<10^{-3}$ and the homology rate, 100%. The conservation between species was also checked. A spot was considered accurately identified as a protein when the cumulated percentage of this protein was >70%.

Statistical Analyses. Spot intensities were normalized using the GLM procedure of the SAS software to take simultaneously into account the technological effects of the bidimensional electrophoresis and the zootechnical effects. The sum of spot intensities of each gel was treated as a covariate, and six fixed effects were defined: (i) crammer effect (3 crammers); (ii) hatching batch effect (2 batches); (iii) general aspect of the gels (3 classes); (iv) first electrophoresis dimension effect (30 isoelectrofocusing series of 12 samples each); (v) second electrophoresis dimension effect (2 SDS-PAGE groups per isoelectrofocusing series); and (vi) interaction of both dimensions (60 levels corresponding to the chronological running order of the samples). Normalized spot intensities are the residual values of this model and will be used for all subsequent statistical analyses.

For each of the four traits considered (LW, MR, LprotCc, and LprotDc), foie gras samples were classified into four quartile groups (Q1, Q2, Q3, and Q4) according to their phenotypic values. For each of the 4 traits and each of the 326 normalized spot intensities, ANOVAs were performed using the GLM procedure of the SAS software across the 294 samples, taking 3 effects into account: the quartile group (4 levels), the F1 family group (3 levels), and the interaction between both, denoted quartile*family (12 levels). p values obtained were corrected by the Benjamini–Hochberg method. For each trait and each fixed effect, the 326 p values were sorted in descending order: the first value had the rank (k) 0 and the last had the rank 325. The corrected p value (q) was then defined as $q = p((326/(326 - k)))$. Effects for a spot were declared significant when $q < 0.1$. For each trait, quartile means were compared pairwise, that is, six tests. The significance threshold was then corrected using the Bonferroni method: the 5% threshold was divided by 6 (the number of tests performed). Spots were considered to be at significantly different levels between two quartiles when the p value was $p < 0.05/6$.

RESULTS

Association between Protein Abundance Levels and Phenotypic Traits. Quartiles of the phenotypic traits are represented in Table 1. For liver weight (LW), values range between 204 and 911 g and quartile means are 394 g for Q1, 531 g for Q2, 621 g for Q3, and 731 g for Q4. Quartiles 1 and 4 are more variable than the other two with values ranging over almost 300 g. For melting rate (MR), values range between 7.4 and 70.9% and quartile means are 18.7% for Q1, 34.8% for Q2, 46.5% for Q3, and 55.2% for Q4. The first quartile is the more variable with values ranging over 20%. For crude liver protein content (LprotCc) values go from 4.98 to 13.66%. Quartile means are 6.2, 7.1, 7.9, and 9.4% from the first to the fourth, respectively. Dry liver protein content (LprotDc) is almost twice higher than crude protein content with values going from 7.23 to 28.02%. Quartile means are 9, 10.7, 12.4, and 16.3% from the first to the fourth, respectively.

Table 1. Repartition in Quartiles of Phenotypic Values[a]

	Q1	Q2	Q3	Q4
LW (g)	394 ± 75	531 ± 27	621 ± 25	731 ± 59
MR (%)	18.7 ± 5.1	34.8 ± 5	46.5 ± 2.5	55.2 ± 3.9
LprotCc (%)	6.2 ± 0.4	7.1 ± 0.2	7.9 ± 0.2	9.4 ± 1.0
LprotDc (%)	9.0 ± 0.7	10.7 ± 0.4	12.4 ± 0.5	16.3 ± 2.9

[a]LW, liver weight; MR, melting rate expressed as a percentage of the liver quantity before cooking; LprotCc, crude liver protein content expressed as a percentage of the fresh liver weight; LprotDc, dry liver protein content expressed as a percentage of the dry liver weight.

For each of the four traits (LW, MR, LprotCc, and LprotDc), the number of spots found at different levels according to the quartile, family, or quartile*family interaction effects was tested by ANOVA, and 1304 statistical tests were performed altogether (4 phenotypic traits × 326 spots each). Thirty-five spots were found significantly affected by the quartile group after correction for multiple testing, only two by the F1 family affiliation of the individuals and one by the quartile*family interaction effect. It is noteworthy that the family affiliation affects the same two spots for each of the four traits and that LprotCc is the only trait for which no spot was affected by the quartile effect. Taken trait by trait, 17, 17, 0, and 16 spots are significantly affected by the LW, MR, LprotCc, and LprotDc quartile groups, respectively. However, some spots are common to several traits (Figure 1A): three spots are affected by the three traits LW, MR, and LprotDc, one spot is affected by both LW and MR, three spots are affected by both LW and LprotDc, and four spots are affected by both MR and LprotDc. Nine spots are affected by only LW, nine by MR, and six by LprotDc.

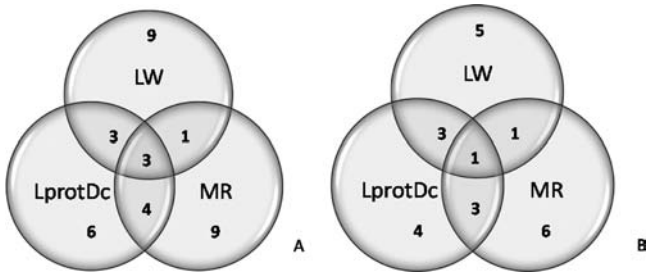

Figure 1. Venn diagram of the 35 differential proteins (A) and of the 23 identified proteins (B) affected by the phenotypic traits. Numbers correspond to the number of spots of protein affected by one, two, or three traits. LW, liver weight; MR, melting rate; LprotDc, dry liver protein rate.

Among the 35 spots affected by the phenotypic traits quartile groups, only 26 could be accurately identified. Three of them were attributed to keratin, which is considered as a contaminant in proteomics analyses, and the 23 remaining ones correspond to 20 unique proteins, 2 of which identified in several spots. α-Enolase was identified in three spots (spots 1403, 1414, and 1427) and annexin A5 in two spots (spots 1854 and 1914). For each protein, the spots were found at the same molecular weight but with different isoelectric points (Figure 2), suggesting different isoforms of the same protein. Among these 23 protein spots, 15 had a variation in abundance following a single trait only (LW, MR, or LprotDc), whereas the 8 remaining spots were differentially present following two or three traits simultaneously (Figure 1B). The 20 proteins showing variation in our data set represent several biological

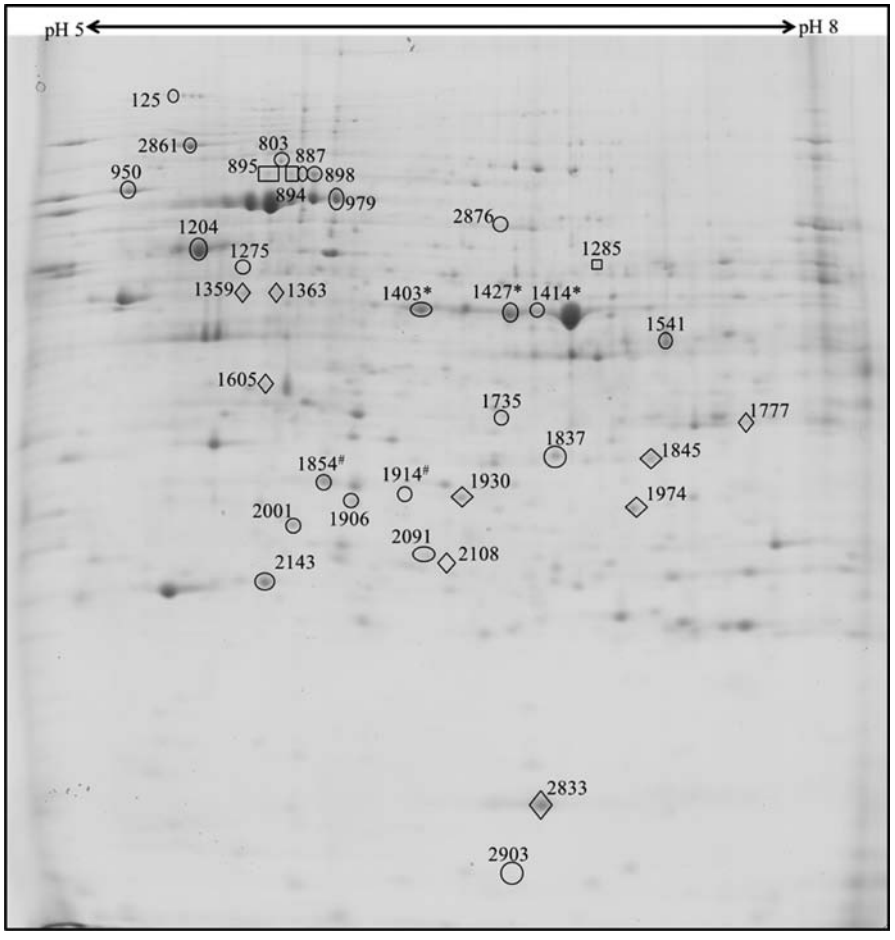

Figure 2. Two-dimensional gel electrophoresis representing a map of duck fatty liver soluble proteins. The first dimension separated the proteins according to their isoelectric point between pH 5 and 8. The second dimension separated the proteins according to their molecular weight in a 12% acrylamide gel. The 35 spots differentially expressed are represented. Spots surrounded by circles correspond to identified proteins, spots surrounded by squares correspond to keratin, and spots surrounded by diamonds correspond to nonaccurately identified spots. The star symbols or the hash symbols after spot numbers indicate that the spots correspond to the same protein.

pathways (Table 2) such as glycolysis, lipid metabolism, oxidative stress, transport, catabolism, and anabolism processes.

Variation of Protein Abundance Specific to a Single Trait. Five unique proteins were found at different levels according to LW values only (Appendix 1 in the Supporting Information). All showed significant differences between the lightest livers (Q1, LW < 486g) and the heaviest ones (Q4, LW > 661g). The hypoxia up-regulated protein 1 (HYOU1), annexin A5 (one of the two spots of ANXA5, spot 1854), and fatty acid binding protein 1 (FABP1) showed higher levels in the heaviest than in the lightest livers, whereas the glutamine synthetase (LOC100545435) and the malic enzyme (ME1) showed conversely lower levels in the heaviest than in the lightest. Of these five proteins, HYOU1 appeared to be particularly specific to LW values because the corrected p values for MR and LprotDc are >50%.

Six unique proteins corresponding to six identified spots were found to be at different levels according to MR values only (Appendix 2 in the Supporting Information). These proteins showed differences between low-melting livers (Q1, MR < 23%) and high-melting ones (Q3 or Q4, MR > 44%). The 70 kDa heat shock protein (HSPA5), the 60 kDa heat shock protein (HSPD1), and the *S*-formylglutathione hydrolase showed higher levels in the highest melting livers than in the lowest melting ones, whereas mitochondrial inner membrane protein-like (IMMT), dihydrolipoamide *S*-acetyltransferase (DLAT), and annexin A5 (the second spot of ANXA5, spot 1914) showed the inverse. With their corrected p value >50% for LW and LprotDc, HSPD1 and IMMT seemed to be specific to MR values.

Three unique proteins corresponding to four spots were found at different levels according to LprotDc values (Appendix 3 in the Supporting Information). Remarkably, all of these proteins show significant differences between the livers with the lowest overall protein content (Q1, LprotDc < 8.5%) and the ones with high content (Q4, Lprotdc >15.5%). α-Enolase was identified in two different spots (ENO1, spots 1414 and 1427), and both spots have lower levels in livers with the overall highest protein content. The two other proteins, trifunctional enzyme subunit α (HADHA) and prohibitin (PHB), showed higher levels in the protein-rich livers than in the protein-poor ones.

Variation of Protein Abundance Common to Two or Three Traits. Eight proteins corresponding to eight spots (Appendix 4 in the Supporting Information) showed different levels of abundance between the first quartile and the third or the fourth, for at least two traits. Among them, seven proteins were found expressed at different levels according to two traits simultaneously. FK506 binding protein 4 (FKBP4) was affected by LW and MR and showed a higher level in the heaviest and

dx.doi.org/10.1021/jf5006963 | J. Agric. Food Chem. 2014, 62, 7140−7150

Table 2. Characteristics of the 35 Spots Differentially Expressed[a]

spot no.	accession no.	gene symbol	protein name	Mascot score	Σ coverage	Σ no. of peptides	no. of AAs	MW[b] (kDa)	pI[b]	%	GO identifier/process
spots accurately identified as protein with an accumulated percentage >70%											
125	F1NY05	HYOU1	hypoxia up-regulated protein 1	331	22.82	17	986	110.8	5.25	100	GO:0006950/response to stress
803	G3UQJ4	IMMT	mitochondrial inner membrane protein-like	204	9.17	6	698	77.9	5.74	63.1	GO:0051560/mitochondrial calcium ion homeostasis
	H0ZKK6	IMMT	mitochondrial inner membrane protein-like	82	3.83	3	757	83.5	7.17	36.9	
887	G1NMS8	HADHA	trifunctional enzyme subunit α	364	18.03	10	771	82.9	9.10	100	GO:0006635/fatty acid β-oxidation
894	G1MVW1	KRT	keratin	81	8.43	4	344	39.9	4.70	60.8	
	G1NEY8	KRT	keratin	255	16.09	8	522	57.0	8.09	39.2	
898	E1C6N5	DLAT	dihydrolipoamide *S*-acetyltransferase	1917	27.37	10	632	66.5	7.84	45.3	GO:0006090/pyruvate metabolic process
	G1MZJ8	DLAT	dihydrolipoyllysine-residue acetyltransferase	1719	32.26	11	530	55.9	6.11	54.8	
950	A0ZT13	HSPA5	heat shock protein 70 kDa	2121	34.36	20	652	71.9	5.22	100	GO:0006950/response to stress
979	I6U3L8	ALB	albumin	1995	45.37	24	615	69.6	5.86	91.2	GO:0006810/transport
1204	I3QII5	HSPD1	heat shock protein 60 kDa	8080	73.24	35	568	60.5	5.64	98.7	GO:0006950/response to stress
1275	H0ZSE5	FKBP4	FK506 binding protein	77	21.75	7	446	50.6	6.18	100	GO:0006463/steroid hormone receptor complex assembly
1285	G1NEY8	KRT	keratin	321	10.92	6	522	57.0	8.09	100	
1403	P19140	ENO1	α-enolase	4700	65.21	28	434	47.2	6.80	92.1	GO:0006096/glycolysis
1414	P19140	ENO1	α-enolase	2427	65.21	28	434	47.2	6.80	72.5	
1427	P19140	ENO1	α-enolase	5356	65.21	28	434	47.2	6.80	69.1	
	P51913	ENO1	α-enolase	4038	53.23	20	434	47.3	6.58	26.0	
1541	G1MW53	LOC100 545 435	glutamine synthetase	466	24.93	8	373	42.2	6.98	77.1	GO:0006542/glutamine biosynthetic process
1735	H0ZRI8	C11orf54	ester hydrolase C11orf54	171	22.15	4	316	34.8	6.24	100	GO:0016788/hydrolase activity
1837	G1NQ47	LOC100 545 718	*S*-formylglutathione hydrolase	402	22.34	5	282	31.5	6.61	100	GO:0046294/formaldehyde catabolic process
1854	G1NDY6	ANXA5	annexin A5	1498	40.57	12	318	35.8	5.80	51.2	GO:0005544/calcium-dependent phospholipid binding
	H0YUM4	ANXA5	annexin A5	1454	37.97	11	316	35.4	5.20	46.9	

dx.doi.org/10.1021/jf5006963 | J. Agric. Food Chem. 2014, 62, 7140−7150

Table 2. continued

spot no.	accession no.	gene symbol	protein name	Mascot score	Σ coverage	Σ no. of peptides	no. of AAs	MW[b] (kDa)	pI[b]	%	GO identifier/process
1906	B8XNP2	FASN	fatty acid synthase	467	59.78	4	92	10.1	5.73	88.3	GO:0004312/fatty acid synthase activity
1914	H0YUM4	ANXA5	annexin A5	72	37.97	11	316	35.4	5.20	100	GO:0005544/calcium-dependent phospholipid binding
2001	P84173	PHB	prohibitin	NA	56.62	14	272	29.9	5.76	100	GO:0006355/regulation of transcription
2091	F1NBV0	PRDX6	peroxiredoxin-6	1703	43.75	8	224	25.1	6.38	75	GO:0006979/response to oxidative stress
2143	O42296	APOA1	apolipoprotein A1	1398	63.64	19	264	30.6	5.54	93.6	GO:0006869/lipid transport
2861	Q5ZMU9	VCP	transitional endoplasmic reticulum ATPase	6502	64.52	40	806	89.3	5.26	100	GO:0006511/ubiquitin-dependent protein catabolic process
2876	G1NLV4	ME1	malic enzyme	162	10.05	4	557	62.0	7.06	100	GO:0006108/malate metabolic process
2903	D7REA1	FABP1	basic fatty acid binding protein	564	64.29	9	126	14.0	8.40	89	GO:0006810/transport
spots presenting a protein mix without any protein of percentage >70%											
895	G1MVW1	KRT	keratin	101	8.43	4	344	39.9	4.70	38.1	
	G1NEY8	KRT	keratin	392	16.09	8	522	57.0	8.09	25.7	
1359	F1NCZ2	GDI2	Rab GDP dissociation inhibitor β	287	18.48	5	433	49.0	5.73	49.8	
	F1P3F1	AHCY	adenosylhomocysteinase	154	32.42	13	438	48.2	7.06	29.2	
	G1MZD6	HMGCS2	hydroxymethylglutaryl-CoA synthase	65	5.35	3	505	55.1	7.36	25.0	
1363	Q2Z1J7	ACTB	β-actin	93	58.18	16	373	41.5	5.48	39.6	
	F1P3F1	AHCY	adenosylhomocysteinase	110	32.42	13	438	48.2	7.06	33.3	
	G1NEY8	KRT	keratin	201	10.92	6	522	57.0	8.09	27.1	
1605	P19140	ENO1	α-enolase	NA	15.44	4	434	47.2	6.80	NA	
	F1NPD1	LOC395933	uncharacterized protein	NA	19.55	4	312	36.1	5.87	NA	
1777	B5G179	MDH	malate dehydrogenase	446	34.73	10	334	36.5	6.58	26.1	
	G1N071	LOC100 539 955	malate dehydrogenase	429	33.53	8	334	36.5	7.36	26	
	B5FXR6		putative aldo-keto reductase family 7 member A2 variant 1	702	28.86	5	246	27.6	8.95	16.9	
	H9H1S2	GPD1	glycerol-3-phosphate dehydrogenase	169	49.19	6	185	20.1	7.88	11.7	
2108	F1NBV0	PRDX6	peroxiredoxin-6	98	43.75	8	224	25.1	6.38	23.8	
	B5FXD0	PSMA	proteasome subunit α type	80	33.74	9	246	27.4	6.89	21.1	
	Q70I43	TPI	triosephosphate isomerase	93	67.30	11	211	22.6	6.64	31.4	

dx.doi.org/10.1021/jf5006963 | J. Agric. Food Chem. 2014, 62, 7140−7150

Table 2. continued

spot no.	accession no.	gene symbol	protein name	Mascot score	Σ coverage	Σ no. of peptides	no. of AAs	MW[b] (kDa)	pI[b]	%	GO identifier/process
	Q5ZKQ2	RCJMB04_9l5	uncharacterized protein	105	18.49	3	238	24.9	6.90	23.8	
2833	D0EKR3	PPI	peptidyl-prolyl cis−trans isomerase	103	10.91	2	165	17.8	8.09	51.7	
	G1NNV7	LOC100 544 220	superoxide dismutase	672	15.67	2	134	13.6	6.60	48.3	
spots with no protein identified											
1845		no protein identified									
1930		no protein identified									
1974		no protein identified									

[a]MW, molecular weight; pI, isoelectric point; GO, gene ontology; NA, not available; %, probability of identifying this protein. [b]pI and molecular are the theoretical ones.

highest melting livers. Ester hydrolase (C11orf54), peroxiredoxin 6 (PRDX6), and α-enolase (one of the three spots of ENO1, spot 1403) were affected by LW and LprotDc. The three proteins showed higher levels in the heaviest livers. Apolipoprotein A1 (APOA1), albumin (ALB), and transitional endoplasmic reticulum ATPase (VCP) were both affected by MR and LprotDc, but their variation profiles of abundance were different. Indeed, VCP showed higher levels both in the high protein content and the high-melting livers, whereas APOA1 and ALB showed similarly higher levels in the high protein content livers, but lower levels in the high-melting ones.

Fatty acid synthase (FASN) was the only protein for which the level of abundance varied with the three traits: it was present at a significantly higher level in the lightest weight and lowest melting livers (first quartile) than in the other ones (second, third, and fourth quartiles) and at a significantly lower expression level in protein-poor livers than in the other ones (first quartile versus second, third, and fourth quartiles).

Biological Pathways. For the eight protein profiles for which variation in protein abundance levels concerns two or three traits, a remarkable opposition appeared between the trend of protein expression with LW and MR levels, on the one hand, and LprotDc level, on the other hand. If the protein expression level increased with LW (FKBP4, C11orf54, PRDX6, ENO1), it also increased with MR or decreased with LprotDc. Inversely, if the protein expression level decreased with MR (APOA1, ALB, and FASN), it increased for LprotDc, with the notable exception of VCP. Using this information, the data set was split into two groups: group A was composed of proteins decreasing with MR or LW and/or increasing with LprotDc, and the "mirror" group B corresponded to proteins increasing with MR or LW and/or decreasing with LprotDc (Figure 3). The submission of the entire data set of proteins identified to IPA (Ingenuity Systems, www.ingenuity.com) helped in highlighting the relationships between protein through a network and in identifying the biological pathways. Proteins of group A represent pathways such as synthesis process (LOC100545435, FASN), anabolism process (DLAT, ME1), transcription regulation (PHB), and transport (APOA1, ALB). Proteins of group B represent biological pathways such as response to stress (HYOU, HSPA5, HSPD1, and PRDX6), transport (FABP1), glycolysis (ENO1), and catabolism process.

DISCUSSION

The aim of this work is to highlight possible differences in liver metabolic state, monitored by the analysis of the variation of protein levels in tissue samples, according to liver quality phenotypes. The primary focus is on four traits related to the quality of foie gras. However, contrary to what could have been expected, no significantly differential protein was identified for the trait LprotCc, whereas nine were found for LprotDc. The difference between the two traits comes from the way the predicted values of protein content are expressed. Indeed, it can be seen at the phenotypic level because values predicted by near-infrared spectroscopy (NIRS) on dry livers are almost twice higher than values predicted on crude livers. The expression of protein content related to the liver dry matter allows us to take partly into account the lipid content of the livers (51.6 ± 5.4%). As no significant result was found for LprotCc, we will therefore focus our discussion on the three other traits, namely, LW, MR, and LprotDc. The genetic correlations between LW and MR are strongly positive (+0.80), and LprotDc is negatively correlated to LW (−0.87) and to MR

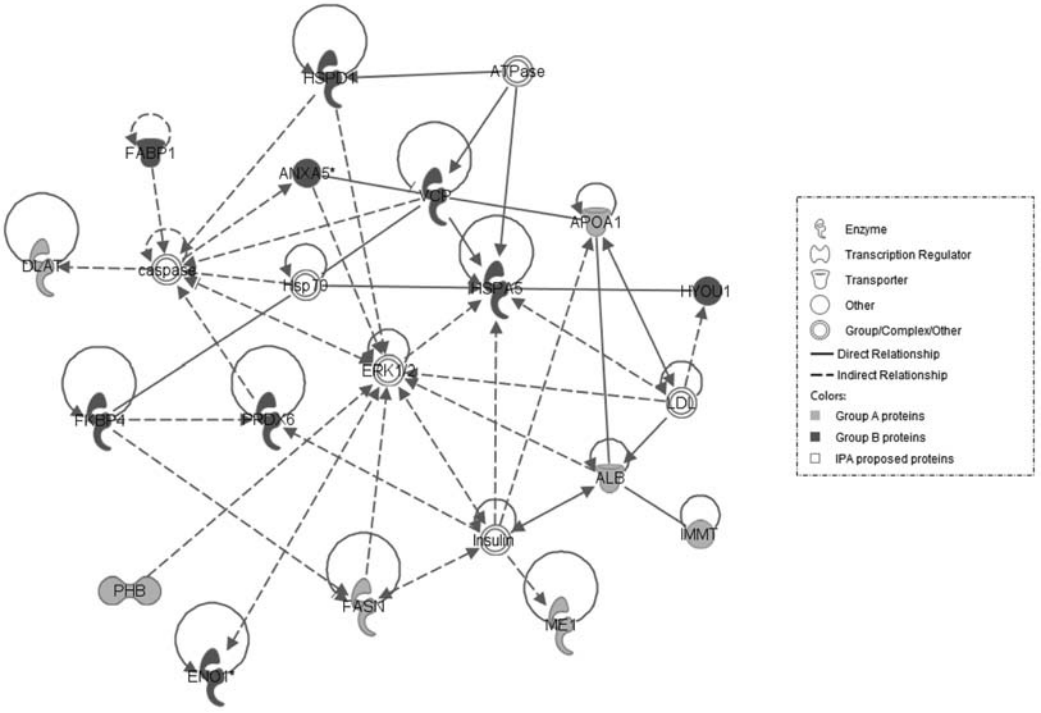

Figure 3. IPA network of hematological disease, immunological disease, and inflammatory disease associated functions representing a subset of 16 of our set of proteins (score of 46). Circled lines indicate self-regulating proteins. ALB, albumin; ANXA5, annexin A5; APOA1, apolipoprotein A1; ATPase, ATP synthase; DLAT, dihydrolipoamide *S*-acetyltransferase; ENO1, α-enolase; ERK1/2, extracellular signal-regulated kinase 1/2; FABP1, fatty acid binding protein 1; FASN, fatty acid synthase; FKBP4, FK506-binding protein 4; HSP70, 70 kDa heat shock protein; HSPA5, 70 kDa heat shock protein 5; HSPD1, 60 kDa heat shock protein; HYOU1, hypoxia up-regulated protein 1; IMMT, mitochondrial inner membrane protein-like; LDL, low-density lipoprotein; ME1, malic enzyme; PHB, prohibitin; PRDX6, peroxiredoxin 6. The proteins included in the network are the proteins included in IPA database.

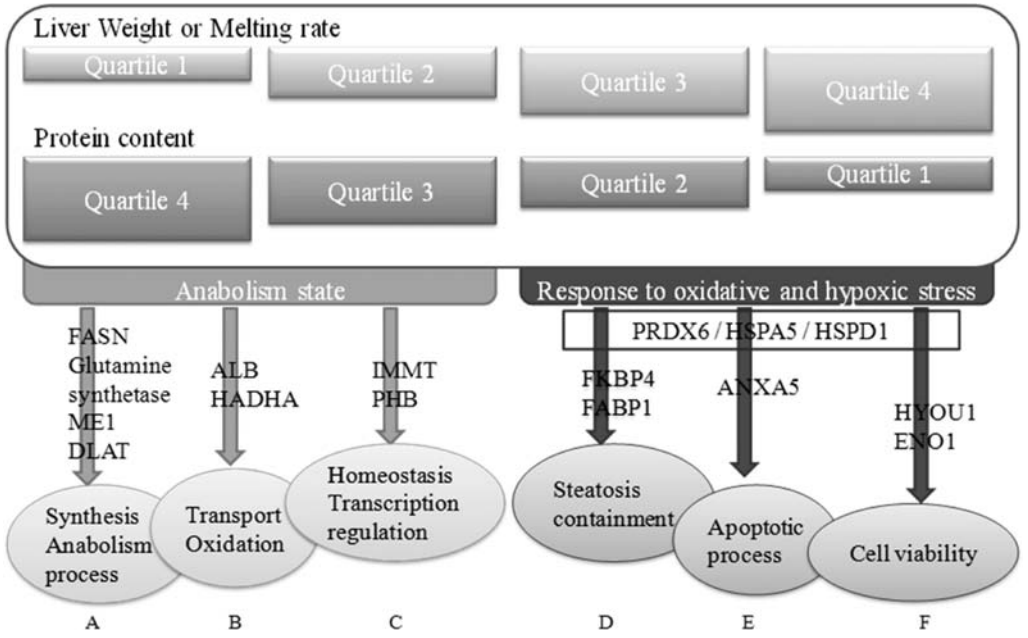

Figure 4. Summary diagram of the different liver protein profiles (from A to F) according to their phenotype. FASN, fatty acid synthase; ME1, malic enzyme; DLAT, dihydrolipoamide *S*-acetyltransferase; ALB, albumin; HADHA, trifunctional enzyme subunit α; APOA1, apolipoprotein A1; IMMT, mitochondrial inner membrane protein-like; PHB, prohibitin; PRDX6, peroxiredoxin 6; HSPA5, 70 kDa heat shock protein 5; HSPD1, 60 kDa heat shock protein; FKBP4, FK506-binding protein 4; FABP1, fatty acid binding protein 1; ANXA5, annexin A5; HYOU1, hypoxia up-regulated protein 1; ENO1, α-enolase.

(−0.87).[11] The phenotypic correlation between LW and MR is +0.67, and the phenotypic correlations between LprotDc and LW or MR are strongly negative (−0.78 or −0.79, respectively) (unpublished data).

dx.doi.org/10.1021/jf5006963 | J. Agric. Food Chem. 2014, 62, 7140−7150

Proteins of group A belong to six gene ontology (GO) processes (Table 2): transport (ALB, APOA1), oxidation (HADHA), transcription regulation (PHB), biosynthetic and metabolic processes (DLAT, glutamine synthase, ME1, FASN), mitochondria homeostasis (IMMT), and phospholipid binding (ANXA5). The biological functions of these proteins are summarized in Figure 4. During overfeeding, duck and geese develop an important steatosis due to an intense lipogenic activity and an insufficient exportation rate of triglycerides in the peripheral tissues. This activity was observed at an enzymatic level by Chartrin et al.,[14] who showed an increased activity of ME1 induced by overfeeding. At the transcriptomic level, studies showed an increased expression of FASN, ME1,[15,16] APOA1,[15] and DLAT[16] due to overfeeding. FASN is the enzyme synthetizing fatty acids. Both ME1 and DLAT are proteins involved in the malate and pyruvate metabolic processes, respectively. APOA1 is a lipid transporter from the liver to the peripheral tissues. Our results are consistent with the biological functions of these enzymes as they are present at higher levels, as well as glutamine synthase (LOC100545435) (proteins of the group A, Figure 4A). FASN, ME1, and glutamine synthase (LOC100545435) were indeed overexpressed in livers of low weight compared to heavy ones. Hérault et al.[15] also reported negative correlations between liver weight and APOA1, FASN, and ME1 gene expressions in duck. These results suggest that when liver weight increases, a negative regulation occurs to reduce lipogenesis. FASN, IMMT, DLAT, APOA1, and ALB were also overexpressed in livers of low melting rate (up to 26%). In a study aiming at determining the proteomic profile of low and high MR livers with the same weight and lipid content, Théron et al.[8] showed that enolase 1, triose phosphate isomerase, malate dehydrogenase, mitochondrial carrier homologue 2, and several ribosomal proteins are present at high levels in low MR livers. In the present study, we do not point out the same proteins. However, the biological functions of the proteins at differential levels are close in both studies. Taken together, these data suggest that livers with low MR are performing anabolic processes. ALB, HADHA, PHB, and FASN were overexpressed in livers with high protein content. To our knowledge, this is the first time that such a differential expression between different liver protein contents is reported. Finally, group A proteins were at high levels in light livers, low-melting ones, and livers rich in proteins; we can hypothesize that these livers were in a higher anabolic state, leading to a more intense lipid synthesis. They also showed a significantly decreased expression when liver weights increased, when melting rate increased, or when protein content decreased. In all three traits (LW, MR, and LprotDc), the significantly decreasing expression of these proteins was followed by the overexpression of proteins of group B (Figure 4).

Proteins of group B belong to six GO processes (Table 2): response to stress (HYOU, HSPA5, HSPD1, PRDX6), glycolysis (ENO1, three isoforms), transport (FABP1), hydrolase activity (C11Orf54), catabolic process (*S*-formylglutathione hydrolase), and steroid receptor (FKBP4). PRDX6 is an antioxidant enzyme induced by the increase of reactive oxygen species (ROS) levels and providing protection against oxidative injury;[17] its level was found higher both in heavy livers (>581 g) and in livers of low protein content (<10%). On the contrary, PRDX6 is underexpressed in simple steatosis compared to normal livers in rat.[18] Other cytoprotective proteins such as HSPA5 and HSPD1 were at higher levels in high-melting livers (>45%), assessing the development of cytoprotection mechanisms. Similarly, Théron et al.[8] reported a higher expression of heat shock protein 27 in high MR livers. Another kind of stress seems to occur only in heavy livers: hypoxia stress is suggested by the overexpression of HYOU1 (also named 150 kDa oxygen-regulated protein (ORP150)) in livers of weight >581 g. This protein seems to be specific to the high-weight livers, as for the two other traits it is highly nonsignificant (p value >50%). This hypoxia-induced protein was described as helping the cell to face stress induced by the lack of oxygen by its protective role to avoid apoptotic cell death.[19] If protein-poor and high-melting livers seem to develop protection against oxidative stress, heavy livers seem to accumulate stresses, with both oxidative and hypoxia stresses.

The proteomics results suggest that the livers are trying to cope with the high amount of lipid synthesized by using different pathways. The first one is by containing the steatosis development (Figure 4D), as suggested by the overexpression of FKBP4 and FABP1 in heavy livers (>581 g). FKBP4 (also known as FKBP52) belongs to the family of immunophilin and plays a role in immunoregulation and basic cellular processes involving protein folding and trafficking. It is also a regulator of glucocorticoid receptor activity. When deficient mice for FKBP52 are fed a high-fat diet, there was a high expression of lipogenic genes such as FASN and an underexpression of gluconeogenic genes in the liver. Finally, the livers of these mice exhibited high lipid content and a steatosis.[20] In our study, FKBP52 is overexpressed when the liver's weight and melting rate increased. On the contrary, FASN and ME expressions decreased. From this, we can speculate that the overexpression of FKBP52 could reduce lipogenesis and, thus, steatosis. FABP1 is the liver isoform of the fatty acid binding protein mainly implicated in lipid transport from liver to peripheral tissues. Results from the literature concerning this protein are inconsistent. Indeed, when comparing normal livers and livers with a simple steatosis by two-dimensional electrophoresis gels, Charlton et al.[21] found an overexpression of FABP1 in simple steatosis in humans, whereas Zhang et al.[18] pointed out an underexpression of the same protein in simple steatosis in rat. Moreover, Théron et al.[8] identified the adipocyte isoform, FABP4, as overexpressed in high melting rate livers. It was shown that FABP1 is a positive regulator of PPARα and of FASN,[22] but because our results do not show any overexpression of both FASN and FABP1 in the same group, we can only speculate that FABP1 has a cytoprotective role in exporting fatty acids.

The second pathway proposed to cope with the intense steatosis is apoptosis (Figure 4E). ANXA5 is a calcium-dependent phospholipid binding protein mainly known as a membrane apoptotic marker. In plasma or extracellular tissues, it also has anticoagulant and antithrombic properties.[23] It is a widely expressed protein in the liver[24] and was overexpressed in the soluble proteome of heavy livers but also in low-melting livers. Even if apoptosis is a common phenomenon for tissues to regenerate, it can be associated with disease such as steatosis in mammals. In the livers of patients suffering from nonalcoholic steatohepatitis (NASH), there is consistently an enhanced Fas expression, activation of caspase-3 and -7, and apoptosis, which positively correlated with biochemical and histopathological markers of liver injury.[23] However, in human livers with a simple steatosis, apoptosis evaluated by a Fas score is not different from normal livers.[25] In the present study, ANXA5 is overexpressed in the heaviest livers and in the lowest

MR ones. The network constructed by IPA (Figure 3) also shows that four proteins (FABP1, ANXA5, VPC, and HSPD1) are linked with caspases. It could emphasized that livers in which these proteins increased with MR or LW and/or decreased with LprotDc could be more prone to develop steatosis.

The third pathway proposed is the stress response to support cell viability (Figure 4F), suggested by both HYOU1 and α-enolase (ENO1). ENO1 is a gluconeogenesis enzyme implicated in growth control and hypoxia tolerance. Its implication in hepatocellular carcinoma (HCC) was described by Hamaguchi et al.:[26] in HCC, ENO1 activation by hypoxia-induced factor 1α (HIF-1α) implicated an increased HCC aggressiveness, whereas ENO1 knockdown inhibited HCC proliferation. ENO1 was overexpressed in livers of low protein content and in heavy livers like HYOU1, described as a suppressor of hypoxia-induced apoptotic cell death.[19] Both proteins promote cell survival and even cell proliferation, suggesting that, despite stress, cell viability is supported.

The high level of proteins of anabolism processes in livers with melting rates up to 26% and of stress response proteins in livers with melting rates >40% confirm what was found by Theron et al.:[8] with a fixed weight and fixed lipid content, livers of low melting rate were in anabolism, whereas livers of high melting rate developed protection mechanisms. Concerning liver weight, we were able to distinguish two different metabolic states according to the liver weight value: an anabolism state in light livers (<600 g) and a cytoprotection state in heavy livers (>600 g). In a kinetic study, Bax et al.[27] reported that during the first half of the overfeeding period, livers were in anabolism (overexpression of FASN), whereas they developed protection mechanisms during the second period. In the present study, similarly, the lightest livers, lowest melting livers, and livers rich in protein still exhibit higher levels of proteins involved in lipogenesis, whereas the heaviest ones show higher expression of stress response proteins. We can wonder if the first group of livers has a better control of steatosis or if steatosis is just delayed. On the contrary, the second group of livers showed a development of protection mechanisms and seemed to have reached an overphysiological point.

■ ASSOCIATED CONTENT

Supporting Information

Appendixes 1−4. This material is available free of charge via the Internet at http://pubs.acs.org.

■ AUTHOR INFORMATION

Corresponding Author

*(C.M.) Phone: +33 5 34 32 39 06. Fax: +33 5 34 32 39 01. E-mail: molette@ensat.fr.

Funding

We thank the Institut National de la Recherche Agronomique and the Institut National Polytechnique Toulouse for funding the research chair of the corresponding author.

Notes

The authors declare no competing financial interest.

■ REFERENCES

(1) Décret no. 93-999 du 09-08-93 du JO du 14-08-93, relatif aux préparations à base de foie gras. *J. Off. Repub. Fr.* **1993**.

(2) Babilé, R.; Auvergne, A.; Setiawan, I.; Joly, E.; Latil, G. Conduite alimentaire au cours du gavage des canards et qualité technologique du foie gras. *1re Journ. Rech. Palmipedes Foie Gras, Bordeaux, Fr.* **1993**, 107−116.

(3) Latil, G.; Auvergne, A.; Babilé, R. Consommation du canard mulard en gavage. Relation avec les performances zootechniques et la qualité du foie gras. *2e Journ. Rech. Palmipedes Foie Gras, Bordeaux, Fr.* **1996**, 93−97.

(4) Rousselot-Pailley, D.; Guy, G.; Gourichon, D.; Sellier, N.; Blum, J. C. Influence des conditions d'abattage et de réfrigération sur la qualité des foies gras d'oie. *INRA, Prod. Anim.* **1992**, *5*, 167−172.

(5) Bouillier-Oudot, M.; Leprettre, S.; Dubois, J. P.; Babilé, R. Itinéraires *post mortem* et caractéristiques technologiques et organoleptiques des foies gras d'oies. *5e Journ. Rech. Palmipedes Foie Gras, Pau, Fr.* **2002**, 172−175.

(6) Baudonnet, C. *Facteurs de Variation de la composition Biochimique et de la Qualité Technologique des Foies Gras de Canard*. Thèse de doctorat, INP, Toulouse, France, 1993.

(7) Molee, W.; Bouillier-Oudot, M.; Auvergne, A.; Babilé, R. Changes in lipid composition of hepatocyte plasma membrane induced by overfeeding in duck. *Comp. Biochem. Physiol. Part B: Biochem. Mol. Biol.* **2005**, *141*, 437−444.

(8) Théron, L.; Fernandez, X.; Marty-Gasset, N.; Pichereaux, C.; Rossignol, M.; Chambon, C.; Viala, D.; Astruc, T.; Molette, C. Identification by proteomic analysis of early post-mortem markers involved in the variability in fat loss during cooking of mule duck "foie gras". *J. Agric. Food Chem.* **2011**, *59*, 12617−12628.

(9) Kileh-Wais, M.; Elsen, J. M.; Vignal, A.; Feves, K.; Vignoles, F.; Fernandez, X.; Manse, H.; Davail, S.; André, J. M.; Bastianelli, D.; Bonnal, L.; Filangi, O.; Baéza, E.; Guéméné, D.; Genêt, C.; Bernadet, M. D.; Dubos, F.; Marie-Etancelin, C. Detection of QTL controlling metabolism, meat quality, and liver quality traits of the overfed interspecific hybrid mule duck. *J. Anim. Sci.* **2013**, *91*, 588−604.

(10) Theron, L.; Cullere, M.; Bouillier-Oudot, M.; Manse, H.; Dalle Zotte, A.; Molette, C.; Fernandez, X.; Vitezica, Z. G. Modeling the relationships between quality and biochemical composition of fatty liver in mule ducks. *J. Anim. Sci.* **2012**, *90*, 3312−3317.

(11) Marie-Etancelin, C.; Basso, B.; Davail, S.; Gontier, K.; Fernandez, X.; Vitezica, Z. G.; Bastianelli, D.; Baéza, E.; Bernadet, M.-D.; Guy, G.; Brun, J.-M.; Legarra, A. Genetic parameters of product quality and hepatic metabolism in fattened mule ducks. *J. Anim. Sci.* **2011**, *89*, 669−679.

(12) Marie-Etancelin, C.; Fernandez, X.; Baéza, E.; Bonnal, L.; Bernadet, M. D.; Manse, H.; Chartrin, P.; Bastianelli, D. Genetic parameters of fatty liver and breast muscle composition predicted by near-infrared spectroscopy. *9th World Congr. Genet. Appl. Livest. Prod., Leipzig, Germany* **2010**, 1−4.

(13) Bradford, M. M. A rapid and sensitive method for the quantitation of microgram quantities of protein utilizing the principle of protein-dye binding. *Anal. Biochem.* **1976**, *72*, 248−254.

(14) Chartrin, P.; Bernadet, M.-D.; Guy, G.; Mourot, J.; Hocquette, J.-F.; Rideau, N.; Duclos, M. J.; Baéza, E. Does overfeeding enhance genotype effects on liver ability for lipogenesis and lipid secretion in ducks? *Comp. Biochem. Physiol. Part A: Mol. Integr. Physiol.* **2006**, *145*, 390−396.

(15) Hérault, F.; Saez, G.; Robert, E.; Al Mohammad, A.; Davail, S.; Chartrin, P.; Baéza, E.; Diot, C. Liver gene expression in relation to hepatic steatosis and lipid secretion in two duck species. *Anim. Genet.* **2010**, *41*, 12−20.

(16) Zhu, L. H.; Meng, H.; Duan, X. J.; Xu, G. Q.; Zhang, J.; Gong, D. Q. Gene expression profile in the liver tissue of geese after overfeeding. *Poult. Sci.* **2011**, *90*, 107−117.

(17) Newton, B. W.; Russell, W. K.; Russell, D. H.; Ramaiah, S.; Jayaraman, A. Liver proteome analysis in a rodent model of alcoholic steatosis. *J. Proteome Res.* **2009**, *8*, 1663−1671.

(18) Zhang, X.; Yang, J.; Guo, Y.; Ye, H.; Yu, C.; Xu, C.; Xu, L.; Wu, S.; Sun, W.; Wei, H.; Gao, X.; Zhu, Y.; Qian, X.; Jiang, Y.; Li, Y.; He, F. Functional proteomic analysis of nonalcoholic fatty liver disease in rat models: enoyl-coenzyme a hydratase down-regulation exacerbates hepatic steatosis. *Hepatology* **2010**, *51*, 1190−1199.

(19) Ozawa, K.; Kuwabara, K.; Tamatani, M.; Takatsuji, K.; Tsukamoto, Y.; Kaneda, S.; Yanagi, H.; Stern, D. M.; Eguchi, Y.; Tsujimoto, Y.; Ogawa, S.; Tohyama, M. 150-kDa oxygen-regulated protein (ORP150) suppresses hypoxia-induced apoptotic cell death. *J. Biol. Chem.* **1999**, *274*, 6397−6404.
(20) Warrier, M.; Hinds, T. D.; Ledford, K. J.; Cash, H. A.; Patel, P. R.; Bowman, T. A.; Stechschulte, L. A.; Yong, W.; Shou, W.; Najjar, S. M.; Sanchez, E. R. Susceptibility to diet-induced hepatic steatosis and glucocorticoid resistance in FK506-binding protein 52-deficient mice. *Endocrinology* **2010**, *151*, 3225−3236.
(21) Charlton, M.; Viker, K.; Krishnan, A.; Sanderson, S.; Veldt, B.; Kaalsbeek, A. J.; Kendrick, M.; Thompson, G.; Que, F.; Swain, J.; Sarr, M. Differential expression of lumican and fatty acid binding protein-1: new insights into the histologic spectrum of nonalcoholic fatty liver disease. *Hepatology* **2009**, *49*, 1375−1384.
(22) He, J.; Tian, Y.; Li, J.; Shen, J.; Tao, Z.; Fu, Y.; Niu, D.; Lu, L. Expression pattern of L-FABP gene in different tissues and its regulation of fat metabolism-related genes in duck. *Mol. Biol. Rep.* **2013**, *40*, 189−195.
(23) Guicciardi, M. E.; Gores, G. J. Apoptosis: a mechanism of acute and chronic liver injury. *Gut* **2005**, *54*, 1024−1033.
(24) Boustead, C. M.; Brown, R.; Walker, J. H. Isolation, characterization and localization of annexin V from chicken liver. *Biochem. J.* **1993**, *291* (Part 2), 601−608.
(25) Feldstein, A. E.; Canbay, A.; Angulo, P.; Taniai, M.; Burgart, L. J.; Lindor, K. D.; Gores, G. J. Hepatocyte apoptosis and fas expression are prominent features of human nonalcoholic steatohepatitis. *Gastroenterology* **2003**, *125*, 437−443.
(26) Hamaguchi, T.; Iizuka, N.; Tsunedomi, R.; Hamamoto, Y.; Miyamoto, T.; Iida, M.; Tokuhisa, Y.; Sakamoto, K.; Takashima, M.; Tamesa, T.; Oka, M. Glycolysis module activated by hypoxia-inducible factor 1α is related to the aggressive phenotype of hepatocellular carcinoma. *Int. J. Oncol.* **2008**, *33*, 725−731.
(27) Bax, M. L.; Chambon, C.; Marty-Gasset, N.; Remignon, H.; Fernandez, X.; Molette, C. Proteomic profile evolution during steatosis development in ducks. *Poult. Sci.* **2012**, *91*, 112−120.

specific soy peptides are responsible for the LDLR modulation.[28−32] Nevertheless, the mechanism at the molecular level has not been investigated in detail yet. These bioactive peptides, initially encrypted in the soy protein sequences, are probably enzymatically released during digestion and absorbed.[33]

The majority of plasma cholesterol is transported by the LDL fraction, and the cellular uptake of LDL is mediated by the LDLR. The circulating level of LDL is determined in large part by its rate of uptake through the hepatic LDLR pathway.[34,35] Moreover, the LDLR plays a crucial role in Apo B turnover, being involved in determining the post-translation fate of apoB by increasing presecretory apoB degradation and mediating re-uptake of nascent lipoprotein particles.[36] In general, LDLR expression is finely tuned by changes in intracellular cholesterol.[37] A transcription factor known as the sterol-responsive element binding protein 2 (SREBP2) plays a critical role in LDLR mRNA expression.[38,39] Among SREBP2 gene targets, the 3-hydroxy-3-methylglutaryl coenzyme A (HMGCoA) reductase (HMGCoAR) is particularly important. This enzyme plays a key role in the intracellular cholesterol biosynthesis, because it is the rate-controlling enzyme in the mevalonate pathway. After synthesis, SREBP2 forms a complex with the SREBP cleavage-activating protein (SCAP) and is localized in the endoplasmic reticulum (ER) as an inactive precursor (pro-SREBP2). Sterol deficiency results in the release of SREBP2/SCAP complex from ER and transport to the Golgi, where pro-SREBP2 is processed further, allowing the N-terminal fragment (mature SREBP2) to enter the nucleus and up-regulate transcription of LDLR and HMGCoAR.[40] In addition to SREBP2, other transcription factors may be involved in a context-dependent fashion in regulating the LDLR expression.

Recent studies[41,42] identify a crucial signaling pathway, via phosphatidylinositol-3-kinase (PI3K)/Akt, as an important player in the regulation of cellular lipid metabolism. This pathway is the best known for its role in promoting cell growth, proliferation, and survival through increased glucose utilization and prevention of apoptosis.[43,44] In particular, Akt has recently been implicated in a novel form of lipid metabolism regulation, through the SREBPs.[45] The physiological coordination between Akt and SREBPs pathways is needed to produce the lipids for new membrane synthesis, which in turn is required for growing and proliferating cells.[41,42] Even though many studies have been focused on the SREBP-1c isoform,[45] new efforts are directed to explore and to investigate the link between Akt and SREBP2.[41,46]

The objective of the present study was to characterize in detail the molecular mechanism at the basis of the cholesterol-lowering properties of *L. albus* protein observed in experimental and clinical investigations. On the basis of the hypothesis that the activity may depend on specific peptides encrypted in the protein sequences, a total protein extract from lupin seed was hydrolyzed either with pepsin (P peptides) or with trypsin (T peptides). The HepG2 cell line was treated with both kinds of peptides, and molecular and functional investigations were performed on the LDLR-SREBP2 and PI3K/Akt pathways, using a combination of techniques.

MATERIALS AND METHODS

Chemicals. Dulbecco's modified Eagle's medium (DMEM), L-glutamine, fetal bovine serum (FBS), phosphate-buffered saline (PBS), penicillin/streptomycin, chemiluminescent reagent, and 96-well plates were purchased from Euroclone (Milan, Italy). Bovine serum albumin (BSA), RIPA buffer, HMGCoAR Assay Kit, 3-(4,5-dimethylthiazol-2-yl)-2,5-diphenyltetrazolium bromide (MTT), and wortmannin were from Sigma-Aldrich (St. Louis, MO, USA). Antibodies against HMGCoAR were bought from Abcam (Cambridge, UK). Antibodies against β-actin, SREBP-2, rabbit Ig-HRP, and mouse Ig-HRP, PMSF, sodium orthovanadate inhibitors, and goat anti-rabbit Ig-HRP were purchased from Santa Cruz Biotechnology Inc. (Santa Cruz, CA, USA). Antibodies against the LDL receptor were from Pierce (Rockford, IL, USA). The inhibitor cocktail Complete Midi was from Roche (Basel, Switzerland). Mini protean TGX precast gel 7.5% and Mini nitrocellulose Transfer Packs were purchased from Bio-Rad (Hercules, CA, USA). LDL-DyLight 549 was from Cayman Chemical (Ann Arbor, MI, USA).

Preparation and Analysis of the Pepsin and Trypsin Peptide Mixtures. Lupin seeds of the species *L. albus* (cultivar Ares) were provided by Terrena (Matrignè-Ferchaud, France). The total protein extracts were obtained as previously reported.[47] Briefly, proteins were extracted from defatted flour with 100 mM Tris-HCl/0.5 M NaCl buffer, pH 8.2, for 2 h at 4 °C. The solid residue was eliminated by centrifugation at 6500*g*, for 20 min at 4 °C, and the supernatant was dialyzed against 100 mM Tris-HCl buffer, pH 8.2, for 24 h at 4 °C. The protein content was assessed according to the method of Bradford, using BSA as standard.

For the hydrolysis, the total protein extract was initially dissolved in Tris-HCl buffer 100 mM at pH 8, and then the pH was adjusted to the optimal hydrolysis conditions for each enzyme (pH 2 for pepsin and pH 8 for trypsin) by adding 1 M NaOH or 1 M HCl. The mixtures were incubated for 18 h, then the enzymes were inactivated, and the mixtures were purified by ultrafiltration through 3000 Da cutoff centrifuge filters (Amicon Ultra-0.5, Millipore, Billerica, MA, USA) at 12000*g* for 30 min at 4 °C. The peptide concentration in the permeates was measured according to a literature method,[48] based on chelating the peptide bonds by Cu(II) in alkaline media and monitoring the change of absorbance at 330 nm. Details are reported in a previous paper.[47]

The hydrolyzed mixtures were acidified with formic acid to a final 10% concentration. Eight microliters of tryptic digest for each band was injected in a nanochromatographic system, UltiMate 3000 RSLC nano-System (Thermo Scientific). The peptide mixtures were loaded on a reversed-phase trap column (Acclaim PepMap100, C18, 100 Å, 100 μm i.d. × 2 cm, Thermo Scientific) for the cleanup and preconcentration. After cleanup, the valve was switched to place the trap column in series with a fused silica reverse-phase column (picoFrit column, C18, 2.7 μm, New Objective). The peptides were eluted with a 30 min gradient from 4% buffer A (2% acetonitrile and 0.1% formic acid in water) to 60% buffer B (2% water and 0.1% formic acid in acetonitrile) at a constant flow rate of 300 nL/min. The chromatographic column was directly connected to an LTQ-XL mass spectrometer (Thermo Scientific) equipped with a nano spray ion source. Full scan mass spectra were acquired in the mass range from m/z 350 to 2000 Da, and the five most intense ions were automatically selected and fragmented in the ion trap. Target ions already selected for mass spectrometry (MS/MS) were dynamically excluded for 30 s. The MS data were analyzed separately by Mascot search engine (version 2.3.01) using Proteome Discover software (v. 1.2.0 Thermo) and consulting Uniprot_viridiplantae (30,264 sequences, 184,678,199 residues). Oxidation of methionine residues was set as variable modifications; two missed cleavages were allowed to trypsin; peptide mass tolerance was set to 1 Da and fragment mass tolerance to 0.8 Da; and an ion source cutoff of 20 was chosen. The false discovery rate obtained by Proteome Discoverer, consulting the Mascot decoy database, was <0.01. Tables 1S and 2S in the Supporting Information list the proteins and the unmatched peptides, with all relevant peptide signals, peptide sequences, ion score, variable modifications and mass errors.

Cell Culture Conditions. HepG2 cell line was bought from ATCC (HB-8065, ATCC from LGC Standards, Milan, Italy). The HepG2 cell line was cultured in DMEM high-glucose with stable L-glutamine supplemented with 10% FBS, 100 U/mL penicillin, and 100 μg/mL streptomycin (complete growth medium) and incubated at 37 °C under 5% CO_2 atmosphere. HepG2 cells were used for no more than 20 passages after thawing because the increase of the number of passages may change the cell characteristics and impair assay results.

MTT. HepG2 cells (3×10^4/well) were seeded in 96-well plates and treated with 0.3, 0.5, 1.0, 2.5, 5.0, and 10.0 mg/mL of P and T peptides, respectively, or vehicle (100 mM Tris) in complete growth media for 48 h. Subsequently, the treatment solvent was aspirated and 100 μL/well of MTT

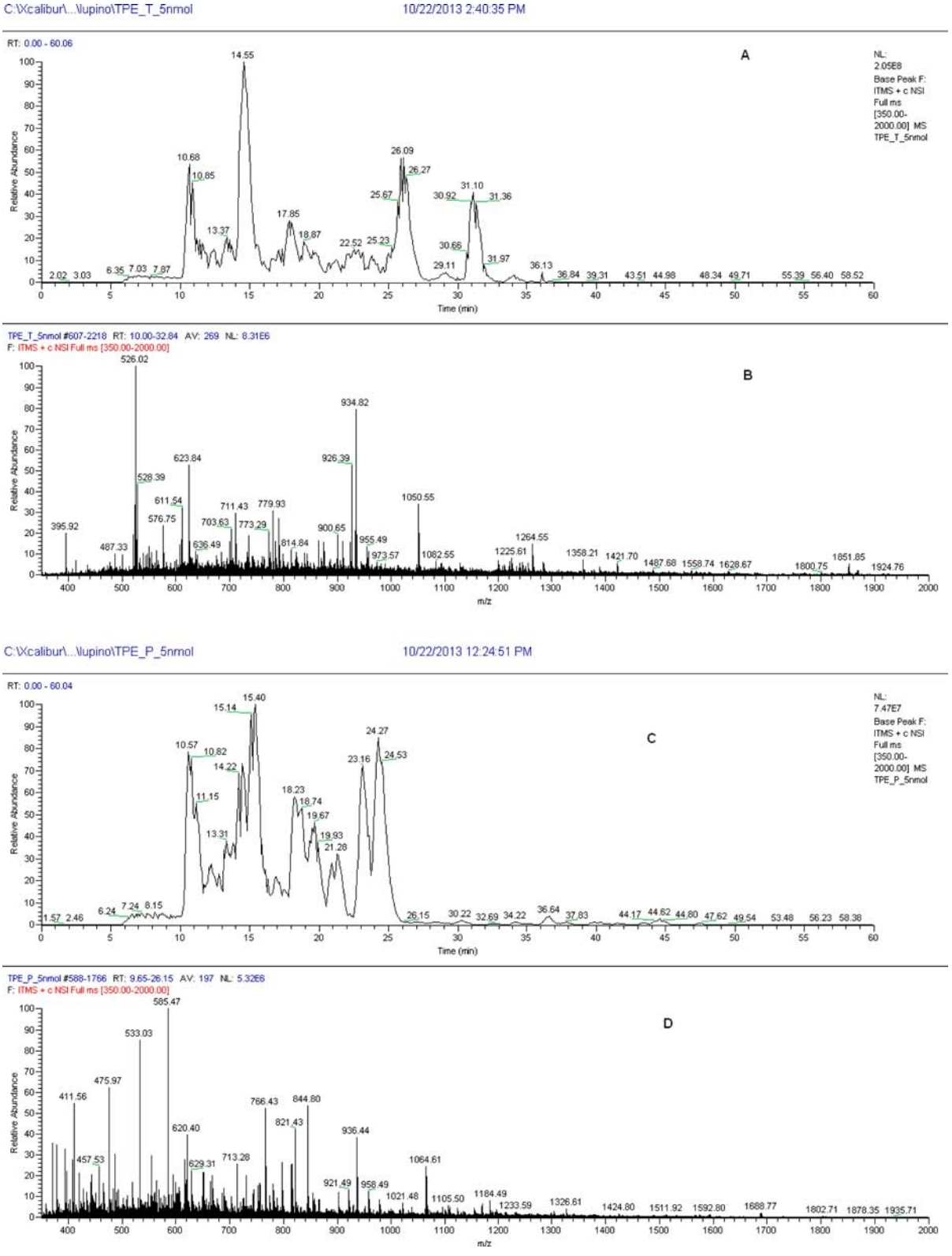

Figure 1. Nano-LC MS/MS of lupin peptide mixtures: (A, B) chromatogram and full scan mass spectrum of T peptides; (C, D) chromatogram and full scan mass spectrum of P peptides.

filtered solution added for 48 h. After the incubation time, 0.5 mg/mL MTT solution was aspirated and 100 μL/well of MTT lysis buffer (8 mM HCl + 0.5% NP-40 in DMSO) added. After 5 min of slow shaking, the absorbance at 575 nm was read on an LT 4000 spectrophotometer.

HMGCoAR Activity Assay. The assay buffer, the NADPH, the substrate solution, and the HMG-CoA reductase were provided in the HMGCoAR Assay Kit (Sigma). The experiments were carried out following the manufacturer's instructions at 37 °C. In particular, each reaction (200 μL) was prepared by adding the reagents in the following order: 1× assay buffer; 0.1, 0.25, 0.5, 1.0, and 2.5 mg/mL of T peptides or 0.5, 1.0, and 2.5 mg/mL of P peptides or vehicle (C); NADPH (4 μL); substrate solution (12 μL); and finally HMG-CoA reductase

(catalytic domain) (2 μL). Subsequently, the samples were mixed and the absorbance at 340 nm read by a Synergy H1 microplate reader from Biotek at times 0 and 10 min. The HMGC-CoA-dependent oxidation of NADPH and the inhibition properties of lupin peptides were measured by the absorbance reduction, which is directly proportional to the enzyme activity.

Western Blot Analysis. HepG2 cells (1.5×10^5/well, 24-well plate) were treated with 0.5, 1, and 2.5 mg/mL of P and T peptides for 24 h. For the experiments in the presence of wortmannin, cells were treated with 1 mg/mL P and 0.5 mg/mL T peptides in the presence or absence of 1 μM inhibitor for 24 h. After each treatment, cells were scraped in 40 μL of ice-cold lysis buffer (RIPA buffer + inhibitor cocktail + 1:100 PMSF + 1:100 sodium orthovanadate) and transferred in an ice-cold microcentrifuge tube. After centrifugation at 13300 rpm for 15 min at 4 °C, the supernatant was recovered and transferred into a new ice-cold tube. Total proteins were quantified according to the Bradford method, and 50 μg of total proteins was loaded on a precast 7.5% sodium dodecyl sulfate−polyacrylamide (SDS-PAGE) gel at 130 V for 45 min. Subsequently, the gel was pre-equilibrated with 0.04% SDS in H_2O for 15 min at room temperature and transferred to a nitrocellulose membrane (Mini nitrocellulose Transfer Packs,) using a Trans-blot Turbo at 1.3 A and 25 V for 7 min. Target proteins, on milk-blocked membrane, were detected by primary antibodies as follows: rabbit anti-SREBP2, rabbit anti-LDLR, anti-HMGCoAR, antipospho-Akt (ser473), antipospho-GSK3α/β (ser21/ser9), and anti-β-actin. Secondary antibodies conjugated with HRP and a chemiluminescent reagent were used to visualize target proteins, and their signal was quantified using ImageJ software. The internal control, β-actin, was used to normalize loading variations. In the case of SREBP2, the band at 70 kDa, corresponding to the N-terminal fragment (mature SREBP2 protein), was detected and quantified.

Fluorescent LDL Uptake Cell-Based Assay. HepG2 cells (3×10^4/well) were seeded in 96-well plates and kept in complete growth medium for 2 days before treatment. The third day, cells were treated with 1.0 mg/mL P peptides and 0.25 mg/mL T peptides, respectively, or vehicle (100 mM Tris) for 24 h. For the experiments in the presence of the PI3K inhibitor, HepG2 cells were treated with 1.0 mg/mL P peptides and 0.5 mg/mL T peptides in the presence or absence of 100 nM wortmannin and in the presence of the only inhibitor, as control, in DMEM without FBS for 24 h. At the end of the treatment periods, the culture medium was replaced with 75 μL/well LDL-DyLight 549 working solution. The cells were additionally incubated for 2 h at 37 °C, and then the culture medium was aspirated and replaced with PBS 100 μL/well. The degree of LDL uptake was measured using the Synergy H1 fluorescent plate reader from Biotek (excitation and emission wavelengths 540 and 570 nm, respectively).

Statistical Analysis. Statistical analyses were carried out by one-way ANOVA (Graphpad Prism 6) followed by Dunnett's test. Values were expressed as means ± SEM; P values <0.05 were considered to be significant.

RESULTS

Preparation and Analysis of the Peptide Mixtures. A total protein extract from lupin seed was hydrolyzed with pepsin and trypsin to produce P peptides and T peptides, respectively. The two samples were analyzed by nano-LC-MS/MS. The chromatograms (Figure 1) showed two diverse profiles due to the different peptide compositions of the digested samples. The number of potentially bioactive peptides is very high in both samples, because more than 2000 peptides were detected in the pepsin-digested mixture and about 3000 in the trypsin-digested one (Tables 1S and 2S in the Supporting Information).

It was possible to assign only a small number of peptides to known lupin proteins by Mascot software consulting the Uniprot_viridiplantae database. The other peptides were sequenced, but not assigned to protein hits, possibly due to the very incomplete sequencing of lupin proteins. The recognized peptides in the P sample belong to the main storage proteins in lupin seed: 21 peptides to the vicilins [*L. albus* vicilin-like protein (Q53HY0) and *L. albus* β-conglutin (Q6EBC1)]; 7 peptides to the legumins [*L. angustifolius* conglutin-α 3 (F5B8V8)], and 8 peptides to γ-conglutin [*L. albus* conglutin-γ (Q9FSH9)], a sulfur-rich basic protein typical of lupin (4−5%).

The identified peptides in the T sample are the following: 16 peptides belong to the vicilins [*L. albus* vicilin-like protein (Q53HY0), *L. albus* β-conglutin precursor (Q6EBC1), and *L. angustifolius* conglutin β (B0YJF8)]; 4 to the legumins [*L. angustifolius* legumin-like protein (Q53I55)], and 2 to δ-conglutin, a 2S protein [*L. albus* conglutin δ seed storage protein precursor (Q99235)]. Two peptides were assigned to other plant proteins, probably because the lupin sequences are not present in the database: *Zea mays* actin partial (ADF3).

HepG2 Cell Viability. MTT experiments were performed to exclude the peptide doses with potential toxic effects on the HepG2 cell line. No significant cell mortality was observed up to 2.5 mg/mL after a 48 h treatment versus vehicle (C, 100 mM Tris), suggesting that neither P nor T peptides induce cell mortality in this dose range, whereas about 20 and 80% cell mortalities were observed at 5.0 and 10 mg/mL, respectively (Figure 2). For this reason, all of the following experiments, aimed at investigating the molecular and functional effects of P and T peptides, were conducted using doses of ≤2.5 mg/mL.

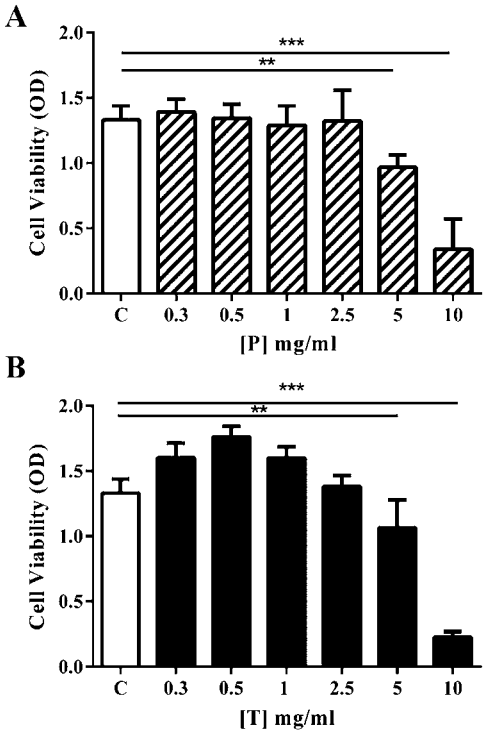

Figure 2. HepG2 cell viability after P and T peptide treatment. Bar graphs indicate the results of MTT cell viability assay of HepG2 cells after P and T peptide treatment for 48 h. Data points represent averages ± SEM of three independent experiments in triplicate. (**) $P < 0.001$ and (***) $P < 0.0001$ versus C. P, pepsin peptides; T, trypsin peptides; C, control.

Effects of P and T Peptides on the Catalytic Domain of HMGCoAR. To check the direct ability of P and T peptides to inhibit HMGCoAR, an in vitro assay was performed using the purified catalytic domain of this enzyme. Both P and T peptides

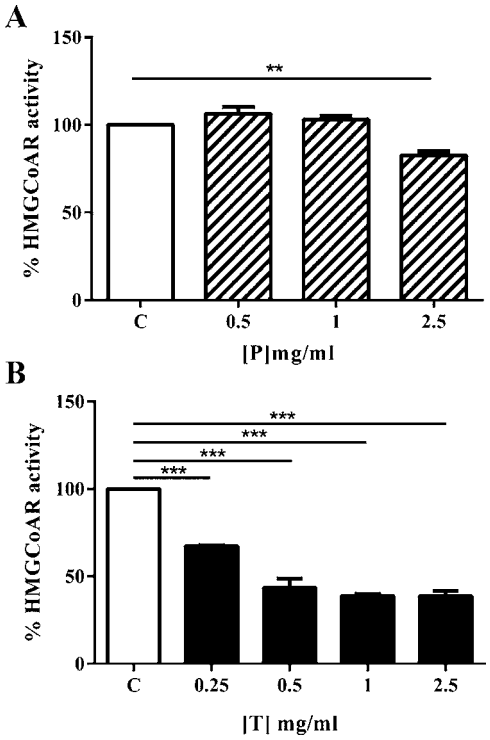

Figure 3. Lupin peptide effect on the catalytic domain of HMGCoAR. Bars indicate the effects of P peptides (0.5, 1.0, and 2.5 mg/mL) (A) and T peptides (0.25, 0.5, 1.0, and 2.5 mg/mL) (B) on HMGCoAR activity. HMGCoAR, physiologically, catalyzes the four-electron reduction of HMG-CoA to coenzyme A (CoA) and mevalonate (HMG-CoA + 2NADPH + $2H^+$ > mevalonate + $2NADP^+$ + CoA-SH). In this assay, the decrease in absorbance at 340 nm, which represents the oxidation of NADPH by the catalytic subunit of HMGCoAR in the presence of the substrate HMG-CoA, was measured spectrophotometrically. Data points represent averages ± SEM of three independent experiments in triplicate. (**) $P < 0.001$ and (***) $P < 0.0001$ versus C. P, pepsin peptides; T, trypsin peptides; C, control.

were capable of inhibiting HMGCoAR, but with very different activities and potencies (Figure 3). In fact, P peptides inhibited the enzyme with a statistical significance (−17%) only at the maximum tested dose (2.5 mg/mL), whereas they are ineffective at 0.5 and 1.0 mg/mL. On the contrary, T peptides showed a statistically significant reduction of the HMGCoAR activity at all tested doses: in fact, the enzyme activity was reduced by 37% at 0.25 mg/mL, by 57% at 0.5 mg/mL, and by 61% at 1.0 and 2.5 mg/mL.

Lupin Peptides Mediate the Up-regulation of LDLR-SREBP2 at HepG2 Cells. HepG2 cells were treated for 24 h with P and T peptides at concentrations of 0.5, 1.0, and 2.5 mg/mL. Immunoblotting experiments showed that the treatments with lupin peptides induce an up-regulation of the SREBP2 protein level. In particular, P peptides up-regulate the SREBP2 protein level by 100, 148, and 162% versus the control, whereas T peptides increase the SREBP2 protein level by 80, 73, and 44% versus the control, after 0.5, 1.0, and 2.5 mg/mL treatments, respectively (Figure 4B).

In the same experiments, also the LDLR and HMGCoAR protein levels were measured by immunoblotting. Figure 4C shows that both P and T peptides are able to induce a statistically significant up-regulation of LDLR protein in HepG2 cells versus the control, but with different behaviors. In particular, at 0.5, 1.0, and 2.5 mg/mL P peptides mediate 147, 136, and 120% inductions of the LDLR protein, whereas T peptides mediate a ∼85% up-regulation at 0.5 and 1.0 mg/mL and a 61% up-regulation at 2.5 mg/mL versus the control (Figure 4C). These results are in agreement with the up-regulation of SREBP2 protein level.

Both P and T peptides affect the HMGCoAR levels (Figure 4D), but with very different behaviors and activities. Precisely, P peptides increase the synthesis of HMGCoAR by 82% at 0.5 mg/mL, by 212% at 1.0 mg/mL, and by 340% at 2.5 mg/mL versus the control, that is, in a dose-dependent manner. On the contrary, treatment with T peptides enhances the production of HMGCoAR by 233% at 0.5 mg/mL and by only 97% at 1.0 mg/mL, whereas it is practically inactive at 2.5 mg/mL.

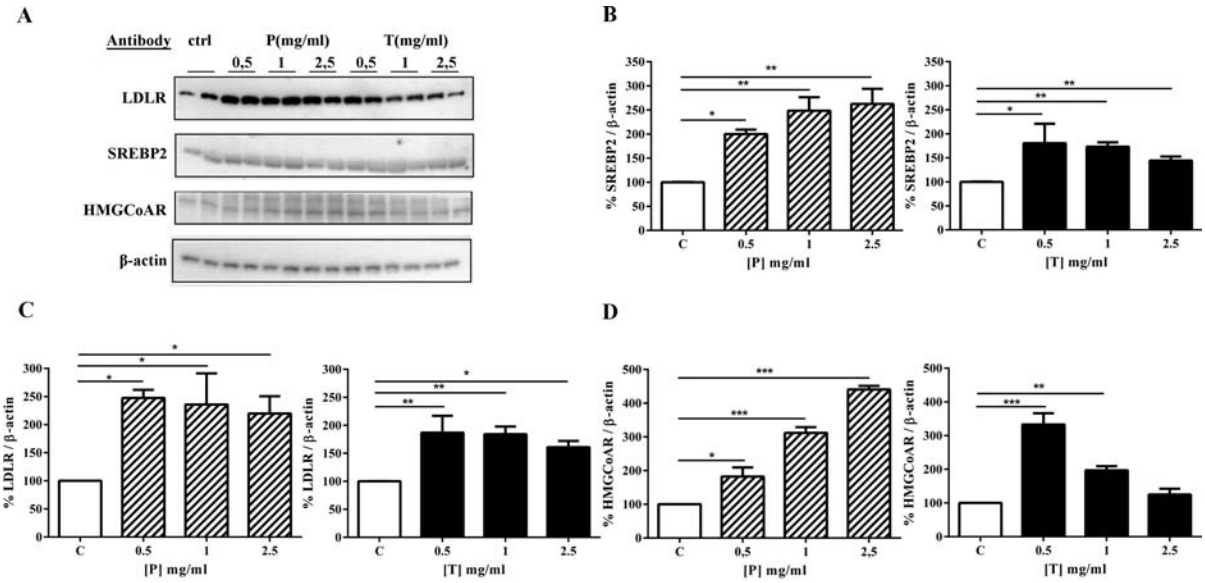

Figure 4. Effect of P and T peptides on the SREBP2, LDLR, and HMGCoAR protein levels. HepG2 cells (1.5×10^5) were treated with 0.5, 1.0, and 2.5 mg/mL of P and T peptides for 24 h, respectively. SREBP2, LDLR, HMGCoAR, and β-actin immunoblotting signals were detected using specific anti-SREBP2, anti-LDLR, anti-HMGCoAR, and anti-β-actin primary antibodies, respectively (A). SREBP2 (B), LDLR (C), and HMGCoAR (D) signals were quantified by ImageJ software and normalized with β-actin signals. Bars represent averages of duplicate samples ± SEM of three independent experiments. (*) $P < 0.05$ and (**) $P < 0.001$ versus C. P, pepsin peptides; T, trypsin peptides; C, control.

dx.doi.org/10.1021/jf500795b | J. Agric. Food Chem. 2014, 62, 7151−7159

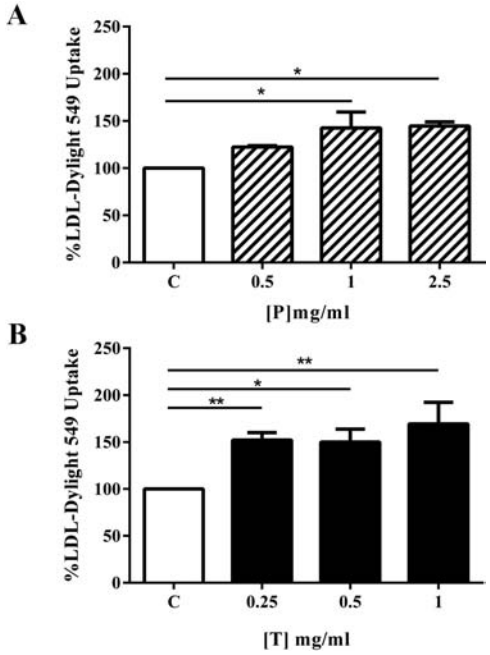

Figure 5. LDL uptake after P and T peptide treatments. HepG2 cells (3×10^4) were treated with P (0.5, 1.0, and 2.5 mg/mL) and T (0.25, 05, and 1.0 mg/mL) peptides for 24 h. LDL-Dylight 549 (10.0 μg/mL) was incubated for an additional 2 h. Excess LDL-Dylight 549 was removed, cells were washed two times with PBS, and specific fluorescent LDL uptake was analyzed by Synergy H1 (Biotek). Data points represent averages ± SEM of three independent experiments in triplicate. (∗) $P <$ 0.05 and (∗∗) $P <$ 0.001 versus C. P, pepsin peptides; T, trypsin peptides; C, control.

Lupin Peptides Increase LDL Uptake at the HepG2 Cell Line. Fluorescent LDL uptake experiments were performed for evaluating the cholesterol-lowering properties of lupin peptides from a functional point of view. Precisely, the fluorescent LDL uptake was examined in HepG2 cells following a 24 h incubation with P and T peptides. Figure 5 shows that both P and T peptides are able to increase the LDL uptake versus the control in a statistically significant way. In particular, treatment with P peptides at concentrations of 1.0 and 2.5 mg/mL increases the LDL uptake by 42 and 45%, respectively, versus the control, whereas the LDL uptake increase was not statistically significant at 0.5 mg/mL. On the other hand, at concentrations of 0.25, 0.5, and 1.0 mg/mL T peptides significantly raise the LDL uptake by 52, 50, and 70%, respectively, versus the control.

Lupin Peptides Mediate LDLR-SREBP2 Up-regulation through the Activation of PI3K/Akt/GSK3β Kinases. To examine the effect of lupin peptides on the activation of Akt and GSK3β (its direct substrate), immunoblot analyses were performed on lysates from treated HepG2 cells using antibodies, which are specific for Akt phosphorylated at serine residue 473 and for GSK3β phosphorylated at serine residue 9. In accordance with the preceding immunoblot experiments, HepG2 cells were treated with P and T peptides at concentrations of 1.0 and 0.5 mg/mL, and the variation of phosphorylated Akt and GSK3β levels was investigated. Figure 6B shows that the treatments with lupin peptides increased the Akt phosphorylation in a dose-dependent manner: by 92 and 125%, respectively, after treatment with P peptides at 0.5 and 1.0 mg/mL and by 144 and 196%, respectively, after treatment with T peptides at 0.5 and 1.0 mg/mL.

Additionally, P peptides mediate a 60% increase of the phosphorylation level of GSK3β at 0.5 mg/mL and a 74% increase at 1.0 mg/mL versus the control. After T peptide treatments, instead, the GSK3β phosphorylation level was increased by 133% at 0.5 mg/mL and by only 75% at 1.0 mg/mL (Figure 6D).

Treatment with 1 μM wortmannin, a PI3K inhibitor, inhibited the Akt phosphorylation either in the presence or in the absence of both lupin peptide mixtures. Figure 7A shows a representative immunoblot and the relative intensity of the phospho-Akt bands. The quantification and normalization against actin bands from

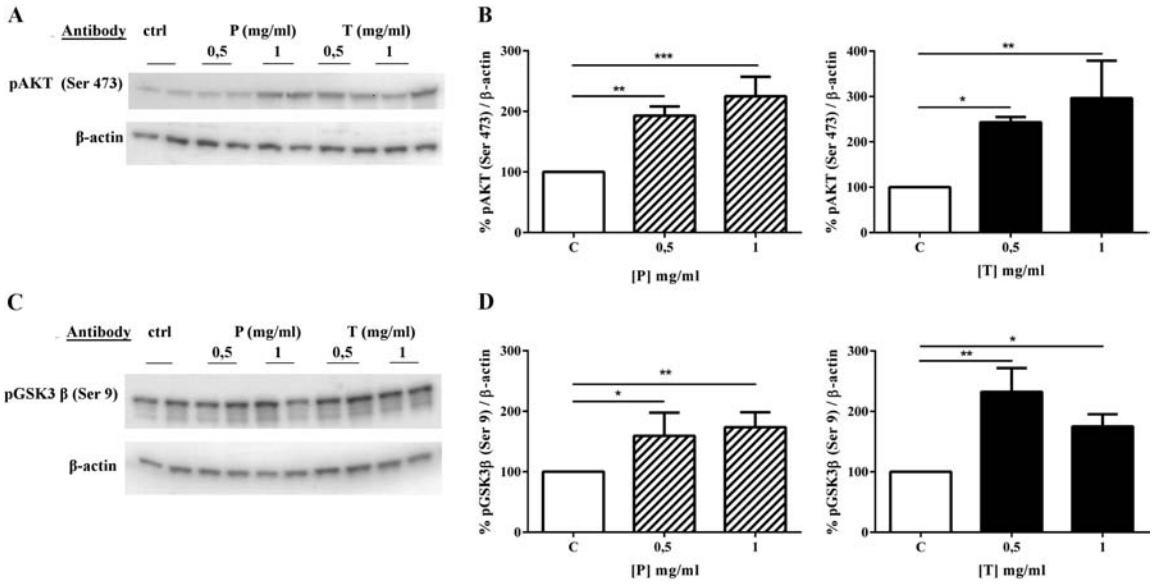

Figure 6. Effect of P and T peptides on the activation of Akt (Ser473) and GSK3 (Ser9). HepG2 cells (1.5×10^5) were treated with 0.5 and 1 mg/mL of P and T peptides for 24 h, respectively. The phosphorylation levels of Akt (Ser473) (A) and GSK3 (Ser9) (C) and β-actin immunoblotting signals were detected using specific anti-posphoAkt (Ser473), anti-posphoGSK3β (Ser9), and anti-β-actin primary antibodies, respectively. PosphoAkt signals (B) and posphoGSK3β (D) were quantified by ImageJ software and normalized with β-actin signals. Bars represent averages of duplicate samples ± SEM of three independent experiments. (∗) $P <$ 0.05, (∗∗) $P <$ 0.001, and (∗∗∗) $P <$ 0.0001 versus C. P, pepsin peptides; T, trypsin peptides; C, control; pAkt, posphoAkt; pGSK3β, posphoGSK3β.

dx.doi.org/10.1021/jf500795b | J. Agric. Food Chem. 2014, 62, 7151−7159

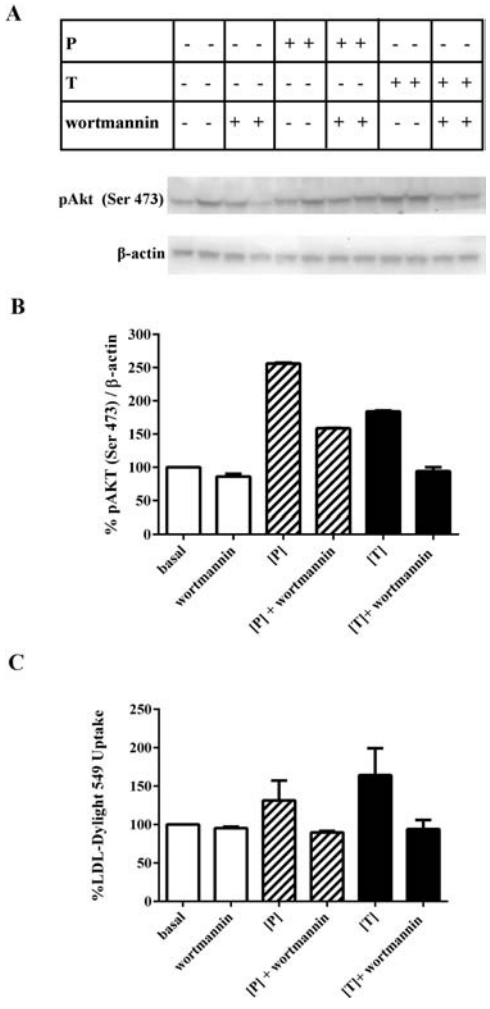

Figure 7. Involvement of PI3K/Akt pathway activation in the regulation of the LDLR−SREBP2 pathway through which lupin peptides mediate the cholesterol-lowering effects. HepG2 cells (1.5×10^5) were treated with 1.0 and 0.5 mg/mL of P and T peptides in the presence or absence of wortmannin for 24 h, respectively. The phosphorylation level of Akt (Ser473) (A) and β-actin immunoblotting signals were detected using specific anti-posphoAkt (Ser473) and anti-β-actin primary antibodies, respectively. Relative intensity of posphoAkt signals (B) was quantified by ImageJ software and normalized with β-actin signals. Panel C shows the LDL uptake after treatment with the PI3K inhibitor. HepG2 cells (3×10^4) were treated with P (1.0 mg/mL) and T (0.5 mg/mL) peptides in the presence or absence of wortmannin and inhibitor alone for 24 h. LDL-Dylight 549 (10.0 μg/mL) was incubated for additional 2 h. Excess LDL-Dylight 549 was removed, and cells were washed two times with PBS. Specific fluorescent LDL uptake was analyzed by Synergy H1 (Biotek). Bars represent averages of duplicate samples ± SEM of three independent experiments. pAkt, posphoAkt; P, pepsin peptides; T, trypsin peptides; C, control.

three different experiments, each performed in duplicate, is shown in Figure 7B. This figure clearly demonstrates that the wortmannin co-incubation with P and T peptides is able to reduce by about 40 and 50% the Akt phosphorylation level, abolishing the Akt phosphorylation induced by lupin peptides.

To confirm the involvement of the PI3K/Akt pathway activation in the regulation of the LDLR-SREBP2 pathway, functional LDL uptake experiments were performed in the presence of wortmannin. As Figure 7C shows, P peptides and T peptides are able to increase the LDL uptake with respect to the basal level, but these uptakes are blocked in the presence of wortmannin. Precisely, the LDL uptake is blocked at the basal level either in the presence of the inhibitor alone or in the co-incubation with P and T peptides, demonstrating that the LDL uptake induced by lupin peptides is abolished by treatment with this well-known PI3K inhibitor.

DISCUSSION

As already indicated in the Introduction, some experimental studies[11−14] and a few clinical trials[17−19] gave clear indications that lupin proteins are able to induce hypocholesterolemic effects in vivo. The present investigation at HepG2 cells was aimed at providing some further information on the mechanism through which the lupin peptides may be responsible of the observed activities.

The main findings of this study are the following: (i) T peptides are able to directly interfere with the HMGCoAR activity, whereas P peptides are much less effective. (ii) Both P and T peptides modulate the cholesterol metabolism at HepG2 cell line, through the up-regulation of the pathway involving the LDLR. (iii) Both P and T peptide treatments increase the LDL-uptake. (iv) Activation of the Akt/GSK3β pathway is involved in the up-regulation of the LDLR-SREBP2 pathway.

HMGCoAR is the rate-controlling enzyme of cellular cholesterol biosynthesis pathway, and therefore it constitutes the target of numerous investigations aimed at lowering the rate of cholesterol biosynthesis.[49] Therefore, initially in vitro experiments were performed using the purified catalytic domain of the enzyme with the objective of clarifying whether lupin peptides were able to directly inhibit the activity of HMGCoAR. As shown in Figure 3, T peptides but not P peptides act as enzyme inhibitors.

The LDLR expression and the receptor protein localization at cellular membranes are strictly correlated to the intracellular cholesterol biosynthesis pathway. In fact, the transcription of the LDLR and the genes required for cholesterol and fatty acid synthesis are controlled by membrane-bound transcription factors called SREBPs,[50] and the intracellular cholesterol acts with a negative feedback inhibition mechanism.[51] The SREBP2 isoform is responsible for the LDLR and HMGCoAR transcription, and the SREBP2 maturation is regulated by the intracellular cholesterol homeostasis. Thus, the up-regulation of LDLR represents a useful strategy to control plasma LDL cholesterol levels. Our findings demonstrate that both lupin peptide mixtures are able to up-regulate the LDLR protein levels through an increase of SREBP2 protein. However, a detailed investigation of the LDLR pathway revealed that lupin peptides produce different effects on the HMGCoAR level. In particular, whereas P peptides are able to increase the enzyme protein level in a dose-dependent manner, T peptides up-regulate the enzyme protein levels in a significant way versus the control at 0.5 mg/mL; the increase remains statistically significant, but it is smaller at 1.0 mg/mL, and it is finally completely abolished at 2.5 mg/mL (Figure 4D).

These pieces of evidence suggest that both peptide mixtures modulate the cholesterol metabolism pathway through the induction of LDLR protein levels due to an increase of SREBP2 protein, although their potencies of induction are different.

In agreement with immunoblotting results, the increase of LDLR protein levels leads to an increase of LDL uptake (Figure 5). Our findings suggest that both P and T peptides are able to significantly induce the LDL clearance, and this result is strictly correlated to an increase of LDLR protein level.

Recently, studies have indicated that there are links between the Akt and the SREBP pathways: in fact, emerging evidence

shows that Akt is implicated in the regulation of lipid metabolism through the activation of SREBPs.[45,52−55] Luu and co-workers[41] showed that insulin-like growth factor-1, an inducer of Akt signaling, acutely increases SREBP2 activation. This study provided evidence that Akt contributes to the regulation of cholesterol metabolism through activating SREBP2.

Even if the precise target or targets of Akt remain elusive and not clarified, part of our investigation was dedicated to evaluating the effects of lupin peptides on the PI3K/Akt pathway. Our study provides experimental evidence that either P or T peptides from lupin protein are able to induce increases of Akt and GSK3β phosphorylation levels, which are completely abolished by treatment with a well-known PI3K inhibitor, such as wortmannin. A constitutively active form of Akt activated the LDLR.[53] Our findings clearly support this study, because both P and T peptides increase the LDLR protein levels and induce an increased fluorescent LDL uptake at HepG2 cells. Moreover, after treatment with both lupin peptides in the presence of wortmannin, LDL uptake is blocked versus the P and T treatments alone, demonstrating that the inhibition of PI3K/Akt has general effects on cellular lipid homeostasis, although the precise Akt target or targets are not definitely assigned yet.

In conclusion, this is the first study providing evidence that peptide mixtures obtained by the hydrolysis of lupin proteins are able to modulate the LDLR/SREBP2 pathway with the final effect of an increased LDL uptake. Because, as indicated above, both P peptides and T peptides are complex mixtures, it appears very difficult to sort out which may be the peptides responsible for the observed activities. It is, however, possible to affirm that the diversity in the behaviors of the two peptide mixtures derives from their different compositions. Further work will be necessary to investigate these aspects in detail. This is also the first study to investigate in detail the mechanism of the hypocholesterolemic activity of peptides deriving from a plant protein, because, even in the case of soy, only partial information is available.[26−32]

■ ASSOCIATED CONTENT

Supporting Information

Tables 1S and 2S. This material is available free of charge via the Internet at http://pubs.acs.org.

■ AUTHOR INFORMATION

Corresponding Author

*(A.A.) Phone: +39 02 503 19372. Fax: +39 02 503 19343. E-mail: anna.arnoldi@unimi.it.

Author Contributions

Ideation and design of experiments: C.L. Experiments: biotechnology, C.L. and C.Z.; mass spectrometry analysis, A.D.; peptide preparation, G.M.S.; analysis of data, C.L., C.Z., and A.D.; figure preparation, C.Z; retrieval of grants, A.A; manuscript writing, C.L. and A.A.

Funding

Research was funded by the European Union Seventh Framework Programme (FP7/2007−2013), under Grant Agreement 285819. We are indebted to Regione Lombardia and HPF-Nutraceutics SRL (Milan, Italy) for the partial funding of a postdoctoral fellowship to C.Z. and to the Carlo Sirtori Foundation (Milan, Italy) for having provided most of the equipment used in this experimentation.

Notes

The authors declare no competing financial interest.

■ ABBREVIATIONS USED

HMGCoAR, 3-hydroxy-3-methylglutaryl CoA reductase; LDL, low-density lipoprotein; LDLR, LDL receptor; *L. albus*, *Lupinus albus*; MTT, 3-(4,5-dimethyl-2-thiazolyl)-2,5-diphenyl-2*H*-tetrazolium bromide; SREBP2, sterol regulatory element binding protein 2; SCAP, SREBP cleavage-activating protein; ER, endoplasmic reticulum; P peptides, pepsin peptides; T peptides, trypsin peptides; PI3K, phosphoinositide 3-kinase; Akt, protein kinase B; GSK3β, glycogen synthase kinase-3β

■ REFERENCES

(1) Sujak, A.; Kotlarz, A.; Strobel, W. Compositional and nutritional evaluation of several lupin seeds. *Food Chem.* **2006**, *98*, 711−719.

(2) Boschin, G.; D'Agostina, A.; Annicchiarico, P.; Arnoldi, A. Effect of genotype and environment on fatty acid composition of *Lupinus albus* L. seed. *Food Chem.* **2008**, *108*, 600−606.

(3) Boschin, G.; Arnoldi, A. Legumes are valuable sources of tocopherols. *Food Chem.* **2011**, *127*, 1199−1203.

(4) Katagiri, Y.; Ibrahim, R. K.; Tahara, S. HPLC analysis of white lupin isoflavonoids. *Biosci., Biotechnol., Biochem.* **2000**, *64*, 1118−1125.

(5) Muzquiz, M.; Pedrosa, M. M.; Cuadrado, C.; Ayet, G.; Burbano, C.; Brenes, A. *Variation of Alkaloids, Alkaloids Esters, Phytic Acid and Phytase Activity in Germinated Seed of Lupinus albus and L. luteus*; Wageningen Pers: Wageningen, The Netherlands, 1998.

(6) Caligari, S.; Chiesa, G.; Johnson, S. K.; Camisassi, D.; Gilio, D.; Marchesi, M.; Parolini, C.; Rubio, L. A.; Sirtori, C. R. Lupin (*Lupinus albus*) protein isolate (L-ISO) has adequate nutritional value and reduces large intestinal weight in rats after restricted and ad libitum feeding. *Ann. Nutr. Metab.* **2006**, *50*, 528−537.

(7) Boschin, G.; Annicchiarico, P.; Resta, D.; D'Agostina, A.; Arnoldi, A. Quinolizidine alkaloids in seeds of lupin genotypes of different origins. *J. Agric. Food Chem.* **2008**, *56*, 3657−3663.

(8) D'Agostina, A.; Antonioni, C.; Resta, D.; Arnoldi, A.; Bez, J.; Knauf, U.; Waesche, A. Optimization of a pilot-scale process for producing lupin protein isolates with valuable technological properties and minimum thermal damage. *J. Agric. Food Chem.* **2006**, *54*, 92−98.

(9) Doxastakis, G.; Papageorgiou, M.; Mandalou, D.; Irakli, M.; Papalamprou, E.; D'Agostina, A.; Resta, D.; Boschin, G.; Arnoldi, A. Technological properties and non-enzymatic browning of white lupin protein enriched spaghetti. *Food Chem.* **2007**, *101*, 57−64.

(10) Boschin, G.; Scigliuolo, G. M.; Resta, D.; Arnoldi, A. Optimization of the enzymatic hydrolysis of lupin (*Lupinus*) proteins for producing ACE-inhibitory peptides. *J. Agric. Food Chem.* **2014**, *62*, 1846−1851.

(11) Sirtori, C. R.; Lovati, M. R.; Manzoni, C.; Castiglioni, S.; Duranti, M.; Magni, C.; Morandi, S.; D'Agostina, A.; Arnoldi, A. Proteins of white lupin seed, a naturally isoflavone-poor legume, reduce cholesterolemia in rats and increase LDL receptor activity in HepG2 cells. *J. Nutr.* **2004**, *134*, 18−23.

(12) Bettzieche, A.; Brandsch, C.; Weisse, K.; Hirche, F.; Eder, K.; Stangl, G. Lupin protein influences the expression of hepatic genes involved in fatty acid synthesis and triacylglycerol hydrolysis of adult rats. *Br. J. Nutr.* **2008**, *99*, 952−962.

(13) Bettzieche, A.; Brandsch, C.; Schmidt, M.; Weisse, K.; Eder, K.; Stangl, G. Differing effect of protein isolates from different cultivars of blue lupin on plasma lipoproteins of hypercholesterolemic rats. *Biosci., Biotechnol., Biochem.* **2008**, *72*, 3114−3121.

(14) Parolini, C.; Rigamonti, E.; Marchesi, M.; Busnelli, M.; Cinquanta, P.; Manzini, S.; Sirtori, C.; Chiesa, G. Cholesterol-lowering effect of dietary *Lupinus angustifolius* proteins in adult rats through regulation of genes involved in cholesterol homeostasis. *Food Chem.* **2012**, *132*, 1475−1479.

(15) Fontanari, G.; Batistuti, J.; da Cruz, R.; Saldiva, P.; Areas, J. Cholesterol-lowering effect of whole lupin (*Lupinus albus*) seed and its protein isolate. *Food Chem.* **2012**, *132*, 1521−1526.

(16) Marchesi, M.; Parolini, C.; Diani, E.; Rigamonti, E.; Cornelli, L.; Arnoldi, A.; Sirtori, C. R.; Chiesa, G. Hypolipidaemic and anti-atherosclerotic effects of lupin proteins in a rabbit model. *Br. J. Nutr.* **2008**, *100*, 707−710.

(17) Naruszewicz, M.; Nowicka, G.; Klosiewicz-Latoszek, L.; Arnoldi, A.; Sirtori, C. Effect of lupin protein (*Lupinus albus*) on cardiovascular risk factors in smokers with mild hypercholesterolemia. *Circulation* **2006**, *114*, 874−874.
(18) Sirtori, C. R.; Triolo, M.; Bosisio, R.; Bondioli, A.; Calabresi, L.; De Vergori, V.; Gomaraschi, M.; Mombelli, G.; Pazzucconi, F.; Zacherl, C.; Arnoldi, A. Hypocholesterolaemic effects of lupin protein and pea protein/fibre combinations in moderately hypercholesterolaemic individuals. *Br. J. Nutr.* **2012**, *107*, 1176−1183.
(19) Bähr, M.; Fechner, A.; Kiehntopf, M.; Jahreis, G. Consuming a mixed diet enriched with lupin protein beneficially affects plasma lipids in hypercholesterolemic subjects: a randomized controlled trial. *Clin. Nutr.* **2014**, DOI: 10.1016/j.clnu.2014.03.008.
(20) Sirtori, C. R.; Agradi, E.; Conti, F.; Mantero, O.; Gatti, E. Soybean-protein diet in the treatment of type-II hyperlipoproteinaemia. *Lancet* **1977**, *1*, 275−277.
(21) Sirtori, C. R.; Eberini, I.; Arnoldi, A. Hypocholesterolaemic effects of soya proteins: results of recent studies are predictable from the Anderson meta-analysis data. *Br. J. Nutr.* **2007**, *97*, 816−822.
(22) Anderson, J. W.; Johnstone, B. M.; Cook-Newell, M. E. Meta-analysis of the effects of soy protein intake on serum lipids. *N. Engl. J. Med.* **1995**, *333*, 276−282.
(23) Harland, J.; Haffner, T. Systematic review, meta-analysis and regression of randomised controlled trials reporting an association between an intake of circa 25 g soya protein per day and blood cholesterol. *Atherosclerosis* **2008**, *200*, 13−27.
(24) FDA. Food labeling health claims: soybean protein and coronary heart disease. Final rule. *Fed. Regist.* **1999**, *64*, 57699−57733.
(25) Sirtori, C. R.; Galli, G.; Lovati, M. R.; Carrara, P.; Bosisio, E.; Kienle, M. G. Effects of dietary proteins on the regulation of liver lipoprotein receptors in rats. *J. Nutr.* **1984**, *114*, 1493−1500.
(26) Lovati, M. R.; Manzoni, C.; Canavesi, A.; Sirtori, M.; Vaccarino, V.; Marchi, M.; Gaddi, G.; Sirtori, C. R. Soybean protein diet increases low density lipoprotein receptor activity in mononuclear cells from hypercholesterolemic patients. *J. Clin. Invest.* **1987**, *80*, 1498−1502.
(27) Baum, J. A.; Teng, H.; Erdman, J. W. J.; Weigel, R. M.; Klein, B. P.; Persky, V. W.; Freels, S.; Surya, P.; Bakhit, R. M.; Ramos, E.; Shay, N. F.; Potter, S. M. Long-term intake of soy protein improves blood lipid profiles and increases mononuclear cell low-density-lipoprotein receptor messenger RNA in hypercholesterolemic, postmenopausal women. *Am. J. Clin. Nutr.* **1998**, *68*, 545−551.
(28) Manzoni, C.; Duranti, M.; Eberini, I.; Scharnag, H.; März, W.; Castiglioni, S.; Lovati, M. Subcellular localization of soybean 7S globulin in HepG2 cells and LDL receptor up-regulation by its alpha′ constituent subunit. *J. Nutr.* **2003**, *133*, 2149−2155.
(29) Duranti, M.; Lovati, M. R.; Dani, V.; Barbiroli, A.; Scarafoni, A.; Castiglioni, S.; Ponzone, C.; Morazzoni, P. The alpha′ subunit from soybean 7S globulin lowers plasma lipids and upregulates liver beta-VLDL receptors in rats fed a hypercholesterolemic diet. *J. Nutr.* **2004**, *134*, 1334−1339.
(30) Consonni, A.; Lovati, M. R.; Parolari, A.; Manzoni, C.; Morazzoni, P.; Magni, C.; Duranti, M. Heterologous expression and purification of the soybean 7S globulin α' subunit extension region: in vitro evidence of its involvement in cell cholesterol homeostasis. *Protein Express. Purif.* **2011**, *80*, 125−129.
(31) Cho, S.; Juillerat, M.; Lee, C. Identification of LDL-receptor transcription stimulating peptides from soybean hydrolysate in human hepatocytes. *J. Agric. Food Chem.* **2008**, *56*, 4372−4376.
(32) Mochizuki, Y.; Maebuchi, M.; Kohno, M.; Hirotsuka, M.; Wadahama, H.; Moriyama, T.; Kawada, T.; Urade, R. Changes in lipid metabolism by soy β-conglycinin-derived peptides in HepG2 cells. *J. Agric. Food Chem.* **2009**, *57*, 1473−1480.
(33) Vermeirssen, V.; van Camp, J.; Verstraete, W. Bioavailability of angiotensin I converting enzyme inhibitory peptides. *Br. J. Nutr.* **2004**, *92*, 357−366.
(34) Brugger, D.; Schuster, H.; Zöllner, N. Familial hypercholesterolemia and familial defective apolipoprotein B-100: comparison of the phenotypic expression In 116 cases. *Eur. J. Med. Res.* **1996**, *1*, 383−386.
(35) Ishibashi, S.; Brown, M. S.; Goldstein, J. L.; Gerard, R. D.; Hammer, R. E.; Herz, J. Hypercholesterolemia in low density lipoprotein receptor knockout mice and its reversal by adenovirus-mediated gene delivery. *J. Clin. Invest.* **1993**, *92*, 883−893.
(36) Twisk, J.; Gillian-Daniel, D. L.; Tebon, A.; Wang, L.; Barrett, P. H.; Attie, A. D. The role of the LDL receptor in apolipoprotein B secretion. *J. Clin. Invest.* **2000**, *105*, 521−532.
(37) Hussain, M. M. Structural, biochemical and signaling properties of the low-density lipoprotein receptor gene family. *Front. Biosci.* **2001**, *6*, D417−D428.
(38) Castoreno, A. B.; Wang, Y.; Stockinger, W.; Jarzylo, L. A.; Du, H.; Pagnon, J. C.; Shieh, E. C.; Nohturfft, A. Transcriptional regulation of phagocytosis-induced membrane biogenesis by sterol regulatory element binding proteins. *Proc. Natl. Acad. Sci. U.S.A.* **2005**, *102*, 13129−13134.
(39) Horton, J. D.; Shimomura, I.; Brown, M. S.; Hammer, R. E.; Goldstein, J. L.; Shimano, H. Activation of cholesterol synthesis in preference to fatty acid synthesis in liver and adipose tissue of transgenic mice overproducing sterol regulatory element-binding protein-2. *J. Clin. Invest.* **1998**, *101*, 2331−2339.
(40) Brown, M. S.; Goldstein, J. L. The SREBP pathway: regulation of cholesterol metabolism by proteolysis of a membrane-bound transcription factor. *Cell* **1997**, *89*, 331−340.
(41) Luu, W.; Sharpe, L. J.; Stevenson, J.; Brown, A. J. Akt acutely activates the cholesterogenic transcription factor SREBP-2. *Biochim. Biophys. Acta* **2012**, *1823*, 458−464.
(42) Nohturfft, A.; Zhang, S. C. Coordination of lipid metabolism in membrane biogenesis. *Annu. Rev. Cell. Dev. Biol.* **2009**, *25*, 539−566.
(43) Whiteman, E. L.; Cho, H.; Birnbaum, M. J. Role of Akt/protein kinase B in metabolism. *Trends Endocrinol. Metab.* **2002**, *13*, 444−451.
(44) Song, G.; Ouyang, G.; Bao, S. The activation of Akt/PKB signaling pathway and cell survival. *J. Cell. Mol. Med.* **2005**, *9*, 59−71.
(45) Krycer, J. R.; Sharpe, L. J.; Luu, W.; Brown, A. J. The Akt-SREBP nexus: cell signaling meets lipid metabolism. *Trends Endocrinol. Metab.* **2010**, *21*, 268−276.
(46) Du, X.; Kristiana, I.; Wong, J.; Brown, A. J. Involvement of Akt in ER-to-Golgi transport of SCAP/SREBP: a link between a key cell proliferative pathway and membrane synthesis. *Mol. Biol. Cell* **2006**, *17*, 2735−2745.
(47) Boschin, G.; Scigliuolo, G. M.; Resta, D.; Arnoldi, A. ACE-inhibitory activity of enzymatic protein hydrolysates from lupin and other legumes. *Food Chem.* **2014**, *145*, 34−40.
(48) Levashov, P. A.; Sutherland, D. S.; Besenbacher, F.; Shipovskov, S. A robust method of determination of high concentrations of peptides and proteins. *Anal. Biochem.* **2009**, *395*, 111−112.
(49) Endo, A. The discovery and development of HMG-CoA reductase inhibitors. *J. Lipid Res.* **1992**, *33*, 1569−1582.
(50) Horton, J. D.; Goldstein, J. L.; Brown, M. S. SREBPs: transcriptional mediators of lipid homeostasis. *Cold Spring Harbor Symp. Quant. Biol.* **2002**, *67*, 491−498.
(51) Edwards, P. A.; Tabor, D.; Kast, H. R.; Venkateswaran, A. Regulation of gene expression by SREBP and SCAP. *Biochim. Biophys. Acta* **2000**, *1529*, 103−113.
(52) Demoulin, J. B.; Ericsson, J.; Kallin, A.; Rorsman, C.; Rönnstrand, L.; Heldin, C. H. Platelet-derived growth factor stimulates membrane lipid synthesis through activation of phosphatidylinositol 3-kinase and sterol regulatory element-binding proteins. *J. Biol. Chem.* **2004**, *279*, 35392−35402.
(53) Zhou, R. H.; Yao, M.; Lee, T. S.; Zhu, Y.; Martins-Green, M.; Shyy, J. Y. Vascular endothelial growth factor activation of sterol regulatory element binding protein: a potential role in angiogenesis. *Circ. Res.* **2004**, *95*, 471−478.
(54) Hegarty, B. D.; Bobard, A.; Hainault, I.; Ferré, P.; Bossard, P.; Foufelle, F. Distinct roles of insulin and liver X receptor in the induction and cleavage of sterol regulatory element-binding protein-1c. *Proc. Natl. Acad. Sci. U.S.A.* **2005**, *102*, 791−796.
(55) Eberlé, D.; Hegarty, B.; Bossard, P.; Ferré, P.; Foufelle, F. SREBP transcription factors: master regulators of lipid homeostasis. *Biochimie* **2004**, *86*, 839−848.

Table 1. Total Soyasaponin B Concentration of 20 Soybean Genotypes Grown in Four Environments in QC, Canada[a]

	environment								average of four environments	
genotype	BEL 2007 (μmol g^{-1})	rank	SHY 2007 (μmol g^{-1})	rank	BEL 2008 (μmol g^{-1})	rank	SMA 2008 (μmol g^{-1})	rank	average (μmol g^{-1})	rank
AC Colibri	3.89	9	4.50	8	3.62	11	3.68	8	3.92	9
AC Orford	3.06	19	3.55	18	2.87	18	2.65	19	3.03	19
AC Proteina	4.50	5	5.26	3	4.41	3	4.02	5	4.55	3
Amasa	3.53	16	3.90	16	3.22	17	2.95	17	3.40	17
Arva	3.84	12	4.12	12	3.26	16	3.24	15	3.61	14
DH3604	4.15	8	4.83	5	4.29	4	4.25	2	4.38	6
Heron	3.59	14	3.85	17	3.62	12	3.34	13	3.60	15
Kamichis	4.85	2	5.50	2	4.19	7	4.02	6	4.64	2
KG41	4.45	6	5.19	4	4.46	2	3.96	7	4.51	4
Micron	4.71	3	4.82	6	4.20	5	4.03	4	4.44	5
OAC Wallace	3.88	11	4.35	11	3.67	10	3.37	12	3.82	11
Ohgata	2.80	20	3.14	20	2.57	20	2.31	20	2.70	20
Pronatto	3.53	17	3.91	15	3.28	15	3.23	16	3.49	16
S00147.40GB	3.76	13	4.36	10	3.70	9	3.50	9	3.83	10
S00147.40GN	3.57	15	4.11	13	3.56	14	3.34	14	3.64	13
S0022.67	4.53	4	4.46	9	4.19	6	4.15	3	4.33	7
S08-80	3.89	10	4.03	14	3.59	13	3.38	11	3.72	12
S14-P6	3.30	18	3.41	19	2.76	19	2.69	18	3.04	18
Toki	5.80	1	6.59	1	5.31	1	5.04	1	5.69	1
Venus	4.32	17	4.73	7	3.75	8	3.42	10	4.06	8
average	3.99		4.43		3.73		3.53		3.92	
$LSD_{0.05}$	0.364		0.387		0.423		0.222		0.248	

[a]BEL, St. Mathieu-de-Beloeil; SHY, St. Hyacinthe; SMA, Ste. Martine.

soyasaponin B concentration is affected by specific environmental factors if soybeans are to be considered a source of saponins for the nutraceutical and functional food industries. Indeed a better understanding of factors affecting concentrations may help ensure the production of soybeans with a more stable and consistent saponin concentration. To our knowledge, the impact of specific environmental or crop management factors on soyasaponin B concentration in mature soybeans has never been researched. The objectives of this study were thus to determine the impact of specific crop management practices, environmental factors, and genotypes on soyasaponin B concentration of early maturing soybean. Three separate experiments, two field experiments and one growth chamber experiment, were conducted to meet these objectives.

MATERIALS AND METHODS

Field Experiment Description. Two distinct field experiments were conducted in 2007 and 2008 at multiple sites in Quebec, Canada to determine the impact of genotype selection and seeding dates on soybean soyasaponin B concentration. The experiments and treatments are only briefly presented here, as these experiments were part of a larger project investigating the impact of agronomic practices on soybean nutraceutical value.[26−28]

The first experiment (i.e., Exp. 1) evaluated 20 early maturing (i.e., maturity groups I to 00) soybean genotypes (AC Colibri, AC Orford, AC Proteina, Amasa, Arva, DH3604, Heron, Kamichis, KG41, Micron, OAC Wallace, Ohgata, Pronatto, S00147.40GB, S00147.40GN, S0022.67, S08-80, S14-P6, Toki, and Venus) in four environments: Saint-Mathieu-de-Beloeil in 2007 and 2008 (BEL; 45°36′N, 73°57′W), Sainte-Hyacinthe in 2007 (SHY; 45°37′ N, 72°58′ W), and Sainte-Martine in 2008 (SMA; 45°14′N, 73°48′ W). All genotypes were replicated twice in each environment. Seguin et al.[26] have previously characterized all genotypes evaluated herein. The second experiment (i.e., Exp. 2) evaluated the impact of four seeding dates (i.e., mid-May, early-June, mid-June, and late-June) of two cultivars (AC Proteina and OAC Vision) in Sainte-Anne-de-Bellevue in 2007 and 2008 (MTL; 45°24′ N, 73°57′ W). Each treatment was replicated four times in each environment.[26]

For both experiments, local recommendations for conventional soybean production were followed.[29] Description of specific management practices and sites used were previously provided in detail by Seguin et al.[26,27] The average plot size across all environments was 1.25 × 5 m. Plots in all experiments and environments were harvested when plants reached physiological maturity. At harvest, subsamples of 50 g were randomly selected from each plot and used for soyasaponin B extraction and quantification.

Growth Chamber Experiment Description. In this experiment (i.e., Exp. 3), two soybean cultivars (i.e., AC Proteina and OAC Champion), were grown in controlled environment growth chambers (model no. E15, Conviron, Winnipeg, MB, Canada). Details regarding growth conditions and seeding were previously described in detail by Chennupati et al.[30] Treatments consisted in the exposure of plants to high temperature at specific stages of development.[31] To generate the stress treatments, growth chambers were set at contrasting temperatures [i.e., stress (33/25 °C, day/night temperatures) and control conditions (23/15 °C)]. The treatments included (i) plants grown during all developmental stages under control conditions or plants grown under control conditions except for specific stages during which stress was imposed and which included (ii) pre-emergence, (iii) vegetative stages, (iv) reproductive stages R1−4 (flowering to early seed formation), (v) reproductive stages R5−8 (seed formation to maturity), and (vi) all stages. Each treatment was replicated four times. Depending on the treatments, the number of days varied for each cultivar to reach specific stage of development.[30] Plants were watered as needed, and a similar level of relative humidity was maintained in all growth chambers. Seeds of a specific treatment were harvested at maturity to determine soyasaponin B concentration.

Soyasaponin Extraction and Quantification. Upon harvest, seeds from all experiments were stored at room temperature for one month and were then finely ground (i.e., to pass through a 1 mm sieve) using a coffee grinder (Black & Decker, Towson, MD, USA)

immediately prior to the extraction of the soyasaponins. Extraction and analysis of soyasaponin B was performed using a modified version of the protocol of Hubert et al.[13] Five hundred milligrams of ground soybean seeds was dissolved in 5 mL of 80% aqueous methanol in a 20 mL vial. Extraction was further carried for 2 h at room temperature followed by vortexing. Then, 1.5 mL of solution was transferred into a 1.5 mL microcentrifuge tube, followed by centrifugation at 12,000*g* for 10 min. Filtration of the extract was done using 0.45 μm filters and 1 mL of clear supernatant was transferred to a HPLC (high performance liquid chromatography) vial. Fifty microliters of potassium hydroxide (5% w/v) was added and allowed to stand for 15 min at room temperature. Neutralization was achieved by the addition of 50 μL of acetic acid and also to maintain the pH of the solution in the range of 4–6.

Separation of soyasaponins was carried out using a Varian HPLC system (Walnut Creek, CA, USA) equipped with a ProStar 210 solvent delivery system, a Model 410 autosampler, and a ProStar 330 photo diode array detector. Twenty microliters of extract was used for each analysis. Separation was carried out on a C18 reversed-phase column (Luna, 5 μm, 4.6 × 250 mm, Phenomenex, Torrance, CA, USA) with a flow rate of 1.0 mL/min and with the column temperature maintained constant at 30 °C. Soyasaponins were detected at 205 nm. Mobile phase solvents, 0.05% trifluoroacetic acid in water (mobile phase A), and HPLC grade acetonitrile (mobile phase B) were used. Soyasaponin elution was carried out using a linear gradient system from 40% solvent B, with a 12 min hold time which then increased to 48% in 25 min followed by reaching up to 100% in 1 min and remaining at 100% for 2 min. The gradient program was recycled back to the initial state of 37% solvent B in 5 min.

Stock solutions of the individual soyasaponins were made by dissolving purified standards (ChromaDex, Irvine, CA, USA) in methanol, followed by serial dilutions. Standard curves were obtained by plotting the soyasaponin concentration as a function of peak area obtained from HPLC at 205 nm. Soyasaponin II standard was used as a reference for individual soyasaponin quantification. Total soyasaponin B concentration was calculated by the addition of the individual soyasaponins.

Statistical Analyses. Plots in each experiment were assigned to a randomized complete block design. The seeding date experiment (Exp. 2) had a split-plot restriction with cultivars as main-plots and seeding date as subplots. Data were analyzed using ANOVA (i.e., PROC GLM) in SAS (version 9.3, Cary, NC, USA) to identify significant model and treatment effects.[32] Data from the genotype evaluation and seeding date experiments (Exps. 1 and 2) were analyzed across environments.[33] Homoscedasticity among environments was confirmed using the chi-square test. Environments and replicates were considered random effects, and other factors were considered fixed. Comparisons between means in all experiments were made using least significant differences at a 0.05 probability level. For the genotype evaluation experiment (Exp. 1), analyses were also performed to determine the stability of genotypes across environments. Values for Francis and Kannenberg[34] mean-CV stability were computed using SAS.

RESULTS AND DISCUSSION

Experiment 1: Genotypes Grown in Multiple Environments. Genotype and environment main effects as well as a genotype × environment (G × E) interaction were observed for total soyasaponin B concentration ($P < 0.001$). Concentration averaged 3.92 μmol g^{-1} across genotypes and environments, ranging between 2.31 and 6.59 μmol g^{-1} (Table 1). This range is in accordance with values previously reported in whole soybean seeds by Hubert et al.[13] and Murphy et al.[14] The presence of a G × E interaction illustrates that the performance of specific genotypes varied across environments (Table 1). The G × E interaction, however, contributed to less than 1% of the total mean square, the environment and genotype contributing to 62 and 38% of the total mean square (data not shown). Ranking of specific genotypes was thus overall remarkably stable across 4 environments, Toki and Ohgata consistently having the highest and lowest concentration of total soyasaponin B, respectively (Table 1). However, these two genotypes also had a larger than average variation across environments (Figure 1). Genotypes with a higher

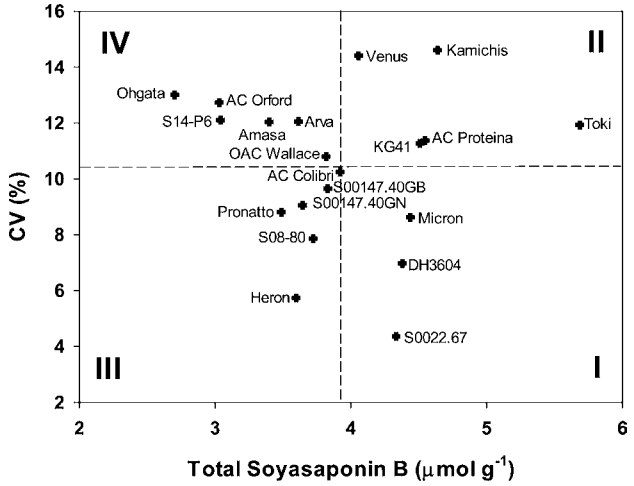

Figure 1. Plot of mean total soyasaponin B concentration versus coefficient of variation (CV) of 20 soybean genotypes grown in four environments in QC, Canada. Dotted lines intersecting the plot indicate the average performance (total soyasaponin B concentration) and average CV.

stability across environments are usually preferable. In Figure 1, genotypes located in quadrant I (i.e., Micron, DH3604, and S0022.67) are more desirable as they have both high concentration and high stability across environments.

Soyasaponin I represented 68% of the total soyasaponin B, the other forms contributing 17 to 2% of the total concentration (i.e., 17, 8, 5, and 2% for soyasaponins II, III, V, and IV, respectively); similar proportions were reported among 7 soybean cultivars from France and the USA.[13] Genotype and environment main effects were also significant ($P < 0.01$) for the concentration of all individual soyasaponin; however, G × E interactions were observed only for soyasaponin I and IV, indicating that the performance of genotypes was relatively stable across environments for the other soyasaponins (Tables S1 to S5, Supporting Information). The G × E interaction contributed to less than 5% of the total mean square for all individual soyasaponin, the environment contributing to more than 50% of the total mean square for soyasaponins II, III, and IV, the genotype contributing to more than 50% of the total mean square for soyasaponins I and V (data not shown). Ranking of genotypes across environments was thus relatively consistent, changes in ranking being minimal for all soyasaponins except for soyasaponin IV for which more variation was observed (Table S4, Supporting Information). Soyasaponin IV was, however, the form found in the lowest concentration. As for total soyasaponin B, genotypes DH3604, Micron, and S0022.67 consistently had high and stable concentrations of most individual soyasaponins with the exception of soyasaponin II (Figures S1 to S5, Supporting Information). Another group of genotypes had high and stable concentrations of soyasaponin II, namely, Toki, S00147.40GB, OAC Wallace, S00147.40GN, S08-80, and KG41.

Table 2. Analysis of Variance of Soyasaponin B Concentrations in Two Soybean Cultivars (AC Proteina and OAC Vision) Seeded at Four Seeding Dates (Mid-May, Early-June, Mid-June, and Late-June), in Two Years (2007 and 2008) in Sainte-Anne-de-Bellevue, QC, Canada

source of variation	soyasaponin I	soyasaponin II	soyasaponin III	soyasaponin IV	soyasaponin V	total
year (Y)	0.56	0.51	0.63	0.45	0.08	0.79
cultivar (C)	**<0.0001**	0.85	0.001	0.41	**<0.0001**	**<0.0001**
Y × C	0.14	0.88	0.32	0.65	**0.03**	0.21
seeding date (SD)	**<0.0001**	**<0.0001**	**0.0006**	**0.03**	0.28	**<0.0001**
SD × C	**0.006**	0.52	**0.04**	0.54	0.60	0.01
Y × SD	0.38	**0.04**	**<0.0001**	0.53	0.33	**0.33**
Y × SD × C	0.12	0.06	**0.02**	0.78	0.83	0.03
CV %	4.5	8.8	9.9	29.6	16.2	4.1
mean	3.15	0.73	0.30	0.06	0.27	4.51

Results thus suggest that the total soyasaponin B concentration, as well as that of most individual soyasaponins, of a given genotype relative to others is relatively stable across environments. The G × E interaction, however, often significantly contributed only minimally to the total variation observed. While this is a desirable characteristic, the large contribution of the environment to the total variation observed emphasizes that the actual soyasaponin B concentration observed at harvest can be greatly affected by environmental factors that remain to be identified.

Experiment 2: Seeding Dates. Seeding date affected total soyasaponin B concentration as well as concentrations of soyasaponins I, II, III, and IV (Table 2); in all cases, earlier seeding dates resulting in the highest concentrations (Figure 2 and Figure S6, Supporting Information). There was an 11% difference in total soyasaponin B concentration of soybeans seeded in mid-May compared to that in late-June, differences being of 9, 22, 11, and 26% for soyasaponins I, II, III, and IV, respectively. The presence of interactions between seeding date and other factors for individual soyasaponins illustrate that the response to seeding date depended on the year and/or the cultivar (Table 2). These interactions, however, only reflect differences in the magnitude of response especially between cultivars, response to seeding date being in some cases slightly greater for AC Proteina than OAC Vision (data not shown). This difference in response might be related to the overall greater concentration of soyasaponin B in AC Proteina, which had 26% more total soyasaponin B compared to that in OAC Vision.

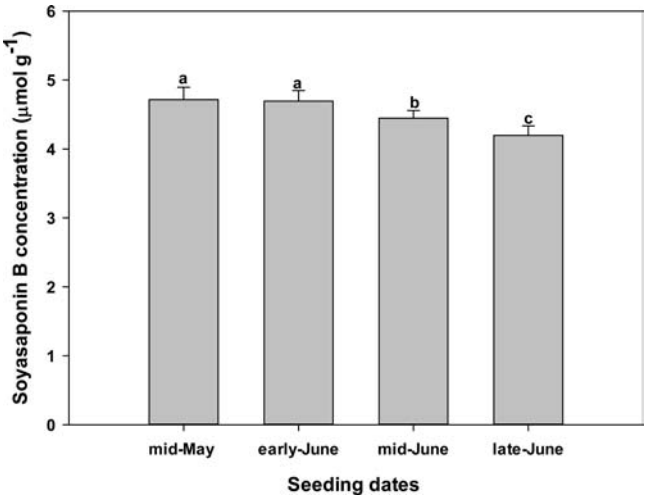

Figure 2. Total soyasaponin B concentrations in soybean seeded at four seeding dates (mid-May, early-June, mid-June, and late-June) in Sainte-Anne-de-Bellevue, QC, Canada. Results are the average for two cultivars (AC Proteina and OAC Vision) and two years (2007 and 2008). Means followed by different letters are significantly different ($P < 0.05$). Vertical bars indicate standard error.

The impact of seeding date on the concentration of other soybean health-beneficial compounds has previously been reported. The response observed herein for soyasaponin B is similar to that reported for α-tocopherol but opposite to that of isoflavones.[15,27,35,36] The response of soybean secondary metabolites to seeding date has often been associated with the impact of resulting temperatures at specific growth stages.[30,37] For example, earlier seeding dates (i.e., in May) compared to later dates (i.e., in June) are usually associated with higher air temperature during seed development. Higher air temperature during seed development has been demonstrated to increase α-tocopherol concentration but also decrease isoflavone concentration.[30,38] It is possible that the observed response of soyasaponin B to seeding date is mediated by a similar response to air temperature during specific growth stages, but this remains to be verified.

Experiment 3: High Temperature Stress at Specific Stages of Development. High temperature stress impacted the concentration of all individual soyasaponin B as well as total concentration ($P < 0.0001$); however, the response to specific treatments depended on the cultivar as illustrated by the presence of temperature stress treatment × cultivar interactions ($P < 0.01$) for all soyasaponin except soyasaponin III (Figure 3 and Figure S7, Supporting Information). High temperature stress restricted to the seed filling stages (i.e., R5−8)[31] increased total soyasaponin B concentration in AC Proteina by 28% when compared to that of control nonstressed plants. However, in OAC Champion, only high temperature applied during all growth stages had an impact reducing the total concentration by 27%.

The impact of specific stress treatments on individual soyasaponin was highly variable depending on the soyasaponin form and the cultivar (Figures 3 and S7, Supporting Information). High temperature stress applied during all growth stages resulted in large reductions (average of 60%) in soyasaponins II, III, and IV in both cultivars and of soyasaponin V in one cultivar (i.e., OAC Champion) when compared to that in the unstressed control. Stress restricted to stages R1−4 (flowering and early seed formation) reduced (average of 11%) the concentration of soyasaponins II, IV, and V of at least one cultivar but increased (average of 36%) that of soyasaponin III in both cultivars. Stress restricted to the R5−8

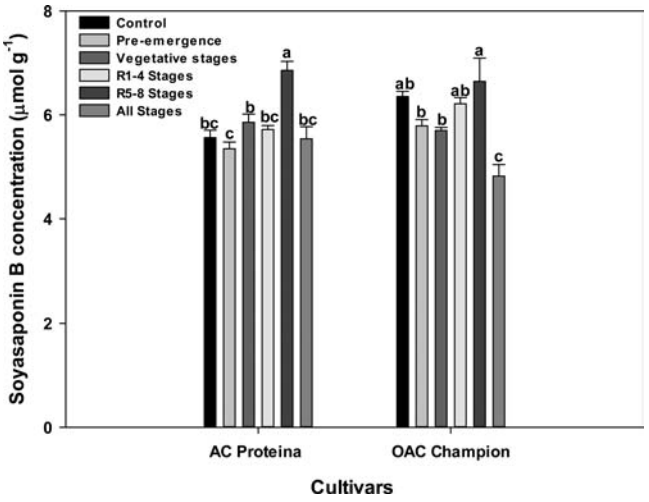

Figure 3. Total soyasaponin B concentrations in mature seeds of two soybean cultivars (AC Proteina and OAC Champion) after exposure to high temperature stress [i.e., 33/25 °C (day/night temperature)] at specific stages of development. Control conditions consisted of day/night temperatures of 23/15 °C. Means for a given cultivar followed by different letters are significantly different ($P < 0.05$). Vertical bars indicate standard error.

(seed filling to maturity stages) strongly reduced (average of 49%) the concentration of soyasaponins III and IV in both cultivars, increased slightly (average of 16%) that of soyasaponins I and II for one cultivar, while the response for soyasaponin V was opposite for the two cultivars. Finally, stress restricted to the pre-emergence stage did not impact any soyasaponin, while the response to stress restricted to vegetative stages postemergence was highly variable. Overall, the total saponin B concentration was comparable in both cultivars evaluated; however, AC Proteina had greater concentrations of soyasaponins I, III, and V, while the reverse was observed for soyasaponins II and IV (Figures 3 and S7, Supporting Information).

The response of soyasaponin B to high temperature is thus complex and appears to be cultivar specific. It is possible that the differential response of the two cultivars studied herein is attributable to differences in the expression of some of the multiple genes involved in the poorly studied saponin biosynthetic pathway in soybeans.[39] The difference in cultivar response might also be attributed to the differential profile of the individual soyasaponin observed between the two cultivars. Indeed, it is possible that the overall cultivar response is linked to its propensity to accumulate particular soyasaponin forms. If the impact of temperature at specific developmental stages has been correlated to the concentration of other heath beneficial compounds in soybean such as isoflavones and tocopherols, the evaluation of a larger number of cultivars will be required before definite conclusions can be made for soyasaponin B.[30,37]

In conclusion, soyasaponin concentration in mature soybeans is mostly determined by genotype and environment main effects. Specific environmental and crop management factors (i.e., air temperature and seeding date) were demonstrated to impact concentrations. The response to air temperature is, however, complex and cultivar specific. A study of soybean response to biotic and abiotic factors at the genetic and/or metabolomic level is now required to increase our understanding of factors determining soyasaponin concentrations in mature seeds. Such an understanding will increase our ability to minimize variation in soyasaponin concentration at harvest and ultimately produce soybeans with high and stable concentrations better suited for the nutraceutical and functional food markets.

■ ASSOCIATED CONTENT

Supporting Information

Plot of mean total soyasaponin B (I, II, III, IV, and V) concentration versus coefficient of variation (CV) of 20 soybean genotypes grown in four environments in QC, Canada; soyasaponin B concentrations in soybean seeded at four seeding dates (mid-May, early-June, mid-June, and late-June) in Sainte-Anne-de-Bellevue, QC, Canada; soyasaponin B concentrations in mature seeds of two soybean cultivars (AC Proteina and OAC Champion) after exposure to high temperature stress [i.e., 33/25 °C (day/night temperature)] at specific stages of development; and soyasaponin B (I, II, III, IV, and V) concentration of 20 soybean genotypes grown in four environments in QC, Canada. This material is available free of charge via the Internet at http://pubs.acs.org.

■ AUTHOR INFORMATION

Corresponding Author

*Tel: 1-514-398-7855. Fax: 1-514-398-7897. E-mail: philippe.seguin@mcgill.ca.

Funding

This research was supported by research grants from the Ministère de l'Agriculture, des Pêcheries, et de l'Alimentation du Québec (MAPAQ) through its Programme de Soutien à l'Innovation en Agroalimentaire, and the Natural Sciences and Engineering Research Council of Canada (NSERC) through a Discovery Grant. Funding from center SEVE is also acknowledged.

Notes

The authors declare no competing financial interest.

■ REFERENCES

(1) Woldemicheal, G. M.; Wink, M. Triterpene glycosides of *Lupinus angustifolius*. *Phytochemistry* **2002**, *60*, 323−327.

(2) Wina, E.; Muetzel, S.; Becker, K. The impact of saponins or saponin−containing plant materials on ruminant production: a review. *J. Agric. Food Chem.* **2005**, *53*, 8093−8105.

(3) Barlie, E.; Bonanomi, G.; Antignani, V.; Zolfaghari, B.; Sajjadi, S. E.; Scala, F.; Lanzotti, V. Saponins from *Allium minutiflorum* with antifungal activity. *Phytochemistry* **2007**, *68*, 596−603.

(4) Liu, K. Soybeans as a Powerhouse of Nutrients and Phytochemicals. In *Soybeans Saponin: Chemistry, Analysis, and Potential Health Effects*; Lin, J., Wang, C., Eds.; AOCS Press: Champaign, IL, 2004; pp 1−53.

(5) Kudou, S.; Tonomura, M.; Tsukamoto, C.; Uchida, T.; Sakabe, T.; Tamura, N.; Okubo, K. Isolation and structural elucidation of DDMP-conjugated soyasaponins as genuine saponins from soybean seeds. *Biosci. Biotechnol. Biochem.* **1993**, *57*, 546−550.

(6) Okubo, K.; Iijima, M.; Kobayashi, Y.; Yoshikoshi, M.; Uchida, T.; Kudou, S. Components responsible for the undesirable taste of soybean seeds. *Biosci. Biotechnol. Biochem.* **1992**, *56*, 99−103.

(7) Lasztity, R.; Hidvegi, M.; Bata, A. Saponins in food. *Food Rev. Int.* **1998**, *14*, 371−390.

(8) Shiraiwa, M.; Harada, K.; Okubo, K. Composition and content of saponins in soybean seed according to variety, cultivation year and maturity. *Agric. Biol. Chem.* **1991**, *55*, 323−331.

(9) Oakenfull, D. G.; Topping, D. L.; Illman, R. J.; Fenwick, D. E. Prevention of dietary hypercholesterolaemia in the rat by soybean and quillaja saponins. *Nutr. Rep. Int.* **1984**, *29*, 1039−1046.

(10) Fournier, D. B.; Erdman, J. W.; Gordon, G. B. Soy, its components, and cancer prevention: a review of invitro, animal and human data. *Cancer Epidemiol., Biomarkers. Prev.* **1998**, *7*, 1055−1065.
(11) Kinjo, J.; Imagire, M.; Udayama, M.; Arao, T.; Nohara, T. Structure-Hepatoprotective relationships study of Soyasaponins I-IV having soyasapogenol B as aglycone. *Planta Med.* **1998**, *64*, 233−236.
(12) Kinjo, J.; Ikeda, J.; Okawa, M.; Udayama, M.; Hirawaka, T.; Shii, Y.; Nohara, T. Hepatoprotective and hepatotoxic activities of sophoradiol analogs on rat primary liver cell cultures. *Biol. Pharm. Bull.* **2000**, *23*, 1118−1121.
(13) Hubert, J.; Berger, M.; Dayde, J. Use of simplified HPLC-UV analysis soyasaponin B determination: study of saponin and isoflavones variability in soybean cultivars and soy-based health food products. *J. Agric. Food Chem.* **2005**, *53*, 3923−3930.
(14) Murphy, P. A.; Hu, J.; Barua, K.; Hauck, C. C. Group B saponins in soy product in the U.S. Department of Agriculture-Iowa State University isoflavone database and their comparison with isoflavone contents. *J. Agric. Food Chem.* **2008**, *56*, 8534−8540.
(15) Tsukamoto, C.; Shimada, S.; Igita, K.; Kudou, S.; Kokubun, M.; Okubo, K.; Kitamura, K. Factors affecting isoflavones content in soybean seeds: changes in isoflavones, saponins and composition of fatty acids at different temperatures during seed development. *J. Agric. Food Chem.* **1995**, *43*, 1184−1192.
(16) Hu, J.; Lee, S. K.; Hendrich, S.; Murphy, P. A. Quantification of the group B soyasaponins by high performance liquid chromatography. *J. Agric. Food Chem.* **2002**, *50*, 2587−2594.
(17) Kim, S. L.; Berhow, M. A.; Kim, J. T.; Chi, H. Y.; Lee, S. J.; Chung, I. M. Evaluation of soyasaponin, isoflavone, protein, lipid, and free sugar accumulation in developing soybean seeds. *J. Agric. Food Chem.* **2006**, *54*, 10003−10010.
(18) Huang, S. S.; Han, Y. P.; Li, C. S.; Tian, J.; Li, W. B.; Wang, J. A. Identification of QTLs associated with total soyasaponin content in soybean [*Glycine max (L.)* Mer]. *J. Integrative Agric.* **2012**, *11*, 1976−1984.
(19) Jang, E. K.; Piao, X.; Hwang, T. Y.; Kim, S. L.; Chung, G. H.; Tsukamato, C.; Choi, Y. M.; Lee, M. C.; Lee, J.; Kim, H. S. Variation of saponin content in Korean native soybean landraces reintroduced from USA to Korea. *Korean J. Crop Sci.* **2012**, *57*, 286−295.
(20) Rupasinghe, H. P.V.; Jackson, C. J. C.; Poysa, V.; Berardo, C. D.; Bewley, J. D.; Jenkinson, J. Soyasapogenol A& B distribution in soybean [*Glycine max L.* Merr.] in relation to seed physiology, genetic variability and growing location. *J. Agric. Food Chem.* **2003**, *51*, 5888−5894.
(21) Szakiel, A.; Paczkowski, C.; Henry, M. Influence of environmental abiotic factors on the content of saponins in plants. *Phytochem. Rev.* **2011**, *10*, 471−491.
(22) Shimoyamada, M.; Okubo, K. Variation in saponin contents in germinating soybean seeds and effect of light irradiation. *Agric. Biol. Chem.* **1991**, *55*, 577−579.
(23) Eswaranandam, S.; Salyer, J.; Chen, P.; Lee, S. K. Effect of elicitor spray at different reproductive stages on saponin content of soybean. *J. Food Sci.* **2012**, *77*, 81−86.
(24) Schwarzbach, A.; Schreiner, M.; Knorr, D. Effect of cultivars and deep freeze storage on saponin content of white asparagus spears (*Asparagus officinalis* L.). *Eur. Food Res. Technol.* **2006**, *222*, 32−35.
(25) Soliz-Guerrero, J. B.; Rodriguez, D. J.; Rodriguez-Garcia, R.; Angulo-Sanchez, J. L.; Mendez-Padilla, G. Quinoa Saponins: Concentration and Composition Analysis. In *Trends in New Crops and New Uses*; Janick, A., Whipkey, A., Eds.; ASHS Press: Alexandria, VA, 2002; pp 110−114.
(26) Seguin, P.; Turcotte, P.; Tremblay, G.; Pageau, D.; Liu, W. Tocopherols concentration and stability in early-maturing soybean genotypes. *Agron. J.* **2009**, *101*, 1153−1159.
(27) Seguin, P.; Tremblay, G.; Pageau, D.; Liu, W. Soybean tocopherol concentrations are affected by crop management. *J. Agric. Food Chem.* **2010**, *58*, 5495−5501.
(28) Seguin, P.; Tremblay, G.; Pageau, D.; Liu, W.; Turcotte, P. Soybean lutein concentration: impact of crop management and genotypes. *Crop Sci.* **2011**, *51*, 1151−1160.
(29) CRAAQ (Centre de Référence en Agriculture et Agro-alimentaire du Québec). *Guide Soya*; CRAAQ: Sainte-Foy, QC, Canada, 2001.
(30) Chennupati, P.; Seguin, P.; Liu, W. Effects of high temperature stress at different development stages on soybean isoflavones and tocopherol concentrations. *J. Agric. Food Chem.* **2011**, *59*, 13081−13088.
(31) Fehr, W. R.; Caviness, C. E.; Burmood, D. T.; Pennington, J. S. Stages of development descriptions for soybeans [*Glycine max (L.)*. Merrill]. *Crop Sci.* **1971**, *11*, 929−931.
(32) SAS Institute. *SAS User Manual*, V.9.1; SAS Institute: Cary, NC, 2003.
(33) McIntosh, M. S. Analysis of combined experiments. *Agron. J.* **1983**, *75*, 153−155.
(34) Francis, T. R.; Kannenberg, L. W. Yield stability studies in short season maize. I: A descriptive method for grouping genotypes. *Can. J. Plant Sci.* **1978**, *58*, 1029−1034.
(35) Al-Tawaha, A. M.; Seguin, P.; Smith, D. L.; Beaulieu, C. Foliar application of elicitors alters isoflavone concentrations and other seed characteristics of field-grown soybean. *Can. J. Plant Sci.* **2006**, *86*, 677−684.
(36) Akagi, I.; Nishihara, M.; Ueda, S.; Yokoyama, A.; Saeki, Y. Effect of late sowing on the isoflavone content of soybean seed in southern Kyushu. *Jpn. J. Crop. Sci.* **2009**, *78*, 250−254.
(37) Morrison, M. J.; Cober, E. R.; Saleem, M. F.; McLaughlin, N. B.; Fregeau-Reid, J.; Ma, B. L.; Woodrow, L. Seasonal changes in temperature and precipitation influence isoflavone concentration in short season soybean. *Field Crop Res.* **2010**, *117*, 113−121.
(38) Chennupati, P.; Seguin, P.; Chamoun, R.; Jabaji, S. H. Effects of high-temperature stress on soybean isoflavones concentration and expression of key genes involved in isoflavone synthesis. *J. Agric. Food Chem.* **2012**, *60*, 12421−12427.
(39) Sayama, T.; Ono, E.; Takagi, K.; Takada, Y.; Horiwaka, M.; Nakamoto, Y.; Hirose, A.; Sasama, H.; Ohashi, M.; Hasegawa, H.; Terakawa, T.; Kikuchi, A.; Kato, S.; Tatsuzaki, N.; Tsukamoto, C.; Ishimoto, M. The Sg-1 glycosyltransferase locus regulates structural diversity of triterpenoid saponins of soybean. *Plant Cell.* **2012**, *24*, 2123−2138.

phenolics in IADFP-CP and (ii) to explore the effects of ultrafine grinding on the antioxidant capacity and phenolic composition of IADFP-CP.

MATERIALS AND METHODS

Materials and Chemicals. Fresh citrus (*Citrus junos* Sieb. ex Tanak) pomace was gifted by the Citrus Research Institute of the Chinese Academy of Agricultural Sciences (Chongqing, China). Chlorogenic acid, ferulic acid, caffeic acid, sinapic acid, gallic acid, naringenin, hesperitin, naringin, hesperidin, and kaempferol (>98.0%) were purchased from Chengdu Biopurify Phytochemicals Co. Ltd. (Chengdu, China). (±)-6-Hydroxy-2,5,7,8-tetramethylchroman-2-carboxylic acid (trolox) and 2,4,6-tris(2-pyridyl)-1,3,5-triazine (TPTZ) were obtained from Sigma-Aldrich Co. Ltd. (Shanghai, China). 2,2-Diphenyl-1-picrylhydrazyl (DPPH) was purchased from Wako Pure Chemical Industries, Co. Ltd. (Tokyo, Japan). Methanol, acetonitrile, ammonium acetate, hexyl hydride, and ethyl acetate of HPLC grade were purchased from Merck Co. Ltd. (Darmstadt, Germany).

IADFP-CP Preparation. After the removal of seeds, fresh citrus pomace was shredded and immediately immersed in a water bath at 90 °C for 30 s to inactivate enzymes; then it was filtered, air-dried (65 °C, 48 h), and ground in a high-speed pulverizer (YS-103, Yongli Pharmaceutical Machinery Co. Ltd., Wenzhou, China) to pass through a 40-mesh sieve. After the resultant powder (350 g) had been defatted in 1.0 L of anhydrous ethanol at room temperature for 1 h, the solid part was recovered by filtering through four layers of cotton gauze. Then it was air-dried at 65 °C for 30 min to remove the solvent. The dried powder was subjected to the removal of soluble components by immersing it in 11.5 L of distilled water at 60 °C for 1 h with continuous stirring. The insoluble fraction was pelleted by centrifuging the suspension at 4000 rpm for 10 min. The pellet was air-dried (60 °C for 48 h) to achieve a moisture content below 6%, and the IADFP-CP was obtained. The dried IADFP-CP was subjected to ordinary grinding, which was performed with a YS-103 high-speed pulverizer. The pulverization process lasted for 3 min.

Ultrafine Grinding of IADFP-CP. The powder obtained by ordinary grinding was used as the starting material for ultrafine grinding (mechanical grinding and jet grinding). The mechanically ground IADFP-CP was prepared in a YSC-701 micronizer (Yanshanzhengde Co. Ltd., Beijing, China) for 8 min by operating the lapping wheel and fan at 4500 and 3500 rpm, respectively. To perform jet grinding, a CBF-250 jet mill (Chengdu, China) was applied and operated at the following parameters: compressor power, 210 kW; nozzle speed, 1 Mach; and rotational speed of classifier, 2100 rpm. The powders obtained by ordinary grinding, mechanical grinding, and jet grinding were denoted by OGP, MGP, and JGP, respectively. All powders were hermetically packaged in plastic bags and stored at room temperature in a brown desiccator with oxygen scavenger until analysis. The particle size was measured with a Mastersizer 2000 E laser particle size analyzer (Malvern Instruments Ltd., UK). In terms of average particle size ($D_{0.5}$), OGP, MGP, and JGP presented particle sizes of 347.25, 59.56, and 24.09 μm, respectively.

Determination of Proximate Composition. Ash, crude fat, and crude protein were determined using AOAC methods.[20] Total sugar was determined by anthrone colorimetry.[21]

HPLC Analysis of Phenolic Extracts. Free and bound phenolics in IADFP-CPs were extracted according to the method previously reported by Okarter et al.[22]

Free phenolics were extracted by blending the powder (1 g) with 50 mL of 80% chilled acetone for 10 min. After centrifugation at 4500 rpm for 10 min, the supernatant was removed. The residues were re-extracted as done for the powder. The supernatants were combined and evaporated at 45 °C to dryness. The remainder was made up to 25 mL with methanol, filtered through 0.45 μm nylon membrane, and frozen at −80 °C until analysis.

Bound phenolics were extracted with the residue from the free phenolic extraction as starting material. The residue was first digested with 2 mol/L sodium hydroxide at room temperature for 1 h while shaking under nitrogen. The mixture was then neutralized with concentrated hydrochloric acid. Hexanes were used to remove lipids in the mixture. The remaining mixture was then successively extracted with ethyl acetate (20 mL with 5 min) five times. The ethyl acetate fractions were combined and evaporated at 45 °C to dryness. The phenolics were reconstituted in 25 mL of methanol, filtered through 0.45 μm nylon membrane, and frozen at −80 °C until analysis.

The determination of phenolics in the extracts was conducted on an Agilent 1260 HPLC (Agilent Technologies, USA) equipped with a diode array detector (DAD). The UV−vis spectra of phenolics were recorded in the range 190−600 nm at an acquisition rate of 2.0 s (peak width = 0.1 min). The phenolics were separated by a reverse phase Thermo BDS Hypersil C18 column (250 × 4.6 mm i.d.; 5 μm) at 30 °C with the mobile phase consisting of A (0.1% ammonium acetate) and B (acetonitrile) at a flow rate of 0.8 mL/min. A linear gradient program was used: 0−3 min, 10% B; 3−15 min, 10−30% B; 15−35 min, 30−50% B; 35−45 min, 50−90% B; 45−48 min, 90−10% B; 48−55 min, 10% B. Each sample injection volume was 20 μL. Absorbance at 280 nm was applied to quantify the eluted phenolics. When a reference compound was not available, the calibration of a structurally related compound was employed with a molecular weight correction factor.[23] The HPLC method applied in the present study was validated and given acceptable values in the correlation coefficients of calibration curves ($R^2 \geqslant 0.9990$) and recovery (⩾80.6%) (Table S1 in the Supporting Information).

Identification of Phenolics by RP-HPLC-DAD/ESI-Q-TOF-MS/MS. To identify phenolics in the extracts, an Agilent 1290 HPLC (Agilent Technologies, Santa Clara, CA, USA) equipped with a binary pump (G4220A), a column compartment (G1316C), a DAD (G4212A), and an autosampler (CTCPAL) was coupled to an Agilent 6540 Q-TOF-MS/MS and applied in the present study. The RP-HPLC-DAD was operated with parameters as described above. The effluent from the column was split using a T-type phase separator before being introduced into the mass spectrometer (split ratio = 1:3). The dual electrospray ionization (ESI) source of the MS was operated in negative mode. Mass spectra were recorded across the m/z range of 100−1100 (scan rate, 1.00 spectra/s). The operating conditions of Q-TOF-MS were as follows: desolvation gas (N_2) temperature, 350 °C; desolvation gas flow rate, 480 L/h; nebulizer, 35 psig; capillary voltage, 3500 V; fragmentor voltage, 125 V; skimmer voltage, 65 V; Oct RFV, 750 V. The parameters of Q-TOF-MS/MS were the same as those for Q-TOF-MS except that the first quadrupole served as a mass filter and the sample injection volume was set as 10 μL. The mass spectra of all analytes were recorded at four collision energies: 10, 20, 30, and 40 V. The mass spectrum with a medium abundance for $[M - H]^-$ and high abundances for ionized fragments was selected and used to identify analytes. The whole system was controlled by MassHunter workstation software (B.05.00, Agilent Technologies).

Antioxidant Capacity of IADFP-CP. *DPPH Radical Scavenging Capacity (DPPH-RSC) Assay.* The DPPH-RSC of IADFP-CP was determined according to the method described by Gadow et al. with some modifications.[24] Briefly, 20 mg of IADFP-CP was weighed into a 10 mL centrifuge tube, and then 3.5 mL of methanol containing DPPH radicals (6×10^{-5} mol/L) was added. The tube was tightly capped and vortexed vigorously for 3 min and repeated twice with a 10 min interval. Then, it was subjected to centrifugation at 10000 rpm for 2 min. The control was prepared by replacing the phenolic extract with the same volume of methanol. The absorbance of the supernatant was recorded at 517 nm using a visible spectrophotometer (722, Shanghai Modern Science Spectral Instrument Co. Ltd., Shanghai, China) against the control. The measurement was performed in the dark and completed within 30 min. Results were expressed as micromoles of trolox equivalent (TE) per 100 g of dw of IADFP-CP.

Ferric Reducing Antioxidant Power (FRAP) Assay. The FRAP of IADFP-CP was determined with the procedure described by Benzie et al. with some modifications.[25] In detail, a fresh FRAP working solution was prepared by blending 25 mL of 300 mmol/L acetate buffer (pH 3.6), 2.5 mL of 10 mmol/L TPTZ in 40 mmol/L hydrochloric acid, and 2.5 mL of 20 mmol/L ferric chloride. To obtain an acceptable decoloring rate for FRAP assay, IADFP-CP was diluted with microcrystalline cellulose at a ratio of 1:4 (w/w). The diluted

Table 1. Proximate Composition and Phenolics in Insoluble Antioxidant Dietary Fiber Powders from Citrus Pomace[a]

component	OGP (g/100 g dw)	MGP (g/100 g dw)	JGP (g/100 g dw)
ash	3.07 ± 0.08b	3.15 ± 0.15b	3.10 ± 0.09b
crude fat	2.31 ± 0.10b	6.22 ± 0.27c	10.33 ± 0.97d
crude protein	5.28 ± 0.18c	4.99 ± 0.24bc	4.67 ± 0.18b
total sugar	2.71 ± 0.12b	2.78 ± 0.12b	3.19 ± 0.16c
free phenolics	1250.41 ± 16.26c	1022.01 ± 7.01b	1412.74 ± 10.95d
bound phenolics	589.69 ± 9.46c	680.01 ± 9.59d	483.46 ± 3.26b
total phenolics	1845.10 ± 25.72c	1712.01 ± 16.76b	1894.2 ± 13.21c

[a]Data in the same row bearing different lower case letters are significantly different ($p < 0.05$). OGP, ordinary-ground powder; MGP, mechanical-ground powder; JGP, jet-ground powder.

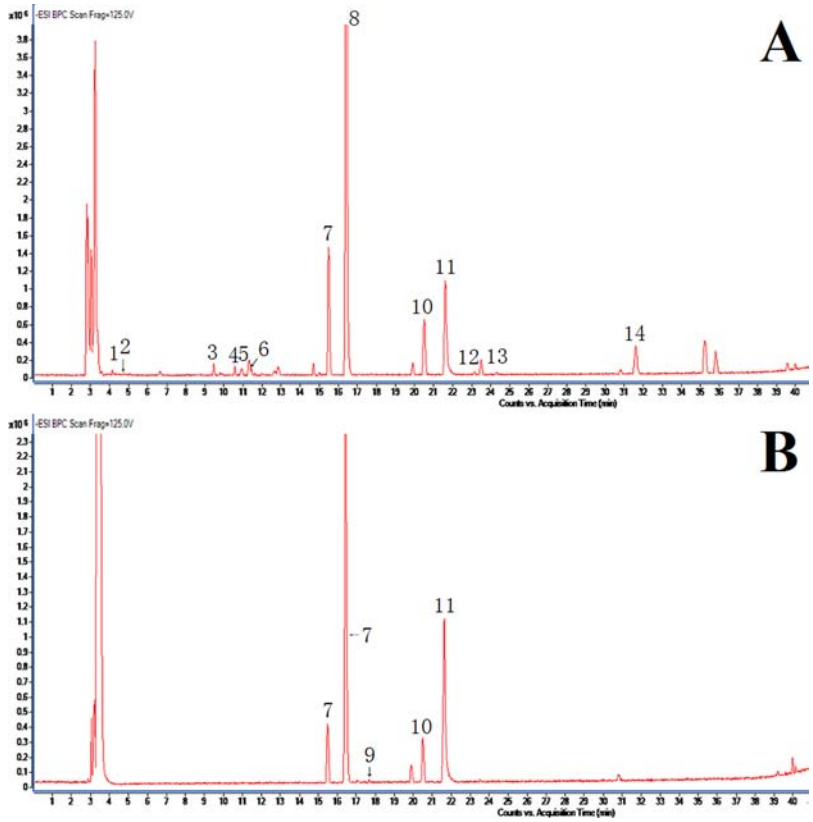

Figure 1. Base peak chromatograms of free (A, jet grinding) and bound (B, mechanical grinding) phenolics in insoluble antioxidant dietary fiber powders from citrus pomace.

IADFP-CP (20 mg) was weighed into a 10 mL centrifuge tube and then 3.5 mL of fresh FRAP working solution was added. The suspension was shaken and kept in a water bath at 37 °C for 5 min, followed by centrifugation at 10000 rpm for 5 min. The absorbance of the resultant supernatant was monitored at 593 nm using a 722 visible spectrophotometer against FRAP working solution. All solutions were used on the day of preparation. Results were expressed as micromoles of $FeSO_4{\cdot}7H_2O$ equivalent (FE) per 100 g of dw of IADFP-CP.

Antioxidant Capacity of Phenolic Extracts. The DPPH and FRAP assays of free and bound phenolic extracts were performed as done with IADFP-CP by omitting vortex and centrifugation treatments.

Statistical Analysis. Results were presented as the mean value ± standard deviation (SD) of triplicate determinations. ANOVA and LSD comparison tests were performed to identify differences between values using SPSS (version 19.0, SPSS Inc., Chicago, IL, USA). Significant differences were declared at $p < 0.05$.

RESULTS AND DISCUSSION

Proximate Composition of IADFP-CP. The proximate composition of IADFP-CP is presented in Table 1. In contrast to ordinary grinding, mechanical grinding generated significant effects only on the contents of crude fat and free, bound, and total phenolics ($p < 0.05$), but jet grinding presented significant changes in the contents of crude fat, crude protein, total sugar, and free and bound phenolics ($p < 0.05$). The contents of crude fat, total sugar, free, and bound and total phenolics in MGP and JGP were significantly different ($p < 0.05$). With regard to the increases in crude fat induced by MGP and JGP and in total sugar induced by JGP, the increases in their extraction efficiencies from micronized powders were assumed to be factual. Ultrafine grindings effectively disrupted the cell structure of the citrus pomace and substantially increased the specific surface of IADFP-CP.[18] The images of IADFP-CP recorded by scanning electron microscope confirmed this fact (Figure S1 in the Supporting Information). Furthermore, the

Table 2. Retention Time, Identification, UV Spectra, Mass Spectrometric Data, and Source of Phenolic Compounds in Insoluble Antioxidant Dietary Fiber Powders from Citrus Pomace

peak	t_R[a] (min)	identity	DAD λ_{max} (nm)	MW[b]	$[M-H]^-$[c] (m/z)	fragment ion (m/z)	source[d]	ref
1	4.2	chlorogenic acid[e]	325	354.1	353.1	191.1; 85.1; 93.1; 161.1; 127.1	FO, FM, FJ	
2	4.6	ferulic acid[e]	322	194.0	193.0	134.0; 178.1; 117.1; 106.1; 149.1	FO, FM, FJ	
3	9.5	kaempferol rutinoside isomer I	283	594.2	593.2	285.0; 309.0; 338.0; 351.0	FO, FM, FJ	26
4	10.5	galloyl HHDP[f] glucoside isomer	284	650.4	649.4	605.7; 347.2; 283.3; 255.3; 236.9	FO, FM, FJ	26
5	11.2	sinapoyl hexoside derivative	224, 267, 334	449.2	448.2	162.0; 223.1; 385.2; 445.2	FO, FM, FJ	27
6	11.5	sinapic acid derivative	223, 272	762.8	761.8	726.0; 696.0; 290.9; 487.0; 264.8	FO, FM, FJ	28
7	15.5	naringin[e]	282	580.0	579.0	460.0; 271.1; 151.1; 119.1	FO, FM, FJ, BO, BM, BJ	
8	16.4	hesperidin[e]	217, 280	610.0	609.0	301.1; 286.3	FO, FM, FJ, BO, BM, BJ	
9	17.7	hesperidin isomer[e]	217, 280	610.0	609.0	301.1; 286.3	BO, BM	
10	20.5	kaempferol rutinoside isomer II	203, 283	594.2	593.2	285.0; 309.0; 338.0; 351.0	FO, FM, FJ, BO, BM, BJ	26
11	21.7	unknown	225, 282	294.2	293.2	236.1; 221.1; 71.0	FO, FM, FJ, BO, BM, BJ	
12	23.2	naringenin[e]	288	272.0	271.0	151.0; 119.1; 107.1; 177.1; 93.1	FO, FM, FJ	
13	24.2	hesperitin[e]	285	302.1	301.1	164.1; 286.1	FO, FM, FJ	
14	31.6	feruloylquinic acid derivative	244, 328	530.2	529.2	154.9; 162.0; 204.9; 248.9; 366.6	FO, FM, FJ	29−31

[a] t_R, retention time. [b] MW, molecular weight. [c] $[M-H]^-$, quasi-molecular ion. [d] FO, free phenolics of ordinary-grinded IADFP-CP; FM, free phenolics of mechanical-grinded IADFP-CP; FJ, free phenolics of jet-grinded IADFP-CP; BO, bound phenolics of ordinary-grinded IADFP-CP; BM, bound phenolics of mechanical-grinded IADFP-CP; BJ, bound phenolics of jet-grinded IADFP-CP. [e] Confirmed with standards. [f] HHDP, hexahydroxydiphenoyl.

results implied that jet grinding was more effective in promoting extraction efficiencies than mechanical grinding, which can be explained by the smaller particle size of JGP (24.09 ± 0.67 μm) than of MGP (59.56 ± 0.66 μm).

Identification of Phenolics. The chromatographic profiles of free (jet grinding) and bound (mechanical grinding) phenolics in IADFP-CP are shown in Figure 1 (for the other four profiles see the Supporting Information, Figure S2). The RP-HPLC-Q-TOF-MS/MS in negative ionization mode allowed the separation and tentative identification of 14 phenolics (9 free, peaks 1−6 and 10−14; 1 bound, peak 9; and 4 free/bound, peaks 7, 8, 10, and 11) in IADFP-CP (Figure S3 in the Supporting Information). The retention time (t_R), molecular weight (MW), quasi-molecular ion $[M-H]^-$, and MS/MS fragment ions for each phenolic compound are summarized in Table 2. Among them, six phenolics including chlorogenic acid (peak 1), ferulic acid (peak 2), naringin (peak 7), hesperidin (peak 8), naringenin (peak 12), and hesperitin (peak 13) were identified using authentic reference compounds. Another eight detected phenolics were tentatively identified by comparing their UV−vis and mass spectra data with the literature data.

Peak 3 and 10, showing an $[M-H]^-$ ion at m/z 593.2 and MS/MS fragment ions at m/z 285.0, 309.0, 338.0, and 351.0, were observed at 9.5 and 20.5 min, respectively. The MS/MS fragment ion at m/z 309 could be assigned as a rutinosyl group.[26] However, fragment ions of glucosyl (−162 amu) or rhamnosyl (−146 amu) groups were absent in the MS/MS chart. In addition, the DAD profiles of peaks 3 and 10 were more similar to that of kaempferol than to that of luteolin. According to the evidence above, peaks 3 and 10 were assigned as kaempferol rutinoside isomers I and II, respectively.

For the identification of peak 4, the deprotonated molecule at m/z 649.4 was in agreement with the data of laggerstannin C (galloyl HHDP glucoside) reported in the literature.[26] Moreover, the MS/MS fragment ions at m/z 605.7 and 283.3 of the peak were in agreement with MS^3 fragment ion data of trisgalloyl HHDP glucoside.[26] Regrettably, the characteristic fragment ions of galloyl HHDP glucoside at m/z 301 and 497 have been not detected in the mass spectrum of peak 4. Thus, we tentatively characterized peak 4 as galloyl HHDP glucoside isomer.

Peak 5 at 11.2 min showed an $[M-H]^-$ ion at m/z 448.2 and MS/MS fragment ions at m/z 223.1, 162.0, and 385.2. According to the literature, the MS/MS fragment ion at m/z 223.1 resulted from the loss of a hexosyl unit (162.0 amu) from the sinapoyl hexoside moiety (385.2 amu).[27] Therefore, peak 5 was tentatively assigned as sinapoyl hexoside derivative.

Peak 6 at 11.5 min showed an $[M-H]^-$ ion at m/z 761.8. The MS/MS fragment ions at m/z 726, 487, and 290.9 were sinapic acid derivatives according to ref28. Moreover, the DAD profile of peak 6 was similar to that of sinapic acid. On the basis of their molecular ions, UV−vis spectra, and literature data, a sinapoyl unit was probably present in the compound, so peak 6 was assigned as a sinapic acid derivative.

Peak 9 at 17.7 min showed identical UV−vis spectra and identical $[M-H]^-$ ion (at m/z 609.0) and MS/MS fragment (at m/z 301.1, hesperitin) patterns to hesperidin. Because the retention time of peak 9 did not match the retention time of hesperidin (16.4 min), peak 9 was tentatively assigned as a hesperidin isomer.

Peak 11 (at 21.7 min), with an $[M-H]^-$ ion at m/z 293.2, was assigned as unknown. Although MS/MS fragments at m/z 236.1 (−57 amu, loss of $-C(CH_3)_3$) and m/z 221.1 (loss of a

dx.doi.org/10.1021/jf501646b | J. Agric. Food Chem. 2014, 62, 7166−7173

Table 3. Free and Bound of Phenolics in Insoluble Antioxidant Dietary Fiber Powders from Citrus Pomace As Affected by Grinding Methods[a]

compound	standards to quantify	free phenolics (mg/100 g dw)			bound phenolics (mg/100 g dw)		
		OGP	MGP	JGP	OGP	MGP	JGP
phenolic acids and their derivatives							
chlorogenic acid	chlorogenic acid	1.88 ± 0.03d	1.88 ± 0.05d	2.15 ± 0.25e	nd[b]	nd	nd
ferulic acid	ferulic acid	0.70 ± 0.14d	1.13 ± 0.13e	1.13 ± 0.23e	nd	nd	nd
galloyl HHDP[c] glucoside isomer	gallic acid	15.00 ± 0.19d	15.09 ± 0.13d	19.58 ± 0.90e	nd	nd	nd
sinapoyl hexoside derivative	sinapic acid	25.56 ± 1.06d	27.67 ± 0.84d	32.06 ± 0.57e	nd	nd	nd
sinapic acid derivative	sinapic acid	6.49 ± 0.26d	6.04 ± 0.11d	7.10 ± 0.49d	nd	nd	nd
unknown	sinapic acid	100.18 ± 3.11e	127.04 ± 1.26f	132.19 ± 1.76g	139.76 ± 1.80h	130.25 ± 4.33fg	76.59 ± 3.25d
feruloylquinic acid derivative	caffeic acid	18.02 ± 1.05d	19.85 ± 0.37d	20.04 ± 0.69d	nd	nd	nd
total (calculation)		167.83 ± 5.84g	198.7 ± 2.89f	214.25 ± 4.89f	139.76 ± 1.80f	130.25 ± 4.33e	76.59 ± 3.25d
flavanones and their derivatives							
naringin	naringin	113.20 ± 2.53g	144.18 ± 1.05h	184.30 ± 1.51i	41.75 ± 0.70e	53.00 ± 0.83f	36.07 ± 0.43d
hesperidin	hesperidin	891.33 ± 10.50g	583.68 ± 3.58f	927.93 ± 6.38h	355.35 ± 5.70d	464.43 ± 6.85e	338.73 ± 2.15d
hesperidin isomer	hesperidin	nd	nd	nd	26.13 ± 0.52e	1.16 ± 0.08d	nd
naringenin	naringenin	0.83 ± 0.10d	0.98 ± 0.28d	1.25 ± 0.28d	nd	nd	nd
hesperitin	hesperitin	0.85 ± 0.07d	0.97 ± 0.04d	1.73 ± 0.12e	nd	nd	nd
total (calculation)		1006.21 ± 13.21h	729.81 ± 4.88g	1115.21 ± 8.22i	423.23 ± 6.99e	518.59 ± 8.49f	374.81 ± 2.58d
flavonols and their derivatives							
kaempferol rutinoside isomer I	kaempferol	15.39 ± 0.32d	16.05 ± 0.18d	21.04 ± 0.58e	nd	nd	nd
kaempferol rutinoside isomer II	kaempferol	51.16 ± 0.75f	63.99 ± 2.02h	59.66 ± 1.5g7	25.09 ± 1.40d	31.15 ± 0.48e	29.71 ± 0.42e
total (calculation)		66.55 ± 1.17f	80.04 ± 2.22g	81.72 ± 2.25g	25.09 ± 1.40d	31.15 ± 0.48e	29.71 ± 0.42e

[a]Data in the same row bearing different lower case letters are significantly different ($p < 0.05$). OGP, ordinary-grinded powder; MGP, mechanical-grinded powder; JGP, jet grinded-powder. [b]nd, not detected. [c]HHDP, hexahydroxydiphenoyl.

methyl group from fragment at m/z 236.1) were observed, MS/MS fragments at m/z 236.1 and 221.1 were unclear. Therefore, peak 11 cannot be identified.

Peak 14 (at 31.6 min) showed an $[M - H]^-$ ion at m/z 529.2 and MS/MS fragments at m/z 154.9, 162, 204.9, 248.9, and 367, respectively. On the basis of the literature data, the fragment ion at m/z 367 resulted from the compound of peak 14 losing a caffeoyl moiety (−162 amu).[29,30] In addition, the MS/MS fragment ion at m/z 154.9 suggested the presence of a feruloyl moiety.[31] Therefore, the compound of peak 14 was assigned to feruloylquinic acid derivative.

Accordingly, phenolics in IADFP-CP mainly consisted of phenolic acids, flavonoids, and their derivatives. All phenolic acids were identified as hydroxycinnamic compounds, including chlorogenic acid (peak 1), ferulic acid (peak 2), sinapic acid derivative (peak 6), peak 11, and feruloylquinic acid derivative (peak 14). Two classes of flavonoids, including five flavanones (peaks 7−9, 12, and 13) and two flavonols (peak 3 and 10), have been characterized. Among the 14 phenolic compounds characterized in the present study, 7 (peaks 1, 2, 7−9, 12, and 13) identified phenolics were reported in citrus peel in the literature.[32−34]

Quantification of Phenolics. The quantitative results of free and bound phenolics in IADFP-CP are presented in Table 3. The free phenolic content (1022.01−1412.74 mg/100 g dw) was much higher than the bound phenolic content (483.46−680.01 mg/100 g dw) in IADFP-CP regardless of the grinding method. The study done by Oboh et al. revealed that the free phenolic content of citrus peels (6.5−13.1 mg/g) was significantly higher than the bound phenolic content (0.7−6.8 mg/g).[35] The total content of phenolic acids and their derivatives (328.95−290.84 mg/100 g) was much lower than that of flavonoids and their derivatives (1359.6−1600.42 mg/100 g). Among phenolic acids and their derivatives, peak 11 presented the highest abundance (257.29−208.78 mg/100 g) and was the unique bound phenolic acid derivative detected in all IADFP-CP samples. Meanwhile, in flavonoids and their derivatives, hesperidin (1048.11−1266.66 mg/100 g) was the most abundant monomer, which accounted for >70% (w/w) in both free and bound phenolics in all samples. It is well documented that flavonoids (mainly naringenin, hesperidin, naringin, and neohesperidin) were the predominant phenolics in citrus peels,[32] and their total content highly exceeded the content of phenolic acids by up to 10 times or more.[14,34] With regard to the effects of ultrafine grinding on free and bound phenolics in IADFP-CP, MGP and JGP presented a bound phenolic content comparable to that of OGP. Contrary to our expectations that the free phenolic content in IADFP-CP would be increased by ultrafine grinding, the free phenolic content in MGP was significantly lower than that in OGP. The possible

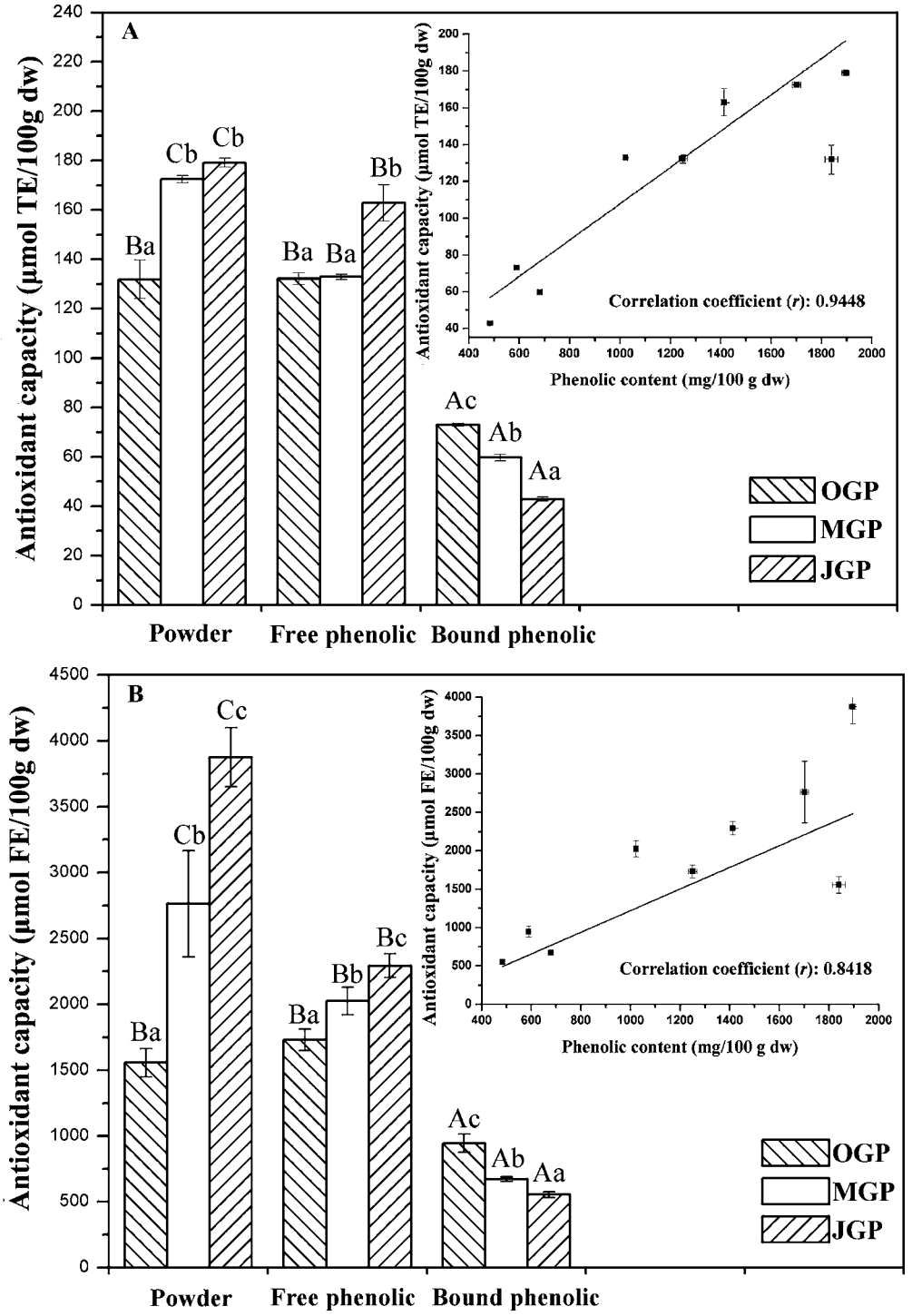

Figure 2. Antioxidant capacities (A, DPPH radical scavenging capacity; B, ferric reducing antioxidant power) of insoluble antioxidant dietary fiber powders from citrus pomace and their phenolic extracts as determined by the DPPH and FRAP assays. Columns bearing different lowercase letters (a–c) with the same sample form (powder, free and bound phenolic) were of significant differences ($p < 0.05$). Columns bearing different capital letters (A–C) with the same grinding method (ordinary (OG), mechanical (MG), and jet grindings (JG)) were of significant differences ($p < 0.05$).

explanation for the result would be the thermal damage of phenolics during mechanical grinding. This was evidenced by the fact that the free phenolic content in JGP was significantly greater than that in OGP. As reported, jet grinding is a good choice in producing thermally sensitive biomaterials. Jet grinding could produce impacting, colliding, and friction among materials by the energy of high-speed or steam and bring about less thermal energy (cavity temperature 32 °C in our study) compared with mechanical grinding.[18] Interestingly, the bound phenolic content in JGP was dramatically lower than that in OGP. Although the reasons for the result were not entirely understood, it is worthwhile noting that a redistribution of bound phenolics to free phenolics possibly happened during jet grinding.[33,36]

Antioxidant Capacity. Numerous studies demonstrated that the DPPH and FRAP assays are simple and cost-effective

dx.doi.org/10.1021/jf501646b | J. Agric. Food Chem. 2014, 62, 7166–7173

spectrophotometric methods to evaluate the potential antioxidant properties of biomaterials.[37,38] Therefore, they were applied in the present study to evaluate the antioxidant capacities of IADFP-CP and their phenolic extracts. The obtained results are presented in Figure 2.

With regard to DPPH-RSC (Figure 2A), in powder form, OGP, MGP, and JGP presented antioxidant values of 131.93, 172.44, and 179.12 μmol TE/100 g dw, respectively. By comparison, the DPPH-RSCs of MGP and JGP were significantly higher than the value of OGP, but no significant difference was observed between the values of MGP and JGP. Te effects of ultrafine grinding on the DPPH-RSC of free phenolics in IADFP-CP revealed that jet grinding significantly improved the antioxidant capacity, whereas mechanical grinding did not significantly change it. Commonly, the decrease in particle size of a powder could facilitate the extraction of antioxidants and increase their activity. This has been confirmed in numerous researche studies.[39,40] However, this law was not effective in comparing the DPPH-RSCs of OGP and MGP. MGP presented a significantly smaller particle size than OGP, but generated an antioxidant value equivalent to that of OGP. This discrepancy was possibly due to the thermal effects of mechanical grinding, which damaged the free phenolic components and thus deteriorated their antioxidant capacities.[18] Without exception, ultrafine grindings significantly decreased the antioxidant capacity of bound phenolics ($p < 0.05$). This should be related to the differences in total bound phenolics induced by the various grindings as mentioned above. With regard to FRAP (Figure 2B), similar results were obtained as with DPPH-RSC. Moreover, significant differences were observed between the antioxidant values of MGP and JGP powder and those from free phenolics in OGP and MGP.

The antioxidant capacity of OGP was lower than that of MGP and JGP, which may be due to the enhanced solubilization of antioxidants, including phenolic and nonphenolic substances, by the decrease in particle size.[19,41] The antioxidant capacities of both ultrafine grinding powders and their phenolic extracts followed the order of powder > free phenolic extract > bound phenolic extract. This sequence reflected that the antioxidant capacity of the powder came not only from its phenolic components but also from other nonphenolic components, such as carotenoids and Maillard compounds.[1] The differences in the antioxidant capacities of free and bound phenolic extracts could be explained by the higher phenolic content in free extracts than in bound extracts, which is reflected by the high correlation coefficients of the relationships between the antioxidant values and phenolic content ($r \geqslant 0.8418$) (Figure 2). Likewise, the DPPH-RSC ($r = 0.939$) and FRAP ($r = 0.906$) of 30 plant extracts were found highly dependent on their total phenolic contents.[42]

The free and bound phenolics in IADFP-CP and their changes induced by two kinds of ultrafine grindings (mechanical grinding and jet grinding) were first investigated in the present study. Fourteen phenolic compounds, mainly including phenolic acids, flavonoids, and their derivatives, were identified and quantified. The free phenolic content was much higher than the bound phenolic content in IADFP-CP. Hesperidin was identified as the component with the highest abundance, which accounted for >57% of total phenolics. As far as the protective effects on phenolics, the redistribution of bound phenolics to free phenolics, and the antioxidant capacity of powders were concerned, jet grinding was superior to mechanical grinding in producing IADFP-CP. For further research, the in vivo antioxidant activity of ultrafine ground IADFP-CP and their potential applications in food systems should be intensively addressed.

■ ASSOCIATED CONTENT

Ⓢ Supporting Information

Figures S1−S3 and Table S1. This material is available free of charge via the Internet at http://pubs.acs.org.

■ AUTHOR INFORMATION

Corresponding Author

*(G.Z.) Phone: +86 23 68 25 03 74. Fax: +86 68 25 19 47. E-mail: zhaogh@swu.edu.cn.

Funding

This work was supported by the National High-tech R&D Program (863 Program) of China (2011AA100805-2) and the National Natural Science Foundation of China (31371737).

Notes

The authors declare no competing financial interest.

■ ACKNOWLEDGMENTS

The citrus pomace was kindly supplied by the Citrus Research Institute of the Chinese Academy of Agricultural Sciences. We are grateful for the helpful assistance from Dr. Yong Tang (College of Food Science, Sichuan Tourism University) in jet grinding.

■ ABBREVIATIONS USED

ADF, antioxidant dietary fiber; DPPH, 2,2-diphenyl-1-picrylhydrazyl; DPPH-RSC, DPPH radical scavenging capacity; DF, dietary fiber; $[M - H]^-$, deprotonated molecule; dw, dry weight; FEAC, $FeSO_4 \cdot 7H_2O$ equivalent antioxidant capacity; FRAP, ferric reducing antioxidant power; GAE, gallic acid equivalent; HHDP, hexahydroxydiphenoyl; IADFP-CP, insoluble antioxidant dietary fiber powder from citrus pomace; IDF, insoluble dietary fiber; JGP, jet ground powder; MGP, mechanical grinded powder; MW, molecular weight; OGP, ordinary ground powder; t_R, retention time; TEAC, trolox equivalent antioxidant capacity

■ REFERENCES

(1) Saura-Calixto, F. Dietary fiber as a carrier of dietary antioxidants: an essential physiological function. *J. Agric. Food Chem.* **2011**, *59* (1), 43−49.

(2) Saura-Calixto, F. Antioxidant dietary fiber product: a new concept and a potential food ingredient. *J. Agric. Food Chem.* **1998**, *46* (10), 4303−4306.

(3) Martinez-Tome, M.; Murcia, M. A.; Frega, L.; Ruggirei, S.; Jimenez, A. M.; Roses, F.; Parras, P. Evaluation of antioxidant capacity of cereal brans. *J. Agric. Food Chem.* **2004**, *52* (15), 4690−4699.

(4) Jiménez-Escrig, A.; Rincón, M.; Pulido, R.; Saura-Calixto, F. Guava fruit (*Psidium guajava* L.) as a new source of antioxidant dietary fiber. *J. Agric. Food Chem.* **2001**, *49* (11), 5489−5493.

(5) Sanchez-Alonso, I.; Borderias, J.; Larsson, K.; Undeland, I. Inhibition of hemoglobin-mediated oxidation of regular and lipid-fortified washed cod mince by a white grape dietary fiber. *J. Agric. Food Chem.* **2007**, *55* (13), 5299−5305.

(6) Vitaglione, P.; Napolitano, A.; Fogliano, V. Cereal dietary fiber: a natural functional ingredient to deliver phenolic compounds into the gut. *Trends Food Sci. Technol.* **2008**, *19* (9), 451−463.

(7) Herrera, E.; Jimenez, R.; Aruoma, O. I.; Hercberg, S.; Sanchez-Garcia, I.; Fraga, C. Aspects of antioxidant foods and supplements in health and disease. *Nutr. Rev.* **2009**, *67* (Suppl.1), S140−S144.

(8) Fontana, A. R.; Antoniolli, A.; Bottini, R. Grape pomace as a sustainable source of bioactive compounds: extraction, characterization, and biotechnological applications of phenolics. *J. Agric. Food Chem.* **2013**, *61* (38), 8987−9003.
(9) He, X. J.; Liu, R. H. Phytochemicals of apple peels: isolation, structure elucidation, and their antiproliferative and antioxidant activities. *J. Agric. Food Chem.* **2008**, *56* (21), 9905−9910.
(10) Marín, F. R.; Soler-Rivas, C.; Benavente-García, O.; Castillo, J.; Pérez-Alvarez, J. A. By-products from different citrus processes as a source of customized functional fibers. *Food Chem.* **2007**, *100* (2), 736−741.
(11) Chantaro, P.; Devahastin, S.; Chiewchan, N. Production of antioxidant high dietary fiber powder from carrot peels. *LWT−Food Sci. Technol.* **2008**, *41* (10), 1987−1994.
(12) Crizel, T. d. M.; Jablonnski, A.; Rios, A. d. O.; Rech, R.; Flôres, S. H. Dietary fiber from orange byproducts as a potential fat replacer. *LWT−Food Sci. Technol.* **2013**, *53* (1), 9−14.
(13) Schieber, A.; Stintzing, F. C.; Carle, R. Byproducts of plant food processing as a source of functional compounds-recent developments. *Trends Food Sci. Technol.* **2001**, *12* (11), 401−413.
(14) Wang, Y. C.; Chuang, Y. C.; Hsu, H. W. The flavonoid, carotenoid and pectin content in peels of citrus cultivated in Taiwan. *Food Chem.* **2008**, *106* (1), 277−284.
(15) Lagha-Benamrouche, S.; Madania, K. Phenolic contents and antioxidant activity of citrus varieties (*Citrus sinensis* L. and *Citrus aurantium* L.) cultivated in Algeria: peels and leaves. *Ind. Crops Prod.* **2013**, *50*, 723−730.
(16) Anagnostopouloua, M. A.; Kefalas, P.; Papageorgiou, V. P.; Assimopoulou, A. N.; Boskou, D. Radical scavenging activity of various extracts and fractions of sweet citrus peel (*Citrus sinensis*). *Food Chem.* **2006**, *94* (1), 19−25.
(17) Chau, C. F.; Wang, Y. T.; Wen, Y. L. Different micronization methods significantly improve the functionality of carrot insoluble fibre. *Food Chem.* **2007**, *100* (4), 1402−1408.
(18) Zhao, X. Y.; Ao, Q.; Yang, L. W.; Yang, Y. F.; Sun, J. C.; Gai, G. S. Application of superfine pulverization technology in biomaterial industry. *J. Taiwan Inst. Chem. Eng.* **2009**, *40* (3), 337−343.
(19) Zhang, Z. P.; Song, H. G.; Peng, Z.; Luo, Q. N.; Ming, J.; Zhao, G. H. Characterization of stipe and cap powders of mushroom (*Lentinus edodes*) prepared by different grinding methods. *J. Food Eng.* **2012**, *109* (3), 406−413.
(20) AOAC. *Official Methods of Analysis of AOAC International*, 16th ed.; Cunniff, P., Ed.; AOAC International: Gaithersburg, MD, USA, 1995.
(21) Llobera, A.; Canñellas, J. Dietary fiber content and antioxidant activity of Manto Negro red grape (*Vitis vinifera*): pomace and stem. *Food Chem.* **2007**, *101* (2), 659−666.
(22) Okarter, N.; Liu, C. S.; Sorrells, M. E.; Liu, R. H. Phytochemical content and antioxidant activity of six diverse varieties of whole wheat. *Food Chem.* **2010**, *119* (1), 249−257.
(23) Chandra, A.; Rana, J.; Li, Y. Q. Separation, identification, quantification, and method validation of anthocyanins in botanical supplement raw materials by HPLC and HPLC-MS. *J. Agric. Food Chem.* **2001**, *49* (8), 3515−3521.
(24) Gadow, A. V.; Joubert, E.; Hansmann, C. F. Comparison of the antioxidant activity of aspalathin with that of other plant phenols of rooibos tea (*Aspalathus linearis*), α-tocopherol, BHT and BHA. *J. Agric. Food Chem.* **1997**, *45* (3), 632−637.
(25) Benzie, I. F. F.; Strain, J. J. The ferric reducing ability of plasma (FRAP) as a measure of "antioxidant powder": the FRAP assay. *Anal. Biochem.* **1996**, *239* (1), 70−76.
(26) Calani, L.; Beghè, D.; Mena, P.; Rio, D. D.; Bruni, R.; Fabbri, A.; Asta, C. D.; Galaverna, G. Ultra-HPLC-MS^n (poly)phenolic profiling and chemometric analysis of juices from ancient *Punica granatum* L. cultivars: a nontargeted approach. *J. Agric. Food Chem.* **2013**, *61* (23), 5600−5609.
(27) Pavlovic, A. V.; Dabic, D. C.; Momirovic, N. M.; Dojcinovic, B. P.; Milojkovic-Opsenica, D. M.; Tesic, Z. L.; Natic, M. M. Chemical composition of two different extracts of berries harvested in Serbia. *J. Agric. Food Chem.* **2013**, *61* (17), 4188−4194.
(28) Obied, H. K.; Song, Y.; Foley, S.; Loughlin, M.; Rehman, A.; Mailer, R.; Masud, T.; Agboola, S. Biophenols and antioxidant properties of Australian canola meal. *J. Agric. Food Chem.* **2013**, *61* (38), 9176−9184.
(29) Clifford, M. N.; Johnston, K. L.; Knight, S.; Kuhnert, N. Hierachical scheme for LC-MS^n identification of chlorogenic acids. *J. Agric. Food Chem.* **2003**, *51* (10), 2900−2911.
(30) Clifford, M. N.; Knight, S.; Kuhnert, N. Discriminating between the six isomers of dicaffeoylquinic acid by LC-MS^n. *J. Agric. Food Chem.* **2005**, *53* (10), 3821−3832.
(31) Kuhnert, N.; Jaiswal, R.; Matei, M. F.; Sovdat, T.; Sagar, D. How to distinguish between feruloyl quinic acids and isoferuloyl quinic acids by liquid chromatography/tandem mass spectrometry. *Rapid Commun. Mass Sepectrom.* **2010**, *24* (11), 1575−1582.
(32) Sawalha, S.; Arráez-Román, D.; Segura-Carretero, A. Quantification of main phenolic compounds in sweet and bitter citrus peel using CE-MS/MS. *Food Chem.* **2009**, *116* (2), 567−574.
(33) Xu, G. H.; Ye, X. Q.; Chen, J. C.; Liu, D. H. Effect of heat treatment on the phenolic compounds and antioxidant capacity of citrus peel extract. *J. Agric. Food Chem.* **2007**, *55* (2), 330−335.
(34) Bocco, A.; Cuvelier, M. E.; Richard, H.; Berset, C. Antioxidant activity and phenolic composition of citrus peel and seed extracts. *J. Agric. Food Chem.* **1998**, *46* (6), 2123−2129.
(35) Oboh, G.; Ademosun, A. O. Characterization of the antioxidant properties of phenolic extracts from some citrus peels. *J. Food Sci. Technol.* **2012**, *49* (6), 729−736.
(36) Li, B.; Xia, J.; Wang, Y.; Xie, B. J. Grain-size effect on the structure and antiobesity of konjac flour. *J. Agric. Food Chem.* **2005**, *53* (19), 7404−7407.
(37) Conde, E.; Moure, A.; Domínguez, H.; Gordon, M. H.; Parajó, J. C. Purified phenolics from hydrothermal treatments of biomass: ability to protect sunflower bulk oil and model food emulsions from oxidation. *J. Agric. Food Chem.* **2011**, *59* (17), 9158−9165.
(38) Nenadis, N.; Wang, L. F.; Tsimidou, M.; Zhang, H. Y. Estimation of scavenging activity of phenolic compounds using the ABTS$^{\bullet+}$ assay. *J. Agric. Food Chem.* **2004**, *52* (15), 4669−4674.
(39) Rosa, N. N.; Barron, C.; Gaiani, C.; Dufour, C.; Micard, V. Ultra-fine grinding increases the antioxidant capacity of wheat bran. *J. Cereal Sci.* **2013**, *57* (1), 84−90.
(40) Zhou, K.; Laux, J. J.; Yu, L. Comparison of Swiss red wheat grain and fractions for their antioxidant properties. *J. Agric. Food Chem.* **2004**, *52* (5), 1118−1123.
(41) Zhu, F. M.; Du, B.; Li, J. Effect of ultrafine grinding on physicochemical and antioxidant properties of dietary fiber from wine grape pomace. *Food Sci. Technol. Int.* **2014**, *20* (1), 55−62.
(42) Dudonné, S.; Vitrac, X.; Coutière, P.; Woillez, M.; Mérillon, J. M. Comparative study of antioxidant properties and total phenolic content of 30 plant extracts of industrial interest using DPPH, ABTS, FRAP, SOD, and ORAC assays. *J. Agric. Food Chem.* **2009**, *57* (5), 1768−1774.

oil (HCO60). Uptake of CoQ in mixed micelles generated during digestion across the brush border membrane (i.e., apical uptake) by Caco-2 human intestinal cells and the extent of transport of CoQ across the monolayer into the basolateral compartment (i.e., basolateral secretion) also were determined. This coupled model has been used previously to compare the micellarization and cellular uptake of ubiquinone from various formulations.[24] The bioaccessibility of ubiquinone was greater for supplements containing solubilized CoQ.

CoQ exists primarily as ubiquinol in extra-mitochondrial cellular compartments and in plasma. Reduction of ubiquinone to ubiquinol has been proposed to be dependent on the activities of a number of enzymes located in various cellular compartments. These include glutathione (GSH) reductase,[25] thioredoxin (Trx) reductase,[26] and NAD(P)H quinone oxidoreductase 1 (NQO1, also commonly referred to as DT-diaphorase)[27] among others. As these enzymes are components of antioxidant systems, it is likely that a balanced redox status is essential for maintaining the elevated ratio of ubiquinol to ubiquinone. The second objective of this study was to examine the effect of disruption of the redox imbalance on the apical uptake and basolateral secretion of CoQ by Caco-2 cells. Cellular redox balance was altered by either decreasing the cellular concentration of GSH or inhibiting the activity of thioredoxin (Trx) reductase in Caco-2 cells.

MATERIALS AND METHODS

Reagents. Ubiquinone, ubiquinol, and polyethylene glycol 60-linked hydrogenated castor oil (HCO60) were provided by Kaneka Corp., Japan. Fetal bovine serum, fungizone, penicillin−streptomycin, L-glutamine, and nonessential amino acids were purchased from Life Technologies Corp. (Grand Island, NY, USA). Bile extract, pepsin, lipase, and pancreatin were purchased from Sigma-Aldrich (St. Louis, MO, USA). All other reagents were purchased from ThermoFisher Scientific (Pittsburgh, PA, USA) unless otherwise indicated.

Preparation of HCO60 Enriched with CoQ. Briefly, 1 g of HCO60 in a 50 mL glass tube was melted at 60 °C in a water bath before the addition of 0.2 g of ubiquinone or ubiquinol. After mixing well and incubating for 10 min at 60 °C, glycerol (0.6 g) was added, and tubes were mixed and incubated for an additional 10 min. Then 1.0 g of the stock solution was transferred to a glass tube (20 mL) containing 7 mL of DI water at 60 °C, mixed well, and incubated for 10 min. Finally, aqueous CoQ solution (1 g) was diluted with hot water to 10 mL to yield yellow and colorless clear solutions of ubiquinone and ubiquinol, respectively. Stock solutions were prepared fresh for each experiment.

Simulated Digestion of CoQ-Enriched HCO60. Details for simulated gastric and small intestinal digestion have been described previously.[28] Initial experiments showed that partitioning of ubiquinol in the filtered aqueous fraction of chyme (i.e., samples at termination of small intestinal phase of simulated digestion) markedly exceeded that of ubiquinone. Thus, the concentration of ubiquinol in 2 mL of HCO60 added to 14.2 g of fat-free yogurt was decreased to generate aqueous fractions of chyme containing similar concentrations of CoQ (sum of ubiquinone + ubiquinol) as that in the aqueous fraction after digestion of HCO60 containing ubiquinone. The total amounts of yogurt, HCO60, ubiquinone, and ubiquinol for in vitro digestion were 2.0 ± 0.1 g, 25 mg, 7.1 μmol, and 2.5 μmol, respectively. α-Tocopherol (50 μmol/L) and ascorbic acid (500 μmol/L) also were added to all tubes containing CoQ-rich yogurt to limit oxidation of ubiquinol during digestion. The efficiencies (%) of micellarization of CoQ during digestion of yogurt supplemented with 7.1 or 2.3 μmol of ubiquinol were similar (62.1 ± 1.8 vs 64.7 ± 3.1%, respectively, $p = 0.197$). Aliquots of the predigestion mixture of yogurt supplemented with CoQ-rich HCO60 (2 mL), after completion of the simulated small intestinal phase of digestion, and filtered (0.2 μm pores) aqueous fraction (2 mL) of chyme were transferred immediately to glass tubes containing 2 mL of 5% potassium hexacyanoferrate(III) in PBS and mixed. Sealed tubes were incubated in a shaking water bath for 10 min at 37 °C at 85 rpm before extraction as described below. Replicate aliquots of starting material, chyme, and its aqueous fraction were transferred to empty glass tubes and immediately extracted. Extracts were analyzed by HPLC with a diode array detector. Ubiquinol content was calculated by the difference in the amount of ubiquinone in tubes lacking potassium hexacyanoferrate and total CoQ in tubes containing potassium hexacyanoferrate. Recovery of CoQ after digestion was calculated as nanomoles of total CoQ in chyme divided by total CoQ in the starting material multiplied by 100%. The efficiency of micellarization was calculated as total CoQ in the aqueous fraction of chyme divided by nanomoles of total CoQ in yogurt matrix multiplied by 100%.

CoQ Uptake and Transport by Caco-2 Cells. Caco-2 HTB37 cells were obtained from American Type Culture Collection (ATCC, Rockville, MD, USA) at passage 19 and maintained as previously described.[28] Cells (2.5×10^5) were seeded on membrane insets (3.0 μm pore diameter; EMD Millipore, Billerica, MA, USA) in six-well dishes. Washed monolayers (passages 20−26) were used for experiments 21−24 days after monolayers became confluent.

Filtered aqueous fraction of chyme generated during in vitro digestion of yogurt containing ubiquinone or ubiquinol solubilized in HCO60 was diluted 1:3 with DMEM (pH 6.5) containing 500 μmol/L phenol red along with oleate (1 mmol/L): taurocholate (0.5 mmol/L) micelles to induce chylomicron assembly and secretion.[29,30] Phenol red-free DMEM (3 mL) containing 1% FBS and 1% NEAA was added to the basolateral compartment. Cultures were incubated for 4 h before apical and basolateral media were collected. Monolayers were washed once with cold PBS containing 2 g/L albumin followed by two additional washes with cold PBS. Cell pellets were collected in cold PBS and centrifuged at 400 × *g* for 5 min at 4 °C. Cell pellets and basolateral medium were stored frozen under nitrogen gas at −80 °C overnight. CoQ uptake was calculated as follows: [(ubiquinone + ubiquinol) in cells of CoQ supplemented cultures − (endogenous ubiquinone + ubiquinol)] + [CoQ] in basolateral compartment. Endogenous CoQ content in monolayers of Caco-2 cells grown on membrane inserts to 21 days postconfluency was 220 ± 12 pmol/mg protein ($n = 10$) with ubiquinol representing 65 ± 2.0% of total CoQ ($n = 10$). To determine possible differences in retrotransport of newly acquired CoQ from medium prepared after digestion of yogurt with ubiquinone or ubiquinol, 100 μmol/L verapamil was added to both apical and basolateral medium to block Pgp-mediated efflux into the apical compartment. The cell monolayer was not adversely affected during the 4 h of incubation with this concentration of verapamil as assessed by phenol red flux from the apical to basolateral compartment and cell protein content per membrane insert.

The effects of altered GSH status and inhibition of Trx reductase activity in Caco-2 cells on uptake and transport of CoQ across the monolayer of Caco-2 cells also were examined to determine the impact of redox imbalance on CoQ flux. For these experiments, cells were treated with inhibitors as described below. Control and treated cells were incubated in DMEM with 500 μmol/L phenol red and Tween-40 micelles containing ubiquinone (80 ± 5 μmol/L) or ubiquinol (65 ± 3 μmol/L) and 10 μmol/L α-tocopherol were prepared as described elsewhere.[28] Apical medium also contained oleate (1.0 mmol/L), sodium taurocholate (0.5 mmol/L), and glycerol (50 μmol/L) to induce chylomicron assembly and secretion into the basolateral compartment.[29] Phenol red-free DMEM containing 1% FBS and 1% NEAA was added to the basolateral compartment. After 4 h, basolateral medium and washed monolayers were collected and extracted immediately for CoQ analysis.

Alteration of Glutathione Status of Caco-2 Cells. The protocol described by Noda et al.[31] was used to decrease the ratio of GSH to GSSG in cells to induce cell redox imbalance without oxidative stress. This involves pretreatment of monolayers with apical medium containing 5 mmol/L DL-buthioninesulfoximine (BSO) for 12.5 h and 30 μmol/L 1,3-bis(2-chloroethyl)-1-nitrosourea (BCNU) for 30 min. Then fresh DMEM containing BSO, BCNU, diamide (30 μmol/L), phenol red (500 μmol/L), Tween-40 micelles containing either

dx.doi.org/10.1021/jf5017829 | J. Agric. Food Chem. 2014, 62, 7174−7182

ubiquinone or ubiquinol, and taurocholate-oleate micelles was added to the apical compartment of cultures. Basolateral medium and washed monolayers were collected after 4 h. To quantify intracellular reduced (GSH) and oxidized (GSSG) glutathione, cell pellets were immediately suspended in ice-cold PBS (0.25 mL) containing an equal volume of 10% PCA and 1 mmol/L DTPA and disrupted with a hand-held homogenizer. Homogenate was centrifuged at 16,000 × *g* at 4 °C for 5 min. Acidified supernatant was collected and stored at −80 °C for glutathione analysis by HPLC-EC using a boron-doped diamond electrode.[32] GSH and GSSG were separated on a Shiseido C_{18} column (5 μm, 250 × 3.0 mm; Phenomenex, Torrance, CA, USA) with a C_{18} guard column containing the identical solid phase. Mobile phase was 6% acetonitrile in 25 mM sodium dihydrogen phosphate containing 1.4 mM 1-octanesulfonic acid, pH 2.5, at a flow rate of 1.0 mL/min. Areas under the curve for cell GSH and GSSG were compared with six-point standard curves using pure GSH and GSSG. GSH reductase activity was measured in cell homogenates by monitoring reduction of GSSG by NADPH coupled to the reaction of GSH with 5,5′-dithiobis(2-nitrobenzoic acid).[25]

Inhibition of Trx Reductase Activity in Caco-2 Cells. Auranofin (10 μmol/L) was added to DMEM containing Tween-40 micelles with CoQ and taurocholate-oleate micelles. This medium (2 mL) was added to the apical compartment of Caco-2 cells grown on membrane inserts. After 4 h of incubation, basolateral medium was collected to quantify CoQ transport across the monolayer. Trx reductase activity and redox status of CoQ in washed monolayers were analyzed to compare with cells identically treated in the absence of auranofin. Trx reductase activity was determined by monitoring the reduction of DTNB substrate in the absence versus in the presence of inhibitor at 412 nm (Thioredoxin Reductase Kit, Abnova, Walnut, CA, USA).

Analysis of Coenzyme Q by HPLC-DAD. CoQ was analyzed by HPLC-DAD as described by Okamoto et al.[33] Briefly, aliquots (1 mL) of either medium or cell pellets resuspended in PBS were extracted in glass tubes with 2 mL of ethanol followed by 6 mL of hexane. The mixture was vortexed for 60 s and centrifuged at 800 × *g* for 10 min at 4 °C. Supernatant was transferred to clean glass vial, and samples were re-extracted. Combined supernatant was dried under a stream of nitrogen gas, the film was resolubilized with 0.4 mL of MeOH/hexane (75:25), and 20−60 μL was injected onto the HPLC column. Because this method lacked sufficient sensitivity for accurate quantification of ubiquinol in cells and basolateral medium, ubiquinol was oxidized by the addition of an equal volume of 5% potassium hexacyanoferrate-(III). After incubation at 37 °C with shaking (85 rpm) for 10 min, ubiquinone was extracted into ethanol and hexane. Ubiquinone was separated on a Sunfire C_{18} column (5 μm, 4.6 × 250 mm; Waters) following elution from a Sunfire C_{18} guard column. Mobile phase was a mixture of methanol and hexane (75:25) flowing at a rate of 1.0 mL/min. Peak area was monitored at 275 nm. A standard curve was prepared for quantification with the limit of detection (signal-to-noise ratio of 5:1) being 58 nmol/L. Ubiquinol was calculated as the difference between total CoQ in samples incubated with potassium hexacyanoferrate and the quantity of ubiquinone in the absence of the oxidant.

Miscellaneous. Cell protein was determined by the bicinchoninic acid assay (Pierce Chemical Co.) using bovine serum albumin as standard. Mean cell protein per insert was 1.2 ± 0.05 mg and independent of the presence or absence of ubiquinone and ubiquinol in the apical compartment. Flux of phenol red from the apical to the basolateral compartment was determined by measuring absorbance at 546 nm at 15 s after the addition of 20 μL of 1 mol/L NaOH to 150 μL of basolateral medium at room temperature.[34]

Analysis of Data. Results are expressed as means ± SD for the number (*n*) of observations indicated. Statistical analyses were performed using Student's paired *t* test and one-way analysis of variance and Tukey's HSD (honestly significant difference). A minimum *p* value of 0.05 was used to determine statistically significant differences among means for all tests.

RESULTS AND DISCUSSION

Bioaccessibility of Ubiquinol Exceeds That of Ubiquinone. We previously reported that the efficiency of micellarization of ubiquinone during simulated digestion was greater for commercial formulations in which the coenzyme was solubilized by incorporation into either γ-cyclodextrin or oils containing emulsifiers.[24] Here ubiquinone and ubiquinol were solubilized in HCO60 to directly compare their micellarization during simulated digestion. HCO60 is polyethylene glycol 60 linked to hydrogenated castor oil and is used as an emulsifier for cosmetic and pharmaceutical formulations.[35,36] Hydroxystearic acid, the most abundant fatty acid in this preparation, appears to have a relatively high affinity for CoQ and the PEG60 moiety facilitates emulsification in the water matrix. Also, PEGylated oils have low toxicity, teratogenicity, and mutagenicity. Preliminary studies showed that the efficiency of micellarization of ubiquinol during the small intestinal phase of digestion of HCO60 added to yogurt was 2−3 times greater than that of ubiquinone. Thus, the concentration of ubiquinone in HCO60 was increased to generate mixed micelles containing similar amounts of ubiquinone and ubiquinol for investigating uptake and transport of CoQ by monolayers of differentiated Caco-2 cells (Table 1).

Table 1. Effect of Redox State of CoQ on Stability and Efficiency of Micellarization during Simulated Digestion of Yogurt Supplemented with Ubiquinone or Ubiquinol in PEG60 Hydrogenated Castor Oil Vehicle[a]

		ubiquinone-rich yogurt	ubiquinol-rich yogurt
starting material (CoQ-enriched yogurt)			
μmol of CoQ	total CoQ[b]	7.1 ± 0.1[a]	2.34 ± 0.05[b]
	ubiquinone	7.1 ± 0.1	0.58 ± 0.02
	ubiquinol	nd	1.78 ± 0.02
chyme generated during digestion			
μmol of CoQ	ubiquinone	5.84 ± 0.26	0.81 ± 0.02
	ubiquinol	nd	1.17 ± 0.03
recovery of CoQ (%)[c]		82.0 ± 3.7[a]	84.5 ± 1.6[a]
filtered aqueous fraction of chyme			
μmol of CoQ	ubiquinone	2.00 ± 0.05	0.66 ± 0.04
	ubiquinol	ND	0.86 ± 0.04
% ubiquinol		0	56.4 ± 2.5
% micellarization of CoQ[d]		28.1 ± 0.7[b]	65.0 ± 2.5[a]

[a]Data are the mean ± SD for four independent digestions. ND, not detected. Different letters in the same row indicate that means differ significantly ($p < 0.01$). [b]Total CoQ = ubiquinone + ubiquinol. [c]Percentage of total CoQ in chyme versus starting material. [d]Percentage of total CoQ in aqueous fraction of chyme versus starting material.

Recovery of ubiquinone after in vitro digestion of the yogurt containing the ubiquinone supplement was 82 ± 3.7% with 28% of the initial content of the coenzyme transferred to the aqueous fraction of chyme during the small intestinal phase of digestion (Table 1). All CoQ in the aqueous fraction, that is, the bioaccessibility, was ubiquinone. After digestion of the yogurt supplemented with ubiquinol, 84% of CoQ (ubiquinone + ubiquinol) in the food matrix was retained and 65% of initial content of CoQ partitioned in the bioaccessible fraction. Partial oxidation of ubiquinol occurred during both preparation of the ubiquinol-enriched yogurt and simulated digestion with

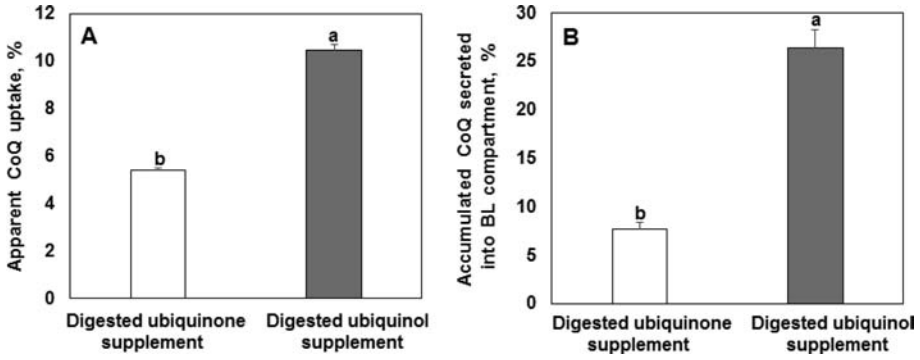

Figure 1. Apparent uptake of CoQ and secretion of the coenzyme into the basolateral compartment by Caco-2 cells incubated with aqueous fraction of chyme generated during digestion of yogurt containing either ubiquinone (20.0 nmol/well) or ubiquinol (15.2 nmol/well) supplement. Apparent uptake (A) represents the percentage of CoQ in the apical compartment present in cells (corrected for endogenous CoQ) and the basolateral compartment (B) of cultures of Caco-2 cells after 4 h of incubation. The percentage of CoQ accumulated by cells that was secreted into the basolateral medium was calculated by dividing the quantity of the coenzyme in the basolateral compartment by the corrected amount in cells plus the quantity in the basolateral compartment. Data are the mean ± SD, $n = 6$. Different letters above bars indicate that means differ significantly ($p < 0.01$).

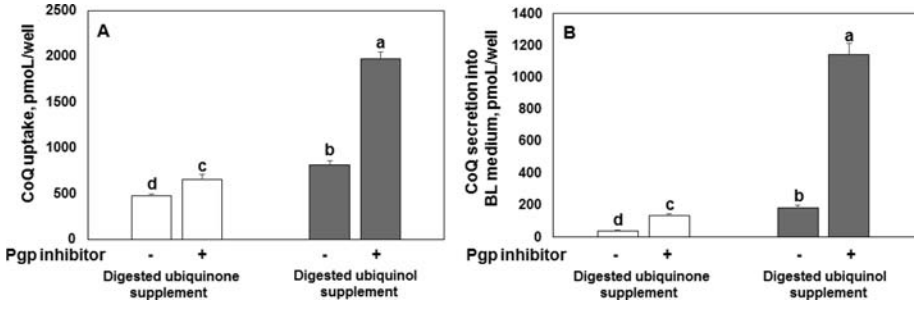

Figure 2. Inhibition of Pgp increases apparent uptake (A) and basolateral secretion (B) of ubiquinone and ubiquinol in apical medium. Caco-2 cells were treated with medium containing verapamil (100 μmol/L) in the apical and basolateral compartments for 30 min before addition of apical medium containing diluted aqueous fractions generated during digestion of yogurt supplemented with either ubiquinone. Apical medium contents of ubiquinone and ubiquinone were 12.8 and 12.3 nmol/well, respectively. Cultures were incubated for 4 h before collection of basolateral medium and washed cells. Data are the mean ± SD, $n = 3$. Different letters above bars indicate significantly ($p < 0.05$) different means.

ubiquinol, accounting for 59 and 56% of total CoQ in chyme and the filtered aqueous fraction, respectively. Nevertheless, the efficiency with which total CoQ partitioned in the aqueous fraction of chyme during digestion of the ubiquinol-supplemented yogurt was more than twice as great as that of CoQ after digestion of yogurt enriched with ubiquinone ($p < 0.001$). The similar recoveries of CoQ after digestion and its more efficient partitioning in the aqueous fraction of chyme demonstrated that solubilized ubiquinol has greater bioaccessibility than solubilized ubiquinone.

The extent of oxidation of ubiquinol during manual manipulations for solubilization in HCO, mixing in the yogurt food matrix, and simulated digestion likely exceeded that in standard commercial preparations of supplements and in situ digestion. The commercial form of ubiquinol is generally a soft-gel capsule. The content of the capsule is prepared in a deoxygenated environment under a blanket of inert gas before the soft-gel capsule shell is filled in the absence of air. These processes result in ≤2% oxidation of ubiquinol. Moreover, the shell of the soft-gel capsule has low oxygen permeability for ubiquinol to stabilize the reduced state until the capsule disintegrates in the stomach. Some oxidation of ubiquinol in the stomach and small intestine is possible as foods contain air and swallowing also introduces air into the stomach. However, oxygen diffuses from the gastrointestinal lumen into gut tissues, resulting in a decreasing oxygen gradient as chyme progresses from the stomach to the anaerobic environment in the colon.[37,38] Therefore, ubiquinol oxidation is expected to be lower in the commercial preparation of the delivery system and in situ environment than we observed in the laboratory.

Apical Uptake and Transepithelial Transport of CoQ by Caco-2 Cells from Micelles Generated during Digestion. Apical uptake of CoQ incorporated into mixed micelles during digestion of yogurt containing either ubiquinone or ubiquinol by Caco-2 cells and subsequent transfer of acquired CoQ to the basolateral compartment were determined. The quantities of CoQ in medium prepared with aqueous fraction of chyme after digestion of yogurt containing ubiquinone and ubiquinol were 20.0 ± 0.4 and 15.2 ± 0.4 nmol/well, respectively. Apparent uptake of CoQ from the apical compartment (%) was calculated as the corrected intracellular CoQ content (i.e., total CoQ minus endogenous CoQ) plus the quantity of CoQ in the basolateral compartment after 4 h of incubation. Apparent uptake of CoQ was twice as great for monolayers exposed to filtered aqueous fraction generated during digestion of yogurt enriched with ubiquinol as for cells incubated with aqueous fraction after digestion of yogurt supplemented with ubiquinone (Figure 1A). The corrected intracellular quantity of CoQ was 17% greater ($p < 0.001$) in cultures incubated with the filtered aqueous fraction of chyme after digestion of the ubiquinol supplement compared to the ubiquinone supplement (1.17 ± 0.02 vs 1.00 ± 0.04

dx.doi.org/10.1021/jf5017829 | J. Agric. Food Chem. 2014, 62, 7174−7182

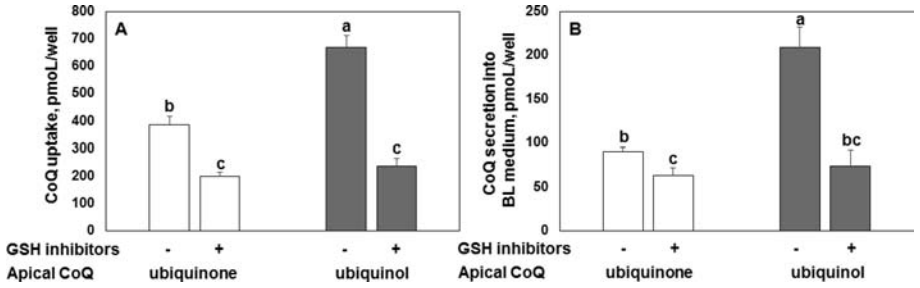

Figure 3. Altered cellular GSH status is associated with decreased apical uptake and basolateral secretion of CoQ. Caco-2 cells were incubated in the absence or presence of a cocktail of inhibitors of GSH synthesis and reduction as described under Materials and Methods. Apical medium containing ubiquinone (5.0 nmol/well) or ubiquinol (4.85 nmol/well) was added and cultures were incubated for 4 h. Data are the mean ± SD, $n = 6$. Different letters above bars indicate that means differ significantly ($p < 0.01$).

nmol/well, respectively). Ubiquinol accounted for 55% of intracellular pool of accumulated CoQ regardless of origin of the mixed micelles delivering CoQ. The quantity of CoQ secreted into basolateral medium was 5 times greater ($p < 0.0001$) in cultures incubated with micellar CoQ generated during digestion of ubiquinol-rich yogurt compared to CoQ incorporated into mixed micelles during digestion of ubiquinone-rich yogurt (0.42 ± 0.04 vs 0.08 ± 0.01 nmol CoQ/well). This represents 2.4-fold greater secretion of the quantity of the coenzyme apparently taken up by cells incubated with micelles generated during digestion of yogurt with ubiquinol compared to ubiquinone (Figure 1B). This difference was not associated with changes in barrier integrity of the monolayers as apical to basolateral flux of the paracellular marker phenol red was not significantly different for monolayers incubated with medium containing filtered aqueous fraction of chyme generated during digestion of yogurt enriched with either ubiquinone (86 ± 5 pmol/cm^2/h, $p = 0.4656$) or ubiquinol (87 ± 4 pmol/cm^2/h, $p = 0.3173$). These rates for paracellular transport of the dye were similar to that across monolayers of control cells, that is, 83.9 ± 8.1 pmol/cm^2/h.

Verapamil-mediated inhibition of the Pgp effluxer increased apparent uptake and basolateral secretion of CoQ from micelles generated during digestion of yogurt supplemented with either ubiquinone or ubiquinol (Figure 2). Apparent apical uptake of CoQ increased 38 and 140% when verapamil-treated Caco-2 cells were incubated with diluted aqueous fraction of chyme after digestion of ubiquinone and ubiquinol supplemented yogurt, respectively (Figure 2A). This change was associated with 19% ($p < 0.01$) and 31% ($p < 0.0001$) increases in intracellular CoQ in verapamil-treated cells incubated in medium containing diluted aqueous fraction from digested yogurt supplemented with ubiquinone and ubiquinol, respectively. Similarly, secretion of CoQ into the basolateral compartment increased 2.4- and 5.3-fold in Pgp-treated cells incubated with micelles generated during digestion of yogurt containing ubiquinone and ubiquinol, respectively (Figure 2B). These data suggest that apical uptake and secretion of CoQ into the basolateral compartment are more efficient for supplemented ubiquinol than for ubiquinone. It is unknown if the redox state of CoQ affects its transfer from mixed micelles to the apical surface of Caco-2 cells, transfer across or incorporation into the plasma membrane, or distribution to other subcellular compartments including the Golgi during chylomicron assembly.

CoQ content and redox status in medium containing the mixed micelles generated during digestion of yogurt with the supplements were stable during 4 h of incubation in cell-free wells. Recovery of total CoQ and ubiquinol exceeded 95 and 90%, respectively. Only ubiquinone was detected in the basolateral medium after collected samples were stored under nitrogen at −80 °C overnight, whereas both ubiquinone and ubiquinol were present in basolateral medium that was analyzed immediately upon termination of the incubation after 4 h. These data suggest that the presence of 19% oxygen (95% air, 5% CO_2) in the cell culture environment, the relative absence of other antioxidants in the basolateral compartment, and overnight storage of medium likely contributed to oxidation of ubiquinol after its transport across the basolateral membrane.

Effect of Altered Cellular Redox Status on Uptake and Basolateral Secretion of CoQ. Because uptake and basolateral secretion of CoQ from micelles generated during digestion of yogurt with ubiquinol exceeded that for micelles containing only ubiquinone, we hypothesized that efficient secretion of CoQ across the basolateral membrane required a reduced intracellular environment. Interactive redox systems are responsible for maintaining a reduced intracellular environment.[39] Reduced glutathione is the most abundant intracellular antioxidant in aerobic cells. Alterations in glutathione status previously have been shown to affect glucose uptake,[40] calcium absorption,[41] and the activity of organic solute transporters and ion channels.[42] The concentration of total glutathione and the high ratio of glutathione to glutathione disulfide are maintained by the activities of γ-glutamyl cysteine synthetase and NADPH-dependent GSH reductase, respectively. GSH reductase also has been reported to directly reduce ubiquinone to ubiquinol in tissue homogenates and cytosol.[25] The protocol of Noda et al.[31] was used to decrease GSH content of Caco-2 cells without inducing oxidative stress. GSH reductase activity and cellular GSH decreased 41 and 99%, respectively, and cell GSSG increased 23% in monolayers incubated with a cocktail. Despite this marked decrease in cellular GSH, there was no overt cytotoxicity as cellular morphology, mitochondrial activity as assessed by reduction of MTT, and cell protein content per well were not significantly different in control cultures and cultures exposed to the cocktail of inhibitors (data not shown). Similarly, there was no significant change in barrier integrity as apical to basolateral flux of phenol red was not significantly different in control in cultures with control and low glutathione status. Finally, the amounts of ubiquinone or ubiquinol in medium were not altered during co-incubation with the inhibitors in the absence of cells.

Apparent uptake of ubiquinone and ubiquinol from micelles in apical medium was decreased 48% ($p < 0.0001$) and 65% ($p < 0.0001$), respectively, in cells with low glutathione status

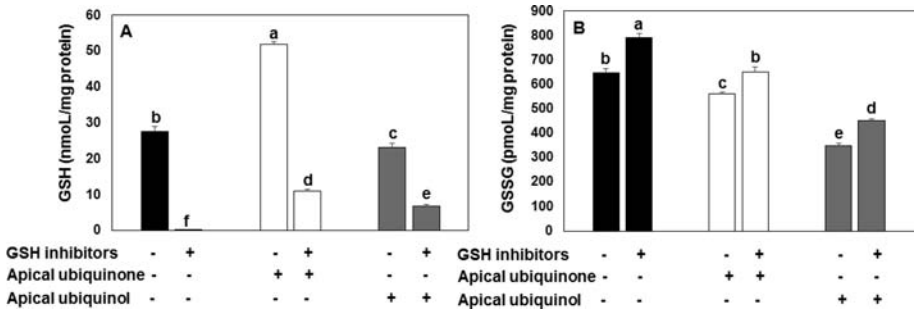

Figure 4. Intracellular GSH (A) and GSSG (B) are altered by exposure of Caco-2 cells to micellar CoQ and inhibitors of GSH status. Cultures were incubated in the absence (control) or presence of inhibitors of GSH status as described under Materials and Methods. Data are the mean ± SD, n = 6. Different letters above error bars indicate that means differ significantly ($p < 0.01$).

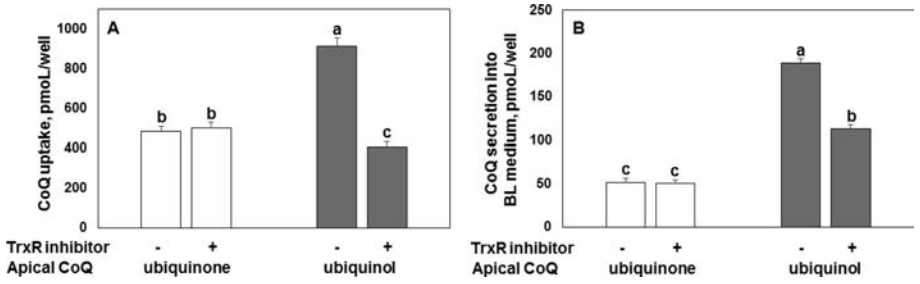

Figure 5. Inhibition of Trx reductase activity decreases apical uptake (A) of ubiquinol and basolateral secretion of CoQ (B) in cultures containing micellar ubiquinol or ubiquinone. Monolayers of Caco-2 grown were co-incubated in apical medium with auranofin (10 μmol/L) and either ubiquinone (6.3 nmol/well) or ubiquinol (6.1 nmol/well) for 4 h. Data are the mean ± SD, n = 6. Different letters above bars indicate significantly ($p < 0.001$) different means.

(Figure 3). Similarly, secretion of CoQ into the basolateral compartment decreased 30 and 65% in cultures incubated in medium with ubiquinone and ubiquinol, respectively. The quantities of CoQ in cells and in basolateral medium were not significantly different in cultures with low GSH status regardless of whether ubiquinone or ubiquinol was present in apical medium. Elucidation of the mechanism by which depletion of cell GSH adversely affects transport of both reduced and oxidized CoQ across the brush border and basolateral membranes of differentiated Caco-2 cells requires investigation.

There were additional interactions between CoQ and glutathione status. The endogenous ratio of ubiquinol to ubiquinone decreased by 20% ($p < 0.05$) in cells treated with the inhibitors of glutathione status in the absence of apical CoQ. The presence of 5.0 nmol of ubiquinone in apical medium was associated with a doubling of cellular GSH (Figure 4A) and a 14% reduction in GSSG (Figure 4B). Similarly, Wagner et al.[43] reported that treatment of C2C12 myotubes with 100 μmol/L ubiquinone plus 250 μmol/L lipoic acid increased expression of γ-glutamyl cysteine synthase and the activities of GSH reductase and glucose-6-phosphate dehydrogenase and phosphogluconate dehydrogenase, the latter two being key enzymes in the synthesis of NADPH. These changes resulted in a 4-fold increase in intracellular GSH. Hwang et al.[44] also reported that addition of 10 μmol/L ubiquinone to medium increased intracellular GSH concentration in UV-A irradiated keratinocytes. In contrast with the stimulatory effect of ubiquinone on cellular GSH content, incubation of cells in apical medium containing 4.85 nmol of ubiquinol per well decreased GSH and GSSG by 16 and 46%, respectively. The basis for the differential effects of ubiquinone and ubiquinol on glutathione status of Caco-2 cells in the present study is unknown. It is also noteworthy that apical medium containing ubiquinone and ubiquinol attenuated the extent of the reduction in cell GSH and increase in GSSG when cells were treated with BSO, BCNU, and diamide (Figure 4).

We next assessed whether the decreased uptake and transport of micellar CoQ in cells with low glutathione status was specific or reflected a more general effect of cell redox status on the greater bioavailability of ubiquinol than of ubiquinone. The thioredoxin/thioredoxin disulfide couple represents the other major intracellular redox system.[41] Trx reductase activity was 7.3−10.0 nmol/min/mg protein in cultures ± apical CoQ, but not detected in cells incubated with 10 μmol/L auranofin for 4 h. Loss of Trx reductase activity was associated with 50 and 40% decreases in the apical uptake (Figure 5A) and basolateral secretion (Figure 5B) of CoQ, respectively, in cultures incubated with apical medium containing ubiquinol. In contrast, cell uptake and basolateral secretion were not altered in auranofin-treated cultures incubated with apical medium containing ubiquinone. Similarly, the intracellular ratio of ubiquinol to ubiquinone also significantly decreased in auranofin-treated cells incubated with micelles containing ubiquinol, but not ubiquinone (Figure 6A). The discrepancy in the response of monolayers to auranofin led us to question whether the presence of the inhibitor in medium was associated with extracellular oxidation of ubiquinol. This interaction was confirmed by comparison of the stability of ubiquinol in Tween-40 micelles in the absence and presence of auranofin in cell-free medium. Ubiquinol decreased 31% during the 4 h of incubation in cell-free medium containing auranofin (Figure 6B). Oxidation of ubiquinol to ubiquinone accounted for only one-third of the total loss. The concentration of ubiquinone in medium ± auranofin incubated for 4 h in the absence of cells was not significantly altered after 4 h (Figure 6B). These results suggest the decreased uptake

dx.doi.org/10.1021/jf5017829 | J. Agric. Food Chem. 2014, 62, 7174−7182

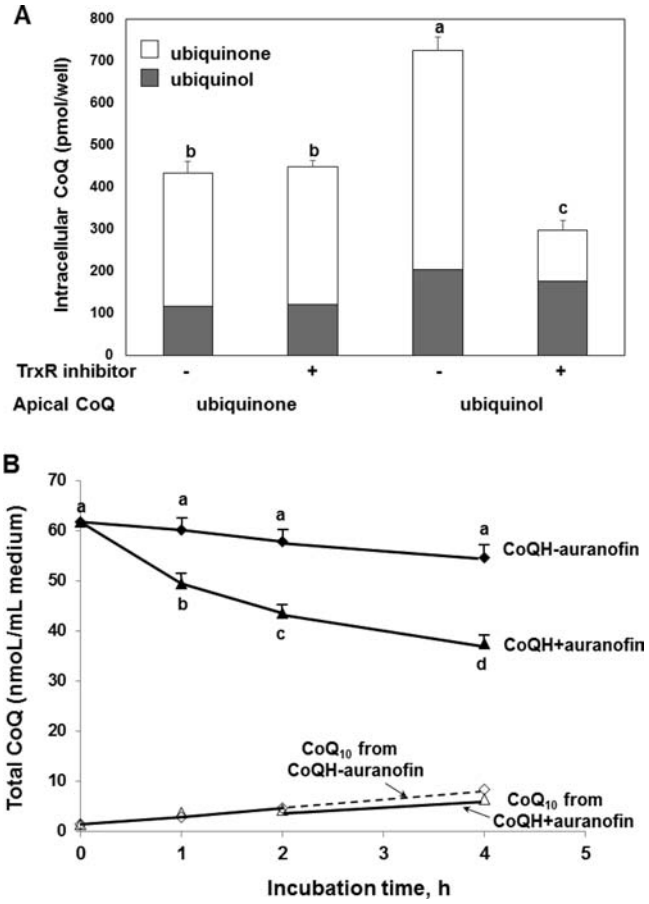

Figure 6. Decreased intracellular CoQ in monolayers co-incubated in apical medium containing 10 μmol/L auranofin and ubiquinol (A) is due to extracellular oxidation and degradation of the reduced coenzyme (B). The amounts of unbiquinone and ubiquinol in apical medium of Caco-2 cell cultures were 6.3 and 5.4 nmol/well, respectively. TrxR, thioredoxin reductase; CoQ_{10}, ubiquinone; CoQH, ubiquinol. Data are the mean ± SD for $n = 6$ and 4 in panels A and B, respectively. Different letters above error bars indicate that means differ significantly different ($p < 0.001$ for panel A and $p < 0.01$ for panel B).

and transport of ubiquinol in medium containing auranofin resulted from both oxidation and degradation of micellar ubiquinol in the apical compartment by an unknown chemical reaction.

NQO1 catalyzes the two-electron reduction of quinones in human tissues and has been suggested to participate in the reduction of ubiquinone.[27] Unlike normal intestinal epithelial cells, Caco-2 cells lack NQO1 activity because they express a mutant form of the enzyme that is rapidly eliminated by the proteosomal degradation pathway.[45−47] Therefore, we were not able to determine whether NQO1 activity affected CoQ uptake, transport, and the redox status of intracellular CoQ using this cell line. We did test the possibility that the enzyme might affect CoQ uptake and redox status using the HT-29 human colonic cell line that expresses wild-type protein. NQO1 activity was decreased by 25% in cells exposed to 10 μmol/L dicoumarol, a specific inhibitor of NQO1.[27] This change did not alter the intracellular content of CoQ or the ratio of ubiquinol to ubiquinone during incubation in medium supplemented with ubiquinone (80 μmol/L) (data not shown). In contrast, there was a 19% decline in intracellular cell CoQ content ($p < 0.05$) without alteration of the ratio of ubiquinol to ubiquinone when cultures were incubated in medium containing ubiquinol and dicoumarol. There was no extracellular interaction between dicoumarol and ubiquinol as recovery of ubiquinol during incubation in cell-free medium with dicoumarol for 6 h was 98%, with 95% of the coenzyme remaining in the reduced state. Together, these data suggest that partial loss of NQO1 activity minimally affected accumulation of ubiquinol by HT-29 cells. Clarity regarding the possible influence of NQO1 activity on the intestinal absorption of ubiquinol will require investigation in an animal model.

In summary, the present in vitro studies suggest that the greater bioavailability of ubiquinol compared to that of ubiquinone is the result of increased efficiency of several processes associated with the absorption of orally administered lipophilic compounds. These included partitioning into mixed micelles during simulated small intestinal digestion, apical uptake by Caco-2 cells, and subsequent secretion of the coenzyme across the basolateral membrane. The extent of the observed differences in these processes between ubiquinol and ubiquinone likely underestimate the situation in situ because oxygen tension in the laboratory exceeded that for commercial preparation of ubiquinol in soft gel capsules, exposure to compounds in the meal prior to ingestion, and during gastric and small intestinal phases of digestion. This led to the partial oxidation of ubiquinol to ubiquinone, resulting in the presence of both ubiquinol and ubiquinone in mixed micelles added to the apical compartment of Caco-2 cells. The present results also show that a reduced intracellular environment is necessary to maintain the elevated ratio of ubiquinol to ubiquinone within cells, which in turn facilitates both the apical uptake and basolateral secretion of CoQ. This was demonstrated by markedly decreasing cellular GSH and the activity of TrxR. Because the actual compartmentalization of the bolus of CoQ taken up by the cell is not known, it is unclear which flavoenzyme or combination of such enzymes shown to reduce extramitochondrial ubiquinone in cell homogenates and once purified are responsible for doing so in absorptive cells lining the gut.

AUTHOR INFORMATION

Corresponding Author

*(M.L.F.) E-mail: failla.3@osu.edu. Phone: (614) 560-9401. Fax: (614) 292-4339.

Notes

The authors declare the following competing financial interest(s): F.A. is an employee of Kaneka North America LLC, the sponsor for this project.

ACKNOWLEDGMENTS

The authors thank Drs. Richard S. Bruno and Eunice Mah for guidance with analysis of GSH and GSSG using the Ultimate HPLC-BDD detector (Thermo Fisher Scientific, Waltham, MA, USA).

ABBREVIATIONS USED

BCNU, 1,3-bis(2 chloroethyl)-1-nitrosourea; BSO, DL-buthionine-sulfoximine; CoQ, coenzyme Q; CoQ_{10}, ubiquinone; CoQH, ubiquinol; DMEM, Dulbecco's modified Eagle's medium; DTNB, 5,5′-dithiobis(2-nitrobenzoic) acid; DTPA, diethylenetriaminepentaacetic acid; FBS, fetal bovine serum; GSH, glutathione; GSSG, glutathione disulfide; HCO, hydro-

genated castor oil; NQO1, NAD(P)H:quinone oxidoreductase family 1; PBS, phosphate buffer saline; PCA, perchloric acid; Pgp, Pgp-glycoprotein; Trx, thioredoxin

REFERENCES

(1) Ernster, L.; Dallner, G. Biochemical, physiological and medical aspects of ubiquinone function. *Biochim. Biophys. Acta* **1995**, *1271*, 195−204.

(2) Littarru, G. P.; Tiano, L. Clinical aspects of coenzyme Q10: an update. *Nutrition* **2010**, *26*, 250−254.

(3) Celik, T.; Iyisoy, A. Coenzyme Q_{10} and coronary artery bypass surgery: what we have learned from clinical trials. *J. Cardiothorac. Vasc. Anesth.* **2009**, *23*, 935−936.

(4) Makhija, N.; Sendasgupta, C.; Kiran, U.; Lakshmy, R.; Hote, M. P.; Choudhary, S. K.; Airan, B.; Abraham, R. The role of oral coenzyme Q_{10} in patients undergoing coronary artery bypass graft surgery. *J. Cardiothorac. Vasc. Anesth.* **2008**, *22*, 832−839.

(5) Henchcliffe, C.; Beal, M. F. Mitochondrial biology and oxidative stress in Parkinson disease pathogenesis. *Nat. Clin. Pract. Neurol.* **2008**, *4*, 600−609.

(6) Naia, L.; Ribeiro, M. J.; Rego, A. C. Mitochondrial and metabolic-based protective strategies in Huntington's disease: the case of creatine and coenzyme Q. *Rev. Neurosci.* **2011**, *23*, 13−28.

(7) Cooke, M.; Losia, M.; Buford, T.; Shelmadine, B.; Hudson, G.; Kerksick, C.; Rasmussen, C.; Greenwood, M.; Leutholtz, B.; Willoughby, D.; Kreider, R. Effect of acute and 14-day coenzyme Q_{10} supplementation on exercise performance in both trained and untrained individuals. *J. Int. Soc. Sports Nutr.* **2008**, *5*, 1−14.

(8) Kon, M.; Tanabe, K.; Akimoto, T.; Kimura, F.; Tanimura, Y.; Shimizu, K.; Okamoto, T.; Kono, I. Reducing exercise-induced muscular injury in kendo athletes with supplementation of coenzyme Q_{10}. *Br. J. Nutr.* **2008**, *100*, 903−909.

(9) Bhagavan, H. N.; Chopra, R. K. Coenzyme Q10: absorption, tissue uptake, metabolism and pharmacokinetics. *Free Radical Res.* **2006**, *40*, 445−453.

(10) Borel, P. Factors affecting intestinal absorption of highly lipophilic food microconstituents (fat-soluble vitamins, carotenoids and phytosterols). *Clin. Chem. Lab. Med.* **2003**, *41*, 979−994.

(11) Miles, M. V.; Horn, P.; Miles, L.; Tang, P.; Steele, P.; DeGrauw, T. Bioequivalence of coenzyme Q10 from over the counter supplements. *Nutr. Res. (N.Y.)* **2002**, *22*, 919−929.

(12) Hosoe, K.; Kitano, M.; Kishida, H.; Kubo, H.; Fuji, K.; Kitahara, M. Study on safety and bioavailability of ubiquinol (Kaneka QH^{TM}) after single and 4-week multiple oral administration to healthy volunteers. *Regul. Toxicol. Pharmacol.* **2007**, *47*, 19−28.

(13) Evans, M.; Baisley, J.; Barss, S.; Guthrie, N. A randomized, double-blind trial on the bioavailability of two CoQ10 formulations. *J. Funct. Food* **2009**, *1*, 65−73.

(14) Itagaki, S.; Ochiai, A.; Kobayashi, M.; Sugawara, M.; Hirano, T.; Iseki, K. Interaction of coenzyme Q10 with the intestinal drug transporter P-glycoprotein. *J. Agric. Food Chem.* **2008**, *56*, 6923−6927.

(15) Xia, S.; Xu, S.; Zhang, X.; Zhong, F.; Wang, Z. Nanoliposomes mediate coenzyme Q_{10} transport and accumulation across the human intestinal Caco-2 cell monolayer. *J. Agric. Food Chem.* **2009**, *57*, 7989−7996.

(16) Beg, S.; Javed, S.; Kohli, K. Bioavailability enhancement of coenzyme Q10: an extensive review of patents. *Recent Pat. Drug Delivery Formulation* **2010**, *4*, 45−257.

(17) Schmelzer, C.; Kohl, C.; Rimbach, G.; Doring, F. The reduced form of coenzyme Q decreases the expression of lipopolysaccharide-sensitive genes in human THP-1 cells. *J. Med. Food* **2010**, *14*, 391−397.

(18) Bruge, F.; Damiani, E.; Puglia, C.; Offerta, A.; Armeni, T.; Littaru, G. P.; Tiano, L. Nanostructured lipid carriers loaded with CoQ10: effect on human dermal fibroblasts under normal and UVA-mediated oxidative conditions. *Int. J. Pharm.* **2013**, *455*, 348−356.

(19) Yan, J.; Fujii, K.; Yao, J.; Kishida, H.; Horose, K.; Sawashita, J.; Takeda, T.; Mori, M.; Higuchi, K. Reduced coenzyme Q_{10} decelerates senescence in SAMP1 mice. *Exp. Gerontol.* **2006**, *41*, 130−140.

(20) Schmelzer, C.; Kubo, M.; Sawashita, J.; Kitano, M.; Hosoe, K.; Boomgaarrden, I.; Doring, F.; Higuchi, K. Supplementation with the reduced form of coenzyme Q_{10} decelerates phenotypic characteristics of senescence and induces a peroxisome proliferator-activated receptor-α gene expression signature in SAMP1 mice. *Mol. Nutr. Food Res.* **2010**, *54*, 805−815.

(21) Peerapanyasut, W.; Thamprasert, K.; Wongmekiat, O. Ubiquinol supplementation protects against renal ischemia and reperfusion injury in rats. *Free Radical Res.* **2013**, *48*, 180−189.

(22) Langsjoen, P. H.; Langsjoen, A. M. Supplemental ubiquinol in patients with advanced congestive heart failure. *Biofactors* **2008**, *32*, 119−128.

(23) Mezawa, M.; Takemoto, M.; Onishi, S.; Ishibashi, R.; Ishikawa, T.; Yamaga, M.; Fujimoto, M.; Okabe, E.; He, P.; Kobayashi, K.; Yokote, K. The reduced form of coenzyme Q10 improves glycemic control in patients with type 2 diabetes. *Biofactors* **2012**, *38*, 416−421.

(24) Bhagavan, H.; Chopra, B. K.; Craft, N. E.; Chitchumroonchokchai, C.; Failla, M. L. Assessment of coenzyme Q_{10} absorption using an in vitro digestion-Caco-2 cell model. *Int. J. Pharm.* **2007**, *333*, 112−117.

(25) Bjornstedt, M.; Nordman, T.; Olsson, J. M. Extramitochondrial reduction of ubiquinone by flavoenzymes. *Methods Enzymol.* **2004**, *378*, 131−138.

(26) Xia, L.; Nordman, T.; Olsson, J. M.; Damdimoupolos, A.; Bjorkhem-Bergman, L.; Nalvarte, I.; Eriksson, L. C.; Arner, E. S. J.; Spyrou, G.; Bjornstedt, M. The mammalian cytosolic selenoenzyme thioredoxin reductase reduces ubiquinone: a novel mechanism for defense against oxidative stress. *J. Biol. Chem.* **2003**, *278*, 2141−2146.

(27) Landi, L.; Fiorentinin, D.; Galli, M.; Segura-Aguilar, J.; Beyer, R. E. DT-diaphorase maintains the reduced state of ubiquinones in lipid vesicles thereby promoting their antioxidant function. *Free Radical Biol. Med.* **1997**, *22*, 329−335.

(28) Chitchumroonchokchai, C.; Schwartz, S. J.; Failla, M. L. Assessment of lutein bioavailability from meals and supplements using simulated digestion and Caco-2 human intestinal cells. *J. Nutr.* **2004**, *134*, 2280−2286.

(29) Luchoomun, J.; Hussain, M. M. Assembly and secretion of chylomicrons by differentiated Caco-2 cells. Nascent triglycerides and preformed phospholipids are preferentially used for lipoprotein assembly. *J. Biol. Chem.* **1999**, *274*, 19565−19572.

(30) During, A.; Hussain, M. M.; Morel, A. W.; Harrison, E. H. Carotenoid uptake and secretion by Caco-2 cells: β-carotene isomer selectivity and carotenoid interactions. *J. Lipid Res.* **2002**, *43*, 1086−1095.

(31) Noda, T.; Iwakiri, R.; Fujimoto, K.; Aw, T. Y. Induction of mild intracellular redox imbalance inhibits proliferation of Caco-2 cells. *FASEB J.* **2001**, *15*, 2131−2139.

(32) Park, J. H.; Mah, E.; Bruno, R. S. Validation of high performance liquid chromatography-boron-doped diamond detector for assessing hepatic glutathione redox status. *Anal. Biochem.* **2010**, *407*, 151−159.

(33) Okamoto, T.; Fukui, K.; Nakamoto, M.; Kishi, T.; Okishio, T.; Yamagami, T.; Kanamori, N.; Kishi, H.; Hiraoka, E. High-performance liquid chromatography of coenzyme Q-related compounds and it application to biological materials. *J. Chromatogr.* **1985**, *342*, 35−46.

(34) Lewis, S. A. Assessing epithelial cell confluence by spectroscopy. In *Methods in Molecular Biology: Epithelial Cell Culture Protocols*; Wise, C., Ed.; Humana Press: Totowa, NJ, USA, 2002; pp 329−336.

(35) Burnett, C.; Heldreth, B. Amended safety assessment of PEGylated oils as used in cosmetics. Amended Report, Cosmetic Ingredient Review 2013, pp 1−29; http://www.cir-safety.org/sites/default/files/pegoil122012final_faa-final%20for%20posting.pdf (accessed Jan 12, 2014).

(36) Committee for Veterinary Medicinal Products. *Summary Report of Polyoxyl Castor Oil, Polyoxylhydrogenated Castor Oil*; The European Agency for the Evaluation of Medicinal Products, Veterinary Medicines Evaluation Unit: London, UK, 1999; pp 1−3.

(37) Forster, R. E. Physiological basis of gas exchange in the gut. *Ann. N.Y. Acad. Sci.* **1968**, *150*, 4−12.
(38) He, G.; Shankar, R. A.; Chzhan, M.; Samouilov, A.; Kuppusamy, P.; Zweier, J. L. Noninvasive measurement of anatomic structure and intraluminal oxygenation in the gastrointestinal tract of living mice with spatial and spectral EPR imaging. *Proc. Natl. Acad. Sci. U.S.A.* **1999**, *96*, 4586−4591.
(39) Circu, M. L.; Aw, T. K. Intestinal redox biology and oxidative stress. *Stem Cell Dev. Biol.* **2012**, *23*, 729−737.
(40) Iantomasi, T.; Favilli, F.; Marracccini, P.; Vincenzini, M. T. Glutathione involvement on the intestinal Na^+-dependent D-glucose active transporter. *Mol. Cell. Biochem.* **1998**, *178*, 387−392.
(41) Xiao, Y.; Cui, J.; Shi, Y. H.; Sun, J.; Wang, Z. P.; Le, G. W. Effects of duodenal redox status on calcium absorption and related genes expression in high-fat diet-fed mice. *Nutrition* **2010**, *26*, 1188−1194.
(42) Hammond, C. L.; Lee, T. K.; Ballatori, N. Novel roles for glutathione in gene expression, cell death, and membrane transport of organic solutes. *J. Hepatol.* **2001**, *34*, 946−954.
(43) Wagner, A.; Ernst, I. M. A.; Birringer, M.; Sancak, O.; Barella, L.; Rimbach, G. A combination of lipoic acid plus coenzyme Q10 induces PGC1α, a master switch of energy metabolism, improves stress response, and increases cellular glutathione levels in cultured C2C12 skeletal muscle cells. *Oxidative Med. Cell. Longevity* **2012**, DOI: 10.1155/2012/835970.
(44) Hwang, T. L.; Tsai, C. K.; Chen, J. L.; Changchien, T. T.; Wang, C. C.; Wu, C. M. Magnesium ascorbyl phosphate and coenzyme Q10 protect keratinocytes against UVA irradiation by suppressing glutathione depletion. *Mol. Med. Rep.* **2012**, *6*, 375−383.
(45) Traver, R.; Horikoshi, T.; Danenberg, K. D.; Stadlbauer, H. W.; Danenberg, P. V.; Ross, D.; Gibson, N. W. NAD(P)H:quinone oxidoreductase gene expression in human colon carcinoma cells: characterization of a mutation which modulates DT-diaphorase activity and mitomycin sensitivity. *Cancer Res.* **1992**, *52*, 797−802.
(46) Karczewski, J. M.; Peters, J. G. P.; Noordhoek, J. Quinone toxicity in DT-diaphorase-efficient and -deficient colon carcinoma cell lines. *Biochem. Pharmacol.* **1999**, *57*, 27−37.
(47) Siegel, D.; Anwar, A.; Winski, S. L.; Kepa, J. K.; Zolman, K. L.; Ross, D. Rapid polyubiquitination and proteosomal degradation of a mutant form of NAD(P)H:quinone oxidoreductase 1. *Mol. Pharmacol.* **2001**, *59*, 263−268.

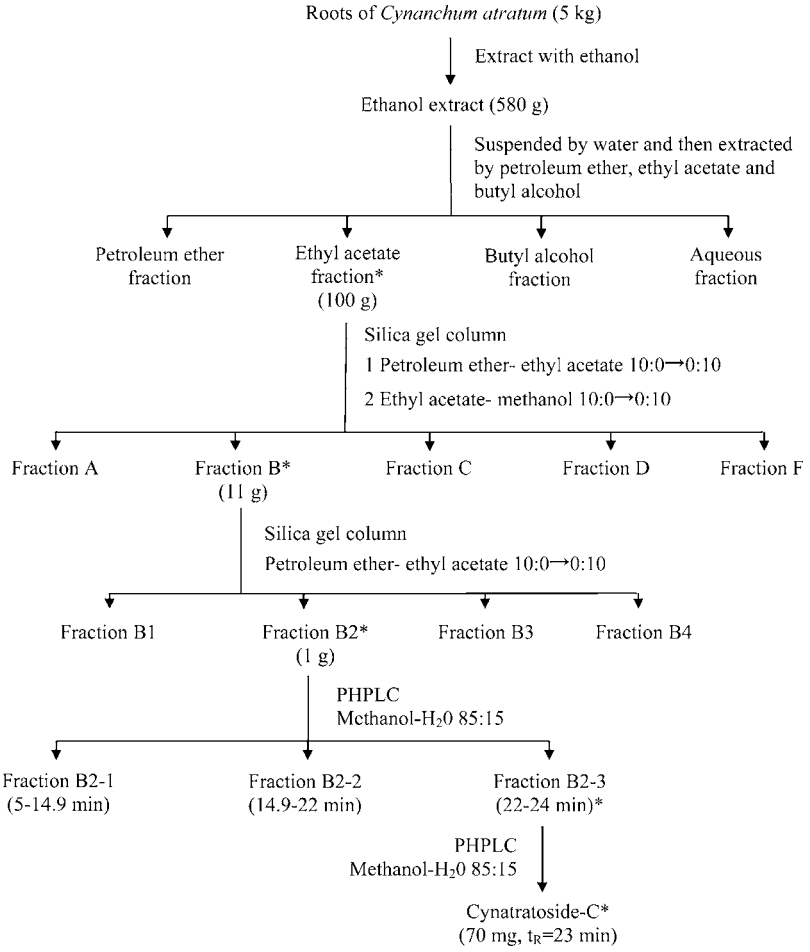

Figure 1. Bioassay-guided fractionation for identification of parasiticidal compound. *: Best antiparasitic activity from the same row.

(Agilent) equipped with a TC-C18 column (5 μm, 4.6 mm × 250 mm, Agilent) was used to analyze the purity of active compound. The thin layer chromatography (TLC) plate was used to identify the obtained semblable fractions with similar TLC patterns for further mixing the similar fractions before bioassay by means of visualizing the plate with a UV lamp (λ_{max} 254 and 365 nm) and anisaldehyde spray reagent (EtOH/anisaldehyde/sulfuricacid, 90:5:10, v/m/v). A Sartorius ME5 microelectronic balance (readability, 0.001 mg) (Sartorius, Niedersachsen, Germany) was used to weigh the fractions and active compound. An inverted microscope (Nikon, Tokyo, Japan) was used to observe and photograph the treated tomonts. Granule feed (Haid, Guangzhou, China) was used to feed grass carp daily to apparent satiation.

Extraction and Isolation of Bioactive Compound. The roots of *C. atratum* (5 kg) were purchased from the Chinese medicinal market at Guangzhou, China, and kept in an oven at 55 °C until completely dried. The dried plant materials were then powdered by a pulverizer with 50 mesh strainer. The root powder was extracted with 95% ethanol (3 × 20 L) at 50 °C. After removal of ethanol in vacuo at 50 °C by a rotary vacuum evaporator, the extract (580 g) was suspended in water (1 L) and partitioned with petroleum ether (3 × 1 L), ethyl acetate (3 × 1 L), and butanol (3 × 1 L).

A bioassay-guided fractionation was designed for the isolation and identification of compounds with anti-*I. multifiliis* effect as shown in Figure 1 and Table 1. Ethyl acetate fraction (100 g) was subjected to column chromatography and continuously eluted using a stepwise gradient of petroleum ether/ethyl acetate (10:0, 4:1, 1:1, and 0:10, v/v) and methanol to get five fractions (A−E). The most active fraction B was further fractionated on a silica gel column and eluted with petroleum ether/ethyl acetate (4:1, 1:1, 1:4, and 0:10, v/v) to obtain fractions B1−B4. The active fraction B2, acquired from the elution of a 1:1 petroleum ether/ethyl acetate, was separated by PHPLC to collect fraction B2-1, fraction B2-2, and fraction B2-3. The mobile phase used

Table 1. Effects of Fractions against *I. multifiliis* Nonencysted Tomonts[a]

	antitomont efficacy (mg/L)			
fraction	100	50	25	0
petroleum ether fraction	+	−	−	−
ethyl acetate fraction	+	+	+	−
butyl alcohol fraction	−	−	−	−
aqueous fraction	−	−	−	−
fraction A	−	−	−	−
fraction B	+	+	+	−
fraction C	+	−	−	−
fraction D	−	−	−	−
fraction E	−	−	−	−
fraction F	−	−	−	−
fraction B1	+	−	−	−
fraction B2	+	+	+	−
fraction B3	−	−	−	−
fraction B4	−	−	−	−
fraction B2-1	−	−	−	−
fraction B2-2	−	−	−	−
fraction B2-3	+	+	+	−

[a]−: The fraction at the listed concentration could not kill 100% nonencysted tomonts after 4 h exposure. +: The fraction at the listed concentration killed 100% of nonencysted tomonts by 4 h exposure.

dx.doi.org/10.1021/jf5018675 | J. Agric. Food Chem. 2014, 62, 7183−7189

for PHPLC was methanol/H_2O (80:20, v/v), applied with a flow rate of 10 mL/min, and ultraviolet detection was a 210 nm. The active fraction B2-3 was further purified by PHPLC under the same condition to yield an active compound (70 mg, t_R = 23 min) at purity >98%. The active compound was recrystallized in methanol and identified by various spectroscopic analyses, including ESI−MS, HR-ESI−MS, and 1D NMR (^1H,^{13}C NMR, and DEPT), and characterized as cynatratoside-C. The other 256 mg of cynatratoside-C was purified from 15 kg of *C. atratum* roots by means of the same method mentioned above (showed in Figure 1) to meet the needs of trials, and stored at 4 °C in a refrigerator prior to use. The spectroscopic data of the active compound are as follows.

ESI−MS (positive) *m/z*: 801.7 $[M + Na]^+$. ESI−MS (negative) *m/z*: 813.8 $[M + Cl]^-$ and 777.9 $[M - H]^-$. HR-ESI−MS *m/z*: $[M + Na]^+$ 801.4039. ^1H NMR (500 MHz, MeOD) δ: 0.96 (3H, s, 19-CH_3), 1.24 (3H, d, *J* = 6.3 Hz, 6′-CH_3), 1.27 (3H, d, *J* = 6.2 Hz, 6″-CH_3), 1.29 (3H, d, *J* = 6.2 Hz, 6‴-CH_3), 1.49 (3H, s, 21-CH_3), 3.44 (3H, s, 3′-O CH_3), 3.45 (3H, s, 3‴-O CH_3), 3.91 (1H, dd, *J* = 9.6, 6.2 Hz, 15-CH_β), 4.13 (1H, dd, 3″-CH), 4.17 (1H, dd, *J* = 8.5, 7.0 Hz, 15-CH_α), 4.67 (1H, dd, *J* = 9.7, 1.8 Hz, 1′-CH), 5.01 (1H, br d, *J* = 3.4 Hz, 1‴-CH), 5.04 (1H, dd, *J* = 9.7, 1.9 Hz, 1″-CH), 5.32 (1H, ddd, *J* = 9.6, 7.5, 7.5 Hz, 16-CH), 5.45 (1H, d, *J* = 5.5 Hz, 6-CH), 6.33 (1H, br s, 18-CH). ^{13}C NMR (125 MHz, MeOD) δ: 18.1 (19-C), 18.4 (6″-C), 18.5 (6‴-C), 18.7 (6′-C), 24.6 (11-C), 24.9 (21-C), 29.1 (12-C), 30.6 (2-C), 30.8 (7-C), 36 (2‴-C), 37.5 (1-C), 38.1 (2′-C), 39.6 (2″-C), 39.7 (10-C), 39.9 (4-C), 41.7 (9-C), 54.5 (8-C), 57.1 (17-C), 57.4 (3‴-OMe), 57.7 (3′-OMe), 68.5 (5″-C), 68.7 (15-C), 69.9 (5‴-C), 69.8 (3″-C), 72.4 (5′-C), 76.5 (16-C), 77.5 (4‴-C), 79 (3-C), 79.2 (3‴-C), 80.1 (3′-C), 82.6 (4″-C), 84.2 (4′-C), 99 (1′-C), 99.6 (1″-C), 101.1 (1‴-C), 115.6 (20-C), 119.4 (13-C), 121.4 (6-C), 141.6 (5-C),144.5 (18-C), 177 (14-C).

Fish and Parasite. Healthy grass carp (*Ctenopharyngodon idellus*) weighing 22.6 ± 3.5 g was obtained from a commercial fish farm at Huadu, Guangzhou City, Guangdong Province. *I. multifiliis* was isolated from goldfish obtained from the ornamental fish market of Guangzhou. The infected goldfish were kept with five naïve grass carp in a 30 L opaque tank for 7 d to allow infection of the grass carp by *I. multifiliis*. The temperature of the water was controlled at 23.0 ± 0.3 °C, and the fish were fed daily with diets at 1% of fish weight. When grass carp were heavily infected with mature trophonts, the skin was gently scraped to dislodge the trophonts after the fish were anesthetized by 150 mg/L tricaine methanesulfonate (MS-222, Sigma). Mature trophonts were rinsed several times with dechlorinated water to wipe off fish mucus. Usage of grass carp was approved by the Animal Experimentation Ethics Committee of Jinan University.

Bioassay of Fractions against *I. multifiliis* Nonencysted Tomonts. Each fraction weighing 5 mg was dissolved in 2.5 mL of dechlorinated freshwater containing 1% (v/v) dimethyl sulfoxide (DMSO) to make a 2000 mg/L stock solution. The stock solution was diluted with dechlorinated freshwater in a 24-well issue culture plate to concentrations of 200, 100, and 50 mg/L. The control (0 mg/L) was made following the method described by Fu et al. (2014)[11] to avoid the influence of residual solvent in each fraction. Briefly, 50 mL of each solvent used in the different fraction was also concentrated under reduced pressure in a vacuum rotary evaporator until the solvent was invisible, and then 50 mL of dechlorinated freshwater containing 1% (v/v) DMSO was added to the evaporator to dissolve the residual solvent, and the solution was used as antitomont trial control.

Nonencysted tomonts came from trophonts obtained above. The average number of nonencysted tomonts per 100 μL of water was determined with the assistance of a microscope (4×) according to Zhang et al. (2013).[12] Approximately 80 nonencysted tomonts in 300 μL of dechlorinated freshwater were placed into each well of a 24-well tissue culture plate. Next, 300 μL of each fraction solution at different concentrations was added to each well in triplicate to make concentrations of 100, 50, 25, and 0 (control) mg/L, respectively. Survival or dead nonencysted tomonts were identified on the basis of movement (live) or no motion (paralysis or dead) of the parasite under a microscope at 4× magnification.

In Vitro Bioactivity of Cynatratoside-C on *I. multifiliis* Tomonts. The stock solution of cynatratoside-C (2000 mg/L) was prepared with the same method mentioned above. The stock solution was diluted with dechlorinated water in a 24-well plate to concentrations of 64, 32, 16, 8, 4, 2, 1, 0.5, 0.25, 0.125, 0.06, and 0.03 mg/L. Next, 300 μL of the cynatratoside-C solution at different concentrations was added to 300 μL of water including about 75 nonencysted tomonts in each well of a 24-well plate in triplicate, and the final concentrations of cynatratoside-C were 32, 16, 8, 4, 2, 1, 0.5, 0.25, 0.125, 0.06, 0.03, and 0.015 mg/L, respectively. The negative control (0 mg/L) was prepared with the method described above, and malachite green at 0.125 and 0.06 mg/L was used as positive control. The duration for killing all nonencysted tomonts was monitored at different time points for 5 h. The numbers of encysted tomonts and released theronts were determined at 6 and 22 h post exposure to cynatratoside-C, respectively. Theronts number in each well were determined under a microscope (10×) according to Zhang et al. (2013).[12]

To evaluate the effect of cynatratoside-C on encysted tomonts, a 300 μL solution that contained about 60 nonencysted tomonts was distributed to each well of a 24-well plate. The nonencysted tomonts were incubated for 6 h, and then encysted tomonts were enumerated in every well. The encysted tomonts were subsequently exposed to cynatratoside-C at concentrations of 32, 16, 8, 4, 2, 1, 0.5, 0.25, 0.125, 0.06, 0.03, 0.015, and 0 (negative control) mg/L, and positive controls (malachite green at 0.125 and 0.06 mg/L), respectively, and then maintained at 23 ± 0.3 °C for 16 h. After 22 h exposure, theronts in each well were counted as described above.

To monitor pathological changes in tomonts after exposure to cynatratoside-C, approximately 50 nonencysted tomonts with 200 μL of dechlorinated freshwater were placed in one well of a 24-well plate, and 200 μL of cynatratoside-C solution at 16 mg/L was added into the well to make a final concentration of 8 mg/L. Fifty nonencysted tomonts with 200 μL of water were put into another well and incubated for 18 h. Next, 200 μL of cynatratoside-C solution was added to the well to make a 0.25 mg/L final concentration. The treated nonencysted and encysted tomonts were observed and photographed under a Nikon ECLIPSE Ti−S inverted microscope at 10×, 20×, and 40× magnification, respectively.

Treatment of Ichthyophthiriasis with Cynatratoside-C. One hundred and twenty grass carp naturally infected with *I. multifiliis* (382 ± 35 trophonts on body surface per fish) were transferred to 12 20-L tanks with 10-L static dechlorinated water at 23 ± 0.3 °C, and randomly divided into four treatments: 0 (control), 0.5, 1, and 2 mg/L cynatratoside-C in triplicate (10 fish/tank). During the trial, water was aerated with air stones, and fish were fed every day. The dead fish were removed twice per day, and mortality was recorded daily. At 48 h post cynatratoside-C treatment, all test fish were moved from each tank, and numbers of trophont on the whole body surface were counted after the fish was anesthetized with 150 mg/L MS-222. Infection intensity was determined and expressed as total numbers of trophont on the fish body surface per infected fish.

Statistical Analysis. All experimental data were expressed as the mean ± SD (standard deviation). Statistical analysis was performed with Student-Newman-Keul's test using a statistical analysis system software package (SPSS 16.0). A probit procedure was used to determine median effective concentration (EC_{50}) with 95% confidence intervals (CI). *p*-values < 0.05 were considered of significant difference.

RESULTS

Isolation and Identification of the Anti-*I. multifiliis* Compound. The anti-*I. multifiliis* effects of different fractions are listed in Table 1. The active component (70 mg), a white amorphous powder, was isolated from fraction B2-3. The compound had a molecular weight of 778, which is consistent with a molecular formula of $C_{41}H_{62}O_{14}$. In the ^{13}C NMR and DEPT spectra, 41 carbons were displayed, including 10 methylene carbons and 5 quaternary carbons. After comparison

of its spectral data with the literature,[22] the compound was identified as cynatratoside-C (glaucogenin C 3-*O*-*α*-D-oleandropyranosyl-(1 → 4)-*β*-D-digitoxopyranosyl-(1 → 4)-*α*-D-oleandropyranoside) (Figure 2).

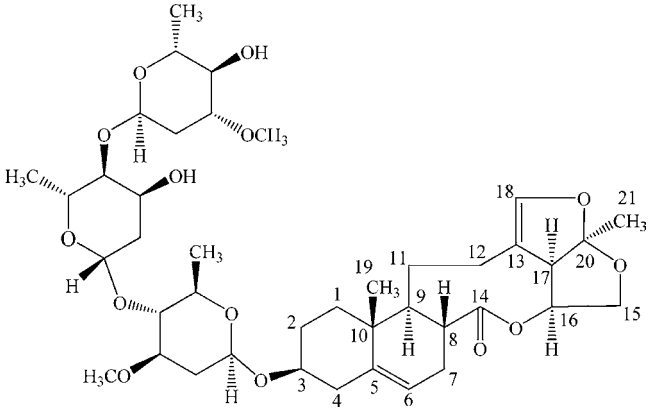

Figure 2. Chemical structure of cynatratoside-C.

In Vitro Bioactivity of Cynatratoside-C on *I. multifiliis* Tomonts. Nonencysted tomonts showed a clear dose−response to cynatratoside-C (Table 2). Mean death duration for killing all nonencysted tomonts ranged from 14.7 min at concentration of 32 mg/L to 270.0 min at concentration of 0.25 mg/L. The mortality of nonencysted tomonts ranged from 63.2% at concentration of 0.125 mg/L to 0% at concentration of 0.015 mg/L or lower (negative control) 5-h post exposure to cynatratoside-C. The 5-h EC_{50} of cynatratoside-C to nonencysted tomonts was 0.083 mg/L with a 95% confidence interval 0.014−0.365. Moreover, the number of theronts released from encysted tomonts sharply decreased from 223 in the negative control to 0 at a concentration of 0.125 mg/L 22 h post exposures. Even though 0.125 mg/L cynatratoside-C killed 63.2% nonencysted tomont 5-h post treatment, the survival nonencysted tomonts did not produce infective theronts. In positive control, malachite green at a concentration of 0.125 mg/L killed all nonencysted tomonts within 89 min and inhabited releasing infective theronts from all encysted tomonts.

Pathological changes of nonencysted tomonts are shown in Figure 3. After exposure to cynatratoside-C at 8 mg/L for 23 min, nonencysted tomonts changed their shape, formed transparent bubbles on plasma membrane, and cytoplasm spilled out from the tomonts (Figure 3b−d). Reproduction of encysted tomonts was significantly ($p < 0.05$) reduced after exposure to cynatratoside-C at concentration of 0.03 mg/L or higher as compared to that in negative control after 16 h treatment (Table 3). When encysted tomonts after incubation for 18 h were treated with 0.25 mg/L cynatratoside-C for about 60 min, the tomites (immature theronts) were released from

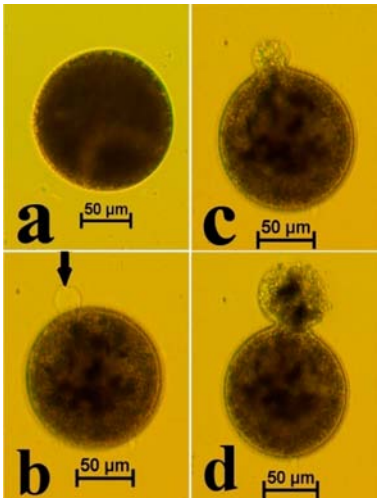

Figure 3. Morphology of nonencysted tomonts. Nonencysted tomont untreated with cynatratoside-C (a). The nonencysted tomont exposed to 8 mg/L cynatratoside-C for 23 min, showing a transparent bubble (black arrow) on plasma membrane (b). Cytoplasm spilled out of the nonencysted tomont from the bubble (c,d).

Table 2. Effect of Cynatratoside-C on Survival and Reproduction of *I. multifiliis* Nonencysted Tomont[a]

concentration (mg/L)	MDDNT[b] (min)	MNT[c] (%)	MNET[d]	MNTLET[e]
0 (control)	−	0.0 ± 0.0 a	72 ± 1.0	223.4 ± 25.5 a
0.015	−	0.0 ± 0.0 a	77 ± 3.5	309.0 ± 103.1 a
0.03	−	11.9 ± 40.3 a	63 ± 11.0	105.2 ± 42.7 b
0.06	−	28.0 ± 12.7 b	32 ± 7.5	33.3 ± 2.4 bc
0.125	−	63.2 ± 8.7 c	15 ± 3.5	0.0 ± 0.0 c
0.25	270.0 ± 20.0 a	100.0 ± 0.0 d	0.0 ± 0.0	0.0 ± 0.0 c
0.5	95.3 ± 6.1 b	100.0 ± 0.0 d	0.0 ± 0.0	0.0 ± 0.0 c
1	56.7 ± 3.5 c	100.0 ± 0.0 d	0.0 ± 0.0	0.0 ± 0.0 c
2	41.7 ± 1.5 d	100.0 ± 0.0 d	0.0 ± 0.0	0.0 ± 0.0 c
4	29.0 ± 2.0 de	100.0 ± 0.0 d	0.0 ± 0.0	0.0 ± 0.0 c
8	20.3 ± 1.5 ef	100.0 ± 0.0 d	0.0 ± 0.0	0.0 ± 0.0 c
16	17 ± 1.0 ef	100.0 ± 0.0 d	0.0 ± 0.0	0.0 ± 0.0 c
32	14.7 ± 0.6 f	100.0 ± 0.0 d	0.0 ± 0.0	0.0 ± 0.0 c
0.125 (malachite green)[f]	89.0 ± 8.5 b	100.0 ± 0.0 d	0.0 ± 0.0	0.0 ± 0.0 c
0.06 (malachite green)[f]	−	58.4 ± 5.0 c	29 ± 2.5	21.9 ± 4.7 bc

[a]Values are expressed as mean ± standard deviation of three replicates. Values with different letters in the same column are significant differences ($p < 0.05$). −: Cynatratoside-C at the listed concentrations could not kill 100% nonencysted tomonts after 5 h exposure. [b]MDDNT: mean death duration for killing all nonencysted tomonts within 5 h exposure. [c]MNT: mortality of *I. multifiliis* nonencysted tomonts at 5 h. [d]MNET: mean number of encysted tomonts transformed from nonencysted tomonts at 6 h. [e]MNTLET: mean number of theronts released from each live encysted tomont at 22 h exposure. [f]Positive control.

dx.doi.org/10.1021/jf5018675 | J. Agric. Food Chem. 2014, 62, 7183−7189

Table 3. Reproduction of *I. multifiliis* Encysted Tomonts Post Cynatratoside-C Treatment[a]

concentration (mg/L)	number of encysted tomonts	number of theronts released from each live encysted tomont
0 (control)	52 ± 5.3	280.1 ± 17.0 a
0.015	47 ± 6.1	310.9 ± 12.2 b
0.03	63 ± 9.0	131.7 ± 16.9 c
0.06	49 ± 7.8	0.0 ± 0.0 d
0.125	54 ± 8.2	0.0 ± 0.0 d
0.25	62 ± 13.7	0.0 ± 0.0 d
0.125 (malachite green)[b]	48 ± 7.6	0.0 ± 0.0 d
0.06 (malachite green)[b]	47 ± 12.7	17.6 ± 2.1 d

[a]Nonencysted tomonts were allowed to attach for 6 h, expose to cynatratoside-C for 16 h, and theronts were counted in every well. Values are expressed as mean ± SD of three replicated wells. Values with different letters in the same column are significant differences ($p < 0.05$). [b]Positive control.

the cyst and subsequently died (Figure 4a–d). The same phenomenon was also observed at concentrations of 0.06 and 0.125 mg/L after 22 h exposure.

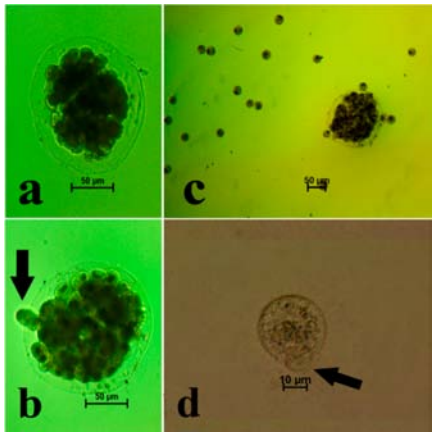

Figure 4. Morphology of encysted tomonts. A normal encysted tomont (a). Encysted tomont exposed to 0.25 mg/L cynatratoside-C for 60 min, showing the first tomite (black arrow) released from the cyst (b). More tomites were released from an encysted tomont (c). Subsequently, a tomite was dead and its cytoplasm (black arrow) was spilled out (d).

Treatment of Ichthyophthiriasis with Cynatratoside-C. Cynatratoside-C at concentration of 2 mg/L completely eliminated all trophonts and cured the infected grass carp within 48 h (100% survival) (Table 4). The infective intensity of grass carp treated with 1 mg/L cynatratoside-C was 184 trophonts/fish, significantly ($p < 0.05$) lower than that of the fish treated with 0.5 mg/L (406 trophonts/fish) and 0 mg/L (357 trophonts/fish).

Table 4. Treatment of Grass Carp Infected by *I. multifiliis* with Cynatratoside-C for 48 h[a]

concentration (mg/L)	infective intensity[b]	survival rate (%)
0 (control)	357 ± 126 a	96.7 ± 5.8 a
0.5	406 ± 48 b	100 ± 0 a
1	184 ± 88 c	100 ± 0 a
2	0 ± 0 d	100 ± 0 a

[a]Values are expressed as mean ± SD of three replicates. In the same column, values with different letters are significant differences ($p < 0.05$). [b]Infective intensity = number of trophonts on grass carp/infected fish number.

DISCUSSION

Medical plants have provided an abundant source of natural products of new parasiticides to control *I. multifiliis*.[8,11,12] Since the crude extracts of *Allium sativum*,[23] *Mucuna pruriens*, and *Carica papaya*[7] were reported to be used to treat *I. multifiliis*, more studies have been conducted to discover new compounds from medical plants.[8−12,24] *C. atratum*, a perennial herb native to East Asia, showed significant parasiticidal effect to *I. multifiliis* in this study. An ethanol extract of *C. atratum* was partitioned with petroleum ether, ethyl acetate, butanol, and water. A bioassay-guided fractionation, a proven method for the discovery of active principles from natural products,[25−27] was used to isolate an anti-*I. multifiliis* compound from *C. atratum*. Finally, the anti-*I. multifiliis* compound was identified as cynatratoside-C by NMR, ESI−MS, and HR-ESI−MS. This is the first report on parasiticidal property of cynatratoside-C. Cynatratoside-C, one of the C-21 steroidal glycosides in *C. atratum*, has a 13,14:14,15-diseco-pregnane-type skeleton. Even though other structurally related analogues, such as cynatratoside-A, cynatratoside-B, cynatratoside-D, and cynatratoside-E, have the same skeleton of 13,14:14,15-diseco-pregnane-type,[22] only cynatratoside-C was isolated by bioassay-guided fractionation. This fact suggested that cynatratoside-C was the main ingredient and the principal compound in *C. atratum* responsible for killing *I. multifiliis*.

Glycosylation plays a key role in the activity of some natural compounds.[28,29] For example, rebeccamycin's inhibition of the topoisomerase I activity by the rebeccamycin analogues is more active than that of the corresponding aglycones lacking the sugar moiety.[28] Compound properties are affected if the glycosyl is changed.[30,31] For example, if the antitumor compound (25S)-ruscogenin 1-*O*-[*O*-*β*-D-glucopyranosyl-(1 → 3)-*O*-*α*-L-rhamnopyranosyl-(1 → 2)-*β*-D-glucopyranoside] from *Brodiaea californica* has a D-xylose added at the C-3 position of its inner glucose, the antitumor activity is significantly reduced.[30] Hence, we expect that the type of carbohydrate chain at C-3 position in the 13,14:14,15-diseco-pregnane-type skeleton of cynatratoside-C will influence the anti-*I. multifiliis* effect.

Once a tomont of *I. multifiliis* settles on a suitable substrate, it reproduces hundreds to thousands of infective theronts.[2,32] Once theronts penetrate into fish skin and gills, the control of the parasite becomes difficult.[33] Therefore, killing the parasite at the reproductive stage is an important way to prevent releasing of infective theronts and protect fish from infection.[12] On the basis of this consideration, trials were conducted to evaluate the parasiticidal effects of cynatratoside-C on nonencysted and encysted tomonts. The results indicated that cynatratoside-C at 0.125 mg/L markedly reduced nonencysted tomonts survival and at 0.06 mg/L completely inhibited encysted tomonts reproduction. Malachite green was used as a positive control, but its concentration of 0.06 mg/L could not completely stop theronts released from the encysted tomonts; the mean number of theronts released from each live tomont was 17. This suggested that cynatratoside-C was more toxic to encysted tomonts than malachite green. Previous studies demonstrated that pentagalloylglucose from *Galla chinensis* at a concentration of 40 mg/L was effective against nonencysted

dx.doi.org/10.1021/jf5018675 | J. Agric. Food Chem. 2014, 62, 7183−7189

tomonts,[12] and chelerythrine and chloroxylonine from *Toddalia asiatica* could be 100% effective against nonencysted tomonts at concentrations of 1.2 and 3.5 mg/L, respectively.[34] As for other chemicals used to treat parasites, potassium ferrate(VI) at a concentration of 19.2 mg/L demonstrated 100% mortality on both nonencysted and encysted tomonts,[35] and a mixture of hydrogen peroxide, peracetic, acetic, and peroctanoic acid at a concentration of 8 mg/L eliminates tomonts.[36] Thus, cynatratoside-C appears to be more effective against *I. multifiliis* than the reported parasiticides.

Published reports demonstrated that nonencysted tomonts were more sensitive to drugs than encysted tomonts, because an encysted tomont secreted a thick cyst wall that prevents drugs from permeating into encysted tomont.[10,35] The methanol extract from *Psoralea corylifolia* at a concentration of 5.00 mg/L kills 100% nonencysted tomonts, but killed only 88.89% encysted tomonts at the same concentration.[10] The acetone extract from *Morus alba* root bark at a dose of 25 and 50 mg/L causes 100% mortality of nonencysted tomonts and encysted tomonts, respectively.[11] However, the encysted tomonts were more susceptible to cynatratoside-C than nonencysted tomonts in this study. The reason for this phenomenon is unclear and needs further study.

The trophonts are more difficult to be killed than the parasite at the free-living stage,[12] because the trophonts are covered by a layer of host epidermis and a thick layer of mucus protects them from drugs in water.[32] In this study, cynatratoside-C at 2 mg/L completely kills all trophonts and cures the infected grass carp within 48 h. The infective intensity of grass carp exposed to 1 mg/L cynatratoside-C was significantly lower than those at 0.5 and 0 mg/L. Other studies on parasiticides, nitazoxanide at 1.5, 2, or 3 mg/L, showed reduction of approximately 98% in the number of trophonts on infected silver catfish (*Rhamdia quelen*) at 96 h exposure.[37] Bronopol utilized once a day for 27 days at concentrations of 2 and 5 mg/L significantly reduced the number of trophonts on juvenile rainbow trout (*Oncorhynchus mykiss*) by 90−98%.[38] The plant-active drugs dihydrosanguinarine and dihydrochelerythrine from *Macleaya microcarpa* were effective against *I. multifiliis* in barbel chub (*Squaliobarbus curriculus*) with median effective concentration (EC_{50}) values of 5.18 and 9.43 mg/L, respectively.[15] Pentagalloylglucose at 20 mg/L was effective for treating *I. multifiliis* infected catfish.[12] These data indicate that concentrations of the therapeutic agents against trophonts are much higher than that of cynatratoside-C. Therefore, cynatratoside-C could be a promising alternative parasiticide against *I. multifiliis*.

Pathological changes occurred after exposure to cynatratoside-C and the plasma membrane of nonencysted tomont was destroyed. This phenomenon was similar to the membrane of nonencysted tomont damaged by pentagalloylglucose.[12] When an encysted tomont was treated with cynatratoside-C, the tomont released abnormal tomites from the cyst. These abnormal tomites were immature theronts, could not infect fish, and finally died. Therefore, we postulate that cyantratoside-C permeates into an encysted tomont across the cyst wall and triggers pathological changes of tomites. Even though the exact mechanism of cynatratoside-C for killing nonencysted tomonts is unknown, it manifests itself microscopically through loss of membrane integrity.

In conclusion, cynatratoside-C isolated from *C. atratum* showed anti-*I. multifiliis* effects in vitro and in vivo. The compound at a very low concentration significantly decreased the survival of nonencysted tomonts and reproduction of encysted tomonts. In addition, the compound can cure the ichthyophthiriasis under laboratory conditions. Therefore, cynatratoside-C is a potential alternative parasiticide to control *I. multifiliis*, and deserves further studies to elucidate the anti-*I. multifiliis* mechanism and evaluate its effectiveness under fish farming conditions.

AUTHOR INFORMATION

Corresponding Author

*Tel.: +86+20+85225808. E-mail: zhangqzdr@126.com.

Funding

This work was supported by the National High Technology Research and Development Program of China (863 Program) (no. 2011AA10A216), Guangzhou Science and Technology Project (no. 2013J4100047), the Marine and Fishery Special Project of Science and Technology in Guangdong Province (A201301B05), and the Fundamental Research Funds for the Central Universities (21612111, 21613105).

Notes

The authors declare no competing financial interest.

REFERENCES

(1) Buchmann, K.; Sigh, J.; Nielsen, C. V.; Dalgaard, M. Host responses against the fish parasitizing ciliate *Ichthyophthirius multifiliis*. *Vet. Parasitol.* **2001**, *100*, 105−116.

(2) Matthews, R. *Ichthyophthirius multifiliis* Fouquet and ichthyophthiriosis in freshwater teleosts. *Adv. Parasitol.* **2005**, *59*, 159−241.

(3) Xu, D. H.; Shoemaker, C. A.; Martins, M. L.; Pridgeon, J. W.; Klesius, P. H. Enhanced susceptibility of channel catfish to the bacterium *Edwardsiella ictaluri* after parasitism by *Ichthyophthirius multifiliis*. *Vet. Microbiol.* **2012**, *158*, 216−219.

(4) Dickerson, H. W.; Findly, R. C. Immunity to *Ichthyophthirius* infections in fish: A synopsis. *Dev. Comp. Immunol.* **2014**, *43*, 290−299.

(5) Shinn, A. P.; Picón-Camacho, S. M.; Bron, J. E.; Conwaya, D.; Yoon, G. H.; Guo, F. C.; Taylor, N. G. H. The anti-protozoal activity of bronopol on the key life-stages of *Ichthyophthirius multifiliis* Fouquet, 1876 (Ciliophora). *Parasitol. Res.* **2012**, *186*, 229−236.

(6) Zhang, C.; Zhang, S.; Diao, H.; Zhao, H.; Zhu, X.; Lu, F.; Lu, Z. Purification and characterization of a temperature- and pH-stable laccase from the spores of *Bacillus vallismortis* fmb-103 and its application in the degradation of malachite green. *J. Agric. Food Chem.* **2013**, *61*, 5468−5473.

(7) Ekanem, A. P.; Obiekezie, A.; Kloas, W.; Knopf, K. Effects of crude extracts of *Mucuna pruriens* (Fabaceae) and *Carica papaya* (Caricaceae) against the protozoan fish parasite *Ichthyophthirius multifiliis*. *Parasitol. Res.* **2004**, *92*, 361−366.

(8) Ling, F.; Wang, J. G.; Lu, C.; Wang, G. X.; Liu, Y. H.; Gong, X. N. Effects of aqueous extract of *Capsicum frutescens* (Solanaceae) against the fish ectoparasite *Ichthyophthirius multifiliis*. *Parasitol. Res.* **2012**, *111*, 841−848.

(9) Yi, Y. L.; Lu, C.; Hu, X. G.; Ling, F.; Wang, G. X. Antiprotozoal activity of medicinal plants against *Ichthyophthirius multifiliis* in goldfish (*Carassius auratus*). *Parasitol. Res.* **2012**, *111*, 1771−1778.

(10) Ling, F.; Lu, C.; Tu, X.; Yi, Y. L.; Huang, A. G.; Zhang, Q. Z.; Wang, G. X. Antiprotozoal screening of traditional medicinal plants: evaluation of crude extract of *Psoralea corylifolia* against *Ichthyophthirius multifiliis* in goldfish. *Parasitol. Res.* **2013**, *112*, 2331−2340.

(11) Fu, Y. W.; Zhang, Q. Z.; Xu, D. H.; Xia, H.; Cai, X. X.; Wang, B.; Liang, J. H. Parasiticidal effects of *Morus alba* root bark extracts against *Ichthyophthirius multifiliis* infecting grass carp. *Dis. Aquat. Org.* **2014**, *108*, 113−127.

(12) Zhang, Q. Z.; Xu, D. H.; Klesius, P. H. Evaluation of an antiparasitic compound extracted from *Galla chinensis* against fish parasite *Ichthyophthirius multifiliis*. *Vet. Parasitol.* **2013**, *198*, 45−53.

(13) Liang, J. H.; Zhang, Q. Z.; Fu, Y. W.; Wang, B. Effect of cinnamaldehyde from *Cinnamomum cassia* on killing *Ichthyophthirius*

multifiliis in vitro. *J. Fish. CHN* **2014**, *38*, 457−463 (Chinese with English abstract).
(14) Yao, J. Y.; Shen, J. Y.; Li, X. L.; Xu, Y.; Hao, G. J.; Pan, X. Y.; Wang, G. X.; Yin, W. L. Effect of sanguinarine from the leaves of *Macleaya cordata* against *Ichthyophthirius multifiliis* in grass carp (*Ctenopharyngodon idella*). *Parasitol. Res.* **2010**, *107*, 1035−1042.
(15) Yao, J. Y.; Zhou, Z. M.; Li, X. L.; Yin, W. L.; Ru, H. S.; Pan, X. Y.; Hao, G. J.; Xu, Y.; Shen, J. Y. Antiparasitic efficacy of dihydrosanguinarine and dihydrochelerythrine from *Macleaya microcarpa* against *Ichthyophthirius multifiliis* in richadsin (*Squaliobarbus curriculus*). *Vet. Parasitol.* **2011**, *183*, 8−13.
(16) Kim, M. G.; Jeon, J. H.; Lee, H. S. Larvicidal activity of the active constituent isolated from *Tabebuia avellanedae* bark and structurally related derivatives against three mosquito species. *J. Agric. Food Chem.* **2013**, *61*, 10741−10745.
(17) Bai, H.; Li, W.; Koike, K.; Satou, T.; Chen, Y. J.; Nikaido, T.; Cynanosides, A.-J. Ten novel pregnane glycosides from *Cynanchum atratum*. *Tetrahedron* **2005**, *61*, 5797−5811.
(18) Bai, H.; Li, W.; Koike, K. Pregnane glycosides from *Cynanchum atratum*. *Steroids* **2008**, *73*, 96−103.
(19) Day, S. H.; Wang, J. P.; Won, S. J.; Lin, C. N. Bioactive constituents of the roots of *Cynanchum atratum*. *J. Nat. Prod.* **2001**, *64*, 608−611.
(20) Lee, K. Y.; Sung, S. H.; Kim, Y. C. New Acetylcholinesterase-inhibitory pregnane glycosides of *Cynanchum atratum* roots. *Helv. Chim. Acta* **2003**, *86*, 474−483.
(21) Bai, H.; Li, W.; Asada, Y.; Satou, T.; Wang, Y.; Koike, K. Twelve pregnane glycosides from *Cynanchum atratum*. *Steroids* **2009**, *74*, 198−207.
(22) Zhang, Z. X.; Zhou, J.; Hayashi, K.; Mitsuhashi, H. Studies on the constituents of Asclepiadaceae plants. LVIII. The structures of five glycosides, cynatratoside-A, -B, -C, -D, and -E, from the Chinese drug "Pai-Wei", *Cynanchum atratum* Bunge. *Chem. Pharm. Bull.* **1985**, *33*, 1507−1514.
(23) Buchmann, K.; Jensen, P. B.; Kruse, K. D. Effects of sodium percarbonate and garlic extract on *Ichthyophthirius multifiliis* theronts and tomocysts. *In vitro* experiments. *N. Am. J. Aquacult.* **2003**, *65*, 21−24.
(24) Chu, C.; Zhang, Q. Z.; Luo, F. Effect of twenty Chinese herbal medicines on killing trophonts, cysts and theronts of *Ichthyophthirius multifiliis in vitro*. *Freshwater Fish* **2010**, *40*, 55−60 (Chinese with English abstract).
(25) Bueno-Silva, B.; Alencar, S. M.; Koo, H.; Ikegaki, M.; Silva, G. V.; Napimoga, M. H.; Rosalen, P. L. Anti-inflammatory and antimicrobial evaluation of neovestitol and vestitol isolated from Brazilian red propolis. *J. Agric. Food Chem.* **2013**, *61*, 4546−4550.
(26) Wang, X.; Radwan, M. M.; Tarawneh, A. H.; Gao, J.; Wedge, D. E.; Rosa, L. H.; Cutler, H. G.; Cutler, S. J. Antifungal activity against plant pathogens of metabolites from the endophytic fungus *Cladosporium cladosporioides*. *J. Agric. Food Chem.* **2013**, *61*, 4551−4555.
(27) Tabanca, N.; Bernier, U. R.; Ali, A.; Wang, M.; Demirci, B.; Blythe, E. K.; Khan, S. I.; Baser, K. H.; Khan, I. A. Bioassay-guided investigation of two *Monarda* essential oils as repellents of yellow fever mosquito *Aedes aegypti*. *J. Agric. Food Chem.* **2013**, *61*, 8573−8580.
(28) Anizon, F.; Belin, L.; Moreau, P.; Sancelme, M.; Voldoire, A.; Prudhomme, M.; Ollier, M.; Sevère, D.; Riou, J. F.; Bailly, C.; Fabbro, D.; Meyer, T. Syntheses and biological activities (topoisomerase inhibition and antitumorand antimicrobial properties) of rebeccamycin analogues bearing modified sugar moieties and substituted on the imide nitrogen with a methyl group. *J. Med. Chem.* **1997**, *40*, 3456−3465.
(29) Teshima, Y.; Ikeda, T.; Imada, K.; Sasaki, K.; El-Sayed, M. A.; Shigyo, M.; Tanaka, S.; Ito, S. Identification and biological activity of antifungal saponins from shallot (*Allium cepa* L. Aggregatum group). *J. Agric. Food Chem.* **2013**, *61*, 7440−7445.
(30) Mimaki, Y.; Nakamura, O.; Sashida, Y.; Koike, K.; Nikaido, T.; Ohmoto, T.; Nishino, A.; Satomi, Y.; Nishino, H. Structures of steroidal saponins from the tubers of *Brodiaea californica* and their inhibitory activity on tumor promoter-induced phospholipid metabolism. *Chem. Pharm. Bull.* **1995**, *43*, 971−976.
(31) Repke, K. R. H.; Megges, R.; Weiland, J.; Schön, R. Digitalis research in berlin-buch-retrospective and perspective views. *Angew. Chem., Int. Ed. Engl.* **1995**, *34*, 282−294.
(32) Dickerson, H. W. In *Ichthyophthirius multifiliis. Fish Parasites: Pathobiology and Protection*; Woo, P. T. K., Buchmann, K., Eds.; CAB International: Wallingford, England, 2012; pp 55−72.
(33) Xu, D. H.; Klesius, P. H. Comparison of serum antibody responses and host protection against parasite *Ichthyophthirius multifiliis* between channel catfish and channel × blue hybrid catfish. *Fish Shellfish Immunol.* **2013**, *34*, 1356−1359.
(34) Shan, X. F.; Meng, Q. F.; Kang, Y. H.; Bian, Y.; Gao, Y. H.; Wang, W. L.; Qian, A. D. Isolation of active compounds from methanol extracts of *Toddalia asiatica* against *Ichthyophthirius multifiliis* in goldfish (*Carassius auratus*). *Vet. Parasitol.* **2014**, *199*, 250−254.
(35) Ling, F.; Wang, J. G.; Wang, G. X.; Gong, X. N. Effect of potassium ferrate(VI) on survival and reproduction of *Ichthyophthirius multifiliis* tomonts. *Parasitol. Res.* **2011**, *109*, 1423−1428.
(36) Picón-Camacho, S. M.; Marcos-Lopez, M.; Beljean, A.; Debeaume, S.; Shinn, A. P. *In vitro* assessment of the chemotherapeutic action of a specific hydrogen peroxide, peracetic, acetic, and peroctanoic acid-based formulation against the free-living stages of *Ichthyophthirius multifiliis* (Ciliophora). *Parasitol. Res.* **2012**, *110*, 1029−1032.
(37) Sutili, F. J.; Gressler, L. T.; Vargas, A. C.; Zeppenfeld, C. C.; Baldisserotto, B.; Cunha, M. A. The use of nitazoxanide against the pathogens *Ichthyophthirius multifiliis* and *Aeromonas hydrophila* in silver catfish (*Rhamdia quelen*). *Vet. Parasitol.* **2013**, *197*, 522−526.
(38) Picón-Camacho, S. M.; Taylor, N. G. H.; Brona, J. E.; Guo, F. C.; Shinn, A. P. Effects of long duration, low dose bronopol exposure on the control of *Ichthyophthirius multifiliis* (Ciliophora), parasitising rainbow trout (*Oncorhynchus mykiss* Walbaum). *Vet. Parasitol.* **2012**, *186*, 237−244.

Table 1. Overview of the Composition and Structural Characteristics of the AXOS Used in This Article[a]

	HBFA-AXOS	HFFA-AXOS	MBFA-AXOS	MFFA-AXOS	LFFA-AXOS
AXOS content (% dm)	73 (±5)	73 (±1)	73 (±1)	74 (±3)	73 (±1)
free ara content (% dm)	<0.1	0.7 (±0.1)	0.1 (±0.1)	0.2 (±0.1)	0.2 (±0.1)
free xyl content (% dm)	<0.1	<0.1	0.7 (±0.1)	0.8 (±0.1)	1.2 (±0.1)
avDPxyl[b]	6.6 (±0.6)	6.6 (±0.1)	3.9 (±0.2)	3.9 (±0.2)	3.8 (±0.1)
avDAS[c]	0.38 (±0.05)	0.39 (±0.01)	0.22 (±0.01)	0.22 (±0.02)	0.19 (±0.01)
oligomeric glucose content (% dm)	12 (±2)	12 (±1)	12 (±1)	13 (±1)	13 (±1)
free FA content (% dm)	0.07 (±0.01)	6.00 (±0.21)	0.01 (±0.01)	1.44 (±0.02)	0.01 (±0.01)
bound FA content (% dm)	7.17 (±0.11)	1.10 (±0.29)	1.67 (±0.06)	0.21 (±0.09)	0.08 (±0.01)
total FA content (% dm)	7.24 (±0.11)	7.11 (±0.12)	1.68 (±0.06)	1.64 (±0.09)	0.09 (±0.01)

[a]Data are expressed as means and standard deviations of triplicate measurements. [b]avDPxyl, average degree of polymerization of the xylan backbone. [c]avDAS, average degree of arabinose substitution.

properties was investigated. Dough properties were studied using the Kieffer dough extensibility rig, and protein extractability was examined for the AXOS enriched breads. Dough pH evolution and the impact of additions on yeast during dough fermentation were studied as well. Furthermore, FA and AXOS recovery from bread and the Trolox Equivalent Antioxidant Capacity (TEAC) values for bread were determined.

MATERIALS AND METHODS

Materials. Commercial wheat flours TB9 (13.9% protein, 0.57% ash, 14.2% moisture content) and Julius (10.3% protein, 0.46% ash, 13.4% moisture content) were provided by Dossche Mills (Deinze, Belgium). All experiments were done using TB9 flour, unless mentioned otherwise. AXOS starting material (MBFA-AXOS) was produced by enzymatic treatment of wheat bran using the procedure described by Swennen et al.[2] with adaptations and obtained from Fugeia (Leuven, Belgium). Other AXOS samples were prepared and characterized as described in Snelders et al.[5] The composition of these samples is presented in Table 1. Throughout the remainder of this Article, AXOS samples are given a code based on their feruloylation. The code consists of "XYFA-AXOS" in which X stands for H, M, or L, indicating that the AXOS sample contained a high, medium, or low level of FA, respectively. The letter B or F at the Y position indicates that most FA was present in a bound or free form, respectively. HBFA-AXOS and HFFA-AXOS had similar carbohydrate structures and high FA level, but differed in the form in which FA was present (bound or free). Also, MBFA-AXOS, MFFA-AXOS, and LFFA-AXOS had similar carbohydrate structures, but specifically differed in the level and/or form in which FA was present. SDS and dithiothreitol were bought from Acros Organics (Geel, Belgium). All other solvents, chemicals, and reagents were of at least analytical grade and purchased from Sigma-Aldrich (Bornem, Belgium).

Methods. *Bread Making.* Bread was made according to a straight-dough method for 10 g of flour.[29] Wheat flour (10.0 g, 14.0% moisture), 0.53 g of compressed commercial yeast (AB Mauri, Merelbeke, Belgium), 0.60 g of sucrose, 0.15 g of NaCl, and 5.60 mL of water were mixed for 240 s in a 10 g pin mixer (National Manufacturing, Lincoln, NE) at 25 °C. Dough was transferred to a fermentation cabinet (National Manufacturing) and fermented for 90 min (30 °C, 90% relative humidity). Doughs were intermediately punched at 52, 77, and 90 min, using a dough sheeter (National Manufacturing). Following the third punch, doughs were molded and proofed (36 min at 30 °C, 90% relative humidity) before baking at 232 °C for 13 min in a rotary oven (Model Hearth, National Manufacturing). Immediately after baking, bread weight and height were measured. Bread volume was analyzed by use of a volumeter based on glass beads displacement.[30] Samples were frozen, freeze-dried, and ground with a laboratory mill (model A10, IKA-Werke GmbH and Co. KG, Staufen, Germany) for further analysis.

To study the effect of the AXOS addition on dough and bread properties, AXOS were added dissolved in the water for bread making. MBFA-AXOS and HBFA-AXOS were added to the bread recipe in different concentrations (1.0−8.0% and 0.25−2.00% AXOS (dm) on flour (dm) basis, respectively), based on their FA content, which corresponded to approximately 200−1800 ppm FA on flour (dm) basis. As the FA content of HBFA-AXOS was not exactly 4 times the FA content of MBFA-AXOS, indicated FA levels (in ppm) are an approximation of the FA levels over the entire range of AXOS additions. Breads were made in triplicate, and control breads were made as described above, without adding AXOS.

Analysis of Dough Extensibility. The Kieffer dough and gluten extensibility rig (Stable Micro Systems Ltd., Surrey, UK) was used for uniaxial dough extensibility measurements as described by Dunnewind et al.[31] Three separate dough samples were prepared by mixing flour (10.0 g, 14.0% moisture) with water (5.6 mL) for 240 s using the above-mentioned pin mixer. Each dough sample was punched, compressed between paraffin oil-coated Teflon plate molds, and rested for 30 min at 30 °C and 90% humidity. As the bottom Teflon plate had grooves, seven to eight dough strands were formed from one dough. For the actual measurement, these strands were clamped at both ends between two plates. The dough strand was pulled upward from the middle until breakage using the Kieffer rig dough extensibility fixture at 3.3 mm/s, attached to an Instron 3342 Single Column Testing System (Instron, Norwood, MA) with a 50 N load cell. From the load−displacement curve, dough extensibility (maximum extension until first point of breakage, mm), resistance to extension (maximum load until breakage, N), and total work needed for breakage (area under curve, mJ) were derived.

When AXOS were added, they were added solubilized in water, similar to described for bread making. Free FA was dissolved in ethanol, and 0.1 mL of this solution was added to flour, together with 5.6 mL of water. HBFA-AXOS and HFFA-AXOS were added in different concentrations ranging from 0.5% to 2.0% AXOS (dm) on flour (dm) basis, and MBFA-AXOS, MFFA-AXOS, and LFFA-AXOS in different concentrations ranging from 1.0% to 8.0% AXOS (dm) on flour (dm) basis, which in each case corresponds to approximately 200−1800 ppm FA on flour (dm) basis. Control samples without added AXOS or FA in the water or ethanol, respectively, were prepared in the same manner. Dough samples were prepared in triplicate, and for each dough, the averages of the above-mentioned rheological properties from 7 to 8 strands were determined.

Doughs with Julius flour were prepared by mixing flour (10.0 g, 14.0% moisture) with water (6.0 mL) for 165 s. Dough extensibility analyses were as described above. MBFA-AXOS was added directly, dissolved in water, and free FA was added in 0.1 mL of ethanol. In a separate experiment, MBFA-AXOS were added in different concentrations [0.0−8.0% AXOS (dm) on flour (dm) basis] together with different levels of free FA (0−1800 ppm FA) to achieve a constant total addition of 1800 ppm FA with varying concentrations of AXOS.

Analysis of Dough Protein Content Extractability and Extract Composition. Protein contents of dough samples, prepared as described above, rested for 30 min, freeze-dried, and ground, were determined by the Dumas method, an adaptation of the AOAC[32] to an automated protein analysis system (EAS Vario Max N/CN, Elt, Gouda, The Netherlands).

Ground freeze-dried dough samples were extracted with a 0.05 M sodium phosphate buffer (pH 6.8) containing 2.0% SDS (1.0 mg dough proteins/mL extraction buffer), centrifuged (10 min, 10 000*g*), and filtered (0.45 μm). Dough protein extractions were also performed under reducing conditions with the above-described buffer containing 1.0% (w/v) dithiothreitol and 2.0 M urea under nitrogen atmosphere to determine total extractability.

Size-exclusion high-performance liquid chromatography (SE-HPLC) on dough extracts was conducted using a LC-2010 system (Shimadzu, Kyoto, Japan) with automatic injection as described by Lagrain et al.[33] To this end, supernatants (60 μL) were loaded on a BioSep SECS4000 column (Phenomenex, Torrance, CA) and eluted with acetonitrile/water (50/50 v/v) containing 0.05% (v/v) TFA. The flow rate was 1.0 mL/min at a column temperature of 30 °C, and eluted proteins were detected at 214 nm. The elution profiles of nonreduced samples were divided into four fractions. First, the elution profile was separated using the lowest extinction value between the two major peaks as the cutoff point.[33] Peak 4 represents lower molecular weight proteins corresponding to SDS-extractable monomeric gluten proteins (mainly gliadins). The other major peak was subdivided into three other peaks based on reoccurring kinks in the profile. Resulting peaks most likely contain SDS-extractable high molecular weight polymeric gluten proteins (peak 1), low molecular weight polymeric gluten proteins (peak 2), and oligomeric gluten proteins (peak 3). SDS-extractability of proteins in the four distinct peaks of a sample in the absence of reducing conditions was expressed as the area under curve relative to the total area under curve of the SDS-extraction profile of the control sample under reducing conditions (100%).

Analysis of Carbon Dioxide Production by Yeast. The Risograph (National Manufacturing) was used to measure carbon dioxide production during 90 min in fermenting dough. Doughs were prepared as described above, with or without AXOS (added in the water phase) or FA (added in an additional 0.1 mL of ethanol).

Determination of pH of AXOS Solutions and Dough. The pH of AXOS solutions used was measured using HI 9126 pH probe (Hanna Instruments, Temse, Belgium). The pH of doughs prepared with and without yeast was measured before and after fermentation and after resting, respectively, by placing the above-mentioned pH probe directly in the dough.

Determination of WE-AX Content. WE-AX content of ground freeze-dried bread samples was determined to calculate the recovery of AXOS added to the bread recipe after baking. Extraction and quantification was done essentially as described by Loosveld et al.[34] Aqueous extracts of ground freeze-dried bread samples (2.00 g) were obtained by suspending them in water (1:10 w/v), shaking (30 min, room temperature), and centrifugation (3000*g*, 15 min, 7 °C). Monosaccharide composition was determined by gas chromatography after hydrolysis (60 min, 2.0 M TFA, 110 °C), reduction with $NaBH_4$, and acetylation of alditols. WE-AX content of one bread was determined in duplicate.

Determination of the FA and 4-Vinylguaiacol Content. Total FA and 4-vinylguaiacol (4-VG) content were analyzed after alkaline hydrolysis as described by Antoine et al.[35] with some modifications. Flour or bread sample (±100 mg) was suspended in 2.0 M sodium hydroxide (4.0 mL) and saponified under slow stirring for 2 h at 35 °C under nitrogen atmosphere and protected from light. Samples were acidified to pH 2.0 with 4.0 M hydrogen chloride, followed by addition of caffeic acid as internal standard. Phenolic acids were extracted twice with diethyl ether (2.0 mL). Ether was evaporated under a nitrogen flow, and phenolic acids were dissolved in methanol and filtered (0.45 μm). Monomeric FA and 4-VG were separated on a Luna Phenyl-Hexyl column (250 mm × 4.6 mm i.d., 5 μm particle size, plus 3 mm × 4.6 mm i.d. guard column; Phenomenex) in a LC-20AT modular high-performance liquid chromatography system (Shimadzu). After injection of 20 μL of sample, a ternary gradient system of 1 mM aqueous TFA (eluent A), acetonitrile/1 mM aqueous TFA [90/10 (v/v)] (eluent B) and methanol/1 mM aqueous TFA [90/10 (v/v)] (eluent C) at 45 °C was used according to Dobberstein and Bunzel[36] with some modifications (Table 2). UV-detection (Shimadzu, UV-10A detector) was carried out at 280 nm. The elution profile was also checked for additional peaks, possibly occurring due to the presence of di-FA in the tested sample.[36]

Table 2. Linear Elution Gradient for the Separation of FA and 4-Vinylguaiacol by Use of Reversed Phase HPLC on a Luna Phenyl-Hexyl Column[a]

time (min)	eluent A (%)	eluent B (%)	eluent C (%)
0.0	87	13	0
10.0	87	13	0
20.0	77	20	3
25.0	70	25	5
40.0	25	50	25
45.0	87	13	0
55.0	87	13	0

[a]Eluent A: 1.0 mM aqueous trifluoroacetic acid. Eluent B: acetonitrile/1.0 mM aqueous trifluoroacetic acid (90/10 v/v). Eluent C: methanol/1.0 mM aqueous trifluoroacetic acid (90/10 v/v).

Determination of Amino Acid Composition. The amino acid composition of flour and ground freeze-dried bread samples was determined after acid hydrolysis as described by Rombouts et al.[37] Samples (10.0 mg dm protein) were hydrolyzed by heating at 110 °C for 24 h in 1.0 mL of 6.0 M hydrogen chloride containing 1.5 mM norleucine (as internal standard) and 0.1% phenol, after the samples were flushed with nitrogen. Bread samples were brought under nitrogen atmosphere prior to hydrolysis by flushing the headspace during 10 s with nitrogen gas to prevent amino acid oxidation. After hydrolysis, samples were subsequently evaporated (110 °C, 180 min), resuspended in 5 mL of water, and diluted 40-fold. For determination of cysteine/cystine levels, cysteine/cystine residues were first converted to cysteic acids as described by Moore[38] with some modifications. Performic acid solution was prepared by mixing 30% hydrogen peroxide and 88% formic acid in a 1/9 volume ratio. This mixture was kept at room temperature for 60 min before cooling on ice (0 °C). Performic acid solution (4.0 mL) was added to flour or ground freeze-dried bread (10.0 mg dm protein), and the mixture was vortexed until the sample was completely dissolved. The reaction mixture was kept on ice for 16 h before reducing the excess of performic acid by adding 0.6 mL of hydrogen bromide (48%). After 5 min, the remaining bromine and formic acid were evaporated (60 °C, 1 mbar, 120 min) using a rotational vacuum concentrator (Q-Lab, Vilvoorde, Belgium).

Samples were filtered (0.22 μm) before separation on a Dionex BioLC system (Sunnyvale, CA) as described by Rombouts et al.[37] The system was equipped with a GS50 gradient pump with online degasser, an AS50 autosampler with a thermal compartment, and an ED50 electrochemical detector containing both a gold working electrode and a pH reference electrode. Separation of 25 μL samples was performed at 30 °C with an AminoPac PA10 guard (Dionex Benelux, 50 × 2 mm) and an analytical (Dionex Benelux, 250 × 2 mm) column at a flow rate of 0.25 mL/min. Chromeleon Version 6.70 software (Dionex Benelux) was used for chromatographic system control, data acquisition, and data analysis. Gradient conditions and pulsed amperometric detection waveform were described in Rombouts et al.[37]

Determination of the Antioxidant Capacity. Determination of the antioxidant capacity of bread samples was based on their ability to scavenge 2,2′-azino-bis(3-ethylbenzothiazoline-6-sulfonic acid) diammonium salt (ABTS) radicals. Prior to analysis, ABTS radicals were generated in McIlvaine buffer (pH 6.5, prepared by mixing appropriate amounts of 0.10 M citric acid and 0.20 M disodium phosphate) as described in Snelders et al.[5] The antioxidant reaction was started by adding 6.0 mL of radical solution to 5.0 mg of freeze-dried bread sample in a centrifuge test tube, as described by Serpen et al.[39] with some modifications. The tubes were vortexed (10 s) and shaken (20 min) to facilitate reaction between the solid particles and the ABTS radicals. When the shaking stopped, the solid particles spontaneously precipitated, and absorbance measurements at 734 nm

(Ultrospec III UV/vis spectrophotometer, GE Healthcare, Piscataway, NJ) were performed exactly 30 min after addition of the radical solution. ABTS radical solution was used as blank. A calibration curve was made between 0.5 and 25.0 μM Trolox (final concentration in cuvette). Therefore, Trolox was dissolved in ethanol and diluted in a range of concentrations. Antioxidant capacity measurements were performed by adding 5.9 mL of radical solution to 0.1 mL of Trolox solution. For the control of the calibration curve, 5.9 mL of radical solution was added to 0.1 mL of ethanol, while the control for the bread samples existed as 6.0 mL of radical solution. Analysis was done in duplicate for all produced breads and flour.

Statistics. Statistical analysis of the results was performed using SAS software 9.2 (SAS Institute, Inc., Cary, NC). Two-way analysis of variation (ANOVA) was performed to compare analysis results. A Tukey multiple comparison procedure was used with a 5% family significance level.

RESULTS AND DISCUSSION

The impact of addition of AXOS and associated FA to the bread recipe on dough and bread properties was investigated. To this end, on the one hand, feruloylated AXOS were produced and added to dough. On the other hand, free FA was added to dough in levels similar to FA levels present in AXOS fortified doughs. The impact of these additions on rheological dough properties, dough pH, gluten network formation, and yeast fermentation was studied. Impact of AXOS addition on (specific) volume of breads was determined. Conversely, the impact of bread making on the antioxidant capacity and extractability of AXOS and associated FA was assessed as well.

Impact of Addition of AXOS and FA on Dough Rheological Properties. Rheological properties of doughs were determined with the Kieffer dough and gluten extensibility rig. Both the level of the added AXOS as well as their FA content influenced the rheological properties of the resulting doughs. In Table 3, rheological properties of doughs with added AXOS with a high FA content (HBFA-AXOS), AXOS with a medium FA content (MBFA-AXOS), and free FA are summarized.

Addition of HBFA-AXOS to dough resulted in an increased dough extensibility and a decreased resistance to extension, already at a low dosage of 0.5%. At higher dosages, when up to 2% of these AXOS samples were added to dough, the extensibility almost doubled, while the resistance to extension was more than halved as compared to the control. The work needed for breakage of the dough was not influenced as the impact on dough extensibility and impact on dough resistance to extension counteracted each other. Only at the highest level of addition (2% in case of HBFA-AXOS), a significant but small decrease in total work needed for breakage was observed. The impact of free FA on dough properties was similar to that of HBFA-AXOS, suggesting that the effect of FA was predominant upon addition of AXOS. The results concerning the impact of free FA on rheological dough properties are in agreement with previous studies.[26−28] Previous research also showed that FA needs to be present in the soluble fraction of the dough to be reactive,[22−24] as is most probably the case for FA esterified to AXOS. HFFA-AXOS, which only differs from HBFA-AXOS in the appearance of FA (free vs bound), had the same effect on dough rheological properties as HBFA-AXOS (Table 4), indicating that the appearance of FA did not matter.

However, the FA-mediated impact on dough rheology as described above was not seen when AXOS with a low to medium FA content were added (MBFA-AXOS, MFFA-AXOS, and LFFA-AXOS) to dough (Table 3 and Table 5). Upon

Table 3. Extensibility (E), Resistance to Extension (R), and Total Work Needed for Breakage (W) of Doughs with Added Free FA or AXOS (HBFA-AXOS and MBFA-AXOS) As Determined with Kieffer Dough and Gluten Extensibility Rig[a]

	free FA			HBFA-AXOS				MBFA-AXOS			
FA equiv (ppm FA/dm flour)[b]	E (mm)	R (N)	W (mJ)	dose (% dm AXOS/dm flour)	E (mm)	R (N)	W (mJ)	dose (% dm AXOS/dm flour)	E (mm)	R (N)	W (mJ)
0	32 (±2) Ba	0.36 (±0.02) Ab	7.6 (±0.4) ABb	0.00	32 (±1) Ca	0.41 (±0.02) Aa	8.7 (±0.4) Aa	0.00	32 (±1) Aa	0.41 (±0.02) Ca	8.7 (±0.4) Ba
200	34 (±1) Ba	0.35 (±0.01) Ab	7.9 (±0.2) Aa	0.25				1.00	30 (±2) ABa	0.48 (±0.01) BCa	9.3 (±1.6) Ba
500	32 (±1) Bb	0.34 (±0.03) ABb	7.5 (±0.6) ABa	0.50	40 (±2) BCa	0.31 (±0.01) Ba	8.5 (±0.4) Aa	2.00	32 (±1) Ab	0.45 (±0.03) BCa	9.2 (±0.5) Ba
750	36 (±4) Bb	0.30 (±0.04) ABa	7.3 (±0.2) ABb	0.75	45 (±2) ABCa	0.27 (±0.02) BCa	8.7 (±0.2) Aa	3.00			
1000	37 (±5) Bb	0.30 (±0.06) ABb	7.8 (±0.1) Aa	1.00	44 (±2) ABCa	0.25 (±0.01) CDb	8.1 (±0.4) ABa	4.00	27 (±1) Bc	0.53 (±0.04) Ba	9.1 (±0.8) Ba
1200	39 (±3) Bb	0.25 (±0.03) BCb	7.1 (±0.1) ABb	1.30	53 (±2) ABa	0.22 (±0.02) DEb	8.2 (±0.6) ABb	5.00	32 (±1) Ac	0.53 (±0.01) Ba	10.7 (±0.5) Ba
1500	57 (±4) Aa	0.16 (±0.02) Cb	6.6 (±0.4) Bb	1.50	56 (±6) Aa	0.19 (±0.03) Eb	7.6 (±0.5) ABb	6.00	28 (±1) Bb	0.55 (±0.03) Ba	10.0 (±1.1) Ba
1800	50 (±4) Aa	0.16 (±0.04) Cb	6.5 (±0.5) Bb	2.00	55 (±10) Aa	0.17 (±0.02) Eb	7.0 (±0.7) Bb	8.00	32 (±1) Ab	0.68 (±0.03) Aa	13.4 (±0.03) Aa

[a]Free FA was added at the same concentration as FA present in the samples with added AXOS. In each row, characteristics of doughs with approximately the same amount of added FA, originating from different AXOS samples or free FA, are compared. Data are expressed as means and standard deviations. Values from the same sample at different doses differ significantly ($p < 0.05$) when not sharing the same uppercase letter. Values from different samples at the same dose (FA content) differ significantly ($p < 0.05$) when not sharing the same lowercase letter. [b]Approximate levels of added FA due to addition of AXOS or free FA (FA/dm flour expressed in ppm).

dx.doi.org/10.1021/jf502315g | J. Agric. Food Chem. 2014, 62, 7190−7199

Table 4. Extensibility (E), Resistance to Extension (R), and Total Work Needed for Breakage (W) of Doughs with Added HBFA-AXOS and HFFA-AXOS As Determined with Kieffer Dough and Gluten Extensibility Rig[a]

		HBFA-AXOS[c]			HFFA-AXOS		
FA equiv (ppm FA/dm flour)[b]	dose (% dm AXOS/dm flour)	E (mm)	R (N)	W (mJ)	E (mm)	R (N)	W (mJ)
0	0	32 (±1) C	0.41 (±0.02) A	8.7 (±0.4) A	32 (±1) C	0.41 (±0.02) A	8.7 (±0.4) A
500	0.50	40 (±2) BC	0.31 (±0.01) B	8.5 (±0.4) A	40 (±5) BC	0.29 (±0.03) B	8.3 (±1.1) A
750	0.75	45 (±2) ABC	0.27 (±0.02) BC	8.7 (±0.2) A	43 (±5) B	0.27 (±0.02) BC	8.4 (±0.5) A
1000	1.00	44 (±2) ABC	0.25 (±0.01) CD	8.1 (±0.4) AB	42 (±3) BC	0.28 (±0.02) B	8.5 (±0.6) A
1200	1.30	53 (±2) AB	0.22 (±0.02) DE	8.2 (±0.6) AB	50 (±4) AB	0.23 (±0.01) CD	8.3 (±0.4) A
1500	1.50	56 (±6) A	0.19 (±0.03) E	7.6 (±0.5) AB	55 (±4) A	0.20 (±0.01) D	8.4 (±0.6) A
1800	2.00	55 (±10) A	0.17 (±0.02) E	7.0 (±0.7) B	50 (±1) AB	0.21 (±0.01) D	7.7 (±0.5) A

[a]In each row, characteristics of doughs with approximately the same amount of added AXOS and FA, originating from different AXOS samples, are compared. Data are expressed as means and standard deviations. Values from the same sample at different doses differ significantly ($p < 0.05$) when not sharing the same uppercase letter. Values from different samples at the same dose did not differ significantly ($p > 0.05$). [b]Approximate levels of added FA due to addition of AXOS or free FA (FA/dm flour expressed in ppm). [c]Values obtained from Table 3.

addition of higher concentrations of these AXOS samples, the maximum extensibility of dough remained more or less constant, while the resistance to extension increased. As a consequence, total work needed for breakage increased as well when 8% of these AXOS was added. Although FA was present in the same levels as tested for free FA or FA-enriched AXOS when MBFA-AXOS or MFFA-AXOS were added, similar effects were hence not observed when also relatively high levels of carbohydrates in the form of AXOS were present. Therefore, addition of MBFA-AXOS, MFFA-AXOS, and LFFA-AXOS, with the latter having a lower FA content, had a similar impact on dough rheology. These observations were confirmed by comparing rheological properties of doughs with different levels of AXOS addition, combined with free FA addition, to obtain a constant combined high level of total FA (1800 ppm FA) (Table 6). Maximum extensibility upon addition of 1800 ppm FA only differed from the control when AXOS were added in concentrations lower than 2% (resulting in higher extensibility) or when 8% (resulting in lower extensibility) was added. Addition of 1800 ppm free FA also led to a reduced resistance to extension as compared to the control dough. However, upon addition of increasing levels of MBFA-AXOS, while keeping a constant total level of 1800 ppm FA addition, dough resistance to extension increased and was significantly higher than that of the control dough when 5% or more MBFA-AXOS were added. There was a trend of increased total work needed for breakage upon increasing levels of AXOS addition, which became significant at 6% and more addition. High levels of AXOS might compete for water or increase dough liquor viscosity. Indeed, maximum resistance to dough extension increases when less water is available for the gluten network[40] and/or when dough viscosity is increased.[41] This dough dehydration or stiffening effect was more dominant than the FA-mediated effect of feruloylated AXOS or free FA when the FA levels of the AXOS were not high.

Impact of Addition of AXOS and FA on Dough pH. As FA, and possibly also AXOS, have a weak acidic nature, they could affect dough pH. Dough pH can influence sulfhydryl−disulfide protein interchange reactions[40] and formation of other covalent bonds between gluten proteins.[42] In addition, charge repulsion of gluten strands and water binding, which influences dough stickiness, depends on dough pH.[40] Solutions with MBFA-AXOS and HBFA-AXOS used in dough and bread making had varying pH values (5.1−6.0), which were lower for the FA-enriched AXOS sample (HBFA-AXOS) and decreased when higher levels of AXOS were dissolved. Despite this, pH values of the obtained doughs were at every stage (before and after fermentation) not significantly different for the control doughs and doughs with added free FA, HBFA-AXOS, or MBFA-AXOS. Before fermentation, dough pH ranged from 5.2 to 5.3 for the different samples, and decreased to about 5.0 after dough fermentation (results not shown). As no significant differences in pH between doughs with different levels of AXOS or free FA were found, the observed differences in dough properties upon addition of AXOS or free FA cannot be explained by acidification.

Impact of Addition of AXOS and FA on Gluten Network Formation. SDS-extractability of dough proteins in the absence of reducing conditions was used to assess the impact of AXOS and FA on gluten network formation, as the extent of reducible disulfide bonds might be affected. The observed increase in SDS-extractability upon addition of higher levels of AXOS or free FA as compared to the SDS-extractability of the control (from approximately 61% to 66%, respectively) was not significant (results not shown). However, the level of SDS-extractable high molecular weight polymeric gluten proteins, as demonstrated by the area under the curve of the first peak, did increase upon increasing AXOS or free FA levels (Figure 1 and Table 7). When MBFA-AXOS, HBFA-AXOS, or free FA were added to the same level of FA, they had a similar effect on SDS-extractability. An increase in SDS-extractable high molecular weight polymeric gluten proteins upon addition of free FA was also observed in previous studies.[26,27]

Limited dough breakdown might be provoked due to reaction of FA (free or bound to AXOS) with thiyl radicals, formed upon disulfide bond breakage during mixing.[43] As a result, reinforcement of the gluten network through reformation of disulfide bonds is hindered.[22] However, the fate of the formed (AXOS esterified) FA radicals is less clear. Jackson and Hoseney[23] proposed the formation of an cysteine-FA adduct. This would explain the reducing effect of the addition of FA, which might act as a sulfhydryl blocking agent, and result in an increased SDS-extractability and formation of a more sticky dough.[44] Another possible fate of FA is the formation of di-FA resulting from FA radicals formed after reaction with thiyl radicals. However, a decrease in monomeric FA and formation of di-FA was not always observed, unless oxidizing conditions were present.[19,20]

The small increase in SDS-extractability of dough proteins might not be the only impact of AXOS or FA on gluten.

Table 5. Extensibility (E), Resistance to Extension (R), and Total Work Needed for Breakage (W) of Doughs with Structurally Related AXOS with Different FA Appearance and/or Content (MBFA-AXOS, MFFA-AXOS, LFFA-AXOS) As Determined with Kieffer Dough and Gluten Extensibility Rig[a]

	MBFA-AXOS[b]			MFFA-AXOS			LFFA-AXOS		
dose (% dm AXOS/dm flour)	E (mm)	R (N)	W (mJ)	E (mm)	R (N)	W (mJ)	E (mm)	R (N)	W (mJ)
0.00	32 (±1) Aa	0.41 (±0.02) Ca	8.7 (±0.4) Ba	32 (±1) Aa	0.41 (±0.02) Ca	8.7 (±0.4) BCa	32 (±1) Aa	0.41 (±0.02) Ba	8.7 (±0.4) Ba
1.00	30 (±2) ABa	0.48 (±0.01) BCa	9.3 (±1.6) Ba	27 (±3) Ba	0.47 (±0.03) BCa	8.3 (±0.5) Ca	29 (±2) Aa	0.47 (±0.05) ABa	9.2 (±1.7) Ba
2.00	32 (±1) Aa	0.45 (±0.03) BCa	9.2 (±0.5) Ba	31 (±1) ABa	0.43 (±0.01) Ca	8.9 (±0.4) BCa	28 (±2) Aa	0.44 (±0.05) Ba	9.2 (±1.3) Ba
4.00	27 (±1) Bb	0.53 (±0.04) Ba	9.1 (±0.8) Ba	30 (±2) ABa	0.49 (±0.01) BCa	9.7 (±0.7) Ba	31 (±2) Aa	0.47 (±0.02) ABa	9.3 (±0.3) Ba
6.00	28 (±1) Bb	0.55 (±0.03) Ba	10.0 (±1.1) Ba	29 (±2) ABa	0.54 (±0.05) Ba	10.1 (±0.7) Ba	29 (±3) Aa	0.56 (±0.11) ABa	10.5 (±0.9) ABa
8.00	32 (±1) Ab	0.68 (±0.03) Aa	13.4 (±0.03) Aa	29 (±1) ABa	0.64 (±0.05) Aa	12.7 (±0.3) Aa	30 (±2) Aa	0.62 (±0.06) Aa	12.2 (±0.3) Aa

[a]Data are expressed as means and standard deviations. Values from the same sample at different doses differ significantly ($p < 0.05$) when not sharing the same uppercase letter. Values from different samples at the same AXOS dose differ significantly ($p < 0.05$) when not sharing the same lowercase letter. [b]Values obtained from Table 3.

The observed changes in rheological properties of doughs might be caused by changes in noncovalent interactions, such as hydrogen bonds or hydrophobic interactions, as well. The hydroxyl group of FA might interact with a carbonyl group of proteins.[45] FA and protein interactions can be further stabilized by hydrophobic interactions between the aromatic ring of FA and certain hydrophobic/aromatic amino acids.[45] Interactions between polyphenols and proline residues of proteins are well established.[46] In this way, AXOS and FA might disturb hydrophobic gluten interactions.

Impact of Addition of AXOS and FA on Yeast Fermentation. As yeast fermentation is a major factor determining bread volume, possible inhibition of yeast in dough by added AXOS and FA was determined using the Risograph. Although it is known that FA might inhibit yeast fermentation,[28,47] similar CO_2 production rates in the control doughs and doughs with AXOS or free FA up to FA levels of about 1800 ppm (corresponding to the addition of 8% MBFA-AXOS or 2% HBFA-AXOS) were observed (results not shown). Yeast inhibition might only occur in the presence of higher levels of FA, or when FA is not esterified.[28]

Impact of Addition of AXOS and FA on Bread Volume and Specific Volume. Because of the different impact of MBFA-AXOS and HBFA-AXOS on dough rheology, breads with different doses of these AXOS [up to 8% and 2% AXOS (dm)/flour (dm), respectively, yielding up to 1800 ppm FA in both cases] were prepared. Volumes of breads made with and without added AXOS varied around 49−50 cm^3 in all cases. The addition of AXOS up to a concentration of 1800 ppm FA equiv hence did not impact bread volume. On sight, there were no observational differences in crumb structure and crust of the produced breads. Doughs with high levels of MBFA-AXOS felt drier during bread making. The specific bread volumes when MBFA-AXOS was added in concentrations of 1−8% on flour dry matter basis decreased from 4.0 to 3.8 cm^3/g ($p < 0.05$), probably as the result of higher levels of dry matter in the AXOS enriched breads (Table 8). Doughs with 2% added HBFA-AXOS were sticky, and higher levels of HBFA-AXOS even led to unmanageable doughs. Nonetheless, neither the specific nor the regular bread volume changed upon addition of HBFA-AXOS up to 2% of flour dry matter. Previous research also showed that the impact of FA on bread volume is nonexistent or limited when less than 850 ppm FA is added to dough.[26,28] In contrast to these results and our results obtained with AXOS addition, lower bread volumes have been reported for doughs supplemented with 250 ppm FA in another study.[27]

A previous study also demonstrated that effects of additives on dough and bread properties can differ. Although glutathione had a weakening effect on the gluten network during the mixing phase, resulting breads did not necessarily have smaller volumes.[48] Glutathione, for example, increased the SDS-extractability of proteins during the mixing phase, which was here also observed to a small extent for FA and AXOS addition, but eventually resulted in the same SDS-extractability of proteins as the control after the fermentation and baking phase. Han and Koh[26] also demonstrated that SDS-extractabilities of proteins were similar for the control breads or breads with 850 ppm FA added to the recipe. If during the baking phase, the initial levels of sulfhydryl groups would be higher, this might facilitate sulfhydryl−disulfide exchange reactions and resulting gluten polymerization. This can only be the case if the sulfhydryl groups are free,[48] which would not be the case if cysteine-FA adducts had formed. However, no loss of cysteine

Table 6. Extensibility (E), Resistance to Extension (R), and Total Work Needed for Breakage (W) of Dough with Different Doses of MBFA-AXOS with a Constant Total FA Addition As Determined with Kieffer Dough and Gluten Extensibility Rig[a]

dose		MBFA-AXOS + free FA (combined total of 1800 ppm FA)		
MBFA-AXOS (% dm AXOS/dm flour)	free FA (ppm/dm flour)	E (mm)	R (N)	W (mJ)
0.00	0	36 (±1) CD	0.19 (±0.01) CD	4.8 (±0.2) CD
0.00	1800	41 (±1) AB	0.13 (±0.01) E	4.0 (±0.1) D
1.00	1600	41 (±2) A	0.16 (±0.01) DE	4.8 (±0.1) CD
2.00	1400	38 (±1) BC	0.19 (±0.01) CDE	4.9 (±0.1) CD
4.00	900	33 (±2) DE	0.22 (±0.03) BC	5.3 (±0.6) BC
5.00	700	33 (±1) DE	0.25 (±0.02) AB	5.6 (±0.3) BC
6.00	400	33 (±1) DE	0.26 (±0.02) AB	6.2 (±0.3) AB
8.00	0	32 (±1) E	0.30 (±0.02) A	6.8 (±0.3) A

[a]Doughs were prepared with Julius flour. Data are expressed as means and standard deviations. Values from different samples differ significantly ($p < 0.05$) when not sharing the same uppercase letter.

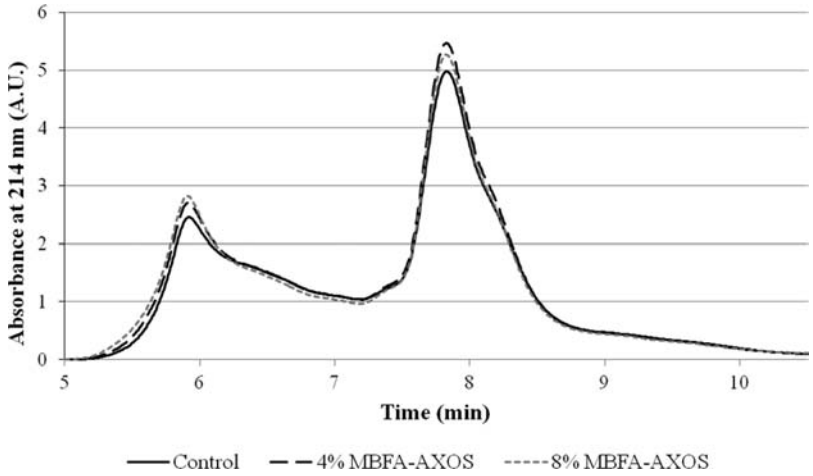

Figure 1. SE-HPLC profile of SDS-extractable dough proteins under nonreducing conditions of doughs with added MBFA-AXOS [%AXOS (dm)/flour (dm)].

Table 7. SDS-Extractability of Gluten Proteins in Doughs with Added Free FA or AXOS (MBFA-AXOS and HBFA-AXOS)[a]

free FA		HBFA-AXOS		MBFA-AXOS	
FA equiv (ppm FA/dm flour)[b]	area under curve peak 1 (%)	dose (% dm AXOS/dm flour)	area under curve peak 1 (%)	dose (% dm AXOS/dm flour)	area under curve peak 1 (%)
0	11.6 (±1.2) B	0.00	10.5 (±1.0) B	0	10.5 (±1.0) B
1000	13.4 (±0.5) AB	1.00	12.7 (±0.6) A	4.00	12.0 (±0.3) AB
1800	14.2 (±0.3) A	2.00	13.9 (±0.5) A	8.00	14.2 (±0.3) A

[a]SDS-extractability of dough proteins eluting in peak 1 of a sample in the absence of reducing conditions was expressed as the area under curve relative to total area under curve of SDS-extraction profile under reducing conditions of the control sample (100%). Data are expressed as means and standard deviations. Values from the same sample at different doses differ significantly ($p < 0.05$) when not sharing the same uppercase letter in the first column. Values from different samples at the same dose (FA content) did not differ significantly ($p > 0.05$). [b]Approximate levels of total added FA due to addition of AXOS or free FA (FA/dm flour expressed in ppm).

or monomeric FA during bread making was observed for any of the tested additions (data not shown).

Impact of the Bread Making Process on Antioxidant Properties and Extractability of AXOS and Associated FA. The antioxidant capacity of breads was measured by use of the TEAC assay. The results are summarized in Table 8. The antioxidant capacity of the control bread without added AXOS was 11.6 μmol Trolox/g dm, and it increased upon addition of AXOS. At the highest level of AXOS addition, that is, 8% of MBFA-AXOS or 2% of HBFA-AXOS on flour dm basis, the antioxidant capacity of bread almost doubled in comparison with that of the control. FA was, as previously demonstrated,[5] the major factor contributing to the antioxidant capacity of AXOS as antioxidant capacities of breads with added MBFA-AXOS were similar to those with added HBFA-AXOS when the level of FA added was similar. The increase in antioxidant capacity of breads due to AXOS addition was a bit lower than expected based on the antioxidant capacity of AXOS, as determined in Snelders et al.,[5] and the control bread. However, the conditions of the assay differed, and the presence of solid particles might influence the reaction between antioxidants and radicals. Cross-linking of FA would lower the antioxidant capacity as well.[5] However, this did not occur during bread making as the level of monomeric FA (sum of endogenous FA and FA from AXOS addition) was not altered after bread making and the areas of some small peaks (about 1% of peak area of monomeric FA) in RP-HPLC profiles, probably representing di-FA moieties, did not differ for breads with or

Table 8. Volume, Specific Volume, and Antioxidant Capacity of Breads with and without the Presence of MBFA-AXOS and HBFA-AXOS As Determined with TEAC[a]

	MBFA-AXOS			HBFA-AXOS		
FA equiv (ppm FA/dm flour)[b]	dose (% dm AXOS/dm flour)	specific volume (cm^3/g)	TEAC (μmol Trolox/g dm flour)	dose (% dm AXOS/dm flour)	specific volume (cm^3/g)	TEAC (μmol Trolox/g dm flour)
0	0.00	4.01 (±0.08) Aa	11.6 (±0.1) E	0.00	4.01 (±0.08) Aa	11.6 (±0.1) E
200	1.00	3.94 (±0.06) ABa	11.9 (±1.7) DE	0.25	3.85 (±0.21) Aa	11.9 (±1.7) DE
500	2.00	3.97 (±0.04) ABa	14.1 (±0.5) CD	0.50	4.13 (±0.09) Aa	14.1 (±0.5) CD
1000	4.00	3.83 (±0.03) ABCb	16.4 (±0.8) BC	1.00	4.11 (±0.05) Aa	16.4 (±0.8) BC
1200	5.00	3.76 (±0.06) BCa	16.7 (±0.8) B	1.30	4.01 (±0.19) Aa	16.7 (±0.8) B
1800	8.00	3.77 (±0.13) BCa	20.7 (±0.3) A	2.00	4.03 (±0.08) Aa	20.7 (±0.3) A

[a]In each row, TEAC values of breads with the same amount of total added FA are presented. Data are expressed as means and standard deviations of triplicate measurements. Values from the same sample at different doses differ significantly ($p < 0.05$) when not sharing the same uppercase letter. Values from different samples at the same dose did not differ significantly ($p > 0.05$). [b]Level of added FA due to addition of AXOS (FA/dm flour expressed in ppm).

without added AXOS (results not shown). Also, formation of 4-VG, which can result from thermal or microbial degradation of FA,[47] or altered levels of amino acids, in particular from cysteine and tyrosine, were not observed after baking (results not shown). Therefore, the bioavailability of FA esterified to AXOS in the obtained breads can be expected to be similar to the bioavailability of FA on feruloylated AXOS as such. FA esterified to AXOS will primarily be metabolized in the colon by means of microbial metabolism.[4] The fate and functionality of these microbial FA metabolites are, however, poorly studied up until now.

Furthermore, AXOS added to the bread recipe remained water-extractable after baking (results not shown). As also their impact on bread volume was limited, AXOS fortified breads can be a promising food product to deliver AXOS for human consumption. Previous research reported that a daily intake of 2.2 g of AXOS beneficially altered the bacterial metabolism in the large bowel of healthy humans.[49] As on average about 178 g, ranging from 90 to 329 g, of bread is consumed daily per capita in Western European countries,[50] breads should be supplemented with about 1.8% AXOS (dm)/flour (dm) to achieve the intake of this AXOS quantity exclusively via bread consumption. The here obtained data show that it is feasible to meet this criterion from a techno-functional point of view. Also, addition of high levels of FA to bread through supplementation with FA-rich AXOS was feasible.

In conclusion, AXOS addition impacted dough rheology probably by a FA-mediated effect. Indeed, the FA content of AXOS, but not the form in which it appeared (free or bound to AXOS), determined to a large extent the effect of AXOS addition on dough rheology. AXOS bound FA caused effects on dough rheology similar to those of free FA. When AXOS contained only low to medium levels of FA, the effects of FA on dough rheological properties were overshadowed by those of the carbohydrate moiety of AXOS. Indeed, addition of higher levels of AXOS might cause decreased hydration of the gluten network, causing dough stiffening, and/or might increase the viscosity of the dough liquor. The mechanism of the FA-mediated effect on dough rheology is not fully understood, as FA was not, or only to a minor extent, involved in cross-linking reactions. Furthermore, the impact on gluten was limited. The influence of added AXOS, and more specific of their esterified FA, on noncovalent interactions, such as hydrogen bonds and hydrophobic interactions, might contribute to their effect on dough rheology. Addition of FA-enriched AXOS was only possible up to 2% AXOS (dm)/flour (dm) as higher levels caused unmanageable doughs. The observed FA-mediated effect on dough rheology could also be involved in the strong impact of WE-AX and WU-AX on dough rheology. Native AX, however, contain only low to medium FA levels, and the effect of their presence might be overshadowed by the increased dough liquor viscosity due to the presence of WE-AX or decreased hydration of the dough gluten network in the presence of WU-AX. Despite the outspoken effects of AXOS addition on dough rheology, no impact on bread volumes was observed in the produced breads. It is hence techno-functionally feasible to provide the daily AXOS dose needed for a beneficial effect on colonic bacterial metabolism via the average consumption of breads supplemented with AXOS, poor or rich in FA. Furthermore, at these addition levels, AXOS associated FA also improved the antioxidant capacity of the produced breads.

AUTHOR INFORMATION

Corresponding Author

*Tel.: + 32 16 32 19 17. Fax: + 32 16 32 19 97. E-mail: christophe.courtin@biw.kuleuven.be.

Funding

Financial support from the "Fonds voor Wetenschappelijk Onderzoek" (FWO, Brussels, Belgium) for the postdoctoral fellowship of E. Dornez and from the European Commission in the Communities seventh Framework Programme (FP7/2007-2013) for the Biocore Project (grant agreement no. FP7-241566) is gratefully appreciated.

Notes

The authors declare no competing financial interest.

ACKNOWLEDGMENTS

This publication reflects only the authors' views, and the Community is not liable for any use that may be made of the information contained in this publication. Mira Beke, Kristien Thoelen, and Hilde Van den Broeck are gratefully thanked for technical assistance. This research is also part of the Methusalem Programme Food for the Future (2007–2014).

ABBREVIATIONS USED

4-VG, 4-vinylguaiacol; AX, arabinoxylan; AXOS, arabinoxylanoligosaccharides; avDAS, average degree of arabinose substitution; avDPxyl, average degree of polymerization of the xylan backbone; FA, ferulic acid; RP-HPLC, reversed-phase high-performance liquid chromatography; SDS, sodium dodecyl sulfate; SE-HPLC, size-exclusion high-performance liquid chromatography; TEAC, Trolox Equivalent Antioxidant Capacity; TFA, trifluoroacetic acid; WE-AX, water-extractable arabinoxylan; WU-AX, water-unextractable arabinoxylan

REFERENCES

(1) Broekaert, W. F.; Courtin, C. M.; Verbeke, K.; Van de Wiele, T.; Verstraete, W.; Delcour, J. A. Prebiotic and other health-related effects of cereal-derived arabinoxylans, arabinoxylan-oligosaccharides, and xylooligosaccharides. *Crit. Rev. Food Sci. Nutr.* **2011**, *51*, 178–194.

(2) Swennen, K.; Courtin, C. M.; Lindemans, G.; Delcour, J. A. Large-scale production and characterisation of wheat bran arabinoxylooligosaccharides. *J. Sci. Food Agric.* **2006**, *86*, 1722–1731.

(3) Izydorczyk, M. S.; Biliaderis, C. G. Cereal arabinoxylans: Advances in structure and physicochemical properties. *Carbohydr. Polym.* **1995**, *28*, 33–48.

(4) Zhao, Z.; Moghadasian, M. Bioavailability of hydroxycinnamates: A brief review of *in vivo* and *in vitro* studies. *Phytochem. Rev.* **2010**, *9*, 133–145.

(5) Snelders, J.; Dornez, E.; Delcour, J. A.; Courtin, C. M. Ferulic acid content and appearance determine the antioxidant capacity of arabinoxylanoligosaccharides. *J. Agric. Food Chem.* **2013**, *61*, 10173–10182.

(6) Diplock, A. T.; Aggett, P. J.; Ashwell, M.; Bornet, F.; Fern, E. B.; Roberfroid, M. Scientific concepts of functional foods in Europe. Consensus document. *Br. J. Nutr.* **1999**, *81*, S1–27.

(7) Damen, B.; Pollet, A.; Dornez, E.; Broekaert, W. F.; Van Haesendonck, I.; Trogh, I.; Arnaut, F.; Delcour, J. A.; Courtin, C. M. Xylanase-mediated *in situ* production of arabinoxylan oligosaccharides with prebiotic potential in whole meal breads and breads enriched with arabinoxylan rich materials. *Food Chem.* **2012**, *131*, 111–118.

(8) Dornez, E.; Verjans, P.; Broekaert, W. F.; Cappuyns, A. M.; Van Impe, J. F.; Arnaut, F.; Delcour, J. A.; Courtin, C. M. *In situ* production of prebiotic AXOS by hyperthermophilic Xylanase B from *Thermotoga maritima* in high-quality bread. *Cereal Chem.* **2011**, *88*, 124–129.

(9) Courtin, C. M.; Delcour, J. A. Arabinoxylans and endoxylanases in wheat flour bread-making. *J. Cereal Sci.* **2002**, *35*, 225–243.

(10) Frederix, S. A.; Van hoeymissen, K. E.; Courtin, C. M.; Delcour, J. A. Water-extractable and water-unextractable arabinoxylans affect gluten agglomeration behavior during wheat flour gluten-starch separation. *J. Agric. Food Chem.* **2004**, *52*, 7950–7956.

(11) Wang, M.; Hamer, R. J.; van Vliet, T.; Gruppen, H.; Marseille, H.; Weegels, P. L. Effect of water unextractable solids on gluten formation and properties: mechanistic considerations. *J. Cereal Sci.* **2003**, *37*, 55–64.

(12) Wang, M.; Oudgenoeg, G.; van Vliet, T.; Hamer, R. J. Interaction of water unextractable solids with gluten protein: Effect on dough properties and gluten quality. *J. Cereal Sci.* **2003**, *38*, 95–104.

(13) Gan, Z.; Ellis, P. R.; Schofield, J. D. Gas cell stabilisation and gas retention in wheat bread dough. *J. Cereal Sci.* **1995**, *21*, 215–230.

(14) Courtin, C. M.; Roelants, A.; Delcour, J. A. Fractionation-reconstitution experiments provide insight into the role of endoxylanases in bread-making. *J. Agric. Food Chem.* **1999**, *47*, 1870–1877.

(15) Courtin, C. M.; Delcour, J. A. Physicochemical and bread-making properties of low molecular weight wheat-derived arabinoxylans. *J. Agric. Food Chem.* **1998**, *46*, 4066–4073.

(16) Hoseney, R. C.; Finney, K. F.; Shogren, M. D.; Pomeranz, Y. Functional (breadmaking) and biochemical properties of wheat flour components. 2. Role of water-solubles. *Cereal Chem.* **1969**, *46*, 117–125.

(17) Delcour, J. A.; Vanhamel, S.; Hoseney, R. C. Physicochemical and functional-properties of rye nonstarch polysaccharides. 2. Impact of a fraction containing water-soluble pentosans and proteins on gluten-starch loaf volumes. *Cereal Chem.* **1991**, *68*, 72–76.

(18) Patil, S. K.; Finney, K. F.; Shogren, M. D.; Tsen, C. C. Water-soluble pentosans of wheat-flour 0.3. Effect of water-soluble pentosans on loaf volume of reconstituted gluten and starch doughs. *Cereal Chem.* **1976**, *53*, 347–354.

(19) Labat, E.; Morel, M. H.; Rouau, X. Effects of laccase and ferulic acid on wheat flour doughs. *Cereal Chem.* **2000**, *77*, 823–828.

(20) Decamps, K.; Joye, I. J.; Rakotozafy, L.; Nicolas, J.; Courtin, C. M.; Delcour, J. A. The bread dough stability improving effect of pyranose oxidase from *Trametes multicolor* and Glucose Oxidase from *Aspergillus niger*: Unraveling the molecular mechanism. *J. Agric. Food Chem.* **2013**, *61*, 7848–7854.

(21) Yeh, Y. F.; Hoseney, R. C.; Lineback, D. R. Changes in wheat-flour pentosans as a result of dough mixing and oxidation. *Cereal Chem.* **1980**, *57*, 144–148.

(22) Labat, E.; Morel, M.-H.; Rouau, X. Wheat gluten phenolic acids: Occurrence and fate upon mixing. *J. Agric. Food Chem.* **2000**, *48*, 6280–6283.

(23) Jackson, G. M.; Hoseney, R. C. Fate of ferulic acid in overmixed wheat flour doughs: Partial characterization of a cysteine-ferulic acid adduct. *J. Cereal Sci.* **1986**, *4*, 87–95.

(24) Jackson, G. M.; Hoseney, R. C. Effect of endogenous phenolic acids on the mixing properties of wheat flour doughs. *J. Cereal Sci.* **1986**, *4*, 79–85.

(25) Piber, M.; Koehler, P. Identification of dehydro-ferulic acid-tyrosine in rye and wheat: Evidence for a covalent cross-link between arabinoxylans and proteins. *J. Agric. Food Chem.* **2005**, *53*, 5276–5284.

(26) Han, H.-M.; Koh, B.-K. Effect of phenolic acids on the rheological properties and proteins of hard wheat flour dough and bread. *J. Sci. Food Agric.* **2011**, *91*, 2495–2499.

(27) Koh, B.-K.; Ng, P. K. W. Effects of ferulic acid and transglutaminase on hard wheat flour dough and bread. *Cereal Chem.* **2009**, *86*, 18–22.

(28) Nicks, F.; Richel, A.; Dubrowski, T.; Whatelet, B.; Whatelet, J.-P.; Blecker, C.; Paquot, M. Effect of new synthetic PEGylated ferulic acids in comparison to ferulic acid and commercial surfactants on the properties of wheat flour dough and bread. *J. Sci. Food Agric.* **2013**, *93*, 2415–2420.

(29) Shogren, M. D.; Finney, K. F. Bread-making test for 10 grams of flour. *Cereal Chem.* **1984**, *61*, 418–423.

(30) Vanhamel, S.; Vandenende, L.; Darius, P. L.; Delcour, J. A. A volumeter for breads prepared from 10-grams of flour. *Cereal Chem.* **1991**, *68*, 170−172.
(31) Dunnewind, B.; Sliwinski, E. L.; Grolle, K.; Van Vliet, T. The Kieffer dough and gluten extensibility rig - An experimental evaluation. *J. Texture Stud.* **2003**, *34*, 537−560.
(32) AOAC. *Official Methods of Analysis, Method 990.03*, 16th ed.; Association of Official Analytical Chemists: Washington, DC, 1995.
(33) Lagrain, B.; Brijs, K.; Veraverbeke, W. S.; Delcour, J. A. The impact of heating and cooling on the physico-chemical properties of wheat gluten-water suspensions. *J. Cereal Sci.* **2005**, *42*, 327−333.
(34) Loosveld, A. M. A.; Grobet, P. J.; Delcour, J. A. Contents and structural features of water-extractable arabinogalactan in wheat flour fractions. *J. Agric. Food Chem.* **1997**, *45*, 1998−2002.
(35) Antoine, C.; Peyron, S.; Mabille, F.; Lapierre, C.; Bouchet, B.; Abecassis, J.; Rouau, X. Individual contribution of grain outer layers and their cell wall structure to the mechanical properties of wheat bran. *J. Agric. Food Chem.* **2003**, *51*, 2026−2033.
(36) Dobberstein, D.; Bunzel, M. Separation and detection of cell wall-bound ferulic acid dehydrodimers and dehydrotrimers in cereals and other plant materials by reversed phase high-performance liquid chromatography with ultraviolet detection. *J. Agric. Food Chem.* **2010**, *58*, 8927−8935.
(37) Rombouts, I.; Lamberts, L.; Celus, I.; Lagrain, B.; Brijs, K.; Delcour, J. A. Wheat gluten amino acid analysis by high-performance anion-exchange chromatography with integrated pulsed amperometric detection. *J. Chromatogr. A* **2009**, *1216*, 5557−5562.
(38) Moore, S. On the determination of cystine as cysteic acid. *J. Biol. Chem.* **1963**, *238*, 235−237.
(39) Serpen, A.; Gökmen, V.; Pellegrini, N.; Fogliano, V. Direct measurement of the total antioxidant capacity of cereal products. *J. Cereal Sci.* **2008**, *48*, 816−820.
(40) Jekle, M.; Becker, T. Effects of acidification, sodium chloride, and moisture levels on wheat dough: I. Modeling of rheological and microstructural Properties. *Food Biophys.* **2012**, *7*, 190−199.
(41) Ognean, M.; Ognean, C. F.; Bucur, A. Rheological effects of some xylanase on doughs from high and low extraction flours. *Procedia Food Sci.* **2011**, *1*, 308−314.
(42) Lagrain, B.; De Vleeschouwer, K.; Rombouts, I.; Brijs, K.; Hendrickx, M. E.; Delcour, J. A. The kinetics of β-elimination of cystine and the formation of lanthionine in gliadin. *J. Agric. Food Chem.* **2010**, *58*, 10761−10767.
(43) MacRitchie, F. Mechanical degradation of gluten proteins during high-speed mixing of doughs. *J. Polym. Sci. Polym. Symp.* **1975**, *49*, 85−90.
(44) Okada, K.; Negishi, Y.; Nagao, S. Factors affecting dough breakdown during overmixing. *Cereal Chem.* **1987**, *64*, 428−434.
(45) Shahidi, F.; Naczk, M. Nutritional and pharmacological effects of food phenolics. In *Food Phenolics: Sources, Chemistry, Effects and Applications*; Shahidi, F., Naczk, M., Eds.; Technomic Publishing Co., Inc.: Lancaster, PA, 1995; pp 171−191.
(46) Siebert, K. J.; Troukhanova, N. V.; Lynn, P. Y. Nature of polyphenol-protein interactions. *J. Agric. Food Chem.* **1996**, *44*, 80−85.
(47) Coghe, S.; Benoot, K.; Delvaux, F.; Vanderhaegen, B.; Delvaux, F. R. Ferulic acid release and 4-vinylguaiacol formation during brewing and fermentation: indications for feruloyl esterase activity in *Saccharomyces cerevisiae*. *J. Agric. Food Chem.* **2004**, *52*, 602−608.
(48) Lagrain, B.; Thewissen, B. G.; Brijs, K.; Delcour, J. A. Impact of redox agents on the extractability of gluten proteins during bread making. *J. Agric. Food Chem.* **2007**, *55*, 5320−5325.
(49) Cloetens, L.; De Preter, V.; Swennen, K.; Brockaert, W. F.; Courtin, C. M.; Delcour, J. A.; Rutgeerts, P.; Verbeke, K. Dose-response effect of arabinoxylooligosaccharides on gastrointestinal motility and on colonic bacterial metabolism in healthy volunteers. *J. Am. Coll. Nutr.* **2008**, *27*, 512−518.
(50) Euromonitor International. *Who Eats What: Identifying International Food Consumption Trends*, 1st ed.; Euromonitor International: London, UK, 2009.

Table 1. Information on the Different Cultivated and Wild Bean Accessions Used in This Study[a]

accession identifier	common name	phaseolin[b]	gene pool[c]	race[d]	status	origin/ country	origin/ locality	seed/weight of 100 seeds (g)	seed/color
PI 201011 (G 12851)		S, Sb, Sd, M11	M		wild	Guatemala	Santa Rosa	6.0	cream, black, other
PI 268110 (G 1459)	Jamapa	S	M	M	landrace	Mexico	Veracruz	18.0	black
PI 313590 (G 2511)	Boyaca 22	B, S	M	M	cultivated	Colombia	Boyaca	16.0	brown, black
PI 417780 (G 12953)		M	M		wild	Mexico	Jalisco	10.5	brown
PI 549695 (G 4498)	Sanilac	S	M	M	cultivated	U.S.		14.0	white
PI 661723			M		wild	Costa Rica	Puntarenas		brown
PI 661840 (G 22837)		M4, Sb	M		wild	Mexico	Chihuahua	11.1	cream, brown
W6 35834 (G 5773)	Ica Pijao	B	M	M	cultivated	Colombia	Valle Del Cauca	24.0	black
G 12053	Nuña	A	A	P	cultivated	Perú	Ayacucho	36.6	purple
G 12588	Huevo de Huanchaco (nuña)	H	A	P	cultivated	Perú	Cajamarca	49.8	white, red
PI 390770 (G 7225)		T	A		wild	Perú	Apurimac	11.0	cream, black
PI 474218 (G 6412)	Contender	C	A	NG	cultivated	U.S.		44.0	cream, brown
PI 549633 (G 7476)	Tendergreen	T	A	NG	cultivated	U.S.		30.0	cream, brown
PI 557465 (G 4474)	Coscorron	S, B	A	C	landrace	Chile		52.0	white, other
PI 638874			A		wild	Argentina	Jujuy		brown, black
PI 640968			A		wild	Argentina	Salta		brown, black
PI 661817			A		wild	Bolivia	Chuquisaca		cream
W6 35784 (G 4494)	Calima	T	A	NG	cultivated	Colombia		54.8	red, cream

[a]Source: Singh et al.[19] and CIAT[28] germplasm collection. [b]Phaseolin types (and subtypes) based on 1-DE banding patterns:[11,20,28] S, Sanilac (Sb, S Brazil; Sd, S Durango 222); M, Mesoamerica (M4, M11); B, Boyaca; A, Ayacucho; H, Huanchaco; T, Tendergreen. [c]Gene pool: M, Mesoamerican; A, Andean. [d]Race: M, Mesoamerica; NG, Nueva Granada; P, Peru; C, Chile.

seed weight across a broad range of genetic backgrounds and environments, tolerance to low soil pH, growth habit, early maturity, and resistance to parasites.[11,20,21] Moreover, the phaseolin is the major seed storage protein that may account for up to ca. 50% of the total seed proteome.[13] It is therefore largely responsible for the seed protein quality. In particular, the levels of phaseolin were found to be positively correlated with the nutritional availability of methionine in total bean seed protein.[22] It has been suggested, therefore, that an improvement of the seed protein quality of the present bean varieties might be accomplished by using types of phaseolin with differences in the number of methionine residues and molar ratio of methionine.[23]

So far, more than 40 different types of phaseolin have been found in domesticated and wild cultivars of beans by 1-DE.[4,5] Nevertheless, 1-DE phaseolin profiles typically have only two to six bands with molecular mass (M_r) ranging from 40 to 54 kDa.[4,24] More informative reference maps of the protein phaseolin have been obtained only recently using high-resolution two-dimensional electrophoresis (2-DE).[25,26] Application of high-resolution 2-DE provides characteristic and reproducible phaseolin profiles for each common bean population, each one constituted by a large number of spots containing differentially glycosylated and phosphorylated α- and β-type polypeptides (see Supporting Information Figures 1 and 2). This surge of information on the variation of the protein phaseolin enables one to obtain quantitative estimates of its degree of diversity across common bean populations based on measures of proteomic distance.[27]

The aim of the present work is to test whether high-resolution 2-DE phaseolin profiles can be useful as molecular markers of the degree of genetic divergence and/or the quality of seed protein in common bean populations. For this purpose, we performed a prospective study on the variation of 2-DE phaseolin profiles over domesticated and wild common bean populations belonging to the Mesoamerican and Andean gene pools. In addition, the quality of the total seed protein in these bean populations was estimated from the content of methionine, an essential amino acid deficient in bean seeds. From the results, we will try to determine whether proteomic distances based on 2-DE phaseolin profiles can efficiently identify populations belonging to each major gene pool, as well as the possible link between proteomic distances and seed protein quality. It might open the way of using the information contained in 2-DE phaseolin profiles for the genetic improvement of common bean populations.

MATERIALS AND METHODS

Plant Material. Dry mature seeds from 8 wild types and 10 cultivars of common bean (*P. vulgaris* L.) from Mesoamerican and Andean gene pools were screened for variability of phaseolin using 2-DE. The cultivars belong to the Mesoamerica, Nueva Granada, Peru, and Chile races. A complete list of the accessions used in this studied together with their passport information, which includes accession identifier, common name, phaseolin type assessed by 1-DE, race type, status (wild, landrace, or cultivar), origin (country and locality), seed

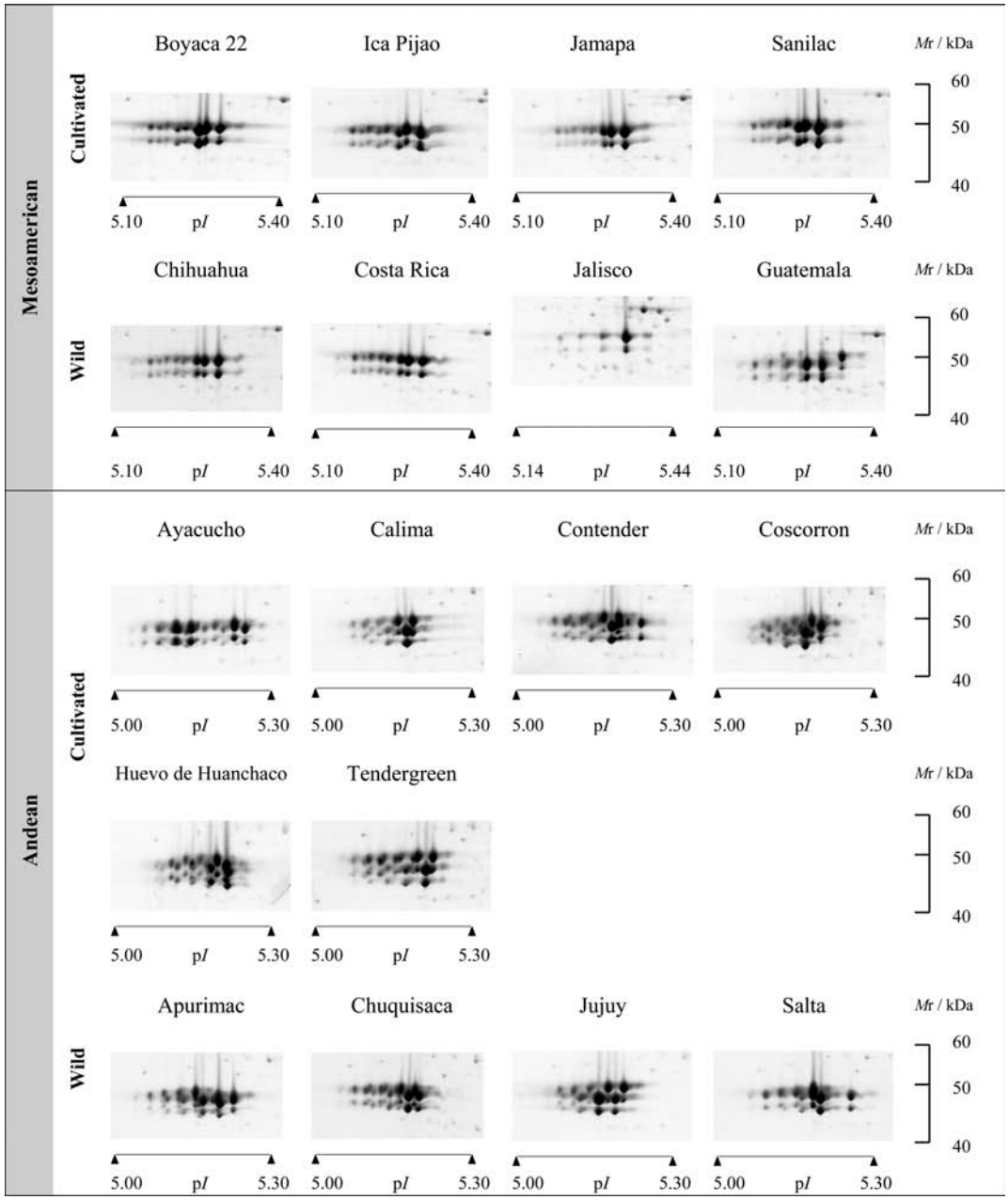

Figure 1. High-resolution 2-DE phaseolin profiles from seeds of 18 cultivated and wild accessions of common bean corresponding to the Mesomerican and Andean gene pools. Positions of the spots according to their isoelectric point (pI) and molecular mass (M_r) are shown.

weight, and seed color is given in Table 1. The seeds were provided by the United States Department of Agriculture (USDA). Ten bean seeds from each accession were lyophilized after previous grinding of the total seed tissue to a powder with liquid nitrogen using a precooled mortar and pestle. The samples were stored at −80 °C until protein extraction.

Seed Protein Extraction. Total seed protein was extracted by the phenol method, which has been proved to give highly satisfactory results for the separation of common bean seed proteins by 2-DE in comparison with other commonly used extraction methods.[29] The phenol method was performed from 100 mg of sample suspended in extraction buffer (500 mM Tris-HCl, 500 mM EDTA, 700 mM sacarose, 100 mM KCl pH = 8.0, 2% DTT, and 1 mM PMSF). Phenol saturated with Tris-HCl (pH 6.6−7.9) was added, and the phenolic phase was recovered after centrifuging (4500 rpm at 4 °C). Proteins were precipitated (0.1 M ammonium acetate in MeOH), and protein pellets were washed (0.1 M ammonium acetate, 10 mM DTT, 80% acetone, and 10 mM DTT) and resuspended in lysis buffer (7 M urea; 2 M thiourea; 4% CHAPS; 10 mM DTT, and 2% Pharmalyte pH 3−10, GE Healthcare, Uppsala, Sweden). Protein quantification was assessed for each extraction using the commercial CB-X protein assay kit (G-Biosciences, St. Louis, MO) following the instructions of the manufacturer for using a microplate reader.

2-DE Phaseolin Patterns. Optimized 2-DE protocol for high-resolution phaseolin patterns was used as previously described.[25,26] 2-DE was carried out from 50 μg of total seed protein extract dissolved in lysis and rehydration (7 M urea, 2 M thiourea, 4% CHAPS, 0,002% Bromophenol Blue) buffers. Protein extracts were loaded on 24 cm-long ReadyStrip IPG Strips with a pH linear gradient of 4.7−5.9 (Bio-Rad Laboratories, Inc., Hercules, CA), together with 0.6% dithiothreitol (DTT) and 1% IPG buffer (Bio-Rad Laboratories). First dimensional isoelectric focusing (IEF) was carried out until reaching 60 kVh after an initial rehydration step for 12 h at 50 V in a PROTEAN IEF cell (Bio-Rad Laboratories). Focused strips were incubated in the equilibration solution (50 mM Tris pH = 8.8, 6 M urea, 30% glycerol, and 2% SDS) with 1% DTT for 15 min at room

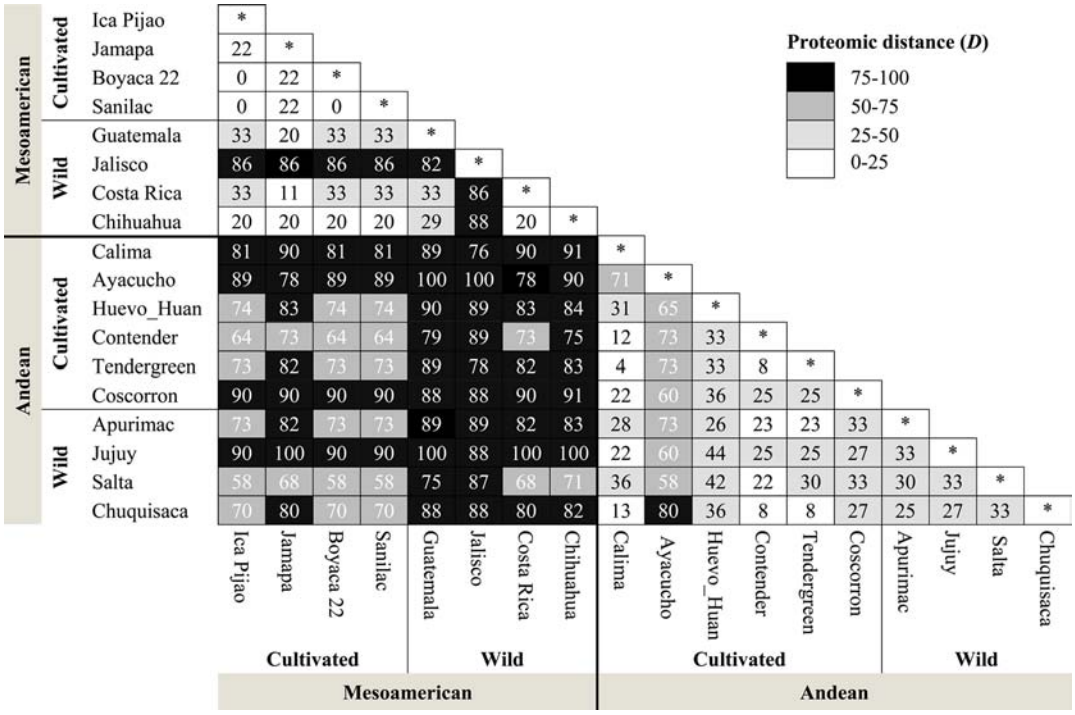

Figure 2. Pairwise proteomic distance (D), expressed as a percentage, based on high-resolution 2-DE phaseolin patterns from seeds of 18 cultivated and wild accessions of common bean.

temperature and then with 2.5% iodoacetamide under the same conditions. For the second dimension (SDS-PAGE), equilibrated strips were placed on 10% (w/v) gels, and they were run vertically in an Ettan DALTsix system (GE, Healthcare, Uppsala, Sweden) using Tris-glycine-SDS (50 mM Tris, 384 mM glycine and 0.2% SDS) as electrode buffer. SDS-PAGE was carried out at a constant current of 16 mA per gel over 15 h. After the run, gels were stained with Sypro Ruby stain (Lonza, Rockland, ME) following the manufacturer's indications.

The 2-DE gel images were acquired with a Gel Doc XR+ system (Bio-Rad Laboratories). Image analysis of digitalized gels was performed through PDQuest Advanced software v. 8.0.1 (Bio-Rad Laboratories). 2-DE gels were matched across wild and cultivated common bean accessions. Only qualitative (presence or absence) differences among spot patterns, detectable under a sensitivity of 1.1, were analyzed.

Seed Amino Acid Composition. Protein hydrolysis was carried out on 100 mg of bean flour (average moisture content 4.32%) with 5 mL of HCl (6 N) in an ampule glass sealed for 24 h at 110 °C. After hydrolysis, the solution was diluted with 200 mL of distilled water and filtered through a 0.45 μm filter (Filter-Lab, Barcelona, Spain). Tryptophan determination was not possible, because acidic hydrolysis transformed it into ammonium.

The derivatization conditions were as follows: 10 μL of sample was buffered to pH 8.8 (AccQFluor borate buffer; Waters, Milford, MA) to yield a total volume of 100 μL. Derivatization was initiated by the addition of 20 μL of AccQ-Fluor (Waters) reagent (3 mg/mL in acetonitrile).

The amino acid analyses were performed by high-performance liquid chromatography (HPLC). Chromatographic analysis conditions were as follows: separations were carried out in a Waters AccQ-Tag column (3.9 mm × 150 mm with a 4 μm of particle size); the pumps were fixed to maintain a flow rate of 1.0 mL/min; and the column heater was fixed to maintain a temperature of 37 °C. The gradient profile and composition of the mobile phase were adapted from methodology developed by Vandelen and Cohen[30] and Waters AccQ-Tag Instruction Manual. Separation and detection were carried out using Alliance model 2695 HPLC Module (Waters) and model 2475 scanning fluorescence detector (Waters). Empower 2 Advanced software (Waters) was used to control system operation and results management. Detection was accomplished by fluorescence with excitation at 250 nm and emission at 395 nm. Amino acids were identified by retention time and quantification using an external calibration, where amino acid standard solution (AA-S-18, Sigma-Aldrich, Saint Louis, MO) was prepared to obtain a calibration curve of five points. Two biological replicate samples were carried out per accession.

Data Analysis. The degree of similarity between 2-DE phaseolin profiles of common bean populations was estimated as the percentage of spots shared through the F (also described in the literature as S) coefficient[31] given by

$$F = 2n_{xy}/(n_x + n_y)$$

where n_{xy} is the number of phaseolin spots shared by populations x and y; and where n_x and n_y are the total numbers of phaseolin spots identified in populations x and y, respectively. Dissimilarity or proteomic distance (D) between pairwise populations was then estimated as

$$D = 1 - F$$

A hierarchical cluster analysis using the unweighted pair-group method with arithmetic averaging (UPGMA) was applied to the matrix of both pairwise proteomic distances and pairwise differences in methionine content. Nonmetric multidimensional scaling (MDS) algorithm was used to construct a two-dimensional plot on the basis of the pairwise proteomic distance matrix. The significance of the relationship between proteomic distance and difference in methionine content across pairs of accessions was assessed using Mantel's matrix-comparison test, which does not require that matrix elements be independent.[32] UPGMA, MDS, and the Mantel test were performed using NTSYSpc v. 2.1 software (Applied Biostatistics, Inc., Setauket, NY).

Standard statistical analyses were performed using the statistical software package IBM SPSS Statistics 20 (SPSS, Chicago, IL). Bootstrapping was used to calculate 95% and 99% confidence intervals (CIs) for the means of proteomic distance. For each set of N estimates of D, bootstrap samples of size N were obtained following a Monte Carlo algorithm putting mass $1/N$ at each one of the observed D

estimates. From distribution of 10 000 bootstrap mean replications of D, the bootstrap CIs (95% and 99%) were obtained by the bias-corrected percentile method.[33] A similar procedure was performed to obtain CIs for the means of methionine content across accessions. Random numbers were obtained using the standard multiplicative linear congruential generator implemented by Schrage,[34] which uses the multiplier 16 807 and prime modulus 2^{31}-1 to give long sequences that have appearance of randomness. Bootstrap CIs were obtained with the software DIANA (C. Zapata, unpublished).

RESULTS AND DISCUSSION

2-DE Phaseolin Patterns. 2-DE phaseolin patterns in 18 wild and cultivated accessions of common bean are shown in Figure 1. It can be seen that 2-DE phaseolin profiles were markedly diverse across accessions. Thus, the number of spots on 2-DE gels across the 18 phaseolin patterns ranged from 10 (Jalisco) to 28 (Huevo de Huanchaco) and averaged (±SE, standard error) 20.4 ± 1.1. Phaseolin patterns were found to be remarkably less complex in Mesoamerican gene pool (M) accessions than in Andean gene pool (A) ones: the mean number of spots for M and A accessions was 16.8 ± 1.4 and 23.4 ± 1.0, respectively (Mann–Whitney U test, $p < 0.01$). It is noteworthy that most of these variations were due to the presence/absence of spots in the first dimension (pI). Recent evidence has shown that differences in the pI of 2-DE phaseolin spots are largely due to differentially phosphorylated α- and β-type polypeptides.[26] The same study revealed that mobilization of the phaseolin in germinating seeds seems to occur through the degradation of highly phosphorylated isoforms. It suggests, therefore, that regulatory mechanisms responsible for the synthesis and subsequent degradation of phaseolin through phosphorylations might undergo variations over common bean populations.

Proteomic Distance. A quantitative estimation of the differences between 2-DE phaseolin profiles was obtained from the matrix of pairwise proteomic distances (D). The D-values (in percentage) between all possible pairwise comparisons of cultivated and wild common bean population are given in Figure 2. We found that proteomic distances were largely heterogeneous: values of D ranged from 0 (three M × M comparisons) to 100% (six M × A comparisons) and averaged 59.9 ± 2.4%. The mean proteomic distance (with 95% and 99% bootstrap CIs) within and between gene pools at different levels of comparison is shown in Table 2. Most of the heterogeneity in proteomic distance can be attributed to between gene pool differences. In fact, proteomic distance between gene pools was statistically significant higher than those proteomic distances within gene pools ($p < 0.01$). Within gene pools, proteomic distances were rather homogeneous over different levels of comparison with a single exception. The Mesoamerican cultivated (MC) populations exhibited indeed the lowest mean proteomic distance score (i.e., 11.0 ± 4.9), which was statistically significantly different from the remaining mean proteomic distances ($p < 0.01$), including Andean cultivated (AC) populations. Lower diversity for phaseolin types in the domesticated Mesoamerican gene pool than in the Andean one has also been reported on the basis of 1-DE analyses.[20] This evidence would support the interpretation that a single domestication event occurred in Mexico, whereas multiple domestication events occurred in the Andes,[20] but the domestication history of the common bean is still a controversial topic.[35]

On the basis of the matrix of pairwise proteomic distances, clustering analysis (UPGMA) and projection of the distances in two-dimensional space (MDS) were used to evaluate the efficiency of 2-DE phaseolin patterns in grouping the populations according to the classification by major gene pools. The UPGMA dendrogram generated from the matrix of pairwise D-values is shown in Figure 3. First, it must be highlighted that proteomic distances were able to reliably reproduce the known separation of the populations into the Mesoamerican and Andean gene pools. The only exception to the double-cluster pattern of Mesoamerican and Andean bean accessions was a well-separated branch containing the wild accession Jalisco. In addition, UPGMA dendrogram was also

Table 2. Proteomic Distance (D) within and between Common Bean Gene Pools Based on 2-DE Phaseolin Profiles

comparison level[a]	n^b	D^c	95% bootstrap CI (CL, CU)[d]	99% bootstrap CI (CL, CU)
Within Gene Pools				
M × M	28	37.8 ± 5.6	27.1, 49.4	23.4, 52.7
A × A	45	34.5 ± 2.9	29.2, 40.0	27.8, 41.5
MC × MC	6	11.0 ± 4.9	3.7, 18.3	0.0, 22.0
MW × MW	6	56.3 ± 13.1	34.0, 77.2	25.8, 86.0
MC × MW	16	40.8 ± 6.9	28.4, 54.9	25.6, 59.5
AC × AC	15	38.1 ± 6.2	26.3, 50.0	23.1, 52.5
AW × AW	6	30.2 ± 1.4	27.5, 32.5	26.8, 33.0
AC × AW	24	33.0 ± 3.8	26.4, 40.6	24.8, 42.7
Between Gene Pools				
M × A	80	81.8 ± 1.1	79.6, 84.1	78.7, 84.7
MC × AC	24	79.5 ± 1.8	76.2, 83.2	74.7, 83.9
MC × AW	16	75.2 ± 3.1	69.3, 81.2	67.6, 83.1
MW × AC	24	86.0 ± 1.4	83.3, 88.8	82.6, 89.5
MW × AW	16	85.6 ± 2.4	81.3, 90.1	79.5, 91.7

[a]M, Mesoamerican gene pool populations; A, Andean gene pool populations; MC, Mesoamerican cultivated populations; MW, Mesoamerican wild populations; AC, Andean cultivated populations; AW, Andean wild populations. [b]Number of accession pairs. [c]Data (expressed in percentage) are means ± standard error. [d]CI, confidence interval; CL, lower bound; CU, upper bound.

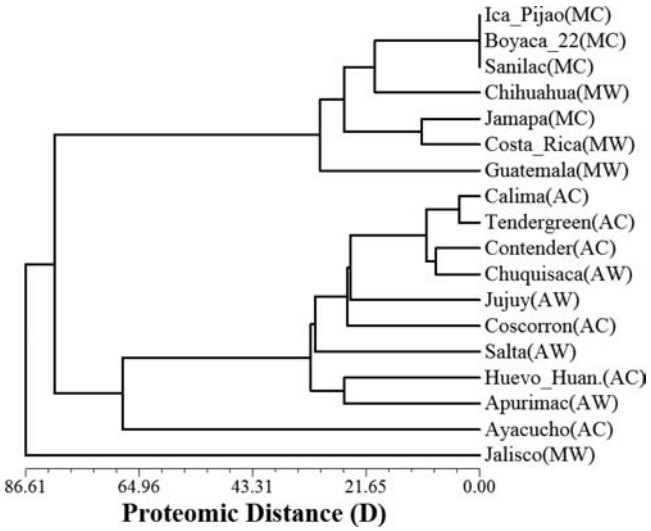

Figure 3. Unweighted pair-group method with arithmetic averaging (UPGMA) dendrogram from the matrix of pairwise proteomic distances (D) based on high-resolution 2-DE phaseolin profiles from seeds of 18 cultivated and wild accessions of common bean.

able to unravel heterogeneity within the two gene pools. In particular, the accession of Ayacucho formed a clearly separated subcluster within Andean cluster. The projection of the proteomic distances between pairs of the 18 common bean accessions in two-dimensional space is shown in Figure 4. The

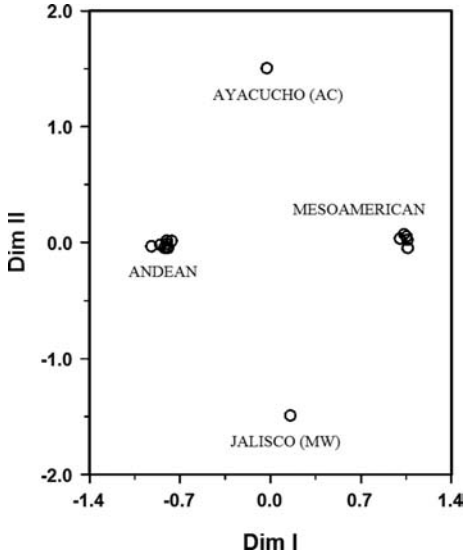

Figure 4. Multidimensional scaling (MDS) projection of the proteomic distance (D) between 18 cultivated and wild populations onto two-dimensional space based on high-resolution 2-DE phaseolin patterns.

stress function value was 0.074, which indicates a good goodness-of-fit of the projected distances in the configuration space to the monotone function of the original distances. The two-dimensional map obtained by MDS reflected essentially the same scenario obtained by the dendrogram. Thus, dimension I showed noticeable differences between two tight clusters of Mesoamerican and Andean gene pools, whereas dimension II separated clearly the bean accessions Ayacucho and Jalisco as two outliers strongly deviating from the two main clusters.

Previous investigations support the highest proteomic distance found for Ayacucho and Jalisco populations.[14,18,35−38] First, it is important to note that Ayacucho is a nuña, a type of cultivar currently restricted to certain parts of the highlands of Peru and Bolivia that exhibits the particular property of popping when exposed to heat. It is considered that nuña beans may represent ancient preceramic landraces descendents of the earliest Andean bean domesticates.[14,36] Second, Jalisco is a possible ancestral wild accession of *P. vulgaris*. Recent evidence using a variety of nuclear and chloroplast DNA markers suggests that the wild forms of *P. vulgaris* originated in Mesoamerica and the Andean gene pool originated through different migration events from central Mexico.[18,35,37] It also seems that Mesoamerican beans were domesticated in the region of Jalisco.[38] Accordingly, analysis of genetic diversity with microsatellite markers in a large number of wild and domesticated common bean accessions from Mesoamerican and Andean gene pools has shown than the race Jalisco constituted a single separated group together with the race Durango.[14] Taken together, our investigations show that proteomic distances obtained from 2-DE phaseolin patterns are a reliable marker of genetic differentiation among cultivated and wild bean populations.

Proteomic Distance and Seed Protein Quality. Essential and nonessential amino acid composition for the 18 cultivated and wild common bean seeds from the Mesoamerican and Andean gene pools is shown in Supporting Information Tables 1 and 2. Figure 5 shows that the values

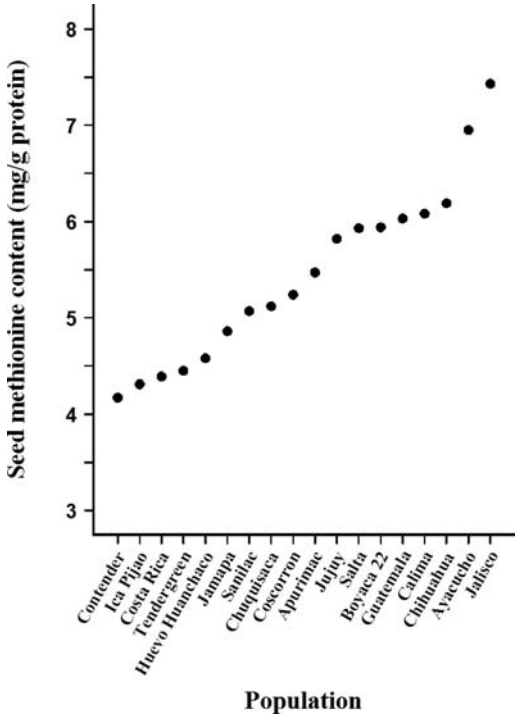

Figure 5. Mean methionine content (mg/g total seed protein) across 18 cultivated and wild populations of common bean.

of the seed methionine content varied markedly across the complete set of accessions: mean values ranged from 4.2 (Contender) to 7.4 mg/g (Jalisco) of protein sample. Despite these oscillations, all accessions contain methionine-cysteine poor proteins as compared to the reference amino acid FAO/WHO requirements recommended in human nutrition (see Supporting Information Figure 3).[7] On the other hand, no statistically significant differences in methionine content were detected between Mesoamerican and Andean gene pools by the Mann−Whitney U test ($p = 0.79$). However, we found a weak relationship between the degree of proteomic distance and the difference in methionine content in total seed protein over pairs of populations (see Supporting Information Figure 4). Specifically, a positive correlation was detected between both variables using both the Pearson product-moment correlation coefficient to assess the strength of association and the Mantel test to assess its probability ($r = 0.176$, $p < 0.05$, $n = 153$). This weak correlation can be understood taking into account that the phaseolin represents about 35−50% of the total seed protein.[6] It seems, therefore, that it is difficult to predict methionine content in total seed protein from individual proteomic distance scores based on 2-DE phaseolin profiles.

Cluster analysis offers a different perspective to the study of the diversity in the methionine content across bean accessions because their degree of similarity/dissimilarity can be analyzed jointly. Cluster analysis using UPGMA from differences in methionine content between pairs of accessions is shown in Figure 6. Interestingly, the accessions Jalisco and Ayacucho appear to be clear outliers distantly related to the rest of the

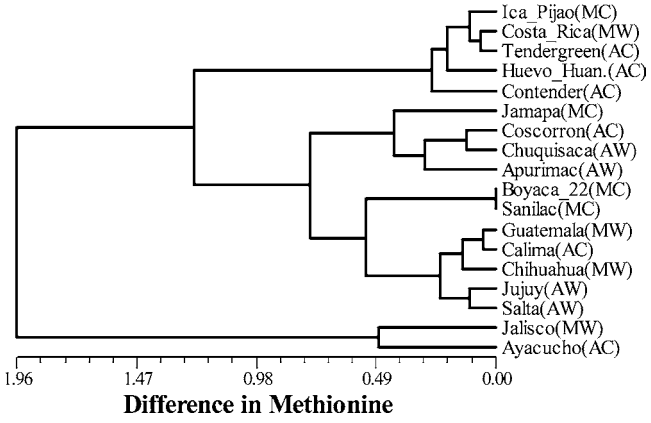

Figure 6. Unweighted pair-group method with arithmetic averaging (UPGMA) dendrogram based on pairwise differences in seed methionine content (mg/g total protein) from 18 cultivated and wild populations of common bean.

accessions in agreement with analyses based on proteomic distances. In addition, the levels of methionine were significantly higher in seeds of Jalisco and Ayacucho than in the remaining accessions used in this study ($p < 0.01$; Table 3),

Table 3. Methionine Content (mg/g protein) in Total Seed Protein of Ayacucho and Jalisco and Other Accessions

accessions	n^a	methionine content[b]	95% bootstrap CI (CL, CU)[c]	99% bootstrap CI (CL, CU)
Ayacucho	2	6.95 ± 0.15	6.94, 7.10	6.80, 7.10
Jalisco	2	7.44 ± 0.45	7.43, 7.88	6.99, 7.88
other accessions	32	5.22 ± 0.13	4.98, 5.47	4.91, 5.52

[a]Number of values. [b]Data are means ± standard error. [c]CI, confidence interval; CL, lower bound; CU, upper bound.

about 70% higher than in the Contender accession (Figure 5). These observations suggest, therefore, that proteomic distances based on 2-DE phaseolin profiles are an informative biomarker to identify outliers with distinct methionine content. Accordingly, phaseolin-based proteomic distances can establish a link between *P. vulgaris* genetic differentiation and methionine content in total seed protein, which has important implications for the genetic improvement of bean seeds with higher nutritional quality.[5,23,39]

The study of natural variation in the protein phaseolin from 2-DE-based patterns can provide additional valuable information to improve bean cultivars. Previous studies suggest that the existing natural variation in phaseolin types could be used for improving the digestibility of common bean. Thus, it is known that the nutritional value of common bean is affected by a high resistance of phaseolin to proteolysis by the digestive enzymes.[4,5,40−43] However, the degree of hydrolysis in vitro of phaseolin seems to be influenced more by the structural characteristics of the phaseolin type determined using 1-DE than by its amino acid composition.[4,5] A number of structural variations can alter the phaseolin susceptibility to proteolysis including differences in the proportion of α- and β-type polypeptides in the whole molecule and post-translational modifications such as glycosylations.[4,5,42,43] At this regard, 2-DE phaseolin profiles have the advantage that they provide more detailed information about the structural differences among phaseolin types than is available via 1-DE banding patterns. In particular, 2-DE profiles allow us to identify differentially glycosylated and phosphorylated α- and β-type phaseolin polypeptides (Supporting Information Figure 2).[25,26] It would be interesting to study as the natural variation in the levels of glycosylation and phosphorylation of α- and β-type polypeptides affects the susceptibility of phaseolin to in vitro and in vivo proteolysis. On the other hand, it is also probable that proteomic distances based on 2-DE phaseolin patterns can provide relevant information about other bean traits. It is well established that phaseolin diversity is associated with several important agronomic traits (seed weight, tolerance to low soil pH, resistance to parasites, etc.).[11,20,21] These associations are likely a byproduct of linkage disequilibrium between alleles at phaseolin coding genes and alleles at quantitative trait loci (QTLs) of agronomic relevance. Linkage disequilibria among functionally unrelated loci could have arisen at any given moment of the history of common bean populations by evolutionary mechanisms such as genetic drift, founder effects, and stratification (or admixture) of populations, and maintained by the self-pollinated nature of *P. vulgaris*.[11]

Overall, our results show that proteomic distances based on high-resolution 2-DE phaseolin profiles are a reliable marker of genetic differentiation of common bean populations. Our study also indicates that phaseolin-based proteomic distances can establish a link between *P. vulgaris* genetic differentiation and seed protein quality as evaluated by the content of the essential amino acid methionine. This link might conceivably include other bean traits of agronomic relevance. Therefore, 2-DE phaseolin patterns might be potentially exploited to speed the process of selection of common bean germplasm in follow-up breeding programs to the improvement of bean cultivars.

■ ASSOCIATED CONTENT

Supporting Information

Tables and figures showing the amino acid composition of seed protein from different bean accessions; the reproducibility of 2-DE phaseolin patterns across biological replicates; the methionine and cysteine content in seed protein samples; and the relationship between proteomic distance and difference in seed methionine content. This material is available free of charge via the Internet at http://pubs.acs.org.

■ AUTHOR INFORMATION

Corresponding Author

*Tel.: +34 881816922. Fax: +34 981528006. E-mail: c.zapata@usc.es.

Funding

This research was supported in part by grant 10PXIB262008PR (Xunta de Galicia, Spain).

Notes

The authors declare no competing financial interest.

■ ABBREVIATIONS USED

1-DE, one-dimensional electrophoresis; 2-DE, two-dimensional electrophoresis; A, Andean gene pool; AC, Andean cultivated accession; AW, Andean wild accession; CI, confidence interval; M, Mesoamerican gene pool; MC, Mesoamerican cultivated accession; MDS, nonmetric multidimensional scaling; M_r, relative molecular mass; MW, Mesoamerican wild accession; pI, isoelectric point; UPGMA, unweighted pair-group method with arithmetic mean

REFERENCES

(1) Gepts, P.; Aragao, F. J. L.; Barros, E.; Blair, M. W.; Brondani, R.; Broughton, W.; Galasso, I.; Hernández, G.; Kami, J.; Lariguet, P.; McClean, P.; Melotto, M.; Miklas, P.; Pauls, P.; Pedrosa-Harand, A.; Porch, T.; Sánchez, F.; Sparvoli, F.; Yu, K. Genomics of *Phaseolus* beans, a major source of dietary protein and micronutrients in the tropics. In *Genomics of Tropical Crop Plants*, 1st ed.; Moore, P. H., Ming, R., Eds.; Springer Science: New York, 2008; pp 113−143.

(2) FAOSTAT. FAO statistical data base for agriculture. Food and Agriculture Organization of the United Nations (FAO). URL http://faostat.fao.org, 2014.

(3) Krupa, U. Main nutritional and antinutritional compounds of bean seeds-A review. *Polym. J. Food Nutr. Sci.* **2008**, *2*, 149−155.

(4) Montoya, C. A.; Leterme, P.; Victoria, N. F.; Toro, O.; Souffrant, W. B.; Beebe, S.; Lallès, J.-P. Susceptibility of phaseolin to in vitro proteolysis is highly variable across common bean varieties (*Phaseolus vulgaris*). *J. Agric. Food Chem.* **2008**, *56*, 2183−2191.

(5) Montoya, C. A.; Lallès, J.-P.; Beebe, S.; Leterme, P. Phaseolin diversity as a possible strategy to improve the nutritional value of common beans (*Phaseolus vulgaris*). *Food Res. Int.* **2010**, *43*, 443−449.

(6) Ma, Y.; Bliss, F. Seed proteins of common bean. *Crop Sci.* **1978**, *18*, 431−437.

(7) FAO/WHO/UNU. Protein and amino acid requirements in human nutrition. *WHO Technical Rep. Ser.* **2007**, 935.

(8) Slightom, J. L.; Drong, R. F.; Klassy, C.; Hoffman, L. M. Nucleotide sequences from phaseolin cDNA clones: The major storage proteins from *Phaseolus vulgaris* are encoded by two unique gene families. *Nucleic Acids Res.* **1985**, *13*, 6483−6498.

(9) Pedrosa-Harand, A.; Porch, T.; Gepts, P. Standard nomenclature for common bean chromosomes and linkage groups. *Annu. Rep. Bean Improv. Coop.* **2008**, *51*, 106−107.

(10) Gepts, P. Phaseolin as an evolutionary marker. In *Genetic Resources of Phaseolus Beans*, 1st ed.; Gepts, P., Ed.; Kluwer Academic Publishers: Dordrech, Holland, 1988; pp 215−241.

(11) Koenig, R. L.; Singh, S. P.; Gepts, P. Novel phaseolin types in wild and cultivated common bean (*Phaseolus vulgaris*, Fabaceae). *Econ. Bot.* **1990**, *44*, 50−60.

(12) Singh, S. P. Broadening the genetic base of common bean cultivars: a review. *Crop Sci.* **2001**, *41*, 1659−1675.

(13) Emani, C.; Hall, T. C. Phaseolin: structure and evolution. *Open Evol. J.* **2008**, *2*, 66−74.

(14) Kwak, M.; Gepts, P. Structure of genetic diversity in the two major gene pools of common bean (*Phaseolus vulgaris* L., Fabaceae). *Theor. Appl. Genet.* **2009**, *118*, 979−992.

(15) Singh, S. P.; Nodari, R.; Gepts, P. Genetic diversity in cultivated common bean. I. Allozymes. *Crop Sci.* **1991**, *31*, 19−23.

(16) Becerra-Velásquez, V. L.; Gepts, P. RFLP diversity in common bean (*Phaseolus vulgaris* L). *Genome* **1994**, *37*, 256−263.

(17) Chacón, S. M. I.; Pickersgill, B.; Debouck, D. G. Domestication patterns in common bean (*Phaseolus vulgaris* L.) and the origin of the Mesoamerican and Andean cultivated races. *Theor. Appl. Genet.* **2007**, *110*, 432−444.

(18) Desiderio, F.; Bitocchi, E.; Bellucci, E.; Rau, D.; Rodríguez, M.; Attene, G.; Papa, R.; Nanni, L. Chloroplast microsatellite diversity in *Phaseolus vulgaris*. *Plant Sci.* **2013**, *3*, 1−15.

(19) Singh, S. P.; Gepts, P.; Debouck, D. G. Races of common bean (*Phaseolus vulgaris* L., Fabaceae). *Econ. Bot.* **1991**, *45*, 379−396.

(20) Gepts, P.; Osborn, C.; Rashka, K.; Bliss, F. A. Phaseolin-protein variability in wild forms and landraces of the common bean (*Phaseolus vulgaris*): evidence for multiple centers of domestication. *Econ. Bot.* **1986**, *40*, 451−468.

(21) Johnson, W. C.; Menéndez, C.; Nodari, R.; Koinange, E. M. K.; Magnusson, S.; Singh, S. P.; Gepts, P. Association of a seed weight factor with the phaseolin seed storage protein locus across genotypes, environments, and genomes in *Phaseolus-Vigna* spp.: Sax (1923) revisited. *J. Agric. Genomics (J. Quant. Trait Loci)* **1996**, *2*, 5.

(22) Gepts, P.; Bliss, F. A. Enhanced available methionine concentration associated with higher phaseolin levels in common bean seeds. *Theor. Appl. Genet.* **1984**, *69*, 47−53.

(23) Kami, J. A.; Gepts, P. Phaseolin nucleotide sequence diversity in *Phaseolus*. I. Intraspecific diversity in *Phaseolus vulgaris*. *Genome* **1994**, *37*, 751−757.

(24) Salmanowicz, B. P. Phaseolin seed variability in common bean (*Phaseolus vulgaris*) by capillary gel electrophoresis. *J. Appl. Genet.* **2001**, *42*, 269−281.

(25) De la Fuente, M.; López-Pedrouso, M.; Alonso, J.; Santalla, M.; de Ron, A. M.; Alvarez, G.; Zapata, C. In-depth characterization of the phaseolin protein diversity of common bean (*Phaseolus vulgaris* L.) based on two-dimensional electrophoresis and mass spectrometry. *Food Technol. Biotechnol.* **2012**, *50*, 315−325.

(26) López-Pedrouso, M.; Alonso, J.; Zapata, C. Evidence for phosphorylation of the major seed storage protein of the common bean and its phosphorylation-dependent degradation during germination. *Plant Mol. Biol.* **2014**, *4*−*5*, 415−428.

(27) Biron, D. G.; Loxdale, H. D.; Ponton, F.; Moura, H.; Marché, L.; Brugidou, C.; Thomas, F. Population proteomics: An emerging discipline to study metapopulation ecology. *Proteomics* **2006**, *6*, 1712−1715.

(28) CIAT (Centro Internacional de Agricultura Tropical). Genetic Resources Program: bean collection. URL http://isa.ciat.cgiar.org/urg/beancollection.do.

(29) De la Fuente, M.; Borrajo, A.; Bermúdez, J.; Lores, M.; Alonso, J.; Santalla, M.; de Ron, A. M.; Zapata, C.; Alvarez, G. 2-DE-based proteomic analysis of common bean (*Phaseolus vulgaris* L.) seeds. *J. Proteomics* **2011**, *74*, 262−267.

(30) Van Wandelen, C.; Cohen, S. Using quaternary high-performance liquid chromatography eluent systems for separating 6-minoquinolyl-N-hydroxysuccinimidyl carbamate-derivatized amino acid mixtures. *J. Chromatogr., A* **1997**, *763*, 11−22.

(31) Nei, M.; Li, W.-H. Mathematical model for studying genetic variation in terms of restriction endonucleases. *Proc. Natl. Acad. Sci. U.S.A.* **1979**, *76*, 5269−5273.

(32) Mantel, N. The detection of disease clustering and a generalized regression approach. *Cancer Res.* **1967**, *27*, 209−220.

(33) Efron, B. *The Jackknife, the Bootstrap and Other Resampling Plans. CBMS-NSF Regional Conference Series in Applied Mathematics No. 38*; Society for Industrial and Applied Mathematics: Philadelphia, PA, 1982; pp 75−92.

(34) Schrage, L. A more portable Fortran random number generator. *ACM Trans. Math. Software* **1979**, *5*, 132−138.

(35) Rossi, M.; Bitocchi, E.; Bellucci, E.; Nanni, L.; Rau, D.; Attene, G.; Papa, R. Linkage disequilibrium and population structure in wild and domesticated populations of *Phaseolus vulgaris* L. *Evol. Appl.* **2009**, *2*, 504−522.

(36) Tohme, J.; Toro, O. C.; Vargas, J.; Debouck, D. G. Variability in Andean nuña common beans (*Phaseolus vulgaris*, Fabaceae). *Econ. Bot.* **1995**, *49*, 78−95.

(37) Bitocchi, E.; Nanni, L.; Bellucci, E.; Rossi, M.; Giardini, A.; Zeuli, P. S.; Logozzo, G.; Stougaard, J.; McClean, P.; Atiene, G.; Papa, R. Mesoamerican origin of the common bean (*Phaseolus vulgaris* L.) is revealed by sequence data. *Proc. Natl. Acad. Sci. U.S.A.* **2012**, *109*, 5148−5149.

(38) Kwak, M.; Kami, J. A.; Gepts, P. The putative Mesoamerican domestication center of *Phaseolus vulgaris* is located in the Lerma-Santiago basin of Mexico. *Crop Sci.* **2009**, *49*, 554−563.

(39) Taylor, M.; Chapman, R.; Beyaert, R.; Hernández-Sebastià, C.; Marsolais, F. Seed storage protein deficiency improves sulphur amino acid content in common bean (*Phaseolus vulgaris* L.): redirection of sulphur from γ-glutamyl-S-methyl-cysteine. *J. Agric. Food Chem.* **2008**, *56*, 5647−5654.

(40) Marinello, L.; Giosaffato, C. V. L.; Di Pierro, P.; Sorrentino, A.; Porta, R. Synthesis and resistance to in vitro proteolysis of transglutaminase cross-linked phaseolin, the major storage protein from *Phaseolus vulgaris*. *J. Agric. Food Chem.* **2007**, *55*, 4717−4721.

(41) Marquez, U. M.; Lajolo, F. M. Composition and digestibility of albumin, globulins and glutelins from *Phaseolus vulgaris*. *J. Agric. Food Chem.* **1981**, *29*, 1068−1074.

(42) Genovese, M. I.; Lajolo, F. M. Influence of naturally acid-soluble proteins from beans (*Phaseolus vulgaris* L.) on in vitro digestibility determination. *Food Chem.* **1998**, *62*, 315−323.
(43) Jivotovskaya, A. V.; Senyuk, V. I.; Rotari, V. I.; Horstmann, C.; Vaintraub, I. A. Proteolysis of phaseolin in relation to its structure. *J. Agric. Food Chem.* **1996**, *44*, 3768−3772.

resistance.[26] Hence, it is of great importance to perform resistance prediction and understand the corresponding mechanism at the molecular level.[27]

In the present study, we have aimed to make a broad prediction of the resistance associated with target mutations in PPO and have acquired a detailed understanding of the resistance mechanisms of typical PPO-inhibiting herbicides by a newly developed computational protocol, computational mutation scanning (CMS).[3] We have computationally studied the resistance mechanism of five most frequently applied PPO-inhibiting herbicides, including acifluorfen (ACJ), fomesafen (FOS), oxadiazon (OXZ), sulfentrazone (SUT), and Chlorphthalim (CHP) (Scheme 1). The computationally determined

Scheme 1. Chemical Structures of PPO Inhibitors

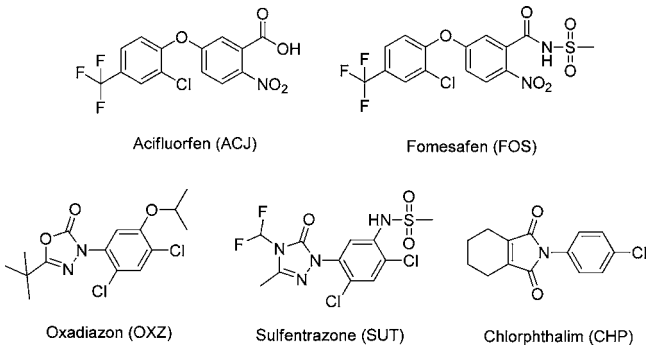

shifts of the binding free energies caused by mutations correlated well with the corresponding experimental data, leading to valuable insights into the potential resistance mechanisms of PPO inhibitors, which will help to reduce the resistance risk of new inhibitors discovered by a structure-based design approach.

MATERIALS AND METHODS

Molecular Docking and Molecular Dynamics (MD) Simulation. The X-ray crystal structure of human PPO used for computation was downloaded from RCSB.[25] Docking calculations were performed on ACJ, FOS, OXZ, SUT, and CHP with AutoDock4.0.[28] Most of the parameters for the docking calculation were set to the default values. Each docked structure was scored by the built-in scoring function and was clustered by 0.8 Å of RMSD criterions. Finally, the enzyme-ligand complex structures were selected according to the criteria for Autodock Score, which were used as initial complex structures for subsequent MD simulations.

Ab initio quantum mechanics (QM) calculations were performed for inhibitor and FAD optimization at the HF/6-31+G* level to determine the electrostatic potential by using the restrained electrostatic potential (RESP) method according to the Merz−Singh−Kollman scheme.[29,30] The RESP charges of ligands (inhibitors and FAD) was produced by using the standard RESP protocol[31,32] implemented in the Antechamber module of the AMBER9 program.[33] To carry out the MD simulations, the topology and coordinate files of the complexes were built with the Leap module of the AMBER9 package. All molecules were solvated by a rectangular box of TIP3P waters extended at least 10 Å in each direction from the solute. Before the MD simulation, some energy minimization steps were applied to the system. First, the solute was kept fixed with a constraint of 500 kcal mol^{-1} $Å^{-2}$ and waters and counterions were minimized; the backbone atoms of the protein were then fixed with the ligand, side chains, and other atoms free to move; finally, the entire system was fully minimized without any constraint. In each step, energy minimization was first performed by using the steepest descent algorithm for 2000 steps and then the conjugated gradient algorithm for another 3000 steps.

The MD simulation was performed under periodic boundary conditions by using the Sander module of the AMBER9 program, as we have done for the same protein before.[27] First, the system was fixed to make the heating only for waters and counterions for 10 ps to make sure the solute was fully solvated; second, the whole system was gradually heated from 10 to 298 K by a weak-coupling method[34] and equilibrated for 100 ps with the protein backbone fixed; last, the system was switched to a constant pressure equilibration for 3 ns. During the MD simulation, the particle mesh Ewald (PME) algorithm[35,36] was used to deal with long-range electrostatic interactions with a cutoff distance of 10 Å, which was also used for the van der Waals (vdW) energy terms. All of the angles and bonds involving hydrogen atoms were constrained by using the SHAKE algorithm.[37] The time step used for the MD simulations was 2.0 fs and the coordinates were collected every 1 ps.

Computational Mutation Scanning. A free energy perturbation approach, computational alanine scanning (CAS), can be used to estimate the free energy shift caused by mutation to alanine, which has been widely used to study protein−protein/ligand interactions. The CMS method, as an extension of the CAS method, has been validated in our previous study and can be applied to all kinds of mutations with the entropy effects taken into account.[3] We saved a total of 100 snapshots from a stable MD trajectory of the last 1000 ps, that is, one structure in every 10 ps, for each MD-simulated complex. We performed mutation automatically on each snapshot with a modified MMTSB Tool Set package.[38] All force field parameters in the topology files for the residue to be mutated were replaced with the parameters of the corresponding new residue. Before the calculation of the binding free energy, the positions of side chain atoms of all residues were energy-minimized by using the Sander module of AMBER9 program via a combined use of the steepest descent/conjugate gradient algorithms, with a convergence criterion of 0.2 kcal mol^{-1} $Å^{-1}$. Then the Gibbs binding free energies between the protein and ligand for each snapshot were calculated by carrying out a modified molecular mechanics/Poisson−Boltzmann surface area (MM/PBSA) energy analysis.[27] The final binding free energy is the average of the calculated values associated with the 100 snapshots.

Kinetic Assays for PPO and Its Mutants. The recombinant plasmid (pHPPO-X) was a generous gift from Dr. Harry A. Dailey (University of Georgia, Athens, GA). *h*PPO (human PPO) mutations were generated from the recombinant plasmid (pHPPO-X) using the DpnI-mediated site-directed mutagenesis kit (Biocrest Manufacturing LP, Cedar Creek, TX), and mutations were confirmed by sequence analysis. Expression and purification methods of *h*PPO were the same as those used in our previous publication.[39,40] The *h*PPO activity was assayed by measuring the velocity of the formation of protoporphyrin from protoporphyrinogen on a 96-well plate using the continuous fluorometric method.[39]

The kinetic parameters were evaluated by Sigma Plot software 10.0 (SPSS, Chicago). IC_{50} was determined by

measuring *h*PPO activity over a range of inhibitor concentrations at a single substrate concentration. IC_{50} values were calculated by fitting v versus [I] data to a single binding site model described by eq 1

$$y = \min + \frac{\max - \min}{1 + 10^{\log IC_{50} - x}} \quad (1)$$

where y is the percentage of maximal rate, max and min are the y values at which the curve levels off, x is the logarithm of inhibitor concentration, and IC_{50} is the inhibitor concentration that elicits 50% of the total inhibition. Calculated K_i value is obtained by applying the following relationship, which exists for competitive inhibition among K_i, K_m, and IC_{50} at any saturating substrate concentration (S).

$$K_i = \frac{IC_{50}}{S/K_m + 1} \quad (2)$$

RESULTS AND DISCUSSION

Structures of PPO–Inhibitors Complexes. Our strategy for the prediction of PPO resistance to herbicides involved determining the binding models of the five inhibitors with PPO. We used molecular docking to examine their possible binding models. Due to docking, the method we used could not fully account for the flexibility of the protein and so the binding models from docking were further studied by molecular dynamics (MD) simulations. We selected the final structures of PPO–inhibitor complexes according to docking scores, the stability of the MD simulation, and geometric matching qualities with the known crystal structures of INH in a complex with tobacco PPO and ACJ in a complex with *Myxococcus xanthus* PPO and also with human PPO.[22,23,39] In addition, obtaining a stable MD trajectory is crucial for subsequent analysis, so the plot of root-mean-square deviation (RMSD) of the protein backbone and inhibitor atoms throughout the whole process of the MD simulation was examined for convergence. According to the RMSD values of the MD trajectories (Figure 1), the simulations have reached equilibrium states. The MD simulations were also repeated with different sets of parameters and force fields to further validate the convergence of the simulations (data not shown).

To further verify the reliability of the MD simulations, the binding free energies of the five inhibitors were calculated by using a modified MM/PBSA method.[27] The results included the overall binding free energy and each energy term (Table 1). The calculated binding affinities were also compared with the experimental data derived from inhibitions studies performed with the mutated PPO enzymes that we prepared. As listed in Table 1, the binding free energies (ΔG_{cal}) of the five inhibitors with respect to wild-type PPO obtained from the MM/PBSA calculations ranged from −11.7 to −23.80 kcal/mol. The corresponding experimentally derived free energies of binding (ΔG_{exp}) using wild-type PPO varied over the narrow range of −5.54 to −8.82 kcal/mol. These data show that the calculation largely overestimated the absolute values of the binding free energies by ∼2.0–2.7-fold. Nevertheless, the qualitative order of the calculated binding affinities for the inhibitors using computational methods was FOS > SUT > ACJ > OXZ > CHP, which is in accordance with the ranking of the binding determined experimentally. Quantitatively, the calculated binding free energies are precisely correlated with the corresponding experimental data, with a correlation coefficient

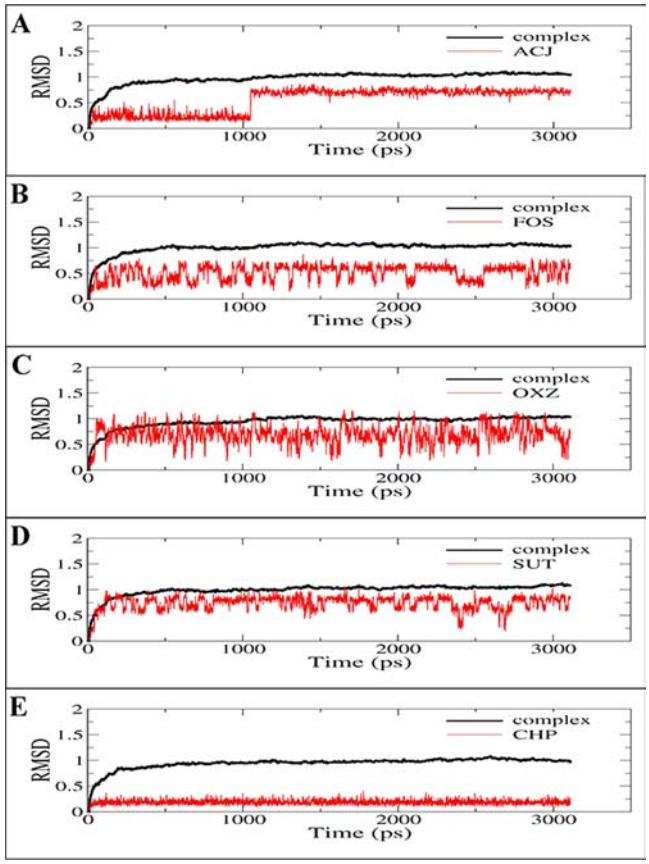

Figure 1. Time dependence of the RMSD of protein backbone atoms (color in black) and inhibitors (color in red). (A) PPO–ACJ, (B) PPO–FOS, (C) PPO–OXZ, (D) PPO–SUT, and (E) PPO–CHP.

r^2 = 0.88. The good agreement between the computational results and the experimental data further confirmed the computational models constructed and tested in this study are reliable.

In addition, the simulated binding models were also compared with available X-ray crystal structures and our previous studies.[27] The interaction between the inhibitor and PPO may occur in the binding pocket defined by seven residues. We have shown that most inhibitors interacted with PPO by establishing strong hydrogen bonds with the highly conserved Arg97 residue and a hydrophobic interaction with Met368, which is similar to that in the X-ray crystal structure of ACJ in a complex with *M. xanthus* PPO and the crystal structure of INH in a complex with tobacco PPO.[22,23] To make a clear view of the interacting pattern, MD simulated models of PPO inhibitors binding with residues in the pocket are shown in Figure 2. The five inhibitors have similar binding modes because they are thought to inhibit PPO activity by mimicking the same part of the substrate. So, the simulated three-dimensional structure of PPO inhibitor complexes obtained in the present investigation should be reasonable.

Selection of Residues for Mutation. The amino acids for mutation in PPO have been the subject of intensive resistance research in agriculture because of the tendency of this enzyme to lose efficacy toward a wide range of pesticides. To make reasonable selection of amino acid residues for mutation, we should compare the key residues interacting with substrate and inhibitors. In light of our earlier studies of both residue mutation experiments and in silico studies, we gained insights

dx.doi.org/10.1021/jf5018115 | J. Agric. Food Chem. 2014, 62, 7209–7215

Table 1. Binding Free Energies Calculated for the WT PPO with Five Inhibitors (kcal/mol)

inhibitor	ΔE_{ele}	ΔE_{vdW}	ΔE_{MM}	ΔG_{PB}	ΔE_{bind}	$-T\Delta S$	ΔG_{bind}[a]	ΔG_{exp}[b]
ACJ	−24.05 (2.06)	−50.24 (1.02)	−74.29 (1.49)	35.82 (1.26)	−38.47 (1.08)	20.55 (0.97)	−17.92 (1.03)	−7.88
FOS	−55.25 (9.19)	−54.97 (1.29)	−110.23 (9.79)	63.84 (8.43)	−46.38 (1.91)	22.50 (1.24)	−23.89 (1.58)	−8.82
OXZ	−10.72 (1.02)	−51.73 (0.79)	−62.45 (1.06)	25.61 (1.02)	−36.84 (1.00)	21.94 (0.65)	−14.90 (0.83)	−7.55
SUT	−27.77 (1.36)	−45.07 (0.89)	−72.84 (1.89)	34.68 (1.56)	−38.16 (1.16)	18.07 (1.02)	−20.09 (1.09)	−8.39
CHP	−11.42 (0.53)	−42.20 (0.46)	−53.62 (0.71)	24.03 (1.04)	−29.60 (1.04)	18.43 (0.56)	−11.17 (0.80)	−5.54

[a]Results determined by the MM−PBSA calculations. The standard deviation (STD) values are included in the parentheses. [b]Experimental values ΔG_{exp} were derived from the experimental K_i values of *h*PPO according to $\Delta G_{exp} = -RT \ln K_i$.

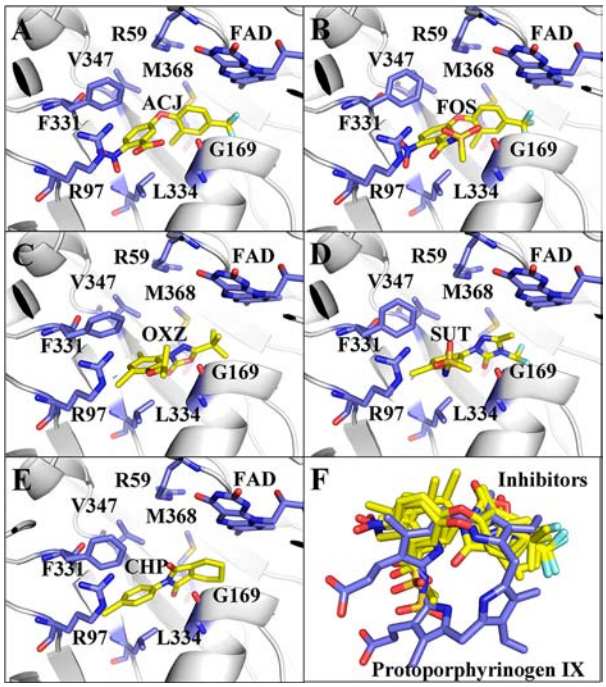

Figure 2. MD simulated models of human PPO in a complex with ACJ, FOS, OXZ, SUT, and CHP. (A) PPO−ACJ, (B) PPO−FOS, (C) PPO−OXZ, (D) PPO−SUT, (E) PPO−CHP, and (F) alignment of the binding conformation of five inhibitors and protoporphyrinogen IX.

into the binding modes of substrate and inhibitors in PPO.[40,41] The residues R59, R97, M368, G169, V347, L334, and F331 comprise the active site of PPO. On the basis of our previously determined binding model of the substrate[41] and site-directed mutagenesis studies of PPO, we identified three mutations, R59Q, R97G, and M368Q, that had no strong effect on the structure and catalytic activity of PPO. This result was at odds with our original idea that the R97G mutation would decrease the catalytic activity of the enzyme through loss of a key hydrogen bond interaction with the substrate. Indeed, the replacement of R97 with glycine improved the enzyme activity.[41] We therefore undertook further studies to understand the mechanism of binding of the five inhibitors to the R59Q, R97G, and M368Q mutants. Hence, site-directed mutagenesis and enzyme kinetic studies were performed on *h*PPO.

Computational Prediction of Resistance. To aid the course of pesticide discovery, the prediction of pesticide resistance by computational methods would be most valuable. Computational methods can provide information about the possible mechanisms of resistance that can be conferred by a target mutation. These mechanisms can be divided into six categories according to thermodynamic parameters: decrease of enthalpy, decrease of entropy, decrease of both the enthalpy and entropy, no significant change in enthalpy and entropy, decrease of enthalpy compensated by the increase of entropy, and decrease of entropy compensated by the increase of enthalpy.

Computational mutation scanning (CMS) calculations were performed to predict the resistance for the five inhibitors and to gain further insight into the contributions of the various energy terms to the differences in the binding free energy of R59Q, R97G, and M368Q, including the changes in the van der Waals and electrostatic interaction energies, as well as the electrostatic and nonpolar desolvation free energies upon mutation. The relative binding free energies calculated by CMS and the corresponding experimental values are given in Table 2. The $\Delta\Delta G$ value can be viewed as an indicator of the resistance level, with the negative and positive values of $\Delta\Delta G_{bind}$ ($\Delta G_{mutant} - \Delta G_{wild\text{-}type}$) indicating favorable and unfavorable outcomes, respectively. Thus, a positive $\Delta\Delta G$ value indicates resistance, whereas a negative $\Delta\Delta G$ value signifies lack of resistance. Most of the calculated relative binding free energies were positive, illustrating that the three mutants usually induced resistance in PPO with respect to the five inhibitors.

To gain further insight into the resistance mechanisms associated with the mutations, contributions of enthalpy and entropy to the binding free energy changes were analyzed by computational methods. As seen in Table 2, all of the mutations, except R97G for OXZ, R59Q for CHP, and R97G for CHP, should result in resistance due to the positive shift in binding free energy.

The resistance prediction results of PPO were validated in vivo, using site-directed mutagenesis and enzyme kinetic studies performed on PPO. We constructed mutant PPO genes, isolated the respective mutant proteins, determined their kinetic parameters via continuous fluorometric method, and compared the results with wild-type (WT) PPO. The three mutations could mostly induce resistance (uppermost 11.63-fold) for the five inhibitors with the exception of R59Q for CHP, R97G for OXZ, and R97G for CHP (Table 2). These outcomes were consistent with the computational studies.

CMS allowed us to further analyze the role of the individual thermodynamic parameters in the mechanism of resistance associated with the mutations. These data are presented as a histogram that compares the effect of the selected mutations in PPO on each parameter affecting the binding of the five inhibitors (Figure 3). R59Q and M368Q appear to function via the same resistance mechanism; they share the common characteristic that the decrease in the enthalpy contribution is mainly responsible for the decrease in binding affinity for the inhibitors. In contrast, R97G led to another mechanism, that the decrease in the enthalpy contribution was compensated by an increase in the entropic contribution. The replacement of

Table 2. Inhibition Constants (K_i) of WT and Mutant Human PPO Activities by Inhibitors, the Relative Resistance Fold, and Calculated Binding Free Energy Changes (kcal/mol)

inhibitors	types	K_i (μM)	RF[a]	$\Delta\Delta H_{cal}$[b]	$-T\Delta\Delta S$	$\Delta\Delta G_{cal}$	result[c]
ACJ	WT	1.71	1	0	0	0	
	R59Q	4.27	2.50	4.06	−0.53	3.53	R
	R97G	9.76	5.71	5.87	−2.97	2.90	R
	M368Q	6.21	3.63	3.88	−0.07	3.81	R
FOS	WT	0.35	1	0	0	0	
	R59Q	0.25	0.70	3.88	−0.78	3.11	R
	R97G	1.15	3.29	8.55	−2.78	5.78	R
	M368Q	1.33	3.81	3.91	−0.16	3.76	R
OXZ	WT	2.96	1	0	0	0	
	R59Q	11.52	3.89	1.00	−0.06	0.94	R
	R97G	0.13	0.04	0.69	−2.30	−1.61	N
	M368Q	11.63	3.93	3.35	0.10	3.45	R
SUT	WT	0.72	1	0	0	0	
	R59Q	4.47	6.21	1.27	0.04	1.31	R
	R97G	8.78	12.19	4.09	−3.13	0.96	R
	M368Q	1.79	2.49	4.41	0.32	4.73	R
CHP	WT	87.87	1	0	0	0	
	R59Q	63.28	0.72	−0.32	0.19	−0.13	N
	R97G	37.33	0.42	0.75	−3.25	−2.50	N
	M368Q	152.79	1.74	4.37	0.13	4.50	R

[a]Resistance fold (RF) = $K_{i,mutant}/K_{i,WT}$. RF > 1 means resistance, whereas RF ≤ 1 means no resistance. [b]$\Delta\Delta G = \Delta G_{MT} - \Delta G_{WT}$ calculated by CMS protocol. [c]Resistance prediction results. R means resistance, whereas N means no resistance.

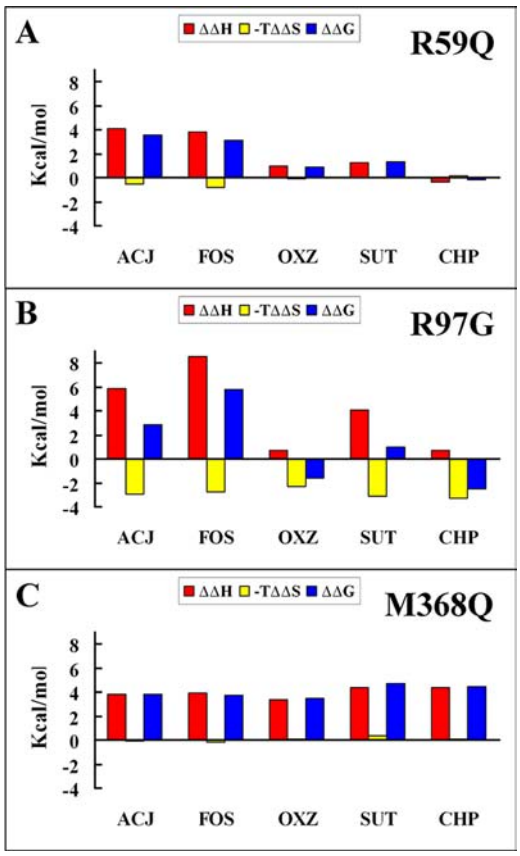

Figure 3. Thermodynamic representation of the resistance mechanism. The histogram means changes of enthalpy, entropy, and binding free energy of the five inhibitors in each mutant. Possible mechanisms of resistance were shown. (A) Resistance mechanism of R59Q. (B) Resistance mechanism of R97G. (C) Resistance mechanism of M368Q.

R97 with glycine could enlarge the mouth of the pocket and could improve the turnover of the inhibitors, which would favor the improvement in the conformational degrees of freedom of the inhibitors in the active site.[41] This structural change could cause an increase in conformational entropy, such that the loss of enthalpy would be offset.

However, R97G confers resistance for ACJ, FOS, and SUT, but not for OXZ and CHP. To explore why the R97G mutation could have such different effects, we further examined the binding models of the five inhibitors (Figure 2). According to a previous study, R97 was located in the pocket between the active site and the binding pathway of the substrate.[41] The inhibitors ACJ, FOS, and SUT can form important hydrogen-bonding interactions with R97 in WT PPO, but OXZ and CHP cannot. The replacement of the salt bridge functionality in R97 by a simple glycine caused ACJ, FOS, and SUT to lose more enthalpy contribution than did OXZ and CHP, which could induce resistance for ACJ, FOS, and SUT. But, the enthalpy loss was compensated by an increase in the entropy component of binding, thereby reducing the level of resistance. It is worth noting that R97G experienced a large enthalpy loss for FOS; such an enthalpy loss should result in over 100-fold rise in resistance if not for the entropic compensation. That is to say, the entropy increase due to the improvement of the conformational degrees of freedom can effectively reduce the resistance level.

The computational studies using the CMS protocol have led to a detailed understanding of the resistance mechanisms and the structure-resistance relation of PPO and five inhibitors associated with the target mutations. Computational simulations based on our developed 3D model of PPO−inhibitor binding structures, followed by resistance prediction, site-directed mutagenesis, and PPO activity assays, have led to a detailed understanding of PPO interaction with herbicides. The computationally determined mutation-caused shifts in the binding free energies are reflected by two resistance

dx.doi.org/10.1021/jf5018115 | J. Agric. Food Chem. 2014, 62, 7209−7215

mechanisms, which provide essential information for structure-based pesticide design. Our computational results demonstrated that the calculated entropy change seems to relate with the conformational degrees of freedom of the inhibitor in the binding pocket. That is to say, inhibitors designed to have more conformational flexibility in the binding site may inhibit both the WT and mutants of a targeted enzyme. The structural and mechanistic insights obtained from the present study provide a valuable base for rational design of novel PPO inhibitors.

AUTHOR INFORMATION

Corresponding Authors

*State Key Laboratory of Elemento-Organic Chemistry, Nankai University, Tianjin 300071, P. R. China. Tel: 86-22-23504782. Fax: 86-22-23504782. E-mail: zhenxi@nankai.edu.cn (Z.X.).

*College of Chemistry, Central China Normal University, 152 Luoyu Road, 430079 Wuhan, Hubei, P.R. China. Tel.: 86-27-67867800. Fax: 86-27-67867141. E-mail: gfyang@mail.ccnu.edu.cn (G.-F.Y.).

Funding

The research was supported in part by the NSFC (No. 21202055), "Specialized Research Fund for the Doctoral Program of Higher Education" (No. 20120144120003), and the "Hong Kong Scholars Program" (No. XJ2012020). This research is also supported in part by the Guangdong Province Key Laboratory of Computational Science and the Guangdong Province Computational Science Innovative Research Team.

Notes

The authors declare no competing financial interest.

ABBREVIATIONS USED

PPO, protoporphyrinogen oxidase; CMS, computational mutation scanning; CAS, computational alanine scanning; ACJ, acifluorfen; FOS, fomesafen; OXZ, oxadiazon; SUT, sulfentrazone; CHP, Chlorphthalim; QM, quantum mechanics; RESP, restrained electrostatic potential; MD, molecular dynamics; PME, particle mesh Ewald; vdW, van der Waals; MM/PBSA, molecular mechanics/Poisson−Boltzmann surface area; RMSD, root-mean-square deviation; WT, wild-type

REFERENCES

(1) Aktar, M. W.; Sengupta, D.; Chowdhury, A. Impact of pesticides use in agriculture: their benefits and hazards. *Interdiscip. Toxicol.* **2009**, *2*, 1−12.

(2) Mithila, J.; Godar, A. S. Understanding Genetics of Herbicide Resistance in Weeds: Implications for Weed Management. *Adv. Crop Sci. Technol.* **2013**, *1*, 1000115.

(3) Hao, G. F.; Yang, G. F.; Zhan, C. G. Computational mutation scanning and drug resistance mechanisms of HIV-1 protease inhibitors. *J. Phys. Chem. B* **2010**, *114*, 9663−9676.

(4) Chellappan, S.; Kiran Kumar Reddy, G. S.; Ali, A.; Nalam, M. N.; Anjum, S. G.; Cao, H.; Kairys, V.; Fernandes, M. X.; Altman, M. D.; Tidor, B.; Rana, T. M.; Schiffer, C. A.; Gilson, M. K. Design of mutation-resistant HIV protease inhibitors with the substrate envelope hypothesis. *Chem. Biol. Drug Des.* **2007**, *69*, 298−313.

(5) Hao, G. F.; Yang, G. F.; Zhan, C. G. Structure-based methods for predicting target mutation-induced drug resistance and rational drug design to overcome the problem. *Drug Discovery Today* **2012**, *17*, 1121−1126.

(6) Zhang, F.; Tang, W. J.; Hedtke, B.; Zhong, L. L.; Liu, L.; Peng, L. W.; Lu, C. M.; Grimm, B.; Lin, R. C. Tetrapyrrole biosynthetic enzyme protoporphyrinogen IX oxidase 1 is required for plastid RNA editing. *Proc. Natl. Acad. Sci. U. S. A.* **2014**, *111*, 2023−2028.

(7) Deybach, J.-C.; Da Silva, V.; Grandchamp, B.; Nordmann, Y. The mitochondrial location of protoporphyrinogen oxidase. *Eur. J. Biochem.* **1985**, *149*, 431−435.

(8) Lermontova, I.; Kruse, E.; Mock, H. P.; Grimm, B. Cloning and characterization of a plastidal and a mitochondrial isoform of tobacco protoporphyrinogen IX oxidase. *Proc. Natl. Acad. Sci. U. S. A.* **1997**, *94*, 8895−8900.

(9) Matringe, M.; Camadro, J. M.; Labbe, P.; Scalla, R. Protoporphyrinogen oxidase as a molecular target for diphenyl ether herbicides. *Biochem. J.* **1989**, *260*, 231−235.

(10) Poulson, R. The enzymic conversion of protoporphyrinogen IX to protoporphyrin IX in mammalian mitochondria. *J. Biol. Chem.* **1976**, *251*, 3730−3733.

(11) Sherman, T. D.; Becerril, J. M.; Matsumoto, H.; Duke, M. V.; Jacobs, J. M.; Jacobs, N. J.; Duke, S. O. Physiological basis for differential sensitivities of plant species to protoporphyrinogen oxidase-inhibiting herbicides. *Plant Physiol.* **1991**, *97*, 280−287.

(12) Li, B.; Lan, Y. M.; Hsu, C. T.; Liu, Z. L.; Song, H. B.; Wu, C.; Yang, H. Z. Three trifluoromethyl-substituted protoporphyrinogen IX oxidase inhibitors. *Acta Crystallogr. C* **2005**, *61*, o122−126.

(13) Li, H. B.; Zhu, Y. Q.; Song, X. W.; Hu, F. Z.; Liu, B.; Li, Y. H.; Niu, Z. X.; Liu, P.; Wang, Z. H.; Song, H. B.; Zou, X. M.; Yang, H. Z. Novel protoporphyrinogen oxidase inhibitors: 3H-pyrazolo[3,4-d]-[1,2,3]triazin-4-one derivatives. *J. Agric. Food Chem.* **2008**, *56*, 9535−9542.

(14) Zhang, L.; Hao, G. F.; Tan, Y.; Xi, Z.; Huang, M. Z.; Yang, G. F. Bioactive conformation analysis of cyclic imides as protoporphyrinogen oxidase inhibitor by combining DFT calculations, QSAR and molecular dynamic simulations. *Bioorg. Med. Chem.* **2009**, *17*, 4935−4942.

(15) Hao, G. F.; Zuo, Y.; Yang, S. G.; Yang, G. F. Protoporphyrinogen oxidase inhibitor: an ideal target for herbicide discovery. *Chimia (Aarau)* **2011**, *65*, 961−969.

(16) Jiang, L. L.; Tan, Y.; Zhu, X. L.; Wang, Z. F.; Zuo, Y.; Chen, Q.; Xi, Z.; Yang, G. F. Design, synthesis, and 3D-QSAR analysis of novel 1,3,4-oxadiazol-2(3H)-ones as protoporphyrinogen oxidase inhibitors. *J. Agric. Food Chem.* **2010**, *58*, 2643−2651.

(17) Jiang, L. L.; Zuo, Y.; Wang, Z. F.; Tan, Y.; Wu, Q. Y.; Xi, Z.; Yang, G. F. Design and syntheses of novel N-(benzothiazol-5-yl)-4,5,6,7-tetrahydro-1H-isoindole-1,3(2H)-dione and N-(benzothiazol-5-yl)isoindoline-1,3-dione as potent protoporphyrinogen oxidase inhibitors. *J. Agric. Food Chem.* **2011**, *59*, 6172−6179.

(18) Yang, Z.; Sheng-Gang, Y.; Yan-Ping, L.; Ying, T.; Ge-Fei, H.; Qiong-You, W.; Zhen, X.; Guang-Fu, Y. Design and synthesis of 1-(benzothiazol-5-yl)-1H-1,2,4-triazol-5-ones as protoporphyrinogen oxidase inhibitors. *Bioorg. Med. Chem.* **2013**, *21*, 3245−3255.

(19) Zhang, L.; Tan, Y.; Wang, N. X.; Wu, Q. Y.; Xi, Z.; Yang, G. F. Design, syntheses and 3D-QSAR studies of novel N-phenyl pyrrolidin-2-ones and N-phenyl-1H-pyrrol-2-ones as protoporphyrinogen oxidase inhibitors. *Bioorg. Med. Chem.* **2010**, *18*, 7948−7956.

(20) Zuo, Y.; Yang, S. G.; Jiang, L. L.; Hao, G. F.; Wang, Z. F.; Wu, Q. Y.; Xi, Z.; Yang, G. F. Quantitative structure-activity relationships of 1,3,4-thiadiazol-2(3H)-ones and 1,3,4-oxadiazol-2(3H)-ones as human protoporphyrinogen oxidase inhibitors. *Bioorg. Med. Chem.* **2012**, *20*, 296−304.

(21) Yang, S. G.; Hao, G. F.; Dayan, F. E.; Tranel, P. J.; Yang, G. F. Insight into the Structural Requirements of Protoporphyrinogen Oxidase Inhibitors: Molecular Docking and CoMFA of Diphenyl Ether, Isoxazole Phenyl, and Pyrazole Phenyl Ether. *Chin. J. Chem.* **2013**, *31*, 1153−1158.

(22) Koch, M.; Breithaupt, C.; Kiefersauer, R.; Freigang, J.; Huber, R.; Messerschmidt, A. Crystal structure of protoporphyrinogen IX oxidase: a key enzyme in haem and chlorophyll biosynthesis. *EMBO J.* **2004**, *23*, 1720−1728.

(23) Corradi, H. R.; Corrigall, A. V.; Boix, E.; Mohan, C. G.; Sturrock, E. D.; Meissner, P. N.; Acharya, K. R. Crystal structure of protoporphyrinogen oxidase from Myxococcus xanthus and its complex with the inhibitor acifluorfen. *J. Biol. Chem.* **2006**, *281*, 38625−38633.

(24) Qin, X. H.; Sun, L.; Wen, X.; Yang, X.; Tan, Y.; Jin, H.; Cao, Q. Y.; Zhou, W. H.; Xi, Z.; Shen, Y. Q. Structural insight into unique properties of protoporphyrinogen oxidase from Bacillus subtilis. *J. Struct. Biol.* **2010**, *170*, 76−82.
(25) Qin, X.; Tan, Y.; Wang, L.; Wang, Z.; Wang, B.; Wen, X.; Yang, G.; Xi, Z.; Shen, Y. Structural insight into human variegate porphyria disease. *FASEB J.* **2011**, *25*, 653−664.
(26) Patzoldt, W. L.; Hager, A. G.; McCormick, J. S.; Tranel, P. J. A codon deletion confers resistance to herbicides inhibiting protoporphyrinogen oxidase. *Proc. Natl. Acad. Sci. U. S. A.* **2006**, *103*, 12329−12334.
(27) Hao, G. F.; Zhu, X. L.; Ji, F. Q.; Zhang, L.; Yang, G. F.; Zhan, C. G. Understanding the mechanism of drug resistance due to a codon deletion in protoporphyrinogen oxidase through computational modeling. *J. Phys. Chem. B* **2009**, *113*, 4865−4875.
(28) Huey, R.; Morris, G. M.; Olson, A. J.; Goodsell, D. S. A semiempirical free energy force field with charge-based desolvation. *J. Comput. Chem.* **2007**, *28*, 1145−1152.
(29) Singh, U. C.; Kollman, P. A. An approach to computing electrostatic charges for molecules. *J. Comput. Chem.* **1984**, *5*, 129−145.
(30) Besler, B. H.; Merz, K. M.; Kollman, P. A. Atomic charges derived from semiempirical methods. *J. Comput. Chem.* **1990**, *11*, 431−439.
(31) Bayly, C. I.; Cieplak, P.; Cornell, W. D.; Kollman, P. A. A well-behaved electrostatic potential based method using charge restraints for deriving atomic charges: the RESP model. *J. Phys. Chem.* **1993**, *97*, 10269−10280.
(32) Cornell, W. D.; Cieplak, P.; Bayly, C. I.; Kollman, P. A. Application of RESP charges to calculate conformational energies, hydrogen bond energies, and free energies of solvation. *J. Am. Chem. Soc.* **1993**, *115*, 9620−9631.
(33) Case, D. A.; Darden, T. A.; Cheatham, T. E.; Simmerling, C. L.; Wang, J.; Duke, R. E.; Luo, R.; Merz, K. M.; Wang, B.; Pearlman, D. A.; Crowley, M.; Brozell, S.; Tsui, V.; Gohlke, H.; Mongan, J.; Hornak, V.; Cui, G.; Beroza, P.; Schafmeister, C.; Caldwell, J. W.; Ross, W. S.; Kollman, P. A. *AMBER 9*; University of California: San Francisco, 2006.
(34) Morishita, T. Fluctuation formulas in molecular-dynamics simulations with the weak coupling heat bath. *J. Chem. Phys.* **2000**, *113*, 2976−2982.
(35) Darden, T.; York, D.; Pedersen, L. Particle mesh Ewald: An N. log(N) method for Ewald sums in large systems. *J. Chem. Phys.* **1993**, *98*, 10089−10092.
(36) Essmann, U.; Perera, L.; Berkowitz, M. L. A smooth particle mesh Ewald method. *J. Chem. Phys.* **1995**, *103*, 8577−8593.
(37) Ryckaert, J. P.; Ciccotti, G.; Berendsen, H. J. C. Numerical integration of the Cartesian equations of mot ion of a system with constraints: molecular dynamics of n-alkanes. *J. Comput. Phys.* **1977**, *23*, 327−341.
(38) Michael, F.; John, K.; Charles, L. B. *MMTSB Tool Set*; MMTSB NIH Research Resource; The Scripps Research Institute: La Jolla, CA, 2001.
(39) Qin, X.; Tan, Y.; Wang, L.; Wang, Z.; Wang, B.; Wen, X.; Yang, G.; Xi, Z.; Shen, Y. Structural insight into human variegate porphyria disease. *FASEB J.* **2010**, *25*, 653−664.
(40) Wang, B.; Wen, X.; Qin, X.; Wang, Z.; Tan, Y.; Shen, Y.; Xi, Z. Quantitative Structural Insight into Human Variegate Porphyria Disease. *J. Biol. Chem.* **2013**, *288*, 11731−11740.
(41) Hao, G. F.; Tan, Y.; Yang, S. G.; Wang, Z. F.; Zhan, C. G.; Xi, Z.; Yang, G. F. Computational and experimental insights into the mechanism of substrate recognition and feedback inhibition of protoporphyrinogen oxidase. *PLoS One* **2013**, *8*, e69198.

fractionated using Sephadex LH-20 gel,[10] and the MW of each tannin fraction is determined based on depolymerization reactions. Estimating the MW of wine tannins using GPC requires the assumption that the hydrodynamic volumes of grape skin tannins equate to those of wine tannins at the same MW and that there is no interaction between the tannins and the gel media. The correlation between the results from GPC and mDP calculations can also be limited[14] as a consequence of low percent yield or differences in hydrodynamic volumes between the tannin sample and the grape tannins of the calibration curve.

Polymers can expand or contract in different solvents[16] and tannins in particular can be more condensed in water than in organic solvents and may change conformation in different hydroalcoholic solutions.[13] The hydrodynamic volumes of tannins in different wine-like conditions (pH 3.0−4.0, 10−15% aqueous ethanol) may therefore be very different to those measured using the GPC conditions. Given that wine tannin size can directly impact astringency,[2,3] it is important to determine if the relative tannin sizes determined using GPC, such as between aged and young wines tannins, are actually representative of relative tannin size in wine. For this reason, the MWs of a selection of tannins were measured using small-angle X-ray scattering (SAXS) with synchrotron radiation in a range of wine-like conditions and compared with those estimated using GPC and mDP. SAXS can be used to measure particle size and shape in a range of solutions[17,18] and has been previously used to measure tannins in aqueous ethanol solutions.[13] The size of macromolecules can be determined for a large range of particle sizes, from less than 1 kDa to several MDa and, although routinely used for model reconstruction from monodisperse systems of biomolecules (e.g., purified proteins),[17] the technique can be applied to the study of polydispersed systems. Previous experiments have measured changes in the MW of polydisperse grape and apple tannins with oxidation by comparing the SAXS forward scattering intensities with mDP,[6,12] highlighting the potential for using this technique for wine tannins. SAXS also provides information on the conformation of tannins in solutions,[19] providing an added advantage over GPC or mDP analysis.

Wine astringency is known to decrease in intensity with aging.[20,21] The underlying cause for this in unclear, and may relate to changes in tannin MW or conformation as no age-related trends have been observed in tannin concentration.[14] Studies that investigate tannin structure in aged wines have reported conflicting results, depending on the method used for analysis. Analyses comparing the mDP of tannins from younger and older wines have suggested that aged wine tannins are smaller than young wine tannins,[22,23] while GPC studies have reported that aged wine tannins are generally larger than younger wine tannins.[14,24] The difference in results produced from these two methods as well as the potential changes in the molecular dimensions of tannins with wine aging highlights the value in measuring aged and young wine tannins in wine-like conditions.

In this study, we determined the relative dimensions of wine tannin samples isolated from a 3 and a 7 year old Cabernet Sauvignon wine using SAXS in a range of wine-like matrixes, including different ethanol concentrations, pH, and ionic strengths. These results were then compared with those of the same wine tannin samples measured using GPC and mDP to assess the usefulness of each method for estimating the relative size of tannins in red wines. Results are also discussed with respect to the potential impact of tannin shape on wine astringency with aging.

MATERIALS AND METHODS

Chemicals. All solvents used were high-performance liquid chromatography (HPLC) grade, all chemicals were analytical reagent grade, and water was obtained from a Milli-Q purification system. Acetic acid (100%), acetonitrile, ethanol, formic acid (98−100%), and HCl (32%), were all purchased from Merck Australia (Kilsyth, VIC, Australia). Ascorbic acid, lithium chloride (LiCl), *N*,*N*-dimethylformamide (DMF), phloroglucinol, sodium acetate, tartaric acid, and sodium chloride (NaCl) were purchased from Sigma-Aldrich (Castle Hill, NSW, Australia).

Tannin Isolation and Fractionation. Tannins were isolated from two Australian Coonawarra Cabernet Sauvignon wines, aged 3 and 7 years, using Toyopearl HW-40F, as previously described.[4] Both isolated tannin samples were then fractionated using liquid−liquid separation with butanol and water as reported previously[4] to give six tannin samples: total tannin samples from each vintage (TT3 and TT7 for the 3 and 7 year old wine tannins, respectively), aqueous fractions from each vintage (Aq3 and Aq7) and butanol-soluble fractions from each vintage (Bu3 and Bu7). The aqueous fractions were more abundant than the butanol-soluble fractions for both vintages, with ratios of 3.6:1 (Aq/Bu) for the 3 year old tannin samples and 2.9:1 (Aq/Bu) for the7 year old tannin samples. Relative water-solubility of the tannin samples were determined using octanol/water assays as previously described.[14]

Tannin Molecular Weight Measurements Using Gel Permeation Chromatography and Depolymerization Reactions. Standard laboratory methods for determining average tannin molecular weight (MW) for each sample were performed using depolymerization reactions with phloroglucinol (phloroglucinolysis)[7] and gel permeation chromatography (GPC).[9] Briefly, for phloroglucinolysis, tannin solutions (25 μL, 10 g/L tannin in methanol) were added to phloroglucinol solution (25 μL, 100 g/L phloroglucinol in methanol with ascorbic acid (20 g/L) and 0.2 N HCl) to give final concentrations of 5 g/L tannin. Reactions were performed at 50 °C for 25 min, after which sodium acetate solution (70 mM, 150 μL) was added to neutralize the reaction. The cleaved subunits were analyzed using HPLC as previously described[7] to give the mean degree of polymerization (mDP, calculated from the proportion of extension to terminal subunits), percent yield (proportion of the tannin weight that was cleaved by acid hydrolysis), percent epigallocatechin subunits (% GC), and percent epicatechin gallate subunits (%ECG). The MW for each sample (MW_{mDP}) was calculated based on the mDP and subunit composition. GPC was performed as described previously[9] using a series of two PLgel columns (500 and 10^3 Å) with an isocratic solvent system of DMF solution (0.15 M LiCl, 1% v/v acetic acid, 5% v/v water in DMF). The retention time of 50% tannin elution of each sample (2 g/L tannin in 1:4 methanol/DMF) was compared with a calibration curve of preveraison grape skin tannins fractions[25] to give an average tannin MW (MW_{GPC}). Tannins are a mixture of polymers and thus the wine tannin samples were polydispersed with MW ranges within the 10−90 percentile range of 900 to 5900 g mol^{-1} for TT3 and from 1100 to 5800 g mol^{-1} for TT7, as measured using GPC.[9] The tannin subfractions were less polydispersed than the total tannin fractions with MW ranges from 1000 to 5000 g mol^{-1} for the butanol subfractions and from 1500 to 6000 g mol^{-1} for the aqueous subfractions.

Sample Preparation for SAXS Analysis. The tannin samples were prepared in 100% ethanol and in model wine solutions for small-angle X-ray scattering (SAXS) analysis. Model wine composition varied depending on the parameters investigated. For the experiments assessing the impacts of different ethanol concentrations, the model wine contained 2% v/v ethanol at pH 3.5 (adjusted with tartaric acid to a final concentration of 0.043 mM). The ethanol concentration was adjusted after tannin addition to give the final concentration range of 5, 10, 12, and 15% v/v ethanol in model wine. For experiments assessing the impacts of pH, the model wine contained 2% v/v ethanol

Table 1. Characteristics of Wine Tannin Samples As Measured from Depolymerization Reactions and Octanol/Water Assays, As Well As the Forward Scattering Intensities Normalized for Concentration ($I(0)/c$) at 12% and 100% Ethanol as Determined Using SAXS

	mDP[a]	% yield[b]	% GC[c]	% ECG[d]	Log P[e]	$I(0)/c$ 12%	$I(0)/c$ 100%
TT3	9.1	33.9	27.9	3.6	−0.61	0.0078	0.0188
TT7	7.7	12.0	29.6	2.1	−0.55	0.0088	0.0178
Aq3	11.1	30.6	33.4	3.0	−1.31	0.0091	0.0204
Aq7	9.6	15.4	34.7	1.8	−1.34	0.0130	0.0237
Bu3	5.8	26.0	21.8	3.5	−0.70	0.0038	0.0079
Bu7	5.7	12.4	24.2	2.0	−0.72	0.0044	0.0073

[a]Mean degree of polymerization. [b]Percent of the tannin mass hydrolyzed using phloroglucinolysis (proportion of tannin analyzed). [c]Percent epigallocatechin subunits. [d]Percent epicatechin gallate subunits. [e]Log of the octanol/water partition coefficients.

for a final concentration of 12% v/v ethanol after tannin addition. The pH was adjusted with tartaric acid at 0.08 mM and 0.01 mM for pH 3.0 and 4.0, respectively. For the ionic strength experiments, the model wine contained 2% v/v ethanol for a final concentration of 12% v/v ethanol after tannin addition. NaCl solution (0.5 M in model wine, pH 3.5) was added to give final concentrations of 25, 50, 100, or 200 mM NaCl. The ionic strength and pH experiments were performed only on the total tannin samples. Blank samples were prepared as the model wine solutions without tannins.

Wine tannin solutions were prepared in 100 μL volumes in 96-well plates at a range of concentrations (1, 2, 5, and 10 g/L). The plates were centrifuged (5 min, 2000 rpm), and the supernatant was transferred to clean 96-well plates prior to SAXS analysis. Tannin samples were first dissolved in ethanol to maximize solubility prior to addition into model wine solutions, however precipitation was observed in some solutions after centrifugation. The relative GPC peak areas of tannin solutions before and after centrifugation indicated that precipitation significantly impacted tannin concentration in Bu3, Aq3, and Aq7 in the 10g/L solutions at 5% ethanol, although there was no significant impact on the MW range of these samples. These samples were not included in the MW calculations as described in the next section.

SAXS Analysis and Data Processing. Small-angle X-ray scattering (SAXS) experiments were performed on the SAXS/WAXS beamline at the Australian Synchrotron (Melbourne, Australia).[26] The incident beam energy was 11.000 ± 0.005 keV (wavelength, λ = 1.0332 Å) with a corresponding scattering vector (q) ranged between 0.015 to 0.7 Å^{-1}, where $q = (4\pi \sin \theta)/\lambda$, and 2θ is the scattering angle. Experiments were performed at 25 °C using a Pilatus 1 M detector (DECTRIS, Switzerland). Samples were loaded using an automatic sample loader with a 2 × 96-well plate capacity (approximately 80 μL volume used per sample). Data collection involved recording successive frames (typically 10) of 2 s each per sample, and the multiple frames averaged as appropriate using ScatterBrain Analysis IDL v8.1 software (Australian Synchrotron) and subtracting the scattering recorded from the solvent blanks. Data were placed on absolute intensity scale using water as an intensity standard. The radiation exposure of the samples under these conditions did not result in sample degradation, as indicated by comparing scattering intensities of successive frames. The cleanliness of the capillary was periodically checked during system washing by monitoring intensity changes during water exposures.

SAXS data were analyzed using the ATSAS software package[27] to give forward scattering intensity, $I(0)$ and radius of gyration, R_g (using PRIMUS[28]), as well as the distance distribution function $P(r)$ (using GNOM[29]) for each tannin sample at each concentration. The $I(0)$ and R_g parameters were extracted from the data by the standard Guinier approach (where $qR_g < 1.3$ in all cases):[19]

$$I_{exp}(q) = I(0)\exp(-q^2 R_g{}^2/3) \quad (1)$$

The $I(0)$ values were normalized for tannin concentration, c, and subsequently averaged for the molecular weight (MW) calculations. Plots of $I(0)$ vs c (1, 2, 5, and 10 g/L tannin), were generally linear and indicated that the scattering results were concentration-independent since the correlation factor, R^2, was greater than 0.99 in most cases[30] (Supporting Information (SI) Table S1). R^2 values were less than 0.99 for Bu3, Aq3, and Aq7 at 10g/L in 5% ethanol (and at 10% ethanol for Aq7), and therefore these values were excluded from the MW calculations. The MW for each wine tannin sample was calculated by comparing the averaged $I(0)$ as a function of concentration ($I(0)/c$) at each ethanol concentration, pH, and ionic strength, with the ($I(0)/c$) values of a calibration curve of preveraison grape skin tannin fractions (MW range 1277 to 8996 g mol^{-1} as determined from depolymerization reactions) in wine-like conditions (12% v/v ethanol, pH 3.5). These were the same grape tannin samples as used in the GPC calibration.[25] This gave the calibration curve for the $I(0)/c$ values:

$$MW_{k.I/c}(\text{g mol}^{-1}) = 518\,396*(I(0)/c) \quad (2)$$

The averaged R_g values of the wine tannins were also compared with those of the grape tannin calibration curve to give a different MW measurement:

$$MW_{Rg}(\text{g mol}^{-1}) = 268.14*R_g \quad (3)$$

The MW of wine tannins was also calculated directly from the $I(0)/c$, independently of the calibration curve, using the equation as per Mylonas et al:[31]

$$MW_{\Delta\rho} = [N_A I(0)/c]/\Delta\rho_M{}^2 \quad (4)$$

where the Avogadro number, $N_A = 6.023 \times 10^{23}$ mol^{-1}. The scattering contrast per mass, $\Delta\rho_M = [\rho_{M.tannin} - (\rho_{solv}\, \upsilon)]r_0$, assumes that $\rho_{M.tannin}$ is similar to that of a flavan-3-ol monomer (3.19×10^{23} electrons/g calculated from the molecular formula and known molecular weight), and that the wine tannin density is 1.57 g/cm^3 as previously reported,[12,32] giving the tannin partial specific volume, υ = 0.637 cm^3/g. The solvent density for water, $\rho_{solv} = 3.34 \times 10^{23}$ e/cm^3 was used for tannins in aqueous solvents and that of ethanol, $\rho_{solv} = 2.68 \times 10^{23}$ e/cm^3 was used only for those samples in ethanol. The scattering length of an electron, $r_0 = 2.8179 \times 10^{-13}$ cm. Information on the conformation of the wine tannin samples was obtained from Kratky plot representations and from the distance distribution functions, $P(r)$, as calculated from the Fourier transformation of the scattering intensity.[19]

RESULTS AND DISCUSSION

Characteristics of Selected Wine Tannins. Wine tannins were isolated from a 3 and a 7 year old Cabernet Sauvignon wine and then separated into two fractions each, one water-soluble (aqueous fraction) and one butanol-soluble (butanol fraction) to give six wine tannin samples. The composition of each tannin sample was determined using phloroglucinolysis and subsequent HPLC analysis of the cleaved subunits (Table 1). This gave the mean degree of polymerization (mDP), proportion of epigallocatechin (%GC), and epicatechin gallate (%ECG) subunits, in addition to the percent yield (proportion of acid-labile interflavan bonds) of the reaction. The aqueous

fractions from both wines were larger (greater mDP) and contained more epigallocatechin subunits than the butanol fractions. The tannin samples isolated from the older wine contained fewer epicatechin gallate subunits and were less susceptible to the depolymerization reactions, with percent yields around half those of the tannin samples from the younger wine. This is likely to be a consequence of gradual oxidation and structural rearrangement reactions leading to intramolecular bond formation, as has been previously shown with grape and apple tannins,[6,12] as well as intermolecular interactions such as the incorporation of pigmented polymers.[4] The difference in water-solubility was demonstrated in the octanol/water partition coefficients (Log *P*) (Table 1). The tannins isolated from the older wine were more hydrophobic than those from the younger wine (−0.61 and −0.55 for TT3 and TT7, respectively), and the total tannin samples were more hydrophobic than the tannin fractions. This potentially suggested that some hydrophobic tannin species were removed from the fractionation process, however the benefit of fractionating the tannins was to enable the analysis of a range of chemically different wine tannins from the same starting wine. The aqueous fractions were more water-soluble than the butanol fractions, as expected.

Comparison of Relative Wine Tannin Sizes in Different Matrixes. Wines of different vintages (3 and 7 years old) were selected to compare wine tannin sizes from young and aged wines in different matrixes. Isolated tannins from each wine were separated into two fractions with distinctly different characteristics that were less polydispersed than the total wine tannins. This gave a range of tannin samples for molecular size analysis. Relative wine tannin sizes were determined using SAXS in 100% ethanol, which has been shown to be a good solvent for tannins,[16,32] and compared to more wine-like conditions: (5−15% ethanol, pH 3.0−4.0, and 2−200 mM NaCl). The forward scattering intensities of wine tannins in 100% ethanol indicated an absence of pronounced aggregation (Figure 1), which concurs with previous reports for grape and apple tannins.[16,32] It must also be noted that the greater $I(0)/c$ values for the tannins is 100% ethanol compared with in the hydroalcoholic solutions (Figure 1 and Table 1) is likely to be influenced by differences in solvent densities (ρ_{solv} = 3.34 × 10^{23} e/cm^3 for water and 2.68 × 10^{23} e/cm^3 for ethanol). This is corrected for in the MW calculations as noted in the next section. The aqueous tannin fractions were consistently larger than butanol fractions, and the aged wine tannins were generally larger than the younger wine tannins.

The major advantage of SAXS analysis over other techniques for tannin characterization is the potential to characterize macromolecules in a range of solvents. Polymer mixtures may expand or contract in different solvent conditions,[16] suggesting that the tannin characterization methods that calculate average MW from relative hydrodynamic volume, such as GPC, may be solvent-dependent. Wine astringency is known to decrease with increasing ethanol concentrations and with increasing wine pH[33] and this may relate to changes in tannin conformation in solution. The forward scattering plots for wine tannins in hydroalcoholic solutions showed aggregation, as indicated by large increases in the scattering intensities at low-*q* (Figure 1) for all measured tannin samples and at all concentrations. The extent of this scattering varied depending on solvent and sample, with tannin fractions from the older wine showing the greatest aggregation. The TT3 and Aq3 samples only aggregated at 5% ethanol, and the Bu3 sample showed some

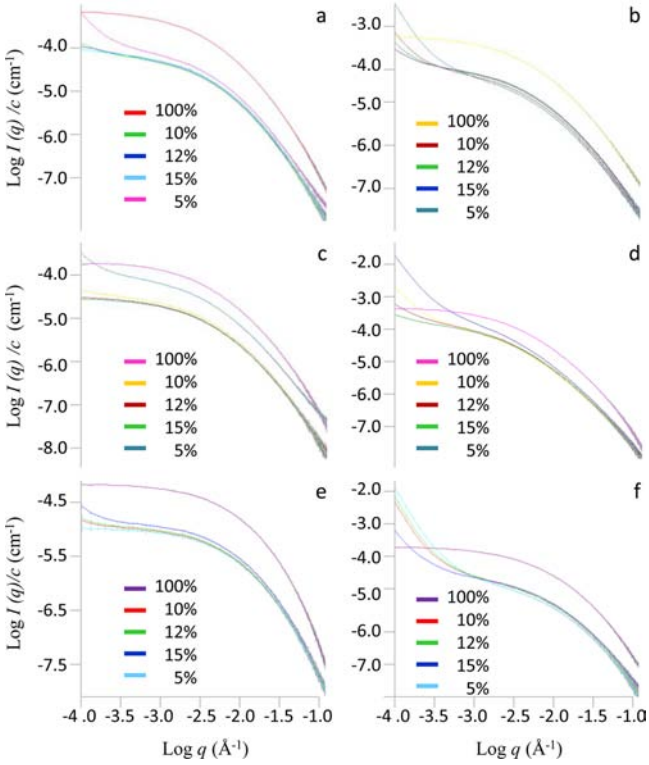

Figure 1. SAXS intensity plots, log $I(q)/c$ vs log q, at each ethanol concentration for (a) TT3; (b) TT7; (c) Aq3; (d) Aq7; (e) Bu3; and (f) Bu7.

aggregation at 15% ethanol. The TT7, Aq7, and Bu7 samples all aggregated in all hydroalcoholic solutions with increasing aggregation at decreasing ethanol concentration. In determining the R_g values for each sample, a shorter *q*-range was used to obtain a linear fit for the Guinier plots (within the qR_g < 1.3 limitation) to minimize the impact of aggregation on this measurement.[19] Some precipitation was observed at higher tannin concentrations (10 g/L) in 5% and 10% ethanol, and this was reflected in a decrease in linearity in the $I(0)$ vs c plots (SI Table S1). This was not the case in 12% ethanol, and these values were used for the MW comparisons as discussed in the next section.

The differences in aggregation between the aged and younger wine tannins are likely to be due to the greater oxidation of the tannins from the older wine, as observed from the comparatively lower percent yield in the phloroglucinol reactions (Table 1). Oxidized wine tannins reportedly have lower water solubility than "native" grape tannins, and are therefore more prone to aggregation in aqueous solutions.[12,32] This potentially contributes to the precipitation of tannins as wines age. The octanol/water partition coefficients (Table 1) also demonstrated that the tannin samples from the older wine were slightly more hydrophobic than the same fractions from the younger wine.

The R_g values were relatively consistent across the measured ethanol concentrations range for most tannin samples (Figure 2). Only the Aq7 fraction increased in R_g with a decrease in ethanol concentration which may relate to a change in tannin size, a change in the solvation layer around the tannin in more aqueous systems or, potentially, interference from aggregation.[13] Previous research has indicated that astringency intensity decreases with increasing ethanol (up to 15%) in

dx.doi.org/10.1021/jf405308m | J. Agric. Food Chem. 2014, 62, 7216−7224

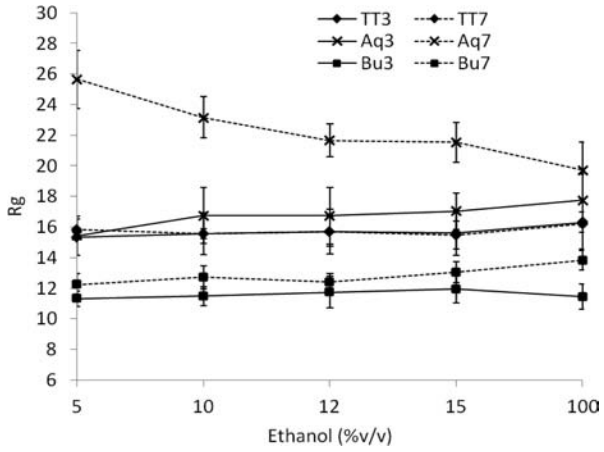

Figure 2. Impact of ethanol concentration on the radii of gyration (R_g, Å) for each tannin sample. Error bars represent the standard deviation of averaged replicates.

model wine solutions containing oliomeric tannins.[33] This study has shown that there is no change in tannin size over wine-like ethanol concentrations. The reported changes in astringency intensity with ethanol concentration may relate to changes in tannin aggregation rather than relative tannin size in solution. Wine pH and ionic strength have been shown to impact wine astringency and protein binding[33,34] and therefore the impact of these characteristics on the relative sizes of the total tannin fractions was also assessed. The $I(0)/c$ and R_g values of the total tannin samples showed no significant change in tannin dimensions across the ionic strength range from 0 to 200 mM NaCl (Figure 3a). Increases in ionic strength have been shown to augment the aggregation of grape and apple tannins[35] potentially due to changes in the solubility of tannins, since ionic strength did not directly alter the wine tannin molecular size. Wine pH also showed negligible impact on wine tannin dimensions with the R_g values remaining fairly consistent across the wine-like pH range (3.0 to 4.0) (Figure 3b). Wine pH has been previously correlated with model wine astringency, with solutions at pH 2.5 and 3.0 producing greater astringency intensity than model wines at 3.5 and 4.0,[33] and this is most likely to be a direct consequence of the wine matrix.

Comparison of Wine Tannin Molecular Weight Using Different Methods. The molecular weight of all wine tannin samples were compared using three different methods: SAXS analysis (from the forward scattering intensities ($I(0)/c$) and radii of gyration (R_g) values as compared to a standard curve, $MW_{k.I/c}$ and MW_{Rg}, respectively, and calculated directly from the $I(0)/c$, $MW_{\Delta\rho}$), GPC analysis (MW_{GPC}), and analysis of tannin subunits from depolymerization reactions (MW_{mDP}) (Table 2). The $I(0)/c$ and R_g of the tannin samples from the

Table 2. Comparison of Wine Tannin Molecular Weights (MW) in g mol^{-1} as Calculated Using Each Method[a]

			12% ethanol			100% ethanol	
	MW_{mDP}	MW_{GPC}	$MW_{\Delta\rho}$ [b]	$MW_{k.I/c}$ [c]	MW_{Rg} [d]	$MW_{\Delta\rho}$	MW_{Rg}
TT3	2730	2930	5242	4043	4207	6485	4376
TT7	2300	2850	5914	4562	4210	6140	4347
Aq3	3340	3030	6115	4717	4486	7037	4757
Aq7	2870	3270	8736	6739	5808	8176	5285
Bu3	1740	1800	2554	1970	3148	2725	3065
Bu7	1700	1930	2857	2281	3325	2518	3708

[a]Depolymerization reactions (MW_{mDP}), gel permeation chromatography (MW_{GPC}) in methanol/DMF, and SAXS ($MW_{k.I/c}$ in 12% ethanol, $MW_{\Delta\rho}$ and MW_{Rg} in 12% and 100% ethanol). [b]Tannin MW calculated directly from $I(0)/c$: $MW_{\Delta\rho} = [N_A I(0)/c]/\Delta\rho_M^2$. [c]Tannin MW calculated from $I(0)/c$ using the calibration curve: $MW_{k.I/c} = 518\,396x$. [d]Tannin MW calculated from R_g using the calibration curve: $MW_{Rg} = 268.14x$.

SAXS analyses in 12% ethanol were compared with those of a calibration curve of fractionated preveraison grape skin tannins measured in 12% ethanol to give the average tannin MW values, $MW_{k.I/c}$ and MW_{Rg}, respectively. The MW_{Rg} values were also determined for the wine tannin samples in 100% ethanol for comparison, however differences in the scattering contrasts of ethanol and aqueous solutions prevented the same comparison for $MW_{k.I/c}$. Instead, MWs were calculated directly from the $I(0)/c$ values to give an independently determined MW of the wine tannins ($MW_{\Delta\rho}$) that corrected for the solvent contrast. For GPC, the retention times of the wine tannin samples (at 50% elution) in a methanol/DMF solvent system were compared to those of a calibration curve in the same solvent to give the average wine tannin MW (MW_{GPC}). The

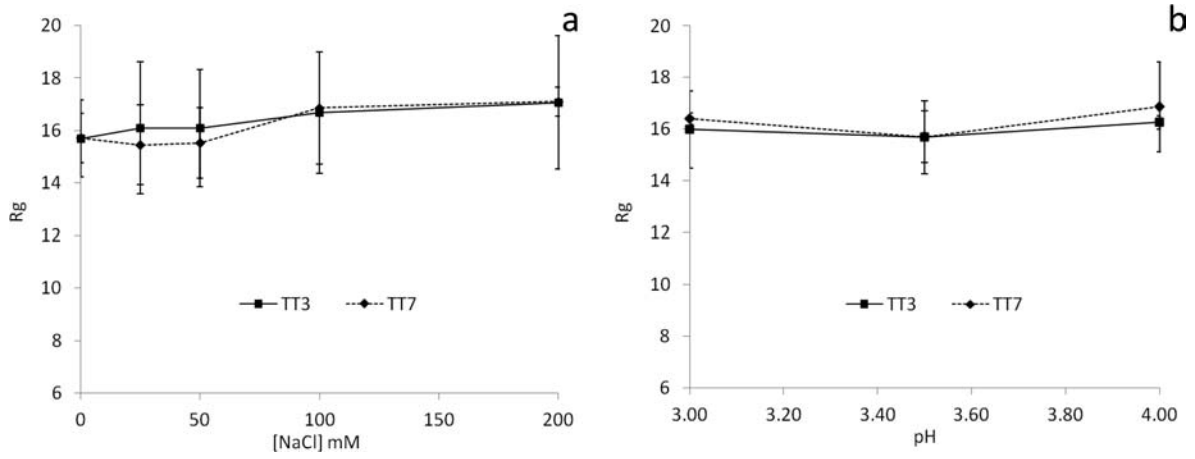

Figure 3. Impact of wine matrix on the radii of gyration (R_g, Å) of the total tannin samples from each vintage wine at (a) varying ionic strength, as NaCl concentration (mM); and (b) varying pH. Error bars represent the standard deviation of averaged replicates.

Table 3. Correlation Factors (R^2) between the Average Wine Tannin Molecular Weights (MW) As Calculated Using Each Method[a]

				12% ethanol			100% ethanol	
	method	MW_{mDP}	MW_{GPC}	$MW_{\Delta\rho}$[b]	$MW_{k.I/c}$[c]	MW_{Rg}[d]	$MW_{\Delta\rho}$	MW_{Rg}
	MW_{mDP}		0.7952	0.6065	0.6018	0.5616	0.8057	0.7122
	MW_{GPC}	0.7952		0. 8857	0.8826	0.8097	0.9866	0.9084
12%	$MW_{\Delta\rho}$	0.6065	0. 8857		0.9998	0.9736	0.9117	0.9208
	$MW_{k.I/c}$	0.6018	0.8826	0.9998		0.9753	0.9067	0.9255
	MW_{Rg}	0.5616	0.8097	0.9736	0.9753		0.8474	0.9006
100%	$MW_{\Delta\rho}$	0.8057	0.9866	0.9117	0.9067	0.8474		0.8894
	MW_{Rg}	0.7122	0.9084	0.9208	0.9255	0.9006	0.8894	

[a]Depolymerization reactions (MW_{mDP}), gel permeation chromatography (MW_{GPC}) in methanol/DMF, and SAXS ($MW_{k.I/c}$ in 12% ethanol, $MW_{\Delta\rho}$ and MW_{Rg} in 12% and 100% ethanol). [b]Tannin MW calculated directly from $I(0)/c$. [c]Tannin MW calculated from $I(0)/c$ using the calibration curve. [d]Tannin MW calculated from R_g using the calibration curve.

same grape-skin tannin fractions were used for the calibration curves in both the SAXS analysis and GPC, enabling a direct comparison between the results obtained in wine-like conditions with SAXS with those from the more widely used tannin characterization technique. The depolymerization reactions involved acid-catalysis of the tannin samples and HPLC analysis of the cleaved subunits to give the tannin subunit composition and mean degree of polymerization (mDP). These results were then used to calculate the average MW for each sample (MW_{mDP}).

The average MWs of all tannin samples as determined using GPC (MW_{GPC}), depolymerization reactions (MW_{mDp}), and with SAXS ($MW_{\Delta\rho}$, $MW_{k.I/c}$, and MW_{Rg}) are shown in Table 2. In all methods, the aqueous fractions (Aq3 and Aq7) were higher in MW than the total tannin fractions (TT3 and TT7), and the butanol-soluble fractions (Bu3 and Bu7) were much smaller. MWs derived from the SAXS data in 12% v/v ethanol were larger than those calculated from GPC analysis or depolymerization reactions (Table 2) indicating that the MWs of wine tannins in wine may be underestimated by the standard methods, particularly for aged-wine tannins. The solvation layer around the tannins in hydroalcoholic solutions would also have contributed to the relative tannin size as measured using SAXS, increasing the calculated MW.[13]

The SAXS-determined MWs and MW_{GPC} values indicated that the tannin samples from the older wine were larger or similar in size to the younger wine tannins. The MW_{mDP} values, however, suggested that the older wine tannins were smaller than the younger wine tannins. This may have be due to the lower percent yield of the older tannin samples (Table 1), which meant that only a very small proportion of the tannin was analyzed (≤15%) and this limited the number of extension subunits that could be cleaved by acid-catalysis. Furthermore, the preveraison grape skin tannin calibration curve used in the SAXS and GPC calculations may have also overestimated the average wine tannin MWs due to differences in spatial distribution between the grape tannin fractions and the wine tannins. The $MW_{\Delta\rho}$ values in 12% ethanol were larger than the MWs determined from the calibration curve ($MW_{k.I/c}$ and MW_{Rg}), suggesting that any differences in dimensions between the wine tannins and the grape tannins had only a limited impact on the determined wine tannin MWs. The calculations used for the $MW_{\Delta\rho}$ values presumed a tannin density of 1.57 g/cm^3 as previously reported for grape seed tannins;[12,32] however, the actual density of wine tannins may be greater given the disparity between these values and those determined with other methods. Further research is required to more accurately determine this value.

The extent to which the determined MWs from each method correlated for the wine tannin samples was measured as R^2 values from correlation plots (Table 3). The MW_{GPC} and MW_{mDP} were compared with the MWs determined using SAXS in 12% ethanol for an example of a wine-like solution and in 100% ethanol to ensure that the aggregation of tannins in hydroalcoholic solutions did not greatly interfere with the correlations. Correlations were strongest between the $MW_{\Delta\rho}$ and $MW_{k.I/c}$ in 12% ethanol (R^2 = 0.9998), providing good support for the MWs derived from the calibration curves, including the MW_{Rg} values in 12% ethanol, which also correlated well with the $MW_{\Delta\rho}$ values (R^2 = 0.9736). The MW_{GPC} values correlated most strongly with the $MW_{\Delta\rho}$ 100% ethanol (R^2 = 0.9866). The strong correlation between the GPC values and those in from both $MW_{\Delta\rho}$ and $MW_{k.I/c}$ in 12% ethanol (R^2 > 0.88) demonstrated that wine tannin MWs as determined with GPC do give a good indication of relative tannin molecular size in wine. The MW_{mDP} values had the weakest correlation with the SAXS methods ($R^2 \approx 0.6$ for MWs determined in 12% ethanol), further highlighting the differences produced from determining tannin MW from average polymer chain length and from relative tannin size.

Overall, there was no significant impact of different wine-like parameters on wine tannin dimensions across the measured ethanol concentration, ionic strength, and pH ranges. Further, the strong correlation between the determined tannin MW in wine-like matrixes as compared with GPC emphasizes that GPC is a useful method for comparing the relative MW of tannins in young and aged wines.

Estimation of Wine Tannin Conformation in Solution. One of the advantages of analyzing samples with SAXS over other techniques for characterizing wine tannins is the potential to obtain information on the conformation of macromolecules in solution. GPC has the advantage over mDP calculations by producing separation profiles, which indicate the proportions of the tannin broadly distributed around the nominal classes of "high", "medium", and "low" MW range, but this does not indicate the shape of the tannin polymer complex. Tannin conformations in solution were estimated for all samples in 100% ethanol, to ensure the complete dissolution of tannin molecules, using a Kratky plot ($q^2\ I(q)$ vs q) representation of the SAXS data and from the real-space distance distributions, $P(r)$. The Kratky plots (Figure 4) for each sample indicated that the tannins were compact but extended structures.[19] Distance distribution functions (Figure 5) indicated that the

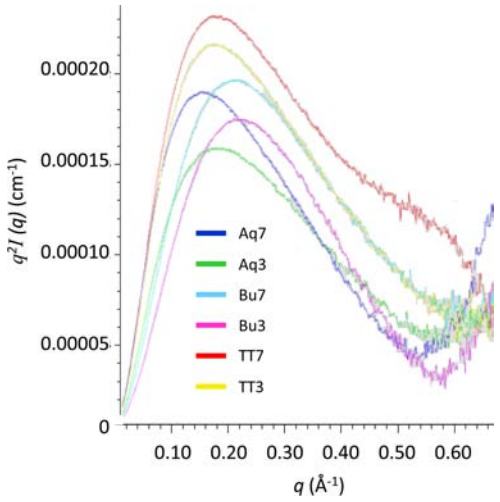

Figure 4. Kratky plots (q^2 $I(q)$ vs q) for each tannin sample in 100% ethanol.

wine tannin samples were not spherical and that the configuration more closely related to elongated ellipsoid structures.[19,36] The $P(r)$ for the wine tannin samples in all hydroalcoholic solutions (data not shown) resembled the elongated ellipsoid conformations that were observed in 100% ethanol.

In summary, the relative molecular dimensions of a range of wine tannins were measured in wine-like conditions using SAXS ($I(0)/c$ and R_g) and the calculated molecular weights (MWs) were compared to the more commonly used methods of GPC (MW_{GPC}) and depolymerization reactions (MW_{mDP}). The MWs determined with SAXS in 12% ethanol correlated well with the MW_{GPC} values, which suggests that GPC can be used to give a good indication of the average MWs of tannins in wines. Variations in wine-like solvent composition, including ethanol concentration, ionic strength, and pH, did not vary the measured tannin dimensions of all samples in solution, although tannin aggregation was influenced by ethanol concentration in the hydroalcoholic solutions. The conformations of the wine tannins resembled elongated ellipsoids in all tested solvent compositions. To our knowledge, SAXS measurements have not previously been attempted for wine tannins. Further research is needed to understand how tannin structures change with wine aging and how tannin aggregation may alter the perceived astringency of red wine.

■ ASSOCIATED CONTENT

Supporting Information

SAXS intensity plots, log $I(q)/c$ vs log q, at each ionic strength for (a) TT3; (b) TT7; and at each pH for (c) TT3; and (d) TT7 (Figure S1); SAXS data for each tannin sample at each ethanol concentration including the forward scattering intensities normalized for concentration ($I(0)/c$), radii of

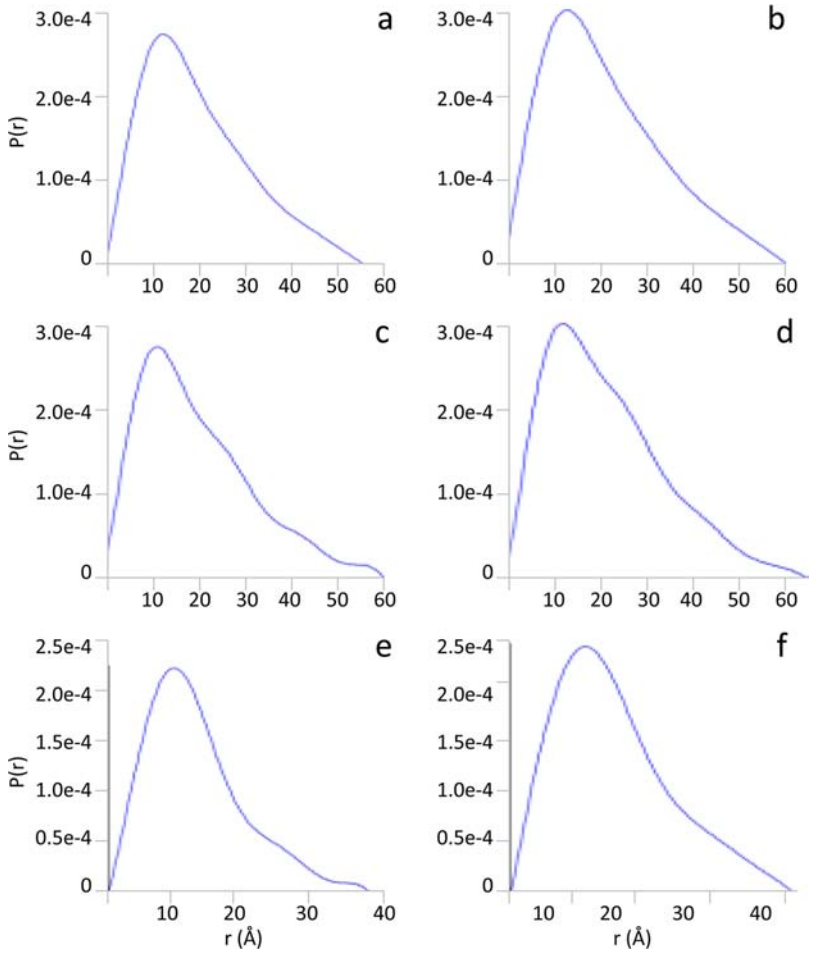

Figure 5. Distance distribution functions for each tannin sample in 100% ethanol. (a) TT3; (b) TT7; (c) Aq3; (d) Aq7; (e) Bu3; and (f) Bu7.

gyration (R_g), calculated molecular weight (MW) values, maximum particle length (D_{max}) and correlations for $I(0)$ vs c (R^2) (Table S1); SAXS data for the total tannin samples (TT3 and TT7) at each ionic strength including the forward scattering intensities normalized for concentration ($I(0)/c$), radii of gyration (R_g), calculated molecular weight (MW) values, maximum particle length (D_{max}) and correlations for $I(0)$ vs c (R^2) (Table S2); SAXS data for the total tannin samples (TT3 and TT7) at each pH including the forward scattering intensities normalized for concentration ($I(0)/c$), radii of gyration (R_g), calculated molecular weight (MW) values, maximum particle length (D_{max}) and correlations for $I(0)$ vs c (R^2) (Table S3). This material is available free of charge via the Internet at http://pubs.acs.org.

AUTHOR INFORMATION

Corresponding Author

*Tel: +61 8313 6600; e-mail: Jacqui.Mcrae@awri.com.au.

Present Address

[§]European Molecular Biology Laboratory-Hamburg Outstation, c/o DESY, Notkestrasse 85, D-22603 Hamburg, Germany.

Notes

The authors declare no competing financial interest.

ACKNOWLEDGMENTS

This research was undertaken on the SAXS/WAXS beamline at the Australian Synchrotron, Victoria, Australia and at The Australian Wine Research Institute, a member of the Wine Innovation Cluster at the Waite Precinct in Adelaide, South Australia, and is supported by Australian grape growers and winemakers through their investment body, the Grape and Wine Research and Development Corporation, with matching funds from the Australian Government.

ABBREVIATIONS

Aq3, aqueous tannin subfraction from the 3 year old wine; Aq7, aqueous tannin subfraction from the 7 year old wine; Bu3, butanol-soluble tannin subfraction from the 3 year old wine; Bu7, butanol-soluble tannin subfraction from the 7 year old wine; GPC, gel-permeation chromatography; mDP, mean degree of polymerization; MW, molecular weight; MW_{GPC}, MW determined using GPC; $MW_{k.I/c}$, MW derived from the $I(0)/c$ values compared to the calibration curve; $MW_{\Delta\rho}$, MW calculated directly from the $I(0)/c$ values; MW_{mDP}, MW determined from the mDP; MW_{Rg}, MW derived from the R_g values compared to the calibration curve; R_g, radius of gyration; SAXS, small-angle X-ray scattering; SEC, size exclusion chromatography; TT3, total tannin sample from the 3 year old wine; TT7, total tannin sample from the 7 year old wine

REFERENCES

(1) Santos-Buelga, C.; Scalbert, A. Proanthocyanidins and tannin-like compounds—Nature, occurrence, dietary intake and effects on nutrition and health. *J. Sci. Food Agric.* **2000**, *80*, 1094−1117.

(2) Chira, K.; Jourdes, M. Cabernet sauvignon red wine astringency quality control by tannin characterization and polymerization during storage. *Eur. Food Res. Technol.* **2012**, *234*, 253−261.

(3) Vidal, S.; Francis, L.; Noble, A.; Kwiatkowski, M.; Cheynier, V.; Waters, E. Taste and mouth-feel properties of different types of tannin-like polyphenolic compounds and anthocyanins in wine. *Anal. Chim. Acta* **2004**, *513*, 57−65.

(4) McRae, J. M.; Schulkin, A.; Kassara, S.; Holt, H.; Smith, P. A. Sensory properties of wine tannin fractions: Implications for in-mouth sensory properties. *J. Agric. Food Chem.* **2013**, *61*, 719−727.

(5) Vidal, S.; Francis, L.; Guyot, S.; Marnet, N.; Kwiatkowski, M.; Gawel, R.; Cheynier, V.; Waters, E. J. The mouth-feel properties of grape and apple proanthocyanidins in a wine-like medium. *J. Sci. Food Agr* **2003**, *83*, 564−573.

(6) Vernhet, A.; Dubascoux, S.; Cabane, B.; Fulcrand, H.; Dubreucq, E.; Poncet-LeGrand, C. Characterization of oxidized tannins: Comparison of depolymerization methods, assymetric flow field-flow fractionation and small-angle X-ray scattering. *Anal. Bioanal. Chem.* **2011**, *401*, 1559−1569.

(7) Koerner, J. L.; Hsu, V. L.; Lee, J.; Kennedy, J. A. Determination of proanthocyanidin A2 content in phenolic polymer isolates by reversed-phase high-performance liquid chromatography. *J. Chromatogr. A* **2009**, *1216*, 1403−1409.

(8) Kennedy, J. A.; Jones, G. P. Analysis of proanthocyanidin cleavage products following acid-catalysis in the presence of excess phloroglucinol. *J. Agric. Food Chem.* **2001**, *49*, 1740−1746.

(9) Kennedy, J. A.; Taylor, A. W. Analysis of proanthocyanidins by high-performance gel permeation chromatography. *J. Chromatogr. A* **2003**, *995*, 99−107.

(10) Bindon, K.; Smith, P.; Kennedy, J. A. Interaction between Grape-Derived Proanthocyanidins and Cell Wall Material. 1. Effect on Proanthocyanidin Composition and Molecular Mass. *J. Agric. Food Chem.* **2010**, *58*, 2520−2528.

(11) Monagas, M.; Bartolome, B.; Gomez-Cordoves, C. Updated knowledge about the presence of phenolic compounds in wine. *Crit. Rev. Food Sci. Nutr.* **2005**, *45*, 85−118.

(12) Poncet-Legrand, C.; Cabane, B.; Bautista-Ortín, A.; Carrillo, S.; Fulcrand, H.; Pérez, J.; Vernhet, A. Tannin oxidation: Intra- versus intermolecular reactions. *Biomacromolecules* **2010**, *11*, 2376−2386.

(13) Zanchi, D.; Konarev, P. V.; Tribet, C.; Baron, A.; Svergun, D. I.; Guyot, S. Rigidity, conformation, and solvation of native and oxidized tannin macromolecules in water−ethanol solution. *J. Chem. Phys.* **2009**, *130*, 245103.

(14) McRae, J. M.; Dambergs, R.; Kassara, S.; Parker, M.; Jeffery, D. W.; Herderich, M.; Smith, P. A. Phenolic compositions of 50 and 30 year sequences of Australian red wines: The impact of wine age. *J. Agric. Food Chem.* **2012**, *60*, 10093−10102.

(15) Jorgensen, E. M.; Marin, A. B.; Kennedy, J. A. Analysis of the oxidative degradation of proanthocyanidins under basic conditions. *J. Agric. Food Chem.* **2004**, *52*, 2292−2296.

(16) Beaucage, G. Small-angle scattering from polymeric mass fractals of arbitrary mass-fractal dimension. *J. Appl. Crystallogr.* **1996**, *29*, 134−146.

(17) Petoukhov, M. V.; Svergun, D. I. Applications of small-angle X-ray scattering to biomacromolecular solutions. *Int. J. Biochem. Cell Biol.* **2013**, *45*, 429−437.

(18) Pérez, J.; Yoshinori, N. Advances in X-ray scattering: From solution SAXS to achievements with coherent beams. *Curr. Opin. Struct. Biol.* **2012**, *22*, 670−678.

(19) Mertens, H. D. T.; Svergun, D. I. Structural characterization of proteins and complexes using small-angle X-ray solution scattering. *J. Struct. Biol.* **2010**, *172*, 128−141.

(20) Lattey, K.; Bramley, B.; Francis, I. L. Consumer acceptability, sensory properties and expert quality judgements of Australian Cabernet Sauvignon and Shiraz wines. *Aust. J. Grape Wine Res.* **2010**, *16*, 189−202.

(21) Herderich, M. J.; Smith, P. A. Analysis of grape and wine tannins: Methods, applications and challenges. *Aust. J. Grape Wine Res.* **2005**, *11*, 1−10.

(22) Chira, K.; Pacella, N.; Jourdes, M.; Teissedre, P.-L. Chemical and sensory evaluation of Bordeaux wines (Cabernet-Sauvignon and Merlot) and correlation with wine age. *Food Chem.* **2011**, *126*, 1971−1977.

(23) Cheynier, V.; Duenas-Paton, M.; Salas, E.; Maury, C.; Souquet, J. M.; Sarni-Manchado, P.; Fulcrand, H. Structure and properties of wine pigments and tannins. *Am. J. Enol. Vitic.* **2006**, *57*, 298−305.

(24) McRae, J. M.; Falconer, R. J.; Kennedy, J. A. Thermodynamics of grape and wine tannin interaction with polyproline: Implications for red wine astringency. *J. Agric. Food Chem.* **2010**, *58*, 12510−12518.
(25) Bindon, K. A.; Smith, P. A.; Holt, H.; Kennedy, J. A. Interaction between grape-derived proanthocyanidins and cell wall material. 2. Implications for vinification. *J. Agric. Food Chem.* **2010**, *58*, 10736−10746.
(26) Kirby, N. M.; Mudie, S. T.; Hawley, A. M.; Cookson, D. J.; Mertens, H. D. T.; Cowieson, N.; Samardzic-Boban, V. A low-background-intensity focusing small-angle X-ray scattering undulator beamline. *J. Appl. Crystallogr.* **2013**, *46*, 1670−1680.
(27) Petoukhov, M. V.; Franke, D.; Shkumatov, A. V.; Trias, G.; Kikhney, A. G.; Gajda, M.; Gorba, C.; Mertens, H. D. T.; Konarev, P. V.; Svergun, D. I. New developments in the ATSAS program package for small-angle scattering data analysis. *J. Appl. Crystallogr.* **2012**, *45*, 342−350.
(28) Konarev, P. V.; Volkov, V. V.; Sokolova, A. V.; Koch, M. H.; Svergun, D. I. PRIMUS: A Windows-PC-based system for small-angle scattering data analysis. *J. Appl. Crystallogr.* **2003**, *36*, 1277−1282.
(29) Semenyuk, A. V.; Svergun, D. I. GNOM—A program package for small-angle scattering data processing. *J. Appl. Crystallogr.* **1991**, *24*, 537−540.
(30) Jacques, D. A.; Guss, J. M.; Svergun, D. I.; Trewhella, J. Publication guidelines for structural modelling of small-angle scattering data from biomolecules in solution. *Acta Crystallogr. D: Biol. Crystallogr.* **2012**, *D68*, 620−626.
(31) Mylonas, E.; Svergun, D. I. Accuracy of molecular mass determination of proteins in solution by small-angle X-ray scattering. *J. Appl. Crystallogr.* **2007**, *40*, s245−s249.
(32) Zanchi, D.; Vernhet, A.; Poncet-Legrand, C.; Cartalade, D.; Tribet, C.; Schweins, R.; Cabane, B. Colloidal dispersions of tannins in water-ethanol solutions. *Langmuir* **2007**, *23*, 9949−9959.
(33) Fontoin, H.; Saucier, C.; Teissedre, P.-L.; Glories, Y. Effect of pH, ethanol and acidity on astringency and bitterness of grape seed tannin oligomers in model wine solution. *Food Qual. Pref.* **2008**, *19*, 286−291.
(34) Kawamoto, H.; Nakatsubo, F. Effects of environmental factors on two-stage tannin-protein co-precipitation. *Phytochemistry* **1997**, *46*, 479−483.
(35) Poncet-Legrand, C.; Cartalade, D.; Putaux, J.-L.; Cheynier, V.; Vernhet, A. Flavan-3-ol aggregation in model ethanolic solutions: Incidence of polyphenol structure, concentration, ethanol content, and ionic strength. *Langmuir* **2003**, *19*, 10563−10572.
(36) Shtykova, E. V.; Kuchkina, N. V.; Shifrina, Z. B.; Bronstein, L. M.; Svergun, D. I. Unusual structural morphology of dendrimer/CdS nanocomposites revealed by synchrotron x-ray scattering. *J. Phys. Chem. C* **2012**, *116*, 8069−8078.

Table 1. Details of the Enzymes That Take Part in the Digestion of Human Milk Proteins Ranked on the Basis of Their Total Number of Cleavages[a]

enzyme[b]	N-terminal cleavage count	C-terminal cleavage count	total cleavage	unique cleavage	no. of expected cleavages within the peptide	no. of proteins cleaved	odds ratio	std error	gene expression given in RPKM
plasmin	120	200	320	0	371	15	4.11	1.08	0
trypsin 1[c]	120	199	319	0	352	14	4.33	1.09	0 (5.81 PRKM for trypsin domain containing protease TYSND1)
cathepsin D	68	62	130	0	846	24	0.61	1.1	365.07
chymotrypsin low 1	68	34	102	0	449	11	0.93	1.12	0
elastase	51	39	90	0	563	13	0.64	1.12	0
pepsin 1 (pH 1.3)	31	47	78	0	479	10	0.66	1.13	0.1
glutamyl endopeptidase[c]	55	21	76	0	930	5	0.31	1.13	0 (75.97 PRKM for proteasome subunit β type-6, responsible for the peptidyl glutamyl-like activity, PSMB6)
pepsin 1 (pH >2)	30	38	68	0	315	8	0.89	1.15	0.1
proline endopeptidase	14	31	45	0	598	18	0.29	1.17	5.52
chymotrypsin low 4	**3**	**12**	**15**	**0**	**102**	**4**	**0.60**	**1.32**	**0**
chymotrypsin low 3	**6**	**6**	**12**	**0**	**79**	**6**	**0.62**	**1.36**	**0**
chymotrypsin low 2	**2**	**0**	**2**	**0**	**0**	**1**	**20.65**	**4.71**	**0**

[a]The corresponding gene expression levels in RPKM are provided for each enzyme. [b]Enzymes in bold represent ones that are not expressed at day 60 of lactation, but low expression of these genes has been detected at earlier stages of lactation (15 and 30 days). [c]Enzymes that do not show expression in milk, but expression data shows the presence of other enzymes that have a similar activity and are expressed.

occurs when samples are frozen. The stage of lactation of the first mother was 3 months and that of the second was 4 months. The mothers providing this milk were instructed to cleanse each breast with water and then use an electronic pump to collect a pool of milk from both breasts. The samples were then stored in the subjects' freezers and delivered to the laboratory on ice where they were stored at −80C.

Sample Preparation. Peptides were extracted from human milk according to the method of Dallas et al.[13] Briefly, 200 μL of each milk sample was thawed on ice and combined. To remove milk fat globules, the milk was centrifuged at 3000*g* for 10 min and the skim infranate was extracted. Centrifugation was repeated on the skim infranate to remove any remaining visible lipid layer. Proteins were then precipitated with the addition of 400 μL of 200 g/L trichloroacetic acid. Samples were vortexed briefly and then centrifuged at 3000*g* for 10 min, and the peptide-containing supernatant was collected, leaving the precipitated protein. This precipitation was repeated for a total of three times. Trichloroacetic acid, salts, oligosaccharides, and lactose were then removed from the peptides by C18 reverse-phase preparative chromatography. Contaminants were eluted with water, and peptides were then eluted with 80% acetonitrile (ACN)/0.1% trifluoroacetic acid (v/v). The peptide solution was then dried down in a vacuum centrifuge at 37 °C. After drying, the sample was rehydrated in 40 μL of nanopure water for MS analysis.

MS Analysis of Human Breast Milk Peptides. Peptides were analyzed via nanoliquid chromatography chip quadrupole time-of-flight tandem MS (Agilent, Santa Clara, CA, USA). Two microliters of sample was injected for each run onto the C18 reverse-phase nanochip. The nanopump flow was 0.3 μL/min, and the capillary pump flow rate was 3 μL/min. Peptides were eluted with the following gradient of solvent A (3% ACN/0.1% formic acid (FA) (v/v)) and solvent B (90% ACN/0.1% FA (v/v)): 0−8% B from 0 to 5 min, 8−26.5% B from 5 to 24 min, 26.5−100% B from 24 to 48 min, followed by 100% B for 2 min and 100% A for 10 min (to re-equilibrate the column). The instrument was run in positive ionization mode. Data collection thresholds were set at 200 ion counts or 0.01% relative intensity for MS spectra and at 5 ion counts or 0.01% relative intensity for MS/MS. Data were collected in centroid mode. The drying gas was 350 °C, and flow rate was 3 L/min. The required chip voltage for consistent spray varied from 1850 to 1920 V. Automated precursor selection based on abundance was employed to select peaks for tandem fragmentation with an exclusion list consisting of all peptides identified in previous analyses in this study. The acquisition rate employed was 3 spectra/s for both MS and MS/MS modes. The isolation width for tandem analysis was 1.3 m/z. The collision energy was set by the formula (slope) × $(m/z)/100$ + offset, with slope = 3.6 and offset = −4.8. Five tandem spectra were collected after each MS spectrum, with active exclusion after 5 MS/MS for 0.15 min. Precursor ions were selected only if they had at least 1000 ion counts or 0.01% of the relative intensity of the spectra. Mass calibration was performed during data acquisition based on an infused calibrant ion with a mass of 922.009789 Da.

Agilent Mass Hunter Qualitative Analysis Software (Santa Clara, CA, USA) was used to analyze the data obtained. Molecules identified in the spectral analysis were grouped into compounds by the Find by Molecular Feature algorithm, which groups together molecules across charge state and charge carrier. All tandem MS from each data file were exported as Mascot Generic Files (.mgf) with a peptide isotope model and a maximum charge state of +9.

Peptide identification was accomplished using both the MS-GFDB (via a command-line interface) and X!Tandem (using the downloadable graphical user interface). The human milk library used in both searches was constructed on the basis of a query to the Uniprot database. The query returned only proteins from *Homo sapiens* and at least one of the following: "tissue specificity" keyword "milk" or "mammary", "tissue" keyword "milk" or "mammary", or gene ontology "lactation". This query returned a list of 1472 proteins. These were exported to FASTA file format. For MS-GFDB, peptides were accepted if p values were ≤0.01 corresponding to confidence levels of 99%. No p values exist in X!Tandem, so a closely related statistic, e value, was used for the X!Tandem search. The e value thresholds selected were again 0.01, reflecting 99% confidence. In both programs, masses were allowed 20 ppm error. No complete (required) modifications were included but up to four potential modifications were allowed on each peptide. Potential modifications allowed were phosphorylation of serine, threonine, or tyrosine and oxidation of methionine. A nonspecific cleavage ([X]|[X]) (where "X" is any amino acid) was used to search against the protein sequences. For MS-GFDB, the fragmentation method selected in the search was collision-induced dissociation and the instrument selected was time-of-flight. For X!Tandem, there was no option for fragmentation type and instrument selection. Because the instrument did not always select the monoisotopic ion for tandem fragmentation, isotope errors were allowed (allowing up to one C13). No model refinement was employed in X!Tandem.

Enzyme Prediction. The web-based software EnzymePredictor[14] was employed to evaluate and predict which enzymes most likely contributed to cleavage of human breast milk proteins (http://bioware.ucd.ie/~enzpred/Enzpred.php). Enzymes were classified on the basis of their total number of performed cleavages, and they were evaluated on the basis of their odds ratio (OR; see Table 1), which is an indicator of their degree of participation in the hydrolysis of the proteins. The OR values indicate that certain enzymes are over-represented and others under-represented. The following information was also collected from EnzymePredictor: number of times an enzyme could have cleaved within the current peptides, total number of proteins cleaved by each enzyme, total number of cleavages performed by an enzyme on the C- and N-termini.

Expression Profiling of Human Milk. *Fresh Milk Sample Collection.* Fresh milk samples were obtained from three healthy females on days 4, 15, 30, and 60 postpartum who gave birth to a term infant (>37 weeks of gestation). In the early morning period, the donor manually pumped one breast until emptied into a collection bag, which was immediately delivered on cold-packs to the laboratory for processing. The Institutional Review Board of University of California, Davis, approved the project.

RNA Extraction for Gene Expression Studies. Somatic cells were pelleted by adding 50 μL of 0.5 M ethylenediaminetetraacetic acid to 20 mL of fresh milk and centrifuged at 2000*g* at 4 °C for 10 min.[15] The pellet of cells was washed with 10 mL of phosphate-buffered saline at pH 7.2 and 10 μL of 0.5 M ethylenediaminetetraacetic acid (final concentration = 0.5 mM) and filtered through sterile cheesecloth to remove any debris. The cells were then centrifuged again at 2000*g* at 4 °C for 10 min. The supernatant was decanted, and RNA was extracted from the milk somatic cell pellet using Trizol (Invitrogen, Carlsbad, CA, USA) according to the manufacturer's instructions. RNA was quantified by an ND-1000 spectrophotometer (Fisher Thermo, Wilmington, MA, USA), and the quality and integrity were assessed by the spectrophotometer 260/280 ratio, gel electrophoresis, and capillary electrophoresis with an Experion Bioanalyzer (Bio-Rad, Hercules, CA, USA).

RNA Sequencing and Data Analysis. Gene expression analysis was conducted on fresh milk samples collected on days 4, 15, 30, and 60 postpartum by RNA sequencing (RNA-Seq). Messenger RNA was isolated and purified using an RNA-Seq sample preparation kit (Illumina, San Diego, CA, USA). The fragments were purified and sequenced at the UC Davis Genome Center DNA Technologies Core Facility using the Illumina Genome Analyzer (GAII) and Illumina HiSeq 2000. Sequence reads were assembled and analyzed in RNA-Seq. Expression analysis was performed with the CLC Genomics Workbench 6.0 (CLC Bio, Aarhus, Denmark). Human genome, GRCh37.69 (ftp://ftp.ensembl.org/pub/release-69/genbank/homo_sapiens/), was utilized as the reference genome for the assembly. Data were normalized by calculating the "reads per kilobase per million mapped reads" (RPKM)[16] for each gene and annotated with ENSEMBL human genome assembly (55203 unique genes).

RESULTS AND DISCUSSION

This project aimed to determine the enzymes responsible for the cleavage patterns identified in milk, examine each enzyme's contribution to the hydrolyses of human milk proteins, and clarify whether these enzymes are expressed in milk or enter milk from other sources.

A novel MS-based peptide search platform using an iterative searching strategy detected a variety of peptides in minor abundances in pooled human breast milk samples.[13] The peptides extracted and identified for the present study were analyzed using EnzymePredictor.[14] The results of this analysis are presented in Table 1. The enzymes are ordered on the basis of their total number of cleavages, from those that have cleaved extensively to those that are predicted to have cleaved one residue. As discussed in the interpretation of EnzymePredictor,[14] the enzymes with a combined high number of total cleavages performed and a high odds ratio are the enzymes that are most likely active in the milk.

Expression profiles from samples of human breast milk were established as the means to investigate if the predicted enzymes originate from the mammary epithelial cells or they enter milk from other sources, such as blood. The samples that were obtained for analysis for peptide detection via MS were pooled from mature milk samples from two mothers, both 3 months postpartum, whereas that of expression data was of 2 month postpartum milk.

Major Cleavage of Proteins in Human Milk Is at Trypsin and Plasmin Target Sites. The natural cleavages of milk proteins showed a strong enrichment for cleavage after K or R, both consistent with plasmin and trypsin cleavage (Tables 1 and 4).

The presence of plasmin, an enzyme that plays a major role in the proteolytic breakdown of blood clots, has been previously reported in milk,[1] but its contribution to human milk proteolytic hydrolysis is unknown. This study found that plasmin potentially cleaved 320 peptides (Figure 1; Table 1)

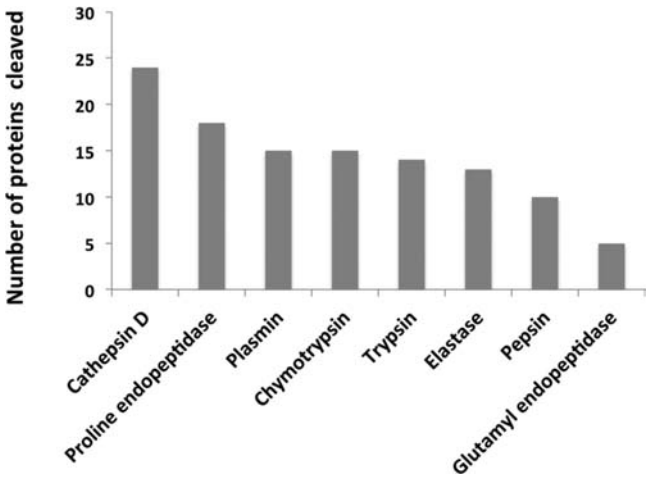

Figure 1. Representation of the total number of cleaved milk proteins per predicted enzyme. Each enzyme name on the *X*-axis is plotted against the total number of proteins it cleaves on the *Y*-axis.

derived from 15 milk proteins (Table 2). Anionic trypsin's presence in human milk was initially identified by Monti et al. and Borulf et al.[3,4] Borulf et al. showed that trypsin's presence in milk is likely in complex with IgA. Whether this enzyme contributes to the hydrolysis of human milk proteins remains unknown.

The two proteins most affected by potential plasmin or trypsin digestion were polymeric immunoglobulin receptor (32 cleavages of peptides) and β-casein (89). Other hydrolyzed proteins included α_{S1}-casein (11), osteopontin (18), butyrophilin subfamily 1 member A1 (15), and κ-casein (7). These analyses found that plasmin cleaves an androgen receptor that trypsin failed to cleave (Q9UN21; Tables 2 and 3). Butyrophilin subfamily 1 member A1 is part of the milk fat globule membrane. Thus, the low number of peptides detected from this protein might be due to the centrifugation for the removal of the milk fat globules. Trypsin can typically not cleave if the K or R is followed by a P, which makes the androgen receptor better fit the plasmin pattern (Table 4). This result would suggest that the cleavage tends to follow the specificity of plasmin more consistently than that of trypsin.

dx.doi.org/10.1021/jf405601e | J. Agric. Food Chem. 2014, 62, 7225−7232

Table 2. Human Milk Proteins Found To Have Been Digested by Plasmin[a]

protein name	Uniprot ID and access name	total no. of cleavages performed
β-casein	P05814 (CASB_HUMAN)	89
polymeric immunoglobulin receptor	P01833 (PIGR_HUMAN)	32
osteopontin	P10451 (OSTP_HUMAN)	18
butyrophilin subfamily 1 member A1	Q13410 (BT1A1_HUMAN)	15
α_{S1}-casein	P47710 (CASA1_HUMAN)	11
κ-casein	P07498 (CASK_HUMAN)	7
mucin-1	P15941 (MUC1_HUMAN)	3
parathyroid hormone-related protein	P12272 (PTHR_HUMAN)	2
bile salt-activated lipase	P19835 (CEL_HUMAN)	2
androgen receptor	Q9UN21 (Q9UN21_HUMAN)	1
protein diaphanous homologue 1	O60610 (DIAP1_HUMAN)	1
complement C4-A	P0C0L4 (CO4A_HUMAN)	1
La-related protein 1	Q6PKG0 (LARP1_HUMAN)	1
NMDA receptor-regulated protein 2	Q659A1 (NARG2_HUMAN)	1
dedicator of cytokinesis protein 1	Q14185 DOCK1_HUMAN	1

[a]The proteins are ordered on the basis of the number of cleavages that plasmin has performed on each. Here we considered only the number of peptides that are unique; if a peptide was not unique, we considered only one copy of the peptide. Proteins exclusively found in milk are presented in bold.

Table 3. Human Milk Proteins Found To Have Been Digested by Trypsin[a]

protein name	Uniprot ID and access name	total no. of cleavages performed
β-casein	P05814 (CASB_HUMAN)	89
polymeric immunoglobulin receptor	P01833 (PIGR_HUMAN)	32
osteopontin	P10451 (OSTP_HUMAN)	18
butyrophilin subfamily 1 member A1	Q13410 (BT1A1_HUMAN)	15
α_{S1}-casein	P47710 (CASA1_HUMAN)	11
κ-casein	P07498 (CASK_HUMAN)	7
mucin-1	P15941 (MUC1_HUMAN)	3
parathyroid hormone-related protein	P12272 (PTHR_HUMAN)	2
bile salt-activated lipase	P19835 (CEL_HUMAN)	2
La-related protein 1	Q6PKG0 (LARP1_HUMAN)	1
protein diaphanous homologue 1	O60610 (DIAP1_HUMAN)	1
NMDA receptor-regulated protein 2	Q659A1 (NARG2_HUMAN)	1
complement C4-A	P0C0L4 (CO4A_HUMAN)	1
dedicator of cytokinesis protein 1	Q14185 (DOCK1_HUMAN)	1

[a]The proteins are ordered on the basis of the number of cleavages that trypsin has performed on each. Here we considered only the number of peptides that are unique; if a peptide was not unique, we considered only one copy of the peptide. Proteins exclusively found in milk are presented in bold.

Table 4. Enzyme Specificity for Plasmin and Trypsin

	cleavage pattern						
enzyme	P4	P3	P2	P1	P1′	P2′	ref
trypsin	–	–	W	K	P	–	22
	–	–	M	R	P	–	22
plasmin	–	–	–	K or R	–	–	23

However, there are too few cleavages representing K or R followed by P (only one in our case) to disambiguate between plasmin and trypsin activities in the milk.

Enzymes Cleaving Hydrophobic Target Sites: Elastase, Cathepsin D, Pepsin, and Chymotrypsin. Whereas the active form of cathepsin D is found in bovine milk,[5] the major form of this enzyme in milk is the inactive zymogen, procathepsin D.[17] In this study, cathepsin D was found to be active in human milk (Table 1), cleaving 130 times. Cathepsin D hydrolyzed the highest number of milk proteins (24 milk proteins) compared to the other enzymes present in milk (Tables 1 and 5; Figure 1). Although the total number of times cathepsin D performed a cleavage is high (130 total cleavages), most of these are located in two proteins: β-casein with 78 cleavages and polymeric immunoglobulin receptor with 21 cleavages. Interestingly, both of these proteins have also been the most digested ones with all five top predicted enzymes.

A high number of potential cleavage sites was predicted for cathepsin D (846; Table 1), which were not observed in the peptide results, with an odds ratio below 1. This failure to produce predicted peptides could be due to the positioning of a subpopulation of these residues in regions difficult for the enzyme to access due to structural constraints. This structural inhibition is more likely for cathepsin D sites, because many potential cleavage sites are strongly hydrophobic, and hydrophobic regions are usually buried within the structured regions of proteins.

Elastase is another enzyme predicted to be active in human milk. Elastase is known to be a major proteinase in polymorphonuclear neutrophils (PMNs), which are phagocytic cells that destroy infectious agents in humans.[18] Elastase activity has been detected in PMNs recovered from milk during experimentally induced mastitis.[19] There is substantial overlap between the cleavage sites of elastase and cathepsin D, and again there are a large number of sites (563) interior to the peptides that were not cleaved. Elastase potentially performed 90 total cleavages of milk peptides (Table 6) over 13 proteins. The proteins that elastase cleaved the most are β-casein (41 cleavages of unique peptides) and polymeric immunoglobulin receptor (25 cleavages of unique peptides). No traces of elastase activity were observed on κ-casein (Table 6), and only one cleavage was observed for cathepsin D (Table 5). This reflects the similar, but not identical, cleavage patterns between elastase and cathepsin D. To resolve the specificity, the number of sites that were cleaved in common between both was determined (60 cleavages of unique peptides) or asa were those specific to only one (69 for cathepsin D of unique peptides, and 28 for elastase of unique peptides). This pattern suggests a role for both enzymes in human milk digestion prior to infant consumption.

Two other enzymes with hydrophobic targets, pepsin and chymotrypsin, are consistent with a number of digestion sites in addition to those digestible by cathepsin D and elastase. Only

Table 5. Human Milk Proteins Found To Have Been Digested by Cathepsin D[a]

protein name	Uniprot ID and access name	total no. of cleavages performed
β-casein	P05814 (CASB_HUMAN)	78
polymeric immunoglobulin receptor	P01833 (PIGR_HUMAN)	21
perilipin-2	Q99541 (PLIN2_HUMAN)	3
osteopontin	P10451 (OSTP_HUMAN)	2
α_{S1}-casein	P47710 (CASA1_HUMAN)	2
deubiquitinating protein VCIP135	Q96JH7 (VCIP1_HUMAN)	2
butyrophilin subfamily 1 member A1	Q13410 (BT1A1_HUMAN)	2
receptor-type tyrosine-protein phosphatase	Q15262 (PTPRK_HUMAN)	2
macrophage mannose receptor 1	P22897 (MRC1_HUMAN)	2
protein CASC3	O15234 (CASC3_HUMAN)	1
flavin containing monooxygenase 5, isoform CRA_c	Q9HA79 (Q9HA79_HUMAN)	1
Abl interactor 1	Q8IZP0 (ABI1_HUMAN)	1
misshapen-like kinase 1	Q8N4C8 (MINK1_HUMAN)	1
La-related protein 1	Q6PKG0 (LARP1_HUMAN)	1
receptor-type tyrosine-protein phosphatase α	P18433 (PTPRA_HUMAN)	1
ubiquitin carboxyl-terminal hydrolase 51	Q70EK9 (UBP51_HUMAN)	1
protein diaphanous homologue 1	O60610 (DIAP1_HUMAN)	1
neural Wiskott−Aldrich syndrome protein	O00401 (WASL_HUMAN)	1
κ-casein	P07498 (CASK_HUMAN)	1
insulin receptor substrate 1	P35568 (IRS1_HUMAN)	1
transcription factor 7-like 2	Q9NQB0 (TF7L2_HUMAN)	1
γ-glutamyltransferase 6	Q6P531 (GGT6_HUMAN)	1
PH domain leucine-rich repeat-containing protein phosphatase 1	O60346 (PHLP1_HUMAN)	1
dedicator of cytokinesis protein 1	Q14185 (DOCK1_HUMAN)	1

[a]The proteins are ordered on the basis of the number of cleavages that trypsin has performed on each. Here we considered only the number of peptides that are unique; if a peptide was not unique, we considered only one copy of the peptide. Proteins exclusively found in milk are presented in bold.

Table 6. Human Milk Proteins Found To Have Been Digested by Elastase[a]

protein name	Uniprot ID and access name	total no. of cleavages performed
β-casein	P05814 (CASB_HUMAN)	41
polymeric immunoglobulin receptor	P01833 (PIGR_HUMAN)	25
butyrophilin subfamily 1 member A1	Q13410 (BT1A1_HUMAN)	8
αS1-casein	P47710 (CASA1_HUMAN)	3
perilipin-2	Q99541 (PLIN2_HUMAN)	3
protein CASC3	O15234 (CASC3_HUMAN)	1
androgen receptor	Q9UN21 (Q9UN21_HUMAN)	1
parathyroid hormone-related protein	P12272 (PTHR_HUMAN)	1
osteopontin	P10451 (OSTP_HUMAN)	1
heat shock protein β-1	P04792 (HSPB1_HUMAN)	1
receptor-type tyrosine-protein phosphatase K	Q15262 (PTPRK_HUMAN)	1
receptor-type tyrosine-protein phosphatase α	P18433 (PTPRA_HUMAN)	1
γ-glutamyltransferase 6	Q6P531 (GGT6_HUMAN)	1

[a]The proteins are ordered on the basis of the number of cleavages that trypsin has performed on each. Here we considered only the number of peptides that are unique; if a peptide was not unique, we considered only one copy of the peptide. Proteins exclusively found in milk are presented in bold.

21 of the 75 total peptide terminal cleavage sites of unique peptides that are predicted to be performed by chymotrypsin are common cleavages with elastase and cathepsin D. For pepsin, only 38 of the 72 cleavages sites predicted from the unique peptides are shared with elastase and cathepsin D. Furthermore, only 16 peptide terminal cleavage sites are shared between both pepsin and chymotryspin. These findings indicate the first support that pepsin- and chymotrypsin-like activities are present in human breast milk (Table 1).

Examination of Gene and Protein Expression Profile of Proteases in Human Milk. Previous work has suggested that plasmin is found in milk but that it originates from blood.[20] This study tested if the enzymes responsible for the observed peptide fragments are produced in the mammary gland or migrate into milk from other origins. Gene expression analysis was carried out for human milk according to the procedure used for bovine milk[15] (Table 1). The expression was analyzed for days 4, 15, 30, and 60 of lactation. For consistency purposes, day 60 gene expression was determined; however, we also took into account the expression levels for the other days of lactation to build Table 1, which shows the possibility of expression of an enzyme at different stages of lactation. The results show that very few of the proteolytic enzymes described in Table 1 are expressed in the mammary gland at these time points (Table 1). In agreement with previous literature, no gene expression of plasmin was detected in the milks. Moreover, no expression was observed for the intestinal enzyme trypsin.

Cathepsin D was highly expressed (365 RPKM, Table 1). Elastase, however, was not expressed in the mammary epithelial cells (Table 1). As mentioned above, the presence of active elastase in milk may be explained by its presence in PMNs. We would expect the vast majority of PMN cells to be pelleted by the centrifugation and, thus, would not participate in any degradation of the milk proteins after centrifugation (see Materials and Methods). However, PMN can secrete elastase

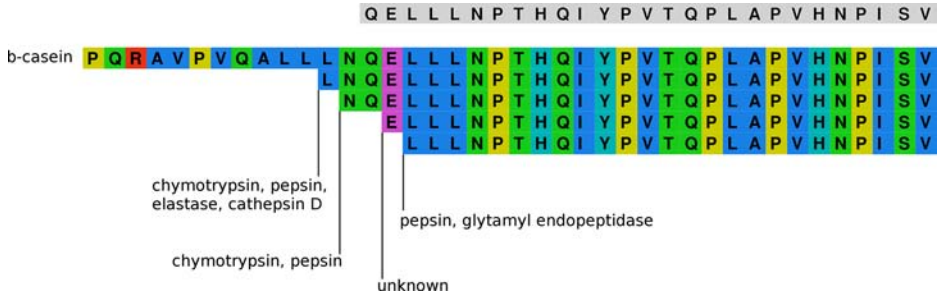

Figure 2. Illustration of antimicrobial-like peptides released in vivo from β-casein in human milk. The peptide QELLLNPTHQIYPVTQPLAPV-HNPISV shown at the top of the figure in gray has been discovered to be an antimicrobial peptide.[21] This peptide is found at the C-terminus of β-casein (positions 199−225). Four overlapping peptides found to be released in vivo in human milk are represented under the β-casein sequence. The in vivo cleavage positions are indicated with gray lines. The enzymes predicted to be responsible for these cleavages are presented beside the gray lines.

while still within the mammary gland, and the predicted elastase activity may derive from it.

Other Predicted Proteases That Were Also Expressed in Human Milk. Most of the other predicted enzymes have a low number of total cleavages, making it difficult to fully support their presence in milk (Table 1; total cleavages $\leq$ 44). Interestingly, some of these enzyme activities predicted in milk seem to be expressed in matching proteases. On the basis of a relatively specific cleavage site not shared by other proteases in these analyses (cleaves after E; with 76 cleavages in total), we predicted a glutamyl endopeptidase-like activity. Transcripts for glutamyl endopeptidase were, however, not detected in mammary epithelial cells. A glutamyl endopeptidase-like protease (proteasome subunit β type-3, PSMB3) is, however, highly expressed (75.9 RPKM; Table 1). This result may explain the high number of cleavage sites (930) predicted to be due to a glutamyl endopeptidase-like enzyme. Indeed, this glutamyl endopeptidase-like protease may have a more specific cleavage pattern explaining the many residues containing glutamic acid (E) that it did not cleave, as this cannot be accounted for by a structural bias, because the charged glutamic acids are not found buried in the core of the proteins. Although the gene expression of a glutamyl endopeptidase (called "a disintegrin and metalloproteinase with thrombospondin motifs 4" (ADAMTS4) was detected, its potential cleavage site, E'[AS], is cleaved only eight times in the data set. Thus, there is no indication for this enzyme playing a role as the major glutamyl endopeptidase activity in milk.

Proline-endopeptidase was found to be expressed in milk (5.52 RPKM; Table 1). Proline-endopeptidase is responsible for the cleavage of 45 residues covering a total of 18 milk proteins (Table 1; Figure 1).

In Vivo Release of Antimicrobial Peptides in Human Milk. Milk proteins may carry encrypted functional peptide sequences that, when released by enzymes from the intact protein, help in the protection and development of the neonate.[12] However, without in vivo results, these concepts remain unproven. This study identified four peptides that overlap (two extra or fewer amino acids on the N-terminus of the peptide) with a known antimicrobial peptide that has been reported previously in the literature.[21] This peptide is present at the C-terminus of β-casein (Figure 2). These four overlapping peptides are naturally released in human milk via the action of several enzymes, including cathepsin D and elastase (Figure 2). The overlapping peptides most likely carry the antibacterial activity, as the amino acid additions compared to the literature-defined sequence are unlikely to abolish the antimicrobial activity of these sequences.

Uneven Distribution of Enzyme Activity in Human Milk. To measure the enzyme activity, we considered the unique cleavages of each (i.e., if an enzyme cleaves out the same peptide from the parent protein multiple times, we will consider this to be only one unique cleavage). This measure highlights more the range of cleavages of an enzyme and makes it possible to compare it with other enzyme ranges rather than comparing its ability to cleave many times the same peptides. Consequently, this measure does not take the abundance of the proteins into account. Using this approach, we find that two proteins, β-casein and polymeric immunoglobulin receptor, show the highest susceptibility to the milk enzyme activity, as shown by the large number of fragments found from these two proteins. β-Casein is a milk-specific protein expressed during lactation. Interestingly, the other two milk-specific proteins, α_{S1}-casein and κ-casein, show little digestion susceptibly within the mammary gland. The possibility of protein structural disorder being the source of variability in degradation susceptibility among these proteins is not supported by these results, as κ-casein and α_{S1}-casein are also highly disordered proteins. The K and R residues are those that show the most susceptibility for the cleavages observed in human milk proteins. However, no enrichment of these amino acids was found in β-casein versus α_{S1}-casein or κ-casein (14 K and R sites in β-casein; 16 in α_{S1}-casein; and 13 in κ-casein). In fact, there are even fewer K and R in β-casein over the sequence length compared to α_{S1}-casein or κ-casein, arguing that this is not the driver behind β-casein susceptibility, nor is it for polymeric immunoglobulin receptor (6% in β-casein, 9% in α_{S1}-casein, 8% κ-casein, and 10% in polymeric immunoglobulin receptor). On the other hand, post-translational modifications may also explain these variations in susceptibility of proteins to degradation. Indeed, large modifications on proteins may prevent enzymes from reaching their target site. However, investigating the potential modification sites using Uniprot shows that all of the casein proteins are slightly/equivalently modified (in terms of numbers of glycosylations and phosphorylations).

The other major milk-specific proteins that have not been affected are α-lactalbumin and lactoferrin. No peptides from these proteins were detected despite the fact that plasmin, trypsin, cathepsin D, and elastase were all predicted to cleave both of these proteins. It is perhaps the particular structure and post-translational modifications of α-lactalbumin and lactoferrin that prevented the enzymes from cleaving them.

Although cathepsin D is highly expressed in milk (Table 1), it does not show a high effectiveness in cleaving milk proteins. This lower cleavage rate may be because cathepsin D is most effective at a more acidic pH (pH 5 for cathepsin D), which is different from the more neutral milk pH.

Independent studies have shown the existence and activity of some enzymes in milk, but the extent to which these enzymes are active relative to each other remained unknown. Likewise, whether or not these enzymes are created in the mammary epithelial cells was unclear. The enzymes that are active in human milk and responsible for protein digestion prior to entry into the infant's digestive system were determined. Using a combination of bioinformatics, peptidomics, transcriptomics, and literature results, we showed that milk begins to be digested even before infant consumption and that this digestion is mainly carried out by four proteolytic enzymes: plasmin, a trypsin-like enzyme, elastase, and cathepsin D (Tables 1−3, 5, and 6). Among these four enzymes, only cathepsin D and elastase are expressed in milk, with elastase showing only weak expression at days 15 and 30 and no expression after that (Table 1). Activity and expression of chymotrypsin and pepsin-like activity were also seen (Table 1). This finding is surprising, given that these enzymes have never been reported in human breast milk. Other enzymes that this analysis predicted from activity and expression are glutamyl endopeptidase and proline endopeptidase (Table 1).

Interestingly, plasmin, trypsin, elastase, and cathepsin D cleave the casein proteins (α_{S1}-, β-, and κ-casein) to various extents. Our novel MS-based peptide search platform using an iterative searching strategy to detect peptides in minor abundances did not detect peptides resulting from α-lactalbumin. Plasmin, a trypsin-like enzyme, elastase, and cathepsin are predicted to cleave this protein, yet none of the predicted peptides could be detected. The mechanism causing this protein selectivity of digestion remains unknown.

We know very little about proteolytic enzyme activity in human milk, which makes the problem of humanizing milk formulas even harder. The work we have carried out here sheds light on the different enzymes we find in human milk and the relative contribution of each of them, in terms of the release of unique peptides, to cleaving milk proteins. The example illustrated in Figure 2 of a known antimicrobial activity being released illustrates how enzyme activity in human milk may be playing a much greater role than previously anticipated, and fully clarifying this role is key to understanding infant needs.

AUTHOR INFORMATION

Corresponding Author

*(N.K.) E-mail: nora.khaldi@ucd.ie. Phone: 00353-1-7165335. Mail: UCD Complex and Adaptive Systems Laboratory, University College Dublin, Dublin 4, Ireland.

Funding

This work was funded by the Irish Research Council for Science, Engineering and Technology, cofunded by Marie Curie Actions under FP7; Enterprise Ireland grant to Food Health Ireland; SFI grant 08/IN.1/B1864; University of California Discovery Program (05GEB01NHB), the National Institutes of Health (HD059127 and HD061923) California Dairy Research Foundation; U.S. Department of Agriculture, National Institute for Food and Agriculture postdoctoral fellowship; National Science Foundation Graduate Research Fellowship Program; and National Institutes of Health Training Program in Biomolecular Technology (2-T3-GM08799).

Notes

The authors declare no competing financial interest.

ACKNOWLEDGMENTS

We thank Prof. Alan Kelly and Kevin Rue for helpful discussions.

ABBREVIATIONS USED

MS, mass spectrometry; FA, formic acid; ACN, acetonitrile; OD, odds ratio; PMN, polymorphonuclear neutrophils; RPKM, reads per kilobase per million mapped reads

REFERENCES

(1) Heegaard, C. W.; Larsen, L. B.; Rasmussen, L. K.; Højberg, K. E.; Petersen, T. E.; Andreasen, P. A. Plasminogen activation system in human milk. *J. Pediatr. Gastroenterol. Nutr.* **1997**, *25*, 159−166.

(2) Nielsen, S. S. Plasmin system and microbial proteases in milk: characteristics, roles, and relationship. *J. Agric. Food Chem.* **2002**, *50*, 6628−6634.

(3) Borulf, S.; Lindberg, T.; Mansson, M. Immunoreactive anionic trypsin and anionic elastase in human-milk. *Acta Paediatr.* **1987**, *76*, 11−15.

(4) Monti, J.; Mermoud, A.; Jolles, P. Trypsin in human milk. *Experientia* **1986**, *42*, 39−41.

(5) Kaminogawa, S.; Yamauchi, K. Acid protease of bovine milk. *Agric. Biol. Chem.* **1972**, *36*, 2351−2356.

(6) Armaforte, E.; Curran, E.; Huppertz, T.; Ryan, C. A.; Caboni, M. F. O.; Connor, P. M.; Ross, R. P.; Hirtz, C.; Sommerer, N.; Chevalier, F. Proteins and proteolysis in pre-term and term human milk and possible implications for infant formulae. *Int. Dairy J.* **2010**, *20*, 715−723.

(7) Ferranti, P.; Traisci, M. V.; Picariello, G.; Nasi, A.; Boschi, V.; Siervo, M.; Falconi, C.; Chianese, L.; Addeo, F. Casein proteolysis in human milk: tracing the pattern of casein breakdown and the formation of potential bioactive peptides. *J. Dairy Res.* **2004**, *71*, 74−87.

(8) Borulf, S.; Lindberg, T.; Mansson, M. Immunoreactive anionic trypsin and anionic elastase in human milk. *Acta Paediatr. Scand.* **1987**, *76*, 11−15.

(9) Monti, J. C.; Mermoud, A. F.; Jolles, P. Trypsin in human milk. *Experientia* **1986**, *42*, 39−41.

(10) Shahani, K.; Kwan, A.; Friend, B. A. Role and significance of enzymes in human milk. *Am. J. Clin. Nutr.* **1980**, *33*, 1861−1868.

(11) Korhonen, H.; Pihlanto, A. Bioactive peptides: production and functionality. *Int. Dairy J.* **2006**, *16*, 945−960.

(12) Dallas, D. C.; Underwood, M. A.; Zivkovic, A. M.; German, J. B. Digestion of protein in premature and term infants. *J. Nutr. Disorders Ther.* **2012**, *2*, 1−9.

(13) Dallas, D. C.; Guerrero, A.; Khaldi, N.; Castillo, P. A.; Martin, W. F.; Smilowitz, J. T.; Bevins, C. L.; Barile, D.; German, J. B.; Lebrilla, C. B. Extensive in vivo human milk peptidomics reveals specific proteolysis yielding protective antimicrobial peptides. *J. Proteome Res.* **2013**, *12*, 2295−2304.

(14) Vijayakumar, V.; Guerrero, A.; Davey, N.; Lebrilla, C. B.; Shields, D. C.; Khaldi, N. EnzymePredictor: a tool for predicting and visualizing enzymatic cleavages of digested proteins. *J. Proteome Res.* **2012**, *11*, 6056−6065.

(15) Wickramasinghe, S.; Rincon, G.; Islas-Trejo, A.; Medrano, J. F. Transcriptional profiling of bovine milk using RNA sequencing. *BMC Genomics* **2012**, *13*, 45−58.

(16) Mortazavi, A.; Williams, B. A.; McCue, K.; Schaeffer, L.; Wold, B. Mapping and quantifying mammalian transcriptomes by RNA-Seq. *Nat. Methods* **2008**, *5*, 621−628.

(17) Larsen, L. B.; Petersen, T. E. Identification of five molecular forms of cathepsin D in bovine milk. In *Aspartic Proteinases*; Springer: Dordrecht, The Netherlands, 1995; pp 279−283.

(18) Travis, J.; Fritz, H. Potential problems in designing elastase inhibitors for therapy. *Am. Rev. Respir. Dis.* **1991**, *143*, 1412−1415.
(19) Prin-Mathieu, C.; Le Roux, Y.; Faure, G.; Laurent, F.; Béné, M.; Moussaoui, F. Enzymatic activities of bovine peripheral blood leukocytes and milk polymorphonuclear neutrophils during intramammary inflammation caused by lipopolysaccharide. *Clin. Diagn. Lab. Immunol.* **2002**, *9*, 812−817.
(20) Kelly, A.; O'Flaherty, F.; Fox, P. Indigenous proteolytic enzymes in milk: a brief overview of the present state of knowledge. *Int. Dairy J.* **2006**, *16*, 563−572.
(21) Hayes, M.; Stanton, C.; Fitzgerald, G. F.; Ross, R. P. Putting microbes to work: dairy fermentation, cell factories and bioactive peptides. Part II: Bioactive peptide functions. *Biotechnol. J.* **2007**, *2*, 435−449.
(22) Wilkins, M. R.; Gasteiger, E.; Bairoch, A.; Sanchez, J.-C.; Williams, K. L.; Appel, R. D.; Hochstrasser, D. F. Protein identification and analysis tools in the ExPASy server. In *2-D Proteome Analysis Protocols*; Springer: Dordrecht, The Netherlands, 1999; pp 531−552.
(23) Christensen, B.; Schack, L.; Kläning, E.; Sørensen, E. S. Osteopontin is cleaved at multiple sites close to its integrin-binding motifs in milk and is a novel substrate for plasmin and cathepsin D. *J. Biol. Chem.* **2010**, *285*, 7929−7937.

ment and, especially, synthesize organic compounds via photosynthesis. However, the functional soybean sprouts should be germinated in artificial dark environment and without any external nutrients except their storage material.[3,4] Up to now, little information is available on the stress responses of soybeans germinating under dark conditions and their response at the proteome level in particular. Identification of distinct proteins has contributed to understanding of the molecular mechanism adopted by soybeans in response to stress, but the regulatory mechanisms of that operation in divergent organs are still unknown without comprehensive organ-specific proteome analyses.

Based on the aforementioned issues, in this study, proteomic responses of dark germinating soybean noncotyledons (hypocotyl and radicle) and cotyledons to NaCl stress, combined with NaCl and AG treatments, was investigated. The objective was to reveal the organ-specific defense strategy, the role of endogenous PAs, and the adaptive mechanisms of dark germinating soybeans against salt stress via identification of the differentially salt-induced endogenous PA-mediated and organ-specific proteins.

MATERIALS AND METHODS

Plant Growth Conditions. Dry soybean seeds (*Glycine max* L. cultivar *Yunhe*) were sterilized, washed, and steeped with distilled water at 30 ± 1 °C for 4 h. The soaked seeds were then placed in a bean sprouting machine to germinate in a dark incubator at 30 ± 1 °C with water containing the following additives: (A) CK, deionized water; (B) NaCl, 50 mM NaCl; (C) NaCl−AG, 50 mM NaCl and 2.5 mM AG. The culture solution was replaced every 1 day. Three independent biological experiments were performed, and 4 days after treatment, the cotyledons and noncotyledons (hypocotyl and radicle) were carefully collected and frozen in liquid nitrogen until analysis.

Malondialdehyde (MDA) Content Determination. The extent of lipid peroxidation in terms of MDA formation was measured following the method of Madhava and Sresty.[16]

GABA and Free PA (*f*PAs) Content Determination. GABA and *f*PA contents were analyzed as described by Yang et al.[11]

Protein Extraction and Two-Dimensional Polyacrylamide Gel Electrophoresis (2-DE). To minimize errors, 10 cotyledons and noncotyledons (hypocotyl and radicle) from ten germinated soybeans, respectively, were pooled for each biological repeat sample. Protein extraction was performed using trichloroacetic acid (TCA)/acetone precipitation with some modifications.[17] Briefly, sample powder was suspended in 10% (w/v) TCA in acetone containing 1 mM dithiothreitol (DTT), and held at −20 °C for 2 h. After centrifugation and rinsing, the pellets were air-dried at room temperature and dissolved at 4 °C in lysis buffer containing 7 M urea, 2 M thiourea, 4% (w/v) 3-[(3-cholamidopropyl)-dimethylammonio]-1-propane sulfonate, 40 mM DTT, and 2% (v/v) Pharmalyte. Insoluble residue was removed through centrifugation, and the protein content was determined according to the Bradford method.[18]

Cotyledon protein (800 μg) was applied onto a 24 cm pH 4−7 linear gradient immobilized pH gradient (IPG) strip (GE Healthcare, Buckinghamshire, UK) and was subjected to electrophoresis at 20 °C for a total of 94850 V·h. Similarly, 800 μg of noncotyledon (hypocotyl and radicle) protein was applied onto an 18 cm pH 4−7 linear gradient IPG strip and was subjected to electrophoresis for a total of 90850 V·h. Subsequently, the strips were equilibrated,[19] and the second electrophoretic dimension was performed by 12% sodium dodecyl sulfate−polyacrylamide gel electrophoresis (SDS-PAGE) and was run on the Ettan Six vertical set (GE Healthcare) in electrophoretic buffer at 15 °C with a cooling device (GE Healthcare). Finally, the gels were stained with Coomassie brilliant blue (CBB) G-250.

Gel Image Analysis. The stained 2-DE gels were digitized with a gel scanner (Imagescanner III, GE Healthcare), and analyzed with PDQuest software package (Version 7.2.0, BIO-RAD, California, USA). Spots were detected, matched, and normalized on the basis of total quantity of valid spots with the parameter of percent volume according to the software guide. For each protein spot, triplicate gels were used for each sample, and the mean relative volume was used to designate the significant and differentially expressed proteins (changed by more than 1.5-fold or less than 0.66-fold and statistically significant as calculated by one-way ANOVA, $P < 0.05$).

Peptide Preparation for Mass Spectrometry Analysis. Protein spots with differential expression patterns were excised from gels, washed with double-distilled water 3 times, destained with 25 mM NH_4HCO_3 for CBB G-250 staining spots, dehydrated with 50% (v/v) acetonitrile (ACN) in 25 mM NH_4HCO_3, reduced with 10 mM DTT in 50 mM NH_4HCO_3 for 1 h at 56 °C, alkylated with 55 mM iodoacetamide in 50 mM NH_4HCO_3 for 1 h at 25 °C, dried twice with 100% ACN, and digested overnight at 37 °C with sequencing grade modified trypsin (Promega, Madison, WI, USA) in 50 mM NH_4HCO_3. The peptides were extracted twice by washing the gel pieces with 0.1% trifluoroacetic acid (TFA) in 67% ACN. Extracts were pooled and lyophilized.

Protein Identification by Nano-Liquid Chromatography−Tandem Mass Spectrometry and Database Search. The lyophilized tryptic peptides were resuspended in 5 mg/mL α-cyano-4-hydroxy-trans-cinnamic acid containing 0.1% trifluoroacetic acid (TFA) and 50% ACN.[20] MALDI-TOF-TOF MS analyses were conducted using an ABI 4800 Plus MALDI-TOF-TOF analyzer (Applied Biosystems, Foster City, CA, USA). Both the MS and MS/MS data were integrated and search was performed using the GPS Explorer software V3.6 (Applied Biosystems, USA) over the NCBI database with the help of the MASCOT search engine V3.5 (Matrix Science Ltd., London, U.K.). The following parameters were used in the search: NCBInr Viridiplantae (Green Plants) database; trypsin as the digestion enzyme; one missed cleavage allowed; cysteine carbamidomethylation as a fixed modification and methionine oxidization as a variable modification; no fixed modifications; 50 ppm for peptide ion tolerance; 0.5 Da for fragment ion tolerance. Only significant hits, as defined by the MASCOT probability analysis ($P < 0.05$) or individual ion score > 49, were accepted.

Identified proteins were annotated to their biological function according to KEGG (http://www.kegg.jp/kegg/pathway.html) and literature. Information on these proteins was obtained from the Universal Protein Resource (http://www.uniprot.org/). Moreover, WOLF PSORT prediction (http://wolfpsort.org/) was used to predict subcellular localization of all identified proteins.

RESULTS

Growth Performance, Sprout Length, and MDA Content in Germinating Soybeans. To evaluate the effect of NaCl stress on germinating soybeans, the growth performance, sprout length, and MDA content in germinating soybeans were measured. Under NaCl stress, the sprouts were significantly shorter ($P < 0.05$) than those of the control at the same germination time, but there was no significant difference ($P > 0.05$) compared with those under NaCl−AG treatment (Figure 1A). The MDA content increased significantly ($P < 0.05$) after 4 days in both organs of the NaCl-stressed and NaCl−AG treated sprouts (Figure 1B). Figure 1C shows that the growth and development of untreated sprouts were better than those of sprouts under NaCl stress and NaCl−AG treatments. The growth was inhibited and membrane integrity was lost after 4 days in both the NaCl-stressed and the NaCl−AG-treated sprouts.

GABA and *f*PA Contents in Germinating Soybeans. The GABA and *f*PA contents in the cotyledons and noncotyledons (hypocotyl and radicle) of 4-day germinating soybeans under NaCl stress and NaCl−AG treatment were analyzed. After germinating for 4 days under NaCl stress,

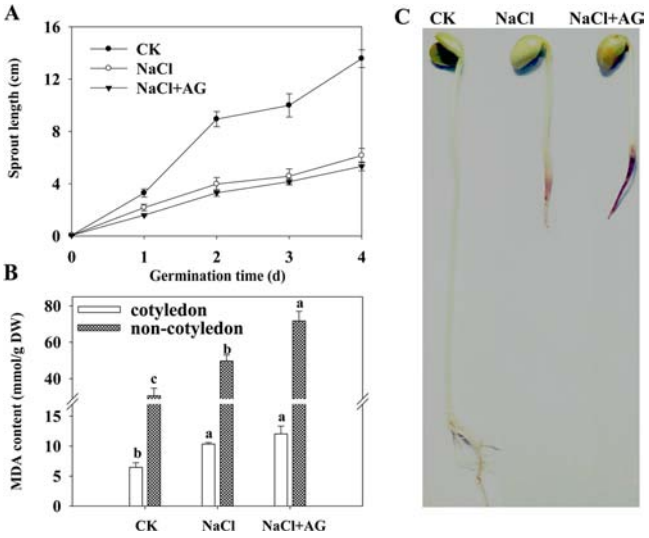

Figure 1. Effect of NaCl stress and NaCl−AG treatment on germinating soybean growth performance, sprout length, and MDA content. Noncotyledons: hypocotyl and radicle. Sprout length (A) and MDA content (B) of germinating soybeans were observed at 0, 1, 2, 3, and 4 days. The photograph of whole germinating soybeans was taken 4 days after treatment (C). Values are the mean ± SE (error bars). The lower case letters reflected the significance of differences in MDA content at germination for 4 days using the Duncan's test ($P < 0.05$).

GABA content was 1.54- and 1.70-fold higher than the control in the cotyledons and noncotyledons, respectively (Figure 2A). The GABA content in the noncotyledons of 4-day germinating soybeans treated with NaCl combined AG was not significantly ($P > 0.05$) different from that of the soybeans under NaCl stress, while the GABA content in cotyledons was significantly ($P < 0.05$) lower than in those under NaCl stress (Figure 2A). The *f*PA content decreased significantly in both organs of the 4-day germinating soybeans under NaCl stress compared with the control (Figure 2B). After treatment with AG, the DAO activity, as the rate limiting enzyme of PA catabolism, was completely inhibited (Supplementary Figure 1, Supporting Information), and the content of *f*PAs in 4-day germinating sprouts were all significantly ($P < 0.05$) higher than those of the sprouts under NaCl stress (Figure 2B).

Identification of Differentially Expressed Proteins Induced in Noncotyledons of 4-Day Germinating Soybeans under NaCl Stress and NaCl−AG Treatment. Comparative proteomic approach was used to determine the changes in protein abundance in noncotyledons of germinating soybeans exposed to NaCl stress and NaCl−AG treatment. The extracted proteins in the noncotyledons of 4-day germinating soybeans were separated using 2-DE and isoelectric focusing (IEF) on 18 cm linear IPG gels stained with CBB (Figure 3A). Three independent experiments were performed as biological replicates (Supplementary Figure 2, Supporting Information). The relative intensities of all the spots were analyzed using the PDQuest software. In total, more than 950 protein spots in germinating soybean noncotyledons were reproducibly detected on the 2-DE gels. A total of 67 proteins showed a less than 0.66-fold or more than 1.5-fold difference ($P < 0.05$) in relative volume in noncotyledons under different treatments. These proteins were excised from the gels for MALDI-TOF/TOF mass spectrometry. Finally, 63 proteins displayed in Table 1 were confidently identified according to the NCBI database (Supplementary Figure 3 and Supplementary Table 1, Supporting Information).

In the NaCl-treated group, 62 differentially expressed proteins were discovered compared with CK, including 37 (59.7%) up-regulated and 25 (40.3%) down-regulated (Figures 4A and 5A). These proteins were divided into 10 functional classes according to KEGG and the literature (Table 1, Figure 5A). Nine identified proteins were annotated as uncharacterized proteins, and six of them were searched for their homologues using BLAST (http://www.ncbi.nih.gov/BLAST/). At the amino acid level, the six proteins showed more than 65% positives, indicating that they might have similar functions (Table 2). All of the energy-related and synthesis-related proteins and most of the disease/defense-related noncotyledon proteins increased significantly under NaCl treatment, but all the transporter-related, signal transduction-related, and secondary metabolism-related and most uncharacterized noncotyledon proteins decreased under NaCl treatment (Figures 4A and 5A). The subcellular localization information of these identified proteins was also analyzed using WOLF PSORT prediction, which revealed that 36 (58%) differentially expressed proteins identified were predicted to be cytoplasmic proteins. All of the endoplasmic reticulum proteins, vacuole proteins, and mitochondrial proteins showed an increased abundance while half of the cytoplasmic proteins and chloroplast proteins showed a decreased abundance under NaCl treatment (Figure 5C).

A total of 51 noncotyledon proteins showed differential responses in the NaCl−AG treated group compared with the group under NaCl stress. Among these identified proteins, 22 were up-regulated proteins and 29 were down-regulated proteins (Figures 4A and 5B). For disease/defense-related

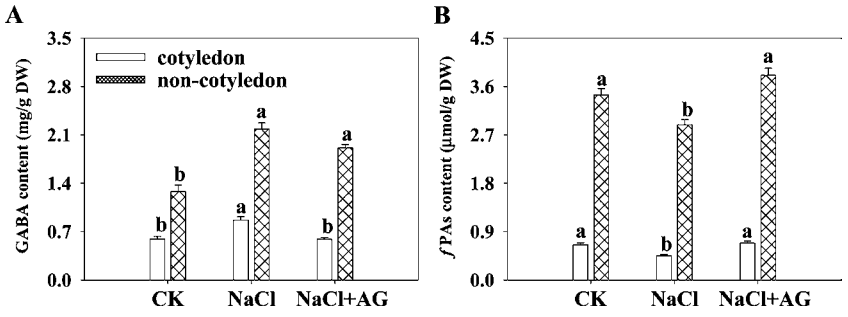

Figure 2. Changes in GABA and *f*PA content in 4-day germinating soybeans. The GABA content (A) and *f*PA content (B) in cotyledons and noncotyledons of germinating soybeans were determined. Noncotyledons: hypocotyl and radicle. Values are the mean ± SE (error bars). Data with the same letters were not significantly different compared with control as was determined using the Duncan's test ($P < 0.05$).

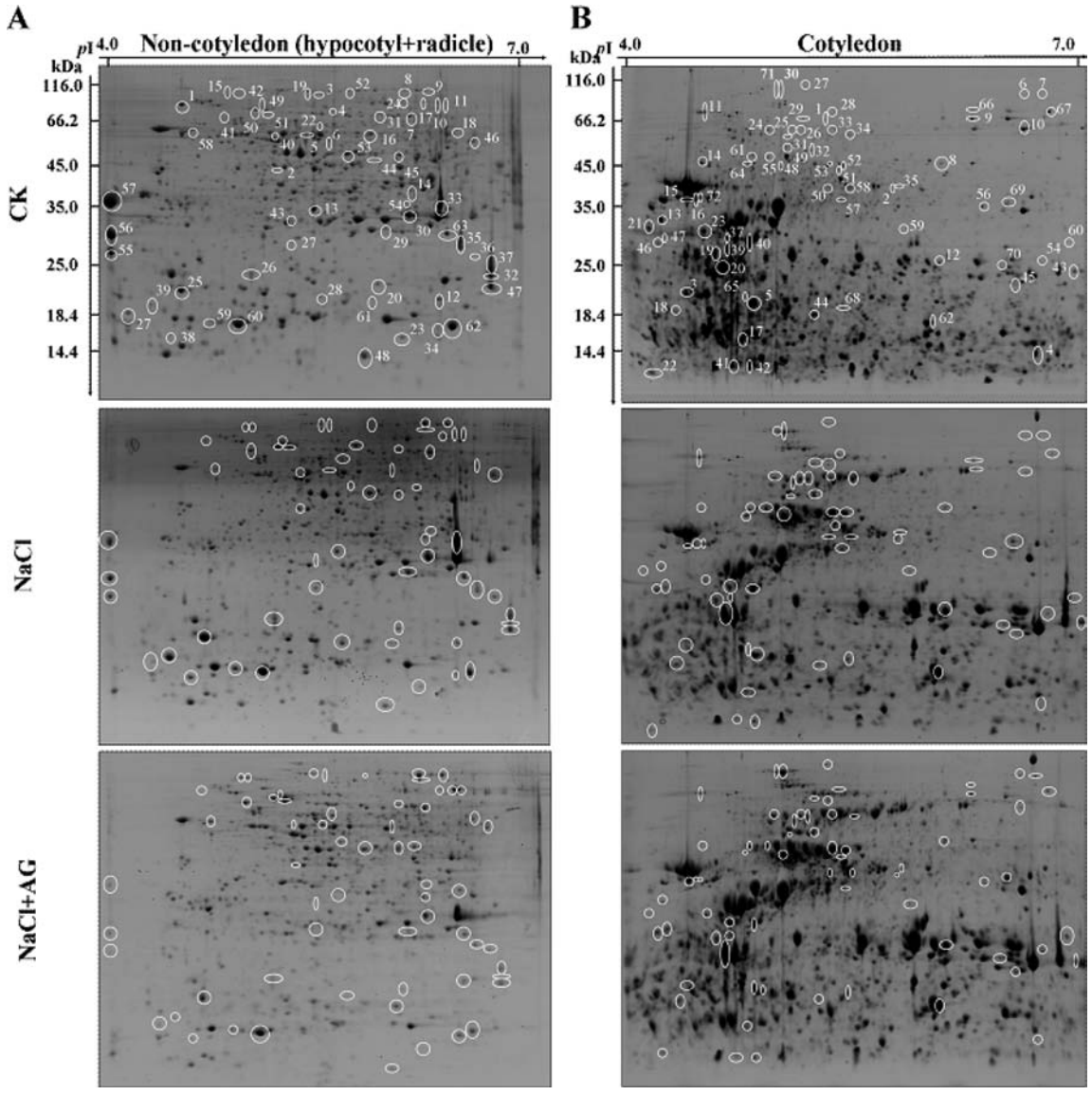

Figure 3. 2-DE pattern of 4-day germinating soybean noncotyledons and cotyledons proteins under NaCl stress or NaCl−AG treatment. Proteins extracted from noncotyledons (A) or cotyledons (B) were separated by 2-DE as described in the Materials and Methods and visualized with CBB staining. Noncotyledons: hypocotyl and radicle. Protein spot numbers are same as those shown in Tables 1 and 3.

proteins, the number of proteins that increased or decreased was equal. In addition, the majority of metabolism-related, energy-related, and protein synthesis-related proteins showed an increased abundance. However, the majority of the proteins involved in secondary metabolism, protein destination/storage, and metabolism showed a decreased abundance (Figures 4A and 5B). Most of the increased noncotyledon proteins were predicted to localize in the chloroplast, vacuole, and endoplasmic reticulum, while the cytoplasmic proteins and mitochondrial proteins were nearly equally increased or decreased (Figure 5D).

Identification of Differentially Expressed Proteins Induced in Cotyledons of 4-Day Germinating Soybeans under NaCl Stress and NaCl−AG Treatment. To analyze the extracted proteins in 4-day germinating soybean cotyledons, 24 cm linear IPG gels were used. Approximately 1150 protein spots were observed in all three biological replicates of stained gels (Supplementary Figure 4, Supporting Information). Among them, 72 protein spots that showed a more than 1.5-fold difference ($P < 0.05$) in abundance were successfully identified (Table 3; Supplementary Figure 4 and Supplementary Table 2, Supporting Information).

For the NaCl-treated group, a total of 72 proteins (45 up-regulated proteins and 27 down-regulated proteins) were significantly altered compared with CK (Figures 4B and 5E). Of these proteins, 45 (62.5%) were involved in the seed storage proteins (SSPs), and the remainder were divided into six functional classes, metabolism, energy, cell growth/division, proteolysis, transporters, and disease/defense (Table 3, Figure 5E). Most of the SSPs and metabolism-related proteins showed an increased abundance, while the energy-related, proteolysis-related, and disease/defense-related proteins showed a decreased abundance under NaCl stress. In total, different from the noncotyledon proteins, 55.5% of identified cotyledon proteins were predicted to localize in cytoplasm, and most of them were up-regulated under NaCl treatment (Figure 5G).

In cotyledons, 29 up-regulated and 13 down-regulated proteins were identified in response to NaCl−AG treatment

Table 1. Differentially Expressed Germinating Soybean Noncotyledon Proteins under NaCl Stress or NaCl Combined with AG Treatment after 4 Days

no.[a]	homolog protein[b]	accession no.[c]	plant species	tmr[d] (kda)	tpi[e]	score[f]	M.P.[g]	SC,[h] %	local[i]
			Metabolism[j]						
1	profilin-2	gil351721630	*Glycine max*	14.20	4.69	205	3	29	Cyto
2	glutamine synthetase PR-2	gil356520651	*Glycine max*	39.29	5.32	165	5	19	Chlo
3	phospholipase D α 1	gil356519347	*Glycine max*	91.94	5.48	219	3	6	Cysk
4	β-amylase	gil169913	*Glycine max*	53.98	5.31	312	3	9	Cyto
5	aminoaldehyde dehydrogenase	gil443294716	*Glycine max*	54.79	5.16	395	1	2	Chlo
6	5-methyltetrahydropteroyltriglutamate–homocysteine methyltransferase	gil356571744	*Glycine max*	84.39	5.97	425	5	7	Cyto
7	lipoxygenase-2	gil126402	*Glycine max*	97.41	6.08	57	1	1	Cyto
8	linoleate 9*S*-lipoxygenase-4	gil585418	*Glycine max*	96.64	5.71	528	10	13	Cyto
9	methionine synthase	gil351724907	*Glycine max*	84.40	5.93	432	3	8	Cyto
10	glutamine synthetase precursor	gil5733730	*Juglans nigra*	48.09	8.34	202	4	10	Chlo
11	UDP-*N*-acetylglucosamine pyrophosphorylase	gil356512205	*Glycine max*	54.69	5.88	54	3	6	Cyto
12	nucleoside diphosphate kinase	gil26245395	*Glycine max*	16.40	6.91	366	4	24	Cyto
			Energy[j]						
13	ATP synthase 24 kDa subunit	gil356512762	*Glycine max*	27.51	6.09	339	4	13	Mito
14	V-type proton ATPase subunit E	gil356528948	*Glycine max*	26.98	5.87	435	7	31	Mito
15	Os01g0654500	gil115438939	*Oryza sativa Japonica*	45.35	6.34	338	7	12	Cyto
16	NADP-dependent malic enzyme	gil356495891	*Glycine max*	65.32	5.83	274	5	12	Cyto
17	NADP-dependent malic enzyme	gil356495891	*Glycine max*	65.32	5.83	307	5	9	Cyto
18	ATPase subunit 1	gil372450254	*Millettia pinnata*	55.60	6.23	660	8	23	Mito
			Cell Growth/Division[j]						
19	cell division cycle protein 48	gil356543494	*Glycine max*	90.53	5.18	440	7	15	Cyto
20	expansin-like B1	gil356563389	*Glycine max*	28.16	6.30	609	8	32	Chlo
21	embryonic protein DC-8	gil356533407	*Glycine max*	48.77	6.12	780	10	25	Nucl
			Protein Synthesis[j]						
22	eukaryotic initiation factor 4A-15	gil356530401	*Glycine max*	47.11	5.46	494	8	25	Cysk
23	eukaryotic translation initiation factor 5A3	gil351721220	*Glycine max*	17.86	5.60	462	7	42	Cyto
24	elongation factor 2	gil356525774	*Glycine max*	94.95	5.80	71	2	3	Cyto
			Protein Destination and Storage[j]						
25	chain A, soybean trypsin inhibitor	gil3318877	*Glycine max*	20.31	4.61	862	9	58	Cyto
26	RuBisCO-associated protein	gil356505863	*Glycine max*	32.76	4.98	486	8	29	Cyto
27	Mcp20	gil18143656	*Matricaria chamomilla*	22.94	5.39	595	7	44	Chlo
28	peptidyl-prolyl isomerase FKBP1	gil357445945	*Matricaria chamomilla*	12.26	7.77	150	5	23	Cyto
29	31kD glycoprotein	gil226866	*Glycine max*	29.80	6.72	660	9	34	Cyto
30	31kD glycoprotein	gil226866	*Glycine max*	29.80	6.72	651	8	34	Cyto
31	subtilisin-like protease	gil356558946	*Glycine max*	82.53	6.24	619	9	17	Cyto
32	peptidyl-prolyl cis−trans isomerase CYP20−2	gil356576933	*Glycine max*	22.93	9.10	100	2	18	Chlo
			Transporters[j]						
33	coatomer subunit β'-2	gil356556044	*Glycine max*	35.38	5.77	586	10	33	Cyto
34	nuclear transport factor 2	gil356512387	*Glycine max*	13.72	5.86	358	4	45	Cyto
35	C nascent polypeptide-associated complex subunit α	gil356509137	*Glycine max*	23.72	4.43	134	3	19	Cyto
			Signal Transduction[j]						
36	auxin-binding protein ABP19a	gil356519747	*Glycine max*	22.00	6.95	73	2	12	Cyto
37	auxin-binding protein ABP19a	gil358248706	*Glycine max*	22.04	6.95	103	2	12	Cyto
			Disease/Defense[j]						
38	pathogenesis-related protein 1	gil356554880	*Glycine max*	17.99	5.14	378	5	45	Vacu
39	pathogenesis-related protein 1	gil356549447	*Glycine max*	19.32	4.54	538	7	69	Vacu
40	nucleoredoxin 1	gil356526803	*Glycine max*	64.97	4.86	885	8	19	Cyto
41	endoplasmin	gil356553371	*Glycine max*	93.62	4.83	74	3	4	Nucl
42	heat shock cognate protein 80	gil356552478	*Glycine max*	80.42	4.98	653	9	16	Cyto
43	ferritin light chain precursor	gil170078	*Glycine max*	28.15	5.73	344	6	18	Mito
44	MnSOD	gil351726054	*Glycine max*	26.69	8.56	317	6	29	Cyto
45	selenium-binding protein 1	gil356568342	*Glycine max*	53.79	5.67	665	9	26	Cyto
46	peroxidase precursor	gil4204759	*Glycine max*	39.23	6.85	444	6	19	Cyto
47	PR-5b protein precursor	gil351727321	*Glycine max*	26.81	6.26	250	4	27	Chlo
48	Hsc70	gil336539018	*Glycine max*	71.43	5.11	657	7	15	Cyto

dx.doi.org/10.1021/jf500851r | J. Agric. Food Chem. 2014, 62, 7233−7244

Table 1. continued

no.[a]	homolog protein[b]	accession no.[c]	plant species	tmr[d] (kda)	tpi[e]	score[f]	M.P.[g]	SC,[h] %	local[i]
			Disease/Defense[j]						
49	Hsc70	gil356505100	*Glycine max*	71.82	5.05	611	8	13	Chlo
50	luminal-binding protein 5	gil356523657	*Glycine max*	73.66	5.08	446	4	8	E.R.
51	endoplasmic reticulum HSC70	gil2642238	*Glycine max*	73.82	5.15	576	5	10	E.R.
			Secondary Metabolism[j]						
52	polyphenol oxidase A1	gil356519570	*Glycine max*	67.41	5.70	510	7	12	Chlo
53	caffeoyl-CoA *O*-methyltransferase	gil356499753	*Glycine max*	28.15	5.46	143	2	11	Cyto
54	isoflavone reductase	gil356518030	*Glycine max*	43.31	6.10	593	3	21	Cyto
			Uncharacterized Protein[j]						
55	uncharacterized protein LOC100783793	gil359806210	*Glycine max*	18.78	3.97	185	1	13	Chlo
56	uncharacterized protein LOC100788703	gil356522047	*Glycine max*	14.56	4.05	165	2	36	Chlo
57	uncharacterized protein LOC100801797	gil358248520	*Glycine max*	13.07	4.00	164	2	41	Chlo
58	uncharacterized protein At5g39570	gil356550983	*Glycine max*	40.86	4.66	512	6	20	Nucl
59	uncharacterized protein LOC100527097	gil351726232	*Glycine max*	16.70	4.80	116	3	24	Cyto
60	uncharacterized protein LOC100783267	gil359807353	*Glycine max*	17.15	5.10	180	3	19	Cyto
61	uncharacterized protein LOC100820359	gil356507945	*Glycine max*	19.00	5.92	368	4	40	Nucl
62	uncharacterized protein LOC100500241	gil351722771	*Glycine max*	11.25	4.95	168	4	43	Cyto
63	uncharacterized protein LOC100500685	gil351727803	*Glycine max*	21.65	6.43	406	5	30	Cyto

[a]Spot number; spot numbering corresponds to the 2-DE gel in Figure 3. [b]Homolog protein name and species obtained via the MASCOT software from the NCBInr database. [c]Accession number according to the NCBInr database. [d]Theoretical molecular weight. [e]Theoretical isoelectric point. [f]MOWSE score probability for the entire protein. [g]Number of query matched peptides. [h]Sequence coverage. [i]Localization category using local classification: Chlo, chloroplast; Mito, mitochondria; Nucl, nuclear; Cyto, cytoplasm; Cysk, cytoplasm skeleton; E.R., endoplasmic reticulum; Vacu, vacuole. [j]Functional classification.

compared with NaCl stress (Figures 4B and 5F). Similarly, the majority of these cotyledon proteins were SSPs. Moreover, all of the metabolism-related and energy-related proteins were up-regulated ones, and most of SSPs were down-regulated ones (Figure 5F). The chloroplast proteins and vacuole proteins were equally increased or decreased while most proteins that localized in cytoplasm, nucleus, and mitochondria increased (Figure 5H).

Proteins Commonly Responsive to Stress in the Noncotyledons and Cotyledons. In the present study, five differentially expressed proteins responsive to NaCl stress were identified in both noncotyledons and cotyledons compared with CK (Tables 1 and 3; Supplementary Figure 6A, Supporting Information). Expansin-like B1 (E20 and C12), coatomer subunit β'-2 (E33 and C69), and endoplasmin (E41 and C71) all showed an increased abundance in noncotyledons and cotyledons under NaCl stress compared with CK. In addition, the embryonic protein DC-8 (E21, C9, and C10) and the soybean trypsin inhibitor (E25 and C20) showed an increased abundance in the noncotyledons but decreased in the cotyledons. Comparison of NaCl treatment with NaCl−AG treatment indicates that coatomer subunit β'-2 (E33 and C69) and endoplasmin (E41 and C71) increased in noncotyledons but decreased in cotyledons (Figure 4B).

DISCUSSION

In the present study, the GABA content was markedly higher in both organs in the NaCl-treated germinating soybeans than in the untreated ones (Figure 2A), which confirmed that soybeans could be good materials for producing functional sprouts. Consistent with previous reports,[11] the DAO activity was completely suppressed by AG, and the GABA content decreased (Figure 2). Additionally, identical negative effects such as inhibited growth of germinating soybeans and destroyed integrity of membrane under NaCl treatment were detected, since soybeans were considered as salt-sensitive plants (Figure 1). In response to NaCl stress, the identified proteins associated with metabolism were involved in amino acid, starch, fatty acid, nitrogen, and nucleotide metabolism pathways. In plant, GABA can be formed through the GABA shunt and the polyamine degradation pathway.[6,11] On the one hand, compared with the control, the abundance of the glutamine synthetase PR-2 (spot E2) and the glutamine synthetase precursor (spot E10) were much lower under NaCl treatment (Figure 6). The glutamine synthetase (GS) catalyzed the assimilation of ammonium to glutamine using glutamate as its substrate. Hence, down-regulated GS implied a higher glutamate content, which was further converted to GABA through the GABA shunt. On the other hand, higher abundance of methionine synthase (MS, spot E9), 5-methyltetrahydropteroyltriglutamate-homocysteine methyltransferase (spot E6), and aminoaldehyde dehydrogenase (spot E5) were observed in the NaCl-treated soybeans (Figure 6). MS and homocysteine methyltransferase, which are involved in the polyamine biosynthesis pathway, catalyze the transfer of a methyl group, resulting in the formation of methionine. Subsequently, the decreased *f*PA content was converted to GABA by the polyamine degradation pathway, since aminoaldehyde dehydrogenase, identified as the indispensable enzyme of polyamine degradation pathway was up-regulated under NaCl stress. The decreased abundance of GS and increased abundance of MS have also been documented on soybeans under other stresses.[19] Compared with NaCl treatment, application of AG decreased GS, and the three enzymes referred to above, which were involved in polyamine biosynthesis, further increased. These facts suggested that more glutamate as substrate was converted to GABA because the polyamine degradation pathway was suppressed. The significantly increased *f*PA content in both organs would in turn promote ion homeostasis and lower the ROS levels. Moreover, the remarkable expression of methionine synthase was an effect

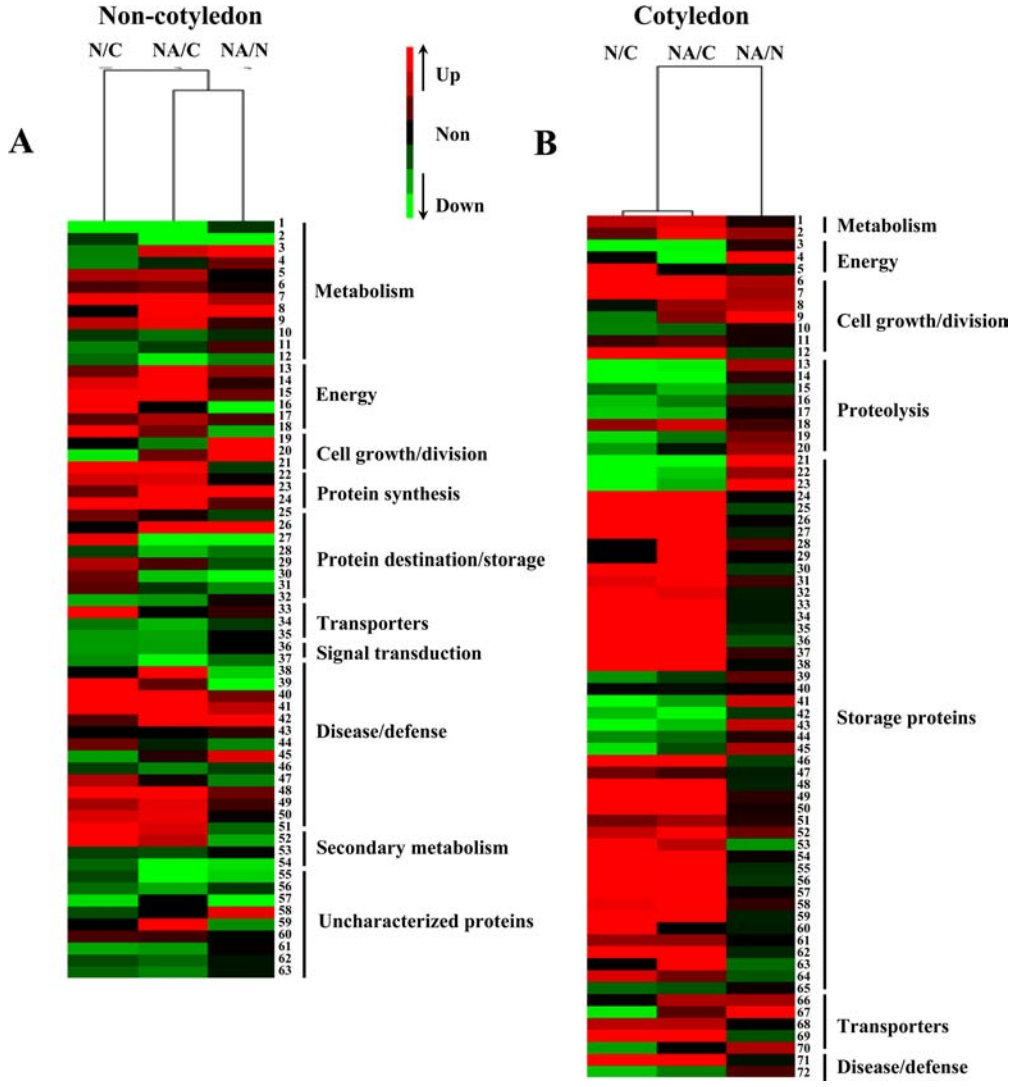

Figure 4. Proteins differentially expressed in response to NaCl stress or NaCl−AG treatment in noncotyledons and cotyledons. The expression change of noncotyledons (A) and cotyledons (B) based on the log2 transformed expression ratios of protein spots was performed using the Gene Cluster 3.0 software. The results were visualized using the JAVA TREEVIEW software. Noncotyledons: hypocotyl and radicle. C, CK; N, NaCl; NA, NaCl−AG treatment. Protein spot numbers are same as those shown in Tables 1 and 3.

of elevated activity of mechanisms that enhanced NaCl stress tolerance, since it was involved in detoxification of ROS.

In our proteome analysis, NaCl stress enhanced expression of all the identified proteins associated with energy metabolism. ATPases are membrane-bound enzymes, and they combine ATP synthesis with the transport of protons. The ATP synthase 24 kDa subunit (spot E13), the V-type proton ATPase subunit E (spot E14), the ATPase subunit 1 (spot E18), and two NADP-dependent malic enzymes (spots E16 and E17) are critical enzymes of glycolysis and the TCA cycle, which support plant growth. The V-type proton ATPase subunit E compartmentalizes Na^+ into the vacuole by generating a proton electrochemical gradient to supply a driving force utilized by the tonoplast Na^+/H^+ antiporter.[21] Studies have proven that increased expression in malate enzyme is an adaptive response to environmental stresses.[22] Up-regulated NADP-dependent malic enzyme in our soybean proteome analysis confirmed its key role in NaCl stress. Contrarily, the NADP-dependent malic enzyme (spot E16) and the ATPase subunit 1 (spot E18) decreased significantly while the other identified energy metabolism related proteins were not significantly different under NaCl−AG treatment compared with those under NaCl stress. This phenomenon suggested that NaCl stress dramatically enhanced energy metabolism in germinating soybeans while AG inhibited energy metabolism under NaCl stress.

Excess generation of reactive oxygen species (ROS), such as superoxide radical, hydroxyl radical, and hydrogen peroxide in plant cells, is an inevitable outcome of all abiotic stresses, especially NaCl stress. These ROS cause membrane damage and attack proteins and nucleic acids. Higher plants have developed an antioxidant enzymatic system to scavenge these toxic compounds. In addition, it has been proven that plant salt tolerance is positively associated with a more efficient antioxidant system. In the present study, Mn-superoxide dismutase (MnSOD, spot E44) increased significantly following its exposure to NaCl stress. This result indicated that MnSOD was the first line defense against the NaCl stress-induced ROS in germinating soybeans and suggested that the antioxidant defense mechanisms were more active in noncotyledons than in cotyledons under NaCl stress. Previous reports demonstrated that exogenous application of PAs improved the antioxidant enzyme system.[10] However, the expression of MnSOD and

dx.doi.org/10.1021/jf500851r | J. Agric. Food Chem. 2014, 62, 7233−7244

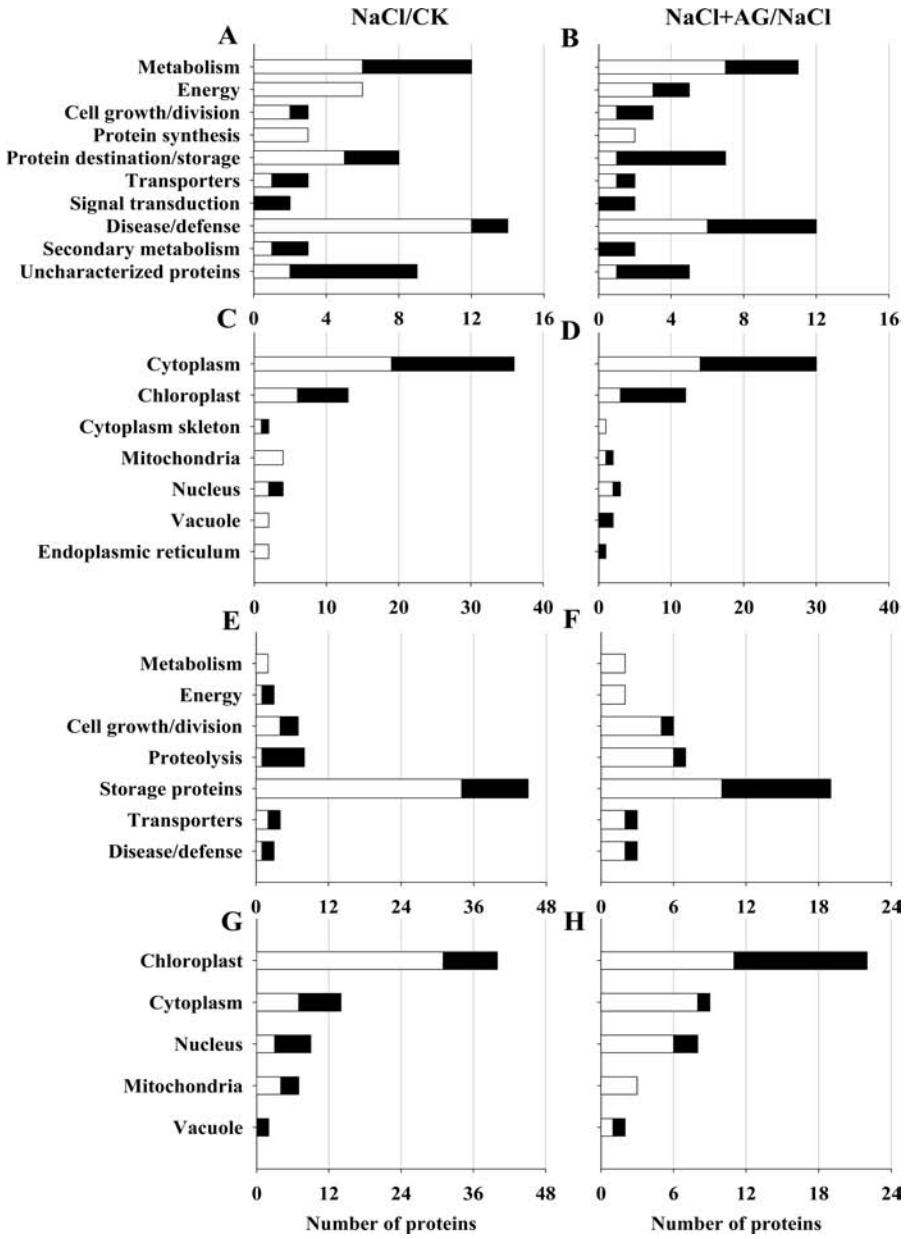

Figure 5. Classification of differentially expressed proteins in noncotyledons and cotyledons of 4-day germinating soybeans treated with NaCl or NaCl−AG. Noncotyledons: hypocotyl and radicle. The functions of differentially expressed proteins in noncotyledons (A, B), and cotyledons (E, F) treated with NaCl (A, E) and NaCl−AG (B, F) were assigned according to KEGG and literature. The localization-based classification of proteins in noncotyledons (C, D) and cotyledons (G, H) treated with NaCl (C, G) and NaCl−AG (D, H) is shown in the lower panels. Identified proteins were classified according to the subcellular localization predicted by WOLFPSORT prediction (http://wolfpsort.org). White and black columns represent increased and decreased proteins, respectively.

Table 2. Homologs of Uncharacterized Proteins in 4-Day Germinating Soybean Noncotyledons

		Homolog Protein					
no.	accession no.[a]	protein name	NCBI accession no.[b]	species	ident,[c] %	pos,[d] %	funct[e]
57	gil358248520	putative cell division protein	BAN18233.1	*Schiedea stellarioides*	64	72	cell growth/division
59	gil351726232	stress-induced protein SAM22	NP_001236038.1	*Glycine max*	92	98	disease/defense
60	gil359807353	MLP-like protein	XP_004489875.1	*Cicer arietinum*	75	88	disease/defense
61	gil356507945	glycine-rich protein 2b	XP_004505774.1	*Glycine max*	65	70	disease/defense
62	gil351722771	small ubiquitin-related modifier 1	XP_004513888.1	*Cicer arietinum*	93	95	metabolism
63	gil351727803	flavoprotein wrbA	XP_003545793.1	*Glycine max*	98	99	disease/defense

[a]The gi number of the uncharacterized proteins. [b]The accession number of homologues. [c]Identities. [d]Positives. [e]Functional classification.

POD decreased under NaCl−AG treatment. Increased endogenous PAs could not enhance the activities of ROS-scavenging enzymes to defend against the damage caused by ROS. This suggested that blocking the normal metabolic

dx.doi.org/10.1021/jf500851r | J. Agric. Food Chem. 2014, 62, 7233−7244

Table 3. Differentially Expressed Germinating Soybean Cotyledon Proteins under NaCl Stress or NaCl Combined with AG Treatment after 4 Days

no.[a]	homolog protein[b]	accession no.[c]	plant species	TMr[d] (kDa)	TpI[e]	score[f]	M.P.[g]	SC,[h] %	local[i]
		Metabolism[j]							
1	UTP-glucose-1-phosphate uridylyltransferase	gil356553237	*Glycine max*	51.55	5.20	171	3	8	Cyto
2	lactoylglutathione lyase	gil356531939	*Glycine max*	33.56	6.14	211	3	14	Cyto
		Energy[j]							
3	ribulose bisphosphate carboxylase	gil224612766	*Asterella macropoda*	21.83	5.14	209	3	10	Cyto
4	RuBisCO small subunit 1	gil132086	*Glycine max*	20.28	8.87	287	6	21	Chlo
5	ribulose-1,5-bisphosphate carboxylase/oxygenase large subunit	gil229464442	*Hylomecon japonica*	52.07	6.00	230	6	13	Cyto
		Cell Growth/Division[j]							
6	seed biotinylated protein 68 kDa	gil351724439	*Glycine max*	67.89	6.10	782	7	18	Mito
7	seed biotinylated protein 68 kDa	gil240254706	*Glycine max*	67.96	6.18	839	8	18	Mito
8	35 kDa seed maturation protein	gil351726750	*Glycine max*	35.32	5.96	450	8	28	Nucl
9	embryonic protein DC-8	gil356533407	*Glycine max*	48.77	6.12	575	8	22	Nucl
10	embryonic protein DC-8	gil356533407	*Glycine max*	48.77	6.12	785	10	21	Nucl
11	calreticulin-1 precursor	gil351726214	*Glycine max*	48.31	4.43	298	4	11	Mito
12	expansin-like B1	gil356563389	*Glycine max*	28.16	6.30	609	8	32	Chlo
		Proteolysis[j]							
13	Gly m Bd 30K	gil3097321	*Glycine max*	43.13	5.63	132	2	4	Nucl
14	cysteine proteinase RD21a	gil356553978	*Glycine max*	55.56	5.70	350	4	16	Chlo
15	Gly m Bd 30K	gil351721011	*Glycine max*	43.09	5.65	109	2	4	Vacu
16	Gly m Bd 30K	gil351721011	*Glycine max*	43.09	5.65	119	2	4	Vacu
17	Kunitz-type trypsin inhibitor B	gil125023	*Glycine max*	20.26	4.66	451	4	21	Cyto
18	soybean trypsin/chymotrypsin Bowman−Birk inhibitor	gil157830209	*Glycine max*	8.66	4.51	141	2	35	Chlo
19	Kunitz trypsin protease inhibitor	gil351722301	*Glycine max*	23.92	5.17	577	8	50	Cyto
20	chain A, soybean trypsin inhibitor	gil3318877	*Glycine max*	20.31	4.61	862	9	58	Cyto
		Storage Proteins[j]							
21	α′ subunit of β-conglycinin	gil9967361	*Glycine max*	65.16	5.23	334	6	12	Chlo
22	α′ subunit of β-conglycinin	gil28629838	*Glycine max*	44.99	5.62	76	2	6	Cyto
23	α′ subunit of β-conglycinin	gil9967357	*Glycine max*	63.18	4.92	317	3	8	Cyto
24	α′ subunit of β-conglycinin	gil9967361	*Glycine max*	65.16	5.23	646	8	16	Chlo
25	α′ subunit of β-conglycinin	gil9967361	*Glycine max*	65.16	5.23	852	9	22	Chlo
26	α′ subunit of β-conglycinin	gil9967361	*Glycine max*	65.16	5.23	886	9	20	Chlo
27	α′ subunit of β-conglycinin	gil9967361	*Glycine max*	65.16	5.23	712	8	20	Chlo
28	α′ subunit of β-conglycinin	gil9967361	*Glycine max*	65.16	5.23	843	9	20	Chlo
29	β-conglycinin, α chain	gil356575853	*Glycine max*	70.55	5.12	715	9	17	Chlo
30	β-conglycinin, α chain	gil121281	*Glycine max*	70.53	5.07	842	10	20	Chlo
31	β-conglycinin, α chain	gil121281	*Glycine max*	70.53	5.07	850	9	20	Chlo
32	β-conglycinin, α chain	gil121281	*Glycine max*	70.53	5.07	792	8	17	Chlo
33	α subunit of β conglycinin	gil9967357	*Glycine max*	63.18	4.92	594	8	16	Cyto
34	α subunit of β conglycinin	gil9967357	*Glycine max*	63.18	4.92	760	8	18	Cyto
35	β-conglycinin, α chain	gil121281	*Glycine max*	70.54	5.07	591	8	17	Chlo
36	β-conglycinin, α chain	gil121281	*Glycine max*	70.54	5.07	834	9	18	Chlo
37	β-conglycinin, α chain	gil121281	*Glycine max*	70.54	5.07	445	5	11	Chlo
38	soybean β-conglycinin β homotrimer complexes with *N*-acetyl-D-glucosamine	gil21465628	*Glycine max*	47.88	5.67	486	6	19	Mito
39	soybean β-conglycinin β homotrimer complexes with *N*-acetyl-D-glucosamine	gil21465628	*Glycine max*	47.88	5.67	396	5	15	Mito
40	soybean β-conglycinin β homotrimer complexes with *N*-acetyl-D-glucosamine	gil21465628	*Glycine max*	47.88	5.67	322	4	12	Mito
41	glycinin G1	gil225651	*Glycine max*	56.28	5.78	183	3	7	Chlo
42	glycinin G1	gil121276	*Glycine max*	56.30	5.89	158	3	6	Chlo
43	glycinin G1	gil121276	*Glycine max*	56.30	5.89	214	4	9	Chlo
44	mutant glycinin subunit A1aB1b	gil254029113	*Glycine max*	44.07	5.51	364	6	16	Chlo
45	glycinin A1bB2−784 precursor	gil351725539	*Glycine max*	54.83	6.01	136	1	5	Chlo
46	glycinin	gil6015515	*Glycine max*	24.35	4.46	901	7	43	Nucl
47	glycinin	gil6015515	*Glycine max*	24.35	4.46	655	4	32	Nucl
48	glycinin A1aBx	gil2225651	*Glycine max*	56.28	5.78	526	9	24	Chlo
49	glycinin A1aBx	gil2225651	*Glycine max*	56.28	5.78	293	4	16	Chlo
50	glycinin A1a subunit	gil121276	*Glycine max*	56.29	5.89	753	9	27	Chlo

dx.doi.org/10.1021/jf500851r | J. Agric. Food Chem. 2014, 62, 7233−7244

Table 3. continued

no.[a]	homolog protein[b]	accession no.[c]	plant species	TMr[d] (kDa)	TpI[e]	score[f]	M.P.[g]	SC,[h] %	local[i]
			Storage Proteins[j]						
51	glycinin A1a subunit	gil121276	*Glycine max*	56.29	5.89	390	5	15	Chlo
52	glycinin A1a subunit	gil121276	*Glycine max*	56.29	5.89	679	8	26	Chlo
53	glycinin A1a subunit	gil121276	*Glycine max*	56.29	5.89	670	9	24	Chlo
54	glycinin A1a subunit	gil121276	*Glycine max*	56.29	5.89	490	9	21	Chlo
55	glycinin G2 precursor	gil351725363	*Glycine max*	54.36	5.46	482	6	15	Chlo
56	glycinin G2 precursor	gil351725363	*Glycine max*	54.36	5.46	819	8	23	Chlo
57	glycinin G2 precursor	gil351725363	*Glycine max*	54.93	5.46	765	9	22	Chlo
58	glycinin G2 precursor	gil351725363	*Glycine max*	54.93	5.46	741	9	22	Chlo
59	glycinin G2 precursor	gil351725363	*Glycine max*	54.93	5.46	354	6	15	Chlo
60	glycinin A3B4 subunit	gil126144646	*Glycine max*	58.12	5.78	482	6	19	Chlo
61	glycinin G4 subunit	gil255224	*Glycine max*	64.09	5.38	695	6	16	Chlo
62	glycinin G4 subunit	gil255224	*Soybeans*	64.10	5.38	309	3	8	Chlo
63	Gy5	gil736002	*Glycine soja*	58.61	5.52	979	8	21	Chlo
64	glycinin A5A4B3 precursor	gil351734402	*Glycine max*	64.21	5.17	1019	8	23	Chlo
65	2S albumin precursor	gil351727517	*Glycine max*	19.02	5.20	149	6	13	Mito
			Transporters[j]						
66	maturation polypeptide	gil351723085	*Glycine max*	50.61	6.33	441	7	25	Nucl
67	maturation polypeptide	gil351723085	*Glycine max*	50.61	6.33	920	10	28	Nucl
68	sucrose-binding protein	gil356536206	*Glycine max*	58.35	6.08	209	4	9	Cyto
69	coatomer subunit β'-2	gil356556044	*Glycine max*	35.38	5.77	586	10	33	Cyto
			Disease/Defense[j]						
70	NAD-dependent formate dehydrogenase	gil4760553	*Oryza sativa*	41.45	6.87	244	3	11	Cyto
71	endoplasmin	gil356553371	*Glycine max*	93.62	4.83	74	3	4	Nucl
72	acidic chitinase	gil4835584	*Glycine max*	32.18	5.01	412	6	12	Chlo

[a]Spot number; spot numbering corresponds to the 2-DE gel in Figure 3. [b]Homolog protein name and species obtained via the MASCOT software from the NCBInr database. [c]Accession number according to the NCBInr database. [d]Theoretical molecular weight. [e]Theoretical isoelectric point. [f]MOWSE score probability for the entire protein. [g]Number of query matched peptides. [h]Sequence coverage. [i]Localization category using local classification: Chlo, chloroplast; Mito, mitochondria; Nucl, nuclear; Cyto, cytoplasm; Cysk, cytoplasm skeleton; E.R., endoplasmic reticulum; Vacu, vacuole. [j]Functional classification.

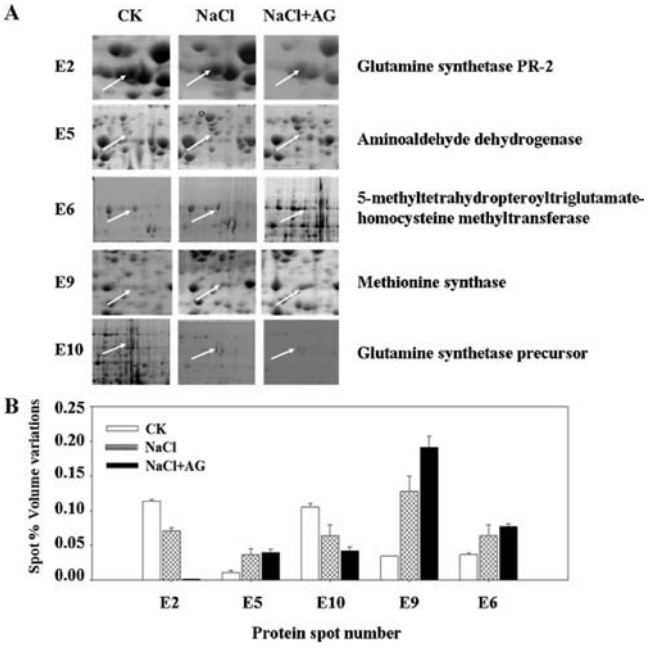

Figure 6. Differentially regulated proteins involved in GABA metabolism upon NaCl stress and NaCl−AG treatment in germinating soybeans. (A) Magnified views of differentially regulated proteins; (B) relative protein levels of differentia regulated proteins. Protein spot numbers are same as those shown in Tables 1 and 3.

processes of endogenous PAs would aggravate the negative effects of NaCl stress. It is noteworthy that nine differentially expressed proteins were associated with protein processing in endoplasmic reticulum, including four heat shock proteins (spots E42, E48, E49, and E51), two endoplasmins (spots E41 and C71), cell division cycle protein 48 (spot E19), luminal-binding protein 5 (spot E50), and calreticulin-1 precursor (spot C11). Almost all the proteins were up-regulated under NaCl stress except the cell division cycle protein 48. These results implied that promotion of protein processing in endoplasmic reticulum might be a very important strategy of germinating soybeans under NaCl stress.

Secondary metabolites play an important role in osmotic adjustment and ROS scavenging in response to environmental stressors.[23] Compared with CK, down-regulated caffeoyl-CoA-*O*-methyltransferase (CCoAOMT, spot E53) and isoflavone reductase (IFR, spot E54) and up-regulated polyphenol oxidase A1 (spot E52) in NaCl-stressed soybeans were detected in the present study. CCoAOMT plays a key role in the supply of substrates for the synthesis of lignin units.[24] Lignification of the cell wall may be one important strategy adopted by plants in response to NaCl stress. The down-regulated CCoAOMT might be linked to the reduced synthesis of monolignols, which was possibly due to stress-imposed growth suppression.[25] However, under NaCl−AG treatment, there was no significant difference in CCoAOMT abundance compared with NaCl treatment. IFR, associated with isoflavonoid biosynthesis pathways, was down-regulated under NaCl stress compared with CK and further significantly decreased under NaCl−AG

treatment. Additionally, polyphenol oxidase increased under NaCl stress but decreased after AG was added. It is well-known that isoflavonoids and polyphenol are potent antioxidants functioning as scavengers of ROS under stressful conditions. Accordingly, the accumulation of isoflavones and polyphenol could play an essential role in regulating the growth response. Taken together, these results indicated that the secondary metabolite synthesis pathways were targets for stress response, possibly altering the development of soybeans.

Auxin-binding protein ABP19a (spot E36 and E37), associated with auxin signaling pathway and mediating the action of auxins, was dramatically down-regulated under NaCl stress compared with the control. Furthermore, compared with NaCl treatment, its abundance decreased after AG was applied. It is known that auxins play a vital role in division and expansion of plant cells.[26] Therefore, the down-regulated auxin-binding protein ABP19a indicated that NaCl and NaCl−AG treatment inhibited plant growth of germinating soybeans, which was fully explained by the reduced sprout length and the inhibited growth performance.

In developing soybean seeds, the expression profiles of SSP are of a complex nature.[27] It has been displayed that SSP may not only function as seed storage reserves but also have additional roles.[28] Under stress conditions, SSP is mobilized and its composition and abundance is changed.[12,25,29,30] In the present study, 62.5% of the differentially expressed proteins (spots C21−C65) in the NaCl-stressed germinating soybean cotyledons represented various kinds of SSPs, almost all of which were assigned to β-conglycinin subunits and glycinin. β-conglycinin and glycinin are the hydrolysis products of globulin and are mobilized to provide carbon and nitrogen for seed germination and growth. GABA-enriched germinating soybeans were germinated in a dark artificial environment, so organic compounds could not be synthesized via photosynthesis. These storage materials were the major source of nutrients for the soybeans. Under NaCl stress, the growth of germinating soybeans was inhibited resulting in soybeans being unable to use SSPs for growth, and therefore they showed higher SSP abundance. However, the expression profiles of different types of subunits of β-conglycinin and glycinin were inconsistent in response to NaCl stress and NaCl−AG treatment. It remains to be seen whether these SSP changes could improve NaCl stress tolerance in germinating soybeans. Furthermore, only two up-regulated SSPs (spots E29 and E30) were detected and identified as 31 kD glycoprotein in noncotyledons. The 31 kD glycoprotein has been proven to accumulate during cell development and serve as a source of amino acids for the developing embryo. The up-regulated glutamine synthetase PR-2 (spot E1), aminoaldehyde dehydrogenase (spot E5), glutamine synthetase precursor (spot E6), methionine synthase (spot E9), and GABA content in the present study might also support the idea that 31 kD glycoprotein can be assumed from the paralleled uptake of amino acids.[25] In conclusion, these results might further indicate an additional role in plant defense of SSPs besides storage reserves.

A group of proteins such as eukaryotic initiation factor 4A-15 (elF, spot E22), eukaryotic translation initiation factor 5A3 (spot E23), and elongation factor 2 (spot E24), associated with protein biosynthesis pathways, were up-regulated by NaCl stress. Studies confirm that eukaryotic translation initiation factors play a key role in the cell division and cell death processes.[31] The elF was up-regulated under NaCl stress and further enhanced under NaCl−AG treatment. This could be caused by endogenous PAs, which were involved in the posttranslation activation of elF and increased significantly after application of AG under NaCl stress. Studies also show that protein synthesis can be enhanced by exogenous PAs.[32] However, our results indicated that increased endogenous PAs had a consistent stimulatory effect on the incorporation of amino acids into protein. The regulated expression response patterns of the three proteins indicated that the promotion of protein biosynthesis was required for germinating soybeans to respond to stress.

It is generally known that soybean seeds contain plenty of allergenic proteins, and thus their extensive usage was limited in the food industry. Gly m Bd 30K proteins (spots C13, C15, and C16) represent a major allergen because more than 65% of soybean-sensitive patients are allergic to the protein, although its content is lower than 1% in soybean seeds.[33] In the present study, Bd 30K protein showed a less than 0.42-fold or even 0.08-fold difference ($P < 0.05$) in abundance in germinating soybean cotyledons under NaCl stress or AG treatment, compared with CK.

The comparative proteomic and physiological analyses indicated that the molecular mechanisms that contributed to tolerance in germinating soybeans were complex. Based on the results of this study, the following conclusions could be drawn: (i) soybean germination under certain stressful conditions would be an effective way to accumulate functional ingredients and to decrease allergens; (ii) most of the differentially expressed proteins in soybean cotyledons were SSPs, and redistribution of SSPs is likely to play an important role in defense; (iii) down-regulated GS and up-regulated MS were responsible for accumulation of GABA and coping with NaCl stress; (iv) enhanced energy metabolism and accelerated protein processing in endoplasmic reticulum were very important strategies for germinating soybean response to NaCl stress; (v) the inhibition of polyamine degradation might further aggravate the negative effects of NaCl stress on germinating soybeans.

■ ASSOCIATED CONTENT

Supporting Information

Changes in DAO activity, 2-DE pattern from non-cotyledon and cotyledon proteins, volume variations of differentially expressed proteins in non-cotyledon and cotyledon, proteins commonly responsive to stress in the non-cotyledon and cotyledon, and peak lists for proteins identified in the non-cotyledon and cotyledon. This material is available free of charge via the Internet at http://pubs.acs.org.

■ AUTHOR INFORMATION

Corresponding Author

*Tel/Fax: 86-25-84396293. E-mail: guzx@njau.edu.cn.

Funding

This project was supported by the Natural Science Foundation of China (Grant 31071581) and was funded by the Priority Academic Program Development of Jiangsu Higher Education Institutions (PAPD).

Notes

The authors declare no competing financial interest.

REFERENCES

(1) Lewis, B.; Sullivan, D. R.; Watts, G. F. Thought for food: Clinical evidence for the dietary prevention strategy in cardiovascular disease. *Int. J. Evidence-Based Healthcare* **2013**, *11* (4), 330−336.

(2) Hawkes, C.; Jewell, J.; Allen, K. A food policy package for healthy diets and the prevention of obesity and diet-related non-communicable diseases: The nourishing framework. *Obes. Rev.* **2013**, *14* (S2), 159−168.

(3) Randhir, R.; Shetty, P.; Shetty, K. L-DOPA and total phenolic stimulation in dark germinated fava bean in response to peptide and phytochemical elicitors. *Process Biochem.* **2002**, *37* (11), 1247−1256.

(4) Guo, Y.; Yang, R.; Chen, H.; Song, Y.; Gu, Z. Accumulation of γ-aminobutyric acid in germinated soybean (*Glycine max* L.) in relation to glutamate decarboxylase and diamine oxidase activity induced by additives under hypoxia. *Eur. Food Res. Technol.* **2012**, *234* (4), 679−687.

(5) Queiroz, H. M.; Sodek, L.; Haddad, C. R. B. Effect of salt on the growth and metabolism of *Glycine max*. *Braz. Arch. Biol. Technol.* **2012**, *55* (6), 809−817.

(6) Xing, S. G.; Jun, Y. B.; Hau, Z. W.; Liang, L. Y. Higher accumulation of gamma-aminobutyric acid induced by salt stress through stimulating the activity of diarnine oxidases in *Glycine max* (L.) Merr. roots. *Plant Physiol. Biochem.* **2007**, *45* (8), 560−566.

(7) Daniele, D. R.; Ana, R. M.; Spencer, J. P.; Tognolini, M.; Borges, G.; Crozier, A. Dietary (poly) phenolics in human health: structures, bioavailability, and evidence of protective effects against chronic diseases. *Antioxid. Redox Signaling* **2013**, *18* (14), 1818−1892.

(8) Shelp, B. J.; Bozzo, G. G.; Trobacher, C. P.; Zarei, A.; Deyman, K. L.; Brikis, C. J. Hypothesis/review: Contribution of putrescine to 4-aminobutyrate (GABA) production in response to abiotic stress. *Plant Sci.* **2012**, *193* (1), 130−135.

(9) Parida, A. K.; Das, A. B. Salt tolerance and salinity effects on plants: A review. *Ecotoxicol. Environ. Saf.* **2005**, *60* (3), 324−349.

(10) Nayyar, H.; Chander, S. Protective effects of polyamines against oxidative stress induced by water and cold stress in chickpea. *J. Agron. Crop Sci.* **2004**, *190* (5), 355−365.

(11) Yang, R.; Guo, Q.; Gu, Z. GABA shunt and polyamine degradation pathway on gamma-aminobutyric acid accumulation in germinating fava bean (*Vicia faba* L.) under hypoxia. *Food Chem.* **2013**, *136* (1), 152−159.

(12) Aghaei, K.; Ehsanpour, A.; Shah, A.; Komatsu, S. Proteome analysis of soybean hypocotyl and root under salt stress. *Amino Acids* **2009**, *36* (1), 91−98.

(13) Xu, X. Y.; Fan, R.; Zheng, R.; Li, C. M.; Yu, D. Y. Proteomic analysis of seed germination under salt stress in soybeans. *J. Zhejiang Univ. Sci. B* **2011**, *12* (7), 507−517.

(14) Komatsu, S.; Han, C.; Nanjo, Y.; Altaf-Un-Nahar, M.; Wang, K.; He, D.; Yang, P. Label-free quantitative proteomic analysis of abscisic acid effect in early-stage soybean under flooding. *J. Proteome Res.* **2013**, *12* (11), 4769−4784.

(15) Mohammadi, P. P.; Moieni, A.; Hiraga, S.; Komatsu, S. Organ-specific proteomic analysis of drought-stressed soybean seedlings. *J. Proteomics* **2012**, *75* (6), 1906−1923.

(16) Madhava Rao, K.; Sresty, T. Antioxidative parameters in the seedlings of pigeonpea (*Cajanus cajan* (L.) Millspaugh) in response to Zn and Ni stresses. *Plant Sci.* **2000**, *157* (1), 113−128.

(17) Natarajan, S.; Xu, C.; Caperna, T. J.; Garrett, W. M. Comparison of protein solubilization methods suitable for proteomic analysis of soybean seed proteins. *Anal. Biochem.* **2005**, *342* (2), 214−220.

(18) Bradford, M. M. A rapid and sensitive method for the quantitation of microgram quantities of protein utilizing the principle of protein-dye binding. *Anal. Biochem.* **1976**, *72* (1), 248−254.

(19) Hossain, Z.; Makino, T.; Komatsu, S. Proteomic study of β-aminobutyric acid-mediated cadmium stress alleviation in soybean. *J. Proteomics* **2012**, *75* (13), 4151−4164.

(20) Shevchenko, A.; Wilm, M.; Vorm, O.; Mann, M. Mass spectrometric sequencing of proteins from silver-stained polyacrylamide gels. *Anal. Chem.* **1996**, *68* (5), 850−858.

(21) Chinnusamy, V.; Jagendorf, A.; Zhu, J. K. Understanding and improving salt tolerance in plants. *Crop Sci.* **2005**, *45* (2), 437−448.

(22) Cheng, L.; Gao, X.; Li, S.; Shi, M.; Javeed, H.; Jing, X.; Yang, G.; He, G. Proteomic analysis of soybean [*Glycine max* (L.) Meer.] seeds during imbibition at chilling temperature. *Mol. Breeding* **2010**, *26* (1), 1−17.

(23) Chalker-Scott, L. Environmental significance of anthocyanins in plant stress responses. *Photochem. Photobiol.* **1999**, *70* (1), 1−9.

(24) Boerjan, W.; Ralph, J.; Baucher, M. Lignin biosynthesis. *Annu. Rev. Plant Biol.* **2003**, *54* (1), 519−546.

(25) Alam, I.; Sharmin, S. A.; Kim, K. H.; Kim, Y. G.; Lee, J. J.; Bahk, J. D.; Lee, B. H. Comparative proteomic approach to identify proteins involved in flooding combined with salinity stress in soybean. *Plant Soil* **2011**, *346* (1−2), 45−62.

(26) Kazan, K. Auxin and the integration of environmental signals into plant root development. *Ann. Bot. (London, U. K.)* **2013**, *112* (9), 1655−1665.

(27) Hajduch, M.; Ganapathy, A.; Stein, J. W.; Thelen, J. J. A systematic proteomic study of seed filling in soybean. Establishment of high-resolution two-dimensional reference maps, expression profiles, and an interactive proteome database. *Plant Physiol.* **2005**, *137* (4), 1397−1419.

(28) Sales, M. c. P.; Gerhardt, I. R.; Grossi-de-Sá, M. F.; Xavier-Filho, J. Do legume storage proteins play a role in defending seeds against bruchids? *Plant Physiol.* **2000**, *124* (2), 515−522.

(29) Rajjou, L.; Belghazi, M.; Huguet, R.; Robin, C.; Moreau, A.; Job, C.; Job, D. Proteomic investigation of the effect of salicylic acid on *Arabidopsis* seed germination and establishment of early defense mechanisms. *Plant Physiol.* **2006**, *141* (3), 910−923.

(30) Danchenko, M.; Skultety, L.; Rashydov, N. M.; Berezhna, V. V.; Mátel, L. u.; Salaj, T.; Pret'ová, A.; Hajduch, M. Proteomic analysis of mature soybean seeds from the Chernobyl area suggests plant adaptation to the contaminated environment. *J. Proteome Res.* **2009**, *8* (6), 2915−2922.

(31) Faurobert, M.; Mihr, C.; Bertin, N.; Pawlowski, T.; Negroni, L.; Sommerer, N.; Causse, M. Major proteome variations associated with cherry tomato pericarp development and ripening. *Plant Physiol.* **2007**, *143* (3), 1327−1346.

(32) Terui, Y.; Tabei, Y.; Akiyama, M.; Higashi, K.; Tomitori, H.; Yamamoto, K.; Ishihama, A.; Igarashi, K.; Kashiwagi, K. Ribosome modulation factor, an important protein for cell viability encoded by the polyamine modulon. *J. Biol. Chem.* **2010**, *285* (37), 28698−28707.

(33) Helm, R.; Cockrell, G.; Herman, E.; Burks, A.; Sampson, H. A.; Bannon, G. Cellular and molecular characterization of a major soybean allergen. *Int. Arch. Allergy Immunol.* **1998**, *117* (1), 29−37.

spectrometry (MS) have been established, facilitating our understanding of glycoconjugate structures.[19]

Electrospray ionization mass spectrometry (ESI-MS) is an ideal tool for structural characterization of various oligosaccharides, especially when coupled with ion trap instruments.[20] Ion trap mass spectrometry (IT-MS^n) allows selective fragmentation of target pseudoglycan ions and detailed elucidation of their sequence and branching and linkage types, but it is impractical for quantitative analysis of isomeric glycans. LC−MS and MS/MS, however, are available for glycan isomer separation and online identification. Hence, the LC−MS technique has been extensively employed as one of the most universal and successful methods for qualitative and quantitative glycan qualitation to date, although its resolving ability is not as powerful as that of MS^n in the analysis of complicated glycan isomer linkages.[21,22] Many researchers prefer online LC−ESI-MS, as it provides the possibility of peak integration, precise determination of retention times, and the principal ability to detect all types of glycans.[23−26]

Stable isotope reagents can be employed to assess rapidly and directly the qualitative and quantitative changes in different samples and to eliminate the variation in instrument response and ionization efficiency of the molecules with the same structures but from different resources. Accordingly, in comparative glycomic analysis, the stable isotopic labeling of glycans via reductive amination[27−29] or hydrazone formation[30] prior to HPLC separation and MS detection is usually involved. A glycan isotopic labeling approach using nondeuterated (d_0-) and deuterated (d_5-) aniline has been developed in our lab. This method is quite suitable for comparative glycomic analysis based on ultraviolet (UV) absorbance and relative ion abundance.[31]

In this article, ovotransferrin was purified from egg whites of chicken (domestic species) and pheasant (wild species), followed by composition profiling of their *N*-glycans released by PNGase F. Aniline stable isotopic labeling combined with ESI−MS analysis were utilized to compare quantitatively the *N*-glycan compositions of COT with those of POT. Online HILIC−MS and MS/MS were employed to identify *N*-glycan isomers and to quantify their relative abundance in COT and POT. This study is the first to reveal, comprehensively and in detail, the *N*-glycan patterns of COT and POT and to give a qualitative and quantitative comparison of COT and POT *N*-glycans.

MATERIALS AND METHODS

Materials. Chicken (*Gallus domesticus*) and pheasant (*Phasianus colchicus*) eggs were purchased from Luozhuang Farm (Xi'an, China). Molecular weight protein markers were purchased from Fermentas (Burlington, Canada). PNGase F was obtained from New England BioLabs (Ipswich, MA, USA). Nonporous graphitized carbon (Carbograph) solid-phase extraction (SPE) columns (150 mg/4 mL) were purchased from Alltech Associates (Deerfield, IL, USA). SepPak C18 SPE columns (100 mg/1 mL) were purchased from Waters (Milford, MA, USA). HPLC-grade methanol and acetonitrile were from Fisher Scientific (Fairlawn, NJ, USA). Other reagents used were of analytical grade.

Preparation of Ovotransferrin. On the basis of the work of Ko and Ahn,[32] the method of Fe^{3+} saturation and two-time ethanol precipitation was utilized to purify ovotransferrin from chicken and pheasant egg whites. Briefly, egg white was diluted with a 1-fold volume of distilled water, and then 2.5 mL of a 20 mM $FeCl_3 \cdot 6H_2O$ solution was added per 100 mL of diluted egg white solution to saturate the Fe^{3+}-bound sites. The obtained mixture was left standing for 1 h after homogenization. The majority of the egg white proteins were precipitated with 43% ethanol, leaving iron-bound ovotransferrin in the supernatant. Crude ovotransferrin was obtained when the ethanol concentration was increased to 59% (v/v). To obtain highly purified products, the crude was dissolved in 43% ethanol and treated again by an increase of the ethanol concentration to 59% (v/v). Finally, the highly purified ovotransferrin products were lyophilized for further use.

Identification of Ovotransferrin by Sodium Dodecyl Sulfate Polyacrylmide Gel Electrophoresis (SDS-PAGE). SDS-PAGE was performed according to the procedure developed by Laemmli,[33] using 4% acrylamide in stacking gels and 12% acrylamide in separating gels. Protein samples were dissolved in loading buffer (1% SDS, 40% glycerol, 0.1% dithiothreitol, and 0.05% bromophenol blue in 10 mM Tris-HCl buffer, pH 8.0) at the concentration of 2 mg/mL and then heated at 100 °C for 10 min. For a maximum visualization of egg white proteins, the amount of protein loaded was 10 μg for all samples. SDS-PAGE molecular weight standards ranging from of 3.4 to 250 kDa were used. Electrophoresis was carried out at 80 V in the stacking gel and 120 V in the separating gel using a Tris-Glycine electrophoretic buffer containing 0.1% SDS (pH 8.3). The gel was stained for 30 min with 1% Coomassie Blue R250 dissolved in a mixture containing 45% methanol, 45% water, and 10% acetic acid and destained with a mixture containing 87.5% water, 5% methanol, and 7.5% acetic acid. The gels were scanned using ImageQuant 350 (GE Healthcare, Milwaukee, WI, USA) and assessed by Gel-Pro Analyzer.

MALDI-TOF-MS Analysis. MALDI-TOF-MS was performed on an AXIMA Performance instrument (Shimadzu, Tokyo, Japan). The MS data acquisition was carried out in positive ion linear mode, using a nitrogen laser with the power level set at 98 and a matrix of 10 mg/mL α-cyano-4-hydroxy-cinnamic acid (CHCA) prepared in 50% acetonitrile containing 0.1% TFA. Two shots accumulated for each profile were acquired for each sample spot. Two milligrams of purified ovotransferrin was dissolved in 100 μL of deionized water, and 1 μL of the sample solution was mixed with 1 μL of matrix solution prior to spotting on a stainless steel target plate and drying at room temperature for analysis.

Release and Clean Up of *N*-Glycans from Ovotransferrin. Ovotransferrin (2 mg) was dissolved in 200 μL of protein denaturing solution (5% SDS, 0.4 M DTT) and denatured at 100 °C for 10 min. After the sample cooled, 20 μL of sodium phosphate buffer (0.5 M, pH 7.5), 20 μL of 10% NP-40, and 1 μL of PNGase F (500 units) were added prior to incubation at 37 °C for 24 h. The sample was boiled for 5 min to stop the reaction and then loaded onto a SepPak C18 SPE column. The released *N*-glycans were not retained on the column and eluted with 10 mL of water. The water fraction containing *N*-glycans was collected and desalted using a graphitized carbon SPE column. The salts were removed by washing with water, and the target *N*-glycans were eluted with 25% acetonitrile containing 0.01% TFA. The eluates were dried under a stream of nitrogen gas for further use.

Derivatization of *N*-Glycans with d_0-Aniline and d_5-Aniline. This procedure was based on a previously reported method.[31] Fifty microliters of d_0- or d_5-aniline, 50 μL of a 1 M $NaCNBH_3$ solution prepared in 30% acetic acid (v/v), and 50 μL of free *N*-glycan solution were mixed and sealed in a screw-capped tube, followed by incubation at 70 °C for 20 min. The resulting sample was purified using a graphitized carbon SPE column. After washing the column with 10−15 mL of distilled water, the target *N*-glycan derivatives were eluted with 30% acetonitrile, dried under a stream of nitrogen, and dissolved in 80% acetonitrile for chromatographic and MS analysis.

ESI−MS Conditions. MS analysis was carried out using an LTQ XL linear ion trap electrospray ionization mass spectrometer coupled with a HPLC system (Thermo Scientific, USA). The samples were injected via a Rheodyne loop with a volume of 2 μL and subsequently brought into the electrospray ion source by a stream of 50% methanol (v/v) at a flow rate of 200 μL/min. The spray voltage was set at 4 kV, with a sheath gas (nitrogen gas) flow rate of 30 arb., an auxiliary gas (nitrogen gas) flow rate of 5.0 arb., a capillary voltage of 37 V, a tube lens voltage of 250 V, and a capillary temperature of 375 °C. For MS/MS analysis, *N*-glycans were subjected to fragmentation by collision induced decomposition (CID), with helium (He) as the collision gas.

Collision parameters were left at default values with a normalized collision energy degree of 60 and an isotope width of m/z 3.00. Activation Q was set at 0.25, and activation time, at 30 ms. The MS and MS/MS data were recorded using LTQ Tune software (Thermo).

Online LC−MS Analysis. Online LC−MS analysis was performed using a Hypersil APS2 (NH_2) column (2.1 mm × 150 mm, 3 μm) (Thermo scientific, USA) on an HPLC system (Thermo) equipped with a photo diode array (PDA) detector and an LTQ XL linear ion trap ESI-MS system. The sample injection volume was 10 μL, and the mobile phase flow rate was 200 μL/min. The elution gradient was as follows: solvent A, acetonitrile; solvent B, water; solvent C, 10 mM ammonium acetate (pH 4.5); time = 0 min (t = 0), 80% A, 16% B, 4% C; t = 45, 27.5% A, 34% B, 38.5% C. The eluates from the chromatographic separation were directly introduced into the ESI-MS system for detection. The MS and MS/MS data were recorded using Xcalibur software (Thermo). The parameters used for LC−MS/MS analysis were the same as those described for ESI−MS/MS analysis in the above section. The obtained date were manually interpreted, and the proposed *N*-glycan compositions and sequences were checked using the software GlycoWorkbench.[34]

RESULTS AND DISCUSSION

Purification and Identification of Ovotransferrin. Highly purified glycoprotein is essential for glycomic analysis.

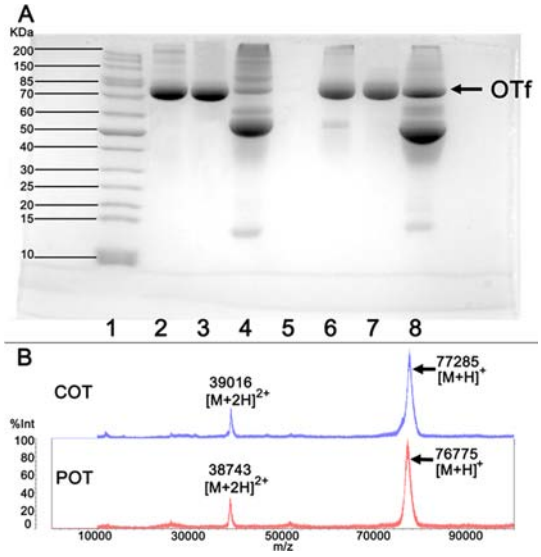

Figure 1. Profiling ovotransferrin (OTf) by SDS-PAGE and MALDI-TOF MS. (A) SDS-PAGE pattern. Lane 1: standard marker; lane 2: COT obtained after the first ethanol precipitation process; lane 3: COT obtained after the second ethanol precipitation process; lane 4: total protein of chicken egg white; lane 5: blank; lane 6: POT obtained after the first ethanol precipitation process; lane 7: POT prepared with a second ethanol precipitation; lane 8: total protein of pheasant egg white. (B) MALDI-TOF MS profiles of highly purified COT (blue mass spectrum) and POT (red mass spectrum).

However, some commercially available samples of egg white proteins such as ovotransferrin and ovalbumin are usually copurified with some other proteins, resulting in difficulties for precisely analyzing their glycosylation.[10,35,36] Thus, to compare the *N*-glycan patterns of COT and POT, a method for the efficient isolation of highly purified ovotransferrin from chicken and pheasant egg whites is needed. The ethanol method for ovotransferrin purification is simple in its operation and produces a high yield. Hence, in this article, we developed a method termed ethanol repeated precipitation to obtain highly purified ovotransferrin. Because iron-saturated ovotransferrin is more stable to chemicals such as ethanol than its iron-free form, the iron-free ovotransferrin in an egg white solution was converted to the iron-bound form by treatment with $FeCl_3$ solution. Almost all egg white proteins except for iron-bound ovotransferrin were denatured and precipitated in 43% ethanol. Iron-saturated ovotransferrin in the 43% ethanol solution started to precipitate as the ethanol concentration increased from 43%, and the optimal conditions for precipitating ovotransferrin occurred when the ethanol concentration reached 59%.[30] Therefore, using 43% ethanol to remove other egg white proteins and 59% ethanol to precipitate ovotransferrin, we obtained COT (lane 2 of Figure 1A) and POT (lane 6 of Figure 1A) with minor impurities. To obtain ovotransferrin that is pure enough for glycosylation analysis, the ethanol (increasing ethanol concentration from 43 to 59%) precipitation process was performed again using the crude COT and POT. As a result, a high purity of COT (lane 3 of Figure 1A) and POT (lane 7 of Figure 1A) was achieved. MALDI-TOF MS (Figure 1B) gave ion signals of COT at m/z 39 016 ($[M + 2H]^{2+}$) and m/z 77 285 ($[M + H]^+$) (blue mass spectrum in Figure 1B) and POT at m/z 38 743 ($[M + 2H]^{2+}$) and m/z 76 775 ($[M + H]^+$) (red mass spectrum in Figure 1B), indicating that the molecular weights of COT and POT are around 77 284 and 78 774 Da, respectively. These results are consistent with those of SDS-PAGE analysis as well as previous literature reports.[37−39]

Moreover, the results from the Gel-Pro Analyzer concerning the SDS-PAGE experiment suggested that the purities of COT and POT were both over 95%. Therefore, this approach proved to be an efficient and simple method for the purification of ovotransferrin. Considering that the variation between species-specific ovotransferrin proteins is related only to the attached glycan moieties,[14] the difference in molecular weights between COT and POT may validate this fact to a certain extent as well as facilitate an understanding of the following comparative glycomic analysis of COT and POT.

Composition Profiling of COT and POT *N*-Glycans. The *N*-glycan structures of COT have been investigated to a certain degree in previous reports.[15−18] However, there is no *N*-glycomic information on POT up to now. In this work, *N*-glycan compositions of COT and POT were analyzed by ESI−MS, where sodiated ions were predominantly produced. Figure 2 presents the MS profiles of the *N*-glycan compositions of COT (Figure 2A) and POT (Figure 2B). The double-sodiated COT glycan ions ($[M + 2Na]^{2+}$) at m/z 782.73 ($Man_3GlcNAc_5$), 884.27 ($Man_3GlcNAc_6$), and 1087.27 ($Man_3GlcNAc_7$) and POT ion of m/z 782.73 ($Man_3GlcNAc_5$) were not annotated here because the corresponding singly charged ions ($[M + Na]^+$) of these glycans were all observed. In total, 12 COT *N*-glycan compositions were observed as the $[M + Na]^+$ type ions at m/z 933.27 ($Man_3GlcNAc_2$), 1136.27 ($Man_3GlcNAc_3$), 1298.27 ($Hex_1Man_3GlcNAc_3$), 1339.27 ($Man_3GlcNAc_4$), 1501.18 ($Hex_1Man_3GlcNAc_4$), 1542.27 ($Man_3GlcNAc_5$), 1663.09 ($Hex_2Man_3GlcNAc_4$), 1704.27 ($Hex_1Man_3GlcNAc_5$), 1745.27 ($Man_3GlcNAc_6$), 1907.27 ($Hex_1Man_3GlcNAc_6$), 1948.09 ($Man_3GlcNAc_7$), and 2151.18 ($Man_3GlcNAc_8$). In contrast, 15 *N*-glycan compositions were found as $[M + Na]^+$ type ions at m/z 771.27 ($Man_2GlcNAc_2$), 933.27 ($Man_3GlcNAc_2$), 1095.27 ($Man_4GlcNAc_2$), 1136.27 ($Man_3GlcNAc_3$), 1257.27 ($Man_5GlcNAc_2$), 1298.27 ($Hex_1Man_3GlcNAc_3$), 1339.27 ($Man_3GlcNAc_4$), 1460.09 ($Man_5GlcNAc_3$), 1501.18 ($Hex_1Man_3GlcNAc_4$), 1542.27 ($Man_3GlcNAc_5$), 1663.09 ($Hex_2Man_3GlcNAc_4$), 1704.27

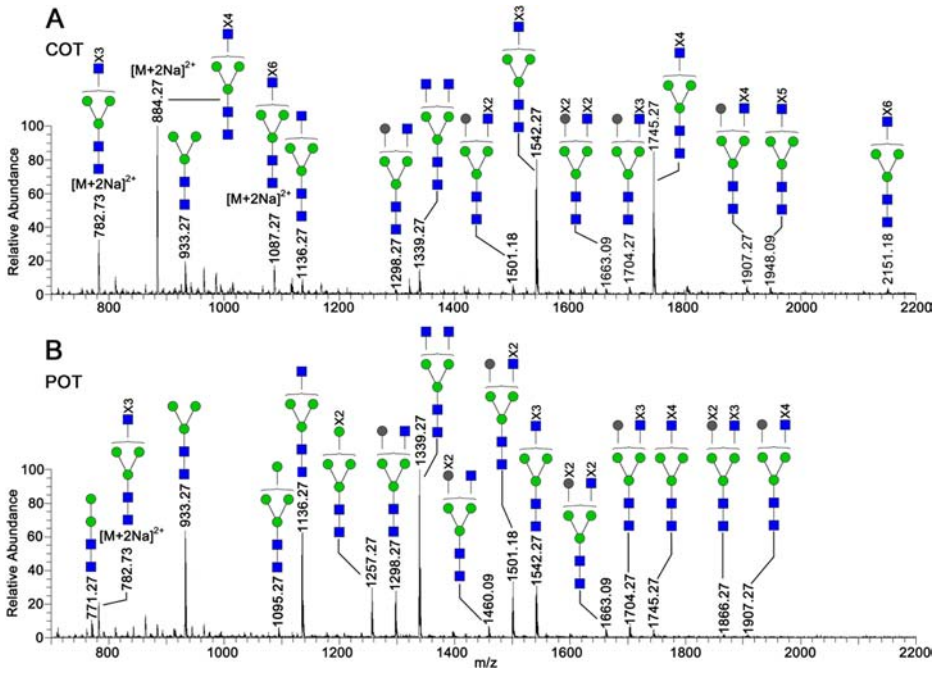

Figure 2. ESI−MS profiles of the *N*-glycans released from (A) COT and (B) POT. Sodiated ions are predominately produced. Putative glycan compositions are presented on the basis of the MS/MS analysis. Structural formulas: blue square, *N*-acetylglucosamine; green circle, mannose; gray circle, hexose.

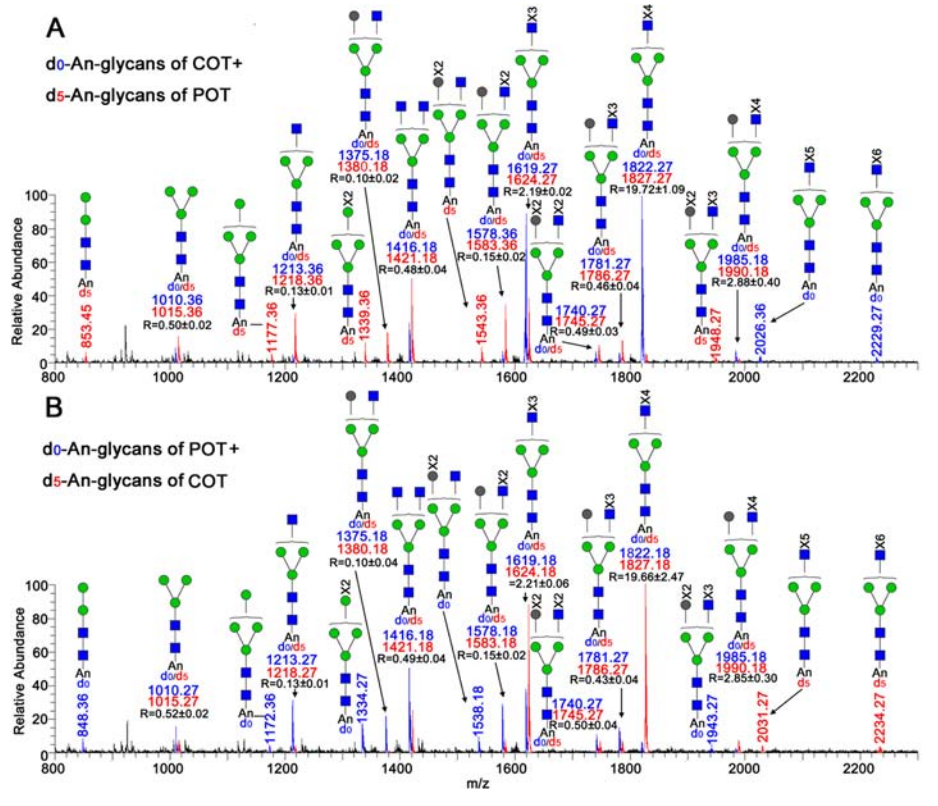

Figure 3. Quantitative comparison of COT and POT *N*-glycan compositions based on stable isotopic labeling using d_0- and d_5-aniline. (A) ESI−MS profile of an equimolar mixture of d_0-aniline derivatives of COT *N*-glycans (d_0-An-COT *N*-glycans) and d_5-aniline derivatives of POT *N*-glycans (d_5-An-POT *N*-glycans). (B) ESI−MS profile of an equimolar mixture of d_0-aniline derivatives of POT *N*-glycans (d_0-An-POT *N*-glycans) and d_5-aniline derivatives of COT *N*-glycans (d_5-An-COT *N*-glycans). The blue and red peaks are the signals of d_0-aniline and d_5-aniline derivatives, respectively. The intensity ratio between the d_0-aniline derivative of each glycan and its corresponding d_5-aniline derivative is shown as R, which consists of the mean value and standard deviation obtained from three repeated experiments. Sodiated ions are predominately produced. Structural formulas: blue square, *N*-acetylglucosamine; green circle, mannose; gray circle, hexose.

dx.doi.org/10.1021/jf501352j | J. Agric. Food Chem. 2014, 62, 7245−7254

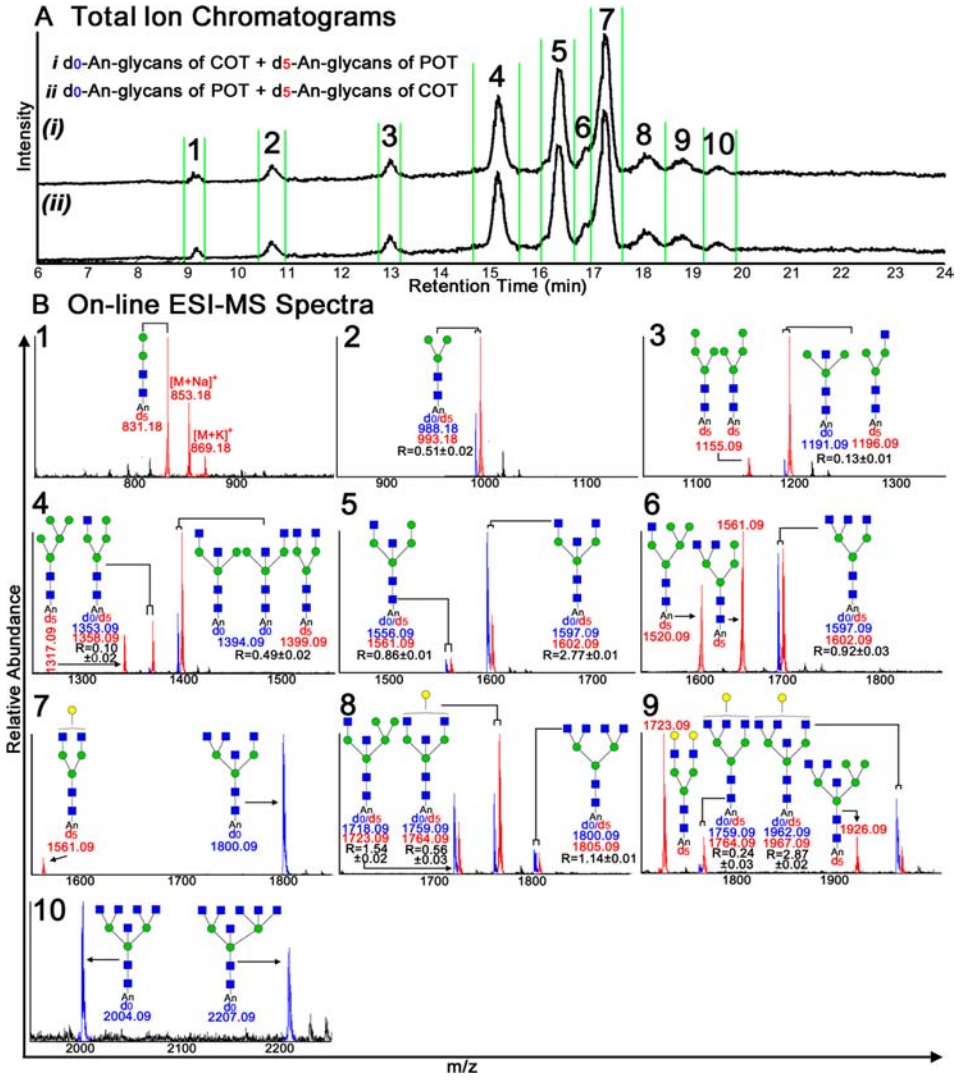

Figure 4. Qualitative and quantitative comparison of the COT and POT *N*-glycan isomers derivatized with d_0- or d_5-aniline via online HILIC−MS. (A) Total ion chromatograms (TICs) showing the elution profiles of (i) the equimolar mixture of d_0-An-COT *N*-glycans and d_5-An-POT *N*-glycans and (ii) the equimolar mixture of d_0-An-POT *N*-glycans and d_5-An-COT *N*-glycans. (B) Online MS spectra of an equimolar mixture of d_0-An-COT *N*-glycans and d_5-An-POT *N*-glycans. The blue and red ion peaks are the signals of d_0- and d_5-aniline derivatives, respectively. The intensity ratio of the d_0-aniline derivative of each glycan to its corresponding d_5-aniline derivative is shown as R, which consists of the mean value and standard deviation obtained from three repeated experiments. Protonated ions are predominately produced. Structural formulas: blue square, *N*-acetylglucosamine; green circle, mannose; yellow circle, galactose.

($Hex_1Man_3GlcNAc_5$), 1745.27 ($Man_3GlcNAc_6$), 1866.27 ($Hex_2Man_3GlcNAc_5$), and 1907.27 ($Hex_1Man_3GlcNAc_6$). Obviously, 10 of these *N*-glycans, at *m*/*z* 993.27, 1136.37, 1298.27, 1339.27, 1501.27, 1542.27, 1663.27, 1704.27, 1745.27, and 1907.27, exist in both COT and POT. All of these *N*-glycan compositions were identified via MS/MS (Supporting Information, Figures S1 and S2) and are supported by the literature.[18]

These results revealed that all of the *N*-glycans of COT and POT are neutral oligosaccharides and that no acidic oligosaccharide or fucosylated oligosaccharide was found in either sample. The *N*-glycan of $Hex_2Man_3GlcNAc_4$ corresponding to *m*/*z* 1663.27 was newly found in COT; however, the COT *N*-glycans including $Man_2GlcNAc_2$, $Man_1GlcNAc_3$, and $Hex_2Man_3GlcNAc_5$ reported in previous work[18] were not detected in our study, which may originate from other chicken egg white glycoproteins mixed in commercially obtained COT. Additionally, we are the first to demonstrate the *N*-glycan composition profile of ovotransferrin derived from wild bird species.

Quantitative Comparison of *N*-Glycan Compositions between COT and POT. For quantitative comparison of the *N*-glycan compositions between COT and POT, two aliquots of *N*-glycans released from COT or POT were separately derivatized with d_0- and d_5-aniline. The equimolar mixture of d_0-aniline-derivatized *N*-glycans of COT (d_0-An-glycans of COT) and d_5-aniline-derivatized *N*-glycans of POT (d_5-An-glycans of POT), as well as the equimolar mixture of d_0-aniline-derivatized *N*-glycans of POT (d_0-An-glycans of POT) and d_5-aniline-derivatized *N*-glycans of COT (d_5-An-glycans of COT), were analyzed by ESI−MS, and the compositions of these glycan derivatives were identified by MS/MS (Supporting Information, Figures S1 and S2).

As shown in Figure 3A, the equal-ratio mixture of d_0-An-glycans of COT and d_5-An-glycans of POT exhibits 12 peaks of d_0-An-glycans of COT and 15 peaks of d_5-An-glycans of POT

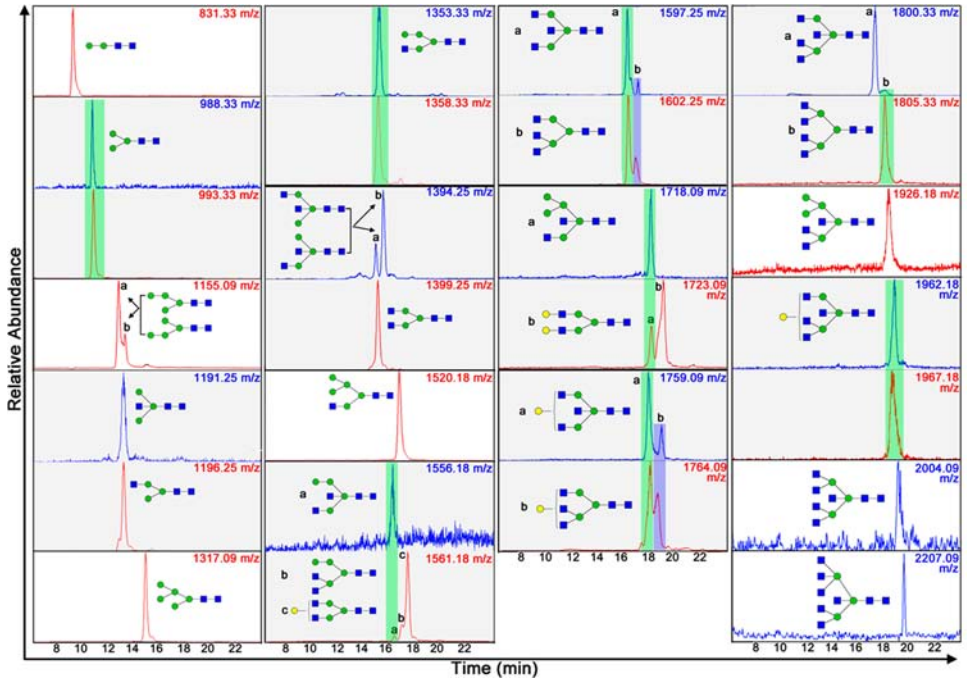

Figure 5. Extracted ion chromatograms (EICs) of d_0-aniline derivatives of COT *N*-glycans (d_0-An-COT *N*-glycans) and d_5-aniline derivatives of POT *N*-glycans (d_5-An-POT *N*-glycans). The blue and red chromatograms represent the EICs of d_0- and d_5-aniline derivatives, respectively. The EICs that share the same glycan compositions were covered with gray shadow. The paired blue (d_0-An-COT *N*-glycan) and red (d_5-An-POT *N*-glycan) EIC peaks that share the same glycan sequences were simultaneously covered with green or blue shadow. Structural formulas: blue square, *N*-acetylglucosamine; green circle, mannose; yellow circle, galactose.

in the ESI−MS profile, giving results that are consistent with those of the *N*-glycan composition profiling. All of those signals are assigned as $[M + Na]^+$ type ions, and their corresponding compositions are all displayed in the figure. In total, 10 pairs of peaks (m/z 1010.36/1015.36, 1213.36/1218.36, 1375.27/1380.27, 1416.18/1421.18, 1578.36/1583.36, 1619.27/1624.27, 1740.27/1745.27, 1781.27/1786.27, 1822.27/1827.27, and 1985.27/1990.27) and seven single peaks (m/z 853.45, 1177.36, 1339.36, 1543.36, and 1948.27 of d_5-aniline derivatives and m/z 2026.36 and 2229.27 of d_0-aniline derivatives) were clearly observed. The peak pairs indicate the coexistence of the corresponding *N*-glycans in both COT and POT, and the MS signal intensity ratio of d_0- to d_5-aniline derivatives of each glycan represents its abundance ratio, namely, the molar ratio between COT and POT. Meanwhile, the single peaks of the d_0- or d_5-aniline derivative indicates the existence of the corresponding *N*-glycans only in COT or POT, respectively. Clearly, 10 *N*-glycans exist in both COT and POT, of which $Man_3GlcNAc_2$, $Man_3GlcNAc_3$, $Hex_1Man_3GlcNAc_3$, $Man_3GlcNAc_4$, $Hex_1Man_3GlcNAc_4$, $Hex_2Man_3GlcNAc_4$, and $Hex_1Man_3GlcNAc_5$ are less abundant (by 0.51, 0.13, 0.10, 0.49, 0.15, 0.50, and 0.46 times, respectively) in COT than in POT, whereas $Man_3GlcNAc_5$, $Man_3GlcNAc_6$, and $Hex_1Man_3GlcNAc_6$ are more abundant (by 2.19, 19.69, and 2.87 times, respectively) in COT than in POT. Figure 3B shows the MS profile of the equal-ratio mixture of d_0-An-glycans of POT and d_5-An-glycans of COT. The results are well-consistent with the results of Figure 3A, confirming the correctness and excellent reproducibility of these results. Therefore, we conclude that the *N*-glycans of POT and COT exhibit conspicuous differences in both composition and abundance, although the two glycoproteins are encoded by identical genes and have the same amino acid sequence. Additionally, although POT possesses more *N*-glycan compositions than COT (15 vs 12), as Figure 3 demonstrates, the average size of oligosaccharides from COT is larger than the oligosaccharides from POT, consistent with the MALDI-TOF-MS analysis result (Figure 1) that demonstrated that the molecular weight of COT (77285 Da) is higher than that of POT (76774 Da).

Qualitative and Quantitative Comparison of COT and POT *N*-Glycan Isomers. Isomers exist extensively within the glycans released from glycoprotein. ESI−MS analysis of a mixture of glycans provides a rapid composition profile but gives little information regarding the isomers. HILIC affords a suitable means for the separation of aniline-labeled *N*-glycan isomers, and online MS/MS allows extensive fragmentation of separated glycan isomers, which provides rich information for differentiation and sequencing of diverse glycan isomers.[29] For the quantitative comparison of *N*-glycan isomers between COT and POT, an equimolar mixture of d_0-An-glycans of COT and d_5-An-glycans of POT and an equimolar mixture of d_0-An-glycans of POT and d_5-An-glycans of COT were separately analyzed by online HILIC−MS and online HILIC−MS/MS (Supporting Information, Figure S2).

The total ion chromatograms (TICs) (Figure 4A) of the two equal-ratio sample mixtures show parallel elution profiles, which exhibit of the derivatives of specific *N*-glycans. The equimolar mixture of d_0-An-glycans of COT and d_5-An-glycans of POT was selected as the example for quantitative comparison analysis. Figure 4B shows the online MS spectra corresponding to the major peaks of the TIC of the equimolar mixture of d_0-An-COT *N*-glycans and d_5-An-POT *N*-glycans. The isomeric sequences of the *N*-glycan derivatives presented in the spectra were proposed on the basis of the data in the extracted ion chromatogram (EIC) (Figure 5) and HILIC−

Table 1. Comprehensive List of COT and POT *N*-Glycans Detailing Monosaccharide Compositions, Proposed Structures, Glycan Types, Relative Quantity (%), and Abundance Ratios Found in Both COT and POT *N*-Glycan Compositions and Isomers

monosaccharide composition[a]	proposed structure	glycan type	relative quantity (%) (Mean) (n=6)		abundance ratio[b] (COT to POT) (Mean ± SD) (n=3)	
			COT	POT	isomer	composition
H2N2		truncated		1.88	-	-
H3N2		core	3.18	6.26	0.51 ± 0.02	0.51 ± 0.02
H4N2		high mannose	-	1.2	-	-
		high mannose	-		-	-
H3N3		complex	1.59	-	-	0.13 ± 0.01
		complex	-	12.24	-	
H5N2		high mannose	-	4.00	-	-
H4N3		hybrid	0.76	7.61	0.10 ± 0.03	0.10 ± 0.03
H3N4	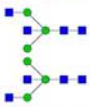	complex	8.40	-	-	0.49 ± 0.05
		complex		-	-	
		complex	-	17.14	-	
H5N3		hybrid	-	1.90	-	-
H4N4	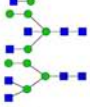	hybrid	2.30	2.67	0.86 ± 0.01	0.15 ± 0.02
		hybrid	-	4.23	-	
		complex	-	11.20	-	
H3N5	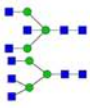	complex	30.54	11.02	2.77 ± 0.01	2.19 ± 0.02
		complex	4.67	5.07	0.92 ± 0.03	
H5N4		hybrid	2.36	1.53	1.54 ± 0.02	0.50 ± 0.03
		complex	-	3.19	-	
H4N5	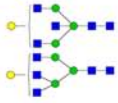	complex	1.83	3.27	0.56 ± 0.03	0.46 ± 0.04
		complex	0.37	1.54	0.24 ± 0.03	
H3N6		complex	36.97	-	-	19.69 ± 1.09
		complex	2.27	1.99	1.14 ± 0.01	
H5N5		hybrid	-	1.22	-	-
H4N6	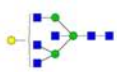	complex	2.46	0.86	2.87 ± 0.40	2.87 ± 0.40
H3N7		complex	1.29	-	-	-
H3N8		complex	1.01	-	-	-

[a]H, hexose; N, *N*-acetylhexosamine. [b]Structural formulas: blue square, *N*-acetylglucosamine; green circle, mannose; yellow circle, galactose. SD, standard deviation.

dx.doi.org/10.1021/jf501352j | *J. Agric. Food Chem.* 2014, 62, 7245−7254

Table 2. Comparison of General Features in Glycosylation between COT and POT

comparison features		COT	POT
total *N*-glycans		16	21
truncated		0	1
core		1	1
high mannose		0	3
hybrid		3	6
complex		12	10
	antennary		
	mono-	1	1
	bi-	2	5
	tri-	4	3
	tetra-	2	1
	penta-	1	0

MS/MS (Suppporting Information, Figure S3). Protonated ions are predominately produced, and very few sodiated and potassiated ions are observed in the mass spectra. Twelve pairs of peaks (*m*/*z* 988.18/993.18, 1191.09/1196.09, 1353.09/1358.09, 1394.09/1399.09, 1556.09/1561.09, 1597.09/1602.09, 1597.09/1602.09, 1718.09/1723.09, 1759.09/1764.09, 1800.09/1805.09, 1759.09/1764.09, and 1962.09/1967.09) were clearly observed. The abundance ratios of the paired d_0-An-COT derivatives and d_5-An-POT derivatives at *m*/*z* 988.18/993.18, 1191.09/1196.09, 1353.09/1358.09, and 1962.09/1967.09 (by 0.51, 0.13, 0.10, and 2.87 times, respectively) are consistent with the results of the glycan composition comparison, and EICs (Figure 5) indicate that there is no isomer for these glycan compositions. Meanwhile, due to the existence of glycan isomers, several pairs of peaks give new molar ratios when compared with those obtained through the above-described *N*-glycan composition comparison analysis. Here, seven pairs of d_0-aniline derivatives and d_5-aniline derivatives at *m*/*z* 1556.09/1561.09, 1597.09/1602.09, 1597.09/1602.09, 1718.09/1723.09, 1759.09/1764.09, 1800.09/1805.09, and 1759.09/1764.09 give corresponding molar ratios of 0.86, 2.22, 0.28, 1.54, 0.56, 1.14, and 0.24, respectively, and each pair of peaks shares the same *N*-glycan sequence. Nevertheless, the pair of peaks at *m*/*z* 1353.09/1358.09 is an exception, as it shares the same composition but different glycan sequences. The molar ratio between the two peaks is 0.49, consistent with the ratio shown in Figure 3. The singly occurring *N*-glycan derivatives from COT or POT were also annotated in the spectra. Some of these *N*-glycans are the isomers of paired *N*-glycans, whereas the others that exist in either COT or POT have no corresponding isomeric structures in POT or COT. The results of HILIC−MS analysis are highly consistent with the data presented in Figure 3.

On the basis of ESI−MS and online HILIC−MS analysis, comprehensive analytical information on COT and POT *N*-glycans is summarized in Table 1, including monosaccharide compositions, proposed structures, glycan types, relative quantity (%) and abundance ratios of *N*-glycan compositions, and isomers found in both COT and POT. In total, 16 *N*-glycans of COT and 21 *N*-glycans of POT were found when glycan isomers were taken into account. Ten of these glycan structures exist in both COT and POT. Additionally, there is no acidic or fucosylated glycans observed in either COT or POT. The COT *N*-glycans with compositions of $Man_3GlcNAc_4$, $Man_3GlcNAc_5$, $Gal_1Man_3GlcNAc_5$, and $Man_3GlcNAc_5$ and POT *N*-glycans with compositions of $Man_4GlcNAc_2$, $Man_3GlcNAc_5$, $Hex_2Man_3GlcNAc_4$, and $Gal_1Man_3GlcNAc_5$ each have two isomers, and the COT *N*-glycan composition of $Hex_1Man_3GlcNAc_4$ has three isomers. The other *N*-glycan compositions have only single structures. As summarized in Table 2 and Figure 6, for COT *N*-glycans, 1 core structure (3.18%), 12 complex type (91.4%), 3 hybrid type (5.42%), and no high mannose type glycan were observed. In contrast, for POT *N*-glycan types, 1 core structure (6.26%), 3 high mannose type (5.20%), 10 complex type (67.52%), 6 hybrid type (19.14%), and 1 truncated structure (1.88%) ($Man_2GlcNAc_2$) were observed. COT contains five types of antennary complex-type structures described as follows: monoantennary (8.4%), biantennary (32.37%), triantennary (44.47%), tetra-antennary (3.56%), and penta-antennary (1.10%). However, POT contains four types of antennary structure including monoantennary (12.24%), biantennary (45.82%), triantennary (7.74%), and tetra-antennary (1.19%); no penta-antennary type structure was observed.

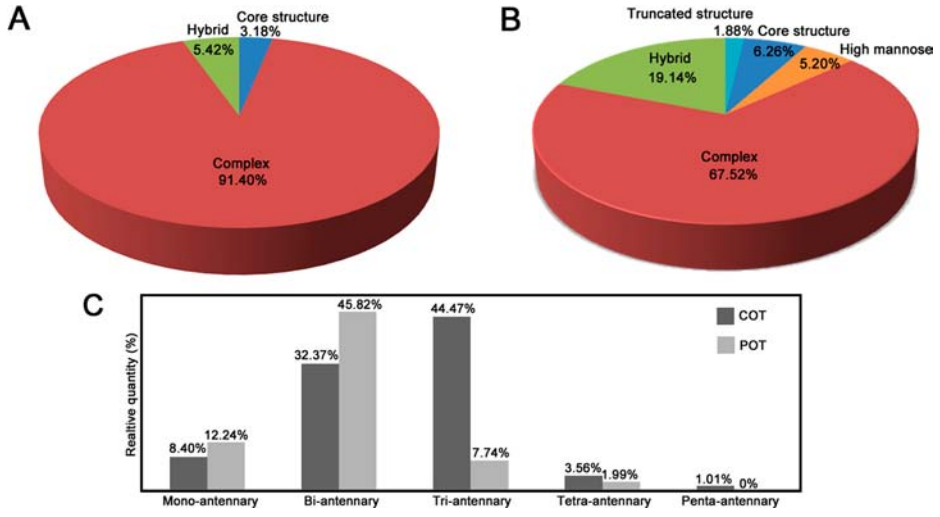

Figure 6. Charts showing the relative quantities of all *N*-glycan types in COT (A) and POT (B) as well as branched patterns of complex type *N*-glycans from COT and POT (C).

dx.doi.org/10.1021/jf501352j | J. Agric. Food Chem. 2014, 62, 7245−7254

This study, to our knowledge, is the first work that comparatively details COT and POT *N*-glycans, especially using qualitative and quantitative analysis of their *N*-glycan isomers through the combination of glycan isotopic aniline labeling, ESI−MS, HILIC−MS, and MS/MS. As the only variable component, attached *N*-glycans contribute to the primary structural differences between COT and POT and may influence the bioactivity of the two glycoproteins. This study provides a foundation for the further elucidation of the specific biofunctions of COT and POT, thereby stimulating, perhaps, their application in the food industry as a novel nutraceutical and functional food ingredient in the future.

■ ASSOCIATED CONTENT

Supporting Information

Figures S1 and S2: ESI-MS/MS spectra for the ions of all free *N*-glycan compositions, d_0-aniline derivatized *N*-glycan compositions, and d_5-aniline derivatized *N*-glycan compositions from COT and POT. Figure S3: Online MS/MS spectra for all d_0- and d_5-aniline derivatives of the glycans from COT or POT. This material is available free of charge via the Internet at http://pubs.acs.org.

■ AUTHOR INFORMATION

Corresponding Authors

*(L.H.) E-mail: huanglj@nwu.edu.cn.

*(Z.W.) E-mail: wangzhf@nwu.edu.cn; Tel.: +86-029-88305853; Fax: +86-029-88303534.

Funding

This work was funded by the National Natural Science Foundation of China (nos. 31170773, 21375103, and 31370804).

Notes

The authors declare no competing financial interest.

■ ABBREVIATIONS USED

COT, chicken ovotransferrin; POT, pheasant ovotransferrin; ESI-MS, electrospray ionization-mass spectrometry; PNGase F, peptide *N*-glycosidase F; UV, ultraviolet; HILIC, hydrophilic interaction liquid chromatography; MS/MS, tandem mass spectrometry; MALDI-TOF, matrix-assisted laser desorption/ionization-time-of-flight; DTT, dithiothreitol; SPE, solid-phase extraction; CID, collision induced decomposition; Hex, hexose; GlcNAc, *N*-acetylglucosamine; Man, mannose; Gal, galactose; Glc, glucose; An, aniline; TIC, total ion chromatogram; EIC, extracted ion chromatograms

■ REFERENCES

(1) Wu, J.; Acero-Lopez, A. Ovotransferrin: structure, bioactivities, and preparation. *Food Res. Int.* **2012**, *46*, 480−487.

(2) *Bioactive Egg Compounds*, 1st ed.; Huopalahti, R.; López-Fandiño, R.; Anton, M.; Schade, R., Eds.; Springer-Verlag: Berlin, Germany, 2007; Vol. *1*, pp 191−293.

(3) Lock, J.; Board, R. Persistence of contamination of hens' egg albumen in vitro with *Salmonella* serotypes. *Epidemiol. Infect.* **1992**, *108*, 389−396.

(4) Valenti, P.; Visca, P.; Antonini, G.; Orsi, N. Antifungal activity of ovotransferrin towards genus *Candida*. *Mycopathologia* **1985**, *89*, 169−175.

(5) Giansanti, F.; Massucci, M. T.; Giardi, M. F.; Nozza, F.; Pulsinelli, E.; Nicolini, C.; Botti, D.; Antonini, G. Antiviral activity of ovotransferrin derived peptides. *Biochem. Biophys. Res. Commun.* **2005**, *331*, 69−73.

(6) Ibrahim, H. R.; Kiyono, T. Novel anticancer activity of the autocleaved ovotransferrin against human colon and breast cancer cells. *J. Agric. Food Chem.* **2009**, *57*, 11383−11390.

(7) Giansanti, F.; Giardi, M. F.; Massucci, M. T.; Botti, D.; Antonini, G. Ovotransferrin expression and release by chicken cell lines infected with Marek's disease virus. *Biochem. Cell Biol.* **2007**, *85*, 150−155.

(8) Del Giacco, G.; Leone, A.; Ferlazzo, A. Total IgE in newborns treated prophylactically with conalbumin. *Int. J. Tissue React.* **1984**, *7*, 535−537.

(9) Huang, W.; Shen, S.; Nimalaratne, C.; Li, S.; Majumder, K.; Wu, J. Effects of addition of egg ovotransferrin-derived peptides on the oxygen radical absorbance capacity of different teas. *Food Chem.* **2012**, *135*, 1600−1607.

(10) Miguel, M.; Manso, M. A.; López-Fandiño, R.; Ramos, M. Comparative study of egg white proteins from different species by chromatographic and electrophoretic methods. *Eur. Food Res. Technol.* **2005**, *221*, 542−546.

(11) Balzarini, J. Inhibition of HIV entry by carbohydrate-binding proteins. *Antiviral Res.* **2006**, *71*, 237−247.

(12) Deepak, A.; Thippeswamy, G.; Shivakameshwari, M.; Salimath, B. P. Isolation and characterization of a 29-kDa glycoprotein with antifungal activity from bulbs of *Urginea indica*. *Biochem. Biophys. Res. Commun.* **2003**, *311*, 735−742.

(13) Bulet, P.; Hegy, G.; Lambert, J.; Van Dorsselaer, A.; Hoffmann, J. A.; Hetru, C. Insect immunity. The inducible antibacterial peptide diptericin carries two *O*-glycans necessary for biological activity. *Biochemistry* **1995**, *34*, 7394−7400.

(14) Jacquinot, P.-M.; Leger, D.; Wieruszeski, J.-M.; Coddeville, B.; Montreuil, J.; Spik, G. Change in glycosylation of chicken transferrin glycans biosynthesized during embryogenesis and primary culture of embryo hepatocytes. *Glycobiology* **1994**, *4*, 617−624.

(15) Williams, J. A comparison of glycopeptides from the ovotransferrin and serum transferrin of the hen. *Biochem. J.* **1989**, *108*, 57−67.

(16) Iwase, H.; Hotta, K. Ovotransferrin subfractionation dependent upon carbohydrate chain differences. *J. Biol. Chem.* **1977**, *252*, 5437−5443.

(17) Dorland, L.; Haverkamp, J.; Vliegenthart, J. F.; Spik, G.; Fournat, B.; Montereuil, J. Investigation by 360-MHz^1 H-nuclear-magnetic-resonance spectroscopy and methylation analysis of the single glycan chain of chicken ovotransferrin. *Eur. J. Biochem.* **1979**, *100*, 569−574.

(18) Hwang, H. S.; Kim, B. S.; Park, H.; Park, H.-Y.; Choi, H.-D.; Kim, H. H. Type and branched pattern of *N*-glycans and their structural effect on the chicken egg allergen ovotransferrin: a comparison with ovomucoid. *Glycoconjugate J.* **2014**, *31*, 41−50.

(19) Geyer, H.; Geyer, R. Strategies for analysis of glycoprotein glycosylation. *Biochim. Biophys. Acta, Proteins Proteomics* **2006**, *1764*, 1853−1869.

(20) Ashline, D. J.; Lapadula, A. J.; Liu, Y.-H.; Lin, M.; Grace, M.; Pramanik, B.; Reinhold, V. N. Carbohydrate structural isomers analyzed by sequential mass spectrometry. *Anal. Chem.* **2007**, *79*, 3830−3842.

(21) Pabst, M.; Bondili, J. S.; Stadlmann, J.; Mach, L.; Altmann, F. Mass + retention time = structure: a strategy for the analysis of *N*-glycans by carbon LC-ESI-MS and its application to fibrin *N*-glycans. *Anal. Chem.* **2007**, *79*, 5051−5057.

(22) Wuhrer, M.; Koeleman, C. A.; Deelder, A. M.; Hokke, C. H. Normal-phase nanoscale liquid chromatography-mass spectrometry of underivatized oligosaccharides at low-femtomole sensitivity. *Anal. Chem.* **2004**, *76*, 833−838.

(23) Pabst, M.; Altmann, F. Influence of electrosorption, solvent, temperature, and ion polarity on the performance of LC-ESI-MS using graphitic carbon for acidic oligosaccharides. *Anal. Chem.* **2008**, *80*, 7534−7542.

(24) Jmeian, Y.; Hammad, L. A.; Mechref, Y. Fast and efficient online release of *N*-glycans from glycoproteins facilitating liquid chromatography−tandem mass spectrometry glycomic profiling. *Anal. Chem.* **2012**, *84*, 8790−8796.

(25) Hua, S.; Jeong, H. N.; Dimapasoc, L. M.; Kang, I.; Han, C.; Choi, J.-S.; Lebrilla, C. B.; An, H. J. Isomer-specific LC/MS and LC/MS/MS profiling of the mouse serum *N*-glycome revealing a number of novel sialylated *N*-glycans. *Anal. Chem.* **2013**, *85*, 4636−4643.
(26) Wang, C.; Yuan, J.; Li, X.; Wang, Z.; Huang, L. Sulfonyl hydrazine-functionalized polymer as a specific capturer of reducing glycans from complex samples for high-throughput analysis by electrospray ionization mass spectrometry. *Analyst* **2013**, *138*, 5344−5356.
(27) Bowman, M. J.; Zaia, J. Tags for the stable isotopic labeling of carbohydrates and quantitative analysis by mass spectrometry. *Anal. Chem.* **2007**, *79*, 5777−5784.
(28) Yuan, J.; Hashii, N.; Kawasaki, N.; Itoh, S.; Kawanishi, T.; Hayakawa, T. Isotope tag method for quantitative analysis of carbohydrates by liquid chromatography−mass spectrometry. *J. Chromatogr. A* **2005**, *1067*, 145−152.
(29) Xia, B.; Feasley, C. L.; Sachdev, G. P.; Smith, D. F.; Cummings, R. D. Glycan reductive isotope labeling for quantitative glycomics. *Anal. Biochem.* **2009**, *387*, 162−170.
(30) Walker, S. H.; Budhathoki-Uprety, J.; Novak, B. M.; Muddiman, D. C. Stable-isotope labeled hydrophobic hydrazide reagents for the relative quantification of *N*-linked glycans by electrospray ionization mass spectrometry. *Anal. Chem.* **2011**, *83*, 6738−6745.
(31) Xue, X.; Zhang, P.; Wang, Z.; Huang, L. Analysis method for relative quantitation and qualitation of reductive glycans via aniline stable isotopic labeling and ESI-MS. *Chem. J. Chin. Univ.* **2010**, *11*, 2173−2180.
(32) Ko, K. Y.; Ahn, D. U. An economic and simple purification procedure for the large-scale production of ovotransferrin from egg white. *Poultry Sci.* **2008**, *87*, 1441−1450.
(33) Laemmli, U. K. Cleavage of structural proteins during the assembly of the head of bacteriophage T4. *Nature* **1970**, *227*, 680−685.
(34) Ceroni, A.; Maass, K.; Geyer, H.; Geyer, R.; Dell, A.; Haslam, S. M. GlycoWorkbench: a tool for the computer-assisted annotation of mass spectra of glycans. *J. Proteome Res.* **2008**, *7*, 1650−1659.
(35) Harvey, D.; Wing, D.; Küster, B.; Wilson, I. Composition of *N*-linked carbohydrates from ovalbumin and co-purified glycoproteins. *J. Am. Soc. Mass Spectrom.* **2000**, *11*, 564−571.
(36) Jiao, J.; Zhang, H.; Reinhold, V. N. High performance IT-MSn sequencing of glycans. *Int. J. Mass Spectrom.* **2011**, *303*, 109−117.
(37) Giansanti, F.; Leboffe, L.; Pitari, G.; Ippoliti, R.; Antonini, G. Physiological roles of ovotransferrin. *Biochim. Biophys. Acta, Gen. Subj.* **2012**, *1820*, 218−225.
(38) Shen, S.; Chahal, B.; Majumder, K.; You, S.-J.; Wu, J. Identification of novel antioxidative peptides derived from a thermolytic hydrolysate of ovotransferrin by LC-MS/MS. *J. Agric. Food Chem.* **2010**, *58*, 7664−7672.
(39) Williams, J.; Elleman, T. C.; Kingston, I. B.; Wilkins, A. G.; Kuhn, K. A. The primary structure of hen ovotransferrin. *Eur. J. Biochem.* **1982**, *122*, 297−303.

temperature and assessing any sensory changes that developed after this storage. The primary aim of this study was to examine the relationship between bottle color and the development of a yellow-golden color, phenolic composition, and sensory characteristics in a Sauvignon Blanc wine after 8 months of storage.

MATERIALS AND METHODS

Reagents and Chemicals. Gallic acid (≥99%), caffeic acid (≥98%), *p*-coumaric acid (≥98%), caftaric acid (≥97%), quercetin (≥98%), and (+)-catechin (≥99%) standards were purchased from Sigma Chemical Co. (St. Louis, MO). Polyethylene membranes of a 0.22 μm pore size were acquired from EMD Millipore (Billerica, MA). Ethyl acetate (≥99.8%), diethyl ether (≥99.7%), anhydrous sodium sulfate (≥98%), glacial acetic acid (100%), ethanol (≥99.9%), hydrochloric acid (37%), and acetonitrile (HPLC-grade) (≥99.9%) were purchased from Merck (Darmstadt, Germany). All reagents were of analytical grade or higher. Ultrapure water was obtained from a Purelab Ultra MK2 purification system (Elga, St Albans, UK).

Wine Bottles. The bottles used (Bordeaux Punted model, 750 mL capacity) were provided by Cristalchile (Santiago, Chile). The bottles used in this study were designated by their trade names (Dead Leaf Green, Antique Green, Amber, and Flint) to describe their color. Groups of 25 bottles were used for each bottle color, for a total of 100 bottles. These colors were chosen because they represent the most commonly used bottles in the wine industry.

White Wine. A commercial Sauvignon Blanc wine (100 L) was provided from "Viña Veramonte" (Casablanca Valley [33°22′14″ S, 71°17′41″ W], Chile). The bottles were filled and capped with roll-on tamper-evident screw caps (Saran Tin liner) (Amcor, Hawthorn, Australia) at "Viña Veramonte". The basic chemical parameters for the wine were as follows: pH, 3.1; titratable acidity, 6.4 g/L (tartaric acid); free sulfur dioxide, 33 mg/L; total sulfur dioxide, 98.1 mg/L, reducing sugars, 1.2 g/L; ethanol, 13.9% (v/v).

Artificial Light Exposure Experiment. During the trial period (8 months), the bottles were stored in a dark room in which small temperature variations were observed (16.8 °C ± 2.9 °C) with a relative humidity of 40−50%, as registered using a VWR-4184 temperature/humidity meter (VMR International, Radnor, PA). Further details regarding the storage temperature will be given later. The bottles only received the light provided by the fluorescent tubes. The wine bottles were placed vertically inside three open cabinets, as shown in Figure 1 (height, 213 cm; width, 110 cm; depth, 52 cm). Each cabinet had four shelves, spaced at 40 cm, with two fluorescent tubes each (T10 40 W 54, standard daylight 6500 K, General Electric, Fairfield, CO), which were located 16 cm from the base of the shelf. The light emitted from the fluorescent tubes was measured using a HD9021 radiometer (Delta OHM, Padua, Italy), placing the radiometer's sensor at a distance of 20 cm from the fluorescent tubes. The incidental radiation at 20 cm from the fluorescent tubes was 68.0 ± 0.1 μmol/m^2·s. These measurements were used to delimit an area of the shelves in which radiation was uniform, to place all of the bottles within that area. The bottles were distributed at a distance of 20 cm from the light source and at a distance of 20 cm from each other. Subsequently, the light exposure regime was adjusted with a Tactic 111.0 timer (Grässlin, St. Georgen, Germany) to 16 h per day (from 8:00 to 24:00 h), with 8 h without light to simulate night-time conditions during the 8-month period of exposure. Furthermore, to assess the ability of each bottle type to limit the light radiation reaching the wine within the bottle, the radiometer recorded the incident radiation in the test room and the transmission inside the bottle. To measure the incident radiation and the transmission of light through the glass, a sensor was placed inside an empty bottle in the medium section, with the bottle located at 20 cm from the light source provided by the fluorescent tubes. All of the bottles were stored for 2 weeks to equilibrate them in the same dark room before the assay was initiated.

Figure 1. Photograph showing the open cabinets with the arrangement of the fluorescent tubes and bottles during the 8 months of storage.

Wine Chemical Analyses. The analyses were performed every month, but considering that the results did not vary much, only the results obtained every 2 months are presented. The chemical analyses at time zero (month 0) were performed after 2 weeks of storage without artificial light exposure. The wine's pH, titratable acidity (g tartaric acid/L), reduced sugar content (g glucose/L), ethanol content (% v/v), and free sulfur dioxide (mg/L) were measured according to OIV methods.[6] The total phenol content was determined by UV absorption at 280 nm using gallic acid as a standard and expressed as mg GAE (gallic acid equivalent)/L.[7] The total tannin content was measured using the method of Ribéreau-Gayon and Stonestreet.[8] Color intensity (CI) was estimated using the method described by Glories.[7] The color coordinates, lightness (L^*), chroma (C^*), hue (h^*), a^* (red-greenness), and b^* (yellow-blueness) were determined according to Ayala et al.[9] All absorbance measurements were taken with a UV−vis spectrophotometer, model UV/vis 1700 Pharmaspec (Shimadzu, Kyoto, Japan).

HPLC-DAD Analyses of Low Molecular Weight Phenolic Compounds. A 50 mL aliquot of white wine was extracted with diethyl ether (3 × 20 mL) and ethyl acetate (3 × 20 mL) to concentrate the phenolic compounds. The organics fractions were combined, dehydrated with 2.5 g of anhydrous sodium sulfate, and evaporated to dryness under a vacuum at 30 °C. The solid residue was dissolved in 2 mL of a methanol/water (1:1, v/v) solution and filtered through a 0.22 μm pore size membrane. A chromatographic system used for identification of individual phenolic compounds consisted of an Agilent Technologies 1100 series (Agilent Technologies, Santa Clara, U.S.) equipped with a diode-array detector (DAD) model G1315B, a quaternary pump model QuatPump G1311A, a degasser model G1379A, and an autosampler model G1329A. Aliquots (25 μL) of the final solution were subjected to reverse-phase chromatographic separation at 20 °C on a reverse-phase Nova Pack C_{18} column (4 μm, 3.9 mm i.d. × 300 mm; Waters Corp.). A photodiode array detector was set from 210 to 360 nm. Two mobile phases were used as follows: A, water/acetic acid (98:2 v/v); and B, water/acetonitrile/acetic acid (78:20:2 v/v/v). A gradient was applied at a flow rate of 1.0 mL/min from 0 to 55 min and 1.2 mL/min from 55 to 90 min as follows: 100−20% A, 20−10% A from 55 to 57 min, 10−0% A from 57 to 90 min. Each major peak in the HPLC chromatograms of the extracts was characterized by both the retention time and the absorption spectrum (from 210 to 360 nm), according to Peña-Neira et al.[10] Quantitative determinations were performed using the external standard method on commercial standards. The calibration curves were produced by injecting the standard solutions before an extraction, under the same conditions as for the samples analyzed, over the range of concentrations observed ($r^2 \geq 0.93$). Quercetin glycosides, for which no standards were available, were quantified using standard curves for quercetin. All of the qualitative and quantitative analyses of phenolic

composition (including their extraction step) were performed in triplicate.[11]

Sensory Evaluation. The sensory panel consisted of personnel (five females and seven males) from the Department of Agro-industry and Enology, ranging in age from 24 to 53 years. All of the judges had previous experience with sensory analysis in white wines. An initial training session was conducted for the recognition of aromatic references. The training consisted of a familiarization exercise with aromatic descriptors by using fresh and processed fruits and vegetables to exemplify the most common aromatic descriptors founded in Sauvignon Blanc wines. The evaluation sessions were performed in individual tasting booths, in a temperature-controlled room set at 20 °C. A total of 20 mL of wine was served at 10−11 °C in wine-tasting glasses (Arcoroc, Arques, France) after being labeled with a three-digit code using a completely randomized order. Each wine was evaluated with regard to two sensory attributes, color intensity, and aromatic intensity, on a 15 cm unstructured linear scale, anchored from "low" to "high" intensity. Furthermore, the judges analyzed the aromatic descriptors of each wine. The flavor descriptors appropriate for discriminating among wines are provided in Table 1. The judges chose a series of flavor descriptors, and the descriptors with the highest scores were chosen after the evaluation and expressed as a percentage. These terms were derived from previous studies of aromatic properties in Sauvignon Blanc wines.[12,13] All judges rated each wine in duplicate. The data were collected using the Fizz software (ver. 2.47b, Biosystemes, Couternon, France). The evaluation sessions lasted approximately 3 h each and were performed every 2 months.

Table 1. Flavor Descriptors and Reference Materials Used in Association with Each Descriptor

typicity	groups	aromas	reference material
vegetal	fresh vegetables	leaves/stems	green leaves
		grass	freshly cut grass
		green capsicum	green capsicum slice
		green pepper	green pepper slice
		tomato stalk	tomato stalks
		boxwood/cat urine	boxwood leaves
	canned/cooked	green beans	fresh green beans
		asparagus	canned asparagus
		green olives	canned green olives
		artichoke	canned artichoke
citric	citrus fruits	grapefruit	grapefruit slices
		lemon	lemon slices
		orange	orange slices
		lemon peel	lemon peel
tropical	tropical fruits	pineapple	pineapple slice
		melon	melon piece
		banana	banana piece
		cherimoya	cherimoya piece
others	stone fruits	apricot	fresh apricot slice
		peach	fresh peach slice
	pome fruits	green apple	fresh green apple slice

Statistical Analyses. Analysis of variance (ANOVA) and the Tukey's Honestly Significant Difference (HSD) test were used to separate the means at a significance level of 95% ($p < 0.05$). All of the chemical and physical analyses were performed in triplicate. The sensory data were analyzed by ANOVA and Least Significance Difference (LSD) test ($p < 0.05$). All statistical analyses were conducted using Statgraphics Centurion (ver. 15.2, Statpoint Technologies, Warranton, VA) and Excel 2007 version 12.0 (Microsoft Corp., Redmond, WA).

RESULTS AND DISCUSSION

Characterization of Bottle Type. To assess the ability of each bottle type to limit the light radiation reaching the wine within the bottle, a radiometer was used to record the incident radiation and the transmission inside the bottle. Table 2 compares the light transmission for the four types of bottles. The Flint bottles had the highest incident radiation with a value of 56.2 μmol/m^2·s. The colored bottles showed a range of incident radiation from 20.3 to 21.5 μmol/m^2·s with slight differences among them. The Flint bottles also had the highest value of transmittance. These results are corroborated by those in the study of Maury et al.,[1] who showed that the highest percentage of transmittance corresponded to the Flint bottles and that the lowest corresponded to the colored bottles. These authors showed that the Flint bottle is capable of transmitting all visible and some UV light; however, darker bottles reduce the amount of visible light reaching the sample and allow only a small amount of UV light to be transmitted.

Table 2. Radiation and Transmittance Percentages in Bottles[a]

bottles	incident radiation (μmol/m^2·s)	transmittance (%)
Dead Leaf Green	20.3 ± 0.2 c	29.9 ± 0.2 c
Antique Green	20.2 ± 0.1 c	29.8 ± 0.2 c
Amber	21.5 ± 0.2 b	31.7 ± 0.2 b
Flint	56.2 ± 0.3 a	82.7 ± 0.4 a

[a]All data are expressed as the mean ± standard deviation ($n = 3$). Different letters among bottle color indicate significant differences ($p < 0.05$) according to Tukey's HSD test.

Chemical Composition of the Wines. Table 3 shows the values of titratable acidity, pH, free sulfur dioxide, and phenolic composition of wine samples. The pH varied from 3.05 to 3.25. With regard to titratable acidity, the values varied from 6.1 to 6.6 g tartaric acid/L. The free SO_2 varied from 27.3 to 33.7 mg/L. These results were in agreement with data from white wines in previous studies.[14,15] No differences were observed in the concentration of total phenols at time 0.

From the second month onward, a slight increase in total phenol concentration was observed in all colored bottles as compared to the Flint ones. The increase in the content of total phenols in the first months could be due to a hydrolysis reaction and complex formation.[16,17] Moreover, the study of Maury et al.[1] on different colors of wine bottles showed a decrease in absorbance at 280 nm in Flint and Green bottles, coinciding with the lowest concentration of total phenols in the Flint bottle.

Regarding the analysis of the total tannins, there was an increase in the concentration across all treatments during wine storage, although an initial decrease was observed in the first month in the dark bottles; however, it is possible that this variation was due to experimental error. The Bate−Smith assay was utilized for the quantification of the total tannins and can be influenced by several variables that might affect the kinetics of color formation. For example, the incomplete transformation of proanthocyanidins into anthocyanidins has reaction yields that depend on both the structure and the polymerization degree of the proanthocyanidins.[18] The medium conditions and the presence of light may also have caused a depolymerization of the more polymerized tannins, leading to the consequent release of less polymerized tannins, procyanidins, and monomers, causing a greater reactivity of these compounds, specifically polymerized tannins and procyanidins in the acid-catalyzed oxidative depolymerization of these compounds.[19]

Table 3. Phenolic Composition and Chemical Parameters in Sauvignon Blanc Wines in Different Bottle Colors under Artificial Light Conditions during the 8 Months of Storage[a]

time (months)	bottles	total phenols (mg GAE/L)	total tannins (mg CE/L)	pH	titratable acidity (g tartaric acid/L)	free SO_2 (mg/L)
0	Dead Leaf Green	199.7 ± 5.2 Ba	60.3 ± 5.4 ABCa	3.21 ± 0.0 Ba	6.4 ± 0.0 Aa	32.0 ± 1.3 Aa
	Antique Green	196.4 ± 2.1 Ba	45.1 ± 4.5 Cb	3.20 ± 0.0 Ba	6.4 ± 0.0 Aa	31.2 ± 0.7 Ba
	Amber	197.5 ± 3.5 ABa	55.9 ± 1.9 ABab	3.22 ± 0.0 Ba	6.4 ± 0.0 Aa	33.3 ± 1.3 Aa
	Flint	191.9 ± 1.8 Ca	55.7 ± 5.4 ABab	3.21 ± 0.0 Ba	6.4 ± 0.0 Aa	33.0 ± 0.7 Aa
2	Dead Leaf Green	210.5 ± 3.8 Aa	49.5 ± 4.7 Cab	3.06 ± 0.0 Da	6.6 ± 0.2 Aa	29.0 ± 0.7 Bab
	Antique Green	205.2 ± 0.3 Ab	62.1 ± 6.0 Aa	3.05 ± 0.0 Da	6.4 ± 0.2 Aa	29.0 ± 0.7 Cab
	Amber	201.0 ± 0.3 Ab	48.9 ± 4.5 Bb	3.05 ± 0.0 Da	6.4 ± 0.0 Aa	30.0 ± 0.7 Ba
	Flint	201.7 ± 0.4 Ab	44.9 ± 4.1 Bb	3.06 ± 0.0 Da	6.4 ± 0.0 Aa	27.3 ± 0.7 Bb
4	Dead Leaf Green	196.3 ± 0.2 Bab	53.4 ± 5.1 BCab	3.17 ± 0.0 Ca	6.6 ± 0.2 Aa	29.0 ± 0.7 Bab
	Antique Green	196.8 ± 0.2 Ba	51.0 ± 2.0 BCb	3.17 ± 0.0 Ca	6.6 ± 0.2 Aa	28.2 ± 0.0 Ca
	Amber	194.3 ± 0.6 Bc	64.4 ± 6.4 Aa	3.16 ± 0.0 Ca	6.6 ± 0.2 Aa	30.0 ± 0.7 Bb
	Flint	195.4 ± 0.6 Bbc	59.0 ± 4.5 Aab	3.16 ± 0.0 Ca	6.4 ± 0.2 Aa	27.3 ± 0.7 Ba
6	Dead Leaf Green	196.3 ± 0.1 Bb	65.9 ± 5.0 ABa	3.24 ± 0.0 Aa	6.4 ± 0.0 Aa	33.3 ± 0.0 Aa
	Antique Green	198.6 ± 0.2 Ba	60.8 ± 2.9 ABa	3.25 ± 0.0 Aa	6.4 ± 0.0 Aa	32.0 ± 1.3 ABa
	Amber	199.9 ± 1.0 Aa	64.2 ± 1.5 Aa	3.25 ± 0.0 Aa	6.4 ± 0.0 Aa	33.3 ± 0.0 Aa
	Flint	192.4 ± 0.2 BCc	58.3 ± 4.9 ABa	3.25 ± 0.0 Aa	6.4 ± 0.0 Aa	29.0 ± 0.7 Bb
8	Dead Leaf Green	198.6 ± 1.3 Ba	70.9 ± 7.0 Aa	3.18 ± 0.0 Ca	6.1 ± 0.0 Ba	27.0 ± 1.3 Bc
	Antique Green	198.4 ± 0.3 Ba	62.1 ± 2.4 Aa	3.17 ± 0.0 Cab	6.1 ± 0.0 Ba	34.0 ± 0.7 Aa
	Amber	199.0 ± 0.3 Aa	62.9 ± 3.2 Aa	3.16 ± 0.0 Cb	6.1 ± 0.0 Ba	31.2 ± 0.7 ABab
	Flint	194.5 ± 0.2 ABb	67.8 ± 6.7 Aa	3.16 ± 0.0 Cb	6.1 ± 0.0 Ba	29.0 ± 1.5 Bbc

[a]All data are expressed as the mean ± standard deviation ($n = 3$). Different lowercase letters indicate significant differences ($p < 0.05$) between bottle colors in each month according to Tukey's HSD test. Different uppercase letters indicate significant difference ($p < 0.05$) for each bottle color during time storage according to Tukey's HSD test. GAE, gallic acid equivalent; CE, (+)-catechin equivalent.

These effects could have resulted in an increase in the value of total tannins quantified by this method.

Table 4 shows the content of some of the major low-molecular-weight phenols in Sauvignon Blanc white wines. The hydroxybenzoic acid quantified was gallic acid, and the hydroxycinnamic acids quantified were caftaric, *cis*-caffeic, *trans*-caffeic, and *p*-coumaric acids. The flavanol quantified was (+)-catechin, and the flavonols quantified were quercetin-3-glucoside, quercetin-3-galactoside, and quercetin. All of these compounds were detected in all of the wines used in this study.

The compounds exhibiting higher concentrations were *trans*-caffeic, caftaric, and *p*-coumaric acids. At time zero (month 0), the greatest differences in concentration were observed, with the highest concentrations of gallic acid, (+)-catechin, caftaric acid, *p*-coumaric acid, and quercetin-3-galactoside being noted in colored bottles, especially in Dead Leaf Green bottles. By contrast, Flint bottles presented a lower content of these compounds.

During storage under artificial light conditions, there was varying behavior in some of the phenolic compounds analyzed. With regards to phenolic acids, *cis*-caffeic acid, a slight increase in concentration during storage was observed, while instead caftaric acid showed a decrease in their concentration. On the other hand, gallic and *trans*-caffeic acids showed a more erratic behavior. The concentration of *p*-coumaric acid decreased substantially in Flint bottles, especially toward the end of the assay. During wine aging, both depolymerization and condensation occur. The storage conditions are expected to strongly affect the content of phenols, because they can undergo modifications during storage, mainly due to hydrolysis (enzymatic or not), oxidations, and complexations that are mainly responsible for the increase of simpler compounds, such as free phenolic acids, especially in colored bottles[16,17] that could support the behavior of some compounds in this assay. Cleavage of interflavan bonds of proanthocyanidins could happen at the pH of wine.[20] According to Schofield et al.,[19] the interflavan links in most condensed tannins may be broken under acid condition. In general, an increase in (+)-catechin concentration during wine storage was observed. This pattern may be due to the medium conditions, in which the combination of low pH (3.05−3.25) and the presence of light were able to cause a depolymerization of the higher molecular mass flavanols (i.e., condensed tannins) and the concomitant release of (+)-catechin monomers.[21] This hypothesis can be supported by the analysis of total tannins, wherein the presence of light and medium conditions could cause the depolymerization of more polymerized condensed tannins and consequent (+)-catechin release (Table 3).

Concerning the flavonols identified, there were different behaviors among them during storage under artificial light conditions. With respect to quercetin-3-glucoside, there were no differences between bottle colors and only minor, erratic differences throughout the time of storage. In contrast, quercetin-3-galactoside showed a clear decrease in concentration during storage that resulted in nondetectable values from the sixth month of storage onward; only in month 0 were differences among bottle color found to occur at a higher concentration in colored bottles. Moreover, quercetin was the predominant flavonol quantified in all samples, demonstrating an increased concentration throughout the wine storage period with no differences among bottle colors. This increase could be due to the hydrolysis reaction (enzymatic or not) that was mainly responsible for the increase in the number of simpler compounds,[16,17] such as quercetin, and was supported by the observed decrease in quercetin-3-galactoside throughout storage. These reactions may be accelerated by the presence of light.

Table 4. Mean and Standard Deviations Values (mg/L) for Wine Phenolic Compounds As a Result of the Exposition of Sauvignon Blanc Wines in Different Bottle Colors under Artificial Light Condition during 8 Months of Storage[a]

compounds	months	Dead Leaf Green	Antique Green	Amber	Flint
gallic acid	0	0.37 ± 0.03 Aa	0.32 ± 0.03 BCab	0.32 ± 0.02 Bab	0.28 ± 0.03 Cb
	2	0.41 ± 0.02 Aa	0.40 ± 0.05 ABa	0.42 ± 0.01 Aa	0.43 ± 0.03 ABa
	4	0.48 ± 0.04 Aa	0.43 ± 0.04 Aa	0.44 ± 0.01 Aa	0.51 ± 0.06 Aa
	6	0.32 ± 0.03 Aab	0.31 ± 0.01 Cb	0.34 ± 0.00 Bab	0.36 ± 0.01 BCa
	8	0.42 ± 0.03 Aa	0.43 ± 0.01 Aa	0.43 ± 0.02 Aa	0.45 ± 0.02 ABa
(+)-catechin	0	0.55 ± 0.12 Aa	0.34 ± 0.01 Cb	0.39 ± 0.03 Bab	0.23 ± 0.02 Db
	2	0.37 ± 0.10 Aa	0.50 ± 0.06 BCa	0.39 ± 0.01 Ba	0.43 ± 0.05 CDa
	4	0.36 ± 0.08 Aa	0.40 ± 0.11 BCa	0.34 ± 0.04 Ba	0.53 ± 0.19 BCa
	6	0.62 ± 0.08 Aa	0.67 ± 0.22 ABa	0.69 ± 0.09 Aa	0.82 ± 0.09 Aa
	8	0.71 ± 0.11 Aa	0.84 ± 0.09 Aa	0.68 ± 0.08 Aa	0.80 ± 0.06 ABa
caftaric acid	0	1.81 ± 0.13 Aa	1.59 ± 0.14 Aab	1.53 ± 0.16 BCab	1.30 ± 0.15 BCb
	2	1.70 ± 0.14 ABa	1.62 ± 0.21 Aa	1.81 ± 0.05 Aa	1.70 ± 0.15 Aa
	4	1.59 ± 0.18 ABa	1.17 ± 0.12 Ba	1.33 ± 0.07 CDa	1.40 ± 0.13 ABCa
	6	1.37 ± 0.16 Ba	1.28 ± 0.08 ABa	1.23 ± 0.06 Da	1.15 ± 0.07 Ca
	8	1.50 ± 0.10 ABa	1.56 ± 0.09 Aa	1.68 ± 0.05 ABa	1.52 ± 0.08 ABa
cis-caffeic acid	0	0.34 ± 0.02 Aa	0.31 ± 0.03 Ba	0.32 ± 0.04 Ba	0.28 ± 0.03 Ba
	2	0.41 ± 0.03 Aa	0.38 ± 0.05 ABa	0.43 ± 0.01 Aa	0.40 ± 0.03 ABa
	4	0.42 ± 0.05 Aa	0.38 ± 0.06 Ba	0.39 ± 0.01 Aa	0.48 ± 0.09 Aa
	6	0.44 ± 0.06 Aa	0.33 ± 0.03 Ba	0.37 ± 0.02 ABa	0.35 ± 0.02 ABa
	8	0.44 ± 0.02 Aa	0.48 ± 0.03 Aa	0.41 ± 0.03 Aa	0.39 ± 0.10 ABa
trans-caffeic acid	0	2.10 ± 0.11 Aa	1.97 ± 0.20 ABa	1.88 ± 0.08 Ba	1.70 ± 0.14 Ba
	2	2.06 ± 0.14 ABa	2.12 ± 0.28 Aa	2.19 ± 0.01 Aa	2.07 ± 0.06 Aa
	4	2.10 ± 0.11 Aa	1.66 ± 0.09 Bb	1.80 ± 0.08 Bab	1.88 ± 0.16 ABab
	6	1.69 ± 0.12 Ca	1.59 ± 0.09 Ba	1.48 ± 0.08 Cab	1.34 ± 0.06 Cb
	8	1.77 ± 0.12 BCa	1.85 ± 0.03 ABa	1.94 ± 0.11 Ba	1.81 ± 0.03 ABa
p-coumaric acid	0	1.40 ± 0.04 Aa	1.32 ± 0.12 ABab	1.30 ± 0.07 Cab	1.16 ± 0.09 Bb
	2	1.36 ± 0.06 ABa	1.40 ± 0.19 Aa	1.50 ± 0.00 ABa	1.37 ± 0.02 Aa
	4	1.06 ± 0.06 Ca	1.04 ± 0.05 Ba	1.51 ± 0.02 ABa	1.02 ± 0.01 Ca
	6	1.18 ± 0.08 Ca	1.17 ± 0.07 ABa	1.44 ± 0.03 Ba	1.10 ± 0.03 BCa
	8	1.19 ± 0.07 BCa	1.31 ± 0.02 ABa	1.57 ± 0.05 Aa	1.21 ± 0.04 Ba
quercetin-3-glucoside	0	0.28 ± 0.03 Aa	0.28 ± 0.03 Ba	0.27 ± 0.03 Ba	0.22 ± 0.02 Ca
	2	0.42 ± 0.09 Aa	0.39 ± 0.07 Aa	0.48 ± 0.02 Aa	0.41 ± 0.03 ABa
	4	0.36 ± 0.02 Aa	0.34 ± 0.04 ABa	0.34 ± 0.05 ABa	0.45 ± 0.10 Aa
	6	0.44 ± 0.11 Aa	0.25 ± 0.02 Ba	0.23 ± 0.07 Ba	0.28 ± 0.02 BCa
	8	0.29 ± 0.06 Aa	0.30 ± 0.02 ABa	0.28 ± 0.09 Ba	0.29 ± 0.04 BCa
quercetin-3-galactoside	0	0.51 ± 0.05 Aa	0.45 ± 0.05 Aab	0.46 ± 0.04 Aab	0.36 ± 0.03 Ab
	2	0.40 ± 0.15 ABa	0.35 ± 0.08 ABa	0.42 ± 0.02 Aa	0.34 ± 0.04 Aa
	4	0.29 ± 0.03 Ba	0.24 ± 0.01 Ba	0.26 ± 0.01 Ba	0.35 ± 0.11 Aa
	6	nd	nd	nd	nd
	8	nd	nd	nd	nd
quercetin	0	0.47 ± 0.06 Ba	0.47 ± 0.07 Ba	0.41 ± 0.03 Ca	0.35 ± 0.05 Ba
	2	0.72 ± 0.06 Aa	0.70 ± 0.06 Aa	0.74 ± 0.00 Ba	0.75 ± 0.13 Aa
	4	0.89 ± 0.16 Aa	0.75 ± 0.04 Aa	0.77 ± 0.02 Ba	0.79 ± 0.02 Aa
	6	0.93 ± 0.31 Aa	0.78 ± 0.04 Aa	0.82 ± 0.05 ABa	0.70 ± 0.06 Aa
	8	0.81 ± 0.15 Aa	0.80 ± 0.05 Aa	0.91 ± 0.05 Aa	0.74 ± 0.03 Aa

[a]All data are expressed as mean ± standard deviation ($n = 3$). Different lowercase letters in a row indicate significant differences ($p < 0.05$) between bottle colors in each month according to Tukey's HSD test. Different uppercase letters in a column indicate significant difference ($p < 0.05$) for each bottle color during time storage according to Tukey's HSD test. nd: not detected.

Regarding wine color, storage under artificial light conditions produced differences in the L^* parameter, which was significantly affected only in the treatments with a lower transmittance percentage, such as Antique Green and Dead Leaf Green bottles (Table 5). The Flint bottle showed a lower value of the parameter C^* throughout the 8 months of storage. This suggests that the higher value of C^* occurring in dark bottles may be linked to the production of pigments that contribute a higher color intensity and browning. The relationship between the loss of luminance (L^*) and the increase of chroma (C^*) is a characteristic of white wines stored for a certain time.[22] The hue values (h^*) differed among all bottle colors in their amounts, suggesting that most of the wines presented a medium yellow color, with a slight tendency toward green.[17,22] Regarding the color coordinates a^* and b^*, the Flint bottle presented the lowest values. The colored bottles showed a greater tendency toward red-greenness or yellow-blueness, especially the Amber bottle, which presented the highest value in coordinate b^*.

dx.doi.org/10.1021/jf501467f | J. Agric. Food Chem. 2014, 62, 7255−7262

Table 5. Color Coordinates in Sauvignon Blanc Wines in Different Bottle Colors under Artificial Light Conditions during the 8 Months of Storage[a]

time (months)	bottle types	L^*	C^*	h^*	a^*	b^*
0	Dead Leaf Green	99.37 ± 0.06 Ca	3.47 ± 0.03 ABa	95.88 ± 0.07 Ca	−0.35 ± 0.01 Bd	3.45 ± 0.03 Ab
	Antique Green	99.30 ± 0.00 Ca	3.46 ± 0.00 Ba	94.84 ± 0.16 Cb	−0.29 ± 0.01 Bb	3.45 ± 0.01 Bb
	Amber	99.30 ± 0.00 Ca	3.58 ± 0.01 Bb	95.34 ± 0.08 Ec	−0.33 ± 0.01 Ac	3.56 ± 0.01 Ba
	Flint	99.37 ± 0.06 Ca	2.84 ± 0.01 Ab	94.30 ± 0.09 Dd	−0.21 ± 0.01 Aa	2.84 ± 0.01 Ac
2	Dead Leaf Green	99.70 ± 0.00 Ab	3.26 ± 0.04 Dc	102.73 ± 0.55 Ab	−0.72 ± 0.03 Da	3.19 ± 0.05 Cc
	Antique Green	99.70 ± 0.00 Ab	3.41 ± 0.02 BCb	103.43 ± 0.12 Aab	−0.79 ± 0.01 Db	3.32 ± 0.02 Cb
	Amber	99.70 ± 0.00 Ab	3.58 ± 0.01 Ba	103.40 ± 0.53 Aab	−0.83 ± 0.03 Eb	3.49 ± 0.01 Ca
	Flint	99.80 ± 0.00 Aa	2.74 ± 0.05 Bd	104.07 ± 0.57 Aa	−0.66 ± 0.02 Da	2.65 ± 0.06 Bd
4	Dead Leaf Green	99.53 ± 0.06 Bb	3.29 ± 0.06 CDb	101.47 ± 0.29 Ba	−0.65 ± 0.03 Cb	3.23 ± 0.06 BCb
	Antique Green	99.70 ± 0.00 Aa	3.36 ± 0.02 Cb	102.93 ± 0.12 Aa	−0.75 ± 0.01 Dc	3.28 ± 0.03
	Amber	99.67 ± 0.06 Aa	3.59 ± 0.01 Ba	102.10 ± 0.44 Ba	−0.75 ± 0.03 Dc	3.50 ± 0.01 Ca
	Flint	99.73 ± 0.06 Aa	2.40 ± 0.05 Dc	101.33 ± 1.25 Ba	−0.47 ± 0.05 Ca	2.35 ± 0.06 Dc
6	Dead Leaf Green	99.60 ± 0.00 ABa	3.38 ± 0.03 BCb	100.7 ± 0.44 Ba	−0.63 ± 0.03 Cc	3.32 ± 0.02 Bc
	Antique Green	99.40 ± 0.00 Bb	3.42 ± 0.03 BCb	97.91 ± 0.70 Bb	−0.47 ± 0.03 Cb	3.40 ± 0.03 Bb
	Amber	99.53 ± 0.06 Ba	3.71 ± 0.01 Aa	100.53 ± 0.51 Ca	−0.68 ± 0.03 Cc	3.65 ± 0.02 Aa
	Flint	99.60 ± 0.00 Ba	2.51 ± 0.02 Cc	98.05 ± 0.47 Cb	−0.35 ± 0.03 Ba	2.48 ± 0.02 Cd
8	Dead Leaf Green	99.03 ± 0.06 Db	3.49 ± 0.02 Ac	89.18 ± 0.33 Dd	0.047 ± 0.01 Aa	3.49 ± 0.02 Ac
	Antique Green	99.10 ± 0.00 Db	3.61 ± 0.04 Aa	91.77 ± 0.20 Dc	−0.11 ± 0.01 Ab	3.61 ± 0.04 Ab
	Amber	99.37 ± 0.06 Ca	3.76 ± 0.04 Ab	99.08 ± 0.29 Da	−0.59 ± 0.02 Bd	3.71 ± 0.04 Aa
	Flint	99.47 ± 0.06 Ca	2.70 ± 0.02 Bd	97.79 ± 0.25 Cb	−0.37 ± 0.01 Bc	2.68 ± 0.01 Bd

[a]All data are expressed as the mean ± standard deviation ($n = 3$). Different lowercase letters indicate significant differences ($p < 0.05$) between bottle colors in each month according to Tukey's HSD test. Different uppercase letters indicate significant difference ($p < 0.05$) for each bottle color during time storage according to Tukey's HSD test.

Surprisingly, the color intensity of the Flint bottles presented values significantly lower ($p < 0.05$) than those of the colored bottles during the 8 months of storage (Figure 2), which is in agreement with the lowest value of C^* in Flint bottles (Table 5). Maury et al.[1] proposed that dark colored glass absorbs and retains more heat, driving pigmentation development in these bottles. Moreover, the higher retention of heat possibly occurring in dark bottle and the high composition of iron oxide[23,24] could result in a higher absorption of UV, visible, and infrared light and a higher production of pigments that increase the color intensity in dark bottles. In our study, the temperature of the dark room was registered at three points at 12:00 pm during the assay, as follows: March, min 17.0 °C, max 20.7 °C; July, min 12.6 °C, max 15.5 °C; October, min 16.0 °C, max 19.2 °C. At the same time, the thermometer probe was placed near of the surface of the bottles to register the temperature. Temperature recording near the bottles (5 cm) showed an average of 18 °C, which was quite variable depending on the temperature of the dark room. Because this experiment was performed with fluorescent tubes, the heat emission was predictably fairly low. In the study of Dias et al.,[4] the use of a mercury vapor lamp under controlled temperature conditions (38 ± 3 °C) produced increased coloration in Flint bottles, although uncontrolled temperature conditions led to the highest development of wine color in Antique Green bottles but the lowest development of wine color in Flint bottles. Moreover, in the study of Maury et al.,[1] a Sauvignon Blanc stored in bottles of different colors exposed to sunlight, with measurement of temperatures between 12.5 and 17.5 °C in the months of May, June, and July at the southeast of Australia, showed greater color development in darker bottles that are in agreement with the results of this work. In that case, the temperatures recorded outside of the bottles in this assay are similar to that exposed by Maury et al.[1] By observing the results of the low molecular weight phenolic compounds (Table 4), in some of them (e.g., caftaric, *p*-coumaric acids) there were a higher concentration in the wines bottled in darker color, especially during the first months of the assay. This slightly significant difference combined with the long storage of these bottles to artificial light conditions may explain the increase in yellow coloration found in the wines from colored bottles. Furthermore, another possibility is that the type of light transmitted by fluorescent tubes (e.g., small quantities of UV light) through the glass in the Flint bottles can degrade the pigments responsible for yellow coloration in white wines, as exposed by other authors.[1,4,25]

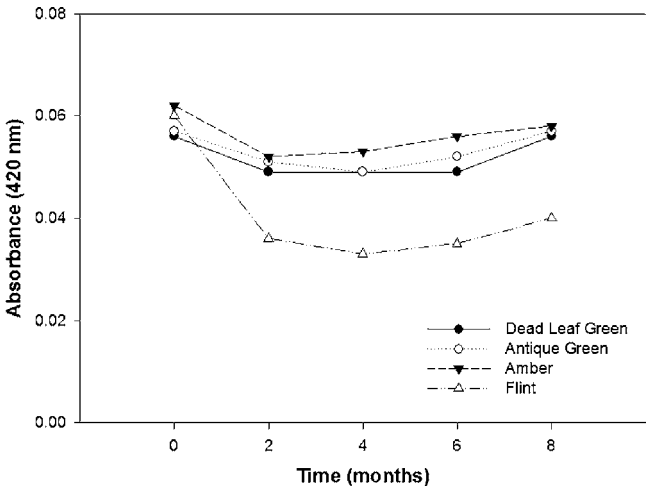

Figure 2. Comparison of color intensity measured at 420 nm for Sauvignon Blanc wines in different bottle colors under artificial light condition over 8 months of storage ($n = 3$).

Sensory Evaluation of Wines. Although within the sensory evaluation, the judges were asked about certain

dx.doi.org/10.1021/jf501467f | J. Agric. Food Chem. 2014, 62, 7255−7262

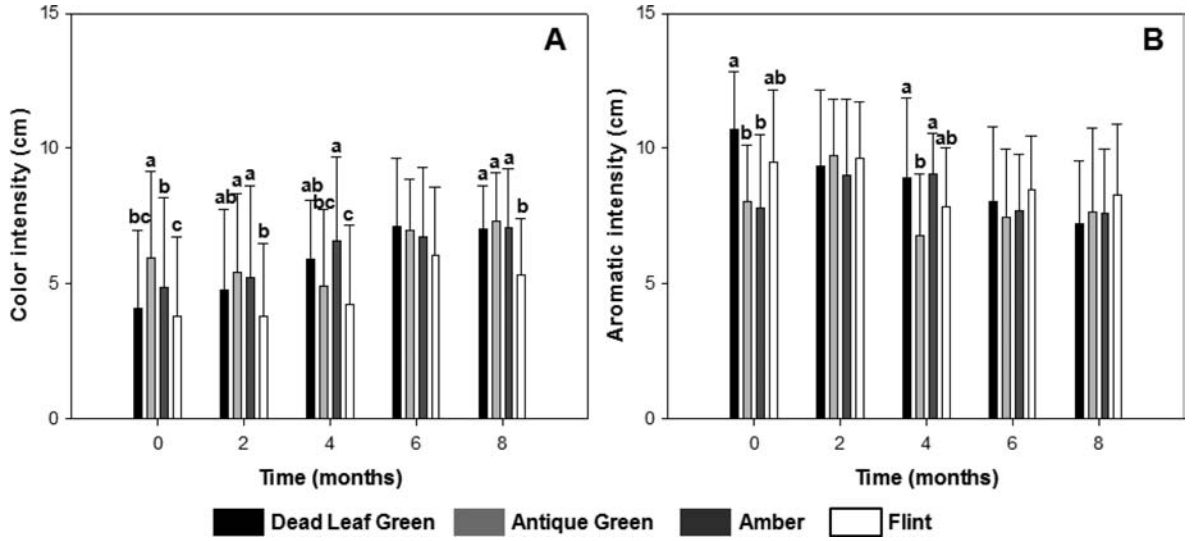

Figure 3. Sensory evaluation of the color intensity (cm) (A) and aromatic intensity (cm) (B) in Sauvignon Blanc wine in different bottle colors under artificial light conditions over 8 months of storage (n = 12). Different letters denote significant differences among bottle colors (p < 0.05, LSD test).

gustatory characteristics, such as bitterness, acidity, and taste intensity, these parameters did not show significant changes throughout the experiment; no differences were found among the treatments. Figure 3 shows the results of color and aromatic intensity. With regards to the perception of color, significant differences were observed among the treatments. The Flint bottles always had the lowest average values of color intensity, with varying differences across the sampling points. Still, only a trend reflecting an increasing color intensity during storage under artificial light conditions was observed. Furthermore, the color intensity by absorbance at 420 nm (Figure 1) and color coordinates (Table 5) correlated well with the sensory data. With regards to the aromatic intensity, only a trend of decreasing intensity was observed during the assay.

With regards to the aromatic descriptors analyzed, clear differences were observed among the treatments. The Sauvignon Blanc grapes are often described as producing wines that have a very distinctive varietal aroma, characterized by descriptors of fruity and vegetable flavors, including passion fruit, green capsicum, and boxwood.[12] In this study, the wines were grouped into four categories that represented the main aromatic characteristics of the Chilean Sauvignon Blanc, as follows: vegetal (e.g., grass, green capsicum, boxwood, asparagus), citric (e.g., lemon, orange), tropical (e.g., pineapple, cherimoya), and others aromas (e.g., apricot, peach, green apple) (Table 1). In general, the wines were described as having an important vegetal and citrus character, with lower notes of tropical fruits and other fruit aromas, specifically, peach and green apple. The analyses of the aromatic descriptors showed that there was a decrease in vegetal aromas in the darker bottles, especially in Antique Green bottles. In general, the storage time and exposure to artificial light produced an increase in citrus and tropical flavors. Clearly, storage under exposure to an artificial light produced significant changes in the aromatic descriptors that depended on the color of bottle used (Figure 4).

Although the principal aromatic descriptor of this cultivar is mainly due to the presence of volatile thiols, esters, and methoxypirazines,[2] further studies are needed to observe whether the use of different conditions of light and temperature

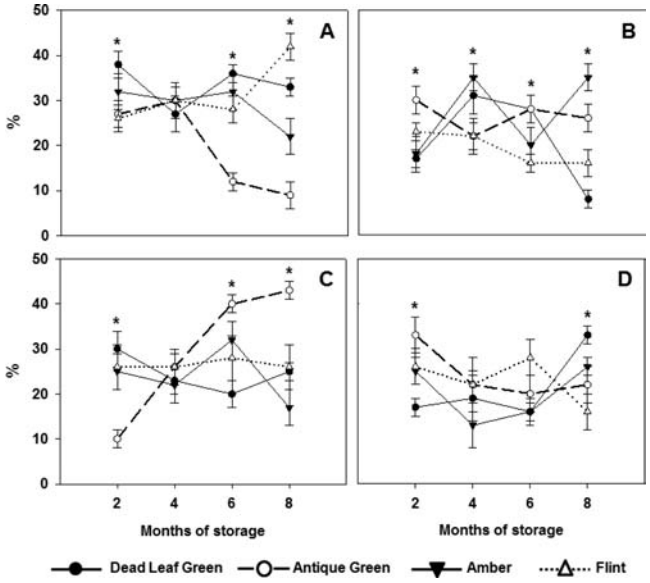

Figure 4. Evolution of the most important aromatic descriptors, such as vegetal (A), citric (B), tropical (C), and others (D), of Sauvignon Blanc wines in different bottle colors under artificial light conditions (n = 12). "*" denotes significant differences among bottle colors in each month (p < 0.05, LSD test).

can affect the concentrations of these compounds during wine storage.

In brief, this artificial light exposure experiment provided important data on the use of Flint and colored bottles and their effects on certain chemical and sensory features of wines. The implications of the results of this study are important to achieve a better comprehension of the principal factors affecting the chemical composition of the wines during storage. The color of the bottles, along with the light used, may affect the chemical composition of the wines. Furthermore, the exposure of the wines under artificial light after a long storage period may produce significant changes in the sensory properties of white wines, especially in the aromatic descriptors. This characteristic and the increase in the yellow coloration of the wines in darker

bottles should be taken into account by wineries and retail shops so that they may improve the safety of their wine storage.

AUTHOR INFORMATION

Corresponding Author

*Phone: 56 2-9785730. E-mail: alecaceres@uchile.cl.

Funding

We are grateful for the funding provided by Conicyt-Chile (grants Fondecyt 1080559, 1110655, and 1140882).

Notes

The authors declare no competing financial interest.

ACKNOWLEDGMENTS

We thank Viña Veramonte (Casablanca Valley, Chile) for providing the wine and permitting our use of their facilities and to Cristalchile for providing the bottles used in this work.

REFERENCES

(1) Maury, C.; Clark, A.; Scollary, G. Determination of the impact of bottle colour and phenolic concentration on pigment development in white wine stored under external conditions. *Anal. Chim. Acta* **2010**, *60*, 81−86.

(2) Blake, A.; Kotseridis, Y.; Brindle, I.; Inglis, D.; Pickering, G. Effect of light and temperature on 3-alkyl-2-methoxypyrazine concentration and other impact odourants of Riesling and Cabernet franc wine during bottle ageing. *Food Chem.* **2010**, *119*, 935−944.

(3) Dias, D.; Smith, T.; Ghiggino, K.; Scollary, G. The role of light, temperature and wine bottle color on pigment enhancement in white wine. *Food Chem.* **2012**, *135*, 2934−2941.

(4) Dias, D.; Clark, A.; Smith, T.; Ghiggino, K.; Scollary, G. Wine bottle colour and oxidative spoilage: Whole bottle light exposure experiments under controlled and uncontrolled temperature conditions. *Food Chem.* **2013**, *138*, 2451−2459.

(5) ODEPA (Oficina de Estudios y Políticas Agrarias). Boletín de vinos y pisco: producción, precios y comercio exterior 2013. URL (http://www.odepa.gob.cl) (4 November 2013).

(6) OIV. *Compendium of International Methods of Wine and Must Analysis*; OIV: Paris, France, 2012; Vols. *I*−*II*, p 419.

(7) Glories, Y. La coleur des vins rouges. 2e partie. Mesure, origine et interpretation. *Connaiss. Vigne Vin* **1984**, *18*, 253−271.

(8) Ribéreau-Gayon, P.; Stonestreet, E. Le dosage des tannins du vin rouge et determination de leur structure. *Chim. Anal.* **1966**, *148*, 188−192.

(9) Ayala, F.; Echávarri, J.; Negueruela, A. A new simplified method for measuring the color of wines. I. Red and rose wines. *Am. J. Enol. Vitic.* **1997**, *48*, 357−363.

(10) Peña-Neira, A.; Hernández, T.; García-Vallejo, C.; Estrella, I.; Suarez, J. A survey of phenolic compounds in Spanish wines from different geographical origins. *Eur. Food Res. Technol.* **2000**, *210*, 445−448.

(11) Peña-Neira, A.; Cáceres, A.; Pastenes, C. Low molecular weight phenolic and anthocyanins composition of grape skins from cv. Syrah (*Vitis vinifera* L.) in the Maipo Valley (Chile): effect of cluster thinning and vineyard yield. *Food Sci. Technol. Int.* **2007**, *13*, 153−158.

(12) Parr, W.; Green, J.; White, K.; Sherlock, R. The distinctive flavour of New Zealand Sauvignon Blanc: Sensory characterization by wine professionals. *Food Qual. Prefer.* **2007**, *18*, 849−861.

(13) Parr, W.; Valentin, D.; Green, J.; Dacremont, C. Evaluation of French and New Zealand wines by experienced French wine assessors. *Food Qual. Prefer.* **2010**, *21*, 56−64.

(14) Maggu, M.; Winz, R.; Kilmartin, P.; Trought, M.; Nicolau, L. Effect of skin contact and pressure on the composition of Sauvignon Blanc must. *J. Agric. Food Chem.* **2007**, *55*, 10281−10288.

(15) Cáceres-Mella, A.; Peña-Neira, A.; Parraguez, J.; López-Solís, R.; Laurie, V. F.; Canals, J. M. Effect of inert gas and prefermentative treatment with Polyvinylpolypyrrolidone on the phenolic composition of Chilean Sauvignon Blanc wines. *J. Sci. Food Agric.* **2013**, *93*, 1928−1934.

(16) Zafrilla, P.; Morillas, J.; Mulero, J.; Cayuela, J.; Martínez-Cachá, A.; Pardo, F.; López Nicolás, J. Changes during storage in conventional and ecological wine: Phenolic content and antioxidant activity. *J. Agric. Food Chem.* **2003**, *51*, 4694−4700.

(17) Recamales, A.; Sayago, A.; González-Miret, M.; Hernanz, D. The effect of time and storage conditions on the phenolic composition and colour of white wine. *Food Res. Int.* **2006**, *39*, 220−229.

(18) Waterman, P.; Mole, S. *Analysis of Phenolic: Plant Metabolites*; Blackwell Scientific: Oxford, UK, 1994; p 256.

(19) Schofield, P.; Mbugua, D.; Pell, A. Analysis of condensed tannins: a review. *Anim. Feed Sci. Technol.* **2001**, *91*, 21−40.

(20) Saucier, C.; Bourgeois, G.; Vitry, C.; Roux, D.; Glories, Y. Characterization of (+)-catechin-Acetaldehyde polymers: A model for colloidal state of wine polyphenols. *J. Agric. Food Chem.* **1997**, *45*, 1045−1049.

(21) Sioumis, N.; Kallithraka, S.; Makris, D.; Kefalas, P. Kinetics of browning onset in white wines: influence of principal redox-active polyphenols and impact on the reducing capacity. *Food Chem.* **2006**, *94*, 98−104.

(22) Hernanz, D.; Gallo, V.; Recamales, A.; Meléndez-Martínez, A.; González-Miret, M.; Heredia, F. Effect of storage on the phenolic content, volatile composition and colour of white wines from the varieties Zalema and Colombard. *Food Chem.* **2009**, *113*, 530−537.

(23) Clark, A.; Vestner, J.; Barril, C.; Maury, C.; Prenzler, P.; Scollary, G. The influence of stereochemistry of antioxidants and flavanols on oxidation processes in a model wine system: Ascorbic acid, erythorbic acid, (+)-catechin and (−)-epicatechin. *J. Agric. Food Chem.* **2010**, *58*, 1004−1011.

(24) Bamford, C. R. Colour generation and control in glass. *Glass Science and Technology 2*; Elsevier: New York, 1977; pp 141−164.

(25) George, N.; Clark, A.; Prenzler, P.; Scollary, G. Factors influencing the production and stability of xanthylium cation pigments in a model white wine system. *Aust. J. Grape Wine Res.* **2006**, *12*, 57−68.

characterized by not only resistance to dye leaching but also rapid color recovery in the presence of oxygen.

MATERIALS AND METHODS

Materials. MB, azure A (AA), thionine (Th), titanium(IV) oxide (TiO_2, AEROXIDE P25, nanopowder, 21 nm particle size), glycerol, zein from maize, and kappa (κ)- and iota (ι)-carrageenans were purchased from Sigma-Aldrich (St. Louis, MO) and used as received without further purification. The film for coating the oxygen indicator ink was a commercial nylon/polyethylene (PE) vacuum packaging film of 0.15 mm thickness (Pack4U, South Korea). All experiments were conducted in triplicate.

Carrageenan-Based Oxygen Indicator Film Preparation. Indicator ink consisted of 40 mg of MB, 1.2 g of TiO_2, and 1.2 g of glycerol. All of these components were added to 3.2 g of aqueous ethanol solution (90%) and then mixed thoroughly by a magnetic stirrer, followed by 5 min of ultrasonic dispersion (Vibra-Cell VCX-750, Sonics and Materials, Inc., Newtown, CT). The packaging film (4 × 4 cm) was spin-coated with the ink at 5000 rpm for 30 s using a spin coater (WS-400B-6NPP-LITE, Laurell Technologies Corporation, North Wales, PA) and dried. The resultant film was then dipped into ι-carrageenan solutions (0.2, 0.3, 0.4, and 0.5%, w/v) using a dip coater (KSV-DC, KSV Instruments, Bridgeport, CT) at an immersion and withdrawal speed of 85 mm/min and finally spun at 2000 rpm for 30 s.

The thickness of the carrageenan-based indicator films was measured using a thickness gauge (ID-S112B, Mitutoyo, Japan) and presented with an average of three samples with eight measurements along the edge of each film.

Zein-Based Oxygen Indicator Film Preparation. Zein (20%)-based indicator ink was prepared by adding 40 mg of MB, 1.2 g of TiO_2, 1.2 g of glycerol, and 0.8 g of zein to 3.2 g of ethanol solution (90%) and then mixing with ultrasonication. The packaging film (4 × 4 cm) was spin-coated with the ink at 5000 rpm for 30 s and then allowed to dry in the dark.

Dye Leaching of Oxygen Indicator Films into Water. The oxygen indicator films were submerged in a beaker filled with distilled water for 1 day, and leached dyes were quantified at 1, 3, 6, 12, and 24 h by measuring the absorbance at λ_{max} of each dye with a Varian Cary 50 UV−vis spectrophotometer. Dye leakage (%) was defined as a ratio of the amount of dye leaching into the water for a given time to the initial amount of dye on the film; thus, dye leakage of 100% indicates that all of the dye leached from the film into the water. The initial dye amounts were determined by measuring the absorbance after immersing the films in vigorously stirred solutions for 3 h: 70% ethanol for the zein-based films and HCl solution (2 M) for the carrageenan-based films.

Activation and Recovery of Oxygen Indicator Films. For bleaching of the oxygen indicator film, UV irradiation was carried out using a CL-1000 UV cross-linker (UVP, Upland, CA) equipped with five tubes of UVC lamps (8 W each). The irradiation intensity measured with a UVX digital radiometer (UVP, Upland, CA) was 5.5 mW/cm^2. For color recovery, the photobleached film was placed in ambient air, and its color change was monitored using a CM-2600d spectrophotometer (Konica Minolta, Tokyo, Japan).

Color Measurement. Several systems for expressing color numerically (i.e., color space) were developed by an international organization concerned with issues of lighting and color, the International Commission on Illumination (usually abbreviated CIE for its French name, Commission Internationale de l'Éclairage). The $L^*a^*b^*$ color space (also referred to as CIELAB) devised in 1976 is the most widely used, owing to the uniform distribution of colors.[25] In this space, L^* indicates lightness, ranging from 0 (black) to 100 (white), while a^* and b^* are the chromaticity coordinates that indicate color directions: $+a^*$ is the red direction; $-a^*$ is the green direction; $+b^*$ is the yellow direction; and $-b^*$ is the blue direction. Because the blue MB-based indicator loses its color during photobleaching and regains the color during recovery, the main color change happens in the b^* axis and can be defined as $-\Delta b^*$:

$$-\Delta b^* = b_0^* - b_t^*$$

where b_0^* is the initial b^* value of samples and b_t^* is their b^* value at a specific time t. The difference of the b^* value has been successfully used as a measure of the MB color.[19]

RESULTS AND DISCUSSION

Preparation of Carrageenan-Based Oxygen Indicator Films. To begin with, we examined whether carrageenans can interact with redox dyes. Two major classes of carrageenans were employed: κ- and ι-carrageenans. Carrageenans are linear, partially sulfated galactans that mainly consist of alternating 3-linked β-D-galactopyranose (G) and 4-linked 3,6-anhydro-α-D-galactopyranose (DA); κ-carrageenan (G4S-DA) has one sulfate group covalently coupled via ester linkage to the carbon atom C-4 of the G residue (G-4), while ι-carrageenan (G4S-DA2S) possesses two sulfate groups at the G-4 and DA-2.[22] Three types of thiazine dyes were used: MB, AA, and Th. When 0.2 mL of each aqueous dye solution (10 mg/mL) was added to 10 mL of ι-carrageenan solution (2.5 mg/mL), insoluble stringy aggregates were formed with all of the dyes tested; however, aggregation with κ-carrageenan was barely observed with the naked eye in all cases (data not shown). This can be explained by the difference in the sulfate content of the carrageenans; typically, commercial κ- and ι-carrageenans contain 22 and 32% (w/w) sulfate, respectively, although they vary considerably according to seaweed species and batches.[23] It was demonstrated that the sulfate moiety of carrageenans is essential for the interaction with cationic dyes, and the binding activity increases when the percentage of sulfate is increased.[26−28] In the present work, only ι-carrageenan was used for further study and carrageenan refers to ι-carrageenan unless otherwise mentioned.

We prepared UV-activated oxygen indicator films using carrageenan as the coating polymer; the packaging film was spin-coated with ink composed of redox dyes, glycerol, and TiO_2 and then dip-coated with carrageenan solutions (see the Materials and Methods). For comparison, the zein-based film was also fabricated in the same manner as the carrageenan-based film. However, little dye remained on the film because the dyes dissolved into the zein solution (90% ethanol) during the dip-coating step.[20] Therefore, the indicator films using zein as the encapsulation polymer were prepared by spin-coating the packaging film with the ink comprising redox dyes, glycerol, TiO_2, and zein, as described in the Materials and Methods. For reference, the carrageenan-based film could not be prepared in this manner because the addition of the dyes to the aqueous carrageenan solution led to the formation of insoluble aggregates as already mentioned.

Leakage Behaviors of Redox Dyes from the Films. Because MB is readily soluble in water, without proper protective polymers, the dye in the indicator film leaches out very quickly when immersed in water.[17] With the water-insoluble zein polymer (5%), the water resistance of the MB-coated indicator film was investigated by immersing the film in water for 24 h. As shown in Figure 1 (closed circles), after MB leached out quite quickly within the first hour of immersion, the dye leakage reached 48% and then remained nearly constant. The resultant MB/TiO_2/glycerol/zein (5%) film was so light-colored that it was not suitable for a colorimetric oxygen indicator. Although water-insoluble zein covered MB, it could not completely prevent the small water-soluble ionic

dx.doi.org/10.1021/jf5014764 | J. Agric. Food Chem. 2014, 62, 7263−7267

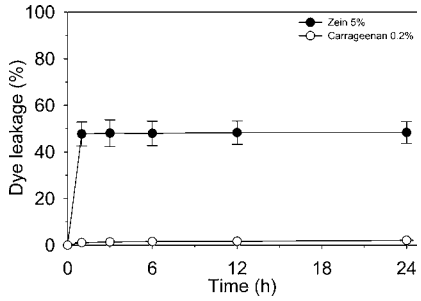

Figure 1. Dye leakage of zein (5%)-based and ι-carrageenan (0.2%)-based oxygen indicator films as a function of the water immersion time.

molecules (about 16.9 Å in length, 7.4 Å in breadth, and 3.8 Å in thickness) from leaking into the water.[29]

The same experiment was carried out using water-soluble carrageenan (0.2%) as the encapsulating polymer; surprisingly, only 2.1% of MB on the film leached into the water (open circles in Figure 1). This high resistance to dye leakage is believed to be attributed to the electrostatic interaction of the anionic polymer and the cationic dye.[26−28] Carrageenan is negatively charged because of the two sulfated groups on the repeating dimer, whereas MB, generally available as chloride salts, exists in cationic form in water.

The concentration effects of each polymer were examined for the protection ability against dye leakage: 5, 10, 15, and 20% for zein and 0.2, 0.3, 0.4, and 0.5% for carrageenan. When the zein concentration was increased from 5 to 20%, the dye leakage gradually declined to around 30% but it was still high (Figure 2a). The dye leakage of the carrageenan-based film slightly decreased from 2.1 to 1.8% when the concentration was increased from 0.2 to 0.5%, indicating that carrageenan is effective enough at as low a concentration as 0.2% (Figure 2b).

We examined whether carrageenan can also prevent dyes other than MB from leaching from the film into water. The carrageenan (0.2%)-based oxygen indicator films were prepared

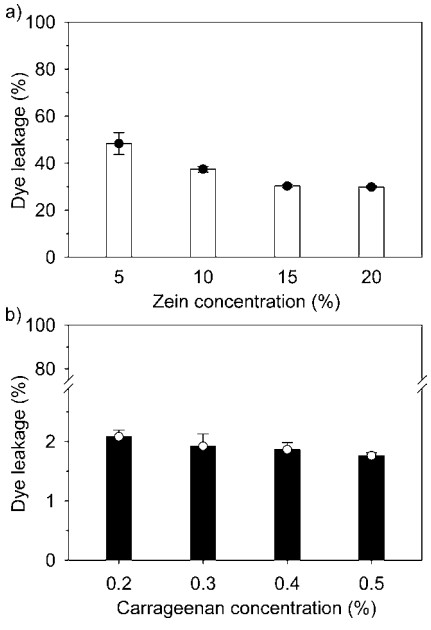

Figure 2. Effect of the polymer concentration on MB leakage after 24 h of (a) zein-based and (b) ι-carrageenan-based oxygen indicator films.

with AA and Th in the same way as with MB; for comparison, the zein (20%)-based films were also fabricated. The leakages of the three dyes after 24 h of immersion in water are shown in Figure 3: zein (open bars) and carrageenan (closed bars).

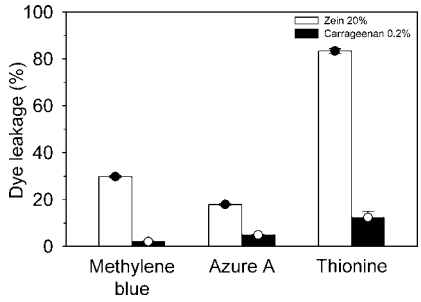

Figure 3. Leaching behaviors of MB, AA, and Th dyes on zein (20%)-based and ι-carrageenan (0.2%)-based oxygen indicator films.

Similar to MB, the leakages of AA and Th were considerable with the zein polymer, particularly Th. The reason why Th showed the highest leakage is not evident, but this could be due to the larger contact area of Th with water; Th (with no methyl group) is more hydrophilic than AA (with two methyl groups) and MB (with four methyl groups).[30] In comparison to zein, carrageenan diminished the leakage of AA and Th as well as MB to a greater degree because of the electrostatic interaction of the anionic carrageenan with the cationic dyes. In addition, the dye leakage might be further lowered by additional optimization (e.g., the employment of carrageenans with higher percentages of sulfate and/or with other molecular weights).[22,23]

Photobleaching and Recovery Process of Carrageenan-Based Indicator Film. An UV-activated indicator film should be bleached when exposed to UV light (photobleaching step) and regain its color in the presence of oxygen (recovery step). Because the strong interaction between carrageenans and dyes might impede the photobleaching and recovery processes of the carrageenan-based indicator film, we investigated this possibility. The oxygen indicator films were prepared using MB and carrageenan (0.2, 0.3, 0.4, and 0.5%) as the redox dye and the coating polymer, respectively. When the carrageenan-coated films were irradiated with UVC light (intensity = 5.5 mW/cm^2) for 4 min, all of the films were completely bleached (data not shown). The finely dispersed TiO_2 nanoparticles (photocatalyst) encapsulated in the polymer generate electron−hole pairs upon UV irradiation. The photogenerated holes oxidize glycerol (a sacrificial electron donor), and the photogenerated electrons reduce MB to its colorless reduced form.[12] The initial rate of photobleaching was also measured as a function of the carrageenan concentration. Figure 4a (circles) shows that the bleaching rate decreased as the polymer concentration increased. This may not be due to the increase in the thickness of the carrageenan film with the increasing concentration because the difference in the thickness was not significant, as shown in Figure 4a (bars); the reason is a question for future research.

Figure 4b shows the recovery behavior of the MB/TiO_2/glycerol/carrageenan (0.2%) indicator film in air under ambient conditions in which $-\Delta b^*$ was plotted against recovery time. The oxygen indicator film was recovered within about 8 h, The colorless reduced form of MB on the film was reoxidized by oxygen, and the original blue color of the indicator film was

dx.doi.org/10.1021/jf5014764 | J. Agric. Food Chem. 2014, 62, 7263−7267

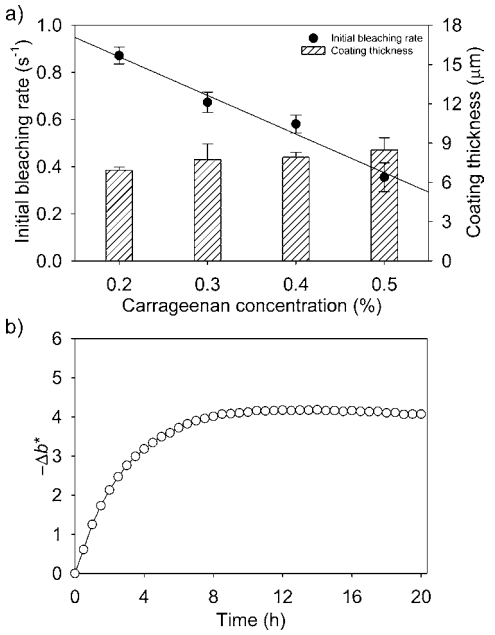

Figure 4. (a) Initial bleaching rate and coating thickness of MB/TiO_2/glycerol/*ι*-carrageenan oxygen indicator films as a function of the carrageenan concentration. (b) Recovery behavior of MB/TiO_2/glycerol/*ι*-carrageenan (0.2%) oxygen indicator film in air under ambient conditions with a sampling time of 30 min.

restored. This recovery time may not be satisfactory if compared to conventional water-susceptible indicator films (~6 min),[12] but it is appreciably short considering that the other waterproof films had recovery times of 5 days using sulfonated polystyrene[17] and 2.5 days using low-density PE.[19] The high recovery rate of the carrageenan-based film is probably attributed to the hydrophilic nature of carrageenans, because hydrophobic films hinder the formation of the charged species, MB^+ and OH^-, for color recovery.[17,19]

In conclusion, we have developed an UV-activated oxygen indicator film resistant to dye leaching by introducing carrageenans, which are natural sulfated polysaccharides. The dye-binding ability of carrageenans substantially lowered the leakage into water of all of the redox dyes tested (MB, AA, and Th). The MB/TiO_2/glycerol/carrageenan oxygen indicator film was successfully bleached upon UV irradiation and regained its color very rapidly in the presence of oxygen. This leaching-resistant colorimetric oxygen indicator film with in-pack activation and irreversibility can be applied to verify that all oxygen is removed using oxygen absorbers/oxygen scavengers, and it can also be used as a seal and leak detector with modified atmosphere packaging; it will be essential for intelligent food packaging.

AUTHOR INFORMATION

Corresponding Author

*Telephone: +82-2-2260-8922. Fax: +82-2-2268-8729. E-mail: keehoon@dongguk.edu.

Funding

This research was supported by the Agriculture Research Center Program of the Ministry of Agriculture, Food, and Rural Affairs (ARC-710003-03-4-SB120), the New and Renewable Energy of the Korea Institute of Energy Technology Evaluation and Planning (KETEP) grant funded by the Korea Government Ministry of Trade, Industry, and Energy (20133030000300), and the Korea Carbon Capture and Sequestration (CCS) Research and Development (R&D) Center (KCRC) Program (2013M1A8A1038187) of the Ministry of Science, Information/Communications Technology (ICT), and Future Planning, Republic of Korea.

Notes

The authors declare no competing financial interest.

REFERENCES

(1) Brody, A. L.; Bugusu, B.; Han, J. H.; Sand, C. K.; Mchugh, T. H. Innovative food packaging solutions. *J. Food Sci.* **2008**, *73*, R107−R116.

(2) De Jong, A. R.; Boumans, H.; Slaghek, T.; van Veen, J.; Rijk, R.; van Zandvoort, M. Active and intelligent packaging for food: Is it the future? *Food Addit. Contam.* **2005**, *22*, 975−979.

(3) Heising, J. K.; Dekker, M.; Bartels, P. V.; van Boekel, M. A. J. S. Monitoring the quality of perishable foods: Opportunities for intelligent packaging. *Crit. Rev. Food Sci. Nutr.* **2014**, *54*, 645−654.

(4) Pereira de Abreu, D. A.; Cruz, J. M.; Paseiro Losada, P. Active and intelligent packaging for the food industry. *Food Rev. Int.* **2012**, *28*, 146−187.

(5) Yam, K. L.; Takhistov, P. T.; Miltz, J. Intelligent packaging: Concepts and applications. *J. Food Sci.* **2005**, *70*, R1−R10.

(6) Kim, K.; Kim, E.; Lee, S. J. New enzymatic time-temperature integrator (TTI) that uses laccase. *J. Food Eng.* **2012**, *113*, 118−123.

(7) Jang, N. Y.; Won, K. New pressure-activated compartmented oxygen indicator for intelligent food packaging. *Int. J. Food Sci. Technol.* **2014**, *49*, 650−654.

(8) Jung, J.; Puligundla, P.; Ko, S. Proof-of-concept study of chitosan-based carbon dioxide indicator for food packaging applications. *Food Chem.* **2012**, *135*, 2170−2174.

(9) Feng, S.; Luo, Z.; Shao, S.; Wu, B.; Ying, T. Effect of relative humidity and temperature on absorption kinetics of two types of oxygen scavengers for packaged food. *Int. J. Food Sci. Technol.* **2013**, *48*, 1390−1395.

(10) Lee, K.-E.; Kim, H. J.; An, D. S.; Lyu, E. S.; Lee, D. S. Effectiveness of modified atmosphere packaging in preserving a prepared ready-to-eat food. *Packag. Technol. Sci.* **2008**, *21*, 417−423.

(11) Mills, A. Oxygen indicators and intelligent inks for packaging food. *Chem. Soc. Rev.* **2005**, *34*, 1003−1011.

(12) Lee, S.-K.; Mills, A.; Lepre, A. An intelligence ink for oxygen. *Chem. Commun.* **2004**, 1912−1913.

(13) Mihindukulasuriya, S. D. F.; Lim, L.-T. Oxygen detection using UV-activated electrospun poly(ethylene oxide) fibers encapsulated with TiO_2 nanoparticles. *J. Mater. Sci.* **2013**, *48*, 5489−5498.

(14) Ghosh, D.; Bhattacharyya, K. G. Adsorption of methylene blue on kaolinite. *Appl. Clay Sci.* **2002**, *20*, 295−300.

(15) Paul, P.; Kumar, G. S. Targeting ribonucleic acids by toxic small molecules: structural perturbation and energetics of interaction of phenothiazinium dyes thionine and toluidine blue O to $tRNA^{phe}$. *J. Hazard. Mater.* **2013**, *263*, 735−745.

(16) Restuccia, D.; Spizzirri, U. G.; Parisi, O. I.; Cirillo, G.; Curcio, M.; Iemma, F.; Puoci, F.; Vinci, G.; Picci, N. New EU regulation aspects and global market of active and intelligent packaging for food industry applications. *Food Control* **2010**, *21*, 1425−1435.

(17) Mills, A.; Hazafy, D.; Lawrie, K. Novel photocatalyst-based colourimetric indicator for oxygen. *Catal. Today* **2011**, *161*, 59−63.

(18) Mills, A.; Lawrie, K. Novel photocatalyst-based colourimetric indicator for oxygen: Use of a platinum catalyst for controlling response times. *Sens. Actuators, B* **2011**, *157*, 600−605.

(19) Mills, A.; Lawrie, K.; Bardin, J.; Apedaile, A.; Skinner, G. A.; O'Rourke, C. An O_2 smart plastic film for packaging. *Analyst* **2012**, *137*, 106−112.

(20) Vu, C. H. T.; Won, K. Novel water-resistant UV-activated oxygen indicator for intelligent food packaging. *Food Chem.* **2013**, *140*, 52−56.

(21) Vu, C. H. T.; Won, K. Bioinspired molecular adhesive for water-resistant oxygen indicator films. *Biotechnol. Prog.* **2013**, *29*, 513−519.

(22) Campo, V. L.; Kawano, D. F.; da Silva Jr., D. B.; Carvalho, I. Carrageenans: biological properties, chemical modifications and structural analysis—A review. *Carbohydr. Polym.* **2009**, *77*, 167−180.
(23) De Ruiter, G. A.; Rudolph, B. Carrageenan biotechnology. *Trends Food Sci. Technol.* **1997**, *8*, 389−395.
(24) Sanchez-Garcia, M. D.; Hilliou, L.; Lagaron, J. M. Nanobiocomposites of carrageenan, zein, and mica of interest in food packaging and coating applications. *J. Agric. Food Chem.* **2010**, *58*, 6884−6894.
(25) Wu, D.; Sun, D.-W. Colour measurements by computer vision for food quality control—A review. *Trends Food Sci. Technol.* **2013**, *29*, 5−20.
(26) Graham, H. D. Quantitative aspects of the interaction of carrageenan with cationic substances. I. Interaction with methylene blue. *J. Food Sci.* **1960**, *25*, 720−730.
(27) Graham, H. D.; Thomas, L. B. Precipitation of food gums by thiazine, oxazine, azine and other cationic dyes: Specificity of the methylene blue carrageenan reaction. *J. Food Sci.* **1961**, *26*, 365−372.
(28) Soedlak, H. S. Colorimetric determination of carrageenans and other anionic hydrocolloids with methylene blue. *Anal. Chem.* **1994**, *66*, 4514−4518.
(29) Hähner, G.; Marti, A.; Spencer, N. D.; Caseri, W. R. Orientation and electronic structure of methylene blue on mica: A near edge X-ray absorption fine structure spectroscopy study. *J. Chem. Phys.* **1996**, *104*, 7749−7757.
(30) Chakraborty, A.; Ali, M.; Saha, S. K. Molecular interaction of organic dyes in bulk and confined media. *Spectrochim. Acta, Part A* **2010**, *75*, 1577−1583.

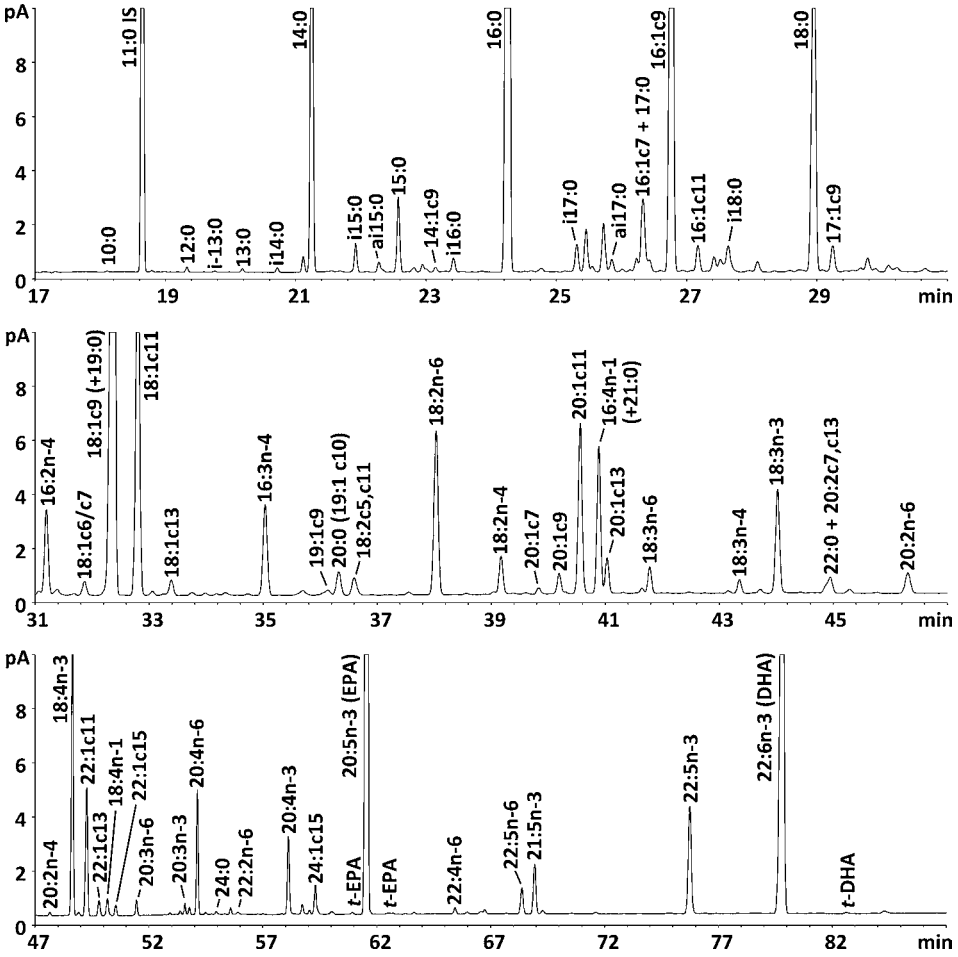

Figure 1. Gas chromatogram of FAME derived from an SO supplement.

conclusive research shows that consumption of EPA and DHA omega-3 fatty acids may reduce the risk of coronary heart disease".[21,22]

MATERIALS AND METHODS

Chemicals and Reagents. ACS reagent grade chemicals and solutions were purchased from Sigma-Aldrich (St. Louis, MO). HPLC grade solvents were purchased from Fisher Scientific (Pittsburgh, PA). FAME (EPA and DHA) and triacylglycerol (TAG; C11:0) standards were purchased from Nu-Chek Prep (Elysian, MN). Our choice of C11:0 TAG as internal standard (IS) was based on the fact that the content of C11:0 is negligible in FO and that the C11:0 FAME isomer is chromatographically resolved from other FAME on the 200 m SLB-IL111 column.[20]

SRM 3275. SRM 3275 was purchased from NIST (Gaithersburg, MD). This reference material consists of three fish oils: SRM 3275-1, a concentrate high in DHA; SRM 3275-2, an anchovy oil high in EPA and DHA; and SRM 3275-3, a concentrate containing nominally 60% omega-3 LCPUFA. The SRM was stored at 4 °C until analysis. Details of the development of SRM 3275 have been reported.[23]

Marine Oil Omega-3 Supplements. Marine oil omega-3 supplements were purchased online between May and July of 2012. Products were included in the study if their ingredient statements listed a source of marine oil and the Supplement Facts panel listed declarations for EPA and DHA. Eighteen of the products listed FO (e.g., anchovy, sardine, and mackerel) as the primary ingredient. Fifteen of the products listed FO concentrate (from anchovy, sardine, mackerel, or species undefined) as the primary ingredient. Nine of the supplements were marketed as salmon oil (SO) supplements. However, two of these products included an additional FO source in their ingredients lists (reportedly added for the purpose of increasing EPA and DHA potency, species undefined) and thus were classified as FO products. The remaining four supplements contained a combination of plant oil (e.g., borage, olive, and flax) and FO (i.e., plant/FO blends). Supplements were purchased in softgel (also referred to on product labels as capsule or minigel; $n = 40$) and liquid ($n = 6$) forms. Softgel products listed gelatin, glycerin, and water as ingredients. Forty-one of the products contained antioxidants (e.g., tocopherols, ascorbyl palmitate, and botanical extracts). Eleven of the products (24%) carried the qualified health claim for EPA and DHA. All products, which were collected for research purposes only, were stored at −80 °C until analysis and were analyzed prior to their expiration dates.

Methylation. Methylation was performed in duplicate according to AOCS Official Method Ce 2-66.[24] This method involves an alkali hydrolysis with 0.5 M NaOH in MeOH followed by methylation with fresh 14% BF_3 in MeOH.[24] For supplements, oil from 2−3 softgels was combined, then ∼50 mg was weighed into 16 × 150 mm glass extraction tubes for methylation. Following derivatization, FAMEs were solubilized in heptane (∼12.5 mg/mL) and stored in silanized, amber-colored autosampler vials.

Preparation of Isomerized EPA and DHA FAME. Standards for the *trans* isomers of EPA and DHA were prepared from all-*cis* EPA and DHA FAME, respectively, by isomerization with *p*-toluenesulfinic acid according to Snyder and Scholfield.[25] Samples were heated for a maximum of 3 min to limit the degree of isomerization. Isomerized EPA and DHA FAMEs were then fractionated by number of *trans* double bonds on silica gel plates impregnated with 10% silver nitrate (Analtech, Newark, DE). Plates were developed at −20 °C in toluene/MeOH (85:15, v/v) according to Fournier et al.[26] Individual bands

dx.doi.org/10.1021/jf5016973 | J. Agric. Food Chem. 2014, 62, 7268−7278

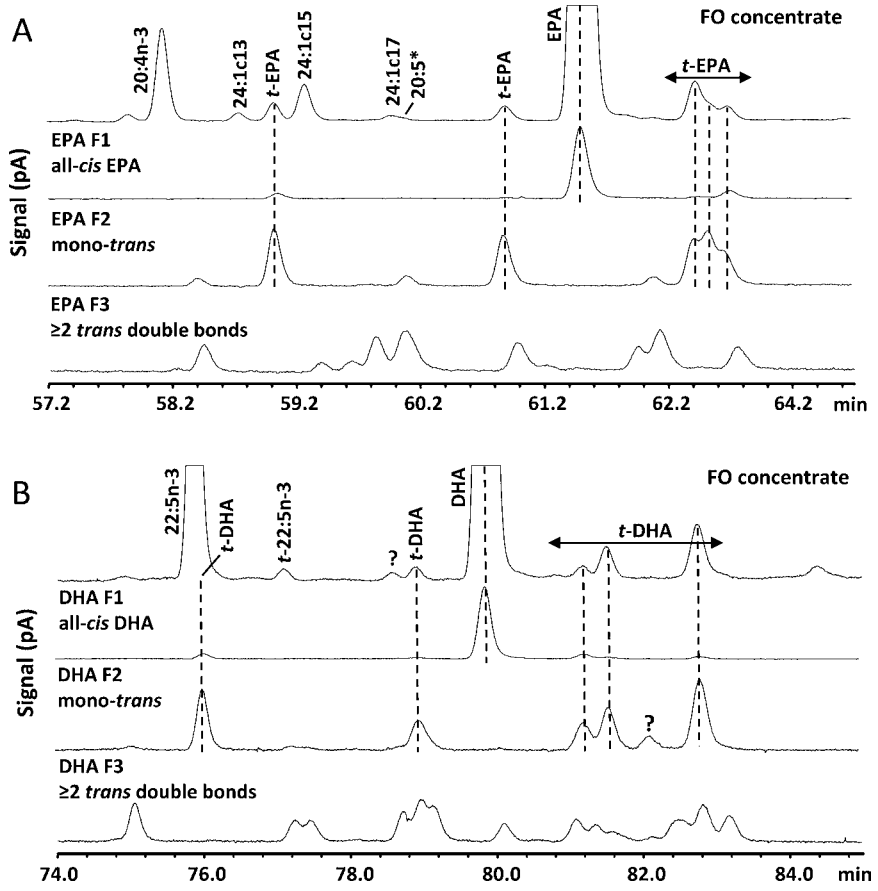

Figure 2. Partial gas chromatograms of FAME derived from an FO concentrate in the regions in which EPA (panel A) and DHA (panel B) elute. For each panel, the top partial gas chromatogram corresponds to FAME derived from the FO concentrate, while the lower partial gas chromatograms correspond to isomerized EPA and DHA FAME fractions (F1−F3). *20:5 contains C20:5n-4 plus *t*-EPA.

were identified by comparison with published thin layer chromatography (TLC) plate images.[27]

GC Instrumentation. Analysis by GC-FID was performed in split mode on a 6890N GC (Agilent Technologies, Wilmington, DE) equipped with a 200 m SLB-IL111 column, which was formed by connecting two 100 m SLB-IL111 columns (Supelco, Bellefonte, PA) using an Agilent press fit quartz column connector. The oven was maintained at 170 °C for 50 min, then ramped at 6 °C/min to 185 °C, held for 50 min, then ramped at 20 °C/min to 220 °C, and held for 5 min. The oven was maintained at 168 °C for the 5 min postrun. A single GC run time was 114.25 min. The flow program for the H_2 carrier gas was as follows: 1.6 mL/min for 35 min, ramped at 0.3 mL/min/min to 3.0 mL/min, and held for ∼70 min. The inlet and FID temperatures were 300 and 235 °C, respectively. The split ratio was 100:1, and the injection volume was 1 μL. A complementary analysis of FAME, which was performed to resolve FAME coeluting on the 200 m SLB-IL111 column, was carried out on the 30 m Supelcowax 10 column (Supelco, Bellefonte, PA) according to AOCS Official Method Ce 1i-07.[14] Calculations for fatty acid content were performed using theoretical correction factors.[14]

GC-mass spectrometry (MS) analysis was performed on a 7890A GC coupled to a 240 MS ion trap mass spectrometer (Agilent Technologies) and equipped with a 200 m SLB-IL111 column. The oven was maintained at 170 °C for 63 min, then ramped at 6 °C/min to 185 °C, held for 20 min, then ramped at 15 °C/min to 220 °C, and held for 22 min. The oven was maintained at 170 °C for a 5 min postrun. The flow of the He carrier gas was held at 1.6 mL/min for 45.5 min, then ramped at 0.3 mL/min/min to 2.0 mL/min, and held for 63 min. FAMEs were identified by covalent adduct chemical ionization (CACI) tandem MS using acetonitrile as the reagent gas.[28]

Calculations for Supplements. Single serving contents of individual fatty acids were calculated based on analyzed fatty acid contents (as % of total weight) and the weight of oil in a single serving. For products for which serving size was reported by volume (e.g., 5 mL), 10 servings were pipetted into tared weighing boats and weighed to the nearest 0.0001 g on an AE100 analytical balance (Mettler-Toledo, Columbus, OH). For products for which serving size was reported by quantity (e.g., two softgels), the weights of 20 servings or a minimum of 1/5 of the contents of the bottle were recorded. Softgel capsules were then punctured, rinsed with hexane, and the weights of the dry capsule shells recorded. The weight of oil in a single serving was calculated as the mean serving weight (capsule shell plus oil) minus the mean capsule shell weight.

Statistical Analysis. Statistical analysis was performed using JMP (version 9.0.0. 2010, SAS Institute, Cary, NC). One way analysis of variance was used to compare mean values, and Student's *t*-test was applied when significant differences were observed ($F < 0.05$). Values are reported as the means ± standard deviations (SD). Statistical outliers were determined using Grubbs' test.[29]

RESULTS

Chromatography. The chromatographic separation of FAME derived from an SO supplement is presented in Figure 1. Seventy-three FAME isomers, accounting for 91.9 ± 3.4% of total fat, were included in this analysis. Chromatographic conditions presented in this article are similar to those reported by Fardin-Kia et al.[20] but included a final temperature ramp to 220 °C, maintained for 5 min. The extended temperature program ensured complete elution of analytes in a single GC run and avoided the occurrence of ghost peaks in subsequent chromatograms due to analyte carryover.

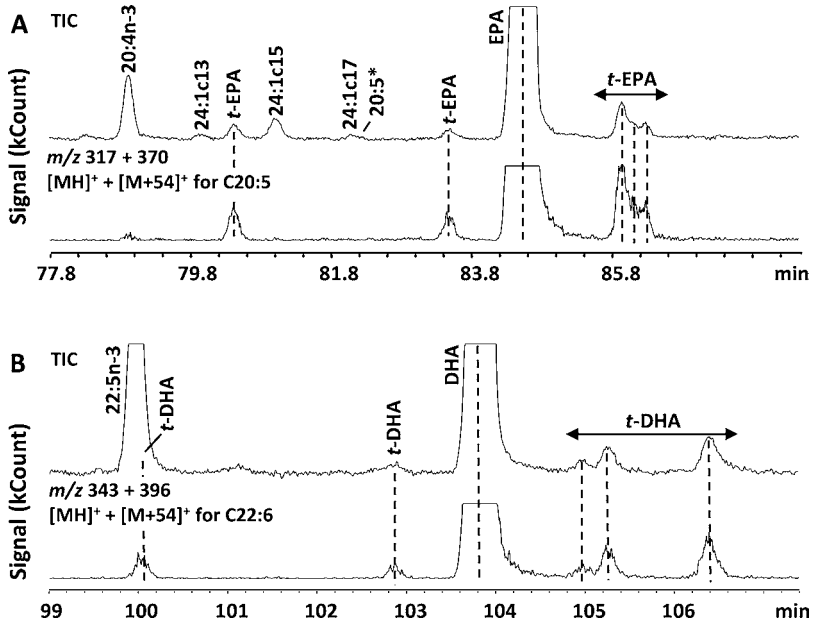

Figure 3. Partial GC-CACI-MS chromatograms of FAME derived from an FO concentrate product in the regions in which EPA (panel A) and DHA (panel B) elute. For each panel, the top partial GC-MS chromatogram corresponds to the TIC. The lower partial GC-MS chromatogram is a reconstructed ion chromatogram specific for ions attributed to C20:5 and C22:6 FAME (molecular ion, $[MH]^+$; m/z 54 adduct ion, $[M+54]^+$).[28]

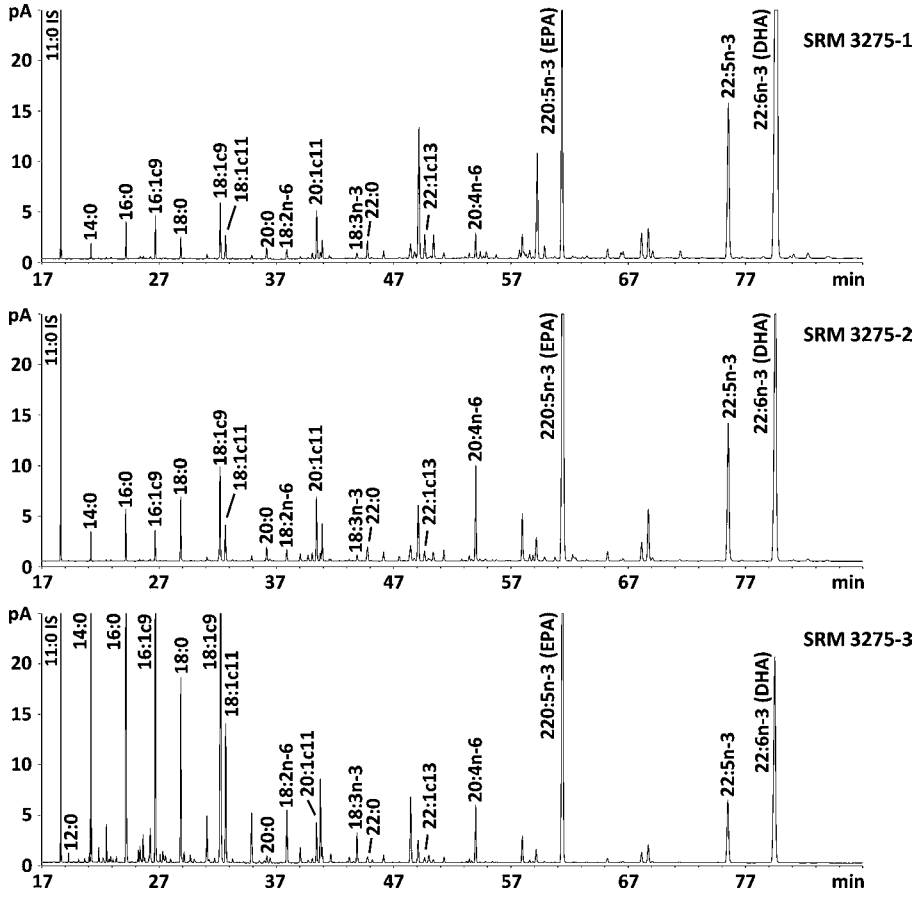

Figure 4. Gas chromatograms of FAME derived from the three fish oils of SRM 3275. FAME for which certified and reference mass fraction values are reported in the Certificate of Analysis are labeled.

Standards for the *trans* isomers of EPA and DHA FAME, which were prepared from all-*cis* EPA and DHA FAME by isomerization with *p*-toluenesulfinic acid, were fractionated on silver ion TLC plates according to the number of *trans* double bonds. Plates were sprayed with 2′,7′-dicholorfluorescein solution (0.1% in isopropanol) and bands identified by

dx.doi.org/10.1021/jf5016973 | J. Agric. Food Chem. 2014, 62, 7268−7278

Table 1. Recoveries of Individual FAME from the Three Fish Oils of NIST SRM 3275[a]

	SRM 3275-1			SRM 3275-2			SRM 3275-3		
FAME	certificate value (mg/g)	analyzed value (mg/g)[b]	recovery (%)[c]	certificate value (mg/g)	analyzed value (mg/g)	recovery (%)	certificate value (mg/g)	analyzed value (mg/g)	recovery (%)
C12:0					0.1 ± 0.0		**0.95 ± 0.12**	1.1 ± 0.0	113
C14:0	**1.094 ± 0.053**	1.9 ± 0.0	174	**3.45 ± 0.40**	4.1 ± 0.0	120	**67.9 ± 1.5**	61.0 ± 0.4	90
C14:1*cis*-9							0.964 ± 0.043	0.5 ± 0.0	49
C16:0	**5.25 ± 0.35**	5.6 ± 0.0	106	**8.01 ± 0.44**	8.8 ± 0.0	109	**186.9 ± 9.4**	155.4 ± 1.3	83
C16:1*cis*-9	**7.43 ± 0.24**	7.6 ± 0.0	102	**5.83 ± 0.45**	6.0 ± 0.0	103	**85.7 ± 3.1**	68.4 ± 0.5	80
C18:0	**4.22 ± 0.13**	4.3 ± 0.0	101	**12.94 ± 0.62**	13.9 ± 0.0	108	**38.0 ± 5.7**	36.4 ± 0.4	96
C18:1*cis*-9	**11.25 ± 0.93**	12.8 ± 0.0	114	**22.1 ± 1.6**	24.2 ± 0.1	109	**112.3 ± 2.6**	106.1 ± 1.0	94
C18:1*cis*-11	**5.33 ± 0.35**	5.4 ± 0.0	102	**9.24 ± 0.77**	9.5 ± 0.0	102	**38.5 ± 2.2**	31.8 ± 0.3	83
C18:2n-6	**2.31 ± 0.19**	2.4 ± 0.0	103	**3.00 ± 0.42**	3.3 ± 0.0	109	**13.49 ± 0.45**	13.3 ± 0.1	99
C18:3n-6	0.344 ± 0.025	0.3 ± 0.0	98	0.507 ± 0.043	0.5 ± 0.0	90	1.771 ± 0.099	2.0 ± 0.0	113
C18:3n-3	1.21 ± 0.05	1.7 ± 0.0	143	1.42 ± 0.12	1.8 ± 0.0	128	6.61 ± 0.31	7.4 ± 0.1	112
C20:0	1.910 ± 0.071	3.0 ± 0.0	154	**0.357 ± 0.027**	4.2 ± 0.1	1182	**1.14 ± 0.26**	1.9 ± 0.0	164
C20:1*cis*-11		11.7 ± 0.0		**6.66 ± 0.69**	16.8 ± 0.1	252	**2.92 ± 0.14**	9.3 ± 0.1	320
C20:4n-6	5.69 ± 0.19	6.4 ± 0.0	112	22.9 ± 1.0	26.6 ± 0.0	116		14.1 ± 0.2	
C20:5n-3 (EPA)	**113 ± 12**	112.0 ± 0.0	99	394 ± 17	407.5 ± 0.4	103	154 ± 9	163.4 ± 2.3	106
C22:5n-3	70.2 ± 1.1	75.5 ± 0.1	107	67.6 ± 2.3	73.9 ± 0.1	109	27.0 ± 1.1	29.0 ± 0.5	107
C22:6n-3 (DHA)	429 ± 15	436.0 ± 0.1	102	187 ± 8	192.4 ± 0.1	103	104 ± 5	106.5 ± 1.3	102
C22:0	**4.02 ± 0.24**	5.2 ± 0.0	129	**1.396 ± 0.046**	2.9 ± 0.0	209	**0.502 ± 0.047**	0.8 ± 0.0	164
C22:1*cis*-13	4.76 ± 0.22	7.7 ± 0.0	162	**3.43 ± 0.32**	3.7 ± 0.0	106	1.61 ± 0.11	1.7 ± 0.0	104
C24:0				0.618 ± 0.028	0.8 ± 0.0	136	0.441 ± 0.013	0.5 ± 0.0	103
C24:1*cis*-15							3.78 ± 0.29	4.4 ± 0.0	116

[a]Mass fraction values for individual FAME are reported in the Certificate of Analysis for SRM 3275. Value assignments are based on two independent methods and the reported mean value represents the mean of the mean values from each method. Certified mass fraction values (bold font) are reported to represent the highest level of confidence in accuracy and account for all known or suspected sources of bias. The associated uncertainty is expressed at a 95% level of confidence and represents the combined standard uncertainty multiplied by a coverage factor *k*. Reference mass fraction values (not bold font) are reported to represent the best estimate of true value based on available data, and the associated uncertainties may reflect only measurement reproducibility. [b]Analyzed values represent the means ± SD of two independent determinations. [c]Recovery calculated as analyzed/certificate value × 100.

comparison with published TLC images.[27] Fractions corresponding to all-*cis* FAME, mono-*trans* FAME, and FAME with two or more *trans* double bonds were collected and analyzed by GC-FID for retention time. Figure 2 presents partial gas chromatograms for the *trans* EPA and DHA FAME standards and for FAME derived from an FO concentrate product. Peaks for five mono-*trans* EPA isomers were observed in both the mono-*trans* EPA standard and the marine oil omega-3 supplements (Figure 2A). The mono-*trans* DHA standard showed five mono-*trans* DHA peaks, but only four mono-*trans* DHA peaks were observed in the supplements (Figure 2B). The first eluting mono-*trans* DHA isomer coeluted with C22:5n-3 in the supplements (Figure 2B). FAMEs with two or more *trans* double bonds, if present in the supplements, were found at or near the level of detection.

The presence of *trans* isomers of EPA and DHA in the supplements was also verified by GC-CACI-MS analysis (Figure 3). The top chromatogram in Figure 3A corresponds to the total ion chromatogram (TIC) for FAMEs derived from an FO concentrate product. The lower chromatogram corresponds to the reconstructed ion chromatogram for *m/z* 317 ($[MH]^+$) and *m/z* 370 ($[M+54]^+$) ions, which are attributed to C20:5 FAME in the FO concentrate product. Peaks in the reconstructed ion chromatogram at 80.3, 82.3, and 85.8 min (Figure 3A) are consistent with those observed in the partial gas chromatogram for the mono-*trans* EPA standard (Figure 2A), providing further confirmation of the presence of mono-*trans* EPA in the supplements. Similarly, in Figure 3B, peaks in the reconstructed ion chromatogram, which correspond to *m/z* 343 ($[MH]^+$) and *m/z* 396 ($[M+54]^+$) ions that are specific to C22:6 FAME in the FO concentrate product, are consistent with those in the partial gas chromatogram for the mono-*trans* DHA FAME standard (Figure 2B). In addition, the first eluting mono-*trans* DHA FAME was found to coelute with C22:5n-3 (Figures 2B and 3B). GC-MS analysis indicated that the area of the first eluting mono-*trans* DHA isomer accounted for 20% of the total peak area for mono-*trans* DHA in the two products with the highest concentrations of *trans* DHA (Figure 3B). Therefore, for all samples, the quantitation of *trans* DHA included a correction factor (i.e., integrated area of mono-*trans* DHA/0.8) to account for the area of the mono-*trans* DHA FAME that coeluted with C22:5n-3.

Analysis of SRM 3275. GC-FID chromatograms for the separation of FAMEs derived from the three SRM fish oils are presented in Figure 4. Analyzed values for 21 FAMEs are presented in Table 1 along with corresponding values reported in the Certificate of Analysis. Recoveries for EPA and DHA, which were calculated as analyzed/certificate values × 100, varied from 99% to 106% and from 102% to 103%, respectively, among the three SRM fish oils. Analyzed values for EPA and DHA were all within the range of mass fraction values covered by the expanded uncertainty. For the remaining FAME, the majority of recoveries were within the range of 80% to 120%, whereas for a few FAMEs, recoveries varied from 49% to 1182%. Analyzed values for three FAMEs (C20:0, C20:1*cis*-11, and C22:0) were significantly greater than the corresponding certificate values, indicating the presence of coeluting peaks on the 200 m SLB-IL111 column.

Table 2. Concentrations of Fatty Acids in the Marine Oil Omega-3 Supplement Groups

fatty acid (% of total fat)[a]	FO	FO concentrate	plant/FO blend	SO	P^b
Σ SFA	17.4 ± 9.2ab	11.7 ± 11.6b	9.5 ± 1.2b	23.0 ± 1.8a	0.03
Σ MUFA	17.0 ± 4.4b	13.3 ± 7.3b	18.0 ± 2.5b	30.6 ± 6.1a	<0.0001
n-6 PUFA					
C18:2n-6	1.0 ± 0.3b	0.8 ± 0.4b	14.2 ± 3.8a	1.8 ± 0.8b	<0.0001
C18:3n-6	0.2 ± 0.1b	0.2 ± 0.1b	4.5 ± 3.0a	0.1 ± 0.2b	<0.0001
C20:2n-6	0.2 ± 0.1b	0.2 ± 0.1b	0.2 ± 0.0c	0.4 ± 0.1a	0.0002
C20:3n-6	0.2 ± 0.1ab	0.2 ± 0.1a	0.1 ± 0.0b	0.1 ± 0.0b	0.02
C20:4n-6	1.4 ± 0.5a	1.5 ± 0.7a	0.6 ± 0.2b	0.5 ± 0.1b	0.0003
C22:5n-6	0.5 ± 0.5	0.6 ± 0.3	0.2 ± 0.1	0.2 ± 0.1	NS
Σ n-6 PUFA	3.5 ± 0.8b	3.7 ± 0.7b	19.9 ± 6.4a	3.3 ± 0.8b	<0.0001
n-4 PUFA					
C16:2n-4	0.6 ± 0.4	0.5 ± 0.5	0.1 ± 0.0	0.4 ± 0.3	NS
C16:3n-4	0.7 ± 0.5a	0.6 ± 0.6ab	0.1 ± 0.0b	0.3 ± 0.3b	0.045
C18:2n-4	0.3 ± 0.1a	0.2 ± 0.1b	0.1 ± 0.1b	0.2 ± 0.1b	0.001
C18:3n-4	0.1 ± 0.0	0.1 ± 0.0	0.0 ± 0.0	0.1 ± 0.1	NS
Σ n-4 PUFA	1.8 ± 1.0	1.5 ± 1.2	0.3 ± 0.1	1.3 ± 1.0	NS
n-3 PUFA (all-*cis*)					
C18:3n-3	0.7 ± 0.2b	0.5 ± 0.2b	18.6 ± 2.9a	1.0 ± 0.2b	<0.0001
C18:4n-3	1.9 ± 0.7	1.8 ± 1.3	0.7 ± 0.2	1.9 ± 0.2	NS
C20:4n-3	0.9 ± 0.3a	1.1 ± 0.4a	0.5 ± 0.1b	1.2 ± 0.3a	0.008
C20:5n-3 (EPA)	19.9 ± 8.3b	26.7 ± 11.4a	10.1 ± 3.8c	9.3 ± 2.0c	0.0002
C21:5n-3	0.9 ± 0.4b	1.2 ± 0.6a	0.5 ± 0.2bc	0.4 ± 0.1c	0.0007
C22:5n-3	2.5 ± 1.0ab	3.2 ± 1.7a	1.5 ± 0.4b	2.1 ± 0.3b	0.04
C22:6n-3 (DHA)	14.3 ± 8.5ab	17.2 ± 8.6a	6.6 ± 2.0b	9.3 ± 0.6b	0.04
Σ n-3 PUFA	41.1 ± 13.3b	51.8 ± 18.1a	38.5 ± 6.0abc	26.8 ± 2.9c	0.003
n-1 PUFA					
C16:4n-1	1.2 ± 0.9	1.0 ± 1.0	0.1 ± 0.1	0.5 ± 0.4	NS
C18:4n-1	0.2 ± 0.1	0.2 ± 0.1	0.1 ± 0.0	0.2 ± 0.1	NS
Σ n-1 PUFA	1.4 ± 0.9	1.2 ± 1.1	0.2 ± 0.1	1.0 ± 0.8	NS
Σ *t*-EPA + *t*-DHA	0.4 ± 0.3ab	0.6 ± 0.4a	0.1 ± 0.0b	0.2 ± 0.2b	0.02

[a]Values represent the means ± SD for all products within a group (FO, $n = 20$; FO concentrate, $n = 15$; plant/FO blend, $n = 4$; SO, $n = 7$). [b]Values within a row with different letters are significantly different ($P < 0.05$); NS, not significant.

Fatty Acid Composition of Omega-3 Supplements. The concentrations of EPA and DHA varied from 7.8% to 45.4% and from 5.5% to 44.1% of total fat, respectively, in the 46 marine oil omega-3 supplements (Table 2). EPA concentrations were highest in the FO concentrates (26.7 ± 11.4% of total fat) and lowest in the plant/FO blends (10.1 ± 3.8% of total fat) and SO supplements (9.3 ± 2.0% of total fat). DHA concentrations were significantly higher in the FO concentrates (17.2 ± 8.6% of total fat) than in the plant/FO blends (6.6 ± 2.0% of total fat) and SO supplements (9.3 ± 0.6% of total fat), while FO products provided intermediate concentrations. The concentration of total SFA, which varied from 0.2 to 26.6% of total fat among all products, was significantly higher in the SO supplements (23.0 ± 1.8%) than in the FO concentrates (11.7 ± 11.6%) and plant/FO blends (9.5 ± 1.2%). SO supplements had the highest mean concentration of MUFA. The plant/FO blends had the highest mean concentration of n-6 PUFA. The sum of the *trans* isomers of EPA plus DHA, which varied from 0.1% to 1.5% of total fat among all products, was significantly higher in the FO concentrates (0.6 ± 0.4%) than in the plant/FO blends (0.1 ± 0.0%) and SO supplements (0.2 ± 0.2%), while FO products provided intermediate concentrations. Concentrations of n-4 and n-1 PUFA, which varied from 0.2% to 3.1% and from 0.1% to 2.6% of total fat, respectively, among all products, were highly correlated ($R^2 = 0.9489$; Supporting Information, Figure 1).

Product Composition. Table 3 presents the contents of fatty acids in single servings within the four supplement groups. One of the FO products was excluded from this analysis because the content of total fat in a single serving of the product (9.2 g total fat) was nearly twice that of the next highest product (4.7 g), causing it to be a statistical outlier. For the remaining 45 products, the overall mean contents of EPA, DHA, and EPA plus DHA in a single serving were 354 ± 247 mg, 239 ± 133 mg, and 592 ± 354 mg, respectively. These values were not significantly different among the four product groups which could be attributed to the large variation in EPA and DHA contents within the FO and FO concentrate groups. Total MUFA were significantly greater in the SO supplements (741 ± 477 mg) than in the FO concentrates (210 ± 172 mg), while FO products and the plant/FO blends provided intermediate contents. Total n-6 PUFA and C18:3n-3 were highest in the plant/FO blends. The mean contents of the n-4 PUFA, n-1 PUFA, and total *trans* EPA plus DHA in a single serving, which were not significantly different among all groups, were 30 ± 31 mg, 23 ± 28 mg, and 8 ± 10 mg, respectively.

Comparison of Analyzed Values with Label Declarations. The measured contents of EPA and DHA (mg/serving) were within ±20% of the declared contents for 38 and 37, respectively, of the 46 products (Supporting Information, Figure 2). For the remaining products, three had EPA and/or DHA contents that exceeded 120% of the declared value, including one FO product that contained EPA at a content that

Table 3. Fatty Acids (mg) in Single Servings within the Marine Oil Omega-3 Supplement Groups

fatty acid (mg/serving)[a]	FO	FO concentrate	plant/FO blend	SO	P^b
Σ SFA	399 ± 369	188 ± 217	204 ± 157	511 ± 237	NS
Σ MUFA	375 ± 264ab	210 ± 172b	394 ± 317ab	741 ± 477a	0.003
n-6 PUFA					
C18:2n-6	23 ± 17b	13 ± 11b	315 ± 251a	41 ± 24b	<0.0001
C18:3n-6	4 ± 3b	2 ± 2b	114 ± 116a	2 ± 1b	<0.0001
C20:2n-6	5 ± 4	4 ± 2	3 ± 2	9 ± 6	NS
C20:3n-6	4 ± 3	3 ± 2	2 ± 1	3 ± 1	NS
C20:4n-6	26 ± 19	21 ± 9	12 ± 8	11 ± 5	NS
C22:5n-6	9 ± 5a	8 ± 4a	5 ± 3ab	3 ± 1b	0.03
Σ n-6 PUFA	74 ± 46b	54 ± 23b	452 ± 381a	73 ± 35b	<0.0001
n-4 PUFA					
C16:2n-4	15 ± 16	7 ± 9	1 ± 0	7 ± 4	NS
C16:3n-4	18 ± 18	10 ± 11	1 ± 0	5 ± 4	NS
C18:2n-4	7 ± 5a	4 ± 3b	3 ± 1ab	3 ± 1b	0.03
C18:3n-4	2 ± 1	1 ± 1	1 ± 0	2 ± 1	NS
Σ n-4 PUFA	43 ± 40	23 ± 23	6 ± 3	22 ± 12	NS
n-3 PUFA (all-*cis*)					
C18:3n-3	13 ± 10b	7 ± 5b	372 ± 221a	24 ± 13b	<0.0001
C18:4n-3	42 ± 33	27 ± 22	13 ± 5	43 ± 23	NS
C20:4n-3	19 ± 13ab	15 ± 8b	9 ± 4b	29 ± 18a	0.046
C20:5n-3 (EPA)	428 ± 318	374 ± 176	186 ± 91	203 ± 91	NS
C21:5n-3	18 ± 11	17 ± 9	9 ± 5	9 ± 4	NS
C22:5n-3	51 ± 31	45 ± 24	28 ± 17	48 ± 26	NS
C22:6n-3 (DHA)	271 ± 149	241 ± 125	124 ± 68	212 ± 110	NS
C20:5n-3 + 22:6n-3	700 ± 438	614 ± 272	310 ± 159	415 ± 200	NS
Σ n-3 PUFA	845 ± 519	727 ± 310	743 ± 402	592 ± 270	NS
n-1 PUFA					
C16:4n-1	30 ± 34	16 ± 19	2 ± 0	10 ± 6	NS
C18:4n-1	4 ± 3	2 ± 2	2 ± 1	3 ± 2	NS
Σ n-1 PUFA	34 ± 37	18 ± 20	3 ± 1	17 ± 10	NS
Σ *t*-EPA + *t*-DHA	10 ± 14	7 ± 4	2 ± 2	4 ± 5	NS
total fat (g)	2.2 ± 1.4	1.5 ± 0.6	2.1 ± 1.4	2.3 ± 1.2	NS

[a]Values represent the means ± SD for all products within a group (FO, n = 19; FO concentrate, n = 15; plant/FO blend, n = 4; SO, n = 7). [b]Values within a row with different letters are significantly different (P < 0.05); NS, not significant.

was three-times greater than its label declaration (i.e., 75 mg vs 24 mg). Six of the products (1 FO, 3 FO concentrates, 1 plant/FO blend, and 1 SO) had EPA and DHA contents that were less than 80% of the declared contents. Of these, one FO concentrate product contained EPA and DHA at 48% and 65%, respectively, of the declared values.

Estimated Intakes. Directions for use of the products, as declared on product labels (e.g., "As a dietary supplement, 1 softgel twice daily..."), varied from one to five servings per day. Half of the products (52%) suggested a daily intake of two or more servings per day. Therefore, products were evaluated on the basis of suggested daily use to facilitate comparisons of the amounts of EPA and DHA the products would be expected to provide (i.e., "estimated daily intake") in a single day. Calculations showed that FO and FO concentrate products provided higher mean estimated intakes of EPA plus DHA (1,036 ± 466 mg/d and 1,026 ± 621 mg/d, respectively) than the plant/FO blends and SO supplements (401 ± 164 mg/d and 533 ± 168 mg/d, respectively) (Figure 5; Supporting Information, Table 1). Estimated intakes of EPA plus DHA, which varied from 255 mg to 3,406 mg among all products, were ≥500 mg/d for 39 of the products, ≥1 g/d for 18 products (39%, 11 FO, 7 FO concentrates), and ≥2 g/d for four of the products (all FO products).

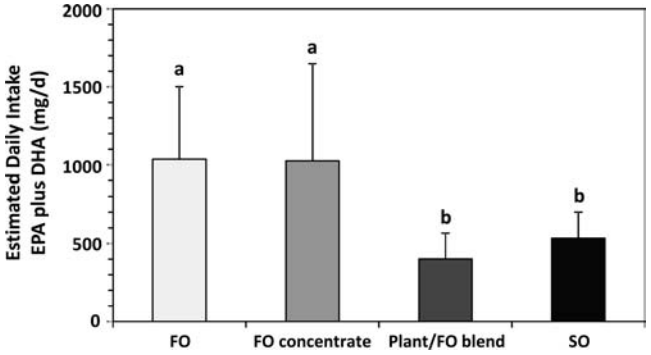

Figure 5. Estimated intakes of EPA plus DHA in the four marine oil omega-3 supplement groups (FO, n = 18; FO concentrate, n = 15; plant/FO blend, n = 4; SO, n = 7). Groups with different letters are significantly different (P < 0.05).

DISCUSSION

Chromatography. The analysis of oils derived from marine sources presents significant challenges due to their complex composition of fatty acids, susceptibility to oxidative changes, and potential for the presence of isomerized fatty acids that are formed during high temperature processing. In addition, many GC column stationary phases (e.g., PEG, cyanopropyl polysiloxane) offer a limited capacity to resolve FAMEs derived

from marine oil in a single-dimension GC run.[15] The present study applied a recently reported gas chromatographic method involving the 200 m SLB-IL111 ionic liquid column[19,20] to the analysis of the content and composition of fatty acids in marine oil omega-3 supplements. The accuracy of this method was confirmed using an SRM for omega-3 and omega-6 fatty acids in FO.

Analysis with the 200 m SLB-IL111 Column. The present study employed the 200 m SLB-IL111 column for the separation of FAME derived from marine oil. A complementary analysis using the 30 m PEG column was performed to resolve C16:1*cis*-7 and C17:0, which were known to coelute on the SLB-IL111 column.[19,20] In addition, Fardin-Kia et al.[20] demonstrated in a sample derived from menhaden oil that C20:0 coelutes with C19:1 FAME, C22:0 coelutes with C20:2*cis*-7,*cis*-13, and C20:1*cis*-11 partially coelutes with C21:0 and C16:4n-1 on the 200 m SLB-IL111 column. In the present study, data for C20:0, C22:0, and 20:1*cis*-11 were not adjusted to correct for coelutions on the SLB-IL111 column because of additional coelutions that were observed on the 30 m PEG column. In a recent study of FO fatty acids, Santercole et al.[15] reported that three GC separations, involving an analysis with the 30 m PEG column and two additional temperature programs using a 100 m cyanopropyl polysiloxane column, were necessary to separate most of the fatty acids derived from menhaden FO. Use of a 100 m cyanopropyl polysiloxane column in the present study may have provided a more appropriate complementary separation of FAMEs.

SRM 3275. The Certificate of Analysis for SRM 3275 reports certified and reference mass fraction values for individual FAMEs. Certified values represent the highest level of confidence in accuracy and account for all known or suspected sources of bias.[23] Reference values represent the best estimate of true value and may reflect only the variability in analytical measurement.[23] We observed recoveries for EPA and DHA FAME in the three SRM fish oils that varied from 99% to 106% and from 102% to 103%, respectively, compared with their respective certified and reference mass fraction values. On the basis of these findings, we determined that the chromatographic method used in the present study was appropriate for the analysis of EPA and DHA in marine oil. These findings are also consistent with those of Khoomrung et al.[30] who demonstrated, using selected FAMEs from SRM 3275-2, the accuracy of a microwave-assisted derivatization method for the preparation of FAME from yeast.

The Certificate of Analysis for SRM 3275 reports a total of 9 to 11 certified mass fraction values for FAMEs present in the three SRM fish oils. NIST selected these FAMEs based on the availability of pure reference standards that could be used to develop GC-MS calibration curves.[23] Our recoveries of FAMEs for which certified mass fraction values were reported were variable with some low abundance FAME having good recoveries (e.g., C18:2n-6 in SRM 3275-1; 103%) and some higher abundance FAMEs having poorer recoveries (e.g., C16:0 in SRM 3275-3; 83%). These discrepancies could be attributed to incomplete resolution of FAMEs with either our method or the NIST method. For example, coelutions on the 200 m SLB-IL111 column may explain the high recoveries that we observed for C20:0 (154%−1182%) and C20:1*cis*-11 (252%−302%). In contrast, NIST, in their characterization of SRM 3275,[23] reported using two cyanopropyl polysiloxane columns of slightly different selectivities for GC-FID and GC-MS analyses, and their conditions were optimized for the separation of 18-carbon omega-3 and omega-6 fatty acids. Representative chromatograms are not presented in the Certificate of Analysis, and it is possible that complementary separations, such as those reported by Santercole et al.,[15] were not performed.[23] Therefore, to our knowledge, chromatograms presented in this article are the first published chromatograms showing the separation of FAMEs derived from the three complex fish oils of SRM 3275.

Marine Oil Omega-3 Supplements. *trans-Isomers of EPA and DHA.* The presence of the *trans* isomers of EPA and DHA in marine oil occurs as the result of the geometrical isomerization of all-*cis* EPA and DHA during high-temperature processing designed to remove unpleasant odors (deodorization[16]) or produce concentrated EPA and DHA formulations (distillation[17]). Fournier et al.[16] demonstrated that deodorization temperature is directly related to the extent of thermal degradation of LCPUFA and the degree of isomerization. At a deodorization temperature of 180 °C, nearly 100% of the *trans* isomers of EPA and DHA were found as the mono-*trans* isomers. However, at a deodorization temperature of 250 °C, more than one-third of the *trans* isomers were present in the di-*trans* configuration.[16] Mono-*trans* isomers of EPA and DHA were the predominant form of the *trans* isomers observed in the marine oil omega-3 supplements analyzed in the present study (Figures 2 and 3). Isomers with two or more *trans* double bonds, if present, were found at or near the level of detection and therefore were not included in the quantitation.

Sciotto and Mjøs[31] reported concentrations for the *trans* isomers of EPA plus DHA that varied from 0.1% to 2.8% of total fat in 77 omega-3 products available in the European market. Products with the highest concentrations of *trans* isomers were those in the "33/23 concentrates" (i.e., products consisting of ∼33% EPA and ∼23% DHA), the "high DHA products", and the "high EPA products" groups.[31] In the present study, concentrations of the *trans* isomers of EPA plus DHA were significantly higher in the FO concentrates than in the plant/FO blends and SO supplements, while FO supplements had intermediate concentrations. Results of the present study are consistent with those of Sciotto and Mjøs,[31] indicating that FO concentrates tend to have higher concentrations of *trans* LCPUFA. However, Sciotto and Mjøs[31] note that because a large number of samples with low levels of *trans* EPA and *trans* DHA were observed in the concentrate groups, the process of deodorization was more likely to be a significant contributor of thermal isomerization than that of distillation.

Few studies of the bioactivity of the *trans* isomers of EPA and DHA can be found in the literature. In a study by Ferreri et al.,[32] six week old male Wistar rats were fed deodorized FO containing 0.1% *trans* EPA (as % of total fat) for 12 weeks. The authors found that the *trans* isomers of EPA were incorporated into liver microsomal membranes, with a *trans* isomeric profile reflecting that of the diet.[32] In the present study, the concentration of the *trans* isomers of EPA and DHA in the supplements varied from 0.1% to 1.5% of total fat, corresponding to a mean content of 8 ± 10 mg/serving (Table 3) and a mean estimated intake of 10 ± 11 mg/d (Supporting Information, Table 1). The nutritional significance of the *trans* EPA and DHA contents currently observed remains unclear.[31]

Significance of Other Fatty Acids. Analysis with the 200 m SLB-IL111 column permitted quantitation of rarely reported fatty acids such as C21:5n-3 and the n-4 and n-1 PUFA. We

observed concentrations of C21:5n-3 that were similar to those previously reported for FO ethyl esters (0.68−1.59% of total fatty acids).[33] Concentrations of n-4 and n-1 PUFA were comparable to those previously reported for FO supplements from Australia.[10] n-4 and n-1 PUFA have also been observed in marine microalgae[34,35] and marine invertebrates.[36,37] The correlation between the concentrations of n-4 and n-1 PUFA observed in the present study (R^2 = 0.9489) was unexpected.

Agreement with Label Declarations. FDA is tasked with, among others, ensuring that dietary supplement labels are truthful and not misleading. This mission is carried out in part through laboratory analysis of products for accuracy of label declarations. More than 80% of the products analyzed in the present study had EPA and DHA contents that were within ±20% of their label declarations. These findings are consistent with those of Ackman et al.[38] who found that the majority of 17 products from the US, Canada, and the United Kingdom had accurate label claims for EPA and DHA. Similarly, analyzed contents of EPA and DHA were within ±20% of label declarations in 15 of the 16 liquid FO products that were analyzed by Ritter et al.[39] In contrast, six of the products analyzed in the present study failed to meet label declarations for EPA and DHA. These findings are consistent with those of Chee et al.[9] who found that two of the nine marine oil capsules analyzed had EPA and DHA contents that were less than 80% of the declared values. Chee et al.[9] speculated that oxidative degradation was the cause of the low EPA and DHA contents. Oxidative degradation may have also been the cause of the low EPA and DHA contents observed in several samples in the present study, but we cannot confirm this.

Estimated Intakes. Half of the products analyzed in the present study had label recommendations for use that included the intake of two or more servings per day. In a similar study of nine marine oil omega-3 supplements from Austria and Germany, Tatarczyk et al.[12] reported that seven of the products had recommendations for daily use that included the intake of two or more servings per day. Only one of the products, a concentrated SO formulation, had a recommendation for intake of EPA plus DHA that exceeded 1 g/d.[12] In contrast, 18 of the products (39%) in the present study had estimated intakes of EPA plus DHA that exceeded 1 g/d. We observed a 13-fold variation in EPA and DHA estimated intakes (255 mg to 3,406 mg) that would be achieved if products were consumed according to their label directions for use.

Use of the Qualified Health Claim for EPA and DHA Omega-3 Fatty Acids. FDA uses its food labeling regulations in part to help consumers make healthful dietary choices. Daily values (% DV), which are used to characterize amounts of specific nutrients present in foods, have been established for many nutrients but remain to be determined for EPA and DHA because there is as yet no consensus among qualified experts regarding recommended daily allowances or dietary reference intakes for EPA and DHA.[1] FDA may also issue regulations authorizing health claims on conventional foods and dietary supplements when it determines that there is significant agreement among qualified experts that available scientific evidence supports such claims. In cases in which scientific evidence is considered supportive but not conclusive, FDA may authorize a "qualified" health claim. This is currently the case with claims regarding the contents of EPA and DHA in conventional foods and dietary supplements. FDA's qualified health claim states that "supportive but not conclusive research shows that consumption of EPA and DHA omega-3-fatty acids may reduce the risk of coronary heart disease".[21,22]

FDA has previously set recommendations for safety that are applicable to products bearing the qualified health claim for EPA and DHA.[21,22] These safety requirements are based on reports that intakes of EPA plus DHA greater than 3 g/d have been associated with adverse effects on bleeding time, glycemic control, and low density lipoprotein cholesterol concentrations.[40] FDA recommends that product labels bearing the qualified health claim suggest a daily intake of EPA plus DHA that is less than 2 g/d. In addition, FDA encourages manufacturers to limit the use of the qualified health claim to products recommending or suggesting daily intakes of 1 g or less of EPA and DHA.[40] In the present study, 11 of the 46 products analyzed (24%) carried the qualified health claim for EPA and DHA. All of these products followed FDA's recommendations, including listing the contents of EPA and DHA on product labels and recommending a daily intake of EPA plus DHA that was 2 g/d or less. In contrast, four of the products not bearing the qualified health claim had estimated intakes for EPA plus DHA that exceeded 2 g/d, including one product that would provide 3.4 g/d of EPA plus DHA if consumed according to label directions for use.

Overall, this study presents the content and composition of fatty acids, including the *trans* isomers of EPA and DHA, in 46 commercially available marine oil omega-3 supplements. We report, for the first time, the chromatographic separation of the *trans* isomers of EPA and DHA on the 200 m SLB-IL111 column and verify the accuracy of our method using an SRM for omega-3 and omega-6 fatty acids in FO. Of the 46 products analyzed, more than 80% had EPA and DHA contents that were consistent with values declared on product labels. In contrast, six of the products failed to meet label declarations for EPA and DHA, which could be attributed to thermal isomerization or oxidative degradation of the omega-3 LCPUFA. Results indicated that a wide range of estimated EPA and DHA intakes (255 mg to 3,406 mg) could be achieved if products are consumed according to label directions for use. However, all products bearing the FDA's qualified health claim for EPA and DHA (24% of analyzed products) met the agency's recommendations for such claims.

■ ASSOCIATED CONTENT

Ⓢ Supporting Information

Estimated fatty acid intakes (mg/day), correlation between concentrations of n-4 and n-1 PUFA, and relative contents of EPA and DHA in single servings from the marine oil omega-3 supplements. This material is available free of charge via the Internet at http://pubs.acs.org.

■ AUTHOR INFORMATION

Corresponding Author

*Tel: 240-402-2360. Fax: 301-436-2332. E-mail: cynthia.srigley@fda.hhs.gov.

Notes

The authors declare no competing financial interest.

†(J.I.R.) Retired.

■ ABBREVIATIONS USED

AOCS, American Oil Chemists' Society; CACI, covalent adduct chemical ionization; DHA, docosahexaenoic acid; DV, daily value; EPA, eicosapentaenoic acid; FAME, fatty acid methyl

ester; FDA, Food and Drug Administration; FID, flame ionization detection; FO, fish oil; GC, gas chromatography; IS, internal standard; LCPUFA, long chain polyunsaturated fatty acid; MS, mass spectrometry; MUFA, monounsaturated fatty acids; NIST, National Institute of Standards and Technology; PEG, polyethylene glycol; SD, standard deviation; SFA, saturated fatty acids; SO, salmon oil; TAG, triacylglycerol; TIC, total ion chromatogram; TLC, thin layer chromatography; US, United States

REFERENCES

(1) Flock, M. R.; Harris, W. S.; Kris-Etherton, P. M. Long-chain omega-3 fatty acids: time to establish a dietary reference intake. *Nutr. Rev.* **2013**, *71*, 692−707.

(2) Cunnane, S. C.; Drevon, C. A.; Spector, A.; Sinclair, A. J.; Harris, W. S. Recommendations for Intake of Polyunsaturated Fatty Acids in Healthy Adults. http://www.issfal.org/statements/pufa-recommendations/statement-3 (accessed Mar 4, 2014).

(3) Gibson, R. A.; Makrides, M.; Koletzko, B. V.; Brenna, J. T. ISSFAL Statement on Dietary Fats in Infant Nutrition. http://www.issfal.org/statements/pufa-recommendations/statement-2 (accessed Mar 4, 2014).

(4) Koletzko, B.; Cetin, I.; Brenna, J. T. Dietary fat intakes for pregnant and lactating women. *Br. J. Nutr.* **2007**, *98*, 873−877.

(5) Kris-Etherton, P. M.; Harris, W. S.; Appel, L. J. Omega-3 fatty acids and cardiovascular disease: new recommendations from the American Heart Association. *Arterioscler., Thromb., Vasc. Biol.* **2003**, *23*, 151−152.

(6) Food and Agriculture Organization/World Health Organization. Fats and fatty acids in human nutrition. Proceedings of the Joint FAO/WHO Expert Consultation. November 10−14, 2008. Geneva, Switzerland. *Ann. Nutr. Metab.* **2009**, *55*, 5−300.

(7) Kris-Etherton, P. M.; Harris, W. S.; Appel, L. J. Fish consumption, fish oil, omega-3 fatty acids, and cardiovascular disease. *Circulation* **2002**, *106*, 2747−2757.

(8) Barnes, P. M.; Bloom, B.; Nahin, R. L. Complementary and alternative medicine use among adults and children: United States, 2007. *Natl. Health Stat. Rep.* **2008**, *12*, 1−23.

(9) Chee, K. M.; Gong, J. X.; Rees, D. M.; Meydani, M.; Ausman, L.; Johnson, J.; Siguel, E. N.; Schaefer, E. J. Fatty acid content of marine oil capsules. *Lipids* **1990**, *25*, 523−528.

(10) Hamilton, K.; Brooks, P.; Holmes, M.; Cunningham, J.; Russell, F. D. Evaluation of the composition of omega-3 fatty acids in dietary oil supplements. *Nutr. Diet.* **2010**, *67*, 182−189.

(11) Fantoni, C. M.; Cuccio, A. P.; Barrera-Arellano, D. Brazilian encapsulated fish oils: Oxidative stability and fatty acid composition. *J. Am. Oil Chem. Soc.* **1999**, *73*, 251−253.

(12) Tatarczyk, T.; Engl, J.; Ciardi, C.; Laimer, M.; Kaser, S.; Salzmann, K.; Lenners, R.; Patsch, J. R.; Ebenbichler, C. F. Analysis of long-chain omega-3 fatty acid content in fish-oil supplements. *Wien. Klin. Wochenschr.* **2007**, *119*, 417−422.

(13) Ahmed, M.; Moazzami, A. A.; Andersson, R.; Pickova, J. Varying quality of fish oil capsules: fatty acids and tocopherol. *Neuroendocrinol. Lett.* **2011**, *32* (Suppl 2), 37−40.

(14) AOCS Official Method Ce 1i-07. In *Official Methods and Recommended Practices of the AOCS*, 6th ed.; Firestone, D., Ed.; AOCS Press: Urbana, IL, 2009.

(15) Santercole, V.; Delmonte, P.; Kramer, J. K. G. Comparison of separations of fatty acids from fish products using a 30-m Supelcowax-10 and a 100-m SP-2560 column. *Lipids* **2012**, *47*, 329−344.

(16) Fournier, V.; Destaillats, F.; Juaneda, P.; Dionisi, F.; Lambelet, P.; Sebedio, J. L.; Berdeaux, O. Thermal degradation of long-chain polyunsaturated fatty acids during deodorization of fish oil. *Eur. J. Lipid Sci. Technol.* **2006**, *108*, 33−42.

(17) Shahidi, F.; Wanasundara, U. Omega-3 fatty acid concentrates: nutritional aspects and production techniques. *Trends Food Sci. Technol.* **1998**, *9*, 230−240.

(18) Ragonese, C.; Sciarrone, D.; Tranchida, P. Q.; Dugo, P.; Mondello, L. Use of ionic liquids as stationary phases in hyphenated gas chromatography techniques. *J. Chromatogr., A* **2012**, *1255*, 130−144.

(19) Delmonte, P.; Fardin-Kia, A. R.; Kramer, J. K. G.; Mossoba, M. M.; Sidisky, L.; Tyburczy, C.; Rader, J. I. Evaluation of highly polar ionic liquid gas chromatographic column for the determination of the fatty acids in milk fat. *J. Chromatogr., A* **2012**, *1233*, 137−146.

(20) Fardin-Kia, A. R.; Delmonte, P.; Kramer, J. K. G.; Jahreis, G.; Kuhnt, K.; Santercole, V.; Rader, J. I. Separation of the fatty acids in menhaden oil as methyl esters with a highly polar ionic liquid gas chromatographic column and identification by time of flight mass spectrometry. *Lipids* **2013**, *48*, 1279−1295.

(21) US Food and Drug Administration. Letter Responding to Health Claim Petition Dated November 3, 2003 (Martek Petition): Omega-3 fatty Acids and Reduced Risk of Coronary Heart Disease (Docket No. 2003Q-0401). http://www.fda.gov/Food/IngredientsPackagingLabeling/LabelingNutrition/ucm072932.htm (accessed Mar 4, 2014).

(22) US Food and Drug Administration. Letter Responding to Health Claim Petition Dated June 23, 2003 (Wellness Petition): Omega-3 Fatty Acids and Reduced Risk of Coronary Heart Disease (Docket No. 2003Q-0401). http://www.fda.gov/Food/IngredientsPackagingLabeling/LabelingNutrition/ucm072936.htm (March 4, 2014).

(23) Schantz, M. M.; Sander, L. C.; Sharpless, K. E.; Wise, S. A.; Yen, J. H.; NguyenPho, A.; Betz, J. M. Development of botanical and fish oil standard reference materials for fatty acids. *Anal. Bioanal. Chem.* **2013**, *405*, 4531−4538.

(24) AOCS Official Method Ce 2-66. In *Official Methods and Recommended Practices of the AOCS*, 6th ed.; Firestone, D., Ed.; AOCS Press: Urbana, IL, 2009.

(25) Snyder, J. M.; Scholfield, C. R. *cis-trans* isomerization of unsaturated fatty acids with *p*-toluenesulfinic acid. *J. Am. Oil Chem. Soc.* **1982**, *59*, 469−470.

(26) Morris, L. J. Separations of lipids by silver ion chromatography. *J. Lipid Res.* **1966**, *7*, 717−732.

(27) Fournier, V.; Juaneda, P.; Destaillats, F.; Dionisi, F.; Lambelet, P.; Sebedio, J. L.; Berdeaux, O. Analysis of eicosapentaenoic and docosahexaenoic acid geometrical isomers formed during fish oil deodorization. *J. Chromatogr., A* **2006**, *1129*, 21−28.

(28) Van Pelt, C. K.; Brenna, J. T. Acetonitrile chemical ionization tandem mass spectrometry to locate double bonds in polyunsaturated fatty acid methyl esters. *Anal. Chem.* **1999**, *71*, 1981−1989.

(29) GraphPad Software. Outlier Calculator. http://graphpad.com/quickcalcs/Grubbs1.cfm (accessed Mar 4, 2014).

(30) Khoomrung, S.; Chumnanpuen, P.; Jansa-ard, S.; Nookaew, I.; Nielsen, J. Fast and accurate preparation fatty acid methyl esters by microwave-assisted derivatization in the yeast *Saccharomyces cerevisiae*. *Appl. Microbiol. Biotechnol.* **2012**, *94*, 1637−1646.

(31) Sciotto, C.; Mjos, S. A. Trans isomers of EPA and DHA in omega-3 products on the European market. *Lipids* **2012**, *47*, 659−667.

(32) Ferreri, C.; Grabovskiy, S. A.; Aoun, M.; Melchiorre, M.; Kabal'nova, N.; Feillet-Coudray, C.; Fouret, G.; Coudray, C.; Chatgilialoglu, C. Trans fatty acids: chemical synthesis of eicosapentaenoic acid isomers and detection in rats fed a deodorized fish oil diet. *Chem. Res. Toxicol.* **2012**, *25*, 687−694.

(33) Azizian, H.; Kramer, J. K. G.; Ehler, S.; Curtis, J. M. Rapid quantitation of fish oil fatty acids and their ethyl esters by FT-NIR models. *Eur. J. Lipid Sci. Technol.* **2010**, *112*, 452−462.

(34) Zhukova, N. V.; Aizdaicher, N. A. Fatty acid composition of 15 species of marine microalgae. *Phytochemistry* **1995**, *39*, 351−356.

(35) Volkman, J. K.; Jeffrey, S. W.; Nichols, P. D.; Rogers, G. I.; Garland, C. D. Fatty acid and lipid composition of 10 species of microalgae used in mariculture. *J. Exp. Mar. Biol. Ecol.* **1989**, *128*, 219−240.

(36) Christie, W. W.; Brechany, E. Y.; Stefanov, K. Silver ion high-performance liquid chromatography and gas chromatography mass

spectrometry in the analysis of complex fatty acid mixtures: application to marine invertebrates. *Chem. Phys. Lipids* **1988**, *46*, 127−135.
(37) Pond, D. W.; Dixon, D. R.; Bell, M. V.; Fallick, A. E.; Sargent, J. R. Occurrence of 16:2(n-4) and 18:2(n-4) fatty acids in the lipids of the hydrothermal vent shrimps Rimicaris exoculata and Alvinocaris markensis: Nutritional and trophic implications. *Mar. Ecol.: Prog. Ser.* **1997**, *156*, 167−174.
(38) Ackman, R. G.; Ratnayake, W. M. N.; Macpherson, E. J. EPA and DHA contents of encapsulated fish oil products. *J. Am. Oil Chem. Soc.* **1989**, *66*, 1162−1164.
(39) Ritter, J. C.; Budge, S. M.; Jovica, F. Quality analysis of commercial fish oil preparations. *J. Sci. Food Agric.* **2013**, *93*, 1935−9.
(40) US Food and Drug Administration. Substanances affirmed as generally recoginized as safe: Menhaden oil [docket no. 86G-0289]. *Fed. Regist.* **1997**, *62*, 30751−30757.

from the two protein mixtures, with 90% purity using hyaluronic acid.

As biodegradable, biocompatible, and environmentally friendly materials, anionic and cationic polysaccharides offer better methods of coacervation-based protein purification. Chitosan (Ch) is the deacetylated form of chitin and is considered to be the most widely distributed cationic biopolymer. Several complex coacervation pairs based on chitosan have been reported, including α-lactalbumin−chitosan and β-lactoglobulin−chitosan,[19] soy globulin−chitosan,[20] pea protein isolate−chitosan,[21] xanthan−chitosan,[22] caseinophosphopeptides−chitosan,[23] and gum arabic−chitosan.[24,25] However, relatively little is known about the interaction between soybean whey proteins and chitosan.

Three types of turbidity titrations had been reported by Dubin et al.[26] The experiment that led to the pH dependence of turbidity at constant ionic strength and protein and polymer concentration was called a "type 1" titration or pH titration. One may also follow the evolution of the turbidity upon addition of either protein to polymer ("type 2") or polymer to protein ("type 3"). In our experiment, type 1 titration was used to study SWP/Ch complexing behavior. Four critical pH values can be observed, which indicated the phase transitions upon changing pH of the system. An initial slight increase in turbidity occurred at pH_c, which corresponded to the soluble complex formation. A sharp elevation in turbidity was found at $pH_{\varphi 1}$, signifying the onset of phase separation. At pH_{max}, maximum turbidity was obtained, whereas at $pH_{\varphi 2}$ the coacervate or precipitate started to redissolove.[27−29]

The aim of this study is to obtain knowledge about the interaction between soybean whey protein and chitosan and to recover proteins from soybean whey. To achieve the goal, protein components in soybean whey were first re-examined. Then, soybean whey protein/chitosan mixtures were brought to complexing conditions by adding NaOH slowly, and effects of pH and protein/chitosan ratio on turbidity and protein recovery were investigated. Finally, protein composition and purity as affected by complexation conditions were studied.

MATERIALS AND METHODS

Materials. Hexane-defatted and flush-desolventized soy flake, provided by Shandong Wonderful Industrial and Commercial Co. Ltd., had a protein content of 52.4% (N × 6.25, dry basis) and a nitrogen solubility index (NSI) of 85%. Food grade chitosan (degree of deacetylation = 80−95%; viscosity average molecular weight = 620 kDa) was purchased from the Sinopharm Chemical Reagent Co., Ltd. (Shanghai, China). All other reagents were of analytical grade.

Preparation of SWP and Ch Stock Solutions. To obtain soybean whey, defatted soybean flake was extracted with distilled water (pH 7.0) with a water-to-meal ratio of 10:1 and blended at room temperature (25 ± 2 °C) for 30 min. After centrifugation of the suspension to remove insoluble precipitate, the supernatant was adjusted to pH 4.5 with hydrochloric acid to precipitate acid-insoluble soy proteins. The supernatant was adjusted to pH 8.0 with 1.0 M NaOH and centrifuged again. The solution was dialyzed for 48 h at 4 °C against water containing 0.02% sodium azide (to prevent microbial growth) and finally preserved at 4 °C. The protein concentration of the laboratory-prepared soybean whey was approximately 0.4% determined by Kjeldahl analysis.

The stock solution of 0.1% chitosan (w/v) was prepared by dispersing chitosan powder in 0.1% acetic acid solution (v/v) with magnetic stirring for 3 h at room temperature (25 ± 1 °C). As for the SWP stock solution, soybean whey was diluted with distilled water to a final concentration 0.1% (calculated by protein content).

Measurement of Turbidity. Both stock solutions were adjusted to a pH of 4.0 separately. Turbidity titration of the SWP/Ch mixture was conducted by first mixing two solutions at the desired ratio (from 100:1 to 1:1) and then adjusting the pH from 4.0 to 10.0. Turbidity was measured using an UV−vis spectrophotometer (Shimadzu, Kyoto, Japan) with a 1 cm cuvette at 600 nm. Turbidimetric titration was carried out by the addition of graded NaOH (1, 0.5, 0.1 M) in increments of ∼0.1 pH unit, to a final pH of 10.0, with gentle stirring and simultaneous monitoring of pH and turbidity. In this way, the added volume could be controlled in the range of 1.5−3% of total volume; thus, the dilution effect was not significant. Titrations were carried out at 25.0 ± 1.0 °C, and the pH (±0.01 pH unit) was monitored with a Mettler Toledo Delta 320 pH-meter that had been carefully calibrated. Homogenous SWP and Ch solutions were used as blanks at their respective concentrations. Homogenous SWP turbidity titration was conducted over the pH range from 3.5 to 7.5. Critical transition points, pH_c, $pH_{\varphi 1}$, pH_{max}, and $pH_{\varphi 2}$, were obtained according to methods reported by Mattison.[30] All measurements were made in triplicate, using separate stock solutions.

Zeta Potential Analyses. Both stock solutions were adjusted to a pH of 4.0 separately. The zeta-potentials (mV) of SWP (0.1%) and chitosan (0.1%) in solution at different pH values ranging from 4.0 to 10.0 were calculated separately from the electrophoretic mobility, at 25.0 ± 0.1 °C, using a Zetasizer Nano ZS instrument (Malvern, UK). All measurements were made in duplicate.

Protein Content Determination and SDS-PAGE Analysis. The phase-separated SWP/Ch mixtures were divided into precipitate and supernatant by centrifugation (4000 rpm, 15 min). Quantitation of protein in the supernatant was determined by using the bicinchoninic acid (BCA) method,[31] and the protein content of the precipitate was calculated by difference from that of the supernatant. BCA reagent was prepared by mixing 50 volumes reagent A (containing BCA (1%), Na_2CO_3 (2%), $Na_2C_4H_4O_6$ (0.16%), NaOH (0.4%), $NaHCO_3$ (0.95%), respectively) with 1 volume reagent B (4% $CuSO_4$) when it will be used. Then, 100 μL of the sample and 2 mL of BCA reagent were pipetted into a test tube and mixed thoroughly. After the mixture had stood for 30 min at 37 °C and then the temperature allowed to drop to room temperature, the change in absorbance was monitored at 562 nm, using 100 μL of water as a control. All measurements were made in triplicate.

Protein compositions of both parts were analyzed using a Tricine−SDS-PAGE method, according to the method of Schagger.[32] Concentrations of stacking and separating gels were 4 and 16%, respectively. 2-Mercaptoethanol was added into the samples to the concentration of 2% (v/v), and samples were heated for 5 min in a boiling water bath. Then 10 μL of each sample was loaded into a sample well, and the samples were electrophoresed at a constant voltage of 30 V until all of protein sample entered into the stacking gel and then at constant voltage of 100 V until the end. The gel was stained using Coomassie Brilliant Blue G-250.

SEC-HPLC Analysis. Contents of major protein component in the complex, supernatant, and soybean whey was determined by SEC-HPLC, using a TSK gel 2000 SWXL (300 mm × 7.8 mm, Tosoh, Tokyo, Japan) column on an Aglient Technologies (USA) 1260 Infinity system equipped with a UV detector, with 20 μL injections. The column was equilibrated and run with ultrapure water containing 45% (v/v) acetonitrile and 0.1% (v/v) trifluoroacetic acid (TFA). The flow rate was 0.5 mL/min, and the wavelength of the UV detector was at 214 nm. Initial sample solutions were directly analyzed after filtration (0.45 μm).

MALDI-TOF/TOF-MS. The verification of reported protein components and the identification of unknown proteins in soybean whey were conducted by the MALDI-TOF/TOF-MS analysis. The MALDI-TOF/TOF-MS analysis of sample was conducted according to the methods of Zhao.[33] The protein spots were excised from a Coomassie Brilliant Blue G-250 stained gel, washed in distilled water, and destained completely in a 30% acetonitrile (v/v) containing 100 mM NH_4HCO_3. After a 100% acetonitrile washing, the destained gel piece was placed into reducing solution (10 μL of 100 mM DTT, 90 μL of 100 mM NH_4HCO_3) for 30 min at 56 °C. After a 100%

acetonitrile washing, 70 μL of 100 mM NH_4HCO_3 and 30 μL of 200 mM iodoacetic acid were added, and the mixture was incubated for 20 min in the dark. After a 100% acetonitrile washing again, 5 μL (10 μg/mL) of trypsin (Promega, V5111) was added, and the mixture was put into a 4 °C refrigerator for 30 min. Then 25 mM NH_4HCO_3 solution was added. The peptides were generated after 20 h of incubation at 37 °C. The solution containing peptides was collected and concentrated at 30 °C to get a dry powder. Three microliters of 0.1% TFA (v/v) was used to dissolve the dry powder. In the final step before MALDI-TOF/TOF analysis, the sample was prepared by mixing 0.7 μL of the sample and 0.7 μL of 4-hydroxy-α-cyanocinnamic acid (used as a matrix) on a MALDI target and air-dried. All mass spectra were obtained with an ultrafleXtreme MALDI-TOF/TOF (Bruker Daltonics, Germany). All mass spectra were analyzed by flexAnalysis software provided by Bruker Daltonics Corp. Protein identification was performed by searching plant proteins in the latest version of the NCBInr database.

Trypsin and Chymotrypsin Inhibitor Activity Assays. Trypsin inhibitor activity (TIA) was measured with 0.04% (w/v) N^{α}-benzoyl-L-arginine 4-nitroanilide hydrochloride (BAPA) as the substrate, which dissolved in 0.05 M, pH 8.2, Tris-HCl buffer (1% dimethyl sulfoxide, v/v; 0.02 M $CaCl_2$). Assay solution was zeroed, and then 2 mL of 0.01% (w/v) trypsin in 0.04 mM HCl solution was added to begin the reaction.[34] Chymotrypsin inhibitor activity (CIA) was determined by using a method modified from that of Tan et al.[35] One milliliter of a diluted sample and 1 mL of deionization water were pipetted into a test tube. Then 4.2 mL of 0.05 M, pH 8.2, Tris-HCl buffer (0.01 M $CaCl_2$) and 2 mL of 0.02% (w/v) α-chymotrypsin in 0.002 M HCl solution were added, followed by 0.8 mL of 0.04% (w/v) *N*-benzoyl-L-tyrosine *p*-nitroanilide (BTpNA) in acetone solution and thorough mixing. Exactly 10 min later, the reaction was terminated by adding 1 mL of 30% (w/v) acetic acid. The change in absorbance was monitored at 410 nm for at least 3 min. Trypsin inhibitor units (TIU) or chymotrypsin inhibitor units (CIU) were calculated as the amount of inhibitor that reduced the absorbance per minute of the standard reaction by 0.01. For accuracy, the reaction was measured in the linear portion in the 40−60% inhibition range.

RESULTS AND DISCUSSION

Protein Components in Soybean Whey. The dialyzed soybean whey without further treatment to increase concentration was first analyzed by Tricine−SDS-PAGE, using 2% 2-ME as disulfide bond reductant, so as to gain an overview of the protein components in the sample. As shown in Figure 1a, five major bands, band 1−5, were obtained. From the molecular marker, it was known that bands 1 and 2 had molecular weights of 56 and 30 kDa, respectively, whereas twin bands 3 and 4 were centered around 20 kDa. Band 5 displayed as a broad smear at a molecular weight around 12 kDa.

To improve the electrophoretic resolution of bands 3, 4, and 5, proteins were enriched by mixing dialyzed soybean whey with chitosan at a ratio of 8:1 and alkalinized to pH 6 (at this condition, there were relatively high amounts of complex). The centrifuging precipitate was recovered and analyzed by Tricine−SDS-PAGE using DTT as disulfide bond reductant. As shown in Figure 1b, bands 1 and 2 were substantially eliminated, but proteins with molecular weight similar to those of bands 3, 4, and 5 were enriched by chitosan complexing. Only one band (4′) was found to correspond with the molecular weight of 20 kDa when using DTT as reductant. Therefore, bands 3 and 4 were actually the same protein showing different electrophoretic mobilities, possibly because of the insufficient reduction of disulfide bonds resulting in inhomogeneous molecular size. In Figure 1b, the original band 5 split in two bands (band 5′ and 5″), and the resolution further improved with the increase of DTT concentration.

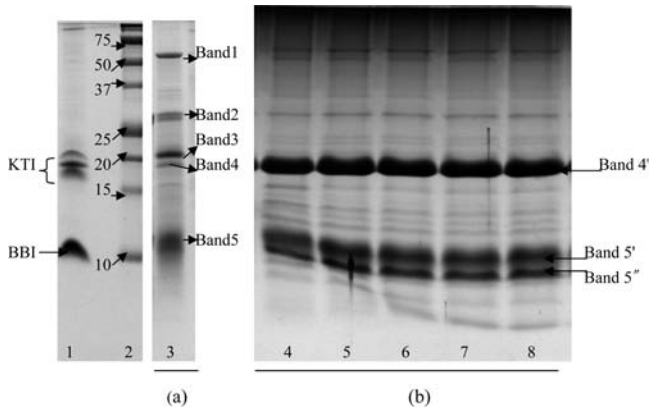

Figure 1. Tricine-SDS-PAGE for SWPs and precipitate proteins: (a) SWP treated with 2-mercaptoethanol (2.0%); (b) precipitate treated with DTT. Lanes 1 and 2 are standards of KTI and BBI; lanes 4−8 represent 200, 300, 600, 800, and 1000 mM DTT treatment, respectively. The DTT treatment samples were chosen as $R_{SWP/Ch}$ = 8:1, which contained the relatively higher content of bands 3−5; all DTT treatment samples were heated for 5 min in a boiling water bath. Band 4′ was derived from bands 3 and 4, and bands 5′ and 5″ were derived from band 5.

Major protein components in soybean whey as separated by Tricine−SDS-PAGE were identified by MALDI-TOF/TOF-MS. As shown in Table 1, bands 1 and 2 in Figure 1a were matched to β-amylase and soybean agglutinin, respectively. As expected, bands 3 and 4 in Figure 1a, as well as band 4′ in Figure 1b, were characterized as the same protein: soybean Kunitz trypsin inhibitor (KTI).

Bands 5′ and 5″, which derive from the 12 kDa protein, were matched to uncharacterized protein LOC100306176 precursor and unnamed protein product, respectively. The latter had a theoretical nominal mass (M_r) of 8807 and a theoretical calculated p*I* of 4.51. The amino acid sequence of the latter was further compared with that of Bowman−Birk protease inhibitor (BBI). It can be found in Table 2 that two specific binding domains existed in soybean BBI (IBBD1_SOYBN), which offers the binding sites for trypsin inhibitors,[36] that is, CTKSNPPQ and CALSYPAQ. Alfonso[37] reported another type of BBI: IBBD2_SOYBN. For this type, CTKSNP was replaced by CTRSMP. It was interesting to find that band 5″ showed a combination of the above: CTRSNP. In addition, there was an extra M residue at the N-terminal. Considering about 30% protein sequence coverage, band 5″ (BBI-U) could be a new member of the BBI family.

Trypsin and Chymotrypsin Inhibitor Activity of the 12 kDa Proteins. At $R_{SWP/Ch}$ = 4:1 and pH 6.39, the 12 kDa proteins distribute in both supernatant and precipitate, and the TIA and CIA activities in both parts (Figure 2) were investigated. It can be seen that there were 31.0% of TIA activity and 41.5% of CIA found in supernatants, due to three proteins in supernatants at the ratio of 4:1: SBA, β-amylase, and the 12 kDa proteins (illustrated under Protein Components of SWP/Ch Complexes). SBA and β-amylase showed no TIA activity; thus, the residual TIA was derived from 12 kDa proteins. As one of the 12 kDa proteins, BBI-U had a structure similar to that of BBI and should contribute part of the inhibitor activities.

SWP/Ch Complexing Behavior as a Function of pH and Mixing Ratio. *Critical Points of SWP/Ch Complexing.* pH affected the charge densities and thus the complexing

Table 1. Identification of Protein Bands in Figure 1 by MALDI-TOF/TOF-MS

band[a]	protein ID	protein score	peptides matched	M_r[b]	NBCInr accession no.
1	β-amylase (*Glycine max*)	396	5 (3)	53983	gil169913
2	soybean agglutinin complexed with 2,6-pentasaccharide	378	4 (4)	27555	gil6729836
3	Kunitz trypsin inhibitor (*Glycine max*)	342	5 (2)	24419	gil13375349
4	Kunitz trypsin inhibitor (*Glycine max*)	154	2 (1)	24419	gil13375349
5	unmatched				
4′	Kunitz trypsin inhibitor (*Glycine max*)	278	5 (3)	24134	gil13375349
5′	protein precursor LOC100306176 (*Glycine max*)	115	4 (2)	19015	gil351722713
5″	unnamed protein	62	2 (0)	8807	gil58059

[a]Band identification numbers correspond to those proteins labeled in Figure 1. [b]Molecular weights (M_r) are given as theoretical values. Searches were performed via Mascot. Peptides matched and accession numbers within NBCI database are given.

Table 2. Amino Acid Sequence Alignment of the 12 kDa Protein[a]

5″	1	*MDDESSKPCC DQCACTRSNP PQCR*CSDIRL NSCHSACKSC ICALSYPAQC
	51	FCVDITDFCY EPCKPSEDDK EN
IBBD1_SOYBN		DDESSKPCC DQCACTKSNP PQCRCSDMRL NSCHSACKSC ICALSYPAQC
		FCVDITDFCY EPCKPSEDDK EN
IBBD2_SOYBN		CTRSMP PQC C MCTRSQPGQC

[a]Amino acid sequences of inhibitory domains are underlined. $P_1-P'_1$ are the reactive peptide bond sites, in bold text. Either K or R at position P1 determines specificity for trypsin, whereas L determines specificity against chymotrypsin. The peptides that contributed to protein identification are indicated in italics.

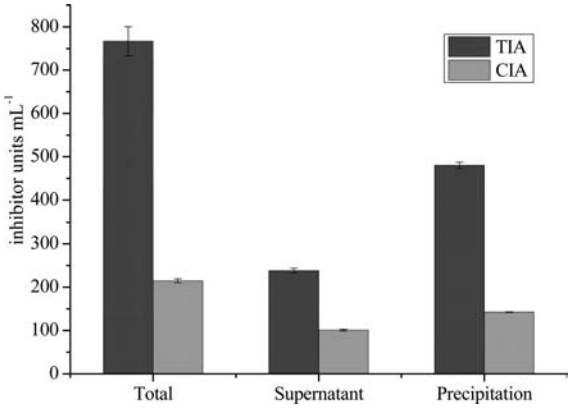

Figure 2. Trypsin and chymotrypsin inhibitor activity of SWP/Ch system at $R_{SWP/Ch}$ = 4:1. At $R_{SWP/Ch}$ = 4:1, the 12 kDa proteins distribute in both supernatant and precipitate. The activity is expressed as inhibitor units and presented as the mean ± SE (n = 3). Lanes: 1, total protein; 2, proteins remained in the supernatant; 3, precipitated proteins.

behavior of soybean whey proteins and chitosan, as shown in Figure 3. On addition of NaOH to SWP/Ch mixtures that had been adjusted to a pH lower than the isoelectric point of SWP (pH 4.3), we first observed the formation of a soluble complex at pH_c, below which electrostatic repulsive forces prohibited the formation of complexes, and the turbidity remained at the baseline. Upon further elevation in alkalinity to $pH_{\varphi 1}$, an abrupt increase in turbidity was observed, indicating the formation of insoluble complex particles. Turbidity rose to the maximum at pH_{max} and decreased rapidly as the pH continued to increase, and a turbidity level-off was found at $pH_{\varphi 2}$. As a control, chitosan was a primary aliphatic amine that can be protonated by selected acids (such as acetic acid), the pK of the chitosan

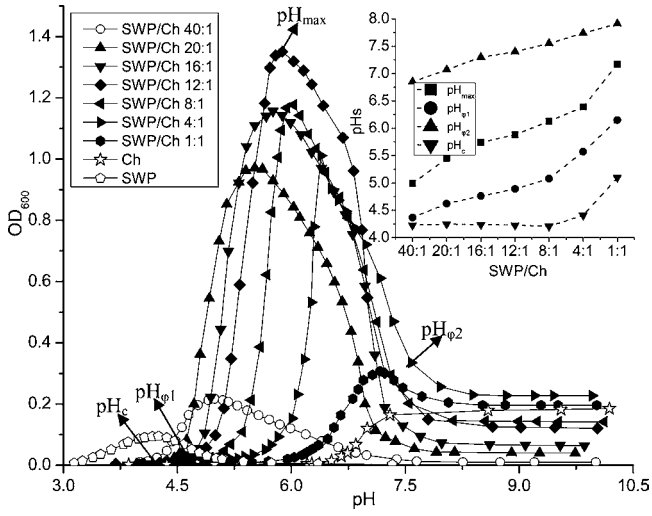

Figure 3. Turbidity curves for the SWP/Ch system (Cp = 0.10%) and homologous SWP solution as a function of $R_{SWP/Ch}$ in the absence of NaCl. The values of pH_c, $pH_{\varphi 1}$, and $pH_{\varphi 2}$ were determined graphically as the intersection point of two tangents to the curve, whereas pH_{max} corresponded to the maximum optical density at 600 nm. (Inset) pH values (pH_c, $pH_{\varphi 1}$, pH_{max}, and $pH_{\varphi 2}$) of SWP/Ch system for different ratios.

amine being 6.3. This made it soluble in acid solution, and deprotonation began at pH >6.3. Therefore, the turbidity curve (Figure 3) for chitosan displayed an abrupt increase in turbidity at pK_a and then reached a maximum at pH around 7.0, followed by the plateaus of turbidity, corresponding to the insolubility of chitosan.

Figure 3 shows that the complexing behavior of SWP/Ch was also substantially affected by the mixing ratio, and the shifts of pH values (pH_c, $pH_{\varphi 1}$, and $pH_{\varphi 2}$) for SWP/Ch system at different ratios are inset in this figure. It was found that a decrease in SWP/Ch ratio resulted in a shift of the turbidity curves to higher pH ranges. Another study done in our laboratory also found the shift of turbidity curves of soy protein−gum arabic mixtures when the mixing ratio changed.[38] The authors noted that, with the increase of soy protein/gum arabic ratio, critical pH values for the formation of insoluble complex shifted to higher values. At the same time, the pH value at which soy proteins and gum arabic carried equal amount but opposite charges also changed in the same way. Therefore, the movement of the turbidity curves seemed to be related to changes of conditions at which the protein/polysaccharide charge compensation was achieved.

To verify the above speculation, a more detailed analysis of electric charge relationships between two biomacromolecules

dx.doi.org/10.1021/jf501904g | J. Agric. Food Chem. 2014, 62, 7279−7286

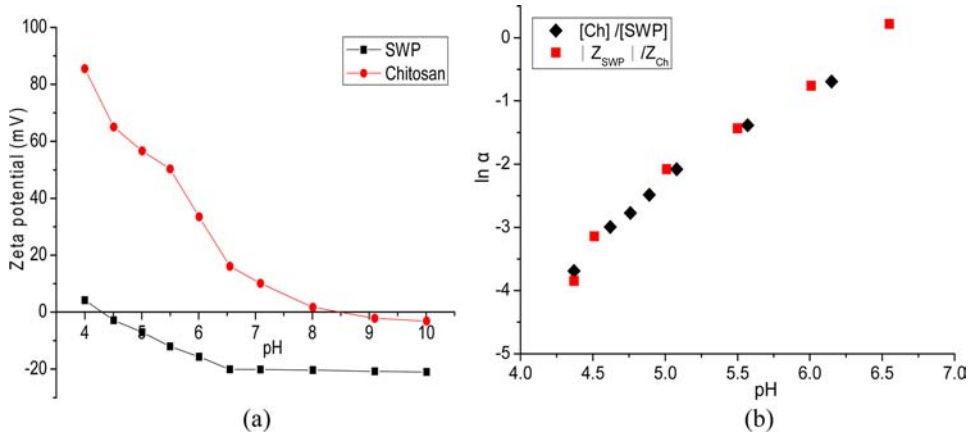

Figure 4. Zeta potential (mV) values for homogeneous SWP (0.1%) and chitosan (0.1%) in the absence of NaCl (a) as a function of pH (n = 2) and the relationship between [Ch]/[SWP] and $|Z_{SWP}|/Z_{Ch}$ as a function of pH (b).

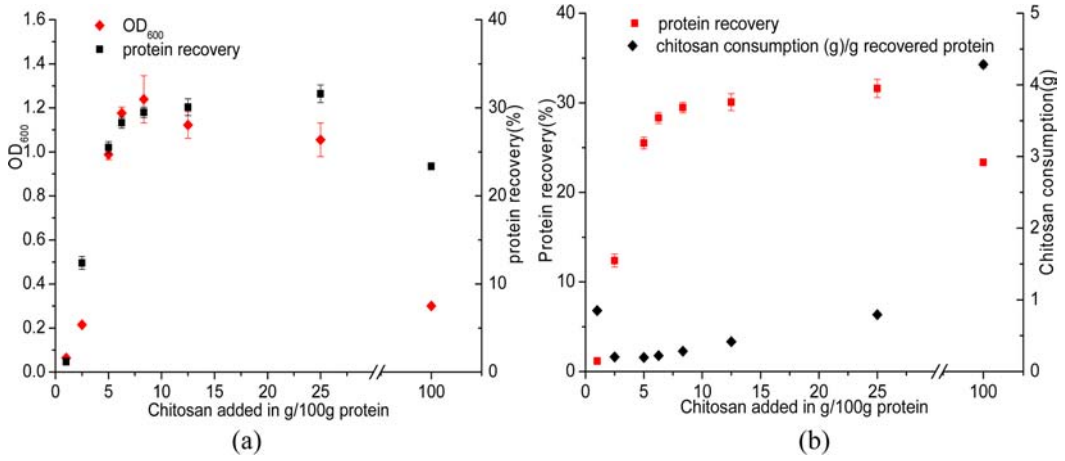

Figure 5. Relationship between turbidity (OD_{600}) and protein recovery (a) and between protein recovery and chitosan consumption (b) for the SWP/Ch (Cp = 0.10%) system. OD_{600} represented the maximum turbidity of given ratios; the protein recovery corresponded to maximum turbidity.

was conducted to get a more quantitative understanding of the effect of mixing ratio on the complexing behavior of SWP/chitosan mixtures. Figure 4a shows that chitosan gave positive zeta potential below about pH 8.3, whereas SWP presented negative zeta potential at pH >4.3. In addition to the nature of electric charges, the absolute value of zeta potentials revealed that the quantities of charges on SWP and Ch, respectively, were also pH dependent. Figure 4b shows the plot of $\ln(|Z_{SWP}|/Z_{Ch})$ as a function of pH. At the same time, $\ln([Ch]/[SWP])$ versus $pH_{\varphi 1}$ was also plotted in the same coordinate system. It was interesting to find that two sets of data can be described by essentially the same curve. We knew that a mixture with a given Ch/SWP ratio started phase separation at $pH_{\varphi 1}$. If we looked at the Ch/SWP mixing ratio of 1:8, or $\ln([Ch]/[SWP]) = -2$, the corresponding $pH_{\varphi 1}$ value was found to be 5.1. At around the same pH (5.05), the natural logarithm of $|Z_{SWP}|/Z_{Ch}$ had almost the same value. Thus, our study indicated that at $pH_{\varphi 1}$, $[SWP] \times |Z_{SWP}| = [Ch] \times Z_{Ch}$ or charge compensation was established. For other mixing ratios, the curve told us that charge compensations were also achieved.

In Figure 3, the maximum turbidity occurred at the pH higher than $pH_{\varphi 1}$, indicating that electric charges on soybean whey proteins and chitosan were not balanced. Most probably, the dissociation of carboxyl groups of proteins and the deprotonation of amino groups of chitosan proceeded more rapidly at higher pH and more complexes were formed in a limited period of time. Therefore, the position and height of maximum turbidity were affected both by thermodynamic and by kinetic factors.

Maximum Turbidity and Protein Recovery. Figure 5a shows the effect of chitosan level on maximum turbidity. It can be observed that turbidity increased rapidly when the amounts of chitosan, which was added into 100 g of soybean whey proteins, increased from 1 to 8.3 g. Further increase in chitosan level resulted in a decrease of turbidity. On the other hand, percent recovery of proteins from soybean whey by centrifugation precipitation of the SWP/Ch complex reflected not only the amount of complex formed but also the deposit ability of the complex. As shown in Figure 5a, protein recovery increased along with turbidity when the chitosan level increased from 1 to 8.33 g/100 g SWP. However, protein recovery kept increasing, although at a slower pace, at higher chitosan level and reached a maximum at 25 g/100 g SWP. A chitosan consumption was defined here as the amount of chitosan used to recover 1 g of proteins in soybean whey. Our experiment (Figure 5b) revealed that although the protein recovery was not very high at a SWP/Ch ratio of 20:1 and pH 5.5, chitosan consumption was lowest (0.196 g Ch/g recovered proteins) under this condition.

Protein Components of SWP/Ch Complexes. Dialyzed soybean whey was mixed at different mixing ratios, and SWP/

dx.doi.org/10.1021/jf501904g | J. Agric. Food Chem. 2014, 62, 7279−7286

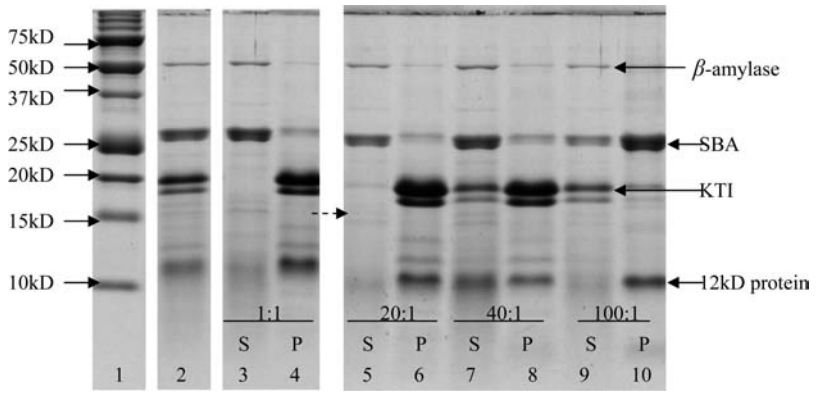

Figure 6. Tricine–SDS-PAGE for proteins in supernatant (S) and precipitate (P). Lanes: 1, marker; 2, SWP; 3, 5, 7, and 9, supernatants for $R_{SWP/Ch}$ 1:1, 20:1, 40:1, 100:1; 4, 6, 8, and 10, precipitates for the same ratios.

Ch complexes were formed by pH titrating to the maximum turbidity using NaOH solution, followed by centrifuging to obtain precipitates and supernatants. Protein compositions of complexes and supernatants were analyzed by SDS-PAGE, and the results are shown in Figure 6. In the case of the SWP/Ch ratio range from 1:1 to 20:1 (the other four ratios 16:1–4:1 are not shown in the figure), a negligible content of KTI in the supernatant and low contents of SBA and β-amylase in the precipitates were observed. For the mixture with a SWP/Ch ratio of 40:1, it was estimated that >80% of KTI transferred into the SWP–Ch complex, whereas >70% of SBA and β-amylase remained in the supernatants. The inability of SBA and β-amylase to form a complex with chitosan could partly be attributed to their higher isoelectric points (pH 5.8 and 5.6). Chitosan started to deprotonate at a pH higher than the pK_a (pH 6.3), at which point SBA and β-amylase were marginally negatively charged. Thus, the electric interaction between proteins and chitosan was weak. From the above, we knew that if the SWP/Ch mixing ratio was less than 20:1, all of the KTI of soybean whey would form a complex with chitosan.

Quite unexpectedly, the precipitate that was formed at very low chitosan level (SWP/Ch =100) and low pH (pH 4.8) displayed a very different protein composition, SBA and 12 kDa protein being the major proteins in addition to a small amount of KTI. The precipitate could not be formed by complexing because both SBA and Ch carried the same positive charge at this pH range. The precipitation of SBA in dialyzed soybean was also found at pH around 4.8. Most possibly, this precipitate was caused by the low solubility of SBA in very low salt concentration. Additionally, it was also remarkable to find that all precipitates seemed to contain essentially the same amount of 12 kDa proteins, regardless of the difference in pH and SWP/Ch ratio.

Selective Complexing of KTI. Protein separation had been achieved by Xu et al.[18] as a consequence of selective protein–polyelectrolyte complexation. This technique may afford the possibility of large-scale protein purification that is fast, efficient, and inexpensive compared to traditional protein separation methods such as chromatography, membrane separation, or centrifugation.[39] In this experiment, dialyzed soybean whey was adjusted to pH 4.0 and centrifuged at 4000 rpm to remove self-aggregated SBA and 12 kDa proteins to increase the selectivity of KTI. Protein content in the supernatant was determined and mixed with chitosan according to different SWP/Ch ratios.

Figure 7 shows that the protein composition of precipitates formed from 4:1 to 40:1. Soybean whey/chitosan mixtures

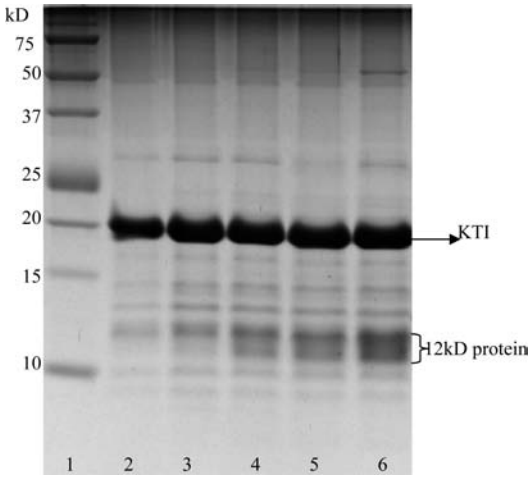

Figure 7. Tricine–SDS-PAGE for proteins in precipitates. Lanes: 1, marker; 2–6, precipitates for $R_{SWP/Ch}$ 100:1 (pH 4.86), 40:1 (pH 4.99), 20:1 (pH 5.52), 12:1 (pH 5.88), and 4:1 (pH 6.39).

were similar to the respective protein composition when soybean whey was not precentrifuged, KTI being the major component together with a small amount of 12 kDa proteins, whereas SBA and β-amylase showed only very faint bands. However, the protein composition for 100:1 precipitate was totally different from the above experiment: before precentrifugation, SBA and 12 kDa proteins were the main components, whereas after precentrifugation, KTI became the major protein. Therefore, the removal of self-aggregated SBA and 12 kDa proteins could increase the availability of chitosan for complexing with KTI. As a lectin, SBA is a nonenzyme, nonantibody, and carbohydrate-binding protein[40] and is well-known for its highly specific interactions with galactose/*N*-acetylgalactosamine.[41] On the other hand, chitosan is composed of randomly distributed β-(1–4)-linked D-glucosamine (deacetylated unit) and *N*-acetyl-D-glucosamine (acetylated unit), which can provide binding sites for SBA. In contrast to protein–polysaccharide complexing, the specific binding of SBA with chitosan at acidic pH range actually stabilized proteins against precipitation. This was confirmed by the fact that, when the isolated SBA was mixed with chitosan and the pH adjusted to the range of phase separation (pH >6.3), the

dx.doi.org/10.1021/jf501904g | J. Agric. Food Chem. 2014, 62, 7279–7286

obtained mixture gave turbidity lower than that of chitosan at the same condition. Therefore, by partly removing SBA through precentrifugation to reduce the consumption of chitosan, KTI was provided the opportunity to be complexed. As to the behavior of 12 kDa proteins, experimental results suggested that they displayed self-aggregating ability at the same pH as that for SBA and the complexing ability with chitosan under the same conditions for KTI complexing. However, it seemed that interaction between 12 kDa proteins and chitosan was weaker than that between KTI and chitosan, which was possibly because 12 kDa proteins had higher isoelectric points than that for KTI. This can explain why these proteins always coexisted with KTI in precipitates but were less enriched.

Kaibara et al.[42] reported that ionic strength, polyelectrolyte charge, and protein charge densities affected the protein purification. In their experiment, the selective coacervation of BSA from the BLG was achieved by the nonmonotonic control of ionic strength to enhance protein charge anisotropy. However, in our experiment, with an environment lacking ionic strength, the selectivity of coacervation depended on the charge of protein and chitosan pairs. The stronger binding affinity to chitosan of KTI than of the 12 kDa protein offered us the possibility to separate them by changing the ratio of protein/polysaccharide. As expected, in the low presence of chitosan, the two proteins showed a significant difference in binding ability, giving the priority of KTI to 12 kDa protein binding to chitosan, and a purified KTI was obtained.

This KTI−Ch complex obtained was adjusted to pH 10 to precipitate chitosan, followed by centrifugation (4000 rpm, 15 min) to collect the supernatant, which was rich in KTI. The purified KTI contained 95.89% protein, 2.02% polysaccharide, 0.87% ash, and 2.2% water. The TIA of the purified KTI was 5901.3 U/mg, higher than that of standard KTI (Sigma) with 5058.08 U/mg, showing that the presence of chitosan may have no effect on the natural activity of KTI.

The purifying effect of KTI by selective complexing with chitosan after precentrifugation was further verified by SEC-HPLC (Figure 8). Several peaks were observed in the dialyzed

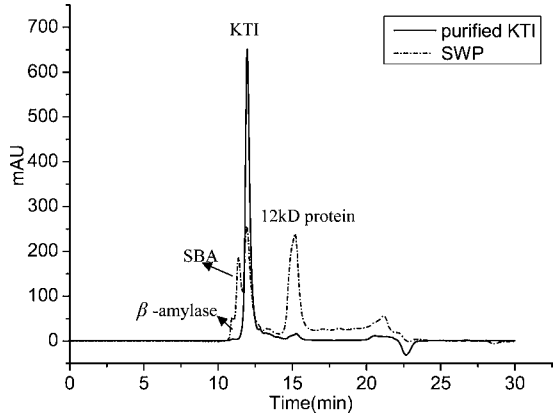

Figure 8. SEC-HPLC analysis for SWP and purified KTI.

soybean whey, and the content of KTI was 33.17% calculated from peak area. After complexing with chitosan, other proteins were substantially removed and the purity of KTI was 92.5%. The problem with the present result was the low (about 10%) recovery of KTI at one time. Two further experiments were also needed to extract the residual KTI in the supernatant, and the average purity of these three prepared samples was also >90%. Therefore, further studies will be conducted to consistently improve the KTI recovery.

In summary, a newly identified protein (12 kDa), which had a structure similar to that of BBI and showed CIA and TIA activities, was found in soybean whey by SDS-PAGE and MALDI-TOF/TOF-MS. The KTI and the 12 kDa protein were the main components to form complexes with chitosan. For different SWP/Ch ratios, charge compensation of system was found to be established at $pH_{\varphi 1}$, at which phase separation began to occur. Selective complexation between KTI and chitosan was observed only at the condition of SWP/Ch = 100:1, pH 4.8 and low ionic strength. After removing chitosan, a high purity KTI (more than 90%) could be obtained.

AUTHOR INFORMATION

Corresponding Author

*(Y.H.) Phone: 0510-85917812. Fax: 0510-85329091. E-mail: yfhua@jiangnan.edu.cn.

Funding

The work received financial support from the National Natural Science Foundation of China (No. 21276107), The National Great Project of Scientific and Technical Supporting Programs funded by the Ministry of Science and Technology of China during the 12th 5-year plan (No. 2012BAD34B04-1), and the 863 Program (Hi-tech research and development program of China, No. 2013AA102204-3).

Notes

The authors declare no competing financial interest.

REFERENCES

(1) Smith, A. K.; Rackis, J. J.; Isnardi, P.; Cartter, J. L.; Krober, O. A. Nitrogen solubility index, isolated protein yield, and whey nitrogen content of several soybean strains. *Cereal Chem.* **1966**, *43*, 261−270.

(2) Iwabuchi, S.; Yamauchi, F. Electrophoretic analysis of whey proteins present in soybean globulin fractions. *J. Agric. Food Chem.* **1987**, *35* (2), 205−209.

(3) Koshiyama, I.; Kikuchi, M.; Fukushima, D. 2S globulins of soybean seeds. II. Physicochemical and biological properties of protease inhibitors in 2S globulins. *J. Agric. Food Chem.* **1981**, *29* (2), 340−343.

(4) Rackis, J. J.; Wolf, W. J.; Baker, E. C. Protease inhibitors in plant foods: content and inactivation. In *Nutritional and Toxicological Significance of Enzyme Inhibitors in Foods*; Friedman, M., Ed.; Plenum: New York, 1986

(5) Kennedy, A. R. Chemopreventive agents: protease inhibitors. *Pharmacol Ther.* **1998**, *78* (3), 167−209.

(6) Armstrong, W. B.; Kennedy, A. R.; Wan, X. S.; Atiba, J.; McLaren, C. E.; Meyskens, F. L. Single-dose administration of Bowman-Birk inhibitor concentrate in patients with oral leukoplakia. *Cancer Epidemiol. Biomarkers Prev.* **2000**, *9* (1), 43−47.

(7) Wang, J.; Shen, W. C. Gastric retention and stability of lipidized Bowman-Birk protease inhibitor in mice. *Int. J. Pharm.* **2000**, *204* (1−2), 111−116.

(8) Smith, A. K.; Nash, A. M.; Eldridge, A. C.; Wolf, W. J. Recovery of soybean whey protein with edible gums and detergents. *J. Agric. Food Chem.* **1962**, *10* (4), 302−304.

(9) Gillberg, L; Tornell, B. Preparation of rapeseed protein isolates. *J. Food Sci.* **1976**, *41*, 1070−1075.

(10) Dickinson, E. Stability and rheological implications of electrostatic milk protein−polysaccharide interactions. *Trends Food Sci. Technol.* **1998**, *9*, 347−354.

(11) Morawetz, H.; Sage, H. The effect of poly(acrylic acid) on the tryptic digestion of hemoglobin. *Arch. Biochem. Biophys.* **1955**, *56*, 103−109.

(12) Larionova, N. I.; Unksova, L. Y.; Mironov, V. A.; Sakharov, I. Y.; Kazanskaya, N. F.; Berezin, I. V. Study of the complex-formation between soluble carboxymethyl ethers of polysaccharides and proteins. *Vysokomol. Soedin., Ser. A* **1981**, *23*, 1823−1829.
(13) Izumrudov, V. A.; Galaev, I. Y.; Mattiasson, B. Polycomplexes − potential for bioseparation. *Bioseparation* **1998**, *7*, 207−220.
(14) Strege, M. A.; Dubin, P. L.; West, J. S.; Flinta, D. In *Protein Purification: From Molecular Mechanisms to Large-scale Processes*; Ladisch, M., et al., Eds.; American Chemical Society: Washington, DC, USA, 1990; Chapter 5.
(15) Du, X. S.; Dubin, P. L.; Hoagland, D. A. Protein-selective coacervation with hyaluronic acid. *Biomacromolecules* **2014**, *15* (3), 726−734.
(16) Hidalgo, J.; Hansen, P. M. T. Selective precipitation of whey proteins with carboxymethylcllulose. *J. Dairy Sci.* **1971**, *54*, 1270−1274.
(17) Dubin, P. L.; Gao, J.; Mattison, K. W. Protein purification by selective phase separation with polyelectrolytes. *Sep. Purif. Methods* **1994**, *23*, 1−16.
(18) Xu, Y.; Mazzawi, M.; Chen, K. Protein purification by polyelectrolyte coacervation: influence of protein charge anisotropy on selectivity. *Biomacromolecules* **2011**, *12*, 1512−1522.
(19) Lee, A. C.; Hong, Y. H. Coacervate formation of α-lactalbumin−chitosan and β-lactoglobulin−chitosan complexes. *Food Res. Int.* **2009**, *42* (5−6), 733−738.
(20) Liu, C.; Yang, X. Q.; Lin, M. G.; Zhao, R. Y.; Tang, C. H.; Luo, L.; Liu, L. Complex coacervation of chitosan and soy globulins in aqueous solution: a electrophoretic mobility and light scattering study. *Int. J. Food Sci. Technol.* **2011**, *46* (7), 1363−1369.
(21) Elmer, C.; Karaca, A. C.; Low, N. H.; Nickerson, M. T. Complex coacervation in pea protein isolate−chitosan mixtures. *Food Res. Int.* **2011**, *44* (5), 1441−1446.
(22) Argin-Soysal, S.; Kofinas, P.; Lo, Y. M. Effect of complexation conditions on xanthan−chitosan polyelectrolyte complex gels. *Food Hydrocolloids* **2009**, *23* (1), 202−209.
(23) Hu, B.; Wang, S. S.; Li, J.; Zeng, X. X.; Huang, Q. R. Assembly of bioactive peptide chitosan nanocomplexes. *J. Phys. Chem. B* **2011**, *115*, 7515−7523.
(24) Coelho, S.; Flores, S. M.; Herrera, J. L. T.; Coelho, M. A. N.; Pereira, M. C.; Rocha, S. Nanostructure of polysaccharide complexes. *J. Colloid Interface Sci.* **2011**, *363* (2), 450−455.
(25) Andrews, H. E.; González, J. G. B.; Sosa, F. C.; Carter, E. J. V. Gum arabic−chitosan complex coacervation. *Biomacromolecules* **2007**, *8* (4), 1313−1318.
(26) Yoshida, K.; Dubin, P. L. Complex formation between polyacrylic acid and cationic: nonionic mixed micelles: effect of pH on electrostatic interaction and hydrogen bonding. *Colloids and Surfaces A: Physicochem. Eng. Aspects* **1999**, *147*, 161−167.
(27) Ru, Q.; Wang, Y.; Lee, J.; Ding, Y.; Huang, Q. Turbidity and rheological properties of bovine serum albumin/pectin coacervates: effect of salt concentration and initial protein/polysaccharide ratio. *Carbohydr. Polym.* **2012**, *88*, 838−846.
(28) Liu, S.; Cao, Y. L.; Ghosh, S. Intermolecular interactions during complex coacervation of pea protein isolate and gum arabic. *J. Agric. Food Chem.* **2010**, *58*, 552−556.
(29) Weinbreck, F.; Nieuwenhuijse, H.; Robijn, G. W.; de Kruif, C. G. Complexation of whey proteins with carrageenan. *J. Agric. Food Chem.* **2004**, *52* (11), 3550−3555.
(30) Mattison, K. W.; Dubin, P. L.; Brittain, I. J. Complex formation between bovine serum albumin and strong polyelectrolytes: effect of polymer charge density. *J. Phys. Chem. B* **1998**, *102*, 3830−3836.
(31) Smith, P. K.; Krohn, R. I.; Hermanson, G. T.; Mallia, A. K.; Gartner, F. H.; Provenzano, M. D.; Fujimoto, E. K.; Goeke, N. M.; Olson, B. J.; Klenk, D. C. Measurement of protein using bicinchoninic acid. *Anal. Biochem* **1985**, *150*, 76−85.
(32) Schagger, H. Tricine-SDS-PAGE. *Nat. Protoc.* **2006**, *1*, 16−22.
(33) Zhao, L. P.; Chen, Y. M.; Cao, Y. Y.; Kong, X. Z.; Hua, Y. F. The integral and extrinsic bioactive proteins in the aqueous extracted soybean oil bodies. *J. Agric. Food Chem.* **2013**, *61*, 9727−9733.
(34) Liu, K. S.; Markakis, P. An improved colorimetric method for determining antitryptic activity in soybean products. *Cereal Chem.* **1989**, *66* (5), 415−422.
(35) Tan, N. H.; Zubaidah, H. A.; Rahim, H. T. K.; Wong, K. C. Chymotrypsin inhibitor activity in winged beans (*Psophocarpus tetragonolobus*). *J. Agric. Food Chem.* **1984**, *32* (1), 163−166.
(36) Yehudith, B. The Bowman-Birk inhibitor trypsin- and chymotrypsin-inhibitor from soybeans. *Int. J. Pept. Protein Res.* **1985**, *25*, 113−131.
(37) Alfonso, C.; Francisco, J. M.; Manzano, M. C. M.; Jiménez, E.; Domoney, C. The cytotoxic effect of Bowman−Birk isoinhibitors, IBB1 and IBBD2, from soybean (*Glycine max*) on HT29 human colorectal cancer cells is related to their intrinsic ability to inhibit serine proteases. *Mol. Nutr. Food Res.* **2010**, *54*, 396−405.
(38) Dong, D; Hua, Y. F.; Chen, Y. M.; Kong, X. Z.; Zhang, C. M.; Wang, Q. Charge compensation, phase diagram, and protein aggregation in soy protein−gum arabic complex formation. *J. Agric. Food Chem.* **2013**, *61*, 3934−3940.
(39) Ladisch, M. R.; Willson, R. C.; Painton, C.; Builder, S. E. In *Protein Purification: From Molecular Mechanisms to Large Scale Processes*; American Chemical Society: Washington, DC, USA, 1990; Chapter 1.
(40) Liener, I. E.; Sharon, N.; Goldstein, I. J. *The Lectins: Properties, Functions, Applications in Biology and Medicine*; Academic: Orlando, FL, 1986; 600 pp.
(41) Sharon, N.; Lis, H. How proteins bind carbohydrate: lessons from legume lectins. *J. Agric. Food Chem.* **2002**, *50*, 6586−6591.
(42) Kaibara, K.; Okazaki, T.; Bohidar, H. B.; Dubin, P. L. pH-induced coacervation in complexes of bovine serum albumin and cationic polyelectrolytes. *Biomacromolecules* **2000**, *1*, 100−107.

Table 1. Content of Selected Metals in Naturally-Contaminated Mn Soil (marked as Mn) and in Control Soil Measured as Pseudo-Total Content and Water-Soluble Fraction

	pseudototal content		water-soluble content	
	control	Mn	control	Mn
Mn (μg g^{-1} DW)	675.1 ± 4.84	6494.3 ± 355.0***	1.50 ± 0.16	280.1 ± 18.6***
K (mg g^{-1} DW)	8.79 ± 0.32	3.04 ± 0.16***	0.063 ± 0.0022	0.038 ± 0.0026***
Ca (mg g^{-1} DW)	0.52 ± 0.014	0.058 ± 0.0016***	0.052 ± 0.0019	0.03 ± 0.00092***
Mg (mg g^{-1} DW)	6.26 ± 0.091	0.64 ± 0.026***	0.029 ± 0.0009	0.015 ± 0.0014***
Zn (μg g^{-1} DW)	143.5 ± 4.78	122.7 ± 6.15*	0.53 ± 0.046	1.36 ± 0.038***
Na (μg g^{-1} DW)	474.3 ± 22.2	176.1 ± 10.4***	23.0 ± 1.59	22.2 ± 1.89
Fe (μg g^{-1} DW)	29566.3 ± 1524.4	22621.7 ± 1134.8*	47.4 ± 4.2	13.2 ± 1.67***
Cu (μg g^{-1} DW)	26.6 ± 1.64	17.5 ± 1.35**	0.23 ± 0.02	0.24 ± 0.012
Ni (μg g^{-1} DW)	42.5 ± 1.82	32.6 ± 2.26*	0.091 ± 0.0072	0.049 ± 0.0031**
Cd (ng g^{-1} DW)	344.8 ± 10.6	514.5 ± 17.4***	13.6 ± 1.52	11.5 ± 1.56
pH (water/1 M KCl)	6.51/7.08	3.74/3.92		

Data are means ± SDs (n = 3). The *, **, and *** indicate significant difference at 0.05, 0.01, and 0.001 level of Student's t-test between control and Mn soil in the given fraction.

impact of pH on Mn uptake in some crops did not match with known fact that "its bioavailability increases with decreasing pH" as for example, potato contained more Mn at less acidic pH.[3] Because control and Mn-soil we used differed in pH, a further solution test was done to verify its involvement in Mn uptake.

MATERIALS AND METHODS

Plant Cultured and Experimental Design. Selected crops were tested in the present study (provided by Josef Hedbavny), namely *Brassica napus* cv. Smaragd, *Hordeum vulgare* cv. Bojos, *Zea mays* cv. Korneli, *Triticum aestivum* cv. Tiguan. Seeds were surface sterilized and sown directly to pots containing 500 g of control or naturally contaminated soil (5 for *Zea*, 10 for cereals and 20 seeds for *Brassica* in order to achieve approximately similar biomass/soil ratio). Control soil, collected on the field (by Jozef Kováčik, western Slovakia, village Bošany), is widely distributed in the Slovak Republic—Eutric Cambisol (with sandy loamy texture) as reported previously.[18] Mn-contaminated soil was collected on the natural locality in the Krušné Hory Mountains (or Ore Mountains) as described in the previous paper.[19] We note that the origin of this soil is not clear, but is probably natural because the composition of plant species around and within this locality is similar (P. Švec, personal visitation). Soil moisture was maintained at 60% of water holding capacity with distilled water to prevent the impact on minerals. Cultivation was realized under laboratory conditions with ∼300 μmol m^{-2} s^{-1} PAR at leaf level supplied by cool white fluorescent tubes L36W/840 (Lumilux, Osram), 25/20 °C day/night temperature and relative humidity of ∼60%.[14] Whole shoots of plants were harvested after 21 days of cultivation because growth retardation was visible. In the subsequent experiment, crops were sown directly on filter paper placed on glass balls in plastic box and supplemented with 5 mM $MnCl_2{\cdot}4H_2O$ solution (deducted from Mn content in water-soluble fraction of Mn-contaminated soil, see discussion) with pH 6.5 or 3.7 (based on pH of water extracts from control and Mn-contaminated soil, see the Results section). Plants were harvested 10 days later because *Brassica* plants showed strong retardation of growth. For fresh mass-requiring parameters, individual plants were powdered using liquid N_2 and fresh material was extracted as described below. Dry samples (dried at 75 °C to constant weight) were analyzed for mineral nutrients including Mn.

Quantification of Mn and Mineral Nutrients. Samples were prepared by mineralization of dry plant material (10−20 mg) in the mixture of concentrated HNO_3 and water (5 + 5 mL) using microwave decomposition (Ethos Sel Microwave Extraction Labstation, Milestone Inc.) at 200 °C over 1 h (complete duration of the mineralization program). The resulting clear solution was placed to glass flasks and diluted to a final volume of 20 mL. Soil samples for total content of metals (more exactly it is pseudototal content because primary HNO_3 concentration in mineralizates is ca. 5 M and traces of metals may remained bound in silicates present in the soil) were prepared by the same way while water-soluble Mn and nutrients were extracted with deionized water as reported earlier.[18] All measurements were carried out using an atomic absorption spectrometer AA30 (Varian Ltd.; Mulgrave, Australia) and the air−acetylene flame. Measurements of mineral nutrients were done as described previously and Mn was quantified at λ_{max} = 279.5 nm, LOD of Mn was 2 μg/L.[14]

Fluorescence Microscopy. For microscopic analyses, cross sections were taken ca. 1 cm above the stem base and were immediately stained with respective reagents. General accumulation of ROS was monitored using two widely used reagents: 2′,7′-dichlorodihydrofluorescein diacetate (DCF-DA, $502_{Ex}/526_{Em}$ nm, Life Technologies, U.S.A.) and CellROX Deep Red Reagent ($644_{Ex}/665_{Em}$ nm, Life Technologies, U.S.A.). Staining procedure was conducted as previously reported.[20] Nitric oxide or reactive nitrogen species (RNS) were visualized with 2,3-diaminonaphthalene (DAN, $365_{Ex}/415_{Em}$ nm, Sigma-Aldrich, U.S.A.) using 250 μM DAN for 1 h at room temperature.[14] Lipid peroxidation was visualized by BODIPY 581/591 C11 lipid peroxidation sensor ($581_{Ex}/591_{Em}$ nm, Life Technologies, U.S.A.) and total thiols by monochlorobimane ($394_{Ex}/490_{Em}$ nm) according to previous protocols.[20,21] Staining solution was always removed by respective buffer and samples were observed using fluorescence microscope and appropriate set of filters (Axioscop 40, Zeiss, Germany).

Assay of Antioxidative Enzymes and Metabolites. For the assay of enzymatic activities, whole shoots were homogenized with inert sand in potassium phosphate buffer containing 1% insoluble PVPP (pH 7.0). Soluble proteins were quantified according to Bradford method[22] and bovine serum albumin as standard (595 nm). Ascorbate peroxidase (APX) and guaiacol peroxidase (GPX) activities were measured as the oxidation of ascorbate and guaiacol at 290 and 470 nm, respectively.[11,12,23] Glutathione reductase (GR) activity was assayed as the reduction of GSSG at 412 nm.[11] Catalase activity was measured as the reduction of H_2O_2 to water monitored at 240 nm.[23] Randomly selected supernatants were boiled and assayed in order to check that reactions were enzymatic.

Total soluble phenols were extracted with 80% methanol and quantified using the Folin−Ciocalteu method with gallic acid as standard and detection at 750 nm.[23]

Quantification of organic and inorganic anions was performed by an Ion-Exchange Chromatography system (DX 600, Dionex Corporation, Sun Valley, CA, U.S.A.) equipped with ED50 Electrochemical detector and conductivity cell installed in DS3 Detection Stabilizer and Anion Self-Regenerating Suppressor−Ultra II (2 mm, ASRS-ULTRA II) operating at 100 mA in AutoSuppression Recycle Mode. Samples were prepared in deionized water (0.1 g FW/1 mL) that was found to be more suitable in comparison with acidified water (data not shown).

Separation was carried out with an IonPac AS 11−HC (2 × 250 mm) analytical column and IonPac AS 11−HC (2 × 50 mm) guard column (Dionex Corporation, Sun Valley, CA, U.S.A.). The mobile phase consisted of deionized water (A) and 100 mM NaOH in deionized water (B). A linear gradient profile of the mobile phase from 1% B (0−4 min), 1−15% B (4−12 min), 15−25% B (12−17 min), 25−45% B (17−20 min), and 45−1% B (20−21 min) was applied at a flow rate 0.35 mL/min. The column was equilibrated for 15 min under initial conditions prior to injection of the next sample. The column temperature was 30 °C and injection loop was 10 μL. The peak identity was confirmed by comparing the retention times with retention time of standards and by spiking standard solutions to the samples. Calibration curves were linear (r^2 > 0.998) for each compound in the concentration range 1−100 μg mL^{-1}. Limit of detection was 0.2−0.9 μg mL^{-1}. Reagents (malic acid, citric acid, ammonium acetate, and ammonium formate) were purchased from Sigma-Aldrich (Chemie GmbH, Steinheim, Germany), sodium hydroxide solution 50%, sodium phosphate and sodium sulfate were supplied by Fluka Chemie (Buchs, Switzerland) and other chemicals (sodium chloride, oxalic acid, potassium nitrate, sodium nitrite) were obtained from Penta Chrudim (Czech Republic). All chemicals used were of analytical grade. Demineralized water with a specific resistance of 18.2 MΩ cm^{-1} (Mili-Q RG, Millipore, Bedford, MA, U.S.A.) was used to prepare all solutions and standards.

Statistical Analyses. Two independent repetitions of the whole experiment were performed in order to check reproducibility. At least six pots were used for each crop and soil. Data were evaluated using ANOVA followed by a Tukey's test (MINITAB Release 11, Minitab Inc.; State College, Pennsylvania) at $P < 0.05$. Additionally, Student's *t*-test was used to compare the difference between control and Mn-soil and biomass production. Number of replications (n) in tables/figures denotes individual soil samples or individual plants analyzed for each parameter. Only for Mn-exposed *Brassica*, several shoots were pooled to achieve enough biomass for measurements.

RESULTS AND DISCUSSION

Uptake of Mn, Alterations of Mineral Nutrients, and Growth of Plants Cultured in Mn-Contaminated Soil. Analysis of soil Mn content revealed ca. 10-times higher amount in Mn-contaminated soil than in control soil in the pseudototal fraction and much higher difference in water-soluble fraction (Table 1). Pseudototal Mn content in Mn-soil is within the range reported previously on the locality from which soil used in the present study originated.[19] Further assay of selected essential and nonessential metallic nutrients showed their higher pseudototal amount in control soil (except for Cd), although it was not observed for all metals in water-soluble fraction (Table 1). The control soil we used is widely distributed in the Slovak Republic−Eutric Cambisol (with sandy loamy texture) with higher Mg content as reported previously for the same soil type from other locality.[18] More acidic pH was the main difference between Mn-soil and control (Table 1) and we therefore subsequently studied the impact of pH on Mn uptake in solution culture (see last paragraph of discussion).

Uptake of Mn, such as in the case of other metals, is affected by soil conditions as well as by plant species. This variability has previously been observed in various plants collected from naturally Mn-contaminated locality.[19] As expected, plants showed similar amount of Mn in control soil because it is an essential micronutrient (Table 2). However, differences of Mn content in Mn-soil were more extensive and suggest species-specific uptake. To our knowledge, this is first laboratory-controlled study using naturally Mn-contaminated soil, and we therefore found no data exactly comparable with the present study. In terms of our crops, it has been reported that shoots of

Table 2. Accumulation of Selected Metals in the Shoots of Four Crops Cultured in Naturally Mn-Contaminated Soil Over 21 Days[a]

	Brassica		*Hordeum*		*Zea*		*Triticum*	
	control	Mn	control	Mn	control	Mn	control	Mn
Mn (μg g^{-1} DW)	53.9 ± 5.17d	13696 ± 1761a	59.2 ± 5.58d	5953 ± 420.1b	62.1 ± 5.73d	5622 ± 476.5b	66.4 ± 6.32d	2363 ± 386.1c
K (mg g^{-1} DW)	36.3 ± 2.69b	39.0 ± 1.10b	56.2 ± 3.25a	32.0 ± 3.20b	54.0 ± 5.57a	19.4 ± 1.50c	54.0 ± 3.84a	21.5 ± 1.57c
Ca (mg g^{-1} DW)	11.7 ± 1.82a	2.12 ± 0.16c	2.83 ± 0.25b	0.91 ± 0.06d	2.25 ± 0.11bc	0.87 ± 0.06d	2.29 ± 0.08bc	0.43 ± 0.05e
Mg (mg g^{-1} DW)	5.63 ± 0.31a	2.90 ± 0.15b	3.40 ± 0.28b	1.81 ± 0.20cd	1.58 ± 0.09de	1.23 ± 0.09ef	2.15 ± 0.11c	0.94 ± 0.11f
Zn (μg g^{-1} DW)	96.5 ± 3.69b	246.9 ± 22.4a	104.4 ± 3.28b	78.9 ± 4.71c	80.1 ± 3.15c	90.5 ± 2.87b	94.6 ± 5.94b	75.1 ± 3.81c
Na (μg g^{-1} DW)	784.4 ± 40.7c	1738.2 ± 102.1b	2765.4 ± 312.1a	1607.7 ± 138.0b	81.4 ± 5.20d	42.6 ± 4.03e	81.1 ± 6.70d	83.6 ± 4.20d
Fe (μg g^{-1} DW)	140.6 ± 13.9b	259.8 ± 26.5a	94.9 ± 8.76c	70.2 ± 5.40d	49.7 ± 3.79e	138.4 ± 11.3b	114.4 ± 10.1bc	101.3 ± 11.7c
Cu (μg g^{-1} DW)	7.17 ± 0.61b	6.80 ± 0.53b	7.53 ± 0.58b	7.05 ± 0.52b	7.18 ± 0.56b	4.52 ± 0.50c	8.96 ± 0.52a	7.11 ± 0.42b
Ni (μg g^{-1} DW)	3.83 ± 0.18bc	7.68 ± 0.37a	2.15 ± 0.18d	2.44 ± 0.30d	1.89 ± 0.32d	3.22 ± 0.30c	4.51 ± 0.38b	4.26 ± 0.51b
Cd (ng g^{-1} DW)	279.3 ± 22.1b	685.0 ± 38.1a	55.2 ± 5.08e	84.0 ± 11.0d	238.4 ± 27.1bc	245.4 ± 31.6b	192.4 ± 12.6c	nd

[a]Data are means ± SDs (n = 3). Species identity is the same as in Figure 1. Values within rows, followed by the same letter(s), are not significantly different according to Tukey's test ($P < 0.05$). nd, not detected.

dx.doi.org/10.1021/jf5010176 | J. Agric. Food Chem. 2014, 62, 7287−7296

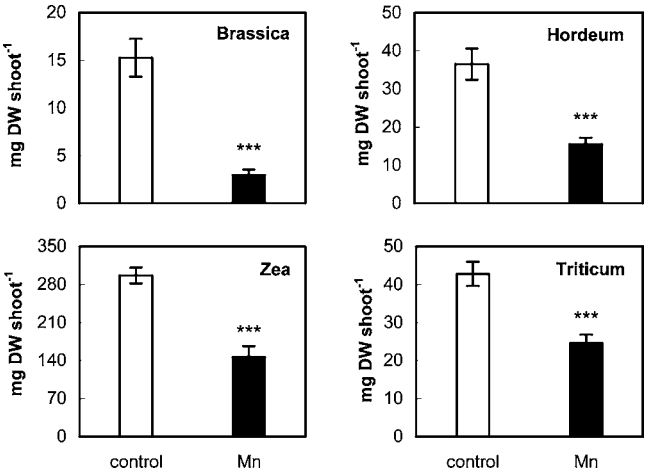

Figure 1. Dry biomass (milligrams per shoot) of four crops cultured in naturally Mn-contaminated soil (shown in Table 1) over 21 days. Data are means ± SDs (n = 10). *** indicates significant difference at 0.001 level of Student's t-test. Brassica, *Brassica napus* cv. Smaragd, Hordeum, *Hordeum vulgare* cv. Bojos, Zea, *Zea mays* cv. Korneli, and Triticum, *Triticum aestivum* cv. Tiguan.

Hordeum contained up to 3500 μg Mn g^{-1} in soil with total Mn concentration 500−2500 μg g^{-1} DW[2]; both these values are lower compared to our data (Tables 1 and 2), although growth depression by ca. 50% (Figure 1) is similar to mentioned study. Another theoretical comparison is possible with barley plants cultured in hydroponics with 1.83 mM Mn^{2+} where bioaccumulation (BAF) value was ca. 6.5:[8] considering that water-soluble Mn was ∼5 mM in our study (280.1 μg g^{-1} DW, Table 1), our BAF value is 21 and indicates similar extent of Mn uptake despite different culture conditions and Mn concentrations. However, BAF values for almost all species analyzed in the present study were calculated with respect to the pseudototal soil metal content, and this value is therefore lower in the case of *Hordeum* (0.92, Table 3). In this sense, only Mn-cultured *Brassica* had BAF higher than 1 but it does not confirm hyperaccumulation potential because growth was extremely suppressed (Figure 1).

Few studies also report Mn uptake in plants from natural localities and BAF can be calculated. For example, BAF in *Vaccinium myrtillus* was lower in the soil from polluted localities (3.6−14.4) in comparison with control localities (27.6−41.3).[10] In a similar study, species *Plantago lanceolata* and *Cardaminopsis arenosa* from a polluted locality (mining and metallurgic activity, where also higher soil Mn content was detected), revealed lower BAF if compared to control site (*P. lanceolata* 0.01−0.03 vs 0.09 in control; *C. arenosa* 0.02−0.1 vs 0.37 in control).[9] Above-mentioned data confirm that various plant species in natural populations do not elevate Mn content, although soil Mn content was higher on polluted localities. On the contrary, our plants had higher BAF values in Mn-soil: there is certainly a "break" of regulatory mechanisms and thus excessive Mn uptake damaged plants visibly in the present study.

Above-mentioned uptake of Mn was therefore reflected in the changes of growth. This was mainly visible in *Brassica* plants where the highest shoot Mn amount correlates with the most depleted growth (cf. Table 2 and Figure 1). Another aspect that certainly affected growth is depletion of some essential nutrients. Mainly Mg and Ca, being quantitatively important divalent cations that could compete with Mn uptake, decreased in plants from Mn-soil (Table 2). Although BAF for these metals was elevated in Mn-soil, indicating that plants effectively cope with their depleted amounts (compared to control, Tables 1 and 3), absolute quantities are probably not high enough for optimal growth (also visible by chlorosis of the leaves that appeared after several days of cultivation). In agreement with our data, Mn excess depleted macronutrients (Ca and Mg) more than the level of micronutrients (Fe, Zn, Cu) in cucumber plants and growth was also affected.[6] Besides, reduction of available Ca led to a dramatic increase in Mn content in *Phytolacca americana*.[24] However, our data also showed that the impact of Mn excess is species-specific and cannot be generalized because some metallic nutrients such as Zn or Fe even increased in Mn-cultured *Brassica* and *Zea*, but not in cereals (Table 2).

Another original aspect arising from the present study is the impact of Mn excess on the uptake of toxic metals. Amount of Cd and Ni was relatively similar in control and Mn-soil (Table 1). Accumulation of Ni was elevated in Mn-soil in *Brassica* and *Zea* plants but not in cereals. On the other hand Cd uptake strongly increased in Mn-cultured *Brassica* plants but was not detected in *Triticum* (Table 2). Owing to absence of similar literature, we are unable to compare these values deeply. Theoretical comparison is possible in relation to studies where polluted and nonpolluted localities in Poland were compared: although polluted localities contained more Mn, they also contained more Cd and therefore sharp increase in shoot Cd

Table 3. Bioaccumulation Factor Calculated as the Ratio of Individual Metals in Tissue (Table 2) to Total Soil Metal Content (Table 1)[a]

	Brassica		*Hordeum*		*Zea*		*Triticum*	
	control	Mn	control	Mn	control	Mn	control	Mn
Mn	0.079	2.11	0.087	0.92	0.092	0.86	0.098	0.36
K	4.13	12.8	6.39	10.5	6.14	6.38	6.14	8.03
Ca	22.5	36.6	5.44	15.7	4.33	15.0	4.40	7.41
Mg	0.899	4.53	0.54	2.83	0.25	1.92	0.34	1.47
Zn	0.67	2.01	0.73	0.64	0.56	0.74	0.66	0.61
Na	1.65	9.87	5.83	9.13	0.17	0.24	0.17	0.47
Fe	0.0047	0.0115	0.0032	0.0031	0.0017	0.0061	0.0039	0.0045
Cu	0.27	0.39	0.28	0.40	0.27	0.26	0.34	0.41
Ni	0.09	0.24	0.051	0.075	0.044	0.098	0.11	0.13
Cd	0.81	1.33	0.16	0.16	0.69	0.48	0.56	nd

[a]According to literature, BAF <1 and >1 indicate excluders and accumulators, respectively (see ref 18 for details).

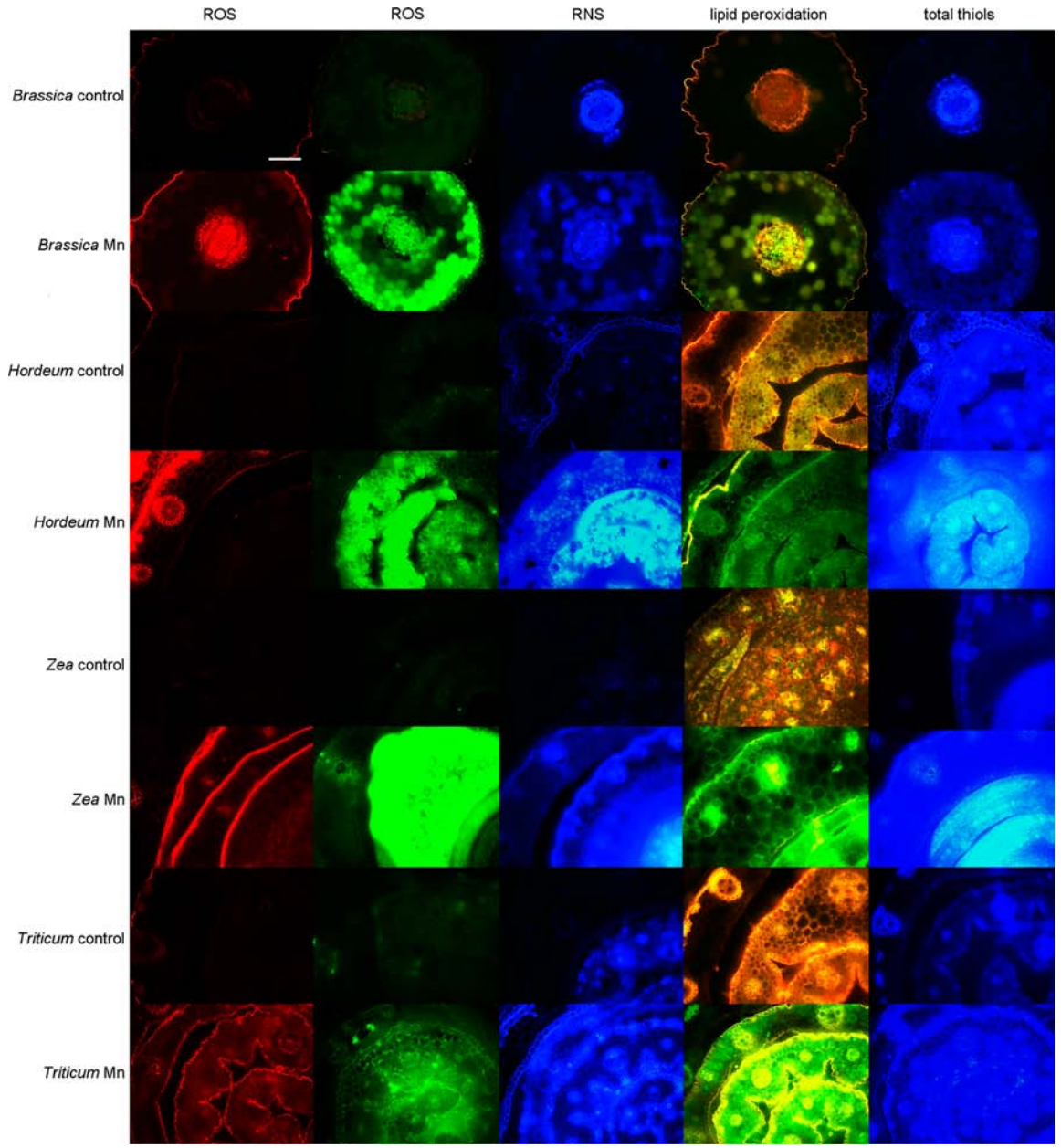

Figure 2. Fluorescence microscopy of selected oxidative stress-related parameters in the shoots of four crops cultured in naturally Mn-contaminated soil over 21 days. Species identity is the same as in Figure 1. Cross sections were taken ca. 1 cm above the stem base and were immediately stained. ROS (reactive oxygen species) were stained with CellROX Deep Red reagent (red signal) and 2′,7′-dichlorodihydrofluorescein diacetate (green signal), RNS (reactive nitrogen species) with 2,3-diaminonaphthalene, lipid peroxidation with BODIPY 581/591 C11 and total thiols with monochlorobimane. Bar indicates 200 μm.

content was found in three species.[9,10] However, our data again confirm that the uptake of toxic metals under Mn excess is not influenced only by pH or Mn itself and cereals (*Hordeum* and *Triticum*) seem to be less effective accumulators.

Oxidative Stress, Antioxidative Enzyme Activities and Metabolites in Plants Cultured in Mn-Contaminated Soil. Appearance of oxidative stress may be detected by various qualitative and quantitative methods. Fluorescence microscopy is sensitive qualitative method owing to use of specific reagents. In fact, visualization of ROS by two staining reagents confirmed that Mn excess evoked increase in ROS in all species investigated (Figure 2). Relatively less pronounced enhancement was observed in *Triticum*, a species with the lowest Mn amount (Table 2 and Figure 2).

Changes of nitric oxide (RNS, Figure 2) were also less extensive in *Triticum*, indicating that the lower level of oxidative stress does not evoke further elevation of nitric oxide. This fits well with our recent study where concentration-dependent stimulation of ROS in response to Mn excess was observed but nitric oxide presence differed in relation to ontogenetic stage; subsequent tests confirmed than exogenous NO ameliorated the appearance of ROS.[14] This is further evidence that NO plays an important role also under Mn excess, although this aspect is only poorly known.[15]

Higher ROS formation may also induce peroxidation of lipids. This peroxidation was confirmed by specific fluorescent reagent, shown as increase in green color within cross sections of tissue (Figure 2). This increase was detected in all species,

dx.doi.org/10.1021/jf5010176 | J. Agric. Food Chem. 2014, 62, 7287−7296

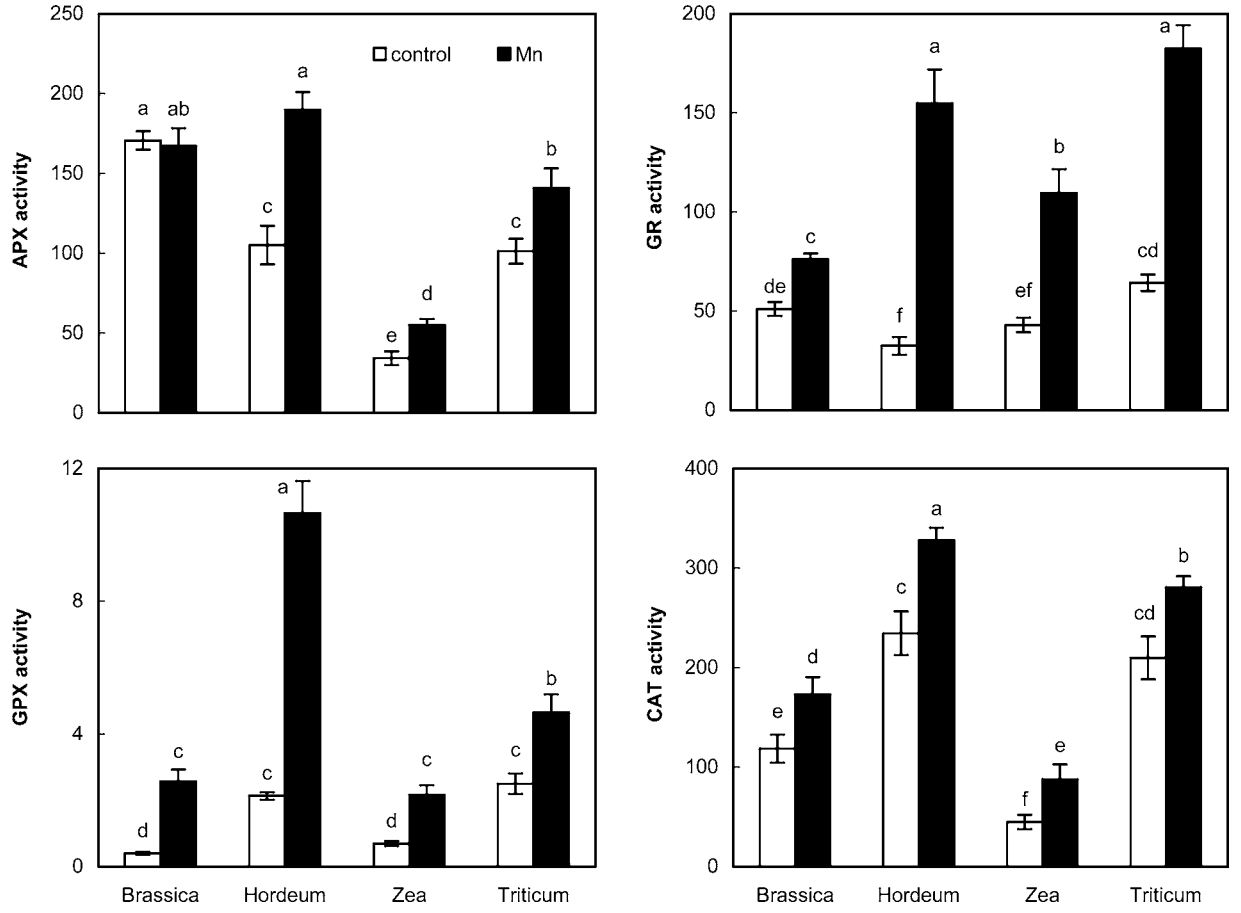

Figure 3. Activities of some antioxidative enzymes in the shoots of four crops cultured in naturally Mn-contaminated soil over 21 days. APX, ascorbate peroxidase, GPX, guaiacol peroxidase; GR, glutathione reductase; and CAT, catalase. Unit is μmol min^{-1} mg^{-1} protein for GPX and nmol min^{-1} mg^{-1} protein for other enzymes. Data are means ± SDs (n = 4). Values within each graph followed by the same letter(s) are not significantly different according to Tukey's test (P < 0.05). Species identity is the same as in Figure 1.

indicating oxidative damage from excessive Mn uptake. This may be explained by the fact that all species contained more Mn in shoots than chamomile plants in our previous study, where also concentration-dependent elevation of lipid peroxidation signal was visible.[14] Species-specific sensitivity is also known, e.g., low Mn excess had no impact on lipid peroxidation in mulberry plants,[25] while high Mn excess evoked only a slight elevation in rice seedlings after 20 days of cultivation.[7]

Antioxidative enzymes did not show any universal trend in relation to Mn amount in individual species (Figure 3). This was also observed in other species, e.g., in cucumber shoots[6] and no concentration dependency was found in pea[5] or chamomile seedlings.[14] In *Hordeum*, activity of enzymes was the most elevated. Peroxidases (APX and GPX) showed significantly enhanced activities in cereals (*Hordeum* and *Triticum*) in response to Mn excess (Figure 3). In agreement with our data, barley plants cultured under Mn excess had higher CAT and GPX activity[8] and rice seedlings showed elevation of GPX and APX activities in response to long-term presence of high Mn (3 and 6 mM)[7] that is similar to our water-soluble Mn fraction (Table 1). However, relatively slight impact of Mn on peroxidases in *Zea* observed in the present study has also been previously reported and even 1 mM of Mn^{2+} had negligible impact on oxidative or peroxidative activities in its roots.[16] Above-mentioned data confirm that antioxidative enzymes are involved in tolerance to Mn excess though responses differ in various species. Despite this increase, overall growth depression and appearance of oxidative damage were detected in all species (Figures 1 and 2). This is in accordance with other crops, e.g., tobacco plants cultured in vitro with 2 or 5 mM Mn contained similar amounts of Mn in leaves (up to 11 000 μg g^{-1} DW) as our plants (Table 2) but GPX and APX activities were considerably suppressed.[17] Glutathione reductase (GR) showed similar basic values in controls among plants and also strong increase in all species in Mn-soil with the exception of *Brassica* that could again indicate its sensitivity. Enhanced activity of GR was also reported in various crops where other antioxidative enzymes were depleted, such as rice,[7] cucumber,[6] and tobacco.[17] This fits well with visualization of total thiols though increase was less visible in some species (Figure 2). However, protein- and nonprotein thiols were variably affected by Mn excess in rice,[7] providing evidence that "total thiols" staining could not always match fully with individual parameters.

Phenolic metabolites are important stress-induced compounds including excess of metals.[26] In the case of Mn excess, it seems that their role is less important because we found significant increase only in *Brassica* plants that could be related to strong growth inhibition (Figure 4). Further studies are needed to analyze profile of phenols in plants under Mn excess. Soluble proteins are typically depleted by excess of metals depending on the given metal and applied concentration.[11] Mn excess in the present study evoked depletion in three species, but not in *Zea* (Figure 4). We assume this is related to high

dx.doi.org/10.1021/jf5010176 | J. Agric. Food Chem. 2014, 62, 7287−7296

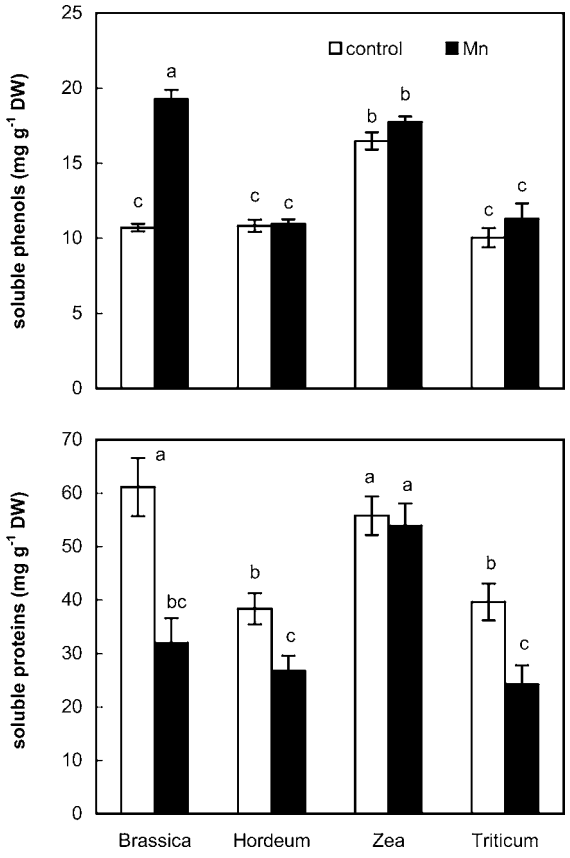

Figure 4. Quantitative changes of total soluble phenols and soluble proteins in the shoots of four crops cultured in naturally Mn-contaminated soil over 21 days. Data are means ± SDs (n = 4). Other details are the same as in Figure 3.

biomass production of *Zea* compared to other species and thus tissue-dilution impact on Mn translocation. Proteomic analyses will be carried out to study detailed changed at proteome level.

Quantitative Changes of Organic and Inorganic Anions in Plants Cultured in Mn-Contaminated Soil. Amount of malate was the highest among organic anions in control shoots of all plants (Table 4). This is in accordance with earlier report e.g. in *Zea*[27] while *Triticum turgidum* contained more oxalic and less malic acid[28] than our species (Table 4). Generally, organic acids such as oxalate, citrate and malate play an important role in the detoxification of various metals through chelation[27,28] or by modulation of rhizosphere pH.[29] In the case of Mn excess, oxalic acid is potentially involved in Mn detoxification in *Phytolacca americana*[30] and citrate enhanced Mn uptake in *Juncus effusus*.[31] Our present data showed decrease or unchanged contents of three above-mentioned acids and their role in the Mn uptake in any species is not expected. This could be related, the most probably, to observed growth depletion (and appearance of oxidative stress) leading to attenuated metabolism including Krebs cycle owing to high Mn excess in Mn-soil we used.

Increase in the nitrate amount in the majority of Mn-cultured species is in accordance with the depleted amount of proteins and indicates suppressed nitrate reduction and incorporation into the organic form. This was not observed in *Zea*, which probably has a higher potential to cope with Mn excess (Figure 4 and Table 4). The lower amount of sulfate in the majority of Mn-cultured crops may be related to elevated signal of thiols (Table 4 and Figure 2), suggesting its conversion into the

Table 4. Accumulation of Selected Organic and Inorganic Anions in the Shoots of Four Crops Cultured in Naturally Mn-Contaminated Soil Over 21 Days

	Brassica		*Hordeum*		*Zea*		*Triticum*	
	control	Mn	control	Mn	control	Mn	control	Mn
malate (mg g^{-1} DW)	29.3 ± 2.83b	4.73 ± 0.38d	40.1 ± 5.71a	7.44 ± 0.87c	7.02 ± 0.59c	2.58 ± 0.24e	8.07 ± 0.45c	0.69 ± 0.05f
citrate (mg g^{-1} DW)	16.5 ± 1.22a	4.59 ± 0.28c	9.53 ± 0.69b	3.35 ± 0.28cd	1.54 ± 0.26ef	0.96 ± 0.06f	2.32 ± 0.20de	0.37 ± 0.04g
oxalate (mg g^{-1} DW)	9.20 ± 0.79a	3.63 ± 0.45b	3.07 ± 0.30b	2.75 ± 0.25bc	3.65 ± 0.43b	2.74 ± 0.22bc	2.36 ± 0.15c	1.12 ± 0.09d
acetate (mg g^{-1} DW)	6.34 ± 0.43a	3.37 ± 0.22b	2.88 ± 0.20bc	1.19 ± 0.24e	0.96 ± 0.13e	2.65 ± 0.11c	1.86 ± 0.11d	1.75 ± 0.09d
formate (μg g^{-1} DW)	205.7 ± 17.4b	118.8 ± 14.2c	44.5 ± 2.92d	5.52 ± 0.54e	112.0 ± 18.3c	562.9 ± 38.6a	239.4 ± 32.1b	181.5 ± 13.8b
nitrate (mg g^{-1} DW)	12.1 ± 1.63c	28.3 ± 3.43a	0.53 ± 0.04g	7.65 ± 0.63d	20.9 ± 2.65b	5.06 ± 0.37e	0.47 ± 0.05g	2.88 ± 0.22f
nitrite (μg g^{-1} DW)	91.4 ± 4.58b	70.9 ± 3.24c	nd	nd	158.6 ± 19.6a	112.3 ± 17.8ab	37.7 ± 4.74d	18.8 ± 1.75e
chloride (mg g^{-1} DW)	5.53 ± 0.19d	2.71 ± 0.26f	14.3 ± 1.45b	2.97 ± 0.32ef	21.6 ± 1.34a	4.23 ± 0.41de	10.3 ± 0.74c	1.64 ± 0.25g
sulfate (mg g^{-1} DW)	11.5 ± 0.84b	8.45 ± 0.49c	15.0 ± 1.10a	8.45 ± 0.64c	3.56 ± 0.40d	3.91 ± 0.26d	8.25 ± 0.22c	2.34 ± 0.21e
phosphate (mg g^{-1} DW)	20.7 ± 1.95a	14.1 ± 1.04b	14.5 ± 2.00b	5.47 ± 0.29d	12.2 ± 1.72b	8.08 ± 0.56c	11.7 ± 1.02b	7.75 ± 0.24c

Data are means ± SDs (n = 3). Species identity is the same as in Figure 1. Values within rows, followed by the same letter(s), are not significantly different according to Tukey's test ($P < 0.05$). nd, not detected.

dx.doi.org/10.1021/jf5010176 | J. Agric. Food Chem. 2014, 62, 7287−7296

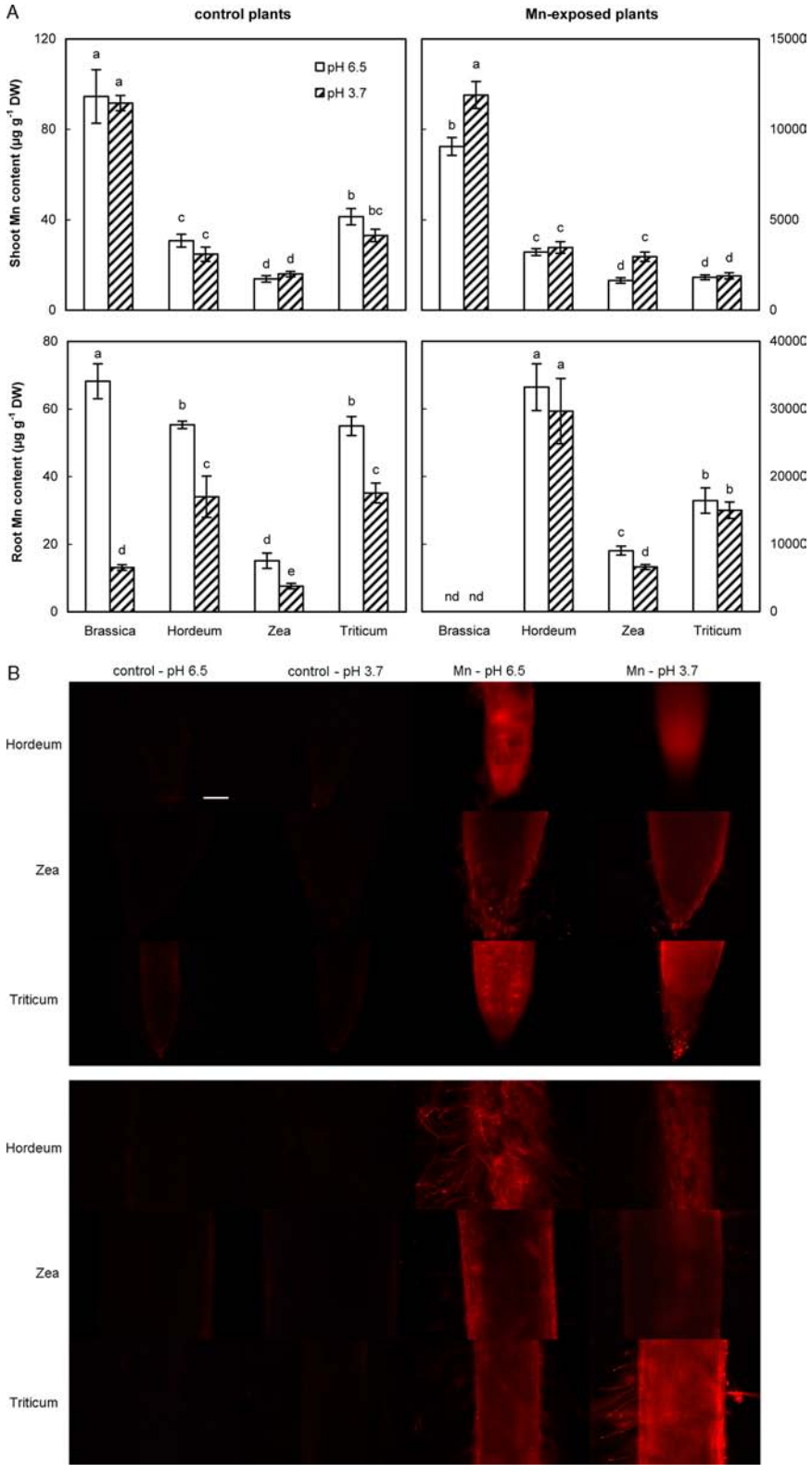

Figure 5. (A) Amount of Mn in the shoots and roots of four crops sown on filter paper and supplemented with deionized water (control plants) or with 5 mM Mn^{2+} solution (Mn-exposed plants) in relation to pH (values were selected based on pH of water extracts of control and Mn-contaminated soil shown in Table 1 and Mn^{2+} concentration based on water-soluble content in Mn-contaminated soil in the same Table). Plants were cultured over 10 days. Data are means ± SDs (n = 3). Other details are the same as in Figure 3. (B) Fluorescence visualization of ROS with CellROX Deep Red reagent in the root tip (above) and upper part of roots (bottom) in relation to pH and Mn absence/presence in the culture solution as mentioned in part A. Bar indicates 100 μm. Note that the root Mn content (nd in graph) and microscopy was not done in Mn-exposed *Brassica* because the roots were strongly rudimentary in the presence of Mn after given exposure time.

dx.doi.org/10.1021/jf5010176 | *J. Agric. Food Chem.* 2014, 62, 7287−7296

organic form under Mn excess. The phosphate quantity was lower in all Mn-exposed species, and its role in Mn uptake is not apparent, although Mn-containing crystals in some species may be formed with phosphate.[24]

Responses of Crops to Mn-Enriched Solution and Various pH. Because control and Mn-contaminated soil differed in pH (Table 1), we further investigated impact of pH on Mn toxicity in solution culture and crops were sown directly on filter paper with treatment solutions. Values of pH were selected based on water extracts (6.5 and 3.7 in control and Mn-soil) and Mn^{2+} concentration was based on water-soluble content in Mn-contaminated soil (Table 1; 280.1 $\mu g\ g^{-1}$ DW = ∼5 mM). Growth (both shoot and root biomass) in control treatments (deionized water only) was reduced only at pH 3.7 in *Zea* (data not shown). In Mn-enriched solutions, growth of *Hordeum* was reduced only by pH 3.7; both pH 3.7 and 6.5 reduced growth of *Zea*, *Triticum*, and *Brassica* (data not shown). Generally, impact of Mn excess on biomass was more negative at lower pH and in the case of *Brassica* it was pH-independent (only rudimentary roots ca. 1 mm long were developed). These are only slight differences in comparison with shoot biomass of plants cultured in Mn-contaminated soil where, e.g., *Triticum* was slightly more tolerant than *Hordeum* (Figure 1). This could be evoked by different exposure conditions and time (10 days in solutions vs 21 days in soil) and it may logically be expected that longer cultivation could lead to restoration of growth after adaptation to Mn excess. However, high sensitivity of *Brassica* to Mn excess (found in soil culture) was confirmed in solution culture and this sensitivity is not therefore pH-dependent but Mn-evoked. In agreement with our observations, growth of potato plants was more negatively affected by lower pH under Mn excess.[3]

Higher toxicity of Mn at lower pH could also be related to its higher solubility, as it is known that various metals are more readily absorbed at more acidic pH. Subsequent analyses of Mn content were therefore carried out to identify if Mn toxicity is related to its uptake in relation to pH. In control plants, decrease of pH depleted Mn content preferentially in the roots while such observation in Mn-exposed plants was only exceptional (Figure 5A). It has been reported that increasing pH increased Mn accumulation in the roots of barley[32] and Mn uptake by potato was also higher at pH 5.8 than at pH 4.0 depending on applied Mn dose.[3] This is partially in contradiction to our data because the Mn content in Mn-exposed plants was slightly higher or unaffected by lower pH in shoots (Figure 5A) but may be explained by concentration dependency of this process because potato treated with 5 mM (approximate concentration of water-soluble Mn in our Mn-soil as mentioned above) showed lower difference between various pH. However, impact of pH on Mn uptake was negligible in our Mn-exposed plants while more pronounced differences in control plants are rather evoked by translocation from seed during growth. This is in accordance with data from *Spiraea* plants where media pH did not affect foliar Mn.[4] It is also visible that shoot Mn content in Mn-treated plants was very similar to that observed in soil culture (cf. Figure 5 and Table 2) with *Brassica* and *Triticum* containing the highest and the lowest value, respectively.

The relatively negligible impact of pH in terms of Mn uptake was further verified at the level of oxidative stress induction. Fluorescence indicator of "general ROS" revealed no extensive or pH-dependent impact either in control or Mn-cultured roots (Figure 5B). It is clear that the appearance of oxidative damage is related to Mn presence, and the same was observed in shoot samples mentioned above (Figure 2).

CONCLUSIONS

Naturally contaminated manganese soil used in the present study had a clearly negative impact on the growth of four crops after prolonged cultivation. High shoot Mn accumulation and the overall trend of its uptake were similar in soil and solution culture, in which *Brassica* and *Triticum* contained the highest and the lowest amounts, respectively. Solution culture also confirmed that the low pH of Mn soil (3.7) is not the main factor affecting Mn uptake or ROS formation. The elevated fluorescent signal of nitric oxide and thiols together with typically enhanced activities of antioxidative enzymes could contribute to protection against Mn excess in soil culture, while the involvement of phenolic metabolites and aliphatic organic acids in this process was not observed. However, the sensitivity of the investigated plants to soil contamination by Mn urges for further selection of a cultivar tolerant to Mn excess, owing to its presence in acidic soils.

AUTHOR INFORMATION

Corresponding Author

*Phone: +420 545 133281; fax: +420 545 212044; e-mail: jozkovacik@yahoo.com.

Funding

The sponsor had no involvement in the present study.

Notes

The authors declare no competing financial interest.

ACKNOWLEDGMENTS

The work was supported by OP Education for Competitiveness (European Social Fund and the state budget of the Czech Republic) CZ.1.07/2.3.00/30.0017 Postdocs in Biological Sciences at MENDELU.

REFERENCES

(1) Millaleo, R.; Reyes-Díaz, M.; Ivanov, A. G.; Mora, M. L.; Alberdi, M. Manganese as essential and toxic element for plants: Transport, accumulation and resistance mechanisms. *J. Soil Sci. Plant Nutr.* **2010**, *10*, 476−494.

(2) Hernandez-Soriano, M. C.; Degryse, F.; Lombi, E.; Smolders, E. Manganese toxicity in barley is controlled by solution manganese and soil manganese speciation. *Soil Sci. Soc. Am. J.* **2012**, *76*, 399−407.

(3) Sarkar, D.; Pandey, S. K.; Sud, K. C.; Chanemougasoundharam, A. In vitro characterization of manganese toxicity in relation to phosphorus nutrition in potato (*Solanum tuberosum* L.). *Plant Sci.* **2004**, *167*, 977−986.

(4) Stanton, K. M.; Mickelbart, M. V. Growth and foliar nutrition of *Spiraea alba* Du Roi and *Spiraea tomentosa* L. in response to root zone pH. *Sci. Hortic.* **2014**, *165*, 23−26.

(5) Gangwar, S.; Singh, V. P.; Prasad, S. M.; Maurya, J. N. Modulation of manganese toxicity in *Pisum sativum* L. seedlings by kinetin. *Sci. Hortic.* **2010**, *126*, 467−474.

(6) Shi, Q.; Zhu, Z. Effects of exogenous salicylic acid on manganese toxicity, element contents and antioxidative system in cucumber. *Environ. Exp. Bot.* **2008**, *63*, 317−326.

(7) Srivastava, S.; Dubey, R. S. Manganese-excess induces oxidative stress, lowers the pool of antioxidants and elevates activities of key antioxidative enzymes in rice seedlings. *Plant Growth Regul.* **2011**, *64*, 1−16.

(8) Demirevska-Kepova, K.; Simova-Stoilova, L.; Stoyanova, Z.; Hölzer, R.; Feller, U. Biochemical changes in barley plants after

excessive supply of copper and manganese. *Environ. Exp. Bot.* **2004**, *52*, 253−266.
(9) Nadgórska-Socha, A.; Ptasiński, B.; Kita, A. Heavy metal bioaccumulation and antioxidative responses in *Cardaminopsis arenosa* and *Plantago lanceolata* leaves from metalliferous and non-metalliferous sites: a field study. *Ecotoxicology* **2013**, *22*, 1422−1434.
(10) Kandziora-Ciupa, M.; Ciepal, R.; Nadgórska-Socha, A.; Barczyk, G. A comparative study of heavy metal accumulation and antioxidant responses in *Vaccinium myrtillus* L. leaves in polluted and non-polluted areas. *Environ. Sci. Pollut. Res.* **2013**, *20*, 4920−4932.
(11) Kováčik, J.; Bačkor, M. Oxidative status of *Matricaria chamomilla* plants related to cadmium and copper uptake. *Ecotoxicology* **2008**, *17*, 471−479.
(12) Kováčik, J.; Klejdus, B.; Hedbavny, J.; Štork, F.; Bačkor, M. Comparison of cadmium and copper effect on phenolic metabolism, mineral nutrients and stress-related parameters in *Matricaria chamomilla* plants. *Plant Soil* **2009**, *320*, 231−242.
(13) Gajewska, E.; Skłodowska, M. Differential effect of equal copper, cadmium and nickel concentration on biochemical reactions in wheat seedlings. *Ecotox. Environ. Safety* **2010**, *73*, 996−1003.
(14) Kováčik, J.; Babula, P.; Hedbavny, J.; Švec, P. Manganese-induced oxidative stress in two ontogenetic stages of chamomile and amelioration by nitric oxide. *Plant Sci.* **2014**, *215*−*216*, 1−10.
(15) Srivastava, S.; Dubey, R. S. Nitric oxide alleviates manganese toxicity by preventing oxidative stress in excised rice leaves. *Acta Physiol. Plant.* **2012**, *34*, 819−825.
(16) Hadži-Tašković Šukalović, V.; Vuletić, M.; Veljović-Jovanović, S.; Vučinić, Z. The effects of manganese and copper in vitro and in vivo on peroxidase catalytic cycles. *J. Plant Physiol.* **2010**, *167*, 1550−1557.
(17) Santandrea, G.; Pandolfini, T.; Bennici, A. A physiological characterization of Mn-tolerant tobacco plants selected by in vitro culture. *Plant Sci.* **2000**, *150*, 163−170.
(18) Kováčik, J.; Grúz, J.; Klejdus, B.; Štork, F.; Hedbavny, J. Accumulation of metals and selected nutritional parameters in the field-grown chamomile anthodia. *Food Chem.* **2012**, *131*, 55−62.
(19) Kula, E.; Hrdlička, P.; Hedbávný, J.; Švec, P. Various content of manganese in selected forest tree species and plants in the undergrowth. *Beskydy* **2012**, *5*, 19−26.
(20) Kováčik, J.; Klejdus, B.; Babula, P. Oxidative stress, uptake and bioconversion of 5-fluorouracil in algae. *Chemosphere* **2014**, *100*, 116−123.
(21) Muller, M.; deKok, L. J.; Weidner, W.; Tausz, M. Differential effects of H_2S on cytoplasmic and nuclear thiol concentrations in different tissues of *Brassica* roots. *Plant Physiol. Biochem.* **2002**, *40*, 585−589.
(22) Bradford, M. M. A rapid and sensitive method for the quantitation of microgram quantities of protein utilizing the principle of protein dye binding. *Anal. Biochem.* **1976**, *72*, 248−254.
(23) Kováčik, J.; Bačkor, M. Changes of phenolic metabolism and oxidative status in nitrogen-deficient *Matricaria chamomilla* plants. *Plant Soil* **2007**, *297*, 255−265.
(24) Dou, C.; Fu, X.; Chen, X.; Shi, J.; Chen, Y. Accumulation and interaction of calcium and manganese in *Phytolacca americana*. *Plant Sci.* **2009**, *177*, 601−606.
(25) Tewari, R. K.; Kumar, P.; Sharma, P. N. Oxidative stress and antioxidant responses of mulberry (*Morus alba*) plants subjected to deficiency and excess of manganese. *Acta Physiol. Plant.* **2013**, *35*, 3345−3356.
(26) Kováčik, J.; Klejdus, B.; Štork, F.; Hedbavny, J. Nitrate deficiency reduces cadmium and nickel accumulation in chamomile plants. *J. Agric. Food Chem.* **2011**, *59*, 5139−5149.
(27) Dresler, S.; Hanaka, A.; Bednarek, W.; Maksymiec, W. Accumulation of low-molecular-weight organic acids in roots and leaf segments of *Zea mays* plants treated with cadmium and copper. *Acta Physiol. Plant.* **2014**, *36*, 1565−1575.
(28) Adeniji, B. A.; Budimir-Hussey, M. T.; Macfie, S. M. Production of organic acids and adsorption of Cd on roots of durum wheat (*Triticum turgidum* L. var. *durum*). *Acta Physiol. Plant.* **2010**, *32*, 1063−1072.
(29) Javed, M. T.; Stoltz, E.; Lindberg, S.; Greger, M. Changes in pH and organic acids in mucilage of *Eriophorum angustifolium* roots after exposure to elevated concentrations of toxic elements. *Environ. Sci. Pollut. Res.* **2013**, *20*, 1876−1880.
(30) Gao, L.; Peng, K.; Xia, Y.; Wang, G.; Niu, L.; Lian, C.; Shen, Z. Cadmium and manganese accumulation in *Phytolacca americana* L. and the roles of non-protein thiols and organic acids. *Int. J. Phytorem.* **2013**, *15*, 307−319.
(31) Najeeb, U.; Xu, L.; Ali, S.; Jilani, G.; Gong, H. J.; Shen, W. Q.; Zhou, W. J. Citric acid enhances the phytoextraction of manganese and plant growth by alleviating the ultrastructural damages in *Juncus effusus* L. *J. Hazard. Mater.* **2009**, *170*, 1156−1163.
(32) Huang, C.; Webb, M. J.; Graham, R. D. Effect of pH on Mn absorption by barley genotypes in a chelate-buffered nutrient solution. *Plant Soil* **1993**, *155*−*156*, 437−440.

supplied by Varian (Agilent Technologies, Winnersh, U.K.), and 1-(heptafluorobutyryl)imidazole (HFBI, >98%) was purchased from Alfa Aesar England. 3-Chloro-1,2-propanediol (3-MCPD), sodium methoxide, filter papers (Whatman No. 4), and potassium bromide were purchased from Sigma-Aldrich (Gillingham, U.K.). MCPD-d_5 and 3-MCPD-palmitate-d_5 were obtained from CDN isotopes and Toronto Research Chemicals, respectively.

Refined wheat flour (standard T55/W150) was kindly supplied by Kraft Foods (Glattpark, Switzerland). Sucrose powder, sodium bicarbonate, ammonium bicarbonate, and sodium chloride were kindly supplied by Eti (Eskişehir, Turkey) and refined corn, canola, hazelnut, olive, and peanut oils by Zade (Konya, Turkey).

Preparation of Biscuits. The biscuits were prepared according to the American Association of Cereal Chemists Method 10-54 with some modifications.[22] The recipe contained 80.0 g of wheat flour, 35.0 g of sucrose powder, 20.0 g of corn oil, 1.0 g of sodium chloride, 0.4 g of ammonium bicarbonate, 0.8 g of sodium bicarbonate, and 17.6 mL of water. All ingredients were thoroughly mixed in accordance with the AACC Method 10-54 procedure using an Artisan Kitchen Aid 5KSM150 dough mixer. The dough was rolled to a 3 mm thickness and cut into three discs 5 cm in diameter and baked in a conventional oven (Memmert, UNE 400).

Two different recipes were prepared with corn oil, namely, a basic recipe and a basic recipe without sodium chloride. Biscuits having the basic recipe were baked at 180, 200, and 220 °C for different times for up to 19 min. The recipe without salt was baked at 220 °C for 7−11 min. Additionally, different refined oils, namely, canola, hazelnut, olive, and peanut, were also used to determine the effect of oil type on MCPD formation by replacing corn oil in the recipe. These sets of biscuits were baked at 220 °C for 10 min. All baking experiments were performed in duplicate. Regardless of the baking condition, all biscuits prepared contained <2% moisture.

Analysis of 3-MCPD and 2-MCPD. *Extraction.* The nonpolar part of the biscuits was isolated by extraction of 4.00 g of the ground biscuit twice with 40 mL of hexane. The combined extracts were kept for MCPD ester analysis; 100 μL of a 10 μg/mL internal standard solution, 3-MCPD-d_5, and 10 mL of 5 M NaCl were added to the defatted biscuits. Then, 7 g of diatomaceous earth sorbent, Hydromatrix, was added, mixed thoroughly, and transferred to a chromatography column (40 cm, 2 cm inside diameter, with a sintered glass disk and a tap at the lower end). Approximately 1 cm of sodium sulfate was added to the top of the column. 3-MCPD and 2-MCPD were eluted over 15 min with 100 mL of diethyl ether. One spatula of anhydrous sodium sulfate was added to the eluent. The extract was then filtered through Whatman No. 4 filter paper and the solvent removed by rotary evaporation to 1−5 mL. The concentrated extract was transferred to a 10 mL flask and made up to volume with diethyl ether.

Derivatization. Four milliliters of the final sample extract was transferred to a 4 mL septum-capped vial. The sample extracts were blown to dryness under a gentle stream of nitrogen before 1 mL of 2,2,4-trimethylpentane was added. A 50 μL aliquot of HFBI was added, and the vial was capped, shaken, and incubated at 70 °C for 20 min. One milliliter of distilled water was added to the cooled mixture; the vial was shaken, and the phases were allowed to separate. The upper 2,2,4-trimethylpentane phase was dried over anhydrous sodium sulfate and carefully transferred to a 2 mL gas chromatography−mass spectrometry vial.

For calibration, 1 mL of appropriate standard solutions was transferred to 4 mL septum cap vials and the same derivatization procedure was performed.

Quantitation. GC−MS determinations were made using an Agilent 6890 Series gas chromatograph with a Gerstel Multipurpose Sampler MPS2 injector interfaced with a 5973N mass selective detector (MSD). For chromatographic separation, a fused silica capillary column [Rxi-5 ms, 30 m × 0.25 mm (inside diameter), 0.25 μm film coated with Crossbond diphenyl dimethyl polysiloxane (Restek)] was used with a helium carrier at a constant flow of 1.1 mL min^{-1}. The following GC oven temperature program was used: 50 °C for 2 min, increase at rates of 2 °C min^{-1} to 80 °C and 50 °C min^{-1} to 270 °C, and hold for 2 min. The total run time was 22.8 min. Injections of 3 μL were made in the splitless mode. The MSD was operated in the selected ion monitoring mode (SIM) using electron impact ionization with an ionizing voltage of 70 eV. The MSD SIM acquisition parameters were m/z 253 (quantifier), 275, and 289 (qualifiers) for 2-MCPD, m/z 253 (quantifier), 275, 289, and 453 (qualifiers) for 3-MCPD, and m/z 257 (quantifier) for 3-MCPD-d_5 with a dwell time of 80 ms. The LOQ was 0.1 mg kg^{-1}. The retention times of 3-MCPD, 2-MCPD, and 3-MCPD-d_5 were 16.215, 16.338, and 16.010 min, respectively.

Analysis of Bound-MCPD. 3-MCPD bound as esters in biscuits was analyzed according to DGF Standard Method C-VI 18(10).[23] The nonpolar extracts of the biscuits, obtained by hexane extraction before 3-MCPD analysis, were evaporated until all the solvent phase was removed; 0.1 g of nonpolar fraction was transferred to a 4 mL vial. MCPD-dipalmitate-d_5 (100 μL) was added and the mixture dissolved in 100 μL of *tert*-butyl methyl ether. Then, 200 μL of CH_3ONa (25 g/L in methanol) was added and vortexed, and the mixture was left for 4 min at room temperature; 600 μL of an acidified chloride-free salt solution [600 g/L KBr, 35 mL of H_2SO_4 (25%) to 1 L of a KBr solution] was added and the aqueous phase was rinsed twice with 1 mL of *n*-hexane. The aqueous phase was extracted twice using 1 mL of a 60/40 ether/ethyl acetate mixture. The combined extract was vortexed, evaporated to dryness under a N_2 stream, dissolved in 2,2,4-trimethylpentane (1 mL), and derivatized as described for free MCPD.

Statistical Analysis. The 3-MCPD and 2-MCPD contents of the samples were statistically analyzed by Duncan and *t*-test (α = 0.05) using the statistical software SPSS.

RESULTS AND DISCUSSION

Kinetics of Formation of 3-MCPD, 2-MCPD, and Bound-MCPD. The corn oil used in the recipe was found to contain 8.7 × 10^{-4} mg of 3-MCPD kg^{-1} and 0.566 mg of bound-MCPD kg^{-1}. The kinetics of formation of 3-MCPD, 2-MCPD, and bound-MCPD were examined in biscuits with a basic formulation baked at 180, 200, and 220 °C for different baking times (Figure 1a−c). The free 3-MCPD content of biscuits was between 0.018 and 0.074 mg kg^{-1}, whereas the 2-MCPD content ranged from 0.002 to 0.008 mg kg^{-1}. From a food safety point of view, the results revealed that the amounts of 3-MCPD formed in biscuits during baking exceeded the maximal level of 20 μg kg^{-1} set for acid-HVP and soy sauce by the European Commission. As shown in panels a and b of Figure 1, both free 3-MCPD and 2-MCPD concentrations increased with an increasing baking time. 3-MCPD and 2-MCPD concentrations in biscuits baked at 220 °C increased by 4.1- and 3.7-fold, respectively, when the baking time increased from 7 to 11 min. Similarly, an increased baking temperature led to an increase in the 3-MCPD and 2-MCPD concentrations of biscuits. As the temperature increased from 200 to 220 °C, 3-MCPD and 2-MCPD concentrations increased 3.2- and 2.6-fold, respectively, in biscuits baked for 11 min. The effect of process parameters on the formation of 3-MCPD and 2-MCPD could be related to the increased thermal load. During the thermal process, water and steam hydrolyze triacylglycerols and phospholipids, producing diacylglycerols, monoacylglycerols, glycerol, and other products, which act as precursors of 3-MCPD and 2-MCPD.[24] Our results also show that the relative proportions of the major chloropropanols (3-MCPD and 2-MCPD) in biscuits were approximately in the ratio ranging from 6.24 to 13.57 in biscuits. The ratio of 10:1 has been reported in acid-HVPs.[21]

On the basis of the assumption that precursors, i.e., lipid and chloride, were present in excess, Hamlet and Sadd reported that formation of 3-MCPD was consistent with zero-order kinetics

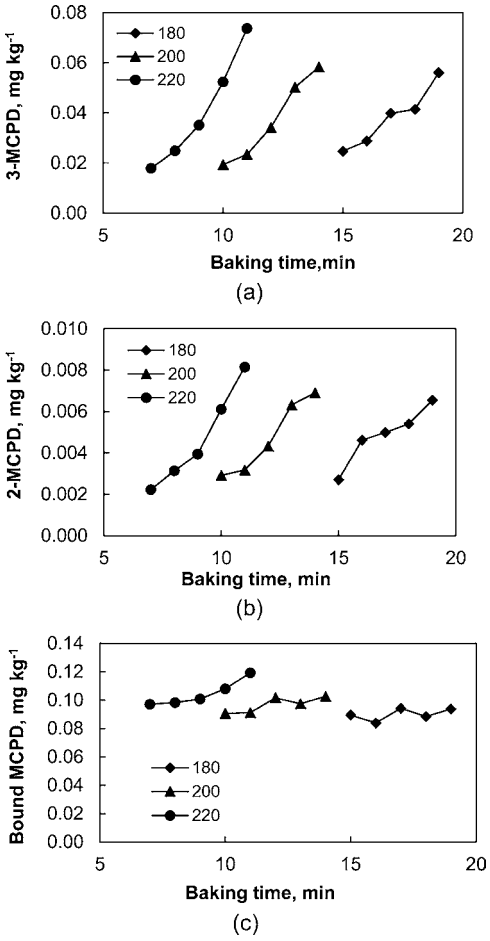

Figure 1. Effect of baking temperature and time on the formation of (a) 3-MCPD, (b) 2-MCPD, and (c) bound-MCPD (milligrams per kilogram of biscuit) in biscuits during baking.

during the baking of wheat flour dough.[16] As the food system studied, i.e., biscuit, suits the same case, the data successfully fit the zero-order kinetic equation. The kinetic rate constants are summarized in Table 1. An increase in temperature led to an increase in the reaction rate constants of both 3-MCPD and 2-MCPD, as the kinetic energy of the system increased. Each 20 °C increase in temperature increased the reaction rate constants of both 3-MCPD and 2-MCPD approximately 1.4-fold. The rate constant of 2-MCPD in biscuits during baking was found to be ~9.4 times lower than that of 3-MCPD. This confirms a previous study that reported that the rate of 2-MCPD formation is lower than rate of 3-MCPD in breads prepared with wheat flour dough.[16] The primary hydroxyl groups of glycerol were reported to be more reactive than the secondary group.[25] It is thought that this might be the reason for the formation of a quantity of 3-MCPD larger than that of 2-MCPD.

Table 1. Calculated Reaction Rate Constants of Formation of 3-MCPD, 2-MCPD, and Bound-MCPD in Biscuits (basic recipe and basic recipe without NaCl) Baked at Different Temperatures According to the Zero-Order Kinetic Equation[a]

	rate constant k ($\times 10^5$ mmol kg^{-1} min^{-1})		
temp (°C)	3-MCPD	2-MCPD	bound-MCPD
	Basic Recipe		
180	6.81 ± 1.71 a	0.77 ± 0.17 a	1.18 ± 0.06 a
200	9.48 ± 0.65 b	1.01 ± 0.06 b	2.71 ± 0.14 b
220	12.59 ± 0.02 c	1.34 ± 0.00 c	4.88 ± 0.24 c
	Basic Recipe without NaCl		
220	5.35 ± 0.91	0.20 ± 0.08	not detected

[a]Values within columns having the same letter are not significantly different ($p > 0.05$).

The temperature dependence of simple chemical reactions was empirically described by Arrhenius' law, which is expressed as

$$k = A \exp\left(-\frac{E_a}{RT}\right) \quad (1)$$

where k (millimoles per kilogram per minute) is the reaction rate constant, A (millimoles per kilogram per minute) is a pre-exponential factor, E_a is the activation energy (joules per mole), R (8.314 J mol^{-1} K^{-1}) is the gas constant, and T (kelvin) is the absolute temperature. Rate constants obtained from both 3-MCPD and 2-MCPD kinetic data fit the Arhenius' equation well (R^2 = 0.999). Finally, the activation energies of both 3-MCPD and 2-MCPD reactions were found to be equal to 29 kJ mol^{-1}, which means that the reactants needed the same amount of energy to start the reaction and carry on spontaneously for both formation reactions.

The initial bound-MCPD concentration of the refined corn oil used in the biscuit formulations was 0.5664 mg (kg of oil)$^{-1}$. This was equivalent to 0.088 mg (kg of biscuit)$^{-1}$, considering that the oil was present at a level of 15% in the uncooked biscuit. Figure 1c shows the bound-MCPD content of the biscuits prepared, which ranged between 0.084 and 0.119 mg kg^{-1}. There was no significant difference between bound-MCPD concentrations of the uncooked biscuit doughs and biscuits baked for the minimal baking time, at all temperatures studied. The U.K. Food Standards Agency reported that both 2- and 3-MPCD could be released from MCPD esters, identified in bread crust and toasted bread.[8] This might lead to a decrease in bound-MCPD concentration. However, after a certain heat load, the concentration of bound-MCPD in biscuits started to increase. This increase could be related to the rate of formation being higher than the rate of degradation during baking. The reaction rate constants of bound-MCPD formation were also calculated. As given in Table 1, an increased baking temperature has an increasing effect on the bound-MCPD formation rate constant in biscuits, which was found to be statistically significant ($p < 0.05$).

Effect of Sodium Chloride on the Formation of 3-MCPD, 2-MCPD, and Bound-MCPD. It is known that chloride is one of the precursors of chloropropanols. Salt (sodium chloride) used in food formulations is the main source of chloride in most foods. The effect of the presence of chloride on the formation of 3-MCPD, 2-MCPD, and bound-MCPD in biscuits was tested. The biscuit recipe described earlier was used without the incorporation of sodium chloride. The results are shown in Figure 2a–c. It was found that eliminating salt had a statistically significant effect on the formation of 3-MCPD and 2-MCPD ($p < 0.05$). When the salt was removed from the recipe, the reaction rate constants of formation of 3-MCPD and 2-MCPD in biscuits decreased by 57.5 and 85.4%, respectively (Table 1). As discussed before, the bound-MCPD content of biscuits baked for 7 min was the same as that of refined corn oil, i.e., 0.088 mg (kg of biscuit)$^{-1}$. Without salt in the recipe, the

dx.doi.org/10.1021/jf502211s | J. Agric. Food Chem. 2014, 62, 7297–7301

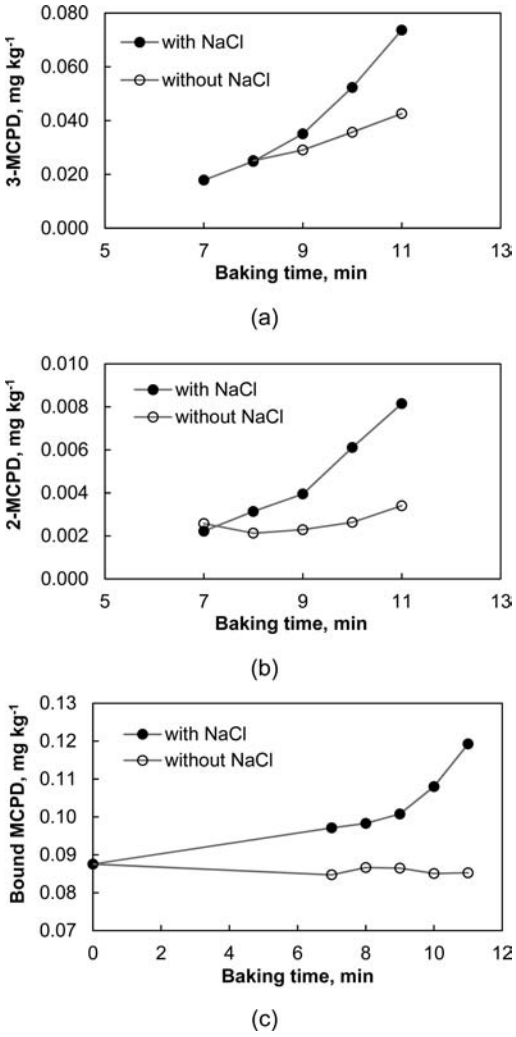

Figure 2. Effect of salt on the formation of (a) 3-MCPD, (b) 2-MCPD, and (c) bound-MCPD (milligrams per kilogram of biscuit) in biscuits during baking at 220 °C.

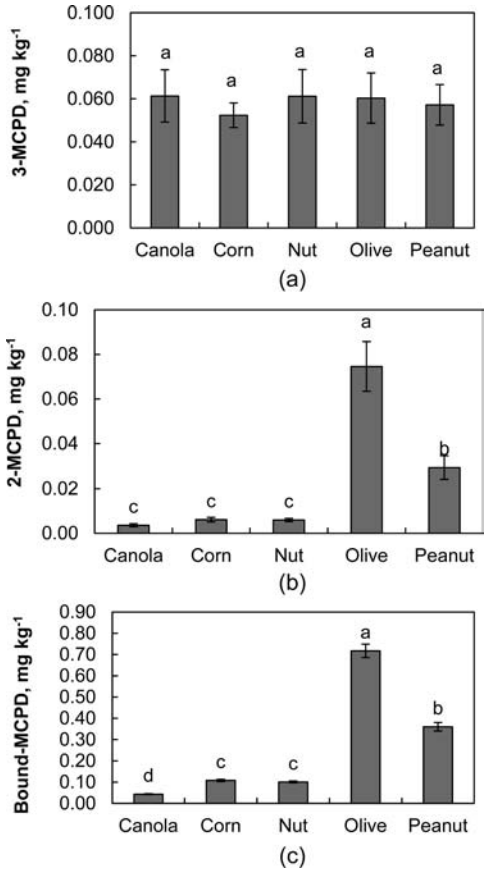

Figure 3. Effect of oil type on the formation of 3-MCPD (a), 2-MCPD (b), and bound-MCPD (c) (milligrams per kilogram of biscuit) in biscuits baked at 220 °C for 10 min. Values having the same letter are not significantly different ($p > 0.05$).

concentration of bound-MCPD in biscuits baked for 7 min was found to be 0.085 ± 0.003 mg (kg of biscuit)$^{-1}$. There was no significant increase in the bound-MCPD concentration during baking ($p < 0.05$). However, the presence of salt as a source of chloride caused an increase in the rate of formation of bound-MCPD in biscuits during baking. The mechanism behind this formation might be a possible reaction between di- and monoacylglycerols of oil and sodium chloride present in the biscuit recipe. In addition, it was reported that sodium chloride acts as a Lewis acid accelerating the hydrolysis of sucrose during heating.[26] In a similar way, it might break the ester bond of acylglycerols, giving available sites to chloride to bind.

Effect of Oil Type on the Formation of 3-MCPD, 2-MCPD, and Bound-MCPD in Biscuits. A range of different vegetable oils, namely, corn oil, canola, nut, olive, and peanut, were used in the biscuit formulation to determine their effect on the formation of 3-MCPD, 2-MCPD, and bound-MCPD (Figure 3a–c). The 3-MCPD content of all biscuits prepared with different oils was found to be ~0.06 mg kg^{-1}. Statistical analysis showed that there was no significant difference between the 3-MCPD contents of these biscuits ($p < 0.05$). Among the refined oils used in this study, 2-MCPD and bound-MCPD concentrations of the biscuit prepared with refined olive oil were found to be the highest, i.e., 0.075 and 0.717 mg kg^{-1}, respectively. Zelinková also reported that the bound-MCPD concentration with refined olive oil was higher than that with other refined edible oils, namely, soybean, sunflower, maize, and rapeseed.[27]

In conclusion, removal of chloride from biscuit formulations controlled the formation of 3-MCPD, 2-MCPD, and bound-MCPD, which could be an effective mitigation strategy in which there are no adverse effects on the biscuit flavor. Careful selection of the type of vegetable oil or shortening and testing for MCPD ester content prior to their use in baking could also reduce the content of these processing contaminants in bakery products.

AUTHOR INFORMATION

Corresponding Author

*Phone: +90 312 2977108. Fax: +90 312 2992123. E-mail: vgokmen@hacettepe.edu.tr.

Funding

This work was conducted within the framework of the PROMETHEUS project (PROcess contaminants: Mitigation and Elimination Techniques for High food quality and their Evaluation Using Sensors & Simulation) funded by the European Commission.

Notes

The authors declare no competing financial interest.

ABBREVIATIONS USED

3-MCPD, 3-chloropropane-1,2-diol; 2-MCPD, 2-chloropropane-1,3-diol; 1,3-DCP, 1,3-dichloro-2-propanol; 2,3-DCP, 2,3-dichloro-1-propanol

REFERENCES

(1) Hamlet, C. G.; Sadd, P. A. In *Process-Induced Food Toxicants. Occurrence, Formation, Mitigation and Health Risks*; Stadler, R. H., Lineback, D. R., Eds.; John Wiley & Sons, Inc.: Hoboken, NJ, 2009.

(2) Davídek, J.; Velíšek, J.; Kubelka, V.; Janiček, G. New chlorine-containing compounds in protein hydrolysates. In *Recent developments in food analysis: Proceedings of the First European Conference on Food Chemistry (EURO FOOD CHEM I), held at Vienna (Austria), 17−20 February 1981*; Baltes, W., Czedik-Eysenberg, P. B., Pfannhauser, W., Eds.; Verlag Chemie: Weinheim, Germany, 1982; pp 322−325.

(3) Joint FAO/WHO Expert Committee on Food Additives (JECFA). *Safety evaluation of certain food additives and contaminants*; Food and Agriculture Organization of the United Nations and World Health Organization, 2002; Vol. *48*, pp 401−432.

(4) Opinion of the Scientific Committee on Food on 3-monochloropropane-1, 2-diol (3-MCPD) updating the SCF opinion of 1994. SCF, 2001.

(5) European Commision. Setting maximum levels for certain contaminants in foodstuffs. In *Official Journal of the European Communities*; Office for Official Publications of the European Communities: Luxembourg, 2001; Vol. Regulation (EC) 466/2001, pp 1−13.

(6) Abraham, K.; Appel, K. E.; Berger-Preiss, E.; Apel, E.; Gerling, S.; Mielke, H.; Creutzenberg, O.; Lampen, A. Relative oral bioavailability of 3-MCPD from 3-MCPD fatty acid esters in rats. *Arch. Toxicol.* **2013**, *87*, 649−659.

(7) Barocelli, E.; Corradi, A.; Mutti, A.; Petronini, P. G. Comparison between 3-MCPD and its palmitic esters in a 90-day toxicological study. EFSA CFP/EFSA/CONTAM/2009/01; European Food safety Authority, University of Parma: Parma, Italy, 2011.

(8) Survey of 3-monochloropropane-1,2-diol (3-MCPD) in selected food groups; Food Standards Agency: London, 2001.

(9) Crews, C.; Hough, P.; Brereton, P.; Harvey, D.; MacArthur, R.; Matthews, W. Survey of 3-monochloropropane-1,2-diol (3-MCPD) in selected food groups, 1999−2000. *Food Addit. Contam.* **2002**, *19*, 22−27.

(10) Massey, R.; Hamlet, C. G. Chloropropanol contaminants in food: The story continues. *Food Sci. Technol.* **2007**, *21*, 32−34.

(11) Massey, R. Fight against 3-MCPD. *Food Manuf.* **2007**, *82*, 35−36.

(12) Discussion paper on chloropropanols derived from the manufacture of acid-HVP and the heat processing of food; FAO, WHO: Beijing, Apr 16−20, 2007.

(13) Hamlet, C. G.; Jayaratne, S. M.; Matthews, W. 3-Monochloropropane-1,2-diol (3-MCPD) in food ingredients from UK food producers and ingredient suppliers. *Food Addit. Contam.* **2002**, *19*, 15−21.

(14) Breitling-Utzmann, C. M. 3-MCPD: Untersuchungen in Lebensmitteln. http://www.lebensmittel.org/wissenswertes/lebensmittel-kosmetika-und-bedarfsgegenstaende/67-3-mcpd-untersuchungen-in-lebensmitteln.html (accessed April 1, 2014).

(15) Breitling-Utzmann, C. M.; Bler, H.; Herzbolzheimer, D.; Maier, A. *3-MCPD: Occurrence in bread crust and various food groups as well as formation in toast*; Behr's Verlag: Hamburg, Germany, 2003; Vol. *99*, p 6.

(16) Hamlet, C. G.; Sadd, P. A.; Gray, D. A. Influence of composition, moisture, pH and temperature on the formation and decay kinetics of monochloropropanediols in wheat flour dough. *Eur. Food Res. Technol.* **2003**, *216*, 122−128.

(17) Hamlet, C. G.; Sadd, P. A.; Gray, D. A. Generation of monochloropropanediols (MCPDs) in model dough systems. 1. Leavened doughs. *J. Agric. Food Chem.* **2004**, *52*, 2059−2066.

(18) Hamlet, C. G.; Sadd, P. A.; Crews, C.; Velisek, J.; Baxter, D. E. Occurrence of 3-chloro-propane-1,2-diol (3-MCPD) and related compounds in foods: A review. *Food Addit. Contam.* **2002**, *19*, 619−631.

(19) Crews, C.; Brereton, P.; Davies, A. The effects of domestic cooking on the levels of 3-monochloropropanediol in foods. *Food Addit. Contam.* **2001**, *18*, 271−280.

(20) Calta, P.; Velíšek, J.; Doležal, M.; Hasnip, S.; Crews, C.; Réblová, Z. Formation of 3-chloropropane-1,2-diol in systems simulating processed foods. *Eur. Food Res. Technol.* **2004**, *218*, 501−506.

(21) Reece, P. The origin and formation of 3-MCPD in foods and food ingredients (final project report); Food Standards Agency: London, 2005.

(22) AACC. *Approved methods of the American Association of Cereal Chemists*; Association of Cereal Chemists: St. Paul, MN, 2000; Vol. *10-54*.

(23) Fatty-acid-bound 3-chloropropane-1,2-diol (3-MCPD) and 2,3-epoxi-propane-1-ol (glycidol). DGF Standard Method C VI 18 (10); Deutsche Einheitsmethoden zur Untersuchung von Fetten, Fettprodukten, Tensiden und verwandten Stoffen, Wissenschaftliche Verlagsgesellschaft: Stuttgart, Germany, 2011.

(24) Svejkovska, B.; Doležal, M.; Velíšek, J. Formation and decomposition of 3-chloropropane-1,2-diol esters in models simulating processed foods. *Czech J. Food Sci.* **2006**, *24*, 172−179.

(25) Chemical Properties and Derivaties of Glycerol; Glycerine Producers' Association: New York, 1964.

(26) Fiore, A.; Troise, A. D.; Mogol, B. A.; Roullier, V.; Gourdon, A.; Jian, S. E. M.; Hamzalıoglu, B. A.; Gökmen, V.; Fogliano, V. Controlling the Maillard reaction by reactant encapsulation: Sodium chloride in cookies. *J. Agric. Food Chem.* **2012**, *60*, 10808−10814.

(27) Zelinkova, Z.; Svejkovska, B.; Velisek, J.; Dolezal, M. Fatty acid esters of 3-chloropropane-1,2-diol in edible oils. *Food Addit. Contam.* **2006**, *23*, 1290−1298.

significantly important to ascertain the validity of their use as substitutes for each other. In our previously published and unpublished work, we have found similarities and differences in metabolite profiles of plant species from same genus grown in China and India.[35−37] Furthermore, study of tissue distribution of metabolites paves a way to unravel the specific tissue sites for metabolic pathways of the plants.[38] Plants of the same species growing in different geographical regions exhibit varying morphological and genetic features, and also differences in the contents of their secondary metabolites are often observed. This is due to the effect of environmental conditions on their metabolic pathways and type of evolution in particular taxa. Evidences to these facts have been provided by various studies. For example, in a study involving broccoli, a variance in the glucosinolate profiles was observed in accessions grown in different environments.[38] In a report including *Brassica oleracea*, dissimilarities in glucosinolate−myrosinase system were found due to different climatic conditions.[39] Genetic diversity was reported in a study involving *Phyllanthus amarus* species grown in different geographical locations.[40,41]

Recently, laser microdissection (LMD) has been recognized as an important tool in isolation of specific plant and animal tissues due to its contamination-free tissue isolation procedures. Combined with hyphenated chromatography techniques like ultra-high-performance liquid chromatography−quadrupole time-of-flight mass spectrometry (UHPLC-QTOF MS) and gas chromatography−mass spectrometry (GC-MS), the LMD method can be exploited for application in tissue-specific metabolite analysis.[35,36]

In consideration of the significance of (+)-nootkatone as a biomarker for important human pathological conditions (like neurodegeneration) and its high demand in various industrial segments, it was selected as a marker for evaluation of the pharmaceutical quality of *C. rotundus* L. in the studied samples. The aim of the current study was to compare the tissue-specific metabolite profiles of *C. rotundus* L. rhizomes collected from various regions of China and India and evaluate the pharmaceutical quality of rhizomes based upon the content of the bioactive sesquiterpenoid (+)-nootkatone.

MATERIALS AND METHODS

Chemicals. For LC-MS analysis, acetonitrile (HPLC-grade) was obtained from E. Merck (Darmstadt, Germany). Formic acid (HPLC-grade, purity 96.0%) was used as a mobile phase modifier, and it was purchased from Tedia Company Inc. Ultrapure water used in various steps of the experiments was obtained from a Milli-Q water purification system (Millipore, Bedford, MA). Standard (+)-nootkatone (purity >95%) used as a reference compound, was procured from Extrasynthese, Genay cedex, France. For GC-MS analysis, *n*-hexane and ethyl acetate used in extraction were procured from ACI Lab Scan Ltd., Thailand.

Plant Material. Dried rhizome samples of *C. rotundus* L., comprising five sample sets from different regions of China and five sample sets from various locations in India, were used for analysis. The samples were authenticated by Professor ZhongZhen Zhao, and voucher specimens (voucher CM/005) were deposited in the Chinese Medicines Centre of Hong Kong Baptist University.

Microscopy Sample Preparation. The sampling of specific microscopic tissues from the *C. rotundus* rhizome samples was carried out as detailed in our previously published reports.[36] Prior to sectioning, the rhizome samples were wrapped in water-soaked noncellulose paper and kept under vacuum at 25 inHg pressure at room temperature for 24 h. After softening by application of vacuum, small sections of the rhizomes were cut and embedded in a cryogel matrix (Leica Microsystems, Germany). Rhizome sections of 25 μm thicknesses were cut with a cryotome and then placed on poly(ethylene terephthalate) (PET) slides at working temperature of −15 °C.

Laser Microdissection and Tissue Extraction. Sections of samples were prepared at −15 °C by use of a Thermo Shandon As620 cryotome. A Leica LMD 7000 system (Leica, Benshein, Germany) was used for laser dissection and investigation of microscopic features. At magnifications of 6.3× and 10×, the target tissues were dissected under a Leica LMD-BGR (blue−green−red) fluorescence filter system. A diode-pumped solid-state (DPSS) laser beam was used with an exposure time of 116.9 ms, aperture size of 1, gain of 2.3×, and speed of 3. The target tissues for investigation were excised by LMD, to obtain tissues with a total area of about 1×10^6 μm^2. The tissues were collected in Eppendorf tube caps, prefixed in the LMD collecting device, and used for further analysis.

For preparation of samples for UHPLC-QTOF MS analysis, the dissected rhizome tissues were centrifuged at 12 000 rpm for 5 min in a 5415Rcentrifuge (Eppendorf, Hamburg, Germany). Following centrifugation, 100 μL of HPLC-grade methanol was added into each sample tube, and the tubes were sonicated for 30 min (Crest 1875HTAG ultrasonic processor). After sonication, the tubes were subjected to centrifugation at 12 000 rpm for 10 min. The resultant supernatants were collected into amber-colored glass HPLC vials containing glass inserts with bottom springs (400 μL, Grace, HK) and stored at 4 °C until analysis.

For analysis of whole rhizome sections, each presoaked sample was sectioned with the cryotome. The sections were collected in Eppendorf tubes and subjected to extraction with 500 μL of methanol by the procedure described above for isolated tissues. The dissected whole sections were used for whole-rhizome metabolite profile analysis. For analysis of raw material, the rhizome samples were coarsely powdered (mesh size 2−8) and extracted as per the procedure used for whole sections.

For GC-MS analysis, the rhizomes were coarsely powdered (mesh size 2−8) and extracted for 1 h with hexane/ethyl acetate mixture (1:1).[39] The obtained extracts were then concentrated by use of a B-480 rotary evaporator from Buchi (Flawil, Switzerland).

Metabolite Profiling by UHPLC-QTOF MS. For ultra high performance liquid chromatography, an Agilent 6540 accurate−mass Q-TOF LC-MS system (Agilent Technologies, Santa Clara, CA) was used. A UPLC C_{18} analytical column [dimensions 2.1 mm × 100 mm, i.d. 1.7 μm, Acquity UPLC ethylene-bridged hybrid (BEH); Waters, Milford, MA] with a C_{18} precolumn (2.1 mm × 5 mm, i.d. 1.7 μm, VanGuard BEH, Waters), was used for separation. The analysis was carried out at room temperature of 20 °C. The operation parameters applied for UHPLC-ESI-MS analysis of adduct ion species generated by electrospray ionization (ESI) were as follows: dry gas temperature 300 °C, fragmentor voltage 150 V, dry gas (N_2) flow rate 6 L/min, Vcap 4500, nozzle voltage 500 V, and nebulizer pressure 40 psi. Mass spectra were acquired in both negative and positive modes. Scanning was carried out for adduct ions of mass to charge ratio (m/z) from 110 to 1700. A mixture of water (A) and acetonitrile (B), both containing 0.1% formic acid, was used as the mobile phase with an optimized linear gradient elution as follows: 0−8 min, 2−15% B; 8−18 min, 15−55% B; 18−23 min, 55−100% B; 23−26 min, 100% B; 26−26.1 min, 100−2% B, 26.1−30 min, 2% B. The injection volume was 2.0 μL. The flow rate was set at 0.4 mL/min. An ESI−low concentration tuning mix solution (Agilent Technologies) was used for accurate molecular mass analysis calibration. The accuracy error threshold of 10 ppm was applied for analysis.

GC-MS-Based Metabolite Profiling and (+)-Nootkatone Quantitation. GC-MS analysis was performed on a Shimadzu GCMS-QP2010 gas chromatograph−mass spectrometer, equipped with a DB-5 capillary column (dimensions 30 m length, 0.25 mm i.d., and film thickness 0.25 μm). An autoinjector (AOC-20i) was employed for sample injection. The oven temperature was programmed from 80 to 280 °C at the rate of 5 °C/min. A splitless injection mode was applied for analysis. The oven temperature was held at 80 °C at the start of the run, then increased to 110 °C at 8 °C/min and 180 °C at 3 °C/min, before being held at 280 °C for 10 min. Helium with a flow rate of 0.95 mL/min was used as a carrier gas. The ion source and interface temperatures were

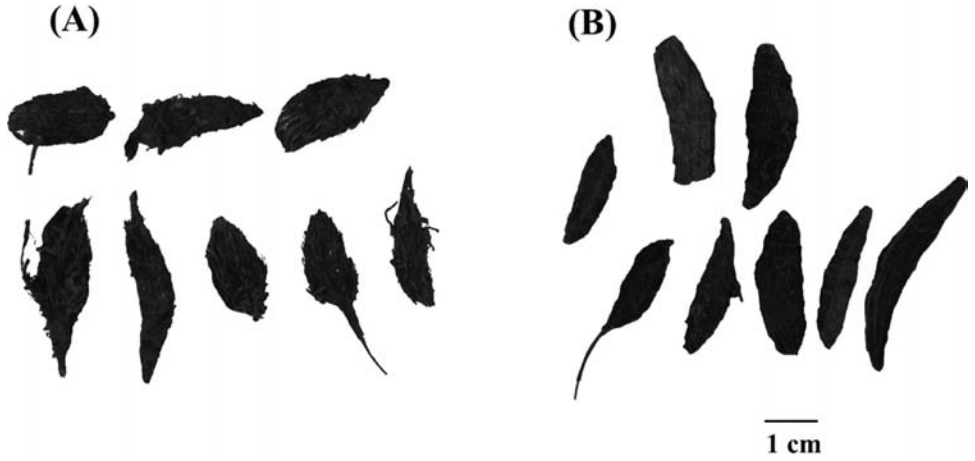

Figure 1. Pictorial representation of *C. rotundus* rhizome samples collected from (A) India and (B) China.

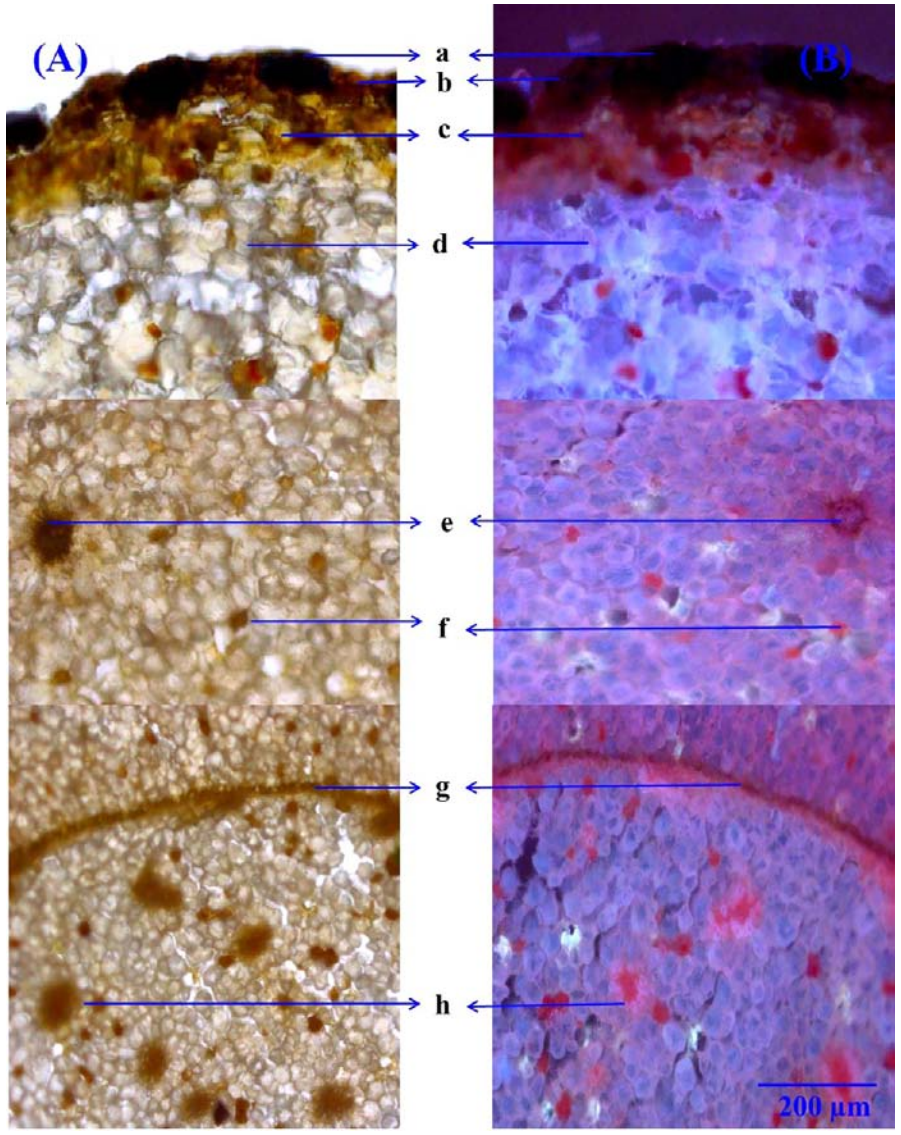

Figure 2. Microscopic characteristics of rhizomes of *C. rotundus*. Leica LMD 7000 system microscope was used with 10× magnification and a 200 μm scale bar. Images were observed under (A) normal light and (B) blue fluorescence. Tissues are denoted as (a) hypodermal fiber bundles, (b) epidermis, (c) hypodermis, (d) cortex, (e) leaf trace-type vascular bundles, (f) secretory cells, (g) endodermis, and (h) vascular bundles (amphivasal type).

held at 200 and 280 °C, respectively. The retention times and characteristic ions for the samples were studied by recording the electron ionization mass spectra of analytes in scan mode (range of m/z 35−425). For quantitative analysis, selected-ion monitoring (SIM)

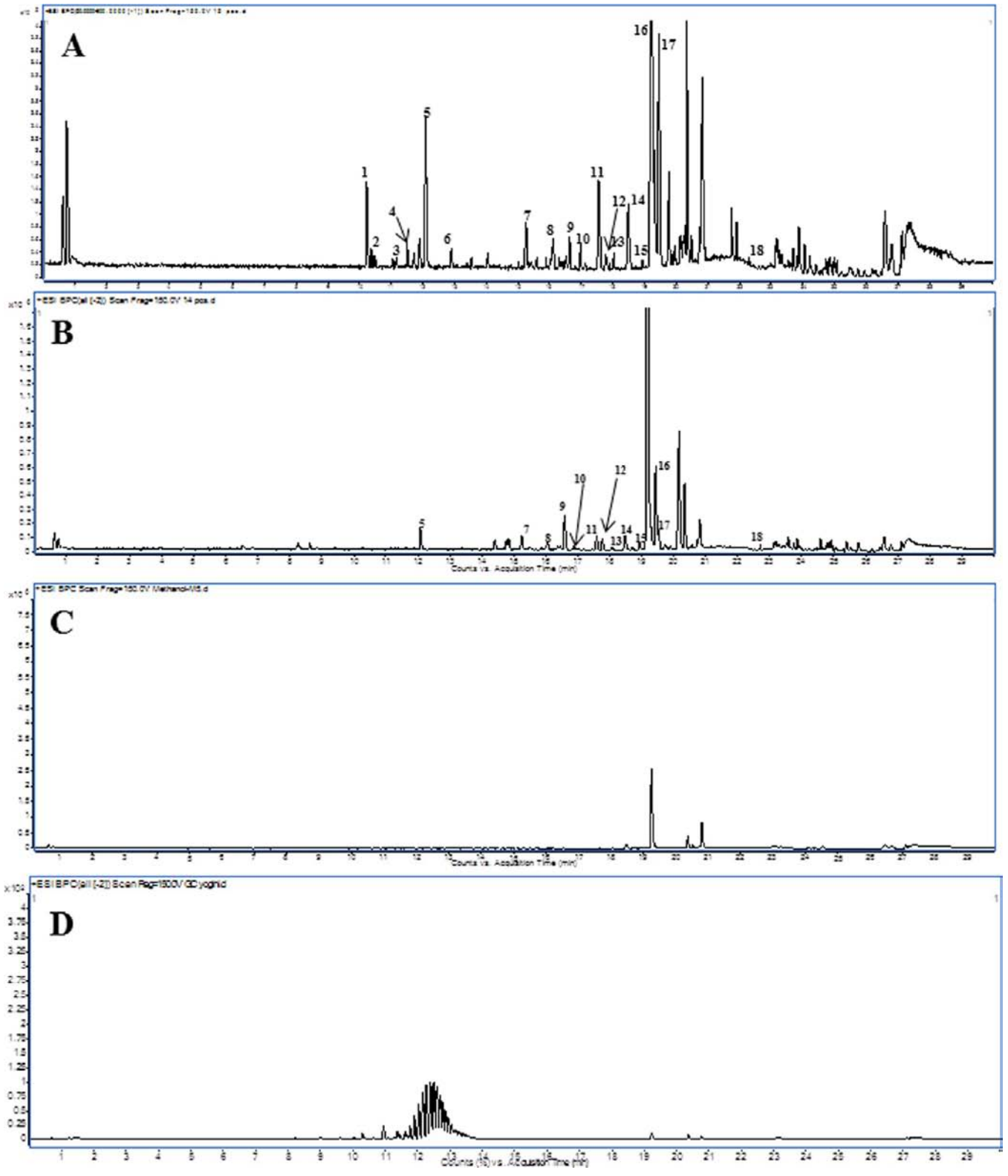

Figure 3. Representative LC-MS base peak chromatograms of *C. rotundus* rhizomes: (A) whole-rhizome sections of samples collected from India; (B) whole-rhizome sections of samples collected from China; (C) methanol used as blank; (D) cryogenic gel. Peak numbers indicating the identified constituents are listed in Table 1.

mode was used and the method was validated.[42] The characteristic ions selected for the analysis had m/z values 190 and 203 for (+)-nootkatone.

Working solutions of standard (+)-nootkatone were prepared by appropriate dilutions of stock of concentration 1.0 mg/mL. Hexane/ethyl acetate mixture (1:1) was used as the solvent for preparation of sample solutions.

Data Analysis. For analysis of LC-MS data, Agilent Mass Hunter Workstation software for qualitative analysis (version B 4.00, Build 4.0.479.5, Service Pack 3, Agilent Technologies, Inc., 2011) was used. Both positive and negative ion modes were applied for analysis with the following settings: peaks with height ≥2000 counts to be used, extraction restricted retention time of 1.0−30.0 min, and charge state of

dx.doi.org/10.1021/jf502494z | J. Agric. Food Chem. 2014, 62, 7302−7316

Table 1. Data for LC-MS-Based Identification of Various Constituents in *C. rotundus* Rhizomes

						m/z			samples[a]									
peak	compd	formula	calcd mass	T_R (min)	species	calcd	obsd	Δ ppm	CW	CA	CB	CC	CD	IW	IA	IB	IC	ID
1	cyperanic acid	$C_{15}H_{22}O_4$	266.1517	10.20	$(M+H)^+ [-H_2O]$	249.1485	249.1483	0.80						+				
2	7-methoxy-2-tetralone	$C_{11}H_{12}O_2$	176.0834	10.36	$(M+H)^+$	177.091	177.0906	2.33						+				
3	sobrerol	$C_{10}H_{18}O_2$	170.1307	11.11	$(M+H)^+$	171.1378	171.138	0.91						+				
3					$(M+Na)^+$	193.1206	193.1199	−3.71						+				
4	sugetriol	$C_{15}H_{24}O_3$	252.1722	11.67	$(M+H)^+$	253.1798	253.1796	1.05						+				
5	ligucyperonol	$C_{15}H_{22}O_2$	234.1681	12.07	$(M+H)^+ [-H_2O]$	217.1587	217.1583	1.75	+					+				
6	(−)-epoxycaryophyllene	$C_{15}H_{24}O$	220.1823	13.09	$(M+H)^+ [-H_2O]$	203.1794	203.1791	1.41						+				
7	calamenene	$C_{15}H_{22}$	202.1716	15.45	$(M+H)^+$	203.1794	203.1788	2.98	+				+	+				
8	mandassidione	$C_{15}H_{22}O_2$	234.1618	16.08	$(M+H)^+$	235.1693	235.1691	0.72	+				+	+				
9	4-cymene	$C_{10}H_{14}$	134.1093	16.55	$(M+H)^+$	135.1168	135.1165	2.06	+				+	+	+	+	+	+
10	sugeonol	$C_{15}H_{22}O_2$	234.1618	16.94	$(M+H)^+$	235.1693	235.1691	0.72	+	+	+	+	+	+	+	+	+	+
10					$(M+Na)^+$	257.1510	257.1512	0.79	+	+	+	+	+	+	+	+	+	+
11	cyperusol B1	$C_{15}H_{24}O_2$	236.1781	17.52	$(M+H)^+$	237.1849	237.1854	−1.98	+	+	+	+	+	+	+	+	+	+
12	cyperusol B2	$C_{15}H_{24}O_2$	236.1782	17.77	$(M+H)^+$	237.1849	237.1855	−2.60	+	+	+			+			+	
13	sitosterol	$C_{29}H_{50}O$	414.3861	18.02	$(M+Na)^+$	437.3754	437.3756	−0.38	+	+	+	+	+	+	+	+	+	+
14	myrcetin	$C_{15}H_{10}O_8$	318.2350	18.44	$(M+H)^+$	319.2843	319.2856	4.15	+	+	+	+	+	+	+	+	+	+
15	cyperotundone	$C_{15}H_{22}O$	218.1673	19.14	$(M+H)^+$	219.1743	219.1745	−0.87	+	+	+		+	+	+	+	+	+
16	valerenal	$C_{15}H_{22}O$	218.1673	19.29	$(M+H)^+$	219.1743	219.1747	−1.77	+					+				
16					$(M+Na)^+$	241.1563	241.1559	1.64	+					+				
17	isolongifolanone	$C_{15}H_{24}O$	220.1839	19.42	$(M+H)^+$	221.1900	221.1912	−5.25	+					+				
18	myristic acid	$C_{14}H_{28}O_2$	228.2099	22.32	$(M+H)^+$	229.2162	229.2173	− 4.79	+	+	+	+	+	+	+	+	+	+
18					$(M+Na)^+$	251.1982	251.1988	−2.75										

[a]CW, extract of sections of whole rhizomes collected from China; CA, CB, CC, and CD represent cortex, hypodermal fiber bundle, endodermis, and amphivisal-type vascular bundle tissues isolated from *C. rotundus* rhizomes collected from China; IW, extract of sections of whole rhizomes collected from India; IA, IB, IC, and ID represent cortex, hypodermal fiber bundle, endodermis, and amphivisal-type vascular bundle tissues isolated from *C. rotundus* rhizomes collected from India. (+) denotes presence of constituents in respective samples.

dx.doi.org/10.1021/jf502494z | J. Agric. Food Chem. 2014, 62, 7302−7316

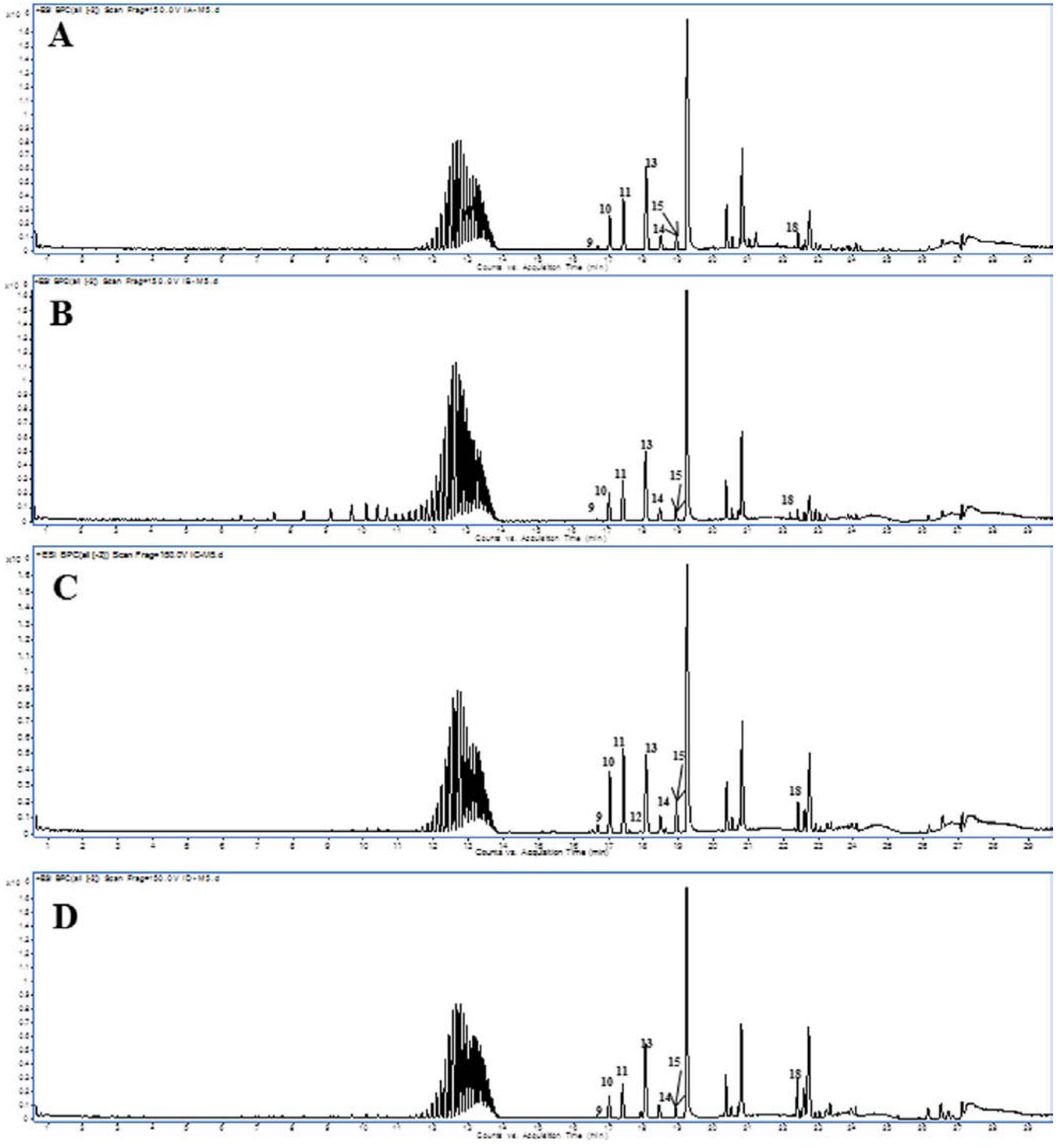

Figure 4. LC-MS base peak chromatograms of various laser-dissected tissues of rhizomes collected from India: (A) cortex, (B) hypodermal fiber bundles, (C) endodermis, and (D) amphivasal-type vascular bundles. Peak numbers indicating the identified constituents are listed in Table 1.

1 and −1 for positive and negative modes, respectively. The compound relative height was ≥2.5%, and absolute height was set to ≥5000 counts with elements of C, H, O, and N from 3−60, 0−120, 0−30, and 0−30, respectively, to generate formulas. The ranges 3−60, 0−120, 0−30, and 0−30 indicate the minimum and maximum limits for the number of elements C, H, O, and N for generation formulas. Peak spacing tolerance was set to 0.0025 m/z plus 7.0 ppm for analysis. The obtained results are depicted as base peak chromatograms (BPC with m/z range 150−950) for each dissected tissue and whole-rhizome tissue analysis. The resultant peak list for LC-MS analysis was processed through Mass Hunter Workstation software and Microsoft Excel software (Microsoft, Redmond, WA). GC-MS analysis data was processed by using the postrun analysis utility of GC-MS solution software (version 2.50 SU3). The results shown in the paper are average values of determinations performed in five sample sets collected from each of the selected countries.

RESULTS AND DISCUSSION

Macroscopic and Microscopic Studies. Pictorial representations of dried *C. rotundus* rhizomes collected from India and

dx.doi.org/10.1021/jf502494z | *J. Agric. Food Chem.* 2014, 62, 7302−7316

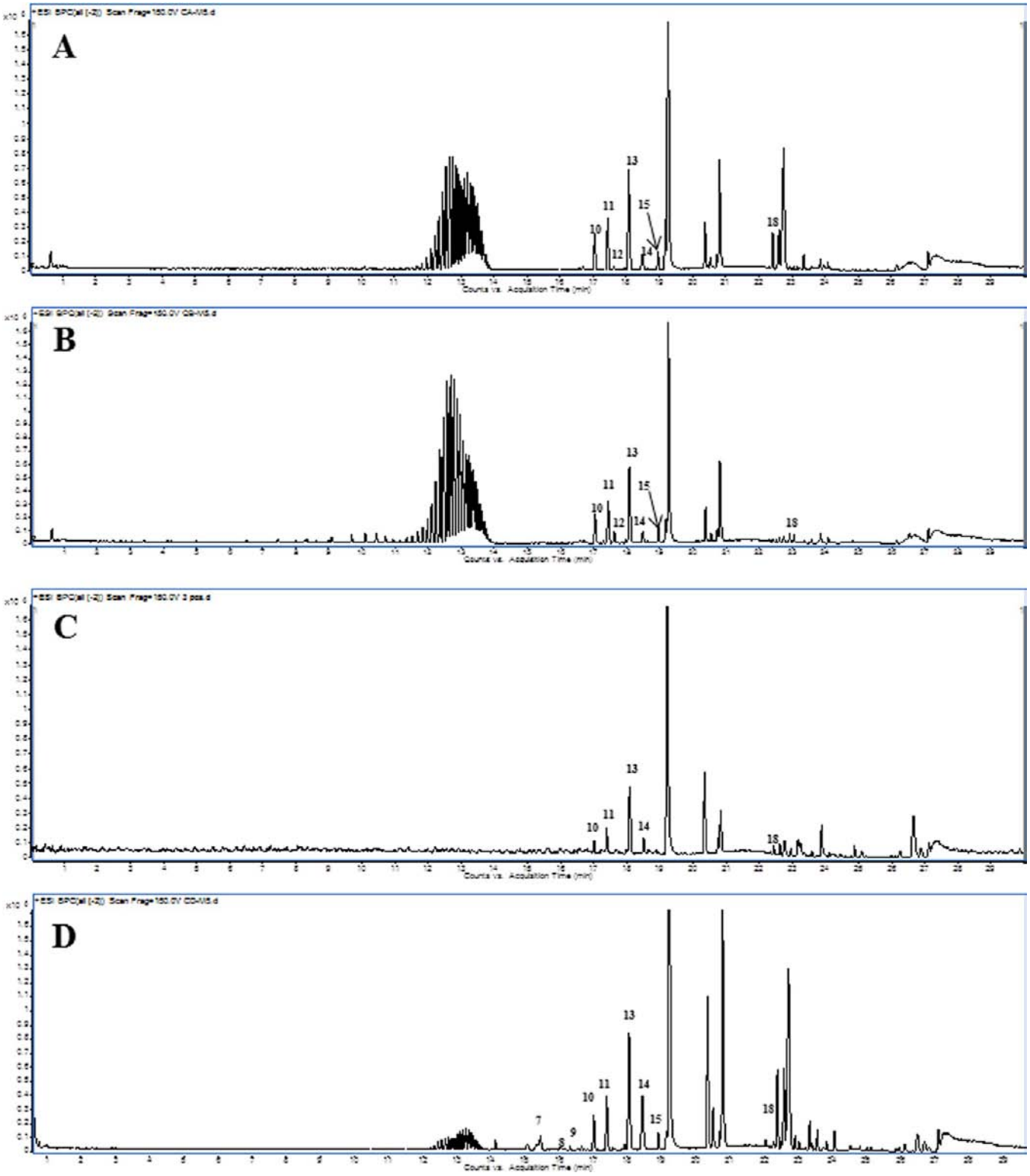

Figure 5. LC-MS base peak chromatograms of various laser-dissected tissues of rhizomes collected from China: (A) cortex, (B) hypodermal fiber bundles, (C) endodermis, and (D) amphivasal-type vascular bundles. Peak numbers indicating the identified constituents are listed in Table 1.

China are shown in Figure 1. The rhizomes of *C. rotundus* are usually spindle-shaped, 2.0−3.0 cm in length and 0.5−1.0 cm in diameter. The outer surface is dark brown or dull black in color. Longitudinal wrinkles are observed on the outer surface along with scars of fibrous roots. The internal surface appears pale cream or yellowish brown in color and has a pleasant odor.

Laser microdissection (LMD) was used to study the microscopic features of rhizomes; a UV laser beam was used to dissect tissues. In the present study, the cortex, hypodermal fiber bundles, endodermis, and amphivasal-type vascular bundles were isolated for analysis of constituents. The microscopic features of transverse sections of rhizomes observed under white light and blue fluorescence for samples from India and China were found

dx.doi.org/10.1021/jf502494z | *J. Agric. Food Chem.* 2014, 62, 7302−7316

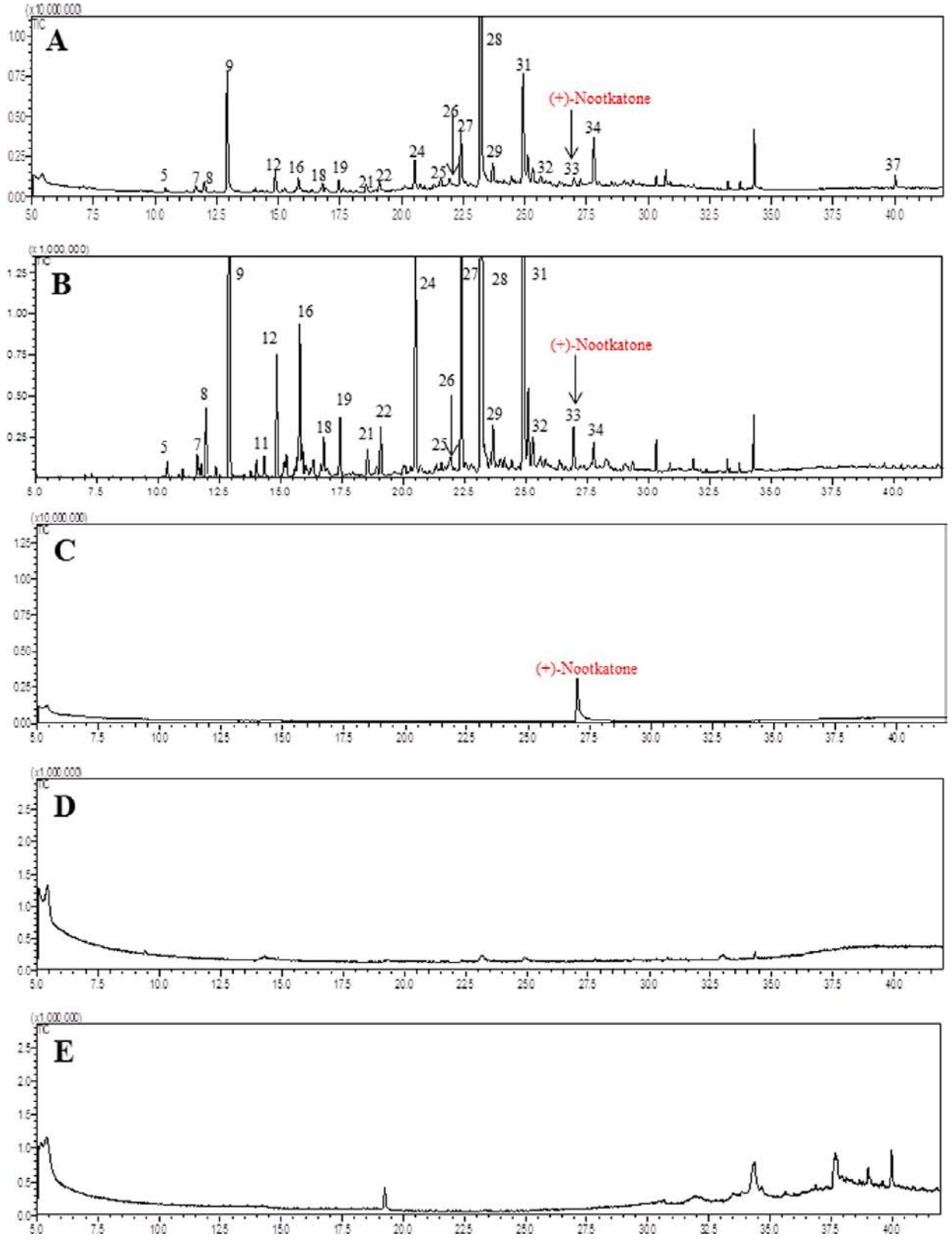

Figure 6. Representative GC-MS chromatograms of *C. rotundus* whole rhizomes: (A) extract of rhizomes collected from India; (B) extract of rhizomes collected from China; (C) (+)-nootkatone standard; (D) blank solvent (hexane/ethyl acetate); (E) cryogenic gel. The peak numbers indicating the identified constituents are listed in Table 2.

to be similar. A representative image indicating various tissues of rhizomes is shown in Figure 2.

A single layer of yellowish-brown epidermis is found to occur with scattered hypodermal fiber bundles (as indicated in Figure 2A). Under blue fluorescence, the epidermis appears blackish-brown (see Figure 2B). Followed by the epidermis, the hypodermis consists of 2−3 layers of fibers filled with dark brownish contents. Under fluorescence, the fibers appear reddish

dx.doi.org/10.1021/jf502494z | J. Agric. Food Chem. 2014, 62, 7302−7316

Table 2. Data for GC-MS-Based Identification of Various Constituents in *C. rotundus* Rhizome Samples

						samples[a]									
peak	compd	obsd m/z	formula	T_R (min)	RI[b]	CW	CA	CB	CC	CD	IW	IA	IB	IC	ID
1	pinocarveol	152.25	$C_{10}H_{16}O$	5.92	1118	−	−	−	−	−	+	−	−	−	−
2	pinocarvone	150.20	$C_{10}H_{14}O$	6.33	1161	−	−	−	−	−	+	−	−	−	−
3	(1*R*)-(−)-myrtenal	150.20	$C_{10}H_{14}O$	7.01	1194	−	−	−	−	−	+	−	−	−	−
4	(+)-verbenone	150.00	$C_{10}H_{14}O$	7.31	1203	+	−	−	−	−	+	−	−	−	−
5	ionone	192.30	$C_{13}H_{20}O$	10.39	1493	+	+	+	+	+	+	+	+	+	+
6	*α*-cubebene	204.35	$C_{15}H_{24}$	11.00	1348	−	−	−	−	−	+	−	−	−	−
7	longipinocarveol	220.35	$C_{15}H_{24}O$	11.65	1169	+	−	−	−	−	+	−	−	−	−
8	copaene	204.35	$C_{15}H_{24}$	11.95	1376	−	−	−	−	−	+	−	−	−	−
9	*β*-cadinene	204.35	$C_{15}H_{24}$	12.91	1538	+	+	+	+	+	+	+	+	+	+
10	*β*-vatirenene	300.45	$C_{20}H_{28}O_2$	14.00	1179	+	−	−	−	−	+	−	−	−	−
11	methylisoeugenol	178.25	$C_{11}H_{14}O_2$	14.48	1453	+	+	+	+	+	+	+	+	+	+
12	*α*-fenchone	152.25	$C_{10}H_{16}O$	14.82	1087	+	+	−	−	−	+	−	+	+	+
13	(+)-cycloisosativene	204.35	$C_{15}H_{24}$	15.24	1381	+	−	−	−	−	+	−	−	−	−
14	germacrene D	204.35	$C_{15}H_{24}$	15.24	1481	+	−	−	−	−	+	−	−	−	−
15	eudesma-4(14),11-diene	204.35	$C_{15}H_{24}$	15.81	1487	+	−	−	−	−	+	−	−	−	−
16	(+)-aromadendrene	204.35	$C_{15}H_{24}$	15.91	1438	+	−	−	−	−	+	−	−	−	−
17	*α*-guaiene	204.35	$C_{15}H_{24}$	16.36	1446	+	−	−	−	−	−	−	−	−	−
18	cycloisolongifolene	202.35	$C_{15}H_{22}$	16.80	1319	+	+	+	+	+	+	+	+	+	+
19	alloaromadendrene oxide-(1)	220.35	$C_{15}H_{24}O$	17.45	1641	+	+	+	+	+	+	+	+	+	+
20	(−)-spathulenol	220.35	$C_{15}H_{24}O$	18.55	1577	−	−	−	−	−	+	−	−	−	−
21	*γ*-gurjunenepoxide-(1)	220.35	$C_{15}H_{24}O$	18.61	1419	+	−	−	−	−	+	−	−	−	−
22	*trans*-*Z*-*α*-bisabolene epoxide	220.35	$C_{15}H_{24}O$	19.12	1671	+	+	+	+	+	+	+	+	+	+
23	caryophyllene oxide	220.35	$C_{15}H_{24}O$	20.11	1573	+	−	−	−	−	−	−	−	−	−
24	9*H*-cycloisolongifolene, 8-oxo-	218.35	$C_{15}H_{22}O$	20.52	1197	+	+	+	+	+	+	+	+	+	+
25	(−)-neoclovene-(II)	206.35	$C_{15}H_{26}$	21.61	1454	+	+	+	+	+	+	−	−	−	−
26	epiglobulol	222.35	$C_{15}H_{26}O$	21.82	1564	+	−	−	−	−	+	−	−	−	−
27	longiverbenone	218.35	$C_{15}H_{22}O$	22.40	1204	+	−	−	−	−	+	−	−	−	−
28	aristolone	218.35	$C_{15}H_{22}O$	23.22	1763	+	+	+	+	+	+	−	−	−	−
29	longipinocarvone	218.35	$C_{15}H_{22}O$	23.66	1559	+	−	−	−	−	+	−	−	−	+
30	isopulegol	154.25	$C_{10}H_{18}O$	24.10	1144	+	−	−	−	−	−	−	−	−	−
31	*α*-cyperone	218.35	$C_{15}H_{22}O$	24.92	1706	+	+	+	+	+	+	−	−	−	−
32	isoaromadendrene epoxide	220.35	$C_{15}H_{24}O$	25.64	1475	+	−	−	−	−	+	+	+	+	+
33	(+)-nootkatone	242.30	$C_{16}H_{18}O_2$	26.99	1810	+	+	+	−	+	+	−	+	−	+
34	menthol	156.25	$C_{10}H_{20}O$	27.79	1171	−	−	−	−	−	+	−	−	−	−
35	corymbolone	236.35	$C_{15}H_{24}O_2$	29.33	1853	+	−	−	−	−	−	−	−	−	−
36	*trans*-9-octadecen-1-ol	268.50	$C_{18}H_{36}O$	37.76	2062	+	−	−	−	−	−	−	−	−	−
37	erucic acid	338.55	$C_{22}H_{42}O_2$	40.00	2473	−	−	−	−	−	+	−	−	−	−

[a]CW, extract of sections of whole rhizomes collected from China; CA, CB, CC, and CD represent cortex, hypodermal fiber bundle, endodermis, and amphivisal-type vascular bundle tissues isolated from *C. rotundus* rhizomes collected from China; IW, extract of sections of whole rhizomes collected from India; IA, IB, IC, and ID represent cortex, hypodermal fiber bundle, endodermis, and amphivisal-type vascular bundle tissues isolated from *C. rotundus* rhizomes collected from India. (+) denotes presence of constituents in respective samples. [b]Calculated Kovats retention indices.

brown. The cortex consists of numerous layers of parenchymatous cells with intercellular spaces. In the cortex, there are numerous secretory cells scattered, and a few leaf trace vascular bundles are also found. When observed under blue fluorescent light, the parenchymatous cells of cortex appear pale blue and secretory cells and endodermis appear reddish brown. An endodermis made of subrectangular cells forming a distinct ring is observed. The stele shows the occurrence of several amphivasal vascular bundles and secretory cells. The samples collected from both India and China belong to the same species, and in the microscopic and morphological investigations carried out in this study, these features were found to be similar between them.

Metabolite Profiling by UHPLC-QTOF MS. *Cyperus* rhizomes are well-known for their terpenoidal constituents.[43] The sesquiterpenoids are a particular class of terpenoids found in this plant. For metabolite profiling of the whole-rhizome tissue sections and the target isolated tissues of *C. rotundus* rhizomes, a database of 86 phytoconstituents reported for *Cyperus* species in scientific publications and mass banks was prepared.[43−48] The constituents found in LC-MS spectra were deduced on the basis of extracted fragment groups and losses in molecular masses of fragment ions.

Representative LC-MS base peak chromatograms of the rhizomes of both Indian and Chinese samples and controls of cryogenic gel and methanol are shown in Figure 3. Retention times, molecular fragment ions, m/z values of measured adduct ions, and calculated molecular masses of all the secondary metabolites detected in samples of *C. rotundus* rhizomes by LC-MS analysis are listed in Table 1. The database of 86 reported constituents was prepared through literature survey and used for identification of components (see Table S1 of Supporting Information). The cryogel used in preparation of tissue sections

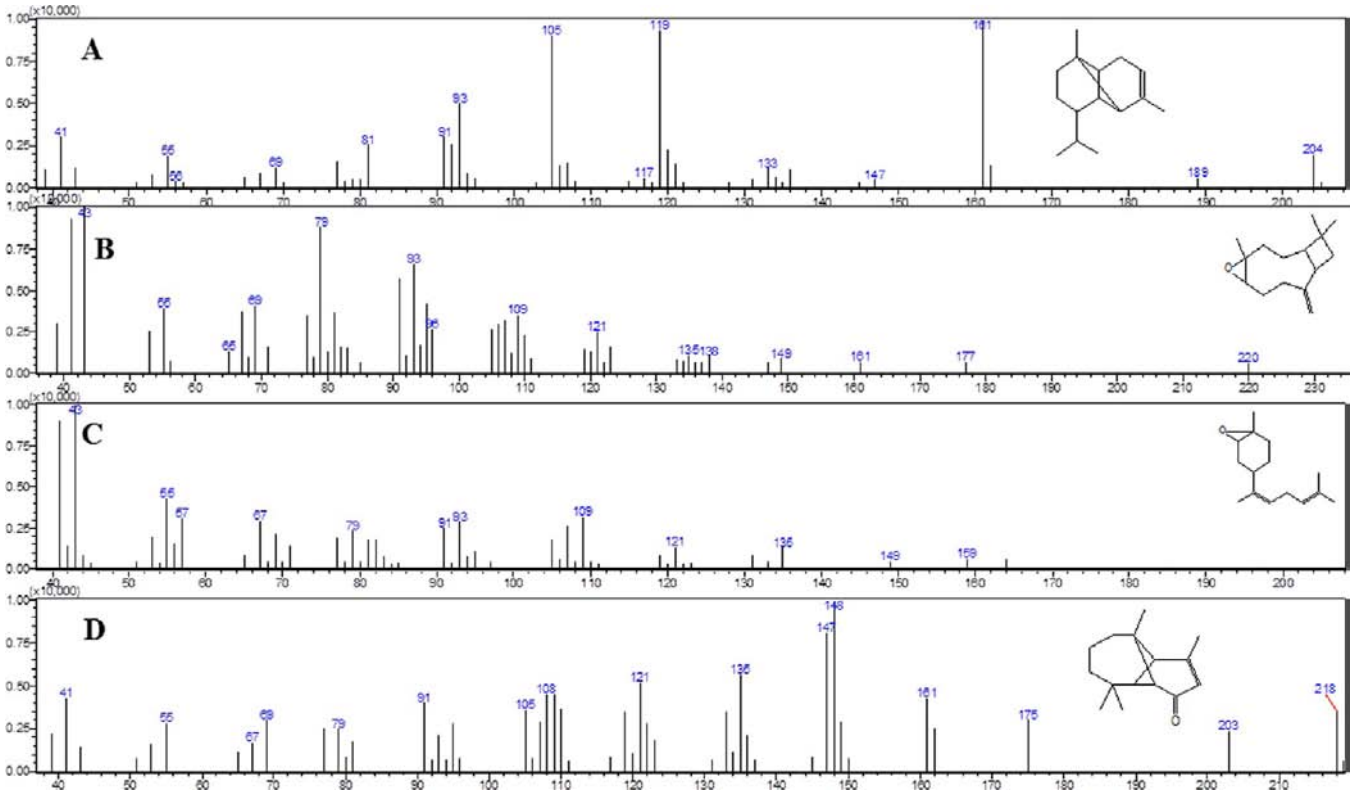

Figure 7. GC-MS mass spectra of some abundant constituents found in whole rhizome samples collected from India: (A) copaene, (B) caryophyllene oxide, (C) *trans-Z-α*-bisabolene epoxide, and (D) longiverbenone.

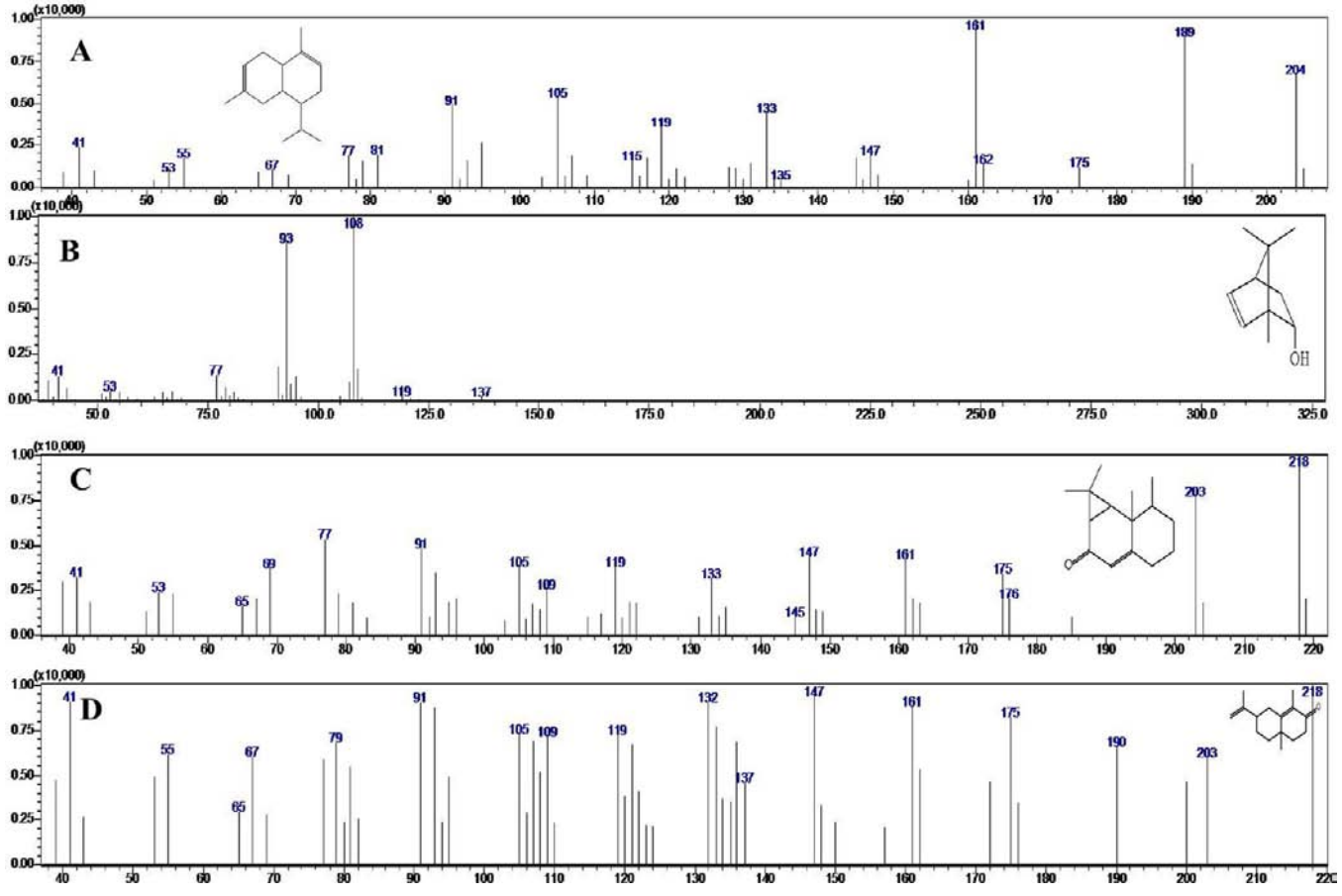

Figure 8. GC-MS mass spectra of some abundant constituents found in whole rhizome samples collected from China: (A) *β*-cadinene, (B) *α*-fenchone, (C) aristolone, and (D) *α*-cyperone.

dx.doi.org/10.1021/jf502494z | J. Agric. Food Chem. 2014, 62, 7302−7316

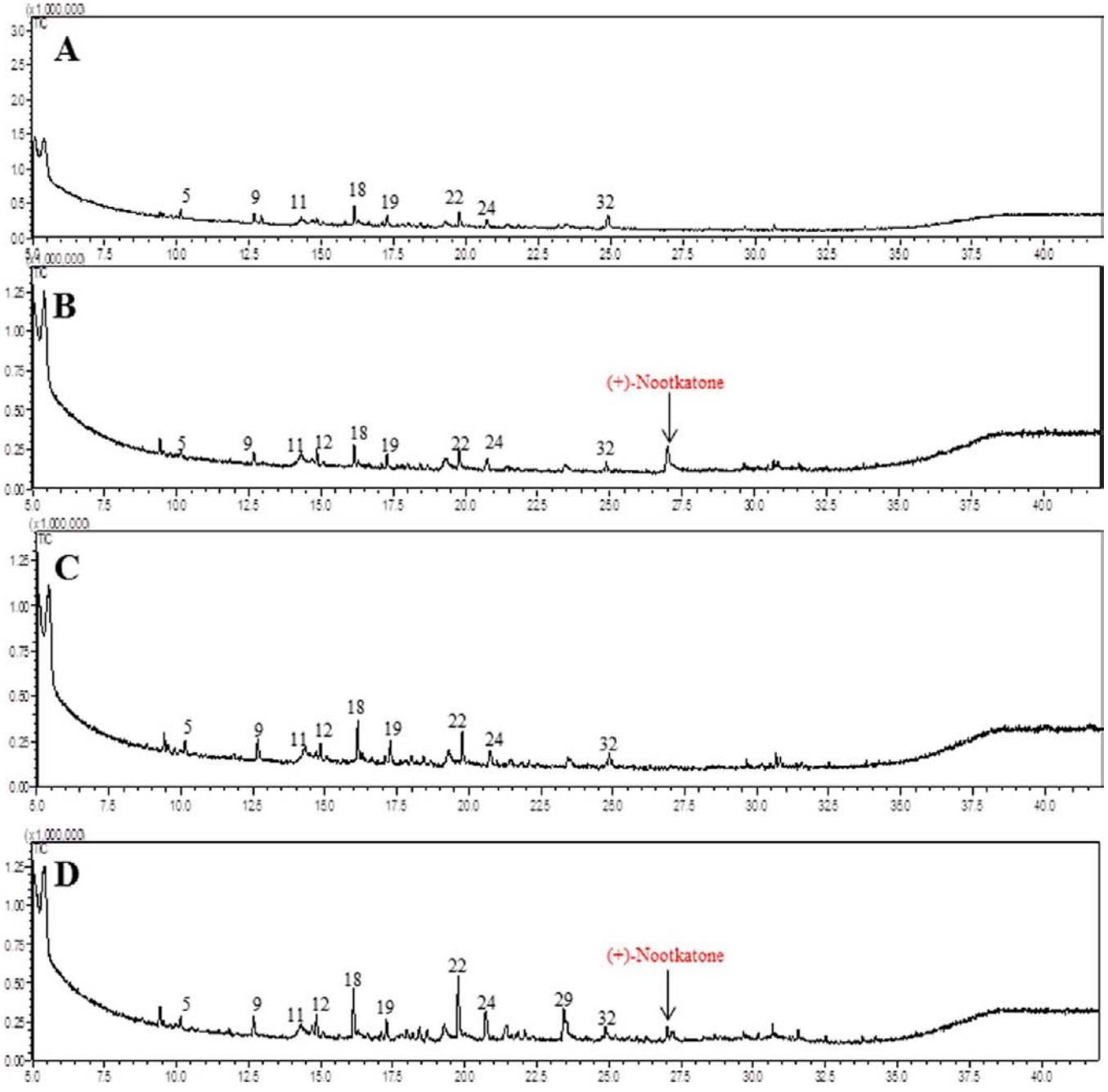

Figure 9. GC-MS base peak chromatograms of various laser-dissected tissues of rhizomes collected from India: (A) cortex, (B) hypodermal fiber bundles, (C) endodermis, and (D) amphivasal-type vascular bundles. Peak numbers indicating the identified constituents are listed in Table 2.

exhibits sharp peaks of glycols and poly(vinyl alcohol) polymers between 11 and 14 min of retention time. Methanol, used as solvent, exhibits few peaks from 18 to 21 min. The positive mode in comparison to negative mode exhibited a better response for profiling of constituents; hence the positive mode was used for analysis.

As seen in the chromatograms of Figure 3, there are several constituents that occur in common between the samples collected from India and China. There were also some constituents that occurred exclusively in each of the samples from India and China. The components cyperanic acid, 7-methoxy-2-tetralone, sobrerol, sugetriol, and (−)-epoxycaryophyllene were found only in samples from India. The common constituents for samples from India and China were ligucyperonol, calamenene, mandassidione, 4-cymene, sugeonol, cyperusol B1 and B2, sitosterol, myrcetin, cyperotundone, isolongifolanone, and valerenal.

Tissue-Specific Metabolite Analysis by UHPLC-QTOF MS. The metabolites present in the selected target tissues were identified by LC-MS analysis. The tissues isolated for analysis were cortex, hypodermal fiber bundles, endodermis, and amphivasal-type vascular bundles. The base peak chromatograms obtained after LC-MS analysis of these tissues of samples from India and China are shown in Figures 4 and 5 respectively. The peak numbers assigned to all the identified secondary metabolites and their occurrence in various tissues is indicated in Table 1, along with the details of their molecular characteristics in LC-MS analysis. Table S1 of Supporting Information lists all the constituents used for profiling.

dx.doi.org/10.1021/jf502494z | J. Agric. Food Chem. 2014, 62, 7302−7316

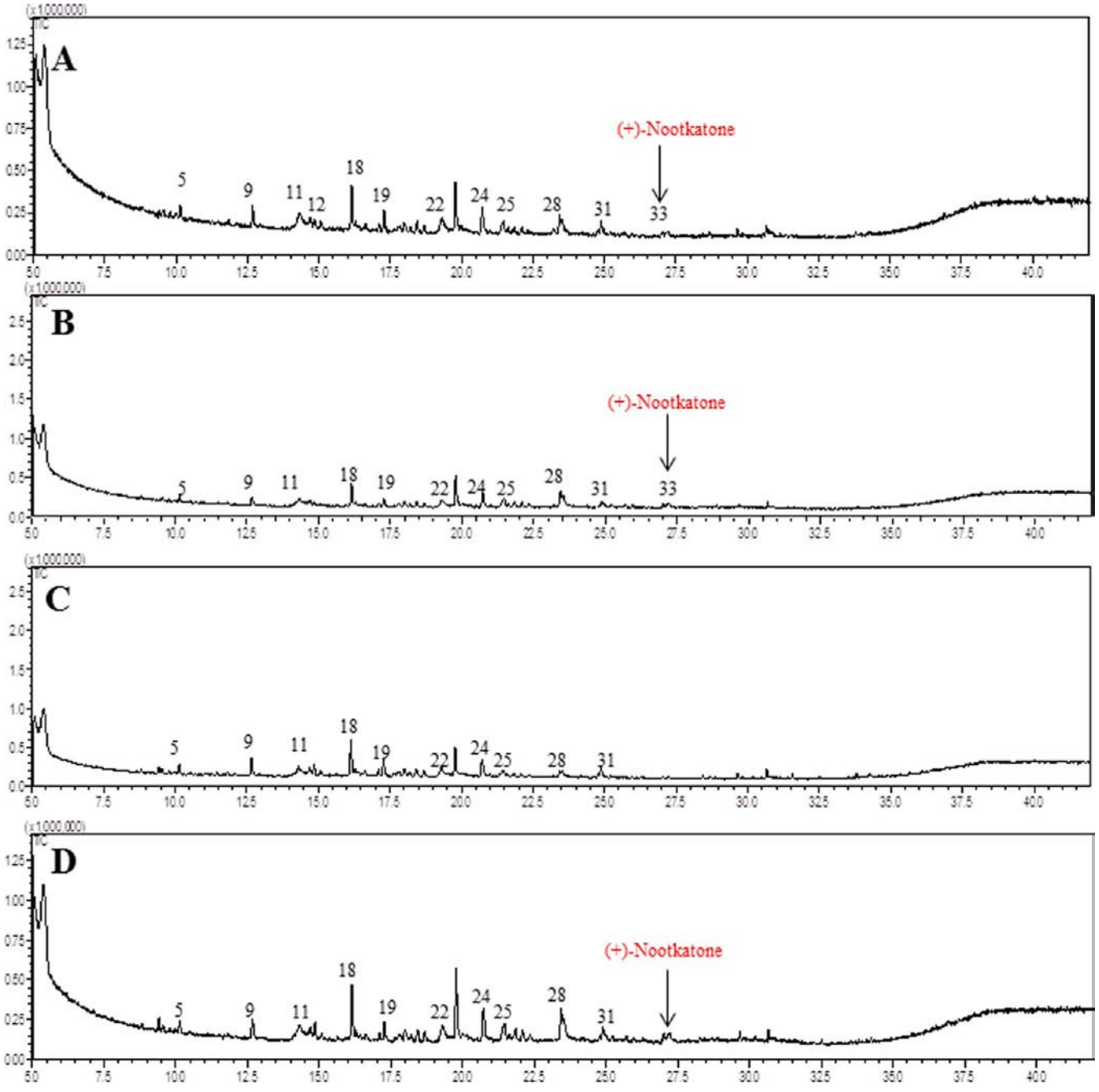

Figure 10. GC-MS base peak chromatograms of various laser-dissected tissues of rhizomes collected from China: (A) cortex, (B) hypodermal fiber bundles, (C) endodermis, and (D) amphivasal-type vascular bundles. Peak numbers indicating the identified constituents are listed in Table 2.

As indicated in Figure 4 and Table 1, the tissues of rhizomes collected from India contained 4-cymene, sugeonol, cyperusol B1, sitosterol, myrcetin, cyperotundone, and myristic acid. The cortex, hypodermal fiber bundles, endodermis, and amphivasal vascular bundles did not differ significantly in constituents except for the endodermis, which contained cyperusol B2 in addition to the common constituents.

With regard to samples collected from China, some differences were observed in the type of constituents in the selected tissues (see Figure 5). The common constituents in all tissues were sugeonol, cyperusol B1, sitosterol, myrcetin, and myristic acid. The cortex and hypodermal fiber bundles also contained cyperusol B2 and cyperotundone in addition to the common constituents. The endodermis contained all the common constituents listed above. The amphivasal vascular bundles, in addition to the common constituents, also had calamenene, mandassidione, 4-cymene, and cyperotundone. On the basis of comparative profiling of tissue metabolites, we infer that the *C. rotundus* rhizome samples collected from both India and China can be used as qualitative substitutes for each other.

GC-MS-Based Metabolite Profiling. As mentioned earlier, several reports indicate the presence of terpenoids, alkaloids, flavonoids, and steroids in rhizomes of *C. rotundus*. In this study, various essential oil constituents present in *C. rotundus* were characterized and the content of the sesquiterpenoid constituent (+)-nootkatone was quantified by GC-MS analysis. Representative chromatograms of extracts of whole rhizome samples from India and China, with hexane/ethyl acetate (1:1) used as blank

dx.doi.org/10.1021/jf502494z | *J. Agric. Food Chem.* 2014, 62, 7302−7316

solvent and (+)-nootkatone standard, are presented in Figure 6. The 37 constituents identified in the study samples through GC-MS analysis are listed in Table 2, along with their retention times and calculated Kovats retention indices. (+)-Nootkatone was found to have a retention time of 26.99 min. The constituents found in common between the samples from India and China are *trans-Z-α*-bisabolene epoxide, longiverbenone, and (+)-nootkatone. From percentage areas it was found that the most abundant constituents in samples from India were copaene (6.96%), *trans-Z-α*-bisabolene epoxide (9.75%), caryophyllene oxide (9.01%), and longiverbenone (8.50%). In samples collected from China, the abundant constituents found were *β*-cadinene (33.45%), *α*-fenchone (7.44%), aristolone (23.31%), and *α*-cyperone (23.31%). Overall, in the optimized experimental conditions used for this study, 23 constituents were detected in samples from India and 20 constituents were detected in samples from China.

Representative mass spectra of some major constituents in samples from India and China are indicated in Figures 7 and 8, respectively, and their occurrence or absence is indicated in Table 2.

GC-MS-Based Tissue-Specific Metabolite Profiling. The presence of nonpolar metabolites in cortex, hypodermal fiber bundle, endodermis, and amphivasal-type vascular bundle tissues of rhizomes was estimated by GC-MS analysis. The base peak chromatograms for tissues of rhizome samples from India and China are shown in Figures 9 and 10, respectively. The peak numbers for all the identified constituents are indicated in the chromatograms are listed in Table 2.

In the rhizome samples collected from India, all the tissues contained ionone, *β*-cadinene, methyl isoeugenol, cycloisolongifolene, alloaromadendrene oxide-(1), *trans-Z-α*-bisabolene epoxide, 9*H*-cycloisolongifolene, and isoaromadendrene epoxide. All these metabolites were found to occur in the cortex. In addition to these common metabolites, the hypodermal fiber bundles and endodermis indicated the presence of *α*-fenchone. The amphivasal-type vascular bundle tissues contained longipinocarvone in addition to *α*-fenchone and the above-mentioned common constituents.

In the rhizome samples collected from China, the common metabolites among all the target tissues were ionone, *β*-cadinene, methyl isoeugenol, cycloisolongifolene, (−)-neoclovene-(II), aristolone, and *α*-cyperone. The cortex, hypodermal fiber bundles and amphivasal-type vascular bundle tissues in addition to the common metabolites contained (+)-nootkatone; however, it was not detected in the endodermis tissues.

Quantitation of (+)-Nootkatone and Method Validation. The content of (+)-nootkatone was determined in the rhizome samples of *C. rotundus* through GC-MS analysis. SIM mode was used for quantitative analysis and the peak areas obtained for the standard analyte in the calibration curve were used for calculation of (+)-nootkatone content in the samples. The content of (+)-nootkatone in samples from India was found to be higher than in samples from China (see Table 3).

The method was validated as per International Conference on Harmonisation (ICH) guidelines (Q2 R1).[42] The results obtained for recovery studies and other parameters of validation are reported in Table 4.

The sesquiterpenoid component (+)-nootkatone has significant insecticidal, anticancer, and antiplatelet activity, and it is an important flavoring agent used in biotechnology, pesticide, and perfume industries.[46−50] Finding sources of rich (+)-nootkatone content like *C. rotundus*, which is an easily available weed and an agricultural waste product, would be of significant importance for the relevant industries.

Table 3. Content of (+)-Nootkatone in *C. rotundus* Rhizome Samples

sample[a]	(+)-nootkatone[b] (μg/10 g)
CW	21.72 ± 0.572
IW	30.47 ± 0.716

[a]CW, extract of whole rhizome samples collected from China; IW, extract of whole rhizome samples collected from India. [b]Contents were calculated on the basis of dry weight of the rhizomes (n = 3) and are presented as mean ± relative standard deviation (RSD).

Table 4. Results of Various Parameters of Validation Studies

parameter	value for (+)-nootkatone
calibration curve equation	y = 109 851x + 56 174
correlation coefficient (r^2)	0.9887
LOD (ng/mL)	0.303
LOQ (ng/mL)	1.0
calibration range (ng)	1.0−100.0
intraday precision (% RSD, n = 5)	0.239
interday precision (% RSD, n = 3)	0.645
repeatability (RSD, n = 5)	0.423
recovery (n = 3)	
low-level spike (50% ± RSD)	56.15 ± 0.203
intermediate-level spike (100% ± RSD)	99.78 ± 0.019
high-level spike (150% ± RSD)	125.73 ± 0.372

In conclusion, our study is the first to compare tissue-specific metabolites and (+)-nootkatone content in *C. rotundus*, which is a common plant species found in China and India. Quantitatively, the samples from both these geographical regions have a difference in their percentage contents of (+)-nootkatone. However, qualitatively they have considerable similarities, which suggests their validity of being used as substitutes for each other.

The plant *C. rotundus* is important not only due to its therapeutic utility in traditional medicine and its applications in food industry but also due to its use as an economic and easily available source of (+)-nootkatone. Thus, its (+)-nootkatone-rich content adds to its beneficial values despite its reputation of being a notorious weed in the agricultural sector.

The experimental approach was designed with a perspective of evaluating the quality of *C. rotundus* rhizome from two different countries in terms of differences in their metabolites and (+)-nootkatone content. Such studies can help in identification of geographical locations for obtaining herbal material of superior quality. Our study provides information that can be utilized for quality control and standardization of *C. rotundus* rhizomes and its products. Furthermore, our study provides a perspective for advantageous utilization of the notorious weed *C. rotundus*, which has been a major concern for the agricultural sector.

■ ASSOCIATED CONTENT

Supporting Information

One table listing constituents identified in *C. rotundus* by UHPLC-QTOF MS analysis. This material is available free of charge via the Internet at http://pubs.acs.org.

■ AUTHOR INFORMATION

Corresponding Author

*E-mail zzzhao@hkbu.edu.hk; phone +852 34112424; fax +852 34112461.

Funding

This work was supported by the Hong Kong Research Grants Council (GRF-HKBU-263412).

Notes

The authors declare no competing financial interest.

REFERENCES

(1) Bendixen, L. E.; Nandihalli, V. B. Worldwide distribution of purple and yellow nutsedge (*Cyperus rotundus* and *C. esculentus*). *Weed Technol.* **1987**, *1*, 61−65.

(2) Bryson, C. T.; Hanks, J. E.; Wills, G. D. Purple nutsedge (*Cyperus rotundus*) control in reduced-tillage cotton (*Gossypium hirsutum* L.) with low volume technology. *Weed Technol.* **1994**, *8*, 28−31.

(3) Seethapathy, G. S.; Balasubramani, S. P.; Venkatasubramanian, P. nrDNA ITS sequence based SCAR marker to authenticate *Aconitum heterophyllum* and *Cyperus rotundus* in Ayurvedic raw drug source and prepared herbal products. *Food Chem.* **2014**, *145*, 1015−1020.

(4) Chen, H. Y.; Lin, Y. H.; Su, I. H.; Chen, Y. C.; Yang, S. H.; Chen, J. L. Investigation on Chinese herbal medicine for primary dysmenorrhea: implication from a nationwide prescription database in Taiwan. *Complementary Ther. Med.* **2014**, *22*, 116−125.

(5) Imam, M. Z.; Sumi, C. D. Evaluation of antinociceptive activity of hydromethanol extract of *Cyperus rotundus* in mice. *BMC Complementary Altern. Med.* **2014**, *14*, 83.

(6) Kumar, K. H.; Razack, S.; Nallamuthu, I.; Khanum, F. Phytochemical analysis and biological properties of *Cyperus rotundus* L. *Ind. Crops Prod.* **2014**, 815−826.

(7) Wriessnegger, T.; Augustin, P.; Engleder, M.; Leitner, E.; Müller, M.; Kaluzna, I.; Schürmann, M.; Mink, D.; Zellnig, G.; Schwab, H.; Pichler, H. Production of the sesquiterpenoid (+)-nootkatone by metabolic engineering of *Pichia pastoris*. *Metab. Eng.* **2014**, *24*, 18−29.

(8) Choi, H.; Lee, J.; Jung, Y. (+)-Nootkatone inhibits tumor necrosis factor α/interferon γ-induced production of chemokines in HaCaT cells. *Biochem. Biophys. Res. Commun.* **2014**, *447*, 278−284.

(9) Davies, K. M.; Deroles, S. C. Prospects for the use of plant cell cultures in food biotechnology. *Curr. Opin. Chem. Biol.* **2014**, *26*, 133−140.

(10) Handore, K. L.; Seetharamsingh, B.; Reddy, D. S. Ready access to functionally embellished *cis*-hydrindanes and *cis*-decalins: protecting group-free total syntheses of (+)-nootkatone and (+)-noreremophilane. *J. Org. Chem.* **2013**, *78*, 8149−8154.

(11) Choi, H. J.; Lee, J. H.; Jung, Y. S. (+)-Nootkatone inhibits tumor necrosis factor α/interferon γ-induced production of chemokines in HaCaT cells. *Biochem. Biophys. Res. Commun.* **2014**, *447*, 278−284.

(12) Schreier, P. Enzymes and flavour biotechnology. In *Biotechnology of Aroma Compounds*. Berger, R. G., Ed.; Springer: Berlin, Heidelberg, and New York, 1997; p 51.

(13) Meena, A.; Yadav, A.; Niranjan, U.; Singh, B.; Nagariya, A.; Verma, M. Review on *Cyperus rotundus* − A potential herb. *Int. J. Pharm. Clin. Res.* **2010**, *2*, 20−22.

(14) Sharma, P.; Yelne, M.; Dennis, T. In *Database on Medicinal Plants Used in Ayurveda*; Central Council for Research in Ayurveda and Siddha: Delhi, India, 2001; pp 404−424.

(15) Eun, J. S.; Dong-Ung, L.; Jong, H. W.; Sun-Mee, L.; Yeong, S. K.; Yi-Sook, J. Antiplatelet effects of *Cyperus rotundus* and its component (+)-nootkatone. *J. Ethnopharmacol.* **2011**, *135*, 48−54.

(16) Hemanth, K. K.; Tamatam, A.; Pal, A.; Khanum, F. Neuroprotective effects of *Cyperus rotundus* on SIN-1 induced nitric oxide generation and protein nitration: Ameliorative effect against apoptosis mediated neuronal cell damage. *Neurotoxicology.* **2013**, *34*, 150−159.

(17) Ladd, W. Fragrance raw material monographs. *Food Chem. Toxicol.* **2000**, *38*, s165−s167.

(18) Oladunni, O. M.; Abass, O. O.; Adisa, A. I. Studies on the physiochemical properties of the oil, minerals and nutritional composition of nut of nut grass (*Cyperus rotundus*). *Am. J. Food Technol.* **2011**, *6*, 1061−1064.

(19) Sánchez-Zapata, E.; Fuentes-Zaragoza, E.; Fernández-López, J.; Sendra, E.; Sayas, E.; Navarro, C.; Pérez-Alvarez, J. A. Preparation of dietary fiber powder from tiger nut (*Cyperus esculentus*) milk ("Horchata") byproducts and its physicochemical properties. *J. Agric. Food Chem.* **2009**, *57*, 7719−7725.

(20) Cantalejo, M. J. Development of new products from earth almond. *Fruit Process.* **1996**, *3*, 87−91.

(21) Chopra, R. N.; Nayar, S. L.; Chopra, I. C. *Glossary of Indian Medicinal Plants*; Publications and Information Directorate: New Delhi, India, 1956.

(22) Messiaen, C. M. *The Tropical Vegetable Garden: Principles for Improvement and Increased Production with Applications to Main Vegetable Types*; Macmillan Press: London, 1992; p 514.

(23) Umerie, S. C.; Ezeuzo, H. O. Physicochemical characterization and utilization of *Cyperus rotundus* starch. *Bioresour. Technol.* **2000**, *72*, 193−196.

(24) Bamgbose, A. M.; Eruvbetine, D.; Dada, W. Utilization of tigernut (*Cyperus rotundus* L.) meal in diets for cockerel starters. *Bioresour. Technol.* **2003**, *89*, 245−248.

(25) Sebastia, N.; Soler, C.; Soriano, J. M.; Manes, J. Occurrence of aflatoxins in tigernuts and their beverages commercialized in Spain. *J. Agric. Food Chem.* **2010**, *58*, 2609−2612.

(26) *The Ayurvedic Pharmacopoeia of India*, 1st ed.; Controller of Publication: Delhi, India, 2001; Vol. *3*, p 129.

(27) Jiangsu New Medical College. *Dictionary of Chinese Materia Medica*; Shanghai People's Publishing House: Shanghai, China, 1971; pp 3441−3443.

(28) Chinese Pharmacopoeia Commission. *The Pharmacopoeia of the People's Republic of China*, English ed.; China Medical Science Press: Beijing, China, 2010; Vol. *1*, p 147.

(29) Weehen, H.; Nkunya, M. H. H.; Bray, D. H.; Mwasumbi, L. B.; Kinabo, L. S.; Kilimali, A. E.; Wijnberg, B. P.A. Antimalarial activity of Tanzanian plants. Part 2. Antimalarial compounds containing an α,β-unsaturated carbonyl moiety from Tanzanian medicinal plants. *Planta Med.* **1990**, *56*, 371−373.

(30) Sayed, H. M.; Mohamed, M. H.; Farag, S. F.; Mohamed, G. A.; Proksch, P. A new steroid glycoside and furochromones from *Cyperus rotundus* L. *Nat. Prod. Res.* **2007**, *21*, 343−350.

(31) Lawal, O. A.; Oyedeji, A. O. Chemical composition of the essential oils of *Cyperus rotundus* L. from South Africa. *Molecules* **2009**, *14*, 2909−2917.

(32) Kilani-Jaziri, S.; Neffati, A.; Limem, I.; Boubaker, J.; Skandrani, I.; Sghair, M. B.; Bouhlel, I.; Bhouri, W.; Mariotte, A. M.; Ghedira, K.; Dijoux Franca, M. G.; Chekir-Ghedira, L. Relationship correlation of antioxidant and antiproliferative capacity of *Cyperus rotundus* products towards K562 erythroleukemia cells. *Chem.-Biol. Interact.* **2009**, *181*, 85−94.

(33) Natarajan, K. S.; Narasimhan, M.; Shanmugasundaran, K. R.; Shanmugasundaram, E. R. Antioxidant activity of salt-spice-herbal mixture against free radical induction. *J. Ethnopharmacol.* **2006**, *105*, 76−83.

(34) Nagulendran, K. R.; Velavan, S.; Mahesh, R.; Begum, H. V. *In vitro* antioxidant activity and total polyphenolic content of *Cyperus rotundus* rhizomes. *e-J. Chem.* **2007**, *4*, 440−449.

(35) Jaiswal, Y.; Liang, Z.; Yong, P.; Chen, H.; Zhao, Z. A comparative study on the traditional Indian shodhana and Chinese processing methods for aconite roots by characterization and determination of the major components. *Chem. Cent. J.* **2013**, *7*, 169.

(36) Jaiswal, Y.; Liang, Z.; Ho, A.; Chen, H.; Zhao, Z. A comparative tissue-specific metabolite analysis and determination of protodioscin content in asparagus species used in traditional chinese medicine and ayurveda by use of laser micro-dissection, UHPLC-QTOF MS and LC-MS/MS. *Phytochem. Anal.* **2014**, DOI: 10.1002/pca.2522.

(37) Zhao, Z.; Liang, Z.; Ping, G. Macroscopic identification of Chinese medicinal materials: Traditional experiences and modern understanding. *J. Ethnopharmacol.* **2011**, *134*, 556−564.

(38) Farnham, M.; Wilson, P.; Stephenson, K.; Fahey, J. Genetic and environmental effects on glucosinolate content and chemoprotective potency of broccoli. *Plant Breed.* **2004**, *123*, 60−65.

(39) Charron, C.; Saxton, A.; Sams, C. Relationship of climate and genotype to seasonal variation in the glucosinolate−myrosinase system.

II. Myrosinase activity in ten cultivars of *Brassica oleracea* grown in fall and spring seasons. *J. Sci. Food Agric.* **2005**, *85*, 682−690.
(40) Jain, N.; Shasany, A.; Sundaresan, V.; Rajkumar, S.; Darokar, M.; Bagchi, G.; Gupta, A.; Kumar, S.; Khanjua, S. Molecular diversity in *Phyllanthus amarus* assessed through RAPD analysis. *Curr. Sci.* **2003**, *10*, 1454−1458.
(41) Williams, H. J.; Sattler, I.; Moyna, G.; Scott, A. L.; Bell, A. A.; Vinson, S. B. Diversity in cyclic sesquiterpene production by *Gossypium hirsutum*. *Phytochemistry* **1995**, *40*, 1633−1636.
(42) ICH, International Conference on Harmonisation of Technical Requirements for Registration of Pharmaceuticals for Human Use. *Validation of Analytical Procedures: Text and Methodology (Q2 R1)*; ICH Harmonised Tripartite Guidelines, Geneva, 2005; pp 6−13.
(43) Khan, S.; Choi, R. J.; Lee, D. U.; Kim, Y. S. Sesquiterpene derivatives isolated from *Cyperus rotundus* L. inhibit inflammatory signalling mediated by NF-κB. *Nat. Prod. Sci.* **2011**, *17*, 250−255.
(44) Bisht, A.; Bisht, G.; Singh, M.; Gupta, R.; Singh, V. Chemical composition and antimicrobial activity of essential oil of tubers of *Cyperus rotundus* Linn. collected from Dehradun (Uttarakhand). *Int. J. Res. Pharm. Biomed. Sci.* **2011**, *2*, 661−665.
(45) Kim, S. J.; Kim, H. J.; Kim, H. J.; Jang, Y. P.; Oh, M. S.; Jang, D. S. New patchoulane-type sesquiterpenes from the rhizomes of *Cyperus rotundus*. *Bull. Korean Chem. Soc.* **2012**, *33*, 3115−3118.
(46) Yang, J. L.; Shi, Y. P. Structurally diverse terpenoids from the rhizomes of *Cyperus rotundus* L. *Planta Med.* **2012**, *78*, 59−64.
(47) Anderson, J.; Coats, J. Acetylcholinesterase inhibition by nootkatone and carvacrol in arthropods. *Pestic. Biochem. Physiol.* **2012**, *102*, 124−128.
(48) Krugener, S.; Krings, U.; Zorn, H.; Berger, R. G. A dioxygenase of *Pleurotus sapidus* transforms (+)-valencene regio-specifically to (+)-nootkatone via a stereo-specific allylic hydroperoxidation. *Bioresour. Technol.* **2010**, *101*, 457−462.
(49) Gliszczyńska, A.; Łysek, A.; Janeczko, T.; Świtalska, M.; Wietrzyk, J.; Wawrzeńczyk, C. Microbial transformation of (+)-nootkatone and the antiproliferative activity of its metabolites. *Bioorg. Med. Chem.* **2011**, *19*, 2464−2469.
(50) Tsoyi, K.; Jang, H. J.; Lee, Y. S.; Kim, Y. M.; Kim, H. J.; Seo, H. G.; Lee, J. H.; Kwak, J. H.; Lee, D. U.; Chang, K. C. (+)-Nootkatone and (+)-valencene from rhizomes of *Cyperus rotundus* increase survival rates in septic mice due to heme oxygenase-1 induction. *J. Ethnopharmacol.* **2011**, *137*, 1311−1317.

that several kinds of soy sauce are assessed. However, this technique is expensive and time-consuming due to the preparation of a huge amount of fraction of soy sauce. Thus, it is difficult to use this technique for several soy sauce samples.

Meanwhile, metabolomics concerning as many metabolites as possible has become an important tool over a wide research area. Specifically, metabolic or compound profiling based on metabolomics technology has recently been receiving much attention for application in the research of the relationship between compounds and food quality.[12,13] Research on metabolic profiling and its relationship to the taste of food has been reported before such as in green tea,[14] tomato,[15] cheese,[16] sake,[17] and soy sauce.[18]

In a previous study[18] about profiling between the compounds and taste of soy sauce, hydrophilic compounds were measured by gas chromatography−mass spectrometry (GC-MS), and its correlation with sensory attribute was assessed. The study focused on the construction of a prediction model of sensory attributes by metabolic profiling that was able to predict the umami taste intensity using metabolite data obtained by GC-MS. In addition, it was reported that glutamic acid, glucose, and sucrose had strong correlation with the umami taste intensity and were suggested as the significant compounds for umami taste. However, the study did not confirm the effect of these compounds on the umami taste of actual soy sauce. Moreover, the compounds' data measured by GC-MS were not likely enough for the aim of the study due to the limitation of measurable compounds by GC-MS.

The aim of the present study was to explore the compounds that affect the umami taste intensity in actual soy sauce by using metabolic profiling and sensory evaluation. We employed two analytical platforms, GC-MS and liquid chromatography−mass spectrometry (LC-MS), for the measurement of compounds. For selection of the candidate compounds related to the umami taste intensity, projection to latent structure (PLS) regression analysis (also known as partial least-squares) was conducted with both the metabolite data and the umami taste intensity data. Additionally, the effect of the candidate compound on the umami taste intensity in soy sauce by sensory evaluation was assessed. On the basis of a metabolic profiling approach, we show that the compound found to be statistically significant to umami taste intensity indeed affects the umami taste of soy sauce.

MATERIALS AND METHODS

Soy Sauce. Twenty-five soy sauce samples were used in this study. The countries of origin of the samples were China (samples 1−6 and 20−22), the United States (samples 7−9), and Japan (samples 10−19 and 23−25). The samples were preserved in a freezer at −30 °C prior to chemical analysis and sensory evaluation.

Chemicals. All chemicals used in this study were of analytical grade. Ribitol was used as internal standard, and pyridine was used as solvent; both were purchased from Wako Pure Chemical Industries (Osaka, Japan). The derivatization reagents methoxyamine hydrochloride and *N*-methyl-*N*-(trimethylsilyl)trifluoroacetamide (MSTFA) were purchased from Sigma-Aldrich (Milwaukee, WI, USA) and GL Science, Inc. (Tokyo, Japan), respectively.

N-(1-Deoxyfructos-1-yl)glutamic acid (Fru-Glu) for compound identification and sensory evaluation was synthesized from food grade glucose and glutamic acid following the literature.[19] Briefly, a mixture of D-glucose (Sanei Sucrochemical Co., Ltd., Aichi, Japan) and L-glutamic acid in a molar ratio of 40:1 in 50 mM phosphate buffer was heated at 60 °C for 3 days under reflux with vigorous stirring. The reaction mixture was purified by passage through a column of cation-exchange resin (DOWEX 50Wx8 200−400 mesh (H) cation exchange resin, Wako Pure Chemical Industries, Osaka, Japan) and ODS-type resin (Daisogel SP-120-40/60-ODS-B, DAISO Co., Ltd., Osaka, Japan). The purity of Fru-Glu (>90%) was confirmed by LC-MS using the same conditions as given below.

Sample Preparation of Soy Sauce for GC-MS Analysis. A previously reported method of sample preparation and derivatization for GC-MS analysis[18] was used with modifications. Soy sauce samples were diluted 10 times, and 20 μL of the diluted sample in a microtube was extracted with 1000 μL of $MeOH/H_2O/CHCl_3$ (5:2:2, v/v/v). Sixty microliters of 0.2 mg/mL ribitol was added to the mixture. The sample was centrifuged at 16000*g*, for 3 min at 4 °C, and then 900 μL of the supernatant was transferred to another microtube. Four hundred microliters of distilled water was added to the sample before mixing. Following centrifugation (16000*g*, 3 min at 4 °C), 900 μL of supernatant was transferred to another microtube and capped. The cap was subsequently pierced and the extract was evaporated, to remove methanol, in a centrifuge vacuum concentrator at room temperature for approximately 2 h. After evaporation, the extract was freeze-dried at room temperature overnight.

Sample Derivatization for GC-MS Analysis. For derivatization, 100 μL of methoxyamine hydrochloride in pyridine (20 mg/mL) was added to the above freeze-dried sample, and the mixture was incubated in a Thermomixer comfort (Eppendorf Ltd., Hamburg, Germany) at 30 °C for 90 min to induce the methoxylation reaction. Fifty microliters of *N*-methyl-*N*-(trimethylsilyl)trifluoroacetamide, the second derivatization agent, was added, and the mixture was incubated at 37 °C for 90 min to induce the silylation reaction. The samples were then used for GC-MS analysis. One microliter of sample was injected in split mode (25:1, v/v).

GC-MS Analysis. A previously reported GC-MS condition[18] was used with modifications. The GC-MS used in this study was a Shimadzu GCMSQP2010 Ultra (Shimadzu, Kyoto, Japan) equipped with a 30 m × 0.25 mm i.d. fused silica capillary column coated with 0.25 μm CP-SIL 8 CB low bleed/MS (Agilent Technologies, Palo Alto, CA, USA). The injection temperature was 230 °C. The carrier gas was helium at a linear velocity of 39 cm/s. The column temperature was held at 80 °C for 2 min isothermally and then raised at 15 °C/min to 330 °C and held for 6 min. The MS conditions were as follows: transfer line temperature, 250 °C; ion source temperature, 200 °C. Ions were generated at 70 eV with electron ionization and were recorded at 20 scan/s over the mass range m/z 85−500. Each sample was measured three times. A standard alkane mixture (C_8−C_{40}) was injected at the beginning and end of the analysis for tentative identification.

Sample Preparation of Soy Sauce for LC-MS Analysis. The sodium chloride (NaCl) level in soy sauce was reduced to below 1.0% by electrodialysis with a Micro Acilyzer S1 (Asahi Chemical Industry, Tokyo, Japan). One hundred microliters of soy sauce sample and 200 μL of methanol were mixed, and 10 μL of the mixed sample was diluted 10 times with distilled water. The sample was filtered before it was placed in a glass vial.

LC-MS Analysis. LC experiments were conducted using an HPLC system (Shimadzu, Japan) consisting of an LC-20AB binary pump, an SIL-20AC autosampler, and a CTO-20AC column oven. Chromatographic separation was achieved using a reversed-phase column (Discovery HS-F5 column, 150 mm × 2.1 mm, 3.5 μm, Sigma-Aldrich, Milwaukee, WI, USA) with a gradient elution with a mobile phase composed of eluents A (0.1% acetic acid in water, v/v) and B (0.1% acetic acid in acetonitrile, v/v). The mobile phase was consecutively programmed as follows: an isocratic elution of 2% B for the first 3 min, followed by linear gradient elutions of 2−50% B from 3 to 16 min and 50−100% B from 16 to 18 min. After the solvent composition of 100% B had been held from 18 to 24 min and then changed to 2% B for the next 10 min, the column was returned to its starting conditions. A 1 μL aliquot of the sample solution was injected onto the column. The flow rate was 0.2 mL/min, and the column temperature was maintained at 40 °C throughout the analysis. The compounds were detected by Shimadzu ion trap/time-of-flight hybrid mass spectrometry (IT-TOF/MS) equipped with an electrospray ionization source (ESI). The MS conditions were as follows: positive ion mode; electrospray voltage, 1.7

kB; CDL temperature, 200 °C; block heater temperature, 200 °C; nebulizing gas (N_2), 1.5 L/min; drying gas (N_2) pressure, 0.1 MPa. Mass spectra were acquired in the range of m/z 100−1000, and ion accumulation time was 200 ms. The calibration of mass accuracy was conducted every 24 h with standard. For quality control, the mixture of all samples was measured every 24 h during the measurement period. Each sample was measured three times.

In MS/MS analysis, MS/MS spectra were acquired in the m/z range of 80−500 under the following conditions: precursor ion isolation in the m/z range of 100−1000 (width, 3 Da); ion accumulation time, 50 ms; tolerance m/z, 0.05; repeat = 2; and CID energy, 50%.

In quantitative analysis, we used synthesized Fru-Glu for external standard and the LC-MS system under the same conditions as above.

Data Processing. A previously reported method for data processing concluding tentative peak identification[18] was used with modifications. MS data obtained by GC-MS were exported in the netCDF format. Peak detection and alignment were performed by MetAlign software (Wageningen UR, The Netherlands; freely available at http://www.pri.wur.nl/UK/products/MetAlign/).[20] The resulting data were exported in the CSV-format file. Then, the CSV-format file was imported by the AIoutput software[21] for tentative peak identification and construction of a data matrix. In tentative peak identification, retention indices of the eluted compounds were calculated on the basis of the standard alkane mixture. Then, by comparing the retention indices and unique mass spectra with our in-house reference library, tentative identifications were obtained. In the construction of the data matrix, spectra were normalized manually by adjusting the peak intensity against the ribitol internal standard before an organized data matrix was generated.

The peak detection and alignment of MS data obtained by LC-MS were performed by Profile solution version 1.0 (Shimadzu). The peak integration parameters were set as default, and the peak alignment parameters were as follows: ion m/z tolerance, 5 mDa; retention time tolerance, 0.5 min; peak intensity threshold, 5000. The resulting data were exported in the CSV-format file. To reduce the risk of ghost peaks, peaks having maximum intensity and minimum relative standard deviation among samples of >300,000 and <15% (n = 3), respectively, were selected for statistics.

Sensory Evaluation of the Umami Taste Intensity of Soy Sauce. Quantitative data of the umami taste intensity were acquired by 13 external panelists who had previous experience in quantity description analysis.[18] Twenty milliliters of each sample in randomized numbered cups covered with a plastic lid were presented to the panelists in random order. Panelists tasted 0.2 mL of the sample and marked the umami taste intensity on a 12 cm line scale. Each sample was evaluated three times.

To assess the influence of Fru-Glu on the umami taste intensity of soy sauce, we evaluated soy sauce samples with or without additional Fru-Glu using 10 in-house panelists who could discriminate between 11.8 and 14.3 mM MSG solutions. In case of the comparison between the two samples, the order effect may be the bias for panelists when the control and test sample are fixed. To remove the order effect, the 10 panelists were randomly divided into two groups of five. In group 1, the Japanese *koikuchi* soy sauce (sample 10) with additional Fru-Glu (5 or 10 mM) was designated as the test sample and the same soy sauce without additional Fru-Glu acted as the control. In group 2, the designation was reversed in which the test sample and control used were the soy sauce without additional Fru-Glu and soy sauce with additional Fru-Glu, respectively. Panelists were not informed which sample was the control.

For both groups, the sensory evaluation for the relative intensity of umami taste was carried out by using a nine-point rating scale (from −4, "very weak compared to the control", to 4, "very strong compared to the control"). Each sample was evaluated three times. In the case of group 2, assuming that a higher umami taste intensity in samples with additional Fru-Glu was observed compared to that without additional Fru-Glu, the sample was rated as "−2, weak". Also, the rating was reversed (i.e., −2 becomes +2,) when counting results.

The same evaluation method was used for the addition of glutamic acid.

Statistics. Multivariate analysis was performed. One-way analysis of variance (ANOVA) and PLS regression analysis were carried out with Excel 2007 and SIMCA-P software (version 12.0, Umetrics, Umeå, Sweden), respectively. For data pretreatment, autoscaling was used so that each variable had a unit variance and zero mean. The number of latent factors (PLS components) in the PLS model was determined by computing the optimum number at the balance between R^2 and Q^2 with the SIMCA-P software algorithm. After fitting the model, R^2 and Q^2 were calculated as the index of model quality. R^2 is the correlation coefficient between actual response variable and predictive value obtained from PLS. Q^2 is an index that reflects the predictive ability of the model.

After construction of the PLS model, the variable importance in the projection (VIP) of each explanatory variable was calculated to select the candidate umami compound. The VIP_{Ak} value of the kth explanatory variable in K variables of PLS with component A was calculated using the equation[22]

$$\mathrm{VIP}_{Ak} = \sqrt{\left(\sum_{A}^{a=1} (w_{ak}^2 \times (\mathrm{SSY}_{a-1} - \mathrm{SSY}_a)) \times \frac{K}{(\mathrm{SSY}_0 - \mathrm{SSY}_A)}\right)}$$

w_{ak} is the PLS weight of the kth variable. SSY_a indicates the amount of Y variance explained by each PLS component, a. The VIP value indicates the contribution of each explanatory variable to the model.[23] The "VIP scores >1" rule is generally used as the criterion for important variable selection.[24]

RESULTS AND DISCUSSION

Metabolite Data Obtained by GC-MS and LC-MS. We employed two analytical platforms, GC-MS and LC-MS, for the measurement of compounds in 25 samples of soy sauce. GC-MS was used to measure low hydrophilic nonvolatiles such as sugar or amino acid with sample derivatization, whereas LC-MS was expected to detect the compounds that are difficult to volatilize with derivatization such as peptides and Maillard compounds. Using the two platforms made it possible to detect a broad range of physical and chemical characteristics of compounds in soy sauce. From the 122 peaks detected in the GC-MS analysis, 68 peaks were tentatively identified by comparing the retention indices and unique mass spectra with our in-house reference library using AIoutput 2.0. The tentatively identified compounds included 26 kinds of amino acids, 23 kinds of sugars or sugar alcohols, 8 kinds of organic acids, 4 kinds of amines, and 7 kinds of other compounds (Supporting Information Table S1). On the other hand, 305 peaks were detected with the positive mode of LC-MS. The m/z range of these peaks was from 110.008 to 671.200. These results suggested that a wide range of compounds were detected by GC-MS and LC-MS analyses. We used the data obtained from LC-MS for explanatory variables of PLS regression analysis before peak identification because identification of all peaks was difficult using only accurate mass. Then, the selected peaks based on VIP values obtained via PLS (described in the succeeding section) were identified by comparison with the MS/MS spectrum and retention time of authentic standard.

Umami Intensity of Soy Sauce by Sensory Evaluation. The umami taste intensity of each soy sauce sample was obtained using sensory evaluation (Figure 1). The highest umami taste intensity was 4.01, and the lowest was 2.79. For evaluation of the significant differences among samples, we conducted one-way ANOVA. The F value was 1.53, and p value was <0.001. Because the data of the umami taste intensity had highly significant differences, we concluded that it is appropriate for the response variable of PLS regression analysis.

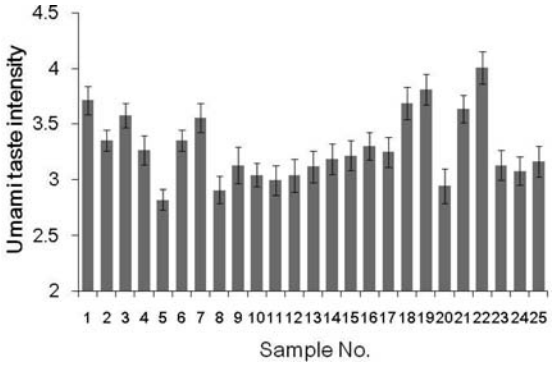

Figure 1. Umami taste intensities of each soy sauce sample. Sensory evaluation was performed by 12 experts using a line scale. Samples 5 and 22 exhibit the weakest and strongest umami taste intensities, respectively, among 25 tested samples. Values are the mean ± standard error.

Metabolic Profiling with PLS Regression Analysis. PLS regression analysis, a supervised multivariate data analysis, summarizes the explanatory variables of the multivariate data into new variables (PLS factors) that maximally correlate with response variables.[25] PLS is often used in metabolomics research due to its ability to cope with a large number of variables and multicollinearity.[26] In addition, the VIP value obtained via PLS is used for the estimation of the relevant explanatory variables to the response variable.[20] To find the relationship between the metabolites data and the umami taste intensity, we conducted PLS regression analysis using the metabolite data obtained from GC-MS and LC-MS as the explanatory variables and the umami taste intensity obtained the sensory evaluation as the response variable. The predicted versus measured figures of the umami taste intensity are shown in Figure 2. R^2 (proportion of explained variance) and Q^2

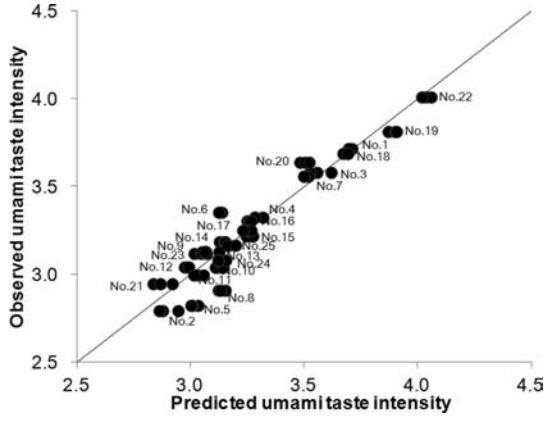

Figure 2. Relationships between predicted and measured umami taste intensity based on projection to latent structure (PLS) model. The numbers of explatanory variables and response variables were 427 and 1, respectively. PLS component was 4. R^2 and Q^2 were 0.914 and 0.877, respectively.

(proportion of predicted variance), which are the diagnostic indices of model quality, were 0.914 and 0.877, respectively. Previously, it has been reported that the accuracy of the prediction model of PLS constructed with only GC-MS is enough.[18] When GC-MS data obtained in this study were used for PLS, R^2 and Q^2 were 0.899 and 0.821, respectively. On the other hand, R^2 and Q^2 from the LC-MS data were 0.909 and 0.816, respectively. Thus, this indicated that the model using both sets of data had the highest quality. In the VIP analysis, the higher quality PLS model was preferred for the relevant variable selection.

Selection of Candidates of Umami Compound Using VIP Value. The explanatory variables were assessed by VIP values for the inference of the compounds that are likely relevant to the umami taste intensity. VIP is an index of the effect of every explanatory variable on the response variable in the model and is used to select the important metabolites in various metabolomics-based research.[26] Whether the effect on response variable is positive or negative was judged by the regression coefficient of each explanatory variable. The compounds with positive coefficients having larger VIP values than glutamic acid (2.14) are shown in Table 1. In the PLS

Table 1. Compounds Selected by Variable Importance in the Projection (VIP) Analysis

RT[a] (min)	m/z	compound	VIP	coefficient[b]	platform
2.20	310.113	*N*-(1-deoxyfructos-1-yl)glutamic acid	2.35	0.045	LC-MS
9.85	174[c]	unknown	2.25	0.036	GC-MS
2.07	349.053	inosinic acid	2.23	0.047	LC-MS
9.47	174[c]	4-aminobutyric acid	2.15	0.044	GC-MS
10.15	246[c]	glutamic acid	2.14	0.038	GC-MS

[a]RT, retention time. [b]Regression coefficient of each compound. [c]The highest fragment mass of peak detected by GC-MS.

model construction, compounds with VIP values >1 were considered to be significant.[24] These compounds in Table 1 have VIP values >1; thus, these compounds are significant explanatory variables for the prediction of the response variable. In the following discussion, we focused on four compounds that had VIP values larger than that of glutamic acid.

In Table 1, both Fru-Glu and inosinic acid were identified using information on both the retention time and MS/MS spectra of authentic standards obtained by LC-MS. Fru-Glu was detected as m/z 310.113 ion and a retention time of 2.20 min. Figure 3 shows the MS/MS spectrum of Fru-Glu obtained by IT-TOF/MS. The m/z 148.06 product ion contained in the mass spectrum corresponded to glutamic acid H^+ adduct. The neutral loss from precursor ion (m/z 310.113) is m/z 162.05 and corresponds to the molecular weight of glucose without one water molecule. Inosinic acid was detected as the m/z

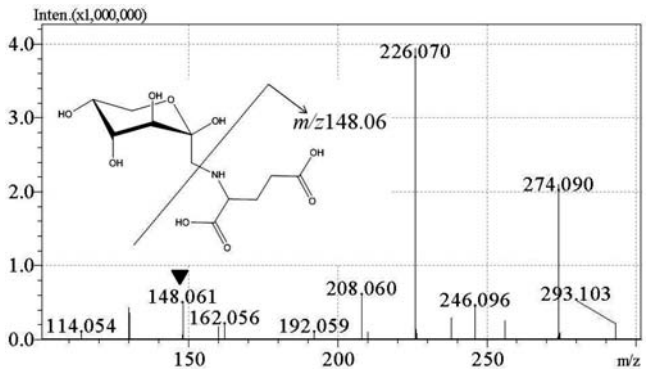

Figure 3. MS/MS spectrum of *N*-(1-deoxyfructos-1-yl)glutamic acid obtained in the positive ionization mode. Triangle symbols indicate m/z 148.061 corresponding to glutamic acid H^+ adduct.

dx.doi.org/10.1021/jf501173r | J. Agric. Food Chem. 2014, 62, 7317−7322

349.053 ion and retention time of 2.07 min by LC-MS via MS/MS analysis (data not shown).

The compound with the largest VIP value was Fru-Glu. It was reported that the umami taste intensity of Fru-Glu was similar to that of MSG in water or NaCl solution,[27] and Fru-Glu was detected in the wheat gluten hydrolysate.[28] However, there has been no report of the umami of Fru-Glu and its taste property in soy sauce.

The compound with the second largest VIP detected by GC-MS could not be identified using our in-house library.

The third largest VIP value was 2.23 for inosinic acid, known as a umami enhancer of MSG.[29] In naturally fermented soy sauce, inosinic acid is not detected because the phosphatase enzymes made by *kouji* mold degrade the inosinic acid in natural soy sauce.[30] Also, some soy sauce products have inosinic acid added as a food additive for umami enhancement after fermentation.[31]

The compound with the fourth largest VIP detected by GC-MS was 4-aminobutyric acid. 4-Aminobutyric acid, which has a VIP value was close to that of glutamic acid, has been reported to give a weak sour taste and a mouth-drying sensation in aqueous solution.[32] It is unclear whether 4-aminobutyric acid has an effect on the umami taste intensity of soy sauce.

This metabolic profiling approach helps in the selection of candidate compounds from a huge number of variables. However, this approach could not substantiate the effect for the umami taste intensity of "actual" soy sauce. We therefore evaluated the effect of Fru-Glu addition, the compound with the highest VIP value, on the umami taste intensity of soy sauce.

Effect of Fru-Glu on the Umami Taste Intensity of Soy Sauce. Using sensory evaluation, we assessed the effect of Fru-Glu addition, the compound with the largest VIP value, on the umami taste intensity of soy sauce. In sensory evaluation, panelists compared the control sample (Japanese *koikuchi* soy sauce (sample 10) without additional Fru-Glu) with the test sample containing the same soy sauce with additional Fru-Glu.

Before sensory analysis, the concentration of Fru-Glu was measured in all samples. We found that the concentration of Fru-Glu in sample 10 was 0.7 mM, and the highest concentration among the samples was 5.5 mM (Figure 4). The additional Fru-Glu concentrations were 5 and 10 mM. The same evaluation method was conducted using glutamic acid. The result of sensory evaluation is shown in Figure 5. The

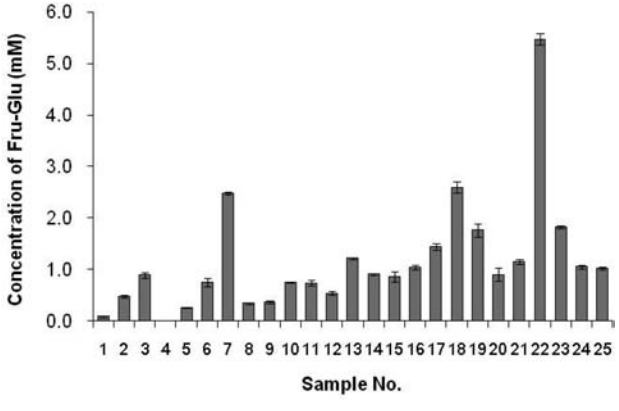

Figure 4. Concentration of *N*-(1-deoxyfructos-1-yl)glutamic acid in each soy sauce sample. Values are the mean ± standard deviation in three replications.

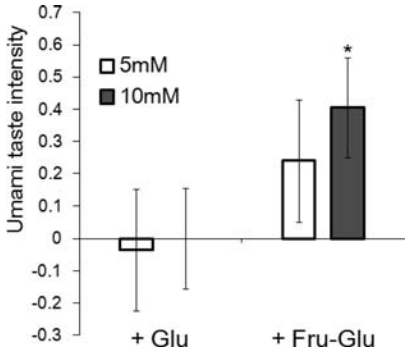

Figure 5. Results of the sensory evaluation of *N*-(1-deoxyfructos-1-yl)glutamic acid (Fru-Glu) in soy sauce. The umami taste intensity was evaluated by comparison between soy sauce with the addition of Fru-Glu and without the addition (control) of Fru-Glu. Sample 10 was used for the evaluation. The 9-point relative categorical scale (comparing control sample −4, "very weak", to 4, "very strong") was used. Intensity was evaluated by 10 selected panelists. The same evaluation method was used for the addition of glutamic acid (Glu). Values are the mean ± standard error. (∗) $p < 0.05$ (sample t test against 0).

umami taste intensity tended to increase with higher Fru-Glu concentration, and there was a significant difference between the sample with added 10 mM Fru-Glu and control sample (one-sample t test $p < 0.05$). On the other hand, there was no significant difference in the umami taste intensity in samples with added 5 and 10 mM glutamic acid. These results indicated that Fru-Glu increased the umami taste intensity of soy sauce at a lower concentration than glutamic acid even though the taste threshold of both compounds in aqueous solutions is the same.[24] Consequently, the evaluation of the taste property of compounds in complex systems such as food may differ from that of model experiment due to the effect of taste interactions such as a synergy effect. Furthermore, these results suggested that Fru-Glu has a stronger synergistic effect than glutamic acid in soy sauce. Glutamic acid did not affect the umami taste intensity at this concentration even though it had a high VIP value. Considering the discrimination threshold of MSG in *koikuchi* soy sauce,[6] a concentration >10 mM is needed for increasing the umami taste intensity of soy sauce. We therefore conclude that to enhance umami taste, at low concentration, Fru-Glu is more essential than glutamic acid in soy sauce. To the best our knowledge, there is no report on the relationship between Fru-Glu and umami in soy sauce.

In summary, the present study explored the compounds related to the umami taste intensity by a metabolic profiling approach. Using this approach, Fru-Glu was found to increase the umami taste intensity of soy sauce more effectively than glutamic acid, the key umami compound. The advantages of the metabolic profiling approach over traditional methods such as sensory-guided fractionation are as follows: (1) metabolic profiling is able to cover a wide variety samples because it is not necessary to prepare fractions; (2) compounds that are difficult to separate from other compounds can also be evaluated. However, the result of statistical analysis such as PLS does not directly substantiate the contribution of each compound to taste; thus, validation of the effect of compounds on taste using sensory evaluation is necessary. The combination of metabolic profiling and sensory evaluation is a useful tool for exploring the compounds that affect taste and may contribute to the

quality assessment or improvement of soy sauce and other foods.

■ ASSOCIATED CONTENT

Supporting Information

Table S1. This material is available free of charge via the Internet at http://pubs.acs.org.

■ AUTHOR INFORMATION

Corresponding Author

*(E.F.) Phone: +81-6-6879-7424. Fax: +81-6-6879-7424. E-mail: fukusaki@bio.eng.osaka-u.ac.jp.

Notes

The authors declare no competing financial interest.

The study represents a portion of the dissertation submitted by K.S. to Osaka University in partial fulfillment of the requirement for his Ph.D.

■ ABBREVIATIONS USED

GC-MS, gas chromatography−mass spectrometry; Fru-Glu, *N*-(1-deoxyfructos-1-yl)glutamic acid; Glu, glutamic acid; LC-MS, liquid chromatography−mass spectrometry; MTSFA, methyl-*N*-(trimethylsilyl)trifluoroacetamide; PLS, projection to latent structures; VIP, variable importance for the projection

■ REFERENCES

(1) Kataoka, T. Functional effects of Japanese style fermented soy sauce (Shoyu) and its components. *J. Biosci. Bioeng.* **2005**, *100* (3), 227−234.

(2) Sun, S. Y.; Jiang, W. G.; Zhao, Y. P. Profile of volatile compounds in 12 Chinese soy sauces produced by a high-salt-diluted state fermentation. *J. Inst. Brew.* **2010**, *116* (3), 316−328.

(3) Lioe, H. N.; Selamat, J.; Yasuda, M. Soy sauce and its umami taste: a link from the past to current situation. *J. Food Sci.* **2010**, *75* (3), 71−76.

(4) Lioe, H. N.; Apriyantono, A.; Takara, K.; Wada, K.; Naoki, H.; Yasuda, M. Low molecular weight compounds responsible for savory taste of Indonesian soy sauce. *J. Agric. Food Chem.* **2004**, *52*, 5950−5956.

(5) Lioe, H. N.; Takara, K.; Yasuda, M. Evaluation of peptide contribution to the intense umami taste of Japanese soy sauces. *J. Food Sci.* **2006**, *71* (3), 277−283.

(6) Imamura, M.; Sato, T.; Hatamoto, O. Effects on thresholds for sweet and umami tastants in soy sauce (in Japanese). *Nippon Shokuhin Kagaku Kogaku Kaishi* **2009**, *56* (7), 384−393.

(7) Lioe, H. N.; Apriyantono, A.; Takara, K.; Wada, K.; Yasuda, M. Umami taste enhancement of MSG/NaCl mixtures by subthreshold L-α-aromatic amino acids. *J. Food Sci.* **2005**, *70*, 401−405.

(8) Oka, S.; Nagata, K. Isolation and characterization of neutral peptides in soy sauce. *Agric. Biol. Chem.* **1974**, *38*, 1185−1194.

(9) Kaneko, S.; Kumazawa, K.; Nishimura, O. Isolation and identification of the umami enhancing compounds in Japanese soy sauce. *Biosci., Biotechnol., Biochem.* **2011**, *75* (7), 1275−1282.

(10) Lioe, H. N.; Wada, K.; Aoki, T.; Yasuda, M. Chemical and sensory characteristics of low molecular weight fractions obtained from three types of Japanese soy sauce (shoyu) − *koikuchi*, *tamari* and *shiro shoyu*. *Food Chem.* **2007**, *100*, 1669−1677.

(11) Keast, R. S. J.; Breslin, P. A. S. An overview of binary taste-taste interactions. *Food Qual. Pref.* **2002**, *14*, 111−124.

(12) Wishart, S. D. Metabolomics: applications to food science and nutrition research. *Trends Food Sci. Technol.* **2008**, *19*, 482−493.

(13) Cevallos-Cevallos, J. M.; Reyes-De-Corcuera, J. J.; Etxeberria, E.; Danyluk, M. D.; Rodrick, G. E. Metabolomic analysis in food science: a review. *Trends Food Sci. Technol.* **2009**, *20*, 557−566.

(14) Pongsuwan, W.; Fukusaki, E.; Bamba, T.; Yonetani, T.; Yamahara, T.; Kobayashi, A. Prediction of Japanese green tea ranking by gas chromatography/ mass spectrometry-based hydrophilic. *J. Agric. Food Chem.* **2007**, *55*, 231−236.

(15) Thissen, U.; Coulier, L.; Overkamp, K. M.; Jetten, J.; van der Werf, B. J. C.; van de Ven, T.; van der Werf, M. J. A proper metabolomics strategy supports efficient food quality improvement: a case study on tomato sensory properties. *Food Qual. Pref.* **2011**, *22*, 499−506.

(16) Ochi, H.; Naito, H.; Iwatsuki, K.; Bamba, T.; Fukusaki, E. Metabolomics-based component profiling of hard and semi-hard natural cheeses with gas chromatography/time-of-flight-mass spectrometry, and its application to sensory predictive modeling. *J. Biosci. Bioeng.* **2012**, *113* (6), 751−758.

(17) Sugimoto, M.; Koseki, T.; Hirayama, A.; Abe, S.; Sano, T.; Tomita, M.; Soga, T. Correlation between sensory evaluation scores of Japanese sake and metabolome profiles. *J. Agric. Food Chem.* **2010**, *58*, 374−383.

(18) Yamamoto, S.; Bamba, T.; Sano, A.; Kodama, Y.; Imamura, M.; Obata, A.; Fukusaki, E. Metabolite profiling of soy sauce using gas chromatography with time-of-flight mass spectrometry and analysis of correlation with quantitative descriptive analysis. *J. Biosci. Bioeng.* **2012**, *114* (2), 170−175.

(19) Roper, H.; Roper, S.; Heyns, K.; Meyer, B. NMR spectroscopy of *N*-(1-deoxy-D-fructos-1-yl)-L-amino acids ("fructose-amino acids"). *Carbohydr. Res.* **1983**, *116*, 183−195.

(20) Lommen, A. MetAlign: interface-driven, versatile metabolomics tool for hyphenated full-scan mass spectrometry data preprocessing. *Anal. Chem.* **2009**, *81*, 3079−3086.

(21) Tsugawa, H.; Tsujimoto, Y.; Arita, M.; Bamba, T.; Fukusaki, E. GC-MS based metabolomics: development of a data mining system for metabolite identification by using soft independent modeling of class analogy (SIMCA). *BMC Bioinf.* **2011**, *12*, 131.

(22) Eriksson, L.; Johansson, E.; Kettaneh-Wold, N.; Wold, S. *Statistical Appendix in Multi- and Megavariate Data Analysis − Principle and Applications*; Umetrics AB: Umea, Sweden, 2001; 504 pp.

(23) Wold, S.; Johansson, E.; Cocchi, M. *3D QSAR in Drug Design; Theory, Methods, and Applications*. ESCOM: Leiden, The Netherlands, 1993; pp 523−550.

(24) Afanador, N. L.; Tran, T. N.; Buydens, L. M. C. Use of the bootstrap and permutation methods for a more robust variable importance in the projection metric for partial least squares regression. *Anal. Chem. Acta* **2013**, *768*, 49−56.

(25) Wold, S.; Sjöström, M.; Eriksson, L. PLS-regression: a basic tool of chemometrics. *Intell. Lab. Syst.* **2011**, *58*, 109−130.

(26) Fonville, J. M.; Richards, S. E.; Barton, R. H.; Boulange, C. L.; Ebbels, T. M. D.; Nicholson, J. K.; Holmes, E.; Dumas, M. E. The evolution of partial least squares models and related chemometric approaches in metabonomics and metabolic phenotyping. *J. Chemom.* **2010**, *24*, 636−649.

(27) Beksan, E.; Schieberle, P.; Robert, F.; Blank, I.; Fay, L. B.; Schlichtherle-Cerny, H.; Hofmann, T. Synthesis and sensory characterization of novel umami-tasting glutamate glycoconjugates. *J. Agric. Food Chem.* **2003**, *51*, 5428−5436.

(28) Schlichtherle-Cerny, H.; Affolter, M.; Cerny, C. Hydrophilic interaction liquid chromatography coupled to electrospray mass spectrometry of small polar compounds in food analysis. *Anal. Chem.* **2003**, *75*, 2349−2354.

(29) Yamaguchi, S. The synergistic taste effect of monosodium glutamate and disodium 5′-inosinate. *J. Food Sci.* **1967**, *32*, 473−478.

(30) Kim, J.; Lee, Y. A study of chemical characteristics of soy sauce and mixed soy sauce: chemical characteristics of soy sauce. *Eur. Food Res. Technol.* **2008**, *227*, 933−944.

(31) Yue, X. Advances in the soy sauce industry in China. *J. Ferment. Bioeng.* **1990**, *70*, 434−439.

(32) Rotzoll, N.; Dunkel, A.; Hofmann, T. Activity-guided identification of (*S*)-malic acid 1-*O*-D-glucopyranoside (morelid) and γ-aminobutyric acid as contributors to umami taste and mouthdrying oral sensation of morel mushrooms (*Morchella deliciosa* Fr.). *J. Agric. Food Chem.* **2005**, *53*, 4149−4156.

and Alan Seawright. Recognizing many of the commonalities between the two countries in livestock poisoning problems, he proposed a Joint U.S.–Australian Symposium on Poisonous Plants, which was held in Logan, Utah, in 1977. A reciprocal meeting took place in Brisbane, Australia, in 1984. At this meeting it was noted that a number of participants were from countries other than the United States or Australia, and a subsequent meeting, held once again in Logan in 1989, was titled the 3rd International Symposium on Poisonous Plants. The fourth such meeting was held in Fremantle, Western Australia, in 1993, and the Chair of that meeting, Dr. Peter Dorling, proposed that the meetings henceforth adopt the name of International Symposium on Poisonous Plants, codified as ISOPP, followed by the meeting number. Subsequent meetings have been held in San Angelo, Texas, in 1997 (ISOPP5); Glasgow, Scotland, in 2001 (ISOPP6); Logan, Utah, in 2005 (ISOPP7); and João Pessoa, Brazil, in 2009 (ISOPP8). The broadening international scope of these symposia has shown that other countries have gone or are going through a progression of poisonous plant research analogous to that experienced by the United States and Australia, albeit at a much more rapid pace. This consists of documentation of poisoning occurrences, identification of the plant and animal species involved, syndromes of toxicity, and ultimately isolation and structural identification of the specific toxins. It is noteworthy that the ISOPP meetings have led to international collaborations, such as that between the research group of Dr. Franklin Riet Correa in Brazil and chemists at the PPRL in Logan, Utah, currently leading to the identification of new plant toxins.

In July 2013, the 9th International Symposium on Poisonous Plants (ISOPP9) was held under the sponsorship of Inner Mongolia Agricultural University and the USDA/ARS Poisonous Plant Research Laboratory at the West Campus of Inner Mongolia Agricultural University in Hohhot, the capital of the Inner Mongolia Autonomous Region of China. After a series of symposia held on the continents of North and South America, Australia, and Europe over more than 30 years, this was the first time that an ISOPP meeting had been held in Asia, a very appropriate venue because the history of poisonous plants in China is well established. It is estimated that there are more than 900 such plant species, belonging to about 100 plant families, affecting livestock. It is noteworthy that many of these species are used in traditional Chinese medicine (TCM). In Inner Mongolia alone, where livestock production is a major economic enterprise, 270 poisonous plant species encompassing 57 plant families have been identified on the extensive grasslands characteristic of the region. The major hazards to grazing livestock are the widespread species *Oxytropis glabra*, *Stellera chamaejasme*, and *Datura stramonium*. *O. glabra* is a member of one of the two plant genera (*Astragalus* and *Oxytropis*) of which certain species have been identified as responsible for locoweed toxicity in the United States, illustrating the common interests in poisonous plant species in disparate parts of the world. In fact, the endophytic toxin, swainsonine, first isolated from *Swainsona* spp. in Australia[15] and subsequently shown to be present in *Astragalus* and *Oxytropis* locoweeds in the United States,[16,17] has recently been identified in *O. glabra* and other Chinese *Astragalus* and *Oxytropis* species.[18] In some areas of western Inner Mongolia 15–30% of the grassland is contaminated by *O. glabra*, and the direct economic loss due to this plant alone has been estimated at RMB 3 million per year (U.S. $0.5 million/year). Its effect on livestock in the region is regarded as being on a par with sandstorms and soil salinization, all three of which can be catastrophic to producers.

Other poisonous plant species, such as *Stellera chamaejasme* (Thymelaeaceae) are unique to China and surrounding regions, or specifically Inner Mongolia. These species have been extensively described and their effects on livestock defined. On the other hand, the role of chemistry in isolating the toxins, elucidating their structures, and determining their mode of action has not become fully integrated into poisonous plant research process. This collection of papers from the ISOPP9 meeting focuses on research that has taken advantage of modern chemistry techniques to fully understand the deleterious nature of plant toxins on animals and perhaps provide structural leads in areas such as pest control, invasive plant management, and new pharmaceuticals. It is anticipated that the presentations at the very successful Hohhot meeting will provide opportunities for collaboration not only within China but also internationally, so that subsequent ISOPP meetings will reveal novel chemistry. A return to Brisbane, Australia, in 2016 is planned for the ISOPP10 meeting, 32 years after the previous meeting there.

Russell J. Molyneux*[,†]
Kip E. Panter[‡]
Mengli Zhao[§]

[†]Daniel K. Inouye College of Pharmacy, University of Hawaii at Hilo, 34 Rainbow Drive, Hilo, Hawaii 96720, United States

[‡]Poisonous Plant Research Laboratory, Agricultural Research Service, U.S. Department of Agriculture, 1150 East 1400 North, Logan, Utah 84341, United States

[§]Inner Mongolia Agricultural University, 306 Zhaowuda Road, Hohhot, Inner Mongolia, People's Republic of China 010018

AUTHOR INFORMATION

Corresponding Author

*(R.J.M.) Phone: (808) 933-1661. Fax: (808) 963-2974. E-mail: molyneux@hawaii.edu.

Notes

The authors declare no competing financial interest.

REFERENCES

(1) Marsh, C. D. *The Locoweed Disease of the Plains*; Bureau of Animal Industry Bulletin 112; U.S. Department of Agriculture: Washington, DC, USA, 1909; 130 pp.

(2) Marsh, C. D.; Clawson, A. B.; Marsh, H. *Larkspur Poisoning of Livestock*; Bureau of Animal Industry Bulletin 365; U.S. Department of Agriculture: Washington, DC, USA, 1916; 91 pp.

(3) Marsh, C. D. *Stock-Poisoning Plants of the Range*; Bureau of Animal Industry Bulletin 1245; U.S. Department of Agriculture: Washington, DC, USA, 1924; 75pp.

(4) Keeler, R. F. Teratogenic compounds of *Veratrum californicum* (Durand). VI. The structure of cyclopamine. *Phytochemistry* **1969**, *8*, 223–225.

(5) Keeler, R. F. Cyclopamine and related steroidal alkaloid teratogens: their occurrence, structural relationship, and biologic effects. *Lipids* **1978**, *13*, 708–715.

(6) Keeler, R. F. Lupin alkaloids from teratogenic and nonteratogenic lupins. III. Identification of anagyrine as the probable teratogen by feeding trials. *J. Toxicol. Environ. Health* **1976**, *1*, 887–889.

(7) Keeler, R. F.; Balls, L. D. Teratogenic effects in cattle of *Conium maculatum* and *Conium* alkaloids and analogs. *Clin. Toxicol.* **1978**, *12*, 49−64.
(8) Keeler, R. F.; Balls, L. D.; Panter, K. E. Teratogenic effects of *Nicotiana glauca* and concentration of anabasine, the suspect teratogen in plants. *Cornell Vet.* **1981**, *71*, 47−53.
(9) Lee, S. T.; Cook, D.; Panter, K. E.; Gardner, D. R.; Ralphs, M. H.; Motteram, E. S.; Pfister, J. A.; Gay, C. C. Lupine induced "crooked calf disease" in Washington and Oregon: identification of the alkaloid profiles in *Lupinus sulfureus*, *Lupinus leucophyllus*, and *Lupinus sericeus*. *J. Agric. Food Chem.* **2007**, *55*, 10649−10655.
(10) Bull, L. B.; Culvenor, C. C. J.; Dick, A. T. *The Pyrrolizidine Alkaloids: Their Chemistry, Pathogenicity and Other Biological Properties*; North-Holland Publishing: Amsterdam, The Netherlands, 1968; 293 pp.
(11) Burrows, G. E.; Tyrl, R. J. *Toxic Plants of North America*, 2nd ed.; Wiley-Blackwell: Ames, IA, USA, 2013; 1390 pp.
(12) McKenzie, R. *Australia's Poisonous Plants, Fungi and Cyanobacteria: A Guide to Species of Medical and Veterinary Importance*; CSIRO Publishing: Melbourne, Australia, 2012; 976 pp.
(13) Kellerman, T. S.; Coetzer, J. A. W.; Naude, T. W.; Botha, C. J. *Plant Poisonings and Mycotoxicoses of Livestock in South Africa*, 2nd ed.; Oxford University Press Southern Africa: Cape Town, South Africa, 2005; 256 pp.
(14) Tokarnia, C. H.; Dobereiner, J.; Peixoto, P. V. *Plantas Toxicas do Brasil*; Editoria Helianthus: Rio de Janeiro, Brazil, 2000; 310 pp.
(15) Colegate, S. M.; Dorling, P. R.; Huxtable, C. R. A spectroscopic investigation of swainsonine: an α-mannosidase inhibitor isolated from *Swainsona canescens*. *Aust. J. Chem.* **1979**, *32*, 2257−2264.
(16) Molyneux, R. J.; James, L. F. Loco intoxication: indolizidine alkaloids of spotted locoweed (*Astragalus lentiginosus*). *Science* **1982**, *216*, 190−191.
(17) Grum, D. S.; Cook, D.; Gardner, D. R.; Roper, J. M.; Pfister, J. A.; Ralphs, M. H. Influence of seed endophyte amounts on swainsonine concentrations in *Astragalus* and *Oxytropis* locoweeds. *J. Agric. Food Chem.* **2012**, *60*, 8083−8089.
(18) Yu, Y.; Zhao, Q.; Wang, J.; Wang, J.; Wang, Y.; Song, Y.; Geng, G.; Li, Q. Swainsonine-producing fungal endophytes from major locoweed species in China. *Toxicon* **2010**, *56*, 330−338.

Table 1. Summary of the *Astragalus*, *Oxytropis*, and *Swainsona* Species Suspected of Causing Locoism and/or Reported To Have Swainsonine, Swainsonine Detection Methods, the Associated *Undifilum* Endophyte (If Known), and Endophyte Detection Methods

				detection		
taxa	country	swainsonine detection	endophyte	culture	PCR	refs
A. allochrous	USA, Mexico	enzyme				14, 15
A. amphioxys	USA	LC-MS	*Undifilum* sp.		x	16
A. asymmetricus	USA	TLC				17
A. bisulcatus	USA	TLC, enzyme				14, 15, 17
A. didymocarpus	USA	TLC				17
A. drummondii	USA	enzyme				14, 15
A. emoryanus	USA	TLC, enzyme, MS				17, 18
A. flavus	USA	TLC				17
A. humistratus	USA					19
A. lentiginosus	USA, Mexico	TLC, LC-MS	*Undifilum fulvum*	x	x	16, 17
A. lonchocarpus	USA	enzyme				14, 15
A. missouriensis	USA	enzyme				14, 15
A. mollissimus	USA, Mexico	TLC, enzyme, LC-MS	*Undifilum cinerum*	x	x	14−17
A. nothoxys	USA, Mexico					20
A. oxyphysus	USA	TLC				17
A. pehuenches	Argentina, Chile	TLC				21
A. praelongus	USA	TLC/enzyme				14, 15, 17
A. pubentissimus	USA	LC-MS	*Undifilum* sp.	x	x	16
A. purshii	USA					19
A. pycnostachyus	USA	TLC				17
A. strictus	China	GC-MS	*Undifilum oxytropis*	x		22
A. tephrodes	USA	enzyme				14, 15
A. thurberi	USA	enzyme				14, 15
A. variabilis	China	GC-MS, LC-MS	*Undifilum oxytropis*	x	x	22, 23
A. wootoni	USA, Mexico	TLC, LC-MS	*Undifilum* sp.	x	x	16, 17
O. besseyi	USA					20
O. campestris	USA, Canada					20
O. glabra	China	GC-MS, LC-MS	*Undifilum oxytropis*	x	x	22, 23
O. glacialis	China	GC-MS	*Undifilum oxytropis*	x		22
O. kansuensis	China	GC-MS	*Undifilum oxytropis*	x		22
O. lambertii	USA, Canada	TLC, enzyme, GC-MS, LC-MS	*Undifilum oxytropis*	x	x	14, 15, 17, 24
O. ochrocephala	China	GC-MS	*Undifilum oxytropis*	x		22
O. sericea	USA, Canada	TLC, enzyme, LC-MS	*Undifilum oxytropis*	x	x	14−17, 24
O. sericopetala	China	GC-MS	*Undifilum oxytropis*	x		22
S. canescens	Australia	GC-FID, LC-MS	*Undifilum* sp.	x	x	25, 37
S. galegifolia	Australia	GC-FID				25
S. greyana	Australia	GC-FID				25

the presence of swainsonine without this verification as the other methods are preliminary and not definitive.

Swainsonine concentrations in locoweeds vary among species, varieties, and populations, often ranging from not detected to >0.2%.[16,24] For example, in *Astragalus amphioxys* mean swainsonine concentrations were <0.001%, whereas in species such as *Astragalus mollissimus* var. *mollissimus* mean concentrations were >0.1%.[16] Additionally, in some varieties of *Oxytropis lambertii* and *A. mollissimus*, such as *O. lambertii* var. *articulata*, *O. lambertii* var. *lambertii*, and *A. mollissimus* var. *thompsonii*, mean swainsonine concentrations were <0.001% in all populations, yet in other varieties within these species mean concentrations were >0.01%.[16,24]

The purpose of this review is to highlight past and current research investigating (1) other swainsonine-containing plants besides those in the Fabaceae family; (2) fungi that produce swainsonine; (3) the plant, endophyte, and swainsonine relationship; (4) environmental factors that influence swainsonine concentrations; and (5) areas for future research.

OTHER SWAINSONINE-CONTAINING PLANTS

In addition to the Fabaceae family, swainsonine has been documented in two other plant families: the Convolvulaceae (Solanales) and the Malvaceae (Malvales) (Figure 2; Table 3). Swainsonine was identified in these plant families after numerous episodes of livestock poisoning by these plants and subsequent economic impact. Many of the species within these families are nontoxic and are important forages. Clinical signs and pathology of animals poisoned by these plants are similar to those of animals poisoned by swainsonine-containing legumes.[6,26−31] Two genera in the morning glory family, *Ipomoea* and *Turbina*, contain swainsonine. Seven taxa among these two genera, *Ipomoea carnea*, *Ipomoea polpha*, *Ipomoea riedelii*, *Ipomoea sericophylla*, *Ipomoea* sp. Q6 (aff. *calobra*), *Ipomoea verbascoidea*, and *Turbina cordata*, contain swainsonine (Table 2).[26−30] Swainsonine concentrations also vary considerably in some of these species.[30] These species are found in South America or Australia with the exception of *I. carnea* and *I. verbascoidea*. *I. carnea* can be found throughout the tropics

dx.doi.org/10.1021/jf501674r | J. Agric. Food Chem. 2014, 62, 7326−7334

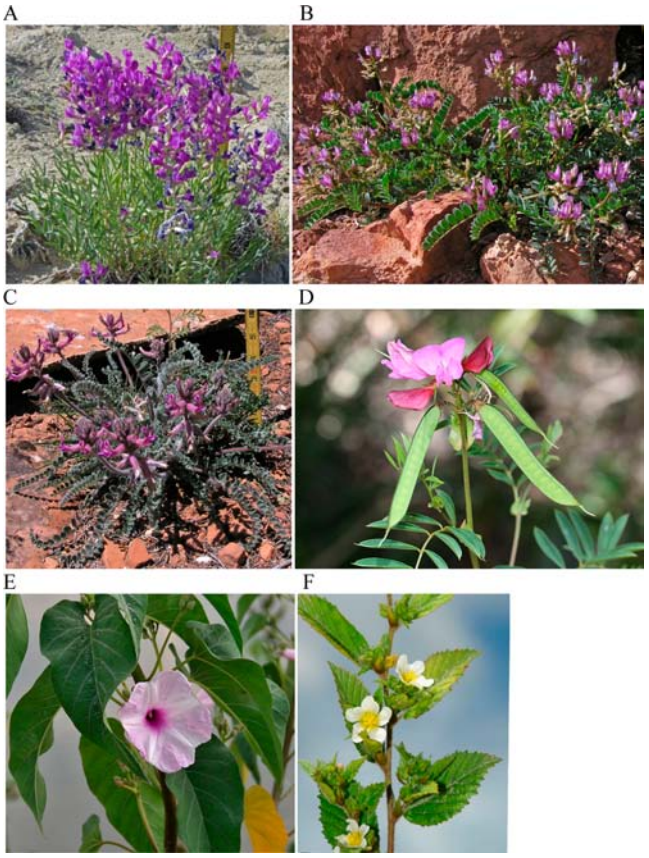

Figure 2. Photographs of swainsonine-containing plants: (A) *Oxytropis lambertii*; (B) *Astragalus lentiginosus*; (C) *Astragalus mollissimus*; (D) *Swainsona galegifolia*; (E) *Ipomoea carnea*; (F) *Sida carpinifolia*. Photographs A, B, and C were provided courtesy and copyright of Al Schneider, http://www.swcoloradowildflowers.com; photograph D was provided courtesy of Moonlight0551, http://commons.wikimedia.org; photograph E was provided courtesy of J. M. Garg, http://commons.wikimedia.org; and photograph F was provided courtesy of Franklin Riet-Correa.

worldwide, whereas *I. verbascoidea* is an African species by herbarium record,[32] although the report of its containing swainsonine comes from Brazil.[29] Only a single species of the Malvaceae, *Sida carpinifolia*, contains swainsonine (Table 2).[31]

SWAINSONINE-PRODUCING FUNGI

For many years it was thought that swainsonine was a plant-derived secondary metabolite; however, recent research suggests otherwise. A swainsonine-producing ascomycete, *Undifilum oxytropis* (Pleosporales), an endophyte associated with *O. lambertii*, *Oxytropis kansuensis*, and *Oxytropis sericea*, is reported to produce swainsonine (Table 1; Figure 2).[33,34] Initial studies described this endophyte as an *Embellisia* species.[35] The *Undifilum* genus (Pleosporales) is phylogenetically related to the genera *Alternaria*, *Embellisia*, and *Ulocladium*.[34] On the basis of molecular and morphological characteristics, three unique *Undifilum* species, *Undifilum cinerum*, *Undifilum fulvum*, and *Undifilum oxytropis*, have been found and identified among the three North American locoweed taxa *A. mollissimus*, *A. lentiginosus*, and *O. sericea*, respectively (Table 1).[34,36] This is in contrast to the swainsonine-containing *Astragalus* and *Oxytropis* species examined to date in China, which all have the same endophyte species, *U. oxytropis* (Table 1).[22] A swainsonine-producing *Undifilum* sp. has also been identified in the Australian species *S. canescens* (Table 1); molecular and morphological data suggest it is a novel species as well.[37] To date, the swainsonine-containing *Astragalus*, *Oxytropis*, and *Swainsona* spp. evaluated for the presence of an *Undifilum* spp. by PCR are associated with an *Undifilum* spp. (Table 1).[16,22,37] *Undifilum* spp. can be cultured from seeds and above-ground plant tissues; however, they have not been cultured from below-ground tissues.[33] *Undifilum* spp. are primarily found in the seed coat as they can be cultured from the seed coat but not the embryo.[38] As a result, plants derived from the embryo where the seed coat has been removed contain little or no swainsonine.[38] Using microscopy, *U. oxytropis* was detected growing between cells in vegetative tissues of *O. sericea*, providing further support that it is an endophyte.[39]

Recently, a swainsonine-producing endosymbiont in the ascomycete order Chaetothyriales was isolated from *I. carnea* (Table 1).[40] This endosymbiont was cultured from seeds and

Table 3. Important Characteristics of Plant–Fungal Symbiota Producing Swainsonine Considered in This Review

	Fabaceae	Convolvulaceae	Malvaceae
host clade	eudicots	eudicots	eudicots
host growth form	herbaceous	mostly woody vines (also shrubs, trees, herbaceous vines)	herbaceous
host genera	*Astragalus*, *Oxytropis*, and *Swainsona*	*Ipomoea* and *Turbina*	*Sida*
fungal order/family	Pleosporales/Pleosporaceae	Chaetothyriales/Chaetothyriaceae (?)	?
endophyte transmission	strictly vertical transmission (?)	strictly vertical transmission (?)	?

Table 2. Summary of the *Ipomoea*, *Turbina*, and *Sida* Species Reported To Have Swainsonine, Swainsonine Detection Methods, the Associated Endosymbiont (If Known), and Endophyte Detection Methods

				detection		
taxa	country	swainsonine detection	endophyte	culture	PCR	refs
I. carnea	tropics worldwide	GC-MS, LC-MS	*Chaetothyriales* sp.	x	x	26, 40
I. polpha	Australia	GC-MS				27
I. riedelii	Brazil	LC-MS				28
I. sericophylla	Brazil	LC-MS				28
I. sp. Q6 (aff. *calobra*)	Australia	GC-MS				27
I. verbascoidea	Brazil and Africa	LC-MS				29, 32
T. cordata	Brazil	LC-MS				30
S. carpinifolia	Brazil	LC-MS				31

dx.doi.org/10.1021/jf501674r | J. Agric. Food Chem. 2014, 62, 7326–7334

plants and detected by PCR in plants containing swainsonine. Unlike the locoweed endophyte, this endosymbiont grows as an epiphyte on the leaf surface of plants containing swainsonine (Figure 3). The epiphyte/endosymbiont was not observed on

Figure 3. Photograph of *Ipomoea carnea* leaf showing the Chaetothyriales fungal endosymbiont that produces swainsonine.

the surface of leaves from plants lacking swainsonine that were derived from fungicide-treated seeds. Plants derived from fungicide-treated seeds did not contain swainsonine but rather contained calystegines, nortropane alkaloids that are also glycosidase inhibitors. The calystegines are also found at similar concentrations in the control non-fungicide-treated plants.[40]

Swainsonine has been detected in other phylogentically disjunct groups of Basidiomycetes and/or Ascomycetes. *Rhizoctonia leguminicola* (Cantharellales), a basidiomycete, is a fungal pathogen of red clover (*Trifolium pratense*) that causes black patch disease.[41] *R. leguminicola* produces swainsonine as well as the indolizidine alkaloid slaframine, which is responsible for the slobbers syndrome in horses.[41,42] Recent data suggest that this fungus is misclassified and is actually an ascomycete (R. Creamer, personal communication). *Metarhizium anisopliae* (Hypocreales), an ascomycete, produces swainsonine and is an entomopathogen that attaches to the outside of an insect, grows internally, and causes death.[43] Lastly, a preliminary study suggests two ascomycetes, *Fusarium trinctum* and a *Schizophyllum* sp., may also produce swainsonine.[44] These fungi were isolated from Chinese swainsonine-containing *Astragalus* and *Oxytropis* species and their rhizosphere soils. More research is needed to determine if *F. trinctum* and the *Schizophyllum* sp. produce swainsonine as there was no detailed analytical work performed such as mass spectrometry coupled to liquid or gas chromatography.

PLANT/ENDOPHYTE RELATIONSHIP

Multiple factors may influence the interaction of plant and endophyte and ultimately determine swainsonine concentrations in planta. Some considerations include, but are not limited to, different plant parts and the phenological stages of the plant. Other factors include, but are not limited to, different plant species, varieties, and populations as well as the respective endophyte associated with each.

Secondary metabolites often differ among plant parts and as a function of plant phenology. Swainsonine is found in all plant parts with greater concentrations in above-ground parts than in below-ground parts in *Astragalus* spp. and *O. sericea* (Figure 4A).[45,46] Furthermore, swainsonine concentrations vary season-

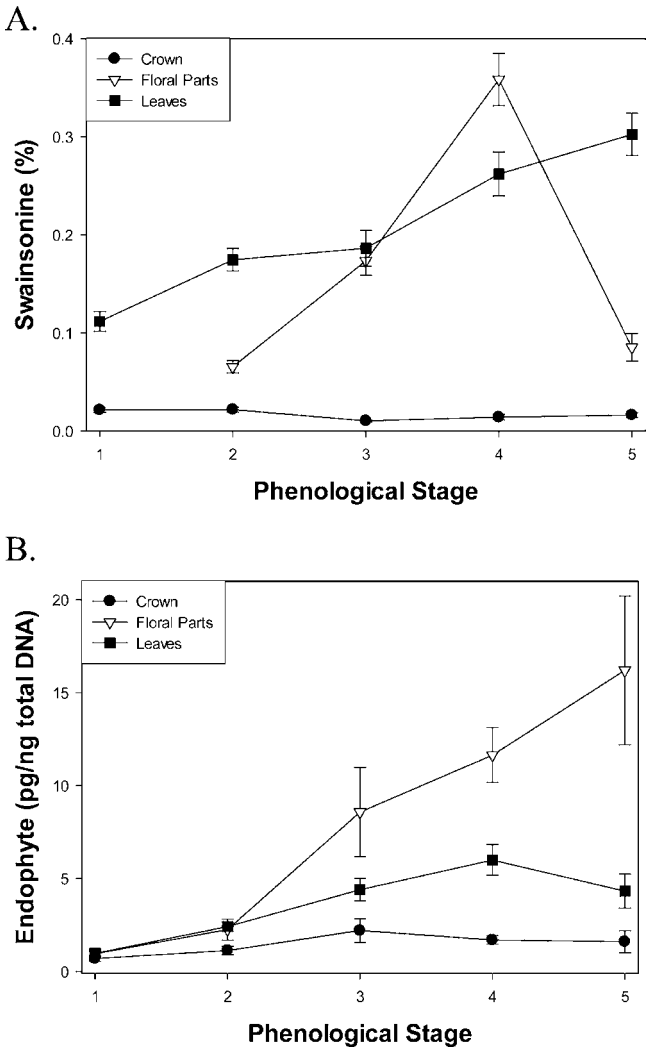

Figure 4. (A) Swainsonine concentrations (%) and (B) endophyte amounts (pg/ng total DNA) in different plant parts of *Oxytropis sericea* from Cuchara, CO, USA, as a function of phenological stage. Mean swainsonine concentrations and endophyte amounts ± the standard error at the different phenological stages (stage 1, vegetative; stage 2, early flower; stage 3, late flower/early pod; stage 4, full pod/mature seed; stage 5, senesced) are shown. Adapted from data presented in Cook et al.[47]

ally or as a function of phenology.[47,48] In *O. sericea*, swainsonine concentrations increase in above-ground tissues throughout the growing season until the plant reaches maturity (Figure 4A).[47] Young newly developing tissues have the least amount of swainsonine, whereas more mature tissues have more swainsonine.[47] As plants senesce, swainsonine concentrations decrease significantly.[47] Likewise, the endophyte *Undifilum* spp. is found in all plant parts, again with greater concentrations in above-ground parts than below-ground parts with the exception

dx.doi.org/10.1021/jf501674r | J. Agric. Food Chem. 2014, 62, 7326−7334

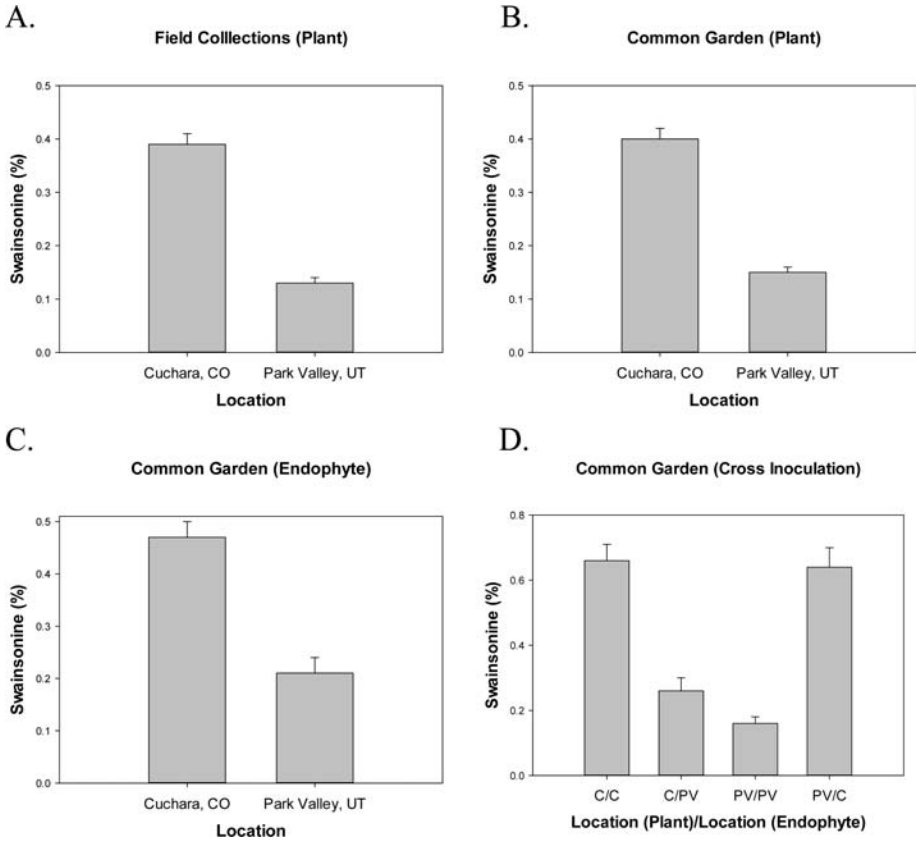

Figure 5. Swainsonine concentrations (%): (A) field collections from two populations, Cuchara, CO, USA (C), and Park Valley, UT, USA (PV), of *Oxytropis sericea*; (B) common garden performed in greenhouse of two *O. sericea* populations; (C) common garden of fungal endophyte isolated from two *O. sericea* populations; (D) common garden of cross inoculation experiment (location: plant/endophyte). Figure adapted from data presented in Cook et al.[49]

of the root crown (Figure 4B).[45,46] The root crown has endophyte amounts more similar to those of above-ground parts, and because many locoweeds are perennial plants, this may serve as a reservoir for the endophyte for the following year's growth.[45,46] In *O. sericea*, endophyte amounts increase in above-ground parts throughout the growing season until the plant reaches maturity (Figure 4B).[47] Swainsonine and endophyte amounts are highly correlated over the growing season in *O. sericea*, indicating that endophyte amount plays a critical role in determining swainsonine concentration in the plant.[47,48]

Environment and genotype of the plant and/or endophyte or an interaction of these factors may influence swainsonine concentrations. Swainsonine concentrations differ spatially among populations of *O. sericea*; for example, mean concentrations were approximately 3 times greater in plants from Cuchara, CO, USA (0.40%), compared to plants from Park Valley, UT, USA (0.15%) (Figure 5A).[47] The following observations suggest that concentration differences between these populations are due to the genotype of the endophyte. First, differences in swainsonine concentrations between populations persisted when plants from these two locations were grown in a common garden (Figure 5B).[49] Second, the respective endophyte, *U. oxytropis*, from each population produced different amounts of swainsonine in vitro when grown under common culture conditions (Figure 5C).[49] Third, a cross inoculation experiment, wherein the endophyte from one population was inoculated onto the embryo from the other location, demonstrated that the endophyte genotype, not the plant genotype nor differences in endophyte amount, were responsible for differences in swainsonine concentration between the two populations (Figure 5D).[49] Although no differences were observed in the internal transcribed spacer sequence between endophyte isolates from the two populations,[49] other genotypic differences may be present that explain the difference in swainsonine production.

Data suggest that the interaction of the plant species and endophyte genotype is a key factor in determining swainsonine concentrations in planta. First, different *Astragalus* and *Oxytropis* species had similar rank order swainsonine concentrations in field collections and greenhouse-grown plants. For example, *Astragalus wootoni* had the highest mean swainsonine concentration followed by similar concentrations in *A. lentiginosus* and *A. mollissimus* var. *mollissimus*, and the lowest concentrations were noted in *O. sericea*.[16,50] Second, similar trends in rank order swainsonine concentrations between field collections and greenhouse-grown plants were observed from the highest to lowest, respectively, in *A. mollissimus* var. *mollissimus*, *O. sericea*, *A. mollissimus* var. *bigelovii*, and *A. mollissimus* var. *matthewsii* or var. *thompsonii*.[51,52] In the latter example the trends in rank order swainsonine concentrations remained the same whether or not the plants were grown under optimum conditions, under water stress, or with a deficiency in nitrogen.[51,52] It is not known if the respective endophyte from each of above species produces different amounts of swainsonine; however, results observed for swainsonine production between the *U. oxytropis* isolates found in the Cuchara, CO, USA, and Park Valley, UT, USA, *O. sericea*

populations suggest this may be the case.[49] Caution should be used not to extrapolate beyond the populations of the highlighted taxa because other populations of these same taxa may have different mean swainsonine concentrations.

Swainsonine concentrations differ among individuals within toxic populations of *Astragalus* and *Oxytropis* spp.[16,24] Swainsonine concentrations segregate into two groups, namely, chemotype 1 plants, which have swainsonine concentrations >0.01%, and chemotype 2 plants, which have concentrations much <0.01% (generally near 0.001% or not detected).[45,46] Initial observations showed a correlation between swainsonine concentrations and the presence of the endophyte, *Undifilum*, as it could be cultured from chemotype 1 plants and was not cultured from chemotype 2 plants.[53] Further studies confirmed these culturing results and demonstrated that the endophyte could be detected by PCR in both groups.[16] These two chemotypes differed significantly in the amount of endophyte they had, further supporting the differences in swainsonine concentrations of the respective host plants.[45,46] Additional studies demonstrated that seeds collected from each corresponding chemotype also differed significantly in swainsonine and endophyte amounts as well.[54]

Endophytes can be horizontally and vertically transmitted.[55] The following observations support the hypothesis that *Undifilum* spp. are vertically transmitted from seed to progeny. Progeny derived from seeds of *Astragalus* and *Oxytropis* chemotype 1 plants had variable swainsonine and endophyte amounts consistent with both chemotype 1 and chemotype 2 plants.[50] Progeny derived from seeds of a chemotype 2 plant had swainsonine and endophyte amounts consistent with chemotype 2 plants.[50] Chemotype 1 seeds and their resulting progeny, with variable amounts of both swainsonine and endophyte, suggest that there is imperfect transmission of the endophyte, resulting in both chemotypes. Chemotype 2 seeds and their resulting progeny suggest that these seeds lack some critical amount of endophyte necessary to produce sufficient swainsonine to be classified as a chemotype 1 plant.[50]

Seed endophyte amounts and/or a plant endophyte by genotype interaction may be important factors in determining swainsonine concentrations in chemotype 1 and 2 plants. The following observations suggest that seed endophyte amounts at germination are a major determinant in the production of swainsonine and thus the classification of a plant as chemotype 1 or 2. First, plants derived from chemotype 1 seeds, in which the amount of endophyte was reduced by seed coat removal or fungicide treatment, had swainsonine and endophyte amounts consistent with those of chemotype 2 plants.[54] Results from the seed coat removal experiment were consistent with previous results reported by Oldrup et al.[38] Second, plants derived from *Undifilum*-inoculated chemotype 1 and chemotype 2 embryos had swainsonine and endophyte amounts consistent with those of chemotype 1 plants.[54] Similar results were observed for both *Astragalus* and *Oxytropis* species. If a plant endophyte by genotype interaction was a key determinant, one would have expected that plants derived from an inoculated chemotype 2 embryo would have had swainsonine and endophyte amounts similar to those of a chemotype 2 plant.[54]

INFLUENCE OF ENVIRONMENTAL FACTORS ON SWAINSONINE CONCENTRATIONS

As swainsonine is an alkaloid, one may suspect that nitrogen availability could influence its production. *Astragalus* and *Oxytropis* species are legumes and are known for forming symbioses with nitrogen-fixing bacteria, thus altering the nitrogen status of plants.[56] Swainsonine concentrations increased in plants inoculated with one strain of *Rhizobium* but not others, suggesting an interaction between the two classes of symbionts.[56] The *Rhizobium*-inoculated plants with the positive swainsonine response had more leaves, more clusters, and greater leaf biomass. These changes in swainsonine and plant physiological measures likely resulted from increased nitrogen availability to the plant and endophyte.[56] However, others have shown that when nitrogen was supplied through fertilizer to locoweed species with different mean swainsonine concentrations, there were no consistent differences in swainsonine concentrations across locoweed taxa either at deficient or optimum nitrogen amounts.[51] All species regardless of mean swainsonine concentration responded positively to nitrogen in terms of biomass and leaf photosynthesis and pigments.[51] Additionally, other experiments showed no differences in swainsonine concentrations in *O. sericea* or *U. oxytropis* when grown under optimum or deficient nitrogen conditions.[38] These results suggest that a given endophyte may produce a defined conentration of swainsonine per unit biomass notwithstanding nitrogen availability. It is critical to note that the total pool of available swainsonine is higher in plants under optimum nitrogen conditions because plant biomass is increased.

Water status of the plant may influence swainsonine concentrations. Swainsonine concentrations were reported to be significantly greater compared to controls in *O. sericea* plants and *U. oxytropis* isolates cultured from these plants that were water-stressed.[38] Further studies by Vallotton et al.[52] demonstrated that swainsonine concentrations increased in some species in response to water deficit but not in others such as *O. sericea*. Swainsonine concentrations increased only in taxa with medium and high swainsonine concentrations. In the species where swainsonine concentrations did change, concentrations changed only after the third water deficit period. Furthermore, in the various plant species there was little evidence for a growth trade-off in physiological measures such as shoot and root biomass, relative growth rate, or photosynthetic rate from taxa differing in mean swainsonine concentrations. The differential effect of water stress in *O. sericea* may be a result of plants being grown in tissue culture on artificial media in one experiment, whereas in the other experiment the plants were grown in soil in pots.[38,52]

It is unclear if herbivory from insects or large ungulates influences swainsonine production. Swainsonine concentrations did not change in response to clipping used to simulate herbivory.[57] There are no reports investigating the bioactivity of swainsonine against insects, fungi, or bacteria, with the exception of one preliminary study that suggested swainsonine had no effect on a native weevil herbivore of locoweeds.[58] Lastly, swainsonine appears not to deter grazing by large ungulates, as animals take 2−3 weeks to show clinical signs and continue grazing locoweeds after becoming intoxicated.[59]

FUTURE DIRECTIONS

In the past 15 years, knowledge concerning swainsonine and fungal relationships has changed dramatically. In summary, the following observations support the assertion that swainsonine is a fungal-endophyte-derived secondary metabolite and is not produced by the host plant in the legume genera and *I. carnea*: (1) Legume species and *I. carnea* that contain swainsonine are infected with *Undifilum* species[22,33−37] or a Chaetothyriales

endosymbiont,[40] respectively. (2) Plants derived from fungicide-treated swainsonine-containing legume and *I. carnea* seeds have no detectable swainsonine or have concentrations <0.001%.[40,54] (3) *Undifilum* species and the Chaetothyriales isolate that were isolated from their respective hosts produce swainsonine in vitro.[22,33,34,37,49] Additional studies on native legumes demonstrate further that swainsonine is a fungal-endophyte-derived secondary metabolite. First, plants derived from *Astragalus* and *Oxytropis* embryos where the seed coat was removed have no detectable swainsonine or have concentrations <0.001%.[38,54] Second, plants derived from *Undifilum*-inoculated embryos have swainsonine concentrations >0.01%.[54]

There are yet unanswered questions that would be important to solving poisoning problems worldwide. The identification of plant taxa containing swainsonine defined to date are primarily a result of episodes of livestock poisoning that result in the plant screening for swainsonine. A systematic examination for swainsonine in taxa from the six plant genera that contain swainsonine, namely, *Astragalus*, *Oxytropis*, *Swainsona*, *Ipomoea*, *Turbina*, and *Sida*, would be valuable to assess future risk. A modified swainsonine extraction method that was recently published[60] allows for the rapid extraction of hundreds of samples simultaneously and could be used to accomplish this objective. Additionally, herbarium specimens in which a small amount of material is removed from a voucher specimen could be screened rather than using field collections. This would facilitate the LC-MS screening of hundreds of taxa in a short amount of time, as verified by a recent paper that shows swainsonine can be detected in herbarium samples.[23] This same material could be screened for the presence of the corresponding fungal endophyte. Furthermore, the presence or absence of swainsonine could be validated in the legumes listed in Table 1. This approach would strengthen the foundation for future work on genetic and environmental factors related to swainsonine and endophyte concentrations.

The biosynthesis of swainsonine should be investigated to identify and characterize the genes that encode the proteins in the swainsonine biosynthetic pathway. To facilitate this work, the biochemical pathway for swainsonine biosynthesis has been investigated in the fungi *R. leguminicola* and *M. anisopliae*.[61,62] Swainsonine is derived from lysine, which is converted into pipecolic acid. Two precursors of swainsonine in the *R. leguminicola* biosynthetic pathway were also detected in the shoots of Diablo locoweed (*Astragalus oxyphysus*).[61,63] As a result, the investigators proposed that the biosynthetic pathway of swainsonine in *R. leguminicola* is similar to the pathway in locoweeds.[63] Subsequently, in *Astragalus* and *Oxytropis* species, swainsonine has been shown to be produced by *Undifilum* species,[33,34,37] which supports the presence of a common pathway in fungi. Investigators have recently developed a transformation system to genetically manipulate *U. oxytropis* that will facilitate this work.[64] These same investigators also knocked out the saccharopine reductase gene from *U. oxytropis*, a protein involved in lysine metabolism, and showed that the fungus had increased swainsonine amounts.[65]

A seed-transmitted endophyte is responsible for the biosynthesis of swainsonine in the legume and morning glory families; thus, methods may be developed to disrupt the transmission of this endophyte to seeds. The swainsonine-containing locoweed and morning glory species are native plants, so following the grass model by developing germplasm that lacks the endophyte or has a nontoxic version of the endophyte is not an option, as these native range plants are not planted in a pasture system like tall fescue and perennial ryegrass.

The preponderance of evidence to date indicates that swainsonine is found in plants due to an interaction between the host and a fungal endosymbiont. Additional research could be performed demonstrating that *Chaetothyriales* spp. are associated with other swainsonine-containing morning glory species as this has been demonstrated only for *I. carnea*. Research could also be performed to determine if the presence of swainsonine in *Sida carpinifolia* is due to a fungal endosymbiont. We anticipate that a fungal endosymbiont will be found in association with other swainsonine-containing morning glory species and *S. carpinifolia*. Lastly, we anticipate that whenever swainsonine is found in a given plant taxa, swainsonine will be associated with a fungal endosymbiont responsible for its production.

AUTHOR INFORMATION

Corresponding Author

*(D.C.) Phone: (435) 752-2941. Fax: (435) 753-5681. E-mail: daniel.cook@ars.usda.gov.

Notes

The authors declare no competing financial interest.

REFERENCES

(1) Marsh, C. D. The locoweed disease of the plains. U.S. Department of Agriculture Bureau Animal Industry Bulletin 112, 1909.

(2) Marsh, C. D.; Clawson, A. B. The locoweed disease. U.S. Department of Agriculture Farmer's Bulletin 1054, July 1919, revised November 1936.

(3) Gardiner, M. R.; Linto, A. C.; Aplin, T. H. E. Toxicity of *Swainsona canescens* for sheep in Western Australia. *Aust. J. Agric. Res.* **1969**, *20*, 87−97.

(4) Huang, Y. Q.; Zhang, E. Y.; Pan, W. F. Current status of locoweed toxicity. *Shandong Sci.* **2003**, *16*, 34−39.

(5) Burrows, G. E.; Tyrl, R. J. *Toxic Plants of North America*, 1st ed.; Iowa State University Press: Ames, IA, USA, 2001.

(6) James, L. F.; Van Kampen, K. R.; Hartley, W. J. Comparative pathology of *Astragalus* (locoweed) and *Swainsona* poisoning in sheep. *Pathol. Vet.* **1970**, *7*, 116−125.

(7) Panter, K. E.; James, L. F.; Stegelmeier, B. L.; Ralphs, M. H.; Pfister, J. A. Locoweeds: effects on reproduction in livestock. *J. Nat. Toxins* **1999**, *8*, 53−62.

(8) Colegate, S. M.; Dorling, P. R.; Huxtable, C. R. A spectroscopic investigation of swainsonine: an α-mannosidase inhibitor isolated from *Swainsona canescens*. *Aust. J. Chem.* **1979**, *32*, 2257−2264.

(9) Molyneux, R. J.; James, L. F. Loco intoxication: indolizidine alkaloids of spotted locoweed (*Astragalus lentiginosus*). *Science* **1982**, *216*, 190−191.

(10) Dorling, P. R.; Huxtable, C. R.; Colegate, S. M. Inhibition of lysosomal α-mannosidase by swainsonine, an indolizidine alkaloid isolated from *Swainsona canescens*. *Biochem. J.* **1980**, *191*, 649−651.

(11) Tulsiani, D. R.; Broquist, H. P.; James, L. F.; Touster, O. Production of hybrid glycoproteins and accumulation of oligosaccharides in the brain of sheep and pigs administered swainsonine or locoweed. *Arch. Biochem. Biophys.* **1988**, *264*, 607−617.

(12) Cook, D.; Ralphs, M. H.; Welch, K. D.; Stegelmeier, B. L. Locoweed poisoning in livestock. *Rangelands* **2009**, *31*, 16−21.

(13) James, L. F.; Nielsen, D. Locoweeds: assessment of the problem on western U.S. rangelands. In *The Ecology and Economic Impact of Poisonous Plants on Livestock Production*; James, L. F., Ralphs, M. H., Nielsen, D. B., Eds.; Westview Press: Boulder, CO, USA, 1988; pp 171−180.

(14) Smith, G. S.; Allred, K. W.; Kiehl, D. E. Swainsonine content of New Mexican locoweeds. *Proc. West. Sec. Am. Soc. Anim. Sci.* **1992**, *43*, 405−407.

(15) Fox, W. E.; Allred, K. W.; Roalson, E. H. A guide to the common locoweeds and milkvetches of New Mexico. *New Mexico Agric. Exp. Stn.* **1998**, *No. 557*.
(16) Ralphs, M. H.; Creamer, R.; Baucom, D.; Gardner, D. R.; Welsh, S. L.; Graham, J. D.; Hart, C.; Cook, D.; Stegelmeier, B. L. Relationship between the endophyte *Embellisia* spp. and the toxic alkaloid swainsonine in major locoweed species (*Astragalus* and *Oxytropis*). *J. Chem. Ecol.* **2008**, *34*, 32−38.
(17) Molyneux, R. J.; James, L. F.; Panter, K. E.; Ralphs, M. H. Analysis and distribution of swainsonine and related polyhydroxyindolizidine alkaloids by thin layer chromatography. *Phytochem. Anal.* **1991**, *2*, 125−129.
(18) Davis, D.; Schwarz, P.; Hernandez, T.; Mitchell, M.; Warnock, B.; Elbein, A. D. Isolation and characterization of swainsonine from Texas locoweed (*Astragalus emoryanus*). *Plant Physiol.* **1984**, *4*, 972−975.
(19) Ralphs, M. H.; Graham, J. D.; James, L. F. A close look at locoweed poisoning on shortgrass prairies. *Rangelands* **2002**, *24*, 30−34.
(20) Kingsbury, J. M. *Poisonous Plants of the United States and Canada*; Prentice Hall: Englewood Cliffs, NJ, USA, 1964; pp 305−313.
(21) Molyneux, R. J.; Gomez-Sosa, E. Presencia del alcaloide indolizidinico swainsonine en *Astragalus pehuenches* (Leguminosae − Galegueae). *Bol. Soc. Argent. Bot.* **1991**, *27*, 59−64.
(22) Yu, Y.; Zhao, Q.; Wang, J.; Wang, J.; Wang, Y.; Song, Y.; Geng, G.; Li, Q. Swainsonine-producing fungal endophyte from major locoweed species in China. *Toxicon* **2010**, *56*, 330−338.
(23) Gao, X.; Cook, D.; Ralphs, M. H.; Yan, L.; Gardner, D. R.; Lee, S. T.; Panter, K. E.; Han, B.; Zhao, M. L. Detection of swainsonine and isolation of the endophyte *Undifilum* from the major locoweeds in Inner Mongolia. *Biochem. Syst. Ecol.* **2012**, *45*, 79−85.
(24) Gardner, D. R.; Molyneux, R. J.; Ralphs, M. H. Analysis of swainsonine: extraction methods, detection, and measurement in populations of locoweeds (*Oxytropis* spp.). *J. Agric. Food Chem.* **2001**, *49*, 4573−4580.
(25) Dorling, P. R.; Colegate, S. M.; Huxtable, C. R. Toxic species of the plant genus *Swainsona*. In *Swainsonine and Related Glycosidase Inhibitors*; James, L. F., Elbein, A. D., Molyneux, R. J., Warren, C. D., Eds.; Iowa State University Press: Ames, IA, USA, 1989; pp 14−22.
(26) de Balogh, K. K.; Dimande, A. P.; van der Lugt, J. J.; Molyneux, R. J.; Naudé, T. W.; Welman, W. G. A lysosomal storage disease induced by *Ipomoea carnea* in goats in Mozambique. *J. Vet. Diagn. Invest.* **1999**, *11*, 266−273.
(27) Molyneux, R. J.; Mckenzie, R. A.; O'Sullivan, B. M.; Elbein, A. D. Identification of the glycosidase inhibitors swainsonine and calystegine B2 in Weir vine (*Ipomoea* sp. Q6 [aff. *calobra*]) and correlation with toxicity. *J. Nat. Prod.* **1995**, *58*, 878−886.
(28) Barbosa, R. C.; Riet-Correa, F.; Medeiros, R. M. T.; Lima, E. F.; Barros, S. S.; Gimeno, E. J.; Molyneux, R. J.; Gardner, D. R. Intoxication by *Ipomoea sericophylla* and *Ipomoea riedelii* in goats in the state of Paraíba, northeastern Brazil. *Toxicon* **2006**, *47*, 371−379.
(29) Mendonça, F. S.; Albuquerque, R. F.; Envêncio-Neto, J.; Freitas, S. H.; Dória, R. G.; Boabaid, F. M.; Driemeier, D.; Gardner, D. R.; Riet-Correa, F.; Colodel, E. M. α-Mannosidosis in goats caused by the swainsonine containing plant *Ipomoea verbascoidea*. *J. Vet. Diagn. Invest.* **2012**, *24*, 90−95.
(30) Dantas, A. F. M.; Riet-Correa, F.; Gardner, D. R.; Medeiros, R. M. T.; Barros, D. O. S.; Anjos, B. L.; Lucena, R. B. Swainsonine-induced lysosomal storage disease in goats caused by the ingestion of *Turbina cordata* in northeastern Brazil. *Toxicon* **2007**, *49*, 111−116.
(31) Colodel, E. M.; Gardner, D. R.; Zlotowski, P.; Driemeier, D. Identification of swainsonine as a glycoside inhibitor responsible for *Sida carpinifolia* poisoning. *Vet. Hum. Toxicol.* **2002**, *44*, 177−178.
(32) *Ipomoea verbascoidea* Choisy; http://tropicos.org/Name/8501355?tab=distribution (accessed March 20, 2014).
(33) Braun, K.; Romero, J.; Liddell, C.; Creamer, R. Production of swainsonine by fungal endophytes of locoweed. *Mycol. Res.* **2003**, *107*, 980−988.
(34) Pryor, B. M.; Creamer, R.; Shoemaker, R. A.; McClain-Romero, J.; Hambleton, S. *Undifilum*, a new genus for endophytic *Embellisia oxytropis* and parasitic *Helminthosporium bornmuelleri* on legumes. *Botany* **2009**, *87*, 178−194.
(35) Wang, Q.; Nagao, H.; Li, Y.; Wang, H.; Kakishima, M. *Embellisia oxytropis*, a new species isolated from *Oxytropis kansuensis* in China. *Mycotaxon* **2006**, *95*, 255−260.
(36) Baucom, D.; Romero, M.; Belfon, R.; Creamer, R. Two new species of *Undifilum*, the swainsonine producing fungal endophyte, from *Astragalus* species of locoweed in the United States. *Botany* **2012**, *90*, 866−875.
(37) Grum, D. S.; Cook, D.; Baucom, D.; Mott, I. W.; Gardner, D. R.; Creamer, R.; Allen, J. G. Production of the alkaloid swainsonine by a fungal endophyte in the host *Swainsona canescens*. *J. Nat. Prod.* **2013**, *76*, 1984−1988.
(38) Oldrup, E.; McLain-Romero, J.; Padilla, A.; Moya, A.; Gardner, D. R.; Creamer, R. Localization of endophytic *Undifilum* fungi in locoweed seed and influence of environmental parameters on a locoweed *in vitro* culture system. *Botany* **2010**, *88*, 512−521.
(39) Reyna, R.; Cooke, P.; Grum, D.; Cook, D.; Creamer, R. Detection and localization of the endophyte *Undifilum oxytropis* in locoweed tissues. *Botany* **2012**, *90*, 1229−1236.
(40) Cook, D.; Beaulieu, W. T.; Mott, I. W.; Riet-Correa, F.; Gardner, D. R.; Grum, D.; Pfister, J. A.; Clay, K.; Marcolongo-Pereira, C. Production of the alkaloid swainsonine by a fungal endosymbiont of the Ascomycete order Chaetothyriales in the host *Ipomoea carnea*. *J. Agric. Food Chem.* **2013**, *61*, 3797−3803.
(41) Schneider, M.; Ungemach, F.; Broquist, H.; Harris, T. (1*S*,2*R*,8*R*,8a*R*)-1,2,8-trihydroxyoctahydroindolizidine (swainsonine), an α-mannosidase inhibitor from *Rhizoctonia leguminicola*. *Tetrahedron* **1983**, *39*, 29−32.
(42) Croom, W. J., Jr.; Hagler, W. M., Jr.; Froetschel, M. A.; Johnson, A. D. The involvement of slaframine and swainsonine in slobbers syndrome: a review. *J. Anim. Sci.* **1995**, *73*, 1499−1508.
(43) Patrick, M.; Adlard, M. W.; Keshavarz, T. Production of an indolizidine alkaloid, swainsonine by the filamentous fungus, *Metarhizium anisopliae*. *Biotechnol. Lett.* **1993**, *15*, 997−1000.
(44) Hao, L.; Chen, J. P.; Lu, W.; Ma, Y.; Zhao, B. Y. Isolation and identification of swainsonine-producing fungi found in locoweeds and their rhizosphere soil. *Afr. J. Microbiol. Res.* **2012**, *6*, 4959−4969.
(45) Cook, D.; Gardner, D. R.; Ralphs, M. H.; Pfister, J. A.; Welch, K. D.; Green, B. T. Swainsonine concentrations and endophyte amounts of *Undifilum oxytropis* in different plant parts of *Oxytropis sericea*. *J. Chem. Ecol.* **2009**, *35*, 1272−1278.
(46) Cook, D.; Gardner, D. R.; Grum, D.; Pfister, J. A.; Ralphs, M. H.; Welch, K. D.; Green, B. T. Swainsonine and endophyte relationships in *Astragalus mollissimus* and *Astragalus lentiginosus*. *J. Agric. Food Chem.* **2011**, *59*, 1281−1287.
(47) Cook, D.; Shi, L.; Gardner, D. R.; Pfister, J. A.; Grum, D.; Welch, K. D.; Ralphs, M. H. Influence of phenological stage on swainsonine and endophyte concentrations in *Oxytropis sericea*. *J. Chem. Ecol.* **2012**, *38*, 195−203.
(48) Achata Böttger, J.; Creamer, R.; Gardner, D. Seasonal changes in *Undifilum* colonization and swainsonine content of locoweeds. *J. Chem. Ecol.* **2012**, *38*, 486−495.
(49) Cook, D.; Grum, D.; Gardner, D. R.; Welch, K. D.; Pfister, J. A. Influence of endophyte genotype on swainsonine concentrations in *Oxytropis sericea*. *Toxicon* **2013**, *61*, 105−111.
(50) Ralphs, M. H.; Cook, D.; Gardner, D. R.; Grum, D. S. Transmission of the locoweed endophyte to the next generation of plants. *Fungal Ecol.* **2011**, *4*, 251−255.
(51) Delaney, K. J.; Klypina, N.; Maruthavanan, J.; Lange, C.; Sterling, T. M. Locoweed dose response to nitrogen: positive for biomass and primary physiology, but inconsistent for an alkaloid. *Am. J. Bot.* **2011**, *98*, 1956−1965.
(52) Vallotton, A. D.; Murray, L. W.; Delaney, K. J.; Sterling, T. M. Water deficit induces swainsonine of some locoweed taxa, but with no swainsonine−growth trade-off. *Acta Oecol.* **2012**, *43*, 140−149.

(53) Gardner, D. R.; Romero, J.; Ralphs, M. H.; Creamer, R. Correlation of an endophytic fungus (*Alternaria* spp.) with the presence of swainsonine in Lambert locoweed (*Oxytropis lambertii*). In *Poisonous Plants and Related Toxins*; Acamovic, T., Stewart, C. S., Pennycott, T., Eds.; CABI: Wallingford, UK, 2004; pp 32−37.
(54) Grum, D. S.; Cook, D.; Gardner, D. R.; Roper, J. M.; Pfister, J. A.; Ralphs, M. H. Influence of seed endophyte amounts on swainsonine concentrations in *Astragalus* and *Oxytropis* locoweeds. *J. Agric. Food Chem.* **2012**, *60*, 8083−8089.
(55) Rodriguez, R. J.; White, J. F.; Arnold, A. E.; Redman, R. S. Fungal endophytes: diversity and functional roles. *New Phytol.* **2009**, *182*, 314−330.
(56) Valdez Barillas, J. R.; Paschke, M. W.; Ralphs, M. H.; Child, R. D. White locoweed toxicity is facilitated by a fungal endophyte and nitrogen-fixing bacteria. *Ecology* **2007**, *88*, 1850−1856.
(57) Ralphs, M. H.; Gardner, D. R.; Graham, J. D.; Greathouse, G.; Knight, A. P. Clipping and precipitation influences on locoweed vigor, mortality, and toxicity. *J. Range Manage.* **2002**, *55*, 394−399.
(58) Parker, J. E. Effects of insect herbivory by the four-lined locoweed weevil, *Cleonidus trivittaus* (Say) (Coleoptera: Curculionidae), on the alkaloid swainsonine in locoweed *Astragalus mollissimus* and *Oxytropis sericea*. MS thesis, New Mexico State University, Las Cruces, NM, USA, 2008; 164 pp.
(59) Pfister, J. A.; Stegelmeier, B. L.; Gardner, D. R.; James, L. F. Grazing of spotted locoweed (*Astragalus lentiginosus*) by cattle and horses in Arizona. *J. Anim. Sci.* **2003**, *81*, 285−293.
(60) Gardner, D. R.; Cook, D. A comparison of alternative sample preparation procedures for the analysis of swainsonine using LC-MS/MS. *Phytochem. Anal.* **2011**, *22*, 124−127.
(61) Harris, C. M.; Schneider, M. J.; Ungemach, F. S.; Hill, J. E.; Harris, T. M. Biosynthesis of the toxic indolizidine alkaloids slaframine and swainsonine in *Rhizoctonia leguminicola*: metabolism of 1-hydroxyindolizidines. *J. Am. Chem. Soc.* **1988**, *110*, 940−949.
(62) Sim, K. L.; Perry, D. Analysis of swainsonine and its early metabolic precursors in cultures of *Metarhizium anisopliae*. *Glycoconjugate J.* **1997**, *14*, 661−668.
(63) Harris, C. M.; Campbell, B. C.; Molyneux, R. J.; Harris, T. M. Biosynthesis of swainsonine in the diablo locoweed (*Astragalus oxyphysus*). *Tetrahedron Lett.* **1988**, *29*, 4815−4818.
(64) Mukherjee, S.; Dawe, A. L.; Creamer, R. Development of a transformation system in the swainsonine producing, slow growing endophytic fungus, *Undifilum oxytropis*. *J. Microbiol. Methods* **2010**, *81*, 160−165.
(65) Mukherjee, S.; Dawe, A. L.; Creamer, R. Potential role for saccharopine reductase in swainsonine metabolism in endophytic fungus, *Undifilum oxytropis*. *Fungal Biol.* **2012**, *116*, 902−909.

explore how secondary compounds isolated from nectar and/or pollen affect the behavior, reproduction, and/or survival of pollinators. Second, because pollinators are often able to survive the consumption of secondary compounds in nectar or pollen, we review the biochemical, physiological, and behavioral mechanisms by which pollinators cope with their consumption. Given that bees are the dominant pollinators globally, we focus most of our review on how bees cope with secondary compound consumption and only touch on other types of pollinators, such as Lepidoptera and birds. Finally, we propose avenues for future research on the chemistry, biochemistry, and ecology of secondary compounds in floral rewards from the plant's and the pollinator's perspectives.

SECONDARY COMPOUNDS IN NECTAR AND POLLEN: CASE STUDIES AND THEIR EFFECTS ON POLLINATORS

Several genera of poisonous plants are found in rangelands throughout the world and the western United States. These plants are typically visited by a suite of generalist pollinators or, more rarely, by select specialists. Here we highlight eight genera of plants (Figure 1), including their pollinators, secondary compounds, and relevant literature describing the presence and concentrations of these secondary compounds in floral rewards as well as their effects on pollinators (Table 1). We focus on alkaloid-containing plants as estimates suggest that 10−25% of angiosperm species contain alkaloids, and alkaloids are well-known to mediate plant−animal interactions.[21]

Figure 1. Floral images of select genera of poisonous plants found in rangelands throughout the world and the western United States: (A) *Zigadenus elegans* (= syn. *Anticlea elegans*); (B) *Veratrum californicum* (= syn *V. tenuipetalum*); (C) *Delphinium barbeyi*; (D) *Aconitum columbianum*; (E) *Nicotiana attenuata*; (F) *Lupinus prunophilus* (= syn. *L. polyphyllus*); (G) *Senecio serra*. Photographs provided courtesy and copyright of Al Schneider (www.swcoloradowildflowers.com).

***Zigadenus* spp. (= syn. *Amianthium*, *Anticlea*, *Stanthium*, and *Toxicoscordion*;[22] Death Camas; Melanthiaceae).** Reports show that several *Zigadenus* species, including *Zigadenus nuttallii* and *Zigadenus paniculatus*, are visited by a single bee, *Andrena astragali*, or a subset of the bee community in the family Halictidae, whereas others such as *Zigadenus elegans* are visited by flies.[23−25] *Zigadenus* spp. contain a group of cevanine-type steroidal alkaloids (Table 1) including esters of germine, protoverine, and zygadenine.[26−28] Zygacine, **1** (Figure 2), an ester of zygadenine, is the major alkaloid in *Z. paniculatus* and *Zigadenus venenosus*.[27,28] These neurotoxic alkaloids bind open voltage-sensitive calcium channels[29] and are toxic to mice, sheep, and cattle.[30,31] Humans have also been poisoned accidentally via consumption of death camas bulbs.[30] Zygacine and related alkaloids can be detected in all above-ground vegetative parts.[28] Moreover, preliminary data suggest that zygacine can be detected in floral rewards, including nectar and pollen of *Z. paniculatus*.[32] In an experiment, adults of the generalist bee *Osmia lignaria* were paralyzed and died soon after feeding on biologically relevant doses of zygacine,[32] matching results suggesting toxicity of nectar and pollen of *Z. venenosus* to honey bees (*Apis mellifera*).[33] Larval progeny of *O. lignaria* also died when they were fed provisions with zygacine.[32] The authors suggest that the presence of zygacine in nectar and pollen may explain the absence of generalist pollinators visiting this plant and that *A. astragali* and pollinating flies may have adaptations to cope with consumption of zygacine.

***Veratrum* spp. (Corn Lily; Melanthiaceae).** The dominant floral visitors of *Veratrum* spp., such as *Veratrum album*, are ants, flies, and beetles.[34] In *V. album* there was also a single record of a bee belonging to the Halictidae visiting the flowers.[34] *Veratrum* spp. contain a series of steroid alkaloids termed azasteroids (Table 1), such as cyclopamine, **2** (Figure 2), of which there are different groups, including veratranine, jervanine, and cevanine; the cevanine types are similar to those found in *Zigadenus* spp.[35] These alkaloids are found in roots as well as vegetative parts and, like zygacine, are also neurotoxins that bind open voltage-sensitive calcium channels.[29] Consuming alkaloids from *V. album* suppresses larval growth in house flies (*Musca vicina*), an effect that dwindles as larvae mature and has been reported in a number of nonpollinating insect species,[36] suggesting negative post-ingestive consequences for

Table 1. Ecology and Secondary Chemistry of Select Poisonous Plants of the Western United States and Impacts on Floral Visitors

plant genus	secondary chemistry	primary pollinators	effects on floral visitors
Zigadenus	cevanine-type steroidal alkaloids	flies, specialized bee *Andrena astragali*, some bees in the Halictidae	zygacine causes mortality in *Osmia lignaria*[32]
Veratrum	azasteroid-type steroidal alkaloids	ants, flies, beetles, rarely bees	induces mortality in house flies and honey bees[36,38,39]
Delphinium	lycoctonine-type C_{19} norditerpene alkaloids	bees (especially bumble bees), hummingbirds	dose-dependent deterrence and reductions in bee activity[4,7]
Aconitum	aconitine-type C_{19} diterpene alkaloids	bees (especially bumble bees), hummingbirds	detected at trace concentrations in bumble bee tissues but effects on bees unknown[48]
Nicotiana	piperidine and pyridine alkaloids	bees, hawkmoths, hummingbirds	dose-dependent deterrence and reductions in bee health and survival[9,15,19]
Lupinus	piperidine and quinolizidine alkaloids	solitary and social bees	sparteine has both deterrent and toxic effects on honey bees[9]

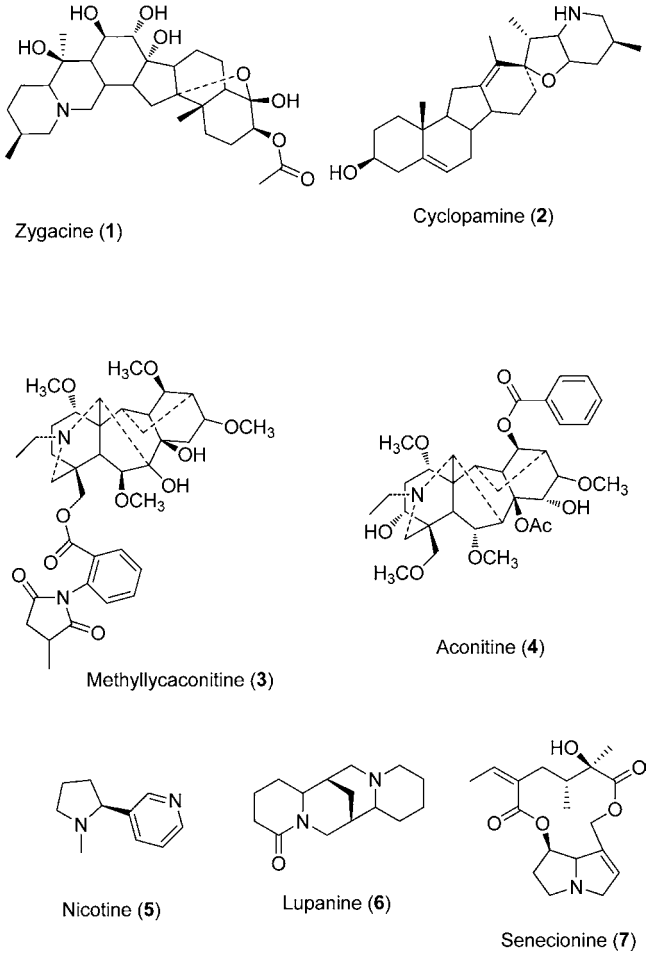

Figure 2. Chemical structures of zygacine, **1**, a steroidal alkaloid from *Zigadenus* spp.; cyclopamine, **2**, a steroidal alkaloid from *Veratrum* spp.; methyllycaconitine, **3**, a norditerpene alkaloid from *Delphinium* spp.; aconitine, **4**, a diterpene alkaloid from *Aconitum* spp.; nicotine, **5**, a pyridine alkaloid from *Nicotiana* spp.; lupanine, **6**, a quinolizidine alkaloid from *Lupinus* spp.; and senecionine, **7**, a pyrrolizidine alkaloid from *Senecio* spp.

pollinator development. Moreover, alkaloids of *V. album* are sequestered by the specialist sawfly *Rhadinoceraea nodicornis*, reducing predation by ants, spiders, and bush crickets.[37] However, no studies to our knowledge have documented the identities and concentrations of alkaloids in *Veratrum* spp. floral rewards, although reports exist of *Veratrum californicum* toxicity to honey bees foraging in the field.[38,39] The structural similarity between some of the *Veratrum* spp. alkaloids and those found in *Zigadenus* spp. leads to speculation of the possibility that these compounds may deter generalist bee pollinators from visiting these plants, as has also been speculated in *Zigadenus* spp. This hypothesis warrants further investigation.

***Delphinium* spp. (Larkspur; Ranunculaceae).** The dominant floral visitors of *Delphinium* spp. are generalists, including a variety of bees, especially bumble bees, as well as hummingbirds.[40,41] The nectar of *Delphinium* flowers is recessed within a nectar spur, so only bees and hummingbirds with a long proboscis or bill can reach the nectar rewards. *Delphinium* spp. contain a series of C_{19} norditerpene alkaloids mainly of the lycoctonine type (Table 1); several of these alkaloids are usually found in any given species. These lycoctonine C_{19} norditerpene alkaloids are divided in two structural classes, the *N*-(methylsuccinimido)anthranoyllycoctonine (MSAL) type, **3** (Figure 2), and the 7,8-methylenedioxylycoctonine (MDL) type, the former being more toxic and the latter less toxic.[42] These alkaloids bind to acetylcholine receptors and are toxic to mammals and insects.[43−45] Consumption of these plants causes significant cattle losses on an annual basis throughout the western United States.[42] *Delphinium barbeyi* and *Delphinium nuttallianum* contain alkaloids in vegetative and floral parts as well as the floral rewards, including nectar and pollen.[4] Alkaloid concentrations differ between floral rewards, vegetative, and floral parts (Figure 3), with alkaloid concentrations in the nectar being at

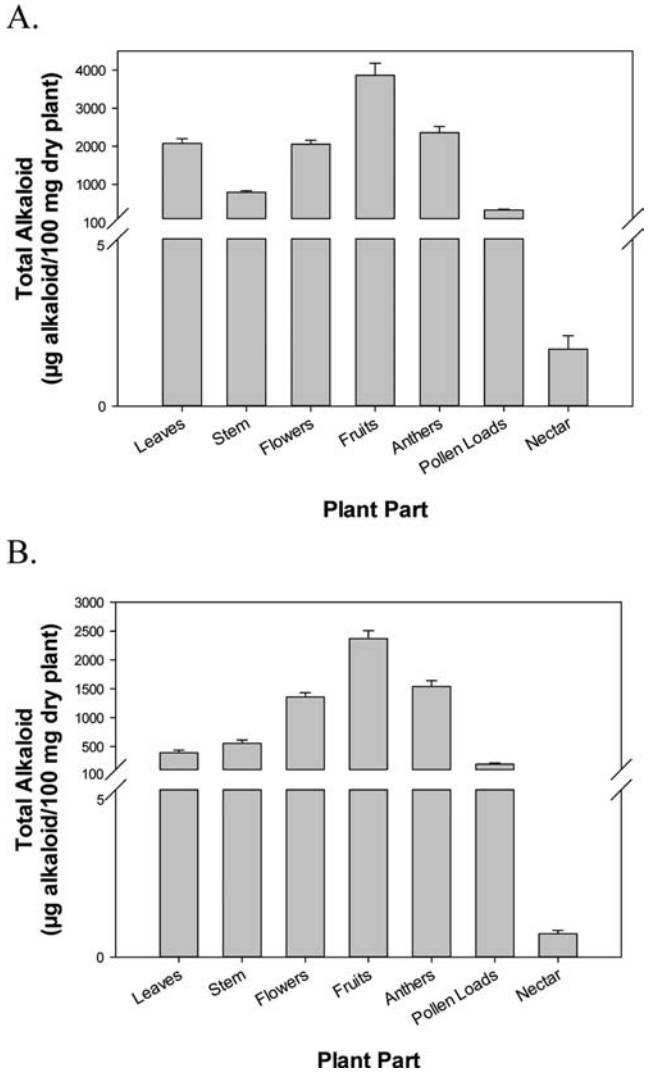

Figure 3. Total alkaloid amounts in different plant parts of (A) *Delphinium barbeyi* and (B) *Delphinium nuttallianum*. Bars are means + SE.

least 450 times less than any vegetative or floral part in both species. Alkaloid concentrations in *Delphinium* pollen are likely to be intermediate to concentrations in pollen loads and anthers as anthers contain other tissues that may overestimate actual pollen concentrations, whereas pollen loads contain nectar that may underestimate pollen concentrations.[4] The alkaloid profile observed in floral rewards is qualitatively similar to the profile found in vegetative parts in both species. Bees fed sugar water supplemented with *Delphinium* alkaloids exhibited

dx.doi.org/10.1021/jf500521w | J. Agric. Food Chem. 2014, 62, 7335−7344

reduced activity, but only at concentrations at least 50 times higher than those detected in floral nectar.[4,7] *D. barbeyi* flowers supplemented with alkaloids had fewer visits by bee pollinators, and bees spent less time per visit, but the effect was concentration dependent.[7] Whereas *D. barbeyi* nectar alkaloid concentrations within the natural range had no effect on bee behavior, alkaloid concentrations higher than reported in nature strongly deterred pollinators, suggesting an adaptive benefit to low nectar alkaloid concentrations to encourage pollination.[7]

***Aconitum* spp. (Monkshood; Ranunculaceae).** *Aconitum* spp. are typically visited by generalist pollinators, including bumble bees and hummingbirds, and in rare instances by specialists.[46−48] The flowers of *Aconitum* spp. are characterized by one of their petaloid sepals forming a hood that holds two nectar spurs on stalks; thus, like *Delphinium* spp., nectar is only accessible to visitors with a long proboscis. *Aconitum* spp. contain a series of C_{19} diterpene alkaloids mainly of the aconitine type, **4** (Table 1; Figure 2). Aconitine-type alkaloids are neurotoxic and cardiotoxic to insects and mammals,[30,49] including livestock; however, there are few livestock morbidity reports from consumption of *Aconitum* as it is seldom eaten in sufficient quantity to cause mortality.[30] Gosselin et al.[48] reported alkaloid concentrations in different plant parts as well as floral rewards in *Aconitum septentrionale*. Alkaloid concentrations in pollen were similar to leaf and flower concentrations, whereas concentrations in nectar were significantly lower. Lappaconitine was the dominant alkaloid in all plant parts investigated including the floral rewards, although some differences were observed in the rank order of abundance of other alkaloids between other tissues and floral rewards. *A. septentrionale* pollen contains alkaloids in concentrations above the LD_{50} concentrations for most alkaloids tested by Detzel and Wink[9] on honey bees, suggesting the potential for post-consumptive effects on pollinator performance. However, effects of *A. septentrionale* alkaloids on bumble bee pollinator larval survival and performance remain unknown. Additionally, Gosselin et al.[48] detected the alkaloid lappaconitine in the tissues of the specialist bumble bee *Bombus consobrinus* but not the generalist *Bombus wurflenii*. Whether this observation has any biological significance or results in a fitness benefit is not known.

***Nicotiana* spp. (Tobacco; Solanaceae).** *Nicotiana* spp. are visited by a suite of generalist pollinators, including bees, hawkmoths, and hummingbirds. *Nicotiana* spp. contain several piperidine and pyridine alkaloids (Table 1), including nicotine, **5** (Figure 2), that can be toxic to insects and mammals.[50,51] Nicotine acts as a stimulant and binds as an agonist to nicotinic acetylcholine receptors. Nicotine is synthesized in the root and transported to all above-ground plant parts, including floral rewards,[50,52,53] with nicotine concentrations in leaves and flowers being greater than that in nectar. In general, species that contain greater concentrations of nicotine in leaves have greater amounts of nicotine in their nectar.[53] Nicotine can reduce the amount of time spent per flower, as well as the amount of nectar removed per visit, by hawkmoth and hummingbird pollinators.[8,54] However, the deterrent effects of nicotine in nectar can be dose-dependent[15,55] and dependent on nectar-sugar concentration,[15] and even at the highest concentrations of nicotine in artificial nectar, there is not complete deterrence.[15] Moreover, Singaravelan et al.[19] found that nectar with low nicotine concentrations is preferred by honey bees over nectar that contains no nicotine, suggesting that low nicotine concentrations may act as attractants or feeding cues. Nicotine consumption also has dose-dependent effects on honey bee health and survival.[9,14,15]

***Lupinus* spp. (Lupine; Fabaceae).** The pea-like flowers of *Lupinus* spp. have an upper banner petal and two lower petals fused into a keel. Pollinators must be strong enough to push down the keel to gain access to the pollen, and in some cases nectar, with bees being the most common pollinators. *Lupinus* spp. contain piperidine and quinolizidine alkaloids (Table 1), such as lupanine, **6** (Figure 2), that bind to nicotinic and muscarinic acetylcholine receptors. These alkaloids are toxic to livestock and are thought to provide protection against natural enemies, including insects.[56−58] Detzel and Wink[9] documented alkaloids in the pollen of *Lupinus polyphyllus*, with pollen alkaloid concentrations being 5 times less than that in flowers and 27 times less than that in leaves. Sparteine, identified in *L. polyphyllus* pollen, has both deterrent and toxic effects on honey bees in the laboratory.[9]

Other Genera. There are several other toxic rangeland plant genera of the western United States, including *Senecio* spp. (Asteraceae) and *Echium* spp. (Boraginaceae). *Senecio* spp. are visited by a suite of generalist pollinators; *Echium* spp. such as *Echium vulgare* can be visited by generalist species of bumble bees in their introduced range in North America but are also the host plants of several oligolectic bees in their native range.[59] *Senecio* and *Echium* spp. both contain pyrrolizidine alkaloids.[30,60] Pyrrolizidine alkaloids, such as senecionine, **7** (Figure 2), are hepatotoxic to livestock and are thought to provide protection to the plants against natural enemies, including insects.[61] These alkaloids have been detected in the pollen and/or flowers (or florets) of different species within each genus.[62] Moreover, pyrrolizidine alkaloids have been detected in honey from *Echium*[62−65] and *Senecio*;[66] whether these alkaloids in honey come from pollen, nectar, or both reward sources remains to be determined. 1,2-Unsaturated tertiary pyrrolizidine alkaloids of *Senecio vernalis* were toxic to honey bees at a concentration of 2% in the laboratory, and honey bees were deterred by pyrrolizidine-*N*-oxides at concentrations >0.2%.[17] How common these effects are on the preference and performance of other pollinators remains to be investigated.

Synthesis. Three general patterns emerge from examination of the case studies. First, secondary compound concentrations in nectar tend to be lower than in pollen or leaves. Second, pollen secondary compound concentrations can, in some cases, be equal to or even higher than those concentrations found in leaves. Third, secondary compounds in floral rewards can act as filters on the community of species visiting flowers, sometimes discouraging visitation by nonspecialist pollinators or nectar robbers or thieves, which could increase the chance of pollen transfer for plants. The ecological and evolutionary implications of these patterns for both plants and pollinators remain to be explored in most cases, and the biochemical and physiological mechanisms behind secondary compounds in nectar are an active area of research.[3]

HOW DO POLLINATORS COPE WITH PLANT SECONDARY COMPOUNDS?

Given that pollinators are exposed to secondary compounds in their diet and frequently survive after consuming these compounds, pollinators, like herbivores, may have mechanisms to cope with the consumption of secondary compounds. Indeed, pollinators and herbivores likely use some of the same biochemical, physiological, and behavioral mechanisms. We focus our review primarily on how bee pollinators survive the

consumption of secondary compounds, but we note that the frugivory literature[67] may also provide testable predictions for how vertebrate pollinators cope with the consumption of not only fruit but also nectar or pollen with secondary compounds. Moreover, we broaden this portion of the review beyond alkaloids to include other classes of secondary compounds that can occur in floral rewards and how pollinators cope with their consumption, including phenolics and terpenoids.

Biochemical and Physiological Mechanisms. There are a variety of biochemical and physiological mechanisms that may help bees survive the consumption of secondary compounds, including detoxification, conjugation, target-site insensitivity, sequestration, rapid excretion, and endosymbionts. Although these mechanisms have been studied in greater depth in herbivores, there is some evidence that bees and/or other pollinators also use some of the same types of mechanisms, with the most literature documenting detoxification.

Detoxification. A common way that animals cope with a variety of potentially toxic compounds is through enzymatic conversion to less toxic forms that can then be eliminated. One of the most prominent superfamilies of enzymes is the cytochrome P450 superfamily of monooxygenases that catalyze the oxidation of organic substances. P450s are present in a wide diversity of prokaryotic and eukaryotic taxa, including pollinating bees. For bees, the diversity and activity of P450s have been studied in the most depth in honey bees and to a lesser extent in bumble bees. Honey and bumble bees contain significantly fewer P450 genes than other insect genomes, such as flies;[68] for example, the honey bee genome contains only 46 P450 genes, almost half that contained in other insect genomes.[69] Why bee genomes are relatively depauperate in detoxification genes relative to other insects remains an active area of research, especially given the generalized foraging strategy of most solitary and social bees. However, one relevant hypothesis is that because nectar and sometimes pollen have lower concentrations of secondary compounds than leaves,[4,6,9] natural selection for detoxification genes in bees may be weaker than that in phytophagous insects,[68] the adults of which may nectar-feed but larvae feed on leaf material.

Nonetheless, a number of P450s in bees have been implicated in the metabolism of secondary compounds found in nectar and pollen as well as xenobiotics, such as acaricides used to control *Varroa* mites,[70] and the CYP6 family of P450s has shown expansion relative to other insect genomes and may be involved in the metabolism of phytochemicals found in nectar, pollen, and honey.[69,71] For example, quercetin, a flavonoid found in honey and pollen, is metabolized by five enzymes in the CYP6AS and CYP9Q subfamilies of P450s.[70,71] In a similar vein, phytochemicals found in pollen and honey, such as *p*-coumaric acid, result in the up-regulation of detoxification genes.[72] *p*-Coumaric acid is ubiquitous in pollen and nonfiltered honey and, although unlikely to be toxic to bees, it may serve as a predictable cue for the up-regulation of detoxification genes against a wide variety of secondary compounds. Honey bees are also exposed to plant secondary compounds when they gather resins from vegetation to produce propolis, a sticky substance used in hive maintenance and architecture.[73] A set of propolis-derived phenolic compounds, such as pinocembrin and pinobanksin, are present in most honeys, where they are considered minor contaminants.[74] These compounds have also been shown to up-regulate P450 detoxification genes.[72]

Along with P450s, other enzyme systems may also play a role in metabolic detoxification, including the carboxylesterases (COEs). COEs catalyze the hydrolysis of esters into amino acids and alcohol. For example, albeit to a lesser extent than P450s, COEs may also be responsible for the detoxification of pyrethroids,[75] insecticides derived from pyrethrins naturally occurring in *Tanacetum* spp. daisies. Like the P450s, there are only about half as many COE protein-coding genes compared to other insect genomes.[69] Additionally, the expression and thus activity of the various detoxification genes may vary as a function of bee sex and/or exposure at a particular life history stage.[68]

Conjugation. Conjugation, another form of detoxification, involves the production of a compound that binds to the secondary compound, which is thus rendered harmless and excreted.[76,77] For example, the superfamily of glutathione *S*-transferases (GSTs) can catalyze the conjugation of exogeneous toxins, including pyrethroids (originally derived from plants) and other xenobiotics.[78,79] Treatment with the pyrethroid flumethrin increased GST activity in larvae, pupae, and nurse honey bees.[80] However, in another study exploring honey bee tolerance to pyrethroids, Johnson et al.[75] found that GSTs did not contribute significantly to honey bee pyrethroid tolerance. To our knowledge, the role of conjugation as a countermeasure for secondary compound consumption is not well explored in bees and warrants further research.

Target-Site Insensitivity. Target-site insensitivity occurs when there is a change at a neuroreceptor site for a particular secondary compound that subsequently inhibits or excludes binding, or when there is a change in the number of receptors for a particular compound, and is a primary mechanism by which herbivores can become resistant to pesticides.[81,82] Although the role of target-site insensitivity to secondary compounds is relatively unexplored in bees, it may play a role in other types of pollinators consuming secondary compounds. For example, target-site insensitivity to milkweed (*Asclepias* spp.) cardenolides occurs in a number of herbivores, including the monarch butterfly (*Danus plexippus*; Lepidoptera) and four other insect orders (Heteroptera, Orthoptera, Coleoptera, and Diptera).[83] Because *D. plexippus* adults can also act as pollinators of milkweed and milkweed nectar can contain toxic cardenolides,[84] it is plausible that target-site insensitivity may also play a role in allowing adults to cope with the consumption of secondary compounds. We should note, however, that target-site insensitivity is not universal in herbivores that feed on cardenolides; for example, arctiid moths feeding on cardenolides may use the perineurium surrounding the nervous tissue as a barrier, preventing cardenolides from reaching the Na^+/K^+-ATPase in the central nerve cord.[85] Nonetheless, adults sometimes nectar feed on the same host plants as their folivorous larvae. These cases may provide insights into the biochemical and physiological mechanisms that adult pollinators use to cope with these compounds.[86]

Sequestration. Some foliar herbivores concentrate and retain secondary compounds from their diets, a phenomenon known as sequestration.[87] As most pollinators consume plant material, it is possible that they too sequester secondary metabolites, but this has been studied for only a few pollination systems. Several species of male ithomiine butterflies (Nymphalidae: Danainae) avidly seek and consume floral nectars containing pyrrolizidine alkaloids, which they sequester.[88] These alkaloids deter predators,[89,90] serve as pheromone

precursors, and operate in a sexual selection mating system.[91] In another example, Southeast Asian *Bulbophyllum* orchids attract their fruit fly (Tephritidae) pollinators with phenylpropanoid secretions including zingerone and methyleugenol; male flies sequester these compounds, converting them to sex pheromones.[92−94]

It is possible that bees might also sequester secondary compounds, because their diet consists almost entirely of nectar and pollen that often contain those compounds, and other herbivorous Hymenoptera such as sawflies commonly sequester compounds such as iridoid glycosides and glucosinolates.[87] In the only study to our knowledge that has investigated sequestration by bees, Gosselin et al.[48] reported trace amounts of six alkaloids in the tissues of a bumble bee species foraging on *Aconitum septentrionale*, including the aconitine-type alkaloid lappaconitine, the major alkaloid in pollen and nectar; however, there was no evidence that bees concentrated the alkaloids. Sequestration is most often found in insects with specialized diets, and given that ∼20% of bees specialize in their pollen collections, the possibility of sequestration of secondary compounds by bees is a research avenue that deserves further attention.

Rapid Excretion. Rapid excretion of secondary compounds either with or without detoxification may serve as another mechanism by which pollinators cope with the consumption of these compounds. One striking example is the reduced gut retention time following consumption of secondary compounds involving Palestine sunbirds (*Nectarinia osea*) feeding on the nectar of tree tobacco (*Nicotiana glauca*). The nectar of *N. glauca* contains the pyridine alkaloids anabasine and nicotine. Gut transit time of a sugar solution containing either of the pyridine alkaloids was significantly lower when compared to that of birds fed a sugar solution without the alkaloids.[55] The authors suggest that consuming pyridine alkaloids may induce a laxative effect, as is observed in mammals that consume plant material containing pyridine alkaloids, which results in accelerated gut transit time due to increased tone and activity of the intestinal smooth muscles.[95] A laxative effect of secondary compounds may be common in other plant-pollinator systems as well but remains to be tested widely.

Endosymbionts. Many species of invertebrates harbor endosymbiotic microbes in their guts, which may play a role in the detoxification of secondary compounds.[96,97] Bees interact with specific suites of horizontally transmitted bacteria[98,99] that mediate immune responses to gut pathogens[100] and may play a role in digestion of plant foods.[101] Some phytophagous beetles interact with endosymbiotic gut fungi that assimilate carbon from their hosts' diets, sometimes detoxifying alkaloids and other potentially toxic compounds to do so.[96,102] Although a detoxifying effect has not been demonstrated for endosymbiotic fungi of pollinators such as bees, the possibility is worth exploring given that bees harbor a diversity of gut fungi.[103]

Behavioral Mechanisms. Behavioral mechanisms may also help pollinators cope with secondary compounds. Here we highlight three strategies: avoidance, diet mixing, and storage.

Avoidance. Biochemical and physiological mechanisms to cope with secondary compounds usually occur or are induced following compound ingestion. In contrast, behavioral mechanisms such as avoidance (or deterrence) can prevent pollinators from consuming or collecting nectar or pollen with secondary compounds prior to tasting their food (i.e., via olfactory or visual cues) as well as reduce feeding once a foraging choice has been made (i.e., via reduced per-flower visit length or the number of flowers visited per plant). For example, the darkly colored nectar of the South African aloe *Aloe vryheidensis* may serve as a warning to some floral visitors of the bitter-tasting phenolic nectar, albeit other visitors might find such coloration attractive.[104] In comparison, high concentrations of nectar alkaloids in *Gelsemium sempervirens* have no effect on whether or not a plant is visited, but do affect floral visitor behavior once pollinators have tasted the nectar, reducing the proportion of flowers visited per plant and the time spent per flower.[6]

Secondary compounds in floral rewards may not only affect adult foragers but also their offspring when bees collect nectar and pollen to provision to their larvae. Just as adult phytophagous insects can avoid exposing their larvae to toxic plants by not ovipositing on them,[105] adult bees could similarly limit larval exposure to secondary compounds by reduced nectar and pollen gathering from sources with floral secondary compounds. In Lepidoptera, the link between oviposition preference and offspring performance can be genetically controlled.[106] The degree to which such preference−performance matches occur and are genetically determined in bees is less explored. One strong difference, however, between phytophagous insects and bees is that, in some cases, adult phytophagous insects are unable to determine which plants are suitable for their larval offspring,[107] but larvae can move between plant species if poor oviposition choices are made.[108] In contrast, bee larvae typically cannot use movement as a behavior to avoid feeding on unsuitable provisions, including those that may have secondary compounds, and thus are forced to eat provisions that may be distasteful and/or toxic.

Diet Mixing. Like many mammalian herbivores, most bees are dietary generalists and are thus exposed to a great diversity of plant secondary compounds. Mixing the products of many plants could dilute the negative effects of any one compound, thereby allowing generalists to exploit a food base that includes nectar and pollen containing secondary compounds.[109] Research with solitary bees (*Osmia* spp.: Megachilidae) demonstrates that foragers will incur greater energetic costs than necessary to assemble pollen loads from a variety of plant species, rather than a single species near the nest,[110] and that bees may develop normally on pollen mixtures that contain up to 50% of a toxic pollen that is lethal when consumed alone.[111] This increased energy expenditure to collect pollen from a variety of plant species may be a mechanism to prevent larval toxicity and/or to balance nutrient acquisition, although such hypotheses warrant further investigation.

Storage. There is evidence that pollinators can avoid negative consequences of secondary compound consumption through social behaviors such as honey production and storage. Honey is the product of enzymatic conversion and dehydration of floral nectar by honey bees and related Apidae.[112] Glucose oxidase, a product of the hypopharyngeal gland of nurse honey bees, may deactivate (or suppress induction of) alkaloids[113] and lower the secondary compound content of plant nectar within the hive.[14,114] Moreover, honey bees maintain a nest homeostasis that is high in temperature and low in CO_2 relative to the environment, which promotes the modification and/or degradation of phenolic compounds.[114] However, toxic honeys have long been known[115] and may also contain unadulterated secondary compounds such as the grayanotoxins of *Rhododendron* (Ericaceae).[116] Although there are reports of nectars that are toxic to bees[117] and some honey is toxic to humans, we do not know whether such "toxic honeys" are toxic to the bees that

produce them. Future research should examine the role of apparently toxic honey in the ecology of social bees.

FUTURE DIRECTIONS

Exciting challenges remain in the study of secondary compounds in floral rewards. Throughout this review we have highlighted a diversity of topics warranting further investigation. Here we highlight three areas that we believe are particularly promising for future research.

Chemistry and Biochemistry of Secondary Compounds in Floral Rewards. Plant secondary compounds have been quintessential in the study of plant−herbivore interactions, and there is growing recognition that these compounds occur in floral rewards.[1,3] A historical survey of plants suggests the commonality of secondary compounds in nectar,[2] with 55% of plants surveyed containing nonprotein amino acids in their nectar, 36% containing phenolics, and 9% containing alkaloids. However, few studies have identified and measured actual concentrations of secondary compounds in nectar and/or pollen rewards and how they relate to secondary compound expression in a whole-plant context.[4,9,48,53,84,118,119] Measuring secondary compounds in floral rewards within a whole-plant context provides an ideal opportunity to test predictions about compound expression related to optimal defense theory.[84,120] A variety of analytical tools are now available to measure both within-species and among-species variation in floral reward chemistry, including large-scale, nontargeted metabolomics approaches.

There is a dearth of information not only on the identities and concentrations of secondary compounds in floral rewards but also of the origin of these reward components. Especially within the context of nectar, where nectar secondary compounds are produced and how they are added to the nectar remain mysteries in most cases. Studies that measure nectar secondary compounds within a whole-plant context should also consider measuring their identities and concentrations in the phloem sap. Doing so may help to identify those compounds that are manufactured by the nectary itself versus those that come from the phloem sap and thus may be a pleiotropic consequence of plant defense against herbivores. Physiological and molecular research into the secretion mechanisms of secondary compounds may also help to identify compounds that serve an adaptive function.

Costs and Benefits of Secondary Compound Consumption for Pollinators. Studies that have focused on the costs and benefits of secondary compounds in floral rewards have in many cases been phytocentric, measuring their effect on plant fitness via changes in pollinator behavior.[6,119] However, as consumers of nectar and pollen, pollinators such as bees are exposed to a diverse array of secondary compounds in their diet. Thus, there is nearly unlimited opportunity to assess how secondary compounds in a pollinator's diet affect performance and fitness and to assess the mechanisms involved. Since the 1800s, there has been recognition that honeys can become contaminated with floral products from nectar and pollen that are harmful to human health, and so it is logical to extend these effects to natural consumers of nectar and pollen. The handful of studies conducted thus far show variable effects of secondary compounds on pollinator performance, even when the same compound is explored. For example, the nectar alkaloid gelsemine reduced oocyte width in subordinate but not dominant bumble bees of *Bombus impatiens*,[13] whereas the same nectar alkaloid had no effect on larval survival or weight of the solitary bee *Osmia lignaria*.[121] Future research should consider that secondary compounds in floral rewards may have not only costs for pollinator preference, performance, and fitness but also potentially benefits and that the relative costs versus benefits may be dependent on the identify and concentration of secondary compound consumed. Moreover, more mechanistic studies are needed from a diversity of approaches, including molecular, biochemical, physiological, and behavioral, that explore how pollinators cope with and benefit from secondary compound consumption and the potential consequences for interactions with other factors, including xenobiotics and parasites. Given widespread concerns over pollinator declines, a mechanistic exploration into how pollinators survive secondary compound consumption may provide insights into how pollinators handle chemical exposure in rangeland and agricultural habitats.

Role of Secondary Compounds in Pollen. Whereas the costs and benefits of nectar secondary compounds are becoming more widely explored,[1,3] research on secondary compounds in pollen has lagged behind. One challenge with the study of pollen is its dual role, both as a gamete for plants and as a reward for pollen-harvesting bees. Nonetheless, research to date suggests that pollen secondary compound concentrations can sometimes mirror or even be higher than those in flowers or leaves, albeit sometimes less chemically diverse.[4,48,118] Whether pollen secondary compounds are simply a pleiotropic consequence of plant defense and development or whether they serve an adaptive function remains to be tested in most cases. Studies that explore pollen secondary compounds using a comparative phylogenetic approach and that incorporate research both from the plant's and the floral visitor's perspective will provide important scientific insights.

AUTHOR INFORMATION

Corresponding Author

*(R.E.I.) Phone: (603) 646-3688. Fax: (603) 646-1347. E-mail: Rebecca.Irwin@Dartmouth.edu.

Funding

L.L.R. was funded by a grant from the National Science Foundation during the writing of this review (DEB-1256817). Any opinions, findings, and conclusions or recommendations expressed in this material are those of the authors and do not necessarily reflect the views of the National Science Foundation.

Notes

The authors declare no competing financial interest.

ACKNOWLEDGMENTS

We thank J. Andicoechea, Z. Gezon, R. Molyneux, G. Pardee, R. Schaeffer, C. Urbanowicz, and two anonymous reviewers for comments on the manuscript and J. Cane for permission to cite unpublished data.

REFERENCES

(1) Adler, L. S. The ecological significance of toxic nectar. *Oikos* **2000**, *91*, 409−420.

(2) Baker, H. G. Non-sugar chemical constituents of nectar. *Apidologie* **1977**, *8*, 349−356.

(3) Heil, M. Nectar: generation, regulation and ecological function. *Trends Plant Sci.* **2011**, *16*, 191−200.

(4) Cook, D.; Manson, J. S.; Gardner, D. R.; Welch, K. D.; Irwin, R. E. Norditerpene alkaloid concentrations in tissues and floral rewards of

larkspurs and impacts on pollinators. *Biochem. Syst. Ecol.* **2013**, *48*, 123−131.
(5) Rhoades, D. F.; Bergdahl, J. C. Adaptive significance of toxic nectar. *Am. Nat.* **1981**, *117*, 798−803.
(6) Adler, L. S.; Irwin, R. E. Ecological costs and benefits of defenses in nectar. *Ecology* **2005**, *86*, 2968−2978.
(7) Manson, J. S.; Cook, D.; Gardner, D. R.; Irwin, R. E. Dose-dependent effects of nectar alkaloids in a montane plant-pollinator community. *J. Ecol.* **2013**, *101*, 1604−1612.
(8) Kessler, D.; Gase, K.; Baldwin, I. T. Field experiments with transformed plants reveal the sense of floral scents. *Science* **2008**, *321*, 1200−1202.
(9) Detzel, A.; Wink, M. Attraction, deterrence or intoxication of bees (*Apis mellifera*) by plant allelochemicals. *Chemoecology* **1993**, *4*, 8−18.
(10) Hagler, J. R.; Buchmann, S. L. Honey bee (Hymenoptera: Apidae) foraging responses to phenolic-rich nectars. *J. Kans. Entomol. Soc.* **1993**, *66*, 223−230.
(11) Stephenson, A. G. Iridoid glycosides in the nectar of *Catalpa speciosa* are unpalatable to nectar thieves. *J. Chem. Ecol.* **1982**, *8*, 1025−1034.
(12) Feinsinger, P.; Swarm, L. A. How common are ant-repellant nectars? *Biotropica* **1978**, *10*, 238−239.
(13) Manson, J. S.; Thomson, J. D. Post-ingestive effects of nectar alkaloids depend on dominance status of bumble bees. *Ecol. Entomol.* **2009**, *34*, 421−426.
(14) Singaravelan, N.; Inbar, M.; Ne'eman, G.; Distl, M.; Wink, M.; Izhaki, I. The effects of nectar-nicotine on colony fitness of caged honeybees. *J. Chem. Ecol.* **2006**, *32*, 49−58.
(15) Köhler, A.; Pirk, C. W. W.; Nicolson, S. W. Honeybees and nectar nicotine: deterrence and reduced survival versus potential health benefits. *J. Insect Physiol.* **2012**, *58*, 286−292.
(16) Sedivy, C.; Piskorski, R.; Müller, A.; Dorn, S. Too low to kill: concentration of the secondary metabolite ranunculin in buttercup pollen does not affect bee larval survival. *J. Chem. Ecol.* **2012**, *38*, 996−1002.
(17) Reinhard, A.; Janke, M.; von der Ohe, W.; Kempf, M.; Theuring, C.; Hartmann, T.; Schreier, P.; Beuerle, T. Feeding deterrence and detrimental effects of pyrrolizidine alkaloids fed to hone bees (*Apis mellifera*). *J. Chem. Ecol.* **2009**, *35*, 1086−1095.
(18) Manson, J. S.; Otterstatter, M. C.; Thomson, J. D. Consumption of a nectar alkaloid reduces pathogen load in bumble bees. *Oecologia* **2010**, *162*, 81−89.
(19) Singaravelan, N.; Nee'man, G.; Inbar, M.; Izhaki, I. Feeding responses of free-flying honeybees to secondary compounds mimicking floral nectars. *J. Chem. Ecol.* **2005**, *31*, 2791−2804.
(20) Wright, G. A.; Baker, D. D.; Palmer, M. J.; Stabler, D.; Mustard, J. A.; Power, E. F.; Borland, A. M.; Stevenson, P. C. Caffeine in floral nectar enhances a pollinator's memory of reward. *Science* **2013**, *339*, 1202−1204.
(21) Aniszewski, T. *Alkaloids − Secrets of Life*; Elsevier: Amsterdam, The Netherlands, 2007.
(22) Zomlefer, W. B.; Judd, W. S. Resurrection of segregates of the polyphyletic genus *Zigadenus* s.l. (Liliales: Melanthiaceae) and resulting new combinations. *Novon* **2002**, *12*, 299−308.
(23) Tepedino, V. J. What's in a name? The confusing case of the death camas bee *Andrena astragali*. *J. Kans. Entomol. Soc.* **2003**, *76*, 194−197.
(24) Tepedino, V. J.; Knapp, A. K.; Eickwort, G. C.; Ferguson, D. C. Death camas (*Zigadenus nuttallii*) in Kansas: pollen collectors and a florivore. *J. Kans. Entomol. Soc.* **1989**, *62*, 411−412.
(25) Bernhardt, P. Anthecology of *Schrankia nuttallii* (Mimosaceae) on the tallgrass prairie. *Plant Syst. Evol.* **1990**, *170*, 247−255.
(26) Kupchan, S. M.; Deliwala, C. V. *Zygadenus* alkaloids. III. Active principles of *Zygadenus venenosus*. Veratroylzygadenine and vanilloylzygadenin. *J. Am. Chem. Soc.* **1953**, *75*, 1025−1029.
(27) Majak, W.; McDiarmid, R. E.; Cristofoli, W.; Sun, F.; Benn, M. Content of zygacine in *Zygadenus venenosus* at different stages of growth. *Phytochemistry* **1992**, *31*, 3417−3418.
(28) Makeiff, D.; Majak, W.; McDiarmid, R. E.; Reaney, B.; Benn, M. H. Determination of zygacine in *Zigdenus venenosus* (death camas) by image analysis on thin layer chromatography. *J. Agric. Food. Chem.* **1997**, *45*, 1209−1211.
(29) Catterall, W. A. Neurotoxins that act on voltage-sensitive sodium channels in excitable membranes. *Annu. Rev. Pharmacol. Toxicol.* **1980**, *20*, 15−42.
(30) Burrows, G. E.; Tyrl, R. J. *Toxic Plants of North America*, 1st ed.; Iowa State University Press: Ames, IA, USA, 2001.
(31) Welch, K. D.; Panter, K. E.; Gardner, D. R.; Stegelmeier, B. L.; Green, B. T.; Pfister, J. A.; Cook, D. The acute toxicity of the death camas alkaloid zygacine in mice, including the effect of methyllycaconitine co-administration on zygacine toxicity. *J. Anim. Sci.* **2011**, *89*, 1650−1657.
(32) Cane, J.; Weber, M.; Yost, M.; Gardner, D. Alkaloids and old lace: pollen toxins exclude generalist pollinators from death camus (*Toxicoscordion* [= *Zigadenus*] *paniculatum*) (Melanthiaceae). In *Botany Conference*, Salt Lake City, UT, USA, 2004; http://2004.botanyconference.org/engine/search/index.php?func=detail&aid=1128.
(33) Hitchcock, J. D. Poisoning of honey bees by death camas blossoms. *Am. Bee J.* **1959**, *99*, 418−419.
(34) Kato, Y.; Araki, K.; Ohara, M. Breeding system and floral visitors of *Veratrum album* subsp. *oxysepalum* (Melanthiaceae). *Plant Species Biol.* **2009**, *24*, 42−46.
(35) Tomko, J.; Voticky, Z. Steroidal alkaloids: the *Veratrum* and *Buxus* groups. In *The Alkaloids: Chemistry and Physiology*; Manske, R. H. F., Ed.; Academic Press: New York, 1973; Vol. 14, pp 1−82.
(36) Bergmann, E. D.; Levinson, Z. H.; Mechoulam, R. The toxicity of *Veratrum* and *Solanum* alkaloids to housefly larvae. *J. Insect Physiol.* **1958**, *2*, 162−177.
(37) Schaffner, U.; Boevé, J.-L.; Gfeller, H.; Schlunegger, U. P. Sequestration of *Veratrum* alkaloids by specialist *Rhadinoceraea nodicornis* konow (Hymenoptera, Tenthredinidae) and its ecoethological implications. *J. Chem. Ecol.* **1994**, *20*, 3233−3250.
(38) Vansell, G. H.; Watkins, W. G. A plant poisonous to adult bees. *J. Econ. Entomol.* **1933**, *26*, 168−170.
(39) Eckert, J. E. Bee diseases as factors in the life and behavior of the honeybee colony. *Insectes Soc.* **1955**, *2*, 187−194.
(40) Inouye, D. W. Resource partitioning in bumblebee guilds: experimental studies of foraging behavior. *Ecology* **1978**, *59*, 672−678.
(41) Waser, N. M.; Price, M. V. Pollinator behavior and natural selection for flower color in *Delphinium nelsonii*. *Nature* **1983**, *302*, 422−424.
(42) Pfister, J. A.; Ralphs, M. H.; Gardner, D. R.; Stegelmeier, B. L.; Manners, G. D.; Panter, K. E.; Lee, S. T. Management of three toxic *Delphinium* species based on alkaloid concentrations. *Biochem. Syst. Ecol.* **2002**, *30*, 129−138.
(43) Jennings, K. R.; Brown, D. G.; Wright, D. P. Methyllycaconitine, a naturally occurring insecticide with a high affinity for the insect cholinergic receptor. *Experientia* **1986**, *42*, 611−613.
(44) Manners, G. D.; Panter, K. E.; Ralphs, H. M.; Pfister, J. A.; Olsen, J. D.; James, L. F. Toxicity and chemical phenology of norditerpenoid alkaloids in the tall larkspurs (*Delphinium* species). *J. Agric. Food Chem.* **1993**, *41*, 96−100.
(45) Manners, G. D.; Panter, K. E.; Pelletier, S. W. Structure-activity relationships of norditerpenoid alkaloids occurring in toxic larkspur (*Delphinium*) species. *J. Nat. Prod.* **1995**, *58*, 863−869.
(46) Fukuda, Y.; Suzuki, K.; Murata, J. The function of each sepal in pollinator behavior and effective pollination in *Aconitum japonicum* var. *montanum*. *Plant Species Biol.* **2001**, *16*, 151−157.
(47) Løken, A. Studies on Scandinavian bumble bees (Hymenoptera, Apidae). *Nor. Entomol. Tidsskr.* **1973**, *20*, 1−218.
(48) Gosselin, M.; Michez, D.; Vanderplanck, M.; Roelants, D.; Glauser, G.; Rasmont, P. Does *Aconitum septentrionale* chemically protect floral rewards to the advantage of specialist bumblebees? *Ecol. Entomol.* **2013**, *38*, 400−407.
(49) Ameri, A. The effects of *Aconitum* alkaloids on the central nervous system. *Prog. Neurobiol.* **1998**, *56*, 211−235.

(50) Steppuhn, A.; Gase, K.; Krock, B.; Halitschke, R.; Baldwin, I. T. Nicotine's defensive function in nature. *PLoS Biol.* **2004**, *2*, e217.
(51) Schmeltz, I. Nicotine and other tobacco alkalioids. In *Naturally Occurring Insecticides*; Jacobson, M., Crosby, D. G., Eds.; Dekker: New York, 1971; pp 99−136.
(52) Steppuhn, A.; Baldwin, I. T. Resistance management in a native plant: nicotine prevents herbivores from compensating for plant protease inhibitors. *Ecol. Lett.* **2007**, *10*, 499−511.
(53) Adler, L. S.; Seifert, M. G.; Wink, M.; Morse, G. E. Reliance on pollinators predicts defensive chemistry across tobacco species. *Ecol. Lett.* **2012**, *15*, 1140−1148.
(54) Kessler, D.; Baldwin, I. T. Making sense of nectar scents: the effects of nectar secondary metabolites on floral visitors of *Nicotiana attenuata*. *Plant J.* **2007**, *49*, 840−854.
(55) Tadmor-Melamed, H.; Markman, S.; Arieli, A.; Distl, M.; Wink, M.; Izhaki, I. Limited ability of Palestine sunbirds (*Nectarinia osea*) to cope with pyridine alkaloids in nectar of tree tobacco, *Nicotiana glauca*. *Funct. Ecol.* **2004**, *18*, 844−850.
(56) Keeler, R. F. Lupin alkaloids from teratogenic and non-teratogenic lupins. III. Identification of anagyrine as the probable teratogen by feeding trials. *J. Toxicol. Environ. Health* **1976**, *1*, 878−889.
(57) Panter, K. E.; Bunch, T. D.; Keeler, R. F.; Sisson, D. V.; Callan, R. J. Multiple congenital contractures (MCC) and cleft palate induced in goats by ingestion of piperidine alkaloid-containing plants: reduction in fetal movement as the probable cause. *Clin. Toxicol.* **1990**, *28*, 69−83.
(58) Wink, M. The role of quinolizidine alkaloids in plant−insect interactions. In *Insect−Plant Interactions*; Bernays, E. A., Ed.; CRC Press: Boca Raton, FL, USA, 1992; pp 131−166.
(59) Sedivy, C.; Dorn, S.; Widmer, A.; Müller, A. Host range evolution in a selected group of osmiine bees (Hymenoptera: Megachilidae): the Boraginaceae-Fabaceae paradox. *Biol. J. Linn. Soc.* **2013**, *108*, 35−54.
(60) Hartmann, T.; Zimmer, M. Organ-specific distribution and accumulation of pyrrolizidine alkaloids during the life history of two annual *Senecio* species. *J. Plant Physiol.* **1986**, *122*, 67−80.
(61) Stegelmeier, B. L.; Edgar, J. A.; Colegate, S. M.; Gardner, D. R.; Schoch, T. K.; Coulombe, R. A.; Molyneux, R. J. Pyrrolizidine alkaloid plants, metabolism and toxicity. *J. Nat. Toxins* **1999**, *8*, 95−116.
(62) Boppré, M.; Colegate, S. M.; Edgar, J. A.; Fischer, O. W. Hepatotoxic pyrrolizidine alkaloids in pollen and drying-related implications for commercial processing of bee pollen. *J. Agric. Food Chem.* **2008**, *56*, 5662−5672.
(63) Culvenor, C. C. J.; Edgar, J. A.; Smith, L. W. Pyrrolizidine alkaloids in honey from *Echium plantagineum* L. *J. Agric. Food. Chem.* **1981**, *29*, 958−960.
(64) Beales, K. A.; Betteridge, K.; Colegate, S. M.; John, A.; Edgar, J. Solid-phase extraction and LC−MS analysis of pyrrolizidine alkaloids in honeys. *J. Agric. Food Chem.* **2004**, *52*, 6664−6672.
(65) Betteridge, K.; Cao, Y.; Colegate, S. M. Improved method for extraction and LC-MS analysis of pyrrolizidine alkaloids and their *N*-oxides in honey: application to *Echium vulgare* honeys. *J. Agric. Food Chem.* **2005**, *53*, 1894−1902.
(66) Deinzer, M. L.; Thomson, P. A.; Burgett, D. M.; Isaacson, D. L. Pyrrolizidine alkaloids: their occurrence in honey from tansy ragwort (*Senecio jacobaea* L.). *Science* **1977**, *195*, 497−499.
(67) Cipollini, M. L.; Levey, D. J. Secondary metabolites of fleshy vertebrate-dispersed fruits: adaptive hypotheses and implications for seed dispersal. *Am. Nat.* **1997**, *150*, 346−372.
(68) Xu, J.; Strange, J. P.; Welker, D. L.; James, R. R. Detoxification and stress response genes expressed in the western North American bumble bee, *Bombus huntii* (Hymenoptera: Apidae). *BMC Genomics* **2013**, *14*, 874.
(69) Claudianos, C.; Ranson, H.; Johnson, R. M.; Biswas, S.; Schuler, M. A.; Berenbaum, M. R.; Feyereisen, R.; Oakeshott, J. G. A deficit of detoxification enzymes: pesticide sensitivity and environmental response in the honeybee. *Insect Mol. Biol.* **2006**, *15*, 615−636.
(70) Mao, W.; Schuler, M. A.; Berenbaum, M. R. CYP9Q-mediated detoxification of acaricides in the honey bee (*Apis mellifera*). *Proc. Natl. Acad. Sci. U.S.A.* **2011**, *108*, 12657−12662.
(71) Mao, W.; Rupasinghe, S. G.; Johnson, R. M.; Zangerl, A. R.; Schuler, M. A.; Berenbaum, M. R. Quercetin-metabolizing CYP6AS enzymes of the pollinator *Apis mellifera* (Hymenoptera: Apidae). *Comp. Biochem. Physiol. B* **2009**, *154*, 427−434.
(72) Mao, W.; Schuler, M. A.; Berenbaum, M. R. Honey constituents up-regulate detoxification and immunity genes in the western honey bee *Apis mellifera*. *Proc. Natl. Acad. Sci. U.S.A.* **2013**, *110*, 8842−8846.
(73) Simone-Finstrom, M.; Spivak, M. Propolis and bee health: the natural history and significance of resin use by honey bees. *Apidologie* **2010**, *41*, 295−311.
(74) Tomás-Barberán, F. A.; Martos, I.; Ferreres, F.; Radovic, B. S.; Anklam, E. HPLC flavonoid profiles as markers for the botanical origin of European unifloral honeys. *J. Sci. Food Agric.* **2001**, *81*, 485−496.
(75) Johnson, R. M.; Wen, Z.; Schuler, M. A.; Berenbaum, M. R. Mediation of pyrethroid insecticide toxicity to honey bees (Hymenoptera: *Apidae*) by cytochrome P450 monooxygenases. *J. Econ. Entomol.* **2006**, *99*, 1046−1050.
(76) Schröder, P.; Collin, C. Conjugating enzymes involved in xenobiotic metabolism of organic xenobiotics in plants. *Int. J. Phytorem.* **2002**, *4*, 247−265.
(77) Strauss, S. Y.; Zangerl, A. R. Plant-insect interactions in terrestrial ecosystems. In *Plant−Animal Interactions*; Herrera, C. M., Pellmyr, O., Eds.; Blackwell: Oxford, UK, 2002.
(78) Kostaropoulos, I.; Papadopoulos, A. I.; Metaxakis, A.; Boukouvala, E.; Papadopoulou-Mourkidou, E. Glutathione S-transferase in the defense against pyrethroids in insects. *Insect Biochem. Mol. Biol.* **2001**, *31*, 313−319.
(79) Enayati, A. A.; Ranson, H.; Hemmingway, J. Insect glutathione transferases and insecticide resistance. *Insect Mol. Biol.* **2005**, *14*, 3−8.
(80) Nielsen, S. A.; Brødsgaard, C. J.; Hansen, H. Effects on detoxification enzymes in different life stages of honey bees (*Apis mellifera* L. Hymenoptera: Apidae) treated with a synthetic phyrethroid (flumethrin). *ATLA* **2000**, *28*, 437−443.
(81) Brattsten, L. B. Enzymatic adaptations in leaf-feeding insects to host-plant allelochemicals. *J. Chem. Ecol.* **1988**, *14*, 1919−1939.
(82) Berenbaum, M. R. Target site insensitivity in insect-plant interactions. In *Molecular Aspects of Insect−Plant Associations*; Brattsten, L. B., Ahmad, S., Eds.; Plenum Press: New York, 1986; pp 257−272.
(83) Agrawal, A. A.; Petschenka, G.; Bingham, R. A.; Weber, M. G.; Rasmann, S. Toxic cardenolides: chemical ecology and coevolution of specialized plant-herbivore interactions. *New Phytol.* **2012**, *194*, 28−45.
(84) Manson, J. S.; Rasmann, S.; Halitschke, R.; Thomson, J. D.; Agrawal, A. A. Cardenolides in nectar may be more than a consequence of allocation to other plant parts: a phylogenetic study. *Funct. Ecol.* **2012**, *26*, 1100−1110.
(85) Petschenka, G.; Offe, J. K.; Dobler, S. Physiological screening for target site insensitivity and localization of Na(+)/K(+)-ATPase in cardenolide-adapted Lepidoptera. *J. Insect Physiol.* **2012**, *58*, 607−612.
(86) Wink, M.; Theile, V. Alkaloid tolerance in *Manduca sexta* and phylogenetically related sphingids (Lepidoptera: Sphingidae). *Chemoecology* **2002**, *12*, 29−46.
(87) Opitz, S.; Müller, C. Plant chemistry and insect sequestration. *Chemoecology* **2009**, *19*, 117−154.
(88) Brown, K. S. Adult-obtained pyrrolizidine alkaloids defend Ithomiine butterflies against a spider predator. *Nature* **1984**, *309*, 707−709.
(89) Trigo, J. R.; Brown, K. S.; Witte, L.; Hartmann, T.; Ernst, L.; Barata, L. E. S. Pyrrolizidine alkaloids: different acquisition and use patterns in Apocynaceae and Solanaceae feeding Ithomiine butterflies (Lepidoptera: Nymphalidae). *Biol. J. Linn. Soc.* **1996**, *58*, 99−123.
(90) Masters, A. R. Pyrrolizidine alkaloids in artificial nectar protect adult *Ithomiine* butterfiles from a spider predator. *Biotropica* **1990**, *22*, 298−304.
(91) Pliske, T. E.; Edgar, J. A.; Culvenor, C. C. J. The chemical basis of attraction of Ithomiine butterflies to plants containing pyrrolizidine alkaloids. *J. Chem. Ecol.* **1976**, *2*, 255−262.

(92) Nishida, R. Sequestration of defensive substances from plants by Lepidoptera. *Annu. Rev. Entomol.* **2002**, *47*, 57−92.
(93) Tan, K. H.; Nishida, R. Zingerone in the floral synomone of *Bulbophyllum baileyi* (Orchidaceae) attracts *Bactrocera* fruit flies during pollination. *Biochem. Syst. Ecol.* **2007**, *35*, 334−341.
(94) Tan, K. H.; Nishida, R. Methyl eugenol: its occurrence, distribution, and role in nature, especially in relation to insect behavior and pollination. *J. Insect Sci.* **2012**, *12*, 1−60.
(95) Bruneton, J. *Pharmacognosy: Phytochemistry, Medicinal Plants*, 2nd ed.; Lavoisier Publishing: Paris, France, 1999.
(96) Dowd, P. F. Insect fungal symbionts: a promising source of detoxifying enzymes. *J. Ind. Microbiol.* **1992**, *9*, 149−161.
(97) Engel, P.; Moran, N. A. The gut microbiota of insects − diversity in structure and function. *FEMS Microbiol. Rev.* **2013**, *37*, 699−735.
(98) Kaltenpoth, M.; Engl, T. Defensive microbial symbionts in Hymenoptera. *Funct. Ecol.* **2014**, *28*, 315−327.
(99) Koch, H.; Abrol, D. P.; Li, J.; Schmid-Hempel, P. Diversity and evolutionary patterns of bacterial gut associates of corbiculate bees. *Mol. Ecol.* **2013**, *22*, 2028−2044.
(100) Koch, H.; Schmid-Hempel, P. Socially transmitted gut microbiota protect bumble bees against an intestinal parasite. *Proc. Natl. Acad. Sci. U.S.A.* **2011**, *108*, 19288−19292.
(101) Koch, H.; Cisarovsky, G.; Schmid-Hempel, P. Ecological effects on gut bacterial communities in wild bumblebee colonies. *J. Anim. Ecol.* **2012**, *81*, 1202−1210.
(102) Shen, S. K.; Dowd, P. F. Detoxification spectrum of the cigarette beetle symbiont *Symbiotaphrina kochii* in culture. *Entomol. Exp. Appl.* **1991**, *60*, 51−59.
(103) Batra, L. R.; Batra, S. W. T.; Bohart, G. E. The mycoflora of domesticated and wild bees (Apoidea). *Mycopathol. Mycol. Appl.* **1973**, *49*, 13−44.
(104) Johnson, S. D.; Hargreaves, A. L.; Brown, M. Dark, bitter-tasting nectar functions as a filter of flower visitors in a bird-pollinated plant. *Ecology* **2006**, *87*, 2709−2716.
(105) Thompson, J. N. Evolutionary ecology of the relationship between oviposition preference and performance of offspring in insects. *Entomol. Exp. Appl.* **1988**, *47*, 3−14.
(106) Thompson, J. N. *The Coevolutionary Process*; University of Chicago Press: Chicago, IL, USA, 1994.
(107) Rodman, J. E.; Chew, F. S. Phytochemical correlates of herbivory in a community of native and naturalized Cruciferae. *Biochem. Syst. Ecol.* **1980**, *8*, 43−50.
(108) Thompson, J. N.; Pellmyr, O. Evolution of oviposition behavior and host preference in Lepidoptera. *Annu. Rev. Entomol.* **1991**, *36*, 65−89.
(109) Williams, N. M. Use of novel pollen species by specialist and generalist solitary bees (Hymenoptera: Megachilidae). *Oecologia* **2003**, *134*, 228−237.
(110) Williams, N. M.; Tepedino, V. J. Consistent mixing of near and distant resources in foraging bouts by the solitary mason bee *Osmia lignaria*. *Behav. Ecol.* **2003**, *14*, 141−149.
(111) Eckhardt, M.; Haider, M.; Dorn, S.; Müller, A. Pollen mixing in pollen generalist solitary bees: a possible strategy to complement or mitigate unfavourable pollen properties? *J. Anim. Ecol.* **2013**, DOI: 10.1111/1365-2656.12168.
(112) Doner, L. W. The sugars of honey − a review. *J. Sci. Food Agric.* **1977**, *28*, 443−456.
(113) Musser, R. O.; Hum-Musser, S. M.; Eichenseer, H.; Peiffer, M.; Ervin, G.; Murphy, J. B.; Felton, G. W. Herbivory: caterpillar saliva beats plant defences. *Nature* **2002**, *416*, 599−600.
(114) Liu, F.; He, J.; Fu, W. Highly controlled nest homeostasis of honey bees helps deactivate phenolics in nectar. *Naturwissenschaften* **2005**, *92*, 297−299.
(115) Ott, J. The Delphic bee: bees and toxic honeys as pointers to psychoactive and other medicinal plants. *Econ. Bot.* **1998**, *52*, 260−266.
(116) Koca, I.; Koca, A. F. Poisoning by mad honey: a brief review. *Food Chem. Toxicol.* **2007**, *45*, 1315−1318.
(117) Clinch, P. G.; Palmer-Jones, T.; Forster, I. W. Effect on honey bees of nectar from the yellow kowhai (*Sophora microphylla* Ait.). *N. Z. J. Agric. Res.* **1972**, *15*, 194−201.
(118) Frolich, C.; Hartmann, T.; Ober, D. Tissue distribution and biosynthesis of 1,2-saturated pyrrolizidine alkaloids in *Phalaenopsis* hybrids (Orchidaceae). *Phytochemistry* **2006**, *67*, 1493−1502.
(119) Kessler, D.; Bhattacharya, S.; Diezel, C.; Rothe, E.; Gase, K.; Schöttner, M.; Baldwin, I. T. Unpredictability of nectar nicotine promotes outcrossing by hummingbirds in *Nicotiana attenuata*. *Plant J.* **2012**, *71*, 529−538.
(120) Kessler, A.; Halitschke, R. Testing the potential for conflicting selection on floral chemical traits by pollinators and herbivores: predictions and case study. *Funct. Ecol.* **2009**, *23*, 901−912.
(121) Elliott, S. E.; Irwin, R. E.; Adler, L. S.; Williams, N. M. Nectar alkaloids do not affect offspring performance of a native solitary bee, *Osmia lignaria* (Megachilidae). *Ecol. Entomol.* **2008**, *33*, 298−304.

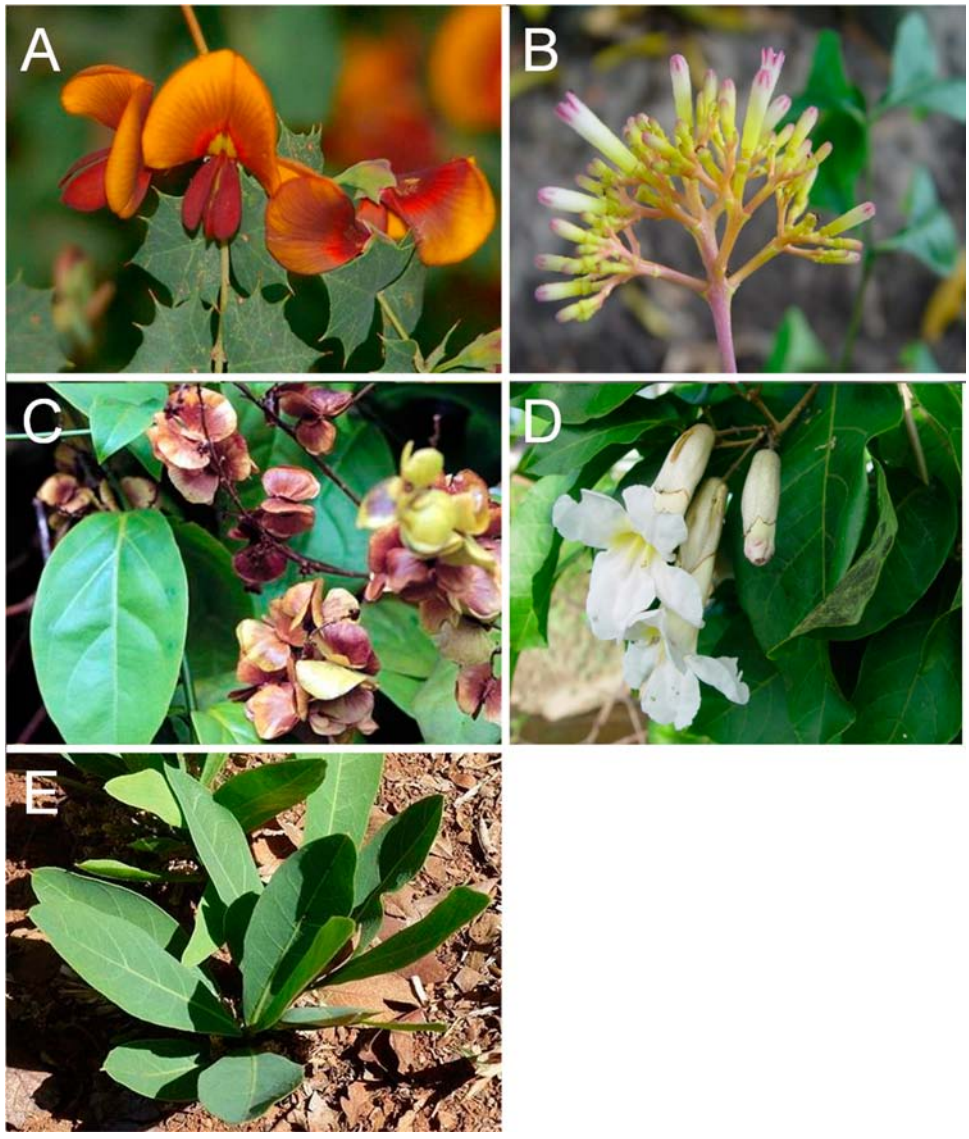

Figure 1. Photographs of representative plants containing monofluoroacetate: (A) *Gastrolobium spinosum*, image courtesy of John E. McLennan; (B) *Palicourea marcgravii*; (C) *Amorimia septentrionalis*; (D) *Arrabidaea bilabiata*; and (E) *Dichapetalum cymosum*, image provided courtesy of JMK (http://commons.wikimedia.org).

concentrations of up to 0.26% in *G. bilobum*, 0.040% in *G. spinosum*, 0.13% in *G. floribundum*, 0.13% in *G. bennettsianum*, and 0.25% in *O. parviflorum*. However, the report warned against extrapolating too much from these values because of the large variation in monofluoroacetate content that was observed within a species. Nonetheless, it was reported that monofluoroacetate concentrations were highest in the reproductive tissues, such as pods, flowers, and young leaves, and much lower in mature leaves and wood.[11−14] Table 1 lists 31 species of *Gastrolobium* and one species of *Acacia* (*A. georginae*) that have been reported to contain monofluoroacetate.[11,13−21] Not listed in Table 1 are five *Gastrolobium* species, *G. appressum*,[11,16] *G. densifolium*,[11,16,17] *G. heterophyllum*,[11,16] *G. ovalifolium*,[9,16] and *G. trilobum*,[16] that have been reported to be toxic but have not been demonstrated to contain monofluoroacetate.

The variability of monofluoroacetate content is documented throughout the *Gastrolobium*/*Acacia* literature. Some of this variation may be due to differences in analysis including the method, the place of analysis, and sampling procedures. However, it is clear that some variation is due to intrinsic biology of the plants. This variation is illustrated by the monofluoroacetate concentration in individual plants within stands of *G. brevipes* (0.0017−0.0099% in leaves and 0.0056−0.030% in pods, expressed as percent dry weight here and all subsequent occurences)[14] and between populations of *G. bilobum* with 0.0010% in leaves and 0.0073% in flowers from one location compared to 0.017% in leaves and 0.11% in flowers from another location.[13] There can be considerable intrastand variability between individual plants growing within meters of each other. For example, the monofluoroacetate concentrations in the leaves of different *G. bilobum* and *G. calycinum* plants within stands ranged from 0.023 to 0.39% and from 0.0029 to 0.058%, respectively.[13] In addition, reports of the presence of high concentrations of monofluoroacetate in leaves of *A. georginae*, *G. bilobum*, *G. calycinum*, *G. oxylobioides*, *G. villosum*, and *G. spinosum* were not confirmed by a ^{19}F NMR analysis. ^{19}F NMR failed to detect monofluoroacetate in leaves from each of these species except *G. bilobum*, for which a concentration 10 times less than reports was measured.[18]

Table 1. Monofluoroacetate-Containing Genera of the Fabaceae (*Acacia*, *Gastrolobium*), Rubiaceae (*Palicourea*), Bignoniaceae (*Arrabidaea*), Malpighiaceae (*Amorimia*), and Dichapetalaceae (*Dichapetalum*, *Tapura*)

genus	species	references	genus	species	references
Acacia	*georginae*	15, 16	*Palicourea*	*aeneofusca*	27, 28
				amapaensis	27
Gastrolobium	*bennettsianum*	11, 15		*grandiflora*	27
	bilobum	11, 13, 16–20		aff. *juruana*	27
	brevipes	14		*longiflora*	27
	brownii	21		aff. *longiflora*	27
	callistachys	16		*macarthurorum*	27
	calycinum	11, 13, 16, 18–20		*marcgravii*	25–27
	crassifolium	11, 16		*nigricans*	27
	crispatum	21		*vacillans*	27
	cuneatum	11, 16, 21			
	floribundum	11, 16, 17	*Tanaecium*	*bilabiatum*[a]	35
	glaucum	11, 16, 17			
	grandiflorum	21	*Amorimia*	*amazonica*	28
	graniticum	11, 16, 17		*camporum*	28
	hamulosum	11, 16, 17		*exotropica*	28
	laytonii	11, 16		*pubiflora*	28
	microcarpum	11, 16–18		*rigida*	28
	oxylobioides	11, 16–18		*septentrionalis*	28
	parviflorum	11, 16–20			
	polystachyum	11, 16–18	*Dichapetalum*	*barteri*	43
	pycnostachyum	11, 16, 17		*braunii*	44
	racemosum	11, 16–19		*cymosum*	45
	rigidum	11, 16, 17		*edule*	44
	rotundifolium	11, 16, 17		*heudelotii*	46
	spathulatum	13, 19, 22		*michelsonii*	44, 47
	spectrabile	11, 17		*toxicarium*	48
	spinosum	11, 13, 17, 19			
	stenophyllum	11, 16–19	*Tapura*	*fischeri*	3
	tetragonophyllum	11, 16–19			
	tomentosum	16			
	vellutinum	11, 16, 17			
	villosum	11, 13, 16–20			

[a] *Tanaecium bilabiatum* was previously known as *Arrabidaea bilabiata*.

A recent re-examination of some *Gastrolobium* spp. from Western Australia using a HPLC-APCI-MS method of analysis again documented variability reported in the literature with respect to their monofluoroacetate content (Table 1).[20] The presence of monofluoroacetate was confirmed in *G. bilobum*, *G. calycinum*, *G. parviflorum*, and *G. villosum*. However, none was detected in *G. spinosum*, *G. laytonii*, or a sample of *G. calycinum* that was collected from the Murdoch University Toxic Plant Garden (Perth, Australia), removed from its native environment over two decades ago.[20]

Rubiaceae. *Palicourea* is a genus composed of approximately 200 species, which range in growth habit from small shrubs to trees. The genus is distributed throughout the tropics of the New World.[22,23] *Palicourea marcgravii* was the first poisonous plant studied in Brazil and is the single most important toxic plant in Brazil due to its acute toxicity, palatability, and broad geographical distribution.[2,24] Three other *Palicourea* species, *P. aeneofusca*, *P. grandiflora*, and *P. juruana*, are also reported to cause sudden death. These plants have less impact due to their restricted distribution.

P. marcgravii is documented to contain monofluoroacetate,[25−27] and a recent report demonstrated that *P. aeneofusca* contains monofluoroacetate.[27,28] A systematic screening of *Palicourea* taxa was recently initiated wherein herbarium specimens were tested for monofluoroacetate (Table 1).[25−28] Monofluoroacetate was confirmed in *P. marcgravii* and *P. aeneofusca* and was detected in *P. grandiflora* and *P.* aff. *juruana*, which is consistent with these species causing sudden death.[29−31] *P.* aff. *juruana* likely corresponds to *P. juruana* as described by Tokarnia,[24] but the identity of *P. juruana* is problematic as this name has been used variously for several different species. Additionally, monofluoroacetate was detected in several other species including *P. amapaensis*, *P. macarthurorum*, and *P. nigricans*[27] (taxonomically similar to *P. grandiflora*[32]), and *P. longiflora*, *P.* aff. *longiflora*, and *P. vacillans*[27] (taxonomically similar to *P. marcgravii* and *P. aeneofusca*[32]).

There are limited data on monofluoroacetate concentrations from *Palicourea* field collections. Studies suggest that monofluoroacetate concentrations in mature leaves are highly variable within populations of *P. marcgravii* and *P. aeneofusca*, ranging from 0.03 to 0.58% and from 0.03 to 0.18%, respectively.[28] Mean concentrations of monofluoroacetate within field collections of mature leaves of *P. marcgravii* and *P. aeneofusca* were approximately 0.20 and 0.10%, respectively.[28] Young leaves from one population of *P. marcgravii* contained monofluoroacetate at concentrations of 0.88 ± 0.08%, in contrast to that in mature leaves at 0.21 ± 0.17%.[28]

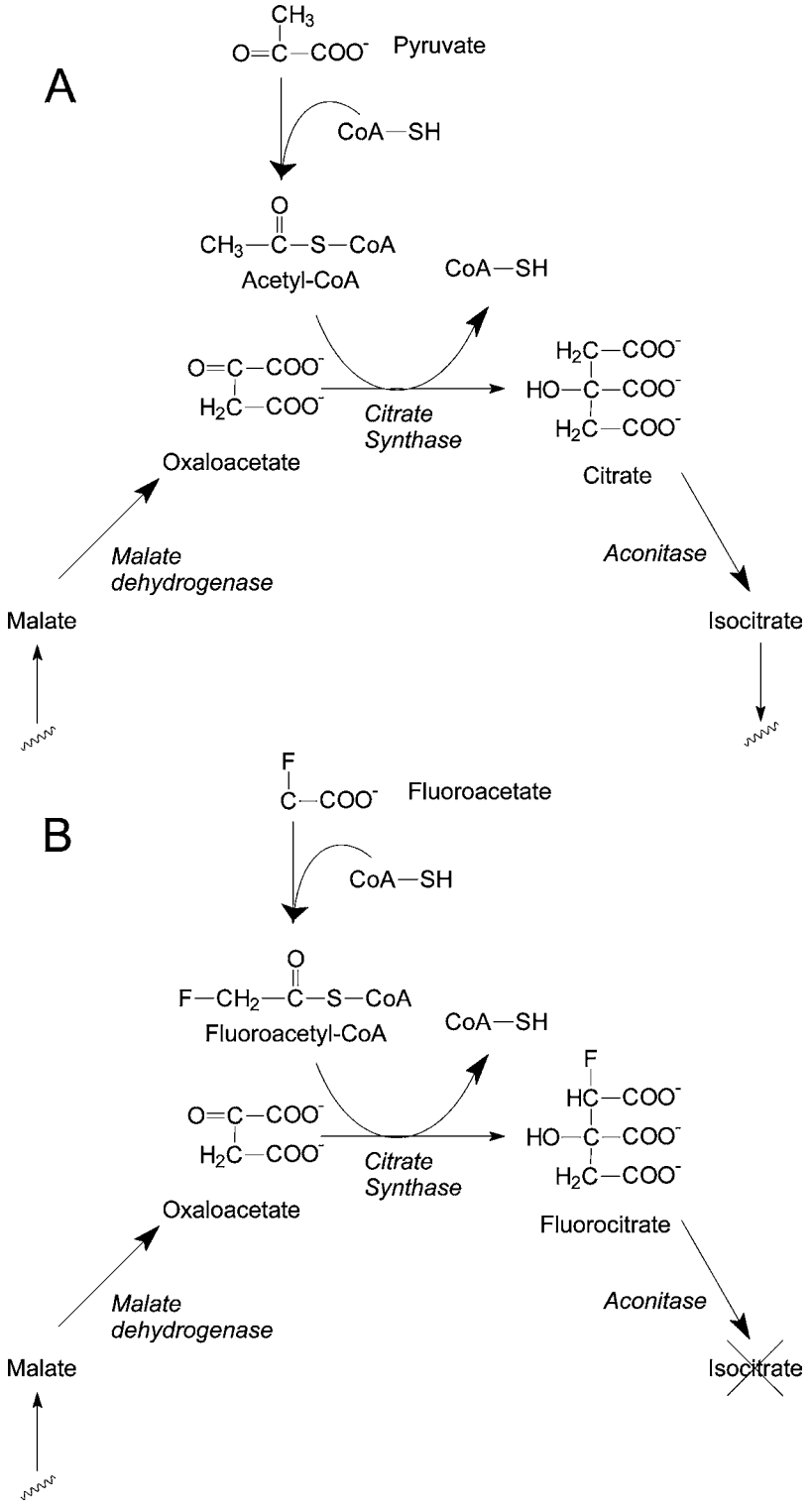

Figure 2. (A) Partial tricarboxylic acid cycle illustrating the incorporation of acetyl-CoA into the cycle. (B) Partial tricarboxylic acid cycle illustrating the incorporation of fluoroacetyl-CoA into the cycle resulting in the formation of fluorocitrate and subsequent inhibition of aconitase.

Bignoniaceae. Several lianas in the family Bignoniaceae, previously classified as *Arrabidaea* and *Pseudocalymma*, are reported to cause sudden death. A recent taxonomic study using molecular and morphological characters has changed the generic circumscriptions in this group.[33] Currently, most *Arrabidaea* and *Pseudocalymma* are now included in *Fridericia* and *Mansoa*, respectively. However, some species such as *Arrabidaea bilabiata* and *Pseudocalymma elgans* were incorrectly classified as to genus and are known as *Tanaecium bilabiatum* and *Fridericia elegans*, respectively. *Fridericia* comprises approximately 70 species that typically grow as high-climbing woody vines or occasionally as small shrubs and trees and is distributed throughout the Neotropics from Mexico and the West Indies to Argentina. *Tanaecium* comprises about 20 species of similar habit found across the same range.[33] Three species of Bignoniaceae have been reported to cause sudden

dx.doi.org/10.1021/jf500563h | J. Agric. Food Chem. 2014, 62, 7345−7354

death, *Arrabidaea bilabiata* (= *Tanaecium bilabiatum*), *A. japurensis* (also sometimes called *Scobinaria japurensis*, = *Fridericia japurensis*), and *Pseudocalymma elgans* (*Fridericia elegans*).[24,34] One species, *A. bilabiata*, has been reported to contain monofluoroacetate (Table 1).[35] Similar concentrations of monofluoroacetate were found in *A. bilabiata* and *P. marcgravii*.[35] The other species have not been confirmed to contain monofluoroacetate, but likely contain this toxin because livestock poisoned with these plants exhibit similar clinical signs.

Malpighiaceae. *Amorimia* is a genus composed of 10 species, which are found in tropical South America and grow as woody vines or sometimes shrubs.[36] *Amorimia* spp. are among the more important poisonous plants of Brazil due to their widespread distribution[24,28] throughout South America from southern Brazil northward.[36] *Amorimia* species were previously included in *Mascagnia*; however, recent taxonomic research using morphological and molecular studies resulted in the separation of the new genus, *Amorimia*.[36,37] Five *Mascagnia* species, *M. elegans*, *M. exotropica*, *M. pubiflora*, *M. rigida*, and *M.* aff. *rigida* have been reported to cause sudden death in livestock.[24,34,38] The latter four are now included in *Amorimia*, whereas *M. elegans* remains in *Mascagnia*.[36,37]

Field collections and a systematic screening of herbarium specimens across these Malpighiaceae were performed to test for monofluoroacetate. Monofluoroacetate was detected in *A. amazonica*, *A. camporum*, *A. exotropica*, *A. pubiflora*, *A. rigida*, and *A. septentrionalis* (Table 1).[28] However, monofluoroacetate was not detected in *A. kariniana*, *A. maritima*, *A. velutina*, and *M. divaricata* (*M. elegans*).[28] This may be due to the limited number of specimens that were available for sampling in some taxa; some of these species have not been reported to be toxic[24] and may not contain monofluoroacetate.

Monofluoroacetate was not detected in *M. elegans*,[28] also known under the synonym *M. divaricata*. This species is reported to have caused sudden death syndrome in Pernambuco state in northeastern Brazil;[38] however, no herbarium collections of *M. divaricata* are known from any of the states of the semiarid area of northeastern Brazil. The plant reported to have caused the sudden death syndrome may have been *A. septentrionalis* or another species that was identified as *M. divaricata*. Another *Mascagnia* sp., *M. sepium*, was reported to cause sudden death syndrome in Rondônia, a state of northwestern Brazil.[39] However, *M. sepium* does not occur in this region of Brazil, but is found in southeastern Brazil. A photograph of the plant responsible for the livestock poisoning was included in the paper and was identified as an *Amorimia* species (W. Anderson, University of Michigan) on the basis of the fruits (i.e., samaras). Because of the location of the case report it is likely that the plant responsible for causing sudden death in this paper was *A. amazonica*; however, this cannot be verified without a voucher specimen.[28] These two examples highlight the need for voucher specimens in plant poisonings and correct identification of plants suspected of toxicity.

Monofluoroacetate was detected in the field collections of *A. septentrionalis* but only in 60% of the plants surveyed.[28] Monofluoroacetate concentrations varied among plant parts with concentrations ranging from approximately 0.001 ± 0.0003% in stems to 0.008 ± 0.004% in flowers and other parts falling within the range reported above.[28] Concentrations of monofluoroacetate in *A. septentrionalis* were significantly less than those reported for *P. marcgravii* and *P. aeneofusca*, which is consistent with the incidence of poisoning and the amount of plant material required to cause sudden death with *Palicourea* and *Mascagnia* species.[40−42]

Dichapetalaceae. *Dichapetalum* spp. occur as trees or shrubs throughout the lowland tropical regions of the world, with more than 80 species reported from Africa.[3] *Dichapetalum cymosum* (Gifblaar) causes sudden death or "Gifblaar poisoning" and is the third most important toxic plant in South Africa.[3] Seven *Dichapetalum* spp., *D. barteri*,[43] *D. braunii*,[44] *D. cymosum*,[45] *D. edule*,[44] *D. heudelotii*,[46] *D. michelsonii*[44,47] (possibly the same as *D. stuhlmanii*), and *D. toxicarium*,[48] have been documented to contain monofluoroacetate (Table 1), and three of these, *D. cymosum*, *D. barteri*, and *D. toxicarium*, are reported to be lethally toxic to livestock.[3] *D. ruhlandii* has also been reported to be lethally toxic, but, apparently, has not been shown to contain monofluoroacetate.[3] Similar to the other species thus far described herein, monofluoroacetate concentrations have been shown to vary between species and plant parts in that young leaves contain greater amounts of monofluoroacetate than do mature leaves. For example, O'Hagan et al.[44] analyzed leaves of three *Dichapetalum* spp. and found concentrations of monofluoroacetate to be 0.72 ± 0.02% in the young leaves of *D. braunii*, 0.012 ± 0.002 and 0.007 ± 0.002% in the young leaves of *D. edule*, and 0.004 ± 0.002% in the young leaves of *D. stuhlmanni*; however, the concentrations in the mature leaves from these three plants were all <0.002%. In addition, *Tapura fischeri*, an African tree of the Dichapetalaceae family, is also reported to contain monofluoroacetate but has not been reported to be involved in livestock poisoning (Table 1).[3]

■ TOXICOLOGY OF MONOFLUOROACETATE

Monofluoroacetate is not toxic per se but requires intracellular metabolism to fluorocitrate that then inhibits aconitase and thereby blocks the cellular respiration tricarboxylic acid cycle (Figure 2).[3] Clinical signs usually take 4−24 h to appear. This is a time-dependent process because the plant material has to be digested in the rumen and the monofluoroacetate absorbed into the bloodstream, transported to the target cells, and then converted to monofluorocitrate, which disrupts cellular respiration.[3] Clinical signs of livestock poisoned by monofluoroacetate-containing plants can include loss of balance, ataxia, tachycardia, and labored breathing.[34] Livestock may attempt to rise after collapsing but immediately fall, sometimes staying in lateral recumbence and pedaling in an attempt to stand up.[34] Death usually occurs shortly after these clinical effects.[34] In sublethal cases, a reluctance to walk or slow movements, lying down frequently, heart palpitations, and a visibly pulsing jugular vein are often observed.[34,38] Clinical signs are usually exacerbated by exercise but, due to the rapidity of death, are rarely seen under field conditions.[3]

Monofluoroacetate poisoning of livestock usually results in no significant gross lesions. Most animals that die of sudden death do not show lesions of any diagnostic significance, although some histological lesions have been observed. Approximately two-thirds of the cattle poisoned by *P. marcgravii* had necrosis and hydropic degeneration of the epithelium of the renal tubules.[38] In some cases of Gifblaar poisoning, myocardial fibrosis and necrosis have been observed.[49] Cardiac fibrosis has also been observed in *Amorimia* spp. from repeated sublethal doses.[39,50]

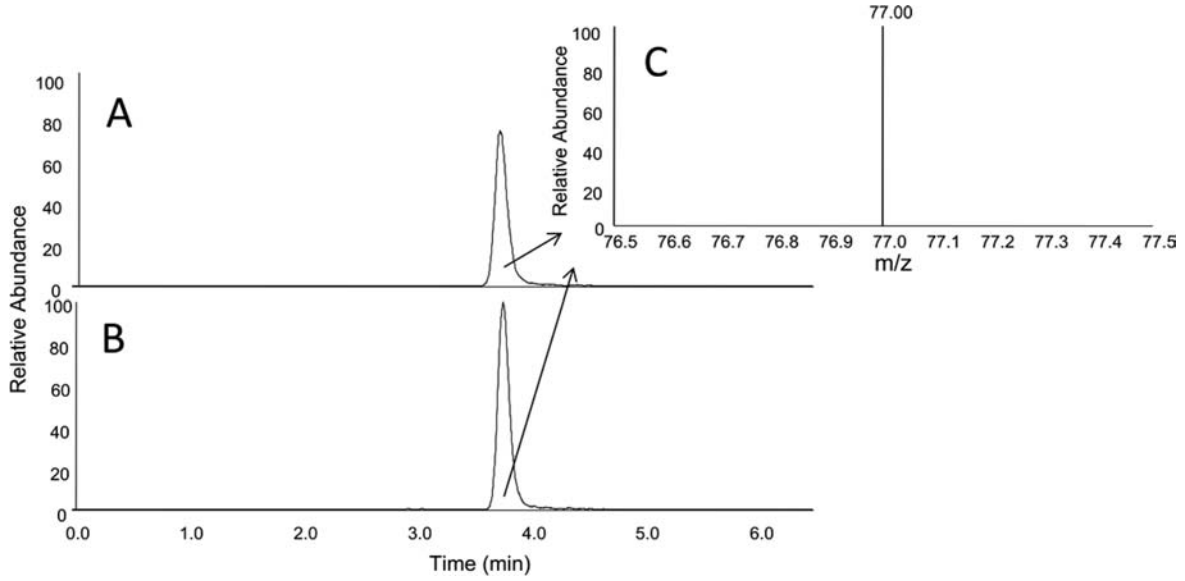

Figure 3. Selected ion monitoring (SIM) at m/z 77 from (A) 2.5 μg/mL standard of sodium monofluoroacetate and (B) water extract of *Palicourea marcgravii* leaves diluted 1:5. (C) Mass spectrum of the peaks.

METHODS OF ANALYSIS FOR MONOFLUOROACETATE

Several methods exist to measure monofluoroacetate in various matrices. Many of these methods require derivatization prior to final analysis by GC,[51−53] GC-MS,[54−56] or HPLC with UV−vis or fluorescence detection.[57,58] A GC method without prior derivatization of monofluoroacetate was developed; however, preparation and frequent replacement of a guard column and intermittent injections of phosphoric acid were required to maintain chromatographic integrity.[59] In addition, capillary zone electrophoresis with UV detection has also been reported for fluoroacetate analysis.[60] Analysis of monofluoroacetate in plant extracts has been accomplished by ^{19}F NMR spectroscopy,[18] ion chromatography with conductivity detection,[44] and HPLC with UV detection at 210 nm.[61] A HPLC-APCI-MS method was developed to measure monofluoroacetate in foods,[62] and this has recently been modified for the analysis of monofluoroacetate in plant samples. Thus, an aliquot of dried, milled plant (10−100 mg) was extracted with water, filtered, appropriately diluted, and analyzed using HPLC-APCI-MS in the selected ion monitoring (SIM) mode at m/z 77 for the $(M - H)^-$ ion of monofluoroacetate. The total HPLC run time was 7.0 min, with monofluoroacetate eluting at 3.8 min (Figure 3).[28]

COEVOLUTION OF NATIVE FLORA AND FAUNA IN SOUTHWESTERN AUSTRALIA

With so many plants containing monofluoroacetate in a small and isolated region of Australia, it might be expected that the fauna that coevolved in the area would develop some tolerance to this poison. Indeed, early settlers in Western Australia were misled about the safety of these plants for their livestock because they observed native animals grazing *Gastrolobium* spp. with impunity.[1] However, it was not until the late 1970s that tolerance to monofluoroacetate was demonstrated in some species of native mammals in Western Australia.[63,64] Subsequently, varying degrees of tolerance has been demonstrated in many insects, reptiles, birds, and mammals that are native to this region.[4,65−72] Within the mammals in particular, this tolerance has been demonstrated by comparing the susceptibility to monofluoroacetate of different populations of the same species, or of closely related species, that live inside and outside the region with these plants. The difference in tolerance can be remarkable, as has been demonstrated in different populations of the bush rat, *Rattus fuscipes*. Populations in eastern Australia are 20−80 times more susceptible to monofluoroacetate poisoning than populations in southwestern Australia.[4,72] Generally, tolerance to monofluoroacetate is greatest in herbivorous species, moderate in omnivores, and least developed in native carnivores.[4] Birds are generally the least sensitive of endothermic vertebrates, and ectotherms are relatively insensitive to monofluoroacetate.[4,73,74]

The high concentration of monofluoroacetate in many *Gastrolobium* spp. seems excessive when it is recognized that most unadapted mammals are fatally poisoned by <2 mg/kg.[74] It is believed that these very high concentrations are the result of a coevolutionary event in which the plants produced monofluoroacetate as a protection against herbivory at the same time as the herbivores developed a resistance to the poison in order to use these plants in their diet.[69] This hypothesis also explains the variation in the levels of tolerance to monofluoroacetate that have been demonstrated. The degree to which the population of any species of animal is tolerant depends on their diet and habitat specialization, the size of their home range, and the length of their evolutionary exposure to the toxic vegetation.[4,64,69,75]

The evolutionary development of tolerance to monofluoroacetate is supported by the development of resistance under artificial situations. The LD_{50} of monofluoroacetate in laboratory rats, *Rattus* sp., was increased from 2.0 to 3.5 mg/kg by dosing the poison over five generations,[76] and in house flies, *Musca domestica*, it was increased from 0.6 to 4.2 μg fly^{-1} by dosing over 25 generations.[77] More recently, Twigg et al.[78] demonstrated a significant reduction in susceptibility to monofluoroacetate in populations of wild rabbits, *Oryctolagus cuniculus*, in Australia that had been subjected to intensive baiting with sodium monofluoroacetate (1080) over a 25 year period.

dx.doi.org/10.1021/jf500563h | J. Agric. Food Chem. 2014, 62, 7345−7354

Several possible mechanisms have been suggested for the tolerance that has developed in native animals in southwestern Western Australia,[4] but none have been proven. In recent times attention has been directed to the aconitase gene *ACO2*, responsible for the aconitate hydratase enzyme. However, the sequencing of the full length *ACO2* transcript has failed to identify a sequence variant between susceptible and tolerant subspecies of the tammar wallaby, *Macropus eugenii*, which would result in an amino acid change in the active site of the enzyme.[79]

METHODS TO MITIGATE LIVESTOCK POISONING FROM MONOFLUOROACETATE

Although the mechanism of toxicity due to monofluoracetate has been known for over 50 years, there is not currently a proven therapy or antidote to reverse or prevent acute intoxication.[5] Remedies such as ethanol, monoacetin (glycerol monoacetate), acetamide, and sodium succinate have been tried with various degrees of success.[5,80] Supportive care for intoxicated animals is important if they survive the initial toxic insult.[5,81]

There are various aspects of animal or pasture management that may prove useful to reduce the incidence of poisoning by monofluoroacetate-containing plants. The most critical aspect is to prevent animal access to the plants. In Australia, Brazil, and southern Africa, fencing is considered the most reliable method to prevent livestock deaths.[34,82] Other possible means of reducing exposure include hand-grubbing to remove the plants, herbicidal control, or grazing management to reduce plant−animal interactions in pastures. Fencing is both expensive and impractical in expansive rangeland settings, but has been used on smaller scales to fence localized patches of monofluoroacetate-containing plants.[3,34,82] Herbicidal control is possible, but is often impractical and expensive.[3,82] Furthermore, many monofluoroacetate-containing plants have extensive underground root systems (e.g., *D. cymosum*), which makes long-term herbicidal control much more difficult.

Reducing grazing livestock selection of monofluoroacetate-containing plants involves both animal and rangeland management. *Palicourea* species are very palatable to livestock,[2] but no studies have documented relative consumption by livestock of *Palicourea* species in overgrazed versus well-managed rangeland situations. In parts of southern Africa, populations of *D. cymosum* are most problematic on overgrazed or degraded rangelands because alternate forage sources are often limited, particularly during the dry season.[3] Livestock losses to *D. cymosum* increase during drought as other nontoxic forage may be scarce;[82] similarly, livestock losses to monofluoroacetate-containing plants in Brazil also increase during drought, particularly in drought-prone northeastern Brazil.[24]

Livestock that consume lethal amounts of monofluoroacetate-containing plants often die suddenly after drinking water or exercising.[3] One critical aspect of management when animals have been exposed to monofluoroacetate-containing plants, particularly plant species with sometimes lower (i.e., less lethal) concentrations of monofluoroacetate, is movement (i.e., exercise) of the animal. Animals that have been consuming nonlethal amounts of monofluoroacetate-containing plants may die suddenly from exercise-induced exacerbation of the intoxication.[38] In Brazil, livestock intoxicated by *Palicourea* or *Arrabidaea* species rarely recover, and many animals are found dead even without exercise.[38] However, livestock intoxicated by monofluoroacetate-containing *Amorimia* species frequently recover if the animals do not exert themselves.[34] The current recommendation is to allow exposed, potentially intoxicated animals in pastures about 7−14 days without access to the plant to allow complete detoxification before moving them to another area.[34] Similarly, if actively grazing animals must be moved during a poisoning episode to prevent further deaths within a herd, the survivors must be moved very cautiously so as to not trigger additional deaths.[3,34]

Managing water intake may attenuate livestock losses. In southern Africa, small holders grazing livestock in communal areas water their animals late in the day to allow increased time for any toxin ingested during the day to be metabolized, thus reducing potentially fatal absorption when animals drink water (I. Zimmermann, Polytechnic of Namibia, personal communication). In South Africa it is recommended that animals that have been exposed to *D. cymosum* be kept from drinking water for 48 h to reduce mortality.[3]

Anecdotal accounts from southern Africa suggest that about 50% of naïve livestock exposed to *D. cymposum* are fatally poisoned, in contrast to a mortality rate of 5% in experienced animals that are raised on rangelands with the toxic plant (I. Zimmermann, personal communication). Furthermore, weaned calves are more likely to be fatally poisoned than are nursing calves grazing alongside their experienced mothers, suggesting that when calves are with mothers who avoid the plant, the calves also avoid the plant.[83] When ruminants consume monofluoroacetate-containing plants such as *A. septentrionalis* or *D. cymosum* and are not fatally poisoned, they appear to acquire a natural aversion to the plant (I. Zimmermann, personal communication).[84] Monofluoroacetate has been used experimentally to induce strong taste aversion learning in rats.[85] Conditioned taste aversion may be a cost-effective way to prevent livestock deaths from some monofluoroacetate-containing plants. Some initial success has been reported in using conditioned taste aversion to reduce consumption of a monofluoroacetate-containing plant, *Mascagnia rigida*.[84,86] It will likely be more difficult to condition livestock to avoid highly toxic monofluoroacetate-containing plants such as *Palicourea* species, because of the difficulty in administering a nonlethal dose to condition the aversion.

It is well documented that some animal species in Australia have evolved resistance to monofluoroacetate.[63,64] In addition to this Australian phenomenon, in South America it appears that water buffalo (*Bubalus bubalis*) are more resistant to monofluoroacetate poisoning than are cattle (*Bos taurus* or *B. indicus*).[87−89] Studies indicate that the lethal dose of monofluoroacetate-containing plants is 4−8 times higher in water buffalo compared to cattle.[87,88] Furthermore, the clinical time course for signs to appear in intoxicated water buffalo is much longer than for cattle.[87] The reason for the difference in susceptibility between bovines and water buffalo is not clear but may involve absorption, ruminal detoxification, or other mechanisms of resistance at the cellular level.[90] For example, in the classic studies on mimosine (3-hydroxy 4(1*H*)-pyridone) toxicity, Jones and Lowry[91] were able to document the bacterial detoxification of mimosine by some ruminants. Furthermore, Jones and Megarrity[92] showed that this detoxification could be transferred from animal to animal in pasture situations, thus alleviating the toxic effects of mimosine.

Recent research has shown that repeated ingestion of nontoxic doses of the monofluoroacetate-containing plants *Amorimia septentrionalis* and *Palicourea aeneofusca* increased the resistance of goats to monofluoroacetate poisoning.[88,93] The

increased resistance was transferred to naïve goats by transfaunation of ruminal fluid. Interestingly, unlike resistance to potentially toxic mimosine in *Leucaena leucocephala*,[92] cohabitation of resistant goats with naïve goats for 6 months did not result in increased resistance in the naïve animals.[93] The increased resistance of subchronically intoxicated ruminants may result from the proliferation of monofluoroacetate-degrading microbes when sufficient substrate is available.[88]

Australian investigators have successfully genetically modified the ruminal bacteria *Butyrivibrio fibrisolvens* by introducing a gene that codes for a dehalogenase, thus rendering the bacteria capable of hydrolyzing monofluoroacetate.[94] The stability of that modified organism has been demonstrated by its retention in the rumen of sheep for over 5 months in vivo.[95] If this modified bacterium could be successfully transferred and maintained in the rumen of grazing animals consuming monofluoroacetate-containing plants, this may provide a method to greatly reduce or eliminate livestock losses.[96]

PERSPECTIVE

Many methods and remedies to mitigate monofluoroacetate plant poisoning have been tried with various degrees of success. Currently, there is no one accepted practice or antidote to eliminate poisoning by monofluoroacetate-containing plants in livestock; however, research in this area is promising, and the solution may be a combination of management strategies and new information or biotechnology. The coevolution of monofluoroacetate-containing plants and fauna in Western Australia may provide some clues to the development of resistance in livestock.

There have been cases when humans have been poisoned by accidental ingestion of monofluoroacetate (1080).[5] However, because monofluoroacetate is highly soluble in water and has a short half-life in livestock, the risk of secondary poisoning by monofluoroacetate in meat intended for human consumption is low.[97] Accidental poisoning of pets by monofluoroacetate (1080) has also been reported.[98−100] Livestock-associated research in poisoning by monofluoroacetate may provide insight into possible treatments for poisoned humans and pets.

AUTHOR INFORMATION

Corresponding Author

*(S.T.L.) Phone: (435) 752-2941. Fax: (435) 797-5681. E-mail: stephen.lee@ars.usda.gov.

Notes

The authors declare no competing financial interest.

REFERENCES

(1) Marchant, N. G. History of plant poisoning in Western Australia. In *Plant-Associated Toxins: Agricultural, Phytochemical and Ecological Aspects*; Colegate, S. M., Dorling, P. R., Eds.; CAB International: Wallingford, UK, 1994; pp 7−12.

(2) Tokarnia, C. H.; Döbereiner, J.; Peixoto, P. V. Poisonous plants affecting livestock in Brazil. *Toxicon* **2002**, *40*, 1635−1660.

(3) Kellerman, T. S.; Coetzer, J. A.W.; Naude, T. W.; Botha, C. J. Cadiovascular system. In *Plant Poisonings and Mycotoxicoses of Livestock in Southern Africa*, 2nd ed.; Oxford University Press: Cape Town, South Africa, 2005; pp 146−153.

(4) Twigg, L. E.; King, D. R. The impact of fluoroacetate-bearing vegetation on native Australian fauna: a review. *OIKOS* **1991**, *61*, 412−430.

(5) Proudfoot, A. T.; Bradberry, S. M.; Vale, J. A. Sodium fluoroacetate poisoning. *Toxicol. Rev.* **2006**, *25*, 213−219.

(6) Eason, C.; Miller, A.; Ogilvie, S.; Fairweather, A. An updated review of the toxicology and ecotoxicology of sodium fluoroacetate (1080) in relation to its use as a pest control tool in New Zealand. *N. Z. J. Ecol.* **2011**, *35*, 1−20.

(7) Green, W. The use of 1080 for pest control, published by the Animal Health Board and the Department of Conservation July 2004; http://www.doc.govt.nz/documents/conservation/threats-and-impacts/animal-pests/use-of-1080-04.pdf (accessed Jan 24, 2014).

(8) Eisler, R. Sodium monofluoroacetate (1080) hazards to fish, wildlife, and invertebrates: a synoptic review; http://www.pwrc.usgs.gov/eisler/CHR_30_Sodium_monofluoroacetate.pdf (accessed Jan 29, 2014).

(9) Chandler, G. T.; Crisp, M. D.; Cayzer, L. W.; Bayer, R. J. Monograph of *Gastrolobium* (Fabaceae: Mirbelieae). *Aust. Syst. Bot.* **2002**, *15*, 619−739.

(10) Chandler, G. T.; Bayer, R. J.; Gilmore, S. R. *Oxylobium*/*Gastrolobium* (Fabaceae: Mirbelieae) condundrum: further studies using molecular data and a reappraisal of morphological characters. *Plant Species Biol.* **2003**, *18*, 91−101.

(11) Aplin, T. H. E. Poison plants of Western Australia: the toxic species of *Gastrolobium* and *Oxylobium*. *Western Australian Department of Agriculture Bulletin 3772*; 1971.

(12) Hall, R. J. The distribution of organic fluorine in some toxic tropical plants. *New Phytol.* **1972**, *71*, 855−871.

(13) Twigg, L. E.; King, D. R.; Bowen, L. H.; Wright, G. E.; Eason, C. T. The fluoroacetate content of some species of the toxic Australian plant genus, *Gastrolobium*, and its environmental persistence. *Nat. Toxins* **1996**, *4*, 122−127.

(14) Twigg, L. E.; Wright, G. E.; Potts, M. D. Fluoroacetate content of *Gastrolobium brevipes* in central Australia. *Aust. J. Bot.* **1999**, *47*, 877−880.

(15) Oelrichs, P. B.; McEwan, T. Isolation of the toxic principle of *Acacia georginae*. *Nature* **1961**, *190*, 808−809.

(16) Everist, S. L. In *Poisonous Plants of Australia*. Angus & Robertson: Melbourne, Australia, 1974.

(17) Twigg, L. E.; Socha, L. V. Physical versus chemical defence mechamisms in toxic *Gastrolobium*. *Oecologia* **1996**, *108*, 21−28.

(18) Baron, M. L.; Bothroyd, C. M.; Rogers, G. I.; Staffa, A.; Rae, I. D. Detection and measurement of fluoroacetate in plant extracts by ^{19}F NMR. *Phytochemistry* **1987**, *26*, 2293−2295.

(19) Peacock, D. E.; Williams, B. D.; Christensen, P. E. "Total fluorine" analysis of seed of Australian *Gastrolobium* spp. showing temporal, spatial and morphological variation. *J. Fluorine Chem.* **2007**, *128*, 631−635.

(20) Lee, S. T.; Cook, D.; Riet-Correa, F.; Allen, J. G.; Pfister, J. A.; Colegate, S. M.; Lima, F. G.; Gardner, D. R. A rapid HPLC-APCI(−)MS method to detect fluoroacetate in plants. In *Poisonous Plants: Proceedings of the Ninth Internationl Symposium*; Zhao, M.-L., Panter, K. E., Weirenga, T. L., Eds.; Watkins Printing: Logan, UT, USA, in press.

(21) McEwan, T. Isolation and identification of the toxic principle of *Gastrolobium grandiflorum*. *Queensland J. Agric. Sci.* **1964**, *21*, 1−14.

(22) Twigg, L. E.; King, D. R.; Bowen, L. H.; Wright, G. E.; Eason, C. T. Fluoroacetate found in *Nemcia spathulata*. *Aust. J. Bot.* **1996**, *44*, 411−412.

(23) Taylor, C. M. Overview of the *Psychotrieae* (Rubiaceae) in the Neotropics. *Opera Bot. Belg.* **1996**, *7*, 261−270.

(24) Tokarnia, C. H.; Brito, M. d. F.; Barbosa, J. D.; Döbereiner, J.; Peixoto, P. V. Plants that affect heart function. In *Plantas Tóxicas do Brasil*, 2nd ed.; Helianthus: Rio de Janeiro, Brazil, 2012; pp 27−68.

(25) Oliveira, M. M. Chromatographic isolation of monofluoroacetic acid from *Palicourea marcgravii* St. Hil. *Experientia* **1963**, *19*, 586−587.

(26) Moraes-Moreau, R. L.; Haraguchi, M.; Morita, H.; Palermo-Neto, J. Chemical and biological demonstration of the presence of monofluoroacetate in the leaves of *Palicourea marcgravii* St. Hil. *Braz. J. Med. Biol. Res.* **1995**, *28*, 658−692.

(27) Cook, D.; Lee, S. T.; Taylor, C. M.; Riet-Correa, F.; Pfister, J. A.; Gardner, D. R. Detection of monofluoroacetate in *Palicourea* species. *Toxicon* **2014**, DOI: 10.1016/j.toxicon.2013.12.003.

(28) Lee, S. T.; Cook, D.; Riet-Correa, F.; Pfister, J. A.; Anderson, W. R.; Lima, F. G.; Gardner, D. R. Detection of monofluoroacetate in *Palicourea* and *Amorimia* species. *Toxicon* **2012**, *60*, 791−796.
(29) Tokarnia, C. H.; Döbereiner, J.; Silva, M. F. Poisoning by *Palicourea grandiflora* (Rubiaceae) in bovines in the territory of Rondonia. *Pesq. Vet. Bras.* **1981**, *1*, 85−94.
(30) Döbereiner, J.; Tokarnia, C. H. Experimental poisoning by *Palicourea grandiflora* (Rubiaceae) in rabbits. *Pesq. Vet. Bras.* **1982**, *1*, 85−94.
(31) Tokarnia, C. H.; Döbereiner, J. Experimental poisoning by *Palicourea juruana* (Rubiaceae) in bovines and rabbits. *Pesq. Vet. Bras.* **1982**, *2*, 17−26.
(32) Taylor, C. M. Conspectus of the genus *Palicourea* (Rubiaceae: Psychotrieae) with the description of some new species from Ecuador and Colombia. *Ann. Mo. Bot. Gard.* **1997**, *84*, 224−262.
(33) Lohmann, L. G.; Taylor, C. M. A new generic classification of Bignonieae (Bignoniaceae) based on molecular phylogenetic data and morphological synapomorphies. *Ann. Mo. Bot. Gard.* **2014**, *99*, in press.
(34) Riet-Correa, F.; Medeiros, R. M. T.; Pfister, J.; Schild, A. L.; Dantas, A. F. M. *Poisonings by Plants, Mycotoxins and Related Substances in Brazilian Livestock*; Sociedade Vicente Pallotti: Patos, Brazil, 2009; pp 15−24
(35) Krebs, H. C.; Kemmerling, W.; Habermehl, G. Qualitative and quantitative determination of fluoroacetic acid in *Arrabidaea bilabiata* and *Palicourea marcgravii* by F-19-NMR spectroscopy. *Toxicon* **1994**, *32*, 909−913.
(36) Anderson, W. R. Eight segregates from the neotropical genus *Mascagnia* (Malpighiaceae). *Novon* **2006**, *16*, 168−204.
(37) Davis, C. C.; Anderson, W. R. A complete generic phylogeny of Malpighiaceae inferred from nucleotide sequence data and morphology. *Am. J. Bot.* **2010**, *97*, 2031−2048.
(38) Tokarnia, C. H.; Peixoto, P. V.; Döbereiner, J. Poisonous plants affecting heart function of cattle in Brazil. *Pesq. Vet. Bras.* **1990**, *5*, 77−91.
(39) Schons, S. S.; de Mello, T. L.; Riet-Correa, F.; Schild, A. L. Poisoning by *Amorimia* (*Mascagnia*) sepium in sheep in northern Brazil. *Toxicon* **2011**, *57*, 781−786.
(40) Gava, A.; Cristani, J.; Branco, J. V.; Neves, D. S.; Mondadori, A. J.; Sousa, R. S. Sudden death in cattle by *Mascagnia* sp (Malpighiaceae) in the state of Santa Catarina, Brazil. *Pesq. Vet. Bras.* **1998**, *18*, 16−20.
(41) Tokarnia, C. H.; Gava, A.; de Farias Brito, M.; Bezerra, P. S.; de Oliveira, K. D. Experimental poisoning in rabbits by *Mascagnia* sp (Malpighiaceae) collected in the state of Santa Catarina, southern Brazil. *Pesq. Vet. Bras.* **1998**, *18*, 61−64.
(42) Medeiros, R. M. T.; Neto, S. A. G.; Barbosa, R. C.; Lima, E. F.; Riet-Correa, F. Sudden bovine death from *Mascagnia rigida* in northeastern Brazil. *Vet. Hum. Toxicol.* **2002**, *44*, 286−288.
(43) Nwude, N.; Parsons, L. E.; Adaudi, A. O. Acute toxicity of the leaves and extracts of *Dichapetalum barteri* (Engl.) in mice rabbits and goats. *Toxicology* **1977**, *7*, 23−29.
(44) O'Hagan, D. O.; Perry, R.; Lock, J. M.; Meyer, J. J. M.; Dasaradi, L.; Hamilton, J. T. G.; Harper, D. B. High levels of monofluoroacetate in *Dichapetalum braunii*. *Phytochemistry* **1993**, *33*, 1043−1045.
(45) Marais, J. S. C. Monofluoroacetic acid, the toxic principle of 'Gifblaar' *Dichapetalum cymosum* (Hook) Engl. *Onderstepoort J. Vet. Sci. Anim. Ind.* **1944**, *20*, 67−73.
(46) Vickery, B.; Vickery, M. L. Analysis of plants for fluoroacetic acids. *Phytochemistry* **1973**, *12*, 145−147.
(47) Esters, V.; Karangwa, C.; Tits, M.; Francotte, P.; Pirotte, B.; Servais, A.-C.; Fillet, M.; Crommen, J.; Robbrecht, E.; Minet, A.; Grisar, T.; Angenot, L.; Frederich, M. Unusual amino acids and monofluoroacetate from *Dichapetalum michelsonii* (Umutambasha), a toxic plant from Rwanda. *Planta Med.* **2013**, *79*, 334−337.
(48) Vickery, B.; Vickery, M. L. Fluoride metabolism in *Dichapetalum toxicarium*. *Phytochemistry* **1972**, *11*, 1905−1909.
(49) Schultz, R. A.; Fourie, N.; Basson, K. M.; Labuschagne, L.; Prozesky, L. Observations on the clinical, cardiac, and histopathological effects of fluoroacetate in sheep. *Onderstepoort J. Vet.* **2001**, *63*, 97−108.
(50) Soares, M. P.; Pavarini, S. P.; Adrien, M. L.; Quevedo, P. S.; Schild, A. L.; Peixoto, P. V.; Farias da Cruz, C. E.; Driemeier, D. *Amorimia exotropica* poisoning as a presumptive cause of myocardial fibrosis in cattle. *J. Vet. Diagn. Invest.* **2011**, *23*, 1226−1229.
(51) Mori, M.; Nakajima, H.; Seto, Y. Determination of fluoroacetate in aqueous samples by headspace gas chromatography. *J. Chromatogr., A* **1996**, *736*, 229−234.
(52) Rompp, A.; Klemm, O.; Fricke, W.; Frank, H. Haloacetates in fog and rain. *Environ. Sci. Technol.* **2001**, *35*, 1294−1298.
(53) Demarchi, A. C. C. O.; Menezes, M. L.; Mercadante, A.; Vassillief, I. Determination of the sodium monofluoroacetate in serum by gas chromatography. *Chromatographia* **2001**, *54*, 402−404.
(54) Vartiainen, T.; Kauranen, P. The determination of traces of fluoroacetic acid by extractive alkylation, pentafluorobenzylation and capillary gas chromatography-mass spectrometry. *Anal. Chim. Acta* **1984**, *157*, 91−97.
(55) Eichhold, T. H.; Hookfin, E. B.; Taiwo, Y. O.; De, B.; Wehmeyer, K. R. Isolation and quantification of fluoroacetate in rat tissues, following dosing of Z-Phe-Ala-CH_2-F, a peptidyl fluoromethyl ketone protease inhibitor. *J. Pharm. Biomed. Anal.* **1997**, *16*, 459−467.
(56) Miki, A.; Tsuchihashi, H.; Yamashita, M. GC and GC-MS determination of fluoroacetic acid and phenoxy acid herbicides via triphasal extractive pentafluorobenzylation using a polymer-bound phase-transfer catalyst. *J. Anal. Toxicol.* **1998**, *22*, 237−245.
(57) Lam, S.; Gruska, E. Labeling of fattyacids with 4-bromomethyl-7-methoxy-coumarin via crown ether catalyst for fluorometric detection in high-performance liquid chromatography. *J. Chromatogr.* **1978**, *158*, 207−214.
(58) Collins, D. M.; Fawcett, J. P.; Rammell, C. G. Determination of sodium fluoroacetate (compound 1080) in poison baits by HPLC. *Bull. Environm. Contam. Toxicol.* **1981**, *26*, 669−673.
(59) Kimball, B. A.; Mishalanie, E. A. Gas chromatographic determination of sodium monofluoroacetate as the free acid in an aqueous solvent. *J. Chromatogr.* **1993**, *634*, 289−296.
(60) Guan, F.; Wu, H.; Luo, Y. Sensitive and selective method for the determination of sodium monofluoroacetate by capillary zone electrophoresis. *J. Chromatogr., A* **1996**, *719*, 421−426.
(61) Minnaar, P. P.; Swan, G. E.; McCrindle, R. I.; de Beer, W. H. J.; Naude, T. W. A high-performance liquid chromatographic method for the determination of monfluoacetate. *J. Chromatogr. Sci.* **2000**, *38*, 16−20.
(62) Noonan, G. O.; Begley, T. H.; Diachenko, G. W. Rapid quantitative and qualitative confirmatory method for the determination of monofluoroacetic acid in foods by liquid chromatography-mass spectrometry. *J. Chromatogr., A* **2007**, *1139*, 271−278.
(63) Oliver, A. J.; King, D. R.; Mead, R. J. The evolution of resistance to fluoroacetate intoxication to mammals. *Search (Syd.)* **1977**, *8*, 130−132.
(64) King, D. R.; Oliver, A. J.; Mead, R. J. The adaptation of some Western Australian mammals to food plants containing fluoroacetate. *Aust. J. Zool.* **1978**, *26*, 699−712.
(65) Oliver, A. J.; King, D. R.; Mead, R. J. Fluoroacetate tolerance, a genetic marker in some Australian mammals. *Aust. J. Zool.* **1979**, *27*, 363−372.
(66) King, D. R.; Oliver, A. J.; Mead, R. J. *Bettongia* and fluoroacetate: a role for 1080 in fauna management. *Aust. Wildlife Res.* **1981**, *8*, 521−536.
(67) McIlroy, J. C. Sensitivity of Australian animals to 1080 poison. III. Marsupial and eutherian herbivores. *Aust. Wildlife Res.* **1982**, *9*, 487−502.
(68) McIlroy, J. C. Sensitivity of Australian animals to 1080 poison. IV. Native and introduced rodents. *Aust. Wildlife Res.* **1982**, *9*, 505−517.
(69) Mead, R. J.; Oliver, A. J.; King, D. R.; Hubach, P. H. The co-evolutionary role of fluoroacetate in plant-animal interaction in Australia. *OIKOS* **1985**, *44*, 55−60.
(70) Twigg, L. E. The sensitivity of some Western Australian caterpillars to fluoroacetate. *Mulga Res. Ctr. J. (Perth, WA)* **1990**, *10*, 14−18.

(71) Martin, G. R.; Twigg, L. E. Sensitivity to sodium fluoroacetate (1080) of native animals from north-western Australia. *Wildlife Res.* **2002**, *29*, 75−83.
(72) Twigg, L. E.; Martin, G. R.; Eastman, A. F.; King, D. R.; Kirkpatrick, W. E. Sensitivity of some Australian animals to sodium fluoroacetate (1080): additional species and populations, and some ecological considerations. *Aust. J. Zool.* **2003**, *51*, 515−531.
(73) McIlroy, J. C.; King, D. R.; Oliver, J. A. The sensitivity of Australian animals to 1080 poison. VIII. Amphibians and reptiles. *Aust. Wildlife Res.* **1985**, *12*, 113−118.
(74) Atzert, S. P. A review of sodium monofluoroacetate (compound 1080), its properties, toxicology and use in predator and rodent control. . *Wildlife Report 146*; Bureau of Sport, Fish and Wildlife Services: Washington, DC, USA, 1971; pp 1−34.
(75) Mead, R. J. The biological arms race. *Proc. Nutr. Soc. Aust.* **1986**, *11*, 55−62.
(76) Howard, W. E.; Marsh, R. E.; Palmateer, S. D. Selective breeding of rats for resistance to sodium monofluoroacetate. *J. Appl. Ecol.* **1973**, *10*, 731−737.
(77) Tahori, A. S. Selection for a fluoroacetate resistant strain of house fly and investigation of its resistance pattern. *J. Econ. Entomol.* **1963**, *56*, 67−69.
(78) Twigg, L. E.; Martin, G. R.; Lowe, T. J. Evidence of pesticide resistance in medium-sized mammalian pests: a case study with 1080 poison and Australian rabbits. *J. Appl. Ecol.* **2002**, *39*, 549−560.
(79) Deakin, J. E.; Cooper, D. W.; Sinclair, J. J.; Herbert, C. A.; Renfree, M. B.; Wakefield, M. Towards an understanding of the genetic basis behind 1080 (sodium fluoroacetate) tolerance and an investigation of the candidate gene *ACO2*. *Aust. J. Zool.* **2013**, *61*, 69−77.
(80) Goncharov, N. V.; Jenkins, R. O.; Radilov, A. S. Toxicology of fluoroacetate: a review with possible directions for therapy research. *J. Appl. Toxicol.* **2006**, *26*, 148−161.
(81) Nogueira, V.; Franca, T. N.; Peixoto, T. C.; Caldas, S. A.; Armien, A. G.; Peixoto, P. V. Experimental poisoning by sodium monofluoroacetate in cattle: clinical and pathological aspects. *Pesq. Vet. Bras.* **2010**, *30*, 533−540.
(82) Phillips, M. C.; Riches, C. R.; Sweet, R. J. Chemical control of the poisonous plant *Dichapetalum cymosum* (Hook) Engl. *Int. J. Pest Manage.* **1993**, *39*, 358−365.
(83) Thorhallsdottir, A. G.; Provenza, F. D.; Balph, D. F. The role of the mother in the intake of harmful foods by lambs. *Appl. Anim. Behav. Sci.* **1990**, *25*, 35−44.
(84) Pacífico da Silva, I.; Soto-Blanco, B. Conditioning taste aversion to *Mascagnia rigida* (Malpighiaceae) in sheep. *Res. Vet. Sci.* **2010**, *88*, 239−241.
(85) Nachman, M.; Hartley, P. L. Role of illness in producing learned taste aversions in rats: a comparison of several rodenticides. *J. Comp. Physiol. Psychol.* **1975**, *89*, 1010−1018.
(86) Barbosa, R. R.; Pacífico da Silva, I.; Soto-Blanco, B. Development of conditioned taste aversion to *Mascagnia rigida* in goats. *Pesq. Vet. Bras.* **2008**, *28*, 571−574.
(87) Barbosa, J. D.; Oliveira, C. M. C.; Tokarnia, C. H.; Riet-Correa, F. Comparison of the susceptibility of cattle and water buffalo to intoxication from *Palicourea marcgravii* (Rubiaceae). *Pesq. Vet. Bras.* **2003**, *23*, 167−172.
(88) Oliveira, M. D.; Riet-Correa, F.; Carvalho, F. K. L.; Silva, G. B.; Pereira, W. S.; Medeiros, R. M. T. Induction of resistance to *Palicourea aeneofusca* (Rubiaceae) poisoning by the continuous administration of non-toxic doses. *Pesq. Vet. Bras.* **2013**, *33*, 731−734.
(89) Tokarnia, C. H.; Barbosa, J. D.; Oliveira, C. M. C.; Brito, M. F.; Oliveira, R. B.; Barbas, L. A. L. Epidemiological aspects and comparative clinical pathology of intoxication by *Arrabidaea bilabiata* (Bignoniaceae) in water buffalo and bovines. *Pesq. Vet. Bras.* **2004**, *24*, 74−79.
(90) Tokarnia, C. H.; Riet-Correa, F.; Barbosa, J. D.; Oliveira, C. M. C. Comparative studies on the susceptibility of buffalo and cattle to three poisonous plants (*Palicourea marcgravii*, *Palicourea juruana* and *Arrabidaea bilabiata*) in the Amazon Region. In *Poisonous Plants: Global Research and Solutions*; Panter, K. E.,Wierenga, T. L., Pfister, J. A., Eds.; CABI: Oxon, UK, 2007; pp 35−39.
(91) Jones, R. J.; Lowry, J. B. Australian goats detoxify the goitrogen 3-hydroxy 4(1*H*) pyridone (DHP) after rumen infusion from an Indonesian goat. *Experientia* **1984**, *40*, 1435−1436.
(92) Jones, R. J.; Megarrity, R. G. Successful transfer of DHP-degrading bacteria from Hawaiian goats to Australian ruminants to overcome the toxicity of *Leucaena*. *Aust. Vet. J.* **1986**, *63*, 259−262.
(93) Duarte, A. L. L.; Medeiros, R. M. T.; Carvalho, F. K. L.; Lee, S. T.; Cook, D.; Pfister, J. A.; Costa, V. M. M.; Riet-Correa, F. Induction and transfer of resistance to poisoning by *Amorimia* (*Mascagnia*) *septentrionalis* in goats. *J. Appl. Toxicol.* **2014**, *34*, 220−223.
(94) Gregg, K.; Cooper, C. L.; Schafer, D. J.; Sharpe, H.; Beard, C. E.; Allen, G.; Xu, J. Detoxification of the plant toxin fluoroacetate by a genetically modified rumen bacterium. *Biotechnology (N.Y.)* **1994**, *12*, 1361−1365.
(95) Gregg, K.; Allen, G.; Beard, C. Genetic manipulation of rumen bacteria: from potential to reality. *Aust. J. Agric. Res.* **1996**, *47*, 247−256.
(96) Padmanabha, J.; Gregg, K.; Ford, M.; Prideaux, C.; McSweeney, C. S. Protection of cattle from fluoroacetate poisoning by genetically modified ruminal bacteria. *Anim. Prod. Aust.* **2004**, *25*, 293.
(97) Eason, C. T.; Gooneratnel, R.; Fitzgerald, H.; Wright, G.; Frampton, C. Persistence of sodium monofluoroacetate in livestock animal and risk to humans. *Hum. Exp. Toxicol.* **1994**, *13*, 119−122.
(98) O'Hagan, B. J. Fluoroacetate poisoning in seven domestic dogs. *Aust. Vet. J.* **2004**, *82*, 756−758.
(99) Goh, C. S. S.; Hodgson, D. R.; Fearnside, S. M.; Helleer, J.; Malikides, N. Sodium monofluoroacetate (compound 1080) poisoning in dogs. *Aust. Vet. J.* **2005**, *83*, 474−479.
(100) Gammie, J. Sodium fluoroacetate poisoning in a cat. *Can. Vet. J.* **1980**, *21*, 64.

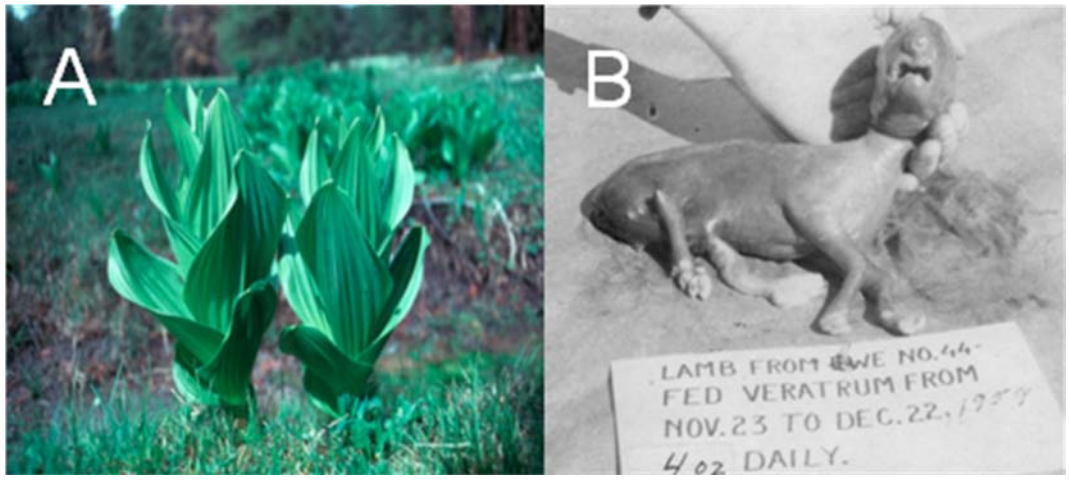

Figure 1. (A) *Veratrum californicum*; (B) the first cyclopic lamb born under controlled feeding conditions.

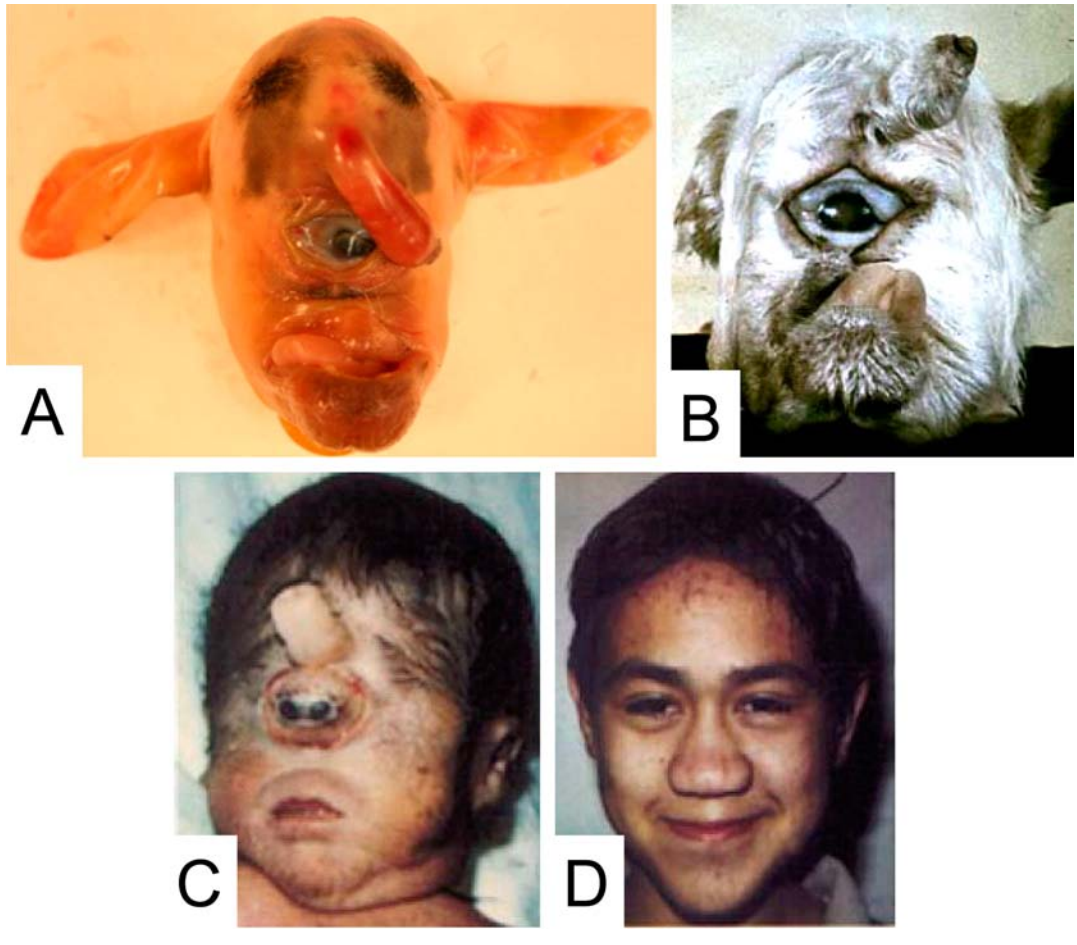

Figure 2. (A, B) Cyclopic lambs from lambs fed *Veratrum californicum* on day 14 of gestation. (C, D) Full brothers from a family with known mutations in the *Shh* gene. Images C and D reprinted with permission from ref 20. Copyright 1999 Oxford University Press.

dendricles resembling a hedgehog, resulting in its being named the hedgehog (*Hh*) gene. In 1993 three mammalian *Hh* counterparts, Desert hedgehog (*Dhh*), Indian hedgehog (*Ihh*), and Sonic hedgehog (*Shh*), were identified in a mouse[14] and named after two hedgehog species and the video game character, Sonic the Hedgehog. In 1995 human *Ihh* and *Shh* genes were identified and their chromosomal locations determined.[15] In 1999 the human *Dhh* gene was identified and its location determined.[16,17] *Shh* is the most broadly expressed and has been the most investigated of the mammalian *Hh* signaling genes. In mammals, *Shh* is responsible for embryonic development of symmetry along the sagittal plane, the central nervous system, skeleton, limbs, eyes, teeth, intestines, lungs, skin, muscles, cartilage, and sperm. Mouse embryos that lacked a *Shh* gene resulted in early embryonic death, holoprosencephaly (failure of the forebrain to develop into hemispheres), cyclopia at the base of an external proboscis, limb mispatterning, and foregut abnormalities, among numer-

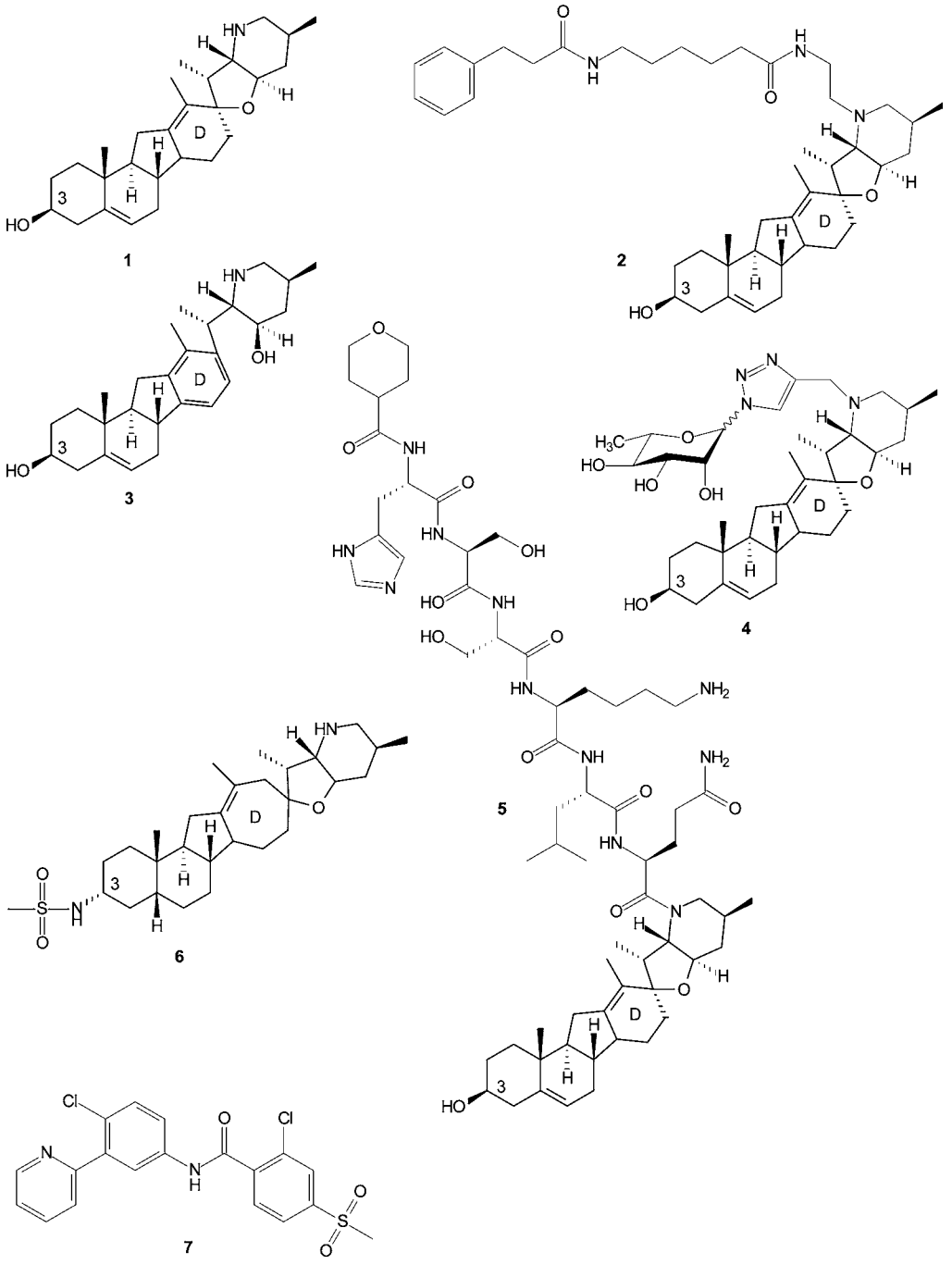

Figure 3. Chemical structures of cyclopamine (**1**), 3-keto-*N*-(aminoethyl-aminocaproyl-dihydrocinnamoyl)cyclopamine (**2**) (KAAD-cyclopamine (**2**)), veratramine (**3**), *N*-(4-L-rhamnopyranosyl-1*H*-1,2,3-triazol-1-yl)-methylcyclopamine (**4**), Mu-SSKLQ-cyclopamine (**5**), IPI-926 (**6**), and GDC-0449 (**7**).

ous other malformations.[18,19] Loss of *Shh* functioning in embryonic human development has also resulted in holoprosencephaly, cyclopia, and proboscis above the eye (Figure 2C).[20] In less severe human cases, flat nose absent of nasal cartilage, decreased distance between the eyes, and underdevelopment of the midface have been observed (Figure 2D).[20]

CYCLOPAMINE AND THE SONIC HEDGEHOG GENE

In 1996 while actively conducting research on the *Shh* gene pathway, Dr. Philip Beachy recalled images of the cyclopic lambs reported in Idaho in 1950−1960s and hypothesized that cyclopamine, **1**, could be used to probe the *Shh* pathway. In 1998 Beachy and co-workers[21] and Incardona et al.[22] established that cyclopamine inhibits the *Shh* signaling pathway. A simplified characterization of the *Shh* signaling pathway is presented in Figure 4. In most adult cells the *Shh* receptor Patched interacts with Smoothened, in effect acting as a molecular brake and inhibiting Smoothened (Figure 4A). During embryonic development, when *Shh* is present, *Shh* binds to Patched and Smoothened is then released from Patched. Smoothened then initiates downstream signaling that results in the binding of *Gli* transcription factors to DNA and subsequent activation of gene expression (Figure 4B). Cyclop-

dx.doi.org/10.1021/jf5005622 | J. Agric. Food Chem. 2014, 62, 7355−7362

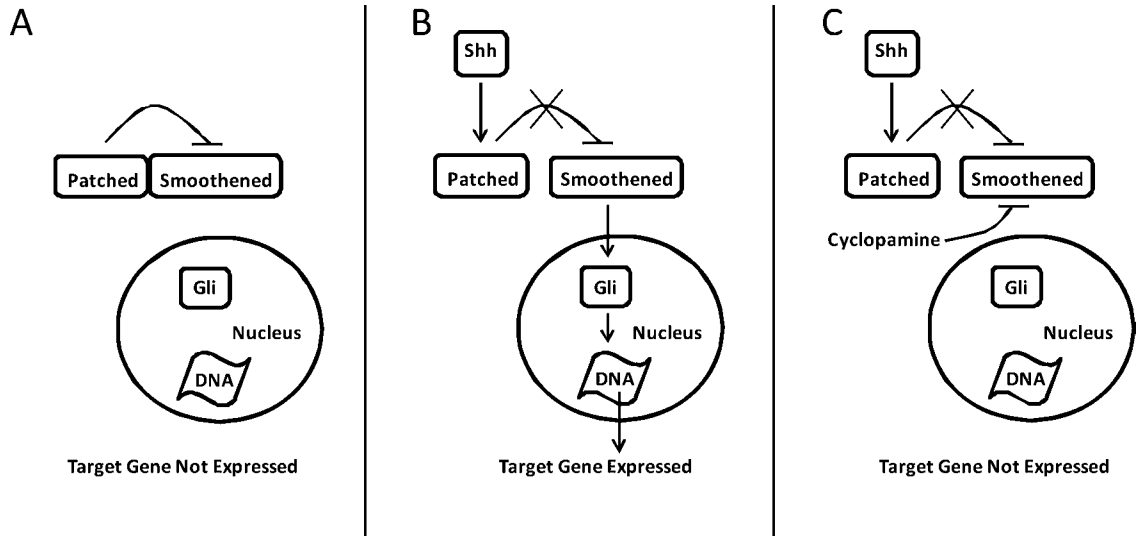

Figure 4. *Shh* signaling pathway. (A) Patched interacts and inactivates Smoothened. (B) When *Shh* is present, *Shh* binds to Patched, Smoothened is released from Patched, and Smoothened leads to downstream signaling via binding of the *Gli* transcription factors to DNA and activation of gene expression. (C) Cyclopamine binds to Smoothened and inhibits the *Shh* pathway downstream from Patched.

amine binds to Smoothened and inhibits the *Shh* pathway downstream from Patched and upstream from *Gli* (Figure 4C).[23,24] Modifications of cyclopamine to improve solubility as well as other pharmacokinetic characteristics have resulted in compounds with enhanced *Shh* signaling pathway inhibitor activity. For example, 3-keto-*N*-(aminoethyl-aminocaproyl-dihydrocinnamoyl)cyclopamine, **2** (KAAD-cyclopamine), a semisynthetic derivative of cyclopamine, was shown to have a 10−20-fold increase in potency compared to cyclopamine.[23]

CYCLOPAMINE DERIVATIVES AND CANCER TREATMENT

In addition to playing a key role in embryonic development, inappropriate activation of the *Shh* signaling pathway in mature cells has been associated with nevoid basal cell carcinoma (Gorlins syndrome) and several cancers, such as basal cell carcinoma, medullablastoma, and rhabdomyosarcoma, that are often driven by inherited mutations in Patched and, less frequently, Smoothened.[24,25] Nevoid basal cell carcinoma is an inherited condition characterized by multiple basal cell carcinomas, other malignant and benign tumors, and malformations.[26] Basal cell carcinoma is the most common type of skin cancer, medulloablastoma is the most common brain tumor in children, and rhabdomyosarcoma is a relatively rare cancer that is most commonly observed in children.[25,27] Other cancers such as colon, glioma, breast, esophageal, gastric, pancreatic, prostate, small cell lung, biliary tract, bladder, ovarian, liver, myeloma, leukemia, and oral cancers have been associated with autocrine- and paracrine-secreted hedgehog protein signaling.[27,28]

The *Shh* signaling pathway plays a critical role in embryonic development and appears to play an important role in a number of cancers in mouse models, because it no longer has a normal biological function in most mature cells. Consequently, inhibition of the *Shh* signaling pathway may be a promising cancer treatment method as it could stop tumor growth without many of the common side effects of traditional cancer therapeutics. Cyclopamine, **1**, has been shown to inhibit tumor growth in a genetic mouse medulloblastoma model,[29] a mouse medulloblastoma allograph model,[30] and mouse xenograft models with human glioma,[31] melanoma,[32] colon cancer,[33] pancreatic cancer,[34−36] prostate cancer,[37] and small cell lung cancer[38] without noticeable side effects in the cyclopamine-treated adult mice.[29−32,34,36] Tumor regression in human patients with basal cell carcinomas was reported after administration of a topical cream containing cyclopamine was applied directly onto the tumors, with no adverse effects to the patient, including the skin surrounding the treated tumors.[39] These results highlight the potential of using cyclopamine and other inhibitors of the *Shh* signaling pathway as therapies for human cancers promoted by aberrant *Shh* signaling and argue for initiation of human clinical trials using inhibitors of the *Shh* signaling pathway for lethal cancers.

Although cyclopamine, **1**, shows promise as a human chemotherapy agent, cyclopamine per se does have some inherent limitations. Cyclopamine has low solubility in water, normal saline, and other physiological solutions. In addition, cyclopamine is not stable under acidic conditions, as would be encountered in the stomach of humans and other monogastric animals. Under acidic conditions, the ether bond in ring E is readily hydrolyzed followed by aromatization of ring D, resulting in veratramine, **3**,[40,41] which is inactive in the *Shh* signaling pathway. These characteristics limit the bioavailability and delivery options of cyclopamine. Previous success in increasing the potency of the *Shh* pathway inhibition with KAAD-cyclopamine, **2**, suggests that other semisynthetic cyclopamine, **1**, compounds could be developed, which would overcome the pharmacokinetic limitations of cyclopamine, **1**, and may even have increased potency as anticancer therapies. In this regard, several different approaches have been undertaken to address the limitations of cyclopamine as a chemotherapeutic agent.

One simple solution to increase the solubility of cyclopamine, **1**, in physiological solutions has been achieved by the creation of a cyclopamine-tartrate salt. The solubility of cyclopamine was increased to approximately 2 mg/mL as cyclopamine-tartrate salt and up to 5 mg/mL with the addition of 1.5 mg of tartaric acid to the solution, as reported by the inventors.[42] Cyclopamine-tartrate salt was used to characterize the pharmacokinetic profile of cyclopamine in sheep[43] and

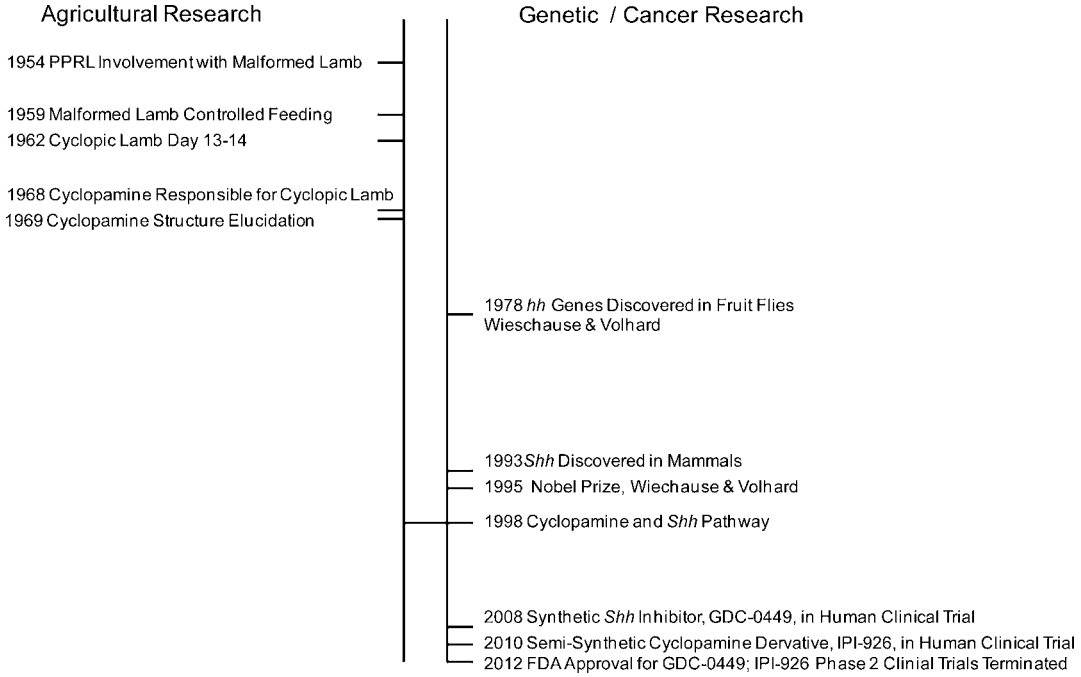

Figure 5. Agricultural, cell biology, and cancer research time line.

induced tumor shrinkage in two mouse basal cell carcinoma models.[44]

Chemists at Utah State University in collaboration with scientists at the PPRL investigated increasing the solubility of cyclopamine, **1**, while retaining or improving its potency by using "click" chemistry to form a series of 11 carbohydrate−cyclopamine conjugates. Most of the conjugates were less potent than cyclopamine; however, the *N*-(4-L-rhamnopyranosyl-1*H*-1,2,3-triazol-1-yl)-methylcyclopamine, **4**, conjugate showed higher potency than cyclopamine in a cytotoxicity assay with lung cancer cells.[45]

Although the *Shh* signaling pathway is inactive in most mature cells, there are select mature cells in which *Shh* signaling is required, such as the gonads, gastrointestinal tract, and bone marrow. To circumvent any possibility of toxicity in these cells, two cyclopamine, **1**, based pro-drugs were developed to target only prostate cancer cells. High levels of enzymatically active prostate specific antigen (PSA) exist in the immediate vicinity of both normal and tumorigenic prostate cells. Enzymatically active PSAs are inactivated by serum protease inhibitors in circulation. Peptide carriers were synthesized that serve as substrates to PSA. Amino acid sequences of His-Ser-Ser-Lys-Leu-Gln (HSSKLQ) and Ser-Ser-Lys-Leu-Gln (SSKLQ) that could be selectively cleaved from cyclopamine in the presence of PSA were conjugated to cyclopamine. The PSA substrate pro-drugs, morpholino (Mu), Mu-HSSKLQ-cyclopamine, and Mu-SSKLQ-cyclopamine, **5**, were evaluated in the presence of enzymatically active PSA, with Mu-SSKLQ-cyclopamine being more efficiently hydrolyzed. In addition, whereas the pro-drugs were minimally effective when cultured in a non-PSA-expressing prostate cancer cell line, the addition of PSA to the culture led to a dramatic 7-fold increase in the efficacy of the pro-drug.[46]

Several pharmaceutical companies have developed *Shh* signaling pathway inhibitors. For example, IPI-926, **6**, is a compound with a number of synthetic modifications to cyclopamine, **1**, which result in improved stability, kinetic profile, and potency. Enlargement of ring D from a six- to a seven-member ring dramatically improved the acid stability and aqueous solubility compared to cyclopamine.[47] The addition of the sulfonamide at the C-3 position further increased the metabolic stability of IPI-926 compared to cyclopamine.[47] IPI-926 was shown to have a longer pharmacokinetic half-life in multiple mammalian species and was more potent in a cellular *Hh* inhibition assay than other semisynthetic lead compounds.[47] Daily oral administration of IPI-926 in a mouse medulloblastoma allograph model led to complete tumor regression during the treatment phase, and tumor regrowth was not observed 21 days post treatment.[47] IPI-926 was also effective in inhibiting tumor growth in lung and pancreatic cancer xenograft models.[47]

A phase I clinical study of IPI-926, **6**, was commenced in 2010 in adult patients with solid tumors. The objectives of this first in-human study were to determine maximum tolerated oral dose and to characterize the pharmacokinetic profile of IPI-926. In addition, an expanded portion of the study evaluated the efficacy of IPI-926 at the maximum tolerated dose in patients with advanced or metastatic basal cell carcinomas. A well-tolerated dose was determined, and IPI-926 showed antitumor activity in patients with basal cell carcinomas.[48]

IPI-926, **6**, was further evaluated in a phase 1b/2 clinical study in patients with previously untreated metastatic pancreatic cancer in 2011. In the phase 1b portion of the study, patients were orally treated with IPI-926 in combination with intravenously administered gemcitabine. This trial evaluated the safety and pharmacokinetics and determined the recommended dose of IPI-926 for phase 2 clinical trials. In this study, a partial response to the therapy was observed in 31% of the patients. The combination of IPI-926 and gemcitabine was well tolerated, and no pharmacokinetic interactions were observed between the two drugs.[49] The phase 2 portion of the study compared IPI-926 in combination with gemcitabine to placebo with gemcitabine in patients with previously untreated metastatic pancreatic cancer with the

dx.doi.org/10.1021/jf5005622 | J. Agric. Food Chem. 2014, 62, 7355−7362

primary end point being overall survival. However, this study was terminated after an interim analysis found that the median survival of patients on the IPI-926 plus gemcitabine arm of the study was <6 months, whereas the median survival of the placebo plus gemcitabine arm was >6 months.[50]

Phase 2 clinical studies were also conducted with IPI-926, **6**, as a single agent in patients with myelofibrosis, an incurable cancer of the bone, and chondrosarcoma, a cancer of the cartilage, with primary end points of progression-free survival. Interim analysis of the chondrosarcoma study concluded that treatment with IPI-926 was similar to placebo and the study was terminated. At the same time, the phase 2 exploratory study with myelofibrosis was discontinued due to unsatisfactory clinical activity in initial patients.[51]

Other small molecules that act as hedgehog pathway inhibitors are currently being studied as anticancer therapies. However, many of these compounds are not based on the steroidal alkaloid structure of cyclopamine, **1**. The most successful of these compounds to date is the synthetically derived GDC-0449, **7**.[52,53] GDC-0449 has completed phase 2 clinical studies in patients with basal cell carcinoma, ovarian, and colorectal cancers and received FDA approval in January 2012 for treatment of adults with metastatic and/or locally advanced basal cell carcinoma.[54−56] In addition, clinical studies with GDC-0449 are active or are recruiting patients with basal cell nevus syndrome, basal cell carcinoma, myeloma, pancreatic, small cell lung, chondrosarcoma, medullablastoma, glioblastoma, prostate, glioma, leukemia, sarcoma, breast, and other solid cancers.[57]

PERSPECTIVE

Dr. Philip Beachy's recollection in 1996 of the research and images of the cyclopic lambs reported in the 1960s led to the correct hypothesis that cyclopamine, **1**, could be used to probe the *Shh* pathway. This observation and hypothesis connected agricultural-based research that had taken place 30 years earlier to current cell biology research. Since this discovery, cyclopamine has served as a valuable tool in elucidating and understanding the *Hh* signaling pathway in embryonic development and in the investigation of the role of the *Hh* pathway in various cancers. In addition, cyclopamine has served as a model compound for new cancer therapy drugs. Figure 5 is a timeline that shows the relationship between agricultural research, cell biology research, and cancer research and the major advances in the research areas that relate to cyclopamine. This long timeline is reminiscent of that involved in the development of Taxol (paclitaxel), which began in 1964 with the discovery that extracts of Pacific yew (*Taxus brevifolia*) bark were cytotoxic.[58] The Taxol time line continued with the identification of Taxol as the active principle in 1971 and the approval by the FDA of Taxol as a treatment for ovarian cancer and breast cancer, respectively, in 1992 and 1994. The use of Taxol has continued to increase and, along with its semisynthetic analogue, Taxotere, has become the best-selling anticancer drug in history.[58] We anticipate that cyclopamine will continue to be an important research tool in the future and additional advances in cancer therapies and the *Hh* pathway will be forthcoming. In addition, other poisonous plants should be investigated as sources for anticancer agents, new drugs, and other biomedical applications.[59]

This review highlights the importance of agricultural/poisonous plant research and the rapid advances that can be made by an interdisciplinary and nonlinear approach to solving important research problems.

AUTHOR INFORMATION

Corresponding Author

*(S.T.L.) Phone: (435) 752-2941. Fax: (435) 797-5681. E-mail: stephen.lee@ars.usda.gov.

Notes

The authors declare no competing financial interest.

REFERENCES

(1) Binns, W.; James, L. F.; Shupe, J. L. Cyclopian-type malformation in lambs. *Arch. Environ. Health* **1962**, *5*, 106−108.

(2) Binns, W.; James, L. F.; Shupe, J. L.; Everett, G. A congenitital−type malformation in lambs induced by maternal ingestion of a range plant *Veratrum californicum*. *Am. J. Vet. Res.* **1963**, *24*, 1164−1175.

(3) James, L. F. Teratological research at the USDA-ARS Poisonous Plant Research Laboratory. *J. Nat. Toxins* **1999**, *8*, 63−80.

(4) Binns, W.; Shupe, J. L.; Keeler, R. F.; James, L. F. Chronologic evaluation of teratogenicity in sheep fed *Veratrum californicum*. *J. Am. Vet. Med. Assoc.* **1965**, *147*, 839−842.

(5) Keeler, R. F. Early embryonic death in lambs induced by *Veratrum californicum*. *Cornell Vet.* **1990**, *80*, 203−207.

(6) Welch, K. D.; Lee, S. T.; Gardner, D. R.; Panter, K. E.; Stegelmeier, B. S.; Cook, D. Dose-response evaluation of *Veratrum californicum* in sheep. In *Poisoning by Plants, Mycotoxins, and Related Toxins*; Riet-Correa, F., Pfister, J. A., Schild, A. L., Wierenga, T. L., Eds.; CAB International: Wallingford, UK, 2011.

(7) Van Kampen, K. R.; Binns, W.; James, L. F.; Balls, L. D. Early embryonic death in ewes given *Veratrum californicum*. *Am. J. Vet. Res.* **1969**, *30*, 517−519.

(8) Keeler, R. F.; Stuart, L. D. The nature of congenital limb defects induced in lambs by maternal ingestion of *Veratrum californicum*. *Clin. Toxicol.* **1987**, *25*, 273−286.

(9) Keeler, R. F.; Young, S.; Smart, R. Congenital tracheal stenosis in lambs induced by maternal ingestion of *Veratrum californicum*. *Teratology* **1985**, *31*, 83−88.

(10) Keeler, R. F.; Binns, W. Teratogenic compounds of *Veratrum californicum* (Durand). V. Comparison of cyclopean effects of steroidal alkaloids from the plant and structurally related compounds from other sources. *Teratology* **1968**, *1*, 5−10.

(11) Keeler, R. F. Teratogenic compounds of *Veratrum californicum* (Durand) − VI. The structure of cyclopamine. *Phytochemistry* **1969**, *8*, 223−225.

(12) Masamune, T.; Mori, Y.; Takasugi, M.; Murai, A.; Ohuchi, S.; Sato, N.; Katsui, N. 11-Deoxojervine, anew alkaloid from *Veratrum* species. *Bull. Chem. Soc. Jpn.* **1965**, *38*, 1374−1378.

(13) Nusslein-Volhard, C.; Wieschaus, E. Mutations affecting segment number and polarity in *Drosophila*. *Nature* **1980**, *287*, 795−801.

(14) Echelard, Y.; Epstein, D. J.; St-Jacques, B.; Shen, L.; Mohler, J.; McMahon, J. A.; McMahon, A. P. Sonic hedgehog, a member of a family of putative signaling molecules, is implicated in the regulation of CNS polarity. *Cell* **1993**, *75*, 1417−1430.

(15) Marigo, V.; Roberts, D. J.; Lee, S. M.; Tuskurov, O.; Levi, T.; Gastier, J. M.; Epstein, D. J.; Gilbert, D. J.; Copeland, H. G.; Seidman, C. E.; Jenkins, N. A.; Seidman, J. G.; McMahon, A. P.; Tabin, C. Cloning, expression, and chromosomal location of *SHH* and *IHH*: two human homologues of the *Drosophilia* segment polarity gene *hedgehog*. *Genomics* **1995**, *28*, 44−51.

(16) Kamisago, M.; Kimura, M.; Furutani, Y.; Furutani, M.; Takao, A.; Momma, K.; Matsuoka, R. Assignment of human desert hedgehog gene (DHH) to chromosome band 12q13.1 by in situ hybridization. *Cytogenet. Cell Genet.* **2000**, *87*, 117−118.

(17) Tate, G.; Satoh, H.; Endo, Y.; Mitsuya, T. Assignment of desert hedgehog (DHH) to human chromosome bands 12q12→q13.1 by in situ hybidization. *Cytogenet. Cell Genet.* **2000**, *88*, 93−94.

(18) Chiang, C.; Litingtung, Y.; Lee, E.; Young, K. E.; Corden, J. L.; Westphal, H.; Beachy, P. A. Cyclopia and defective axial patterning in mice lacking sonic hedgehog gene function. *Nature* **1996**, *383*, 407−413.
(19) Litingtung, Y.; Lei, L.; Westphal, H.; Chiang, C. Sonic hedgehog is essential to foregut development. *Nat. Genet.* **1998**, *20*, 58−61.
(20) Nanni, L.; Ming, J. E.; Bocian, M.; Steinhaus, K.; Bianchi, D. W.; de Die-Smulders, C.; Giannotti, A.; Imaizumi, K.; Jones, K. L.; Del Campo, M.; Martin, R. A.; Meinecke, P.; Peirpont, M. E. M.; Robin, N. H.; Young, I. D.; Roessler, E.; Muenke, M. The mutational spectrum of the Sonic hedgehog gene in holoproencephaly: SHH mutations cause a significant proportion of autosomal dominant holoprosencephaly. *Hum. Mol. Genet.* **1999**, *8*, 2479−2488.
(21) Cooper, M. K.; Porter, J. A.; Young, K. E.; Beachy, P. A. Teratogen-mediatied inhibition of target tissue response to Shh signaling. *Science* **1998**, *5*, 1603−1607.
(22) Incardona, J. P.; Gaffield, W.; Kapur, R. P.; Roelink, H. The teratogenic *Veratrum* alkaloid cyclopamine inhibits Sonic hedgehog signal transduction. *Development* **1998**, *125*, 3553−3562.
(23) Taipale, J.; Chen, J. K.; Cooper, M. K.; Wang, B.; Mann, R. K.; Milenkovic, L.; Scott, M.; Beachy, P. A. Effects of oncogenic mutations in smoothened and patched can be reversed by cyclopamine. *Nature* **2000**, *406*, 1005−1008.
(24) Chen, J. K.; Taipale, J.; Cooper, M. K.; Beachy, P. A. Inhibition of hedgehog signaling by direct binding of cyclopamine to smoothened. *Genes Dev.* **2002**, *16*, 2743−2748.
(25) Heretsch, P.; Tzagkaroulaki, L.; Giannis, A. Cyclopamine and hedgehog signaling: chemistry, biology, medical perspectives. *Angew. Chem., Int. Ed.* **2010**, *49*, 2−12.
(26) Bale, A. E.; Yu, K.-p. The hedgehog pathway and basal cell carcinomas. *Hum. Mol. Genet.* **2001**, *10*, 757−762.
(27) Varjosalo, M.; Taipale, J. Hedgehog: functions and mechanisms. *Genes Dev.* **2008**, *22*, 2454−2472.
(28) Mas, C.; Altaba, A. R. i. Small molecule modulation and HH-GLI signaling: current leads, trial and tribulations. *Biochem. Pharmacol.* **2010**, *80*, 712−723.
(29) Sanchez, P.; Altaba, A. R. i. In vivio inhibition of endogenous brian tumors through systemic interference of Hedgehog signaling in mice. *Mech. Dev.* **2005**, *122*, 223−230.
(30) Berman, D. M.; Karhadkar, S. S.; Hallahan, A. R.; Pritchard, J. I.; Eberhart, C. G.; Watkins, D. N.; Chen, J. K.; Cooper, M. K.; Taipale, J.; Olson, J. M.; Beachy, P. A. Medulloblastoma growth inhibition by hedgehog pathway blockage. *Nature* **2002**, *297*, 1559−1561.
(31) Clement, V.; Sanchez, P.; de Tribolet, N.; Radovanovic, I.; Altaba, A. R. i. Hedgehoge-GLi1 signaling regulates human glioma growth, cancer stem cell self-renewal, and tumorigenicity. *Curr. Biol.* **2007**, *17*, 165−172.
(32) Stecca, B.; Mas, C.; Clement, V.; Zbinden, M.; Correa, R.; Piquet, V.; Beermann, F.; Altaba, A. R. i. Melanomas require Hedgehog-GLi signaling regulated by interactions between GLi1 and the RAS-MEK/AKT pathways. *Proc. Natl. Acad. Sci. U.S.A.* **2007**, *104*, 5895−5900.
(33) Varnat, F.; Duquet, A.; Malerba, M.; Zbinden, M.; Mas, C.; Gervas, P.; Altaba, A. R. i. Human colon cancer epithelial cells harbor active hedgehoge-GLi signaling that is essential for tumor growth, recurrence, metastasis and stem cell survival and expansion. *EMBO Mol. Med.* **2009**, *1*, 338−351.
(34) Berman, D. M.; Karhadkar, S. S.; Maitra, A.; de Oca, R. M.; Gerstenblith, M. R.; Briggs, K.; Parker, A. R.; Shimada, Y.; Eshlemann, J. R.; Watkins, D. N.; Beachy, P. A. Widespread requirement for hedgehog ligand growth of digestive tract tumors. *Nature* **2003**, *425*, 846−851.
(35) Thayer, S. P.; di Magliano, M. P.; Heiser, P. W.; Neilsen, C. M.; Roberts, D. J.; Lauwers, G. Y.; Qi, Y. P.; Glysin, S.; Castillo, C. F-d.; Yajnik, V.; Antoniu, B.; McMahon, M.; Warchaw, A. W.; Hebrok, M. Hedgehog is an early and late mediator of pancreatic cancer tumorigenesis. *Nature* **2003**, *425*, 851−856.
(36) Feldmann, G.; Dhara, S.; Fendrich, V.; Bedja, D.; Beaty, R.; Mullendore, M.; Karikari, C.; Alverez, H.; Iacobuzio-Donahue, C.; Jimeno, A.; Gabrielson, K. L.; Matsui, W.; Maitra, A. Blockade of hedgehog signaling inhibits pancreatic cancer invasion and metastases: a new paradigm for combination therapy in solid cancers. *Cancer Res.* **2007**, *67*, 2187−2196.
(37) Karhadkar, S. S.; Bova, G. S.; Abdallah, N.; Dhara, S.; Gardner, D.; Maltra, A.; Isaacs, J. T.; Berman, D. M.; Beachy, P. A. Hedgehog signaling in prostate regeneration, neoplasis and metastasis. *Nature* **2004**, *431*, 107−712.
(38) Watkins, N. D.; Berman, D. M.; Burkholder, S. G.; Wang, B.; Beachy, P. A.; Baylin, S. B. *Nature* **2003**, *422*, 313−317.
(39) Sinan, S.; Oktay, A. Induction of the differentiation and apoptosis of tumor cells *in vivo* with efficiency and selectivity. *Eur. J. Dermatol.* **2004**, *14*, 96−102.
(40) Keeler, R. F. Teratogenic compounds in the *Veratrum californicum* (Durand) IX. Structure-activity relation. *Teratology* **1970**, *3*, 169−173.
(41) Tremblay, M. R.; Nevalainen, M.; Nair, S. J.; Porter, J. R.; Castro, A. C.; Behnke, M. L.; Yu, L.-C.; Hagel, M.; White, K.; Faia, K.; Grenier, L.; Campbell, M. J.; Cushing, J.; Woodward, C. N.; Hoyt, J.; Foley, M. A.; Read, M. A.; Sydor, J. R.; Tong, J. K.; Palombella, V. J.; McGovern, K.; Adams, J. Semisynthetic cyclopampaine analogues as potent and orally bioavailable hedgehog pathway antagonists. *J. Med. Chem.* **2008**, *51*, 6646−6649.
(42) Logan Natural Products. http://www.logannaturalproducts.com/cyclopamine_tartrate.php (accessed Jan 8, 2014).
(43) Welch, K. D.; Panter, K. E.; Gardner, D. R.; Stegelmeier, B. L.; Cook, D. Cyclopamine-induced synopthalmia in sheep: defining a critical window and toxicokinetic evaluation. *J. Appl. Toxicol.* **2009**, *29*, 414−421.
(44) Fan, Q.; Gu, D.; He, M.; Liu, H.; Sheng, T.; Xie, G.; Li, C-x.; Zhang, X.; Wainwright, B.; Garrossian, A.; Garrossian, M.; Gardner, D. R.; Xie, J. Tumor shrinkage by cyclopamine tartrate through inhibiting hedgehog signaling. *Chin. J. Cancer* **2011**, *30*, 472−481.
(45) Zhang, J.; Garrossian, M.; Gardner, D.; Garrossian, A.; Chang, Y.-T.; Kim, Y. K.; Chang, C-W. T. Synthesis and anticancer activity studies of cyclopamine derivatives. *Bioorg. Med. Chem. Lett.* **2008**, *18*, 1359−1363.
(46) Kumar, S. K.; Roy, I.; Anchoori, R. K.; Fazli, S.; Maitra, A.; Beachy, P. A.; Khan, S. R. Targeted inhibition of hedgehog signaling by cyclopamine prodrugs for advanced prostate cancer. *Bioorg. Med. Chem.* **2008**, *16*, 2764−2768.
(47) Tremblay, M. R.; Lescarbeau, A.; Grogan, M. J.; Tan, E.; Lin, G.; Austad, B. C.; Yu, L.-C.; Behnke, M. L.; Nair, S. J.; Hagel, M.; White, K.; Conley, J.; Manna, J. D.; Alvarez-Diez, T. M.; Hoyt, J.; Woodward, C. N.; Sydor, J. R.; Pink, M.; MacDougall, J.; Campbell, M. J.; Cushing, J.; Ferguson, J.; Curtis, M. S.; McGovern, K.; Read, M. A.; Palombella, V. J.; Adams, J.; Castro, A. C. Discovery of potent and orally active hedgehog pathway antagonist (IPI-926). *J. Med. Chem.* **2009**, *52*, 4400−4418.
(48) Jimeno, A.; Weiss, G. J.; Miller, W. H., Jr.; Gettinger, S.; Eigl, B. J. C.; Chang, A. L. S.; Dunbar, J.; Devens, S.; Faia, K.; Skliris, G.; Kutok, J.; Lewis, K. D.; Tibes, R.; Sharfman, W. H.; Ross, R. W.; Rudin, C. M. Phase I study of hedgehog pathway inhibitor IIPI-926 in adult patients with solid tumors. *Clin. Cancer Res.* **2013**, *19*, 2766−2774.
(49) Infinity reports results from phase 1b clinical trial of IPI-926, an oral smoothened antagonist, in pancreatic cancer at ASCO meeting. http://globenewswire.com/news-release/2011/06/04/448749/223661/en/Infinity-Reports-Results-From-Phase-1b-Clinical-Trial-of-IPI-926-an-Oral-Smoothened-Antagonist-in-Pancreatic-Cancer-at-ASCO-Meeting.html (accessed Jan 7, 2014).
(50) Infinity reports update from phase 2 study of Saridegib plus Gemcitabine in patients with metastatic pancreatic cancer. http://www.businesswire.com/news/home/20120127005146/en (accessed Jan 7, 2014).
(51) Infinity stops phase 2 trials of Saridegib in chondrosarcoma and myelofibrosis. http://www.businesswire.com/news/home/20120618005411/en/Infinity-Stops-Phase-2-Trials-Saridegib-Chondrosarcoma (accessed Jan 7, 2014).

(52) Robarge, K. D.; Brunton, S. A.; Castanedo, G. M.; Cui, Y.; Dina, M. S.; Goldsmith, R.; Gould, S. E.; Guichert, O.; Gunzerner, J. L.; Halladay, J.; Jia, W.; Khojasteh, C.; Koehler, M. F.; Kotkow, K.; La, H.; LaLonde, R. L.; Lau, K.; Lee, L.; Marshall, D.; Marsters, J. C., Jr.; Murray, L. J.; Qian, C.; Rubin, L. L.; Salphati, L.; Stanley, M. S.; Stibbard, J. H. A.; Sutherlin, D. P.; Ubhayaker, S.; Wang, S.; Wong, S.; Xie, M. GDC-0449-A potent inhibitor of the hedgehog pathway. *Bioorg. Med. Chem. Lett.* **2009**, *19*, 5576−5581.

(53) LoRusso, P. M.; Rudin, C. M.; Reddy, J. C.; Tibes, R.; Weiss, G. J.; Borad, M. J.; Hann, C. L.; Brahmer, J. R.; Chang, I.; Darbonne, W. C.; Graham, R. A.; Zervitz, K. L.; Low, J. A.; Von Hoff, D. D. Phase 1 trial of hedgehog pathway inhibitor Vismodegib (GDC-449) in patients with refractory, locally advanced or metastatic solid tumors. *Clin. Cancer Res.* **2011**, *17*, 2502−2511.

(54) National Cancer Institute Clinical Trials Search Results. http://www.cancer.gov/clinicaltrials/search/results?protocolsearchid=10366832 (accessed Jan 8, 2014).

(55) Vismodegib. http://www.fda.gov/Drugs/InformationOnDrugs/ApprovedDrugs/ucm289571.htm (accessed Jan 8, 2014).

(56) Erivedge development timeline. http://www.gene.com/media/product-information/erivedge-development-timeline (accessed Jan 8, 2014).

(57) National Cancer Institute Clinical Trials Search Results. http://www.cancer.gov/clinicaltrials/search/results?protocolsearchid=6235953 (accessed Jan 8, 2014).

(58) Kingston, D. G. I. Recent advances in the chemistry of Taxol. *J. Nat. Prod.* **2000**, *63*, 726−734.

(59) James, L. F.; Panter, K. E.; Gaffield, W.; Molyneux, R. J. Biomedical applications of poisonous plant research. *J. Agric. Food Chem.* **2004**, *52*, 3211−3230.

behavior is one of the most common results of drug−drug interactions.[7]

Interactions involving drug metabolism can have profound effects on the concentration of active drugs by affecting the rate at which the drug is either bioactivated or detoxified. Many drugs inhibit, or induce, key drug-metabolizing enzymes including cytochrome P450s (CYP). For example, dietary substances such as grapefruit juice will inhibit CYP 3A4, a ubiquitous drug-metabolizing enzyme, whereas some herbal remedies such as St. John's wort will induce CYP3A.[6,8] Thus, cotreatment with dietary, herbal, or additional drugs can result in altered metabolism of the drugs and subsequently alter the concentration of the bioactive drugs. In this regard, studies have shown the potential for negative effects from concomitant use of certain herbs and drugs.[9] For example, St. John's wort, by inducing CYPs, may affect the bioavailability of many conventional drugs[10] including the efficacy of drugs such as warfarin.[11] Clinical studies have suggested the risk for adverse reactions increases when herbal and conventional drugs are taken at the same time.[12] For example, rutaecarpine, an alkaloid found in *Evodia rutaecarpa*, a plant used in traditional Chinese medicine, affects CYP-mediated metabolism, glucuronidation, and transport pathways, which results in altered metabolism and elimination of caffeine, theophylline, and acetaminophen.[13−15] Similarly, the furanocoumarins in grapefruit juice, which inhibit CYP3A4, are known to interact with at least 85 drugs, resulting in adverse effects in many instances.[16] Although this phenomenon is most commonly associated with grapefruit juice, furanocoumarin derivatives have been found in numerous other plants.[17] In this regard, the furanocoumarins that are known to inhibit CYP3A4 have also been detected in eight other citrus fruits.[18] Consequently, the ingestion of many citrus fruits and/or other plants may adversely affect drug therapies by altering CYP3A4-mediated metabolism.

■ CHEMICAL MIXTURES OF PLANT TOXINS

In most cases where livestock are poisoned by plants in a range setting, there is more than one potential poisonous plant in that area. Additionally, many poisonous plants contain more than one toxin. Often, much is known regarding the toxicity of the individual plants and their toxins; however, little is known regarding the effect of coexposure to multiple toxic plants or even multiple toxins from an individual plant. For the remainder of this review, we will focus on the effect of chemical mixtures of plant toxins. We will discuss results from experiments in which we investigated the role of two different types of alkaloids from larkspur (*Delphinium* species) plants on the overall toxicity of the larkspur plant. We will also consider results from experiments characterizing the effect of coexposure to two different plants, each containing different classes of toxins. These experiments provide examples of the mixture effects that result from exposure to multiple toxins, either from an individual plant species or from two different plant species.

■ LARKSPUR: MDL- AND MSAL-TYPE ALKALOIDS

Larkspurs are placed into one of three categories based upon the mature plant height and distribution: low, tall, and plains larkspurs.[19] Larkspurs contain numerous (>18) norditerpenoid alkaloids, which are structurally delineated as 7,8-methylenedioxylycoctonine (MDL)-type alkaloids, such as deltaline, **1**, and 14-*O*-acetyldictyocarpine (14-OAD), **2**, and *N*-(methylsuccinimido)anthranoyllycoctonine (MSAL)-type alkaloids, such as methyllycaconitine (MLA), **3** (Figure 1).[19] Each of the different larkspur classes and species contains the

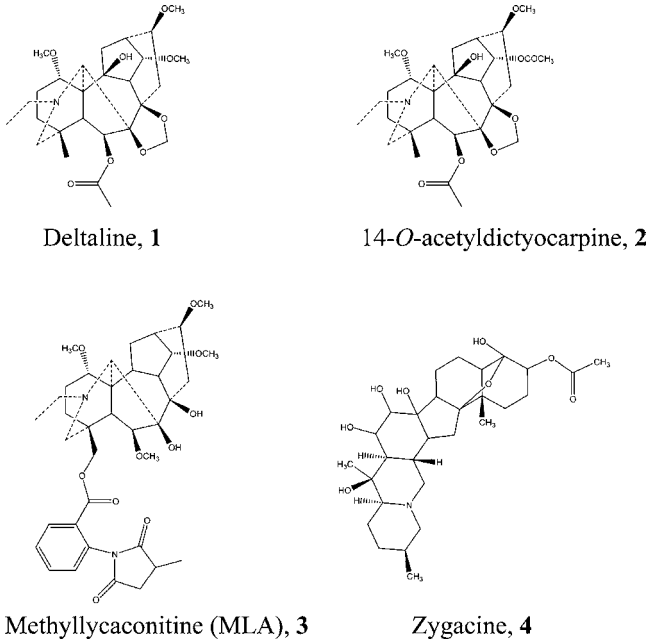

Figure 1. Chemical structures of selected norditerpenoid alkaloids in larkspur (*Delphinium* spp.) plants and zygacine, the main toxic alkaloid in death camas (*Zigadenus paniculatus*). Larkspurs contain numerous (>18) norditerpenoid alkaloids, which are structurally delineated as 7,8-methylenedioxylycoctonine (MDL), including deltaline and 14-*O*-acetyldictyocarpine (14-OAD), and *N*-(methylsuccinimido)anthranoyllycoctonine (MSAL)-type alkaloids, including methyllycaconitine (MLA).

norditerpenoid alkaloids, with MLA occurring to some degree in most larkspurs.[19] Although the MSAL-type alkaloids are more toxic (typically >20 times) than the MDL-type alkaloids,[20,21] the MDL-type alkaloids are generally more abundant in the tall larkspur *Delphinium barbeyi* and *Delphinium occidentale* populations.[19,22,23] If a risk analysis of tall larkspur species is performed on the basis of the MSAL-type alkaloid content only, then *Delphinium glaucum* is considered the most toxic tall larkspur species followed by *D. barbeyi* and *Delphinium glaucescens*, with *D. occidentale* being the least toxic tall larkspur species.[24] In this regard, current management recommendations for grazing cattle on larkspur-infested ranges are in fact based primarily on the concentration of the MSAL-type alkaloids,[25,26] in part because research has demonstrated that tall larkspur populations with only MDL-type alkaloids are of low risk to cattle.[27]

D. barbeyi is one of the more problematic species of tall larkspur plants due to its high concentration of MLA. However, the most abundant norditerpenoid alkaloids in most *D. barbeyi* populations are the less toxic MDL-type alkaloids, either deltaline or 14-OAD.[19,21,23] Although the toxicities of MLA, 14-OAD, and deltaline have been determined individually,[28] it is not known what effects the proportionally higher concentration of deltaline or 14-OAD in these plants have on the toxicity of MLA. To understand what contributions MDL-type alkaloids make to the overall toxicity of larkspurs, the effects of deltaline and 14-OAD on the toxicity of MLA were assessed by comparing the lethality, in mice, of these alkaloids administered individually and in combination. Both deltaline and 14-OAD

caused an increase in toxicity when co-administered with MLA (Figure 2). The effect of these two MDL-type alkaloids on the

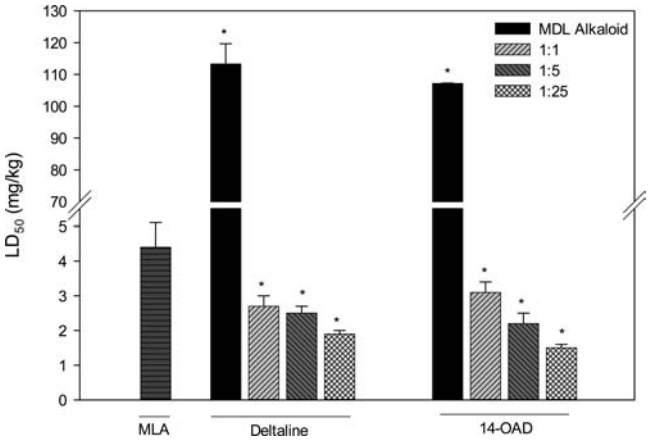

Figure 2. Effect of co-administration of various 7,8-methylenedioxylycoctonine (MDL)-type alkaloids on the toxicity of methyllycaconitine (MLA) in mice. The data represent the LD_{50} of MLA alone, MDL-type alkaloids alone, and MLA plus MDL-type alkaloids at ratios of 1:1, 1:5, and 1:25 MLA to MDL-type alkaloids. Results represent the mean ± SD of 24−86 mice per group; ∗, $P < 0.05$ as compared to the MLA group. (Adapted from Welch et al.[29])

toxicity of MLA was greater than additive, as their co-administration with MLA at 1:1, 1:5, and 1:25 ratios resulted in decreases in the LD_{50} (more toxic) by approximately 25, 50, and 60%, respectively, versus that of MLA alone. Solutions containing both MLA- and a MDL-type alkaloid showed increased toxicity compared to MLA alone, suggesting that MDL-type alkaloids exacerbate MSAL toxicity and therefore play an important part in the toxicity of larkspur plants.[29]

We examined the role of MDL-type alkaloids in the overall toxicity of larkspur plants to cattle with the hypothesis that if the MDL-type alkaloids affect the toxicity of the larkspur plant material in an additive manner, then a larkspur population with a high MDL-type alkaloid concentration would be more toxic than a larkspur population with a low MDL-type alkaloid concentration when both have a similar MSAL-type alkaloid content.[30] The results of that study (Table 1) clearly demonstrate that as the ratio of MDL- to MSAL-type alkaloids

Table 1. Effects of Single Doses of Three Tall Larkspur Populations on Heart Rate in Steers

	dose (mg alkaloid/kg)			heart rate[a] (beats/min)	
tall larkspur population (MDL:MSAL)	MSAL-type	MDL-type	total alkaloid	baseline	24 h
D. barbeyi (3:1)	8	25	33	75 ± 9	102 ± 16*
D. barbeyi (1:1)	12	12	24	70 ± 5	82 ± 12
	13	13	26	68 ± 14	100 ± 18*
D. glaucescens (0.6:1)	12	8	20	62 ± 10	73 ± 17
	14	9	23	61 ± 14	69 ± 5
	15	10	25	55 ± 3	74 ± 18
	18	11	29	65 ± 14	100 ± 21*

[a]Data represent the mean ± SD heart rate from three to six steers. (*) Value is significantly ($P < 0.05$) different from the baseline value. (Adapted from Welch et al.[30])

decreased, the amount of plant material required to raise heart rate, a clinical sign of poisoning in larkspur-poisoned cattle, increased.[31] A decrease in the MDL- to MSAL-type alkaloid ratio from 3.1:1 to 0.6:1 required the dose to be increased from 8 to 18 mg MSAL/kg to achieve an elevated heart rate. Coincidentally, the dose that was observed to elevate heart rate was >26 mg total alkaloid/kg for each population. Consequently, it could be argued that surpassing a threshold of total alkaloid is all that is required to elevate heart rate. However, we found a correlation between the increase in heart rate associated with larkspur intoxication and serum MLA concentrations ($P = 0.0001$) but not deltaline ($P = 0.2$).[32] Additionally, we observed that cattle dosed at 37.6 mg total alkaloid/kg with a tall larkspur population that contains almost exclusively MDL-type alkaloids showed no elevation in heart rate.[27] These results are in agreement with the mouse experiments[29] and demonstrate that MDL-type alkaloids increase the toxicity of MSAL-containing larkspur plants.

In the study using cattle, animals were dosed with different populations of tall larkspur that naturally have different ratios of MDL- to MSAL-type alkaloids.[30] A drawback with that study was that as the ratio of MDL- to MSAL-type alkaloids changed, so did the amount of MSAL-type alkaloids dosed, which made it difficult to differentiate the role of the MDL-type alkaloids from that of the MSAL-type alkaloids. Therefore, we also examined the role of MDL-type alkaloids on the overall toxicity of tall larkspur plants to cattle while controlling for the exact dose of MSAL-type alkaloids.[33] Cattle were dosed with plant material from two different populations of tall larkspur containing either almost exclusively MDL- or MSAL-type alkaloids (Figure 3). A more detailed description of the alkaloids in *Delphinium* species is provided by Gardner et al.[34] These two plant populations were combined to create mixtures with ratios of 0.3:1, 1:1, 5:1, and 10:1 MDL- to MSAL-type alkaloids. The dose that elicited similar clinical signs of poisoning was determined for each mixture based on the MSAL-type alkaloid content (Figure 4). As the ratio of MDL- to MSAL-type alkaloids increased, the amount of MSAL-type alkaloids required to elicit clinical signs decreased.

The results from these studies indicate that MDL-type alkaloids exacerbate the overall toxicity of the MSAL-type alkaloids and should be considered when predicting potential toxicity of larkspur populations. Therefore, when chemical analyses are performed on larkspur plants to assess their toxic potential, the concentration of both the MSAL- and MDL-type alkaloids should be determined, with more weight given to the effect of the MSAL-type alkaloids. Finally, the results from this study indicate that larkspur plants containing large amounts of MDL-type alkaloids, in addition to high MSAL-type alkaloid content, should be considered potentially more dangerous to cattle than plants with only high MSAL-type alkaloids.

■ DEATH CAMAS AND LOW LARKSPUR

There are many species of death camas (*Zigadenus* spp.) located in North America.[35,36] Death camas is one of the first plant species to emerge in the spring. Poisonings generally occur during the spring when death camas is abundant and while other forage species show little growth. Poisonings also occur on overgrazed ranges where better quality forage has been depleted or when management errors result in hungry animals being moved into death camas-infested areas.[37] Livestock losses due to death camas have been reported in numerous species, with the largest losses generally occurring in

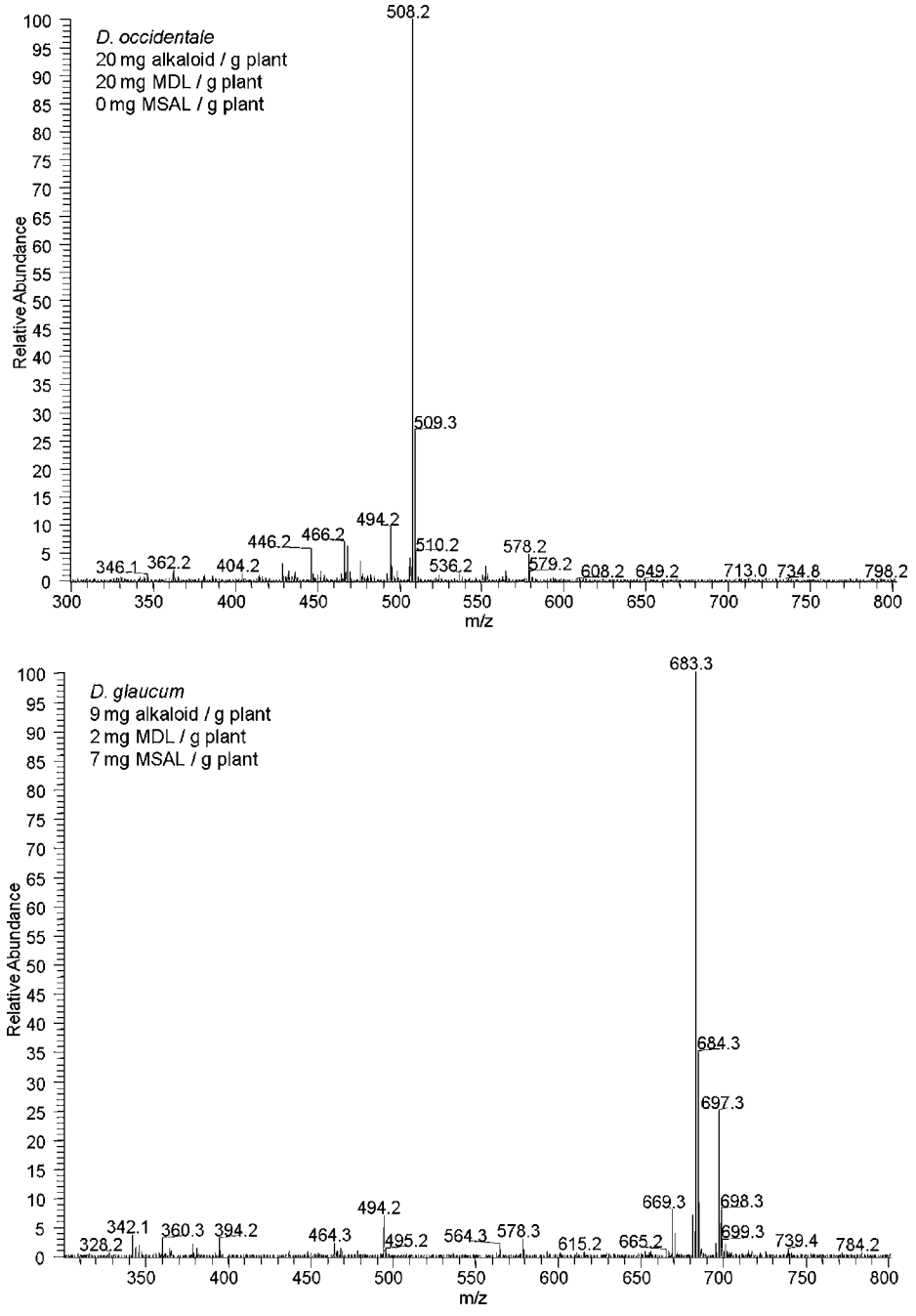

Figure 3. Mass spectra of alkaloids from the *Delphinium occidentale* and *Delphinium glaucum* plant populations used for these experiments. Spectra include protonated molecules (MH^+) for the different alkaloids in the plants. The major alkaloid in the *D. occidentale* population was deltaline (*m*/*z* 508), whereas the major alkaloid in the *D. glaucum* population was methyllycaconitine (MLA; *m*/*z* 683). (Adapted from Welch et al.[33])

sheep[38] and some reported losses in cattle.[39] Sheep are primarily affected because of their tendency to select forbs, particularly in the early spring when there is little other plant growth. Clinical signs of poisoning are similar for all animal species studied, including excessive salivation, with foamy froth around the nose and muzzle that persists, followed by nausea and occasionally vomition in ruminants. Intestinal peristalsis is dramatically increased, accompanied by frequent defecation and urination, muscular weakness with accompanying ataxia, muscular fasciculations, prostration, and eventual death.[37,40] Zygacine, **4** (Figure 1), is often the most abundant alkaloid in death camas and is consequently believed to be the primary toxic component.[41,42]

One common poisonous plant found growing simultaneously in the same area as death camas is low larkspur (*Delphinium nuttallianum*). *D. nuttallianum* is known to contain a high concentration of MLA.[43,44] In fact, MLA is one the more abundant alkaloids in many low larkspur species.[45,46] Additionally, the kinetic profile of MLA and the other toxic alkaloids in low larkspur have been shown to be similar when the alkaloids are dosed to cattle as either tall or low larkspur.[32,47,48] Consequently, the objective of our studies was to determine if co-administration of low larkspur will exacerbate the toxicity of death camas. We first characterized the effects of coexposure of the primary toxin from each of these plants in a mouse model.[42] The LD_{50} values of purified zygacine and MLA in mice were 2.0

dx.doi.org/10.1021/jf500086u | J. Agric. Food Chem. 2014, 62, 7363−7369

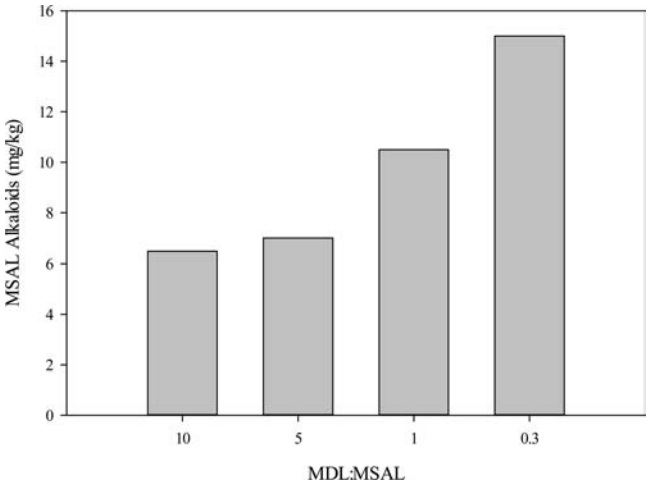

Figure 4. Effect of ratios of 7,8-methylenedioxylycoctonine (MDL)- to *N*-(methylsuccinimido)anthranoyllycoctonine (MSAL)-type alkaloids on lethal dose determination. Data represent the amount of MSAL-type alkaloids required to kill at least one steer per group; n = 2−4 steers per group. (Adapted from Welch et al.[33])

± 0.2 and 4.6 ± 0.5 mg/kg, respectively (Figure 5).[42] In comparison, the LD_{50} of a 1:1 mixture of MLA to zygacine was

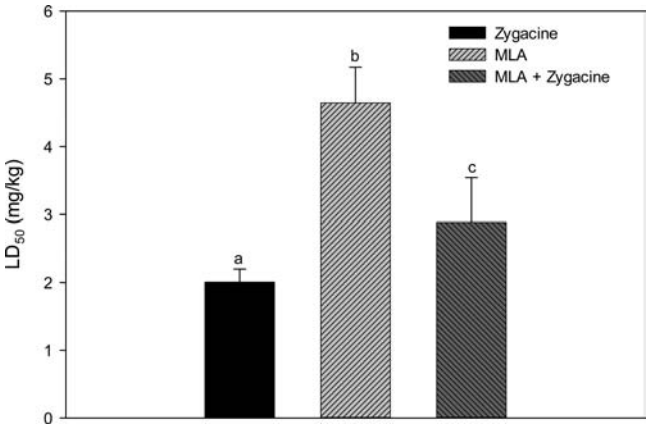

Figure 5. Comparison of the acute toxicity of zygacine, MLA, and a 1:1 mixture of zygacine and MLA. The data represent the median lethal doses (LD_{50}) of zygacine, methyllycaconitine (MLA), and a 1:1 mixture of zygacine and MLA. Results represent the mean ± SD of 28−39 mice per group. Different letters above bars designate significant difference between groups, $P < 0.05$. Each group was significantly different from the other two groups. (Adapted from Welch et al.[42])

2.9 ± 0.7 mg/kg. The LD_{50} value for the mixture is almost halfway between the LD_{50} values for the individual compounds, suggesting that both alkaloids contributed to the toxicity. Similar results were observed when the toxicity of a 1:1 mixture of a death camas total alkaloid extract and a low larkspur total alkaloid extract was compared to the toxicities of the individual total alkaloid extracts.[42]

The alkaloids in low larkspur inhibit normal neuromuscular function, causing muscle weakness and collapse in poisoned animals. This muscle weakness can be exacerbated by physically stressing the animals. Consequently, we evaluated the effect of low larkspur and death camas coexposure on exercise-induced muscle weakness and fatigue in sheep.[49] For this experiment, four groups of four sheep each were used, including control (alfalfa), death camas alone, death camas plus low larkspur, and low larkspur alone. The sheep were exercised by walking them back and forth across a 100 m alley at approximately 3 km/h for 10 min at 4, 8, and 24 h postdosing. The number of sheep in each group that were physically unable to maintain this pace was noted (Table 2). Statistically there was no difference in the

Table 2. Effect of Death Camas and Low Larkspur Cotreatment on Exercise-Induced Muscle Weakness[a] in Sheep

	4 h		8 h		24 h	
group	yes	no	yes	no	yes	no
control	0	4	0	4	0	4
death camas	1	3	1	3	0	4
death camas + low larkspur	0	4	2	2	1	3
low larkspur	0	4	0	4	0	4

[a]Data represent the number of sheep that collapsed due to muscle weakness (yes) or did not collapse (no) at each time point. Statistical comparisons were performed using Fisher's exact test, using a 2 × 2 contingency table; none of the comparisons of treated and control animals were significantly different ($P > 0.05$). (Adapted from Welch et al.[49])

number of sheep that collapsed in each group at each time point. An important note was that no sheep receiving low larkspur alone demonstrated any clinical signs of poisoning, which supports previous findings that sheep are very resistant to larkspur poisoning. Consequently, the results from this study suggest that low larkspur does not potentiate the toxicity of death camas in sheep. However, due to the fact that there was an additive effect in mice, future experiments will be conducted to determine what effect coexposure of low larkspur and death camas has in cattle, a livestock species known to be susceptible to both death camas and low larkspur poisoning.

■ ISOBOLOGRAMS OF MULTIPLE PLANT TOXINS

The isobologram, introduced by Loewe and Muischnek,[50] provides a convenient graphical method to visually characterize the effect of co-administration of two compounds in relation to their individual effects.[51] The isobologram consists of a set of discrete, experimentally determined points, the location of which allows a classification of the interaction. Points on the isobologram that are significantly below the additivity line indicate synergistic, or potentiating, combinations (sometimes referred to as greater than additive), whereas those significantly above this line are antagonistic (sometimes referred to as less than additive). We evaluated the interaction of multiple plant toxins in mice by performing an isobolographic analysis for the different combinations. For characterization of the co-administration of MDL- and MSAL-type alkaloids, the isobologram was constructed by connecting the mouse LD_{50} of the corresponding MDL-type alkaloid deltaline, plotted on the x-axis, with the mouse LD_{50} of the MSAL-type alkaloid MLA, plotted on the y-axis, to obtain the additivity line. The corresponding values for mixtures of the two types of alkaloids were also plotted, and their location was compared to the additivity line (Figure 6A). It is very evident that co-administration of these two types of alkaloid has a greater than additive effect.

For characterization of the co-administration of zygacine and MLA to mice, an isobologram was constructed by connecting the LD_{50} of the zygacine plotted on the x-axis with the LD_{50} of

dx.doi.org/10.1021/jf500086u | J. Agric. Food Chem. 2014, 62, 7363−7369

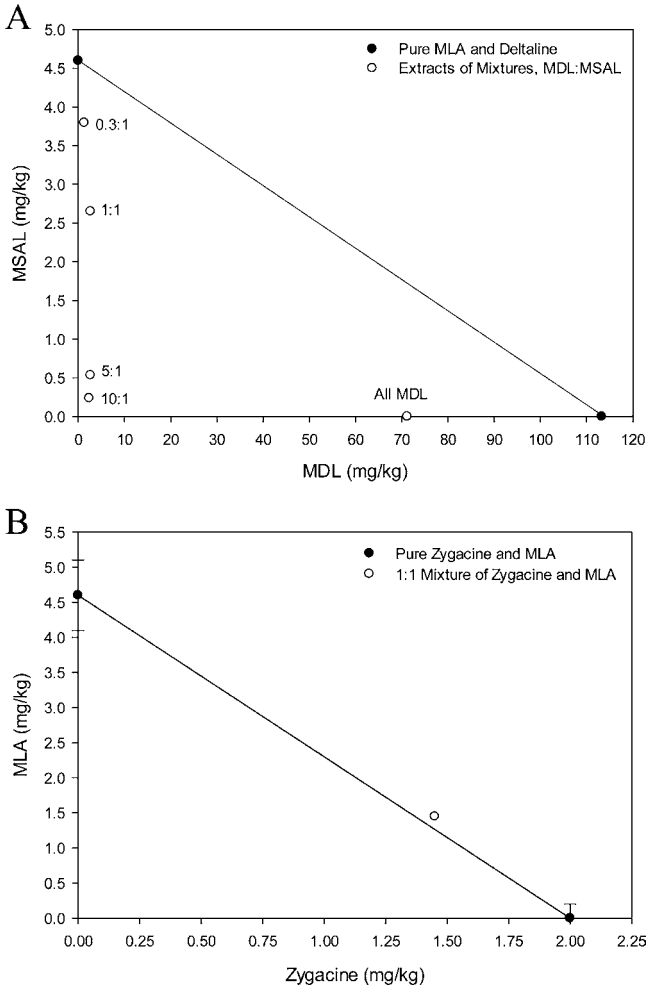

Figure 6. Isobologram analysis for the effect of simultaneous administration of multiple toxins. Panel A represents the effect of simultaneous administration MSAL- and MDL-type alkaloids in mice. Solid circles correspond to the LD_{50} of pure MDL- and MSAL-type alkaloids dosed individually. The line connecting the two points represents the additivity line. Open circles correspond to the LD_{50} of mixtures of MDL- and MSAL-type alkaloids at the indicated ratios. Panel B represents the effect of simultaneous administration of MLA and zygacine in mice. Solid circles correspond to the LD_{50} of zygacine and MLA dosed individually. The line connecting the two points represents the additivity line. The open circle corresponds to the LD_{50} of the 1:1 mixture of zygacine and MLA.

the MLA plotted on the *y*-axis to obtain the additivity line. The corresponding value for the 1:1 mixture of zygacine and MLA was also plotted and its location compared to the additivity line (Figure 6B). The close proximity of the value for the 1:1 mixture to the additivity line suggests that co-administration of these two alkaloids to mice has an additive effect.

In conclusion, the results from our experiments dosing animals with multiple plant toxins demonstrate that there can be a mixture effect. The experiments with tall larkspur indicate that MDL-type alkaloids exacerbate the overall toxicity of the MSAL-type alkaloids and should be accounted for in the prediction of potential toxicity of larkspur populations. The results from the experiments with mice using MLA and zygacine suggest that there could be an additive effect with death camas and low larkspur. However, low larkspur cotreatment does not potentiate the toxicity of death camas in sheep. This information will be useful in further developing livestock management recommendations for ranchers and in designing additional experiments to study the toxicity of multiple plant toxins in livestock species.

AUTHOR INFORMATION

Corresponding Author

*(K.D.W.) E-mail: Kevin.Welch@ars.usda.gov. Phone: (435) 752-2941. Fax: (435) 753-5681.

Funding

This work was supported by direct congressional appropriations via the U.S. Department of Agriculture to the Poisonous Plant Research Laboratory, which is part of the Agricultural Research Service.

Notes

The authors declare no competing financial interest.

ABRREVIATIONS USED

CYP, cytochrome P450; MLA, methyllycaconitine; LD_{50}, median lethal dose; MDL, 7,8-methylenedioxylycoctonine; MSAL, *N*-(methylsuccinimido)anthranoyllycoctonine; 14-OAD, 14-*O*-acetyldictyocarpine

REFERENCES

(1) National Research Council. *Principles of Toxicological Interactions Associated with Multiple Chemical Exposures*; National Academy Press: Washington, DC, USA, 1980.

(2) Eaton, D. L.; Gilbert, S. G. Principles of toxicology. In *Casarett & Doull's Toxicology: The Basic Science of Poisons*, 7th ed.; Klaassen, C. D., Ed.; McGraw Hill Medical: New York, 2008; pp 11−44.

(3) Feron, V. J.; Groten, J. P. Toxicological evaluation of chemical mixtures. *Food Chem. Toxicol.* **2002**, *40*, 825−839.

(4) SCHER; SCCS; SENIHR Opinion on the toxicity and assessment of chemical mixures; http://ec.europa.eu/health/scientific_committees/consultations/public_consultations/scher_consultation_06_en.htm (accessed Feb 14, 2014).

(5) Hutson, S. Researchers sound alarm on 'silent' drug interactions. *Nat. Med.* **2011**, *17*, 6−6.

(6) Nies, A. S. Principles of therapeutics. In *Goodman & Gilman's The Pharmacological Basis of Therapeutics*, 10th ed.; Hardman, J. G., Limbird, L. E., Gilman, A. G., Eds.; McGraw-Hill: New York, 2001; pp 45−66.

(7) Borgert, C. J.; Quill, T. F.; McCarty, L. S.; Mason, A. M. Can mode of action predict mixture toxicity for risk assessment? *Toxicol. Appl. Pharmacol.* **2004**, *201*, 85−96.

(8) Hafner, V.; Jager, M.; Matthee, A. K.; Ding, R.; Burhenne, J.; Haefeli, W. E.; Mikus, G. Effect of simultaneous induction and inhibition of CYP3A by St John's wort and ritonavir on CYP3A activity. *Clin. Pharmacol. Ther.* **2009**, *87*, 191−196.

(9) Cheng, C. W.; Fan, W.; Ko, S. G.; Song, L.; Bian, Z. X. Evidence-based management of herb-drug interaction in cancer chemotherapy. *Explore (N.Y.)* **2010**, *6*, 324−329.

(10) Mills, E.; Montori, V. M.; Wu, P.; Gallicano, K.; Clarke, M.; Guyatt, G. Interaction of St John's wort with conventional drugs: systematic review of clinical trials. *BMJ* **2004**, *329*, 27−30.

(11) Henderson, L.; Yue, Q. Y.; Bergquist, C.; Gerden, B.; Arlett, P. St John's wort (*Hypericum perforatum*): drug interactions and clinical outcomes. *Br. J. Clin. Pharmacol.* **2002**, *54*, 349−356.

(12) Jeong, T. Y.; Park, B. K.; Cho, J. H.; Kim, Y. I.; Ahn, Y. C.; Son, C. G. A prospective study on the safety of herbal medicines, used alone or with conventional medicines. *J. Ethnopharmacol.* **2012**, *143*, 884−888.

(13) Noh, K.; Seo, Y. M.; Lee, S. K.; Bista, S. R.; Kang, M. J.; Jahng, Y.; Kim, E.; Kang, W.; Jeong, T. C. Effects of rutaecarpine on the metabolism and urinary excretion of caffeine in rats. *Arch. Pharm. Res.* **2011**, *34*, 119−125.

(14) Ueng, Y. F.; Tsai, T. H.; Don, M. J.; Chen, R. M.; Chen, T. L. Alteration of the pharmacokinetics of theophylline by rutaecarpine, an alkaloid of the medicinal herb *Evodia rutaecarpa*, in rats. *J. Pharm. Pharmacol.* **2005**, *57*, 227−232.
(15) Lee, S.; Bista, S.; Jeong, H.; Kim, D.; Kang, M.; Jahng, Y.; Jeong, T. The effects of rutaecarpine on the pharmacokinetics of acetaminophen in rats. *Arch. Pharmacal Res.* **2007**, *30*, 1629−1634.
(16) Bailey, D. G.; Dresser, G.; Arnold, J. M. Grapefruit-medication interactions: forbidden fruit or avoidable consequences? *CMAJ* **2013**, *185*, 309−316.
(17) Pathak, M. A.; Daniels, F., Jr.; Fitzpatrick, T. B. The presenhpy known fistrixuhion of furocoumarins (psoralens) in plants. *J. Invest. Dermatol.* **1962**, *39*, 225−239.
(18) Saita, T.; Fujito, H.; Mori, M. Screening of furanocoumarin derivatives in citrus fruits by enzyme-linked immunosorbent assay. *Biol. Pharm. Bull.* **2004**, *27*, 974−977.
(19) Pfister, J. A.; Gardner, D. R.; Panter, K. E.; Manners, G. D.; Ralphs, M. H.; Stegelmeier, B. L.; Schoch, T. K. Larkspur (*Delphinium* spp.) poisoning in livestock. *J. Nat. Toxins* **1999**, *8*, 81−94.
(20) Manners, G. D.; Panter, K. E.; Pelletier, S. W. Structure-activity relationships of norditerpenoid alkaloids occurring in toxic larkspur (*Delphinium*) species. *J. Nat. Prod.* **1995**, *58*, 863−869.
(21) Manners, G. D.; Panter, K. E.; Ralphs, M. H.; Pfister, J. A.; Olsen, J. D.; James, L. F. Toxicity and chemical phenology of norditerpenoid alkaloids in the tall larkspurs (*Delphinium* species). *J. Agric. Food Chem.* **1993**, *41*, 96−100.
(22) Cook, D.; Gardner, D. R.; Pfister, J. A.; Welch, K. D.; Green, B. T.; Lee, S. T. The biogeographical distribution of duncecap larkspur (*Delphinium occidentale*) chemotypes and their potential toxicity. *J. Chem. Ecol.* **2009**, *35*, 643−652.
(23) Gardner, D. R.; Ralphs, M. H.; Turner, D. L.; Welsh, S. L. Taxonomic implications of diterpene alkaloids in three toxic tall larkspur species (*Delphinium* spp.). *Biochem. Syst. Ecol.* **2002**, *30*, 77−90.
(24) Ralphs, M. H. Toxic alkaloid concentration in tall larkspur species in the western U.S. *J. Range Manage.* **1997**, *50*, 497−502.
(25) Pfister, J. A.; Ralphs, M. H.; Gardner, D. R.; Stegelmeier, B. L.; Manners, G. D.; Panter, K. E.; Lee, S. T. Management of three toxic *Delphinium* species based on alkaloid concentrations. *Biochem. Syst. Ecol.* **2002**, *30*, 129−138.
(26) Ralphs, M. H.; Gardner, D. R.; Turner, D. L.; Pfister, J. A.; Thacker, E. Predicting toxicity of tall larkspur (*Delphinium barbeyi*): measurement of the variation in alkaloid concentration among plants and among years. *J. Chem. Ecol.* **2002**, *28*, 2327−2341.
(27) Cook, D.; Green, B. T.; Welch, K. D.; Gardner, D. R.; Pfister, J. A.; Panter, K. E. Comparison of the toxic effects of two duncecap larkspur (*Delphinium occidentale*) chemotypes in mice and cattle. *Am. J. Vet. Res.* **2011**, *72*, 706−714.
(28) Panter, K. E.; Manners, G. D.; Stegelmeier, B. L.; Lee, S.; Gardner, D. R.; Ralphs, M. H.; Pfister, J. A.; James, L. F. Larkspur poisoning: toxicology and alkaloid structure−activity relationships. *Biochem. Syst. Ecol.* **2002**, *30*, 113−128.
(29) Welch, K. D.; Panter, K. E.; Gardner, D. R.; Green, B. T.; Pfister, J. A.; Cook, D.; Stegelmeier, B. L. The effect of 7,8-methylenedioxylycoctonine-type diterpenoid alkaloids on the toxicity of methyllycaconitine in mice. *J. Anim. Sci.* **2008**, *86*, 2761−2770.
(30) Welch, K. D.; Green, B. T.; Gardner, D. R.; Cook, D.; Pfister, J. A.; Stegelmeier, B. L.; Panter, K. E.; Davis, T. Z. Influence of 7,8-methylenedioxylycoctonine-type alkaloids on the toxic effects associated with ingestion of tall larkspur (*Delphinium* spp) in cattle. *Am. J. Vet. Res.* **2010**, *71*, 487−492.
(31) Green, B. T.; Pfister, J. A.; Cook, D.; Welch, K. D.; Stegelmeier, B. L.; Lee, S. T.; Gardner, D. R.; Knoppel, E. L.; Panter, K. E. Effects of larkspur (*Delphinium barbeyi*) on heart rate and electrically evoked electromyographic response of the external anal sphincter in cattle. *Am. J. Vet. Res.* **2009**, *70*, 539−546.
(32) Green, B. T.; Welch, K. D.; Gardner, D. R.; Stegelmeier, B. L.; Davis, T. Z.; Cook, D.; Lee, S. T.; Pfister, J. A.; Panter, K. E. Serum elimination profiles of methyllycaconitine and deltaline in cattle following oral administration of larkspur (*Delphinium barbeyi*). *Am. J. Vet. Res.* **2009**, *70*, 926−931.
(33) Welch, K. D.; Green, B. T.; Gardner, D. R.; Cook, D.; Pfister, J. A.; Panter, K. E. The effect of 7,8-methylenedioxylycoctonine-type diterpenoid alkaloids on the toxicity of tall larkspur (*Delphinium* spp.) in cattle. *J. Anim. Sci.* **2012**, *90*, 2394−2401.
(34) Gardner, D. R.; Panter, K. E.; Pfister, J. A.; Knight, A. P. Analysis of toxic norditerpenoid alkaloids in *Delphinium* species by electrospray, atmospheric pressure chemical ionization, and sequential tandem mass spectrometry. *J. Agric. Food Chem.* **1999**, *47*, 5049−5058.
(35) Burrows, G. E.; Tyrl, R. J. *Toxic Plants of North America*; Iowa State University Press: Ames, IA, USA, 2001.
(36) Knight, A. P.; Walter, R. G. *A Guide to Plant Poisoning of Animals in North America*; Teton NewMedia: Jackson Hole, WY, USA, 2001.
(37) Panter, K. E.; Ralphs, M. H.; Smart, R. A.; Duelke, B. Death camas poisoning in sheep: a case report. *Vet. Hum. Toxicol.* **1987**, *29*, 45−48.
(38) Kingsbury, J. M. *Poisonous Plants of the United States and Canada*; Prentice-Hall: Englewood Cliffs, NJ, USA, 1964.
(39) Smith, R. A.; Lewis, D. Death camas poisoning in cattle. *Vet. Hum. Toxicol.* **1991**, *33*, 615−616.
(40) Panter, K. E.; Gardner, D. R.; Lee, S. T.; Pfister, J. A.; Ralphs, M. H.; Stegelmeier, B. L.; James, L. F. Important poisonous plants of the United States. In *Veterinary Toxicology, Basic and Clinical Principles*; Gupta, R. C., Ed.; Elsevier: New York, 2007; pp 1031−1079.
(41) Majak, W.; McDiarmid, R. E.; Cristofoli, W.; Sun, F.; Benn, M. Content of zygacine in *Zygadenus venenosus* at different stages of growth. *Phytochemistry* **1992**, *31*, 3417−3418.
(42) Welch, K. D.; Panter, K. E.; Gardner, D. R.; Stegelmeier, B. L.; Green, B. T.; Pfister, J. A.; Cook, D. The acute toxicity of the death camas (*Zigadenus* species) alkaloid zygacine in mice, including the effect of methyllycaconitine coadministration on zygacine toxicity. *J. Anim. Sci.* **2011**, *89*, 1650−1657.
(43) Majak, W.; McDiarmid, R. E.; Benn, M. H. Isolation and HPLC determination of methyllycaconitine in a species of low larkspur (*Delphinium nuttallianum*). *J. Agric. Food Chem.* **1987**, *35*, 800−802.
(44) Gardner, D. R.; Manners, G. D.; Panter, K. E.; Lee, S. T.; Pfister, J. A. Three new toxic norditerpenoid alkaloids from the low larkspur *Delphinium nuttallianum*. *J. Nat. Prod.* **2000**, *63*, 1127−1130.
(45) Majak, W.; Engelsjord, M. Levels of a neurotoxic alkaloid in a species of low larkspur. *J. Range Manage.* **1988**, *41*, 224−226.
(46) Gardner, D. R.; Pfister, J. A. HPLC-MS analysis of toxic norditerpenoid alkaloids: refinement of toxicity assessment of low larkspurs (*Delphinium* spp.). *Phytochem. Anal.* **2009**, *20*, 104−113.
(47) Green, B. T.; Welch, K. D.; Gardner, D. R.; Stegelmeier, B. L.; Pfister, J. A.; Cook, D.; Panter, K. E. Toxicokinetics of norditerpenoid alkaloids from low larkspur (*Delphinium andersonii*) orally administered to cattle. *Am. J. Vet. Res.* **2012**, *73*, 1318−1324.
(48) Green, B. T.; Welch, K. D.; Gardner, D. R.; Stegelmeier, B. L.; Lee, S. T. A toxicokinetic comparison of two species of low larkspur (*Delphinium* spp.) in cattle. *Res. Vet. Sci.* **2013**, *95*, 612−615.
(49) Welch, K. D.; Green, B. T.; Gardner, D. R.; Stonecipher, C. A.; Panter, K. E.; Pfister, J. A.; Cook, D. The effect of low larkspur (*Delphinium* spp.) co-administration on the acute toxicity of death camas (*Zigadenus* spp.) in sheep. *Toxicon* **2013**, *76C*, 50−58.
(50) Loewe, S.; Muischnek, H. Über Kombinationswirkungen. *Naunyn−Schmiedeberg's Arch. Pharmacol.* **1926**, *114*, 313−326.
(51) Tallarida, R. J.; Porreca, F.; Cowan, A. Statistical analysis of drug-drug and site-site interactions with isobolograms. *Life Sci.* **1989**, *45*, 947−961.

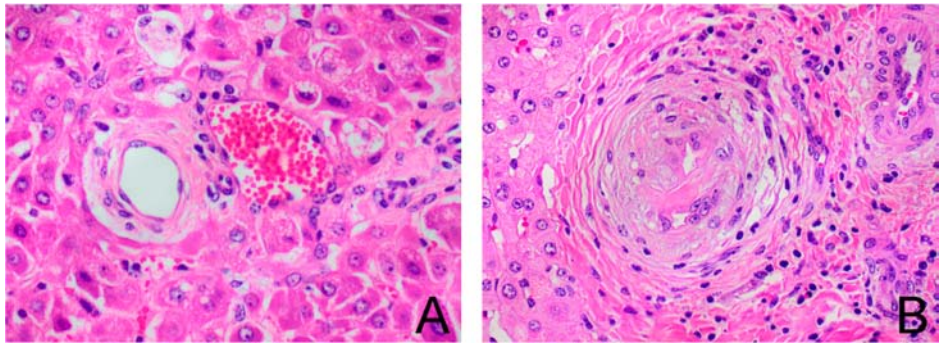

Figure 1. (A) Photomicrograph of the liver of a cow that had grazed a turnip crop and that had been photosensitive for 9 days. The dilated small bile duct (left of center) is lined by an abnormally thin, attenuated epithelium and surrounded by a thin band of concentric fibrosis. A normal portal vein (right of center) and a small arteriole between the vein and bile duct are also visible. (B) Photomicrograph of the liver of another cow that had grazed a turnip crop and that had been photosensitive for 16 days. Two small bile ducts are present in the center, and both are surrounded by a moderately thick band of concentric fibrosis. A normal arteriole is visible top right. H&E 40×.

GLUCOSINOLATES (GSLS) AND THEIR DEGRADATION PRODUCTS

GSLs (mustard oil glucosides) are biosynthesized from certain amino acids and are composed of a β-D-thioglucose group linked to a sulfonated aldoxime. Nearly 130 unique glucosinolates with elongated and modified amino acid-derived side chains[4] have been described. GSLs are classified as aliphatic, aromatic, or indolic depending on whether the derived amino acids are aliphatic (methionine, alanine, valine, leucine, isoleucine), aromatic (tyrosine, phenylalanine), or indolic (tryptophan).[5] There are a large number of GSLs in turnip and rape varieties grown around the world, but the six that occur in the highest concentrations are (i) progoitrin (2-hydroxy-3-butenyl GSL), (ii) gluconapin (3-butenyl GSL), and (iii) glucobrassicanapin (4-pentenyl GSL), all three of which are in the alkenyl (terminally unsaturated carbon in the side-chain) subgroup of the aliphatic GSL, plus (iv) gluconasturtiin (2-phenylethyl), an aromatic GSL, as well as the indolic GSLs (v) glucobrassicin and (iv) neoglucobrassicin.[6−11] In New Zealand, progoitrin would appear to be the dominant GSL,[12] whereas gluconapin, glucobrassicanapin, and gluconasturtiin tend to be more dominant elsewhere.[8,10] Another aliphatic GSL worth mentioning is sinigrin (2-propenyl GSL), which is found in high concentrations in *Brassica oleracea* (kale, cabbage, cauliflower, broccoli, Brussels sprouts) and *Brassica nigra* (black mustard), and in small amounts in turnips and rape.[9]

Intact GSLs are stable, nontoxic compounds found in all plant tissues in *Brassica* spp. When plant cells are crushed during cutting or chewing, the GSLs come in contact with the myrosinase enzyme system, leading to rapid generation of unstable thiohydroximate-*O*-sulfonate intermediates and spontaneous Lossen rearrangement of the core structure to form the isothiocyanate and, in the case of progoitrin GSL, the oxazolidine-2-thione (goitrin). This process is sometimes called the "mustard oil bomb".[4] In vitro experiments have shown that the interaction of nitrile-specifier protein, epithiospecifier protein, and epithiospecifier-modifier protein act as non-enzymic cofactors that, in the presence of ferrous ions, drive the hydrolysis of specific GSLs toward the production of nitriles (organic cyanides) and epithionitriles.[13−16] As far as is known, however, no in vivo work has yet been done to establish whether these proteins are functional in the rumen. Low pH (4−6) also favors nitrile formation.[17,18] Conceivably, it is also possible that microbiota with myrosinase activity, such as lactic acid bacteria, could further contribute to heightened nitrile/epithionitrile production in the rumen.[19] Other hydrolysis derivatives include thiocyanates, glucose, elemental sulfur, and ascorbigens.[18,20−22] Isothiocyanates are regarded as the most active GSL derivatives but are often volatile, highly reactive, and unstable; nitriles, on the other hand, are less reactive but more stable.[23] A diagrammatic representation of this process is shown in Figure 2.

The majority of the degradation products that result from the presence of intact GSLs in the rumen under weakly acid pH conditions are nitriles.[24] Furthermore, nitriles can be produced from GSLs by the action of Fe^{2+} under similar pH conditions.[23] Epithionitriles, characterized by the cyclic thiirane (episulfide)

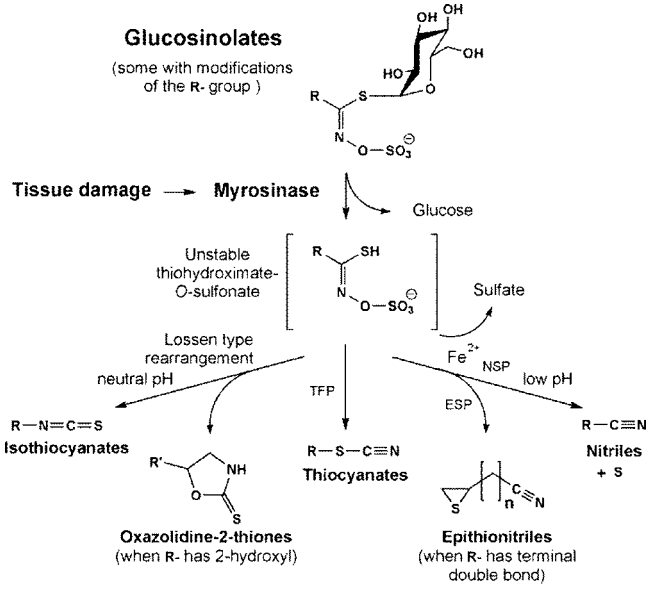

Figure 2. Generic diagram of glucosinolate (GSL) hydrolysis following tissue damage and myrosinase enzyme activity ("the mustard oil bomb") with the respective derivatives (based on Wittstock and Halkier).[5] At neutral pH the unstable thiohydroximate-*O*-sulfonate rearranges to form the isothiocyanate or the oxazolidine-2-thione (goitrin) if the R-group is hydroxylated at carbon 3. In some GSL, a thiocyanate-forming protein (TFP) drives the formation of thiocyanate. Nitriles and epithionitriles tend to be derived when certain cofactors, such as nitrile-specifier protein (NSP), epithiospecifier protein (ESP), and ferrous ions, plus low pH, are present.

dx.doi.org/10.1021/jf500526u | J. Agric. Food Chem. 2014, 62, 7370−7375

Table 1. Parent Glucosinolates, Together with Their Nitrile and Epithionitrile Derivatives[a]

Glucosinolate R-group	Glucosinolate name, synonym(s), formula and structure	Nitrile name, synonym(s), formula and structure	Epithionitrile name, synonym(s), formula and structure
Alkenyl	Progoitrin, (Glucorapiferin, 2(R)-hydroxy-3-butenyl GSL) $C_{11}H_{19}NO_{10}S_2$ 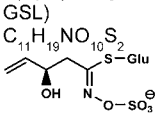	3-hydroxy-4-pentenenitrile, (1-cyano-2-hydroxy-3-butene, crambene) C_5H_7NO 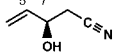	β-hydroxy-thiiranepropanenitrile, ((2R)-1-cyano-2-hydroxy-3,4-epithiobutane, (2R)-3-hydroxy-3-(thiiran-2-yl)-propanenitrile) C_5H_7NOS [diastereoisomers] 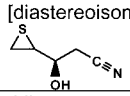
	Sinigrin, (2-propenyl GSL, allyl GSL) $C_{10}H_{17}NO_9S$ 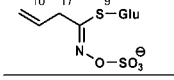	3-butenenitrile, (allyl cyanide) C_4H_5N 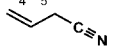	thiiraneacetonitrile, (3,4-epithiobutanenitrile, 1-cyano-2,3-epithiopropane) C_4H_5NS (3(R,S)-isomers) 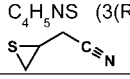
	Gluconapin, (3-butenyl GSL) $C_{11}H_{18}NO_9S_2$ 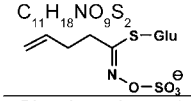	4-pentenenitrile, (1-cyano-3-butene) C_5H_7N 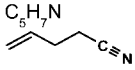	thiiranepropanenitrile, (1-cyano-3,4-epithiobutane, 4,5-epithiovaleronitrile) C_5H_7NS (4(R,S)-isomers) 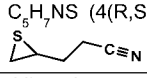
	Glucobrassicanapin, (4-pentenyl GSL) $C_{12}H_{20}NO_9S_2$ 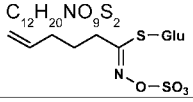	5-hexenenitrile, (1-cyano-4-pentene) C_6H_9N 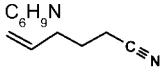	thiiranebutanenitrile, (5,6-epithiohexylnitrile, 1-cyano-4,5-epithiopentane) C_6H_9NS (5(R,S)-isomers) 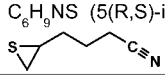
Aromatic	Gluconasturtiin, (2-phenylethyl GSL) $C_{15}H_{21}NO_9S_2$ 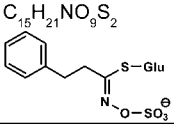	phenyl-3-propanenitrile (2-phenylethyl cyanide) C_9H_9N 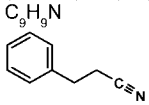	
Indolic	Glucobrassicin (indol-3-ylmethyl GSL) $C_{16}H_{20}N_2O_9S_2$ 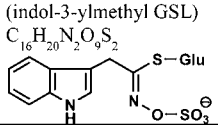	indole-3-acetonitrile $C_{10}H_8N_2$ 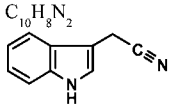	

[a]The first name for each compound is the systematic name[26] and the one used in the text. One or more synonyms, sometimes used in references, for each compound, together with the chemical formula and structure are also shown.

moiety, can be derived only from the alkenyl subgroup of the aliphatic GSLs.[16,25] The following nitriles and epithionitriles, using systematic nomenclature,[26] are potentially derived: (*R*)-3-hydroxy-4-pentenenitrile plus two diastereomeric (2*R*)-*β*-hydroxy-thiiranepropanenitriles from progoitrin; 4-pentenenitrile and thiiranepropanenitrile from gluconapin; and 5-hexenenitrile and thiiranebutanenitrile from glucobrassicanapin.[21,27−30] Additional nitrile derivatives potentially derived from turnips and rape include phenyl-3-propanenitrile from gluconasturtiin and indole-3-acetonitrile from glucobrassicin.[31−33] Of these nitriles, the most stable is 3-hydroxy-4-pentenenitrile from progoitrin.[21] The class, trivial name, synonym(s), and formula of the GSLs in turnips and rape, as well as the systematic names, synonyms, formulas, and structures of their respective nitrile and epithionitrile derivatives are shown in Table 1.

NITRILE AND EPITHIONITRILE TOXICITY STUDIES IN RATS AND MICE

In mice, the nitrile derivatives of progoitrin GSL are about 8 times as toxic as the oxazolidinethione derivative, goitrin.[34] Rats fed diets containing mixed nitriles developed liver lesions (bile duct hyperplasia, fibrosis, megalocytosis, and zonal necrosis) and kidney lesions (megalocytosis of renal tubular epithelial cells).[35] Similar dose-dependent lesions, associated with serum biochemical alterations indicative of hepatocellular damage and cholestasis, were induced in rats that were fed diets containing the diastereoisomers of (2*S*)-*β*-hydroxy-thiiranepropanenitrile for 3 months.[36] The authors in this study described hepatic changes similar to those seen after ingestion of aflatoxin or pyrrolizidine alkaloids, as well as biliary hyperplastia with "flattened epithelium and dilated lumina"[36] of affected bile ducts. The latter changes are reminiscent of the microscopic cholangiectasis seen in a turnip-poisoned cow (Figure 1A).

dx.doi.org/10.1021/jf500526u | J. Agric. Food Chem. 2014, 62, 7370−7375

The derivatives responsible for the nephrotoxicity in rats were identified as (2*S*)-*β*-hydroxy-thiiranepropanenitrile and thiiranepropanenitrile.[37−39] It is not clear whether the renal lesions are due to released cyanide, terminal hypoxia, the epithio group, the nitrile itself, or oxidation products of the aliphatic moiety.[38−40] In another experiment, administration of thiiranepropanenitrile to rats caused severe toxicity, characterized by periacinar hepatic necrosis and renal tubular degeneration.[40] Degeneration and necrosis of the forestomach epithelium of rats dosed with thiiranepropanenitrile have also been described.[39]

Another less potent nitrile derived from progoitrin, 3-hydroxy-4-pentenenitrile, is a selective pancreatotoxin, causing apoptosis and necrosis in individual exocrine acinar cells in rats treated for 4 days.[41] This may be related to the duration and route of exposure as subcutaneous injections of this nitrile into pregnant rats induced liver necrosis and bile duct hyperplasia after 12 days.[37] In contrast, the closely related 4-pentenenitrile derivative from gluconapin GSL appears to be nontoxic in rats.[40]

A large number of aliphatic nitrile compounds are utilized in industrial applications and manufacturing, and some of these products produce central nervous system, hepatic, cardiovascular, renal, or gastrointestinal toxicity. Acrylonitrile, for example, is a known mutagen, animal carcinogen, and suspected human carcinogen. It and the structurally similar methacrylonitrile are eliminated unchanged in expired air, as well as via a variety of urinary metabolites. The principal metabolites in bile are glutathione conjugates, whereas oxidation by cytochrome P450 enzymes to an epoxide intermediate could lead to the release of cyanide.[42]

With regard to nitrile compounds that could potentially be hepato- or cholangiotoxic in cattle, attention is drawn to the epithionitrile derivatives. The latter are thiirane molecules (1,2-episulfides) that are rarely encountered in nature.[43] Chemically, they are similar to epoxides and would be expected to bind covalently to proteins and to DNA and thus could act as alkylating agents with cytotoxic, mutagenic, and carcinogenic effects.[40,44−46] In addition, they could react with a wide variety of electrophilic and nucleophilic compounds, as well as undergo polymerization.[40,47] Polymerized thiiranepropanenitrile appeared to be relatively nontoxic when administered in high doses to rats.[40] In the rat, thiiranepropanenitrile is rapidly absorbed irrespective of route of administration. It is bioactivated following conjugation to glutathione and excreted predominantly as a mercapturic acid in urine with smaller amounts in bile.[46,48,49] It has been suggested that the three-membered thiirane ring is partially responsible for the toxicity of the epithionitriles.[50]

In addition, it is possible that the slow liberation of hydrogen cyanide may make some contribution to the toxicity of epithionitriles.[46] In humans, there are reports of convulsions and fatalities following respiratory arrest ascribed to a variety of aliphatic nitriles that are structurally similar to 3-hydroxy-4-pentenenitrile.[51] Experiments with mice inoculated intraperitoneally show that these nitriles release free cyanide after hepatic microsomal biotransformation of the cyano group.[51] It has been suggested that cyanide levels in the brain play an important role in mortality.[52] For aliphatic nitriles, the length of the carbon chain, the position of a double bond, and the presence of an *α*-hydrogen atom are determinants of the extent of metabolism of nitriles to CN^-.[53,54]

NITRILE AND EPITHIONITRILE STUDIES IN RUMINANTS

3-Butenenitrile, a derivative of the glucosinolate sinigrin, has been shown to cause minor liver damage as indicated by slightly raised GGT activities when given orally to sheep. The liver lesions were not characterized histologically.[55,56]

The analysis of samples of fat, liver, kidney, and muscle from slaughtered beef cattle that had been fed a ration containing up to 10% crambe (*Crambe abyssinica*) seed meal, which would be expected to contain high levels of crambene (3-hydroxy-4-pentenenitrile),[57] failed to detect any GSL derivatives.[58]

In ruminants grazing brassica crops, the dose of derived nitriles and epithionitriles will depend both on the amount produced via enzymatic hydrolysis during chewing and rumination and on the amount produced nonenzymatically in the presence of low rumen pH and ferrous ions. Certainly, additional metabolism including microbial degradation in the rumen and the nature, concentration, and reactivity of, and host tolerance to, the respective compounds will influence disease development.[23,24] Further work on the mechanism by which nitriles and epithionitriles exert potentially noxious effects on hepatocytes and biliary epithelium is needed. An aspect that will also need investigation in future cases is whether a lowered rumen pH, associated with subacute ruminal acidosis induced by the low neutral detergent fiber and high water-soluble carbohydrate content of forage brassica, contributes to greater nitrile or epithionitrile elaboration in the rumen.[12,59]

In conclusion, distinctive bile duct lesions can occur in cattle that develop photosensitization following grazing on turnip or rape forage crops. To date, the identity of the hepato- or cholangiotoxic phytochemical(s) in such toxic forage brassica remains undiscovered. Various nitrile and epithionitrile derivatives of GSL found in crop plants have been shown to be hepatic, renal, pancreatic, and/or gastric toxins in rats. Because of this, it is hypothesized that one or more of these GSL derivatives, in particular those with the thiirane episulfide moiety (the epithionitriles), could be toxic to the livers of cattle under certain circumstances, such as when rumen pH is acidic. Research on the potential toxicity of these compounds, either through the dosing of pure compounds or through the creation of rumen conditions conducive to their formation in high concentrations (low pH, ferrous ions) from ingested brassica forage, is warranted.

AUTHOR INFORMATION

Corresponding Author

*(M.G.C.) Phone: +64 6 356 9099. Fax: +64 6 350 5714. E-mail: m.g.collett@massey.ac.nz.

Notes

The authors declare no competing financial interest.

ACKNOWLEDGMENTS

Stimulating discussions on the possible roles of epithionitriles in the induction of bile duct and/or hepatocyte lesions in cows were held with Rex Munday, AgResearch Hamilton, New Zealand. We thank Colleen Blair, Hayley Dann, and John Munday for assistance.

ABBREVIATIONS USED

GGT, *γ*-glutamyl transferase; GDH, glutamate dehydrogenase; GSL, glucosinolate

REFERENCES

(1) Morton, J. M.; Campbell, P. H. Disease signs reported in south-eastern Australian dairy cattle while grazing *Brassica* species. *Aust. Vet. J.* **1997**, *75*, 109−113.

(2) Collett, M. G.; Matthews, Z. M. Photosensitivity in cattle grazing *Brassica* crops. *Int. J. Poisonous Plant Res.* **2013**, *3*, xx−yy (in press).

(3) Collett, M. G. Bile duct lesions associated with turnip (*Brassica rapa*) photosensitization compared to those due to sporidesmin toxicosis in dairy cows. *Vet. Pathol.* **2014**, DOI: 10.1177/0300985813513042.

(4) Grubb, C. D.; Abel, S. Glucosinolate metabolism and its control. *Trends Plant Sci.* **2006**, *11*, 89−100.

(5) Wittstock, U.; Halkier, B. A. Glucosinolate research in the *Arabidopsis* era. *Trends Plant Sci.* **2002**, *7*, 263−270.

(6) Carlson, D. G.; Daxenbichler, M. E.; VanEtten, C. H.; Tookey, H. L.; Williams, P. H. Glucosinolates in crucifer vegetables: turnips and rutabagas. *J. Agric. Food Chem.* **1981**, *29*, 1235−1239.

(7) Carlson, D. G.; Daxenbichler, M. E.; Tookey, H. L.; Kwolek, W. F.; Hill, C. B.; Williams, P. H. Glucosinolates in turnip tops and roots: cultivars grown for greens and/or roots. *J. Am. Soc. Hortic. Sci.* **1987**, *112*, 179−183.

(8) Matthäus, B.; Luftmann, H. Glucosinolates in members of the family Brassicaceae: separation and identification by LC/ESI-MS-MS. *J. Agric. Food Chem.* **2000**, *48*, 2234−2239.

(9) Kim, S.-J.; Ishida, M.; Matsuo, T.; Watanabe, M.; Watanabe, Y. Separation and identification of glucosinolates of vegetable turnip rape by LC/APCI-MS and comparison of their contents in ten cultivars of vegetable turnip rape (*Brassica rapa* L.). *Soil Sci. Plant Nutr.* **2001**, *47*, 167−177.

(10) Zukalová, H.; Vašák, J.; Nerad, D.; Štranc, P. The role of glucosinolates of *Brassica* genus in the crop system. *Rostlinna Vyroba* **2002**, *48*, 181−189.

(11) Padilla, G.; Cartea, M. E.; Velasco, P.; De Haro, A.; Ordás, A. Variation of glucosinolates in vegetable crops of *Brassica rapa*. *Phytochemistry* **2007**, *68*, 536−545.

(12) Barry, T. N. The feeding value of forage brassica plants for grazing ruminant livestock. *Anim. Feed Sci. Technol.* **2013**, *181*, 15−25.

(13) Tookey, H. L. *Crambe* thioglucoside glucohydrolase (EC 3.2.3.1): separation of a protein required for epithiobutane formation. *Can. J. Biochem.* **1973**, *51*, 1654−1660.

(14) MacLeod, A. J.; Rossiter, J. T. The occurrence and activity of epithiospecifier protein in some Cruciferae seeds. *Phytochemistry* **1985**, *24*, 1895−1898.

(15) Bernardi, R.; Negri, A.; Ronchi, S.; Palmieri, S. Isolation of the epithiospecifier protein from oil-rape (*Brassica napus* ssp. *oleifera*) seed and its characterization. *FEBS Lett.* **2000**, *467*, 296−298.

(16) Kissen, R.; Bones, A. M. Nitrile-specifier proteins involved in glucosinolate hydrolysis in *Arabidopsis thaliana*. *J. Biol. Chem.* **2009**, *284*, 12057−12070.

(17) Gil, V.; MacLeod, A. J. The effects of pH on glucosinolate degradation by a thioglucoside glucohydrolase preparation. *Phytochemistry* **1980**, *19*, 2547−2551.

(18) Agerbirk, N.; Olsen, C. E.; Sørensen, H. Initial and final products, nitriles, and ascorbigens produced in myrosinase-catalyzed hydrolysis of indole glucosinolates. *J. Agric. Food Chem.* **1998**, *45*, 1563−1571.

(19) Mullaney, J. A.; Kelly, W. J.; McGhie, T. K.; Ansell, J.; Heyes, J. A. Lactic acid bacteria convert glucosinolates to nitriles efficiently yet differently from Enterobacteriaceae. *J. Agric. Food Chem.* **2013**, *61*, 3039−3046.

(20) Daxenbichler, M. E.; VanEtten, C. H.; Brown, F. S.; Jones, Q. Oxazolidinethiones and volatile isothiocyanates in enzyme-treated seed meals from 65 species of Cruciferae. *J. Agric. Food Chem.* **1964**, *12*, 127−130.

(21) Paik, I. K.; Robblee, A. R.; Clandinin, D. R. Products of the hydrolysis of rapeseed glucosinolates. *Can. J. Anim. Sci.* **1980**, *60*, 481−493.

(22) Cartea, M. E.; Velasco, P. Glucosiniolates in *Brassica* foods: bioavailability in food and significance for human health. *Phytochem. Rev.* **2008**, *7*, 213−229.

(23) Bellostas, N.; Sørensen, A. D.; Sørensen, J. C.; Sørensen, H. Fe^{2+} catalyzed formation of nitriles and thionamides from intact glucosinolates. *J. Nat. Prod.* **2008**, *71*, 76−80.

(24) Forss, D. A.; Barry, T. N. Observations on nitrile production during autolysis of kale and swedes, and their stability during incubation with rumen fluid. *J. Sci. Food Agric.* **1983**, *34*, 1077−1084.

(25) Bones, A. M.; Rossiter, J. T. The myrosinase-glucosinolate system, its organization and biochemistry. *Physiol. Plant.* **1996**, *97*, 194−208.

(26) U.S. National Library of Medicine, ChemID*plus*, http://www.chem.sis.nlm.nih.gov/chemidplus (accessed Jan 30, 2014).

(27) Daxenbichler, M. E.; VanEtten, C. H.; Tallent, W. H.; Wolff, I. A. Rapeseed meal autolysis. Formation of diastereomeric (2*R*)-1-cyano-2-hydroxy-3,4-epithiobutanes from progoitrin. *Can. J. Chem.* **1967**, *45*, 1971−1974.

(28) Daxenbichler, M. E.; VanEtten, C. H.; Wolff, I. A. Diastereomeric episulfides from *epi*-progoitrin upon autolysis of crambe seed meal. *Phytochemistry* **1968**, *7*, 989−996.

(29) VanEtten, C. H.; Daxenbichler, M. E. Formation of organic nitriles from progoitrins in leaves of *Crambe abyssinica* and *Brassica napus*. *J. Agric. Food Chem.* **1971**, *19*, 194−195.

(30) Kirk, J. T. O.; MacDonald, C. G. 1-Cyano-3,4-epithiobutane: a major product of glucosinolate hydrolysis in seeds from certain varieties of *Brassica campestris*. *Phytochemistry* **1974**, *13*, 2611−2615.

(31) Cole, R. A. Isothiocyanates, nitriles and thiocyanates as products of autolysis of glucosinolates in Cruciferae. *Phytochemistry* **1976**, *15*, 759−762.

(32) Daxenbichler, M. E.; VanEtten, C. H.; Spencer, G. F. Glucosinolates and derived products in cruciferous vegetables. Identification of organic nitriles from cabbage. *J. Agric. Food Chem.* **1977**, *25*, 121−124.

(33) McDanell, R.; McLean, A. E. M.; Hanley, A. B.; Heaney, R. K.; Fenwick, G. R. Chemical and biological properties of indole glucosinolates (glucobrassicins): a review. *Food Chem. Toxicol.* **1988**, *26*, 59−70.

(34) VanEtten, C. H.; Daxenbichler, M. E.; Wolff, I. A. Natural glucosinolates (thioglucosides) in foods and feeds. *J. Agric. Food Chem.* **1969**, *17*, 483−491.

(35) VanEtten, C. H.; Gagne, W. E.; Robbins, D. J.; Booth, A. N.; Daxenbichler, M. E.; Wolff, I. A. Biological evaluation of crambe seed meals and derived products by rat feeding. *Cereal Chem.* **1969**, *46*, 145−155.

(36) Gould, D. H.; Gumbmann, M. R.; Daxenbichler, M. E. Pathological changes in rats fed the crambe meal-glucosinolate hydrolytic products, 2*S*-1-cyano-2-hydroxy-3,4-epithiobutanes (*erythro* and *threo*) for 90 days. *Food Cosmet. Toxicol.* **1980**, *18*, 619−625.

(37) Nishie, K.; Daxenbichler, M. E. Toxicology of glucosinolates, related compounds (nitriles, *R*-goitrin, isothiocyanates) and vitamin U found in Cruciferae. *Food Cosmet. Toxicol.* **1980**, *18*, 159−172.

(38) Gould, D. H.; Fettman, M. J.; Daxenbichler, M. E.; Bartuska, B. M. Functional and structural alterations of the rat kidney induced by the naturally occurring organonitrile 2*S*-1-cyano-2-hydroxy-3,4-epithiobutane. *Toxicol. Appl. Pharmacol.* **1985**, *78*, 190−201.

(39) Wallig, M. A.; Gould, D. H.; Fettman, M. J.; Willhite, C. C. Comparative toxicities of the naturally occurring nitrile 1-cyano-3,4-epithiobutane and the synthetic nitrile *n*-valeronitrile in rats: differences in target organs, metabolism and toxic mechanisms. *Food Chem. Toxicol.* **1988**, *26*, 149−157.

(40) Dietz, H. M.; Panigrahi, S.; Harris, R. V. Toxicity of hydrolysis products from 3-butenyl glucosinolate in rats. *J. Agric. Food Chem.* **1991**, *39*, 311−315.

(41) Wallig, M. A.; Gould, D. H.; Fettman, M. J. Selective pancreatotoxicity in the rat induced by the naturally occurring plant nitrile 1-cyano-2-hydroxy-3-butene. *Food Chem. Toxicol.* **1988**, *26*, 137−147.

(42) Ghanayem, B. I.; Burka, L. T. Excretion and identification of methacrylonitrile in the bile of male F344 rats. *Drug Metab. Dispos.* **1996**, *24*, 390−394.
(43) Brocker, E. R.; Benn, M. H. The intramolecular formation of epithioalkanenitriles from alkenylglucosinolates by *Crambe abyssinica* seed flour. *Phytochemistry* **1983**, *22*, 770−772.
(44) Benn, M. Glucosinolates. *Pure Appl. Chem.* **1977**, *49*, 197−210.
(45) Lüthy, J.; Benn, M. Cyanoepithioalkanes: some chemical and toxicological studies. In *Natural Sulfur Compounds*; Cavallini, D., Gaull, G. E., Zappia, V., Eds.; Plenum Press: New York, 1980; pp 381−389.
(46) Brocker, E. R.; Benn, M. H.; Lüthy, J.; Von Däniken, A. Metabolism and distribution of 3,4-epithiobutanenitrile in the rat. *Food Chem. Toxicol.* **1984**, *22*, 227−232.
(47) Fokin, A. V.; Kolomiets, A. F. The reactivity of epithio-compounds. *Russ. Chem. Rev.* **1976**, *45*, 25−42.
(48) VanSteenhouse, J. L.; Fettman, M. J.; Gould, D. H. Sequential changes in hepatic and renal glutathione and development of renal karyomegaly in 1-cyano-3,4-epithiobutane toxicity in rats. *Food Chem. Toxicol.* **1989**, *27*, 731−739.
(49) VanSteenhouse, J. L.; Prescott, J. S.; Barker, S. A. Identification of the 1-cyano-3,4-epithiobutane-derived urinary mercapturic acid *n*-acetyl-*s*-(4-cyano-2-thio-1-butyl)-cysteine in male Fischer 344 rats. *J. Appl. Toxicol.* **2000**, *20*, 1−10.
(50) VanSteenhouse, J. L.; Prescott, J. S.; Swenson, D. H. Protection from 1-cyano-3,4-epithiobutane nephrotoxicity by aminooxyacetic acid and effect on xenobiotic-metabolizing enzymes in male Fischer 344 rats. *J. Appl. Toxicol.* **1999**, *19*, 237−249.
(51) Willhite, C. C.; Smith, R. P. The role of cyanide liberation in the acute toxicity of aliphatic nitriles. *Toxicol. Appl. Pharmacol.* **1981**, *59*, 589−602.
(52) Tanii, H.; Hashimoto, K. Studies on the mechanism of acute toxicity of nitriles in mice. *Arch. Toxicol.* **1984**, *55*, 47−54.
(53) Ahmed, A. E.; Farooqui, M. Y. H. Comparative toxicities of aliphatic nitriles. *Toxicol. Lett.* **1982**, *12*, 157−163.
(54) Silver, E. H.; Kuttab, S. H.; Hasan, T.; Hassan, M. Structural considerations in the metabolism of nitriles to cyanide *in vivo*. *Drug Metab. Dispos.* **1982**, *10*, 495−498.
(55) Duncan, A. J.; Milne, J. A. Effect of long-term intra-ruminal infusion of the glucosinolate metabolite allyl cyanide on the voluntary food intake and metabolism of lambs. *J. Sci. Food Agric.* **1992**, *58*, 9−14.
(56) Duncan, A. J.; Milne, J. A. Effects of oral administration of brassica secondary metabolites, allyl cyanide, allyl isothiocyanate and dimethyl disulphide, on the voluntary food intake and metabolism of sheep. *Br. J. Nutr.* **1993**, *70*, 631−645.
(57) Niedoborski, T. E.; Klein, B. P.; Wallig, M. A. Rapid isolation and purification of 1-cyano-2-hydroxy-3-butene (crambene) from *Crambe abyssinica* seed meal using immiscible solvent extraction and high-performance liquid chromatography. *J. Agric. Food Chem.* **2001**, *49*, 3594−3599.
(58) VanEtten, C. H.; Daxenbichler, M. E.; Schroeder, W.; Princen, L. H.; Perry, T. W. Tests for *epi*-progoitrin, derived nitriles, and goitrin in body tissues from cattle fed crambe meal. *Can. J. Anim. Sci.* **1977**, *57*, 75−80.
(59) Westwood, C. T.; Mulcock, H. Nutritional evaluation of five species of forage brassica. *Proc. N.Z. Grassland Assoc.* **2012**, *74*, 31−38.

NOTE ADDED AFTER ASAP PUBLICATION

The structures in Table 1 have been revised from the original posting of April 11, 2014. The correct version was posted July 8, 2014.

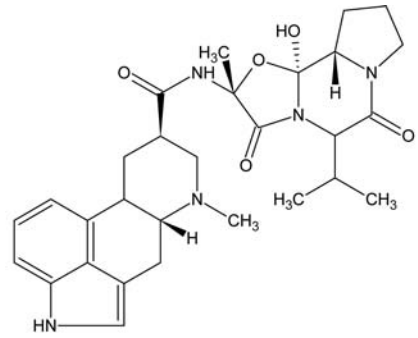

Ergovaline = **1**

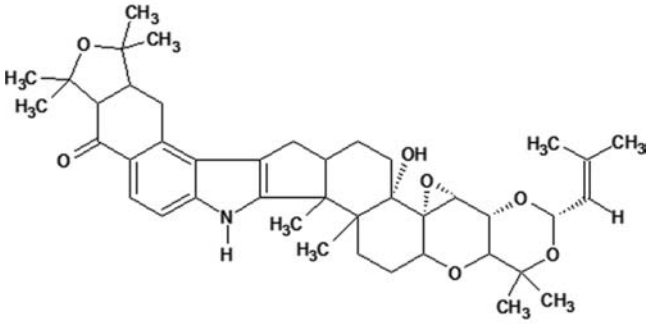

Lolitrem B = **2**

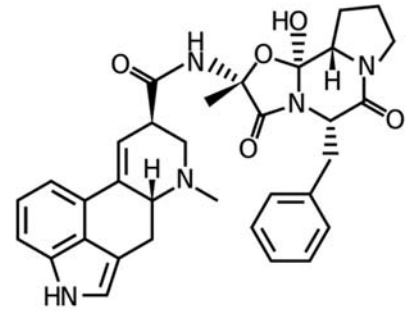

Ergotamine = **3**

Figure 1. Chemical structures of the compounds ergovaline (**1**), lolitrem B (**2**), and ergotamine (**3**).

and perennial ryegrass straw, with particular attention paid to replicating the environmental conditions in which these animals exist; such a study has been conducted for camelids.[6]

The OSU Endophyte Service Laboratory[13] receives an average of 3497 test requests per year (years 2005−2013) to test feed material for the alkaloids discussed above. During 2005−2013, an average of 226 accessions/year were clinical cases submitted principally by veterinarians who suspected feed material was causing vasoconstrictive disease, reproductive problems, or ryegrass staggers. The remaining majority of the samples were submitted by the Ag-Fiber industry with the goal of ensuring "safe feed". A summary of the extraction and HPLC detection methodologies currently in use and six examples of clinical cases follow.

EXTRACTION AND DETECTION METHODOLOGY

Extraction of Endophyte Mycotoxins from Plant Material. *Ergovaline and the Ergot Alkaloids.* A method for the extraction of ergot alkaloids from plant material was developed on the basis of previous studies for subsequent analysis by HPLC-fluorescence.[2,3,10,14] As "neat" standard is expensive and difficult to synthesize, ground seed or straw is mixed in large batches at four target concentrations to generate reference material for use in a calibration curve, which is validated using >98% pure ergovaline, **1**, provided by Forrest Smith, Auburn University. Seed and straw samples are ground in a Cyclotec 1093 sample mill and passed through a 0.5 mm screen. To each tube containing 1 g of sample, control, or reference material are added 10 mL of chloroform plus 1 mL of internal standard (0.661 mg/L ergotamine, **3**, in chloroform) and 1 mL of 0.001 M NaOH; the tubes are capped and mixed for 18−24 h in the dark and then centrifuged at 650*g*. Five milliliters of organic supernatant is applied to a 500 mg/6 mL solid phase extraction (SPE) column containing 0.5 g of Ergosil and 0.5 g of anhydrous sodium sulfate. Ergovaline, **1**, and the ergot alkaloids are extracted by adding 5 mL of sample eluent to the SPE contained in a positive pressure manifold, followed by a 2 mL 4:1 acetone/chloroform (v/v) wash and elution with 2.5 mL of methanol. The eluent is dried under nitrogen at 50 °C and then reconstituted in 0.5 mL of methanol. Samples are mixed for 10 s, sonicated for 10 s, and centrifuged at 650*g* for 5 min. Samples are transferred to amber HPLC vials and sealed for analysis. The percent recovery for this method is 91% for seed and plant material; inter- and intra-assay variations are 5.7 and 3.8%, respectively.

Extraction of Lolitrem B. Lolitrem B, **2**, quantitation involves solvent extraction and filtering before HPLC analysis.[4,10] Plant material is ground as described above, and then 3 mL of a 2:1 chloroform/methanol (v/v) mixture is added to 0.200 g of sample, control or reference material, capped, and mixed for 18−24 h in the dark. Due to the same cost and availability circumstances described above, the Endophyte Service Laboratory uses straw or seed reference material mixed in large batches at four concentrations that is validated using purified lolitrem B, **2**, provided by Ag Research, Ltd., New Zealand, to establish a calibration curve. Next, the samples are centrifuged at 650*g* for 10 min, and 1.6 mL of supernatant is dried under nitrogen at ambient temperature. One milliliter of dichloromethane (CH_2Cl_2) is added to the evaporated supernatant, capped, and sonicated for 10 s, followed by vortexing for 10 s. An additional 1 mL of CH_2Cl_2 is added, and the sample is again sonicated and vortexed for 20 s each to ensure the entire sample is dissolved. CUSIL 500 mg/6 mL SPE cartridges are loaded onto a positive pressure manifold and preconditioned with 2 mL of CH_2Cl_2. The samples are loaded onto the SPE, followed by a 2 mL CH_2Cl_2 wash. A 0.5 mL wash of elution solution (4:1 CH_2Cl_2/acetonitrile (CH_3CN) (v/v)) is added to the cartridges, and positive pressure is applied. The sample is then eluted with 3 mL of elution solution; SPE columns are dried to force all remaining liquid out of the columns. The eluent is mixed, and 1.5 mL is transferred to amber HPLC vials and sealed for analysis. The percent recovery for this method is 91.5% for plant material. Inter- and intra-assay variations are 8.1/8.5 and 6.2/6.8% for straw/seed, respectively.

HPLC-Fluorescence Analysis for Ergot Alkaloids. *Ergovaline, 1.* The current protocol in our laboratory for HPLC analysis of ergovaline, **1**, involves reversed-phase chromatography with fluorescence detection (excitation and emission wavelengths of 250 and 420 nm, respectively) and a gradient pump program run at a flow rate of 1.8 mL/min with 35% CH_3CN and 2 mM ammonium carbonate in purified water as mobile phase A and CH_3CN as mobile phase B, as follows:

dx.doi.org/10.1021/jf5027229 | J. Agric. Food Chem. 2014, 62, 7376−7381

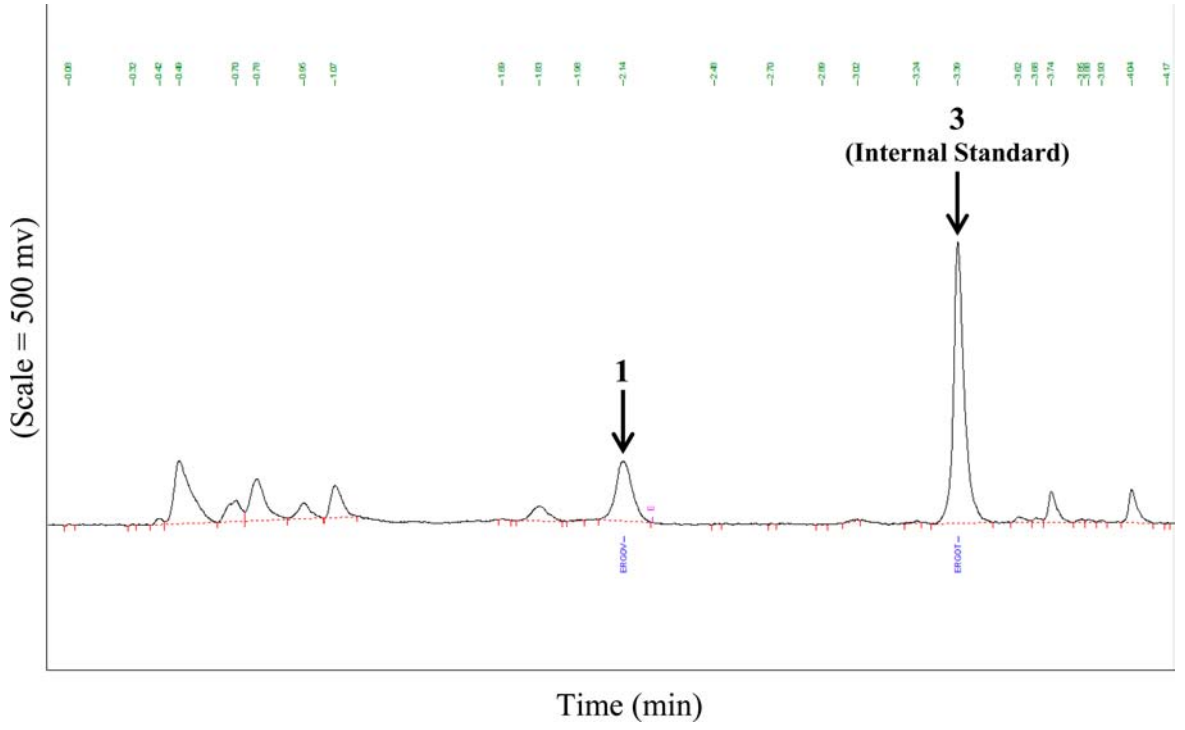

Figure 2. HPLC-fluorescence chromatogram of tall fescue seed (500 ppb) extracted for ergovaline, **1**, by the Endophyte Service Laboratory, Oregon State University. Ergotamine, **3**, is added as an internal standard to all materials being tested.

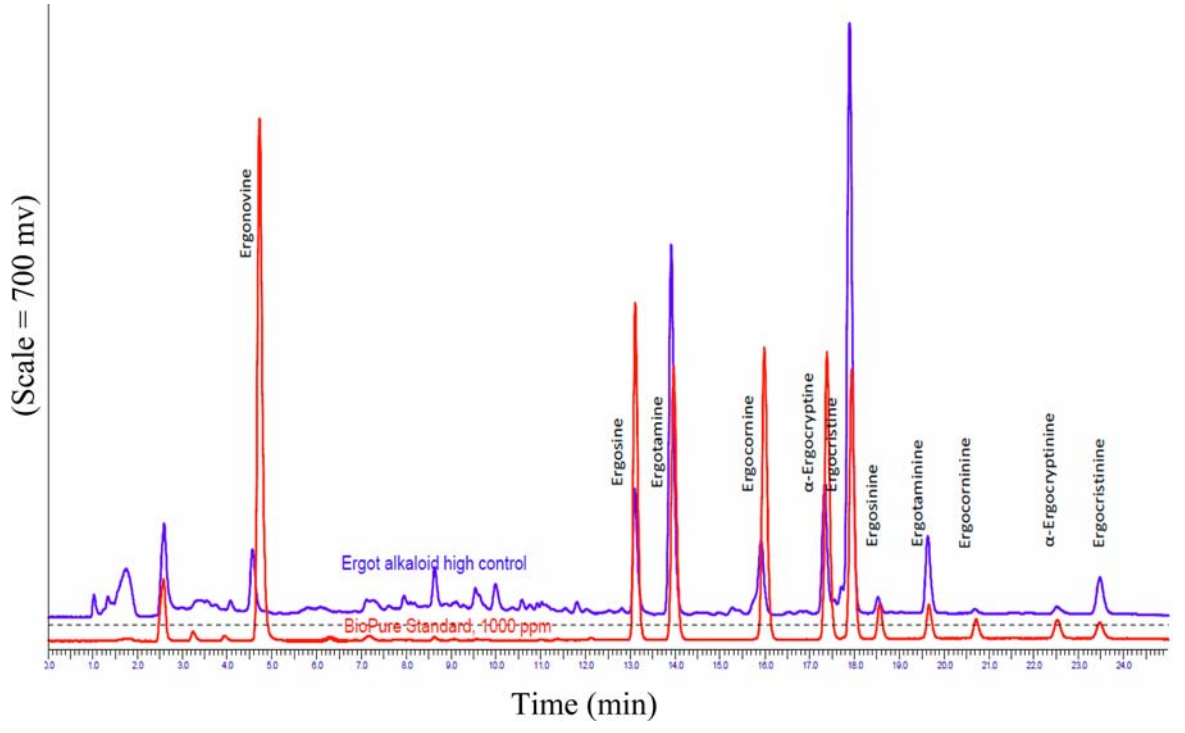

Figure 3. HPLC-fluorescence chromatogram of pure standard (red trace) and tall fescue high control seed (blue trace) extracted for the five ergot alkaloids associated with ergot (ergosine, ergotamine, **3**, ergocornine, α-ergocryptine, and ergocristine) by the Endophyte Service Laboratory, Oregon State University. (The -inine epimers for these five alkaloids elute subsequent to the main compounds.)

equilibrate from 0 to 0.5 min at 99% A, hold at 99% A for 1.0 min, then decrease linearly from 1.5 to 2.3 min to 35% A, hold at 35% A from 2.3 to 3.1 min, then raise linearly to 99% A from 3.1 to 3.4 min, and hold for another 1.3 min before cycling to the next sample. A column (either 100 mm × 4.6 mm i.d., 2.6 μm, Kinetex C18 or 100 mm × 4.6 mm i.d., 2.7 μm, Brownlee SPP C18) is used in conjunction with a guard column cartridge of similar packing. The retention time for ergovaline, **1**, is 2 min, whereas that for ergotamine, **3**, is 3 min. The limit of detection (LOD) of ergovaline, **1**, is 31 ppb, whereas the limit of quantitation (LOQ) is 100 ppb. Figure 2 shows an example of a HPLC-fluorescence chromatogram for ergovaline, **1**, produced using this assay.

dx.doi.org/10.1021/jf5027229 | *J. Agric. Food Chem.* 2014, 62, 7376−7381

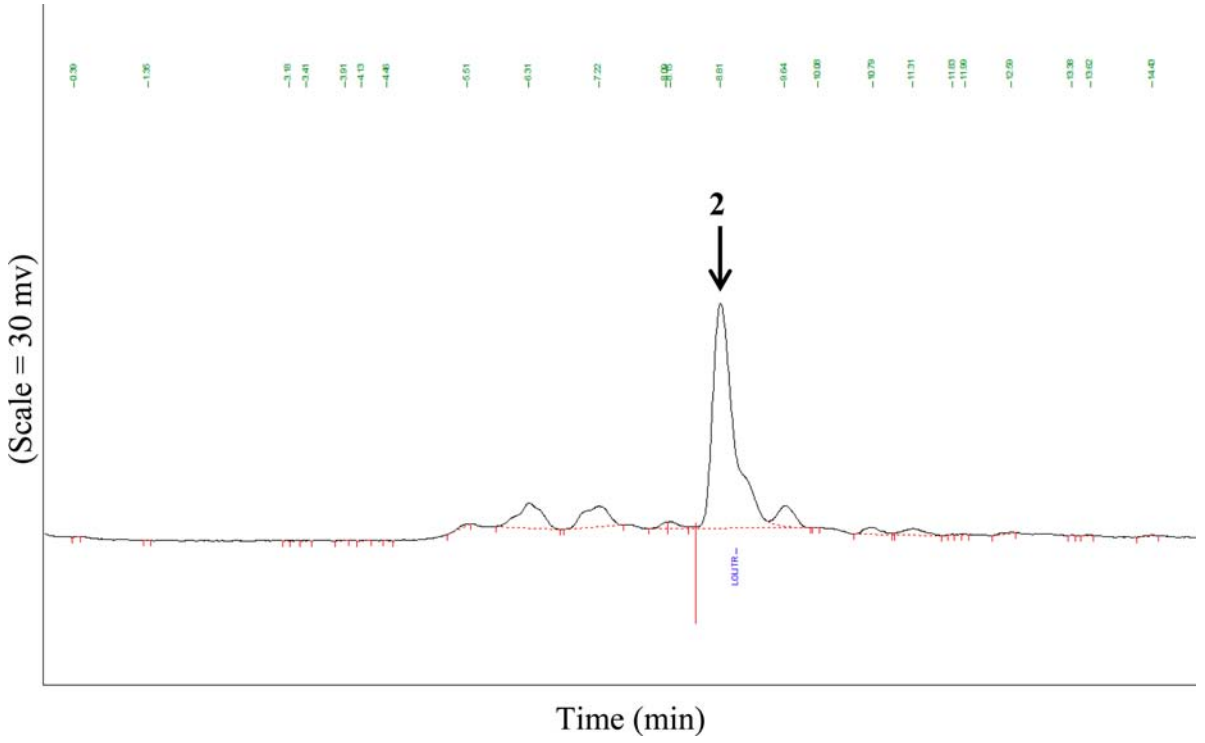

Figure 4. HPLC-fluorescence chromatogram of perennial ryegrass straw (2500 ppb) extracted for lolitrem B, **2**, by the Endophyte Service Laboratory, Oregon State University.

Ergot Alkaloids. For ergot analysis, fluorescence detection is the same as above but a different chromatography configuration is used. At a flow rate of 0.9 mL/min, mobile phases of 1 mM ammonium carbonate (A) and CH_3CN (B) are run through a gradient pump program as follows: equilibrate from 0 to 5 min at 75% A, then decrease linearly to 65% A from 5 to 15 min, hold at 65% A from 15 to 20 min, and then decrease linearly to 25% A from 20 to 25 min. Compounds analyzed in this assay and their LOD/LOQ values are ergosine, ergotamine, **3** (11/38 ppb), ergocristine (14/50 ppb), ergocornine (11/41 ppb), and α-ergocryptine (13/49 ppb). Figure 3 illustrates an example of a HPLC-fluorescence chromatogram for the ergot alkaloids examined for cases of ergot using this assay.

HPLC Analysis Protocol for Lolitrem B, 2. The Endophyte Service Laboratory performs lolitrem B, **2**, quantitation by HPLC-fluorescence detection using normal phase separation and an isocratic mobile phase ($CH_2Cl_2/CH_3CN/H_2O$ 4:1:0.02 (v/v)) run at 0.5 mL/min for 15 min.[15−17] Lolitrem B, **2**, is detected using a fluorescence detector set with an excitation wavelength of 268 nm and an emission wavelength of 440 nm. A 250 mm × 4.6 mm i.d., 5 μm, Zorbax RX-SIL analytical column is used in conjunction with a hand-packed silica guard column. The retention time of lolitrem B, **2**, is 8.3 min. The LOD is 30 ng/mL and the LOQ, 100 ng/mL, for plant material. Figure 4 shows an example HPLC-fluorescence chromatogram of straw reference material extracted for lolitrem B, **2**, using this method.

CASE REPORTS

The following documents six clinical cases of endophyte toxicoses in herds of cattle in the Pacific Northwest, USA and Canada, coupled with toxin levels analyzed by the Endophyte Service Laboratory. Often, these values were confirmatory of the tentative diagnosis. In addition, these values helped validate the threshold levels that had been determined by experimental feeding trials.

Case 1. A crossbred beef cow/calf operation of 1800 head from Harney County, eastern Oregon, was supplemented in January with endophyte-infected tall fescue straw in addition to their winter range. They were owned by the same family but were kept divided into three herds, A, B, and C. Two of the three herds with 1040 animals (herd A) and 260 cows (herd B) were fed from common stacks of tall fescue straw. Tall fescue straw was fed initially as the sole source of fiber, supplemented with residual fall pasture grazing starting November 25. Herd A had added alfalfa hay at 20% of the ration to their younger cows and at a 50:50 ratio to the older cows from December 1 to January 17. Herd B had free access to a protein supplement (28%), and both herds A and B had access to mineral salts. On January 17, all feeding of the tall fescue stopped. Herd C with 500 cows was fed 100% fine fescue straw until November 27 and then changed on December 10 to 50% meadow hay and 50% fine fescue. This herd returned to a full ration of fine fescue from December 31 to January 15. Clinical signs of lameness and swollen feet were first noted by the owners in cows from herds A and B on December 25, but the cause was not yet understood. These signs progressed to dry gangrene of the feet, often with subsequent fracture of the necrotic toes or lower limbs. By March 5 in herd A, 449 animals had died or were euthanized due to fescue foot, 56 were lame, and 12 had uterine prolapses. In herd B, 36 were dead or destroyed, 49 were lame, and 3 had uterine prolapses. Abortions and birth of weak or dead calves occurred in the majority of the pregnant cows that were affected. Herd C had no clinical problems. The minimum environmental temperatures from November 25 to December 25 ranged from 1 to 30 °F, with 16 days of minimum temperatures below 10 °F. Core samples of the remaining tall fescue were taken on January 17, with subsequent analyses for ergovaline, **1**, concentration. The mean of 10 core

dx.doi.org/10.1021/jf5027229 | J. Agric. Food Chem. 2014, 62, 7376−7381

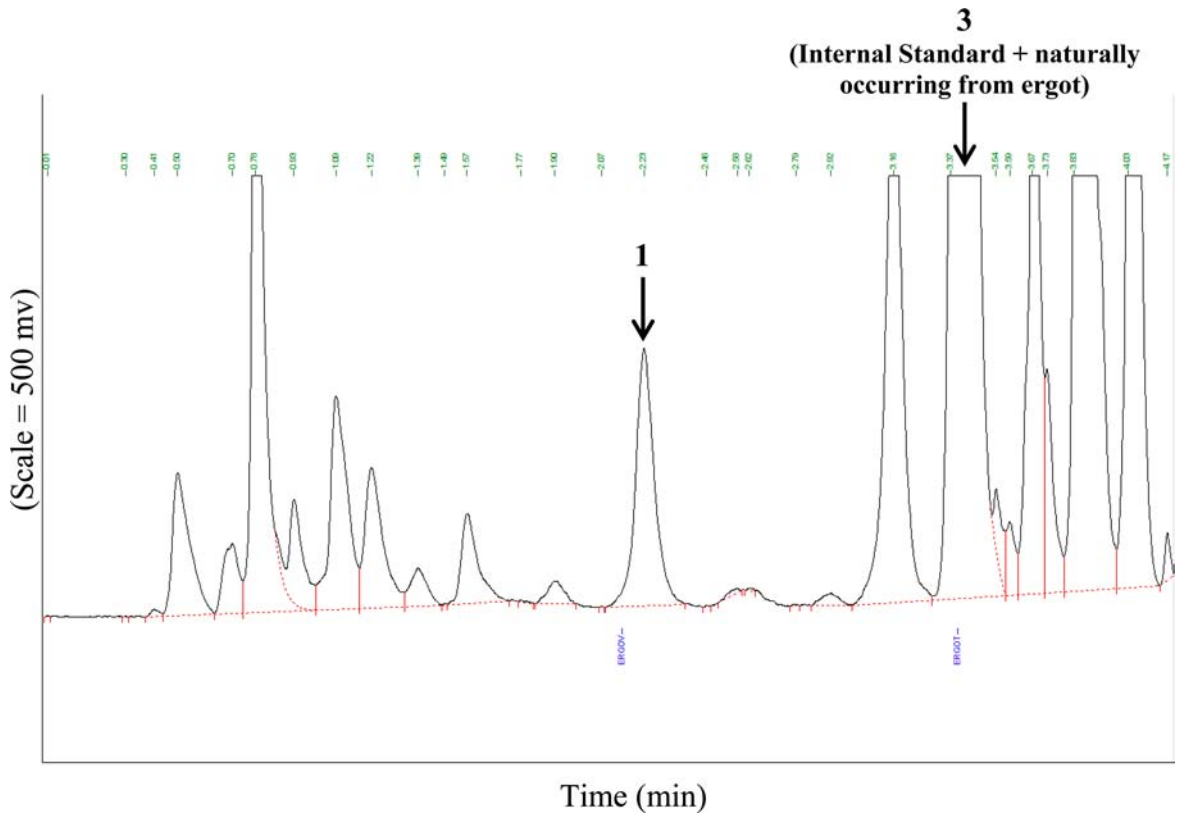

Figure 5. HPLC-fluorescence chromatogram of pellets associated with loss of 13/40 cattle (case 4). Sample was flagged for suspected ergot contamination by the Endophyte Service Laboratory, Oregon State University, due to the large ergotamine, **3**, peak eluting in the ergovaline, **1**, assay.

samples was 329.7 ppb, with a standard deviation of 90.7 ppb. Whereas some core samples had low levels of 116 and 222 ppb, eight samples had values from 340 ppb to a high of 406 ppb. Forty tons of tall fescue straw had been consumed in November and December, prior to testing. Within a month, a total of 600 cows had died, were humanely euthanized, or aborted.

Case 2. During January, 1500 steers in Lethbridge, Alberta, Canada, were supplemented with silage and wheat and barley grain. Clinical signs of dry gangrene of the ears and feet were evident, with sloughing of the hooves being the most serious. In sum, 45 steers were euthanized or died. The grain was infected with *C. purpurea* and contained 3473 ppb total ergot alkaloids. This total was derived from peaks of 262 ppb of ergosine, 545 ppb of ergotamine, **3**, 753 ppb of ergocornine, 613 ppb of α-ergocryptine, and 1299 ppb of ergocristine.

Case 3. In January, 330 steers, bulls, and pregnant beef cows, on frozen pastureland in Coburg, OR, USA, were supplemented with tall fescue straw plus pellets. The pellets were said to be made from perennial ryegrass screenings combined with steamed corn. Five bins of pellets were tested, as well as the straw bales. The straw bales had <100 ppb of ergovaline, **1**, which is below the LOD for our method. It was determined that the five bins of pellets had more than ryegrass screenings, as evidenced by chromatographic analyses, which showed ergovaline, **1**, concentrations ranging from 800 to 1100 ppb; these values are more consistent with tall fescue screenings. One bin of pellets underwent an ergot analysis, which had a value of 820 ppb of ergotamine, **3**. Initial examination of the lameness by a local veterinarian was mistaken for wire cuts on the lower limbs. Within days, multiple cows were affected with vasoconstrictive dry gangrene. Eventually, 44 animals lost hooves, ears, and tails, resulting in their deaths.

Case 4. Forty cattle in a cow/calf operation were housed in a pen in rural Oregon in early January. They were being fed pellets, seed screenings, and haylage. Thirteen of these developed lameness and dry gangrene of their distal limbs and were euthanized. It was determined that the vasoconstrictive lesions were due to ergot toxicosis caused by *C. purpurea*. Pellets were contaminated with 54916 ppb total ergot alkaloids. These included ergotamine, **3** (36858 ppb), ergocristine (8016 ppb), α-ergocryptine (3494 ppb), and ergosine (4684 ppb) (Figure 5).

Case 5. Thirty pregnant cows in their second trimester were on grass seed fields in late December. Pellets made of tall fescue grass seed screenings were spread in piles over the field. After 2 weeks of ingestion, two animals aborted and three animals had open bleeding from their distal limbs and were in extreme pain. Feeding of the pellets was stopped and samples were sent to the Endophyte Service Laboratory for analysis. The affected animals also developed vasoconstrictive lesions in their feet; five were euthanized, four lost their tails, two became lame, and two aborted. Analysis of the screenings detected ergovaline, **1**, at 2096 ppb.

Case 6. Seventeen Hereford × Red Angus male and female calves weighing between 136 and 181 kg had been weaned and moved into confinement in the Willamette Valley, Oregon. They were fed free-choice perennial ryegrass straw and started on a grain ration, the amount of which was gradually increased over a 1.5 week period to 1.82 kg/calf/day. After 1 week, some of the calves developed head tremors and a staggering, stiff gait. The owner incorrectly suspected grain overload and treated them with a mineral oil drench, procaine penicillin G (IM), and dexamethasone (20 mg IM). Response to this treatment was minimal. The calves were not removed from the perennial ryegrass straw until day 23 following the initiation of feeding and

dx.doi.org/10.1021/jf5027229 | *J. Agric. Food Chem.* 2014, 62, 7376−7381

the death of one of the calves. Samples of the turf-quality perennial ryegrass straw being fed contained 3711 ± 243 ppb of lolitrem B, **2** (the threshold of toxicity in cattle is between 1800 and 2000 ppb of lolitrem B, **2**). The ruminal contents of the necropsied calf had a lolitrem B, **2**, concentration of 185 ppb, as compared to a clinically normal calf from the same herd with 25 ppb of lolitrem B, **2**, in its ruminal fluid. Eight of 17 of the calves developed concurrent acute pulmonary emphysema, which had not been reported. An experimental study with four healthy calves fed perennial ryegrass straw with a similar lolitrem B, **2**, concentration showed ryegrass staggers in all animals after 5 days of the feeding trial, but no lung lesions.[18]

SUMMARY

The overriding importance of the Endophyte Service Laboratory is to ensure "safe feed" is exported throughout the world, as well as to local markets. The clinical cases presented here of lameness, dry gangrene, sloughing of ears and tails, and abortions in livestock highlight the fact that, only through feed analysis, can the causative agent of disease be determined. In a similar manner, definitive diagnosis of ryegrass staggers requires analysis of feed even though cessation of feeding does result in remission of clinical signs. For tall fescue toxicosis, levels of ergovaline, **1**, at 300−350 ppb are the threshold for development of clinical disease in horses and cattle.[5] With extreme low environmental temperatures during winter months, these values may be lower. Care should be taken not to feed endophyte-infected tall fescue straw or seed screenings in the winter months unless they have been analyzed for ergot alkaloid toxins. Threshold values for cattle of lolitrem B, **2**, in feed are between 1500 and 2000 ppb;[8] camels have shown clinical signs in experimental feeding trials at 1000 ppb when fed continuously for 60 days.[6] Table 1 details current threshold levels for livestock species for these two endophyte toxicoses. In addition, in the Pacific Northwest, cases of ergotism due to *C. purpurea* contamination of feed have been increasing. Feeding trials need to be conducted to establish threshold of toxicity levels in livestock species for the collection of ergot alkaloids that cause this disease.

Table 1. Threshold Levels for Fescue Toxicosis (Ergovaline, 1) and Perennial Ryegrass Staggers (Lolitrem B, 2)

	ergovaline, **1**	lolitrem B, **2**
camels	not determined	500 ppb
cattle	300−500 ppb[a]	1800−2000 ppb
horses	300−500 ppb[b]	not determined
sheep	500−800 ppb[a]	1800−2000 ppb

[a]Depending on weather. [b]Brood mares should have no detectable ergovaline, **1**, in their feed.

AUTHOR INFORMATION

Corresponding Author

*(A.M.C.) Phone: (541) 737-3036. Fax: (541) 737-2730. E-mail: a.morrie.craig@oregonstate.edu.

Notes

The authors declare no competing financial interest.

REFERENCES

(1) Strickland, J. R.; Oliver, J. W.; Cross, D. L. Fescue toxicosis and its impact on animal agriculture. *Vet. Hum. Toxicol.* **1993**, *35*, 454−464.

(2) Rottinghaus, G. E.; Garner, G. B.; Cornell, C. N.; Ellis, J. L. HPLC method for quantitating ergovaline in endophyte-infested tall fescue: Seasonal variation of ergovaline levels in stems with leaf sheaths, leaf blades, and seed heads. *J. Agric. Food Chem.* **1991**, *39*, 112−115.

(3) Craig, A. M.; Bilich, D.; Hovermale, J. T.; Welty, R. E. Improved extraction and HPLC methods for ergovaline from plant material and rumen fluid. *J. Vet. Diagn. Invest.* **1994**, *6*, 348−352.

(4) Hovermale, J. T.; Craig, A. M. Correlation of ergovaline and lolitrem B levels in endophyte-infected perennial ryegrass (*Lolium perenne*). *J. Vet. Diagn. Invest.* **2001**, *13*, 323−327.

(5) Tor-Agbidye, J.; Blythe, L. L.; Craig, A. M. Correlation of endophyte toxins (ergovaline and lolitrem B) with clinical disease: fescue foot and perennial ryegrass staggers. *Vet. Hum. Toxicol.* **2001**, *43*, 140−146.

(6) Alabdouli, K.; Blythe, L. L.; Duringer, J. M.; Elkhouly, A.; Kassab, A.; Askar, M.; Mohammed, E. E.; Al-Juboori, A.; Craig, A. M. Physiological effects of endophyte-infected perennial ryegrass straw on female camels in the Middle East. *Emirates J. Food Agric.* **2014**, *26*, 82−92.

(7) Miyazaki, S.; Fukumura, M.; Yoshioka, M.; Yamanaka, N. Ryegrass staggers in Japan induced by consumption of ryegrass straw imported from America. From the International Symposium on Mycotoxicology; *Mycotoxin Contamination: Health Risk and Prevention Project*; Kumagai, S., Ed.; Chiba University: Chiba, Japan, 1999; pp 138−144

(8) Blythe, L. L.; Estill, C.; Males, J.; Craig, A. M. Determination of the toxic threshold of lolitrem B in cattle eating endophyte-infected perennial ryegrass. *Fungal Endophytes Grasses* **2007**, 399−402.

(9) Saiga, S. Livestock poisoning caused by ryegrass straw produced in Oregon, USA. *J. Tohoku Livest. Sci. Technol.* **1998**, *47*, 44−46.

(10) Duringer, J. M.; Murty, L. D.; Craig, A. M. Endophyte mycotoxins in animal health. In *Phytchemicals, Plant Growth, and the Environment*; Gang, D. R., Ed.; Springer: New York, 2012; Vol. 42, pp 37−58.

(11) Klotz, J. L.; Kirch, B. H.; Aiken, G. E.; Bush, L. P.; Strickland, J. R. Effects of selected combinations of tall fescue alkaloids on the vasoconstrictive capacity of fescue-naive bovine lateral saphenous veins. *J. Anim. Sci.* **2008**, *86*, 1021−1028.

(12) Klotz, J. L.; Kirch, B. H.; Aiken, G. E.; Bush, L. P.; Strickland, J. R. Bioaccumulation of ergovaline in bovine lateral saphenous veins in vitro. *J. Anim. Sci.* **2009**, *87*, 2437−2447.

(13) Oregon State University Endophyte Service Laboratory. www.oregonstate.edu/endophyte-lab (accessed June 16, 2014).

(14) Hill, N. S.; Rottinghaus, G. E.; Agee, C. S.; Schultz, L. M. Simplified sample preparation for HPLC analysis of ergovaline in tall fescue. *Crop Sci.* **1993**, *33*, 331−333.

(15) Miyazaki, S.; Ishizaki, I.; Ishizaka, M.; Kanbara, T.; Ishiguro-Takeda, Y. Lolitrem B residue in fat tissues of cattle consuming endophyte-infected perennial ryegrass straw. *J. Vet. Diagn. Invest.* **2004**, *16*, 340−342.

(16) Gallagher, R. T.; White, E. P.; Mortimer, P. H. Ryegrass staggers − isolation of potent neurotoxins lolitrem A and lolitrem B from staggers-producing pastures. *N. Z. Vet. J.* **1981**, *29*, 189−190.

(17) Gallagher, R. T.; Hawkes, A. D.; Stewart, J. M. Rapid-determination of the neurotoxin lolitrem B in perennial ryegrass by high-performance liquid-chromatography with fluorescence detection. *J. Chromatogr.* **1985**, *321*, 217−226.

(18) Blythe, L. L.; Andreasen, C. B.; Pearson, E. G.; Craig, A. M. Atypical pneumonia associated with ryegrass staggers in calves. In *Toxic Plants and Other Natural Toxicants*; Garland, T., Barr, A. C., Eds.; CAB International: New York, 1998; pp 69−72.

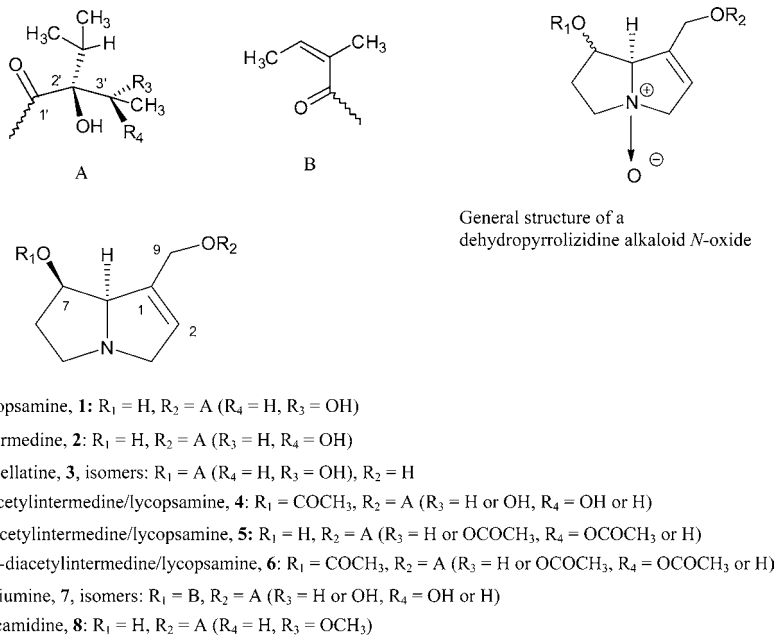

Figure 1. Structures of dehydropyrrolizidine alkaloids detected in *Amsinckia* species or discussed in the text.

and a putative deoxylycopsamine-*N*-oxide. The latter has also been observed in *Cryptantha crassipes*[13] and may correspond to the monoester dehydropyrrolizidine alkaloid amabiline previously identified in some *Amsinckia* species.[7] Also described in the same study of collections of *Amsinckia intermedia* from Arizona and Washington states were some pan-seasonal changes in dehydropyrrolizidine alkaloid levels and, in contrast to Johnson et al.,[3] the presence of **1** as its free base in the seeds of plants collected in Arizona and a significant increase in the quantity and diversity of alkaloids produced by the plants collected in Washington relative to the Arizona plants.[5] This difference once again raises the issue of potential taxonomic misassignment based upon very similar morphologic features.

A continued concern about taxonomic differentiation based on subtle morphologic features, combined with the HPLC-esi(+)MS capacity to directly detect and quantitate both the free base and *N*-oxide forms of the dehydropyrrolizidine alkaloids, prompted this current investigation of annotated herbarium specimens of *Amsinckia*. The objectives included a more accurate profiling of the free base/*N*-oxide ratios, a correlation of the alkaloid profiles with the species, and a determination of the potential usefulness of herbarium-preserved specimens with respect to detection of dehydropyrrolizidine alkaloids and their *N*-oxides.

MATERIALS AND METHODS

Chemicals and Reagents. Methanol was reagent ACS/USP/NF grade (Pharmaco Products; Brookfield, CT). Acetonitrile was the HPLC-certified solvent (Honeywell Burdick and Jackson; Muskegon, MI), and water was Milli-Q-purified (18.2 MΩ/cm) (Millipore; USA). Formic acid, was "For Analysis" grade (>99%) (Acros Organics/Thermo Fisher Scientific; NJ). Lycopsamine, **1**, and intermedine, **2**, and their *N*-oxides (Figure 1) and lasiocarpine (all >99% pure based on HPLC-esi(+)MS and NMR analysis) were sourced from the stocks of extracted and purified pyrrolizidine alkaloids kept by the USDA/ARS Poisonous Plant Research Laboratory.

Plant Specimens. One or two leaves from geographically- and/or temporally differentiated specimens of annotated *Amsinckia douglasiana*, *A. tessellata*, *Amsinckia retrorsa*, *A. menziesii*, *Amsinckia lycopsoides*, *Amskinckia eastwoodiae*, and *A. intermedia* were harvested from the Stanley L. Welsh Herbarium, Brigham Young University. Additionally, leaf samples of similarly differentiated specimens of *A. eastwoodiae*, *A. douglasiana*, *A. lunaris*, and *A. vernicosa* were obtained from the Botany Herbarium and the Agronomy Herbarium of the University of California, Davis. Samples of specimens of *A. menziesii* var. *intermedia*, *A. intermedia* and *A. retrorsa* were harvested from the USDA/ARS Poisonous Plant Research Laboratory Herbarium. Finally, five samples each of *A. eastwoodiae*, *Amsinckia lunaris*, and *Amsinckia vernicosa*, and four samples each of *Amsinckia grandiflora* and *A. douglasiana* were supplied by the Jepson Herbarium at the University of California, Berkeley (Table 1).

Sample Preparation and Extraction. The entire sample for each specimen was transferred to a weighed microcentrifuge tube (2 mL Graduated Free Standing) (Fisherbrand, Pittsburgh, PA) to which was added a 4.5 mm Copperhead copper-coated steel pellet (Crosman Corporation, Bloomfield, NY). The capped tubes were then shaken using a MM301 Retsch shaker (Retsch Inc., Newtown, PA) for 5 min at 17 cps. The grinding pellet was carefully removed from the centrifuge tube that was then recapped and weighed to afford the residual plant weight (ca. 7−70 mg). Methanol (0.5 mL) was added to each tube and the powdered plant gently extracted by inversion mixing at room temperature for 16 h. After centrifugation (15000*g*, 5 min), analytical samples were prepared by adding a 10 μL aliquot of the supernatant to 90 μL of a solution of 0.1% formic acid/methanol (1:1, v/v) containing lasiocarpine (ca. 10 μg/mL) as an internal standard. In some cases, a more concentrated sample was prepared by dilution of 50 μL of the supernatant with 50 μL of the formic acid/methanol solution.

HPLC-esi(+)MS and MS/MS Analysis. Analytical samples (5 μL) were injected using a model 1260 Infinity HPLC system (Agilent Technologies, CA) onto a 150 mm × 2 mm i.d., 4 μm, Synergi Hydro RP column (Phenomenex, Torrence, CA) fitted with a 2 mm × 4 mm i.d. AC C18 guard column (Security Guard cartridge system, Phenomenex, Torrence, CA). A gradient flow (400 μL/min) of 0.1% formic acid in water (mobile phase A) and acetonitrile (mobile phase B) was used to elute sample components from the column. Mobile phase B was held at 3% for 2 min before linearly increasing to 70% by 10 min. After holding at 70% for another 5 min, the column was re-equilibrated to 3% mobile phase B over 2 min and held for a further 7 min before the next injection.

Eluate from the column was monitored using a Velos Pro LTQ mass spectrometer (Thermo Scientific, USA) in a two-scan, positive ion mode and equipped with a heated electrospray ionization (HESI)

Table 1. Specimens of *Amsinckia* Species Harvested from Various Herbaria

Amsinckia species	collection: state	county	date	herbarium and voucher no.[a]
A. douglasiana				
1	CA	Monterey	April 15, 1964	UCB61045
2	CA	San Louis Obispo	March 22, 2011	UCB8147
3	CA	Santa Clara	April 8, 1938	UCB2007
4	CA	Monterey	April 9, 1938	UCB2094
5	CA	San Louis Obispo	April 10, 1938	UCB2088
6	CA	Merced	March 16, 1941	AHUC 038259
7	CA	San Luis Obispo	March 26, 1962	DAV 32015
8	CA	Fresno	March 9, 1952	AHUC 038496
9	CA	Tulare	February 3, 1952	AHUC 038426
10	CA	Monterey	May 12, 1970	UCB7442
11	CA	Monterey	April 2, 1938	UCB2970
12	CA	San Bernito	April 1, 1932	UCB16,142
A. tessellata				
1	UT	Washington	April 10, 2010	BYU28877
2	UT	Washington	March 21, 1986	BYU2212
3	UT	Washington	April 13, 2001	BYU1698
4	UT	Washington	April 5, 1978	BYU357
5	UT	Washington	April 24, 1988	BYU23962
A. retrorsa				
1	UT	Cache	June 27, 2005	BYU21095
2	UT	Box Elder	June 24, 1989	BYU6704
3	UT	Wasatch	July 19, 1983	BYU13946
4	ND	Humboldt	June 5, 2008	BYU15565
5	WA	Benton	April 23, 2006	BYU49
6	WA	Adams	June 21, 2002	PPRL2778
7 leaves	WA	Adams	June 21, 2002	PPRL1999
8 flowers	WA	Adams	June 21, 2002	PPRL1999
A. menziesii				
1	UT	Washington	April 12, 1932	BYUxxxx
2	UT	Washington	May 26, 1978	BYU11938
3	UT	Tooele	May 13, 1971	BYU4097
4	UT	Rich	June 13, 1981	BYU1272
5	UT	Rich	July 3, 1983	BYU13877
A. lycopsoides				
1	Canada	Quebec	August 26, 1967	BYU26446
2	WA	Benton	June 13, 1984	BYU1086
3	WA	Klikilat	May 1, 1989	BYU3808
4	WY	Albany	August 11, 1946	BYU4090
5	WA	Benton	April 28, 1984	BYU527
6	WA	Lincoln	June 11, 1958	BYU2051
A. eastwoodiae				
1	CA	Kern	April 5, 1953	UCB588
2	CA	Kern	March 21, 1996	UCB19161
3	CA	Kern	March 21, 1996	UCB19165
4	CA	Tulare	April 14, 1938	UCB2104
5	CA	Stanislaus	March 27, 1986	BCB3117
6	CA	Calaveras	May 9, 1967	AHUC 33811
7	CA	Fresno	March 20, 2002	DAV 151803
8	CA	Kern	April 21, 1965	DAV 37826
9	CA	Kern	April 9, 1927	UCB11616
10	CA	Fresno	March 28, 1939	UCB15136
11	CA	Tulare	February 29, 2013	UCB736
12	CA	Kern	April 7 1941	UCB286
13	CA	Contra Costa	March 27 1957	UCB5765
A. intermedia				
1	UT	Washington	April 28, 1986	BYU870
2	UT	Washington	May 31, 1985	BYU15520
3	UT	Washington	March 18, 1987	BYU17090
4	UT	Washington	April 15, 1983	BYU21616
5	UT	Washington	June 6, 1985	BYU1635
6	WA	Adams	May 16, 2012	PPRL4362
7	WA	Adams	May 16, 2012	PPRL4361
8	WA	Adams	May 15, 2012	PPRL4363
9	AZ	Mohave	February 16, 2012	PPRL4377
10	AZ	Mohave	February 16, 2012	PPRL4378
A. menziesii var. *intermedia*				
1	AZ	Mohave	March 13, 2012	PPRL4364
2	AZ	Mohave	February 16, 2012	PPRL4351
A. vernicosa				
1	Ca	San Luis Obispo	April 14, 1985	DAV 141038
2	CA	San Joaquin	April 2, 1935	UCB16951
3	CA	Alameda	April 21, 1935	UCB548
4	CA	Alameda	April 3, 1937	UCB1751
5	CA	Stoneslaus	April 13, 1940	UCB4341
6	CA	Merced	March 20, 1938	UCB2879
A. lunaris				
1	CA	Contra Costa	April 14, 1986	UCB539
2	CA	Contra Costa	April 25, 1976	UCB507−2
3	CA	Contra Costa	April 19, 1899	UCB21083
4	CA	Contra Costa	April 20, 1938	UCB3178
5	CA	San Mateo	April 3, 2008	DAV 182419
A. grandiflora				
1	CA	San Joaquin	April 9 1938	UCB3021
2	CA	San Joaquin	March 19 1938	UCB2866
3	CA	San Joaquin	May 7 1938	UCB3397
4	CA	San Joaquin	April 5 1956	UCB664

[a]DAV (Botany Herbarium) and AHUC (Agronomy Herbarium): Crampton Herbarium at the UC Davis Center for Plant Diversity. UCB: Jepson Herbarium, University of California, Berkley. BYU: Stanley L Welsh Herbarium, Brigham Young University.

source. The first full scan (m/z 200−800) was followed by a data dependent, collision-induced dissociation (CID) scan using a generic CID energy of 32%, activation Q of 0.25, and an activation time of 10.0 ms. The capillary temperature was set at 275 °C, the ionization spray voltage at 3.45 kV, the HESI source heater temperature at 305 °C, and the sheath gas flow was 40 units with an auxiliary flow of 5 units.

Identification and Quantitation of Dehydropyrrolizidine Alkaloids. Reconstructed ion chromatograms (RICs) displaying the mass to charge ratio (m/z) of the protonated molecule (MH^+) for dehydropyrrolizidine alkaloids previously identified in *Amsinckia* spp. were used in the first instance to identify potential alkaloids (Figure 2). The retention times and MS/MS data of significant peaks thereby observed were compared to standards where available. Otherwise, the MS/MS data were examined for fragment ions characteristic of dehydropyrrolizidine alkaloids or their *N*-oxides and, further, compared to literature reports of the suspected alkaloids.[12,14]

To account for intrinsic inconsistencies between analytical ion chromatograms, the peak area for a dehydropyrrolizidine alkaloid or its *N*-oxide was divided by the peak area of the internal standard, lasiocarpine, to afford an "adjusted area". Every HPLC sample was analyzed twice to provide an average "adjusted area". This process immediately highlighted any machine or user errors that could be

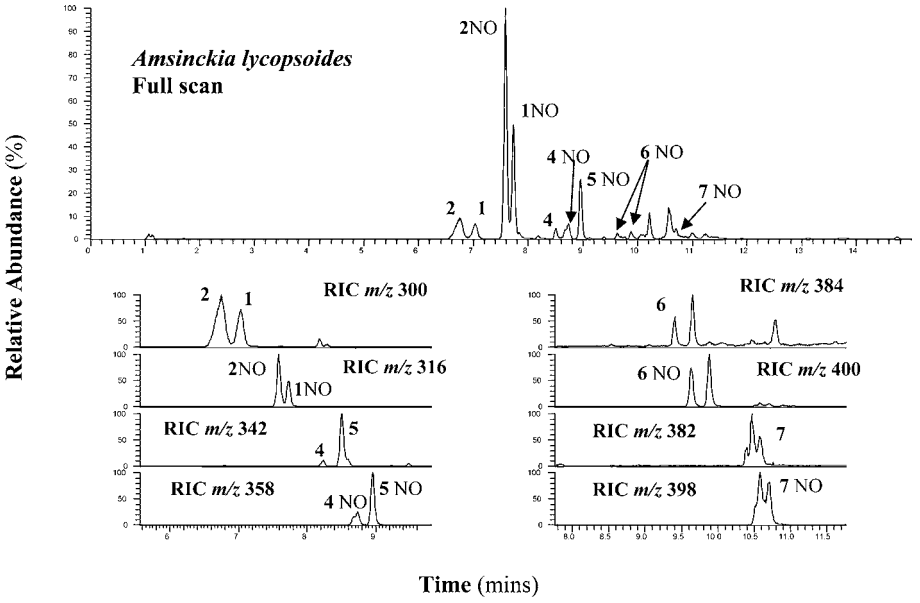

Figure 2. HPLC-esi(+)MS base ion (m/z 200−1000) and reconstructed ion chromatograms for specimen 5 of *Amsinckia lycopsoides* (Table 1). Peaks are annotated with the structure numbers (bold) (Figure 1).

corrected. Relative quantitative estimates of the dehydropyrrolizidine alkaloid and *N*-oxide content of most samples were then based on an eight-point calibration curve (adjusted area = 1.35 × concentration in μg/mL: R^2 = 0.9983) generated using seven 1:1 serial dilutions of intermedine, **2**, from 14.15 to 0.12 μg/mL. In more dilute samples, the quantitative estimate was completed using an eight-point calibration curve (adjusted area = 0.0023 × concentration in μg/mL: R^2 = 0.9993) generated using seven 1:1 serial dilutions of **2** from 2.2 to 0.016 μg/mL). Therefore, concentrations of alkaloids and their *N*-oxides are expressed as "μg equivalents of intermedine/g plant material".

RESULTS AND DISCUSSION

CalFlora recognizes 11 species and five additional varieties of *Amsinckia*,[10] while the USDA plants database describes 10 species with six varieties and many synonyms.[11] It appears that of those, only *A. intermedia*, *A. lycopsoides*, *A. menziesii*, and *A. tessellata* are widely distributed and have been carried from their historical ranges, mainly in the states of California, Oregon, and Washington, with lesser representation east onto the Columbia Plateau and Great Basin regions. The remaining species and varieties are distributed mainly in coastal California and nearby desertic ranges, some into the Great Valley, and others along the U.S. coast northward as far as Skagway, Alaska. The weedy representatives of this genus have been spread, by whatever means (feed, autos, planes, people, etc.), widely within the U.S. and to other parts of the world including Europe and Australia.

However, the taxonomic differentiation within the genus *Amsinckia* (Boraginaceae) is somewhat suspect in many cases, due mainly to the minor morphological distinctions upon which such differentiation is based. Therefore, in an attempt to discover any useful chemotaxonomic indicators, the dehydropyrrolizidine alkaloid profiles of leaf samples collected from herbarium specimens of *Amsinckia* species, including some of doubtful assignation, were acquired from crude methanolic extracts of the samples. Because only small samples of leaves from herbarium specimens could be taken for analysis, detection of only the major dehydropyrrolizidine alkaloids present in each sample was expected. For similar reasons, replicate analyses of the same specimen were not possible and thus potential intraspecimen variation could not be accounted for or addressed.

Dehydropyrrolizidine alkaloids, usually present mainly as their *N*-oxides, were detected in every sample analyzed (Figure 1). The efficiencies of recovery of dehydropyrrolizidine alkaloids and their *N*-oxides from these small samples were not determined. However, because all samples were treated the same way, it is assumed that the relative profiles determined for each specimen will be an accurate reflection of alkaloid content. Estimated total levels of dehydropyrrolizidine alkaloids were usually quite variable within and between species and varied from about 1 to 4500 μg equivalents of intermedine/g plant material (Table 2). The predominant dehydropyrrolizidine alkaloids observed were the *N*-oxides of lycopsamine, **1**, and

Table 2. Total Dehydropyrrolizidine Alkaloid Content Summary

		total dehydropyrrolizidine alkaloid content (μg equivalents intermedine/g dry weight plant)			
Amsinckia species	no. of specimens	median	average	range	standard deviation
A. douglasiana	12	13	139	1−1412	403
A. tessellata	5	57	87	4−192	76
A. retrorsa	7[a]	351	640	16−2269	822
A. menziesii	5	134	405	4−1670	711
A. lycopsoides	6	144	1055	2−3991	1640
A. eastwoodiae	13	22	175	1−1216	362
A. intermedia	10	263	1061	12−4584	1557
A. menziesii var. *intermedia*	2	2088	2088	352−3824	2455
A. vernicosa	6	6	10	2−26	9
A. lunaris	5	364	607	4−1875	777
A. grandiflora	4	69	111	19−287	126

[a]Specimen 8 was a flower sample and is excluded from these estimates of leaf content.

dx.doi.org/10.1021/jf500425v | J. Agric. Food Chem. 2014, 62, 7382−7392

intermedine, **2**, in varying relative amounts from almost exclusively **1** in specimen 2 of *A. tessellata* to almost exclusively **2** in specimen 2 of *A. lunaris* (Figure 3). In extracts that

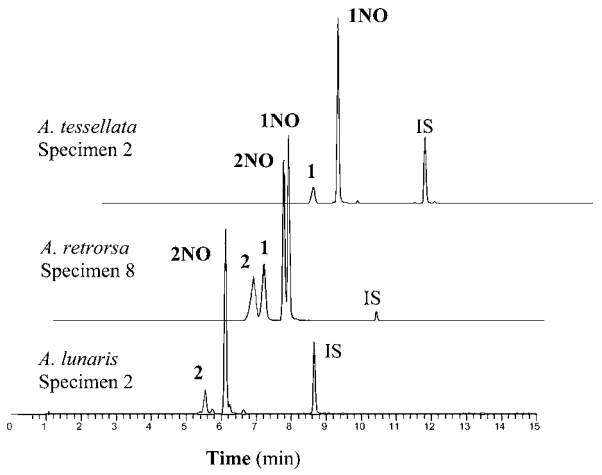

Figure 3. HPLC-esi(+)MS reconstructed base ion chromatograms showing differences in the production of lycopsamine, **1**, intermedine, **2**, and their *N*-oxides in samples of three species of *Amsinckia*. Peaks are annotated with the structure numbers (bold) (Figure 1). "IS" is the internal standard lasiocarpine.

contained larger amounts of alkaloids several trace to minor levels of components were observed that revealed MS/MS profiles strongly indicative of dehydropyrrolizidine alkaloids. However, their contribution to the overall dehydropyrrolizidine alkaloid content and profile was considered negligible. Additionally, minor amounts of the 1,2-dihydro analogues of the dehydropyrrolizidine alkaloids were observed that displayed very similar MS/MS profiles, albeit with fragment ions 2 Da greater than their dehydro counterparts.

The relative abundance profile of dehydropyrrolizidine alkaloids could be quite different between species and even within a designated species (Table 3). It remains to be determined whether these differences represent natural diversity or whether taxonomic misassignments have occurred. For example, specimen 1 of *A. retrorsa*, collected in 2005 from Cache County, Utah (Tables 1 and 3), was an intermedine chemotype with about 95% (of total dehydropyrrolizidine alkaloids identified) intermedine-*N*-oxide, **2**NO, (Figure 4A), whereas the other seven specimens of the same species collected in neighboring counties in Utah, or from sites in the states of Nevada and Washington, all showed a more even ratio of **1NO** and **2NO** (Figure 4B–H). Also noted are the relative differences in the *N*-oxides of the two 3′-monoacetylated derivatives, **5**NO(1) and **5**NO(2), described in detail later in the text, between the specimens of this species (Figure 4).

When comparing the specimens annotated as *A. menziesii*, *A. intermedia*, or *A. menziesii* var. *intermedia* (Table 3) it appears as though four out of five specimens of *A. menziesii* and seven out of 10 of the *A. intermedia* specimens produce both **1**NO and **2**NO in various relative amounts (from predominantly **1**NO, through approximately equal amounts, to predominantly **2**NO), whereas *A. menziesii* specimen 3 and *A. intermedia* specimens 4, 9, and 10, and both samples annotated *A. menziesii* var. *intermedia*, only produce **1**NO. Therefore, it is possible that the sole production of **1** and its *N*-oxide can characterize *A. menziesii* var. *intermedia* and that the *A. menziesii* and *A. intermedia* specimens with the inconsistent profiles may be misassigned.

Three minor abundance ions, isobaric with lycopsamine, **1**, and intermedine, **2**, were deduced, on the basis of the MS/MS data, to be tessellatine, **3**, and related isomers (Table 4). In particular, the base ion peak at m/z 156 in the MS/MS profile for the putative tessellatine isomers is in contrast to the base peak at m/z 138 that is observed with the C9 monoesters **1** and **2** and is consistent with a C7 monoester dehydropyrrolizidine alkaloid analyzed under these esi(+)MS conditions.[15] A corresponding *N*-oxide was only observed for the putative tessellatine peak that eluted earlier than the other two isomers. The putative tessellatine (as its *N*-oxide) is only a major contributor in one specimen analyzed, i.e., *A. eastwoodiae* specimen 1 (Tables 1 and 3). Similar to the lack of tessellatine detected in the preparative chromatography work by Cooper et al.,[8] no significant amount of the putative tessellatine, its isobaric isomers or any other peak that might be assigned to tessellatine on the basis of its MS/MS data were observed for any of the other samples analyzed. This included *A. grandiflora*, *A. douglasiana*, and *A. tessellata* in the section Tessellatae and which were previously reported to contain significant amounts of tessellatine, **3**.[7]

Echiumine, **7**, an open chain diester dehydropyrrolizidine alkaloid more commonly observed in *Echium* species,[12] has been previously reported to be restricted to the section Muricatae and has been detected in one of three specimens of *A. eastwoodiae* and four of 14 specimens of *A. menziesii* var. *intermedia* examined using GC-MS.[7] In this present HPLC-esi(+)MS/MS examination, up to three closely eluting echiumine-*N*-oxide isomers (Figure 2) with identical MS/MS profiles were observed to occur in various relative abundances. In addition to both specimens of *A. menziesii* var. *intermedia* and one of 13 specimens of *A. eastwoodiae*, echiumine (as its *N*-oxide)[12] has also been detected in one of eight specimens of *A. retrorsa*, one of five specimens of *A. menziesii*, three of six specimens of *A. lycopsoides* and five of 10 specimens of *A. intermedia*, all in the section Muricatae, but also in three of five specimens of *A. tessellata* in the section Tessellatae.

Within some specimens examined in this study, four monoacetylated derivatives of lycopsamine-*N*-oxide isomers (i.e., MH^+ m/z 358) were detected in various relative abundances ranging from one, two, three, or through to all four being present in a specimen. The characters of the four isomers are illustrated by comparison of the MS/MS profiles (Table 4) for m/z 358 in *A. intermedia* specimen 2 and specimen 5 (Figure 5). In *A. intermedia* specimen 2, two major monoacetylation peaks are observed at ca. 8.70 and 8.92 min. They have near identical MS/MS profiles (peaks 3 and 4, Figure 5) that include a strong loss of 60 Da (m/z 358 → m/z 298) indicative of a 3′-acetyl derivative. In *A. intermedia* specimen 5, three major monoacetylation peaks are observed at ca. 8.68, 8.73, and 8.92 min. While the third, later eluting peak is the same as described for specimen 2, the early eluting peaks (peaks 1 and 2, Figure 5) again have near identical MS/MS profiles that include a minor ion at m/z 298, a base ion peak at m/z 214, and an ion at m/z 180 indicative of a C7 acetylated derivative.[14] Because of the near coelution of the peaks at ca. 8.68, 8.7, and 8.73 min, there is some mixing of the MS/MS data when all three are present, but scans at the beginning, middle, and end of the coeluting peak envelope help distinguish the three eluants. It is suggested that the four isomers represent 3′- and 7-acetyl derivatives of lycopsamine-*N*-oxide and intermedine-*N*-oxide. The largest

Table 3. Estimated Total Dehydropyrrolizidine Alkaloid Content and Relative Concentrations of Lycopsamine, 1, and Intermedine, 2, and Their *N*-Oxides, Along with the Levels of the *N*-Oxides of Other Major to Minor Dehydropyrrolizidine Alkaloids Observed in Extracts of Several *Amsinckia* Species

		dehydropyrrolizidine alkaloid (% relative abundance)										
Amsinckia species	mass extracted (mg)	**1**[b]	**1**NO	**2**	**2**NO	**3**NO	2[c] × **4**NO	**5**NO (1)	**5**NO (2)	2 × **6**NO	3 × **7**NO	total[a]
A. douglasiana												
1	57.3	4	96									10
2	49.8	7	28		16	17	16	15				3
3	60.8	52	33		15							1
4	31.8	48	51			1						19
5	45.8	33	61			6						3
6	15.4	27	16		15							3
7	22.7	34	63									1412
8	13.7	10	40	4	17		13	1	6	3		136
9	8.4	42	17									4
10	11.1	15	81	4	+[d]	+						38
11	21.8	34	66									20
12	7.1	67	21	9	3							16
A. tessellata												
1	77.2	4	95				+		+			44
2	65	12	74								+	192
3	57.8	1	69				+		+		6	57
4	59.7	10	74						+		3	139
5	55.7	9	40									4
A. retrorsa												
1	37.7				95			5				64
2	57.2		37		48			2	14			59
3	30.1	6	13	7	17	10		34	6			16
4	17.7		37		27				32		2	2269
5	55.7	2	22	1	12			11	38	10		351
6	23.9	3	42	3	39				12			579
7	11.9	7	43	5	29				14			1145
8	66.1	18	31	18	28				4			4061
A. menziesii												
1	6.4	6	30	10	52							134
2	21.5	15	14	28	24							4
3	37.1	11	72								3	35
4	9.8	4	29	5	34		24					180
5	27.7	3	26	6	46				13			1670
A. lycopsoides												
1	49.6	14	14	36	15							2
2	42.4	3	19	10	58				1	1	1	3991
3	30.3	3	27	6	36		17		4	8		212
4	44	9	20	20	46							13
5	42.6	5	21	9	40		1		12	2	5	2035
6	41.7	5	28	8	39		2		9		10	75
A. eastwoodiae												
1	25.6	14	13		6	55						9
2	50.2	2	21	5	50	2	15				6	79
3	39.1	3	39	4	38	2	8		4			113
4	58.8	16	39	8	37							1
5	33.5	4	34	6	46		4		6			682
6	15	9	27	17	45							66
7	18.5	3	19	11	60		2		3			1216
8	9.1	15	8	44	20							22
9	33.2	27	20	24	6	19						6
10	31.5	29	10	30	6	11						14
11	22		51		19	30						2
12	19	31	14	12	3	7	17					66
13	20.5	44		56								2
A. intermedia												
1	55	10	60		10		18		+			12

dx.doi.org/10.1021/jf500425v | J. Agric. Food Chem. 2014, 62, 7382−7392

Table 3. continued

		dehydropyrrolizidine alkaloid (% relative abundance)									
Amsinckia species	mass extracted (mg)	**1**[b]	**1**NO	**2**	**2**NO	**3**NO	2[c] × **4**NO	**5**NO (1)	**5**NO (2)	2 × **6**NO	3 × **7**NO	total[a]
2	55.8	1	28	3	58			6	3			100
3	57.1	4	28	7	48		7		3	2		66
4	44.9	9	90				+		+			22
5	43.2	1	25	2	54		10		6			426
6	14.9	1	14	1	17		+	+	36	3	27	549
7	12.8	4	27	2	24		+	+	22		19	79
8	17.8		13	2			2	5	12	3	10	2094
9	26.5	4	83				+		2		1	4584
10	26.1	8	79				+		2		2	2680
A. menziesii var. *intermedia*												
1	26.6	4	93								0.3	3824
2	33.4	4	86						5		3	352
A. vernicosa												
1	57.4	6	5	47	28							5
2	16.8			99	+							16
3	25.8	15	17	34	34							6
4	57.3			95	5							26
5	43.2			83	17							3
6	36.3			99	+							2
A. lunaris												
1	33.4			5	35		54					1875
2	18.3			12	74		3		6			364
3	39.9			66	34				+			10
4	25.3	13	29	15	26	17			+			4
5	40.6			7	70			20				774
A. grandiflora												
1	12.4	33	64			3						287
2	37.7	43	54			2						19
3	26.4	51	33	9	4	4						21
4	25.5	11	82			6						117

[a]Concentration shown as μg intermedine equivalents/g plant material. [b]Structures shown in Figure 1: **1**, lycopsamine; **2**, intermedine; **3**, tessellatine; **4**, 7-acetyllycopsamine and/or 7-acetylintermedine; **5**, 3′-acetyllycopsamine and/or 3′-acetylintermedine; **6**, 3′,7-diacetyllycopsamine and/or 3′,7-diacetylintermedine; **7**, echiumine and isomers. [c]isomers with the same MS/MS profiles and eluting close together. [d]"+" indicates nonquantitated, low level detection of alkaloid.

effect of acetylation might be expected at the epimeric C3′ position and thus have more effect on retention time of the lycopsamine- and intermedine-based compounds as observed in this HPLC system.

Even though the first five specimens annotated as *A. intermedia* were all collected in Washington County, Utah, between 1983 and 1987 (Table 1), they displayed somewhat different *N*-oxide profiles for lycopsamine isomers and acetyllycopsamine isomers (Figure 6). This may serve as a further example of the variation observed in the HPLC-esi(+)MS profiles of some of the *Amsinckia* species examined or an indication of possible misassignment on morphologic grounds. Specimens 2, 3, and 5 (Table 1) contained similar amounts and ratios of **1**NO and **2**NO. However, specimen 2 was found to produce both of the 3′-acetyl isomers, **5**NO, whereas specimens 3 and 5 produced both of the 7-acetyl isomers, **4**NO, and only the **5**NO isomer 2 (Rt ca. 8.9 min). Specimen 1 produced mainly **1**NO relative to **2**NO, whereas specimen 4 was a lycopsamine chemotype similar to *A. intermedia* specimens 9 and 10.[5]

In accord with an earlier observation,[9] diacetylation of **1** and/or **2** was sometimes evident as two well resolved peaks (Figure 7) with MS/MS profiles (Table 4) that included the presence of ions at *m*/*z* 180 and 214 as well as a loss of 60 Da (*m*/*z* 400 → *m*/*z* 340), consistent with acetylation at both C7 and C3′. The data did not allow specific assignment of the peaks to either diacetyllycopsamine-*N*-oxide or its epimer diacetylintermedine-*N*-oxide. For example, no relative abundance correlation was observed between the similar relative abundances of **1**NO and **2**NO in specimen 9 of *A. douglasiana* and specimen 5 of *A. retrorsa* and their C3′ and C7 monoacetylated derivatives or the two diacetylated derivatives (Figure 7).

Four of the specimens of *A. lunaris* were collected (in 1899, 1938, 1976, and 1986) from Contra Costa County in California while the fifth was collected (in 2008) from San Mateo County in the same state. Similar to four of six specimens of *A. vernicosa*, four of the five *A. lunaris* specimens were also intermedine, **2**, chemotypes with the *N*-oxide predominating except for the oldest specimen collected in 1899. In contrast, *A. lunaris* specimen 4, despite being collected in the same county, produced equal amounts of intermedine and lycopsamine, and their *N*-oxides, in addition to significant levels of the putative tessellatine-*N*-oxide, **3**NO. Another source of contrast between the *A. lunaris* specimens was the production of the monoacetylated derivatives. The oldest two specimens (3 and 4) showed unquantified traces (confirmed by the MS/MS profiles) of the 3′-acetyllycopsamine/intermedine isomer 2,

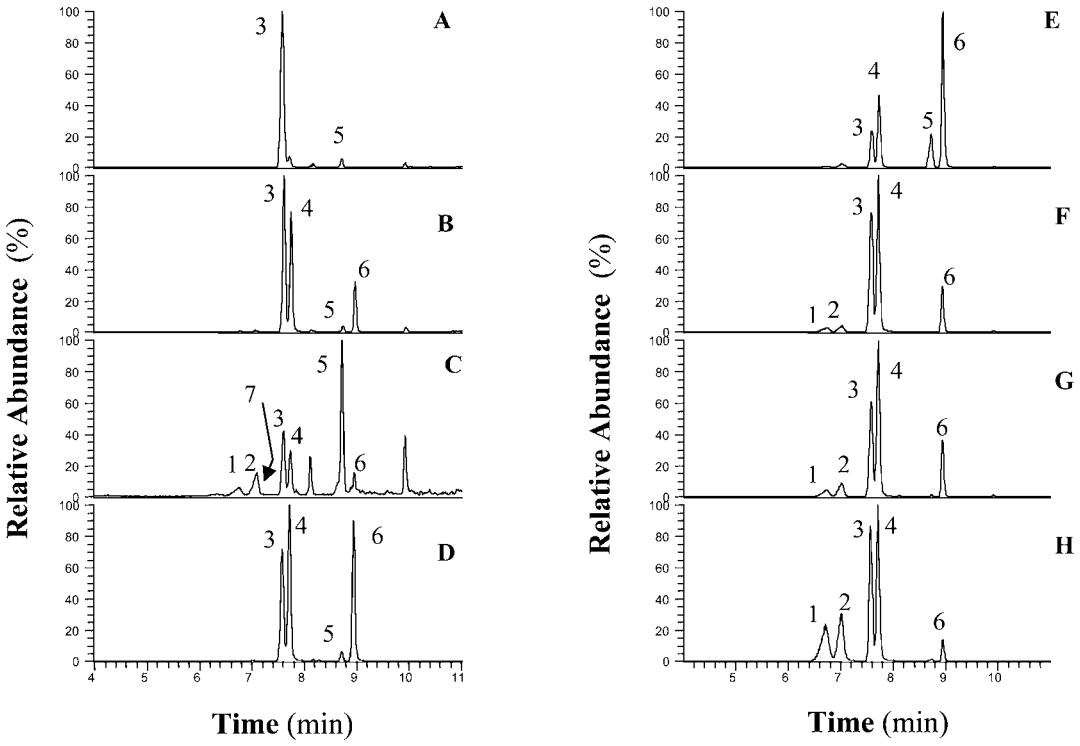

Figure 4. Comparison of HPLC-esi(+)MS reconstructed ion chromatograms displaying (A–H) the major ions *m/z* 300, 316, and 358 for the specimens 1–8, respectively, of *Amsinckia retrorsa* (Table 1). Peak 1 = intermedine, **2**; peak 2 = lycopsamine, **1**; peak 3 = intermedine-*N*-oxide, **2**NO; peak 4 = lycopsamine-*N*-oxide, **1**NO; peak 5 = 3′-acetyllycopsamine-*N*-oxide isomer 1, **5**NO(1); peak 6 = 3′-acetyllycopsamine-*N*-oxide isomer 2, **5**NO(2); peak 7 = putative tessellatine-*N*-oxide, **3**NO.

Table 4. MS and MS/MS Data for Pyrrolizidine Alkaloids Detected in Methanol Extracts of Various *Amsinckia* Species[a]

pyrrolizidine alkaloid	retention time (min)	$MH^+/(2M + H)^+$ *m/z* (% relative abundance)[b]	MS/MS *m/z* (% relative abundance)
lycopsamine (**1**) and intermedine (**2**)	7.0 and 6.7	300	282(0.5), 256(3), 210(2) 156(6), 138(100), 120(22), 94(48),
lycopsamine-*N*-oxide and intermedine-*N*-oxide	7.7 and 7.6	316(100)/631(17)	298(8), 272(19), 254(3), 226(28), 210(4), 172(100), 155(8), 154(7), 138(27), 137(6), 136(12), 120(2), 112(2), 108(2), 94(7)
putative tessellatine (**3**) or isomer	6.4	300	282(1), 256(5), 238(1), 210(1), 192(1), 156(100), 139(1), 138(3), 120(1), 108(2),
putative tessellatine-*N*-oxide or isomer	6.8	316(100)/631(2)	298(3), 272(5), 238(3), 226(3), 172(100), 171(8), 170(6), 154(5), 153(2), 138(1), 137(3), 136(2), 111(1), 106(3)
unidentified tessellatine (**3**)-like isomers (no corresponding *N*-oxides observed)	8.18 and 8.3	300	300(2), 282(9), 256(23), 238(2), 210(36), 194(5), 184(2), 156(100), 139(16), 138(9), 122(8), 120(14), 110(3), 108(2), 94(3)
3′-acetyllycopsamine and/or 3′-acetylintermedine (**5**)	8.22	342	324(2), 297(20), 282(80), 187(3), 156(1), 138(100), 136(3), 120(14)
3′-acetyllycopsamine and/or 3′-acetylintermedine (**5**) isomer	8.5	342	324(2), 282(40), 187(3), 156(1), 138(100), 136(3), 120(14)
3′-acetyllycopsamine-*N*-oxide and/or 3′-acetylintermedine-*N*-oxide	8.7 and 8.9	358 (100)/715(10)	340(10), 316(9), 298(100), 280(2), 172(15), 154(2), 138(5), 137(1), 136(3)
7-acetyllycopsamine and/or 7-acetylintermedine (**4**)	8.6	342	324(1), 282(5), 198(3), 180(57), 162(4), 138(13), 136(1), 124(1), 120(100), 118(2)
7-acetyllycopsamine-*N*-oxide and/or 7-acetylintermedine-*N*-oxide	8.67 and 8.72	358(100)/715(5)	340(12), 314(25), 298(6), 268(23), 252(4), 242(3), 214(100), 197(4), 180(11), 178(5), 154(3), 137(6), 136(3), 120(3)
3′,7-diacetyllycopsamine and/or 3′,7-diacetylintermedine (**6**)	9.4 and 9.65	384	366(6), 352(1), 342(2), 338(1), 324(100), 240(1), 198(2), 180(79), 162(5), 120(90), 118(2)
3′,7-diacetyllycopsamine-*N*-oxide and/or 3′,7-diacetylintermedine-*N*-oxide	9.63 and 9.88	400(100)/799(5)	382(12), 358(11,) 340(100), 322(4), 214(9), 197(2), 180(3), 137(2), 136(1), 120(1)
echiumine (**7**)	10.4, 10.47, and 10.58	382	364(2), 338(1), 300(1), 238(2), 220(27), 138(1), 120(100), 118(2)
echiumine-*N*-oxide	10.53, 10.58, and 10.71	398(100)/795(5)	380(10), 354(22), 308(18), 298(6), 292(4), 282(2), 254(100), 238(2), 237(5), 236(1), 220(12), 218(4), 154(2), 137(4), 136(2), 120(3)

[a]Where indicated by bold numbers, structures are shown in Figure 1. [b]Depending upon the intensity of the protonated molecule (MH^+), weak to moderate dimer ions $(2M + H)^+$ were observed for *N*-oxides

dx.doi.org/10.1021/jf500425v | J. Agric. Food Chem. 2014, 62, 7382–7392

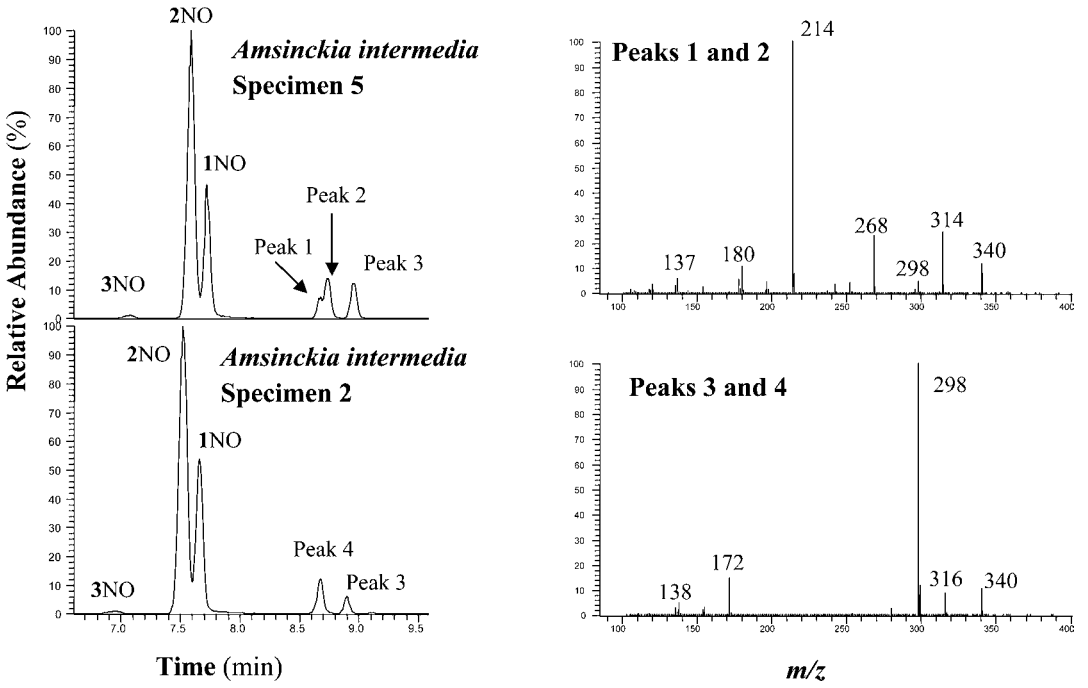

Figure 5. MS/MS differentiation of four monoacetyllycopsamine isomers detected at varying relative amounts in the *Amsinckia* species analyzed. Shown, for example, are the HPLC-esi(+)MS reconstructed ion chromatograms (displaying *m*/*z* 316 and 358) for *Amsinckia intermedia* specimens 5 and 2 (Table 1) and the MS/MS spectra for each pair of monoacetylated *N*-oxide derivatives (peaks 1 and 2 = C7 acetylation (**4**), and peaks 3 and 4 = C3′ acetylation (**5**)). Also annotated are the peaks for lycopsamine-*N*-oxide, **1**NO; intermedine-*N*-oxide, **2**NO; and the putative tessellatine-*N*-oxide, **3**NO.

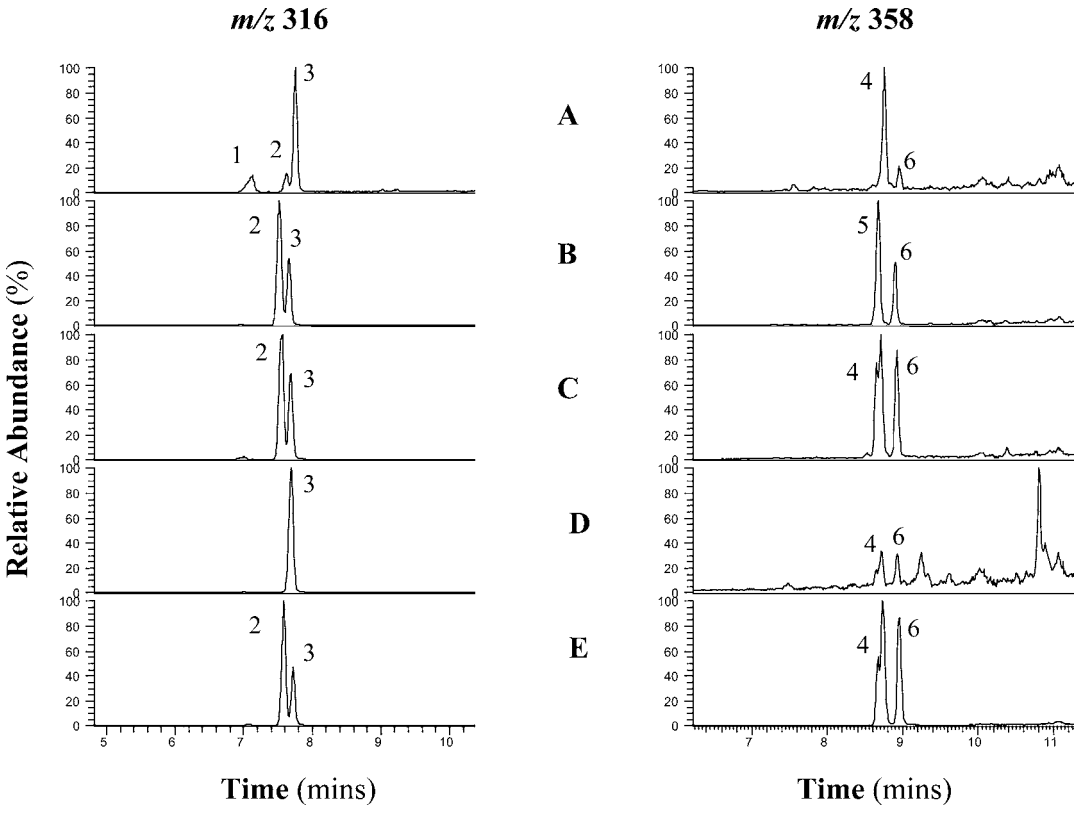

Figure 6. HPLC-esi(+)MS comparison of *N*-oxide profiles of the lycopsamine isomers (*m*/*z* 316) and acetylated isomers (*m*/*z* 358) produced by: (A–E) specimens 1–5 (Table 1) identified as *Amsinckia intermedia*, all collected in Washington County, Utah, between 1983 and 1987. Peak 1 = putative tessellatine-*N*-oxide, **3**NO; peak 2 = intermedine-*N*-oxide, **2**NO; peak 3 = lycopsamine-*N*-oxide, **1**NO; peak 4 = two 7-acetyllycopsamine-*N*-oxide isomers, **4**NO; peak 5 = a 3′-acetyllycopsamine-*N*-oxide isomer, **5**NO (1); and peak 6 = a 3′-acetyllycopsamine-*N*-oxide isomer, **5**NO (2).

dx.doi.org/10.1021/jf500425v | J. Agric. Food Chem. 2014, 62, 7382–7392

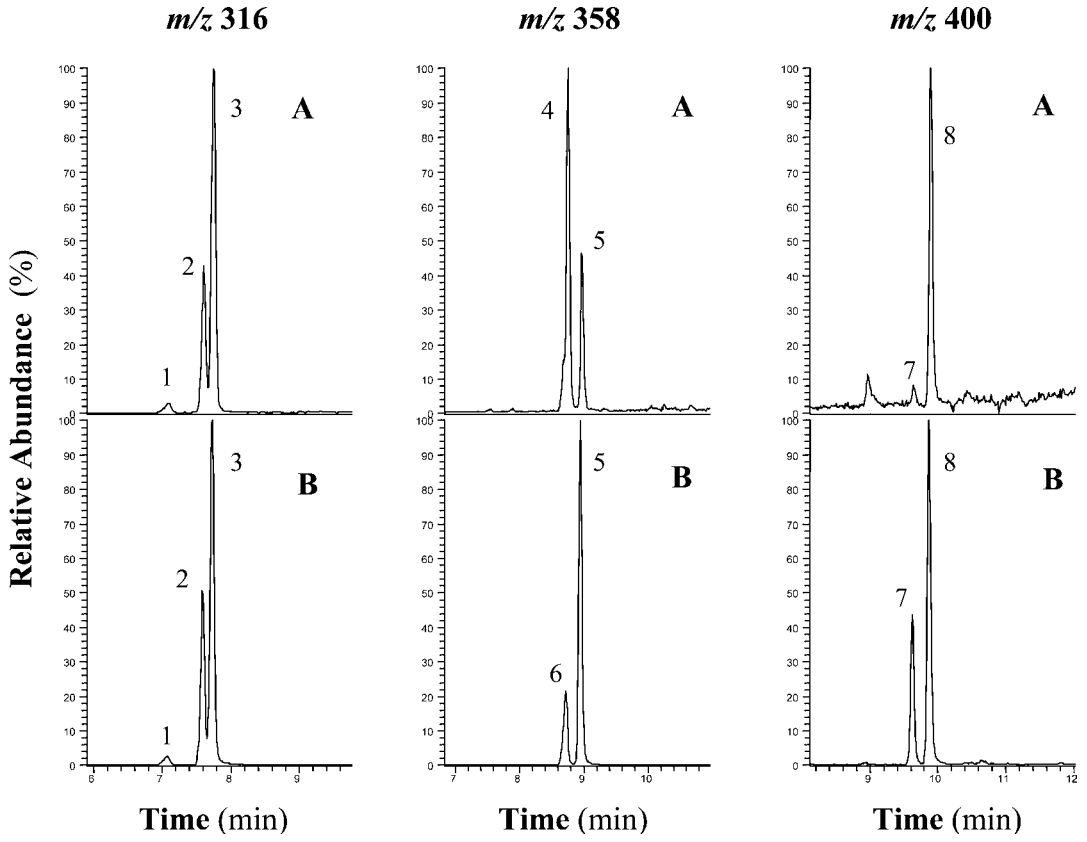

Figure 7. HPLC-esi(+)MS reconstructed ion chromatogram comparison of lycopsamine-*N*-oxide and intermedine-*N*-oxide (*m*/*z* 316) with their mono- (*m*/*z* 358) and diacetylated (*m*/*z* 400) derivatives detected in specimen 9 of *Amsinckia douglasiana* (A) and specimen 5 of *Amsinckia retrorsa* (B). Peak 1 = putative tessellatine-*N*-oxide, **3**NO; peak 2 = intermedine-*N*-oxide, **2**NO; peak 3 = lycopsamine-*N*-oxide, **1**NO; peak 4 = two 7-acetyllycopsamine-*N*-oxide isomers, **4**NO; peak 5 = a 3′-acetyllycopsamine-*N*-oxide isomer, **5**NO (2); peak 6 = mainly 3′-acetyllycopsamine-*N*-oxide isomer, **5**NO (1), with minor presence of 7-acetyllycopsamine-*N*-oxide isomers, **4**NO; peaks 7 and 8 = 3′,7-diacetyl derivatives of lycopsamine and intermedine *N*-oxides, **6**NO.

5NO (2). Specimen 1 produced a single 7-acetyl derivative, presumably of intermedine, while specimen 2 produced both the 7-acetyl derivative, **4**NO, and the second 3′- acetyl derivative, **5**NO (2). In stark contrast, the specimen collected in San Mateo County, although still an intermedine chemotype, only produced the first 3′- acetyl derivative, **5**NO (1).

The levels of dehydropyrrolizidine alkaloids in the six specimens of *A. vernicosa* were all quite low, ranging from 2−26 μg equivalents intermedine/g plant. In contrast to most of the other species examined the level of free base exceeded the level of corresponding *N*-oxide. Three of the *A. grandiflora* specimens were clearly lycopsamine/lycopsamine-*N*-oxide chemotypes, with the fourth presenting with a significant level of intermedine and its *N*-oxide.

The levels of dehydropyrrolizidine alkaloids observed did not uniquely reflect the date of specimen collection and herbarium-mounting. There were some consistencies within a species collected in the same area but decades apart, for example *A. eastwoodiae* specimens 4 and 11 collected in 1938 and 2013 in Tulare County, California both returned very low (ca. 1−2 μg equivalents intermedine/g plant material) total levels of dehydropyrrolizidine alkaloids. However, there were also some inconsistencies such as *A. douglasiana* specimens 2, 5, and 7 collected from San Louis Obispo County, California, in 2011, 1938, and 1962, respectively, that showed total alkaloid levels of about 3, 3, and 1412 μg equivalents intermedine/g plant material. Of these, only specimen 2 produced about equal levels of the *N*-oxides of **1**, **2**, and the monoacetyl derivative(s) of **1** and/or **2**. The other two only showed **1** (about 33% total dehydropyrrolizidine alkaloid content) and its *N*-oxide (ca. 61%). Of the 12 specimens annotated as *A. douglasiana*, six were lycopsamine/lycopsamine-*N*-oxide chemotypes, whereas the other six produced both lycopsamine-*N*-oxide and its epimer, intermedine-*N*-oxide, in various relative levels.

It is clear that the application of HPLC-esi(+)MS and MS/MS to the analysis of mass-limited samples harvested from herbarium-preserved specimens is a useful approach to simultaneous profiling of the dehydropyrrolizidine alkaloids and their *N*-oxides. It is important to consider that intraspecies (as designated in this study by the herbaria) variations in profiles may reflect differences in degradation of the alkaloids and their *N*-oxides that were influenced by different collection, storage, and preservation processes. Notwithstanding this caveat, and although the dehydropyrrolizidine alkaloid data have not yet been correlated to an in-depth examination of morphology for the species examined, it seems evident that there are either: (1) few, robustly unambiguous differences in the dehydropyrrolizidine alkaloid profiles that would facilitate or support species differentiation or (2) that the observed, inconsistent profiles of dehydropyrrolizidine alkaloids within a species may reflect taxonomic misassignment. For example, it is possible that the lack of significant, or any, intermedine-*N*-oxide in samples annotated as *A. menziesii* var. *intermedia*, compared to four of the five *A. menziesii* samples and eight of the 10 *A. intermedia* samples

dx.doi.org/10.1021/jf500425v | *J. Agric. Food Chem.* 2014, 62, 7382−7392

may well support a differentiation between the three and indicate possible taxonomic misassignment of the samples with inconsistent profiles. Future work should also attempt to correlate the dehydropyrrolizidine alkaloid profiles of the herbarium-preserved specimens with profiles determined for collections of fresh plant from the same sites to determine any significant changes of profile with age of the preserved specimen or the potential for specimen collection and storage artifacts.

AUTHOR INFORMATION

Corresponding Author

*Phone: 1-435-752-2941. Fax: 1-435-753-5681. E-mail: steven.colegate@ars.usda.gov.

Funding

This research is supported by the Agricultural Research Service of the U.S. Department of Agriculture and an Interagency Agreement with the Office of Dietary Supplements of the National Institutes of Health.

Notes

The authors declare no competing financial interest.

ACKNOWLEDGMENTS

We gratefully acknowledge Scott Larsen and Katie Lotte (USDA/ARS Poisonous Plant Research Laboratory, Logan, Utah) who, respectively: prepared and extracted all leaf samples prior to HPLC-esiMS analysis and interacted with personnel from the various herbaria to acquire samples. The study could not have been contemplated without the support of the curators of the various herbaria from which samples were sourced. The constructive comments from the reviewers are gratefully acknowledged.

REFERENCES

(1) Molyneux, R. J.; Gardner, D. R.; Colegate, S. M.; Edgar, J. A. Pyrrolizidine alkaloid toxicity in livestock: a paradigm for human poisoning? *J. Food Addit. Contam.* **2011**, *28*, 293−307.

(2) Hooper, P. T. Pyrrolizidine Alkaloid Poisoning—pathology with Particular Reference to Differences in Animal and Plant Species. In *Effects of Poisonous Plants on Livestock*; Keeler, R. F., Van Kampen, K. R., James, L. F., Eds.; Academic Press: New York, 1798; pp 161−176.

(3) Johnson, A. E.; Molyneux, R. J.; Merrill, G. B. Chemistry of toxic range plants. Variation in pyrrolizidine alkaloid content of *Senecio*, *Amsinckia*, and *Crotalaria* species. *J. Agric. Food Chem.* **1985**, *33*, 50−55.

(4) Edgar, J. A.; Colegate, S. M.; Boppré, M.; Molyneux, R. J. Pyrrolizidine alkaloids in food: a spectrum of potential health consequences. *J. Food Addit. Contam.* **2011**, *28*, 308−324.

(5) Colegate, S. M.; Gardner, D. R.; Davis, T. Z.; Welsh, S. L.; Betz, J. M.; Panter, K. E. Identification of a lycopsamine-*N*-oxide chemotype of *Amsinckia intermedia*. *Biochem. Syst. Ecol.* **2103**, *48*, 132−135.

(6) Culvenor, C. C. J.; Smith, L. W. The alkaloids of *Amsinckia* species: *A. intermedia* Fisch. & Mey., *A. hispida* (Ruiz. & Pav.) Johnst. and *A. lycopsoides* Lehm. *Aust. J. Chem.* **1966**, *19*, 1955−1964.

(7) Kelley, R. B.; Seiber, J. N. Pyrrolizidine alkaloid chemosystematics in *Amsinckia*. *Phytochemisty* **1992**, *31*, 2369−2387.

(8) Cooper, R. A.; Bowers, R. J.; Beckham, C. J.; Huxtable, R. J. Preparative separation of pyrrolizidine alkaloids by high-speed counter-current chromatography. *J. Chromatogr., A* **1996**, *732*, 43−50.

(9) Roitman, J. N. The pyrrolizidine alkaloids of *Amsinckia menziesii*. *Aust. J. Chem.* **1983**, *36*, 769−778.

(10) *Amsinckia Plant Search Result*; Calflora: Berkeley, CA; http://www.calflora.org/cgi-bin/specieslist.cgi?orderby=taxon&where-genus=Amsinckia (accessed January 25, 2014).

(11) *USDA, NRCS: The PLANTS Database*; National Plant Data Team: Greensboro, NC, 2014; http://plants.usda.gov/java/nameSearch (accessed January 25th 2014).

(12) Colegate, S. M.; Edgar, J. A.; Knill, A. M.; Lee, S. T. Solid phase extraction and LCMS profiling of pyrrolizidine alkaloids and their *N*-oxides: a case study of *Echium plantagineum*. *Phytochem. Anal.* **2005**, *16*, 108−119.

(13) Williams, M. T.; Warnock, B. J.; Betz, J. M.; Beck, J. J.; Gardner, D. R.; Lee, S. T.; Molyneux, R. J.; Colegate, S. M. Detection of high levels of pyrrolizidine-*N*-oxides in the endangered plant *Cryptantha crassipes* (Terlingua Creek Cat's-eye) using HPLC-ESI-MS. *Phytochem. Anal.* **2011**, *22*, 532−540.

(14) Boppré, M.; Colegate, S. M.; Edgar, J. A. Pyrrolizidine alkaloids of *Echium vulgare* honey found in pure pollen. *J. Agric. Food Chem.* **2005**, *53*, 594−600.

(15) Colegate, S. M.; Gardner, D. R.; Joy, R. J.; Betz, J. M.; Panter, K. E. Dehydropyrrolizidine alkaloids, including monoesters with an unusual esterifying acid, from cultivated *Crotalaria juncea* (Sunn Hemp cv.'Tropic Sun'). *J. Agric. Food Chem.* **2012**, *60*, 3541−3550.

the tube but not tightened completely. The tube was placed on the heat block (90 °C) for a minimum of 2 h or until all of the hair sample was digested. Following digestion the contents of the tube were transferred to a clean 10 mL graduated cylinder, and the sample volume was increased to 1 mL using nitric acid. Then 0.5 mL of digested sample was transferred to a 15 mL polypropylene, colorless, metal-free centrifuge tube containing 9.5 mL of ultrapure water. Appropriate dilutions were made when necessary, and after vortexing, the samples were analyzed using an ELAN 6000 inductively coupled plasma mass spectrometer (ICP-MS) (PerkinElmer, Shelton, CT, USA) at the Utah Veterinary Diagnostic laboratory at Utah State University. Quantification of Se was performed by the standard addition method, using a four-point standard curve. A quality control sample (in similar matrix) was analyzed after every five samples, and analysis was considered acceptable if the Se concentration of the quality control sample fell within ±5% of the standard/reference value for the quality control.

Plant Digests. Plant samples of aster (*Symphyotrichum ascendens*), sedge (*Cyperaceae* spp.), and water cress (*Nasturtium* spp.) as well as a mixture of grasses were collected from various locations in the pasture, dried, and ground with a Wiley mill to pass through a 0.5 mm screen. The ground plant material (0.50 g) was placed into a labeled 30 mL Oak Ridge Teflon digestion tube (Nalge Nunc International). Trace metal grade nitric acid (9.0 mL) (Fisher Scientific) was added to the digestion tubes. The tubes were then heated at 90 °C for 2 h with the caps loose on the tubes. After digestion, tubes were allowed to cool and contents were quantum satis to 10 mL and then transferred to another trace metal-free tube. Five hundred microliters of sample was transferred into another trace metal-free tube containing 9.5 mL of ultrapure water, to make up a 5% nitric acid matrix. After vortexing, the samples were analyzed using an ELAN 6000 ICP-MS (PerkinElmer) at the Utah Veterinary Diagnostic Laboratory at Utah State University. Quantitation and quality control were performed as described above.

RESULTS

Three of the four horses that grazed on a Se-contaminated pasture were chronically poisoned by Se. The diagnosis of chronic Se poisoning was made in May, 6 months after the horses were removed from the pasture. ICP-MS analysis of forage samples from various locations in the pasture, collected during the following year, demonstrated that the forages which contained >5 μg/g Se were found within 7 m of the stream in the pasture. None of the six mixed forages that were collected from other locations in the pasture, that were >7 m from the stream, contained >1.31 μg/g Se. Some of the forages growing in the stream and in the meadow portion of the pasture contained up to 127.4 μg/g Se (dry weight) and are reported in Table 1. Water samples were also collected from the stream at various times the following year. On May 18 the Se concentration in the stream was 0.82 μg/L and by August 30 the Se concentrations had dropped to 0.06 μg/L (Table 1).

None of the horses had alopecia of mane, tail, or body hair. The predominant lesions in the three horses that grazed the pasture for the entire previous grazing season were hoof lesions (Figure 1). Mane and tail samples were collected approximately 6 months after the horses were removed from the pasture, the ends were aligned, and the samples were segmented into 2.5 cm segments and analyzed for Se content. The lengths of the mane and tail samples collected from each horse are reported in Table 2. The Se concentrations in mane samples ranged from 0.7 to 27.6 μg/g Se and showed an increase and decrease in Se concentrations for each of the horses sampled (Figure 2A). The Se concentrations in the tail samples ranged from 0.6 to 47.6 μg/g Se, and for each of the longer tail samples the Se concentrations followed a cyclic pattern (Figure 2B).

Table 1. Selenium Concentrations of Forages and Water in the Selenium-Contaminated Pasture Where Horses Were Poisoned[a]

plants in pasture	collection date	Se (μg/g)
sedge from meadow	May 18	60.82
watercress from meadow	May 18	127.40
sedge from meadow	June 10	30.64
watercress from meadow	June 10	91.13
aster, 7 m from stream	June 10	14.29
grass, >7 m from stream	June 10	<1.31
water in pasture	collection date	Se (μg/L)
stream	May 18	0.82
stream	June 10	0.33
stream	July 29	0.09
stream	Aug 30	0.06
stream	Sept 29	0.04
stream	Oct 28	0.04

[a]All plant values are the Se concentration in μg/g on a dry weight basis of a composite sample of 5−7 plants.

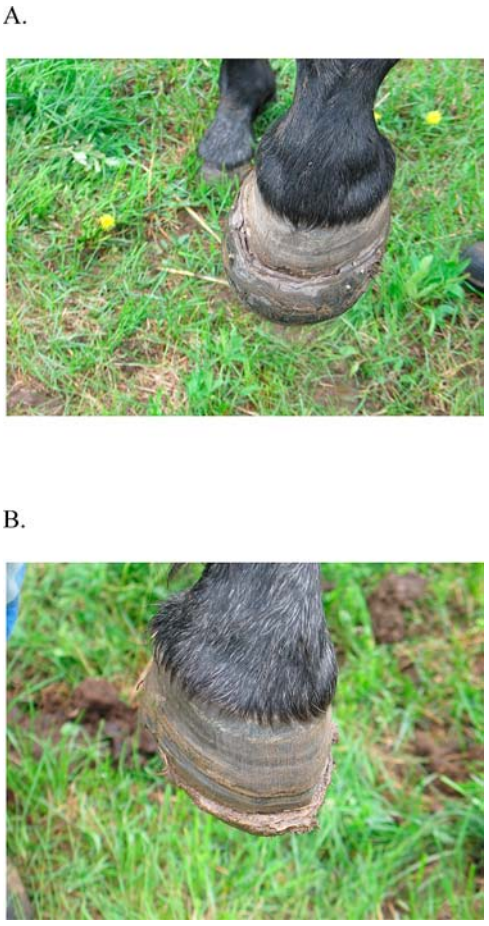

Figure 1. Photographs of (A) left front and (B) right front hooves of a horse chronically poisoned on selenium 7 months after being removed from the pasture containing high-selenium forage and water. The horse had been shod 6 weeks previously and had sloughed part of the right front hoof 1 day prior to this photograph being taken.

Horse 1 developed severe hoof lesions (Figure 1). Clinically his condition deteriorated and he became lame and was fitted with pads to help relieve the pain. However, within 4 months of his last exposure he became reluctant to bear weight on both

Table 2. Description of Horses Chronically Poisoned on Selenium and the Length of Their Mane and Tail Samples Collected and Analyzed for Selenium Content

			first sampling (May 15)		second sampling (Oct 15)	
horse	description	time in contaminated pasture	length of mane (cm)	length of tail (cm)	length of mane (cm)	length of tail (cm)
1	5-year-old gelding	~May 15 to Nov 15 for 3 years	24.5	68.5	NA	NA
2	9-year-old mare	~May 15 to Nov 15 for 3 years	35.5	87.6	35.5	101.6
3	11-year-old mare	~May 15 to Nov 15 for 3 years	20.3	33.0	38.1	91.4
4	15-year-old gelding	Sept 1 to Nov 15 for 1 year	30.4	69.8	NA	NA

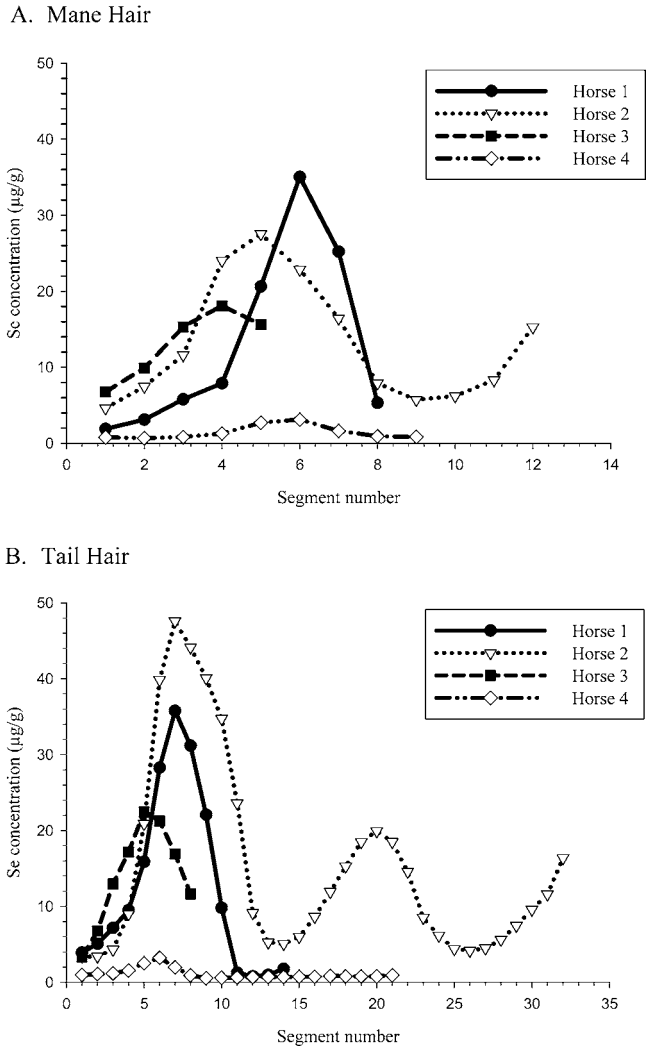

Figure 2. Selenium (Se) concentrations in (A) mane segments (2.5 cm) and (B) tail segments (2.5 cm) from four horses that grazed in a pasture with high-Se forages and water. The hair segments were numbered sequentially with the most recent growth (closest to skin) being number 1. Horses 1−3 grazed the pasture from May 15 to November 15 for three consecutive years. Horse 4 was in the pasture for 1.5 months during the third year only.

front feet. Seven months postexposure there was severe necrosis of the laminae of both front feet and the hoof wall sloughed away from underlying laminae up to the hyperplastic circular band of new growth that had developed around the hooves postexposure. The peak Se concentrations in the tail of horse 1 were from segment seven and were 35.8 μg/g Se. The mane of horse 1 was only 24.5 cm long, and the peak Se concentration in his mane was in segment six and contained 34.2 μg/g Se. Horse 1 required nearly 18 months to recover as he was rested as the hoof laminae healed and regrew. He was returned to normal work, although the prognosis of complete recovery with normal hoof strength and growth is questionable.

Horse 2 had hoof lesions that included vertical cracks in the hoof walls and prominent circular bands below the coronary band. The horse periodically exhibited minor signs of lameness but was able to be used for light ranch work. The mane of horse 2 was divided into 12 segments that could be analyzed, and the Se concentration of each segment plotted as a curve showed the complete increase and decrease of Se concentrations over one grazing season and the decrease of Se from a second grazing season (Figure 2A). The tail of horse 2 was 87.6 cm long and had increased Se concentrations during two grazing seasons that were flanked by lower Se concentrations marking the growth during months without high-Se exposure (Figure 2B). Horse 2 also had the highest peak Se concentration found in any of the hair from the horses with segment seven of the tail containing 47.6 μg/g Se.

Horse 3 had the shortest mane and tail samples but the cyclic pattern was the same as observed in horses 1 and 2. The peak Se concentrations in the mane and tail were both in segment five and were 18.1 and 22.5 μg/g Se, respectively. Horse 3 had minor vertical hoof wall cracks with some circular laminae disruption below the coronary band. She did not become lame at any time and was therefore able to be used for normal work on the ranch.

Horse 4 was in the pasture for approximately 45 days during one grazing season from the first of October until the middle of November. The horse did not develop hoof lesions, nor did it become lame at any time. The peak Se concentrations in the mane and tail of horse 4 were both in segments six and were 3.1 and 3.2 μg/g Se, respectively.

A second collection of tail and mane samples was made from horses 2 and 3 at 5 months after the first hair collections. The hair samples were segmented in the same manner as the hair from the first collection, and the Se concentrations were determined and are shown in Figures 3 and 4, respectively.

DISCUSSION

The horses were diagnosed with chronic Se poisoning on the basis of hoof lesions and mane and tail Se concentrations. On the basis of the cyclic pattern that was observed in the longer tail samples and forage and water analysis, it was determined that the forage and water during 6 months of each year were likely the toxic sources of Se. Mineral supplements were eliminated as a possible source of excessive Se because the horses were on the same mineral supplement on a year-round basis. The Se concentrations in streams contaminated by Se in the mining area are generally elevated during the spring months when runoff is high; thus, forages growing in or near the water source can also contain elevated Se concentrations.

The lesions observed in this case are typical of those reported for chronic selenosis in horses.[4,6] Horses that lose hair will eventually grow their mane and tail to normal lengths over a

dx.doi.org/10.1021/jf500861p | J. Agric. Food Chem. 2014, 62, 7393−7397

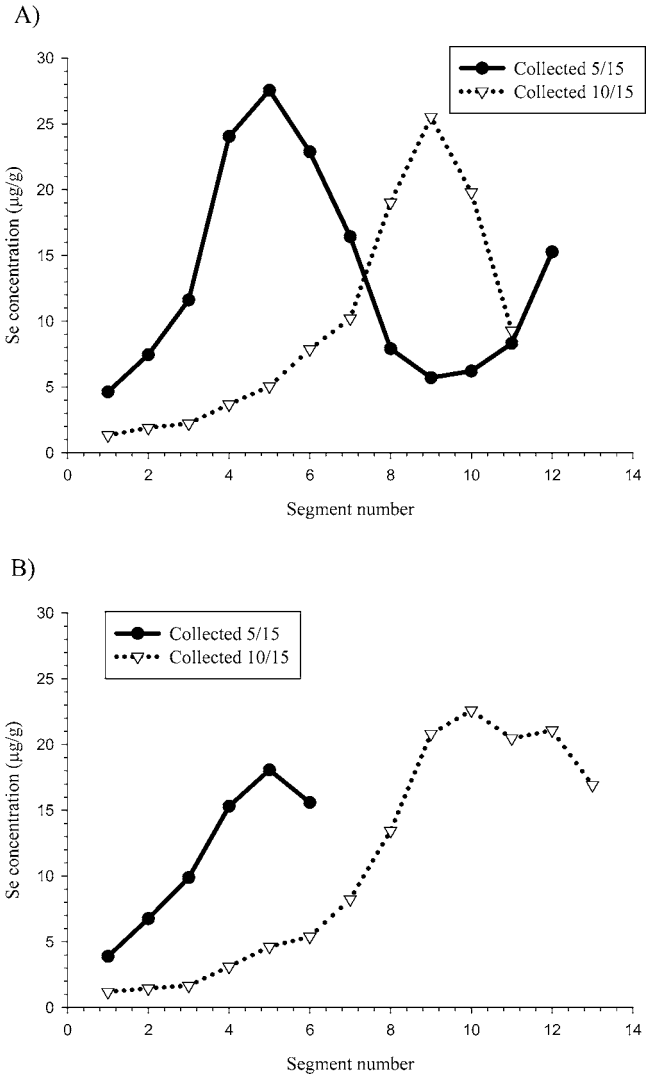

Figure 3. Selenium (Se) concentrations in mane segments (2.5 cm) from horse 2 (A) and horse 3 (B) that grazed in a pasture with high-Se forages and water. The hair segments were numbered sequentially with the most recent growth (closest to the skin) being number 1. The samples were collected 6 and 11 months postremoval from the pasture.

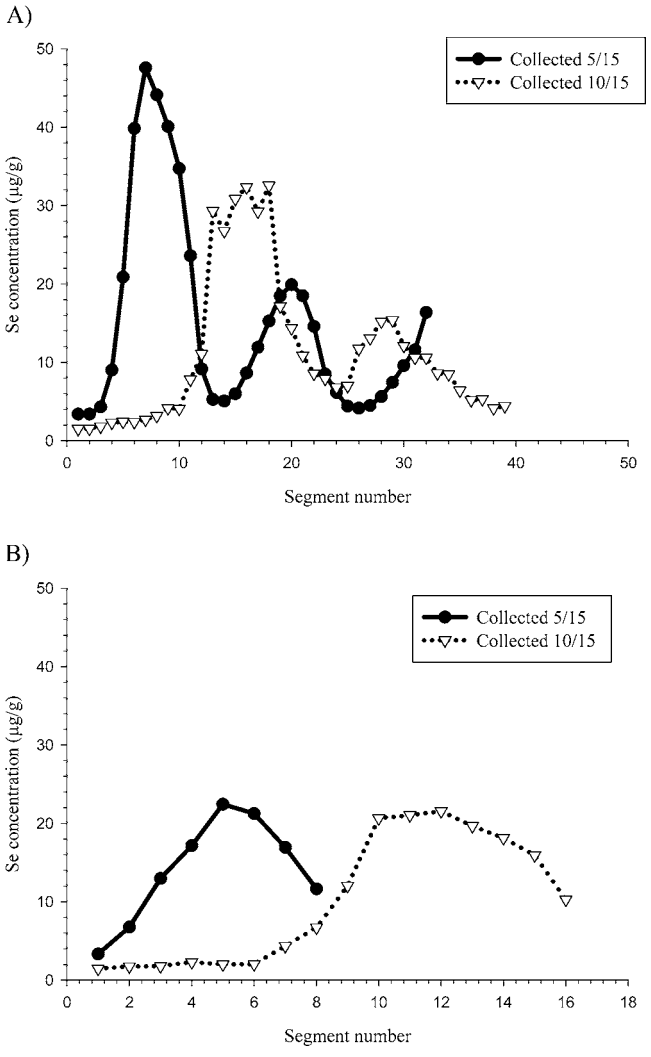

Figure 4. Selenium (Se) concentrations in tail segments (2.5 cm) from horse 2 (A) and horse 3 (B) that grazed in a pasture with high-Se forages and water. The hair segments were numbered sequentially with the most recent growth (closest to the skin) being number 1. The samples were collected 6 and 11 months postremoval from the pasture.

period of 1−2 years. However, horses that suffer severe hoof lesions and slough their hoofs often suffer from severe laminitis and may need to be euthanized to alleviate their suffering.

To avoid similar problems in the future the recommendation was made to use the pasture as a holding pasture for yearling steers for durations of 1−3 days when steers are received and shipped. The ranchers were told to avoid using the pasture for horses for any length of time because horses are more susceptible to Se toxicosis than many other livestock species.

Selenium accumulates in the hair of horses when exposed to forage with high Se content, and the concentrations of Se in the forage have been previously correlated with Se concentration in the mane and tail.[4] Hair analysis has been used to track human exposure to toxic metals.[10] Previous studies have demonstrated that there is a continual growth in the permanent hair of equine mane and tail. These studies indicate a relatively constant rate of growth of manes and tails over periods of time up to 12 months.[11,12] Dunnet and Lees[12] reported that tail and mane (medial) grew at 0.792 and 0.746 mm/day, respectively. In our study the horses were in the contaminated pasture for approximately 6 months each year. The distance between the peak Se concentrations and lowest Se concentration in each hair sample was very symmetrical, indicating that the growth rate of the hair was relatively the same over the time period during which the hair grew. Our data also support previous studies[12] that tail hair grows more rapidly than mane hair as the distance between the peak Se concentrations and the closest low Se concentration before concentration increased again was generally one segment less.

Often horses chronically poisoned on Se will have alopecia of the mane and tail. The reason for alopecia in some cases and not others is unknown. However, we speculate that it may be due to the forms and amounts of Se to which the horses are exposed. It may also be due to the Se and nutritional status of the horse at the time of the exposure.

In cases in which Se-exposed horses do not have mane and tail alopecia, the data from this study demonstrate that hair samples can be taken 1−3 years postexposure to document exposure to seleniferous forages, diets, or contaminated water.

dx.doi.org/10.1021/jf500861p | J. Agric. Food Chem. 2014, 62, 7393−7397

Additionally, the data presented in Figures 3 and 4 in which two of the horses were sampled a second time, 5 months after the first sampling, demonstrate that the concentrations of the Se in the mane and tail are relatively stable. The plotted curves of Se concentration in the mane and tail from the second sampling of horses 2 and 3 contain the same pattern with nearly the same Se concentrations as the hair contained when the final samples were collected. However, the curves are shifted to the right as the hair has grown longer and the high Se-containing segments have moved farther down the hair samples. The sampling is repeatable because the Se has been incorporated into the hair.

Cases of chronic selenosis in horses continue to occur in horses grazing seleniferous forages or when forage produced on soils with high concentrations of available Se is harvested and fed to horses. The cost of poisoning can be high because some trained horses are very valuable and are often treated as companion animals. Some animals may need to be euthanized. However, in some cases such as this one, even though the animal is not functional for an extended period of time because of lameness, the poisoned horse may be able to recover and be used for normal work.

In conclusion, sampling and segmenting of equine tail and mane can be a valuable tool to document or determine exposure to excessive Se in the diet for up to 3 years postexposure in some cases. Additionally, this study demonstrates that the concentrations of Se in mane and tail hair remain relatively stable over time.

AUTHOR INFORMATION

Corresponding Author

*(T.Z.D.) Phone: (435) 752-2941. Fax: (435) 753-5681. E-mail: zane.davis@ars.usda.gov.

Funding

This research was supported by USDA/ARS and the Utah Agriculture Experiment Station, Utah State University.

Notes

The authors declare no competing financial interest.

ACKNOWLEDGMENTS

We thank Katie Lott, Mary Hubbard, and Harold Winger for their assistance with this research.

REFERENCES

(1) Asano, K.; Suzuki, K.; Chiba, M.; Sera, K.; Asano, R.; Sakai, T. Twenty-eight element concentrations in mane hair samples of adult riding horses determined by particle-induced x-ray emission. *Biol. Trace Elem. Res.* **2005**, *107*, 135−140.

(2) Crinion, R. A.; O'Conner, J. P. Selenium intoxication in horses. *Ir. Vet. J.* **1978**, *32*, 81−86.

(3) McLauglin, J. G.; Cullen, J. Clinical cases of chronic selenosis in horses. *Ir. Vet. J.* **1986**, *40*, 136−138.

(4) Witte, S. T.; Will, L. A.; Olsen, C. R.; Kinker, J. A.; Miller-Graber, P. Chronic selenosis in horses fed locally produced alfalfa hay. *J. Am. Vet. Med. Assoc.* **1993**, *202*, 406−409.

(5) Martin, J. L. Selenium compounds in nature and medicine. In *Organic Selenium Compounds: Their Chemistry and Biology*; Klayman, D. L., Gunther, W. H. H., Eds.; Wiley: New York, 1973; pp 663−691.

(6) Kingsbury, J. M. Selenium. In *Poisonous Plants of the United States and Canada*; McElroy, W. D., Swanson, C. P., Eds.; Prentice-Hall: Englewood Cliffs, NJ, USA, 1964; pp 44−50.

(7) Raisbeck, M. F. Selenosis. *Vet. Clin. North Am. Food Anim. Pract.* **2000**, *16*, 465−480.

(8) Tiwary, A. K.; Stegelemeier, B. L.; Panter, K. E.; James, L. F.; Hall, J. O. Comparative toxicosis of sodium selenite and selenomethionine in lambs. *J. Vet. Diagn. Invest.* **2006**, *18*, 61−70.

(9) Davis, T. Z.; Stegelmeier, B. L.; Panter, K. E.; Cook, D.; Gardner, D. R.; Hall, J. O. Toxicokinetics and pathology of plant-associated acute selenium toxicosis in steers. *J. Vet. Diagn. Invest.* **2012**, *24*, 319−327.

(10) Chatt, A.; Katz, S. A. *Hair Analysis: Applications in the Biomedical and Environmental Sciences*; VCH Publications: New York, 1989; pp 14−16.

(11) Popot, M. A.; Stojiljkovic, N.; Garcia, P.; Richard, C. A.; Bonnaire, Y.; Tabet, J. C. Additional studies on the detection of drugs in horse hair. In *14th International Conference of Racing Analysts and Veterinarians*; R&W Publications: Orlando, FL, USA, 2002.

(12) Dunnett, M.; Lees, P. Trace element, toxin and drug elimination in hair with particular reference to the horse. *Res. Vet. Sci.* **2003**, *75*, 89−101.

Table 1. Number of Dams, Number of Pups/Dam, and the Proportion (Mean Percent ± SEM) of Rat Pups with Various Malformations When Pregnant Dams Were Dosed with Various *Mimosa tenuiflora* Plant Parts, Extracts, or Purified Compounds

treatment	no. of dams	mean no. of pups/dam	NMT in feed ration (μg/g)	DMT in feed ration (μg/g)	cleft palate (soft tissue) (%)	hard palate damage[a] (%)	skeletal deformities[b] (%)	scoliosis[c] (%)
control	7	12.8			0 ± 0	0 ± 0	9.0 ± 5.9	1.2 ± 1.0
leaf	9	12.1	149	154	27.5 ± 5.0	0 ± 0	25.3 ± 5.9	1.2 ± 1.1
leaf (MeOH)[d]	7	13.1	134	139	24.9 ± 4.8	0 ± 0	38.4 ± 6.6	3.47 ± 2.5
leaf alkaloid	6	10.8	120	108	25.1 ± 3.6	0 ± 0	53.2 ± 8.9	0 ± 0
seed	11	13.7	11	8	26.5 ± 5.9	0 ± 0	37.9 ± 6.2	4.0 ± 1.7
seed MeOH	7	14.0	8	6	3.1 ± 2.2	0 ± 0	50.3 ± 7.2	1.3 ± 1.3
seed alkaloid	7	11.6	9	4	10.1 ± 4.6	0 ± 0	40.2 ± 4.4	2.8 ± 2.1
DMT (**1**)	7	11.8		60	5.8 ± 3.1	0 ± 0	48.2 ± 11.2	4.8 ± 2.1
NMT (**2**)	8	11.5	61		18.6 ± 3.4	0 ± 0	36.1 ± 9.5	0 ± 0
DMT/NMT	10	11.7	93	116	58.6 ± 6.8	7.7 ± 3.9	13.4 ± 5.5	13.4 ± 5.5

[a]Hard palate damage consisted of overlapping or missing bone. [b]The bones included in this column include sternebrae, the caudal, lumbar, sacral, and thoracic vertebrae, metacarpals, ribs, and parietal bones. Deformities include fewer than normal number of bones, greater than normal number of bones, or misaligned bones. [c]S- or C-shaped curvature of the spine in rat pups. [d]MeOH, methanol; NMT, *N*-methyltryptamine; DMT, *N,N*-dimethyltryptamine.

10% *M. tenuiflora* plant material or the components therefrom, extracted or synthesized, during gestation days 6–21. Rats were humanely euthanized (CO_2 asphyxiation) on gestation day 21, and pups were examined for cranial–facial defects including cleft palate and cleft lip and skeletal malformations. Nine different experimental diets were tested including *M. tenuiflora* leaf and seed material, crude methanol extracts of leaf and seed, crude alkaloid extracts of leaf and seed, and the purified alkaloids *N*-methyltryptamine (**2**) and *N,N*-dimethyltryptamine (**1**). The concentrations of **1** and **2** in each of the different diets were measured and reported in Table 1. The use of all animals was approved by the Institutional Animal Care and Use Committee (Utah State University, IACUC approval 1527) and conducted under veterinary supervision.

Preparation of Methanol and Crude Alkaloid Extracts. For an experimental group of 10 animals approximately 4 kg of feed was needed over a period of 15 days (gestation days 6–21). Therefore, for a 10% concentration in the feed, 400 g of *M. tenuiflora* leaf, seed, or extract from the equivalent amount of plant material was used in the formulation of the experimental group ration. Thus, 400 g of plant material was extracted with methanol (3 L) by Soxhlet extraction for 48 h. The methanol extracts were concentrated by rotoevaporation and transferred to a glass storage vessel by dilution in methanol at a concentration of 50 g of plant material equivalents per 100 mL. For preparation of the rations, 44 g of plant or the equivalent extract (88 mL) was combined with 360 g of rat chow (the methanol was removed by evaporation) and 36 g of corn starch and formulated as previously described.[3]

To obtain a crude base (alkaloid) fraction, an 88 mL aliquot of the methanol extract (equivalent to 44 g of plant material) was evaporated by rotoevaporation, the flask rinsed twice with 1% H_2SO_4 (50 and 25 mL), and the acid solution saved. The flask was then rinsed three times with dichloromethane (3 × 50 mL), the dichloromethane was subsequently extracted with 1% H_2SO_4 (2 × 100 mL), and all acid extracts were combined. The acid solution was applied to a Strata XC solid phase extraction column (5 g) (Phenomenex, Torrance, CA, USA) prerinsed with methanol (50 mL) and water (50 mL). The SPE column was then rinsed with water (150 mL) and methanol (150 mL). The crude alkaloid fraction was then eluted with ammoniated methanol (150 mL; methanol saturated with ammonia then diluted with methanol 1:10). The ammoniated methanol was removed by rotoevaporation and the residue then dissolved in methanol (50 mL) and stored at 2 °C until used in rat chow formulation. This procedure was repeated approximately nine times to provide the total alkaloid fraction to formulate the rat chow for one experimental group of 10 rats.

Synthesis of *N,N*-Dimethyltryptamine (1). *N,N*-Dimethyltryptamine (**1**) was prepared by synthesis from tryptamine using reductive amination,[4] with modifications, followed by cleanup with flash chromatography. Tryptamine (4.7 mmol, 750 mg) was combined with sodium triacetoxyborohydride (18.4 mmol, 3.9 g) and glacial acetic acid (9 mmol; 0.54 mL) in 40 mL of THF. The solution was stirred at room temperature, and 1.89 mL of formaldehyde (37%) (~23 mmol) was added dropwise; the reaction continued with stirring for 2 h. The reaction solution was transferred to a round-bottom flask and the THF solvent removed by rotoevaporation at 40 °C. The flask was then rinsed with 1 N HCl (2 × 40 mL) and the acid solution extracted with ethyl acetate (2 × 50 mL). The ethyl acetate extract was discarded, and the pH of the acid solution was increased to a pH value of 10 with a 20% KOH solution and the basic solution extracted with ethyl acetate (2 × 70 mL). The ethyl acetate extract was dried over anhydrous sodium sulfate and filtered, and the solvent was removed by rotoevaporation to give crude **1**. The crude reaction mixture was purified by flash chromatography over silica gel (50 g) (Biotage) using a solvent gradient of ethyl acetate (A) and methanol (B) at a flow rate of 50 mL/min. Solvent gradient was 5% B (4 min), 5–40% linear gradient (26 min), 40% B (5 min). Fractions (20 mL) were collected throughout the run, and fractions selected on the basis of the UV detection at 280 nm were further analyzed by HPLC-UV-MS. The purest fractions were combined to give the final product (**1**) (380 mg; 43% yield). The reaction was repeated as needed to supply sufficient product for rat chow formulations. The final product was characterized by NMR and MS analyses and purity estimated to be >95%. UV (acetonitrile/water with 0.5% acetic acid/0.05% TFA) 233, 273, 279 nm; MS (LC-APCI-MS) 189 (100%; MH^+), 144 (20), 130 (40); ^{1}H NMR (300 MHz, $CDCl_3$) δ 8.05 (br s, NH), 7.62 (d, 1H, J = 7.5 Hz, H-1), 7.34 (d, 1H, J = 8.2 Hz, H-4), 7.16 (dt, 1H, J = 7.9, 1.0 Hz, H-2 or H-3), 7.12 (dt, 1H, J = 7.9, 1.0 Hz, H-2 or H-3), 7.02 (br s, 1H, H-8), 2.95 (m, 2H, H-11), 2.64 (m, 2H, H-10), 2.34 (s, 6H, $N(CH_3)_2$) in agreement with previously reported ^{1}H NMR data.[1]

Quantitative Analysis of *N*-Methyl- and *N,N*-Dimethyltryptamine by LC-MS in Formulated Rat Chow Pellets. Samples of the formulated rat chow were analyzed for the concentrations of **1** and **2** by LC-MS. Six random pellets from each formulation were ground separately with a mortar and pestle. A 100 mg aliquot of each pellet was placed into a 15 mL screw-cap test tube and extracted with 4 mL of dichloromethane and 4 mL of 1% H_2SO_4 for 3 h by mechanical rotation. The samples were centrifuged and the upper aqueous layer removed and saved. The samples were then extracted a second time with 2 mL of 1% H_2SO_4 for 5 min and centrifuged and the upper aqueous layer removed and combined with first extraction. The total aqueous acid extract (~6 mL) was added to a prepared 200 mg Strata SCX SPE cartridge, prerinsed with 2 mL of methanol and 2 mL of water. The SPE column was rinsed with 2 mL of water and 2 mL of methanol. The analytes were eluted with 4 mL of an ammoniated methanol solution. The samples were evaporated to dryness under a flow of nitrogen at 60 °C and then dissolved in 1.0 mL of 50%

dx.doi.org/10.1021/jf5005176 | J. Agric. Food Chem. 2014, 62, 7398–7401

methanol/0.1% TFA, and 5 μL injections were analyzed by LC-APCI-MS using a Betasil C18 column, 100 mm × 2.1 mm i.d. (Thermo Fisher, Waltham, MA, USA) and a linear gradient of acetonitrile (A) and water (0.05% TFA/0.5% acetic acid) (B). Flow rate was 0.300 mL/min with a gradient of 10% A (0−3 min), 10−70% A (3−10 min), and 70% A (10−15 min). Detection was by APCI-MS, and peak areas were measured from reconstructed ion chromatograms of the protonated molecules (*m*/*z* 175 and 189). Calibration curves were composed of a set of five standards prepared from the *N*-methyltryptamine and *N*,*N*-dimethyltryptamine at concentration levels of 40, 30, 20, 10, and 2 μg/mL.

RESULTS AND DISCUSSION

In the original work, Medeiros[3] clearly demonstrated the acceptable characteristics of the rat model for testing of teratogenic effects of *M. tenuiflora*. Data were presented showing no adverse effects on animals receiving the ration containing 10% *M. tenuiflora* seed as to feed consumption, weight gain, clinical signs of sickness, abnormal behavior, and organ weights, and no significant histological lesions were produced in the treated pregnant rats. However, significant fetal malformations were observed, clearly demonstrating the teratogenic effects of the *M. tenuiflora* seed. In the most recent experiments presented here, the *M. tenuiflora* seed formulation was repeated, but the investigation extended to leaf material and then to chemical extracts and purified compounds found in *M. tenuiflora* in an attempt to identify and further understand the active chemical components in the plant material responsible for the teratogenic effects.

As in the prior work, rats accepted the prepared diets and showed no significant differences between control and treated animals as to feed consumption, weight gain, and overall health (data not presented). For the analysis of the current experiments fetal malformations were assessed in three categories: (1) soft tissue cleft palate; (2) hard palate anomalies; and (3) skeletal deformities. The skeletal deformities were grouped together and included analysis of spinal column alignment (scoliosis) and development of the sternebrae, the caudal, lumbar, sacral, and thoracic vertebrae, metacarpals, ribs, and parietal bones.

From the current experiment groups, rat pups from mothers who received *M. tenuiflora* plant material, methanol extracts, alkaloid extracts, and purified *N*-methyltryptamines had a higher incidence of soft tissue cleft palate in all treatments (Table 1). The soft tissue cleft palate was the most consistent and significant observed deformity in pups from treated dams. This soft tissue cleft palate was characterized by incomplete closure or overlap of the tissue (Figure 1). Deformities of the hard palate were observed only in the combined dose of **1** and **2**.

Skeletal deformities, including missing, extra, or misaligned bones, were observed in all treatment groups to some degree (Table 1). An extreme example was a pup with missing vertebrae (Figure 2). Minor skeletal aberrations were noted in a few control animals and were considered in the treatment evaluations. In general, the skeletal deformities were highly random in type and frequency, but when added together were considerably higher in frequency in comparison to the control group.

Specifically noted was the frequency of observed scoliosis in Table 1 to highlight an observed difference in the results of the rat pups from mothers receiving the mixed *N*-methyl- and *N*,*N*-dimethyltryptamine treatments. The frequency of induced scoliosis was higher at 13.4 ± 5.5% in pups from the *N*-methyl- and *N*,*N*-dimethyltryptamine group compared to all other treatments (2.1 ± 1.7%).

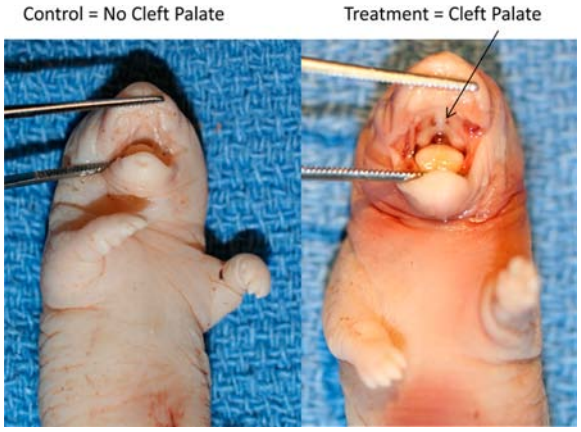

Figure 1. Observed induced soft-tissue cleft palate in a rat pup from a dam treated with *Mimosa tenuiflora* leaf and a control.

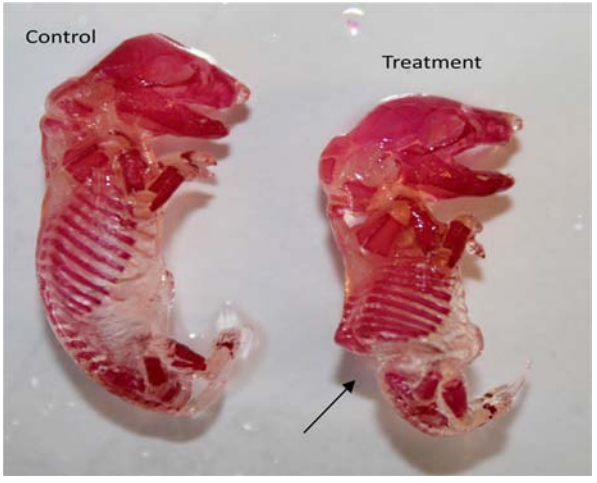

Figure 2. Observed skeletal malformation in a rat pup from a dam receiving a ration containing 10% *Mimosa tenuiflora* leaf and a control. Note complete lack of lower vertebrae.

In using the rat model, the teratogenic compounds were found to be extractable in methanol and not lost during further cation ion exchange solid phase procedures giving a teratogenic active crude base fraction. In previous work[5] the alkaloid content of *M. tenuiflora* was examined, and the major alkaloid fraction was found to be composed of *N*,*N*-dimethyltryptamine (**1**), 2-methyltetrahydro-β-carboline (**3**), and an unidentified alkaloid with a proposed molecular weight of 174. The unknown alkaloid has since been identified as *N*-methyltryptamine (**2**) (Figure 3). It was thus followed here with experimental diets using the two major alkaloids (**1** and **2**) in purified form, first in separate formulations and then in a combined (**1** and **2**) fortified ration.

Dams receiving **1** or **2** only rations resulted in pups with a slightly lower frequency of induced cleft palate compared to the original plant material or even the methanol or crude base extracts; however, skeletal deformities were of similar frequency (Table 1). In the final experiment using a combined **1** and **2** fortified ration, an increase in cleft palate and skeletal deformities was expected. Cleft palate induction frequency indeed increased (58.6%), and in a few cases there was even observed hard palate damage. An unexpected finding was the

dx.doi.org/10.1021/jf5005176 | J. Agric. Food Chem. 2014, 62, 7398−7401

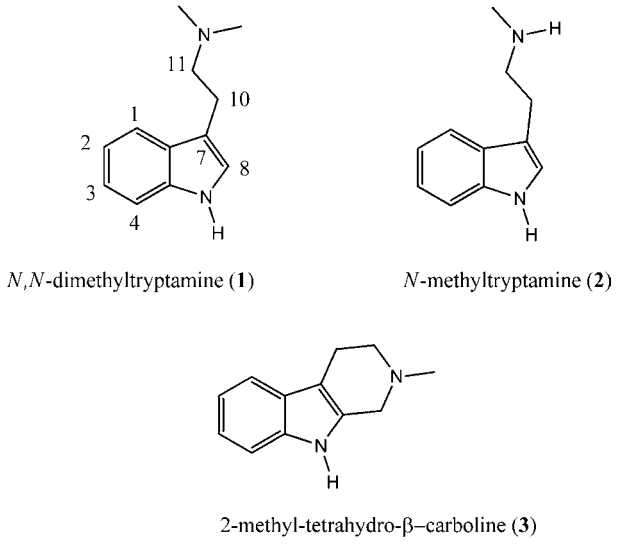

Figure 3. Structures of alkaloids in *Mimosa tenuiflora*.

total lack of skeletal deformities such as missing or misaligned or extra bones in this series of pups, although the frequency of induced scoliosis increased. There are no prior reports of any teratogenic effects of **1** or **2**. They are best known for their psychoactive properties.[6−8] There is currently insufficient information to allow speculation on the possible teratogenic mechanism of action at this time.

In summary, the use of the pregnant rat model for the testing of crude chemical extracts, semipurified extracts, and even purified compounds for teratogenic effects of *M. tenuiflora* seems plausible. The results confirmed that the active principles could be extracted from the plant with methanol and were carried through an ion exchange procedure to what would be considered a crude alkaloid fraction. However, other compounds of basic characteristics, for example, basic amino acids, would also be present in this crude alkaloid fraction. Both **1** and **2** were found to be teratogenic in the rat model as they induced cleft palates and skeletal malformations. Future work should include confirmation of the teratogenic activity of *N*-methyl- and *N,N*-dimethyltryptamine in a small ruminant model.

AUTHOR INFORMATION

Corresponding Author

*(D.G.) Phone: (435) 752-2941. Fax: (435) 797-5681. E-mail: dale.gardner@ars.usda.gov.

Funding

Partial funding was provided by the Brazilian National Institute for Science and Technology for the Control of Plant Poisonings, Grant 573534/2008-0.

Notes

The authors declare no competing financial interest.

ACKNOWLEDGMENTS

We thank Ed Knoppel (USDA, ARS, Poisonous Plant Research Laboratory) for assistance in animal care and post-mortem analyses.

REFERENCES

(1) Gaujac, A.; Martinez, S. T.; Gomes, A. A.; Andrade, S. J.; Pinto, A. C.; David, J. M.; Navickiene, N.; Andrade, J. B. Application of analytical methods for the structural characterization and purity assessment of *N,N*-dimethyltryptamine, a potent psychedelic agent isolated from *Mimosa tenuiflora* inner barks. *Microchem. J.* **2013**, *109*, 78−83.

(2) Pimentel, L. A.; Riet-Correa, F.; Gardner, D. R.; Panter, K. E.; Dantas, A. F. M.; Medeiros, R. M. T.; Mota, R. A.; Araujo, J. A. S. *Mimosa tenuiflora* as a cause of malformations in ruminants in the northeastern Brazilian semiarid rangelands. *Vet. Pathol.* **2007**, *44*, 928−931.

(3) Medeiros, R. M. T.; de Figueiredo, A. P. M.; Benicio, T. M. A.; Dantas, F. P. M.; Riet-Correa, F. Teratogenicity of *Mimosa tenuiflora* seeds to pregnant rats. *Toxicon* **2008**, *51*, 316−319.

(4) Brandt, S. D.; Moore, S. A.; Freeman, S.; Kanu, A. B. Characterization of the synthesis of *N,N*-dimethyltryptamine by reductive amination using gas chromatography ion trap mass spectrometry. *Drug Test. Anal.* **2010**, *2*, 330−338.

(5) Gardner, D. R.; Riet-Correa, F.; Panter, K. E. Alkaloid profiles of *Mimosa tenuiflora* and associated methods of analysis. In *Poisoning by Plants, Mycotoxins and Related Toxins*; Riet-Correa, F., Pfister, J., Schild, A., Wierenga, T., Eds.; CAB International: Wallingford, UK, 2011; pp 600−605.

(6) Sai-Halasz, A. The effect of antiserotonin on experimental psychosis induced by dimethyltryptamine. *Experientia* **1962**, *18*, 137−139.

(7) Rosenberg, D. E.; Isbeel, H.; Miner, E. J. Comparison of a placebo, *N,N*-dimethyltryptamine, and 6-hydroxy-*N,N*-dimethyltryptamine in man. *Psychopharmacology* **1963**, *4*, 39−42.

(8) Moussatche, H.; Carlini, E. A.; Santos, M. Behavioral effects of *N,N*-dimethyltryptamine n rats and mice. *Rev. Bras. Biol.* **1970**, *30*, 483−489.

onset of clinical signs, initially manifest as severe diarrhea. Appropriate analytical technology was not then available, and plant toxin levels were not reported for any of these feeding trials.

Analysis of simplexin levels in *Pimelea* plant material by liquid chromatography−tandem mass spectrometry (LC-MS/MS) has demonstrated that toxin levels are dependent on *Pimelea* species, growth stage, weathering, and the particular plant parts utilized.[2,3] In previous feeding trials it was common to utilize material collected from a number of different sites, but this now causes complications in the interpretation of data due to subsequent reclassification of *Pimelea* species.[2] For instance, Clark[8] dosed cattle with *Pimelea* material from multiple field collections from different locations, with no record of whether individual collections were combined or administered separately. Herbarium voucher specimens lodged for these individual collections have now been re-examined and determined to represent multiple different *Pimelea* species.[2] Given the composite nature of these collections, it is now not possible to make any realistic estimate of the dosage of toxin in plant material administered in these previous trials. Our present study utilizes a single collection of *P. trichostachya* of measured simplexin content and was undertaken to ascertain the minimum toxin intake required to induce *Pimelea* poisoning in cattle. Animal tissues arising from the feeding trial were also analyzed for simplexin to determine whether this toxin intake results in detectable simplexin residues in animal tissues.

MATERIALS AND METHODS

Plant Material. Young flowering *P. trichostachya* plants (Queensland Herbarium voucher AQ751764) were collected from a single location 40 km south of Roma (Queensland). The composite aerial portion (seeds, flower heads, small stems, and leaves) of the air-dried plant material was milled and kept frozen at −20 °C until required. Simplexin levels of the composite sample (6 kg) were determined by LC-MS/MS analysis.[2]

Calf Feeding Trial. Four weaned, ruminating calves (130−180 kg) with no previous exposure to *Pimelea* were housed in individual enclosed, low-security cattle pens at the Animal Research Institute, Yeerongpilly (Queensland), and fed a base diet of Rhodes grass (*Chloris gayana*) and lucerne (*Medicago sativa*). Thawed *Pimelea* plant material was mixed with molasses (approximately 50 mL) and added to a small amount of Rhodes grass and lucerne, which was consumed by the calves prior to provision of their basic daily feed of lucerne/Rhodes grass. *Pimelea* plant material was introduced incrementally over the initial 4 days (days 1−4; 25, 50, 75, and 100% of the daily dose, respectively) to an initial dose of 7.5 mg dried *Pimelea* plant/kg bw/day. This daily dose was maintained until day 14, when the dose was incremented to 10.0 mg dried *Pimelea* plant/kg bw/day, and increased thereafter in 2.5 mg increments every 14 days. This feeding trial was conducted taking full account of the welfare of the calves under DAFF Animal Ethics Committee Approval SA 2008/03/239. The health of the animals was monitored daily throughout the trial, with feed intake, demeanor, scours, rectal temperature, and heart and respiratory rates recorded daily. Scouring by animals was assessed and scored (1−5): 1 = regular dung pat; 2 = moist pat; 3 = wet pat; 4 = scour; 5 = watery scour.

Jugular blood samples (3 × 10 mL) were obtained weekly and immediately before euthanasia. Blood for hematology was collected into EDTA anticoagulant; that for clinical biochemistry testing and toxin assay was collected into lithium heparin and frozen (−40 °C) for toxin analysis. Hematological values measured by ABX VET ABC Hematology Analyzer (ABX Diagnostics, Montpellier, France) were hemoglobin concentration, packed cell volume, erythrocyte count, total leucocyte counts, and erythrocyte indices; enzyme activities and chemical concentrations measured in plasma using an Olympus AU400 (Olympus, Tokyo, Japan) were aspartate aminotransferase, creatine phosphokinase, glutamate dehydrogenase, γ-glutamyl transferase, total protein, albumin, globulin, calcium, sodium, magnesium, potassium, chloride, β-hydroxybutyrate, total bilirubin, urea, and creatinine. At 2-week intervals, muscle biopsy samples were excised from the rump muscle as previously described[12] and frozen (−40 °C) for assay.

Animals were killed at day 125 by stunning with a captive bolt pistol and exsanguination and immediately necropsied. At necropsy, samples of liver, kidney, heart, skeletal muscle, and renal fat were collected, frozen, and stored at −40 °C before assay. Tissues were also collected at necropsy into 10% buffered neutral formalin for histopathology.

Extraction of Lyophilized Blood. Freeze-dried blood (0.5 g) was shaken with chloroform/methanol (2:1, 15 mL) for 30 min and centrifuged at 3200*g* for 10 min; the supernatant was decanted, and the residue was re-extracted by the same process. The combined decanted supernatant was washed once with brine (6 mL) and then with methanol/brine (1:1, 6 mL). The organic layer was dried (Na_2SO_4) and evaporated under reduced pressure. The residue was partitioned between hexane (4 mL) and acetonitrile (4 mL). The hexane layer was extracted with further acetontrile (2 × 2 mL), and the combined acetonitrile extract was evaporated.

Extraction of Adipose Tissue. Adipose tissue (1.0 g) was homogenized by IKA T25 Ultra Turrax (In Vitro, Brisbane, Australia) in chloroform/methanol (2:1, 15 mL) and the resultant solution filtered, washed with brine (0.73%, 4.5 mL), dried (Na_2SO_4); the solvent was removed under reduced pressure. The oily residue was redissolved in hexane (20 mL) and extracted with acetonitrile (3 × 5 mL), and the combined acetonitrile extract was evaporated.

Extraction of Other Tissues. Methanol (10 mL) was added to other animal tissues (1.0 g), cooled in ice (5 min), and homogenized by Ultra Turrax. Chloroform (20 mL) was added and the suspension shaken for 30 min and centrifuged at 3200*g* for 20 min. The filtered supernatant was washed with brine (6 mL) and then with methanol/brine (1:1, 6 mL). The organic layer was dried (Na_2SO_4) and evaporated under reduced pressure. The residue was partitioned between hexane (5 mL), acetonitrile (2 mL), and methanol (1 mL). The hexane layer was extracted with further acetontrile (2 × 2 mL), and the combined acetonitrile extract was evaporated.

LC-MS/MS Analysis. For each tissue, the evaporated residue was taken up in methanol (0.5 mL) and filtered (0.22 μm PVDF), and the simplexin content was determined by LC-MS/MS analysis as previously described.[2]

RESULTS AND DISCUSSION

LC-MS/MS quantification of simplexin in positive-ion atmospheric pressure chemical ionization (APCI) mode comprises multiple reaction monitoring (MRM) transitions 533 → 253 (for quantification) and 533 → 267 (for verification),[2] which represent the two most dominant daughter ions from the fragmentation of the protonated molecular ion (Figure 2). LC-MS/MS analysis of the milled dried *P.*

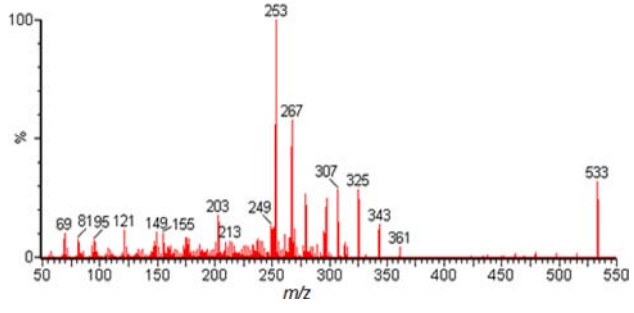

Figure 2. Positive ion APCI-MS fragmentation of the protonated molecular ion of simplexin, *m/z* 533.

dx.doi.org/10.1021/jf5005644 | J. Agric. Food Chem. 2014, 62, 7402−7406

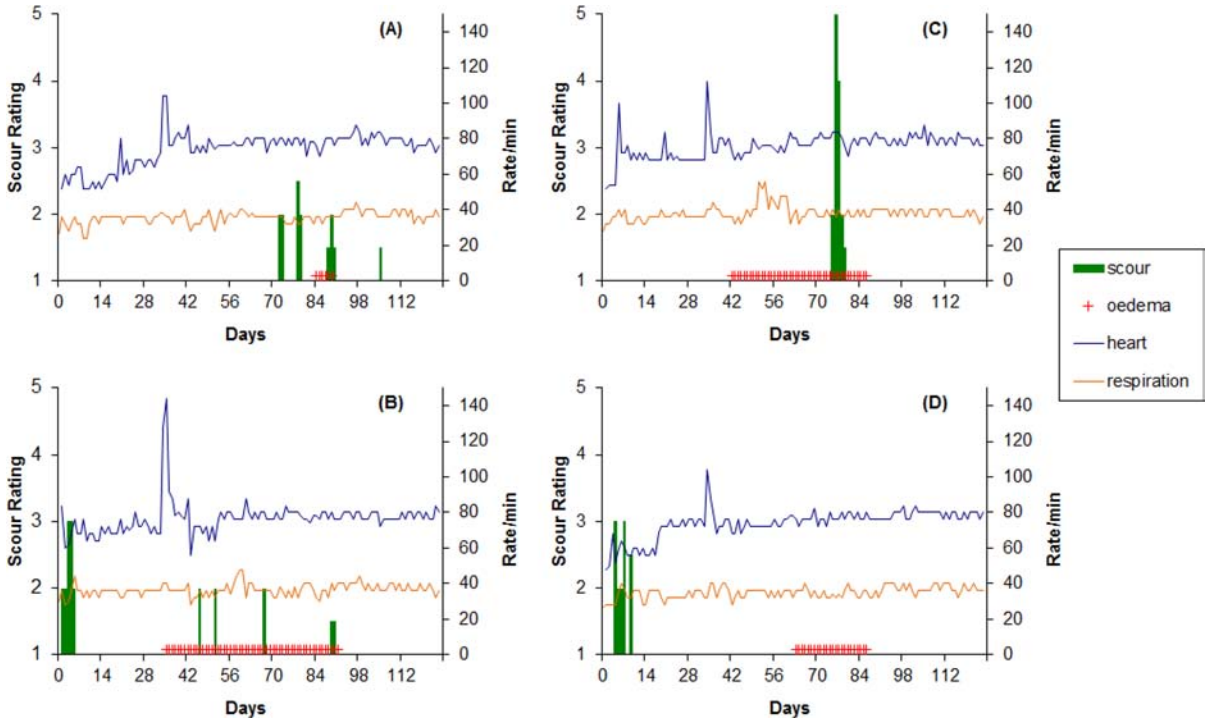

Figure 3. Plots for calves (A–D) showing days during the *Pimelea* feeding trial on which edema was recorded, scour rating (1–5), and heart and respiration rates (per minute).

trichostachya plant material used in this feeding trial provided a simplexin content of 227 mg simplexin/kg plant, comparable to average simplexin concentrations measured in flowering *P. trichostachya* or *P. elongata* of 225 and 239 mg simplexin/kg plant, respectively.[3] By comparison, the simplexin content of *P. simplex* flowering foliage is generally lower, with an average concentration of only 116 mg simplexin/kg plant.[3] Simplexin is a quite stable molecule, and the simplexin levels in the milled plant material were relatively unchanged during the feeding trial, with 195 mg simplexin/kg determined after 4 months at −20 °C.

Previous feeding trials by Clark[8] have shown that a high oral dose rate of 50–100 mg/kg bw/day dried *Pimelea* caused acute intoxication characterized by profuse watery diarrhea, emaciation, and jugular vein distension within 1 week but without edema. Kelly[9] induced similar subacute symptoms without jugular distension with dried *Pimelea* stems at 40–80 mg/kg bw/day for 6–14 days. Lower feeding dose rates over extended periods produced a more chronic syndrome with "subcutaneous edema, hydrothorax and jugular pulsation in addition to the features of subacute intoxication".[9] In his work, Clark[8] demonstrated that intravenous injection of plant extracts caused pulmonary venule constriction and proposed that prolonged constriction of these vessels is the basic cause of the classic *Pimelea* poisoning edema through increased pulmonary vascular resistance. The *Pimelea* toxin simplexin was later isolated[13] and subsequently demonstrated to constrict bovine pulmonary venules in vitro,[14] consistent with the proposed cause of the disease.

In previous *Pimelea* feeding trials,[6−11] the simplexin content of plant material employed was not known, and the toxin dosage rate is therefore unknown. Without this prior knowledge, the dosing regimen employed in our feeding trial erred on the side of caution with 2-week dose increments to avoid unintended adverse effects. The initial daily dose of 7.5 mg dried *Pimelea* plant/kg bw (equal to only 1.7 μg simplexin/kg bw) was incremented by 2.5 mg dried *Pimelea* plant/kg bw (or 0.57 μg simplexin/kg bw) every 14 days to a final dose of 27.5 mg dried *Pimelea* plant/kg bw (or 6.2 μg simplexin/kg bw) at day 125. The calves tolerated the daily intake of *P. trichostachya* with no adverse effects, other than initial mild diarrhea in two of four animals, until day 35, when increased heart rates were noted and one animal had mild subcutaneous edema under the jaw. In the remaining calves similar fluid accumulation under the jaw developed at days 42, 63, and 84, respectively (Figure 3). Although still being fed *P. trichostachya*, the subcutaneous edema progressively diminished, and all four animals appeared normal from day 91 until the end of the experiment at 125 days. All four calves developed diarrhea on at least one occasion for up to 5 days, and all showed a trend to elevated heart rates after a few weeks, which were sustained for the duration of the feeding (Figure 3).

Previous *Pimelea* feeding trials have reported falls in white cell count and reduction in packed cell volume and hemoglobin concentration preceding the onset of acute diarrhea.[9] A full range of biochemical and clinical parameters were studied during the current trial. The mean corpuscular volume increased in three of the four animals during the trial period (Figure 4i), whereas the red cell counts (Figure 4ii) tended to decline initially with a trough around days 35–42, followed by a mild to moderate increase over the next 7–14 days and then a gradual recovery during the remainder of the trial.

Similar to the mild clinical and hematological effects of *Pimelea* seen in the feeding trial animals, necropsy examinations showed little pathology. Subjectively, all four animals appeared to have a mild increased volume of pericardial fluid. Histopathology of lung tissues did not show convincing evidence of constriction of pulmonary venules, the primary pathological effect of the toxin simplexin. The lack of inclusion of a control animal in the experiment meant comparisons could

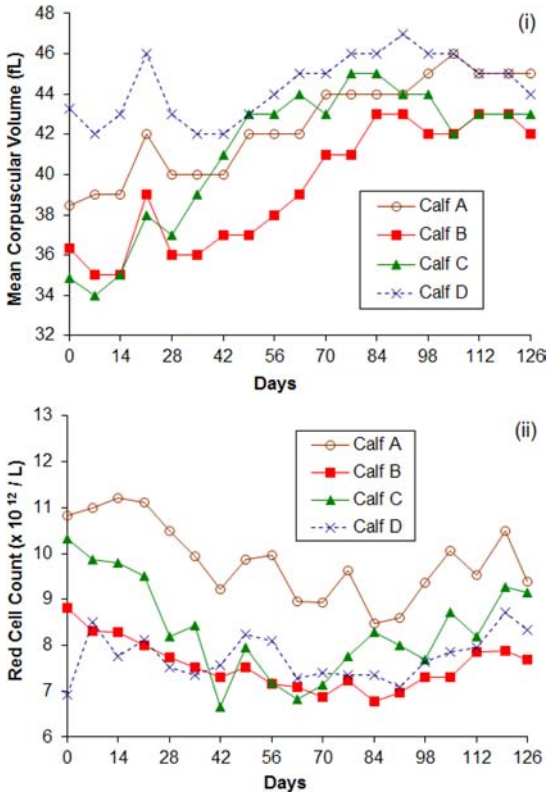

Figure 4. (i) Mean corpuscular volume (fL) and (ii) red cell count ($\times 10^{12}$/L) in each of the four calves (A–D) measured during the *Pimelea* feeding trial.

not be made, therefore reducing the chance of recognizing any very subtle changes. However, there was no evidence of significant gross pulmonary or subcutaneous edema, cardiac dilation, or liver changes (namely, peliosis hepatis) as seen in severely affected natural cases of *Pimelea* poisoning.[15]

Due to its hydrophobic nature, the potential for simplexin to form tissue residues in animals consuming this plant has also been considered. Our LC-MS/MS method for simplexin was adapted to analyze the toxin in animal tissues with good recoveries from a range of tissues spiked at 0.028 and 0.055 mg/kg (skeletal muscle, 90–104%; heart, 88–97%; liver, 63–81%; kidney, 76–93%) and at 0.055 and 0.088 mg/kg in dried blood (60–84%), with a limit of detection (LOD) of 17 μg/kg in dried blood and 8 μg/kg in other tissues. Tissues (heart, muscle, liver, kidney, fat, and blood) collected at necropsy together with weekly blood samples collected throughout the trial were analyzed by using this method. The simplexin concentration in all samples was below the LOD. Fortnightly rump muscle biopsy samples were also collected throughout the trial, but the sample quantity proved insufficient to provide a reliable simplexin result.

Earlier experimental work postulated that cattle exposed to the *Pimelea* toxin predominantly through inhalation of plant debris developed the circulatory failure and edema signs, whereas those ingesting plant material (and toxin) developed diarrhea.[6−8] Current knowledge, however, suggests that most inhaled particles are likely to be trapped in the mucosa of the upper respiratory tract and ultimately swallowed. Hence, regardless of the mode of exposure (ingestion or inhalation), we consider the digestive tract as the major route of toxin absorption from *Pimelea* plant material. In the present study, incorporation of the *Pimelea* plant material in molasses excluded inhalation as a means of exposure, and cattle developed both circulatory signs and diarrhea, consistent with the digestive system as the major route of toxin absorption.

At day 35 when the initial signs of edema were evident, the calves were each consuming 12.5 mg *Pimelea*/kg bw/day (equivalent to 2.8 μg simplexin/kg bw/day). For 160 kg calves this equates to a daily intake of approximately 2 g *Pimelea* per day (approximately 0.07% of their daily ration), and a total intake at that point of only 55 g *Pimelea* (12.5 mg simplexin) from the commencement of the feeding trial. This relatively small dose of plant material required to induce signs of mild *Pimelea* poisoning demonstrates the potent toxicity of these plant species and is consistent with field observations where only minor, inadvertent consumption of *Pimelea* plant material by cattle seems sufficient to result in poisoning. The time required to induce visible symptoms in this trial is also consistent with producer observations, which indicate that naive animals introduced into a *Pimelea*-infested pasture do not develop poisoning symptoms rapidly and generally noticeable symptoms take several weeks to appear.

It is particularly noteworthy that edema effects in all four calves diminished as the feeding trial progressed, despite being fed increasing doses of *Pimelea* plant material of the same simplexin content and, hence, corresponding increasing simplexin doses. These calves were sourced from south east Queensland, which is geographically distant from the arid inland regions where *Pimelea* occurs, and these animals would not previously have encountered these plant species or toxin. It was concluded that these calves, when exposed to prolonged low simplexin doses, developed mechanisms within a matter of 5–12 weeks for detoxifying or metabolizing simplexin, possibly through rumen microbial adaptation or activation of liver enzymes. The exact mechanism by which the observed tolerance is induced has not yet been determined, but it is noted that structurally similar phorbol esters are not degraded by rumenal microbes[16] but are metabolized by carboxylesterase and other microsomal liver enzymes.[17] Possibly such enzymes would be induced by prolonged low toxin doses. Regardless of the mechanism for the induced tolerance of simplexin, if similar low simplexin doses could be artificially maintained in field animals, then this could possibly provide an effective protective mechanism to prevent significant stock losses from *Pimelea* poisoning.

AUTHOR INFORMATION

Corresponding Author

*(M.T.F.) Phone 61 7 3276 6089. Fax 61 7 3216 6565. E-mail: mary.fletcher@uq.edu.au.

Funding

This study was funded by the Australian Government Natural Heritage Trust through AgForce Queensland.

Notes

The authors declare no competing financial interest.

ACKNOWLEDGMENTS

Plant identification was determined by staff of Queensland Herbarium (Environmental Protection Agency, Queensland). Technical assistance was provided by Claire McNeale, Matt Pyke, Michael Somerville, Brian Burren, and Alan McManus. Andrew Kelly and other DAFF farm staff provided invaluable assistance in daily management of the calves.

REFERENCES

(1) Fletcher, M.; Silcock, R.; Ossedryver, S.; Milson, J.; Chow, S. *Understanding Pimelea Poisoning of Cattle*; Collins, A., Ed.; Department of Employment Economic Development and Innovation: Brisbane, Australia, 2009; available at http://www.futurebeef.com.au/wp-content/uploads/2011/09/Understanding_pimelea_poisoning_of_cattle.pdf (accessed Jan 16, 2014).

(2) Chow, S.; Fletcher, M. T.; McKenzie, R. A. Analysis of daphnane orthoesters in poisonous Australian *Pimelea* species by liquid chromatography-tandem mass spectrometry. *J. Agric. Food Chem.* **2010**, *58*, 7482−7487.

(3) Fletcher, M. T.; Chow, K. Y. S.; Silcock, R. G.; Milson, J. A. LCMSMS analysis of the daphnane orthoester simplexin in poisonous *Pimelea* species of Australian rangelands. In *Poisonings by Plants, Mycotoxins and Related Toxins*; Riet-Correa, F., Pfister, J., Schild, A. L., Wierenga, T., Eds.; CABI: Wallingford, Oxfordshire, UK, 2011; pp 550−556.

(4) Silcock, R. G.; Mann, M. B. Poisonous pimeleas on inland farming lands of Queensland and New South Wales. *Trop. Grasslands* **2009**, *43*, 249−252.

(5) *Pimelea Poisoning in Cattle*; Meat and Livestock Australia: Sydney, Australia, 2006; available at http://www.mla.com.au/News-and-resources/Publication-details?pubid=2700 (accessed Jan 16, 2014).

(6) Clark, I. A. A note on the pathogenesis of St. George disease of cattle. *Aust. Vet. J.* **1971**, *47*, 285−286.

(7) Clark, I. A. St. George disease of cattle. *Aust. Vet. J.* **1971**, *47*, 123.

(8) Clark, I. A. The pathogenesis of St. George disease of cattle. *Res. Vet. Sci.* **1973**, *14*, 341−349.

(9) Kelly, W. R. The pathology and haematological changes in experimental *Pimelea* spp. poisoning in cattle ("St. George Disease"). *Aust. Vet. J.* **1975**, *51*, 233−243.

(10) McClure, T. J.; Farrow, B. R. Chronic poisoning of cattle by desert rice flower (*Pimelea simplex*) and its resemblance to St. George disease as seen in north-western New South Wales. *Aust. Vet. J.* **1971**, *47*, 100−102.

(11) Roberts, H. B.; Healy, P. J. *Pimelea simplex* and St. George disease of cattle. *Aust. Vet. J.* **1971**, *47*, 123−124.

(12) Fletcher, M. T.; Reichmann, K. G.; Brock, I. J.; McKenzie, R. A.; Blaney, B. J. Residue potential of norsesquiterpene glycosides in tissues of cattle fed Austral bracken (*Pteridium esculentum*). *J. Agric. Food Chem.* **2011**, *59*, 8518−8523.

(13) Freeman, P. W.; Ritchie, E.; Taylor, W. C. The constituents of Australian *Pimelea* spp. I. The isolation and structure of the toxin of *Pimelea simplex* and *P. trichostachya* Form B responsible for St. George disease of cattle. *Aust. J. Chem.* **1979**, *32*, 2495−2506.

(14) Oberoi, G.; D'Occhio, M. J.; Hoey, A.; Pegg, G. G. *Nux Vomica* attenuates constriction of bovine pulmonary venules induced by *Pimelea* toxins. *Clin. Exp. Pharmacol. Physiol.* **1993**, *Suppl. 1*, 53.

(15) Seawright, A. A.; Francis, J. Peliosis hepatis − a specific liver lesion in St. George disease of cattle. *Aust. Vet. J.* **1971**, *47*, 91−99.

(16) Makkar, H. P. S.; Becker, K. Are *Jatropha curcas* phorbol esters degraded by rumen microbes? *J. Sci. Food Agric.* **2010**, *90*, 1562−1565.

(17) Goel, G.; Makkar, H. P. S.; Francis, G.; Becker, K. Phorbol esters: structure, biological activity, and toxicity in animals. *Int. J. Toxicol.* **2007**, *26*, 279−288.

Figure 2. *O. kansuensis* distributed in Qinghai.

shady place after air-drying and grinding. Swainsonine was analyzed by TLC and GC-MS methods.[9] Swainsonine content was determined by gas chromatography as 0.021% by weight of the total plant. The plant was identified by the Institute of Botany (College of Life Science, Northwest A&F University).

Animals and Animal Feed. The animals and protocols used in this study were approved by the Animal Care Committee of Xi'an Jiaotong University. Sprague−Dawley rats were purchased from the Experimental Animal Center of College of Medicine, Xi'an Jiaotong University (Xi'an, China). The aerial portion of *O. kansuensis* was ground completely and sifted through a 200 mesh screen. The resulting *O. kansuensis* meal was mixed with whole feed (25% flour, 28% cornmeal, 20% soybean cake, 10% wheat bran, 10% fish meal, 1% vegetable oil, 1% yeast powder, 2% bone meal, 1% cooking salt, 1% cod-liver oil, 0.9% mineral additive, 0.1% vitamin additive)[10] to reach 15, 30, and 45% plant content (0.003, 0.006, and 0.009% swainsonine, respectively).[11] Water was then added to this mixture and stirred into 1−3 cm^3 diced mixed rations, dried for preservation.

Chemical Reagents and Apparatuses. NRNAiso Plus Total RNA Extraction kit, RT-PCR kit, and Real-Time PCR Kit were obtained from TaKaRa Bio Inc. (Dalian, China). DNA marker (Topsun, Jiangmen, China), PCR-mix (TransGen, Beijing, China), PCR primers (GenScript, Nanjing, China), EB (RUNDE, Sichuan, China), APES (Boster, Wuhan, China), DAB (Boster, Wuhan, China), IHC Antibody Diluent (Beyotime, Shanghai, China), S-P Ultra-Sensitive SAP kit (Maixin, Fuzhou, China),and primary antibody (MAN2A1, Abcam, London, UK) were obtained as noted.

Establishment of a Chronic Poisoning Model of *O. kansuensis* in SD Rats. Experiments were performed on male and female SD rats (200−220 g total body weight). After a week-long adaptation period in a room with controlled temperature (21 ± 1 °C) and lighting (12 h light/12 h dark), 24 SD rats were assigned to either a control group (complete feed) or experimental groups I (15% *O. kansuensis* containing 0.003% swainsonine), II (30% *O. kansuensis* containing 0.006% swainsonine), or III (45% *O. kansuensis* containing 0.009% swainsonine), and the 6 SD rats of each group were fed in three cages separately. All treated rats were fed for 119 days and showed neurological disorders to different degrees, which was considered to be successful establishment of a chronic poisoning model of *O. kansuensis*. All SD rats were anesthetized with ether vapor and sacrificed by decapitation. The cerebrum and cerebellum were collected and divided into two parts: one was preserved in liquid nitrogen, whereas the other was fixed in 4% paraformaldehyde.

Immunohistochemistry. Immunohistochemistry was performed according to instructions of the S-P UltraSensitive SAP kit (Maixin, Fuzhou, China). Paraformaldehyde fixed brain tissues were paraffin-embedded and sliced at 6 μm thickness onto slides. Tissue slices were deparaffinized, rehydrated, treated using microwave heat-induced epitope retrieval, and incubated in 3% hydrogen peroxide to block endogenous peroxidases with healthy nonimmune goat serum to block endogenous biotin. Subsequently, tissues were incubated in a 1:100 dilution of primary antibody for 12 h at 4 °C. A negative control slice was incubated with antibody diluent alone. Tissues were then incubated with a biotin-labeled secondary antibody for 10 min at room temperature, followed by treatment with streptavidin−peroxidase and staining by DAB. The stained tissues were observed through a light microscope, and the resulting images were analyzed using Image-Pro Plus 6.0 (Media Cybernetics).

Real-Time Quantitative PCR. PCR primers were designed by Primer 5.0. The primer sequences for MAN2A1 were as follows: forward primer, 5′-TCAGCTACCCTTCCCTCCTC-3′; reverse primer, 5′-TGCCCACCTTTGACTGTATTG-3′. The length of the PCR amplicon was 189 bp. β-Actin was used as an internal reference with primer sequences as follows: forward primer, 5′-GACAGGATG-CAGAAGGAGATTACT-3′; reverse primer, 5′-ATAGAGCCACCA-ATCCACACAG-3′. The length of the PCR amplicon was 104 bp. All primers were synthesized by GenScript Co. (Nanjing, China).

The tissues preserved in liquid nitrogen were prepared as tissue homogenate for total RNA extraction according to the manufacturer's instructions for the NRNAiso Plus kit. RT-PCR was performed following the manufacturer's instructions for the PrimeScript RT Reagent Kit with gDNA Eraser; the resulting cDNA was then used as input for real-time PCR performed as described by the manufacturer's protocol for SYBR Premix Ex *Taq*II. The reaction mixture was 1 μL of cDNA, 0.3 μL of forward primer (10 μM), 0.3 μL of reverse primer (10 μM), 7.5 μL of SYBR, premix *Ex Taq*II (2×), and ddH_2O up to 15 μL. The reaction conditions were as follows: initial denaturation for 3 min at 95 °C, followed by 40 cycles of denaturation at 94 °C for 3 s, annealing at 58 °C for 30 s, and extension at 72 °C for 30 s. After cycling, a final step was performed at 72 °C for 10 min.

Statistical Analysis. Results are expressed as the mean ± standard deviation. All data were analyzed in SPASS 18.0 using one-way analysis of variance (ANOVA) followed by Duncan's test for multiple comparisons. $P < 0.05$ was considered statistically significant.

RESULTS AND DISCUSSION

Effects of *O. kansuensis* on the Distribution and Expression of MAN2A1 in Brain Tissues of SD Rats. MAN2A1 was expressed in all areas of the brain except the molecular layer of the cerebral cortex and certain hippocampal layers (the stratum radiatum, the stratum oriens, and the molecular layer of the gyrus dentatus). The strongest expression levels were observed in the pyramidal cell layer of the cerebral cortex, the mesencephalon, the mesocephalon, the cerebellar nuclei or nerve cells of the medulla oblongata, and the Purkinje cells. The expression level of MAN2A1 in neurons is higher when compared to other cell types. Among neurons, MAN2A1 expression was strongest in cells located in the nucleus of the facial nerve and the pyramidal cell layer of the cerebral cortex, followed by Purkinje cells. The lowest expression was in the hippocampus cells. The expression of MAN2A1 decreased proportionally with increasing doses of

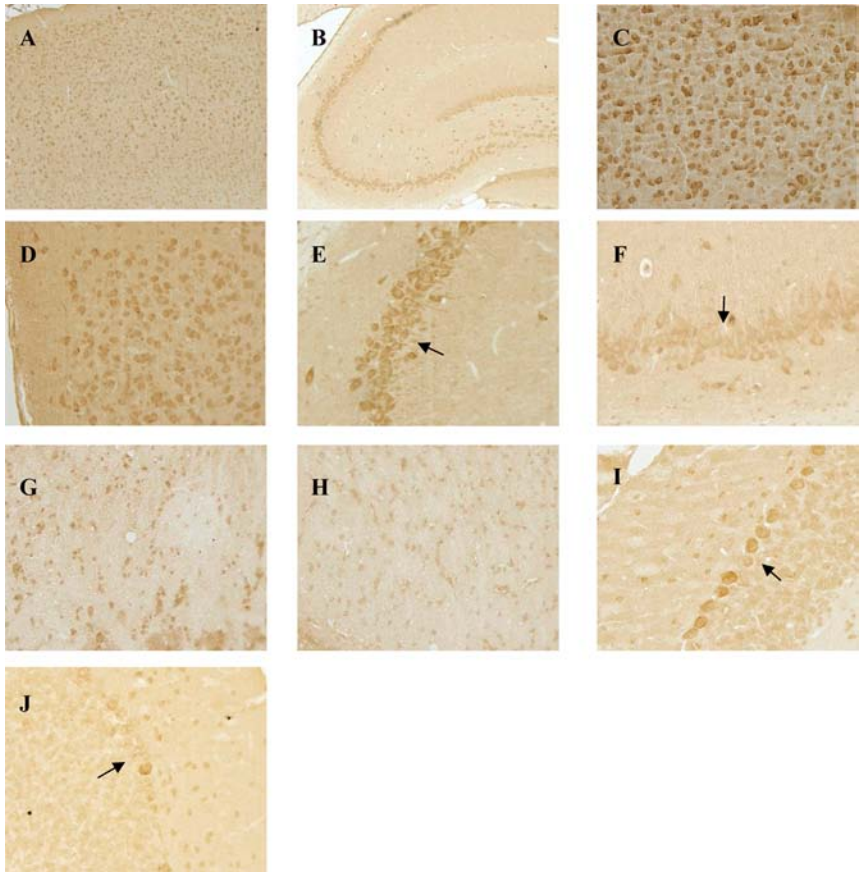

Figure 3. MAN2A1 expression in different areas of the cerebrum and cerebellum: (A) cerebral cortex in the control group (IHC × 100); (B) hippocampal formation in the control group (IHC × 100); (C) external granular cells in the control group (IHC × 400); (D) external granular cells in experimental group III (IHC × 400); (E) hippocampus of the control group (IHC × 400); (F) hippocampus of experimental group III (the arrow indicates pyramidal cells) (IHC × 400); (G) corpus callosum of the control group (IHC × 400); (H) corpus callosum of experimental group III (IHC × 400); (I) cerebellar cortex of the control group (the arrow indicates Purkinje's layer) (IHC × 400); (J) cerebellar cortex of experimental group III (some of the Purkinje cells turned pale) (IHC × 400).

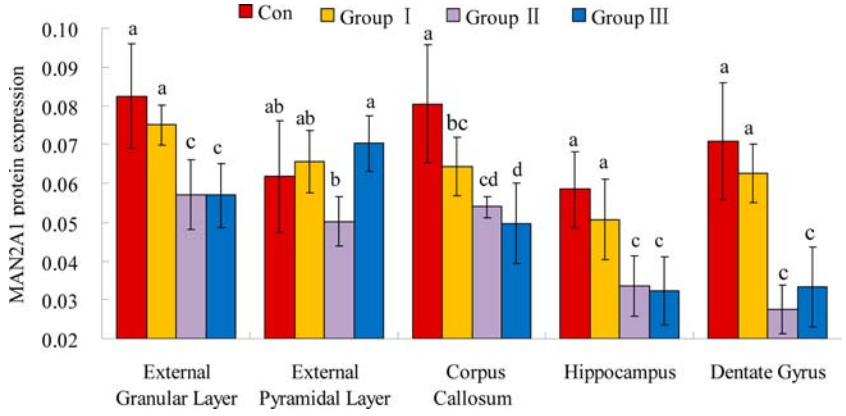

Figure 4. MAN2A1 expression in different areas of the cerebrum. MAN2A1 expression was detected in the cerebrum of SD rats by immunohistochemistry. The stained tissues were observed through a light microscope, and the resulting images were analyzed using Image-Pro Plus 6.0. Results are the mean ± SD. Identical letters denote nonsignificant deviation ($P > 0.05$); adjacents denote significant deviation ($P < 0.05$), and alternates denote extreme significance ($P < 0.01$) versus the control group.

swainsonine, and it significantly decreased in the external granular layer of the cerebral cortex, nerve cells in the hippocampus, cerebellar medulla, and molecular layer.

Expression of MAN2A1 in Different Areas of the Cerebrum. We found MAN2A1 was widely distributed in the cerebral cortex, with expression in all regions except the molecular layer (Figure 3A). It was most strongly expressed in the granular layer and the external pyramidal layer, whereas its expression was relatively weaker in the polymorphic layer. In the hippocampus, MAN2A1 was expressed most strongly in the stratum pyramidale, followed by the molecular layer; however, there was almost no expression in the hippocampal medulla, and the expression level was even lower in the dentate gyrus (Figure 3B). When the poisoning dose was increased, the

dx.doi.org/10.1021/jf501299d | J. Agric. Food Chem. 2014, 62, 7407−7412

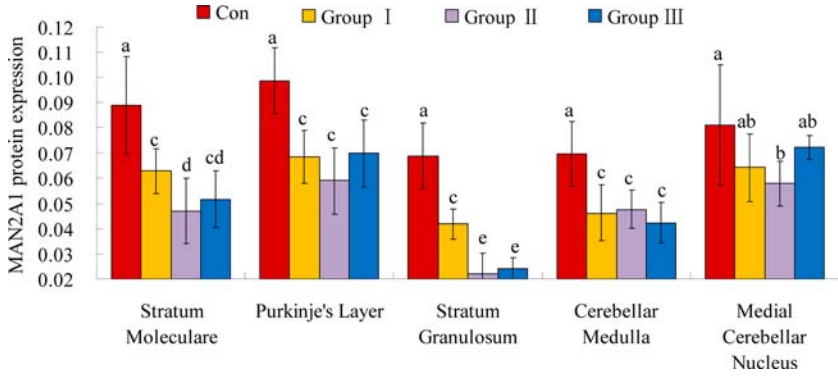

Figure 5. MAN2A1 expression in different areas of the cerebellum. MAN2A1 expression was detected in the cerebellum of SD rats by immunohistochemistry. The stained tissues were observed through a light microscope, and the resulting images were analyzed using Image-Pro Plus 6.0. Results are the mean ± SD. Identical letters denote nonsignificant deviation ($P > 0.05$); adjacents denote significant deviation ($P < 0.05$), and alternates denote extreme significance ($P < 0.01$) versus the control group.

expression of MAN2A1 decreased in the cerebrum; the decrease in expression was more obvious in the external granular layer of the cerebral cortex than in either the external pyramidal layer, ganglion cell layer, or polymorphic layer. Furthermore, the difference in expression in the polymorphic layer was more significant than that in the ganglion cell layer (Figure 3C,D). MAN2A1 was expressed at much lower levels in the hippocampus of experimental groups when compared to the control group (Figure 3E,F). MAN2A1 was more strongly and widely expressed in the corpus callosum (Figure 3G), and its expression in this region was much weaker in experimental groups when compared to the control group (Figure 3G,H).

The expression of MAN2A1 in different groups is shown in Figure 4. When compared with the control group, the expression of MAN2A1 showed a tendency to decrease in the external granular layer of the cerebral cortex in the experimental groups. The expression levels of experimental groups II and III decreased by 30.8 and 31.0%, respectively, and this difference was found to be extremely significant ($P < 0.01$). When compared with the control group, the expression of MAN2A1 in the external pyramidal layer of the cerebral cortex was 18.7% lower in experimental group II and 5.9 and 13.6% higher in experimental groups I and III, respectively. However, these differences were not significant ($P > 0.05$). The expression of MAN2A1 fell by 13.1, 42.4, and 44.8% in the hippocampus and by 11.7, 61.1, and 52.9% in the gyrus dentatus in the experimental groups, respectively. The differences between the control group and experimental groups II and III were extremely significant ($P < 0.01$), as were those between experimental group I and experimental groups II and III ($P < 0.01$). In the corpus callosum, the expression of MAN2A1 decreased by 20.1, 33.0, and 38.2% in experimental groups, respectively, and these differences were either significant or extremely significant when compared with the control group ($P < 0.05$ or $P < 0.01$) (Figure 3G,H).

Expression of MAN2A1 in Different Areas of the Cerebellum. The Purkinje cell layer had the highest expression, whereas the molecular layer and the granular layer had the lowest (Figure 3I). With increasing locoweed doses, the expression of MAN2A1 in the cerebellum decreased clearly and uniformly in the cerebellar medulla and the molecular layer, whereas in the Purkinje cell layer, parts of Purkinje cells showed decreased or complete loss of expression, but in some cells the expression level tended to increase (Figure 3I,J).

The expression of MAN2A1 of the different groups is shown in Figure 5. Upon increasing the locoweed dose, MAN2A1 expression tended to decrease in the molecular layer of the cerebellum, the Purkinje cell layer, the granular layer, and the medulla. When compared with the control group, the expression in groups I, II, and III, respectively, decreased by 30.7, 40.3, and 29.3% in the molecular layer; by 29.4, 47.2, and 42.0% in the Purkinje cell layer; by 38.9, 67.8, and 64.9% in the granular layer; and by 33.7, 31.5, and 39.0% in the medulla, and all differences were extremely significant with respect to the control group ($P < 0.01$); however, differences between experimental groups were either significant or nonsignificant ($P < 0.05$ or $P > 0.05$). The expression in the medial cerebellar nucleus of experimental groups I, II, and III dropped by 20.8, 29.9, and 10.8%, respectively, when compared with the control group; these differences were either significant or extremely significant ($P < 0.05$ or $P < 0.01$).

Effects of *O. kansuensis* on the Expression of MAN2A1 mRNA in Brain Tissues of SD Rats. *Expression of MAN2A1 mRNA in the Cerebrum.* The MAN2A1 mRNA expression showed a decreasing trend in the cerebrum of SD rats as the poisoning dose increased in experimental groups (Figure 6). When compared with the control group, MAN2A1 mRNA expression was reduced by 8.1, 11.8, and 21.3% in the cerebrum of experimental groups I, II, and III, respectively. However, these differences were not significant ($P > 0.05$).

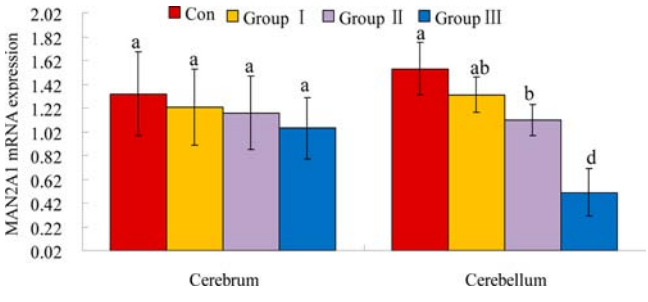

Figure 6. MAN2A1 mRNA expression in the cerebrum and cerebellum. MAN2A1 mRNA expression was measured using real-time quantitative PCR. Swainsonine treatment decreased the expression of MAN2A1 at mRNA levels. Results are the mean ± SD. Identical letters denote nonsignificant deviation ($P > 0.05$); adjacents denote significant deviation ($P < 0.05$), and alternates denote extreme significance ($P < 0.01$) versus the control group.

dx.doi.org/10.1021/jf501299d | J. Agric. Food Chem. 2014, 62, 7407−7412

Expression of MAN2A1 mRNA in the Cerebellum. Expressions of MAN2A1 mRNA also had a decreasing trend in the cerebellum of SD rats as the poisoning dose increased in experimental groups (Figure 6). When compared with the control group, MAN2A1 mRNA expression was reduced by 14.2, 27.7, and 67.1% in the cerebellum of experimental groups, respectively. The difference was not significant for experimental group I ($P > 0.05$), whereas differences were either significant or extremely significant in experimental groups II and III ($P < 0.05$ or $P < 0.01$).

MAN2A1 contains an amino acid sequence from family 38 of the glycoside hydrolases that distributes it to the Golgi apparatus, but its location within the Golgi apparatus can vary in different cell types.[12] It plays a key catalytic role during the N-glycosylation process of proteins, specifically cleaving mannose α-1,3 and α-1,6 glycosidic bonds.[13,14] Immunohistochemical staining showed that MAN2A1 is widely distributed throughout brain of SD rats, consistent with reports that N-linked glycoprotein is also widely distributed throughout the brain.[8] The expression level of MAN2A1 is variable in different kinds of cells: it is high in cells involved in information transmission and low in cells that do not participate in information transmission. These differences may due to the important role of N-linked glycoprotein in mediating signal transduction and intracellular communication.[4]

Swainsonine can specifically inhibit MAN2A1;[14] therefore, it can interfere with the glycosylation pathway, leading to abnormal N-glycosylation of proteins and effects on the processing, modification, and transport of proteins, which subsequently affect cell functions.[7,15] The results from this study clearly showed that swainsonine can inhibit the expression of MAN2A1 in external granular layer cells, stratum pyramidale cells, granular cells of the dentate gyrus, Purkinje cells in the cerebellum, and cerebellar granular cells. The hippocampus plays an important role in the process of memory formation and, when damaged, may cause dysmnesia. The Purkinje cell, originating from the cerebellar cortex, is the only neuron that can transmit the efferent impulses from the cerebellum. Its axon goes through the granular layer and white substance, reaching the cerebellar central nuclei, and plays a significant role in the motor coordination of animals.[16] Abnormal N-glycosylation may affect signal transmission and, as a result, produce clinical symptoms such as ataxia in animals. MAN2A1 mRNA levels decreased in the cerebrum and cerebellum of SD rats from experimental groups, but the absence of significant differences when compared to the control group shows that swainsonine can weakly inhibit the expression of MAN2A1 at the transcriptional level.

Swainsonine inhibited the expression of MAN2A1 in many areas of the cerebrum and cerebellum of rats, potentially causing abnormal N-glycosylation that would decrease the synthesis of complex N-linked oligosaccharides while increasing the synthesis of hybrid N-linked oligosaccharides.[17] Proteins that undergo N-glycosylation include receptors, secreted proteins, hormones, and intracellular proteins, and abnormal N-glycosylation can affect the bioactivity, folding, and location of these proteins. The complex N-linked oligosaccharide chain of glycoproteins participates in the posttranslational modification of intracellular and secreted proteins, and their inhibition can cause cellular dysfunction.[17−19] Tomoya et al.[20] found that rats that are deficient in Golgi α-mannosidase II genes die quickly during the postnatal period due to dyspnea, proving that complex N-linked oligosaccharide chains play an important role in the respiratory system of newborn animals. The effects of MAN2A1 on the CNS of animals have not been reported.

Researchers have also shown that the development and metastasis of cancer cells are related to abnormal N-glycosylation of glycoprotein on the surface of these cells. Finding an inhibitor of the key enzyme in this process has clinical significance, and MAN2A1 is one of the key enzymes in catalyzing N-glycosylation.[15] It has been reported that giving terminal cancer patients a specific inhibitor of MAN2A1, swainsonine, could inhibit tumor growth and metastasis with relatively minor side effects.[21−24] At the same time, ongoing research highlighted the search for a MAN2A1inhibitor with lower toxicity.[25,26]

mRNA is translated into polypeptide chains in the ribosome; these polypeptide chains are then folded and modified by processes such as acylation and hydroxylation in the endoplasmic reticulum. Subsequently, these chains undergo further processing, such as glycosylation and are packaged into the Golgi apparatus, before mature proteins are finally transported to the lysosome and cytomembrane or secreted as extracellular proteins.[27] If a protein is folded incorrectly, it will be degraded through the ubiquitin pathway. When compared with the control group, differences in MAN2A1 expression of the experimental group at mRNA level were not as significant as differences at the protein level. This may be due to the abnormal metabolism and processing of glycoproteins after swainsonine poisoning, which can affect the translation and posttranslational modification of MAN2A1, ultimately leading to MAN2A1 being degraded because it cannot mature or is incorrectly folded. Furthermore, the differences could also be due to how much swainsonine each cell type is exposed to.

In this study, the influence of swainsonine on the expression of MAN2A1 in the cerebrum is not as significant as in the cerebellum. These data are consistent with the fact that clinical signs in poisoned rats are characterized by dyskinesia. Our results further demonstrate the inhibition of MAN2A1 by swainsonine in SD rats and provide experimental evidence for the underlying neurotoxicological mechanism of swainsonine.

AUTHOR INFORMATION

Corresponding Author

*(B.Z.) Phone: +86 29 87092429. Fax: +86 29 87091032. E-mail: zhaobaoyu12005@163.com.

Funding

This work was cofinanced by grants from the National Natural Science Foundation (Grants 31072175, 31201958), the Ph.D. Programs Foundation of Ministry of Education of China (Grant 20100204120018), and the Special Scientific Research Fund of Agriculture Public Welfare industry (Grant 201203062).

Notes

The authors declare no competing financial interest.

REFERENCES

(1) Zhang, S. M.; Gao, Q. D.; Hou, D. H.; Li, O.; Chen, J. M.; Zhu, X. W. *O. kansuensis* Bunge intoxication. *Acta. Vet. Zootech. Sinica* **1981**, *12*, 145−149.

(2) Wu, D.; Liang, B.; Shi, Y. P.; Wang, J. H. Research progress on *Oxytropis kansuensis* Bunge. *China Herbivores* **2003**, *1*, 37−39.

(3) Zhao, B. Y. *The Systematic Analysis and Toxic Comparative Pathology Research of Locoweed (Oxytropis kansuensis) Alkaloid Composition*. Ph.D. thesis, Northwest A&F University, Yangling, Shaanxi, China, 2001.

(4) Hueza, I. M.; Gorniak, S. L. The immunomodulatory effects of *Ipomoea carnea* in rats vary depending on life stage. *Hum. Exp. Toxicol.* **2011**, *30*, 1690−1700.
(5) Cholich, L. A.; Gimeno, E. J.; Teibler, P. G.; Jorge, N. L.; Acosta de Perez, O. C. The guinea pig as an animal model for *Ipomoea carnea* induced α-mannosidosis. *Toxicon* **2009**, *54*, 276−282.
(6) Douglas, A.; Kuntz, D.; Shinichi, N.; Kayla, S.; Hitoshi, H.; Yoshihiro, U.; Hideko, N.; David, R. R. Structural investigation of the binding of 5-substituted swainsonine analogues to Golgi α-mannosidase II. *ChemBioChem* **2010**, *5*, 673−680.
(7) Stegelmeier, B. L.; Molyneux, R. J.; Elbein, A. D.; James, L. F. The lesions of locoweed (*Astragalus mollissimus*), swainsonine, and castanospermine in rats. *Vet. Pathol.* **1995**, *2*, 289−298.
(8) Tulsiani, D. R.; Broquist, H. P.; James, L. F.; Touster, O. Production of hybrid glycoproteins and accumulation of oligosaccharides in the brain of sheep and pigs administered swainsonine or locoweed. *Arch. Biochem. Biophys.* **1988**, *2*, 607−617.
(9) Lu, H.; Wang, S. S.; Zhao, B. Y. Isolation and identification of swainsonine from *Oxytropis glabra* and its pathological lesions to SD rats. *Asian J. Anim. Vet. Adv.* **2012**, *7*, 822−831.
(10) Sun, Y. F.; Bai, D. C.; Zhang, W. H. *Laboratory Animal Science*; Zhengzhou University Press: Zhengzhou, China, 1998; pp 33−34.
(11) Shi, Z. C. *Important Poisonous Plants of China Grassland*; China Agriculture Press: Beijing, China, 1997; pp 49−50.
(12) Cobucci-Ponzano, B.; Conte, F.; Strazzulli, A.; Capasso, C.; Fiume, I.; Pocsfalvi, G.; Rossi, M.; Moracci, M. The molecular characterization of a novel GH38 α-mannosidase from the crenarchaeon *Sulfolobus solfataricus* revealed its ability in demannosylating glycoproteins. *Biochimie* **2010**, *12*, 1895−1907.
(13) Velasco, A.; Hendricks, L.; Moremen, K. W.; Tulsiani, D. R. P.; Touster, O.; Farquhar, M. G. Cell-type dependent variations in the subcellular distribution of α-mannosidase IA and II. *J. Cell. Biol.* **1993**, *122*, 39−51.
(14) Young, W. W. Organization of Golgi glycosyltransferases in membranes: complexity via complexes. *J. Membr. Biol.* **2004**, *1*, 1−13.
(15) Yang, Y. Y.; Li, Y. Q.; Yi, Y. F.; He, T. T.; Xiao, Z. Significance of Golgi α-mannosidases II, E-cadherin, galectin-3 expression and their correlation in human gastric carcinoma. *J. Chongqing Med. Univ.* **2010**, *9*, 1313−1317.
(16) Zhu, C. G. *Neuroanatomy*, 2nd ed.; People's Medical Press: Beijing, China, 2009; pp 473−556.
(17) Chui, D.; Sellakumar, G.; Green, R.; Sutton-Smith, M.; McQuistan, M. T.; Morris, W. K.; Dell, R. H.; Marth, A. Genetic remodeling of protein glycosylation in vivo induces autoimmune disease. *Proc. Natl. Acad. Sci. U.S.A.* **2001**, *3*, 1142−1147.
(18) William, G. D.; James, E. R. Compartmentation of asparagine-linked oligosaccharide processing in the Golgi apparatus. *J. Cell. Biol.* **1983**, *97*, 270−275.
(19) Moremen, K. W. Golgi α-mannosidase II deficiency in vertebrate systems: implications for asparagine-linked oligosaccharide processing in mammals. *Biochim. Biophys. Acta−-Biomembranes* **2002**, *3*, 225−235.
(20) Tomoya, O. A.; Michiko, N. F. Processing enzymes involved in N-glycan biosynthesis and related genes: the Golgi N-glycan processing α-mannosidase II and α-mannosidase II. *Exp. Glycosci.* **2008**, Part 1, Section IV, 111−114.
(21) Dennis, J. W.; Laferte, S. Recognition of asparagine-linked oligosaccharides on murine tumor cells by natural killer cells. *Cancer Res.* **1985**, *45*, 6034−6040.
(22) Kiyohara, T.; Dennis, J. W.; Roder, J. C. Double restriction in NK cell recognition is linked to transmethylation and can be triggered by asparagine-linked oligosaccharides on tumor cells. *Cell. Immunol.* **1987**, *106*, 223−233.
(23) Goss, P. E.; Baker, M. A.; Carver, J. P.; Dennis, J. W. Inhibitors of carbohydrate processing: a new class of anticancer agents. *Clin. Cancer Res.* **1995**, *1*, 935−944.
(24) Goss, P. E.; Reid, C. L.; Bailey, D.; Dennis, J. W. Phase IB clinical trial of the oligosaccharide processing inhibitor swainsonine in patients with advanced malignancies. *Clin. Cancer Res.* **1997**, *3*, 1077−1086.
(25) Poláková, M.; Šesták, S.; Lattová, E.; Petruša, L.; Muchaa, J.; Tvaroškaa, I.; Kóňa, J. α-D-Mannose derivatives as models designed for selective inhibition of Golgi α-mannosidase II. *Eur. J. Med. Chem.* **2011**, *3*, 944−952.
(26) Gerber-Lemaire, S.; Juillerat-Jeanneret, L. Studies toward new anti-cancer strategies based on α-mannosidase inhibition. *Chimia* **2010**, *9*, 634−639.
(27) Zhai, Z. H.; Wang, X. Z.; Ding, M. X. *Cell Biology*, 3rd ed.; Higher Education Press: Beijing, China, 2007; pp 200−205.

Gross and Histopathology. SHNW1−3 and SHNW7−10 were subjected to necropsy within 12 h of death at the Veterinary Diagnostic Laboratory, University of Adelaide. Representative tissues were collected and fixed in 10% neutral buffered formalin or frozen for storage and future analysis. Tissues fixed in 10% neutral buffered formalin were routinely processed for examination by light microscopy.[5]

Haematology, Serum Biochemistry, and Urinalysis. Blood samples were analyzed within 24 h of collection. Hematological analysis was conducted on EDTA whole blood, using a Cell Dyne 3500 automated analyzer (Abbott Diagnostics, Abbott Park, IL, USA). Blood films were made from EDTA-preserved whole blood, stained with a Wright−Giemsa stain using a Hema-tek Slide Stainer (Ames Division of Miles Laboratories, Elkhart, IN, USA), and examined under light microscopy for WBC differential counts and morphological evaluation. Biochemical analysis was performed using extracted serum samples in a Beckman Coulter AU480 (Beckman Coulter, Brea, CA, USA) analyzer.

Plant Material for Analysis. *Heliotropium europaeum* samples were collected from a paddock where affected wombats had been found approximately 10 km southwest of Blanchetown in South Australia. Field-collected plant material was transported to the laboratory, where the material was freeze-dried, milled, and stored frozen at −20 °C prior to analysis. A separate pressed mature plant sample was submitted for species identification by the State Herbarium of South Australia and confirmed as *H. europaeum* (Voucher AD255584).

Plant, Gastrointestinal, and Fecal Toxicology. Milled plant material (2 g) was extracted to provide both a free pyrrolizidine alkaloid extract and a total alkaloid extract (after Zn reduction of pyrrolizidine alkaloid *N*-oxides) as previously described.[6] Pyrrolizidine alkaloid analysis was conducted by GC-MS on a 30 m × 0.25 mm i.d. HP-5MS column (Agilent Technologies) with retrorsine added as an internal standard. Retention indices for each alkaloid were calculated with respect to co-injected standard hydrocarbons[6] and are slightly greater than those measured on a similar DB-5MS column, but with similar relative retention order. Individual alkaloids were identified by comparison of mass spectra and retention index with a laboratory mass spectra database and literature data.

Fecal and gastrointestinal contents from SHNW7−10 were collected during necropsy examinations. Samples were also freeze-dried, milled, and similarly analyzed by GC-MS for pyrrolizidine alkaloids. Initial analysis indicated negligible alkaloids were present, and sample extracts were concentrated 20-fold and reanalyzed.

RESULTS AND DISCUSSION

Gross Pathology and Histopathology. Most significant pathological findings were identified in the three juvenile female wombats (SHNW1−3). Wombats were jaundiced, in poor to emaciated body condition, and had extensive patchy to diffuse hair loss over the dorsal and lateral body walls and head. Elevation of total bilirubin in either the blood or urine was present in two wombats. Grossly, the livers of all animals were decreased in size with scalloped lobar borders, orange-yellow, and firm on palpation and had an enhanced lobular pattern, and one liver (SHNW1) had multifocal white foci <2 mm in diameter over the capsular and cut surfaces. In SHNW3, the gall bladder walls were thickened and inflamed. SHNW7−10 were adult female wombats in poor to emaciated body condition with extensive bilaterally symmetrical patchy alopecia and dermatitis.

Histologically, a spectrum of changes was observed in the livers of juvenile female wombats (SHNW1−3) including marked and often atypical ductular proliferation and disrupted sinusoidal architecture (Figure 1A), hepatocellular megalocytosis and multinucleation (Figure 1B), cholestasis, periportal and bridging hepatic fibrosis, nodular regeneration, multifocal

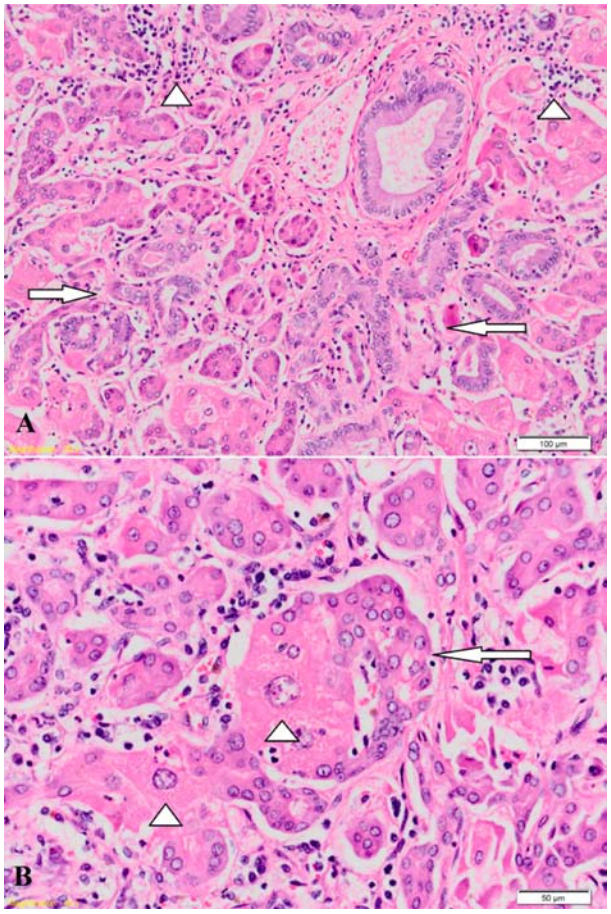

Figure 1. (A) Atypical ductular proliferation (arrows) and markedly disrupted sinusoidal architecture observed in the livers of affected wombats (SHNW1). Lymphomonocytic infiltrates (arrowheads) were seen in periportal regions in some sections. (B) Hepatocellular multinucleation (arrow), megalocytosis (arrowheads), anisocytosis (variation in cell size), and anisokaryosis (variation in nuclear size), frequent abnormalities in wombat livers (SHNW1).

necrosuppurative hepatitis, and lymphomononuclear infiltrates. Hepatocellular degeneration and necrosis, megalocytosis, bile ductile proliferation, nodular regeneration, and portal fibrosis are features of pyrrolizidine alkaloid toxicity.[7−10] Toxic hepatopathies associated with the grazing of toxic weeds have not been reported in wombats previously; however, they are well characterized in domestic grazing species such as the cow, sheep, and horse.[4,8,11,12] Both acute and chronic forms of pyrrolizidine alkaloid toxicosis can occur in animals, often reflecting variation in species susceptibility to toxic effects[8,13] as well as chemotype of plant ingested. Cattle, horses, pigs, chickens, ducks, rats, and mice are susceptible to pyrrolizidine alkaloid intoxication, whereas sheep, goats, rabbits, and guinea pigs are relatively resistant to toxicity.[12,14−17] The susceptibility of the wombat to toxic alkaloids relative to other species is uncertain. In other marsupial species, hepatic lesions typical of pyrrolizidine alkaloid toxicity have been reported in red kangaroos from free-ranging regions in which pyrrolizidine alkaloid-containing plants occur, and hepatotoxicity and secondary photosensitization have been reported in captive red kangaroos following ingestion of *Lantana camara*.[18,19] Hepatosis in pygmy possums has circumstantially been related to the feeding of honey from regions with heavy ragwort (*Senecio jacobea*) infestations.[20]

In SHNW1 and SHNW2 there was severe bilaterally symmetrical exudative and necrohemorrhagic dermatitis of facial extremities and sun-exposed alopecic dorsal and lateral body skin. Histologically, skin lesions were characterized by vascular degeneration, hemorrhage, thrombosis, and infarction in the superficial layers of sun-exposed skin. Eyelid and ear lesions were characterized by locally extensive exudative necrosuppurative and hemorrhagic dermatitis with superficial vascular degeneration, thrombosis, and infarction. Features that support hepatogenous photosensitization as the underlying cause of these skin lesions include the distribution of lesions (dorsal and lateral body wall, eyelids, and ears, with sparing of ventral abdomen and medial aspects of legs), superficial vascular degeneration, hemorrhage, thrombosis, infarction restricted to superficial layers of sun-exposed skin, and the presence of a severe cholestatic hepatopathy in both wombats.[21−24] Significant hair loss and pigmentary incontinence in skin from these animals in conjunction with unusual diurnal grazing habits may have rendered them more susceptible to photosensitization and solar skin damage (superficial dermal sclerosis).

Clinical Pathology. Clinicopathological data were available for two live juvenile and one adult female wombats (SHNW4−6) and from antemortem samples collected from a juvenile wombat subjected to necropsy examination (SHNW3). SHNW4−6 were in thin or emaciated body condition with patchy bilaterally symmetrical noninflammatory alopecia. Serum biochemical analysis in SHNW3−6 identified elevated hepatocellular leakage enzymes (GLDH, AST) and/or hepatobiliary enzymes (GGT, ALP). Elevations in hepatic leakage (cytosolic) enzymes GLDH and AST suggest either sublethal or lethal hepatocyte damage, and elevations in hepatobillary liver enzymes GGT and ALP are induced enzymes suggestive of inflammation or irritation within the hepatobiliary tree and/or intra- or extrahepatic cholestasis.[25,26] Similar patterns of hepatic enzyme elevations are observed in horses and ruminants with pyrrolizidine alkaloid toxicity.[12,13,27] Elevated total bilirubin was seen in antemortem blood samples collected from SHNW3, consistent with jaundice and intrahepatic cholestasis observed post-mortem.

Hematological analysis identified a moderate poorly regenerative (normocytic normochromic) anemia in the three juvenile wombats (SHNW3−5) and leukocytosis characterized by a mature neutrophilia in SHNW3. The normocytic normochromic nonregenerative anemia observed was typical of findings seen in malnourished free-ranging wombats during drought conditions[28,29] and with starvation or malnutrition in domestic animal species.[30]

Habitat Botanical Survey. Botanical surveys of habitat from where affected wombats were found revealed a scarcity of native grasses and invasion by introduced weed species with a dominance of and sometimes monoculture of onion weed (*Asphodelus fistulosus*), with lesser Wards weed (*Carrichtera annua*) and horehound (*Marrubium vulgare*). *Echium* spp. and *Heliotropium europaeum* were also present, sometimes in close proximity to wombat warrens. Southern hairy-nosed wombats are herbivorous, feeding mostly on native grasses (*Austrastipa*, *Poa* spp.), fresh shoots, and bulbs when available[31,32] and will also graze introduced grasses and sedges.[33] They will dig up grass and plant roots and eat bulbs if vegetative sources are not available, particularly during drought. A scarcity of wombat-preferred herbivory and predominance of poorly palatable introduced weed species in areas of the Murraylands in which affected wombats were found likely contributed to their poor body condition and health status, as well as their tendency toward consumption of toxic weeds.

Plant, Gastrointestinal, and Fecal Toxicology. Toxicological analysis performed on scats and gastrointestinal contents from wombats from habitat in which affected wombats were found (SHNW7−10) identified a number of toxic alkaloids consistent with ingestion of *H. europaeum*. Plant material collected in March 2012 (autumn) at the site from which affected wombats were identified was confirmed as *H. europaeum* by State Herbarium of South Australia Voucher AD255584. The plant sample was freeze-dried, milled, and analyzed for pyrrolizidine alkaloids by GC-MS with individual alkaloids, **1**−**5** (Figure 2), identified by comparison of retention index (RI) and mass spectra.[34−36] Pyrrolizidine alkaloids can occur as either the free alkaloids or the *N*-oxides, with the latter not detected by GC-MS analysis unless chemically reduced to the free alkaloid prior to analysis. GC-MS analysis of the plant extract with and without zinc reduction thus enables the alkaloid content of both free alkaloids and total alkaloids to be determined.[6]

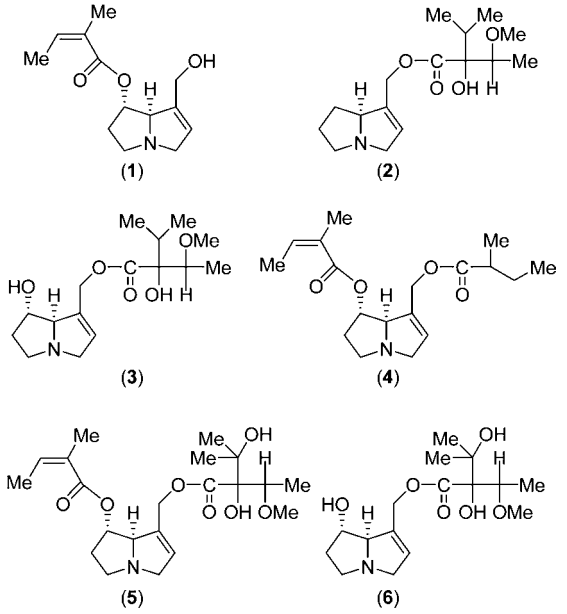

Figure 2. Pyrrolizidine alkaloids identified in plant and animal extracts: 7-angeloylheliotridine (**1**), heleurine (**2**), heliotrine (**3**), 7-angeloyl-9-(2-methylbutyryl)heliotridine (**4**), lasiocarpine (**5**), and europine (**6**).

Alkaloids present were identified as lasiocarpine, **5** (RI 2652, M^+ 411), and 7-angeloyl-9-(2-methylbutyryl)heliotridine, **4** (RI 2258, M^+ 321), with lesser amounts of 7-angeloylheliotridine, **1** (RI 1888, M^+ 237), heleurine, **2** (RI 2036, M^+ 297), heliotrine, **3** (RI 2198, M^+ 313), and three further components tentatively identified as heliotridine diesters, with all alkaloids present predominantly as free alkaloids. Mass spectra were consistent with depicted structures and with previously reported data for 7-angeloylheliotridine, **1**,[34,36] heliotrine, **3**,[35,36] 7-angeloyl-9-(2-methylbutyryl)heliotridine, **4**,[34] and lasiocarpine, **5**.[35,36] It is not possible to definitively distinguish between retronecine/heliotridine isomers from mass spectra,[36] but on biosynthetic grounds alkaloids **1** and **4** are assumed to be heliotridine alkaloids. This analysis contrasts with previous analysis of *H. europaeum* in which europine, heliotrine, and lasiocarpine were major alkaloids with lesser amounts of heleurine and supinine,

with all alkaloids present primarily as *N*-oxides.[37] These authors noted wide variations in this species between site, sampling periods, and following rainfall, but none as markedly different as seen in AD255584, which may represent a different chemotype of this plant species. Neither 7-angeloylheliotridine, **1**, nor 7-angeloyl-9-(2-methylbutyryl)heliotridine, **4**, has previously been reported in *H. europaeum*. Both alkaloids, **1** and **4**, have however been reported as components of *Cynoglossum officinale* and *Cynoglossum amabile* within the same family, Boraginaceae.[34] Trace amounts of lasiocarpine, **5**, and 7-angeloyl-9-(2-methylbutyryl)heliotridine, **4**, were also detected in three of four wombat fecal samples collected from the same location as *H. europeaum* AD255584.

Stomach, small intestinal, colonic, and/or fecal contents collected from four wombats (SHNW7−10) from a different site, euthanized in April 2012 (autumn), were also analyzed for pyrrolizidine alkaloids (Table 1). Concentrated extracts of the stomach contents from two wombats (SHNW8 and SHNW9) showed lasiocarpine, **5**, heliotrine, **3**, europine, **6**, and heleurine, **2**. Levels of alkaloids were too low to be quantitated (LOQ = 1 μg/g), but relative amounts are shown in Table 1. Alkaloids were identified from background-subtracted mass spectra and retention index, which provided good matches with mass spectra from plant extracts, match quality 90 or better. Europine, **6** (RI 2327, M^+ 329), was identified by comparison with literature mass spectra.[35] In each of SHNW8 and SHNW9, alkaloids were predominantly present in the zinc-reduced extracts, indicating the presence of *N*-oxides rather than free alkaloids in these stomach contents. This alkaloid profile is more consistent with previously reported analyses of *H. europaeum* plant material[37] and with previous unpublished analysis of this species in our laboratory. Intestinal and colonic contents from SHNW10 contained europine, **6**, with lesser amounts of other alkaloids. Feces from this animal contained europine, **6**, with negligible amounts of other alkaloids. Europine, **6**, was present in both free and reduced extracts, indicating the presence of the free alkaloid in the fecal sample. Alkaloids **1**−**6** are all 1,2-dehydropyrrolizidine ester alkaloids (dehydroPAs) and as such have the requisite structure to be metabolized to hepatotoxic intermediates.[38] Only alkaloids with this 1,2-dehydro bond are hepatotoxic.

Table 1. Relative Presence of Heleurine, Heliotrine, Europine, and Lasiocarpine as Free and Total Alkaloids As Measured by GC-MS Analysis of Wombat Gastrointestinal Samples[a]

	heleurine (2)		heliotrine (3)		lasiocarpine (5)		europine (6)	
	free	total	free	total	free	total	free	total
SHNW7 SC	−	−	−	−	−	−	−	−
SHNW8 SC	−	+	−	+++	+	+++	+	++
SHNW9 SC	−	+	−	+++	+	++	−	+++
SHNW10 FC	−	−	−	+	−	−	+++	+++
SHNW10 IC	−	−	−	−	−	−	−	+
SHNW10 CC	−	−	−	+	−	+	+	++

[a]SC, stomach contents; F, fecal contents; IC, intestinal contents; CC, colon contents.

Managing the Risk to Wombat Populations. *H. europaeum* (also known as common heliotrope or potato weed) is a summer-growing annual with widespread prevalence in southeastern Australia. Through this study and additional work we have observed a distinct bias toward hepatotoxicity occurring more frequently in juvenile wombats. Although this weed is generally unpalatable, ingestion may have occurred in these juvenile animals due to decreased availability of preferred forages in the severely degraded habitat in which these animals were found and due to the emergence of weeds around the time of weaning of naive animals. Furthermore, it has been shown elsewhere that young of other animal species exhibit higher susceptibility to the toxic effects of pyrrolizidine alkaloids than do adults;[10,12] therefore, similar mechanisms for susceptibility may also exist in wombats.

There is clear evidence that the wombats are consuming *H. europaeum*. There is wide variation in the alkaloid profile of this introduced heliotrope species, but whether the alkaloid profile looks like that reported here in AD255584 or that detected in the stomach contents of SHNW8 and SHNW9, it would make little difference to toxicity. Both free alkaloids and *N*-oxides are hepatotoxic if consumed, with *N*-oxides reduced to free alkaloids in the gut. Individual alkaloids have differing toxicity with lasioscarpine > heliotrine > europine,[37] but, regardless, all are hepatotoxic; consequently, if wombats are consuming this plant species, it may well be responsible for the observed toxicosis.

Hepatotoxicity due to ingestion of a pyrrolizidine alkaloid-containing plant in juvenile Murraylands wombats is supported by characteristic histopathological changes in the liver, detection of pyrrolizidine alkaloid-containing plants during botanical surveys, and gastrointestinal toxicology performed on wombats from the same habitat. Habitat degradation leading to malnutrition and ingestion of weed species is a significant welfare issue in the Murraylands southern hairy-nosed wombats. It appears that ingestion of *H. europaeum* is the most likely cause of the observed hepatotoxicity in juvenile wombats; however, the contribution of other weeds with known or proposed hepatotoxicity such as *Carrichtera annua* and *Echium* spp. is presently unknown. It is not known whether wombats will graze *Echium*, and although found during botanical surveys of affected habitat, it was noted to be less prevalent than *H. europaeum*. However, as toxic *Echium* spp. contain pyrrolizidine alkaloids and therefore have a similar mechanism of action to *H. europaeum*,[4] it cannot be excluded as a contributor to hepatotoxicity in wombats. The toxic principles in *C. annua*, or Wards weed, are unknown, but thought to be glucosinolates.[4] Hepatic lesions have been observed in cattle thought to have died following ingestion of *C. annua*;[39] therefore, contribution of this plant to hepatotoxicity in wombats cannot be definitely excluded either. Exposure to such a number of weeds containing toxic principles (*H. europaeum*, *Echium* spp., *C. annua*, and also *Asphodelus* spp.) has significant welfare implications for the animals that inhabit this degraded habitat, and the full spectrum of adverse effects in wombats due to ingestion of toxic plants may be broader than currently appreciated.

Due to the often close interaction between agricultural enterprises and wildlife, the findings of this study have implications for the management of both conservation areas and agricultural land. The habitat described in this study was previously a livestock grazing enterprise, in which wombats had coexisted with livestock. Loss of preferred forage, weed overgrowth, and health problems in wombats attributable to habitat degradation arose soon after the land was destocked and land management practices abandoned, highlighting the need for consideration of the impact that changes in agricultural

management may have on native species that coexist in the region. Future research directions focus on the clarification of underlying ecological and land management factors that have led to these problems in Murraylands southern hairy-nosed wombats, as well as the best methods to manage and prevent this problem becoming more widespread.

AUTHOR INFORMATION

Corresponding Author

*(L.W.) Phone: +61 8 313 7632. E-mail: lucy.woolford@adelaide.edu.au.

Funding

This study was funded by a grant from the Nature Foundation of South Australia.

Notes

The authors declare no competing financial interest.

ACKNOWLEDGMENTS

We extend our gratitude to Benita Dillon, Mike Greig, Fiona Fuhlbohm, Greg Drogemuller, and Ellen Ryan-Colton of the Department of Environment, Water and Natural Resources (South Australia); Chien Cao of Queensland Department of Agriculture, Fisheries and Forestry; Brigitte Stevens and all staff at the Wombat Awareness Organisation; Dr. David Taggart, Ron Dibbin and family, and Jessica Strauss of Ecoknowledge; Conservation Volunteers Australia and Brookfield Conservation Reserve; Nature Foundation SA; the Natural History Society of South Australia; and the Murraylands Local Action Planning group.

ABBREVIATIONS USED

ALT, alanine aminotransferase; ALP, alkaline phosphatase; AST, aspartate aminotransferase; GGT, γ-glutamyl transferase; GLDH, glutamate dehydrogenase

REFERENCES

(1) Taggart, D. A.; Robinson, T. *Lasiorhinus latifrons*; International Union for Conservation of Nature: Gland, Switzerland, 2008.

(2) Taggart, D. A.; Temple-Smith, P. D. Southern hairy-nosed wombat: *Lasiorhinus latifrons*. In *Mammals of Australia*; Van Dyck, S., Strahan, R., Eds.; Reed New Holland: Sydney, Australia, 2008.

(3) Woolford, L.; Dillon, B.; Boardman, W. *NFSA Grant Report: Investigating the Causes of a Newly Emerging Disease Syndrome (Alopecia, Weight Loss and Mortality) in Southern Hairy-Nosed Wombats (Lasiorhinus latifrons) in the Murraylands District of South Australia*; University of Adelaide: Roseworthy, SA, Australia, 2012.

(4) McKenzie, R. *Australia's Poisonous Plants, Fungi and Cyanobacteria: A Guide to Species of Medical and Veterinary Importance*; CSIRO Publishing: Collingwood, VIC, Australia, 2012.

(5) Bancroft, J. D.; Gamble, M. *Theory and Practice of Histological Techniques*, 6th ed.; Churchill Livingstone Elsevier: Philadelphia, PA, USA, 2008.

(6) Fletcher, M. T.; McKenzie, R. A.; Blaney, B. J.; Reichmann, K. G. Pyrrolizidine alkaloids in *Crotalaria taxa* from northern Australia: risk to grazing livestock. *J. Agric. Food Chem.* **2009**, *57*, 311−319.

(7) Mattocks, A. R. *Chemistry and Toxicology of Pyrrolizidine Alkaloids*; Academic Press: London, UK, 1986.

(8) Stalker, M. J.; Hayes, M. A. Liver and biliary system. In *Jubb, Kennedy and Palmer's Pathology of Domestic Animals*; Maxie, M. G., Ed.; Elsevier: Philadelphia, PA, USA, 2007; Vol. 2, pp 297−388.

(9) Bull, L. B.; Culvenor, C. C.; Dick, A. J. *The Pyrrolizidine Alkaloids. Their Chemistry, Pathogenicity and Other Biological Properties*; North-Holland: Amsterdam, The Netherlandds, 1968; Vol. 9.

(10) Fu, P. P.; Xia, Q.; Lin, G.; Chou, M. W. Pyrrolizidine alkaloids—genotoxicity, metabolism enzymes, metabolic activation, and mechanisms. *Drug Metab. Rev.* **2004**, *36*, 1−55.

(11) Seaman, J. T. Pyrrolizidine alkaloid poisoning of horses. *Aust. Vet. J.* **1978**, *54*, 150.

(12) Stegelmeier, B. L. Pyrrolizidine alkaloid−containing toxic plants (*Senecio*, *Crotalaria*, *Cynoglossum*, *Amsinckia*, *Heliotropium*, and *Echium* spp.). *Vet. Clin. North Am. Food Anim. Pract.* **2011**, *27*, 419−428.

(13) Craig, A. M.; Pearson, E. G.; Meyer, C.; Schmitz, J. A. Clinicopathologic studies of tansy ragwort toxicosis in ponies: sequential serum and histopathological changes. *J. Equine Vet. Sci.* **1991**, *11*, 261−271.

(14) Castagnoli, N., Jr.; Rimoldi, J. M.; Bloomquist, J.; Castagnoli, K. P. Potential metabolic bioactivation pathways involving cyclic tertiary amines and azaarenes. *Chem. Res. Toxicol.* **1997**, *10*, 924−940.

(15) Huan, J. Y.; Miranda, C. L.; Buhler, D. R.; Cheeke, P. R. Species differences in the hepatic microsomal enzyme metabolism of the pyrrolizidine alkaloids. *Toxicol. Lett.* **1998**, *99*, 127−137.

(16) Stegelmeier, B. L.; Edgar, J. A.; Colegate, S. M.; Gardner, D. R.; Schoch, T. K.; Coulombe, R. A.; Molyneux, R. J. Pyrrolizidine alkaloid plants, metabolism and toxicity. *J. Nat. Toxins* **1999**, *8*, 95−116.

(17) White, I. N.; Mattocks, A. R.; Butler, W. H. The conversion of the pyrrolizidine alkaloid retrorsine to pyrrolic derivatives in vivo and in vitro and its acute toxicity to various animal species. *Chem.−Biol. Interact.* **1973**, *6*, 207−218.

(18) Johnson, H.; Jensen, J. M. Hepatotoxicity and secondary photosensitisation in a red kangaroo (*Megaleia rufus*) due to ingestion of *Lantana camara*. *J. Zoo Wildlife Med.* **1998**, *29*, 203−207.

(19) Ladds, P. *Pathology of Australian Native Wildlife*, 1st ed.; CSIRO Publishing: Melbourne, Australia, 2009.

(20) Munday, B. L., Marsupial diseases. In *Proceedings 104 Australian Wildlife. Refresher Course for Veterinarians*; Post Graduate Foundation in Veterinary Science, University of Sydney: Sydney, Australia, 1988.

(21) Rowe, L. D. Photosensitization problems in livestock. *Vet. Clin. North Am. Food Anim. Pract.* **1989**, *5*, 301−23.

(22) Scott, D. W.; Miller, W. H.; Griffin, C. E., Nutritional skin diseases. In *Muller & Kirk's Small Animal Dermatology*, 6th ed.; Elsevier: Philadelphia, PA, USA, 2001.

(23) Stegelmeier, B. L. Equine photosensitization. *Clin. Tech. Equine Prac.* **2002**, *1*, 81.

(24) Maxie, M. G.; Robinson, W. F. Cardiovascular system. In *Jubb, Kennedy and Palmer's Pathology of Domestic Animals*, 5th ed.; Maxie, M. G., Ed.; Elsevier: Philadelphia, PA, USA, 2007; Vol. 1.

(25) Stockham, S. L.; Scott, M. A. *Fundamentals of Veterinary Clinical Pathology*; Blackwell Publishing: Ames, IA, USA, 2008.

(26) Bain, P. J. Liver. In *Duncan & Prasse's Veterinary Laboratory Medicine: Clinical Pathology*, 5th ed.; Latimer, K. S., Ed. Wiley-Blackwell: Chichester, UK, 2011.

(27) Curran, J. M.; Sutherland, R. J.; Peet, R. L. A screening test for subclinical liver disease in horses affected by pyrrolizidine alkaloid toxicosis. *Aust. Vet. J.* **1996**, *74*, 236−240.

(28) Gaughwin, M. D.; Judson, G. J.; Macfarlane, W. V.; Siebert, B. D. Effect of drought on the health of wild hairy-nosed wombats, *Lasiorhinus latifrons*. *Aust. Wildlife Res.* **1984**, *11*, 455−463.

(29) Gaughwin, M. D.; Judson, G. J. Haematology and clinical-chemistry of hairy nosed wombats (*Lasiorhinus latifrons*). *J. Wildlife Dis.* **1980**, *16*, 275.

(30) Valli, V. E. O. Hematopoietic system. In *Jubb, Kennedy and Palmer's Pathology of Domestic Animals*; Maxie, M. G., Ed.; Elsevier: Philadelphia, PA, USA, 2007; Vol. 3, pp 107−324.

(31) St John, B. J.; Saunders, G. M. *Plan of Management for the Hairy-Nosed Wombat (Lasiorhinus latifrons) in South Australia*; National Parks and Wildlife Service SA: Adelaide, SA, Australia, 1989.

(32) Wells, R. T. Vombatidae. In *Fauna of Australia*; Walton, D. W., Richardson, B. J., Eds.; Australian Government Publishing Service: Canberra, Australia, 1989; Vol. 1B: Mammalia.

(33) Hume, I. D.; Barboza, P. S. The gastrointestinal tract and digestive physiology of wombats. In *Wombats*; Wells, R. T., Pridmore,

P. A., Eds.; Surrey Beatty and Sons: Chipping Norton, NSW, Australia, 1998.
(34) El-Shazly, A.; Sarg, T.; Ateya, A.; Abdel Aziz, E.; Witte, L.; Wink, M. Pyrrolizidine alkaloids of *Cynoglossum officinale* and *Cynoglossum amabile* (family boraginaceae). *Biochem. Syst. Ecol.* **1996**, *24*, 415−421.
(35) Zalkow, L. H.; Bonetti, S.; Gelbaum, L.; Gordon, M. M.; Patil, B. B.; Shani, A.; Van Derveer, D. Pyrrolizidine alkaloids from Middle Eastern plants. *J. Nat. Prod.* **1979**, *42*, 603−614.
(36) Pedersen, E.; Larsen, E. Mass spectrometry of some pyrrolizidine alkaloids. *Org. Mass Spectrom.* **1970**, *4*, 249−256.
(37) O'Dowd, D. J.; Edgar, J. A. Seasonal dynamics in the pyrrolizidine alkaloids of *Heliotropium europaeum*. *Aust. J. Ecol.* **1989**, *14*, 95−105.
(38) Molyneux, R. J.; Gardner, D. L.; Colegate, S. M.; Edgar, J. A. Pyrrolizidine alkaloid toxicity in livestock: a paradigm for human poisoning? *Food Addit. Contam. Part A, Chem., Anal., Control, Exposure Risk Assess.* **2011**, *28*, 293−307.
(39) Curran, G. *New South Wales Animal Health Sureveillance: Suspect Ward's Weed Poisoning in Cattle and Sheep in the Western Division*; NSW Department of Primary Industries: Orange, NSW, Australia, 2007; 1.

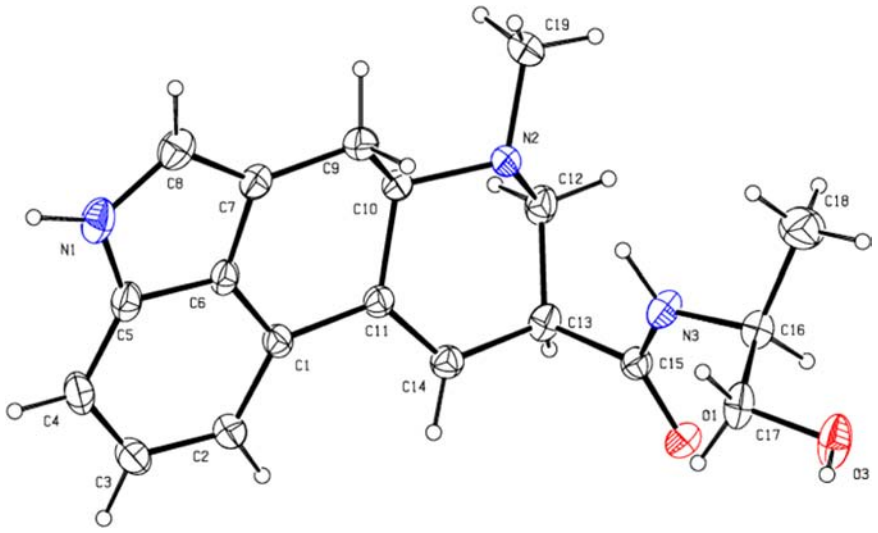

Figure 1. Single-crystal X-ray diffraction analysis for ergonovinine.

TLC. The chloroform extract (fraction 4) was further purified by silica gel column chromatography (CC; ⌀ 46 × 630 mm, 200−300 mesh, 270 g) and eluted with a step gradient of chloroform/methanol (100:1, 50:1, 30:1, 20:1, 10:1, 5:1, 2:1, 1:1, 9.7 L), followed by repeated CC ($CHCl_3$/MeOH, 3:1) on silica gel, Sephadex LH-20, and preparative TLC. Compound **1** (ergonovinine, 23.2 mg) was produced by recrystallization and further Sephadex LH-20 CC ($CHCl_3$/MeOH, 1:1). Compound **2** (ergonovine, 17.8 mg) was fully purified and obtained by repeated CC on silica gel eluted with a step gradient of chloroform/methanol (20:1, 10:1).

Cytotoxicity Assay of the Ergot Alkaloids. The 96-well nanoculture plates with a microsquare pattern [NCP-L-MS (96)] were provided by NUNC Corp. (Roskilde, Denmark).

Vascular smooth muscle cells (VSMC) from cattle (*Bos taurus*) were purchased from the Shanghai cell bank of the Chinese Academy of Sciences and maintained at 35 °C under an atmosphere of 95% air and 5% CO_2 in Dulbecco's modified Eagle's medium (DMEM; Mediatech, Herndon, VA, USA) containing 10% fetal bovine serum (FBS), 100 IU/mL penicillin, and 100 μg/mL streptomycin.

The cytotoxicity of the ergot alkaloids was determined by measuring the cell viability of cultured cells after exposure to different concentrations of extract from the grass. The cytotoxicity of ergot alkaloids was assessed according to the methyl thiazolyl tetrazolium assay (MTT) method.[23] To initiate cell culture, VSMC cells were seeded at a density of 1×10^4 cells/well on a conventional monolayer 96-well plate for expanding propagation. Each of the two ergot alkaloids (1 mg) was dissolved in 0.1% dimethyl sulfoxide (DMSO) (10 μL) and then diluted to concentrations of 125, 100, 75, 50, 12.5, 6.25, and 3.175 μg/mL with the medium and filtered using 0.22 μm syringe filters. These were then added to 24 h cultured cells in 96-well tissue culture plates. Logarithmic phase VSMC cells with a density of 1×10^5 cells/well were inoculated into 96-well plates for 18 h, and then the various concentrations of ergot alkaloids were added as the treatments. Media with 0.1% DMSO in DMEM was used as the blank group, and the cell cultures without added ergot served as the control, each treatment being repeated eight times, independently. The cells were then exposed to different concentrations of the above alkaloids. The cells in the control wells received medium containing the same volume of DMSO (0.1%). Twenty-four hours after the incubation, 20 μL of MTT reagent (5 mg/mL in PBS) was added and cells were incubated for an additional 4 h. The formazan produced by the viable cells was solubilized by the addition of 100 μL of DMSO. The suspension was placed on a microvibrator for 15 min, and absorbance at 490 and 570 nm was quantitated after subsequent addition of MTT solution and DMSO and was also read using a Versamax + Multiwash III ELISA reader (Molecular Devices, Sunnyvale, CA, USA). The experiment was performed three times for each alkaloid concentration treatment. The percentage of growth inhibition was calculated with respect to vehicle control using the following formula:

$$\text{inhibition rate } (\%) = (A_{\text{control}} - A_{\text{test}})/A_{\text{control}} - A_{\text{blank}} \times 100\%$$

Statistical Analysis. All values are expressed as the mean ± SE. Analysis of variance (ANOVA) using SPSS software (SPSS 13.0 Inc., Chicago, IL, USA) was conducted for the cell inhibition rate that resulted from various concentrations of the two ergot alkaloids. Analysis of regression was also carried out between the cell inhibition rate and concentrations of the ergot alkaloids.

RESULTS AND DISCUSSION

Isolation and Identification of the Alkaloids from E+ Plant Compounds. Single-crystal X-ray diffraction for ergonovinine is shown in Figure 1, and ^1H and ^{13}C NMR spectral data for ergonovine and ergonovinine are shown in the Supporting Information. Two ergot alkaloids, ergonovinine and ergonovine, were identified (Figure 2).

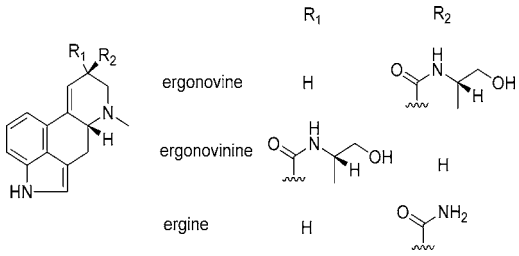

Figure 2. Structures of ergonovinine, ergonovine, and ergine and their C-8 epimers.

Ergonovine (25 mg from 2 kg) and ergonovinine (30 mg from 7 kg) were first isolated from dry powdered drunken horse grass, but without studying the biological activity.[24] Ergonovine and ergine (i.e., lysergic acid amide) were the major ergot alkaloids in drunken horse grass from Xinjiang province.[18] Previous research also investigated the ergonovine and ergine levels and their temporal variation within E+ and E− drunken horse grass grown in Gansu province.[19] Furthermore, seven alkaloids were also detected from drunken horse grass growing naturally near the Jinqiang River, Tianzhu county, Gansu province.[25] Ergine was reported as the main alkaloid, but we did not isolate it during this experiment because of its instability

dx.doi.org/10.1021/jf502264j | J. Agric. Food Chem. 2014, 62, 7419−7422

under high temperature. Ren[26] first reported that animals produced symptoms of intoxication after grazing on drunken horse grass. However, sheep were not significantly intoxicated[27,28] when gavaged with drunken horse grass powder, contrary to equines and rabbits (*Oryctolagus cuniculus*).[29] Research showed that the *Neotyphodium* endophyte was the cause of drunken horse grass toxicity in rabbits.[20] Recently, it was also reported that the *Neotyphodium* endophyte was apparently responsible for the toxicity of drunken horse grass on sheep (*Ovis aries*), which was especially harmful to kidney and liver function.[30]

Cytotoxicity of the Two Ergot Alkaloids. Each of the two ergot alkaloids exhibits cytotoxicity on animal smooth muscle cells, the cell inhibition rate increasing with alkaloid concentration in a significantly ($P < 0.05$) positive correlation (Figure 3). The regression equations for these two alkaloids

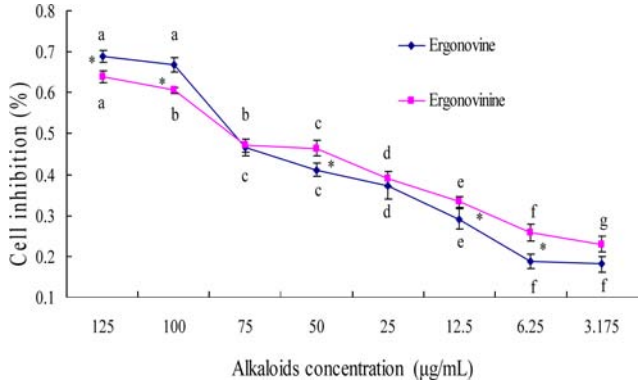

Figure 3. Cytotoxicity of the two ergot alkaloids on VSMC.

were $Y_{ergonovine} = 0.0041x + 0.205$ ($R^2 = 0.945$, $P < 0.05$) and $Y_{ergonovinine} = 0.0032x + 0.2672$ ($R^2 = 0.9411$, $P < 0.05$). The median inhibitory concentrations (IC_{50}) for ergonovine and ergonovinine were 71.95 and 72.75 μg/mL, respectively.

In conclusion, to the best of our knowledge, the present work represents the first study on the cytotoxic effect on animal smooth muscle cells of the pure ergot alkaloids isolated from E+ drunken horse grass. These alkaloids may be the cause of E+ drunken horse grass poisoning and elicit its clinical symptoms. The absence of detection of these chemicals could indicate plants that are safe for grazing animals.

■ ASSOCIATED CONTENT

Supporting Information

Tables 1 and 2, ^{1}H NMR and ^{13}C NMR spectroscopy of ergonovine and ergonovinine. This material is available free of charge via the Internet at http://pubs.acs.org.

■ AUTHOR INFORMATION

Corresponding Author

*(Z.N.) Phone: +86 931 8661047. Fax: +86 931 8910979. E-mail: zhibiao@lzu.edu.cn.

Funding

This research was financially supported by the National Basic Research Program (973) of China (2014CB138702), the National Nature Science Foundation of China (30771531), the Fundamental Research Funds for the Central Universities (lzujbky-2014-75), and the Program for Changjiang Scholars and Innovative Research Team in University (IRT13019).

Notes

The authors declare no competing financial interest.

■ REFERENCES

(1) White, J. F. J.; Morgan-Jones, G. Endophyte-host associations in forage grass. X. Culture studies on some species of *Acremonium* sect. *albo-lanosa*, including a new species *A. starrii*. *Mycotaxon* **1987**, *30*, 87−95.

(2) Schardl, C. L.; Leuchtmann, A. The *Epichloë* endophytes of grasses and the symbiotic continuum. In *The Fungal Community*, 3rd ed.; Dighton, J., White, J. F., Oudemans, P., Eds.; CRC Press: Boca Raton, FL, USA, 2004; pp 475−503.

(3) Faeth, S. H.; Bultman, T. L. Endophytic fungi and interactions among host plants, herbivores and natural enemies. In *Multitrophic Level Interactions*; Tscharnfre, T., Hawkins, B. A., Eds.; Cambridge University Press: Cambridge, UK, 2002; pp 89−123.

(4) Meister, B.; Krauss, J.; Härri, S. A.; Schneider, M. V.; Müller, C. B. Fungal endophyte symbionts affect aphid population size by reduction of adult lifespan and fecundity. *Basic Appl. Ecol.* **2006**, *7*, 244−252.

(5) Li, C. J.; Zhang, X. X.; Li, F.; Nan, Z. B.; Schardl, C. L. Disease and pests resistance of endophyte infected and non-infected drunken horse grass. In *Proceedings of the 6th International Symposium on Fungal Endophytes of Grasses*; Popay, A., Thom, E. R., Eds.; New Zealand Grassland Association: Dunedin, New Zealand, 2007; pp 111−114.

(6) Malinowski, D. P.; Belesky, D. P.; Lewis, G. C. Abiotic stresses in endophyte grasses. In *Neotyphodium in Cool-Season Grasses*; Roberts, C. A., West, C. P., Spiers, D. E., Eds.; Wiley: Hoboken, NJ, USA, 2005; pp 187−199.

(7) Müller, C. B.; Krauss, J. Symbiosis between grasses and asexual fungal endophytes. *Curr. Opin. Plant Biol.* **2005**, *8*, 450−456.

(8) Shi, Z. C. *Important Poisonous Plants of China Grassland*; Agriculture Press: Beijing, China, 1997 (in Chinese with some English content).

(9) Li, C. J.; Nan, Z. B.; Gao, J. H.; Tian, P. Detection and distribution of *Neotyphodium-Achnatherum inebrians* association in China. In *Proceedings of 5th International Neotyphodium/Grass Interactions Symposium*; Fayetteville, AR, USA, 2004; p 210.

(10) Li, C. J.; Nan, Z. B.; Paul, V. H.; Dapprich, P.; Liu, Y. A new *Neotyphodium* species symbiotic with drunken horse grass (*Achnatherum inebrians*) in China. *Mycotaxon* **2004**, *90*, 141−147.

(11) Li, C. J.; Gao, J. H.; Nan, Z. B. Interactions of *Neotyphodium gansuense*, *Achnatherum inebrians*, and plant-pathogenic fungi. *Mycol. Res.* **2007**, *111*, 1220−1227.

(12) Li, C. J.; Li, F.; Gou, X. Y.; Nan, Z. B. Effects of abiotic stresses on *Achnatherum inebrians* by symbiotic endophyte of *Neotyphodium gansuense*. In *Multifunctional Grasslands in a Changing World*; Organizing Committee of 2008 IGC/IRC Congress; Guangdong People's Publishing House: Guangzhou, China, 2008; p 819.

(13) Chen, N. *Molecular Mechanism Involved in Low Temperature Resistance of Endophyte-Infected Drunken Horse Grass during Seed Germination*. Ph.D. Dissertation, Lanzhou University, China, 2011.

(14) Zhang, X. X.; Li, C. J.; Nan, Z. B. Effects of cadmium stress on growth and anti-oxidative systems in *Achnatherum inebrians* symbiotic with *Neotyphodium gansuense*. *J. Hazard. Mater.* **2010**, *175*, 703−709.

(15) Zhang, X. X.; Fan, X. M.; Li, C. J.; Nan, Z. B. Effects of cadmium stress on seed germination, seedling growth and antioxidative enzymes in *Achnatherum inebrians* plants infected with a *Neotyphodium* endophyte. *Plant Growth Regul.* **2010**, *60*, 91−97.

(16) Zhang, X. X.; Li, C. J. Effects on bird cherry-oat aphid resistance to drunken horse grass by *Neotyphodium* endophyte infection. In *Multifunctional Grasslands in a Changing World*; Organizing Committee of 2008 IGC/IRC Conference, Huhhot, Inner Mongolia, China, 2008; Vol. II, p 833.

(17) Zhang, X. X.; Li, C. J.; Nan, Z. B.; Cory, M. *Neotyphodium* endophyte increases drunken horse grass (*Achnatherum inebrians*) resistance to herbivores and seed predators. *Weed Res.* **2012**, *52*, 70−78.

(18) Miles, C. O.; Lane, G. A.; Menna, M. E. High levels of ergonovine and lysergic acid amide in toxic *Achnatherum inebrians* accompany infection by an *Acremonium* like endophytic fungus. *J. Agric. Food Chem.* **1996**, *5*, 1285−1290.
(19) Li, C. J.; Nan, Z. B.; Schardl, C. L. Levels and temporal variation of ergot alkaloids in endophyte-infected drunken horse grass, *Achnatherum inebrians,* in China. APS, CPS and MSA Joint Meeting Abstracts; Quebec City, Canada, 2006; pp 203−204.
(20) Li, C. J.; Nan, Z. B.; Zhang, C. J.; Zhang, C. Y.; Zhang, Y. H. Effects of endophyte infected drunken horse grass on Chinese rabbit. *J. Agric. Sci. Technol.* **2009**, *11*, 90−96 (in Chinese with English abstract).
(21) Zhang, X. X.; Li, C. J.; Nan, Z. B. Effects of cutting frequency and height on alkaloid production in endophyte-infected drunken horse grass (*Achnatherum inebrians*). *Sci. China Life Sci.* **2011**, *54*, 567−571.
(22) Zhang, X. X.; Li, C. J.; Nan, Z. B. Effects of salt and drought stress on alkaloid production in endophyte-infected drunken horse grass (*Achnatherum inebrians*). *Biochem. Syst. Ecol.* **2011**, *39*, 471−476.
(23) Carmichael, J.; DeGraff, W. G.; Gazdar, A. F.; Minna, J. D.; Mitchell, J. B. Evaluation of a tetrazolium-based semiautomated colorimetric assay-assessment of chemosensitivity testing. *Cancer Res.* **1987**, *47*, 936−942.
(24) Zhang, Y.; Chu, T. Studies on the chemical compositions of *Achnatherum inebrians*. *Chem. J. Chin. Univ.* **1982**, *3* (Special Issue), 150−152.
(25) Sang, M.; Zhang, J.; Yao, J.; Yang, Y. L.; Huan, G. L.; Zeng, F. L.; Wei, R. H.; Wang, Y.; Wei, P. F. Abstraction and analysis of poisonous components of *Achnatherumn inebrians*. *Livest. Poult. Ind.* **2006**, *200*, 9−11 (in Chinese with English abstract).
(26) Ren, J. Z. *Northwest Grasslands Several Common Poisonous Weeds*; Gansu Agricultural University Press: Lanzhou, China, 1959; p 16.
(27) Dang, X. P. Experimental animal drunken horse grass poisoning case. *Vet. Sci. Technol.* **1990**, *11*, 20.
(28) Cao, G. R.; Dang, X. P. Drunken horse grass poisoning experiment. *Vet. Sci. Technol.* **1991**, *21*, 27.
(29) Dang, X. P.; Cao, G. R.; Duan, D. X.; Li, S. J.; Zhao, X. W.; Zhou, J. H. Studies on the toxic constituent of *Achnatherum inebrians*. *Acta Vet. Zootechnol. Sinica* **1992**, *4*, 366−371 (in Chinese with English abstract).
(30) Liang, Y., Li, C. J.; Nan, Z. B.; Wang, H. C.; Li, F. D. *Neotyphodium gansuense* symbiotic within *Achnatherum inebrians* produces clinical symptoms and physiological effects on small-tailed Han sheep (*Ovis aries*). In *Proceedings of the 8th International Symposium on Fungal Endophytes of Grasses*; Nan, Z. B., Li, C. J., Eds.; Lanzhou, China, 2012; pp 163−166.

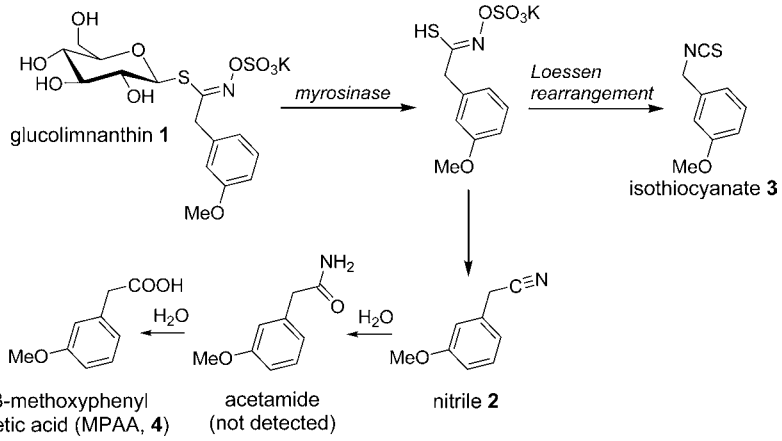

Figure 1. Production of glucolimnanthin breakdown products in soil amendment with meadowfoam seed meal.

another glucolimnanthin **1**-related compound and evaluated the phytotoxicity of soil amended with either nonactivated or activated MSM on seed emergence and growth.

MATERIALS AND METHODS

Chemicals. Glucolimnanthin **1** (1-*S*-(2-(3-methoxyphenyl)-*N*-(sulfonatooxy)ethanimidoyl)-1-thio-β-D-glucopyranose) was extracted from MSM.[11] 3-Methoxyphenylacetonitrile (nitrile **2**) (Sigma-Aldrich Chemicals, St. Louis, MO), 3-methoxybenzyl isothiocyanate (isothiocyanate **3**) (Oakwood Products, West Columbia, SC), and 3-methoxyphenylacetic acid (MPAA **4**) (TCI America, Portland, OR) were purchased from the indicated commercial sources.

Materials. MSM (Natural Plant Products, Salem, OR) was processed using a coffee grinder (Proctor Silex E160B, Southern Pines, NC) and sieved through 1 mm mesh before use. MSM was used at 3:100 MSM/dry soil. Activated MSM was produced by adding 1:100 freshly ground meadowfoam seed/MSM to provide active myrosinase.[11] Nonactivated MSM contained only ground MSM.

Soil was collected at 0−20 cm in 2010 from a site near Sweet Home, Oregon, USA (44°25′5″ N, 122°42′43″ W), where no herbicide application had been made for at least 4 years. The soil was a Newburg sandy loam (coarse-loamy, mesic Fluventic Haploxerolls) with an organic matter content of 3.2% and pH of 6.1. The soil was ground, passed through a 2 mm sieve, air-dried for 7 days, and kept in a closed container until use.

Isolation and Identification of a Compound 4. Compound **4** was detected in soil amended with MSM and activated MSM and was not found in the untreated control during the analyses of glucolimnanthin **1** and its breakdown products. Isolation and identification of compound **4** were performed using the following procedures. Soil amended with 3% by weight of MSM was mixed thoroughly in an 11 cm × 11 cm × 3.5 cm plastic box, and H_2O was added to reach 30% moisture content. The MSM amended soil was incubated in the sealed box at room temperature for 4 days before extraction. The moist soil was transferred into a glass centrifuge tube, and CH_2Cl_2 was added (1.5 mL/g of moist soil). The tube was shaken, sonicated for 3 min, and allowed to stand for 15 min. The supernatant was transferred to a glass tube, and the extraction was repeated for two more cycles. The supernatants were combined and then dried using a rotary evaporator. The resultant residue was redissolved in MeOH (2 mL/g dry soil). The methanolic resuspension was extracted with hexane three times to remove nonpolar compounds. The remaining MeOH suspension was evaporated using a rotary evaporator, and resuspended in MeOH before purification using a 2.5 cm × 50 cm column of Sephadex LH-20 (Sigma-Aldrich Chemicals, St. Louis, MO) eluted with 100% degassed MeOH at a flow rate of 1.6 mL/min. Elution was monitored using high performance liquid chromatography (HPLC) as previously described.[11]

The fractions containing compound **4** were collected and concentrated using a rotary evaporator. The fractions were redissolved in acetonitrile and separated on a 250 mm × 4.6 mm Phenomenex Luna 5 μm C18 column (Phenomenex, Torrance, CA) eluted with a linear gradient of 35−40% of 0.1% formic acid in acetonitrile and aqueous 0.1% formic acid in H_2O at 1 mL/min. The eluted compound **4** was identified using LC-UV at λ 274 nm (SPD-10Avp UV−vis detector, Shimadzu Scientific Instruments, Columbia, MD) and high resolution LC-MS/MS (Triple TOF 5600, AB SCIEX, Framingham, MA). Mass spectrometric analysis utilized negative full scan and product ion scan modes. A DuoSpray source was operated at 550 °C and −4.5 kV using a declustering potential of −80 V and a collision energy of 20 eV. The commercial standard was analyzed using LC-UV and high resolution LC-MS/MS under the same conditions as the suspension extract. The retention times and mass spectra of the standard and compound **4** were compared.

Glucolimnanthin and Its Breakdown Products in Soil. Soil incubations were conducted in 15 mL centrifuge tubes using a completely randomized design with three replications. Dry soil (1.94 g) was incubated with either 0.06 g of MSM or activated MSM in a tube. After addition of 750 μL of deionized H_2O to thoroughly hydrate the seed meal amended soil, the tubes were laid horizontally. Nonamended soil was used as a control. The extraction method for glucolimnanthin **1** and its breakdown products from the soil was developed by modifying the method of Stevens et al.[11]

Each incubated soil tube received 6 mL of 70% MeOH. The tube was shaken, sonicated for 10 min, and allowed to stand for 60 min. The mixture was centrifuged for 5 min at 3000 rpm. The supernatant was centrifuged for 10 min at 13 000 rpm. The MeOH concentration in the supernatant was increased to 90% to prevent further enzymatic degradation of glucolimnanthin **1**. The analyses of glucolimnanthin **1** and GBPs were performed using HPLC.[11] The injection volume was 30 μL. A Waters 2996 photodiode array detector (Waters Corporation, Milford, MA) at λ 274 nm was used to calculate peak areas for all compounds. Analyte concentrations were determined from calibration curves constructed for each analyte using the external standard method. The glucolimnanthin **1** and GBPs were quantified on 0, 1, 2, 3, 6, 12, and 18 DAI. The experiment was repeated.

Petri Plate Bioassay. In a comparative assay of relative toxicity, each GBP was used to test the response of lettuce germination and growth. A 10 cm diameter Petri plate (VWR International, Visalia, CA) served as a bioassay study chamber. Test compounds were dissolved in EtOH and diluted in various concentrations. Test solutions (480 μL) were added on top of an 8.3 cm diameter germination blotter paper. Based on preliminary testing, the following concentrations were chosen for dose−response study of the test compounds. Concentrations of test compounds were adjusted by considering the potential losses during the evaporative period. Nitrile **2** solutions were prepared to give 0, 0.38, 3.77, 7.54, 15.1, 22.6, 30.1, 37.7, and 75.4 μmol/plate. Isothiocyanate **3** was prepared to deliver 0, 0.033, 0.33, 0.67, 1.33, 2, 2.66, and 3.33 μmol/plate, and MPAA **4** was prepared at 0, 0.048, 0.48, 4.8, 9.6, 19.2, 28.8, 38.4, and 48 μmol/plate.

dx.doi.org/10.1021/jf5018687 | J. Agric. Food Chem. 2014, 62, 7423−7429

Control plates received EtOH only. Plates were placed in a fume hood for a 3-h evaporative period to remove EtOH.

After 3 h, each plate received 6 mL of deionized H_2O. Sixteen lettuce seeds (*Lactuca sativa* L. "Black Seeded Simpson", Plantation Products, Norton, MA) were placed in a 4 × 4 grid on top of a germination blotter paper. The Petri plate was sealed with a layer of Parafilm (American National Can, Menasha, WI). Lettuce seeds were grown in the incubator at 20/15 °C day/night temperature with a 14 h photoperiod. Seeds were counted as germinated when the hypocotyl, radicle, or hypocotyl plus radicle measured 2 mm, and seedling growth was evaluated by measuring radicle and hypocotyl length on day 7. The experiment was performed in a completely randomized design with three replications of each test compound and was repeated.

Phytotoxicity of Meadowfoam Seed Meal. Filter paper was placed at the bottom of a 132 mL pot to prevent soil loss. Pots were filled with 116.4 g of soil and amended with 3.6 g of either MSM or activated MSM. The untreated control was 120 g of soil without amendment. Lettuce seeds were sown nine seeds per pot at an approximate depth of 0.4 cm on 0, 6, and 12 days after MSM incorporation (DAI). Each pot was watered daily. Soil moisture in each pot was maintained at 37.5% by weighing the pots. The experiments were conducted in the greenhouse with 25/20 °C day/night temperature and a 14 h photoperiod. Seedling emergence was counted, and shoot biomass was harvested 21 days after planting. The biomass was dried at 60 °C for 72 h and weighed. The experiment was structured in a randomized complete block design with three replications and was repeated.

Statistical Analyses. Concentrations of glucolimnanthin **1** and GBPs and lettuce germination, emergence, hypocotyl and radicle growth, and biomass were analyzed using analysis of variance (ANOVA) with means separated using a least significant difference (LSD) test at a 0.05 level. For the phytotoxicity of GBPs in the lettuce germination study, dose−response curves were obtained by a nonlinear regression using a log−logistic equation (eq 1),[26,27]

$$y = C + (D - C)/[1 + (x/I_{50})^b] \quad (1)$$

where y represents germination (percent of untreated control) at GBP concentration x, C is the mean response at the greatest GBP concentration (lower limit), D is the mean response when the GBP concentration is zero (upper limit), b is the slope of the line at I_{50}, and I_{50} is the GBP concentration required for 50% germination reduction.

The regression parameters, 95% confidence interval for each GBP, and lack of fit test were obtained using the package drc in the statistical program R.[28] The relative I_{50} level was calculated by the ratio of one GBP to another GBP. The statistical program R v. 3.0.2 was used for all the statistical analyses.[29]

RESULTS AND DISCUSSION

Glucolimnanthin 1 and Its Breakdown Products. The analytical data of the composition of MSM and activated MSM are provided in Supporting Information, Figure S1. When MSM was incubated with soil, a previously unknown metabolite **4** of glucolimnanthin **1** was observed (Figure 1). Its identity was confirmed by LC-UV and by high resolution LC-MS/MS with a 4.2 ppm error compared with the exact mass of MPAA **4** (Figure 2). The observed spectrum of an MPAA **4** standard had 2.4 ppm error compared with the calculated mass of MPAA **4** (Supporting Information, Figure S2).

Glucolimnanthin **1** was converted into isothiocyanate **3** by active myrosinase from freshly ground meadowfoam seed (Figure 3B). The production of isothiocyanate **3** occurred quickly within 30 min after soil incorporation with activated MSM. Maximal concentrations of isothiocyanate **3** were observed at 1 DAI, after which they decreased >90% of the maximum by 2 DAI. Within 6 days, glucolimnanthin **1** in MSM (Figure 3A) degraded slower to trace amounts compared with activated MSM (Figure 3B), and isothiocyanate **3** was not detected. Isothiocyanate **3** was the major degradation product and was produced rapidly. Similar findings were observed in soil incorporation of Brassicaceous plants. Brown et al.[30]

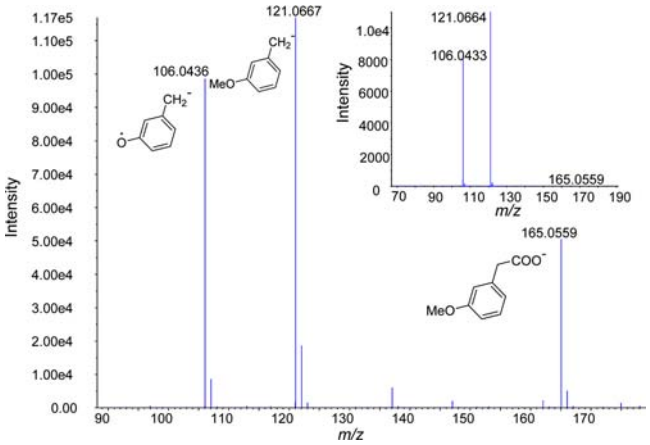

Figure 2. Time-of-flight (TOF) mass spectrum of 3-methoxyphenylacetic acid (MPAA) produced from soil amended with 3% by weight of meadowfoam seed meal, showing the molecular ion (observed m/z 165.0559, calculated m/z 165.0552, 4.2 ppm error). The inset shows an MS−MS fragmentation of the parent peak at m/z 165.

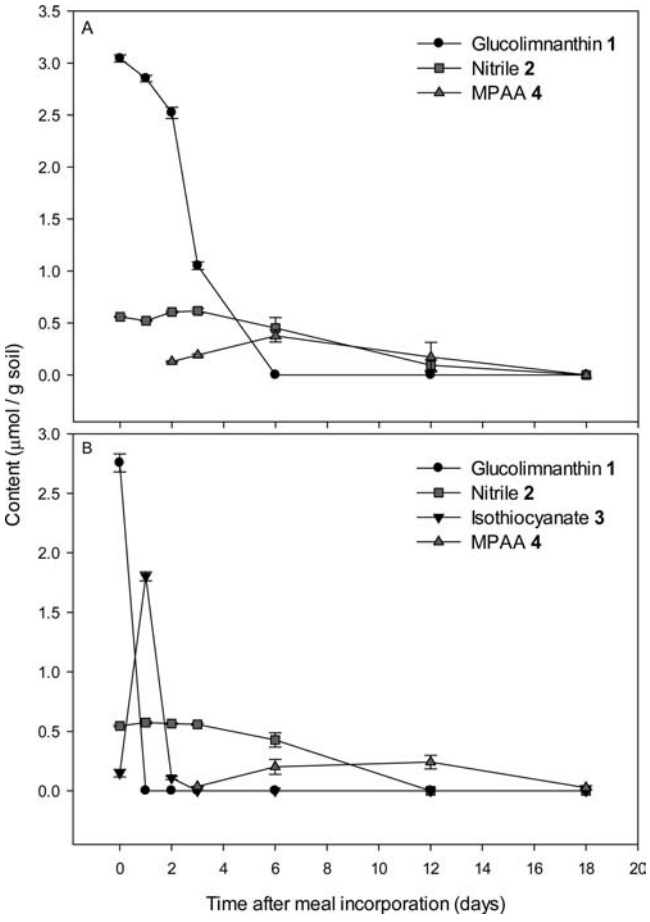

Figure 3. Concentrations of glucolimnanthin and its breakdown products in soil amended with meadowfoam seed meal (A) and activated meadowfoam seed meal (B). On day 0, the extraction started 30 min after meal incorporation. Symbols and bars represent means and standard errors of two studies (n = 6).

dx.doi.org/10.1021/jf5018687 | J. Agric. Food Chem. 2014, 62, 7423−7429

reported the isothiocyanate degradation from soil amended with rapeseed (*Brassica napus* L.) meal, which was detected in 2 h but decreased to trace amounts at 2 DAI. The maximum concentrations of detected meadowfoam isothiocyanate **3** were similar to allyl isothiocyanate from sinigrin decomposition in soil.[31] Allyl isothiocyanate reached maximum levels within 1 DAI and remained detectable until 7 DAI. Morra and Kirkegaard[32] suggested that greater isothiocyanate production and its retention could occur by disruption of glucosinolate-containing tissue to provide greater contact between glucosinolate-containing tissue and myrosinase. However, isothiocyanate disappeared rapidly, possibly because it easily binds with free amino acids and proteins.[13]

Nitrile **2** occurs in MSM because of the heat involved in the commercial process, but it is minimally produced by enzymatic degradation of glucolimnanthin **1**.[11] From 0 to 3 DAI, nitrile **2** concentrations with MSM or activated MSM were not different ($p > 0.05$) (Figure 3). Nitrile **2** concentrations decreased from 3 to 18 DAI in MSM and from 3 to 12 DAI in activated MSM. Vaughn et al.[22] reported that the large amount of nitrile **2** in MSM was possibly a driving factor for its phytotoxicity.

MPAA **4** appeared on 2 DAI of MSM and 3 DAI of activated MSM (Figure 3). While nitrile **2** decreased after 3 DAI, MPAA **4** increased. MPAA **4** occurred last and remained detectable at 12 DAI. Soil was amended with nitrile **2** alone to determine whether nitrile **2** was the parent compound of MPAA **4**. The metabolite mass was consistent with the calculated mass of standard MPAA **4** (mass error 4.8 ppm; Supporting Information, Figure S3). A possible pathway for MPAA **4** formation from glucolimnanthin **1** via nitrile **2** involves hydrolytic conversion of nitrile **2** to its corresponding amide followed by hydrolysis of the amide into its corresponding carboxylic acid, MPAA **4** (Figure 1). However, MPAA **4** was detected when soil was incubated with either MSM or activated MSM within 3 DAI, when nitrile **2** concentration had not decreased. A potential explanation is that the MPAA **4** formation may not have been only from nitrile **2** degradation but also derived from glucolimnanthin **1** through nitrile **2**. MPAA **4** was not detected in incubation of MSM in the absence of soil. It was also possible that MPAA **4** was not present as a simultaneous metabolite but occurred through enzymatic activity mediated by soil microbes. MPAA **4** production may have been facilitated by nitrilases from soil microorganisms, which are known to catalyze nitriles into their corresponding carboxylic acids.[33]

Petri Plate Bioassay. Herbicidal efficacy of each GBP was of interest. Commercially available GBPs were used to evaluate their phytotoxicity. The required concentrations of GBPs for suppression of seed germination and growth are important for developing MSM as a bioherbicide. Nitrile **2**, isothiocyanate **3**, and MPAA **4** showed potent inhibition of lettuce germination and growth (Figures 4 and 5). Isothiocyanate **3** had the most effective herbicidal activity followed by MPAA **4** and nitrile **2**. The amounts required to reduce germination by 50% (I_{50}) were 1.4 μmol/plate for isothiocyanate **3**, 11.9 μmol/plate for MPAA **4**, and 20.2 μmol/plate for nitrile **2**. I_{50} values for the GBPs were different from each other ($p < 0.05$). The relative potency of isothiocyanate **3** was 8.5- and 14.4-fold greater than MPAA **4** and nitrile **2**, respectively. The relative potency of MPAA **4** was 1.7-fold greater than nitrile **2**. Both hypocotyl and radicle length decreased with increasing concentrations of GBPs (Figure 5). Isothiocyanate **3** provided the greatest inhibition of hypocotyl and radicle length followed by MPAA **4** and nitrile **2**,

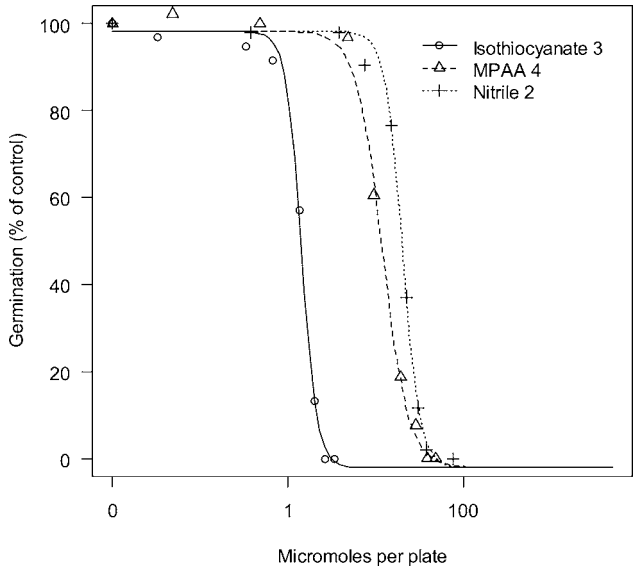

Figure 4. Phytotoxicity of glucolimnanthin breakdown products on lettuce germination. Symbols represent means of samples of two studies ($n = 6$).

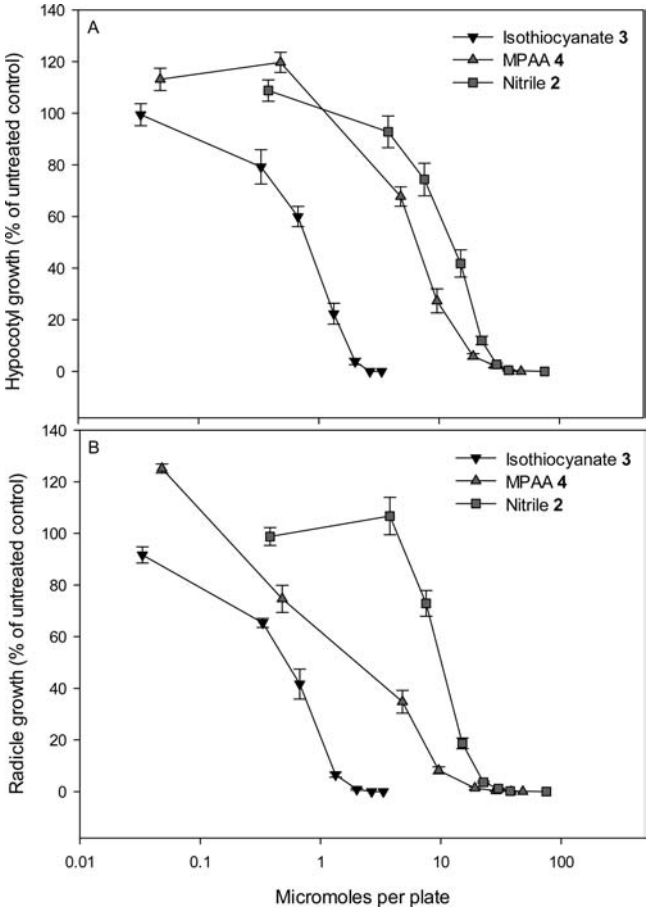

Figure 5. Phytotoxicity of glucolimnanthin breakdown products on lettuce hypocotyl length (A) and radicle length (B). Symbols and bars represent means and standard errors of samples of two studies ($n = 6$).

respectively ($p < 0.05$), which was the same as for germination inhibition.

Several published studies of Brassicaceae glucosinolates[9,32] and meadowfoam glucolimnanthin **1**[23−25] have shown

dx.doi.org/10.1021/jf5018687 | J. Agric. Food Chem. 2014, 62, 7423−7429

isothiocyanates to be the major phytotoxic metabolites. Vaughn et al.[22] reported that meadowfoam isothiocyanate **3** had phytotoxic effects on velvetleaf and wheat (*Triticum aestivum* L.) radicle growth, but they were unable to detect isothiocyanate **3** in nonactivated MSM. However, Stevens et al.[11] reported that meadowfoam nitrile **2** had greater activity than the isothiocyanate **3** in preventing coleoptile emergence of downy brome. The difference between the studies may have been due to experimental conditions and target species. In our study, isothiocyanate **3** had the greatest phytotoxic effects on lettuce germination and growth. It is possible that phytotoxicity does not depend on a single chemical compound. A combination of all GBPs may result in phytotoxicity. A synergistic or antagonistic response of GBP combinations for herbicidal activity may exist.

Phytotoxicity of Meadowfoam Seed Meal in Soil. Greenhouse studies were conducted to evaluate the direct use of MSM as a soil amendment material for inhibition of seed emergence and growth. Lettuce emergence and growth were different among amendment materials and planting times (Table 1). Activated MSM had greater phytotoxicity on lettuce

Table 1. Greenhouse Studies on Lettuce Emergence and Growth in Soil Amended with 3% by Weight of Meadowfoam Seed Meal (MSM) or Activated MSM

treatments	lettuce emergence[a] (% of sown seeds)	lettuce biomass (mg/plant)
	Planted on 0 DAI[b]	
unamended	57.4 ± 5.30 a	9.7 ± 1.30 a
MSM	50.0 ± 10.24 a	4.1 ± 0.87 b
activated MSM[c]	25.9 ± 4.68 b	2.7 ± 1.00 b
	Planted on 6 DAI	
unamended	79.6 ± 5.30 ns[d]	9.4 ± 0.89 ns[d]
MSM	70.4 ± 9.37	13.9 ± 3.29
activated MSM[c]	77.8 ± 2.87	8.5 ± 2.61
	Planted on 12 DAI	
unamended	81.5 ± 8.45 ns[d]	10.0 ± 0.65 b
MSM	77.8 ± 7.03	19.3 ± 2.44 a
activated MSM[c]	75.9 ± 3.41	10.9 ± 1.83 b

[a]Data are from two experiments, with each value representing the mean of six replicates ± the standard error of the mean. Different letters within a column indicate significant differences at the 0.05 level within a planting date. [b]Planting dates after meal incorporation (DAI). [c]1:100 freshly ground meadowfoam seed/total meadowfoam seed meal. [d]Not significant.

emergence than MSM when lettuce seeds were sown on 0 DAI ($p < 0.05$). Lettuce emergence was reduced by 55% in activated MSM compared with the untreated control. On the 0 DAI planting date, the lettuce seedling biomass was reduced by 58% in MSM and 72% in activated MSM treatments compared with the untreated control. Adding active myrosinase from freshly ground meadowfoam seed to MSM increased phytotoxicity and suppression of lettuce growth. Similar results were reported in another study where activated MSM with 18-h incubation or addition of iron provided greater inhibition on coleoptile emergence of downy brome compared with MSM.[11] Other glucosinolate-containing seed meals such as brown mustard (*Brassica juncea* (L.) Czern.)[18,34,35] and white mustard (*Sinapis alba* L.)[35,36] have been reported to have potential uses as bioherbicides without requiring activation.

No differences in lettuce emergence and biomass were found among treatments when lettuce seeds were planted 6 days after seed meal incorporation so waiting before planting into MSM treatments was necessary to prevent crop injury. A study conducted by Rice et al.[18] suggested that lettuce sown into 3% white mustard seed meal-amended soil required approximately 35 DAI for crop safety. The length of phytotoxicity varied depending on glucosinolate-containing species, application methods, and environmental conditions such as soil moisture and soil temperature.[37]

On the 12 DAI planting date, there was no difference in lettuce emergence but there was a difference in lettuce biomass. The lettuce biomass was greater in MSM compared with untreated control and activated MSM. These results were possibly due to the protein and fiber content in MSM,[6] which may be utilized as N and C sources by soil microorganisms. Similar fertilizer effects were found after other Brassicaceae seed meal applications.[18] However, the reduced lettuce biomass in activated MSM compared with MSM was potentially due to greater phytotoxicity and nonselective inhibition of soil microorganisms. When the concentration of the remaining phytotoxic compounds was no longer toxic to lettuce seeds, it still may have inhibited soil microbial activity. Snyder et al.[38] suggested the mixed effects of different glucosinolate-containing Brassicaceae seed meals on plants and soil microbes involved with the N cycle. The soil microbes may not have completely recovered and utilized the C and N sources provided by the activated MSM application. Intanon[37] reported that between 0 and 7 days after activated MSM incorporation, microbial biomass C and N increased. Microorganisms immobilized C and N sources, and then C and N became available to plants during microbial turnover.[39] The harvest time at 21 days after seeding may not be long enough to observe the fertilizer effect from the activated MSM application.[37]

The low number of emerged lettuce seedlings in all treatments on the 0 DAI planting date possibly was due to seeds being buried during the initial irrigation. When seeds were planted 6 and 12 days later, the soil was more settled so seeds were not buried as deep. Other possible reasons were a CO_2 flush or microbial respiration. Andalo et al.[40] suggested that the response on seed germination to elevated CO_2 as a result of wetting dry soil is species specific. Lettuce seed germination was inhibited with increasing the concentration of CO_2 to 6.4% and 12.8%.[41] The increase of CO_2 concentration during germination had no effect on seed germination in mouse-ear cress (*Arabidopsis thaliana* (L.) Heynh.).[40] After wetting of the soil, the moisture can induce metabolic processes such as respiration by seeds and microbes. During the respiration process, heat was released, which possibly reduced germination.[42]

Although isothiocyanate **3** was shown to have the greatest toxicity, its presence in the soil amended with activated MSM was very short-lived (Figure 3B). The rapid degradation of this bioactive compound in the soil should allow the use of activated MSM for weed control preplant. After the loss of MSM phytotoxicity, subsequent fertilizer effects were observed. Thus, planting crops in the field at least 6 days after MSM application may protect the crop from allelochemicals and increase competitiveness against emerging weeds.

The results of this study improve the current knowledge that activated MSM has greater herbicidal activity compared with nonactivated MSM. The temporal change in biodegradation of glucolimnanthin **1** and GBPs under soil conditions were evaluated. In addition, the newly identified metabolite, MPAA **4**, was discovered as a breakdown product of glucolimnanthin

1, and it has phytotoxic activity. The study benefits meadowfoam growers as well as provides an alternative bioherbicide for use on organic farms and other high value crops for which reduced synthetic herbicide applications are desired.

■ ASSOCIATED CONTENT

Supporting Information

HPLC analysis of MSM and activated MSM, mass spectrum of an MPAA **4** standard, and an extraction of soil incubated with nitrile **2**. This material is available free of charge via the Internet at http://pubs.acs.org.

■ AUTHOR INFORMATION

Corresponding Author

*Telephone (541) 737-5754; fax (541) 737-1589; e-mail suphannika.intanon@oregonstate.edu.

Notes

The authors declare no competing financial interest.

■ REFERENCES

(1) Kleiman, R. Chemistry of new industrial oilseed crops. In *Advances in New Crops*; Janick, J., Simon, J. E., Eds.; Timber Press: Portland, OR, 1990; pp 198−199.

(2) Knapp, S. J.; Crane, J. M. Fatty-acid diversity of section inflexae *Limnanthes* (meadowfoam). *Ind. Crops Prod.* **1995**, *4*, 219−227.

(3) Burg, D. A.; Kleiman, R. Preparation of meadowfoam dimer acids and dimer esters, and their use as lubricants. *J. Am. Oil Chem. Soc.* **1991**, *68*, 600−603.

(4) Hirsinger, F. New annual oil crops. In *Oil Crops of the World*; Röbbelen, G., Downey, R. K., Ashri, A., Eds.; McGraw-Hill: New York, 1989; pp 518−532.

(5) Steiner, J. J.; Griffith, S. M.; Mueller-Warrant, G. W.; Whittaker, G. W.; Banowetz, G. M.; Elliott, L. F. Conservation practices in western Oregon perennial grass seed systems: II. Meadowfoam rotation crop manament. *Agron. J.* **2006**, *98*, 177−186.

(6) Purdy, R. H.; Craig, C. D. Meadowfoam: New source of long-chain fatty acids. *J. Am. Oil Chem. Soc.* **1987**, *64*, 1161−1174.

(7) Fahey, J. W.; Zalcmann, A. T.; Talalay, P. The chemical diversity and distribution of glucosinolates and isothiocyanates among plants. *Phytochemistry* **2001**, *56*, 5−51.

(8) Agerbirk, N.; Olsen, C. E. Glucosinolate structures in evolution. *Phytochemistry* **2012**, *77*, 16−45.

(9) Brown, P. D.; Morra, M. J. Hydrolysis products of glucosinolates in *Brassica napus* tissues as inhibitors of seed germination. *Plant Soil* **1996**, *181*, 307−316.

(10) VanEtten, C. H.; Tookey, H. L. Glucosinolates in cruciferous plants. In *Effects of Poisonous Plants on Livestock*; Keeler, R. F., Van Kampen, K. R., James, L. F., Eds.; Academic Press: New York, 1978; pp 507−520.

(11) Stevens, J. F.; Reed, R. L.; Alber, S.; Pritchett, L.; Machado, S. Herbicidal activity of glucosinolate degradation products in fermented meadowfoam (*Limnanthes alba*) seed meal. *J. Agric. Food Chem.* **2009**, *57*, 1821−1826.

(12) Borek, V.; Morra, M. J.; McCaffrey, J. P. Myrosinase activity in soil extracts. *Soil Sci. Soc. Am. J.* **1996**, *60*, 1792−1797.

(13) Fenwick, G. R.; Heaney, R. K.; Mullin, W. J.; VanEtten, C. H. Glucosinolates and their breakdown products in food and food plants. *Crit. Rev. Food Sci. Nutr.* **1982**, *18*, 123−201.

(14) Thangstad, O. P.; Evjen, K.; Bones, A. Immunogold-EM localization of myrosinase in Brassicaceae. *Protoplasma* **1991**, *161*, 85−93.

(15) Gimsing, A.; Kirkegaard, J. Glucosinolates and biofumigation: Fate of glucosinolates and their hydrolysis products in soil. *Phytochem. Rev.* **2009**, *8*, 299−310.

(16) Rakariyatham, N.; Butrindr, B.; Niamsup, H.; Shank, L. Screening of filamentous fungi for production of myrosinase. *Braz. J. Microbiol.* **2005**, *36*, 242−245.

(17) Sakorn, P.; Rakariyatham, N.; Niamsup, H.; Nongkunsarn, P. Rapid detection of myrosinase-producing fungi: A plate method based on opaque barium sulphate formation. *World J. Microbiol. Biotechnol.* **2002**, *18*, 73−74.

(18) Rice, A. R.; Johnson-Maynard, J. L.; Thill, D. C.; Morra, M. J. Vegetable crop emergence and weed control following amendment with different Brassicaceae seed meals. *Renew. Agric. Food Syst.* **2007**, *22*, 204−212.

(19) Borek, V.; Morra, M. J. Ionic thiocyanate (SCN^-) production from 4-hydroxybenzyl glucosinolate contained in *Sinapis alba* seed meal. *J. Agric. Food Chem.* **2005**, *53*, 8650−8654.

(20) Linderman, R. G.; Davis, E. A.; Masters, C. J. Response of conifer seedlings to potting medium amendment with meadowfoam seed meal. In *Issues in New Crops and New Uses*; Janick, J., Whipkey, A., Eds.; ASHS Press: Alexandria, VA, 2007; pp 138−142.

(21) Machado, S. Allelopathic potential of various plant species on downy brome: Implications for weed control in wheat production. *Agron. J.* **2007**, *99*, 127−132.

(22) Vaughn, S. F.; Boydston, R. A.; Mallory-Smith, C. A. Isolation and identification of (3-methoxyphenyl)acetonitrile as a phytotoxin from meadowfoam (*Limnanthes alba*) seedmeal. *J. Chem. Ecol.* **1996**, *22*, 1939−1949.

(23) Vaughn, S. F.; Palmquist, D. E.; Duval, S. M.; Berhow, M. A. Herbicidal activity of glucosinolate-containing seedmeals. *Weed Sci.* **2006**, *54*, 743−748.

(24) Zasada, I. A.; Weiland, J. E.; Reed, R. L.; Stevens, J. F. Activity of meadowfoam (*Limnanthes alba*) seed meal glucolimnanthin degradation products against soilborne pathogens. *J. Agric. Food Chem.* **2012**, *60*, 339−345.

(25) Bartelt, R. J.; Mikolajczak, K. L. Toxicity of compounds derived from *Limnanthes alba* seed to fall armyworm (Lepidoptera: Noctuidae) and European corn borer (Lepidoptera: Pyralidae) larvae. *J. Econ. Entomol.* **1989**, *82*, 1054−1060.

(26) Seefeldt, S. S.; Jensen, J. E.; Fuerst, E. P. Log-logistic analysis of herbicide dose-response relationships. *Weed Technol.* **1995**, *9*, 218−227.

(27) Streibig, J. C.; Rudemo, M.; Jensen, J. E. Dose-response curves and statistical models. In *Herbicide Bioassay*; Streibig, J. C., Kudsk, P., Eds.; CRC Press: Boca Raton, FL, 1993; pp 29−53.

(28) Knezevic, S. Z.; Streibig, J. C.; Ritz, C. Utilizing R software package for dose-response studies: the concept and data analysis. *Weed Technol.* **2007**, *21*, 840−848.

(29) R Core Team *R: A language and environment for statistical computing*; R Foundation for Statistical Computing: Vienna, Austria, 2013.

(30) Brown, P. D.; Morra, M. J.; McCaffrey, J. P.; Auld, D. L.; Williams, L. Allelochemicals produced during glucosinolate degradation in soil. *J. Chem. Ecol.* **1991**, *17*, 2021−2034.

(31) Borek, V.; Morra, M. J.; Brown, P. D.; McCaffrey, J. P. Allelochemicals produced during sinigrin decomposition in soil. *J. Agric. Food Chem.* **1994**, *42*, 1030−1034.

(32) Morra, M. J.; Kirkegaard, J. A. Isothiocyanate release from soil-incorporated *Brassica* tissues. *Soil Biol. Biochem.* **2002**, *34*, 1683−1690.

(33) O'Reilly, C.; Turner, P. D. The nitrilase family of CN hydrolysing enzymes − a comparative study. *J. Appl. Microbiol.* **2003**, *95*, 1161−1174.

(34) Earlywine, D. T.; Smeda, R. J.; Teuton, T. C.; Sams, C. E.; Xiong, X. Evaluation of oriental mustard (*Brassica juncea*) seed meal for weed suppression in turf. *Weed Technol.* **2010**, *24*, 440−445.

(35) Handiseni, M.; Brown, J.; Zemetra, R.; Mazzola, M. Herbicidal activity of Brassicaceae seed meal on wild oat (*Avena fatua*), Italian ryegrass (*Lolium multiflorum*), redroot pigweed (*Amaranthus retroflexus*), and prickly lettuce (*Lactuca serriola*). *Weed Technol.* **2011**, *25*, 127−134.

(36) Hansson, D.; Morra, M. J.; Borek, V.; Snyder, A. J.; Johnson-Maynard, J. L.; Thill, D. C. Ionic thiocyanate (SCN) production, fate, and phytotoxicity in soil amended with Brassicaceae seed meals. *J. Agric. Food Chem.* **2008**, *56*, 3912−3917.

(37) Intanon, S. Bioherbicide use of plant defensive compounds in meadowfoam seed meal. Ph.D. Dissertation, Oregon State University, Corvallis, OR, 2013.
(38) Snyder, A.; Morra, M. J.; Johnson-Maynard, J.; Thill, D. C. Seed meals from Brassicaceae oilseed crops as soil amendments: influence on carrot growth, microbial biomass nitrogen, and nitrogen mineralization. *HortScience* **2009**, *44*, 354−361.
(39) Brookes, P. The soil microbial biomass: Concept, measurement and applications in soil ecosystem research. *Microbes Environ.* **2001**, *16*, 131−140.
(40) Andalo, C.; Godelle, B.; Lefranc, M.; Mousseau, M.; Till-Bottraud, I. Elevated CO_2 decreases seed germination in *Arabidopsis thaliana*. *Global Change Biol.* **1996**, *2*, 129−135.
(41) Negm, F. B.; Smith, O. E. Effects of ethylene and carbon dioxide on the germination of osmotically inhibited lettuce seed. *Plant Physiol.* **1978**, *62*, 473−476.
(42) Justice, O. L.; Bass, L. N. *Principles and Practices of Seed Storage*; USDA: Washington, D. C., 1978; p 289.

Scheme 2. Illustration for the Production of Furfural from Xylose in [BMIM]Cl

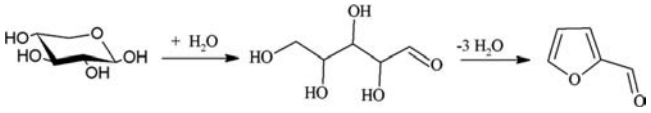

xylose in IL has received much attention.[6,27,28] The aim of this work was to perform the conversion of xylose using IL ([BMIM]Cl) as a pertinent solvent and LS as catalyst. The combination of using biomass-based feedstock and catalyst as well as green solvent presents a pathway to realize the green conversion of xylose into high value-added chemicals.

MATERIALS AND METHODS

Chemicals and Reagents. *Dendrocalamus membranaceus* (*Dm*M) was obtained from Kunming, China. The composition (%, w/w) of *Dm*M was 45.68% cellulose, 25.60% hemicelluloses, 26.33% lignin, 1.53% ash, and 1.40% wax on a dry weight basis. Xylose was supplied by J&K Scientific Ltd. Furfural standard, *N*,*N*-dimethylformamide (DMF), *N*,*N*-dimethylacetamide (DMA), dimethyl sulfoxide (DMSO), tetrahydrofuran (THF), and *N*-methylpyrrolidone (NMP) were purchased from Aladdin Reagent Co., Ltd. [BMIM]Cl (99%) was purchased from Zhongke Kate Industry & Trade Co., Ltd. Acidic ion-exchange resin, acetonitrile, and 1,4-dioxane were purchased from Shanghai Chemical Reagent co., Ltd. Toluene and methanol were supplied by National Medicine Group Chemical Reagent Co., Ltd. Lignosulfonate was prepared by sulfonating the lignin according to the former literature;[29] lignin was obtained by bamboo kraft pulping process and purified from black liquor as reported.[29,30] The M_w of the obtained lignosulfonate was about 534 g/mol determined by gel permeation chromatography (GPC). THF was used as eluent with the flow rate of 1.0 mL/min. The lignosulfonate concentration was 1.0 g/L. Distilled and deionized water was obtained in-house from a Heal Force Smart ultrapure water system.

Catalyst Preparation. The synthesis of LS was prepared according to the literature[23] with slight modifications. The acidic resin was activated in a saturated aqueous solution of NaCl for 1 day, followed by the treatment of 2.5 wt % NaOH aqueous solution for 80 min, and then washed with distilled water until pH 7.0, and finally it was treated with 5.0 wt % HCl aqueous solution for 12 h. Afterward, the resin was transferred to a column and washed with deionized water until the eluent reached pH 7.0. The sodium salt of LS (3.0 g) was dissolved in water (50 mL), and the solution was allowed to flow through the acidic resin column at a speed of 20 drops per minute. The acidic eluent was collected and then freeze-dried for 12 h to obtain LS product.

Catalyst Characterizations. Fourier transform infrared (FT-IR) spectra was conducted on a Vector-33 FT-IR spectrometer in the wavenumber range of 400–4000 cm^{-1}. The thermal stability of lignosulfonate and LS was determined by using an SDT-Q500 thermogravimetric analyzer (TGA) with temperature varying from room temperature to 700 °C in a nitrogen atmosphere and at a heating rate of 20 °C/min. A Zeiss EVO 18 (Jena, Germany) scanning electron microscope (SEM) was also used to investigate the morphology of lignosulfonate and LS. An Agilent 1100 (Santa Clara, CA, USA) high-performance liquid chromatograph (HPLC) was used to determine the yields of furfural.

Titration of −SO3H in LS. LS (100 mg) was added into a NaCl (2.00 mol/L, 20 mL) aqueous solution, sonicated for 1 h, and then centrifuged. The solution was titrated by standard NaOH solution (0.05 mol/L) with phenophthalein as indicator. The average value of $-SO_3H$ content was determined to be 1.87 mmol/g. The sulfur content in LS was determined to be 1.93 mmol/g by elemental analysis, which was very similar to the result of titration. These results showed that sulfur species on the sample were mainly in the form of sulfonic acids.[31]

Catalyst Reactions. In a typical procedure, LS (50 mg) was added into [BMIM]Cl (2 g) to obtain a well-proportioned and stable LS–IL solution in 15 min at 80 °C. Then xylose (200 mg) was added into the mixture and oil-bathed at 120 °C for 1 h. The reaction mixture was diluted with deionized water/methanol (1:4 by volume) to a certain concentration for HPLC detection range.

Identification and Quantitation with HPLC. Furfural was quantified by external standard calibration curve method, which was performed on an Agilent 100 HPLC system. The sample was separated by using a reversed-phase C_{18} column (200 × 4.6) at 40 °C with a detection wavelength of 283.40 nm. The optimized mobile phase consisted of methanol and deionized water with a volume ratio of 30:70. The flow rate was fixed at 1.0 mL/min. The seven concentrations of furfural (0.005, 0.0025, 0.001, 0.0005, 0.00025, 0.0001, and 0.00005 mol/L) were selected for HPLC analysis to determine the standard calibration curve. The content of furfural was obtained directly by calibration curves.

RESULTS AND DISCUSSION

Characterization of LS Catalyst. The FT-IR spectrum of LS is shown in Figure 1. Three new bands appeared at 1200–

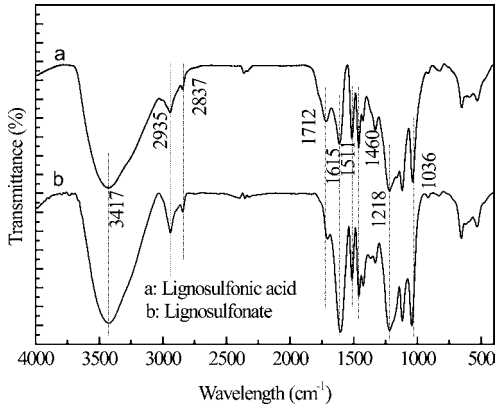

Figure 1. FT-IR spectrum for the lignosulfonic acid and lignosulfonate.

1250, 1010–1100, and 650 cm^{-1}, which were attributed to the O═S═O asymmetric and symmetric stretching vibration and S–O stretching vibration of sulfonic groups ($-SO_3H$), respectively.[32] The peak at 1712 cm^{-1} is attributed to −COOH. The absorbance at 3200–3500 cm^{-1} can be assigned to the O–H stretching vibration of LS, which is consistent with the former literature.[31] The peaks at 2837 and 2935 cm^{-1} belonged to the extensional vibration of −CH−, indicating that the phenol structure of LS is connected by methylene of the aldehyde structure.[33] The absorptions at 1460, 1511, and 1615 cm^{-1} are characteristic peaks of benzene rings.

The results of TGA are illustrated in Figures 2 and 3. Because of the evaporation of water, when the temperature was >100 °C, the TG curves of LS and lignosulfate fell slowly. LS began to pyrolyze when the temperature was >140 °C and decomposed quickly at higher temperature. The thermal stability of lignosulfonate was much better when the temperature was <170 °C.

Figures 4 and 5 show the SEM images of the lignosulfate and lignosulfonic acid. It was indicated that lignosulfonate exhibited spheres, which was different from fragmentary LS. The particle size of LS was much finer than that of lignosulfonate. It was found that LS was easier to dissolve in [BMIM]Cl than lignosulfonate.

dx.doi.org/10.1021/jf502404g | J. Agric. Food Chem. 2014, 62, 7430–7435

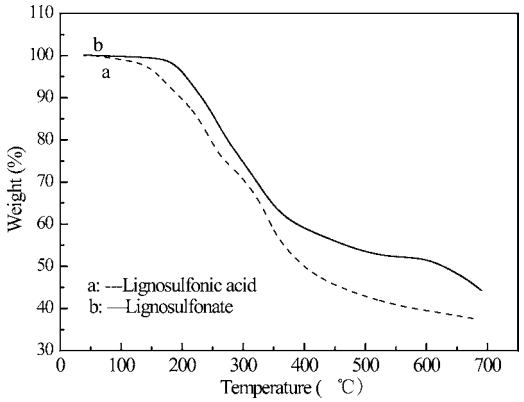

Figure 2. TG curves of lignosulfonic acid and lignosulfonate.

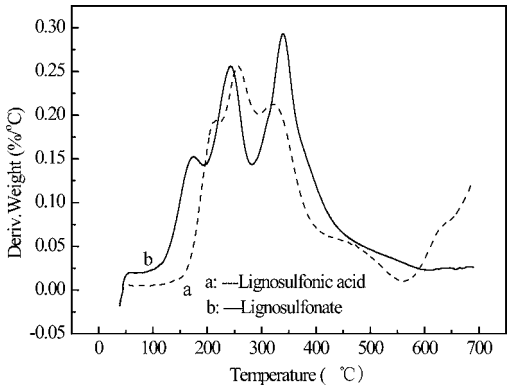

Figure 3. DTG spectrum of lignosulfonic acid and lignosulfonate.

Influence of Reaction Conditions on Catalytic Conversion of Xylose into Furfural. The influence of solvents on the formation of furfural is shown in Table 1 and Figure 6. It was found that it was easy to prepare a 2.5 wt % solution of LS in [BMIM]Cl at 80 °C for 15 min, and a brown-red solution was obtained. In this study, conversion of xylose into furfural catalyzed by LS was carried out in [BMIM]Cl and various organic solvents to investigate the influence of solvent. As shown in Table 1 and Figure 6, furfural yields were 3.4% in 1,4-dioxane, 3.2% in DMSO, 2.8% in toluene, and 10.3% in [BMIM]Cl, indicating that [BMIM]Cl was a better reaction solvent for furfural conversion catalyzed by LS. Clearly, DMF, DMA, and NMP were less effective reaction media in this study, with furfural yields of 0.7, 0.7, and 0.6%, respectively. The results demonstrated that the homogeneous catalysis of LS in [BMIM]Cl accelerated the conversion of xylose into furfural.[23] Furthermore, [BMIM]Cl could suppress the formation of humins during the conversion of xylose into furfural catalyzed by LS.

The effect of reaction temperature on the conversion of xylose into furfural was also studied. The conversion of xylose in [BMIM]Cl catalyzed by LS was carried out at 80, 100, 120, and 140 °C to study the influence of reaction temperature on furfural formation. The effect of reaction temperature on the hydrolysis of xylose is shown in Figure 7. It was found that the reaction temperature had a significant influence on the conversion of xylose.[6] Furfural yield (1 h) first increased from 8.7 to 15.0% as the temperature increased from 80 to 100 °C and then decreased to 12.4% when the temperature rose to 120 °C. The results indicated that high temperature not only facilitated the conversion of xylose into furfural but also facilitated the formation of humins.[16,28,34] Additionally, when the temperature increased to, or above, 100 °C, the thermal stability of LS was not so good. Therefore, 100 °C was the optimal temperature for the conversion of xylose into furfural catalyzed by LS.

To illustrate the relationship between reaction time and the yield of furfural, the experiments were carried out for 0.5, 1.0, 1.5, 2.0, and 2.5 h at 100 °C, respectively. As can be seen from Figure 8, the furfural yield increased from 8.2 to 18.3% as the reaction time increased from 0.5 to 2.5 h. With the increase of reaction time, the furfural yield increased first significantly, and then the increasing trend became slow. The reason may be ascribed to the decrease of furfural selectivity. Zhang and Lima[11,28] reported that the formation of humins led to low furfural selectivity, especially at high pentose conversions. The side reactions (dehydration of furfural, condensation between furfural and intermediates, and resinification of furfural) at longer reaction time formed undesired byproducts and decreased furfural yield. Therefore, the suitable reaction time was 1.5 h.

Besides solvents, reaction temperature, and time, the effect of catalyst loading on the conversion of xylose was also investigated. The reactions were carried out at 100 °C with LS loadings of 50, 100, 150, 200, 250, and 300 mg, respectively. As shown in Figure 9, the catalyst loading displayed a remarkable effect. A general trend was that the furfural yield increased with the increase of LS loading during the time course of reaction process. It was noted that with the increase of LS dosage from 50 to 250 mg, the yield of furfural increased from 10.3 to 18.1%. This improvement can be attributed to more active sites at higher catalyst loading. However, further increase in the catalyst loading to 300 mg did not result in a significant increase in furfural yield, which implied that the catalytic active sites available for the substrate in the system under the experimental condition were saturated, and a higher catalyst concentration could also facilitate both the dehydration

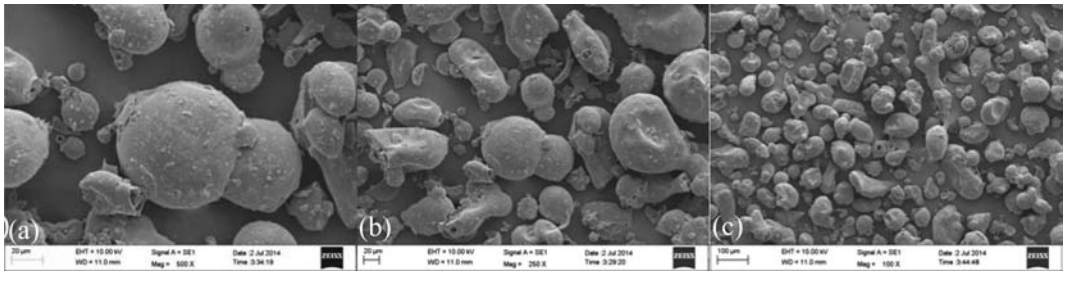

Figure 4. SEM of lignosulfate.

dx.doi.org/10.1021/jf502404g | J. Agric. Food Chem. 2014, 62, 7430−7435

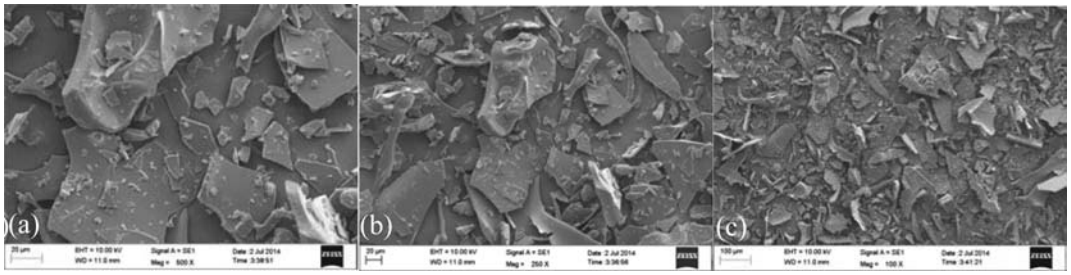

Figure 5. SEM of lignosulfonic acid.

Table 1. HPLC Results of Furfural Yields in Various Solvents

solvent	[BMIM]Cl	1,4-dioxane	DMSO	toluene	acetonitrile (CH_3CN)
yield (%)	10.3	3.4	3.2	2.8	1.7
solvent	THF	DMF	DMA	NMP	
yield (%)	1.3	0.7	0.7	0.6	

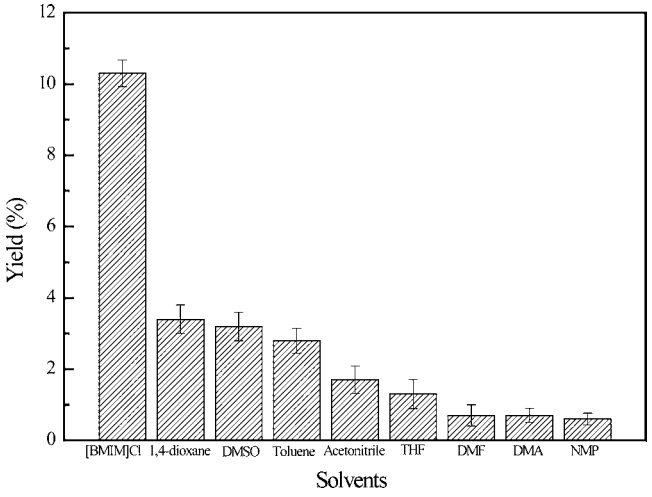

Figure 6. Influence of solvent on the catalytic conversion of xylose into furfural by LS. Experimental conditions: 2 g of solvent, 200 mg of xylose, 50 mg of LS, 120 °C, 1 h.

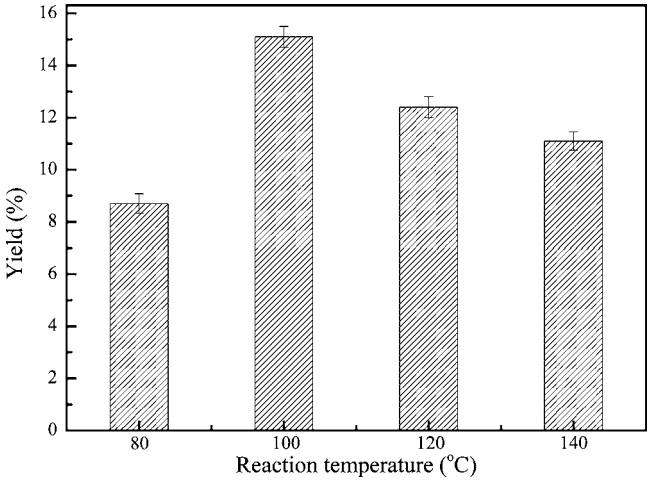

Figure 7. Influence of reaction temperature on xylose conversion into furfural. Experimental conditions: 2 g of [BMIM]Cl, 200 mg of xylose, 100 mg of LS, 1 h.

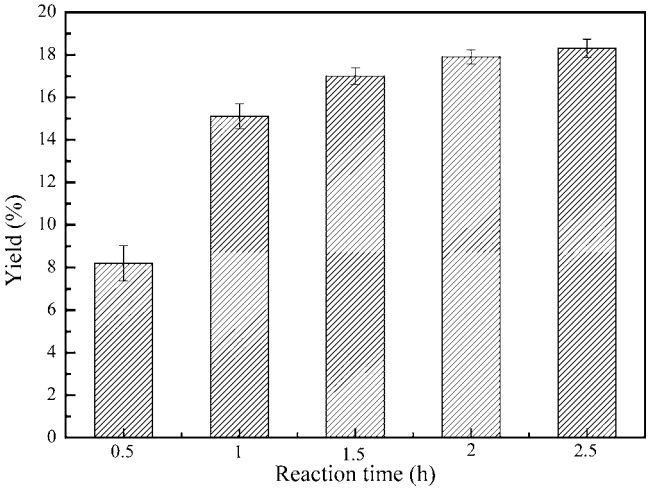

Figure 8. Influence of reaction time on conversion of xylose into furfural. Experimental conditions: 2 g of [BMIM]Cl, 200 mg of xylose, 100 mg of LS, 100 °C.

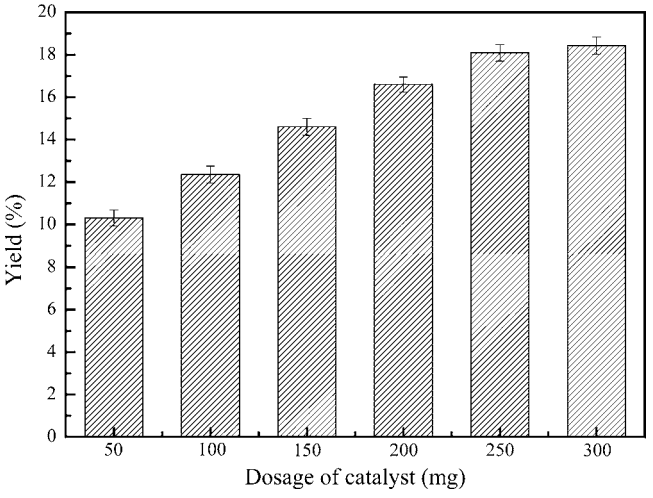

Figure 9. Effect of LS dosage on conversion of xylose into furfural. Experimental conditions: 2 g of [BMIM]Cl, 200 mg of xylose, 120 °C, 1 h.

of xylose and the dehydration of furfural. Further increasing the loading of LS could not facilitate the conversion. According to the results discussed above, the optimum reaction conditions were 250 mg of LS, 100 °C, and 1.5 h.

Recycling of LS Catalyst. The humins can be precipitated from the IL phase by ethanol. Therefore, the lifetime of LS was studied for the conversion of xylose into furfural by extracting furfural with ethyl acetate and then the precipitated humins were filtered and the catalytic system was used for the next

dx.doi.org/10.1021/jf502404g | J. Agric. Food Chem. 2014, 62, 7430−7435

process. The furfural yields for each reaction run are shown in Figure 10. It was found that the furfural yield decreased from

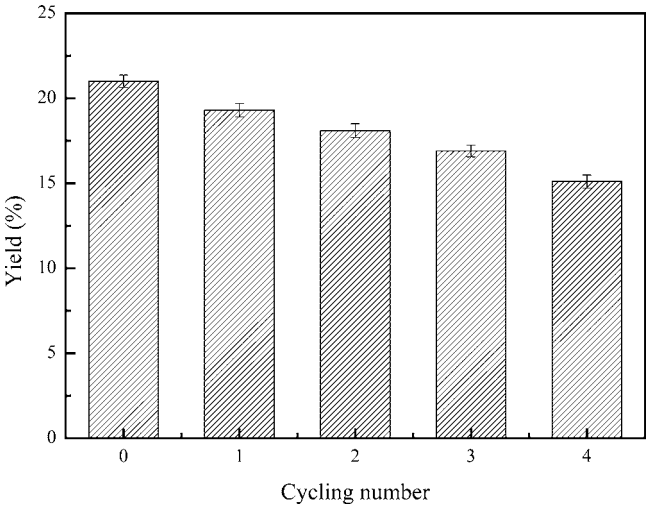

Figure 10. Reusability of LS in conversion of xylose into furfural. Experimental conditions: 2 g of [BMIM]Cl, 200 mg of xylose, 250 mg of LS, 100 °C, 1.5 h.

21.0% for the first time to 15.1% for the fifth time. This demonstrated that the humins may form and accumulate during the reaction, which affected the catalytic activity of LS in IL.

In summary, the homogeneous catalysis of LS in IL was successfully utilized as an efficient and environmentally friendly system for the conversion of xylose to furfural. The conversion yield of furfural from xylose was up to 21.0% for 1.5 h under mild conditions. LS was stable in the reaction process. The reusability study of the LS−IL catalytic system illustrated that the furfural yield decreased from 21.0 to 15.1% after five cycles, and the catalytic activity could be recovered after removal of the accumulated humins. For the integration of using sustainable lignocelluloses, renewable catalyst, and environmentally friendly solvent, this study shows a promising furfural production process that followed the concept of green chemistry.

AUTHOR INFORMATION

Corresponding Authors

*(X.P.) E-mail: fexwpeng@scut.edu.cn. Phone: +86-020-87111860. Fax: +86-020-87111860.

*(R.S.) E-mail: rcsun3@bifu.edu.cn

Funding

The project is supported by the State Key Program of National Natural Science Foundation of China (No. 21336002), Guangdong Natural Science Foundation (S2013040015055), Fundamental Research Funds for the Central Universities (2013ZM0050), Science and Technology Project of Guangzhou City in China (2014J2200063), National Natural Science Foundation of China (31110103902), and Major State Basic Research Projects of China (973-2010CB732204).

Notes

The authors declare no competing financial interest.

ABBREVIATIONS USED

*Dm*M, Dendrocalamus membranaceus; LS, lignosulfonic acid; IL, ionic liquid

REFERENCES

(1) Menon, V.; Rao, M. Trends in bioconversion of lignocellulose: biofuels, platform chemicals and biorefinery concept. *Prog. Energy Combust.* **2012**, *38*, 522−550.

(2) Sanders, J. P. M.; Clark, J. H.; Harmsen, G. J.; Heeres, H. J.; Heijnen, J. J.; Kersten, S. R. A.; van Swaaij, W. P. M.; Moulijn, J. A. Process intensification in the future production of base chemicals from biomass. *Chem. Eng. Process.* **2012**, *51*, 117−136.

(3) Kim, E. S.; Liu, S.; Abu-Omar, M. M.; Mosier, N. S. Selective conversion of biomass hemicellulose to furfural using maleic acid with microwave heating. *Energy Fuels* **2012**, *26*, 1298−1304.

(4) Wang, R.; Shi, W. Production and application of furfural. *Henan Chem. Ind.* **2008**, *25*, 14−15.

(5) Kemp, L. C.; Hamilton, G. B.; Gross, H. H. Furfural as a selective solvent in petroleum refining. *Ind. Eng. Chem.* **1948**, *40*, 220−227.

(6) Zhang, L. X.; Yu, H. B.; Wang, P.; Dong, H.; Peng, X. H. Conversion of xylan, D-xylose and lignocellulosic biomass into furfural using $AlCl_3$ as catalyst in ionic liquid. *Bioresour. Technol.* **2013**, *130*, 110−116.

(7) Russo, P. A.; Lima, S.; Rebuttini, V.; Pillinger, M.; Willinger, M. G.; Pinna, N.; Valente, A. A. Microwave-assisted coating of carbon nanostructures with titanium dioxide for the catalytic dehydration of D-xylose into furfural. *RSC Adv.* **2013**, *3*, 2595.

(8) Ordomsky, V. V.; Schouten, J. C.; van der Schaaf, J.; Nijhuis, T. A. Biphasic single-reactor process for dehydration of xylose and hydrogenation of produced furfural. *Appl. Catal., A: Gen.* **2013**, *451*, 6−13.

(9) Chareonlimkun, A.; Champreda, V.; Shotipruk, A.; Laosiripojana, N. Catalytic conversion of sugarcane bagasse, rice husk and corncob in the presence of TiO_2, ZrO_2 and mixed-oxide TiO_2-ZrO_2 under hot compressed water (HCW) condition. *Bioresour. Technol.* **2010**, *101*, 4179−4186.

(10) Marcotullio, G.; de Jong, W. Furfural formation from D-xylose: the use of different halides in dilute aqueous acidic solutions allows for exceptionally high yields. *Carbohydr. Res.* **2011**, *346*, 1291−1293.

(11) Lima, S.; Antunes, M. M.; Fernandes, A.; Pillinger, M.; Ribeiro, M. F.; Valente, A. A. Catalytic cyclodehydration of xylose to furfural in the presence of zeolite H-Beta and a micro/mesoporous Beta/TUD-1 composite material. *Appl. Catal., A: Gen.* **2010**, *388*, 141−148.

(12) Lessard, J.; Morin, J. F.; Wehrung, J. F.; Magnin, D.; Chornet, E. High yield conversion of residual pentoses into furfural via zeolite catalysis and catalytic hydrogenation of furfural to 2-methylfuran. *Top. Catal.* **2010**, *53*, 1231−1234.

(13) Sadaba, I.; Lima, S.; Valente, A. A.; Lopez Granados, M. Catalytic dehydration of xylose to furfural: vanadyl pyrophosphate as source of active soluble species. *Carbohydr. Res.* **2011**, *346*, 2785−2791.

(14) Dias, A. S.; Lima, S.; Pillinger, M.; Valente, A. A. Modified versions of sulfated zirconia as catalysts for the conversion of xylose to furfural. *Catal. Lett.* **2007**, *114*, 151−160.

(15) Rong, C.; Ding, X.; Zhu, Y.; Li, Y.; Wang, L.; Qu, Y.; Ma, X.; Wang, Z. Production of furfural from xylose at atmospheric pressure by dilute sulfuric acid and inorganic salts. *Carbohydr. Res.* **2012**, *350*, 77−80.

(16) Yang, Y.; Hu, C. W.; Abu-Omar, M. M. Synthesis of furfural from xylose, xylan, and biomass using $AlCl_3{\cdot}6H_2O$ in biphasic media via xylose isomerization to xylulose. *ChemSusChem* **2012**, *5*, 405−410.

(17) Zhang, J. H.; Zhuang, J. P.; Lin, L.; Liu, S. J.; Zhang, Z. Conversion of D-xylose into furfural with mesoporous molecular sieve MCM-41 as catalyst and butanol as the extraction phase. *Biomass Bioenergy* **2012**, *39*, 73−77.

(18) Agirrezabal-Telleria, I.; Larreategui, A.; Requies, J.; Guemez, M. B.; Arias, P. L. Furfural production from xylose using sulfonic ion-exchange resins (Amberlyst) and simultaneous stripping with nitrogen. *Bioresour. Technol.* **2011**, *102*, 7478−7485.

(19) Zhang, X.; Glusen, A.; Garcia-Valls, R. Porous lignosulfonate membranes for direct methanol fuel cells. *J. Membrane Sci.* **2006**, *276*, 301−307.

(20) Milczarek, G. Lignosulfonate-modified electrodes: electrochemical properties and electrocatalysis of NADH oxidation. *Langmuir* **2009**, *25*, 10345−10353.
(21) Hirai, N.; Kubo, S.; Magara, K. Combined cyclic voltammetry and in situ electrochemical atomic force microscopy on lead electrode in sulfuric acid solution with or without lignosulfonate. *J. Power Sources* **2009**, *191*, 97−102.
(22) Wang, Z.; Xue, J. W.; Zhang, J. S.; Liu, W. X. Concrete superplasticizer prepared from catalytic oxidation of lignosulfonate. *Adv. Mater. Res.* **2012**, *424*, 1088−1092.
(23) Xie, H.; Zhao, Z. K.; Wang, Q. Catalytic conversion of inulin and fructose into 5-hydroxymethylfurfural by lignosulfonic acid in ionic liquids. *ChemSusChem* **2012**, *5*, 901−905.
(24) Sun, P.; Armstrong, D. W. Ionic liquids in analytical chemistry. *Anal. Chim. Acta* **2010**, *661*, 1−16.
(25) Renner, R. Ionic liquids: an industrial cleanup solution. *Environ. Sci. Technol.* **2001**, *35*, 410−413.
(26) Brennecke, J. F.; Maginn, E. J. Ionic liquids: innovative fluids for chemical processing. *J. AIChE* **2001**, *47*, 2384−2389.
(27) Sievers, C.; Musin, I.; Marzialetti, T.; Olarte, M. B.; Agrawal, P. K.; Jones, C. W. Acid-catalyzed conversion of sugars and furfurals in an ionic-liquid phase. *ChemSusChem* **2009**, *2*, 665−671.
(28) Zhang, L.; Yu, H.; Wang, P. Solid acids as catalysts for the conversion of D-xylose, xylan and lignocellulosics into furfural in ionic liquid. *Bioresour. Technol.* **2013**, *136*, 515−521.
(29) Abu-Dalo, M. A.; Al-Rawashdeh, N. A. F.; Ababneh, A. Evaluating the performance of sulfonated Kraft lignin agent as corrosion inhibitor for iron-based materials in water distribution systems. *Desalination* **2013**, *313*, 105−114.
(30) Beramendi-Orosco, L. E.; Castro-Díaz, M.; Snape, C. E.; Vane, C. H.; Large, D. J. Application of catalytic hydropyrolysis for the rapid preparation of lignin concentrates from wood. *Org. Geochem.* **2004**, *35*, 61−72.
(31) Liu, B.; Zhang, Z.; Huang, K. Cellulose sulfuric acid as a bio-supported and recyclable solid acid catalyst for the synthesis of 5-hydroxymethylfurfural and 5-ethoxymethylfurfural from fructose. *Cellulose* **2013**, *20*, 2081−2089.
(32) Koukabi, N.; Kolvari, E.; Zolfigol, M. A.; Khazaei, A.; Shaghasemi, B. S.; Fasahati, B. A magnetic particle-supported sulfonic acid catalyst: tuning catalytic activity between homogeneous and heterogeneous catalysis. *Adv. Synth. Catal.* **2012**, *354*, 2001−2008.
(33) Zhang, X.; Zhang, Z.; Wang, F.; Wang, Y.; Song, Q.; Xu, J. Lignosulfonate-based heterogeneous sulfonic acid catalyst for hydrolyzing glycosidic bonds of polysaccharides. *J. Mol. Catal. A: Chem.* **2013**, *377*, 102−107.
(34) Shi, X. J.; Wu, Y. L.; Li, P. P.; Yi, H. F.; Yang, M. D.; Wang, G. H. Catalytic conversion of xylose to furfural over the solid acid SO_4^{2-}/ZrO_2-Al_2O_3/SBA-15 catalysts. *Carbohydr. Res.* **2011**, *346*, 480−487.

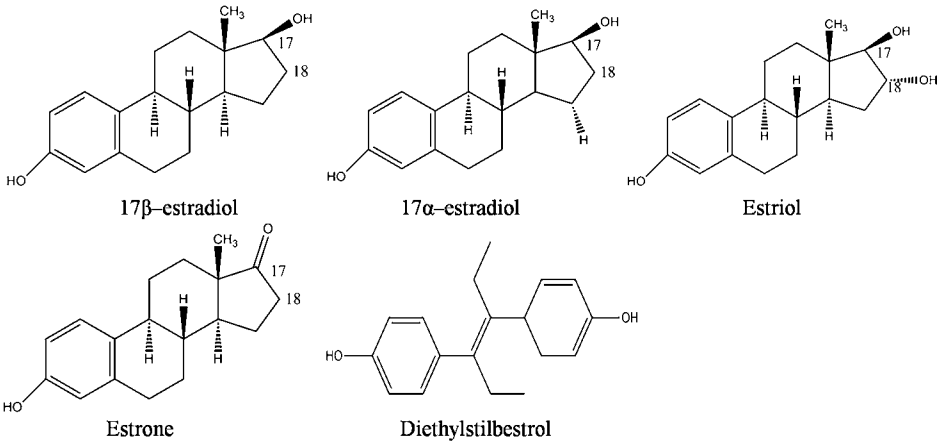

Figure 1. Chemical structures of 17β-estradiol, 17α-estradiol, estriol, estrone, and diethylstilbestrol.

(GO) has an extremely large specific surface area and small dimension,[19] and these characteristics make GO an excellent candidate as a support material for preparing surface MIPs.[20] Using MIPs on GO surface (MIPs-GO) has been proposed with high loading capacity and short binding time for the template molecule.[20,21] However, MIPs-GO homogeneously disperses in solution and is difficult to separate via traditional centrifugation and filtration methods, which restricted the application of MIPs-GO to some extent. Magnetic nanoparticles (Fe_3O_4) have properties of superparamagnetic and magnetic susceptibility, which means Fe_3O_4 can easily be separated from solutions by an external magnetic field.[22,23] On the basis of the advantages of GO and Fe_3O_4, the GO-Fe_3O_4 composites have been developed and widely applied in MIPs fields.[24,25] However, information is lacking on the development of 17β-E_2-based MIPs by using GO-Fe_3O_4 composites as the supporting material.

In the present paper, 17β-E_2-based MIPs were coated on the GO-Fe_3O_4 surface to achieve high imprinting efficiency and binding capacity. This study was the first demonstration for the preconcentration of 17β-E_2 in a food matrix using MIPs-GO-Fe_3O_4. The characteristics and binding capacity of 17β-E_2-based MIPs-GO-Fe_3O_4 were investigated in detail. The efficacy of MIPs-GO-Fe_3O_4 in extracting 17β-E_2 from food samples was also evaluated.

EXPERIMENTAL PROCEDURES

Reagents and Materials. 17β-Estradiol (17β-E_2), 17α-estradiol (17α-E_2), estrone (E_1), estriol (E_3), and diethylstilbestrol (DES) were purchased from Aladdin (Shanghai, China), and Figure 1 shows their chemical structures. Graphite powder, hexahydrate ferric chloride ($FeCl_3{\cdot}6H_2O$), sodium acetate, and ethylene glycol were purchased from Sinopharm Chemical Reagent Co., Ltd. (Shanghai, China). Acrylic acid (AA) and 2,2′-azobis(isobutyronitrile) (AIBN) were purchased from Aladdin. Acrylamide (AM) and ethylene glycol dimethacrylate (EGDMA) were obtained from Sigma-Aldrich (Shanghai, China). Other reagents were analytically pure and used without further purification.

Synthesis of Graphene Oxide. GO was prepared using natural graphite powders according to the modified Hummers method.[26] Five grams of graphite powders and 2.5 g of $NaNO_3$ were added into a flask containing 120 mL of H_2SO_4 (95%) and cooled in an ice bath with stirring. After the graphite powders dispersed, 15 g of $KMnO_4$ was added gradually under stirring, and the temperature of the mixture was kept at 35 °C for 60 min. H_2O_2 (3 mL, 30%) and deionized water (100 mL) were added slowly into the above reaction mixture at 90 °C with vigorous agitation for 30 min. Finally, the resultant yellow-brown GO was washed with a 10% HCl aqueous solution and distilled water until the pH was 7.0 and then was dried at 40 °C for 24 h.

Synthesis of Magnetic Graphene Oxide (GO-Fe_3O_4). The GO-Fe_3O_4 nanocomposites were synthesized according to the solvothermal method as follows:[27] 0.45 g of GO was completely dispersed in 70 mL of ethylene glycol via ultrasound for more than 3 h; then 1.4 g of $FeCl_3{\cdot}6H_2O$ and 2.8 g of NaOAc were added into the above mixture. After stirring for about 30 min, the mixture was transferred into a 100 mL Teflon stainless steel autoclave and reacted at 200 °C for 8 h. The obtained GO-Fe_3O_4 nanocomposites were thoroughly washed with distilled water and ethanol and then freeze-dried.

Modification of GO-Fe_3O_4 Nanocomposites. The surface of GO-Fe_3O_4 nanocomposites was grafted with AA by the following procedures:[28] Briefly, 5 mL of the suspension containing 100 mg of GO-Fe_3O_4 nanocomposites was added into 15 mL of ethanol with ultrasonication, and 1 mL of AA was then added into the above mixture with shaking at a rate of 300 rpm for 2 h.

Preparation of MIPs-GO-Fe_3O_4. The 17β-E_2-based MIPs-GO-Fe_3O_4 was prepared using AM as functional monomer, EGDMA as cross-linker, and AIBN as initiator in acetonitrile containing surface supporting materials of GO-Fe_3O_4-AA. 17β-E_2 (0.272 g, 1 mmoL), AM (0.517 g, 6 mmoL), EGDMA (170 μL, 0.90 mmoL), and AIBN (0.062 g, 0.381 mmoL) were added into 60 mL of acetonitrile containing GO-Fe_3O_4-AA (80 mg) in a 250 mL thick-walled glass tube. The prepolymerization mixture was degassed by using an ultrasonic bath for 10 min, then purged with nitrogen for 15 min to remove oxygen, and polymerized at 60 °C for 24 h. The MIPs-GO-Fe_3O_4 particles were washed with methanol/acetic acid solution (9:1, v/v) to remove completely the template molecules and residual monomers. Finally, the particles were dried to constant weight under vacuum at 55 °C. As control, non-imprinted polymers (NIPs-GO-Fe_3O_4) were synthesized simultaneously under identical conditions but omitting the template in the reaction system.

Characterization. Fourier transform infrared (FT-IR) spectra were recorded by using a FT-IR spectrophotometer (Nicolet 5700, Thermo Electron Corp., Waltham, MA, USA). The X-ray diffractometer (XRD) patterns were recorded using an XRD analyzer (D8-FOCUS, Bruker, Karlsruhe, Germany). Transmission electron microscopy (TEM) images were obtained on a JEOL (JEM-2010HR, Japan) transmission electron microscope. The magnetic properties were examined by vibrating specimen magnetometer (VSM) (7407; Lake Shore Cryotronics, Westerville, OH, USA). Raman spectra were collected using INVIA spectrophotometer (Renishaw, UK).

Adsorption Experiments. To investigate the binding capacity of MIPs-GO-Fe_3O_4 particles, a static adsorption test was conducted in acetonitrile solutions as follows:[15] 20 mg of MIPs-GO-Fe_3O_4 particles was dispersed in a 10 mL flask containing 2.0 mL of 17β-E_2 solutions of various concentrations within 0.1−1.0 mmol L^{-1}, respectively. After shaking for 12 h at room temperature, the samples were separated by

dx.doi.org/10.1021/jf501845w | J. Agric. Food Chem. 2014, 62, 7436−7443

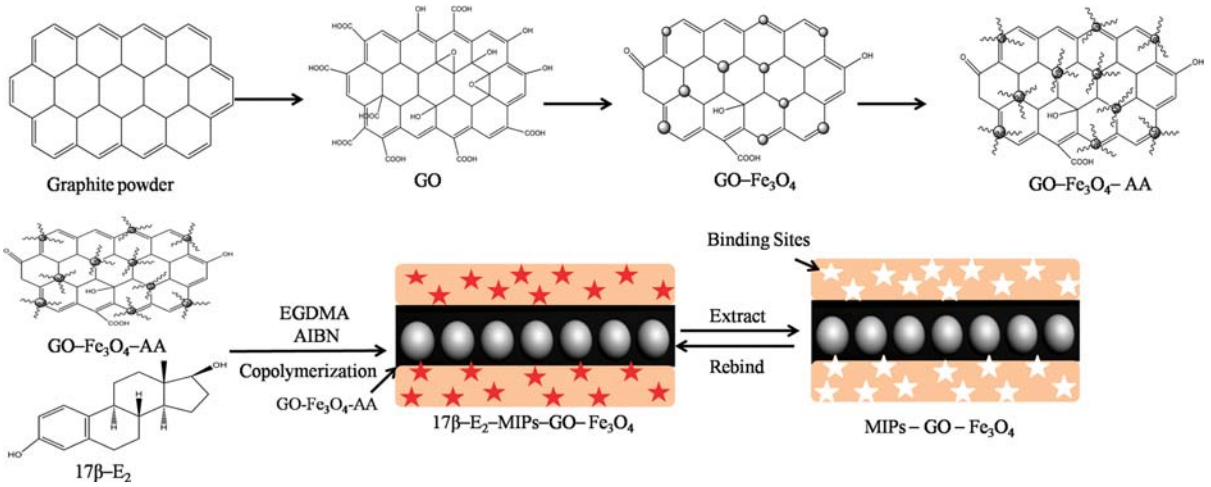

Figure 2. Schematic illustration of the preparation processes of MIPs-GO-Fe_3O_4.

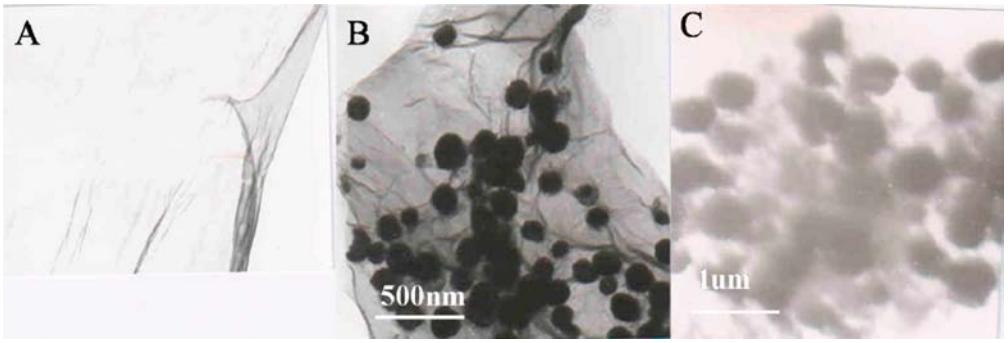

Figure 3. TEM images of GO (A), GO-Fe_3O_4 (B), and MIPs-GO-Fe_3O_4 (C).

an external magnet. The free concentration of 17β-E_2 in the supernatant solutions was determined using a UV spectrometer at 280.0 nm (TU-1810; Beijing Purkinje General Instrument Co., Ltd.). The adsorption amount of 17β-E_2 on MIPs-GO-Fe_3O_4 particles (Q) was calculated according to the following equation; Q tests were performed in triplicate with data reported as the mean values:

$$Q = (C_0 - C_F)V/M$$

C_0 (mg mL^{-1}) and C_F (mg mL^{-1}) are the initial and final 17β-E_2 solution concentrations, respectively. V (mL) is the sample volume, and M (g) is the mass of MIPs-GO-Fe_3O_4 particles.

Dynamic adsorption experiments were also performed. MIPs-GO-Fe_3O_4 (20 mg) or NIPs-GO-Fe_3O_4 (20 mg) were dispersed into 2.0 mL acetonitrile solutions containing 17β-E_2 (0.5 mmol L^{-1}), respectively. The solution was separated, and the free concentration of 17β-E_2 in the supernatant solutions was determined using UV spectrometry at 280.0 nm after 5, 10, 15, 20, 25, 30, 35, and 40 min of stirring, respectively.

Selectivity experiments were conducted using 17α-E_2, E_1, E_3, and DES as structural analogues. MIPs-GO-Fe_3O_4 (20 mg) or NIPs-GO-Fe_3O_4 (20 mg) were dispersed into 2.0 mL acetonitrile solutions containing 0.5 mmol L^{-1} of 17β-E_2, 17α-E_2, E_1, E_3, and DES, respectively. The amount of 17β-E_2, 17α-E_2, E_1, E_3, and DES in the supernatant was determined by UV after shaking for 12 h at room temperature. The recognition ability of MIPs-GO-Fe_3O_4 was evaluated by imprinting factor (α), which is defined in the equation

$$\alpha = Q_{MIP}/Q_{NIP}$$

where Q_{MIP} and Q_{NIP} are the adsorption amounts of the template or analogues on MIPs-GO-Fe_3O_4 and NIPs-GO-Fe_3O_4, respectively.

Analysis of 17β-E_2 in Real Samples. Milk powder samples were purchased from a local market. The milk powder samples (2 g) without spiking or spiked with 17β-E_2 standard solutions (2 mL; 0.2, 0.5, or 1.0 μmol L^{-1}) were first extracted using acetonitrile (20 mL) for 30 min. Then the solutions were centrifuged and filtered, and the extract solutions were obtained. MIPs-GO-Fe_3O_4 particles (20 mg) were added to the extract solution. The solution was shaken at room temperature for 1 h. A magnet (N_{35} model) was used to separate MIPs-GO-Fe_3O_4 particles from the solution, and the supernatant was measured by UV to determine the amounts of 17β-E_2. Simultaneously, the 17β-E_2 adsorbed onto MIPs-GO-Fe_3O_4 sorbent was subsequently eluted with 2 mL of methanol/acetic acid (9:1, v/v). After desorption for 2 h, the template molecule 17β-E_2 and adsorbent were easily rapidly separated by the magnet. The solution containing template molecule 17β-E_2 was dissolved in 2 mL of acetonitrile solvent, and the recovery amount of 17β-E_2 was determined by UV at 280.0 nm. All tests were performed in triplicate with data reported as the mean values. It should be noted that matrix interferences could be excluded by using the selective MIPs-GO-Fe_3O_4 as extracting agent. Moreover, the absorbance values were measured by deducting the blank values.

RESULTS AND DISCUSSION

Fabrication of MIPs-GO-Fe_3O_4. Figure 2 illustrates the synthesis route of MIPs-GO-Fe_3O_4. GO was prepared according to the classic Hummers method using graphite powders as starting material. GO-Fe_3O_4 nanocomposites were fabricated by a solvothermal method, GO was dissolved in ethylene glycol solution, and $FeCl_3 \cdot 6H_2O$ and NaOAC were used as the iron source and reductant, respectively. The Fe^{3+} could be absorbed by oxygen-containing functional groups of GO, and the Fe^{3+} was reduced to Fe_3O_4 by NaOAC during the reaction. GO-Fe_3O_4 nanocomposites were functionalized by a simple coordination reaction of the carboxyl group of AA with

dx.doi.org/10.1021/jf501845w | J. Agric. Food Chem. 2014, 62, 7436−7443

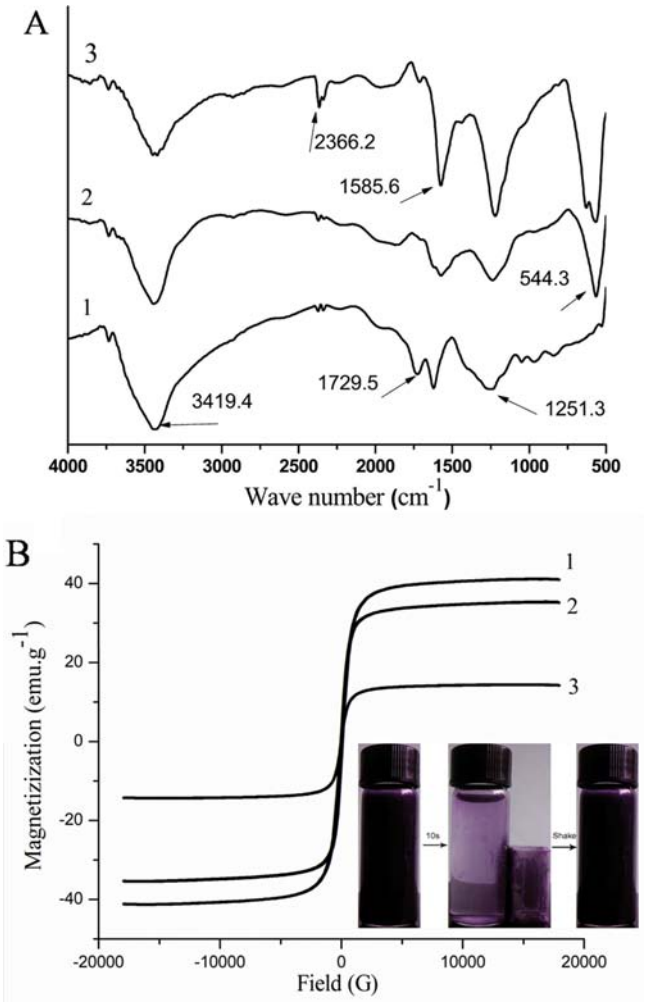

Figure 4. FT-IR spectra (A) of GO, GO-Fe_3O_4, and MIPs-GO-Fe_3O_4 (1, GO; 2, GO-Fe_3O_4; 3, MIPs-GO-Fe_3O_4) and VSM (B) (1, Fe_3O_4; 2, GO-Fe_3O_4; 3, MIPs-GO-Fe_3O_4).

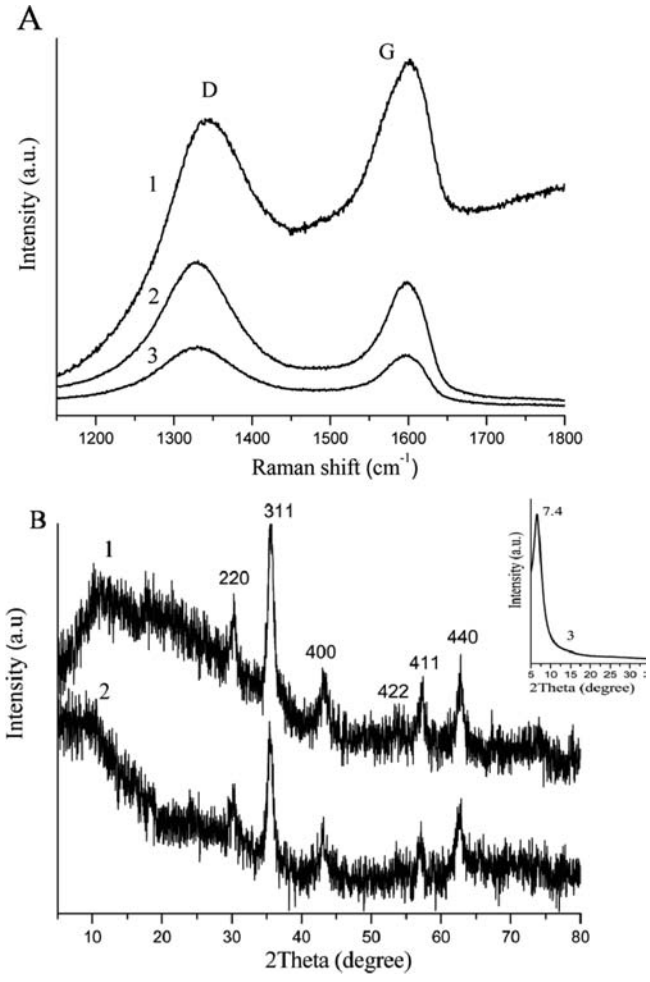

Figure 5. Raman (A) (1, GO; 2, GO-Fe_3O_4; 3, MIPs-GO-Fe_3O_4) and XRD (1, GO-Fe_3O_4; 2, MIPs-GO-Fe_3O_4; 3, GO).

the oxygen-containing functional groups of GO and particle surface residual Fe^{3+}. AA monomer grafted to GO-Fe_3O_4 surfaces and formed GO-Fe_3O_4-AA with vinyl end groups.[29,30] The 17β-E_2-based MIPs-GO-Fe_3O_4 was developed at 60 °C for 24 h in the presence of nanosized supporting materials (GO-Fe_3O_4-AA), template molecule (17β-E_2), functional monomer (AM), and cross-linking agent (EGDMA). The imprinted monolayer will polymerize at the GO-Fe_3O_4 surface by the reaction between AA and AM.[31,32] Finally, MIPs-GO-Fe_3O_4 was fabricated after washing with methanol/acetic acid (9:1, v/v) to remove the template molecule of 17β-E_2.

Characterization of MIPs-GO-Fe_3O_4. The prepared samples were characterized by TEM, FT-IR, Raman, XRD, and VSM. Figure 3 shows the morphologies of GO, GO-Fe_3O_4, and MIPs-GO-Fe_3O_4, respectively. GO displays a thin and irregular paper-like morphology with some wrinkles (Figure 3A). Fe_3O_4 nanoparticles were formed and homogeneously anchored onto the GO sheet (Figure 3B). As shown in Figure 3C, the MIPs were firmly attached on the surface of GO-Fe_3O_4 after polymerization.

Figure 4A shows the FT-IR spectra results of GO, GO-Fe_3O_4, and MIPs-GO-Fe_3O_4. The three samples have the same adsorption peak at 3419.4 cm^{-1} because of the O−H stretching vibration. For the FT-IR spectra of GO, the peak at 1251.3 cm^{-1} characterized C−O stretching vibration of the epoxy groups. A strong Fe−O characteristic stretching vibration peak of 544.0 cm^{-1} appeared for GO-Fe_3O_4, which indicated that Fe_3O_4 nanoparticles were successfully anchored onto the GO sheets. For the FT-IR spectra of MIPs-GO-Fe_3O_4, the absorption peaks of 2366.2 and 1585.6 cm^{-1} were attributed to C═O stretching vibration of AA monomer.[28] The intensity of C═O stretching (1728.0 cm^{-1}) was remarkably increased when Fe_3O_4 particles were covered with MIPs containing a large number of C═O groups in polyacrylamide units, which indicated the formation of imprinted polymers on the GO-Fe_3O_4 surface.

Figure 4B shows the magnetic property of Fe_3O_4, GO-Fe_3O_4, and MIPs-GO-Fe_3O_4, and the inset illustrates the dispersion and agglomeration processes of MIPs-GO-Fe_3O_4. The remanence and coercivity of samples almost disappeared, indicating that Fe_3O_4, GO-Fe_3O_4, and MIPs-GO-Fe_3O_4 have superparamagnetic characteristics. The saturation magnetization of Fe_3O_4, GO-Fe_3O_4, and MIPs-GO-Fe_3O_4 gradually decreased 41.14, 35.37, and 11.11 emu g^{-1}, respectively. Saturation magnetization decreased for MIPs-GO-Fe_3O_4 because of the presence of the GO and MIPs polymers on the Fe_3O_4 surface. Fortunately, the saturation magnetization value of MIPs-GO-Fe_3O_4 (11.11 emu g^{-1}) was sufficient to ensure the easy and quick separation of the compounds from solutions. As shown in the inset of Figure 4B, the MIPs-GO-

dx.doi.org/10.1021/jf501845w | J. Agric. Food Chem. 2014, 62, 7436−7443

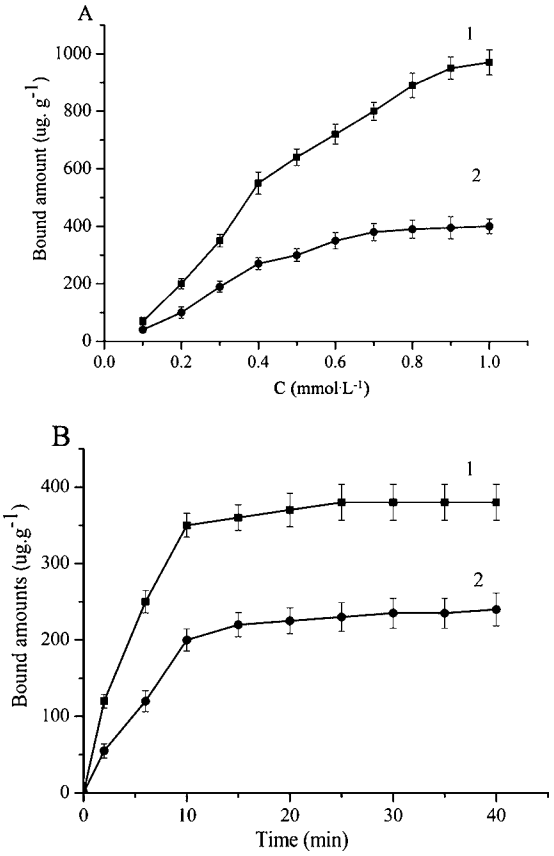

Figure 6. Static adsorption isotherms (A) and kinetic binding curves (B) of 17β-E_2 onto MIPs-GO-Fe_3O_4 (1) and NIPs-GO-Fe_3O_4 (2). Data are represented as the mean ± standard deviation (SD) (n = 3).

Fe_3O_4 can homogeneously disperse in aqueous solutions and is also sensitive to the magnetic field, showing MIPs-GO-Fe_3O_4 can be separated easily by the external magnet.

Figure 5A shows the Raman spectra of GO, GO-Fe_3O_4, and MIPs-GO-Fe_3O_4. All Raman spectra showed that three samples had G (approximately 1580 cm^{-1}) and D bands (approximately 1340 cm^{-1}), which agreed with the usual features of carbon materials in the Raman spectra. The valued of I_D/I_G wrtr approximately 0.923, 1.24, and 1.38 for GO, GO-Fe_3O_4, and MIPs-GO-Fe_3O_4, respectively.[33] The average size of the in-plane graphitic crystallite sp^2 domains increased, and such increase may be due to the small partial reduction of GO during synthesis.

The corresponding (XRD) patterns of GO, GO-Fe_3O_4, and MIPs-GO-Fe_3O_4 are presented in Figure 5B. GO showed a very sharp diffraction peak at 2θ = 7.40 corresponding to a d-spacing of 12.45 nm. However, the sharp peak of 2θ = 7.40 decreased for GO-Fe_3O_4 and MIPs-GO-Fe_3O_4, showing that GO was reduced to some extent by NaOAC during preparation. Typical XRD pattern peaks of Fe_3O_4 were observed at 2θ values of 30.0, 35.7, 42.9, 53.6, 56.8, and 62.7 for GO-Fe_3O_4 and MIPs-GO-Fe_3O_4, which are consistent with the standard XRD data of Fe_3O_4 (JCPDS Card 019-0629). The XRD pattern results showed that MIPs-GO-Fe_3O_4 comprised Fe_3O_4 nanoparticles, and the synthesized processes did not change the XRD phase of Fe_3O_4.

Binding Studies of MIPs-GO-Fe_3O_4. The static, dynamic, and selective binding abilities of MIPs-GO-Fe_3O_4 were investigated. Figure 6A shows the static binding isotherms of 17β-E_2 on MIPs-GO-Fe_3O_4. The adsorption capacity of MIPs-GO-Fe_3O_4 for 17β-E_2 increased quickly with increasing concentration. When the equilibrium concentration reached 0.9 mmol L^{-1}, the adsorption amounts of MIPs-GO-Fe_3O_4 appeared stable, and such stability may be due to the recognition sites, which were almost completely occupied by 17β-E_2. Figure 6A also shows that the NIPs-GO-Fe_3O_4 had lower saturated adsorption amounts than MIPs-GO-Fe_3O_4 because of the nonspecific recognition sites in NIPs-GO-Fe_3O_4. Moreover, the equilibrium dissociation constant (k_d) and maximum adsorption capacity (q_{max}) of the Scatchard equation were calculated, as follows: 12.68 μg mL^{-1} and 5.44 μmol g^{-1} for MIPs-GO-Fe_3O_4 and 7.65 μg mL^{-1} and 1.42 μmol g^{-1} for NIPs-GO-Fe_3O_4, respectively. The obtained q_{max} well

Table 1. Parameters Obtained of 17β-E_2 Adsorption onto MIPs-GO-Fe_3O_4 and NIPs-GO-Fe_3O_4 from Four Adsorption Isotherm Models

isotherm model	equation	parameter	MIPs-GO-Fe_3O_4	NIPs-GO-Fe_3O_4
Langmuir	$\frac{C_e}{Q_e} = \frac{1}{Q_{max}}C_e + \frac{1}{k_L Q_{max}}$	R^{2a}	0.9143	0.9276
		$Q_{max}{}^b$	2.154 ± 0.543	0.965 ± 0.038
		$k_L{}^c$	0.021 ± 0.003	0.034 ± 0.003
Freundlich	$\ln Q_e = \frac{1}{n}\ln C_e + \ln k_F$	R^2	0.9430	0.9287
		$k_F{}^d$	0.168 ± 0.028	0.069 ± 0.009
		$1/n^e$	0.689 ± 0.042	0.586 ± 0.037
Scatchard	$\frac{Q_e}{C_e} = \frac{(Q_{max} - Q_e)}{k_d}$	R^2	0.9172	0.9236
		Q_{max}	5.437 ± 0.489	1.415 ± 0.049
		$k_d{}^f$	12.68 ± 12. 41	7.65 ± 0.98
Langmuir–Freundlich	$\frac{1}{B} = \frac{1}{N_t\alpha}\left(\frac{1}{F}\right)^m + \frac{1}{N_t}$	R^2	0.9872	0.9743
		$N_t{}^g$	59.28 ± 14.31	6.365 ± 1.128
		α^h	0.038 ± 0.003	0.034 ± 0.001
		m^i	0.682 ± 0.034	0.825 ± 0.028

[a]Correlation coefficient. [b]Maximum absorption capacity. [c]Langmuir constant. [d]Freundlich constant. [e]Related to adsorption intensity and surface heterogeneity. [f]Scatchard constant. [g]Total number of binding sites. [h]Related to the median binding affinity constant K_0 via $K_0 = \alpha_1/m$. [i]Heterogeneity index, ranging from 0 to 1,equal to 1 for homogeneous materials.

dx.doi.org/10.1021/jf501845w | J. Agric. Food Chem. 2014, 62, 7436–7443

Table 2. Parameters Obtained of 17β-E_2 Adsorption toward MIPs-GO-Fe_3O_4 and NIPs-GO-Fe_3O_4 from Two Kinetic Adsorption Models

kinetic model	equation	parameters	MIPs-GO-Fe_3O_4	NIPs-GO-Fe_3O_4
pseudo-first-order	$\ln(Q_e - Q_t) = \ln Q_e - k_1 t$	R^{2a}	0.9675	0.9376
		$k_1{}^b$	0.034 ± 0.003	0.042 ± 0.004
		$Q_e{}^c$	1.926 ± 0.325	0.872 ± 0.024
pseudo-second-order	$\frac{t}{Q_t} = \frac{1}{k_2 Q_e{}^2} + \frac{t}{Q_e}$	R^2	0.9912	0.9864
		$k_2{}^d$	0.0062 ± 0.0023	0.0473 ± 0.0028
		Q_e	4.378 ± 0.154	0.952 ± 0.024

[a]Correlation coefficient. [b]Rate constant of adsorption in pseudo-first-order model. [c]Saturated adsorption amount of template molecule at equilibrium. [d]Rate constant of adsorption in pseudo-second-order model.

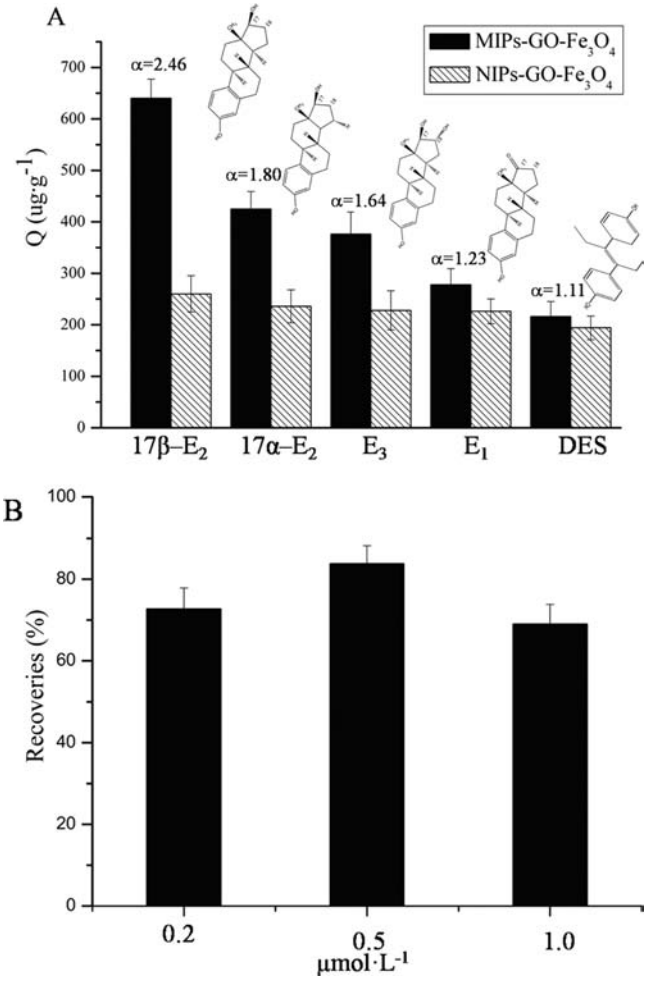

Figure 7. Competitive binding of 17β-E_2, 17α-E_2, E_3, E_1, and DES on MIPs-GO-Fe_3O_4 and NIPs-GO-Fe_3O_4 (A), and recoveries (%) and RSD (%) of MIPs-GO-Fe_3O_4 obtained from analysis of milk powder samples spiked with different concentrations (0.2, 0.5, and 1.0 mmol L^{-1}) 17β-E_2 (B). Data are represented as the mean ± SD (n = 3).

agreed with the experimental result (3.95 μmol g^{-1}). The results suggested that the MIPs-GO-Fe_3O_4 had excellent binding capacity for the template molecule.

Moreover, the adsorption process was further studied by four classical isotherm models including Langmuir, Freundlich, Scatchard, and Langmuir–Freundlich.[34] The corresponding equations and parameters of these models for adsorption of 17β-E_2 onto the MIPs-GO-Fe_3O_4 and NIPs-GO-Fe_3O_4 are listed in Table 1. The best fit was obtained from the Langmuir–Freundlich model, which resulted in a correlation coefficient of 0.9872. The parameters N_t, α, and m were 59.28, 0.038, and 0.682 for MIPs-GO-Fe_3O_4 and 6.365, 0.034, and 0.825 for NIPs-GO-Fe_3O_4, respectively. An excellent imprinting effect was observed from the presence of a number of specific binding sites on the MIPs-GO-Fe_3O_4 surface.

Dynamic binding experiments were performed to investigate the mass transfer properties of MIPs-GO-Fe_3O_4, and the results are shown in Figure 6B. The adsorption amounts of MIPs-GO-Fe_3O_4 for 17β-E_2 increased and reached equilibrium within 10 min. The rapid adsorption and high equilibrium binding capacity (381.2 μg g^{-1}) were due to the high ratio of surface-imprinted sites and large surface-to-volume ratio of MIPs-GO-Fe_3O_4, which allow high binding capacity and fast mass transfer. To investigate the mechanism underlying the biosorption process, such as mass transfer and chemical reaction, the pseudo-first-order and pseudo-second-order kinetic models were used to test the experimental data of MIPs-GO-Fe_3O_4 and NIPs-GO-Fe_3O_4.[35] The results are shown in Table 2. The pseudo-second-order model could better fit the time effect on the adsorption system than other kinetic models. The pseudo-second-order model provided the most suitable correlation for the adsorption, with the highest correlation coefficient of 0.9912. The obtained rate constant (k_2) was 0.0062 g (mg·min)$^{-1}$, and the equilibrium adsorption capacity (Q_e) was 4.378 μmol g^{-1}. Therefore, the adsorption could be deduced to follow the pseudo-second-order kinetic model.

To investigate the binding specificity of the MIPs-GO-Fe_3O_4, a selectivity test was conducted using structural analogues of 17β-E_2, being 17α-E_2, E_3, E_1, and DES, as control compounds. As shown in Figure 7A, the adsorption capacity of NIPs-GO-Fe_3O_4 is very close and nonselective for the five compounds because selective recognition sites are absent in NIPs-GO-Fe_3O_4. However, MIPs-GO-Fe_3O_4 showed a significantly higher binding capacity for 17β-E_2 than for these competitive analogues. The binding capacities of MIPs-GO-Fe_3O_4 for 17β-E_2, 17α-E_2, E_3, E_1, and DES were 640, 425, 376, 278, and 216 μg g^{-1}, respectively. Accordingly, the imprinting factor values (α) of MIPs-GO-Fe_3O_4 for 17β-E_2, 17α-E_2, E_3, E_1, and DES were 2.46, 1.80, 1.64, 1.23, and 1.11, respectively. These results indicated that MIPs-GO-Fe_3O_4 has highly specific recognition ability for 17β-E_2. The high selectivity for 17β-E_2 may be based on two factors. The first factor is the difference in chemical structures between 17β-E_2, 17α-E_2, E_3, E_1, and DES. The second factor is that only 17β-E_2 can specifically match the binding sites with the template in terms of size and shape.

Method Validation and Application to Analysis of 17β-E_2 in Food Samples. To further assess the practical applicability of MIPs-GO-Fe_3O_4, milk powder samples were

dx.doi.org/10.1021/jf501845w | J. Agric. Food Chem. 2014, 62, 7436–7443

used as real sample in the analysis. Figure 7B shows the extraction recoveries of MIPs-GO-Fe_3O_4 at three spiked 17β-E_2 concentrations of 0.2, 0.5, and 1.0 μmol L^{-1}, that is, 72.63, 84.20, and 68.93% with relative standard deviations (RSDs) of 5.26, 4.67, and 4.92%, respectively. The limits of detection and quantification were determined to be 0.035 and 0.10 μmol L^{-1} on the basis of signal-to-noise ratios of 3 and 10, respectively, and the regression equation was attained, $y = 0.0933x + 0.2152$ ($R^2 = 0.9928$) within 0.1−1.0 mmol L^{-1}. It is noted that the separation process was finished quickly within 10 s when a magnet was used. Compared to conventional MIPs extraction, a simpler, faster, and more economical magnetic separation procedure was provided, dispensing with pretreatment such as filtration or centrifugation. Thus, MIPs-GO-Fe_3O_4 can be used for preconcentration, separation, extraction, and removal of 17β-E_2 in real food samples.

In conclusion, a new type of molecularly imprinted nanomaterial (MIPs-GO-Fe_3O_4) was developed for the specific recognition and highly effective removal of 17β-E_2 in complicated matrices. MIPs-GO-Fe_3O_4 was prepared using GO-Fe_3O_4, AM, and 17β-E_2 as the supporting material, monomer, and template molecule, respectively. The magnetic property of MIPs-GO-Fe_3O_4 allowed the simple, rapid, and efficient separation of 17β-E_2 from matrices. Owing to the extremely large area of GO-Fe_3O_4, MIPs-GO-Fe_3O_4 has faster desorption and adsorption dynamics and higher selectivity than other traditional MIPs. MIPs-GO-Fe_3O_4 also showed excellent selectivity toward template molecules. In addition, MIPs-GO-Fe_3O_4 displayed satisfactory 17β-E_2 recovery when used for enrichment and removal of 17β-E_2 from food samples. We have provided an excellent platform for pretreatment and removal of 17β-E_2 from contaminated environmental and food samples.

AUTHOR INFORMATION

Corresponding Author

*(H.X.) Phone: +86-791-86634810. Fax: +86-791-86634810. E-mail: huaxiong100@126.com.

Author Contributions

‖F.N. and H.P. equally contributed to this work and should be regarded as co-first authors.

Funding

This work was supported by the National Natural Science Foundation of China (21266020, 21201098, 31160317, and 21105117), the Planning Subject of "the Twelfth Five-Year-Plan" National Science and Technology for the Rural development of China (2013AA102203-05), and the Jiangxi Department of Education Fund (GJJ13039).

Notes

The authors declare no competing financial interest.

REFERENCES

(1) Noppe, H.; Le Bizec, B.; Verheyden, K.; De Brabander, H. F. Novel analytical methods for the determination of steroid hormones in edible matrices. *Anal. Chim. Acta* **2008**, *611*, 1−16.

(2) Holgerm, K.; Karlhein, Z. C. Determination of endocrine-disrupting phenolic compounds and estrogens in surface and drinking water by HRGC-(NCI)-MS in the picogram per liter range. *Environ. Sci. Technol.* **2001**, *35*, 3201−3206.

(3) Tanaka, T.; Takeda, H.; Ueki, F.; Obata, K.; Tajima, H.; Takeyama, H.; Goda, Y.; Fujimoto, S.; Matsunaga, T. Rapid and sensitive detection of 17β-estradiol in environmental water using automated immunoassay system with bacterial magnetic particles. *J. Biotechnol.* **2004**, *108*, 153−159.

(4) Wang, S.; Li, Y.; Wu, X.; Ding, M.; Yuan, L.; Wang, R.; Wen, T.; Zhang, J.; Chen, L.; Zhou, X.; Li, F. Construction of uniformly sized pseudo template imprinted polymers coupled with HPLC-UV for the selective extraction and determination of trace estrogens in chicken tissue samples. *J. Hazard. Mater.* **2011**, *186*, 1513−1519.

(5) Vega-Morales, T.; Sosa-Ferrera, Z.; Santana-Rodriguez, J. Determination of alkylphenol polyethoxylates, bisphenol-A, 17α-ethynylestradiol and 17β-estradiol and its metabolites in sewage samples by SPE and LC/MS/MS. *J. Hazard. Mater.* **2010**, *183*, 701−711.

(6) Janssens, G.; Mangelinckx, S.; Courtheyn, D.; Prevost, S.; De Poorter, G.; De Kimpe, N.; Le Bizec, B. Application of gas chromatography−mass spectrometry/combustion/isotope ratio mass spectrometry (GC-MS/C/IRMS) to detect the abuse of 17β-estradiol in cattle. *J. Agric. Food Chem.* **2013**, *61*, 7242−7249.

(7) Wang, S.; Quan, Y.; Lee, N.; Kennedy, Ivanr Rapid determination of fumonisin B_1 in food samples by enzyme-linked immunosorbent assay and colloidal gold immunoassay. *J. Agric. Food Chem.* **2006**, *54*, 2491−2495.

(8) Ahn, Y. G.; Shin, J. H.; Kim, H. Y.; Khim, J.; Lee, M. K.; Hong, J. Application of solid-phase extraction coupled with freezing-lipid filtration clean-up for the determination of endocrine-disrupting phenols in fish. *Anal. Chim. Acta* **2007**, *603*, 67−75.

(9) Carpinteiro, J.; Quintana, J. B.; Rodríguez, I.; Carro, A. M.; Lorenzo, R. A.; Cela, R. Applicability of solid-phase microextraction followed by on-fiber silylation for the determination of estrogens in water samples by gas chromatography-tandem mass spectrometry. *J. Chromatogr., A* **2004**, *1056*, 179−185.

(10) Cormack, P. A.; Elorza, A. Z. Molecularly imprinted polymers: synthesis and characterisation. *J. Chromatogr., B* **2004**, *804*, 173−182.

(11) Chen, L.; Xu, S.; Li, J. Recent advances in molecular imprinting technology: current status, challenges and highlighted applications. *Chem. Soc. Rev.* **2011**, *40*, 2922−2942.

(12) Haupt, K. Molecularly imprinted polymers in analytical chemistry. *Analyst* **2001**, *126*, 747−756.

(13) Masqueè, N.; Marceè, R. M.; Borrull, F. Molecularly imprinted polymers: new tailor-made materials for selective solid-phase extraction. *TrAC−Trends Anal. Chem.* **2001**, *20*, 477−485.

(14) Huang, X. D.; Zou, H. F.; Chen, X. M.; Luo, Q. Z.; Kong, L. Molecularly imprinted monolithic stationary phases for liquid chromatographic separation of enantiomers and diastereomers. *J. Chromatogr., A* **2003**, *984*, 273−282.

(15) Jiang, T.; Zhao, L.; Chu, B.; Feng, Q.; Yan, W.; Lin, J. M. Molecularly imprinted solid-phase extraction for the selective determination of 17β-estradiol in fishery samples with high performance liquid chromatography. *Talanta* **2009**, *78*, 442−447.

(16) Yan, H.; Cheng, X.; Yang, G. Dummy molecularly imprinted solid-phase extraction for selective determination of five phthalate esters in plastic bottled functional beverages. *J. Agric. Food Chem.* **2012**, *60*, 5524−5531.

(17) Xu, S.; Li, J.; Chen, L. Molecularly imprinted core-shell nanoparticles for determination of trace atrazine by reversible addition-fragmentation chain transfer surface imprinting. *J. Mater. Chem.* **2011**, *21*, 43−46.

(18) Ma, J.; Yuan, L.; Ding, M.; Wang, S.; Ren, F.; Zhang, J.; Du, S.; Li, F.; Zhou, X. The study of core-shell molecularly imprinted polymers of 17β-estradiol on the surface of silica nanoparticles. *Biosens. Bioelectron.* **2011**, *26*, 2791−2795.

(19) Geim, A. K. Graphene: status and prospects. *Science* **2009**, *324*, 1530−1534.

(20) Li, Y.; Li, X.; Dong, C.; Qi, J.; Han, X. A graphene oxide-based molecularly imprinted polymer platform for detecting endocrine disrupting chemicals. *Carbon* **2010**, *48*, 3427−3433.

(21) Luo, J.; Jiang, S.; Liu, X. Efficient one-pot synthesis of mussel-inspired molecularly imprinted polymer coated graphene for protein-specific recognition and fast separation. *J. Phys. Chem. C* **2013**, *117*, 18448−18456.

(22) Chen, L.; Li, B. Magnetic molecularly imprinted polymer extraction of chloramphenicol from honey. *Food Chem.* **2013**, *141*, 23−28.
(23) Chen, F. F.; Xie, X. Y.; Shi, Y. P. Magnetic molecularly imprinted polymer for the selective extraction of sildenafil, vardenafil and their analogs from herbal medicines. *Talanta* **2013**, *115*, 482−489.
(24) Qiu, H.; Luo, C.; Sun, M.; Lu, F.; Fan, L.; Li, X. A chemiluminescence sensor for determination of epinephrine using graphene oxide-magnetite-molecularly imprinted polymers. *Carbon* **2012**, *50*, 4052−4060.
(25) Han, Q.; Wang, X.; Yang, Z.; Zhu, W.; Zhou, X.; Jiang, H. Fe_3O_4@rGO doped molecularly imprinted polymer membrane based on magnetic field directed self-assembly for the determination of amaranth. *Talanta* **2014**, *123*, 101−108.
(26) Wang, C.; Feng, C.; Gao, Y.; Ma, X.; Wu, Q.; Wang, Z. Preparation of a graphene-based magnetic nanocomposite for the removal of an organic dye from aqueous solution. *Chem. Eng. J.* **2011**, *173*, 92−97.
(27) Ai, L.; Zhang, C.; Chen, Z. Removal of methylene blue from aqueous solution by a solvothermal-synthesized graphene/magnetite composite. *J. Hazard. Mater.* **2011**, *192*, 1515−1524.
(28) Liu, B.; Han, M.; Guan, G.; Wang, S.; Liu, R.; Zhang, Z. Highly-controllable molecular imprinting at superparamagnetic iron oxide nanoparticles for ultrafast enrichment and separation. *J. Phys. Chem. C* **2011**, *115*, 17320−17327.
(29) Jeong, U. Y.; Teng, X. W.; Wang, Y.; Yang, H.; Xia, Y. N. Superparamagnetic colloids: controlled synthesis and niche applications. *Adv. Mater.* **2007**, *19*, 33−60.
(30) Shen, J. F.; Yan, B.; Li, T.; Long, Y.; Li, N.; Ye, M. X. Mechanical, thermal and swelling properties of poly(acrylic acid)-graphene oxide composite hydrogels. *Soft Matter* **2012**, *8*, 1831−1836.
(31) Kim, D. J.; Park, K. Swelling and mechanical properties of superporous hydrogels of poly(acrylamide-co-acrylic acid)/polyethylenimine interpenetrating polymer networks. *Polymer* **2004**, *45*, 189−196.
(32) Huang, Y. W.; Zeng, M.; Ren, J.; Wang, J.; Fan, L. R.; Xu, Q. Y. Preparation and swelling properties of graphene oxide/poly(acrylic acid-co-acrylamide) super-absorbent hydrogel nanocomposites. *Colloids Surf. A: Physicochem. Eng. Aspects* **2012**, *401*, 97−106.
(33) Li, X. L.; Wang, H. L.; Robinson, J. T.; Sanchez, H.; Diankov, G.; Dai, H. J. Simultaneous nitrogen doping and reduction of graphene oxide. *J. Am. Chem. Soc.* **2009**, *131*, 15939−15944.
(34) Chen, Z.; Ma, W.; Han, M. Biosorption of nickel and copper onto treated alga (*Undaria pinnatifida*): application of isotherm and kinetic models. *J. Hazard. Mater.* **2008**, *155*, 327−333.
(35) Zhu, J.; Wei, S.; Gu, H.; Rapole, S. B.; Wang, Q.; Luo, Z.; Haldolaarachchige, N.; Young, D. P.; Guo, Z. One-pot synthesis of magnetic graphene nanocomposites decorated with core@double-shell nanoparticles for fast chromium removal. *Environ. Sci. Technol.* **2012**, *46*, 977−985.

evidence of toxicity to GT has been reported. Patients have shown tolerance to drug complaints of gastrointestinal distress, even at high doses (72 g/kg body weight).[14] GT derivatives may thus be useful as additional or adjuvant preventive and therapeutic agents for hypercholesterolemia. The lipid-lowering effect of GT derivatives is considered to be associated with the increased excretion of bile acids.[13] However, the metabolic effects of 1,4-GL in hypercholesterolemia are yet to be reported.

Metabonomics, an emerging subject of the postgenome era, deals with the quantitative understanding of metabolites in biological fluids and their dynamic responses to changes in endogenous and exogenous factors. Metabonomics can thus provide the information on what is actually happening. Furthermore, this technology adopts a "top-down" strategy to determine the function of organisms from the terminal symptoms of the metabolic network and to elucidate the metabolic changes in a complete system caused by interventions in a holistic context.[15] Therefore, metabonomics provides important information on the possible model of action of nutritional agents.[16,17] The present study reveals that 1,4-GL significantly prevents or delays the onset and development of hypercholesterolemia when rats were coadministered with a high-fat, high-cholesterol (HFHC) emulsion. The metabolic mechanism of 1,4-GL in hypercholesterolemia prevention was quantitatively investigated via nuclear magnetic resonance (^{1}H NMR)-based metabonomic analysis and colonic flora tests.

MATERIALS AND METHODS

Chemicals. 1,4-GL and the sodium salt of (trimethylsilyl)-propionic-2,2,3,3-d_4 acid (TSP) were purchased from Sigma (USA). All chemicals used were of analytical reagent grade. The HFHC emulsion was prepared as previously described,[18] and it was composed of 20% lard, 10% cholesterol, and 2% sodium cholate.

Animal Experiment. Forty female Sprague–Dawley (SD) rats weighing 180–200 g were randomly divided into five groups (n = 8 each) after acclimating to the environment for 7 d. The control group received water via oral gavage for 12 d once daily. Rats in the HFHC group were administered with 1.0 mL of HFHC for 12 d once daily to induce hypercholesterolemia. The 1,4-GL treatment group received 1,4-GL (30.0 mg/kg) via oral gavage for 12 d once daily. The HFHC +1,4-GL1 and HFHC+1,4-GL2 groups were treated with HFHC (1.0 mL) in combination with 30.0 or 10.0 mg/kg 1,4-GL, respectively, via oral gavage daily for 12 d. All animals were housed in approved facilities by group at a controlled relative humidity (50–70%) and temperature (22 ± 2 °C). Water and regular rodent chow were available ad libitum. On the 13th day, all rats were placed in individual metabolism cages and fasted for 12 h. Urine and blood samples were collected after 24 h. The rats were immediately sacrificed following the treatment. Rat livers were removed and stored at −20 °C. All urine samples were immediately diluted after collection with H_2O to 15.0 mL. About 1.2 mL of the aliquots of the solution were centrifuged at 8000 rpm for 10 min. The obtained supernatant was stored at −20 °C until analysis.

Animal experiments were carried out in accordance with the Guidelines for Animal Experiments at Nanchang University (Nanchang, China). The protocol was approved by the Animal Ethics Committee at Nanchang University.

Measurement of Lipids in Serum and Extraction of Liver. In this experiment, 0.2 g of liver tissue was homogenized. The lipid was extracted by 4.0 mL of 2-propanol. The lipid levels in the serum and liver extracts, which include total cholesterol, triglyceride, and high- and low-density lipoprotein cholesterol, were measured in duplicate by using commercial kits from Jiancheng Biotechnology Institute (Nanjian, China).

^{1}H NMR Spectroscopy of Urine Samples. Urine samples were prepared for NMR spectroscopy by diluting 300 μL of rat urine with 200 μL of 0.2 M sodium phosphate buffer (pH 7.4) and 50 μL of TSP in D_2O to a final concentration of 0.1 mM to calibrate the chemical shift. NMR spectroscopy was carried out using a Bruker AvanceII-600 MHz spectrometer (Germany). All spectra were recorded at 298 K. 1D proton spectra were obtained from 32 scans over a spectral width of 14 ppm. The presaturation method was used to suppress the proton signal of the solvent.

All ^{1}H NMR spectra were processed using Topspin 2.1 (Bruker Biospin GmbH, Rheinstetten, Germany). The spectra were processed to a size of 64 k after multiplying with an exponential window function. The spectra were phase and baseline corrected manually. The chemical shifts were referenced to the TSP signal. Full-resolution spectra from 0.2 to 9.5 ppm were saved. Data from 4.5 to 6.5 ppm were excluded to eliminate the effects of imperfect water suppression and cross-saturation of urea. Each spectral intensity data set was normalized to the total spectral intensity over the whole spectrum.

The metabolites were identified in the ^{1}H NMR spectra by comparing their chemical shifts and coupling patterns with the corresponding values from the literature and publicly accessible databases (http://www.bmrb.wisc.edu, http://www.hmdb.ca). Total correlation spectroscopy (TOCSY), ^{13}C-heteronuclear single-quantum correlation (^{13}C-HSQC), statistical total correlation spectroscopy (STOCSY), and some standard compounds were also utilized to identify the metabolites.

Data Processing. Principal component analysis (PCA) and orthogonal partial least-squares discriminant analysis (OPLS-DA) were performed using SIMCA-P (version 12.0, Umetrics, Umeå, Sweden). The quality of OPLS-DA models was described by R^2X, R^2Y, and Q^2. The parameters were calculated using the default leave 1/7 out cross validation. R^2X and R^2Y represent the fraction of the sum of squares for the selected component. Q^2 represents the predictive ability of the model. To investigate model predictability and data overfitting, a 200-iteration permutation test was performed in the PLS-DA model with the same number of components as that in the OPLS-DA model.[19] Score and loading plots combined with variable importance in the projection (VIP) were used to interpret the model.

Gut Microflora Cultivation. After thawing at room temperature, the samples taken from colonic contents were accurately weighed and immediately homogenized using glass beads into a sterile saline solution (1.0 g/10.0 mL). The solution was serially diluted in 10-fold steps. Then 0.1 mL of the aliquots of the diluents (10- and 100-fold) was inoculated in the middle of agar plates containing eosin methylene blue agar, *Enterococcus* selective agar, *Lactobacillus* selective agar, and BBL agar media. The sample was spread over the surface of the plate by using an L-rod. Each diluent was inoculated in duplicate. *Escherichia coli* was aerobically incubated at 37 °C for 48 h. *Lactobacillus* and *Enterococcus* were incubated at 37 °C for 48 h in a microaerophilic environment; *Bifidobacterium* was incubated in an anaerobic glovebox at 37 °C for 72 h. Bacterial colonies were counted after incubation.

Quantification of Significant Metabolites in Urine and Serum. The contents of lactate, acetate, formate, creatinine, and bile acid in urine samples were quantified based on their individual ^{1}H NMR spectra. At least six concentrations of the standard solutions were analyzed. The calibration curves were constructed by plotting the ratio of the analyte peak area to TSP area against each analyte. The contents of lactate and creatinine in serum were quantified using commercial kits from the Jiancheng Biotechnology Institute (Nanjian, China). The acetate in serum was measured using commercial kits from R-Biopharm (Germany).

Creatinine clearance (CC) was calculated using the formula given as follows: CC = Urine creatinine concentration × Urine volume (24 h)/Serum creatinine concentration.

RESULTS

HFHC-Induced Hypercholesterolemia in Rats. Animal models have provided fundamental contributions to the analysis of the onset and progression of complex multifactorial

Table 1. Serum (and/or Liver) Lipid Levels for Various Treatments[a]

biochemical indexes	control	1,4-GL1 treatment	HFHC group	HFHC coadministered with 1,4-GL1	HFHC coadministered with 1,4-GL2
LDL-C (mmol/L)	0.70 ± 0.09	0.94 ± 0.16	5.45 ± 0.74[b]	1.78 ± 0.39[c]	2.58 ± 0.33[c]
HDL-C (mmol/L)	1.76 ± 0.08	1.73 ± 0.10	1.68 ± 0.14	1.45 ± 0.15	1.68 ± 0.13
TC (mmol/L)	3.06 ± 0.26	3.08 ± 0.18	6.51 ± 0.09[b]	3.44 ± 0.29[c]	4.32 ± 0.32[c]
(liver, μmol/g)	6.04 ± 1.21	6.34 ± 2.11	15.3 ± 2.41[b]	7.42 ± 2.12[c]	10.6 ± 1.33[c]
TG (mmol/L)	0.82 ± 0.08	0.93 ± 0.10	1.58 ± 0.56	1.04 ± 0.15	0.95 ± 0.17
(liver, μmol/g)	0.21 ± 0.02	0.18 ± 0.04	0.78 ± 0.04[b]	0.38 ± 0.01[c]	0.53 ± 0.04[c]

[a]1,4-GL1 and 1,4-GL2 respectively denote the doses of 1,4-GL, which are 30.0 and 10.0 mg/kg. The values are expressed by mean ± SEM, $n = 8$. Abbreviations: LDL-C: low-density lipoprotein cholesterol; HDL-C: high-density lipoprotein cholesterol; TC: total cholesterol; TG: triglyceride. [b]Significant difference from the control group ($p < 0.05$, one-way ANOVA). [c]Significant difference from the HFHC group ($p < 0.05$, one-way ANOVA).

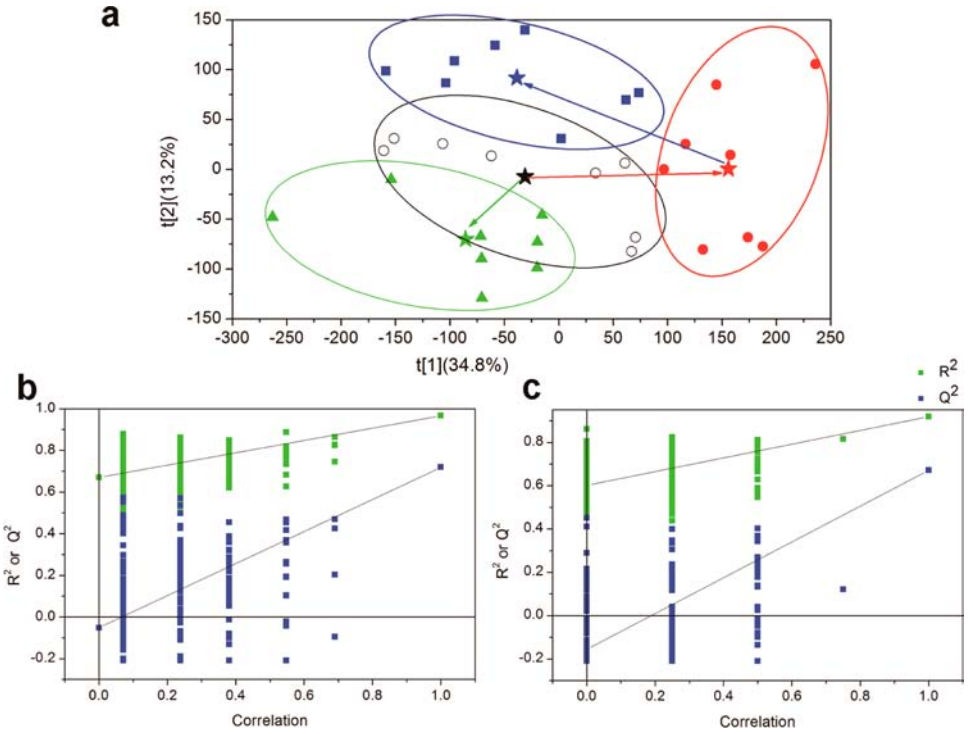

Figure 2. Results of PCA and (O)PLS-DA generated by data from ^{1}H NMR spectroscopy of rat urine. (a) PCA score plot; the variables were scaled by unit variance (UV). ●: HFHC group; ■: HFHC coadministered with 1,4-GL (30.0 mg/kg); ○: control group; ▲: 1,4-GL treatment (30.0 mg/kg). ★: Mean score of $t[1]$ (or $t[2]$) for each group. (b) Statistical validation of the OPLS-DA model by PLS-DA for the HFHC group and the control group. (c) Statistical validation of the OPLS-DA model by PLS-DA for the 1,4-GL treatment group and the control group.

diseases, such as cardiovascular diseases.[20] Animal models have smaller interindividual variation in their genetic and metabolic factors in each strain than in humans. In addition, experiments can be carried out at the same environmental and feeding conditions. In this study, the rats were administered with HFHC[18] or coadministered with 1,4-GL for 12 successive days. Table 1 reveals that the biochemical indicators of hypercholesterolemia, particularly serum LDL-c and total cholesterol (TC), significantly increase in the HFHC group compared with those in the control group. Furthermore, notable increases in TC and triglyceride (TG) in the liver are observed in the HFHC group. The dose-dependent decreases in LDL-c, TC, and TG in the serum are detected upon coadministration of HFHC with 1,4-GL (10.0 and 30.0 mg/kg), which suggests strongly that 1,4-GL prevents or delays the onset and development of HFHC-induced hypercholesterolemia.

^{1}H NMR-Based Metabonomic Analysis for Rat Urine. A ^{1}H NMR-based metabonomic experiment was carried out to explore the possible mechanisms of 1,4-GL in preventing the development of HFHC-induced hypercholesterolemia at metabolic levels. PCA is a statistical approach to facilitate an understanding of the relationships of a number of complex objects in a multivariate data set. The resulting data were displayed as "score plots", which represent the distribution of samples in multivariate space. The score plots of the first two principal components allowed visualization of the data and to establish whether there was any intrinsic difference in the ^{1}H NMR-based metabolic profiling of rat urine. The PCA score plot (Figure 2a) shows that the HFHC group is isolated from other groups; however, the group of HFHC coadministered with 1,4-GL is closer to the normal groups. The result indicates that 1,4-GL restores the urinary ^{1}H NMR phenotype that is disturbed by HFHC-induced hypercholesterolemia.

OPLS-DA, a supervised model, can be considered as a modification of the traditional PLS-DA, particularly in extracting information on changes in the metabolic profiling of samples. Thus, in this study, the ^{1}H NMR data of rat urine were employed to establish pairwise OPLS-DA models of the

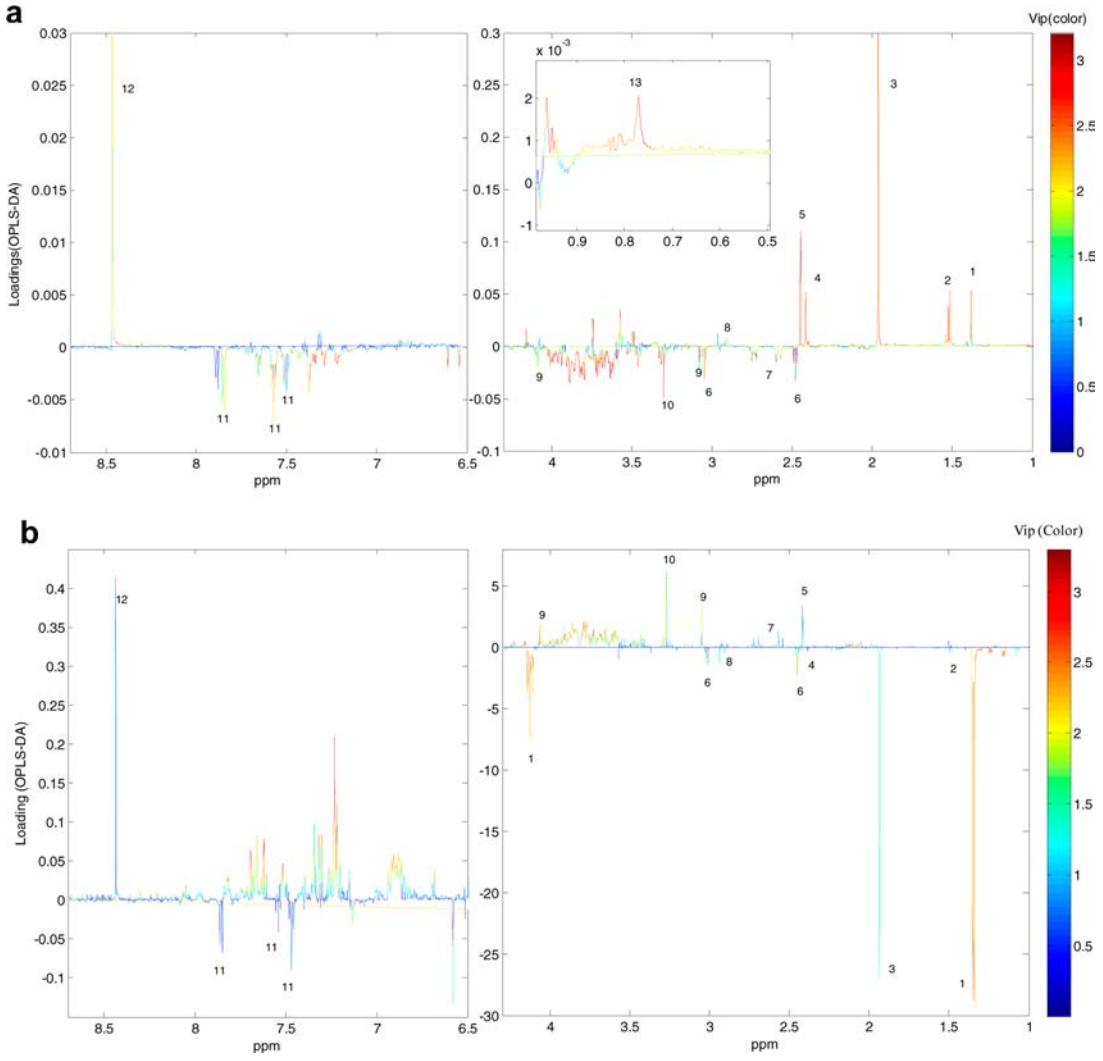

Figure 3. VIP-coded loadings plot. The color scales (VIP values) show variable importance in the OPLS-DA projection generated by the urinary ^{1}H NMR data of the HFHC and the control group (a: R^2X, 0.878, R^2Y, 1.0; Q^2, 0.89) or the 1,4-GL treatment and the control group (b: R^2X, 0.72, R^2Y, 0.97; Q^2, 0.73). Metabolite keys: 1, lactate; 2, alanine; 3, acetate; 4, pyruvate; 5, succinate; 6, 2-oxoglutarate; 7, citrate; 8, TMA; 9, creatinine; 10, TMAO; 11, hippurate; 12, formate; 13, cholate.

HFHC group (and the 1,4-GL treatment group) to the control group, aiming to single out statistically and potentially significant variables (metabolites) responsible for the difference between the HFHC group (and 1,4-GL treatment group) and the control group. Successful discrimination is achieved with a goodness-of-prediction Q^2 of more than 0.70. The OPLS-DA models reveal that the HFHC and 1,4-GL treatment groups are statistically distinguishable from the control group (p = 0.031 and p = 0.018, respectively; CV-ANOVA). The validation plot from the PLS-DA model (Figure 2b and c) demonstrates that the original OPLS-DA model is not random and overfitted because the permutated R^2 and Q^2 values are significantly lower than the corresponding original values; hence, the OPLS-DA model is robust.

A bivariate plot, which combines the loading coefficients and VIP, was generated based on the OPLS-DA model[21] (Figure 3). The plot characterizes the variation of a peak with changes in intensity and its importance to classification (color code). Upward- and downward-oriented peaks in the bivariate plot reflect the increased and decreased intensities from the intervention of HFHC or 1,4-GL, respectively. Figure 3 lists the important metabolites for classification.

1,4-GL Modifies Gut Flora Intervened by HFHC. Figure 3 reveals the significant downregulation and upregulation of trimethylamine-*N*-oxide (TMAO) in the HFHC and 1,4-GL groups, respectively, upon comparison with the control group. The excretion of trimethylamine (TMA) is also found to be opposite the alteration by HFHC compared with the 1,4-GL treatment. Metabolites (e.g., TMAO and TMA) are directly related to the statuses of gut microbiota and are urinary biomarkers of the alteration of gut flora.[22,23] We therefore presume the differences between the effects of 1,4-GL treatment and HFHC on gut flora. To clarify the hypothesis, the contents in rat colon underwent aseptic manipulation to culture the enterobacteria. The results show that the levels of gut bacteria, such as *Bifidobacterium*, *Lactobacillus*, and *Enterococcus*, markedly decrease in the HFHC group compared with the control group (Figure 4). Similar results to *Bifidobacterium* species in high-fat-feeding mice have been previously reported.[24,25] However, the quantities of *Bifidobacterium*, *Lactobacillus*, and *Enterococcus* significantly increase when the rats with hypercholesterolemia were coadministered with 1,4-GL. 1,4-GL significantly increases the quantities of *Bifidobacterium* (1.7-fold) and *Lactobacillus* (4.2-fold) but

dx.doi.org/10.1021/jf501744d | J. Agric. Food Chem. 2014, 62, 7444−7451

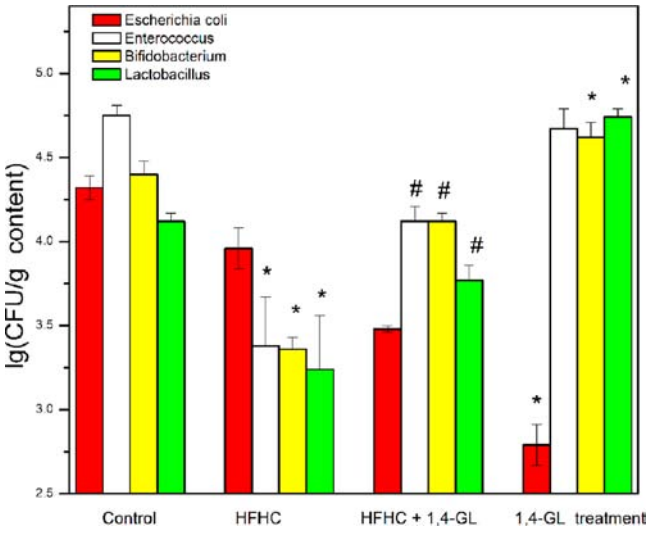

Figure 4. Levels of bacterial flora in rat colon after various interventions. CFU: colony forming units. The bar graph represents the mean ± SE for samples derived from five rats in each group. *Significant difference from the control group ($p < 0.05$, one-way ANOVA). #Significant difference from the HFHC group ($p < 0.05$, one-way ANOVA).

reduces that of *E. coli* (31.2-fold) in 1,4-GL-treated rats (Figure 4). The findings indicate that 1,4-GL restores the HFHC-induced imbalance of gut flora and affects their conversion to probiotics (e.g., *Bifidobacterium* and *Lactobacillus*).

Elevation of Serum Lactate and Acetate in Hypercholesterolemic Rats. NMR-based metabonomic results (Figure 3) indicate that the alterations of particular metabolites (e.g., lactate, creatinine, acetate, and formate) in urine were significantly opposite the direction of regulation caused by HFHC intervention compared with 1,4-GL treatment. To comprehend the possible biological effects of 1,4-GL in preventing hypercholesterolemia, the contents of the key metabolites were determined in the urine and serum samples (Table 2). The HFHC group exhibits higher serum (lactate: 1.77-fold, $p < 0.01$; acetate: 1.50-fold, $p < 0.01$) and urinary excretion (lactate: 1.47-fold, $p > 0.05$; acetate: 4.87-fold, $p < 0.01$) of lactate and acetate than the control group.

The quantitative results (Table 2) also show that the concentrations of lactate and acetate in serum fall to normal levels when the rats were coadministered with HFHC and 1,4-GL. Meanwhile, urinary excretions of lactate and acetate after rats were treated with HFHC and 1,4-GL were found to be about 2 to 3 times higher than those treated with HFHC alone. Kidneys excrete waste products from the body through urine and regulate the concentration of metabolites in the blood. The data indicate that the increased urinary excretion of lactate and acetate by 1,4-GL treatment contributes to the prevention of hypercholesterolemia.

Increased Creatinine Clearance after 1,4-GL Treatment. Metabonomic and quantitative results likewise reveal that 1,4-GL treatment significantly increases the urinary excretion of creatinine. Creatinine is constantly produced at a rate proportional to the muscle mass; this substance is then filtered from the blood by the kidneys. In this study, no statistical differences were observed in rat weight between different groups during the experiment. This result suggests that the increased urinary excretion of creatinine during 1,4-GL treatment is not attributed to changes in muscle mass. The excretion of creatinine is primarily determined by glomerular filtration and proximal tubular secretion. Therefore, creatinine levels in blood and urine can be used to calculate the creatinine clearance, which reflects renal function.[26] Our results show that the creatinine clearance of 1,4-GL treatment exceeds that of the control group by 77.4%. Creatinine clearance was reduced by 33.6% in the HFHC group and was not statistically significant in the group coadministered with HFHC and 1,4-GL compared with that of the control group (Table 2). The increased creatinine clearance after 1,4-GL treatment increases the urinary elimination of metabolites (e.g., lactate and acetate) and maintains the concentration of metabolites in the blood.

DISCUSSION

Mammals are "superorganisms" with karyomes, chondriomes, and microbiomes. Research has suggested that the microbiome–host relationship contributes to diabetes, obesity, and increased blood pressure.[27,28] The results from metabonomic analysis show that particular urinary biomarkers (e.g., hippurate, TMAO, and TMA) of the changes in gut microbiota are significantly altered after 1,4-GL treatment. Thus, counts of some general gut bacteria in rat colonic contents were

Table 2. Quantitative Results of Particular Metabolites in the Urine (from 0 to 24 h) and Serum of Rats (n = 6–8 in Each Group, Mean ± SE)[a]

metabolite	control	HFHC group	HFHC coadministered with 1,4-GL	1,4-GL treatment
lactate (U, μmol)	271 ± 48.3	397 ± 79.5	750 ± 126[c]	146 ± 37.2[b]
acetate (U, μmol)	299 ± 40.6	1461 ± 292[c]	4384 ± 608[c]	179 ± 50.7[b]
formate (U, μmol)	81.2 ± 8.90	540 ± 135[c]	2158 ± 431[c]	72.4 ± 25.5
creatinine (U, μmol)	13.5 ± 1.30	12.5 ± 2.30	13.9 ± 3.20	22.2 ± 2.10[b]
cholate (U, μmol)	not detected	19.4 ± 1.70	28.5 ± 3.60[d]	not detected
lactate (S, μmol/L)	189 ± 20.9	335 ± 47.1[c]	219 ± 31.5	167 ± 18.7
acetate (S, μmol/L)	15.1 ± 1.40	23.8 ± 1.20[c]	15.5 ± 1.50	15.3 ± 1.50
creatinine (S, μmol/L)	30.5 ± 2.90	40.4 ± 5.70	30.7 ± 3.45	26.7 ± 2.70
CC (mL/h)	20.8 ± 3.30	13.8 ± 3.0[b]	19.8 ± 2.20	36.9 ± 3.40[c]

[a]Abbreviations: U, urine; S, serum; CC, creatinine clearance; control, rats were administered with water; HFHC, rats were administered with high-fat, high-cholesterol emulsion; HFHC coadministered with 1,4-GL, rats were administered with 1,4-GL (30.0 mg/kg) and administered with high-fat, high-cholesterol emulsion afterward; 1,4-GL treatment, rats were administered with 1,4-GL (30.0 mg/kg). [b]Significant difference from the control group by $p < 0.05$ (one-way ANOVA). [c]significant differences from the control group by <0.01 (one-way ANOVA). [d]Significant difference from the HFHC group ($p < 0.05$, one-way ANOVA).

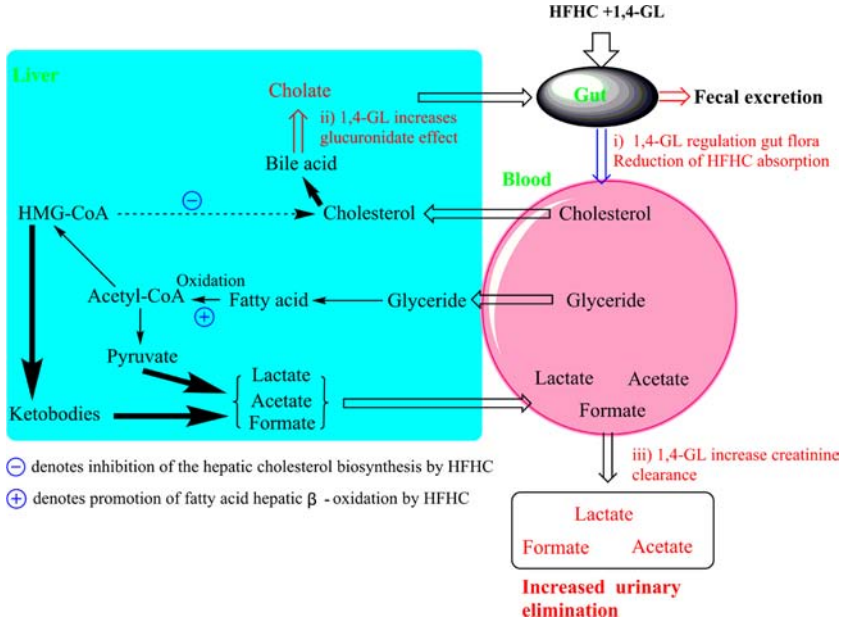

Figure 5. Putative mechanism of 1,4-GL in preventing HFHC-induced hypercholesterolemia.

measured. The results reveal that 1,4-GL treatment regulates gut flora by notably decreasing the colonic quantity of *E. coli* but increases the quantities of probiotics *Bifidobacterium* and *Lactobacillus*, which contribute to reduction in cholesterol in vivo. The probiotics bind cholesterol in the small intestines and decrease the absorption of dietary cholesterol absorption.[29,30] Indeed, since *β*-glucuronidase is mainly produced by *E. coli* in the gastrointestinal tract,[31,32] part of the reason for the reduction in colonic quantity of *E. coli* after 1.4-GL treatment lies in the inhibitory effect of 1,4-GL on the enzyme. The decreasing of *E. coli* could affect gut microbiota balance and lead to an elevated colonic quantity of probiotics. Our results imply that there exists a high correlation between prevention of hypercholesterolemia by 1,4-GL and gut microbial community.

The amount of particular metabolites (e.g., lactate, pyruvate, and acetate) in urine and blood samples increases in the HFHC group. A previous study in mice has suggested that the increase in serum lactate and pyruvate is strongly associated with a high fat diet,[33] which is in agreement with our results. During absorption of dietary fat, fatty acids and monoglycerides that are enzymatically digested in the intestines are transported into the endoplasmic reticulum. These substances are used to synthesize triglycerides. The provision of dietary triglyceride in the blood promotes fatty acid hepatic *β*-oxidation.[34] Lactate and acetate are also produced when acetyl-CoA derived from lipid *β*-oxidation exceeds the capacity of the TCA cycle.[35] Furthermore, the biosynthesis of hepatic cholesterol is inhibited by high dietary cholesterol.[36] As a result, HMG-CoA may produce ketobodies and then convert into lactate *in vivo*.[37] Given these processes, the metabolites such as lactate and acetate after the administration of HFHC are, at least in part, the breakdown products from dietary fat/cholesterol catabolism.

The products are accumulated in the blood if the production rate from successive administration of HFHC exceeds the removal rate by tissues or urinary excretion. The increase in metabolites in the blood yields a new equilibrium in the synthesis. Catabolism of fat and cholesterol is established from the interconversion among lactate, glucose, cholesterol, and fatty acid.[34,38] The high correlation of increased urinary excretions of lactate and acetate with prevention of hypercholesterolemia by 1,4-GL treatment suggests that the increased urinary excretion of the breakdown products of fat/cholesterol from the increase in creatinine clearance after 1,4-GL treatment prevents hypercholesterolemia.

Bile acids are water-soluble end products synthesized by cholesterol in the liver and conjugate with glucuronic acid (glucuronidation), are excreted through the biliary tract, and are transported to the intestine for the enterohepatic cycle. The inhibition of *β*-glucuronidase by 1,4-GL increases the glucuronidation and catabolism of cholesterol in the liver.[7] The results show that the urinary excretion of cholate increases (Table 2), which supports the hypothesis.

We propose the putative mode of action of 1,4-GL in preventing HFHC-induced hypercholesterolemia on metabolic levels based on the results (Figure 5), which involve the following: (i) increased gut bacteria (e.g., *Bifidobacterium* and *Lactobacillus*), which reduces the absorption of cholesterol;[29,30] (ii) increased bile acid glucuronidate to inhibit *β*-glucuronidase, thereby enhancing the conversion of cholesterol into bile acid; (iii) increased urinary elimination of breakdown products (e.g., lactate and acetate) from fat catabolism because of increased creatinine clearance. One limitation of this study is the limited information on enzymes related to the production of lactate and acetate after HFHC administration and 1,4-GL treatment. This work will be performed by combining molecular biology and metabonomics.

In conclusion, we demonstrate that 1,4-GL significantly prevents HFHC-induced hypercholesterolemia in rats, which supports the benefits of the use of 1,4-GL in treating cardiovascular diseases. Metabonomic analysis and colonic flora test results reveal the increased quantities of probiotics (e.g., *Bifidobacterium* and *Lactobacillus*) and urinary excretion of breakdown products of fat/cholesterol because of increased creatinine clearance after 1,4-GL treatment. This procedure contributes to the cholesterol-lowering effects. We first reported on the direct link between the development of HFHC-induced hypercholesterolemia and gut flora as well as

the breakdown products of fat/cholesterol, which provides insights in the treatment and prevention of hypercholesterolemia based on systemic considerations.

AUTHOR INFORMATION

Corresponding Author

*(B.-G. Xie) Fax and phone: +8679186361839. E-mail: xiebaogang@ncu.edu.cn.

Funding

This work was supported by a grant from the Natural Science Foundation of China (Grant No. 30960456).

Notes

The authors declare no competing financial interest.

REFERENCES

(1) Dolan, L. C.; Potter, S. M.; Burdock, G. A. Evidence-based review on the effect of normal dietary consumption of fructose on blood lipids and body weight of overweight and obese individuals. *Crit Rev. Food Sci. Nutr.* **2010**, *50*, 889−918.

(2) Lee, S. H.; Park, S.; Kang, S. M.; Jang, Y.; Chung, N.; Choi, D. Effect of atorvastatin monotherapy and low-dose atorvastatin/ezetimibe combination on fasting and postprandial triglycerides in combined hyperlipedemia. *J. Cardiovasc. Pharmacol. Ther.* **2012**, *17*, 65−71.

(3) Gao, S.; Kinzig, K. P.; Aja, S.; Scott, K. A.; Keung, W.; Kelly, S.; Strynadka, K.; Chohnan, S.; Smith, W. W.; Tamashiro, K. L.; Ladenheim, E. E.; Ronnett, G. V.; Tu, Y.; Birnbaum, M. J.; Lopaschuk, G. D.; Moran, T. H. Leptin activates hypothalamic acetyl-CoA carboxylase to inhibit food intake. *Proc. Natl. Acad. Sci. U.S.A.* **2007**, *104*, 17358−17363.

(4) Executive summary of the third report of the National Cholesterol Education Program (NCEP) expert panel on detection, evaluation, and treatment of high blood cholesterol in adults (adult treatment panel III). *JAMA* **2001**, *285*, 2486−2497.

(5) Walaszek, Z.; Szemraj, M. H.; Adams, A. K.; Sherman, U. D-Glucaric acid content of various fruits and vegetables and cholesterol lowering effects of dietary D-glucarate in the rat. *Nutr. Res. (N.Y.)* **1996**, *16*, 673−682.

(6) Heerdt, A. S.; Young, C. W.; Borgen, P. I. Calcium glucarate as a chemopreventive agent in breast cancer. *Isr. J. Med. Sci.* **1995**, *31*, 101−105.

(7) Simone, C. B.; Simone, N. L.; Pallante, M.; Simone, C. B. Cancer, lifestyle modification and glucarate. *J. Orthomol. Med,* **2001**, *16*, 83−90.

(8) Bhattacharya, S.; Manna, P.; Gachhui, R.; Sil, P. C. D-Saccharic acid 1,4-lactone protects diabetic rat kidney by ameliorating hyperglycemia-mediated oxidative stress and renal inflammatory cytokines via NF-kappaB and PKC signaling. *Toxicol. Appl. Pharmacol.* **2013**, *267*, 16−29.

(9) Bhattacharya, S.; Gachhui, R.; Sil, P. C. The prophylactic role of D-saccharic acid-1,4-lactone against hyperglycemia-induced hepatic apoptosis via inhibition of both extrinsic and intrinsic pathways in diabetic rats. *Food Funct.* **2013**, *4*, 283−296.

(10) Macfadyen, A.; Ho, K. J. D-Glucaro-1,4-lactone: its excretion in the bile and urine and effect on the biliary secretion of beta-glucuronidase after oral administration in rats. *Hepatology* **1989**, *9*, 552−6.

(11) Horton, D.; Walaszek, Z. Conformations of the D-glucarolactones and D-glucaric acid in solution. *Carbohydr. Res.* **1982**, *105*, 95−109.

(12) Walaszek, Z.; Szemraj, J.; Narog, M.; Adams, A. K.; Kilgore, J.; Sherman, U.; Hanausek, M. Metabolism, uptake, and excretion of a D-glucaric acid salt and its potential use in cancer prevention. *Cancer Detect. Prev.* **1997**, *21*, 178−90.

(13) Walaszek, Z.; Hanausek, M.; Adams, A. K.; Sherman, U. Cholesterol-lowering effects of dietary D-glucarate. *Faseb J.* **1991**, *5*, A930−A930.

(14) Simone, C. B.; Simone, N. L.; Pallante, M.; Simone, C. B. Cancer, lifestyle modification and glucarate. *J. Orthomol. Med.* **2001**, *16*, 83−90.

(15) Dumas, M. E.; Barton, R. H.; Toye, A.; Cloarec, O.; Blancher, C.; Rothwell, A.; Fearnside, J.; Tatoud, R.; Blanc, V.; Lindon, J. C.; Mitchell, S. C.; Holmes, E.; McCarthy, M. I.; Scott, J.; Gauguier, D.; Nicholson, J. K. Metabolic profiling reveals a contribution of gut microbiota to fatty liver phenotype in insulin-resistant mice. *Proc. Natl. Acad. Sci. U.S.A.* **2006**, *103*, 12511−12516.

(16) Yang, H.; Pang, W.; Lu, H.; Cheng, D.; Yan, X.; Cheng, Y.; Jiang, Y. Comparison of metabolic profiling of cyanidin-3-O-galactoside and extracts from blueberry in aged mice. *J. Agric. Food Chem.* **2011**, *59*, 2069−2076.

(17) Van Dorsten, F. A.; Daykin, C. A.; Mulder, T. P.; Van Duynhoven, J. P. Metabonomics approach to determine metabolic differences between green tea and black tea consumption. *J. Agric. Food Chem.* **2006**, *54*, 6929−6938.

(18) Liu, M.; Dong, C. R.; Su, J. Y. Development of a simple and practical hyperlipedemia rat model. *Chin. Pharmacol. Bull.* **1989**, *5*, 119−120.

(19) Zheng, P.; Gao, H. C.; Li, Q.; Shao, W. H.; Zhang, M. L.; Cheng, K.; Yang, D. Y.; Fan, S. H.; Chen, L.; Fang, L.; Xie, P. Plasma metabonomics as a novel diagnostic approach for major depressive disorder. *J. Proteome Res.* **2012**, *11*, 1741−1748.

(20) Speakman, J.; Hambly, C.; Mitchell, S.; Krol, E. The contribution of animal models to the study of obesity. *Lab Anim.* **2008**, *42*, 413−432.

(21) Cloarec, O.; Dumas, M. E.; Trygg, J.; Craig, A.; Barton, R. H.; Lindon, J. C.; Nicholson, J. K.; Holmes, E. Evaluation of the orthogonal projection on latent structure model limitations caused by chemical shift variability and improved visualization of biomarker changes in ^{1}H NMR spectroscopic metabonomic studies. *Anal. Chem.* **2005**, *77*, 517−26.

(22) Wang, Z.; Klipfell, E.; Bennett, B. J.; Koeth, R.; Levison, B. S.; Dugar, B.; Feldstein, A. E.; Britt, E. B.; Fu, X.; Chung, Y. M.; Wu, Y.; Schauer, P.; Smith, J. D.; Allayee, H.; Tang, W. H.; DiDonato, J. A.; Lusis, A. J.; Hazen, S. L. Gut flora metabolism of phosphatidylcholine promotes cardiovascular disease. *Nature* **2011**, *472*, 57−63.

(23) al-Waiz, M.; Mikov, M.; Mitchell, S. C.; Smith, R. L. The exogenous origin of trimethylamine in the mouse. *Metabolism* **1992**, *41*, 135−136.

(24) Cani, P. D.; Neyrinck, A. M.; Fava, F.; Knauf, C.; Burcelin, R. G.; Tuohy, K. M.; Gibson, G. R.; Delzenne, N. M. Selective increases of bifidobacteria in gut microflora improve high-fat-diet-induced diabetes in mice through a mechanism associated with endotoxaemia. *Diabetologia* **2007**, *50*, 2374−2383.

(25) Hekmatdoost, A.; Feizabadi, M. M.; Djazayery, A.; Mirshafiey, A.; Eshraghian, M. R.; Yeganeh, S. M.; Sedaghat, R.; Jacobson, K. The effect of dietary oils on cecal microflora in experimental colitis in mice. *Indian J. Gastroenterol.* **2008**, *27*, 186−189.

(26) Lew, S. W.; Bosch, J. P. Effect of diet on creatinine clearance and excretion in young and elderly healthy subjects and in patients with renal disease. *J. Am. Soc. Nephrol.* **1991**, *2*, 856−65.

(27) Ley, R. E.; Turnbaugh, P. J.; Klein, S.; Gordon, J. I. Microbial ecology: human gut microbes associated with obesity. *Nature* **2006**, *444*, 1022−1023.

(28) Nicholson, J. K.; Holmes, E.; Lindon, J. C.; Wilson, I. D. The challenges of modeling mammalian biocomplexity. *Nat. Biotechnol.* **2004**, *22*, 1268−1274.

(29) Usman; Hosono, A. Bile tolerance, taurocholate deconjugation, and binding of cholesterol by Lactobacillus gasseri strains. *J. Dairy Sci.* **1999**, *82*, 243−248.

(30) Rump, L. V.; Meng, J.; Strain, E. A.; Cao, G.; Allard, M. W.; Gonzalez-Escalona, N. Complete DNA sequence analysis of enterohemorrhagic Escherichia coli plasmid pO157_2 in beta-glucuronidase-positive E. coli O157:H7 reveals a novel evolutionary path. *J. Bacteriol.* **2012**, *194*, 3457−3463.

(31) Fricker, C. R.; DeSarno, M.; Warden, P. S.; Eldred, B. J. False-negative beta-D-glucuronidase reactions in membrane lactose glucur-

onide agar medium used for the simultaneous detection of coliforms and Escherichia coli from water. *Lett. Appl. Microbiol.* **2008**, *47*, 539−542.
(32) Xiang, L.; Qi, F.; Dai, D.; Li, C.; Jiang, Y. Simulated microgravity affects growth of Escherichia coli and recombinant beta-D-glucuronidase production. *Appl. Biochem. Biotechnol.* **2010**, *162*, 654−661.
(33) Shearer, J.; Duggan, G. E.; Hittel, D. S.; Hughey, C. C.; Weljie, A.; Vogel, H. J. Differentiating short- and long-term effects of diet in the obese mouse using (1)H-nuclear magnetic resonance metabolomics. *Diabetes Obes. Metab.* **2011**, *13*, 859−862.
(34) Randle, P. J. Regulatory interactions between lipids and carbohydrates: the glucose fatty acid cycle after 35 years. *Diabetes Metab. Rev.* **1998**, *14*, 263−283.
(35) McGarry, J. D.; Foster, D. W. Regulation of hepatic fatty acid oxidation and ketone body production. *Annu. Rev. Biochem.* **1980**, *49*, 395−420.
(36) Wang, Y.-M.; Zhang, B.; Xue, Y.; Li, Z.-J.; Wang, J.-F.; Xue, C.-H.; Yanagita, T. The mechanism of dietary cholesterol effects on lipids metabolism in rats. *Lipids Health Dis.* **2010**, *9*, 1−6.
(37) Piloquet, H.; Ferchaud-Roucher, V.; Duengler, F.; Zair, Y.; Maugere, P.; Krempf, M. Insulin effects on acetate metabolism. *Am. J. Physiol. Endocrinol. Metab.* **2003**, *285*, E561−E565.
(38) Akanji, A. O.; Ng, L.; Humphreys, S. Plasma acetate levels in response to intravenous fat or glucose/insulin infusions in diabetic and non-diabetic subjects. *Clin. Chim. Acta* **1988**, *178*, 85−94.

MATERIAL AND METHODS

Chemicals. DMSO (dimethyl sulfoxide), MtBE (methyl-*tert*-butyl ether), and all other solvents used were of HPLC grade. Pure DL-α-tocopherol (100% analytical grade) was used from Calbiochem (Darmstadt, Germany). All carotenoids (97−99% analytical grade) were purchased from CaroNature (Ostermundigen, Switzerland). HPLC grade water (18 MΩ) was prepared using a Millipore Milli-Q purification system (Millipore GmbH, Schwalbach, Germany). Carbonate buffer, polar aprotic mixture, photosensitizer, and all other chemicals were of analytical grade. Special reagent was 2.2-azinobis-(3-ethylbenzothiazoline-6-sulfonic acid)diammonium salt (ABTS) (Sigma-Aldrich, Taufkirchen, Germany).

Standard Preparation. Stock solutions of each carotenoid standard were prepared in the specific solvent and stored at −30 °C. The exact concentrations of the stock solutions were determined spectrophotometrically at their specific absorption maxima as described in ref 10.

Food Samples. Fresh tomatoes, tomato ketchup, tomato passata, tomato pesto, and tomato puree were bought in a local supermarket and stored in the refrigerator until analysis.

Food Extraction. All examinations were performed under subdued light conditions. All products were each weighed into an Erlenmeyer flask and extracted with methanol/tetrahydrofuran (1/1, v/v) by homogenization using an ultra turrax (type T25, IKA-Werke, Staufen, Germany) for 30 s on ice. The extract was filtered under vacuum through filter paper no. 390 (Filtrak, Niederschlag, Germany) on a Büchner funnel with magnesium hydroxide carbonate. This extraction was repeated until colorlessness. The combined extracts were rotary-evaporated under reduced pressure at 30 °C to a small volume. The dried residues were dissolved in a defined volume of MeOH/THF (50/50, v/v) using an ultrasonic bath. After centrifugation (18407 rcf, 5 min), the samples were used for PCL and HPLC measurement. For the α-TEAC assay the samples were extracted with *n*-hexane.

PCL. Carotenoid stock solutions and food extracts were dried under nitrogen and dissolved in MtBE/DMSO (1/4, v/v). The carotenoid concentrations were prepared to 25, 50, and 75 μmol/L, and the food samples were diluted in different concentrations. α-Tocopherol (dissolved in methanol) at concentrations of 2.5−125 μmol/L was used for calibration. Hence, AOA and AOC were expressed as α-tocopherol equivalents (α-TE). The measurement was performed in a special cuvette apparatus (Analytik Jena AG, Jena, Germany). A polar aprotic mixture, carbonate buffer, photosensitizer and sample were pipetted in a quartz glass cuvette (Hellma GmbH, Müllheim, Germany). Methanol and MtBE/DMSO (1/4, v/v), were used as blank.

α-TEAC Assay. The lipophilic α-TEAC assay was performed according to (ref 10) by using a V-530 spectrophotometer (Jasco, Gross-Umstadt, Germany). The α-TEAC procedure is based on the decolorization of the $ABTS^{\bullet+}$ to determine the lipophilic antioxidant properties of the samples. The method was described by Miller et al.[11] and was modified slightly by numerous researchers. Briefly, the radical cation $ABTS^{\bullet+}$ was prepared by filtering an ABTS solution (tip of a spatula ABTS dissolved in PBS) covered with manganese dioxide powder. Afterward, the particles of manganese dioxide were removed by 0.2 μm membrane filtration. The stable radical cation $ABTS^{\bullet+}$ was produced daily by diluting with 75 mM phosphate buffer (pH 7.4) to an absorbance of 0.70 ± 0.05 at 730 nm in a cuvette spectral photometer and preincubated at room temperature for 2 h. For the measurement, 100 μL of lipophilic extract of the antioxidants and 1000 μL of the adjusted $ABTS^{\bullet+}$ solution were shaken for 30 s in reaction tubes. Following, the solution was transferred completely in half-micro cuvettes and was centrifuged for 30 s at 200 rcf to separate the phases. Exactly 2 min after initiation of mixing, the absorbance of the lower phase was measured at 734 nm. The lipophilic antioxidant potential was expressed in mmol α-tocopherol equivalents per 100 g.

Analysis of Carotenoids and Vitamin E. The analysis of carotenoid compounds was performed on an HPLC apparatus with diode array detection at 450 nm (Merck Hitachi, Darmstadt, Germany). The chromatographic separation was performed at 13 °C on a Develosil RP-Aqueous (250 mm × 4.6 mm, 5 μm) C_{30}-column (Phenomenex, Aschaffenburg, Germany) by using the following gradient procedure of MeOH (solvent A) and MtBE (solvent B): initial conditions 90% solvent A and 10% solvent B; 40 min linear gradient to 50% solvent B; 2 min linear gradient to 60% solvent B, 40% solvent A and 60% solvent B for 23 min; 5 min linear gradient to 10% solvent B; and 90% solvent A and 10% solvent B for 5 min. The flow rate was 1 mL/min. The carotenoid standards were diluted daily 1:50 with MeOH/THF (50/50, v/v) modified to Werner et al.[12]

Tocopherols and tocotrienols were analyzed with a fluorescence detector (excitation: 292 nm, emission: 330 nm) (Merck Hitachi, Darmstadt, Germany) according to the method of Franke et al.[13] The column was a normal-phase Eurospher 100 Diol (250 mm × 4.0 mm, 7 μm, Knauer, Berlin, Germany) and was heated to 35 °C. Elution was carried out using a mixture of *n*-hexane/MtBE (98/2, v/m) at a flow rate of 1.5 mL/min, and the run time was 45 min. Calibration curves were done for α-, δ-, γ-tocopherol, and γ-tocotrienol in the range 0.1−3 μg/mL, for β-tocopherol 0.1−1 μg/mL, for α- and β-tocotrienol 0.1−2 μg/mL, and for δ-tocotrienol 0.3−6 μg/mL.

Carotenoids and tocopherols as well as tocotrienols were identified and quantified by comparison with external standards.

Statistical Analysis. All experiments were done in triplicate. The data are expressed as means ± SD (n = 3). The data were analyzed with ANOVA using SPSS statistical software (version 19.0; SPSS, Chicago, USA). The homogeneity of variances for all data was assumed by Levene's test. The antioxidant activities of carotenoids and the antioxidant capacities of tomato products were tested with Student−Newmann−Keuls procedure. Differences were considered statistically significant at $p < 0.05$. Tests on correlation between the carotenoid content and the antioxidant capacity were made using the Pearson procedure $p < 0.01$.

RESULTS AND DISCUSSION

AOA of Carotenes and Xanthophylls. The antioxidant activities of 6 carotenes and 11 xanthophylls were measured in three different concentrations on three different days. Table 1 shows the results of the antioxidant activity of α-carotene. The highest concentration (75 μmol/L) resulted in reproducible values. In contrast, the variation in results of the smaller concentrations was higher. This trend was observed for all carotenes and xanthophylls used. One reason for this phenomenon could be adsorption effects of carotenoids at the surface of the quartz glass cuvettes. Therefore, we did experiments to check adsorption effects by using photometric spectra and measured different concentrations. However, there were no results indicating absorption effects. We looked also for the solubility of the carotenoids in MtBE/DMSO (1/4, v/v) and for α-tocopherol in MeOH. The concentrations of capsanthin, antheraxanthin, and α-tocopherol were measured in stock solutions and in MtBE/DMSO (1/4, v/v) respectively MeOH. All carotenoids investigated were completely dissolved in the solvent mixture for PCL as well as α-tocopherol in MeOH.

Table 1. Antioxidant Activity (mol α-TE/mol) of Different Concentrations of α-Carotene, Measured on Three Different Days by Using PCL; Different Letters within Columns Indicate Significant Differences between Days, Determined by ANOVA with *post hoc* S−N−K ($p < 0.05$)

	antioxidant activity [mol α-TE/mol] of α-carotene		
day	25 μmol/L	50 μmol/L	75 μmol/L
1	0.48 ± 0.02^{F}	0.33 ± 0.05^{D}	0.34 ± 0.01^{B}
2	0.44 ± 0.04^{F}	0.38 ± 0.04^{D}	0.28 ± 0.01^{A}
3	0.11 ± 0.02^{E}	0.17 ± 0.03^{C}	0.28 ± 0.01^{A}
mean ± SD	0.34 ± 0.18	0.29 ± 0.10	0.30 ± 0.03

dx.doi.org/10.1021/jf502019r | J. Agric. Food Chem. 2014, 62, 7452−7459

Concentration-dependent effects, which were described in the literature[14−16] for hydrophilic substances, could be one reason for the different values of 25, 50, and 75 μmol/L. The AOA of pure substances and food extracts was dependent on their concentration and dilution.

The antioxidant activities of all carotenoids investigated were calculated by using the highest concentrations (75 μmol/L) (Figure 2). α-Tocopherol, used as calibration standard, expressed

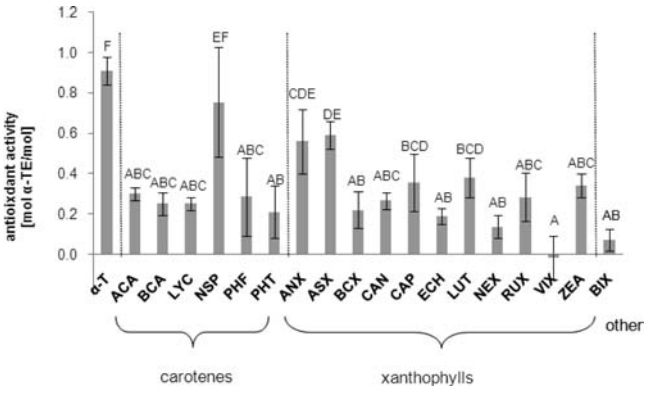

Figure 2. Antioxidant activities (mol α-TE/mol) of carotenoids ((all-E)-isomers), measured by PCL on three different days at 75 μmol/L. Bars with different letters differ significantly (ANOVA, $n = 3$, *post hoc* S−N−K, $p < 0.05$). α-T = α-tocopherol; ACA = α-carotene; ANX = antheraxanthin; ASX = astaxanthin; BCA = β-carotene; BCX = β-cryptoxanthin; BIX = bixin; CAN = canthaxanthin; CAP = capsanthin; ECH = echinenone, LUT = lutein; LYC = lycopene; NEX = neoxanthin; NSP = neurosporene; PHT = phytoene; PHF = phytofluene; RUX = rubixanthin; VIX = violaxanthin; ZEA = zeaxanthin.

the highest antioxidant power compared to all analyzed carotenoids. Within the carotenes, neurosporene (0.76 ± 0.27 mol α-TE/mol) presented the highest and phytoene (0.21 ± 0.13 mol α-TE/mol) the lowest activity. β-Carotene (0.25 ± 0.06 mol α-TE/mol) and lycopene (0.25 ± 0.03 mol α-TE/mol) were similar as well α-carotene (0.30 ± 0.03 mol α-TE/mol) and phytofluene (0.29 ± 0.19 mol α-TE/mol). Astaxanthin (0.59 ± 0.07 mol α-TE/mol) showed the maximum antioxidant activity of all xanthophylls investigated followed by antheraxanthin (0.56 ± 0.16 mol α-TE/mol), lutein (0.38 ± 0.10 mol α-TE/mol), capsanthin (0.36 ± 0.14 mol α-TE/mol), and zeaxanthin (0.34 ± 0.06 mol α-TE/mol). The AOA of rubixanthin (0.28 ± 0.12 mol α-TE/mol) and canthaxanthin (0.27 ± 0.04 mol α-TE/mol) did not differ significantly. Echinenone (0.19 ± 0.04 mol α-TE/mol) showed a small activity as well as neoxanthin (0.14 ± 0.06 mol α-TE/mol), which showed only 15% of the activity of that of α-tocopherol. Bixin was just as little (0.07 ± 0.05 mol α-TE/mol) and violaxanthin (−0.02 ± 0.11 mol α-TE/mol) did not show any activity using the PCL method.

Comparison of PCL Data with Results of FRAP, α-TEAC, DPPH, and LPSC Assay. The AOA values of the PCL method were compared to the results of Müller et al. (2011) (Table 2).[10] Generally, the AOAs of PCL were lower than the results of FRAP, LPSC, and α-TEAC for most of the investigated carotenoids. Neither carotenes nor xanthophylls demonstrated any DPPH scavenging activity. Only α-tocopherol showed an activity (1.0 mol α-TE/mol). In FRAP assay, rubixanthin (3.3 mol α-TE/mol) indicated the highest antioxidant activity. β-Cryptoxanthin, capsanthin, lutein, and lycopene had the second highest activity (2.1 mol α-TE/mol) with no differences between these compounds. However, all carotenes, excluding lycopene, did not show remarkable ferric reducing activity. In the α-TEAC assay, the highest $ABTS^{\bullet+}$ reducing activity was observed for lycopene (3.9 mol α-TE/mol) followed by β-cryptoxanthin (3.2 mol α-TE/mol), rubixanthin (3.3 mol α-TE/mol), α-carotene (3.3 mol α-TE/mol), and β-carotene (3.1 mol α-TE/mol). Phytoene and phytofluene showed the same reducing potential as α-tocopherol (1.0 mol α-TE/mol). The lowest values in the α-TEAC assay with no differences were shown for astaxanthin and canthaxanthin (0.8 mol α-TE/mol).

Table 2. Comparison of Antioxidant Activities of Carotenoids ((all-*E*)-Isomers) and α-Tocopherol in PCL to Other AOA Assays (Data from Müller et al. 2011[10]); Different Letters Indicate a Significant Difference within the Column, Determined by ANOVA ($p < 0.05$) with *post hoc* S−N−K

cmpd	PCL mol α-TE/mol	FRAP mol α-TE/mol	α-TEAC mol α-TE/mol	DPPH mol α-TE/mol	LPSC mol α-TE/mol
α-tocopherol	0.91^{F}	1.0^{A}	1.0^{A}	1.0	1.0^{A}
neurosporene	0.76^{EF}	0.0^{B}	2.1^{B}	0.0	0.0^{B}
astaxanthin	0.59^{DE}	0.5^{E}	0.8^{E}	0.0	26.3^{E}
antheraxanthin	0.56^{CDE}	1.8^{I}	2.0^{B}	0.0	24.7^{E}
lutein	0.38^{BCD}	2.1^{C}	2.0^{B}	0.0	19.6^{D}
capsanthin	0.36^{BCD}	2.1^{C}	2.0^{B}	0.0	25.3^{E}
zeaxanthin	0.34^{ABC}	2.0^{C}	1.9^{B}	0.0	20.3^{D}
α-carotene	0.30^{ABC}	0.0^{B}	3.3^{D}	0.0	19.0^{D}
phytofluene	0.29^{ABC}	0.0^{B}	1.0^{A}	0.0	0.1^{B}
rubixanthin	0.28^{ABC}	3.3^{F}	3.3^{D}	0.0	8.9^{G}
canthaxanthin	0.27^{ABC}	0.3^{D}	0.8^{E}	0.0	21.0^{D}
β-carotene	0.25^{ABC}	0.0^{B}	3.1^{D}	0.0	19.1^{D}
lycopene	0.25^{ABC}	2.1^{C}	3.9^{C}	0.0	13.3^{C}
β-cryptoxanthin	0.22^{AB}	2.1^{C}	3.2^{D}	0.0	19.3^{D}
phytoene	0.21^{AB}	0.1^{B}	1.0^{A}	0.0	0.1^{B}
echinenone	0.19^{AB}	0.3^{D}	2.2^{B}	0.0	26.3^{E}
neoxanthin	0.14^{AB}	1.3^{G}	1.1^{G}	0.0	20.6^{D}
bixin	0.07^{AB}	1.7^{I}	1.3^{H}	0.0	29.1^{H}
violaxanthin	-0.02^{A}	1.5^{H}	1.6^{F}	0.0	22.5^{F}

dx.doi.org/10.1021/jf502019r | J. Agric. Food Chem. 2014, 62, 7452−7459

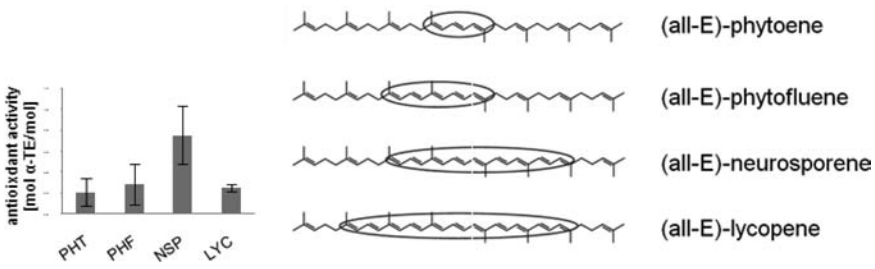

Figure 3. AOA of selected carotenes related to their structures.

Table 3. Antioxidant Capacities Based on Fresh Weight As Well As on Dry Weight of Selected Tomato Products Measured by PCL, α-TEAC, Calculated AOC of PCL; the Single Carotenoids and Vitamin E Compounds Are Listed, Too[a]

	fresh tomatoes	tomato ketchup	tomato passata	tomato pesto	tomato puree
PCL [μmol α-TE/100 g]	26.3 ± 9.4$^{\times A}$	456.0 ± 104.7$^{\times C}$	36.7 ± 14.7$^{\times A}$	309 ± 27$^{\times B}$	271 ± 63$^{\times B}$
PCL (dry weight) [μmol α-TE/100 g]	411 ± 147^{A}	1714 ± 394^{B}	528 ± 212^{A}	518 ± 45^{A}	852 ± 198^{A}
AOC$_{calculated}$ (PCL) [μmol α-TE/100 g]	14.51	17.59	15.48	78.91	54.89
α-TEAC [μmol α-TE/100 g]	95.0 ± 2.4$^{\times A}$	414.4 ± 19.4$^{\times BC}$	593.7 ± 65.0$^{\times C}$	343.8 ± 20.3$^{\times B}$	2562 ± 238$^{\times D}$
α-TEAC (dry weight) [μmol α-TE/100 g]	1484 ± 37^{A}	1558 ± 73^{A}	8555 ± 937^{B}	577 ± 34^{A}	8046 ± 749^{B}
Carotenoids [mg/100 g]					
(all-*E*)-lycopene	14.77 ± 2.10	27.21 ± 3.60	20.02 ± 1.55	14.69 ± 1.8	73.34 ± 11.2
∑ (*Z*)-lycopene	1.95 ± 0.42	2.06 ± 0.08	1.73 ± 0.22	19.33 ± 0.7	7.93 ± 1.29
(all-*E*)-β-carotene	1.38 ± 0.18	0.53 ± 0.05	0.36 ± 0.03	1.58 ± 0.09	1.85 ± 0.09
(9*Z*)-β-carotene	0.05 ± 0.01	–	–	0.32 ± 0.06	0.32 ± 0.03
(13*Z*)-β-carotene	–	–	–	–	0.33 ± 0.03
(all-*E*)-lutein	0.13 ± 0.01	–	–	0.63 ± 0.01	0.14 ± 0.02
(all-*E*)-zeaxanthin	0.03 ± 0.00	–	–	0.36 ± 0.06	–
∑ [mg/100 g]	**18.3 ± 1.9** ^{A}	**29.8 ± 3.7** ^{AB}	**22.1 ± 1.6** ^{A}	**36.9 ± 2.3** ^{B}	**83.9 ± 12.5** ^{C}
∑ [μmol/100g]	**34.1**	**55.5**	**41.2**	**68.6**	**156.3**
Vitamin E [mg/100 g]					
α-tocopherol	0.85 ± 0.07	1.20 ± 0.14	1.68 ± 0.18	26.14 ± 1.09	5.36 ± 0.22
β-tocopherol	–	–	–	1.04 ± 0.09	
γ-tocopherol	–	0.14 ± 0.02	0.12 ± 0.01	1.00 ± 0.19	0.47 ± 0.07
δ-tocopherol	0.16 ± 0.01	–	–	–	
α-tocotrienol	–	–	–	0.89 ± 0.14	
β-tocotrienol	1.32 ± 0,19	0.81 ± 0.01	0.90 ± 0.08	1.35 ± 0.18	3.11 ± 0.11
γ-tocotrienol	0.43 ± 0,04	–	–	–	–
δ-tocotrienol	–	–	–	–	–
∑ [mg/100 g]	**2.8 ± 0.3**^{A}	**2.2 ± 0.2**^{A}	**2.7 ± 0.3**^{A}	**30.4 ± 1.2**^{C}	**9.0 ± 0.4**^{B}
∑ [μmol/100g]	**6.6**	**5.1**	**7.4**	**71.0**	**21.1**

[a]All results presented are calculated by taking the dilution factors and means (± SD) of three independent analyzes. Values with different capital letters within rows differ significantly (ANOVA, $n = 3$, *post hoc* S−H−K, $p > 0.05$). ^{X}concentration-dependent effect.

The AOA measured by LPSC showed 10 times higher values than using the PCL method. The highest luminol-chemiluminescence peroxyl radical scavenging capacity was measured for bixin (29.1 mol α-TE/mol). All xanthophylls, excluding rubixanthin, showed comparable LPSC values, ranging between 19.3 and 26.3 mol α-TE/mol. Astaxanthin and echinenone demonstrated the same activity with 26.3 mol α-TE/mol. The carotenes phytoene, phytofluene, and neurosporene did not react in the LPSC assay.

The AOAs of β-cryptoxanthin, lutein, capsanthin, zeaxanthin, rubixanthin, and violoxanthin analyzed by PCL differed significantly compared to the LPSC assay. β-Cryptoxanthin had 10 times higher antioxidant activity in FRAP and 100 times higher in LPSC than in PCL. Using FRAP and α-TEAC assay, lutein, capsanthin, zeaxanthin as well as rubixanthin and violaxanthin did not show significant differences in the antioxidant activity. These xanthophylls showed considerably higher values compared to the measured activity in PCL assay (five times for lutein, capsanthin and zeaxanthin, 12−15 times for rubixanthin and violaxanthin). No statistically significant differences were observed for astaxanthin, antheraxanthin, neoxanthin, canthaxanthin, or bixin in PCL, FRAP, and α-TEAC. In the carotene group neurosporene indicated the highest activity in PCL but in α-TEAC, FRAP, and LPSC was among the lowest activities. Phytofluene and phytoene differed only in α-TEAC, whereas the values for FRAP, LPSC, and PCL were similarly low. Lycopene had significantly different values in all AOA assays.

Relationship of AOA of Carotenoids and Their Structure. The chemical structures of some carotenes are illustrated in Figure 3. The antioxidant activity of the carotenes increased with the number of conjugated double bonds with the exclusion of lycopene. A relationship could be established between the AOA of the carotenes and their structure. Consequently, the following order can be presented, depending on the antioxidant activity and the number of conjugated double bonds: phytoene < phytofluene < neurosporene. Additionally,

dx.doi.org/10.1021/jf502019r | J. Agric. Food Chem. 2014, 62, 7452−7459

the presence of functional groups, e.g. carbonyl-, hydroxyl-, epoxy-groups also affect the AOA of xanthophylls. The antioxidant activities of carotenoids are based on their singlet oxygen ($^1O_2$) quenching properties and their ability to trap peroxyl radicals.[17] The quenching ability is based on the number of conjugated double bonds and is influenced to a lesser extent by carotenoid end groups (cyclic or acyclic) or the nature of substituents in carotenoids containing cyclic end groups.[17] Carotenoids that contain more than seven conjugated double bonds were reported to have stronger antioxidant activity.[18] The conjugated system delocalizes the electrons along the chromophore.[19] This property gives the carotenoids their distinctive molecular shape, chemical reactivity, and light-absorption properties.[20] Carotenoids lose their color when exposed to radicals or to oxidizing species. This process involves interruption of the conjugated double bond system either by cleavage or by addition to one of the double bonds.[1] Lycopene, which has 11 conjugated and two nonconjugated double bonds and gives tomatoes their red color, had the highest singlet oxygen quenchers activity of the natural carotenoids.[17,21−23] Hence, we expected that lycopene had the highest AOA compared to the other carotenes measured by PCL. But lycopene is very susceptible to oxidation because of the high unsaturated chemical structure.[24] Furthermore, lycopene is also very sensitive to light, heat, oxygen, and acids in degradation, and some metallic ions such as Cu^{2+}, Fe^{3+} catalyze its oxidation.[25] In nature, lycopene exists in all-*trans*- form and seven of these bonds can isomerize from the *trans*-form ((all-*E*)-lycopene) to the mono- or poly *cis*-form ((*Z*)-isomers) under the influence of heat, light, or certain chemical reactions.[25] Traces of metallic ions in solvents as well as the influence of the pH of the carbonate buffer (10.6) could be reasons for the low AOA of lycopene.

AOC, Carotenoid and Vitamin E Contents of Various Tomato Food Products. Fresh tomatoes, tomato ketchup, tomato passata, tomato pesto, and tomato puree were investigated on their lipophilic antioxidant capacity by photochemiluminescence and α-TEAC assay. All extracted samples were analyzed in different concentrations and in triplicate. To quantify the carotenoid and vitamin E contents, HPLC methods were used (Table 3). The results measured for the tomato samples depended on the assay used, but in general the AOC of fresh tomatoes was lower than that of other tomato product samples in PCL and α-TEAC assay as well as in the carotenoid content. In PCL assay fresh tomatoes and tomato passata did not differ significantly as well as tomato pesto and tomato puree. The highest value was shown for tomato ketchup followed by tomato pesto, tomato puree, tomato passata, and fresh tomatoes. The contained herbs and spices could explain the highest antioxidant potential of tomato ketchup. The composition of the tomato pesto was basil, garlic, pine nut, different oils (e.g. sunflower oil and olive oil), hard cheese and ascorbic acid which also had a positive influence on the antioxidant capacity. In contrast to tomato passata, tomato puree is a more concentrated tomato product, and the order of the antioxidant potential, which was assumed, could be demonstrated. The raw material fresh tomato was estimated to have the smallest AOA of the measured tomato products. Because the fresh tomato is a raw material without concentration steps, and no substances like herbs or spices and no oils were added, which can have positive influence on the AOC. To date, it is very difficult to compare our results because publications about the lipophilic antioxidant capacity of tomato products measured by PCL are scare in the literature.

The theoretically calculated antioxidant capacity in μmol α-TE/100 g for PCL could be generated with measured single substances measured by PCL. The lowest antioxidant potential was expected for fresh tomatoes and the highest for tomato pesto. Noticeably, the experimental values were higher than the calculated values. For example, the experimental AOC of tomato ketchup was much higher than calculated (2592%). Reasons could be interaction between single substances which was described in the literature. Researchers observed synergistic effects between lycopene and α-tocopherol,[26,27] lycopene and β-carotene,[26,28] lycopene and lutein,[27,28] lutein and β-carotene,[27] α-tocopherol and β-carotene.[28,29] However, Zanfini et al. described that significant synergistic acts do not take place when compounds are combined.[27] All four substances (lycopene, β-carotene, lutein, and α-tocopherol) which have the ability to make synergism were detected in our tomato samples. Synergistic effects were dependent on the type of antioxidant and on their concentration.[30] Mixtures of carotenoids could be more effective than single substances.[31] Matrix effects (for example interactions between antioxidants and polysaccharides) should not be disregarded.

To check if the water content of samples had an influence on the antioxidant capacity, we calculated the dry weight-based antioxidant capacity. The differences between the fresh tomatoes and the tomato products were mainly due to the water content. In the PCL as well as in the α-TEAC assay the antioxidant capacities were dependent on the water content.

For all results in the PCL assay and α-TEAC, concentration-dependent effects on the measured AOC were detected. Hengst et al.[14] described first the influence of the sample concentration on determination of the hydrophilic antioxidant capacity. The hydrophilic PCL assay was investigated as well as TEAC, FRAP, ORAC, and total phenolics assays. The measured antioxidant activities/capacities of pure substances (gallic acid, uric acid, Trolox, ascorbic acid) and food extracts (strawberry nectar, tomato extract, white tea) decreased or increased with increasing sample concentration. Hence, the values depended significantly on the applied sample concentration. The basic causes of these dilution effects are hardly unknown.[14−16] The AOC of tomato pesto and tomato puree measured by PCL increased with increasing dilutions (Figure 4). The opposite was shown for tomato ketchup, having the highest polysaccharide content, the values decreased with decreasing concentrations. For fresh tomatoes and tomato passata not any relation between their concentration and their results was observed. In addition, for the three samples with high antioxidant capacity, a good linear

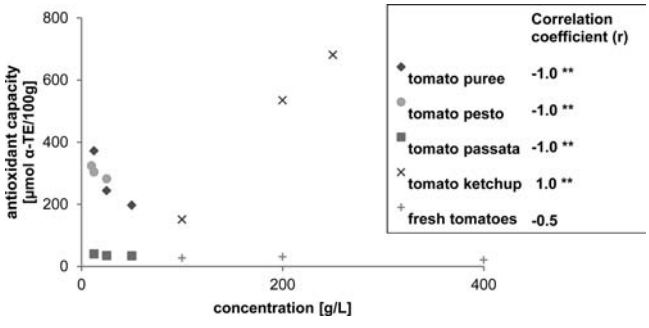

Figure 4. Correlation between the concentration of the tomato samples and their antioxidant capacity. Data were statistically analyzed using the Spearman correlation coefficient test. ** Indicates a significant correlation at the level of $p < 0.01$.

correlation between concentrations and antioxidant capacity was registered. On the basis of the concentration-dependent effects it is suggested to measure different sample dilution factors/concentrations, for the analysis to detect and to discuss the influence of concentrations.

It is assumed that the range in the α-tocopherol calibration (2.5−125 μmol/L) had also an influence on the results. If the values were smaller than 25 μmol/L, the standard deviation of the determined tomato products became higher. For example the tomato pesto dilutions were measured in an α-tocopherol concentration range between 50 μmol/L and 75 μmol/L. Therefore, the variation and the concentration-dependent effects were smaller. In contrast, for the tomato passata, the concentration area analyzed was <25 μmol/L α-tocopherol, and the variation was higher. Consequentially, the sample concentration should not be smaller than 25 μmol/L α-tocopherol calibration.

According to Navas et al.,[32] chemiluminescence not only has advantages such as superior sensitivity, safety, and controllable emission rate but also has some disadvantages such as poor reproducibility. Furthermore, Barni et al.[33] described that photosensitizer solutions can be sensitive to light and the presence of metal cations (e.g., iron and copper). In addition, the light-producing pathway for the oxidation of photosensitizers is a complex multiple process and depends on several factors, including pH, temperature, and ionic strength of the reaction medium and reactive species that can be present in solution and interact with photosensitizer metal catalyst or hydroxide ions.

The lipophilic extract of the tomato puree, characterized by a high carotenoid and vitamin E content, showed the highest antioxidant capacity (2562 ± 238 μmol α-TE/100 g) measured using ABTS radical cation decolorization assay. Tomato passata (594 ± 65 μmol α-TE/100 g) and tomato ketchup (414 ± 19 μmol α-TE/100 g) were significantly different from tomato pesto (344 ± 20 μmol α-TE/100 g). Fresh tomatoes had significantly the lowest lipophilic antioxidant capacity in the TEAC assay.

A significantly linear correlation between the antioxidant potential measured by α-TEAC and the contents of carotenoids could be observed (R = 0.939). An increase of the carotenoid content led to an increase of the lipophilic antioxidant capacity using the α-TEAC. Only a low correlation between the PCL values and the carotenoid contents was observed (R = 0.333).

The PCL and the α-TEAC assays are based on different reaction mechanisms. The pH value can also have an influence. While the PCL reaction is in an alkaline the α-TEAC is in a neutral milieu. Matrix effects should not be disregarded.

The antioxidant capacity of all tested tomato products showed different results. All methods to determine the antioxidant capacity are based on different principles. The α-TEAC assay is based on the single electron transfer reaction (SET).[9,34] The mechanism of PCL is still unclear.[35] The antioxidant capacity is being measured by individual, different methods and reflects only the chemical reactivity under the specific conditions applied in that assay. It is inappropriate and misleading to generalize the data as indicators of "total antioxidant activity". No single assay will reflect the "total antioxidant capacity" of the samples. Diverse methods which are based on different reaction mechanisms as well as the lipophilic and hydrophilic capacities should be used.[10,14,34]

Our results have shown that lycopene is the main carotenoid in tomatoes, which was expected from the literature. The total lycopene contents in the tomato samples investigated ranged between 16.7 mg/100 g (tomato fresh) and 81.3 mg/100 g (tomato puree). The total lycopene content in processed tomatoes was higher than that in the raw tomatoes. The content of carotenoids measured in this study is in good agreement with the results of Baranska et al. (2006)[36] who measured lycopene and β-carotene in tomatoes, ketchup, and puree. On the other hand, the lycopene values, determined by Fröhlich et al.[37] are about 45−23% lower for tomatoes, ketchup, and tomato passata. Sass-Kiss et al.[38] recorded that lycopene represented 90−95% of the total carotenoid content in tomatoes. Our lycopene contents also ranged between 91 and 98% of the total carotenoid composition in the variety of tomato products. Lower abundance for lycopene was determined by Kotíková et al.[39] with 67% and Burns et al.[40] with 58%. Otherwise, a much higher contribution was detected for lutein in fresh tomatoes and ketchup by Gama et al.[41] Total β-carotene in fresh tomatoes and in tomato products amounted 0.36−2.17 mg/100 g and was comparable with the results of Fröhlich et al.[37] and Baranska et al.[36] Differences between the carotenoids contents can be affected by many factors such as variety, growing conditions and time of harvest, climatic conditions, and geographical locations. Warmer and south-oriented areas may promote the production of lycopene at the expense of other carotenoids.[37,39]

Tomato pesto has shown the highest total tocopherol content of all samples, because of containing olive and sunflower oils, which have a high α-tocopherol concentration.[42] Tomato puree had the highest β-tocotrienol content (3.11 ± 0.11 mg/100 g) compared to the other samples. Tomato passata, tomato ketchup, and fresh tomatoes did not differ significantly in their vitamin E content. δ-Tocotrienol was not found in the analyzed samples. Only β-tocopherol and α-tocotrienol were determined in tomato pesto as well as δ-tocopherol and γ-tocotrienol in fresh tomatoes. In comparison to the data of Pinela et al.,[43] the α-tocopherol content of fresh tomatoes was similar to our results. However, β- and γ-tocopherol were not detected in our fresh tomatoes, and Pinela et al. did not determine the content of tocotrienols. The main form of vitamin E determined in the tomato samples was α-tocopherol with relative contents between 31% for fresh tomatoes and 86% for tomato pesto. A much higher contribution of α-tocopherol for raw tomatoes (78%), ketchup (92%) and puree (94%) was measured by Chun et al.[44] A reason for the high content of α-tocopherol could be that only α-tocotrienol was found in trace amounts in raw tomatoes and no other tocotrienols were found in ketchup and puree.

AUTHOR INFORMATION

Corresponding Author

*Tel.: +49 3641 949633. Fax: +49 3641 949702. E-mail: volker.boehm@uni-jena.de (V. B.).

Funding

The funding of this research within the project "BioOptiSens" is gratefully acknowledged.

Notes

The authors declare no competing financial interest.

ACKNOWLEDGMENTS

We thank Jana Hesse for her assistance in laboratory work.

ABBREVIATIONS USED

AOA, antioxidant activity; AOC, antioxidant capacity; DPPH, 2,2′-diphenylpicrylhydrazyl scavenging activity; FRAP, ferric reducing antioxidant power; LPSC, luminol-chemiluminescence peroxyl radical scavenging capacity; PCL, photochemilumines-

cence; α-TE, α-tocopherol equivalents; α-TEAC, α-tocopherol equivalent antioxidant capacity

REFERENCES

(1) Eldahshan, O. A. E. O. A. Carotenoids: A review. *(Advance Research in Pharmaceuticals and Biologicals) ARPB* **2013**, *3* (I), 345−352.

(2) Lakshminarayana, R.; Baskaran, V. Influence of olive oil on carotenoids bioavailability - A review. *Eur. J. Lipid Sci. Technol.* **2013**, *115* (10), 1085−1093.

(3) Stahl, W.; Sies, H. Antioxidant activity of carotenoids. *Mol. Aspects Med.* **2003**, *24*, 345−351.

(4) Popov, I. N.; Lewin, G. Photochemiluminescent detection of antiradical activity: II. Testing of nonenzymic water-soluble antioxidants. *Free Radical Biol. Med.* **1994**, *17*, 267−271.

(5) Popov, I. N.; Lewin, G. Photochemiluminescent detection of antiradical activity; IV: Testing of lipid-soluble antioxidants. *J. Biochem. Biophys. Methods* **1996**, *31*, 1−8.

(6) Popov, I.; Lewin, G. Photochemiluminescent detection of antiradical activity. VII. Comparison with a modified method of thermo-initiated free radical generation with chemiluminescent detection. *Luminescence* **2005**, *20*, 321−325.

(7) Schlesier, K.; Harwat, M.; Böhm, V.; Bitsch, R. Assessment of antioxidant activity by using different in vitro methods. *Free Radical Res.* **2002**, *36*, 177−187.

(8) Bauerfeind, J.; Hesse, J.; Killenberg, M.; Böhm, V. Comparison of antioxidant activities of carotenoids measured. *Ann. Nutr. Metab.* **2012**, *60*, 132.

(9) Prior, R. L.; Wu, X.; Schaich, K. Standardized methods for the determination of antioxidant capacity and phenolics in foods and dietary supplements. *J. Agric. Food Chem.* **2005**, *53*, 4290−4302.

(10) Müller, L.; Fröhlich, K.; Böhm, V. Comparative antioxidant activities of carotenoids measured by ferric reducing antioxidant power (FRAP), ABTS bleaching assay (alpha TEAC), DPPH assay and peroxyl radical scavenging assay. *Food Chem.* **2011**, *129*, 139−148.

(11) Miller, N. J.; Sampson, J.; Candeias, L. P.; Bramley, P. M.; Rice-Evans, C. A. Antioxidant activities of carotenes and xanthophylls. *FEBS Lett.* **1996**, *384*, 240−242.

(12) Werner, S.; Böhm, V. Bioaccessibility of carotenoids and vitamin E from pasta: evaluation of an in vitro digestion model. *J. Agric. Food Chem.* **2011**, *59*, 1163−1170.

(13) Franke, S.; Fröhlich, K.; Werner, S.; Böhm, V.; Schöne, F. Analysis of carotenoids and vitamin E in selected oilseeds, press cakes and oils. *Eur. J. Lipid Sci. Technol.* **2010**, *112*, 1122−1129.

(14) Hengst, C.; Werner, S.; Müller, L.; Fröhlich, K.; Böhm, V. Determination of the antioxidant capacity: influence of the sample concentration on the measured values. *Eur. Food Res. Technol.* **2009**, *230*, 249−254.

(15) Apak, R.; Gorinstein, S.; Böhm, V.; Schaich, K. M.; Özyürek, M.; Güçlü, K. Methods of measurement and evaluation of natural antioxidant capacity/activity (IUPAC Technical Report). *Pure Appl. Chem.* **2013**, *85*, 957−998.

(16) Sipel, A.; Kevers, C.; Pincemail, J.; Grygiel, P.-G.; Defraigne, J.-O.; Dommes, J. Sample dilution influences the determination of antioxidant capacity in food: How to minimize it? *Food Anal. Method.* **2013**, 1−7.

(17) Stahl, W.; Sies, H. Lycopene: A Biologically Important Carotenoid for Humans? *Arch. Biochem. Biophys.* **1996**, *336*, 1−9.

(18) Khoo, H.-E.; Prasad, K. N.; Kong, K.-W.; Jiang, Y.; Ismail, A. Carotenoids and their isomers: Color pigments in fruits and vegetables. *Molecules* **2011**, *16*, 1710−1738.

(19) Meléndez-Martínez, A. J.; Britton, G.; Vicario, I. M.; Heredia, F. J. Relationship between the colour and the chemical structure of carotenoid pigments. *Food Chem.* **2007**, *101*, 1145−1150.

(20) Britton, G. Structure and properties of carotenoids in relation to function. *FASEB J.* **1995**, *9*, 1551−1558.

(21) Maiani, G.; Periago Castón, M. J.; Catasta, G.; Toti, E.; Cambrodón, I. G.; Bysted, A.; Granado-Lorencio, F.; Olmedilla-Alonso, B.; Knuthsen, P.; Valoti, M.; Böhm, V.; Mayer-Miebach, E.; Behsnilian, D.; Schlemmer, U. Carotenoids: Actual knowledge on food sources, intakes, stability and bioavailability and their protective role in humans. *Mol. Nutr. Food Res.* **2009**, *53*, S194−S218.

(22) Conn, P. F.; Schalch, W.; Truscott, T. G. The singlet oxygen and carotenoid interaction. *J. Photochem. Photobiol. B* **1991**, *11*, 41−47.

(23) Di Mascio, P.; Kaiser, S.; Sies, H. Lycopene as the most efficient biological carotenoid singlet oxygen quencher. *Arch. Biochem. Biophys.* **1989**, *274*, 532−538.

(24) Henry, L. K.; Catignani, G. L.; Schwartz, S. J. Oxidative degradation kinetics of lycopene, lutein, and 9-cis and all-trans β-carotene. *J. Am. Oil Chem. Soc.* **1998**, *75*, 823−829.

(25) Shi, J. Lycopene in tomatoes: Chemical and physical properties affected by food processing. *Crit. Rev. Biotechnol.* **2000**, *20*, 293−334.

(26) Liu, D.; Shi, J.; Colina Ibarra, A.; Kakuda, Y.; Jun Xue, S. The scavenging capacity and synergistic effects of lycopene, vitamin E, vitamin C, and β-carotene mixtures on the DPPH free radical. *LWT Food Sci. Technol.* **2008**, *41*, 1344−1349.

(27) Zanfini, A.; Corbini, G.; La Rosa, C.; Dreassi, E. Antioxidant activity of tomato lipophilic extracts and interactions between carotenoids and α-tocopherol in synthetic mixtures. *LWT Food Sci. Technol.* **2010**, *43*, 67−72.

(28) Kotikova, Z.; Lachman, J.; Hejtmankova, A.; Hejtmankova, K. Determination of antioxidant activity and antioxidant content in tomato varieties and evaluation of mutual interactions between antioxidants. *LWT Food Sci. Technol.* **2011**, *44*, 1703−1710.

(29) Palozza, P.; Krinsky, N. I. β-Carotene and α-tocopherol are synergistic antioxidants. *Arch. Biochem. Biophys.* **1992**, *297*, 184−187.

(30) Shi, J.; Qu, Q.; Kakuda, Y.; Xue, S. J.; Jiang, Y.; Koide, S.; Shim, Y.-Y. Investigation of the antioxidant and synergistic activity of lycopene and other natural antioxidants using LAME and AMVN model systems. *J. Food Compos. Anal.* **2007**, *20*, 603−608.

(31) Stahl, W.; Junghans, A.; de Boer, B.; Driomina, E. S.; Briviba, K.; Sies, H. Carotenoid mixtures protect multilamellar liposomes against oxidative damage: synergistic effects of lycopene and lutein. *FEBS Lett.* **1998**, *427*, 305−308.

(32) Navas, M. J.; Jiménez, A. M. Review of chemiluminescent methods in food analysis. *Food Chem.* **1996**, *55*, 7−15.

(33) Barni, F.; Lewis, S. W.; Berti, A.; Miskelly, G. M.; Lago, G. Forensic application of the luminol reaction as a presumptive test for latent blood detection. *Talanta* **2007**, *72*, 896−913.

(34) Huang, D.; Ou, B.; Prior, R. L. The chemistry behind antioxidant capacity assays. *J. Agric. Food Chem.* **2005**, *53*, 1841−1856.

(35) Ozgen, M.; Reese, R. N.; Tulio, A. Z.; Scheerens, J. C.; Miller, A. R. Modified 2,2-azino-bis-3-ethylbenzothiazoline-6-sulfonic acid (ABTS) method to measure antioxidant capacity of selected small fruits and comparison to ferric reducing antioxidant power (FRAP) and 2,2′-diphenyl-1-picrylhydrazyl (DPPH) methods. *J. Agric. Food Chem.* **2006**, *54*, 1151−1157.

(36) Baranska, M.; Schütze, W.; Schulz, H. Determination of lycopene and β-Carotene content in tomato fruits and related products: Comparison of FT-Raman, ATR-IR, and NIR spectroscopy. *Anal. Chem.* **2006**, *78*, 8456−8461.

(37) Fröhlich, K.; Burkhardt, S.; Böhm, V. Bioactive compounds in tomatoes and tomato products-investigations of different commercially available foodstuffs. *Schubert, R., Flachowsky, G., Jahreis, G., Bitsch, R. (Hrsg.): Vitamine und Zusatzstoffe in der Ernährung von Mensch und Tier (Vitamins and Additives in the Nutrition of Man and Animal), Informations- und Datenzentrum der FAL* **2005**, 240−243.

(38) Sass-Kiss, A.; Kiss, J.; Milotay, P.; Kerek, M. M.; Toth-Markus, M. Differences in anthocyanin and carotenoid content of fruits and vegetables. *Food Res. Int.* **2005**, *38*, 1023−1029.

(39) Kotíková, Z.; Lachman, J.; Hejtmánková, A.; Hejtmánková, K. Determination of antioxidant activity and antioxidant content in tomato varieties and evaluation of mutual interactions between antioxidants. *LWT Food Sci. Technol.* **2011**, *44*, 1703−1710.

(40) Burns, J.; Fraser, P. D.; Bramley, P. M. Identification and quantification of carotenoids, tocopherols and chlorophylls in commonly consumed fruits and vegetables. *Phytochemistry* **2003**, *62*, 939−947.

(41) Gama, J.; Tadiotti, A.; Sylos, C. Comparison of carotenoid content in tomato, tomato pulp and ketchup by liquid chromatography. *Braz. J. Food Nutr.* **2009**, *17*, 353−358.
(42) Monge-Rojas, R.; Campos, H. Tocopherol and carotenoid content of foods commonly consumed in Costa Rica. *J. Food Compos. Anal.* **2011**, *24*, 202−216.
(43) Pinela, J.; Barros, L.; Carvalho, A. M.; Ferreira, I. C. F. R. Nutritional composition and antioxidant activity of four tomato (Lycopersicon esculentum L.) farmer' varieties in Northeastern Portugal homegardens. *Food Chem. Toxicol.* **2012**, *50*, 829−834.
(44) Chun, J.; Lee, J.; Ye, L.; Exler, J.; Eitenmiller, R. R. Tocopherol and tocotrienol contents of raw and processed fruits and vegetables in the United States diet. *J. Food Compos. Anal.* **2006**, *19*, 196−204.

that CO_2 enriched atmospheres, which are used widely to reduce the incidence of decay of strawberries, resulted in the degradation of fruit internal color, which is manifested in a remarkable decrease in the anthocyanin content.[15] In another study, it was found that arils of pomegranates, which were stored in air enriched with 10 kPa CO_2, had a lower anthocyanin concentration than air-stored fruit.[16] In addition, Harb et al.[10] reported a dramatic loss in ascorbic acid and lower antioxidative capacity of water-soluble antioxidants in blueberries stored under CA conditions. In another study that addressed superatmospheric O_2 treatments with 'Duke' blueberries, researchers found significant increases in the antioxidant levels of blueberries that were stored at 60−100% O_2.[17]

Despite the above-mentioned findings, detailed studies that address quantitative and qualitative changes of polyphenols during storage of blueberries, as well as changes in the expression levels of selected genes that have roles in the biosynthesis of polyphenols, are limited. Accordingly, this study aims to quantify changes in polyphenols in blueberries in addition to the relative quantification of expression levels of some related genes. The findings of this study provide new insights into the postharvest biology of blueberries which may have implications on storage technologies for these fruits.

MATERIALS AND METHODS

Plant Material, Storage Conditions, and Determination of Quality Parameters. Blueberries (cultivar: Duke) were obtained from a private orchard located at Lake of Constance region, Germany. Directly after picking, fruits were stored at 1 °C (±0.3 °C) under the following CA-storage conditions (kPa O_2 + kPa CO_2): 21 + 0.03 (air-storage = control), 3 + 6, 3 + 12, 3 + 18, 10 + 6, 10 + 12, and 10 + 18. Storage containers were 26.4 L hermitic jars that were continuously monitored by gas analyzers. After 4 and 8 weeks of storage, portions of the stored blueberries were assessed for firmness, total soluble solids, and titratable acidity. For each treatment and sampling date, there were three biological replicates, each with 250 g (125 fruits) of berries. All measurements were conducted on the same sampling day after 2 h conditioning period at room temperature. Firmness of 20 fruits for each replicate was measured using a nondestructive device (FirmTech2, BioWorks, Wamego, KS) designed for soft fruits. Readings obtained are expressed in g mm^{-1}. The same fruits used for firmness measurements plus another 30 fruits (a total of 50 fruit per each biological replicate) were used for total soluble solids (TSS) and titratable acidity (TA) measurements. TSS of the juice was determined using a digital refractometer (PR-1; Atago Co. Ltd., Tokyo, Japan) and expressed as °Brix. TA was determined through titration of 10 mL juice plus 50 mL distilled water with 0.1 N NaOH to pH 8.1 using a fully automatic titration robot (Metrohm 702 SM Titrino, Filderstadt, Germany). TA was expressed in meq

Extraction and Determination of Individual Polyphenols Using LC−MS. Twenty fruits per biological replicate (60 fruits for each treatment with three biological replicates) were obtained after a storage period of 8 weeks to be rapidly frozen in liquid nitrogen. The samples were freeze-dried to powder, and 100 mg of the lyophilized tissue (from each biological replicate) was added to 500 μL of absolute methanol and 250 μL of the internal standard solution (50 mg biochanin A in 250 mL absolute methanol). After vortexing for 1 min and sonicating for 5 min, the mixed solutions were centrifuged at 13 200 rpm for 10 min. Supernatants were collected in fresh tubes, and pellets were extracted, vortexed, sonicated, and centrifuged once again as mentioned above. Supernatants were pooled and placed in a Speed-Vac for 2 h. The dried residue from each replicate was dissolved in 35 μL of water, sonicated for 10 min, and finally centrifuged at 13 200 rpm for 10 min. For each replicate, 20 μL of the clear supernatant was placed in a HPLC vial for final analysis using an LC−MS instrument (Agilent HPLC 1100; MS: Bruker Daltonics esquire3000plus, Santa Clara, CA) which was equipped with a Phenomenex column (Luna 3u C18 (2) 100A″, 150 mm × 2.0 mm (Part-Nr. 00F-4251-B0); Aschaffenburg, Germany). The analysis conditions were as follows: column temperature, 28 °C; injection volume, 5 μL; flow rate, 0.2 $mL.min^{-1}$. Solvents were as follows: A, 0.1% formic acid in water; B, 0.1% formic acid in methanol; gradient 0−30 min, 0−50% B; 30−35 min, 50−100% B; 35−50 min, 100% B; 50−55 min, 100−0% B; 55−65 min, 0% B; detection wavelength, 280 nm. MS details are as follows: dry gas, nitrogen at 330 °C; flow rate of 10 L min^{-1}; capillary, −4000 V; end plate offset, −500 V. The electrospray ionization voltage of the capillary was set to −4000 V and the end plate to −500 V. The full scan mass spectra were measured in a scan range from m/z 100 to 800. Tandem mass spectrometry was carried out using helium as collision gas (3.5−6 mbar) with the collision voltage set at 1 V. Spectra were acquired in both positive and negative ionization modes. Data analysis was performed using the DataAnalysis 5.1 software (Bruker Daltonics, Bremen, Germany). Relative concentrations of polyphenols were calculated on the basis of the values of the internal standard (Biochanin A; Sigma-Aldrich, Seelze, Germany).

Gene Expression Analysis. Samples were taken from berries that were stored for 8 weeks at the designated conditions. The gene expression analyses were conducted according to Harb et al.[18] with minor modifications. Ten berries per each biological replicate were randomly selected after 2 h conditioning period at room temperature, shock-frozen in liquid nitrogen, and ground to powder. RNA extraction was conducted according to the protocol of Chang[19] with modifications. Eight grams of powdered tissue were added to 20 mL prewarmed (65.0 °C) CTAB-based extraction buffer and incubated for 15 min at 65.0 °C. After centrifugation at 7740*g* for 10 min at room temperature, 15 mL from the clear supernatant was added to an equal volume of chloroform/isoamylalcohol (24:1), vortexed, and centrifuged at 7740*g* for 20 min at room temperature. This step was repeated twice, and RNA was precipitated overnight at 4.0 °C using 1 volume of LiCl (2.5 M). After pellets were washed, RNA was suspended in water. Quality and quantity of extracted RNA were assessed using gel-electrophoresis and the NanoDrop, respectively. The extracted RNAs were purified using RNeasy MinElute Cleanup Kit (Qiagen, Valencia, CA) and subsequently subjected to DNase treatment (RNase-Free DNase Set; Qiagen, Valencia, CA).

The qPCR analyses were conducted using a LightCycler 480II from Roche Diagnostics Deutschland GmbH (Mannheim, Germany) and SensiMix kit from Bioline GmbH (Luckenwalde, Germany). Taqman RT-PCR reagents from Applied Biosystems (Foster City, CA) were used to synthesize cDNA (2 μg DNA-digested RNA from each sample using random hexamer primers). Sequences from the NCBI database and also from the available literature, in particular Zifkin et al.,[20] served to design the following gene-specific primers using Primer3 software: *VcCHS*-F, 5′-cttgactgaggaaatcttgaagg-3′; *VcCHS*-R, 5′-agcctctttgcc-caatttg-3′ (GenBank: JN654702.1); *VcF3′H*-F, 5′-cgagattcgatg-cgtttctgagtg-3′; *VcF3′H*-R, 5′-gatttcggtatcggtgagcttcc-3′; *VcDFR*-F, 5′-cactgagtttaaggggattcctaagg-3′; *VcDFR*-R, 5′-cccttctccctacaagtgtcaatgg-3′; *VcANS*-F, 5′-cttcatcctccacaacatggt-3′; *VcANS*-R, 5′-gctcttgta-cttcccattgctc-3′ (GenBank: JN654701.1); *VcGAPDH*-F, 5′-ggttatcaatgataggtttggca-3′; *VcGAPDH*-R, 5′-cagtccttgcttgatggacc-3′ (GenBank: AY123769.1). *VcGAPDH* served as a reference gene. For each treatment and sampling date, there were two biological replicates, each with three technical replicates. The quantification of the expression levels of the targeted genes were calculated relative to the transcript abundance of the reference gene employing relative quantification with efficiency correction.[21]

Statistical Analysis. The experimental design was completely randomized with a single factor, namely the storage conditions. The CoStat statistical package (CoHort Software, Monterey, CA) was used for the analysis of variance (ANOVA). Comparisons of means were conducted using Student−Newman−Keuls test at $P \leq 0.05$. Moreover, the standrad error (SE) values were calculated and included ($n = 3$ for all parameters, except gene expression analyses; for those analyses $n = 2$ (two biological replicates, each with three technical replicates).

Table 1. Influence of Controlled Atmosphere Storage Condition (kPa O_2 + kPa CO_2) on Fruit Firmness (g × mm^{-1}), Total Soluble Solids (TSS, °Brix), and Titratable Acidity (meq) of Blueberries (cv. Duke) after Harvest (HT) and after Four and Eight Weeks Storage at 1 °C[a]

	firmness (g × mm^{-1}) (197.4 ± 10.1 at HT)		total soluble solids (°Brix) (9.0 ± 0.3 at HT)		titratable acidity (meq) (18.6 ± 1.0 at HT)	
storage condition	4 weeks	8 weeks	4 weeks	8 weeks	4 weeks	8 weeks
air-storage	215.0 ± 9.8 a	179.9 ± 9.2 c	9.2 ± 0.3	8.7 ± 0.0	18.2 ± 0.7	16.3 ± 0.1 b
03 + 06	228.5 ± 7.0 a	262.5 ± 3.5 a	9.2 ± 0.3	8.7 ± 0.0	19.4 ± 1.2	20.0 ± 0.3 a
03 + 12	190.6 ± 5.4 b	162.6 ± 8.3 c	8.9 ± 0.1	8.3 ± 0.0	19.2 ± 0.5	18.4 ± 0.8 a
03 + 18	153.1 ± 5.8 c	123.7 ± 1.1 d	9.05 ± 0.1	8.4 ± 0.2	18.6 ± 0.2	17.4 ± 0.8 a
10 + 06	224.2 ± 8.0 a	230.8 ± 14.8 b	9.6 ± 0.6	8.8 ± 0.1	19.5 ± 0.9	17.1 ± 0.4 a
10 + 12	188.6 ± 7.0 b	214.2 ± 12.4 b	9.2 ± 0.1	8.6 ± 0.1	18.4 ± 0.1	19.4 ± 0.0 a
10 + 18	168.9 ± 11.7 bc	136.6 ± 11.2 d	9.2 ± 0.0	8.3 ± 0.1	19.2 ± 0.0	18.0 ± 0.6 a
ANOVA	***	***	ns	ns	ns	**

[a]Mean separations were conducted using Student−Newman−Keuls test (n = 3). ± are SE values. Values followed by the same letter do not differ significantly in the column at $p \leq 0.05$.

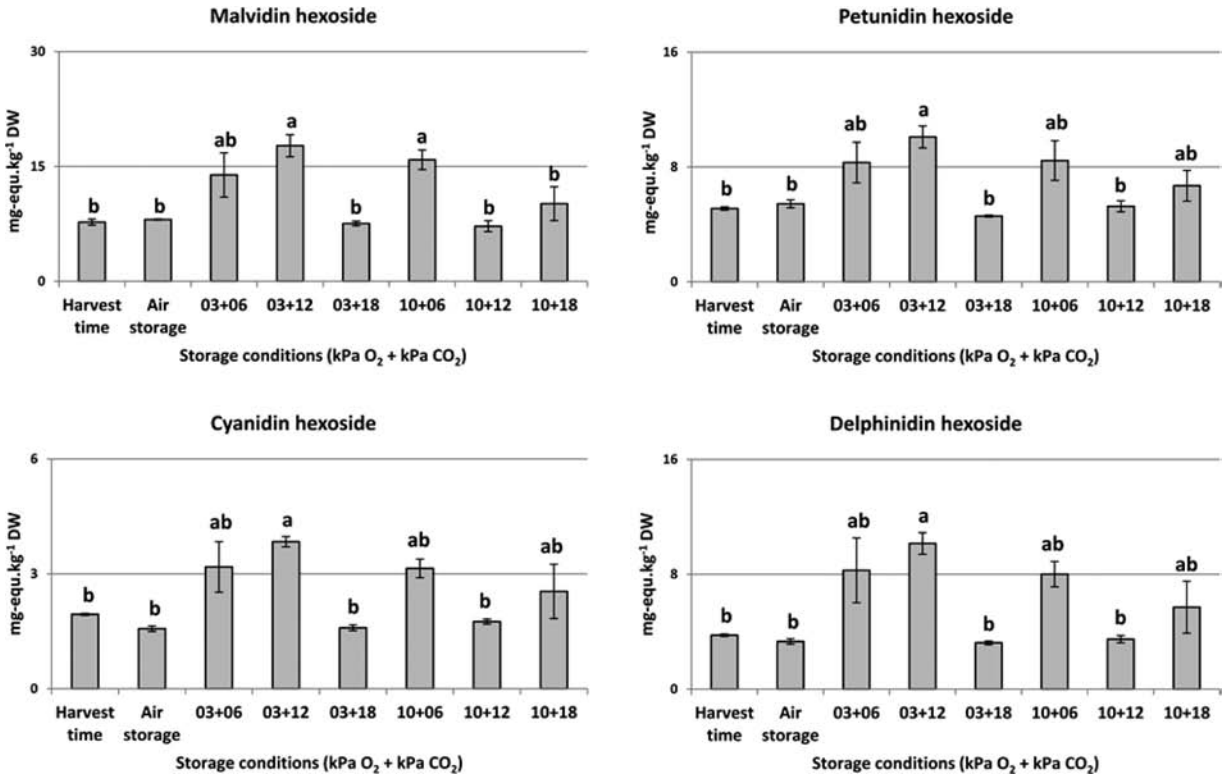

Figure 1. Influence of controlled atmosphere storage condition (kPa O_2 + kPa CO_2) on the relative content (mg-equ kg^{-1} DW) of malvidin hexoside, petunidin hexoside, cyanidin hexoside, and delphinidin hexoside of blueberries (cv. Duke) after 8 weeks storage at 1 °C. Mean separations were conducted using Student−Newman−Keuls test at $p \leq 0.05$ (n = 3). Values followed by the same letter do not differ significantly at $p \leq 0.05$. Error bars are SE values. Contents (Y-axis) are calculated relative to the internal standard (Biochanin A).

RESULTS

Quality Parameters. Storing blueberries for 8 weeks resulted in an accelerated softening of fruits that were stored under high CO_2 partial pressure (18 kPa) (Table 1), but with no significant differences between treatments in respect to total soluble solids contents. However, air-stored berries showed significant decrease in titratable acidity (TA) after 8 weeks of storage. Moreover, the sensory evaluation by the end of the storage trial revealed that berries stored under 3 + 6, 3 + 12, 10 + 6, and 10 + 12 (kPa O_2 + kPa CO_2) storage conditions tasted "good", whereas berries stored under 3 + 18 and 10 + 18 (kPa O_2 + kPa CO_2) had alcoholic off-flavor (data not shown).

Semiquantitative Changes in Polyphenols. The effects of various storage conditions on sets of polyphenols are shown in Figures 1−4. Figure 1 shows changes in the first group of polyphenols (hexosides of malvidin, petunidin, cyanidine, and delphinidin), and it is evident that the storage condition with very high CO_2 partial pressure (18 kPa) and low O_2 prevented the increase in the levels of these polyphenols. Moreover, it was found that blueberries had significantly lower levels of these polyphenols at harvest time as compared to berries that were stored at 3 kPa O_2 with 6 or 12 kPa CO_2. In addition, it is evident that the 3 kPa O_2 + 12 kPa CO_2 storage condition resulted in the highest levels for all compounds of the first group, whereas the levels of these compounds in air-stored

dx.doi.org/10.1021/jf5024774 | J. Agric. Food Chem. 2014, 62, 7460−7467

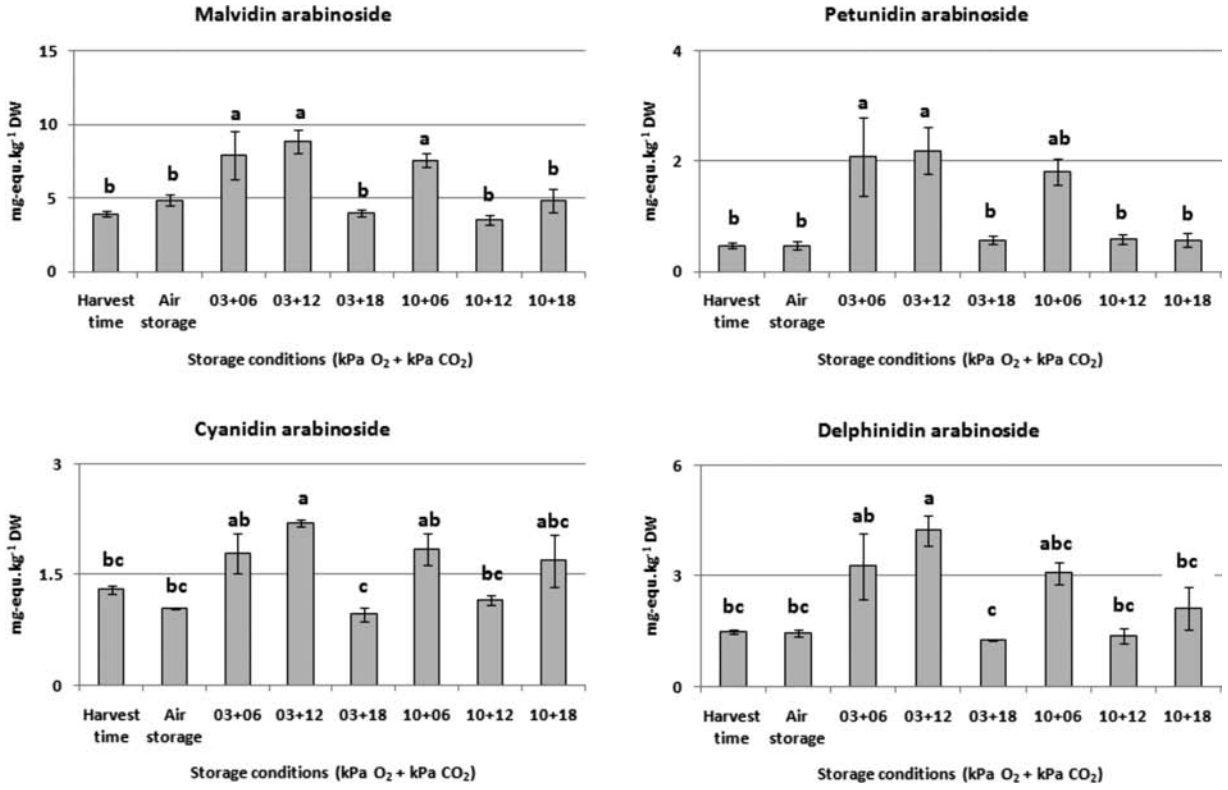

Figure 2. Influence of controlled atmosphere storage condition (kPa O_2 + kPa CO_2) on the content (mg-equ kg^{-1} DW) of malvidin arabinoside, petunidin arabinoside, cyanidin arabinoside, and delphinidin arabinoside of blueberries (cv. Duke) after 8 weeks storage at 1 °C. Mean separations were conducted using Student−Newman−Keuls test at $p \leq 0.05$ ($n = 3$). Values followed by the same letter do not differ significantly at $p \leq 0.05$. Error bars are SE values. Contents (*Y*-axis) are calculated relative to the internal standard (Biochanin A).

berries remained low with no significant differences with regard to harvest time.

The second group of polyphenols (arabinosides of malvidin, petunidin, cyanidine, and delphinidin; Figure 2) shows a similar trend to the first group, but with slight differences. Increasing O_2 partial pressure to 10 kPa led mostly to lower levels of the compounds. With this group of compounds, the influence of the highest CO_2 partial pressure (18 kPa) was more pronounced than with compounds of the first group.

The polyphenols of the third group (Figure 3) behaved differently. The highest CO_2 partial pressure (18 kPa) had less influence on their content. Moreover, it is clear that most storage conditions significantly induced, in comparison to harvest time, the biosynthesis of chlorogenic acid.

As for the compounds of the last group (Figure 4), two trends are clear: catechin (and also epicatechin; data not shown) levels were already high at harvest time, and declined steadily with all storage conditions, except under regular air-storage. The decrease was most noticeable under 3 kPa O_2 + 18 kPa CO_2. The second trend is for the unknown compounds (only unknown 1 is shown; Figure 4). It is clear that the highest partial pressure of CO_2 (18 kPa), irrespective of O_2 level, resulted in highly elevated levels of these compounds.

Expression of Polyphenol-Related Genes. Figure 5 depicts the expression levels of a few genes that encode enzymes involved in the biosynthesis of various polyphenols. The expression levels of chalcone synthase (*VcCHS*) and dihydroflavonol-4-reductase (*VcDFR*) were already high at harvest time, but declined significantly and drastically upon storage under very high CO_2 partial pressure levels. For both *VcCHS* and *VcDFR*, the decrease in the expression levels correlates well with the increasing partial pressure of CO_2, especially when combined with 3 kPa O_2. For both flavonoid 3′-hydroxylase (*VcF3′H*) and anthocyanidin synthase (*VcANS*) genes, berries at harvest time showed the highest expression levels, and differences between storage treatments are minimal with no clear trends between storage conditions.

DISCUSSION

A CO_2 enriched storage atmosphere is highly recommended to control decay in various fruits, including strawberry and blueberry.[17] Blanch et al.[22] attributed this antifungal efficacy of high CO_2 atmosphere to the induction of the biosynthesis of catechin, which is believed to reduce fungal decay. Despite this positive effect, our previous studies[23] showed that CO_2 partial pressure (above 12 kPa) led to an accelerated softening of fruits that renders them to be unmarketable. In the current study, several polyphenols (Figures 1 and 2) showed significant increases following storage under nonstressful CO_2 partial pressure (6−12 kPa), in particular when coupled with low O_2 partial pressure (3 kPa). Similar trends were reported by Kalt et al.,[24] who found that anthocyanins continued to be synthesized during storage. Schotsmans et al.[25] also found that blueberries showed the highest antioxidant activity after 6 days at 20 °C (shelf life), which indicates that the enzymatic machinery for flavonoids biosynthesis is still active during storage. Our results reveal also that medium to high (6 or 12 kPa) CO_2 partial pressure as well as low O_2 (3 kPa) partial pressure preserved the capacity of cells to synthesize flavonoids. This was clear with the major polyphenols, in particular malvidin hexoside, which is considered one of the major polyphenols in blueberry.[6] In contrast, Beaudry[26] set the lower O_2 limits for the storage of

dx.doi.org/10.1021/jf5024774 | J. Agric. Food Chem. 2014, 62, 7460−7467

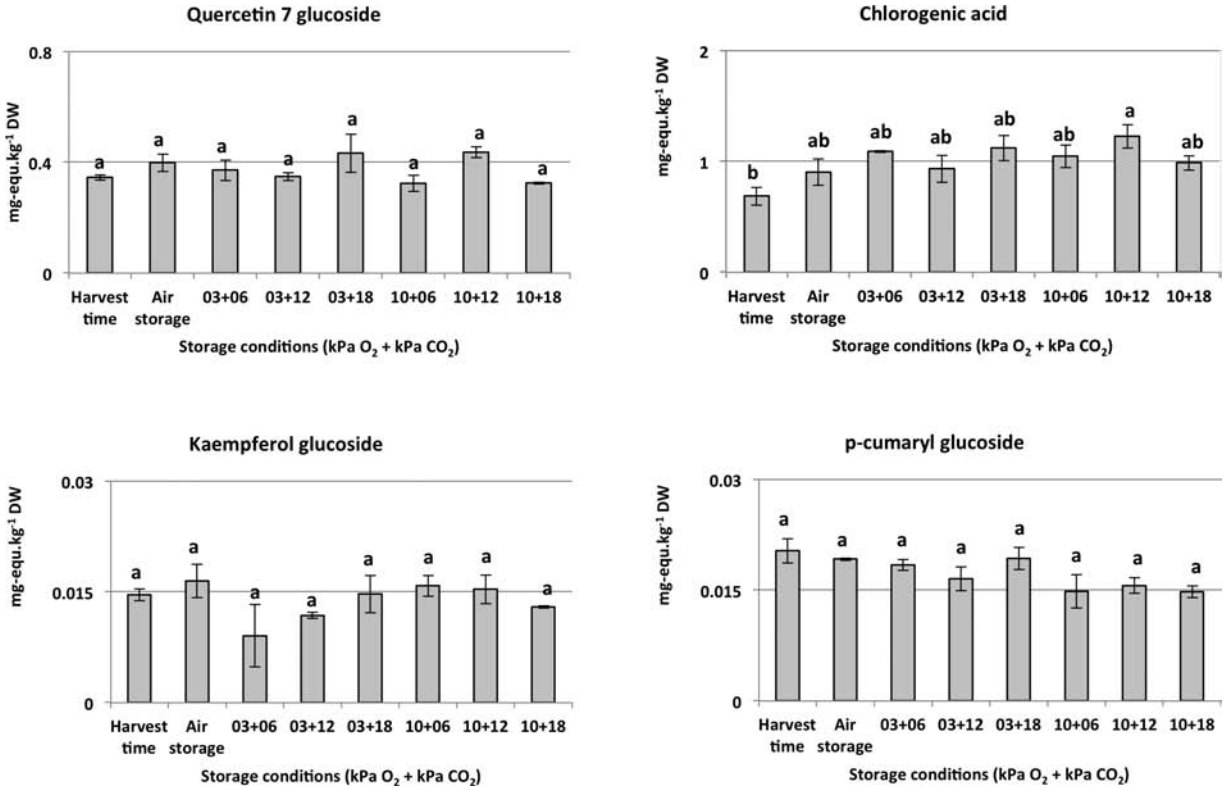

Figure 3. Influence of controlled atmosphere storage condition (kPa O_2 + kPa CO_2) on the content (mg-equ kg^{-1} DW) of quercetin-7-glucoside, chlorogenic acid, kaempferol glucoside, and p-coumaryl glucoside of blueberries (cv. Duke) after 8 weeks storage at 1 °C. Mean separations were conducted using Student−Newman−Keuls test at $p \leq 0.05$ ($n = 3$). Values followed by the same letter do not differ significantly at $p \leq 0.05$. Error bars are SE values. Contents (*Y*-axis) are calculated relative to the internal standard (Biochanin A).

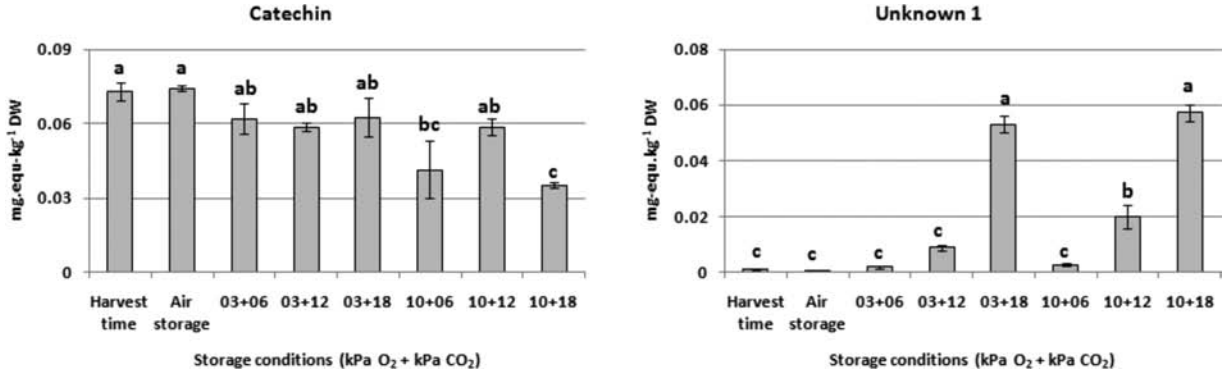

Figure 4. Influence of controlled atmosphere storage condition (kPa O_2 + kPa CO_2) on the content (mg-equ kg^{-1} DW) of catechin, and unknown 1 of blueberries (cv. Duke) after 8 weeks storage at 1 °C. Mean separations were conducted using Student−Newman−Keuls test at $p \leq 0.05$ ($n = 3$). Values followed by the same letter do not differ significantly at $p \leq 0.05$. Error bars are SE values. Contents (*Y*-axis) are calculated relative to the internal standard (Biochanin A).

blueberry (cvs 'Bluecrop' and 'Elliot') at 6, 7, and 11 kPa O_2 for the 5, 20, and 40 kPa CO_2 treatments, respectively. Taking into account that 'Duke' blueberries were used in our study, and that 3 kPa O_2 caused no negative effect, it is possible to predict that genotypes differ in their tolerance.

Referring to the above-mentioned impact of medium to high CO_2 partial pressure and low O_2 partial pressure on the biosynthesis of flavonoids, it is hard to elucidate the possible mechanism for such impact. Earlier studies showed that elevating CO_2 partial pressures in storage resulted usually in the prevention of significant increases in the levels of polyphenols. Since studies addressing blueberry, a nonclimacteric fruit, are rare, studies with other nonclimacteric fruits (e.g., strawberry and table grapes) will be used for further comparison and interpretation of the current results. With strawberry, it was found that air-storage, as well as storage under low CO_2 concentrations, resulted in higher levels of anthocyanin and intense red coloration compared to strawberries stored under elevated CO_2 concentrations.[14,15] In addition, it was reported that arils of pomegranates stored under 10 kPa CO_2 had lower anthocyanin concentration than air-stored fruit.[16] Moreover, various studies reported significant reductions in organic acids, mainly malic acid, upon storage at high CO_2 atmospheres.[14,27] Regarding anthocyanins, Holcroft and Kader[28] assumed that the slight changes in pH may affect the biosynthesis of anthocyanins. In this sense, it is worth

dx.doi.org/10.1021/jf5024774 | J. Agric. Food Chem. 2014, 62, 7460−7467

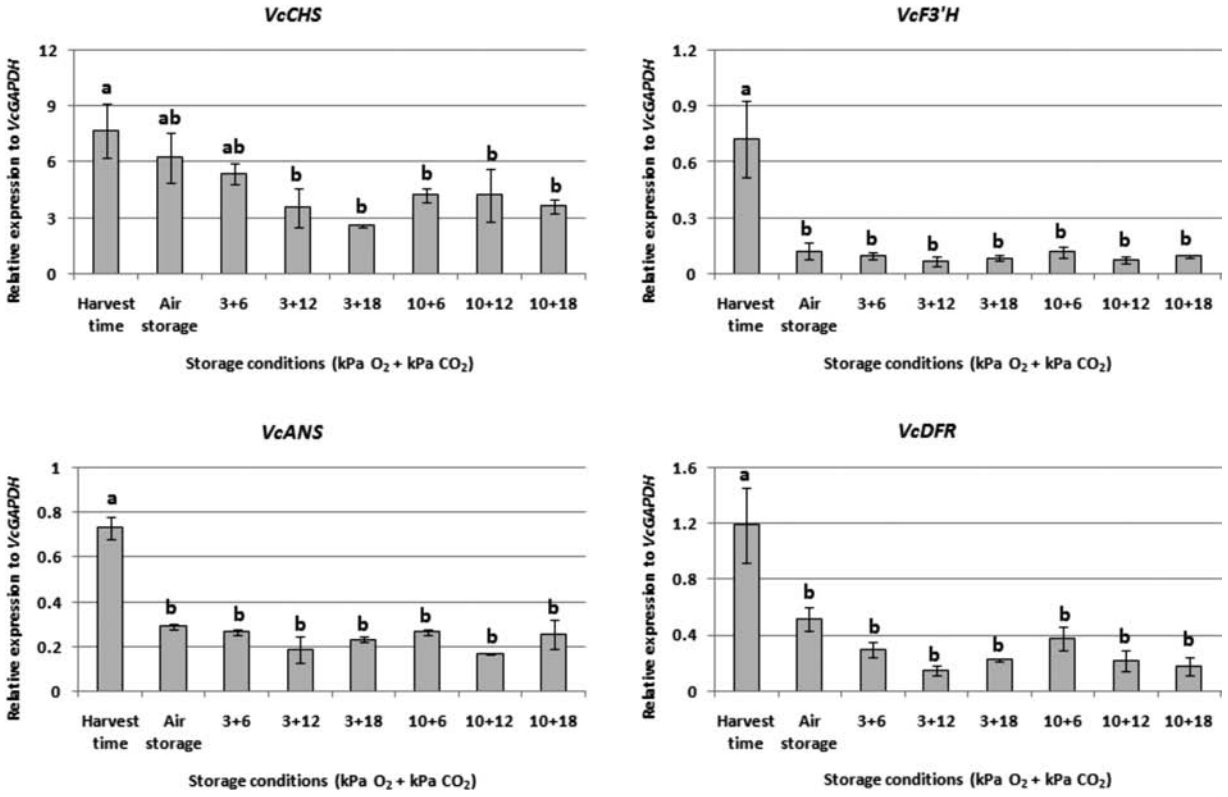

Figure 5. Influence of controlled atmosphere storage condition (kPa O_2 + kPa CO_2) on the expression levels of chalcone synthase (*VcCHS*), flavonoid 3′-hydroxylase (*VcF3′H*), anthocyanidin synthase (*VcANS*), and dihydroflavonol-4-reductase (*VcDFR*) of blueberries (cv. Duke) normalized to *VcGAPDH* (reference gene) after 8 weeks storage at 1 °C. Mean separations were conducted using Student−Newman−Keuls test at $p \leq 0.05$ ($n = 2$). Values followed by the same letter do not differ significantly at $p \leq 0.05$. Error bars are SE values.

mentioning that pH is an important factor in maintaining the stability of anthocyanins,[29] and lowering pH values improved the stability of strawberry color more than any other factor.[30] Concerning the slightly negative impact of 10 kPa O_2, compared to 3 kPa, it is most probable that the high O_2 partial pressure promoted the oxidation of polyphenols. Odriozola-Serrano et al.[31] reported that high O_2 concentrations around stored strawberries promoted greater losses of phenolic acids and vitamin C compared to low O_2 levels. Moreover, it was evident that oxygenation had a detrimental effect on bioactive phenolic compounds of red wine.[32]

In addition to the above-mentioned reductions in flavonoids under the highest CO_2 levels, changes in chlorogenic acid levels deserve special attention. This is due to the fact that chlorogenic acid is the main representative of the chlorogenic acid pathway and the major hydroxycinnamic acid in blueberries.[5,17] In the current study, high CO_2 coupled with either low or high O_2 levels had no negative impact on chlorogenic acid contents. In contrast, these conditions led to significant increases in chlorogenic levels during storage. Similar trends were also observed with loquat fruits, either during fruit ripening[33] or under CA-storage.[34] With pears, the chlorogenic acid content was the lowest by air-stored fruits, compared to fruits stored in CO_2 enriched environment.[35] In another study with 'Red d'Anjou' pear, 1-MCP treatment inhibited the transcription of key flavonoid biosynthetic genes with the concomitant decrease of chalcone synthase activity, which resulted in the diversion of the carbon flux from flavonoid pathway to chlorogenic acid pathway.[36]

Our results, as well as results from the above-mentioned studies, clearly indicate that the biosynthesis of chlorogenic acid through the chlorogenic acid pathway is independent from other polyphenols (Figures 1 and 2) that are synthesized by the flavonoid pathway. Accordingly, we hypothesize that high CO_2 may have negative impact on the expression of certain enzymes (e.g., chalcone synthase (*VcCHS*)) that are involved in flavonoid biosynthesis. In the current study, the expression level of *VcCHS* by freshly harvest blueberries is significantly higher than that for blueberries that were stored for 8 weeks under 18 kPa CO_2 condition (Figure 5); comparing storage treatments alone (without the harvest time) reveals that the expression level by air-stored blueberries is also significantly higher than those stored under 18 kPa CO_2 (data not shown). With grapes, a nonclimacteric fruit, storage under air at 0 °C increased phenylalanine ammonia-lyase, chalcone synthase and stilbene synthase mRNA levels in the skin, whereas the accumulation of these transcripts was lower in the skin of grapes that were stored for 3 days under high CO_2 level.[37] Taking into account that chalcone synthase is the first committed enzyme in flavonoid biosynthesis that catalyzes the formation of naringenin chalcone from 4-coumaroyl-CoA and malonyl-CoA to naringenin chalcone, its expression is crucial for the biosynthesis of a large set of polyphenols (e.g., malvidin hexoside). Although the start points for the control of anthocyanin differ between plant species,[38−40] we assume that the reduction in the expression of *VcCHS* is significant and may contribute highly to lower levels of polyphenols that are synthesized through the flavonoid pathway. In this respect, Gil et al.[15] reported that elevated CO_2 atmospheres led to bleaching of the strawberry internal flesh.

In conclusion, it is evident that storing 'Duke' blueberries under 18 kPa CO_2 significantly retarded, in comparison to

dx.doi.org/10.1021/jf5024774 | J. Agric. Food Chem. 2014, 62, 7460−7467

other conditions with lower CO_2 partial pressures, the biosynthesis and accumulation of polyphenols from the flavonoid pathway. Such an effect was not recorded on polyphenols from the chlorogenic pathway. Further investigations are planned to assess changes at metabolome and transcriptome levels to elucidate the causes of the rapid loss of polyphenols upon storage under high CO_2 partial pressure. In addition, the interaction between the low levels of polyphenols and the rapid softening of blueberries, which were stored under 18 kPa CO_2, deserves further investigations.

AUTHOR INFORMATION

Corresponding Author

*Phone: 00970 2 2982003. Fax: 00970 2 2982084. E-mail: jharb@birzeit.edu.

Funding

Financial support by the joint USIAS-FRIAS grant META-BEVO and by the European Regional Development Fund via the INTERREG Upper Rhine program in the framework of the Trinational Institute for Plant Research is gratefully acknowledged.

Notes

The authors declare no competing financial interest.

ACKNOWLEDGMENTS

Special thanks to Mr. Baraa Tartouri and Miss Zein Najjar for the technical support

REFERENCES

(1) Wu, X.; Beecher, G. R.; Holden, J. M.; Haytowitz, D. B.; Gebhardt, S. E.; Prior, R. L. Concentrations of anthocyanins in common foods in the United States and estimation of normal consumption. *J. Agric. Food Chem.* **2006**, *54*, 4069−4075.

(2) Basu, A.; Rhone, M.; Lyons, T. J. Berries: Emerging impact on cardiovascular health. *Nutr. Rev.* **2010**, *68*, 168−177.

(3) Neto, C. C. Cranberry and blueberry: Evidence for protective effects against cancer and vascular diseases. *Mol. Nutr. Food Res.* **2007**, *51*, 652−664.

(4) Gordillo, G.; Fang, H.; Khanna, S.; Harper, J.; Phillips, G.; Sen, C. K. Oral administration of blueberry inhibits angiogenic tumor growth and enhances survival of mice with endothelial cell neoplasm. *Antioxid. Redox Signaling* **2009**, *11*, 47−58.

(5) Gavrilova, V.; Kajdzanoska, M.; Gjamovski, V.; Stefova, M. Separation, characterization and quantification of phenolic compounds in blueberries and red and black currants by HPLC-DAD-ESI-MSn. *J. Agric. Food Chem.* **2011**, *59*, 4009−4018.

(6) Burdulis, D.; Sarkinas, A.; Jasutiene, I.; Stackevicene, E.; Nikolajevas, L.; Janulis, V. Comparative study of anthocyanin composition, antimicrobial and antioxidant activity in bilberry (*Vaccinium myrtillus* L.) and blueberry (*Vaccinium corymbosum* L.) fruits. *Acta Pol. Pharm.* **2009**, *66*, 399−408.

(7) Rodríguez-Mateos, A.; Cifuentes-Gómez, T.; Tabatabaee, S.; Lecras, C.; Spencer, J. P. Procyanidin, anthocyanin, and chlorogenic acid contents of highbush and lowbush Blueberries. *J. Agric. Food Chem.* **2012**, *60*, 5772−5778.

(8) Huang, W. Y.; Zhang, H. C.; Liu, W. X.; Li, C. Y. Survey of antioxidant capacity and phenolic composition of blueberry, blackberry, and strawberry in Nanjing. *J. Zhejiang Univ., Sci., B* **2012**, *13*, 94−102.

(9) Castrejón, A.; Eichholz, I.; Rohn, S.; Kroh, L.; Huyskens-Keil, S. Phenolic profile and antioxidant activity of highbush blueberry (*Vaccinium corymbosum* L.) during fruit maturation and ripening. *Food Chem.* **2008**, *109*, 564−572.

(10) Harb, J.; Khraiwesh, B.; Streif, J.; Reski, R.; Frank, W. Characterization of blueberry monodehydroascorbate reductase gene and changes in levels of ascorbic acid and the antioxidative capacity of water soluble antioxidants upon storage of fruits under various conditions. *Sci. Hortic.* **2010**, *125*, 390−395.

(11) Remberg, S.; Haffner, K.; Blomhoff, R. Total antioxidant capacity and other quality criteria in blueberries cvs 'Bluecrop', 'Hardyblue', 'Patriot', 'Putte' and 'Aron' after storage in cold store and controlled atmosphere. *Acta Hortic.* **2003**, *600*, 595−598.

(12) Connor, A.; Luby, J.; Tong, C. Variability in antioxidant activity in blueberry and correlations among different antioxidant activity assays. *J. Am. Soc. Hortic. Sci.* **2002**, *127*, 238−244.

(13) Kalt, W.; Forney, C. F.; Martin, A.; Prior, R. L. Antioxidant capacity, vitamin C, phenolics, and anthocyanins after fresh storage of small fruits. *J. Agric. Food Chem.* **1999**, *47*, 4638−4644.

(14) Holcroft, D.; Kader, A. Carbon dioxide-induced changes in color and anthocyanin synthesis of stored strawberry fruit. *HortScience* **1999**, *34*, 1244−1248.

(15) Gil, M.; Holcroft, D.; Kader, A. Changes in strawberry anthocyanins and other polyphenols in response to carbon dioxide treatments. *J. Agric. Food Chem.* **1997**, *45*, 1662−1667.

(16) Holcroft, D.; Gil, M.; Kader, A. Effect of carbon dioxide on anthocyanins, phenylalanine ammonia lyase and glucosyltransferase in the arils of stored pomegranates. *J. Am. Soc. Hortic. Sci.* **1998**, *123*, 136−140.

(17) Zheng, Y.; Wang, C. Y.; Wang, S. Y.; Zheng, W. Effect of high-oxygen atmospheres on blueberry phenolics, anthocyanins, and antioxidant capacity. *J. Agric. Food Chem.* **2003**, *51*, 7162−7169.

(18) Harb, J.; Saleh, O.; Kittemann, D.; Neuwald, D.; Frank, W.; Reski, R. Upregulation of polyphenol-related genes prevents 'skin burning' by well-colored 'Cameo' apples stored under stressful controlled atmosphere conditions. *Postharvest Biol. Technol.* **2013**, *77*, 121−127.

(19) Chang, S.; Puryear, J.; Cairney, J. A simple and efficient method for isolating RNA from pine trees. *Plant Mol. Biol. Rep.* **1993**, *11*, 113−116.

(20) Zifkin, M.; Jin, A.; Ozga, J. A.; Zaharia, L. I.; Schernthaner, J. P.; Gesell, A.; Abrams, S. R.; Kennedy, J. A.; Constabel, C. P. Gene expression and metabolite profiling of developing highbush blueberry fruit indicates transcriptional regulation of flavonoid metabolism and activation of abscisic acid metabolism. *Plant Physiol.* **2012**, *158*, 200−224.

(21) Livak, K. J.; Schmittgen, T. D. Analysis of relative gene expression data using real-time quantitative PCR and the $2^{-\Delta\Delta CT}$ method. *Methods* **2001**, *25*, 402−408.

(22) Blanch, M.; Álvarez, I.; Sánchez-Ballesta, M. T.; Escribano, M. I.; Merodio, C. Increasing catechin and procyanindin accumulation in high-CO_2-treated *Fragaria vesca* strawberries. *J. Agric. Food Chem.* **2012**, *60*, 7489−7496.

(23) Harb, J.; Bisharat, R.; Streif, J. Einfluß verschiedende kontrolliertem Atmosphere Lagerbedingungen auf die Qualitätsmerkmale von Heidelbeeren Sorte "Bluecrop". *Erwerbs-Obstbau* **2006**, *48*, 115−120.

(24) Kalt, W.; Lawand, C.; Ryan, D.; McDonald, J.; Donner, H.; Forney, C. Oxygen radical absorbing capacity, anthocyanin and phenolic content of highbush blueberries (*Vaccinium corymbosum* L.) during ripening and storage. *J. Am. Soc. Hortic. Sci.* **2003**, *128*, 917−923.

(25) Schotsmans, W.; Molan, A.; MacKay, B. Controlled atmosphere storage of rabbiteye blueberries enhances postharvest quality aspects. *Postharvest Biol. Technol.* **2007**, *44*, 277−285.

(26) Beaudry, R. Effect of carbon dioxide partial pressure on blueberry fruit respiration and respiratory quotient. *Postharvest Biol. Technol.* **1993**, *3*, 249−258.

(27) Fernández-Trujillo, J.; Nock, J.; Watkins, C. Fermentative metabolism and organic acid concentrations in fruit of selected strawberry cultivars with different tolerance to carbon dioxide. *J. Am. Soc. Hortic. Sci.* **1999**, *124*, 696−701.

(28) Holcroft, D.; Kader, A. Controlled atmosphere-induced changes in pH and organic acid metabolism may affect color of stored strawberry fruit. *Postharvest Biol. Technol.* **1999**, *17*, 19−32.

(29) Macheix, J.; Fleuriet, A.; Billot, J. Importance and roles of phenolic compounds in fruit. In *Fruit Phenolics*; CRC Press: Boca Raton, FL, 1990; pp 239−358.
(30) Wrolstad, R.; Putnam, T.; Varseveld, G. Color quality of frozen strawberries: effect of anthocyanin, pH, total acidity and ascorbic acid variability. *J. Food Sci.* **1970**, *35*, 448−452.
(31) Odriozola-Serrano, I.; Soliva-Fortuny, R.; Martín-Belloso, O. Changes in bioactive composition of fresh-cut strawberries stored under superatmospheric oxygen, low-oxygen or passive atmospheres. *J. Food Compos. Anal.* **2010**, *23*, 37−43.
(32) Castellari, M.; Matricardi, L.; Arfelli, G.; Galassi, S.; Amati, A. Level of single bioactive phenolics in red wine as a function of the oxygen supplied during storage. *Food Chem.* **2000**, *69*, 61−67.
(33) Ding, C. K.; Chachin, K.; Ueda, Y.; Imahori, Y.; Wang, C. Y. Metabolism of phenolic compounds during loquat fruit development. *J. Agric. Food Chem.* **2001**, *49*, 2883−2888.
(34) Ding, C. K.; Chachin, K.; Ueda, Y.; Imahori, Y.; Kurooka, H. Effects of high CO_2 concentration on browning injury and phenolic metabolism in loquat fruits. *J. Jpn. Soc. Hortic. Sci.* **1999**, *68*, 275−282.
(35) Galvis-Sánchez, A.; Morais, A.; Malcata, F.; Gil, M. Quantification of chlorogenic acid and polyphenol oxidase activity in 'Rocha' pear after CA-long storage. *Acta Hortic.* **2003**, *600*, 405−408.
(36) MacLean, D.; Murr, D.; Deell, J.; Mackay, A.; Kupferman, E. Inhibition of PAL, CHS, and ERS1 in 'Red d'Anjou' pear (*Pyrus communis* L.) by 1-MCP. *Postharvest Biol. Technol.* **2007**, *45*, 46−55.
(37) Sánchez-Ballesta, M.; Romero, I.; Bernardo Jiménez, J.; Orea, J.; González-Ureña, A.; Escribano, M.; Merodio, C. Involvement of the phenylpropanoid pathway in the response of table grapes to low temperature and high CO_2 levels. *Postharvest Biol. Technol.* **2007**, *46*, 29−35.
(38) Boss, P. K.; Davies, C.; Robinson, S. P. Analysis of the expression of anthocyanin pathway genes in developing *Vitis vinifera* L. cv Shiraz grape berries and the implications for pathway regulation. *Plant Physiol.* **1996**, *111*, 1059−1066.
(39) Martin, C.; Gerats, T. The control of flower coloration. In *The Molecular Biology of Flowering*; Jordan, B. R., Ed.; CAB International: Wallingford, CT, 1993; pp 219−255.
(40) Quattrocchio, F.; Wing, J. F.; Leppen, H.; Mol, J.; Koes, R. E. Regulatory genes controlling anthocyanin pigmentation are functionally conserved among plant species and have distinct sets of target genes. *Plant Cell* **1993**, *5*, 1497−1512.

2. MATERIALS AND METHODS

2.1. Materials. *Plant Material.* The outer fresh leaves, a byproduct from the cauliflower harvest, were collected from a local farm in West-Flanders, Belgium, during the harvesting of cauliflowers from one field in July 2012. The leaves were kept frozen at −18 °C until further analysis.

Chemicals and Reagents. Folin-Ciocalteu reagent and sodium carbonate (Na_2CO_3) were purchased from VWR International (Leuven, Belgium), and gallic acid, hesperetin, and rutin were from Sigma-Aldrich (Bornem, Belgium). Viscozyme L and Rapidase vegetable juice were purchased from Novozyme (Bagsvaerd, Denmark) and DSM Food Specialties (Delft, The Netherlands), respectively.

Viscozyme L, produced by *Aspergillus aculeatus*, contains different polysaccharide-degrading enzymes, including beta-glucanase, cellulase, hemicellulase, and xylanase. The specific enzyme activity of Viscozyme L, as given by the supplier, is 120 Fungal Beta-Glucanase units (FBG)/mL, in which 1 FBG is the amount of enzyme required under standard conditions (30 °C, pH 5.0, and 30 min reaction time) to degrade barley α-glucan to reducing carbohydrates with a reducing power corresponding to 1 μmol glucose/min.

Rapidase vegetable juice is an enzyme mixture produced by both *Aspergillus niger* and *Trichoderma longibrachiatum*. As stated by the supplier, it contains pectinase and hemicellulase (optimal pH 4.0−5.0, optimal temperature 10−55 °C).

2.2. Experimental Procedure. *Enzyme-Assisted Pretreatment.* The frozen outer leaves of cauliflower were cut into pieces (2 × 5 cm), followed by 3 min mixing using a kitchen homogenizer. Enzymes were first dissolved in water taking into account the appropriate concentrations to obtain a correct E/S (cauliflower outer leaves) ratio. The cabbage mixture (60 g) then was placed in a 500 mL glass vial, and 90 mL of aqueous enzyme solution was added. In a first series of experiments, we searched for the optimal conditions for the two enzyme pretreatments. A first set of incubations was done at 40 °C, pH 4.0 with different enzyme concentrations (0−5% E/S ratio). In the second set with the optimal enzyme concentrations (E/S ratio of 0.2% for Viscozyme L and 0.5% for Rapidase), the incubation temperature varied from 30 to 50 °C, always at pH 4.0. In a last step, the optimal enzyme concentrations and optimal temperature (35 °C) were used, while the pH value varied from 3.0 to 6.0. All incubations were performed in a temperature-controlled water bath with agitation. Samples of the treated cabbage were taken at 0, 6, and 24 h for methanol extract, and a sample of the supernatans was taken at 24 h, representing the aqueous extract. All samples were stored at −18 °C for further analysis of total phenolic content. All incubations were done in triplicate.

Using the optimal conditions for both enzymes obtained in the first experiment, a second series of experiments was performed to investigate the enzymatic kinetics of the two enzymes. All of the experimental parameters were the same as in the first series of experiments, except that samples were taken at 2 h intervals during the first 12 h and then at 30 h. All incubations were done in triplicate. Samples were stored at −18 °C for analysis of total phenolic content, and to profile the individual phenolic compounds.

Extraction of Phenolic Compounds. Samples were divided into two parts. Supernatant from the liquid phase, after 24 h of incubation, was obtained by centrifugation (13 000*g*, 10 min, 4 °C) and filtered through filter paper (VWR, grade 413) (aqueous extract, AE). The solid samples at 0, 6, 12, and 24 h of incubation were extracted by the method according to Olsen et al.[23] In brief, 15 mL of methanol was added to 5 g of sample, and the suspension was homogenized at 9500 rpm using an ultraturrax for 40 s, followed by incubation in ice water for 15 min. Supernatant was collected after centrifugation (13 000*g*, 10 min, 4 °C). The pellet obtained was then re-extracted by the same procedure, using 10 mL of methanol/water (80/20; v/v). Both extracts were pooled and filtered through filter paper (VWR, grade 413) before adding methanol to a final volume of 25 mL (methanolic extract, ME).

2.3. Analytical Methods. *Determination of Total Phenolic Content.* Total phenolic content was determined according to Folin−Ciocalteu,[24] with slight modifications. In brief, 1.8 mL of deionized water was added to 0.2 mL of sample. After thorough mixing, Folin−Ciocalteu reagent (0.5 mL) was added, and the tube was shaken vigorously. After 6 min, 1.5 mL of sodium carbonate solution (20%) was added, followed by adding deionized water to a final volume of 5 mL and mixing well again. The solution was then allowed to stand in the dark for 2 h at ambient temperature, and the absorbance was read at 760 nm. Total phenolic content (TPC) was expressed as milligrams of gallic acid equiv per 100 g of dry weight (mg GAE/100 g DW) by using a standard curve of gallic acid in the range of 10−100 mg/L. The blank was prepared with 0.2 mL of methanol instead of sample solution.

Sample Purification Using SPE. In brief, 1 mL of sample was diluted in water (0.1% formic acid) up to 20 mL of total volume, followed by adding 100 μL of 100 μg/mL hesperetin as internal standard. The mixture was slowly loaded onto a solid-phase extraction (SPE) C18 column (50 mg, 4 mL; Davison Discover Science, Deerfield, IL), which was previously preconditioned with methanol (0.1% formic acid). The column then was washed with 5 mL of water (0.1% formic acid) prior to loading 3 mL of methanol (0.1% formic acid). The eluent obtained was evaporated under nitrogen flux. After drying, the residue of the sample was redissolved in 100 μL of methanol (0.1% formic acid) prior to adding 900 μL of water (0.1% formic acid). The sample obtained was kept at −18 °C until UPLC-DAD-HDMS-TOF-MS analysis.

Quantification and Identification of Phenolic Compounds by UPLC-DAD-HDMS-TOF-MS. UPLC-DAD analysis was performed on a bride ethylene hybrid (BEH) C18 column (150 × 2.1 mm, 1.7 μm particle size) by using an Ultimate U(H)PLC (Dionex, Breda, The Netherlands). The column and autosampler temperatures were kept at 40 and 4 °C, respectively. The mobile phase was formed by two solvents, solvent A (water containing 0.1% formic acid; v/v) and solvent B (methanol containing 0.1% formic acid; v/v). A stable flow rate of 250 μL/min was applied at 0 min, 90% A; followed by linear and isocratic gradient of eluting solvents as 0−6 min, 20% B linear; 6−12 min, 20% B isocratic; 12−13 min, 30% B linear; 13−23 min, 50% B linear, 23−30 min, 90% B linear; 30−35 min, 90% isocratic; 35−40 min, 10% B linear; and 40−45 min 10% B isocratic. Quantification was achieved by comparing the peak areas to a calibration curve made using rutin. Quantities of the compounds were expressed as rutin equivalents (RE).

Identification was achieved using an ACQUITY UPLC system (Waters, Milford, MA) coupled to a Synapt HDMS-TOF mass spectrometer (Micromass, Manchester, UK), equipped with an electrospray ionization source. The working conditions of MS analysis were: capillary voltage, 2 kV; sampling cone voltage, 40 V; extraction cone voltage, 4 V; source temperature 150 °C; desolvation temperature, 350 °C; cone gas flow rate, 50 L/h; desolvation gas flow rate, 550 L/h. Collision energies for the trap and transfer were set at 6 and 4 V for low energy, while a ramp of 15−45 V was applied for the high energy collision-induced dissociation. The instrument was operated in negative and positive continuum mode, and data were acquired using Waters MassLynx software. Detailed information on the MS analysis and peak identification is described by Gonzales et al.[25]

2.4. Statistical Analysis. The data are given as mean ± standard deviation (SD) for the optimization of the enzyme treatment and as mean with the standard error of mean (SEM) for the individual phenolic compounds. One-way and two-way ANOVA were used to determine significant differences between individual means using Tukey posthoc test for P values < 0.05. Principal component analysis (PCA) was applied to visualize differences in effects between treatments as well as incubation times based on the contents of individual phenolic compounds. The SPSS software v.22 (IBM, Chicago, IL) was used for all statistical analyses.

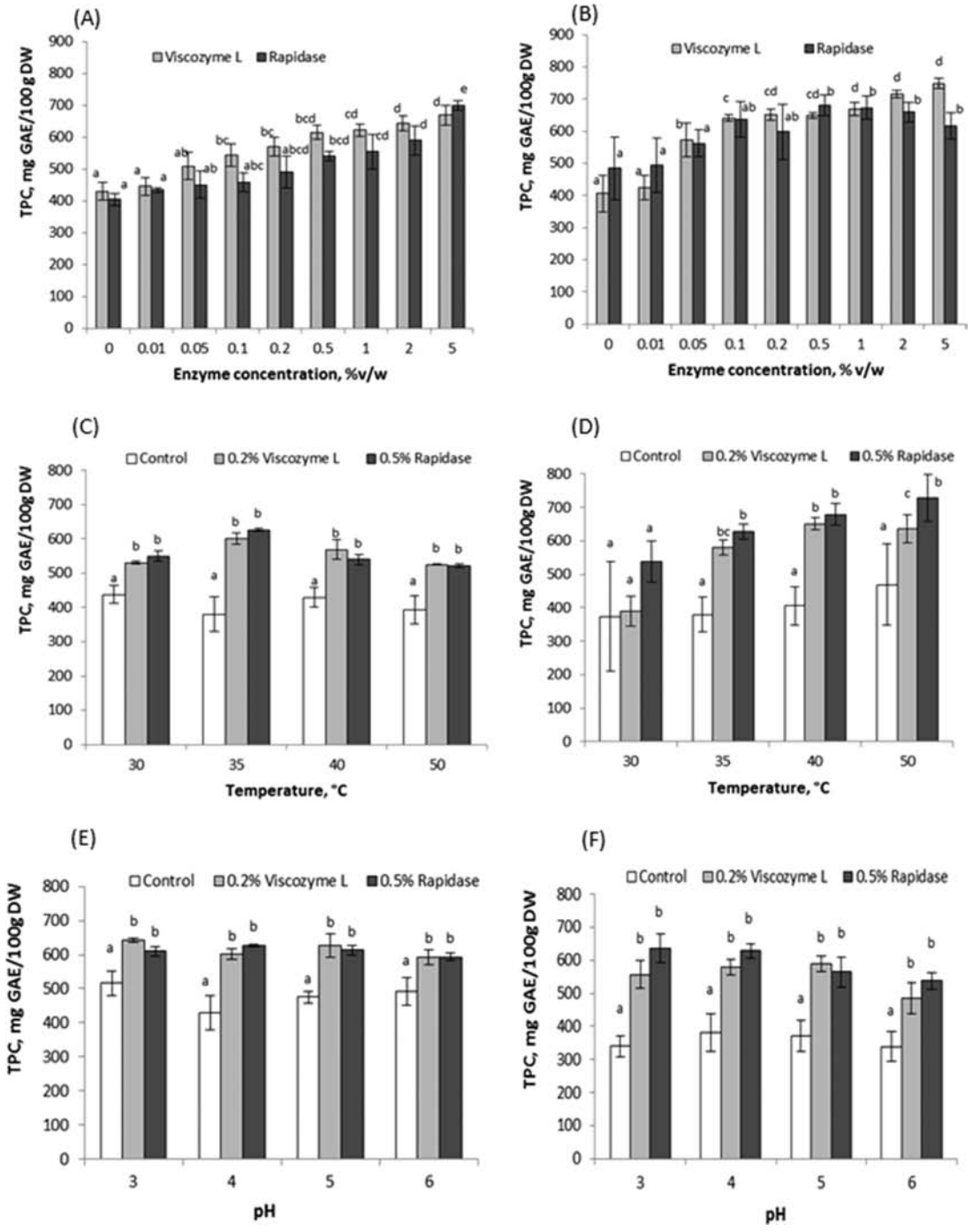

Figure 1. Effect of enzyme concentration (A,B), temperature (C,D), and pH (E,F) on the extraction of phenolic compounds from outer leaves of cauliflower after 24 h of incubation. (A,C,E) Total phenolic content in AE assisted by enzymes. (B,D,F) Total phenolic content in ME after enzymatic pretreatment. Different letters (a−e) indicate significant difference (P value < 0.05) within the same color column. The total phenolics of methanolic extract from cabbage solid residue at 0 h of incubation (control sample): 336 ± 30 mg GAE/100 g DW (n = 3).

3. RESULTS

3.1. Optimization of Enzyme-Assisted Extraction of Phenolic Compounds. Independent of the treatment (type of enzyme, concentration of enzyme, temperature, and pH), the TPC at 0 h of incubation in the ME was 336 ± 30 mg GAE/100 g DW. During 24 h of incubation, it was observed that enzyme dosages, temperature, and pH, as well as their two-way interaction term with time significantly affected the total phenolic release (P-value < 0.001), with an exception for Rapidase concentration × time.

Effect of Enzyme Concentration. The total phenolic contents of AE (Figure 1A) and of ME (Figure 1B) after 24 h enzyme-assisted extraction at 40 °C and pH 4.0 of the cauliflower outer leaves were measured in response to the different concentrations of enzymes (Viscozyme L and Rapidase) used. The level of phenolic compounds in both extracts was significantly increased after 24 h of incubation as compared to the control incubation, when 0.1% Viscozyme L and 0.5% Rapidase were added. Viscozyme L resulted in a higher concentration of phenolic compounds in AE, ranging

dx.doi.org/10.1021/jf502543c | J. Agric. Food Chem. 2014, 62, 7468−7476

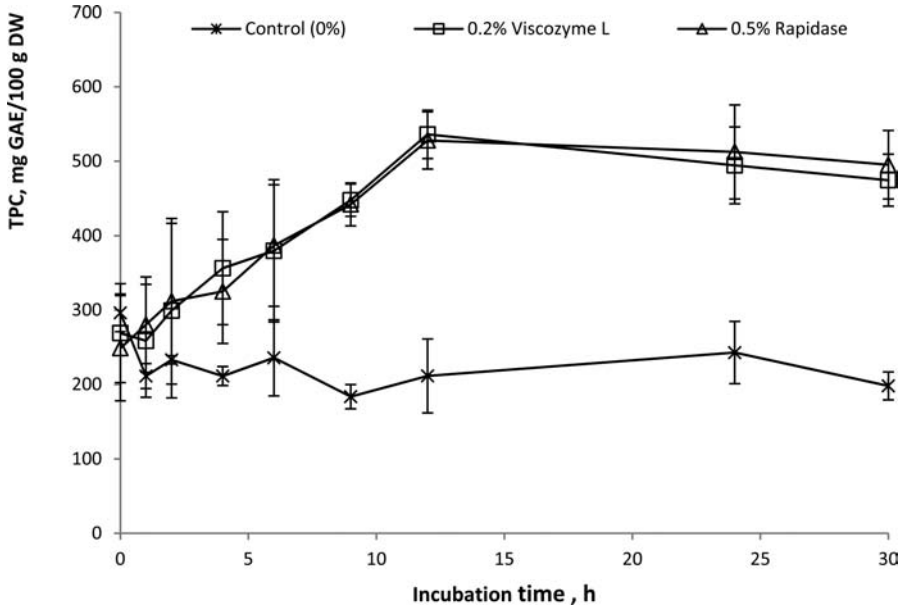

Figure 2. Changes in total phenolic content in ME from solid residue incubated with Viscozyme L and Rapidase at 35 °C, pH 4.0, during 30 h (n = 3).

Table 1. Identification of Flavonoid Glycosides from Cauliflower Byproduct Extract[a]

peak	Rt (min)	molecular ion mass	fragments	λ max (nm)	identity
1	7.8	359.07	359.07	213, 307	unknown 1
2	9.9	950.23	771, 609, 285	nd	kaempferol-C-glucoside-3-glucose units
3	10.8	963.25	963, 609, 771, 801, 284	nd	kaempferol-3-glucoside-7-hydroxyferuloyldiglucoside
4	11.11	933.21	933, 609, 285	265, 345	kaempferol-3-diglucoside-7-diglucoside
5	11.79	785	nd	nd	unknown 2
6	12.16	nd	nd	269, 318	unknown 3
7	13.26	977.35	977, 815, 609, 284, 446	268, 338	kaempferol-3-sinapoyldiglucoside-7-glucoside
8	13.59	1109.30	1109, 947, 771, 609, 447, 285	268, 331	kaempferol-3- feruloyltriglucoside-7-glucoside
9	13.92	947.24	947, 785, 609, 284	269, 322	kaempferol-3-feruloylglucoside-7-diglucoside
10	19.46	787.18	787, 625, 462, 300	254, 348	kaempferol-3- diglucoside-7-glucoside
11	20.07	609.12	609, 284	265	kaempferol-3-diglucoside
12	20.75	785.18	785, 609, 284	329	kaempferol-3-feruloyldiglucoside
13	21.08	755.18	755, 609, 284	320	kaempferol-3-coumaroyldiglucoside
14	23.39	447.07	447, 284	nd	kaempferol-3-glucoside
15	24.28		623, 447, 284	nd	kaempferol-C-feruloylglucoside/kaempferol-3-feruloylglucoside

[a]Rt, retention time; nd, not detected.

from 429 ± 28 mg GAE/100 g DW at 0% E/S (control) to 614 ± 23 mg GAE/100 g DW at 0.5% E/S, with no further significant increase in TPC at higher enzyme concentrations (Figure 1A). Similar results were found for the ME, whereby the TPC in ME significantly increased to 650 ± 18 mg GAE/100 g DW at 0.2% E/S, without further significant improvement between 0.2% and 5% E/S (Figure 1B). The Rapidase treatment with 0.5% E/S resulted in a greater release of phenolic compounds, mainly in the ME and to a lesser extent in the AE, as compared to the control sample (Figure 1A,B), whereas an increased Rapidase concentration from 0.5% to 5% did not enhance the TPC in AE and ME, except for AE from sample treated with 5% Rapidase (Figure 1B). On the basis of the results of the different enzyme concentrations, it was chosen to work further with 0.2% Viscozyme L and 0.5% Rapidase.

Temperature. The influence of incubation temperature on the extraction of phenolic compounds from cauliflower outer leaves using 0.2% Viscozyme L or 0.5% Rapidase at a pH of 4 is given in Figure 1C and D. The treatments with Viscozyme L and Rapidase resulted in a significant improvement of TPC at all temperature points examined, ranging from 30 to 50 °C, as compared to the control (no enzyme) incubation, except for ME at 30 °C, where no difference between enzymatic treatment and control sample was found (Figure 1D). Although a trend toward a higher release of phenolic compounds with higher temperatures was observed in the ME, this was not observed in AE. The TPC in ME was significantly higher at 35 °C than at 30 °C for Viscozyme L and Rapidase treatment, whereas no further increase in total phenolic release between 35 to 50 °C was observed for both ME and AE. Even the TPC at 50 °C was lower than that at 40 °C with Viscozyme L treatment. Therefore, 35 °C was chosen as the optimal incubation temperature for both enzymes.

Effect of pH. During enzymatic treatment, the pH values were varied from 3 to 6 to investigate its effect on extraction

dx.doi.org/10.1021/jf502543c | J. Agric. Food Chem. 2014, 62, 7468−7476

Table 2. Effect of Different Treatments on the Profile of Phenolic Release in ME from Cauliflower Outer Leaves (n = 3)[a]

methanol extraction							
			treatment				
peak	individual compound (mg RE/100 g DW)	Rt (min)	control	viscozyme	rapidase	SEM	P value
1	unknown 1	7.8	10.1 a	16.0 b	12.2 ab	1.1	0.003
2	kaempferol-C-glucoside-3-glucose units	9.9	10.0	19.4	15.0	3.9	0.250
3	kaempferol-3-glucoside-7-hydroxyferuloyldiglucoside	10.8	6.1 a	10.8 b	8.1 ab	1.2	0.034
4	kaempferol-3-diglucoside-7-diglucoside	11.11	5.7 a	8.1 b	6.0 a	0.5	0.007
5	unknown 2	11.79	5.0 a	6.8 b	5.1 ab	0.5	0.030
6	unknown 3	12.16	5.0	6.4	4.8	0.6	0.125
7	kaempferol-3-sinapoyldiglucoside-7-glucoside	13.26	6.5 a	11.5 b	8.2 ab	1.2	0.026
8	kaempferol-3-feruloyltriglucoside-7-glucoside	13.59	9.0 a	21.0 b	14.8 ab	3.2	0.046
9	kaempferol-3-feruloylglucoside-7-diglucoside	13.92	5.8 a	10.0 b	7.3 ab	0.8	0.007
10	kaempferol-3-diglucoside-7-glucoside	19.46	7.1 a	12.5 b	11.8 ab	1.5	0.033
11	kaempferol-3-diglucoside	20.07	48.0	52.8	43.6	4.5	0.369
12	kaempferol-3-feruloyldiglucoside	20.75	17.2 a	37.8 b	28.7 ab	3.5	0.002
13	kaempferol-3-coumaroyldiglucoside	21.08	10.0 a	16.7 b	13.1 ab	1.3	0.004
14	kaempferol-3-glucoside	23.39	8.1 a	58.4 b	29.9 c	5.4	<0.001
15	kaempferol-C-feruloylglucoside/kaempferol-3-feruloylglucoside	24.28	7.1 a	12.2 b	10.7 a	1.1	0.012
	total compounds		160.3 a	300.0 b	219.2 a	19.8	<0.001

[a]Different letters (a, b, c) indicate significant difference (P value < 0.05) within a row. SEM, standard error of mean.

Table 3. Effect of Incubation Time on the Profile of Phenolic Release in ME from Cauliflower Outer Leaves (n = 3)[a]

methanol extraction								
			incubation time (h)					
peak	individual compound (mg RE/100 g DW)	Rt (min)	0	6	12	24	SEM	P value
1	unknown 1	7.8	13.0	12.7	13.7	11.6	1.3	0.732
2	kaempferol-C-glucoside-3-glucose units	9.9	32.8 b	10.9 a	8.6 a	6.9 a	4.5	0.001
3	kaempferol-3-glucoside-7-hydroxyferuloyldiglucoside	10.8	12.3 b	8.8 ab	6.6 a	5.7 a	1.4	0.011
4	kaempferol-3-diglucoside-7-diglucoside	11.11	6.1	7.7	7.0	6.1	0.6	0.441
5	unknown 2	11.79	5.0	6.2	6.2	5.2	0.6	0.364
6	unknown 3	12.16	4.4	5.9	6.1	5.1	0.7	0.276
7	kaempferol-3-sinapoyldiglucoside-7-glucoside	13.26	9.2	9.7	8.1	7.8	1.4	0.757
8	kaempferol-3-feruloyltriglucoside-7-glucoside	13.59	23.2 b	15.7 ab	12.6 ab	8.1 a	3.7	0.051
9	kaempferol-3-feruloylglucoside-7-diglucoside	13.92	9.6 b	8.5 ab	7.1 ab	5.7 a	1.0	0.047
10	kaempferol-3-diglucoside-7-glucoside	19.46	8.0	12.8	9.4	11.6	1.7	0.230
11	kaempferol-3-diglucoside	20.07	31.6 b	61.2 a	59.6 a	39.9 b	5.2	0.001
12	kaempferol-3-feruloyldiglucoside	20.75	12.0 b	26.2 ab	33.7 a	39.7 a	4.1	<0.001
13	kaempferol-3-coumaroyldiglucoside	21.08	6.6 b	15.3 a	16 a	15 a	1.5	<0.001
14	kaempferol-3-glucoside	23.39	6.1 c	26.3 bc	37.2 ab	59.0 a	6.3	<0.001
15	kaempferol-C-feruloylglucoside/kaempferol-3-feruloylglucoside	24.28	5.7 b	10.7 a	11.6 a	11.6 a	1.3	0.008
	total compounds		185.6	237.9	243.6	239.1	22.9	0.258

[a]Different letters (a, b, c) indicate significant difference (P value < 0.05) within a row. SEM, standard error of mean.

yields of total phenolic compounds (Figure 1E and F). The results obtained showed that the TPC did not significantly change in response to the difference in pH values during extraction for both AE and ME, within one enzymatic treatment.

3.2. Identification and Quantification of Phenolic Compounds. Using the optimal conditions for the enzyme treatment, the individual phenolic compounds released from the cauliflower outer leaves were identified and quantified. The shift in the phenolic profile during time of incubation and type of enzyme was studied.

Kinetics of the Release of TPC at Optimal Conditions. Selecting the optimal conditions obtained for enzyme treatment (0.2% Viscozyme L or 0.5% Rapidase, temperature 35 °C, and pH 4), we evaluated the effects of incubation time on the phenolic extraction from outer leaves of cauliflower (Figure 2). The TPC in ME of the control incubation remained stable. A significant increase in the TPC in the ME after enzyme treatment was observed, with a more than 100% increase after 12 h of incubation for the enzyme-treated incubations as compared to the control ones. The TPC of ME increased as a function of incubation time. No difference in TPC in the ME extract was observed between the two enzyme treatments. After 12 h of incubation, the TPC in the ME remained constant, and this trend was observed for both enzymes. The enzymatic treatments also caused significant effects on released phenolic compounds in AE after 30 h of incubation, increasing to 581 ± 16 mg GAE/100 g DW (with Viscozyme L) and to 604 ± 9 mg GAE/100 g DW (with Rapidase) as compared to 457 ± 23 mg GAE/100 g DW for the control without enzyme treatment.

Identification and Quantification of Individual Compounds by UPLC-DAD-HDMS-TOF-MS. The phenolic com-

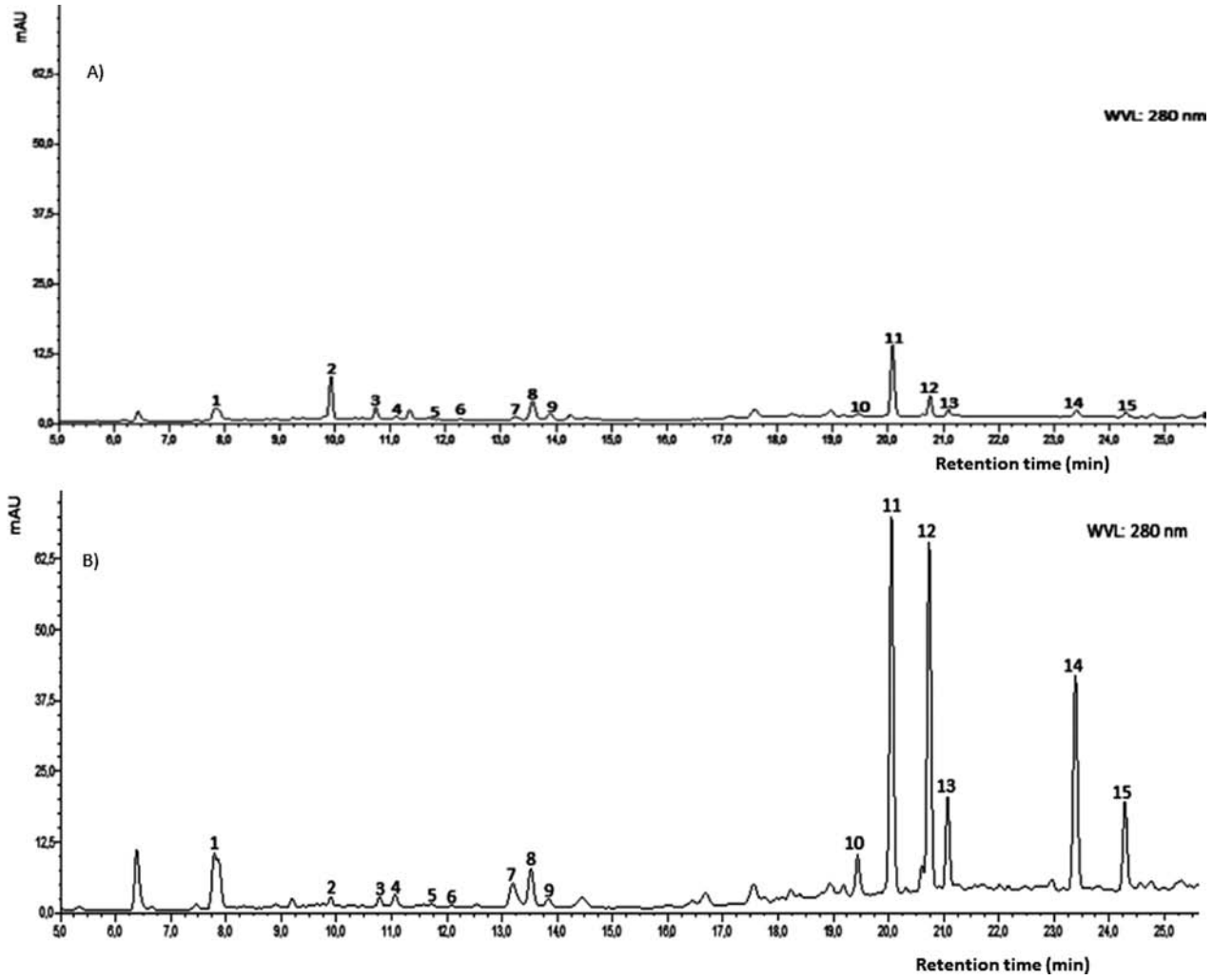

Figure 3. U(H)PLC profile of phenolic compounds from cauliflower byproduct extracts obtained by an incubation of 0 h (A) and 12 h (B) with Rapidase, recorded at 280 nm (see Table 1 for identification of peaks).

pounds in cauliflower outer leaves extracts were quantified by UPLC-DAD and identified by the UPLC-MS/MS method. As there was no interaction effect between treatment and time of incubation on the content of the individual phenolic compounds, results are presented for the main factors separately, that is, treatment and time of incubation in Tables 2 and 3, respectively.

As shown in Figure 3 and Table 1, 15 individual compounds were identified, of which three components in the extracts could not be identified by our protocol (unknown 1, 2, and 3). All individual phenolic compounds present in the extracts and identified by our analysis belonged to different derivatives of kaempferol. The results also indicated that the treatment with Rapidase did not enhance the amount of all identified compounds released as compared to the control with an exception for kaempferol-3-glucoside. In contrast, there was a clear increase in identified compounds by Viscozyme L treatment. The release of kaempferol-3-feruloyltriglucoside-7-glucoside (compound 8; 21.0 mg RE/100 g DW), kaempferol-3-feruloyldiglucoside (compound 12; 37.8 mg RE/100 g DW), and kaempferol-3-glucoside (compound 14; 58.4 mg RE/100 g DW) was sharply improved by Viscozyme L treatment, as compared to the control sample (9.0, 17.2, and 8.1 mg RE/100 g DW, respectively) (Table 1). As shown in Table 2, in general the release of the total phenolic compounds increased during time of incubation, although the increase was not significant. However, the amounts of individual components including kaempferol-3-feruloyldiglucoside (compound 12), kaempferol-3-coumaroyldiglucoside (compound 13), kaempferol-3-glucoside (compound 14), and kaempferol-*C*-feruloylglucoside/kaempferol-3-feruloylglucoside (compound 15) were significantly increased after 12 or 24 h of incubation in comparison with nontreatment samples (0 h).

The changes in profiles of phenolic compounds affected by different treatments were visualized by using PCA (Figure 4). The PC 1 (86.69%) described the distinct difference between the samples without adding enzymes (control-AE) and the samples treated by enzymes, which are mostly localized on the positive axis of PC1, except for control-ME. All of the phenolic components released were positively related to the Viscozyme L and Rapidase used. The PC2 (13.20%) can be expressed as a factor associated with the profile of individual compounds in ME, as compared to AE. The observation from the graph indicated that the high values of compounds 7, 8, 12, 13, 14, and 15 are associated with AE (cluster of Viscozyme-AE, Rapidase-AE), while the phenolic profile in ME exhibited higher content of compounds 2, 4, 5, 6, 9, and 11.

dx.doi.org/10.1021/jf502543c | *J. Agric. Food Chem.* 2014, 62, 7468−7476

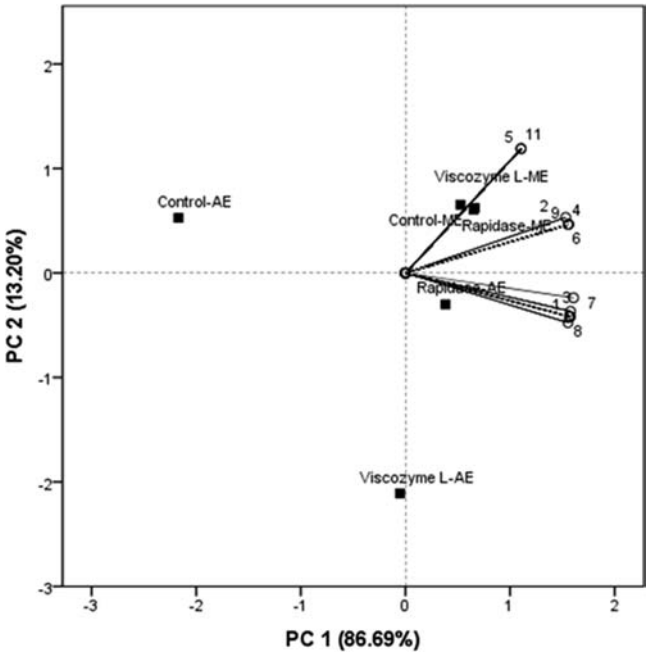

Figure 4. Principal component analysis of the individual phenolic compounds in AE and ME by different treatments (n = 3). The numbers in the PCA plot represent the different phenolic compounds as described in Table 1. Control-AE, aqueous extract obtained by an incubation of 30 h without enzyme; Viscozyme L-AE, aqueous extract obtained by an incubation of 30 h with Viscozyme L; Rapidase-AE, aqueous extract obtained by an incubation of 30 h with Rapidase; Control-ME, methanolic extract obtained by an incubation of 12 h without enzyme; Viscozyme L-ME, methanolic extract obtained by an incubation of 12 h with Viscozyme L; Rapidase-MA, methanolic extract obtained by an incubation of 12 h with Rapidase.

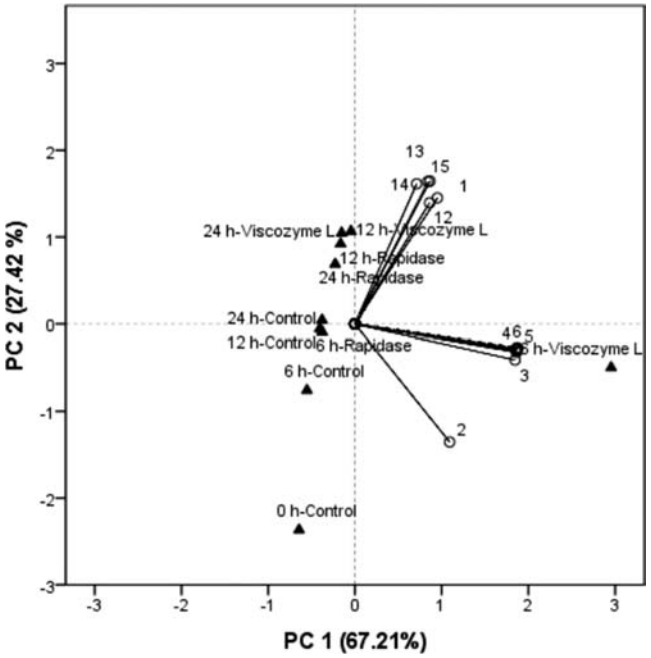

Figure 5. Principal component analysis of the individual phenolic compounds in ME from different time of treatments (n = 3). The numbers in the PCA plot represent the different phenolic compounds as described in Table 1. 0 h-Control, 6 h-Control, 12 h-Control, 24 h-Control represent methanolic extracts obtained by an incubation of 0, 6, 12, and 24 h without enzyme, respectively; 0 h-Viscozyme L, 6 h-Viscozyme L, 12 h-Viscozyme L, 24 h-Viscozyme L represent methanolic extracts obtained by an incubation of 0, 6, 12, and 24 h with Viscozyme L, respectively; 0 h-Rapidase, 6 h-Rapidase, 12 h-Rapidase, 24 h-Rapidase represent methanolic extracts obtained by an incubation of 0, 6, 12, and 24 h with Rapidase, respectively.

Figure 5 shows the effect of incubation time on the profile of phenolic release. Two PCs are responsible for 94.63% of the total variance of data. An incubation of 6 h with Viscozyme L was characterized for the high amount of compounds 2, 3, 4, 5, and 6, while the longer period of Viscozyme L and Rapidase treatments (12 h, 24 h) positively contributed to the high content of compounds 1, 12, 13, 14, and 15.

4. DISCUSSION

The enzyme-assisted extraction yield of phenolic compounds depends on multiple variables including type of enzyme and concentration, incubation temperature, pH, and incubation time. In this experiment, the optimization of Viscozyme L and Rapidase-assisted enzymatic pretreatment was studied on cauliflower outer leaves, with the focus on the identification of the released phenolic compounds. The significantly improved release of total phenolic compounds in both AE and ME for Viscozyme L (0.2%) and Rapidase (0.5%) treatment as compared to the control treatment clearly indicated that the hydrolysis of cell-wall components of cabbage improves the extraction yields of phenolic compounds. This observation could be explained by an increased degradation of the cell-wall structure as a result of the hydrolysis of cell-wall components, especially glycosidic bonds/linkages between phenolic compounds and cell-wall polysaccharides.[12,26] In addition, it is known that the permeability and porosity of plant cells increase by the breakdown of cell-wall polymers, improving the solubility of cell internal components, and in turn this results in an increase in concentration of phenolic compounds present in the extracts.[10,16] The treatments with higher enzyme doses did not increase the release of total phenolic compounds (p > 0.05), which could be due to competitive adsorption to the cell-wall polysaccharide when a higher enzyme concentration is applied. This leads to steric hindrance of binding positions of enzymes to the substrate, which negatively influences the breakdown of cell-wall components.[27,28] The lack of improvement at higher enzyme concentrations is in accordance with previous studies, for example, on black currant pomace,[27] or on unripened apples.[22]

The increased phenolic concentration in both AE and ME at all temperature incubations in comparison with the control sample demonstrates the importance of enzymatic catalysis to release phenolic compounds from cauliflower leaves. The significant enhancement of TPC in ME by treatments with 0.2% Viscozyme L and 0.5% Rapidase at higher temperature (35, 40, and 50 °C) could be caused by an increase of the hydrolysis activity and overall porosity of cell-wall structure, improving hydrolysis of the linkages between bound-phenolics and cell-wall compositions.[12,29] However, at 50 °C for Viscozyme L, there was a significant decrease in TPC in ME, as compared to 40 °C. This finding might be explained by a decreased activity of one of the enzymes in Viscozyme L, which is lower at 50 °C. Also, a possible loss of phenolic compounds has been observed due to thermal degradation,[26] which is mainly attributed to an increased oxidation.[30] This observation is consistent with results of Kapasakalidis et al.,[27] who reported a reduction of phenolic concentration by cellulase-assisted

dx.doi.org/10.1021/jf502543c | J. Agric. Food Chem. 2014, 62, 7468−7476

extraction at 50 °C as compared to 40 °C. As the different pH values tested did not affect the level of TPC in both AE and ME, it can be concluded that the commercial enzyme mixture has a broad pH activity range.

The kinetic study of phenolic release at optimal conditions (Figure 2) indicates that the TPC in ME greatly increased during the first 12 h of enzymatic treatment with the maximum level reached at 12 h of incubation. This finding can be attributed to the catalytic action of carbohydrate-cleaving enzymes[31] as a pretreatment process. It can also be concluded that an incubation of 12 h is sufficient for Viscozyme L and Rapidase to hydrolyze the substrate. The stable level of total phenolic content in ME between 12 and 30 h incubation can be attributed to deactivation, even inactivation, of cellulase, hemicellulase, and pectinase by bioactive inhibitors, such as phenolic compounds and lignin, released from the substrate.[32] Indeed, Berlin et al.[33] and Tejirian et al.[34] reported that phenolics, flavonoids, and polymeric lignin could strongly adsorb onto cellulase and pectinase, limiting the enzyme activity and/or precipitation of enzyme. Our results confirm the possibility of enzymes as an effective method to improve the yield of phenolic compounds released from waste material. However, it is also important to know if the enzyme treatment resulted in the release of specific phenolic compounds or in a change in their structure, as compared to the nonenzymatic treated outer leaves. As far as we know, the effect of enzymatic treatment on the release of individual phenolic compounds from vegetable waste material has not been reported before.

The LC−MS analysis revealed that the main components found in ME and AE from controls (no-enzyme treatment) were kaempferol glycosides. This indicates that most phenolic compounds, naturally produced by cauliflower plants, are present in conjugated form, as was also reported on cauliflower byproducts by Llorach et al.[35,36] and Gonzales et al.[37] Similar results were also observed after the enzymatic treatment with Viscozyme L and Rapidase, meaning that no aglycones were formed. This is probably due to the insufficiency or absence of β-glycosidase, which is known for its capacity of deglycosylation by hydrolyzing the β-1,4 glycosidic bonds in aryl and alkyl β-D-glucosides as well as glycosides containing disaccharides and oligosaccharides.[38,39] The presence of the β-glycosidase was not specified by the supplier for the enzyme mixtures used. Viscozyme L was more efficient in hydrolyzing the substrate to obtain higher amounts of kaempferol-3-feruloyldiglucoside (compound 12) and kaempferol-3-glucoside (compound 14). The large increase in kaempferol-3-feruloyldiglucoside (compound 12) can be the result of the deglycosylation of two glucose molecules from kaempferol-3-feruloyltriglucoside-7-glucoside (compound 8). The large increase of kaempferol-3-glucoside (compound 14) by both enzymatic treatments is probably the result of removing one glucose molecule from kaempferol-3-diglucoside (compound 11). These cleavages may be caused by the presence of cellobiase activity or other unknown enzymatic actions in the commercial enzymes Viscozyme L and Rapidase. However, a full characterization of these commercial enzyme mixtures and their activity is not available. This behavior has also been confirmed by the results on time of incubation in the profile of phenolic release. The longer the samples were treated, the lower was the concentration of compounds 2, 8, and the higher was the amount of compounds 11, 12, and 14. However, no difference in the individual components of AE was observed as a function of the treatment, although a substantial increase in TPC was measured by Folin−Ciocalteu assay for the enzymatic treatments as compared to the control. This apparent difference can be attributed to the reaction of Folin−Ciocalteau reagent with other interfering components such as protein, enzymes, sugars, as well as ascorbic acid present in AE.[24,27,40]

Although no phenolic aglycones were found in comparison with extract from native cauliflower byproduct, the study showed that the use of Viscozyme L or Rapidase enzyme mixture results in a higher yield of kaempferol-glucosides extracted from the cauliflower outer leaves. Further treatment with β-glycosidase, either with or without Viscozyme L or Rapidase, could result in the release of kaempferol as aglycone form, a flavonoid that is characterized by several bioactivities.[41,42]

AUTHOR INFORMATION

Corresponding Author

*Tel.: +3256241255. Fax: +3256241224. E-mail: katleen.raes@ugent.be.

Funding

H.T.N. is grateful for the Ph.D. grant financed by MOET-Vietnam. We thank the Special Research Fund (BOF) of Ghent University (BOF05 V02512) and the Hercules foundation (AUGE028 and AUGE014) for financial support.

Notes

The authors declare no competing financial interest.

ABBREVIATIONS USED

AE, aqueous extract; ME, methanolic extract; TPC, total phenolic content; SPE, solid-phase extraction; DW, dry weight; GAE, gallic acid equivalent; RE, rutin equivalent; E/S, enzyme/substrate; PCA, principal component analysis

REFERENCES

(1) Cabello-Hurtado, F.; Gicquel, M.; Esnault, M.-A. Evaluation of the antioxidant potential of cauliflower (Brassica oleracea) from a glucosinolate content perspective. *Food Chem.* **2012**, *132*, 1003−1009.

(2) Hodges, D. M.; Munro, K. D.; Forney, C. F.; McRae, K. B. Glucosinolate and free sugar content in cauliflower (Brassica oleracea var. botrytis cv. Freemont) during controlled-atmosphere storage. *Postharvest Biol. Technol.* **2006**, *40*, 123−132.

(3) Picchi, V.; Migliori, C.; Lo Scalzo, R.; Campanelli, G.; Ferrari, V.; Di Cesare, L. F. Phytochemical content in organic and conventionally grown Italian cauliflower. *Food Chem.* **2012**, *130*, 501−509.

(4) Podsędek, A. Natural antioxidants and antioxidant capacity of Brassica vegetables: A review. *LWT-Food Sci. Technol.* **2007**, *40*, 1−11.

(5) Iñiguez-Covarrubias, G.; Lange, S. E.; Rowell, R. M. Utilization of byproducts from the tequila industry: part 1: agave bagasse as a raw material for animal feeding and fiberboard production. *Bioresour. Technol.* **2001**, *77*, 25−32.

(6) Nilnakara, S.; Chiewchan, N.; Devahastin, S. Production of antioxidant dietary fibre powder from cabbage outer leaves. *Food Bioprod. Process.* **2009**, *87*, 301−307.

(7) Tanongkankit, Y.; Chiewchan, N.; Devahastin, S. Physicochemical property changes of cabbage outer leaves upon preparation into functional dietary fiber powder. *Food Bioprod. Process.* **2012**, *90*, 541−548.

(8) Puri, M.; Sharma, D.; Barrow, C. J. Enzyme-assisted extraction of bioactives from plants. *Trends Biotechnol.* **2012**, *30*, 37−44.

(9) Wijngaard, H.; Hossain, M. B.; Rai, D. K.; Brunton, N. Techniques to extract bioactive compounds from food by-products of plant origin. *Food Res. Int.* **2012**, *46*, 505−513.

(10) Cerda, A.; Martínez, M. E.; Soto, C.; Poirrier, P.; Perez-Correa, J. R.; Vergara-Salinas, J. R.; Zúñiga, M. E. The enhancement of antioxidant compounds extracted from Thymus vulgaris using

enzymes and the effect of extracting solvent. *Food Chem.* **2013**, *139*, 138−143.
(11) Pinelo, M.; Arnous, A.; Meyer, A. S. Upgrading of grape skins: Significance of plant cell-wall structural components and extraction techniques for phenol release. *Trends Food Sci. Technol.* **2006**, *17*, 579−590.
(12) Yadav, G.; Singh, A.; Bhattacharya, P.; Yuvraj, J.; Banerjee, R. Comparative analysis of solid-state bioprocessing and enzymatic treatment of finger millet for mobilization of bound phenolics. *Bioproc. Biosyst. Eng.* **2013**, *36*, 1−7.
(13) Gómez-García, R.; Martínez-Ávila, G. G.; Aguilar, C. Enzyme-assisted extraction of antioxidative phenolics from grape (*Vitis vinifera* L.) residues. *3 Biotech* **2012**, *2*, 297−300.
(14) Li, B. B.; Smith, B.; Hossain, M. M. Extraction of phenolics from citrus peels: II. Enzyme-assisted extraction method. *Sep. Purif. Technol.* **2006**, *48*, 189−196.
(15) Kim, Y. J.; Kim, D.-O.; Chun, O. K.; Shin, D.-H.; Jung, H.; Lee, C. Y.; Wilson, D. B. Phenolic extraction from apple peel by cellulases from *Thermobifida fusca*. *J. Agric. Food Chem.* **2005**, *53*, 9560−9565.
(16) Chen, S.; Xing, X.-H.; Huang, J.-J.; Xu, M.-S. Enzyme-assisted extraction of flavonoids from Ginkgo biloba leaves: Improvement effect of flavonol transglycosylation catalyzed by Penicillium decumbens cellulase. *Enzyme Microb. Technol.* **2011**, *48*, 100−105.
(17) Hansson, T.; Andersson, M.; Wehtje, E.; Adlercreutz, P. Influence of water activity on the competition between β-glycosidase-catalysed transglycosylation and hydrolysis in aqueous hexanol. *Enzyme Microb. Technol.* **2001**, *29*, 527−534.
(18) Alrahmany, R.; Tsopmo, A. Role of carbohydrases on the release of reducing sugar, total phenolics and on antioxidant properties of oat bran. *Food Chem.* **2012**, *132*, 413−418.
(19) Maier, T.; Göppert, A.; Kammerer, D.; Schieber, A.; Carle, R. Optimization of a process for enzyme-assisted pigment extraction from grape (*Vitis vinifera* L.) pomace. *Eur. Food Res. Technol.* **2008**, *227*, 267−275.
(20) Saulnier, L.; Marot, C.; Elgorriaga, M.; Bonnin, E.; Thibault, J. F. Thermal and enzymatic treatments for the release of free ferulic acid from maize bran. *Carbohydr. Polym.* **2001**, *45*, 269−275.
(21) Pimpao, R. C.; Dew, T.; Oliveira, P. B.; Williamson, G.; Ferreira, R. B.; Santos, C. N. Analysis of phenolic compounds in Portuguese wild and commercial berries after multienzyme hydrolysis. *J. Agric. Food Chem.* **2013**, *61*, 4153−4162.
(22) Zheng, H. Z.; Hwang, I. W.; Chung, S. K. Enhancing polyphenol extraction from unripe apples by carbohydrate-hydrolyzing enzymes. *J. Zhejiang Univ., Sci., B* **2009**, *10*, 912−919.
(23) Olsen, H.; Aaby, K.; Borge, G. I. A. Characterization and quantification of flavonoids and hydroxycinnamic acids in curly kale (Brassica oleracea L. Convar. acephala Var. sabellica) by HPLC-DAD-ESI-MSn. *J. Agric. Food Chem.* **2009**, *57*, 2816−2825.
(24) Singleton, V. L.; Orthofer, R.; Lamuela-Raventós, R. M. Analysis of total phenols and other oxidation substrates and antioxidants by means of folin-ciocalteu reagent. *Methods Enzymol.* **1999**, *299*, 152−178.
(25) Gonzales, G. B.; Raes, K.; Coelus, S.; Struijs, K.; Smagghe, G.; Van Camp, J. High performance liquid chromatography-electrospray ionization quadrupole time-of-flight-ion mobility high definition mass spectrometry for the rapid identification and structural characterisation of flavonoid glycosides from cauliflower waste. *J. Chromatogr., A* **2014**, *1323*, 39−48.
(26) Bagger-Jørgensen, R.; Meyer, A. B. S. Effects of different enzymatic pre-press maceration treatments on the release of phenols into blackcurrant juice. *Eur. Food Res. Technol.* **2004**, *219*, 620−629.
(27) Kapasakalidis, P. G.; Rastall, R. A.; Gordon, M. H. Effect of a cellulase treatment on extraction of antioxidant phenols from black currant (*Ribes nigrum* L.) pomace. *J. Agric. Food Chem.* **2009**, *57*, 4342−4351.
(28) Norsker, M.; Bloch, L.; Adler-Nissen, J. Enzymatic degradation of plant cell wall polysaccharides: The kinetic effect of competitive adsorption. *Mol. Nutr. Food Res.* **1999**, *43*, 307−310.
(29) Landbo, A.-K.; Meyer, A. S. Effects of different enzymatic maceration treatments on enhancement of anthocyanins and other phenolics in black currant juice. *Innovative Food Sci. Emerging Technol.* **2004**, *5*, 503−513.
(30) Patras, A.; Brunton, N. P.; O'Donnell, C.; Tiwari, B. K. Effect of thermal processing on anthocyanin stability in foods: mechanisms and kinetics of degradation. *Trends Food Sci. Technol.* **2010**, *21*, 3−11.
(31) Jamal, P.; Idris, Z. M.; Alam, M. Z. Effects of physicochemical parameters on the production of phenolic acids from palm oil mill effluent under liquid-state fermentation by *Aspergillus niger* IBS-103ZA. *Food Chem.* **2011**, *124*, 1595−1602.
(32) Gamble, G.; Snook, M.; Henriksson, G.; Akin, D. Phenolic constituents in flax bast tissue and inhibition of cellulase and pectinase. *Biotechnol. Lett.* **2000**, *22*, 741−746.
(33) Berlin, A.; Balakshin, M.; Gilkes, N.; Kadla, J.; Maximenko, V.; Kubo, S.; Saddler, J. Inhibition of cellulase, xylanase and β-glucosidase activities by softwood lignin preparations. *J. Biotechnol.* **2006**, *125*, 198−209.
(34) Tejirian, A.; Xu, F. Inhibition of enzymatic cellulolysis by phenolic compounds. *Enzyme Microb. Technol.* **2011**, *48*, 239−247.
(35) Llorach, R.; Gil-Izquierdo, A.; Ferreres, F.; Tomás-Barberán, F. A. HPLC-DAD-MS/MS ESI characterization of unusual highly glycosylated acylated flavonoids from cauliflower (*Brassica oleracea* L. var. botrytis) agroindustrial byproducts. *J. Agric. Food Chem.* **2003**, *51*, 3895−3899.
(36) Llorach, R.; Espín, J. C.; Tomás-Barberán, F. A.; Ferreres, F. Valorization of cauliflower (Brassica oleracea L. var. botrytis) by-products as a source of antioxidant phenolics. *J. Agric. Food Chem.* **2003**, *51*, 2181−2187.
(37) Gonzales, G. B.; Smagghe, G.; Raes, K.; Van Camp, J. Combined alkaline hydrolysis and ultrasound-assisted extraction for the release of nonextractable phenolics from cauliflower (*Brassica oleracea* var. *botrytis*) waste. *J. Agric. Food Chem.* **2014**, *62*, 3371−3376.
(38) Turner, C.; Turner, P.; Jacobson, G.; Almgren, K.; Waldeback, M.; Sjoberg, P.; Karlsson, E. N.; Markides, K. E. Subcritical water extraction and [small beta]-glucosidase-catalyzed hydrolysis of quercetin glycosides in onion waste. *Green Chem.* **2006**, *8*, 949−959.
(39) Zheng, Z.; Shetty, K. Solid-state bioconversion of phenolics from Cranberry Pomace and role of Lentinus edodes β-Glucosidase. *J. Agric. Food Chem.* **2000**, *48*, 895−900.
(40) Roura, E.; Andrés-Lacueva, C.; Estruch, R.; Lamuela-Raventós, R. M. Total polyphenol Intake Estimated by a modified Folin−Ciocalteu assay of urine. *Clin. Chem.* **2006**, *52*, 749−752.
(41) Ferreres, F.; Fernandes, F. t.; Sousa, C.; Valentão, P. c.; Pereira, J. A.; Andrade, P. B. Metabolic and bioactivity Insights into Brassica oleracea var. acephala. *J. Agric. Food Chem.* **2009**, *57*, 8884−8892.
(42) Spencer, J. P. E.; Abd El Mohsen, M. M.; Rice-Evans, C. Cellular uptake and metabolism of flavonoids and their metabolites: implications for their bioactivity. *Arch. Biochem. Biophys.* **2004**, *423*, 148−161.

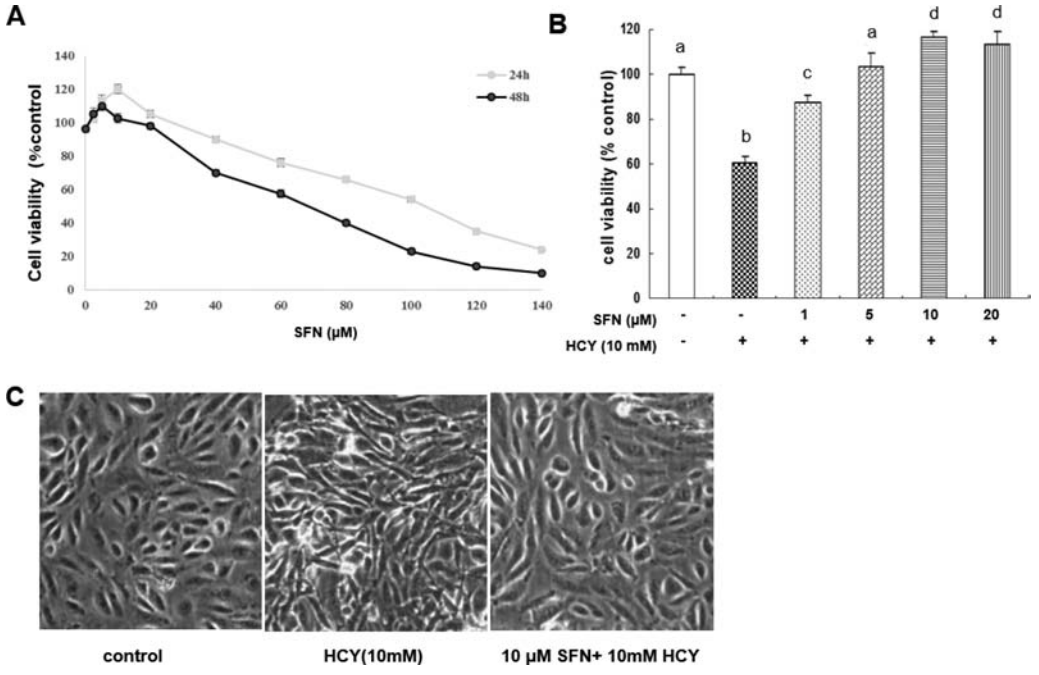

Figure 1. Dual-growth control and morphological improvement in HHL-5 cells by SFN. (A) Cells (10^4/well) were seeded in a 96-well plate and incubated with 1−140 μmol/L SFN for 24 and 48 h. (B) HHL-5 cells were preincubated with 1, 5, 10, and 20 μmol/L SFN for 24 h and then incubated with 10 mmol/L HCY for 24 h. The absorbance was measured by a microplate reader at 490 nm. Data are presented as the mean ± SD (n = 6). (C) Cells were grown in DMEM/F12 medium, 10 mmol/L HCY, or 10 μmol/L SFN plus 10 mmol/L HCY for 24 h. Cell morphological changes were observed under an inverted microscope (×100). Bars with no letters in common are significantly different ($p < 0.05$).

antioxidants and phase II enzymes.[18] Accordingly, impaired Nrf-2 signaling heightens ER stress response in the lungs of patients with chronic obstructive pulmonary disease.[19]

Given the potent antioxidant effects of SFN, it is of keen interest to determine whether SFN can protect against the HCY-induced injuries of which HCY is responsible for the mechanisms of numerous disorders. Our present results demonstrate that SFN improves both the ER swelling and reactive oxygen species (ROS) production by HCY. The underlining mechanism may be involved with enhancing phase II enzymes and reversing ER stress, all of which may be related to the activation of Nrf-2.

MATERIALS AND METHODS

Chemicals and Reagents. Sulforaphane (1-isothiocyanato-4-(methylsulfinyl) butane, SFN, purity ⩾98%) was purchased from LKT laboratories (St. Paul, MN), dissolved in dimethyl sulfoxide (DMSO) and stored as a stock solution of 100 mmol/L at −20 °C.[20] DL-homocysteine (purity ⩾ 95%), 2′,7′-dichlorofluorescin diacetate (H_2DCFDA), and 3-[4,5-dimethylthiazol-2-yl]-2, 5-diphenyl tetrazolium bromide (MTT) were obtained from Sigma (St. Louis, MO). Dulbecco's modified Eagle's medium−Ham's F-12 medium (DMEM-F12) and fetal bovine serum (FBS) were from Hyclone (Logan, UT). Antibodies against glucose-regulated protein-78 (GRP78), protein kinase RNA (PKR)-like ER kinase (PERK), phospho (p)-PERK, thioredoxin reductase-1 (TrxR-1), NAD(P)H:quinone oxidoreductase 1 (NQO1), Nrf-2, LaminB1, and β-actin were from Santa Cruz Biotechnology (Santa, CA). Other chemicals and solvents used were of the highest analytic grade. The nuclear extraction kit was purchased from Chemicon International (UK).

Cell Culture and Treatments. Immortalized human hepatocytes (defined as HHL-5) were kindly supplied by Professor Duncan McGeoch, Medical Research Council (MRC) Virology Unit, UK. Immortalized human hepatocytes HHL-5 were maintained in DMEM/F12 medium supplemented with 10% FBS, 2 mmol/L L-glutamine, 100 U/mL penicillin, and 100 μg/mL streptomycin in a humidified atmosphere of 5% CO_2 at 37 °C. SFN was dissolved in dimethyl sulfoxide (DMSO), with a final concentration in the medium was ⩽0.1% (v/v).[20]

DL-HCY was freshly prepared in serum-free medium and sterilized by 0.22 μm filtration. The range of DL-HCY concentrations was selected on the basis of other research[21] and our preliminary tests. HHL-5 cells were pretreated with 1−20 μmol/L SFN for 24 h (for dose course) or 20 μmol/L SFN for 6−48 h (for time course) followed by 10 mmol/L HCY for 6 h.

Cell Survival Assay. MTT assay was performed according to the manufacturer's protocol (Sigma) and our previous method.[22] Briefly, cells (1×10^4/well) were seeded in 96-well plates and grown to 80% confluence. Various concentrations of SFN or HCY were exposed to HHL-5 cells or vehicle for the desired time. Afterward, MTT (5 mg/mL in PBS) was added to each well and incubated at 37 °C for 4 h. Formazan crystals formed were dissolved by DMSO, and its optical density was measured with a microplate reader (Bio-Tek Instruments, Inc., USA) at 490 nm. Cell viability was calculated from the optical density readings, when vehicle-treated cells were taken as 100% viable. The experiment was repeated three times, and the IC_{50} value was calculated with the SPSS13.0 software.

Morphological Changes. HHL-5 cells were seeded in a 6-well plate and attached overnight. Then, the cells were grown in DMEM/F12 medium, 10 mmol/L HCY, or 10 μmol/L SFN with 10 mmol/L HCY for 24 h. Cell morphological changes were observed under an inverted microscope and photographed (Olympus Optical Co., Ltd., Japan).

Determination of ROS Generation. The membrane-permeable probe 2′,7′-dichlorofluorescin diacetate (H_2DCFDA) enters the cells and produces fluorescence after intracellular oxidation by ROS such as hydrogen peroxide (H_2O_2) and hydroxyl radical. Intracellular oxidant stress was monitored by changes in fluorescence intensity resulting from intracellular probe oxidation.[23] Following treatment, cells were incubated with 5 μmol/L DCFH-DA at 37 °C for 30 min in the dark and then rinsed with PBS three times. Intracellular ROS was imaged using an Olympus X70 fluorescence microscope with ultraviolet (UV)

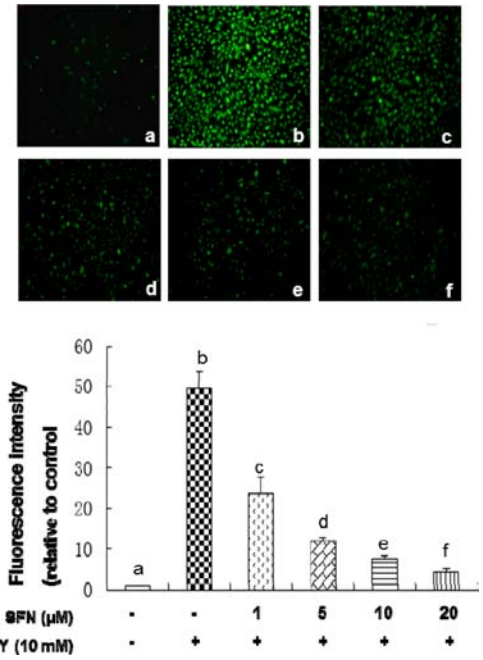

Figure 2. Protective effect of SFN on ROS production by HCY. HHL-5 cells were seeded in a 6-well plate and incubated with or without SFN (1−20 μmol/L) for 24 h, followed by exposure to 10 mmol/L HCY for 6 h. (Top) ROS fluorescence intensity was visualized using a confocal fluorescence microscope (×100). (a) Control; (b) HCY; (c) 1 μmol/L SFN + HCY; (d) 5 μmol/L SFN + HCY; (e) 10 μmol/L SFN + HCY; (f) 20 μmol/L SFN + HCY. (Bottom) The relative fluorescence densities of ROS were analyzed with image analysis software (ImageJ 1.45 s, USA) and standardized by the control. The data are representative of at least three independent experiments with a microscope (×100). Bars with no letters in common are significantly different ($p < 0.05$).

excitation at 300−500 nm. Fluorescence images were analyzed with image analysis software (ImageJ 1.45s, USA).[24]

Aminotransferases Activities Assays. Activities of alanine aminotransferase (ALT) and aspartate aminotransferase (AST) were measured in the culture medium.[25] Preincubated with various concentrations of SFN for 24 h or 20 μmol/L SFN for different times, the cells were then exposed to 10 mmol/L HCY for 6 h. After treatment, the supernatant medium was collected for ALT and AST activity measurement immediately using E-test kits (Biosino Biotechnology Company Ltd., via a Hitachi Automatic Analyzer (Hitachi, Inc., Japan)). All procedures were performed according to the manufacturer's instructions.

Determination of Malondialdehyde (MDA). Lipid peroxidation was determined by measuring the level of MDA.[26] The concentration of protein was determined by the method of Bradford. The MDA content in cell lysates was spectrophotometrically measured by using thiobarbituric acid-reacting substance (TBARS) production at 532 nm, according to the manufacturer's instruction from Jiancheng Bioengineering Institute (Nanjing, China). The results were expressed as nmol MDA produced per mg protein.

Transmission Electron Microscope Examination of ER. Transmission electron microscopy was performed on HHL-5 cells pretreated with 10 μmol/L SFN for 24 h and then replaced with 10 mmol/L HCY for 6 h. Transmission electron microscopy of cells was done as described previously.[27] Briefly, samples were fixed with 3% glutaraldehyde dissolved in 0.1 mol/L sodium cacodylate, postfixed in osmium tetroxide, dehydrated with graded acetone series, and finally embedded in Epon. Ultrathin sections were stained with uranyl acetate and lead citrate, examined in a JEM 1220 transmission electron microscope operated at 80 kV.

Preparation of Cell Lysates and Western Blotting. After various treatments, cells were washed twice with ice-cold PBS and subjected to whole cell lysis buffer [50 mmol/L Tris-HCl (pH 7.4), 150 mmol/L NaCl, 2 mmol/L EDTA, 10% glycerol, 1% Nonidet P-40 containing 0.1 mol/L PMSF, and 1× protease inhibitor cocktail (Sigma)] for 30 min on ice. After centrifugation at 16,000g for 10 min at 4 °C, the supernatants were collected for Western blot analysis. Equal amounts of protein (40−60 μg) were separated on 8% to 10% SDS−PAGE and transferred to polyvinylidene difluoride (PVDF) membranes (Millipore, Bedford, MA). The membrane was blocked with 5% nonfat milk for 30 min at room temperature and were then incubated at 4 °C overnight with the following primary antibodies: NQO1, TrxR-1, GRP78, PERK, P-PERK, Nrf-2, LaminB1, and β-actin. The membrane was then incubated with the secondary alkaline phosphatase-conjugated IgG and detected with Western Blue Stabilized Substrate for alkaline phosphatase (Promega). The relative densities of the individual bands were analyzed densitometrically using the ChemiImager 4000 instrument (Alpha Innotech, USA).

Nuclear Extraction. Nuclear protein extraction was regularly performed as previously described.[28] After SFN treatments, cells were harvested and washed with phosphate-buffered saline (PBS). Nuclear and cytoplasmic extractions were isolated using Chemicon Nuclear Extraction Kit. Then, each pellet was suspended in cell lysis buffer containing 1% Nonidet P-40, 50 mmol/L Tris (pH 7.4), 150 mM NaCl, 1 mmol/L PMSF, and 1× protease inhibitor cocktail, then incubated on ice for 30 min. Lysates were centrifuged at 10,000g for 10 min at 4 °C, and the supernatant was used for Western blot analysis.

Statistical Analysis. All results shown are representative of at least three independent experiments. Data are presented as the mean ± SD. Statistical analysis was performed by one-way ANOVA, followed by Dunnett's test and SNK test using the SPSS 13.0 software. Probability values of <0.05 were considered to be statistically significant.

RESULTS

Cell Proliferation and Morphology of HHL-5 Pretreated with SFN. Cells were treated with 1−140 μmol/L SFN in six replicate wells for 24 or 48 h. Dual regulation of cell growth by SFN was observed (Figure 1A). Lower doses of SFN ($\leqslant$20 μmol/L) promoted the proliferation of HHL-5 cells. At the dose of 10 μmol/L, for instance, cell viabilities were even achieved to 120 ± 2.3% (24 h) and 108 ± 2.6% (48 h). The IC_{50} values were 106.3 ± 2.6 μmol/L (24 h) and 60.9 ± 1.5 μmol/L (48 h). Therefore, the range of SFN concentrations (1−20 μmol/L) was selected for the following experiments.

To confirm whether SFN presents the protective effects on HHL-5 cells against HCY, the MTT assay and morphological examination were performed. As shown in Figure 1B, after challenging with 10 mmol/L HCY for 24 h, the cell viability significantly declined to 60.4 ± 3.1%. However, preincubation with SFN (1−20 μmol/L) for 24 h before HCY exposure cell viabilities were increased to 87.7 ± 2.9%, 103.7 ± 5.7%, 116.3 ± 2.8%, and 113.4 ± 5.5%. The statistical analysis showed that significant differences in any two groups among 1 μmol/L, 5 μmol/L, 10 μmol/L, and 20 μmol/L SFN except for the two groups between 10 μmol/L and 20 μmol/L SFN ($p < 0.05$).

Under light microscopy, cells in the control group appeared spindle-shaped (Figure 1C). When exposed to 10 mmol/L HCY for 24 h, a large number of cells displayed morphological changes such as shrinkage, rounding up, floating, or death. However, upon preincubation with 10 μmol/L SFN for 24 h the injured cells became narrower and had clear cell boundaries. Apparently, SFN enables the improvement of the morphological defect of HHL-5 cells injured by HCY.

Protective Effect of SFN on Oxidative Injury by HCY in HHL-5 Cells. Oxidative stress due to excessive production of

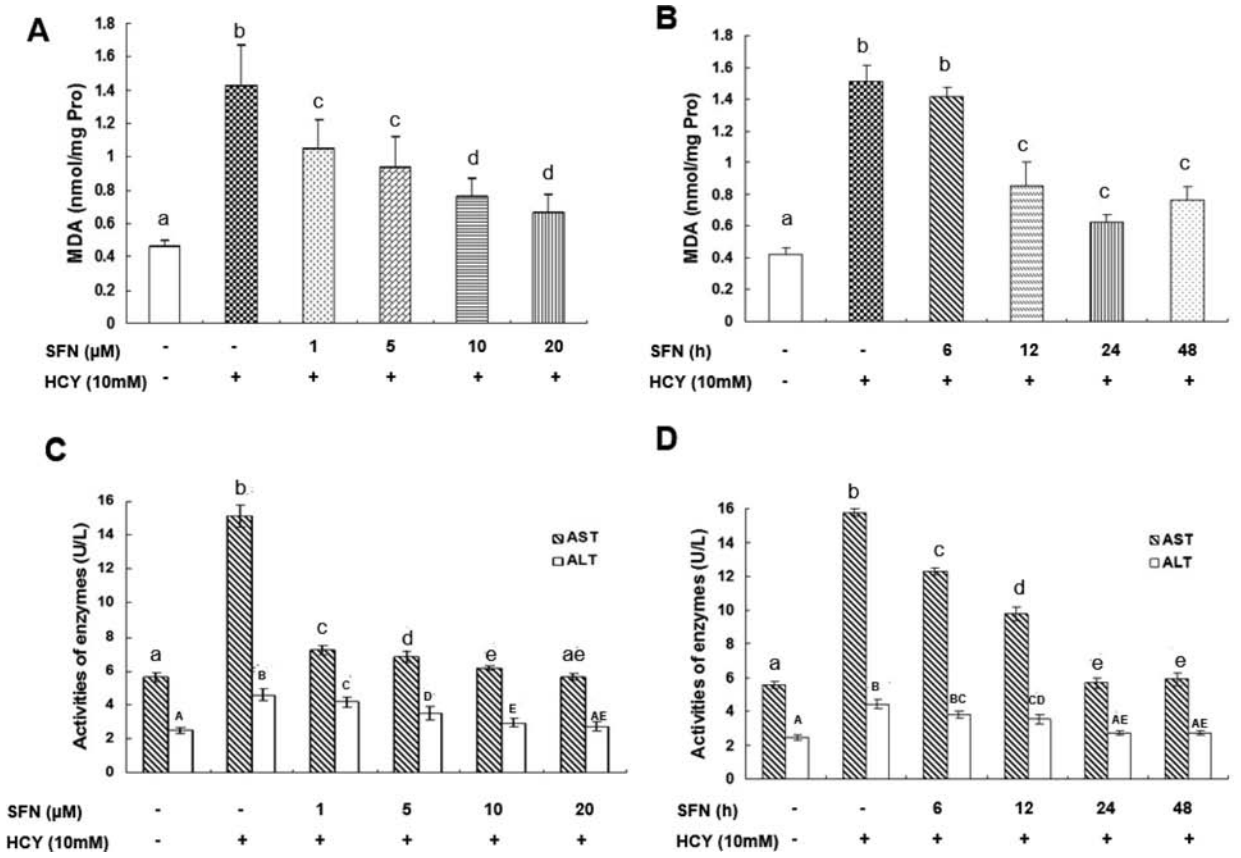

Figure 3. Protective effect of SFN on oxidative damage by HCY. Cells were pretreated with graded concentrations of SFN for 24 h (A and C) or 20 μmol/L SFN for 6−48 h (B and D), then exposed to 10 mmol/L HCY for 6 h. The supernatant was collected for quantifying the contents of MDA and activities of AST and ALT. All results represent the mean values ± SD from three independent experiments. Bars with no letters in common are significantly different ($p < 0.05$).

ROS has been suggested as one of the important mechanisms for HCY-induced injury.[29] After incubation with HCY (10 mmol/L) for 1 h, intracellular ROS was significantly enhanced (Figure 2b), whereas these fluorescent signals were rarely detected in nontreated cells (Figure 2a). Treatment of the cells with SFN (1−20 μmol/L) for 24 h prior to HCY exposure effectively nullified ROS accumulation (Figure 2c−f). Compared to the HCY group (Figure 2b), the lowest dose of SFN (1 mmol/L) significantly decreased the fluorescence intensity (Figure 2c and bottom panel), while higher SFN entirely abolished ROS generation (Figure 2d−f and bottom panel). Statistical analysis showed the significant differences in any two groups among 1 μmol/L SFN, 5 μmol/L SFN, 10 μmol/L SFN, 20 μmol/L SFN, and HCY group ($p < 0.05$). These results indicated that SFN could antagonize HCY-induced oxidative stress.

MDA, an indicator of lipid peroxidation, was drastically elevated after 6 h of incubation with HCY (10 mmol/L) by more than 3-fold as compared with the control, which indicated that the cells had suffered severe oxidative stress conditions (Figure 3A−B). The results in Figure 3A showed that preincubation with 1−20 μmol/L SFN decreased the enhanced levels of MDA by 45−75% significantly ($p < 0.05$). Similarly, the increased levels of MDA by HCY were reduced significantly by 43−65% after pretreatment with 20 μmol/L SFN by 6−48 h (Figure 3B, $p < 0.05$). To confirm the hepato-protective effects of SFN on HHL-5 cells against HCY, the enzymatic activities of ALT and AST in the medium were tested. Compared to the control group, HCY increased the AST and ALT activities by 3-fold and 2-fold, respectively (Figure 3C and D). The lowest dose of SFN (1 μmol/L) significantly inhibited the enhanced AST activity by HCY by 1.7-fold. The activity of ALT was noticeably decreased by 5−20 μmol/L SFN (Figure 3C). After pretreatment with 20 μmol/L SFN for 6−48 h, the increased activities of AST and ALT were decreased to 37%−77% and 62%−86%, respectively (Figure 3D, $p < 0.05$).

Phase II Enzymes Were Involved in the Protection of SFN against HCY Injury. After treatment with 10 mmol/L HCY for 6 h, both NQO1 and TrxR-1 were decreased almost to half of the control (Figure 4). SFN ameliorated the decreasing expression of TrxR-1 and NQO1 in a dose- and time-course. Compared to the HCY group, preincubation with 1−20 μmol/L SFN increased the levels of TrxR-1 by 1.68- to 4.31-fold (Figure 4A, $p < 0.05$) and of NQO1 by 1.5-fold to 2.9-fold (Figure 4B, $p < 0.05$). TrxR-1 showed a time-dependent manner until 48 h, whereas NQO1 reached a plateau at 24 h. Preincubation with 20 μmol/L SFN for 6−48 h increased the levels of TrxR-1 by 2.7-fold to 5-fold (Figure 4C, compare with HCY, $p < 0.05$) and increased the levels of NQO1 by 2.7-fold to 3-fold (Figure 4D, compare with HCY, $p < 0.05$).

SFN Minimizes the Injuries of the ER and Abrogates the Aberrant Expression of GRP78 and PERK Protein by HCY. According to the results in Figure 5, HCY (10 mmol/L) treatment severely damaged the structure of ER with visible swelling; conversely, pretreatment with SFN significantly improved ER dilation. To obtain further evidence for ER

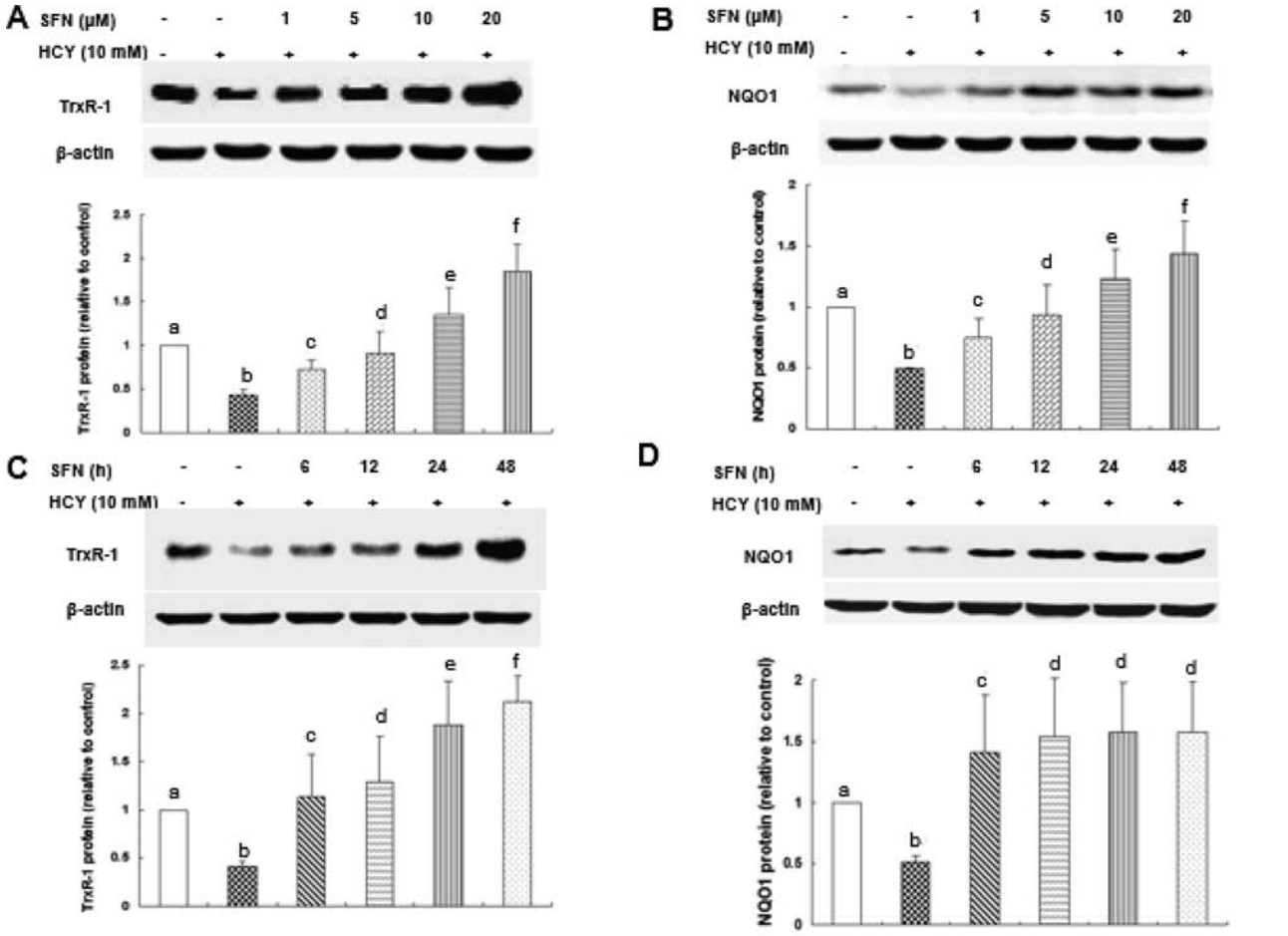

Figure 4. SFN enhanced the expressions of TrxR-1 and NQO1 weakened by HCY. Cells were pretreated with 1−20 μmol/L SFN for 24 h (A and B) or treated with 20 μM SFN for the indicated times (C and D), then followed with 10 mmol/L HCY for 6 h. Cytosolic protein was isolated and subjected to Western blot analysis. The relative densities of the target proteins were scanned with a ChemiImager 4000 digital system (Alpha Innotech Corporation, USA) and standardized by the control (β-actin). The data are representative of at least three independent experiments. Bars with no letters in common are significantly different ($p < 0.05$).

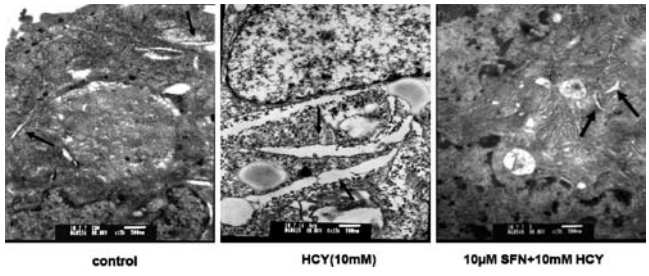

Figure 5. SFN improved ER dilation caused by HCY in HHL-5 cells. Cells were pretreated without or with 10 μmol/L SFN for 24 h then eventually with 10 mmol/L HCY for 6 h. After a series of washing, dehydration, and staining, cells were visualized for the structure of the ER with electron microscopy. Arrows refer to the individual ER in the cells. The data are representative of at least three independent experiments.

stress, we investigated the expressions of ER stress specific proteins. GRP78, an ER molecular chaperone serving as a central regulator of ER stress, was up-regulated by 10 mmol/L HCY with 2.5-fold of the control. SFN abrogated GRP78 up-regulation caused by HCY (Figure 6A and C). PERK, an ER resident sensor associating with GRP78 in the absence of ER stress, was investigated. PERK phosphorylation was strongly increased by HCY with 6.5-fold of the control, while it was strikingly abolished by preincubation with SFN (Figure 6B and D). Compared with the HCY group, preincubation with 1−20 μmol/L SFN for 24 h decreased the levels of GRP78 by 38% to 69% (Figure 6A, $p < 0.05$) and of p-PERK by 30% to 47% (Figure 6B, $p < 0.05$). Similarly, preincubation with 20 μmol/L SFN for 6−48 h decreased the levels of GRP78 by 45% to 73% (Figure 6C, $p < 0.05$) and of p-PERK by 30% to 70% (Figure 6D, $p < 0.05$).

Effect of SFN on Nrf-2 Translocation to the Nucleus. Nrf-2 regulates many of the antioxidant and phase II detoxifying enzymes, including TrxR-1 and NQO1.[30,31] The nuclear protein was extracted to test the translocation of Nrf-2 into the nucleus, and LaminB1 was chosen as the internal control instead of β-actin.[32,33] As shown in Figure 7, the expression of p-Nrf-2 was decreased to nearly 85% after treatment with HCY (Figure7A and B). Pretreatment with SFN abolished the inhibition of p-Nrf-2 by HCY, and phosphorylation of Nrf-2 (p-Nrf-2) in the nucleus was no longer decreased by HCY but increased by 3−4-fold after preincubation with SFN (Figure 7A and B).

DISCUSSION

The present findings show that SFN presents its protective effects on hepatic injury caused by HCY in immortalized

dx.doi.org/10.1021/jf501944u | J. Agric. Food Chem. 2014, 62, 7477−7485

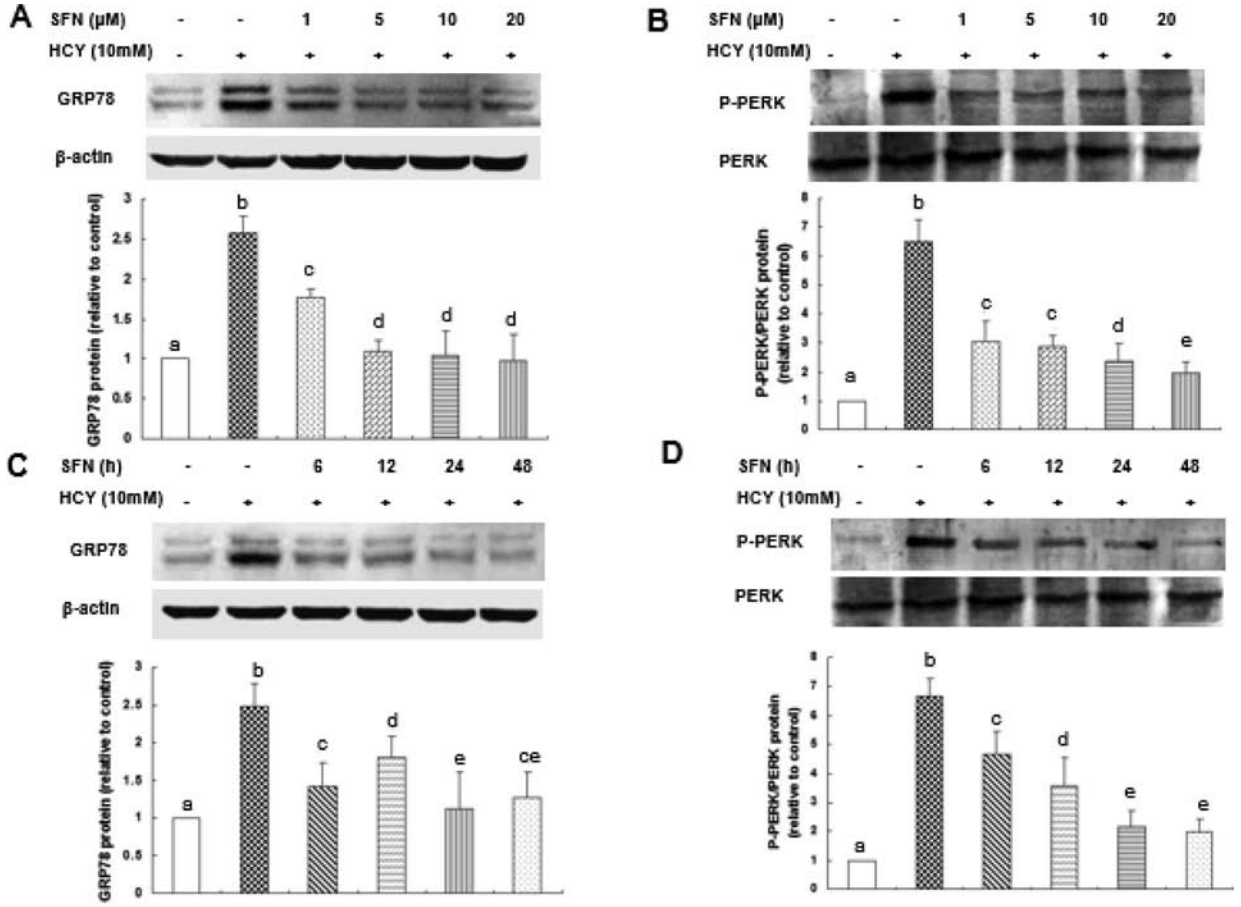

Figure 6. SFN inhibited the expression of GRP78 and phosphorylation of PERK induced by HCY in HHL-5 cells. Cells were preincubated with 1, 5, 10, and 20 μmol/L SFN for 24 h (A and B) or 20 μmol/L SFN for 6, 12, 24, and 48 h (C and D), then treated with 10 mmol/L HCY for 6 h. Protein was isolated and subjected to Western blot analysis. The relative densities of the target proteins were scanned with a ChemiImager 4000 digital system and standardized by a control. Data were from three independent experiments. Bars with no letters in common are significantly different ($p < 0.05$).

human hepatocyte line HHL-5 through inducing antioxidant enzymes and reducing ER stress. Furthermore, the results suggest that Nrf-2 activation might be a key factor in attenuating oxidative damage caused by HCY. On the basis of these findings, our results have strongly implied the potential roles of SFN in the prevention of HHCY-related disorders.

It is well established that Nrf-2 protects against oxidative stress-mediated damage to cells through activating the basic zipper (bZIP) transcription factor and binding to ARE-dependent gene expression.[34,35] Nrf-2 activator attenuated the histological injury induced by α-naphthylisothiocynate (ANIT) in mice.[36] Chemicals and drugs have been shown to reduce oxidative stress through activating the Nrf-2 regulatory pathway, which indicates a hepatoprotective role of Nrf-2 activation against various liver diseases.[37,38] Our previous research also demonstrated that SFN exhibited its potential in the prevention of human bladder cancer by targeting Nrf-2 activation.[39]

ER stress plays a pathogenic role in a variety of diseases, including Alzheimer's, Parkinson's diseases, cancer, cardiac and cerebral ischemia/reperfusion injury, diabetes, and atherosclerosis.[36,37,40,41] Chemicals that function through the ER stress pathways have been proved to be effective, building enthusiasm for the therapeutic potentials of ER stress response augmentation. For instance, *trans*-4,5-dihydroxy-1,2-dithiane (DTTox) stimulated an increase in GRP78 expression and protected the proximal tubular epithelium against a nephrotoxic chemical.[42]

To date, few studies have implicated the underlining relationship between Nrf-2 and ER stress regulation. Unfolded protein response (UPR), a well-conserved intracellular signaling invoked by ER stress, modulates the oxidative stress-inducible Nrf-2 pathway or the hypoxia-inducible factor (HIF) pathway to enhance the expression of the target genes, which support cell survival. Importantly, the accumulation of intracellular ROS caused by ER stress is attenuated by the double-stranded RNA-activated PERK pathway of UPR, which simultaneously activates oxidative stress-inducible transcription factor Nrf-2 and maintains redox homeostasis, thereby ensuring cell survival.[43] In the present findings, the expression of p-Nrf-2 was decreased to 85% by HCY treatment compared with that of the control group ($p = 0.052$). These results showed that, to some extent, HCY attenuated the phosphorylation of Nrf2, although no significant difference was observed. As far as we know, a few of the mechanisms were involved in HCY-stressed cells. Apart from oxidative injury, the inflammatory signal also takes the predominant role.[44] Moreover, NF-κB has been reported to be an important target of HCY.[45,46] Our previous studies have confirmed that NF-κB is a targeting transcription factor controlled by SFN.[28] Therefore, we postulate that Nrf-2 plays a part in the effect. During the early phase of ER stress,

dx.doi.org/10.1021/jf501944u | J. Agric. Food Chem. 2014, 62, 7477−7485

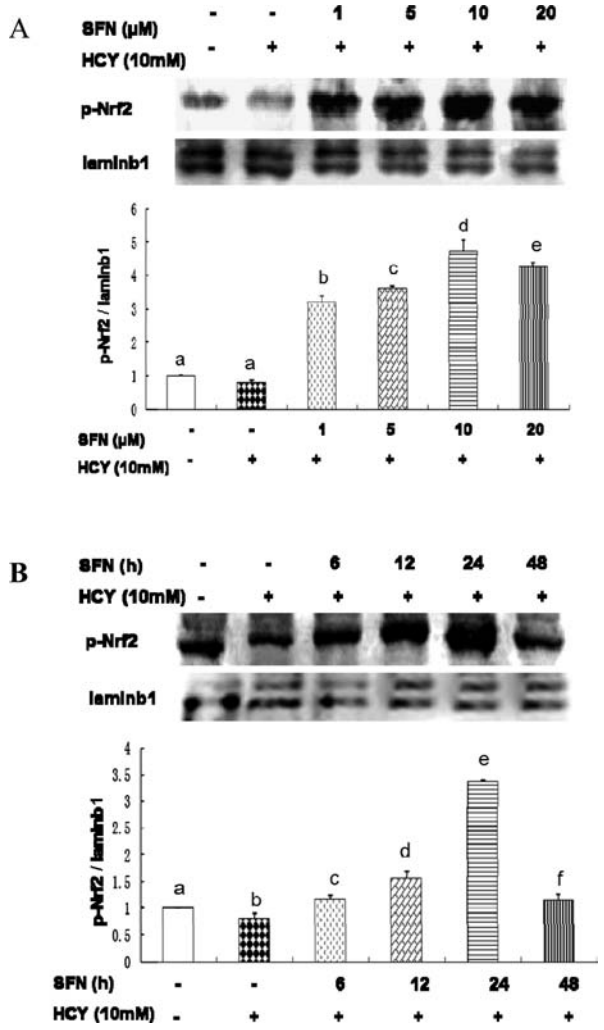

Figure 7. SFN activated Nrf-2 translocation into the nucleus. Cells were preincubated with 1, 5, 10, and 20 μM SFN for 24 h (A) or 20 μM SFN for 6, 12, 24, and 48 h (B), then treated with 10 mM HCY for 6 h. Protein was isolated and subjected to Western blot analysis. The relative densities of the target proteins were scanned with a ChemiImager 4000 digital system and standardized by a control. Data were from three independent experiments. Bars with no letters in common are significantly different ($p < 0.05$).

PERK activation may be beneficial for the cell's self-defenses.[47,48] However, continuous activation of PERK was phosphorylated by the initiation of apoptosis signaling and/or abnormal redox state and will lead to the cell injury and even death.[49−51] As shown in the present findings, the translocation of Nrf-2 was activated by SFN (Figure 7), accompanied by the lower phosphorylates of PERK (Figure 6), which suggested the potential regulation of PERK phosphorylation through Nrf-2 signaling. It should be noted that Nrf-2 activation plays a vital role in UPR activation and functions like an effector of PERK cell survival signaling during the process of ER stress.[43] Therefore, more studies should be done to expose their relationships. Taken together, SFN prevents oxidative injury induced by HCY through attenuating ER stress and initiating Nrf-2 translocation and subsequently enhancing the expressions of TrxR-1 and NQO1 in the immortalized human hepatocyte line HHL-5 (Figure 8). These findings suggest that SFN may be a powerful agent for relieving liver injury caused by HCY.

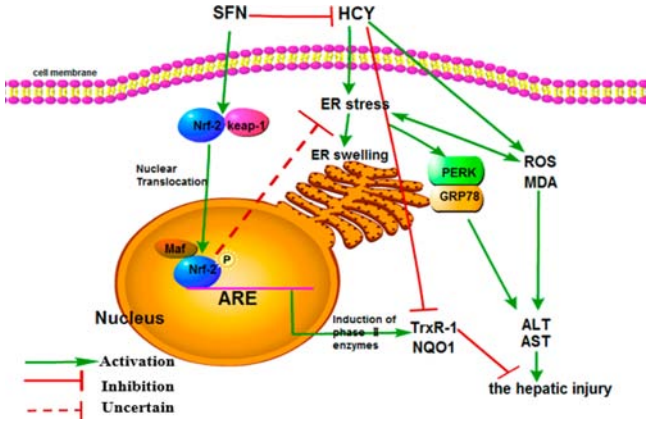

Figure 8. A proposed mechanism of SFN protect the oxidative injury-induced by HCY in immortalized human hepatocyte line HHL-5. SFN improved the oxidative injuries that were caused by HCY in immortalized human hepatocyte line HHL-5, such as ER swelling, excessive ROS generation, increased MDA levels, and increased activities of ALT and AST. The hepatoprotective effect of SFN was through attenuating the ER stress and inducing Nrf-2/phase II enzymes in immortalized human hepatocyte line HHL-5.

AUTHOR INFORMATION

Corresponding Authors

*(S.W.) Tel: +86 432-64560095. Fax: +86 432-64560095. E-mail: shuranwang@163.com.

*(Y.S.) Tel: +86 451 86282021. Fax: +86 451 862822906. E-mail: yujuan72@163.com.

Author Contributions

‖C.H. and B.L. contributed equally to this work.

Funding

This work was supported by the China-UK science network funding, jointly administrated by the Royal Society and the China Scholarship Council (CSC) (No. Z6530573), and the Fundamental Research Funds for the Central Universities (Grant No. HIT. IBRSEM. 201335).

Notes

The authors declare no competing financial interest.

ACKNOWLEDGMENTS

We thank Dr. Nditange Shigwedha from University of Namibia (Windhoek, Namibia) for carefully reading the manuscript. We also thank Dr. Yongping Bao from University of East Anglia (Norwich, UK) for the critical revision of the manuscript.

REFERENCES

(1) Ji, C.; Kaplowitz, N. Hyperhomocysteinemia, endoplasmic reticulum stress, and alcoholic liver injury. *World J. Gastroenterol.* **2004**, *10*, 1699−1708.

(2) Refsum, H.; Ueland, P. M.; Nygard, O.; Vollset, S. E. Homocysteine and cardiovascular disease. *Annu. Rev. Med.* **1998**, *49*, 31−62.

(3) Wilson, F. A.; van den Borne, J. J.; Calder, A. G.; O'Kennedy, N.; Holtrop, G.; Rees, W. D.; Lobley, G. E. Tissue methionine cycle activity and homocysteine metabolism in female rats: impact of dietary methionine and folate plus choline. *Am. J. Physiol. Endocrinol. Metab.* **2009**, *296*, E702−713.

(4) Seshadri, S.; Beiser, A.; Selhub, J.; Jacques, P. F.; Rosenberg, I. H.; D'Agostino, R. B.; Wilson, P. W.; Wolf, P. A. Plasma homocysteine as a risk factor for dementia and Alzheimer's disease. *New Engl. J. Med.* **2002**, *346*, 476−483.

(5) Garcia-Tevijano, E. R.; Berasain, C.; Rodriguez, J. A.; Corrales, F. J.; Arias, R.; Martin-Duce, A.; Caballeria, J.; Mato, J. M.; Avila, M. A. Hyperhomocysteinemia in liver cirrhosis: mechanisms and role in vascular and hepatic fibrosis. *Hypertension* **2001**, *38*, 1217−1221.
(6) Ji, C.; Kaplowitz, N. Betaine decreases hyperhomocysteinemia, endoplasmic reticulum stress, and liver injury in alcohol-fed mice. *Gastroenterology* **2003**, *124*, 1488−1499.
(7) Lu, S. C.; Tsukamoto, H.; Mato, J. M. Role of abnormal methionine metabolism in alcoholic liver injury. *Alcohol* **2002**, *27*, 155−162.
(8) Woo, C. W.; Siow, Y. L.; Pierce, G. N.; Choy, P. C.; Minuk, G. Y.; Mymin, D.; O, K. Hyperhomocysteinemia induces hepatic cholesterol biosynthesis and lipid accumulation via activation of transcription factors. *Am. J. Physiol. Endocrinol. Metab.* **2005**, *288*, E1002−1010.
(9) Hotamisligil, G. S. Endoplasmic reticulum stress and the inflammatory basis of metabolic disease. *Cell* **2010**, *140*, 900−917.
(10) Young, I. S.; Woodside, J. V. Homocysteine–what does it mean and have we been led astray? *Int. J. Clin. Pract.* **2010**, *64*, 281−284.
(11) Marti-Carvajal, A. J.; Sola, I.; Lathyris, D.; Karakitsiou, D. E.; Simancas-Racines, D. Homocysteine-lowering interventions for preventing cardiovascular events. *Cochrane Database Syst. Rev.* **2013**, *1*, CD006612.
(12) Doshi, S. N.; McDowell, I. F.; Moat, S. J.; Payne, N.; Durrant, H. J.; Lewis, M. J.; Goodfellow, J. Folic acid improves endothelial function in coronary artery disease via mechanisms largely independent of homocysteine lowering. *Circulation* **2002**, *105*, 22−26.
(13) Dinkova-Kostova, A. T.; Talalay, P. Direct and indirect antioxidant properties of inducers of cytoprotective proteins. *Mol. Nutr. Food Res.* **2008**, *52* (Suppl 1), S128−138.
(14) Fahey, J. W.; Talalay, P. Antioxidant functions of sulforaphane: a potent inducer of Phase II detoxication enzymes. *Food Chem. Toxicol.* **1999**, *37*, 973−979.
(15) Miao, X.; Bai, Y.; Sun, W.; Cui, W.; Xin, Y.; Wang, Y.; Tan, Y.; Miao, L.; Fu, Y.; Su, G.; Cai, L. Sulforaphane prevention of diabetes-induced aortic damage was associated with the up-regulation of Nrf2 and its down-stream antioxidants. *Nutr. Metab.* **2012**, *9*, 84.
(16) Wu, L.; Noyan Ashraf, M. H.; Facci, M.; Wang, R.; Paterson, P. G.; Ferrie, A.; Juurlink, B. H. Dietary approach to attenuate oxidative stress, hypertension, and inflammation in the cardiovascular system. *Proc. Natl. Acad. Sci. U.S.A.* **2004**, *101*, 7094−7099.
(17) Angeloni, C.; Leoncini, E.; Malaguti, M.; Angelini, S.; Hrelia, P.; Hrelia, S. Modulation of phase II enzymes by sulforaphane: implications for its cardioprotective potential. *J. Agric. Food Chem.* **2009**, *57*, 5615−5622.
(18) Zhu, H.; Jia, Z.; Strobl, J. S.; Ehrich, M.; Misra, H. P.; Li, Y. Potent induction of total cellular and mitochondrial antioxidants and phase 2 enzymes by cruciferous sulforaphane in rat aortic smooth muscle cells: cytoprotection against oxidative and electrophilic stress. *Cardiovasc. Toxicol.* **2008**, *8*, 115−125.
(19) Malhotra, D.; Thimmulappa, R.; Vij, N.; Navas-Acien, A.; Sussan, T.; Merali, S.; Zhang, L.; Kelsen, S. G.; Myers, A.; Wise, R.; Tuder, R.; Biswal, S. Heightened endoplasmic reticulum stress in the lungs of patients with chronic obstructive pulmonary disease: the role of Nrf2-regulated proteasomal activity. *Am. J. Respir. Crit. Care Med.* **2009**, *180*, 1196−1207.
(20) Shan, Y.; Zhao, R.; Geng, W.; Lin, N.; Wang, X.; Du, X.; Wang, S. Protective effect of sulforaphane on human vascular endothelial cells against lipopolysaccharide-induced inflammatory damage. *Cardiovasc. Toxicol.* **2010**, *10*, 139−145.
(21) Werstuck, G. H.; Lentz, S. R.; Dayal, S.; Hossain, G. S.; Sood, S. K.; Shi, Y. Y.; Zhou, J.; Maeda, N.; Krisans, S. K.; Malinow, M. R.; Austin, R. C. Homocysteine-induced endoplasmic reticulum stress causes dysregulation of the cholesterol and triglyceride biosynthetic pathways. *J. Clin. Invest.* **2001**, *107*, 1263−1273.
(22) Shan, Y.; Sun, C.; Zhao, X.; Wu, K.; Cassidy, A.; Bao, Y. Effect of sulforaphane on cell growth, G(0)/G(1) phase cell progression and apoptosis in human bladder cancer T24 cells. *Int. J. Oncol.* **2006**, *29*, 883−888.
(23) Gomes, A.; Fernandes, E.; Lima, J. L. Fluorescence probes used for detection of reactive oxygen species. *J. Biochem. Biophys. Methods* **2005**, *65*, 45−80.
(24) Kondo, Y.; Murayama, Y.; Konishi, H.; Morimura, R.; Komatsu, S.; Shiozaki, A.; Kuriu, Y.; Ikoma, H.; Kubota, T.; Nakanishi, M.; Ichikawa, D.; Fujiwara, H.; Okamoto, K.; Sakakura, C.; Takahashi, K.; Inoue, K.; Nakajima, M.; Otsuji, E. Fluorescent detection of peritoneal metastasis in human colorectal cancer using 5-aminolevulinic acid. *Int. J. Oncol.* **2014**, *45*, 41−46.
(25) Lubberstedt, M.; Muller-Vieira, U.; Biemel, K. M.; Darnell, M.; Hoffmann, S. A.; Knospel, F.; Wonne, E. C.; Knobeloch, D.; Nussler, A. K.; Gerlach, J. C.; Andersson, T. B.; Zeilinger, K. Serum-free culture of primary human hepatocytes in a miniaturized hollow-fibre membrane bioreactor for pharmacological in vitro studies. *J. Tissue Eng. Regener. Med.* **2012**, DOI: 10.1002/term.1652.
(26) Lu, K. H.; Tseng, H. C.; Liu, C. T.; Huang, C. J.; Chyuan, J. H.; Sheen, L. Y. Wild bitter gourd protects against alcoholic fatty liver in mice by attenuating oxidative stress and inflammatory responses. *Food Funct.* **2014**, *5*, 1027−1037.
(27) Carew, J. S.; Nawrocki, S. T.; Xu, R. H.; Dunner, K.; McConkey, D. J.; Wierda, W. G.; Keating, M. J.; Huang, P. Increased mitochondrial biogenesis in primary leukemia cells: the role of endogenous nitric oxide and impact on sensitivity to fludarabine. *Leukemia* **2004**, *18*, 1934−1940.
(28) Shan, Y.; Wu, K.; Wang, W.; Wang, S.; Lin, N.; Zhao, R.; Cassidy, A.; Bao, Y. Sulforaphane down-regulates COX-2 expression by activating p38 and inhibiting NF-kappaB-DNA-binding activity in human bladder T24 cells. *Int. J. Oncol.* **2009**, *34*, 1129−1134.
(29) Perna, A. F.; Ingrosso, D.; De Santo, N. G. Homocysteine and oxidative stress. *Amino Acids* **2003**, *25*, 409−417.
(30) Yu, S.; Khor, T. O.; Cheung, K. L.; Li, W.; Wu, T. Y.; Huang, Y.; Foster, B. A.; Kan, Y. W.; Kong, A. N. Nrf2 expression is regulated by epigenetic mechanisms in prostate cancer of TRAMP mice. *PLoS One* **2010**, *5*, e8579.
(31) Barve, A.; Khor, T. O.; Nair, S.; Reuhl, K.; Suh, N.; Reddy, B.; Newmark, H.; Kong, A. N. Gamma-tocopherol-enriched mixed tocopherol diet inhibits prostate carcinogenesis in TRAMP mice. *Int. J. Cancer* **2009**, *124*, 1693−1699.
(32) Kang, H. J.; Hong, Y. B.; Kim, H. J.; Bae, I. CR6-interacting factor 1 (CRIF1) regulates NF-E2-related factor 2 (NRF2) protein stability by proteasome-mediated degradation. *J. Biol. Chem.* **2010**, *285*, 21258−21268.
(33) Mobasher, M. A.; Gonzalez-Rodriguez, A.; Santamaria, B.; Ramos, S.; Martin, M. A.; Goya, L.; Rada, P.; Letzig, L.; James, L. P.; Cuadrado, A.; Martin-Perez, J.; Simpson, K. J.; Muntane, J.; Valverde, A. M. Protein tyrosine phosphatase 1B modulates GSK3beta/Nrf2 and IGFIR signaling pathways in acetaminophen-induced hepatotoxicity. *Cell Death Dis.* **2013**, *4*, e626.
(34) Krajka-Kuzniak, V.; Paluszczak, J.; Szaefer, H.; Baer-Dubowska, W. Betanin, a beetroot component, induces nuclear factor erythroid-2-related factor 2-mediated expression of detoxifying/antioxidant enzymes in human liver cell lines. *Br. J. Nutr.* **2013**, *110*, 2138−2149.
(35) Liang, L.; Gao, C.; Luo, M.; Wang, W.; Zhao, C.; Zu, Y.; Efferth, T.; Fu, Y. Dihydroquercetin (DHQ) induced HO-1 and NQO1 expression against oxidative stress through the Nrf2-dependent antioxidant pathway. *J. Agric. Food Chem.* **2013**, *61*, 2755−2761.
(36) Tanaka, Y.; Aleksunes, L. M.; Cui, Y. J.; Klaassen, C. D. ANIT-induced intrahepatic cholestasis alters hepatobiliary transporter expression via Nrf2-dependent and independent signaling. *Toxicol. Sci.* **2009**, *108*, 247−257.
(37) Okada, K.; Shoda, J.; Taguchi, K.; Maher, J. M.; Ishizaki, K.; Inoue, Y.; Ohtsuki, M.; Goto, N.; Takeda, K.; Utsunomiya, H.; Oda, K.; Warabi, E.; Ishii, T.; Osaka, K.; Hyodo, I.; Yamamoto, M. Ursodeoxycholic acid stimulates Nrf2-mediated hepatocellular transport, detoxification, and antioxidative stress systems in mice. *Am. J. Physiol. Gastrointest. Liver Physiol.* **2008**, *295*, G735−747.
(38) Okada, K.; Shoda, J.; Taguchi, K.; Maher, J. M.; Ishizaki, K.; Inoue, Y.; Ohtsuki, M.; Goto, N.; Sugimoto, H.; Utsunomiya, H.; Oda, K.; Warabi, E.; Ishii, T.; Yamamoto, M. Nrf2 counteracts cholestatic

liver injury via stimulation of hepatic defense systems. *Biochem. Biophys. Res. Commun.* **2009**, *389*, 431−436.
(39) Shan, Y.; Wang, X.; Wang, W.; He, C.; Bao, Y. p38 MAPK plays a distinct role in sulforaphane-induced up-regulation of ARE-dependent enzymes and down-regulation of COX-2 in human bladder cancer cells. *Oncol. Rep.* **2010**, *23*, 1133−1138.
(40) Zhang, Y.; Talalay, P.; Cho, C. G.; Posner, G. H. A major inducer of anticarcinogenic protective enzymes from broccoli: isolation and elucidation of structure. *Proc. Natl. Acad. Sci. U.S.A.* **1992**, *89*, 2399−2403.
(41) Prochaska, H. J.; Santamaria, A. B.; Talalay, P. Rapid detection of inducers of enzymes that protect against carcinogens. *Proc. Natl. Acad. Sci. U.S.A.* **1992**, *89*, 2394−2398.
(42) Asmellash, S.; Stevens, J. L.; Ichimura, T. Modulating the endoplasmic reticulum stress response with trans-4,5-dihydroxy-1,2-dithiane prevents chemically induced renal injury in vivo. *Toxicol. Sci.* **2005**, *88*, 576−584.
(43) Cullinan, S. B.; Zhang, D.; Hannink, M.; Arvisais, E.; Kaufman, R. J.; Diehl, J. A. Nrf2 is a direct PERK substrate and effector of PERK-dependent cell survival. *Mol. Cell. Biol.* **2003**, *23*, 7198−7209.
(44) Papatheodorou, L.; Weiss, N. Vascular oxidant stress and inflammation in hyperhomocysteinemia. *Antioxid. Redox Signaling* **2007**, *9*, 1941−1958.
(45) Mikael, L. G.; Rozen, R. Homocysteine modulates the effect of simvastatin on expression of ApoA-I and NF-kappaB/iNOS. *Cardiovasc. Res.* **2008**, *80*, 151−158.
(46) Ferlazzo, N.; Condello, S.; Curro, M.; Parisi, G.; Ientile, R.; Caccamo, D. NF-kappaB activation is associated with homocysteine-induced injury in Neuro2a cells. *BMC Neurosci.* **2008**, *9*, 62.
(47) Shen, J.; Chen, X.; Hendershot, L.; Prywes, R. ER stress regulation of ATF6 localization by dissociation of BiP/GRP78 binding and unmasking of Golgi localization signals. *Dev. Cell* **2002**, *3*, 99−111.
(48) Liu, C. Y.; Wong, H. N.; Schauerte, J. A.; Kaufman, R. J. The protein kinase/endoribonuclease IRE1alpha that signals the unfolded protein response has a luminal N-terminal ligand-independent dimerization domain. *J. Biol. Chem.* **2002**, *277*, 18346−18356.
(49) Harding, H. P.; Zhang, Y.; Bertolotti, A.; Zeng, H.; Ron, D. Perk is essential for translational regulation and cell survival during the unfolded protein response. *Mol. Cell* **2000**, *5*, 897−904.
(50) Kammoun, H. L.; Hainault, I.; Ferre, P.; Foufelle, F. Nutritional related liver disease: targeting the endoplasmic reticulum stress. *Curr. Opin. Clin. Nutr. Metab. Care* **2009**, *12*, 575−582.
(51) Yoshida, H. ER stress and diseases. *FEBS J.* **2007**, *274*, 630−658.

strain culture; yeast encapsulation requires special technology that can be difficult to use; and the flocculation yeast must be recycled, resulting in high power consumption and a complex process. *A. nidulans* does not have the ability to convert xylose into ethanol, and its ethanol productivity is lower than that of *S. cerevisiae* with regard to glucose utilization.[19] Hence, microbial and in situ detoxification technology should be further investigated as an inexpensive and convenient alternative.

A modified method is proposed in this study. Rice straw was first pretreated by SE or BSE, and then the exploded rice straw was immediately fermented without the separate detoxification procedure. The proposed technology includes detoxification, saccharification, and fermentation as a single step, and the exploded material is gradually added into the fermented mash to overcome the inhibitors, which has not been previously performed. After optimizing the simultaneous saccharification and cofermentation (SSCF) of detoxified material, the SSCF of non-detoxified material was investigated to determine the possibility of omitting the advance detoxification and strain pre-adaptation steps. A 10 L fermenter was employed because of its larger scale, better accuracy, and practical application.

MATERIALS AND METHODS

Materials. Dried rice straw was obtained from a rural area (Meisan, Sichuan, China). The dried rice straw was sheared into 2 mm long straw pieces that were stored at room temperature and used as feedstock for the explosions. The compositions of the rice straw, the SE rice straw, and the BSE rice straw are listed in Table 1.

Table 1. Compositions of the Different Rice Straws (%, w/w)[a]

component	rice straw	SE[b] rice straw	BSE[c] rice straw
crude protein	4.7 ± 0.3	1.8 ± 0.2	3.2 ± 0.3
crude fat	1.4 ± 0.3	0.8 ± 0.4	1.1 ± 0.3
ash	18.1 ± 0.5	19.3 ± 0.5	18.8 ± 0.6
moisture content (% total)	9.8 ± 0.4	21.3 ± 0.6	47.8 ± 1.4
lignin	19.3 ± 0.5	17.2 ± 0.3	18.5 ± 0.5
starch	4.9 ± 0.4	0.6 ± 0.3	1.9 ± 0.3
hemicellulose	21.9 ± 0.5	14.8 ± 0.6	17.7 ± 0.6
cellulose	33.6 ± 0.8	34.7 ± 0.9	36.2 ± 0.7
glucose[d]	36.6 ± 0.6	31.4 ± 0.5	34.6 ± 0.8
xylose[d]	24.1 ± 0.4	18.7 ± 0.3	21.3 ± 0.4
total sugar[d]	67.3 ± 1.1	55.1 ± 1.2	61.8 ± 1.0

[a]All values are reported as a % dry basis except when otherwise noted. [b]SE, steam explosion. [c]BSE, butanone solution explosion. [d]The glucose, xylose, and total sugar contents were determined from the material hydrolysate, which was prepared using concentrated acid hydrolysis, as recommended by the National Renewable Energy Laboratory of Biomass Analysis Technology (NREL BAT).

The enzyme activities per milligram of protein of cellulase, xylanase, and β-glucosidase, purchased from commercial corporations (Sigma products agented by Gensheng Biology Technology Co. Ltd., Shang Hai, China), were 2.76 filter paper activity units (FPU), 45 units units of xylanase activity, and 0.55 cellobiose units (CBU), respectively. The filter paper activity and β-glucosidase activity were determined according to standard International Union of Pure and Applied Chemistry (IUPAC) procedures.[20] One FPU is defined as the amount of enzyme able to release 1 μmol of glucose equivalents from Whatman no. 1 filter paper per minute. One CBU in international units (IU) is defined as the amount of enzyme that converts 1 μmol of cellobiose to 2 μmol of glucose per minute. Xylanase activity was assayed by using Chinese standard GB/T23874-2009. One unit (1 U) of xylanase activity is defined as the enzymatic loading that releases 1 μmol of reducing sugar from a 5 mg/mL xylan solution per minute at 37 °C and pH 5.5. The total protein was measured using a Bio-Rad Protein Assay, and bovine serum albumin was used as the standard.

Butanone, $(NH_4)_2SO_4$, and H_2SO_4 were analytically pure.

Explosion and Detoxification. The conditions of the BSE were as follows:[4] butanone concentration, 0.9 mol/L; explosive pressure, 3.1 MPa (170 °C); residence time, 7 min; and rice straw dry matter-to-water ratio, 1:3 (w/w). Following the explosion, the feedstock was stored in the explosion machine for 2 h, using the residual heat to evaporate the butanone. The conditions for the SE were as follows: pressure, 3.7 MPa (245 °C); residence time, 3 min; and water content of the rice straw, 5.5% (w/w, as will be used throughout this paper). The exploded rice straws were stored and used as feedstocks for in situ detoxification and SSCF.

To produce the detoxified feedstocks for SSCF comparison, the SE rice straw was detoxified by washing until the 65 °C deionized water was colorless,[5] and the BSE rice straw was detoxified by drying at 90 °C for 8 h.[4] The water contents of the detoxified feedstocks were 73.4 ± 2.4% after washing and 18.6 ± 0.6% after drying.

Optimized SSCF Technology of Detoxified Feedstocks. On the basis of a previous study,[21] we set up an optimized SSCF technology for the detoxified feedstocks using the following procedures. The detoxified BSE rice straw (860 g) or 2500 g of detoxified SE rice straw was mixed with a 0.05 mol/L citrate buffer solution, and the resulting dry matter content was adjusted to 10% in a 10 L ventilated fermenter (model SFY-C-10L, Zhengjiang Jianggong Bioengineering Equipment Co., Ltd., China). After the pH of the mixture was adjusted to 5.0 with 0.1 mol/L H_2SO_4 followed by sterilization at 100 °C for 35 min, the slurry was cooled to 50 °C, and the mixed enzymes were added, using cellulase of 12 FPU/g dry matter, β-glucosidase of 5 IU/g dry matter, and xylanase of 10 U/g dry matter. The mixture was maintained at 50 °C and 180 rpm for 25 h (BSE rice straw) or 27 h (SE rice straw), and then the first *S. cerevisiae* fermentation of the SSCF was initiated at 37 °C by transferring 8% inoculum into the culture. The fermentation was performed at 37 °C for 34 h. The temperature of the fermented mash was subsequently adjusted to 35 °C,[22] and the *C. shehatae* starter was then inoculated into the fermented mash at an inoculum concentration of 8%. The second or mixed fermentation was performed at 35 °C and 0.3 L/(min·L) of air volume for 144 h (BSE rice straw) or for 147 h (SE rice straw).

Studying the SSCF Technology of the Non-detoxified Feedstocks. The SSCF of the non-detoxified feedstocks was designed and investigated according to the amounts of materials used in the previously optimized SSCF. The water contents differed between the non-detoxified materials (Table 1) and the detoxified materials. Therefore, to maintain the same level of total dry matter as in the fermentation of the detoxified feedstocks, 1341 g of non-detoxified BSE rice straw or 845 g of non-detoxified SE rice straw was used as the total amount. Part of the exploded rice straw, $(NH_4)_2SO_4$, and citrate buffer solution (containing all of the water and part of the citrate from the 0.05 mol/L citrate buffer solution used in the optimized SSCF of the detoxified feedstocks) were blended into the 10 L ventilated fermenter. The pH of the mixed slurry was adjusted to 5.0 by adding 0.1 mol/L H_2SO_4. After the mixed slurries were sterilized at 100 °C for 35 min and then cooled to 35 °C, all three enzymes and all of the *S. cerevisiae* and *C. shehatae* starters were added to the slurries (the amounts were the same as those used in the detoxified feedstock fermentation). The mixed fermentation was performed at 35 °C and 0.3 L/(min·L) of air volume, as in the optimized SSCF of detoxified feedstocks. An added feedstock was then gradually introduced into the mash. Here, the rest of the non-detoxified and exploded rice straw, 0.1 mol/L H_2SO_4, citrate (based on the optimized SSCF technology), and $(NH_4)_2SO_4$ were blended and used as the added feedstocks, which was sterilized at 100 °C for 35 min. After the feedstock increase was complete, the fermentation time was determined as the point at which the ethanol concentration ceased to increase, as measured at 4 h intervals.

A solid material feeder constructed by our laboratory was used to add the feedstocks from 0 to 200 mg/min, on the basis of the amount

of exploded rice straw. The amounts of citrate and 0.1 mol/L H_2SO_4 were divided into two parts with an initial dosage and an added dosage in the same proportion to the dry matter amount of exploded rice straw as in the optimized SSCF of the detoxified materials. Therefore, after the addition of feedstock was finished, the dry matter content of the exploded rice straws, the citrate concentration, the enzyme loadings, and the H_2SO_4 concentration were purposefully maintained at the same level as the optimized SSCF of detoxified materials, except that $(NH_4)_2SO_4$ was added in the proportion to the dry matter amount of exploded rice straw, too.

This in situ detoxification and SSCF were divided into three stages, including the adaptation time from inoculation to the beginning of feedstock addition, the addition time of feedstocks from beginning to end, and the secondary fermentation time from the end of the feedstock addition to the end of the fermentation. On the basis of the SSCF parameters of the detoxified material, an additional five factors must still be explored, including the initial dry matter content, the yeast adaptation time, the required amount of additional $(NH_4)_2SO_4$, the addition time (or addition rate), and the secondary fermentation time.

Starter Preparation. *C. shehatae* (No. 1967) from the China Center of Industrial Culture Collection (CICC) was prepared in four stages. The activation medium was composed of 3 g/L yeast extract, 3 g/L malt extract, 5 g/L peptone, and 15 g/L xylose, and deionized water was added to reach a final volume of 1000 mL. After the activation medium had been sterilized at 125 °C for 25 min, ethanol was added at 15 g/L, and the medium was then inoculated with *C. shehatae*. The activation culture was incubated in a 250 mL shake flask at 25 °C and 160 rpm for 48 h. This procedure was repeated four times, and the temperature of the subsequent stages was raised by 2 °C at each stage. An inoculum concentration of 10% (w/w) was used, and the incubations were set at 160 rpm for 96 h at each stage. The culture from the fourth stage was reserved as the starter for xylose fermentations.

S. cerevisiae was obtained from Sichuan Swellfun Co., Ltd. (Chendu, Sichuan, China). Liquid potato medium was prepared for the yeast as follows. Peeled and crushed potatoes (200 g) were added to 1000 mL of tap water. After boiling for 30 min, the mixture was filtered, and tap water was added to the filtrate to a final volume of 1000 mL. After sterilization of the activation medium at 125 °C for 25 min, it was inoculated with the yeast at a concentration of 10%. The activated culture was subsequently prepared using the four-stage method outlined above. In accordance with the four-stage process, the first-stage culture temperature was 26 °C, and the temperature was raised by 2 °C at each subsequent stage. The inoculum concentration and culture time for each stage were 8% and 72 h, respectively. The culture from the fourth stage was reserved as the starter for the glucose fermentations.

Analysis Methods. The starch, crude protein, crude fat, crude ash, and moisture contents were determined according to Chinese standards GB/T 20194-2006, GB/T 6432-1994, GB/T 6433-2006, GB/T 6438-2007, and GB/T 6435-2006, respectively. The glucose, xylose, and total sugar contents were determined from material hydrolysates. To hydrolyze the cellulose, the hydrolysate was prepared by concentrated acid hydrolysis at room temperature followed by dilute acid hydrolysis at 121 °C, as recommended by the National Renewable Energy Laboratory Biomass Analysis Technology (NREL BAT).[23] The glucose, xylose, and total sugar contents of the hydrolysate were determined using a Glucose Assay Kit II (Biovision), a D-Xylose Assay Kit (Megazyme), and a 3,5-dinitrosalicylic acid (DNS) method,[20] respectively. The cellulose, hemicellulose, and lignin contents were determined using the NREL method.[23] The lignin contained acid-soluble and acid-insoluble lignin and lignin ash.

Fermented mash (20 mL) was centrifuged at 5000 rpm for 10 min, and the supernatant was used to determine the sugar contents as described above.

The ethanol and butanone concentrations were determined by gas chromatography (GC) analysis. Fermented mash (1.5 mL) was centrifuged at 13000 rpm for 10 min, and the supernatant was analyzed using a GC model GC7890 equipped with an AE. An SE-54 column (15 m × 0.25 m × 0.33 μm, Lanzhou Atech Technologies Co., Ltd., Lanzhou, China) was used. The analysis conditions were as follows: column temperature, 145 °C; detector temperature, 260 °C; sample injection temperature, 240 °C; measuring range, 10; attenuation, 0; and sample volume, 1 μL.

The furfural, 5-HMF, and acetic acid contents were determined by high-performance liquid chromatography (HPLC). The exploded slurries (1 mL) were centrifuged at 13000 rpm for 10 min; the residual solid matter was washed with deionized water at 65 °C until the wash water was colorless; and then the wash water and the supernatant were mixed for HPLC analysis. The fermented mash (15 mL) was filtered prior to HPLC analysis. A model LC-10AT HPLC equipped with an SPD-$10A_{vp}$ visible−ultraviolet detector, a Synergi Hydro RP column (4 μm, 4.6 × 250 mm, FLM Inc., Guangzhou, China), and an SCL-$10A_{vp}$ analysis system was used. The analysis conditions were as follows: reactor temperature, 50 °C; column temperature, 60 °C; detected wavelength, 250 nm; mobile phase, 0.005 M H_2SO_4; velocity, 1.2 mL/min; and sample volume, 10 μL.

Data Processing. The ethanol yield was based on the rice straw dry matter, as calculated using the following equation.

$$\text{ethanol yield (g/100 g rice straw dry matter)} = [(\text{ethanol (g) produced from SSCF})/\text{rice straw dry matter (g)}] \times 100$$

Triplicate samples were used for all analytical determinations, and the data were presented as the means of the three replicates. Differences between the samples and orthogonal tests were statistically analyzed by SPSS software (version 19). Design expert software (version 8.0.5.0) was used for the central composite design (CCD) and response surface methodology (RSM) experiments.

RESULTS

SSCF of Detoxified and Exploded Rice Straw. The BSE rice straw was dried for detoxification and then used for SSCF. The SSCF parameters were optimized using the Plackett−Burman (PB) method, the steepest ascent method, CCD, and RSM. Some of the changes introduced over the course of fermentation are shown in Figure 1. The whole SSCF was divided into three stages as follows: enzymatic hydrolysis (EH),

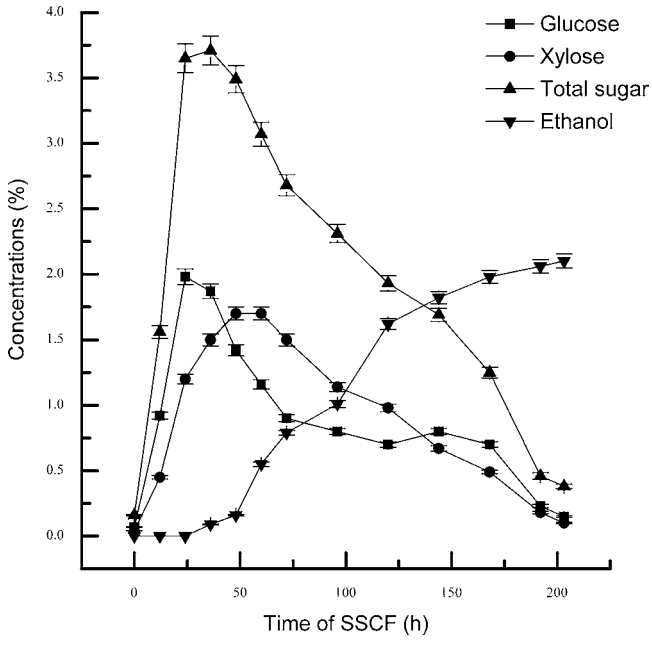

Figure 1. Substance changes over the course of SSCF for the detoxified rice straw exploded by 0.9 mol/L butanone solution.

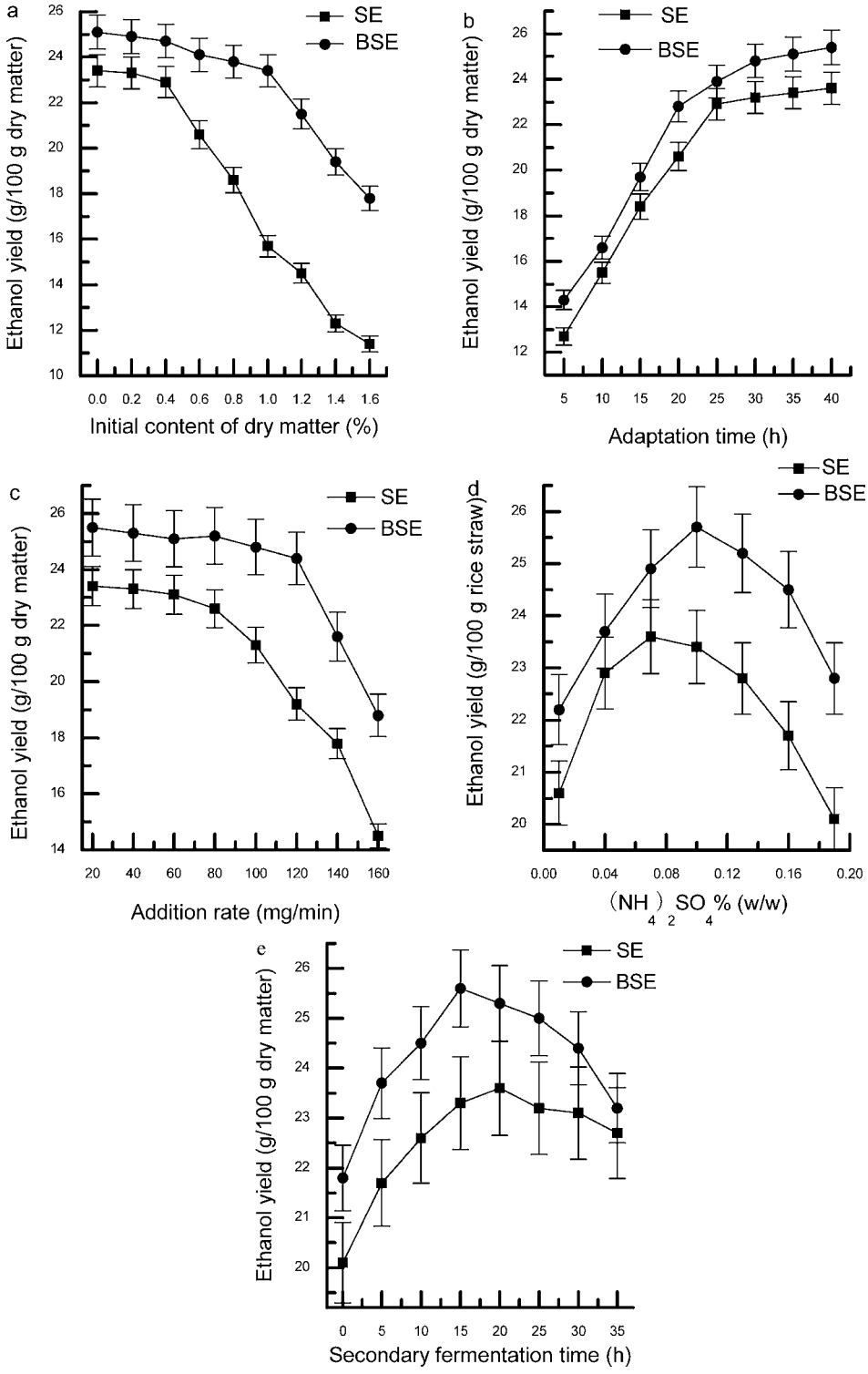

Figure 2. Key factor effects on the ethanol yield of in situ detoxification and SSCF. The two lines in panel a were drawn using the following conditions: adaptation time, 25 h; addition rate, 80 mg/min for SE rice straw and 100 mg/min for BSE rice straw; $(NH_4)_2SO_4$%, 0.1%; and secondary fermentation time, 20 h. The lines in panel b were drawn using the following conditions: initial content, 0.4% for SE rice straw and 0.8% for BSE rice straw; addition rate, 80 mg/min for SE rice straw and 100 mg/min for BSE rice straw; $(NH_4)_2SO_4$%, 0.1%; and secondary fermentation time, 20 h. In panel c, the addition rate was expressed using the amount of exploded rice straw. The lines in panel c were drawn using the following conditions: initial content, 0.4% for SE rice straw and 0.8% for BSE rice straw; adaptation time, 25 h; $(NH_4)_2SO_4$%, 0.1%; and secondary fermentation time, 20 h. In panel d, the $(NH_4)_2SO_4$ dose was expressed as $(NH_4)_2SO_4$% (w/w) = [(total amount of $(NH_4)_2SO_4$) (g)]/[(total amount of fermented mash) (g)] × 100%. Here, the total amount of fermented mash was referred to as the total of all matter introduced into the fermentation. The lines in panel d were drawn using the following conditions: initial content, 0.4% for SE rice straw and 0.8% for BSE rice straw; adaptation time, 25 h; addition rate, 80 mg/min for SE rice straw and 100 mg/min for BSE rice straw; and secondary fermentation time, 20 h. The lines in panel e were drawn using the following conditions: initial content, 0.4% for SE rice straw and 0.8% for BSE rice straw; adaptation time, 25 h; addition rate, 80 mg/min for SE rice straw and 100 mg/min for BSE rice straw; and $(NH_4)_2SO_4$%, 0.1%.

dx.doi.org/10.1021/jf501703j | J. Agric. Food Chem. 2014, 62, 7486−7495

first fermentation (*S. cerevisiae* fermentation), and second fermentation (mixed yeast fermentation). According to the optimized result (Figure 1), the total SSCF time was 203 h. The sugars and ethanol were estimated at 12 h intervals during the initial 72 h and at 24 h intervals after 72 h.

The glucose and total sugar concentrations increased with time from 0 to 36 h and then decreased after 36 h ($P < 0.05$). The xylose concentration simultaneously increased with time from 0 to 60 h and then decreased after 60 h ($P < 0.05$). After the *C. shehatae* was inoculated into the fermented mash at 59 h, the xylose concentration decreased. The ethanol concentration increased from 0 to 2.63% with increasing time ($P < 0.05$). The solid residue of the fermented mash was analyzed to determine the glucose, xylose, and total sugar contents using the rice straw analysis method. The results showed that after the SSCF, the glucose, xylose, and total sugar in the rice straw could be used at 91.4 ± 2.3, 84.7 ± 1.9, and 87.3 ± 2.5%, respectively, and the ethanol yield was 26.2 ± 0.8 g/100 g rice straw dry matter.

The SSCF course of the detoxified SE rice straw was similar to the course shown in Figure 1, but the sugar and ethanol yields were lower than the yields of the BSE ($P < 0.05$). Because the SE condition was harsher than the BSE condition, the sugar loss was greater with SE, as shown in Table 1. When SE rice straw was used as feedstock, the glucose, xylose, and total sugar in the rice straw dry matter could be used at 83.0 ± 2.1, 73.4 ± 1.3, and 79.1 ± 2.7%, respectively, and the ethanol yield was 23.7 ± 0.6 g/100 g rice straw dry matter after a total fermentation time of 208 h.

Factor Effects on in Situ Detoxification and SSCF. The impacts of five factors on ethanol yield for the non-detoxified materials are shown in Figure 2.

The ethanol yields decreased with increasing initial dry matter contents (Figure 2a). The dry matter content increased from 0 to 1.6%, whereas the ethanol yield of the SE rice straw significantly decreased from 23.4 to 11.4 g/100 g dry matter ($P < 0.05$) and the ethanol yield of the BSE rice straw significantly decreased from 25.1 to 17.8 g/100 g dry matter ($P < 0.05$). According to the analysis of variance, 0.4 and 1.0% of the dry matter contents were inflection points for SE rice straw and BSE rice straw ($P < 0.05$), respectively. The various inhibitor amounts continued to increase with increasing dry matter contents. However, the yeasts exhibited some ability to resist the inhibitors only if the inhibitor concentration was less than a specific value, as confirmed by the existence of the inflection points. There were different inflection points between SE rice straw and BSE rice straw, which could be explained by the fact that the amounts of inhibitors were different in the two types of exploded rice straw. A lower dry matter content might provide a high ethanol yield, but the lower the dry matter content, the longer the fermentation time. Therefore, 0.4 and 1.0% dry matter contents were selected as the center levels for the next orthogonal tests.

In Figure 2b, the ethanol yield increased from 12.7 to 23.6 g/100 g dry matter with an increase in the adaptation time from 5 to 40 h for SE feedstock ($P < 0.05$), and the ethanol yield increased from 14.3 to 25.4 g/100 g dry matter with an increased adaptation time from 5 to 40 h for BSE feedstock ($P < 0.05$). At an adaptation time of 25 h, the ethanol yields were 22.8 and 23.9 g/100 g dry matter for SE rice straw and BSE rice straw, respectively. The 25 h of adaptation time might have served as the inflection points for the two types of exploded rice straws. Although the initial dry matter content was lower than in the traditional method, the yeasts still needed time to adapt to the environment. An adaptation time of >25 h might be beneficial for the ethanol yield at the cost of delaying the total fermentation time, but the increased ethanol yield was insignificant ($P > 0.05$). However, the inflection points exhibited no great difference between the two types of exploded rice straw, which demonstrated the stability of the yeasts with respect to the different explosion pretreatments. If the adaptation time was not sufficient, the additional feedstock could seriously damage the yeasts and reduce the ethanol yield.

The ethanol yields of the two exploded rice straws decreased with increasing addition rate (Figure 2c) ($P < 0.05$). At addition rates of 80 and 120 g/min, the ethanol yields were 22.6 and 24.4 g/100 g dry matter for SE rice straw and for BSE rice straw, respectively, and the two points could be used as inflection points in the analysis. The ethanol yields of the two feedstocks could be maintained at a high level until the addition rate was increased to a specific level, which illustrated that an excessively fast addition rate resulted in yeast inhibition. The gradual feedstock increase differs from traditional fed-batch technology because the traditional method generally employed an added substrate and the feedstock content of the substrate was not greatly different from that of fermented mash. However, because of the technical feature of the added feedstock, this in situ and SSCF technology may be suitable for an exploded material and not for an acid-pretreated material. As shown in Figure 2c, a lower addition rate might lead to a high-level ethanol yield, but the total fermentation time could be greatly delayed. Therefore, 80 and 120 g/min addition times were selected as the center levels for the orthogonal tests.

An additional N source was not necessary in the SSCF of the detoxified and exploded rice straws because the added $(NH_4)_2SO_4$ did not greatly increase the ethanol yield in a previous study ($P > 0.05$). An excessive N source could result in cell growth with the consumption of fermentable sugars. However, as shown in Figure 2d, the ethanol yields peaked only when $(NH_4)_2SO_4$ was added to the fermented mash at a specific concentration ($P < 0.05$). At $(NH_4)_2SO_4$ addition values of 0.07 and 0.1%, the ethanol yield peaks were 23.4 and 25.7 g/100 g dry matter for SE rice straw and BSE rice straw, respectively. Using the same type of exploded rice straw as feedstock, the ethanol yield peaks obtained from SSCF exhibited no significant difference between the detoxified feedstock and non-detoxified feedstock ($P > 0.05$). It can be concluded that the additional N source can be used to grow the cells without exhausting the fermentable sugars. Too little N may weaken the yeasts' ability to digest the inhibitors, and too much N may cause more sugars to be consumed during cell growth. Therefore, the 0.07 and 0.1% $(NH_4)_2SO_4$ doses were selected as the center levels for the next orthogonal tests.

As shown in Figure 2e, the yeasts needed a period of time after the feedstock addition to ferment before the ethanol yield began decreasing (BSE rice straw) ($P < 0.05$) or was maintained at a higher level without an obvious decrease (SE rice straw) ($P < 0.05$). Therefore, fermentable sugars could still be released from the feedstocks, and the saccharification process was not finished, although the feedstock addition procedure was finished. The 15−20 h of secondary fermentation time was acceptable and suitable for the two types of feedstocks ($P < 0.05$).

Optimized Technology of in Situ Detoxification and SSCF. The five factors, with three levels for each factor, and the results of the orthogonal tests are listed in Table 2.

Table 2. Results of the Orthogonal Test for BSE and SE Rice Straws[a]

no.	*A*, initial dry matter content (%)	*B*, adaptation time (h)	*C*, addition rate (mg/min)	*D*, $(NH_4)_2SO_4$ addition amount (%)	*E*, secondary fermentation time (h)	ethanol yield (g/100 g dry matter)
1	0.4 (1.0)[b]	25 (25)	80 (120)	0.07 (0.10)	13 (13)	23.1 ± 0.7 (25.3 ± 0.8)
2	0.4 (1.0)	20 (20)	100 (140)	0.05 (0.08)	23 (23)	19.7 ± 0.4 (23.5 ± 0.6)
3	0.2 (0.8)	25 (25)	100 (140)	0.05 (0.08)	18 (18)	20.6 ± 0.6 (24.1 ± 0.5)
4	0.6 (1.2)	30 (30)	100 (140)	0.09 (0.12)	13 (13)	19.5 ± 0.5 (22.9 ± 0.7)
5	0.2 (0.8)	20 (20)	60 (100)	0.05 (0.08)	13 (13)	19.4 ± 0.6 (23.1 ± 0.8)
6	0.2 (0.8)	20 (20)	80 (120)	0.09 (0.12)	13 (13)	19.1 ± 0.3 (22.3 ± 0.6)
7	0.6 (1.2)	20 (20)	80 (120)	0.05 (0.08)	23 (23)	19.5 ± 0.5 (22.6 ± 0.7)
8	0.2 (0.8)	30 (30)	60 (100)	0.07 (0.10)	23 (23)	23.5 ± 0.8 (25.9 ± 0.9)
9	0.2 (0.8)	30 (30)	80 (120)	0.05 (0.08)	18 (18)	23.0 ± 0.4 (24.6 ± 0.7)
10	0.4 (1.0)	30 (30)	60 (100)	0.05 (0.08)	13 (13)	20.3 ± 0.3 (23.8 ± 0.5)
11	0.6 (1.2)	20 (20)	60 (100)	0.07 (0.10)	18 (18)	22.4 ± 0.5 (24.5 ± 0.4)
12	0.4 (1.0)	20 (20)	60 (100)	0.09 (0.12)	18 (18)	21.8 ± 0.3 (23.7 ± 0.6)
13	0.2 (0.8)	20 (20)	100 (140)	0.07 (0.10)	13 (13)	20.7 ± 0.5 (22.5 ± 0.7)
14	0.6 (1.2)	25 (25)	60 (100)	0.05 (0.08)	13 (13)	19.8 ± 0.4 (22.0 ± 0.7)
15	0.2 (0.8)	20 (20)	60 (100)	0.05 (0.08)	13 (13)	19.6 ± 0.3 (22.8 ± 0.5)
16	0.2 (0.8)	25 (25)	60 (100)	0.09 (0.12)	23 (23)	20.3 ± 0.6 (23.4 ± 0.8)
k_1[c]	21.271 (23.946)	20.604 (23.329)	21.421 (24.029)	20.554 (23.579)	20.488 (23.279)	
k_2	21.721 (24.433)	21.279 (23.904)	21.708 (24.079)	22.742 (24.817)	22.250 (24.417)	
k_3	20.796 (23.358)	21.904 (24.504)	20.658 (23.629)	20.492 (23.342)	21.050 (24.042)	
signif	0.168 (0.173)	0.034 (0.087)	0.103 (0.595)	0.003 (0.049)	0.011 (0.083)	

[a]SE, steam explosion; BSE, butanone solution explosion. [b]Values in parentheses are the values for butanone solution-exploded rice straw, and values outside parentheses are the values for steam-exploded rice straw. [c]k_1, k_2, and k_3 are the mean levels for the factors.

By employing SE rice straw as feedstock, the optimum result was $A_2B_3C_2D_2E_2$ according to the mean levels of k_1, k_2, and k_3; that is, the highest ethanol yield could be obtained when the SSCF conditions were set at an initial dry matter content of 0.4%, an adaptation time of 30 h, an addition rate of 80 mg/min, an $(NH_4)_2SO_4$ addition amount of 0.07%, and a secondary fermentation time of 18 h. From a variance analysis of the orthogonal test, the marked order of the factors was *D* (addition amount of $(NH_4)_2SO_4$, %) > *E* (secondary fermentation time, h) > *B* (adaptation time, h) > *C* (addition rate, mg/min) > *A* (initial dry matter content, %). Among these factors, *B*, *D*, and *E* were significant ($P < 0.05$), whereas *C* and *A* were not significant ($P > 0.05$).

Using BSE rice straw as feedstock, the optimum result was also $A_2B_3C_2D_2E_2$; that is, the highest ethanol level was obtained when the SSCF conditions were set at an initial dry matter content of 1.0%, an adaptation time of 30 h, an addition rate of 120 mg/min, an $(NH_4)_2SO_4$ addition amount of 0.1%, and a secondary fermentation time of 18 h. However, the marked order of the factors was *D* (addition amount of $(NH_4)_2SO_4$, %) > *E* (secondary fermentation time, h) > *B* (adaptation time, h) > *A* (initial dry matter content, %) > *C* (addition rate, mg/min), which had a slight difference in the placement of *A* and *C* when compared with the order for SE rice straw. Furthermore, *D* was the only significant factor ($P < 0.05$), and the others were not significant ($P > 0.05$). Hence, these differences indicated that the SSCF of the SE rice straw was more easily influenced by changes in parameters than that of the BSE rice straw.

These optimized parameters were used for confirmation, and the resulting ethanol yields were 23.3 ± 0.7 and 25.8 ± 0.6 g/100 g dry matter for SE rice straw and BSE rice straw, respectively. In comparison with the SSCF of the detoxified feedstocks, the ethanol yields were not significantly different from the feedstocks that were exploded by the same method ($P > 0.05$). Therefore, in situ detoxification and SSCF are effective.

According to the in situ detoxification and SSCF experiment, the total fermentation time was 224 h for SE rice straw and 234 h for BSE rice straw. In comparison with the SSCF of detoxified feedstocks, the fermentation time was delayed by approximately 31 h for BSE rice straw and by 16 h for SE straw. $(NH_4)_2SO_4$ was used at 0.10% for BSE rice straw and at 0.07% for SE rice straw, and a fermentation temperature of 35 °C and an air volume of 0.3 L/(min·L) were maintained from start to finish. The other loadings, including the feedstock, enzymes, H_2SO_4, and citrate, were used at the same levels as the SSCF of detoxified feedstocks.

Substance Changes during the Course of the in Situ Detoxification and SSCF. The changes in several inhibitors in the fermented mash are shown in Figure 3. The concentrations of furfural, 5-HMF, and acetic acid significantly increased as fermentation time increased ($P < 0.05$) regardless of whether the feedstock was SE rice straw or BSE rice straw, except during the initial 30 h and the secondary fermentation time ($P > 0.05$). After fermentation, the furfural, 5-HMF, and acetic acid concentrations were 197, 136, and 330 ppm (w/w in all cases) for SE rice straw, respectively. However, if all of the non-detoxified feedstocks were immediately introduced for fermentation, the initial inhibitor concentrations would be 1615 ppm of furfural, 803 ppm of 5-HMF, and 2651 ppm of acetic acid. Therefore, most of the inhibitors were removed by the fermented mash through the gradual increase in feedstock.

For the BSE rice straw, the furfural, 5-HMF, and acetic acid concentrations were 204, 152, and 312 ppm, respectively, after the completion of the fermentation. If all of the non-detoxified feedstock was immediately introduced, the initial inhibitor concentrations would be 503 ppm of furfural, 378 ppm of 5-HMF, and 1122 ppm of acetic acid, respectively. Decreases also occurred. The BSE rice straw contained more butanone than the SE rice straw because of the additional butanone in the explosion. Although the butanone content was reduced by drying with the residual heat of explosion, the content still

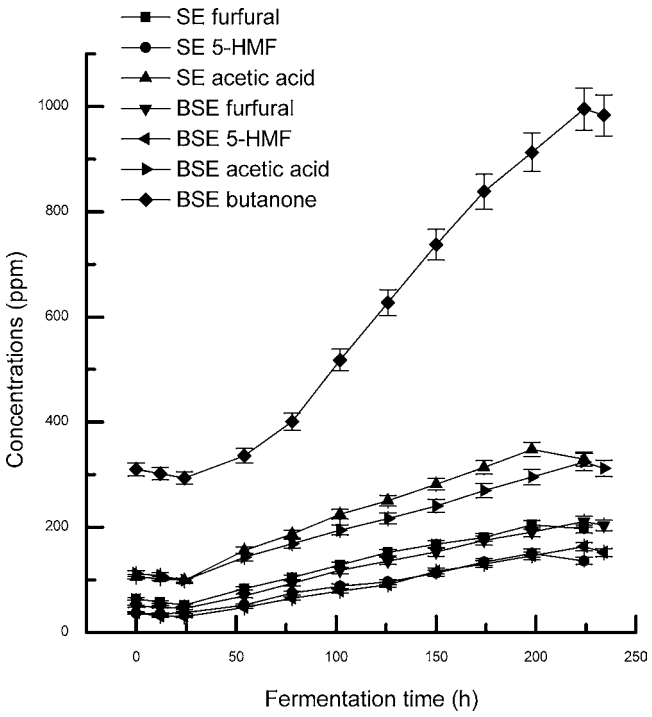

Figure 3. Concentration changes of certain inhibitors during in situ detoxification and SSCF. The parts per million of the vertical axis units is expressed as the mass ratio.

reached 3.1 ± 0.1% in the exploded rice straw. Approximately two-thirds of the butanone was removed during the in situ detoxification and SSCF.

Over the course of the fermentation, three types of sugar and ethanol concentration changes occurred, as shown in Figure 4. The ethanol concentrations significantly increased with increasing fermentation time ($P < 0.05$), and the maximum concentration was obtained at 2.55 ± 0.06%. This maximum ethanol concentration was slightly lower than in the detoxified feedstock SSCF, but the difference was not statistically significant ($P > 0.05$). Sugar changes were different between Figures 1 and 4. First, the highest sugar concentrations were significantly lower in Figure 4 ($P < 0.05$). The enzyme loadings were high enough that the feedstock could be quickly degraded into sugars, and then the sugars could be immediately used by the yeasts without great accumulation. Second, the highest sugar concentrations appeared during late fermentation (Figure 4) rather than during early fermentation (Figure 1). These differences can be attributed to the technical features of the gradual increase in feedstock. However, one of the same points regarding the sugars between Figures 1 and 4 was the change in the increasing trend and then the decline ($P < 0.05$). In addition, the three types of sugar and ethanol concentration changes for SE rice straw were similar to the ones in Figure 4 and are not shown.

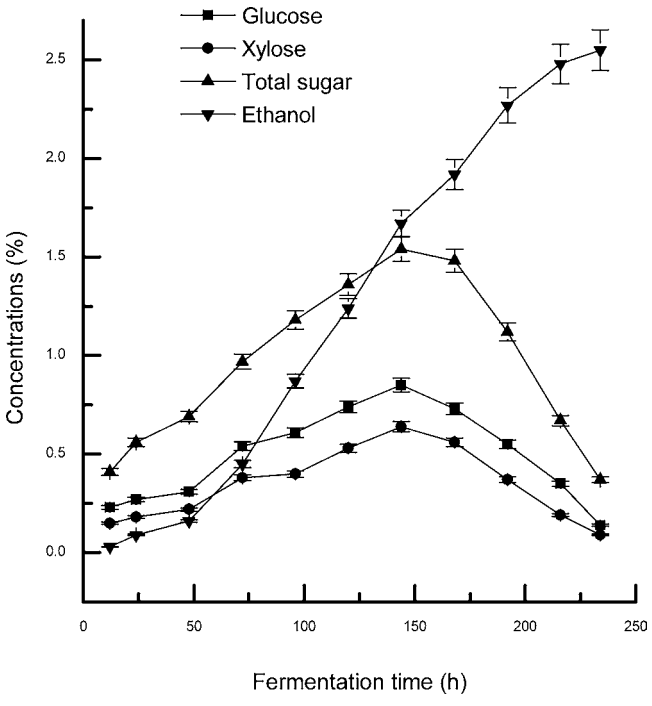

Figure 4. Substance changes during the in situ detoxification and SSCF for BSE rice straw.

DISCUSSION

The Current State of the SSCF for Bioethanol Production. Because *S. cerevisiae* normally lacks the ability to produce ethanol by fermenting the xylose obtained from hemicellulose,[24,25] there are extensive studies underway to develop yeasts that can produce high bioethanol yields from xylose. To this end, genetic improvement strategies have been based on the metabolism of wild yeasts, such as *S. cerevisiae*[26] or *C. shehatae*,[27] and a coculture process, such as a coculture of *Zymomonas mobilis* and *P. stipitis*[28] or of *S. cerevisiae* and *P. stipitis*,[29] has also been reported as an effective way to ferment both glucose and xylose. However, the recombinant yeasts are still far from industrial use because of the defective stability of the strains and because the coculture methods always exclude saccharification and detoxification; thus, saccharification and detoxification must be performed before fermentation. To overcome the mutual inhibition between strains in mixed fermentation, some co-immobilized fermentation methods were examined with *S. cerevisiae* and *C. shehatae*.[30,31] However, the methods did not obviously improve xylose utilization and were difficult to apply.

In addition, previous studies of certain single factors, such as temperature control,[32] dissolved oxygen,[33] feedstock concentration,[34] and the mixed enzymes system,[35] have provided a basis for this study, although the reported technologies are completely different from the in situ detoxification and SSCF technology. The literature[3,4] has recently reported a SSCF technology. However, its details were unclear, and the parameters were not optimized. More importantly, the reported SSCF was not an in situ detoxification technology because it required a pre-detoxification procedure and strain pre-adaptation for subsequent fermentation, resulting in higher cost and more complex procedures. Therefore, the combination of biodetoxification and SSCF is rarely observed and must be further explored.

Technical Characterisations of the SSCF for Detoxified and Non-detoxified Feedstocks. As shown in Figure 1, the highest concentrations of glucose and ethanol were below 1.98 and 2.63%, respectively, which should not inhibit *C. shehatae* from converting xylose into ethanol.[33,36] In addition, although an aerobic fermentation condition was beneficial for *C. shehatae*,[33] *S. cerevisiae* could still compete with *C. shehatae* to obtain glucose for producing ethanol under a micro-oxygenated

condition.[37,38] Therefore, this condition should support a higher ethanol yield. Glucose and xylose could be simultaneously fermented by *C. shehatae*[39] if the glucose and ethanol concentrations of the fermented mash were limited to below a specific level.[40,41] However, the theoretical ethanol productivity of *C. shehatae* is lower than the theoretical productivity of *S. cerevisiae*[42] if an equal number of glucose molecules were consumed by each strain. Therefore, the SSCF of detoxified feedstock could be completed as follows. *S. cerevisiae* was first inoculated into the hydrolysate to ferment glucose into ethanol, and most of the glucose was used by *S. cerevisiae*. However, with the accumulation of xylose released from the feedstocks, *C. shehatae* was required because of xylose's inhibition of enzymes.[43,44] Afterward, cofermentation was conducted through the competition of *S. cerevisiae* and *C. shehatae*. Because of the low glucose concentration, the glucose could not inhibit *C. shehatae* from converting xylose into ethanol and *S. cerevisiae* could ferment glucose into ethanol. Hence, some key points of the detoxified feedstock SSCF are as follows: limitations in dissolved oxygen and the N source, lower concentrations of glucose and xylose, and separate glucose and xylose fermentation for different strains as much as possible.

The SSCF of non-detoxified materials have some of the same features as the detoxified feedstocks of SSCF, for example, dissolved oxygen limitations under a micro-oxygenated condition, low glucose and xylose concentrations, and separate glucose and xylose fermentation for different strains as much as possible. However, the technology has certain intrinsic features attributable to the added detoxification within the process.

The decreases in these inhibitors (Figure 3) may be primarily attributed to the role of the micro-organisms. For example, furfural and 5-HMF were consumed by *S. cerevisiae*,[10] and this yeast was able to use phenolic and furan compounds.[45] When the acetic acid concentration was below a limited level, *S. cerevisiae* could remove the acetic acid through metabolic consequences.[46] A higher butanone concentration may result in *S. cerevisiae* aneuploidy[47,48] and may confer quantitative proteome changes and phenotypic variation.[49] Therefore, these changes may reduce the butanone concentration during the fermentation process. However, because the inhibitors were controlled at a very slow addition rate, abnormal changes may not occur in all cells, and the yeasts may have time to adapt to the environment, resulting in normal cells that can employ fermentable sugars to produce ethanol. In addition, although there are few reports about how *C. shehatae* responds to the inhibitors, it could be concluded that the micro-organism can also attempt to negate the harmful effects of the environment. This finding would be confirmed by the pre-adaptation of the micro-organisms.[50,51]

Therefore, in situ detoxification and SSCF technology have the following intrinsic features. Sufficient proportions of enzymes and yeasts were employed to gradually overcome the inhibition and to maintain their advantage without overdosing or multiple additions, in contrast to traditional fermentation methods. Very low sugar concentrations and the addition of a nitrogen source impelled some of the cells to seek other carbon sources and resulted in metabolic change, but the extended fermentation time kept most cells normal by virtue of yeast self-adaptation.

Potential Applications of the in Situ Detoxification and SSCF. The ethanol yields displayed no significant difference between the detoxified materials and non-detoxified materials, indicating that the in situ detoxification and SSCF were effective in terms of the fermentation time cost and the N source but eliminated the need for a separate detoxification procedure and the pre-adaptation of strains. If all of the glucose and xylose contained in the rice straw were calculated, 86.7% of the theoretical ethanol yield for BSE rice straw could be obtained. Few studies can be compared for ethanol yields because of their different analyses, and ,thus, the calculation and methods criteria in various literature regarding acid-pretreated material greatly differ for exploded materials. This study supplies a reference for the further study of in situ detoxification and SSCF technology for converting lignocellulosic material into ethanol in scale applications. Furthermore, given an increased scale, the addition procedure will become simpler, as in the 10 L example.

AUTHOR INFORMATION

Corresponding Author

*(J.Z.) Phone: +86 831 3545069. Fax: +86 831 3545057. E-mail: zhangranjian@aliyun.com.

Funding

We are grateful to the key program of the Key Laboratory of Fermentation Resource and Application of Institutes of Higher Learning in Sichuan of Yibin University of the People's Republic of China (No. 2012KFZ002), the program of the Science and Technology Department of Sichuan Province of the People's Republic of China (No. 2014JY0028), and the project supported by Scientific Research Fund of SiChuan Provincial Education Department of the People's Republic of China (No. 14ZA0275).

Notes

The authors declare no competing financial interest.

REFERENCES

(1) Ballesteros, I.; Oliva, J. M.; Negro, M. J.; Manzanares, P.; Ballesteros, M. Enzymic hydrolysis of steam exploded herbaceous agricultural waste (*Brassica carinata*) at different particule sizes. *Process Biochem.* **2002**, *38*, 187−192.

(2) Oliva, J. M.; Sáez, F.; Ballesteros, I.; González, A.; Negro, M. J.; Manzanares, P.; Ballesteros, M. Effect of lignocellulosic degradation compounds from steam explosion pretreatment on ethanol fermentation by thermotolerant yeast *Kluyveromyces marxianus*. *Appl. Biochem. Biotechnol.* **2003**, *105*−*108*, 141−153.

(3) Zhang, J.; Zhang, W. X.; Yang, J.; Liu, Y. H.; Zhong, X.; Deng, Y. A comparison of different dilute solution explosions pretreatment for conversion of distillers' grains into ethanol. *Prep. Biochem. Biotechno.* **2013**, *l43*, 1−21.

(4) Zhang, J.; Zhang, W. X.; Yang, J.; Liu, Y. H.; Zhong, X.; Wu, Z. Y.; Kida, K.; Deng, Y. Pretreatment of rice straw using a butanone or an acetaldehyde dilute solution explosion for producing ethanol. *Appl. Biochem. Biotechnol.* **2012**, *166*, 1856−1870.

(5) Li, H. Q.; Chen, H. Z. Detoxification of steam-exploded corn straw produced by an industrial-scale reactor. *Process Biochem.* **2008**, *43*, 1447−1451.

(6) Silva, C. J.; Roberto, I. C. Statistical screening method for selection of important variables on xylitol biosynthesis from rice straw hydrolysate by *Candida guilliermon* dii FTI 20037. *Biotechnol. Technol.* **1999**, *13*, 743−747.

(7) Jönsson, L. J.; Palmqvist, E.; Nilvebrant, N. O. Detoxiatcation of wood hydrolysates with laccase and peroxidase from the white-rot fungus *Trametes versicolor*. *Appl. Microbiol. Biotechnol.* **1998**, *49*, 691−697.

(8) Okuda, N.; Soneura, M.; Ninomiya, K.; Katakura, Y.; Shioya, S. Biological detoxification of waste house wood hydrolysate using for bioethanol production. *J. Biosci. Bioeng.* **2008**, *106*, 128−133.

(9) Shiho, T.; Kevin, S.; Pedram, F.; Yonghao, N. Ethanol production via in-situ detoxification of spent sulfite liquor. *J. Bioprocess Eng. Biorefinery* **2012**, *1*, 105−112.
(10) Keating, J. D.; Panganiban, C.; Mansfield, S. D. Tolerance and adaptation of ethanologenic yeasts to lignocelulosic inhibitory compounds. *Biotechnol. Bioeng.* **2006**, *93*, 1196−l206.
(11) Gao, J.; Zhang, Y.; Ntoni, J.; Begonia, M. F. T.; Lee, K. S.; Hicks, L.; Hwang, W. W.; Hwang, H. M. Effects of selected by-products of an acid hydrolyzate on cell growth and ethanol fermentation by *Saccharomyces cerevisiae*. *J. Mississippi Acad. Sci.* **2006**, *51*, 220−230.
(12) Zhu, J. J.; Yong, Q.; Xu, Y.; Chen, S. X.; Yu, S. Y. Adaptation fermentation of *Pichia stipitis* and combination detoxification on steam exploded lignocellulosic prehydrolyzate. *Nat. Sci.* **2009**, *1*, 47−54.
(13) Palmqvist, E.; Grage, H.; Meinander, N. Q.; Hahn-Hägerdal, B. Main and interaction effects of acetic acid, furfural, and *p*-hydroxybenzoic acid on growth and ethanol productivity of yeasts. *Biotechnol. Bioeng.* **1999**, *63*, 46−55.
(14) Limtong, S.; Sumpradit, T.; Kitpreechavanich, V.; Tuntirungkij, M.; Seki, T.; Yoshida, T. Effect of acetic acid on growth and ethanol fermentation of xylose fermenting yeast and *Saccharomyces cerevisiae*. *Kasetsart J. (Nat. Sci.)* **2000**, *34*, 64−73.
(15) Chung, I. S.; Lee, Y. Y. Ethanol fermentation of crude acid hydrolyzate of cellulose using high-level yeast inocula. *Biotechnol. Bioeng.* **1985**, *27*, 308−315.
(16) Cantarella, M.; Cantarella, L.; Gallifuoco, A.; Spera, A.; Alfani, F. Comparison of different detoxification methods for steam-exploded poplar wood as a substrate for the bioproduction of ethanol in SHF and SSF. *Process Biochem.* **2004**, *39*, 1533−1542.
(17) Talebnia, F.; Taherzadeh, M. J. In situ detoxification and continuous cultivation of dilute-acid hydrolyzate to ethanol by encapsulated *S. cerevisiae*. *J. Biotechnol.* **2006**, *125*, 377−384.
(18) Purwadi, R.; Brandberg, T.; Taherzadeh, M. J. A. Possible industrial solution to ferment lignocellulosic hydrolyzate to ethanol: continuous cultivation with flocculating yeast. *Int. J. Mol. Sci.* **2007**, *8*, 920−932.
(19) Yu, Y.; Feng, Y.; Xu, C.; Liu, J.; Li, D. Onsite bio-detoxification of steam-exploded corn stover for cellulosic ethanol production. *Bioresour. Technol.* **2011**, *102*, 5123−5128.
(20) Ghose, T. K. Measurement of cellulase activities. *Pure Appl. Chem.* **1987**, *59*, 257−268.
(21) Zhang, J.; Zhang, W. X.; Wu, Z. Y.; You, L.; Yang, J.; Wei, Q.; Zhu, W. Y. Optimization of a simultaneous saccharification and co-fermentation with *Saccharomyces cerevisiae* and *Candida shehatae* for converting exploded rice straw to ethanol. *Food Fermentation Ind.* **2013**, *39*, 48−54.
(22) Öhgren, K.; Bengtsson, O.; Gorwa-Grauslund, M. F.; Galbe, M.; Hahn-Hägerdal, B.; Zacchi, G. Simultaneous saccharification and co-fermentation of glucose and xylose in steam-pretreated corn stover at high fiber content with *Saccharomyces cerevisiae* TMB3400. *J. Biotechnol.* **2006**, *126*, 488−498.
(23) Sluiter, A.; Hames, B.; Ruiz, R.; Scarlata, C.; Sluiter, J.; Templeton, D. *Determination of Structural Carbohydrates and Lignin in Biomass*; Laboratory Analytical Procedure from the Biomass Analysis Technology (NREL BAT) Team; Technical Report NREL/TP-510-42618; National Renewable Energy Laboratory: Golden, CO, USA, 2008.
(24) Jeffries, T. W.; Jin, Y. S. Metabolic engineering for improved fermentation of pentoses by yeasts. *Appl. Microbiol. Biotechnol.* **2004**, *63*, 495−509.
(25) Kuhad, R. C.; Gupta, R.; Khasa, Y. P.; Singh, A.; Zhang, Y. H. P. Bioethanol production from pentose sugars: current status and future prospects. *Renew Sust. Energy Rev.* **2011**, *15*, 4950−4962.
(26) Madhavan, A.; Tamalampudi, S.; Srivastava, A.; Fukuda, H.; Bisaria, V. S.; Kondo, A. Alcoholic fermentation of xylose and mixed sugars using recombinant *Saccharomyces cerevisiae* engineered for xylose utilization. *Appl. Microbiol. Biotechnol.* **2009**, *82*, 1037−1047.
(27) Li, Y.; Park, J. Y.; Shiroma, R.; Ike, M.; Tokuyasu, K. Improved ethanol and reduced xylitol production from glucose and xylose mixtures by the mutant strain of *Candida shehatae* ATCC 22984. *Appl. Biochem. Biotechnol.* **2012**, *166*, 1781−1790.
(28) Fu, N.; Peiris, P.; Markham, J.; Bavor, J. A novel co-culture process with *Zymomonas mobilis* and *Pichia stipitis* for efficient ethanol production on glucose/xylose mixtures. *Enzyme Microb. Technol.* **2009**, *45*, 210−217.
(29) Yadav, K. S.; Naseeruddin, S.; Prashanthi, G. S.; Sateesh, L.; Rao, L. V. Bioethanol fermentation of concentrated rice straw hydrolysate using co-culture of *Saccharomyces cerevisiae* and *Pichia stipitis*. *Bioresour. Technol.* **2011**, *102*, 6473−6478.
(30) Lebeau, T.; Jouenne, T.; Junter, G. A. Long-term incomplete xylose fermentation, after glucose exhaustion, with *Candida shehatae* co-immobilized with *Saccharomyces cerevisiae*. *Microbiol. Res.* **2007**, *162*, 211−218.
(31) Lebeau, T.; Jouenne, T.; Junter, G. A. Continuous alcoholic fermentation of glucose/xylose mixtures by co-immobilized *Saccharomyces cerevisiae* and *Candida shehatae*. *Appl. Microbiol. Biotechnol.* **1998**, *50*, 309−313.
(32) Abdel-Banat, B. M. A.; Hoshida, H.; Ano, A.; Nonklang, S.; Akada, R. High temperature fermentation: how can processes for ethanol production at high temperatures become superior to the traditional process using mesophilic yeast? *Appl. Microbiol. Biotechnol.* **2010**, *85*, 861−867.
(33) Laplace, J. M.; Delgenes, J. P.; Moletta, R.; Navarro, J. M. Alcoholic fermentation of glucose and xylose by *Pichia stipitis*, *Candida shehatae*, *Saccharomyces cerevisiae* and *Zymomonas mobilis*: oxygen requirement as a key factor. *Appl. Microbiol. Biotechnol.* **1991**, *36*, 158−162.
(34) Sun, W. L.; Tao, W. Y. Comparison of cell growth and ethanol productivity on different pretreatment of rice straw hemicellulose hydrolysate by using *Candida shehatae* CICC 1766. *Afr. J. Microbiol. Res.* **2010**, *4*, 1105−1109.
(35) Banerjee, G.; Car, S.; Scott-Craig, J. S.; Borrusch, M. S.; Walton, J. D. Rapid optimization of enzyme mixtures for deconstruction of diverse pretreatment/biomass feedstock combinations. *Biotechnol. Biofuels* **2010**, *3*, 22.
(36) Panchal, C. J.; Bast, L.; Russell, I.; Stewart, G. G. Repression of xylose utilization by glucose in xylose-fermenting yeasts. *Can. J. Microbiol.* **1988**, *34*, 1316−1320.
(37) Emily, L. W. T.; Nandong, J.; Samyudia, Y. Experimental investigation on the impact of aeration rate and stirrer speed on micro-aerobic batch fermentation. *J. Appl. Sci.* **2009**, *9*, 3126−3130.
(38) Grosz, R.; Stephanopoulos, G. Physiological, biochemical, and mathematical studies of micro-aerobic continuous ethanol fermentation by *Saccharomyces cerevisiae* I: hysteresis, oscillations, and maximum specific ethanol productivities in chemostat culture. *Biotechnol. Bioeng.* **1990**, *36*, 1006−1019.
(39) Sreenath, H. K.; Jeffries, T. W. Production of ethanol from wood hydrolyzate by yeasts. *Bioresour. Technol.* **2000**, *72*, 253−260.
(40) du-Preez, J. C.; Bosch, M.; Prior, B. A. Temperature profiles of growth and ethanol tolerance of the xylose-fermenting yeasts *Candida shehatae* and *Pichia stipitis*. *Appl. Microbiol. Biotechnol.* **1987**, *25*, 521−525.
(41) Sánchez, S.; Bravo, V.; Castro, E.; Moya, A. J.; Camacho, F. The fermentation of mixtures of D-glucose and D-xylose by *Candida shehatae*, *Pichia stipitis* or *Pachysolen tannophilus* to produce ethanol. *J. Chem. Technol. Biotechnol.* **2002**, *77*, 641−648.
(42) Hahn-Hagerdal, B.; Jeppsson, H.; Skoog, K.; Prior, B. A. Biochemistry and physiology of xylose fermentation by yeasts. *Enzyme Microb. Techno1.* **1994**, *16*, 933−943.
(43) Xiao, Z. Z.; Zhang, X.; Gregg, D. J.; Saddler, J. N. Effects of sugar inhibition on cellulases and β-glucosidase during enzymatic hydrolysis of softwood substrates. *Appl. Biochem. Biotechnol.* **2004**, *113−116*, 1115−1126.
(44) Qing, Q.; Yang, B.; Wyman, C. E. Xylooligomers are strong inhibitors of cellulose hydrolysis by enzymes. *Bioresour. Technol.* **2010**, *101*, 9624−9630.
(45) Fonseca, B. G.; Puentes, J. G.; Mateo, S.; Sánchez, S.; Moya, A. J.; Roberto, I. C. Detoxification of rice straw and olive tree pruning

hemicellulosic hydrolysates employing *Saccharomyces cerevisiae* and its effect on the ethanol production by *Pichia stipitis*. *J. Agric. Food Chem.* **2013**, *61*, 9658−9665.
(46) Vasserot, Y.; Mornet, F.; Jeandet, P. Acetic acid removal by *Saccharomyces cerevisiae* during fermentation in oenological conditions. Metabolic consequences. *Food Chem.* **2010**, *119*, 1220−1223.
(47) Zimmermann, F. K.; Mayer, V. W.; Scheel, I.; Resnick, M. A. Acetone, methyl ethyl ketone, ethyl acetate, acetonitrile and other polar aprotic solvents are strong inducers of aneuploidy in *Saccharomyces cerevisiae*. *Mutat. Res.* **1985**, *149*, 339−351.
(48) Zimmermann, F. K. A test for uniparental disomy in *Saccharomyces cerevisiae*. *Mutat. Res.* **1994**, *306*, 187−196.
(49) Pavelka, N.; Rancati, G.; Zhu, J.; Bradford, W. D.; Saraf, A.; Florens, L.; Sanderson, B. W.; Hattem, G. L.; Li, R. Aneuploidy confers quantitative proteome changes and phenotypic variation in budding yeast. *Nature* **2010**, *468*, 321−325.
(50) Parekh, S. R.; Yu, S.; Wayman, M. Adaptation of *Candida shehatae* and *Pichia stipitis* to wood hydrolysates for increased ethanol production. *Appl. Microbiol. Biotechnol.* **1986**, *25*, 300−304.
(51) Almeida, J. R. M.; Modig, T.; Petersson, A.; Hähn-Hägerdal, B.; Lidén, G.; Gorwa-Grauslund, M. F. Increased tolerance and conversion of inhibitors in lignocellulosic hydrolysates by *Saccharomyces cerevisiae*. *J. Chem. Technol. Biotechnol.* **2007**, *82*, 340−349.

Those cells anchoring mini-scaffoldins were optimized to produce approximately 1138 mg/L ethanol from microcrystalline cellulose within 4 days. However, it should be noted that the ethanol titer and cellulose consumption were lower than those obtained when using a yeast self-assembled mini-cellulosome.[13] Attending to the length of scaffoldin II, Fan and colleagues[12,13] reported a higher display level on yeasts with smaller scaffoldin II (lower amount of cohesin II), as well as a maximum ethanol production when the mini-cellulosome had only two cohesins II. Considering the number of cohesin I domains, Jaeho et al.[14] obtained a little difference in the effects on cellulosic and hemicellulosic substrates produced by three different *C. cellulovorans* recombinant mini-cellulosomes containing either endoglucanase EngB or endoxylanase XynA bound to mini-CbpA with one (mini-CbpA1), two (mini-CbpA12), or four (mini-CbpA1234) cohesin domains when the cellulosomal enzyme concentration was held constant, regardless of the copy number of cohesins in the cellulosome. However, a synergistic effect was observed when the enzyme concentration was increased to be proportional to the number of cohesins in the mini-cellulosome. Comparing mini-cellulosome with free cellulosomal enzymes, Murashima et al.[15] reported an enhanced activity toward crystalline cellulose when using mini-cellulosomes.

Cereal-based diets may contain high levels of soluble nonstarch polysaccharides (NSPs) that significantly affect the digestive process, impairing animal performance. It is now well-known that barley incorporation in poultry diets is limited by its high content in soluble β-1,3−1,4-glucans that upon solubilization lead to an increase in digesta viscosity, reducing digesta passage rate and affecting the interaction of the endogenous digestive enzymes with their target substrates.[16−18] In addition, higher viscosities also lead to prolonged digesta passage rates, promoting modifications in gut physiology such as the enlargement of gastrointestinal organs, which are detrimental to the final carcass yields.[16] High digesta viscosity also favors the proliferation of anaerobic microbes in the upper parts of the gastrointestinal (GI) tract, thus affecting the animal's health.[18] To reduce the negative effects associated with the presence of barley β-glucans, commercial enzyme mixtures expressing high levels of β-glucanase activity are currently added to broiler diets.[19] Exogenous enzymes added to poultry diets reduce the degree of polymerization of soluble glucans, leading to a reduction in digesta viscosity and improvements of diet digestibility and feed intake, thus contributing to improved animal performance.[19] However, little is known about the mechanisms affecting the efficiency of exogenous enzymes used to improve the nutritive value of cereal-based diets in vivo.

Here we aim to produce mini-cellulosomes expressing β-1,3−1,4-glucanase activity and use the engineered nanomachines to improve the nutritive value of barley-based diets for broilers. These mini-cellulosomes are based on *C. thermocellum* CipA scaffoldin and incorporate one or three *Ct*Glc16A enzymes in a single nanomachine.

MATERIALS AND METHODS

Bacterial Strains and Plasmid. Genomic DNA of *C. thermocellum* ATCC 27405 was purchased from DSMZ (Braunschweig, Germany). *E. coli* DH5α cells were used for cloning, and *E. coli* BL21 (DE3) was used as the expression host. The plasmids used for cloning and expression were pET-21a (+) derivatives. All of the above-mentioned items were procured from Novagen (Madison, WI, USA).

Gene Isolation and Cloning. The thermostable β-1,3−1,4-glucanase of *C. thermocellum*, termed *Ct*Glc16A,[20] is a modular enzyme containing an N-terminal glycoside hydrolase family 16 catalytic domain followed by a C-terminal type I dockerin. The gene encoding mature *Ct*Glc16A (residues 30−334) was amplified from *C. thermocellum* genomic DNA through PCR using the NZYProof DNA polymerase (NZYTech Ltd., Lisboa, Portugal) and the following primers: 5′-CACACACA**GCTAGC**ACTGTGGTAAATACGCC-3′ and 5′-CACACACA**GGATCC**TCAAAGTGACGGAATTG-3′ (NZYTech Ltd.). Primers included engineered *Nhe*I and *Bam*HI restriction sites (in bold) that allowed the subsequent cloning of the resulting nucleic acid into similarly restricted pET21a, generating the plasmid pGH16-Doc21a. pGH16-Doc21a encodes the bimodular *Ct*Glc16A, containing aN N-terminal GH16 β-1,3−1,4-glucanase catalytic domain and a C-terminal type I dockerin. Previously we observed that dockerins are highly unstable when expressed in *E. coli* cells. However, cellulosomal enzymes are stabilized once dockerins bind their cohesin counterpart.[21] Thus, cohesin−dockerin complexes are usually assembled in vivo in cells coexpressing the genes encoding the dockerin- and cohesin-containing proteins. Previously we produced a *C. thermocellum* mini-cellulosome containing three CtCel8A cellulases bound to a mini-scaffoldin comprising cohesin modules 3, 4, and 5 of CipA (residues 562−1030).[21] The mini-cellulosome was produced in *E. coli* cells transformed with a pET21a derivative containing the genes encoding the cellulase and the tricohesin mini-scaffoldin organized in tandem and under the control of separate T7 promoters (the plasmid was termed pG8D3C21a;[21] for details). Here we used pG8D3C21a construct and replaced the gene encoding CtCel8A by *Ct*Glc16A gene through restriction digestion. Thus, pGH16-Doc21a was digested with *Sph*I and *Bam*HI, and the DNA fragment containing the β-glucanase gene and the 5′-region of pET21a was cloned into a truncated version of pG8D3C21a from which the CtCel8A gene was excised after a *Sph*I−*Bgl*II digestion, generating pG16D3C21a. pG16D3C21a contains the genes encoding the *Ct*Glc16A glucanase and the three-cohesin mini-scaffoldin organized in tandem. to prepare a protein−protein complex resulting from the binding of a single-cohesin domain protein to *Ct*Glc16A, to use as a control in the biochemical experiments described below, the same approach was employed to produce plasmid pGH16Doc-1Coh21a by replacing CtCel8A with *Ct*Glc16A in plasmid pG8D1C21a, which contains the gene encoding CtCel8A followed by the gene encoding a single cohesin, cohesin 3, of CipA scaffoldin. The two resulting plasmids used in this study, pGH16Doc-3Coh21a (GH16-3C) and pGH16Doc-1Coh21a (GH16-1C), were subsequently sequenced to confirm that no mutations were accumulated during gene amplification and the resulting subcloning steps. The engineered cohesin-containing proteins (3Coh and 1Coh) contain a C-terminal His tag, allowing the direct purification of the assembled complex and unbound scaffoldins by immobilized metal affinity chromatography (IMAC). Because cohesin-containing proteins are usually expressed at low levels in *E. coli*, it is expected that in both cases the majority of the proteins recovered by affinity chromatography will constitute the protein complexes.

Expression and Purification of *Ct*Glc16A Mini-cellulosomes. *E. coli* BL-21(DE3) cells were transformed with pGH16Doc-3Coh21a and pGH16Doc-1Coh21a as described elsewhere.[22] Recombinant cells were grown in Luria−Bertani medium supplemented with ampicillin (100 μg mL^{-1}) at 37 °C, 200 rpm, until midexponential phase ($A_{600\ nm} \approx 0.4$). Recombinant gene expression was induced by adding 1.0 mM isopropyl-1-thio-β-D-galactopyranoside (NZYTech), and cells were further incubated at 19 °C for 16 h. The cells were harvested at 5000*g*, and the resulting pellet was resuspended in 10 mM imidazole buffer (10 mM imidazole, 50 mM NaHepes, 1 M NaCl, 5 mM $CaCl_2$, at pH 7.5), submitted to ultrasonication, and centrifuged at 4 °C and 17000*g* during 30 min; finally, the obtained His_6-tagged recombinant protein extracts were purified by IMAC using 5 mL HiTrap chelating columns (GE Healthcare, Piscataway, NJ, USA) as described by Fontes et al.[23] The purity of the protein complexes was analyzed by SDS-PAGE.[24]

Analytical Procedures. Unless otherwise stated, enzyme assays were determined following the method described by Fontes et al.[25] by measuring the release of reducing sugars resulting from carbohydrate

hydrolysis in phosphate citrate (PC) buffer (64 mM K_2HPO_4 and 12 mM citric acid; pH 6.5) at 40 °C. The substrates used in this study were barley β-glucan, hydroxyethylcellulose, carboxymethylcellulose, arabinoxylan, xyloglucan, galactomannan, and glucomannan (Megazyme, Wicklow, Ireland) at a 0.3% (w/v) final concentration. Reactions were stopped by adding a DNSA-based solution (1% DNSA, 1% NaOH, and 0.2% phenol) following the method described by Miller.[26] To explore the pH profiles of pGH16Doc-3Coh21a and pGH16Doc-1Coh21a plasmids and compare them with *Ct*Glc16A, 50 mM 2-*N*-morpholinoethanesulfonic acid (MES) (pH 4.5−7), 50 mM Tris-HCl (pH 7−9.5), and 50 mM $NaHCO_3$ (pH 9.5−11) buffers were used in enzyme assays employing 0.25% barley β-glucan as the substrate. For thermostability experiments, the three proteins were incubated at temperatures ranging from 60 to 90 °C. After 20 min at the required temperature, samples were withdrawn and residual activity was determined at 50 °C by measuring the amount of reducing sugar released from barley β-glucan as described above. Determination of the temperature of maximal enzyme activity was performed by incubating the enzyme at temperatures ranging from 50 to 90 °C and measuring reducing sugar release as previously described. One unit of catalytic activity is defined as the amount of enzyme required to release 1 μmol of product per minute.

In a previous study it was shown that levels of endogenous β-glucanase activity affect the efficacy of exogenous enzymes used to improve the nutritive value of barley-based diets for poultry.[27] To select barley batches expressing lower levels of endogenous β-glucanases, five different barley lots available commercially were selected. The barley lots were milled at 0.5 mm, and enzyme extraction was performed by adding 1 mL of PC buffer into 0.75 g of barley. The supernatant was recovered and used to quantify the β-glucanase activity using a β-glucanase commercial assay kit (Megazyme), following the manufacturer's protocol. The incubation period was extended to 3 h. The barley lot expressing the lowest endo-β-glucanase activity was used as the main component of the basal diet described below.

To standardize the number of enzyme units used to supplement the animal diets, the catalytic activity of the recombinant enzymes, including the commercial enzyme mixture (Rovabio Excel AP), was determined in parallel at 40 °C by measuring the release of reducing sugars.[25] The extract containing the commercial enzyme was prepared by ressuspending 250 mg of the enzyme in 10 mL of PC buffer, followed by an overnight incubation at room temperature with gentle agitation and centrifugation at 16000*g* for 10 min.

To evaluate the levels of β-glucanase activity present in the four animal diets and in digesta samples collected in different parts of the broilers' GI tract, samples were initially centrifuged at 16000*g* for 5 min, and the supernatants were recovered for analysis. The barley and feed samples (0.75 g) were previously mixed in 1 mL of PC buffer. The mixed samples were subjected to vigorous stirring during 30 min and centrifuged, and the supernatant was analyzed. Qualitative analysis of β-glucanase activity was assessed in agar plates, using barley β-glucan at 0.1% (w/v) mixed with agar at 2% (w/v) final concentration, in 10 mM Tris-HCl (pH 8.0). Catalytic activity was detected on the basis of the method described by Ponte and colleagues[28] with some modifications. Briefly, a Pasteur pipet was used to create wells in the agar plates, which were filled with 20 μL of enzyme extract from digesta samples. Subsequently, the plates were incubated for 16 h at 37 °C and dyed with 1% Congo Red (E. Merck, Darmstadt, Germany) in10 mM Tris-HCl (pH 8) for 30 min. To observe regions where the polysaccharides were degraded, the plates were subjected to three 15 min washes with 1 M NaCl in 10 mM Tris-HCl (pH 8). For measuring the viscosity of small intestine contents, samples collected from the duodenum plus jejunum and from the ileum were centrifuged for 10 min at 10867*g*, and the viscosity of sample supernatant was measured at 6 rpm using a viscometer (model LVDVCP-II, Brookfield Engineering Laboratories, Middleboro, MA, USA) with a cup maintained at 24 °C.

Incorporating Mini-cellulosomes in Poultry Diets. Bird experiment was conducted in accordance with the Ethics Committee of CIISA, Faculdade de Medicina Veterinária, and approved by the Animal Care Committee of the National Veterinary Authority (Direcção Geral de Veterinária, Lisboa, Portugal), following the appropriate European Union guidelines (Council Directive 86/609/EEC). One hundred and sixty 1-day-old Ross 308 male broiler birds were assigned to 40 pens of 4 birds each. Chicks were wing-banded for individual identification. The 40 pens were randomly assigned to four treatments consisting of four different diets provided to the animals. A barley-based diet was not supplemented (treatment NC) or supplemented with the commercial enzyme Rovabio Excel AP (Adisseo, Antony, France; treatment Rov), supplemented with pGH16Doc-1Coh21a (treatment 1C), or supplemented with pGH16Doc-3Coh21a (treatment 3C). The commercial enzyme manufacturers guarantee activity of endo-1,4-β-xylanase and endo-1,3(4)-β-glucanase. All three enzymes were incorporated at a calculated dose of 1500 U/kg feed. The calculated 1500 U/kg feed of the commercial enzyme corresponded to the manufacturer's recommended dose of 50 g of enzyme per ton of feed. The duration of the trial was 28 days. The basal diet (Table 2) contained 618 g/kg of barley and was formulated to ensure a nutrient availability as defined by the NRC.[29] Throughout the experiment, chicks were given free access to water and feed, which were provided with drinking nipples and hanging feeders, respectively. Broilers were raised in wired floor pens that were located in an environmentally controlled room adjusted daily to the recommended temperatures, according to standard brooding practices.[30] Feed consumption and body weight (BW) were determined weekly throughout the experiment, and mortality was recorded daily. At 28 days of age, one bird per pen was slaughtered by cervical dislocation. The weight of the crop, gizzard, and liver, and the length of the duodenum, jejunum, ileum, and cecum were determined. Digesta samples were collected at duodenum and jejunum and ileum compartments to determine contents viscosity as described above.

Zymogram Analysis and Resistance of Mini-cellulosomes to Proteinase Attack. Zymogram analysis was performed as described by Fontes et al.[23] and Ribeiro et al.[31] In brief, digesta proteins were separated through SDS-PAGE in 14% acrylamide gels containing 0.1% of barley β-glucan (Megazyme), according to the method of Laemmli.[24] After electrophoresis, polypeptides were renatured by subjecting the gel to five 30 min washes in 100 mM sodium succinate, pH 6.3, 10 mM $CaCl_2$, and 1 mM DTT. The gels were incubated for 16 h at 37 °C in the same buffer, and proteins were stained in a solution comprising 40% (v/v) methanol, 10% (v/v) glacial acetic acid, and 0.4% (w/v) Coomassie Brilliant Blue R. After destaining, gels were washed in 0.1 M Tris-HCl (pH 8) for 20 min. β-Glucanase activity was detected using a 0.1% (w/v) Congo Red solution for 15 min and washing with 1 M NaCl in 10 mM Tris-HCl (pH 8) until excess dye was removed. After Congo Red staining, the gels were counterstained with 1 N HCl as described elsewhere.[32] Areas of catalytic activity appeared as colorless zones in a gray background.

The ability of mini-cellulosomes to resist protease degradation was evaluated by incubating the two protein complexes (approximately 30 μg) with50 μg of pancreatin from porcine pancreas (Sigma, P-1500) in buffer A (50 mM Hepes, 50 mM NaCl, 5 mM $CaCl_2$, pH 7.5) at 37 °C during 30 min. Negative controls consisting of the reaction without pancreatin were prepared, as well as a reaction only with pancreatin in buffer A. Mini-cellulosome integrity was evaluated by SDS-PAGE, as described above.

Statistical Analyses. Data related to bird performance from each experiment were subjected to ANOVA according to the general linear models procedure of SAS.[33] The least-squared means procedure was used to detect significant differences between treatment groups. The experimental unit was the cage of fpur animals (n = 10). Differences were considered significant when $p < 0.05$.

RESULTS AND DISCUSSION

Construction of Mini-cellulosomes Expressing β-1,3−1,4-Glucanase Activity. The open reading frame of *Ct*Glc16A, amplified by polymerase chain reaction, was used to replace the gene encoding CtCel8A in plasmids previously prepared to produce a mini-cellulosome containing CtCel8A

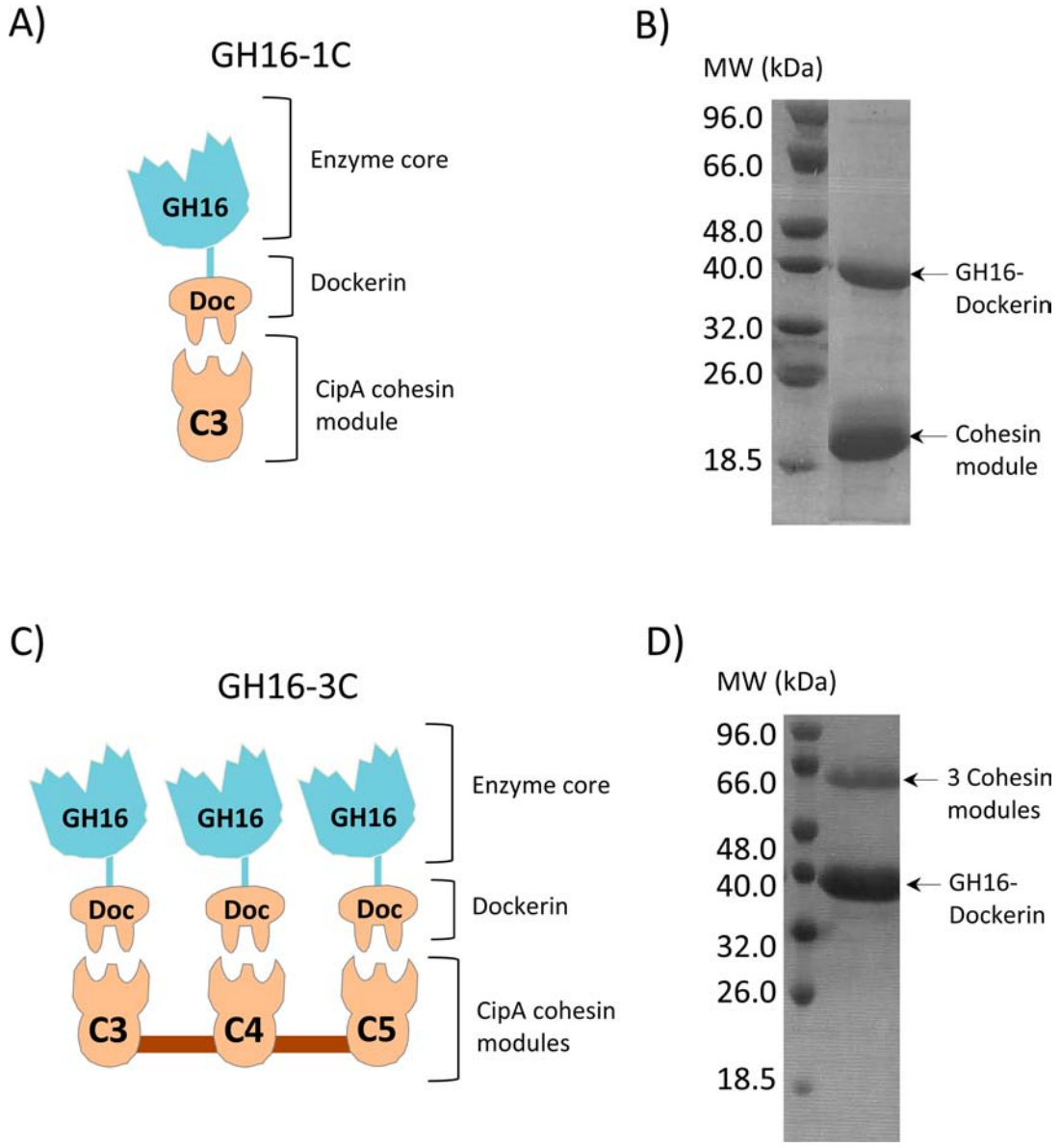

Figure 1. Molecular architecture of mini-cellulosomes (A, C) and protein purification (B, D). The molecular architectures of mini-cellulosomes containing one cohesin fused to one *Ct*Glc16A enzyme or three cohesin domains fused to three *Ct*Glc16A enzymes are displayed in panels A and C, respectively. The two complexes were expressed and assembled in vivo in *E. coli* and purified through IMAC using a polyhistidine tag located at the C-terminus of the mini-scaffoldins as the affinity tag. SDS-PAGE was used to confirm complex homogeneity as observed in panels B (GH16-1C) and D (GH16-3C), respectively.

bound to mini-scaffoldins containing either one or three cohesin domains.[21] Two *C. thermocellum* mini-cellulosome protein complexes (Figure 1a) of roughly 52 and 156 kDa, respectively, were produced. The complexes comprising one (C3; 16.5 kDa) or three cohesin modules (C3−C4−C5; 51.2 kDa) derived from CipA bound to one or three cellulosomal *Ct*Glc16A glucanases (34.9 kDa), respectively, were purified from *E. coli* via nickel affinity chromatography (Figure 1b). The genes encoding the truncated versions of CipA (C3 or C3−C4−C5) and *Ct*Glc16A were coexpressed in the bacterium under the control of separate T7 promoters (see Materials and Methods). The recombinant CipA derivatives, C3 and C3−C4−C5, were engineered to contain a C-terminal His6-tag. The levels of expression of *Ct*Glc16A were estimated to be at least 5 times higher than the levels of expression of C3 or C3−C4−C5 mini-scaffoldins (not shown). Thus, during expression, the mini-scaffolds became saturated with the cellulosomal glucanase, allowing the purification of homogeneous complexes through affinity chromatography that targeted the C-terminal His6-tag of C3 or C3−C4−C5, respectively.

Assembly of *Ct*Glc16A in Mini-cellulosomes Does Not Affect pH and Temperature Stability of the Enzyme. *Ct*Glc16A is a typical β-glucanase as it does not exhibit any activity against soluble cellulosic substrates and hemicelluloses but displays specificity for β-1,3−1,4-glucans, such as lichenan and barley β-glucan.[20] The enzyme displays a broad pH optimum (pH 6−9), with maximal activity at pH 8.0, and is thermostable at temperatures of ~70 °C. In addition, *Ct*Glc16A was found to be completely resistant to proteolytic inactivation.[20] Thus, *Ct*Glc16A biochemical properties suggest that the enzyme is particularly suited to resist the harsh conditions observed during feed processing and poultry

dx.doi.org/10.1021/jf502157y | J. Agric. Food Chem. 2014, 62, 7496−7506

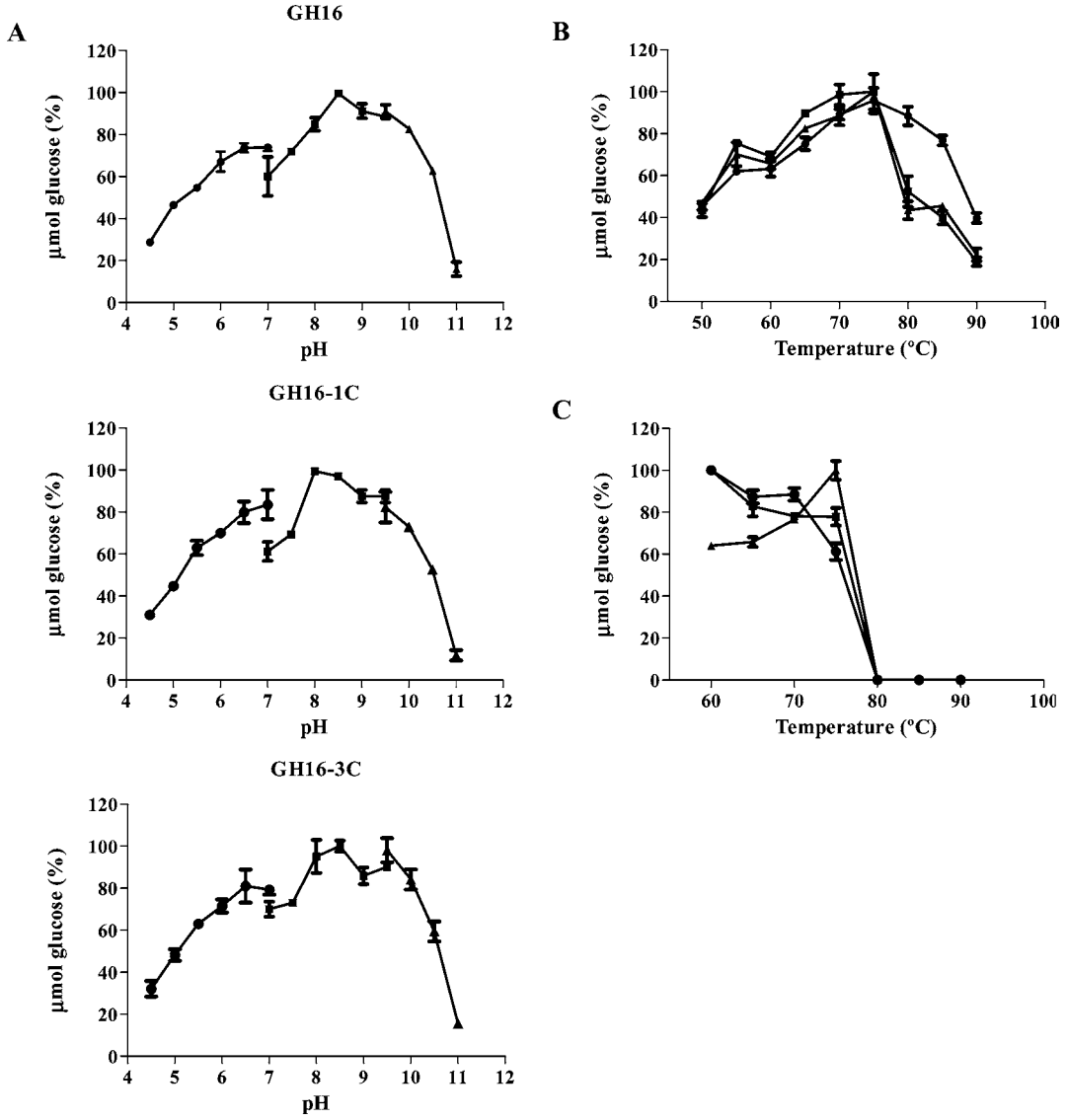

Figure 2. pH (A), temperature (B), and thermostability (C) profiles of unbound *Ct*Glc16A (GH16) or the enzyme when organized in mini-cellulosomes GH16-1C and GH16-3C. In panel A, the enzymes were incubated at standard conditions in MES (●), Tris (■), or $NaHCO_3$ (▲) buffer with different pH values, and β-glucanase activity was determined (% of glucose released). In panel B, *Ct*Glc16A (GH16) (●), GH16-1C (■), and GH16-3C (▲) activities were determined against barley β-glucan at different temperatures. In panel C, the thermostability of the enzyme and enzyme complexes was determined by incubating the proteins for 30 min at different temperatures, and residual activity was determined at 55 °C (symbols are the same as in panel B).

Table 1. Substrate Specificity of *Ct*Glc16A, GH16-1C, and GH16-3C, Measured at 70 °C and pH 8.0[a]

substrate	*Ct*Glc16A	GH16-1C	GH16-3C
barley β-glucan	2845.1 ± 35.98	2859.4 ± 98.39	2321.2 ± 139.50
hydroxyethylcellulose	0	0	0
carboxymethylcellulose	0	0	0
arabinoxylan	0	0	0
xyloglucan	0	0	0
galactomannan	0	0	0
glucomannan	0	0	0

[a] *Ct*Glc16A and mini-cellulosomes were incubated with a variety of carbohydrates (0.25%), and release of reducing sugars was measured through the DNSA assay as described under Materials and Methods. Enzyme activity is expressed in number of enzyme units per milligram of *Ct*Glc16A. Values are the average of three independent assays ± standard error of mean.

digestion,[20] and thus *Ct*Glc16A constitutes an ideal candidate to be assembled in mini-cellulosomes. In fact, *Ct*Glc16A is a cellulosomal enzyme isolated from the anaerobic thermophilic bacterium *C. thermocellum*.

dx.doi.org/10.1021/jf502157y | J. Agric. Food Chem. 2014, 62, 7496−7506

Organization of cellulases and hemicellulases in mini-cellulosomes is supposed to confer additional stability to the enzyme complex and improve activity on the hydrolysis of recalcitrant substrates.[1] Here we investigate the biochemical properties of *Ct*Glc16A when organized in mini-cellulosomes containing one (GH16-1C) or three cohesin (GH16-1C) mini-cellulosomes. The data, presented in Figure 2, reveal that mini-cellulosomes GH16-1C and GH16-3C displayed optimum temperature and pH similar to those expressed by uncomplexed *Ct*Glc16A. The mini-cellulosomes expressed a broad pH optimum (6−9) and displayed unaltered optimum temperatures and thermostability when compared with *Ct*Glc16A. The substrate specificities of GH16-1C and GH16-3C were also probed against a range of natural substrates at optimized pH and temperatures. The data, presented in Table 1, reveal that the two mini-cellulosomes retained a strict specificity for β-1,3−1,4-glucans. Thus, reflecting the specificity displayed by *Ct*Glc16A, the mini-cellulosomes were unable to degrade cellulosic substrates and a range of the most frequent hemicelluloses. In addition, the capacity of the enzyme to degrade β-glucans is not affected by the binding to the mini-scaffoldins, although a slight reduction of the activity of GH16-3C during the hydrolysis of barley β-glucan is observed. This might reflect a restriction of *Ct*Glc16A flexibility upon its organization in mini-cellulosomes. This flexibility is of primary importance in the hydrolysis of soluble substrates. In contrast, organization of mini-cellulosomes is of primary importance to improve the catalytic efficiency of hydrolysis of recalcitrant substrates such as cellulose.

Using Mini-cellulosomes To Improve the Nutritive Value of Barley-Based Diets for Poultry. The effect of assembling *Ct*Glc16A in mini-cellulosomes organized by scaffoldins containing one (GH16-1C) or three (GH16-3C) cohesins, respectively, in improving the nutritive value of barley-based diets for poultry was analyzed in an animal trial using 160 broiler chicks. Mini-cellulosome GH16-1C was used as a control mini-cellulosome as it contains exclusively one enzyme per protein complex and should thus behave as a typical single enzyme. Basal diet (Table 2) containing a major proportion of barley (>60%) was formulated to provide nutrients to requirements as defined by the NRC.[29] Barley contains a significant proportion of β-glucans, which, due to its intrinsic viscosity, displays considerable antinutritive properties for monogastric animals, in particular for poultry. Thus, the basal diet was fed without the addition of exogenous enzymes (negative control group, NC) or with the addition of one of three different β-glucanase preparations, the mini-cellulosome GH16-1C (GH16-1C), the mini-cellulosome GH16-3C (GH16-3C), and a commercial enzyme (Rov). The four diets were fed to broiler chicks during a 28 day trial. Animal performance data, presented in Table 3, revealed that as early as day 7 and during the entire trial animals from the NC group had lower ($p < 0.05$) body weight than animals fed diets supplemented with the exogenous enzyme preparations. At days 7 and 14, animals from the Rov group presented the highest body weights, which were similar to the animals from the GH16-1C treatment ($p > 0.05$). In addition, although GH16-3C animals had body weights similar to those of animals from the GH16-1C group ($p > 0.05$), they presented lower weights ($P < 0.05$) than animals supplemented with the commercial enzyme. These data suggest that in the initial period of the broiler growing cycle assembling *Ct*Glc16A in a three cohesin mini-cellulosome might restrict the efficacy of the exogenous β-glucanase. Weekly weight gains were only significantly different until day 14 (Table 3). During the first week of the trial, animals from the NC group displayed the lowest weight gains, whereas broiler chicks of the Rov and GH16-1C groups displayed the best performances. In addition, during this initial trial period GH16-3C broilers presented an intermediate weight gain, suggesting a lower efficacy resulting from enzyme assembly. Overall, the data suggest that exogenous enzymes act predominantly during the initial period of the broilers' growth (before day 14). This has previously been observed in other studies using barley-based diets for poultry,[18] suggesting that as birds age the capacity of the endogenous enzymatic repertoire is improved and can face the inherent increase in digesta viscosity resulting from the presence of high levels of β-glucans (see below). Data presented in Table 3 also reveal that supplemented animals presented higher feed intakes ($p < 0.05$) when compared with nonsupplemented animals, and this difference predominates at the initial periods of the trial. In addition, the feed conversion ratio (FCR) was lower for animals of the supplemented groups during the first 2 weeks of the experiment. Thus, the better performance revealed by animals supplemented with microbial β-glucanases results not only from a higher feed intake but also from an improved efficacy of nutrient digestibility as reflected by the improved FCR revealed by animals receiving exogenous enzymes. The mortality rate of the experiment was 1.25% and was not related to treatments. Taken together, the data suggest that exogenous enzymes improve the nutritive value of barley-based diets for broilers. This effect operates during the first 2 weeks of broiler growth. In addition, assembling of β-glucanases in mini-cellulosomes seems to restrict their initial efficacy as a

Table 2. Ingredient Composition and Calculated Analysis of the Cereal-Based Feed

ingredient	g/kg
barley	618
soybean meal 47%	294
soybean oil	59
salt	2.5
calcium carbonate	8.4
dicalcium phosphate 18%	17.4
DL-methionine	1.7
mineral and vitamin premix[a]	2.5
nutrient content	
energy (MJ ME/kg DM)	12.1
crude protein	208
ether extract	75
crude cellulose	51
methionine	0.469
methionine + cysteine	0.820
lysine	1.09
threonine	0.758
calcium	0.920
available phosphorus	0.410
total phosphorus	0.713

[a]Mineral−vitamin premix provided the following per kilogram of feed: retinol, 2.7 mg; cholecalciferol, 0.05 mg; α-tocopherol, 20 mg; nicotinic acid, 30 mg; cyanocobalamin, 0.12 mg; calcium pantothenate, 10 mg; menadione, 2 mg; thiamin, 1 mg; riboflavin, 4.2 mg; pyridoxine hydrochloride, 1.7 mg; folic acid, 0.5 mg; biotin, 0.5 mg; Fe, 80 mg; Cu, 10 mg; Mn, 100 mg; Zn, 80 mg; Co, 0.2 mg; I, 1.0 mg; Se, 0.3 mg; monensin, 100 mg/kg.

dx.doi.org/10.1021/jf502157y | J. Agric. Food Chem. 2014, 62, 7496−7506

Table 3. Growth Performance Parameters of Broilers Fed a Barley-Based Diet Nonsupplemented (NC) or Supplemented with a Commercial Enzyme (Rov) or with the GH16-1C or GH16-3C Construct

	NC	Rov	GH16-1C	GH16-3C	SEM	p (F)
body weight (g)						
0 days	42.3	42.0	42.0	42.2	0.16	0.3059
7 days	126 c	150 a	146 ab	140 b	2.32	0.0001
14 days	298 c	393 a	394 ab	370 b	7.26	0.0001
21 days	664 b	784 a	766 a	749 a	13.5	0.0001
28 days	1105 b	1234 a	1229 a	1227 a	22.4	0.0004
weight gain (g)						
0–7 days	81.6 c	108 a	104 a	96.5 b	2.33	0.0001
7–14 days	174 b	243 a	245 a	232 a	5.60	0.0001
14–21 days	363	386	375	379	9.17	0.3447
21–28 days	443	450	465	478	12.8	0.1494
0–28 days	1063	1192	1188	1185	42.7	0.0621
feed intake (g)						
0–7 days	111 b	129 a	128 a	120 a	3.60	0.0028
7–14 days	254 c	329 ab	331 a	312 b	5.99	0.0001
14–21 days	529 b	575 a	558 ab	547 ab	10.4	0.0129
21–28 days	746	765	786	774	17.5	0.3553
0–28 days	1608 b	1798 a	1780 a	1753 a	33.7	0.0012
feed conversion ratio						
0–7 days	1.36 a	1.19 b	1.24 b	1.24 b	0.035	0.0110
7–14 days	1.46 a	1.36 b	1.36 b	1.36 b	0.024	0.0048
14–21 days	1.46	1.49	1.49	1.45	0.020	0.3044
21–28 days	1.69	1.74	1.70	1.62	0.031	0.0866
0–28 days	1.53	1.56	1.50	1.48	0.028	0.2389

Table 4. Relative Weight and Length of Gastrointestinal Tract Compartments and Viscosity of Digesta Samples of Broilers Fed a Barley-Based Diet Nonsupplemented (NC) or Supplemented with the Commercial Enzyme (Rov) or with the GH16-1C or GH16-3C Construct

	NC	Rov	GH16-1C	GH16-3C	SEM	p (F)
relative weight (g/kg bw)						
crop	3.08	3.47	3.79	3.59	0.232	0.1904
gizzard	11.8 b	15.3 a	12.4 b	13.4 ab	0.84	0.0315
liver	27.5	30.0	29.1	28.4	1.06	0.3890
duodenum	10.5	10.4	9.02	8.70	0.861	0.3477
jejunum	17.0	14.6	14.5	14.5	0.77	0.0637
ileum	13.5 a	10.6 b	11.6 b	11.6 b	0.66	0.0339
cecum	3.14	3.08	2.94	2.98	0.178	0.8539
relative length (cm/kg bw)						
duodenum	24.5 a	20.1 b	22.1 ab	20.9 b	1.08	0.0366
jejunum	58.4 a	52.6 b	52.4 b	50.2 b	1.95	0.0327
ileum	59.9	53.6	53.7	55.1	2.39	0.2197
cecum	14.8	14.2	13.2	13.3	0.65	0.3032
content viscosity (cP)						
duodenum + jejunum	9.08 a	7.27 b	5.50 c	5.07 c	0.676	0.0001
ileum	14.9 a	11.4 a	7.03 b	7.47 b	1.396	0.0005

result of a lower enzyme flexibility imposed by cellulosome assembly upon the hydrolysis of a predominantly soluble substrate.

The relative weight and length of the bird's GI compartments, as well as digesta viscosity, are presented in Table 4. The relative weight of the bird's GI compartments was affected by treatment for the ileum ($p < 0.05$) and jejunum ($p < 0.1$). Ileum and jejunum from supplemented animals were lighter than those from animals not subjected to feed supplementation. In addition, the relative length of a bird's duodenum and jejunum was affected by enzyme supplementation. Animals from supplemented groups had shorter duodenum and jejunum when compared with the nonsupplemented animals. Several studies have reported a lower overall size of the GI tract in birds subjected to supplementation with exogenous plant cell wall degrading enzymes.[34,35] Exogenous enzymes contribute to decrease digesta viscosity, which is the main factor contributing to the enlargement of the birds' GI tract. Hence, data presented in Table 4 reveal that digesta viscosity in the duodenum + jejunum and ileum was different among birds fed the different diets. Digesta viscosity in the duodenum + jejunum and in the ileum was lowest ($p < 0.05$) for animals of the GH16-1C and GH16-3C groups. However, duodenum + jejunum and ileum viscosity was also significantly lower in the animals from the

dx.doi.org/10.1021/jf502157y | J. Agric. Food Chem. 2014, 62, 7496–7506

Rov group in comparison with the nonsupplemented animals, for which the viscosity reached the highest values.

Molecular Integrity of Minicellulosomes upon Passage through the GI Tract. Data concerning the qualitative detection of β-glucanase activity in digesta samples collected in various GI compartments are presented in Table 5, and the qualitative β-glucanase activity present in the feed is presented in Figure 3. The results revealed that β-glucanase activity could be detected in the crop and also in the cecum of animals in all treatments. However, only supplemented animals, in particular those of the GH16-1C and GH16-3C treatments, presented significant levels of β-glucanase activity in the gizzard, duodenum, jejunum, and ileum. This observation suggests an improved stability of *Ct*Glc16A when compared with the commercial enzymes upon passage through the GI tract. It is intriguing that β-glucanase activity was detected in digesta samples collected in the crop of the nonsupplemented animals. However, the intensity of the halos corresponding to β-glucanase crop activity of nonsupplemented animals was considerably weaker when compared with the supplemented groups. Although a barley lot expressing lower levels of endogenous β-glucanase activity was selected for this study, the sensitivity of the plate assay implemented to screen for exogenous enzymes was sufficient to detect it.

Table 5. Number of Birds, of 10 Animals Analyzed, Fed a Barley-Based Diet Not Supplemented (NC) or Supplemented with a Commercial β-Glucanase (Rov), the GH16-1C Construct, or the GH16-3C Construct, Presenting β-Glucanase Activity in Digesta Samples Collected from Various Gastrointestinal Compartments

	NC	Rov	GH16-1C	GH16-3C	chi-square	*p* value
crop	9	7[a]	10	10	2.401	0.4934
gizzard	0	2	9[b]	10	32.6	0.0001
duodenum	0[b]	0	10	10	39.0	0.0001
jejunum	2	0[b]	9[b]	10	31.5	0.0001
ileum	0	0	10	10	40.0	0.0001
cecum	8[a]	9[b]	8[a]	8[a]		

[a] $n = 8$. [b] $n = 9$.

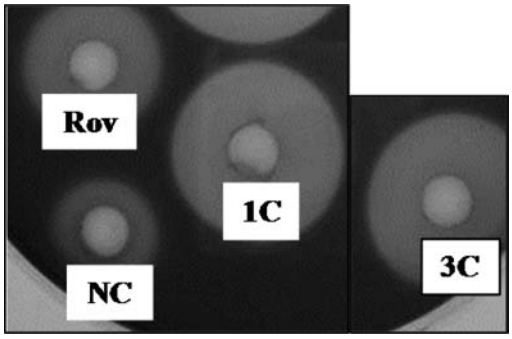

Figure 3. Qualitative plate assay for detection of β-glucanase activity in the barley-based diet not supplemented (NC) or supplemented with a commercial β-glucanase (Rov) or with mini-cellulosome GH16-1C (1C) or GH16-3C (3C).

The integrity of exogenous enzymes during passage through the GI tract was verified through zymogram analysis. The data, presented in Figure 4, reveal that the cecum of all animals is populated with a large range of β-glucanases presenting molecular masses ranging from 20 to 100 kDa. In contrast, a limited number of polypeptides expressing β-glucanase activity are present in other portions of the GI tract. In particular, a prominent 96 kDa protein is present in the majority of the digesta samples collected in both supplemented and nonsupplemented animals, and this might constitute an endogenous enzyme expressed in barley seeds. In addition, a second potentially endogenous but nonetheless less prominent polypeptide is identified in samples of the majority of the animals and presents approximately 34 kDa (Figure 4A). Digesta samples collected in the gizzard, duodenum, jejunum, and ileum of supplemented animals display the presence of highly active polypeptides. The majority of the β-glucanase activity expressed by birds supplemented with the commercial enzyme mixture seems to be represented by two polypeptides of 32 and 36 kDa, respectively (Figure 4B). These proteins are clearly visible in the small intestine of supplemented animals, although in some GI fractions they seem to be absent. This may result from a partial inactivation of the polypeptides due to pH denaturation or proteolysis.

With the exception of the gizzard, zymogram analysis of digesta samples of animals supplemented with mini-cellulosome preparations revealed the presence of β-glucanase activity. Zymogram analysis is preceded by SDS-PAGE. During SDS-PAGE protein denaturation will lead to the disassembling of mini-cellulosomes. Thus, zymogram analysis of mini-cellulosomes should reveal exclusively the polypeptide bands corresponding to the cellulosomal catalytic units. The data, presented in Figure 4, panels C (GH16-1C) and D (GH16-3C), suggest that in the crop of animals receiving the GH16-1C and GH16-3C mini-cellulosomes, *Ct*Glc16A is present in two forms, with molecular masses of 28 and 35 kDa, respectively. These two bands in the crop are present approximately in similar proportions. In contrast, when duodenum, jejunum, and ileum digesta fractions are analyzed (Figure 4C,D), *Ct*Glc16A is observed exclusively in the 28 kDa form. *Ct*Glc16A used in this study is a bimodular enzyme containing an N-terminal GH16 β-glucanase catalytic domain and a C-terminal dockerin module, which is responsible for anchoring the enzyme into the cellulosome. The two modules are separated by a proline-rich linker region. Data presented in Figure 4C,D suggest that the linker sequence separating the two *Ct*Glc16A modules is prone to proteolysis in the avian GI tract, and the 28 kDa band corresponds in size to a *Ct*Glc16A truncated derivative lacking the C-terminal dockerin. Proteolytic cleavage of the bimodular exogenous β-glucanase starts in the crop, where only 50% of the enzyme was present in the intact form. Taken together, the data presented here suggest that proteolysis affects the integrity of mini-cellulosomes used to supplement barley-based diets for poultry by removing the dockerin sequence of *Ct*Glc16A, most probably through cleavage of the linker region separating the two sequences.

To confirm that endogenous proteases are contributing to unbound *Ct*Glc16A from mini-cellulosomes through the removal of the enzyme C-terminal dockerin, the two protein complexes were incubated in vitro with a pancreatic mixture of proteases (see Materials and Methods for details). After 30 min of incubation at 37 °C, the proteins were separated through SDS-PAGE to evaluate mini-cellulosome integrity. The data, presented in Figure 5, confirm that *Ct*Glc16A is indeed susceptible to proteolysis and that proteases cleave the full-length enzyme to generate a truncated version of the recombinant β-glucanase consisting exclusively of the enzyme's

dx.doi.org/10.1021/jf502157y | J. Agric. Food Chem. 2014, 62, 7496−7506

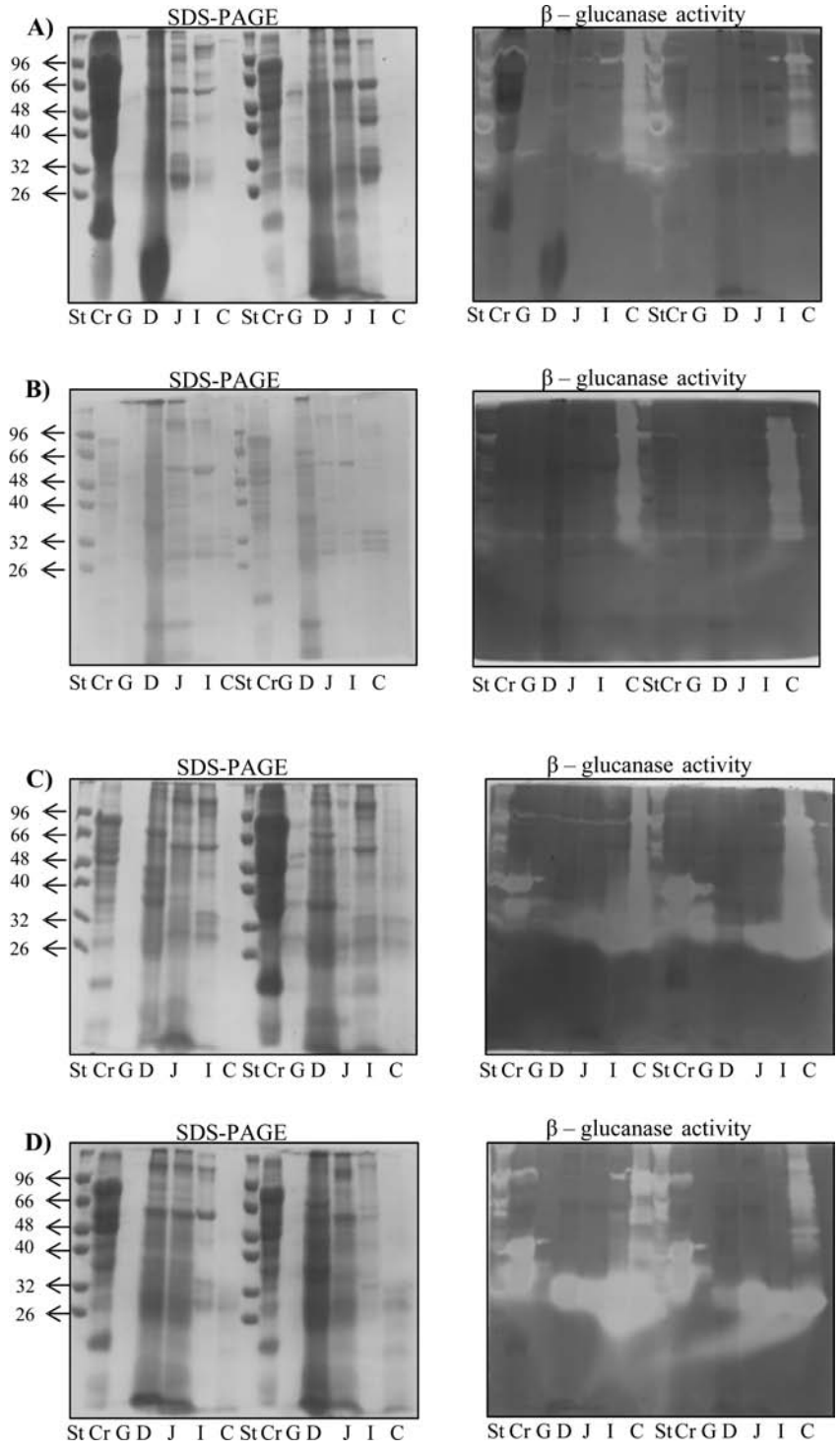

Figure 4. Zymogram analysis of digesta contents of broilers fed a barley-based diet not supplemented (A) or supplemented with a commercial enzymatic mixture (B), with the GH16-1C (C), or with the GH16-3C (D). St, low molecular protein marker; Cr, crop; G, gizzard; D, duodenum; J, jejunum; I, ileum; C, cecum.

catalytic domain (28 kDa). Linker regions play an important function in the efficacy of CAZYmes and cellulosomes by contributing to the flexibility of the modular enzymes and the quaternary structure of protein complexes.[36] Glycosylation of protein linker regions is known to protect them from proteolytic cleavage.[37] *Ct*Glc16A was recombinantly produced in *E. coli* that is unable to glycosylate proteins.[38,39] It is presently unknown if *C. thermocellum* cellulosomal enzymes are glycosylated at their linkers. However, this study clearly indicates that protection of linker regions of cellulosomal enzymes from proteolytic cleavage is fundamental to maintain cellulosome integrity. Finally, cohesin domains seem to resist the protease attack, although mini-scaffoldin C3−C4−C5 was susceptible to proteolysis at its linkers (Figure 5, lane 4).

In conclusion, this study reports the in vivo construction of two mini-cellulosomes based on scafoldins with one or three CipA-derived cohesin domains. The protein complexes were purified, and protein stability studies revealed that *Ct*Glc16A

dx.doi.org/10.1021/jf502157y | J. Agric. Food Chem. 2014, 62, 7496−7506

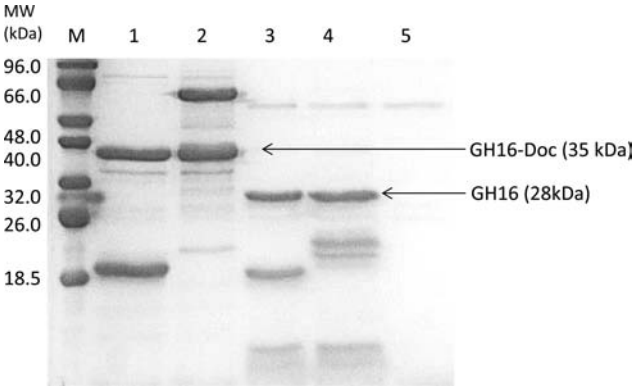

Figure 5. SDS-PAGE analysis of mini-cellulosomes GH16-1C (lane 1) and GH16-3C (lane 2) after incubation with a pancreatic mixture of proteases, lanes 3 and 4, respectively. In lane 5 the pancreatic mixture of enzymes was analyzed. M represents the low molecular protein marker.

biochemical properties are not significantly affected by protein complexation. However, the catalytic efficacy of GH16-3C mini-cellulosomes seems to be slightly reduced. This may represent a decrease in enzyme flexibility resulting from the assembling in a multiprotein complex. Protein flexibility is highly important for the hydrolysis of soluble carbohydrates. The two mini-cellulosomes are shown to be very effective in improving the nutritive value of barley-based diets for poultry. However, the efficacy of the recombinant nanomachines is not improved when compared with that of commercially available enzyme mixtures. Whether this represents a comparable efficacy of the three enzyme systems under analysis (commercial unbound enzymes, GH16-1C, and GH16-3C) or a saturation of the animal feed with exogenous enzymes remains to be established. In addition, endogenous proteases were shown to affect the integrity of the recombinant mini-cellulosomes by cleaving the linker region that separates *Ct*Glc16A catalytic and dockerin domains. Thus, in future studies protection of linker regions needs to be improved as the molecular integrity of mini-cellulosomes is critical to potentiate its use in a variety of biotechnological applications.

AUTHOR INFORMATION

Corresponding Author

*(T.R.) Mail: Faculdade de Medicina Veterinária, Universidade Técnica de Lisboa, Avenida da Universidade Técnica, 1300-477 Lisboa, Portugal. Phone: +351 213652876. Fax: +351 213652889. E-mail: teresaribeiro@fmv.ulisboa.pt.

Author Contributions

‖M.C., V.O.F., and T.R. contributed equally.

Funding

V.O.F., M.C., and T.R. were supported by Fundação para a Ciência e a Tecnologia (Lisbon, Portugal) through the individual fellowships SFRH/BDE/51101/2010, SFRH/BD/90468/2012, and SFRH/BPD/80280/2011, respectively. This work was supported by Grant PTDC/CVT/103942/2008 from Fundação para a Ciência e a Tecnologia (Lisbon, Portugal).

Notes

The authors declare no competing financial interest.

ACKNOWLEDGMENTS

We thank Sociedade Agrícola da Quinta da Freiria SA (Bombarral, Portugal) for supplying the 1-day-old broilers used in this experiment.

REFERENCES

(1) Fontes, C. M. G. A.; Gilbert, H. J. Cellulosomes: highly efficient nanomachines designed to deconstruct plant cell wall complex carbohydrates. *Annu. Rev. Biochem.* **2010**, *79* (1), 655−681.

(2) Carvalho, A. L.; Dias, F. M.; Prates, J. A.; Nagy, T.; Gilbert, H. J.; Davies, G. J.; Ferreira, L. M. A.; Romao, M. J.; Fontes, C. M. G. Cellulosome assembly revealed by the crystal structure of the cohesin-dockerin complex. *Proc. Natl. Acad. Sci. U.S.A.* **2003**, *100*, 13809−13814.

(3) Adams, J. J.; Webb, B. A.; Spencer, H. L.; Smith, S. P. Structural characterization of type II dockerin module from the cellulosome of *Clostridium thermocellum*: calcium-induced effects on conformation and target recognition. *Biochemistry* **2005**, *44*, 2173−2182.

(4) Carvalho, A. L.; Dias, F. M.; Nagy, T.; Prates, J. A.; Proctor, M. R.; Smith, N.; Smith, N.; Bayer, E. A.; Davies, G. J.; Ferreira, L. M. A.; Romão, M. J.; Fontes, C. M. G. A.; Gilbert, H. J. Evidence for a dual binding mode of dockerin modules to cohesins. *Proc. Natl. Acad. Sci. U.S.A.* **2007**, *104*, 3089−3094.

(5) Malça, J.; Freire, F. Renewability and life-cycle energy efficiency of bioethanol and bio-ethyl tertiary ether (bioETBE): assessing the implications of allocation. *Energy, Int. J.* **2006**, *31* (15), 3326−3380.

(6) Nordon, R. E.; Craig, S. J.; Foong, F. C. Molecular engineering of the cellulosome complex for affinity and bioenergy applications. *Biotechnol. Lett.* **2009**, *31* (4), 465−476.

(7) Tamaru, Y.; Miyake, H.; Kuroda, K.; Ueda, M.; Doi, R. H. Comparative genomics of the mesophilic cellulosome-producing *Clostridium cellulovorans* and its application to biofuel production via consolidated bioprocessing. *Environ. Technol.* **2010**, *31*, 889−903.

(8) Sheridan, C. Making green. *Nat. Biotechnol.* **2009**, *27*, 1074−1076.

(9) Lynd, L. R.; Weimer, P. J.; van Zyl, W. H.; Pretorius, I. S. Microbial cellulose utilization: fundamentals and biotechnology. *Microbiol. Mol. Biol. Rev.* **2002**, *66* (3), 506−577.

(10) Lynd, L. R.; Laser, M. S.; Bransby, D.; Dale, B. E.; Davison, B.; Hamilton, R.; Himmel, M.; Keller, M.; McMillan, J. D.; Sheehan, J.; Wyman, C. E. How biotech can transform biofuels. *Nat. Biotechnol.* **2008**, *26* (2), 169−172.

(11) Tsai, S. L.; Goyal, G.; Chen, W. Surface display of a functional minicellulosome by intracellular complementation using a synthetic yeast consortium and its application to cellulose hydrolysis and ethanol production. *Appl. Environ. Microbiol.* **2010**, *76*, 7514−7520.

(12) Fan, L. H.; Zhang, Z. J.; Yu, X. Y.; Xue, Y. X.; Wang, M. M.; Tan, T. W. In vitro assembly of minicellulosomes with two scaffoldins on the yeast cell surface for cellulose saccharification and bioethanol production. *Process Biochem.* **2013**, *48* (3), 430−437.

(13) Fan, L. H.; Zhang, Z. J.; Yu, X. Y.; Xue, Y. X.; Tan, T. W. Self-surface assembly of cellulosomes with two miniscaffoldins on *Saccharomyces cerevisiae* for cellulosic ethanol production. *Proc. Natl. Acad. Sci. U.S.A.* **2012**, *109* (33), 13260−13265.

(14) Jaeho, C.; Matsuoka, S.; Chan, H.; Yukawa, H.; Inui, M.; Doi, R. H. Effect of multiple copies of cohesins on cellulase and hemicellulase activities of clostridium cellulovorans mini-cellulosomes. *J. Microbiol. Biotechnol* **2007**, *17* (11), 1782−1788.

(15) Murashima, K.; Kosugi, A.; Doi, R. H. Synergistic effects on crystalline cellulose degradation between cellulosomal cellulases from *Clostridium cellulovorans*. *J. Bacteriol.* **2002**, *184* (18), 5088−5095.

(16) Smits, C. H. M.; Annison, G. Non-starch plant polysaccharides in broiler nutrition − towards a physiologically valid approach to their determination. *World Poult. Sci.* **1996**, *52*, 203−221.

(17) Pettersson, D.; Aman, P. Enzyme supplementation of a poultry diet containing rye and wheat. *Br. J. Nutr.* **1989**, *62*, 139−149.

(18) Jozefiak, D.; Rutkowski, A.; Jensen, B. B.; Engberg, R. M. The effect of β-glucanase supplementation of barley- and oat-based diets on

growth performance and fermentation in broiler chicken gastrointestinal tract. *Br. Poult. Sci.* **2006**, *47*, 57−64.
(19) Bedford, M. R.; Morgan, A. J. The use of enzymes in poultry diets. *World Poult. Sci.* **1996**, *52*, 61−68.
(20) Ribeiro, T.; Lordelo, M. M. S.; Prates, J. A. M.; Falcão, L.; Freire, J. P. B.; Ferreira, L. M. A.; Fontes, C. M. G. A. The thermostable *β*-1,3−1,4-glucanase from *Clostridium thermocellum* improves the nutritive value of highly viscous barley-based diets for broilers. *Br. Poult. Sci.* **2012**, *53* (2), 224−234.
(21) García-Alvarez, B.; Melero, R.; Dias, F. M. V.; Prates, J. A. M.; Fontes, C. M. G. A.; Smith, S. P.; Romão, M. J.; Carvalho, A. L.; Llorca, O. Molecular architecture and structural transitions of a *Clostridium thermocellum* mini-cellulosome. *J. Mol. Biol.* **2011**, *407* (4), 571−580.
(22) Das, S. P.; Ravindran, R.; Ahmed, S.; Das, D.; Goyal, D.; Fontes, C. M. G. A.; Goyal, A. Bioethanol production involving recombinant *C. thermocellum* hydrolytic hemicellulase and fermentative microbes. *Appl. Biochem. Biotechnol.* **2012**, *127*, 1475−1488.
(23) Fontes, C. M. G. A.; Ponte, P. I. P.; Reis, T. C.; Soares, M. C.; Gama, L. T.; Dias, F. M. V.; Ferreira, L. M. A. A family 6 carbohydrate-binding module potentiates the efficiency of a recombinant xylanase used to supplement cereal-based diets for poultry. *Br. Poult. Sci.* **2004**, *45*, 648−656.
(24) Laemmli, U. K. Cleavage of structural proteins during the assembly of the head of bacteriophage T4. *Nature* **1970**, *227*, 680−685.
(25) Fontes, C. M. G. A.; Gilbert, H. J.; Hazelwood, G. P.; Clarke, J. H.; Prates, J. A. M.; McKie, V. A.; Nagy, T.; Fernandes, T. H.; Ferreira, L. M. A. A novel *Cellvibrio mixtus* family 10 xylanase that is both intracellular and expressed under non-inducing conditions. *Microbiology* **2000**, *146*, 1959−1967.
(26) Miller, G. L. The use of dinitrosalicylic acid reagent for determination of reducing sugar. *Anal. Chem.* **1959**, *31*, 426−428.
(27) Ribeiro, T.; Lordelo, M. M. S.; Ponte, P. I. P.; Macas, B.; Prates, J. A. M.; Aguiar Fontes, M.; Falcao, L.; Freire, J. P. B.; Ferreira, L. M. A.; Fontes, C. M. G. A. Levels of endogenous *β*-glucanase activity in barley affect the efficacy of exogenous enzymes used to supplement barley-based diets for poultry. *Poult. Sci.* **2011**, *90* (6), 1245−1256.
(28) Ponte, P. I. P.; Ferreira, L. M. A.; Soares, M. A. C.; Gama, L. T.; Fontes, C. M. G. A. Xylanase inhibitors affect the action of exogenous enzymes used to supplement *Triticum durum*-based diets for broiler chicks. *J. Appl. Poult. Res.* **2004**, *13*, 660−666.
(29) NRC. *Nutrient Requirements of Poultry*, 9th ed.; National Academy Press: Washington, DC, USA, 1994.
(30) *Ross Broiler Management Manual*; Aviagen: Midlothian, Scotland, 2009.
(31) Ribeiro, T.; Ponte, P. I.; Guerreiro, C. I. P. D.; Santos, H. M.; Falcao, L.; Freire, J. P. B.; Ferreira, L. M. A.; Prates, J. A. M.; Fontes, C. M. G. A.; Lordelo, M. M. A family 11 carbohydrate-binding module (CBM) improves the efficacy of a recombinant cellulase used to supplement barley-based diets for broilers at lower dosage rates. *Br. Poult. Sci.* **2008**, *49* (5), 600−608.
(32) Ruijssennars, H. J.; Hartmans, S. Plate screening method for the detection of polysaccharide-producing microorganisms. *Appl. Microbiol. Biotechnol.* **2001**, *55*, 143−149.
(33) SAS. *SAS User's Guide: Statistics*; SAS Institute: Cary, NC, USA, 2004.
(34) Choct, M.; Annison, G. Anti-nutritive activity of wheat pentosans in broiler diets. *Br. Poult. Sci.* **1990**, *30*, 811−821.
(35) Choct, M. Feed non-starch polysaccharides: chemical structures and nutritional significance. *Feed Milling Int.* **1997**, No. June, 13−26.
(36) Coutinho, P. M.; Reilly, P. J. Structure function relationships in the catalytic and starch binding domains of glucoamylase. *Protein Eng.* **1994**, *7* (3), 393−400.
(37) Tomme, P.; Warren, R. A. J.; Gilkes, N. R.; Poole, R. K. Cellulose hydrolysis by bacteria and fungi. In *Advances in Microbial Physiology*; Elsevier: Amsterdam, The Netherlands, 1995; Vol. 37, pp 1−81.
(38) Demaina, A. L.; Vaishnav, P. Production of recombinant proteins by microbes and higher organisms. *Biotechnol. Adv.* **2009**, *27*, 297−306.
(39) Kamionka, M. Engineering of therapeutic proteins production in *Escherichia coli*. *Curr. Pharm. Biotechnol.* **2011**, *12*, 268−274.

Table 1. Effects of Different Concentrations of the Free Radical-Generating System on Contents [dry weight (%)] and Fatty Acid Profiles of Lipids of Myofibrils

	control[a]	0 mM	0.2 mM	1.0 mM	3.0 mM	5.0 mM	10.0 mM
lipid content[b]	3.38 ± 0.70 a	3.46 ± 0.49 a	3.41 ± 0.65 a	3.84 ± 0.36 a	3.64 ± 0.69 a	4.01 ± 0.45 a	4.16 ± 0.92 a
fatty acid profile (%)							
C14:0	0.62	0.38	0.38	0.54	0.60	0.66	0.44
C16:1	1.35	1.56	1.39	1.59	1.87	1.51	1.89
C16:0	30.19	28.96	30.04	30.49	30.66	31.80	31.19
C18:2	15.17	14.75	12.53	10.67	7.86	7.00	9.97
C18:1	37.23	38.70	41.40	43.35	46.43	45.64	41.66
C18:0	12.25	11.68	11.86	11.27	11.58	12.66	13.28
C20:4	3.19	3.97	2.40	2.09	1.00	0.73	1.57

[a]Values in this row indicate the concentrations of the free radical-generating system. [b]Values in this row followed by different letters are significantly different ($P < 0.05$).

μm mesh), and collagen was eliminated by filtration on the sifter. The filtrate was centrifuged at 2000g for 15 min at 4 °C. The pellet was washed twice with 100 mL of a 50 mM KCl solution at pH 6.4 and once with 100 mL of 20 mM phosphate buffer at pH 6.0. Myofibrils were adjusted to a certain concentration (12 mg/mL) for use.

The protein contents of myofibrils were 88 ± 2% (dry basis). The water contents of myofibrils were 4.1 ± 0.6% (after freeze-drying).

Lipid Extraction and Analysis of the Fatty Acid Composition by Gas Chromatography and Mass Spectrometry (GC−MS). Lipids were extracted from myofibrils with a chloroform/methanol mixture [2:1 (v/v)] according to the method described by Qiu et al.[19] The extracts were dried under vacuum on a rotary evaporator and finished with a nitrogen flow.

The fatty acid composition of lipids from myofibrils was determined by gas liquid chromatography of methyl esters prepared using the method described by Qiu et al.[19] The GC−MS system consisted of a Trace Ultra gas chromatograph (ThermoFinnigan, San Jose, CA), a Trisplus automated sampler, and a quadropole DSQ II mass spectrometer. GC was performed on a TR-5MS capillary column [30 m × 0.2 mm, 0.25 μm (Thermo)]. Chromatograms and mass spectra were evaluated using Xcalibur software bundle version 2.0 (ThermoFinnigan). The relative percentages of fatty acids were determined by the peak areas.

Chemical Induction of Myofibril Oxidation. Chemical oxidation was conducted according to the method described by Morzel et al.[17] Myofibrils (final concentration of 10 mg/mL) were incubated for 3 h at 37 °C in 20 mM phosphate buffer at pH 6.0 with an $FeSO_4$/diethylenetriaminepentaacetic acid (DETAPAC)/H_2O_2 (Fenton's reagent) mixture at various concentrations (from 0 to 10 mM). The H_2O_2 concentration was adjusted by the absorbance at 240 nm. Phosphate was used in this study because, as opposed to other buffers commonly used for protein studies, it has no marked effects on protein oxidation.[20] After 3 h, no residual H_2O_2 could be detected by absorbance at 240 nm ($\varepsilon = 43.6\ M^{-1}\ cm^{-1}$), but to prevent subsequent oxidation, butylated hydroxyl toluene (BHT, at a final concentration of 1 mM) was added to the incubation medium. Samples were centrifuged at 4000g for 10 min, and the pellets were washed extensively with corresponding buffers. The pellet was washed twice with 100 mL of distilled water. The washed myofibril pellet was freeze-dried for XPS (which can investigate the surface chemical composition of biological powders obtained by freeze-drying). The protein oxidation level was evaluated by the carbonyl content and free thiol group content. Results (not shown) were similar to those of previous studies[16,17] and indicated that protein oxidation did occur.

Particle Size Distributions. Particle size distributions of myofibrils were measured by an integrated-laser light scattering instrument (Mastersizer 2000, Malvern Instruments Co. Ltd., Worcestershire, U.K.). The relative refractive index and absorption were set as 1.414 and 0.001, respectively. $D_{4,3}$ is the mean diameter in volume, whereas $D_{3,2}$ is the mean diameter in surface called the "Sauter diameter". The specific surface area (square meters per gram) was also recorded. $D_{v,0.5}$ is the size for which 50% of the sample particles have a lower size and 50% have an upper size. These indexes of protein were analyzed using Malvern Mastersizer software (version 5.12c, Malvern Instruments Co. Ltd.).

Sodium Dodecyl Sulfate−Polyacrylamide Gel Electrophoresis (SDS−PAGE). SDS−PAGE was performed on myofibrils according to the method described by Flores et al.[21] Briefly, 2 mg lyophilized samples were dissolved in 500 μL of sample buffer with and without 5% β-mercaptoethanol (β-ME), and the samples with β-ME were boiled for 3 min before centrifugation (10000g for 10 min). Then, 9 μL samples were loaded onto the polyacrylamide gel made of a 13.5% running gel and a 5% stacking gel and subjected to electrophoresis at a constant current of 25 mA per gel using a Mini-PROTEAN 3 Cell apparatus (Bio-Rad Laboratories, Hercules, CA).

Salt Solubility. The concentration of KCl in the myofibril stock suspension was increased to 0.6 M by adding 2.0 M KCl containing 20 mM sodium phosphate buffer (pH 6.5), and the solution (1 mg/mL) was kept at 0 °C for 2 h and centrifuged at 5000g and 4 °C for 30 min to separate salt-soluble fractions (supernatants) from the insolubles. Protein contents were determined by the Biuret method using bovine serum albumin as a standard. Salt solubility was expressed as the percentage of total protein.

X-ray Photoelectron Spectroscopy (XPS). X-ray photoelectron spectroscopy data were collected with an AXis Ultra DLD spectrometer (Kratos Analytical) using Al Kα monochromic X-ray radiation ($h\upsilon$ = 1486.6 eV, 150 W). The X-ray source was run at 15.0 kV and 10 mA. Samples were placed in a vacuum chamber (5.0×10^{-10} Torr). The takeoff angle of the photoelectrons was perpendicular to the sample. Elemental compositions were determined from spectra acquired at a pass energy of 160 eV. High-resolution spectra were recorded using an analyzer pass energy of 40 eV. The binding energy was set by fixing the C−(C,H) component of the C 1s peak at 284.8 eV. Data analysis was performed using PeakFit version 4.12 (SPSS Inc., Chicago, IL). Atomic concentrations were calculated from photoelectron peak areas. The areas of the bands were calculated by integration of the corresponding fitted band with a Gaussian−Lorentzian fitting procedure and after subtraction of a linear baseline (full width at half-maximum of 1.4 eV and a maximal resolution factor).

Microstructure. The microstructure of the myofibril sample was observed with a scanning electron microscope (S-3700N, Hitachi Co., Tokyo, Japan) at an operating voltage of 10 kV. The samples were deposited on silicon wafers and coated with a conductive material (gold) to ensure sufficient electron refraction. They were then mounted on an aluminum stub with epoxy and coated with a gold platinum alloy in a sputter-coating device.

Statistical Analysis. Statistical calculation was investigated using SPSS version 11.5 (SPSS Inc.) for one-way analysis of variance. The least-squares difference was used for comparison of mean values among treatments and to identify significant differences ($P < 0.05$) among treatments.

RESULTS AND DISCUSSION

Lipid Analysis. During the isolation of myofibrils, proteins are co-extracted with a certain amount of lipid. As shown in Table 1, lipid contents in dry myofibrils were between 3.38 ± 0.70 and 4.16 ± 0.92%. Oleic acid (C18:1) was the most abundant fatty acid followed by palmitic acid (C16:0). With the addition of an increasing amount of oxidizing agent, the proportions of linoleic acids (C18:2) and arachidonic acid (C20:4) decreased, but the proportions of oleic acid increased except at 10.0 mM. The decrease in the contents of these fatty acids (polyunsaturated fatty acids) might be due to the occurrence of oxidation. This result was in agreement with the report of Qiu et al.,[19] showing that the polyunsaturated fatty acids are more oxidized than the monounsaturated fatty acids.

Particle Size Distributions. The particle size distributions of myofibrils as a function of free radical-generating system concentration are shown in Figure 1. Compared with that of the control, the volume of large particles (100−1000 μm) of myofibrils treated with 37 °C decreased slightly. Promeyrat et al.[22] have found that cooking can produce a decrease in the volume of large particles of myofibrils. Addition of an oxidizing agent between 0.2 and 1.0 mM also led to a decrease in the volume of large particles in a concentration-dependent manner. However, at 3.0 mM oxidizing agent, the particle size distribution showed a relatively obvious double peak, indicating that the distributions of large particles and small particles increased simultaneously. At 5.0 and 10.0 mM oxidizing agent, the particle size range between 10 and 100 μm increased remarkably, while the particle size range between 100 and 1000 μm decreased correspondingly.

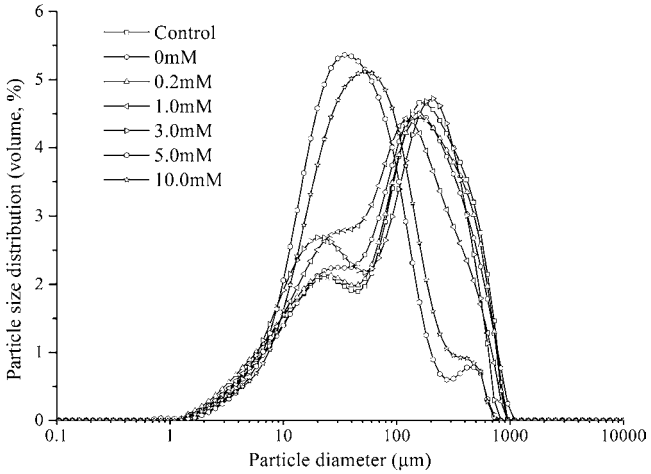

Figure 1. Effect of different concentrations of the free radical-generating system on particle size distributions of myofibrils.

As shown in Table 2, the $D_{3,2}$ value of myofibrils treated with 37 °C showed no significant difference ($P > 0.05$) compared to that of the control, while the value of $D_{4,3}$ decreased significantly ($P < 0.05$). Because large droplets or droplet aggregates have weights in the calculation of $D_{4,3}$ higher than that in the calculation of $D_{3,2}$, samples with similar $D_{3,2}$ values but different $D_{4,3}$ values would differ mainly in the amount of large droplets or droplet aggregates. Addition of an oxidizing agent could produce a decrease in $D_{3,2}$ and $D_{4,3}$, but not in a concentration-dependent manner. Under poorly oxidative conditions (0.2 and 0.5 mM), $D_{3,2}$ and $D_{4,3}$ decreased significantly ($P < 0.05$). Between 1.0 and 3.0 mM oxidizing agent, $D_{3,2}$ increased significantly ($P < 0.05$), whereas the value of $D_{4,3}$ further decreased at 1.0 mM. The lowest values of $D_{3,2}$ and $D_{4,3}$ (21.33 and 63.93 μm, respectively) were observed at 5.0 mM oxidizing agent. At 10.0 mM oxidizing agent, $D_{3,2}$ and $D_{4,3}$ increased slightly compared to the values at 5.0 mM. Changes in $D_{v,0.5}$ were similar to changes in $D_{4,3}$. For a specific surface area, a reciprocal change compared to $D_{3,2}$ was also found during the oxidative process. Span is the width of the distribution regardless of the median size, indicating the uniformity of the measured system.[23] Compared to that of the control, a significant increase in span (from 3.57 to 3.81) was observed after incubation for 3 h at 37 °C without an oxidizing agent. Span increased to a maximum at 1.0 mM and thereafter decreased continuously during the later stage.

Protein oxidation can lead to changes in the physical properties of the proteins, including cleavage of peptide bonds (fragmentation), modification of amino acid side chains, and formation of intra- and intermolecular cross-links.[12,13] The hydrophobic surfaces frequently act as the interfaces between the interacting molecules. Protein oxidation can enhance protein surface hydrophobicity by exposing hydrophobic amino acids, which are buried inside in native status.[16] The heat treatment also can induce partial unfolding of the proteins, thereby exposing certain sites that are normally hidden within proteins.[24] A decrease in the particle size due to heat treatment and oxidation could be explained by the formation of intermolecular cross-links and protein aggregates, and these aggregates look like a disorganized stack of fibers with no preferential orientation.[22] Bityrosine and Schiff base formation between protein molecules can also lead to polymerization and aggregation.[16,20] An increase in span after incubation for 3 h at 37 °C without an oxidizing agent or under poorly oxidative conditions confirmed this cross-link process.

Table 2. Effects of Different Concentrations of the Free Radical-Generating System on Average Particle Size, Specific Surface Area, and Span of Myofibrils[a]

	$D_{3,2}$ (μm)	$D_{4,3}$ (μm)	$D_{v,0.5}$ (μm)	specific surface area (m^2/g)	span
control[b]	28.14 ± 0.05 e	166.82 ± 1.34 f	114.39 ± 1.44 f	0.213 ± 0.001 a	3.57 ± 0.03 b
0 mM	28.44 ± 0.49 e	157.29 ± 1.83 e	101.45 ± 1.62 e	0.211 ± 0.004 a	3.81 ± 0.04 c
0.2 mM	25.10 ± 0.26 c	157.96 ± 0.97 e	104.27 ± 0.73 e	0.239 ± 0.003 c	3.79 ± 0.02 c
1.0 mM	25.42 ± 0.17 c	129.20 ± 0.81 c	77.90 ± 0.87 c	0.236 ± 0.002 c	4.17 ± 0.03 d
3.0 mM	27.01 ± 1.46 d	137.82 ± 6.49 d	92.98 ± 7.08 d	0.222 ± 0.012 b	3.60 ± 0.16 b
5.0 mM	21.33 ± 0.35 a	63.93 ± 4.84 a	36.43 ± 2.37 a	0.281 ± 0.005 e	3.29 ± 0.17 a
10.0 mM	23.73 ± 0.06 b	74.94 ± 2.36 b	44.61 ± 1.73 b	0.253 ± 0.001 d	3.45 ± 0.05 ab

[a]Values in the same column followed by different letters are significantly different ($P < 0.05$). [b]Values in this column are the concentrations of the free radical-generating system.

SDS−PAGE and Salt Solubility Analysis. As shown in Figure 2, in the absence of β-ME, myosin heavy chain (MHC)

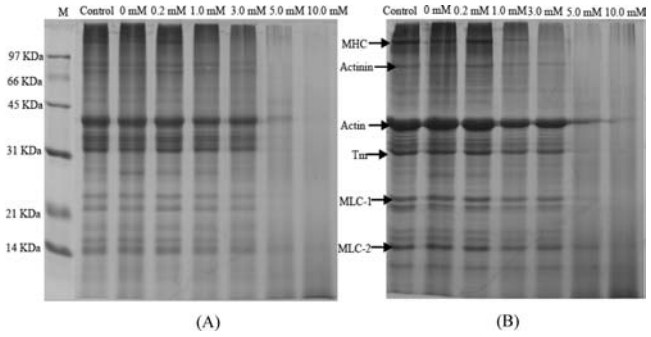

Figure 2. Effect of different concentrations of the free radical-generating system on the SDS−PAGE pattern of myofibrils in the absence (A) and presence (B) of 5% β-mercaptoethanol.

gradually showed a decreased band intensity and even vanished after the addition of an oxidizing agent. All bands were lost upon addition of excess oxidizing agent (>5.0 mM), indicating over-cross-linking of myofibrillar proteins. MHC under highly oxidative conditions could not be recovered in the presence of β-ME. This indicated that most cross-linking that originated from myosin was not only through disulfide bonds. The actin band was relatively more stable, and their band intensity exhibited a progressive decrease at higher oxidant concentrations. These results were in accordance with a previous work.[17] Under highly oxidative conditions, the band appeared to be much more diffused, indicating the degradation or fragmentation of myofibrils. As shown in Figure 3, salt solubility

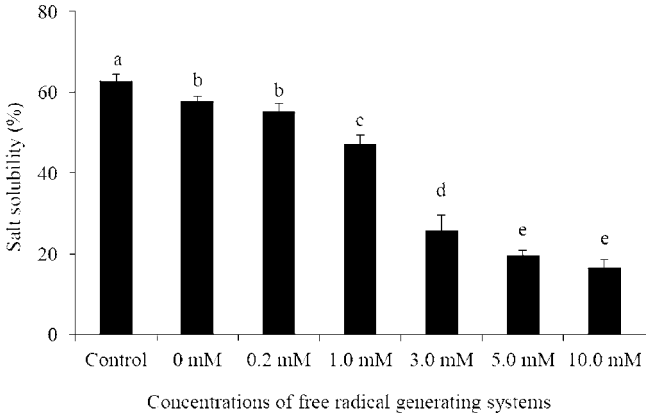

Figure 3. Effect of different concentrations of the free radical-generating system on the salt solubility of myofibrils.

decreased with an oxidizing agent ($P < 0.05$). Salt solubility can reflect the extent of myofibril aggregation after oxidation.[25] Protein aggregates induced by hydroxyl radicals can be formed mainly via bityrosine formation and carbonyl formation.[17] Aggregation due to disulfide cross-linkages is also involved. Fragmentation of the protein is a consequence of the direct attack by hydroxyl radicals on the polypeptide backbone or on the side chains of glutamyl or prolyl residues.[26]

XPS Analysis. XPS analysis was used to identify the chemical functions and the components located at the surface of myofibrils and to try to quantify the surface concentrations of components.

Surface Composition. As expected, XPS survey scans obtained from myofibrils give major signals corresponding to C, O, N, and P (Table 3). It was notable that the detection of S 2p elements was possible due to the very good detectivity of the XPS equipment, but this element was neglected because of its very low content and high noise level. The relative atomic concentrations of carbon, nitrogen, oxygen, and phosphorus measured for myofibrils are listed in Table 3. The relative atomic concentrations of carbon showed no significant difference after heat treatment and oxidation. The relative atomic concentrations of nitrogen and oxygen changed significantly ($P < 0.05$). These results indicate that the surface properties of myofibrils have changed after oxidation. Zhao et al.[27] showed the correlation was found between the elemental composition and particle size of ginger powder. Differences in particle size distributions could lead to slight differences in elemental composition.[27] However, in this work, no statistically significant correlation was found between the elemental composition and particle size of myofibrils. This discrepancy might be attributed to not only changes in particle sizes but also oxidation and structural changes that involved changes in elemental composition during the oxidative process. Myofibril aggregation induced by oxidation, heat treatment, and freeze-drying could also contribute to this phenomenon. The P 2p element was detected in this work, which confirmed the presence of phospholipids at the myofibril surface. However, no statistically significant correlation was found between the P 2p element atomic concentration at the surface and the lipid content of myofibrils. In addition, N2/P was changed during the oxidative processing. These results indicated that only a portion of the phospholipids are located at the surface layers of myofibrils, and the phospholipid distribution was altered during the oxidative processing.

Because of the presence of the lipid within the surface layers of myofibrils and different amino acids that are prone to being located in the surface layers of myofibrils, the decreased N/C atom ratios and O/C ratios (0.111 and 0.222, respectively) were compared to the theroitcial chemical composition of $C_1H_{1.88}O_{0.45}N_{0.27}S_{0.005}$ [according to amino acid analysis (data not shown)]. The changes in N/C atom ratios might be caused by protein structural changes, oxidation, and phospholipid distribution. Protein oxidation can result in conformational changes in the myofibrillar protein.[12,28] Under highly oxidative conditions, protein fragmentation led to more amino groups exposed, resulting in increases in N/C ratios. Oxidation of the myofibril surface[29] and a change in the interaction between myofibrils yield increases in lipid-induced O/C ratios. Decreases in O/C ratios might be due to protein fragmentation.

C 1s Spectra. The XPS survey scans for myofibrils were analyzed to assign the C 1s peaks to chemical functions. As shown in Figure 4, four main protein functional groups for the C 1s peak were identified. The major component at 284.8 eV (C1) was due to C making a single bond with C or H (C−C or C−H, respectively) and indicated the presence of aliphatic lateral chains of amino acids and lipid in the myofibrils.[7,30,31] The peak (C2) at 286.1−286.2 eV was attributed to C making a single bond with O or N (C−O or C−N, respectively) in amide functions in proteins.[7,30] The peak (C3) at 287.5−287.7 eV was identified as C making two single bonds or one double bond with O (O−C−O, O=C−N, or O=C) in ester and amide functions in proteins.[30,32] Lastly, the carboxyl group was found at 288.7−288.9 eV (C4), which was C making one double or single bond with O (O=C−OH or O=C−OR).[7,32]

Table 3. Surface Chemical Compositions Determined by XPS and Peak Assignments of Control Myofibrils and Oxidized Myofibrils[a]

	atomic abundance (%) of elements at the surface of myofibrillar proteins						
function	control[b]	0 mM	0.2 mM	1.0 mM	3.0 mM	5.0 mM	10.0 mM
C	74.70 ± 2.02 a	75.86 ± 1.97 a	73.74 ± 2.41 a	71.85 ± 1.17 a	75.23 ± 2.45 a	73.83 ± 0.12 a	73.68 ± 1.52 a
N	8.31 ± 0.94 bc	8.59 ± 0.81 bc	6.93 ± 1.01 ab	7.60 ± 0.98 ab	6.12 ± 1.04 a	8.41 ± 1.20 bc	9.61 ± 0.66 c
O	16.54 ± 1.46 ab	15.00 ± 1.12 a	18.86 ± 1.77 bc	20.19 ± 1.29 c	18.00 ± 1.39 bc	17.20 ± 1.20 ab	16.27 ± 1.16 ab
P	0.46 ± 0.05 ab	0.57 ± 0.06 bc	0.47 ± 0.06 ab	0.36 ± 0.07 a	0.66 ± 0.09 c	0.56 ± 0.05 bc	0.45 ± 0.06 ab
O/C	0.222 ± 0.025 ab	0.198 ± 0.020 a	0.256 ± 0.032 bc	0.281 ± 0.021 c	0.240 ± 0.026 abc	0.233 ± 0.016 abc	0.221 ± 0.020 ab
N/C	0.111 ± 0.015 ab	0.113 ± 0.014 ab	0.094 ± 0.016 a	0.106 ± 0.015 ab	0.081 ± 0.017 a	0.114 ± 0.016 ab	0.130 ± 0.011 b
P/C × 100	0.62 ± 0.08 ab	0.75 ± 0.09 bc	0.64 ± 0.06 ab	0.50 ± 0.10 a	0.88 ± 0.13 c	0.76 ± 0.07 bc	0.61 ± 0.09 ab
C−C,C−H	284.8	284.8	284.8	284.8	284.8	284.8	284.8
C1	69.63 ± 2.58 b	69.04 ± 1.59 b	68.04 ± 2.85 b	66.39 ± 2.26 ab	62.45 ± 1.63 a	69.37 ± 2.99 b	67.98 ± 2.05 b
C−O,C−N	286.1	286.2	286.1	286.2	286.2	286.1	286.1
C2	18.62 ± 2.01 a	18.71 ± 1.61 a	20.09 ± 1.16 a	18.96 ± 0.89 a	23.00 ± 1.88 b	18.03 ± 1.3 a	19.71 ± 0.93 a
O−C−O,C=O	287.7	287.6	287.6	287.5	287.5	287.6	287.7
C3	8.06 ± 1.36 ab	8.34 ± 1.00 ab	7.22 ± 0.84 a	8.64 ± 0.42 ab	9.66 ± 1.21 b	7.35 ± 1.18 a	7.65 ± 1.52 a
O=C−OH,O=C−OR	288.7	288.7	288.8	288.8	288.9	288.8	288.9
C4	3.69 ± 0.52 a	3.90 ± 0.92 a	4.66 ± 0.89 ab	6.01 ± 0.96 b	4.89 ± 1.49 ab	5.25 ± 0.84 ab	4.66 ± 0.62 ab
NH,NH2	399.9	399.8	399.8	399.9	399.8	399.7	399.9
N1	92.28 ± 0.86 c	91.50 ± 1.22 bc	92.31 ± 1.18 c	91.29 ± 1.46 bc	91.41 ± 1.05 bc	89.45 ± 1.56 ab	89.10 ± 1.16 a
NH3	401.3	401.1	401.1	401.3	401.2	401.1	401.3
N2	7.72 ± 0.86 a	8.50 ± 1.22 ab	7.69 ± 1.18 a	8.71 ± 1.46 ab	8.59 ± 1.05 ab	10.55 ± 1.56 bc	10.90 ± 1.16 c
O=C−OR,O=C−N	531.4	531.4	531.2	531.2	531.4	531.3	531.4
O1	44.71 ± 2.00 b	47.15 ± 2.60 b	33.44 ± 1.58 a	32.44 ± 4.55 a	36.58 ± 2.56 a	43.86 ± 4.19 b	47.81 ± 4.00 b
C−OH,C−O−C,C−O	532.5	532.5	532.4	532.3	532.4	532.3	532.5
O2	39.40 ± 3.60 a	38.22 ± 3.95 a	47.19 ± 3.29 b	46.91 ± 2.23 b	41.89 ± 4.18 ab	41.19 ± 1.77 a	38.13 ± 2.62 a
O=C−OR	533.8	533.7	533.7	533.7	533.8	533.6	533.8
O3	15.89 ± 1.61 a	14.63 ± 1.35 a	19.37 ± 2.16 b	20.66 ± 2.31 b	21.53 ± 1.92 b	14.95 ± 2.42 a	14.06 ± 1.42 a
O1/C	0.099 ± 0.007 a	0.093 ± 0.004 a	0.086 ± 0.014 a	0.092 ± 0.020 a	0.087 ± 0.006 a	0.102 ± 0.003 a	0.106 ± 0.019 a
O2/C	0.088 ± 0.018 a	0.076 ± 0.016 a	0.120 ± 0.007 bc	0.132 ± 0.004 c	0.101 ± 0.021 ab	0.096 ± 0.011 ab	0.084 ± 0.002 a
O3/C	0.035 ± 0.001 a	0.029 ± 0.001 a	0.050 ± 0.012 b	0.058 ± 0.003 b	0.051 ± 0.001 b	0.035 ± 0.008 a	0.031 ± 0.001 a
N1/C	0.103 ± 0.014 bc	0.103 ± 0.011 bc	0.087 ± 0.015 ab	0.096 ± 0.012 ab	0.075 ± 0.015 a	0.102 ± 0.016 bc	0.116 ± 0.009 c
N2/P	1.39 ± 0.17 bc	1.29 ± 0.23 ab	1.12 ± 0.14 ab	1.89 ± 0.44 c	0.81 ± 0.26 a	1.57 ± 0.14 bc	2.33 ± 0.12 d
O1/N1	0.971 ± 0.12 ab	0.902 ± 0.056 a	0.998 ± 0.148 ab	0.966 ± 0.251 ab	1.194 ± 0.181 b	1.012 ± 0.139 ab	0.915 ± 0.155 ab

[a]Values in the same row followed by different letters are significantly different ($P < 0.05$). [b]Values in this row indicate the concentrations of the free radical-generating system. [c]The atomic abundance of C, N, O, and P is shown as a percentage of total elements (%). O/C, N/C, etc., represent the ratios of the corresponding element atoms. Values (electronvolts) of O=C−OR,O=C−N, C−O,C−N, etc., represent the binding energies of the corresponding element components. Values of C1, C2, etc., represent the percentages of the total corresponding element (%).

dx.doi.org/10.1021/jf501272p | J. Agric. Food Chem. 2014, 62, 7507−7514

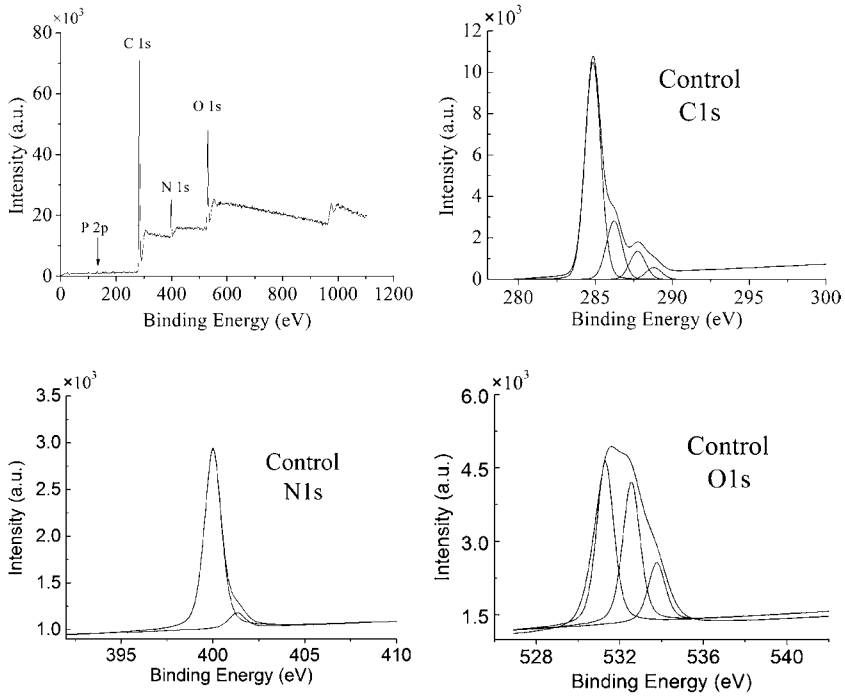

Figure 4. XPS survey spectra and typical deconvoluted C 1s, N 1s, and O 1s high-resolution XPS spectra of myofibrils.

The corresponding results of the curve fitting analysis are listed in Table 3. The binding area of C1 showed no significant difference ($P > 0.05$) under oxidative conditions from 0 and 1.0 mM. At 3.0 mM oxidizing agent, it decreased significantly ($P < 0.05$) and increased to the former value at 5.0 and 10.0 mM oxidizing agent. The key points for the change in the binding area of C2 and C3 were also observed at 3.0 mM oxidizing agent ($P < 0.05$). Reciprocal changes in the binding area of C4 were found during oxidative processing.

Amino acids with the NH or NH_2 moiety on their side chains can react with free oxygenated radicals (such as $OH^{\bullet}$ generated by Fenton reaction) that involves the formation of carbonyl moieties.[33] Protein carbonyl derivatives can be generated through oxidative cleavage of proteins by either the α-amidation pathway or oxidation of glutamyl side chains, leading to the formation of a peptide in which the N-terminal amino acid is blocked by an α-ketoacyl derivative.[12,13] The changes in C 1s binding area, especially for C3 and C4 during oxidative processing, could be due to the formation of carbonyl groups. Protein fragmentation might result in the C3 and C4 binding area decreasing during the last oxidative processing. In addition, myofibril particle size variations due to aggregation could also contribute to changes in C 1s spectra.[7] Myofibril aggregation might alter their surface properties by exposure of different amino acid residues.

N 1s Spectra. Figure 4 shows the peak decomposition for the N 1s peak, decomposed into two peaks. The peak (N1) at 399.7−399.9 eV was attributed to uncharged nitrogen, typical of amine (C−NH2)[7] or amide (O═C−NH2 and O═C−NH−C) in proteins.[7,30] The peak (N2) at 401.1−401.3 eV was attributed to positively charged N ($C-\underline{N}H_3^+$) in protonated amine or quaternary ammonium functions in proteins.[32]

As shown in Table 3, upon addition of an increasing amount of oxidizing agent, the binding area of N1 decreased slightly to the minimum of 89.10% ($P > 0.05$) at 10.0 mM oxidizing agent. Reciprocal changes in the binding area of N2 were found during oxidative processing. An increase for positively charged N ($C-\underline{N}H_3^+$) of N2 indicated that amino acid residues in proteins were attacked by $OH^{\bullet}$. Protonated nitrogen was formatted during protein carbonylation.[12,13,34] Phospholipids are also attributed to protonated amine. Alteration of the phospholipid distribution could partially explain changes in N2.

O 1s Spectra. The O 1s peak is decomposed into three peaks. The peak (O1) at 531.2−531.4 eV is attributed to O doubly bound to C (O═C−O, O═C−N, or O═C−OH), due to amide, ester, and carboxyl in proteins.[7,31] Two oxygen atoms bound to phosphorus (P═O and $P-O^-$) in phospholipids also contribute below 532 eV.[8] The peak (O2) at 532.3−532.5 eV is attributed to O making single bonds with C (C−OH, C−O, or C−O−C) in amino acid side chains of proteins.[7,30] The peak (O3) at 533.6−533.8 eV is attributed to O singly bound to C (O═C−O−R) in ester and carboxyl functions in proteins.[7] However, O2 may be due to the overlapping of carboxyl groups,[30] peptide groups,[30] or C−O groups,[32] and O1 may be due to similar functional groups.[31]

As shown in Table 3, the binding area of O1 decreased first and then increased during the later stage. Reciprocal changes in the binding area of O2 and O3 were found during the oxidative processing. Some researchers suggested that the O 1s spectra did not provide useful chemical-state information because so many O-containing species were present, which could not be resolved by XPS because of their closely spaced binding energies,[5,35] but using these values, the results in this study suggested that O-containing functional groups of the myofibril surface changed significantly after oxidation. In addition, a significant correlation between the binding area of O1 and N2/C was observed. However, no significant correlations between N2/C and C3 and P were found. These results might imply that protein carbonylation and phospholipid alteration are involved in changes in O 1s spectra.

Microstructure. To understand the effect of oxidation on the surface characterization of myofibrils, the microstructure

dx.doi.org/10.1021/jf501272p | J. Agric. Food Chem. 2014, 62, 7507−7514

was observed by scanning electron microscopy (SEM) at a magnification factor of 300-fold. Figure 5 shows a set of SEM images of myofibrils. Myofibrils (control) showed a complex heterogeneous structure consisting of clumps with different sizes and shapes. Incubation for 3 h at 37 °C without an oxidizing agent led to a slight increase in clump size. This observation was consistent with particle size analysis. Addition of 0.2−1.0 mM oxidizing agent could induce the appearance of the filaceous curliness structure. In particular, fibrous curliness was observed at 0.2 mM oxidizing agent. Formation of the structures described above on the surface of oxidized myofibrils had been attributed to modification of amino acid side chains that rendered protein intra- and intermolecular cross-links and aggregates. Some relative homogeneous flake or clumps structures were exhibited in the samples of 3.0, 5.0, and 10.0 mM oxidizing agent. These structural features suggested protein fragmentation due to cleavage of peptide bonds. These results of the microstructure analysis were in agreement with span (Table 2).

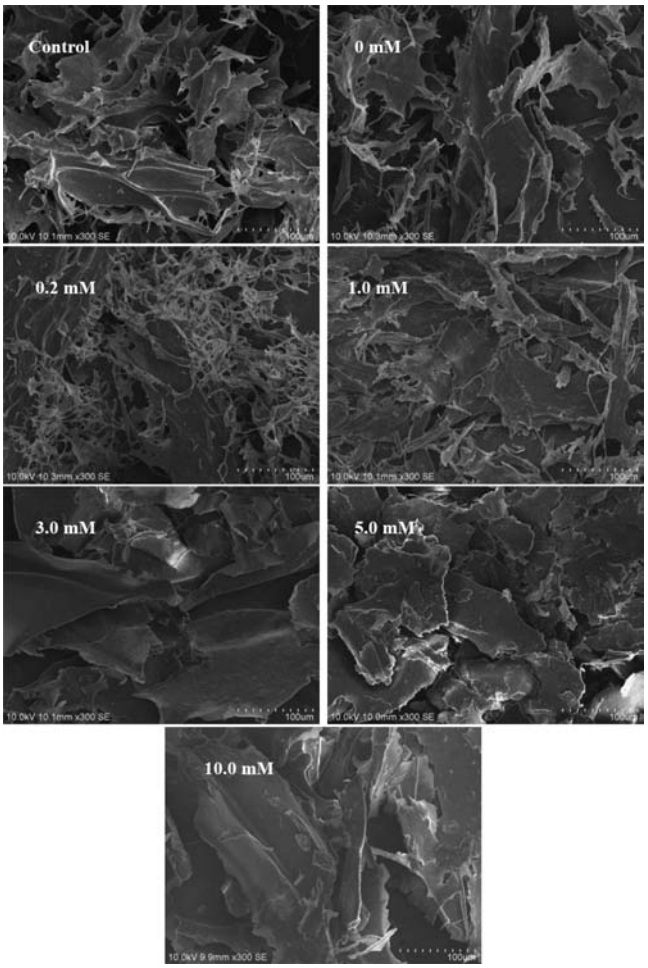

Figure 5. Scanning electron micrographs of control myofibrils and oxidized myofibrils.

In this investigation, particle size, XPS, and SEM analysis yielded complementary and essential information for the evaluation of myofibril surface changes during oxidative processing. Results presented as XPS data, including the C 1s, N 1s, and O 1s spectra, led to the conclusion that surface compositions were modified during oxidative processing, which correlate with cleavage of peptide bonds, modification of amino acid side chains, formation of intra- and intermolecular cross-links, and phospholipid alteration. The results of SEM analysis further confirmed it. This study would be helpful for understanding the relationship between surface characterization and functional properties of myofibrils after oxidation.

AUTHOR INFORMATION

Corresponding Authors

*Telephone and fax: +86 20 87113914. E-mail: femmzhao@scut.edu.cn.

*Telephone and fax: +86 20 22236089. E-mail: hfzhao@scut.edu.cn.

Funding

We are grateful to the National Natural Science Foundation of China (31201387), the Natural Science Foundation of Guangdong Province (S2012040007533), and the Doctoral Fund of the Ministry of Education of China (20120172120017) for their financial support.

Notes

The authors declare no competing financial interest.

REFERENCES

(1) Razumovsky, L.; Damodaran, S. Surface activity-compressibility relationship of proteins at the air-water interface. *Langmuir* **1999**, *15*, 1392−1399.

(2) Goto, S.; Nishioka, T.; Kanehisa, M. LIGAND: Chemical database for enzyme reactions. *Bioinformatics* **1998**, *14*, 591−599.

(3) Spolar, R. S.; Record, M. T. Coupling of local folding to site-specific binding of proteins to DNA. *Science* **1994**, *263*, 777−784.

(4) Poirrette, A. R.; Artymiuk, P. J.; Rice, D. W.; Willett, P. Comparison of protein surfaces using a genetic algorithm. *J. Comput.-Aided Mol. Des.* **1997**, *11*, 557−569.

(5) Zhao, X.; Chen, J.; Zhu, Q.; Du, F.; Ao, Q.; Liu, J. Surface characterization of 7S and 11S globulin powders from soy protein examined by X-ray photoelectron spectroscopy and scanning electron microscopy. *Colloids Surf., B* **2011**, *86*, 260−266.

(6) Faldt, P.; Bergenstahl, B.; Carlsson, G. The surface coverage of fat on food powders analyzed by ESCA (electron spectroscopy for chemical analysis). *Food Struct.* **1993**, *12*, 225−234.

(7) Saad, M.; Gaiani, C.; Mullet, M.; Scher, J.; Cuq, B. X-ray Photoelectron Spectroscopy for Wheat Powders: Measurement of Surface Chemical Composition. *J. Agric. Food Chem.* **2011**, *59*, 1527−1540.

(8) Rouxhet, P.; Misselyn-Bauduin, A.; Ahimou, F.; Genet, M.; Adriaensen, Y.; Desille, T.; Bodson, P.; Deroanne, C. XPS analysis of food products: Toward chemical functions and molecular compounds. *Surf. Interface Anal.* **2008**, *40*, 718−724.

(9) Chelh, I.; Gatellier, P.; Santé-Lhoutellier, V. Characterisation of fluorescent Schiff bases formed during oxidation of pig myofibrils. *Meat Sci.* **2007**, *76*, 210−215.

(10) Sun, W.; Cui, C.; Zhao, M.; Zhao, Q.; Yang, B. Effects of composition and oxidation of proteins on their solubility, aggregation and proteolytic susceptibility during processing of Cantonese sausage. *Food Chem.* **2011**, *124*, 336−341.

(11) Sun, W.; Zhao, Q.; Zhao, M.; Yang, B.; Cui, C.; Ren, J. Structural evaluation of myofibrillar proteins during processing of Cantonese sausage by Raman spectroscopy. *J. Agric. Food Chem.* **2011**, *59*, 11070−11077.

(12) Estévez, M. Protein carbonyls in meat systems: A review. *Meat Sci.* **2011**, *89*, 259−279.

(13) Lund, M. N.; Heinonen, M.; Baron, C. P.; Estévez, M. Protein oxidation in muscle foods: A review. *Mol. Nutr. Food Res.* **2011**, *55*, 83−95.

(14) Park, D.; Xiong, Y. L.; Alderton, A. L.; Ooizumi, T. Biochemical changes in myofibrillar protein isolates exposed to three oxidizing systems. *J. Agric. Food Chem.* **2006**, *54*, 4445−4451.
(15) Park, D.; Xiong, Y. L.; Alderton, A. L. Concentration effects of hydroxyl radical oxidizing systems on biochemical properties of porcine muscle myofibrillar protein. *Food Chem.* **2007**, *101*, 1239−1246.
(16) Sante-Lhoutellier, V.; Aubry, L.; Gatellier, P. Effect of oxidation on in vitro digestibility of skeletal muscle myofibrillar proteins. *J. Agric. Food Chem.* **2007**, *55*, 5343−5348.
(17) Morzel, M.; Gatellier, P.; Sayd, T.; Renerre, M.; Laville, E. Chemical oxidation decreases proteolytic susceptibility of skeletal muscle myofibrillar proteins. *Meat Sci.* **2006**, *73*, 536−543.
(18) Martinaud, A.; Mercier, Y.; Marinova, P.; Tassy, C.; Gatellier, P.; Renerre, M. Comparison of oxidative processes on myofibrillar proteins from beef during maturation and by different model oxidation systems. *J. Agric. Food Chem.* **1997**, *45*, 2481−2487.
(19) Qiu, C.; Zhao, M.; Sun, W.; Zhou, F.; Cui, C. Changes in lipid composition, fatty acid profile and lipid oxidative stability during Cantonese sausage processing. *Meat Sci.* **2013**, *93*, 525−532.
(20) Davies, K. Protein damage and degradation by oxygen radicals. I. General aspects. *J. Biol. Chem.* **1987**, *262*, 9895−9901.
(21) Flores, M.; Barat, J. M.; Aristoy, M.; Peris, M. M.; Grau, R.; Toldrá, F. Accelerated processing of dry-cured ham. Part 2. Influence of brine thawing/salting operation on proteolysis and sensory acceptability. *Meat Sci.* **2006**, *72*, 766−772.
(22) Promeyrat, A.; Gatellier, P.; Lebret, B.; Kajak-Siemaszko, K.; Aubry, L.; Santé-Lhoutellier, V. Evaluation of protein aggregation in cooked meat. *Food Chem.* **2010**, *121*, 412−417.
(23) Palazolo, G. G.; Sorgentini, D. A.; Wagner, J. R. Emulsifying properties and surface behavior of native and denatured whey soy proteins in comparison with other proteins. Creaming stability of oil-in-water emulsions. *J. Am. Oil Chem. Soc.* **2004**, *81*, 625−632.
(24) Chelh, I.; Gatellier, P.; Santé-Lhoutellier, V. Technical note: A simplified procedure for myofibril hydrophobicity determination. *Meat Sci.* **2006**, *74*, 681−683.
(25) Ooizumi, T.; Xiong, Y. L. Biochemical susceptibility of myosin in chicken myofibrils subjected to hydroxyl radical oxidizing systems. *J. Agric. Food Chem.* **2004**, *52*, 4303−4307.
(26) Liu, G.; Xiong, Y. L. L. Electrophoretic pattern, thermal denaturation, and in vitro digestibility of oxidized myosin. *J. Agric. Food Chem.* **2000**, *48*, 624−630.
(27) Zhao, X.; Ao, Q.; Du, F.; Zhu, J.; Liu, J. Surface characterization of ginger powder examined by X-ray photoelectron spectroscopy and scanning electron microscopy. *Colloids Surf., B* **2010**, *79*, 494−500.
(28) Sun, W.; Zhou, F.; Sun, D.-W.; Zhao, M. Effect of Oxidation on the Emulsifying Properties of Myofibrillar Proteins. *Food Bioprocess Technol.* **2013**, *6*, 1703−1712.
(29) Salaita, G. N.; Ma, F.; Parker, T. C.; Hoflund, G. B. Weathering properties of treated southern yellow pine wood examined by X-ray photoelectron spectroscopy, scanning electron microscopy and physical characterization. *Appl. Surf. Sci.* **2008**, *254*, 3925−3934.
(30) Xiao, S.; Textor, M.; Spencer, N.; Wieland, M.; Keller, B.; Sigrist, H. Immobilization of the cell-adhesive peptide Arg-Gly-Asp-Cys (RGDC) on titanium surfaces by covalent chemical attachment. *J. Mater. Sci.: Mater. Med.* **1997**, *8*, 867−872.
(31) Premathilaka, S.; Hyland, M.; Chen, X.; Bansal, B. A study of the effects of surface chemistry on the initial deposition mechanisms of dairy fouling. *Food Bioprod. Process.* **2006**, *84*, 265−273.
(32) Vinnichenko, M.; Chevolleau, T.; Pham, M.; Poperenko, L.; Maitz, M. Spectroellipsometric, AFM and XPS probing of stainless steel surfaces subjected to biological influences. *Appl. Surf. Sci.* **2002**, *201*, 41−50.
(33) Butterfield, D. A.; Stadtman, E. R. Protein oxidation processes in aging brain. *Adv. Cell Aging Gerontol.* **1997**, *2*, 161−191.
(34) Hawkins, C. L.; Davies, M. J. Hypochlorite-induced damage to proteins: Formation of nitrogen-centred radicals from lysine residues and their role in protein fragmentation. *Biochem. J.* **1998**, *332*, 617−625.
(35) Beamson, G.; Briggs, D. *High resolution XPS of organic polymers: The Scienta ESCA300 database*, 1st ed.; John Wiley & Sons: New York, 1992; Vol. *4*, p 96.

wines produced from the hybrid grapes Corot noir and Marechal Foch, as compared to an average of 500 mg/L in *vinifera* wines.[18−20] Furthermore, vinification techniques aimed at increasing hybrid wine condensed tannin, including extended maceration, pectinase enzyme addition, and exogenous tannin addition, were shown to be ineffective.[8] However, concentrations of tannin in the skin and seeds of the hybrid grapes were comparable to literature reports of tannin in red *vinifera* grapes.[18,19] Although interpretation of these results is complicated by the fact that the studies were performed in different regions and with different winemaking protocols, they suggest that variation in wine tannin may result from differences in grape tannin extractability rather than grape tannin concentration. The impact of tannin extractability on final wine tannin concentrations has been recognized in studies on *vinifera*. In contrast to anthocyanin pigments, tannins in grapes are reported to be uncorrelated with tannins in finished wines, even under identical winemaking conditions.[21] Multiple authors have reported that a significant portion of grape tannin remains bound to insoluble cell wall materials after fermentation and that the ability of both berry skin and flesh cell walls to bind tannin could account for the incomplete extraction of tannin into wine.[21,22] Potentially, greater tannin−cell wall interactions and thus poorer tannin extractability could also explain low tannin concentrations in red hybrid wines.

In this work, we first confirmed that tannin concentrations were significantly lower in wines produced from hybrid grapes in comparison to *vinifera*, as had been observed in limited previous studies. We then evaluated two separate hypotheses to explain these differences, either that the grape species differed in tannin concentration or that they differed in tannin extractability. The latter was investigated by quantifying tannin binding by grape cell wall material and appeared to be the more important explanation. Finally, we hypothesized that differences in tannin binding among cell wall fractions could be related to differences in the major tannin-binding macromolecular classes, protein and pectin.

MATERIALS AND METHODS

Chemical Reagents. Ethanol (reagent grade), (+)-catechin hydrate, albumin from bovine serum, iron(III) chloride, triethanolamine (TEA), sodium dodecyl sulfate (SDS), Viscozyme L, sodium tetraborate, 3-phenylphenol, sulfamic acid, and D-(+)-galacturonic acid monohydrate were obtained from Sigma-Aldrich (St. Louis, MO, USA). Acetic acid, sodium hydroxide, hydrochloric acid, potassium metabisulfite, acetone, L-(+)-tartaric acid, Clinitest tablets (Bayer, Pittsburgh, PA, USA), sodium acetate anhydrous, and sulfuric acid were sourced from Fisher Scientific (Waltham, MA, USA). A grape tannin extract, BioTan, was provided by Laffort (Petaluma, CA, USA). Diammonium hydrogen phosphate (DAP) was purchased from Presque Isle Wine Cellars (North East, PA, USA). GoFerm Protect, Fermaid K, and Lalvin ICV-GRE yeast were obtained from Lallemand (Santa Rosa, CA, USA).

Survey of Tannins in *V. vinifera* versus Hybrid (*Vitis* spp.) Wines. Ten commercial *vinifera* varietal wines and 10 interspecific hybrid wines from the Finger Lakes (NY) American Viticultural Area (AVA) were purchased from a local store (Geneva, NY, USA). Wines covered the vintages 2010−2012. Additionally, two *V. vinifera* varietals and two interspecific hybrid wines from these vintages were provided by the Cornell Vinification and Brewing facility (Geneva, NY, USA). Protein-precipitable tannin was measured using the Adams−Harbertson assay, as described elsewhere.[23]

Grape Sample Collection. Six *vinifera* cultivars (Pinot noir, Merlot, Lemberger, Sangiovese, Cabernet Sauvignon, and Cabernet franc) and six *Vitis* spp. hybrids (French−American hybrids Baco noir, Leon Millot, Maréchal Foch, and DeChaunac; neo-American hybrids Corot noir and Noiret) were hand harvested across two vineyard locations within the Finger Lakes AVA in New York state at commercial harvest time points in 2012. Three kilograms of each cultivar was collected, from which 50 berries were randomly selected and pressed for juice analysis. Titratable acidity was measured using a Titrino Plus 848 doser and 869 autosampler (Metrohm USA, Riverview, FL, USA), soluble solids were determined with an Atago digital pocket refractometer (Japan), and pH was analyzed using an Accumet Excel XL25 pH meter (Thermo Fisher Scientific, Waltham, MA, USA). Harvested fruit not used for winemaking was kept frozen at −20 °C for further analyses.

Winemaking. From each harvested sample, fresh berries were manually destemmed, and 750 g was crushed into 1 L fermenters in duplicate. Musts were treated with 100 mg/L sulfur dioxide, added as potassium metabisulfite, before inoculation with yeast (0.2 g/L, rehydrated with GoFerm according to the manufacturer's instructions). Fermaid K and DAP were added at rates of 0.25 and at 0.3 g/kg, respectively, after 48 h. All samples were fermented at 18 °C on the skins with daily punch downs. After 7 days, residual sugar was determined to be below 0.5 g/L in all fermentations by Clinitest, and wines were pressed manually using cheesecloth. Wines were supplemented with 60 mg/L sulfur dioxide, bottled in 187 mL glass bottles under nitrogen, and crown capped (Waterloo Container, Waterloo, NY, USA). Bottled wine was stored in the dark at 2 °C until analyzed.

Condensed Tannin Measurements in Experimental Wine and Grape Samples. Condensed tannin in wine was measured by the Adams−Harbertson protein precipitation assay as described elsewhere.[23] Samples that fell below the limit of quantification (100 mg/L, or an absorbance change of <0.3 AU[24]) were concentrated in an Eppendorf vacufuge (Hamburg, Germany) until the volume was reduced by half, and the protein precipitation assay was rerun. To determine condensed tannin in fruit, a frozen 50 berry subsample (in duplicate) was dissected on ice into skin, flesh, and seed fractions using forceps and a scalpel. Freshly dissected sample weights of each tissue were recorded. An extract was prepared from the skins by agitation in 100 mL of 70% acetone overnight, and solids were separated by vacuum filtration and saved for cell wall material preparation. Acetone was removed from 1 mL of extract under reduced pressure at 30 °C, and volumes were adjusted to 1 mL with filtered water (Millipore Corp., Billerica, MA, USA) before measurement of protein-precipitable tannin. Seeds were extracted with 25 mL of 70% acetone overnight with agitation. Solids were filtered as for skins, acetone was removed from a 1 mL aliqout and the final volumes were adjusted to 1 mL with Milli-Q filtered water before measurement of protein-precipitable tannin. Tannin extractability was calculated as the ratio of protein-precipitable tannin quantities (mg) in a volume of wine (L) to protein-precipitable tannin quantities in a corresponding weight of berries (mg/g, skin plus seed):

$$\text{tannin extractability} = \left[\frac{\text{wine tannin } \frac{\text{mg}}{\text{L}}\ \text{CE} \times \text{wine yield (L)}}{\left(\text{seed} + \text{skin tannin } \frac{\text{mg}}{\text{g}}\ \text{CE}\right) \times \text{initial must wt (g)}}\right] \times 100\% \quad (1)$$

Preparation of Alcohol-Insoluble Cell Wall Material. Cell wall material was prepared as alcohol-insoluble solids in a manner similar to that of de Vries and co-workers.[25] For each 50 berry subsample replicate, acetone-extracted skins (from above) were extracted in 200 mL of hot 95% ethanol for 10 min and vacuum filtered. The procedure was repeated twice for each replicate. The alcohol-insoluble cell wall material was then rinsed with acetone and allowed to dry overnight in a 40 °C oven, weighed, ground to a fine powder using a Genogrinder 2000 (Spex SamplePrep, Metuchen, NJ, USA), and stored at −20 °C until use. This procedure was repeated for the grape flesh fractions, isolated as described in the previous section.

Evaluation of Tannin Binding by Cell Wall Material. Tannin binding experiments were performed in model wine, consisting of 1500 mg/L BioTan, 12% (v/v) ethanol, 5 g/L tartaric acid, and Milli-Q filtered water with the pH adjusted to 3.3 using NaOH. Ten milligrams of each skin or flesh cell wall fraction was weighed into a 1.5 mL microcentrifuge tube in duplicate. To each tube was added 1 mL of the BioTan model wine solution. Controls containing only the BioTan model wine and no cell wall material were prepared in triplicate. Microcentrifuge tubes were sealed with Parafilm and incubated overnight at room temperature (23 °C) on a shaker in the dark to allow for tannin−cell wall binding, after which insoluble material was pelleted by centrifugation at 10000*g* for 5 min. The protein-precipitable tannin was then measured for the supernatant from each tube. For each tube, the amount of condensed tannin bound to cell wall material was calculated as the difference between the protein-precipitable tannins measured in the controls and the tube's supernatant. For this paper, a distribution coefficient, *K*, was used to quantify the degree of tannin binding, where a lower *K* value indicates stronger binding. *K* was calculated by dividing the concentration of tannin remaining in the model wine solution after incubation with cell wall materials by the apparent concentration of tannin bound to cell wall material:

$$K = \frac{[\text{tannin in supernatant}]}{[\text{tannin in control} - \text{tannin in supernatant}]} \quad (2)$$

Protein and Pectin in Cell Wall Materials. Percent nitrogen was determined for all cell wall samples using a Thermo Delta V isotope ratio mass spectrometer interfaced to an NC2500 element analyzer at the Cornell Isotope Laboratory (Ithaca, NY, USA). Crude protein was calculated as milligrams per gram nitrogen × 5.27.[26] Pectin was measured as the uronic acid content following enzymatic digestion. Enzymatic digestion was selected because it yields superior galacturonic acid recovery with less degradation in comparison to traditional hot acid hydrolysis.[27] Briefly, 5 mg of cell wall material was incubated in 950 μL of 25 mM acetate buffer, pH 4.8, in a screw-capped 1.5 mL microcentrifuge tube. Ten microliters of Viscozyme was added to each tube. Samples were mixed by vortexing and incubated at 30 °C for 18 h on a shaker. After incubation, samples were centrifuged at 13000 rpm for 5 min, and supernatant containing uronic acids was collected for analysis. Uronic acids were quantified using a spectrophotometric method with D-galacturonic acid as standard, as previously described.[28]

Statistical Analysis. For the Finger Lakes wine survey, samples that fell below the limit of quantification (100 mg/L CE, or an absorbance change <0.3 AU[24]) were assigned a value of half the quantification limit (50 mg/L CE) for statistical testing.[29,30] A similar approach was taken for experimental wines with unquantifiable tannin, except that the quantification limit was 50 mg/L CE because of the concentration step, and a value of 25 mg/L CE was assigned to these wines for statistical purposes.[29,30] JMP Pro 10 (by SAS, Cary, NC, USA) was used to perform all statistical testing and modeling for this study, with a type 1 error rate set to 0.05. Student's *t* test was performed to compare *vinifera* and hybrid wine tannin in the commercial wine survey. One-way ANOVA was performed on grape tissue weights, cell wall yields, skin tannin, seed tannin, total tannin, tannin extractability, and tannin binding cell wall experiments and for measurements of protein and pectin. When significant differences were observed following ANOVA, Tukey's range test was performed to determine if differences existed between individual groups. To investigate the effects of cultivar, harvest location, and grape classification on wine tannin, a multivariate fixed-effects modeling approach was used to identify significant variables. Graphics were generated using GraphPad Prism version 5.0c (GraphPad Software, San Diego, CA, USA).

RESULTS AND DISCUSSION

Recent papers have indicated that hybrid-based wines have low tannin concentrations as compared to literature papers for *vinifera* varietal wines, but these studies have been limited in scope.[8,18,19] We performed a survey consisting of hybrid- and *vinifera*-based wines, mostly commercial, using the Adams−Harbertson protein precipitation assay[31] to quantify condensed tannins (Supporting Information Figure S1). One challenge to using the Adams−Harbertson assay is its relatively high limit of quantification (LOQ), and several wines had nonquantifiable tannin even after preconcentration. The average protein-precipitable tannin was significantly higher in *vinifera*- than hybrid-based wines (255 vs 61 mg/L CE, $p < 0.05$). Furthermore, 10 of 12 of these wines fell below the LOQ (100 mg/L CE[24]), and only one hybrid-based wine contained >200 mg/L CE tannin. By comparison, only 3 of 12 *vinifera*-based wines in our survey had <200 mg/L CE of tannin, and a larger survey of red *vinifera*-based wines observed only about 8% had <200 mg/L CE of tannin.[20]

The tannin concentrations of *vinifera* wines in our commercial wine survey were approximately 50% of that measured by the same assay in red wines from California, Washington, Oregon, and Australia, 544 mg/L CE.[20] Although the distribution of varietal wines included in the two surveys was different, lower concentrations were typically observed for the same varietal wine. For example, the average protein-precipitable tannin in Cabernet Sauvignon wines from Washington State averaged 660 mg/L CE, whereas the Cabernet Sauvignon wines included for this survey from the Finger Lakes averaged 266 mg/L CE. The Finger Lakes region of New York is a cool-climate region having fewer growing degree-days, heat summation, and sunlight and more precipitation than many of the aforementioned warmer regions.[32] Several of these factors are reported to decrease grape or wine tannin concentrations. For example, increases in heat summation between fruit set and veraison have been associated with increased tannin in Pinot noir berries and their respective wines,[11] and greater water availability has been linked to decreases in flavonoid biosynthesis.[33]

Tannin in Experimental Wines Produced from Different Cultivars. Because winemaking protocols can have a profound effect on wine tannins, an alternative explanation for observed differences in tannins between *vinifera*- and hybrid-based wines could be that commercial wineries utilize different practices for these grapes. Additionally, U.S. labeling laws allow the addition of 25% of varieties other than those listed on the label. To control these variables, we collected fruit from 12 cultivars (4 French−American hybrids, 2 neo-American hybrids, and 6 *vinifera* cultivars), with each cultivar collected from two different sites for a total of 24 grape lots. Basic fruit chemistry is shown in Supporting Information Table S2. Fruit was then vinified using a standardized small-scale winemaking protocol and tannin quantified in the finished wines using the Adams−Harbertson assay (Figure 1A).

A multivariable fixed-effects model fitting wine tannin with variables "classification" (French−American hybrid, neo-American hybrid, or *vinifera*), "cultivar" nested within classification, and "location" revealed that location did not have a significant influence on wine tannin ($p = 0.51$). Cultivar was a significant factor ($p < 0.05$) in the model, similar to other findings.[34] Additionally, belonging to a classification group of "French−American hybrid", "neo-American hybrid", or "*vinifera*" was a significant determinant of wine tannin ($p < 0.05$). Wines produced from classic French−American hybrid grapes had significantly lower tannin concentrations than *vinifera*-based wines based on mean values, 45 versus 248 mg/L CE, respectively (5.5-fold lower, $p < 0.05$). Even though wine-

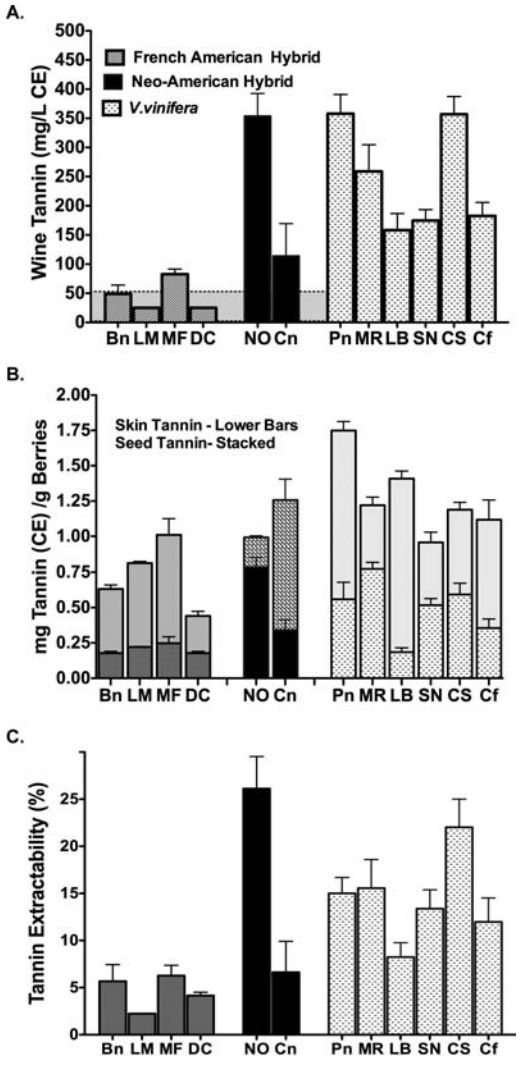

Figure 1. (A) Protein-precipitable wine tannin by variety (n = 4 per variety, bars indicate standard error of the mean) Bn, Baco noir; LM, Leon Millot; MF, Marechal Foch; DC, DeChaunac; NO, Noiret; Cn, Corot noir; Pn, Pinot noir; MR, Merlot; LB, Lemberger; SN, Sangiovese; CS, Cabernet Sauvignon; Cf, Cabernet franc. (B) Protein-precipitable tannin per gram of berries by cultivar. (C) Tannin extractability by variety.

making practices were kept constant, the range in wine tannin from these two classes reached a maximum variation of >17.4-fold. Notably, tannins in both *vinifera*- and hybrid-based wines were comparable to data for commercial wines in Supplementary Figure 1, indicating that our experimental wines were comparable to commercial wines.

The neo-American hybrids had higher tannin concentrations than the classic French–American hybrids. Noiret had the highest amount of tannin of all hybrid-based wines, averaging 354 mg/L CE. The other neo-American hybrid in this study, Corot noir, was variable, with Corot noir wine produced from fruit from one site having 203 mg/L CE wine tannin, whereas Corot noir from the second site had tannin below the LOQ for the protein precipitation assay.

Although the neo-American hybrids investigated have a percentage of *vinifera* in their background similar to that in the French–American hybrids (~50%), the pedigrees of most neo-American hybrids involve several backcrosses, including Corot noir, Noiret, and Vincent (wine 22 from Figure 1).[3] In contrast, many classic French–American hybrids result from a direct cross (F1) of *vinifera* with a wild *Vitis* species (or crosses of wild *Vitis*). A potential explanation for low wine tannin in the classic French–American grapes is that traits that lead to higher wine tannin are derived from *vinifera* and recessive and that backcrossing is necessary for hybrid grapes to yield high wine tannin.

Relationship of Grape Tannin and Tannin Extractability to Wine Tannin in Experimental Wines. To evaluate if differences in wine tannin concentrations arose from differences in grape tannin, the tannin in skins or seeds was quantified. These data are reported on a per berry weight basis in Figure 1B. Skin and seed tannin among grape classes were evaluated by a one-way ANOVA and were significantly different ($p < 0.05$). Total tannin (skin + seed) concentrations were significantly higher in *vinifera* grapes (mean = 1.27 mg CE/g berry) as compared to French–American hybrid grapes (0.71 mg CE/g berry). Tannin concentrations in *vinifera* grapes were similar to previous reports using the same protein precipitation method. Harbertson and colleagues reported values from Cabernet Sauvignon, Pinot noir, and Syrah ranging from 0.99 to 1.44 mg CE/g berry.[23] Although the 1.8-fold higher total tannin concentrations in *vinifera* grapes may serve as a partial explanation for differences in wine tannin, it cannot fully account for the 5.5-fold higher tannin concentrations (and 17-fold maximum difference in wine tannin vs 6.1-fold maximum difference in berry tannin) between *vinifera*- and French–American hybrid-based wines. This indicates that the cultivar classifications must also vary in tannin extractability.

Tannin extractability was calculated as described in eq 1, and data are shown in Figure 1C. Extractability from French–American hybrids was lower than that of the other two classes (one-way ANOVA, $p < 0.05$) and ranged from 2.2 to 5.7% in French–American hybrids, from 6.6 to 26.1% in neo-American hybrids, and from 8 to 22% in *vinifera*. The low tannin extractability observed from French–American hybrids is comparable to previous reports from our group,[18,19] and the extractability observed for *vinifera* is on the lower end reported by others (4.9–61%).[23]

We observed that skin tannin was better correlated with final wine tannin across cultivars ($r^2 = 0.73$, $p < 0.05$), as compared to total tannin ($r^2 = 0.44$, $p < 0.05$) and seed tannin (ns) (Table 1). Thus, differences in grape skin tannin may partially explain

Table 1

	wine tannin			tannin extractability		
predictor	p value	r^2	RMSE	p value	r^2	RMSE
total tannin	0.0179	0.44	99.7	0.21	0.15	7.08
skin tannin	0.0004	0.73	69.1	0.0001	0.79	3.52
seed tannin	0.75	0.01	133	0.51	0.04	7.52

both differences in wine tannin and apparent tannin extractability during fermentation. The median concentration of skin tannin in *vinifera* is 2.7-fold higher than in French–American hybrids (0.54 vs 0.20 mg CE/g berry). Skin tannin is extracted more quickly than seed tannin, with one paper stating that skin tannin extraction reaches a maximum after 5 days, whereas seed tannin extraction occurs more slowly and does not reach equilibrium by the time the fermentation is at dryness.[11] Assuming 29% skin tannin and 6% seed tannin extraction during maceration (excluding any other calculated binding effects) as previously reported by Kennedy,[35] the

Table 2. Fresh Weight, Dry Cell Wall Material, Protein Content of Cell Wall Material, and Pectin Content of Cell Wall Material in Skin and Flesh Fractions of Grape Cultivars[a]

cultivar	tissue	fresh wt (mg/g berries)	cell wall yield (mg/g FW)	crude protein (mg/g CW)	pectin (as uronic acids) (mg/g CW)	distribution coefficient (K)
			French–American Hybrid			
Baco noir	skin	212 ± 5.5 c	38.7 ± 0.91 e	113 ± 2.5 a	178 ± 3.6 a b c	6.13 ± 0.052 d
	flesh	705 ± 5 w x y z	11.7 ± 0.59 y z	98.7 ± 0.92 z	71.3 ± 2.1 y z	8.48 ± 0.73 y
Leon Millot	skin	230 ± 17 a b c	45.8 ± 2.8 b c d e	106 ± 3.3 a	192 ± 11 a b	8.40 ± 0.57 c d
	flesh	667 ± 19 y z	9.25 ± 0.96 y z	102 ± 5.0 y z	91 ± 3 y	7.78 ± 0.86 y
Marechal Foch	skin	211 ± 17 c	48.3 ± 1.4 b c	116 ± 2.5 a	173 ± 9.4 a b c	8.30 ± 0.088 c d
	flesh	672 ± 23 w x y z	15.1 ± 1.0 x	119 ± 4.2 y	71.5 ± 2.2 y z	8.75 ± 0.60 y
DeChaunac	skin	199 ± 11 c	46.7 ± 0.97 b c d e	103 ± 3.1 a	227 ± 8.0 a	9.74 ± 0.71 b c d
	flesh	737 ± 16 w	13.0 ± 0.48 y	90 ± 2.6 z	68.3 ± 4.5 x y z	10.1 ± 0.52 w x y
average	skin	213 ± 6.7 B	44.9 ± 2.1 B	110 ± 1.9 A	193 ± 6.6 A	8.14 ± 0.40 B
	flesh	695 ± 11 X	12.3 ± 0.66 X	102 ± 6 X Y	75.5 ± 2.7 Y	8.78 ± 0.38 Y
			Neo-American Hybrid			
Noiret	skin	279 ± 7.8 a	47.5 ± 0.85 b c d	103 ± 4.6 a	159 ± 20 b c	15.6 ± 1.1 b c d
	flesh	665 ± 7.8 y z	10.7 ± 0.97 y z	84.7 ± 4.1 z	99 ± 5 x	11.8 ± 0.99 w x y
Corot noir	skin	200 ± 8.3 c	64.4 ± 1.8 a	111 ± 4.8 a	172 ± 11 a b c	10.8 ± 0.70 b c d
	flesh	731 ± 9.8 w x	11.5 ± 1.7 y z	138 ± 6.7 x	84.5 ± 2.4 y z	2.99 ± 1.1 z
average	skin	239 ± 16 A B	56.0 ± 8.5 A	107 ± 3.4 A B	166 ± 11 A B	13.2 ± 1.1 B
	flesh	698 ± 14 X	11.2 ± 0.92 X Y	112 ± 27 X	91.8 ± 3.8 X	7.39 ± 1.8 Y
			Vinifera			
Pinot noir	skin	270 ± 7.8 a b	49.7 ± 1.3 b	102 ± 6.2 a	121 ± 5.0 c	36.5 ± 9.1 a
	flesh	668 ± 8.9 y z	8.47 ± 1.3 z	103 ± 4.5 y z	62.9 ± 3.7 y z	9.59 ± 0.86 w x y
Merlot	skin	252 ± 21 a b c	39.4 ± 2.7 d e	100 ± 3.4 a	168 ± 5.0 b c	17.9 ± 1.6 b c d
	flesh	675 ± 24 w x y z	10.1 ± 0.68 y z	84.0 ± 2.5 z	62.7 ± 1.0 y z	11.6 ± 0.82 w x y
Lemberger	skin	212 ± 4.5 c	61.2 ± 1.7 a	107 ± 5.8 a	140 ± 6.6 b c	20.5 ± 0.74 b c
	flesh	733 ± 7.3 w x	10.9 ± 0.56 y z	98.7 ± 3.6 z	67.4 ± 5.3 y z	13.4 ± 0.83 w
Sangiovese	skin	220 ± 12 b c	44.5 ± 1.7 b c d e	104 ± 0.84 a	177 ± 27 a b c	22.8 ± 2.0 a b
	flesh	726 ± 14 w x y	8.10 ± 0.36 z	87.0 ± 2.1 z	73.0 ± 4.6 y z	12.8 ± 1.3 w x
Cabernet Sauvignon	skin	274 ± 3.9 a b	41.1 ± 0.69 c d e	104 ± 3.4 a	148 ± 6.1 b c	19.5 ± 2.0 b c d
	flesh	659 ± 4.0 y z	10.7 ± 0.61 y z	99.2 ± 4.7 z	54.6 ± 4.2 z	13.3 ± 0.94 w
Cabernet franc	skin	272 ± 4.5 a b	44.1 ± 1.5 b c d e	95.6 ± 7.0 a	171 ± 6.2 a b c	15.5 ± 0.60 b c d
	flesh	641 ± 7.4 z	13.1 ± 0.89 y	98.3 ± 2.8 z	87.1 ± 18 y	10.5 ± 0.31 w x y
average	skin	250 ± 6.5 A	46.7 ± 3.2 B	102 ± 1.9 B	154 ± 6.1 B	22.1 ± 2.0 A
	flesh	684 ± 8.5 X	10.2 ± 0.45 Y	95 ± 3 Y	68.0 ± 3.6 Y	11.9 ± 0.44 X

[a]Significant differences ($p < 0.05$) by Tukey–Kramer HSD among cultivars are denoted by not sharing lower case letters for skin tissue (a, b, c, d) or flesh tissues (w, x, y, z). Significant differences among classes (French–American, neo-American, *V. vinifera*) are indicated by capital letters for skin tissue (A, B, C) or flesh tissue (X, Y, Z).

predicted average French–American hybrid wine would be 126 mg/L CE, whereas the average *vinifera* wine would be 261 mg/L CE, a 2.1-fold difference. However, *vinifera*-based wines averaged 5.5-fold higher tannin concentrations than French–American hybrids (Figure 1A), indicating that other factors beyond skin tannin likely contribute to differences in tannin extractability.

Tannin Binding by Cell Wall Material. Factors that contribute to variation in tannin extraction among grape sources under consistent winemaking conditions are not fully understood, but binding of tannins by cell wall material has been proposed.[22] We observed 17% more skin tissue by weight for *vinifera* versus French–American hybrids, whereas cell wall yields from skins by fresh weight were not significantly different (Table 2). A small, but significant, increase in flesh cell wall material yield was observed for French–American hybrids relative to *vinifera* (12.3 vs 10.2 mg/g fresh weight, Table 2). The neo-American hybrid grapes had significantly more skin cell wall material, but not flesh cell wall material, than both *vinifera* and French–American hybrid fruit by fresh tissue weight (56.0 vs 46.7 and 44.9 mg/g, respectively; Table 2). Because differences in cell wall material quantity were small, they were thought unlikely to affect extractability.

To investigate if tannin binding affinity rather than cell wall material concentration could contribute to differences in wine tannin among the classes, alcohol-insoluble residues were prepared from skins and flesh from each grape source. The protocol selected was previously employed for preparing cell wall material samples from *vinifera* grapes and results in isolation of carbohydrates, proteins, phenolic compounds, and cell wall microstructure with lower cost and preparation time per sample than comparable methods.[36]

Equal masses (10 mg) of cell wall material were incubated with a commercial tannin product (BioTan) in a winelike medium to evaluate tannin binding of each fraction. BioTan was selected for this study on the basis of previous work that showed it had the highest concentration of iron-reactive protein-precipitable tannin (48%) for commercial grape-derived products.[37] In close agreement with Harbertson and co-workers, we calculated the iron-reactive protein-precipitable tannin to be 47% by weight.[37] Phloroglucinolysis analysis by other authors indicates that BioTan is more similar to seed tannin than skin in size (mDP = 6.93[38]).

dx.doi.org/10.1021/jf5023274 | J. Agric. Food Chem. 2014, 62, 7515–7523

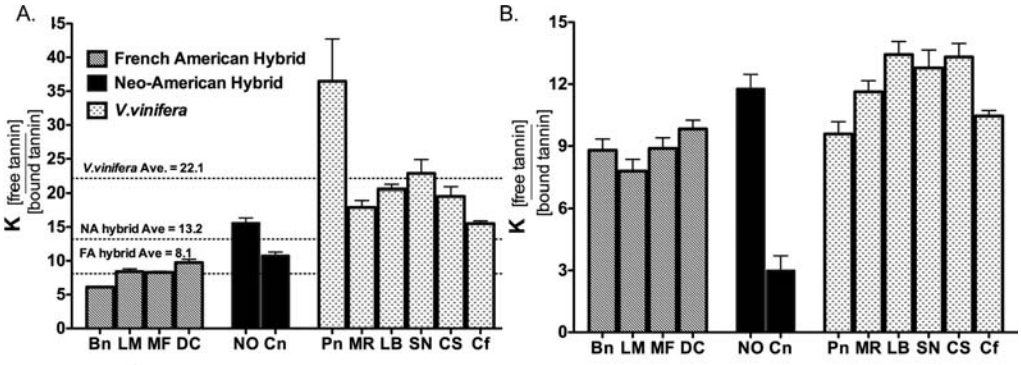

Figure 2. Distribution coefficients, calculated as ratio of free to bound tannin, after an 18 h incubation of tannin with skin cell wall (A) and flesh cell wall (B) materials from different cultivars (n = 8, bars indicate standard error of the mean).

Skin cell wall materials from French–American hybrid grapes were able to bind significantly more tannin on a by weight basis than *vinifera* ($p < 0.05$, Figure 2A). For this paper, we define the binding affinity of skin cell wall material as a distribution coefficient (K), calculated as the ratio of tannin in model wine versus the skin cell wall material during incubation experiments. K was 2.7-fold greater in *vinifera* than in French–American hybrids. The ability of neo-American hybrid skin materials to bind tannins was not significantly different from that of *vinifera* or the French–American hybrids, and the average distribution coefficient fell between the other two groups. Flesh cell wall materials from all three classes were not significantly different in their binding ability (Figure 2B, $p > 0.05$). Although tannin binding by cell wall material from neo-American grapes did not differ significantly from that of French–American or *vinifera* grapes, Noiret flesh demonstrated significantly less binding than both Corot noir and the French–American hybrids (Figure 2). We also observed that the Corot noir flesh cell wall sample with the highest binding affinity corresponded to the Corot noir wine with undetectable tannin. Whereas cell wall binding could potentially explain the greater tannin extractability observed in Noiret as compared to Corot noir (Figure 1C), Noiret also had significantly greater skin tannin (Figure 1B), and it is not currently possible to decouple which of these effects is more important.

As a caveat, these distribution coefficients are specific for the test conditions employed. Tannin–cell wall interactions do not follow simple Langmuir or Freundlich binding patterns and may involve cooperative binding.[39] Using a different tannin preparation (e.g., a skin-derived tannin fraction) would be expected to lead to different absolute K values and may reveal additional differences in the tannin binding behavior between cell wall fractions.[40] Given that skin tannin was found to be a significant factor in determining final wine tannin, further characterizing the interaction of cell wall material with skin tannin would benefit our current understanding of tannin extractability. Additionally, we used cell wall materials from grapes, which may not account for cell wall changes that occur during fermentation. However, our work does appear comparable to that of Bindon and colleagues, who recently reported on tannin binding by Shiraz cell wall material.[41] In agreement with their work, *vinifera* flesh cell wall materials in our study bound significantly more tannin than skin cell wall material. Although this previous work expressed binding in different units than in our current study, it was possible to determine distribution coefficients from the data presented.[41] We calculate that the Shiraz-derived cell wall material incubated with seed tannins had K values of 17 (flesh) and 30 (skin), comparable to the values reported here for *vinifera*.

Characterization of Cell Wall Material: Protein and Pectin Content. Because the reasons for differences in tannin binding among classes or cultivars could arise from differences in grape composition and/or structure, we quantified the two major classes of tannin-binding macromolecules, pectin and protein.[40,42,43] Pectin was quantified as uronic acids (in galacturonic acid equivalents) presuming galacturonic acid is the main constituent of grape pectin and glucuronic acid is a minor constituent of grape cell walls.[44,45] Results are reported in Table 2. The gravimetric recovery of cell wall materials reported here is within the range of values previously reported.[26] Pectin and crude protein quantities in both skin and flesh cell wall materials are also within the range of other studies using similar methods of quantification.[26] We observed that French–American hybrid grape skin cell walls had significantly more pectin (as uronic acids). Pectin has been shown to bind tannin more efficiently than other less flexible carbohydrates,[26,46,47] and pectin differences may contribute to observed differences in extraction from French–American hybrids. We also observed that pectin content was weakly correlated with K distribution coefficients ($p < 0.05$, $r^2 = 0.255$). As a caveat, the pectin molecular weight and degree of substitution were not analyzed in this study and may account for additional small differences in tannin binding affinity.

An even stronger correlation was observed between K values and flesh protein ($p < 0.05$, $r^2 = 0.597$, Figure 3). As a specific example, Corot noir flesh contained the highest amount of protein by weight and the lowest K values (strongest binding). This is in agreement with Bindon et al., who observed that

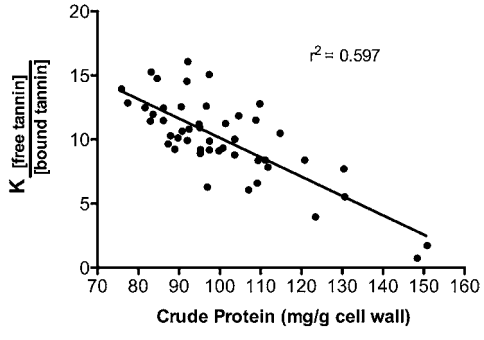

Figure 3. Flesh cell wall distribution coefficients (K) versus corresponding cell wall crude protein content.

dx.doi.org/10.1021/jf5023274 | J. Agric. Food Chem. 2014, 62, 7515–7523

crude protein was higher in Cabernet Sauvignon cell wall fractions possessing greater tannin affinity.[26] French−American hybrid skin cell walls also had higher crude protein than *vinifera*, although differences were small and the correlation of *K* and skin protein was worse ($p < 0.05$, $r^2 = 0.19$). Protein concentrations in our study ranged from 8 to 14%, although these values may be higher due to precipitation of cytoplasmic proteins with the ethanol precipitation method of cell wall preparation.[22,48] Interactions between structural cell wall proteins, such as the hydroxyproline-rich extensin, and tannin have been recently discussed, but their impact on wine tannin has not been thoroughly investigated.[22] Because of the nature of this study, it is not possible to determine if flesh protein content is a direct cause of low tannin extractability or merely correlated.

In agreement with previous studies using *vinifera* cultivars, flesh cell walls bound more tannin than skin cell walls in this classification, but had less pectin and protein by weight in comparison in this study.[40] This could be due to the presumably more flexible nature of flesh cell wall material facilitating stronger tannin interactions, but additional information is needed to address this. Bindon and colleagues reported that cell wall flexibility was an important aspect for tannin adsorption, and increased adsorption with decreasing acid-insoluble fiber and insoluble bound tannin was reported for Cabernet Sauvignon,[26] but these two parameters were not quantified in this study. An increase in cell wall porosity and surface area has also been reported to increase tannin binding.[49,50] Thus, although pectin and protein contents may contribute to tannin extraction differences among cultivars, more detailed compositional analysis may be necessary to understand differences in tannin binding between tissues.

This publication did not evaluate all possible factors that could affect tannin extractability. For example, the French−American hybrids are reported to have high anthocyanin concentrations as compared to *vinifera*.[51,52] Although anthocyanins can bind cell walls,[53] a competitive binding effect seems unlikely because low anthocyanin concentrations are reported to decrease tannin extraction.[54,55] Differences in tannin composition, particularly tannin size (mDP) and, to a lesser extent, degree of galloylation, could also decrease extraction by increasing binding efficiency to cell wall material.[41] Differences in tannin composition between hybrids and *vinifera* were not investigated in this work, but may be of interest to future studies.

Potential Consequences to Winemaking with Hybrid Grapes. Our data indicate that lower tannin concentrations (5.5-fold, up to a maximum of 17.4-fold) are present in hybrid-based wines as compared to *vinifera*-based wines both in commercial wines and in wines produced under standardized winemaking conditions. Although these differences can be partially explained by differences in berry tannin (particularly skin tannin), differences in tannin binding by cell wall material appear to explain an equal or greater amount of the variation. The demonstrated importance of skin tannin to final wine tannin in this study, in conjunction with the timing of skin tannin extraction during winemaking reported elsewhere, emphasizes the critical impacts of cell wall interactions on final wine tannin. The high tannin binding of hybrid grapes may explain the lack of success observed with winemaking approaches designed to increase wine tannin, especially in the early stages of winemaking. For example, recent work on hybrid grapes observed that prefermentation tannin additions to must resulted in a less than expected increase in wine tannin.[8] Additionally, the mDP of hybrid wine condensed tannin in this previous work was low as compared to *vinifera*-based wines (mDP < 4) and decreased throughout the course of fermentation. These low molecular weight tannins are anticipated to contribute more bitterness than astringency. Other work on *vinifera* has demonstrated selective removal of high mDP tannins by cell wall materials, resulting in lower mDP for tannins remaining in solution.[41] Because skin tannin both has higher mDP and is extracted more rapidly than seed tannin during fermentation, there will be a preferential loss of skin tannin due to cell wall binding.[40] Thus, the higher binding affinity of hybrid grape cell wall material may account not only for low tannin but also for a reduction in mDP. Furthermore, removing or degrading the tannin-binding compounds may prove more effective for increasing the final tannin concentrations in these wines (hybrid or *vinifera*) than commercial tannin addition. As our data indicate that the protein content of grape flesh is correlated with tannin binding, one strategy for increasing tannin extractability may be to use proteases during maceration. Pectin content was also correlated with tannin binding, although previous work has shown that pectinase enzyme additions are ineffective at increasing tannin concentrations in wines produced from by hybrid grapes.[8]

Finally, identification of grape components that limit tannin extractability may make for an interesting target to facilitate breeding of high-quality winegrapes. Interspecific hybrids are of interest to the grape and wine industries due to their better economic and environmental sustainability. Modern genetic tools, such as marker-assisted selection, have been used to facilitate grape breeding, especially for viticulturally important traits such as disease resistance. Whereas a few genetic markers for wine quality related attributes have been identified, such as for herbaceous-smelling methoxypyrazines,[56] wine tannin concentrations pose a particular challenge because they are poorly correlated with grape concentrations and thus are not currently well suited for high-throughput phenotyping in grape-mapping populations. Future work to identify compounds that limit tannin extraction from grapes could facilitate these studies.

■ ASSOCIATED CONTENT

Supporting Information

Additional figure and tables. This material is available free of charge via the Internet at http://pubs.acs.org.

■ AUTHOR INFORMATION

Corresponding Author

*(G.L.S.) E-mail: gls9@cornell.edu. Phone: (315) 787-2458. Fax: (315) 787-2397.

Funding

This project was funded by USDA SCRI Project 2011-51181-3063.

Notes

The authors declare no competing financial interest.

■ ACKNOWLEDGMENTS

We gratefully acknowledge the assistance of Emily Defnet, Avery Stahlecker, and Christian Deakin for their contributions to sample processing and laboratory support. We thank David Manns and Lauren Thomas for performing phloroglucinolysis on the commercial tannin used in this study. We also thank Sawmill Creek Vineyards, Lakewood Vineyards, Fulkerson

Winery, Knapp Winery, Anthony Road Wine Co., and Prejean Winery for their generous fruit donations.

REFERENCES

(1) Riaz, S.; Doligez, A.; Henry, R. J.; Walker, M. A. Grape. In *Genome Mapping and Molecular Breeding in Plants*; Kole, C., Ed.; Springer Verlag: Berlin, Germany, 2007; Vol. 4.
(2) Reisch, B.; Owens, C. L.; Cousins, P. S. Grape. In *Fruit Breeding*; Badenes, M. L., Byrne, D. H., Eds.; Springer: New York, 2012; pp 225−262.
(3) Warmund, M. R.; Guinan, P.; Fernandez, G. Temperatures and cold damage to small fruit crops across the eastern United States associated with the April 2007 freeze. *HortScience* **2008**, *46*, 1643−1647.
(4) Rice, A. C. Chemistry of winemaking from Nnative American grape varieties. In *Chemistry of Winemaking*; American Chemical Society: Washington, DC, USA, 1974; Vol. 137, pp 88−115.
(5) Sun, Q.; Gates, M. J.; Lavin, E. H.; Acree, T. E.; Sacks, G. L. Comparison of odor-active compounds in grapes and wines from *Vitis vinifera* and non-foxy American grape species. *J. Agric. Food Chem.* **2011**, *59*, 10657−10664.
(6) Acree, T. E.; Lavin, E. H.; Nishida, R.; Watanabe, S. *o-Aminoacetophenone, the Foxy Smelling Component of Labruscana Grapes*; Wiley: Chichester, UK, 1990; pp 49−52.
(7) Nelson, R. R.; Acree, T. E.; Lee, C. Y.; Butts, R. M. Methyl anthranilate as an aroma constituent of American wine. *J. Food Sci.* **1977**, *42*, 57−59.
(8) Manns, D. C.; Coquard Lenerz, C. T.; Mansfield, A. K. Impact of processing parameters on the phenolic profile of wines produced from hybrid red grapes Marechal Foch, Corot noir, and Marquette. *J. Food Sci.* **2013**, *78*, C696−C702.
(9) Spada, P. Tannin additions in red hybrid wines. In *Midwest Wine Press*; www.midwestwinepress.com/2013/07/07/tannin-addition-in-red-hybrids/, 2013; Vol. 2013.
(10) Vidal, S.; Francis, L.; Guyot, S.; Marnet, N.; Kwiatkowski, M.; Gawel, R.; Cheynier, V.; Waters, E. J. The mouth-feel properties of grape and apple proanthocyanidins in a wine-like medium. *J. Sci. Food Agric.* **2003**, *83*, 564−573.
(11) Pastor del Rio, J. L.; Kennedy, J. A. Development of proanthocyanidins in *Vitis vinifera* L. cv. Pinot noir grapes and extraction into wine. *Am. J. Enol. Vitic.* **2006**, *57*, 125−132.
(12) Busse-Valverde, N.; Bautista-Ortin, A. B.; Gomez-Plaza, E.; Fernandez-Fernandez, J. I.; Gil-Munoz, R. Influence of skin maceration time on the proanthocyanidin content of red wines. *Eur. Food Res. Technol.* **2012**, *235*, 1117−1123.
(13) Lea, A. G. H.; Arnold, G. M. Phenolics of ciders − bitterness and astringency. *J. Sci. Food Agric.* **1978**, *29*, 478−483.
(14) Vidal, S.; Cartalade, D.; Souquet, J. M.; Fulcrand, H.; Cheynier, V. Changes in proanthocyanidin chain length in wine-like model solutions. *J. Agric. Food Chem.* **2002**, *50*, 2261−2266.
(15) Bajec, M. R.; Pickering, G. J. Astringency: mechanisms and perception. *Crit. Rev. Food Sci. Nutr.* **2008**, *48*, 858−875.
(16) du Toit, W. J. Micro-oxidation, oak alternatives and added tannins and wine quality. In *Mangaing Wine Quality*; Reynolds, A. C., Ed.; Woodhead Publishing: Cambridge, UK, 2010; Vol. 2, pp 226−254.
(17) Fanzone, M.; Pena-Neira, A.; Gil, M.; Jofre, V.; Assof, M.; Zamora, F. Impact of phenolic and polysaccharidic composition on commercial value of Argentinean Malbec and Cabernet Sauvignon wines. *Food Res. Int.* **2012**, *45*, 402−414.
(18) Sun, Q.; Sacks, G.; Lerch, S.; Heuvel, J. E. V. Impact of shoot thinning and harvest date on yield components, fruit composition, and wine quality of Marechal Foch. *Am. J. Enol. Vitic.* **2011**, *62*, 32−41.
(19) Sun, Q.; Sacks, G. L.; Lerch, S. D.; Vanden Heuvel, J. E. Impact of shoot and cluster thinning on yield, fruit composition, and wine quality of Corot noir. *Am. J. Enol. Vitic.* **2012**, *63*, 49−56.
(20) Harbertson, J. F.; Hodgins, R. E.; Thurston, L. N.; Schaffer, L. J.; Reid, M. S.; Landon, J. L.; Ross, C. F.; Adams, D. O. Variability of tannin concentration in red wines. *Am. J. Enol. Vitic.* **2008**, *59*, 210−214.
(21) Adams, D. O.; Scholtz, R. C. Tannins − the problem of extraction. In *Thirteenth Annual Australian Wine Industry Technical Conference*, Adelaide, Australia; 2007; pp 160−164.
(22) Hanlin, R. L.; Hrmova, M.; Harbertson, J. F.; Downey, M. O. Review: condensed tannin and grape cell wall interactions and their impact on tannin extractability into wine. *Aust. J. Grape Wine Res.* **2010**, *16*, 173−188.
(23) Harbertson, J. F.; Kennedy, J. A.; Adams, D. O. Tannin in skins and seeds of Cabernet Sauvignon, Syrah, and Pinot noir berries during ripening. *Am. J. Enol. Vitic.* **2002**, *53*, 54−59.
(24) Jensen, J. S.; Werge, H. H. M.; Egebo, M.; Meyer, A. S. Effect of wine dilution on the reliability of tannin analysis by protein precipitation. *Am. J. Enol. Vitic.* **2008**, *59*, 103−105.
(25) De Vries, J. A.; Voragen, A. G. J.; Rombouts, F. M.; Pilnik, W. Extraction and purification of pectins from alcohol insoluble solids from ripe and unripe apples. *Carbohydr. Polym.* **1981**, *1*, 117−127.
(26) Bindon, K. A.; Bacic, A.; Kennedy, J. A. Tissue-specific and developmental modifications of grape cell walls influence the adsorption of proanthocyanidins. *J. Agric. Food Chem.* **2012**, *60*, 9249−9260.
(27) Garna, H.; Mabon, N.; Nott, K.; Wathelet, B.; Paquot, M. Kinetic of the hydrolysis of pectin galacturonic acid chains and quantification by ionic chromatography. *Food Chem.* **2006**, *96*, 477−484.
(28) Filisetticozzi, T. M. C. C.; Carpita, N. C. Measurement of uronic-acids without interference from neutral sugars. *Anal. Biochem.* **1991**, *197*, 157−162.
(29) Helsel, D. R. Less than obvious: statistical treatment of data below the detection limit. *Environ. Sci. Technol.* **1990**, *24*, 1767−1774.
(30) Office of Pesticide Programs. *Assigning Values to Non-Detected/Non-Quantified Pesticide Residues in Human Health Food Exposure Assessments*; Item 6047; U.S. Environmental Protection Agency: Washington, DC, USA, March 23, 2000.
(31) Kennedy, J. A.; Ferrier, J.; Harbertson, J. F.; Gachons, C. P. D. Analysis of tannins in red wine using multiple methods: correlation with perceived astringency. *Am. J. Enol. Vitic.* **2006**, *57*, 481−485.
(32) Newman, J. L. Vines, wines, and regional identity in the Finger Lakes region. *Geographical Rev.* **1986**, *76*, 301−316.
(33) Castellarin, S. D.; Matthews, M. A.; Di Gaspero, G.; Gambetta, G. A. Water deficits accelerate ripening and induce changes in gene expression regulating flavonoid biosynthesis in grape berries. *Planta* **2007**, *227*, 101−112.
(34) Harbertson, J. F.; Wran, S.; Mireles, M.; Keller, M. Rootstock and scion influences on grape and wine composition. *Am. J. Enol. Vitic.* **2009**, *60*, 401A−401A.
(35) Kennedy, J. A. Grape and wine phenolics: observations and recent findings. *Cienc. Invest. Agraria* **2008**, *35*, 107−120.
(36) Apolinar-Valiente, R.; Romero-Cascales, I.; Lopez-Roca, J. M.; Gomez-Plaza, E.; Ros-Garcia, J. M. Application and composition of four selected procedures for the isolation of cell-wall material from the skin of grapes cv. Monastrell. *Anal. Chim. Acta* **2010**, *660*, 206−210.
(37) Harbertson, J. F.; Parpinello, G. P.; Heymann, H.; Downey, M. O. Impact of exogenous tannin additions on wine chemistry and wine sensory character. *Food Chem.* **2012**, *131*, 999−1008.
(38) Thomas, L. M. *Phenolic Extraction from Red Hybrid Winegrapes*; Cornell University: Ithaca, NY, USA, 2013.
(39) Renard, C. M. G. C.; Baron, A.; Guyot, S.; Drilleau, J. F. Interactions between apple cell walls and some native apple polyphenols: quantification and some consequences. *Int. J. Biol. Macromol.* **2001**, *29*, 115−125.
(40) Bindon, K. A.; Smith, P. A.; Holt, H.; Kennedy, J. A. Interaction between grape-derived proanthocyanidins and cell wall material. 2. Implications for vinification. *J. Agric. Food Chem.* **2010**, *58*, 10736−10746.
(41) Bindon, K. A.; Smith, P. A.; Kennedy, J. A. Interaction between grape-derived proanthocyanidins and cell wall material. 1. Effect on

proanthocyanidin composition and molecular mass. *J. Agric. Food Chem.* **2010**, *58*, 2520−2528.
(42) Ortega-Regules, A.; Ros-Garcia, J. M.; Bautista-Ortin, A. B.; Lopez-Roca, J. M.; Gomez-Plaza, E. Changes in skin cell wall composition during the maturation of four premium wine grape varieties. *J. Sci. Food Agric.* **2008**, *88*, 420−428.
(43) Ortega-Regules, A.; Ros-Garcia, J. M.; Bautista-Ortin, A. B.; Lopez-Roca, J. M.; Gomez-Plaza, E. Differences in morphology and composition of skin and pulp cell walls from grapes (*Vitis vinifera* L.): technological implications. *Eur. Food Res. Technol.* **2008**, *227*, 223−231.
(44) Nunan, K. J.; Sims, I. M.; Bacic, A.; Simon, P. R.; Fincher, G. B. Changes in cell wall composition during ripening of grape berries. *Plant Physiol.* **1998**, *118*, 783−792.
(45) Vidal, S.; Williams, P.; O'Neill, M. A.; Pellerin, P. Polysaccharides from grape berry cell walls. Part I: Tissue distribution and structural characterization of the pectic polysaccharides. *Carbohydr. Polym.* **2001**, *45*, 315−323.
(46) Le Bourvellec, C.; Bouchet, B.; Renard, C. M. G. C. Non-covalent interaction between procyanidins and apple cell wall material. Part III: Study on model polysaccharides. *Biochim. Biophys. Acta−Gen. Subj.* **2005**, *1725*, 10−18.
(47) Watrelot, A. A.; Le Bourvellec, C.; Imberty, A.; Renard, C. M. G. C. Interactions between pectic compounds and procyanidins are influenced by methylation degree and chain length. *Biomacromolecules* **2013**, *14*, 709−718.
(48) Carpita, N. C.; Gibeaut, D. M. Structural models of primary cell walls in flowering plants: consistency of molecular structure with the physical properties of the walls during growth. *Plant J.* **1993**, *3*, 1−30.
(49) Bindon, K. A.; Madani, S. H.; Pendleton, P.; Smith, P. A.; Kennedy, J. A. Factors affecting skin tannin extractability in ripening grapes. *J. Agric. Food Chem.* **2014**, *62*, 1130−1141.
(50) Le Bourvellec, C.; Watrelot, A. A.; Ginies, C.; Imberty, A.; Renard, C. M. G. C. Impact of processing on the noncovalent interactions between procyanidin and apple cell wall. *J. Agric. Food Chem.* **2012**, *60*, 9484−9494.
(51) Auw, J. M.; Blanco, V.; O'Keefe, S. F.; Sims, C. A. Effect of processing on the phenolics and color of Cabernet Sauvignon, Chambouricin, and Noble wines and juices. *Am. J. Enol. Vitic.* **1996**, *47*, 279−286.
(52) Thimothe, J.; Bonsi, I. A.; Padilla-Zakour, O. I.; Koo, H. Chemical characterization of red grape (*Vitis vinifera* and *Vitis* interspecific hybrids) and pomace phenolic extracts and their biological activity against *Streptococcus mutans*. *J. Agric. Food Chem.* **2007**, *55*, 10200−10207.
(53) Padayachee, A.; Netzel, G.; Netzel, M.; Day, L.; Zabaras, D.; Mikkelsen, D.; Gidley, M. Binding of polyphenols to plant cell wall analogues − Part 1: Anthocyanins. *Food Chem.* **2012**, *134*, 155−161.
(54) Kilmister, R. L.; Mazza, M.; Baker, N. K.; Faulkner, P.; Downey, M. O. A role for anthocyanin in determining wine tannin concentrations in Shiraz. *Food Chem.* **2014**, *152*, 475−482.
(55) Singleton, V. L.; Trousdale, E. K. Anthocyanin-tannin interactions explaining differences in polymeric phenols between white and red wines. *Am. J. Enol. Vitic.* **1992**, *43*, 63−70.
(56) Dunlevy, J. D.; Dennis, E. G.; Soole, K. L.; Perkins, M. V.; Davies, C.; Boss, P. K. A methyltransferase essential for the methoxypyrazine-derived flavor of wine. *Plant J.* **2013**, *75*, 606−617.

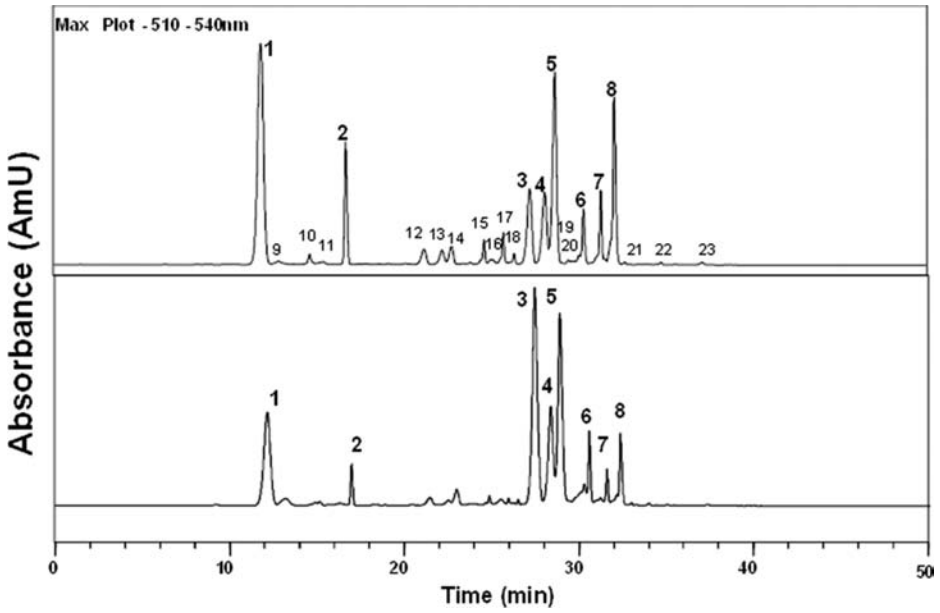

Figure 1. HPLC chromatograms of two representative red cabbage anthocyanin extracts: second-harvested Cairo (top) and first-harvested Integro (bottom) red cabbage at 510−540 nm. Refer to Table 1 for major peak identifications. HPLC conditions: solvent A, 4.5% formic acid in LC-MS grade water; solvent B, LC-MS acetonitrile; gradient, 0−50 min, 0−30% B. The major peaks (1−8) were found in all other red cabbage samples.

and the anthocyanins were recovered with acidified methanol (0.1% formic acid). The methanol was removed using the rotavapor, and the volume was taken to 25 mL with acidified water (0.1% formic acid).

Anthocyanins Content. The total monomeric anthocyanin was determined by using the pH differential method according to Giusti and Wrolstad.[29] The extract was diluted using pH 1 (0.025 M potassium chloride) and pH 4.5 (0.4 M sodium acetated) buffers with a dilution factor of 100. The solutions were allowed to equilibrate for 15 min in the dark. Absorbance was read on 1 cm path length cuvettes at 520 and 700 nm using a Shimadzu UV−visible spectrophotometer (Shimadzu, Columbia, MD, USA). The total monomeric anthocyanin was calculated on the basis of the dry matter (DM) and fresh matter (FM) and reported as milligrams of cyanidin-3-glucoside (Cy3G) per 100 g of sample using the equation

$$\text{total monomeric anthocyanin (mg/L)} = [((A_{520} - A_{700})_{\text{pH1}} - (A_{520} - A_{700})_{\text{pH4.5}}) \times \text{DF} \times 1000 \times \text{MW}]/(\varepsilon \times P)$$

where DF is the dilution factor, MW is the molecular weight (449.2 for Cy3G), ε is the molar absorptivity coefficient (26900 cm^{-1} mg^{-1} for Cy3G), and P is the cuvette path length.

Alkaline Hydrolysis of Anthocyanins. Alkaline hydrolysis (saponification) was adopted from the method of Giusti and Wrolstad.[28] Purified red cabbage anthocyanin extract (10 mL) was mixed with 10 mL of 10% KOH in a capped test tube and set aside for 15 min at room temperature in the dark. The solution was neutralized using 2 N HCl until the color turned pink. The neutralized sample was then purified using a Sep-Pak C18 cartridge (Waters Corp., Milford, MA, USA) and prepared for HPLC analysis.

Chromatographic Analysis. A Shimadzu Prominence reverse phase high-pressure LC-MS was coupled to an SPD-M20-A photodiode array and a single-quadrupole electrospray ionization (ESI) mass spectrophotometer (Shimadzu Scientific, Inc.). For data analysis, LC-MS Solution software was used (Shimadzu Scientific, Inc.). The column was a 100 × 4.5 mm Kinetex PFP 2.6 μm (Phenomenex Inc., Torrance, CA, USA). The solvents were phase A, 4.5% formic acid in LC-MS grade water, and phase B, LC-MS acetonitrile (Fisher Scientific Inc., Fair Lawn, NJ, USA), and the gradient was 0−50 min, 0−30% B. Injection volume was 20 μL. Spectral data were obtained from 250 to 700 nm, and elution of anthocyanins was monitored at 510−540 nm. Peak areas at this region were then integrated and normalized. The proportion of the total peak area of each individual anthocyanin was calculated and reported as percentage of total peak area at 510−540 nm.

For MS analyses, a 0.2 mL/min volume was diverted into the MS and ionized under positive ion condition using an electrospray probe. Data were monitored using total ion scan (SCAN) (m/z 200−1200) and selected ion monitoring at m/z 271 (pelargonidin), m/z 287 (cyanidin), m/z 301 (peonidin), m/z 303 (delphinidin), m/z 317 (petunidin), and m/z 331 (malvidin).

Color and Spectrophotometric Analyses. A ColorQuest XE colorimeter (HunterLab, Hunter Associates Laboratories Inc., Reston, VA, USA) was used to measure the color characteristics (Hunter CIE LCh) of the samples. The equipment was set for transmittance with specular included, and D65/10° was used for the measurements. Samples were placed in a 1 cm path length plastic cuvette and CIE L^*, a^*, b^*, chroma (c^*), and hue angle ($h°$) were measured.

To measure the color in acidic condition, the extract was mixed (in triplicate) with distilled (DI) water (1:20 v/v). The pH of the solutions were measured after 30 min of equilibration and was 3.5. To measure the color in neutral conditions, the extract was diluted with water (1:2 v/v, in triplicate). The diluted solutions were then mixed with 0.1 M potassium phosphate buffer (pH 7) with a dilution factor (DF) of 20. The maximum absorbances (λ_{max}) in the visible range of the neutral solutions were recorded using a Shimadzu UV−visible spectrophotometer 2450.

FD&C Red No. 3, FD&C No. 40, and FD&C Blue No. 2 (Noveon Hilton Davis, Inc., Cincinnati, OH, USA) were also dissolved in DI water to concentrations that most closely matched the lightness (L^*) and chroma (c^*) of the samples.

Statistical Analysis. Seven different cultivars at two maturity stages (three heads each) for a total of 42 samples were analyzed using principal component analysis (PCA). PCAs for total monomeric anthocyanin, nonacylated, monoacylated, and diacylated pigments (based on the proportional peak areas shown in Table 2) were performed. Autoscaling was used to normalize each variable before the analysis.

To compare the anthocyanin contents and profile, normality of the variables were first checked using the Kolmogorov−Smirnov test (α = 0.05). Analysis of variance (ANOVA) was then used to analyze the total monomeric anthocyanin and the proportion of each group of pigments separately using the following model: $Y_{ijk} = \mu + v_i + t_j + vt_{ij} +$

$\alpha_k + \varepsilon_{ijk}$, where Y is the individual variable, μ is the grand mean, v_i is the cultivar effect, t_j is the harvesting time effect, vt_{ij} is the interaction between the main factors, α_k is the heads effect defined as random factor, and ε_{ijk} is the random error of the model. When a significant difference was obtained (P value < 0.05), the Tukey means-comparison test was used to compare each pair of means.

All statistical analyses were done on the basis of at least three independent replicate samples from each individual head. Results were analyzed by using Minitab 16 statistical software (Minitab Inc.).

RESULTS AND DISCUSSION

HPLC-PDA-MS and Identification of Major Pigments. According to the HPLC-PDA data obtained at 510−540 nm, up to 23 peaks were observed. In previous studies, up to 36 different anthocyanins have been detected in red cabbage.[29−31] Figure 1 shows examples of anthocyanin profiles (Cairo and Integro extracts) obtained by HPLC-PDA. The eight major peaks, representing ≃90% of the total anthocyanins and common to all seven cultivars at both maturity stages, were selected for further identification and analyses. The λ_{max} at the UV and vis ranges, molecular ions, and fragments along with tentative identification of each peak are presented in Table 1. The pigments were identified using HPLC-PDA and HPLC-MS and compared with data reported in the literature.[11,12]

Table 1. PDA Absorbance and MS Data for Red Cabbage Anthocyanins[a]

peak	RT[b] (min)	λ_{vis}[c] (nm)	λ_{acyl}[d] (nm)	M^{+}[e]	identification
1	12.13	513		773 (287)	Cy-3diG-5G
2	16.95	528	334	979 (287)	Cy-3diG-5G + sinapic[f]
3	27.41	523	313	919 (287)	Cy-3diG-5G + *p*-coumaric
4	28.33	523	326	949 (287)	Cy-3diG-5G + ferulic
5	28.85	524	329	979 (287)	Cy-3diG-5G + sinapic
6	30.53	536	319	1125 (287)	Cy-3diG-5G + ferulic and ferulic
7	31.55	536	330	1155 (287)	Cy-3diG-5G + sinapic and ferulic
8	32.31	536	331	1185 (287)	Cy-3diG-5G + sinapic and sinapic

[a] m/z 287 was the major fragment in all eight peaks. Cy-3diG-5G, cyanidin-3-diglucoside-5-glucoside. [b] Retention time. [c] λ vis−max. [d] λ of acylation. [e] Mass ion. [f] Tentative identification.

As shown in Table 1, m/z 287 was the fragment in all eight anthocyanins indicating that cyanidin derivatives were the major aglycon as reported in previous studies.[12,30,32−34] All of the pigments were nonacylated, monoacylated, and diacylated derivatives of cyanidin-3-diglucoside-5-glucoside (Cy-3diG-5G), which was also confirmed by saponification (results are not shown). The acylating groups were aromatic acids: sinapic, ferulic, and *p*-coumaric acids (Table 1).

Anthocyanin Content and Proportion of the Pigments. *Principal Component Analysis of Red Cabbage Anthocyanin Extracts.* The analysis of the objects (i.e., red cabbage cultivars at two maturity stages) is performed visually using the scores plot (Figure 2), where the objects are represented as a function of the principal components (PCs). As shown in Figure 2, PC1 correlated positively with monoacylated pigments as opposed to the diacylated pigments. PC2, on the other hand, was more affected by the nonacylated pigments and the total monomeric anthocyanin. PC1 and PC2 extracted 83.7 and 12.8% of the total variances, respectively.

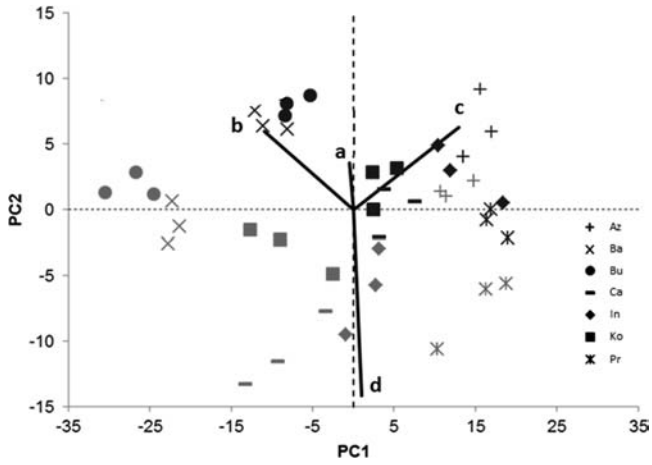

Figure 2. Correlation between the first two principal components and the variables as well as score plot with respect to cultivars and harvesting time for seven different red cabbage cultivars: a, total monomeric anthocyanin; b, diacylated pigments; c, monoacylated pigments; d, nonacylated pigments. AZ, Azurro; Ba, Bandolero; Bu, Buscaro; Ca, Cairo; In, Integro; Ko, Kosaro; Pr, Primero. Symbols in black and gray represent harvest times after 13 or 21 weeks, respectively.

According to this analysis, the samples were clearly separated diagonally on the basis of their maturation time. With maturation the percentage of diacylation increased for most samples, so for most of the second-harvested samples PC1 is negative. Also, because the early mature samples (week 13) had slightly higher amounts of total monomeric anthocyanin, PC2 tend to be more positive (Figure 2).

PCA is a proper way to obtain relevant information from the original variables into fewer new latent variables (PCs). According to our results, this analysis was helpful in classification of the samples at two maturity stages. Most samples with different maturity times were separated on the basis of the first two principal components. Azurro and Primero cultivars, however, were exceptions because their pigment profiles were not significantly changed with maturation.

Anthocyanin Content. The average anthocyanin contents for the 13- and 21-week-harvested plants were ≃1442 and 1269 mg Cy3G/100 g DM respectively, and these values for the fresh matter were ≃150 and 145 mg Cy3G/100 g FM, respectively. Piccaglia et al. also reported the anthocyanin content of three red cabbage cultivars in Italy to be >1000 mg/100 g DM.[10] The anthocyanin content for the fresh weight red cabbage reported by Oregon State University database and Wu et al. were, however, 25 and 322 ± 40.8 mg/100 g FW, respectively.[35,36] According to our findings, cultivar made a difference in anthocyanin contents at both maturity stages.

As shown in Table 2, Buscaro and Integro harvested after 13 weeks had the highest anthocyanin contents. Anthocyanin contents, however, did not change significantly from the first to the second harvest except for the Buscaro (DM) cultivar, which showed a lower anthocyanin content when plants were left longer on the ground (Table 2). Accumulation of anthocyanins can be explained by developmental factors, which could be different in different varieties.[23]

Proportion of Major Pigments. Although red cabbage is known to have more than 20 different anthocyanins, relative proportions of 8 of them (Figure 1 and Table 1) represented ≃90% of the total anthocyanins and were measured and

dx.doi.org/10.1021/jf501991q | J. Agric. Food Chem. 2014, 62, 7524−7531

Table 2. Anthocyanin Contents (Total Monomeric Anthocyanin) and Percentage of Major Pigments (Percent Total Peak Area at 510−540 nm) in Seven Red Cabbage Cultivars at Two Different Harvesting Times[a]

		total monomeric anthocyanin (mg Cy3G/100 g)				
cultivar	harvest time (week)	DM[b]	FM[c]	nonacylated pigments[d] (%)	monoacylated pigments[e] (%)	diacylated pigments[f] (%)
Primero	13	1111 e	109 gh	21.24 bc	67.63 a	4.56 g
	21	1026 e	104 h	26.84 a	63.71 ab	4.09 g
Integro	13	1660 ab	185 a	18.17 cde	65.22 ab	7.23 fg
	21	1637 ab	188 a	25.59 ab	53.32 cde	12.28 ef
Azurro	13	1392 bcd	144 bcdef	15.85 def	69.33 a	9.19 fg
	21	1217 de	137 cdef	19.33 cde	65.01 ab	9.21 fg
Kosaro	13	1247 cde	128 efgh	15.51 ef	55.43 cd	11.42 f
	21	1001 e	115 fgh	20.25 cd	46.74 ef	19.41 cd
Cairo	13	1389 bcd	153 bcde	20.08 cde	58.23 bc	12.87 ef
	21	1256 cde	168 ab	28.5 a	43.96 fg	17.74 de
Bandolero	13	1517 abc	165 abcd	13.1 f	48.67 def	24.54 bc
	21	1512 abc	165 abcd	19.07 cde	36.75 gh	29.1 b
Buscaro	13	1780 a	170 abcd	13.36 f	52.1 cde	23.59 bcd
	21	1236 de	137 defg	17.04 cdef	35.48 h	35.45 a

[a]Different letters in the same column indicate significant differences ($p < 0.05$). [b]Dry matter. [c]Fresh matter. [d]Peak 1 (Table 1). [e]Peaks 2, 3, 4, and 5 (Table 1). [f]Peak 6, 7, and 8 (Table 1).

Table 3. CIE $L^*a^*b^*$, Chroma (c^*), Hue ($h°$), and λ_{max} of Seven Red Cabbage Cultivar Extracts at Two Different Harvesting Times at pH 3.5 and Their Comparison with Two FD&C Synthetic Red Dyes

cultivar	HT[a] (week)	L^*	a^*	b^*	c^*	$h°$	λ_{max} (nm)	ΔE_1[b]	ΔE_2[c]
Primero	13	76.2 ± 0.8	45.3 ± 0.6	−3.5 ± 0.7	47.4 ± 3.5	359.2 ± 4.4	520 ± 1.2	15.9 ± 2	18 ± 0.7
	21	77.1 ± 2	42.1 ± 4	−2.7 ± 0.7	42.2 ± 4	356.3 ± 0.9	520 ± 1.4	18.5 ± 4.2	17.9 ± 1
Integro	13	67.4 ± 2.6	59.5 ± 1.7	−0.5 ± 0.3	59.6 ± 4.6	357.5 ± 2.6	520 ± 0.8	8.8 ± 3.1	23.4 ± 1.3
	21	66.2 ± 1.8	61 ± 2.5	−1.9 ± 1.2	61 ± 2.5	358.2 ± 1.2	520 ± 1.1	9.3 ± 2.2	24.8 ± 1.4
Azurro	13	69.6 ± 3	56.1 ± 1	−2.8 ± 2	56.6 ± 5.3	357.7 ± 2.7	520 ± 0.6	6.8 ± 2.9	20.7 ± 2
	21	71.2 ± 2.9	53.2 ± 4.7	−2.9 ± 1.4	53.3 ± 4.6	356.7 ± 1.9	520 ± 0.5	9.1 ± 2.2	20.2 ± 1.4
Kosaro	13	69 ± 3.2	57 ± 3.5	−5.9 ± 1.2	57.3 ± 5	354.1 ± 2.6	520 ± 0.3	6.1 ± 2.7	23.7 ± 3.7
	21	69.5 ± 1.5	55.5 ± 2.4	−7.1 ± 0.9	56 ± 2.4	352.7 ± 1	520 ± 0.8	7 ± 0.8	24.8 ± 1.6
Cairo	13	68.9 ± 3.5	57.1 ± 1.6	−4.5 ± 0.6	55.9 ± 3.6	357 ± 1.4	520 ± 1.4	6.6 ± 3.2	23 ± 1.3
	21	64.9 ± 1.5	63 ± 2	−4.3 ± 0.4	63.2 ± 2	356.1 ± 0.5	520 ± 0.6	10.1 ± 2	28.1 ± 1.6
Bandolero	13	62.5 ± 1.6	67.3 ± 4.3	−4.7 ± 1.3	68.4 ± 1.5	356.8 ± 4.4	520 ± 0.8	14.8 ± 3	32 ± 1.5
	21	60.7 ± 1.8	68.2 ± 2.1	−4.8 ± 1.5	68.4 ± 2	356 ± 1.4	530 ± 1.2	15.9 ± 2.7	33.6 ± 1.3
Buscaro	13	62.9 ± 4.1	66.9 ± 2.3	−3.7 ± 1	64.5 ± 1.2	357.9 ± 1.4	520 ± 0.9	12.8 ± 3	29.9 ± 4.4
	21	61.7 ± 4.2	66 ± 4.5	−6.4 ± 2.9	66.4 ± 4.2	354.4 ± 2.8	530 ± 1.5	14.2 ± 5.7	33 ± 3
FD&C Red No. 3		74.2	59.99	−6.1	60.3	354.19	520		
FD&C Red No. 40		75.64	45.11	14.48	47.38	17.79	500		

[a]Harvesting time. [b]Color difference with FD&C Red No. 3. [c]Color difference with FD&C Red No. 40.

compared among cultivars and maturation stages as they are more likely to affect the color and stability of the extract. The pigments were also grouped into nonacylated, monoacylated, and diacylated.

According to our results, nonacylated pigments represented an average of ≃19.6% (±4.5) of the major pigments (Table 2). Charron et al. also found the percentage of nonacylated pigment in red cabbage to be 21.3%.[31] Among the major pigments identified, the amounts of mono- and diacylated

dx.doi.org/10.1021/jf501991q | J. Agric. Food Chem. 2014, 62, 7524−7531

anthocyanins were on average 54.4 (±12.6) and 15.8% (±8.7), respectively (Table 2). Red cabbage has been identified as a highly acylated anthocyanin source according to previous research.[30,31]

Before the percentages of each group of pigments were compared using ANOVA, the normality test was done to verify the validity of the test, and none of the variables had a p value smaller than 0.05.

Cultivar had a significant (p value < 0.05) impact on pigment profile. The proportions of monoacylated and diacylated pigments were the major differences found among the cultivars. Primero and Azurro had the highest proportions of monoacylated pigments and the lowest proportions of diacylated pigments, whereas Buscaro and Bandolero varieties had the lowest proportions of monoacyltaed pigments and the highest proportion of diacylated pigments. The effect of maturity on pigment profile was largely dependent on the cultivar for monoacylated and diacylated pigments (p value < 0.05); this interaction was not observed for the nonacylated pigments.

As shown in Table 2, the proportion of nonacylated pigments increased significantly in the 21-week-mature plants except for Azurro and Buscaro cultivars, which did not show a significant increase. More mature Primero, Cairo, and Integro had highest amounts of nonacylated pigments.

The proportions of monoacylated anthocyanins were, however, decreased with longer maturation time, except for Primero and Azurro cultivars, which did not show a significant decrease on monoacylated pigments. The proportion of monoacylated pigments was highest (≃67%) for cultivar Primero, Integro, and Azurro first harvests as compared to the other cultivars (≃54%) harvested at the same time (Table 2).

The proportion of diacylated pigments varied remarkably among cultivars. They increased significantly in Kosaro and Buscaro due to maturation. Buscaro and Bandolero, harvested after 21 weeks, had the highest (≃30%) proportion of diacylated pigments, whereas Primero (≃4%) had the lowest at both maturity stages (Table 2).

Because the plants were grown side by side, the main reason for the profile differences could arise from intrinsic factors such as plant genetics and enzymes and their activities throughout the maturation, which influence the anthocyanin synthesis within the plant. Variation in anthocyanin structures can be correlated with alteration of single genes, which influence the enzymatic step of anthocyanin synthesis pathways.[37] The reason for accumulation of certain anthocyanins in certain cultivars could be due to the difference in the activities of different genes. Also, during the maturation, the activity of the genes controlling the synthesis of monoacylated pigments could have slowed, whereas those responsible for the synthesis of nonacylated anthocyanins or for the addition of a second acyl group may have remained active.

Color Characteristics and Stability. *Color in Acidic pH.* Table 3 shows the color characteristics of solutions colored with red cabbage anthocyanin extracts from the different cultivars at pH 3.5 and their color comparisons to synthetic colorants FD&C Red No. 3 and No. 40. The lightness of the samples was approximately between 60 and 77 (Table 3). The synthetic colorant solutions were also adjusted to have a similar lightness. Extracts from all seven cultivars produced a deep pink color at pH 3.5 with a hue angle close to 350°. Chroma values of the samples were higher for solutions prepared with Bandolero and Buscaro extracts as opposed to Primero. The wavelengths of maximum absorbances (λ_{max}) of the samples were similar to that of Red No. 3 (≃520 nm) except for late-harvested Bandolero and Buscaro cultivars ($\lambda_{max} \simeq 530$ nm). Generally, samples showed more similar color characteristics to FD&C Red No. 3 than to FD&C Red No. 40 synthetic dyes ($\Delta E_1 < \Delta E_2$). Under acidic pH, maturation of the plants did not seem to significantly affect the color of the solutions. Early-harvested Azurro, Kosaro, Cairo, and Integro at the tested concentrations were the samples that produced colors most similar to FD&C Red No. 3 with similar λ_{max} and ΔE between 6.1 and 8.8 (Table 3).

Stability in Neutral pH. The spectral characteristics of the samples at pH 7 were monitored over 72 h of refrigerated storage. Figure 3 shows the changes in λ_{max} for three

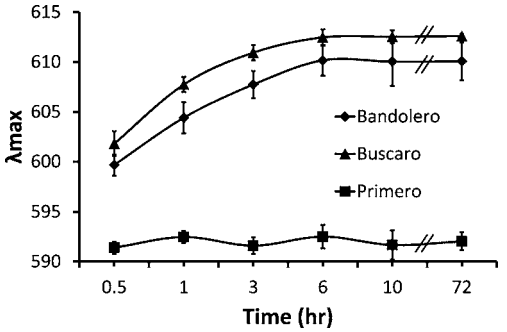

Figure 3. Change in λ_{max} for the second-harvested Buscaro, Bandolero, and Primero at pH 7 over 72 h of refrigeration. Most color changes happened during the first 6 h of storage.

representative samples. Solutions colored with Buscaro and Bandolero red cabbage extracts showed the highest variations in the λ_{max}, whereas solutions colored with Primero extract showed the least changes over the 72 h. Most of the changes observed happened during the first 5−6 h (Figure 3). Table 4 shows the λ_{max} of all seven varieties 30 min after the extracts were mixed with buffer pH 7 and 6 h afterward (refrigerated storage). The λ_{max} for samples containing significantly higher amounts of diacylated anthocyanins (Buscaro and Bandolero) at this pH seemed to be the highest (≃600 nm) compared to the other samples. Torskangerpoll and Andersen also investigated the absorbance and color change in cyanidin 3-(2″-(2‴-sinapoylglucosyl)-6″-sinapoylglucoside)-5-glucoside (a diacylated pigment isolated from red cabbage) at different pH values. They also found out that at pH 7.2 the pigment had λ_{max} of ≃605 nm.[38] A bathochromic effect of up to 7 nm was observed for most samples after 6 h of refrigerated storage. More mature Buscaro and Bandolero varieties produced a λ_{max} (≃610 nm) similar to that of FD&C Blue No. 2. For other samples such as Primero and Integro, however, minute bathochromic effects were observed (Table 4).

Anthocyanins tend to have lower stabilities at neutral to alkaline pH values.[14,39] After mixing with buffer pH 7 followed by 6 h of refrigeration, the color degradation was highest (≃53%) and lowest (≃19%) for the second-harvested Primero and Buscaro, respectively (Table 4). Higher stabilities of the Buscaro and Bandolero cultivars at the tested pH values could be explained by the larger number of diacylated anthocyanins, which have higher stabilities due to the pigments intramolecular and/or intermolecular copigmentation and self-association reactions.[15] Torskangerpoll and Andersen also demonstrated

Table 4. Maximum Absorbance (λ_{max}) of Red Cabbage Extracts at Two Different Harvesting Times Measured after 30 min and 6 h of Refrigeration Storage in Buffer pH 7 Compared to FD&C Synthetic Blue No. 2 and Stabilities (Percent Degradation) during This Time[a]

		λ_{max} (nm)		
cultivar	HT[b] (weeks)	30 min	6 h	% degradation
Primero	13	591.4 ± 0.6	591.6 ± 0.8	50.1 ± 5.5
	21	591.3 ± 0.4	591.9 ± 1	53.3 ± 8.9
Integro	13	591.4 ± 1.1	592.1 ± 0.1	38.9 ± 5.4
	21	598.6 ± 2.3	599.7 ± 2	44 ± 9.9
Azurro	13	590.8 ± 0.8	593.5 ± 0.5	41.5 ± 4.9
	21	595.9 ± 0.7	597.8 ± 2.1	49.3 ± 7.9
Kosaro	13	596.3 ± 1	599.9 ± 1.4	31 ± 3.3
	21	602 ± 0.3	604.8 ± 0.8	39.5 ± 5.2
Cairo	13	593.6 ± 0.2	595.3 ± 4.2	42.1 ± 8.4
	21	599.7 ± 2.4	602.9 ± 0.5	36.7 ± 8.2
Bandolero	13	601.8 ± 1.2	609.4 ± 1.2	27.1 ± 4
	21	599.7 ± 2.3	610.1 ± 1.6	22.5 ± 3.8
Buscaro	13	600.1 ± 0.7	606.7 ± 1.9	28.6 ± 2.3
	21	601.8 ± 0.4	610.1 ± 1.8	19.1 ± 3.8
FD&C Blue No. 2		610	610	

[a]Percent degradation was calculated by dividing the absorbance at λ_{max} after 6 h by the absorbance at λ_{max} after 30 min in buffer pH 7 × 100. [b]Harvesting time.

that diacylation of anthocyainins increases their color stabilities.[38]

The color characteristics of pH 7 buffer solutions colored with the different red cabbage extracts after 6 h of refrigeration compared to FD&C Blue No. 2 are shown in Table 5. The lightness of the samples ranged between ≃60 and 85. Chroma values were higher for Bandolero and Buscaro cultivars at the tested pH value (Table 5). The synthetic FD&C Blue No. 2 was diluted until the lightness was similar to that of the evaluated samples. ΔE values of the samples when compared to this synthetic dye were between 17.6 and 26.4 (Table 5). The color difference with FD&C Blue No. 2 at the tested concentration for the late-harvested Kosaro sample was the smallest; however, the λ_{max} values for the second-harvested Buscaro and Bandolero cultivars were closer to this value for FD&C Blue No. 2 (Tables 4 and 5). Acylation of anthocyanins with aromatic acids (e.g., cinnamic acid) has proven to increase the λ_{max} and shift the hue angle to purple color under acidic conditions.[16,17] As shown in Table 1, late-harvested Buscaro and Bandolero cultivars, with the highest percentages of diacylated pigments, also exhibited the highest λ_{max} under neutral conditions.

In conclusion, anthocyanin content varied among red cabbage cultivars, and leaving the cabbages in the ground for additional time did not increase the pigment content. The pigment profiles changed among the cultivars and maturation stages. For most cultivars, the amount of nonacylated and diacylated pigments increased as opposed to the monoacylated pigments. Cultivars with lower proportions of diacylated pigments better reproduced the color of FD&C Red No. 3 under acidic conditions, whereas cultivars with higher proportions of diacylated pigments better matched the colors of FD&C Blue No. 2 at neutral pH. Pigment profile also affected the color stability at neutral pH. For future studies,

Table 5. CIE $L^*a^*b^*$, Chroma (c^*), and Hue ($h°$) of Seven Red Cabbage Extracts at Two Different Harvesting Times after 6 h of Refrigeration Storage at pH 7 Compared to FD&C Blue No. 2

cultivar	HT[a] (weeks)	L^*	a^*	b^*	c^*	$h°$	ΔE^b
Primero	13	83.6 ± 0.6	2.6 ± 0.2	−9.9 ± 0.6	10.2 ± 2.4	284.6 ± 1.5	25.7 ± 0.5
	21	84.8 ± 2	2.1 ± 0.6	−8.7 ± 2.2	9 ± 2.2	284.5 ± 5.1	26.4 ± 2
Integro	13	70.5 ± 2.9	1.7 ± 2.2	−22.4 ± 2.8	22.5 ± 2.7	274.7 ± 5.8	21.4 ± 1
	21	69.9 ± 3.2	−0.2 ± 0.6	−23.5 ± 2.6	23.5 ± 2.6	269.5 ± 1.3	19.8 ± 0.7
Azurro	13	77.7 ± 1.5	1.4 ± 0.2	−15.8 ± 1.5	15.9 ± 1.4	275.3 ± 1.3	21.2 ± 1.3
	21	78.5 ± 3.7	1.2 ± 0.4	−15.2 ± 3.1	15.3 ± 3.1	274.7 ± 1.9	21.5 ± 1.3
Kosaro	13	72.1 ± 1.5	−1.3 ± 0.7	−22.1 ± 1.9	22.1 ± 2.4	266.7 ± 1.3	17.9 ± 2.3
	21	71.9 ± 2.5	−1.8 ± 1.8	−22.5 ± 2	22.6 ± 2.2	265.6 ± 4.2	17.6 ± 1.1
Cairo	13	69.3 ± 4.4	−0.5 ± 1.7	−24.7 ± 4.2	24.7 ± 4.2	269.2 ± 3.5	20.2 ± 1.1
	21	66.2 ± 3.4	−2.3 ± 0.6	−27.9 ± 3	28 ± 3	265.3 ± 0.8	20.2 ± 1.8
Bandolero	13	60.8 ± 1.8	−4.9 ± 0.7	−31.9 ± 2.7	32.3 ± 4.3	261.2 ± 1.4	22.9 ± 1.2
	21	59.6 ± 3.1	−5.7 ± 0.6	−33.2 ± 2.6	33.7 ± 2.5	260.2 ± 1.6	23.9 ± 3.6
Buscaro	13	63.4 ± 3	−3.8 ± 1.5	−29.9 ± 2.9	30.2 ± 2.1	262.9 ± 2.9	21.2 ± 1.6
	21	63.4 ± 1.4	−5.4 ± 0.2	−30.6 ± 0.8	31 ± 0.8	260 ± 0.7	20.3 ± 1.4
FD&C Blue No. 2		78.06	−17.95	−24.28	30.19	233.52	

[a]Harvesting time. [b]Color difference with FD&C Blue No. 2.

dx.doi.org/10.1021/jf501991q | J. Agric. Food Chem. 2014, 62, 7524−7531

however, year-to-year variability of these cultivars should be investigated.

AUTHOR INFORMATION

Corresponding Author

*(M.M.G.) Phone: (614) 247-8016. Fax: (614) 292-0218. E-mail: giusti.6@osu.edu.

Funding

We are thankful to MARS Global Chocolate, Hackettstown, NJ, USA, for providing funding for the project.

Notes

The authors declare no competing financial interest.

ACKNOWLEDGMENTS

We thank Ken McCammon and Bejo Seeds, Inc., for providing the plant materials. Also, we especially thank Marçal Plans Pujolras from Universitat Politècnica de Catalunya for his help with data statistical analysis.

ABBREVIATIONS USED

DM, dry matter; FM, fresh matter; AZ, Azurro; Ba, Bandolero; Bu, Buscaro; Ca, Cairo; In, Integro; Ko, Kosaro; Pr, Primero

REFERENCES

(1) Giusti, M. M.; Schwartz, S.; Elbe, H. V. Colorants. In *Fennema's Food Chemistry*, 4th ed.; Damodaran, S., Parkin, K., Fennema, O. R., Eds.; CRC Press/Taylor & Francis: Boca Raton, FL, USA, 2008; pp 571−638.

(2) Henry, B. S. Natural food colours. In *Natural Food Colorants*, 2nd ed.; George, A. F., Hendry, J. D., Eds.; Blackie Chapman & Hall: London, UK, 1996; pp 40−79.

(3) Wrolstad, R. E.; Smith, D. E. Color analysis. In *Food Analysis*, 4th ed.; Nielsen, S. S., Ed.; Springer Science+Business Media: Berlin, Germany, 2010; pp 573−586.

(4) Socaciu, C. *Food Colorants: Chemical and Functional Properties*; Taylor & Francis: Boca Raton, FL, USA, 2008.

(5) Wrolstad, R. E. Symposium 12: Interaction of natural colors with other ingredients − anthocyanin pigments − bioactivity and coloring properties. *J. Food Sci.* **2004**, *69*, C419−C421.

(6) Kong, J.-M.; Chia, L.-S.; Goh, N.-K.; Chia, T.-F.; Brouillard, R. Analysis and biological activities of anthocyanins. *Phytochemistry* **2003**, *64*, 923−933.

(7) Heins, A.; Stockmann, H.; Schwarz, K. Designing "anthocyanin-tailored" food composition. In *Biologically-Active Phytochemicals in Food*; Pfannhauser, W., Fenwick, G. R., Khokhar, S., Eds.; Springer: Berlin, Germany, 2001; pp 378−381.

(8) He, J. A.; Giusti, M. M. Anthocyanins: natural colorants with health-promoting properties. Doyle, M. P., Klaenhammer, T. R., Eds. *Annu. Rev. Food Sci. Technol.* **2010**, *1*, 163−186.

(9) Ghosh, D.; Konishi, T. Anthocyanins and anthocyanin-rich extracts: role in diabetes and eye function. *Asia Pac. J. Clin. Nutr.* **2007**, *16*, 200−208.

(10) Piccaglia, R.; Marotti, M.; Baldoni, G. Factors influencing anthocyanin content in red cabbage (*Brassica oleracea* var *capitata* L f *rubra* (L) Thell). *J. Sci. Food Agric.* **2002**, *82*, 1504−1509.

(11) McDougall, G. J.; Fyffe, S.; Dobson, P.; Stewart, D. Anthocyanins from red cabbage − stability to simulated gastro-intestinal digestion. *Phytochemistry* **2007**, *68*, 1285−1294.

(12) Wiczkowski, W.; Szawara-Nowak, D.; Topolska, J. Red cabbage anthocyanins: profile, isolation, identification, and antioxidant activity. *Food Res. Int.* **2013**, *51*, 303−309.

(13) Mazza, G.; Miniati, E. *Anthocyanins in fruits, vegetables, and grains*; CRC Press: Boca Raton, FL, USA, 1993.

(14) Cabrita, L.; Fossen, T.; Andersen, O. M. Colour and stability of the six common anthocyanidin 3-glucosides in aqueous solutions. *Food Chem.* **2000**, *68*, 101−107.

(15) Giusti, M. M.; Wrolstad, R. E. Acylated anthocyanins from edible sources and their applications in food systems. *Biochem. Eng. J.* **2003**, *14*, 217−225.

(16) Stintzing, F. C.; Stintzing, A. S.; Carle, R.; Frei, B.; Wrolstad, R. E. Color and antioxidant properties of cyanidin-based anthocyanin pigments. *J. Agric. Food Chem.* **2002**, *50*, 6172−6181.

(17) Giusti, M. M.; Rodriguez-Saona, L. E.; Wrolstad, R. E. Molar absorptivity and color characteristics of acylated and non-acylated pelargonidin-based anthocyanins. *J. Agric. Food Chem.* **1999**, *47*, 4631−4637.

(18) Walkowiak-Tomczak, D.; Czapski, J. Colour changes of a preparation from red cabbage during storage in a model system. *Food Chem.* **2007**, *104*, 709−714.

(19) Tamura, H.; Yamagami, A. Antioxidative activity of mono-acylated anthocyanins isolated from Muscat Bailey A grape. *J. Agric. Food Chem.* **1994**, *42*, 1612.

(20) Dyrby, M.; Westergaard, N.; Stapelfeldt, H. Light and heat sensitivity of red cabbage extract in soft drink model systems. *Food Chem.* **2001**, *72*, 431−437.

(21) Chalker-Scott, L. Environmental significance of anthocyanins in plant stress responses. *Photochem. Photobiol.* **1999**, *70*, 1−9.

(22) Connor, A. M.; Luby, J. J.; Tong, C. B. S.; Finn, C. E.; Hancock, J. F. Genotypic and environmental variation in antioxidant activity, total phenolic content, and anthocyanin content among blueberry cultivars. *J. Am. Soc. Hortic. Sci.* **2002**, *127*, 89−97.

(23) Awad, M. A.; de Jager, A.; van der Plas, L. H. W.; van der Krol, A. R. Flavonoid and chlorogenic acid changes in skin of 'Elstar' and 'Jonagold' apples during development and ripening. *Sci. Hortic.−Amsterdam* **2001**, *90*, 69−83.

(24) Solomon, A.; Golubowicz, S.; Yablowicz, Z.; Grossman, S.; Bergman, M.; Gottlieb, H. E.; Altman, A.; Kerem, Z.; Flaishman, M. A. Antioxidant activities and anthocyanin content of fresh fruits of common fig (*Ficus carica* L.). *J. Agric. Food Chem.* **2006**, *54*, 7717−7723.

(25) Fawole, O. A.; Opara, U. L. Effects of maturity status on biochemical content, polyphenol composition and antioxidant capacity of pomegranate fruit arils (cv. 'Bhagwa'). *S. Afr. J. Bot.* **2013**, *85*, 23−31.

(26) Josuttis, M.; Verrall, S.; Stewart, D.; Krueger, E.; McDougall, G. J. Genetic and environmental effects on tannin composition in strawberry (*Fragaria* × *ananassa*) cultivars grown in different European locations. *J. Agric. Food Chem.* **2013**, *61*, 790−800.

(27) Wrolstad, R. E.; Durst, R. W.; Giusti, M. M.; Rodriguez-Saona, L. E. Analysis of anthocyanins in nutraceuticals. In *Quality Management of Nutraceuticals*; American Chemical Society: Washington, DC, USA, 2001; Vol. 803, pp 42−62.

(28) Giusti, M. M.; Wrolstad, R. E. Characterization of red radish anthocyanins. *J. Food Sci.* **1996**, *61*, 322−326.

(29) Arapitsas, P.; Sjoberg, P. J. R.; Turner, C. Characterisation of anthocyanins in red cabbage using high resolution liquid chromatography coupled with photodiode array detection and electrospray ionization-linear ion trap mass spectrometry. *Food Chem.* **2008**, *109*, 219−226.

(30) Wu, X. L.; Prior, R. L. Identification and characterization of anthocyanins by high-performance liquid chromatography-electrospray ionization-tandem mass spectrometry in common foods in the United States: vegetables, nuts, and grains. *J. Agric. Food Chem.* **2005**, *53*, 3101−3113.

(31) Charron, C. S.; Clevidence, B. A.; Britz, S. J.; Novotny, J. A. Effect of dose size on bioavailability of acylated and nonacylated anthocyanins from red cabbage (*Brassica oleracea* L. var. *capitata*). *J. Agric. Food Chem.* **2007**, *55*, 5354−5362.

(32) Park, S.; Arasu, M. V.; Lee, M. K.; Chun, J. H.; Seo, J. M.; Lee, S. W.; Al-Dhabi, N. A.; Kim, S. J. Quantification of glucosinolates, anthocyanins, free amino acids, and vitamin C in inbred lines of cabbage (*Brassica oleracea* L.). *Food Chem.* **2014**, *145*, 77−85.

(33) Scalzo, R. L.; Genna, A.; Branca, F.; Chedin, M.; Chassaigne, H. Anthocyanin composition of cauliflower (*Brassica oleracea* L. var.

botrytis) and cabbage (*B. oleracea* L. var. *capitata*) and its stability in relation to thermal treatments. *Food Chem.* **2008**, *107*, 136−144.
(34) Sun, J. H.; Xiao, Z. L.; Lin, L. Z.; Lester, G. E.; Wang, Q.; Harnly, J. M.; Chen, P. Profiling polyphenols in five brassica species microgreens by UHPLC-PDA-ESI/HRMSn. *J. Agric. Food Chem.* **2013**, *61*, 10960−10970.
(35) Wu, X. L.; Beecher, G. R.; Holden, J. M.; Haytowitz, D. B.; Gebhardt, S. E.; Prior, R. L. Concentrations of anthocyanins in common foods in the United States and estimation of normal consumption. *J. Agric. Food Chem.* **2006**, *54*, 4069−4075.
(36) Linus Pauling Institute: Micronutrient Research for Optimum Health, Oregon State University; http://lpi.oregonstate.edu/infocenter/phytochemicals/flavonoids/flavtab2.html (accessed July 15, 2013).
(37) Holton, T. A.; Cornish, E. C. Genetics and biochemistry of anthocyanin biosynthesis. *Plant Cell* **1995**, *7*, 1071−1083.
(38) Torskangerpoll, K.; Andersen, Ø. M. Colour stability of anthocyanins in aqueous solutions at various pH values. *Food Chem.* **2005**, *89*, 427−440.
(39) Fossen, T.; Cabrita, L.; Andersen, O. M. Colour and stability of pure anthocyanins influenced by pH including the alkaline region. *Food Chem.* **1998**, *63*, 435−440.

stirrer input power (IP) on the loading of curcumin in OSG micelles using response surface methodology (RSM). Moreover, the curcumin-loaded OSG was characterized by using dynamic light scattering (DLS), transmission electron microscopy (TEM), atomic force microscopy (AFM), Fourier transform infrared (FT-IR) spectroscopy, differential scanning calorimetry (DSC), and X-ray diffraction (XRD).

MATERIALS AND METHODS

Materials. Commercial soluble β-glucan (80 wt% β-glucan content) extracted from oats was purchased from Zhangjiakou Yikang Biological Technology Co., Ltd. (China). 2-Octen-1-ylsuccinic anhydride (product no. 416487) was purchased from Sigma Chemical Co. (USA). Curcumin (bis(4-hydroxy-3-methoxyphenyl)-1,6-heptadiene-3,5-dione, 98% purity) was supplied by Adamas Reagent Co., Ltd. (China). IR spectroscopy grade KBr was purchased from Guangfu Reagent Chemical Co., Ltd. (China). Chromatographic grade acetonitrile and formic acid were also used. All chemicals were used in this study without further purification.

Oat β-Glucan Solution Preparation and Hydrolysis. Oat β-glucan (2.500 g) was dispersed in 1 L of distilled water and heated at 80 °C with magnetic stirring for 2 h. The resultant dispersion was cooled to room temperature with tap water. An oat β-glucan solution (1.953 ± 0.075 g/L) was obtained as the supernatant by centrifuging the dispersion at 3000g for 10 min. Oat β-glucan was hydrolyzed according to a previously described method.[29] Two hydrolysates of oat β-glucan (OG1 and OG2) were prepared in the present study. In detail, 100 μL (OG1) and 200 μL (OG2) of hydrochloric acid (6 M) were mixed with 100 mL of the above-prepared oat β-glucan solution (0.195 g oat β-glucan), respectively. Then, the mixtures were inoculated at 50 °C for 10 min to allow the intended hydrolysis. After hydrolysis was completed, hydrolysates were rapidly cooled to room temperature and neutralized (pH 6~7) with 2 M NaOH. The hydrolysates were successively dialyzed against tap water and distilled water for 24 h in a dialysis bag (MD44-14, Union Carbide Co., Seadrift, TX, USA) with a size exclusion of 14 000 g/mol for globular molecules. Then, they were subjected to lyophilization to obtain OG1 (0.192 ± 0.007 g) and OG2 (0.188 ± 0.004 g). The M_w values of oat β-glucan, OG1, and OG2 were determined as 16.8×10^4, 11.9×10^4, and 7.3×10^4 g/mol, respectively, on a high-performance size-exclusion chromatography (HPSEC) system.[30] Different M_w values (4×10^4, 7×10^4, 10×10^4, and 200×10^4 g/mol) of standard dextrans (Pharmacia Fine Chemicals, Uppsala, Sweden) were used as M_w standard reference.

Synthesis of Octenylsuccinate of Oat β-Glucan and Its Hydrolysates. Oat glucan, OG1, and OG2 were octenylsuccinated according to our previously proposed method, and the DS of each was determined by elemental analysis using an Elementar CHNS analyzer (Vario EL III, Elementar Analysensysteme, Germany).[28,31] Detailed information on reaction conditions and DS of the resultant products was shown in Table 1.

Loading Curcumin into OSG Micelles. Freeze-dried OSG powder (40 mg) was dissolved in 20 mL of distilled water by heating at 100 °C for 2 min continuous stirring. After complete cooling at room temperature, the volume of the resultant solution was complemented to 20 mL by adding distilled water. Curcumin powder (10 mg) was introduced into the solution, and the suspension was homogenized at 12 000 rpm for 1 min in a homogenizer (IKA T18 basic, IKA-Werke GmbH & Co., Staufen, Germany). Then, the resultant homogenate was continuously stirred under different input power of the stirrer (IP) (Table 2) at 25 °C for 24 h to complete the transfer of curcumin into OSG micelles. Finally, the suspension was centrifuged at 5600g for 10 min to recover the supernatant for determining the CLC of OSG micelles. The CLC values of OSG micelles were determined as described previously and calculated by using the following equation:[28]

Table 1. Degree of Substitution (DS) and Reaction Condition for Preparing Octenylsuccinate Oat β-Glucan (OSG)[a]

no.	oat β-glucan[b]	OSA[c] (mL)	time (h)	DS	M_w[d] (g/mol)
1	OG	0.3	2	0.0076 ± 0.0010	17.0×10^4
2	OG	0.6	2	0.0169 ± 0.0038	17.1×10^4
3	OG	0.6	3	0.0266 ± 0.0022	17.3×10^4
4	OG1	0.3	2	0.0085 ± 0.0007	12.0×10^4
5	OG1	0.6	2	0.0175 ± 0.0032	12.2×10^4
6	OG1	0.6	3	0.0281 ± 0.0021	12.3×10^4
7	OG2	0.3	2	0.0080 ± 0.0005	7.4×10^4
8	OG2	0.6	2	0.0172 ± 0.0025	7.5×10^4
9	OG2	0.6	3	0.0273 ± 0.0015	7.5×10^4

[a]All reactions were carried out at 45 °C. [b]The molecular weights of oat β-glucan (OG), OG1, and OG2 were 16.8, 11.9 and 7.3×10^4 g/mol. The molecular weights of OG, OG1, and OG2 were determined before derivatization with OSA. [c]OSA, 2-octen-1-ylsuccinic anhydride. [d]The molecular weight of octenylsuccinate oat β-glucan was calculated according to the DS and molecular weight of oat β-glucan.

Table 2. Level of Various Independent Variables at Coded Values of Response Surface Methodology Experimental Design

		coded values		
independent variable	symbol	−1	0	1
degree of substitution	X_1	0.0080	0.0172	0.0273
molecular weight (10^4 g/mol)	X_2	7.3	11.9	16.8
stirrer input power (W)	X_3	3.3	3.8	4.4

$$\text{curcumin loading capacity (μg/mg)} = \frac{\text{mass of loaded curcumin in 1 mL of OSG solution (μg)}}{\text{mass of used OSG in 1 mL of OSG solution (mg)}} \quad (1)$$

Experimental Design. RSM based on the Box−Behnken design was adopted to observe the effects of DS and M_w of OSG as well as IP of operation on CLC of OSG micelles. A three-level, three-variable design was used in the present study. The three independent variables are DS (X_1), M_w (X_2), and IP (X_3), and CLC was used as the dependent variable response. The factorial design consisted of 12 factorial points and 5 central points. The coded and uncoded independent variables used in the RSM design are listed in Table 3. To fulfill this experiment, totally, nine OSG should be synthesized. Theoretically, as the requirement of the experiment design, nine OSG could be evenly divided into three groups, and the OSGs in the same group own the identical DS but the differentiated M_w. Actually, it is an impossible task to obtain an identical DS for oat β-glucans with different M_w. Therefore, three OSG with different M_w and non-significantly differentiated DS were grouped in the present study (Table 3). All trials were performed in triplicate. A Design-Expert software version 7.0 (STAT-EASE Inc., Minneapolis, MN, USA) was used to generate the experimental designs, statistical analysis, and regression model. A second-order polynomial equation was used to express the predicted responses (CLC) as functions of the independent variables, as shown in the following equation:

$$Y_i = a_0 + a_1X_1 + a_2X_2 + a_3X_3 + a_{12}X_1X_2 + a_{13}X_1X_3 + a_{23}X_2X_3 + a_{11}X_1^2 + a_{22}X_2^2 + a_{33}X_3^2$$

where X_i represents the independent variables, a_0 is a constant, and a_i, a_{ii}, and a_{ij} are the linear, quadratic, and interactive coefficients, respectively.

Characterization of OSG Micelles. OSG micelles (2 mg/mL OSG) and curcumin-loaded OSG (2 mg/mL OSG) were prepared

Table 3. Box–Behnken Design Matrix, Experimental Values for Three-Level, Three-Factor Response Surface Analysis[a]

	decoded values[c]				
no.[b]	X_1	X_2	X_3	experiment values (μg/mg)	predicted values (μg/mg)
1	0.0076 ± 0.0010a	7.3	3.8	1.28 ± 0.04	1.11
2	0.0266 ± 0.0022c	7.3	3.8	0.55 ± 0.05	0.63
3	0.0080 ± 0.0005a	16.8	3.8	1.59 ± 0.13	1.51
4	0.0273 ± 0.0015c	16.8	3.8	1.78 ± 0.12	1.95
5	0.0085 ± 0.0007a	11.9	3.3	0.15 ± 0.07	0.20
6	0.0281 ± 0.0021c	11.9	3.3	0.04 ± 0.01	0.20
7	0.0085 ± 0.0007a	11.9	4.4	0.30 ± 0.16	3.22
8	0.0281 ± 0.0021c	11.9	4.4	3.22 ± 0.16	3.17
9	0.0169 ± 0.0038b	7.3	3.3	0.20 ± 0.02	0.32
10	0.0172 ± 0.0025b	16.8	3.3	0.65 ± 0.11	0.68
11	0.0169 ± 0.0038b	7.3	4.4	2.86 ± 0.11	2.83
12	0.0172 ± 0.0025b	16.8	4.4	4.30 ± 0.19	4.18
13	0.0175 ± 0.0032b	11.9	3.8	1.99 ± 0.12	1.91
14	0.0175 ± 0.0032b	11.9	3.8	2.22 ± 0.11	1.91
15	0.0175 ± 0.0032b	11.9	3.8	1.78 ± 0.12	1.91
16	0.0175 ± 0.0032b	11.9	3.8	1.80 ± 0.09	1.91
17	0.0175 ± 0.0032b	11.9	3.8	1.78 ± 0.08	1.91

[a]Values bearing different on-line lowercase letters in the same column are significantly different ($p < 0.05$) by Tukey's HSD test. [b]Experiments were conducted in a random order. [c]X_1 = degree of substitution, X_2 = weight-average molecular weight (10^4 g/mol), X_3 = stirrer input power (W).

under above obtained optimal conditions (DS = 0.0199, M_w =16.8 × 10^4 g/mol, and IP = 4.4 W) and subjected to DLS, TEM, and AFM analyses. Moreover, the lyophilized micelles were analyzed by FT-IR spectroscopy, DSC, and XRD.

DLS. The size and ζ potential of OSG micelles in aqueous solution were determined based on DLS and laser doppler electrophoresis by using a Zetasizer Nano ZS90 (Malvern Instruments Ltd., UK) equipped with a He–Ne laser (633 nm) and 90° collecting optics. The results of size and ζ potential were expressed as nanometers and millivolts, respectively. The particle size distribution is reported as a polydispersity index (PDI). The temperature was maintained at 25 °C during the measurement. These measurements were performed in triplicate.

TEM. The appearance of the samples was determined by TEM measurements. A drop of the curcumin-loaded OSG solution was placed in a carbon-coated copper TEM grid, negatively stained with 1% uranyl acetate (w/v) for 10 min, and air-dried. Imaging was performed at 200 kV using a JEOL JEM-2100 instrument (JEOL, Japan) equipped with a Gatan 94 Ultrascan 1k charge-coupled device camera.[32]

AFM. The shape of curcumin-loaded OSG micelles (COMs) were further characterized by AFM (Dimension Icon, Bruker, Germany).[33] A drop of the curcumin-loaded OSG solution (2 mg/mL) was placed on freshly cleaved mica. After 5 min of incubation at room temperature, the surface of the mica was gently rinsed with 5 mL of deionized water and blown with dry nitrogen. The sample was air-dried at room temperature and mounted on the microscope scanner. The shape was observed and imaged in a noncontact mode.

FT-IR Spectroscopy. FT-IR spectra of native curcumin, OSG, their physical mixture (OSG/curcumin =100:1), and curcumin-loaded OSG were obtained using an FT-IR spectrophotometer (Spectrum 100, Perkin–Elmer, Akron, OH, USA) in the range 500–4000 cm^{-1} through the KBr method.

DSC. DSC measurements were carried out with a thermal analyzer (DSC 4000, Perkin–Elmer). Up to 5 mg of native curcumin, OSG, their physical mixture (OSG/curcumin = 100:1), and curcumin-loaded OSG were placed in an aluminum sample pan, which were hermetically sealed, and were quickly transferred to the sample holder of the instrument. Then, the pans were heated from 30 to 200 °C with a heating rate of 10 °C min^{-1} in a nitrogen atmosphere. The recorded DSC curve of a sealed empty pan was used as reference.

XRD. The patterns of native curcumin, OSG, their physical mixture (OSG/curcumin = 100:1), and curcumin-loaded OSG were obtained using an X-ray diffractometer (D8 Advance, Bruker, Germany). The measurements were performed with 40 kV and 25 mA. The scanned angle (2θ) was set from 5° to 40°, and the scan rate was 2° min^{-1}.

UV Stability Study. To verify the effective loading of curcumin by OSG micelles, a methanol–water (5:95, v/v) solution of curcumin and curcumin-loaded OSG micelles were subjected to UV light (253 nm) using a superclean bench (SW-CJ-1F, China). Sampling was carried out at various time points (10, 20, 30, 40, 50, and 60 min), and the amount of curcumin in the samples was determined by high-performance liquid chromatography.[28] The percent of curcumin refers to the ratio of the content of curcumin retained in the sample after UV irradiation to the original one in the sample.

Statistical Analysis. Results were expressed as the mean with standard deviation of at least three measurements. SPSS 19.0 was used to analyze the data. Analysis of variance (ANOVA) was utilized to determine the least significance at $p < 0.05$ by Tukey's HSD test.

RESULTS AND DISCUSSION

Results of RSM. The data of 17 experiments represented in Table 1 relating the CLC value of OSG micelles were fitted to multiple regressions. A second-order polynomial function was built to describe the effects of independent factors, namely, DS (X_1), M_w (X_2), and IP (X_3), on the dependent variable *CLC* (Y), which was given as follows:

$$Y = 1.914 - 0.0113X_1 - 0.4595X_1^2 + 0.4288X_2 - 0.1545X_2^2 + 1.5X_3 + 0.243X_3^2 + 0.23X_1X_2 - 0.0125X_1X_3 + 0.2475X_2X_3$$

The coefficients of the response surface model as described above were evaluated. The ANOVA was shown in Table 4. In

Table 4. Analysis of Variance of the Regression Coefficients of the Fitted Quadratic Equations for the Curcumin Loading Capacity of Curcumin-Loaded Octenylsuccinate Oat β-Glucan Micelles

source[a]	sum of squares	df	mean	F value	p value	model fit
model	21.1375	9	2.3486	48.19	<0.0001[b]	R^2 = 0.9844
DS	0.0010	1	0.0010	0.02	0.8883	R_{adj} = 0.9644
DS^2	0.8890	1	0.8890	18.62	0.0035[c]	
M_w	1.4706	1	1.4706	30.80	0.0009[b]	
M_w^2	0.1005	1	0.1005	2.11	0.1901	
IP	18.0000	1	18.0000	377.03	<0.0001[b]	
IP^2	0.2486	1	0.2486	5.21	0.0565	
DS × M_w	0.2116	1	0.2116	4.43	0.0733	
DS × IP	0.0006	1	0.0006	0.01	0.9121	
M_w × IP	0.2450	1	0.2450	5.13	0.0579	
residual	0.3342	7	0.0477			
lack of fit	0.1859	3	0.0620	1.67	0.3091	
pure error	0.1483	4	0.0371			
cor total	21.4717	16				

[a]DS = degree of substitution, M_w = molecular weight, IP = stirrer input power. [b]Statistically significant at $p < 0.001$. [c]Statistically significant at $p < 0.05$.

dx.doi.org/10.1021/jf5014692 | J. Agric. Food Chem. 2014, 62, 7532–7540

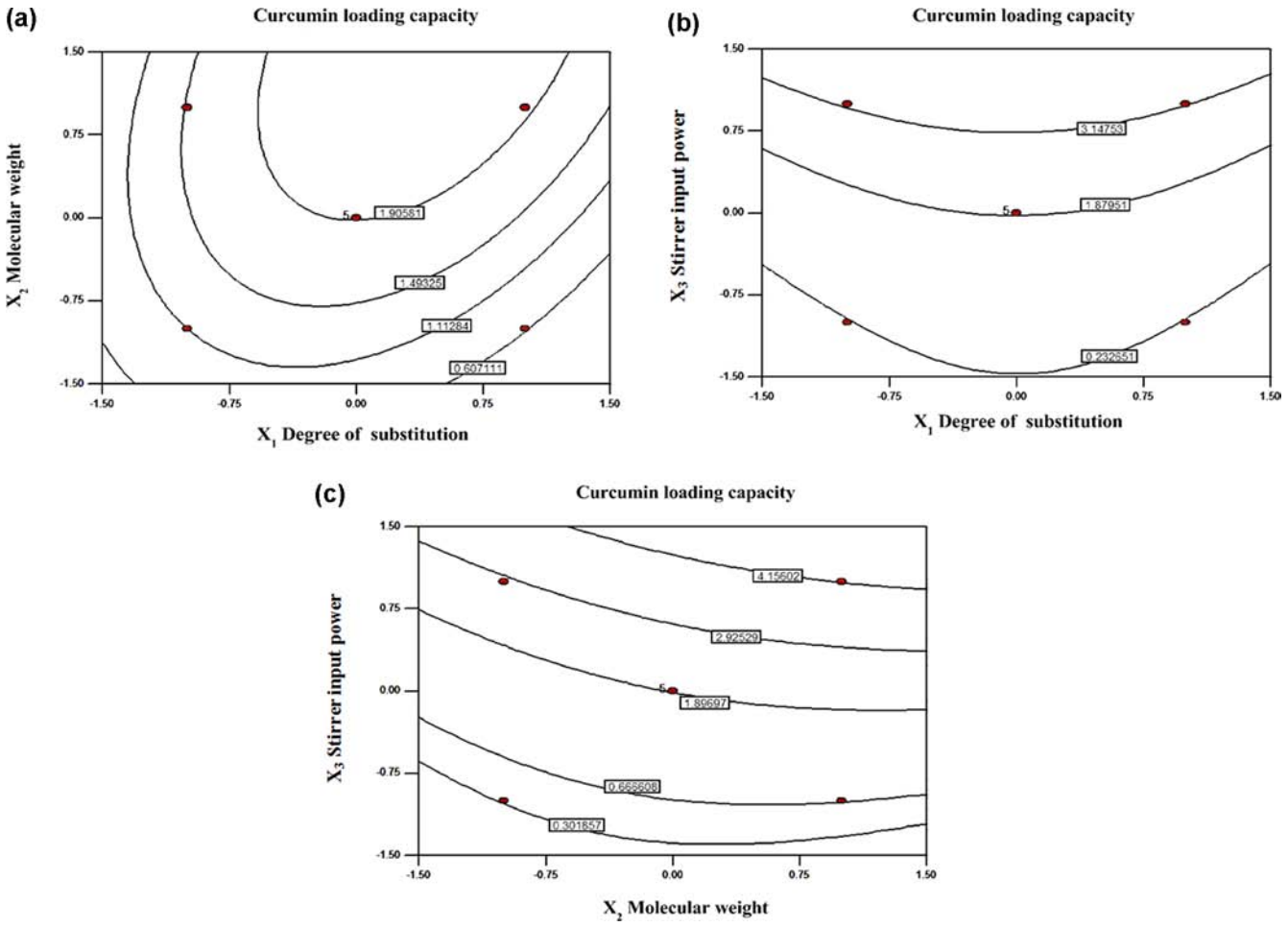

Figure 1. Response surface plots showing the interactive effects of degree of substitution (X_1), molecular weight (X_2), and stirrer input power (X_3) on the curcumin loading capacity (a–c) of octenylsuccinate oat β-glucan (OSG) micelles.

the present study, a preliminary screening experiment was first fulfilled in order to rank the significance of three key parameters on the resultant CLC of OSG micelles. The total of three parameters consisted of two structural and one process related factors: DS and M_w of OSG and IP of process, respectively. The p values are used as an indicator to judge the significance of each of the coefficients, which in turn, are necessary to reveal the pattern of mutual interactions between the test variables. The smaller the magnitude of the p value, the more significant is the corresponding coefficient. The coefficient with a p value less than 0.05 was significant. The coefficient estimates and the corresponding linear p values implied that M_w and IP were significant variables and the variable of DS (p = 0.8883) was insignificant in the present study. In addition, IP (p < 0.0001) posed a higher effect on CLC than M_w (p = 0.0009).

Effects of DS on CLC. Concerning DS, it presented extremely significant quadratic effects (DS^2) on the CLC value of OSG micelles (p < 0.01). However, its linear effect (DS) and interactive effects with M_w (DS × M_w) and IP (DS × IP) were insignificant (p > 0.05) (Table 4). The contour plots of DS versus M_w and DS versus IP revealed (Figure 1a, b) that CLC maximized at medium DS (0.0172) and decreased as DS increased or lowered. This could be explained by the effects of DS on the hydrophobic nature of OSG molecules and the particle size of OSG micelles. The higher the DS, the more the physically entrapped curcumin in the micelles, which mainly resulted from hydrophobic interactions through interaction between the aromatic groups of curcumin and octenyl succinate groups of OSG. Thus, hydrophobic interaction was the driving force for the OSG micelle to encapsulate curcumin. Besides the hydrophobic interactions, hydrogen bonding and π–π stacking interactions were also observed in the physical entrapment of curcumin.[32,34−39] However, the lower CLC was observed as the DS of OSG increased from 0.0172 to 0.0273. This result can be attributed to two related factors. First, the less accommodation of curcumin could be caused by the smaller micelle cavity. Our previous study revealed that increase in DS could cause a significant decrease in the OSG micelle size (476 to 267 nm, DS from 0.0172 to 0.0387).[28] Second, highly substituted OSG with amounts of octenyl succinate groups presenting in the core of micelles may further hinder the loading of curcumin. The complexation of sulfoalkyl ether β-cyclodextrins with steroids also showed the same observation.[40]

Effects of M_w on CLC. As revealed by the ANOVA (Table 4), the linear term of M_w had a significant (p < 0.01) effect on the CLC of OSG micelles. However, its quadratic effect and interactive effects with IP (M_w × IP) were insignificant (p > 0.05). The contour plots of M_w versus DS and M_w versus IP (Figure 1a, c) revealed that CLC increased with the increase of M_w. Compared with molecular chains of OSG with higher M_w, the chains of OSG with lower M_w are relatively short, and possibly make the physical entrapment of curcumin difficult.[41] The encapsulation of curcumin in the pluronic block copolymer

dx.doi.org/10.1021/jf5014692 | J. Agric. Food Chem. 2014, 62, 7532−7540

Table 5. Size, ζ Potential, and Polydispersity Index (PDI) of β-Glucan and Octenylsuccinate Oat β-Glucan (OSG) before and after Curcumin Loading.

sample	DS	size (nm)	ζ potential (mV)	PDI
β-glucan[a]	–	691.0 ± 10.5a	−8.7 ± 0.2c	0.459 ± 0.020a
OSG	0.0199	404.2 ± 3.5b	−12.4 ± 0.5b	0.356 ± 0.012b
curcumin-loaded OSG	0.0199	308.0 ± 10.2c	−10.8 ± 0.2a	0.233 ± 0.014c

[a]Size, ζ potential, and PDI of β-glucan was reported by Liu et al.[28]

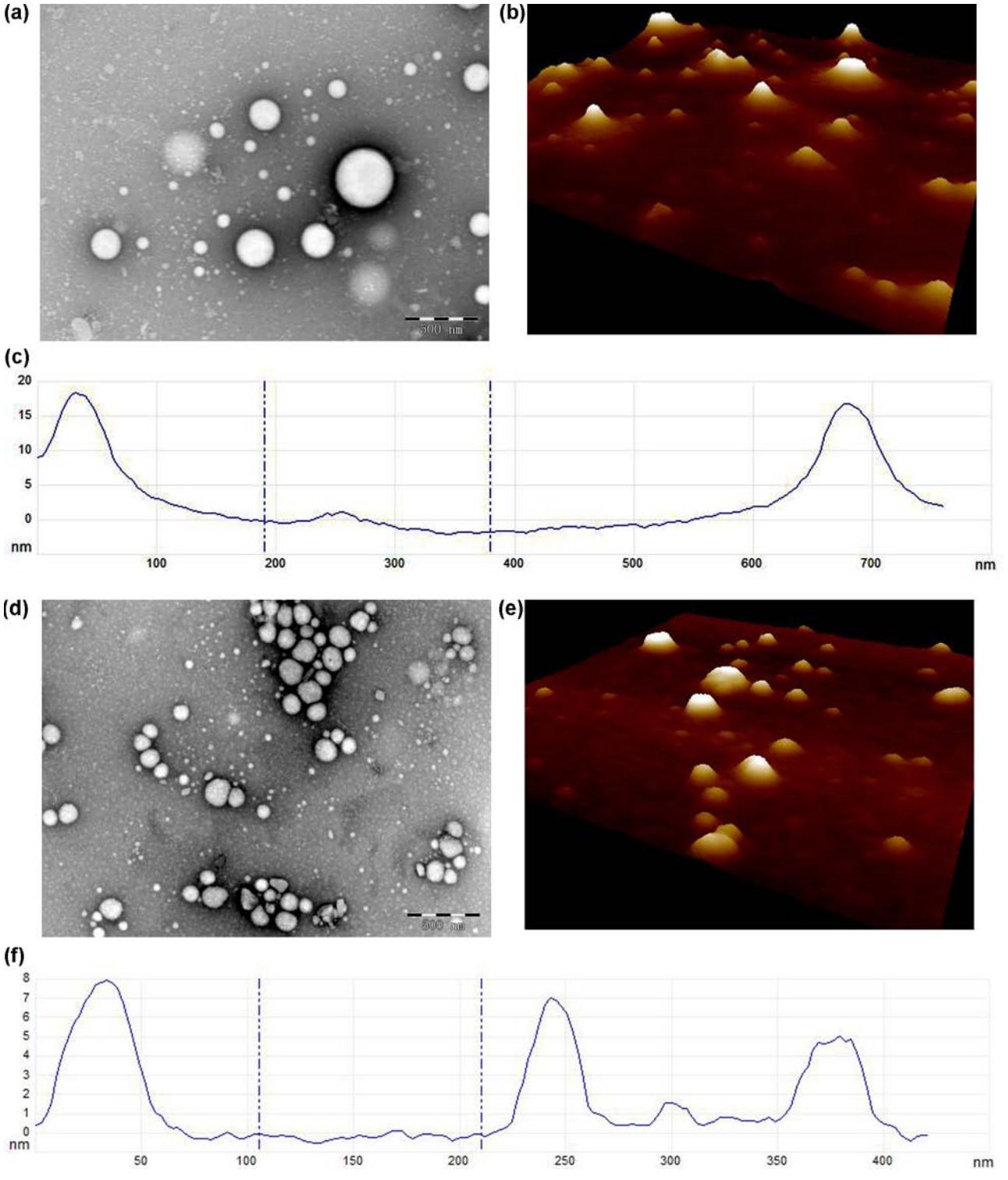

Figure 2. Transmission electron micrograph, three-dimensional view, and size distribution of octenylsuccinate oat β-glucan (OSG) micelles before (a–c) and after (d–f) curcumin loading.

dx.doi.org/10.1021/jf5014692 | J. Agric. Food Chem. 2014, 62, 7532–7540

and PEO-PCL micelles also showed that polymers with higher molecular weights had a better CLC.[42,43]

Effects of IP on CLC. As revealed by the ANOVA (Table 4), the linear term of IP had a significant effect ($p < 0.01$) on the CLC of OSG micelles. However, its quadratic effect was insignificant ($p > 0.05$). CLC of OSG micelles increased as IP increased from low input power levels to high input power levels (Figure 1b, c). The OSG micelles underwent a process of disassembly and reassembly during the agitation, which allowed the loading of curcumin into the OSG micelle core. Thus, increasing IP can increase the contact opportunity of curcumin and OSG micelles. More importantly, an increase of IP can promote the diffusion of the hydrophobic compounds toward the dispersed phase.[44]

Predicted Model and ANOVA. ANOVA results in Table 4 indicated that the regression model was adequate for the prediction. The coefficient of determination R^2 was found to be 0.9844, indicating that 98.44% of the variability in the response could be explained by the obtained model. The value of R^2 was always in the range 0∼1.0, and the closer the R^2 was to 1.0, the stronger the model and the better it predicted the response. The adjusted R^2 (0.9644) is in good agreement with the coefficient of determination R^2 (0.9844), suggesting an excellent correlation between the predicted values and the experimental results. The model showed that the p value for CLC (0.3091) was higher than 0.05, which implied that the lack-of-fit was not significant relative to the pure error. Verification of the model equation was conducted using the selected optimal conditions. Under optimal conditions (DS = 0.0199, $M_w = 16.8 \times 10^4$ g/mol, and IP = 4.4 W), the maximum CLC of OSG micelle was 4.21 ± 0.16 μg/mg, which agreed with the predicted value of 4.20 μg/mg. No significant difference ($p > 0.05$) was observed between the experimental and predicted values. Therefore, the results indicated the suitability of the model employed and the success of RSM in the optimization of CLC.

Characterization of Curcumin-Loaded OSG. *Particle Size, ζ Potential, and Morphology.* Particle characteristics of β-glucan and OSG before and after curcumin loading were shown in Table 5. After derivatization (OSG), the size, PDI, and ζ potential of micelles decreased due to the strong intra- and intermolecular hydrophobic interactions among octenylsuccinic groups, causing the hydrophobic substituent groups to self-assemble and form a uniform distribution of size.[28] DLS results (Table 5) revealed that the mean diameter and PDI of the OSG micelles were decreased from 404.2 to 308 nm and 0.356 to 0.234 after curcumin loading. The size and PDI of micelles formed by monomethoxyl poly(ethylene glycol)-poly(1,3-bis(*p*-carboxy-phenoxy)propane) also showed a significant decrease after curcumin incorporation.[45] Hong et al. ascribed the decreased size of micelles to the stronger hydrophobic interaction between curcumin and polymers.[45] After loading of curcumin into OSG micelles, ζ potential values of COMs were increased from −12.4 to −10.8 mV. Furthermore, TEM showed that smooth spherical and irregular-shaped particles were observed for the OSG micelles before and after curcumin loading. AFM results confirmed that both OSG micelles and COMs were elliptical in shape with a horizontal size of 20−200 nm and a vertical size of 5−18 nm (Figure 2 b, c and e, f). The mean diameter of COMs determined by DLS was slightly larger than the size observed by TEM and AFM. The difference of reported diameter between DLS and TEM was probably due to the process of the sample preparation. DLS determined the size in the hydrated state of the sample, whereas TEM and AFM observed the size in the dried state of the sample.

FT-IR Spectra. The FT-IR spectra of curcumin, OSG, their physical mixture, and curcumin-loaded OSG were shown in Figure 3. The characteristic peaks at 1727 and 1574 cm^{-1} in

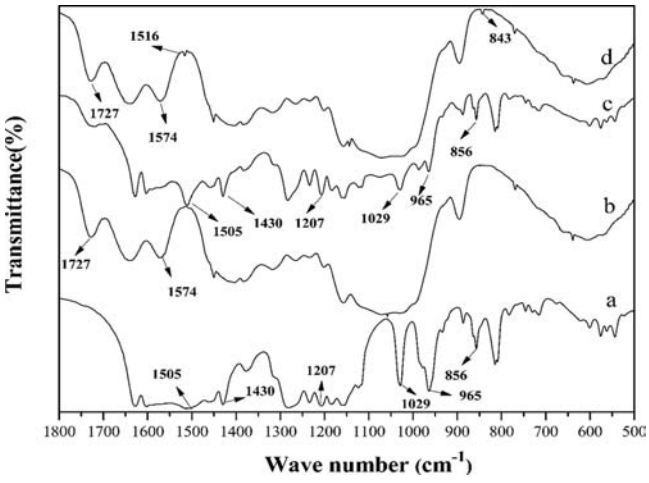

Figure 3. FT-IR spectra of curcumin (a), octenylsuccinate oat β-glucan (b), their physical mixture (c), and curcumin-loaded octenylsuccinate oat β-glucan (OSG) (d).

OSG and curcumin-loaded OSG are attributed to the OSG carbonyl group (−CO−) and the asymmetric stretch of vibration of the carboxylate group ($RCOO^-$). Several absorbance peaks are observed in the spectra of curcumin. Six of them are also observed in the physical mixture (curcumin and OSG). These peaks at 1505, 1430, 1207, 1029, 965, and 856 cm^{-1} are assigned to the vibration of C═O stretching, C—C stretching, (trans) olefinic C—H bending stretching, and asymmetric C—O—C stretching. The spectra of curcumin-loaded OSG nearly overlapped with that of OSG. This observation indicates that the curcumin is loaded into the micelle and no free curcumin is observed.[46,47] Nevertheless, the peaks at 1505 and 856 cm^{-1} shifted toward 1516 and 843 cm^{-1} in the spectra of curcumin-loaded OSG. The peaks at 1430, 1206, 1029, and 965 cm^{-1} disappeared in the spectra of curcumin-loaded OSG. These shifted and disappeared vibrations in the spectra of curcumin-loaded OSG compared with curcumin and the mixture are an evidence for the successful loading of curcumin into OSG micelles.

DSC. DSC studies were employed to investigate the crystal transformation of the curcumin-loaded OSG (Figure 4). The results showed that the endothermic peak of native curcumin was found at approximately at 182 °C. OSG showed a broad endothermic peak at around 75 °C. However, a weak endothermic peak at 182 °C indicates that the crystalline structure of curcumin is still present in the physical mixture of OSG and curcumin. More interestingly, the characteristic peak was not observed in the lyophilized powder of curcumin-loaded OSG. This observation indicates that curcumin is dispersed by loading into OSG micelles forming an amorphous state.[48]

XRD. To study the interactions between curcumin and OSG polymer, XRD was used. The characteristic peaks at a diffraction angle of 2θ (8.89°, 14.48°, 17.22°, 18.18°, 23.3°, 24.60°, and 25.52°) suggested the high crystalline structure of curcumin (Figure 5a). A weak peak at 8.89° and 17.22°

dx.doi.org/10.1021/jf5014692 | J. Agric. Food Chem. 2014, 62, 7532−7540

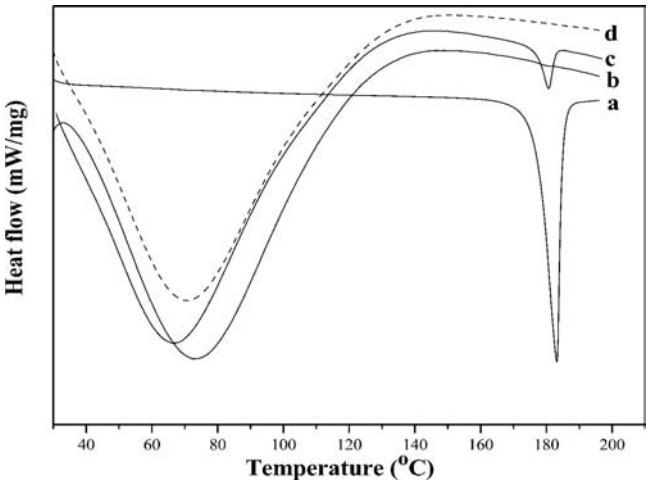

Figure 4. DSC curves of curcumin (a), octenylsuccinate oat β-glucan (b), their physical mixture (c), and curcumin-loaded octenylsuccinate oat β-glucan (OSG) (d).

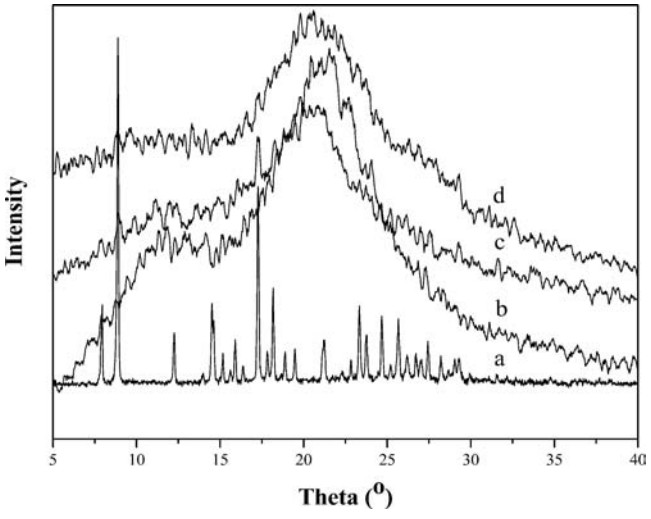

Figure 5. XRD patterns of curcumin (a), octenylsuccinate oat β-glucan (b), their physical mixture (c), and curcumin-loaded octenylsuccinate oat β-glucan (OSG) (d).

indicated that the crystalline structure of curcumin was still present in the physical mixture of the OSG micelles. However, no characteristic curcumin peaks were observed in the spectrum of curcumin-loaded OSG (Figure 5d). The absence of the crystalline order of curcumin in the curcumin-loaded OSG indicated that the formation of an amorphous complex through the intermolecular interactions between curcumin and OSG.[49]

UV Stability Study. The data from the UV stability study were summarized in Figure 6. More than 90% of curcumin was unchanged in OSG micelles as compared to less than 20% for curcumin in methanol−water (5:95, v/v) solution at the end of 6 h. Obviously, the curcumin loaded in OSG micelles showed a better stability under UV irradiation than in methanol−water (5:95, v/v) solution. This is due to the OSG cavity originates a sort of "shield" effect of the curcumin against the UV irradiation. This phenomenon strongly supports the successful loading of curcumin into OSG micelles.

In summary, the dependence of CLC of OSG micelles on the structural parameters of OSG and the characterization of

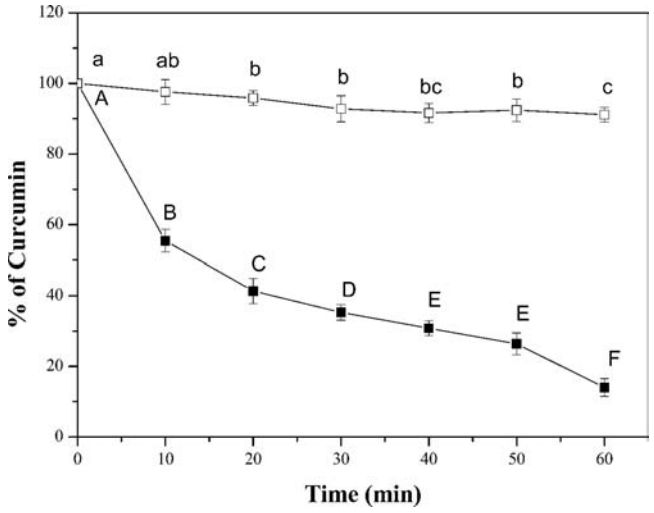

Figure 6. UV stability study of curcumin (■) and curcumin-loaded octenylsuccinate oat β-glucan (OSG) micelles (□). Values are given as the mean of three independent experiments, and error bars represent the SD. Different lower case letters indicate a significant difference ($p < 0.05$).

curcumin-loaded OSG were first investigated in this work. CLC highly depended on the structural characteristics of OSG. The CLC increased with an increase in the DS of OSG from 0.0080 to 0.0172, indicating that the hydrophobic interaction was the driving force for the increased dispersibility of curcumin. However, a decrease in the CLC was observed as further increase in the DS, due to the smaller micelle cavity of OSG micelles and the hindrance of curcumin loading into the micelle by amounts of octenyl succinate groups on the highly substituted OSG. OSG with higher M_w, offering a longer chain to encapsulate curcumin, also resulted in a higher CLC. The FT-IR, DSC, and XRD analyses confirmed that curcumin was loaded in OSG micelles to form an amorphous complex through the intermolecular interactions. Besides, the UV stability study supported the successful loading of curcumin into OSG micelles. This study suggested that OSG could be used as a nanovehicle for the loading of hydrophobic bioactive compounds.

AUTHOR INFORMATION

Corresponding Author

*Phone: +86 23 68 25 19 02; fax: +86 23 68 25 19 47; e-mail: zhaogh@swu.edu.cn.

Funding

We gratefully acknowledge the financial support from the National Natural Science Foundation of China (no. 31371737).

Notes

The authors declare no competing financial interest.

REFERENCES

(1) Day, L.; Seymour, R. B.; Pitts, K. F.; Konczak, I.; Lundin, L. Incorporation of functional ingredients into foods. *Trends Food Sci. Technol.* **2009**, *20*, 388−395.

(2) Benshitrit, R. C.; Levi, C. S.; Tal, S. L.; Shimoni, E.; Lesmes, U. Development of oral food-grade delivery systems: Current knowledge and future challenges. *Food Funct.* **2012**, *3*, 10−21.

(3) Huang, Q.; Yu, H.; Ru, Q. Bioavailability and delivery of nutraceuticals using nanotechnology. *J. Food Sci.* **2010**, *75*, R50−R57.

(4) Acosta, E. Bioavailability of nanoparticles in nutrient and nutraceutical delivery. *Curr. Opin. Colloid Interface Sci.* **2009**, *14*, 3−15.

(5) Rekharsky, M. V.; Inoue, Y. Complexation and chiral recognition thermodynamics of 6-amino-6-deoxy-β-cyclodextrin with anionic, cationic, and neutral chiral guests: Counterbalance between van der Waals and coulombic interactions. *J. Am. Chem. Soc.* **2002**, *124*, 813−826.
(6) Kaya-Celiker, H.; Mallikarjunan, K. Better nutrients and therapeutics delivery in food through nanotechnology. *Food Eng. Rev.* **2012**, *4*, 114−123.
(7) Anderson, A. M.; Mitchell, M. S.; Mohan, R. S. Isolation of curcumin from turmeric. *J. Chem. Educ.* **2000**, *77*, 359−360.
(8) Lantz, R. C.; Chen, G. J.; Solyom, A. M.; Jolad, S. D.; Timmermann, B. N. The effect of turmeric extracts on inflammatory mediator production. *Phytomedicine* **2005**, *12*, 445−452.
(9) Ruby, A. J.; Kuttan, G.; Babu, K. D.; Rajasekharan, K. N.; Kuttan, R. Anti-tumour and antioxidant activity of natural curcuminoids. *Cancer Lett.* **1995**, *94*, 79−83.
(10) Esmaili, M.; Ghaffari, S. M.; Moosavi-Movahedi, Z.; Atri, M. S.; Sharifizadeh, A.; Farhadi, M.; Yousefi, R.; Chobert, J. M.; Haertlé, T.; Moosavi-Movahedi, A. A. Beta casein-micelle as a nano vehicle for solubility enhancement of curcumin; food industry application. *LWT Food Sci. Technol.* **2011**, *44*, 2166−2172.
(11) Yu, H. L.; Huang, Q. R. Enhanced *in vitro* anti-cancer activity of curcumin encapsulated in hydrophobically modified starch. *Food Chem.* **2010**, *119*, 669−674.
(12) Bisht, S.; Feldmann, G.; Soni, S.; Ravi, R.; Karikar, C.; Maitra, A.; Maitra, A. Polymeric nanoparticle-encapsulated curcumin ("nanocurcumin"): A novel strategy for human cancer therapy. *J. Nanobiotechnol.* **2007**, *5*, 1−18.
(13) Lin, Y. L.; Liu, Y. K.; Tsai, N. M.; Hsieh, J. H.; Chen, C. H.; Lin, C. M.; Liao, K. W. A Lipo-PEG-PEI complex for encapsulating curcumin that enhances its antitumor effects on curcumin-sensitive and curcumin-resistance cells. *Nanomedicine* **2012**, *8*, 318−327.
(14) Song, L. L.; Shen, Y. Y.; Hou, J. W.; Lei, L.; Guo, S. R.; Qian, C. Y. Polymeric micelles for parenteral delivery of curcumin: Preparation, characterization and *in vitro* evaluation. *Colloids Surf., A* **2011**, *390*, 25−32.
(15) Zhao, L.; Du, J.; Duan, Y.; Zang, Y. N.; Zhang, H.; Yang, C.; Cao, F.; Zhai, G. Curcumin loaded mixed micelles composed of Pluronic P123 and F68: Preparation, optimization and *in vitro* characterization. *Colloids Surf., B* **2012**, *97*, 101−108.
(16) Dhule, S. S.; Penfornis, P.; Frazier, T.; Walker, R.; Feldman, J.; Tan, G.; He, J; Alb, A.; John, V.; Pochampally, R. Curcumin-loaded γ-cyclodextrin liposomal nanoparticles as delivery vehicles for osteosarcoma. *Nanomedicine* **2012**, *8*, 440−451.
(17) Shelma, R.; Sharma, C. P. *In vitro* and *in vivo* evaluation of curcumin loaded lauroyl sulphated chitosan for enhancing oral bioavailability. *Carbohydr. Polym.* **2013**, *95*, 441−448.
(18) Boruah, B.; Saikia, P. M.; Dutta, R. K. Binding and stabilization of curcumin by mixed chitosan-surfactant systems: A spectroscopic study. *J. Photochem. Photobiol. A* **2012**, *245*, 18−27.
(19) Tapal, A.; Tiku, P. K. Complexation of curcumin with soy protein isolate and its implications on solubility and stability of curcumin. *Food Chem.* **2012**, *130*, 960−965.
(20) Patel, A.; Hu, Y. C.; Tiwari, J. K.; Velikov, K. P. Synthesis and characterisation of zein-curcumin colloidal particles. *Soft Matter* **2010**, *6*, 6192−6199.
(21) Manju, S.; Sreenivasan, K. Gold nanoparticles generated and stabilized by water soluble curcumin-polymer conjugate: Blood compatibility evaluation and targeted drug delivery onto cancer cells. *J. Colloid Interface Sci.* **2012**, *368*, 144−151.
(22) Dey, S.; Sreenivasan, K. Conjugation of curcumin onto alginate enhances aqueous solubility and stability of curcumin. *Carbohydr. Polym.* **2014**, *99*, 499−507.
(23) Wu, Z.; Ming, J.; Gao, R. P.; Wang, Y. X.; Liang, Q.; Yu, H. G.; Zhao, G. H. Characterization and antioxidant activity of the complex of tea polyphenols and oat β-glucan. *J. Agric. Food Chem.* **2011**, *59*, 10737−10746.
(24) Wu, Z.; Li, H.; Ming, J.; Zhao, G. H. Optimization of adsorption of tea polyphenols into oat β-glucan using response surface methodology. *J. Agric. Food Chem.* **2011**, *59*, 378−385.
(25) Gao, R. P.; Liu, H.; Peng, Z.; Wu, Z.; Zhao, G. H. Adsorption of (−)-epigallocatechin-3-gallate (EGCG) onto oat β-glucan. *Food Chem.* **2012**, *132*, 1936−1943.
(26) Gao, R. P.; Wang, Y.; Wu, Z.; Ming, J.; Zhao, G. H. Interaction of barley β-glucan and tea polyphenols on glucose metabolism in streptozotocin-induced diabetic rats. *J. Food Sci.* **2012**, *77*, H128−H134.
(27) Wang, Y.; Liu, J.; Chen, F.; Zhao, G. H. Effects of molecular structure of polyphenols on their noncovalent interactions with oat β-glucan. *J. Agric. Food Chem.* **2013**, *61*, 4533−4538.
(28) Liu, J.; Li, J.; Ma, Y.; Chen, F.; Zhao, G. H. Synthesis, characterization and aqueous self-assembly of octenylsuccinate oat β-glucan. *J. Agric. Food Chem.* **2013**, *61*, 12683−12691.
(29) Tosh, S. M.; Wood, P. J.; Wang, Q.; Weisz, J. Structural characteristics and rheological properties of partially hydrolyzed oat β-glucan: The effects of molecular weight and hydrolysis method. *Carbohydr. Polym.* **2004**, *55*, 425−436.
(30) Lazaridou, A.; Biliaderis, C. G.; Izydorczyk, M. S. Molecular size effects on rheological properties of oat β-glucans in solution and gels. *Food Hydrocolloids* **2003**, *17*, 693−712.
(31) Shin, M. S; Lee, S.; Lee, K. Y.; Lee, H. G. Structural and biological characterization of aminated derivatized oat β-glucan. *J. Agric. Food Chem.* **2005**, *53*, 5554−5558.
(32) Podaralla, S.; Averineni, R.; Alqahtani, M.; Perumal, O. Synthesis of novel biodegradable methoxy poly (ethylene glycol)-zein micelles for effective delivery of curcumin. *Mol. Pharm.* **2012**, *9*, 2778−2786.
(33) Das, R. K.; Kasoju, N.; Bora, U. Encapsulation of curcumin in alginate-chitosan-pluronic composite nanoparticles for delivery to cancer cells. *Nanomed. Nanotechnol.* **2010**, *6*, 153−160.
(34) Sanoj Rejinold, N.; Muthunarayanan, M.; Divyarani, V. V.; Sreerekha, P. R.; Chennazhi, K. P.; Nair, S. V.; Tamura, H.; Jayakumar, R. Curcumin-loaded biocompatible thermoresponsive polymeric nanoparticles for cancer drug delivery. *J. Colloid Interface Sci.* **2011**, *360*, 39−51.
(35) Mangalathillam, S.; Rejinold, N. S.; Nair, A.; Lakshmanan, V. K.; Nair, S. V.; Jayakumar, R. Curcumin loaded chitin nanogels for skin cancer treatment via the transdermal route. *Nanoscale* **2012**, *4*, 239−250.
(36) Gou, M. L.; Men, K.; Shi, H. S.; Xiang, M. L.; Zhang, J.; Song, J.; Long, J. L.; Wan, Y.; Luo, F.; Zhao, X.; Qian, Z. Y. Curcumin-loaded biodegradable polymeric micelles for colon cancer therapy *in vitro* and *in vivo*. *Nanoscale* **2011**, *3*, 1558−1567.
(37) Ke, D.; Wang, X.; Yang, Q.; Niu, Y.; Chai, S.; Chen, Z.; An, X.; Shen, W. Spectrometric study on the interaction of dodecyltrimethylammonium bromide with curcumin. *Langmuir* **2011**, *27*, 14112−14117.
(38) Tripodo, G.; Mandracchia, D.; Dorati, R.; Latrofa, A.; Genta, I.; Conti, B. Nanostructured polymeric functional micelles for drug delivery applications. *Macromol. Symp.* **2013**, *334*, 17−23.
(39) Song, Z.; Feng, R.; Sun, M.; Guo, C.; Gao, Y.; Li, L.; Zhai, G. Curcumin-loaded PLGA-PEG-PLGA triblock copolymeric micelles: Preparation, pharmacokinetics and distribution *in vivo*. *J. Colloid Interface Sci.* **2011**, *354*, 116−123.
(40) Zia, V.; Rajewski, R. A.; Bornancini, E. R.; Luna, E. A.; Stella, V. J. Effect of alkyl chain length and degree of substitution on the complexation of sulfoalkyl ether β-cyclodextrins with steroids. *J. Pharm. Sci.* **1997**, *86*, 220−224.
(41) Xu, Y.; Du, Y. Effect of molecular structure of chitosan on protein delivery properties of chitosan nanoparticles. *Int. J. Pharm.* **2003**, *250*, 215−226.
(42) Sahu, A.; Kasoju, N.; Goswami, P.; Bora, U. Encapsulation of curcumin in pluronic block copolymer micelles for drug delivery applications. *J. Biomater. Appl.* **2011**, *25*, 619−639.
(43) Ma, Z.; Haddadi, A.; Molavi, O.; Lavasanifar, A.; Lai, R.; Samuel, J. Micelles of poly (ethylene oxide)-*b*-poly(ε-caprolactone) as vehicles

for the solubilization, stabilization, and controlled delivery of curcumin. *J. Biomed. Mater. Res. A* **2008**, *86*, 300−310.
(44) Tirucherai, G. S.; Mitra, A. K. Effect of hydroxypropyl beta cyclodextrin complexation on aqueous solubility, stability, and corneal permeation of acyl ester prodrugs of ganciclovir. *AAPS PharmSciTech* **2003**, *4*, 124−135.
(45) Hong, D. W.; Liu, T. H.; Chu, I. Encapsulation of curcumin by methoxy poly (ethylene glycol-*b*-aromatic anhydride) micelles. *J. Polym. Sci.* **2011**, *122*, 898−907.
(46) Teng, Z.; Luo, Y.; Wang, Q. Nanoparticles synthesized from soy protein: Preparation, characterization, and application for nutraceutical encapsulation. *J. Agric. Food Chem.* **2012**, *60*, 2712−2720.
(47) Sahu, A.; Kasoju, N.; Goswami, P.; Bora, U. Encapsulation of curcumin in pluronic block copolymer micelles for drug delivery applications. *J. Biomater. Appl.* **2011**, *25*, 619−639.
(48) Yen, F. L.; Wu, T. H.; Tzeng, C. W.; Lin, L. T.; Lin, C. C. Curcumin nanoparticles improve the physicochemical properties of curcumin and effectively enhance its antioxidant and antihepatoma activities. *J. Agric. Food Chem.* **2010**, *58*, 7376−7382.
(49) Xie, X.; Tao, Q.; Zou, Y.; Zhang, F.; Guo, M.; Wang, Y.; Wang, H.; Zhou, Q.; Yu, S. Q. PLGA nanoparticles improve the oral bioavailability of curcumin in rats: Characterizations and mechanisms. *J. Agric. Food Chem.* **2011**, *59*, 9280−9289.

Acetonitrile and methanol (HPLC gradient grade) were purchased from VWR (Darmstadt, Germany). Silica gel for column chromatography (0.06−0.2 mm) was obtained from Roth (Karlsruhe, Germany). Diethylenetriaminepentaacetic acid (DTPA) was obtained from Merck (Darmstadt, Germany). Methanol-d_4 (CD_3OD) and trichloromethane-d ($CDCl_3$) were purchased from Armar Chemicals (Döttingen, Switzerland). 4-Methyl-2-pentenoic acid and isovaleryl chloride were obtained from Alfa Aesar (Karlsruhe, Germany). The hop extract was kindly provided by the Hasseröder brewery (Wernigerode, Germany).

4-Methyl-3-pentenoic Acid. 4-Methyl-3-pentenoic acid was prepared according to the literature with some modifications.[20] One milliliter of 4-methyl-2-pentenoic acid (8.4 mmol) was dissolved in 20 mL of 6 M potassium hydroxide solution and heated to 105 °C for 48 h. After cooling to room temperature, the reaction mixture was acidified to pH 1 with 2 M hydrochloric acid and extracted three times with dichloromethane (30 mL). The combined organic layers were dried with sodium sulfate, and the solvent was removed under reduced pressure to afford a mixture of the target compound and the educt as a colorless liquid (90% 4-methyl-3-pentenoic acid, determined by gas chromatography as its trimethylsilyl derivative and NMR). ^{1}H NMR (400 MHz, $CDCl_3$), δ 1.65 (s, 3H), 1.79 (d, 3H, ^4J = 0.9 Hz), 3.08 (d, 2H, ^3J = 7.2 Hz), 5.30 (m, 1H); ^{13}C NMR (400 MHz, $CDCl_3$), δ 18.1, 25.8, 33.6, 115.2, 136.5, 178.3.

General Method for the Preparation of *N*-Acyl-L-proline Derivatives. The preparation was based on a method described in the literature with some modifications.[21] One equivalent of L-proline was suspended with 1.1 equiv of triethylamine in 10 mL of dry dichloromethane. The mixture was flushed with argon and cooled to 0 °C. Then 1 equiv of carboxylic acid chloride dissolved in 5 mL of dry dichloromethane was added dropwise. The reaction mixture was then stirred at room temperature for 15 h. After completion, the reaction mixture was washed two times with 15 mL of 1 M hydrochloric acid. The aqueous phase was re-extracted with 25 mL of dichloromethane. The combined organic layers were dried with sodium sulfate, and the solvent was removed under reduced pressure. The crude product was purified using flash chromatography (silica gel 60, *n*-hexane/acetone/trifluoroacetic acid 66:33:1). Fractions containing the desired product (TLC (silica gel 60, *n*-hexane/acetone/trifluoroacetic acid 66:33:1); detection, mixture of ninhydrine and *p*-toluenesulfonic acid (1%, 3%) in isopropanol) were collected and concentrated in vacuo.

***N*-Isovaleryl-L-proline (3-Methylbutyric Acid Proline Amide).** Six hundred and thirty-three milligrams of L-proline (5.5 mmol), 837 μL of triethylamine (6 mmol), and 671 μL of isobutyryl chloride (5.5 mmol) were used according to the general procedure. The product (TLC, R_f 0.31) was yielded as a yellowish oil (98%) from which the *trans* derivative was precipitated as colorless crystals at room temperature. ^{1}H NMR (500 MHz, $CDCl_3$, *trans* derivative), δ 0.97−0.99 (2d, 6H, ^3J = 6.4 Hz), 1.85−2.35 (m, 7H), 3.45−3.68 (m, 2H), 4.54−4.59 (m, 1H), 11.00 (s br, 1H); ^{13}C NMR (125 MHz, $CDCl_3$, *trans* derivative), δ 22.6. 22.7, 24.8, 25.7, 43.2, 48.0, 59.6, 173.9, 174.4; HR-MS, m/z 198.1135 (found), m/z 198.1135 (calcd for $C_{10}H_{17}NO_3$ $[M - H]^-$).

***N*-4-Methyl-3-pentenoyl-L-proline (4-Methyl-3-pentenoic Acid Proline Amide).** One milliliter of 4-methyl-3-pentenoic acid (7.6 mmol) was dissolved in 1 mL of thionyl chloride (13.8 mmol) and refluxed for 2 h. Excess thionyl chloride was removed under reduced pressure. The product, 967 mg of L-proline (8.4 mmol), and 1.25 mL of triethylamine (9 mmol) were used according to the general procedure. The product (TLC, R_f 0.31) was yielded as a brown oil (74%). ^{1}H NMR (500 MHz, $CDCl_3$, *trans* derivative), δ 1.63 (s, 3H), 1.73 (s, 3H), 1.88−2.17 (m, 2H), 2.18−2.35 (m, 2H), 3.10 (d, 2H, ^3J = 6.5 Hz), 3.38−3.68 (m, 2H), 4.48−4.57 (m, 1H), 5.23 (t, 1H, ^3J = 6.3 Hz), 10.30 (s br, 1H); ^{13}C NMR (125 MHz, $CDCl_3$, *trans* derivative), δ 18.2, 24.8, 25.7, 28.4, 34.5, 47.8, 59.7, 115.2, 136.3, 173.7, 174.2; HR-MS, m/z 210.1135 (found), m/z 210.1136 (calcd for $C_{11}H_{17}NO_3$ $[M - H]^-$).

Preparation of *n*-Humulone and *trans*-Isohumulone. A mixture of α-acids was obtained by multilayer coil countercurrent chromatography (MLCCC) using *n*-hexane, methanol, and water as tertiary system (10:8.2, v/v/v). The crude MLCCC product was further purified by preparative HPLC as described below (water/methanol (25:75, v/v)) to give pure humulone. To obtain *trans*-isohumulone, humulone was isomerized by using a modified literature protocol.[22] One gram of pure humulone was dissolved in 250 mL of methanol and flushed with argon before the isomerization was begun. The solution was radiated with a mercury-vapor lamp until the educt was completely vanished (monitored by HPLC). After removal of the solvent under reduced pressure, the crude product was purified by preparative HPLC as described below (water/methanol (50:50, v/v)) to yield *trans*-isohumulone with a purity of 98% (HPLC-DAD). Structure was confirmed by NMR experiments (^{1}H, ^{13}C; CD_3OD) in accordance with literature data.[23]

Preparation of *trans*-Humulinic Acid. Pure humulone was converted into *trans*- and *cis*-humulinic acid by using a modified literature protocol.[24] Humulone was stirred in 2 M aqueous sodium hydroxide at 95 °C for 2 h to give a mixture of *trans*- and *cis*-humulinic acid (89:11). After acidification with hydrochloric acid, the solution was extracted with diethyl ether and concentrated under reduced pressure. The individual isomers were isolated by preparative HPLC as described below (water/methanol (65:35, v/v)) to yield pure *trans*-humulinic acid. NMR spectra (^{1}H, ^{13}C; CD_3OD) were in line with the literature.[24,25]

Preparation of Hydroxy-*trans*-alloisohumulone. Pure *trans*-isohumulone was incubated in 0.1 M phosphate buffer at pH 7 after the addition of 10% vol ethanol for 1 week at 50 °C. After acidification with hydrochloric acid, the incubation was extracted with ethyl acetate, dried over sodium sulfate, and concentrated in vacuo. The crude extract was further processed by preparative HPLC (water/methanol (80:20, v/v)) to give hydroxy-*trans*-alloisohumulone with a purity of 95% (HPLC-DAD). NMR spectra (^{1}H, ^{13}C; CD_3OD) were in line with the literature.[6]

MLCCC. The MLCCC system (Ito, multilayer separator-extractor model, P. C. Inc., Potomac, MD, USA) was equipped with a constant-flow pump (Waters 510, Waters Corp., Milford, MA, USA) and a Jasco UV-2075 detector (Jasco, Gross-Umstadt, Germany) operating at 250 nm. Eluted liquids were collected in fractions of 16 mL with a fraction collector (LKB Ultrorac 7000). Chromatograms were recorded on a plotter (Servogor 200). The multilayer coil was prepared from a 1.6 mm inner diameter polytetrafluoroethylene (PTFE) tubing. The total capacity was 270 mL. The MLCCC was run at a revolution speed of 790 rpm and a flow rate of the mobile phase of 2 mL/min in head-to-tail modus. Separation was performed by using binary solvent systems (upper phase as stationary phase and lower phase as mobile phase). The sample was dissolved in a 1:1 mixture of upper and lower phase (10 mL) and injected into the system. The collected fractions were dried for further processing.

Preparative HPLC-UV. A Besta HD 2-200 pump (Wilhelmsfeld, Germany) was used at a flow rate of 20 mL/min. Elution of material was monitored by a UV detector (Jasco UV-2075). Detection wavelength for α-acids, iso-α-acids, and *trans*-humulinic acid was set at 270 and 250 nm for hydroxy-*trans*-alloisohumulone. Chromatographic separations were performed on a stainless steel column (KNAUER, Berlin, Germany; Eurospher-100-10 C18, 250 × 20 mm, 10 μm). All target substances were separated isocratically with mixtures of water and methanol containing 0.2% formic acid. The fractions containing target material were combined and dried under reduced pressure.

***trans*-Isohumulone Incubation Setup.** Individual iso-α-acids were incubated in 0.1 M ethanolic phosphate buffer (10% vol. ethanol) at two different pH values (5 and 7) with 25 mM L-proline for up to 21 days at 50 °C. The final iso-α-acids concentration was 5 mM. The incubations were performed under aerated and deaerated conditions. Deaerated conditions were achieved by adding diethylenetriaminepentaacetic acid (1 mM), degassing the buffer with helium, and flushing the residual headspace with argon. All samples were prepared in triplicate.

Incubation of *trans*-Isohumulone with $H_2{}^{18}O$. The buffer (300 μL) described above (aerated, pH 7) was lyophilized and redissolved with 270 μL of $H_2{}^{18}O$ (97 atom % ^{18}O). Thirty microliters of an ethanolic *trans*-isohumulone solution (50 mM) was added to meet the

conditions described above. Samples were incubated for 21 days at 50 °C.

Analytical HPLC-UV for Determination of Residual Iso-α-acid Levels. Analyses were performed on a Jasco HPLC system (PU-2089plus, AS-2055plus, UV-2075plus; Gross-Umstadt, Germany). Chromatographic separations were performed on a stainless steel column (KNAUER; Eurospher 100-5 C18, 250 × 4.0 mm, 5 μm) using a flow rate of 1 mL/min at 20 °C. The mobile phase used consisted of eluent A (water, 20 mg/L DTPA, 0.2% formic acid) and eluent B (acetonitrile/water (90:10, v/v), 0.2% formic acid). The incubation solutions were diluted with methanol and injected at 50% B. After 20 min, B was raised to 100% within 5 min (held for 5 min) and returned to starting conditions within 2 min (held for 8 min). The detection wavelength was set at 270 nm.

Extraction and Derivatization of Carboxylic Acids from Iso-α-acid Incubations. First, all of the samples (200 μL) were spiked with 100 μL of aqueous butyric acid solution (0.1 mM) as internal standard. After acidification with concentrated hydrochloric acid (25 μL), the precipitate was removed by centrifugation. An aliquot of the supernatant (200 μL) was saturated with sodium chloride and extracted with 300 μL of toluene. Two hundred microliters of the organic layer was dried with sodium sulfate. An aliquot was then derivatized with an equal volume of hexamethyldisilazane at 50 °C for 3 h prior to GC-MS analysis. External calibration samples were prepared in the same manner.

GC-LCI-MS Determination of Carboxylic Acid Trimethylsilyl Derivatives. One microliter of the samples described above was injected to a Thermo Finnigan Trace GC Ultra coupled to a Thermo Trace DSQ (Thermo Fisher Scientific, Bremen, Germany). Separation was carried out on a DB-5MS GC column (30 m × 0.25 mm × 0.25 μm; Agilent Technologies, Palo Alto, CA, USA). Helium 5.0 was used as carrier gas in constant flow mode (linear velocity = 28 cm/s, flow = 1 mL/min). The split flow was set at 20 mL/min. Injector and transfer lines were heated to 220 and 250 °C, respectively. The oven program was as follows: 40 °C (1 min), 4 °C/min to 100 °C (0 min), 20 °C/min to 270 °C (10 min). LCI mass spectra were obtained at 70 eV (source, 190 °C; emission current, 50 μA) in SIM mode using methanol as reagent gas. The retention times and SIM parameters for the silylated acid derivatives were as follows: butyric acid at 7.7 min (m/z 161), isovaleric acid at 9.2 min (m/z 175), and 4-methyl-3-pentenoic acid at 14.3 min (m/z 187).

LC-MS/MS Analyses of Humulinic Acid and Hydroxy-*trans*-alloisohumulone. Analyses were performed on a Jasco HPLC system (AS2057plus and PU-2080plus). Chromatographic separations were performed on a stainless steel column (KNAUER; Eurospher 100-5 C18, 250 × 4.6 mm) using a flow rate of 1 mL/min at 25 °C. The mobile phase used consisted of eluent A (30 mM ammonium formate buffer, pH 5.5) and eluent B (methanol). For analyses of incubations, samples were diluted with methanol (1:1). The respective samples (20 μL) were injected to the LC system at 25% B. After 10 min, B was raised to 30% within 12 min and then to 70% within 3 min (held for 5 min) and returned to starting conditions within 1 min (held 5 min). The LC system was connected to the probe of the mass spectrometer. The mass analyses were performed using an Applied Biosystems API 4000 quadrupole instrument (Applied Biosystems, Foster City, CA, USA) equipped with an API source using an electrospray ionization (ESI) interface. Nitrogen was used as sheath and auxiliary gas. For electrospray ionization in negative mode the following specifications were used: sprayer capillary voltage, −4.5 kV; nebulizing gas flow, 50 mL/min; heating gas, 60 mL/min at 500 °C; and curtain gas, 40 mL/min. For multiple reaction monitoring (MRM), declustering potential (DP), collision energy (CE), and cell exit potential (CXP) were optimized by syringe injection of reference compounds. Quantitation was based on matrix-assisted calibration. The LC-MS/MS parameters are given in Table 1A.

LC-MS/MS Analyses of Amides. Analyses were performed on a Jasco HPLC system (AS2057plus and PU-2080plus). Chromatographic separations were performed on a stainless steel column (Vydac 218TP54, RP18, 5 μm 250 × 4.6 mm; Hesperia, CA, USA) using a flow rate of 1 mL/min at 25 °C. The mobile phase used consisted of eluent A (water, 1.2 mL/L heptafluorobutyric acid) and eluent B (methanol/water (70:30, v/v), 1.2 mL/L heptafluorobutyric acid). For analyses the samples were diluted with methanol (1:1) and injected to the LC system at 20% B. After 10 min, B was raised to 70% within 20 min and then to 100% within 2 min (held for 13 min) and returned to starting conditions within 5 min for equilibration (10 min). The LC system was connected to the probe of the mass spectrometer. The mass analyses were performed using an Applied Biosystems API 4000 quadrupole instrument equipped with an API source using an electrospray ionization (ESI) interface. Nitrogen was used as sheath and auxiliary gas. For electrospray ionization in positive mode the following specifications were used: sprayer capillary voltage, 4 kV; nebulizing gas flow, 70 mL/min; heating gas, 70 mL/min at 500 °C; and curtain gas, 50 mL/min. For MRM, declustering potential (DP), collision energy (CE), and cell exit potential (CXP) were optimized by syringe injection of reference compounds. Quantitation was based on matrix-assisted calibration. The LC-MS/MS parameters are given in Table 1B. Proline amides were extracted from Pilsener type beer after acidification to pH 2 with hydrochloric acid by means of solid phase extraction (Bakerbond C_{18} Polar Plus; Avantor, Deventer, The Netherlands). After elution with methanol, the extract was concentrated and redissolved in methanol/water (7:3, v/v). The crude extract was filtered and fractionated by analytical HPLC runs with the setup described above to isolate 3-methylbutyric acid proline amide. Fractions were collected by an automated fraction collector (1 min/fraction; CHF122SB, Advantec, Japan). Fractions containing the desired amide were dried and redissolved in a mixture of methanol and water (1:1) for LC-MS analysis. MS^2 spectra were generated by using the parameters described above (collision energy = 19 eV). The same experiment was performed with the authentic reference compound.

Table 1. Mass Spectrometer Parameters for Quantitation (MRM Mode)

	t_R (min)	mass (amu) Q1	mass (amu) Q3	DP (V)	CE (eV)	CXP (V)
		A				
trans-humulinic acid	21.2	265.1	154.9	−75	−30	−24
hydroxy-*trans*-alloisohumulone	23.5	377.1	195.2	−90	−41	−16
		B				
3-methylbutyric acid proline amide	22.0	200.2	116.1	50	20	6
4-methyl-3-pentenoic acid proline amide	24.7	212.1	116.2	56	25	10

Nuclear Magnetic Resonance Spectroscopy (NMR). NMR spectra were recorded on a Varian VXR 400 spectrometer operating at 400 MHz for ^1H and 100 MHz for ^{13}C or on a Varian Unity Inova 500 instrument operating at 500 MHz for ^1H and 125 MHz for ^{13}C, respectively. Chemical shifts are given relative to external $SiMe_4$.

Accurate Mass Determination (HR-MS). The high-resolution positive ion ESI mass spectra (HR-MS) were obtained from a Bruker Apex III Fourier transform ion cyclotron resonance (FT-ICR) mass spectrometer (Bruker Daltonics, Billerica, MA, USA) equipped with an Infinity cell, a 7.0 T superconducting magnet (Bruker, Karlsruhe, Germany), a radio frequency (RF)-only hexapole ion guide, and an external electrospray ion source (Apollo; Agilent, off-axis spray). Nitrogen was used as drying gas at 150 °C. The samples were dissolved in methanol, and the solutions were introduced continuously via a syringe pump at a flow rate of 120 μL/h. The data were acquired with 256K data points and zero filled to 1024K by averaging 32 scans.

RESULTS

Preparation of *N*-Acyl-L-proline Derivatives. For the analyses of the amino acid amides authentic reference material was necessary. In the case of proline the synthesis led to *cis*- and *trans*-configured amides due to the partial double character of

dx.doi.org/10.1021/jf501826h | J. Agric. Food Chem. 2014, 62, 7541−7549

the amide moiety. In this context the *trans* isomer is considered to be the thermodynamically more stable species, which was confirmed by the performed syntheses.[26,27] The proline-originated α-methine proton was used as a probe for the *cis*/*trans* ratio (1:5.7−6.5, Figure 1). The crystals precipitated from

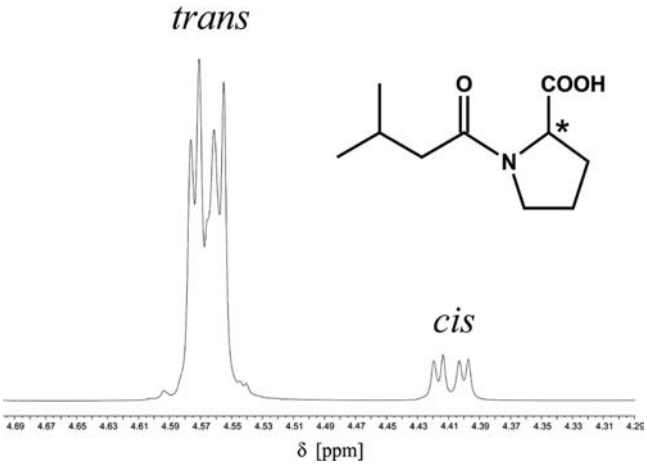

Figure 1. 3-Methylbutyric acid proline amide ^{1}H NMR spectra (excerpt) showing the α-methine proton of the *trans* (4.57 ppm) and *cis* (4.41 ppm) isomer.

3-methylbutyric acid proline amide were identified as the *trans* derivative by crystal structure analysis (data not shown). Interestingly, redissolution of *trans* crystals in deuterated chloroform, followed by NMR analysis, resulted in the reconstitution of the isomeric ratio stated above. Furthermore, the isomers could not be distinguished by LC-MS analyses.

Determination of Carboxylic Acids in Incubations. For quantitation the carboxylic acids had to be separated from the matrix. Residual *trans*-isohumulone led to artifacts during derivatization with hexamethyldisilazane and thus had to be removed by precipitation through acidification with hydrochloric acid. The carboxylic acids were extracted from the isohumulone-free supernatant (verified by HPLC-UV) with toluene. Butyric acid was used as internal standard because it cannot be formed from *trans*-isohumulone. The optimized workup provided a minimization of matrix effects and led to reproducible results.

Formation of *trans*-Isohumulone Degradation Products. *trans*-Isohumulone was incubated from 3 to 21 days at two different pH values under aerated and deaerated conditions. An overview of the substances analyzed in incubations is given in Figure 2.

Figure 3 (**1**) shows the degradation of *trans*-isohumulone. At acidic pH values it was almost completely vanished after 3 weeks (up to 97% degradation), although slightly more slowly at deaerated conditions (95%). On the contrary, relatively high amounts of unaltered *trans*-isohumulone were remained at pH 7, at which 72% was degraded in deaerated samples and 85% under oxidative conditions.

Along with the degradation of *trans*-isohumulone, the levels of 3-methylbutyric acid (MBA) increased over the incubation time in all incubation setups, preferably at neutral and aerated conditions with concentrations up to 86 mmol/mol *trans*-isohumulone (Figure 3, **2a**). The concentrations found in deaerated samples (35 mmol/mol) were approximately 3 times lower. At pH 5 the highest concentrations were also observed under oxidative conditions (34 mmol/mol), that is, about one-

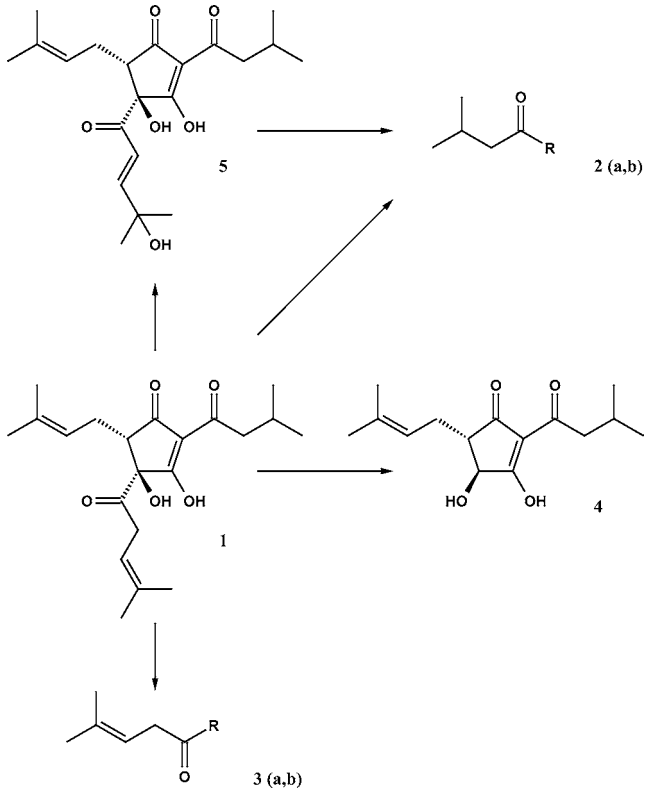

Figure 2. Overview of the structures analyzed in *trans*-isohumulone (**1**) incubations: 3-methylbutyric acid (**2a**, R = OH), 3-methylbutyric acid proline amide (**2b**, R = L-proline), 4-methyl-3-pentenoic acid (**3a**, R = OH), 4-methyl-3-pentenoic acid proline amide (**3b**, R = L-proline), *trans*-humulinic acid (**4**), hydroxy-*trans*-alloisohumulone (**5**).

third of the level determined at pH 7. A pH of 5 and deaeration led to concentrations of 24 mmol/mol after 3 weeks. The results for the formation of 4-methyl-3-pentenoic acid (MPA) (Figure 3, **3a**) revealed an almost identical pattern as seen for MBA. However, MPA levels were about 4−6 times lower compared to MBA concentrations. Again, the maximum was found at pH 7 and oxidative conditions (20 mmol/mol), whereas under deaeration half as much MPA was formed (10 mmol/mol). At pH 5 the levels were about 3 times lower after 3 weeks (4.1 mmol/mol for deaerated vs 6.6 mmol/mol for aerated samples). The carboxylic acids in the stable isotope experiment with $H_2{}^{18}O$ were analyzed analogously to the regular incubations. The incorporation of ^{18}O was monitored by analyzing additionally the [M + 2] molecular ion. For pH 7 and oxidative conditions about 90% of both carboxylic acids incorporated ^{18}O. As an example, the SIM chromatograms for the unlabeled (m/z 175) and labeled (m/z 177) MBA are given in Figure 4. Additional incubations were also performed without proline. However, there were no significant differences in the levels of carboxylic acids (data not shown).

On the basis of isolated authentic reference compounds, *trans*-humulinic acid and hydroxy-*trans*-alloisohumulone were also quantitated in the incubations. *trans*-Humulinic acid was preferentially formed at a pH of 7 under deaerated conditions (Figure 3, **4**; 11.6 mmol/mol after 3 weeks). Oxidative conditions led to levels up to 9.4 mmol/mol at the same pH. In contrast, in acidic incubations *trans*-humulinic levels were significantly higher at oxidative conditions (4.9 vs 3.0 mmol/mol in deaerated incubations). Hydroxy-*trans*-alloisohumulone had its maximum for pH 5 and oxidative conditions after 3 days

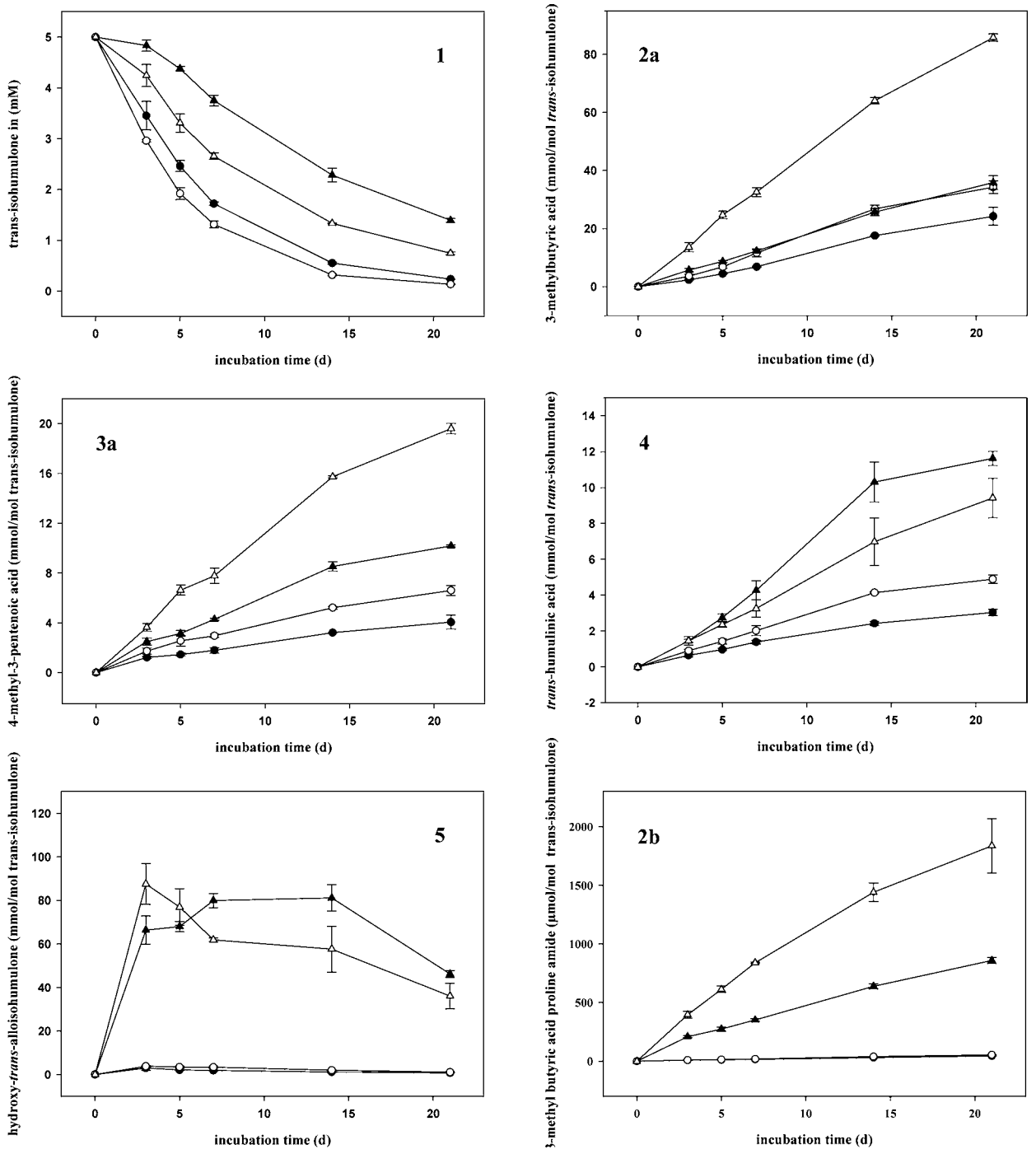

Figure 3. Degradation of *trans*-isohumulone (**1**) and formation of 3-methylbutyric acid (**2a**), 4-methyl-3-pentenoic acid (**3a**), *trans*-humulinic acid (**4**), hydroxy-*trans*-alloisohumulone (**5**), and 3-methylbutyric acid proline amide (**2b**) at pH 7 (aerated, △; deaerated, ▲) and pH 5 (aerated, ○; deaerated, ●).

(3.9 mmol/mol) and then started slowly to decrease to a final level of 1.1 mmol/mol (Figure 3, **5**). The curve for deaerated incubation was similar, although concentrations were slightly lower (maximum, 3.0 mmol/mol; 0.7 mmol/mol after 3 weeks). At pH 7 levels of hydroxy-*trans*-alloisohumulone were considerably higher. The maximum at aerated conditions was reached after 3 days at 87 mmol/mol. Thereafter, the level decreased to 36 mmol/mol within 3 weeks. At nonoxidative conditions the maximum was reached after 2 weeks at 80 mmol/mol and decreased to 46 mmol/mol afterward.

In parallel to the carboxylic acids, the analogous L-proline amides were found in the incubations. The results for 3-methylbutyric acid amide (MBA amide) are given in Figure 3 (**2b**). Whereas for pH 7 relatively high concentrations of MBA amide were found (up to 1800 µmol/mol), about 50 times lower compared to MBA itself, only minor amounts (up to 54 µmol/mol) were found at pH 5. The ratio of the MBA amide levels between aeration and deaeration at pH 7 were almost identical to the ratio found for the analogous acid (2.4 to 2.1). In contrast, 4-methyl-3-pentenoic acid proline amide (MPA amide) reached a plateau after 3 days regardless of the presence

dx.doi.org/10.1021/jf501826h | J. Agric. Food Chem. 2014, 62, 7541−7549

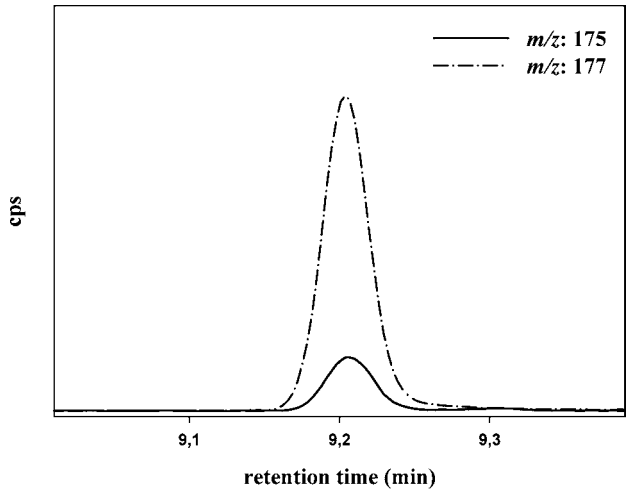

Figure 4. GC-LCI-MS chromatogram (SIM) of unlabeled (m/z 175; $[M + H]^+$) and labeled (m/z 177; $[M + H]^+$) 3-methylbutyric acid from *trans*-isohumulone incubation with $H_2{}^{18}O$. The ratio of 1:9 (unlabeled vs labeled) was calculated on the basis of the peak areas.

of oxygen and remained constant at levels around 170 μmol/mol at pH 7. An additional experiment showed that MPA amide was stable at these conditions. Analogous to MBA amide, MPA amide levels at pH 5 were extremely low (1.8 μmol/mol). MBA amide was also verified in beer by LC-MS/MS experiments (Figure 5). Although the spectrum of the isolate

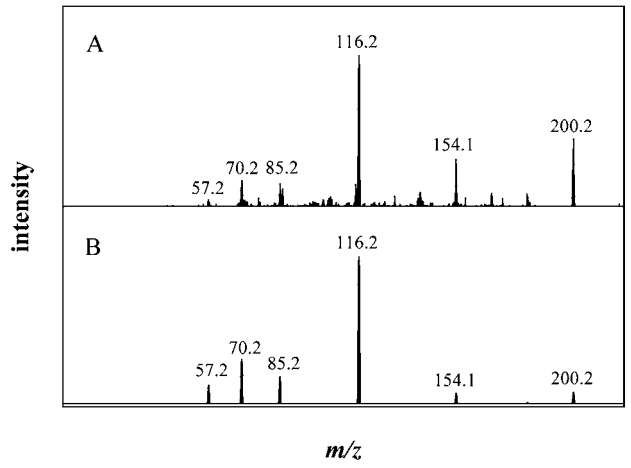

Figure 5. MS^2 of 3-methylbutyric acid proline amide (**2b**) isolated from beer (A) and synthesized reference standard (B) (product ion scan of m/z 200.2, collision energy of 19 eV).

(A) was much less intense, the fragmentation pattern was virtually identical to that of the authentic standard (B). For MPA amide, only traces were found in beer.

DISCUSSION

For the first time the degradation of *trans*-isohumulone in the presence of L-proline was thoroughly investigated in a model experiment. The clear impact of pH and oxidative conditions on the formation of carboxylic acids provided insights into the molecular mechanisms. In general, oxidative and hydrolytic reactions increased with higher pH. The question was whether the formation of carboxylic acids is based on hydrolytic or oxidative mechanisms or even a combination of both. Strong evidence for a hydrolytic cleavage was the formation of carboxylic acid amides. The nucleophilic L-proline nitrogen can react analogously to water or hydroxide, respectively. Obviously because of its weaker nucleophilicity compared to water, the amounts of the amides remain low. However, from a mechanistic point of view their formation is very important. As MBA amide was preferentially formed at oxidative conditions and the ratio between aerated and deaerated conditions was almost equal to that of the free acids, an identical mechanism must be assumed. To strengthen the postulated hydrolytic mechanism a stable isotope experiment with $H_2{}^{18}O$ was performed, revealing the incorporation of approximately 90% ^{18}O into the carboxylic acids, which supported the proposed hydrolytic cleavage. Incorporation of ^{18}O into free carboxylic acids was excluded by incubation of MBA and MPA with $H_2{}^{18}O$, resulting in no enrichment of the heavy isotope into the acids at these conditions. The remaining 10% must be explained by incorporation of molecular oxygen by yet unknown pathways, presumably including reactive oxygen species as intermediates. Thus, the difference in the formation of MBA under aeration versus deaeration is mainly not caused by the incorporation of molecular oxygen to the acid. Obviously there is an upstream oxidation step promoting the hydrolytic cleavage of *trans*-isohumulone.

trans-Isohumulone is a β-dicarbonyl structure and also a carboxylic acid with a pK_a of 3.23 and is almost completely deprotonated at pH 5 and entirely at pH 7.[28] Because of the β,β′-tricarbonyl system a negative charge after deprotonation is distributed over seven atoms. Thus, the anticipated carbonyl activity at the alkanoic side chain is limited in deprotonated isohumulones and does not support the preferred generation of carboxylic acid by hydrolytic β-dicarbonyl cleavage at neutral pH. Considering the given hydrolytic cleavage at oxidative conditions, we therefore postulate the mechanism shown in Figure 6.

After deprotonation, the isohumulate ion is oxidized via a one-electron oxidation, according to Huavere et al., giving a carbon-centered *trans*-isohumulone radical.[29] Reaction with molecular oxygen leads to the formation of the corresponding hydroperoxy radical. After abstraction of hydrogen, the hydroperoxide undergoes a Fenton-like redox reaction to form the alkoxy radical and subsequently the alcohol after a second abstraction of hydrogen. The now oxidized isohumulone has lost its ability to enolize, which comes along with a significantly increased carbonyl activity. Nucleophilic attack of water or L-proline at the carbonyl function at the alkanoic or alkenoic side chain then gives the free carboxylic acid or the carboxylic acid amide based on β-dicarbonyl cleavage, respectively. The difference between the concentrations of MBA and MPA is likely caused by lower reactivity of the alkenoic side chain compared to the β,β′-tricarbonyl system, a potential steric hindrance due to the prenyl side chain at the C5 of the isohumulone and the coinciding oxidation to hydroxy-*trans*-alloisohumulone. Hydrolytic cleavage of the latter would give 4-hydroxy-4-methyl-2-pentenoic acid.

The identification of the remaining cleavage products with intact ring structure would have been unambiguous proof for the present mechanism. Unfortunately, it was not possible to isolate these compounds. In contrast to the carboxylic acids and their amides, which represent stable reaction endproducts, the remaining isohumulone structures must be evaluated as highly reactive and thus can be further degraded. For instance, the cleavage of MBA gives a reductone structure, which is highly

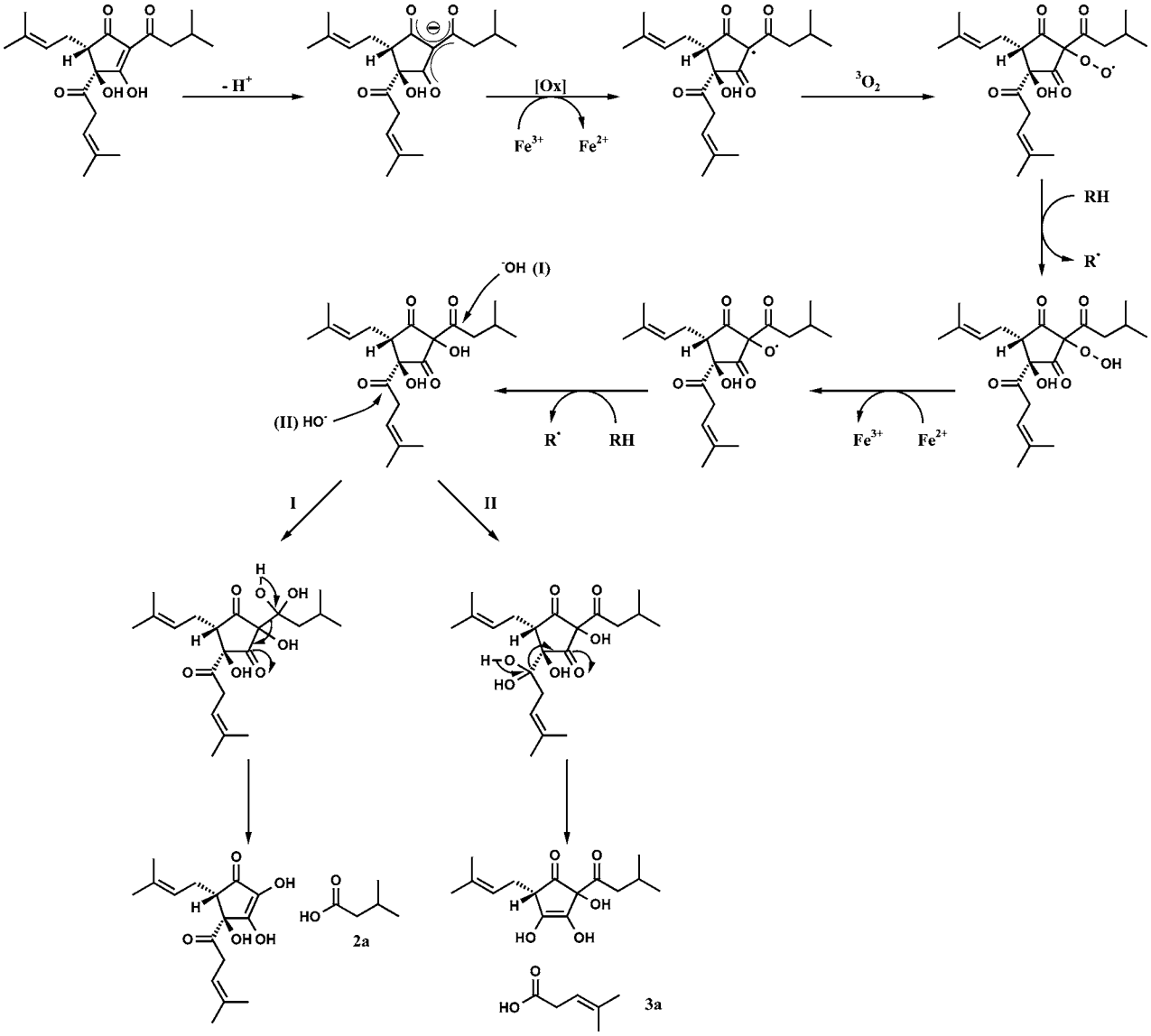

Figure 6. Proposed mechanism leading to the formation of 3-methylbutyric acid (**2a**) and 4-methyl-3-pentenoic acid (**3a**) from *trans*-isohumulone (**1**) by hydrolytic β-dicarbonyl cleavage after oxidation of the isohumulone ring structure.

susceptible to oxidation. This would also entail a loss or change of chromophoric properties to withdraw the products from the given detection systems. Therefore, in the present work, only *trans*-humulinic acid and hydroxy-*trans*-alloisohumulone were monitored as degradation products of *trans*-isohumulone.

Humulinic acids are known to form under harsh alkaline treatment. Here, we were able to detect *trans*-humulinic acid under mild conditions, preferably at pH 7. This per se nonoxidized structure must be formed by direct hydrolysis of the alkenoic side chain, which is not part of the tricarbonyl system and maintains its carbonyl activity. *trans*-Humulinic acid appeared to be stable under oxidative conditions and was not degraded significantly in an independent incubation (data not shown). Interestingly, higher amounts of *trans*-humulinic acid were generated at pH 7 under deaeration than in aerated incubations. This is reasonable considering the oxidation of *trans*-isohumulone according to above proposed mechanism leading to MBA and MPA. However, at pH 5 the picture is reversed and may be the result of a suppression of the initial oxidative step. Nevertheless, from our experiments the hydrolytic cleavage is evident at least for the alkenoic chain without previous oxidation. This is further supported by the fact that the levels of *trans*-humulinic acid and MPA were almost equal at pH 5, whereas MPA levels were significantly higher than *trans*-humulinic concentrations at pH 7 on the contrary. Obviously the oxidation of *trans*-isohumulone decreases the yield of *trans*-humulinic acid.

As a major degradation product under oxidative conditions at pH 7, 4-hydroxy-*trans*-alloisohumulone was isolated and analyzed in incubations. Together with its precursor, 4-hydroperoxy-*trans*-alloisohumulone, it has already been described by Intelmann et al.[6] The structure was relatively unstable and degraded after reaching a maximum more quickly under aerated conditions. In support, independent incubations of hydroxy-*trans*-alloisohumulone indeed revealed the formation of significant amounts of MBA, most likely according to our proposed mechanism (data not shown). We therefore must assume that MBA is not generated by only one precursor structure. As an alternative mechanism for the degradation of

dx.doi.org/10.1021/jf501826h | J. Agric. Food Chem. 2014, 62, 7541−7549

hydroxy-*trans*-alloisohumulone, Intelmann et al. assumed the formation of polycyclic compounds.[4]

In conclusion, we present a novel degradation mechanism that comprehensively explains the so far unknown formation of carboxylic acids from isohumulones. Stable isotope experiments with $H_2{}^{18}O$ as well as the generation of carboxylic acid amides unambiguously revealed a dominant hydrolytic mechanism. We showed that this reaction is relevant to brewing by the verification of MBA amide in beer. The lacking fragmentation counterparts and other reactive intermediates are subjects of current research. The actual influence of carboxylic acids derived from hops on the staling flavor of beer still has to be clarified. Nevertheless, our results are in good agreement with Williams and Wagner, who found increased levels of fatty acids during beer aging caused by the addition of hops.[14] Alternatively, MBA can also be formed by Strecker degradation of leucine, and molecular mechanisms may not be distinguishable in the aging of beer. It is very likely that the hydrolytic cleavage of isohumulones is also occurring during wort boiling after the addition of hops. High temperatures and exposure to oxygen would support the hydrolytic cleavage of isohumulones based on the proposed mechanism. Consequently, the formation of carboxylic acids from isohumulones at this stage would also promote the so-called staling esters during fermentation or beer storage. As we proved for L-proline, other nucleophiles besides water are able to react with isohumulones. Thus, also sulfur-containing substances may lead to potent odor-active compounds, such as *S*-methylthioisovalerate.[30]

AUTHOR INFORMATION

Corresponding Author

*(M.A.G.) Phone: ++049-345-5525784. E-mail: marcus.glomb@chemie.uni-halle.de.

Notes

The authors declare no competing financial interest.

ACKNOWLEDGMENTS

We thank Dr. D. Ströhl from the Institute of Organic Chemistry, Halle, Germany, for recording NMR spectra and Dr. J. Schmidt from the Leibniz Institute of Plant Biochemistry, Halle, Germany, for performing accurate mass determination.

REFERENCES

(1) Vanderhaegen, B.; Neven, H.; Verachtert, H.; Derdelinckx, G. The chemistry of beer aging − a critical review. *Food Chem.* **2006**, *95*, 357−381.

(2) Jaskula, B.; Kafarski, P.; Aerts, G.; de Cooman, L. A kinetic study on the isomerization of hop α-acids. *J. Agric. Food Chem.* **2008**, *56*, 6408−6415.

(3) de Cooman, L.; Aerts, G.; Overmeire, H.; de Keukeleire, D. Alterations of the profiles of iso-α-acids during beer ageing, marked instability of trans-iso-α-acids and implications for beer bitterness consistency in relation to tetrahydroiso-α-acids. *J. I. Brewing.* **2000**, *106*, 169−178.

(4) Intelmann, D.; Haseleu, G.; Dunkel, A.; Lagemann, A.; Stephan, A.; Hofmann, T. Comprehensive sensomics analysis of hop-derived bitter compounds during storage of beer. *J. Agric. Food Chem.* **2011**, *59*, 1939−1953.

(5) Intelmann, D.; Demmer, O.; Desmer, N.; Hofmann, T. O-18 stable isotope labeling, quantitative model experiments, and molecular dynamics simulation studies on the trans-specific degradation of the bitter tasting iso-α-acids of beer. *J. Agric. Food Chem.* **2009**, *57*, 11014−11023.

(6) Intelmann, D.; Hofmann, T. On the autoxidation of bitter-tasting iso-α-acids in beer. *J. Agric. Food Chem.* **2010**, *58*, 5059−5067.

(7) Taniguchi, Y.; Matsukura, Y.; Ozaki, H.; Nishimura, K.; Shindo, K. Identification and quantification of the oxidation products derived from α-acids and β-acids during storage of hops (*Humulus lupulus* L.). *J. Agric. Food Chem.* **2013**, *61*, 3121−3130.

(8) Burns, C. S.; Heyerick, A.; de Keukeleire, D.; Forbes, M. D. E. Mechanism for formation of the lightstruck flavor in beer revealed by time-resolved electron paramagnetic resonance. *Chem.−Eur. J.* **2001**, *7*, 4553−4561.

(9) Vermeulen, C.; Lejeune, I.; Tran, T. T. H.; Collin, S. Occurrence of polyfunctional thiols in fresh lager beers. *J. Agric. Food Chem.* **2006**, *54*, 5061−5068.

(10) Hashimoto, N.; Eshima, T. Oxidative-degradation of isohumulones in relation to flavor stability of beer. *J. Inst. Brew.* **1979**, *85*, 136−140.

(11) de Clippeleer, J.; de Rouck, G.; de Cooman, L.; Aerts, G. Influence of the hopping technology on the storage-induced appearance of staling aldehydes in beer. *J. Inst. Brew.* **2010**, *116*, 381−398.

(12) Green, C. P. The volatile water-soluble fraction of hop oil. I. Formation by the oxidation of soft resins. *J. Inst. Brew.* **1970**, *76*, 36−40.

(13) Clarke, B. J.; Hildebrand, R. P. The isomerization of humulone II. Preparation of reference compounds. *J. Inst. Brew.* **1967**, *73*, 60−70.

(14) Williams, R. S.; Wagner, H. P. Contribution of hop bitter substances to beer staling mechanisms. *J. Am. Soc. Brew. Chem.* **1979**, *37*, 13−19.

(15) Davidek, T.; Devaud, S.; Robert, F.; Blank, I. Sugar fragmentation in the Maillard reaction cascade: isotope labeling studies on the formation of acetic acid by a hydrolytic β-dicarbonyl cleavage mechanism. *J. Agric. Food Chem.* **2006**, *54*, 6667−6676.

(16) Voigt, M.; Glomb, M. A. Reactivity of 1-deoxy-D-erythro-hexo-2,3-diulose: a key intermediate in the Maillard chemistry of hexoses. *J. Agric. Food Chem.* **2009**, *57*, 4765−4770.

(17) Smuda, M.; Glomb, M. A. Novel insights into the Maillard catalyzed degradation of maltose. *J. Agric. Food Chem.* **2011**, *59*, 13254−13264.

(18) Smuda, M.; Voigt, M.; Glomb, M. A. Degradation of 1-deoxy-D-erythro-hexo-2,3-diulose in the presence of lysine leads to formation of carboxylic acid amides. *J. Agric. Food Chem.* **2010**, *58*, 6458−6464.

(19) Vanderhaegen, B.; Neven, H.; Verstrepen, K. J.; Delvaux, F. R.; Verachtert, H.; Derdelinckx, G. Influence of the brewing process on furfuryl ethyl ether formation during beer aging. *J. Agric. Food Chem.* **2004**, *52*, 6755−6764.

(20) Caspi, E.; Varma, K. R. Synthesis of (−)-(3*S*)- and (+)-(3*R*)-4-methyl-3D_1-pentan-1-ols and (−)-(3*S*)- and (+)-(3*R*)-3D_1-isocaproic acids. *J. Org. Chem.* **1968**, *33*, 2181−2188.

(21) Kim, B. H.; Lee, H. B.; Hwang, J. K.; Kim, Y. G. Asymmetric induction in the conjugate addition of thioacetic acid to methacrylamides with chiral auxiliaries. *Tetrahedron Asymm.* **2005**, *16*, 1215−1220.

(22) Sharpe, F. R.; Ormrod, I. H. L. Fast isomerization of humulone by photo-reaction − preparation of an HPLC standard. *J. Inst. Brew.* **1991**, *97*, 33−37.

(23) Intelmann, D.; Haseleu, G.; Hofmann, T. LC-MS/MS quantitation of hop-derived bitter compounds in beer using the ECHO technique. *J. Agric. Food Chem.* **2009**, *57*, 1172−1182.

(24) Tynan, P. J. T.; Murrough, I. M.; Byrne, J. Preparation, purification and separation by high-performance liquid-chromatography of humulinic acids, dehydrohumulinic acids, and hulupones. *J. Inst. Brew.* **1990**, *96*, 137−141.

(25) Borremans, F.; Depotter, M.; Dekeukeleire, D. C-13 NMR-spectroscopy of hop bitter substances. *Magn. Reson. Chem.* **1975**, *7*, 415−417.

(26) Nishihara, H.; Nishihara, K.; Uefuji, T.; Sakota, N. Conformation and circular dichroism of several N-acyl-L-prolines. *Bull. Chem. Soc. Jpn.* **1975**, *48*, 553−555.

(27) Pauling, L.; Corey, R. B. Configurations of polypeptide chains with favored orientations around single bonds − 2 new pleated sheets. *Proc. Natl. Acad. Sci. U.S.A.* **1951**, *37*, 729−740.
(28) Simpson, W. J. Ionization behavior of hop compounds and hop-derived compounds. *J. Inst. Brew.* **1993**, *99*, 317−326.
(29) Huvaere, K.; Andersen, M. L.; Olsen, K.; Skibsted, L. H.; Heyerick, A.; de Keukeleire, D. Radicaloid-type oxidative decomposition of beer bittering agents revealed. *Chem.−Eur. J.* **2003**, *9*, 4693−4699.
(30) Lermusieau, G.; Bulens, M.; Collin, S. Use of GC-olfactometry to identify the hop aromatic compounds in beer. *J. Agric. Food Chem.* **2001**, *49*, 3867−3874.

where $C_{\text{molecular binding}}$ refers to the retained water that is molecularly bound to the globular protein (0.06−0.07 g of water/g of protein, where typically already 0.04 g of water is required to hydrate peptide bonds) and is, in this research, assumed to be constant. $C_{\text{submicron structure}}$ includes water held by building blocks dictated by protein−protein and protein−water interactions. $C_{\text{microstructure}}$ refers to porosity, connectivity, and deformability of the spatial gel microstructure and covers micrometer length scales. $C_{\text{disruption}}$ is determined by gel−water surface boundaries creating the rupture events, which could be on sub(micron) or supra(micron) length scales.

The aim of this paper is to show which length scales are most contributing to WH of soy protein-based gels when centrifugal compression is applied. In the presence of divalent salts and by varying their concentration during the gelation process, a variety of different gel structures can be obtained, of which the morphology was analyzed by confocal scanning laser microscopy (CSLM) and large deformation rheological responses were determined in relation to the WH for different centrifugal forces.

MATERIALS AND METHODS

Materials. Defatted soy flour was provided by Cargill BV (Amsterdam, The Netherlands). Anhydrous magnesium sulfate ($MgSO_4$) and magnesium chloride ($MgSO_4$) were obtained from Sigma−Aldrich (Steinheim, Germany). Reagents were of analytical grade and used without further purification.

Preparation of Enriched Soy Protein Solution. Defatted soy flour was suspended in reverse osmosis (RO) water at a ratio 1:10 (w/w) at 45 °C and stirred for 30 min. Then, the pH was adjusted to 8.0 with 5 M NaOH and stirred for an additional 30 min. The supernatant was collected by centrifugation (30 min, 6000*g*, 13 °C). Isolation of the globulins (glycinin and *β*-conglycinin) was achieved by isoelectric precipitation (pH 4.5, 6 M HCl). After mild stirring of precipitate overnight at 4 °C, the suspension was centrifuged (30 min, 6000*g*, 7 °C). The pellet was resuspended three times at pH 4.5 in RO water at a ratio 1:3 (w/w) to remove impurities followed by centrifugation (30 min, 6000*g*) and was finally suspended in RO water at ratio 1:4 (w/w) at pH 7.0 using 5 M NaOH. This material was denoted as enriched soy protein solution (SP). Protein content of SP was determined by Kjeldahl (calculated using N × 6.25) and was between 11% and 12% (w/w). The ratio of glycinin/*β*-conglycinin was estimated to be 50:50 by gel electrophoresis and reversed-phase high-performance liquid chromatography (results are not shown). SP was stored at 4 °C in solution in the presence of 0.02% sodium azide and used within a month after preparation. The enthalpy change, indicative for the protein nativity, was 15.2 J/g of protein measured by differential scanning calorimetry (DSC) (Q1000, TA Instruments, New Castle, DE, USA).

Preparation of Soy Protein Aggregates. Soy protein aggregates were prepared in 20 mM MOPS buffer pH 7.0 by mixing 0.1% (v/v) SP with 0.1−1.5 mM $MgSO_4$ or $MgCl_2$ salt at (i) 25 °C for 15 min, (ii) 25, 50, and 70 °C for 25 min, or (iii) 95 °C for 30 min and cooled to 25 °C. Prior to the experiments, all solutions were filtered with disposable syringe filters before mixing (Machery−Nagel Chromafil RC-20/25, pore size 0.2 *μ*m).

Turbidity. Turbidity was measured with a Hewlett−Packard 8435 diode array spectrophotometer (HP, Waldbronn, Germany) with integrated heating element and magnetic stirrer at 600 nm. Cuvettes with a light path of 10 mm were used. Samples were stirred at 200 rpm during measurements. Two different measurements were performed: (1) change in turbidity as a function of increased salt concentration after 15 min mixing protein with salt, and (2) 25 min measurements at fixed protein and salt concentrations, immediately after the addition of salt. Samples were measured at least in duplicate.

Aggregate Size. The size of protein aggregates was determined using a Zetasizer Nano ZS (Malvern Instruments, Worcestershire, UK) by 173° angle backward scattering. Measurements were performed at 25 °C and repeated 10 times per sample; data were analyzed using the general purpose model.

Preparation of Gels. SP was diluted to 10% (w/w) protein at pH 7.0 using Tris buffer to a final Tris concentration of 20 mM. The protein solution was mixed with different concentrations of $MgSO_4$ or $MgCl_2$. Gelation was performed in 20 mL syringes (20 mm in diameter), lubricated with paraffin oil, closed airtight to reduce air bubble formation during heating at 95 °C for 30 min in the water bath, and subsequently, cooled overnight at room temperature. Every sample was prepared in triplicate.

Water Holding Measurements. The centrifugation procedure was adapted from Kocher and Foegeding.[11] A microcentrifuge filtration unit was composed of an inner spin tube and a 2 mL Eppendof tube (Axygen Biosciences, Inc., Union City, CA, USA). Gels were cut in 10 mm height and 4.8 mm diameter cylinders using a cork borer and carefully placed on the bottom of the spin tube. The bottom of the spin tube was covered with a 5.5 mm diameter filter paper to reduce grid size. Centrifugation was performed at different maximal *g*-force ranging from 20 to 1000*g* for 10 min at 20 °C. No changes in WH were seen above 1000*g*. Exuded serum from the gel was collected at the bottom of the Eppendorf tube. Some samples exposed to high *g*-forces fractured in a number of pieces of which part co-eluted in the exuded serum. In that case, a strip of filter paper was used to carefully remove serum from the bottom of Eppendorf tube to eliminate the contribution of gel residue, and the removed weight was determined. The WH was calculated as the remaining water (%) in the gel after centrifugation (eq 1), where W_T is the total amount of water in the sample (g) and W_g is removed water from the sample at a given centrifugal force (*g*). Measurements were performed in duplicate.

$$\text{WH} = \frac{W_T - W_g}{W_T} \cdot 100 \quad [\%] \tag{1}$$

Obtained WH (%) at various centrifugal forces were fitted using an exponential decay (eq 2) analogous to the exponential decay as a function of time at constant force as reported by Kocher and Foegeding.[11] *A* represents the maximum amount of water that can leave the system between applied 0 and 1000*g* force, *B* (equals 100 − *A*) refers to the amount of water remaining in the gel, and *k* represents the coefficient reflecting how easy water leaves the system under applied force (in units of the gravitational acceleration, *g*):

$$\text{WH} = A \cdot e^{-kg} + B \tag{2}$$

Parameters *A* and *k* were obtained by least-squares minimization fitting of the experimented data on WH as a function of applied *g* force with Excel optimization tool Solver. Fitting the curves using two exponential decay did not give an improvement.

Confocal Laser Scanning Microscopy. Samples for microstructural analysis were stained with 0.1% fluorescent dye Rhodamine B to visualize proteins. Imaging of the samples was performed using a Leica TCS-SP5 confocal laser scanning microscope (Leica Microsystems (CMS) GmbH., Mannheim, Germany). Leica objective lenses HC PL APO 20×/0.70 IMM/CORR CS and HCX PL APO 63×/1.20 W CORR CS were used. The excitation wavelength and emission spectral regime of Rhodamine B was 561 nm and 570−725 nm, respectively.

Large Deformation Rheology. Gels were sliced with a gel slicer into cylinders of 20 mm in height and 20 mm in diameter. Fracture stress and fracture strain were measured by uniaxial compression with an AP-501 rheometer (Anton Paar, Graz, Austria) mounted with the 5 kg load cell. Paraffin oil was applied on top and bottom of the gel to prevent friction during compression. Gel samples were compressed to 90% of their initial height between two parallel plates at a constant deformation rate of 1 mm/s. Measurements were performed at 20 °C in triplicate, and mean values of fracture stress and strain were calculated. The compressive stress and strain was recalculated to true Hencky's stress and strain. True Hencky's strain ε_h is defined as

$$\varepsilon_h = \ln \frac{h(t)}{h_0} \quad [-] \tag{3}$$

where h_0 is the initial height of the gel sample and $h(t)$ is the height after certain deformation time t. The true strain is negative for compression but is expressed as an absolute value. It was assumed that the volume of gel samples did not change during deformation and that the cylindrical shape was retained. Therefore, the contact surface area A of the gel sample at compression time t can be defined as

$$A(t) = \frac{h_0}{h(t)} \cdot A_0 \quad [m^2] \tag{4}$$

where A_0 is the initial contact surface area of the gel sample. The true stress σ in the gel sample at time t is defined as

$$\sigma(t) = \frac{F(t)}{A(t)} \quad [Pa] \tag{5}$$

in which $F(t)$ is the force per unit of area $A(t)$. Fracture of the gel is described as a peak or discontinuity of the stress over strain curve. Young's modulus E_u was calculated from the linear part of the stress over strain curve within the region 0.05−0.15 of the fracture strain and is defined as

$$E_u = \left(\frac{d\sigma}{d\varepsilon_h}\right) \quad [Pa] \tag{6}$$

Recoverable energy was measured by compressing each gel to 50% of its fracture strain with a deformation speed of 1 mm/s. The measure that was used for the recoverable elastic energy (RE) was defined as the ratio of the released energy during decompression over the applied energy during compression. The areas below the stress over time curve (before and after the transition point between compression and decompression) were used to calculate the recoverable energy:

$$RE = \frac{\int_{t_{end}}^{t_{trans}} \sigma \, dt}{\int_{0}^{t_{trans}} \sigma \, dt} \times 100 \quad [\%] \tag{7}$$

We note that the measure we have defined for recoverable energy is a ratio and does not have a unit. We nonetheless refer to it as recoverable energy.

Fracture Events (Centrifugation). Over a range of centrifugal forces used (10−1000g), the gel either fractures on microscopic and/or macroscopic scales, depending on gel morphology and centrifugal speed used. To estimate which centrifugal force, F, leads to macrofracture of a gel, applied centrifugal acceleration (RFC) were transformed to uniaxial compression pressure (Pa) as follows:

$$F = m \cdot RCF \cdot 9.807 \tag{8}$$

where m is the effective mass of protein network (kg) (eq 9)

$$m = \Delta\rho \cdot V \tag{9}$$

with $\Delta\rho$ = 350 kg/m^3,[15] and V is the volume of the cylinder shaped gel (m^3). The calculated force (N) was converted to pascal (force/area) using the following definition:

$$P = F/A \tag{10}$$

where A is the area of the cylinder top surface (m^2).

Obtained values were plotted on a true strain over true stress curve to estimate in which region (linear, nonlinear, fracture, or above fracture) recalculated centrifugal force appears on the fracture curve. To make it more explicit, 200g used in centrifugation would be similar to 7 kPa in TA for compression of a 10% (w/w) soy protein gel. Compression speed in both the texture analyzer and the centrifuge tube were comparable, but time under compression differed.

RESULTS

The ability of a protein gel to retain or hold water has often been correlated to rheological properties, such as gel strength, and is suggested to be related to gel morphology. However, a concise study where it is attempted to link the macroscopic ability to retain water to properties at different length scales has not been reported. In this study, the aim was to create a variety of soy protein gels, based on either different microstructural building blocks or different gel morphologies. These gels were then subjected to WH measurements, microscopic imaging, and rheological characterization.

Variation in Aggregate Size. To investigate the contribution to WH of a gel determined by the aggregate level $C_{submicron\ structure}$, we studied the effect of $MgSO_4$ or $MgCl_2$ salts on soy protein aggregation. By varying salt concentrations, different types of aggregates can be created, as measured by turbidity. Results of 0.1% SP (v/v) mixed with 0.1−1.5 mM $MgSO_4$ or $MgCl_2$ salts at ambient temperature are shown in Figure 1. At a concentration higher than about 0.1 mM, a proportional dependence of turbidity with increasing salt addition was observed, suggesting larger or higher number of aggregates. Both salts showed the same salt concentration−turbidity dependence; however, $MgCl_2$ showed slightly higher turbidity above 0.7 mM concentration compared to $MgSO_4$.

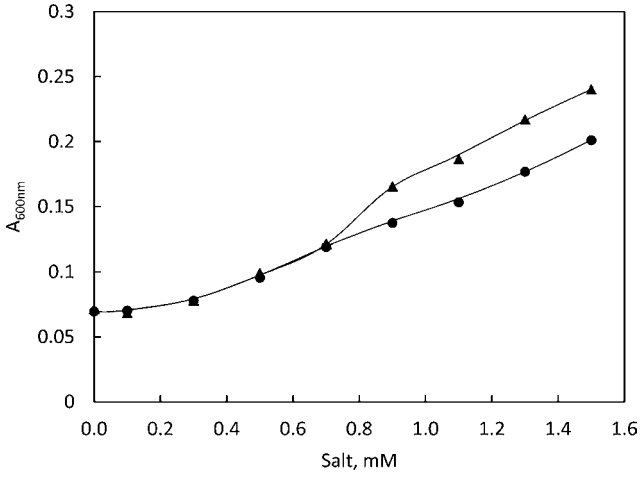

Figure 1. Turbidity measurement of 0.1% (v/v) SP mixed with 0.1−1.5 mM $MgSO_4$ or $MgCl_2$ (25 °C, reaction time 15 min): (●) $MgSO_4$; (▲) $MgCl_2$. The solid lines are fits to guide the eye.

Heat-induced soy protein aggregation kinetics in the presence of magnesium salts was monitored by changes in turbidity over time: first, to investigate the effect of anions (SO_4^{2-} or Cl^-) on aggregate formation, and second, to mimic the initial aggregation during heating and the gel formation. The protein to salt ratio was kept the same in both aggregation and gelation experiments. Results of 0.1% SP (v/v) mixed with 1.0 mM $MgSO_4$ or $MgCl_2$ at 25, 50, and 70 °C in time are shown in Figure 2. The major change in turbidity was completed within the first 5 min. At 50 and 70 °C, higher turbidity was measured indicating the formation of aggregates either larger or higher in number. Samples containing $MgCl_2$ salt showed a significant turbidity increase compared to those containing $MgSO_4$. With increasing temperatures, the impact on turbidity of chloride over sulfate became more pronounced.

The above-described effect of different salts on aggregate size was confirmed by Zetasizer measurements (Figure 3). In Figure 3a, protein aggregate sizes in 0.1% SP (v/v) mixed with or without 0.5 mM $MgSO_4$ or $MgCl_2$ at 25 °C (no heating) are shown. The addition of $MgSO_4$ increased the aggregate size

dx.doi.org/10.1021/jf501728t | J. Agric. Food Chem. 2014, 62, 7550−7558

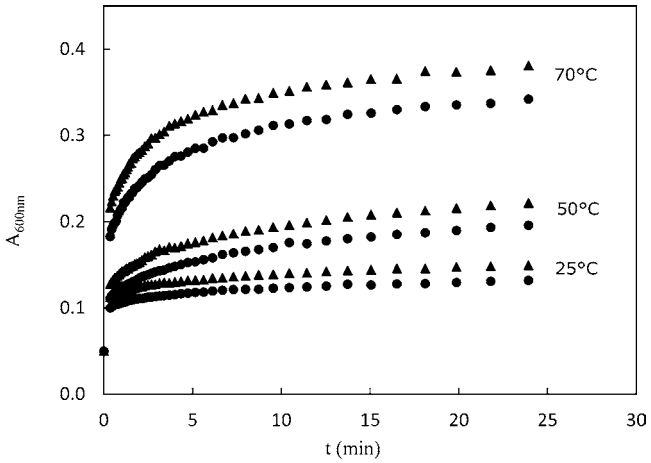

Figure 2. Turbidity measurements of 0.1% (v/v) SP with 1.0 mM salt in time at 25, 50, and 70 °C: (●) $MgSO_4$; (▲) $MgCl_2$.

from approximately 14 to 22 nm, while $MgCl_2$ resulted in a mixture of 20−65 nm aggregates. Effect of heating on soy protein aggregate size is shown in Figure 3b. Heating of 0.1% SP (v/v) in the absence of salt increased aggregate size from approximately 14 to 50 nm, while the addition of 0.5 mM $MgCl_2$ salt resulted in aggregate size of approximately 110 nm. From these results, it can be concluded that heating of SP in the presence of $MgSO_4$ and $MgCl_2$ results in typical different aggregates that will serve (at higher concentrations) as building blocks for network formation.

Soy Protein Gels: Variation in Morphology. To study the effect of the $C_{microstructure}$ contribution to WH of 10% (w/w) SP gels, we aimed to create a range of different morphologies of self-supporting gels without observable syneresis. As discussed above, by varying the type of salt ($MgCl_2$ and $MgSO_4$), different building blocks were created, and by varying the salt concentration (5−100 mM), different gel morphologies were obtained. With increasing salt concentration, the visual appearance of these gels changed. These varied from being translucent to white. Typically, $MgSO_4$ gels appeared smoother and more homogeneous compared to chloride gels. The 40−60 mM $MgCl_2$ gels showed syneresis, and therefore, these gels were discarded in this study.

Gel morphology was visualized with confocal laser scanning microscopy (CLSM) and imaged at 250 and 25 μm length scales (Figure 4a, b) (scale bars are indicated in the top left parts only). Heating in the presence of salts resulted in mixed

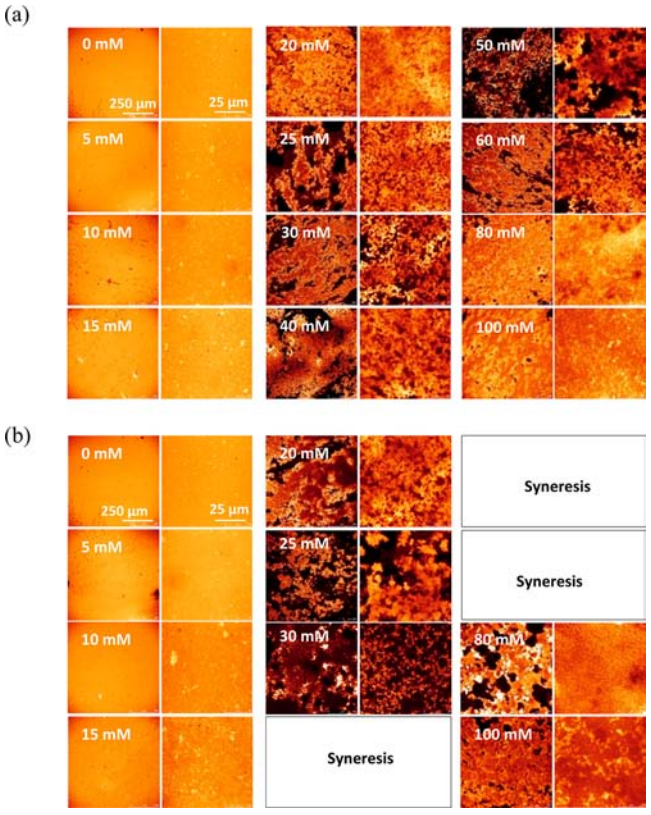

Figure 4. CLSM images of 10% (w/w) SP gels in the presence of 0−100 mM (a) $MgSO_4$ and (b) $MgCl_2$. Left image side stands for 250 μm scale, right side for 25 μm.

or particulate soy protein networks with different microstructures in terms of pore size, strand thickness, and homogeneity. As intended, a wide range of microstructures varying from fine to very coarse were obtained by using either $MgSO_4$ or $MgCl_2$ salts.

Rheological Gel Characteristics. Large deformation rheology measurements were performed to obtain mechanical characteristics of the formed gels. Young's modulus, which reflects the stiffness of the material, was determined from the

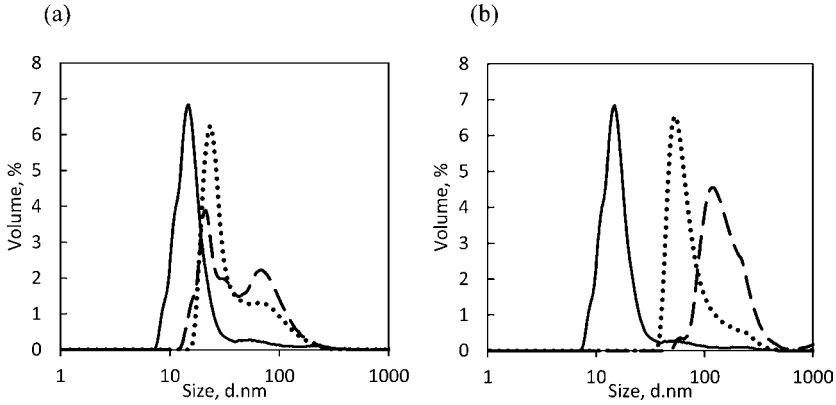

Figure 3. (a) Aggregate size of 0.1% (v/v) SP (solid line), 0.1% (v/v) SP with 0.5 mM $MgSO_4$ (dotted line), and 0.1% (v/v) SP with 0.5 mM $MgCl_2$ mixed for 30 min at 25 °C (dashed line). (b) Aggregate size of 0.1% (v/v) SP (solid line), 0.1% (v/v) SP heated at 95 °C for 30 min (dotted line), and 0.1% (v/v) SP with 0.5 mM $MgCl_2$ heated at 95 °C for 30 min (dashed line). All measurements were performed at 25 °C.

dx.doi.org/10.1021/jf501728t | J. Agric. Food Chem. 2014, 62, 7550−7558

initial slope of the resulting stress by applying a strain deformation. Figure 5a shows that both $MgSO_4$ and $MgCl_2$ SP gels increased in Young's moduli with increasing salt concentration indicating the formation of firmer structures, reaching a maximum around 30−40 mM salt and decreased again with further salt increment. The fracture stress (Figure 5b) followed the same pattern as the Young's moduli indicating harder structures formed with increasing salt concentration, and upon further increase softer structure were formed. All gels were comparable in fracture strain with the exception of 40−50 mM $MgSO_4$ gels with the higher fracture strain and 30 and 80 mM $MgCl_2$ SP gels with the lower fracture strain (Figure 5c). Typically, SP gels in the presence of $MgCl_2$ had lower fracture stress and strain compared to those with a similar concentration $MgSO_4$.

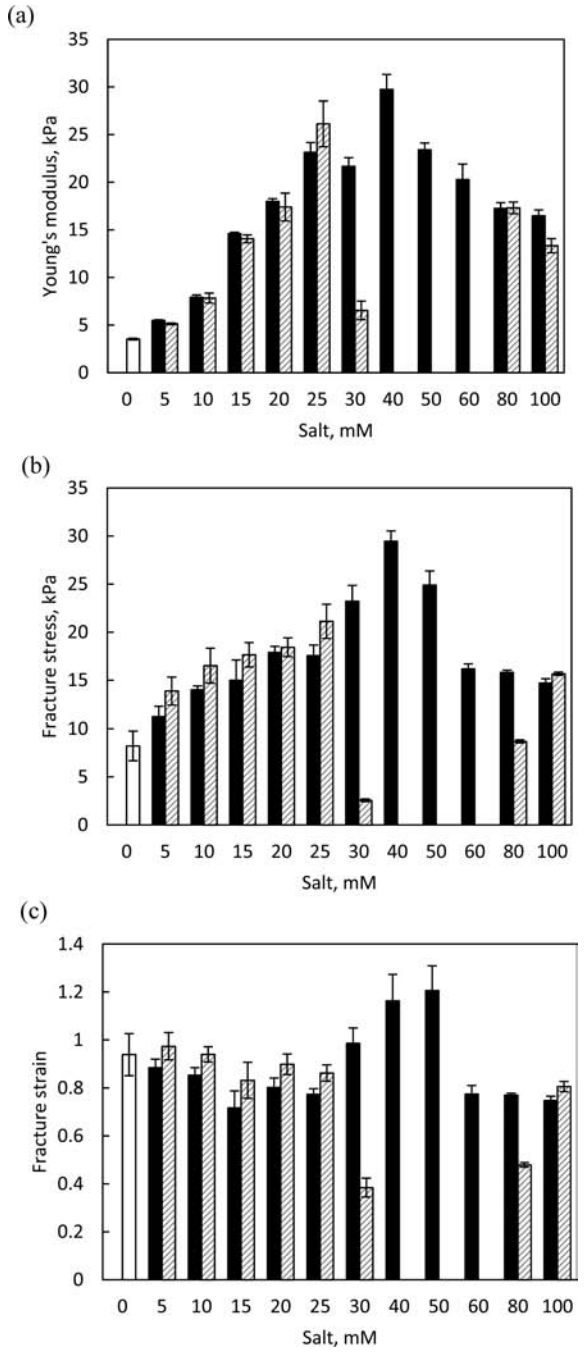

Figure 5. Large deformation rheology measurements of 10% (w/w) SP gels without salt (open bars) and mixed with 5−100 mM $MgSO_4$ (filled bars) or with 5−100 mM $MgCl_2$ (striped bars).

Recoverable Energy. Recoverable energy represents the energy that is elastically stored during deformation. Recoverable energy was measured by compressing a gel to half of its fracture strain followed by decompression. Recoverable energy results of $MgSO_4$ and $MgCl_2$ SP gels are shown in Figure 6.

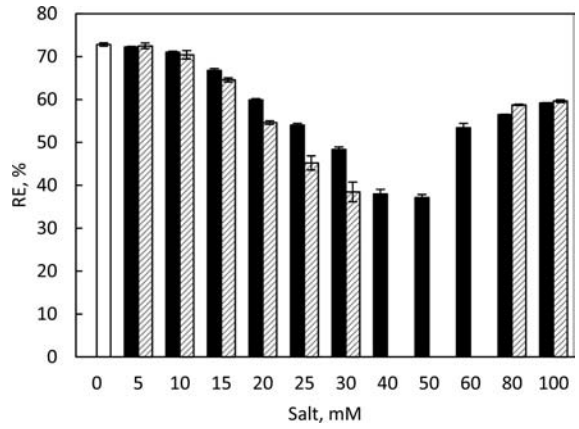

Figure 6. Recoverable energy 10% (w/w) SP gels measured at half of fracture strain: without salt (open bar) and mixed with 5−100 mM $MgSO_4$ (filled bars) or with 5−100 mM $MgCl_2$ (striped bars).

Recoverable energy decreased from approximately 70% to 40% with increasing salt concentration and increased with higher salt concentration (80−100 mM) up to 60%. Between 15 and 60 mM $MgSO_4$ gels gave significantly higher RE compared to $MgCl_2$ gels.

Water Holding Measurements. To measure WH, SP gels were centrifuged from 20 to 1000*g* for fixed time (10 min). The WH results of 10% (w/w) SP gels with 0−100 mM $MgSO_4$ and $MgCl_2$ salts are shown in Figure 7. Large differences in WH were observed by varying type of salt and its concentration. These data were further analyzed using eq 2 (dashed lines, Figure 7). The results of the obtained fitting parameters A and k are plotted in Figure 8. Up to 30 mM salt concentration, both k and A increased, indicating easier water removal (k) from the gel under applied force, as well as increased amount or removable water (A) from the gel. The 30−60 mM $MgSO_4$ gels were comparable in values of k and A. At higher salt concentrations, k slightly decreased as well as the amount of removable water (A).

DISCUSSION

In this work, the aim was to show which length scales are most contributing to WH of soy protein-based gels when centrifugal compression is applied. More specifically, it was attempted to differentiate between the contributions of submicron (aggregate level) and supramicron length scales (morphology) to WH by varying salt concentration and by employing the salt specificity ($MgSO_4$ and $MgCl_2$) on protein aggregation. Moreover, by applying different *g*-forces, the influence of macroscopic gel disruption on WH could be assessed.

Gel Microstructure and Water Holding. CSLM and scanning electron microscopy (SEM) imaging has been used to visualize gel microstructure on a (sub)micron scale, and observed differences in coarseness have been linked to WH

dx.doi.org/10.1021/jf501728t | J. Agric. Food Chem. 2014, 62, 7550−7558

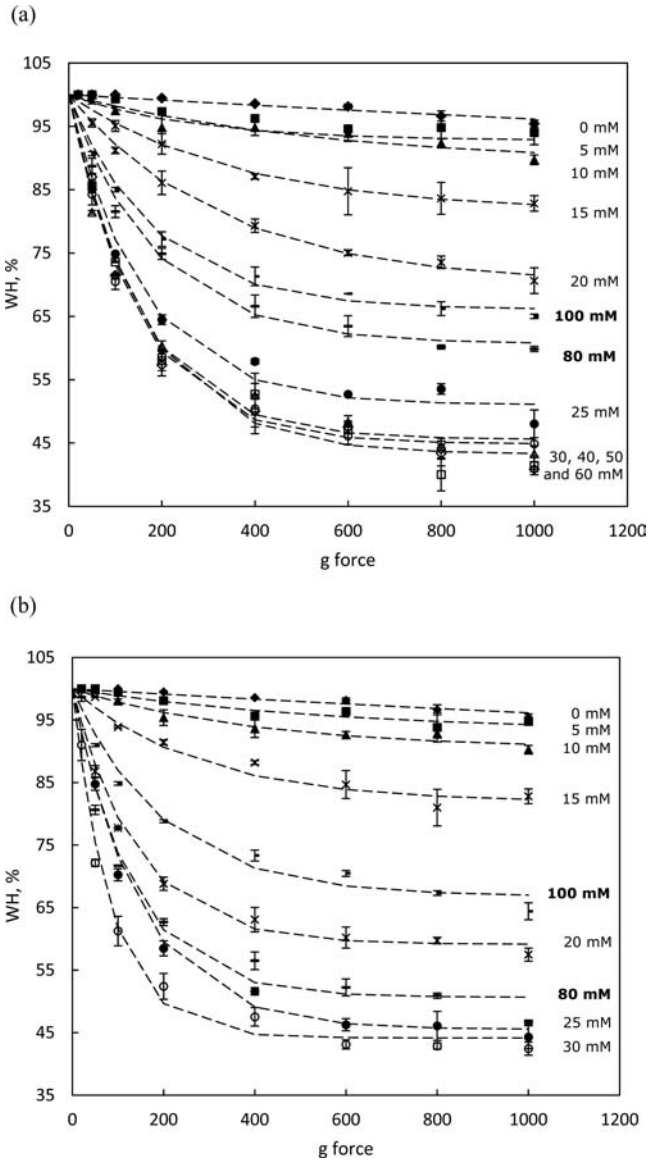

Figure 7. WH of 10% (w/w) SP gels with 0−100 mM (a) $MgSO_4$ gels and (b) $MgCl_2$ gels. The dashed lines represent the fits following the analysis as described in the text.

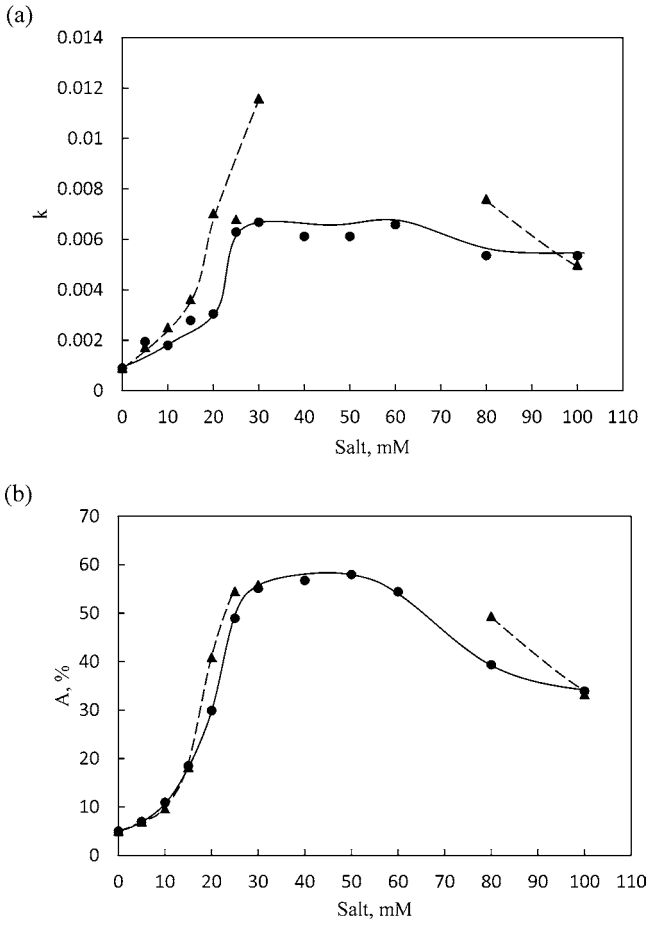

Figure 8. Fitting parameters as a function of salt concentration: (a) k parameter and (b) A parameter, where (●) $MgSO_4$ and (▲) $MgCl_2$. The lines are fits to guide the eye.

results[4,16−18] or used to estimated capillary pressure.[12,14] Fine stranded gels are homogeneous through different length scales, whereas coarse gels can be homogeneous on a (sub)micron scale but may be heterogeneous on submillimeter level. It was shown that addition up to 15 mM magnesium salt yielded gels with comparable microstructures on submicron to submillimeter length scales (Figure 4) but displayed different WH properties (Figure 7). Alternatively, for example, 30−60 mM $MgSO_4$ gels were different in microstructure but had a comparable WH. This illustrates that WH cannot be simply explained by a single length scale evaluation of gel microstructure. To ensure that the differences in coarseness provide a differentiation in porosity and pore dimensions, leading to differences in capillary pressures especially when salts are present as well, a more detailed study on WH was performed using capillary suction measurements. This has been reported in the Supporting Information. The outcome of that study is that capillary pressures in the different gels do not relate to the observed water holding capacities described for the various SP gels under the type of centrifugal deformation we applied.

Gel Stiffness or Fracture Properties and Water Holding. A correlation plot of WH (Figure 7) against the Young's moduli (Figure 5a) of the various SP gels is shown in Figure 9. A clear negative relation can be observed. The stiffer the gel, the more energy is needed to deform the network for a given deformation. The correlation shown in Figure 9 illustrate that such higher stiffness coincides with the inability of a gel network to hold water well. Correlation plots between WH and the fracture stress (Figure 5b) or fracture strain (Figure 5c) did not show any correlation (not shown), illustrating that the ability of a protein network to retain water in its structure under applied force does not show a relation to the inability of the network to withstand stress build-up leading to fracture events. Also Hermansson and Lucisano suggested that WH and rheological properties of blood plasma gels are not related.[10] Yet, few other studies on blood plasma gels indicated that stronger gels can lose more water than weaker ones,[10,19] in contrast to another study by Hu et al. on SP gels.[20] Alternatively, Pares et al. reported on gels with different strengths but comparable in WH.[17] Yang et al. found a positive correlation of G' and WH of SP emulsion filled gels.[21]

Recoverable Elastic Energy and Water Holding. Once energy is applied to the system, the energy can be stored in the system or dissipated by fracture, friction, or serum flow. RE can be regarded as the difference between applied and dissipated

dx.doi.org/10.1021/jf501728t | J. Agric. Food Chem. 2014, 62, 7550−7558

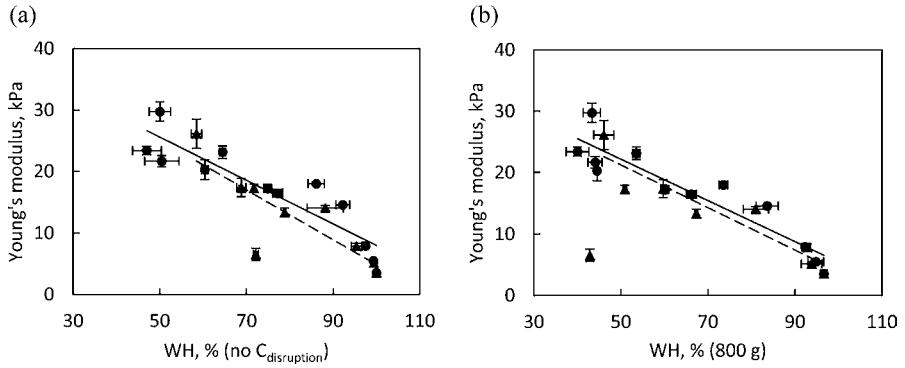

Figure 9. Correlation plots of WH as a function of Young's moduli, where (●) $MgSO_4$ and (▲) $MgCl_2$. (a) WH results when $C_{disruption}$ is eliminated; (b) WH results when fracture events are present. Horizontal error bars stand for WH, vertical for Young's moduli. Linear fitting was done as a guide to guide the eye, where solid line stands for $MgSO_4$ and dashed line for $MgCl_2$.

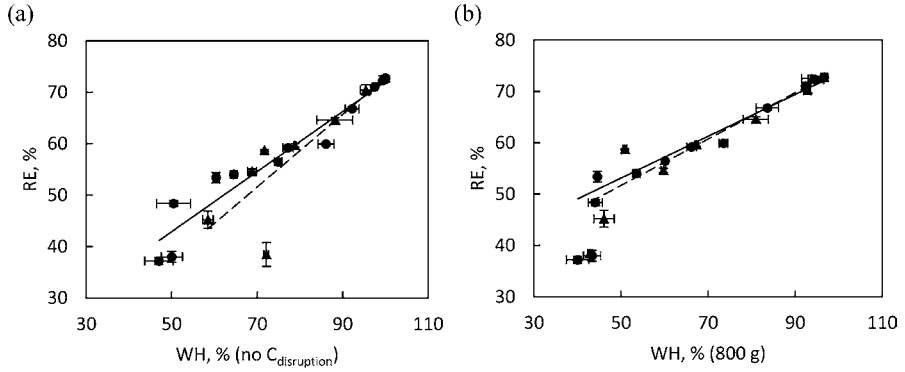

Figure 10. Correlation plots of WH as a function of RE, where (●) $MgSO_4$ and (▲) $MgCl_2$. (a) WH results when $C_{disruption}$ is eliminated; (b) WH results when fracture events are present. Horizontal error bars stand for WH, vertical for RE. Linear fitting was done as a guide to guide the eye, where solid line stands for $MgSO_4$ and dashed line for $MgCl_2$.

energy. When limited deformation is applied while determining the RE, macroscopic fracture events can be neglected, and a loss of RE might reflect predominantly the energy required to displace serum within the gel. Figure 10 shows RE (Figure 6) as a function of the WH (Figure 7) for the various SP gels. A clear positive correlation can be observed, showing an extrapolated intercept close to zero. This latter would imply that, when a protein gel would not be able to retain any water during mechanical deformation, it would also not be capable to store energy in the gel that can be regained after decompression. A comparable finding was obtained by Chantrapornchai and McClements for WPI gels.[12] The slope of the correlation shown in Figure 10 could be a measure for the efficiency by which a deformed protein network transduces its energy to viscous flow of the serum phase and thereby dissipates the applied energy.

Influence of Gel Disruption on Water Holding. A positive correlation of fracture strain to WH was reported in gellan gels,[22,23] but thus far, no information is available of fracture properties in relation to WH for protein-based gels. As already stipulated above, no correlations were found between gel fracture stress or fracture strain and WH for these gels (results are not shown). Comparing the correlation plots shown in Figures 9 and 10 at relatively low applied *g*-force (panel a) where the exerted stress in the systems is much lower than the recorded fracture stress (see the Materials and Methods section for the pressure-to-stress conversion) with those at high *g*-force (panel b) may provide insight in the contribution of gel disruption on the WH of these gels. When looking at the RE, the correlation with WH at higher applied *g*-force (Figure 10b) illustrates a general shift to lower WH and an offset in RE at zero WH. It can thus be suggested that the generation of microcracks introduces a small reduction in WH of a few percentage. Rupture of the protein network has thus a limited effect on WH, and the fragmented pieces (either at macro- of microlength scale) of the network still behave predominantly as an ensemble of intact smaller gel pieces.

Alternatively, when the stiffness of the gel under non-rupturing conditions is correlated to WH as determined at high *g*-force (Figure 9b), a similar dependence is found as compared to low applied *g*-force (Figure 9a). This supports the idea that, upon rupturing of the gel, the individual fragmented pieces behave as smaller intact gel pieces where the stiffness sets the WH ability of the gel pieces.

Discrimination of Sub- and Supramicron Contributions to Water Holding. In this work, the aim was to show which length scale was most important for WH of SP gels under compression as defined WH consisted of four different contributions covering from molecular to macro length scales. To this end, different gel morphologies (supramicron) were created based on different protein aggregates (submicron). The correlation graphs shown in Figures 9 and 10 show the data sets of both $MgSO_4$ (dashed lines) and $MgCl_2$ (solid lines) containing gels, where the first ones were based on smaller aggregates (Figures 1−3). It can be concluded that, when considering the Young's modulus (Figure 9), the aggregate level has no significant impact. But, also for the RE (Figure 10),

dx.doi.org/10.1021/jf501728t | J. Agric. Food Chem. 2014, 62, 7550−7558

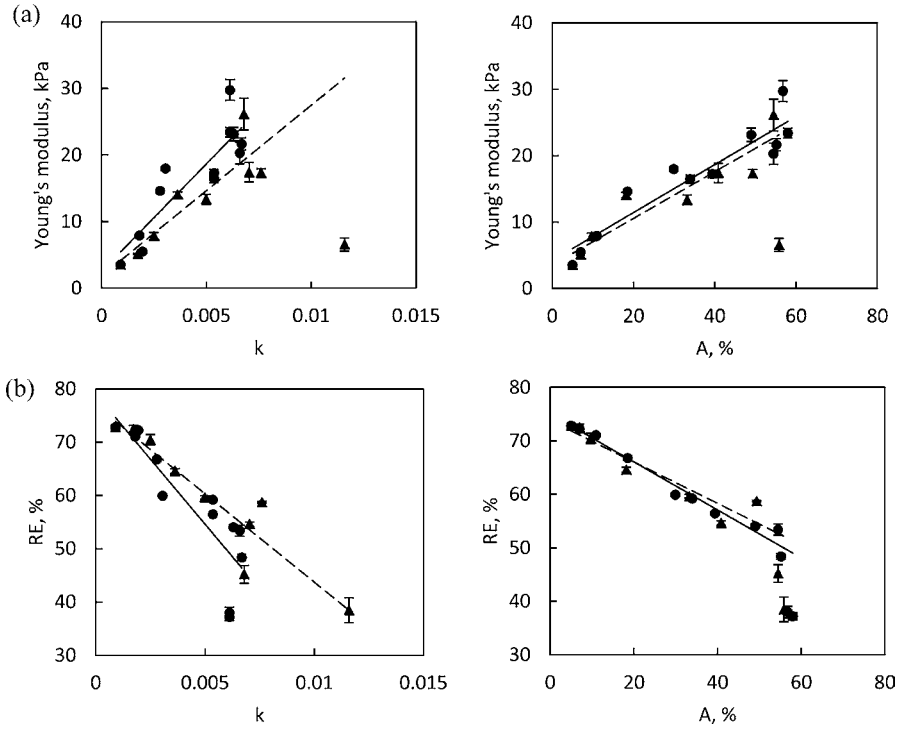

Figure 11. Correlation plots of fitting parameters k and A against (a) Young's moduli and (b) RE, where (●) $MgSO_4$ and (▲) $MgCl_2$. Vertical error bars stand for moduli and RE. Linear fitting was done as a guide to guide the eye, where solid line stands for $MgSO_4$ and dashed line for $MgCl_2$.

it cannot be concluded that there is an obvious effect when the outlier around a WH of around 72% for $MgCl_2$ is discarded.

It is then interesting to evaluate whether there might be a submicron differentiation when the kinetics is considered, as described in Figure 8 from fitting of the *g*-force curves. This is shown in Figure 11 for both the Young's modulus (panel a) and the RE (panel b) as a function of the k and A factors. It can be observed that the $MgCl_2$ gels show less steep dependence compared to the $MgSO_4$ gels when the ease by which water is removed from the gel (k) is considered. The physical implication of this finding is still unclear. On the other hand, the maximum quantity of water that can be removed (A) does not show a clear discrimination between the two different types of aggregates.

In summary, this work shows that straightforward microstructural analysis (CSLM or SEM) does not predict the WH of SP gels. The stiffness of the gels does show a negative correlation with WH, which in turn might set the propensity of the gel to reversibly store energy in the system during mechanical deformation. Fracturing characteristics, such as fracture stress and strain, have no correlation with the ability of the gel to hold water, while the occurrence of rupture events, either as micro- or macroscopic cracks, has only a limited impact on WH, as the WH of the gel fragments is still dominated by the inherent stiffness of these pieces. Comparison of gels derived from differently sized soy protein aggregates did not provide an indication that length scales at the submicron level are a determinant factor for WH of soy protein gels and that this latter property is predominantly set by larger length scales. The ease by which water may be removed from the gel (not the total amount) seems to be related to the initial building block size, which could be speculated to be related to the fine-structure of the microstructure elements that set up the network. Different aggregate characteristics might of course directly influence the gel morphology (coarseness) that can be derived and thereby set the WH capacity of the gels.

■ ASSOCIATED CONTENT

Supporting Information

Additional materials and methods; SEM images; and figures of salt concentration dependency on WH−RE relation, WH measurements by the static capillary suction method, and WH_{CS} as a function of Young's moduli and RE. This material is available free of charge via the Internet at http://pubs.acs.org.

■ AUTHOR INFORMATION

Corresponding Author

*Phone: +31 317 486160; e-mail: vaida.urbonaite@wur.nl.

Notes

The authors declare no competing financial interest.

■ ACKNOWLEDGMENTS

Joost van Eijndhoven is acknowledged for his contribution towards the completion of this work.

■ REFERENCES

(1) Van Vliet, T.; Walstra, P. Large deformation and fracture behaviour of gels. *Faraday Discuss.* **1995**, *101*, 359−370.

(2) Kao, F.-J.; Su, N.-W.; Lee, M.-H. Effect of calcium sulfate concentration in soymilk on the microstructure of firm tofu and the protein constitutions in tofu whey. *J. Agric. Food. Chem.* **2003**, *51*, 6211−6216.

(3) Maltais, A.; Remondetto, G. E.; Gonzalez, R.; Subirade, M. Formation of soy protein isolate cold-set gels: Protein and salt effects. *J. Food Sci.* **2005**, *70*, C67−C73.

(4) Puppo, M. C.; Añón, M. C. Structural properties of heat-induced soy protein gels as affected by ionic strength and pH. *J. Agric. Food. Chem.* **1998**, *46*, 3583−3589.

(5) Campbell, L. J.; Gu, X.; Dewar, S. J.; Euston, S. R. Effects of heat treatment and glucono-δ-lactone-induced acidification on characteristics of soy protein isolate. *Food Hydrocolloids* **2009**, *23*, 344−351.
(6) Furukawa, T.; Ohta, S. Mechanical and water-holding properties of heat-induced soy protein gels as related to their structural aspects. *J. Texture Stud.* **1982**, *13*, 59−69.
(7) Gu, X.; Campbell, L. J.; Euston, S. R. Influence of sugars on the characteristics of glucono-δ-lactone-induced soy protein isolate gels. *Food Hydrocolloids* **2009**, *23*, 314−326.
(8) Molina, E.; Defaye, A. B.; Ledward, D. A. Soy protein pressure-induced gels. *Food Hydrocolloids* **2002**, *16*, 625−632.
(9) Wu, W.; Hua, Y.; Lin, Q.; Xiao, H. Effects of oxidative modification on thermal aggregation and gel properties of soy protein by peroxyl radicals. *Int. J. Food Sci. Technol.* **2011**, *46*, 1891−1897.
(10) Hermansson, A.-M.; Lucisano, M. Gel characteristics—Water-binding properties of blood plasma gels and methodological aspects on the waterbinding of gel systems. *J. Food Sci.* **1982**, *47*, 1955−1959.
(11) Kocher, P. N.; Foegeding, E. A. Microcentrifuge-based method for measuring water-holding of protein gels. *J. Food Sci.* **1993**, *58*, 1040−1046.
(12) Chantrapornchai, W.; McClements, D. J. Influence of NaCl on optical properties, large-strain rheology and water holding capacity of heat-induced whey protein isolate gels. *Food Hydrocolloids* **2002**, *16*, 467−476.
(13) Labuza, T. P.; Lewicki, P. P. Measurement of gel water-binding capacity by capillary suction potential. *J. Food Sci.* **1978**, *43*, 1264−1269.
(14) Stevenson, C. D.; Dykstra, M. J.; Lanier, T. C. Capillary pressure as related to water holding in polyacrylamide and chicken protein gels. *J. Food Sci.* **2013**, *78*, C145−C151.
(15) Fischer, H.; Polikarpov, I.; Craievich, A. F. Average protein density is a molecular-weight-dependent function. *Protein Sci.* **2004**, *13*, 2825−2828.
(16) Picone, C. S. F.; da Cunha, R. L. Interactions between milk proteins and gellan gum in acidified gels. *Food Hydrocolloids* **2010**, *24*, 502−511.
(17) Parés, D.; Saguer, E.; Saurina, J.; Suñol, J. J.; Carretero, C. Functional properties of heat induced gels from liquid and spray-dried porcine blood plasma as influenced by pH. *J. Food Sci.* **1998**, *63*, 958−961.
(18) He, J.-S.; Azuma, N.; Yang, H. Effects of pH and ionic strength on the rheology and microstructure of a pressure-induced whey protein gel. *Int. Dairy J.* **2010**, *20*, 89−95.
(19) Hermansson, A.-M. Gel characteristics—Structure as related to texture and waterbinding of blood plasma gels. *J. Food Sci.* **1982**, *47*, 1965−1972.
(20) Hu, H.; Fan, X.; Zhou, Z.; Xu, X.; Fan, G.; Wang, L.; Huang, X.; Pan, S.; Zhu, L. Acid-induced gelation behavior of soybean protein isolate with high intensity ultrasonic pre-treatments. *Ultrason. Sonochem.* **2013**, *20*, 187−195.
(21) Yang, M.; Liu, F.; Tang, C.-H. Properties and microstructure of transglutaminase-set soy protein-stabilized emulsion gels. *Food Res. Int.* **2013**, *52*, 409−418.
(22) Mao, R.; Tang, J.; Swanson, B. G. Water holding capacity and microstructure of gellan gels. *Carbohydr. Polym.* **2001**, *46*, 365−371.
(23) Huang, Y.; Tang, J.; Swanson, B. G.; Rasco, B. A. Effect of calcium concentration on textural properties of high and low acyl mixed gellan gels. *Carbohydr. Polym.* **2003**, *54*, 517−522.

light has rarely been specified. Most precisely, "exposure to sunlight" was applied, although these experimental conditions might not reflect retail or consumer handling. In retail stores and households, cold fluorescent lights are most abundant, whereas exposure to sunlight might be more prevalent in developing countries where the oil is scooped into polyethylene terephthalate (PET) bottles from large open containers stored outside. Sunlight-exposed storage of RP-fortified soybean oil in closed PET bottles for 4 weeks at room temperature has been demonstrated to reduce the initial vitamin A concentration by 27.1 ± 12.1%, whereas additional oxygen exposure, induced by intermittent opening of the PET bottles, augmented the vitamin A loss to 88.6 ± 1.97%.[10] When the same oil samples were stored at room temperature in opened PET bottles in the dark, the mean retention of vitamin A was 97.4 ± 1.28%, clearly demonstrating that, at room temperature, protection from sunlight is more critical for preserving the vitamin A stability in edible oils than exclusion of oxygen. Whether the impact of cold fluorescent light, commonly installed in retail stores and households, is comparable to that of sunlight has not yet been studied.

Besides the need to study the vitamin A stability, the stability of vitamin E (total tocopherols) in soybean oil stored under household conditions needs also to be investigated as tocopherols were shown to affect the stability of vitamin A.[11] The presence of α-tocopherol, at a concentration of 156 μM, led to retention of 91 ± 4% of RP after air oxidation of the ethanolic RP solution for 4 h, compared to only 69 ± 4% retention of RP in the absence of α-tocopherol. However, the literature studying the stability of vitamins E and A in vegetable oils stored under domestic handling is scarce.

Thus, the current study investigated, for the first time, the stability of RP and vitamin E in vitamin A fortified soybean oil stored under household conditions in the presence of cold fluorescent light at 22 and 32 °C. Soybean oil was filled in transparent PET bottles, which were reopened periodically for sampling to mimic consumer handling. Mildly and highly oxidized soybean oil was used for fortification with RP to elucidate the effect of oxidative oil quality on RP stability.

MATERIALS AND METHODS

Chemicals. Transparent PET bottles (0.5 L; 19.4 ± 0.05 g) and corresponding screw caps were kindly provided by Rauch Fruchtsäfte GmbH, Rankweil, Austria. Refined soybean oil was purchased from Henry Lamotte Oils GmbH, Bremen, Germany. For illumination of the oil with visible daylight, a cold cathode fluorescent lamp (Philips Tornado 1450 lm, 103 W) was obtained from Philips, Eindhoven, The Netherlands. d_{12}-Hexanal was ordered from C/D/N Isotopes, Quebec, Canada. The internal standard *all-rac*-tocol was obtained from Matreya, Pleasant Gap, PA, USA. RP, which was stabilized with tocopherols, was kindly provided by DSM Nutritional Products, Kaiseraugst, Switzerland. All other chemicals were ordered from Sigma-Aldrich, Vienna, Austria, and Carl Roth, Karlsruhe, Germany.

Study Design. Soybean oil was homogenized and partly fortified with 31.6 IU/g (17.4 mg/kg) RP. To ensure a homogeneous distribution of RP in the oil, RP was premixed in 50 g of oil before it was slowly added under agitation to 20 kg of soybean oil. A total of 460 ± 1 g fortified soybean oil was filled in each of the 0.5 L transparent PET bottles, which were closed with a screw cap afterward. The soybean oil was stored at 22 ± 1 or 32 ± 1 °C following a 12 h dark/light cycle in the presence of cold fluorescent light for 56 days (Figure 1). To expose soybean oil to visible light, a 103 W (1450 lm) lamp was installed 34 cm above the bottles. A distance of 15 cm was kept between the bottles to ensure access to illumination. To investigate the influence of the oxidative status of soybean oil at the time of fortification on the stability of RP, a nonfortified soybean oil, which was exposed to cold fluorescent light at 22 ± 1 or 32 ± 1 °C, was stored until a POV of >10 mequiv O_2/kg was reached on day 28. Then, this oil was fortified with 31.6 IU/g RP and stored until the end of the study (day 56). To mimic consumer handling, the bottles were reopened on days 1, 7, 14, 21, 28, and 56, and sample volumes of 51.4 mL, 42.4 mL, 42.4 mL, 37.0 mL, 42.4 mL, and 51.4 mL, respectively, were withdrawn. On day 56, a headspace volume of 334 mL was determined. On days 1, 7, 14, 28, and 56, samples were withdrawn for analyses after gently agitating the bottles. Thus, the samples, which were withdrawn on day 21 to mimic consumer handling, were not subjected to further analyses.

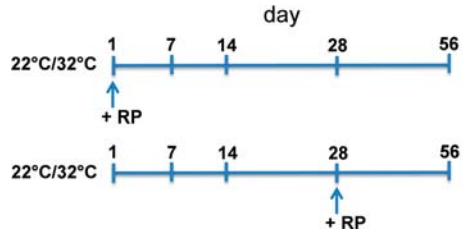

Figure 1. Study design. Fortified soybean oil was stored under different household conditions at 22 and 32 °C. Samples were withdrawn on the indicated days.

Quantification of Copper in Soybean Oil. Copper concentrations in oil samples were determined by means of atomic absorption spectrometry using a PinAAcle 900Z graphite furnace atomic absorption spectrometer (PerkinElmer, Vienna, Austria) as described previously.[12] A volume of 8 mL of 34% HNO_3 (TraceSELECT Fluka) was added to 0.2 g of oil sample and heated to 180 °C in a microwave MARS XPRESS system (CEM Corp., Kamp-Lintfort, Germany). After treatment in the microwave oven, double-distilled water was added, leading to a final volume of 20 mL, which was passed through a 0.2 μm PTFE filter prior to measurement. The limit of detection for copper was determined to be 0.02 μg/g.

Quantification of Retinol in Soybean Oil. Retinyl palmitate was analyzed as retinol after saponification. The quantification of retinol in soybean oil was performed according to the method of Bognar.[13] Sample preparation was conducted under nitrogen atmosphere in the dark. For saponification, 1 g of oil sample was mixed with 30 mL of double-distilled water, 20 mL of KOH (10.7 M), 100 mL of ethanol, 1 g of sodium ascorbate, and 2 mL of sodium sulfide (0.51 M) and heated to 80 °C under reflux for 30 min. Afterward, the reflux apparatus was rinsed with 20 mL of water. The mixture was cooled to 15 °C before 28 mL of cold, double-distilled water and 100 mL of *n*-hexane were added. The extraction was repeated twice with 100 mL of *n*-hexane and twice with 50 mL of *n*-hexane. The pooled hexane extracts were washed four times with 100 mL of cold, double-distilled water and dried with sodium sulfate. The solvent was removed from the dried extract under nitrogen by means of a rotating evaporator. The residue was dissolved in 5 mL of methanol before HPLC analysis. HPLC analysis was carried out on a Dionex Ultimate 3000 LC system (Thermo Fisher Scientific, Vienna, Austria), coupled to a diode array detector set to 325 nm. A volume of 20 μL of the samples was separated on a C18 column (Luna, 250 × 3.00 mm, 5 μm, Phenomenex, Aschaffenburg, Germany) with a flow rate of 0.5 mL/min at 25 °C. A mixture of methanol and double-distilled water (98:2, v/v) was used to elute retinol after 5.05 min. Quantification of retinol was performed by applying external calibration. Calibration curves for retinol ($y = 4.64x + 0.06$) were prepared in the beginning, middle, and end of the study. To determine the limit of detection the signal-to-noise method was applied by measuring the peak height of the analyte and the noise in proximity of the analyte. A signal-to-noise ratio of 3 was considered as the lowest amount for detection. The limit of detection for retinol was 3.27 ± 0.25 ng/mL. The corresponding limit of quantification for retinol was calculated to be 10.9 ± 0.84 ng/mL, corresponding to a signal-to-noise ratio of 10. The recovery of retinol was determined by spiking oil samples with 30.5 μM retinyl palmitate

followed by sample preparation as described above. The loss of vitamin A was evaluated by comparing the retinol content after sample preparation with 30.5 μM retinol standard. The recovery was determined to be 75.5 ± 7.78%.

Iodometric Quantification of the Peroxide Value. To quantify the peroxidic oxygen in the oil samples, the POV was determined according to AOCS official method Cd 8-53.[14] Briefly, a total of 5 g of oil sample was mixed with 18 mL of glacial acetic acid and 12 mL of chloroform. A volume of 0.5 mL of saturated solution of potassium iodide was added to the solution. After mixing for 1 min, 30 mL of double-distilled water and 2 drops of a saturated starch solution were added. The iodine was reduced with 0.1 N sodium thiosulfate until discoloration of the solution was obtained. The difference between the volumes of sodium thiosulfate needed to reduce the iodine in the oil samples and the control without the oil was multiplied by the concentration of the sodium thiosulfate and related to the amount of oil sample in kilograms. The unit of the POV corresponds to milliequivalents of O_2 per kilogram of oil.

Quantification of Hexanal in Soybean Oil. Analysis of hexanal in soybean oil was performed by applying static headspace GC-MS. Samples were prepared with slight modifications according to the method of Giuffrida et al.[15] A total of 2.5 g of oil sample was mixed with 2.72 mL of methanol/double-distilled water (1:1, v/v) filled in 20 mL glas vials sealed with gastight screw caps before 4 μg/mL of the internal standard, d_{12}-hexanal, was added. The mixture was incubated at 70 °C and agitated at 750 rpm on a CTC Combi Pal (CTC Analytics AG, Zwingen, Switzerland) for 15 min. A headspace volume of 1000 μL was injected with a syringe preheated at 90 °C using a split ratio of 1:5 into a Shimadzu GCMS-QP 2010 Ultra (Shimadzu, Vienna, Austria) at 250 °C. The samples were separated on a capillary column (ZB-WAX Zebron (PEG), 30 m × 0.25 mm × 0.25 μm, Phenomenex), at a column flow rate of 1.31 mL/min with an initial temperature of 35 °C held for 2 min. A temperature increase to 65 °C at 15 °C/min was followed by an increase to 80 °C at 2 °C/min. The final temperature of 230 °C, which was held for 5 min, was reached at 30 °C/min. Quantification of hexanal was performed by stable isotope dilution analysis using d_{12}-hexanal as internal standard. Mixtures of known amounts of hexanal and d_{12}-hexanal with different mass ratios (1:10−35:1) were analyzed to calculate the response factor. A response factor of 1.09 ± 0.08 was obtained. The concentration of hexanal was quantified using the linear equation $y = 1.07x + 0.12$, which was calculated by analyzing the mixtures of labeled and unlabeled hexanal. Hexanal and d_{12}-hexanal eluted after 5.21 and 5.12 min, respectively. Hexanal was identified with the corresponding standard and the NIST11 database for MS spectra by comparing the retention time and the fragmentation pattern with the reference spectrum. For quantification in the SIM mode, m/z of 72 and 80 were selected for hexanal and d_{12}-hexanal.[16] The limits of detection and quantification were 0.03 ± 0.02 and 0.10 ± 0.01 μg/mL, respectively.

Quantification of Total Tocopherols in Soybean Oil. Total tocopherols were analyzed according to the procedure of Gliszczynska-Swiglo and Sikorska.[17] Briefly, 0.05 g of oil sample was dissolved in 995 μL of 2-propanol and mixed with 5 μL of tocol (1 mg/mL). Prior to UHPLC analysis on a Dionex Ultimate 3000 LC system (Thermo Fisher Scientific, Vienna, Austria), samples were passed through a 0.22 μm nylon filter. Separation of the tocopherols was carried out on a C18 column (PFP Kinetex, 100 × 2.10 mm, 1.7 μm, Phenomenex) with a flow rate of 0.5 mL/min at 25 °C. After injection of 5 μL of sample, the tocopherol isomers and the internal standard were eluted at 5.59 min (δ), 6.10 min (β), 6.24 min (γ), 6.71 min (α), and 4.92 min (tocol), respectively. A methanol gradient, starting from 75% and finishing at 100% within 10 min, was used for proper separation. Pure methanol was held for 3 min before starting conditions with 75% methanol and 25% double-distilled water were reached again. Total tocopherols were detected at 295 nm and quantified using tocopherol standards for external calibration, with corresponding calibration curves for α- ($y = 0.05x - 0.08$), β- ($y = 0.04x + 0.01$), γ- ($y = 0.06x + 0.41$), and δ- ($y = 0.06x + 0.19$) tocopherols. The sum of the individual tocopherol isomers calculated corresponds to total tocopherols. The recovery of total tocopherols was analyzed by adding 0.5 μg/mL tocol as internal standard to the samples. By comparing the area under the curve of tocol in 2-propanol with the area under the curve of tocol in the samples, a recovery of 94.4 ± 12.1% could be determined. The limits of detection for α-, β-, γ-, and δ-tocopherols were calculated to be 0.24 ± 0.02, 0.20 ± 0.02, 0.04 ± 0.01, and 0.02 ± 0.01 μg/mL, respectively, according to the signal-to-noise method described above. The corresponding limits of quantification for α-, β-, γ-, and δ-tocopherols were calculated to be 0.80 ± 0.07, 0.67 ± 0.07, 0.13 ± 0.03, and 0.07 ± 0.03 μg/mL, corresponding to a signal-to-noise ratio of 10.

Statistical Analysis. All experiments were performed in quadruplets with two technical replicates. The results are shown as the mean value ± standard deviation after exclusion of outliers by applying the Nalimov outlier test. To analyze time effects and differences between storage conditions, one-way ANOVA followed by the Holm−Sidak post hoc test was applied using SigmaPlot 11 (Systat Software Inc., Chicago, IL, USA). To study the relationship between retinol or tocopherols and hexanal or POV, the Pearson product-moment correlation coefficient was calculated. Differences were considered statistically significant when the p value was <0.05.

RESULTS

Stability of Retinyl Palmitate in Soybean Oil. The impact of cold fluorescent light and ambient temperatures of 22 and 32 °C on RP stability was studied in fortified soybean oil filled in closed transparent bottles, which were reopened once a week within the first month of storage. The stability of RP in soybean oil was determined after saponification of RP as unesterified retinol. Figure 2 shows a significant decrease of

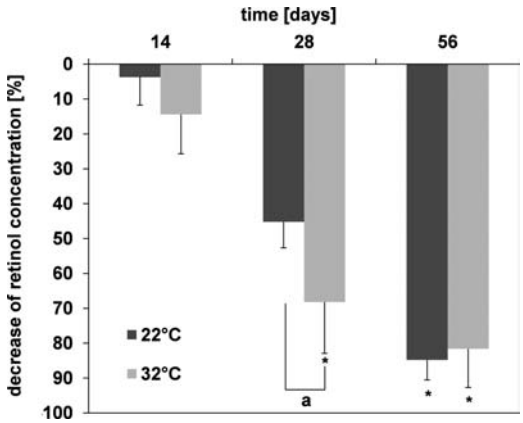

Figure 2. Percent decrease of retinol concentration in soybean oil after storage at 22 and 32 °C in the presence of cold fluorescent light for up to 56 days. Data are expressed as the mean ± SD ($n = 4$). Small letter (a) indicates statistically significant difference between storage temperatures ($p < 0.05$). Asterisks indicate statistically significant difference versus day 1 ($p < 0.05$).

retinol concentration by a maximum of 84.8 ± 5.76% after 56 days of storage under household-representative handling conditions. A significant decline of retinol concentration by 68.2 ± 14.7% was already obtained after 28 days for soybean oil exposed to cold fluorescent light at 32 °C. Thus, an accelerated degradation of RP was observed during storage of soybean oil under household conditions and handling, which was affected by an elevated ambient temperature of 32 °C on day 28.

Stability of Vitamin E in Soybean Oil. The decrease of vitamin A stability in fortified soybean oil stored under domestic conditions might also be associated with the degradation of vitamin E. With an initial concentration of 465 ± 5.25 μg/mL on day 1, total tocopherols decreased to

dx.doi.org/10.1021/jf502109j | J. Agric. Food Chem. 2014, 62, 7559−7566

46.7 ± 0.87 and 47.7 ± 1.46% of the initial content after storage at 22 and 32 °C, respectively, for 56 days (Figure 3A). After 28 days of storage, already a decrease of total tocopherols to about 86% of their initial content on day 1 was determined.

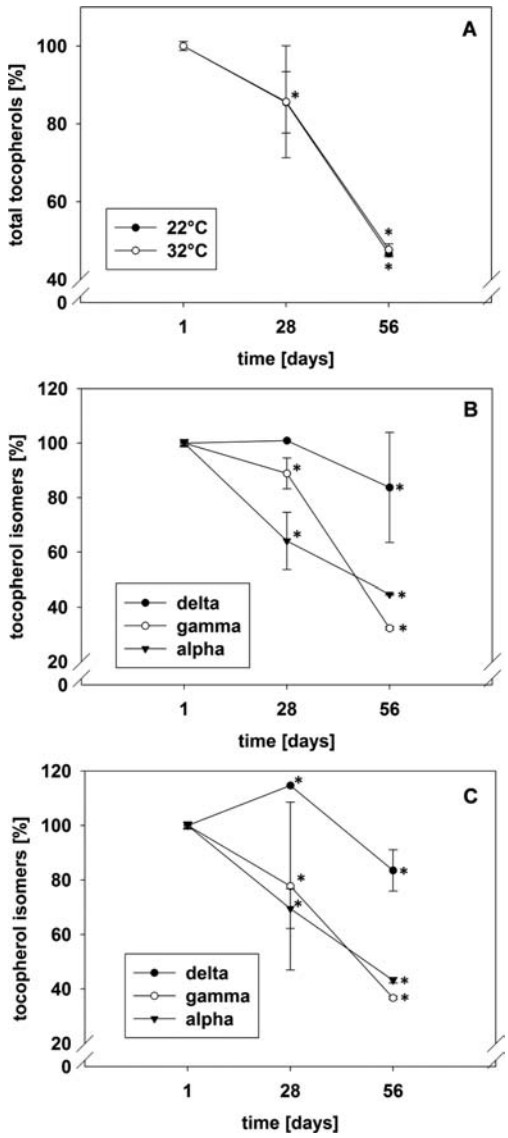

Figure 3. Decrease of total tocopherols (A) in soybean oil exposed to cold fluorescent light in the presence of RP at 22 or 32 °C for 56 days; decrease of tocopherol isomers in soybean oil exposed to cold fluorescent light in the presence of RP at 22 (B) or 32 °C (C) for 56 days. Data are expressed as the mean ± SD (n = 4). Asterisks indicate statistically significant differences versus the concentration of tocopherols on day 1 ($p < 0.05$).

Panels B and C of Figure 3 show the contribution of the individual tocopherol isomers to the loss of the total tocopherols during storage of soybean oil under consumer-representative handling at 22 and 32 °C, respectively. α- and γ-tocopherols exhibited the most pronounced decrease of tocopherol isomers. With initial values of 128 ± 1.31 and 227 ± 3.07 μg/mL, mean losses of 55.3 ± 0.29 and 67.7 ± 0.59% for α- and γ-tocopherol, respectively, were detected after storage of soybean oil at 22 °C for 56 days. Similar losses of 56.8 ± 1.01 and 63.2 ± 0.57% for α- and γ-tocopherols were obtained when the oil was stored at 32 °C. The decomposition of tocopherols differed between the tocopherol isomers during storage days 28−56 compared to the first 28 days. Whereas α-tocopherol decreased rapidly during the first 28 days of storage, the decomposition of γ-tocopherol was accelerated during the last 4 weeks of the study period. Compared to α- and γ-tocopherols, only moderate changes of the initial concentration of 103 ± 1.35 μg/mL of δ-tocopherol were observed throughout the study. β-tocopherol could be detected only on day 1 (0.67 ± 0.04 mg/100 g), whereas on the other sampling days β-tocopherol was below the limit of detection (0.20 ± 0.02 μg/mL).

Lipid Oxidation in Soybean Oil Stored under Domestic Conditions Correlates with Vitamin A and E Stability. To elucidate whether the low stability of vitamins A and E is associated with an increased oxidative deterioration of the study oil, lipid oxidation products were monitored. The formation of lipid oxidation products might be favored by the presence of transition metals, such as iron or copper. According to the analysis certificate of the manufacturer, the content of transition metals is <0.001%. However, even traces of metals might initiate lipid oxidation. Thus, soybean oil was characterized by its content of copper. Atomic absorption spectroscopic analyses revealed that the copper content was below the limit of detection of 0.02 μg/g, thereby limiting copper-induced autoxidation processes. The impact of traces of other metals, such as iron, on lipid oxidation cannot be excluded. Domestic storage of soybean oil for 56 days fortified with RP affected not only the stability of RP and vitamin E but also its susceptibility to lipid oxidation. Lipid oxidation was monitored by determining early and late oxidation markers. For analysis of early events in lipid oxidation, the POV was analyzed. An increase of the POV from 1.20 ± 0.004 to 24.3 ± 0.02 and 27.9 ± 0.33 mequiv O_2/kg was determined in soybean oil exposed to cold fluorescent light at 22 and 32 °C, respectively, after 56 days of storage (Figure 4).

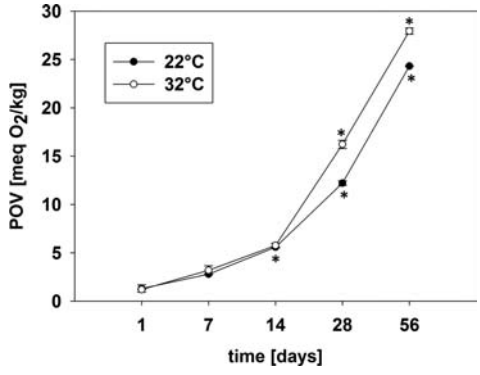

Figure 4. Increase of the POV (mequiv O_2/kg) in soybean oil exposed to cold fluorescent light in the presence of RP at 22 or 32 °C for 56 days. Data are expressed as the mean ± SD (n = 4). Asterisks indicate statistically significant differences versus the POV on day 1 ($p < 0.05$).

For analysis of the effects of soybean oil storage on late events in lipid oxidation, hexanal was chosen as a marker. Peak concentrations of hexanal of 2.13 ± 0.21 and 3.35 ± 0.69 μg/mL were reached after 28 days of storage at 22 and 32 °C, respectively, which differed significantly from the initial hexanal concentration of 0.91 ± 0.29 μg/mL on day 1 (Figure 5). Hexanal can be formed via degradation of hydroperoxides in linoleic acid-rich oils. However, an increased hexanal concentration does not necessarily lead to an decreased

dx.doi.org/10.1021/jf502109j | J. Agric. Food Chem. 2014, 62, 7559−7566

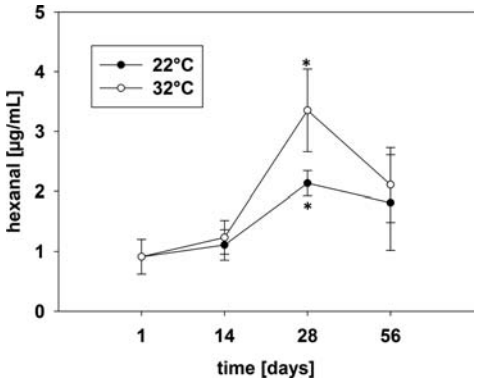

Figure 5. Alterations of the formation of hexanal (μg/mL) in soybean oil exposed to cold fluorescent light in the presence of RP at 22 or 32 °C for 56 days. Data are expressed as the mean ± SD (n = 4). Asterisks indicate statistically significant differences versus the hexanal concentration on day 1 (p < 0.05).

peroxide value, because the rate of peroxide formation might not be equal to the rate of peroxide decomposition. In the present study, the rate of peroxide formation might be higher than the rate of peroxide degradation, explaining the simultaneous increase in the peroxide value and the hexanal concentration.

To reveal any association between the RP stability and the progress of lipid oxidation, correlation analyses were performed. The relationship between RP stability and the lipid oxidation in soybean oil stored under domestic conditions was demonstrated by the negative correlation between lipid oxidation markers and retinol concentration (Figure 6). A significant correlation with a correlation coefficient of r = −0.930 (p < 0.001) and r = −0.725 (p < 0.01) was obtained between retinol concentration and the POV (Figure 6A) and the hexanal concentration (Figure 6B), respectively.

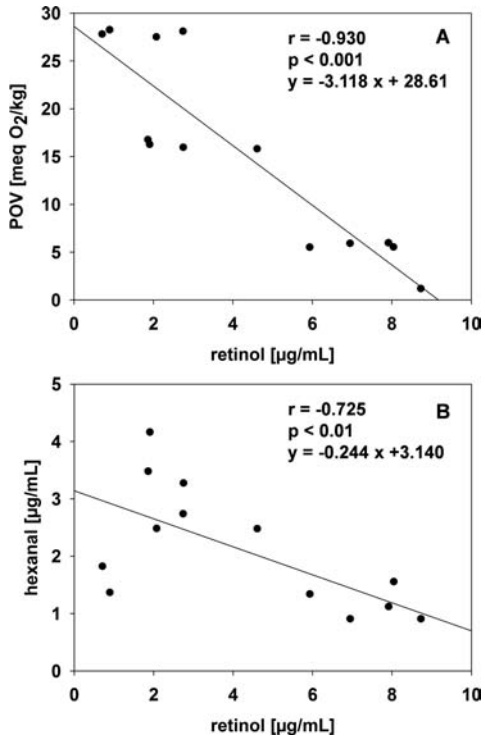

Figure 6. Correlation analyses between retinol and lipid oxidation markers, such as POV (A) and hexanal (B), as detected in soybean oil exposed to cold fluorescent light in the presence of RP at 32 °C for 56 days.

Besides the association between vitamin A stability and lipid oxidation, the stability of vitamin E was shown to depend on the oxidative status of the soybean oil (Figure 7). The storage-induced increase of the POV in mildly oxidized oil from 1.30 ± 0.38 to 24.3 ± 0.02 mequiv O_2/kg at 22 °C was associated with a decrease in total tocopherols from 465 ± 5.25 to 398 ± 6.21 μg/mL. In highly oxidized oil, characterized by a POV of 12.2 ± 0.23 mequiv O_2/kg and a tocopherol content of 398 ± 6.21 μg/mL, the 28 day storage period resulted in a tocopherol degradation to 177 ± 26.8 μg/mL.

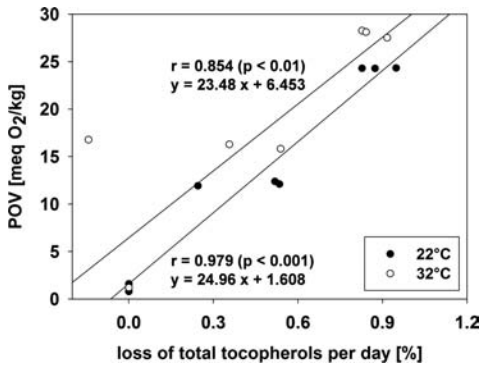

Figure 7. Loss of total tocopherols per day (%) in soybean oil with specific POV (mequiv O_2/kg). Data are expressed as the mean ± SD (n = 3).

Preoxidized Oil Lowered the Stability of RP. To confirm the correlation between RP stability and the progress of lipid oxidation, the impact of highly oxidized soybean oil, characterized by a POV of >10 mequiv O_2/kg, on the stability of RP was investigated. Besides the inverse association of RP and tocopherol concentration with lipid oxidation markers, RP stability was shown to depend on the oxidative oil quality at the time of RP fortification (Table 1). Domestic storage and handling of mildly oxidized soybean oil, which was fortified with RP at a POV of 1.43 ± 0.24 mequiv O_2/kg at day 1, led to average daily decreases of retinol concentration of 1.52 ± 0.10 and 1.46 ± 0.19% at 22 and 32 °C, respectively (p > 0.05). When highly oxidized soybean oil samples with POVs of 12.1 ±

Table 1. Percent Decrease of Retinol Concentration in Mildly and Highly Oxidized Soybean Oil, Which Was Fortified with RP on Days 1 and 28, Respectively, after Storage under Light Exposure at 22 and 32°C for 56 Days[a]

	POV at RP fortification (mequiv O_2/kg)	total decrease of retinol concentration at day 56 (%)	average decrease of retinol concentration per day (%)
mildly oxidized oil fortified with RP at day 1 (POV < 2 mequiv O_2/kg)			
22 °C	1.43 ± 0.24	84.8 ± 5.76*a	1.52 ± 0.10a
32 °C	1.43 ± 0.24	81.6 ± 11.1*a	1.46 ± 0.19a
highly oxidized oil fortified with RP at day 28 (POV > 10 mequiv O_2/kg)			
22 °C	12.1 ± 0.23	72.0 ± 1.72*a	2.57 ± 0.06b
32 °C	17.3 ± 0.18	80.3 ± 13.6*a	2.87 ± 0.49b

[a]Data are expressed as the mean ± SD (n = 4). Distinct letters within a column indicate statistically significant difference (p < 0.05). Asterisks indicate statistically significant difference with regard to the day of fortification with RP (p < 0.05).

dx.doi.org/10.1021/jf502109j | J. Agric. Food Chem. 2014, 62, 7559−7566

0.23 mequiv O_2/kg (stored at 22 °C) and 17.3 ± 0.18 mequiv O_2/kg (stored at 32 °C) were fortified with RP on day 28 and stored for another 28 days, average decreases of retinol concentration of 2.57 ± 0.06 and 2.87 ± 0.49% per day were determined. Thus, the daily decrease of retinol concentration was accelerated when highly oxidized soybean oil with a POV of >10 mequiv O_2/kg was used for fortification with RP, compared to mildly oxidized soybean oil with a POV of 1.43 ± 0.24 mequiv O_2/kg ($p < 0.05$). No statistically significant difference was reached with regard to the overall decrease of retinol concentration on day 56 between the highly oxidized oil fortified with RP on day 28 of the study compared to the mildly oxidized oil, which was fortified already on day 1 of the study ($p > 0.05$). However, the rate of RP degradation was approximately 2-fold higher ($p < 0.05$) in the highly oxidized oil compared to the mildly oxidized oil.

DISCUSSION

Consumption of vegetable oils fortified with RP is considered to prevent and combat vitamin A deficiency in populations at risk. Soybean oil is one of the most abundant vegetable oils used in vitamin A fortification programs. Storage conditions of edible oils affect not only the oxidative deterioration of the oil but also the stability of vitamin A. However, the effect of the oxidative status of soybean oil used for fortification with RP and the effect of domestic handling and storage conditions of the oil on the stability of RP are not yet clear. Besides the stability of vitamin A, other vitamins such as vitamin E might be affected by the oxidative status of the oil.

The current study demonstrated a remarkable loss of RP during storage under household-simulated conditions, yielding a maximal decrease of retinol concentration in soybean oil after 56 days of storage at 22 and 32 °C and a daily 12 h exposure to cold fluorescent light of 84.8 ± 5.76 and 81.6 ± 11.1%, respectively. After 28 days of storage, the decrease of retinol concentration was significantly enhanced from 45.2 ± 7.44% at a storage temperature of 22 °C to 68.2 ± 14.7% when the oil was stored at 32 °C. An even higher loss of vitamin A was obtained by Puysuwan et al.,[10] who detected a vitamin A loss of 88.61 ± 1.97% in fortified soybean oil that was stored with intermittent openings for sampling in closed PET bottles at room temperature in Thailand in the presence of sunlight on a kitchen shelf for 4 weeks. Comparable results were also obtained by Viana et al.,[18] showing high degradation of vitamin A to 21 and 9% of initial values in soybean oil stored at 25 and 40 °C, respectively, and exposed to light (2400 lm/m^2) for 4 weeks. Although the experimental conditions were quite similar to our approach, Puysuwan et al.[10] did not investigate the vitamin A decrease in fortified soybean oil under controlled light exposure. In the current study, the low stability of vitamin A in soybean oil exposed to light at room temperature might also be associated with a low content of antioxidant vitamins, such as tocopherols. The concentration of tocopherols in vegetable oils depends on the processing steps applied.[19] It could be shown that refined soybean oil contained 1438 μg/mL tocopherols, corresponding to a loss of 7.43% of tocopherols compared to the crude soybean oil.[19] The refined soybean oil in the current study contained only 50.7 mg/100 g (465 ± 5.25 μg/mL) tocopherols, consisting of 14.0 ± 0.14 mg/100 g α-tocopherol, 0.67 ± 0.04 mg/100 g β-tocopherol, 24.8 ± 0.33 mg/100 g γ-tocopherol, and 11.2 ± 0.15 mg/100 g δ-tocopherol. The comparatively low total tocopherol concentration might be one reason for the instability of RP in soybean oil stored for 56 days in this study. The reference values reported by the European Food Safety Agency (EFSA) are 7.5, 1.5, 79.7, and 26.6 mg/100 g for α-, β-, γ-, and δ-tocopherol, respectively.[20] Another reason for the instability of vitamin A might be the exposure of the oil to cold fluorescent light and/or the storage-induced progress of lipid oxidation. Photooxidative deterioration of vegetable oils was demonstrated to be induced by natural pigments in vegetable oils.[21] In the current study, storage of the oil, which was exposed to cold fluorescent light, for 14 days did not change the RP concentration independent of the conditions applied, likely due to sufficient availability of not yet degraded tocopherols or the less pronounced progress of lipid oxidation at the beginning of the study. The content of total tocopherols significantly decreased to almost 50% of its initial value after storage of the soybean oil for 56 days. These results are in agreements with findings reported by Player et al.,[22] demonstrating a remarkable loss of individual tocopherols when the soybean oil was stored in a forced-air oven at 50 °C for 24 days: whereas α-tocopherol was completely degraded after 16 days of storage in the oven, γ- and δ-tocopherols decreased by 28 and 17% after 24 days of storage at 50 °C. In the current study, α-tocopherol was rapidly degraded to 64.1 ± 10.5% of its initial value in soybean oil after the first 28 days of storage under domestic conditions at 22 °C, whereas γ-tocopherol was degraded to 88.9 ± 5.65% of its initial concentration ($p < 0.05$). The slight increase of δ-tocopherol in soybean oil after 28 days of storage might indicate antioxidant activity of δ-tocopherol on day 1 because its original concentration might be regenerated between days 1 and 28. δ-Tocopherol might be regenerated by phytosterols in soybean oil, such as brassicasterin. The certificate of analysis of the study oil confirmed the presence of brassicasterins (<0.3%) in the soybean oil. Kadoma et al.[23] also concluded that regeneration by flavonoids of δ-tocopherol was favored over other tocopherol isomers due to the lower steric effect of δ-tocopherol. Because it was reported that the stability of tocopherols is associated with its hydrogen-donating ability,[24] we hypothesize that the different decrease of tocopherol isomers during the storage days 28−56 and the first 28 days and the difference of the decrease between the isomers in the current study might be explained by the varying hydrogen-donating ability throughout the storage of soybean oil for 56 days.

Besides the low initial content of vitamin E and its low stability, which was shown to be associated with an increasing POV in soybean oil, the oxidative deterioration of the oil during storage might have contributed to the low stability of vitamin A as well. The current study demonstrated a progressive increase of lipid oxidation markers in soybean oil stored under household conditions applied. The POV increased from 1.20 ± 0.004 to 24.3 ± 0.02 mequiv O_2/kg, corresponding to a mean 20-fold increase, in RP-fortified soybean oil stored at 22 °C for 56 days. Recently, it was reported that household storage of non-RP-fortified soybean oil led to a comparable mean 15% rise of the POV.[25]

In the current study, hexanal, which represents a marker for late-stage lipid oxidation in linoleic acid-rich oils, was significantly enhanced from 0.91 ± 0.29 μg/mL on day 1 to 2.13 ± 0.21 and 3.35 ± 0.69 μg/mL in soybean oil after storage for 28 days at 22 and 32 °C, respectively. Despite the low RP stability in fortified soybean oil in the current study, RP could be shown to ameliorate the oxidative status of fortified soybean oil as evidenced by the hexanal formation, which is

approximately 16% lower in fortified soybean oil. Others proved that the beneficial effect of retinol on the oxidative status of vegetable oils is a result of the chain-breaking effect of retinol by forming carbon-centered radical adducts or by inducing one-electron reduction of peroxyl radicals.[26,27] Although the POV is regarded as a sensitive marker for assessing lipid oxidation, no lipid oxidation lowering effect of RP was detected by monitoring the POV in fortified soybean oil. RP might have a higher scavenging activity for radicals derived from decomposition of lipid hydroperoxides compared to lipid radicals formed during initiation of lipid oxidation. By scavenging the alkoxy radical derived from the decomposition of linoleic acid hydroperoxide, the formation of hexanal might be reduced by RP. Alkoxy radicals have been suggested to be 4 orders of magnitude more reactive toward lipids than peroxyl radicals, which might also be valid for the reaction between RP and alkoxy radicals.[27]

Due to the potential radical scavenging effect of RP, the remarkable loss of vitamin A is likely to be associated with the progress of lipid oxidation. The current study revealed a significant correlation between retinol stability and lipid oxidation markers. Laillou et al.[7] also identified a negative association between vitamin A concentration and the POV, as evidenced by a slope of −1.23 ($p < 0.001$). Ahmed et al.[28] showed a comparable relationship between carotenoids and POV in 100 mL soybean oil exposed to fluorescent light for 5 weeks. The POV in soybean oil increased from 3.89 to 20.8 mequiv O_2/kg, while the content of carotenoids decreased from approximately 19 to 5 μg/g, after 5 weeks of storage in the presence of fluorescent light. The present study confirmed the negative correlation between retinol concentration and the POV in soybean oil, as indicated by the correlation coefficient of $r = -0.930$ ($p < 0.001$). Thus, the vitamin A loss in soybean oil during household storage and consumer handling depends on the progress of lipid oxidation. To further prove this hypothesis for the vitamin A loss in soybean oil during storage conditions applied, the average daily decrease of retinol concentration was calculated for soybean oil with a low (POV < 2 mequiv O_2/kg) and a high (POV > 10 mequiv O_2/kg) oxidative status at RP fortification. It could be demonstrated that the RP concentration in soybean oil depends not only on the storage duration under domestic conditions and handling but also on the oxidative quality of the oil at the time of fortification with RP. Whereas fortification of the mildly oxidized soybean oil, characterized by a POV of 1.43 ± 0.24 mequiv O_2/kg at day 1, led to average decreases of retinol concentration of 1.52 ± 0.10 and 1.46 ± 0.19% per day at 22 and 32 °C, respectively, fortification of oxidized oil, characterized by a POV of 12.1 ± 0.23 or 17.3 ± 0.18 mequiv O_2/kg, induced more pronounced decreases of retinol concentrations of 2.57 ± 0.06 and 2.87 ± 0.49% per day at 22 and 32 °C, respectively. Thus, the decay of RP was approximately twice as high when oxidized soybean oil was used for fortification. Comparable results were obtained by Laillou et al.,[7] who demonstrated a higher loss of vitamin A of 23.1% in an oxidized (POV = 5.8 mequiv O_2/kg) oil mixture of soybean oil and sunflower oil (1:1), which was exposed to uncontrolled light during domestic storing on a shelf at 30 ± 5 °C for 4 weeks compared to a mildly oxidized oil mixture (POV = 0.4 mequiv O_2/kg) with a loss of vitamin A of only 7.3%. There, the degradation of vitamin A was about 3 times higher in the highly oxidized than in the mildly oxidized oil mixture. The relative loss of vitamin A in highly oxidized compared to mildly oxidized oil was slightly higher than in the present study, which might be attributed to different tocopherol concentrations. Laillou et al.[7] showed a 3 times higher loss of vitamin A, whereas in the present study, the loss of vitamin A was only twice as high in highly oxidized oil compared to mildly oxidized oil. The more pronounced loss of vitamin A in highly oxidized oil might also be due to different sample volumes withdrawn throughout storage compared to the current study. Whereas Laillou et al.[7] withdrew a total volume of 900 mL of oil from 1 L PET bottles, only 334 mL of oil was withdrawn from 0.5 L PET bottles in this study, the latter leading to a less pronounced increase of the headspace in the current study.

In conclusion, household-representative storage and handling of soybean oil fortified with RP at 22 or 32 °C in the presence of cold fluorescence light led to a pronounced decrease of RP. The remarkable loss of RP in fortified soybean oil was accompanied by a significant loss of vitamin E and an enhanced oxidative deterioration of the oil. It could be shown that the RP stability was influenced not only by storage duration but also by the oxidative status of soybean oil at the time of RP fortification. Fortifying highly oxidized soybean oil with RP enhanced RP loss by almost doubling the average decrease of retinol concentrations per day compared to fortified mildly oxidized soybean oil. Fortification programs should carefully consider the oxidative quality of the edible oil to be fortified and the use of a light-protecting container to ensure maximum stability and delivery of vitamins A and E throughout the intervention.

AUTHOR INFORMATION

Corresponding Author

*(V.S.) Mail: Althanstraße 14, 1090 Vienna, Austria. Phone: +43 1 4227 70601. Fax: +43 1 4227 9706. E-mail: veronika.somoza@univie.ac.at.

Funding

This study was financially supported by Sight and Life, a humanitarian nutrition think tank of DSM.

Notes

The authors declare the following competing financial interest(s): This study was financially supported by Sight and Life, a humanitarian nutrition think tank of DSM. Dr. Klaus Kraemer, one of the authors, is heading Sight and Life. The author Georg Steiger is an employee of DSM.

ABBREVIATIONS USED

PET, polyethylene terephthalate; POV, peroxide value; RP, retinyl palmitate

REFERENCES

(1) World Health Organization. Global prevalence of vitamin A deficiency in populations at risk 1995−2005. *WHO Global Database on Vitamin A Deficiency*, 2009.

(2) Allen, L.; de Benoist, B.; Dary, O.; Hurrell, R. *Guidelines on Food Fortification with Micronutrients*; WHO and FAO: Geneva, Switzerland, 2006.

(3) Bagriansky, J.; Ranum, P. Vitamin A fortification of P.L. 480 vegetable oil. *SUSTAIN*; Washington, DC, USA, 1998; www.sustaintech.org.

(4) Dary, O.; Mora, J. O. Food fortification to reduce vitamin A deficiency: international vitamin A consultative group recommendations. *J. Nutr.* **2002**, *132*, 2927s−2933s.

(5) Gogia, S.; Sachdev, H. S. Vitamin A supplementation for the prevention of morbidity and mortality in infants six months of age or less. *Cochrane Database Syst. Rev.* **2011**, No. CD007480.
(6) Gopal, S.; Ketyum, F. Vitamin A and D in ghee and vanaspati. *J. Sci. Ind. Res.* **1956**, *15c*, 48−51.
(7) Laillou, A.; Hafez, S. A.; Mahmoud, A. H.; Mansour, M.; Rohner, F.; Fortin, S.; Berger, J.; Ibrahim, N. A.; Moench-Pfanner, R. Vegetable oil of poor quality is limiting the success of fortification with vitamin A in Egypt. *Food Nutr. Bull.* **2012**, *33*, 186−193.
(8) Favaro, R. M. D.; Ferreira, J. F.; Desai, I. D.; Dutra de Oliveira, J. E. Studies on fortification of refined soybean oil with all-trans-retinyl palmitate in Brazil: stability during cooking and storage. *J. Food Compos. Anal.* **1991**, *4*, 237−244.
(9) Atwood, S. J.; Sanghvi, T. G.; Sharma, V.; Carolan, N. Stability of vitamin A in fortified vegetable oil and corn soy blend used in child feeding programs in India. *J. Food Compos. Anal.* **1995**, *8*, 32−44.
(10) Puysuwan, L.; Chavasit, V.; Sungpuag, P.; Hediger, D.; Punvichai, T. Feasibility and use of vitamin A-fortified vegetable oils among consumers of different socioeconomic status in Thailand. *Food Nutr. Bull.* **2007**, *28*, 181−188.
(11) Ihara, H.; Hashizume, N.; Hirase, N.; Suzue, R. Esterification makes retinol more labile to photolysis. *J. Nutr. Sci. Vitaminol.* **1999**, *45*, 353−358.
(12) Otachi, E. O.; Korner, W.; Avenant-Oldewage, A.; Fellner-Frank, C.; Jirsa, F. Trace elements in sediments, blue spotted tilapia *Oreochromis leucostictus* (Trewavas, 1933) and its parasite *Contracaecum multipapillatum* from Lake Naivasha, Kenya, including a comprehensive health risk analysis. *Environ. Sci. Pollut. Res. Int.* **2014**, *21*, 7339−7349.
(13) Bognar, A. Bestimmung von Vitamin A in Lebensmitteln mittels Hochleistungs-Flüssigchromatographie (HPLC). *Z. Lebensm. Unters. Forsch.* **1986**, *182*, 492−497.
(14) Firestone, D. Method Cd 8-53. In *Official Methods and Recommended Practices of the American Oil Chemists' Society*; Firestone, D., Ed.; American Oil Chemists' Society: Champaign, IL, USA, 1997.
(15) Giuffrida, F.; Golay, P. A.; Destaillats, F.; Hug, B.; Dionisi, F. Accurate determination of hexanal in beef bouillons by headspace solid-phase microextraction gas-chromatography mass-spectrometry. *Eur. J. Lipid Sci. Technol.* **2005**, *107*, 792−798.
(16) Panseri, S.; Soncin, S.; Chiesa, L. M.; Biondi, P. A. A headspace solid-phase microextraction gas-chromatographic mass-spectrometric method (HS-SPME-GC/MS) to quantify hexanal in butter during storage as marker of lipid oxidation. *Food Chem.* **2011**, *127*, 886−889.
(17) Gliszczynska-Swiglo, A.; Sikorska, E. Simple reversed-phase liquid chromatography method for determination of tocopherols in edible plant oils. *J. Chromatogr. A* **2004**, *1048*, 195−198.
(18) Viana, M.; Boy, E.; Boutilieir, Z.; Furr, H. C.; Craft, N. E. Stability of vitamin A in Bolivian fortified cooking oil. *FASEB J.* **2007**, *21* (Suppl. A682), 674−679.
(19) Jung, M. Y.; Yoon, S. H.; Min, D. B. Effects of processing steps on the contents of minor compounds and oxidation of soybean oil. *J. Am. Oil Chem. Soc.* **1989**, *66*, 118−120.
(20) Scientific Opinion of the Panel on Food Additives, Flavourings, Processing Aids and Materials in Contact with Food on a request from the Commission on mixed tocopherols, tocotrienol tocopherol and tocotrienols as sources for vitamin E. *EFSA J.* **2008**, *640*, 1−34.
(21) Khan, M. A.; Shahidi, F. Rapid oxidation of commercial extra virgin olive oil stored under fluorescent light. *J. Food Lipids* **1999**, *6*, 331−339.
(22) Player, M. E.; Kim, H. J.; Lee, H. O.; Min, D. B. Stability of α-, γ-, or δ-tocopherol during soybean oil oxidation. *J. Food Sci.* **2006**, *71*, C456−C460.
(23) Kadoma, Y.; Ishihara, M.; Okada, N.; Fujisawa, S. Free radical interaction between vitamin E (α-, β-, γ- and δ-tocopherol), ascorbate and flavonoids. *In Vivo* **2006**, *20*, 823−827.
(24) Jung, M. Y.; Min, D. B. Effects of α-, γ- and δ-tocopherols on oxidative stability of soybean oil. *J. Food Sci.* **1990**, *55*, 1464−1465.
(25) Pignitter, M.; Stolze, K.; Gartner, S.; Dumhart, B.; Stoll, C.; Steiger, G.; Kraemer, K.; Somoza, V. Cold fluorescent light as major inducer of lipid oxidation in soybean oil stored at household conditions for eight weeks. *J. Agric. Food Chem.* **2014**, *62*, 2297−2305.
(26) Livrea, M.; Tesoriere, L.; Freisleben, H. J. Vitamin A as an antioxidant. In *Handbook of Antioxidants*; Livrea, M., Tesoriere, L., Freisleben, H. J., Eds.; Dekker: New York, 1996; pp 371−405.
(27) Rozanowska, M.; Cantrell, A.; Edge, R.; Land, E. J.; Sarna, T.; Truscott, T. G. Pulse radiolysis study of the interaction of retinoids with peroxyl radicals. *Free Radical Biol. Med.* **2005**, *39*, 1399−1405.
(28) Ahmed, T.; Atta, S.; Sohail, M.; Khan, A. R.; Akhtar, S. Effect of fluorescent light on quality and stability of edible fats and oils. *J. Chem. Soc. Pak.* **2011**, *33*, 233−237.

incompatible for strong electrostatic interaction. In this work, we attempt to investigate and understand in detail the structural changes and thermal stability of β-LG as a result of interacting with SBP using circular dichroism (CD), Fourier transform infrared (FTIR), and steady-state and time-resolved fluorescence spectroscopic techniques.

2. MATERIALS AND METHODS

2.1. Materials. Purified β-lactoglobulin (β-LG) powder (Lot no. JE001-0-415) was kindly donated by Davisco Foods International (Le Sueur, MN, USA). The reported composition (expressed as dry weight percent unless otherwise indicated) of the powder was as follows: >95% protein (of which 90% was β-lactoglobulin); <3.5% ash; <1.0% fat; < 1.0% lactose; <6.5% moisture (wet weight). HPLC analysis using previously published methods[29] revealed that the sample contains a total of 93.1% β-LG, distributed nearly evenly between genetic variants A and B, 51.2% and 48.8%, respectively.

Sugar beet pectin (Lot no. 30091) was donated by CP Kelco (San Diego, CA, USA). The composition of the pectin was supplied as the following: galacturonic acid (GalA), 58.5 ± 5.4%; degree of methyl esterification (DME), 57.4 ± 1.0%; degree of acetyl esterification (DAE), 21.7 ± 0.1%; neutral sugar, 37.3 ± 1.1% using previously published methods.[30,31] Ferulic acid (*trans*-4-hydroxy-3-meth- oxy-cinnamic acid) content in the pectin was determined to be 4.3 ppm by measuring the UV absorbance (Varian spectrophotometer Bio100 UV−visible, Agilent, Santa Clara, CA, USA). A molar extinction coefficient of 18.6 $mM^{-1}\cdot cm^{-1}$ at 322 nm (in ethanol) was used for ferulic acid (Sigma-Aldrich, St. Louis, MO, USA) to obtain the estimation.

Diluted hydrochloric acid solutions were prepared from a 12.1 N hydrochloric acid solution (Fisher Scientific, Fairlawn, NJ, USA). All other chemicals including ferulic acid (trans isomer), sodium hydroxide (NaOH), and sodium phosphate (monobasic and dibasic) were purchased from Sigma-Aldrich, reagent grade and used directly. All solutions were made with Millipore water (double-distilled/deionized) and filtered with a 0.45 μm syringe filter (Millex-HV, PVDF, Millipore Corp., Billerica, MA, USA).

2.2. Amino Acid and Protein Composition Analysis of SBP. SBP used in this work was subjected to amino acid composition analysis. Powdered sample (∼100 mg) was hydrolyzed in 6 N HCl containing a small amount of phenol. The hydrolysis flasks were extensively purged of oxygen using a PicoTag workstation (Waters Corp., Milford, MA, USA) and then incubated at 110 °C for 20 h. Hydrolyzed samples were filtered, dried under vacuum, and derivatized with AccQFluor reagent (Waters) following the manufacturer's directions. Chromatography was performed using procedures described as "system 1" in Cohen and De Antonis,[32] with α-aminobutyric acid as an internal standard. Separation was achieved using an AccQTag C18 reverse-phase column (Waters), and a fluorescence detector was used with 250 nm as the excitation and 395 nm as the emission wavelengths. Hydrolysis, derivitization, and analysis of each sample were performed in triplicate. The total protein content of the SBP was determined to be 4.78 ± 0.08%.

2.3. Preparation of Stock Solution. Dried β-LG and SBP samples were dissolved at 10.0 and 4.0 mg/mL respectively, in a 33 mM sodium phosphate buffer, pH 6.75. β-LG was easily soluble at the specified concentration. Dissolving SBP, on the other hand, required an overnight stirring followed by centrifugation at 27000*g* and 20 °C in a Sorval RC-5B centrifuge (DuPont Co., Wilmington, DE, USA) for 20 min. Only the SBP supernatant was removed and used in subsequent experiments. All β-LG and SBP solutions were filtered through a 0.45 μm syringe-driven filter (Millex HV, PVDF, Millipore). Appropriate dilution using the same phosphate buffered saline (PBS) buffer was made to obtain either individual β-LG or SBP or the mixture at specified concentrations as described in subsequent text.

Preheating treatment involved holding each solution of β-LG and SBP at the concentrations of 10.0 and 4.0 mg/mL respectively, at 80 °C for 10 min in a water bath. Heated solution was then allowed to cool to room temperature prior to subsequent analysis or mixing. The mixture of β-LG and SBP was prepared by either mixing the two untreated or preheated solutions, denoted as β-LG-h and SBP-h respectively, to obtain the final mixture containing 0.3 mg/mL of β-LG and 0.1 mg/mL of SBP for the CD and fluorescence experiments unless otherwise noted. All solutions were made fresh prior to each use.

2.4. Circular Dichroism Spectroscopy. CD spectroscopy was performed at 20 °C with an Aviv Model 420 CD spectrometer (Aviv Biomedical, Inc., Lakewood, NJ, USA). Spectra in the far-UV region (190−260 nm) were measured at the concentration of 0.3 mg/mL for β-LG and/or 0.1 mg/mL for SBP in a 0.05 cm path length quartz cell. The CD spectra in the near-UV region (250−320 nm) were acquired using β-LG concentration at 1.0 mg/mL and/or SBP at 0.33 mg/mL in a path length of 1 cm rectangular cuvette. All spectra were recorded with 0.5 nm step and 5 s average time. Spectra were corrected for buffer (33 mM sodium phosphate, pH 6.75) contribution and for SBP signal when present. The mean residue ellipticity, $[\theta]$ (degree cm^2 $dmol^{-1}$), was calculated from the formula $[\theta] = (M_w\theta)/(10Cln)$, where θ is the measured ellipticity (millidegrees), M_w is the molecular weight (M_w = 18320 Da, an average for a mixture of β-LG A and B variants), l is the path length of the cuvette (cm), C is the protein concentration (mg/mL), and n is the number of amino acid residues in β-LG (n = 162).

Analysis of the secondary structure of β-LG (untreated and heated) in the presence and absence of SBP (untreated and heated) in phosphate buffer (33 mM, pH 6.75) from the far-UV CD spectra was carried out using the software CDNN (v.2.1, Applied Photophysics, Ltd., Leatherhead, United Kingdom) developed by Dr. Gerald Böhm.[33] A database consisting of 33 reference proteins was used in the deconvolution analysis. The standard deviation (SD) was ±0.4% based on a set of triplicate CD experiments and followed by CDNN analysis.

Temperature dependence of far-UV CD (190−260 nm) spectra was carried out on solutions containing 0.3 mg/mL β-LG or/and 0.1 mg/mL SBP in the buffer containing 33 mM PBS (pH 6.75) in a 0.05 cm path length quartz cell. Temperature was adjusted using a solid-state Pelletier element, and a minimum of 30 min equilibration time was used between each temperature point. Each spectrum at each temperature was corrected for buffer and SBP (when present) contributions before being subjected to deconvolution using CDNN program.

2.5. FTIR Spectroscopic Measurements and Analysis. Infrared spectra were collected with a FTIR spectrometer (Nexus 670, Thermo Electron, Madison, WI, USA) equipped with a DTGS KBr detector and a KBr beam splitter. PBS buffer at reduced concentration, 20 mM, was used due to its IR contribution at the higher concentration (33 mM) used in all other experiments. β-LG and SBP samples were dissolved at 15 and 5 mg/mL respectively, and followed by subsequent mixing or/and preheating and then mixing. Aliquots of 200 μL each of the solutions investigated in this work were placed on a CaF_2 plate, allowed to air-dry overnight, and then vacuum-dried for 30 min prior to measurement. The thin film was scanned from 4000 to 1000 cm^{-1} at 20 °C with a nominal resolution of 2 cm^{-1} and 128 accumulative scans.

Analysis of the secondary structure of β-LG (untreated and heated) in the presence and absence of SBP (untreated and heated) from the FTIR spectra was carried out as previously reported.[34] The baselines were corrected automatically using the built-in software of the spectrophotometer (OMNIC v.7.3). By means of the second derivative in the amide I region, 1600−1700 cm^{-1}, eight and nine major peaks for β-LG in the absence and presence of SBP and β-LG-h in the absence and presence of SBP-h were resolved, respectively, and fitted using Peak Resolve (OMNIC v.7.3). A Gaussian function was used during the fitting routine for all peaks corresponding to α-helix (∼1660 cm^{-1}), unordered (∼1550 cm^{-1}), β-sheet (1610−1620 cm^{-1}), β-turn (1670−1690 cm^{-1}), and β-antiparallel sheet (∼1690 and 1630−1640 cm^{-1}) according to the assignments by Barth,[35] Dong et al.,[36] and Hasni et al.[37] A separate Fourier self-deconvolution procedure (OMNIC v.7.3)[38] was also used to independently confirm the positions of overlapping peaks (±2 cm^{-1}). The areas of all of the

component bands assigned to a given secondary structural element were then summed and divided by the total integrated area to yield the percentage of the element. The standard deviation of this analysis procedure was ±2%.

2.6. Fluorescence Spectroscopy. Fluorometric experiments were carried out on a FluoroLog-3 spectrometer (Horiba Scientific, Edison, NJ, USA) capable of both steady-state and time-correlated single-photon counting (TCSPC) lifetime measurements. Solutions containing either β-LG (0.3 mg/mL) or SBP (0.1 mg/mL), or a mixture, were prepared in 33 mM sodium phosphate buffer, pH 6.75, as described in section 2.3. The fluorescence spectra of β-LG in the absence and presence of SBP were recorded at 20 °C using λ_{ex} = 282 and 295 nm, and λ_{em} scanned from 320 to 450 nm. The fluorescence emission spectra (λ_{em}) of all solutions containing SBP were also recorded from 380 to 600 nm using excitation λ_{ex}= 330 nm. The bandwidths used for the excitation and the emission were 5 nm. The quartz cuvettes had 1 cm optical path lengths.

Temperature dependence analysis of Trp intrinsic and feruloyl fluorescence was carried out on solutions containing 0.3 mg/mL β-LG and 0.1 mg/mL SBP in the same buffer containing 33 mM PBS, pH 6.75, using λ_{ex} = 295 nm, λ_{em} = 330 and λ_{ex} = 330 nm, λ_{em} = 440 nm for the β-LG and SBP solutions, respectively. Ferulic acid solution (at 0.002 mg/mL) in the same buffer was also recorded as a comparison. Temperature was adjusted using a solid-state Pelletier element, and a minimum of 20 min equilibration time was used between each temperature point.

For the fluorescence lifetime measurements, the concentration of β-LG and SBP was adjusted to 3.0 and 1.0 mg/mL respectively, in 33 mM sodium phosphate buffer (I = 50 mM), pH 6.75. The excitation was performed using 296 nm or/and 331 nm NanoLEDs, and the corresponding emission was set at 340 and 440 nm, respectively. A Ludox solution was used as a scatter. Each fluorescence lifetime decay was analyzed with one, two, three, and four lifetime components, and then values of χ^2 were compared in order to determine the best fit using the software FluorEssence (v.2.5.2, Horiba Scientific). A minimal value of χ^2 indicates the best fit. A χ^2 value that approaches 1 indicates a good fit.

3. RESULTS AND DISCUSSION

3.1. Composition of the Sugar Beet Pectin. Figure 1 shows the UV−vis absorption spectrum of SBP in a 33 mM PBS buffer, pH 6.75, in comparison with that of ferulic acid (FA). It has a broad absorption band with a maximum at ∼325 nm and a shoulder of less intensity at ∼290 nm, which is consistent with the spectrum previously reported for other beet pectin.[39] In comparison, pure FA exhibited two distinctive sharp peaks at 312 and 287 nm with nearly equal intensity (see Figure 1). This difference in the overall absorption behavior of ferulic acid between its free form and its existence in SBP along with the obvious red shift, from 312 to 325 nm, of the main absorption peak provided further evidence for its covalent bonding nature with SBP, as demonstrated previously by other methods such as mass spectrometry.[40] In addition, we recently reported[28] the coexistence of a small amount of noncovalently bound ferulic acid in SBP, which clearly contributes to its absorbance behavior.

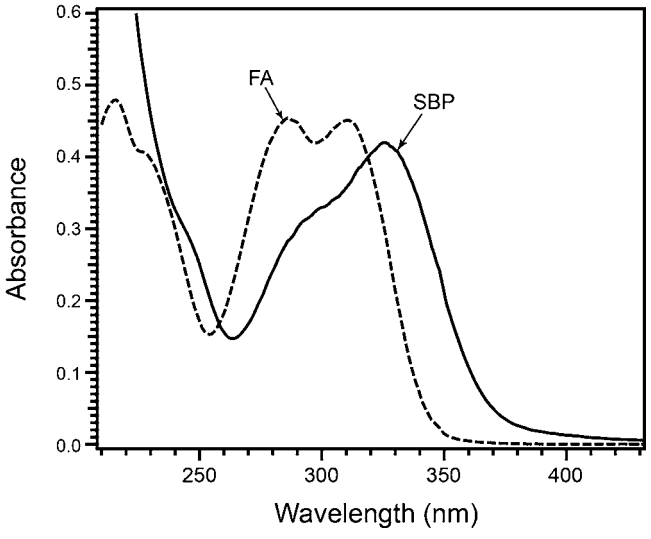

Figure 1. UV−vis absorption spectra of SBP and ferulic acid (FA) in 33 mM phosphate buffer at pH 6.75 and 20 °C. The concentration was 0.5 mg/mL for SBP and 0.005 mg/mL for FA.

Similar to previously published results for other sugar beet pectin,[39] no detectable Trp was found in the SBP used in this work as Trp may interfere with fluorescence measurements. However, it is possible that a trace amount of Trp may exist and was destroyed during the acid hydrolysis of the amino acid analysis procedure. As discussed below in detail, no Trp fluorescence contribution from SBP was evident in this work. Considerable amounts (number of amino acids) of Phe and Tyr residues were measured in the total protein moieties (4.78%) in SBP. These aromatic residues evidently contributed significantly to the broadening of the absorption peak of the SBP, in the area of ∼280 nm.

The high level of methyl esterification (57%) of the sugar beet pectin (SBP) used in this work makes it an effective binding partner for β-LG according to Sperber et al.[41] due to its low block charge density (at low ionic strength). Although both β-LG and SBP remain negatively charged at pH 6.75, the patches of positive charges localized on the surface of β-LG can attract the negative charges of SBP. The attraction force can be stronger than the incompatible forces between the two components repelled.[42] The formation of complexes between β-LG and SBP of varying sizes has been demonstrated using HPSEC.[28] At I = 50 mM, the binding process is expected to be mainly driven by entropy released upon local counterion binding,[43] which results in lowered free energy. Favorable enthalpy contribution was also an important factor as well.[44] In addition other weaker forms of interactions including localized hydrophobic interaction and hydrogen binding between the side chains of β-LG and SBP also play a role in stabilizing the interacting complexes as discussed below.

3.2. Secondary Structural Changes of β-LG upon Interacting with SBP. *Far-UV CD Spectroscopy.* Figure 2 shows far-UV CD spectra of β-LG, native and heat-treated in the absence and presence of SBP at pH 6.75 and 20 °C. It should be noted that SBP, untreated and heat-treated, exhibits negligible circular dichroism activity in the same region. When it was present, the CD spectrum of SBP was subtracted from that of the mixture. Consistent with both X-ray crystallography[11] and NMR[13] studies, the CD spectrum of native β-LG shows predominantly a β-sheet protein at neutral pH exhibiting a wide minimum around 215 nm. Furthermore, a deconvolution procedure was carried out using the software CDNN[45] and a database consisting of 33 reference proteins. The results are given in Table 1. Comparable to the analyses in the literature,[36,46] native β-LG contains predominately over 50% β-sheet with the majority in antiparallel form (∼45%). The relative amounts of other structural elements including α-helix, parallel β-sheet, turn, and unstructured are also in close agreement with the analyses by X-ray crystallography[11] and other spectroscopic techniques.[36,46]

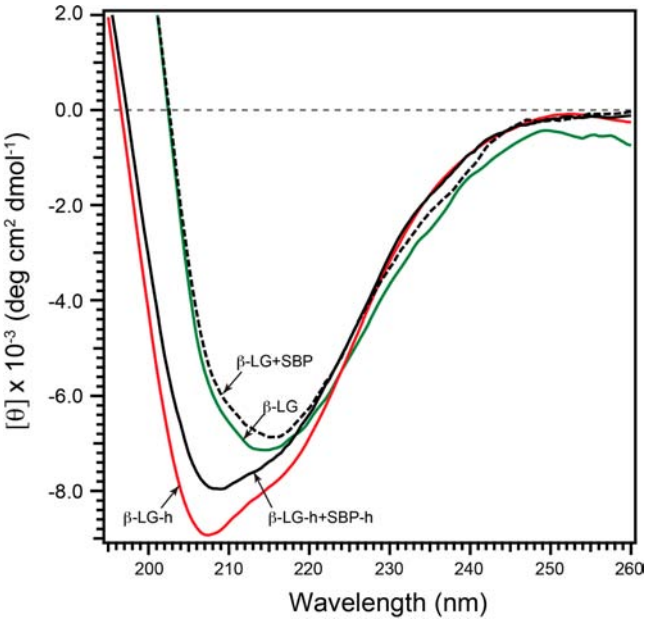

Figure 2. Far-UV CD spectra of β-LG, β-LG + SBP, β-LG-h, and β-LG-h + SBP-h in 33 mM phosphate buffer at pH 6.75 and 20 °C. The concentrations were 0.3 and 0.1 mg/mL for β-LG and SBP, respectively, using a 0.05 cm path length cell. All spectra were corrected against buffer and SBP (when present).

Table 1. Secondary Structure Analysis (%)[a] from Far-UV CD Spectra of Untreated and Heated β-LG in the Absence and Presence of SBP at pH 6.75 (33 mM Sodium Phosphate Buffer)

	antiparallel β-sheet	turn	α-helix	unordered	β-sheet
β-LG	43.3	16.1	10.5	25.6	4.5
β-LG +SBP	33.1	17.6	11.2	32.3	5.8
β-LG-h	29.4	20.5	10.9	34.3	5.1
β-LG-h +SBP-h	30.5	19.9	10.6	33.9	5.1

[a]Analyzed by deconvolution using the CDNN program and a database consisting of 33 proteins.[45]

When combined with SBP, the CD spectrum of β-LG underwent a rather unremarkable change as evidenced by a small decrease in the magnitude of its mean molar ellipticity $[\theta]$ (Figure 2). Quantitative analysis by CDNN deconvolution (see Table 1), however, revealed significant changes in the secondary structure of β-LG caused by interacting with SBP, noticeably ~10% loss in antiparallel β-sheet accompanied by increase (~7%) in unordered structure. Slight increases in other elements including α-helix, parallel β-sheet, and turn accounted for the remaining 4% secondary structural change from native β-LG. This secondary structural change appeared to be greater than our recent report by HPSEC studies[28] in which 6% of native β-LG was found to bind to SBP. This apparent higher level of structural re-distribution can be attributed to the fact that the mixture of β-LG and SBP (in the CD experiments) allowed more direct and efficient interaction than the complexes detected by HPSEC in which case only those surviving the columns and detectors were analyzed.

Preheat treatment (at 80 °C and pH 6.75 for 10 min) of β-LG significantly affected all secondary structural elements compared to native β-LG, particularly, a ~14% reduction in antiparallel β-sheet, as shown in Figure 2 and Table 1. This loss resulted in the apparent 10% increase in unstructured and 4% in turn forms, respectively. Interestingly, this relatively mild treatment did not cause much change in the amounts of α-helix and parallel β-sheet. The addition of preheated SBP apparently caused a small degree of the secondary structural elements to recover in β-LG, noticeably the amount of antiparallel β-sheet, by ~1.0% (±0.4%), compared to the preheated β-LG alone (β-LG-h). The amounts of unstructured and turn were only reduced slightly to account for this slight but noticeable recovery. On the other hand, our HPSEC studies[28] identifying ~16% of preheated β-LG was involved in the complex with preheated SBP. Clearly the pre-heat-treatment did indeed facilitate more effective interaction and lead to largely irreversible structural changes in β-LG.

FTIR Spectroscopy. FTIR spectra in the amide I region (1600−1700 cm^{-1}), known for its sensitivity to protein secondary conformational change, were deconvoluted and analyzed following the band assignments by Barth.[35] The results are shown in Figure 3 and Table 2 and compared with the analyses for native β-LG by Dong et al. and Hasni et al.[37] It should be noted that SBP (at 5 mg/mL) contributes less than ~4% in absorbance in this region compared to that of β-LG (at 15 mg/mL), and mainly centered at the bands 1634 and 1618 cm^{-1}. To obtain only changes in the spectrum of β-LG, the spectra of SBP and SBP-h only were subtracted from that of the mixture, respectively. Table 2 shows that the results for native β-LG were in close agreement with previously published analyses and reveals that the addition of SBP indeed caused statistically significant secondary structural shifts in β-LG. Consistent with the analyses by far-UV CD spectroscopy as discussed previously, the amount of antiparallel β-sheet suffered nearly 10% loss. Instead of the marked increase in unordered form as analyzed by the far-UV CD, an increase of 9% (±2%) in turn structure apparently compensated for the majority of this loss. The difference between the unordered (by the far-UV CD analysis) and turn structure (by the FTIR analysis) is perhaps dictated by the difference in these techniques followed by difference in the deconvolution process. Both turn and random structural elements signify structural irregularity and instability. In addition, the amount of α-helix also increased ~4% (±2%) in the presence of SBP by FTIR analysis, which may be due to the spectral overlap with the adjacent unordered structure.

As expected, when β-LG was subjected to heat treatment (β-LG-h), its secondary structure, especially antiparallel β-sheet, suffered a significant loss, ~8%. As a result, the levels of unstable structures, turn and unordered, increased by ~4% (±2%), whereas the amounts of α-helix and parallel β-turn remained virtually unchanged. In contrast, past work by Eissa et al.[47] found a complete loss of intramolecular β-sheet at 1634 and 1621 cm^{-1} when β-LG was heated at 80 °C for 1 h. In this work, the increase in the absorption band at 1620 cm^{-1} is statistically insignificant for β-LG-h and is likely due to the shortened heating time (10 min) employed. The addition of preheated SBP (SBP-h) increased the amount of antiparallel β-sheet, ~4% (±2%), and decreased the same amount of turn structure, suggesting that interacting with SBP-h resulted in a small level of recovery in the secondary structure of β-LG-h. This is consistent with the analyses by far-UV CD spectroscopy as discussed previously.

3.3. Tertiary Structural Change of β-LG upon Binding to SBP. *Near-UV CD Spectroscopy.* The CD spectrum in the near-UV region (see Figure 4) of native β-LG shows

dx.doi.org/10.1021/jf502699g | J. Agric. Food Chem. 2014, 62, 7567−7576

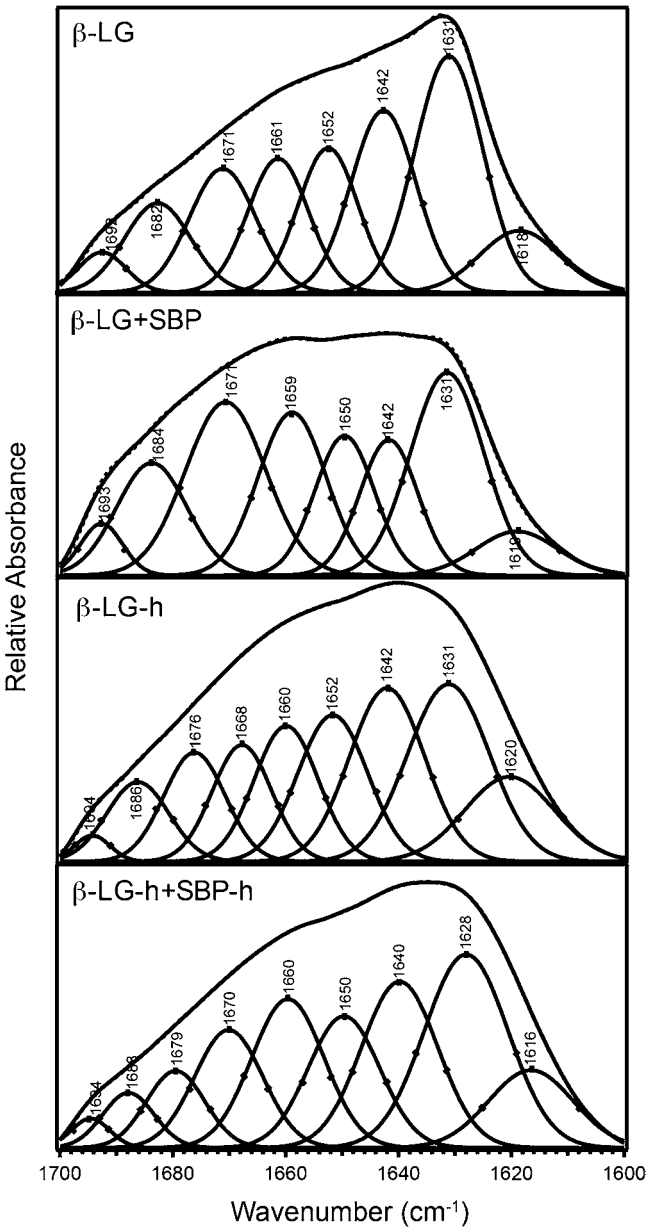

Figure 3. FTIR spectra of *β*-LG, *β*-LG + SBP, *β*-LG-h, and *β*-LG-h + SBP-h and the deconvoluted components in hydrated film made from solution in 20 mM phosphate buffer, pH 6.75. The concentration was 15 and 5 mg/mL for *β*-LG and SBP, respectively. The spectra of SBP and SBP-h were subtracted from those of *β*-LG + SBP and *β*-LG-h + SBP-h, respectively.

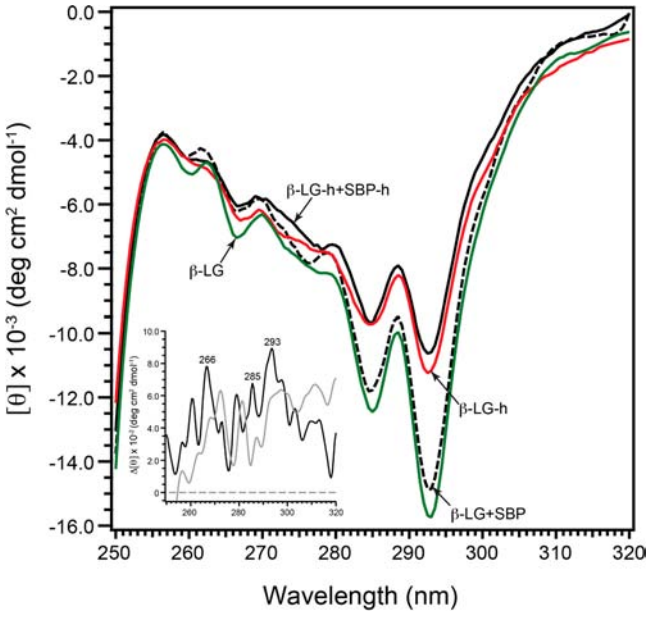

Figure 4. Near-UV spectra of *β*-LG, *β*-LG + SBP, *β*-LG-h, and *β*-LG-h + SBP-h in a 33 mM phosphate buffer at pH 6.75 and 20 °C. The concentrations were 0.9 and 0.3 mg/mL for *β*-LG and SBP, respectively, using a 1 cm path length cell. The insert is the difference spectra between *β*-LG + SBP and *β*-LG (dark line), and between *β*-LG-h + SBP-h and *β*-LG-h (gray line). All spectra were corrected against buffer and SBP (when present).

pronounced negative ellipticity values at 293, 285, and 266 nm. It has been well established[48] that the 293 nm peak belongs to Trp residues, the 285 nm to Tyr plus a small contribution by Trp, and the peaks below 270 nm to Phe. Preheat treatment clearly significantly interrupted the environment and reduced the molar ellipiticity of Trp and Tyr residues, in the form of peak intensity loss at 285 and 293 nm.

When the difference spectrum of *β*-LG in the presence of SBP against native *β*-LG alone was analyzed (the light gray line in the inset of Figure 4), changes in this region broadly reflect the effect of interacting with SBP on the environment of the Trp, Tyr, and Phe residues in *β*-LG. This disruption is particularly prominent for the Phe residues of *β*-LG (four total) upon interacting with SBP as signified by the loss in its intensity at 270 nm and below. When *β*-LG-h was combined with SBP-h, its tertiary structural elements remained roughly unchanged compared to that in the absence of SBP-h except for the slight reversal in 285 nm peak (∼2%) showing as a negative residual peak (the dark line in the inset of Figure 4). This would suggest

Table 2. Secondary structure analysis (%)[a] from the Amide I Region (cm^{-1}) of Untreated and Heated *β*-LG in the Presence and Absence of SBP in Hydrated Film at pH 6.75 (20 mM Sodium Phosphate Buffer)

	1690 and 1630−1640 antiparallel *β*-sheet	1670−1690 turn	∼1660 *α*-helix	∼1650 unordered	1610−1620 *β*-sheet
β-LG[b]		27	10	9	54
β-LG[c]	19	13	12		56
β-LG	45	22	12	13	8
β-LG + SBP	36	31	16	12	5
β-LG-h	37	26	12	15	10
β-LG-h + SBP-h	41	22	15	13	9

[a]The assignments were made based on the publication by Barth.[35] [b]Results were analyzed in H_2O by Dong et al..[36] [c]Analyzed in hydrated film by Hasni et al.[37]

dx.doi.org/10.1021/jf502699g | J. Agric. Food Chem. 2014, 62, 7567−7576

a slight recovery in either the environment of Trp residues (mainly Trp19) or/and the five Tyr residues in β-LG.

Fluorescence Spectroscopy. Trp intrinsic fluorescence was used to probe possible tertiary structural interruption of β-LG upon interacting with SBP because of its sensitivity to the polarity of its environment. It is known[49,50] that the major fluorescence contribution of β-LG comes from Trp19, buried within the hydrophobic β-barrel whereas Trp61 is located on the surface of the protein. Figure 5A shows steady-state Trp fluorescence spectra of native and heat-treated β-LG in the absence and presence of SBP at pH 6.75. It should be pointed out that excitation at 282 nm produced the same fluorescence spectrum of β-LG as that using 295 nm as the excitation wavelength.

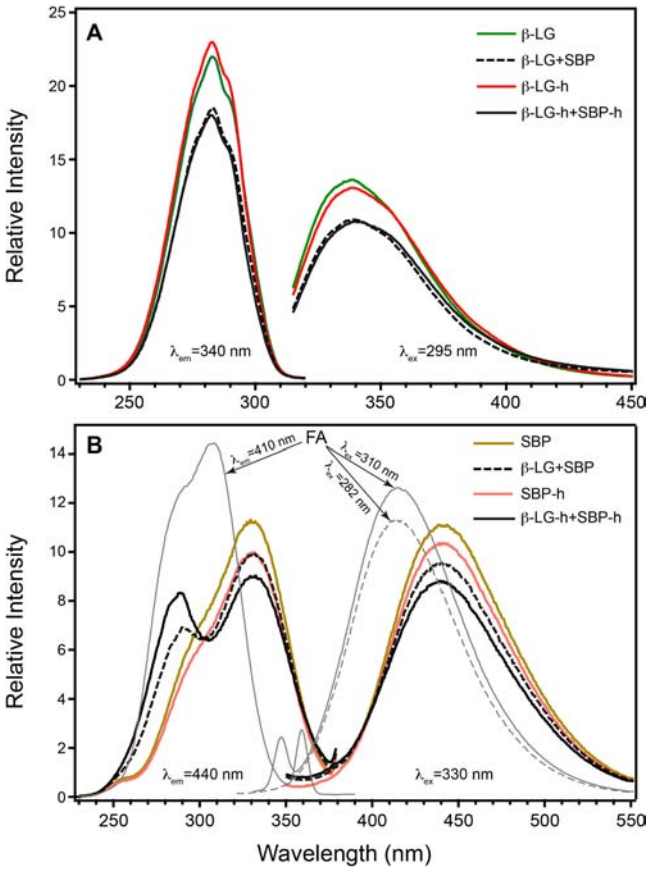

Figure 5. Fluorescence emission and excitation spectra of solutions containing 0.3 mg/mL β-LG or/and 0.1 mg/mL SBP in 33 mM phosphate buffer at pH 6.75 and 20 °C. All λ_{ex} and λ_{em} were as noted. (A) Trp intrinsic fluorescence spectra of β-LG, β-LG + SBP, β-LG-h, and β-LG-h + SBP-h; (B) fluorescence spectra of the feruloyl groups of SBP, β-LG + SBP, SBP-h, and β-LG-h + SBP-h.. The emission (λ_{ex} = 310 nm and λ_{ex} = 282 nm) and excitation (λ_{em} = 410 nm) spectra of ferulic acid (0.0.002 mg/mL) in the same buffer were also plotted as a comparison.

To limit the absorption interference (at 282 nm) from other aromatic residues such as Phe and Tyr than Trp in β-LG, excitation at 295 nm was used in this work. The relatively short time (10 min) heating at 80 °C appeared to have caused only slight reduction and peak broadening in the fluorescence of the single fluorescent Trp residue (Trp19) β-LG, typical for protein denaturation. The addition of SBP and SBP-h, however, greatly quenched the fluorescence of β-LG and β-LG-h, respectively, demonstrating that the Trp19 environment was severely perturbed upon interacting with SBP. Furthermore, this denaturation effect of SBP on β-LG reached a similar level in each case (native and preheated) at the same concentration of β-LG.

Figure 5B shows the fluorescence spectra of the feruloyl groups of SBP as a result of interacting with β-LG. Free ferulic acid displayed a strong fluorescence emission at 415 nm (see Figure 5B); however, the maximum emission of the feruloyl groups in SBP red-shifted to 440 nm. The maximum excitation of the feruloyl groups also red-shifted to 345 nm from 330 nm (for ferulic acid), illustrating changes in the molecular electronic and vibrational states of ferulic acid when present in and covalently bound to SBP than its free form. It should be noted, when excitation was set at λ_{ex} = 287 nm, the other strong absorption shoulder peak for FA (see Figure 1), the same emission peak at λ_{em} = 415 nm as that for λ_{ex} = 345 nm was obtained and the intensity was much reduced.

Combining with β-LG significantly reduced the fluorescence intensity of feruloyl groups present in SBP, more than by the pre-heat-treatment used in this work (Figure 5B). Even though the maximum emission wavelength from β-LG (λ_{em} ~ 340 nm) overlaps with the maximum excitation wavelength for feruloyl groups in SBP (λ_{ex} ~ 330 nm), no fluorescence resonance transfer (FRET) was observed between the two chromophores in this work. This is likely due to the distance between them being greater than 100 Å according to Wu and Brand,[51] which is clearly attributable to the relatively low concentrations of β-LG and SBP used.

3.4. Involvement of Feruloyl Groups of SBP in Interaction with β-LG. To further quantify the effect of binding to SBP on the Trp intrinsic fluorescence of β-LG and vice versa, fluorescence lifetime decays were analyzed. Table 3 summarizes the lifetime decays (τ_i) and their corresponding preexponential factors (α_i) for Trp19 fluoresecence of β-LG and the feruloyl groups of SBP by selectively applying their excitation and emission wavelengths. A double-exponential lifetime of nearly equal magnitude (α), but with different decay times τ_1 = 1.93 ns and τ_2 = 0.94 ns, was obtained for native β-LG. As elucidated comprehensively by Beechem and Brand,[52] the lifetime characteristics of Trp residues in proteins is strictly pH-dependent. At neutral pH, used in this work, Trp typically exhibits biexponential decay.[52]

Nearly only one lifetime decay, τ_1 = 93 ps, was determined for the untreated SBP as the much longer decay τ_2 = 3.46 ns was only less than 1% (Table 3). Free ferulic acid, however, contains strictly a single short lifetime, τ_1 = 44 ps. The delayed fluorescence emission time upon the excitation of the feruloyl groups in SBP than that of its free form further supported the covalent nature of the feruloyl groups in SBP.

One of the two measured Trp fluorescence lifetime decays, i.e., τ_1 for native β-LG, was visibly affected by the interaction with SBP (see Table 3) whereas τ_2 remained unchanged. τ_1 was extended by ~20 ps in its value and also with increased presence, ~4%, demonstrating the disruption of the environment of Trp19, which is consistent with both our near-UV CD and steady-state fluorescence results as discussed previously. The fluorescence lifetime decays of the feruloyl groups of SBP, on the other hand, also underwent significant change in the presence of β-LG, i.e., τ_1 shifted ~10 ps shorter than its counterpart in the absence of β-LG, suggesting profound involvement of the feruloyl groups in the interaction. This is consistent with our findings from HPSEC.[28] The minor but

Table 3. Time Components (τ_i, ns)[a] and Preexponential Factors (α_i, %) Obtained from the Fit of Fluorescence Decays of the Trp Residues of β-LG and the Feruloyl Groups of SBP (pH 6.75, 33 mM Sodium Phosphate Buffer), Measured by TCSPC at Selected Excitation (λ_{ex}) and Emission (λ_{em}) Wavelengths

sample	τ_1	τ_2	τ_3	α_1	α_2	α_3	λ_{ex} (nm)	λ_{em} (nm)
β-LG	0.94(0.01)	1.93(0.02)		49.9(1.4)	50.1(1.4)		296	340
SBP	0.093(0.002)	3.46(0.34)		99.4(0.0)	0.63(0.02)		331	440
ferulic acid	0.044(0.003)			100			331	415
β-LG + SBP	0.96(0.00)	1.95(0.02)		53.9(1.1)	46.1(1.1)		296	340
	0.084(0.004)	3.77(1.25)		99.3(0.1)	0.68(0.05)		331	440
β-LG-h	0.68(0.04)	1.81(0.08)	5.50(0.12)	20.4(2.3)	56.1(1.8)	23.6(1.0)	296	340
SBP-h	0.083(0.003)	3.16(0.25)		99.3(0.0)	0.67(0.03)		331	440
β-LG-h + SBP-h	0.79(0.01)	1.86(0.02)	5.60(0.23)	26.3(0.2)	53.2(0.4)	20.4(0.4)	296	340
	0.095(0.009)	5.27(0.06)		92.9(0.1)	7.11(0.10)		331	440

[a]Average and standard deviations (in parentheses) were obtained through a set of triple experiments.

longer lifetime component (τ_2) of SBP and the preexponential factors (α_1 and α_2) remained virtually unchanged.

When β-LG was subjected to heating at its denaturation temperature (80 °C) for 10 min, a third much longer lifetime decay, τ_3 = 5.5 ns was resolved in addition to the two (τ_1 and τ_2), already existed in the untreated β-LG. Heat-induced self-aggregation of β-LG as a result of denaturation is attributed to this additional decay component. Furthermore, it is clear that τ_1 has become notably shorter, ~0.30 ns, whereas τ_2 remained roughly the same as in native β-LG within the range of standard deviation. The distribution of the triple exponential lifetimes was 20%, 56%, and 24%, respectively. It is apparent that τ_2 is the dominating one among the three and saw a 6% increase from native β-LG whereas τ_1 is the most heat-sensitive component, and τ_3 is the result of denaturation and aggregation at the cost of ~30% reduction in τ_1. The dominating decay component of SBP-h, τ_1, became ~10 ps shorter than that of untreated SBP and to about the same level as that of untreated SBP in the presence of β-LG.

When combined with SBP-h, the thermal sensitivity marker, τ_1 of β-LG became 0.1 ns longer than β-LG-h alone and with an ~6% increased level of contribution as well. In the mean time, both τ_2 and τ_3 showed reduced levels of participation, ~3% for each. Changes in the triple lifetime decays of β-LG suggested a limited level of restoration of the tertiary structure of β-LG-h upon binding to SBP-h.

Both lifetime components of the feruloyl groups of SBP-h, τ_1 and τ_2 also featured an interesting response to the binding interaction with β-LG-h. The main component τ_1 was returned to its untreated value, ~95 ps, but reduced contribution, ~6%, whereas the minor one τ_2 nearly doubled, from ~3.5 to 5.3 ns. Taken all together, it is evident that feruloyl groups of SBP are directly involved in the complex formation with β-LG, more prominent for the preheated mixture. As a result, ~4% of the total loss (24%) in tertiary structural contacts in β-LG caused by heat-induced aggregation and denaturation was recovered due to the presence of SBP-h, mostly in the environment of Trp19 with increased stabilization. This result is clearly in close agreement with the temperature dependence of Trp fluorescence of β-LG in the presence of SBP and the protective effect on which it imparted, as discussed in subsequent text.

3.5. Thermal Stability of Secondary Structure of β-LG as a Result of Interaction with SBP. To investigate the effect of interacting with SBP on the structural stability of β-LG, we conducted far-UV CD experiments as a function of temperature. A deconvolution procedure was performed on each spectrum at each temperature using the software CDNN,[45] and a database consisting of 33 reference proteins was used. Parts A–E of Figure 6 show the content of each secondary structural element of β-LG as a function of temperature. For native β-LG, temperature-induced denaturation behavior (open circles and solid lines) closely resembled a two-state unfolding model[53] for all five individual elements as deconvoluted in this work. The presence of SBP (open triangles and dotted lines) did not significantly alter the unfolding process of β-LG except for the initial denaturation effect upon interaction. Pre-heat-treated β-LG still retained a good amount of secondary structural elements as discussed above, and underwent further temperature-induced denaturation (closed circles and dashed lines). The addition of pre-heat-treated SBP only initially restored a limited amount of

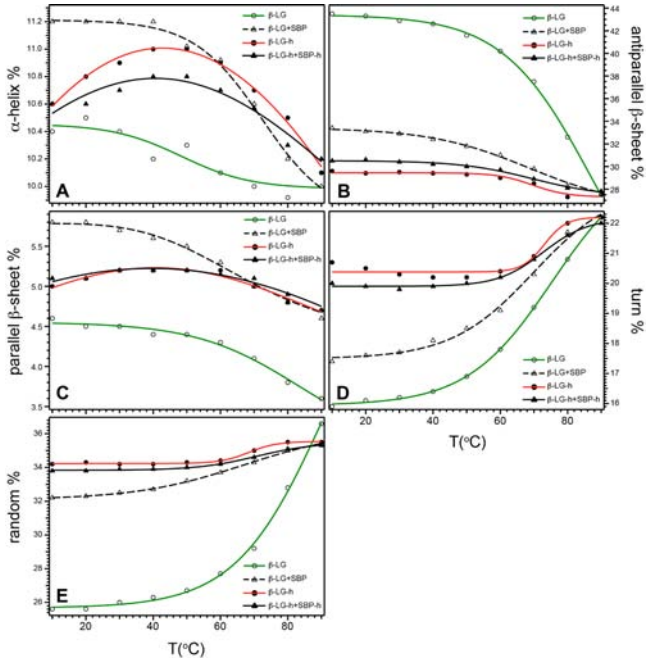

Figure 6. Temperature dependence of secondary structural elements: (A) α-helix, (B) antiparallel β-sheet, (C) β-sheet, (D) turn, and (E) random coil of β-LG, β-LG + SBP, β-LG-h, and β-LG-h + SBP-h obtained by deconvolution of far-UV CD spectra of β-LG, β-LG + SBP, β-LG-h, and β-LG-h + SBP-h in 33 mM phosphate buffer at pH 6.75. The concentrations were 0.3 and 0.1 mg/mL for β-LG and SBP, respectively, using a 0.05 cm path length cell. All spectra were corrected against buffer and SBP (when present). Various lines were used to make it easier to visualize all data points.

dx.doi.org/10.1021/jf502699g | J. Agric. Food Chem. 2014, 62, 7567–7576

secondary structures but did not significantly affect the temperature dependence behavior of β-LG-h under the conditions employed in this work.

In addition, all secondary structural elements of β-LG arrived at a similar level at the highest temperature used (90 °C) in the absence and presence of SBP.

3.6. Thermal Stability of Tertiary Structure of β-LG as a Result of Interaction with SBP. To further understand the effect of interacting with SBP on the tertiary contact and stability of β-LG, experiments were carried out on the Trp intrinsic fluorescence and feruloyl fluorescence at varying temperatures (10−90 °C), and the results are shown in Figure 7. As expected, the intrinsic Trp (mainly Trp19) fluorescence

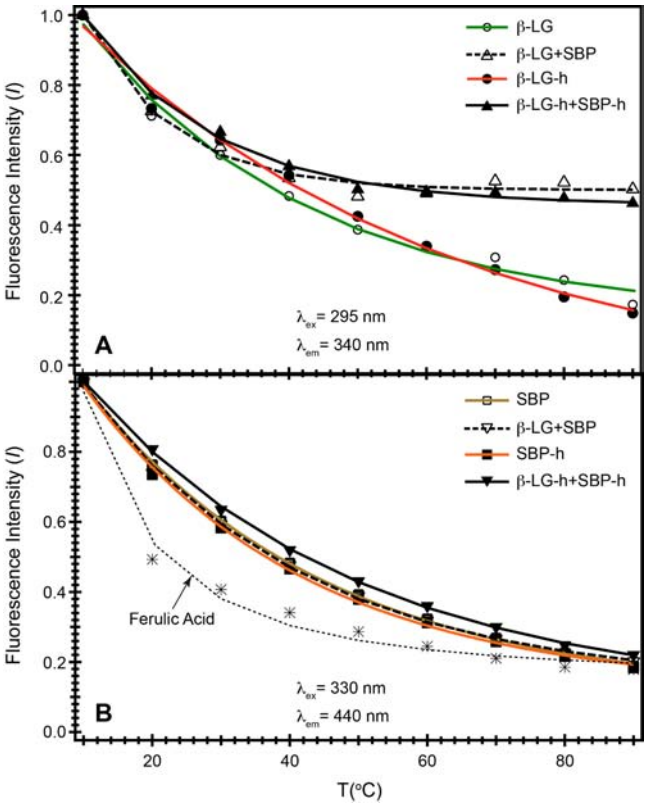

Figure 7. Temperature dependence of fluorescence intensity of all solutions containing 0.3 mg/mL β-LG or/and 0.1 mg/mL SBP in 33 mM phosphate buffer at pH 6.75. All λ_{ex} and λ_{em} were used as specified. (A) Trp intrinsic fluorescence spectra of β-LG, β-LG + SBP, β-LG-h, and β-LG-h + SBP-h. (B) Fluorescence spectra of the feruloyl groups of SBP, β-LG + SBP, SBP-h, and β-LG-h + SBP-h. The fluorescence intensity of FA as a function of temperature is also compared using λ_{ex} = 310 nm and λ_{em} = 410 nm. The intensity (I) at each temperature was normalized against its value at 10 °C.

intensities of both native and preheated β-LG (β-LG-h; Figure 7A) underwent a continuous decline in a fashion similar to the temperature increase and eventually arrived at ∼20% of their initial intensity at the highest temperature used (90 °C).

In the presence of SBP, the intensity of the Trp fluorescence of native β-LG first saw an accelerated reduction and then at ∼40 °C it began to level off to ∼55%. This level was maintained thereafter as temperature increased even as high as 90 °C. Clearly, SBP first acted as a quencher but then functioned as a shield and helped preserve the Trp residue from undergoing further thermal-induced solvent exposure. Although the Trp fluorescence intensity of pre-heat-treated β-LG (β-LG-h) was diminished compared to its native form, further temperature treatment imposed little or no visible effect, attesting the protective role that SBP-h played for β-LG-h against thermal treatment.

On the other hand, the temperature dependence of fluorescence intensity of the feruloyl groups of SBP was virtually unaffected by interacting with β-LG (Figure 7B) and decreased to nearly 10% of its initial intensity at 90 °C. The fluorescence of FA also displayed a sharply different temperature dependence behavior. For example, even at room temperature (20 °C), its fluorescence intensity already reduced by nearly half compared to 10 °C whereas changes in its fluorescence were much slower when present as feruloyl groups in SBP against temperature increase (Figure 7B), suggesting a possible "shielded" environment for the feruloyl groups in SBP.

In this work, we have demonstrated that interacting with SBP caused a significant amount of antiparallel β-sheet structure, up to 10%, to turn into random or turn structure in native β-LG. Tertiary structural contacts, for all aromatic residues, Trp, Tyr, and Phe, also suffered considerable loss in the presence of SBP. A limited level, ∼4%, of lost secondary and tertiary structures of β-LG caused by pre-heat-treatment (80 °C for 10 min) was restored by interacting SBP. Furthermore, thermal stability of all secondary structure elements of β-LG was not significantly affected by the presence of SBP. However, the Trp19 environment of β-LG was greatly protected by interacting with SBP against thermal denaturation. All evidence gathered in this work further demonstrated that the interaction between β-LG and SBP occurred near the calyx and at the outer surface region of β-LG involving the β-barrel area formed mainly by the antiparallel β-sheets. Results from this work provided an in-depth understanding of the functional properties (e.g., emulsion) of protein-based food products containing polysaccharides as an additive and correlated these properties with the detailed molecular structures of the protein.

AUTHOR INFORMATION

Corresponding Author

*Tel.: 215-233-6438. Fax: 215-233-6597. E-mail: Phoebe.Qi@ars.usda.gov.

Notes

Mention of trade names or commercial products in this publication is solely for the purpose of providing specific information and does not imply recommendation or endorsement by the U.S. Department of Agriculture. USDA is an equal opportunity provider and employer.

The authors declare no competing financial interest.

REFERENCES

(1) George, M.; Abraham, T. E. Polyionic hydrocolloids for the intestinal delivery of protein drugs: Alginate and chitosan—A review. *J. Controlled Release* **2006**, *114*, 1−14.

(2) Dickinson, E. Interfacial structure and stability of food emulsions as affected by protein-polysaccharide interactions. *Soft Matter* **2008**, *4*, 932−942.

(3) Turgeon, S. L.; Laneuville, S. I. Protein + polysaccharide coacervates and complexes: From scientific background to their application as functional ingredients in food products. In *Modern Biopolymer Science: Bridging the Divide between Fundamental Treatise and Industrial Application*; Kasapis, S., Norton, I. T., Ubbink, J. B., Eds.; Academic Press: Burlington, MA, USA, 2009; Chapter 11, pp 327−364.

(4) Jones, O. G.; McClements, D. J. Recent progress in biopolymer nanoparticle and microparticle formation by heat-treating electrostatic protein-polysaccharide complexes. *Adv. Colloid Interface Sci.* **2011**, *167*, 49−62.
(5) Evans, M.; Ratcliffe, I.; Williams, P. A. Emulsion stabilisation using polysaccharide-protein complexes. *Curr. Opin. Colloid Interface Sci.* **2013**, *18*, 272−282.
(6) Cho, Y.; Batt, C. A.; Sawyer, L. Probing the retinol-binding site of bovine β-lactoglobulin. *J. Biol. Chem.* **1994**, *269*, 11102−11107.
(7) Liang, L.; Subirade, M. β-Lactoglobulin/folic acid complexes: Formation, characterization, and biological implication. *J. Phys. Chem. B* **2010**, *114*, 6707−6712.
(8) Teng, Z.; Li, Y.; Luo, Y.; Zhang, B.; Wang, Q. Cationic β-lactoglobulin nanoparticles as a bioavailability enhancer: Protein characterization and particle formation. *Biomacromolecules* **2013**, *14*, 2848−2846.
(9) Livney, Y. D. Milk proteins as vehicles for bioactives. *Curr. Opin. Colloid Interface Sci.* **2010**, *15*, 73−83.
(10) Sawyer, L. β-Lactoglobulin. In *Advanced Dairy Chemistry, Vol. 1A: Proteins*, 3rd ed.; Fox, P. F., McSweeney, P. L. H., Eds.; Kluwer Academic/Plenum: New York, NY, USA, 2003; Chapter 7, pp 319−363.
(11) Brownlow, S.; Morais Cabral, J. H.; Cooper, R.; Flower, D. R.; Yewdall, S. J.; Polikarpov, I.; North, A. C. T.; Sawyer, L. Bovine β-lactoglobulin at 1.8 A resolution—Still an enigmatic lipocalin. *Structure* **1997**, *5*, 481−495.
(12) Qin, B. Y.; Bewley, M. C.; Creamer, L. K.; Baker, H. M.; Baker, E. N.; Jameson, G. B. Structural basis of the Tanford transition of bovine β-lactoglobulin. *Biochemistry* **1998**, *37*, 14014−14023.
(13) Kuwata, K.; Hoshino, M.; Forge, V.; Era, S.; Batt, C. A.; Goto, Y. Solution structure and dynamics of bovine β-lactoglobulin A. *Protein Sci.* **1999**, *8*, 2541−2545.
(14) Sakai, K.; Sakurai, K.; Sakai, M.; Hoshino, M.; Goto, Y. Conformation and stability of thiol-modified bovine β-lactoglobulin. *Protein Sci.* **2000**, *9*, 1719−1729.
(15) Wu, S. Y.; Perez, M. D.; Puyol, P.; Sawyer, L. β-Lactoglobulin binds palmitate within its central cavity. *J. Biol. Chem.* **1999**, *274*, 170−174.
(16) Kontopidis, G.; Holt, C.; Sawyer, L. The ligand-binding site of bovine β-lactoglobulin: Evidence for a function? *J. Mol. Biol.* **2002**, *318*, 1043−1055.
(17) Perez, M. D.; Calvo, M. Interaction of β-lactoglobulin with retinol and fatty acids and its role as a possible biological function for this protein: A review. *J. Dairy Sci.* **1995**, *78*, 978−988.
(18) Kampa, M.; Alexaki, V. I.; Notas, G.; Nifli, A. P.; Nistikaki, A.; Hatzoglou, A.; Bakogeorgou, E.; Kouimtzoglou, E.; Blekas, G.; Boskou, D.; Gravanis, A.; Castanas, E. Antiproliferative and apoptotic effects of selective phenolic acids on T47D human breast cancer cells: Potential mechanisms of action. *Breast Cancer Res.* **2004**, *6*, R63−R74.
(19) Zhao, Z.; Moghadasian, M. H. Chemistry, natural sources, dietary intake and pharmacokinetic properties of ferulic acid: A review. *Food Chem.* **2008**, *109*, 691−702.
(20) Riihimaki, L. H.; Vainio, M. J.; Heikura, J. M.; Valkonen, K. H.; Virtanen, V. T.; Vuorela, P. M. Binding of phenolic compounds and their derivatives to bovine and reindeer β-lactoglobulin. *J. Agric. Food Chem.* **2008**, *56*, 7721−7729.
(21) Voragen, A. G. J.; Pilnik, W.; Thibault, J. F.; Axelos, M. A. V.; Renard, C. M. G. C. Pectins. In *Food Polysaccharides and Their Applications*; Stephen, A. M., Ed. Marcel Dekker: New York, NY, USA, 1995; pp 287−339.
(22) Chen, T.; Small, D. A.; Wu, L. Q.; Rubloff, G. W.; Ghodssi, R.; Vazquez-Duhalt, R.; Bentley, W. E.; Payne, G. F. Nature-inspired creation of protein-polysaccharide conjugate and its subsequent assembly onto a patterned surface. *Langmuir* **2003**, *19*, 9382−9386.
(23) Oliver, C. M.; Melton, L. D.; Stanley, R. A. Creating proteins with novel functionality via the Maillard reaction: A review. *Crit. Rev. Food Sci. Nutr.* **2006**, *46*, 337−350.
(24) Jung, J.; Wicker, L. Laccase mediated conjugation of heat treated β-lactoglobulin and sugar beet pectin. *Carbohydr. Polym.* **2012**, *89*, 1244−1249.
(25) Mariniello, L.; Porta, R.; Sorrentino, A.; Giosafatto, C. V. L; Rossi Marquez, G.; Esposito, M.; Di Pierro, P. Transglutaminase-mediated macromolecular assembly: Production of conjugates for food and pharmaceutical applications. *Amino Acids* **2014**, *46*, 767−776.
(26) de Kruif, C. G.; Tuinier, R. Polysaccharide protein interactions. *Food Hydrocolloids* **2001**, *15*, 555−563.
(27) Cooper, C. L.; Dubin, P. L.; Kayitmazer, A. B.; Turksen, S. Polyelectrolyte-protein complexes. *Curr. Opin. Colloid Interface Sci.* **2005**, *10*, 52−78.
(28) Qi, P. X.; Chau, H. K.; Fishman, M. L.; Wickham, E. D.; Hotchkiss, A. T., Jr. Investigation of molecular interactions between β-lactoglobulin and sugar beet pectin by multi-detection HPSEC. *Carbohydr. Polym.* **2014**, *107*, 198−208.
(29) Qi, P. X.; Nunez, A.; Wickham, E. D. Reactions between β-lactoglobulin and genipin: Kinetics and characterization of the products. *J. Agric. Food Chem.* **2012**, *60*, 4327−4335.
(30) DuBois, M.; Gilles, K. A.; Hamilton, J. K.; Rebers, P. A.; Smith, F. D. Colorimetric method for determination of sugars and related substances. *Anal. Chem.* **1956**, *28*, 350−356.
(31) Yoo, S. H.; Fishman, M. L.; Savary, B. J.; Hotchkiss, A. T., Jr. Monovalent salt-induced gelation of enzymatically deesterified pectin. *J. Agric. Food Chem.* **2003**, *51*, 7410−7417.
(32) Cohen, S. A.; De Antonis, K. M. Applications of amino acid derivatization with 6-aminoquinolyl-N-hydroxysuccinimidyl carbamate: Analysis of feed grains, intravenous solutions and glycoproteins. *J. Chromatogr. A* **1994**, *661*, 25−34.
(33) Böhm, G.; Jaenicke, R. Correlation functions as a tool for protein modeling and structure analysis. *Protein Sci.* **1992**, *1*, 1269−1278.
(34) Byler, D. M.; Susi, H. Examination of the secondary structure of proteins by deconvolved FTIR spectra. *Biopolymers* **1986**, *25*, 469−487.
(35) Barth, A. Infrared spectroscopy of proteins. *Biochim. Biophys. Acta* **2007**, *1767*, 1073−1101.
(36) Dong, A.; Matsuura, J.; Allison, S. D.; Chrisman, E.; Manning, M. C.; Carpenter, J. F. Infrared and circular dichroism spectroscopic characterization of structural differences between β-lactoglobulin A and B. *Biochemistry* **1996**, *35*, 1450−1457.
(37) Hasni, I.; Bourassa, P.; Tajmir-Riahi, H.-A. Binding of cationic lipids to milk β-lactoglobulin. *J. Phys. Chem. B* **2011**, *115*, 6683−6690.
(38) Kauppinen, J. K.; Moffatt, D. J.; Mantsch, H. H.; Cameron, D. G. Fourier Self-Deconvolution: A method for resolving intrinsically overlapped bands. *Appl. Spectrosc.* **1981**, *35*, 271−276.
(39) Williams, P. A.; Sayers, C.; Viebke, C.; Senan, C.; Mazoyer, J.; Boulenguer, P. Elucidation of the emulsification properties of sugar beet pectin. *J. Agric. Food Chem.* **2005**, *53*, 3592−3597.
(40) Levigne, S. V.; Ralet, M.-C. J.; Quemener, B. C.; Pollet, B. N.-L.; Lapierre, C.; Thibault, J.-F. J. Isolation from sugar beet cell walls of arabinan oligosaccharides esterified by two ferulic acid monomers. *Plant Physiol.* **2004**, *134*, 1173−1180.
(41) Sperber, B. L. H. M.; Cohen Stuart, M. A.; Schols, H. A.; Voragen, A. G.; Norde, W. Overall charge and local charge density of pectin determines the enthalpic and entropic contributions to complexation with β-lactoglobulin. *Biomacromolecules* **2010**, *11*, 3578−3583.
(42) Becker, A. L.; Henzler, K.; Welsch, N.; Ballauff, M. Proteins and polyelectrolytes: A charged relationship. *Curr. Opin. Colloid Interface Sci.* **2012**, *17*, 90−96.
(43) de Kruif, C. G.; Weinbreck, F.; de Vries, R. Complex coacervation of proteins and anionic polysaccharides. *Curr. Opin. Colloid Interface Sci.* **2004**, *9*, 340−349.
(44) Turgeon, S. L.; Schmitt, C.; Sanchez, C. Protein−polysaccharide complexes and coacervates. *Curr. Opin. Colloid Interface Sci.* **2007**, *12*, 166−178.

(45) Böhm, G.; Muhr, R.; Jaenicke, R. Quantitative analysis of protein far UV circular dichroism spectra by neural networks. *Protein Eng.* **1992**, *5*, 191−195.
(46) Casal, H. L.; Kohler, U.; Mantsch, H. H. Structural and conformational changes of β-lactoglobulin B: An infrared spectroscopic study of the effect of pH and temperature. *Biochim. Biophys. Acta* **1988**, *957*, 11−20.
(47) Eissa, A. S.; Puhl, C.; Kadla, J. F.; Khan, S. A. Enzymatic cross-linking of β-lactoglobulin: Conformational properties using FTIR spectroscopy. *Biomacromolecules* **2006**, *7*, 1707−1713.
(48) Townend, R.; Kumosinski, T. F.; Timasheff, S. N. The circulation dichroism of variants of β-lactoglobulin. *J. Biol. Chem.* **1967**, *242*, 4538−4545.
(49) Sakurai, K.; Konuma, T.; Yagi, M.; Goto, Y. Structural dynamics and folding of β-lactoglobulin probed by heteronuclear NMR. *Biochim. Biophys. Acta* **2009**, *1790*, 527−537.
(50) Halder, U. C.; Chakraborty, J.; Das, N.; Bose, S. Tryptophan dynamics in the exploration of micro-conformational changes of refolded β-lactoglobulin after thermal exposure: A steady state and time-resolved fluorescence approach. *J. Photochem. Photobiol.* **2012**, *109*, 50−57.
(51) Wu, P. G.; Brand, L. Resonance energy transfer: Methods and applications. *Anal. Biochem.* **1994**, *218*, 1−13.
(52) Beechem, J. M.; Brand, L. Time-resolved fluorescence of proteins. *Annu. Rev. Biochem.* **1985**, *54*, 43−71.
(53) Pace, C. N. Determination and analysis of urea and guanidine hydrochloride denaturation curves. *Methods Enzymol.* **1986**, *131*, 266−280.

al.[10] were adapted to determine penicillin G concentrations at injection sites, serum, urine, kidney, and skeletal muscle. Liver and adipose tissue residues were not measured because neither is a regulatory target tissue for detecting penicillin G residues. Depletion kinetics of penicillin G subsequently were modeled to determine preslaughter withdrawal period recommendations for kidney and muscle.

MATERIALS AND METHODS

Study Overview. To determine the effect of intramuscular (IM) administration pattern on penicillin G depletion, 126 heavy sows were administered a 5× label dose of penicillin G procaine for 3 consecutive days. The three penicillin G treatments differed in injection volume and pattern. Animals were serially slaughtered with 5, 10, 15, 20, 25, 32, and 39 day withdrawal periods, and urine, serum, kidney, skeletal muscle, and injection site were collected for penicillin G analyses by liquid chromatography−mass spectrometry (LC−MS/MS). Because of the large number of animals, the study was conducted in two identical trials of 63 animals each.

Animals. Prior to the initiation of the study, an animal use protocol was approved by the North Dakota State University (NDSU) Animal Care and Use Committee. One-hundred sixty heavy sows, in lots of 80 each, were purchased from the North Dakota Pig Cooperative (Larimore, ND). Sows were group housed in concrete-floored pens covered with ample quantities of straw as bedding. Animals were ear tagged and group-fed approximately 2 kg of a corn−soybean ration (Table 1) per animal at approximately 0800 h each day; pens were cleaned daily, and water was available on an ad libitum basis. At delivery, sows were sorted into groups that were lame, had visible abscesses, or other visible anomalies. These animals were separated from the other sows and were not considered for inclusion in the study. Within the pool of healthy animals, sows were randomly allocated to treatment and pen so that each pen contained 21 sows. At this time, individual sows were randomly allocated to withdrawal period.

Table 1. Sow Diets Fed on a Restricted Basis (2 kg/animal per day)

ingredient	kg	percentage
corn, ground	723.6	79.6
soybean meal (46.0%)	123.2	13.5
malt sprouts	45.5	5.0
monocal, 21%	0.9	0.1
limestone	7.8	0.9
salt	3.6	0.4
RalCo sow	4.5	0.5
	909.1	100.0

Approximately 7 days prior to the initiation of penicillin G treatment, sows were tattooed according to their treatment assignment. An apparatus allowed multiple patterns of 2 cm "O"s to be tattooed onto necks of sows according to treatment (Figure 1). Tattooing allowed a consistent adherence to treatment protocols and designations for dose delivery.

Treatments. All sows were dosed with penicillin G procaine (Norocillin; Norbrook Laboratories, Lenexa, KS) at 33 000 U/kg BW. Treatments (illustrated in Figure 1) were designed to mimic the extra-label administration of penicillin G procaine thought to be used by veterinarians and swine producers during the treatment of infected sows.[6] Thus, each treatment differed in the volume and pattern of penicillin G procaine administration:

- Treatment 1: "10 mL; Single Site". A maximum injection volume of 10 mL using multiple injection sites within day to deliver the total required drug volume; across day, injections were administered into the same site as the previous day (Figure 1, top panel).
- Treatment 2: "10 mL; Multiple Sites". A maximum injection volume of 10 mL using multiple injection sites within day to deliver the total required drug volume; across day, injection sites were separated by approximately 5 cm (Figure 1, middle panel).
- Treatment 3: "20 mL; Multiple Sites". A maximum injection volume of 20 mL using multiple injection sites within day to deliver the total required drug volume; across day, injections were separated by approximately 5 cm (Figure 1, lower panel).

The day prior to penicillin G procaine administration, sows were weighed. At dosing, penicillin G Procaine was administered via intramuscular injection through 3.8 cm, 16-gauge needles. Dosing was uneventful.

In addition to treatment animals, two positive control hogs received the label dose of penicillin G procaine by IM (6600 U/kg BW) injection for 3 consecutive days; during both trials, a single positive control sow was euthanized after a 7-day withdrawal period, consistent with the product label instructions. The other positive control sows were scheduled to be slaughtered after a 15-day withdrawal period; however, in trial 1, the 15 withdrawal day positive control sow died 12 days after penicillin G administration due to a ruptured spleen, so both 15-day withdrawal positive controls were obtained during trial 2. For both trials, untreated control sows were administered saline via intramuscular administration at 1 mL per 45.5 kg BW for 3 consecutive days and slaughtered after 5 days.

Slaughter and Tissue Sampling. Sows were euthanized according to American Veterinary Medicine Association recommendations[12] after 5, 10, 15, 20, 25, 32, or 39 day withdrawal periods relative to the last dosing day. Approximately 15 h prior to slaughter, sows designated for slaughter were withheld from access to feed. Sows were stunned by electrocution and captive bolt, after which they were quickly exsanguinated. Viscera were removed, and kidney and skeletal muscle (mid portion of the *longissimus dorsi*) were collected as well as urine and blood samples. At collection, samples were placed on dry ice; they were subsequently transported to the Biosciences Research Laboratory and stored at −80 °C until processing and analysis.

Tissue Processing. Frozen tissue samples were homogenized with dry ice using a Waring 1 L stainless steel blender (Torrington, CT) at a sample to dry ice ratio of approximately 1 to 1. Homogenized samples were subsequently placed at −20 °C to allow overnight sublimation; after sublimation of CO_2, samples were moved to a −80 °C freezer until analysis.

Extraction. Apley et al.'s[10] analytical method was adapted to accommodate larger volumes for serum and urine analyses. One milliliter of serum or urine and 4 mL of HPLC-grade acetonitrile were mixed for 15 min. Samples were then centrifuged for 20 min at 3000*g* (4 °C); supernatants were transferred to clean labeled tubes and were evaporated under N_2 at 45 °C to a volume of 0.5 mL. Concentrated extracts were quantitatively transferred to 1.5 mL microcentrifuge tubes, diluted to the 1 mL mark with HPLC-grade water, fortified with deuterated penicillin G standard (d_7, 100 ng; Sigma-Aldrich), and vortexed for 15 s. Extracts were then centrifuged at 17 000*g* for 20 min and aliquoted into glass vials for same-day LC−MS/MS analysis. Matrix-matched standard curves were prepared with each sample set having a concentration range of 2−500 pg/μL. Samples having penicillin G concentrations greater than the highest calibration standard were diluted with water into the quantitative range of the calibration curve as were contemporaneously run matrix-matched calibration standards. The extraction efficiency for serum was 88.7 ± 8% (n = 16) with method limits of detection (mLOD) and quantification (mLOQ) of 1.5 and 5.0 pg/μL, respectively. The urine extraction efficiency was 98.1 ± 8.0% (n = 16) with mLOD and mLOQ of 1.1 and 4.1 pg/μL, respectively.

Kidney, muscle, and injection site samples were extracted following the FSIS method CLG-BLAC.02 for β-lactam screening and confirmation[11] with minimal modifications. To kidney samples (2 g) was added 10 mL of an 80/20 mixture of HPLC-grade acetonitrile/nanopure water, and tubes were shaken for 15 min and centrifuged at 3000*g* for 15 min (4 °C). Sample extracts were then added to a

dx.doi.org/10.1021/jf501492v | J. Agric. Food Chem. 2014, 62, 7577−7585

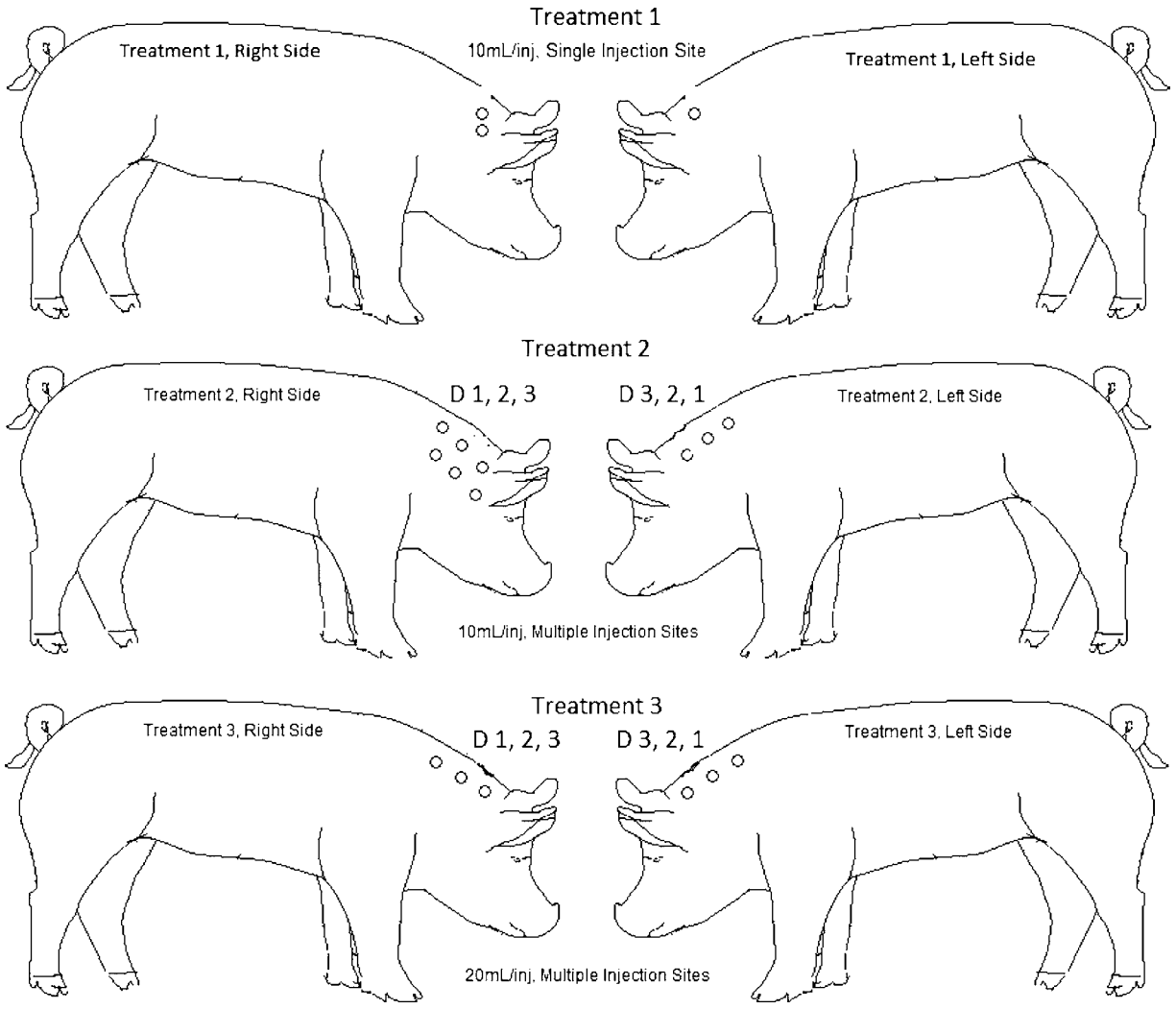

Figure 1. Penicillin G procaine treatments. Sows were administered 5× doses (33 000 IU/kg BW) of penicillin G procaine on each of three consecutive days as either 10 mL injections (treatments 1 and 2) or 20 mL injections (treatment 3). Across day, treatment 1 sows received injections in a single location; sows in treatments 2 and 3 received consecutive injections at locations separated by approximately 5 cm intervals. Because sows were very large, total injection volumes were typically greater than 20 mL; thus, for treatments 1 and 2, the pattern of injections was 10 mL right, 10 mL left, and the remaining volume (for total doses greater than 20 mL) would be injected into the right side approximately 5 cm below the initial 10 mL injection. The injection pattern for treatment 3 was 20 mL in the right side with overflow injections occurring in the left neck muscles. Injection sites were marked by tattoos 7 days prior to the initial treatment.

prepared (5 mL of acetonitrile and 2 × 5 mL of nanopure water) Bakerbond Octadecyl (C18, 1000 mg; JT Baker) solid-phase extraction (SPE) cartridge. Samples were allowed to flow through SPE cartridges by gravity; SPE cartridges were dried under vacuum. Unretained eluents were subsequently evaporated to 1 mL under N_2, syringe filtered through a PTFE 0.45 μm filter, and 100 ng of deuterated penicillin G was added. Extracts were centrifuge-filtered through a Millipore Amicon Ultra centrifuge filter (3000 nominal molecular weight limit) at 14 500*g* for 30 min, and 100 μL was placed into an autoinjector vial for LC−MS/MS analysis. The extraction efficiency for kidney was 72.7 ± 10.7% (n = 26) with mLOD and mLOQ of 1.8 and 6.1 ng/g, respectively.

Muscle and injection site samples were extracted with 10 mL of an 80/20 mixture of HPLC-grade acetonitrile/water saturated with hexane. Samples were then shaken for 15 min and centrifuged at 3000*g* for 15 min at 4 °C. The supernatants were decanted into a clean 50 mL tube, 5 mL of hexane was added, and extracted for 5 min with shaking. Samples were then centrifuged at 3000*g* for 15 min at 4 °C, the hexane layer was removed, and the extracts were processed as described for kidney by SPE and filtration. The extraction efficiency for muscle and injection site was 55.8 ± 9.4% with mLOD and mLOQ of 0.7 and 2.4 ng/g, respectively.

Duplicate blank (negative control) and fortified samples (25 ng/g penicillin G procaine) were extracted with each sample set. Trial samples were extracted in duplicate by withdrawal day. Before analysis, a penicillin G-d7 internal standard was added to each sample extract at an end concentration of 100 pg/μL. Blank sample extracts were utilized to prepare matrix matched standard curves ranging from 2 to 500 pg/μL. A new standard curve was made fresh for each sample set to avoid any penicillin G degradation. Samples and curves were analyzed by UPLC−MS/MS within 24 h of extraction. Samples with penicillin G concentrations above the highest standard in the curve were re-extracted and diluted with water before analysis. Blank matrices for standard curves of diluted samples were diluted with water to ensure equivalent matrix-matching.

Ultra High Performance Liquid Chromatography−Mass Spectrometry. A modified version of the UHPLC−MS/MS method described by Apley et al.[10] was used to determine penicillin G concentrations. Extracts were analyzed using a Waters (Milford, MA) ultra high performance liquid chromatograph coupled to a tandem quadrupole mass spectrometer (Acquity). The chromatography was modified slightly to be a slower gradient to affect a longer retention of

dx.doi.org/10.1021/jf501492v | J. Agric. Food Chem. 2014, 62, 7577−7585

Table 2. Depletion of Penicillin G Residues (mean ± std dev) from Skeletal Muscle, Kidney, Serum, and Injection Site of Heavy Sows[a]

	treatment				
WD period (d)	1 (ng/g or ng/mL)	2 (ng/g or ng/mL)	3 (ng/g or ng/mL)	P^b	overall average (ng/g or ng/mL)
			Skeletal Muscle[c]		
5	20.0 ± 6.3	20.1 ± 10.5	30.4 ± 11.9	0.14†	23.5 ± 10.5
10	4.8 ± 5.9 x,y	*1.3 ± 2.1 x*	9.8 ± 6.4 y	0.004†	5.3 ± 6.1
15	*0.8 ± 0.7*	*1.0 ± 1.2*	*0.7 ± 0.6*	0.81‡	0.8 ± 0.8
20	*1.1 ± 1.0*	*1.0 ± 1.4*	*0.6 ± 0.4*	NC	0.9 ± 1.0
25	**0.4**	**0.4**	**0.4**	NC	**0.4**
32	**0.4**	*0.6 ± 0.3*	**0.4**	NC	0.5 ± 0.2
39	**0.4**	**0.4**	**0.4**	NC	**0.4**
			Kidney[d]		
5	3751 ± 676	3238 ± 1110	4298 ± 3219	0.81†	3762 ± 1932
10	782 ± 1034 x,y	100 ± 210 x	1119 ± 919 y	0.03†	667 ± 875
15	183 ± 315	42.1 ± 65.5	133 ± 138	0.61‡	119 ± 199
20	65.4 ± 140	22.0 ± 51.7	46.2 ± 111	0.42‡	44.5 ± 103
25	25.6 ± 60.4	15.7 ± 23.1	**0.9**	0.36‡	14.1 ± 36.6
32	16.1 ± 26.0	28.5 ± 67.6	**0.9**	NC	15.2 ± 41.0
39	**0.9**	*4.5 ± 8.9*	*3.6 ± 6.6*	NC	*3.0 ± 6.2*
			Serum[e]		
5	466 ± 169	368 ± 120	486 ± 122	0.33†	440 ± 141
10	89.6 ± 116	9.7 ± 17.1	164 ± 170	0.02†	87.8 ± 129
15	12.0 ± 18.5	7.6 ± 11.2	15.2 ± 13.9	0.51‡	11.6 ± 14.3
20	5.3 ± 11.1	*1.0 ± 0.6*	6.7 ± 14.6	0.98‡	4.3 ± 14.6
25	*3.0 ± 5.6*	**0.8**	**0.8**	NC	*1.5 ± 3.2*
32	*1.0 ± 0.7*	*2.0 ± 3.0*	**0.8**	NC	*1.2 ± 1.7*
39	**0.8**	*1.4 ± 1.5*	**0.8**	NC	*1.0 ± 0.8*
			Injection Site[c]		
5	2 910 000 ± 1 230 000	1 600 000 ± 1 680 000	3 570 000 ± 3 150 000	0.18†	2 690 000 ± 2 220 000
10	428 000 ± 686 000	787 ± 1860	500 000 ± 430 000	0.01‡	310 000 ± 494 000
15	118 000 ± 286 000	80.0 ± 121	493 ± 581	0.63†	39 400 ± 165 000
20	2350 ± 5720	30 700 ± 75 100	16.5 ± 24.0	0.52†	11 000 ± 43 300
25	98 300 ± 241 000	4120 ± 10 100	2.9 ± 5.8	0.54‡	34 200 ± 139 000
32	20 600 ± 50 500	**0.4**	**0.4**	NC	6880 ± 29 200
39	3.5 ± 7.6	*1.0 ± 1.3*	212 ± 511	NC	72.2 ± 295

[a]Data are expressed as ng of penicillin G per g of tissue. Individual values below each matrix limit of quantitation (LOQ), but above the method limit of detection (LOD), were included in means as nominal values returned by the LC−MS/MS assay. Values below the matrix LOD were included in mean calculations at 1/2 of the LOD. Mean values shown in italic font were below the method limit of quantification (LOQ) but above the method limit of detection (LOD); mean values shown in bold font were below the method LOD and are expressed at one-half the LOD. Means within a row with differing letters (x, y) differ ($P < 0.05$). Means within withdrawal period and treatment were calculated from six animals each. Data from individual animals are included in the Supporting Information. [b]Within withdrawal period means were ln transformed and compared using one-way ANOVA using parametric (†) or nonparametric (‡) tests; NC, not compared. [c]Skeletal muscle and injection site data are not corrected for recovery, which averaged 55.8 ± 9.4% across all skeletal muscle assays ($n = 14$); method LOQ, 2.4 ng/g LOD, 0.7 ng/g; one-half LOD, 0.4 ng/g. [d]Kidney data are not corrected for recovery, which averaged 72.7 ± 10% across all kidney assays ($n = 26$); method LOQ, 6.1 ng/g; LOD, 1.8 ng/g; one-half LOD, 0.9 ng/g. [e]Serum data are not corrected for recovery, which averaged 88.7 ± 9.4% across all serum assays ($n = 14$); method LOQ, 5.0 ng/g; LOD, 1.5 ng/g; one-half LOD, 0.8 ng/g.

penicillin G relative to the Apley et al.[10] method. Penicillin G was separated from matrix on a Waters BEH C18 column (2.1 × 50 mm, 1.8 μm) using a mobile phase gradient consisting of: 0 to 1.5 min, isocratic 80/20 10 mM ammonium acetate in water/10 mM ammonium acetate in acetonitrile (A/B); 1.5 to 1.75 min, linear gradient to 20/80 A/B; 1.75 to 4 min, isocratic 20/80 A/B; flow rate of 0.8 mL/min. Penicillin G and deuterated penicillin G eluted at 0.45 min. Analytes were ionized in positive electrospray mode using a capillary voltage of 3.5 kV at a desolvation temperature of 500 °C and a nitrogen flow rate of 800 L/h. Other parameters included a source temperature of 150 °C and a cone voltage of 35 V.

The detection method was also modified to monitor additional fragment ions for penicillin G to improve confirmation and quantification of residues. Fragment ion isolation and detection was accomplished in the multiple reaction monitoring mode. For penicillin G and deuterated penicillin G, two fragments were monitored. The precursor ion for penicillin G was 335 m/z; using a collision energy of 10, fragment ions at 160 m/z and 176 m/z were produced. For dueterated penicillin G, the precursor ion was 342 m/z; with a collision energy of 12, fragment ions at 160 m/z and 183 m/z were produced. If sample duplicate concentrations differed by more than 25%, they were re-extracted and reanalyzed in duplicate to achieve better agreement between replicates. Reported data are not corrected for recovery.[13] Method LODs were calculated as the standard deviation of seven replicates of fortified samples (2 ng/mL or ng/g) multiplied by the Student's t value (99% confidence) with $n - 1$ degrees of freedom; mLOQs are 10 times the standard deviation of the seven replicates.[14]

Statistical Comparisons. Within withdrawal period and matrix, data were natural log (ln) transformed prior to analyses by simple one-way ANOVA. For time points in which assumptions of normality (tested using the Shapiro−Wilk method) were met, differences in

Table 3. Depletion of Penicillin G Residues (mean ± std dev) from Urine of Heavy Sows[a]

	treatment				
WD period (d)	1 (ng/mL)	2 (ng/mL)	3 (ng/mL)	P^b	overall average (ng/mL)
5	338 000 ± 473 000	378 000 ± 252 000	282 000 ± 234 000	0.62‡	332 000 ± 320 000
10	41 100 ± 57 600 x,y	6490 ± 10 200 x	78 600 ± 70 400 y	0.04†	42 100 ± 58 200
15	11 000 ± 20 700	9960 ± 17 000	26 400 ± 27 000	0.35‡	15 800 ± 22 000
20	2870 ± 4580	2220 ± 5440	4410 ± 10 800	0.87‡	3170 ± 7080
25	2800 ± 6840	487 ± 1040	*0.8 ± 0.6*	NC	1090 ± 3950
32	2270 ± 3770	8030 ± 19 700	**0.6**	NC	3430 ± 11 400
39	**0.6**	585 ± 1430	880 ± 2150	NC	489 ± 1450

[a]Data are expressed as ng of penicillin G per mL of urine. Individual values below each matrix limit of quantitation (LOQ; 4.1 ng/mL), but above the method limit of detection (LOD; 1.1 ng/mL), were included in means as nominal values returned by the LC−MS/MS assay. Values below the matrix LOD were included in mean calculations at 1/2 of the LOD. Means within a row with differing letters (x, y) differ ($P < 0.05$). Means within withdrawal period and treatment were calculated from six animals each. Data from individual animals are included in the Supporting Information. [b]Within withdrawal period means were ln transformed and compared using one-way ANOVA using parametric (†) or nonparametric (‡) tests; NC, not compared.

treatment means were determined using standard parametric methods (i.e., Holm−Sidak). In instances in which normality was not met, nonparametric analysis was conducted using the Kruskal−Wallis one-way ANOVA on ranks. Specific details on the use parametric or nonparametric tests for any tissue/withdrawal period combination are shown within each data table.

Estimation of Withdrawal Period. Withdrawal periods were estimated using the method described by the US FDA-CVM[13] with some modification. In the estimation of withdrawal periods for kidney, the following criteria were used. These criteria are a combination of European Union and US FDA approaches to handling data from residue depletion trials. First, for tissue residue data for a given withdrawal day to be included in the analysis, at least three animals had to have returned residues above the method limit of quantification.[13] Second, nominal values below the limit of quantification, but above the limit of detection, were used as returned by the assay if there were at least three points at the withdrawal period above the limit of quantification. Third, values falling below the limit of detection were included at one-half the method limit of detection.[15]

For kidney, data obtained from withdrawal days 10, 15, 20, and 25 were used for the calculation of withdrawal period. Data from day 32 were not employed even though there were three animals with penicillin residues above the LOQ because the 32-day data were not linear ($P = 0.45$) with respect to withdrawal day 20 and 25 data. It should be noted, however, that the 10, 15, 20, and 25 day data set violated the statistical assumptions of normality and equal variance.

To estimate the withdrawal period for skeletal muscle, only one animal out of 18 had residues above the LOQ at the 15-d withdrawal period, with three animals having residues above the LOD, but below the LOQ. Because a minimum of three time points are required to determine the terminal, linear elimination period, the 15-d withdrawal period data were used to estimate a withdrawal period for skeletal muscle. In doing so, the day 15 data included one value that was above the LOQ, four animals that had residue values between the LOQ and LOD, and 13 animals in which no detectable residue was present; for the latter animals, a value of one-half the LOD was used for calculations. Skeletal muscle data also violated the statistical assumptions of normality and equal variance.

Estimations of withdrawal period were completed for kidney and skeletal muscle tissues using the procedure described by the US-FDA CVM in guideline no. 3, "General Principles for Evaluating the Safety of Compounds used in Food Producing Animals".[13] Excel 7.0 was used in conjunction with the tables of Owen[16] to calculate the critical values of the noncentral *t*-distribution used in FDA calculations.

RESULTS AND DISCUSSION

Weights of sows dosed with penicillin G procaine averaged 234.2, 223.8, and 226.8 kg for treatments 1, 2, and 3, respectively (±4.5 kg; pooled SEM) and did not differ ($P = 0.24$). Average slaughter weights were 237.4, 226.5, and 228.9 kg (±4.4 kg; pooled SEM) and did not differ ($P = 0.19$).

Mean residues of penicillin G in skeletal muscle, kidney, serum, and injection site are shown in Table 2. Table 3 shows mean urinary depletion of penicillin G by treatment and withdrawal period. Raw (individual animal) data are presented as Supporting Information.

The depletion of penicillin G residues from kidneys of heavy sows is presented in Figure 2. The pattern of penicillin G administration had no discernible effect on residue depletion, so treatments were pooled. Quantifiable residues were present in kidneys of all 18 animals 5 days after the final penicillin G procaine injection, but by 10 days 6 of 18 (33%) animals had residues below the assay LOD (1.8 ng/g). By 20 days of withdrawal, 5 of 18 animals had residues above the LOQ with three of these animals having kidney residues above 100 ng/g and one animal with penicillin G residues greater than 300 ng/g. Penicillin G residues were present in the kidneys of two hogs after a 39-d withdrawal period. The presence of penicillin G residues in 11% of animals (2 of 18 animals) at withdrawal day 39 suggests that an extensive withdrawal period would be required for the complete depletion of penicillin from kidneys of a population of treated animals.

Regulatory organizations in the European Union and the United States estimate preslaughter withdrawal periods using nearly identical techniques.[13,15] That is, withdrawal periods are calculated by determining the time required for tissue residues in 99% (U.S.) or 95% (Europe) of a population of animals to deplete to an established tolerance with 95% confidence. Tolerance limits are calculated using linear regression of the natural logs (ln) of tissue residues in the linear depletion phase of the residue depletion curve. In calculating the 95th percentile confidence interval, the U.S. assumes a noncentral *t*-distribution,[13] whereas the European Union allows the 95th percentile confidence interval to be calculated using the standardized normal distribution.[15] The two methods generally return similar results,[15,17] depending upon a number of variables, the most important being the handling of data which fall below the method limit of quantification.[17] Both the U.S. and the CVMP methods of establishing withdrawal periods have been criticized[18,19] because of the difficulty with which residue data collected over time meet assumptions of normality and equal variance.

A withdrawal period was estimated for kidney tissues using the ln-linear approach promulgated by the US-FDA CVM[13]

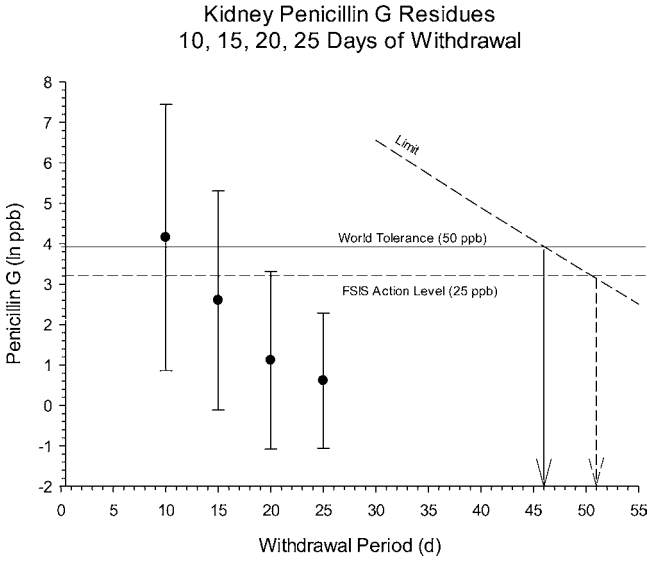

Figure 2. Estimation of preslaughter withdrawal period in heavy sows treated with a 5× dose of penicillin G procaine, based on depletion of penicillin G residues from kidney tissues. Data taken from the linear portion of the depletion curve were analyzed as described by FDA Guidance Document no. 3 (US FDA CVM, 2006). In contrast to US FDA guidance, 15-d withdrawal data below the method LOD were assigned values of 1/2 the LOD (CMVP, 1995). Kidney penicillin G concentrations that were between the LOQ and LOD were included in the analysis as their nominal concentration. The residue tolerance used by most of the world (50 ng/g or ln 3.91 ng/g) crossed the 99th percentile with a 95th percent confidence interval tolerance limit at approximately 46.5 days (solid vertical arrow). The kidney withdrawal period for a tolerance of 50 ng/g was established at 47 days after rounding up to the nearest whole-day. In the United States, the tolerance level is zero for penicillin G in swine tissues, but FSIS has established an action limit of 25 ng/g for penicillin residues detected in swine tissues (FSIS, 2013). For penicillin residues to deplete below the action limit of 25 ng/g in a population of swine, just over 50 days would be required; rounding up to the nearest whole-day, the withdrawal period would be 51 days.

with modifications suggested by the CVMP.[15] In making a withdrawal period estimation, the essential assumptions of equal variance and normal distributions (Shapiro−Wilk) of data were violated ($P < 0.001$). That is, because the withdrawal period estimate is based on the assumption that the variance of the upper 1% of a population is known, the withdrawal period parameter is sensitive to assumptions associated with the variance model.[20] As discussed by Concordet and Toutain[18] and Riviere,[20] and as documented by Sanquer et al.[19] and Chiesa et al.,[21] assumptions of equal variances are difficult, and sometimes impossible to meet. Nonparametric approaches to withdrawal period calculations proffered by Sanquer et al.[19] and Concordet and Toutain[19] were not attempted on this data set.

Poor confidence in the variance estimates governing the withdrawal parameter notwithstanding, Figure 2 shows that an estimated 47-day withdrawal period would be required for kidney residues to deplete to 50 ng/g in 99% of the animals (with 95% certainty) in a population of heavy sows treated with a 5× dose of penicillin G procaine for 3 consecutive days. For residues to fall below the FSIS action level of 25 ng/g[22] in a population of treated sows, an estimated 51-day withdrawal period would be required. Again, these estimates are not statistically valid because the data from which they were calculated were not normally distributed and did not have an equal variance. Nevertheless, the empirical evidence itself suggests that had a statistically sound data set been generated, an actual withdrawal period based on kidney residues would be prohibitively long with regards to commercial sow production systems in the United States.

In contrast to kidney tissues, penicillin G residues depleted quickly from skeletal muscle (Table 2, Figure 3). Residues in

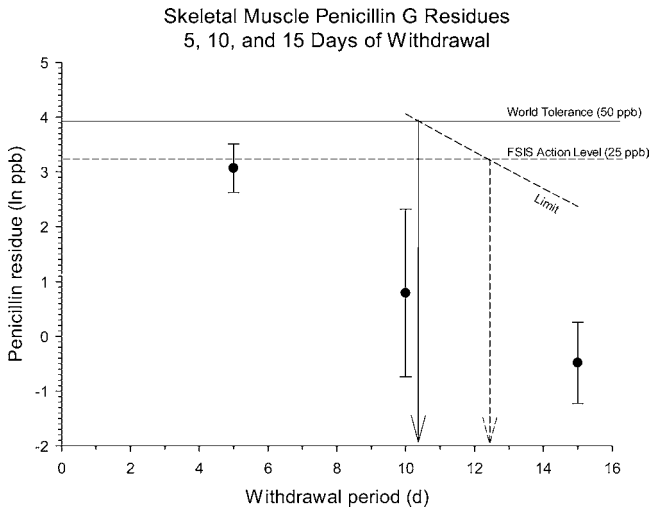

Figure 3. Estimation of preslaughter withdrawal period in heavy sows treated with a 5× dose of penicillin G procaine, based on depletion of penicillin G residues from skeletal muscle. Data taken from the linear portion of the depletion curve were analyzed as described by FDA Guidance Document no. 3 (US FDA CVM, 2006). In contrast to US FDA guidance, withdrawal data below the method LOD were assigned values of 1/2 the LOD (CMVP, 1995). Skeletal muscle penicillin G concentrations that were between the LOQ and LOD were included in the analysis as their nominal concentrations. The residue tolerance used by most of the world (50 ng/g or ln 3.91 ng/g) crossed the 99th percentile with a 95th percent confidence interval tolerance limit at approximately 10.4 days (solid vertical arrow). The skeletal muscle withdrawal period for a tolerance of 50 ng/g was estimated to be 11 days after rounding up to the nearest whole-day. In the United States, the tolerance level is zero for penicillin G in swine tissues, but FSIS has established an action limit of 25 ng/g for penicillin residues detected in swine tissues (FSIS, 2013). For penicillin residues to deplete below the action limit of 25 ng/g in a population of swine, an estimated 13 days would be required.

skeletal muscle at 5 days of withdrawal averaged only 23.5 ± 10.5 ng/g and depleted rapidly thereafter. By the 15th day of withdrawal, only 1 sow of 18 dosed had skeletal muscle residues greater than the method LOQ (2.4 ng/g), with 4 other sows having residues greater than the method LOD (0.7 ng/g), but less than the method LOQ. Thus, the estimated withdrawal periods for skeletal muscle were 11 days (Figure 3) for the worldwide tolerance of 50 ng/g, and 13 days for the FSIS action level of 25 ng/g. Regardless of dosing pattern, the Food Animal Residue Avoidance Database-estimated withdrawal time of 15 days proposed by Payne et al.[23] in 2006 (and at the time this study was conducted) was sufficient for penicillin residues to deplete from skeletal muscle. Again, it should be noted that an 11-day withdrawal period does not represent a regulatory withdrawal period because the normality assumption inherent in regression analyses was not met.

Table 2 contains residue depletion data from day three (last exposure) injection sites collected at slaughter. Across all treatments, residues in injection sites collected 5 days after the

dx.doi.org/10.1021/jf501492v | J. Agric. Food Chem. 2014, 62, 7577−7585

last administration of penicillin G were very high, averaging over 2.6 million ng/g of tissue; however, the data also indicate that injection site residues were highly variable. At withdrawal day 15 and later, the relative variation in residue concentration was approximately 400% of the mean. Such variation at injection sites has been described previously[19] and is typical of injection site residue data. Because of this variability, no long-term-effect of injection pattern was discerned from the data. Kosrud et al.[9] suggest that the proportion of an intramuscular dose that is delivered intramuscularly will influence the kinetics of penicillin depletion. In practice, however, ensuring uniform, intramuscular delivery of injectable penicillin G is difficult in heavy sows, especially when injected into the neck.

From a broad perspective, the actual method that a producer uses to deliver extra-label doses of penicillin G to a sow is unknown by regulators. Therefore, pooling injection site data, or residue data from other tissues, across treatments may provide the best indication of how penicillin residues deplete in the larger swine population, which, no doubt, is subject to a variety of injection techniques. The pooled data ("overall average" column of Table 2) clearly indicate that injection site residues are greater than skeletal muscle residue. Supporting Information tables showing residues from individual animals, however, indicate that high average residues usually occurred through the contributions of only a few animals per withdrawal period.

For penicillin, the target tissue for regulatory monitoring is kidney.[24] While kidneys are not commonly consumed in the U.S., it is possible that muscle from injection sites could be consumed.[25] Injection sites are not typically defined as a target tissue because they are difficult to locate on an animal carcass, injection sites containing drug residues are applicable to only a small number of market animals, and injection sites are not a reliable tissue for monitoring drug exposure in a population of animals.[26] In addition, residues from injection sites deplete at inconsistent rates and are highly variable, which makes calculating withdrawal periods based on injection site residues difficult.[19] Finally, the probability of a consumer actually being exposed to an injection site in a food product is extremely low. Because tolerances are based on acceptable daily intakes of a given residue over assumed lifetime exposures,[25,27] and because tolerances are established with several inherent safety factors, the probability of an adverse toxic effect occurring, even in the event of exposure to residue at an injection site, is extremely low.

Actual probability of risk notwithstanding, food animal producers would generally distance themselves from marketing products containing residues that may be perceived as risky. For penicillin, overt toxicity to the general population is not a concern because penicillin is of low toxicity;[28] in individuals with allergic hypersensitivity to penicillin, however, residue might initiate an allergic reaction. For example, use of penicillin in dairy cows and delivery of penicillin residues in milk to sensitive individuals was a problem in the decade after the introduction of penicillin to veterinary use.[29−31] The degree of allergic reaction to penicillin, ranging from mild to severe, depends upon the sensitivity of presensitized individuals, the route of penicillin exposure, and the dose of penicillin residue received.[30,32] Estimates of the doses of penicillin required to initiate allergic response range from 3 to 6 μg[28,32] with doses required to sensitize individuals being much greater. While the probability of delivering sufficient penicillin to sensitized individuals is very low, examples of allergic reactions in intentionally[33] and unintentionally[34] penicillin-exposed (via meat) individuals have been documented. For unintentional exposures, documented reactions are exceedingly rare.[28,35]

For swine producers, the presence of penicillin residues in food products could be mitigated by several practices. First, producers using extra-label penicillin could observe the estimated withdrawal periods of 50 days or greater in all treated sows, which would allow residues in edible tissues to deplete. However, observation of a 7-week withdrawal period would not be economical in sows destined for market.

A second option would be to discontinue penicillin use altogether. Such action, however, is not likely justifiable based on combined animal welfare and human food safety considerations. As pointed out by the European Food Safety Authority,[36] β-lactam antibiotics (including penicillin) "are among the most important group of antimicrobial agents in veterinary medicine", and they have been used in animal agriculture for decades. For example, the first U.S. approval for penicillin occurred in 1951,[37] and currently approximately 99.5% of all penicillin use in swine is administered for disease prophylaxis and treatment.[38] It is telling that with regards to food safety, the main criticism of penicillin use resides not with toxicity concerns or even allergic responses to residues, but to the hypothesis that β-lactam use in food animals could contribute to the transmission of antimicrobial resistance.[37,38] Thus, the elimination of penicillin use in food animals is not likely justified on the basis of food safety.

A third option would be to market penicillin-treated animals with a withdrawal period sufficient for muscle residues to deplete, and to discard the kidneys with inedible offal for rendering. While kidney is the target tissue for penicillin in swine carcasses,[24] residues in kidney do not represent a risk if they are not available for human consumption. In the United States, only a small percentage of the value of a market sow is associated with kidney; therefore, discard of kidney for rendering would not likely represent a hardship for processing plants that handle heavy sows. Admittedly, such discard might not be economically viable in markets in which sow kidney has a greater relative value.

As attractive as kidney discard would appear to be in the United States for solving penicillin residue issues, regulatory agencies will not likely allow such action because kidney is also the target tissue for a number of other drugs. For example, in the United States, the Food Safety and Inspection Service's screening and confirmatory method for a multitude of residues is based on kidney.[22] Even with the retention of renal tissue at slaughter, producers do have the option, suggested by Payne et al.,[23] of screening animals to ensure that they are penicillin-free prior to marketing. Table 3 shows that urinary penicillin residues are substantially more concentrated than kidney residues (Table 2) at any given slaughter time. Thus, the presence of penicillin in urine is an excellent predictor that the antibiotic has not completely depleted from tissues, whereas there is little evidence (Table 2) that serum would serve in such capacity. Using instrumental analysis such as LC−MS/MS to perform urinary penicillin residues analysis, however, would be difficult to provide timely feedbacks to producers to ensure that the animals are penicillin G free. Using urine and kidney samples from the current study, Shelver et al.[39] demonstrated that the kidney inhibition swab test (KIS test, Charm Sciences, Inc.; Lawrence, MA) rapid screening assay, employed by the FSIS to screen kidney tissues at slaughter facilities, when used with urine samples very accurately predicted Charm-KIS

positive kidney samples and was an excellent predictor of residues greater than the 25 ng/g action limit in use by the US FSIS.[22] Figure 4 demonstrates the within-animal relationship

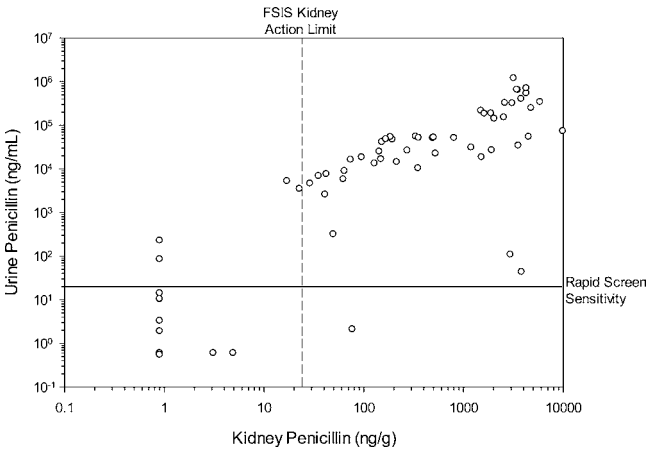

Figure 4. Within-animal relationship between urinary penicillin G residues (*Y*-axis) and renal penicillin G concentrations across all slaughter times. The horizontal solid line represents the limits of detection of the Charm-KIS rapid screening assay in urine,[39] and the vertical hatched line shows the FSIS "minimal level of applicability" for penicillin G residues in swine kidney (FSIS-2013). Points below the solid line would not be detected by a urinary rapid screening assay; points to the left of the vertical hatched line would not be flagged by the FSIS. Use of the urinary assay would be conservative due to the fact that the screen would have flagged four animals as "positive" when the kidney results would have been flagged as negative. A single sample would have passed the urine screen while kidney residues remained above the FSIS action level.

between renal and urinary penicillin concentrations. With one exception, urinary penicillin concentrations were excellent predictors of potentially violative kidney residues (n = 121). Such data suggest that the kidney inhibition swab test, when used with a urine matrix, is a viable option for a timely (<5 h run time) on-farm screen for the presence of penicillin residues.

Data presented in this study clearly demonstrate that penicillin residues deplete at disparate rates in edible tissues in swine treated with extra-label doses. From a human food safety perspective, the earlier FARAD 15-day withdrawal period that is commonly observed for extra-label penicillin doses[23] is sufficient for residue depletion from skeletal muscle. It would take approximately 50 days for residue to deplete to nondetectable levels in kidneys from a population of sows treated with an extra-label penicillin dose, concurring with the current FARAD recommendation (which is based on these data). This study demonstrates the disparity between residue depletion in tissues sometimes selected for regulation of drug residues (kidney) and tissues for which the majority of the value of a carcass resides (skeletal muscle). This disparity could leave valuable animal-health drugs vulnerable to discontinuation, not due to human food safety concerns, but due to regulatory inflexibility.

■ ASSOCIATED CONTENT

Supporting Information

Results on an individual animal basis. This material is available free of charge via the Internet at http://pubs.acs.org.

■ AUTHOR INFORMATION

Corresponding Author

*Tel.: (701) 239-1238. E-mail: david.j.smith@ars.usda.gov.

Funding

This study was collaboratively funded by the National Pork Board (58-5442-2-404), the USDA ARS (project no. 5442-32000-014), North Dakota State University, and in-kind contributions provided by Charm Sciences (agreement no. 58-5442-32000-014-07n).

Notes

The use of trade, firm, or corporation names in this publication is for the information and convenience of the reader. Such use does not constitute an official endorsement or approval by the United States Department of Agriculture or the Agricultural Research Service of any product or service to the exclusion of others that may be suitable. USDA is an equal opportunity employer.

The authors declare no competing financial interest.

■ ACKNOWLEDGMENTS

The technical expertise of Roberta Dahlen, Dee Ellig, Austen Germolous, Justin Gilbertson, Nathaniel Grosz, Kelsey Heiberg, Grant Herges, Dillon Hoffsommer, Jason Holthusen, Benjamin Klinkner, Erin Loeb, Amy McGarvey, Richelle Miller, Colleen Pfaff, and Terry Skunberg is greatly appreciated as are the efforts of student employees of the North Dakota State University Meats Laboratory and Animal Physiology and Nutrition Center.

■ REFERENCES

(1) USDA Agricultural Marketing Service. 2012 Annual Meat Trade Review. http://www.ams.usda.gov/mnreports/lsancmtr.pdf, accessed 6/25/2014.

(2) Salvage, B. Most US sausage categories are growing, thanks to product diversity and bold business moves. MeatPoultry.com, January 8, 2014. http://www.meatpoultry.com/Writers/Bryan%20Salvage/Sausage%20tsunami.aspx, accessed 6/25/2014.

(3) Meyer, S. R. Sausage market fundamentals taking hold. National Hog Farmer, September 8, 2009. http://nationalhogfarmer.com/weekly-preview/0908-sausage-market-fundamentals, accessed 6/25/2014.

(4) JAVMA. Tissue tests locate penicillin G residues, JAVMA news, October 1, 2011. https://www.avma.org/News/JAVMANews/Pages/111001j.aspx, accessed 1/8/2014.

(5) National Hog Farmer. Warning Issued for Penicillin Residues in Sows. National Hog Farmer, July 21, 2011. http://nationalhogfarmer.com/health-diseases/warning-issued-penicillin-residues-sows, accessed 1/8/2014.

(6) Hoover, T. C. Health and performance improvements of pigs treated with DRAXXIN (tulathromycin) injectable solution for swine respiratory disease under field conditions. March 31, 2009. The Pig Site. http://www.thepigsite.com/articles/1/pig-health/2674/health-and-performance-of-pigs-treated-with-draxxin, accessed 1/8/2014.

(7) Code of Federal Regulations. Twenty-one CFR Part 530.

(8) Moats, W. A.; Harris, E. W.; Steele, N. C. Depletion of intramuscularly injected procaine penicillin G from tissue of swine. A comparison of HPLC and bioassay procedures. *J. Agric. Food Chem.* **1986**, *34*, 452−456.

(9) Kosrud, G. O.; Salisbury, C. D. C.; Rhodes, C. S.; Papich, M. G.; Yates, W. D. G.; Bulmer, W. S.; MacNeil, J. D.; Landry, D. A.; Lambert, G.; Yong, M. S.; Ritters, L. Depletion of penicillin G residues in tissues, plasma and injection sites of market pigs injected intramuscularly with procaine penicillin G. *Food Addit. Contam.* **1998**, *15*, 421−426.

(10) Apley, M., Coetzee, H.; Gehring, R.; Karriker, L. Pharmacokinetics and tissue residues of procaine penicillin G in sows after administration of 33,000 IU/kg intramuscularly and by needle-free injection in the hip. National Pork Board Research Report NPB #07-234, 2009.
(11) USDA FSIS. 2011. Screening and Confirmation of β-Lactam Antibiotics by HPLC-MS/MS, CLG-BLAC.02. Effective 07/02/2011.
(12) AVMA. *AVAMA Guidelines for the Euthanasia of Animals*, 2013 ed.; American Veterinary Medical Association: Schaumburg, IL, 2013.
(13) US FDA CVM. 2006. Guidance for Industry, #3. General principles for evaluating the safety of compounds used in food-producing animals. U.S. Dept. Health and Human Services. http://www.fda.gov/downloads/AnimalVeterinary/GuidanceComplianceEnforcement/GuidanceforIndustry/UCM052180.pdf.
(14) Harris, D. C. *Quantitative Chemical Analysis*, 8th ed.; W. H. Freeman and Co.: New York, NY, 2010.
(15) CVMP. Note for guidance: Approach towards harmonisation of withdrawal periods. European Agency for the Evaluation of Medicinal Products, Veterinary Medicines Evaluation Unit, Committee for Veterinary Medicinal Products, 1995.
(16) Owen, D. B. *Handbook of Statistical Tables*; Addision-Wesley Publishing Co., Inc.: Reading, MA, 1962.
(17) Damte, D.; Jeong, H.-J.; Lee, S.-J.; Cho, B.-H.; Kim, J.-C.; Park, S.-C. Evaluation of linear regression statistical approaches for withdrawal time estimation of veterinary drugs. *Food Chem. Toxicol.* **2012**, *50*, 773−778.
(18) Concordet, D.; Toutain, P. L. The withdrawal time estimation of veterinary drugs revisited. *J. Vet. Pharmacol. Ther.* **1997**, *20*, 380−386.
(19) Sanquer, A.; Wackowiez, G.; Havrileck, B. Critical review on the withdrawal period calculation for injection site residues. *J. Vet. Pharmacol. Ther.* **2006**, *29*, 355−364.
(20) Riviere, J. *Comparative Pharmacokinetics. Principles, Techniques, and Applications*, 2nd ed.; Wiley-Blackwell: Ames, IA, 2011.
(21) Chiesa, O. A.; Li, H.; Kijak, P. J.; Li, J. X.; Lancaster, V.; Smith, M. L.; Heller, D. N.; Thomas, M. H.; von Bredow, J. Tissue /fluid correlation study for the depletion of sulfadimethoxine in bovine kidney, liver, plasma, urine, and oral fluid. *J. Vet. Pharmacol. Ther.* **2011**, *35*, 249−258.
(22) US FSIS. Screening and confirmation of animal drug residues by UHPLC-MS-MS. CLG-MRM1.02, 2013.
(23) Payne, M. A.; Craigmill, A.; Riviere, J. E.; Webb, A. I. Extralabel use of penicillin in food animals. *J. Am. Vet. Med. Assoc.* **2006**, *229*, 1401−1403.
(24) NADA 065-010. Freedom of Information Summary: Norocillin, Penicillin G procaine injectable suspension cattle, sheep, swine, and horses. http://www.fda.gov/downloads/AnimalVeterinary/Products/ApprovedAnimalDrugProducts/FOIADrugSummaries/UCM218419.pdf.
(25) Reeves, P. T. Residues of veterinary drugs at injection sites. *J. Vet. Pharmacol. Ther.* **2007**, *30*, 1−17.
(26) CVMP. Revised reflection paper on injection site residues: Considerations for risk assessment and residue surveillance. European Mecicines Agency, Committee for Medicinal Products of Veterinary Use. (http://www.ema.europa.eu/docs/en_GB/document_library/Scientific_guideline/2013/10/WC500152656.pdf), 2013.
(27) Oriani, J. US Food and Drug Administration's perspective on aquaculture drug residues. In *Xenobiotics in Fish*; Smith, D. J., Gingerich, W. H., Beconi-Barker, M. G., Eds.; Kluwer Academic/Plenum Publishers: New York, 1999.
(28) CVMP. Penicillins, Summary Report. European Medicines Agency, Veterinary Medicines and Inpsection, Committee for Veterinary Medicinal Products. http://www.ema.europa.eu/docs/en_GB/document_library/Maximum_Residue_Limits_-_Report/2009/11/WC500015568.pdf, 2008.
(29) Ormerod, A.; Reid, T.; Main, R. A. Penicillin in milk: its importance in urticaria. *Clin. Exp. Allergy* **1987**, *17*, 229−234.
(30) Siegel, B. B. Hidden contacts with penicillin. *Bull. W. H. O.* **1959**, *21*, 703−713.
(31) Wicher, K.; Reisman, R. E.; Arbesman, C. E. Allergic reaction to penicillin in milk. *JAMA, J. Am. Med. Assoc.* **1969**, *208*, 143−145.
(32) Dewdney, J. M.; Maes, L.; Raynaud, J. P.; Blanc, F.; Scheid, J. P.; Jackson, T.; Lens, S.; Verschueren, C. Risk assessment of antibiotic residues of β-lactams and macrolides in food products with regard to their immuno-allergic potential. *Food Chem. Toxicol.* **1991**, *29*, 477−483.
(33) Lindemayr, H.; Knobler, R.; Kraft, D.; Baumgartner, W. Challenge of penicillin-allergic volunteers with penicillin-contaminated meat. *Allergy* **1981**, *36*, 471−478.
(34) Raison-Peyron, N.; Messaad, D.; Bousquet, J.; Demoly, P. Anaphylaxis to beef in penicillin-allergic patient. *Allergy* **2001**, *56*, 796−797.
(35) Dayan, A. D. Allergy to antimicrobial residues in food: assessment of risk to man. *Vet. Microbiol.* **1993**, *35*, 213−226.
(36) European Food Safety Authority. Scientific opinion on the public health risks of bacterial strains producing extended β-lactamases and/or AmpC β-lactamases in food and food-producing animals. *EFSA J.* **2011**, *9*, 2322.
(37) Institute of Medicine. Human health risks with the subtherapeutic use of penicillin or tetracyclines in animal feed. *Report by the Committee of Human Health Risk Assessment of Using Subtherapeutic Antibiotics in Animal Feeds, Institute of Medicine, IOM-88-89*; National Academy Press: Washington, DC, 1989.
(38) Cox, L. A.; Popken, D. A.; Mathers, J. J. Human health risk assessment of penicillin/aminopenicillin resistance in enterococci due to penicillin use in food animals. *Risk Anal.* **2009**, *29*, 796−805.
(39) Shelver, W. L.; Lupton, S.; Newman, D. J.; Larsen, S.; Smith, D. J. Depletion of penicillin G residues in heavy sows after intramuscular injection Part II: Application of kidney inhibition swab tests. *J. Agric. Food Chem.* **2014**, DOI: 10.1021/jf501494w.

the limits of quantitation (LOQ) (50 μg/kg). This contrasts with animals slaughtered after 6 days of withdrawal where five of five animals had quantifiable (>50 μg/kg) penicillin G residues in kidney. Skeletal muscle residues were generally lower than kidney, with residues ranging from 0 to 34 μg/kg (LOQ 10 μg/kg for muscle). Considerable penicillin G remained at the injection site even after 8 days (2970−190 000 μg/kg). The maximum withdrawal day used by Apley et al.[7] was 8 days, a time period insufficient to allow residues in all animals to deplete to nondetectable levels. As a consequence, they recommended use of a 28 day withdrawal period based on a 95% confidence interval that 99% of treated animals would have residue levels below detection limits in kidney.

The USDA-Food Safety and Inspection Service (FSIS) changed the on-site screening method they use for antimicrobial drug residues by switching from the Fast Antimicrobial Screen Test (FAST) to the Kidney Inhibition Swab (KIS) test with a phase III effective date of September 11, 2011 for swine carcasses in slaughter establishments in which KIS tests were used for cattle.[10] On August 19, 2012, all livestock species slaughter establishments were switched to KIS test for carrying out on-site carcass antimicrobial residues screening.[11] This article describes the detection of penicillin G procaine residues with the KIS test from kidney, liver, plasma, urine, skeletal muscle, and injection site of heavy sows after an extra-label penicillin G procaine administration. Sows were treated IM with 33 000 IU/kg for 3 consecutive days and were slaughtered with withdrawal periods extending to 39 days post-treatment. Although the dosage used in this study is 5× the FDA-CVM approved penicillin G procaine dose, it is in the middle of levels (2×−10×) typically administered to swine under the auspices of AMDUCA.[12] Three patterns of drug administration were studied; each was designed to mimic patterns of administration thought to be used in the industry.

MATERIALS AND METHODS

Chemicals and Supplies. Penicillin G procaine (300 000 IU/mL; Norocillin; Norbrook Pharmaceuticals, Lenexa, KS) injection solution was purchased from Ivesco, LLC (Iowa Falls, IA). Penicillin G procaine monohydrate reference standard was purchased from U.S. Pharmacopeia, Rockville, MD. Kidney inhibition swabs, positive and negative controls, and heating blocks were obtained from Charm Laboratories (Lawrence, MA). Driploss containers were purchased from the Danish Meat Research Institute, Taastrup, Denmark.

Animal Housing and Treatment Assignment. A study protocol was approved by the North Dakota State University Institutional Animal Care and Use Committee prior to the initiation of the live-phase of the study. Heavy sows (80 animals per trial for a total of two trials) were purchased from the North Dakota Pig Cooperative (Larimore, ND) and delivered to the North Dakota State University Animal Research Center (Fargo, ND). Sows were group fed an unmedicated corn−soybean ration at 2 kg per animal per day and had ad libitum access to clean water. During the 14-day acclimation period, animals were each provided unique identification numbers by ear tag and were randomly assigned to one of three treatments to deliver 33 000 IU/kg bw; treatment details are described in the accompanying paper.[13]

Treatment 1. A maximum injection volume of 10 mL using multiple injection sites within day to deliver the total required drug volume; across day, injections were administered into a single muscle location.

Treatment 2. A maximum injection volume of 10 mL using multiple injection sites within day to deliver the total required drug volume; across day, injection sites were separated by approximately 5 cm.

Treatment 3. A maximum injection volume of 20 mL using multiple injection sites within day to deliver the total required drug volume; across day, injections were separated by approximately 5 cm.

Controls. Positive control hogs (n = 2 per withdrawal period) were treated with the label dose (6600 IU/kg bw) of penicillin G procaine via IM administration for 3 consecutive days and were euthanized after a 7-day withdrawal period, consistent with the product label; or a 15-day withdrawal period, representing extended withdrawal period. Untreated control sows (n = 2) were dosed IM with sterile saline (1 mL per 45.5 kg) for 3 consecutive days and were slaughtered 5 days after the last saline injection.

Injection Site Identification and Treatment. Approximately 7 days prior to the initiation of penicillin treatment, sows were tattooed according to their treatment assignment. A device was machined at the North Dakota State University machine shop, which allowed multiple patterns of 2 cm "O"s to be tattooed onto necks of sows according to treatment. Such tattooing allowed a consistent adherence to treatment protocols and treatment designations.

Sows were weighed and penicillin G procaine was administered via intramuscular injection through 3.8 cm, 16-gauge needles according to treatment assignments. Sows were dosed in a modified metal crate that allowed for elevation to facilitate dose administration. Dosing was uneventful.

Slaughter and Sampling. Sows were slaughtered at the NDSU abattoir with 5, 10, 15, 20, 25, 32, and 39 day withdrawal periods relative to the last dosing day. Control sows treated with the label dose were slaughtered at 7 and 15 days of withdrawal. Sows were sequentially stunned by electrocution and captive bolt, and then quickly exsanguinated. Viscera were removed, and kidney, skeletal muscle (mid portion of the *longissimus dorsi*), injection site, and liver sample aliquots were collected and stored at −80 °C until analysis. In addition, urine and blood samples were collected. Blood was allowed to clot at 37 °C in a heating block for approximately 1 h, and serum was collected after centrifuging at 1200*g* for 15 min. Serum and urine aliquots were stored at −80 °C until analysis.

On-Site Analysis of Kidneys. Kidney samples were screened for penicillin residues on the kill floor using the KIS microbial inhibition test according to FSIS procedures;[14] the manufacturer's recommended incubation time, without the automatic shut-off option, was followed. The other option in the FSIS procedure, which allows a 15 min shorter incubation time with automatic shut-off, was not used in this study. Briefly, cotton swabs were saturated with kidney juice after perforating kidneys with the KIS test wand. Swabs were placed into test media and incubated at 64 ± 2 °C for the prescribed time (batch dependent, 2 h 45 min to 3 h 20 min for kidney). The presence of penicillin G was indicated by the development of a purple/blue color; samples testing negative for penicillin G were indicated by a yellow/green color. Samples containing penicillin G residues below the sensitivity threshold (see below) could produce ambiguous results, and such samples were defined as "cautions" as described by the FSIS[14] (Figure 1). In instances in which "caution" results were returned at the prescribed incubation time, tubes were reread several hours later but within the allowed 16 h KIS test "grace" period.[14,15]

Analysis of Injection Site, Muscle, and Kidney Samples. At collection, injection site, skeletal muscle, and additional kidney samples were collected using a 3 cm diameter tissue coring device driven by a cordless drill and trimmed to approximately 3 × 3 cm (d × l). Samples were placed into Driploss (Danish Meat Research Institute, Taastrup, Denmark) containers and were frozen at −80 °C until analysis. Samples were thawed at room temperature for 1 h, and the tissue juices were collected from the drip tubes after centrifuging at 1200*g* for 10 min. The collected tissue juices were used to saturate KIS test swabs. Microbial inhibition tests for tissues were then conducted as described by the FSIS[14] for determination of the presence of penicillin G.

Analysis of Liver Samples. Liver samples were cored, placed into Driploss tubes, frozen, thawed, and juice collected as described for kidney and muscle samples. However, liver liquid isolation required the addition of an equal volume of water followed by boiling (1 min) and centrifugation at 14 000*g* for 10 min. After centrifugation, the KIS

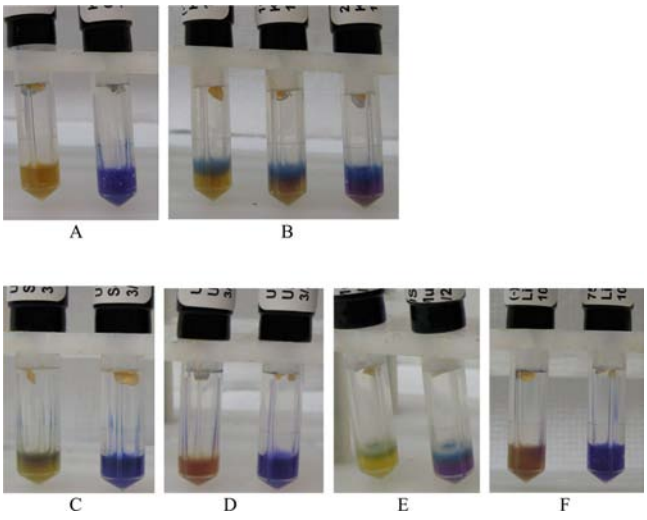

Figure 1. Typical negative control (left) and positive control (right) results returned from the KIS test rapid screening assay. (A) KIS negative control and KIS positive control; (B) negative (left), caution (middle), and positive (right) from kidney swabs; notice there is a blue cover on top of the negative kidney swab; the blue cover was not observed in the negative control provided by Charm; (C) serum negative control and serum positive control; (D) urine negative control and urine positive control; (E) muscle negative control and muscle positive control; (F) liver negative control and liver positive control.

test cotton applicator was immersed in the liver juice supernatant for 10 s prior to performing the KIS microbial inhibition assay as described previously. The effect of boiling on penicillin G residues in liver liquid is described below.

Analysis of Serum and Urine Samples. Urine or serum aliquots (500 μL) were combined with a single KIS test neutralization tablet and mixed using a vortex mixer; particulates were allowed to settle for 1 min. Serum/urine supernatant was adsorbed for 10 s with a cotton swab, after which the KIS microbial inhibition assay was performed.

Assay Sensitivity Determination. Control serum, urine, skeletal muscle juice, and kidney juice were prepared as previously described. Tissue matrix aliquots were fortified with 0, 10, 20, 30, 40, and 50 ppb of penicillin G, while liver liquid samples were fortified at 0, 10, 25, 50, 75, and 100 ppb of penicillin G due to low sensitivity. Fortified liver liquid samples were also analyzed with, and without, boiling for 1 min before analysis. Swab tests were conducted for each given matrix described above. Fortification of each matrix was repeated on three separate days. Typical color indication for positive, negative, and "caution" KIS test results is shown in Figure 1.

Statistical Analysis. The matrix differences were compared employing McNemar's square test using negative results as 0 and positive results as 1 and processed using SigmaPlot 11.2 (Systat Software, Inc., San Jose, CA). Missing collection points obtained from urine samples were recorded as blanks in the data file. Significant differences between the two treatments were defined as $p \leq 0.05$.

RESULTS AND DISCUSSION

Assay Sensitivity. The penicillin concentrations that produced positives in a minimum of three replicates in kidney juice, muscle juice, urine, serum, and liver juice were 20, 30, 20, 30, and 100 ppb, respectively, accounting for liver juice dilution, based on a single lot. The assay sensitivity for kidney appeared to be slightly higher than reported by the manufacturer (30−35 ppb for cattle and swine kidney, dependent on source of reports),[14,15] with similar sensitivity of serum and urine as reported by the manufacturer (20−30 ppb).[16] However, our results are slightly less sensitive than the assay sensitivity reported by Schneider et al.[17] of 10 ppb for beef kidney juice and 15 ppb for serum. Nevertheless, both species had the same trend; that is, the KIS test is more sensitive for kidney juice than for serum. In this study, kidney juice used for the assay sensitivity determination was prepared from frozen kidney rather than from unfrozen kidney used by the manufacturer. The results generated by our laboratory indicate kidney and urine are the matrices allowing for the most sensitive KIS test analyses followed by assay sensitivities returned by muscle juice and serum; the liver returned relatively insensitive KIS test results, with much lower assay sensitivity than the other tissues because a dilution step is needed. Our results indicated a short boiling period of 1 min did not reduce the penicillin G threshold of the KIS test when assayed using the liver liquid with or without reboiling after penicillin G was spiked into control liver liquid. This observation confirms the results of Moats et al.[18] who reported that penicillin G only lost 10% of its potency when heated at 100 °C for 10 min for both milk and water and required at least 30 min at 121 °C to completely inactivate penicillin G in meat homogenate.

Effects of Incubation Period. Samples containing penicillin residues near the assay sensitivity threshold could produce ambiguous results, defined as "cautions" by the FSIS.[14] In instances in which "caution" results were returned at the prescribed incubation time, which ranged from 2 h 45 min to 3 h 20 min for kidney, based on the manufacturer's lot-specific recommendation, the same tubes were also read several hours into the 16 h "grace" period at room temperature allowed in the FSIS method.[14] On some occasions the "caution" results darkened during the extended time period (Figure 2). Thus, even though a 15 min automatic shut off option was applied, additional "positive" results could occur if the samples were left at room temperature without immediate scoring.

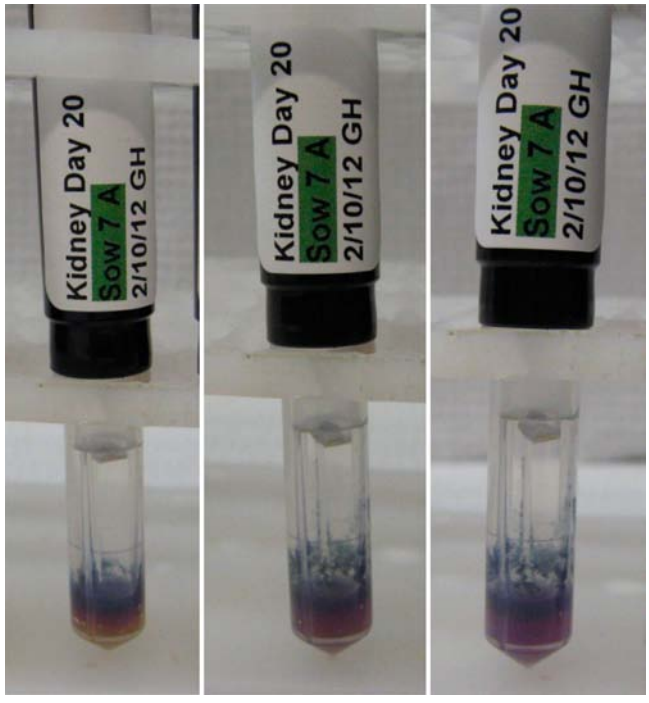

Figure 2. Example of a kidney sample that darkened sequentially with time as it proceeded from the prescribed incubation time at 64 °C (left), to 1 h post incubation at room temperature (middle), and after 2 h post incubation at room temperature (right).

Table 1. Results Expressed as Positive and Negative for the KIS Test in Tissues of Heavy Sows Treated with a 5× Penicillin G Procaine Dose for 3 Consecutive Days and Slaughtered with Varying Withdrawal Periods

		treatment[a]									
		1			2			3			
tissue	day	trial 1	trial 2	total	trial 1	trial 2	total	trial 1	trial 2	total	pooled treatments
kidney on-site[b]	5	+ + +	+ + +	6/6	+ + +	+ + +	6/6	+ + +	+ + +	6/6	18/18
	10	− − +	+ + +	4/6	− − +	− − +	2/6	+ + +	+ + +	6/6	12/18
	15	− − +	− + +	3/6	− − −	− + +	2/6	− + +	c[c] + +	4/6	9/18
	20	− − +	− + +	3/6	− − −	− − +	1/6	− − −	− − +	1/6	5/18
	25	− − +	− − −	1/6	∼[d] − −	− + +	2/6	− − −	− − −	0/6	3/18
	32	− − −	− + +	2/6	− − −	− − +	1/6	− − −	− − −	0/6	3/18
	39	− − −	− − −	0/6	− − +	− − −	1/6	− − −	− − +	1/6	2/18
frozen kidney[e]	5	+ + +	+ + +	6/6	+ + +	+ + +	6/6	+ + +	+ + +	6/6	18/18
	10	− − +	+ + +	4/6	− − +	∼[d] − +	2/6	+ + +	+ + +	6/6	12/18
	15	− − +	− + +	3/6	∼[d] − −	− + +	2/6	− + +	− + +	4/6	9/18
	20	− − c[c]	− + +	2/6	− − −	− − +	1/6	− − −	− − +	1/6	4/18
	25	− − +	− − −	1/6	− − −	− + +	2/6	∼[d] − −	− − −	0/6	3/18
	32	− − −	− + +	2/6	− − −	− − +	1/6	− − −	− − −	0/6	3/18
	39	− − −	− − −	0/6	− − +	− − −	1/6	− − −	− − +	1/6	2/18
frozen muscle[e]	5	+ + +	+ + +	6/6	+ + ∼[d]	+ + +	5/6	+ + +	c[c] + +	5/6	16/18
	10	− − ∼[d]	− − ∼[d]	0/6	− − −	− ∼[d] ∼[d]	0/6	− − −	− − +	1/6	1/18
	15	− − −	− − −	0/6	∼[d] − −	− − −	0/6	− − −	− − ∼[d]	0/6	0/18
	20	− − −	− − −	0/6	FP[f] − −	− − −	0/6	− − −	− − −	0/6	0/18
	25	− − −	− − −	0/6	− − −	− − −	0/6	− − −	− − −	0/6	0/18
	32	− − −	− − −	0/6	− − −	− − ∼[d]	0/6	− − −	− − −	0/6	0/18
	39	− − −	− − −	0/6	FP[f] − −	− − −	0/6	− − −	− − −	0/6	0/18
injection site	5	+ + +	+ + +	6/6	+ + +	+ + +	6/6	+ + +	+ + +	6/6	18/18
	10	− − +	+ + +	4/6	− + +	− − +	3/6	c[c] + +	+ + +	5/6	12/18
	15	− − +	− − −	1/6	− − −	− − −	0/6	− − −	− + +	2/6	3/18
	20	− − +	− + +	3/6	− − +	− + +	3/6	− − −	− − −	0/6	6/18
	25	− − −	− − −	0/6	− − −	− − −	0/6	c[c] − −	− − −	0/6	0/18
	32	− − −	− − +	1/6	− − −	− − −	0/6	− − −	− − −	0/6	1/18
	39	− − −	− − −	0/6	− − +	− − −	1/6	− ∼[d] +	− − +	2/6	3/18

[a]Treatments: (1) maximum of 10 mL of penicillin G procaine per injection; injections on consecutive days were in the same location as the previous day; (2) maximum of 10 mL of penicillin G procaine per injection site; injections on consecutive days were separated by approximately 5 cm; (3) maximum injection volumes of 20 mL of penicillin G procaine; injections on consecutive days were separated by approximately 5 cm. [b]KIS tests of kidney swabs were performed on the kill floor; results were obtained 3−4 h after animal harvest. [c]"c" Duplicate, simultaneously run KIS tests each returned "caution" results. FSIS regards cautions as a negative result. [d]A tilde (∼) represents ambiguous results in which duplicate KIS assays of the tissue scored either ±, ∓, −/c, c/−, +/c, or c/+ or in which independent analyst interpretations of the KIS assay were in disagreement. Ambiguous results were never clearly positive, so they were regarded as a negative result. [e]Aliquots of injection site; kidney and skeletal muscle were placed in Driploss tubes and stored at −80 °C until use. KIS tests were performed on kidney and muscle juice. [f]False positive. Presence of penicillin in positive KIS test results could not be verified with mass spectral analysis.

Kidney On-Site and Frozen Kidney Comparison. There was excellent agreement between KIS test positive on-site kidney and frozen kidney samples (Table 1). This consistency suggests the assay of frozen kidney tissue could be valuable for research purposes or for screening where testing fresh tissue is not possible. The assay of frozen tissues could also be used to verify results obtained on fresh tissues.

Effect of Withdrawal Time on the Detection of Penicillin G Procaine by the Rapid Screening Assay. Table 1 summarizes the effects of treatment and withdrawal period on KIS test positive results from regulated tissues (kidney and skeletal muscle) as a function of withdrawal time. Penicillin G residues were detected by the KIS test in kidney swab samples for the duration of the study, but with decreasing frequency as the withdrawal time increased. In the earlier withdrawal days (up to day 15), treatment 3 (high volume injection) gave the most positives followed by treatment 1 (same site injection) and treatment 2. However, when all withdrawal days were considered, there appeared to be no clear effects of treatment (penicillin G administration pattern) on the depletion of penicillin G from the kidney, as assessed by KIS test detection (Figure 3). When KIS test detection frequency (% positive) data were plotted against time for each treatment and fit with a monoexponential decay curve, no difference ($P > 0.05$) in the decay rate constants among the three treatments was observed; data among treatments were therefore pooled, and all of the frequency of detection data were fit to a monoexponential decay curve. Figure 3 demonstrates that penicillin G residues had not depleted from kidneys of all animals even after 39 days of withdrawal as also shown in Table 1.

Confirmation of the KIS test results by LC−MS/MS analysis indicated that the KIS test returned no false positive results for kidney despite the wide range of concentrations obtained from LC−MS/MS analysis (with samples above mLOQ from 17−9900 ng/g tested as positive by KIS test). Kidney LC−MS/MS concentrations <4.92 ng/g were returned as either "caution" or negative by the KIS test. Details of LC−MS/MS analysis for

dx.doi.org/10.1021/jf501494w | J. Agric. Food Chem. 2014, 62, 7586−7592

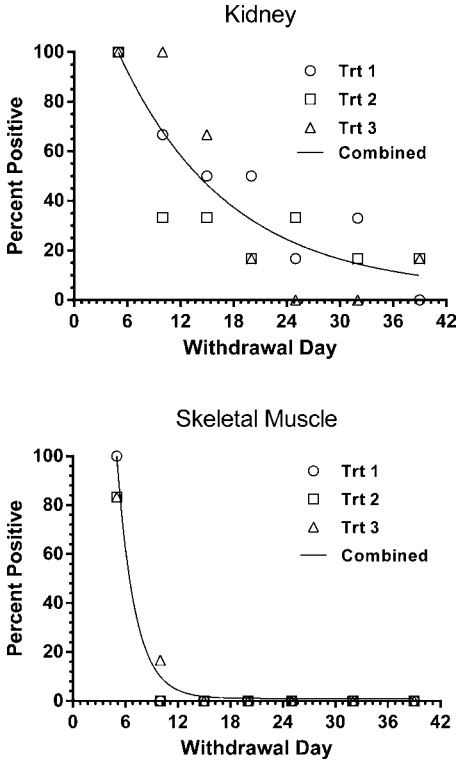

Figure 3. Depletion of penicillin G residues in kidneys (upper panel) and muscle (lower panel) of heavy sows as detected by the KIS rapid screening assay. Line is a first-order depletion fit of combined data from treatments; false positive results were removed from the skeletal muscle data prior to plotting.

penicillin G in sows are available in the accompanying paper.[13] The KIS test analysis of kidney indicated that approximately 50% of the animals administered a 5× labeled dose would show positive penicillin residues when slaughtered at day 15. The Food Animal Residue Avoidance Database (FARAD) had recommended a preslaughter withdrawal period of 15 days for swine administered a 10× penicillin G procaine dose,[12] but this has since been revised to a 50 day withdrawal interval for swine dosed with 2×−10× penicillin G procaine.[19] On the basis of the kidney results, a 15-d withdrawal period is insufficient. Even after a 39 day withdrawal period, approximately 11% of the animals tested positive for penicillin G, indicating that a prolonged period (50 days) would be required for animals to have kidneys free of penicillin residue.

Muscle. It was difficult to obtain muscle juice on-site from fresh pork, which is in apparent contrast to the cattle study reported by Schneider et al.[20] A simple freeze and thaw cycle, however, allowed sufficient quantities of muscle juice to be collected. There were no distinguishable effects of treatment on skeletal muscle detection frequency, so further analysis was conducted with results from the three treatments pooled (Table 1, Figure 3). For skeletal muscle, 16 of 18 hogs returned positive KIS test results after a 5 day withdrawal period, but by 10 days, only 1 of 18 hogs tested returned a positive KIS test result. Despite the difficulty in using the KIS test for muscle determination of penicillin G, the results clearly indicate more rapid elimination of penicillin G from muscle than kidney. The data also demonstrate the variability between animals, which has been previously observed with IM injection of penicillin G.[21] From market hog penicillin results reported by Korsrud et al.,[6] penicillin concentrations in kidney were approximately 40−70 times greater than residues in corresponding muscle samples. In agreement with their findings, the KIS test assay returned smaller numbers of muscle positives than in kidneys for the same animal and time point.

Scoring of samples derived from muscle juice was more difficult than for kidney juice. For example, of the 132 samples tested (5× treated animals plus controls), eight needed to be repeated due to ambiguous results for a 6% repeat rate. In one incidence with a "caution" result in a muscle sample on withdrawal day 5, treatment 3 had a corresponding LC−MS/MS concentration of 33 ng/g,[13] which is above the FSIS minimum applicability level (25 ng/g)[22] and would be considered a false negative. Two instances occurred in which the KIS test returned positive assay results in muscle (treatment 2, days 20 and 39; Table 1), but the corresponding LC−MS/MS results were nondetects,[13] confirming that these two KIS test results are false positives. In general terms, skeletal muscle was a more difficult matrix for use with the KIS test with regards to sample treatment and when comparing assay results with the LC−MS/MS data.

KIS Test Results from Serum, Urine, and Liver Juice. Applicability of using the KIS test for preslaughter screening of treated animals was tested with assays of serum and urine (Table 2). When compared to LC−MS/MS results, serum and urine samples did not return false positives. The urine was a much better surrogate matrix for detecting potential violative penicillin G residues in kidney (Figure 4) than serum; statistical evaluation using the McNemar's test showed no difference between kidney and urine (P = 0.48). Serum results clearly demonstrate that serum is an inadequate surrogate for kidney because serum is more rapidly cleared of penicillin G than kidney, and McNemar's test showed a significant difference between kidney and serum ($P \leq 0.001$).

The KIS test assays of liver returned fewer positive results than the assays of other tissues, even at day 5 (Table 2). These results could be caused by the much poorer assay sensitivity of liver as compared to other matrices. However, these results could also have been obtained from a lower retention of penicillin G in liver, relative to other tissues, as reported by some researchers.[6] The penicillin G in liver was not performed using LC−MS/MS analysis for this study because liver was not a tissue of interest for regulatory agencies or industry and was not suitable for ante-mortem purposes.

Serum showed more positive samples than muscle on day 10, but from day 20 on these matrices showed only one positive reflecting little retention in this matrices. Surprisingly, serum levels do not correlate to muscle levels, and McNemar's test showed significant difference between muscle and serum ($P \leq 0.001$).

Injection Sites. The injection site KIS tests returned a pattern similar to that of kidney with relatively few exceptions. For example, the two positive kidney samples at day 39 also had corresponding positive responses in their injection site samples reflecting prolonged exposure (Table 1). An additional sow had a positive KIS test result from the injection site without a corresponding positive KIS test result from the kidney at withdrawal day 39. All three KIS test injection site positives from withdrawal day 39 had penicillin G residues as determined by LC−MS/MS analysis (3.7, 9.6, and 1254 ng/g).[13] However, there were 5 false positives and 13 false negatives among the 126 injection site samples when compared to the LC−MS/MS data, indicating difficulty in analysis of injection sites. The wide range of penicillin G levels found in injection sites could be one

Table 2. Results of the KIS Test in Serum, Urine, and Liver Expressed as Positive or Negative from Heavy Sows Treated with a 5× Penicillin G Procaine Dose for 3 Consecutive Days and Slaughtered with Varying Withdrawal Periods

		treatment[a]									
		1			2			3			
tissue	day	trial 1	trial 2	total	trial 1	trial 2	total	trial 1	trial 2	total	pooled treatments
serum[b]	5	+ + +	+ + +	6/6	+ + +	+ + +	6/6	+ + +	+ + +	6/6	18/18
	10	− − +	+ + +	4/6	∼[c] − −	− − +	1/6	− + +	+ + +	5/6	10/18
	15	∼[c] − −	− − +	1/6	− − −	− c[d] c[d]	0/6	∼[c] − −	c[d] c[d] −	0/6	1/18
	20	∼[c] − −	c[d] − −	0/6	− − −	∼[c] − −	0/6	− − −	− ∼[c] +	1/6	1/18
	25	c[d] − −	∼[c] − −	0/6	− − −	− − −	0/6	− − −	− − −	0/6	0/18
	32	− − −	− − −	0/6	− − −	∼[c] ∼[c] −	0/6	− − −	∼[c] − −	0/6	0/18
	39	− − −	− − −	0/6	− − −	− − −	0/6	− − −	− − −	0/6	0/18
urine[b]	5	+ + +	+ + +	6/6	+ + +	+ + +	6/6	+ + +	+ + +	6/6	18/18
	10	− + +	+ + +	5/6	c + +	− − +	3/6	+ + +	+ + +	6/6	14/18
	15	− − +	− + +	3/6	− − −	− + +	2/6	− + +	− + +	4/6	9/18
	20	− − −	− + +	2/6	∼[c] − −	− − +	1/6	− − −	− − +	1/6	4/18
	25	x[e] − +	− − −	1/5	x[e] c[d] −	− + +	2/5	∼[c] − −	− − −	0/6	3/16
	32	x[e] − −	− + +	2/5	− − −	− − +	1/6	− − −	− − −	0/6	3/17
	39	x[e] − −	− − −	0/5	∼[c] − x[e]	− − −	0/5	− − −	− − +	1/6	1/16
liver[f]	5	− − +	− + +	3/6	− + +	− − −	2/6	∼[c] − −	− − +	1/6	6/18
	10	− − −	− − −	0/6	− − −	− − −	0/6	− − −	− − +	1/6	1/18
	15	− − −	− − +	1/6	− − −	− − −	0/6	− − −	− − −	0/6	1/18
	20	− − −	− − −	0/6	− − −	− − −	0/6	− − −	− − −	0/6	0/18
	25	− − −	− − −	0/6	− − −	− − −	0/6	− − −	− − −	0/6	0/18
	32	− − −	− − −	0/6	− − −	− − −	0/6	− − −	− − −	0/6	0/18
	39	− − −	− − −	0/6	− − −	− − −	0/6	− − −	− − −	0/6	0/18

[a]Treatments: (1) maximum of 10 mL of penicillin G procaine per injection; injections on consecutive days were in the same location as the previous day; (2) maximum of 10 mL of penicillin G procaine per injection site; injections on consecutive days were separated by approximately 5 cm; (3) maximum injection volumes of 20 mL of penicillin G procaine; injections on consecutive days were separated by approximately 5 cm. [b]Serum and urine aliquots were combined with KIS serum/urine neutralizing tablets, mixed, and supernatant was used for KIS tests. [c]A tilde (∼) represents ambiguous results in which duplicate KIS assays of the tissue scored either ±, ∓, −/c, c/−, +/c, or c/+ or in which independent analyst interpretations of the KIS assay were in disagreement. Ambiguous results were never clearly positive, so they were regarded as a negative result. [d]"c" Duplicate, simultaneously run KIS tests each returned "caution" results. FSIS regards cautions as a negative result. [e]x, Urine sample unobtainable. [f]Aliquots of liver were placed in Dripless tubes and were frozen at sampling; KIS tests were performed on liver juice after thawing and 1 min boil.

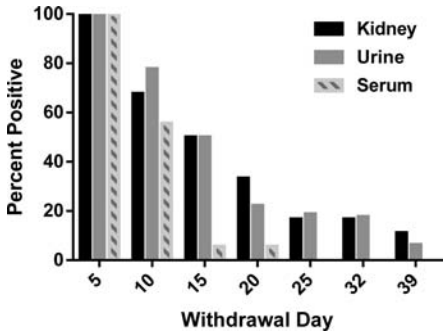

Figure 4. Comparison of KIS test results in urine, serum, and kidneys of treated sows as a function of withdrawal day.

of the contributing factors resulting in these inconsistencies. For example, for treatment 1 withdrawal day 10, the penicillin G concentrations returned by LC−MS/MS ranged from 3.2 to 1 580 000 ng/g among the six sows. Another difficulty was the performance of the KIS test analysis in muscle tissue and particularly interferences caused by fat. Problems in uniform injections (intermuscular vs intramuscular) have been previously noted[6] and could cause increased variability of penicillin G concentration at the injection site. Finally, difficulties in obtaining appropriate samples at the injection site could produce diversity due to the heterogeneity expected at this site.

Positive and Negative Control Sows. Negative control sows that received normal saline and that were slaughtered on withdrawal day 5 had negative KIS readings for all matrices tested for both trials 1 and 2. The positive control sows, which received the label dose and were slaughtered at withdrawal day 7, showed positive KIS test results for both trials (data not shown) from on-site kidney samples and the kidney samples that were frozen and thawed once. Results from LC−MS/MS gave 461 and 202 ng/g of penicillin G in the kidney of the positive control animals. Urine, injection sites, and serum also tested positive, with the exception of a "caution" result in serum for trial 2 withdrawal day 7. Muscle and liver samples tested negative for withdrawal day 7 positive control animals. For withdrawal day 15, one out of two positive control animals tested positive using the KIS test in kidney, injection site, and urine samples, but the rest of the matrices returned negative results. The LC−MS/MS results had penicillin G concentrations of 190 ng/g, 2090 ng/g, and 17 760 ng/mL for kidney, injection site, and urine, respectively, from the positive control sow on withdrawal day 15 that tested positive by KIS test. Thus, use of the KIS test as a screen could return a positive kidney result even though the main tissue of human consumption, muscle (meat), would probably be negative when the prescribed dose and withdrawal period are observed. These results would produce an unnecessary condemnation due to slow elimination of penicillin G in the kidney.

dx.doi.org/10.1021/jf501494w | J. Agric. Food Chem. 2014, 62, 7586−7592

Collectively, these data suggest along with other studies that the earlier recommended 15 day withdrawal period for swine dosed with up to 10× the labeled penicillin G procaine dose[12] is insufficient for residues to deplete to levels nondetectable by the KIS test assay in kidney. Specifically, approximately 50% of the heavy sows treated with a 5× dose of penicillin G procaine on each of three consecutive days had kidneys that would test positive with the regulatory on-site screening assay. Indeed, the KIS test detection system indicated the probability that greater than 39 days of withdrawal would be required for residues to deplete sufficiently to ensure that treated animals be free of renal penicillin G prior to slaughter, supporting the current FARAD recommendation.[19] In contrast, the KIS test data seemed to indicate that penicillin G depleted very rapidly from muscle, relative to kidney, and that the 2006 FARAD recommended 15-day withdrawal period[12] for muscle would be adequate to ensure the safety of skeletal muscle. Skeletal muscle was a more difficult matrix to analyze than kidney when using the KIS test, but using our modified procedure the results indicate rapid clearance from muscle. Muscle required a freeze and thaw step to produce sufficient liquid for the KIS test; hence muscle is not particularly useful for on-site monitoring to determine whether an animal had been exposed to penicillin G. The data indicate that urine would be a very useful antemortem matrix for on-farm or preslaughter testing with which veterinarians or pork producers could predict the presence of kidney penicillin G residues.

AUTHOR INFORMATION

Corresponding Author

*Tel.: (701) 239-1425. E-mail: weilin.shelver@ars.usda.gov.

Funding

Financial support was partially provided by the National Pork Board, agreement no. 58-5442-2-404, and in-kind support provided by Charm Sciences, agreement no. 58-5442-32000-014-07N.

Notes

Names are necessary to report factually on available data; however, the USDA neither guarantees nor warrants the standard of the product, and the use of the name by USDA implies no approval of the product to the exclusion of others that may also be suitable. USDA is an equal opportunity provider and employer.

The authors declare no competing financial interest.

ACKNOWLEDGMENTS

We wish to thank Amy McGarvey, Grant Herges, and Erin Loeb for performing KIS tests; Dillon Hofsommer, Kelsey Heiberg, and Nathaniel Grosz for LC−MS/MS sample preparation; and Jason Holthusen for LC−MS/MS analysis. The animal care, slaughter, and sampling assistance provided by Roberta Dahlen, Dee Ellig, Austen Germolus, Justin Gilbertson, Benjamin Klinkner, Richelle Miller, Colleen Pfaff, and Terry Skunberg is gratefully acknowledged. Manuscript reviews provided by Drs. Pat Basu, Louis Bluhm, and Joseph Hill from USDA-FSIS are greatly appreciated.

REFERENCES

(1) NADA 065-010, Freedom of information summary, supplemental new animal drug application, Norocillin, Penicillin G procaine, injectable suspension cattle, sheep, swine, and horses. Approval date: April 23, 2010.

(2) 21 CFR Section 556.510(b).

(3) Hoover, T. C. Health and Performance Improvements of Pigs Treated with DRAXXIN (tulathromycin) Injectable Solution for Swine Respiratory Disease Under Field Conditions. http://www.thepigsite.com/articles/1/pig-health/2674/health-and-performance-of-pigs-treated-with-draxxin, accessed 1/3/2014.

(4) 21 CFR Section 530.

(5) Moats, W. A.; Harris, E. W.; Steele, N. C. Depletion of intramuscularly injected procaine penicillin G from tissues of swine. A comparison of HPLC and bioassay procedures. *J. Agric. Food Chem.* **1986**, *34*, 452−456.

(6) Korsrud, G. O.; Salisbury, C. D. C.; Rhodes, C. S.; Papich, M. G.; Yates, W. D. G.; Bulmer, W. S.; MacNeil, J. D.; Landry, D. A.; Lambert, G.; Yong, M. S.; Ritter, S. L. Depletion of penicillin G residues in tissues, plasma, and injection sites of market pigs injected intramuscularly with procaine penicillin G. *Food Addit. Contam.* **1998**, *15*, 421−426.

(7) Apley, M.; Goetzee, H.; Gehring, R.; Karriker, L. Pharmacokinetics and tissue residues of procaine penicillin G in sows after administration of 33,000 IU/kg intramuscularly and by needle-free injection in the hip. National Pork Board Research Report NPB #07-234, 2009.

(8) KuKanich, B.; Gehring, R.; Webb, A. I.; Craigmill, A. L.; Riviere, J. E. Effect of formulation and route of administration on tissue residues and withdrawal times. *J. Am. Vet. Med. Assoc.* **2005**, *227*, 1574−1577.

(9) Riviere, J. E. *Comparative Pharmacokinetics: Principles, Techniques, and Applications*, 2nd ed.; Wiley-Blackwell: Chichester, West Sussex, UK, 2011.

(10) Food Safety and Inspection Service Notice 45-11, Using the kidney inhibition swab (KIS) test to detect antimicrobial drug residues in swine in selected establishments - phase III.

(11) Food Safety and Inspection Service Notice 43-12, Using the kidney inhibition swab (KIS) test to detect antimicrobial drug residues in all livestock in slaughter establishments-Phase IV.

(12) Payne, M. A.; Craigmill, A.; Riviere, J. E.; Webb, A. I. Extralabel use of penicillin in food animals. *J. Am. Vet. Med. Assoc.* **2006**, *229*, 1401−1403.

(13) Lupton, S. J.; Shelver, W. L.; Newman, D. J.; Larsen, S.; Smith, D. J. Depletion of penicillin G residues in heavy sows after intramuscular injection. *J. Agric. Food Chem.***2014**, 10.1021/jf501492v.

(14) Food Safety and Inspection Service, Swab test for antimicrobial drug detection, CLG-ADD 3.01. Effective 05/29/2011.

(15) Kidney inhibition swab brochure, http://www.charm.com/en/products/charm-inhibition/kis-kidney-inhibition-swab/kis-kidney-inhibition-swab-learn-more.html, accessed 10/25/13.

(16) Operator's Manual: Charm kidney inhibition swab (KIS) test for antimicrobial drugs in cattle serum and urine. OM-519-001, Charm Sciences, Inc.

(17) Schneider, M. J.; Lehotay, S. J. A comparison of the FAST, Premi, and KIS tests for screening antibiotic residues in beef kidney juice and serum. *Anal. Bioanal. Chem.* **2008**, *390*, 1775−1779.

(18) Moats, W. A. Inactivation of antibiotics by heating in foods and other substrates − a review. *J. Food Prot.* **1988**, *51*, 491−497.

(19) http://www.farad.org/WDIlookup/DigestResults.asp, accessed 1/7/14.

(20) Schneider, M. J.; Mastovska, K.; Solomon, M. B. Distribution of penicillin G residues in culled dairy cow muscles: implications for residue monitoring. *J. Agric. Food Chem.* **2010**, *58*, 5408−5413.

(21) Ranheim, B.; Ween, H.; Egeli, A. K.; Hormazabal, V.; Yndestad, M.; Soli, N. E. Benzathine penicillin G and procaine penicillin G in piglets: comparison of intramuscular and subcutaneous injection. *Vet. Res. Commun.* **2002**, *26*, 459−465.

(22) Food Safety and Inspection Service, Screening and confirmation of animal drug residues by UHPLC-MS-MS, CLG-MRM 1.01. Effective 02/22/2013.

MATERIALS AND METHODS

Collection of Fish Samples. *Marine Fish Sampling.* The list of marine fishes to be collected was based on the individual dietary consumption analysis of the 996 adult high-seafood consumers of the CALIPSO study,[38] recruited in four coastal areas in metropolitan France between October and December 2004. The fish consumption habits of the population of these four areas and their surrounding 20−25 km, namely, La Rochelle in Gironde-Charente Maritime Sud, Le Havre in Normandy-Baie de Seine, Lorient in South Brittany, and Toulon in Mediterranean-Var, match the highest fish consumption habits in metropolitan France.[38] Five primary samples were bought in each region for each species between January and April 2005 to take into account the purchase habits of the considered population (fresh or frozen products; purchase locations of fishmarket, supermarket, etc.). For example, if a fish species is purchased 80% of the time in a supermarket and 20% of the time in a fishmarket, then four of the five primary samples were purchased in a supermarket and one primary sample was purchased in a fishmarket. The sex and fish body weight and length were not available and consequently not taken into account in the sampling and analyses. However, it should be remembered that the purpose of the present study was to perform an exposure assessment study at populational scale and not to study the determinant factors associated with the observed levels of chemicals. The used sampling process respected the purchase habits of the study population, and it has been considered as fairly representative of what is bought and consumed by the CALIPSO population. Each sample finally considered for analysis was a composite one of 1000 g, made up of five 200 g portions of the primary sample raw edible parts (fillets without skin or entrails). Twenty-three composite samples were then constituted in La Rochelle, 22 in Le Havre, 26 in Lorient, and 23 in Toulon. The sampling period ranged between January and April 2005, and a total of 94 fish composite samples were prepared, corresponding to 29 species, which reflect the regional consumption and contamination differences. This sampling procedure allowed covering 89−96% of the total consumption of fish according to the four areas. Recruiting strategy, consumption survey development, and marine fish sampling methodology have already been described.[38]

Freshwater Fish Sampling. The list of freshwater fishes to be collected was based on the individual dietary consumption analysis of the 606 anglers or their family members of the ICAR-PCB study, initially designed to assess French freshwater fish contamination in PCBs along with angler's PCB internal exposure (i.e., serum level). Seven hundred and forty-seven freshwater fishes were collected in 2008 and 2009 covering different seasons by ONEMA (French National Agency for Water and Aquatic Environments) in six major French rivers, each river being divided in three or four sections. The dietary consumption analysis and the freshwater fish sampling methodology have already been described elsewhere.[39,40] Briefly, each sample had to contain at least 400 g of fish muscle for analysis purposes. If one fish was not enough to reach this amount, then several fishes from the same species and the same location were pooled to form a composite sample, as was the case for half of the samples. The consequence is the loss of some raw data such as sex, body weight, and body length, but as the fishes were sampled randomly, it was considered that they were fairly representative of what could be caught and consumed by the anglers. Although this study was designed for PCBs, we assessed that PCB and PFAA contamination levels in freshwater fishes were not statistically associated. Indeed, due to their physicochemical properties, PCBs are lipophilic and accumulate in fat, whereas PFAAs are amphiphibic and tend to accumulate in liver and blood.[41,42] It is assumed that our samples offer a representative view of freshwater fish contamination in metropolitan France. The 16 most consumed fish species among the remaining samples after multiple analyses (for PCBs, dioxins, hexachlorobenzene, etc.) were selected, resulting in 387 samples being analyzed for PFAAs.

The samples for lipid and FA analysis were extracted from the same ONEMA freshwater fish sample library constituted between 2008 and 2010. The number of fish included per composite sample of the same freshwater fish species was determined based on availability of material in the library and was also linked to the weight of individual fish, more fishes being needed per composite for small fish. Among the 32 freshwater fish groups sampled, the 11 most consumed were selected with at least 10 individual fishes per sample, resulting in 28 composite samples.

Analysis of Lipid and Fatty Acid Composition and PFAA Contamination. *Analysis of PFAAs.* The used methodology targeted 15 PFAAs: perfluorobutanoic acid (PFBA), perfluoropentanoic acid (PFPA), perfluorohexanoic acid (PFHxA), perfluoroheptanoic acid (PFHpA), perfluorooctanoic acid (PFOA), perfluorononanoic acid (PFNA), perfluorodecanoic acid (PFDA), perfluoroundecanoic acid (PFUnA), perfluorotridecanoic acid (PFTrDA), perfluorotetradecanoic acid (PFTeDA), perfluorobutane sulfonate (PFBS), perfluorohexanane sulfonate (PFHxS), perfluoroheptane sulfonate (PFHpS), perfluorooctane sulfonate (PFOS), and perfluorodecane sulfonate (PFDS). The analytical procedure used for PFAA determination was described elsewhere.[43] Briefly, samples were pretreated by freeze-drying and liquid/solid extraction with methanol. A dispersive solid phase extraction (SPE) based on charcoal particles was then applied. Final purified extracts were analyzed by liquid chromatography coupled to tandem mass spectrometry (LC-MS/MS) with negative electrospray ionization on a triple-quadrupole system. Two diagnostic signals (MRM transitions) were recorded for each targeted analyte. Quantification was performed according to the isotope dilution principles: each sample was supplemented by 11 ^{13}C-labeled internal standards ($^{13}C_4$-PFBA, $^{13}C_5$-PFHxA, $^{13}C_4$-PFHpA, $^{13}C_4$-PFOA, $^{13}C_5$-PFNA, $^{13}C_2$-PFDA, $^{13}C_7$-PFUnA, $^{13}C_2$-PFDoA, $^{18}O_2$-PFHxS, $^{13}C_4$-PFOS, and $^{13}C_4$-PFOSi). Limits of detection (LOD), depending on the considered fish species and target compound, were determined on the basis of the signal-to-noise ratio (S/N > 3) and ranged from 0.005 to 0.3 ng g^{-1} for PFOA and PFOS and from 0.007 to 0.95 ng g^{-1} for other PFAA substances. Repeatability of the signal was also dependent on the matrix but was globally estimated below 18.6% for all compounds.

The generated exposure data were produced under the Quality Assurance system (ISO.IEC 17025:2005 and ISO 9001:2008 standards) and using validated analytical methods, including interlaboratory comparison tests, that have proven the fitness-for-purpose of this method.

Blank and quality control samples were analyzed and monitored in parallel with the samples to be characterized: the signal of each compound in the blanks was checked to ensure the absence of contamination throughout the analytical procedure, and concentrations of analytes in quality control were monitored to check the method repeatability.

Analysis of Lipids and Fatty Acids. The total lipids and 48 free FAs were analyzed for the 40 marine fish composite samples. The protocol was detailed elsewhere.[44] Briefly, the total lipids were analyzed by two different laboratories with two different methods for the same samples. One of the laboratories freeze-dried the samples before powdering and transfer into accelerated solvent extraction with a 70:30 (v/v) mixture of toluene/acetone. Then the samples were evaporated and the total lipids were determined by gravimetry. The second laboratory followed the AFNOR NF V04-403 standard for meat, meat products, and fish products for the extraction, purification, and esterification of the free fat.[45] Then the extracts were dried, extracted with a mixture of hexane/isopropanol 3:2 (v/v) before filtration on a Na_2SO_4 and Celite column, and weighed. For the free FA analysis, the FAs were extracted with hexane, filtered, esterified with a mixture of methanol/sulfuric acid 13:2 (v/v), and analyzed using a gas phase chromatograph equipped with a flame ionization detector. Their identification was based on retention time obtained for standard esters. The part of each free FA was based on the area of the corresponding peaks, in relation with a standard solution.

The total lipids and 40 free FAs were analyzed for the 28 freshwater fish composite samples. For each sample, the free fat was extracted, purified, and esterified by reaction with boron trifluoride according to the NF EN ISO 5509 standards.[46] The esters were then analyzed using a gas phase chromatograph equipped with a flame ionization detector according to the NF EN ISO 5508 standards[47] and identified in the same way as for the marine fish samples.

Data and Statistical Analysis. All statistical analyses were performed using the SAS software 9.3 (SAS Institute Inc., Cary, NC, USA). Normality of the distributions was tested with the Kolmorogov−Smirnov test and homoscedasticity with the Bartlett test. The Kruskal−Wallis test was used to compare fish PFAA contamination between the

Table 1. PFAA Contamination of Fresh and Frozen Marine Fish LB-UB If LB Value Different from UB Value (Nanograms per Gram ww)[a]

species	*n*	PFBA	PFPA	PFHxA	PFHpA	PFOA	PFNA	PFDA	PFUnA
anchovy, *Engraulis encrasicolus*	1	0−0.08	0−0.07	0−0.05	0−0.06	0−0.07	0−0.06	0−0.09	0−0.09
monkfish, *Lophius piscatorius, Lophius budegassa*	4	0.45−0.46	0.14−0.16	0.4−0.43	0.36−0.39	0.98−0.99	0.09−0.11	0.06−0.08	0.16−0.16
catshark *Scyliorhinus canicula, Scyliorhinus stellaris*	4	0.17	0.14−0.16	0.25−0.27	0.26−0.28	0.41−0.43	0.06−0.08	0.04−0.07	0.14−0.15
cod, *Gadus morhua*	4	0.34−0.38	0.11−0.13	0.43	0.36	1.05−1.06	0.15	0.13−0.13	0.19−0.19
common dab *Limanda limanda, Microstomus kitt*	4	0.17	0.12−0.13	0.33−0.34	0.28−0.29	0.8−0.81	0.09−0.1	0.09−0.09	0.03−0.06
orange roughy, *Hoplostethus atlanticus*	3	0.44	0.32−0.33	1.2	0.73	1.69	0.19	0.35−0.35	0.13−0.15
plaice/witch *Pleuronectes platessa, Glyptocephalus cynoglossus*	2	0.48	0.46	0.87	0.6	1.21	0.16	0.17−0.17	0.01−0.04
goatfish, *Mullus barbatus barbatus, Mullus surmelutus*	3	0.74−0.77	0.48−0.5	0.65−0.66	0.43−0.45	0.87−0.89	0.15−0.19	0.1−0.1	0.02−0.07
grenadier, *Coryphaenoides rupestris*	4	0.26	0.07−0.08	0.19	0.22	0.3−0.31	0.05−0.07	0.03−0.05	0.07−0.07
gurnard *Trigla lucerna*	1	0.27	0.03	0−0.05	0−0.06	0−0.01	0−0.04	0−0.05	0.07−0.07
haddock *Melanogrammus aeglefinus*	2	0.6	0.23	1.01	0.4	1.3	0.17	0.3−0.3	0.07−0.07
hake *Merluccius merluccius*	4	0.41	0.14−0.15	0.33−0.34	0.26−0.28	0.74−0.76	0.05−0.06	0.07−0.07	0−0.05
halibut *Hippoglossus hippoglossus, Reinhardtius hippoglossoides*	4	0.08−0.12	0.05−0.09	0.13−0.15	0.1−0.13	0.29−0.33	0.03−0.06	0.03−0.06	0.14−0.14
John Dory, *Zeus faber*	2	0.37	0.25	0.53	0.51	0.48	0.08−0.1	0.08−0.08	0.24−0.24
ling, *Molva molva, Molva dypterygia*	4	0.21	0.04−0.05	0.13	0.17	0.29−0.3	0.03−0.07	0.03−0.05	0.09−0.09
mackerel, *Scomber scombrus*	4	0.12−0.17	0.32−0.38	0.34−0.38	0.22−0.26	0.31−0.34	0.03−0.06	0.02−0.05	0.21−0.23
pollack, *Pollachius pollachius*	3	0.19	0.21	0.67	0.55	1.58	0.19	0.15−0.15	0.13−0.13
pout, *Trisopterus luscus*	1	0.51	0.32	1.06	0.88	1.44	0.12	0.04−0.04	0.04−0.04
ray ,*Raja clavata, Raja naevus, Raja circularis*	4	0.14−0.16	0.11−0.12	0.36−0.37	0.28−0.3	0.88−0.91	0.13	0.22−0.22	0.74−0.74
saithe, *Pollachius virens*	4	0.11−0.14	0.07−0.09	0.16−0.17	0.15	0.47−0.48	0.04−0.06	0.05−0.05	0.15−0.15
salmon, *Salmo salar*	4	0.06−0.13	0.09−0.12	0.26−0.27	0.18−0.19	0.66−0.68	0.05−0.07	0.05−0.06	0−0.14
sardine, *Sardina pilchardus*	4	0.67−0.71	0−0.09	0.11−0.14	0.1−0.13	0.26−0.29	0−0.07	0.02−0.09	0.42−0.54
scorpionfish, *Scorpaena porcus, Scorpaena scrofa, Helicolenus dactylopterus*	1	0.29	0.23	1.6	0.16	0.92	0.12	0.55−0.55	0.18−0.18
seabass, *Dicentrarchus labrax*	4	0.44	0.25−0.28	0.42−0.44	0.35−0.38	0.76−0.79	0.21−0.24	0.13−0.14	1.56−1.56
sea bream, *Spondyliosoma cantharus, Sparus aurata, Pagellus bogaraveo*	4	0.23−0.25	0.25−0.29	0.35−0.37	0.3−0.35	0.41−0.44	0.07−0.09	0.05−0.08	0−0.07
sole, *Solea solea*	4	0.8	0.12−0.13	0.5	0.39−0.4	0.92	0.27	0.11−0.11	0.04−0.06
swordfish, *Xiphias gladius*	4	0.06−0.14	0−0.07	0−0.08	0.04−0.08	0.18−0.22	0−0.06	0−0.08	0−0.08
tuna, *Thunnus thunnus*	4	0−0.09	0−0.04	0.08−0.1	0.06−0.07	0.21−0.24	0−0.04	0.01−0.03	0.35−0.4
whiting, *Merlangius merlangus*	4	0.34−0.35	0.13−0.14	0.41−0.42	0.32−0.33	0.92−0.93	0.07−0.1	0.07−0.09	0.05−0.05
mean (std)	LB	0.31 (0.22)	0.16 (0.18)	0.44 (0.39)	0.3 (0.21)	0.7 (0.46)	0.09 (0.07)	0.1 (0.12)	0.18 (0.31)
	UB	0.33 (0.21)	0.18 (0.12)	0.46 (0.38)	0.32 (0.2)	0.72 (0.45)	0.11 (0.06)	0.12 (0.11)	0.21 (0.3)
min−max	LB	0−0.8	0−0.48	0−1.6	0−0.88	0−1.69	0−0.27	0−0.55	0−1.56
	UB	0.08−0.8	0.03−0.5	0.05−1.6	0.06−0.88	0.01−1.69	0.04−0.27	0.03−0.55	0.04−1.56

[a]Std, standard deviation; min, minimum contamination value; max, maximum contamination value.

coastal sites or major river sections. Ward's method has been applied for the hierarchical cluster analysis to define three groups of freshwater fishes (low, medium, and high levels of PFAA contamination). A multiple regression analysis was conducted to assess the association between PFAA contamination and content of lipids, FAs, n-3 PUFAs, and n-6 PUFAs. Differences were considered as significant for an α risk below 5%.

The percentage of left-censored data (i.e., data below the limit of detection, LOD) for the PFAA contamination was above 60%, and the LOD was low enough for the WHO GEMS/Food-EURO workshop recommendations to be applied.[48] Two scenarios were defined. In the lower bound (LB) scenario, the values below the LOD were replaced by 0, and in the upper bound (UB) scenario, the values below the LOD were replaced by the value of the LOD.

RESULTS AND DISCUSSION

PFAA Contamination. The 15 PFAAs analyzed in both marine and freshwater fishes were considered to describe PFAA contamination. The results are expressed with the sum of the 15 following PFAAs: PFBA, PFPA, PFHxA, PFHpA, PFOA, PFNA, PFDA, PFUnA, PFTrDA, PFTeDA, PFBS, PFHxS, PFHpS, PFOS, and PFDS. The percentage of censored data ranged from 9.5% (for PFOS) to 100% (for PFBS and PFHpS) for marine fishes and from 0.26% (for PFOS) to 100% (for PFPA) for freshwater fishes with mean percentages of, respectively, 69.9 and 64.3%. Contamination under UB hypothesis is about 4% higher

Table 2. PFAA Contamination of Fresh and Frozen Marine Fish LB-UB If LB Value Different from UB Value (Nanograms per Gram wet weight)[a]

species	*n*	PFTrDA	PFTeDA	PFBS[b]	PFHxS	PFHpS[b]	PFOS	PFDS	ΣPFAAs
anchovy, *Engraulis encrasicolus*	1	0−0.07	0−0.07	0.03	0−0.03	0.05	0.34	0−0.05	0.34−1.19
monkfish, *Lophius piscatorius, Lophius budegassa*	4	0.02−0.05	0−0.06	0.02	0−0.02	0.03	0.43	0−0.03	3.1−3.41
catshark, *Scyliorhinus canicula, Scyliorhinus stellaris*	4	0.12−0.13	0−0.05	0.02	0.02−0.04	0.03	1.01	0−0.03	2.62−2.92
cod, *Gadus morhua*	4	0−0.08	0−0.04	0.02	0−0.02	0.01	0.63	0−0.01	3.38−3.63
common dab, *Limanda limanda, Microstomus kitt*	4	0−0.04	0−0.04	0.02	0−0.02	0.03	0.37	0−0.03	2.29−2.55
orange roughy, *Hoplostethus atlanticus*	3	0−0.05	0−0.04	0.02	0−0.03	0.03	0.18	0−0.03	5.23−5.45
plaice/witch *Pleuronectes platessa, Glyptocephalus cynoglossus*	2	0−0.04	0−0.07	0.02	0−0.02	0.03	1.15	0−0.03	5.1−5.34
goatfish, *Mullus barbatus barbatus, Mullus surmelutus*	3	0−0.05	0−0.04	0.03	0−0.03	0.04	0.96	0−0.04	4.4−4.81
grenadier, *Coryphaenoides rupestris*	4	0.02−0.05	0−0.03	0.02	0−0.02	0.03	0.05	0−0.03	1.26−1.5
gurnard, *Trigla lucerna*	1	0−0.05	0−0.01	0.03	0.03	0.04	0.97	0−0.04	1.37−1.73
haddock, *Melanogrammus aeglefinus*	2	0−0.04	0−0.06	0.02	0−0.02	0.03	0.6	0−0.03	4.68−4.88
hake, *Merluccius merluccius*	4	0−0.04	0−0.03	0.02	0−0.02	0.03	0.08	0−0.03	2.07−2.39
halibut, *Hippoglossus hippoglossus, Reinhardtius hippoglossoides*	4	0−0.06	0−0.05	0.02	0−0.03	0.04	0.33	0−0.04	1.19−1.64
John dory, *Zeus faber*	2	0−0.05	0−0.04	0.02	0.02−0.04	0.03	1.04	0−0.03	3.59−3.8
ling, *Molva molva, Molva dypterygia*	4	0.01−0.05	0−0.04	0.02	0−0.02	0.03	0.14	0−0.03	1.15−1.4
mackerel, *Scomber scombrus*	4	0−0.05	0−0.05	0.02	0−0.03	0.04	1.01	0−0.04	2.58−3.12
pollack, *Pollachius pollachius*	3	0−0.08	0−0.05	0.02	0−0.02	0.01	0.71	0−0.01	4.38−4.56
pout, *Trisopterus luscus*	1	0−0.05	0−0.04	0.03	0−0.03	0.04	0.25	0−0.04	4.67−4.89
ray, *Raja clavata, Raja naevus, Raja circularis*	4	0.12−0.14	0−0.05	0.02	0−0.02	0.03	1.24	0.17−0.19	4.38−4.63
saithe, *Pollachius virens*	4	0−0.08	0.01−0.07	0.02	0−0.02	0.01	0.18	0−0.01	1.38−1.67
salmon, *Salmo salar*	4	0−0.13	0−0.04	0.03	0−0.03	0.02	0.05−0.07	0−0.01	1.39−1.98
sardine, *Sardina pilchardus*	4	0−0.05	0.03−0.07	0.02	0−0.03	0.04	1.4	0−0.04	3.01−3.71
scorpionfish, *Scorpaena porcus, Scorpaena scrofa, Helicolenus dactylopterus*	1	0−0.05	0−0.01	0.02	0−0.03	0.04	0.1	0−0.04	4.14−4.32
seabass, *Dicentrarchus labrax*	4	0.06−0.1	0−0.04	0.02	0−0.03	0.04	2.6	0−0.04	6.79−7.13
sea bream, *Spondyliosoma cantharus, Sparus aurata, Pagellus bogaraveo*	4	0−0.06	0−0.03	0.02	0−0.03	0.04	0.03	0−0.04	1.7−2.2
sole, *Solea solea*	4	0−0.04	0−0.04	0.02	0−0.02	0.03	0.62	0−0.03	3.77−4.01
swordfish, *Xiphias gladius*	4	0−0.07	0−0.05	0.03	0−0.03	0.05	0−0.03	0−0.05	0.28−1.11
tuna, *Thunnus thunnus*	4	0−0.1	0−0.05	0.03	0−0.03	0.01	0.15−0.16	0−0.01	0.86−1.38
whiting, *Merlangius merlangus*	4	0−0.04	0−0.05	0.02	0−0.02	0.03	0.32	0−0.03	2.64−2.9
mean (std)	LB	0.01 (0.03)	0.00 (0.01)	0 (0)	0.00 (0.01)	0 (0)	0.58 (0.57)	0.01 (0.03)	2.89 (1.66)
	UB	0.06 (0.03)	0.04 (0.01)	0.02 (0.00)	0.03 (0.01)	0.03 (0.01)	0.59 (0.57)	0.04 (0.03)	3.25 (1.56)
min−max	LB	0−0.12	0−0.03	0−0	0−0.03	0−0	0−2.6	0−0.17	0.28−6.79
	UB	0.04−0.14	0.01−0.07	0.02−0.03	0.02−0.04	0.01−0.05	0.03−2.6	0.01−0.19	1.11−7.13

[a]Std, standard deviation; min, minimum contamination value; max, maximum contamination value [b]Null contamination level under LB hypothesis. Only UB contamination level is shown.

than in LB hypothesis for freshwater fishes and about 17% for marine fishes. This difference between freshwater and marine fishes is linked to the level of PFAA contamination: the lower the contamination is, the higher the censored-data part under UB is. Indeed, marine fishes are about 18 times less contaminated than freshwater fishes in mean (Tables 1−3). The LB contamination range is 0.3−6.8 ng g^{-1} for marine fishes and 9.4−168.4 ng g^{-1} for freshwater fishes (1.1−7.1 and 10.3−169.9 ng g^{-1} under the UB hypothesis). Swordfish *Xiphias gladius* and brown trout *Salmo trutta fario* appear to be the less contaminated species, both being marine fishes, whereas seabass *Dicentrarchus labrax* and gudgeon *Gobio gobio* are the most contaminated ones, both being freshwater fishes.

The differences between marine and freshwater species are based not only on contamination levels but also on their contamination profile. Whereas PFOS is clearly the prevailing PFAA for the freshwater fishes (LB, 74% of the total contamination), for marine fishes the latter is shared between PFOA (24%), PFOS (20%), PFHxA (15%), PFHpA (11%), and PFBA (11%). The percentages between the LB and UB hypotheses are similar.

These differences are to date not well documented. Nevertheless, our results are consistent with the literature,[49−51]

Table 3. PFAA Contamination of Fresh Freshwater Fish LB-UB (Nanograms per Gram ww)

		n	PFBA	PFPA[a]	PFHxA	PFHpA	PFOA	PFNA	PFDA	PFUnA	PFTrDA	PFTeDA	PFBS[a]	PFHxS	PFHpS	PFOS	PFDS	ΣPFAAs
barbel, *Barbus barbus*		5	0−0.57	0.25	0−0.38	0−0.18	0−0.1	1.19−1.21	5.26	43.64	36.3	0.8−0.91	0.06	0.19−0.22	0−0.19	41.7	0.23−0.34	129.3−131.3
bleak, *Alburnus alburnus*		9	0−0.14	0.24	0−0.32	0−0.08	0−0.04	0.01−0.03	1.24	0.85	0.16−0.19	0−0.08	0.06	0.02−0.41	0.02−0.11	28.11	0.16−0.25	30.4−32
brown trout, *Salmo trutta fario*		31	0.02−0.12	0.17	0.07−0.21	0.01−0.07	0.04−0.11	0.08−0.13	1.94	0.95	0.29−0.32	0.03−0.05	0.09	0.06−0.17	0−0.08	7.27	0.04−0.08	9.4−10.3
chub, *Squalius cephalus*		9	0−0.51	0.22	2.2−2.47	0.22−0.35	1.08−1.15	0.68−0.7	3.71	18.32	5.03	0.06−0.22	0.07	0.05−0.16	0−0.17	35.5	0.14−0.28	67−68.9
common carp, *Cyprinus carpio*		7	0−0.12	0.18	0−0.14	0−0.1	0.03−0.08	0.03−0.1	0.82	0.39	0−0.08	0−0.08	0.07	0.67−0.76	0.42−0.46	32.28	0.1−0.14	34.6−35.7
common roach, *Rutilus rutilus*		67	0.02−0.18	0.13	0.11−0.24	0.01−0.09	0.07−0.12	0.34−0.38	1.18	12.58	12.44−12.49	0.14−0.19	0.07	0.06−0.18	0.24−0.3	17.63	0.1−0.17	44.6−45.7
minnow, *Phoxinus phoxinus*		1	0−0.56	0.24	0−0.37	0−0.17	0−0.1	0.19	7.07	6.17	0.42	0−0.23	0.06	0.4	0.68	134.81	0−0.23	149.7−151.7
European eel, *Anguilla anguilla*		137	0.07−0.36	0.27	0.05−0.34	0.01−0.18	0.09−0.2	0.12−0.26	2.12	1.84	0.22−0.33	0.09−0.18	0.16	0.67−0.77	0.08−0.21	39.55	0.1−0.25	44.6−46.6
European perch, *Perca fluviatilis*		9	0−0.12	0.09	0.03−0.13	0−0.05	0.02−0.07	0.12−0.13	2.79	2.51	0.42−0.43	0.1−0.16	0.08	0.11−0.2	0.28−0.3	82.52	0.27−0.28	88.8−89.5
freshwater bream, *Abramis brama*		34	0.03−0.18	0.12	0.08−0.21	0.01−0.08	0.05−0.09	0.11−0.13	1−1.02	0.46−0.47	0.11−0.17	0.07−0.12	0.07	0.1−0.24	0.07−0.12	22.3	0.11−0.14	24.5−25.5
gudgeon, *Gobio gobio*		5	0−0.58	0.25	3.88−4.1	0.33−0.43	1.75−1.81	0.21−0.24	8.27	23.19	1.18	0.06−0.25	0.06	0.36−0.39	0.6	128.06	0.5	168.4−169.9
northern pike, *Esox lucius*		8	0−0.13	0.14	0−0.13	0−0.08	0−0.04	0.04−0.07	1.46	2.87	0.46−0.48	0.02−0.04	0.08	0.02−0.18	0−0.08	14.73	0.06−0.12	19.3−20.3
white bream, *Blicca bjoerkna*		22	0.01−0.16	0.14	0−0.15	0−0.09	0.04−0.08	0.06−0.11	0.97−0.99	1.13−1.14	0.14−0.23	0.07−0.14	0.07	0.21−0.3	0.09−0.13	35.6	0.13−0.16	38.4−39.5
thicklip grey mullet, *Chelon labrosus*		6	0−0.14	0.13	0−0.21	0−0.11	0.01−0.05	0.15*	1.27	0.56	0−0.04	0−0.01	0.12	0.01−0.16	0−0.06	13.71	0−0.04	15.7−16.7
wels catfish, *Silurus glanis*		14	0−0.15	0.13	0−0.13	0−0.08	0.01−0.05	0.08−0.1	1.27	2.01	0.33−0.34	0.02−0.08	0.1	0.01−0.12	0−0.07	7.78	0.04−0.08	11−11.9
western vairone, *Telestes souffia*		1	0−0.61	0.26	0−0.41	0−0.19	0−0.1	0−0.08	2.52	2.45	0.38	0−0.25	0.06	0−0.17	0−0.2	41.78	0−0.25	47.1−49.7
pike-perch, *Sander lucioperca*		22	0−0.17	0.11	0−0.14	0−0.08	0−0.05	0.03−0.08	1.34	0.82	0.02−0.11	0.01−0.08	0.08	0.06−0.16	0.08−0.11	31.2	0.26−0.27	33.8−34.8
fishes with low level of PFAA contamination and $n > 5$ (freshwater bream, northern pike, thicklip grey mullet, wels catfish, brown trout)																		
mean	LB		0.01	0.00	0.03	0.00	0.02	0.09	1.15	1.26	0.23	0.04	0.00	0.04	0.02	13.05	0.05	16
	UB		0.14	0.14	0.18	0.08	0.07	0.12	1.17	1.27	0.26	0.07	0.09	0.17	0.08	13.05	0.09	17
std	LB		0.01	0.00	0.04	0.00	0.02	0.04	0.28	0.94	0.19	0.04	0.00	0.04	0.03	6.25	0.04	6.2
	UB		0.02	0.02	0.05	0.01	0.03	0.03	0.25	0.94	0.18	0.06	0.02	0.04	0.02	6.24	0.04	6.1
fishes with medium level of PFAA contamination and $n > 5$ (European perch, chub, common roach, European eel, silver bream, common carp, pike-perch, bleak)																		
mean	LB		0.01	0.00	0.30	0.03	0.16	0.17	1.65	4.76	2.30	0.06	0.00	0.23	0.15	37.80	0.16	47.8
	UB		0.22	0.17	0.49	0.13	0.22	0.22	1.69	4.77	2.36	0.14	0.08	0.37	0.22	37.80	0.23	49.1
std	LB		0.02	0.00	0.77	0.08	0.37	0.23	1.00	6.76	4.44	0.05	0.00	0.28	0.15	19.23	0.07	20.1
	UB		0.14	0.07	0.80	0.10	0.38	0.22	1.00	6.76	4.43	0.06	0.03	0.26	0.12	19.23	0.06	20.1
fishes with high level of PFAA contamination and $n > 5$ (gudgeon, barbel)																		
mean	LB		0.00	0.00	1.94	0.16	0.88	0.70	6.76	33.42	18.74	0.43	0.00	0.27	0.30	84.88	0.36	148.9
	UB		0.58	0.25	2.24	0.30	0.95	0.73	6.76	33.42	18.74	0.58	0.06	0.31	0.40	84.88	0.42	150.6
std	LB		0.00	0.00	2.74	0.23	1.24	0.69	2.13	14.46	24.84	0.52	0.00	0.12	0.43	61.06	0.19	27.6
	UB		0.01	0.00	2.63	0.18	1.21	0.68	2.13	14.46	24.84	0.46	0.00	0.12	0.30	61.06	0.12	27.3

[a]Null contamination level under LB hypothesis. Only UB contamination level is shown.

dx.doi.org/10.1021/jf501113j | J. Agric. Food Chem. 2014, 62, 7593−7603

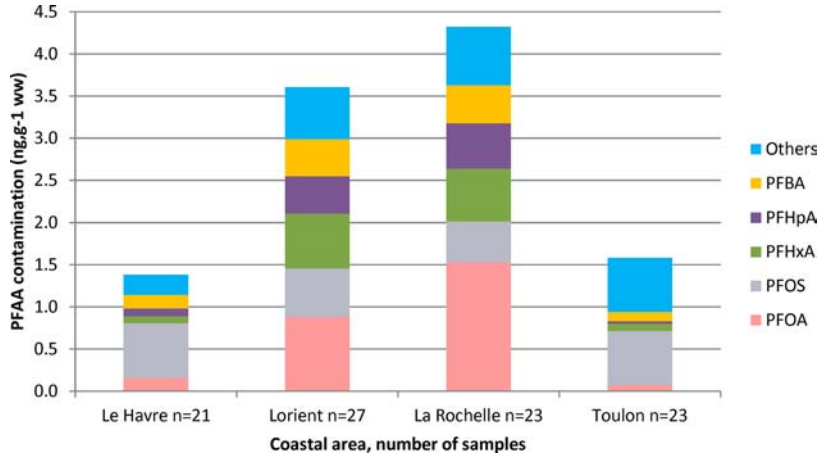

Figure 1. Mean marine fish PFAA contamination by coastal area (ng g^{-1} ww), LB hypothesis.

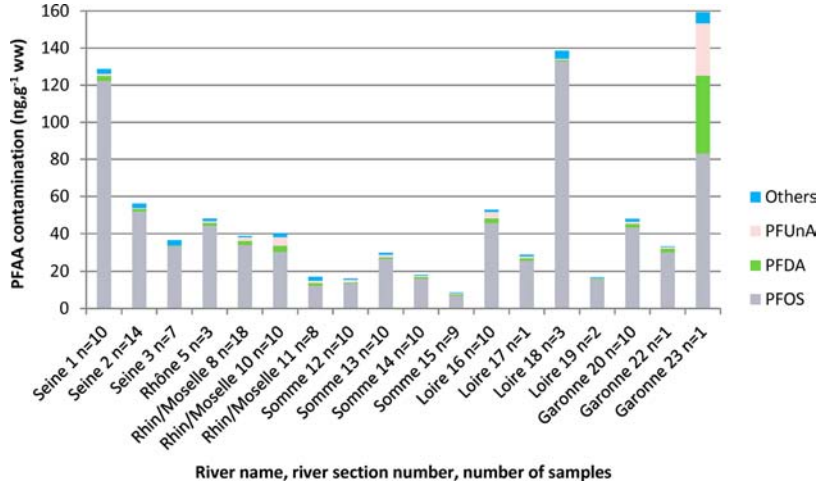

Figure 2. Mean European eel PFAA contamination by river section (ng g^{-1} ww), LB hypothesis.

which also finds a higher PFAA contamination in freshwater fish than in marine ones. One of the hypotheses about this observation is the water contamination level difference between rivers/lakes and seas/oceans, where the pollutants are diluted in a larger amount of water. Whereas the contamination levels in seawaters seem to range from a few picograms per liter to a few nanograms per liter,[52] except in coastal waters and industrialized bays such as Tokyo Bay, where a maximum level of 192 ng L^{-1} was found for PFOA,[53] the levels in rivers can reach from nanograms per liter to micrograms per liter,[54−56] a thousand times higher than in seawaters. Another hypothesis is a difference in the bioaccumulation potency between marine and freshwater fishes. However, comprehensive studies are still lacking in this field. No association was found between feeding behavior, living depth (demersal, pelagic, etc.), or climate (temperate, subtropical environment, etc.) and PFAA contamination levels.

Moreover, it seems that marine fish PFAA contamination levels are different among the four coastal areas. Indeed, the fresh and frozen fishes collected in Lorient and La Rochelle are twice more contaminated than those collected in Le Havre or Toulon as presented in Figure 1. Even if the Kruskal−Wallis test revealed a significant difference ($p < 0.001$), it remains difficult to draw a conclusion, as some species are specific from some sampling sites. For example, the gurnard *Trigla lucerne* was sampled only in Lorient, as it was the only site among the four where it was sufficiently consumed.

Spatial trend of freshwater fish PFAA contamination was also investigated. The European eel *Anguilla anguilla* was chosen to illustrate this part of the study because of the importance of the size of this group ($n = 137$). European eel contamination was mostly driven by PFOS as is the case for the freshwater fishes in general, except for one sample caught in the Garonne river, which shows a contamination split among PFOS (52%), PFDA (26%), and PFUnA (18%). With regard to the sum of the 15 PFAAs, the contamination was significantly different among the 18 river sections (Kruskal−Wallis test, $p < 0.0001$) (Figure 2). The results are deliberately presented by river section and not by major river because of the contamination heterogeneity within some rivers such as the Seine. This heterogeneity could be explained by the presence of a point source of PFAA discharge such as wastewater treatment plants and plants producing or processing PFASs, for instance. Our colleagues from the Nancy laboratory of hydrology are currently working on this subject.[57,58]

Table 4 presents a few PFOS contamination data from the literature to be compared to the results of the present study. It can be noted that the PFAA contamination data from this study are consistent with the existent data, with PFOS being the most frequently detected PFAA, often dominating the contamination pattern. In Babut and co-workers' study, gudgeon, common roach, European eel, and barbel *Barbus barbus* were the species with the highest PFAA levels.[59] Our fishes from the low contamination level group are 2.7 times more contaminated when

Table 4. PFOS Contamination Level of Freshwater Fishes (Nanograms per Gram wet weight)

country	species	*n*	median	mean	reference
France	low level	93	13.71	13.05	this study
	medium level	282	33.89	37.8	
	high level	10	84.88	84.88	
	Rhône−Mediterranean drainage basin	823	5		Babut et al.[59]
Germany	perch (*Perca fluviatilis*)	15	96		Hölzer et al.[61]
	pike (*Esox lucius*)	6	37		
	eel (*Anguilla anguilla*)	5	77		
	roach (*Rutilus rutilus*)	10	6.1		
US	northern pike (*Esox lucius*)	21	9.6	9.9	Xiao et al.[67]
China	grey mullet	5		1.2	Zhao et al.[60]
	catfish	4		0.49	
	catfish	21		0.51	

the median value is considered and 17 times more contaminated for the high contamination level group. However, the authors mentioned that their fishes were globally less contaminated than anywhere in France. Our thicklip grey mullet samples (mean PFOS level = 13.7 ng g^{-1} ww) and our wels catfish *Silurus glanis* samples (mean PFOS level = 7.8 ng g^{-1} ww) were surprisingly 10 and 15 times more contaminated in mean by PFOS than those purchased in local markets in Xiamen, China,[60] even if China is still known for their PFAS production. A German study collected and analyzed European perch (n = 15), northern pike *Esox lucius* (n = 6), European eel (n = 5), and roach (n = 10) fillets for PFOS contamination in Lake Möhne.[61] The median contaminations were, respectively, 96, 37, 77, and 6.1 ng g^{-1} ww. Our mean PFOS contaminations were 83 ng g^{-1} ww for European perch (n = 9), 15 ng g^{-1} ww for northern pike (n = 8), 40 ng g^{-1} ww for European eel (n = 137), and 18 ng g^{-1} ww for roach (n = 67). Globally, our data were consistent with those published in the literature, even if some fishes were probably sampled in "hotspots" of environmental contamination.

Lipid and Fatty Acid Composition. Table 5 shows the marine and freshwater fish composition for lipids, eicosapentaenoic acid (EPA), docosahexaenoic acid (DHA), n-3 LC-PUFA, n-6 LC-PUFA, and total PUFA for the 29 marine fish species and for 11 of the 16 freshwater fish species. Results for marine fish were already published and compared with the existing literature data.[44] Marine fish n-3 LC-PUFA level distribution is wider than the freshwater fish one, with ranges of, respectively, 46−4472 mg for 100 g ww (mean = 708 mg for 100 g ww) and 4−3895 mg for 100 g ww (mean = 368 mg for 100 g ww). As expected, for the marine fish, the oiliest species are also the richest in PUFA. The three oiliest marine fishes are salmon *Salmo salar* (13.5% of lipids ww in mean), swordfish (12.4% of lipids in ww in mean), and halibut *Hippoglossus hippoglossus* (11.7% of lipids in ww in mean), which are also the richest in PUFAs and n-3 LC-PUFAs, including EPA. The DHA-rich marine fishes are salmon (2164 mg for 100 g ww), swordfish (1750 mg for 100 g ww), and mackerel *Scomber scombrus* (1404 mg for 100 g ww), and the n-6 LC-PUFA-rich marine fishes are anchovy *Engraulis encrasicolus* (682 mg for 100 g ww), salmon (671 mg for 100 g ww), and swordfish (5410 mg for 100 g ww). For freshwater fishes, lipid and PUFA amounts are not so clearly related. Indeed, if European eel, the oiliest freshwater fish, is also the richest in n-3 LC-PUFAs, n-6 LC-PUFAs, and PUFAs, common carp *Cyprinus carpio*, the second oiliest fish, is relatively poor in PUFAs. Our data are consistent for European eel, wels catfish, pike-perch, trout, common carp, and bream *Abramis brama* in recent German and Polish studies.[62,63] The differences between the studies could be explained by the difference of sampling season, fish size, and intraspecies variability.

PFAA Contamination and LC-PUFA Balance. According to the multiple regression analysis, no positive or negative relationship has been highlighted between PFAA contamination and muscle protein rate, lipid content, and n-3 and n-6 LC-PUFA composition of the studied fishes (R^2 = 0.26, p = 0.86), which is not surprising considering the physicochemical properties of PFAAs. PFAAs are amphiphibic and are mostly found in the liver and blood,[64,65] not in fat tissues, as are organic persistent compounds such as PCB or dioxins. As PFAAs seem to bind preferentially to serum proteins rather than to muscle proteins, the results would surely be interesting to measure these contaminants in the liver and blood.

The most interesting fishes with high n-3 LC-PUFA content and low PFAA contamination are the swordfish, anchovy, halibut, salmon, and mackerel, all of them being marine fishes, whereas the potentially risky fishes to consume with high PFAA contamination and low n-3 LC-PUFA content are common carp, pike-perch *Sander lucioperca*, European perch *Perca fluviatilis*, thicklip grey mullet *Chelon labrosus*, and common roach *Rutilus rutilus*, all of them being freshwater fishes. If consumed regularly, these fishes could largely contribute to increase the PFAA level found in human serum. This hypothesis is consistent with Hölzer's study, which observed that anglers who consume fish two to three times per month have a higher PFOS serum concentration. Those fishes, caught in Lake Möhne, present a PFAA contamination similar to of the fishes of the present study.[61]

Our data tried to reflect an extended view of PFAA contamination along with n-3 and n-6 LC-PUFA composition of marine and freshwater fishes in metropolitan France. However, for some species such as western vairone *Telestes souffia* (n = 1), minnow *Phoxinus phoxinus* (n = 1), or marine fishes (n = 1−4), the size of the group is a limit of this study, even if the samples are composite ones made up of a homogeneous mix of several individual fishes. This concern leads to the question of the spatial trend of PFAA contamination. In this study, we chose to work on mean PFAA contamination of fishes because our FA composition data were available only by species, but there are obviously some differences between the river sections or the coastal areas, probably due to the differences in environmental contamination. Further studies could include a comparison between river sediment/water contamination and the corresponding fish contamination. Another weakness of our study is the lack of information available concerning the age, weight, and seasonality effect during the freshwater fish sampling. The French agency for food, environmental, and occupational health and safety (Anses) recently published an overview of all their recommendations since 2002 concerning the risk−benefit balance of fishery and aquaculture products for the general population, elderly, immunodepressed people, children, and pregnant or breastfeeding and child-bearing age women.[66] However, these recommendations take into account only dioxins, methylmercury, and PCBs. It could be suggested to add pike-perch, European perch, thicklip grey mullet, and common roach in the list of species that should be consumed with limitation, common carp already being in this list, as they do not present such a positive profile as far as the lowest n-3 LC-PUFA levels and the highest PFAA level were

Table 5. Mean Free Fatty Acid Composition of Fresh and Frozen Marine Fish and Fresh Freshwater Fish (Milligrams per 100 g ww)[a]

species	*n*	lipids (g/100 g)	C20:5 n-3 (EPA)	C22:6 n-3 (DHA)	LC-PUFA n-3	LC-PUFA n-6	PUFA
marine fish[b]							
anchovy	1	7.51	701	1365	3241	682	3923
monkfish	4	0.21	26	37	66	7	71
catshark	4	0.55	113	66	195	23	219
cod	4	0.30	28	75	112	8	121
common dab	4	0.72	84	131	250	30	281
European eel	1	20.4	432	716	1880	1285	3205
orange roughy	3	5.78	471	742	1940	201	2141
plaice	2	0.37	46	41	97	15	111
goatfish	3	3.75	348	669	1147	148	1295
grenadier	4	0.44	41	78	160	8	168
gurnard	1	0.73	43	3	46	10	54
haddock	2	0.25	18	60	84	10	94
hake	4	0.59	28	123	180	14	193
halibut	4	11.7	969	1400	3960	191	4186
John Dory	2	0.59	32	156	203	13	217
ling	4	0.33	45	65	112	4	117
mackerel	4	7.07	662	1404	2585	259	2845
pollack	3	0.27	15	76	97	5	103
pout	1	0.29	36	30	77	14	91
ray	4	0.61	17	156	195	23	216
saithe	4	1.04	71	173	262	126	391
salmon	4	13.5	1112	2164	4472	671	5146
sardine	4	5.72	638	1269	2270	130	2407
scorpionfish	1	2.27	121	507	890	57	949
seabass	4	2.99	357	617	1090	125	1221
sea bream	4	4.89	497	773	1507	350	1859
sole	4	0.40	14	72	109	19	128
swordfish	4	12.4	1265	1750	3764	541	4331
tuna	4	0.73	35	131	179	31	211
whiting	4	0.25	15	69	93	5	98
mean (std)		3.56 (5.05)	276 (361)	399 (535)	708 (1195)	167 (286)	1,213 (1563)
min−max		0.2	14	3	46	4	54
		120.4	1265	2164	4472	1285	5146
freshwater fish							
bleak	2	9.69	131	196	556	868	1464
brown trout	5	11.03	50	108	271	296	583
common carp	3	16.74	45	54	168	300	516
common roach	6	6.08	155	190	530	322	885
European eel	6	46.38	958	632	3895	2511	6702
European perch	1	4.39	165	274	563	309	894
bream	5	7.59	228	247	740	594	1376
northern pike	2	2.08	59	204	332	127	467
thicklip grey mullet	2	8.44	57	39	131	47	208
wels catfish	3	4.32	132	228	542	275	850
pike-perch	3	1.57	41	132	209	91	305
mean (std)		10.76(12.59)	184(264)	209(160)	368(231)	294(252)	429(352)
min−max		1.57	41	39	4	3	1
		46.38	958	632	3895	2511	6702

[a]Std, standard deviation; min, minimum contamination value; max, maximum contamination value. [b]From Sirot et al.[44]

found compared to other fish species analyzed in this study. As a further step, additional data on marine and fish species could be interpreted in terms of fish consumption recommendation by an expert committee and the food safety recommendations to French consumers updated, if needed, according to the last recommendations of the French agency for food, environmental, and occupational health and safety.

AUTHOR INFORMATION

Corresponding Author

*(A.Y.) Mail: LUNAM Université, Oniris, Laboratoire d'Etude des Residus et Contaminants dans les Aliments (LABERCA), USC INRA 1329, Nantes 44307, France. Phone: +33 (0) 611169833. E-mail: ami.s.yamada@gmail.com.

Funding

This work was partially supported by the ANR (Agence Nationale de la Recherche/French National Research Agency) within the framework of the CONTREPERF program "Emerging perfluorinated contaminants: contribution to the human exposure assessment, to the study of their metabolism and to the characterization of their toxicological impact" (Grant ANR-10-CESA-008). For the ICAR-PCB study, samples provided from ONEMA national PCB action plan and freshwater fish analyses were funded by the French Ministry of Health. The CALIPSO study was funded by the French Ministry of Agriculture.

Notes

The authors declare no competing financial interest.

■ ACKNOWLEDGMENTS

We thank Florence Ramdin for her kind help.

■ ABBREVIATIONS USED

DHA, docosahexaenoic acid; EPA, eicosapentaenoic acid; FA, fatty acid; LB, lower bound; LOD, limit of detection; LC-PUFA, long-chain polyunsaturated fatty acid; ONEMA, French national agency for water and aquatic environments; PCB, polychlorobiphenyl; PFAA, perfluoroalkyl acid; PFBA, perfluorobutanoic acid; PFBS, perfluorobutanesulfonate; PFDA, perfluorodecanoic acid; PFDS, perfluorodecanesulfonate; PFHxA, perfluorohexanoic acid; PFHxS, perfluorohexanesulfonate; PFHpA, perfluoropentanoic acid; PFHpS, perfluoropentanesulfonate; PFNA, perfluorononanoic acid; PFOA, perfluorooctanoic acid; PFOS, perfluorooctanesulfonate; PFPA, perfluoropentanoic acid; PFTeDA, perfluorotetradecanoic acid; PFTrDA, perfluorotridecanoic acid; PFUnA, perfluoroundecanoic acid

■ REFERENCES

(1) Ruiter, A. Fish and fishery products: composition, nutritive properties and stability. In *Fish and Fishery Products: Composition, Nutritive Properties and Stability*; CAB International: Wallingford, UK, 1995.

(2) AFSSA. *The Omega 3 Fatty Acids and the Cardiovascular System: Nutritional Benefits and Claims*; Maisons-Alfort, France, 2003; p 123.

(3) Baum, S. J.; Kris-Etherton, P. M.; Willett, W. C.; Lichtenstein, A. H.; Rudel, L. L.; Maki, K. C.; Whelan, J.; Ramsden, C. E.; Block, R. C. Fatty acids in cardiovascular health and disease: a comprehensive update. *J. Clin. Lipidol.* **2012**, *6*, 216−234.

(4) Riediger, N. D.; Othman, R. A.; Suh, M.; Moghadasian, M. H. A systemic review of the roles of n-3 fatty acids in health and disease. *J. Am. Diet. Assoc.* **2009**, *109*, 668−679.

(5) Matsuoka, Y. Clearance of fear memory from the hippocampus through neurogenesis by omega-3 fatty acids: a novel preventive strategy for posttraumatic stress disorder? *BioPsychoSoc. Med.* **2011**, *5*, 3.

(6) Mahaffey, K. R.; Sunderland, E. M.; Chan, H. M.; Choi, A. L.; Grandjean, P.; Marien, K.; Oken, E.; Sakamoto, M.; Schoeny, R.; Weihe, P.; Yan, C. H.; Yasutake, A. Balancing the benefits of n-3 polyunsaturated fatty acids and the risks of methylmercury exposure from fish consumption. *Nutr. Rev.* **2011**, *69*, 493−508.

(7) Sirot, V.; Leblanc, J. C.; Margaritis, I. A risk-benefit analysis approach to seafood intake to determine optimal consumption. *Br. J. Nutr.* **2012**, *107*, 1812−1822.

(8) Dewailly, E.; Ayotte, P.; Lucas, M.; Blanchet, C. Risk and benefits from consuming salmon and trout: a Canadian perspective. *Food Chem. Toxicol.* **2007**, *45*, 1343−1348.

(9) Posner, S.; Roos, S.; Brunn Poulsen, P.; Jörundsdottir, H. Ó.; Gunnlaugsdottir, H.; Trier, X.; Astrup Jensen, A.; Katsogiannis, A. A.; Herzke, D.; Bonefeld-Jörgensen, E. C.; Jönsson, C.; Pedersen, G. A.; Ghisari, M.; Jensen, S. *Per and Polyfluorinated Substances in the Nordic Countries*; Nordic Council of Ministers: Copenhagen, Denmark, 2013.

(10) Prevedouros, K.; Cousins, I. T.; Buck, R. C.; Korzeniowski, S. H. Sources, fate and transport of perfluorocarboxylates. *Environ. Sci. Technol.* **2006**, *40*, 32−44.

(11) Giesy, J. P.; Kannan, K.; Jones, P. D. Global biomonitoring of perfluorinated organics. *Sci. World J.* **2001**, *1*, 627−629.

(12) Calafat, A. M.; Kuklenyik, Z.; Reidy, J. A.; Caudill, S. P.; Tully, J. S.; Needham, L. L. Serum concentrations of 11 polyfluoroalkyl compounds in the U.S. population: data from the national health and nutrition examination survey (NHANES). *Environ. Sci. Technol.* **2007**, *41*, 2237−2242.

(13) Inoue, K.; Okada, F.; Ito, R.; Kato, S.; Sasaki, S.; Nakajima, S.; Uno, A.; Saijo, Y.; Sata, F.; Yoshimura, Y.; Kishi, R.; Nakazawa, H. Perfluorooctane sulfonate (PFOS) and related perfluorinated compounds in human maternal and cord blood samples: assessment of PFOS exposure in a susceptible population during pregnancy. *Environ. Health Perspect.* **2004**, *112*, 1204−1207.

(14) Gallo, V.; Leonardi, G.; Genser, B.; Lopez-Espinosa, M. J.; Frisbee, S. J.; Karlsson, L.; Ducatman, A. M.; Fletcher, T. Serum perfluorooctanoate (PFOA) and perfluorooctane sulfonate (PFOS) concentrations and liver function biomarkers in a population with elevated PFOA exposure. *Environ. Health Perspect.* **2012**, *120*, 655−660.

(15) Yamaguchi, M.; Arisawa, K.; Uemura, H.; Katsuura-Kamano, S.; Takami, H.; Sawachika, F.; Nakamoto, M.; Juta, T.; Toda, E.; Mori, K.; Hasegawa, M.; Tanto, M.; Shima, M.; Sumiyoshi, Y.; Morinaga, K.; Kodama, K.; Suzuki, T.; Nagai, M.; Satoh, H. Consumption of seafood, serum liver enzymes, and blood levels of PFOS and PFOA in the Japanese population. *J. Occup. Health* **2013**, *55*, 184−194.

(16) Knox, S. S.; Jackson, T.; Frisbee, S. J.; Javins, B.; Ducatman, A. M. Perfluorocarbon exposure, gender and thyroid function in the C8 Health Project. *J. Toxicol. Sci.* **2011**, *36*, 403−410.

(17) Lin, C.-Y.; Wen, L.-L.; Lin, L.-Y.; Wen, T.-W.; Lien, G.-W.; Hsu, S. H. J.; Chien, K.-L.; Liao, C.-C.; Sung, F.-C.; Chen, P.-C.; Su, T.-C. The associations between serum perfluorinated chemicals and thyroid function in adolescents and young adults. *J. Hazard. Mater.* **2013**, *244*−*245*, 637−644.

(18) Jain, R. B. Association between thyroid profile and perfluoroalkyl acids: data from NHNAES 2007−2008. *Environ. Res.* **2013**, *126*, 51−59.

(19) Lin, C.-Y.; Lin, L.-Y.; Wen, T.-W.; Lien, G.-W.; Chien, K.-L.; Hsu, S. H. J.; Liao, C.-C.; Sung, F.-C.; Chen, P.-C.; Su, T.-C. Association between levels of serum perfluorooctane sulfate and carotid artery intima−media thickness in adolescents and young adults. *Int. J. Cardiol.* **2013**, *168*, 3309−3316.

(20) Min, J.-Y.; Lee, K.-J.; Park, J.-B.; Min, K.-B. Perfluorooctanoic acid exposure is associated with elevated homocysteine and hypertension in US adults. *Occup. Environ. Med.* **2012**, *69*, 658−662.

(21) Shankar, A.; Xiao, J.; Ducatman, A. Perfluorooctanoic acid and cardiovascular disease in US adults. *Arch. Int. Med.* **2012**, *172*, 1397−1403.

(22) Fei, C.; McLaughlin, J. K.; Tarone, R. E.; Olsen, J. Perfluorinated chemicals and fetal growth: a study within the Danish National Birth Cohort. *Environ. Health Perspect.* **2007**, *115*, 1677−1682.

(23) Chen, M.-H.; Ha, E.-H.; Wen, T.-W.; Su, Y.-N.; Lien, G.-W.; Chen, C.-Y.; Chen, P.-C.; Hsieh, W.-S. Perfluorinated compounds in umbilical cord blood and adverse birth outcomes. *PLoS One* **2012**, *7*, No. e42474.

(24) Darrow, L. A.; Stein, C. R.; Steenland, K. Serum perfluorooctanoic acid and perfluorooctane sulfonate concentrations in relation to birth outcomes in the Mid-Ohio Valley, 2005−2010. *Environ. Health Perspect.* **2013**, *121*, 1207−1213.

(25) Halldorsson, T. I.; Rytter, D.; Haug, L. S.; Bech, B. H.; Danielsen, I.; Becher, G.; Henriksen, T. B.; Olsen, S. F. Prenatal exposure to perfluorooctanoate and risk of overweight at 20 years of age: a prospective cohort study. *Environ. Health Perspect.* **2012**, *120*, 668−673.

(26) Maisonet, M.; Terrell, M. L.; McGeehin, M. A.; Christensen, K. Y.; Holmes, A.; Calafat, A. M.; Marcus, M. Maternal concentrations of polyfluoroalkyl compounds during pregnancy and fetal and postnatal growth in British girls. *Environ. Health Perspect.* **2012**, *120*, 1432−1437.

(27) Knox, S. S.; Jackson, T.; Javins, B.; Frisbee, S. J.; Shankar, A.; Ducatman, A. M. Implications of early menopause in women exposed to perfluorocarbons. *J. Clin. Endocrinol. Metab.* **2011**, *96*, 1747−1753.
(28) Fei, C.; McLaughlin, J. K.; Lipworth, L.; Olsen, J. Maternal levels of perfluorinated chemicals and subfecundity. *Hum. Reprod.* **2009**, *24*, 1200−1205.
(29) Vested, A.; Ramlau-Hansen, C. H.; Olsen, S. F.; Bonde, J. P.; Kristensen, S. L.; Halldorsson, T. I.; Becher, G.; Haug, L. S.; Ernst, E. H.; Toft, G. Associations of in utero exposure to perfluorinated alkyl acids with human semen quality and reproductive hormones in adult men. *Environ. Health Perspect.* **2013**, *121*, 453−458 (458e1−5).
(30) Bonefeld-Jorgensen, E. C.; Long, M.; Bossi, R.; Ayotte, P.; Asmund, G.; Kruger, T.; Ghisari, M.; Mulvad, G.; Kern, P.; Nzulumiki, P.; Dewailly, E. Perfluorinated compounds are related to breast cancer risk in Greenlandic Inuit: a case control study. *Environ. Health* **2011**, *10*, 88.
(31) Hardell, E.; Kärrman, A.; van Bavel, B.; Bao, J.; Carlberg, M.; Hardell, L. Case−control study on perfluorinated alkyl acids (PFAAs) and the risk of prostate cancer. *Environ. Int.* **2014**, *63*, 35−39.
(32) Joensen, U. N.; Veyrand, B.; Antignac, J. P.; Blomberg Jensen, M.; Petersen, J. H.; Marchand, P.; Skakkebaek, N. E.; Andersson, A. M.; Le Bizec, B.; Jorgensen, N. PFOS (perfluorooctanesulfonate) in serum is negatively associated with testosterone levels, but not with semen quality, in healthy men. *Hum. Reprod.* **2013**, *28*, 599−608.
(33) Mundt, D. J.; Mundt, K. A.; Luippold, R. S.; Schmidt, M. D.; Farr, C. H. Clinical epidemiological study of employees exposed to surfactant blend containing perfluorononanoic acid. *Occup. Environ. Med.* **2007**, *64*, 589−594.
(34) Christensen, K. Y.; Maisonet, M.; Rubin, C.; Holmes, A.; Calafat, A. M.; Kato, K.; Flanders, W. D.; Heron, J.; McGeehin, M. A.; Marcus, M. Exposure to polyfluoroalkyl chemicals during pregnancy is not associated with offspring age at menarche in a contemporary British cohort. *Environ. Int.* **2011**, *37*, 129−135.
(35) Savitz, D. A.; Stein, C. R.; Bartell, S. M.; Elston, B.; Gong, J.; Shin, H. M.; Wellenius, G. A. Perfluorooctanoic acid exposure and pregnancy outcome in a highly exposed community. *Epidemiology* **2012**, *23*, 386−392.
(36) Specht, I. O.; Hougaard, K. S.; Spanò, M.; Bizzaro, D.; Manicardi, G. C.; Lindh, C. H.; Toft, G.; Jönsson, B. A. G.; Giwercman, A.; Bonde, J. P. E. Sperm DNA integrity in relation to exposure to environmental perfluoroalkyl substances − a study of spouses of pregnant women in three geographical regions. *Reprod. Toxicol.* **2012**, *33*, 577−583.
(37) Vestergaard, S.; Nielsen, F.; Andersson, A.-M.; Hjøllund, N. H.; Grandjean, P.; Andersen, H. R.; Jensen, T. K. Association between perfluorinated compounds and time to pregnancy in a prospective cohort of Danish couples attempting to conceive. *Hum. Reprod.* **2012**, *27*, 873−880.
(38) Bemrah, N.; Sirot, V.; Leblanc, J. C.; Volatier, J. L. Fish and seafood consumption and omega 3 intake in French coastal populations: CALIPSO survey. *Public Health Nutr.* **2009**, *12*, 599−608.
(39) Desvignes, V.; de Bels, F.; Aubert, L.; Volatier, J. L.; Favrot, M. C.; Marchand, P.; Le Bizec, B.; Leblanc, J. C.; Merlo, M. National study on polychlorinated biphenyl blood levels in French consumers of freshwater fish (ICAR-PCB) (1): description of the study population. *Organohalogen Compd.* **2012**, *74*, 827−836.
(40) Desvignes, V.; Merlo, M.; Volatier, J. L.; Bechaux, C.; Denys, S.; Marchand, P.; Le Bizec, B.; Leblanc, J. C. National study on blood PCB levels in French consumers of freshwater fish (ICAR-PCB) (3): effect of different risk management measures on the dietary exposure assessment. *Organohalogen Compd.* **2012**, *74*, 832−836.
(41) Hundley, S. G.; Sarrif, A. M.; Kennedy, G. L. Absorption, distribution, and excretion of ammonium perfluorooctanoate (APFO) after oral administration to various species. *Drug Chem. Toxicol.* **2006**, *29*, 137−145.
(42) Kudo, N.; Sakai, A.; Mitsumoto, A.; Hibino, Y.; Tsuda, T.; Kawashima, Y. Tissue distribution and hepatic subcellular distribution of perfluorooctanoic acid at low dose are different from those at high dose in rats. *Biol. Pharm. Bull.* **2007**, *30*, 1535−1540.
(43) Kadar, H.; Veyrand, B.; Antignac, J. P.; Durand, S.; Monteau, F.; Le Bizec, B. Comparative study of low- versus high-resolution liquid chromatography-mass spectrometric strategies for measuring perfluorinated contaminants in fish. *Food Addit. Contam., Part A* **2011**, *28*, 1261−1273.
(44) Sirot, V.; Oseredczuk, M.; Bemrah-Aouachria, N.; Volatier, J.-L.; Leblanc, J.-C. Lipid and fatty acid composition of fish and seafood consumed in France: CALIPSO study. *J. Food Compos. Anal.* **2008**, *21*, 8−16.
(45) AFNOR Group (French Normalisation Association). *French standard NF V04-403: meat, meat products and fishery products − determination of free fat content*, 2001.
(46) AFNOR Group (French Normalisation Association). *NF EN ISO 5509: animal and vegeable fats and oils − preparation of methyl esters of fatty acids*, 2000.
(47) AFNOR Group (French Normalisation Association). *NF EN ISO 5508: animal and vegetable fats and oils − analysis by gas chromatography of methyl esters of fatty acids*, 1995.
(48) GEMS/Food-EURO − World Health Organization. Reliable evaluation of low-level contamination of food. In *Workshop in the Frame of GEMS/Food-EURO*; World Health Organization: Kulmbach, Germany, 1995.
(49) Berger, U.; Glynn, A.; Holmström, K. E.; Berglund, M.; Ankarberg, E. H.; Törnkvist, A. Fish consumption as a source of human exposure to perfluorinated alkyl substances in Sweden − analysis of edible fish from Lake Vättern and the Baltic Sea. *Chemosphere* **2009**, *76*, 799−804.
(50) Schuetze, A.; Heberer, T.; Effkemann, S.; Juergensen, S. Occurrence and assessment of perfluorinated chemicals in wild fish from northern Germany. *Chemosphere* **2010**, *78*, 647−652.
(51) European Food Safety Authority. *Perfluoroalkylated Substances in Food: Occurrence and Dietary Exposure*; EFSA: Luxembourg, 2012; pp 2743−2792.
(52) Wei, S.; Chen, L. Q.; Taniyasu, S.; So, M. K.; Murphy, M. B.; Yamashita, N.; Yeung, L. W. Y.; Lam, P. K. S. Distribution of perfluorinated compounds in surface seawaters between Asia and Antarctica. *Mar. Pollut. Bull.* **2007**, *54*, 1813−1818.
(53) Yamashita, N.; Kannan, K.; Taniyasu, S.; Horii, Y.; Petrick, G.; Gamo, T. A global survey of perfluorinated acids in oceans. *Mar. Pollut. Bull.* **2005**, *51*, 658−668.
(54) Loos, R.; Locoro, G.; Huber, T.; Wollgast, J.; Christoph, E. H.; de Jager, A.; Manfred Gawlik, B.; Hanke, G.; Umlauf, G.; Zaldívar, J.-M. Analysis of perfluorooctanoate (PFOA) and other perfluorinated compounds (PFCs) in the River Po watershed in N-Italy. *Chemosphere* **2008**, *71*, 306−313.
(55) Loos, R.; Locoro, G.; Contini, S. Occurrence of polar organic contaminants in the dissolved water phase of the Danube River and its major tributaries using SPE-LC-MS2 analysis. *Water Res.* **2010**, *44*, 2325−2335.
(56) Sánchez-Avila, J.; Meyer, J.; Lacorte, S. Spatial distribution and sources of perfluorochemicals in the NW Mediterranean coastal waters (Catalonia, Spain). *Environ. Pollut.* **2010**, *158*, 2833−2840.
(57) Dauchy, X.; Boiteux, V.; Rosin, C.; Munoz, J.-F. Relationship between industrial discharges and contamination of raw water resources by perfluorinated compounds. Part I: Case study of a fluoropolymer manufacturing plant. *Bull. Environ. Contam. Toxicol.* **2012**, *89*, 525−530.
(58) Dauchy, X.; Boiteux, V.; Rosin, C.; Munoz, J.-F. Relationship between industrial discharges and contamination of raw water resources by perfluorinated compounds. Part II: Case study of a fluorotelomer polymer manufacturing plant. *Bull. Environ. Contam. Toxicol.* **2012**, *89*, 531−536.
(59) Babut, M.; Roy, A.; Lopes, C.; Pradelle, S. *Contamination des poissons d'eau douce par les PCB et d'autres contaminants persistants dans le bassin Rhône-Méditerranée [Freshwater fish contamination by PCBs and other persistent organic pollutants in Rhône-Mediterranean basin]*; Cemagref DREAL Rhône-Alpes: France, 2011.
(60) Zhao, Y. G.; Wan, H. T.; Law, A. Y. S.; Wei, X.; Huang, Y. Q.; Giesy, J. P.; Wong, M. H.; Wong, C. K. C. Risk assessment for human consumption of perfluorinated compound-contaminated freshwater and

marine fish from Hong Kong and Xiamen. *Chemosphere* **2011**, *85*, 277−283.
(61) Hölzer, J.; Göen, T.; Just, P.; Reupert, R.; Rauchfuss, K.; Kraft, M.; Müller, J.; Wilhelm, M. Perfluorinated compounds in fish and blood of anglers at Lake Möhne, Sauerland Area, Germany. *Environ. Sci. Technol.* **2011**, *45*, 8046−8052.
(62) Luczynska, J.; Paszczyk, B.; Borejszo, Z.; Tarkowski, L. Fatty acid profile of muscles of freshwater fish from Olsztyn markets. *Polym. J. Food Nutr. Sci.* **2012**, *62*, 51−55.
(63) Strobel, C.; Jahreis, G.; Kuhnt, K. Survey of n-3 and n-6 polyunsaturated fatty acids in fish and fish products. *Lipids Health Dis.* **2012**, *11*, 144.
(64) Greaves, A. K.; Letcher, R. J.; Sonne, C.; Dietz, R.; Born, E. W. Tissue-specific concentrations and patterns of perfluoroalkyl carboxylates and sulfonates in East Greenland polar bears. *Environ. Sci. Technol.* **2012**, *46*, 11575−11583.
(65) Pérez, F.; Nadal, M.; Navarro-Ortega, A.; Fàbrega, F.; Domingo, J. L.; Barceló, D.; Farré, M. Accumulation of perfluoroalkyl substances in human tissues. *Environ. Int.* **2013**, *59*, 354−362.
(66) Anses. *Anses Opinion Concerning Recommendations on the Benefits and Risks of Fishery Product Consumption in the Context of the PNNS Nutritional Guideline Update*; Anses: Maisons-Alfort, France, 2013.
(67) Xiao, F.; Gulliver, J. S.; Simcik, M. F. Perfluorooctane sulfonate (PFOS) contamination of fish in urban lakes: a prioritization methodology for lake management. *Water Res.* **2013**, *47*, 7264−7272.

To the authors knowledge, no scientific data showing increased deamidation in microbial transglutaminase treated food have been published. However, when incubating immunodominant α-gliadin-peptides p56−68 (13mer) and p56−88 with MTG in buffer at pH 8.5 as well as in water no deamidated 13mer has been found.[19] The same observation has been made when analyzing gliadin extracted from dough treated with MTG in the presence of lysine methyl ester.[20]

Furthermore, gliadin cross-linking by MTG may even reduce immunotoxicity, because the substrate glutamine now is not available for TG2-catalyzed deamidation in the intestinal mucosa anymore. In this context, it has been shown that immunodominant 13mer loses its stimulatory effect on IFNγ-expression by gliadin-specific intestinal T-cell-lines (iTCL) when cross-linked by MTG to lysine-methyl-ester at the deamidation site (Q65). The observation that MTG-catalyzed modification of gliadin results in reduced stimulatory effects on iTCLs or spleen cells from gliadin-immunized DQ8-transgenic mice was confirmed by gliadin extracted from wheat flour treated with MTG and lysine methyl ester. Gliadin from dough treated with MTG alone also showed a reduction of cytokine-expression in iTCLs, although less efficient than gliadin from lysine-methyl-ester and MTG-treated dough.[19,22] Further PT-Gluten (peptic-tryptic digest of gluten) treated with MTG in the presence of MTG-substrate lysine showed no stimulatory effect on IFNγ, antibodies to TG2, transglutaminase activity and TG2-expression in cultured biopsies taken from celiac disease patient's duodenum, while nontreated PT-Gluten increased IFNγ-expression 13−15-fold and also clearly increased the other parameters mentioned above.[23]

Currently, there is a public discussion on the potential impact of MTG-treated food on celiac disease patients. In this context, the German federal institute of risk assessment (BfR) states that due to the deamidation activity of MTG a potential risk for celiac disease patients consuming MTG-treated gliadin containing food is possible, as long as there are no satisfactory clinical studies.[24] Cabrera-Chavez et al. state that TG2 is homologous to MTG (which in fact is not the case as has been explained above) and deduce that MTG in foodstuff could elicit the immune response of celiac patients. The authors further state a latent risk in celiac patient's to elicit or increase their immune response by MTG-treated gluten-free bakery products in consequence to modified glutamine residues.[25]

There are only few scientific data on this topic available. Cabrera-Chavez et al. reported a higher antibody titer to gliadin extracted from MTG-treated wheat bread for two out of nine celiac disease patient's sera they analyzed.[25] They further reported an increased immunoreactivity for gliadin extracted from MTG-bread with sera from patients older than 8 years.[26] Bread wheat gliadin treated in vitro with MTG also increased immunoreactivity to IgA antibodies from celiac patients.[27]

The aim of this study was to analyze the immunoreactivity of gliadins extracted from pasta prepared with and without MTG-treatment with IgA and IgG-type antibodies in CD patient's sera and to elucidate the catalytic effect of MTG on durum wheat-gliadin when applied in pasta production.

MATERIALS AND METHODS

Materials. Gluten (Amygluten 160) was a gift from Tereos Syral (Marckolsheim, France). Commercial Durum wheat semolina (Nisshin DF) was purchased from the Nisshin Flour Milling (Tokyo, Japan). Microbial transglutaminase (1,000 units/g) was from Ajinomoto (Tokyo, Japan). Pronase (EC 3.4.24.4) was from Roche, Aminopeptidase M (EC 3.4.11.2.) from Merck, Carboxypeptidase A (EC 3.4.17.1.) and Prolidase (E.C.3.4.13.9.) from Sigma, Ortho-phthalaldehyde (OPA) from Agilent and 9-fluorenylmethyloxycarbonyl (FMOC) was from Weblio, Japan. Deamidated gliadin peptide DGPx2 (for description, see the Results section), antigliadin monoclonal antibody A011 and monoclonal antibody to deamidated gliadin-peptide A057 were from Zedira, Darmstadt, Germany.

Sera. Celiac disease patients' sera and blood donor's sera have been purchased from The Binding Site, (Schwetzingen, Germany) and SLR Research (Carlsbad, U.S.A.), respectively.

Pasta Preparation. Two kilograms of semolina and 540 g of tap water with or without 0.4 units microbial transglutaminase per gram of semolina were mixed for 15 min at room temperature by a mixing machine, Vacuum Mixer Model VU-2 (Ogu Leaves Machinery Works Plant Co., Ltd.) to make dough samples. The dough samples were then applied to a pasta machine, Vacuum Extruder Model FPV-2 (Nippon Engineering Co., Ltd.) with a die (diameter: 1.80 mm) to form the shape of spaghetti. The spaghetti were refrigerated immediately and dried by a drier, Model LH21-13P Temperature and Humidity Chamber (Nagano Science Machinery Co., Ltd.). The dried spaghetti samples were used and referred to MTG-pasta (dough prepared with transglutaminase) and pasta (based on dough prepared without transglutaminase) in the following.

Analysis of Moisture, Fat and Protein Content. Moisture, fat and total nitrogen content were determined for 3 independent samples in duplicate according to the Japan's Specifications and Standards for Food Additives by Japan Food Research Laboratories.[28] Briefly, moisture content was determined by the heat drying method with 105 °C for 4 h. Fat content was measured by the acid hydrolysis method. Total nitrogen was determined by the Kjeldahl method and protein content was calculated as total nitrogen × 6.25. Generally, mean values are given.

Analysis of ε-(γ-Glutamyl)lysine Content. Quantitative analysis of ε-(γ-glutamyl)lysine was performed in 3 independent pasta samples each according to the method of Kumazawa et al. with modifications.[29] Ten mg of crushed pasta sample was suspended in 1 mL of 50 mM potassium phosphate (pH7.0). Pronase (2.8 units) was added to the suspension and incubated at 40 °C for 24 h. After heat inactivation of Pronase by boiling for 10 min, aminopeptidase M (8.0 units), carboxypeptidase A (8.4 units) and prolidase (4.0 units) were added and kept at 40 °C for 24 h. The sample was boiled for 10 min to terminate the enzymatic digestion and then centrifuged at 10000*g* for 5 min. The supernatant was diluted 5-fold with 50 mM potassium phosphate (pH7.0) and used as the analysis sample. One μL of the sample was mixed with 0.5 μL of OPA and 0.4 μL of FMOC to make fluorescence derivative and applied to HPLC (Agilent ZORBAX Eclipse Plus C18 3.0 × 100 mm) with fluorescence detector (Agilent 1290 Infinity DAD). The content of ε-(γ-glutamyl)lysine was determined using the synthetic ε-(γ-glutamyl)Iysine (Sigma-Aldrich, St. Louis, U.S.A.) as standard.

Gliadin Extraction. A modified method according to Wieser et al.[30] was used to extract gliadin from commercial gluten as well as from pasta samples. Briefly 100 mg gluten or 200 mg pasta meal/MTG-pasta meal (produced using a mortar) have been added to 10 mL 0.4 M NaCl, 0.067 mM $HKNaPO_4$ pH 7.6. Albumins and globulins have been extracted at room temperature (approximately 24 °C) two times by vortexing for 2 min and gentle stirring for 10 min followed by 15 min centrifugation at 6000*g*. Gliadins have then been extracted from the resulting nonsoluble fraction by adding 5 mL 60% ethanol, vortexing for 2 min and gently stirring for 10 min followed by 20 min centrifugation at 6000*g*. The extraction procedure has been repeated twice, the supernatants including soluble gliadin combined and filtered through a 0.45 μM membrane.

If necessary, the extracts have been concentrated using Microcon Ultracel YM-10 centrifugal filter devices (Millipore, Darmstadt, Germany).

Gel Electrophoresis and Immunoblotting. SDS-PAGE was performed according to Laemmli.[31] Briefly samples have been mixed with 5× SDS-PAGE loading buffer (128 mM Tris-HCl pH 6.8, 10% ß-mercaptoethanol, 10% gycerol, 4% SDS, 13% bromophenole blue), heated for 10 min and loaded on a 10% or 12.5% SDS-PAGE gel,

Table 1. Moisture, Protein and Fat-Content per 100 g Pasta and MTG-Pasta

	pasta [g]	MTG-pasta [g]
moisture	10.0	09.9
protein	12.3	12.4
fat	1.7	1.6

except otherwise mentioned. The following amounts of protein have been loaded on the gels: pasta or MTG-pasta gliadin-extracts: 2.2 μg; bread-wheat gliadin: 2.0 μg; DGPx2: 0.19 μg. Gels have been stained with silver nitrate according to Blum et al.[32] Electro-blotting has been performed in a Trans Blot SD Semi Dry Transfer Cell (Bio-Rad, Hercules, U.S.A.) for 80 min at 20 V. After electro-blotting, the nitrocellulose membranes have been presoaked in 48 mM Tris, 39 mM glycine, 1.3 mM SDS, 20% (v/v) methanol. Residual binding sites were blocked in 5% skimmed milk powder in TBST (10 mM Tris, 150 mM NaCl, 0.05% (v/v) Tween 20, pH 8.0) for 60 min at RT. The membrane was then briefly washed in TBST wash buffer and incubated for 1 h at room temperature with primary antibody/serum (diluted 1000 fold in TBST). After washing for 3 × 5 min with large volumes of TBST buffer the secondary antibodies (antihuman IgA (Thermoscientific, Karlsruhe, Germany) antihuman IgG, antimouse IgG (both Sigma, Schnelldorf, Germany), each conjugated to alkaline phosphatase and diluted 10,000 fold in TBST buffer) has been added to the membrane followed by a 1 h incubation at room temperature. After intensive washing, the membrane has been placed in detection reagent (100 fold dilution of AP color reagent in color development buffer, BioRad, Hercules, U.S.A.) and incubated for 30 to 60 s at room temperature. Excess detection reagent has been drained off and the staining reaction was stopped with 20 mM Tris-HCl, 5 mM EDTA, pH 8. All washing steps were performed at room temperature on a shaker.

ELISA. Sera have been analyzed for the following antibody titers (IgA and IgG) using commercial ELISA-kits according to the manufacturer's instructions: TG2 and DGP (Zedira, Darmstadt, Germany), Gliadin (Steffens Biotechnische Analysen, Ebringen, Germany).

For coating of 96-well microtiter plates (ThermoFisher, Karlsruhe, Germany), 100 μL gliadin-extracts (diluted to 2 μg/mL in coating buffer (20 mM Tris-HCl, pH 7.4, 150 mM NaCl)) per well have been incubated at 4 °C overnight, and washed five times with coating buffer containing 0.01% Tween 20. For blocking 250 μL coating buffer containing 3% bovine serum albumin have been added and incubated for 1 h at room temperature. After washing for 5 times with coating buffer the dry plates have been stored at 4 °C.

For further procedure, the components of the ELISA for the determination of antibodies (IgG or IgA) against gliadin from Steffens Biotechnische Analysen (Ebringen, Germany) have been used. The ELISA has been performed according to the manufacturer's instructions.

Measurements have been performed in quadruplicate.

RESULTS AND DISCUSSION

Determination of ε-(γ-Glutamyl)lysine in Pasta and MTG-Pasta. MTG-treatment did not affect general pasta-properties like moisture, fat, and protein content, as no significant differences for these properties could be observed for pasta and MTG-pasta (Table 1). In pasta, the content of transglutaminase cross-linking reaction product ε-(γ-glutamyl)-lysine was below the detection limit of 0.001 μmol/g protein. In contrast, ε-(γ-glutamyl)lysine content in MTG-pasta (having the same protein content as pasta) was determined with 0.45 μmol/g pasta, corresponding to 3.63 μmol/g protein (Table 2). Thus, the cross-linking activity of MTG on pasta dough was clearly proven. The increased amount of cross-links is in agreement with an improved breaking energy, or firmness described earlier for MTG-pasta.[16] The ε-(γ-glutamyl)lysine content in food treated with MTG (∼4 U/g) has been reported with 0.2 μmol/g for soy protein isolate or egg white and 1.5 μmol/g for surimi.[33,34] Therefore, wheat proteins are about 2- to 20-fold better cross-linking substrates within the respective reaction conditions than the before mentioned proteins.

Table 2. ε-(γ-Glutamyl)lysine Content in Pasta and MTG-Pasta Measured in 3 Independent Samples[a]

	pasta		MTG-pasta	
sample	ε-(γ-glutamyl)lysine [μmol/g pasta]	ε-(γ-glutamyl)lysine [μmol/g protein]	ε-(γ-glutamyl)lysine [μmol/g pasta]	ε-(γ-glutamyl)lysine [μmol/g protein]
1	<0.0001	<0.001	0.44	3.53
2	<0.0001	<0.001	0.48	3.85
3	<0.0001	<0.001	0.43	3.49
mean	<0.0001	<0.001	**0.45**	**3.63**
STDEV			0.02	0.20
CV			5.5%	5.5%

[a](STDEV: Standard deviation; CV: Coefficient of Variation).

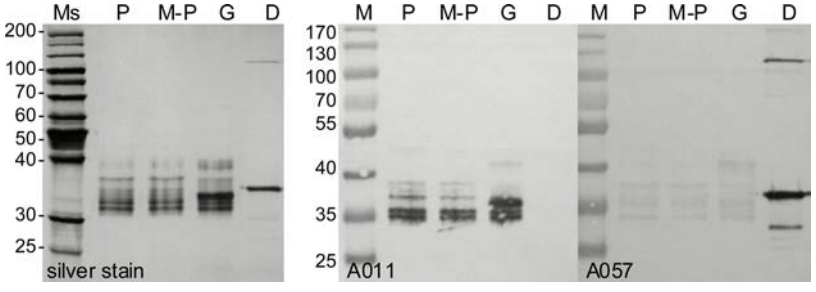

Figure 1. SDS-PAGE and Western Blot of gliadin-extracts from pasta (P) or MTG-pasta (M-P), from wheat gluten (G) and of deamidated gliadin peptide DGPx2 (D). Left: silver stained gel. Middle and right: Western blots using monoclonal antibodies to gliadin (A011) and deamidated gliadin (A057). Ms: molecular weight marker (200, 150, 120, 100, 85, 70, 60, 50, 40, 30, and 25 kDa) silver stained gel. M: molecular weight marker immunoblotted gel (170, 130, 100, 70, 55, 40, 35, and 25 kDa).

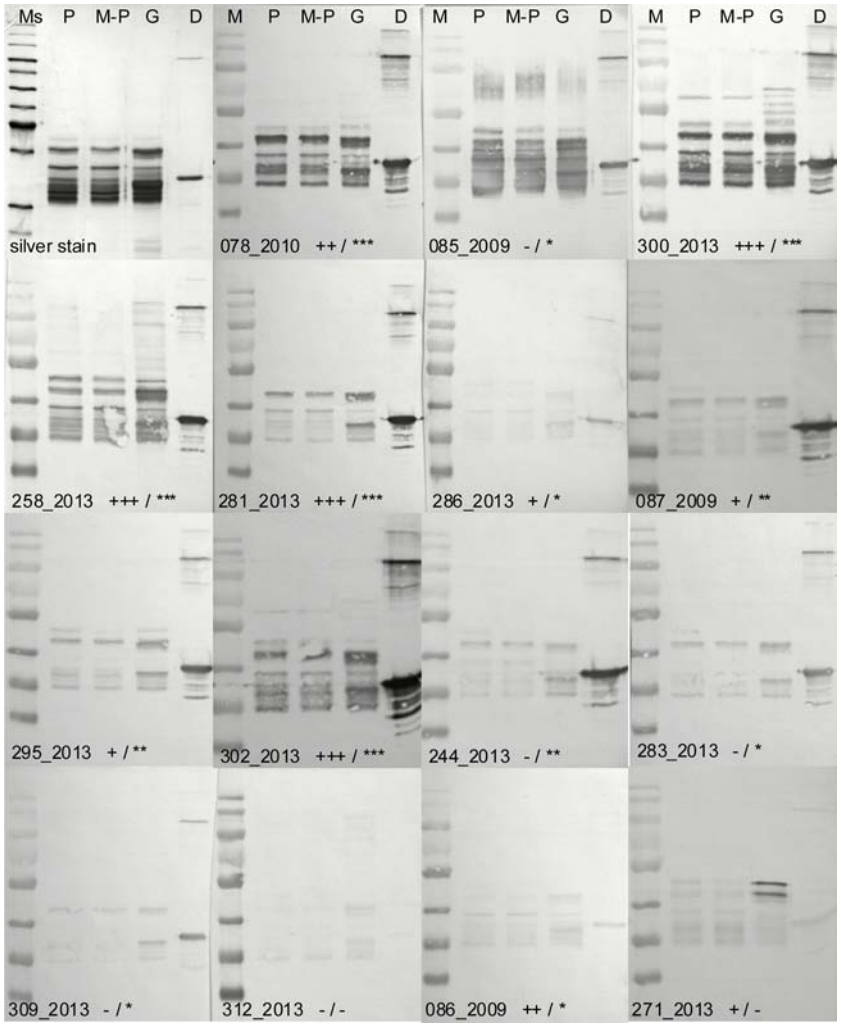

Figure 2. SDS-PAGE (silver stained) and immunoblot (IgG) of gliadin-extracts from pasta prepared without (P) or with (M-P) MTG, from wheat gluten (G) and of deamidated gliadin peptide DGPx2 (D). Ms and M: molecular weight markers, see Figure 1. The celiac disease patient's serum used as primary antibody is indicated. Antihuman IgG-alcaline phosphatase-conjugate was used as secondary antibody. The ELISA-IgG-titers measured for the sera have been added according to the following classification: Gliadin-Ab: −: < 14 U/mL; +: 15−30 U/mL; ++: 30−65 U/mL; and +++: > 65 U/mL. DGPx1-Ab: −: < 3 U/mL; *: 3−30 U/mL; **: 30−65 U/mL; and ***: > 65 U/mL.

Preparation and Analysis of Gliadin Extracts from Pasta and MTG-Pasta. Gliadin has been extracted as ethanolic fraction from pasta and MTG-pasta as well as from a commercial bread-gluten-preparation serving as a positive control in immunoblotting. The silver-stained SDS-PAGE (Figure 1) reveals no differences with respect to pattern and intensity for the two pasta gliadin-extracts and no polymerized gluten has been observed. A similar result is described for gliadin extracted from MTG-bread.[25] Other reports show polymerized proteins in acidic extracts of MTG-treated gluten or and in complete gluten.[35,36] This different observations may be explained by polymer amounts below the detection limit or the insolubility of high molecular weight polymers in the ethanolic fraction.

The bread-gluten derived gliadin shows a different band pattern characterized by a dominant band not present in pasta gliadins. This may be ascribed to different cultivars: Pasta is based on durum wheat, whereas the commercial gluten preparation has been obtained from bread wheat. The recombinant deamidated gluten peptide DGPx2, which is composed by the α2-gliadin-derived 33mer and γ-gliadin derived 26mer, both in their deamidated form fused to a carrier protein has been added as positive control for immunoreactivity of deamidated gliadin.[37] It yields a dominant band at the expected size of 31 kDa as well as two minor bands, which are presumably a fragment and a multimer of the recombinant DGPx2.

The gliadin-extracts have been further analyzed by immunoblotting (Figure 1). Using gliadin specific monoclonal antibody A011, the band patterns and intensities for both pasta gliadins are identical, while in agreement with the silver stained gel the pattern of bread-wheat gliadin differs. A011 is not able to bind to the deamidated gluten peptide DGPx2. Deamidated gliadin specific antibody A057, raised against deamidated (Q66E) α-gliadin peptide 58−73 (KLQPFPQPELPYPQPQ) recognizes both gliadin extracts from pasta as well as the extract from gluten very weakly. The deamidated gliadin peptide DGPx2 is recognized by A057 as a major band and two minor bands, in agreement to the silver stained gel. For the silver stained gel as well as both immunoblots, no differences in band pattern or in intensity could be observed for gliadin extracts from pasta and MTG-pasta. In particular, the antibody specific to deamidated gliadin did not yield additional or more intensive bands for the MTG-pasta gliadin extract.

While MTG-treatment clearly increases the number of ε-(γ-glutamyl)lysine-bonds there is no change in the ethanol-extractable

dx.doi.org/10.1021/jf501275c | J. Agric. Food Chem. 2014, 62, 7604−7611

gliadin fraction in SDS-PAGE and immunoblotting. No deamidation products can be detected using an antibody specific to deamidated gliadin.

Characterization of Sera for Antibody Titers. A collection of 40 celiac disease patients' sera covering a broad range of IgA-type autoantibodies to tissue transglutaminase (TG2) according to the distributors certificates have been analyzed for their antibody titers (IgA and IgG) to TG2, gliadin and deamidated gliadin. The results presented in Table 3 confirm the broad range of TG2-IgA-titers. Fourteen sera were also positive for anti-TG2-IgG. More sera were positive for anti-DGP than for antigliadin-antibodies (IgA: 28 vs 35 sera; IgG: 20 vs 33 sera). This observation as well as the overall ratio of positive sera (gliadin-IgA: 70%; IgG: 50%; DGP-IgA: 88%; IgG: 83%) is in good agreement with an earlier study on 128 untreated celiac disease patients (gliadin-IgA: 73%; IgG: 74%; DGP-IgA: 84%; IgG: 84%), where only the antigliadin-IgG positive ratio has been found higher (84% vs 59%).[38] There is a trend that sera with high anti-TG2-IgA-titers are strong positive for antigliadin and anti-DGP (both IgA and IgG), while for anti-TG2-IgG titers, such a correlation is not given. This observation confirms the data from an earlier study.[39] Nevertheless Table 3 also shows that individual sera do not follow this trend. E.g. sera with low anti-TG2-titer may show a negative (093_2009), intermediate (270_2013) or high (078_2010) antigliadin-titer. Sera negative or weak-positive for antigliadin are positive or even strong positive for anti-DGP (085_2009, 120_2010). In summary, despite a common trend, there is an individual composition of patient's sera with respect to antibodies to TG2, gliadin and DGP.

As a negative control, 20 arbitrarily chosen blood donor's sera have been characterized for antibodies to TG2, gliadin, and DGP. All these sera have been negative for TG2-autoantibodies

Table 3. Autoantibody and Antibody Titers of 40 Celiac Disease Patients' Sera for TG2, Gliadin and Deamidated Gliadin[a]

serum	immuno-blotting	TG2-ab cut-off: 3.0 U/mL		gliadin-ab cut-off: 14.0 U/mL		DGP-ab cut-off: 3.0 U/mL	
		IgA	IgG	IgA	IgG	IgA	IgG
268_2013		**3**	1	5	10	3	1
275_2013		**3**	1	7	**70**	**3**	**10**
255_2013		**4**	1	4	4	2	3
270_2013		**4**	**4**	7	**41**	**5**	7
093_2009		**5**	1	10	4	7	1
120_2010		**5**	1	**16**	2	**100**	0
078_2010	IgG	**5**	1	**100**	**64**	**100**	**100**
088_2009		**8**	1	**100**	**68**	**100**	**100**
266_2013		**10**	1	4	8	3	**3**
085_2009	IgG, IgA	**10**	2	13	9	**12**	**26**
293_2013		**13**	**6**	**22**	9	**12**	**17**
312_2013	IgG, IgA	**15**	2	**18**	6	1	0
244_2013	IgG	**15**	**4**	13	9	**13**	**57**
086_2009	IgG	**19**	**3**	**25**	**56**	**12**	**4**
254_2013		**20**	2	11	8	**5**	1
080_2009		**25**	**5**	7	**15**	2	7
083_2009		**25**	1	**100**	4	**100**	**97**
252_2013		**29**	**7**	14	8	**11**	**100**
281_2013	IgG	**31**	**100**	**100**	**100**	**100**	**100**
300_2013	IgG	**31**	**17**	**100**	**100**	**100**	**100**
075_2009		**32**	2	**36**	3	**59**	**64**
251_2013		**33**	0	13	9	**6**	**8**
084_2009		**34**	1	**82**	2	**100**	**6**
081_2009		**35**	3	**24**	13	**27**	**11**
295_2013	IgG	**37**	**7**	**39**	**15**	**35**	**49**
106_2009	IgA	**39**	2	**61**	1	**52**	**31**
309_2013	IgG	**47**	1	**66**	5	**83**	**10**
271_2013	IgG	**49**	1	**100**	**28**	**100**	2
089_2009		**69**	**42**	**21**	**100**	**12**	**100**
305_2013		**69**	2	**87**	**15**	**100**	**100**
310_2013		**72**	**6**	**38**	**34**	**59**	**96**
079_2009		**100**	**12**	**39**	**63**	**43**	**100**
087_2009	IgG	**100**	3	**100**	**16**	**40**	**45**
103_2009		**100**	**9**	**100**	**18**	**100**	**100**
258_2013	IgG	**100**	1	**100**	**100**	**100**	**100**
280_2013		**100**	1	**100**	14	**100**	**34**
283_2013	IgG, IgA	**100**	2	**100**	2	**100**	**10**
286_2013	IgG	**100**	2	**26**	**26**	**8**	**8**
287_2013		**100**	2	**32**	**33**	**10**	**100**
302_2013	IgG, IgA	**100**	**100**	**100**	**100**	**100**	**100**

[a]Sera have been listed according to increasing TG2-ab (IgA) titers. Positive sera according to the manufacturers cut-offs are written in bold. Sera used as detection antibody in immunoblotting are marked within the column "immunoblotting" as IgG or IgA. Note: 100 U/mL corresponds to a titer equivalent or higher than the maximal calibrator.

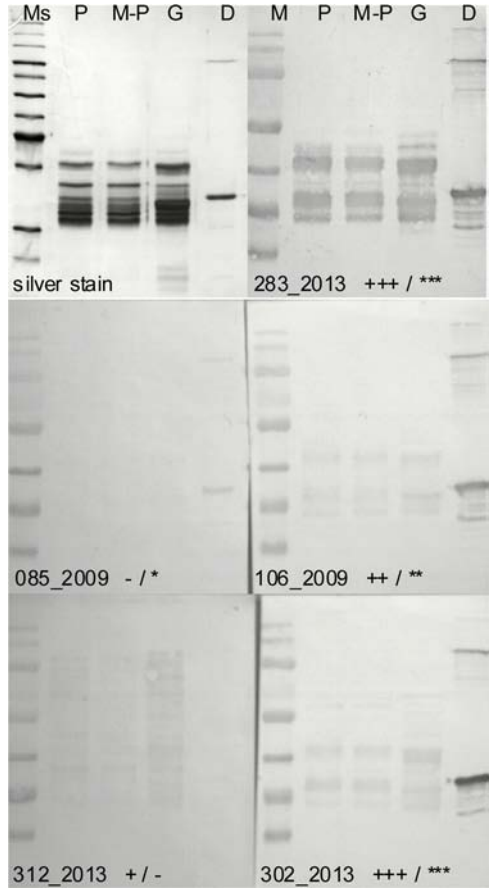

Figure 3. SDS-PAGE (silver stained) and immunoblot (IgA) of gliadin-extracts from pasta prepared without (P) or with (M-P) MTG, from wheat gluten (G) and of deamidated gliadin peptide DGPx2 (D). Ms and M: molecular weight markers, see Figure 1. The celiac disease patient's serum used as primary antibody is indicated. Antihuman IgA-alcaline phosphatase-conjugate was used as secondary antibody. The ELISA-IgA-titers measured for the sera have been added according to the classification given in Figure 2.

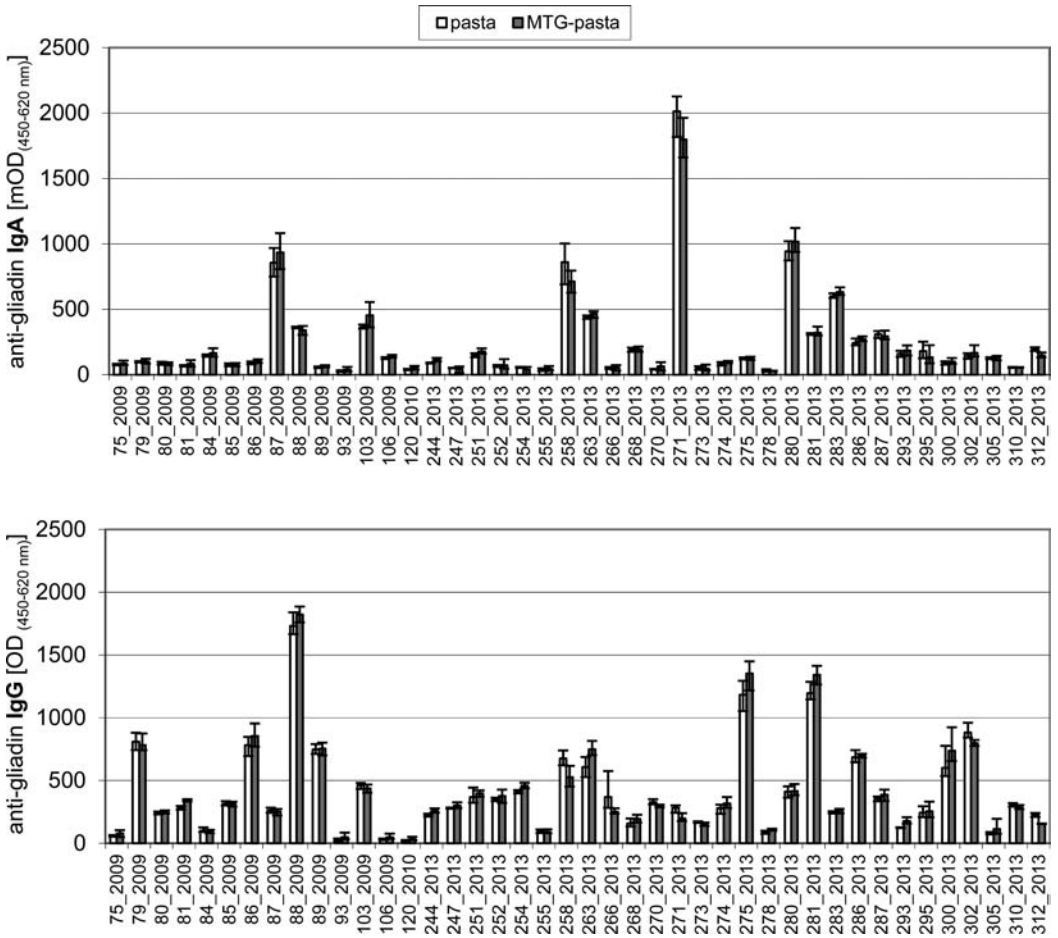

Figure 4. Antibody titers (IgA: upper part, IgG: lower part) of celiac disease patients' sera determined by ELISA using microtiter plates coated with gliadin extracts from pasta (white columns) and MTG-pasta (gray columns). $mOD_{(450-620\ nm)} = (\Delta E_{450} - \Delta E_{620})$ *1000.

(both IgA and IgG-type). Nine sera found positive for anti-DGP or antigliadin-antibodies in the IgA- or IgG-assay have not been used for control experiments.

Analysis of Gliadin Extracts by Immunoblotting. Immunoblotting of gliadin extracts from pasta and MTG-pasta as well as from bread wheat-gluten and DGPx2 as controls has been performed as described above, but by using 15 celiac disease patient's sera (see column "immunoblotting" in Table 3) as primary antibody. The 15 sera cover the whole range from weak to strong titers for anti-TG2-IgA, the primary serological marker in celiac disease. The sera also cover the whole range from negative over mild to strong positive antigliadin-IgG and anti-DGP-IgG antibody-titers (Table 3). IgG-detection has been chosen, as in celiac disease diagnostics measurement of anti-DGP-IgG-titers is recommended.[40] The resulting blots presented in Figure 2 at a look show, that the antigliadin and anti-DGP antibody-compositions of celiac patient's sera are not only individual with respect to their titers, but also with respect to their specificities. Individual sera are therefore composed by a differing oligoclonal antibody population. While some sera recognize gliadins as well as deamidated gliadin in a strong manner (e.g., 078_2010–258_2013 in Figure 2) there are sera which yield an intensive signal only for DGP (e.g., 281_2013, 087_2009, or 244_2013). Other sera yield weak to very weak signals for all antigens (286_2013, 309_2013, or 312_2013). Serum 286_2013 only recognizes DGP. It does not recognize gliadins including gliadin from MTG-pasta. Serum 271_2013 shows a strong preference for two gliadins from bread wheat, but only weak bands for gliadins from pasta and MTG-pasta.

In summary, the recognition patterns differ from serum to serum, and the recognition pattern for gliadin extracts from pasta and MTG-pasta is identical for every individual serum. Also sera which bind to DGP in a strong manner do not show a different or more intensive recognition pattern for gliadin from MTG-pasta compared to gliadin from pasta.

Immunoblotting using anti-DGP-antibody A057 and serum 302_2013 (IgG) as primary antibodies of the albumin/globulin-fractions and the glutenin-fractions from pasta and MTG-pasta revealed no difference in recognition patterns (data not shown). Therefore, a shift of deamidated gliadin to the other wheat protein-fractions can be excluded.

Five antigliadin-/anti-DGP-negative over weak to strong positive celiac disease patient's sera have also been analyzed for their IgA-type antibodies to gliadin and DGP by immunoblotting (Figure 3). The observations obtained for the IgG-type antibodies could be confirmed: The antibody composition of the sera is individual. No difference in pattern and intensity for gliadin from pasta and MTG-pasta can be seen, even if titers for anti-DGP-antibodies are high (sera 283_2013, 106_2009, 302_2013).

Blood donor's sera, negative for gliadin and deamidated gliadin antibodies in ELISA have also been negative in Western blots run as controls (data not shown).

dx.doi.org/10.1021/jf501275c | J. Agric. Food Chem. 2014, 62, 7604–7611

Celiac disease patient's sera recognize gliadin and deamidated gliadin sensitively. Above results suggest that there is no increased deamidation in pasta-gliadin by MTG.

In contrast to our data different immunoblotting pattern (IgA) for MTG-treated bread has been reported using a pool of 9 celiac patients' sera.[25] This may be due to different wheat-cultivars for bread and pasta. While a proper comparison in immunoblotting requires analysis of both extracts on a single blot, the authors obviously used different blots, which might also explain their observation.

Analysis of Gliadin Extracts by ELISA. The titer of celiac disease patient's sera for antibodies against gliadin extracts from pasta and MTG-pasta has been determined using microtiter plates (MTP) coated with the respective gliadin extracts in the ELISA-format (Figure 4). In order to avoid plate to plate discrepancies, every single serum has been analyzed in quadruplicate on single plates coated with gliadin from pasta and MTG-pasta. Generally, the extinction-values are lower for the pasta-gliadin ELISAs compared to the commercial anti-bread-wheat-gliadin-ELISA, which might be explained by differences in the coating efficiency. As can be seen in the SDS-PAGE (Figure 1), gliadin from pasta (durum wheat) differs from bread wheat gliadin.

When considering tendency rather than absolute values, the titers of the homemade gliadin-ELISA are in rough agreement with the commercial gliadin-ELISA, although some sera differ significantly. For example, serum 302_2013 shows a weak IgA titer in the homemade ELISA, which is in line with the weak bands the serum yields in immunoblotting, but is highly positive in the commercial ELISAs. Besides coating efficacy changes in structure upon adhesion on the MTPs polystyrene surface may also explain these differences. The results given in Figure 4 show that there are no differences in immunoreactivity of celiac disease patients' sera to gliadin extracts from pasta and MTG-pasta, neither for IgA nor for IgG-type antibodies. It has to be emphasized that sera characterized by a significantly higher DGP-antibody titer also do not show differences for the gliadin extracts from pasta and MTG-pasta. In this context, the ELISA-results are in line with the immunoblots shown in Figure 2 (IgG) and Figure 3 (IgA).

Cabrera-Chavez reported an increased immunoreactivity of a pool of 9 CD-sera to gliadin from MTG-bread. For two individual sera they observed no difference for a high titer serum, but an increased imunoreactiviy to MTG-bread-gliadin for a low titer serum.[25] This difference to our results may be due to different wheat cultivars used for pasta and bread production but it may also be a consequence to different conditions in bread and pasta production. Further, the same group reported an increased immunoreactivity in ELISAs for gliadin from MTG-bread for sera from 5 CD patient's older than 8 years, while sera for up to 3 years old patients did not show increased IgA-titers.[26] In contrast, we did not observe age-related differences with respect to IgA or IgG-titers against MTG-pasta-gliadin in our sera taken from patients well distributed from 1 to 81 years.

Antibodies to gliadin or deamidated gliadin are of diagnostic significance. Especially DGP-specific antibodies support celiac disease diagnostics when TG2-autoantibody titers are negative.[41] Despite the diagnostic relevance, a pathogenic role for (deamidated) gliadin antibodies is not described. Therefore, with respect to reports of increased immunoreactivity of celiac disease patients' sera following MTG-treatment, it has to be emphasized that this cannot be considered by itself a sign of enhanced gluten toxicity.

On the basis of our results, we consider immunoblotting to be more suitable than ELISA for the characterization of immunoreactivity of gliadin-extracts from food samples with celiac disease patient's sera.

In summary, treatment of pasta dough with MTG leads to an increase in cross-links (ε-(γ-glutamyl)lysine-bonds). This does not lead to a changed immunoreactivity of the gliadin-extracts for celiac disease patients' sera by immunoblotting and ELISA.

AUTHOR INFORMATION

Corresponding Author

*Phone: +49 (6151) 325100; fax: +49 (6151) 325119; e-mail: hils@zedira.com.

Notes

The authors declare the following competing financial interest(s): R.P., M.H., T.R., and J.O. are shareholders and/or employees of Zedira. K.Y. and Y.K. are employees of Ajinomoto. Zedira received financial support from Ajinomoto for this study. Ajinomoto did not participate in the analysis and interpretation of the data.

ABBREVIATIONS USED

CD, celiac disease; DGP, deamidated gliadin peptide; ELISA, enzyme linked immune sorbent assay; MTG, microbial transglutaminase; MTP, micro titer plate; TG2, tissue transglutaminase; PAGE, poly acrylamide gelelectrophoresis

REFERENCES

(1) Reilly, N. R.; Green, P. H. R. Epidemiology and clinical presentations of celiac disease. *Semin. Immunopathol.* **2012**, *34*, 473−478.

(2) Dewar, D.; Pereira, S. P.; Ciclitira, P. J. The pathogenesis of coeliac disease. *Int. J. Biochem. Cell Biol.* **2004**, *36*, 17−24.

(3) Schuppan, D.; Junker, Y.; Barisani, D. Celiac disease: from pathogenesis to novel therapies. *Gastroenterology* **2009**, *137*, 1912−1933.

(4) Shan, L.; Molberg, Ø.; Parrot, I.; Hausch, F.; Filiz, F.; Gray, G. M.; Sollid, L. M.; Khosla, C. Structural basis for gluten intolerance in celiac sprue. *Science* **2002**, *297*, 2275−2279.

(5) Vader, L. W.; de Ru, A.; van der Wal, Y.; Kooy, Y. M. C.; Benckhuijsen, W.; Mearin, M. L.; Drijfhout, J. W.; van Veelen, P.; Koning, F. Specificity of tissue transglutaminase explains cereal toxicity in celiac disease. *J. Exp. Med.* **2002**, *195*, 643−649.

(6) Stamnaes, J.; Fleckenstein, B.; Sollid, L. M. The propensity for deamidation and transamidation of peptides by transglutaminase 2 is dependent on substrate affinity and reaction conditions. *Biochim. Biophys. Acta* **2008**, *1784*, 1804−1811.

(7) Molberg, O.; Mcadam, S. N.; Körner, R.; Quarsten, H.; Kristiansen, C.; Madsen, L.; Fugger, L.; Scott, H.; Norén, O.; Roepstorff, P.; Lundin, K. E.; Sjöström, H.; Sollid, L. M. Tissue transglutaminase selectively modifies gliadin peptides that are recognized by gut-derived T cells in celiac disease. *Nat. Med.* **1998**, *4*, 713−717.

(8) Dieterich, W.; Ehnis, T.; Bauer, M.; Donner, P.; Volta, U.; Riecken, E. O.; Schuppan, D. Identification of tissue transglutaminase as the autoantigen of celiac disease. *Nature* **1997**, *3*, 797−801.

(9) Aleanzi, M.; Demonte, A. M.; Esper, C.; Garcilazo, S.; Waggener, M. Celiac disease: Antibody recognition against native and selectively deamidated gliadin peptides. *Clin. Chem.* **2001**, *47*, 2023−2208.

(10) Hill, I. D. What are the sensitivity and specificity of serologic tests for celiac disease? Do sensitivity and specificity vary in different populations? *Gastroenterology* **2005**, *128*, S25−S32.

(11) Lindfors, K.; Kaukinen, K. Contribution of celiac disease autoantibodies to the disease process. *Exp. Rev. Clin. Immunol* **2012**, *8*, 151−154.

(12) Lindfors, K.; Mäki, M.; Kaukinen, K. Transglutaminase 2-targeted autoantibodies in celiac disease: Pathogenetic players in addition to diagnostic tools? *Autoimmun. Rev.* **2010**, *9*, 744−749.
(13) Teesalu, K.; Panarina, M.; Uibo, O.; Uibo, R.; Utt, M. Autoantibodies from patients with celiac disease inhibit transglutaminase 2 binding to heparin/heparan sulfate and interfere with intestinal epithelial cell adhesion. *Amino Acids* **2012**, *42*, 1055−1064.
(14) Ando, H.; Adachi, M.; Umeda, K.; Matsuura, A.; Nonaka, M.; Uchio, R.; Tanaka, H.; Motoki, M. Purification and characteristics of a novel transglutaminase derived from microorganisms. *Agric. Biol. Chem.* **1989**, *53*, 2613−2617.
(15) Kanaji, T.; Ozaki, H.; Takao, T.; Kawajiri, H.; Ide, H.; Motoki, M.; Shimonishi, Y. Primary structure of microbial transglutaminase from *Streptoverticillium* sp. Strain s-8112. *J. Biol. Chem.* **1993**, *268*, 11565−11572.
(16) Kuraishi, C.; Yamazaki, K.; Susa, Y. Transglutaminase: Its utilization in the food industry. *Food Rev. Int.* **2001**, *17*, 221−2456.
(17) Kieliszek, M.; Misiewicz, A. Microbial transglutaminase and its application in the food industry. A review. *Folia Microbiol. (Praha).* **2014**, *59*, 241−250.
(18) Soeda, T., Yamazaki, K., Murase, K. *A method for producing long-shelf-life noodles distributed at room temperture. Japan Pat.* 5,244,887 1993.
(19) Gianfrani, C.; Siciliano, R. a; Facchiano, A. M.; Camarca, A.; Mazzeo, M. F.; Costantini, S.; Salvati, V. M.; Maurano, F.; Mazzarella, G.; Iaquinto, G.; Bergamo, P.; Rossi, M. Transamidation of wheat flour inhibits the response to gliadin of intestinal T cells in celiac disease. *Gastroenterology* **2007**, *133*, 780−789.
(20) Mazzeo, M. F.; Bonavita, R.; Maurano, F.; Bergamo, P.; Siciliano, R.; Rossi, M. Biochemical modifications of gliadins induced by microbial transglutaminase on wheat flour. *Biochim. Biophys. Acta* **2013**, *1830*, 5166−5174.
(21) Skovbjerg, H.; Koch, C.; Anthonsen, D.; Sjöström, H. Deamidation and cross-linking of gliadin peptides by transglutaminases and the relation to celiac disease. *Biochim. Biophys. Acta* **2004**, *1690*, 220−230.
(22) Lombardi, E.; Bergamo, P.; Maurano, F.; Bozzella, G.; Luongo, D.; Mazzarella, G.; Rotondi Aufiero, V.; Iaquinto, G.; Rossi, M. Selective inhibition of the gliadin-specific, cell-mediated immune response by transamidation with microbial transglutaminase. *J. Leukoc. Biol.* **2013**, *93*, 479−488.
(23) Elli, L.; Roncoroni, L.; Hils, M.; Pasternack, R.; Barisani, D.; Terrani, C.; Vaira, V.; Ferrero, S.; Bardella, M. T. Immunological effects of transglutaminase-treated gluten in coeliac disease. *Hum. Immunol.* **2012**, *73*, 992−997.
(24) Bundesinstitut für Risikobewertung. Transglutaminase in Fleischerzeugnissen. 2011, *52*, 1−6.
(25) Cabrera-Chávez, F.; Rouzaud-Sández, O.; Sotelo-Cruz, N.; Calderón de la Barca, A. M. Transglutaminase treatment of wheat and maize prolamins of bread increases the serum IgA reactivity of celiac disease patients. *J. Agric. Food Chem.* **2008**, *56*, 1387−1391.
(26) Cabrera-Chávez, F.; Rouzaud-Sández, O.; Sotelo-Cruz, N.; Calderón de la Barca, A. M. Bovine milk caseins and transglutaminase-treated cereal prolamins are differentially recognized by IgA of celiac disease patients according to their age. *J. Agric. Food Chem.* **2009**, *57*, 3754−3759.
(27) Berti, C.; Roncoroni, L.; Falini, M. L.; Caramanico, R.; Dolfini, E.; Bardella, M. T.; Elli, L.; Terrani, C.; Forlani, F. Celiac-related properties of chemically and enzymatically modified gluten proteins. *J. Agric. Food Chem.* **2007**, *55*, 2482−2488.
(28) *Japan's Specifications and Standards for Food Additives*, 7th ed.; The Ministry of Health and Welfare Reproduced by Japan Food Additives Association: Tokyo, Japan; pp 19−35.
(29) Kumazawa, Y.; Seguro, K.; Takamura, M.; Motoki, M. Formation of ε-(γ-glutamyl)lysine cross-link in cured horse mackerel meat induced by drying. *J. Food Sci.* **1993**, *58*, 1062−1064.
(30) Wieser, H.; Antes, S.; Seilmeier, W. Quantitative determination of gluten protein types in wheat flour by reversed-phase high-performance liquid chromatography. *Cereal Chem.* **1998**, *75*, 644−650.
(31) Laemmli, U. K. Cleavage of structural proteins during the assembly of the head of bacteriophage T4. *Nature* **1970**, *227*, 508−585.
(32) Blum, H.; Beier, H.; G, H. J. Improved silver staining of plant protein, RNA & DNA in PAA gels. *Electrophoresis* **1987**, *8*, 93−99.
(33) Sakamoto, H.; Kumazawa, Y.; Motoki, M. Strength of protein gels prepared with microbial transglutaminase as related to reaction conditions. *J. Food Sci.* **1994**, *59*, 866−871.
(34) Sakamoto, H.; Kumazawa, Y.; Toiguchi, S.; Seguro, K.; Soeda, T.; Motoki, M. Gel strength enhancement by addition of microbial transglutaminase during onshore Surimi manutacture. *J. Food Sci.* **1995**, *60*, 300−304.
(35) Larré, C.; Denery-Papini, S.; Popineau, Y.; Deshayes, G.; Desserme, C.; Lefebvere, J. Biochemical analysis and rheological properties of gluten modified by transglutaminase. *Cereal Chem.* **2000**, *77*, 32−38.
(36) Basman, A.; Köksel, H.; NG, P. K. W. Effects of tranglutaminse on SDS-PAGE patterns of wheat, soy, and barley proteins and their blends. *J. Food Sci.* **2002**, *67*, 2654−2658.
(37) Dørum, S.; Qiao, S.-W.; Sollid, L. M.; Fleckenstein, B. A quantitative analysis of transglutaminase 2-mediated deamidation of gluten peptides: Implications for the T-cell response in celiac disease. *J. Proteome Res.* **2009**, *8*, 1748−1755.
(38) Volta, U.; Granito, A.; Fiorini, E.; Parisi, C.; Piscaglia, M.; Pappas, G.; Muratori, P.; Bianchi, F. B. Usefulness of antibodies to deamidated gliadin peptides in celiac disease diagnosis and follow-up. *Dig. Dis. Sci.* **2008**, *53*, 1582−1588.
(39) Marietta, E.-V.; Rashtak, S.; Murray, J. A. Correlation analysis of celiac sprue tissue transglutaminase and deamidated gliadin IgG/IgA. *World J. Gastroenterol.* **2009**, *15*, 845−848.
(40) Husby, S.; Koletzko, S.; Korponay-Szabó, I. R.; Mearin, M. L.; Phillips, A.; Shamir, R.; Troncone, R.; Giersiepen, K.; Branski, D.; Catassi, C.; Lelgeman, M.; Mäki, M.; Ribes-Koninckx, C.; Ventura, A.; Zimmer, K. P. European Society for Pediatric Gastroenterology, Hepatology, and Nutrition guidelines for the diagnosis of coeliac disease. *J. Pediatr. Gastroenterol. Nutr.* **2012**, *54*, 136−160.
(41) Rubio-Tapia, A.; Hill, I. D.; Kelly, C. P.; Calderwood, A. H.; Murray, J. A. American college of gastroenterology clinical guideline: Diagnosis and management of celiac disease. *Am. J. Gastroenterol.* **2013**, *108*, 656−677.

the viability of *P. caribbica* under oxidative stress; (iv) the effect of VC on ROS accumulation; (v) the effect of VC on induction of antioxidant enzymes, including catalase (CAT), superoxide dismutase (SOD), and glutathione peroxidase (GPX) in *P. caribbica*; (vi) the effect of VC on population dynamics of *P. caribbica* both in wounds and on the surface of apple fruit; and (vii) the biological function of the differentially expressed proteins of *P. caribbica* combined with VC and *P. caribbica* as sole treatment.

MATERIALS AND METHODS

Yeast. *P. caribbica* was obtained from the culture collection maintained by our laboratory at 4 °C on nutrient yeast dextrose agar (NYDA; 8 g of nutrient broth, 5 g of yeast extract, 10 g of glucose, and 20 g of agar, 1 L of distilled water; Sangon, Shanghai, China). A loop of the culture was inoculated in nutrient yeast dextrose broth (NYDB) and incubated on a rotary shaker at 180 rpm at 28 °C for 24 h. After incubation, cells were centrifuged at 5000 rpm for 10 min and washed twice with sterile distilled water to remove the residual medium.[15] Cell pellets were then resuspended in sterile distilled water and adjusted to an appropriate concentration with a hemocytometer for experiments.

Pathogen. *Penicillium expansum* was isolated from infected apples and maintained on potato dextrose agar (PDA; extract of boiled potatoes, 200 mL; dextrose, 20 g; agar, 20 g; and distilled water, 800 mL) at 4 °C. Spore suspensions were harvested by removing the spores from a 7-day-old culture and suspending them in sterile distilled water. With a hemocytometer, spore concentrations were determined and adjusted as required.

Fruits. Apple (*Malus domestica* Borkh.) fruits at commercial maturity without wounds or rot were selected on the basis of uniformity of size and color, disinfected with 1% (w/v) sodium hypochlorite for 1−2 min, rinsed with tap water, air-dried, and prepared for subsequent experiments.

Efficacy of *P. caribbica* in Controlling Blue Mold Decay of Apples. Three wounds were made on the equator of each apple with a sterile cork borer (approximately 5 mm diameter and 3 mm deep) and treated with 30 μL of different treated solutions as follows: (1) cell suspensions of *P. caribbica* (1×10^8 cells/mL); (2−6) cell suspensions of *P. caribbica* alone (1×10^8 cells/mL) supplemented with different concentrations of VC at 150, 200, 250, 300, or 350 μg/mL separately; and (7) sterile distilled water as the control. Biocontrol activity of *P. caribbica* was tested according to the procedure of Cao et al. [16] with some modifications. Three hours later, 30 μL of *P. expansum* suspension (5×10^4 spores/mL) was inoculated into each wound. After being air-dried, fruits were placed in enclosed plastic trays to maintain a high relative humidity (about 95%) and incubated at 25 °C. Disease incidences of apple fruits caused by *P. expansum* were determined after 15 days. There were three replications of each treatment that consisted of 12 fruits. The entire experiment was repeated three times, and the overall percentage of infection was calculated.

Evaluation of Survival of *P. caribbica* under Oxidative Stress. The survival of *P. caribbica* under oxidative stress was determined according to the method of Liu et al.,[3] with a slight modification. Yeasts was prepared as described, and 4 mL of yeast cell suspension at a final concentration of 1×10^8 cells/mL was placed in a 20 mL of test tube. Then the same volume of H_2O_2 was added at different concentrations (0, 5, 10 and 20 mM) into the test tube, exposing the yeast cells to oxidative stress at 28 °C on a shaker at 190 rpm for 0, 20, 40, or 60 min. At the described time points, 100 μL of serial 10-fold dilutions (from 5×10^7 to 5×10^3 cells/mL) of the samples were spread on NYDA. Colonies were counted after incubation at 28 °C for 3 days and expressed as the $\log_{10}$ colon-forming units per milliliter (CFU/mL) of each wound. There were three replicates of each treatment, and the entire experiment was conducted three times.

Effect of VC on Oxidative Stress Tolerance of *P. caribbica*. The effect of VC on survival of *P. caribbica* after H_2O_2 treatment was determined according to the method of Deveau et al.[17] with some modifications. Yeasts was prepared as described and adjusted to a final concentration of 1×10^8 cells/mL, and the non-VC-treated (NVC-treated) and 250 μg/mL VC-treated yeast suspensions were respectively exposed to 10 mM H_2O_2 according to the previous study and incubated at 28 °C at 190 rpm. After 20 min, colonies were evaluated with the same method as described above to test the survival of *P. caribbica* under oxidative stress. There were three replicates of each treatment, and the experiment was conducted three times.

Determination of Intracellular Reactive Oxygen Species. 2,7-Dichlorodihydrofluorescein diacetate (H_2DCFDA), the oxidant-sensitive probe, was used to determine the intracellular ROS production of *P. caribbica* according to the procedure of Liu et al.,[3] with a slight modification. Non-VC-treated and VC-treated yeast cells (the final concentration of VC was 250 μg/mL) were collected and then exposed to 10 mM H_2O_2 at 0, 20, 40, and 60 min, and cells without H_2O_2 treatment was considered as control. After exposure, cells were harvested quickly by centrifugation and washed twice with phosphate-buffered saline (PBS) buffer (pH 7.0) and resuspended in the same buffer containing 25 μM H_2DCFDA (dissolved in dimethyl sulfoxide). The suspension was incubated in the dark at 30 °C for 1 h. After washing twice with PBS buffer, intracellular ROS were examined with a fluorospectrophotometer using $\lambda_{excitation}$ = 504 nm and $\lambda_{emission}$ = 522 nm. The higher relative intensity indicates a higher ROS level. There were three replicates of each treatment, and the entire experiment was repeated three times.

Determination of the Enzyme Activities of CAT, SOD, and GPX. Yeasts were prepared as described and then supplemented with VC at the final concentration of 250 μg/mL. The yeast cells without VC treatment were considered as control. Cells were exposed to 10 mM H_2O_2 at 28 °C at 190 rpm for 1 h, then harvested by centrifugation at 10000 rpm for 10 min, and washed three times with sterile distilled water to remove residual VC and H_2O_2. The yeast samples at each time point (before H_2O_2 treatment and 0, 20, 40 and 60 min after exposure to H_2O_2) were harvested by centrifugation at 10000 rpm for 10 min and washed three times with sterile distilled water. Cells were disintegrated in liquid nitrogen and suspended in chilled potassium phosphate buffer (50 mM, pH 7.8, containing 5 mM DL-dithiothreitol and 5% PVPP). The cell suspension was centrifuged at 10000 rpm for 20 min at 4 °C, and the supernatant was used for enzyme assays.

SOD activity was evaluated by spectrophotometric assay according to the method of Bernstein et al. [18] A reaction mixture containing no protein extract was used as the control. Test tubes with the reaction mixture were irradiated under fluorescent lights at 4000 lx for 20 min. Then the absorbance of each solution was measured at 560 nm. One unit of enzyme activity was defined as the amount of enzyme inhibiting 50% of NBT photoreduction. Results were analyzaed from three independent replicates.

CAT activity was measured by monitoring at 240 nm with the decrease in absorbance due to the decomposition of H_2O_2 according to the method of Reverberi et al.[19] The reaction solution (3 mL) contained 2.8 mL of 30 mM H_2O_2 (dissolved in phosphate buffer (pH 7.8)) and 200 μL of extracted solution. After addition of the enzyme solution, the reaction was initiated, and one unit was defined as a decrease in A_{240} of 0.01 per minute. Results were analyzed from three independent replicates.

GPX was assayed by monitoring at 422 nm with the decrease in absorbance due to the reduction of GSH at 37 °C. The reaction mixture (1 mL) contained 0.4 mM GSH, 0.3 mM H_2O_2, and 0.3 mL of enzyme solution. The mixture was placed in an electrically heated thermostatic water bath at 37 °C for 5 min. Subsequently, 4 mL of 1.67% (w/v) meta-phosphoric acid (containing 0.05% (w/v) EDTA; 28% (w/v) NaCl) was quickly added to terminate the reaction followed by centrifugation for 10 min at 3000 rpm. Two milliliters of supernatant was added with 0.32 M Na_2HPO_4 (2.5 mL) and 0.5 mL of DTNB for 5 min. One unit was defined as a decrease of 1 μM GSH in 37 °C per minute. Results were analyzed from three independent replicates

The activities of SOD, CAT, and GPX were expressed as units per milligram of protein. Protein content was measured as described by Bradford,[20] bovine serum albumin (BSA) being used as standard.

Population Dynamics of *P. caribbica* in Apple Fruits. *Population Dynamics of P. caribbica on the Surface of Apple Fruits.* Four circles (approximately 14 mm diameter) were made on the upper part of each apple fruit with a marker pen. Two treatment solutions were used, VC-treated and non-VC-treated suspensions of *P. caribbica*. Three drops of 10 μL of these solutions were added evenly in each circle. Treated fruits in plastic trays were stored at 20 and 4 °C, respectively. Fruit samples were collected at different time points after treatment. At each time point, yeasts were harvested by removing the circled tissues with a sterilized knife. Samples were then ground with a mortar and pestle in 50 mL of sterile distilled water. Then, 100 μL of serial 10-fold dilutions were spread on NYDA plates. One hour after samples had been taken served as time 0. Fruits stored at 20 °C were assessed at 0 (1 h after the apples were inoculated with *P. caribbica*), 12, 24, 36, 48, 60, 72, 84, and 96 h, whereas those stored at 4 °C were assessed at 0 (1 h after the apples were inoculated with *P. caribbica*), 4, 5, 6, 7, 8, 9, 10, and 11 days. Colonies were counted after incubation at 28 °C for 48 h and expressed as the $\log_{10}$ CFU per wound. Each treatment contains three replications that consisted of 24 fruits, and the experiment was repeated three times.

Population Dynamics of P. caribbica in Wounds of Apple Fruits. Apples were prepared and wounded as described above. A 30 μL suspension of *P. caribbica* (1×10^8 cells/mL) alone (NVC) or *P. caribbica* (1×10^8 cells/mL) added with VC at a final concentration of 250 μg/mL (VC) was applied to each wound. Treated fruits were placed in enclosed plastic trays and stored at 20 and 4 °C, respectively. Fruit samples were collected with a sterile cork borer (9 mm diameter) to a depth of 10 mm[21] at different time points after treatment as described above. Fruits stored at 20 °C were assessed each day for 10 days, whereas those stored at 4 °C were assessed every 3 days for 33 days (1 h after the apples were inoculated with *P. caribbica* served as time 0). Colonies were counted after incubation at 28 °C for 48 h and expressed as the $\log_{10}$ CFU per wound. There were three replications of each treatment, and the entire experiment was repeated three times.

Biological Function of the Differentially Expressed Proteins of *P. carbbica* Combined with VC and *P. caribbica* as Sole Treatment. *Protein Sample Preparation.* Non-VC-treated and VC-treated yeast cells were collected and then exposed to 10 mM H_2O_2 for 60 min. The yeast cells were harvested by centrifuging at 10000*g* for 10 min (4 °C) and washed three times with cold double-distilled water to remove residual VC and H_2O_2. Protein sample preparation was performed as described by Li et al.[22]

Two-Dimensional Electrophoresis (2-DE) and Image Analysis. 2-DE and image analysis were performed as described by Wang et al.[23] using the vertical electrophoresis systems, Image Scanner III and Image Master 2D Platinum 7.0 software (GE Healthcare Bio-Science, Uppsala, Sweden), respectivly.

Protein In-Gel Digestion. Differentially expressed protein spots were excised from the gel and prepared for MS analysis according to the procedure of Zhang et al.[24]

Protein Identification by MALDI-TOF/TOF and Database Query. The peptide solution was analyzed using MALDI TOF/TOF mass spectrometer (Bruker, Germany). The resulting monoisotopic peptide masses were queried against protein database in NCBInr using MASCOT software according to the procedure of Majoul et al.[25]

Data Analysis. All statistical analyses were performed by analysis of variance (ANOVA) using the statistical program SPSS/PC version 16.0 (SPSS Inc., Chicago, IL, USA), and Duncan's multiple-range test was used for means separation. Differences at $p < 0.05$ were considered significant.

RESULTS

Efficacy of *P. caribbica* in Controlling Blue Mold Decay of Apples. As shown in Figure 1, *P. caribbica* effectively controlled postharvest blue mold decay of apples caused by *P. expansum* after 15 days of storage at 25 °C compared with the control fruits ($p < 0.05$). However, VC-treated yeast exhibited a better biocontrol efficacy compared to non-VC-treated yeast. Disease incidences in apple fruits treated with yeast alone and yeast combined with 250 μg/mL VC were 38.9 and 19.4%, respectively, whereas disease incidence in the control fruits (inoculated with water followed by the pathogen) reached 94.4%.

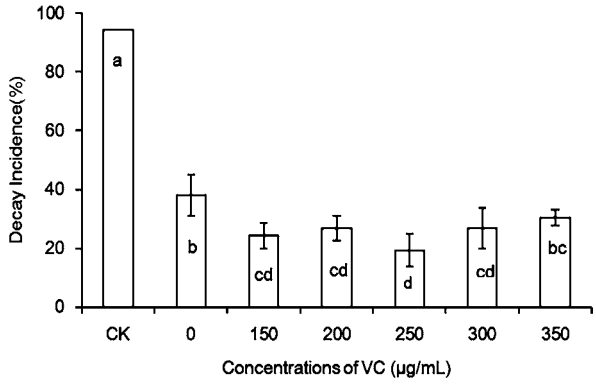

Figure 1. Efficacy of *P. caribbica* in controlling blue mold decay of apples stored at 25 °C. Sterilized water was used as control. Each value is the mean of three experiments. Bars represent the standard error of the mean. Data in columns with different letters are significantly different according to Duncan's multiple-range test at $p < 0.05$.

Evaluation of Survival of *P. caribbica* under Oxidative Stress. The viability of *P. caribbica* cells decreased with increasing H_2O_2 concentration and exposure time within each concentration (Figure 2). At 0 min, the yeast with all treatments had the same population level, whereas quite different levels were recorded at other time points. Furthermore, the population of *P. caribbica* cells reduced dramatically with a higher H_2O_2 concentration, particularly under the oxidative stress condition induced by 20 mM H_2O_2 for 60 min, in which yeast cells were nearly all dead. On the basis of the result of the viability assay, 10 mM H_2O_2 was chosen to be the appropriate stress condition for the following experiments.

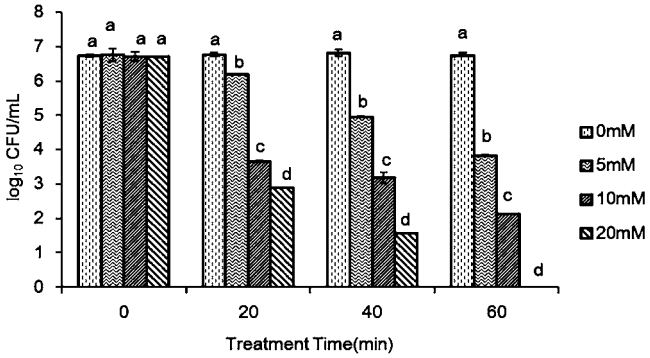

Figure 2. Population of *P. caribbica* under oxidative stress induced by H_2O_2. Each value is the mean of three experiments. Bars represent the standard error of the mean. Data in columns with different letters at the same time point are significantly different according to Duncan's multiple-range test at $p < 0.05$

Effect of VC on Oxidative Stress Tolerance of *P. caribbica*. As indicated in Figure 3, VC treatment had a significant effect on *P. caribbica* viability ($p < 0.05$); supplementation of VC improved the yeast viability from 2.73×10^4 cells/mL to 4.15×10^4 cells/mL.

ROS Accumulation of *P. caribbica* under Oxidative Stress. As illustrated in Figure 4, the ROS accumulation of

dx.doi.org/10.1021/jf501984n | J. Agric. Food Chem. 2014, 62, 7612−7621

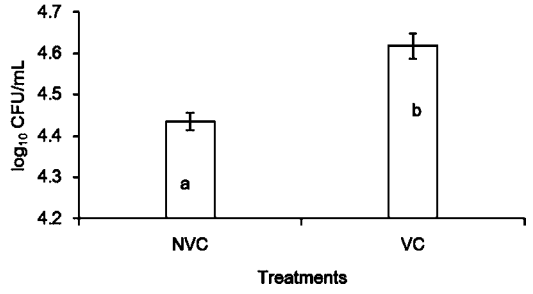

Figure 3. Effect of VC on oxidative stress tolerance of *P. caribbica*. Each value is the mean of three experiments. Bars represent the standard error of the mean. Data in columns with different letters are significantly different according to Duncan's multiple-range test at $p < 0.05$.

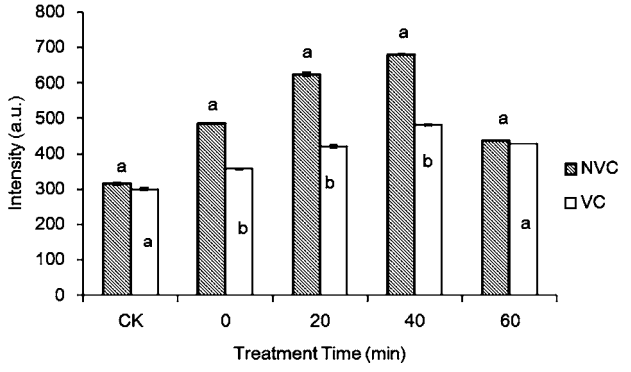

Figure 4. ROS accumulation in non-VC-treated and VC-treated cells of *P. caribbica* exposed to oxidative stress (10 mM H_2O_2) for various periods of time. Sterilized water was used as control. Each value is the mean of three experiments. Bars represent the standard error of the mean. Data in columns with different letters at the same time point are significantly different according to Duncan's multiple-range test at $p < 0.05$.

both treatments reached the highest level at 40 min. VC-treated cells showed significantly lower reactive oxidative stress (ROS) level compared to non-VC-treated cells at all tested time points except 60 min.

Activities of Antioxidant Enzymes. Adding exogenous VC enhanced the enzyme activities of SOD, CAT, and GPX of *P. caribbica* at some time point under oxidative stress. H_2O_2 induced the SOD activity, and VC improved its activity after exposure (Figure 5A). At 20 min, VC had the most obvious efficacy, and at 40 min, both treatments had the highest level of SOD activity, but all decreased at 60 min. VC did not increase CAT activity significantly until 40 min. However, CAT activity in non-VC-treated cells decreased greatly, whereas the CAT activity in VC-treated cells increased markedly at 40 min, and both of them exhibited a decreasing trend at 60 min (Figure 5B). When exposed to H_2O_2, GPX decreased tremendously before 20 min and then increased (Figure 5C). GPX activity of VC-treated *P. caribbica* was significantly higher than that of non-VC-treated *P. caribbica* at all tested times.

Population Dynamics of *P. caribbica* in Apple Fruits. *Population Dynamics of P. caribbica on the Surface of Apple Fruits.* The population of *P. caribbica* on the surface of apple fruits decreased quickly at the first stage at both temperatures (20 and 4 °C) and then increased (Figure 6A,B). However, irrespective of the storage temperature, the population of VC-

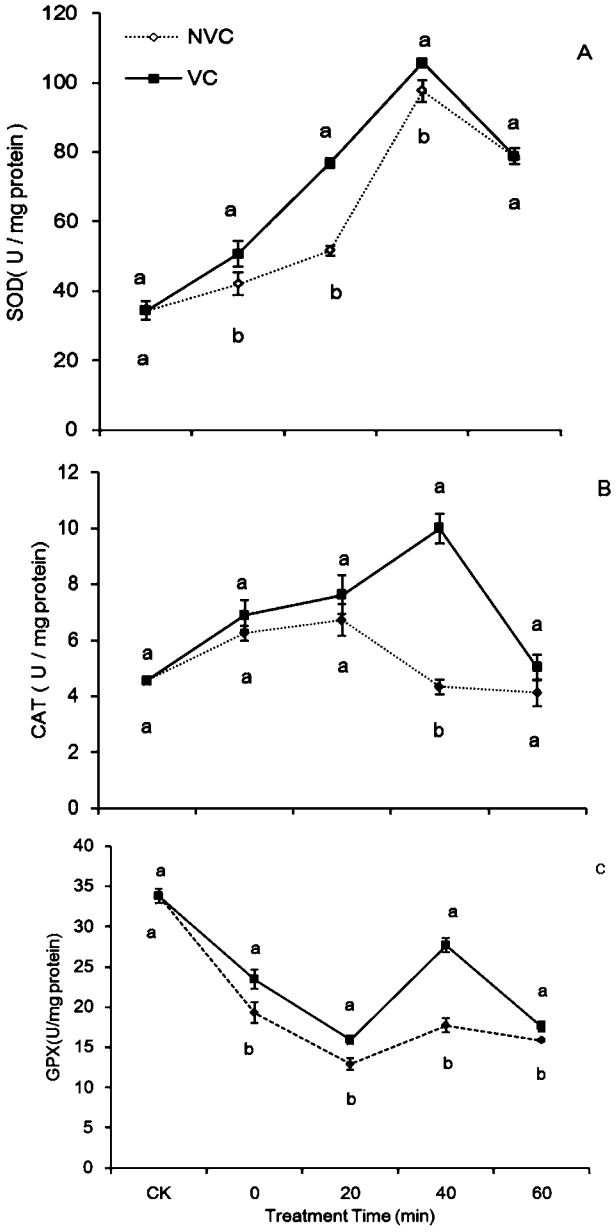

Figure 5. Change of SOD (A), CAT (B), and GPX (C) activities in control and VC-treated cells of *P. caribbica*. Cells without VC treatment served as control. Sterilized water was used as control. Data in columns with different letters are significantly different according to Duncan's multiple-range test at $p < 0.05$.

treated cells was significantly higher than that of non-VC-treated cells at all tested times.

Population Dynamics of P. caribbica in Wounds of Apple Fruits. Population dynamics of cells in the wounds compared with those on the fruit surfaces indicated a quite different trend (Figure 6). *P. caribbica* multiplied quickly in apple fruit wounds, and the number of yeast cells increased almost 10-fold at the first day (Figure 6C). The population of *P. caribbica* reached the maximum at days 7 and 8 for non-VC-treated cells and VC-treated cells, respectively. Although the yeast in wounds of apple fruits stored at 4 °C grew more slowly than that stored at 20 °C, rapid colonization of *P. caribbica* was observed during the first 3 days (Figure 6D). Although during all time points this population trend showed little fluctuation, it remained at a high level and did not fall below 1×10^6 CFU/wound at 4 °C.

dx.doi.org/10.1021/jf501984n | J. Agric. Food Chem. 2014, 62, 7612−7621

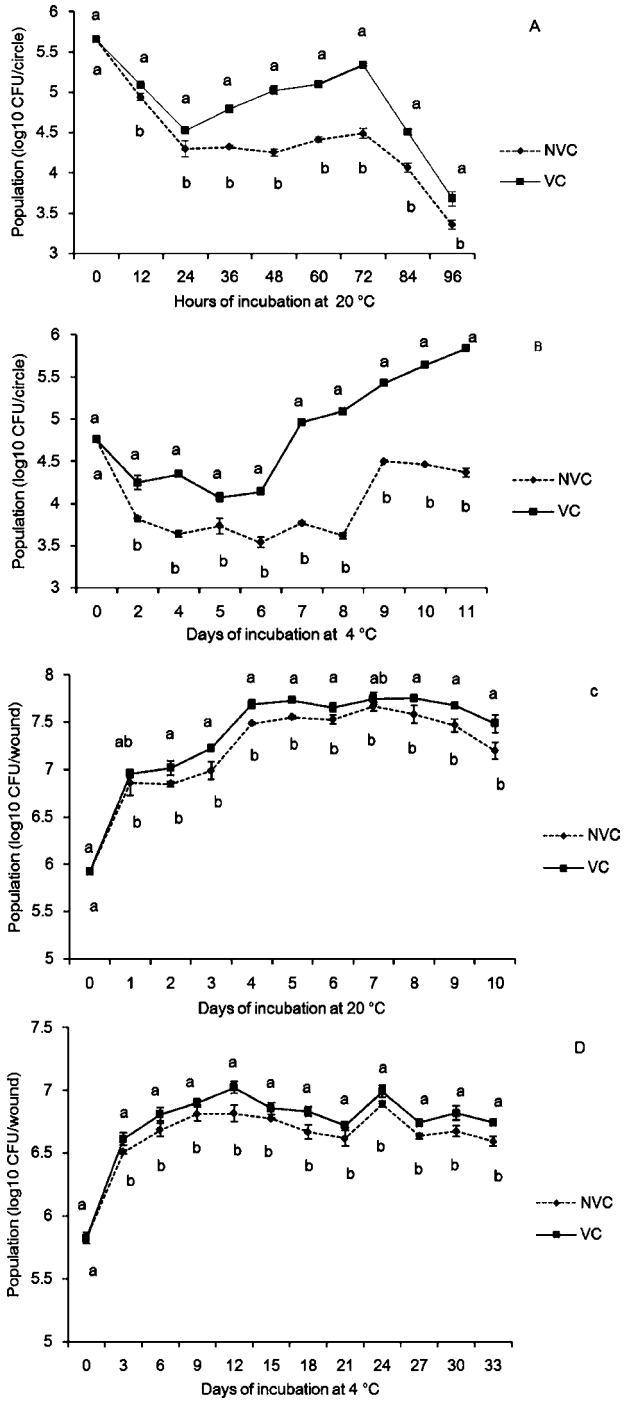

Figure 6. Population dynamics of *P. caribbica* both on the surface and in wounds of apple fruits stored at 20 and 4 °C, respectively. Each value is the mean of three experiments. Bars represent the standard error of the mean. Data in columns with different letters are significantly different according to Duncan's multiple-range test at $p < 0.05$. (A, B) Fruits were circled and inoculated with three 10 μL drops of non-VC-treated (NVC) or VC-treated (VC) cell suspension of *P. caribbica* at 1×10^8 cells/mL. Yeast colonies were counted after incubation at 28 °C for 36−48 h and expressed as the $\log_{10}$ CFU per circle. (C, D) Fruits were wounded and inoculated with 30 μL of non-VC-treated (NVC) or 250 μg/mL VC-treated (VC) cell suspension of *P. caribbica* at 1×10^8 cells/mL. Population levels at 20 °C were assessed each day for 10 days; meanwhile, the levels at 4 °C were assessed every 2 days for 33 days. Yeast colonies were counted after incubation at 28 °C for 36−48 h and expressed as the $\log_{10}$ CFU per wound.

Furthermore, irrespective of the temperature, the population of VC-treated *P. caribbica* was higher than the population of non-VC-treated *P. caribbica* at all tested times.

Identification of Differentially Expressed Proteins. Two aspects, changes in abundance of common spots between the two treatments (non-VC-treated and VC-treated) and appearance or absence of spots specifically, were considered when the differentially expressed proteins were evaluated. More than 200 protein spots were detected in each gel using IMP7.0 (Figure 7). Among them, 61 protein spots showing statistically significant ($p < 0.05$) changes of >1.5-fold in relative abundance between the two treatments were selected. Of the 61 proteins, 41 proteins were up-regulated and 20 proteins were down-regulated. All 61 proteins were focused on differences in degree of peak protein (Table 1). Most of the proteins were related to basic metabolism. Besides, there are proteins that correlate with protein synthesis, transportation, and stress response.

DISCUSSION

New methods to control postharvest decay have been found as an alternative to the use of synthetic fungicides; biocontrol agents were considered to be one of the most effective means.[26] In the present study, the results indicated that *P. caribbica* has showed control efficacy against postharvest blue mold decay of apples. This observation is in agreement with the one reported by Lahlali et al.,[27] but there are many differences between laboratory tests with host/parasite systems and performance of biocontrol agents/products under practical conditions,[28,29] which have great impact on the efficacy of controlling the postharvest disease of fruits. Oxidative stress, a crucial environmental factor, influenced the survival and efficacy of biocontrol yeasts.[30,31] Consequently, to maintain or increase the biocontrol activity of antagonists under commercial conditions, improving its stress tolerance is a useful strategy.[32,33] *P. caribbica* at 1×10^8 cells/mL combined with 250 μg/mL VC was demonstrated to be more effective in reducing *P. expansum* infection in apple fruit wounds than treatment with *P. caribbica* alone in this present study.

Combining antagonists with some food additives has drawn researchers' attention recently.[34] Previous studies have demonstrated the efficacy of NH_4Mo on improving the biocontrol ability of the yeast *Pichia membranifaciens* in fruit.[34] Ascorbic acid (VC) has been reported in various fruits and vegetables,[35] is an essential nutrient for physiological function of most animal species,[36] and plays an important role as a water-soluble antioxidant. From our experiments, we have got a similar result that VC is a potential approach to enhance the biocontrol efficacy of the antagonistic yeast *P. caribbica*. Specifically, the biological control activity of *P. caribbica* was greatly enhanced when the yeast was amended with VC at a final concentration range from 150 to 300 μg/mL, compared with the performance of *P. caribbica* used alone (Figure 1). It was found that 250 μg/mL VC showed the greatest enhancement for the biocontrol efficacy of *P. caribbica* (Figure 1).

With regard to oxidative stress, yeasts subjected to oxidative stress produce ROS. ROS can initiate cataract reactions leading to the production of $OH^{\bullet}$ and other destructive species such as lipid peroxides, which do serious harm to the cells.[37] Hydroxyl radicals are known to be very reactive and can damage vital cellular macromolecules, resulting in a decrease in cell viability.[18] As a consequence, in Figure 2 it was observed that *P. caribbica* was susceptible to oxidative stress, which led to a

dx.doi.org/10.1021/jf501984n | J. Agric. Food Chem. 2014, 62, 7612−7621

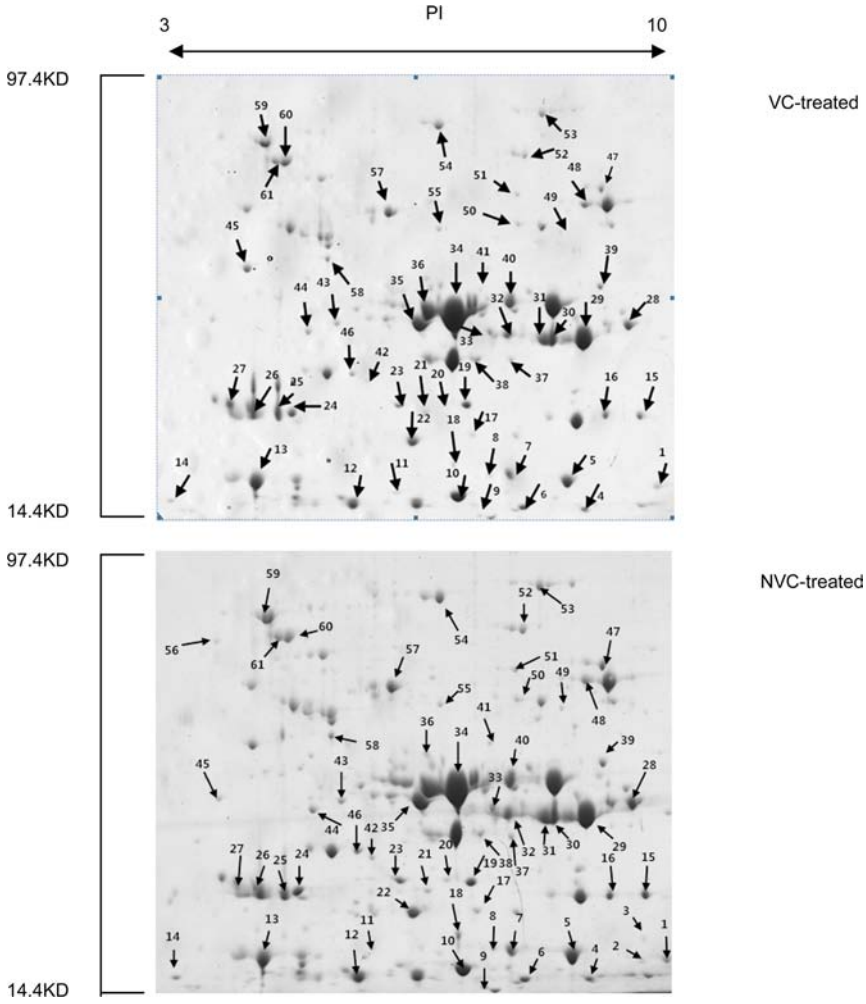

Figure 7. Two-dimensional pattern of intracellular proteins of non-VC-treated (NVC) or 250 μg/mL VC-treated (VC) cell under oxidative stress. Proteins were separated by 2D gel electrophoresis using 24 cm IPG strips with a pH 3−10 nonlinear gradient. After electrophoresis, proteins were visualized by Coomassie blue staining.

low viability that influenced its biocontrol efficacy. This observation is in agreement with that reported by Liu et al.,[3] who indicated that with the increasing H_2O_2 concentration and exposure time, the viability of *Cystofilobasidium infirmominiatum* decreased rapidly.[3] At the same time, the integration with VC is an effective measurement to improve the oxidative tolerance of the antagonistic yeast (Figure 3) .

Further studies showed that lower ROS accumulation was exhibited in VC-treated cells compared to non-VC-treated cells (Figure 4). Compared with the yeast viability presented under oxidative stress in Figure 2, the decreasing survival ability of the yeast with high concentrations of H_2O_2 might be caused by the higher accumulation of intracellular ROS. However, at 60 min, the ROS accumulation decreased tremendously compared with 40 min. This result is different from that achieved by Liu et al.,[3] who observed much higher ROS accumulation at 60 min. This may be attributed to cell death including cell apoptosis and necrocytosis. ROS produced under stress will induce cell apoptosis and lead to necrocytosis. Besides, a high concentration of ROS will cause necrocytosis directly. Cells release the cell content such as mitochondria and cytoplasm due to necrocytosis. This will be a possible mechanism leading to the decrease of ROS level. From the results of this present study, it is possible to conclude that the trend of ROS accumulation is negatively correlated with cell viability. Thus, the application of VC was capable of reducing the intracellular ROS accumulation, which could improve the population level of antagonistic yeast.

To reduce the excess of ROS, yeasts have developed an antioxidant defense system during evolution, which comprises various enzymatic and nonenzymatic components. The antioxidant enzymes that can directly react with ROS and scavenge ROS include SOD, CAT, and various peroxidases. In the present study, it was found that the activities of the three enzymes (SOD, CAT, and GPX) of *P. caribbica* cells were increased by VC treatment when exposed to H_2O_2 (Figure 5) at all tested time points. The results suggested that the induction of antioxidant enzyme activity in *P. caribbica* by VC treatment may be a key factor in lowering ROS levels, thus improving the viability of yeast cells exposed to oxidative stress.

It has been confirmed that there is a direct relationship between the population and the biocontrol efficacy of the antagonists.[5] The expected biocontrol efficacy will be achieved if antagonistic yeasts are able to survive and proliferate on the surface of the fruits.[5] There are many differences between laboratory tests and practical conditions,[29] which have great impact on the efficacy of controlling postharvest diseases of fruits. Oxidative stress, a crucial environmental factor,

dx.doi.org/10.1021/jf501984n | J. Agric. Food Chem. 2014, 62, 7612−7621

Table 1. . Identification of Cellular Proteins of *P. caribbica* Showing Differential Expression under Oxidative Stress Using MS/MS Analysis

protein name	NCBI accession no.	mass	PI	species	score	SC (%)	matches
guanyl-nucleotide exchange factor	gil528061614	168581	5.51	*Schizosaccharomyces octosporus* yFS286	71	8	10
hypothetical protein BC1G_10068	gil154301833	73084	4.32	*Botryotinia fuckeliana* B05.10	69	11	8
small GTPase Rac1	gil299755668	21794	8.22	*Coprinopsis cinerea okayama* 7#130	75	35	5
GTP-binding nuclear protein GSP1/Ran	gil146421317	24413	6.52	*Meyerozyma guilliermondii* ATCC 6260	97	45	8
polyketide synthase	gil296808807	41053	9.41	*Arthroderma otae* CBS 113480	61	14	4
hypothetical protein SMAC_00264	gil336273934	16556	5.55	*Sordaria macrospora* k-hell	68	43	4
hypothetical protein PGUG_05024	gil146414197	32118	7.77	*Meyerozyma guilliermondii* ATCC 6260	124	34	10
conserved hypothetical protein	gil115384822	140175	5.51	*Aspergillus terreus* NIH2624	75	11	12
hypothetical protein TRIATDRAFT_51448	gil358400748	110004	4.99	*Trichoderma atroviride* IMI 206040	70	8	7
phosphoglycerate mutase-like protein	gil512200498	37855	5.06	*Glarea lozoyensis* ATCC 20868	70	17	8
short-chain dehydrogenase reductase	gil320585844	39123	5.36	*Grosmannia clavigera* kw1407	65	25	7
malate dehydrogenase [*Aspergillus oryzae* RIB40]	gil317148785	32665	6.85	*Aspergillus oryzae* RIB40	63	14	5
CYP52A16	gil29469871	62054	6.88	*Candida tropicalis*	46	11	4
hypothetical protein CaO19.11314	gil68477373	77594	8.63	*Candida albicans* SC5314	47	9	5
glyceraldehyde-3-phosphate dehydrogenase	gil146419367	35831	6.6	*Meyerozyma guilliermondii* ATCC 6260	111	44	10
KLTH0E13530p	gil255715569	76761	8.9	*Lachancea thermotolerans*	77	19	11
hypothetical protein BN14_11504	gil471868712	55505	8.73	*Rhizoctonia solani* AG-1 IB	68	33	14
hypothetical protein PGUG_05024	gil146414197	32118	7.77	*Meyerozyma guilliermondii* ATCC 6260	95	31	7
hypothetical protein PGUG_04204	gil190347768	37468	5.42	*Meyerozyma guilliermondii* ATCC 6260	86	25	8
RNA helicase	gil405118839	75720	9.83	*Cryptococcus neoformans* var. *grubii* H99	63	13	8
hypothetical protein PGUG_02783	gil146418176	33223	5.22	*Meyerozyma guilliermondii* ATCC 6260	60	31	4
hypothetical protein F503_06451	gil512187970	85551	8.21	*Ophiostoma piceae* UAMH 11346	64	12	9
xylose reductase	gil4103055	36247	5.58	*Meyerozyma guilliermondii*	129	41	12
inorganic pyrophosphatase	gil344232670	31666	5.18	*Candida tenuis* ATCC 10573	69	25	6
malate dehydrogenase	gil317148785	32665	6.85	*Aspergillus oryzae* RIB40	63	14	5
conserved hypothetical protein	gil189191866	71626	6.57	*Pyrenophora tritici-repentis* Pt-1C-BFP	67	11	6
40S ribosomal protein S0	gil146417344	28665	4.77	*Meyerozyma guilliermondii* ATCC 6260	70	31	6
conserved hypothetical protein	gil146415847	42169	6.08	*Meyerozyma guilliermondii* ATCC 6260	89	36	12
hypothetical protein TPHA_0N00980	gil367007166	96418	5.8	*Tetrapisispora phaffii* CBS 4417	60	14	6
nicotinate phosphoribosyltransferase	gil344230982	47536	5.51	*Candida tenuis* ATCC 10573	42	15	4
putative high-affinity nicotinic acid transporter protein	gil500252021	64344	9.51	*Togninia minima* UCRPA7	69	24	7
50S ribosomal protein l19	gil405124304	21403	11.6	*Cryptococcus neoformans* var. *grubii* H99	65	27	5
putative oligopeptide transporter	gil328863365	79177	8.41	*Melampsora larici-populina* 98AG31	70	20	8
enolase 1	gil146415384	46951	5.42	*Meyerozyma guilliermondii* ATCC 6260	147	34	13
hypothetical protein COCHEDRAFT_1157214	gil451997726	55174	10.22	*Bipolaris maydis* C5	59	18	6
enolase 1	gil146415384	46915	5.42	*Meyerozyma guilliermondii* ATCC 6260	154	34	13
hypothetical protein BN14_07940	gil471884071	21986	9.82	*Rhizoctonia solani* AG-1 IB	53	34	4
MCM7	gil359294723	22843	5.97	*Trichosporon laibachii*	74	32	5
hypothetical protein CANTEDRAFT_128012	gil344228724	51735	6.53	*Candida tenuis* ATCC 10573	82	20	9
hypothetical protein ASPNIDRAFT_44377	gil350632783	30733	6.15	*Aspergillus niger* ATCC 1015	69	24	6
phosphoglycerate kinase	gil146416915	44452	5.9	*Meyerozyma guilliermondii* ATCC 6260	71	24	7
T-complex protein 1 subunit α Short=TCP-1-α	gil471909326	38733	7.62	*Rhizoctonia solani* AG-1 IB	71	22	8
homogentisate 1,2-dioxygenase	gil494828579	51230	5.56	*Coniosporium apollinis* CBS 100218	65	20	5
DEHA2F09570p	gil50424381	44438	6.3	*Debaryomyces hansenii* CBS767	135	36	13
conserved hypothetical protein	gil146414762	35538	4.54	*Meyerozyma guilliermondii* ATCC 6260	81	20	8
hypothetical protein PGUG_00294	gil146421948	35991	5.22	*Meyerozyma guilliermondii* ATCC 6260	60	15	5

Table 1. continued

protein name	NCBI accession no.	mass	PI	species	score	SC (%)	matches
isocitrate lyase	gil146413757	61937	6.31	*Meyerozyma guilliermondii* ATCC 6260	172	35	14
pyruvate kinase	gil146422809	55672	6.62	*Meyerozyma guilliermondii* ATCC 6260	154	30	17
hypothetical protein PGUG_01180	gil190345229	53074	7.23	*Meyerozyma guilliermondii* ATCC 6260	90	27	11
hypothetical protein PGUG_01180	gil146423756	53100	7.23	*Meyerozyma guilliermondii* ATCC 6260	67	20	7
acetyl-CoA hydrolase	gil146417797	58385	5.96	*Meyerozyma guilliermondii* ATCC 6260	107	28	13
hypothetical protein PGUG_01282	gil146419296	73680	5.91	*Meyerozyma guilliermondii* ATCC 6260	80	21	9
conserved hypothetical protein	gil146420955	85853	5.68	*Meyerozyma guilliermondii* ATCC 6260	253	47	27
conserved hypothetical protein	gil146421560	84975	5.92	*Meyerozyma guilliermondii* ATCC 6260	173	32	19
hypothetical protein PGUG_03032	gil146418675	69418	8.31	*Meyerozyma guilliermondii* ATCC 6260	117	31	18
heat shock protein 60, mitochondrial precursor	gil190348913	60586	5.17	*Meyerozyma guilliermondii ATCC 6260*	258	45	26
hypothetical protein SEPMUDRAFT_147302	gil453087363	83575	5.94	*Sphaerulina musiva* SO2202	80	23	11
hypothetical protein PGUG_00667	gil146422710	56048	5.44	*Meyerozyma guilliermondii* ATCC 6260	101	21	13
heat shock protein 70 2	gil146413777	70177	5.04	*Meyerozyma guilliermondii* ATCC 6260	213	43	22
hypothetical protein PGUG_04143	gil190347716	81682	6.69	*Meyerozyma guilliermondii* ATCC 6260	247	45	28
hypothetical protein PGUG_04143	gil190347716	81682	6.69	*Meyerozyma guilliermondii* ATCC 6260	92	24	13

influenced the survival and efficacy of biocontrol yeasts.[31] Hence, the improvement of oxidative tolerance has an important significance for adequate biological effectiveness.[33]

It was observed that VC improved the oxidative stress tolerance of *P. caribbica* and so did the population dynamics both on the surface and in the wounds of apples. The biocontrol activity of the antagonist is based on its capacity for rapid colonization and competition for space and nutrients.[5] In this study, 250 μg/mL VC improved the oxidative stress tolerance of *P. caribbica* and the population of *P. caribbica* both in the wounds and on the surface of the apple fruit (Figure 6), which probably explains the enhancement of the efficacy of *P. caribbica* exhibited in a previous assay. Similar results for other antagonist yeasts have been reported by Bencheqroun et al.[38] and Zhang et al.[39] In addition, the first 2 days after inoculation into apple wounds are quite important for *P. expansum* germination and infection.[40] As shown in Figure 6, it is notable that VC-treated cells of *P. caribbica* had a relatively higher population level than non-VC-treated cells both in wounds and on the surface of apple fruits during the first 2 days after inoculation. Thus, the higher population of VC-treated yeast cells compared to non-VC-treated cells in the early days may have produced the better biocontrol ability.

As to the molecular mechanism, most differentially expressed proteins in response to oxidative stress by the addition of VC were related to basic metabolism, which indicated that the basic metabolism of *P. caribbica* was improved by application of VC, so as to improve its biocontrol efficacy. Enolase 1, which can catalyze 2-phosphoglyceric acid to phosphoenolpyruvic acid, is a key enzyme in the glycolytic pathway; polyketide synthase is the key enzyme mediating polyketide formation; and malate dehydrogenase corresponded to the tricarboxylic acid cycle. According to these, we can conclude that the higher basic metabolic activity can induce higher oxidative tolerance.

In conclusion, the results of the present study showed that the oxidative stress tolerance of the antagonist can be improved markedly by the application of VC. Application of VC was also efficient in reducing the ROS level and inducing the activities of antioxidant enzymes. Consequently, VC can increase the population dynamics and the biocontrol efficacy of *P. caribbica* against postharvest blue mold decay of apples. This may offer great practical potential in reducing postharvest diseases of apples. However, according to results reported by Macarisin et al.,[4] the appropriate concentration of ROS production stimulated by these biomicrobial biocontrol agents is important for fruits to initiate their protective effect, so the interation among the ROS production, antagonist, pathogen, and host fruits/vegetables should be investigated in the future.

AUTHOR INFORMATION

Corresponding Author

*(H.Z.) Phone: +86-511-88780174. Fax: +86-511-88780201. E-mail: zhanghongyin126@126.com.

Funding

This research was supported by the National Natural Science Foundation of China (31271967), the Technology Support Plan of Jiangsu Province (BE2014372), the Research Fund for the Doctoral Program of Higher Education of China (20123227110015), and the Technology Support Plan of Zhenjiang (NY2013004).

Notes

The authors declare no competing financial interest.

■ ACKNOWLEDGMENTS

We thank Qingzhi Ding for technical assistance. We also acknowledge Dr. Yanhua Yang for help with mass spectrometry analysis.

■ REFERENCES

(1) Droby, S.; Wisniewski, M.; Macarisin, D.; Wilson, C. Twenty years of postharvest biocontrol research: is it time for a new paradigm? *Postharvest Biol. Technol.* **2009**, *52*, 137−145.

(2) Zhao, L. N.; Zhang, H. Y.; Li, J. H.; Cui, J.; Zhang, X. Y.; Ren, X. F. Enhancement of biocontrol efficacy of *Pichia carribbica* to postharvest diseases of strawberries by addition of trehalose to the growth medium. *Int. J. Mol. Sci.* **2012**, *13*, 3916−3932.

(3) Liu, J.; Wisniewski, M.; Droby, S.; Vero, S.; Tian, S.; Hershkovitz, V. Glycine betaine improves oxidative stress tolerance and biocontrol efficacy of the antagonistic yeast *Cystofilobasidium infirmominiatum*. *Int. J. Food Microbiol.* **2011**, *146*, 76−83.

(4) Macarisin, D.; Droby, S.; Bauchan, G.; Wisniewski, M. Superoxide anion and hydrogen peroxide in the yeast antagonist−fruit interaction: a new role for reactive oxygen species in postharvest biocontrol? *Postharvest Biol. Technol.* **2010**, *58*, 194−202.

(5) Janisiewicz, W. J.; Korsten, L. Biological control of postharvest diseases of fruits. *Annu. Rev. Phytopathol.* **2002**, *40*, 411−441.

(6) Macarisin, D.; Cohen, L.; Eick, A.; Rafael, G.; Belausov, E.; Wisniewski, M.; Droby, S. *Penicillium digitatum* suppresses production of hydrogen peroxide in host tissue during infection of citrus fruit. *Phytopathology* **2007**, *97*, 1491−1500.

(7) Tolaini, V.; Zjalic, S.; Reverberi, M.; Fanelli, C.; Fabbri, A. A.; Del Fiore, A.; De Rossi, P.; Ricelli, A. *Lentinula edodes* enhances the biocontrol activity of *Cryptococcus laurentii* against *Penicillium expansum* contamination and patulin production in apple fruits. *Int. J. Food Microbiol.* **2010**, *138*, 243−249.

(8) Sharma, R. R.; Singh, D.; Singh, R. Biological control of postharvest diseases of fruits and vegetables by microbial antagonists: a review. *Biol. Control* **2009**, *50*, 205−221.

(9) Sandermann, H., Jr. Ozone and plant health. *Annu. Rev. Phytopathol.* **1996**, *34*, 347−366.

(10) Inzé, D.; Van Montagu, M. Oxidative stress in plants. *Curr. Opin. Biotechnol.* **1995**, *6*, 153−158.

(11) GalvisSá nchez, A. C.; Gil-Izquierdo, A.; Gil, M. 1. I. Comparative study of six pear cultivars in terms of their phenolic and vitamin C contents and antioxidant capacity. *J. Sci. Food Agric.* **2003**, *83*, 995−1003.

(12) Shewfelt, R.; del Rosario, B. The role of lipid peroxidation in storage disorders of fresh fruits and vegetables. *HortScience* **2000**, *35*, 575−579.

(13) Pintó, E.; Lentheric, I.; Vendrell, M.; Larrigaudière, C. Role of fermentative and antioxidant metabolisms in the induction of core browning in controlled-atmosphere stored pears. *J. Sci. Food Agric.* **2001**, *81*, 364−370.

(14) Jelodar, G.; Akbari, A.; Nazifi, S. The prophylactic effect of vitamin C on oxidative stress indexes in rat eyes following exposure to radiofrequency wave generated by a BTS antenna model. *J. Radiat. Biol.* **2013**, *89*, 128−131.

(15) Li, B. Q.; Tian, S. P. Effects of trehalose on stress tolerance and biocontrol efficacy of *Cryptococcus laurentii*. *Appl. Microbiol.* **2006**, *100*, 854−861.

(16) Cao, S.; Yang, Z.; Hu, Z.; Zheng, Y. The effects of the combination of *Pichia membranefaciens* and BTH on controlling of blue mould decay caused by *Penicillium expansum* in peach fruit. *Food Chem.* **2011**, *124*, 991−996.

(17) Deveau, A.; Piispanen, A.; Jackson, A.; Hogan, D. Farnesol induces hydrogenperoxide resistance in *Candida albicans* yeast by inhibiting the Ras-cyclic AMP signaling pathway. *Eukaryotic Cell* **2010**, *9*, 569−577.

(18) Bernstein, N.; Shoresh, M.; Xu, Y.; Huang, B. Involvement of the plant antioxidative response in the differential growth sensitivity to salinity of leaves vs roots during cell development. *Free Radical Biol. Med.* **2010**, *49*, 1161−1171.

(19) Reverberi, M.; Fabbri, A. A.; Zjalic, S.; Ricelli, A.; Punelli, F.; Fanelli, C. Antioxidant enzymes stimulation in *Aspergillus parasiticus* by *Lentinula edodes* inhibits aflatoxin production. *Appl. Microbiol. Biotechnol.* **2005**, *69*, 207−215.

(20) Bradford, M. M. A rapid and sensitive method for the quantitation of microgram quantities of protein utilizing the principle of protein-dye binding. *Anal. Biochem.* **1976**, *72*, 248−254.

(21) Li, R.; Zhang, H.; Liu, W.; Zheng, X. Biocontrol of postharvest gray and blue mold decay of apples with *Rhodotorula mucilaginosa* and possible mechanisms of action. *Int. J. Food Microbiol.* **2011**, *146*, 151−156.

(22) Li, B. Q.; Lai, T. F.; Qin, G. Z.; Tian, S. P. Ambient pH stress inhibits spore germination of *Penicillium expansum* by impairing protein synthesis and folding: a proteomic-based study. *J. Proteome Res.* **2010**, *9*, 298−307.

(23) Wang, Y.; Yang, L. M.; Xu, H. B.; Li, Q. F.; Ma, Z. Q.; Chu, C. G. Differential proteomic analysis of proteins in wheat spikes induced by *Fusarium graminearum*. *Proteomics* **2005**, *5*, 4496−4503.

(24) Zhang, L.; Yu, Z. F.; Jiang, L.; Jiang, J.; Luo, H. B.; Fu, L. R. Effect of post-harvest heat treatment on proteome change of peach fruit during ripening. *J. Proteomics* **2011**, *74*, 1135−1149.

(25) Majoul, T.; Bancel, E.; Tribol, E.; Hamida, J. B.; Branlard, G. Proteomic analysis of the effect of heat stress on hexaploid wheat grain: characterization of heat-responsive proteins from total endosperm. *Proteomics* **2003**, *3*, 175−183.

(26) Wilson, C. L.; Wisniewski, M. E. Biological control of postharvest diseases of fruits and vegetables: an emerging technology. *Annu. Rev. Phytopathol.* **1989**, *27*, 425−441.

(27) Lahlali, R.; Massart, S.; Clercq, D.; Serrhini, M. N.; Creemers, P.; Jijakli, M. H. Assessment of *Pichia anomala* (strain K) efficacy against blue mould of apples when applied pre- or post-harvest under laboratory conditions and in orchard trials. *Eur. J. Plant Pathol.* **2008**, *123*, 37−45.

(28) Droby, S.; Chalutz, E.; Hofstein, R.; Wilson, C. L.; Wisniewski, M. E.; Fridlender, B.; Cohen, L.; Weiss, B.; Daus, A. Pilot testing of *Pichia guilliermondiui*: a biocontrol agent of postharvest diseases of citrus fruit. *Biol. Control* **1993**, *3*, 47−52.

(29) Wisniewski, M.; Wilson, C.; El Ghaouth, A.; Droby, S. Non-chemical approaches to postharvest disease control. *Acta Hortic.* **2001**, *553*, 407−412.

(30) Castoria, R.; Caputo, L.; De Curtis, F.; De Cicco, V. Resistance of postharvest biocontrol yeasts to oxidative stress: a possible new mechanism of action. *Phytopathology* **2003**, 564−572.

(31) Patiño-Vera, M.; Jiménez, B.; Balderas, K.; Ortiz, M.; Allende, R.; Carrillo, A.; Galindo, E. Pilot-scale production and liquid formulation of *Rhodotorula minuta*, a potential biocontrol agent of mango anthracnose. *J. Appl. Microbiol.* **2005**, *99*, 540−550.

(32) Teixidó, N.; Cañamás, T. P.; Abadias, M.; Usall, J.; Solsona, C.; Casals, C.; Viñas, I. Improving low water activity and desiccation tolerance of the biocontrol agent *Pantoea agglomerans* CPA-2 by osmotic treatments. *J. Appl. Microbiol.* **2006**, *101*, 927−937.

(33) Wang, Y.; Wang, P.; Xia, J.; Yu, T.; Lou, B.; Wang, J.; Zheng, X. D. Effect of water activity on stress tolerance and biocontrol activity in antagonistic yeast*Rhodosporidium paludigenum*. *Int. J. Food Microbiol.* **2010**, *143*, 103−108.

(34) Cao, S.; Yuan, Y.; Hu, Z.; Zheng, Y. Combination of *Pichia membranifaciens* and ammonium molybdate for controlling blue mould caused by *Penicillium expansum* in peach fruit. *Int. J. Food Microbiol.* **2010**, *141*, 173−176.

(35) Vanderslice, J. T.; Higgs, D. J.; Hayes, J. M.; Block, G. Ascorbic acid and dehydroascorbic acid content of foods-as-eaten. *J. Food Compos. Anal.* **1990**, *3*, 105−118.

(36) Lim, C.; Lovell, R. T. Pathology of the vitamin C deficiency syndrome in channel catfish (*Ictalurus punctatus*). *J. Nutr.* **1978**, *108*, 1137−1146.

(37) Dat, J.; Vandenabeele, S.; Van Montagu, M.; Van Breusegem, F. Dual action of the active oxygen species during plant stress responses. *Cell. Mol. Life Sci.* **2000**, *5*, 779−795.
(38) Bencheqroun, S. K.; Bajji, M.; Massart, S.; Labhilili, M.; El-jafari, S.; Jijakli, M. H. *In vitro* and *in situ* study of postharvest apple bluemold biocontrol by *Aureobasidium pullulans*: evidence for the involvement of competition for nutrients. *Biol. Technol.* **2007**, *46*, 128−135.
(39) Zhang, H. Y.; Zheng, X. D.; Fu, C. X.; Xi, Y. F. Postharvest biological control of gray mold rot of pear with *Cryptococcus laurentii*. *Postharvest Biol. Technol.* **2005**, *35*, 79−86.
(40) Li, B. Q.; Zhou, Z. W.; Tian, S. P. Combined effects of endo- and exogenous trehalose on stress tolerance and biocontrol efficacy of two antagonistic yeasts. *Biol. Control* **2008**, *46*, 187−139.

and dried fruit production to enhance color stability. The presence of vitamin C in apple products has implications on disulfide bridges and may lead to increased IgE reactivity or even enhanced allergenicity for sensitized individuals.

The present study focused on the influence of heat treatment and vitamin C or sulfur addition to purified Mal d 2. The conformational stability of Mal d 2 in the presence of vitamin C was investigated using IgE Western blot, mass spectrometry (MS), and attenuated total reflectance Fourier transform infrared (ATR-FTIR) spectroscopy. Furthermore, the characterization of the in vivo reactivity to vitamin C-treated Mal d 2 was performed using patients with clinically confirmed allergy to apples.

MATERIALS AND METHODS

Chemicals. Trichloroacetic acid (TCA), acetone, sodium bicarbonate (Na_2CO_3), diethyldithiocarbamic acid (DIECA), sodium chloride (NaCl), potassium chloride (KCl), disodium phosphate (Na_2HPO_4), potassium dihydrogen phosphate (KH_2PO_4), sodium hydrogen carbonate ($NaHCO_3$), sodium hydrogen phosphate ($NaH_2PO_4{\cdot}H_2O$), hydrochloric acid (HCl), glycerol, sodium borate decahydrate($Na_2B_4O_7{\cdot}10H_2O$), magnesium chloride (Mg_2Cl_2), sodium disulfite ($Na_2S_2O_5$), acetic acid, 2-mercaptoethanol, calcium chloride ($CaCl_2$), ammonia (NH_4HCO_3), D-glucose, and ethylenediaminetetraacetic acid (EDTA) were purchased from Merck (Darmstadt, Germany). Urea, poly(vinylpyrrolidone) K25, Tris base, sodium dodecyl sulfate (SDS), goat antirabbit IgG conjugated with alkaline phosphatase, goat antihuman IgE antibodies conjugated with horseradish peroxidase, bromochloroindolyl phosphate (BCIP), nitro blue tetrazolium (NBT), bovine serum albumin (BSA), L-glutamine, sodium pyruvate, 2-(4-(2-hydroxyethyl)-1-piperazinyl)ethanesulfonic acid (HEPES), citric acid, dithiothreitol (DTT), 4-methylumbelliferyl *N*-acetyl-β-D-glucosaminide, polyvinyl polypyrrolidone (PVPP), and Triton X-100 were obtained from Sigma-Aldrich (Steinheim, Germany). Skim milk and iodoacetamide were obtained from Fluka (Steinheim, Germany). Formic acid (FA) was obtained from Roth (Karlsruhe, Germany). The Micro BCA protein assay kit was purchased from Pierce (Rockford, IL). Acetonitrile (ACN) and vitamin C were purchased from BDH Prolabo (Leuven, Belgium). The ECL-Advanced Western blot kit was obtained from GE Healthcare (Buckinghamshire, U.K.). RPMI medium was obtained from Invitrogen (Carlsbad, CA). Trypsin and GluC were purchased from Roche (Basel, Switzerland).

Apple Material. Seven different apple breeding lines and cultivars were harvested from an experimental field with drip irrigation near the Adriatic seaside at cultivar-specific dates and stored at 4 °C before extraction: G198, Braeburn, Topaz, Fuji, Golden Delicious, Granny Smith and Pilot, and Pink Lady. Protein extraction was performed as previously described.[17] Five apples per cultivar were peeled (5 mm) with a paring machine, shock frozen, and powdered in liquid nitrogen. Frozen powder was mixed in a blender with extraction buffer (10 mM K_2HPO_4, 10 mM KH_2PO_4, 0.27 mM EDTA, 13.3 mM DIECA, 2% PVPP, pH 7) in a ratio of 1:2 (w/v) and extracted by stirring at 4 °C. The mixture was filtered through two layers of Miracloth (Calbiochem, United States) and centrifuged at 10000*g* for 30 min at 4 °C and the supernatant immediately frozen at −80 °C. Additional parameters such as the firmness and sugar and titratable acid contents, which indicate the maturity of the apples, were measured. The firmness of the apples is measured by a peneterometer, sugar content by refractometry, and titratable acid content by titration with 0.1 M HCl (Table 1).

Apple-derived food products were obtained from the local market: (1) dried apple chips, (2) sulfured apple rings, (3) nonsulfured apple rings, (4) baby apple puree, (5) clear apple juice, (6) cloudy apple juice, (7) clear organic apple juice. Dried apple samples (2 g) were precipitated by phenol, and the obtained protein pellets were resolved in 8 N urea.[18] Due to the low protein contents of apple juices, the enrichment of proteins required a precipitation step with 10% TCA/acetone. A 20 mL volume of apple juice was incubated with the same volume of 10% TCA/acetone overnight. The pellet was washed three times with pure acetone and dried at −20 °C. The total protein content was determined using the BCA kit (Pierce) according to the manufacturer's instructions.

Table 1. Parameters Such as Firmness and Sugar and Titratable Acid Contents Were Measured in Tested Apple Cultivars as Indicators of Maturity and Physiological State

cultivar	firmness (kgf)	sugar content (%)	titratable acid content (g/L)
G198	9.1	14.5	7.5
Braeburn	7.5	12.1	6.7
Fuji	7.2	13.8	3.7
Golden Delicious	6.6	14.9	5.2
Granny Smith	7.7	11.8	6.8
Pink Lady	8.7	15.1	6.7
Topaz	7.8	12.8	2.3

Purification of Apple Allergens. Apple cultivar Topaz was used for extraction of Mal d 2 and Mal d 1.[8] A 1 kg mass of apple peels was homogenized in carbonate extraction buffer (20 mM Na_2CO_3, 13.3 mM diethyldithiocarbamic acid, 1 mM ethylenediaminetetraacetic acid, 2 mg/mL PVP, pH 9.0) and stirred for 30 min at 4 °C.[8] The extract was filtered through two layers of Calbiochem Miracloth and centrifuged at 28000*g* (Beckman Coulter, Avanti J-25, JLA-10500) for 30 min at 4 °C. The supernatant was lyophilized and stored at −20 °C. The lyophilizate was dissolved in carbonate extraction buffer at a ratio of 1:10 (w/v), centrifuged for 30 min at 4000*g* and 4 °C, and buffer-exchanged using PD-10 columns (GE Healthcare) into equilibration buffer (10 mM Tris, 2 mg/mL PVP, pH 8). The obtained samples were loaded onto an anion exchange column, 30Q HR 10/10 (GE Healthcare). The purification was performed by an ÄKTA 100 Explorer chromatography system (GE Healthcare). Elution was carried out with a linear gradient from 0 to 1 M NaCl and the product fractionated for further analyses. To identify which fraction contained Mal d 1 and Mal d 2, IgE Western blotting was performed using Mal d 1- or Mal d 2-reactive patient sera. Fractions containing Mal d 1 and Mal d 2 were subjected to size-exclusion column chromatography on a Superdex 75 column (GE Healthcare) equilibrated with 25 mM sodium phosphate buffer, pH 7.0.

The identity and purity of purified Mal d 2 were confirmed by mass spectrometry. For the tryptic and GluC digestions of Mal d 2, 10 μL of the protein solution (1 mg/mL H_2O) was adjusted to 50 mM NH_4HCO_3 and 7.5 mM DTT (final concentration) by addition of 10 μL of 100 mM NH_4HCO_3 containing 15 mM DTT and incubated for 45 min at 56 °C to reduce disulfide bridges. Trypsin cleaves proteins and peptides at the amino acids arginine and lysine, and GluC cleaves proteins and peptides at glutamate. Thiol groups were carbamidomethylated by the addition of 40 μL of 55 mM iodoacetamide in 50 mM NH_4HCO_3. Proteins were precipitated by the addition of acetone (4:1), and the pellet was resuspended in 20 μL of NH_4HCO_3 buffer containing 0.1 μg of trypsin and GluC. All proteolytic reactions were performed at 37 °C overnight. The digested samples were directly injected into the LC−MS system (LC, Dionex Ultimate 3000 LC instrument; MS, Bruker, AmaZon ETD, equipped with the online nanosource). The peptides were separated on a C-18 column (Dr. Maisch GmbH, C-18 HPLC column, ReproSil-Pur, 200 × 0.1 mm, 3 μm packing, 200 Å pore diameter, flow 0.4 μL/min). A gradient from 95% solvent A and 5% solvent B (solvent A, 0.1% FA in water; solvent B, 0.1% FA in ACN) to 32% B in 40 min was applied, followed by a 15 min gradient from 32% B to 75% B that facilitates elution of large peptides. The peptides were analyzed by MS with data-dependent acquisition. Data were processed using the freeware program X!-tandem combined with GPM (Global Proteome Machine). The purity of Mal d 2 was determined by mass spectrometric analysis of the whole protein. A 1 μg mass of Mal d 2 was directly injected into the LC−MS system (LC, Dionex Ultimate 3000 LC instrument; MS, Bruker, Maxis

dx.doi.org/10.1021/jf5020878 | J. Agric. Food Chem. 2014, 62, 7622−7630

4G, equipped with the standard ESI source). The protein solution was eluted by developing a linear gradient from 10% to 60% ACN (Supelco Discovery Bio wide-pore C5 column, 50 × 0.32 mm, 3 μm packing). Data were processed using Data Analysis 4.0 (Bruker), and the spectrum was deconvoluted by the maximum entropy equation.

Polyclonal antibodies were raised in rabbits by immunization with 500 μg of native Mal d 1 and Mal d 2 and Freund's adjuvant.[8,17] The specificity of the Mal d 2 antiserum was confirmed by Western blotting.

SDS–PAGE and Western Blotting. All samples were diluted in sample buffer (0.125 M Tris/HCl, pH 6.8, 20% (v/v) glycerol, 2% (w/v) SDS, 0.005% (v/v) bromophenol blue) in a ratio of 1:2 (v/v) and denatured for 10 min at 90 °C or chemically reduced by 50 mM DTT. Total protein was determined via BCA assay after buffer exchange using PD-10 columns (GE Healthcare). For cultivar screening, 10 μg of total protein per lane was loaded to precast 4–20% Tris–glycine gel (Novex System, Invitrogen). As positive controls, two different concentrations of purified Mal d 2 (0.5 and 1 μg) were applied to each gel. Gels were electroblotted onto nitrocellulose membranes using a blotting buffer containing 50 mM $Na_2B_4O_7{\cdot}10H_2O$, 0.1% (w/v) SDS, and 20% (v/v) methanol. After overnight blocking with 3% skim milk powder, polyclonal antibodies against purified Mal d 2 were diluted to a ratio of 1:1000 (v/v) in dilution buffer (1% skim milk, 0.1% Tween 20 in PBS, 137 mM NaCl, 2.7 mM KCl, 4.3 mM Na_2HPO_4, 1.47 mM KH_2PO_4, pH 7.4) and added to the membranes. The immunoreaction was detected using goat antirabbit IgG conjugated with alkaline phosphatase in dilution buffer in a ratio of 1:2000 (v/v), followed by visualization with BCIP and NBT in alkaline phosphate buffer (100 mM NaCl, 5 mM $MgCl_2$, 100 mM Tris).

Influence of Different Processing Conditions on Purified Mal d 2. To study the influence of food preservatives on the immunoreactivity of Mal d 2, purified Mal d 2 was treated by reducing agents such as vitamin C (1% and 5%, w/v) as well as sulfur (1% and 5% (w/v) $Na_2S_2O_5$) in 10% (v/v) acetic acid at pH < 3 and different temperatures. Room temperature (rt) and 90 °C were selected, since they simulate the processing conditions in dried fruit production. Lowered pH is able to increase the effectivity of the treatments. Additionally, the purified Mal d 2 was treated for three incubation times: (i) 2 min, (ii) 20 min, and (iii) overnight (>16 h). Purified Mal d 2 reduced with 50 mM dithiotreithol for 1 h at rt was used as a control for positive IgE-binding.

Patient Selection. Six of eighteen apple-allergic patients showing positive reactivity to Mal d 2 in IgE Western blotting were selected for these studies. These patients, who were enrolled for in vivo testing, gave written informed consent for participating in the study, which was approved by the local Medical Ethical Committee of Vienna and conducted according to guidelines for Good Clinical Practice.

IgE Western Blots Using Patient Sera. Electroblotted membranes were blocked with 3% BSA for 2 h at 37 °C and incubated overnight at 4 °C with sera in a ratio of 1:10 (v/v). Goat antihuman IgE antibodies conjugated with horseradish peroxidase (1:20000, v/v) were used for visualization. Purified Mal d 2 was applied to the gel in reduced and not reduced form. Reacting protein bands were detected with the ECL-Advanced Western blotting kit according to the manufacturer's guidelines. In summary, horseradish peroxidase present on a Western blot is detected by its reaction with peroxide, an enhancer molecule, and the chemoluminescent substrate, all of which are present in the substrate reagents provided and visualized with a chemoluminescence imager.

Skin Prick and Oral Smear Tests. Only the influence of vitamin C addition on altered allergenicity of Mal d 2 could be examined by skin prick and oral smear tests. Due to severe skin irritations caused by DTT and $Na_2S_2O_5$ on healthy skin, sulfur-treated Mal d 2 could not be used for patient skin testing. Skin prick tests (SPTs) were performed on the forearm with different concentrations of purified Mal d 2 (100, 20, 10, and 5 μg/mL). The samples were provided as native, heat-denatured (20 min at 90 °C), and treated (2 min at 90 °C, 1% vitamin C). Positive skin reactions were recorded after 20 min by copying the wheal reaction onto a transparent adhesive tape, and wheal diameters were measured as soon as a positive reaction was visible. Fresh apple and histamine (10 mg/mL) were used as positive controls and 1% vitamin C in saline solution and saline solution as negative controls. Oral smear tests (OSTs) were applied as a minivariant of oral provocation to test the mucosal reaction inside the mouth. OSTs were performed using increasing concentrations of purified Mal d 2 (10, 20, and 100 μg/mL) in 1% vitamin C saline solution. To start, a 1% vitamin C saline solution (negative control) soaked cotton swab was smeared for 1 min on the mucosal side of the lower lip, and after 20 min native Mal d 2 was smeared on the inner side of the upper lip. Thereafter, increasing concentrations of native Mal d 2 were smeared, alternating on the lower and upper lips until the highest concentration was reached.

β-Hexosaminidase Secretion Assay from Human FcεRI Receptor Protein Transfected Rat Basophilic Leukemia Cells. The binding of treated and untreated Mal d 2 to IgE receptor FceRI was studied using cell-based the rat basophilic leukemia assay (RBL assay) in vitro. RBL-703/21 cells, derived from RBL-2H3, contained genes of the human high-affinity IgE receptor FceRI (kindly provided by Dr. Lothar Vogel, Paul-Ehrlich Institute, Langen, Germany). Cells were cultured in RPMI medium supplemented with 10% fetal calf serum, 4 mM L-glutamine, 2 mM sodium pyruvate, 10 mM HEPES, 1% penicillin/streptomycin, and 100 μM 2-mercaptoethanol at 37 °C and 5% CO_2. RBL cells (4×10^4 cells per well in 100 μL of medium) were seeded in a 96-well round-bottom microtiter plate (Nunc) and incubated overnight at 37 °C and 5% CO_2. Cells were passively sensitized with sera from six patients (diluted 1:25) for 2 h at 37 °C and 5% CO_2. Cells were washed twice with Tyrode's buffer (137 mM NaCl, 2.68 mM KCl, 1.4 mM $CaCl_2$, 1.7 mM $MgCl_2$, 5 mM D-glucose, 10 mM HEPES, 0.42 mM $NaH_2PO_4{\cdot}H_2O$, 12 mM $NaHCO_3$) at pH 7.2 supplemented with 0.1% BSA. Native Mal d 2 (0.05 μg in 100 μL of Tyrode's buffer per well), heat-denatured Mal d 2 (90 °C for 5 min, 0.05 μg in 100 μL of Tyrode's buffer per well), Mal d 2 with 1% vitamin C (90 °C for 5 min, 0.05 μg in 100 μL of Tyrode's buffer per well), and 1% vitamin C solution alone as the control were added to control wells and incubated for 30 min at 37 °C in a 5% CO_2 atmosphere. As a negative control, RBL cells were incubated with Tyrode's buffer to calculate spontaneous release of β-hexosaminidase. Cell lysis was performed by addition of 10 μL of 10% Triton-X in Tyrode's buffer for 5 min for total release of β-hexosaminidase (100% release) as a positive control. A 50 μL volume of supernatant was mixed with 50 μL of assay solution (5 mL of 0.1 M citric acid, pH 4.5, and 80 μL of 4-methylumbelliferyl *N*-acetyl-β-D-glucosaminide) and incubated at 37 °C for 1 h. The reaction was terminated by addition of 100 μL of glycine buffer (200 mM glycine, 200 mM NaCl, pH 10.7). Fluorescence signals were read at 360 nm/465 nm (Cytofluor 2350, Millipore), and the results were calculated as a percentage of total release. The values of the negative controls were subtracted.

Attenuated Total Reflectance Fourier Transform Infrared Spectroscopy. ATR-FTIR measurements were performed using a VERTEX 70 spectrometer (Bruker) and a BioATRcell IITM (Harrick). The BioATRcell IITM was cooled with a Haake K20 water bath at 20 ± 0.05 °C. The sample chamber of the spectrometer was continuously purged with dry air. Spectra of 20 μL volume samples from 4000 to 850 cm^{-1} were acquired by using a nitrogen-cooled MCT (photovoltaic mercury cadmium telluride) detector (spectral resolution 4 cm^{-1}, 64 scans, forward–backward). A Blackman-Harris three-term apodization function was used along with a zero-filling factor of 1. Purified Mal d 2 at a concentration of 1.8 mg/mL was dissolved in 15 mM phosphate buffer at pH 7.0 containing 0%, 1%, and 5% (w/w) vitamin C. Samples were incubated for 1 h at rt before the measurements. For background measurements 15 mM phosphate buffer at pH 7.0 without vitamin C and the same buffer with 1% (w/w) or 5% (w/w) vitamin C in Milli-Q water (SGWater) were used. The samples were prepared so that the concentrations of the buffer and the vitamin C were identical to those of the blank used for the background. Sample preparation with identical buffer concentrations for the sample and blank is a critical error-prone step. However, a correction of small differences between sample and background concentrations is possible. For each sample three to five spectra were collected, and the averages were used for

A

```
  1  MMKSQVASLLGLTLAILFFSGAHAAKITFTNNCPNTVWPGTLTGDQKPQLSLTGFELASK  60
 61  ASRSVDAPSPWSGRFWGRTRCSTDAAGKFTCETADCGSGQVACNGAGAVPPATLVEITIA 120
121  ANGGQDYYDVSLVDGFNLPMSVAPQGGTGECKPSSCPANVNKVCPAPLQVKAADGSVISC 180
181  KSACLAFGDSKYCCTPPNNTPETCPPTEYSEIFEKQCPQAYSYAYDDKNSTFTCSGGPDY 240
241  VITFCP                                                        246
```

B

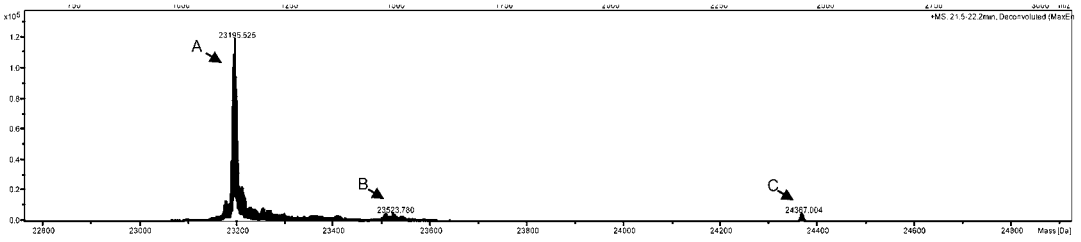

Figure 1. (A) Sequence coverage of identified peptide fragments obtained by trypsin and GluC digestion of Mal d 2. The fragments in bold were found by MS/MS analyses and showed high sequence coverage of Mal d 2. (B) Mass spectrometry of the Mal d 2 molecule. The measured mass of the major peak corresponds to the theoretical mass of 23 195.7 Da beginning from the N-terminal sequence AKITFTNNCPN (UniProt accession no. Q9FSG7). Key: (A) main peak, (B) Mal d 2 isoform, (C) glycosylated Mal d 2.

analysis. OPUS software (version 7.2, www.brukeroptics.de) was used for signal processing. An atmospheric correction of the full spectrum and a rubber-band baseline correction of the resulting spectrum were performed in the wavelength ranges between 1100 and 1900 cm^{-1}.

RESULTS AND DISCUSSION

Characterization of Purified Mal d 2. To perform in vivo and in vitro experiments under simulated food processing conditions, Mal d 2 was purified from the apple cultivar Topaz due to its high content of Mal d 2.[8] Mass spectrometry and peptide sequencing were used for the verification of the identity, molecular mass, and purity of purified Mal d 2 (Figure 1). The results showed high sequence coverage (UniProt accession no. Q9FSG7) and confirmed the purity of the protein at 23 195 Da. The peak at about 23 500 Da is a Mal d 2 isoform which is present in trace amounts (Figure 1B). One minor peak is detected at 24 367 Da which may contain a single glyco-MMXF residue and compared to the major Mal d 2 peak is of very low quantity. In fact, Mal d 2 was found to possess one putitative N-glycosylation site.[4] Purified Mal d 2 was used for raising specific anti-Mal d 2 polyclonal antibodies and for in vitro and in vivo experiments.

Influence of Different Processing Conditions on Purified Mal 2. SDS−PAGE and the Western blotting technique were applied to investigate the influence of different temperatures and addition of sulfur or vitamin C at different concentrations (Figure 2). A temperature of 90 °C was used for the chemical reduction of Mal d 2. Mal d 2 was not detected by Coomassie after heat treatment at 90 °C and with sulfur (1% or 5% (w/v) $Na_2S_2O_5$, Figure 2A). Considering that the detection limit of Coomassie staining for Mal d 2 is 1.0 ng or 50 fmol,[19] under these conditions, the protein was completely degraded and only traces of a protein band could be visualized. In IgG Western blot and SDS−PAGE only faint bands of sulfur-treated Mal d 2 indicate the presence of only traces of intact protein (Figure 2B). Purified Mal d 2 was stable after treatments with sulfur at rt, and in Western blotting the 23 kDa band of native Mal d 2 remained constantly reactive with polyclonal antibodies, indicating the integrity of IgG epitopes (Figure 2B). No significant band migration shift was detected after

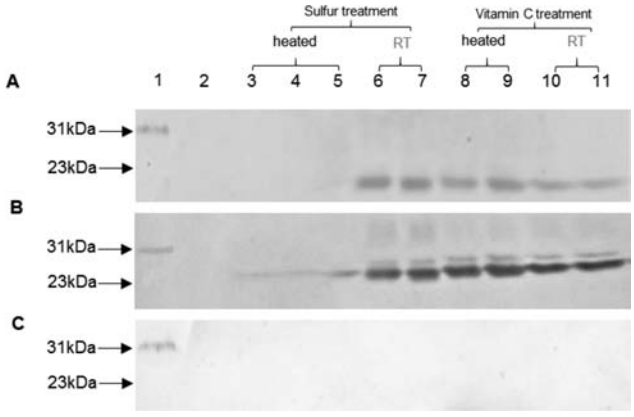

Figure 2. Influence of different treatments on immunoreactivity of Mal d 2: (A) Coomassie-stained gel, (B) Western blot using polyclonal rabbit antibody against Mal d 2, (C) IgE Western blot using the serum pool of the six selected patients. Lane 1: chemically reduced Mal d 2 as positive control. Lane 2: negative control. Lanes 3−11: Mal d 2 with different treatments: (3) 5% $Na_2S_2O_5$, 20 min at 90 °C and 1 h at rt, (4) 5% $Na_2S_2O_5$, 2 min at 90 °C, (5) 1% $Na_2S_2O_5$, 20 min at 90 °C and 1 h at rt, (6) 5% $Na_2S_2O_5$, 2 min at rt, (7) 1% $Na_2S_2O_5$, 2 min at rt, (8) 5% vitamin C at 90 °C for 2 min, (9) 1% vitamin C incubated at 90 °C for 2 min, (10) 5% vitamin C incubated overnight at rt, (11) 1% vitamin C incubated overnight at rt.

treatment at rt with sulfur or with vitamin C at different temperatures. In IgG Western blotting a diffuse faint band at approximately 28−31 kDa can be visualized after treatments with 1% or 5% sulfur at rt and 1% or 5% vitamin C at 90 °C or rt and might be attributed to a minimal denaturation of Mal d 2. The diffuse faint band was not detectable in Coomassie staining or reactive with serum pool IgE's (Figure 2).

The results showed that neither sulfur nor vitamin C is able to reduce or linearize Mal d 2, so the mobility of the Mal d 2 band in the SDS−PAGE gel is shifted to the level of a 31 kDa protein. IgE Western blotting confirmed that Mal d 2 remained in its native conformation in all treatments and therefore was not reactive with the serum pool of the selected patients (Figure 2C). The absence of in vitro IgE reactivity to treated

dx.doi.org/10.1021/jf5020878 | J. Agric. Food Chem. 2014, 62, 7622−7630

Mal d 2 can be explained by the presence of the protein in its natural conformation (Figure 2C). Taking into consideration that Mal d 2 can refold very quickly almost to its natural conformation after heat denaturation, it is unlikely to bind to serum IgE's.[8]

Conformational Stability of Mal d 2 in the Presence of Vitamin C. Biophysical measurements were performed to analyze the stability of Mal d 2 in the presence of vitamin C. Circular dichroism (CD) and differential scanning calorimetry (DSC) failed to determine the conformational stability of Mal d 2 in the presence of vitamin C because of the high ellipticity of vitamin C that overlapped with the maxima and minima of the protein. DSC could not be performed since vitamin C is destroyed by heat treatment and the thermograms were not reproducible.

ATR-FTIR spectroscopy was, therefore, used as an independent methodology to detect possible conformational changes of Mal d 2 protein by the addition of vitamin C at rt. Purified Mal d 2 at a concentration of 1.8 mg/mL was dissolved in 15 mM phosphate buffer at pH 7.0 containing 1% and 5% (w/w) vitamin C. ATR-FTIR spectra of purified Mal d 2 in the absence and presence (1% or 5%, w/w) of vitamin C were recorded in the wavenumber range between 1100 and 1900 cm^{-1} (Figure 3A). Upon normalization (Figure 3B), vitamin C-induced spectral changes are obvious. The band of the amide I position around 1650 cm^{-1} is shifted to lower wavenumbers, which might reflect some loss of α-helical structure. It was shown by using electronic CD spectrometry that the secondary structure of Mal d 2 is dominated by β-sheets and has some contributions from α-helices,[8] which could also be confirmed by ATR-FTIR-spectroscopy with a peak at about 1650 cm^{-1} (α-helices) and a shoulder at about 1630 cm^{-1}, highlighted by a black arrow (Figure 3A,B). This is due to the unfolding of the α-helices by the addition of vitamin C, comparable to thermal unfolding.[8] As there is still a shoulder visible at about 1655 cm^{-1} in the spectrum of Mal d 2 with 5% (w/w) vitamin C (Figure 3B), the α-helical secondary structure remains intact to some extent.

The standard reduction potential of the redox couple cystine/cysteine is around −0.21 V at pH 7.0.[20,21] DTT is a powerful reducing agent with a reduction potential at pH 7.0 of −0.33 V.[22] Thus, in its presence all intramolecular disulfide bridges are in the reduced state.[20] DTT was used in a previous study to reduce Mal d 2.[8] The calculated redox potential of vitamin C at pH 7.0 of $E° = -0.066$ V is too low to reduce cysteine.[23]

The Cys ν (stretching vibration of S−H) typically appears around 2551 cm^{-1} [24] in a region without overlap by any other protein absorptions.[25] Strong hydrogen bonding between an SH group and a peptide carbonyl might shift the band to lower wavenumbers. In Mal d 2 no evidence for the existence of an SH group was found. The small peak at about 1760 cm^{-1} (Figure 3A) might derive from the small difference in vitamin C content between the sample and reference cell. Oxidized vitamin C (dehydroascorbic acid) has a peak at 1795 cm^{-1} which is also completely missing in the spectra. This confirms additionally that no oxidation of vitamin C and therefore most probably also no reduction of the cysteine groups of Mal d 2 took place.

Verification of Mal d 2 Allergenicity in the Cell-Based RBL Assay. To verify the allergenicity of native and heat-treated purified Mal d 2, 18 patients were screened by the means of anamnesis, positive OAS minutes after consumption of apples, and serum reactivity to native and reduced Mal d 2. Six patient sera reacted positively with chemically reduced Mal d 2 in Western blotting, but none of the sera reacted with native Mal d 2. These patients were selected for in vitro RBL assay and in vivo experiments using skin prick and oral smear tests (Table 2 and Figure 4).

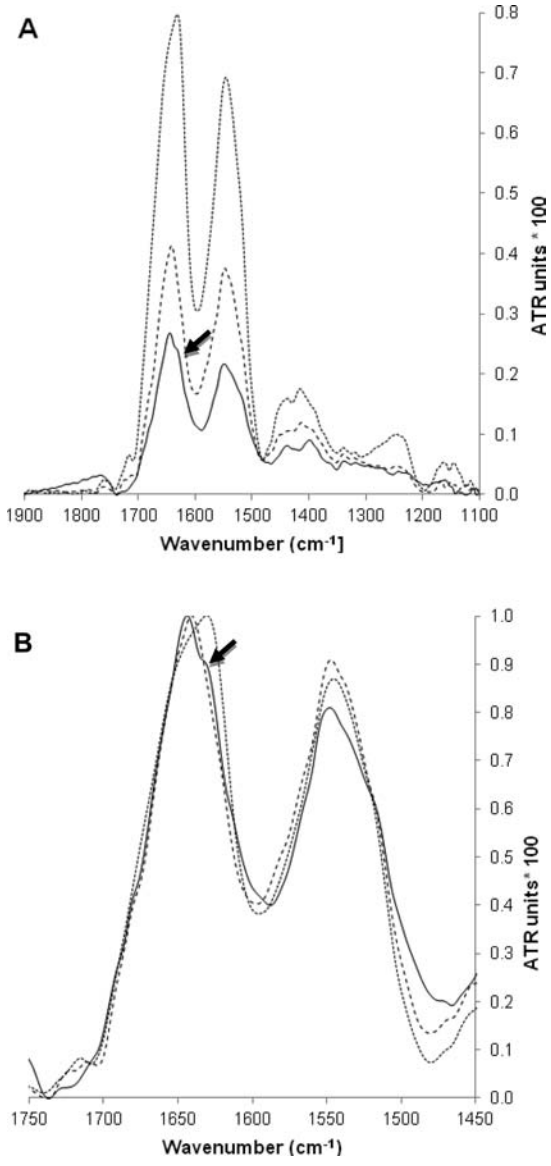

Figure 3. Spectroscopy of Mal d 2 in the absence/presence of vitamin C: (A) measured ATR-FTIR spectra in the wavenumber range from 1100 to 1900 cm^{-1} of Mal d 2 (continuous line), Mal d 2 with 1% vitamin C (dashed line), and Mal d 2 with 5% vitamin C (dotted line) using the corresponding buffer without or with vitamin C as the background, (B) ATR-FTIR spectra in the wavenumber range from 1450 to 1750 cm^{-1} which have been normalized to the amide I peak.

The RBL assay allowed the characterization of individual and specific IgE response of each selected patient to native and differently treated Mal d 2. Each serum was tested, and the results were presented separately to demonstrate the individual patient response in a component-resolved manner. Sera of all patients showed no to only very weak affinity for native Mal d 2, which is in correspondence with IgE Western blotting (Figures 4 and 5). Stimulation of the RBL cells with heat-denatured as well as vitamin C heat-treated Mal d 2 induced an

Table 2. Clinical History of Six Patients with Positive OAS or SPT for Apple Whose Sera Were Selectively Reactive to Reduced Mal d 2 in IgE Western Blotting

patient no.	OAS	asthma	urticaria	SPT to inhalative allergens	SPT to nutritive allergens
I	apple, hazelnut, plum	+	−	birch	apple, hazelnut
II	apple, banana, carrot, nuts, soybean	+	−	birch, grasses	carrot, hazelnut, peanut, tomato
III	apple carrot, nuts, plum	−	−	birch, grasses, mugwort, rye	almond, apple, carrot, nuts, peach
IV	apple, kiwi, nuts	−	−	birch	apple, fig, nuts, peach
V	apple, celery, kiwi, nuts	−	−	birch, mugwort, ragweed	almond, apple, nuts, soybean, celery
VI	apple, stone fruits, nuts	+	+	ash, birch, plantain	apple, peach, hazelnut, soybean

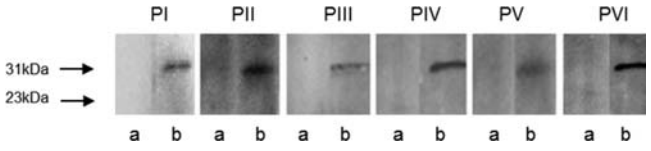

Figure 4. Screening of patient sera by IgE Western blotting. The IgE Western blots of (a) native Mal d 2 and (b) reduced Mal d 2 with sera of six patients (I–VI) show a positive reaction to chemically reduced Mal d 2.

increased β-hexosaminidase release, while native Mal d 2 did not increase the mediator release (Figure 5). Heat-treated Mal d 2 caused a β-hexosaminidase release with patient sera I, II, IV, V, and VI which is higher compared to the response induced by native Mal d 2 (Figure 5). The serum of patient VI showed the highest β-hexosaminidase release by heat-treated Mal d 2 (Figure 5). The results showed that heat treatment and addition of vitamin C could not influence the IgE reactivity to Mal d 2. Due to the high toxicity of sulfur, its addition could not be examined in the RBL assay.

Previously it was shown that conformational changes of Mal d 2 induced by chemical reduction of disulfide bridges are responsible for enhanced binding to IgE molecules.[8] In the cell-based RBL assay the hexosaminidase release is lightly increased in the majority of sera by heat-denatured and vitamin C-treated Mal d 2 compared to native Mal d 2, although remaining at low levels, <10% (Figure 5). The low affinity of Mal d 2 for the patients' RBL cell receptor-bound IgE can be explained by the rapid refolding as described previously.[8]

Skin Prick Test and Oral Smear Test. To examine the clinical relevance of native and heat-treated purified Mal d 2, SPTs and OSTs were performed. Patients developed neither a skin nor an oral reaction to native, heat-treated, or vitamin C-treated Mal d 2. The lack of skin reaction in SPTs to heat- and vitamin C-treated Mal d 2 can be attributed to the stability of Mal d 2.[8] The refolding kinetic study of Mal d 2 via CD showed that the molecule refolds after a few minutes, and the refolding spectrum overlaps almost exactly with the spectrum of the native protein.[8]

High prevalence of IgE reactivity to Mal d 2 strengthened the assumption that it might also be involved in the development of severe reactions due to high structural stability.[6−9] However, it was reported that five out of six Mal d 2-sensitized patient sera reacted exclusively with carbohydrate epitopes on the upper glycosylated variants of the allergen.[9] Whereas the impact of sensitization to glycosylated Mal d 2 still remains unclear, only 15% of patient sera reacted with the nonglycosylated recombinant Mal d 2, which supports the crucial role of

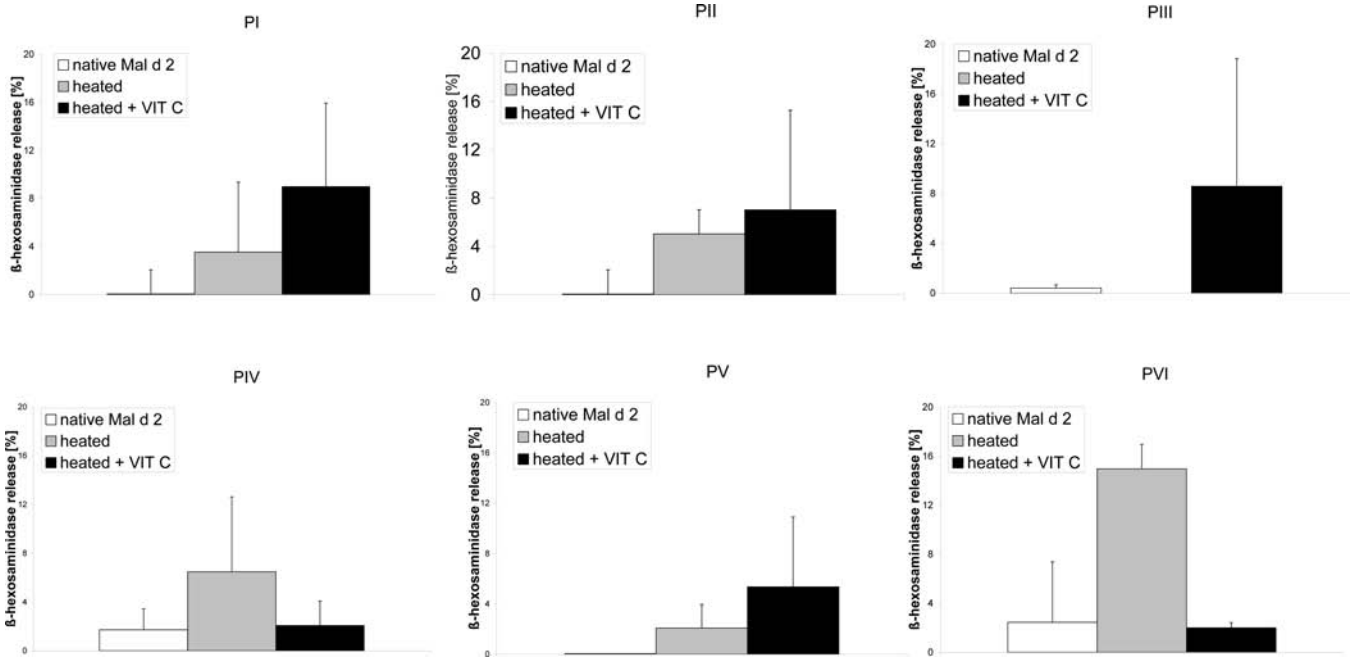

Figure 5. Results of β-hexosaminidase release in RBL assay from six tested patient sera (PI–PVI). The RBL cells are assayed using Tyrode's buffer as a negative control, native Mal d 2, heated Mal d 2, and heated Mal d 2 supplemented with 1% vitamin C. The patient sera showed variable reactivity if Mal d 2 was heated in the presence of vitamin C. The serum of patient VI displayed 2 times more reactivity to heated Mal d 2 than the other sera.

dx.doi.org/10.1021/jf5020878 | J. Agric. Food Chem. 2014, 62, 7622−7630

glycosylation in sensitization and IgE reactivity.[9] The obtained MS results demonstrate that a minor fraction of Mal d 2 is glycosylated to a low extent (Figure 1B).

For patient sensitization and production of IgE's reactive to Mal d 2, natural exposure to other TLPs must also be taken into consideration since Mal d 2 shares >50% identity with other TLPs. For example, Pru p 2 from peach shows the closest homology of almost 85% with Mal d 2.[24] In this context, the presence of common epitopes, offering the molecular basis for cross-reactivity, is of crucial importance.[26] Previous observations showed that Mal d 2 reacts with human IgE's mainly after complete denaturation by destruction of disulfide bridges, which fix the intramolecular α-helical domain II.[8,9] Lack of skin reactivity to native and heat- and vitamin C-treated Mal d 2 confirmed the previous assumption that allergenic epitopes of native Mal d 2 must be cryptic within molecular structures[8] and the conformationally intact protein is not presenting reactive epitopes for an in vivo reaction.

Detection of Mal d 2 and Mal d 1 in Different Cultivars. To demonstrate the variations in the content of Mal d 2 and Mal d 1 in different apple cultivars, Western blotting and SDS−PAGE using polyclonal antibodies directed to these allergens under reducing conditions were performed. Bands with different intensities indicated the variable and relative allergen contents among different cultivars (Figure 6). The

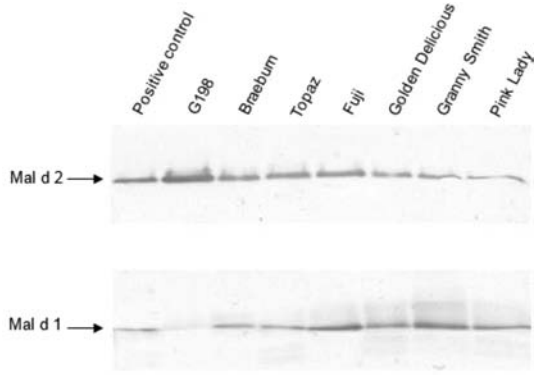

Figure 6. Semiquantitative determination of Mal d 1 and Mal d 2 in different apple cultivars (G198, Braeburn, Topaz, Fuji, Golden Delicious, Granny Smith, Pink Lady) grown under conventional conditions analyzed by reducing SDS−PAGE and Western blot. Mal d 2 and Mal d 1 were detected with polyclonal anti-Mal d 1 and anti-Mal d 2 antibodies. The positive control is 0.5 μg of native Mal d 2 and Mal d 1.

obtained results revealed a cultivar-dependent variability of the Mal d 2 content, comparable to the previously known variation of Mal d 1, determined quantitatively by a specific enzyme-linked immunosorbent assay (ELISA).[17] The protein bands for both apple allergens Mal d 2 and Mal d 1 showed almost identical intensities in the cultivars Braeburn, Topaz, Fuji, Golden Delicious, Granny Smith, and Pink Lady.

However, the band intensity of Mal d 2 was highest for the breeding line G198, which was shown previously to have a significantly lower content of Mal d 1 (3.47 μg/g) compared to the known cultivars Braeburn, Fuji, Golden Smith, Granny Smith, and Pink Lady (Figure 6).[17] Pathogen attack was reported to increase the expression of TLPs in apple apoplasts, which means that pathogen resistance is related to and responsible for the TLP content.[28,29] Additionally, factors such as climate and environmental changes and storage and cultivation practice influence the expression levels of TLPs in apples.[30]

Mal d 1, the major allergen of apple, belongs to the PR-10 family and is also expressed in response to fungal or bacterial infection and stress.[17] In a previous study the content of Mal d 1 was shown to be rather high in Braeburn, Fuji, Golden Delicious, Granny Smith, and Pink Lady.[17] The high levels of PR-10's were considered an indication of longevity and high stress or pathogen resistance during storage.[27] Experimental down-regulation of PR-10 proteins in *Medicago truncatula* resulted in an antagonistic induction of TLPs and an increased tolerance to pathogens.[31]

Detection of Mal d 2 and Mal d 1 in Different Apple Products. To investigate the availability of the minor apple allergen Mal d 2 and the major apple allergen Mal d 1, Western blots were performed with extracts of different apple products obtained from local markets (Figure 7).

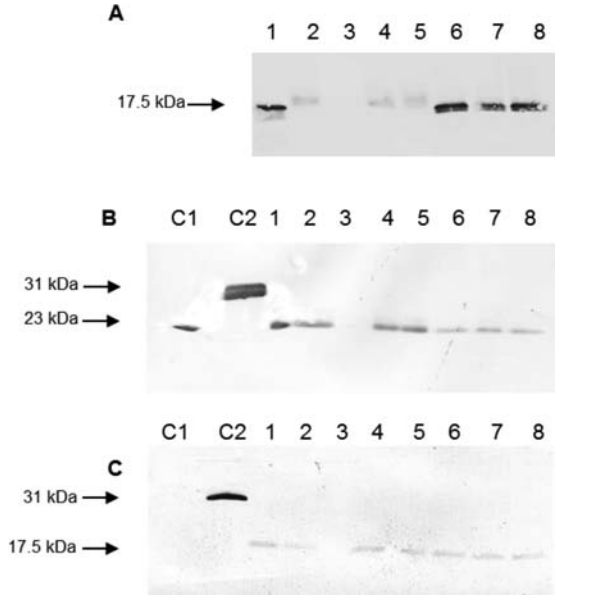

Figure 7. SDS−PAGE and Western blot analyses of different apple products: (A) Western blot using polyclonal rabbit antibody against Mal d 1, (B) Western blot using polyclonal rabbit antibody against Mal d 2, (C) IgE Western blot using the patient serum pool. Key: (C1) native Mal d 2, (C2) chemically reduced Mal d 2, (1) positive control "apple extract Topaz", (2) apple chips nonsulfured, (3) apple rings sulfured, (4) apple rings nonsulfured, (5) apple baby food, (6) clear apple juice, (7) cloudy apple juice, (8) clear organic apple juice.

Analyses of apple-derived foods revealed that Mal d 2 can be detected as the native 23 kDa band in nonsulfured dried apple products (Figure 7B). Mal d 2 was previously detected on two-dimensional electrophoresis (2-DE) gel maps of reduced and not reduced apple extracts.[10] It was shown that chemically reduced Mal d 2 migrated as a protein band at 31 kDa in SDS−PAGE and was reported as IgE reactive.[5,10] The same altered mobility was also reported for the homologous allergen Pru ap 2 from peach.[32] However, the correlation between denaturation of Mal d 2 by reduction of disulfide bridges and its allergenicity is unclear so far. It could be demonstrated that the IgE reactivity of the reduced form of Mal d 2 was recovered after reoxidization of Mal d 2.[8] In fact, the results indicate that Mal d 2 is mostly available as nonreduced native protein in nonsulfured apple products and is not reactive to patients'

IgE's (Figure 7B,C). The same samples were analyzed using patient sera to characterize the patient reactivity to Mal d 2 in the apple-derived products (Figure 7C). The sera reacted strongly only to the positive control, a reduced Mal d 2 band at 31 kDa, and weakly to Mal d 1 at 17.5 kDa in all apple products except sulfured apple rings.

Within the experiment, the major allergen from apple Mal d 1 was also investigated in parallel due to its significant susceptibility to heat treatment and high processing pressure.[27,33] Detection of Mal d 1 is an indication that none of the analyzed products were heated or treated by pressure except sulfured apple rings (Figure 7A). The reactive bands to Mal d 1 polyclonal antibodies are diffuse and shifted in apple samples such as dried and nonsulfured products as well as baby food (Figure 7A), which show protein degradation or aggregation.

Sulfurization is used in the manufacturing of dried food as a pretreatment before hot and cold drying processes to increase the shelf life and to act as an antimicrobial agent.[34] Due to health risks for consumers, the addition of sulfur to food is currently limited by regulations.[34] The investigation of commercially available apple products confirmed the assumption that nonsulfured apple products contain detectable amounts of native Mal d 2. However, the food allergy is mediated through IgE's bound to the surface of mast cells and basophils.[35,36] If the allergen protein binds to the specific IgE's, it can potentially cause the release of histamine and other mediators responsible for the clinical symptoms. Food pretreatments such as sulfurization and subsequent hot drying in combination with food preservatives such as vitamin C were shown to denature food allergens and lead to a reduction or an enhancement of binding to IgE-reactive epitopes.[37,38] It has been demonstrated that irreversible heat-denatured allergens can cause increased binding to immunoglobulin by the exposure of different sets of epitopes in a mouse model.[35,36] Remarkable structural stability and resistance to proteolysis has been linked to potentially increased risks of peptide allergens which survive food treatments and the digestive tract.[39] However, a prerequisite for sufficient IgE reactivity remains the presentation of IgE-binding epitopes.[35]

In conclusion, sulfur is able to degrade or modify Mal d 2 only in combination with heat treatment. Vitamin C, however, is too weak as a reducing agent to cause breakage of the disulfide bridges or protein defolding. The result of the RBL assay confirmed that the individual patient sera can bind to heat-treated purified Mal d 2 to various extents, but the overall affinity for Mal d 2 remained significantly low to nonexistent. The ATR-FTIR results confirmed only minimal changes at α-helices comparable to those observed during thermal unfolding.[8] However, the molecule remained tightly held by eight disulfide bridges and resisted defolding in the presence of vitamin C.

The results of our studies confirm that (a) only the treatment with hot sulfites is able to destroy Mal d 2 and (b) the lack of patient symptom development to apple Mal d 2 is attributed to the absence of defolded IgE-reactive Mal d 2 in fresh and processed apple products. Additionally, current data substantiate that Mal d 2 is present mainly in its native nonreactive conformation in the apple products and cannot be seen as a major health risk for sensitized consumers.

AUTHOR INFORMATION

Corresponding Author

*Phone: +43-1-47654-6560. Fax: +43-1-47654-6675. E-mail: margit.laimer@boku.ac.at.

Funding

This work was supported by EU Project SAFE QLK1-CT-2000-03194.

Notes

The authors declare no competing financial interest.

ACKNOWLEDGMENTS

We thank Prof. W. Hemmer from Floridsdorfer Allergie Zentrum (FAZ) for providing the patient sera and Dr. A. Martinelli and Dr. M. Zaccharini (Centro Innovazione Varietale (CIV), Ferrara, Italy) for the apple cultivars.

DEDICATION

This work is dedicated to Manfred Schwanninger.

REFERENCES

(1) Breiteneder, H. Thaumatin-like protein—a new family of pollen and fruit allergens. *Allergy* **2004**, *59*, 485−490.

(2) Ghosh, R.; Chakrabarti, C. Crystal structure analysis of NP24-1: a thaumatin-like protein. *Planta* **2008**, *228*, 883−890.

(3) Oh, D. H.; Song, K. J.; Shin, Y. U.; Chung, W. I. Isolation of a cDNA encoding a 31-kDa, pathogenesis-related thaumatin-like (PR5/TL) protein abundantly expressed in apple fruit (*Malus domestica* cv. Fuji). *Biosci., Biotechnol., Biochem.* **2006**, *64*, 355−362.

(4) Krebitz, M.; Wagner, B.; Ferrreira, F.; Peterbauer, C.; Campillo, N.; Witty, M.; Kolarich, D.; Steinkellner, H.; Scheiner, O.; Breiteneder, H. Plant-based heterologous expression of Mal d 2, a thaumatin-like protein and allergen of apple (*Malus domestica*), and its characterisation as an antifungal proteins. *J. Mol. Biol.* **2003**, *329*, 721−730.

(5) Smole, U.; Bubin, M.; Radauer, C.; Ebner, C.; Breiteneder, H. Mal d 2, the thaumatin-like allergen from apple, is highly resistant to gastrointestinal digestion and thermal processing. *Int. Arch. Allergy Immunol.* **2008**, *147*, 289−298.

(6) Hsieh, L. S.; Moos, M.; Lin, Y. Characterisation of apple 18 and 31 kDa allergens by micro sequencing and evaluation of their content during storage and ripening. *J. Allergy Clin. Immunol.* **1995**, *96*, 960−970.

(7) Fernandez-Rivas, M.; Bolhaar, S.; Gonzalez-Mancebo, E.; Asero, R.; van Leeuwen, A.; Bohle, B.; Ma, Y.; Ebner, C.; Rigby, N.; Sancho, A. I.; Miles, S.; Zuidmeer, L.; Knulst, A.; Breiteneder, H.; Mills, C.; Hoffmann-Sommergruber, K.; van Ree, R. Apple allergy across Europe: how allergen sensitization profiles determine the clinical expression of allergies to plant foods. *J. Allergy Clin. Immunol.* **2006**, *118*, 481−488.

(8) Marzban, G.; Herndl, A.; Pietrozotto, S.; Banerjee, S.; Obinger, C.; Maghuly, F.; Hahn, R.; Boscia, D.; Katinger, H.; Laimer, L. Conformational changes of Mal d 2, a thaumatin-like apple allergen, induced by food processing. *Food Chem.* **2009**, *112*, 803−811.

(9) Oberhuber, C.; Ma, Y.; Marsh, J.; Smole, U.; Radauer, C.; Alessandri, S.; Briza, P.; Zuidmeer, L.; Maderegger, B.; Himly, M.; Sancho, A. I.; van Ree, R.; Knulst, A.; Ebner, C.; Shewry, P.; Mills, E. N.; Wellner, K.; Breiteneder, H.; Hoffmann-Sommergruber, K.; Bublin, M. Purification and characterisation of relevant natural and recombinant apple allergens. *Mol. Nutr. Food Res.* **2008**, *52*, 208−219.

(10) Herndl, A.; Marzban, G.; Kolarich, D.; Hahn, R.; Boscia, D.; Hemmer, W.; Maghuly, F.; Stoyanova, E.; Katinger, H.; Laimer, M. Mapping of *Malus domestica* allergens by two-dimensional electrophoresis and IgE-reactivity. *Electrophoresis* **2007**, *28*, 437−448.

(11) Gavrović-Jankulović, M.; Irković, T.; Vucković, O.; Atanasković-Marković, M.; Petersen, A.; Gojgic, G.; Burazer, L.; Jankov, R. M. Isolation and biochemical characterization of a thaumatin-like kiwi allergen. *J. Allergy Clin. Immunol.* **2002**, *110*, 805−810.

(12) Kamisili, F.; Karatas, F. Effects of sulfurisation on vitamins (A, C and E) and malondialdehyde in apricots. *Int. J. Food Sci. Technol.* **2009**, *44*, 987−993.
(13) Koksal, N.; Hasanoglu, H. C.; Gokirmak, M.; Yildirim, Z.; Gutlek, A. Apricot sulfurization: An occupation that induce an asthma-like syndrome in agricultural environments. *Am. J. Ind. Med.* **2003**, *43*, 447−453.
(14) Daniels, D. L.; Joe, F. L.; Warner, C. R.; Longfellow, S. D.; Fazio, T.; Diachenko, G. W. Survey of sulfites determined in a variety of foods by the optimized Monier-Williams method. *Food Addit. Contam.* **1992**, *9*, 283−289.
(15) Zaubermann, G.; Ronen, R.; Akerman, K.; Fuchs, Y. Low pH treatment protects litchi fruit colour. *Acta Hortic.* **1990**, *269*, 309−314.
(16) Meister, A. Gluthation-ascorbic acid atioxidant system in animals. *J. Biol. Chem.* **1994**, *269*, 9397−9400.
(17) Marzban, G.; Puehringer, H.; Dey, R.; Brynda, S.; Ma, Y.; Martinelli, A.; Zaccarini, M.; Kolarich, D.; Altmann, F.; Katinger, H.; Laimer, M. Localization and distribution of the major allergens in apple fruits. *Plant Sci.* **2005**, *169*, 387−394.
(18) Wang, W.; Scali, M.; Vignani, R.; Spadafora, A.; Sensi, E.; Mazzuca, S.; Cresti, M. Protein extraction for two-dimensional electrophoresis from olive leaf, a plant tissue containing high levels of interfering compounds. *Electrophoresis* **2003**, *24*, 2369−75.
(19) Winkler, C.; Denker, K.; Wortelkamp, S.; Sickermann, A. Silver- and Coomassie-staining protocols: detection limits and compatibility with ESI MS. *Electrophoresis* **2007**, *28*, 2095−2099.
(20) Cleland, W. W. Dithiothreitol, a new protective reagent for SH groups. *Biochemistry* **1964**, *3*, 480−482.
(21) Fruton, J. S.; Clarke, H. T. J. Chemical reactivity of cyctein and its derivatives. *Biol. Chem.* **1934**, *106*, 667−691.
(22) Aitken, C. E.; Marshall, R. A.; Puglisi, J. D. An oxygen scavenging system for improvement of dye stability in single-molecule fluorescence experiments. *Biophys. J.* **2008**, *94*, 1826−1835.
(23) Borsook, H.; Keighley, G. Oxidation reduction potential of ascorbic acid (vitamin C). *Proc. Nat. Acad. Sci. U.S.A.* **1933**, *19*, 875−878.
(24) Susi, H.; Byler, D. M.; Gerasimowicz, W. V. Vibrational analysis of amino acids: cysteine, serine, *β*-chloroalanine. *J. Mol. Struct.* **1983**, *102*, 63−79.
(25) Alben, J. O. Fourier transform infrared spectroscopy of enzyme systems. In *Infrared Spectroscopy of Biomolecules*; Mantsch, H. H., Chapman, D., Eds.; Wiley-Liss: New York, 1996; pp 19−37.
(26) Leone, P.; Menu-Bouaouiche, L.; Peumans, W. J.; Payan, F.; Barre, A.; Roussel, A.; Van Damme, E. J. M.; Rougé, P. Resolution of the structure of the allergenic and antifungal banana fruit thaumatin-like protein at 1.7-A. *Biochimie* **2005**, *88*, 45−52.
(27) Sancho, A. I.; Foxal, R.; Browne, T.; Dey, R.; Zuidmeer, L.; Marzban, G.; Waldron, K. W.; van Ree, R.; Hoffmann-Sommergruber, K.; Laimer, M.; Mills, C. E. N. Effect of postharvest storage on the expression of apple allergen Mal d 1. *J. Agric. Food Chem.* **2006**, *54*, 5917−5923.
(28) Biggs, A.; Miller, S. Comparative relative susceptibility of NE-183 apple cultivars to fruit rot pathogens in West Virginia. *J. Am. Pomol. Soc.* **2005**, *59*, 72−77.
(29) Gau, A. E.; Koutb, M.; Piotrowski, M.; Kloppstech, K. Accumulation of pathogenesis-related proteins in the apoplast of a susceptible cultivar of apple (*Malus domestica* cv. Elstar) after infection by *Venturia inaequalis* and constitutive expression of PR genes in the resistant cultivar Remo. *Eur. J. Plant Pathol.* **2004**, *110*, 703−711.
(30) Botton, A.; Lezzer, P.; Dorigoni, A.; Barcaccia, G.; Ruperti, B.; Ramina, A. Genetic and environmental factors affecting allergen-related gene expression in apple fruit (*Malus domestica* L. Borkh). *J. Agric. Food Chem.* **2008**, *56*, 6707−6717.
(31) Colditz, F.; Niehaus, K.; Krajinski, F. Silencing of PR-10-like proteins in *Medicago truncatula* results in an antagonistic induction of the other PR proteins and in an increased tolerance upon infection with the oomycete *Aphanomyces euteiches*. *Planta* **2007**, *226*, 57−71.
(32) Palacin, A.; Tordesillas, L.; Gamboa, P.; Cuesta-Herranz, J.; Sanz, M. L.; Barber, D.; Salcedo, G.; Diaz-Perales, A. Characterisation of peach thaumatin-like proteins and their identification as major peach allergens. *Clin. Exp. Allergy* **2010**, *40*, 1422−1430.
(33) Somkuti, J.; Houska, M.; Smeller, L. Pressure and temperature stability of the main apple allergen Mal d 1. *Eur. Biophys. J.* **2011**, *40*, 143−151.
(34) DiPersio, P. A.; Kendall, P. A.; Calicioglu, M.; Sofos, J. N. Inactivation of *Salmonella* during drying and storage of apple slices treated with acidic or sodium metasulfite. *J. Food Prot.* **2003**, *66*, 2245−51.
(35) Johansen, P.; Senti, G.; Martinez Gomez, J. M.; Wütrich, B.; Bot, A.; Kündig, T. M. Heat denaturation, a simple method to improve the immunotherapeutic potential of allergens. *Eur. J. Immunol.* **2005**, *35*, 3591−3598.
(36) Storni, T.; Kundig, T. M.; Senti, G.; Johansen, P. Immunity in response to particulate antigen-delivery systems. *Adv. Drug Delivery Rev.* **2005**, *57*, 333−355.
(37) Untersmayr, E.; Vestergaard, H.; Malling, H.-J.; Jensen, L. B.; Platzer, M. H.; Boltz-Nitulescu, G.; Poulsen, L. K. Incomplete digestion of codfish represents a risk factor for anaphylaxis in patients with allergy. *J. Allergy Clin. Immunol.* **2007**, *119*, 711−717.
(38) Breiteneder, H.; Mills, C. E. N. Molecular properties of food allergens. *J. Allergy Clin. Immunol.* **2005**, *115*, 14−23.
(39) Asero, R.; Mistrello, G.; Roncarolo, D.; Amato, S.; Falagiani, P. Analysis of the heat stability of lipid transfer protein from apple. *J. Allergy Clin. Immunol.* **2003**, *112*, 1009−1011.

could enter the colon with the potential to influence colonic health.[16,18]

MATERIALS AND METHODS

Chemicals. Cyanidin 3-*O*-glucoside was purchased from Apin Chemicals (Abingdon, Oxford, U.K.), cyanidin 3-*O*-sambubioside 5-*O*-glucoside was supplied by Polyphenols (Sandnes, Norway), morin and ellagic acid were obtained from Sigma-Aldrich (Poole, Dorset, U.K.), and punicalagin was obtained from Chromadex (United States). HPLC-grade solvents were obtained from Rathburn Chemicals (Walkerburn, U.K.). Formic acid and sodium diethyldiothiocarbamate were purchased from Sigma-Aldrich, and acetic acid was purchased from BDH (Poole, U.K.).

Plant Material and Processing. Raspberries (30 kg, *R. idaeus* variety Glen Ample) were purchased from Peter Marshall & Co., Alyth, Perthshire, U.K. The raspberries were picked as commercially ripe and transported to the James Hutton Institute on the day of picking, where they were washed in distilled water, left to drain on sieves, and then pureed in 10 kg batches using a catering homogenizer (Fimar MX40S fixed speed stick blender). The procedure did not homogenize the seeds. The purees were combined and continually stirred using an overhead paddle stirrer at 75 rpm (to prevent settlement) and ladled into food-grade bags in 300 ± 1 g amounts. The purees were frozen, transported to the University of Ulster, and stored at −20 °C prior to use in the ileostomy feeding studies.

Ileostomy Feeding Study. The study (11/NI/0112) was conducted with the prior approval of the Office for Research Ethics Committees Northern Ireland (ORECNI) and the University of Ulster Ethical Committee and with the informed consent of participants who were recruited from clinics at Altnagelvin Area Hospital, with the assistance of a colorectal consultant (Dr. R. Lawther) and nurse specialist (Dr. G. O'Connor). Eleven ileostomists (six males, five females, mean age 44 ± 12 yr) who had undergone terminal ileostomies and were at least 1.5 years postoperative prior to the study and were nonsmokers undertook the study. Participants were required to follow a diet low in polyphenolic compounds as described previously,[14] avoiding fruits and vegetables, nuts, high-fiber products, and beverages such as tea, coffee, and fruit juices, as well as abstaining from consumption of alcohol for 48 h prior to the beginning of the study. Following an overnight fast, the participants provided an ileal fluid sample (T 0 h), then consumed 300 g of homogenized raspberries within 10 min, and continued the low polyphenolic diet, with provision of a standard lunch, for a further 8 h until provision of the second ileal fluid sample (T 8 h). The ileal fluid samples were collected and processed within 30 min. The volumes and pH values of the ileal fluid were recorded, before dilution with ice-cold distilled water as required, dependent on the viscosity, and before the fluid was homogenized in a chilled Waring blender for 30 s and storage of aliquots at −80 °C in preparation for subsequent analysis.

Targeted Analysis of Raspberry Phenolics in Ileal Fluids. Duplicate samples of ileal fluid (2 ± 0.1 g) were spiked with 10 μg of cyanidin 3-*O*-sambubioside 5-*O*-glucoside as an internal standard and homogenized in 3 mL of 1% aqueous formic acid (FA) containing 20 mM sodium diethyldiothiocarbamate (DDC) for 1 min at 24 000 rpm using an Utra-Turrax homogeneizer. The samples were centrifuged for 20 min at 4000*g* at 4 °C, and the supernatants were collected. The pellet was re-extracted twice with 1% formic acid in methanol containing 20 mM DDC, and the three supernatants were pooled. Portions (4 mL) of this extract were reduced to dryness in vacuo using a SpeedVac concentrator. The residues were resuspended in 50 μL of 1% formic acid in methanol and 450 μL of 1% formic acid, and 100 μL aliquots were analyzed by HPLC-PDA−MS^2 (PDA = photodiode array).

The samples were analyzed on a Surveyor HPLC system comprised of an HPLC pump, a PDA detector, scanning from 200 to 700 nm, and an autosampler cooled to 4 °C (Thermo Finnigan, San Jose, CA). Separations of ellagic acid derivatives, ellagitannins, and anthocyanins from raspberry were performed using a Synergi 4 μm RP-POLAR 80 Å 250 × 4.6 mm i.d. reversed-phase column (Phenomenex, Macclesfield, U.K.) maintained at 40 °C. The mobile phase, pumped at a flow rate of 1 mL/min, was 1% aqueous formic acid (A) and 99% methanol containing 1% formic acid (B), establishing a linear gradient from 10% to 40% B over 60 min. Chromatograms were recorded at 280, 325, 365, and 520 nm. After passing through the flow cell of the diode array detector, the column elute was split, and 0.3 mL/min was directed to an LCQ DecaXP ion trap mass spectrometer fitted with an electrospray interface (ESI) operating in either positive ionization mode for anthocyanins or negative ionization mode for ellagic acid and ellagitannins. Analyses were carried out using full-scan, data-dependent MS^2 scanning from m/z 150 to m/z 2000. With the ESI in positive ionization mode, the capillary temperature was 300 °C, the amount of sheath gas was 50 units, the amount of auxiliary gas was 35 units, and the source voltage was 2 kV. For negative ionization, the capillary temperature was 325 °C, the amounts of the sheath and auxiliary gases were both 40 units, and the source voltage was 4 kV.

Anthocyanins were quantified from their chromatographic peak areas recorded at 520 nm and expressed as cyanidin 3-*O*-glucoside equivalents, ellagitannins detected at 260 nm were expressed as punicalagin equivalents, and ellagic acid and ellagic acid conjugates monitored at 365 nm were quantified in ellagic acid equivalents.

Untargeted Analysis of Raspberry Metabolites in Ileal Fluids. Ileal samples were extracted by the procedure described above with small differences. The frozen samples were thawed and vortexed, and duplicate 2.0 ± 0.1 g samples were weighed into 15 mL centrifuge tubes. These samples were extracted using 3 mL of UPW containing 1% formic acid and 20 mM DDC. The tubes were vortex-mixed for 3 × 30 s and then sonicated in a water bath for 1 min. All procedures were carried out at 5 °C. After centrifugation (2500*g*, 10 min, 5 °C), the supernatants were transferred to new tubes. The pellets were extracted twice using 3 mL of 1% formic acid in methanol containing 20 mM DDC and the supernatants combined and vortex-mixed. A subsample of 4 mL was removed and dried in a Speed-Vac. The dried samples were resuspended in 10% acetonitrile containing 0.2% formic acid and prepared in filter vials prior to analysis using the orbitrap LC−MS system.

Untargeted analysis of the ileal fluids was performed on an HPLC system consisting of a quaternary pump (Thermo Fisher Scientific, Accella 600) and a PDA detector (Thermo Fisher Scientific, Accella) coupled to an LTQ orbitrap mass spectrometer (Thermo Fisher Scientific, Stafford House, Boundary Way, Hemel Hempstead, U.K.). Replicate 10 μL samples were injected onto a 2 × 150 mm (4 μm) Synergy Hydro-RP 80 fitted with a C18 4 × 2 mm Security Guard cartridge (Phenomenex Ltd.). Sample and column temperatures were maintained at 6 and 30 °C, respectively. The samples were analyzed at a flow rate of 0.3 mL/min using a binary mobile phase of (A) 0.1% aqueous formic acid and (B) 0.1% formic acid in acetonitrile/water (1:1, v/v) and the following gradient: 0−4 min, 5% B; 4−22 min, 5−50% B; 22−32 min, 50−100% B. Mass detection was carried out using an LTQ orbitrap mass spectrometer in negative ESI mode.

Two scan events were employed; full-scan analysis was followed by data-dependent MS/MS of the three most intense ions using collision energies of 45 eV source voltage (set at 3.4 kV) in wide-band activation mode. The instrument was optimized (tuned) against morin at a resolution of 30 000 (to maximize the number of scans across peaks but retain a reasonable resolution) in a range of 80−2000 mass units. For optimal electrospray ionization, the source conditions were set at a source temperature of 300 °C, a sheath gas amount of 60 arbitrary units, and an auxiliary gas amount of 5 arbitrary units. Prior to analysis, the mass accuracy of the instrument was assured by calibrating using a preparative ESI negative ion calibration tuning solution (containing 2.9 μg/mL sodium dodecyl sulfate, 5.4 μg/mL sodium taurocholate, and 0.001% Ultramark 1621) following the manufacturer's protocols.

SIEVE Analysis. Mass spectral data from the orbitrap analysis were applied to the SIEVE software program (Thermo Fisher Scientific, Hemel Hempstead, U.K; http://www.thermoscientific.com/en/product/sieve-software-differential-expression.html). The SIEVE method compares and contrasts multiple samples on the basis of the nature of the experimental setup. In this case, the samples were labeled

either before or after, and the program was set to discern which MS signals were consistently present and increased in the after-supplementation samples. As the SIEVE software automatically detects and integrates peaks, it can also provide lists of peaks that are consistently decreased after feeding. SIEVE parameters were chosen which have been shown in our laboratory to be effective for this pairwise comparison of samples. These parameters define the optimum and maximum numbers of peaks, peak threshold values, a delayed retention start of 5 min to dismiss unbound material, and suitable peak width parameters to allow for drifts in retention time between runs and samples. These settings have been used to accurately align and "bin" signals from mass spectral data from multiple chromatograms. The output, as peak areas for the detected peaks, can be accessed in Excel file format and used to develop principal component analysis (PCA) plots and other models.

Data Analysis and Conditions. Statistical analysis was carried out on all the variables collected from the LC−MS analysis of the samples. Data were obtained as peak areas from the SIEVE automatic integration software and consisted of 862 variables or potential peaks. Three approaches were taken: First, PCA, using univariate scaling, was applied to all the samples, and components 1−4 described 42% of the variation in the data set, with component 1 describing almost 17%. Second, a discriminant analysis (optimized partial least squares, OPLS) was performed with two classifications (before feeding and after feeding), resulting in a model that described 33% of the variation, 14% of which described the after feeding classification. The Q^2 score for this model was 0.974. These analyses were performed using SIMCA-P 12.0.1.0 software. The third analysis performed was pairwise metabolite−metabolite correlations (using Genstat for Windows, 16th ed., VSN International Ltd., Hemel Hempstead, U.K.), determined by Pearson's correlation coefficient (r) test using two sample sets, first all samples and then a subset consisting of the "after feeding" samples. This technique was used to define components whose patterns of abundance matched those of components identified by the targeted analysis and provide a subset which was likely to have arisen from the berry material.

Extraction and Analysis of Extracts from Raspberry Seeds. Raspberry seeds were isolated from the purees by repeated sieving and washing using ice-cold distilled water. The seeds, which were free of attached material, were dried using paper tissues and stored at −18 °C. The extraction procedure was essentially the same as noted above for the untargeted study, but only 200 mg of seeds was extracted and the volumes were reduced to 1 mL. After the 1 mL extracts were dried in the Speed-Vac, they were resuspended in 5% acetonitrile containing 0.1% FA and prepared in filter vials.

Samples of resolubilized extracts were analyzed using an LCQ-DECA system, comprising a Surveyor autosampler, pump, and PDA detector, and a Thermo-Finnigan ion trap mass spectrometer controlled by Xcalibur software. A 2 mm × 150 mm C18 column (Synergi Hydro C18 with polar end-capping, Phenomenex Ltd.) was eluted with a binary solvent of (A) 0.1% aqueous formic acid and (B) 0.1% formic acid in acetonitrile at a flow rate of 200 μL/min using a 30 min gradient of 5−40% B. The PDA detector scanned three discrete channels at 280, 365, and 520 nm. The mass data were collected in negative or positive mode scanning over the mass range m/z 80−2000. The MS detector was tuned against morin in negative mode and cyanidin 3-*O*-glucoside in positive mode. Two scan events were employed; full-scan analysis was followed by data-dependent MS/MS of the most intense ions using collision energies of 45% of the source voltage (set at 3 kV) in wide-band activation mode. The capillary temperature was set at 250 °C, with the sheath gas pressure at 60 psi and auxiliary gas pressure at 15 psi.

RESULTS AND DISCUSSION

This study confirms and extends previous research that examined the fate of anthocyanins, the major ellagitannins, and ellagic acid derivatives from raspberries excreted in ileal fluid by subjects with an ileostomy.[14] The 11 ileostomists participating in the current study had a mean age of 44 ± 12 yr, and the group mean ileal fluid sample mass at baseline (T 0 h) was 187.8 ± 73 g (range 107.4−318.0 g) with a group mean pH value of 5.6 ± 0.4 (range 5.0−6.3). The group mean ileal fluid mass for the T 8 h sample (post berry consumption) was 268. ± 108 g (range 62−470 g) with a group mean pH value of 6.6 ± 0.6 (range 5.3−7.5). In both cases the group mean ileal fluid masses and pH values were significantly ($p < 0.05$) increased compared to those of the baseline fasted samples.

Eight anthocyanins were detected in Glen Ample raspberries (Table 1). Although the composition was comparable to that detected previously in this variety of raspberries,[14,19,20] the amounts of anthocyanins and the ellagic acid derivatives were lower than in the berries used in a previous feeding study.[14] The overall levels of ellagitannins were similar, but the profile was different, with lower levels of sanguiin H-6 and higher amounts of sanguiin H-10 and lambertianin C. These differences may reflect differences in growing location or year-to-year variation, but the lower content of anthocyanins could indicate that the raspberries were not as ripe as those used in the previous study, which were picked directly from the field as opposed to being part of a shipment of raspberries to be delivered to a supermarket.

Table 1. Identification and Quantification of Phenolic Compounds Detected in Raspberries

peak	compd	t_R (min)	$[m/z]^+$	MS^2 m/z	concn[a] (μmol/300 g)
1	cyanidin 3,5-*O*-diglucoside	18.1	611	449, 287	0.6 ± 0.1
2	cyanidin 3-*O*-sophoroside	18.9	611	449, 287	22 ± 1
3	cyanidin 3-*O*-(2″-*O*-glucosyl) rutinoside	19.9	757	611, 287	4.2 ± 0.3
4	pelargonidin 3-*O*-sophoroside	23.5	595	271	0.25 ± 0.01
5	cyanidin 3-*O*-glucoside	24.2	449	287	9 ± 1
6	cyanidin 3-*O*-(2″-*O*-xylosyl) rutinoside	25.2	727	581, 287	0.3 ± 0.1
7	cyanidin 3-*O*-rutinoside	27.1	595	287	2.2 ± 0.2
8	pelargonidin 3-*O*-glucoside	28.9	433	271	0.1 ± 0.1
				total anthocyanins	38.2 ± 3.2
9	ellagic acid *O*-pentoside	34.6	433[b]	257, 229	1.2 ± 0.1
10	ellagic acid	35.6	301[b]	257, 229	4.8 ± 0.1
				total ellagic acid	6.0 ± 0.2
11	sanguiin H-10	18.9	783[b]	1265, 1103, 933, 631	43 ± 3
12	sanguiin H-6	26.0	1869[b]	1567, 1265, 933, 631	61 ± 3
13	lambertianin C	29.2	1401[b]	1869, 1567, 1265, 933, 631	20 ± 2
				total ellagitannins	124 ± 8

[a]Data expressed as mean values ± SD ($n = 2$). [b]$[m/z]^-$.

Table 2. Recovery of Anthocyanins, Ellagic Acid, and Ellagitannins in Ileal Fluid Collected 0−8 h after Consumption of 300 g of Raspberries[a]

compd	S1		S2		S3		S4		S5		S6	
cyanidin 3-*O*-sophoroside	8.0 ± 0.7	36	4.2 ± 0.4	19	7 ± 2	33	6.6 ± 0.8	30	0.41 ± 0.06	2	6 ± 2	27
cyanidin 3-*O*-(2″-*O*-glucosyl) rutinoside	1.7 ± 0.5	40	1.6 ± 0.1	38	1.7 ± 0.7	39	1.7 ± 0.3	40	0.11 ± 0.01	3	1.6 ± 0.4	38
pelargonidin 3-*O*-sophoroside	0.1 ± 0.1	40	0.10 ± 0.01	40	0.10 ± 0.02	40	0.08 ± 0.01	32	nd	0	0.08 ± 0.02	32
cyanidin 3-*O*-glucoside	0.1 ± 0.1	1	0.4 ± 0.1	4	0.06 ± 0.01	1	0.12 ± 0.03	1	nd	0	0.09 ± 0.01	1
cyanidin 3-*O*-rutinoside	0.3 ± 0.1	14	0.10 ± 0.01	4	0.04 ± 0.01	2	0.03 ± 0.01	1	0.03 ± 0.02	1	0.2 ± 0.03	9
total anthocyanins	10.2 ± 1.5	27	6.4 ± 0.6	17	8.9 ± 2.7	23	8.5 ± 1.1	22	0.55 ± 0.09	1	7.9 ± 2.5	21
ellagic acid *O*-pentoside	0.3 ± 0.1	25	0.5 ± 0.1	42	0.50 ± 0.03	42	0.6 ± 0.3	50	0.05 ± 0.01	42	0.5 ± 0.2	42
ellagic acid	7.2 ± 0.6	150	10 ± 3	208	14.6 ± 0.1	304	12 ± 6	250	0.8 ± 0.1	17	12 ± 3	250
total ellagic acid	7.5 ± 0.7	125	10.5 ± 3.1	175	15.1 ± 0.1	252	12.6 ± 6.3	210	0.85 ± 0.11	14	12.5 ± 3.2	208
sanguiin H-10	13.5 ± 0.6	31	6 ± 1	14	8 ± 4	19	6.5 ± 0.2	15	0.6 ± 0.04	1	8 ± 2	19
sanguiin H-6	8.5 ± 1.7	14	17 ± 7	28	32 ± 2	52	29 ± 19	47	0.4 ± 0.06	1	19 ± 3	31
lambertianin C	nd	0	0.7 ± 0.6	4	2.4 ± 0.7	12	4 ± 2	20	nd	0	nd	0
total ellagitannins	22.0 ± 2.3	18	23.7 ± 8.6	19	42.4 ± 8.7	34	39.5 ± 21.2	32	1.0 ± 0.1	0.8	27 ± 5	22

compd	S8		S9		S10		S11		S12	
cyanidin 3-*O*-sophoroside	4 ± 1	18	6.8 ± 0.2	31	6.3 ± 0.5	29	3.5 ± 0.8	16	4.03 ± 2.1	19
cyanidin 3-*O*-(2″-*O*-glucosyl)rutinoside	1.0 ± 0.2	24	1.66 ± 0.01	39	1.51 ± 0.03	36	0.9 ± 0.4	21	1 ± 0.55	24
pelargonidin 3-*O*-sophoroside	0.05 ± 0.01	20	0.10 ± 0.01	40	0.07 ± 0.01	28	0.04 ± 0.01	16	0.02 ± 0.01	8
cyanidin 3-*O*-glucoside	0.3 ± 0.1	3	0.07 ± 0.01	1	0.06 ± 0.01	1	0.11 ± 0.08	1	0.09 ± 0.05	0.3
cyanidin 3-*O*-rutinoside	0.4 ± 0.1	18	0.11 ± 0.02	5	0.9 ± 0.1	41	0.02 ± 0.01	1	0.57 ± 0.3	23
total anthocyanins	5.7 ± 1.4	15	8.7 ± 0.2	23	8.8 ± 0.6	23	4.6 ± 1.3	12	5.7 ± 1.7	15
ellagic acid *O*-pentoside	0.5 ± 0.1	40	0.4 ± 0.1	33	0.5 ± 0.1	40	0.13 ± 0.01	11	0.8 ± 0.3	33
ellagic acid	8.6 ± 0.5	179	13 ± 1	271	9 ± 1	187	7.3 ± 0.7	152	7 ± 2	83
total ellagic acid	9.1 ± 0.6	152	13.4 ± 1.1	223	9.5 ± 1.1	158	7.4 ± 0.7	124	8 ± 2.3	134
sanguiin H-10	4 ± 2	9	7 ± 2	16	7.4 ± 0.3	17	6 ± 1	14	5 ± 3	13
sanguiin H-6	23 ± 4	38	39 ± 5	64	19 ± 7	31	26 ± 2	43	12 ± 8	20
lambertianin C	0.4 ± 0.2	2	7 ± 5	35	2.3 ± 0.6	12	1 ± 1	5	1.1 ± 0.8	6
total ellagitannins	27.4 ± 6.2	22	53 ± 9	43	28.7 ± 7.9	23	33 ± 4	27	27 ± 5	15

[a]In the first column for each subject, the data are expressed as mean values in micromoles ± standard error (n = 2). The numbers in the second column for each subject represent the amounts recovered as a percentage of the quantity ingested. nt = not detected. Anthocyanins, ellagic acid, and ellagitannins were not detected in ileal fluid samples collected at time 0 h before raspberry intake. S1 = subject 1, S2 = subject 2, and so on. Subject 7 did not complete the study, and therefore 11 subjects are described.

Five of the major anthocyanins in the raspberries were consistently detected in the ileal fluids collected from the 11 donors after supplementation (Table 2). The most abundant anthocyanin in the raspberries, cyanidin 3-*O*-sophoroside, was also the main anthocyanin in the ileal fluids, but the recovery varied greatly between the subjects (from 2% to 36% of intake, mean 21.7%, Table 3). Other anthocyanins that were less abundant in the raspberries, such as cyanidin 3-*O*-(2″-glucosyl)rutinoside and pelargonidin 3-*O*-sophoroside, often had higher precentage recoveries than cyanidin 3-*O*-sophoroside. The order of recovery was cyanidin 3-*O*-(2″-glucosyl)-rutinoside > pelargonidin 3-*O*-sophoroside > cyanidin 3-*O*-sophoroside > cyanidin 3-*O*-rutinoside > cyanidin 3-*O*-glucoside (mean recoveries 28.6%, 24.0%, 21.7%, 9.2%, and 1.3%, respectively), but again with substantial interindividual variation. These recoveries were lower than but showed the same order as those observed previously.[14]

The major ellagitannins detected in raspberries were also detected in the ileal samples after supplementation (Tables 2 and 3). Sanguiin H-6 was the most abundant in the ileal samples, but as with the anthocyanins, there was a large interindividual variation in recoveries (1−64%, mean 30.5%). Sanguiin H-10 was generally recovered at higher levels (1−31%, mean 13.8%) than lambertianin C (0−35%, mean 8.2%), but again with large interindividual variation. The recovery figures may reflect their innate relative stability to the conditions of the upper gastrointestinal tract, but it also possible that some components are formed through degradation of larger ellagitannins. For example, sanguiin H-6 is a potential degradation product of lambertianin C, and sanguiin H-10 could be formed during the degradation of sanguiin H-6. Indeed, in vitro digestion studies indicated an increased recovery of sanguiin H-10 isomers which was suggested to be due to breakdown of the larger ellagitannins.[21,22]

Table 3. Mean Recovery of Anthocyanins, Ellagic Acid, and Ellagitannins in Ileal Fluid Collected from 11 Volunteers 0−8 h after Consumption of 300 g of Raspberries

compd	recovery	
	μmol (mean ± SE)	% of intake
cyanidin 3-*O*-sophoroside	4.7 ± 0.8	21.7
cyanidin 3-*O*-(2″-*O*-glucosyl)rutinoside	1.2 ± 0.3	28.6
pelargonidin 3-*O*-sophoroside	0.06 ± 0.02	24.0
cyanidin 3-*O*-glucoside	0.11 ± 0.04	1.3
cyanidin 3-*O*-rutinoside	0.23 ± 0.06	9.2
total anthocyanins	6.30 ± 1.22	16.3
ellagic acid *O*-pentoside	0.4 ± 0.1	33.0
ellagic acid	8.4 ± 1.5	175.7
total ellagic acid	8.8 ± 1.6	146.6
sanguiin H-10	6.0 ± 1.3	13.8
sanguiin H-6	18.7 ± 4.9	30.5
lambertianin C	1.6 ± 0.9	8.2
total ellagitannins	26.3 ± 7.1	21.2

Although the levels of ellagic acid pentoside were generally reduced (recoveries 11−50%, mean 33%, Tables 2 and 3), ellagic acid was detected in the ileal fluids from all subjects at levels generally higher than in the raspberries (17−304%, mean 175.7%). This increase in ellagic acid most probably is a result of the degradation of ellagitannins and/or ellagic acid pentosides and release of ellagic acid as noted in model studies.[23] However, in the previous study[14] only sanguiin H-6 and ellagic acid were detected.

It is very noticeable that the recoveries of (poly)phenols in certain subjects were relatively high (e.g., subject 4) whereas those in other subjects (e.g., subject 5) were very low. This interindividual variation may be related to the differing physiology of the subjects. In particular, subject 5 had the lowest output of ileal fluid, which may indicate slow passage of the berries through the intestine or lower levels of intestinal secretions. Subject 1 had the highest ileal output and had higher than average recovery of anthocyanins but poorer recovery of sanguiin H-6 (Table 2). Overall, the targeted analysis provided evidence for the differential stability of the anthocyanin, ellagitannin, and ellagic acid derivatives following consumption of raspberries and largely confirmed previous findings.[14]

For the nontargeted approach, the ileal samples were examined by LC−MS/MS using an orbitrap mass spectrometer capable of exact mass determination. This confirmed the presence of the major anthocyanins, ellagitannins, and ellagic acid derivatives detected by the targeted analysis as can be seen in a characteristic absorbance profile of the "before"- and "after"-supplementation samples (Figure 1a). The presence of anthocyanins could be detected by examining the elution profiles at 520 nm (Figure 1b). There was a good association between the targeted and nontargeted analyses as indicated by a comparison of the levels of anthocyanins and the levels of the major ellagitannin peak, sanguiin H-6 (see the Supporting Information, Figure S1). Indeed, it was apparent that the interindividual variabilities in recoveries were similar between the targeted and nontargeted analyses. However, it also became clear that certain subjects had very different profiles. In particular, subjects 1 and 5, and to a lesser extent subject 10, gave a different PDA profile in the after-supplementation samples (Supporting Information, Figure S2). Their profiles

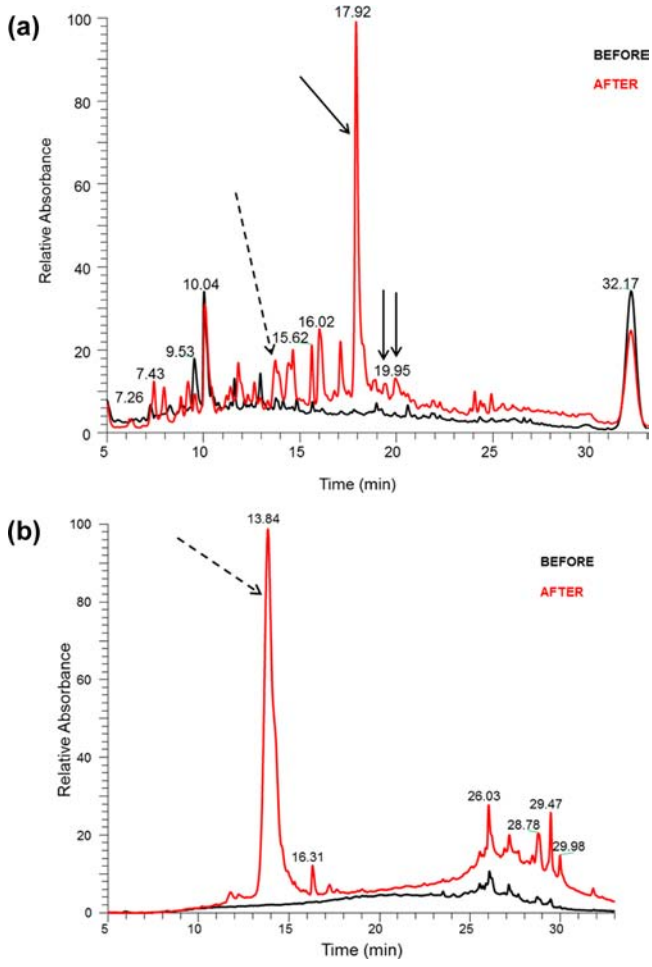

Figure 1. (a) Characteristic UV traces for ileal samples before and after supplementation. Traces from subject 6 are shown before and after (red) supplementation with raspberries. The black arrows denote the positions of the sanguiin H-6, ellagic acid pentose, and ellagic acid peaks. The dashed arrow denotes the position of the main anthocyanin peak. The figure in the top right corner is the full-scale deflection of the PDA detector at 280 nm. (b) Traces at 520 nm of ileal samples before and after supplementation. Traces from subject 6 are shown before and after (red) supplementation with raspberries. The dashed arrow denotes the position of the main anthocyanin peak. The figure in the top right corner is the full-scale deflection of the PDA detector at 520 nm.

were dominated by two peaks (t_R = 9.72 and 13.76 min) with PDA and m/z data characteristic of caffeoylquinic acids (PDA maximum ∼320 nm; [M − H], m/z 353; MS^2, m/z 191), arguably indicative of coffee intake by the subjects during the supplementation period.[24]

The chromatographic profiles were examined visually to discern peaks that consistently increased after supplementation, but the human element was supplemented by a nontargeted method. The MS data from all of the samples including blanks and the quality control samples were examined using the SIEVE software program, which selects peaks that increase or decrease significantly after supplementation. The SIEVE approach is completely unbiased and provides data to produce principal component analysis plots illustrating the differences and similarities between the samples (see Figure 2). The before and after samples were separated mainly on the t[1] axis (which explains 17% of the variation). Certain before and after samples

dx.doi.org/10.1021/jf502259j | J. Agric. Food Chem. 2014, 62, 7631−7641

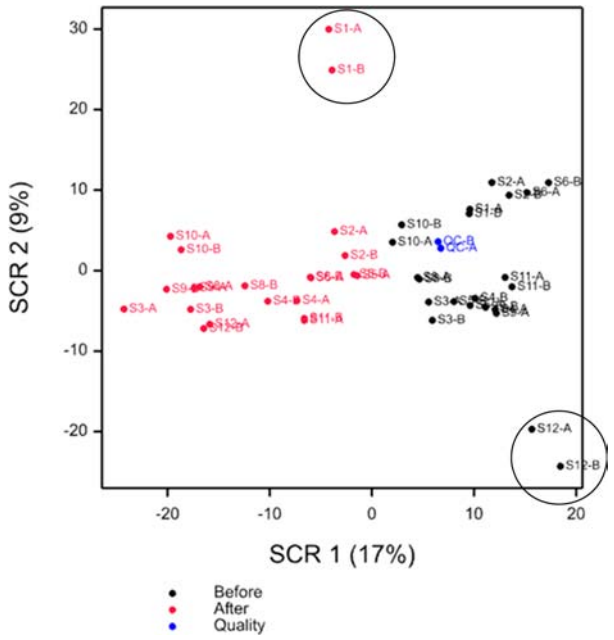

Figure 2. Principal component analysis of the samples from the ileostomy study using the SIEVE process. Black markers represent the before samples, and the red markers represent the after samples. The blue markers are the quality control samples, which were prefeeding samples (subject 10) given blind before extraction. Axis t[1] explains 17% of the variation and t[2] 9%. The double-headed arrow shows the separation of replicate samples along axis t[1]. The circles annotate samples discussed in the text.

were separated from the others; e.g., the S1-2 (after) replicates were displaced from the other after samples, and the S12-1 (before) samples were also separated from the other before samples. In most cases, the replicate extractions were tightly bunched, but some replicates (e.g., S3-2) were slightly but definitely separated (see the arrows, Figure 2). The SIEVE output data were also plotted as bar charts to illustrate peaks/metabolites that show similar patterns of increased or decreased levels across the subjects. For example, the first approach taken was to select peaks that not only increased after supplementation but also had a pattern of recovery similar to that of the main ellagitannin peak, sanguiin H-6, across the subjects (see Figure S3a, Supporting Information). This subjective approach should focus on components that have arisen from the supplementation. However, when we analyzed the SIEVE data using an unbiased approach, a near-identical list of peaks was generated (results not shown). It is also possible to select for peaks that systematically decreased across the subjects after raspberry intake, but although this may be very interesting, this was not a priority in this study. Using this approach, we identified peaks such as ellagic acid pentose (Figure S3b) and an unidentified component with m/z = 355 (Figure S3c). Once this subset of peaks had been identified and the quality of the peaks was checked to ensure that they were not artifacts, this subset of peaks was assessed against previous reports and the m/z, MS^2, and exact mass data were employed to putatively identify the components (Table 4).

It was noted that the ileal samples contained intact raspberry seeds that had survived the digestion process. Although the ileal samples were well mixed before extraction, they were not milled in a fashion that would homogenize the seeds, as this does not occur in vivo. Therefore, it is possible that some of the variation between replicate extractions as illustrated in the PCA plot (Figure 2) could have been caused by different numbers of seeds being present in replicate samples. To examine which components could be extracted from the raspberry seeds, the seeds were separated from some of the original raspberry puree, then extracted under identical conditions, and examined using similar LC conditions but using an ion-trap MS detector (Figure 3). A number of components were identified in the seed extracts that had been identified in the ileal samples. The major component was the ellagitannin sanguiin H-6, but there were also other ellagitannins and some proanthocyanidin (PAC) components (see Table 5). In particular, the seeds contained a peak with PDA and MS properties consistent with a proanthocyanidin dimer composed of (epi)afzelchin and (epi)catechin (peak 12, Table 5; PDA maximum 275 nm; [M − H], m/z 561; MS^2, m/z 543, 435, 289) and a proanthocyanidin dimer composed of (epi)catechin units (peak 8, Table 5; PDA maximum 275 nm; [M − H], m/z 577; MS^2, m/z 559, 533, 289). There was also evidence for larger PACs containing (epi)afzelchin groups which was supported by further analyses of different extracts of the seeds (results not shown).

These findings highlight the possible contribution of raspberry seeds to the availability of phenolic components in ileal fluids. Raspberry seeds can make a considerable contribution to the total berry mass. Seed/flesh ratios of 20% have been reported, although values of ∼5% are more common for cultivated varieties, such as Glen Ample (Dr. Nikki Jennings, The James Hutton Institute, personal communication). Of course, the components extractable from the seeds (or the pulp) in the ileal fluid may not be equivalent to those extractable during digestion in the gastrointestinal tract. Such components may only become accessible during colonic digestion of the raspberry material and would be subject to degradation by fermentation. Raspberry seeds have evolved to survive gastrointestinal digestion. and it would be interesting to compare the components extractable from seeds after ileal digestion with those that are expelled in feces.

In essence, the components found by this nontargeted approach to be increased after raspberry supplementation can be split into four classes: (1) those that were also identified by targeted analysis, (2) those which are related to the targeted components, but may have been extracted from the seeds (Table 5), (3) components present in the raspberries which have become more abundant due to their stability in the gastrointestinal tract, and (4) unknown components which may also encompass some potential breakdown products or metabolites of the original berry polyphenols (Table 4).

Components suggestive of breakdown of ellagitannins include ellagic acid, which was identified in the targeted approach (Table 1). The presence of (epi)catechin and derivatives in the ileal fluid after supplementation (see Table 4) suggests breakdown of the proanthocyanidins, perhaps from the raspberry seeds (Table 5). Indeed, it is notable that epicatechin and (epi)afzelchin were not detected in the raspberry seed extracts. Components such as dihydroxybenzoic acid and hydroxybenzoic acid could appear due to anthocyanin degradation as the B-ring fragments from cyanidin and pelargonidin aglycons, respectively.[25,26] The putatively identified hydroxybenzoic acid glucoside and benzoic acid components could also arise from anthocyanin degradation. The hydroxycinnamic acids *p*-coumaric and caffeic acids have also been reported to be formed through the degradation of anthocyanins.[26] However, these hydroxycinnamic acids were

Table 4. Putative Identification of Elevated MS Signals in Ileal Samples after Raspberry Supplementation[a]

Rt (min)	*m/z*	MS^2	Exact mass	Mass deviation (ppm)	Predicted formula and Putative Identity
8.0	181.0	151.0	181.04980 150.99824	0.185	$C_9H_9O_4$ - unknown $C_7H_3O_4$ (loss of 30 – loss of methoxy group)
8.4	232.9	188.98, 152.99	232.97492 153.01462	0.150 3.615	$C_7H_5O_7S$ – dihydroxybenzoic acid-sulphate $C_7H_5O_4$ - dihydroxybenzoic acid
8.6	299.1	209.04, 137.00	299.07549 137.01277	0.001	$C_{13}H_{15}O_8$ - hydroxybenzoic acid-glucoside
8.7	153.0	108.99	153.01863 108.98715	0.395	$C_7H_5O_4$ - dihydroxybenzoic acid
9.3	783.1*	481.10, 301.01	783.06336 300.95297	N/A	$C_{23}H_{27}O_{30}$ - *doubly charged species $[M-2H]^{2-}$ Sanguiin H10 isomer (Gasperotti et al., 2010)[33]
10.3	355.1	337.01, 209.03, 191.03,	355.06478 337.03748 209.03677 191.02192	1.003 2.361	$C_{15}H_{15}O_{10}$ $C_{13}H_{13}O_8$ (loss of H_2O) $C_6H_9O_8$ (loss of 146) $C_6H_7O_7$ - citric acid - (loss of 164)
10.4	355.1	337.01, 209.03, 191.03,	355.06472 209.03677 191.02192	1.125	$C_{15}H_{15}O_{10}$ as above
10.6	187.0	143.01	187.02389 143.02376	0.096	$C_7H_7O_6$ - 2-methyl aconitate – (Sun et al. 2013)[29] (http://www.hmdb.ca/metabolites/HMDB06357)
12.3	355.1	337.01, 209.03, 191.03,	335.06497 209.04999 191.00498	1.333	$C_{15}H_{15}O_{10}$ as above
13.3 &14.0	259.0	229.1, 179.1	259.02661, 179.03873	0.161 4.845	$C_9H_7O_7S$ – caffeic acid sulphate – (Borges et al., 2013)[27] $C_9H_7O_4$ – caffeic acid
14.2	369.1	289.1, 233.0, 205.1	369.08054 289.06792	0.909 2.745	$C_{15}H_{13}O_9S$ – catechin-sulphate? $C_{15}H_{13}O_6$ –catechin?
14.3	355.1	No MS^2	355.10114	1.219	$C_{16}H_{19}O_9$ – possibly feruloyl-*O*-glycoside http://metlin.scripps.edu/metabo_info.php?molid=91926 (Sun et al. 2013)[29]
14.4	121.1	109.0 93.0	121.02910 93.01939	0.694	$C_7H_5O_2$ – benzoic acid
14.5	577.1	559.15, 451.10, 425.06, 407.11, 289.13	577.13183	2.223	$C_{30}H_{25}O_{12}$ Procyanidin dimer (http://www.hmdb.ca/metabolites/HMDB33973) (Sun et al., 2013)[29]
14.6	273.0	229.01, 193.02	273.00575	0.600	$C_{10}H_9O_7S$ - ferulic acid-sulphate – (Borges et al., 2013)[27]
15.7	289.1 335.1 369.0	245.01 289.11 289.01	289.07313 335.07511 369.02627	0.635 1.034 1.389	$C_{15}H_{13}O_6$ – (epi)catechin $C_{16}H_{15}O_8$ – (epi)catechin formate adduct $C_{15}H_{16}O_9S$– (epi)catechin sulphate
16.1	561.1	543.1, 435.1, 289.1, 271.1	561.13625 289.09197	2.538	$C_{30}H_{25}O_{11}$- epi-afzelechin-catechin (Sun et al. 2013)[29] $C_{15}H_{13}O_6$ - catechin
17.2	167.0	152.01, 108.01	167.03417	0.285	$C_8H_7O_4$ Methylated diOHBA - possibly isovanillic acid but 3,4-dihydroxybenzene acetic acid is equally good fit http://www.hmdb.ca/metabolites/HMDB01336
17.4	337.1	191.05	337.09070 191.05548	1.194	$C_{16}H_{17}O_8$ - *p*-coumaroyl quinic acid
17.8	163.0	119.01	163.03936 119.00201	0.159	$C_9H_7O_3$ *p*-coumaric acid Loss of 44, 119 fragment characteristic for *p*-isomer http://www.massbank.jp/jsp/FwdRecord.jsp?id=KO000408
17.9	551.0* 551.5 552.0 552.5	935.01, 897.02, 633.01, 469.0, 301.01	551.03626	N/A	ET derivative at 1103 – Sanguiin H2 (Gasperotti et al., 2010)[33]- *doubly charged species $[M-2H]^{2-}$
18.0	934.0*	1566.82, 1264.87, 1234.89, 914.91, 633.01, 301.01	934.06516	N/A	ET Sanguiin H6 @ 1869 - *doubly charged species $[M-2H]^{2-}$ (Gasperotti et al., 2010)[33]

dx.doi.org/10.1021/jf502259j | J. Agric. Food Chem. 2014, 62, 7631−7641

Table 4. continued

Rt (min)	*m/z*	MS^2	Exact mass	Mass deviation (ppm)	Predicted formula and Putative Identity
18.1	258.1*, 258.5, 259.1	436.09 <u>218.10</u> 210.60 79.93	258.01886	N/A	*Doubly charged species therefore *m/z* =517 436-sulphate?
18.8	441.2	423.2, 411.1, 397.1, 381.1, <u>331.0</u> <u>330.1</u>,	441.17363	1.943	$C_{21}H_{29}O_{10}$. Unknown Some matches i.e. http://www.hmdb.ca/metabolites/HMDB34120 but MS^2 does not fit
18.4 & 19.3	317.1	269.1	317.13769 269.13315	1.020	$C_{18}H_{21}O_5$ – hydroxyenterodiol? http://www.phenol-explorer.eu/metabolites/1024
18.9	347.1	329.1 235.1 135.0	347.11164 329.06152 235.09784 135.00714	1.309	$C_{18}H_{19}O_7$ – gibberellin derivative? http://www.hmdb.ca/metabolites/HMDB35043
18.9	363.1	<u>345.11</u> <u>165.05</u>	363.14242	1.409	$C_{19}H_{23}O_7$- gibberellin derivative? http://www.hmdb.ca/metabolites/HMDB35038 http://msue.anr.msu.edu/news/gibberellin_to_increase_blueberry_fruit_set
19.2	289.1	245.1	289.08111	0.808	$C_{14}H_{13}O_5N_2$ – indole-3-yl-acetyl aspartic acid (www.ams.usda.gov/AMSv1.0/getfile?dDocName=STELPRDC5101065)
19.7	433.0	301.02	433.03841	1.742	$C_{19}H_{13}O_{12}$ - EA pentose (Gasperotti et al., 2010)[33]
19.7	549.1	531.18 373.09 <u>355.12</u> <u>343.13</u> 175.02	549.15779	2.477	$C_{26}H_{29}O_{13}$ - 4'-Hydroxyacetophenone 4'-[4-hydroxybenzoyl-apiosyl-(1-2)-glucoside]? http://www.hmdb.ca/metabolites/HMDB36332
19.8	383.0	303.05, 285.07	383.00522 303.04711 285.07359	1.204	$C_{15}H_{11}O_{10}S$ – methyl epicatechin sulphate $C_{15}H_{11}O_7$ (Neutral loss of 80 amu - SO_3) (Borges et al., 2012)
19.9	300.9	284.121, 257.01, 229.01	300.99731	0.584	$C_{14}H_5O_8$ Ellagic acid (Gasperotti et al., 2010)[33]
20.2	477.1	301.05	447.06461 301.05094	1.917 2.328	$C_{21}H_{17}O_{13}$ Quercetin GlcA (Mullen et al. 2010)[37] $C_{12}H_{13}O_9$ – no match
21.4	567.2	520.7 341.2 179.0	567.20472 341.19491 179.03556	0.005 0.955 1.675	$C_{27}H_{35}O_{13}$ losses of 46 – formic acid? – caffeic acid derivative? $C_{18}H_{29}O_6$ – caffeic acid hexose? $C_9H_7O_4$ – caffeic acid?
22.6	437.1	357.12 151.05	437.08823	1.849	$C_{20}H_{21}O_9S$ 357 -$C_{20}H_{21}O_6$ 151 – $C_5H_{11}O_5$ Matairesinol sulphate? http://www.hmdb.ca/metabolites/HMDB35789

[a]Shading indicates the compounds were also found in the extracts of raspberry seeds. Asterisks denote doubly charged species, $[M - 2H]^{2-}$. Underlined masses are the main MS^2 fragments. Formulas in italics are predicted for MS^2 fragments.

also detected in ileal fluid after intake of a mixed fruit juice,[27] where they may have arisen from intake of hydroxycinnamic acid derivatives. Some other components, such as *p*-coumaroylquinic acid, indole 3-acetylaspartic acid, and the putative gibberellin-like derivatives, were present in raspberry in relatively low amounts, but became more apparent due to their stability in the small intestine.

The stringency of the SIEVE approach is illustrated in the case of the putative identification of a methylepicatechin sulfate derivative. Although three signals with *m/z* 383 can be discerned in most ileal samples after supplementation, only one peak was consistently and significantly increased. In addition, a peak putatively attributable to dihydrocaffeic acid sulfate (t_R = 5.1 min; *m/z* 261; MS^2, *m/z* 181 and 143) could be discerned in many after samples but was not selected by the SIEVE method. However, a set of three peaks with *m/z* 355 were identified by the SIEVE approach. These peaks all gave an exact mass that yielded a predicted formula of $C_{15}H_{15}O_{10}$ with a low mass deviation (~1 ppm). This formula matches that of a caffeic acid glucuronide, which has been identified in urine and plasma after coffee intake.[28] Indeed, the METLIN database provides this compound as a potential hit (http://metlin.scripps.edu/metabo_info.php?molid=96063). However, the MS^2 data do not fit, and in particular, there is no fragment at *m/z* 179 as expected for caffeic acid. Therefore, this component remains unidentified. Recent work by Sun et al. identified *m/z*

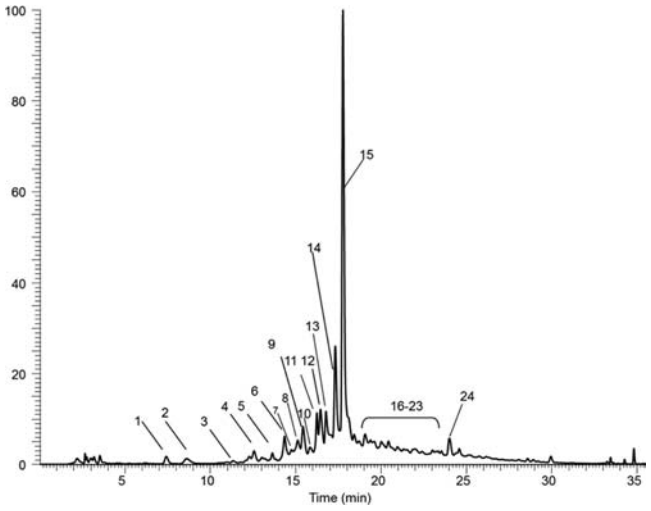

Figure 3. UV trace of components extracted from isolated raspberry seeds. The peaks denoted are described in Table 5. The figure in the top right corner is the full-scale deflection of the PDA detector at 280 nm.

signals at 191.0193 in strawberry extracts as citric acid,[29] and the main MS^2 fragment of the m/z 355 component is a good match for this structural formula ($C_6H_7O_7$, mass deviation <2 ppm). Therefore, this could be a citric acid metabolite.

As well as the sulfated metabolites already discussed, there is evidence for the apparently sulfated derivatives of dihydroxybenzoic acid, (epi)catechin, maitiresinol, caffeic acid, and ferulic acid. Sulfated derivatives of phenolic components of fruit juices have been identified in ileal fluid after juice intake.[27] However, further studies are required to confirm the identity of these derivatives. Such phase II metabolites could be produced in the wall of the small intestine, efflux back into the lumen, and as a consequence appear in ileal fluid. An alternative route could involve their absorption into the bloodstream and return to the small intestine via enterohepatic recirculation in the bile. However, recent studies with (−)-epicatechin metabolites indicate that recycling by the bile is at best a minor event.[30,31]

In conclusion, targeted and nontargeted LC−MS^n techniques have been used to identify components in ileal fluid that increase after raspberry intake. These components have survived digestion in the upper gastrointestinal tract and in healthy subjects with an intact functioning colon would enter the large intestine where they may influence gut function and health.[19] Understanding which components enter the colon is of benefit to estimate the possible health effects that may occur. Previous work has shown that components that enter the colon are subject to degradation by resident microbiota, usually to a simpler set of metabolites which may have their own potential bioactive effects.[22,32] This study confirmed previous work[14] that illustrated that considerable amounts of ellagitannins, ellagic acid derivatives, and anthocyanins survive and may enter the colon. However, the untargeted approach has extended the list of "known" components and identified new compounds that may arise from the seeds present in the raspberry purees as breakdown products of the original berry anthocyanins (e.g., hydroxybenzoic acid derivatives), a set of components that are enriched due to their stability, and unknown components yet to

Table 5. Phenolic Components in Extracts of Raspberry Seeds[a]

peak	t_R (min)	PDA max	[M − H] m/z	MS^2 m/z	putative ID
1	7.43	280	no distinct m/z		unknown
2	8.63	270	783.1, 301.2	481.1, 301.2	peduncalagin-like ET
3	12.29	260	933.0	896.9, 631.0, 451.0, 315.2	castalagin
4	12.57	270	783.1, 301.2	481.1, 301.1	peduncalagin-like ET
5	13.04	270	950.9	906.9, 783.1, 604.9, 469.0, 301.0	unknown ellagitannin
6	14.36	280	1716.9, 1566.9, 933.0, 858.9, 783.2, 301.2	1414.9, 1234.9, 1113.0, 932.9, 783.1, 631.1	sanguiin H-6 minus gallic group
7	14.80	270	1869.0, 1717.0	1414.9, 1234.9, 1113.0, 932.9, 783.1, 631.1	sanguiin H-6-like ET
8	15.13	270	577.1	451.0, 425.0, 407.1, 289.1	EC dimer
9	15.44	270	1716.9	1414.9, 1235.0, 1113.1, 950.9, 932.9, 631.0	sanguiin H-6 minus gallic group
10	15.85	270	1325.5	poor MS^2	unknown
11	16.25	270	1567.1, 932.9, 783.2	1415.1, 1264.9, 932.9, 897.0, 631.0	sanguiin H-10
12	16.47	365, 260	561.1, 289.1	435.0, 425.0, 417.0, 407.0, 289.0, 271.0	EF/EC dimer
13	16.75	270	1869.0, 1717.0, 1566.9, 934.2, 301.2	1717.0, 1569.0 and multiple others	sanguiin H-6-like ET
14	17.33	270	1401.2 and 0.5 amu variants	1869.2, 1566.9, 1250.9, 935.0, 897.0, 633.0	lambertianin C-like ET
15	17.78	270	1868.9, 1566.9, 1235.0, 1103.0, 934.2, 301.2	1566.9, 1264.9, 1234.9, 932.9, 896.9, 631.0	sanguiin H-6-like ET
16	18.27	275	833.1, 289.1	707.1, 679.0, 561.0, 543.0, 435.0, 407.1, 289.1, 271.1	EF/EF/EC trimer
17	19.01	355	433.1	301.1	EA pentoside 1
18	19.07	270	1121.0	1077.1, 1092.8, 577.2, 543.1, 435.0	EF/EF/EC/EC tetramer
19	19.40	355	433.1	301.1	EA pentoside 2
20	19.62	270	1409.2	1119.1, 865.1, 849.1, 559.1, 577.1	EF/EF/EF/EC/EC pentamer
21	21.33	270	833.0, 289.1	707.1, 679.0, 561.0, 543.0, 435.0, 407.1, 289.1, 271.1	EF/EF/EC trimer
22	22.04	270	1085.0	932.9, 897.0, 783.0, 633.1, 451.1	galloyl castalagin
23	23.02	270	1377.0	1251.0, 1087.0, 978.9, 833.1, 815.0, 707.0, 689.0, 561.0, 543.0	EF/EF/EF/EF/EC pentamer

[a]ET = ellagitannin, EC = epicatechin, and EF = epiafzelechin. Most putative identities for ellagitannins supported by refs 33 and 34 Identities for PACs supported by refs 29 and 35−37.

be identified. In addition, there is evidence for the presence of phase II sulfated and glucuronidated phenolic components, arguably produced in the enterocytes of the small intestine and effluxed back into the lumen.

Future work will focus on the identification of these metabolized components but will also examine the effect of in vitro fermentation of the ileal sample by colonic microflora before assessment of their bioactivities in cell models of colon cancer.[22]

■ ASSOCIATED CONTENT

Supporting Information

Figures showing comparisons of total anthocyanin and sanguiin H-6 levels between the targeted and nontargeted approaches, noncharacteristic PDA traces for before and after supplementation ileal samples, and peak areas for m/z 934, 433, and 355 extracted from MS data by SIEVE. This material is available free of charge via the Internet at http://pubs.acs.org.

■ AUTHOR INFORMATION

Funding

C.I.R.G., R.L., and A.C. acknowledge funding from the National Processed Raspberry Council, Western Health and Social Care Trust, and University of Ulster. D.S. and G.J.M. acknowledge funding from the Scottish Government's Rural and Environment Science and Analytical Services Division (RESAS). G.P.-C. was supported by a postdoctoral fellowship from IFAPA (Programa Operativo del Fondo Social Europeo 2007−2013 de Andaluc1a).

Notes

The authors declare no competing financial interest.

■ ACKNOWLEDGMENTS

G.J.M. is a member of the INFOGEST Cost Action (https://www.cost-infogest.eu/ABOUT-Infogest).

■ REFERENCES

(1) Ezzati, M.; Riboli, E. GLOBAL HEALTH: Behavioral and dietary risk factors for non-communicable diseases. *N. Engl. J. Med.* **2013**, *369*, 954−964.

(2) Johnson, C. M.; Wei, C.; Ensor, J. E.; Smolenski, D. J.; Amos, C. I.; Levin, B.; Berry, D. A. Meta-analyses of colorectal cancer risk factors. *Cancer Causes Control* **2013**, *24*, 1207−1222.

(3) Pérez-Jiménez, J.; Fezeu, L.; Touvier, M.; Arnault, N.; Manach, C.; Hercberg, S.; Galan, P.; Scalbert, A. Dietary intake of 337 polyphenols in French adults. *Am. J. Clin. Nutr.* **2011**, *93*, 1220−1228.

(4) Ovaskainen, M. L.; Törrönen, R.; Koponen, J. M.; Sinkko, H.; Hellström, J.; Reinivuo, H.; Mattila, P. Dietary intake and major food sources of polyphenols in Finnish adults. *J. Nutr.* **2008**, *138*, 562−566.

(5) Deighton, N.; Brennan, R.; Finn, C.; Davies, H. V. Antioxidant properties of domesticated and wild *Rubus* species. *J. Sci. Food Agric.* **2000**, *80*, 1307−1313.

(6) Anttonen, M. J.; Karjalainen, R. O. Environmental and genetic variation of phenolic compounds in red raspberry. *J. Food Compos. Anal.* **2005**, *18*, 759−769.

(7) Mikulic-Petkovsek, M.; Schmitzer, V.; Slatnar, A.; Stampar, F.; Veberic, R. Composition of sugars, organic acids, and total phenolics in 25 wild or cultivated berry species. *J. Food Sci.* **2012**, *77*, C1064−1070.

(8) Määttä-Riihinen, K. R.; Kamal-Eldin, A.; Törrönen, A. R. Identification and quantification of phenolic compounds in berries of *Fragaria* and *Rubus* species (family Rosaceae). *J. Agric. Food Chem.* **2004**, *52*, 6178−6187.

(9) Veberic, R. Composition of sugars, organic acids, and total phenolics in 25 wild or cultivated berry species. *J. Food Sci.* **2012**, *77*, 1064−1070.

(10) Castrejon, A. D. R.; Eichholz, I.; Rohn, S.; Kroh, L. W.; Huyskens-Keil, S. Phenolic profile and antioxidant activity of highbush blueberry (*Vaccinium corymbosum* L.) during fruit maturation and ripening. *Food Chem.* **2008**, *109*, 564−572.

(11) Häkkinen, S. H.; Kärenlampi, S. O.; Mykkänen, H. M.; Törrönen, A. R. Influence of domestic processing and storage on flavonol contents in berries. *J. Agric. Food Chem.* **2000**, *48*, 2960−2965.

(12) Borges, G.; Mullen, W.; Mullan, A.; Lean, M. E.; Roberts, S. A.; Crozier, A. Bioavailability of multiple components following acute ingestion of a polyphenol-rich juice drink. *Mol. Nutr. Food Res.* **2010**, *54*, S268−277.

(13) Gill, C. I. R.; McDougall, G. J.; Glidewell, S.; Steward, D.; Tuohy, K.; Shen, Q.; Dobbin, A.; Boyd, A.; Brown, E. M.; Haldar, S.; Rowland, I. Profiling of phenols in human fecal water after raspberry supplementation. *J. Agric. Food Chem.* **2010**, *58*, 10389−10395.

(14) González-Barrio, R.; Borges, G.; Mullen, W.; Crozier, A. Bioavailability of anthocyanins and ellagitannins following consumption of raspberries by healthy humans and subjects with an ileostomy. *J. Agric. Food Chem.* **2010**, *58*, 3933−3939.

(15) Del Rio, D.; Borges, G.; Crozier, A. Berry flavonoids and phenolics: Bioavailability and evidence of protective effects. *Br. J. Nutr.* **2010**, *104*, S67−90.

(16) Del Rio, D.; Rodriguez-Mateos, A.; Spencer, J. P.; Tognolini, M.; Borges, G.; Crozier, A. Dietary (poly)phenolics in human health: Structures, bioavailability, and evidence of protective effects against chronic diseases. *Antioxid. Redox Signaling* **2013**, *18*, 1818−1892.

(17) González-Barrio, R.; Edwards, C. A.; Crozier, A. Colonic catabolism of ellagitannins, ellagic acid, and raspberry anthocyanins: in vivo and in vitro studies. *Drug Metab. Dispos.* **2011**, *39*, 1680−1688.

(18) Brown, E. M.; Latimer, C.; Allsopp, P.; Ternan, N. G.; McMullan, G.; McDougall, G. J.; Stewart, D.; Crozier, A.; Rowland, I.; Gill, C. I. In vitro and in vivo models of colorectal cancer: Antigenotoxic activity of berries. *J. Agric. Food Chem.* **2014**, *62*, 3852−3866.

(19) McDougall, G.; Dobson, P.; Smith, P.; Blake, A.; Stewart, D. Assessing potential bioavailability of raspberry anthocyanins using an in vitro digestion system. *J. Agric. Food Chem.* **2005**, *53*, 5896−5904.

(20) Coates, E. M.; Popa, G.; Gill, C. I.; McCann, M. J.; McDougall, G. J.; Stewart, D.; Rowland, I. Colon-available raspberry polyphenols exhibit anti-cancer effects on in vitro models of colon cancer. *J. Carcinog.* **2007**, *18*, 1−6.

(21) McDougall, G. J.; Dobson, P.; Fyffe, S.; Shapiro, F.; Stewart, D. Assessing bioavailability of soft fruit polyphenols in vitro. *Acta Hortic.* **2007**, *744*, 135−148.

(22) Brown, E. M.; McDougall, G. J.; Stewart, D.; Pereira-Caro, G.; González-Barrio, R.; Allsopp, P.; Magee, P.; Crozier, A.; Rowland, I.; Gill, C. I. Persistence of anticancer activity in berry extracts after simulated gastrointestinal digestion and colonic fermentation. *PLoS One* **2012**, *7*, e49740.

(23) Daniel, E.; Ratnayake, S.; Kinstle, T.; Stoner, G. The effects of pH and rat intestinal contents on the liberation of ellagic acid from purified and crude ellagitannins. *J. Nat. Prod.* **1991**, *54*, 946−952.

(24) Stalmach, A.; Steiling, H.; Williamson, G.; Crozier, A. Bioavailability of chlorogenic acids following acute ingestion of coffee by humans with an ileostomy. *Arch. Biochem. Biophys.* **2010**, *501*, 98−105.

(25) Vitaglione, P.; Donnarumma, G.; Napolitano, A.; Galvano, F.; Gallo, A.; Scalfi, L.; Fogliano, V. Protocatechuic acid is the major human metabolite of cyanidin glucosides. *J. Nutr.* **2007**, *137*, 2043−2048.

(26) Nurmi, T.; Mursu, J.; Heinonen, M.; Nurmi, A.; Hiltunen, R.; Voutilainen, S. Metabolism of berry anthocyanins to phenolic acids in humans. *J. Agric. Food Chem.* **2009**, *57*, 2274−2281.

(27) Borges, G.; Lean, M. E.; Roberts, S. A.; Crozier, A. Bioavailability of dietary (poly)phenols: A study with ileostomists to discriminate between absorption in small and large intestine. *Food Funct.* **2013**, *4*, 754−762.

(28) Fumeaux, R.; Menozzi-Smarrito, C.; Stalmach, A.; Munari, C.; Kraehenbuehl, K.; Steiling, H.; Crozier, A.; Williamson, G.; Barron, D.

First synthesis, characterization, and evidence for the presence of hydroxycinnamic acid sulphate and glucuronide conjugates in human biological fluids as a result of coffee consumption. *Org. Biomol. Chem.* **2010**, *8*, 5199−5211.
(29) Sun, J.; Liu, X.; Yang, T.; Slovin, J.; Chen, P. Profiling polyphenols of two diploid strawberry (*Fragaria vesca*) inbred lines using UHPLC-HRMS^n. *Food Chem.* **2014**, *146*, 289−298.
(30) Actis-Goretta, L.; Lévèques, A.; Rein, M.; Teml, A.; Schäfer, C.; Hofman, U.; Li, H.; Schwab, M.; Eichelbaum, M.; Williamson, G. Intestinal absorption, metabolism, and excretion of (−)-epicatechin in healthy humans assessed by using an intestinal perfusion technique. *Am. J. Clin. Nutr.* **2013**, *98*, 924−933.
(31) Crozier, A. Absorption, metabolism and excretion of (−)-epicatechin in humans: An evaluation of recent findings. *Am. J. Clin. Nutr.* **2013**, *98*, 861−862.
(32) Williamson, G.; Clifford, M. N. Colonic metabolites of berry polyphenols: The missing link to biological activity? *Br. J. Nutr.* **2010**, *104*, S48−66.
(33) Gasperotti, M.; Masuero, D.; Vrhovsek, U.; Guella, G.; Mattivi, F. Profiling and accurate quantification of *Rubus* ellagitannins and ellagic acid conjugates using direct UPLC-Q-TOF HDMS and HPLC-DAD analysis. *J. Agric. Food Chem.* **2010**, *58*, 4602−4616.
(34) Mullen, W.; Yokota, T.; Lean, M. E.; Crozier, A. Analysis of ellagitannins and conjugates of ellagic acid and quercetin in raspberry fruits by LC-MS^n. *Phytochemistry* **2003**, *64*, 617−624.
(35) Aaby, K.; Skrede, G.; Wrolstad, R. E. Phenolic composition and antioxidant activities in flesh and achenes of strawberries (*Fragaria ananassa*). *J. Agric. Food Chem.* **2005**, *53*, 4032−4040.
(36) Gu, L.; Kelm, M. A.; Hammerstone, J. F.; Zhang, Z.; Beecher, G.; Holden, J.; Haytowitz, D.; Prior, R. L. Liquid chromatographic/electrospray ionization mass spectrometric studies of proanthocyanidins in foods. *J. Mass Spectrom.* **2003**, *38*, 1272−1280.
(37) Mullen, W.; Borges, G.; Lean, M. E.; Roberts, S. A.; Crozier, A. Identification of metabolites in human plasma and urine after consumption of a polyphenol-rich juice drink. *J. Agric. Food Chem.* **2010**, *58*, 2586−2595.

Table 1. Incidence, Range, and Median Concentration of OTA in Beer

country (ref)	product	no. of samples	incidence (%)	range (ng/mL)	median (ng/mL)
Spain[24]	beer	31	77	0.205[a]	0.044
	with alcohol	21	67	0.205[a]	0.038
	without alcohol	10	100	0.152	0.056
Spain[20]	beer	88	82.9	0.007−0.204	ni[b]
	from Spain	31	83.8	0.007−0.147	0.036
	imported	57	82.5	0.007−0.204	0.046
Spain[19]	beer	69	100	0.008−0.498	0.070
	from Spain	35	100	ni	0.085
	imported	34	100	ni	0.055
Italy[25]	beer	106	67.9	0.002−0.189	0.019
Italy[55]	beer	30	16.7	<0.2	ni
Turkey[21]	beer	35	14	0.012−0.045	0.02
	from Turkey	31	13	0.012−0.045	ni
	imported	4	25	0.012	ni
Czech Republic[17]	beer	115	39	0.001−0.244	ni
Hungary[23]	beer	25	100	0.030−0.250	0.13

[a]Maximum value. [b]ni, not indicated.

Arch, in the period of 2005−2013, and comparing those results with the legislation available in the European Union (EU).

PRESENCE OF OTA IN BEER

Beer is a drink obtained from must alcoholic fermentation, mainly elaborated from germ barley solely or mixed with other cereals, starchy substances, yeast, and water. It is the third most consumed drink around the world after water and tea. In 2012, there were 182.69 million of kiloliters consumed, Asia being the continent that registered the highest consumption (33.6%), followed by Europe (27.7%), Latin America (16.215%), and North America (14.5%); nonetheless, the highest beer consumers per capita are found in the Czech Republic followed by Germany.[15]

In the past two decades there have been several studies confirming the presence of OTA mycotoxin in beers from all over the world. It has been stated in the European Commission's report that beer consumption contributes 5% of OTA intake.[16]

The origin of OTA mycotoxin in beer comes from contamination of prime material used for its processing as barley, malt, or cereal derivatives. Contaminated barley grains contain ochratoxigenic strains from *A. ochraceus* and *P. verrucosum*, which are transferred to beer. OTA provided by these strains on cereals is stable through the cooking process, but it suffers a reduction during beer production and, as a consequence, during fermentation it is the yeast that retains the original content of OTA (eliminating between 2 and 19% of OTA) and the rest is transmitted to the final consumable beer.[17]

The EU has not established limits for OTA in beer, because its presence in this drink should be controlled in another more appropriate phase of its production chain, specifically in malt prime material (Directive (UE) No. 105/2010);[18] however, several countries have established maximum permitted limits of OTA in beer, for example, The Netherlands (0.3 ng/mL), Finland (0.5 ng/mL), or Italy (0.2 ng/mL), and in research studies several authors have assumed a recommended limit of 0.2 ng/mL.[19,20]

Incidence and Presence of OTA in Beer. In this review, only published papers related to OTA in beer or wine from southern Europe, and more specifically from the Mediterranean Arch, from the past 10 years have been collected. The incidence of OTA in beer, as well as the range and OTA median concentrations found in this matrix in different studies, is summarized in Table 1.

Recent studies of OTA in beer show values of incidence varying from 14%[21] to 100%,[19] although in most of them the incidence was higher than those obtained by the European Commission[16] (set at 39% incidence in beer). The reason for these differences in the studies might be a consequence of the different detection methods and the malt quality used for its elaboration.

When studies are examine per country, the highest presence (100%) of OTA in beer samples was found in a study carried out in Spain,[19], compared with other published studies; however, only five samples presented concentrations above the assumed value of 0.2 ng/mL. These levels were similar to those reported by the European Commission[16] for Spain, where OTA was detected in 97% of the analyzed samples, but different from results obtained in other studies,[22] where no sample analyzed was OTA positive.

Another study carried out on beers from Navarra markets in Spain[24] reported that 77% of samples were OTA positive, but no sample exceeded the proposed legal limit and only one almost reached the proposed value (see Table 1).

Several studies reveal that the presence of OTA in beers from Italy is around 70%,[25,55] although the concentration levels detected were lower than those obtained in beers from Spain[24] (see Table 1). By relating these values with beers from other countries, such as Turkey, the presence of OTA decreases to 14%, with values below the one assumed as reference.[21]

To compare these results with studies carried out in other European countries, and turning to eastern Europe, data analysis of beer from Hungary[23] showed that all samples were contaminated by small amounts of OTA (presence of 100%) but only one sample was detected at levels >0.2 ng/mL (see Table 1). A beer study from the Czech Republic[17] reveals that the incidence (39%) correlates with data obtained from the European Commission (2002) and only one pale beer sample presented the highest value: 0.2438 ng/mL.

Other studies outside the region of interest in this review have been consulted, and it is interesting to observe that in a study in which beers from different origins (United States,

Table 2. OTA Intake Estimation for Beer Consumed (Data Taken from Table 1)

country (ref)	body wt (kg)	consumption (mL/day)	OTA median (ng/g)	OTA DI[a] median (ng/kg bw/day)	% OTA TDI[b] (17.2 ng/kg bw/day)	% SCF[c]
Spain[24]	60	500	0.044	0.36	2.09	7.2
Spain[20]	60	500[d]	0.036	0.29	1.7	5.9
Spain[19]	60	500[d]	0.070	0.58	3.4	11.6
Italy[25]	60	197	0.019	0.06	0.36	1.24
Turkey[21]	60	200	0.02	0.011	2.44	8.4
Hungary[23]	60	33	0.127	0.42	0.06	0.22

[a]DI, daily intake. [b]TDI, tolerable daily intake. [c]SCF, Scientific Committee on Food. [d]Collected from Araguas et al.[24]

Europe, Australia, Canada, Mexico, South America, and Asia) were analyzed, no OTA levels were detected,[26] coinciding with results obtained in studies performed on beers from China.[27]

OTA Levels in Beer. According to the published studies, OTA mean concentrations obtained in beer present few variations. The lowest OTA mean value achieved was <0.2 ng/mL, except for samples analyzed by Medina et al.,[20] who found a maximum value for one sample of 0.5 ng/mL.

When the median levels of contamination obtained from samples of different studies are compared with those from the European Commission,[16] where the OTA mean value of 496 beer samples was 0.03 ng/g, contamination median levels are slightly higher, although always below 0.1 ng/mL.

Studies can be found where levels of contamination in beers mainly from southern European countries (Italy, Spain, Turkey, Germany, and The Balkans) were detected below 0.04 ng/mL, showing different statistical significances with respect to all other analyzed beers; the highest level of contamination (0.189 ng/mL) was found for one beer from Denmark.

The reason for these low OTA values in beers from southern Europe might be explained by the fact that *P. verrucosum* involved in OTA's production is important in northern European countries where conditions of temperature and humidity are optimum for its growth[25] but not in the south.

Analyses of alcoholic and nonalcoholic beers have been performed, and data show that no differences in OTA levels can be found;[21,24] nonetheless, incidence and mean levels of contamination are higher in nonalcoholic beers than in alcoholic, most probably due to the different procedures in both types of beer production. In nonalcoholic beer production, the fermentation step does not occur or it occurs under controlled conditions; as a consequence, if it is considered that the fermentation step reduces OTA content, it is expected to have higher contamination in this type of beer.

These results differ from the European Commission report,[16] because the presence of OTA (39%) and OTA levels of contamination detected (0.03 ng/g) were low. In summary, contamination mean values found never were above the value assumed (0.2 ng/mL) and differences among beers from different origins were detected.

Estimation of OTA Intake in Beer. An evaluation of the OTA intake associated with beer consumption demonstrates that even considering the highest values, beer contributes only 3% OTA intake as its maximum,[20] (<5% reported by the European Commission). Nevertheless, these values are much lower than the tolerable daily intake (TDI) established by the European Food Safety Authorities (EFSA).[28]

Table 2 collects the calculation of human OTA intake related to beer consumption for recently published studies and for adults.

When studies of beers from outside Europe were examined, such as a study carried out in Korea,[15,63] OTA intake associated with beer consumption was very low, but it was recommended to develop a new evaluation attending to actual consumption data in recent years as the Asian population has experienced a remarkable increase of consumption in beer.[15]

In summary, beer seems not to constitute an important factor for OTA exposure in the population, but it is an additional source to control and consider for OTA mycotoxin intake calculation.

PRESENCE OF OTA IN WINE

In this review, wine has been considered a drink of importance for OTA intake evaluation in the past ten years. Wine, besides being one of the most important subproducts obtained from the grape, is consumed worldwide in developed and developing countries. According to an estimation carried out by the Wine and Vineyard International Organization (OIV) world wine production in 2011 reached 265.8 million of hectoliters (without counting grape juice or must), 600,000 hectoliters more than in 2010.[29] Spain contributed 12.9% of this production with 34.3 million hectoliters.[30]

The presence of OTA in the grape can be shifted from grain grapes to wine during its brewing. After cereals, wine represents the principal source of OTA daily intake for the European population, comprising 13% of the OTA daily intake. OTA levels in wine depend on different factors such as vineyard location (latitude), weather (rain, temperature, relative humidity in the vineyards), period of harvest, pesticide treatments, and the wine brewing technique employed. The European Union allows a maximum limit for OTA in wine of 2 ng/g.

There is a huge variety of wine typologies, which gives place to a very complicated classification. Most of the studies show that OTA levels are higher in red wines than in rosé wines, followed by white wines, mostly due to the must maceration with the skin of the grain grape, which could enhance OTA extraction. In sweet or special wines, enological practices are highly diverse compared with dry wines, which originates different OTA concentrations. In general, sweet wines present higher OTA concentrations than dry wines.[31] These wines can be classified according to their brewing as (i) biological brewing, during which must is protected from direct air contact through the formation of a natural flower veil (fino wine and chamomile wine follow this process), or (ii) oxidative or physicochemical brewing, during which must is in direct contact with the air, giving rise to flavored wines.

Wines can also be classified according to the type of fermentation: (i) complete fermentation in fortified or dry wines or (ii) partial fermentation, as in natural sweet wines, using must from mature grapes with high glucose content and

Table 3. Percentage Detected and Median and Maximum Concentrations of OTA in Wines

	red wine			rosé wine			white wine			
country	% detected	median (ng/mL)	max[a] (ng/mL)	% detected	median (ng/mL)	max[a] (ng/mL)	% detected	median (ng/mL)	max[a] (ng/mL)	ref
Spain							75	1.81	3.42	Hernández et al. (2006)[35]
							100	2.86	7.30	
							97	0.5		Burdaspal and Legarda (2007)[36]
							99	0.65	4.63	
							50	1.49	27.79	Valero et al. (2008)[32]
							80	0.138	0.642	Murillo-Arbizu et al. (2010)[37]
	57	0.035	0.179	33	0.007		67	0.014	0.015	Quintela et al. (2011)
	53	0.037	0.179							
	88	0.051	0.237							Quintela et al. (2012)[40]
	88	0.085	0.138							
Italy	82[b]	0.29	1.4	71.4	0.32	0.82	62	0.16	0.42	Bacaloni et al. (2005)[48]
	100[c]	0.33	0.87				66	0.14	0.17	
	84	ni[d]	4.0	56	ni	1.04	19	ni	0.21	Brera et al. (2005)[52]
	55	0.72	2.9	50	0.34	0.40	40	0.9	1.95	Aresta et al. (2006)[53]
	ni.	0.18[e]	0.75	ni	nd[f]	ni	ni	0.06	0.18	Chiodini et al. (2006)[54]
		0.16[g]	0.72		0.09			0.08	0.22	
	69	0.34	7.5	92	0.5	4.07	44.3	0.08	1.95	Brera et al. (2008)[49]
	69	0.12	2.630				61.3	0.08	1.36	Spadaro et al. (2010)[64]
	6.7	0.23	ni							Prelle et al. (2013)[55]
Greece	66.7	0.17	1.5				81.5	0.57	2	Labrinea et al. (2011)[57]
Turkey	86	0.11	0.82	90	0.052	0.16	85	0.108	0.62	Var and Kabak (2007)[58]
Hungary	0	nd								Berente et al. (2005)[62]
	97.7	0.01	0.53							Varga et al. (2005)[23]
Croatia	80	ni	0.02							Flajs et al. (2009)[59]
	80		0.05							
China	57.1	0.8	5.65	25	0.22	0.22	2.9	0.07	0.07	Zhang et al. (2013)[45]
	53	0.013	0.043							Mao et al. (2013)[46]

[a]OTA maximum concentration. [b]Bottle. [c]Box. [d]ni, not indicated. [e]Conventional. [f]nd, not detected. [g]Organic.

the fermentation is interrupted by the addition of wine alcohol. Different techniques provoke grape maturation such as late harvesting, sun exposure (such as Pedro Ximénez wine), dehydration in closed places in either cold or warm rooms, fungus colonization by *Botrytis cinerea* (which it gives rise to noble rot and consequently rot wines), or grape dehydration due to winter harvest (which gives rise to ice wines).[32]

In the Council Regulation (EC) No. 1493/1999 of May 17, 1999, on the common organization of the market in wine,[33] "liqueur wine" is defined as the wine product with an actual alcoholic strength by volume of (i) not less than 15% vol and not more than 22% vol or (ii) an overall alcoholic strength by volume of not less than 17.5% vol, except for certain quality liqueur wines produced in specified regions, where natural sweet wines are included in this category.

The EU has not established OTA levels for wines (excluding liqueur wines and wines with an alcoholic strength by volume of not less than 15% vol), and although there are many OTA studies in dry wines from different Mediterranean countries, only a few reviews approach the presence of OTA in sweet or special wines.[32]

Four countries reveal the highest production of wines in Europe: France, Italy, Spain, and Portugal. Another point of view to consider is its consumption.

In this review three different countries of wine production have been studied: (i) Spain, as the third country in the world with the highest production of wine after France and Italy (OIV, 2012);[34] (ii) Portugal, as the country with the greatest ideal conditions for *Aspergillus* and *Penicillium* fungus growth and OTA production; and (iii) Italy, as the second country with the highest wine production according to OIV data[29] and the one with the highest index of consumption per habitant.

In the following sections, studies by countries are compiled and discussed.

OTA Studies in Spanish Wines. Spain has 69 registered designations of origin (RDO).[34] Recently, a few studies regarding OTA presence in typical Spanish wines have been published, especially on Jerez and chamomile wines and Rioja Alavesa wines, as reported in Table 3.

The presence of OTA in muscatel sweet wines and Pedro Ximénez wines goes from 75 to 100%, respectively.[35] In a study where a pool of sweet wine samples formed by 65% of Spanish samples, OTA mycotoxin was present in 97% of the samples,

showing the general presence of this mycotoxin in this wine typology throughout the world.[36] A total of 9.6% of those Spanish wine samples presented levels above the legislated limits of the EU appropriate for liqueur wines (2 ng/g).

Special wines, obtained with different winemaking techniques and from different European countries, have been compared as the literature allows. With regard to OTA content, the data show that 50% of these samples were OTA positive;[32] with a median level of 1.49 ng/mL (Table 3). Wines with the highest presence and concentration corresponded to fortified must (mistela and muscatel) with values of 91% of OTA positive sample wines, 4.48 ng/mL OTA median levels, and 27.79 ng/mL OTA maximum value; wines from sun grape maturation (Pedro Ximénez, Malvasía) showed 91% OTA positive samples, 2.77 ng/mL OTA median level, and 15.62 ng/mL maximum OTA value.[32]

One might expect to find higher OTA levels in fortified musts due to the fermentation interruption occurring during its brewing. The reason is because if the fermentation step is avoided, the possibility of OTA reduction and/or elimination can occur. Also, wines from a sun grape drying process demonstrated higher OTA levels than those obtained with brewing wines. All of this could be explained because the fermentation step progresses slowly, as a consequence of the high sugar content present in must, and because the aging process carried out in these wines is performed in wood barrels. It has to be mentioned that dehydrated grapes used were obtained in cold and warm rooms; however, it is usual that the sun grape dehydration process, used in sweet wines, is carried out in an open environment where conditions for *Aspergillus carbonarius* spp. growth are favorable as well as OTA production.[32] In summary, variations of OTA content in wine mainly depend on the grape dehydration process.

Long-aged fortified wines obtained through wood barrels (Oporto, Jerez, etc.) have been demonstrated to be OTA contaminated (presence in 52% of the samples), whereas late harvest wines, ice wines, and noble wines were OTA free.[32] Among these, almost 20% of the OTA-contaminated wines had values above the European maximum permitted levels established for wine. The reason for this finding was attributed to the origin of the wines, most of them from cold regions of Europe.

OTA content in fortified Jereź wine RDO reveals (fino, amontillado, flavored, and Sanlúcar de Barrameda chamomile) its presence in 80% of the samples[37] (Table 3) (<2 ng/g), with an OTA median concentration of 0.138 ng/mL, which was similar to that detected in white wines and starting wines by other authors. Nonetheless, a relationship was observed between aging wine typology, OTA's presence, and its concentration as follows: biological aging wines had the lowest OTA rate and OTA concentration.

Wines from the Rioja Alavesás RDO are some of the oldest wines in Spain, and four weather conditions can be distinguished in this zone: semiarid, dry, subhumid, and humid. Besides that, this region receives the influence of the Atlantic Ocean and the Mediterranean Sea. All wines produced in this zone are red wines, and depending on the brewing process, four different wine typologies can be distinguished: young wine, aging wine, reserve wine, and large reserve wine. OTA existence in wine samples the from Rioja Alavesás RDO has been detected in 57% of the analyzed samples, in a concentration range of 0.004−0.179 ng/mL and with an OTA concentration median of 0.035 ng/mL[38] (below the EU established limits). The number of OTA positive samples was higher in semiarid zones than in dry zones, and different statistical significances have been obtained. This fact could be explained as a consequence of the lower amount of rain and higher temperatures reached in semiarid zones than in dry zones. However, there were no different statistical significances in OTA concentrations detected, most probably due to the accurate brewing and harvest process carried out. There were no different statistical significances in the different wine typologies and production processes, a fact that differs from other papers in which red wines present the highest contamination. Romero-González et al.[39] determined OTA in different alcoholic drinks, and the incidence obtained was 11% at a concentration of 1.1 ng/g.

Studies performed on exported wines from the Riojás RDO, but in different years, demonstrated that the presence of OTA and OTA contamination in the latest year (2012) presented statistical differences higher than those same wines analyzed earlier (2011).[38,40] OTA median level found in wines from 2012 was 0.077 ng/mL, whereas in 2011 it was 0.037 ng/mL. Higher OTA levels and greater incidence were detected in southern European wine samples.

In summary, it can be concluded that OTA incidence detected in Spanish wines is elevated (as shown in Figure 2),

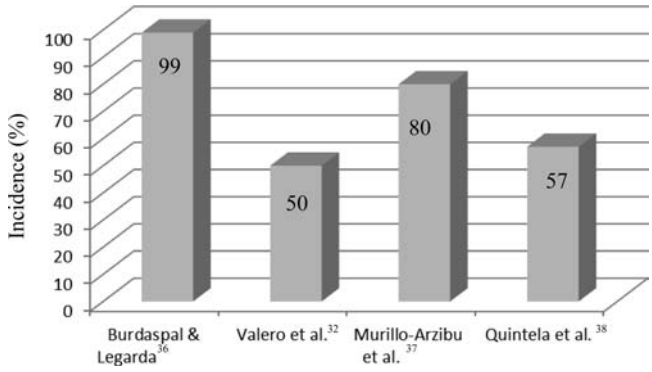

Figure 2. Presence of OTA in Spanish wines.

reaching values of 100% in Pedro Ximenéz wines, but OTA median concentration did not exceed the EU established limits. Incidences collected in previous studies exceeded those recorded in the report from the CE (2002) (59%) and were proximal to OTA detected in southern European wines (72%). OTA contamination median values in wines were higher than that collected in the above-mentioned report for Spanish wines (0.03 ng/mL). Besides, it is confirmed that sweet wines (fortified musts such as mistela and sun grape maturation precedent process) showed higher OTA presence and concentration than for the other wines, reaching a maximum value of 27.79 ng/mL for fortified musts.[32]

Besides the studies performed on the presence of OTA in wines, it has been jointly studied with its analogues: ochratoxin B (OTB), ochratoxin C (OTC), methylochratoxin A (MeOTA), methylochratoxin B (MeOTB), and ethylochratoxin B (EtOTB).[41] Spanish samples belonging to the Mediterranean zone showed OTA, OTB, and MeOTB positive in 100% followed by OTC and EtOTB in 91.7% and, finally, MeOTA in 75%. All six compounds appeared simultaneously in 44.8% of wine samples. The OTA mean value detected in that study was 25.1 ng/L, similar to that declared by other authors.[42−44] It was concluded that there is no evidence that

Table 4. OTA Intake Estimation in Spanish and Italian Wines

country	body wt (kg)	consumption[a] (mL/day)	OTA median (ng/g)	OTA DI[b] median (ng/kg bw/day)	% OTA TDI[c] (17.2 ng/kg bw/day)	ref
Spain	60	58.2(a)	0.65	0.63	3.6	Burdaspal and Legarda (2007)[36]
		4.93(b)		0.05	0.3	
	60	4.93	1.49	0.12	0.7	Valero et al. (2008)[32]
	60	50	0.138	0.115	0.66	Murillo-Arbizu et al. (2010)[37]
	70	24.22	0.035	0.012	0.06	Quintela et al. (2011)[38]
	70	65.75	0.051	0.048	0.28	Quintela et al. (2012)[40]
	70	56.7	0.085	0.069	0.40	
	70	105.75	0.149	0.225	1.31	
	70	25.72	0.125	0.046	0.27	
Italy	70	250	0.14−0.33	0.5−1.2	2.9−6.9	Bacaloni et al. (2005)[48]
	70	159.7(a)	0.4−0.6	0.9−1.4	5.6−8	Brera et al. (2005)[52]
	70	83.7(b)	0.28[d]	0.3	1.9	Brera et al. (2008)[49]
	70	83.7	0.12[e]	0.14−0.09	0.8	Spadaro et al. (2010)[64]
			0.08[f]		0.5	

[a]Data from consumption obtained from different studies: (a) value reported in CE (2002) for consumers; (b) population in general. [b]DI, daily intake. [c]TDI, tolerable daily intake. [d]Total wine samples. [e]Red wine. [f]White wine.

OTA from southern Europe presents greater levels than those detected in northern Europe, which coincides with the reported results in SCOOP.[16]

When the latest studies of OTA in wines outside Spain, for example, wines from different regions of China,[45] are compared, results showed that dry red wine samples were OTA positive (57.1%), followed by dry rosé and ice wines (25% each) and, finally, dry white wines (2.9%). OTA concentrations detected were 0.80, 0.22, 0.10, and 0.07 μg/L in red, rosé, ice, and white wines, respectively. All of these values were higher than those obtained in Spanish wines declared by other authors. Red wines from Chinese markets presented OTA range values from 0.0028 to 0.0437 μg/L.[41]

Estimation of OTA Intake in Spanish Wines. Evaluation of OTA intake by consumption of Spanish wines is collected in Table 4. It can be observed that OTA intake by consumption of wines in a population is below 0.1 ng/kg bw/day, which represents 1.31% of the maximum of the TDI. Levels of exposure, either for the general population or for consumers of sweet wine, are lower than the TDI established by EFSA.[28] These values are above those reported in the EC,[16] where OTA intake collected for wine in Spain was 0.07 ng/kg bw/day. Some studies assume that the intake for starter wines is 50 mL/day,[37] a value higher than that reported by the EU in the above-mentioned report (2.93 g/person/day). This OTA intake could be higher in those cases where the consumer was below 60 kg and wine consumed had the highest detected levels.

As a consequence, wine is an OTA source for humans, and it is necessary to adopt an alert attitude to avoid human OTA consumption.

OTA Studies in Portuguese Wines. Portugal presents several weather conditions according to its location. It receives influences from the Atlantic Ocean and Mediterranean Sea. As mentioned previously, weather conditions and geographical positions determine fungus growth and contamination of the grape by OTA. Assays on wines from different regions in Portugal[47] (35 red wines, 25 white wines) revealed that 26% of red wine samples and 12% of white wine samples were OTA positive, and only 1 sample of white wine exceeded the EU's permitted level of 2 ng/g. In general, white wines present levels of OTA below those obtained in red or rosé wines; in fact, the highest level found in white wine sample differed between studies, and it was attributed to the possibility of the low quality of the analyzed sample. The OTA tolerable weekly intake (TWI) has been also calculated by considering (i) the highest OTA concentrations obtained (1.23 ng/mL in red wine and 2.4% in white wine), (ii) a wine consumption of 49.9 L/habitant/year (136.7 mL/person/day), and (iii) a body weight of 60 kg. OTA's TWI ranged from 20 to 38 ng/kg bw (from 2.8 to 5.5 ng/kg bw/day). These values represent between 17 and 32% of the TWI.

OTA Studies in Italian Wines. Italy has the second highest wine production according to OIV data[29] and the highest index of consumption per habitant. There are a high number of publications in which the presence of OTA in wine has been studied. Table 3 reports the most recent studies of this mycotoxin in Italian wines.

In general, most of the Italian wines are contaminated with OTA, although the levels detected are low. The detection of OTA oscillates between 51 and 77% for its presence in Italian wines, but when the different wine typologies are compared, its presence reaches 100% for red wines[48] and 92% for rosé wines.[49] In other publications, focused on developing new methods of detection, OTA was not detected for any of the analyzed samples.[50,51]

All studies carried out to detect the presence of OTA and its concentration in wines concluded that those values decrease in the following order: red wines, dessert wines, rosé wines, and white wines. This could be explained by the different technological conditions used during their brewing. Nonetheless, an exception has been reported for rosé wines where the highest value of OTA has been detected[49] (Table 3).

Results of OTA analysis in Italian wines reveal that 0.01% of them are OTA positive, with levels above the limits established by the EU.[52] The literature demonstrates that red wine presents the major detection and concentration of OTA, reaching its maximum at 2.92 ng/mL and exceeding the limits fixed by the EU.[53]

There are studies in which no wine sample exceeded OTA levels established by the EU (2 ng/mL) and also where no different statistical significances have been observed for OTA levels when organic and conventional wines were compared.[54]

Related to this, it has been postulated that the use of fungicides in conventional agriculture can provoke stress in fungus and as a consequence increase the production of mycotoxins; fungicides could fight pathogen fungus but enhance the production of OTA fungus producers, due to the absence of rivalry, which favors the conditions of fungus growth and OTA production. On the other hand, there are other studies in which 2.2% of all analyzed samples exceeded the OTA levels established limits by the EU, reaching the highest values for red wine samples (7.5 ng/mL).[49]

When the influence of the latitude and the presence of OTA in Italian wines is studied, it is observed that there is a gradient of concentration from north to south, especially in red wines, as a consequence of the warm temperatures and humid weather conditions, which favor fungus growth and OTA production. The literature puts into evidence that the OTA median concentration gradually increases from northern (0.01 ng/mL) to southern Italy (0.54 ng/mL).[49]

Prelle et al.[55] carried out a study of 30 wine samples from Italy, and only 6.7% of samples exceeded the European OTA threshold. These wines were from southern Italy, a fact in agreement with the latitude influence described for OTA contamination.

Recently, Comuzzo et al.[56] published a database regarding OTA pollution in 199 organic wines, most of them collected from Italy (specifically from two regions, Sicily and Puglia). Among all wines studied, 10 showed OTA levels above the EU limits (2.5−6 μg/L) and 3 showed levels close to the limit. After relating all parameters in wines, they concluded that in wines from southern European countries the OTA contamination risk might be higher.

Estimation of OTA Intake in Italian Wines. Evaluation of OTA intake for Italian wines is reported in Table 4. It can be observed that the maximum OTA intake for Italian wines is 1.4 ng/kg bw/day, which represents 5.6−8% of the TDI established by EFSA.[28] In the worst evaluated case, calculating OTA intake in regular wine consumers from southern Italy (including Italian islands) and considering the median of consumption, the exposure obtained was very low, representing 9.8% of the TDI (1.68 ng/kg bw/day).[49]

These values are similar to those reported in the EC,[16] where OTA intake through wines is declared as 0.86 ng/kg bw/day for the general population and 2.94 ng/kg bw/day for consumers.

In summary, OTA intake through wine consumption does not suppose a health risk in the Italian population.

OTA Studies in Wines from Inside and Outside the EU. Table 3 collects the most recent studies carried out in wines from inside and outside EU countries. It can be observed that there are a high number of positive samples, which increases the incidence of contamination, reaching 98%, although OTA levels detected were low.

Greek wine data show high presence of OTA among all samples analyzed (69%);[57] however, the levels of contamination were low (OTA median value 0.26 ng/mL), 91% of the samples presented OTA values below 1.0 ng/mL, and only one sample achieved the maximum value established by the EU. With regard to OTA incidence and OTA concentration, it was higher in sweet wines (dessert wines) than in dry wines, coinciding with other authors who found OTA detection in sweet wines exceeding 90% of the analyzed samples compared with dry wines.[32]

Results obtained from a study carried out in Turkish wines showed that all samples had OTA levels below the limits established by the EU;[58] however, when Hungarian wines were analyzed, none of the 87 samples analyzed were OTA positive.[62] This confirms the gradient north−south theory: OTA contamination is less probable in northern regions than in southern. However, in a study performed also in Hungarian wines by another research group,[23] OTA was detected in 97.7% of analyzed samples and one sample had a level >0.5 ng/mL.

When the geographical origin of the wine was evaluated, an increased grade of contamination in wines from northern to southern Greece, especially in sweet wines or dessert wines (0.08 ng/mL was the OTA median value in wines from northern, western, and central Greece and 0.23 ng/mL was the OTA median value in wines from southern Greece), was detected.[57] This coincides with other published results from which it was concluded that the geographical origin of the wine had a strong influence on the OTA levels detected; in fact, wines from northwestern and western Turkey presented higher OTA values than those from the central Turkey;[58] however, it differs from results showing wines from Hungary do not evidence the north−south gradient.[23]

It has been mentioned that there is a gradient of OTA concentration depending on the color of the wine. In general, the highest OTA values have been detected in red wines,[23,58] and also the incidence is higher in red wines than in white wines;[57] nonetheless, OTA median values measured were similar.

Differences regarding OTA levels in conventional or organic wines have not been detected.[57] OTA incidence in wine obtained through conventional culture was 70.9%, whereas in organic wine it was 63%; it was also observed that OTA concentration in conventional wine was 0.28 ng/mL and in organic wine 0.12 ng/mL, without observing in any case different statistical significances, coinciding with results obtained by other authors.[54] It was concluded that there are no differences related with the typology of cultured wine.

There is a published study carried out on wine samples from Croatia.[59] Samples studied were six red must, six wines obtained from the previous red must samples, and four bottled wine samples from 2007. It was detected that all must samples were OTA positive, differing from wine samples. The presence of OTA in must was related to the contamination of grape during pressing and maceration, and its concentration decreased during fermentation, although it was not completely eliminated. There were no strains of the most prolific OTA mycotoxin producer, *Aspergillus carbonarius* spp., neither in the must nor in the wine, most probably due to the presence of other OTA fungus producers such as *Aspergillus tubingensis*, *Aspergillus ochraceus*, or *Aspergillus niger* spp., which allowed its detection.

A survey carried out for 11 mycotoxins, in 143 red and white wines, has been also performed, with wines from United States, Europe, Australia, and South America.[26] OTA was detected in 8.3% of the red wines at concentrations ranging from 0.11 to 0.43 ng/mL. The greater contamination detected in red versus white wines was attributed to the longer processing time of red wines as reported by other authors, because once red grapes are mashed, the skin and juice are set aside for several days, aerobic conditions and high temperatures are reached, and growth of OTA mold producers is favored.

Lately, 35 Chilean wine samples along with 18 imported wines (from Spain and Australia) have been analyzed.[60] OTA

was present in 23% of the samples, whereas the percentage in imported wines was 28%. Nonetheless, OTA levels were in general 7 times lower (0.15−0.26 ng/mL) than the EU limit.

In an Asian study carried out in 20 red wine and grape juice samples, OTA levels ranged from 0.26 to 0.63 ng/mL. These limits did not exceed the legal limits; however, it the large consumption of these products was pointed out along with attention to strategies to manage the contamination of raw materials for beverages during harvest and postharvest.[27]

Estimation of OTA intake of Wines. Studies of OTA intake in wines have shown that for a person with a body weight of 60 kg and a consumption of 100 mL of wine per day, OTA intake was 0.18 ng, which is 3.6% of the daily intake established by the Scientific Committee on Food (SCF) (5 ng/kg bw/day).[23]

OTA daily intake calculation of Chilean wines, using the formula of Breás et al.,[52] was 0.24 ng/kg bw/day, which is 70 and 58 times lower than the current TDI established by the SCF of the EC.[60,61] It was concluded that wines commercialized in Chile can be considered safe and not associated with a toxicological risk.

It is difficult to compare the percentage of positive samples and OTA levels in wines from different countries due to the great variety of wines analyzed and the differences between the limits of detection used in each analytical method; however, red and sweet wines seem to be the most contaminated wines, and wine samples from southern regions presented higher incidences and concentrations of this mycotoxin.

AUTHOR INFORMATION

Corresponding Author

*(A.J.-G.) E-mail: ana.juan@uv.es. Phone: 0034 96 354 49 57. Fax: 0034 96 354 49 54.

Funding

This research has been supported by the Ministry of Science and Innovation (AGL2010-17024).

Notes

The authors declare no competing financial interest.

REFERENCES

(1) Juan-García, A.; Manyes, L.; Ruiz, M. J.; Font, G. Involvement of enniatins-induced cytotoxicity in human HepG2 cells. *Toxicol. Lett.* **2013**, *218*, 166−173.

(2) Follman, W.; Behm, C.; Degen, G. H. The emerging Fusarium toxin enniatin B: in-vitro studies on its genotoxic potential and cytotoxicity inV79 cells in relation to other mycotoxins. *Mycotoxin Res.* **2009**, *25*, 11−19.

(3) Nicholson, P.; Simpson, D. R.; Wilson, A. H.; Chandler, E.; Thomsett, M. Detection and differenciation of trichotecene and enniatin-producing fusarium species on small-grain cereals. *Eur. J. Plant Pathol.* **2004**, *110*, 503−514.

(4) Bennett, J. W.; Klich, M. Mycotoxins. *Clin. Microbiol. Rev.* **2003**, *16*, 497−516.

(5) Juan-García, A.; Manyes, L.; Ruiz, M. J.; Font, G. Applications of flow cytometry to toxicological mycotoxin effects in cultured mammalian cells: a review. *Food Chem. Toxicol.* **2013**, *56*, 40−59.

(6) Juan, C.; Mañes, J.; Raiola, A.; Ritieni, A. Evaluation of beauvericin and enniatins in Italian cereal products and multicereal food by liquid chromatography coupled to triple quadrupole mass spectrometry. *Food Chem.* **2013**, *140*, 755−762.

(7) Prosperini, A.; Juan-García, A.; Font, G.; Ruiz, M.J. Reactive oxygen species involvement in apoptosis and mitochondrial damage in Caco-2 cells induced by enniatins A, A1, B and B1. *Toxicol. Lett.* **2013**, *222*, 36−44.

(8) Peraica, M.; Radic, B.; Lucić, P.; Pavlovic, M. Toxic effects of mycotoxins in humans. *Bull. WHO: Int. J. Public Health* **1999**, *77*, 754−766.

(9) Amezqueta, S.; González-Peñas, E.; Murillo-Arbizu, M.; López de Cerain, A. Ochratoxin A decontamination: a review. *Food Control* **2009**, *20* (4), 326−333.

(10) Battilani, P.; Magan, N.; Logrieco, A. European research on ochratoxin A in grapes and wine. *Int. J. Food Microbiol.* **2006**, *111*, S2−S4.

(11) Murphy, P. A.; Hendrich, S.; Landgre, C.; Bryant, C. M. Food mycotoxins: an update. *J. Food Sci.* **2006**, *71*, 51−65.

(12) FAO. Basic facts on the world cereal situation. *Food Outlook* **1996**, *5/6*.

(13) FAO. *Manual sobre la aplicación del sistema de Análisis de Peligros y de Puntos de Críticos de Control (APPCC) en la prevención y control de las micotoxinas*, No. 73; Estudio FAO Alimentación y Nutrición: Rome, Italy, 2003.

(14) Shephard, G. S. Determination of mycotoixns in humans foods. *Chem. Soc. Rev.* **2008**, *37* (11), 2468−2477.

(15) Kirin Institute of Food and Lifestyle. Global beer consumption by country in 2010, report 33; available at http://www.kirinholdings.co.jp/english/news/2011/1221_01.html.

(16) EU. Assessment of dietary intake of ochratoxin A by the population of EU member states, reports on tasks for scientific cooperation, task 3.2.7; SCOOP Directorate-General Health and Consumer Protection, 2002.

(17) Bêlakova, S.; Benesova, K.; Mikulikova, R.; Svoboda, Z. D. Determination of ochratoxin A in brewing materials and beer by ultra performance liquid chromatography with fluorescence detection. *Food Chem.* **2011**, *126*, 321−325.

(18) Reglamento (UE) no. 105/2010 de la Comisión de 5 de febrero de 2010 que modifica el Reglamento (CE) no. 1881/2006, por el que se fija el contenido máximo de determinados contaminantes en los productos alimenticios por lo que se refiere a la ocratoxina A (DOUE L50/8).

(19) Medina, Á.; Valle-Algarra, F. M.; Gimeno-Adelantado, J. V.; Mateo, R.; Mateo, F.; Jiménez, M. New method for determination of ochratoxin A in beer using zinc acetate and solid-phase extraction silica cartridges. *J. Chromatogr., A* **2006**, *1121*, 178−183.

(20) Medina, A.; Jimenez, M.; Gimeno-Adelantado, J. V.; Valle-Algarra, F. M.; Mateo, R. Determination of ochratoxin A in beer marketed in Spain by liquid chromatography with fluorescence detection using lead hydroxyacetate as a clean-up agent. *J. Chromatogr., A* **2005**, *1083*, 7−13.

(21) Kabak, B. Ochratoxin A in cereal-derived products in Turkey: occurrence and exposure assessment. *Food Chem. Toxicol.* **2009**, *47*, 348−352.

(22) Romero-Gonzalez, R.; Frenich, A. G.; Vidal, J. L. M.; Aguilera-Luiz, M. M. Determination of ochratoxin A and T-2 toxin in alcoholic beverages by hollow fiber liquid phase microextraction and ultra-high-pressure liquid chromatography coupled to tandem mass spectrometry. *Talanta* **2010**, *82*, 171−176.

(23) Varga, J.; Kiss, R.; Matrai, T.; Matrai, T.; Teren, J. Detection of ochratoxin A in Hungarian wines and beers. *Acta Aliment.* **2005**, *34*, 381−392.

(24) Araguas, C.; González-Penas, E.; López de Cerain, A. L. Study on ochratoxin A in cereal-derived products from Spain. *Food Chem.* **2005**, *92*, 459−464.

(25) Bertuzzi, T.; Rastelli, S.; Mulazzi, A.; Donadini, G.; Pietri, A. Mycotoxin occurrence in beer produced in several European countries. *Food Control* **2011**, *22*, 2059−2064.

(26) Al-Taher, F.; Banaszewski, K.; Jackson, L.; Zweiggenbaum, J.; Ryu, D.; Cappozzo, J. Rapid method for the determination of multiple mycotoxins in wines and beers by LC-MS/MS using a stable isotope dilution assay. *J. Agric. Food Chem.* **2013**, *61*, 2378−2384.

(27) Cao, J.; Kong, W.; Zhou, S.; Yin, L.; Wan, L.; Yang, M. Molecularly imprinted polymer-based solid phase clean-up for analysis of ochratoxin A in beer, red wine, and grape juice. *J. Sep. Sci.* **2013**, *36*, 1291−1297.

(28) EFSA. Opinion of the Scientific Panel on Contaminants in the food chain on a request from the Comission related to ochratoxin A in food (EFSA-Q-2005-154), 2006.
(29) OIV. International Organisation of Vine and Wine. Organización Intergugernamental. Analisis de la coyuntura mundial, 2012; available at http://www.oiv.int/oiv/cms/index.
(30) OEMV. Observatorio Español del Mercado del Vino. El vino en cifras, estudio elaborado para wines from Spain − ICEX, edición actualizada a 30-03-2012; available at www.winesfromspain.com.
(31) Covarelli, L.; Beccari, G.; Marini, A.; Tosi, L. A review on the occurrence and control of ochratoxigenic fungal species and ochratoxin A in dehydrated grapes, non-fortified dessert wines and dried vine fruit in the Mediterranean area. *Food Control* **2012**, *26*, 347−356.
(32) Valero, A.; Marín, S.; Ramos, A. J.; Sanchis, V. Survey: Ochratoxin A in European special wines. *Food Chem.* **2008**, *108*, 593−599.
(33) EU. Reglamento (CE) no. 1493/1 999 del Consejo, de 17 de mayo de 1999, por el que se establece la organización común del mercado vitivinícola (DOCE L179, 14.07.1999).
(34) MAGRAMA. Denominaciones de origen protegidas (DOP). Indicaciones geográficas protegidas (IGP), 2012; available at http://www.magrama.gob.es/es/_tcmlinkfilter.aspx?tcmuri=141862.
(35) Hernández, M. J.; García-Moreno, M. V.; Durán, E.; Guillén, D.; Barroso, C. G. Validation of two analytical methods for the determination of ochratoxin A by reversed-phased high-performance liquid chromatography coupled to fluorescence detection in musts and sweet wines from Andalusia. *Anal. Chim. Acta* **2006**, *566*, 117−121.
(36) Burdaspal, P.; Legarda, T. Occurrence of ochratoxin A in sweet wines produced in Spain and other countries. *Food Addit. Contam.* **2007**, *24*, 976−986.
(37) Murillo-Arbizu, M. T.; Amezqueta, S.; González-Penas, E.; López de Cerain, A. Ocurrence of ochratoxin A in southerm Spanish generous wines under the denomination of origin "jerez-xerez-Sherry and manzanilla Sanlucar de Barrameda". *Toxin* **2010**, *2* (5), 1054−1064.
(38) Quintela, S.; Villarán, M. C.; López de Armentia, I.; Elejalde, E. Occurrence of ochratoxin A in Rioja Alavesa wines. *Food Chem.* **2011**, *126* (1), 302−305.
(39) Romero-Gonzalez, R.; Martínez, J. L.; Aguilera-Luiz, M. M.; Garrido, A. Application of conventional solid-phase extraction for multimycotoxin analysis in beers by ultrahigh-performance liquid chromatography-tandem mass spectrometry. *J. Agric. Food Chem.* **2009**, *57*, 9385−9392.
(40) Quintela, S.; Villarán, M. C.; López de Armentia, I.; Elejalde, E. Ochratoxin A in Spanish exportation wine market. *Food Control* **2012**, *25*, 501−504.
(41) Remiro, R.; Irigoyen, A.; Gónzalez-Peñas, E.; Lizarraga, E.; Lopez de Cerain, A. Levels of ochratoxins in Mediterranean wines. *Food Control* **2013**, *32*, 63−68.
(42) Belli, N.; Marin, S.; Duaigües, A.; Ramos, A. J.; Sanchis, V. Ochratoxin a in wines, musts and grape juices from Spain. *J. Sci. Food Agric.* **2004**, *84*, 591−594.
(43) Blesa, J.; Soriano, J. M.; Moltó, J. C.; Mañes, J. Concentration of ochratoxin A in wines from supermarkets and stores of Valencia community (Spain). *J. Chromatogr., A* **2004**, *1054*, 397−401.
(44) López de Cerain, A.; González-Peñas, E.; Jiménez, A. M.; Bello, J. Contribution to the study of ochratoxin A in Spanish wines. *Food Addit. Contam.* **2002**, *19*, 1058−1064.
(45) Zhang, X.; Chen, L.; Li, J.; Zhu, B.; Ma, L. Occurrence of ochratoxin A in Chinese wines: influence of local meteorological parameters. *Eur. Food Res. Technol.* **2013**, *236*, 277−283.
(46) Mao, J.; Lei, S.; Yang, X.; Xiao, D. Quantification of ochratoxin A in red wines by commercial HPLC-FLD using a column packed with core-shell particles. *Food Control* **2013**, *32*, 505−511.
(47) Pena, A.; Cerejo, F.; Silva, L. J. G.; Lino, C. M. Ochratoxin A survey in Portuguese wine by LC−FD with direct injection. *Talanta* **2010**, *82* (4), 1556−1561.
(48) Bacaloni, A.; Cavaliere, C.; Faberi, A.; Pastorini, E.; Samperi, R.; Lagana, A. Automated on-line solid-phase extraction-liquid chromatography-electrospray tandem mass spectrometry method for the determination of ochratoxin A in wine and beer. *J. Agric. Food Chem.* **2005**, *53* (14), 5518−5525.
(49) Brera, C.; Debegnach, F.; Minardi, V.; Prantera, E.; Pannunzi, E.; Faleo, S. Ochratoxin A contamination in Italian wine samples and evaluation of the exposure in the Italian population. *J. Agric. Food Chem.* **2008**, *56*, 10611−10618.
(50) Anfossi, L.; Giovannoli, C.; Biagioli, F.; Passini, C.; Baggiani, C. A lateral flow immunoassay for the rapid detection of ochratoxin A in wine and grape must. *J. Agric. Food Chem.* **2012**, *60*, 11491−11497.
(51) Longobardi, F.; Iacovell, V.; Catucci, L.; Panzarini, G.; Pascale, M.; Visconti, A.; Agostiano, A. Determiantion of ochratoxin A in wine by means of immunoaffinity and aminopropyl solid-phase column cleanup and fluorometric detection. *J. Agric. Food Chem.* **2013**, *61*, 1604−1608.
(52) Brera, C.; Soriano, J. M.; Debegnach, F.; Miraglia, M. Exposure assessment to ochratoxin A from the consumption of Italian and Hungarian wines. *Microchem. J.* **2005**, *79*, 109−113.
(53) Aresta, A.; Vatinno, R.; Palmisano, F.; Zambonin, C. G. Determination of ochratoxin A in wine at sub ng/mL levels by solid-phase microextraction coupled to liquid chromatography with fluorescence detection. *J. Chromatogr., A* **2006**, *1115*, 196−201.
(54) Chiodini, A. M.; Scherpenisse, P.; Bergwerff, A. A. Ochratoxin A contents in wine: comparison of organically and conventionally produced products. *J. Agric. Food Chem.* **2006**, *54*, 7399−7404.
(55) Prelle, A.; Spadaro, D.; Denca, A.; Garibaldi, A.; Gullino, M. L. Comparison of clean-up methods for ochratoxin A on wine, beer, roasted coffee and chili commercialized in Italy. *Toxins* **2013**, *5*, 1827−1844.
(56) Comuzzo, P.; Rauhut, D.; Werner, M.; Lagazio, C.; Zironi, R. A survey on wines from organic viticulture from different European countries. *Food Control* **2013**, *34*, 274−282.
(57) Labrinea, E. P.; Natskoulis, P. I.; Spiropoulos, A. E.; Magan, N.; Tassou, C. C. A survey of ochratoxin A occurence in Greek wines. *Food Addit. Contam. Part B−Surveillance* **2011**, *4* (1), 61−66.
(58) Var, I.; Kabak, B. Occurrence of ochratoxin A in Turkish wines. *Microchem. J.* **2007**, *86*, 241−247.
(59) Flajs, D.; Domijan, A.; Ivić, D.; Cvjetković, B.; Peraica, M. ELISA and HPLC analysis of ochratoxin A in red wines of Croatia. *Food Control* **2009**, *20*, 590−592.
(60) Alvarado, M.; Galarce-Bustos, O.; Vega, M.; Aranda, M. Fast and selective determiantion of ochratoxin a in wines using an optimized and validated liquid chromatographic method. *Food Anal. Methods* **2013**, *6*, 621−629.
(61) SCF. CE: Opinion of the Scientific Committee on Food on ochratoxin A, expressed Sept 17, 1998.
(62) Berente, B.; Moricz, A.; H-Otta, K.; Zaray, G.; Leko, L.; Racz, L. Determination of ochratoxin A in Hungarian wines. *Microchem. J.* **2005**, *79*, 103−107.
(63) Park, J.; Chung, S.; Kim, Y. Ochratoxin A in Korean food commodities: occurrence and safety evaluation. *J. Agric. Food Chem.* **2005**, *53*, 4637−4642.
(64) Spadaro, D.; Lorè, A.; Garibaldi, A.; Gullino, M. L. Occurrence of ochratoxin A before bottling in DOC and DOCG wines produced in Piedmont (northern Italy). *Food Control* **2010**, *21*, 1294−1297.

Table 1. Carvacrol Bioactivities Described in the Text Listed Alphabetically

Bioactivity	References
acaricidal	183, 184
analgesic	2, 32, 202, 206, 209
antiallergic	59
antiarthritic	213
antibiotic, animal feed	59, 148, 150−152
antibiotic, animal waste	156−158
antibiotic, food bacteria	55, 63, 64, 70, 71, 78, 79, 96, 102, 103, 150, 152, 257, 258
antibiotic, human bacteria	37, 60, 78, 94, 130, 141
antibiotic, resistant bacteria	90, 91, 93−95, 99, 100, 103
anticarcinogenic	4, 7, 31, 37, 215, 216, 223−225, 227−229
anticholesterol	147, 148, 159, 231, 237
antidiabetic	237, 238, 250
antiendotoxemic	240, 241
antifungal	4, 11, 14, 34, 112, 164, 165, 167−172, 176, 215
anti-inflammatory	32, 198−202, 208, 213, 239, 245
antileishmanial	185, 186, 189
antimicrobial films	45, 55, 70−74, 100, 139
antioxidant	13, 16, 18, 31, 35, 46, 50, 51, 53, 54, 56−58, 69, 85, 86, 138, 139, 159, 181, 195, 248
antitoxins	79, 167, 174−176, 257, 258
antiviral	11, 55, 103, 141, 177−182, 257, 258
cardioprotective	229, 232, 234−236
gastroprotective	2, 243
hepatoprotective	2, 4, 159, 194, 200, 213, 217−219, 221, 224, 228, 231, 245−248, 258
insecticidal	34, 160−163
nematocidal	187
neuroprotective	204, 227, 250, 251, 255, 256
trypanocidal	188, 189

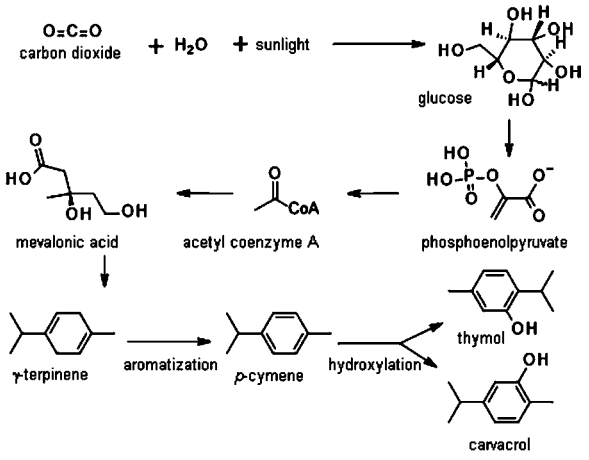

Figure 1. Biosynthesis of carvacrol in aromatic plants. Adapted from refs 5−7.

major steps involve cleavage of glucose to phosphoenolpyruvate followed by decarboxylation and acetylation to acetyl coenzyme A (acetyl CoA) and transformation to the key intermediate, mevalonic acid. The latter is then transformed to γ-terpinene, which then undergoes aromatization to *p*-cymene and hydroxylation to carvacrol and thymol. Not all intermediates are shown in Figure 1. The enzymes and cofactors that catalyze the individual transformations are given in the cited references. The discovery of genes that govern the biosynthesis of carvacrol and other monoterpenes via the γ-terpinene intermediate is currently an active area of research.[9]

Ramak et al.[10] discovered that inhibition of the mevalonate pathway enhances the biosynthesis of carvacrol in shoot cultures of the Iranian plant *Satureja khuzistanica*. They found that expression of the methylerythritol-4-phosphate (MEP) pathway provides the precursor isopentenyl diphosphate (IPP) for the multistep biosynthetic transformation to carvacrol with a yield of ∼90%. The authors suggest that a better understanding of the regulation of carvacrol biosynthesis could result in an increased yield of carvacrol in this and other plants.

Carvacrol is present in large amounts in numerous aromatic essential oil producing plants.[11−17] Although the growing season seems to influence yields, chemical composition, and antioxidant properties of Turkish oregano (*Origanum onites* L.) plants, the carvacrol content of the oils from plants harvested in four different seasons was >80%.[18]

An investigation of the biotransformation of carvacrol in cultured plant cells of *Eucalyptus perriniana* showed that the monoterpene is transformed to glycoside derivatives that are accumulated in the cells.[19] It would be of interest to determine antimicrobial and other bioactivities of the carvacrol glycosides, which are probably more soluble than carvacrol in water and body fluids.

Carvacrol is not only produced by plants, but its presence in the soil seems to act as a selective agent on different plant species, with the response ranging from negative to neutral to positive, suggesting that carvacrol and other thyme monoterpenes can influence plant−plant interactions that might affect the dynamics and stability of plants.[20]

Physical Properties. Carvacrol (liquid; mol wt, 150.22; boiling point, 237−238 °C; density, 0.967 mL/g; melting point, ∼0 °C; UV max in 95% ethanol, 277.5 nm; log extinction coefficient ε, 3.262; pK_a phenolic OH group, ∼10.9; practically insoluble in water; soluble in ethanol; oral rat LD50, 810 mg/kg; oral rabbit LD50, 100 mg/kg) is a major constituent of oregano oil, widely used as a salad dressing, and numerous other essential oils with concentrations up to ∼86%.[21−25] Carvacrol has a pleasant tangy taste and smells like marjoram.[10] Carvacrol is considered to be a generally accepted-as-safe (GRAS) compound used commercially as a food flavor.[26] Standard pure carvacrol for analysis characterized by quantitative NMR (qNMR) is available from a commercial source.[27]

Carvacrol is included in the list of chemical flavorings by the European Commission[28] and approved by the Food and Drug Administration for use as a flavoring in food.[29]

Synthesis. Yadav and Kamble,[30] describe a kinetically controlled synthesis of carvacrol with an 82% yield without the use of solvent (green chemistry) that involves a one-step alkylation of *ortho*-cresol with propylene or isopropyl alcohol over solid acid catalysts. Synthetic carvacrol may be less expensive than the plant-derived natural form.

Several studies report on the synthesis and bioactivities of carvacrol derivatives. These include the following: (a) antioxidative and antimicrobial hydroxymethyl carvacrols;[31] (b) the anti-inflammatory and antinociceptive carvacryl acetate formed by esterification of the carvacrol OH group;[32] (c) other antimicrobial carvacryl esters formed by esterification of the phenolic OH group with different organic acids;[33] (d)

dx.doi.org/10.1021/jf5023862 | J. Agric. Food Chem. 2014, 62, 7652−7670

antifungal and insecticidal hybrid molecules of carvacrol and benzoyl urea/thiourea prepared by structurally modifying carvacrol with benzoyl urea;[34] (e) Schiff's bases with high antioxidant activity formed by introduction of an NH_2 group into the benzene ring of carvacrol followed by reaction with structurally different aldehydes;[35] and (f) antimicrobial chlorocarvacrol formed by chloroperoxidase-catalyzed halogenation of carvacrol.[36] The carvacrol derivatives need to be evaluated for safety before use in agriculture, food, and medicine.

It is also worth noting that the phosphate form of carvacrol solubilized in liposomes has been reported to inhibit tumor growth in a murine tumor model.[37]

Analysis. Several HPLC and GC/MS analytical methods are described to measure the carvacrol content in plants, essential oils, food, pharmaceuticals, and plasma. Here, we briefly mention highlights of selected analyses.

Viñas et al.[38] found that a monolithic HPLC column with fluorometric detections and gradient elution with an acetonitrile−water mixture permitted good separation of chromatographic peaks of carvacrol and thymol in different types of honey with a limit of detection (LOD) of 1−4 ng/g.

Hajimehdipoor et al.[12] validated an HPLC method for the analysis of carvacrol and thymol in the medicinal plant *Thymus vulgaris* using an ACE C18 column and isocratic acetonitrile water (50:50, v/v) at a flow rate of 1 mL/min as the elution solvent. The authors suggest that the method can be used for quality control of pharmaceutical samples for which GC methods may not be effective.

Aleksseva[39] developed a chromatographic system consisting of a reverse-phase (RP) Diasorb 130-C18T column eluted with MeOH:H_2O:THF (50:50:22, v/v) for the analysis of carvacrol and thymol and in plant and medicinal samples.

Horváth et al.[40] describe a method for analysis of carvacrol and other essential oil compounds based on direct bioautography with TLC. The method was used to screen for microorganisms that grow on the TLC plate, suggesting that bioautography can quickly determine which component of an essential oil exhibits antimicrobial activity.

Cantalapiedra et al.[17] developed a reversed-phase high-performance liquid chromatographic (RP-HPLC) method for the simultaneous determination of phenolic compounds (carvacrol, eugenol, thymol, and vanillin) of aromatic plants using spectrophotometric detection with diode-array and electrochemical detection with amperometric and coulometric detectors, suggesting that the low detection limits (LODs) obtained make the method more useful for quality control than more expensive GC-MS methods.

In related studies, Chaieb et al.[11] and Vale-Silva et al.[14] used GC/MS to characterize multiple components of essential oils, Kirkin et al.[41] used the same technique to study the gamma-irradiation-induced degradation of carvacrol and other monoterpenes, and Nostro et al.[42] used gas chromatography to determine residual carvacrol in carvacrol-treated microbial biofilms.

Hallier et al.[43] describe a GC/MS method without the use of solvents to determine carvacrol, thymol, cinnamaldehyde, and dially disulfide residues in cow milk. Lejonklev et al.[44] describe a GC/MS method for analysis of the transfer of carvacrol and other terpenes from oregano and caraway essential oils into cow milk by gastrointestinal or respiratory exposure.

Other studies used HPLC for carvacrol analysis: Du et al.[45] determined the storage stability of carvacrol in edible antimicrobial apple films using an HPLC system that consisted of a Beckman 110B pump, a Thermo Separation Products AS3500 Autosampler, a UV 3000HR scanning detector with both deuterium and tungsten lamps, and an eluent consisting of 50% acetonitrile, 50 mM ammonium phosphate, and 0.05% phosphoric acid at pH 3.1 (Figure 2). Hadad et al.[46] measured

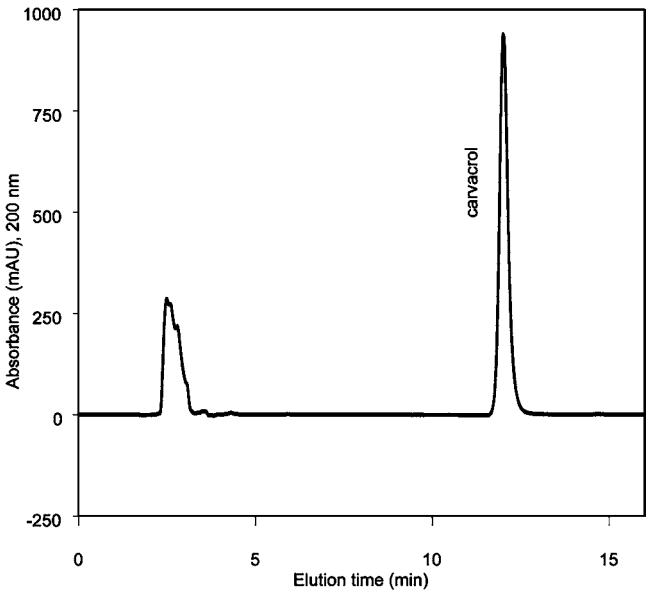

Figure 2. HPLC chromatogram of carvacrol extracted from a carvacrol-containing antimicrobial apple-based film. Adapted with permission from ref 45. Copyright 2008 American Chemical Society.

carvacrol and other compounds in black seed phytopharmaceuticals. Keawchaoon and Yoksan[47] measured carvacrol released from chitosan nanoparticles using UV−vis spectroscopy over the wavelength range 250−400 nm. Shakeri et al.[48] determined carvacrol in polyhydroxylate nanoparticles at 275 nm. Finally, Fiori et al.[49] used GC/MS and headspace solid-phase microextraction to measure carvacrol and thymol in plasma and milk of dairy cows with an LOD of 0.5 and 2.0 ng/mL, respectively.

Sensitive analytical methods seem to be available for the analysis of carvacrol in different milieus.

Antioxidative Properties. A kinetic investigation of the antioxidant effects showed that carvacrol and thymol inhibit autoxidation in purified triacylglycerols, lard, and sunflower oil at room temperature, suggesting their possible use to extend the shelf life of lipid-containing food.[50] Related studies found that carvacrol was highly effective in inhibiting the oxidation of sunflower seeds,[51] that it protected blueberries against storage-induced spoilage,[52,53] and that carvacrol grafted to chitosan nanoparticles via the Schiff's base reaction exhibited greater antioxidant and antibacterial activities and was less cytotoxic to mammalian cells than free carvacrol, suggesting that the method can be applied to chitosan films, membranes, and fibers for biomedical and food packaging applications.[54,55] In another study, carvacrol and thymol were shown to exhibit moderate antioxidant activity in vitro and no clastogenic effects in vivo at biologically relevant concentrations.[56] In addition, DPPH antioxidant values of 73 active essential oils ranged from 14 to 340 μg/mL, suggesting that supplementing of food with spices containing high levels of essential oils may counteract and retard oxidative damage and lipid oxidation and enhance

the antioxidant effects of the food products. These findings suggest the need to determine which components provide maximal antioxidative effects with minimal toxicity and whether combinations of oil components exhibit synergistic effects.[57] Antioxidant properties of essential oil components often differ from those of the oils from which they are derived.[58] Carvacrol in chicken feed exhibited in vivo antioxidative and immunostimulating (antiallergic) properties.[59]

INHIBITION OF FOODBORNE PATHOGENS

Generalities. Foodborne diseases result from ingesting food that is contaminated with either infectious microorganisms or toxins produced by the organisms. Foodborne pathogenic bacteria include *Bacillus cereus, Campylobacter jejuni, Clostridium botulinum, Clostridium perfringens, Escherichia coli, Listeria monocytogenes, Salmonella enterica*, and *Vibrio cholerae*. Bacteria can exert adverse effects in animals and humans by adhering to cells as biofilms and releasing cellular toxins. Understanding the molecular basis of bacteria and toxins will facilitate the development of food-compatible approaches to mitigate the burden of pathogenic bacteria. A key objective of worldwide research efforts in this area is to develop unexplored ways to reduce the human pathogen burden of foods with the aid of naturally occurring safe compounds. The ultimate goal is to develop a better understanding of the structural features that govern antimicrobial activities as well as to devise food formulations that use the active compounds and plant extracts to reduce pathogens in foods, feeds, animals, and humans after consumption. Studies with food need to assess safety and palatability and the effect of the food matrix and storage conditions on antibacterial activities.

Here, we present brief overviews of reported efforts to define the potential of carvacrol to meet these needs.

Inhibition of Foodborne Pathogenic Bacteria in Vitro and in Food. Carvacrol has been shown to have broad-spectrum antibiotic effects against bacteria involved in upper respiratory tract infections,[60] and it also inhibits *Shigella sonnei and S. flexneri* in an agar well diffusion assay with MIC values of 0.1−1.0%, suggesting it has the potential to be used as a disinfectant in the washing water of minimally processed vegetables.[61] It was also highly active against multiple pathogens in an in vitro bactericidal assay,[1] and it inhibited *Mycobacterium avium* subsp. paratuberculosis that causes the virulent Johne's disease in livestock, with a MIC value of 72.2 μg/mL.[62]

With these activities in mind, carvacrol-containing recipes for antimicrobial wine marinades against four foodborne pathogens have the potential to improve the microbial safety of food.[63] Indeed, carvacrol could also improve the safety and shelf life of fruit juices because it has been shown to inactivate *E. coli* and *Salmonella* in freshly prepared apple juices.[64,65]

Many studies have been carried out on the antimicrobial properties of carvacrol on meat and meat products. The bacterium *Clostridium perfringens* is a common cause of foodborne illness. Carvacrol and cinnamaldehyde were shown to inhibit spore germination and outgrowth of *C. perfringens* in ground turkey during chilling, suggesting their value for inhibiting *C. perfringens* in commercial products.[66] The two antimicrobials also facilitated the thermal destruction of *E. coli* in ground beef, suggesting that their use could allow shorter times and lower temperatures for heating beef products safely.[67]

In another study, carvacrol vapor inhibited the growth of *S. enterica* and inhibited and eliminated the pathogen on the surface of raw chicken, suggesting the vapors diffused into the agar and into the moisture layer and/or cell membranes on the surface of the chicken substrate, possibly affecting the flavor and aroma of the chicken breast.[68]

Studies have also been conducted on the use of carvacrol in antimicrobial films. An HPLC method that was used to measure the stability of carvacrol in apple-based antimicrobial films during storage showed that optimal antimicrobial effects against *E. coli* occurred with a carvacrol concentration of ∼1.0% added to the apple purees prior to film preparation and that carvacrol in the films and the film weights remained unchanged for up to 7 weeks of storage, suggesting that the apple films merit use as antimicrobial food coatings.[45]

El Abed et al.[69] showed that *Thymus capitata* essential oil (0.25−1.0%) with a carvacrol content of 89.9% inhibited *Listeria monocytogenes* in contaminated minced beef.

Apple films containing carvacrol or cinnamaldehyde also inactivated *E. coli* and *Salmonella* inoculated on chicken breast and *L. monocytogenes* inoculated on ham, suggesting that the food industry could use the edible antimicrobial apple films as wrappings to control surface contamination by pathogenic microorganisms.[70] Related studies found that apple, carrot, and hibiscus edible carvacrol-containing films were effective against *L. monocytogenes* on ham and bologna,[71] and against *Salmonella* on iceberg lettuce in sealed plastic bags, which could perhaps lead to their potential use in commercial salad bags.[72] As far as palatability is concerned, chicken wrapped with antimicrobial apple and tomato films was acceptable to a human sensory panel.[73] Carvacrol released from microencapsulated gum arabic polymer films inactivated a broad spectrum of pathogenic bacteria, suggesting that gum arabic has good edible-film-forming and flavor-enhancing potential.[74]

Carvacrol facilitated the simultaneous heat inactivation of *E. coli* and inhibition of formation carcinogenic heterocyclic amines in grilled ground beef patties (hamburgers), suggesting that the compound can impart dual health benefits to meat products cooked at lower temperatures.[75]

Combinations of carvacrol cinnamaldehyde, eugenol, and thymol acted synergistically against *E. coli* at physiological pH, indicating that using them in combination might minimize the unpleasant flavors of some of the individual compounds.[76] Carvacrol exhibited dose-dependent inhibition against *Vibrio cholerae* in inoculated carrot juice more efficiently at 25 °C than at 4 or 15 °C, suggesting its potential value to mitigate the virulent cholera disease.[77] Subinhibitory levels of carvacrol inhibited *C. jejuni* motility and infection of epithelial cells by interfering with flagellar function, suggesting the potential use of the compound in infection prevention strategies.[78]

As mentioned, carvacrol can act against many pathogens. It has been shown that the efficacy of carvacrol against cultures of multiple pathogens in corn flour dough is influenced by the complexity of the microbial populations and the relationship between individual populations.[79]

Carvacrol and lauric alginate acted synergistically in reducing *Salmonella* counts in ground turkey by 4 log cfu/g, a much greater value than was found with the individual compounds.[80]

Predictive models can be useful when considering the action of antimicrobials on food and in vitro. For example, a three-factor polynomial predictive model can be used to estimate the processing times and temperatures needed to achieve recommended 7.0-log reduction of *Salmonella* by carvacrol and cinnamaldehyde in ground chicken.[81] A related in vitro

study describes carvacrol-induced death kinetics of *L. monocytogenes*.[82]

Carvacrol and citral potentiated the antibiotic activity of bacitracin, colistin, and erythromycin by reducing MIC values of *Listeria* strains, suggesting that such combinations may help reduce the required dosages of antibiotics and may be of value against both Gram-negative and Gram-positive bacteria.[83,84]

Carvacrol microencapsulated in hydroxypropyl-β-cyclodextrin inhibited *E. coli* and *Salmonella* at lower concentrations than free carvacrol, suggesting that encapsulation can enhance antimicrobial action and decrease the concentration of antimicrobial for inhibition, and indicating that carvacrol inclusion complexes could be useful antimicrobial delivery systems.[85]

It is also worth noting that combinations of compounds may have detrimental effects. For example, combinations of carvacrol with the food antioxidant BHA (2-isobutyl-4-methxyphenol) exhibited antagonistic antimicrobial effects against *S. aureus*, suggesting that these interactions could affect food safety.[86] A possible explanation is that carvacrol and structurally similar BHA compete for the same microbial membrane receptor sites.

The cited studies demonstrate worldwide interest in defining the antimicrobial potential of carvacrol in vitro, in antimicrobial films, in encapsulated form, and in food. It seems that combinations of carvacrol with other plant-derived antimicrobials and with medical antibiotics enhance activity and require lower amounts of each component for the same effect, with the additional possible benefit of better sensory properties. This promising aspect merits further study with foods, feeds, and medicine.

Carvacrol Inhibits Antibiotic-Resistant Bacteria. Antibiotics are widely used as animal feed supplements to fight infection, to promote growth of livestock and poultry, and to reduce production costs as well as to treat human infections. Resistant microorganisms that often arise from use of antibacterial soaps and sanitizers, administration of subtherapeutic levels and overprescription of antibiotics, and widespread use in livestock are a worldwide concern.[87−90] In the United Sates, infections of about 2 million people annually cannot be treated with antibiotics, resulting in about 23,000 deaths.[88] Because of the need to develop new alternatives to standard antibiotics that can be effective against antibiotic-resistant bacteria, we evaluated several natural products, including carvacrol, for their ability to inhibit resistant *Bacillus cereus, E. coli, and S. aureus*.[91] All substances were active against the resistant organisms, suggesting that natural compounds can provide candidates to reduce both susceptible and resistant pathogens. Here, we briefly mention published studies on the efficacy of carvacrol against resistant bacteria in vitro and in food.

An evaluation of the susceptibility of methicillin-susceptible and methicillin-resistant Staphylococci by Nostro et al.[92] to oregano oil, carvacrol, and thymol showed that all three substances inhibited both types of pathogens to the same extent, with MIC values for carvacrol of 0.015−0.03%.

In another study, it was shown that essential oils from the Korean *Thymus* and their components carvacrol and thymol inhibited both susceptible and resistant strains of *Streptococcus pneumoniae, S. aureus, S.* Enteritidis, *and S.* Typhimurium with MIC values ranging from 0.125 to 8 mg/mL.[93]

Carvacrol inhibited seven nalidixic acid-resistant bacteria species, with MIC values of 125−500 μg/mL.[94] Combinations of carvacrol or methyl gallate isolated from an essential oil were more effective than the individual compounds, suggesting that the two natural compounds have the potential to restore the efficacy of nalidixic acid against resistant bacteria.

Carvacrol and thymol were highly effective in reducing the resistance of microbes, including *Salmonella* and *E. coli*, to several medicinal antibiotics; some combinations of the plant and medical antibiotics acted synergistically, suggesting that natural antibiotics can decrease the MIC of a diverse group of drug-resistant bacteria.[95]

A subinhibitory concentration of five natural antimicrobials including carvacrol individually and synergistically increased the susceptibility of multidrug resistant *S. Typhimurium* to five medical antibiotics, suggesting the potential value of the natural compounds as feed supplements to reduce the antibiotic resistance of *Salmonella* in food animals.[96]

In other studies, it was found that tea tree oil did not induce bacterial resistance to antimicrobial agents including carvacrol,[97] and that *Thymus maroccanus* essential oil and its major components carvacrol and thymol modified the susceptibility of resistant bacteria to antibiotics by a membrane-associated mechanism, thereby conferring protection to bacteria.[98]

Carvacrol and cinnamaldehyde rapidly inactivated susceptible and resistant *Campylobacter jejuni* strains, suggesting that the same mechanism probably governs the inactivation of both types of pathogens.[99] These two compounds also inhibited resistant *Campylobacter* on chicken breast,[100] and resistant *S. enterica* on celery and oysters,[101] suggesting that these plant antimicrobials have the potential to be used to decontaminate resistant pathogens on seafood, salads, and oysters. Carvacrol, cinnamaldehyde, and eugenol decreased a five-strain mixture of nalidixic-acid-resistant *Salmonella* on shell eggs from log 8.0 cfu/mL to undetectable levels, suggesting that the natural antimicrobials could be used as a wash treatment to reduce *Salmonella* Enteritidis on shell eggs.[102] Our studies also indicate that the antimicrobial efficacy of carvacrol is similar to that of oregano oil with a ∼80% carvacrol content, suggesting that the minor components of the oil do not seem to contribute to the bioactivity.[1,103]

The availability of plant-derived antibiotics provides more options for the treatment of livestock and poultry and reduces the exposure of humans to resistant bacteria.

Mechanism of Antimicrobial Effects. Here, we briefly mention results of experimental approaches designed to define possible mechanisms that might govern the antimicrobial effects of carvacrol.

It has been shown that exposure of *B. cereus* to carvacrol results in the depletion of the intracellular ATP pool, a change in membrane potential, and an increase in the permeability of the cytoplasmic to membrane for protons and potassium ions.[104] The loss of the ion gradient impairs essential metabolic processes in the cell and consequently leads to cell death.

We used autofluorescence spectra to determine the effect of carvacrol on *E. coli*.[103] The autofluorescence spectra and data showed significant changes at much lower concentrations of carvacrol (0.01 mM) than changes in membrane potential or release of ATP (ATP flux) after disruption of the bacterial cell membrane (1−2 mM), suggesting that autofluorescence detects physiological responses to carvacrol more efficiently than do changes in membrane potential or release of ATP. Difference spectra also make it possible to differentiate between autofluorescence associated with native bacterial cells and those exposed to carvacrol.

A Langmuir trough equipped with a computer-controlled microbalance was used to measure the effect of carvacrol and four other natural antimicrobials on monolayers of model membranes composed of bacterial phospholipids.[105] Surface pressure−area (π−A) and surface potential−area ($\Delta\psi$−A) isotherms were measured to monitor changes in the thermodynamic and physical properties of the lipid monolayers. Results indicated that carvacrol modified the three lipid monolayer structures by integrating into the monolayer, forming aggregates of antimicrobial−lipid complexes, reducing the packing effectiveness of the lipids, increasing the membrane fluidity, and altering the total dipole moment in the monolayer membrane model. These results provide insight into the mechanism of the molecular interactions between naturally occurring antimicrobial compounds and phospholipids of the bacterial cell membrane that govern activities.

Related studies reported that (a) exposure of *B. cereus* to subinhibitory, nonlethal concentrations of carvacrol resulted in increased resistance of the bacteria to inhibition that was accompanied by a lowering of membrane fluidity associated with changes in their fatty acid and headgroup composition;[106] (b) similar changes in membrane fatty acid profiles observed by Di Pasqua et al.[107] and by Luz Ida et al.[108] suggest that the mechanism of the antimicrobial effect is associated with an alteration in membrane lipid profiles and damage to the cell envelope; (c) a whole-cell biosensor assay suggests that the antimicrobial mechanism of action of carvacrol and related compounds involves damage to cell membranes and disruption to cellular metabolism and energy production in the evaluated five pathogens;[109] (d) carvacrol and low doses of γ-radiation synergistically inhibited *B. cereus* via disruption of cell membranes, suggesting that the combined treatment could be effective in contaminated food;[110,111] (e) carvacrol and thymol seem to induce antimicrobial activity via a mechanism that involves production of formaldehyde and its reaction products;[112] (f) bacterial membrane proteins are promising therapeutic targets of potential antibacterial therapy;[98,113,114] and (g) carvacrol and thymol bind to DNA via H-bonding of the OH group to the guanine N7, cytosine N3, and backbone phosphate group, with binding constants $K = 1.55 \times 10^3$/M and 2.43×10^3/M, respectively, suggesting that the mechanism of formation of the DNA complexes can serve as a model for drug−DNA interactions.[115]

A better understanding of the mechanisms that govern the antimicrobial activities of carvacrol will help in the design of better approaches to inhibit pathogenic bacteria in different environments.

Inhibition of Microbial Biofilms. Biofilms occur both at infection sites and during environmental growth of bacteria. They inhibit the diffusion and penetration of antibiotics into the microbial cells, and in vivo, they inhibit the penetration of immune cells to the microbes.[116] The composition of biofilms is a mixture of extracellular polymeric matrices mostly synthesized by the microorganisms that are responsible for the cohesion and three-dimensional architecture of the biofilms.[117]

The presence of biofilms on food and on food contact surfaces negatively impacts food quality and safety, and compared to nonattached cells, biofilm-associated bacteria are more resistant to inactivation by antimicrobial compounds and biocides.[118] Annous et al.[119] describe biofilm formation by *E. coli* and other pathogens on fruits and vegetables, including on leafy greens, apples, and cantaloupes. The authors note that while planktonic bacterial pathogens are easily controlled by low levels of washing water disinfectant, the degree to which leafy greens are sanitized is highly limited and is dependent on diverse intrinsic factors and on the effectiveness of the commercial unit. Washing with hypochlorite or other sanitizing agents can achieve only limited pathogen reduction (1−2 logs) and therefore cannot ensure microbial safety; greater reduction of the pathogen is not possible, owing to strong microbial attachment and internalization of the organisms and biofilm formation.[119] Bodur et al.[120] and Shen et al.[121] describe biofilms on stainless steel surfaces, and Gião et al.[122] describe biofilms in tap water.

GC-MS methods show that the biofilm matrix of *Streptococcus pneumoniae* is composed of extracellular DNA, proteins, and polysaccharide, suggesting that the web-like biofilm matrix links bacterial cells to one another and to their underlying substrate. We do not know to what extent the composition of biofilms varies among different pathogens.[117] Continuous exposure to carvacrol was as effective as a commercial sanitizer in inhibiting biofilm formation by *Staphylococcus aureus* and *S. enterica* pathogens.[123]

In a series of studies, Nostro et al.[42,124,125] found that (a) the concentrations of carvacrol and thyme required to eradicate biofilms produced by *S. aureus* and *Staphylococcus epidermidis* were 2- to 4-fold greater than those required to inhibit planktonic groups and that subinhibitory concentrations of the antimicrobials attenuated biofilm formation on polystyrene microtiter plates; (b) acidic formulations of carvacrol were more effective than neutral ones in inhibiting the formation of the biofilms; and (c) carvacrol- and cinnamaldehyde-containing polymeric films progressively released the antimicrobial that then inhibited both the bacteria and biofilm formation by *Staphylococci* and *E. coli*, possibly by reducing attachment ability and interfering with flagellar motility. In a related study, Zodrow et al.[126] found that a biodegradable FDA-approved polymer containing carvacrol or cinnamaldehyde delayed biofilm formation by Gram-positive *S. aureus*, Gram-negative *E. coli*, and spoilage bacteria *Pseudomonas aeruginosa*, suggesting that these films might be used in polymer coatings for medical and other devices to delay colonization by bacteria.

Subinhibitory concentration ratios of carvacrol, *trans*-cinnamaldehyde, eugenol, and thymol inhibited biofilm formation and inactivated mature biofilms of *Listeria monocytogenes* on microtiter plates and stainless steel coupons, suggesting that these compounds could be used to control the biofilms in food processing environments.[127]

A GFP-promoter fusion library with 79 *Salmonella* biofilm genes was used to study gene expression in the biofilms under experimental conditions, and that might facilitate study of biofilm inhibition in different environments.[128] Carvacrol, thymol, and carvacrol−thymol combinations limited biofilm formation in paper mill machines, suggesting that the natural (green) compounds are promising alternatives or supplements to the currently applied treatments.[129]

A test of the effect of carvacrol against the oral pathogens *Fusobacterium nucleatum*, *Porphyromonas gingivalis*, and *Streptococcus mutans* and their preformed biofilms on a titanium disc surface showed that carvacrol has the potential to serve as a useful hygiene formulation to prevent periodontal disease in implanted patients.[130] Inhibition of biofilm formation by *Chromobacterium violaceum*, *S. enterica*, and *S. aureus* but not by *P. aeruginosa* on polystyrene microplates by subinhibitory concentrations of carvacrol seems to be related to the

disruption of quorum sensing, an essential part of biofilm formation, not by bactericidal activity.[131]

INHIBITION OF HUMAN PATHOGENIC BACTERIA

Although foodborne pathogens cause human infections, carvacrol also inhibits nonfoodborne pathogens. This section presents brief overviews of reported studies on the inhibition of growth and/or destruction of a variety of pathogenic foodborne and human pathogenic bacteria that can cause human illness. These pathogens are listed in alphabetical order.

Campylobacter jejuni. *C. jejuni* is a widely distributed human pathogen that is implicated in abortion of sheep and induces emetic and diarrheal syndromes in humans. There also seems to be an apparent association between outbreaks of *Campylobacter*-induced diarrhea and the development of Guillain−Barre syndrome in humans.[132] As mentioned previously, carvacrol inhibited the motility of *C. jejuni* and thus infection of epithelial cells.[78]

Helicobacter pylori. This bacterium in gastric mucosa might contribute to gastritis and peptic ulcer. Carvacrol and 15 essential oils inhibited the bacterium in vitro with MIC values ranging from 0.02 to 0.1 g/L but were not effective when administered orally to infected mice, suggesting that essential oils are unlikely to be efficient anti-*Helicobacter* compounds.[133] Another in vitro study using a disc diffusion assay found that essential oils from the Iranian *Thymus caramanicus* plant inhibited ten clinical isolates of *H. pylori* with MIC values that ranged from 14.5 to 58.0 μg/mL.[134]

Klebsiella pneumoniae. Several studies reported that carvacrol-containing plant essential oils inhibited pneumonia-causing bacterium *K. pneumoniae*.[135−139] Iten et al.[140] found that an increase in carvacrol concentration in the oils enhanced the kill-rate and that the combination of carvacrol and linalool has additive antimicrobial effects.

Mycobacterium tuberculosis. Carvacrol-containing aromatic and medicinal plants from Columbia exhibited antitubercular activity,[141] and carvacrol derivatives inhibited the *Mycobacterium tuberculosis* chorismate mutase enzyme,[142] suggesting that these substances might help alleviate tuberculosis symptoms.

Salmonella enterica. Oral iron therapy can increase the level of bacterial pathogens in the large intestine of African children. To help overcome this problem, Kortman et al.[143] discovered that carvacrol inhibited iron-induced epithelial intestinal cell adhesion of *S. enterica* at high iron concentrations, suggesting its potential value to prevent pathogenic overgrowth and colonization in the large intestine during oral iron therapy.

Oral Pathogenic Bacteria. Several studies describe the anticariogenic effects of carvacrol. For example, the essential oil from *Lippia sidoides* and its major components carvacrol and thymol exhibited potent antimicrobial activity against the cariogenic species *Streptococcus mutans* and *Candida albicans*, with MIC values from 0.625 to 10.0 mg/mL, suggesting their value in combating oral microbial growth.[144] In addition, mucoadhesive patches consisting of bilayers containing carvacrol, and the antibiotic tetracycline exhibited antimicrobial activity against oral bacteria and the yeast *C. albicans*, indicating the potential use of carvacrol in combination to treat local mouth bacterial infections and candidiasis.[145] Related studies reported that carvacrol inhibited oral biofilms and planktonic cultures,[130] that a carvacrol gel protected rats against induced periodontitis,[146] and that carvacrol has the potential to serve as a dietary supplement to prevent pathogenic overgrowth and colonization during oral iron therapy. The cited observations suggest that carvacrol inhibits dental caries, indicating the need for further human studies.

Impact of Carvacrol on Animal Feed, Milk Production, and Waste Odors. The following observations suggest carvacrol can improve the quality and safety of animal feed. (a) The addition of up to 200 mg of carvacrol + thymol to a viscose poultry feed resulted in a decrease in digesta viscosity, in improvement of feed conversion and growth performance, and in reduced serum cholesterol level, suggesting that monoterpenes might alleviate the negative effects of viscous compounds in poultry diets.[147] (b) Carvacrol-containing oregano leaves improved the growth performance of turkeys.[148] (c) A mixture of carvacrol, capsicum, and cinnamaldehyde added to a poultry diet increased feed efficiency and carcass protein but not fat retention, suggesting that the additives improved the metabolic utilization of absorbed nutrients, possibly by inhibiting pathogenic bacteria.[149,150] (d) Carvacrol inhibited the growth of *Brachyspira intermedia*, which chronically infects laying hens, causing spirochetosis.[151] (e) Four natural antimicrobials including carvacrol acted synergistically with two antibiotics in inhibiting the growth of antibiotic-resistant microorganisms from animal feed, suggesting that the natural antimicrobials have the potential to control the development of antibiotic-resistant bacteria as substitutes for antibiotics.[152]

In the area of milk production, a study has shown that carvacrol/thymol and carvacrol/thyme/*p*-cymene mixtures inhibit the growth of multiple bacterial strains responsible for livestock mastitis. The incidence of mastitis, an inflammatory reaction of the mammary gland induced by pathogens in the udder that produce toxins, can be a problem for livestock and milk production, so the essential oil compounds might have use as a preventive herbal treatment.[153]

Hallier et al.[43] developed a method to determine carvacrol and other essential residues in cow milk samples, enabling a measure of the transfer of the compounds from feed to milk and to evaluate their effect on sensory perception on raw milk and milk processing. No residues of these compounds were detected in the milk samples. By contrast, Lejonklev et al.[44] found that carvacrol and other terpenes are transferred unaltered into milk within hours of exposure, regardless of whether the animals receive the compounds by gastrointestinal or respiratory exposure. Giannenas et al.[154] found that supplementation of the feed with essential oils resulted in improved feed utilization and in increased production of milk by dairy ewes (sheep), suggesting the need for long-term trials to validate these results on dairy sheep.

A study on goats found that supplementation of the diet with carvacrol resulted in reduced methane emissions.[155] Carvacrol and thymol reduced livestock and swine waste odors and pathogens.[156−158]

A study on mice revealed that dietary *Thymbra spicata* essential oil containing 44.1% carvacrol reduced total and LDL and increased HDL serum cholesterol as well as GSH and oxidative enzyme levels, explaining the ethnomedical use of this oil.[159] Will this oil also beneficially impact livestock and human cholesterol?

Insecticidal Activities. A fumigation bioassay found that carvacrol and related compounds exhibited good larvicidal activity against *Lycoriella ingénue*, similar to that of the synthetic pesticide dichlorovos.[160] Carvacrol was an effective fumigant against *Culex pipiens pallens* adult insects[161] and showed a

concentration-dependent inhibition of nicotine binding in a membrane preparation of housefly heads containing the nicotinic acetylcholine receptor, suggesting that insect N-acetylcholine receptors could serve as a novel target for monoterpenoid insecticides.[162,163]

Antifungal Activities. The following capsule summaries of published studies show that low concentrations of carvacrol inhibit the growth or inactivate phytopathogenic and pathogenic fungi.

Carvacrol was effective against both susceptible (MIC = 75−90 mg/L) and fluconazole-resistant (MIC = 75−100) *Candida albicans* and other fungal isolates.[164] Thymol was shown to have similar antifungal effects, suggesting that both compounds could serve as an alternative fluconazole therapy for the treatment and prevention of human candidiasis.

A study on fruit decay found that an application of carvacrol- or thymol-containing waxes to lemons inoculated with *Penicillium digitatum* and *P. italicum* fungi reduced the decay of the citrus fruit, indicating that perhaps such waxes could be used in citrus packing lines to replace synthetic fungicides.[165]

Candida lusitaniae is a pH-tolerant yeast that contaminates fruit juices. Carvacrol at concentrations >1 mM inhibited the growth of *C. lusitaniae*, suggesting carvacrol could be used for preserving minimally processed food.[166]

Carvacrol inhibited the following pathogenic and toxinogenic fungi with MIC50 values of 37−76 μg/mL and MIC100 values of 131−262 μg/mL: *Aspergillus flavus*, *A. fumigatus*, *Fusarium oxysporum*, *F. verticillioides*, *Penicillium brevicompactum*, and *P. expansum*.[167] Carvacrol and thymol were the most promising of the 22 tested compounds, indicating their potential as effective fungicides. A study on the inhibition of 11 food-decaying fungi found that carvacrol exhibited high efficacy with an average MIC value of 154.5 μg/mL, suggesting that the in vitro study may serve as a guide for future studies of the inhibition of the foodborne fungal pathogens on/in food.[168]

Essential oils from *Origanum vulgare* from Southern Italy showed both significant compositional variability and antifungal activity, and their antifungal potencies increased with carvacrol content. All the oils were the carvacrol/thymol chemotypes. At 1000 ppm, the three oils completely inhibited fungal growth of *Monilinia laxa*, *M. fructicola*, and *M. fructigena* species without any hemolytic effect on the cell membranes of bovine erythrocytes.[169]

A quantitative structure−activity relationship (QSAR) analysis of natural phenolic compounds including carvacrol against fluconazole-resistant *Candida* species based on steric descriptors can be used to predict the anti-*Candida* activity of new phenolic compounds.[170] Related studies on the effects of carvacrol against *Candida albicans* are described by Ahmad et al.[171] and Lima et al.[172]

In a study of fungal infection of the tree *Ulmus minor*, it was shown that carvacrol imparts resistance to *U. minor* xylem tissues against the fungal pathogen *Ophiostoma novo-ulmi*, the cause of Dutch elm disease in trees.[173]

The cited studies indicate that carvacrol and thymol, as well as essential oils that contain high levels of carvacrol, strongly inhibit both human pathogenic and phytopathogenic fungi. Further studies are needed to define their usefulness in fungal-contaminated food.

Inhibition of Microbial and Fungal Toxin Production. Hospital-acquired *Clostridium difficile* is the most common cause of antibiotic-associated colitis and diarrhea that affects about 300,000 individuals in the United States.[132] Carvacrol and *trans*-cinnamaldehyde substantially reduced toxin production by this pathogen in Vero cells, down-regulated toxin genes, and did not inhibit the growth of beneficial gut bacteria, suggesting the potential of the plant compounds to reduce *C. difficile* virulence.[174]

A structure−activity study of ten natural phenolic compounds including carvacrol found that a mathematical expression obtained was able to predict the release of the highly toxic mycotoxin fumonisin from the *Fusarium verticillioides* fungal strain, suggesting that lipophilicity is the key property that allowed the target molecule to reach inside the fungal cells.[175] The authors suggest that the mathematical analysis can be used to predict the antifumonisin activity of structurally related molecules, so it will be interesting to find out whether carvacrol can inactivate the biological (toxicological) activities of these and other pure toxins.[176]

Antiviral Activities. Viral contamination of food and infection of animals and humans is a major cause of numerous diseases. The mechanism of antiviral action of plant compounds is based on their abilities to act as antioxidants, to inhibit enzymes, to disrupt cell membranes, to prevent viral binding and penetration into cells, and to induce the host cell defense mechanism. Here, we present brief summaries of reported studies on the antiviral activities of carvacrol against several pathogenic viruses.

Carvacrol and thymol had significant antiviral activity with an IC50 value of 7 μM against herpes simplex virus type 1 (HSV-1) that causes orofacial and genital infections, suggesting that the topical application of these monoterpenes for the treatment of the viral infections merits study.[177] An evaluation of thymol-related monoterpenes showed that the aliphatic side chains had a minor effect, while the hydrophilic OH group on the benzene ring was sufficient for activity. Carvacrol and thymol were reported to be responsible for the antiviral activity against HSV-1 in supercritical carbon dioxide oregano and sage oil extracts.[178] Mexican oregano oils exhibited high antiviral activity against acyclovir-resistant HSV-1, bovine herpesvirus type 2 (BoHV-2), bovine viral diarrhea virus (BVDV), and human rotavirus.[179] Carvacrol inactivates murine norovirus, a human norovirus surrogate after 1 h of exposure via direct action on the viral capsid followed by the RNA.[180] Carvacrol at concentrations of ∼0.5% induced an up to 3.87 log reduction within 1 h, acting directly on the virus capsid and then on the RNA. Surprisingly, oregano oil was less effective than carvacrol. Sökmen et al.[181] and Schnitzler et al.[182] describe viricidal effects of monoterpenes derived from essential oils and essential oil extracts. An unanswered question is whether carvacrol in pure form and in carvacrol-containing essential oils will inactivate pathogenic viruses in contaminated food and water and in a clinical setting.

Acaricidal, Antileishmanial, Nematicidal, and Trypanocidal Effects. Treatment with carvacrol (2.5 μL/mL) induced 100% death of larvae of the cattle parasite *Rhipicephalus microplus* and the tropical horse tick parasite *Dermacentor nitens*, suggesting the potential of the monoterpene to control these two tick species in the field.[183] A related study on the acaricidal efficacy of carvacrol and related compounds on larvae of nymphs of *Amblyomma cajennense* (Cayenne tick) and *Rhipicephalus sanguineous* parasites that afflict horses and other animals found that similar low concentrations of carvacrol and thymol (2.5 μL/mL) also cause 100% lethality in these parasites, indicating the value of further studies to evaluate these acaricides under natural conditions.[184]

Leishmaniasis caused by the tropical parasite *Leishmania amazonensis* affects more than 12 million people worldwide. A comparison of the antileishmanial activity of the essential oil from *Chenopodium ambrosioides* and its main components carvacrol and caryophyllene oxide in mice showed that oil prevented lesion development, the individual compounds were not effective, and the mixture of the pure compounds caused death of the animals after 3 days of treatment, suggesting the superiority of the oil against experimental leishmaniasis.[185] An in vitro study found that carvacrol and thymol from the essential oil *Lippia sidoides* inhibited *Leishmania chagasi* with IC50 values of 58.4 and 74.1 μg/mL, respectively, suggesting that this oil is a promising source of leishmanicidal compounds.[186] Carvacrol also showed antileishmanial activity against experimental cutaneous leishmaniasis caused by *L. amazonensis*.[185]

At a concentration of 1000 μL/L, 12 of 27 essential oils and active components evaluated immobilized more than 80% of juveniles of the root-knot nematode *Meloidogyne javanica* and inhibited nematode hatching and root galling of cucumber seedlings in pot experiments, indicating that the oils and components could serve as nematicides. Carvacrol immobilized the juveniles and inhibited hatching at 125 μL/L.[187]

Human African trypanosomiasis (sleeping sickness) is caused by *Trypanosoma brucei* and poses a risk of infection for about 60 million people living in sub-Saharan countries.[188] The cited investigators discovered that *Hagenia abyssinica* essential oils and their bioactive components including carvacrol strongly inhibited the parasite with an IC50 value of 11.25 μg/mL, with minimal toxicity on human leukemia cells. The order of decreasing trypanocidal effects of phenolic monoterpenes, carvacrol > thymol > eugenol, paralleled acute oral toxicities in rats (LD50 in mg/kg): carvacrol, 810; thymol, 980; eugenol, 2680. The relative potencies are similar to those we reported for antimicrobial activities of these compounds.[1] The most active compounds have the potential to protect against or treat human and animal trypanosomiasis.

Another study[189] reported that 13 essential oils from different species of Columbian *Lippia* plants containing an average of 46.2% carvacrol inhibited *Leishmania chagasi* and *Trypanosoma cruzi* parasites with IC50 values of 5.5−12.2 μg/mL. The corresponding values for pure carvacrol were 3.0−38.0 μg/mL, suggesting that some of oils and carvacrol could be useful in the treatment and prevention of Chagas and leishmaniasis protozoan diseases, which are a major public health problem in Latin America. Carvacrol and nootkatone suppressed *Ixodes scapularis* and *Amblyomma americanum parasites* in a Lyme disease endemic in New Jersey.[190]

ADDITIONAL BIOACTIVITIES AND HEALTH-PROMOTING PROPERTIES OF CARVACROL

Metabolism. After consumption, carvacrol is metabolized by cytochrome enzymes, mostly hydroylated derivatives that has unknown safety. Here, we briefly mention selected studies on carvacrol metabolism.

A metabolic study of carvacrol in rats showed that only a small amount is excreted in urine 24 h after oral administration.[191,192] Figure 3 shows the structures of the characterized metabolic products that result from the in vivo enzyme-catalyzed hydroxylation of the benzene ring and hydroxylation and oxidation of the aliphatic isopropyl and methyl groups of carvacrol. These compounds seem to be excreted as the glucoronide and sulfate derivatives.

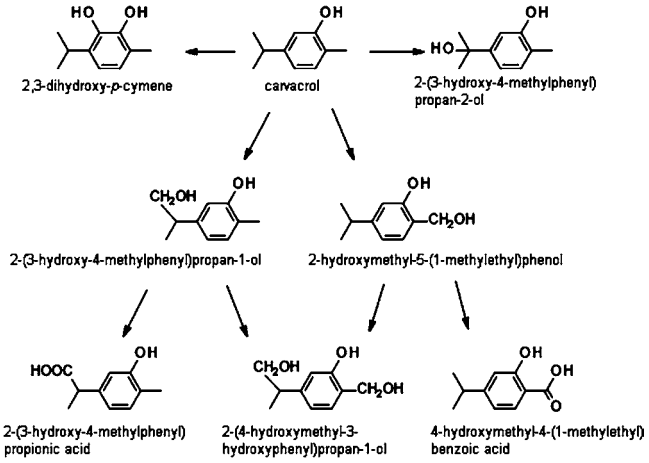

Figure 3. Metabolism and urinary excretion of carvacrol in rats. Adapted from refs 191 and 192.

Using human microsomes, Dong et al.[193] detected two new hydroxylated metabolites that resulted from the cytochrome isoform CYP2A6-induced oxidation of carvacrol to new hydroxylated metabolites, suggesting that carvacrol could impact pharmacokinetic and clinical outcomes when coadministered with other compounds undergoing CYP2A6 metabolism. Related studies found that (a) carvacrol acted in a dose-dependent manner as a liver mitochondrial antioxidant and protected against reactive-oxygen-species (ROS)-generating mitochondrial enzymes and DNA damage in D-galactosamine-induced hepatotoxicity in rats, suggesting that the antioxidant effect of carvacrol could be responsible for the observed hepatoprotective effects;[194] (b) in vitro and parallel in vivo studies in the hippocampus of mice revealed that synthetic carvacrol acetate reduced lipid peroxidation, GSH levels, catalase activity, and nitrite content and that the antioxidative potential correlated between these two parameters;[195] and (c) plant enzymes in germinating wheat seeds partly converted carvacrol and other monoterpenes to corresponding less toxic oxidation and reduction products and partly to degradation products, suggesting that such changes might also take place in other foods.[196] Noma and Asakawa[197] comprehensively reviewed biotransformation pathways of monoterpenes by microorganisms, insects, and mammals.

Anti-inflammatory Mechanisms. The strong anti-inflammatory properties of carvacrol provide a scientific basis for many of its beneficial bioactivities. Here, we will mention some of the cellular events that seem to be associated with these properties.

An investigation on the cytokine modulation induced in paw inflammation in mice showed that carvacrol at 100 μg/kg attenuated the paw edema and reduced the pro-inflammatory COX-2 and IL-1ß mRNA expression and enhanced the levels of IL-10 and IL-10 mRNA anti-inflammatory cytokines, suggesting that the treatment reduced the production of inflammatory mediators, possibly through induction of IL-10 release.[198] Carvacrol did not produce an antidermatogenic effect in IL-10 deficient mice.

In related studies, Silva et al.[199] found that carvacrol induced reduction of mouse ear edema and significantly up-regulated mRNA and protein expressions of TNF-α, IL-6, iNOS, COX-2, and NF-κB in D-galactosamine-induced hepatotoxic rats and

dx.doi.org/10.1021/jf5023862 | J. Agric. Food Chem. 2014, 62, 7652−7670

down-regulated the expression of these genes,[200] confirming the mechanistic basis for the anti-inflammatory activity of carvacrol. A review on anti-inflammatory effects of monoterpenes further expands on the proposed mechanisms that seem to govern anti-inflammatory effects of monoterpenes.[201]

Analgesia. Pain that occurs in response to tissue injury results from activation of peripheral pain receptors (nociceptors) and their sensory fibers. Many studies have been designed to demonstrate the antinociceptive (analgesic) properties of carvacrol. For example, carvacrol attenuates carrageenan-induced hypernociception and inflammation in mice, suggesting that carvacrol is a candidate in the treatment of painful conditions associated with inflammation.[202] The beneficial effects seem to be associated with inhibition of pro-inflammatory cytokine TNF-α production and NO release.

Related studies found that (a) carvacrol enhanced warmth and heat pain on the human tongue;[203,204] (b) synthetic carvacrol propionate attenuates nociception, mechanical hyperalgesia, and inflammation in male Swiss mice through inhibition of cytokines;[205] (c) oral administration of carvacrol in mice models of pain resulted in significant inhibition of nociception without impairment of motor performance, suggesting that the antinociceptive activity might not act through the opioid system;[206] (d) results of a study of orofacial analgesic-like activity of carvacrol in rodents suggest that the compound might represent an important tool for the treatment of orofacial pain;[207] (e) carvacrol in drinking water was more effective than the steroidal drug dexamethasone in mitigating adverse effects in sensitized guinea pigs, suggesting the monoterpene could be used to treat asthma in humans;[208] and (f) Guimarães et al.[209] reviewed mechanisms that might govern analgesic aspects of structurally different monoterpenes.

These observations indicate that carvacrol could benefit individuals suffering from inflammatory-related allergies.

Arthritis. The folate antagonist methotrexate is an anti-inflammatory drug with many side effect used to treat human rheumatoid arthritis and cancer. We previously reported that both folic acid and methotrexate protected frog embryos against organ malformations (teratogenicity) induced by the potato glycoalkaloid α-chaconine.[210,211]

The following observations suggest that carvacrol has the potential to ameliorate adverse side effects of methotrexate: (a) carvacrol overcame methotrexate-induced oxidative stress and the pro-inflammatory response in the sciatic nerve tissue of the rat, indicating that carvacrol has the potential to reduce the toxic side effects;[212] (b) carvacrol enhanced the antiarthritic action and reduced liver toxicity of methotrexate in a rat model, suggesting that carvacrol might promote the safe use of methotrexate in the management of arthritis;[213] and (c) carvacrol partially abrogated methotrexate-induced kidney damage in male rats.[214] The cited observations suggest the need to evaluate the potential of carvacrol to ameliorate methotrexate-associated toxicity in human patients.

Cancer. Cancer that can develop in any tissue organ at any age is an unregulated proliferation of cells due to loss of normal control, resulting in unregulated growth and, often, metastasis.[132] Because multiple genes are involved in carcinogenesis, there is a need for therapies that target multiple signaling pathways. The following observations suggest that carvacrol might act additively or synergistically with other cancer cell inhibitors.

Incubation of human nonsmall cell lung cancer cells (A549) with carvacrol in DMSO for 24 h resulted in a decrease in cell number and protein content and in degeneration of cell morphology, suggesting that the monoterpene is a potent inhibitor cell associated with about 75% of lung cancers.[215]

Carvacrol also induced a 30% decrease of 3,4-benzopyrene-induced in vivo carcinogenicity in Wistar rats and exhibited anticarcinogenic effects against the cells in vitro, with IC50 values of 90 μM and 67 μM after 24 and 48 h incubations.[216]

In a series of studies, Slameňová et al.[217−220] found that carvacrol protected human hepatoma (HepG2) and human colonic (Caco-2) and other cell lines against DNA strand breaks induced by hydrogen peroxide and methylene blue, and reduced DNA lesions in hepatocytes and testicular cells in rats given carvacrol in drinking water for 7 days, suggesting that the beneficial effects might be associated with an increase in antioxidant activity in liver and testicular cells in the animals.

Carvacrol was also shown to inhibit human hepatoma HepG2 cell growth by inducing apoptosis by the direct activation of the mitochondrial and mitogen-activated protein kinases (MAPK) pathways; thus, it might help prevent liver cancer.[221]

Carvacrol inhibited the proliferation of porcine lymphocytes in the MTT assays that measure cell viability, with an IC50 value of 182 μM, suggesting that the reduced lymphocyte proliferation was due to apoptotic cell death, as determined by Annexin-V binding and caspase-3 activation.[222] These authors also mention that because the antimicrobial concentrations of carvacrol (5−100 mM) are much higher than concentrations that are toxic to leucocytes and epithelial cells (100−1000 μM), caution should be exercised when using carvacrol as a feed additive in pigs.

In another cancer cell death study, carvacrol exhibited antiproliferative effects in metastatic breast cancer, MDA-MB231, cells with an IC50 value of 100 μM, suggesting that carvacrol could be a potent antitumor molecule against metastatic breast cancer cells.[223] The induction of apoptosis seems to have been mediated by cell cycle arrest at S phase, increases in Annexin V positive cells, caspase activity, cytochrome c release from mitochondria, decreases in mitochondrial membrane potential and in the Bcl2Bax protein ratio, cleavage of PARP, and fragmentation of DNA.

Carvacrol (15 mg/kg BW) protected rats against diethylnitrosamine-induced hepatocellular carcinoma. Reduction in liver cancer progression was associated with prevention of liver peroxidation, hepatic cell damage, and protection of the liver antioxidant system.[224]

Carvacrol-induced ROS-associated apoptosis in OC2 human oral cancer cells was triggered by caspase-3 activity and the release of calcium ions from the endoplasmic reticulum.[225] A related study on periodontal inflammation used a focused microarray analysis of apoptosis-related genes, and the results suggest that caspase-3 is a target protein for carvacrol in the inhibition of periodontitis apoptosis of HaCaT epithelial cells.[226]

On the basis of the results from a study of the effect of carvacrol on healthy neurons and N2a neuroblastoma cells, Aydin et al.[227] conclude that the efficacy of anticancer chemotherapy seems to be limited by the cytotoxic effect on healthy cells, owing to the lack of selectivity of carvacrol and poor uptake by the neuroblastoma cells.

Overall, the in vitro and rodent studies suggest that the food ingredient carvacrol alone or in combination with cancer drugs such as methotrexate and doxorubicin merits further study for the potential to mitigate human breast, liver, and other cancers.

Moreover, because other widely consumed food ingredients and foods are also reported to inhibit cancer cells in vitro and in vivo, combinations of carvacrol with anticarcinogenic tea catechins and theaflavins,[228] the tomato compounds lycopene and α-tomatine,[229] and pigmented rice brans[230] also merit study.

Cardioprotection. The protective effect of carvacrol against risk factors associated with heart disease has also been reported. For example, the administration of carvacrol for 21 days to hepatotoxic rats increased levels of good very low density (VLDL) and low density lipoprotein (LDL) and decreased bad high density lipoprotein (HDL) serum levels, suggesting that carvacrol affords a significant hepatoprotective and hypolipidemic effect against induced hepatotoxicity.[231]

Carvacrol induces relaxation of the arteries by activating TRPV cation channels and suppressing calcium ion currents in the endothelium, which may account for some of the cardioprotective effects of the Mediterranean diet.[232−234]

Carvacrol has also been shown to decrease the heart rate and blood pressure of anesthetized rats[235] and protected rats against myocardial infarction,[236] suggesting that the compound seems to be a promising cardioprotective agent for the treatment of myocardial infarction. The beneficial effects of carvacrol seem to be modulated by its antioxidative and antiapoptotic properties.

Diabetes and Obesity. Here, we briefly examine the beneficial properties of carvacrol against obesity and diabetes in rodents.

Orally administered carvacrol at doses of 25 and 50 mg/BW to diabetic rats for 7 days after the onset of streptozotocin-induced diabetes did not significantly reduce serum glucose or insulin levels. The treatments did, however, have a protective effect against the negative effects of streptozotocin on liver enzymes, suggesting that the compound would be useful in the diet of diabetics.[237]

Co-administration of carvacrol (20 mg/kg BW) and the antidiabetic drug rosiglitazone (4 mg/kg BW) for 35 days to rats on a high-fat diet prevented changes in metabolic enzymes associated with obesity and diabetes, thus indicating that the combination had a better antihyperglycemic effect than the individual compounds.[238] The results of the histopathology of the islet cells of the pancreas support the biochemical findings.

It has also been reported that mice fed a 0.1% carvacrol-supplemented diet had reduced body weight gain, visceral fad-pad weights, and plasma lipid levels compared with mice fed a high-fat diet.[239] Inhibition of adipogenesis seems to occur by suppression of bone marrow protein-, fibroblast growth factor 1-, and galanin-mediated signaling and reduction of the of pro-inflammatory cytokines in visceral adipose tissues by inhibiting toll-like receptor 2 (TLR2)- and TLR4-mediated signaling. The cited findings suggest that carvacrol might help prevent obesity in humans.

Endotoxemia. Endotoxemia is an infection-related virulent disease with a high mortality rate.[240] Intraperitoneal administration of carvacrol improved the survival of mice during induced lethal endotoxemia and attenuated lung injury.[241] The protective effect seems to be related to inhibition of activation of NF-κB and MAPK signaling pathways, thereby inhibiting inflammatory cytokines TNF-α, IL-6, and IL-1ß; thus, it seems that carvacrol might be useful in preventing endotoxemia-associated adverse effects. Possible synergistic antiendotoxemia effects of carvacrol with other natural compounds[240,242] merit study.

Gastroprotection. The protection of drug-induced gastric lesions in mice and rats seems to be mediated by endogenous prostaglandins, K(ATP) channel openings, NO synthase activation, and antioxidant properties, suggesting that carvacrol has the potential to be an effective gastroprotective agent.[243] A related study found that carvacrol helps heal induced gastric ulcers in mice by interfering with the release and/or synthesis of pro-inflammatory mediators.[199] By contrast, an in vitro study found that exposure of human intestinal Caco-2 cells to carvacrol and thymol resulted in vacuolated cytoplasm, altered organelles, and other evidence of morphological cellular damage.[244]

Hepatoprotection. Pretreatment with carvacrol ameliorates thioacetamide-induced liver injury in rats. This is mediated by the inhibitory effect of carvacrol on nuclear factor NFκB activation of Bax and Bcl-2 protein expression, and the restoration of histopathological changes, suggesting that the beneficial effect is associated with the inhibition of apoptosis.[245] Related studies show that carvacrol: (a) increases the regeneration rate of rat livers undergoing partial hepatectomy;[246] (b) protects rat livers against hepatic ischemia, a risk factor in liver surgery and transplantation;[247] and (c) protects rats against D-galactosamine-induced hepatotoxicity.[231,248] It seems that carvacrol has the potential to help overcome liver injuries in clinical settings.

Neuroprotection. Carvacrol was 10 times stronger than the isomeric thymol in inhibiting acetylcholinesterase, a key compound involved in neurotransmission.[249] An investigation of the effect of carvacrol on diabetes-associated cognitive deficit (DACD) in a rat model showed that the compound dose-dependently prevented behavioral, biochemical, and molecular changes associated with diabetes, indicating that it might be useful for treating diabetes and DACD.[250] The cognitive impairment was associated with oxidative stress, inflammation, and apoptotic cascades.

An investigation of the effect of carvacrol on induced cerebral edema in a mouse model showed that the molecule reduced the edema and neurological deficits, suggesting that it might protect against intracerebral hemorrhage injury by ameliorating aquaporin-4 (AQP4)-mediated edema.[251] Carvacrol also enhanced the recovery of traumatic brain injury in mice by altering permeable calcium ion channels that are involved in neuronal cell death, suggesting the monoterpene should be further evaluated in animals and humans.[252] Related studies reported that carvacrol protected against methotrexate-induced neurotoxicity in rats,[212] and alleviated cognitive impairment in scopolamine-treated rats caused by increased amyloid-ß-pathology (Aß) levels associated with Alzheimer's disease or cholinergic hypofunction.[253] Orally administered carvacrol, up to 50 mg/kg BW, induced antidepressant effects that seem to be dependent on an interaction with the dopaminergic brain pathways.[254] The cited and related studies[255,256] imply that carvacrol merits further study in humans to establish its potential to treat neurological disorders, including Alzheimer's disease and depression.

OUTLOOK

Carvacrol-containing aromatic plants and spices are a major source of essential oils that are widely used in the human diet. Carvacrol can be isolated from a large number of essential oil producing plants. The results of the cited studies indicate that the antioxidative properties associated with the phenolic OH group, the hydrophobic properties associated with the benzene

ring and the methyl and isopropyl substituents, the binding affinity to the guanine moiety of DNA, and the anti-inflammatory and apoptotic and cell membrane disruptive properties of carvacrol all seem to contribute to the observed diverse bioactivities. These bioactivities have the potential to contribute to the prevention and therapy of several chronic human diseases, including allergic response, cancer, diabetes, and infectious, cardiovascular, and neurological syndromes. Future studies should further explore the beneficial synergistic properties of combinations of carvacrol with other natural antimicrobials, including tea compounds,[257] seashell-derived chitosans,[55] and wine flavonoids.[258] Such dietary combinations in which the individual components might exert their effects by different mechanisms could make it possible to use lower amounts of each component, thus minimizing possible adverse sensory properties, antibiotic resistance, and toxicity.

AUTHOR INFORMATION

Notes

The authors declare no competing financial interest.

ACKNOWLEDGMENTS

I am most grateful to my colleagues whose names appear on the cited references for excellent scientific collaboration, to Carol E. Levin for facilitating the preparation of the manuscript, and to journal reviewers for helpful comments.

ABBREVATIONS USED

ATP, adenosine triphosphate; Bcl2/Bax, cancer biomarker signaling proteins; BoHV-2, bovine herpesvirus type 2; BVDV, bovine viral diarrhea virus; BW, body weight; COX-2, cyclooxygenase-2; CYP2A6, cytochrome P450 2A6; DPPH, 2,2-diphenyl-1-picrylhydrazyl; GFP, green fluorescent protein; DACD, diabetes-associated cognitive deficit; HDL, high-density lipoprotein; HSV-1, herpes simplex virus type 1; IL, interleukin; LD50, concentration of test substance that kills 50% of the animals; LDL, low-density lipoprotein; LOD, limit of detection; GC/MS, gas chromatography/mass spectrometry; iNOS, inducible nitric oxide synthase; MIC, minimum inhibitory concentration; MAPK, mitogen-activated protein kinases; MTT, tetrazol 3-(4,5-dimethylthiazol-2-yl)-2.5-diphenyltetrazolium bromide; NF-κB, nuclear factor kappa B; NO, nitric oxide; PARP, poly(ADP-ribose) polymerase; RT-HPLC, reversed-phase high-performance liquid chromatography; QSAR, quantitative structure–activity relationship; RNA, ribonucleic acid; ROS, reactive oxygen species; TNF-α, tumor necrosis factor alpha; TRPV, transient receptor potential vanilloid; VLDL, very low density lipoprotein

REFERENCES

(1) Friedman, M.; Henika, P. R.; Mandrell, R. E. Bactericidal activities of plant essential oils and some of their isolated constituents against *Campylobacter jejuni, Escherichia coli, Listeria monocytogenes,* and *Salmonella enterica*. *J. Food Prot.* **2002**, *65*, 1545–1560.

(2) Baser, K. H. C. Biological and pharmacological activities of carvacrol and carvacrol bearing essential oils. *Curr. Pharm. Des.* **2008**, *14*, 3106–3119.

(3) Nostro, A.; Papalia, T. Antimicrobial activity of carvacrol: current progress and future prospectives. *Recent Pat Anti-Infect. Drug Discovery* **2012**, *7*, 28–35.

(4) Suntres, Z. E.; Coccimiglio, J.; Alipour, M. The bioactivity and toxicological actions of carvacrol. *Crit. Rev. Food Sci. Nutr.* **2013**, available online May 14; doi: 10.1080/10408398.2011.653458.

(5) Sell, C. Chemistry of essential oils. In *Handbook of Essential Oils: Science, Technology, and Applications*; Baser, K. H. C., Buchbauer, G., Eds.; CRC Press, Taylor & Frances Group: Boca Raton, FL, 2010; pp 121–150.

(6) Nhu-Trang, T. T.; Casabianca, H.; Grenier-Loustalot, M. F. Deuterium/hydrogen ratio analysis of thymol, carvacrol, gamma-terpinene and p-cymene in thyme, savory and oregano essential oils by gas chromatography-pyrolysis-isotope ratio mass spectrometry. *J. Chromatogr., A* **2006**, *1132*, 219–227.

(7) Loza-Tavera, H. Monoterpenes in essential oils: biosynthesis and properties. *Adv. Exp. Med. Biol.* **1999**, *464*, 49–62.

(8) Smith, C. A.; Wood, E. J. *Biosynthesis*; Chapman & Hall: London, 1992; p 226.

(9) Mendes, M. D.; Barroso, J. G.; Oliveira, M. M.; Trindade, H. Identification and characterization of a second isogene encoding γ-terpinene synthase in *Thymus caespititius*. *J. Plant Physiol.* **2014**, *171*, 1017–1027.

(10) Ramak, P.; Kazempour Osaloo, S.; Ebrahimzadeh, H.; Sharifi, M.; Behmanesh, M. Inhibition of the mevalonate pathway enhances carvacrol biosynthesis and DXR gene expression in shoot cultures of *Satureja khuzistanica* Jamzad. *J. Plant Physiol.* **2013**, *170*, 1187–1193.

(11) Chaieb, K.; Hajlaoui, H.; Zmantar, T.; Kahla-Nakbi, A. B.; Rouabhia, M.; Mahdouani, K.; Bakhrouf, A. The chemical composition and biological activity of clove essential oil, *Eugenia caryophyllata* (*Syzigium aromaticum* L. Myrtaceae): a short review. *Phytother. Res.* **2007**, *21*, 501–506.

(12) Hajimehdipoor, H.; Shekarchi, M.; Khanavi, M.; Adib, N.; Amri, M. A validated high performance liquid chromatography method for the analysis of thymol and carvacrol in *Thymus vulgaris* L. volatile oil. *Pharmacogn. Mag.* **2010**, *6*, 154–158.

(13) Hadad, G. M.; Salam, R. A.; Soliman, R. M.; Mesbah, M. K. High-performance liquid chromatography quantification of principal antioxidants in black seed (*Nigella sativa* L.) phytopharmaceuticals. *J. AOAC Int.* **2012**, *95*, 1043–1047.

(14) Vale-Silva, L.; Silva, M. J.; Oliveira, D.; Gonçalves, M. J.; Cavaleiro, C.; Salgueiro, L.; Pinto, E. Correlation of the chemical composition of essential oils from *Origanum vulgare* subsp. virens with their in vitro activity against pathogenic yeasts and filamentous fungi. *J. Med. Microbiol.* **2012**, *61*, 252–260.

(15) Ghassemi, N.; Ghanadian, M.; Ghaemmaghami, L.; Kiani, H. Development of a validated HPLC/photodiode array method for the determination of isomenthone in the aerial parts of *Ziziphora tenuior* L. *Jundishapur J. Nat. Pharm. Prod.* **2013**, *8*, 180–186.

(16) Jaberian, H.; Piri, K.; Nazari, J. Phytochemical composition and in vitro antimicrobial and antioxidant activities of some medicinal plants. *Food Chem.* **2013**, *136*, 237–244.

(17) Cantalapiedra, A.; Gismera, M. J.; Sevilla, M. T.; Procopio, J. R. Sensitive and selective determination of phenolic compounds from aromatic plants using an electrochemical detection coupled with HPLC method. *Phytochem. Anal.* **2014**, *25*, 247–254.

(18) Ozkan, G.; Baydar, H.; Erbas, S. The influence of harvest time on essential oil composition, phenolic constituents and antioxidant properties of Turkish oregano (*Origanum onites* L.). *J. Sci. Food Agric.* **2010**, *90*, 205–209.

(19) Shimoda, K.; Kondo, Y.; Nishida, T.; Hamada, H.; Nakajima, N.; Hamada, H. Biotransformation of thymol, carvacrol, and eugenol by cultured cells of *Eucalyptus perriniana*. *Phytochemistry* **2006**, *67*, 2256–2261.

(20) Jensen, C. G.; Ehlers, B. K. Genetic variation for sensitivity to a thyme monoterpene in associated plant species. *Oecologia* **2010**, *162*, 1017–1025.

(21) Yannai, S. *Dictionary of Food Compounds—Additives, Flavors, and Ingredients*; Chapman & Hall/CRC Press: Boca Raton, FL, 2004; p 835.

(22) O'Neil, M. J. *The Merck Index*, 15th ed; Royal Society of Chemistry: Oxford, U.K., 2013.

(23) Teuscher, E. *Medicinal Spices—A Handbook of Culinary Herbs, Spices, Spice Mixtures and Their Essential Oils*; Medpharm Scientific Publishers: Stuttgart, Germany, 2006; p 459.

(24) Parthasarathy, V. A.; Chempakam, B.; Zachariah, T. J. *Chemistry of Spices*; CABI: Oxfordshire, U.K., 2008; p 464.
(25) Baser, K. H. C.; Buchbauer, G. *Handbook of Essential Oils: Science, Technology, and Applications*; CRC Press, Taylor & Frances Group: Boca Raton, FL, 2010; p 991.
(26) Smith, R. L.; Cohen, S. M.; Doull, J.; Feron, V. J.; Goodman, J. I.; Marnett, L. J.; Portoghese, P. S.; Wadddell, W. J.; Wagner, B. M.; Hall, R. L.; Higley, N. A.; Lucas-Gavin, C.; Adams, T. B. A procedure for the safety evaluation of natural flavor complexes used as ingredients in food: essential oils. *Food Chem. Toxicol.* **2005**, *43*, 345−363.
(27) Nold, M. New standards for the anlysis of herbal medicinal drugs. In *Analytix*; Sigma-Aldrich: 2014; p 13.
(28) European Commission. Regulations: commission implementing regulation (EU) No 872/2012. *Official Journal of the European Union, L: Legislation* **2012**, *55*, 24.
(29) Code of Federal Regulations Title 21, Food additives permitted for direct addition to food for human consumption; flavoring agents and related substances; synthetic flavoring substances and adjuvants. In *21CFR172.515*, U.S. Food and Drug Administration, Ed. revised as of April 1, 2013.
(30) Yadav, G. D.; Kamble, S. B. Synthesis of carvacrol by Friedel-Crafts alkylation of *o*-cresol with isopropanol using superacidic catalyst UDCaT-5. *J. Chem. Technol. Biotechnol.* **2009**, *84*, 1499−1508.
(31) Mastelic, J.; Jerkovic, I.; Blazevic, I.; Poljak-Blazi, M.; Borovic, S.; Ivancic-Bace, I.; Smrecki, V.; Zarkovic, N.; Brcic-Kostic, K.; Vikic-Topic, D.; Muller, N. Comparative study on the antioxidant and biological activities of carvacrol, thymol, and eugenol derivatives. *J. Agric. Food Chem.* **2008**, *56*, 3989−3996.
(32) Damasceno, S. R.; Oliveira, F. R.; Carvalho, N. S.; Brito, C. F.; Silva, I. S.; Sousa, F. B.; Silva, R. O.; Sousa, D. P.; Barbosa, A. L.; Freitas, R. M.; Medeiros, J. V. Carvacryl acetate, a derivative of carvacrol, reduces nociceptive and inflammatory response in mice. *Life Sci.* **2014**, *94*, 58−66.
(33) Mathela, C. S.; Singh, K. K.; Gupta, V. K. Synthesis and in vitro antibacterial activity of thymol and carvacrol derivatives. *Acta Polym. Pharm.* **2010**, *67*, 375−380.
(34) Pete, U. D.; Zade, C. M.; Bhosale, J. D.; Tupe, S. G.; Chaudhary, P. M.; Dikundwar, A. G.; Bendre, R. S. Hybrid molecules of carvacrol and benzoyl urea/thiourea with potential applications in agriculture and medicine. *Bioorg. Med. Chem. Lett.* **2012**, *22*, 5550−5554.
(35) Beena; Kumar, D.; Rawat, D. S. Synthesis and antioxidant activity of thymol and carvacrol based Schiff bases. *Bioorg. Med. Chem. Lett.* **2013**, *23*, 641−645.
(36) Getrey, L.; Krieg, T.; Hollmann, F.; Schrader, J.; Holtmann, D. Enzymatic halogenation of the phenolic monoterpenes thymol and carvacrol with chloroperoxidase. *Green Chem.* **2014**, *16*, 1104−1108.
(37) Coimbra, M.; Isacchi, B.; van Bloois, L.; Torano, J. S.; Ket, A.; Wu, X.; Broere, F.; Metselaar, J. M.; Rijcken, C. J.; Storm, G.; Bilia, R.; Schiffelers, R. M. Improving solubility and chemical stability of natural compounds for medicinal use by incorporation into liposomes. *Int. J. Pharm.* **2011**, *416*, 433−442.
(38) Viñas, P.; Soler-Romera, M. J.; Hernández-Córdoba, M. Liquid chromatographic determination of phenol, thymol and carvacrol in honey using fluorimetric detection. *Talanta* **2006**, *69*, 1063−1067.
(39) Alekseeva, L. I. Determining thymol and carvacrol by reversed-phase high-performance liquid chromatography. *Pharm. Chem. J.* **2009**, *43*, 665−667.
(40) Horváth, G.; Jámbor, N.; Végh, A.; Böszörményi, A.; Lemberkovics, É.; Héthelyi, É.; Kovács, K.; Kocsis, B. Antimicrobial activity of essential oils: the possibilities of TLC-bioautography. *Flavour Fragrance J.* **2010**, *25*, 178−182.
(41) Kirkin, C.; Mitrevski, B.; Gunes, G.; Marriott, P. J. Combined effects of gamma-irradiation and modified atmosphere packaging on quality of some spices. *Food Chem.* **2014**, *154*, 255−261.
(42) Nostro, A.; Cellini, L.; Zimbalatti, V.; Blanco, A. R.; Marino, A.; Pizzimenti, F.; Giulio, M. D.; Bisignano, G. Enhanced activity of carvacrol against biofilm of *Staphylococcus aureus* and *Staphylococcus epidermidis* in an acidic environment. *APMIS* **2012**, *120*, 967−973.
(43) Hallier, A.; Noirot, V.; Medina, B.; Leboeuf, L.; Cavret, S. Development of a method to determine essential oil residues in cow milk. *J. Dairy Sci.* **2013**, *96*, 1447−1454.
(44) Lejonklev, J.; Løkke, M. M.; Larsen, M. K.; Mortensen, G.; Petersen, M. A.; Weisbjerg, M. R. Transfer of terpenes from essential oils into cow milk. *J. Dairy Sci.* **2013**, *96*, 4235−4241.
(45) Du, W. X.; Olsen, C. W.; Avena-Bustillos, R. J.; McHugh, T. H.; Levin, C. E.; Friedman, M. Storage stability and antibacterial activity against *Escherichia coli* O157:H7 of carvacrol in edible apple films made by two different casting methods. *J. Agric. Food Chem.* **2008**, *56*, 3082−3088.
(46) Hadad, G. M.; Abdel Salam, R. A.; Soliman, R. M.; Mesbah, M. K. HPLC-DAD determination of seven antioxidants and caffeine in different phytopharmaceuticals. *J. Chromatogr. Sci.* **2014**, *52*, 617−623.
(47) Keawchaoon, L.; Yoksan, R. Preparation, characterization and in vitro release study of carvacrol-loaded chitosan nanoparticles. *Colloids Surf., B: Biointerfaces* **2011**, *84*, 163−171.
(48) Shakeri, F.; Shakeri, S.; Hojjatoleslami, M. Preparation and characterization of carvacrol loaded polyhydroxybutyrate nanoparticles by nanoprecipitation and dialysis methods. *J. Food Sci.* **2014**, *79*, N697−705.
(49) Fiori, G. M. L.; Bonato, P. S.; Pereira, M. P. M.; Contini, S. H. T.; Pereira, A. M. S. Determination of thymol and carvacrol in plasma and milk of dairy cows using solid-phase microextraction. *J. Braz. Chem. Soc.* **2013**, *24*, 837−846.
(50) Yanishlieva, N. V.; Marinova, E. M.; Gordon, M. H.; Raneva, V. G. Antioxidant activity and mechanism of action of thymol and carvacrol in two lipid systems. *Food Chem.* **1999**, *64*, 59−66.
(51) Quiroga, P. R.; Asensio, C. M.; Nepote, V., Antioxidant effects of the monoterpenes carvacrol, thymol and sabinene hydrate on chemical and sensory stability of roasted sunflower seeds. *J. Sci. Food Agric.* **2014**, available online May 19; doi: 10.1002/jsfa.6744.
(52) Sun, X.; Narciso, J.; Wang, Z.; Ference, C.; Bai, J.; Zhou, K. Effects of chitosan-essential oil coatings on safety and quality of fresh blueberries. *J. Food Sci.* **2014**, *79*, M955−960.
(53) Wang, C. Y.; Wang, S. Y.; Chen, C. Increasing antioxidant activity and reducing decay of blueberries by essential oils. *J. Agric. Food Chem.* **2008**, *56*, 3587−3592.
(54) Chen, F.; Shi, Z.; Neoh, K. G.; Kang, E. T. Antioxidant and antibacterial activities of eugenol and carvacrol-grafted chitosan nanoparticles. *Biotechnol. Bioeng.* **2009**, *104*, 30−39.
(55) Friedman, M.; Juneja, V. K. Review of antimicrobial and antioxidative activities of chitosans in food. *J. Food Prot.* **2010**, *73*, 1737−1761.
(56) Ündeğer, Ü.; Başaran, A.; Degen, G. H.; Başaran, N. Antioxidant activities of major thyme ingredients and lack of (oxidative) DNA damage in V79 Chinese hamster lung fibroblast cells at low levels of carvacrol and thymol. *Food Chem. Toxicol.* **2009**, *47*, 2037−2043.
(57) Anthony, K. P.; Deolu-Sobogun, S. A.; Saleh, M. A. Comprehensive assessment of antioxidant activity of essential oils. *J. Food Sci.* **2012**, *77*, C839−843.
(58) Dawidowicz, A. L.; Olszowy, M. Does antioxidant properties of the main component of essential oil reflect its antioxidant properties? The comparison of antioxidant properties of essential oils and their main components. *Nat. Prod. Res.* **2014**, DOI: 10.1080/14786419.2014.918121.
(59) Hashemipour, H.; Kermanshahi, H.; Golian, A.; Veldkamp, T. Effect of thymol and carvacrol feed supplementation on performance, antioxidant enzyme activities, fatty acid composition, digestive enzyme activities, and immune response in broiler chickens. *Poult. Sci.* **2013**, *92*, 2059−2069.
(60) Didry, N.; Dubreuil, L.; Pinkas, M. Activity of thymol, carvacrol, cinnamaldehyde and eugenol on oral bacteria. *Pharm. Acta Helv.* **1994**, *69*, 25−28.
(61) Bagamboula, C. F.; Uyttendaele, M.; Debevere, J. Inhibitory effects of spices and herbs towards *Shigella sonnei* and *S. flexneri*. *Meded. Rijksuniv. Gent Fak. Landbouwkd. Toegep. Biol. Wet.* **2001**, *66*, 523−530.

(62) Wong, S. Y. Y.; Grant, I. R.; Friedman, M.; Elliott, C. T.; Situ, C. Antibacterial activities of naturally occurring compounds against *Mycobacterium avium* subsp. *paratuberculosis*. *Appl. Environ. Microbiol.* **2008**, *74*, 5986−5990.
(63) Friedman, M.; Henika, P. R.; Levin, C. E.; Mandrell, R. E. Recipes for antimicrobial wine marinades against *Bacillus cereus*, *Escherichia coli* O157:H7, *Listeria monocytogenes*, and *Salmonella enterica*. *J. Food Sci.* **2007**, *72*, M207−M213.
(64) Friedman, M.; Henika, P. R.; Levin, C. E.; Mandrell, R. E. Antibacterial activities of plant essential oils and their components against *Escherichia coli* O157:H7 and *Salmonella enterica* in apple juice. *J. Agric. Food Chem.* **2004**, *52*, 6042−6048.
(65) Kisko, G.; Roller, S. Carvacrol and *p*-cymene inactivate *Escherichia coli* O157:H7 in apple juice. *BMC Microbiol.* **2005**, *5*, 36.
(66) Juneja, V. K.; Friedman, M. Carvacrol, cinnamaldehyde, oregano oil, and thymol inhibit *Clostridium perfringens* spore germination and outgrowth in ground turkey during chilling. *J. Food Prot.* **2007**, *70*, 218−222.
(67) Juneja, V. K.; Friedman, M. Carvacrol and cinnamaldehyde facilitate thermal destruction of *Escherichia coli* O157:H7 in raw ground beef. *J. Food Prot.* **2008**, *71*, 1604−1611.
(68) Burt, S. A.; Fledderman, M. J.; Haagsman, H. P.; van Knapen, F.; Veldhuizen, E. J. A. Inhibition of *Salmonella enterica* serotype Enteritidis on agar and raw chicken by carvacrol vapour. *Int. J. Food Microbiol.* **2007**, *119*, 346−350.
(69) El Abed, N.; Kaabi, B.; Smaali, M. I.; Chabbouh, M.; Habibi, K.; Mejri, M.; Marzouki, M. N.; Ben Hadj Ahmed, S. Chemical composition, antioxidant and antimicrobial activities of *Thymus capitata* essential oil with Its preservative effect against *Listeria monocytogenes* inoculated in minced beef meat. *Evid. Based Complement. Alternat. Med.* **2014**, *2014*, No. 152487.
(70) Ravishankar, S.; Zhu, L.; Olsen, C. W.; McHugh, T. H.; Friedman, M. Edible apple film wraps containing plant antimicrobials inactivate foodborne pathogens on meat and poultry products. *J. Food Sci.* **2009**, *74*, M440−M445.
(71) Ravishankar, S.; Jaroni, D.; Zhu, L.; Olsen, C. W.; McHugh, T. H.; Friedman, M. Inactivation of *Listeria monocytogenes* on ham and bologna using pectin-based apple, carrot, and hibiscus edible films containing carvacrol and cinnamaldehyde. *J. Food Sci.* **2012**, *77*, M377−M382.
(72) Zhu, L.; Olsen, C.; McHugh, T.; Friedman, M.; Jaroni, D.; Ravishankar, S. Apple, carrot, and hibiscus edible films containing the plant antimicrobials carvacrol and cinnamaldehyde inactivate *Salmonella* Newport on organic leafy greens in sealed plastic bags. *J. Food Sci.* **2014**, *79*, M61−M66.
(73) Du, W.-X.; Avena-Bustillos, R. J.; Woods, R. D.; Breksa, A. P.; McHugh, T. H.; Friedman, M.; Levin, C. E.; Mandrell, R. Sensory evaluation of baked chicken wrapped with antimicrobial apple and tomato edible films formulated with cinnamaldehyde and carvacrol. *J. Agric. Food Chem.* **2012**, *60*, 7799−7804.
(74) Guarda, A.; Rubilar, J. F.; Miltz, J.; Galotto, M. J. The antimicrobial activity of microencapsulated thymol and carvacrol. *Int. J. Food Microbiol.* **2011**, *146*, 144−150.
(75) Friedman, M.; Zhu, L.; Feinstein, Y.; Ravishankar, S. Carvacrol facilitates heat-induced inactivation of *Escherichia coli* O157:H7 and inhibits formation of heterocyclic amines in grilled ground beef patties. *J. Agric. Food Chem.* **2009**, *57*, 1848−1853.
(76) Pei, R. S.; Zhou, F.; Ji, B. P.; Xu, J. Evaluation of combined antibacterial effects of eugenol, cinnamaldehyde, thymol, and carvacrol against *E. coli* with an improved method. *J. Food Sci.* **2009**, *74*, M379−383.
(77) Rattanachaikunsopon, P.; Phumkhachorn, P. Assessment of factors influencing antimicrobial activity of carvacrol and cymene against *Vibrio cholerae* in food. *J. Biosci. Bioeng.* **2010**, *110*, 614−619.
(78) van Alphen, L. B.; Burt, S. A.; Veenendaal, A. K.; Bleumink-Pluym, N. M.; van Putten, J. P. The natural antimicrobial carvacrol inhibits *Campylobacter jejuni* motility and infection of epithelial cells. *PLoS One* **2012**, *7*, e45343.
(79) Morente, E. O.; Abriouel, H.; Lopez, R. L.; Ben Omar, N.; Galvez, A. Antibacterial activity of carvacrol and 2-nitro-1-propanol against single and mixed populations of foodborne pathogenic bacteria in corn flour dough. *Food Microbiol.* **2010**, *27*, 274−279.
(80) Oladunjoye, A.; Soni, K. A.; Nannapaneni, R.; Schilling, M. W.; Silva, J. L.; Mikel, B.; Bailey, R. H.; Mahmoud, B. S.; Sharma, C. S. Synergistic activity between lauric arginate and carvacrol in reducing *Salmonella* in ground turkey. *Poult. Sci.* **2013**, *92*, 1357−1365.
(81) Juneja, V. K.; Gonzales-Barron, U.; Butler, F.; Yadav, A. S.; Friedman, M. Predictive thermal inactivation model for the combined effect of temperature, cinnamaldehyde and carvacrol on starvation-stressed multiple *Salmonella* serotypes in ground chicken. *Int. J. Food Microbiol.* **2013**, *165*, 184−199.
(82) Kamdem, S. S.; Belletti, N.; Magnani, R.; Lanciotti, R.; Gardini, F. Effects of carvacrol, (E)-2-hexenal, and citral on the thermal death kinetics of *Listeria monocytogenes*. *J. Food Prot.* **2011**, *74*, 2070−2078.
(83) Zanini, S. F.; Silva-Angulo, A. B.; Rosenthal, A.; Rodrigo, D.; Martínez, A. Effect of citral and carvacrol on the susceptibility of *Listeria monocytogenes* and *Listeria innocua* to antibiotics. *Lett. Appl. Microbiol.* **2014**, *58*, 486−492.
(84) Langeveld, W. T.; Veldhuizen, E. J.; Burt, S. A. Synergy between essential oil components and antibiotics: a review. *Crit. Rev. Microbiol.* **2013**, *40*, 76−94.
(85) Kamimura, J. A.; Santos, E. H.; Hill, L. E.; Gomes, C. L. Antimicrobial and antioxidant activities of carvacrol microencapsulated in hydroxypropyl-beta-cyclodextrin. *LWT–Food Sci. Technol.* **2014**, *57*, 701−709.
(86) Fernández-Álvarez, L.; del Valle, P.; de Arriaga, D.; García-Armesto, M. R.; Rúa, J. Binary combinations of BHA and other natural and synthetic phenolics: antimicrobial activity against *Staphylococcus aureus* and antioxidant capacity. *Food Control* **2014**, *42*, 303−309.
(87) Xue, K., Superbug, an epidemic begins. *Harvard Magazine* **2014**; May−June, pp 40−49.
(88) Park, A. Man vs. microbe: we're losing the battle against bacteria. Can we win the war? *Time* **2014**; May 19, p 20.
(89) Blaser, M. J. *Missing Microbes: How the Overuse of Antibiotics Is Fueling Our Modern Plagues*; Henry Holt and Co.: New York, 2014; p 288.
(90) Yap, P. S. X.; Yiap, B. C.; Ping, H. C.; Lim, S. H. E. Essential oils, a new horizon in combating bacterial antibiotic resistance. *Open Microbiol. J.* **2014**, *8*, 6−14.
(91) Friedman, M.; Buick, R.; Elliott, C. T. Antibacterial activities of naturally occurring compounds against antibiotic-resistant *Bacillus cereus* vegetative cells and spores, *Escherichia coli*, and *Staphylococcus aureus*. *J. Food Prot.* **2004**, *67*, 1774−1778.
(92) Nostro, A.; Blanco, A. R.; Cannatelli, M. A.; Enea, V.; Flamini, G.; Morelli, I.; Roccaro, A. S.; Alonzo, V. Susceptibility of methicillin-resistant *staphylococci* to oregano essential oil, carvacrol and thymol. *FEMS Microbiol. Lett.* **2004**, *230*, 191−195.
(93) Shin, S.; Kim, J. H. In vitro inhibitory activities of essential oils from two Korean *Thymus* species against antibiotic-resistant pathogens. *Arch. Pharm. Res.* **2005**, *28*, 897−901.
(94) Choi, J. G.; Kang, O. H.; Lee, Y. S.; Oh, Y. C.; Chae, H. S.; Jang, H. J.; Shin, D. W.; Kwon, D. Y. Antibacterial activity of methyl gallate isolated from Galla Rhois or carvacrol combined with nalidixic acid against nalidixic acid resistant bacteria. *Molecules* **2009**, *14*, 1773−1780.
(95) Palaniappan, K.; Holley, R. A. Use of natural antimicrobials to increase antibiotic susceptibility of drug resistant bacteria. *Int. J. Food Microbiol.* **2010**, *140*, 164−168.
(96) Johny, A. K.; Hoagland, T.; Venkitanarayanan, K. Effect of subinhibitory concentrations of plant-derived molecules in increasing the sensitivity of multidrug-resistant *Salmonella enterica* serovar Typhimurium DT104 to antibiotics. *Foodborne Pathog. Dis.* **2010**, *7*, 1165−1170.
(97) Thomsen, N. A.; Hammer, K. A.; Riley, T. V.; Van Belkum, A.; Carson, C. F. Effect of habituation to tea tree (*Melaleuca alternifolia*) oil on the subsequent susceptibility of *Staphylococcus* spp. to

antimicrobials, triclosan, tea tree oil, terpinen-4-ol and carvacrol. *Int. J. Antimicrob. Agents* **2013**, *41*, 343−351.
(98) Fadli, M.; Chevalier, J.; Hassani, L.; Mezrioui, N. E.; Pages, J. M. Natural extracts stimulate membrane-associated mechanisms of resistance in Gram-negative bacteria. *Lett. Appl. Microbiol.* **2014**, *58*, 472−477.
(99) Ravishankar, S.; Zhu, L.; Law, B.; Joens, L.; Friedman, M. Plant-derived compounds inactivate antibiotic-resistant *Campylobacter jejuni* strains. *J. Food Prot.* **2008**, *71*, 1145−1149.
(100) Mild, R. M.; Joens, L. A.; Friedman, M.; Olsen, C. W.; McHugh, T. H.; Law, B.; Ravishankar, S. Antimicrobial edible apple films inactivate antibiotic resistant and susceptible *Campylobacter jejuni* strains on chicken breast. *J. Food Sci.* **2011**, *76*, M163−M168.
(101) Ravishankar, S.; Zhu, L.; Reyna-Granados, J.; Law, B.; Joens, L.; Friedman, M. Carvacrol and cinnamaldehyde inactivate antibiotic-resistant *Salmonella enterica* in buffer and on celery and oysters. *J. Food Prot.* **2010**, *73*, 234−240.
(102) Upadhyaya, I.; Upadhyay, A.; Kollanoor-Johny, A.; Baskaran, S. A.; Mooyottu, S.; Darre, M. J.; Venkitanarayanan, K. Rapid inactivation of *Salmonella* Enteritidis on shell eggs by plant-derived antimicrobials. *Poult. Sci.* **2013**, *92*, 3228−3235.
(103) Friedman, M. Antibiotic activities of plant compounds against non-resistant and antibiotic-resistant foodborne human pathogens. *ACS Symp. Ser.* **2006**, *931*, 167−183.
(104) Ultee, A.; Kets, E. P.; Smid, E. J. Mechanisms of action of carvacrol on the food-borne pathogen *Bacillus cereus*. *Appl. Environ. Microbiol.* **1999**, *65*, 4606−4610.
(105) Nowotarska, S.; Nowotarski, K.; Friedman, M.; Situ, C. Effect of structure on the interactions between five natural antimicrobial compounds and phospholipids of bacterial cell membrane on model monolayers. *Molecules* **2014**, *19*, 7497−7515.
(106) Ultee, A.; Kets, E. P.; Alberda, M.; Hoekstra, F. A.; Smid, E. J. Adaptation of the food-borne pathogen *Bacillus cereus* to carvacrol. *Arch. Microbiol.* **2000**, *174*, 233−238.
(107) Di Pasqua, R.; Betts, G.; Hoskins, N.; Edwards, M.; Ercolini, D.; Mauriello, G. Membrane toxicity of antimicrobial compounds from essential oils. *J. Agric. Food Chem.* **2007**, *55*, 4863−4870.
(108) Luz Ida, S.; de Melo, A. N.; Bezerra, T. K.; Madruga, M. S.; Magnani, M.; de Souza, E. L. Sublethal amounts of *Origanum vulgare* L. essential oil and carvacrol cause injury and changes in membrane fatty acid of *Salmonella* Typhimurium cultivated in a meat broth. *Foodborne Pathog. Dis.* **2014**, *11*, 357−361.
(109) Chan, A. C.; Ager, D.; Thompson, I. P. Resolving the mechanism of bacterial inhibition by plant secondary metabolites employing a combination of whole-cell biosensors. *J. Microbiol. Methods* **2013**, *93*, 209−217.
(110) Ayari, S.; Dussault, D.; Millette, M.; Hamdi, M.; Lacroix, M. Response of *Bacillus cereus* to gamma-irradiation in combination with carvacrol or mild heat treatment. *J. Agric. Food Chem.* **2010**, *58*, 8217−8224.
(111) Ayari, S.; Dussault, D.; Hayouni, E.; Hamdi, M.; Lacroix, M. Radiation tolerance of *Bacillus cereus* pre-treated with carvacrol alone or in combination with nisin after exposure to single and multiple sub-lethal radiation treatment. *Food Control* **2013**, *32*, 693−701.
(112) Altintas, A.; Tabanca, N.; Tyihak, E.; Ott, P. G.; Moricz, A. M.; Mincsovics, E.; Wedge, D. E. Characterization of volatile constituents from *Origanum onites* and their antifungal and antibacterial activity. *J. AOAC Int.* **2013**, *96*, 1200−1208.
(113) Patil, S. D.; Sharma, R.; Srivastava, S.; Navani, N. K.; Pathania, R. Downregulation of yidC in *Escherichia coli* by antisense RNA expression results in sensitization to antibacterial essential oils eugenol and carvacrol. *PLoS One* **2013**, *8*, e57370.
(114) Ait-Ouazzou, A.; Espina, L.; Gelaw, T. K.; De Lamo-Castellví, S.; Pagán, R.; García-Gonzalo, D. New insights in mechanisms of bacterial inactivation by carvacrol. *J. Appl. Microbiol.* **2013**, *114*, 173−185.
(115) Nafisi, S.; Hajiakhoondi, A.; Yektadoost, A. Thymol and carvacrol binding to DNA: model for drug-DNA interaction. *Biopolymers* **2004**, *74*, 345−351.
(116) Wax, R. G.; Lewis, K.; Salyers, A. A.; Taber, H. *Bacterial Resistance to Antimicrobials*, 2nd ed.; CRC Press: Boca Raton, FL, 2008; available online 2nd, p 448.
(117) Domenech, M.; Garcia, E.; Prieto, A.; Moscoso, M. Insight into the composition of the intercellular matrix of *Streptococcus pneumoniae* biofilms. *Environ. Microbiol.* **2013**, *15*, 502−516.
(118) Fratamico, P. M.; Annous, B. A.; Guenther, N. W., IV *Biofilms in the Food and Beverage Industries*, 1st ed.; Woodhead Publishing Limited and CRC Press LLC: Boca Raton, FL, USA, 2009; available online 1st, p 600.
(119) Annous, B. A.; Smith, J. L.; Fratamico, P. M.; Solomon, E. B., Biofilms in fresh fruit and vegetables. In *Biofilms in the Food and Beverage Industry*, 1st ed.; Fratamico, P. M., Annous, B. A., Gunther, N. W., IV, Eds. Woodhead Publishing Limited and CRC Press LLC: Boca Raton, FL, USA, 2009; available online 1st, pp 517−535.
(120) Bodur, T.; Cagri-Mehmetoglu, A. Removal of *Listeria monocytogenes*, *Staphylococcus aureus* and *Escherichia coli* O157: H7 biofilms on stainless steel using scallop shell powder. *Food Control* **2012**, *25*, 1−9.
(121) Shen, C.; Luo, Y.; Nou, X.; Bauchan, G.; Zhou, B.; Wang, Q.; Millner, P. Enhanced inactivation of *Salmonella* and *Pseudomonas* biofilms on stainless steel by use of T-128, a fresh-produce washing aid, in chlorinated wash solutions. *Appl. Environ. Microbiol.* **2012**, *78*, 6789−6798.
(122) Gião, M. S.; Keevil, C. W. *Listeria monocytogenes* can form biofilms in tap water and enter into the viable but non-cultivable state. *Microb. Ecol.* **2014**, *67*, 603−611.
(123) Knowles, J. R.; Roller, S.; Murray, D. B.; Naidu, A. S. Antimicrobial action of carvacrol at different stages of dual-species biofilm development by *Staphylococcus aureus* and *Salmonella enterica* serovar Typhimurium. *Appl. Environ. Microbiol.* **2005**, *71*, 797−803.
(124) Nostro, A.; Roccaro, A. S.; Bisignano, G.; Marino, A.; Cannatelli, M. A.; Pizzimenti, F. C.; Cioni, P. L.; Procopio, F.; Blanco, A. R. Effects of oregano, carvacrol and thymol on *Staphylococcus aureus* and *Staphylococcus epidermidis* biofilms. *J. Med. Microbiol.* **2007**, *56*, 519−523.
(125) Nostro, A.; Scaffaro, R.; D'Arrigo, M.; Botta, L.; Filocamo, A.; Marino, A.; Bisignano, G. Study on carvacrol and cinnamaldehyde polymeric films: mechanical properties, release kinetics and anti-bacterial and antibiofilm activities. *Appl. Microbiol. Biotechnol.* **2012**, *96*, 1029−1038.
(126) Zodrow, K. R.; Schiffman, J. D.; Elimelech, M. Biodegradable polymer (PLGA) coatings featuring cinnamaldehyde and carvacrol mitigate biofilm formation. *Langmuir* **2012**, *28*, 13993−13999.
(127) Upadhyay, A.; Upadhyaya, I.; Kollanoor-Johny, A.; Venkitanarayanan, K. Antibiofilm effect of plant derived antimicrobials on *Listeria monocytogenes*. *Food Microbiol.* **2013**, *36*, 79−89.
(128) Robijns, S. C.; Roberfroid, S.; Van Puyvelde, S.; De Pauw, B.; Uceda Santamaria, E.; De Weerdt, A.; De Coster, D.; Hermans, K.; De Keersmaecker, S. C.; Vanderleyden, J.; Steenackers, H. P. A GFP promoter fusion library for the study of *Salmonella* biofilm formation and the mode of action of biofilm inhibitors. *Biofouling* **2014**, *30*, 605−625.
(129) Neyret, C.; Herry, J. M.; Meylheuc, T.; Dubois-Brissonnet, F. Plant-derived compounds as natural antimicrobials to control paper mill biofilms. *J. Ind. Microbiol. Biotechnol.* **2014**, *41*, 87−96.
(130) Ciandrini, E.; Campana, R.; Federici, S.; Manti, A.; Battistelli, M.; Falcieri, E.; Papa, S.; Baffone, W. In vitro activity of carvacrol against titanium-adherent oral biofilms and planktonic cultures. *Clin. Oral Investig.* **2014**, available online Jan 24; doi: 10.1007/s00784-013-1179-9.
(131) Burt, S. A.; Ojo-Fakunle, V. T.; Woertman, J.; Veldhuizen, E. J. The natural antimicrobial carvacrol inhibits quorum sensing in *Chromobacterium violaceum* and reduces bacterial biofilm formation at sub-lethal concentrations. *PLoS One* **2014**, *9*, e93414.
(132) Beers, M. H. *The Merck Manual of Diagnosis and Therapy*, 18th ed.; Merck Research Laboratories: Whitehouse Station, NJ, 2006.
(133) Bergonzelli, G. E.; Donnicola, D.; Porta, N.; Corthesy-Theulaz, I. E. Essential oils as components of a diet-based approach to

management of *Helicobacter* infection. *Antimicrob. Agents Chemother.* **2003**, *47*, 3240−3246.
(134) Eftekhar, F.; Nariman, F.; Yousefzadi, M.; Hadiand, J.; Ebrahimi, S. N. Anti-*Helicobacter pylori* activity and essential oil composition of *Thymus caramanicus* from Iran. *Nat. Prod. Commun.* **2009**, *4*, 1139−1142.
(135) Rasooli, I.; Mirmostafa, S. A. Bacterial susceptibility to and chemical composition of essential oils from *Thymus kotschyanus* and *Thymus persicus*. *J. Agric. Food Chem.* **2003**, *51*, 2200−2205.
(136) Marwah, R. G.; Fatope, M. O.; Deadman, M. L.; Ochei, J. E.; Al-Saidi, S. H. Antimicrobial activity and the major components of the essential oil of *Plectranthus cylindraceus*. *J. Appl. Microbiol.* **2007**, *103*, 1220−1226.
(137) Cosge, B.; Turker, A.; Ipek, A.; Gurbuz, B. Chemical compositions and antibacterial activities of the essential oils from aerial parts and corollas of *Origanum acutidens* (Hand.-Mazz.) *Ietswaart*, an endemic species to Turkey. *Molecules* **2009**, *14*, 1702−1712.
(138) Saidi, M.; Ghafourian, S.; Zarin-Abaadi, M.; Movahedi, K.; Sadeghifard, N. In vitro antimicrobial and antioxidant activity of black thyme (*Thymbra spicata* L.) essential oils. *Roum. Arch. Microbiol. Immunol.* **2012**, *71*, 61−69.
(139) Altiok, D.; Altiok, E.; Tihminlioglu, F. Physical, antibacterial and antioxidant properties of chitosan films incorporated with thyme oil for potential wound healing applications. *J. Mater. Sci. Mater. Med.* **2010**, *21*, 2227−2236.
(140) Iten, F.; Saller, R.; Abel, G.; Reichling, J. Additive antmicrobial effects of the active components of the essential oil of *Thymus vulgaris*—Chemotype carvacrol. *Planta Med.* **2009**, *75*, 1231−1236.
(141) Bueno-Sánchez, J. G.; Martínez-Morales, J. R.; Stashenko, E. E.; Ribón, W. Anti-tubercular activity of eleven aromatic and medicinal plants occurring in Colombia. *Biomedica* **2009**, *29*, 51−60.
(142) Alokam, R.; Jeankumar, V. U.; Sridevi, J. P.; Matikonda, S. S.; Peddi, S.; Alvala, M.; Yogeeswari, P.; Sriram, D. Identification and structure-activity relationship study of carvacrol derivatives as *Mycobacterium tuberculosis* chorismate mutase inhibitors. *J. Enzyme Inhib. Med. Chem.* **2014**, *29*, 547−554.
(143) Kortman, G. A. M.; Roelofs, R. W. H. M.; Swinkels, D. W.; de Jonge, M. I.; Burt, S. A.; Tjalsma, H. Iron-induced virulence of *Salmonella enterica* serovar Typhimurium at the intestinal epithelial interface can be suppressed by carvacrol. *Antimicrob. Agents Chemother.* **2014**, *58*, 1664−1670.
(144) Botelho, M. A.; Nogueira, N. A.; Bastos, G. M.; Fonseca, S. G.; Lemos, T. L.; Matos, F. J.; Montenegro, D.; Heukelbach, J.; Rao, V. S.; Brito, G. A. Antimicrobial activity of the essential oil from *Lippia sidoides*, carvacrol and thymol against oral pathogens. *Braz. J. Med. Biol. Res.* **2007**, *40*, 349−356.
(145) Obaidat, R. M.; Bader, A.; Al-Rajab, W.; Abu Sheikha, G.; Obaidat, A. A. Preparation of mucoadhesive oral patches containing tetracycline hydrochloride and carvacrol for treatment of local mouth bacterial infections and candidiasis. *Sci. Pharm.* **2011**, *79*, 197−212.
(146) Botelho, M. A.; Martins, J. G.; Ruela, R. S.; Rachid, I.; Santos, J. A.; Soares, J. B.; França, M. C.; Montenegro, D.; Ruela, W. S.; Barros, L. P.; Queiroz, D. B.; Araujo, R. S.; Sampio, F. C. Protective effect of locally applied carvacrol gel on ligature-induced periodontitis in rats: a tapping mode AFM study. *Phytother. Res.* **2009**, *23*, 1439−1448.
(147) Hashemipour, H.; Kermanshahi, H.; Golian, A.; Khaksar, V. Effects of carboxy methyl cellulose and thymol + carvacrol on performance, digesta viscosity and some blood metabolites of broilers. *J. Anim. Physiol. Anim. Nutr. (Berl.)* **2014**, *98*, 672−679.
(148) Bampidis, V. A.; Christodoulou, V.; Florou-Paneri, P.; Christaki, E.; Chatzopoulou, P. S.; Tsiligianni, T.; Spais, A. B. Effect of dietary dried oregano leaves on growth performance, carcase characteristics and serum cholesterol of female early maturing turkeys. *Br. Poult. Sci.* **2005**, *46*, 595−601.
(149) Bravo, D.; Pirgozliev, V.; Rose, S. P. A mixture of carvacrol, cinnamaldehyde, and capsicum oleoresin improves energy utilization and growth performance of broiler chickens fed maize-based diet. *J. Anim. Sci.* **2014**, *92*, 1531−1536.
(150) Venkitanarayanan, K.; Kollanoor-Johny, A.; Darre, M. J.; Donoghue, A. M.; Donoghue, D. J. Use of plant-derived antimicrobials for improving the safety of poultry products. *Poult. Sci.* **2013**, *92*, 493−501.
(151) Verlinden, M.; Pasmans, F.; Mahu, M.; Vande Maele, L.; De Pauw, N.; Yang, Z.; Haesebrouck, F.; Martel, A. In vitro sensitivity of poultry *Brachyspira intermedia* isolates to essential oil components and in vivo reduction of *Brachyspira intermedia* in rearing pullets with cinnamaldehyde feed supplementation. *Poult. Sci.* **2013**, *92*, 1202−1207.
(152) Zhang, D.; Hu, H.; Rao, Q.; Zhao, Z. Synergistic effects and physiological responses of selected bacterial isolates from animal feed to four natural antimicrobials and two antibiotics. *Foodborne Pathog. Dis.* **2011**, *8*, 1055−1062.
(153) Fratini, F.; Casella, S.; Leonardi, M.; Pisseri, F.; Ebani, V. V.; Pistelli, L.; Pistelli, L. Antibacterial activity of essential oils, their blends and mixtures of their main constituents against some strains supporting livestock mastitis. *Fitoterapia* **2014**, *96*, 1−7.
(154) Giannenas, I.; Skoufos, J.; Giannakopoulos, C.; Wiemann, M.; Gortzi, O.; Lalas, S.; Kyriazakis, I. Effects of essential oils on milk production, milk composition, and rumen microbiota in Chios dairy ewes. *J. Dairy Sci.* **2011**, *94*, 5569−5577.
(155) Martinez-Fernandez, G.; Abecia, L.; Martin-Garcia, A. I.; Ramos-Morales, E.; Hervas, G.; Molina-Alcaide, E.; Yanez-Ruiz, D. R. In vitro-in vivo study on the effects of plant compounds on rumen fermentation, microbial abundances and methane emissions in goats. *Animal* **2013**, *7*, 1925−1934.
(156) Varel, V. H. Carvacrol and thymol reduce swine waste odor and pathogens: stability of oils. *Curr. Microbiol.* **2002**, *44*, 38−43.
(157) Varel, V. H.; Miller, D. N. Effect of carvacrol and thymol on odor emissions from livestock wastes. *Water Sci. Technol.* **2001**, *44*, 143−148.
(158) Varel, V. H.; Miller, D. N.; Lindsay, A. D. Plant oils thymol and eugenol affect cattle and swine waste emissions differently. *Water Sci. Technol.* **2004**, *50*, 207−213.
(159) Akkol, E. K.; Avci, G.; Kucukkurt, I.; Keles, H.; Tamer, U.; Ince, S.; Yesilada, E. Cholesterol-reducer, antioxidant and liver protective effects of *Thymbra spicata* L. var. spicata. *J. Ethnopharmacol.* **2009**, *126*, 314−319.
(160) Park, I. K.; Kim, J. N.; Lee, Y. S.; Lee, S. G.; Ahn, Y. J.; Shin, S. C. Toxicity of plant essential oils and their components against *Lycoriella ingenua* (Diptera: Sciaridae). *J. Econ. Entomol.* **2008**, *101*, 139−144.
(161) Ma, W. B.; Feng, J. T.; Jiang, Z. L.; Wu, H.; Ma, Z. Q.; Zhang, X. Fumigant activity of eleven essential oil compounds and their selected binary mixtures against *Culex pipiens pallens* (Diptera: Culicidae). *Parasitol. Res.* **2014**, available online Jul 13; doi: 10.1007/s00436-014-4028-0.
(162) Anderson, J. A.; Coats, J. R. Acetylcholinesterase inhibition by nootkatone and carvacrol in arthropods. *Pestic. Biochem. Physiol.* **2012**, *102*, 124−128.
(163) Tong, F.; Gross, A. D.; Dolan, M. C.; Coats, J. R. The phenolic monoterpenoid carvacrol inhibits the binding of nicotine to the housefly nicotinic acetylcholine receptor. *Pest Manage. Sci.* **2013**, *69*, 775−780.
(164) Ahmad, A.; Khan, A.; Akhtar, F.; Yousuf, S.; Xess, I.; Khan, L. A.; Manzoor, N. Fungicidal activity of thymol and carvacrol by disrupting ergosterol biosynthesis and membrane integrity against *Candida*. *Eur. J. Clin. Microbiol. Infect. Dis.* **2011**, *30*, 41−50.
(165) Perez-Alfonso, C. O.; Martinez-Romero, D.; Zapata, P. J.; Serrano, M.; Valero, D.; Castillo, S. The effects of essential oils carvacrol and thymol on growth of *Penicillium digitatum* and *P. italicum* involved in lemon decay. *Int. J. Food Microbiol.* **2012**, *158*, 101−106.
(166) Aznar, A.; Fernández, P. S.; Periago, P. M.; Palop, A., Antimicrobial activity of nisin, thymol, carvacrol and cymene against growth of *Candida lusitaniae*. *Food Sci. Technol. Int.* **2013**, available online Nov 29; doi: 10.1177/1082013213514593.

(167) Zabka, M.; Pavela, R. Antifungal efficacy of some natural phenolic compounds against significant pathogenic and toxinogenic filamentous fungi. *Chemosphere* **2013**, *93*, 1051−1056.
(168) Abbaszadeh, S.; Sharifzadeh, A.; Shokri, H.; Khosravi, A. R.; Abbaszadeh, A. Antifungal efficacy of thymol, carvacrol, eugenol and menthol as alternative agents to control the growth of food-relevant fungi. *J. Mycol. Med.* **2014**, *24*, e51−56.
(169) Mancini, E.; Camele, I.; Elshafie, H. S.; De Martino, L.; Pellegrino, C.; Grulova, D.; De Feo, V. Chemical composition and biological activity of the essential oil of *Origanum vulgare* ssp. hirtum from different areas in the southern Apennines (Italy). *Chem. Biodivers.* **2014**, *11*, 639−651.
(170) Gallucci, M. N.; Carezzano, M. E.; Oliva, M. M.; Demo, M. S.; Pizzolitto, R. P.; Zunino, M. P.; Zygadlo, J. A.; Dambolena, J. S. In vitro activity of natural phenolic compounds against fluconazole-resistant *Candida* species: a quantitative structure-activity relationship analysis. *J. Appl. Microbiol.* **2014**, *116*, 795−804.
(171) Ahmad, A.; Khan, A.; Manzoor, N. Reversal of efflux mediated antifungal resistance underlies synergistic activity of two monoterpenes with fluconazole. *Eur. J. Pharm. Sci.* **2013**, *48*, 80−86.
(172) Lima, I. O.; De Oliveira Pereira, F.; De Oliveira, W. A.; De Oliveira Lima, E.; Menezes, E. A.; Cunha, F. A.; De Fátima Formiga Melo Diniz, M. Antifungal activity and mode of action of carvacrol against *Candida albicans* strains. *J. Essent. Oil Res.* **2013**, *25*, 138−142.
(173) Martin, J. A.; Solla, A.; Garcia-Vallejo, M. C.; Gil, L. Chemical changes in *Ulmus minor* xylem tissue after salicylic acid or carvacrol treatments are associated with enhanced resistance to *Ophiostoma novo-ulmi*. *Phytochemistry* **2012**, *83*, 104−109.
(174) Mooyottu, S.; Kollanoor-Johny, A.; Flock, G.; Bouillaut, L.; Upadhyay, A.; Sonenshein, A. L.; Venkitanarayanan, K. Carvacrol and trans-cinnamaldehyde reduce *Clostridium difficile* toxin production and cytotoxicity in vitro. *Int. J. Mol. Sci.* **2014**, *15*, 4415−4430.
(175) Dambolena, J. S.; Zygadlo, J. A.; Rubinstein, H. R. Antifumonisin activity of natural phenolic compounds. A structure-property-activity relationship study. *Int. J. Food Microbiol.* **2011**, *145*, 140−146.
(176) Friedman, M.; Rasooly, R. Review of the inhibition of biological activities of food-related selected toxins by natural compounds. *Toxins (Basel)* **2013**, *5*, 743−775.
(177) Lai, W. L.; Chuang, H. S.; Lee, M. H.; Wei, C. L.; Lin, C. F.; Tsai, Y. C. Inhibition of herpes simplex virus type 1 by thymol-related monoterpenoids. *Planta Med.* **2012**, *78*, 1636−1638.
(178) Santoyo, S.; Jaime, L.; García-Risco, M. R.; Ruiz-Rodríguez, A.; Reglero, G. Antiviral properties of supercritical CO2 extracts from oregano and sage. *Int. J. Food Prop.* **2014**, *17*, 1150−1161.
(179) Pilau, M. R.; Alves, S. H.; Weiblen, R.; Arenhart, S.; Cueto, A. P.; Lovato, L. T. Antiviral activity of the *Lippia graveolens* (Mexican oregano) essential oil and its main compound carvacrol against human and animal viruses. *Braz. J. Microbiol.* **2011**, *42*, 1616−1624.
(180) Gilling, D. H.; Kitajima, M.; Torrey, J. R.; Bright, K. R. Antiviral efficacy and mechanisms of action of oregano essential oil and its primary component carvacrol against murine norovirus. *J. Appl. Microbiol.* **2014**, *116*, 1149−1163.
(181) Sökmen, M.; Serkedjieva, J.; Daferera, D.; Gulluce, M.; Polissiou, M.; Tepe, B.; Akpulat, H. A.; Sahin, F.; Sokmen, A. In vitro antioxidant, antimicrobial, and antiviral activities of the essential oil and various extracts from herbal parts and callus cultures of *Origanum acutidens*. *J. Agric. Food Chem.* **2004**, *52*, 3309−3312.
(182) Schnitzler, P.; Astani, A.; Reichling, J. Antiviral effects of plant-derived essential oils and pure oil components. In *Lipids and Essential Oils as Antimicrobial Agents*; Thormar, H., Ed.; John Wiley & Sons, Ltd: Chichester, UK, 2011; pp 239−254; doi: 10.1002/9780470976623.ch10.
(183) de Oliveira Souza Senra, T.; Zeringota, V.; de Oliveira Monteiro, C. M.; Calmon, F.; Maturano, R.; Gomes, G. A.; Faza, A.; de Carvalho, M. G.; Daemon, E. Assessment of the acaricidal activity of carvacrol, (E)-cinnamaldehyde, trans-anethole, and linalool on larvae of *Rhipicephalus microplus* and *Dermacentor nitens* (Acari: Ixodidae). *Parasitol. Res.* **2013**, *112*, 1461−1466.
(184) Senra, T. O.; Calmon, F.; Zeringota, V.; Monteiro, C. M.; Maturano, R.; da Silva Matos, R.; Melo, D.; Gomes, G. A.; de Carvalho, M. G.; Daemon, E. Investigation of activity of monoterpenes and phenylpropanoids against immature stages of *Amblyomma cajennense* and *Rhipicephalus sanguineus* (Acari: Ixodidae). *Parasitol. Res.* **2013**, *112*, 3471−3476.
(185) Monzote, L.; Pastor, J.; Scull, R.; Gille, L. Antileishmanial activity of essential oil from *Chenopodium ambrosioides* and its main components against experimental cutaneous leishmaniasis in BALB/c mice. *Phytomedicine* **2014**, *21*, 1048−1052.
(186) Farias-Junior, A. P.; Rios, M. C.; Moura, T. A.; Almeida, R. P.; Alves, P. B.; Blank, A. F.; Fernandes, R. P. M.; Scher, R. Leishmanicidal activity of carvacrol-rich essential oil from *Lippia sidoides* Cham. *Biol. Res.* **2012**, *45*, 399−402.
(187) Oka, Y.; Nacar, S.; Putievsky, E.; Ravid, U.; Yaniv, Z.; Spiegel, Y. Nematicidal activity of essential oils and their components against the root-knot nematode. *Phytopathology* **2000**, *90*, 710−715.
(188) Nibret, E.; Wink, M. Trypanocidal and antileukaemic effects of the essential oils of *Hagenia abyssinica*, *Leonotis ocymifolia*, *Moringa stenopetala*, and their main individual constituents. *Phytomedicine* **2010**, *17*, 911−920.
(189) Escobar, P.; Leal, S. M.; Herrera, L. V.; Martinez, J. R.; Stashenko, E. Chemical composition and antiprotozoal activities of Colombian *Lippia* spp essential oils and their major components. *Mem. Inst. Oswaldo Cruz.* **2010**, *105*, 184−190.
(190) Dolan, M. C.; Jordan, R. A.; Schulze, T. L.; Schulze, C. J.; Manning, M. C.; Ruffolo, D.; Schmidt, J. P.; Piesman, J.; Karchesy, J. J. Ability of two natural products, nootkatone and carvacrol, to suppress *Ixodes scapularis* and *Amblyomma americanum* (Acari: Ixodidae) in a Lyme disease endemic area of New Jersey. *J. Econ. Entomol.* **2009**, *102*, 2316−2324.
(191) Austgulen, L. T.; Solheim, E.; Scheline, R. R. Metabolism in rats of *p*-cymene derivatives: carvacrol and thymol. *Pharmacol. Toxicol.* **1987**, *61*, 98−102.
(192) Jäger, W. Metabolism of terpenoids in animal models and humans. In *Handbook of Essential Oils: Science, Technology, and Applications*; Baser, K. H. C., Buchbauer, G., Eds. CRC Press, Taylor & Frances Group: Boca Raton, FL, 2010; pp 209−234.
(193) Dong, R. H.; Fang, Z. Z.; Zhu, L. L.; Ge, G. B.; Cao, Y. F.; Li, X. B.; Hu, C. M.; Yang, L.; Liu, Z. Y. Identification of CYP isoforms involved in the metabolism of thymol and carvacrol in human liver microsomes (HLMs). *Pharmazie* **2012**, *67*, 1002−1006.
(194) Aristatile, B.; Al-Numair, K. S.; Al-Assaf, A. H.; Pugalendi, K. V. Pharmacological effect of carvacrol on D-galactosamine-induced mitochondrial enzymes and DNA damage by single-cell gel electrophoresis. *J. Nat. Med.* **2011**, *65*, 568−577.
(195) Pires, L. F.; Costa, L. M.; de Almeida, A. A.; Silva, O. A.; Cerqueira, G. S.; de Sousa, D. P.; de Freitas, R. M. Is there a correlation between in vitro antioxidant potential and in vivo effect of carvacryl acetate against oxidative stress in mice hippocampus? *Neurochem. Res.* **2014**, *39*, 758−769.
(196) Veldhuizen, E. J.; Creutzberg, T. O.; Burt, S. A.; Haagsman, H. P. Low temperature and binding to food components inhibit the antibacterial activity of carvacrol against *Listeria monocytogenes* in steak tartare. *J. Food Prot.* **2007**, *70*, 2127−2132.
(197) Noma, Y.; Asakawa, Y. Biotransformation of monoterpenoids by microorganisms, insects, and mammals. In *Handbook of Essential Oils: Science, Technology, and Applications*; Baser, K. H. C., Buchbauer, G., Eds.; CRC Press, Taylor & Frances Group: Boca Raton, FL, 2009; pp 585−736.
(198) Lima, M. d. S.; Quintans-Júnior, L. J.; de Santana, W. A.; Martins Kaneto, C.; Pereira Soares, M. B.; Villarreal, C. F. Anti-inflammatory effects of carvacrol: evidence for a key role of interleukin-10. *Eur. J. Pharmacol.* **2013**, *699*, 112−117.
(199) Silva, F. V.; Guimaraes, A. G.; Silva, E. R.; Sousa-Neto, B. P.; Machado, F. D.; Quintans-Junior, L. J.; Arcanjo, D. D.; Oliveira, F. A.; Oliveira, R. C. Anti-inflammatory and anti-ulcer activities of carvacrol, a monoterpene present in the essential oil of oregano. *J. Med. Food* **2012**, *15*, 984−991.

(200) Aristatile, B.; Al-Assaf, A. H.; Pugalendi, K. V. Carvacrol suppresses the expression of inflammatory marker genes in D-galactosamine-hepatotoxic rats. *Asian Pac. J. Trop. Med.* **2013**, *6*, 205−211.
(201) de Cassia da Silveira e Sa, R.; Andrade, L. N.; de Sousa, D. P. A review on anti-inflammatory activity of monoterpenes. *Molecules* **2013**, *18*, 1227−1254.
(202) Guimarães, A. G.; Xavier, M. A.; De Santana, M. T.; Camargo, E. A.; Santos, C. A.; Brito, F. A.; Barreto, E. O.; Cavalcanti, S. C. H.; Antoniolli, Â. R.; Oliveira, R. C. M.; Quintans-Júnior, L. J. Carvacrol attenuates mechanical hypernociception and inflammatory response. . *Naunyn-Schmiedeberg's Arch. Pharmacol.* **2012**, *385*, 253−263.
(203) Klein, A. H.; Carstens, M. I.; Carstens, E. Eugenol and carvacrol induce temporally desensitizing patterns of oral irritation and enhance innocuous warmth and noxious heat sensation on the tongue. *Pain* **2013**, *154*, 2078−2087.
(204) Klein, A. H.; Joe, C. L.; Davoodi, A.; Takechi, K.; Carstens, M. I.; Carstens, E. Eugenol and carvacrol excite first- and second-order trigeminal neurons and enhance their heat-evoked responses. *Neuroscience* **2014**, *271*, 45−55.
(205) de Santana, M. T.; Silva, V. B.; de Brito, R. G.; Dos Santos, P. L.; de Holanda Cavalcanti, S. C.; Barreto, E. O.; de Souza Ferro, J. N.; Dos Santos, M. R.; de Sousa Araujo, A. A.; Quintans-Junior, L. J., Synthesis and pharmacological evaluation of carvacrol propionate. *Inflammation* **2014**, available online Apr 8; doi: 10.1007/s10753-014-9884-3.
(206) Cavalcante Melo, F. H.; Rios, E. R. V.; Rocha, N. F. M.; Citõ, M. D. C. D. O.; Fernandes, M. L.; De Sousa, D. P.; De Vasconcelos, S. M. M.; De Sousa, F. C. F. Antinociceptive activity of carvacrol (5-isopropyl-2-methylphenol) in mice. *J. Pharm. Pharmacol.* **2012**, *64*, 1722−1729.
(207) Guimarães, A. G.; Silva, F. V.; Xavier, M. A.; Santos, M. R. V.; Oliveira, R. C. M.; Oliveira, M. G. B.; Oliveira, A. P.; De Souza, C. C.; Quintans-Júnior, L. J. Orofacial analgesic-like activity of carvacrol in rodents. *Z. Naturforsch. C* **2012**, *67 C*, 481−485.
(208) Boskabady, M. H.; Jalali, S. Effect of carvacrol on tracheal responsiveness, inflammatory mediators, total and differential WBC count in blood of sensitized guinea pigs. *Exp. Biol. Med. (Maywood)* **2013**, *238*, 200−208.
(209) Guimarães, A. G.; Quintans, J. S. S.; Quintans-Júnior, L. J. Monoterpenes with analgesic activity—a systematic review. *Phytother. Res.* **2013**, *27*, 1−15.
(210) Friedman, M.; Burns, C. F.; Butchko, C. A.; Blankemeyer, J. T. Folic acid protects against potato glycoalkaloid α-chaconine-induced disruption of frog embryo cell membranes and developmental toxicity. *J. Agric. Food Chem.* **1997**, *45*, 3991−3994.
(211) McWilliams, M. L.; Blankemeyer, J. T.; Friedman, M. The folic acid analogue methotrexate protects frog embryo cell membranes against damage by the potato glycoalkaloid α-chaconine. *Food Chem. Toxicol.* **2000**, *38*, 853−859.
(212) Celik, F.; Gocmez, C.; Bozkurt, M.; Kaplan, I.; Kamasak, K.; Akil, E.; Dogan, E.; Guzel, A.; Uzar, E. Neuroprotective effects of carvacrol and pomegranate against methotrexate-induced toxicity in rats. *Eur. Rev. Med. Pharmacol. Sci.* **2013**, *17*, 2988−2993.
(213) Banji, O. J.; Banji, D.; Soumya, N.; Chilipi, K. K.; Kalpana, C. H.; Kranthi Kumar, C. H.; Annamalai, A. R. Combination of carvacrol with methotrexate suppresses Complete Freund's Adjuvant induced synovial inflammation with reduced hepatotoxicity in rats. *Eur. J. Pharmacol.* **2014**, *723*, 91−98.
(214) Bozkurt, M.; Em, S.; Oktayoglu, P.; Turkcu, G.; Yuksel, H.; Sariyildiz, M. A.; Caglayan, M.; Batmaz, I.; Nas, K.; Bozkurt, Y.; Kuyumcu, M. Carvacrol prevents methotrexate-induced renal oxidative injury and renal damage in rats. *Clin. Invest. Med.* **2014**, *37*, E19−25.
(215) Koparal, A. T.; Zeytinoglu, M. Effects of carvacrol on a human non-small cell lung cancer (NSCLC) cell line, A549. *Cytotechnology* **2003**, *43*, 149−154.
(216) Karkabounas, S.; Kostoula, O. K.; Daskalou, T.; Veltsistas, P.; Karamouzis, M.; Zelovitis, I.; Metsios, A.; Lekkas, P.; Evangelou, A. M.; Kotsis, N.; Skoufos, I. Anticarcinogenic and antiplatelet effects of carvacrol. *Exp. Oncol.* **2006**, *28*, 121−125.
(217) Slameňová, D.; Horváthová, E.; Chalupa, I.; Wsólová, L.; Navarová, J. Ex vivo assessment of protective effects of carvacrol against DNA lesions induced in primary rat cells by visible light excited methylene blue (VL+MB). *Neoplasma* **2011**, *58*, 14−19.
(218) Slameňová, D.; Horváthová, E.; Maršálková, L.; Wsólová, L. Carvacrol given to rats in drinking water reduces the level of DNA lesions induced in freshly isolated hepatocytes and testicular cells by H(2)O(2). *Neoplasma* **2008**, *55*, 394−399.
(219) Slameňová, D.; Horváthová, E.; Šramkovóá, M.; Maršálková, L. DNA-protective effects of two components of essential plant oils carvacrol and thymol on mammalian cells cultured *in vitro*. *Neoplasma* **2007**, *54*, 108−112.
(220) Slameňová, D.; Kozics, K.; Hunáková, L.; Melusova, M.; Navarová, J.; Horváthová, E. Comparison of biological processes induced in HepG2 cells by tert-butyl hydroperoxide (t-BHP) and hydroperoxide (H_2O_2): The influence of carvacrol. *Mutat. Res.* **2013**, *757*, 15−22.
(221) Yin, Q.-H.; Yan, F.-X.; Zu, X.-Y.; Wu, Y.-H.; Wu, X.-P.; Liao, M.-C.; Deng, S.-W.; Yin, L.-L.; Zhuang, Y.-Z. Anti-proliferative and pro-apoptotic effect of carvacrol on human hepatocellular carcinoma cell line HepG-2. *Cytotechnology* **2012**, *64*, 43−51.
(222) Bimczok, D.; Rau, H.; Sewekow, E.; Janczyk, P.; Souffrant, W. B.; Rothkotter, H. J. Influence of carvacrol on proliferation and survival of porcine lymphocytes and intestinal epithelial cells in vitro. *Toxicol. In Vitro* **2008**, *22*, 652−658.
(223) Arunasree, K. M. Anti-proliferative effects of carvacrol on a human metastatic breast cancer cell line, MDA-MB 231. *Phytomedicine* **2010**, *17*, 581−588.
(224) Jayakumar, S.; Madankumar, A.; Asokkumar, S.; Raghunandhakumar, S.; Gokula dhas, K.; Kamaraj, S.; Divya, M. G.; Devaki, T. Potential preventive effect of carvacrol against diethylnitrosamine-induced hepatocellular carcinoma in rats. *Mol. Cell. Biochem.* **2012**, *360*, 51−60.
(225) Liang, W.-Z.; Chou, C.-T.; Lu, T.; Chi, C.-C.; Tseng, L.-L.; Pan, C.-C.; Lin, K.-L.; Kuo, C.-C.; Jan, C.-R. The mechanism of carvacrol-evoked [Ca2+]i rises and non-Ca2+-triggered cell death in OC2 human oral cancer cells. *Toxicology* **2013**, *303*, 152−161.
(226) Zeidán-Chuliá, F.; Gursoy, M.; de Oliveira, B. H.; Gelain, D. P.; Könönen, E.; Gursoy, U. K.; Moreira, J. C.; Uitto, V. J. Focussed microarray analysis of apoptosis in periodontitis and its potential pharmacological targeting by carvacrol. *Arch. Oral Biol.* **2014**, *59*, 461−469.
(227) Aydin, E.; Turkez, H.; Keles, M. S. The effect of carvacrol on healthy neurons and N2a cancer cells: some biochemical, anticancerogenicity and genotoxicity studies. *Cytotechnology* **2014**, *66*, 149−157.
(228) Friedman, M.; Mackey, B. E.; Kim, H.-J.; Lee, I.-S.; Lee, K.-R.; Lee, S.-U.; Kozukue, E.; Kozukue, N. Structure-activity relationships of tea compounds against human cancer cells. *J. Agric. Food Chem.* **2007**, *55*, 243−253.
(229) Friedman, M. Anticarcinogenic, cardioprotective, and other health benefits of tomato compounds lycopene, α-tomatine, and tomatidine in pure form and in fresh and processed tomatoes. *J. Agric. Food Chem.* **2013**, *61*, 9534−9550.
(230) Nam, S. H.; Choi, S. P.; Kang, M. Y.; Kozukue, N.; Friedman, M. Antioxidative, antimutagenic, and anticarcinogenic activities of rice bran extracts in chemical and cell assays. *J. Agric. Food Chem.* **2005**, *53*, 816−822.
(231) Aristatile, B.; Al-Numair, K. S.; Veeramani, C.; Pugalendi, K. V. Antihyperlipidemic effect of carvacrol on D-galactosamine-induced hepatotoxic rats. *J. Basic Clin. Physiol. Pharmacol.* **2009**, *20*, 15−27.
(232) Earley, S.; Gonzales, A. L.; Garcia, Z. I. A dietary agonist of transient receptor potential cation channel V3 elicits endothelium-dependent vasodilation. *Mol. Pharmacol.* **2010**, *77*, 612−620.
(233) Peixoto-Neves, D.; Silva-Alves, K. S.; Gomes, M. D. M.; Lima, F. C.; Lahlou, S.; Magalhães, P. J. C.; Ceccatto, V. M.; Coelho-De-Souza, A. N.; Leal-Cardoso, J. H. Vasorelaxant effects of the

monoterpenic phenol isomers, carvacrol and thymol, on rat isolated aorta. *Fundam. Clin. Pharmacol.* **2010**, *24*, 341−350.
(234) Magyar, J.; Szentandrassy, N.; Banyasz, T.; Fulop, L.; Varro, A.; Nanasi, P. P. Effects of terpenoid phenol derivatives on calcium current in canine and human ventricular cardiomyocytes. *Eur. J. Pharmacol.* **2004**, *487*, 29−36.
(235) Aydin, Y.; Kutlay, Ö.; Ari, S.; Duman, S.; Uzuner, K.; Aydin, S. Hypotensive effects of carvacrol on the blood pressure of normotensive rats. *Planta Med.* **2007**, *73*, 1365−1371.
(236) Yu, W.; Liu, Q.; Zhu, S. Carvacrol protects against acute myocardial infarction of rats via anti-oxidative and anti-apoptotic pathways. *Biol. Pharm. Bull.* **2013**, *36*, 579−584.
(237) Bayramoglu, G.; Senturk, H.; Bayramoglu, A.; Uyanoglu, M.; Colak, S.; Ozmen, A.; Kolankaya, D. Carvacrol partially reverses symptoms of diabetes in STZ-induced diabetic rats. *Cytotechnology* **2014**, *66*, 251−257.
(238) Ezhumalai, M.; Radhiga, T.; Pugalendi, K. V. Antihyperglycemic effect of carvacrol in combination with rosiglitazone in high-fat diet-induced type 2 diabetic C57BL/6J mice. *Mol. Cell. Biochem.* **2014**, *385*, 23−31.
(239) Cho, S.; Choi, Y.; Park, S.; Park, T. Carvacrol prevents diet-induced obesity by modulating gene expressions involved in adipogenesis and inflammation in mice fed with high-fat diet. *J. Nutr. Biochem.* **2012**, *23*, 192−201.
(240) Kim, S. P.; Park, S. O.; Lee, S. J.; Nam, S. H.; Friedman, M. A polysaccharide isolated from the liquid culture of *Lentinus edodes* (Shiitake) mushroom mycelia containing black rice bran protects mice against a *Salmonella* lipopolysaccharide-induced endotoxemia. *J. Agric. Food Chem.* **2013**, *61*, 10987−10994.
(241) Feng, X.; Jia, A. Protective effect of carvacrol on acute lung injury induced by lipopolysaccharide in mice. *Inflammation* **2014**, *37*, 1091−1101.
(242) Kim, S. P.; Nam, S. H.; Friedman, M. Rice hull smoke extract protects mice against a *Salmonella* lipopolysaccharide-induced endotoxemia. *J. Agric. Food Chem.* **2014**, Accepted July 19, 2014, doi: 10.1021/jf501533s.
(243) Oliveira, I. S.; Da Silva, F. V.; Viana, A. F. S. C.; Dos Santos, M. R. V.; Quintans-Júnior, L. J.; Martins, M. D. C. C.; Nunes, P. H. M.; Oliveira, F. D. A.; Oliveira, R. D. C. M. Gastroprotective activity of carvacrol on experimentally induced gastric lesions in rodents. *Naunyn-Schmiedeberg's Arch. Pharmacol.* **2012**, *385*, 899−908.
(244) Llana-Ruiz-Cabello, M.; Gutiérrez-Praena, D.; Pichardo, S.; Moreno, F. J.; Bermúdez, J. M.; Aucejo, S.; Cameán, A. M. Cytotoxicity and morphological effects induced by carvacrol and thymol on the human cell line Caco-2. *Food Chem. Toxicol.* **2014**, *64*, 281−290.
(245) Nafees, S.; Ahmad, S. T.; Arjumand, W.; Rashid, S.; Ali, N.; Sultana, S. Carvacrol ameliorates thioacetamide-induced hepatotoxicity by abrogation of oxidative stress, inflammation, and apoptosis in liver of Wistar rats. *Hum. Exp. Toxicol.* **2013**, *32*, 1292−1304.
(246) Uyanoglu, M.; Canbek, M.; Aral, E.; Husnu Can Baser, K. Effects of carvacrol upon the liver of rats undergoing partial hepatectomy. *Phytomedicine* **2008**, *15*, 226−229.
(247) Canbek, M.; Uyanoglu, M.; Bayramoglu, G.; Senturk, H.; Erkasap, N.; Koken, T.; Uslu, S.; Demirustu, C.; Aral, E.; Husnu Can Baser, K. Effects of carvacrol on defects of ischemia-reperfusion in the rat liver. *Phytomedicine* **2008**, *15*, 447−452.
(248) Aristatile, B.; Al-Numair, K. S.; Veeramani, C.; Pugalendi, K. V. Effect of carvacrol on hepatic marker enzymes and antioxidant status in D-galactosamine-induced hepatotoxicity in rats. *Fundam. Clin. Pharmacol.* **2009**, *23*, 757−765.
(249) Jukic, M.; Politeo, O.; Maksimovic, M.; Milos, M.; Milos, M. In vitro acetylcholinesterase inhibitory properties of thymol, carvacrol and their derivatives thymoquinone and thymohydroquinone. *Phytother. Res.* **2007**, *21*, 259−261.
(250) Deng, W.; Lu, H.; Teng, J. Carvacrol attenuates diabetes-associated cognitive deficits in rats. *J. Mol. Neurosci.* **2013**, *51*, 813−819.
(251) Zhong, Z.; Wang, B.; Dai, M.; Sun, Y.; Sun, Q.; Yang, G.; Bian, L. Carvacrol alleviates cerebral edema by modulating AQP4 expression after intracerebral hemorrhage in mice. *Neurosci. Lett.* **2013**, *555*, 24−29.
(252) Peters, M.; Trembovler, V.; Alexandrovich, A.; Parnas, M.; Birnbaumer, L.; Minke, B.; Shohami, E. Carvacrol together with TRPC1 elimination improve functional recovery after traumatic brain injury in mice. *J. Neurotrauma* **2012**, *29*, 2831−2834.
(253) Azizi, Z.; Ebrahimi, S.; Saadatfar, E.; Kamalinejad, M.; Majlessi, N. Cognitive-enhancing activity of thymol and carvacrol in two rat models of dementia. *Behav. Pharmacol.* **2012**, *23*, 241−249.
(254) Melo, F. H. C.; Moura, B. A.; de Sousa, D. P.; de Vasconcelos, S. M. M.; Macedo, D. S.; Fonteles, M. M. D. F.; Viana, G. S. D. B.; de Sousa, F. C. F. Antidepressant-like effect of carvacrol (5-Isopropyl-2-methylphenol) in mice: involvement of dopaminergic system. *Fundam. Clin. Pharmacol.* **2011**, *25*, 362−367.
(255) Yu, H.; Zhang, Z.-L.; Chen, J.; Pei, A.; Hua, F.; Qian, X.; He, J.; Liu, C.-F.; Xu, X. Carvacrol, a food-additive, provides neuroprotection on focal cerebral ischemia/reperfusion injury in mice. *PLoS One* **2012**, *7*, e33584.
(256) Zotti, M.; Colaianna, M.; Morgese, M. G.; Tucci, P.; Schiavone, S.; Avato, P.; Trabace, L. Carvacrol: from ancient flavoring to neuromodulatory agent. *Molecules* **2013**, *18*, 6161−6172.
(257) Friedman, M. Overview of antibacterial, antitoxin, antiviral, and antifungal activities of tea flavonoids and teas. *Mol. Nutr. Food Res.* **2007**, *51*, 116−134.
(258) Friedman, M. Antibacterial, antiviral, and antifungal properties of wines and winery byproducts in relation to their flavonoid content. *J. Agric. Food Chem.* **2014**, *62*, 6025.

identification of individual phenolic compounds was based on their diode array detector spectra and electrospray ionization mass spectrometry fragmentation patterns compared with those of authentic standards and reported data (see Figure S1 and Table S1 of the Supporting Information). The chemical structure of identified chlorogenic acid isomers is shown in Figure 1 (compounds **1**–**3**).

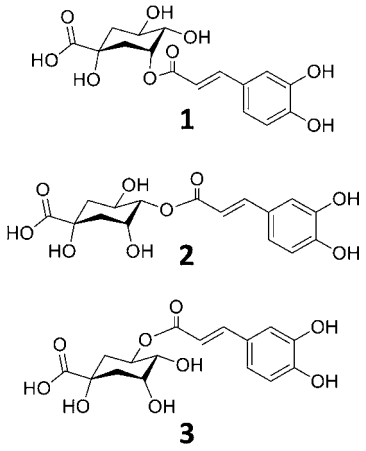

Figure 1. Chemical structures of chlorogenic acid isomers identified in potato tubers subjected to wounding stress and exogenous amylolytic enzymes: (**1**) chlorogenic acid (3-*O*-caffeoylquinic acid), (**2**) cryptochlorogenic acid (4-*O*-caffeoylquinic acid), and (**3**) neochlorogenic acid (5-*O*-caffeoylquinic acid).

To quantitate the chlorogenic acid isomers, a standard curve of chlorogenic acid at a range of 5–250 ppm was obtained. The concentrations of chlorogenic acid isomers were expressed as milligrams of compound per kilogram of potato DW. Results are expressed as chlorogenic acid equivalents.

Statistical Analysis. Statistical analyses were performed using five repetitions. Data represent the mean values of repetitions, and bars indicate their standard error. Analyses of variance were conducted using JMP version 11.0 (SAS Institute Inc., Cary, NC), and mean separation was performed using the LSD test ($p < 0.05$).

RESULTS AND DISCUSSION

Total reducing sugars were evaluated during storage of wounded potatoes treated with or without enzymes (Figure 2A). As expected, control samples (without enzymes) showed a significant increase in reducing sugar content during the first 72 h of storage; thereafter, from 96 to 168 h, the content remained stable, and at 192 h, a significant decline ($p < 0.05$) was observed. Wounded potatoes treated with enzymes at either 0 (E0h) or 48 h (E48h) showed a level of hydrolysis of starch higher than that of the control. These treatments (E0h and E48h) presented a rapid increase in the content of reducing sugars after enzyme application for 24 h. Interestingly, for the E96h treatment, the addition of amylolytic enzymes induced a significant decrease ($p < 0.05$) in the content of reducing sugars during the following storage time. Because sugars accumulate when their production rate exceeds their utilization rate,[25,26] it is likely that for the E96h treatment although the rate of production of reducing sugars could be enhanced by exogenous amylolytic enzymes, their utilization rate in a metabolic process such as cellular respiration[22] or for the production of aromatic amino acids needed for the biosynthesis of phenolic compounds[27] was higher.

To evaluate the effect of wounding stress and the addition of amylolytic enzymes on the wound-induced accumulation of phenolic compounds in potato tubers, quantification of

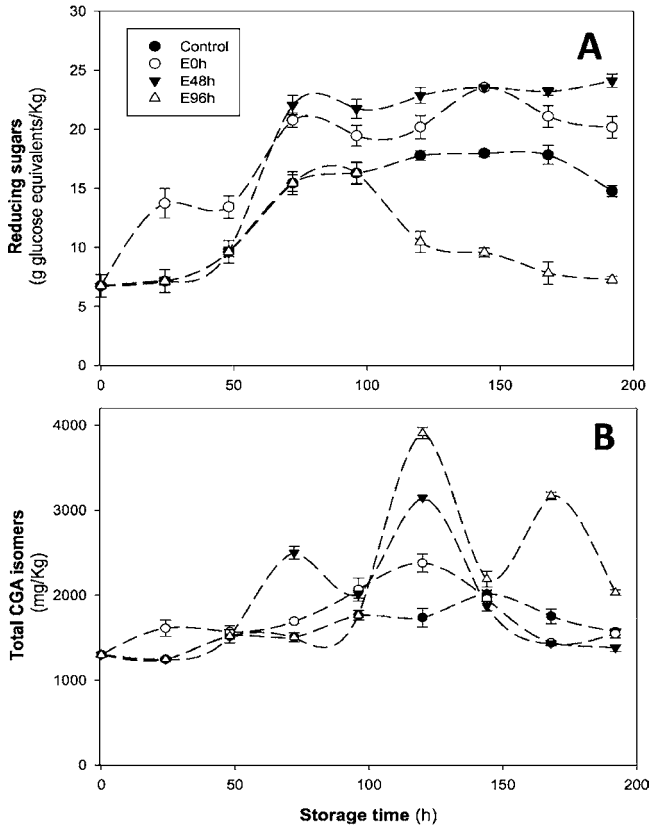

Figure 2. (A) Total reducing sugars and (B) chlorogenic acid isomer content during storage (192 h at 20 °C) of pie cut potatoes with and without (control) amylolytic enzymes. For each treatment, amylolytic enzymes were added after storage for 0 (E0h), 48 (E48h), or 96 h (E96h). Values represent the mean of five repetitions with their standard error bars.

chlorogenic acid and its isomers cryptochlorogenic acid and neochlorogenic acid was performed (Figure 2B) because these compounds represent ~75% of the total phenolic compounds in potato tubers.[3,28−32] The highest level of accumulation of total chlorogenic acid isomers in control samples was observed after storage for 144 h, a content that was ~60% higher than that of time zero samples (Figure 2B). For the subsequent storage time, the concentration started to decrease. All samples treated with enzymes showed the highest level of accumulation of total chlorogenic acid isomers after storage for 120 h compared with the control (Figure 2B). The treatment that showed the highest total chlorogenic acid content was E96h followed by E48h and E0h, with increases of ~210, ~150, and ~90%, respectively, compared with the time zero samples (Figure 2B). After 120 h, the total chlorogenic acid content decreased for all treatments (Figure 2B). In general, the application of amylolytic enzymes caused a significant increase ($p < 0.05$) in the content of total chlorogenic acid isomers just 24 h after their addition in potato tubers, suggesting that the higher availability of sugars could result in a higher level of synthesis of phenolic compounds, and these observations are associated with higher levels of reducing sugars detected in E0h and E48h samples 24 h after the addition of the enzyme (Figure 2A). However, this trend was not observed for the E96h sample. Because the E96h sample showed the highest content of chlorogenic acid isomers (Figure 2B), the results indicate that sugars are rapidly utilized as a carbon source for the

dx.doi.org/10.1021/jf5026983 | J. Agric. Food Chem. 2014, 62, 7671−7675

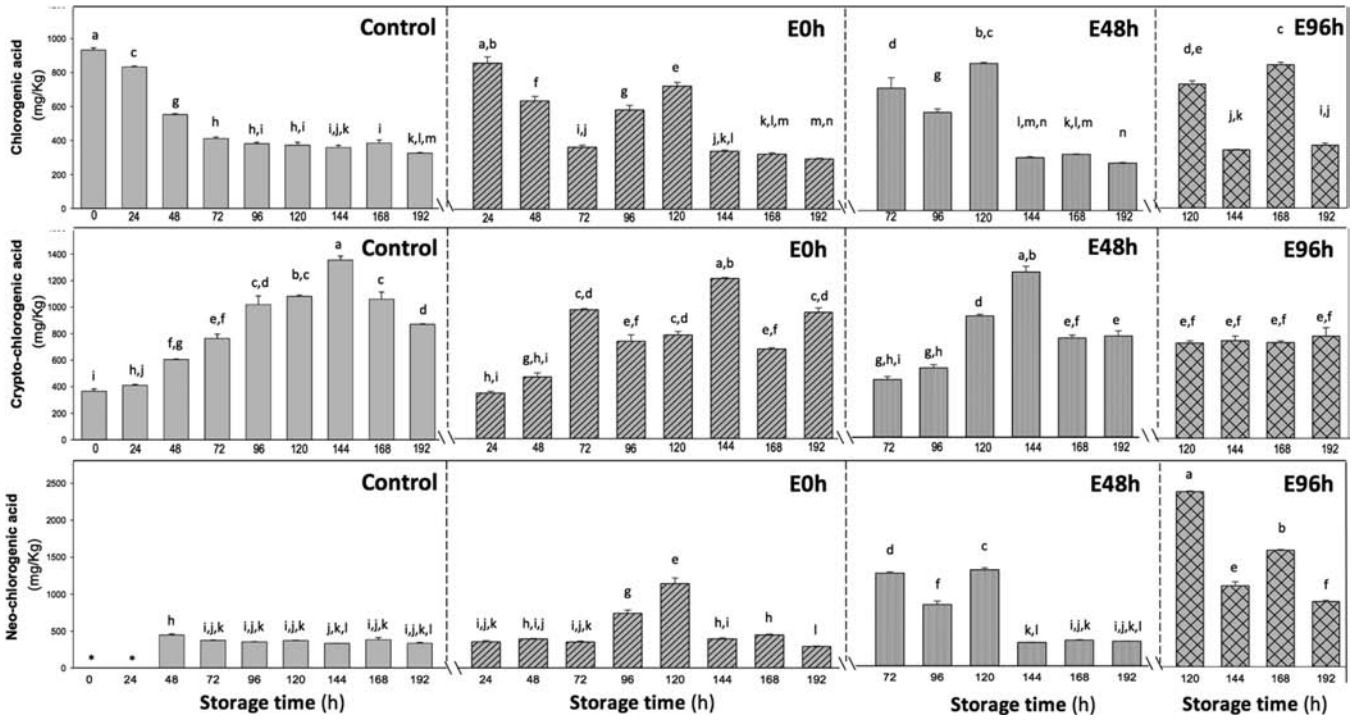

Figure 3. Accumulation of individual chlorogenic acid isomers during storage (192 h at 20 °C) of pie cut potatoes with and without (control) amylolytic enzymes. Amylolytic enzymes were added after storage for 0 (E0h), 48 (E48h), or 96 h (E96h). Asterisks denote not detected. Values represent the means of five repetitions with their standard error bars. Different letters in the same compound indicate statistical differences determined by the LSD test ($p < 0.05$).

biosynthesis of phenolic compounds, and thus as discussed earlier, their utilization rate is higher than their production rate.

The quantification of individual chlorogenic acid isomers (compounds **1**–**3**) during storage (20 °C) of wounded potatoes with or without enzymes is shown in Figure 3. In the particular case of chlorogenic acid (compound **1**), no accumulation was observed in control samples. Instead, a significant ($p < 0.05$) decrease was observed over time. Wounded potatoes with amylolytic enzymes showed chlorogenic acid levels after the addition of enzymes higher than that of the control; however, the levels did not exceed those observed at time zero in control samples. The results obtained herein are in contrast with those of a previous report, in which the accumulation of chlorogenic acid was observed in wounded potatoes stored for 96 h at 10 °C.[3] The difference in the results obtained here and those previously reported could be attributed to the storage temperature, because in this study a temperature of 20 °C was selected to maintain the activity of exogenous amylolytic enzymes. Previous reports indicated that 20 °C is the optimal temperature for suberin and lignin biosynthesis.[33,34] Thus, the results suggest that in control samples the chlorogenic acid content decreases during storage because chlorogenic acid is rapidly utilized for the production of lignin and suberin.

With regard to cryptochlorogenic acid (compound **2**), the levels were increased by 260% in control samples during the first 144 h of storage; however, the addition of amylolytic enzymes did not enhance its wound-induced accumulation. Likewise, the increase in cryptochlorogenic acid content observed in the control suggests that this compound accumulates while chlorogenic acid is available. In addition, as previously reported, chlorogenic acid seems to be preferred over cryptochlorogenic acid for lignin biosynthesis,[35] because its concentration is rapidly decreased after wounding. The accumulation of compound **2** agrees with a previous report in which its highest concentration in potato pie cuts was observed after storage for 144 h at 10 °C.[3] However, at 10 °C, the observed increase (~80%) was smaller than that observed herein, suggesting that temperature can be used as an abiotic stress to selectively induce a higher rate of accumulation of cryptochlorogenic acid in wounded potatoes.

Neochlorogenic acid (compound **3**) was not detected in time zero potatoes (Figure 3). In the control, compound **3** was detected after storage for 48 h and the content remained constant until 72 h. The application of amylolytic enzymes significantly increased the rate of accumulation of neochlorogenic acid in all samples 24 h after their addition, where the highest levels (~2400 mg/kg) were obtained in E96h samples after storage for 120 h.

On the basis of the results presented herein and a previous work (unpublished results), a procedure for the production of chlorogenic isomers in potato tubers, which is based on the application of wounding stress and amylolytic enzymes as well as on the selection of storage time and temperature, is proposed. If the production of chlorogenic acid is pursued, pie cut potatoes should be stored for 96 h at 10 °C. For cryptochlorogenic acid production, the optimal storage conditions should be 144 h at 20 °C. Finally, to obtain high levels of neochlorogenic acid, pie cut potatoes should be stored at 20 °C for 96 h, amylolytic enzymes should be added, and the enzyme-treated samples should be stored for an additional 24 h at 20 °C. The stressed potato tubers with a high concentration of chlorogenic acid isomers could be used as the starting material for the extraction of antioxidant phenolic compounds with potential applications in the pharmaceutical and dietary supplement industries.

dx.doi.org/10.1021/jf5026983 | J. Agric. Food Chem. 2014, 62, 7671–7675

Ana Mariel Torres-Contreras[†]
Vimal Nair[‡]
Luis Cisneros-Zevallos[‡]
Daniel A. Jacobo-Velázquez*[,†]
[†]Department of Biotechnology and Food Engineering, Centro de Biotecnología-FEMSA, Tecnológico de Monterrey-Campus Monterrey, E. Garza Sada 2501 Sur, C.P. 64849 Monterrey, NL, México
[‡]Vegetable & Fruit Improvement Center, Department of Horticultural Sciences, Texas A&M University, College Station, Texas 77843-2133, United States

■ ASSOCIATED CONTENT

Supporting Information

Typical high-performance liquid chromatography (HPLC)−PDA chromatogram (shown at 320 nm) from methanol extracts of potato pie cuts stored for 120 h and treated with amylolytic enzymes after storage for 96 h (E96h) (Figure S1) and tentative identification of chlorogenic acid isomers in potato tissue by HPLC−diode array detection and HPLC−electrospray ionization mass spectrometry (Table S1). This material is available free of charge via the Internet at http://pubs.acs.org.

■ AUTHOR INFORMATION

Corresponding Author

*Telephone: +52-818-358-20-00, ext. 4820. Fax: +52-818-328-4136. E-mail: djacobov@itesm.mx.

Funding

This study is based upon research supported by research funds from the Tecnológico de Monterrey-Research Chair iniciative (CAT 161), Cátedra de Nutrigenómica-FEMSA, and Consejo Nacional de Ciencia y Tecnología (CONACYT, México) (Grant 177012). A.M.T.-C. acknowledges the scholarship (279532) from CONACYT.

Notes

The authors declare no competing financial interest.

■ REFERENCES

(1) U.S. Department of Agriculture. Potatoes 2012 Summary. http://usda01.library.cornell.edu/usda/current/Pota/Pota-09-19-2013.pdf (accessed May 28, 2014).
(2) Food and Agricultural Organization of the United Nations statistical database. http://faostat.fao.org (accessed May 28, 2014).
(3) Torres-Contreras, A. M. The effect of Wounding Intensity and Exogenous Amylolytic Enzymes on the Accumulation of Chloroenic Acid Isomers in Potato Tubers. M.S. Thesis, Tecnólogico de Monterrey, Monterrey, NL, Mexico, 2014.
(4) McCarty, M. F. A chlorogenic acid-induced increase in GLP-1 production may mediate the impact of heavy coffee consumption on diabetes risk. *Med. Hypotheses* **2005**, *64*, 848−853.
(5) Thom, E. The effect of chlorogenic acid enriched coffee on glucose absorption in healthy volunteers and its effect on body mass when used long-term in overweight and obese people. *J. Int. Med. Res.* **2007**, *35*, 900−908.
(6) Cho, A. S.; Jeon, S. M.; Kim, M. J.; Yeo, J.; Seo, K. I.; Choi, M. S.; Lee, M. K. Chlorogenic acid exhibits anti-obesity property and improves lipid metabolism in high-fat diet-induced-obese mice. *Food Chem. Toxicol.* **2010**, *48*, 937−943.
(7) Wang, G. F.; Shi, L. P.; Ren, Y. D.; Liu, Q. F.; Liu, H. F.; Zhang, R. J.; Li, Z.; Zhu, F. H.; He, P. L.; Tang, W.; Tao, P. Z.; Li, C.; Zhao, W. M.; Zuo, J. P. Anti-hepatitis B virus activity of chlorogenic acid, quinic acid and caffeic acid in vitro and in vivo. *Antiviral Res.* **2009**, *83*, 186−190.
(8) Yagasaki, K.; Miura, Y.; Okauchi, R.; Furuse, T. Inhibitory effects of chlorogenic acids and its related compounds on the invasion of hepatoma cells in culture. *Cytotechnology* **2000**, *33*, 229−235.
(9) Noratto, G.; Porter, W.; Byrne, D.; Cisneros-Zevallos, L. Polyphenolics from peach (*Prunus persica* var. Rich Lady) inhibit tumor growth and metastasis of MDA-MB-435 breast cancer cells *in vivo*. *J. Nutr. Biochem.* **2014**, *25*, 796−800.
(10) Gamborg, O. L. Aromatic metabolism in plants: V. The biosynthesis of chlorogenic acid and lignin in potato cell cultures. *Can. J. Biochem.* **1967**, *45*, 1451−1457.
(11) Dean, B. B.; Kolattukudy, P. E. Biochemistry of suberization: Incorporation of [1-^{14}C] oleic acid and [1-^{14}C] acetate into the aliphatic components of suberin in potato tuber disks (*Solanum tuberosum*). *Plant Physiol.* **1977**, *59*, 48−54.
(12) Whetten, R.; Sederoff, R. Lignin biosynthesis. *Plant Cell* **1995**, *7*, 1001−1013.
(13) Friedman, M. Chemistry, biochemistry, and dietary role of potato polyphenols. A review. *J. Agric. Food Chem.* **1997**, *45*, 1523−1540.
(14) Lulai, E. C.; Corsini, D. L. Differential deposition of suberin phenolic and aliphatic domains and their roles in resistance to infection during potato tuber (*Solanum tuberosum* L.) wound-healing. *Physiol. Mol. Plant Pathol.* **1998**, *53*, 209−222.
(15) Bernards, M. A.; Susag, L. M.; Bedgar, D. L.; Anterola, A. M.; Lewis, N. G. Induced phenylpropanoid metabolism during suberization and lignification: A comparative analysis. *J. Plant Physiol.* **2000**, *157*, 601−607.
(16) Bernards, M. A.; Razem, F. A. The poly(phenolic) domain of potato suberin: A non-lignin cell wall bio-polymer. *Phytochemistry* **2001**, *57*, 1115−1122.
(17) Yoshida, S. Biosynthesis and conversion of aromatic amino acids in plants. *Annu. Rev. Plant Physiol.* **1969**, *20*, 41−62.
(18) Umbarger, H. E. Amino acid biosynthesis and its regulation. *Annu. Rev. Biochem.* **1978**, *47*, 533−606.
(19) Hopkins, E. F. Variation in sugar content in potato tubers caused by wounding and its possible relation to respiration. *Bot. Gaz. (Chicago)* **1927**, *84*, 75−88.
(20) Passam, H. C.; Read, S. J.; Rickard, J. E. Wound repair in yam tubers: Physiological processes during repair. *New Phytol.* **1976**, *77*, 325−331.
(21) Linask, J.; Laties, G. G. Multiphasic absorption of glucose and 3-O-methyl glucose by aged potato slices. *Plant Physiol.* **1973**, *51*, 289−294.
(22) Burton, W. G. The sugar balance in some British potato varieties during storage. I. Preliminary observations. *Eur. Potato J.* **1965**, *8*, 80−91.
(23) Miller, G. L. Modified DNS method for reducing sugars. *Anal. Chem.* **1959**, *31*, 426−428.
(24) Becerra-Moreno, A.; Benavides, J.; Cisneros-Zevallos, L.; Jacobo-Velázquez, D. A. Plants as biofactories: Glyphosate-induced production of shikimic acid and phenolic antioxidants in wounded carrot tissue. *J. Agric. Food Chem.* **2012**, *60*, 11378−11386.
(25) Hertog, M. L. A. T. M.; Tijskens, L. M. M.; Hak, P. S. The effects of temperature and senescence on the accumulation of reducing sugars during storage of potato (*Solanum tuberosum* L.) tubers: A mathematical model. *Postharvest Biol. Technol.* **1997**, *10*, 67−79.
(26) Kumar, D.; Singh, B. P.; Kumar, P. An overview of the factors affecting sugar content of potatoes. *Ann. Appl. Biol.* **2004**, *145*, 247−256.
(27) Hilal, M.; Parrado, M. F.; Rosa, M.; Gallardo, M.; Orce, L.; Massa, E. M.; González, J. A.; Prado, F. E. Epidermal lignin deposition in quinoa cotyledons in response to UV-B radiation. *Photochem. Photobiol.* **2004**, *79*, 205−210.
(28) Malmberg, A. G.; Theander, O. Determination of chlorogenic acid in potato tubers. *J. Agric. Food Chem.* **1985**, *33*, 549−551.
(29) Ramamurthy, M. S.; Maiti, B.; Thomas, P.; Nair, P. M. High-performance liquid chromatography determination of phenolic acids in potato tubers (*Solanum tuberosum*) during wound healing. *J. Agric. Food Chem.* **1992**, *40*, 569−572.

(30) Fernandes, J. B.; Griffiths, D. W.; Bain, H.; Fernandes, F. A. N. The development and evaluation of capillary electrophoretic methods for the determination of the major phenolic constituents of potato (*Solanum tuberosum*) tubers. *Phytochem. Anal.* **1996**, *7*, 253−258.
(31) Leo, L.; Leone, A.; Longo, C.; Lombardi, D. A.; Raimo, F.; Zacheo, G. Antioxidant compounds and antioxidant activity in "early potatoes". *J. Agric. Food Chem.* **2008**, *56*, 4154−4163.
(32) Navarre, D. A.; Pillai, S. S.; Shakya, R.; Holden, M. J. HPLC profiling of phenolics in diverse potato genotypes. *Food Chem.* **2011**, *127*, 34−41.
(33) Dean, B. B. Deposition of aliphatic suberin monomers and associated alkanes during aging of *Solanum tuberosum* L. tuber tissue at different temperatures. *Plant Physiol.* **1989**, *89*, 1021−1023.
(34) Cai, C.; Xu, C.; Li, X.; Ferguson, I.; Chen, K. Accumulation of lignin in relation to change in activities of lignification enzymes in loquat fruit flesh after harvest. *Postharvest Biol. Technol.* **2006**, *40*, 163−169.
(35) Chabannes, M.; Barakate, A.; Lapierre, C.; Marita, J. M.; Ralph, J.; Pean, M.; Danoun, S.; Halpin, C.; Grima-Pettenati, J.; Boudet, A. M. Strong decrease in lignin content without significant alteration of plant development is induced by simultaneous down-regulation of cinnamoyl CoA reductase (CCR) and cinnamyl alcohol dehydrogenase (CAD) in tobacco plants. *Plant J.* **2001**, *28*, 257−270.

Finally, a traceless method of spiking is investigated, after a finding that solvent-based spiking of standards led to significant influences on the release of the analytes from the soil.

MATERIALS AND METHODS

General. Apparatus used in this study includes: Zx[3] vortexer (Velp Scientifica, Italy); sonicator (FungiLab, Barcelona, Spain); centrifuge (Eppendorf centrifuge 5415D, Hamburg, Germany); gastight Hamilton GC syringes (Seelze, Germany); gas chromatograph−mass spectrometer (Shimadzu QP2010, Kyoto, Japan) equipped with a Zebron 35MS column with 30 m × 0.25 mm × 0.25 μm dimensions (Phenomenex, Torrance, U.S.).

The pesticides metolachlor (Met), atrazine (Atrz), and their deuterated (^{2}H) analogues (each being 100 μg/mL in 1 mL ampules) were obtained from Dr. Ehrenstorfer GmbH (Augsburg, Germany). A 10-component standard mixture of triazines, mixture TP-619, was obtained from Chem Service (PA) (prometron, atraton, atrazine, propazine, simazine, terbuthylazine, prometryn, ametryn, simetryn, and terbutryn with individual triazine concentrations of 500 mg/L). Diphenylamine, desethylatrazine, and desisopropylatrazine (100 μg/mL) were purchased from Chem Service (PA), while chloroform, methanol, and water (all HPLC grade) were purchased from Riedel de Haën (Seelze, Germany). Sodium chloride (AR grade) was obtained from Sigma-Aldrich (Seelze, Germany). Helium (99.999%) was from Afrox, South Africa. The agricultural soil samples were collected from a farming area in the North West Province near the small town of Derby about 150 km West of Johannesburg, South Africa. In each case, collections were made at various depths (0−5 cm, 20−25 cm cm), and three samples of each were collected from a single agricultural field at distances 15−20 m apart. The soil in the field is classified as red-brown humic sandy soil with approximately 20% silt content, pH 6, cation exchange capacity of around 70 mmol/kg, and bulk density around 1300 kg/m^3.[23]

Standard Solutions. The H-standards of 100 μg/mL atrazine and metolachlor were combined, diluted to 1 μg/mL in MeOH, and kept in a freezer at −18 °C. The deuterated (^{2}H) standards for the same herbicides were prepared and stored similarly. The atrazine breakdown products desethylatrazine and desisopropylatrazine were also mixed with atrazine and metolachlor to prepare a 1 μg/mL standard mixture in MeOH, and the mixture was kept in the same freezer. The working solutions were prepared by dilution of these stock solutions. Reference solutions were prepared by dilution of the stock solution with methanol and were injected directly (1 μL) into the instrument. For the extraction procedure, 10% NaCl aqueous solutions were used, in light of the efficiencies gained using this medium as determined in our previous work.[20] A 100 ng/mL diphenylamine solution was prepared by dilution from a 100 μg/mL solution with chloroform. This was used as the extracting solvent for the BID-SDME method with the diphenylamine employed as internal standard.

Preparation of Soil Samples. Soil suspensions were prepared by adding 2 g of air-dried soil to 2 mL of water (1 g/mL). This suspension was treated by vortexing it at 30 Hz, followed by sonication for 15 min, and thereafter centrifugation at 8165*g*. Given portions of the clear supernatant liquid were transferred into a gas chromatograph (GC) vial containing 0.1 g of NaCl, after which BID-SDME extraction was applied as previously described.[20]

Different extraction methods were used to solubilize the pesticides from the soil, and the results were compared to room temperature sonication. These techniques included heating the suspension, or using boiling/hot water to prepare the suspension, as well as superheating the suspension in a closed vessel.

GC−MS Setup. A calibrated gastight syringe (10 μL) was used for sampling and injections. Analyses were carried out using a gas chromatograph coupled to a mass spectrometer (GC−MS). Pure helium at a constant flow rate of 1 mL/min was used as the carrier gas. Injections (1 μL) were carried out in the splitless mode; after 2 min, a split ratio of 1:10 was maintained throughout the runs. The injector and transfer line were maintained at 250 °C. The oven programming included an initial temperature of 100 °C (held for 4 min), the temperature increased by 50 °C/min to 200 °C, then ramped by 10 °C/min to 280 °C and held for 5 min. The total time for one GC run was 17 min.

The MS (EI 70 eV, 200 °C ion source temperature, 1.5 kV detector potential) was set up in scanning mode with mass range m/z 50−350 mass units. The ions of interest were extracted out of the total ion chromatogram as follows: m/z 162 (166, 4 × ^{2}H), 169, 172, 187, and 200 (205, 5 × ^{2}H) for metolachlor, diphenylamine, desethylaztrazine, desisopropylatrazine, and atrazine, respectively (the values in the parentheses represent the ^{2}H analogues). For quantitative analysis at trace level (lower ng/mL range), the MS was set to the selected ion monitoring (SIM) mode using the same ions as listed above together with their qualifying ions (m/z 215 and 238 for atrazine and metolachlor, respectively); otherwise, the MS was always used on scanning mode using the extracted ion monitoring (EIM) facility.

Microextraction Procedure. The setup for the BID-SDME extraction protocol was reported in detail in our earlier paper.[20] Briefly, 1 μL of the extracting solution was drawn into the syringe, followed by 0.5 μL of air. These contents were introduced into the aqueous solution by gentle depression of the plunger, causing the air to form a bubble contained within the microdroplet. Following a period of 20 min (under static conditions), the total solvent volume was carefully retracted into the syringe, and injected into the GC−MS.

Performance of the Analytical Method for Metolachlor. Only a limited amount of development and validation work was carried out as part of the present study, given the backdrop of our prior work.[20] The main thrust included an assessment of the chromatographic separation of metolachlor in the same TP-619 mixture of 10 triazines reported in our earlier study.[20] The extraction efficiency was evaluated using three aqueous solutions (prepared in 10% aqueous NaCl) at concentrations of 1, 50, and 100 ng/mL for each pesticide together with the corresponding organic solutions. Linearity and LOD were determined using aqueous mixtures of atrazine and metolachlor in the concentration range 0.01−1.0 ng/mL.

Evaluation of Extraction Recovery. Soil samples were air-dried, ground, and sieved through a 0.0035 in. (0.089 mm) mesh. Subsamples (2 g) were wet with 1 mL of HPLC grade water and spiked with 50 μL of a 1 μg/mL solution of the ^{2}H-standard so as to prepare concentrations of 25 ng/g of the pesticide standards in the soil samples. The suspension was allowed to air-dry. Following complete drying, the soil residue was suspended in 2 mL of hot water to dissolve and release the spiked herbicides. The extracts were then subjected to the BID-SDME extraction protocol as described above. The effect of organic solvents in spiking was also evaluated using different spiking solutions, being 100% water, 3:1 water/MeOH, 1:1 water/MeOH, 1:3 water/MeOH, and pure MeOH, respectively. The extraction values from these solutions, especially those from the herbicides existing in the soil from the farming activities (metolachlor and atrazine), were compared to those obtained with the spiked HPLC grade water (spiked to the same concentration as the samples).

All soil samples were sampled in triplicate and each sample analyzed in triplicate, so every analysis was carried out for $n = 9$ as a minimum. Following assessment of recovery, quantitation of the amounts of the herbicides in the soil was calculated from the calibration curve using the extraction efficiency factor.

RESULTS AND DISCUSSION

Assessment of Linearity of the Extraction Method for Metolachlor and Atrazine. The linearity of the method was determined in the concentration range 0.01−1 ng/mL by BID-SDME extraction under optimum conditions established for triazines[20] and analysis using GC−MS: 1 mL of a 10% aqueous NaCl solution of the herbicides was extracted for 20 min with a 1 μL chloroform droplet containing diphenylamine as an internal standard, and a 0.5 μL air bubble, with no stirring. The calibration curves give the following data for atrazine, R^2 0.999 and LOD 0.013 ng/L, and for metolachlor, R^2 0.999, LOD 0.024 ng/L. LOD values were determined using LOD = 3 ×

standard deviation$_{Intercept}$/slope[24] (see also Supporting Information, Figure S3). For purposes of comparison, LOD values for the US FDA Method 302 for metolachlor and atrazine are both 0.010 μg/mL,[25] while the LOD values applied in the EPA Method 507 from water samples are 0.19 and 0.015 ng/mL for metolachlor and atrazine, respectively.[26] The data above indicate that the present approach falls well within the FDA and EPA method requirements for testing these analytes, while following an easy-to-use protocol. Indirectly, the data in Table 1 also fall within these parameters: these were generated from liquid extracts of the soils and converted into mass-basis information.

Table 1. Hot Water Extraction and Analysis of Herbicides at 25 cm Soil Depth for Different Dates

week no.	metolachlor (ng/g)[a]	atrazine (ng/g)
9	n.d.[b]	n.d.
10	n.d.	n.d.
11	4	3
15	4	1.5
26	2	n.d.

[a]The calculation is based on the outcomes of the later section on quantification. [b]n.d. means not detected.

Analysis of Soil Samples. *Monitoring of Soil Pesticide Concentration over Time.* Following method refinement, the dissipation of the herbicides over time in agricultural soil samples was investigated, making use of samples collected from the upper 5 cm of the soil. Interviews with the farmer had revealed that metolachlor had been sprayed on the farmland in week 1 while atrazine had been sprayed on the farmland during week 4 (the fourth week postspraying of metolachlor). The collected samples were sonicated[27,28] for 15 min, after which they were subjected to BID-SDME. GC−MS analysis of extracts made from farm soils over a period of 15 weeks postspraying showed only the presence of metolachlor (Figure 1: the "sonication" curve shows the depletion of metolachlor

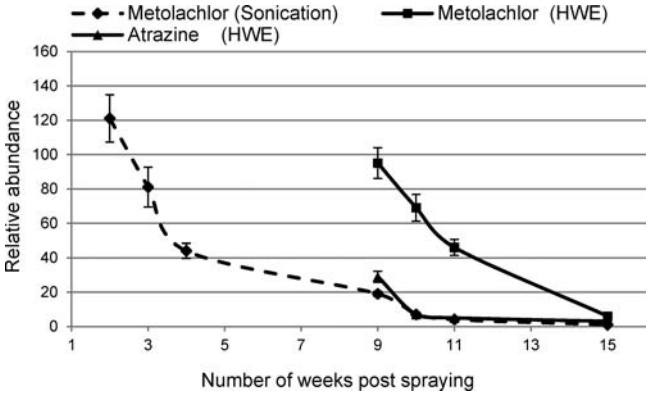

Figure 1. Dissipation−time profile of the herbicides in farmland soil over a 15 week period using sonication and hot water extraction (HWE).

over time). Discovering that neither atrazine nor its breakdown products desethylatrizine and desisopropylatrazine could be detected, we investigated more forcing dissolution methods than sonication (see below).

Throughout and for consistency, subsamples of a given soil sample were employed. Different extraction conditions were explored: the use of vortexing, sonication, hot water (adding freshly boiled water to the sample), heating the sample to boiling, hot water + sonication, and superheated water. The superheated water scenario was achieved by heating the sample in a sealed small stainless steel autoclave to a temperature of 140 °C. In all cases, the allocated time for extraction was 20 min. The results are given below (Figure 2).

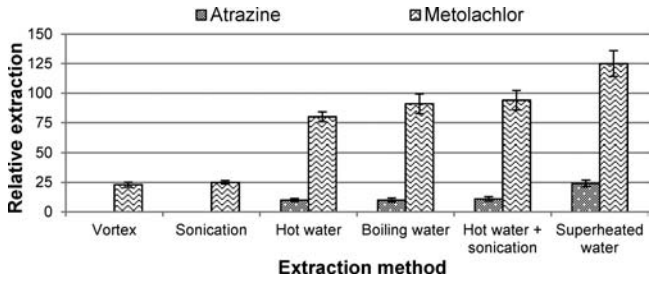

Figure 2. Evaluation of different extraction methods for a given soil sample.

As can be seen in Figure 2, only metolachlor was detected using vortexing or sonication-assisted extraction followed by BID-SDME and GC−MS analysis. However, when using the other more vigorous extraction methods with higher temperatures, atrazine was detected. As can be seen in Figure 2, hot water (96 °C) and heating the sample in water to boiling do not offer much difference in extraction efficiency. Also, sonication is no longer important when using hot water extraction. Although superheated water extraction gave higher extraction of both analytes (Figure 2), this method was not considered useful for wide application due to the difficulty in sample handling and the high pressure equipment required.

Having shown quite good improvements to the solubilization protocols when employing hot water (96 °C) extraction, it was decided to revisit the analysis of the soil samples with the view to improving sensitivity for the detection of metolachlor in the latter part of the sampling period and reassessing the samples for the presence of atrazine. Figure 1 shows the dissipation profiles obtained for the two extraction methods, room temperature sonication versus hot water (96 °C) extraction. Room temperature sonication had extracted only metolachlor (between weeks 2 and 9), while the hot water (denoted in Figure 1 legend as HWE) extracted both analytes, thereby allowing their detection. The improvements secured with hot water extraction are clearly evident with respect to metolachlor with extractability rising from about 20 to 90 in relative abundance (representing about a 4.5-fold improvement in the amount extracted).

Given the improvements achieved in detecting both metolachlor and atrazine, the subsurface layers of soil were also assessed for the presence of the two herbicides of interest there. Table 1 below shows results obtained using samples lying about 25 cm deep and using different time periods following spraying. Evidently, neither herbicide suffers significant leaching from the top layer into lower soil strata as an intact entity, because they were present only at low levels in the subsurface soil. This is a contrast to prior work, which describes metolachlor as "transient" (meaning substantial leaching, in the context of the cited work) in soils, leading to diminished herbicidal efficacy.[29]

One of the two major breakdown products of atrazine, desethylatrazine, could be detected at low levels when

combining BID-SDME preconcentration with GC–MS analysis. No breakdown products for metolachlor could be identified in the extracts. Additional future work will provide robust data on the usefulness of the methods described here to the monitoring of breakdown products of these herbicides.

Recovery of Herbicides from the Soil. While the data generated above provide good relative information, absolute data based on recovery experiments are important for the quantification of analytes. To assess the level of recovery, labeled analogues of the analytes of interest are usually spiked into the sample.[30] Such labeled surrogate materials are readily quantified as separate entities by detectors such as mass spectrometers.[31] Given their physical characteristics that are essentially identical to those of the analyte in question, this approach is widely used to establish quantitative recovery of analytes from samples.[32] The spiking solution is usually added with the organic analyte dissolved in an appropriate organic solvent such as methanol,[33,34] and the influence of the spiking solvent is ignored. In other instances, aqueous spiking solutions are used.[35,36]

Figure 3 shows the effect of the spiking solvent to recovery of the herbicides (see also Supporting Information, section S3).

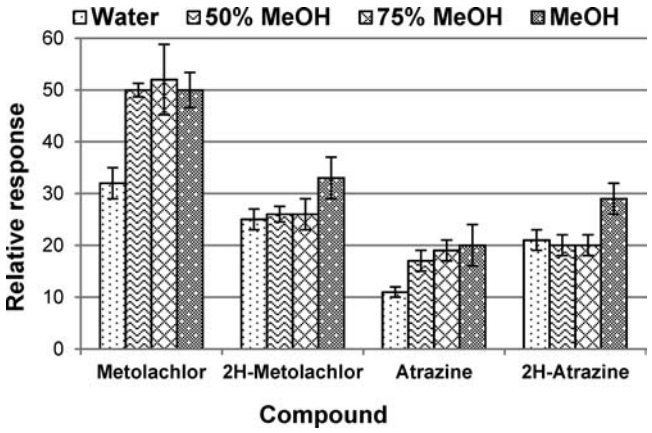

Figure 3. Effect of solvent composition of the spiking solution on extraction.

Clearly, the spiking solvent has an effect on the release of the pre-existing herbicides as demonstrated by the varying extractabilities thereof. Concomitantly, the deuterated spiking surrogate materials showed little changes to their levels of extraction (with the exception of the use of 100% MeOH). Bearing in mind that only 50 μL of spiking solution was used with 2 g of soil, the influence is rather dramatic.

Given the limited scope of our work in terms of soil types, it is not yet known whether this is a general phenomenon or not. Nevertheless, the implication of this exercise is that the suspension of the soils in methanol-containing solutions enhances the extractability of the analytes in question, despite the samples being air-dried and putatively solvent-free at the time of analysis. This implies that the method of choice for the application of spiking solutions to soil samples is to use aqueous spiking solutions where practicable and to allow the samples to dry completely before further manipulation.

This organic solvent effect is consistent with the results obtained by Merini et al.,[37] who reported recoveries of 49% when using an aqueous surrogate and 81% when using methanol surrogate for 2,4-dichlorophenoxyacetic acid. This observation is very important because most of the spiking reported in literature is carried out using an organic solvent in which the surrogates are dissolved, and the influence of the spiking solvent is often overlooked.

Traceless Spiking Method. The composition of the spiking solution was found to influence the extractability of analytes. To avoid this variable, it was decided to use strictly aqueous solutions even for spiking. For this purpose, a 1 μg/mL aqueous spiking solution containing the surrogate deuterated samples was prepared by dilution of 100 μg/mL solutions into 1 mL with HPLC grade water. This solution (50 μL) was used to spike the soil samples (2 g, wet with 1 mL of HPLC grade water), vortexing to ensure equal distribution of the spiking solution over the soil sample and air drying as described above. The application of hot water extraction, BID-SDME, and GC–MS analysis afforded the set of results contained in Table 2, which demonstrate the recovery of the both the analyte and the surrogate herbicides from differently treated soils and from water used as a reference solution.

Table 2. Recoveries of the Analytes (ng/g) from Different Samples Spiked with Aqueous Solutions

	atrazine	metolachlor	^{2}H-atrazine	^{2}H-metolachlor
water (ref)			34 (16)[a]	21 (12)[a]
control soil[b]	3 (6)[a]	13 (8)[a]		
control treated soil[c]	2.8 (8)[a]	12.8 (5)[a]		
spiked soil[d]	3 (9)[a]	13 (5)[a]	33 (10)[a]	22 (8)[a]
% recovery	100%[e]	100%[e]	97%[f]	105%[f]

[a]Values in parentheses are %RSD based on n = 9. [b]The soil sample was used without spiking or suspension in water. [c]The soil sample was wet with water to mimic spiking but without the use of the spiking solution. [d]The spiking solution contained ^{2}H-atrazine and ^{2}H-metolachlor. [e]The % recovery was calculated on the basis of the control soil sample as the reference. [f]The % recovery was calculated on the basis of the water sample as the reference.

These results show that water indeed provided a suitable vehicle for the deuterated surrogates, as the control, treated control, and spiked samples gave the same extractability for the H-analytes. The recoveries obtained for the two deuterated herbicides are 97% and 105%, respectively, for atrazine and metolachlor using the spiked water sample set at 100% for comparison.

Quantitation of the Amounts of the Herbicides in the Soil. Having determined the recoveries of the analytes from the soil samples, the actual concentrations observed at different times were calculated as shown in Table 3. The soil samples were collected over several months from the upper 5 cm layer of soil, right up to the time of harvesting. The data clearly demonstrate that the method can be used to track the concentration of the herbicides in question in agricultural soils.

In summary, this work demonstrates the applicability of the BID-SDME preconcentration technique as an efficient tool for application to the environmental monitoring of the herbicides atrazine and metolachlor using a method that demonstrates sub ng/mL LOD values (0.013 and 0.024 ng/mL, respectively). We identify highly influential effects of the spiking solvent used to prepare the surrogate solutions of the analytes of interest and the care that should be taken to ensure that traceless spiking is employed. Finally, the beneficial effect of hot water extraction over standard techniques such as sonication has been demonstrated. The data generated in this study provide a

Table 3. Quantitative Data for Different Samples[a] Obtained from the Calibration Curves Using Recovery Values

week no.	atrazine	metolachlor
	Calculated Concentrations (ng/g)[b,c]	
18	0.144 (2.9)[c]	1.585 (6.2)[c]
22	0.087 (8.4)[c]	1.295 (2.0)[c]
26	0.048 (3.5)[c]	1.231 (0.8)[c]
30	0.031 (7.3)[c]	0.930 (6.8)[c]
	Adjusted Concentration (ng/g) Using the Recovery Data[d]	
18	0.15 ± 0.01	1.51 ± 0.13
22	0.09 ± 0.01	1.23 ± 0.04
26	0.05 ± 0.01	1.17 ± 0.02
30	0.03 ± 0.01	0.89 ± 0.11

[a]Soil samples were collected from the upper 5 cm of soil. [b]Calculated using the calibration equations: $y_{Met} = 47.966x + 3.8069$ and $y_{Atrz} = 56.147x + 0.2193$. [c]The values in parentheses depict the %RSD. [d]Recovery values used: 97% (atrazine) and 105% (metolachlor).

good platform from which decision making as far as herbicide residues in the soils is concerned (environmental and farming perspective) can be performed. In the agricultural context, crop rotation is routinely performed, for example, for maintenance of soil productivity. Because crops show varied sensitivities toward given herbicides, intimate knowledge relating to herbicide residues may be critical information in deciding which crops may or should not be planted in a particular field. This work expands the BID-SDME and associated extraction protocols, which now underpin this method, to become more widely applicable in assessing the transport and fate of pesticides in the environment.

■ ASSOCIATED CONTENT

Supporting Information

Miscellaneous data covering chromatographic and recovery experiments. This material is available free of charge via the Internet at http://pubs.acs.org.

■ AUTHOR INFORMATION

Corresponding Author

*Tel.: (644) 463-0065. Fax: (644) 931-3055. E-mail: bradley.williams@vuw.ac.nz.

Funding

We gratefully acknowledge the University of Johannesburg, NRF, and THRIP for funding of this project.

Notes

The authors declare no competing financial interest.

■ ACKNOWLEDGMENTS

We gratefully acknowledge the Derby farmer for allowing access to his farm and for information related to his spraying program. M.J.G. thanks the National University of Lesotho for study leave.

■ REFERENCES

(1) WHO. *Guidelines for Drinking-Water Quality*, 2nd ed.; World Health Organization: Geneva, 1993; Chapter 3, Vol. *1*.

(2) Extoxnet, Extension Toxicology Network: Pesticide Information Profiles-Metolachlor, Oregon State University, http://extoxnet.orst.edu/pips/metolach.htm (09 April 2014).

(3) EPA. Special Report on Environmental Endocrine Disruption: An effects Assessment Analysis, 1997 (EPA document number EPA/630/R-96/012).

(4) Hayes, T.; Haston, K.; Tsui, M.; Hoang, A.; Haeffele, C.; Vonk, A. Atrazine-induced hermaphroditism at 0.1 ppb in American leopard frogs (*Rana pipiens*): laboratory and field evidence. *Environ. Health Perspect.* **2003**, *111*, 568−575.

(5) Hartzler, B. *Absorption of Soil-Applied Herbicides, Department of Agronomy*; Iowa State University, 2002; http://www.weeds.iastate.edu/mgmt/2002/soilabsorption.htm (09 April 2014).

(6) Singh, N.; Kloeppel, H.; Klein, W. Movement of metolachlor and terbuthylazine in core and packed soil columns. *Chemosphere* **2002**, *47*, 409−415.

(7) Zambonin, C. G.; Palmisano, F. Determination of triazines in soil leachates by solid-phase microextraction coupled to gas chromatography-mass spectrometry. *J. Chromatogr., A* **2000**, *874*, 247−255.

(8) Accinelli, C.; Dinelli, G.; Vicari, A.; Catizone, P. Atrazine and metolachlor degradation in subsoils. *Biol. Fertil. Soils* **2001**, 495−500.

(9) Kochany, J.; Maguire, R. J. Sunlight photodegradation of metolachlor in water. *J. Agric. Food Chem.* **1994**, *42*, 406−412.

(10) Munoz, A.; Koskinen, W. C.; Cox, L.; Sadowsky, M. J. Biodegradation and mineralization of metolachlor and alachlor by *Candida xestobii*. *J. Agric. Food Chem.* **2011**, *59*, 619−627.

(11) Krause, A.; Hancock, W. G.; Minard, R. D.; Freyer, A. J.; Honeycutt, R. C.; Lebaron, H. M.; Paulson, D. L.; Liu, S. Y.; Bollag, J. M. Microbial transformation of the herbicide metolachlor by a soil actinomycete. *Environ. Toxicol. Water Qual.* **1985**, *33*, 584−589.

(12) Liu, D.; Maguire, R. J.; Pacepavicius, G. J.; Aoyama, I.; Okamura, H. Microbial transformation of metolachlor. *Environ. Toxicol. Water Qual.* **1995**, *10*, 249−258.

(13) Frías, S.; Rodríquez, M. S.; Conde, J. E.; Pérez-Trujillo, J. P. Optimisation of a solid-phase microextraction procedure for the determination of triazines in water with gas chromatography-mass spectrometry detection. *J. Chromatogr., A* **2003**, *1007*, 127−135.

(14) Di Muccio, A.; Pelosi, P.; Camoni, I.; Barbini, D. A.; Dommarco, R.; Generali, T.; Ausili, A. Selective, solid-matrix dispersion extraction of organophosphate pesticide residues from milk. *J. Chromatogr., A* **1996**, *754*, 497−506.

(15) Payá, P.; Anastassiades, M.; Mack, D.; Sigalova, I.; Tasdelen, B.; Oliva, J.; Barba, A. Analysis of pesticide residues using the Quick Easy Cheap Effective Rugged and Safe (QuEChERS) pesticide multiresidue method in combination with gas and liquid chromatography and tandem mass spectrometric detection. *Anal. Bioanal. Chem.* **2007**, *389*, 1697−1714.

(16) Rasmussen, K. E.; Petersen-Bjergaard, S.; Krogh, M.; Ugland, H. G.; Gronhaug, T. Development of a simple in-vial liquid-phase microextraction device for drug analysis compatible with capillary gas chromatography, capillary electrophoresis and high-performance liquid chromatography. *J. Chromatogr., A* **2000**, *873*, 3−9.

(17) Rezaee, M.; Assadi, Y.; Hosseini, M.-R. M.; Aghaee, E.; Ahmadi, F.; Berijani, S. Determination of organic compounds in water using dispersive liquid−liquid microextraction. *J. Chromatogr., A* **2006**, *1116*, 1−9.

(18) Jeannot, M. J.; Cantwell, F. F. Solvent microextraction into a single drop. *Anal. Chem.* **1996**, *68*, 2236−2240.

(19) Xie, H.-Y.; Yan, J.; Jahan, S.; Zhong, R.; Fan, L.-Y.; Xiao, H.; Jin, H.-Q.; Cao, C.-X. A new strategy for highly efficient single-drop microextraction with a liquid-gas compound pendant drop. *Analyst* **2014**, *139*, 2545−2550.

(20) Williams, D. B. G.; George, M. J.; Meyer, R.; Marjanovic, L. Bubbles in solvent microextraction: the influence of intentionally introduced bubbles on extraction efficiency. *Anal. Chem.* **2011**, *83*, 6713−6716.

(21) Ozcan, S.; Tor, A.; Aydin, M. M. Application of miniaturised ultrasonic extraction to the analysis of organochlorine pesticides in soil. *Anal. Chim. Acta* **2009**, *640*, 52−57.

(22) Lambropoulou, D. A.; Albanis, T. A. Determination of the fungicides vinclozolin and dicloran in soils using ultrasonic extraction coupled with solid-phase microextraction. *Anal. Chim. Acta* **2004**, *514*, 125−130.

(23) Information gathered from the International Soil Reference and Information Centre via http://www.isric.org/data/soil-property-maps-africa-1-km (accessed 10 July 2014).
(24) Ribani, M.; Collins, C. H.; Bottoli, C. B. G. J. Validation of chromatographic methods: evaluation of detection and quantification limits in the determination of impurities in omeprazole. *J. Chromatogr., A* **2007**, *1156*, 201−205.
(25) Peterson, D. *Analytical Report to eXfuze, LLP*; Environmental Micro Analysis Inc., 2009.
(26) Munch, J. *Method 507, Determination of Nitrogen- and Phosphorus-containing pesticides in water by gas chromatography with a nitrogen-phosphorus detector*; US EPA, 1995; pp 1−31.
(27) Gonçalves, C.; Alpendurada, M. F. Assessment of pesticide contamination in soil samples from an intensive horticulture area, using ultrasonic extraction and gas chromatography−mass spectrometry. *Talanta* **2005**, *65*, 1179−1189.
(28) US EPA. *Method 3550C*; U.S. Environmental Protection Agency, Feb. 2007.
(29) Caracciolo, A. B.; Giuliano, G.; Grenni, P.; Guzzella, L.; Pozzoni, F.; Bottoni, P.; Fava, L.; Crobe, A.; Orrù, M.; Funari, E. Degradation and leaching of the herbicides metolachlor and diuron: a case study in an area of Northern Italy. *Environ. Pollut.* **2005**, *134*, 525−534.
(30) LGC Standards, 2008, http://www.lgcstandards.com/corpinfo/isotope_en.aspx (16 April 2014).
(31) van de Merbel, N. C. Quantitative determination of endogenous compounds in biological samples using chromatographic techniques. *Trends Anal. Chem.* **2008**, *27*, 924−933.
(32) Morgan, L.; Dike, L.; Dandeneau, A.; Crespi, C. L.; Stresser, D. M. *BD Biosciences − Discovery Labware*, Woburn, MA.
(33) D'Agostino, P. A.; Hancock, J. R.; Provost, L. R. Determination of sarin, soman and their hydrolysis products in soil by packed capillary liquid chromatography−electrospray mass spectrometry. *J. Chromatogr., A* **2001**, *912*, 291−299.
(34) Saifuddin, N.; Chua, K. H. Extraction of Tetrachloroethylene from weathered soils: a comparison between soxhlet extraction and microwave-assisted extraction. *Mal. J. Chem.* **2003**, *5*, 30−33.
(35) Psillakis, E.; Naxakis, G.; Kalogerakis, N. Detection of TNT-contamination in spiked-soil samples using SPME and GC/MS. *Global Nest J.* **2000**, *2*, 227−236.
(36) D'Agostino, P. A.; Hancock, J. R.; Chenier, C. L. Packed capillary liquid chromatography−electrospray ionization (tandem) mass spectrometry of mustard hydrolysis products in soil. *J. Chromatogr., A* **2004**, *1058*, 97−105.
(37) Merini, L. J.; Cuadrado, V.; Giulietti, A. M. Spiking solvent, humidity and their impact on 2,4-D and 2,4-DCP extractability from high humic matter content soils. *Chemosphere* **2008**, *71*, 2168−2172.

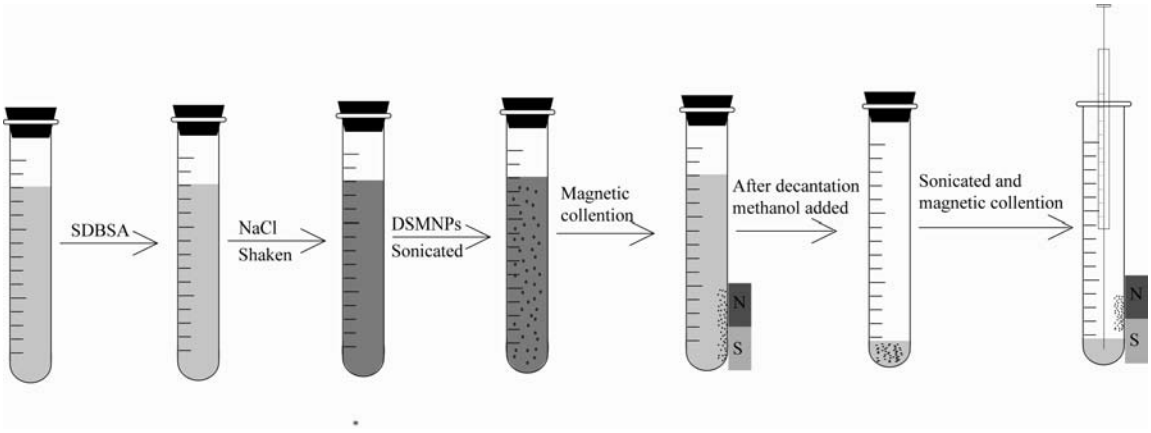

Figure 1. Simplified scheme of the two-step extraction process.

CPE can be used to determine PEs in environmental water samples by high-performance liquid chromatography (HPLC) and ultraviolet (UV) detection, using the nonionic surfactant Trinton X-114 as the extraction solvent.[26] However, the nonionic surfactants most frequently used for extraction and preconcentration prior to HPLC analysis have high background absorbance in the UV region and long retention times.[30] The results also overlap between the chromatographic peaks of the surfactant and the analytes, thereby requiring a cleanup step to obtain adequate selectivity.[31] Gradient elution has also been used to separate the surfactant and PEs to obtain quality chromatograms.[26] In 1999, Casero et al.[30] proposed the acid-induced CPE using anionic surfactants to overcome the aforementioned problems because anionic surfactants have appropriate ionic groups that lead to low retention times. Anionic surfactant solutions exhibiting phase separation in the presence of electrolytes is a phenomenon called coacervation.[32]

In this work, anionic surfactants were used as extraction solvents, and then electrolytes were added to separate the two phases, coacervation phase (CAP) and aqueous phase. The CAP was found to be loose solid instead of liquid, which became the top part and cannot be accurately transferred after centrifugation. For the complete separation of the CAP, a two-step extraction technique that combines the CAP and further dispersive microsolid phase extraction (D-μ-SPE) was developed. The diatomaceous earth-supported magnetite nanoparticles (DSMNPs) were used as the D-μ-SPE material to retrieve the anionic surfactant CAP instead of centrifugation. The new method was used for preconcentration of PEs in water prior to HPLC-UV determination.

MATERIALS AND METHODS

Reagents and Materials. All PE standards including dimethyl phthalate (DMP; 98%), diethyl phthalate (DEP; 99.9%), butylbenzyl phthalate (BBP; 99%), dibutyl phthalate (DBP; 96.8%), and DEHP (99.6%) were obtained from AccuStandard, Inc. (New Haven, USA). Sodium dodecylbenzenesulfonic acid (SDBSA) (Acros Organics, New Jersey, USA) accounted for 88% and sodium dodecyl sulfate (SDS) (Acros Organics, New Jersey, USA) accounted for 99% of the main component and were used as received. A 7% (w/v) surfactant solution was prepared by dissolving the reagents in water. Individual stock solutions of each PE compound were prepared in methanol, and a standard mixture solution of all target compounds was prepared in methanol at a final concentration of 0.1 mg mL^{-1}. The working solution was freshly prepared daily by appropriately diluting the methanolic stock standard solution. All standard solutions were stored at 4 °C and brought to ambient temperature prior to use. For the convenience of the analysis and for minimizing reagent consumption, 10 mL aqueous standard solutions containing each analyte at 50 ng mL^{-1} were used for the optimization study

Methanol and acetonitrile (HPLC grade) were purchased from J&K Scientific Ltd. (Beijing, China). Iron(III) chloride hexahydrate ($FeCl_3 \cdot 6H_2O$) (Acros Organics, New Jersey, USA), ethylene glycol (EG; Acros Organics, New Jersey, USA), 1,2-ethylenediamine (ETH; J&K Scientific Ltd., Beijing, China), sodium acetate (NaAc, J&K Scientific Ltd., Beijing, China), and diatomaceous earth (Qingdao, China) were used to prepare the DSMNPs. Milli-Q water (Millipore, Bedford, MA, USA) was used throughout the study. All solutions prepared for HPLC were filtered through 0.45 μm membranes (Tianjing Jinteng Instrument Factory, Tianjin, China) before use, and all labware are glass products that do not come into contact with any plastic products. All tubes in HPLC are made of Teflon and stainless steel.

Synthesis and Characterization of DSMNPs. Raw diatomaceous earth from Qingdao, China was purified by a previously described method.[33] In a typical synthesis, purified diatomaceous earth (0.3 g) was added to 24 mL of EG. Subsequently, 0.6 g of $FeCl_3 \cdot 6H_2O$ and 1.2 g of NaAc were dissolved in the EG solution at ambient temperature. After stirring for about 30 min, the solution was transferred to a 50 mL Teflon-lined stainless-steel autoclave kept at 200 °C for 8 h and then naturally cooled to ambient temperature. The black precipitate was isolated using an external magnetic field, and the supernatant was decanted. The obtained solid part was washed with ethanol several times and then dried at 60 °C in a vacuum oven. Using this method, 100 g of DSMNPs could be synthesized simultaneously using multiple Teflon-lined stainless-steel autoclaves. The non-modified MNPs were prepared according to the literature.[34] The photography of scanning electronic microscope for MNPs and DSMNPs has been shown in Figure S1 in the Supporting Information.

Liquid Chromatography Analysis. The chromatography equipment was a 1525 binary HPLC pump and a 2489 dual λ UV detector from Waters (Waters Corporation, USA). Waters Breeze software was used to control the instruments and collect the data. Chromatographic separation of the analytes was carried out on a Gemini C18 column (5 μm; 4.6 mm × 250 mm; Phenomenex, Torrance, CA, USA) maintained at 25 °C. The mobile phases A and B were water and acetonitrile. The gradient conditions are as follows: 0−15 min, 70% B; 15−20 min, 70%−100% B; 20−30 min, 100% B. The flow rate of the mobile phase was maintained at 1.0 mL/min; the sample injection volume was 10 μL; and the detection wavelength was 280 nm.

Extraction Procedure. In a typical procedure, 0.8 mL of SDBSA solution was put into a 10 mL glass tube containing 10 mL of sample and was thoroughly mixed. Afterward, 1.2 g of NaCl was added, and the tube was sealed and shaken for 4 min. Then, 25 mg of DSMNPs was added to the tube that was sonicated for another 2 min. The DSMNPs were rapidly collected from the tube wall using an magnetic field provided by a strong Nd−Fe−B magnet (Supporting Information Figure S2), and the sample solution was discarded by decanting. After removing the magnet, 0.2 mL of methanol was introduced to the tube

dx.doi.org/10.1021/jf502364x | J. Agric. Food Chem. 2014, 62, 7682−7689

to desorb the SDBSA by sonication for 2 min. Finally, the magnet was again placed next to the tube, and the supernatant was collected into an Eppendorf tube. All optimized experiments were performed in triplicate. A schematic of the two-step extraction process is shown in Figure 1.

Real Samples. To evaluate the feasibility of the developed method, four real-world water samples were used, including tap, river, tanked, well, and bottled water. Tap water was obtained from a water tap after flowing for 10 min in our laboratory. River water was obtained from the Fen River (Linfen, China) in May 2013. Tanked and well water were simultaneously collected from a local area (Linfen, China). Bottled water was obtained from a local market (Linfen, China). All water samples were collected into precleaned, light-colored glass bottles, and each sample was filtered through 0.45 μm micropore membranes to remove suspended solids. All samples were stored in a refrigerator (at 4 °C) in the dark until analysis.

Calibration of the EF and Extraction Recovery Percentage (ER%). To evaluate the performance of the proposed method, EF and ER% were determined using eqs 1 and 2

$$\mathrm{EF} = \frac{C_{\mathrm{des}}}{C_0} \tag{1}$$

where C_{des} and C_0 are the concentrations of the analytes in the desorbed phase and the initial concentration of the analytes in the sample solution, respectively.

$$\mathrm{ER\%} = \frac{C_{\mathrm{des}} \times V_{\mathrm{des}}}{C_0 \times V_0} \times 100\% = \mathrm{EF} \times \frac{V_{\mathrm{des}}}{V_0} \times 100\% \tag{2}$$

where V_{des} and V_0 are the volumes of the desorbed phase and sample solution, respectively.

RESULTS AND DISCUSSION

Optimization of CAP Extraction Parameters. Selecting an appropriate extraction solvent is important for optimizing the extraction process. Thus, the inexpensive and highly water-soluble anionic surfactants, SDBSA and SDS, were used. The working solution concentration of the surfactants was 7% (w/v). The experimental results showed (Figure 2) that the percentage of the extracted PEs was high for SDBSA with a phenyl group. This effect was consistent with the affinity of PEs to a more hydrophobic CAP. Thus, SDBSA was selected as the extraction solvent.

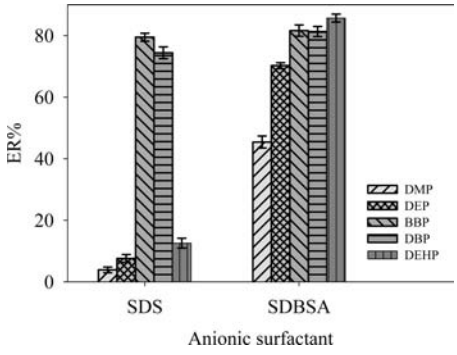

Figure 2. Effect of types of anionic surfactants. Experiment conditions: volume of surfactants, 0.8 mL; amount of DSMNs, 25 mg; extraction time, 4 min; amount of NaCl, 1.2 g; sonication time, 2 min; volume of methanol, 0.2 mL.

To study the effect of the extraction solvent volume of 7% SDBSA on the extraction efficiency (EE) of PEs, other experimental conditions were fixed, and different SDBSA volumes were tested (0.3−1.2 mL). The results are shown in Figure 3. ER% increased with increased SDBSA volumes up to 0.8 mL, beyond which the ER% remained constant. Thus, 0.8 mL of SDBSA solution was used in the subsequent experiments.

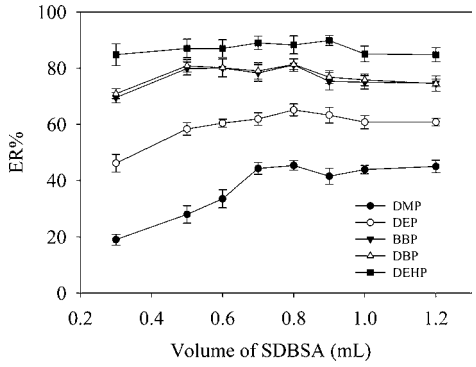

Figure 3. Effect of volume of SDBSA. Experiment conditions: amount of DSMNPs, 25 mg; extraction time, 4 min; amount of NaCl, 1.2 g; sonication time, 2 min; volume of methanol, 0.2 mL.

The coacervation of anionic surfactants is achieved only at a certain salt concentration. Addition of NaCl to the water sample may have various effects (salting out, salting in, or no effect) on extraction. The effect of NaCl on the coacervation of the system was investigated. The effect of NaCl was studied within the quality range of 0.6−1.8 g to 10 mL of sample. The results showed (Supporting Information Figure S3) that the ER % of the four PEs increased with increased NaCl until the amount was 1.2 g, beyond which ER% remained almost constant. Thus, 1.2 g of NaCl was deemed optimum.

The pH of the working solutions or samples has an important role in the extraction because it determines the existing state of the analytes and the EE of the target analytes. In this experiment, the effect of pH was studied within the range of 2.0−11.0, and the results show (Supporting Information Figure S4) the EE almost had no significant change within pH 4.0−9.0 of the sample solution. Therefore, the sample solution pH was not adjusted because the pH of the normal water samples ranged within 6.0−8.0.

Extraction time is also an important parameter affecting EE. Increasing the extraction repeatability necessitates an extraction period within which the equilibrium between the aqueous phase and CAPs is reached. The effect of the extraction time was examined within the range of 0−10 min, whereas other experimental conditions were kept constant. The results showed (Supporting Information Figure S5) that the EE of PEs increased with increased extraction time within 0−4 min and remained almost constant within 4−10 min. Therefore, 4 min was selected as the optimum extraction time.

Magnetic Material Selection. The magnetic material used in this method has a strong interaction effect on the SDBSA CAP so that target analytes extracted by SDBSA can be completely transferred. Two types of magnetic material, i.e., nonmodified MNPs and DSMNPs, were chosen in terms of their adsorption behavior to the CAP. Compared with MNPs, DSMNPs can completely retrieve the SDBSA CAP and have better dispersion and less coaggregation.[35] Thus, DSMNPs were chosen for further experiments.

Sonication was performed for the complete adsorption of CAP to DSMNPs. The sonication time was studied within the time range of 0.5−5 min in 0.5 min intervals. The results showed (Supporting Information Figure S6) that the EE increased with increased sonication time from 0.5 to 2 min.

Table 1. Analytical Performance of the Proposed Method for Determination of PEs

compounds	retention time (min)	calibration equation (ng/mL)	LRs (ng/mL)	LODs (ng/mL)	LOQs (ng/mL)	R^2	ER%	EFs	RSD (%, n = 10)
DMP	4.1	$y = 599x + 1503$	5−1000	1.0	3.0	0.9952	48.6	14.6	4.6
DEP	5.4	$y = 800x + 2300$	2−1000	0.5	1.5	0.9987	72.7	21.8	3.9
BBP	12.5	$y = 538x + 3834$	5−1000	1.0	3.0	0.9992	82.5	24.8	5.5
DBP	14.1	$y = 699x + 2514$	5−1000	1.0	3.0	0.9991	82.7	24.8	4.7
DEHP	26.7	$y = 348x + 1607$	10−1000	5.0	10.0	0.9965	84.8.	25.4	5.7

Table 2. Intra- and Interday Precision

		intraday precision[a]			interday precision[a]		
added PAEs	concentration (ng/mL)	found (ng/mL)	RSD (%)	recovery (%)	found (ng/mL)	RSD (%)	recovery (%)
DMP	10	8.8	3.2	88.2	8.9	5.1	89.2
	20	20.9	2.9	104.7	19.1	4.7	95.7
DEP	10	9.4	4.4	94.4	10.6	5.6	105.6
	20	20.2	2.6	101.1	20.0	4.4	99.9
BBP	10	8.7	3.5	86.5	10.1	3.8	101.3
	20	19.3	1.8	96.7	18.4	4.2	92.2
DBP	10	10.3	2.4	102.6	8.6	5.8	86.2
	20	18.3	3.9	91.4	20.7	4.4	103.3
DEHP	10	8.7	3.8	87.3	9.4	4.3	93.8
	20	20.8	2.3	103.9	19.7	3.9	98.7

[a]Based on five sample extractions.

Table 3. Comparison of the Presented Method with Other Microextraction Techniques[a]

extraction mehod	determination technique	extracting solvent/material	consumption of organic solvent (μL)	extraction time (min)[b]	LRs (ng mL^{-1})	LODs (ng mL^{-1})	R^2	ref
SPE	HPLC/UV	bamboo charcoal	2000	50	1−200	0.35−0.43	0.9974−0.9999	9
SPME	GC/FID	calix(6)arene fiber	-	60	0.8−8000	0.06−3.429	0.9965−0.9998	16
SPME	GC/FID	Fe_3O_4@ polythiophene MNPs	-	>10	0.4−100	0.4	0.998	19
SDME	GC/FID	dichloromethane:hexane:toluene	2	25	0.1−50	0.02−0.21	-	20
LPME	GC/MS	1-dodecanol	7	25	0.05−100	0.02−0.05	0.9940−0.9971	21
HFM-LPME	GC/MS	toluene	3	20	0.02−10	0.005−0.01	0.9984−0.9999	22
IL-CIA-DLLME	HPLC/VWD	1-octyl-3-methylimidazolium hexafluorophosphate	750	13	2−100	0.68−1.36	0.9968−0.9994	24
LDS-VSLLME	GC/MS	toluene	30	6	0.05−25	0.008−0.020	0.9823−0.9984	25
CPE	HPLC/UV	triton X-114	-	65	5−200	1.0−3.8	0.9964−0.9998	26
CAP-D-μ-SPE	HPLC/UV	SDBSA	-	8	2−1000	0.5−1.0	0.9952−0.9992	this work

[a]UV, ultraviolet detector; FID, flame ionization detector; HFM, Hollow-fiber membrane; VWD, variable wavelength detector; IL-CIA-DLLME, Ionic liquid cold-induced aggregation dispersive liquid−liquid microextraction; LDS−VSLLME, low-density solvent-based vortex-assisted surfactant-enhanced-emulsification liquid−liquid microextraction. LPME, liquid-phase microextraction; SDME, single-drop microextraction. [b]The time interval between added extraction agent to before chromatographic analysis.

Prolonged sonication time had little effect on EE. Thus, the sonication time of 2 min was deemed suitable for subsequent experiments.

The effect of the amount of DSMNPs was studied using 15, 20, 25, 30, 35, and 40 mg amounts of retrieval agent. The results showed (Supporting Information Figure S7) that, with increased amount of DSMNPs from 15 to 40 mg, the maximum EE was obtained at 25 mg of DSMNPs (corresponding to its concentration of 2.5 mg mL^{-1} in the sample). When the amount of the adsorbents was >25 mg, the plots were flat, and no distinct increase in EE was observed. Therefore, 25 mg of DSMNPs was used in the subsequent experiments.

Desorption Conditions. Different organic solvents were studied including methanol, ethanol, and acetonitrile. The results (Supporting Information Figure S8) showed that methanol gave the highest overall EE for the five PEs, followed by ethanol and acetonitrile. Therefore, methanol was used for the desorption of the target analytes from the DSMNP surface. The methanol volume investigated ranged from 0.1 to 0.6 mL. The results showed (Supporting Information Figure S9) that the increase in methanol volume from 0.1 to 0.2 mL increased the EE, whereas the ER% remained almost constant, except when the volume was 0.2 mL. However, in this case, EF decreased because the volume of the desorption solvent increased. The application of 0.2 mL of methanol was finally chosen, and the total volume of the desorption solution was almost 0.33 mL.

Influence of Interfering Substances for CAP-D-μ-SPE. Aliquots of aqueous solutions containing 50 ng mL^{-1} PEs and certain amounts of other chemical species were obtained, and the proposed procedure was followed to study the selective separation and determination of PEs from the water samples with various chemical species. The tolerance limit was defined as the concentration of the added interfering substance that

Table 4. Determination of PEs in Water Samples

water sample	DMP	DEP	BBP	DBP	DEHP
tap water					
found[a] (ng mL^{-1})	nd[b]	nd[b]	nd[b]	nd[b]	nd[b]
recovery[a] (%)	86.0 ± 2.1	103.1 ± 2.8	101.7 ± 2.7	93.0 ± 2.1	90.1 ± 4.5
river water					
found[a] (ng mL^{-1})	nd[b]	nd[b]	nd[b]	nd[b]	nd[b]
recovery[a] (%)	87.7 ± 2.4	97.6 ± 2.3	89.8 ± 3.8	89.0 ± 2.1	97.1 ± 2.4
well water					
found[a] (ng mL^{-1})	nd[b]	nd[b]	nd[b]	nd[b]	nd[b]
recovery[a] (%)	85.7 ± 0.9	94.8 ± 2.4	95.7 ± 1.3	98.9 ± 2.3	90.8 ± 3.2
tanked water					
found[a] (ng mL^{-1})	nd[b]	nd[b]	nd[b]	6.13 ± 0.32	nd[b]
recovery[a] (%)	93.0 ± 3.6	87.5 ± 2.2	92.2 ± 2.0	93.2 ± 5.1	93.1 ± 3.4
bottled water 1					
found[a] (ng mL^{-1})	nd[b]	nd[b]	nd[b]	5.51 ± 0.18	nd[b]
recovery[a] (%)	91.7 ± 5.1	93.7 ± 1.4	105.8 ± 4.0	102.5 ± 2.1	88.9 ± 2.4
bottled water 2					
found[a] (ng mL^{-1})	nd[b]	3.24 ± 0.14	nd[b]	nd[b]	nd[b]
recovery[a] (%)	87.1 ± 1.8	95.8 ± 3.3	103.7 ± 1.6	91.9 ± 1.3	95.8 ± 3.2
bottled water 3					
found[a] (ng mL^{-1})	6.38 ± 0.29	nd[b]	nd[b]	5.24 ± 0.24	nd[b]
recovery[a] (%)	104.1 ± 3.8	103.2 ± 4.0	94.7 ± 2.7	105.5 ± 2.0	89.8 ± 1.4
bottled water 4					
found[a] (ng mL^{-1})	nd[b]	2.77 ± 0.11	nd[b]	6.03 ± 0.23	nd[b]
recovery[a] (%)	104.1 ± 2.2	91.9 ± 3.5	93.3 ± 2.5	100.4 ± 3.8	90.1 ± 3.0
bottled water 5					
found[a] (ng mL^{-1})	5.36 ± 0.17	nd[b]	nd[b]	nd[b]	nd[b]
recovery[a] (%)	88.7 ± 4.3	99.5 ± 3.3	89.3 ± 2.4	91.8 ± 1.3	89.4 ± 2.9
bottled water 6					
found[a] (ng mL^{-1})	nd[b]	nd[b]	nd[b]	7.43 ± 0.32	nd[b]
recovery[a] (%)	94.4 ± 5.1	86.5 ± 3.8	93.3 ± 3.5	91.5 ± 3.5	86.4 ± 2.0
bottled water 7					
found[a] (ng mL^{-1})	5.94 ± 0.21	nd[b]	nd[b]	nd[b]	nd[b]
recovery[a] (%)	94.4 ± 3.1	104.6 ± 1.9	90.3 ± 2.3	97.9 ± 1.8	89.6 ± 2.7
bottled water 8					
found[a] (ng mL^{-1})	nd[b]	nd[b]	nd[b]	6.18 ± 0.25	nd[b]
recovery[a] (%)	92.9 ± 4.1	97.1 ± 2.1	95.8 ± 2.2	94.2 ± 2.9	96.6 ± 3.1
bottled water 9					
found[a] (ng mL^{-1})	nd[b]	nd[b]	nd[b]	5.71 ± 0.16	nd[b]
recovery[a] (%)	87.2 ± 3.6	95.6 ± 2.2	98.4 ± 4.7	103.1 ± 3.2	87.1 ± 4.0
bottled water 10					
found[a] (ng mL^{-1})	nd[b]	nd[b]	nd[b]	6.46 ± 0.27	nd[b]
recovery[a] (%)	89.7 ± 2.0	95.3 ± 2.1	95.3 ± 3.4	90.3 ± 3.2	95.0 ± 1.8

[a]Based on five sample extractions. [b]Not detected.

caused less than ±5% relative error in the determination of the PEs. The results show that 1500-fold Na^+, K^+, Ba^{2+}, Ca^{2+}, Mg^{2+}, Al^{3+}, Ni^{2+}, Cu^{2+}, Cd^{2+}, Hg^{2+}, Co^{2+}, Cr^{3+}, NH_4^+, Cl^-, NO_2^-, CH_3O^-, CrO_4^{2-}, $Cr_2O_7^{2-}$, F^-, Br^-, I^-, NO_3^-, SO_4^{2-}, $S_2O_3^{2-}$, $S_2O_8^{2-}$, BO_3^{3-}, $B_4O_7^{2-}$, CH_3COO^-, CO_3^{2-}, HCO_3^-, $C_2O_4^{2-}$, HPO_4^{2-}, and $H_2PO_4^-$, and 500-fold Zn^{2+} and Sr^{2+}, and 100-fold Sn^{2+}, and 50-fold Pb^{2+}, Fe^{2+}, and Fe^{3+}, and 8-fold MnO^{4-} did not interfere with the determination, indicating the high selectivity of the proposed method.

Determination by HPLC-UV. The background chromatograms of the blank water, reagent blank, and spiked water samples were determined. The results (Supporting Information Figure S10) show the absence of interfering peaks in the background chromatograms and highlight the selectivity of the HPLC-UV method. The matrix effect during HPLC-UV determination was studied by comparing the slopes of two calibration sets prepared in methanol and in the matrix extract. The results (Supporting Information Table S1) show no significant differences between the slopes. Therefore, HPLC-UV determination is not affected by matrix effects.

Method Validation. The external calibration curves were prepared by 10 concentration levels from 0.02 μg mL^{-1}, 0.05 μg mL^{-1}, or 0.1 μg mL^{-1} to 10 μg mL^{-1} of analytes to blank water samples with working solutions, calibration equations calculated using the peak areas of the substances, linear ranges (LRs), determination coefficient (R^2), limits of detection (LODs), limits of quantification (LOQs), and ER%, and EFs for PE determination were obtained under optimum conditions (Table 1). The linearity of the method was explored at PE concentrations from 2.0 ng mL^{-1}, 5.0 ng mL^{-1}, or 10.0 ng mL^{-1} to 1000 ng mL^{-1} with R^2 between 0.9952 and 0.9991. The LODs based on a signal-to-noise ratio (S/N) of 3 ranged

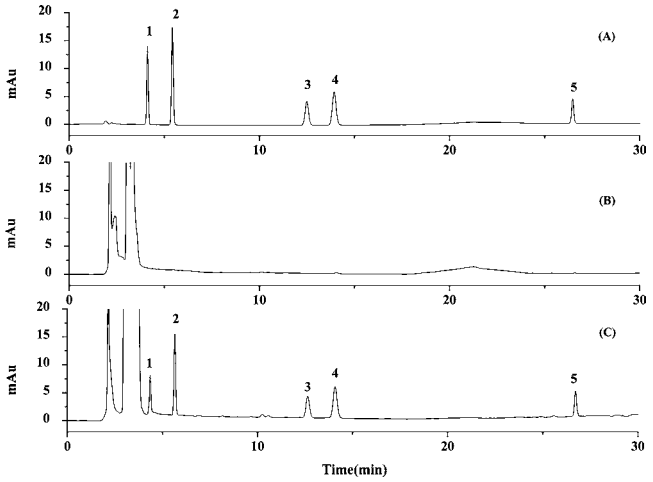

Figure 4. Typical chromatograms for determination of PEs in river water. (A) Standard solution; (B) river water after extraction; (C) spiked river water after extraction, PEs, 10 ng mL^{-1}. Peak 1, DMP; 2, DEP; 3, BBP; 4, DBP; 5, DEHP.

between 0.5 and 5.0 ng mL^{-1}. The repeatability study was carried out by extracting spiked water samples at a concentration of 5 ng mL^{-1} for the DMP, DEP, DBP, and BBP and of 10 ng mL^{-1} for the DEHP, and the relative standard deviations (RSDs) were between 3.9% and 5.7% (n = 10). The results confirmed that the proposed method had good reproducibility and stability and potential for use in the analysis of PEs at trace levels.

Intra- and interday variations were chosen to measure the precision of the developed method by analyzing spiked water samples at a concentration of 10 and 20 ng mL^{-1}. Intraday precision was assessed by five extractions and determinations in 1 day, whereas interday precision was evaluated by five extractions and determinations in different days. The RSDs obtained for both of them presented acceptable precisions (Table 2); i.e., they were obtained in the range of 1.8−4.4% and 3.8−5.8% for intra- and interday assay, respectively.

Comparison of the Proposed Technique with Other Methods. The performance of the proposed method in extracting and determining PEs in water samples was compared with those of other methods, and the results are shown in Table 3. The analytical performance of the proposed method has the following advantages. First, the utilization of the anionic surfactant SDBSA as an extractant without adding any toxic organic solvent and dispersant enabled true "green" microextraction. Second, SDBSA is a front eluting compound than nonionic surfactants and did not interfere with the analytes. Third, using DSMNPs as an adsorbent of the CAP simplified the phase-separation procedures that commonly use centrifugation or filtration during extraction. Although the LOD and linear range of the proposed method are poorer than GC methods,[16,19−22,25] especially the LOD of DEHP (10 ng mL^{-1}) is higher than the maximum limit established by the EPA (6 ng mL^{-1})[3] but similar to other HPLC methods.[9,24,26] These results revealed that this technique was environmentally friendly, simple, rapid, and effective. Moreover, this technique can also be used for PE preconcentration in water samples and extended to other applications.

Analysis of Real Water Samples. The practical applicability of the developed method was evaluated by the extraction of DMP, DEP, BBP, DBP, and DEHP from water samples collected from various sources, including tap, river, tanked, well, and bottled water. All water samples were spiked with standards of the 10 ng mL^{-1} of PEs to assess the matrix effect. The results in Table 4 show that DMP, DEP, and DBP may be detected in tank and bottled water; here, the containers were made of polyethylene terephthalate (PET). PAEs with low molecular weights are fairly soluble in water and are not chemically bonded to the polymer.[36] Thus, PAEs easily migrate from bottles, especially PET ones, to the water.[37] Table 4 also shows that the average results of the five replicate analyses of each water sample obtained by the proposed method satisfactorily agreed with one another (relative recoveries between 85.7% and 105.5%). This result indicated that the method was feasible for the determination of PEs in water samples. The HPLC chromatograms of river water are shown in Figure 4.

A simple, low-cost, and reliable method for enriching and determining four PEs in environmental water samples was established using SDBSA as an extraction solvent and DSMNPs as an adsorption solvent in a two-step extraction technique. Compared with the nonionic surfactant which due to the nonpolar character and large retention times causes the chromatographic overlapping between the surfactant and the analytes, the anionic surfactant SDBSA had an ionic group which resulted in low retention time and did not interfere with the determination of analytes. No toxic organic solvent or dispersant was used throughout the entire extraction procedure, in addition to diatomaceous earth. The DSMNPs used to retrieve the SDBSA CAP in the magnetic field simplified the phase-separation process, rendering unnecessary the use of time-consuming procedures of centrifugation. Overall, the proposed method can expand the applicability of anionic surfactants as extraction solvents because of their low toxicity, high preconcentration factors, and low retention time. The automation of such an extraction procedure is possible, and related work by our group is underway.

■ ASSOCIATED CONTENT

Ⓢ Supporting Information

The SEM figure for the MNPs and DSMNPs (Figure S1), the figure of Nd−Fe−B magnet (Figure S2), the figures of optimization steps (Figure S3−S9), the background chromatogram of the blank water sample, reagent blank sample and spiked water sample (Figure S10), and the comparison of the slopes (Table S1). This material is available free of charge via the Internet at http://pubs.acs.org.

■ AUTHOR INFORMATION

Corresponding Author

*Tel.: +86 357 2057969. Fax: +86 357 2057969. E-mail: lmd@dns.sxnu.edu.cn.

Funding

Financial support by the National Natural Science Foundation of China (No. 21171110), the Research Fund for the Doctoral Program of Higher Education of China (No.20091404110001), and the Shanxi Province Natural Science Foundation for Youths (No. 2014021018−3) is gratefully acknowledged.

Notes

The authors declare no competing financial interest.

REFERENCES

(1) Cai, Y.-Q.; Jiang, G.-B.; Liu, J.-F.; Zhou, Q.-X. Multi-walled carbon nanotubes packed cartridge for the solid-phase extraction of several phthalate esters from water samples and their determination by high performance liquid chromatography. *Anal. Chim. Acta* **2003**, *494*, 149−156.

(2) Balafas, D.; Shaw, K. J.; Whitfield, F. B. Phthalate and adipate esters in Australian packaging materials. *Food Chem.* **1999**, *65*, 279−287.

(3) EPA, Basic information about Di(2-ethylhexyl) phthalate in drinking water, http://water.epa.gov/drink/contaminants/basicinformation/di_2-ethylhexyl_phthalate.cfm (accessed July 13, 2014).

(4) Liang, P.; Xu, J.; Li, Q. Application of dispersive liquid−liquid microextraction and high-performance liquid chromatography for the determination of three phthalate esters in water samples. *Anal. Chim. Acta* **2008**, *609*, 53−58.

(5) Serôdio, P.; Nogueira, J. M. F. Considerations on ultra-trace analysis of phthalates in drinking water. *Water Res.* **2006**, *40*, 2572−2582.

(6) Li, J.; Cai, Y.; Shi, Y.; Mou, S.; Jiang, G. Analysis of phthalates via HPLC-UV in environmental water samples after concentration by solid-phase extraction using ionic liquid mixed hemimicelles. *Talanta* **2008**, *74*, 498−504.

(7) Castillo, M.; Oubiña, A.; Barceló, D. Evaluation of ELISA Kits Followed by Liquid Chromatography-Atmospheric Pressure Chemical Ionization-Mass Spectrometry for the Determination of Organic Pollutants in Industrial Effluents. *Environ. Sci. Technol.* **1998**, *32*, 2180−2184.

(8) Jara, S.; Lysebo, C.; Greibrokk, T.; Lundanes, E. Determination of phthalates in water samples using polystyrene solid-phase extraction and liquid chromatography quantification. *Anal. Chim. Acta* **2000**, *407*, 165−171.

(9) Zhao, R.-S.; Wang, X.; Yuan, J.-P.; Lin, J.-M. Investigation of feasibility of bamboo charcoal as solid-phase extraction adsorbent for the enrichment and determination of four phthalate esters in environmental water samples. *J. Chromatogr., A* **2008**, *1183*, 15−20.

(10) Liu, Y.; Wang, S.; Wang, L. Development of Rapid Determination of 18 Phthalate Esters in Edible Vegetable Oils by Gas Chromatography Tandem Mass Spectrometry. *J. Agric. Food Chem.* **2013**, *61*, 1160−1164.

(11) Sun, H.; Yang, Y.; Li, H.; Zhang, J.; Sun, N. Development of Multiresidue Analysis for Twenty Phthalate Esters in Edible Vegetable Oils by Microwave-Assisted Extraction−Gel Permeation Chromatography−Solid Phase Extraction−Gas Chromatography−Tandem Mass Spectrometry. *J. Agric. Food Chem.* **2012**, *60*, 5532−5539.

(12) Yan, H.; Cheng, X.; Yang, G. Dummy Molecularly Imprinted Solid-Phase Extraction for Selective Determination of Five Phthalate Esters in Plastic Bottled Functional Beverages. *J. Agric. Food Chem.* **2012**, *60*, 5524−5531.

(13) Yasuhara, A.; Shiraishi, H.; Nishikawa, M.; Yamamoto, T.; Uehiro, T.; Nakasugi, O.; Okumura, T.; Kenmotsu, K.; Fukui, H.; Nagase, M.; Ono, Y.; Kawagoshi, Y.; Baba, K.; Noma, Y. Determination of organic components in leachates from hazardous waste disposal sites in Japan by gas chromatography−mass spectrometry. *J. Chromatogr., A* **1997**, *774*, 321−332.

(14) Zhou, X.; Xie, P.-F.; Wang, J.; Zhang, B.-B.; Liu, M.-m.; Liu, H.-L.; Feng, X.-H. Preparation and characterization of novel crown ether functionalized ionic liquid-based solid-phase microextraction coatings by sol−gel technology. *J. Chromatogr., A* **2011**, *1218*, 3571−3580.

(15) Feng, J.; Sun, M.; Li, J.; Liu, X.; Jiang, S. A novel silver-coated solid-phase microextraction metal fiber based on electroless plating technique. *Anal. Chim. Acta* **2011**, *701*, 174−180.

(16) Ye, C.-W.; Gao, J.; Yang, C.; Liu, X.-J.; Li, X.-J.; Pan, S.-Y. Development and application of an SPME/GC method for the determination of trace phthalates in beer using a calix[6]arene fiber. *Anal. Chim. Acta* **2009**, *641*, 64−74.

(17) Dalby, O.; Birkett, J. W. The evaluation of solid phase microextraction fibre types for the analysis of organic components in unburned propellant powders. *J. Chromatogr., A* **2010**, *1217*, 7183−7188.

(18) Cao, X.-L. Determination of phthalates and adipate in bottled water by headspace solid-phase microextraction and gas chromatography/mass spectrometry. *J. Chromatogr., A* **2008**, *1178*, 231−238.

(19) Elham, T.; Yadollah, Y.; Morteza, M.; Ali, E. Polythiophene-coated Fe_3O_4 superparamagnetic nanocomposite: Synthesis and application as a new sorbent for solid-phase extraction. *Anal. Chim. Acta* **2013**, *770*, 68−74.

(20) Batlle, R.; Nerín, C. Application of single-drop microextraction to the determination of dialkyl phthalate esters in food simulants. *J. Chromatogr., A* **2004**, *1045*, 29−35.

(21) Farahani, H.; Ganjali, M. R.; Dinarvand, R.; Norouzi, P. Screening method for phthalate esters in water using liquid-phase microextraction based on the solidification of a floating organic microdrop combined with gas chromatography−mass spectrometry. *Talanta* **2008**, *76*, 718−723.

(22) Psillakis, E.; Kalogerakis, N. Hollow-fibre liquid-phase microextraction of phthalate esters from water. *J. Chromatogr., A* **2003**, *999*, 145−153.

(23) Yao, J.; Xu, H.; Lv, L.; Song, D.; Cui, Y.; Zhang, T.; Feng, Y.-Q. A novel liquid-phase microextraction method combined with high performance liquid chromatography for analysis of phthalate esters in landfill leachates. *Anal. Chim. Acta* **2008**, *616*, 42−48.

(24) Zhang, H.; Chen, X.; Jiang, X. Determination of phthalate esters in water samples by ionic liquid cold-induced aggregation dispersive liquid−liquid microextraction coupled with high-performance liquid chromatography. *Anal. Chim. Acta* **2011**, *689*, 137−142.

(25) Zhang, Y.; Lee, H. K. Low-density solvent-based vortex-assisted surfactant-enhanced-emulsification liquid−liquid microextraction combined with gas chromatography−mass spectrometry for the fast determination of phthalate esters in bottled water. *J. Chromatogr., A* **2013**, *1274*, 28−35.

(26) Wang, L.; Jiang, G.-B.; Cai, Y.-Q.; He, B.; Wang, Y.-W.; Shen, D.-Z. Cloud point extraction coupled with HPLC-UV for the determination of phthalate esters in environmental water samples. *J. Environ. Sci.-China* **2007**, *19*, 874−878.

(27) Giokas, D. L.; Zhu, Q.; Pan, Q.; Chisvert, A. Cloud point−dispersive μ-solid phase extraction of hydrophobic organic compounds onto highly hydrophobic core−shell Fe2O3@C magnetic nanoparticles. *J. Chromatogr., A* **2012**, *1251*, 33−39.

(28) Watanabe, H.; Tanaka, H. A non-ionic surfactant as a new solvent for liquid—liquid extraction of zinc(II) with 1-(2-pyridylazo)-2-naphthol. *Talanta* **1978**, *25*, 585−589.

(29) Pytlakowska, K.; Kozik, V.; Dabioch, M. Complex-forming organic ligands in cloud-point extraction of metal ions: A review. *Talanta* **2013**, *110*, 202−228.

(30) Casero, I.; Sicilia, D.; Rubio, S.; Pérez-Bendito, D. An Acid-Induced Phase Cloud Point Separation Approach Using Anionic Surfactants for the Extraction and Preconcentration of Organic Compounds. *Anal. Chem.* **1999**, *71*, 4519−4526.

(31) Ferrer, R.; Beltrán, J. L.; Guiteras, J. Use of cloud point extraction methodology for the determination of PAHs priority pollutants in water samples by high-performance liquid chromatography with fluorescence detection and wavelength programming. *Anal. Chim. Acta* **1996**, *330*, 199−206.

(32) Rubio, S.; Pérez-Bendito, D. Supramolecular assemblies for extracting organic compounds. *TrAC, Trends Anal. Chem.* **2003**, *22*, 470−485.

(33) Yuan, P.; Yang, D.; Lin, Z.; He, H.; Wen, X.; Wang, L.; Deng, F. Influences of pretreatment temperature on the surface silylation of diatomaceous amorphous silica with trimethylchlorosilane. *J. Non-Cryst. Solids* **2006**, *352*, 3762−3771.

(34) Guo, S.; Li, D.; Zhang, L.; Li, J.; Wang, E. Monodisperse mesoporous superparamagnetic single-crystal magnetite nanoparticles for drug delivery. *Biomaterials* **2009**, *30*, 1881−1889.

(35) Yuan, P.; Liu, D.; Fan, M.; Yang, D.; Zhu, R.; Ge, F.; Zhu, J.; He, H. Removal of hexavalent chromium [Cr(VI)] from aqueous solutions

by the diatomite-supported/unsupported magnetite nanoparticles. *J. Hazard. Mater.* **2010**, *173*, 614−621.
(36) Cao, X. Phthalate esters in foods: sources, occurrence, and analytical methods. *Compr. Rev. Food Sci. Food Saf.* **2010**, *9*, 21−43.
(37) Montuori, P.; Jover, E.; Morgantini, M.; Nayona, J. M.; Triassi, M. Assessing human exposure to phthalic acid and phthalate esters from mineral water stored in polyethylene terephthalate and glass bottles. *Food Addit. Contam.* **2008**, *25*, 511−518.

Table 1. Structures of β-Acids and Their Transformation Products

no.	structure		side chain	compound	summary formula
1	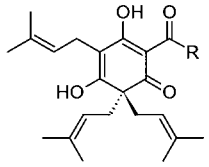	a		colupulone (**1a**)	$C_{25}H_{36}O_4$
		b		lupulone (**1b**)	$C_{26}H_{38}O_4$
		c		adlupulone (**1c**)	$C_{26}H_{38}O_4$
		d		postlupulone (**1d**)	$C_{24}H_{34}O_4$
		e		prelupulone (**1e**)	$C_{27}H_{40}O_4$
2	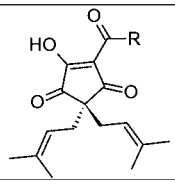	a		cohulupone (**2a**)	$C_{19}H_{26}O_4$
		b	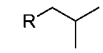	hulupone (**2b**)	$C_{20}H_{28}O_4$
		c	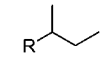	adhulupone (**2c**)	$C_{20}H_{28}O_4$
3	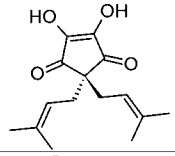			hulupinic acid (**3**)	$C_{15}H_{20}O_4$
4	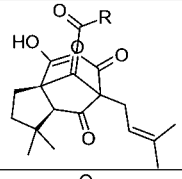	a		norticyclocolupone (**4a**)	$C_{22}H_{30}O_4$
		b	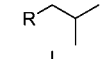	norticyclolupone (**4b**)	$C_{23}H_{32}O_4$
		c	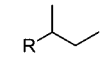	norticycloadlupone (**4c**)	$C_{23}H_{32}O_4$
5	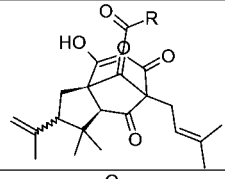	a		dehydrotricyclocolupone (**5a**, **5′a**)	$C_{25}H_{34}O_5$
		b	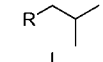	dehydrotricyclolupone (**5b**, **5′b**)	$C_{26}H_{36}O_5$
		c	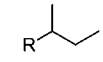	dehydrotricycloadlupone (**5c**, **5′c**)	$C_{26}H_{36}O_5$
7	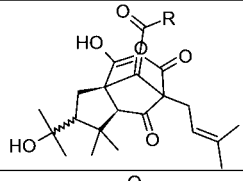	a		hydroxytricyclocolupone (**7a**, **7′a**)	$C_{25}H_{36}O_5$
		b	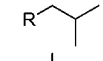	hydroxytricyclolupone (**7b**, **7′b**)	$C_{26}H_{38}O_5$
		c	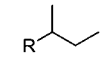	hydroxytricycloadlupone (**7c**, **76′c**)	$C_{26}H_{38}O_5$
8	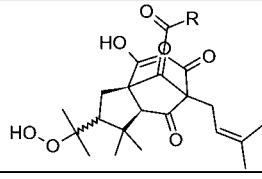	a		hydroperoxytricyclocolupone (**8a**, **8′a**)	$C_{25}H_{36}O_6$
		b	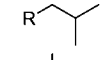	hydroperoxytricyclolupone (**8b**, **8′b**)	$C_{26}H_{37}O_6$
		c	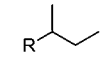	hydroperoxytricycloadlupone (**8c**, **8′c**)	$C_{26}H_{37}O_6$

transformation products of β-acids. Exact mass measurement of product ions allowed us to assign predicted fragments of known/previously identified transformation products to the product ions obtained by fragmentation of precursor ions with molecular mass corresponding to the transformation products of β-acid. This approach thus allowed us to identify well-described compounds at least in model mixtures without the necessity of having an individual standard of each compound. The efficiency of this approach was demonstrated in the pilot study of β-acids and their transformation products in hops and beer.

MATERIALS AND METHODS

Chemicals and Materials. Commercial CO_2 hop extract of Magnum variety (Hopsteiner, Mainburg, Germany) kept at 4 °C was used for preparation of β-acids. The following chemicals were obtained commercially: acetic acid, acetonitrile of LC-MS grade, ammonium formate, cellulose powder for column chromatography, formic acid (Fluka, St. Louis, MO, USA); acetonitrile of HPLC grade (LiChrosolv, Merck, Darmstadt, Germany); hulupinic acid (HWI Analytic GmbH, Ruelzelheim, Germany); disodium carbonate, diethyl ether, sodium hydroxide (Lach-Ner, Brno, Czech Republic); toluene (LiChrosolv, Merck); ethanol (LiChrosolv, Merck), methanol (Penta, Prague, Czech Republic). Deionized water used for chromatography was purified by means of a Milli-Q purification system (Millipore, Bilerrica, MA, USA).

Hop Samples. Two real samples of Sládek variety T90 hop pellets were analyzed to verify the newly developed method. Sládek is an aroma variety with a balanced content of α-acids and β-acids in an amount of about 4−7% w/w. The pellets were in evacuated barrier packaging as in commercial packages. The first sample (S1) was fresh pellets of the 2012 harvest, the second sample (S2) was aged pellets of the 2008 harvest. These pellets were stored in conditions simulating those in unconditioned warehouses of hop merchants or breweries. Hop samples were selected on the basis of a similar content of β-acids in fresh hops

dx.doi.org/10.1021/jf501852r | J. Agric. Food Chem. 2014, 62, 7690−7697

Table 2. MS Parameters of Compounds of Interest[a]

compound	no.[b]	summary formula	$[M-H]^-$ m/z	t_R (min)	NCE (%)	daughter ions of $[M-H]^-$ presented in fragmentation spectra[c]
colupulone	**1a**	$C_{25}H_{36}O_4$	399.3	12.1	35	194.0576, 219.0657, 275.1290, **287.1289**
cohulupone	**2a**	$C_{19}H_{26}O_4$	317.2	3.4	35	111.0436, 180.0418, 184.0367, 205.0499, 220.1099, 233.0814, **248.1052**
hulupinic acid	**3**	$C_{15}H_{20}O_4$	263.1	4.4	35	124.9868, 151.0026, 165.0548, 181.0498, 193.0499, **209.0450**, 263.1291
norticyclocolupone	**4a**	$C_{22}H_{30}O_4$	357.2	12.8	35	**219.1749**, 287.1653
dehydrotricyclocolupone	**5a**, **5′a**	$C_{25}H_{34}O_5$	397.2	13.7, 13.9	45	95.0487, 111.0437, 189.1276, 232.0437, **259.2067**, 264.0639, 327.1964
hydroxytricyclocolupone	**7a**, **7′a**	$C_{25}H_{36}O_5$	415.3	10.9, 11.1	35	**277.2172**, 345.2068
hydroperoxytricyclocolupone	**8a**, **8′a**	$C_{25}H_{36}O_6$	431.2	11.0, 11.1	35	111.0437, 233.0814, 287.1289, **341.1757**
epoxycohulupone	**9a**	$C_{19}H_{26}O_5$	333.2	4.8	40	124.9868, 151.0026, 165.0548, 181.0498, 193.0499, **209.0450**, 263.1291
lupulone	**1b**	$C_{26}H_{38}O_4$	413.3	12.6	35	208.0734, 233.0815, 289.1446, **301.1445**
hulupone	**2b**	$C_{19}H_{26}O_4$	331.2	3.9	35	125.0594, 194.0576, 198.0525, 219.0657, 234.1257, 247.0973, **262.1210**
norticyclolupone	**4b**	$C_{23}H_{32}O_4$	371.2	13.3	45	**217.1749**, 287.1653
dehydrotricyclolupone	**5b**, **5′b**	$C_{26}H_{36}O_5$	411.3	14.2, 14.4	45	95.0487, 125.0594, 189.1276, 246.0895, **259.2066**, 287.94, 327.1965
hydroxytricyclolupone	**7b**, **7′b**	$C_{26}H_{38}O_5$	429.3	11.5, 11.8	45	**277.2172**, 345.2070
hydroperoxytricyclolupone	**8b**, **8′b**	$C_{26}H_{38}O_6$	445.3	11.5, 11.7	35	125.0594, 247.0974, 301.1446, **355.1916**
epoxyhulupone	**9b**	$C_{20}H_{20}O_{20}$	347.2	5.8	40	124.9868, 151.0026, 165.0548, 181.0498, 193.0499, **209.0450**, 263.1291

[a]Name, summary formula, numbering of compound, molecular ions $[M-H]^-$, retention times (t_R), normalized collision energy (NCE), and mass spectrometric fragments of the β-acids and their transformation products are given. [b]Numbering of the compound refers to the literature.[18] [c]HR-MS/MS fragment in bold.

analyzed according to the EBC 7.7 method.[19] Both samples were used in a brewing test.

Preparation of Reference Compounds. *Isolation of Pure β-Acids from Hop Extracts (**1a**–**1c**, Table 1).* The β-acids were isolated from CO_2 hop extracts by two purification steps according to the schedule elaborated by the Hop Research Institute.[18] In the first step, a solution of 20 g of hop extract in 75 mL of toluene was stepwise extracted by disodium carbonate (c = 0.2 mol/L) and sodium hydroxide (c = 1 mol/L). In the second step, crude extract of β-acids containing up to 5% w/w of residual α-acids was recrystallized from the mixed solvent acetonitrile/water. The final mixture of β-acids was entirely free of α-acid residues. Pure β-acids were reconditioned in a refrigerator for 24 h to remove residual solvent and were then kept at −18 °C until use.

Oxidation of β-Acids on Solid Carrier's Surface. The transformation products of β-acids were prepared by oxidation by air oxygen. The purified isolate of β-acids (15 g) was dissolved in pure ethanol (300 mL) and mixed with the cellulose powder (65 g) used as a solid carrier. After thorough mixing, ethanol was removed on a rotary vacuum evaporator. The theoretical amount of β-acids on the carrier was 18.7% w/w. The dry powder with the mixture of β-acids applied on the cellulose surface was afterward kept for 48 h in the dark at room temperature. The HPLC analysis confirmed that about 99% of β-acids were converted by oxidation decomposition to transformation products. Ten milligrams of cellulose powder containing oxidized β-acids was weighed into an Eppendorf tube, and 1 mL of acetonitrile was added. The solid material was removed by centrifugation, and supernatant was diluted 1:10 before injection to the mass spectrometer by adding 0.1 mL of the sample to 0.9 mL of acetonitrile.

High-Performance Liquid Chromatography (HPLC). A Shimadzu Prominence LC 20A HPLC system, equipped with an LC-20 AD pump, an SIL-20A automated sample injector, a thermostated column compartment CTO-20AC, and an SPD-M20A photodiode array detector, was used to analyze the products of oxidation of β-acids. Data acquisition was performed by means of the Class LC20 software package. Analyses were performed on a Nucleodur C18ec column (250 × 4 mm i.d.; particle size, 5 μm; Macherey-Nagel, Düren, Germany) with a mobile phase flow rate of 0.8 mL/min and a column temperature of 40 °C. The mobile phase consisted of (A) water/formic acid (99:1, v/v) and (B) acetonitrile/formic acid (99:1, v/v) with the following gradient elution (min/% A): 0/30, 5/30, and 25/20, followed by a 10 min equilibration. Time of analysis was 45 min. The effluent flow was monitored at the wavelengths of 260, 290, 314, and 355 nm. Injection volume was 10 μL.

High-Performance Liquid Chromatography–High-Resolution MS (HPLC-HR/AM-MS). The studies were performed on a hybrid quadrupole-Orbitrap (Q-Exactive) mass spectrometer (Thermo Fisher Scientific, San Jose, CA, USA) coupled with a Dionex UltiMate 3000 UHPL system, consisting of a pump, a degasser, a column oven, and an autosampler (Dionex, Sunnyvale, CA, USA). Analyses were performed on an XSelect HSS T3 C18 column (100 × 2.1 mm i.d.; particle size 3 μm; Waters, Milford, MA, USA) with a mobile phase flow rate of 0.4 mL/min and a column temperature of 40 °C. The mobile phase consisted of (A) water containing 10 mM ammonium formate plus 0.1% formic acid and (B) methanol containing 0.1% formic acid with the following gradient elution (min/% A): 0/70, 0.2/70, 13/5, and 16.5/5, followed by a 5 min equilibration. The samples were kept at 10 °C, and the injection volume was 2 μL.

The electrospray operated in negative mode using the following parameters: electrospray voltage, 2.5 kV; sheath gas, 48 arbitrary units; auxiliary gas, 11 arbitrary units; sweep gas, 2 arbitrary units. The heater in source was set to 413 °C, and the heated capillary in the mass spectrometer was operated at 256 °C. Data were acquired by targeted MS/MS. Precursor ions from the inclusion list were selected one by one on the quadrupole, collected in the C-trap and transferred to an HCD collision cell. There, the fragmentation took place at appropriate collision energy (Table 2), after which all ions were sent back to the C-trap and from there forwarded to the Orbitrap mass analyzer. The resolving power for MS/MS scan was 70,000. The automatic gain control target was set to 2×10^5 ions and an isolation width of 2 m/z. The LC and mass spectrometer were controlled by Xcalibur 2.2 coupled with Dionex Chromatography MS Link v. 2.14. Calibration of the mass spectrometer was done with external calibration.

Sample Preparation. *Preparation of Hop Samples.* Ten grams (10 ± 0.01 g) of ground hops at a time was mixed in a Duran GLS 80 laboratory bottle with 20 mL of methanol, 100 mL of diethyl ether (temperature = 20 ± 3 °C), and 40 mL of acetic acid (c = 0.1 mol/L). The bottle was tightly closed, placed on an orbital shaker, and treated for 40 min. After shaking, the dispersion of hops particles was left for 10 min

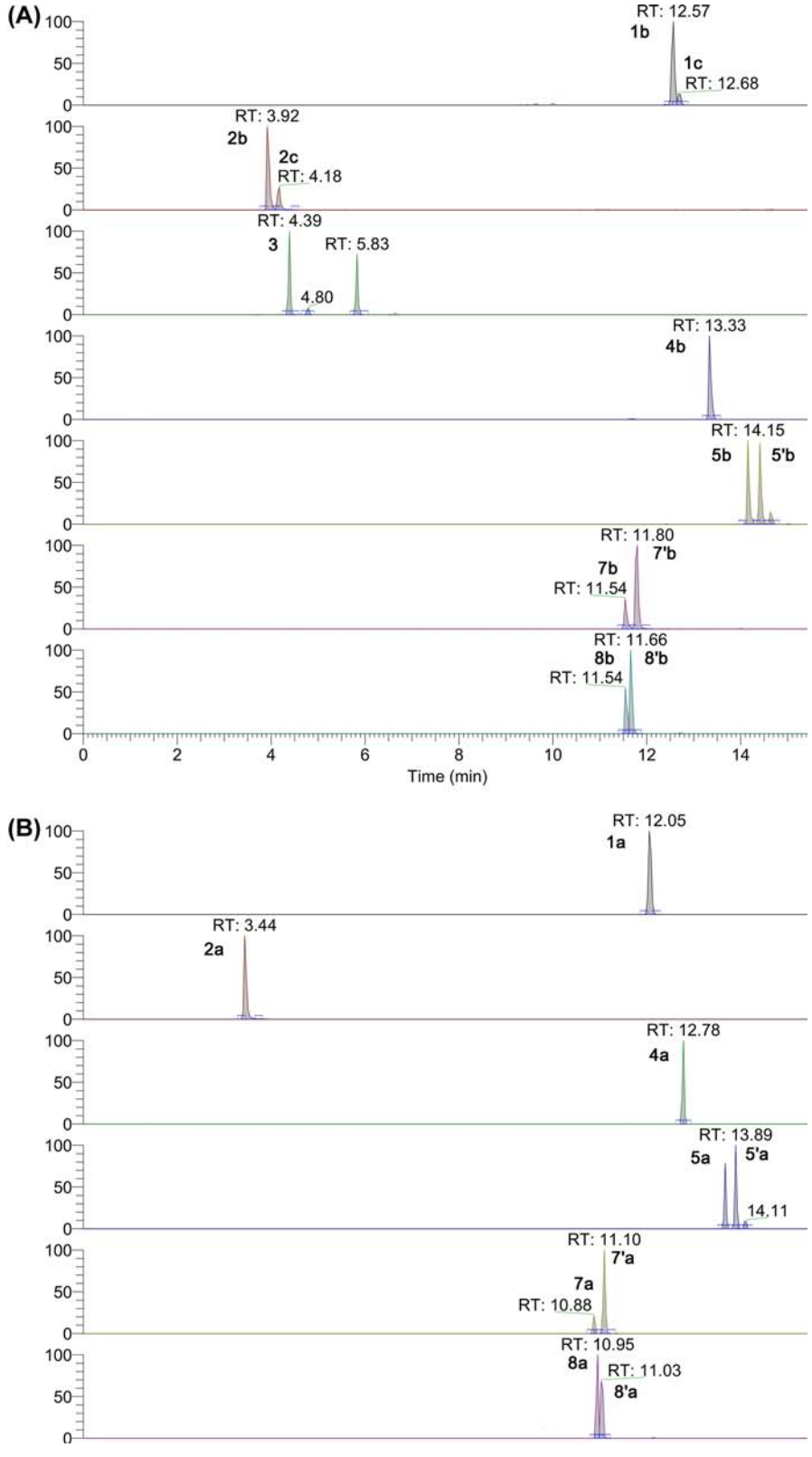

Figure 1. High-resolution extracted ion chromatograms (XICs) associated with selected product ions of transformation products of (A) colupulone (**1a**) and (B) lupulone (**1b**) after oxidation of purified extract of β-acids. The list of used product ions is given in Table 2.

to settle in the bottle. Afterward, 1 mL of extract without any solid particles was transferred into a 50 mL volumetric flask and filled with methanol.

Preparation of Beer Samples by the QuEChERS Method. Extraction of β-bitter acids and their transformation products from samples of beer was carried out according to the original buffered QuEChERS method.[20] Ready-to-use QuEChERS extraction kits (Agilent, Santa Clara, CA, USA) used for sample preparation contained 4 g of magnesium sulfate, 1 g of sodium chlorine, 1 g of sodium citrate tribasic dihydrate, and 0.5 g of sodium hydrogencitrate sesquihydrate for buffered extraction of the

dx.doi.org/10.1021/jf501852r | J. Agric. Food Chem. 2014, 62, 7690−7697

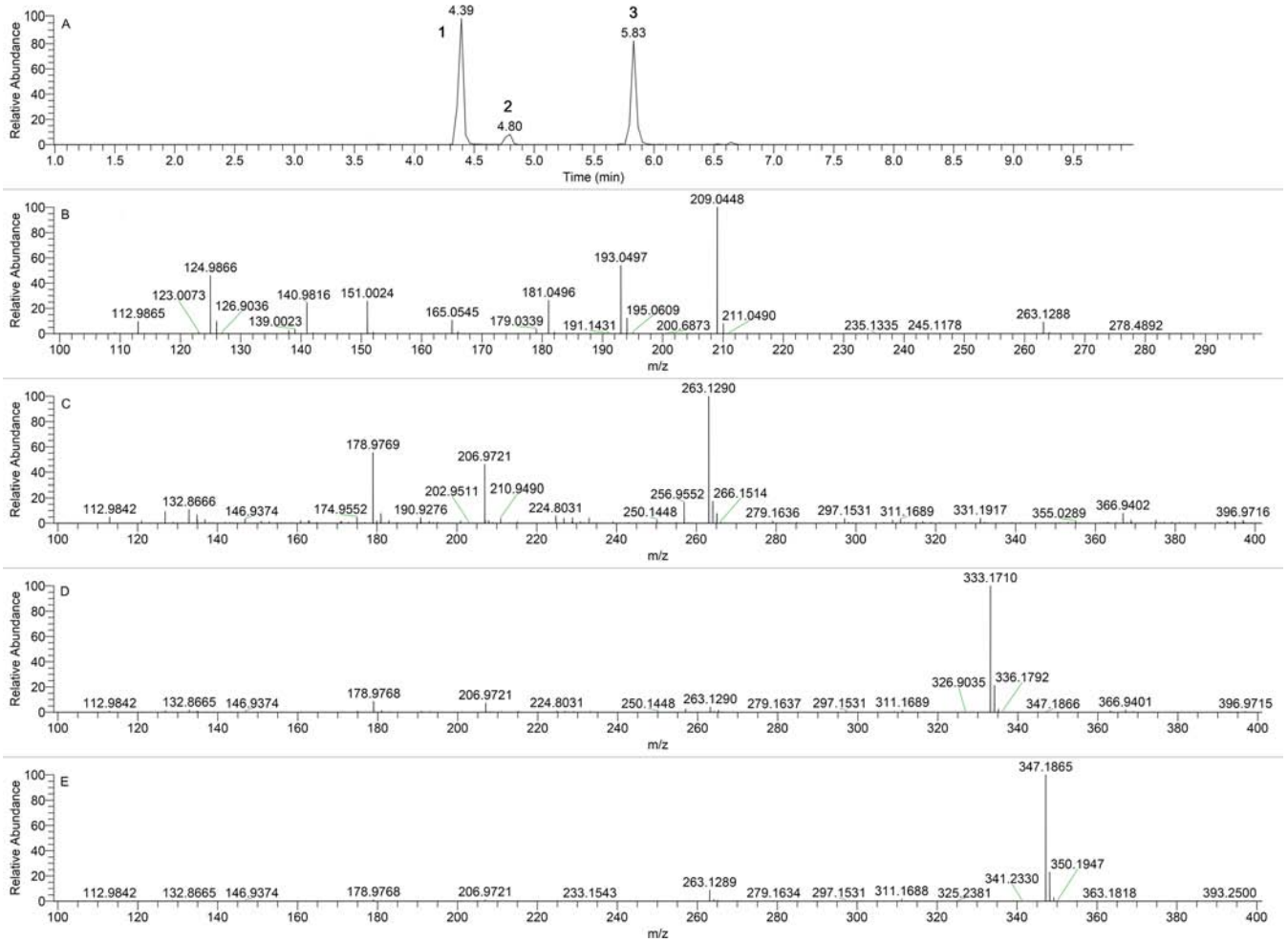

Figure 2. Elucidation of unknown compounds found in oxidized test material: (A) extracted ion chromatogram of (−)SRM 263.1/209.045 m/z with three unidentified peaks numbered 1−3; (B) MS/MS fragmentation spectrum of the peak eluted at 4.8 min; (C) full MS spectrum of peak 2 eluted at 4.8 min; (D) full MS spectrum of peak 1 eluted at 4.4 min; (E) full MS spectrum of peak 3 eluted at 5.8 min.

target. A brief description of the extraction procedure used is as follows: (a) pour 10 mL of degassed beer into a 50 mL centrifuge tube; (b) add salt mixture—whole content of one package; (c) seal the tube, shake vigorously for 1 min by hand, and centrifuge at 4000 rpm for 7 min; (d) transfer 200 μL of the extract to an autosampler vial and add 800 μL of water.

Beer-Brewing Trial. Two pilot-scale (60 L) brews of 12 °P all malt pale lager beer were carried out. Sweet wort was prepared using double-decoction mashing. The following wort boiling technology was used: hop dose was divided into three portions: 30% at the beginning, 50% after 30 min, and 20% after 15 min before the end of the 90 min wort boiling. The primary fermentation was performed in cylindrical−conical tanks (CCT), and a 40 day beer maturation took place in lager tanks. The beer was filtered, bottled, and pasteurized.

RESULTS AND DISCUSSION

Preparation of Pure β-Acid Extract. The final isolate of pure β-acids was entirely free of α-acid residues. Its purity was approximately 99% and was confirmed by HPLC analysis under previously described conditions. The isolation procedure allowed the preparation of β-acids in amounts of several tens of grams in a relatively short time. Pure isolate of β-acids was used for brewing tests in laboratory and pilot scales.

Identification of Hulupones in Oxidized Material. Previously in the literature[17] described compounds generated upon transformation of β-acids, colupulone (**1a**) and lupulone (**1b**), were extracted by acetonitrile from cellulose powder containing oxidized β-acids, diluted, and analyzed using the high-resolution MRM (MRM-HR) technique. Summary formulas of parent compounds (**1a**, **1b**) and their transformation products were used for creating the software inclusion list. Each m/z value from the inclusion list was isolated one by one in quadrupole and consequently fragmented in an HCD cell, collected in a C trap, and analyzed in an Orbitrap. The HR-MS/MS spectra of parent compounds so obtained provide enough specific fragments for building a MRM-HR qualification method and could also be used for confirmation of proposed structure on the basis of the fragmentation pattern of the parent compound. Generally, the MRM-HR method showed better sensitivity compared to the scan method, and in comparison with MRM on QqQ mass analyzers it provided structural information as a benefit. This approach is useful (a) when the structure of transformation products has been previously described in the literature[17] and (b) when these compounds are determined in a model mixture. It could be used for identification of the transformation products of β-acids with a high level of confidence without the presence of the standards for individual compounds of the basis of two facts. (i) The specificity of fragments found in the HR-MS/MS spectra could be compared with the proposed fragmentation pattern by applying a mass window of 5 ppm to the theoretical mass of the fragments. (ii) The mass difference of molecular weight between

dx.doi.org/10.1021/jf501852r | J. Agric. Food Chem. 2014, 62, 7690−7697

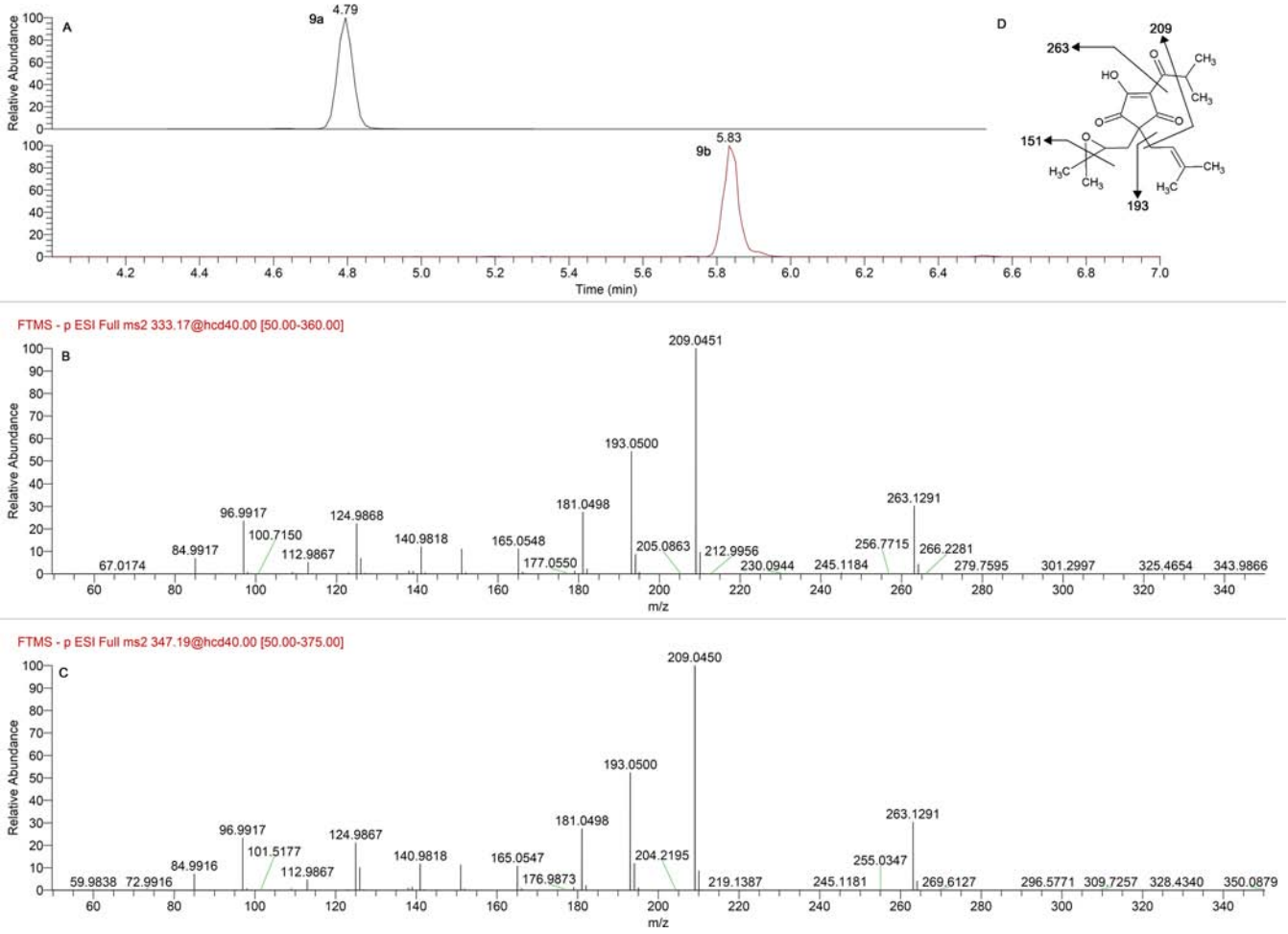

Figure 3. Fragmentation spectra of newly identified compounds (**9a**, **9b**): (A) extracted ion chromatograms of (−)SRM traces 333.2/209.045 and 347.2/209.045; (B) product ion mass spectra of parent ion at *m*/*z* 333 (**9a**); (C) product ion mass spectra of parent ion at *m*/*z* 347 (**9b**); (D) structure proposals for some of the fragments in the product ion mass spectra of parent ion at *m*/*z* 333 (**9a**).

colupulone and lupulone is 14 Da, and the structures of lupulone and colupulone are almost identical, the difference being only in the length of the side chain (see Table 1). The same difference could be expected between transformation products of these two compounds. This fact could be a clue to matching suitable fragments in the MS/MS spectra to the corresponding parent compound. The same mass difference, 14 Da, between the parent compounds colupulone and lupulone could be readily observed also for the fragments of these compounds in the MS/MS spectrum (see Table 1).

Figure 1 shows the MRM-HR chromatograms of colupulone (**1a**) and lupulone (**2b**) and their transformation products found in oxidized test material. Although a different procedure has been used for the preparation of transformation products, the distribution of individual β-acid transformation products corresponds to the literature source[17] except for SRM corresponding to the hulupinic acid. In this case not only was this SRM trace (*m*/*z* 263→209) found to contain three peaks having only one common fragment, but the whole spectrum was almost identical. It was necessary to compare this SRM trace with the HR-MS scan and identify the parent ions because it was obvious that the seeming parent ion (*m*/*z* 263) arose during in-source fragmentation of some other precursor ion. Figure 1 shows the SRM trace (*m*/*z* 263→209) including three peaks at retention times of 4.4, 4.8, and 5.8 min and the MS/MS fragmentation spectrum. As mentioned above, this spectrum was identical for these three peaks. Besides this, Figure 2 also includes three HR-MS spectra corresponding to the retention of these three peaks. The HR-MS spectrum of the peak at a retention time of 4.4 min shows an $[M - H]^-$ ion at *m*/*z* 263.1290, indicating the molecular formula $C_{15}H_{19}O_4^-$, which corresponds to the hulupinic acid with 0.45 ppm accuracy. The HR-MS spectra of the peaks at retention times of 4.8 and 5.8 min show $[M - H]^-$ ions at *m*/*z* 333.1710 and 347.1865, indicating the molecular formulas $C_{19}H_{26}O_5^-$ (0.8 ppm) and $C_{20}H_{28}O_5^-$ (0.3 ppm), respectively. The difference between these summary formulas is one carbon atom plus two hydrogen atoms, which represent a mass difference of 14 Da, which is the same as the difference between lupulone and colupulone. Therefore, these two compounds are most likely the unknown transformation products of β-acids because these molecular masses or summary formulas have not been described in the literature. These unknown compounds have been found in the material treated by oxidation by air oxygen, and, first, the summary formulas of known transformation products were compared with these two unknowns. The difference between the summary formula of cohulupone (**2a**, $C_{19}H_{26}O_4$) and the unknown compound ($C_{19}H_{26}O_5$) is one oxygen atom. The molecule of cohulupone has three double bonds in the side isoprenyl chains, and one of these bonds was most probably oxidized. Figure 3 shows the

dx.doi.org/10.1021/jf501852r | J. Agric. Food Chem. 2014, 62, 7690−7697

tentative structure proposed for this newly detected compound. The second step in the elucidation of the structure of this compound was confirmation of the tentative structure on the basic HR-MS/MS fragmentation pattern (see Figure 3). The fragments (m/z 263.1291, 209.0450, 193.0499, 151.0026, and 124.9869) matched predicted fragments proposed on the basis of the tentative structure of the newly identified compound. Although the structure was not confirmed by NMR, the high-resolution MS/MS spectra could provide satisfactory confidence for the confirmation of the tentative structure of these two oxidation products. These two newly identified compounds were named epoxycohulupone and epoxyhulupone.

Identification of Hulupones in Hops and Beer. The HPLC-HR/AM-MS technique operating on the basis of a MRM approach was used to investigate the compounds derived from the β-acids in hops and beer. The molecular masses for all previously described and newly identified transformation products of β-acids were added to a scheduled inclusion list, and the most intensive or most specific daughter ion was selected for each individual compound. Specificity of analysis was achieved by applying the 5 ppm mass window for extraction of daughter ions from HR-MS/MS spectra. Table 2 shows the characteristic mass transition of each individual transformation product and also the list of other characteristic ions found in the HCD fragmentation spectra. To check the separation of the transformation products that existed as two epimers, they were detected as two separate peaks. The newly identified transformation products were also observed in samples of hops, but only the compound tentatively named epoxyhulupone was found in traces.

Table 3 shows the results of analysis of two hop pellet samples of Sládek variety, harvested in 2012 (S1) and 2008 (S2) and stored for 24 and 60 months, respectively, to promote oxidation of β-acid analogues. Results are expressed as the ratio of the peak areas corresponding to each of the substances found in hops from the 2012 harvest (S1) relative to the hop harvest of 2008 (S2). The relative difference was expressed as a percentage, and these values are in parentheses. A positive sign indicates that a compound is presented in higher amount in freshly harvested hops. A negative sign indicates that a compound, in this case mainly a transformation product, is presented in higher amount in aged hops. Both hop pellets were used for the preparation of beer, and the relationship between β-acids and their transformation products found in beer samples was expressed in the same way; these results are also presented in Table 3.

Table 3. β-Acids and Their Transformation Products in Hops and Beer[a]

compound	hops R (±%)	beer R (±%)
colupulone (**1a**)	1.19 (+71%)	0.48 (−52%)
cohulupone (**2a**)	0.30 (−70%)	0.35 (−65%)
hulupinic acid (**3**)	0.65 (−35%)	0.48 (−52%)
norticyclocolupone (**4a**)	0.29 (−71%)	0.33 (−67%)
dehydrotricyclocolupone (**5a**, **5′a**)	0.29 (−71%)	
hydroxytricyclocolupone (**7a**, **7′a**)	0.29 (−71%)	
hydroperoxytricyclocolupone (**8a**, **8′a**)	0.39 (−61%)	
lupulone (**1b**)	1.38 (+38%)	0.55 (−45%)
hulupone (**2a**)	0.30 (−70%)	0.46 (−54%)
norticyclolupone (**4b**)	0.39 (−61%)	0.23 (−77%)
dehydrotricyclolupone (**5b**, **5′b**)	0.29 (−71%)	
hydroxytricyclolupone (**7b**, **7′b**)	0.29 (−71%)	
hydroperoxytricyclolupone (**8b**, **8′b**)	0.39 (−61%)	

[a]Ratio between responses of corresponding compounds found in hops harvested in 2012 and in 2008 or between two beers prepared from these hops (R); relative difference is expressed in percentage (± %).

The results of analyses of hop samples clearly show that the amount of starting materials, lupulone and colupulone, in fresh hops was higher (by 71 and 38%, respectively) than in long-term stored hops. Simultaneously, lower levels of degradation products were found in fresh hops. The differences ranged from 61 to 71%. The content and composition of β-acids in fresh hops were comparable. Thus, the results suggest that long-term storage of hops leads to appreciable changes in β-acids even under anaerobic conditions in an evacuated container. The content of individual transformation products found in beer produced from freshly harvested hops was about 45−77% lower than that in beer produced from hops harvested in 2008. In contrast to hops, no measurable concentration of cyclic (dehydrotricyclo-, hydroxytricyclo-, and hydroperoxytricyclo-) products was found in beers.

In summary, this study presents an alternative approach, based on high-resolution accurate mass spectroscopy, for the qualitative determination of β-acids and their transformation products. Apart from the fact that we were able to find all transformation products described in the literature,[17] two newly identified compounds with tentative structures have been found. The method could be utilized for a wide range of research applications. Many issues associated with the formation of transformation products of β-acids in hops during aging and in the production of beer, as well as issues related to the importance of the individual compounds for the bitterness of beer, are not yet satisfactorily resolved. Results of demonstration analysis of real samples of hops and beer were satisfactory and thoroughly confirmed our expectations. Future work will focus on the isolation of individual transformation products, and these compounds will be subsequently used for quantification of transformation products and the study of their impact on beer bitterness and its characteristics.

AUTHOR INFORMATION

Corresponding Author

*(M.D.) E-mail: dusek@beerresearch.cz. Phone: +420 224 900 184.

Funding

This study was supported by the Ministry of Agriculture of the Czech Republic, project QI91B227, "Importance of beta acids for Czech beer".

Notes

The authors declare no competing financial interest.

ACKNOWLEDGMENTS

We thank Petr Verner and Jaroslav Pól (Thermo Fisher Scientific Prague) for helpful comments and advice.

REFERENCES

(1) Biendl, M. Hops and health. *MBAA Tech. Q.* **2009**, *46*, 1−7.
(2) Biendl, M.; Pinzl, C. *Arzneipflanze Hopfen*; Deutsches Hopfenmuseum: Wolnzach, Germany, 2007; 18 pp.
(3) Jaskula, B.; Aerts, G.; De Cooman, L. Hop α-acids isomerization and utilisation: an experimental review. *Cerevisia* **2010**, *35*, 57−70.
(4) Haseleu, G.; Lagemann, A.; Stephan, A.; Intelmann, D.; Dunkel, A.; Hofmann, T. Quantitative sensomic profiling of hop-derived bitter compounds throughout a full-scale beer manufactoring process. *J. Agric. Food Chem.* **2010**, *58*, 7930−7939.

(5) Hughes, P. S.; Simpson, W. J. Bitterness of congeners and stereoiso-mers of hop-derived bitter acids found in beer. *J. Am. Soc. Brew. Chem.* **1996**, *54*, 234−237.
(6) Malowicki, M. G.; Shellhammer, T. H. Isomerization and degradation kinetics of hop (*Humulus lupulus* L.) acids in a model wort-boiling system. *J. Agric. Food Chem.* **2005**, *53*, 4434−4439.
(7) Fritsch, A.; Shellhammer, T. H. Relative bitterness of reduced and non-reduced iso-α-acids in lager beer. *J. Am. Soc. Brew. Chem.* **2008**, *66*, 88−93.
(8) Intelmann, D.; Hofmann, T. On the autoxidation of bitter-tasting iso-α-acids in beer. *J. Agric. Food Chem.* **2010**, *58*, 5059−5067.
(9) Spetsig, L. O.; Steninger, M. Hulupones, a new group of hop bitter substances. *J. Inst. Brew.* **1960**, *66*, 413−417.
(10) Van Cleemput, M.; Cattoor, K.; De Bosscher, K.; Haegeman, G.; De Keukeleire, D.; Heyerick, A. Hop (*Humulus lupulus*)-derived bitter acids as multipotent bioactive compounds. *J. Nat. Prod.* **2009**, *72*, 1220−1230.
(11) Krofta, K.; Vrabcová, S.; Mikyška, A.; Jurková, M.; Čajka, T.; Hajšlová, T. Stability of hop beta acids and their decomposition products during natural ageing. *Proceedings of the Third International Humulus Symposium*, Zatec, Czech Republic, Sept 9−14, 2012; ISHS: Leuven, Belgium, 2013.
(12) Mikyška, A.; Krofta, K. Assessment of changes in hop resins and polyphenols during long-term storage. *J. Inst. Brew.* **2012**, *118*, 269−279.
(13) Krofta, K.; Vrabcová, S.; Mikyška, A.; Jurková, M. The effect of hop beta acids oxidation products on beer bitterness. *Kvasny Prum.* **2013**, *59*, 296−305.
(14) Kowaka, M.; Kokubo, E. Composition of bitter substances of hops and characteristics of beer bitterness. *J. Am. Soc. Brew. Chem.* **1977**, *35*, 16−21.
(15) Haseleu, G.; Intelmann, D.; Hofmann, T. Structure determination and sensory evaluation of novel bitter compounds formed from β-acids of hop (*Humulus lupulus* L.) upon wort boiling. *Food Chem.* **2009**, *116*, 71−81.
(16) Taniguchi, Y.; Matsukura, Y.; Ozaki, H.; Nishimura, K.; Shindo, K. Identification and quantification of the oxidation products derived from α-acids and β-acids during storage of hops (*Humulus lupulus* L.). *J. Agric. Food Chem.* **2013**, *61*, 3121−3130.
(17) Haseleu, G.; Intelmann, D.; Hofmann, T. Identification and RP-HPLC-ESI-MS/MS quantitation of bitter-tasting β-acids transformation products in beer. *J. Agric. Food Chem.* **2009**, *57*, 7480−7489.
(18) Krofta, K.; Vrabcová, S.; Lišková, H. The method of preparation of pure β-acids. CZ Patent 303,017, Jan 18, 2012.
(19) *Analytica-EBC*, 5th ed.; European Brewery Convention; Carl-Hans Verlag: Nürenberg, Germany, 1998; Section 7 Hops, Method 7.7.
(20) EN 15662, Foods of Plant Origin-Determination of Pesticide Residues Using GC-MS and/or LC-MS/MS Following Acetonitrile Extraction/Partitioning and Clean-up by Dispersive SPE−QuEChERS method.

and sulfate forms of monomeric flavanols) after the ingestion of proanthocyanidins,[17,21−25] but only a few studies have been focused on colonic microbial metabolites and the use of proanthocyanidins.[13,16,20,21,26,27]

Therefore, the aim of this study was to develop and validate a method that uses improved off-line μ-SPE followed by HPLC-MS/MS detection for quantification of colonic metabolites derived from grape flavanols in the plasma collected from rats.

MATERIALS AND METHODS

Grape Seed Proanthocyanidin Extract. Grape seed proanthocyanidin extract (GSPE) was obtained from Les Dérives Résiniques et Terpéniques (Dax, France). The individual flavanols and phenolic acids contained in the grape seed extract that were used in this study are detailed in Table 1 (adapted from Quiñones et al.[9]).

Table 1. Individual Phenolic Compounds of Grape Seed Proanthocyanidin Extract (Flavanols and Phenolic Acids)[a]

compd	concn[b] (mg/g)
catechin	90.7 ± 7.6
epicatechin	55.0 ± 0.8
procyanidin dimer[c]	144.2 ± 32.2
procyanidin trimer[c]	28.4 ± 2.0
procyanidin tetramer[c]	2.0 ± 0.2
dimer gallate[d]	39.7 ± 7.1
epigallocatechin gallate	0.4 ± 0.1
epicatechin gallate[d]	55.3 ± 1.5
p-coumaric acid	0.1 ± 0.0
gallic acid	17.7 ± 2.0
3,4-dihydroxybenzoic acid	1.0 ± 0.1
vanillic acid	0.1 ± 0.0
quercetin	0.3 ± 0.0
quercetin 3-*O*-gallate	0.2 ± 0.0
naringenin 7-glucoside	0.1 ± 0.0
kaempferol 3-glucoside	0.1 ± 0.0

[a]Determined by reverse-phase HPLC-ESI-MS/TOF. Values are expressed as milligrams of compound per gram of fresh extract and are the means of three samples. [b]Data adapted from Quiñones et al.[9] [c]Quantified by use of the calibration curve of procyanidin B2. [d]Quantified by use of the calibration curve of epigallocatechin gallate.

Chemicals and Reagents. Acetone (HPLC analytical grade), methanol (HPLC analytical grade), and phosphoric acid were purchased from Sigma-Aldrich (Barcelona, Spain). Ultrapure water was obtained from a Milli-Q Advantage A10 system (Madrid, Spain). Glacial acetic acid was purchased from Panreac (Barcelona, Spain). (+)-Catechin, (−)-epicatechin, benzoic acid, phloroglucinol, 3-hydroxybenzoic acid, 4-hydroxybenzoic acid, 3,4-dihydroxybenzoic acid, 2-(4-hydroxyphenyl)acetic acid, 2-(3,4-dihydroxyphenyl)acetic acid, 3-(4-hydroxyphenyl)propionic acid, vanillic acid, gallic acid, hippuric acid, and ferulic acid (all from Fluka/Sigma−Aldrich, Madrid, Spain) were individually dissolved in methanol at 4000 mg/L. Procyanidin B2, epigallocatechin gallate (EGCG), and pyrocatechol (internal standard, IS) (all from Fluka/Sigma−Aldrich, Madrid, Spain) and 5-(3′,4′-dihydroxyphenyl)-γ-valerolactone (MicroCombiChem e.K., Wiesbaden, Germany) were individually dissolved in methanol at 2000 mg/L. All standard stock solutions were prepared every 3 months and stored in dark-glass flasks at −20 °C.

A mixed standard stock solution in methanol of all these compounds [(+)-catechin, (−)-epicatechin, benzoic acid, phloroglucinol, 3-hydroxybenzoic acid, 4-hydroxybenzoic acid, 3,4-dihydroxybenzoic acid, 2-(4-hydroxyphenyl)acetic acid, 2-(3,4-dihydroxyphenyl)-acetic acid, 3-(4-hydroxyphenyl)propionic acid, vanillic acid, gallic acid, hippuric acid, ferulic acid, EGCG, and 5-(3′,4′-dihydroxyphenyl)-γ-valerolactone] at 200 mg/L and procyanidin B2 at 100 mg/L was prepared weekly and stored in dark-glass flasks at −20 °C. This mixed standard stock solution was diluted daily to the desired concentration by use of an acetone/Milli-Q water/acetic acid (70/29.5/0.5 v/v/v) solution and stored under the same conditions until chromatographic analysis.

Animal and Plasma Collection. Male Wistar rats, weighing between 226 and 260 g, were obtained from Charles River Laboratories (Barcelona, Spain). All of the animals were housed at 22 °C with a light/dark cycle of 12 h (lights on at 9:00 a.m.) and were fed a standard chow diet (AO4, Panlab, Barcelona, Spain) ad libitum during the experiment. The animals were randomly divided into two groups: the control group (n = 6) and the GSPE group (n = 6). On the day of the experiment, the rats were starved for 12 h. To the GSPE group, a dose of 1000 mg of GSPE/kg of body weight (1 mL) was administered by oral gavage. Water (1 mL) was orally administered to the control group. In both groups, oral administration was performed by gastric intubation to the fasted rats between 9:00 and 10:00 a.m. Blood samples were obtained via saphenous vein extraction by use of heparin vials (Starsted, Barcelona, Spain) 7 h after GSPE or water administration. Plasma samples were obtained by centrifugation (2000g, 15 min, 4 °C). The plasma was pooled (n = 6) to obtain sufficient sample volume to perform three replicate chromatographic analyses. The pooled plasma samples were stored at −80 °C until chromatographic analysis was performed. The study was performed in accordance with the institutional guidelines for the care and use of laboratory animals, and the experimental procedures were approved by the Ethical Committee for Animal Experimentation of Universitat Rovira i Virgili.

Off-line μ-SPE Extraction. *Optimization of Plasma Volume.* To determine the minimum sample volume with good recovery values, four different spiked blank plasma volumes were tested (350, 250, 200, and 150 μL) at three different levels of concentration (50, 500, and 5000 μg/mL) for all the standards. Briefly, the Oasis HLB μ-Elution Plates 30 μm (Waters, Barcelona, Spain) were conditioned sequentially with 250 μL of methanol and 250 μL of 0.2% acetic acid. To ensure full contact of the compounds with the sorbent column, plasma aliquots were mixed with different volumes of 4% phosphoric acid (300 μL for 350- and 250-μL plasma samples, 350 μL for 200-μL plasma sample, and 400 μL for 150-μL plasma sample) and 50 μL of IS (200 μg/mL). The loaded plates were washed with 200 μL of Milli-Q water and 200 μL of 0.2% acetic acid. The retained polyphenols were then eluted with 2 × 50 μL of acetone/Milli-Q water/acetic acid solution (70/29.5/0.5 v/v/v). The eluted solution was directly injected into the HPLC-MS/MS.

Optimization of Cleanup Steps. The cleanup steps were further evaluated following the procedure described under Optimization of Plasma Volume) for a plasma volume of 250 μL. In this case, the loaded plates were washed with 100 μL each or 150 μL each of Milli-Q water and 0.2% acetic acid.

Optimization of Elution Steps. The elution steps were further evaluated following the procedure described under Optimization of Plasma Volume for a plasma volume of 250 μL. In this case, the retained polyphenols were eluted with 2 × 25 μL of acetone/Milli-Q water/acetic acid solution (70/29.5/0.5 v/v/v).

Plasma Flavanol Metabolite Extraction. Prior to extraction, the plasma samples were centrifuged (1500g, 5 min, 4 °C) to remove aggregates. The plasma extraction was performed by off-line μ-SPE as described under Optimization of Plasma Volume for a plasma volume of 250 μL The eluted solution was directly injected into the HPLC-MS/MS.

Analysis of Plasma Flavanols and Their Metabolites. *Instrumental Conditions.* The HPLC system consisted of a 1200 LC Series (Agilent Technologies, Palo Alto, CA) using Zorbax SB-Aq (150 mm × 2.1 mm i.d., 3.5 μm particle size) chromatographic column, from Agilent Technologies, Palo Alto, CA. The mobile phase was 0.2% acetic acid (solvent A) and acetonitrile (solvent B). The flow rate was 0.4 mL/min. The elution gradient was 5−55% B (0−10 min), 55−80% B (10−12 min), 80% B isocratic (12−15 min), and 80−5% B (15−16 min). A 10 min post run was applied. The sample injection volume used was 2.5 μL.

Table 2. Retention Times, Exact Masses, and Optimized MRM Conditions[a]

		TOF/MS[b]		MS/MS quantification[c]			MS/MS confirmation[c]			
compd	MW	$[M-H]^-$	RT (min)	MRM_1	F (V)	CE (V)	MRM_2	F (V)	CE (V)	ref
catechin	290.27	289.0735	6.6	289 > 203	120	20	289 > 245	120	20	
epicatechin	290.27	289.0735	6.9	289 > 245	130	10	289 > 203	130	20	
procyanidin B1	578.52	577.1360	6.5	577 > 425	130	10	577 > 407	130	30	41
procyanidin B2	578.52	577.1360	6.7	577 > 425	130	10	577 > 407	130	30	
procyanidin B3	578.52	577.1360	6.1	577 > 425	130	10	577 > 407	130	30	41
gallic acid	170.12	169.0147	2.8	169 > 125	90	10	169 > 79	90	40	
vanillic acid	168.15	167.0358	7.09	167 > 152	80	10	167 > 123	80	5	
epigallocatechin gallate	458.37	457.0780	7.3	457 > 169	110	20	457 > 305	110	20	
1-(3′,4′-dihydroxyphenyl)-3-(2″,4″,6″-trihydroxyphenyl)propan-2-ol	292.28	291.088	7.1	291 > 247	70	20	291 > 96	70	20	27
5-(3′,4′-dihydroxyphenyl)-γ-valerolactone	208.21	207.0669	7.8	207 > 85	120	10	207 > 121	120	10	
4-hydroxy-5-(3′,4′-dihydroxyphenyl)valeric acid	226.23	225.0779	9.2	225 > 163	70	10	225 > 181	70	10	27
4-hydroxy-5-(3′-hydroxyphenyl)valeric acid	210.23	209.0830	11.9	209 > 147	150	0				27
4-hydroxy-5-phenylvaleric acid	194.23	193.0880	9.8	193 > 175	60	10				27
3-(3,4-dihydroxyphenyl)propionic acid	182.17	181.0512	6.2	181 > 137	60	10				20
3-(3-hydroxyphenyl)propionic acid	166.17	165.0558	6.9	165 > 121	90	10	165 > 59	90	0	20,27
3-(4-hydroxyphenyl)propionic acid	166.17	165.0558	7.2	165 > 121	90	10	165 > 59	90	0	
phenylpropionic acid	150.17	149.0615	9.5	149 > 105	90	10				27
2-(3,4-dihydroxyphenyl)acetic acid	168.15	167.0357	4.6	167 > 123	50	10	167 > 95	50	30	20
2-(3-hydroxyphenyl)acetic acid	152.15	151.0409	6.1	151 > 107	60	5	151 > 93	60	20	27
2-(4-hydroxyphenyl)acetic acid	152.15	151.0409	6.5	151 > 107	60	5	151 > 65	60	30	
phenylacetic acid	136.15	135.0451	9.2	135 > 91	90	5	135 > 100	90	5	20
3,4-dihydroxybenzoic acid	154.12	153.0201	4.1	153 > 109	80	10	153 > 62	80	40	20
3-hydroxybenzoic acid	138.12	137.0243	6.5	137 > 93	70	10				
4-hydroxybenzoic acid	138.12	137.0243	6.8	137 > 93	70	10				20
benzoic acid	122.12	121.0296	7.9	121 > 77	60	5	121 > 59	60	5	
3-*O*-methylgallic acid	184.15	183.0308	5.6	183 > 168	90	10	183 > 124	90	10	20
homovanillic acid	182.17	181.0512	4.5	181 > 163	90	10	181 > 134	90	20	42
homovanillyl alcohol	168.19	168.0715	6.3	167 > 152	150	10	167 > 133	150	10	42
ferulic acid	194.18	193.0510	8.2	193 > 134	60	10	193 > 178	60	10	
hippuric acid	179.17	178.0512	5.5	178 > 134	80	5	178 > 77	80	10	
phloroglucinol	126.11	125.0250	2.27	125 > 57	90	10	125 > 125	90	0	

[a]Abbreviations: MW, molecular weight; RT, retention time; F, fragmentor; CE, collision energy; MRM, multiple reaction monitoring. [b]For compounds studied by HPLC-ESI-TOF/MS. [c]For analysis of phenolic compounds studied by HPLC-ESI-MS/MS.

This HPLC system was coupled to a 6210 time-of-flight (TOF) mass spectrometer (Agilent Technologies, Palo Alto, CA) system or coupled to a 6410 MS/MS (Agilent Technologies, Palo Alto, CA) system. Ionization was done by electrospray (ESI) in the negative mode. When HPLC-ESI-TOF/MS was performed, the ESI conditions were drying gas temperature of 350 °C, flow of 12 L/min, rnebulizer gas pressure of 45 psi, and capillary voltage of 4000 V. Moreover, when HPLC-ESI-MS/MS was performed, the acquisition was done by multiple reaction monitoring (MRM). The ESI working conditions were as follows: capillary voltage, 3 kV; source temperature, 150 °C; cone gas flow rate, 80 L/h; desolvation gas flow rate, 800 L/h; and desolvation temperature, 400 °C. Nitrogen (>99% purity) was used as a nebulizing and collision gas. Cone voltages and collision energies were optimized by infusing a standard solution of 10 mg/L of each standard or treated rat plasma for expected analytes in a mixture of acetone/Milli-Q water/acetic acid (70/29.5/0.5 v/v/v) at a flow rate of 0.4 μL/min. The full-scan mode was first acquired to select the most abundant m/z value, and the fragmentor was optimized. Main $[M-H]^-$ ions were selected as precursor ions. The collision energies were then studied to find the most abundant product ions, and the most sensitive transition was selected for subsequent quantification. The second transition was used for confirmation purposes. All of the HPLC-MS/MS conditions are outlined in Table 2. The dwell time established for each transition was 30 ms. Data were acquired by use of MassHunter qualitative analysis software B.02.00 (Agilent Technologies, Palo Alto, CA). All of the expected product transitions were confirmed in the literature.

Method Validation. To validate the quantitative method, the calibration curves, linearity, extraction recovery, matrix effect, precision, and method detection and quantification limits were studied by analyzing standard solutions and blank plasma samples spiked with the standard polyphenols. Blank plasmas were obtained at 7 h from rats that ingested water (without GSPE); no phenolic acid basal metabolites were present in blank plasmas. The calibration curves were obtained by plotting the analyte/IS peak abundance ratio and the corresponding analyte/IS concentration ratio.

Method precision was determined as the relative standard deviation (% RSD) of the concentration in a triplicate analysis of three different spiked samples (50, 500, and 5000 μg/mL) randomly distributed intraday. Recovery values were calculated by comparing the responses of the abundance ratio analyte/IS spiked in pretreated plasma matrices by adding the standards before and after pretreatment (off-line μ-SPE) at three different concentration levels (50, 500, and 5000 μg/mL). Matrix effects were evaluated by comparing the relative analyte/IS abundance obtained from spiked blank plasma after off-line μ-SPE with those obtained from commercial standard solutions at three different concentration levels (50, 500, and 5000 μg/mL). Sensitivity was evaluated by determining LOD, defined as the concentration corresponding to 3 times the signal/noise ratio, and LOQ, defined as the concentration corresponding to 10 times the signal/noise ratio. Method detection and quantification limits (MDL and MQL,

Table 3. Recovery Values for Analysis of Phenolic Compounds in Different Volumes of Spiked Plasma Samples by Off-line μ-SPE

	recovery (%)											
	150 μL[a]			200 μL[a]			250 μL[a]			350 μL[b]		
compd	50 μg/mL	500 μg/mL	5000 μg/mL	50 μg/mL	500 μg/mL	5000 μg/mL	50 μg/mL	500 μg/mL	5000 μg/mL	50 μg/mL	500 μg/mL	5000 μg/mL
catechin	60	55	60	97	99	91	98	104	107	97	99	101
epicatechin	36	32	38	85	80	88	95	102	100	101	104	106
procyanidin B2	51	48	42	83	78	79	92	102	102	98	107	106
epigallocatechin gallate	54	51	63	82	80	82	93	94	96	90	84	101
gallic acid	54	50	36	65	68	86	85	83	96	97	95	91
vanillic acid	84	77	83	106	96	84	100	103	99	95	98	95
5-(3,4-dihydroxyphenyl)-γ-valerolactone	57	52	70	82	76	75	93	93	96	95	99	109
3-(4-hydroxyphenyl)propionic acid	63	69	65	88	84	81	106	97	92	113	112	94
2-(3,4-dihydroxyphenyl)acetic acid	40	47	49	79	81	76	95	99	98	99	94	97
2-(3-hydroxyphenyl)acetic acid	67	61	57	81	90	100	101	99	97	96	95	88
2-(4-hydroxyphenyl)acetic acid	63	57	78	62	65	79	83	85	100	96	92	110
3-hydroxybenzoic acid	89	76	86	81	78	86	95	98	101	99	102	98
benzoic acid	67	64	78	96	92	90	94	93	90	109	97	101
ferulic acid	17	27	26	75	77	86	102	103	94	108	99	108
hippuric acid	46	51	82	96	92	82	100	99	94	94	92	94
phloroglucinol	25	27	14	86	80	83	100	93	92	96	103	92

[a]Total volume added into μ-SPE sorbent was 600 μL. [b]Total volume added into μ-SPE sorbent was 700 μL.

respectively) were calculated for the analysis of 250-μL plasma sample following the procedure described previously.

RESULTS AND DISCUSSION

Currently, the common approach for quantification of flavanol metabolites is to quantify the phase II metabolites from the small intestine and liver in plasma or other tissues at short times after the intake of proanthocyanidins.[17−19] Additionally, there are a few studies where microbial metabolites derived from flavanols are analyzed in biological samples.[16,21,26] However, recent investigations revealed that the majority of ingested polyphenols reach the colon, where the enzymes of gut bacteria are able to convert polyphenols and their metabolites into a wide variety of low molecular weight compounds, which can then be absorbed in situ.[11,28] Therefore, since colonic metabolites could be responsible for many of the health benefits attributed to flavanols, complete characterization of the colonic metabolism of flavanols will help to elucidate the bioavailability and metabolism of proanthocyanidins and identify the derivatives responsible for the beneficial health effects attributed to proanthocyanidins.[11] Nevertheless, to our knowledge, there are no validated chromatographic methodologies for the analysis of flavanol-derived microbial metabolites in biological samples.[16,20,21,29] Indeed, only a few studies have analyzed colonic microbial metabolites in biological samples after the ingestion of flavanols.[16,21,26] Currently, the most commonly used method for the study of colonic metabolites is based on in vitro models using batch-culture fecal fermentations.[13,27,30] Hence, in this study we set up an improved methodology for analysis of flavanols and their microbial metabolites.

Improved Off-line μ-SPE for Plasma Sample Pretreatment. The off-line μ-SPE method, previously reported for plasma samples treatment prior to analysis of proanthocyanidins, anthocyanins, and their phase II metabolites,[15,17] was here improved to further reduce plasma volume and to enable extraction of colonic metabolites derived from flavanols. The μ-SPE method enabled concentration of the compounds prior to chromatographic analysis, since they are present in plasma samples at very low levels. Furthermore, the plasma samples had a large number of interferences, mainly proteins, which were removed in this methodology by precipitation with-phosphoric acid.[15] In addition, in this study μ-SPE with hydrophilic−lipophilic balanced (HLB) sorbent allowed the extraction of flavanols and their colonic metabolites. Furthermore, previous studies using this sorbent extracted phase II metabolites derived from flavanols (i.e., the glucuronidated, methylated and sulfated forms of catechin and epicatechin).[16,17] However, in this study phase II metabolites were not analyzed, as the methodology was already reported, and phase II metabolites should not be expected to occur in significant amount in plasma 7 h after polyphenol administration.[16,17]

A major limitation for the analysis of biological samples such as plasma or serum is the sample volume.[15] Especially for the study of small subjects such as rats or mice, the sample volume becomes the most critical parameter to consider. Moreover, reducing the plasma volume will enable experimentation without the sacrifice of animals. Hence, in this study the sample volume for μ-SPE was reduced from 350 to 250 μL with preservation of the recovery values (Table 3). All of the recovery values for 350 μL of plasma sample were similar to reported values of Martí et al.[15] When the extraction recovery was tested with 250 μL of plasma sample, its related rates were also suitable and ranged from 83% to 107%. However, when the extraction recovery was tested with 200 or 150 μL, some compounds showed poorer recovery percentages than when a volume of 250 μL was evaluated. Specifically, recoveries showed

dx.doi.org/10.1021/jf5019752 | J. Agric. Food Chem. 2014, 62, 7698−7706

Table 4. Recovery Values Obtained after Testing Different Volumes of Clean-up and Elution Solutions[a]

	recovery (%)								
	100 μL clean-up step			150 μLclean-up step			50 μL elution step		
compd	50 μg/mL	500 μg/mL	5000 μg/mL	50 μg/mL	500 μg/mL	5000 μg/mL	50 μg/mL	500 μg/mL	5000 μg/mL
catechin	63.1	9.9	3.3	57.9	20.1	2.6	61.3	86.3	83.8
epicatechin	45.0	60.9	19.0	52.0	58.4	19.6	35.5	89.6	90.1
procyanidin B2	61.4	47.1	19.6	73.0	44.5	20.7	66.8	82.8	97.1
epigallocatechin gallate	5.8	0.8	0.0	9.2	2.9	0.1	50.4	62.5	70.1
gallic acid	0.0	0.0	0.0	0.0	0.0	0.0	43.2	26.8	92.8
vanillic acid	66.1	14.3	2.2	68.6	15.1	2.5	23.5	84.7	79.6
5-(3,4-dihydroxyphenyl)-γ-valerolactone	57.3	4.5	0.1	26.7	7.9	2.4	54.9	82.0	64.5
3-(4-hydroxyphenyl)propionic acid	0.0	0.0	44.5	0.0	0.0	37.5	0.0	99.7	90.9
2-(3,4-dihydroxyphenyl)acetic acid	0.0	0.0	0.0	0.0	0.0	0.0	53.3	73.4	88.5
2-(3-hydroxyphenyl)acetic acid	38.5	59.2	26.7	55.1	77.2	17.8	62.1	52.4	93.6
2-(4-hydroxyphenyl)acetic acid	68.9	65.0	17.7	69.1	69.2	20.6	58.8	15.8	35.2
3-hydroxybenzoic acid	71.7	10.0	7.7	71.7	11.6	1.9	26.5	66.9	75.3
benzoic acid	68.4	73.0	61.4	70.6	78.6	40.6	52.4	96.2	64.9
ferulic acid	20.3	3.4	0.7	14.2	3.1	0.2	15.3	84.9	86.9
hippuric acid	30.1	55.3	94.6	38.0	55.8	95.7	23.5	24.0	103.4
phloroglucinol	0.0	0.0	0.0	0.0	0.0	0.0	0.0	39.9	19.8

[a]Results are expressed as a percentage after comparing the spiked blank plasma response at three different levels (50, 500, and 5000 μg/mL) before and after off-line μ-SPE.

Table 5. Parameters for Quantification of Phenolic Compounds in Spiked Plasma Samples by HPLC-ESI-MS/MS[a]

					precision (% RSD, $n = 3$)			% matrix effect						
compd	RT (min)	calibration curve	determ coeff (R^2)	working linearity range (μM)	50 μg/mL	500 μg/mL	5000 μg/mL	50 μg/mL	500 μg/mL	5000 μg/mL	LOD (nM)	LOQ (nM)	MDL[b] (nM)	MQL[b] (nM)
catechin	6.4	$y = 0.799x$	0.997	0.007−17.225	0.8	3.9	6.6	7.7	3.1	2.7	2.30	7.66	0.66	2.19
epicatechin	6.9	$y = 1.674x$	0.996	0.007−17.225	1.6	5.6	0.8	−1.0	0.3	1.2	1.66	5.52	0.47	1.58
procyanidin B2	6.7	$y = 34.138x$	0.991	0.008−4.321	0.6	3.6	5.4	−0.4	1.6	0.0	1.95	6.49	0.56	1.85
epigallocatechin gallate	7.3	$y = 8.399x$	0.990	0.004−10.908	1.1	4.2	2.0	2.2	1.5	6.0	0.76	2.52	0.22	0.72
gallic acid	2.8	$y = 1.035x$	0.991	0.059−29.391	1.6	4.6	4.2	0.7	0.8	1.4	11.75	39.22	3.36	11.20
vanillic acid	6.7	$y = 0.862x$	0.996	0.012−29.762	1.7	6.0	2.7	2.4	−0.2	2.5	4.29	14.29	1.22	4.08
5-(3,4-dihydroxyphenyl)-γ-valerolactone	7.2	$y = 0.746x$	0.998	0.048−24.038	3.8	3.4	4.9	5.5	4.7	1.8	14.42	48.08	4.12	13.74
3-(4-hydroxyphenyl)propionic acid	7.3	$y = 0.063x$	0.997	0.060−30.120	3.6	2.6	0.5	2.8	−1.7	0.5	24.10	80.32	6.88	22.95
2-(3,4-dihydroxyphenyl)acetic acid	4,3	$y = 0.389x$	0.996	0.060−29.762	3.2	4.5	3.4	0.6	0.8	0.3	11.90	39.68	3.40	11.34
2-(3-hydroxyphenyl)acetic acid	5.8	$y = 0.775x$	0.995	0.013−32.895	2.2	2.2	1.7	5.4	2.9	0.4	3.29	10.96	0.94	3.13
2-(4-hydroxyphenyl)acetic acid	6.1	$y = 0.534x$	0.994	0.013−32.895	5.0	8.5	2.4	0.1	4.1	−1.5	8.87	29.90	2.56	8.54
3-hydroxybenzoic acid	6.3	$y = 0.690x$	0.998	0.072−36.232	3.1	1.1	2.8	3.2	2.7	4.2	39.13	130.43	11.28	37.37
benzoic acid	7.8	$y = 0.510x$	0.995	0.016−40.984	3.4	5.6	3.5	−0.2	1.2	3.2	3.78	12.61	1.08	3.60
ferulic acid	8.1	$y = 5.658x$	0.995	0.010−25.773	0.5	5.4	2.7	4.9	2.0	7.3	2.13	7.11	0.61	2.03
hippuric acid	5.5	$y = 1.981x$	0.986	0.011−27.933	2.4	5.0	4.5	−2.7	0.3	−0.1	0.10	0.34	0.03	0.10
phloroglucinol	2.3	$y = 0.157x$	0.990	0.079−39.683	2.5	6.2	1.7	2.1	1.3	−0.2	23.81	79.37	6.80	22.68

[a]Abbreviations: RT, retention time; LOD, limit of detection; LOQ, limit of quantification; MDL, method detection limit; MQL, method quantification limit. [b]Method detection and quantification limits are given as nanomoles per liter of fresh sample, calculated for analysis of 250-μL plasma sample.

values lower than 80% when the plasma volume was 150 μL. Thus, 250 μL is the lowest plasma sample volume required to achieve acceptable recovery values for all compounds and, hence, was the plasma volume used in this study. On the other hand, decreasing the cleanup solution volume from 200 μL to either 150 or 100 μL did not improve the extraction recovery, as some compounds, like 2-(3,4-dihydroxyphenyl)acetic acid or gallic acid, were not detected by HPLC-ESI-MS/MS. In the same way, decreasing the volume of elution solution from 100 to 50 μL also showed poor recovery values for all compounds tested (Table 4), which indicate that more volume is needed to elute all the compounds. Thus, from all the assessed factors, it

dx.doi.org/10.1021/jf5019752 | J. Agric. Food Chem. 2014, 62, 7698−7706

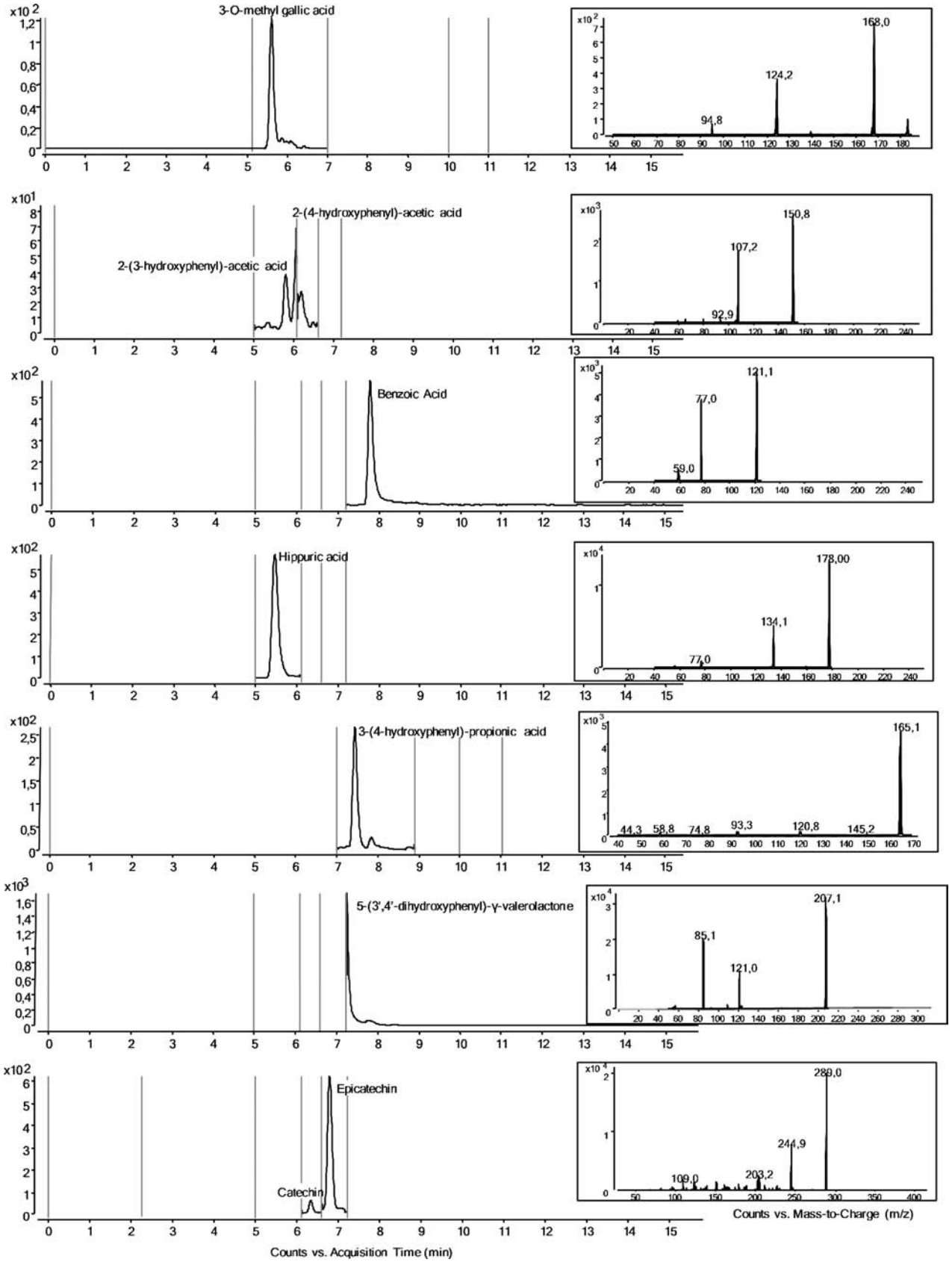

Figure 1. Extracted ion chromatograms of plasma microbial metabolites and their respective mass spectra fragmentation 7 h after ingestion of GSPE (1000 mg/kg).

can be concluded that, for off-line μ-SPE, the plasma volume can be reduced to 250 μL but the cleanup needs to be realized with 200 μL of Milli-Q water and 200 μL of 0.2% acetic acid and the elution volume should be 100 μL.

dx.doi.org/10.1021/jf5019752 | J. Agric. Food Chem. 2014, 62, 7698−7706

Quality Parameters. Basal plasma spiked with a range of different concentrations of flavanols and phenolic acids was analyzed via off-line μ-SPE coupled to HPLC-ESI-MS/MS to determine the matrix effect, working linearity range, calibration curves, reproducibility, LODs, and LOQs (Table 5). The linearity of flavanols and phenolic acids was between 0.004 and 41 μM. All of the compounds possessed a R^2 value equal or higher than 0.99, even taking into account that the standards present in the spiked blank plasma and the interactions between compounds could have an adverse effect on the working linearity range.[31] The relative standard deviation (% RSD) was calculated at three concentration levels (50, 500, and 5000 μg/mL) for all the standards in three randomly distributed intraday analyses. For the flavanols and phenolic acids studied, RSD values were between 0.51% and 8.5%. The higher percent RSD values are correlated with a higher dispersion; therefore, these RSD percentages indicate a large variance between the compounds. However, all the percent RSD results were considered the correct values because they did not exceed 20%.[32] Furthermore, no matrix effect was observed with rates close to 0% for all the flavanols and phenolic acids evaluated. For all of the phenolic compounds studied, the LODs and LOQs were lower than 40 nM and 131 nM, respectively. The MDL and MQL values were 0.03−11.28 nM and 0.10−37.37 nM, respectively. The use of 5-(3′,4′-dihydroxyphenyl)-γ-valerolactone as a standard for quantification of all valerolactone and valeric acids metabolites was an important improvement for the methodology developed in our study, as these metabolites were previously quantified as (−)-epicatechin equivalents.[20]

Identification of Colonic Microbial Metabolites Derived from Grape Seed Proanthocyanidins in Rat Plasma. The strategy applied in this study to determine colonic metabolites derived from GSPE was to identify all of the colonic metabolites, including glucuronidated or sulfated phenolic acids, present in the rat plasma from the exact mass of all potential molecular ions by HPLC-ESI-TOF/MS. For this, we analyzed a pool of rat plasma (n = 6) 7 h after GSPE ingestion. The pooled plasma was necessary to collect enough volume of plasma for three replicate chromatographic analyses without the rat sacrifice (i.e., plasma obtained from saphenous vein). Moreover, pooled plasma increases homogeneity and sensitivity in order to allow the detection of all potential metabolites.[33,34] The 7 h time point was selected to allow the flavanols to reach the colon, to be metabolized by gut bacteria, and to be absorbed.

Of the 43 metabolites described in the literature from human[13,20,28] or rat,[14,16,20] 30 colonic metabolites were detected in the plasma after 7 h. Interestingly, at 7 h post-GSPE administration, no glucuronide or sulfate derivatives of the phenolic acids were detected. The fragmentation pattern and retention behavior were subsequently determined by a literature search for all of the compounds identified (i.e., the exact mass and retention time detected), and the compound parameters were then optimized to be quantified by HPLC-ESI-MS/MS (Table 2). Searching the literature for potential compound fragmentation that could occur is very important because the ionization conditions may vary depending on the equipment used in the analysis. Therefore, all of the compounds quantified that did not have their own commercial standard were confirmed in the literature.[20,29] All of the MRM conditions and quality parameters for quantification by HPLC-ESI-MS/MS are listed in Tables 2 and 5, respectively.

Application to Flavanol Bioavailability. The major breakthrough of the method reported in this study was the ability to analyze more than 20 different rat colonic metabolites and additional nonmetabolized flavanols by the same plasma extraction pretreatment and same chromatographic analysis, with a large number of commercial standards (16) for the most specific and accurate quantification possible.

The method developed was applied to analyze rat plasma obtained from the saphenous vein after administration of 1000 mg/kg GSPE. This dose was selected because it was the previously reported acute dose necessary to reach appropriate levels of metabolized forms in the plasma.[17] However, although the high dose was used in rats, these methodologies are usually further extended to the analysis of human plasma with more physiological concentrations of polyphenols.[26,35−37] HPLC-ESI-MS/MS chromatograms of flavanol colonic products in the plasma from treated rats and the respective mass spectra fragmentations are shown in Figure 1. All of the compound concentrations in rat plasma analyzed by HPLC-ESI-MS/MS are shown in Table 6.

The plasma concentrations of catechin, epicatechin, and procyanidin dimer B2, present in the GSPE, were 0.087, 0.532, and 0.013 μM, respectively. The catechin and epicatechin monomers are rapidly absorbed and appear in plasma between 1 and 2 h after ingestion.[17] In this study, we showed that these nonmetabolized compounds can still be quantified in the plasma 7 h after GSPE ingestion, at even lower concentrations than at the 2 h time point.[16] However, EGCG was not detected, which can be attributed to the low concentration in the GSPE more than the poor solubility of the gallate forms of flavanols.[38] Gallic and vanillic acids were two phenolic acids present in GSPE (Table 1) and in plasma that reached concentrations of 0.745 and 0.555 μM, respectively. This high concentrations at 7 h after GSPE ingestion can be attributed to formation of these phenolic acids as products of microbial metabolism.[12,13,27]

Regarding valerolactone or valeric acid compounds, the results show that the only metabolite found in plasma 7 h after administration of GSPE was 5-(3′,4′-dihydroxyphenyl)-γ-valerolactone, although other in vitro experiments performed in human feces with GSPE reported the presence of 5-(3′-hydroxyphenyl)-γ-valerolactone and γ-valerolactone.[13,39] On the other hand, the phenolic acids that presented the highest concentration in rat plasma were 3-(3,4-dihydroxyphenyl)-propionic acid and 3-(4-hydroxyphenyl)propionic acid (9.467 and 7.605 μM, respectively). The rest of the studied phenolic acids were found in concentrations lower than 1 μM. However, it is important to take into account that when microbial metabolites reach the liver, they can be subjected to phase II enzymes and can be conjugated to different final products,[12] as has been observed for 3-*O*-methylgallic acid, the methyl conjugate product from gallic acid[28] whose rat plasma concentration after GSPE intake was 0.217 μM, or ferulic acid, a methyl-conjugated derivative of 3-(3,4-dihydroxyphenyl)propionic acid,[28] which was quantified in the rat plasma at a concentration of 0.241 μM. Unfortunately, no comparable experiments exist in the literature for GSPE colonic metabolites, as they differ in their experimental approach and/or the composition of the extracts. Specifically, when microbial metabolites were analyzed in the plasma, the studies were performed with extracts from cocoa and almonds.[21,26] Almond polyphenols differ considerably in composition from polyphenols found in grapes,[21] and the cocoa-derived polyphenols, which are very similar to grape-

Table 6. Quantified Levels of Flavanols and Their Colonic Metabolites in Rat Plasma (n = 6) at 7 h after an Acute Intake of Grape Seed Proanthocyanidin Extract (1000 mg/kg)[a]

	total concn ± SEM[b] (μM)
Flavanols	
catechin	0.087 ± 0.000
epicatechin	0.532 ± 0.001
procyanidin dimer B1[c]	nq
procyanidin dimer B2	0.013 ± 0.000
procyanidin dimer B3[c]	nq
gallic acid	0.745 ± 0.001
vanillic acid	0.555 ± 0.000
epigallocatechin gallate	nq
Metabolites	
1-(3′,4′-dihydroxyphenyl)-3-(2″,4″,6″-trihydroxyphenyl)-propan-2-ol[d]	nq
5-(3′,4′-dihydroxyphenyl)-γ-valerolactone	1.276 ± 0.005
4-hydroxy-5-(3′,4′-dihydroxyphenyl)valeric acid[d]	nq
4-hydroxy-5-(3′-hydroxyphenyl)valeric acid[d]	nq
4-hydroxy-5-phenylvaleric acid[d]	nq
3-(3,4-dihydroxyphenyl)propionic acid[e]	9.467 ± 0.180
3-(3-hydroxyphenyl)propionic acid[e]	0.135 ± 0.004
3-(4-hydroxyphenyl)propionic acid	7.605 ± 0.084
3-phenylpropionic acid[e]	0.175 ± 0.000
2-(3,4-dihydroxyphenyl)acetic acid	0.637 ± 0.001
2-(3-hydroxyphenyl)acetic acid	0.111 ± 0.000
2-(4-hydroxyphenyl)acetic acid	0.140 ± 0.001
2-phenylacetic acid[f]	0.034 ± 0.000
3,4-dihydroxybenzoic acid[g]	nq
3-hydroxybenzoic acid	0.117 ± 0.000
4-hydroxybenzoic acid[g]	nq
benzoic acid	0.502 ± 0.002
3-*O*-methylgallic acid[h]	0.217 ± 0.000
homovanillic acid[i]	0.137 ± 0.000
homovanillyl alcohol[i]	nd
ferulic acid	0.241 ± 0.000
hippuric acid	0.669 ± 0.001
phloroglucinol	nd

[a]Data are given as the concentration (micromolar) ± standard error of the mean (SEM) from a triplicate chromatographic analysis. [b]Abbreviations: nd = not detected; nq = not quantified. [c]Quantified as procyanidin B2. [d]Quantified as 5-(3′,4′-dihydroxyphenyl)-γ-valerolactone. [e]Quantified as 3-(4-hydroxyphenyl)propionic acid. [f]Quantified as 2-(4-hydroxyphenyl)acetic acid. [g]Quantified as 3-hydroxybenzoic acid. [h]Quantified as gallic acid. [i]Quantified as vanillic acid.

derived polyphenols in composition, were used for chronic treatment in the study.[26] On the other hand, all of the studies performed with grape seed polyphenol extract,[13] its fractions,[40] or a red wine extract[27] were performed in in vitro systems by fecal fermentations.

In conclusion, the present study describes a rapid, simple, and sensitive method for measuring flavanol colonic metabolites in plasma samples by HPLC-ESI-MS/MS. The improved method for off-line μ-SPE plasma pretreatment allowed the flavanols and their colonic metabolites to be determined at low concentrations in a reduced plasma volume, which is an important factor to develop a complete in vivo study. In total, 30 flavanols and their colonic derivatives could be analyzed by a unique pretreatment extraction and chromatographic analysis. Hence, the method developed could be used for completed pharmacokinetics and bioavailability studies in animals.

AUTHOR INFORMATION

Corresponding Author

*Phone +34 977559566; fax +34 977558232; e-mail begona.muguerza@urv.cat.

Funding

This work was supported by the European Union Seventh Framework Programme FP7 2007-2013 under Grant Agreement 244995 (BIOCLAIMS Project) and by the Universitat Rovira i Virgili-Banco Santander (2011 LINE-13 and 2011 LINE-12).

Notes

The authors declare no competing financial interest.

ACKNOWLEDGMENTS

We gratefully acknowledge Dr. Manuel Suárez and Dr. Rosa-Maria Ras for their scientific and technical assistance.

REFERENCES

(1) Aherne, S. A.; O'Brien, N. M. Dietary flavonols: Chemistry, food content, and metabolism. *Nutrition* **2002**, *18*, 75−81.

(2) Hollman, P. C.; Katan, M. B. Dietary flavonoids: Intake, health effects and bioavailability. *Food Chem. Toxicol.* **1999**, *37*, 937−942.

(3) Aron, P. M.; Kennedy, J. A. Flavan-3-ols: Nature, occurrence and biological activity. *Mol. Nutr. Food Res.* **2008**, *52*, 79−104.

(4) Puiggros, F.; Llópiz, N.; Ardévol, A.; Bladé, C.; Arola, L.; Salvadó, M. J. Grape seed procyanidins prevent oxidative injury by modulating the expression of antioxidant enzyme systems. *J. Agric. Food Chem.* **2005**, *53*, 6080−6086.

(5) Baselga-Escudero, L.; Bladé, C.; Ribas-Latre, A.; Casanova, E.; Salvadó, M. J.; Arola, L.; Arola-Arnal, A. Grape seed proanthocyanidins repress the hepatic lipid regulators miR-33 and miR-122 in rats. *Mol. Nutr. Food Res.* **2012**, *56*, 1636−1646.

(6) Guerrero, L.; Margalef, M.; Pons, Z.; Quiñones, M.; Arola, L.; Arola-Arnal, A.; Muguerza, B. Serum metabolites of proanthocyanidin-administered rats decrease lipid synthesis in HepG2 cells. *J. Nutr. Biochem.* **2013**, *24*, 2092−2099.

(7) Pinent, M.; Bladé, M. C.; Salvadó, M. J.; Arola, L.; Hackl, H.; Quackenbush, J.; Trajanoski, Z.; Ardévol, A. Grape-seed derived procyanidins interfere with adipogenesis of 3T3-L1 cells at the onset of differentiation. *Int. J. Obes.* **2005**, *29*, 934−941.

(8) Pinent, M.; Blay, M.; Bladé, M. C.; Salvadó, M. J.; Arola, L.; Ardévol, A. Grape seed-derived procyanidins have an antihyperglycemic effect in streptozotocin-induced diabetic rats and insulinomimetic activity in insulin-sensitive cell lines. *Endocrinology* **2004**, *145*, 4985−4990.

(9) Quiñones, M.; Guerrero, L.; Suarez, M.; Pons, Z.; Aleixandre, A.; Arola, L.; Muguerza, B. Low-molecular procyanidin rich grape seed extract exerts antihypertensive effect in male spontaneously hypertensive rats. *Food Res. Int.* **2013**, *51*, 587−595.

(10) Terra, X.; Pallarés, V.; Ardèvol, A.; Bladé, C.; Fernández-Larrea, J.; Pujadas, G.; Salvadó, J.; Arola, L.; Blay, M. Modulatory effect of grape-seed procyanidins on local and systemic inflammation in diet-induced obesity rats. *J. Nutr. Biochem.* **2011**, *22*, 380−387.

(11) Del Rio, D.; Rodriguez-Mateos, A.; Spencer, J. P. E.; Tognolini, M.; Borges, G.; Crozier, A. Dietary (poly)phenolics in human health: Structures, bioavailability, and evidence of protective effects against chronic diseases. *Antioxid. Redox Signal.* **2013**, *18*, 1818−1892.

(12) Monagas, M.; Urpi-Sarda, M.; Sánchez-Patán, F.; Llorach, R.; Garrido, I.; Gómez-Cordovés, C.; Andres-Lacueva, C.; Bartolomé, B. Insights into the metabolism and microbial biotransformation of dietary flavan-3-ols and the bioactivity of their metabolites. *Food Funct.* **2010**, *1*, 233−253.

(13) Sánchez-Patán, F.; Cueva, C.; Monagas, M.; Walton, G. E.; Gibson, G. R.; Martín-Álvarez, P. J.; Moreno-Arribas, M. V.; Bartolomé, B. Gut microbial catabolism of grape seed flavan-3-ols by human faecal microbiota. Targetted analysis of precursor compounds, intermediate metabolites and end-products. *Food Chem.* **2012**, *131*, 337−347.
(14) Serra, A.; Macià, A.; Romero, M. P.; Reguant, J.; Ortega, N.; Motilva, M. J. Metabolic pathways of the colonic metabolism of flavonoids (flavonols, flavones and flavanones) and phenolic acids. *Food Chem.* **2012**, *130*, 383−393.
(15) Martí, M. P.; Pantaleón, A.; Rozek, A.; Soler, A.; Valls, J.; Macià, A.; Romero, M.-P.; Motilva, M.-J. Rapid analysis of procyanidins and anthocyanins in plasma by microelution SPE and ultra-HPLC. *J. Sep. Sci.* **2010**, *33*, 2841−2853.
(16) Serra, A.; Macià, A.; Rubió, L.; Anglès, N.; Ortega, N.; Morelló, J. R.; Romero, M. P.; Motilva, M. J. Distribution of procyanidins and their metabolites in rat plasma and tissues in relation to ingestion of procyanidin-enriched or procyanidin-rich cocoa creams. *Eur. J. Nutr.* **2013**, *52*, 1029−1038.
(17) Serra, A.; Macià, A.; Romero, M. P.; Valls, J.; Bladé, C.; Arola, L.; Motilva, M. J. Bioavailability of procyanidin dimers and trimers and matrix food effects in in vitro and in vivo models. *Br. J. Nutr.* **2010**, *103*, 944−952.
(18) Arola-Arnal, A.; Oms-Oliu, G.; Crescenti, A.; Del Bas, J. M.; Ras, M. R.; Arola, L.; Caimari, A. Distribution of grape seed flavanols and their metabolites in pregnant rats and their fetuses. *Mol. Nutr. Food Res.* **2013**, *57*, 1741−1752.
(19) Serra, A.; Macià, A.; Romero, M. P.; Anglès, N.; Morelló, J. R.; Motilva, M. J. Distribution of procyanidins and their metabolites in rat plasma and tissues after an acute intake of hazelnut extract. *Food Funct.* **2011**, *2*, 562−568.
(20) Urpi-Sarda, M.; Monagas, M.; Khan, N.; Lamuela-Raventos, R. M.; Santos-Buelga, C.; Sacanella, E.; Castell, M.; Permanyer, J.; Andres-Lacueva, C. Epicatechin, procyanidins, and phenolic microbial metabolites after cocoa intake in humans and rats. *Anal. Bioanal. Chem.* **2009**, *394*, 1545−1556.
(21) Urpi-Sarda, M.; Garrido, I.; Monagas, M.; Gómez-Cordovés, C.; Medina-Remón, A.; Andres-Lacueva, C.; Bartolomé, B. Profile of plasma and urine metabolites after the intake of almond [*Prunus dulcis* (Mill.) D.A. Webb] polyphenols in humans. *J. Agric. Food Chem.* **2009**, *57*, 10134−10142.
(22) Donovan, J. L.; Lee, A.; Manach, C.; Rios, L.; Morand, C.; Scalbert, A.; Rémésy, C. Procyanidins are not bioavailable in rats fed a single meal containing a grapeseed extract or the procyanidin dimer B3. *Br. J. Nutr.* **2002**, *87*, 299−306.
(23) Ottaviani, J. I.; Kwik-Uribe, C.; Keen, C. L.; Schroeter, H. Intake of dietary procyanidins does not contribute to the pool of circulating flavanols in humans. *Am. J. Clin. Nutr.* **2012**, *95*, 851−858.
(24) Shoji, T.; Masumoto, S.; Moriichi, N.; Akiyama, H.; Kanda, T.; Ohtake, Y.; Goda, Y. Apple procyanidin oligomers absorption in rats after oral administration: analysis of procyanidins in plasma using the porter method and high-performance liquid chromatography/tandem mass spectrometry. *J. Agric. Food Chem.* **2006**, *54*, 884−892.
(25) Tsang, C.; Auger, C.; Mullen, W.; Bornet, A.; Rouanet, J.-M.; Crozier, A.; Teissedre, P.-L. The absorption, metabolism and excretion of flavan-3-ols and procyanidins following the ingestion of a grape seed extract by rats. *Br. J. Nutr.* **2005**, *94*, 170−181.
(26) Urpi-Sarda, M.; Monagas, M.; Khan, N.; Llorach, R.; Lamuela-Raventós, R. M.; Jáuregui, O.; Estruch, R.; Izquierdo-Pulido, M.; Andrés-Lacueva, C. Targeted metabolic profiling of phenolics in urine and plasma after regular consumption of cocoa by liquid chromatography−tandem mass spectrometry. *J. Chromatogr. A* **2009**, *1216*, 7258−7267.
(27) Sánchez-Patán, F.; Cueva, C.; Monagas, M.; Walton, G. E.; Gibson, G. R. M.; Quintanilla-López, J. E.; Lebrón-Aguilar, R.; Martín-Álvarez, P. J.; Moreno-Arribas, M. V.; Bartolomé, B. In vitro fermentation of a red wine extract by human gut microbiota: Changes in microbial groups and formation of phenolic metabolites. *J. Agric. Food Chem.* **2012**, *60*, 2136−2147.
(28) Selma, M. V.; Espín, J. C.; Tomás-Barberán, F. A. Interaction between phenolics and gut microbiota: role in human health. *J. Agric. Food Chem.* **2009**, *57*, 6485−6501.
(29) Sánchez-Patán, F.; Monagas, M.; Moreno-Arribas, M. V.; Bartolomé, B. Determination of microbial phenolic acids in human faeces by UPLC-ESI-TQ MS. *J. Agric. Food Chem.* **2011**, *59*, 2241−2247.
(30) Gonthier, M. P.; Cheynier, V.; Donovan, J. L.; Manach, C.; Morand, C.; Mila, I.; Lapierre, C.; Rémésy, C.; Scalbert, A. Microbial aromatic acid metabolites formed in the gut account for a major fraction of the polyphenols excreted in urine of rats fed red wine polyphenols. *J. Nutr.* **2003**, *133*, 461−467.
(31) Matuszewski, B. K.; Constanzer, M. L.; Chavez-Eng, C. M. Strategies for the assessment of matrix effect in quantitative bioanalytical methods based on HPLC−MS/MS. *Anal. Chem.* **2003**, *75*, 3019−3030.
(32) Shah, V. P.; Midha, K. K.; Findlay, J. W. A.; Hill, H. M.; Hulse, J. D.; McGilveray, I. J.; McKay, G.; Miller, K. J.; Patnaik, R. N.; Powell, M. L.; Tonelli, A.; Viswanathan, C. T.; Yacobi, A. Bioanalytical method validation: A revisit with a decade of progress. *Pharm. Res.* **2000**, *17*, 1551−1557.
(33) McGaw, E. A.; Phinney, K. W.; Lowenthal, M. S. Comparison of orthogonal liquid and gas chromatography−mass spectrometry platforms for the determination of amino acid concentrations in human plasma. *J. Chromatogr. A* **2010**, *1217*, 5822−5831.
(34) Demelbauer, U. M.; Plematl, A.; Josic, D.; Allmaier, G.; Rizzi, A. On the variation of glycosylation in human plasma derived antithrombin. *J. Chromatogr. A* **2005**, *1080*, 15−21.
(35) Day, A. J.; Mellon, F.; Barron, D.; Sarrazin, G.; Morgan, M. R. A.; Williamson, G. Human metabolism of dietary flavonoids: Identification of plasma metabolites of quercetin. *Free Radical Res.* **2001**, *35*, 941−952.
(36) Rein, D.; Lotito, S.; Holt, R. R.; Keen, C. L.; Schmitz, H. H.; Fraga, C. G. Epicatechin in human plasma: In vivo determination and effect of chocolate consumption on plasma oxidation status. *J. Nutr.* **2000**, *130*, 2109S−2114S.
(37) Holt, R. R.; Lazarus, S. A.; Sullards, M. C.; Zhu, Q. Y.; Schramm, D. D.; Hammerstone, J. F.; Fraga, C. G.; Schmitz, H. H.; Keen, C. L. Procyanidin dimer B2 [epicatechin-(4{beta}-8)-epicatechin] in human plasma after the consumption of a flavanol-rich cocoa. *Am. J. Clin. Nutr.* **2002**, *76*, 798−804.
(38) Chu, K. O.; Wang, C. C.; Chu, C. Y.; Chan, K. P.; Rogers, M. S.; Choy, K. W.; Pang, C. P. Pharmacokinetic studies of green tea catechins in maternal plasma and fetuses in rats. *J. Pharm. Sci.* **2006**, *95*, 1372−1381.
(39) Déprez, S.; Brezillon, C.; Rabot, S.; Philippe, C.; Mila, I.; Lapierre, C.; Scalbert, A. Polymeric proanthocyanidins are catabolized by human colonic microflora into low-molecular-weight phenolic acids. *J. Nutr.* **2000**, *130*, 2733−2738.
(40) Cueva, C.; Sánchez-Patán, F.; Monagas, M.; Walton, G. E.; Gibson, G. R.; Martín-Álvarez, P. J.; Bartolomé, B.; Moreno-Arribas, M. V. In vitro fermentation of grape seed flavan-3-ol fractions by human faecal microbiota: Changes in microbial groups and phenolic metabolites. *FEMS Microbiol. Ecol.* **2013**, *83*, 792−805.
(41) Serra, A.; Macià, A.; Romero, M. P.; Piñol, C.; Motilva, M. J. Rapid methods to determine procyanidins, anthocyanins, theobromine and caffeine in rat tissues by liquid chromatography-tandem mass spectrometry. *J. Chromatogr. B* **2011**, *879*, 1519−1528.
(42) Suárez, M.; Romero, M. P.; Macià, A.; Valls, R. M.; Fernández, S.; Solà, R.; Motilva, M. J. Improved method for identifying and quantifying olive oil phenolic compounds and their metabolites in human plasma by microelution solid-phase extraction plate and liquid chromatography−tandem mass spectrometry. *J. Chromatogr. B* **2009**, *877*, 4097−4106.

saponins,[26] and pharmaceutical drugs.[30] Currently, there are no reports on the application of CAD to the analysis of FOS.

Here, a HPLC-CAD and microwave-assisted extraction method was developed for simultaneous determination of 11 FOS with DP 3−13 in 12 different plants in Compositae, Campanulaceae, and Rubiaceae families. The methods were validated and demonstrated for use in analysis of inulin-type FOS and are potentially useful for other plants.

MATERIALS AND METHODS

Materials, Reagents, and Chemicals. The analyzed plants belonged to Compositae, Campanulaceae, and Rubiaceae families, and their detailed characteristics are presented in Table 1. Species identification was performed by Dr. C. F. Qiao. Voucher specimens of these samples were deposited at the Institute of Chinese Medical Sciences, University of Macau, Macao SAR, China.

Inulin-type FOS with DP between 3 and 13 (all purities determined by HPLC-DAD-ELSD were more than 95%) were separated and purified in our laboratory (Figure 1). The structures were confirmed by comparing their methylation, MS, and NMR data with the literature.[17,22] Acetonitrile for HPLC was purchased from Merck (Darmstadt, Germany). Purified water for HPLC was prepared on a Millipore Milli-Q Plus system (Millipore, Bedford, MA). All other chemicals and reagents were of analytical grade.

Table 1. Characteristics of Analyzed Samples

producing area	place of purchase	codes
Atractylodes lancea (Thunb.) DC., family Compositae		
Jiangsu	Shenzhen	A1
Hebei	Zhuhai	A2
unknown	Macau	A3
Codonopsis pilosula (Franch.) Nannf., family Campanulaceae		
Gansu	Shenzhen	B1
Shanxi	Zhuhai	B2
unknown	Macau	B3
Atractylodes macrocephala Koidz., family Compositae		
Anhui	Shenzhen	C1
Hunan	Zhuhai	C2
unknown	Macau	C3
Taraxacum mongolicum Hand.-Mazz., family Compositae		
Hunan	Shenzhen	D1
Shanxi	Zhuhai	D2
Unkonwn	Macau	D3
Platycodon grandiflorus (Jacq.) A.DC., family Campanulaceae		
Anhui	Shenzhen	E1
unknown	Zhuhai	E2
unknown	Macau	E3
Aucklandia lappa Decne., family Compositae		
Guangdong	Shenzhen	F1
Yunnan	Zhuhai	F2
unknown	Macau	F3
Smallanthus sonchifolius (Poepp. & Endl.) H. Robinson, family Compositae		
Guangdong	Zhuhai	G1
Guangdong	Macau	G2
Carthamus tinctorius L., family Compositae		
Sichuan	Shenzhen	H1
Sichuan	Zhuhai	H2
unknown	Macau	H3
Adenophora tetraphylla (Thunb.) Fisch., family Campanulaceae		
Anhui	Shenzhen	I1
unknown	Macau	I2
Morinda officinalis How., family Rubiaceae		
unknown	Zhuhai	J1
unknown	Meizhou	J2
Deqing	Deqing	J3
Helianthus tuberosus L., family Compositae		
Hunan	Hunan	K1
Arctium lappa L., family Compositae		
Korea	Macau	L1
Shandong	Shandong	L2
Jilin	Jilin	L3

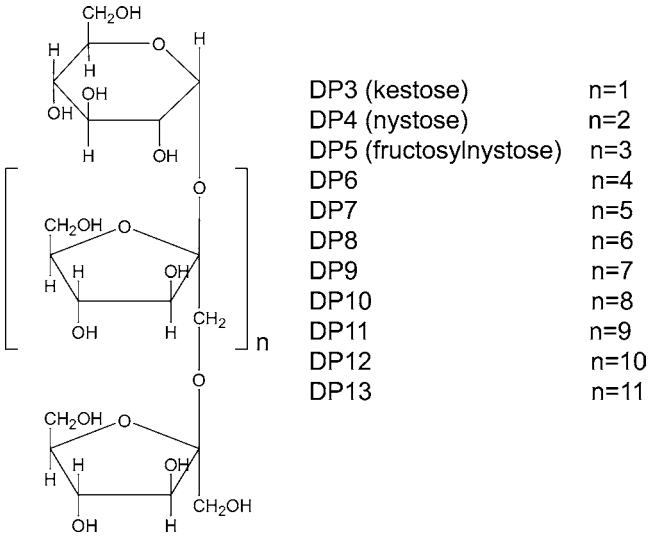

Figure 1. Structures of inulin-type fructooligosaccharides (FOS).

Preparation of Standard Solutions. Mixed standard stock solution containing inulin-type FOS (DP3−DP13) was prepared in 60% ethanol. The concentrations of DP3−DP13 were about 20 mg/mL. The standard stock solution was stored in a refrigerator at 4 °C before use. Working standard solutions were prepared from the stock solution by dilution with the appropriate volume of 60% ethanol.

Sample Preparation. Extraction experiments were carried out with a Multiwave 3000 reaction system (Anton Paar GmbH, Graz, Austria) equipped with a 64-position extraction rotor. The herbal medicine powder (0.1 g, 40 mesh) and 2 mL of ethanol−water (60:40 v/v) were transferred into 5 mL extraction vessels made of borosilicate glass. After the vessels were closed and capped, the rotor was placed inside the microwave oven. The extractions were performed in temperature-controlled mode. After a heating ramp of 1 min, the microwave program was stated as 400 W for 5 min at the temperature of 80 °C. Immediately after the temperature program had finished, all vessels were cooled down to ambient temperature. All extractions were performed with magnetic stirring. After extraction, an aliquot was taken and centrifuged for 5 min at 5000*g*. After centrifugation, 1 mL of supernatant was transferred into a 10 mL volumetric flask and made up to the volume with extraction solvent. Then the solution was filtered through a 0.45 μm filter before injection into the HPLC system for analysis.

HPLC-CAD Analysis. Chromatographic analyses were performed on a Dionex (Germering, Germany) Ultimate 3000 UHPLC system equipped with Ultimate 3000 degasser, pump, RS autosampler, and RS column compartment, coupled with a Corona charged aerosol detector (CAD) instrument (ESA, Chelmsford, MA). Data processing was carried out with Chromeleon 6.8 software (Dionex). The N_2 pressure of the CAD was adjusted to 35 psi and the response range was set to 100 pA. Separations were carried out on a Waters XBridge Amide column (4.6 × 250 mm id, 3.5 μm). The column temperature was set at 30 °C. The mobile phase was consist of water (A) and acetonitrile

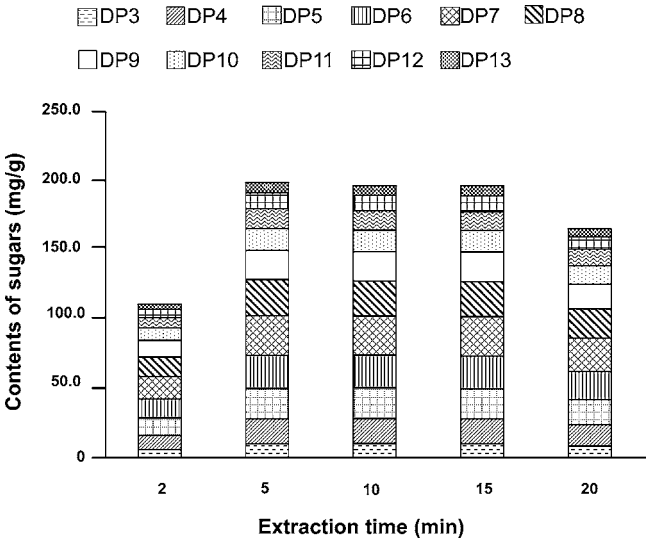

Figure 2. Effect of extraction time on extraction efficiency of FOS with different degrees of polymerization (DP).

Table 2. Linear Regression Data and Limits of Detection and Quantitation for Fructooligosaccharides DP3−DP13

analyte	regression eq	R^2	linear range (μg/mL)	LOD (μg/mL)	LOQ (μg/mL)
DP3	$y = 1.3400x - 2.3594$	0.9993	1.4−53.8	0.4	2.3
DP4	$y = 1.3437x - 2.2999$	0.9979	1.6−58.5	0.6	1.9
DP5	$y = 1.3309x - 2.2231$	0.9978	1.4−52.5	0.6	1.4
DP6	$y = 1.3285x - 2.1593$	0.9983	1.5−36.7	0.4	1.5
DP7	$y = 1.3112x - 2.232$	0.9968	1.5−38.3	0.5	1.5
DP8	$y = 1.2913x - 2.1935$	0.9962	1.5−38.0	0.4	1.6
DP9	$y = 1.3084x - 2.2270$	0.9967	1.5−37.5	0.4	1.6
DP10	$y = 1.3165x - 2.2200$	0.9981	1.4−34.7	0.4	1.4
DP11	$y = 1.2250x - 2.1673$	0.9971	1.4−106.5	0.4	1.4
DP12	$y = 1.2024x - 2.2063$	0.9978	1.3−96.0	0.6	1.6
DP13	$y = 1.1955x - 2.2064$	0.9981	1.5−221.0	0.5	1.5

(B) with gradient elution: 75%−45% B at 0−30 min, 45%−75% B at 30−32 min, and then equilibrated with 75% B for 10 min. The flow rate was 1.0 mL/min and injection volume was 5 μL.

Calibration Curves and Limits of Detection and Quantification. Standard stock solutions containing reference compounds were prepared and diluted to appropriate concentrations for construction of calibration curves. Six concentrations of 11 analyte solutions were injected in triplicate, and then the calibration curves were constructed and their linear ranges determined. Since CAD response was nonlinear and it can be represented by $y = ax^b$, where y refers to peak area, while x is the analyte amount, a is the constant term, and b is the exponential response factor.[31] Therefore, calibration of CAD was constructed by a double logarithmic plot as in previous reports.[26,29,31]

Stock solutions were diluted to a series of appropriate concentration with 60% ethanol, and aliquots of the diluted solutions were injected into HPLC for determining the limit of detection (LOD) and limit of quantification (LOQ). The LOD and LOQ under the present chromatographic conditions were determined at a signal-to-noise ratio (S/N) of 3 and 10, respectively.

Table 3. Precision (Intra- and Interday) for Fructooligosaccharides DP3−DP13

	peak area (% RSD)		retention time (% RSD)	
analyte	intraday (n = 6)	interday[a] (n = 6)	intraday (n = 6)	interday[a] (n = 6)
DP3	2.75	11.10	1.50	0.05
DP4	2.40	10.20	1.30	0.06
DP5	2.10	9.90	1.13	0.05
DP6	1.48	9.56	1.03	0.06
DP7	1.67	11.76	0.95	0.07
DP8	1.58	11.64	0.89	0.06
DP9	1.57	13.05	0.85	0.05
DP10	1.80	13.57	0.81	0.07
DP11	1.72	13.17	0.76	0.06
DP12	1.90	17.33	0.75	0.05
DP13	2.62	15.74	0.72	0.06

[a]Interday precision was determined over a period of 5 days (3 measurements on each day).

Table 4. Repeatability, Stability, and Accuracy for Fructooligosaccharides DP3−DP13

	repeatability		stability	accuracy	
analyte	content (mg/g)	RSD (%)	RSD (%)	recovery (%)	RSD (%)
DP3	19.28	2.44	2.21	99.0	3.92
DP4	29.74	2.18	2.36	100.4	4.43
DP5	31.72	2.11	3.53	95.9	5.26
DP6	30.14	2.07	3.49	97.5	4.44
DP7	35.25	2.03	3.36	94.0	5.18
DP8	32.51	2.25	3.48	94.1	5.07
DP9	28.52	2.28	3.71	95.6	5.00
DP10	23.45	2.44	3.54	98.7	5.17
DP11	25.62	3.09	4.46	113.3	5.36
DP12	24.37	2.93	4.97	114.4	5.40
DP13	19.39	2.94	4.88	99.5	7.25

Precision, Repeatability, Accuracy, and Stability. Precision of the HPLC-CAD method was determined by evaluating the repeatability of intraday and interday measurements. Intraday precision was determined by repeating the analysis of the mixed standards solution for six replicates within 1 day, while interday precision was determined in duplicates on three successive days. Repeatability of the developed method was confirmed with preparation and analysis of six parallel samples. Stability was tested and analyzed at 0, 1, 2, 4, 8, 12, and 24 h. In order to check the accuracy of the developed method, recovery experiments were carried out as follows: accurate amounts of the standards were spiked into the samples (0.05 g) in the form of solution. The spiked samples were extracted, processed, and quantified in accordance with methods mentioned above. Average recoveries were determined by the equation recovery (percent) = 100 × (observed amount − original amount)/spiked amount, and relative standard deviation (RSD, percent) = 100 × standard deviation (SD)/mean.

Liquid Chromatography−Tandem Mass Spectrometric Analyses. LC-MS/MS analyses were carried out on an Agilent 1100 Series LC/MSD Trap system (Agilent Technologies, Palo Alto, CA), equipped with vacuum degasser, quaternary pump, autosampler, column compartment, diode-array detector (DAD), and ion-trap mass spectrometer with electrospray ionization (ESI) interface, connected to Agilent LC/MSD Trap software. ESI-MS conditions were as follows: drying gas N_2 at 7 L/min, temperature 325 °C, pressure of nebulizer 25 psi, source voltage 3.5 kV. ESI-MS/MS

dx.doi.org/10.1021/jf502329n | J. Agric. Food Chem. 2014, 62, 7707−7713

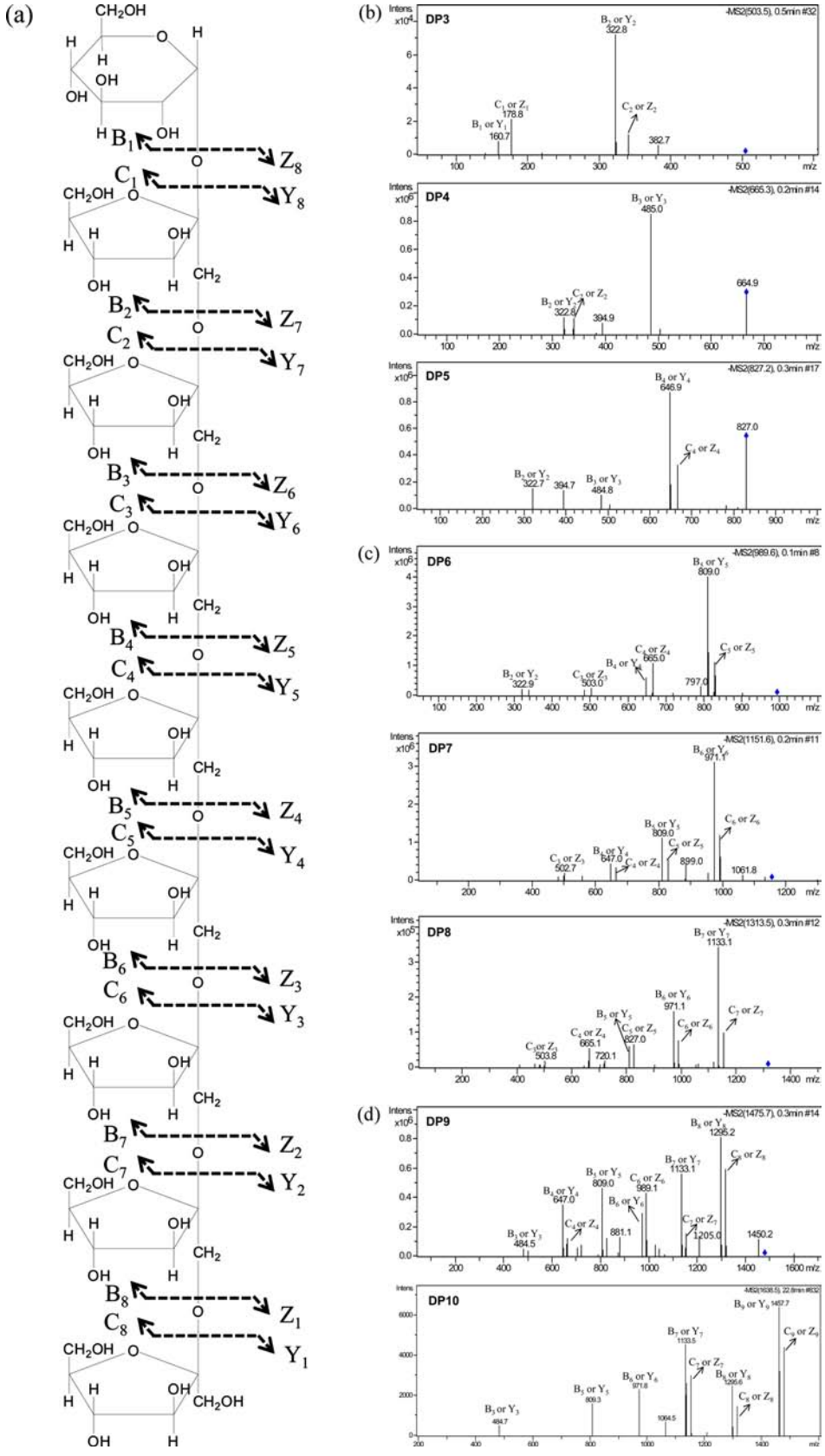

Figure 3. (a) LC−MS/MS spectra and (b−d) Domon and Costello nomenclature for the fragmentation of separated FOS (DP3−DP10).

conditions included isolation width 4 and fragment amplification 1.5. Scan ranges of both MS and MS/MS were 200−2200 m/z. The liquid chromatographic conditions for LC-MS/MS were the same as described for HPLC-CAD analysis.

RESULTS AND DISCUSSION

Optimization of Sample Preparation. In order to obtain quantitative extraction, the extraction method, extraction solvents,

dx.doi.org/10.1021/jf502329n | J. Agric. Food Chem. 2014, 62, 7707−7713

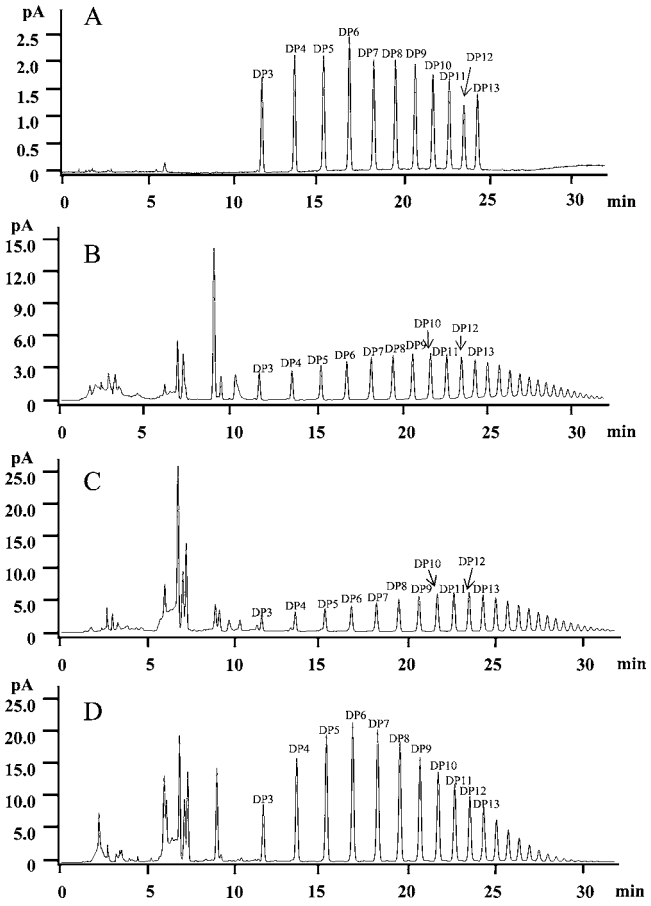

Figure 4. HPLC-CAD chromatograms of (A) mixed standards and (B–D) samples of (B) *Atractylodes macrocephala*, (C) *Platycodon grandiflorum*, and (D) *Morinda officinalis*.

extraction solvent volume, extraction time, and temperature were optimized. Solvent choices, solvent volumes, and temperature used in this study were fixed according to our previous study.[23] We investigated the effect of extraction time, which directly influence the extraction yields of FOS.

In order to get the optimal reaction time, we performed the extraction by microwave extraction in a range from 2 to 20 min at 80 °C, using a sample (*Morinda officinalis*, sample J3) of approximately 0.1 g. Results (Figure 2) showed that the optimal extraction time of FOS was 5 min, whereas longer extraction time did not significantly increase extraction yields and FOS degradation was observed at 20 min. We therefore selected 5 min as the optimal extraction time.

Optimization of HPLC Conditions. Analysis of FOS is a challenge due to their high polarity and complexity and lack of specific UV absorptivity. Therefore, the HPLC-CAD method was selected for analysis of FOS. Several different commercial columns were tested, and finally the Waters XBridge Amide column (4.6 × 250 mm id, 3.5 μm) was selected for separation of 11 investigated inulin-type FOS because of its high resolution and good signal-to-noise performance. The analytes in both mixed standard solution and sample solutions can be well separated by gradient elution with water and acetonitrile.

Method Validation. Linearity, regression, and linear ranges of the 11 analytes were determined by the developed HPLC method. The data indicated the calibration curves of the 11 analytes had good linearity (R^2 > 0.9962), and their LODs and LOQs were in the ranges 0.4–0.6 μg/mL and 1.4–2.3 μg/mL, respectively (Table 2). For intraday precision, RSDs of the peak area was 1.48–2.75% and RSD of the retention time was 0.72–1.50%; for interday precision, the corresponding RSDs were 9.56–17.33% and 0.05–0.07% (Table 3). Recoveries ranged from 94.0% to 114.4%, and the analytes were very stable in 60% ethanol solution during the tested period (Table 4). The high recoveries (113.3% and 114.4%) of DP11 and DP12 might be attributed to the variation of their purities, and more attention should be paid in future.

LC-MS/MS Analysis. Molecular mass information on the standards and the extracted samples were determined in negative ion mode. In the negative ion mode, the $[M - H]^-$ of FOS (DP3–DP13) were detected at m/z 503, 665, 827, 989, 1151, 1313, 1475, 1637, 1799, 1961, and 2123. ESI-MS/MS of their $[M - H]^-$ ions was performed to obtain the individual fragment patterns. Their MS/MS spectra are shown in Figure 3. The fragment ions of FOS include glycosidic cleavages between two sugar residues and cross-ring cleavages of two bonds within the sugar ring. In our MS/MS spectra, the fragment ions of FOS mainly result from glycosidic cleavages between two sugar residues, which were as the same as those reported in previous literature.[17] That little fragments with low abundance of the cross-ring cleavages of two bonds within the sugar ring were found might be derived from the low collision energy or few sodium ions in mobile phase.[17,32] FOS (DP11–DP13) with high molecular weights are difficult to ionize for LC-MS/MS analysis, so the characteristic MS/MS spectra of FOS (DP11–DP13) could not be shown. However, in the MS spectrum of FOS (DP11–DP13), the characteristic ions at m/z 161, 179, 323, 341, 485, 503, 647, 665, 809, 827, 971, 989, 1133, 1151, 1313, 1475, 1457, 1638, and 1800 were obtained. In summary, all the results suggested that FOS should consist of the corresponding number of hexoses.

Quantitative Determination of FOS in Plants. The established HPLC-CAD method was applied for analysis of inulin-type FOS (DP3–DP13) in different samples of Compositae, Campanulaceae, and Rubiaceae families. HPLC-CAD chromatograms of the mixed standards and different samples are shown in Figure 4. Besides the investigated 11 oligosaccharides, many oligosaccharides with DP of more than 13 were also found in these samples. Unfortunately, we could not quantitatively determine these oligosaccharides because of the absence of related reference compounds, which should be performed in the future. The contents of the 11 investigated FOS in different samples are summarized in Table 5 and Figure 5. The results showed that the three samples with highest contents of FOS were *Morinda officinalis*, *Helianthus tuberosus* and *Arctium lappa*, and both *H. tuberosus* and *A. lappa* belong to the Compositae family. The data also indicated there was no FOS detected in *Taraxacum mongolicum* and *Carthamus tinctorius*, which are also of the Compositae family. That is because FOS are usually the chemical compounds for storing energy in organs such as bulbs, tubers, and tuberous roots. The flowers contain little FOS.

In summary, there are many reports on the existence of FOS in plants of Liliaceae, Compositae, Campanulaceae, and Rubiaceae families, but few reports on their contents in these samples. This is the first report for quantitative analysis of inulin-type FOS (DP3–DP13) in different samples of plants in Compositae, Campanulaceae, and Rubiaceae families, which is helpful to improve their qualities. The developed HPLC-CAD method, which is accurate and specific, can also be used for determination of inulin-type FOS in other plants.

Table 5. Contents of the 11 Analytes in Tested Samples

	analyte content(mg/g)											
sample	DP3	DP4	DP5	DP6	DP7	DP8	DP9	DP10	DP11	DP12	DP13	total
A1	6.01	4.05	3.27	4.22	5.08	5.44	5.59	5.59	6.63	7.56	7.46	60.89
A2	4.68	2.86	1.96	3.24	3.85	2.96	3.08	3.02	3.48	3.88	3.3	36.32
A3	2.69	2.14	1.66	1.7	2.09	2.22	2.5	2.75	3.63	4.33	4.64	30.36
B1	1.49	0.8	0.75	1.34	1.48	1.48	1.59	1.64	2.13	2.46	2.35	17.52
B2	3.59	1.62	1.25	3.01	3.15	2.81	2.49	1.99	2.19	2.2	1.91	26.21
B3	0.65	0.42	0.39	0.4	0.48	0.51	0.64	0.76	1.05	1.34	1.38	8.01
C1	4.29	4.08	4.39	4.42	5.61	5.77	6.03	6.06	7.32	8.41	8.24	64.62
C2	4.52	4.36	4.78	4.91	6.28	6.57	6.89	6.69	7.79	8.76	8.3	69.84
C3	7.15	5.65	5.4	5.22	6.68	6.7	6.92	6.7	7.83	8.72	8.41	75.38
D1[a]												
D2[a]												
D3[a]												
E1	4.02	4.71	4.93	5.67	7.47	8.01	8.78	8.97	11.19	12.93	12.65	89.34
E2	4.8	4.67	4.28	4.52	5.55	5.61	5.48	5.93	7.47	9.22	9.38	66.91
E3	8.49	6.58	6.56	7.14	9.42	10.07	10.74	10.75	13.52	15.65	15.6	114.52
F1	4.5	2.97	1.96	2.23	2.28	2.33	2.74	2.85	3.47	4.22	4.32	33.86
F2	4.28	2.59	1.85	1.78	1.89	1.83	2.05	2.36	3.14	4.28	4.51	30.55
F3	2.92	2.25	1.65	2.13	2.5	2.46	2.74	3.2	4.21	5.17	5.49	34.72
G1	29.43	27.17	19.8	14.17	13.04	11.09	9.36	7.1	6.06	4.75	3.17	145.13
G2	23.8	24.54	18.91	13.92	15.25	14.32	13	10.35	9.61	7.89	5.57	157.17
H1[a]												
H2[a]												
H3[a]												
I1	4.28	4.69	4.22	4.47	4.81	4.21	4.13	4.11	5.22	6.59	7.31	54.04
I2	5.17	4.98	5.65	5.97	8.11	9.01	10.11	10.62	13.92	16.7	17.08	107.31
J1	22.28	28.97	30.34	29.16	32.11	27.47	22.93	18.36	19.35	18.62	15.52	265.11
J2	11.92	18.02	20.53	20.08	23.93	22.5	20.3	17.39	19.6	19.88	17.11	211.24
J3	19.58	29.24	31.61	29.89	35.06	32.44	28.46	23.61	25.56	24.47	19.54	299.44
K1	36.42	28.58	23.82	19.6	19.85	18.57	16.16	15.13	15.54	14.54	11.81	220.02
L1	24.05	22.08	15	15.7	18.54	17.68	15.81	13.54	14.76	14.74	13.22	185.13
L2	22.8	18.59	16.06	14.86	17.21	14.57	13.52	11.72	12.06	12.82	11.37	165.59
L3	16.52	13.33	12.87	11.71	13.97	13.72	13.11	11.87	13.93	15.44	14.78	151.26

[a]Not detected.

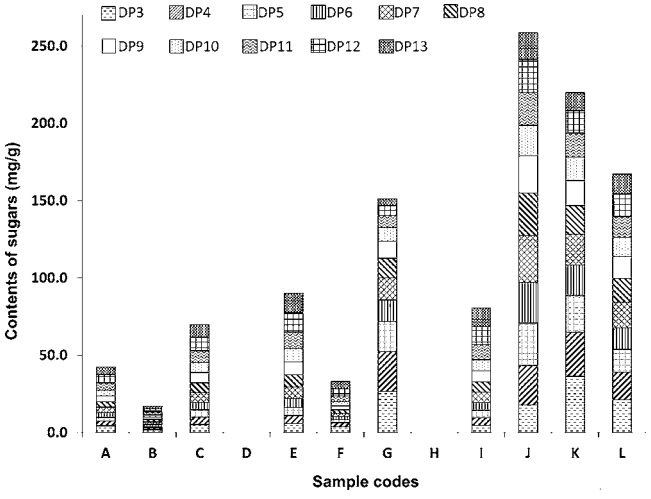

Figure 5. Average contents of FOS with different degree of polymerization (DP) in different edible plants. A–L mean the average of three related samples in Table 1.

AUTHOR INFORMATION

Corresponding Authors

* Phone +853-8397-4692; fax +853-2884-1358; e-mail zhaojing.cpu@163.com.

* Phone +853-8397-4692; fax +853-2884-1358; e-mail spli@umac.mo.

Author Contributions

[†]J.L., D.H., and W.Z. contributed equally to this work

Funding

This research was supported by grants from the Science and Technology Development Fund of Macao (FDCT059/2011/A3), and the University of Macau (MYRG140 and MYRG085).

Notes

The authors declare no competing financial interest.

ABBREVIATIONS

HPLC, high-performance liquid chromatography; CAD, charged aerosol detector; FOS, fructooligosaccharides; DP, degree of polymerization; ELSD, evaporative light scattering detector; HPAEC, high-performance anion-exchange chromatography; PAD, pulsed amperometric detection; RID, refractive index detector; MS, mass spectrometry; LOD, limit of detection; LOQ, limit of quantification; S/N, signal-to-noise ratio

REFERENCES

(1) Milani, E.; Koocheki, A.; Golimovahhed, Q. A. Extraction of inulin from Burdock root (*Arctium lappa*) using high intensity ultrasound. *Int. J. Food Sci. Technol.* **2011**, *46*, 1699–1704.

(2) Van Loo, J.; Coussement, P.; De Leenheer, L.; Hoebregs, H.; Smits, G. On the presence of inulin and oligofructose as natural ingredients in the Western diet. *Crit. Rev. Food Sci.* **1995**, *35*, 525−552.
(3) Moshfegh, A. J.; Friday, J. E.; Goldman, J. P.; Chug Ahuja, J. K. Presence of inulin and oligofructose in the diets of Americans. *J. Nutr.* **1999**, *129*, 1407S−1411S.
(4) Pool-Zobel, B. L. Inulin-type fructans and reduction in colon cancer risk: review of experimental and human data. *Br. J. Nutr.* **2005**, *93*, S73−S90.
(5) Sangeetha, P. T.; Ramesh, M. N.; Prapulla, S. G. Recent trends in the microbial production, analysis and application of fructooligosaccharides. *Trends Food Sci. Technol.* **2005**, *16*, 442−457.
(6) Lou, Z.; Wang, H.; Wang, D.; Zhang, Y. Preparation of inulin and phenols-rich dietary fibre powder from burdock root. *Carbohydr. Polym.* **2009**, *78*, 666−671.
(7) Zhang, R.; Zhou, J.; Jia, Z.; Zhang, Y.; Gu, G. Hypoglycemic effect of *Rehmannia glutinosa* oligosaccharide in hyperglycemic and alloxan-induced diabetic rats and its mechanism. *J. Ethnopharmacol.* **2004**, *90*, 39−43.
(8) Li, Y.-F.; Li, Y.; Xu, Y.-K.; Yang, M.; Zhao, Y.-M.; Luo, Z.-P. Antistress effect of oligosaccharides extracted from *Morinda officinalis* in mice and rats. *Acta Pharmacol. Sin.* **2001**, *22*, 1084−1088.
(9) Li, Y.-F.; Liu, Y.-Q.; Yang, M.; Wang, H.-L.; Huang, W.-C.; Zhao, Y.-M.; Luo, Z.-P. The cytoprotective effect of inulin-type hexasaccharide extracted from *Morinda officinalis* on PC12 cells against the lesion induced by corticosterone. *Life Sci.* **2004**, *75*, 1531−1538.
(10) Sun, F.; Zhang, P.; Guo, M.; Yu, W.; Chen, K. Burdock fructooligosaccharide induces fungal resistance in postharvest Kyoho grapes by activating the salicylic acid-dependent pathway and inhibiting browning. *Food Chem.* **2013**, *138*, 539−546.
(11) Kaur, N.; Gupta, A. K. Applications of inulin and oligofructose in health and nutrition. *J. Biosci.* **2002**, *27*, 703−714.
(12) Flamm, G.; Glinsmann, W.; Kritchevsky, D.; Prosky, L.; Roberfroid, M. Inulin and oligofructose as dietary fiber: A review of the evidence. *Crit. Rev. Food Sci.* **2001**, *41*, 353−362.
(13) Roberfroid, M. B. Functional foods: Concepts and application to inulin and oligofructose. *Br. J. Nutr.* **2002**, *87*, S139−S143.
(14) Zhu, H.-T.; Chen, J.-Y.; Chen, L.; Tu, Z.-L.; An, Z.-B. Pharmacognosy studies on *Atractylodes macrocephala* Koidz. *Lishizhen Med. Mater. Med. Res.* **2006**, *17*, 1019−1020.
(15) Fu, W.-W.; Dou, D.-Q.; Pei, Y.-H. Review on chemical components and bioactivities of *Platycodon grandiflorum*. *J. Shenyang Pharm. Univ.* **2006**, *23*, 184−191.
(16) Yang, H.; Xie, J.-L.; Sun, H.-D. Research progress on the medicinal plant *Saussurea lappa*. *Nat. Prod. Res. Dev.* **1997**, *10*, 90−98.
(17) Yang, Z.; Yi, Y.; Gao, C.; Hou, D.; Hu, J.; Zhao, M. Isolation of inulin-type oligosaccharides from Chinese traditional medicine: *Morinda officinalis* How. and their characterization using ESI-MS/MS. *J. Sep. Sci.* **2010**, *33*, 120−125.
(18) Ishiguro, Y.; Ueno, K.; Onodera, S.; Benkeblia, N.; Shiomi, N. Effect of temperatures on inulobiose and inulooligosaccharides in burdock roots during storage. *J. Food Compos. Anal.* **2011**, *24*, 398−401.
(19) Ishiguro, Y.; Onodera, S.; Yoshihira, T.; Kosaka, S.; Benkeblia, N.; Shiomi, N. Variation of 1-kestose, nystose and higher fructooligosaccharides in burdock root stored under different temperature regimes. *Agric. Biol. J. N. Am.* **2010**, *1*, 491−494.
(20) Ishiguro, Y.; Onodera, S.; Benkeblia, N.; Shiomi, N. Variation of total FOS, total IOS, inulin and their related-metabolizing enzymes in burdock roots (*Arctium lappa* L.) stored under different temperatures. *Postharvest Biol. Technol.* **2010**, *56*, 232−238.
(21) Imahori, Y.; Kitamura, N.; Kobayashi, S.; Takihara, T.; Ose, K.; Ueda, Y. Changes in fructooligosaccaride composition and related enzyme activities of burdock root during low-temperature storage. *Postharvest Biol. Technol.* **2010**, *55*, 15−20.
(22) Yang, Z.; Hu, J.; Zhao, M. Isolation and quantitative determination of inulin-type oligosaccharides in roots of *Morinda officinalis*. *Carbohydr. Polym.* **2011**, *83*, 1997−2004.
(23) Li, J.; Liu, X.; Zhou, B.; Zhao, J.; Li, S. Determination of fructooligosaccharides in burdock using HPLC and microwave-assisted extraction. *J. Agric. Food Chem.* **2013**, *61*, 5888−5892.
(24) Brokl, M.; Hernández-Hernández, O.; Soria, A. C.; Sanz, M. L. Evaluation of different operation modes of high performance liquid chromatography for the analysis of complex mixtures of neutral oligosaccharides. *J. Chromatogr. A* **2011**, *1218*, 7697−7703.
(25) Dixon, R. W.; Peterson, D. S. Development and testing of a detection method for liquid chromatography based on aerosol charging. *Anal. Chem.* **2002**, *74*, 2930−2937.
(26) Eom, H. Y.; Park, S.-Y.; Kim, M. K.; Suh, J. H.; Yeom, H.; Min, J. W.; Kim, U.; Lee, J.; Youm, J.-R.; Han, S. B. Comparison between evaporative light scattering detection and charged aerosol detection for the analysis of saikosaponins. *J. Chromatogr. A* **2010**, *1217*, 4347−4354.
(27) Vervoort, N.; Daemen, D.; Török, G. Performance evaluation of evaporative light scattering detection and charged aerosol detection in reversed phase liquid chromatography. *J. Chromatogr. A* **2008**, *1189*, 92−100.
(28) Inagaki, S.; Min, J. Z.; Toyo'oka, T. Direct detection method of oligosaccharides by high-performance liquid chromatography with charged aerosol detection. *Biomed. Chromatogr.* **2007**, *21*, 338−342.
(29) Khoomrung, S.; Chumnanpuen, P.; Jansa-Ard, S.; Staiŝhlman, M.; Nookaew, I.; Borén, J.; Nielsen, J. Rapid quantification of yeast lipid using microwave-assisted total lipid extraction and HPLC-CAD. *Anal. Chem.* **2013**, *85*, 4912−4919.
(30) Pistorino, M.; Pfeifer, B. A. Polyketide analysis using mass spectrometry, evaporative light scattering, and charged aerosol detector systems. *Anal Bioanal. Chem.* **2008**, *390*, 1189−1193.
(31) Bai, C.-C.; Han, S.-Y.; Chai, X.-Y.; Jiang, Y.; Li, P.; Tu, P.-F. Sensitive determination of saponins in Radix et Rhizoma notoginseng by charged aerosol detector coupled with HPLC. *J. Liq. Chromatogr. Relat. Technol.* **2008**, *32*, 242−260.
(32) Reis, A.; Coimbra, M. A.; Domingues, P.; Ferrer-Correia, A. J.; Rosário, M.; Domingues, M. Structural characterisation of underivatised olive pulp xylo-oligosaccharides by mass spectrometry using matrix-assisted laser desorption/ionisation and electrospray ionisation. *Rapid Commun. Mass Spectrom.* **2002**, *16*, 2124−2132.

based infant formula samples were powder. Fruit and vegetable pure samples were selected in the similar manner and they were all semiliquid. Jarred foods that were gels grouped as pudding and they were also containing milk or milk products. The main ingredients (fruits, vegetables, and cereals etc.) of these foods are given in Table 1.

Analysis of α-Dicarbonyl Compounds. *Extraction.* One gram of sample (infant formula, fruit puree, vegetable puree, and pudding) was extracted with water in three stages (10−5−5 mL) by vortexing 3 min. After centrifugation (5000*g* for 5 min) in each stage, supernatants were collected in a test tube. The coextracted colloids were precipitated by mixing with acetonitrile. Two hundred μL of the combined extract was diluted 5 fold with 800 μL of the mixture of acetonitrile:water (5:3, v/v), and centrifuged at 15 000*g* for 5 min. All samples were extracted in duplicates.

Derivatization. Derivatization of α-dicarbonyl compounds was carried out with *o*-phenylenediamine according to the published procedures with minor modifications [18,21,22]. Five hundred μL of supernatant was mixed with 150 μL of 0.2% *o*-phenylenediamine solution containing 11 mM diethylenetriaminepenta acetic acid and 150 μL of 0.5 M sodium phosphate buffer (pH 7). The mixture was immediately filtered through 0.45 μm syringe filter into an auto sampler vial. It was kept at room temperature, at dark for 2 h prior to HPLC-ESI-MS measurement.

HPLC-ESI-MS Measurement. α-Dicarbonyl compounds were determined by using an Agilent 1200 series HPLC system coupled with an Agilent 6130 single quadrupole mass spectrometer. The chromatographic separation was performed on a Merck Purospher Star RP-18e column (150 × 4.6 mm^2 id., 5 μm) using a gradient mixture of (A) 1% formic acid in water and (B) 1% formic acid in methanol as the mobile phase at a flow rate of 1 mL/min at 30 °C. The gradient mixture was started from 30% B and increased to 60% B in 10 min, then it was decreased to 30% B in 2 min and the 30% B remained for 3 min. The chromatographic run was completed in 15 min. The injection volume was 10 μL. The electrospray source had the following settings: drying gas (N_2) flow of 13 L/min at 300 °C, nebulizer pressure of 40 psig and capillary voltage of 4000 V. Fragmentor voltage was set to 100 V. MS data were acquired in the positive mode and α-dicarbonyl compounds were identified by selected ion monitoring (SIM) mode. The SIM ions $[M + H]^+$ were as follows for the quinoxaline derivatives of glucosone: 251; 1- or 3-deoxyglucosone: 235; dimethylglyoxal: 159; methylglyoxal: 145; and glyoxal: 131. A dwell time was set at 97 ms for each.

The SIM ions of the quinoxaline derivatives of α-dicarbonyl compounds were used for quantitation. The concentrations of quinoxaline, 2-methylquinoxaline and 2,3-dimethylquinoaxaline were calculated by means of external calibration curves in the range between 0.01 and 0.2 mg/L. Working solutions of 3-deoxyglucosone in the concentration range between 0.01 and 2.0 mg/L were derivatized and analyzed as described above to build its external calibration curve. Also, this calibration curve was used for semiquantitation of glucosone and 1-deoxyglucosone quinoxaline derivatives since both have same proton accepting groups. All working solutions were prepared in acetonitrile−water (50:50, v/v). Limit of detection (LOD) and limit of quantitation (LOQ) were determined at a signal-to-noise ratio of 3 and 10, respectively. Repeatability of the method was determined by analyzing three replicates in three consecutive days.

Analysis of Furfurals. The previously reported methods were used with some modifications.[23,24] The same extract of the samples was used for HMF and furfural analysis. A part of the extract was precipitated by Carrez clarification and centrifuged at 10 000*g* for 5 min. The supernatant was filtered through 0.45 μm syringe filter into an autosampler vial prior to analysis. The analysis was performed by Shimadzu UFLC system (Kyoto, Japan) consisting of a quaternary pump, an autosampler, a diode array detector and a temperature-controlled column oven. The chromatographic separations were performed on an Waters Atlantis dC18 column (250 × 4.6 mm^2 i.d., 5 μm) using the isocratic mixture of 10 mM aqueous formic acid solution and acetonitrile (90:10) at a flow rate of 1.0 mL/min at 25 °C. Data acquisition was performed by recording chromatograms at 285 nm. Concentrations of HMF and furfural were calculated by means of external calibration curves built in the range between 0.1 and 5 mg/L.

Table 1. Manufacturers' Declared Ingredients in the Baby Food Samples

samples		ingredients
infant formulas		
	1	Corn semolina and rice flour (37%), nonfat dry milk, whey powder, vegetable oils, pear powder (2.7%), orange powder (0.9%)
	2	Rice flour (37%), nonfat dry milk, whey powder, vegetable oils
	3	Wheat semolina (18%), rice flour (11%), nonfat dry milk, whey powder, vegetable oils, honey (0.9%)
	4	Mixture of cereal flours (27%), biscuit flour mix with butter, nonfat dry milk, whey powder
	5	Wheat semolina (34%), nonfat dry milk, whey powder, vegetable oils
	6	Rice flour (39%), nonfat dry milk, whey powder, vegetable oils, banana powder (0.3%)
	7	Hydrolyzed wheat semolina (53%), nonfat dry milk, lactose, vegetable oils, honey (5%)
	8	Rice flour (32%), nonfat dry milk, whey powder, apple concentrate (11%)
	9	Mixture of cereal flours, nonfat dry milk, whey powder, cheese powder, grape molasses (15.6%)
fruit purees		
	1	Pear (30%), peach (20%), pineapple (10%), grape juice concentrate (9%)
	2	Plum (50%)
	3	Grape juice (29%), banana (27%), peach (23%), carrot (10%), starch (4%)
	4	Apple (35%), apple juice concentrate (26%), pear (25%), carrot (10%), starch (4%)
	5	Apple (62%), carrot (33%), concentrated apple juice (5%)
	6	Apple (67%), apricot (14%), carrot (9%), grape juice concentrate (7.5%)
	7	Grape juice (33%), apple (14%), banana (9%), apricot (6%), whole oat flour (2.5%)
	8	Grape juice (34%), apple (17%), carrot (10%), mandarin juice (6%), banana (4%), rice flour (6%), whole oat flour (2.5%)
	9	Grape juice (33%), apple (14%), banana (9%), apricot (6%), whole oat flour (2.5%)
	10	Apple (35%), peach (27%), apple juice (23%), carrot (10%), rice flour (5%)
	11	Apple juice (40%), banana (30%), apricot (15%), carrot (10%), rice flour (5%)
vegetable purees		
	1	Potato (40%), spinach (26%), apple juice (11%), rice (10%)
	2	Carrot (%28), potato (15%), zucchini (12%), rice flour
	3	Carrot (90%)
	4	Rice (30%), green beans (28%), tomato (23%), apple juice (10%), potato (9%)
	5	Carrot, potato, green beans, cauliflower
	6	Rice (26%), carrot (20%), cauliflower (20%), potato (13%), apple juice (13%)
puddings		
	1	Milk (%54), rice (34%), sugar cane (4.5%)
	2	Yogurt (20%), banana (14%), orange juice (6%), starch (5%), sugar (5%)
	3	Yogurt (20%), skimmed milk (10%), pineapple juice (8%), sugar (5%), starch (6%), concentrated lemon juice (1%)
	4	Apple puree (35%), milk (30%), rice flour, sugar

Measurement of pH. Infant formula samples (0.2 g of powder) were mixed with 10 mL of deionized water and the tubes were put onto an orbital shaker for 10 min. After centrifugation (5000*g* for 5

dx.doi.org/10.1021/jf502418n | J. Agric. Food Chem. 2014, 62, 7714−7720

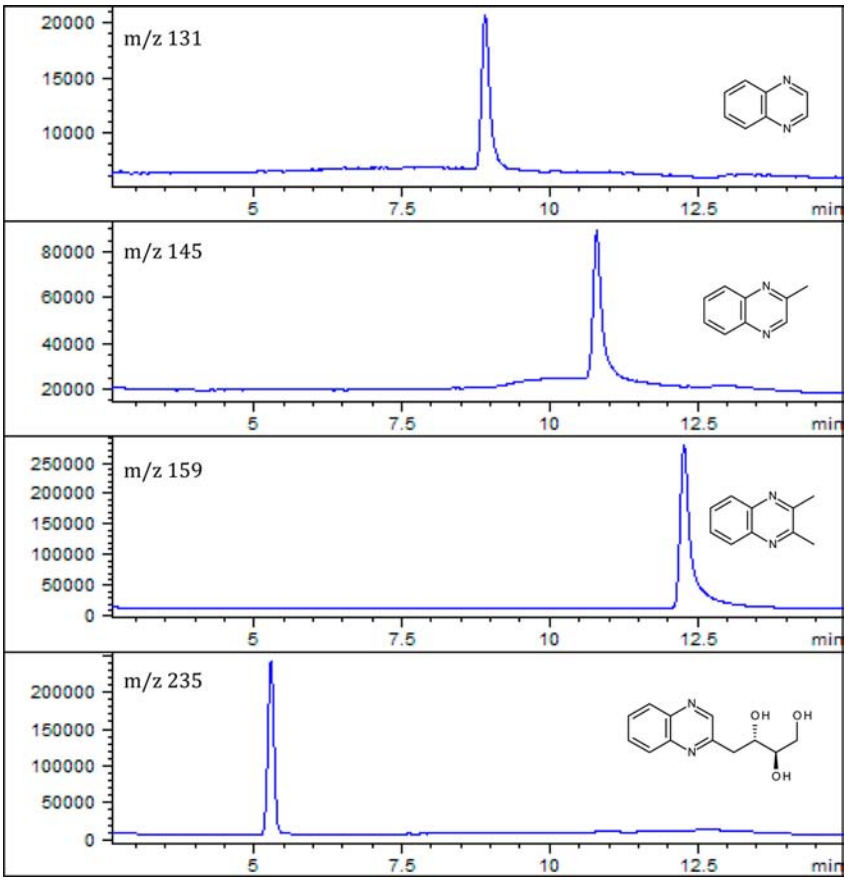

Figure 1. Extracted ion chromatograms of the quinoxaline derivatives of 1 mg/L of glyoxal (m/z 131), methylglyoxal (m/z 145), dimethylglyoxal (m/z 159), and 3-deoxyglucosone (m/z 235).

min) pH of the supernatant was measured by using a pH meter (MeterLab PHM210, France). Fruit and vegetable puree samples were centrifuged and pH of the supernatant was measured without another treatment. Pudding samples were diluted with water 1:1 ratio and the pH of the supernatant was measured after centrifugation.

Statistical Analysis. Comparison of different groups was analyzed with independent samples t test by using SPSS Statistics 21.0 program.

RESULTS AND DISCUSSION

Evaluation of the Analytical Method. In this study, an HPLC-ESI-MS method was developed and validated for the determination of α-dicarbonyl compounds in baby foods. Figure 1 illustrates the extracted ion chromatograms of the quinoxaline derivatives of glyoxal (m/z 131), methylglyoxal (m/z 145), dimethylglyoxal (m/z 159), and 3-deoxyglucosone (m/z 235). The quinoxaline derivatives of these α-dicarbonyl compounds could be successfully resolved within 15 min under the stated chromatographic conditions. There was very good linearity between the concentration and the ESI-MS signal intensity for all α-dicarbonyl compounds studied. Day-to-day reproducibility of the ESI-MS signal intensities of the ions was high with a coefficient of variation of less than 5.0%.

Figure 2 illustrates the HPLC-ESI-MS chromatogram of a baby food with corresponding extracted ion chromatograms of different α-dicarbonyl compounds. Expectedly, the quinoxaline derivative of glucosone eluted first as identified at m/z of 251. It followed by the quinoxaline derivatives 3-deoxyglucosone and 1-deoxyglucosone as both identified at m/z of 235. However, 3-deoxygalactosone, the epimer of 3-deoxyglucosone, could not be resolved in this chromatographic run. Therefore, the data given might include 3-deoxygalactosone in the concentration of 3-deoxglucosone. The ESI-MS conditions applied in this study allowed detecting low ppb levels of α-dicarbonyl compounds in baby food matrices. The LOD and LOQ values of α-dicarbonyl compounds calculated for fruit puree, vegetable puree and infant formula matrices are given in Table 2.

Percentage recoveries of 3-deoxyglucosone, glyoxal and methylglyoxal were determined by analyzing the spiked infant formula and fruit puree samples (Table 3). The mean recoveries of 3-deoxyglucosone, glyoxal and methylglyoxal were found to be 102.4%, 103.6%, and 99.5% from infant formula, and 91.2%, 101.7%, and 101.4% from fruit puree, respectively.

Profiling α-Dicarbonyl Compounds in Baby Foods. The HPLC-ESI-MS method was used to analyze α-dicarbonyl compounds in baby foods including cereal based infant formula (n = 9), jarred fruit puree (n = 11), jarred vegetable puree (n = 6), and pudding (n = 4). The concentrations of α-dicarbonyl compounds along with furfurals are given in Table 4. 3-Deoxyglucosone was the most abundant α-dicarbonyl compound in each subcategory of the samples analyzed. The highest levels of 3-deoxyglucosone were found in cereal-based infant formula with the mean concentration of 152.5 ± 2.78 mg/kg. The concentrations of other α-dicarbonyl compounds and furfurals were rather low in comparison to 3-deoxyglucosone.

Infant Formula. Differences in the total concentrations of α-dicarbonyl compounds were compared statistically between cereal-based infant formula samples from different brands, as

dx.doi.org/10.1021/jf502418n | J. Agric. Food Chem. 2014, 62, 7714−7720

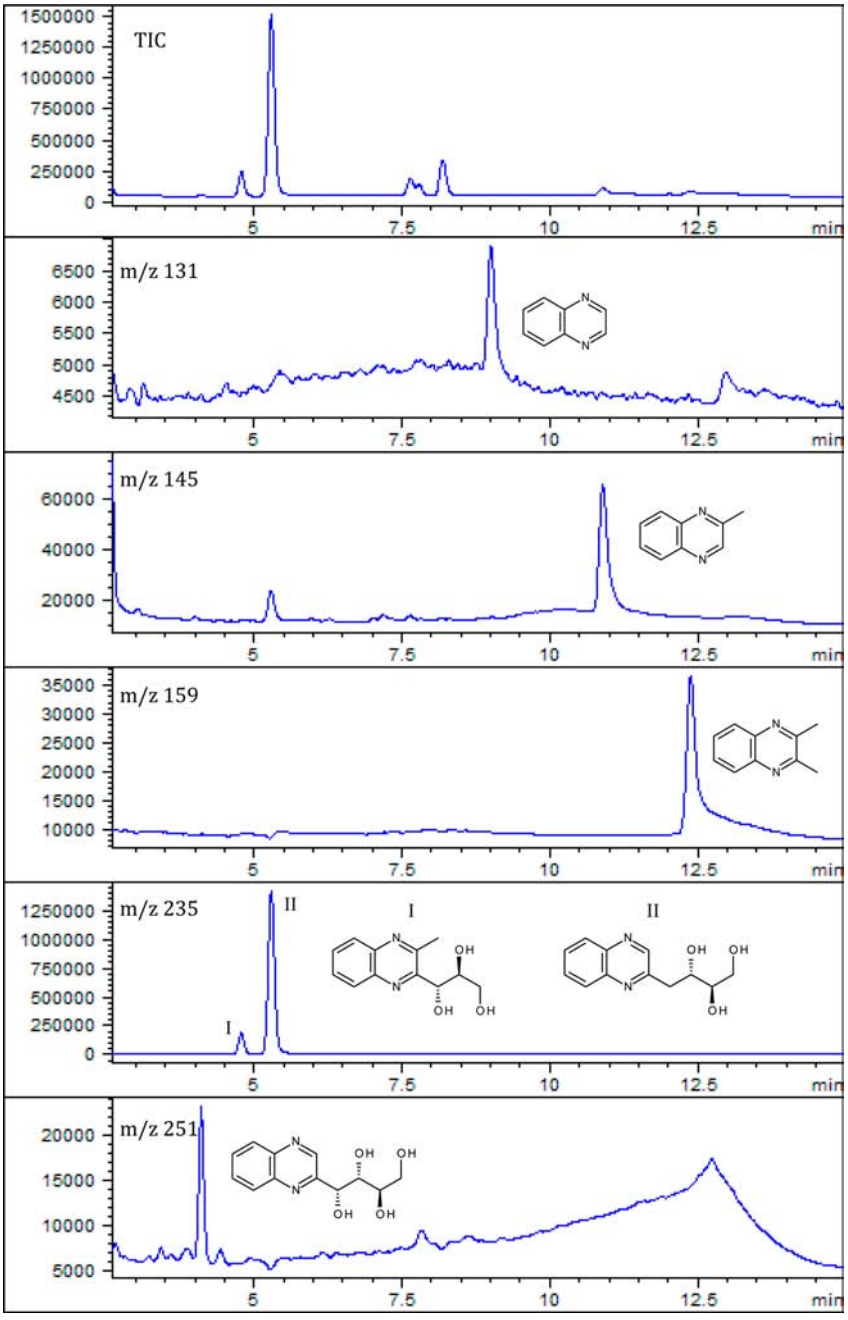

Figure 2. Total and extracted ion chromatograms of an infant formula; glyoxal (*m*/*z* 131), methylglyoxal (*m*/*z* 145), dimethylglyoxal (*m*/*z* 159), 3-deoxyglucosone and 1-deoxyglucosone (*m*/*z* 235), and glucosone (*m*/*z* 251).

Table 2. LOD and LOQ Values in μg/kg Calculated for α-Dicarbonyl Compounds in Different Baby Food Matrices

α-dicarbonyl compound	fruit puree		vegetable puree		infant formula	
	LOD	LOQ	LOD	LOQ	LOD	LOQ
3-deoxyglucosone	2.9	9.6	1.6	5.2	4.3	14.2
glucosone	2.8	9.4	4.2	14.0	10.2	34.1
glyoxal	27.1	90.3	21.8	72.7	23.5	78.4
methylglyoxal	7.5	25.0	7.3	24.4	6.0	20.1
dimethylglyoxal	2.6	8.8	2.7	9.0	2.7	9.2

well as between the samples from same brand containing different ingredients such as honey and grape molasses. There was no significant difference ($p > 0.05$) in the total α-dicarbonyl compounds in infant formulas from the same brand. However, the difference was statistically significant ($p < 0.05$) for infant formulas from different brands (Table 5). It is thought that this might be indicating differences in the thermal input of these samples during processing. Moreover, it was apparent from the results that infant formulas containing honey or grape molasses had significantly more total α-dicarbonyl compounds ($p < 0.05$). This means that sugar rich ingredients might be an important contamination source for α-dicarbonyl compounds in cereal-based infant formulas. Mechanistic studies are rather needed to control the formation of α-dicarbonyl compounds during thermal treatment, and to understand the effect of certain ingredients.

dx.doi.org/10.1021/jf502418n | J. Agric. Food Chem. 2014, 62, 7714−7720

Table 3. Percentage Recoveries with Standard Deviations (SD) of α-Dicarbonyl Compounds in an Infant Formula and a Fruit Puree Sample

α-dicarbonyl compound	spiking level (mg/kg)	recovery ± SD (%)	
		infant formula	fruit puree
3-deoxyglucosone	10	100.6 ± 2.01	95.1 ± 2.40
	20	99.6 ± 2.98	88.9 ± 3.02
	50	106.9 ± 1.07	89.6 ± 1.06
glyoxal	2	108.4 ± 4.07	104.3 ± 1.28
	5	92.6 ± 2.03	99.3 ± 0.83
	10	109.8 ± 3.36	101.4 ± 1.72
methylglyoxal	2	103.4 ± 2.04	101.6 ± 1.25
	5	96.7 ± 1.06	98.7 ± 0.93
	10	98.4 ± 0.98	103.9 ± 1.78

Lower concentrations of short chain ($<C_6$) α-dicarbonyl compounds were also detected in infant formula. Concentration of glyoxal was not reported in this study because de novo formation was observed during derivatization. This was also demonstrated by other researchers.[19,21,22] However, it should be mentioned that lower ppm levels already present in infant formula. Methylglyoxal concentrations were found between 0.4 and 17.3 mg/kg. Dimethylglyoxal concentrations were generally below LOQ except in 3 samples with a mean value of 0.2 ± 0.02 mg/kg (data not shown). Higher concentrations of glyoxal and methylglyoxal are generally found in honey, high fructose corn syrup or bread and biscuits, which are baked at higher temperatures.[18−20] Cleavage of C—C bond requires higher temperatures and it is favored in alkaline pH. However, lower pH favors sugars to dehydrate yielding mainly 3-deoxyglucosone and HMF.

Table 4. Concentration (mg/kg) of α-Dicarbonyl Compounds and Furfurals Found in Baby Foods[a]

	sugar (%)[b]	pH	concentration, mg/kg						
			glucosone	3-DG	1-DG	MG	HMF	furfural	total α-dicarbonyls
infant formulas									
1	33	6.8	3.3 ± 0.20	128.8 ± 15.85	2.2 ± 1.15	1.0 ± 0.08	3.2 ± 0.04	nd	136.7 ± 16.80
2	39	7.2	0.3 ± 0.02	82.2 ± 3.60	1.2 ± 0.69	0.7 ± 0.12	1.2 ± 0.03	nd	85.4 ± 4.39
3	43	6.9	1.1 ± 0.07	115.2 ± 16.13	1.7 ± 1.02	0.8 ± 0.05	2.7 ± 0.15	2.6 ± 0.28	119.7 ± 16.95
4	36	7.3	nd	3.9 ± 0.52	nd	2.5 ± 0.26	nd	5.9 ± 0.21	9.6 ± 1.17
5	43	7.1	0.3 ± 0.05	28.1 ± 9.78	0.2 ± 0.10	0.6 ± 0.02	1.9 ± 0.65	4.6 ± 0.15	30.3 ± 10.6
6	37	7.3	0.1 ± 0.02	6.9 ± 0.48	nd	0.4 ± 0.00	nd	nd	8.4 ± 0.49
7	28	7.0	1.3 ± 0.03	73.2 ± 1.21	9.2 ± 1.08	4.8 ± 0.03	1.9 ± 0.02	nd	90.6 ± 0.33
8	41	6.5	4.8 ± 0.08	107.2 ± 1.86	2.6 ± 0.20	2.9 ± 0.20	8.2 ± 0.02	nd	118.9 ± 2.50
9	47	6.7	4.2 ± 0.13	827.1 ± 21.94	50.6 ± 7.04	17.3 ± 0.35	19.6 ± 0.05	1.0 ± 0.08	902.7 ± 14.38
average			1.7 ± 0.01	152.5 ± 2.78	7.5 ± 1.25	3.5 ± 0.09	4.3 ± 0.1	1.6 ± 0.03	166.9 ± 4.18
fruit purees									
1	16	3.9	4.8 ± 0.24	92.3 ± 5.55	0.5 ± 0.18	nd	6.9 ± 0.03	0.7 ± 0.03	97.6 ± 5.49
2	11	3.7	1.2 ± 0.08	26.7 ± 1.53	nd	nd	2.5 ± 0.28	1.8 ± 0.14	27.9 ± 0.01
3	16	3.9	7.4 ± 0.47	68.0 ± 5.43	nd	nd	3.8 ± 0.08	0.6 ± 0.13	75.7 ± 5.89
4	15	3.4	4.5 ± 0.20	64.0 ± 0.96	0.6 ± 0.08	nd	5.2 ± 0.14	0.9 ± 0.03	69.1 ± 1.08
5	12	3.7	0.8 ± 0.05	64.1 ± 1.52	0.5 ± 0.06	nd	5.5 ± 0.04	1.4 ± 0.05	65.5 ± 0.09
6	13	3.8	4.3 ± 0.12	61.8 ± 2.85	0.5 ± 0.09	nd	6.8 ± 0.30	0.9 ± 0.03	66.5 ± 3.07
7	13	3.8	7.6 ± 1.21	50.9 ± 1.84	nd	nd	4.3 ± 0.03	0.8 ± 0.08	58.5 ± 3.15
8	15	3.8	3.5 ± 0.74	42.2 ± 0.77	nd	nd	5.2 ± 0.04	0.6 ± 0.05	45.8 ± 1.67
9	13	3.8	3.8 ± 0.68	46.4 ± 1.83	nd	nd	5.1 ± 0.02	0.8 ± 0.08	50.3 ± 1.35
10	14	3.6	4.2 ± 0.93	57.3 ± 4.02	nd	nd	5.6 ± 0.07	0.9 ± 0.05	61.9 ± 3.35
11	16	3.9	5.4 ± 1.54	65.1 ± 3.38	0.7 ± 0.14	nd	3.5 ± 0.08	2.2 ± 0.10	71.0 ± 2.07
average			4.3 ± 0.16	61.8 ± 2.85	0.4 ± 0.10	nd	4.9 ± 0.06	1.1 ± 0.01	62.7 ± 0.83
vegetable purees									
1	9	5.3	0.9 ± 0.40	31.3 ± 0.96	nd	nd	1.6 ± 0.29	1.0 ± 0.07	32.2 ± 0.55
2	9	5.3	0.2 ± 0.00	26.7 ± 0.98	nd	nd	1.6 ± 0.07	0.3 ± 0.00	26.9 ± 0.97
3	4	5.0	0.4 ± 0.02	46.8 ± 2.89	nd	1.4 ± 0.27	3.0 ± 0.07	0.3 ± 0.02	48.6 ± 2.59
4	10	4.8	0.6 ± 0.09	49.3 ± 4.88	nd	nq	4.0 ± 0.04	0.3 ± 0.01	49.9 ± 4.80
5	5	5.5	0.3 ± 0.01	9.9 ± 0.10	nd	1.3 ± 0.25	0.6 ± 0.03	0.3 ± 0.03	11.3 ± 0.60
6	9	5.1	0.4 ± 0.00	40.7 ± 2.20	nd	nq	1.6 ± 0.16	0.3 ± 0.03	41.1 ± 2.20
average			0.4 ± 0.09	34.1 ± 2.00	nd	0.4 ± 0.04	2.1 ± 0.06	0.4 ± 0.01	35.0 ± 2.0
puddings									
1	15	6.6	nd	1.9 ± 0.14	nd	nd	0.3 ± 0.01	nd	1.9 ± 0.14
2	14	4.0	0.5 ± 0.36	7.4 ± 0.18	nd	nd	0.3 ± 0.03	0.2 ± 0.01	7.9 ± 0.18
3	16	3.8	0.5 ± 0.08	11.1 ± 1.19	nd	nd	0.8 ± 0.05	0.2 ± 0.02	11.6 ± 1.04
4	21	4.1	3.2 ± 2.21	98.1 ± 3.44	0.7 ± 0.09	nd	0.8 ± 0.02	nd	102.7 ± 1.12
average			1.4 ± 0.06	29.4 ± 0.01	0.2 ± 0.03	nd	0.5 ± 0.01	0.11 ± 0.00	31.0 ± 0.06

[a]3-DG: 3-deoxyglucosone, 1-DG: 1-deoxyglucosone, MG: methylglyoxal, HMF: 5-hydroxy-2-methylfurfural, nd: not detected, and nq: not quantified. [b]According to manufacturers' declaration on the label.

Table 5. Comparison of Total α-Dicarbonyl Compounds Content of Certain Baby Food Samples According to Their Brands and Composition[a]

baby food	brand	no.	total α-dicarbonyls (mg/kg)
infant formula	brand 1	3	114.0 ± 26.13 [a]
	brand 2	3[b]	16.1 ± 12.31 [b]
	brand 1	2	111.1 ± 10.60 [a]
	brand 1 containing honey	1	131.7 ± 16.95 [a]
	brand 2	2	9.0 ± 0.83 [a]
	brand 2 containing honey	1	30.3 ± 10.06 [b]
	brand 2 containing grape molasses	1	902.7 ± 14.38 [c]
fruit puree	brand 1	5	60.9 ± 19.21 [a]
	brand 2	5	57.5 ± 9.91 [a]

[a]Different superscript letters indicate statistical significance for each comparison ($p < 0.05$). [b]Grape molasses containing sample was excluded.

Jarred Baby Foods. Impact of lower pH on sugar dehydration was more apparent in jarred fruit puree. Even they have lower sugar concentration than infant formula, remarkably high 3-deoxyglucosone was observed in jarred fruit puree samples. The concentrations of 3-deoxyglucosone were found between 26.7 and 92.3 mg/kg with a mean value of 61.8 mg/kg. Glucosone and 1-deoxyglucosone were found between 0.8 and 7.6 mg/kg and none-0.6 mg/kg, respectively. No methylglyoxal was detected in jarred fruit puree samples. There was no significant difference in the total α-dicarbonyl concentrations of two different brands of jarred fruit purees ($p > 0.05$). Jarred vegetable purees were generally found to contain lesser amounts of α-dicarbonyl compounds and furfurals (Table 4).

The results revealed that approximately 90% of the total α-dicarbonyl compounds in baby foods were composed of 3-deoxyglucosone. The average amount of dicarbonyls was estimated to be 8.3 mg per serving (50 g powder) for cereal-based infant formula. While average amounts for fruit and vegetable puree were estimated to be 7.3 and 4.3 mg per jar (125 g), respectively. Degen et al. (2012) reported the concentrations of α-dicarbonyl compounds and HMF in several foodstuffs.[18] According to their results higher quantities per serving were reported to be 8.8, 7.3, and 7.7 mg for fruit juice, bread and cookies in staple foods (excluding vinegar, beer, honey and candies, some of which could contain up to 23.5 mg/serving).

Studies about the bioavailability and intestinal absorption of α-dicarbonyl compounds are limited. However, recent studies demonstrated that certain detoxifying systems might be efficient in adults, such as glyoxalase, aldehyde reductase, and aldehyde dehydrogenase systems.[25,26] 3-Deoxyglucosone has shown to transform 3-deoxyfructose and 3-deoxy-2-keto-gluconic acid, which are less reactive and secreted in urine.[27−30] Degen et al. (2014) demonstrated that only 10−15% of the dietary 3-deoxyglucosone recovered as metabolites in urine.[26] However, the fate of the remaining is unknown. In the very low pH of the stomach, 3-deoxyglucosone is most probably dehydrated to HMF, which is another concern due to its metabolite 5-sulphoxymethyl-2-furfural. 3-Deoxyglucosone might also react with proteins and amino acids during gastrointestinal digestion. Since 3-deoxyglucosone in particular is very high in baby foods, its biological consequences should be evaluated with respect to infant gastrointestinal conditions and intestinal absorption.

In conclusion, the HPLC-ESI-MS method was successfully used for profiling α-dicarbonyl compounds in various baby foods. Use of mass spectrometry provided lower quantitation limits and precise results. The results of present study addressed the following points some of which needed to be clarified. Since baby foods contain high amount of sugars, treatments like sterilization or spray drying applied during their processing result in the formation of reactive carbonyl species in high amounts, especially 3-deoxyglucosone. In addition to processing conditions, ingredients like grape molasses and honey may be an important source of contamination. These results recommend investigating in detail the effects of processing conditions and type of ingredients on the occurrence of α-dicarbonyl compounds in baby foods.

AUTHOR INFORMATION

Corresponding Author

*Tel: +90-312-2977108; fax: +90-312-2992123; e-mail: vgokmen@hacettepe.edu.tr.

Notes

The authors declare no competing financial interest.

REFERENCES

(1) Kroh, L. W. Caramelisation in food and beverages. *Food Chem.* **1994**, *51*, 373−379.

(2) Thornalley, P. J.; Langborg, A.; Minhas, H. S. Formation of glyoxal, methylglyoxal and 3-deoxyglucosone in the glycation of proteins by glucose. *Biochem. J.* **1999**, *344*, 109−116.

(3) Singh, R.; Barden, A.; Mori, T.; Beilin, L. Advanced glycation end-products: a review. *Diabetologia* **2001**, *44*, 129−146.

(4) Abordo, E. A.; Minhas, H. S.; Thornalley, P. J. Accumulation of alpha-oxoaldehydes during oxidative stress: A role in cytotoxicity. *Biochem. Pharmacol.* **1999**, *58*, 641−648.

(5) Igaki, N.; Sakai, M.; Hata, H.; Oimomi, M.; Baba, S.; Kato, H. Effects of 3-deoxyglucosone on the Maillard reaction. *Clin. Chem.* **1990**, *36*, 631−634.

(6) Mera, K.; Takeo, K.; Izumi, M.; Maruyama, T.; Nagai, R.; Otagiri, M. Effect of reactive-aldehydes on the modification and dysfunction of human serum albumin. *J. Pharm. Sci-Us.* **2010**, *99*, 1614−1625.

(7) Linden, T.; Cohen, A.; Deppisch, R.; Kjellstrand, P.; Wieslander, A. 3,4-Dideoxyglucosone-3-ene (3,4-DGE): A cytotoxic glucose degradation product in fluids for peritoneal dialysis. *Kidney Int.* **2002**, *62*, 697−703.

(8) Amoroso, A.; Maga, G.; Daglia, M. Cytotoxicity of alpha-dicarbonyl compounds submitted to in vitro simulated digestion process. *Food Chem.* **2013**, *140*, 654−659.

(9) Daglia, M.; Amoroso, A.; Rossi, D.; Mascherpa, D.; Maga, G. Identification and quantification of alpha-dicarbonyl compounds in balsamic and traditional balsamic vinegars and their cytotoxicity against human cells. *J. Food Compos. Anal.* **2013**, *31*, 67−74.

(10) Cerny, C. The aroma side of the Maillard reaction. *Ann. N.Y. Acad. Sci.* **2008**, *1126*, 66−71.

(11) Yaylayan, V. A. Recent advances in the chemistry of Strecker degradation and Amadori rearrangement: Implications to aroma and color formation. *Food Sci. Technol. Res.* **2003**, *9*, 1−6.

(12) Gobert, J.; Glomb, M. A. Degradation of glucose: reinvestigation of reactive alpha-dicarbonyl compounds. *J. Agric. Food Chem.* **2009**, *57*, 8591−8597.

(13) Locas, C. P.; Yaylayan, V. A. Isotope labeling studies on the formation of 5-(hydroxymethyl)-2-furaldehyde (HMF) from sucrose by pyrolysis-GC/MS. *J. Agric. Food Chem.* **2008**, *56*, 6717−6723.

(14) Marceau, E.; Yaylayan, V. A. Profiling of alpha-dicarbonyl content of commercial honeys from different botanical origins:

Identification of 3,4-dideoxyglucoson-3-ene (3,4-DGE) and related compounds. *J. Agric. Food Chem.* **2009**, *57*, 10837−10844.
(15) Weenen, H. Reactive intermediates and carbohydrate fragmentation in Maillard chemistry. *Food Chem.* **1998**, *62*, 393−401.
(16) Belitz, H. D.; Grosch, W.; Schieberle, P. *Food Chemistry*, 4th ed.; Springer-Verlag: Berlin, Germany, 2009.
(17) Weigel, K. U.; Opitz, T.; Henle, T. Studies on the occurrence and formation of 1,2-dicarbonyls in honey. *Eur. Food Res. Technol.* **2004**, *218*, 147−151.
(18) Degen, J.; Hellwig, M.; Henle, T. 1,2-Dicarbonyl compounds in commonly consumed foods. *J. Agric. Food Chem.* **2012**, *60*, 7071−7079.
(19) Gensberger, S.; Mittelmaier, S.; Glomb, M. A.; Pischetsrieder, M. Identification and quantification of six major alpha-dicarbonyl process contaminants in high-fructose corn syrup. *Anal. Bioanal. Chem.* **2012**, *403*, 2923−31.
(20) Arribas-Lorenzo, G.; Morales, F. J. Analysis, distribution, and dietary exposure of glyoxal and methylglyoxal in cookies and their relationship with other heat-induced contaminants. *J. Agric. Food Chem.* **2010**, *58*, 2966−2972.
(21) Gensberger, S.; Glomb, M. A.; Pischetsrieder, M. Analysis of sugar degradation products with alpha-dicarbonyl structure in carbonated soft drinks by UHPLC-DAD-MS/MS. *J. Agric. Food Chem.* **2013**, *61*, 10238−10245.
(22) Glomb, M. A.; Tschirnich, R. Detection of alpha-dicarbonyl compounds in Maillard reaction systems and in vivo. *J. Agric. Food Chem.* **2001**, *49*, 5543−5550.
(23) Gökmen, V.; Açar, Ö. Ç.; Serpen, A.; Morales, F. J. Effect of leavening agents and sugars on the formation of hydroxymethylfurfural in cookies during baking. *Eur. Food Res. Technol.* **2008**, *226*, 1031−1037.
(24) Gökmen, V.; Şenyuva, H. Z. Improved method for the determination of hydroxymethylfurfural in baby foods using liquid chromatography-mass spectrometry. *J. Agric. Food Chem.* **2006**, *54*, 2845−2849.
(25) Degen, J.; Vogel, M.; Richter, D.; Hellwig, M.; Henle, T. Metabolic transit of dietary methylglyoxal. *J. Agric. Food Chem.* **2013**, *61*, 10253−60.
(26) Degen, J.; Beyer, H.; Heymann, B.; Hellwig, M.; Henle, T. Dietary influence on urinary excretion of 3-deoxyglucosone and its metabolite 3-deoxyfructose. *J. Agric. Food Chem.* **2014**, *62*, 2449−56.
(27) Kato, H.; van Chuyen, N.; Shinoda, T.; Sekiya, F.; Hayase, F. Metabolism of 3-deoxyglucosone, an intermediate compound in the Maillard reaction, administered orally or intravenously to rats. *Biochim. Biophys. Acta* **1990**, *1035*, 71−76.
(28) Collard, F.; Vertommen, D.; Fortpied, J.; Duester, G.; Van Schaftingen, E. Identification of 3-deoxyglucosone dehydrogenase as aldehyde dehydrogenase 1A1 (retinaldehyde dehydrogenase 1). *Biochimie* **2007**, *89*, 369−373.
(29) Kanazu, T.; Shinoda, M.; Nakayama, T.; Deyashiki, Y.; Hara, A.; Sawada, H. Aldehyde reductase is a major protein associated with 3-deoxyglucosone reductase-activity in rat, pig and human livers. *Biochem. J.* **1991**, *279*, 903−906.
(30) Vander Jagt, D. L.; Hunsaker, L. A. Methylglyoxal metabolism and diabetic complications: Roles of aldose reductase, glyoxalase-1, betaine aldehyde dehydrogenase, and 2-oxoaldehyde dehydrogenase. *Chem-Biol. Interact.* **2003**, *143*, 341−351.

The separation and determination of proanthocyanidins of sea buckthorn is problematic because they occur as highly complex mixtures. The aim of this work was to establish a method for identification of the key PA oligomers in the berries. The crude extract was fractionated by Sephadex LH-20 column chromatography, PAs of the fractions were separated according to molecular weight by NP-UPLC-ESI-SIR and HILIC-ESI-SIR, and the isomers were analyzed by RP-HPLC-ESI-SIR. Quantification of the dimers, trimers, and tetramers was carried out using a HILIC-ESI-SIR method.

MATERIALS AND METHODS

Plant Materials. Wild sea buckthorn berries (*Hippophaë rhamnoides* ssp. *rhamnoides* L.) were harvested on September 28, 2011, at Pyhämaa, southern Finland, on the coast of the Gulf of Bothnia and stored at −18 °C.

Chemicals and Reagents. Methanol, dichloromethane, and formic acid (all HPLC grade) were purchased from J. T. Baker (Deventer, Holland), acetone and acetonitrile (HPLC grade) from VWR International Oy (Espoo, Finland). Water was obtained from a Millipore system (Billerica, MA). The reference compound procyanidin B2 was purchased from from Extrasynthese (Genay, France).

Sample Preparation. Fifty grams of sea buckthorn berries were crushed and extracted three consecutive times with 200 mL of a mixture of acetone, water, and acetic acid (80:19.5:0.5, v/v) by sonicating each time for 15 min. After centrifugation and combining of the supernatants, acetone was removed by rotary evaporator. The final volume of ca. 100 mL was used for Sephadex LH-20 column chromatography (CC).

Isolation and Purification of Proanthocyanidin. A 15 mm i.d. × 250 mm glass column packed with 5 g of Sephadex LH-20 (Pharmacia, Uppsala, Sweden) was used for column chromatography. The column was activated and rinsed with 100 mL of water. The crude extract was loaded in the column and washed with 60 mL of water. Three fractions were collected with 250 mL of methanol and water (20:80, v/v, fraction I), 200 mL of acetone and water (70:30, v/v, fraction II), and 250 mL of acetone and water (70:30, v/v, fraction III) in sequence. The flow of elution was maintained at 1 mL/min by Alitea-XV peristaltic pump (Bioengineering, Wald, Switzerland). All the fractions were dried by vacuum rotary evaporator, redissolved in 1 mL of methanol, and clarified through a polytetrafluoroethylene (PTFE) filter (13 mm i.d., 0.45 μm, VWR International, West Chester, PA) before analyses.

LC-DAD-MS Apparatus. A Waters Acquity ultrahigh performance LC system (Waters Corp., Milford, MA), which consisted of a sample manager, binary solvent delivery system, and Waters 2996 PDA detector, was used. In addition, a Waters Quattro Premier tandem quadrupole mass spectrometer (Waters Corp., Milford, MA) equipped with an electrospray ionization (ESI) source was combined with the system. The chromatograph was operated using MassLynx 4.1 software.

Reversed-Phase HPLC Analyses. The crude extract and its fractions I to III were analyzed by reversed-phase HPLC-DAD to define the content of proanthocyanidins. A Phenomenex Luna RP-C18 column (5 μm, 250 × 4.60 mm, Torrance, CA) combined with a Phenomenex Prodigy guard column (5 μm, 30 × 4.60 mm, Torrance, CA) was used. The mobile phase was run as gradient elution of formic acid/water (0.5:99.5, v/v) as solvent A and acetonitrile/methanol (80:20, v/v) as solvent B at a flow rate of 1 mL/min. The gradient program of solvent B in A (v/v) was 0−5 min 10% B, 5−15 min 10−18% B, 15−25 min 18% B, 25−30 min 18−25% B, 30−35 min 25% B, 35−40 min 25−35% B, 40−45 min 35−60% B, 45−50 min with 60−10% B, and 50−55 min with 10% B.[35] The injection volume was 20 μL. The peaks were monitored at two different wavelengths, 280 nm for all the phenolic compounds and 360 nm for the flavonol glycosides. UV spectra of the compounds were recorded. A split joint was used after the UV detector, directing a flow of 0.3 mL/min to the mass spectrometer and the rest to a waste bottle.

Normal-Phase UPLC Analyses. The proanthocyanidin-rich fraction II was analyzed by normal-phase ultrahigh performance liquid chromatography (NP-UPLC). A Restek Pinnacle DB silica UPLC column (1.9 μm, 100 × 2.1 mm, Bellefonte, PA) was used for resolution of sea buckthorn proanthocyanidin clusters for mass spectrometric analysis. The analyses were carried out by a gradient elution of dichloromethane, methanol, water, and acetic acid (82:14:2:2 v/v) as solvent A and methanol, water, and acetic acid (96:2:2 v/v) as solvent B at the mobile phase flow rate of 0.4 mL/min. The gradient program of solvent B in A (v/v) was 0−15 min 0−15% B, 15−20 min 15−30% B, 20−25 min 30−80% B, 25−30 min 80−0% B, and 30−35 min with 0% B. The injection volume was 10 μL. The parameter of the UV detector was set as used in the reversed-phase HPLC analyses. The whole flow of 0.4 mL/min was led to the mass spectrometer after the UV detector.

HILIC Analyses. A Phenomenex Luna HILIC 200A column (3 μm, 150 × 3.00 mm, Torrance, CA) combined with a Phenomenex Security Guard Cartridge Kit (Torrance, CA) was used for the analysis of fraction II. Acetonitrile was used as solvent A and formic acid/water (0.5:99.5, v/v) as solvent B with gradient elution. The gradient program of solvent B in A (v/v) was 0−5 min 5−20% B, 5−10 min 20−30% B, 10−12 min 30−40% B, 12−15 min 40−65% B, 15−17 min with 65−5% B, and 17−30 min with 5% B. The injection volume was 10 μL. The total flow rate was 0.6 mL/min, and the whole flow was led to the mass spectrometer after the UV detector. The LC-UV chromatograms were recorded at 280 and 360 nm.

Mass Spectrometry. The electrospray ionization (ESI) source was operated in negative ion mode. The ESI inlet conditions were as follows: capillary voltage, 3.5 kV; cone voltage, 15 V; extractor voltage, 8 V; source temperature, 120 °C; and the desolvation temperature, 300 °C.

Both full scan and SIR functions were used. The total ion ESI-MS analysis of proanthocyanidins was carried out by scanning the ions from m/z 500 to 3000 for oligomer size screening. The total ion spectra were recorded to elucidate the PA groups with different molecular weights. A smoothing process with a window of $m/z \pm 3$ was operated in the MassLynx 4.1 software to combine the peaks of various isotope combinations of the proanthocyanidins in the spectrum. The m/z signals chosen for the selected ion recording (SIR) function were those of the most abundant deprotonated proanthocyanidin ions calculated based on the nominal masses. According to the isotope distribution, the most abundant deprotonated proanthocyanidin ions only consist of ^{12}C, ^{1}H, and ^{16}O. In the SIR model, the m/z ions which were $m/z \pm 0.5$ out of the range were discarded. Therefore, the PA molecular ions containing ^{13}C and ^{14}C were not recorded. The actual molar proportions were estimated by correcting the SIR peak areas by taking the isotopic abundances of ^{13}C, ^{14}C, ^{2}H, ^{3}H, ^{17}O, and ^{18}O into account.

Quantitative Analysis. The quantive analysis of proanthocyanidin dimers was carried out using the HILIC-ESI-SIR method and an external standard. The calibration curves were constructed by analyzing standard solutions of procyanidin B2 in methanol in the concentration range of 0.01−0.05 mg/mL by plotting the peak areas against the concentrations. The contents of proanthocyanidin dimers and trimers were calculated with the calibration curve of procyanidin B2 and correction factors.[36]

RESULTS AND DISCUSSION

Purification by Column Chromatography. For the extraction of proanthocyanidins from sea buckthorn berries, a mixture of acetone, water, and acetic acid (80:19.5:0.5, v/v) was found to serve as an optimal solvent system. A purification step was needed due to the presence of flavonols and other impurities in the extract disturbing the chromatographic and mass spectrometric analyses. Thus, the crude extract and the Sephadex fractions I−III were analyzed by RP-HPLC at 280

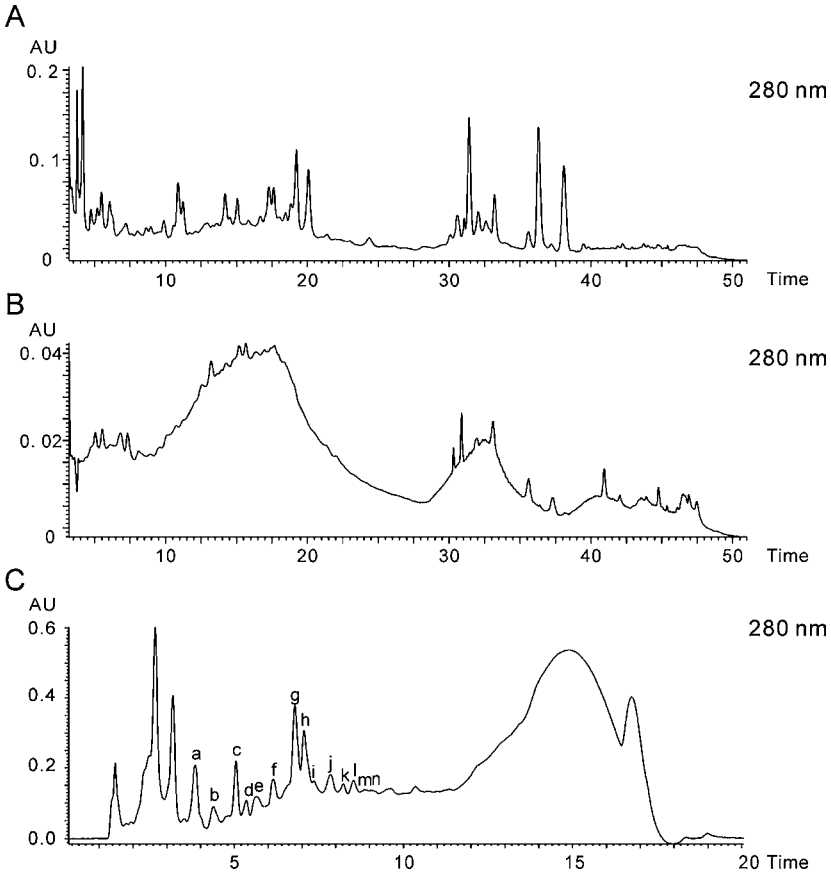

Figure 1. RP-HPLC-DAD chromatograms measured at 280 nm of (A) the crude extract of sea buckthorn berries and of (B) the Sephadex-purified fraction II. The HILIC-DAD chromatogram of (C) fraction II measured at 280 nm.

and 360 nm, and the UV spectra were obtained by DAD. Chromatograms of the crude extract and fraction II recorded at 280 nm are presented in Figures 1A and 1B. It was found that the non-tannin substances were mainly eluted in fraction I, and proanthocyanidins were recovered in fraction II. In fractions I and III hardly traces of proanthocyanidins were recognized, and fraction II was used for mass spectrometric analyses of the target compounds. The UV spectra of all the proanthocyanidins were highly similar throughout the chromatogram in Figure 1B, from 2.5 to 45 min at 280 nm. The compounds had pronounced and symmetrical maxima at around 240 and 280 nm without band broadening beyond 300 nm.

Identification of Proanthocyanidins. The PA fraction II was analyzed by RP-HPLC, NP-UPLC, and HILIC combined with DAD and electrospray ionization mass spectrometry.

Complexity of the extract and fractions of sea buckthorn resulted in unsatisfactory separation of PAs in the chromatograms recorded by both RP-HPLC-DAD and NP-UPLC-DAD at 280 nm. The peaks overlapped seriously with each other, forming only broad humps of PAs instead of proper resolution as seen in the chromatogram of RP-HPLC-DAD in Figure 1B. However, on the HILIC-DAD chromatogram recorded at 280 nm, 14 peaks eluting between 3.5 and 9 min were legible (peaks a to n, Figure 1C). The UV spectra revealed all of them to be PAs, and they were tentatively identified based on their ESI mass spectra. Each peak displayed may contain several pronthocyanidins as presented in Table 1. No legible chromatographic peaks and thus no proper spectra of individual PAs were obtained by RP-HPLC- or NP-UPLC-ESI-MS.

In addition, full scan mode of ESI-MS was applied to obtain the oligomeric profiles of fraction II. The mass spectra of HILIC and NP chromatography are shown in Figures 2A and 2B, respectively. The best results were obtained with the HILIC method, and oligomers up to 11 PA units were recorded. Dichloromethane commonly used in normal-phase methods is a harmful solvent both for LC instruments and for the sensitivity of the analysis and is recommended to be replaced by other solvents, e.g., such as used in the HILIC analyses.

Identification of Proanthocyanidins by Total Ion Spectra. Fraction II was analyzed by RP-HPLC, NP-UPLC, and HILIC coupled with electrospray ionization mass spectrometry in negative ion mode.

The total ion spectra over the whole chromatogram of the isolated fractions were recorded. Scanning from m/z 500 to 3000 in 14 min (from 3.6 to 17.6 min) in HILIC, 22 min (from 3 to 25 min) in NP-UPLC, and 37 min (from 3 to 40 min) in RP-UPLC were used to recognize the PAs in fraction II. The total ion spectra obtained from the HILIC- and NP-ESI-MS are shown in Figure 2. The low molecular weight parts of the total ion spectra were highly similar, however, the HILIC-ESI-MS was the most sensitive and revealed also the existence of higher oligomers up to DP11 (Figure 2A). This may be due to the lower water content in the HILIC solvents enhancing the ionization. The $[M - H]^-$ ions of PAs with DP from 2 to 7 and $[M - 2H]^{2-}$ ions of PAs with DP from 7 to 11 with the HILIC method are collected in Table 1.

The ions from m/z 577.52 to 1828.03, 2115.64, 2130.49 of the individual compounds as well as the corresponding full-scan spectra are the deprotonated, average molecular weight

dx.doi.org/10.1021/jf502056f | J. Agric. Food Chem. 2014, 62, 7721−7729

Table 1. Composition of Oligomeric Proanthocyanidins Estimated from the Total Ion Spectrum Obtained by HILIC-ESI-MS

		no. of subunits[b]			detected mass	
DP[a]	molecular formula	(E)C	(E)GC	exact mass	$[M-H]^-$	$[M-2H]^{2-}$
2	$C_{30}H_{26}O_{12}$	3	0	578.14	577.52	
2	$C_{30}H_{26}O_{13}$	2	1	594.14	593.52	
2	$C_{30}H_{26}O_{14}$	0	3	610.13	609.52	
3	$C_{45}H_{38}O_{18}$	3	0	866.21	865.77	
3	$C_{45}H_{38}O_{19}$	2	1	882.20	881.77	
3	$C_{45}H_{38}O_{20}$	1	2	898.20	897.77	
3	$C_{45}H_{38}O_{21}$	0	3	914.19	913.77	
4	$C_{60}H_{50}O_{24}$	4	0	1154.27	1154.97	
4	$C_{60}H_{50}O_{25}$	3	1	1170.26	1170.34	
4	$C_{60}H_{50}O_{26}$	2	2	1186.25	1186.02	
4	$C_{60}H_{50}O_{27}$	1	3	1202.25	1202.06	
4	$C_{60}H_{50}O_{28}$	0	4	1218.25	1217.88	
5	$C_{75}H_{62}O_{32}$	3	2	1474.32	1473.89	
5	$C_{75}H_{62}O_{33}$	2	3	1490.32	1490.04	
5	$C_{75}H_{62}O_{34}$	1	4	1505.31	1505.34	
5	$C_{75}H_{62}O_{35}$	0	5	1522.31	1522.16	
6	$C_{90}H_{74}O_{40}$	2	4	1794.38	1794.07	
6	$C_{90}H_{74}O_{41}$	1	5	1810.37	1811.01	
6	$C_{90}H_{74}O_{42}$	0	6	1826.37	1828.03	
7	$C_{105}H_{86}O_{45}$	4	3	2066.44		1032.84
7	$C_{105}H_{86}O_{46}$	3	4	2082.43		1041.91
7	$C_{105}H_{86}O_{47}$	2	5	2098.43		1049.18
7	$C_{105}H_{86}O_{48}$	1	6	2114.43	2115.64	1057.13
7	$C_{105}H_{86}O_{49}$	0	7	2130.42	2130.49	1065.00
8	$C_{120}H_{98}O_{50}$	6	2	2337.51		1168.25[c]
8	$C_{120}H_{98}O_{52}$	4	4	2369.49		1184.24[c]
8	$C_{120}H_{98}O_{53}$	3	5	2386.50		1193.29
8	$C_{120}H_{98}O_{54}$	2	6	2402.49		1200.24[c]
8	$C_{120}H_{98}O_{55}$	1	7	2418.49		1209.18
8	$C_{120}H_{98}O_{56}$	0	8	2434.48		1216.23[c]
9	$C_{135}H_{110}O_{56}$	7	2	2626.58		1312.95
9	$C_{135}H_{110}O_{57}$	6	3	2642.57		1319.95
9	$C_{135}H_{110}O_{58}$	5	4	2658.57		1328.61
9	$C_{135}H_{110}O_{59}$	4	5	2674.56		1336.64
9	$C_{135}H_{110}O_{60}$	3	6	2690.56		1344.59
9	$C_{135}H_{110}O_{61}$	2	7	2706.55		1353.51
9	$C_{135}H_{110}O_{62}$	1	8	2722.54		1361.31
9	$C_{135}H_{110}O_{63}$	0	9	2738.54		1369.33
10	$C_{150}H_{122}O_{64}$	6	4	2945.62		1472.31[d]
10	$C_{150}H_{122}O_{66}$	4	6	2978.62		1488.30[d]
10	$C_{150}H_{122}O_{67}$	3	7	2994.61		1496.57
10	$C_{150}H_{122}O_{68}$	2	8	3010.61		1504.30[d]
10	$C_{150}H_{122}O_{69}$	1	9	3026.60		1513.96
10	$C_{150}H_{122}O_{70}$	0	10	3042.60		1520.29[d]
11	$C_{165}H_{134}O_{75}$	2	9	3314.67		1657.09
11	$C_{165}H_{134}O_{76}$	0	11	3330.66		1665.49

[a]DP = degree of polymerization. [b](E)C = (epi)catechin, (E)GC = (epi)gallocatechin. [c]$[M-2H]^{2-}$ ions of DP8 overlapped with the $[M-H]^-$ ions of DP4. [d]$[M-2H]^{2-}$ ions of DP10 overlapped with the $[M-H]^-$ ions of DP5.

proanthocyanidins of DP from 2 to 7. All the compounds represent the B-type proanthocyanidins, dimers (MW 578.14, 594.14, and 610.13), trimers (866.20, 882.20, 898.19, and 914.19), tetramers (1154.27, 1170.26, 1186.26, 1202.25, and 1218.25), pentamers (1474.32, 1490.32, 1505.31, and 1522.31), hexamers (1793.37, 1809.37, and 1825.36), and heptamers (2114.43 and 2130.42). The molecular weights are the exact masses with all the isotope abundances taken into account.

No single-charged molecular ions of proanthocyanidins with DP higher than 7 were found. As indicated in Table 1, the ions from m/z 1032.84 to 1665.49 were the $[M-2H]^{2-}$ ions of heptamers (MW 2066.44, 2082.43, 2098.43, 2114.43, and 2129.42), octamers (2385.49 and 2417.48), nonamers (2626.58, 2642.57, 2658.57, 2674.56, 2690.56, 2706.55, 2722.54, and 2738.54), decamers (2994.61 and 3026.60), and undecamers (3314.67 and 3330.66).

No A-type oligomers with molar masses of two units lower than corresponding B-type PA were found. Tentative identification of all the proanthocyanidins is also presented in Table 1.

dx.doi.org/10.1021/jf502056f | J. Agric. Food Chem. 2014, 62, 7721−7729

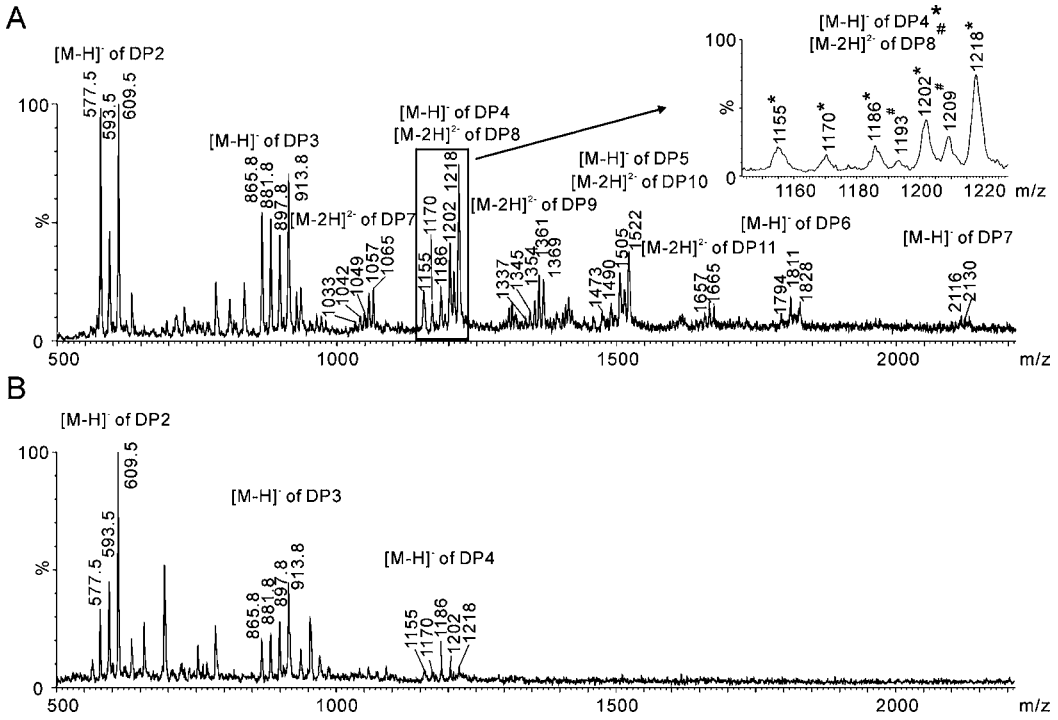

Figure 2. Total ion spectrum of fraction II (A) from 3.6 to 17.6 min analyzed by HILIC-ESI-MS and (B) from 3 to 25 min analyzed by NP-UPLC-ESI-MS. The PA signals in the spectrum are marked as deprotonated calculated molar masses where the isotope abundances have been taken into account.

Identification of Proanthocyanidins by NP-UPLC- and HILIC-ESI-MS-SIR. Because of the high complexity of the sea buckthorn extract and fractions, neither the UV analysis nor mass spectrometry in full scan mode gave results detailed enough. The molecular weights of proanthocyanidins are relatively close to each other in each group of the low-DP oligomers, and the NP-UPLC and HILIC resolutions were not sufficient for quantitative analysis. Instead, the NP-UPLC-, HILIC-, and even RP-HPLC-ESI-MS in the SIR mode provided highly selective methods for determination of proanthocyanidins in sea buckthorn, and the three methods complemented well each other.

All the 12 $[M - H]^-$ ions of the nominal mass proanthocyanidin dimers, trimers, and tetramers were scanned in 12 channels by HILIC-, NP-UPLC-, and RP-HPLC-ESI-MS-SIR analyses and are displayed in Figure 3. The HILIC and NP chromatograms showed rather systematic difference in retention times based on molecular weight within each of the three oligomer groups. The higher the MW, the longer the retention time within a group, but the rule did not apply when all peaks in the 12 molecular weight classes were taken into account. All the PA dimers, trimers, and tetramers defined earlier (Table 1) were eluted in 4 to 12 min as shown in Figure 3. Combinations of the monomeric units as well as retention times of the major peaks in each MW group from both the HILIC-ESI-MS-SIR and the NP-UPLC-ESI-MS-SIR analyses are shown in Table 2. Both methods showed relatively low chromatographic resolution in each channel, and only poorly resolved peaks were recorded. The HILIC method was more sensitive than the NP method.

Identification of Proanthocyanidins by RP-HPLC-ESI-MS-SIR. As an effective separation technique for phenolic compounds, RP-HPLC is widely used in routine analysis.[35,37] The RP-HPLC method coupled to ESI-MS-SIR was used to distinguish the major proanthocyanidin isomer groups with different monoisotopic nominal masses in the 12 channels.

Fraction II was analyzed by RP-HPLC-DAD by monitoring at 280 nm, and by RP-HPLC-ESI-MS-SIR at the 12 channels (m/z 577, 593, and 609 for proanthocyanidin dimers, m/z 865, 881, 897, and 913 for trimers, and m/z 1153, 1169, 1185, 1201, and 1217 for tetramers, respectively) as in NP-UPLC and HILIC-SIR methods. The chromatograms obtained by the RP-HPLC method are shown in Figures 3C, 3F, and 3I, and the peaks are listed in Table 2. The analysis provided sufficient separation of proanthocyanidin isomers with same molecular weights among the dimeric and trimeric PAs. Resolution was less good in the case of tetrameric isomers, and individual peaks were only occasionally visible. Unlike in NP-UPLC and HILIC chromatography the oligomers with higher MW eluted in the RP analyses on average faster than the smaller counterparts within one polymer group.

In the chromatogram of RP-HPLC-ESI-MS-SIR at m/z 577, five peaks (from 1 to 5) were found to display at least five characteristic dimeric procyanidin isomers with composition of [(E)C-(E)C]. At m/z 593 the 11 isomers (from 6 to 16) consisted of one (epi)catechin and one (epi)gallocatechin subunit. Based on the UV spectra recorded, the clear peak at 45 min was not a proanthocyanidin. The 12 peaks from 17 to 28 in the chromatogram at m/z 609 represent the dimeric prodelphinidins of two (E)GC units (Figure 3C).

Among the trimers, the peaks from 29 to 36 in the SIR chromatogram at m/z 865 revealed at least eight isomeric structures of [(E)C-(E)C-(E)C]. The m/z 881 suggested at least 12 isomers consisting of two (epi)catechin and one (epi)gallocatechin subunits, and m/z 897 also 12 compounds of one (epi)catechin and two (epi)gallocatechins. The less resolved peaks from 56 to 62 in the chromatograms at m/z 913 were the isomers of trimeric prodelphinidins (Figure 3F).

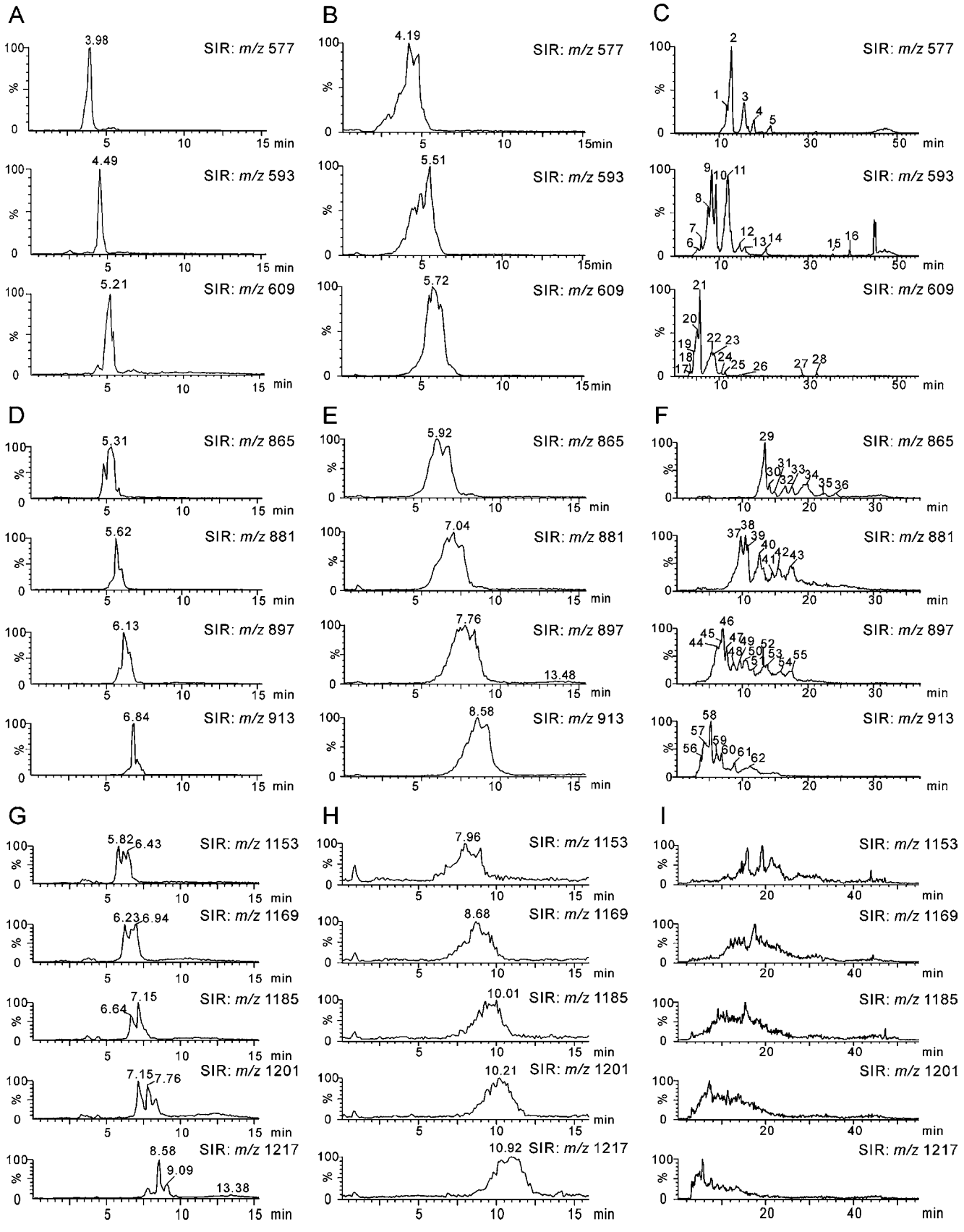

Figure 3. Selected ion recording (SIR) chromatograms of proanthocyanidins analyzed by ESI-MS in fraction II: dimers (A) HILIC, (B) NP-UPLC, and (C) RP-HPLC; trimers (D) HILIC, (E) NP-UPLC, and (F) RP-HPLC; tetramers (G) HILIC, (H) NP-UPLC, and (I) RP-HPLC.

It is clear that many of the trimeric isomers overlap in the chromatograms.

The numerous isomers of proanthocyanidin tetramers overlapped each other significantly. The ion peaks $[M - H]^-$

dx.doi.org/10.1021/jf502056f | J. Agric. Food Chem. 2014, 62, 7721−7729

Table 2. Identification and Quantification of Oligomeric Proanthocyanidins (DP ≤ 4) in Fraction II of Sea Buckthorn Berries by NP-UPLC-, RP-HPLC-, and HILIC-ESI-MS-SIR

							MS-SIR				total ion spectrum		
DP[a]	$[M-H]^-$ m/z[b]	t_{R1}[c]	t_{R2}[d]	peak[e]	peak[f]	structure assignment[g]	peak area[h]	%[i]	CF[j]	%[k]	peak area[l]	%[m]	contents (mg/100 g)
PA dimers	577	3.98	4.19	a	1−5	(E)C-(E)C	65653	23.6	1.42	20.6	22670	16.2	0.45
	593	4.49	5.51	b	6−16	(E)C-(E)GC	38037	13.7	1.43	12.0	14083	10.0	0.35
	609	5.21	5.72	c	17−28	(E)GC-(E)GC	24031	8.7	1.43	7.6	17231	12.3	0.18
PA trimers	865	5.31	5.92	d	29−36	(E)C-(E)C-(E)C	19856	7.1	1.70	7.5	11580	8.3	0.25
	881	5.62	7.04	e	37−43	(E)C-(E)C-(E)GC	20937	7.5	1.71	8.0	8609	6.1	0.27
	897	6.13	7.76	f	44−55	(E)C-(E)GC-(E)GC	26843	9.7	1.71	10.1	10866	7.7	0.35
	913	6.84	8.58	g−i	56−62	(E)GC-(E)GC-(E)GC	41191	14.8	1.72	15.6	16790	12.0	0.54
PA tetramers	1153	5.82	7.96			(E)C-(E)C-(E)C-(E)C	5853	2.1	2.04	2.6	6367	4.5	0.11
	1169	6.94	8.68			(E)C-(E)C-(E)C-(E)GC	7891	2.8	2.04	3.6	4244	3.0	0.16
	1185	7.15	10.01			(E)C-(E)C-(E)GC-(E)GC	5487	2.0	2.05	2.5	5727	4.1	0.11
	1201	7.76	10.21	j		(E)C-(E)GC-(E)GC-(E)GC	6947	2.5	2.05	3.1	7927	5.6	0.14
	1217	8.58	10.92	k−n		(E)GC-(E)GC-(E)GC-(E)GC	14998	5.4	2.06	6.8	14236	10.1	0.32

[a]DP = degree of polymerization. [b]Deprotonated nominal masses. [c]Retention times (min) in HILIC-ESI-MS-SIR shown in Figures 3A, 3D, and 3G. [d]Retention times (min) in NP-UPLC-ESI-MS-SIR shown in Figures 3B, 3E, and 3H. [e]Peaks in HILIC-DAD as shown in Figure 1C. [f]Peaks in RP-HPLC-ESI-MS-SIR shown in Figures 3C and 3F. [g]Alternative sequences possible for heterogeneous proanthocyanidins, (E)C = (epi)catechin, (E)GC = (epi)gallocatechin. [h]Peak areas in HILIC-ESI-MS-SIR shown in Figures 3A, 3D, and 3G. [i]Proportions of PA oligomer peak areas in SIR mode. [j]Correction factors for isotopic abundances. [k]Proportions of PA oligomer peak areas corrected by isotopic abundances. [l]Peak areas calculated in total ion spectrum. [m]Proportions of PA oligomer peak areas in full scan mode.

from m/z 1153 to 1217 are suggested to consist of tetrameric procyanidins, three (epi)catechin and one (epi)gallocatechin subunits, two (epi)catechin and two (epi)gallocatechin subunits, one (epi)catechin and three (epi)gallocatechin subunits, and tetrameric prodelphinidins, respectively (Figure 3I).

Quantitative Profiling of Oligomeric Proanthocyanidins. Due to the lack of reference compounds, determination of the ratios of different PA classes of sea buckthorn berries was not possible. It has to be highlighted that all three mass spectrometric methods are useful for profiling and comparisons between different samples but none of them give correct proportions. The tentative identification of PA oligomers was based on chromatographic and mass spectral data as well as on UV spectra and literature reports.[10,38] However, neither exact structural elucidation of the bonds between the monomeric units nor the steroisomerism of the B-ring and hydroxyl group at position 3 could be determined.

The HILIC-ESI-MS in full scan mode and in SIR function methods were used as the two most sensitive methods to study the quantitative profiles of proanthocyanidins in sea buckthorn. Based on MS analyses illustrated in Figures 2 and 3, it was possible to get an overview of distribution of the compounds in different oligomeric classes in wild, Nordic *Hippophaë rhamnoides* berries summarized in Table 2.

The peak areas of at least the dimeric and trimeric proanthocyanidins in the HPLC-ESI-MS-SIR chromatograms show typically close to linear molar responses regardless of the slight differences in the structures.[36] Thus, among the dimers, the compounds of two (epi)catechin subunits ($[M-H]^-$ at m/z 577) were the most abundant. Their content was close to three times that of [(E)GC-(E)GC] ($[M-H]^-$ at m/z 609) and almost twice the content of [(E)C-(E)GC] ($[M-H]^-$ at m/z 593) (Table 2). Overall, in the dimeric PAs, (epi)catechin was the main subunit.

(Epi)gallocatechins with m/z 913 formed the most abundant combination (>30%) within the trimeric PAs. The tetrameric (epi)gallocatechins with m/z 1217 comprised analogously 1/3 of the tetrameric PAs.

Information of the two HILIC methods applied gave quite consistent results despite the different calibration profiles. The bigger the molecule was, the more isotope ions were lost in the SIR model due to the MW window parameters set in the method. Thus, proportions of the peak areas of the trimeric and tetrameric PAs in the full scan mode were higher than those in the SIR analysis. Results after the isotope correction are shown in Table 2, and they are quite close to the full scan results. Both ESI-MS-SIR analysis and the total ion spectra with the HILIC method showed the molar proportion of the dimeric and trimeric PAs to approach the level of 40% of the three PA classes studied. The higher oligomers than tetramers were found in the MS analyses in low amounts, and all the compounds identified were of type-B proanthocyanidin oligomers.

Procyanidin B2 reference compound was used as an external standard for quantification of the procyanidin dimers. Their total content was 0.45 mg/100 g (Table 2). Our earlier studies showed that the efficiencies of ionization of procyanidin dimers and trimers are very similar in the ESI mode calculated on molar bases.[36] Based on this principle, we listed in Table 2 the contents of all PA oligomers with DP ≤ 4, and the contents of proanthocyanidin dimers, trimers, and tetramers were 0.98 mg/100 g, 1.41 mg/100 g, and 0.84 mg/100 g, respectively.

It is worth noticing that the proanthocyanidins of DP2 to DP4 quantified in Table 2 represent only a small part of all the PA oligomers and polymers of sea buckthorn. Figure 1C reveals that based on the UV recording at 280 nm there is a huge hump of polymeric PAs, which were not recognized in the MS analyses.

Proanthocyanidins in wild sea buckthorn of *H. r.* ssp. *rhamnoides* berries were analyzed by RP-, NP-, and hydrophilic interaction (HILIC) liquid chromatography (HILIC). HILIC provided separation mainly by PA size and provided the highest sensitivity of the methods applied. PAs with degree of polymerization from 2 to 11 were detected by HILIC-ESI-MS. More than 60 combinations of (epi)catechins and (epi)gallocatechins of proanthocyanidin dimers and trimers were found. All of them were B-type compounds, and (epi)gallocatechins were the main monomeric units. Quantification of dimeric, trimeric, and tetrameric PAs was carried out with ESI-MS-SIR by reference compound.

AUTHOR INFORMATION

Corresponding Author

*Tel: +35823336870. Fax: +35822317666. E-mail: heikki.kallio@utu.fi.

Funding

This work was financed by the China Scholarship Council (CSC), China.

Notes

The authors declare no competing financial interest.

ACKNOWLEDGMENTS

Inkeri Peltomaa and Markku Peltomaa are acknowledged for the sea buckthorn berries.

REFERENCES

(1) Sun, K.; Chen, X.; Ma, R.; Li, C.; Wang, Q.; Ge, S. Molecular phylogenetics of *Hippophae* L.(Elaeagnaceae) based on the internal transcribed spacer (ITS) sequences of nrDNA. *Plant Syst. Evol.* **2002**, *235*, 121−134.

(2) Rousi, A. The genus *Hippophae* L. A taxonomic study. *Ann. Bot. Fenn.* **1971**, *8*, 177−227.

(3) Gao, X.; Ohlander, M.; Jeppsson, N.; Bjork, L.; Trajkovski, V. Changes in antioxidant effects and their relationship to phytonutrients in fruits of sea buckthorn (*Hippophae rhamnoides* L.) during maturation. *J. Agric. Food Chem.* **2000**, *48*, 1485−1490.

(4) Ganju, L.; Padwad, Y.; Singh, R.; Karan, D.; Chanda, S.; Chopra, M. K.; Bhatnagar, P.; Kashyap, R.; Sawhney, R. C. Anti-inflammatory activity of sea buckthorn (*Hippophae rhamnoides*) leaves. *Int. Immunopharmacol.* **2005**, *5*, 1675−1684.

(5) Xing, J.; Yang, B.; Dong, Y.; Wang, B.; Wang, J.; Kallio, H. P. Effects of sea buckthorn (*Hippophaë rhamnoides* L.) seed and pulp oils on experimental models of gastric ulcer in rats. *Fitoterapia* **2002**, *73*, 644−650.

(6) Yang, B.; Kalimo, K. O.; Mattila, L. M.; Kallio, S. E.; Katajisto, J. K.; Peltola, O. J.; Kallio, H. P. Effects of dietary supplementation with sea buckthorn (*Hippophaë rhamnoides*) seed and pulp oils on atopic dermatitis. *J. Nutr. Biochem.* **1999**, *10*, 622−630.

(7) Michel, T.; Destandau, E.; Le Floch, G.; Lucchesi, M. E.; Elfakir, C. Antimicrobial, antioxidant and phytochemical investigations of sea buckthorn (*Hippophaë rhamnoides* L.) leaf, stem, root and seed. *Food Chem.* **2012**, *131*, 754−760.

(8) Suryakumar, G.; Gupta, A. Medicinal and therapeutic potential of sea buckthorn (*Hippophae rhamnoides* L.). *J. Ethnopharmacol.* **2011**, *138*, 268−278.

(9) Dhyani, D.; Maikhuri, R. K.; Dhyani, S. Seabuckthorn: an underutilized resource for the nutritional security and livelihood improvement of rural communities in Uttarakhand Himalaya. *Ecol. Food Nutr.* **2011**, *50*, 168−180.

(10) Rösch, D.; Krumbein, A.; Kroh, L. W. Antioxidant gallocatechins, dimeric and trimeric proanthocyanidins from sea buckthorn (*Hippophaë rhamnoides*) pomace. *Eur. Food Res. Technol.* **2004**, *219*, 605−613.

(11) Hosseinian, F. S.; Li, W.; Hydamaka, A. W.; Tsopmo, A.; Lowry, L.; Friel, J.; Beta, T. Proanthocyanidin profile and ORAC values of manitoba berries, chokecherries, and seabuckthorn. *J. Agric. Food Chem.* **2007**, *55*, 6970−6976.

(12) Hellström, J. K.; Törrönen, A. R.; Mattila, P. H. Proanthocyanidins in common food products of plant origin. *J. Agric. Food Chem.* **2009**, *57*, 7899−7906.

(13) Hsieh, M. C.; Shen, Y. J.; Kuo, Y. H.; Hwang, L. S. Antioxidative activity and active components of longan (*Dimocarpus longan* Lour.) flower extracts. *J. Agric. Food Chem.* **2008**, *56*, 7010−7016.

(14) Zang, X.; Shang, M.; Xu, F.; Liang, J.; Wang, X.; Mikage, M.; Cai, S. A-Type proanthocyanidins from the stems of *Ephedra sinica* (Ephedraceae) and their antimicrobial activities. *Molecules* **2013**, *18*, 5172−5189.

(15) Cheng, H.; Lin, T.; Yang, C.; Shieh, D.; Lin, C. *In vitro* anti-HSV-2 activity and mechanism of action of proanthocyanidin A-1 from *Vaccinium vitis-idaea*. *J. Sci. Food Agric.* **2005**, *85*, 10−15.

(16) Cortes, S. F.; Valadares, Y. M.; de Oliveira, A. B.; Lemos, V. S.; Barbosa, M. P.; Braga, F. C. Mechanism of endothelium-dependent vasodilation induced by a proanthocyanidin-rich fraction from *Ouratea semiserrata*. *Planta Med.* **2002**, *68*, 412−415.

(17) Manach, C.; Williamson, G.; Morand, C.; Scalbert, A.; Rémésy, C. Bioavailability and bioefficacy of polyphenols in humans. I. Review of 97 bioavailability studies. *Am. J. Clin. Nutr.* **2005**, *81*, 230−242.

(18) Holt, R. R.; Lazarus, S. A.; Sullards, M. C.; Zhu, Q. Y.; Schramm, D. D.; Hammerstone, J. F.; Fraga, C. G.; Schmitz, H. H.; Keen, C. L. Procyanidin dimer B2 [epicatechin-(4β-8)-epicatechin] in human plasma after the consumption of a flavanol-rich cocoa. *Am. J. Clin. Nutr.* **2002**, *76*, 798−804.

(19) Sano, A.; Yamakoshi, J.; Tokutake, S.; Tobe, K.; Kubota, Y.; Kikuchi, M. Procyanidin B1 is detected in human serum after intake of proanthocyanidin-rich grape seed extract. *Biosci., Biotechnol., Biochem.* **2003**, *67*, 1140−1143.

(20) Naczk, M.; Shahidi, F. Extraction and analysis of phenolics in food. *J. Chromatogr. A* **2004**, *1054*, 95−111.

(21) Callemien, D.; Collin, S. Use of RP-HPLC-ESI (−)-MS/MS to differentiate various proanthocyanidin isomers in lager beer extracts. *J. Am. Soc. Brew. Chem.* **2008**, *66*, 109−115.

(22) Karonen, M.; Loponen, J.; Ossipov, V.; Pihlaja, K. Analysis of procyanidins in pine bark with reversed-phase and normal-phase high-performance liquid chromatography-electrospray ionization mass spectrometry. *Anal. Chim. Acta* **2004**, *522*, 105−112.

(23) Gu, L.; Kelm, M.; Hammerstone, J. F.; Beecher, G.; Cunningham, D.; Vannozzi, S.; Prior, R. L. Fractionation of polymeric procyanidins from lowbush blueberry and quantification of procyanidins in selected foods with an optimized normal-phase HPLC-MS fluorescent detection method. *J. Agric. Food Chem.* **2002**, *50*, 4852−4860.

(24) Karonen, M.; Ossipov, V.; Sinkkonen, J.; Loponen, J.; Haukioja, E.; Pihlaja, K. Quantitative analysis of polymeric proanthocyanidins in birch leaves with normal-phase HPLC. *Phytochem. Anal.* **2006**, *17*, 149−156.

(25) Buszewski, B.; Noga, S. Hydrophilic interaction liquid chromatography (HILIC) -a powerful separation technique. *Anal. Bioanal. Chem.* **2012**, *402*, 231−247.

(26) Karonen, M.; Liimatainen, J.; Sinkkonen, J. Birch inner bark procyanidins can be resolved with enhanced sensitivity by hydrophilic interaction HPLC-MS. *J. Sep. Sci.* **2011**, *34*, 3158−3165.

(27) Kelm, M. A.; Johnson, J. C.; Robbins, R. J.; Hammerstone, J. F.; Schmitz, H. H. High-performance liquid chromatography separation and purification of cacao (*Theobroma cacao* L.) procyanidins according to degree of polymerization using a diol stationary phase. *J. Agric. Food Chem.* **2006**, *54*, 1571−1576.

(28) Yanagida, A.; Murao, H.; Ohnishi-Kameyama, M.; Yamakawa, Y.; Shoji, A.; Tagashira, M.; Kanda, T.; Shindo, H.; Shibusawa, Y. Retention behavior of oligomeric proanthocyanidins in hydrophilic interaction chromatography. *J. Chromatogr. A* **2007**, *1143*, 153−161.

(29) Kalili, K. M.; de Villiers, A. Off-line comprehensive 2-dimensional hydrophilic interaction × reversed phase liquid

chromatography analysis of procyanidins. *J. Chromatogr. A* **2009**, *1216*, 6274−6284.
(30) Montero, L.; Herrero, M.; Prodanov, M.; Ibáñez, E.; Cifuentes, A. Characterization of grape seed procyanidins by comprehensive two-dimensional hydrophilic interaction × reversed phase liquid chromatography coupled to diode array detection and tandem mass spectrometry. *Anal. Bioanal. Chem.* **2012**, *405*, 4627−4638.
(31) Montero, L.; Herrero, M.; Ibáñez, E.; Cifuentes, A. Profiling of phenolic compounds from different apple varieties using comprehensive two-dimensional liquid chromatography. *J. Chromatogr. A* **2013**, *1313*, 275−283.
(32) Engström, M. T.; Pälijärvi, M.; Fryganas, C.; Grabber, J. H.; Mueller-Harvey, I.; Salminen, J. Rapid qualitative and quantitative analysis of proanthocyanidin oligomers and polymers by UPLC-MS/MS. *J. Agric. Food Chem.* **2014**, *62*, 3390−3399.
(33) Luo, X.; Chen, B.; Ding, L.; Tang, F.; Yao, S. HPLC-ESI-MS analysis of Vitamin B 12 in food products and in multivitamins-multimineral tablets. *Anal. Chim. Acta* **2006**, *562*, 185−189.
(34) Mondy, N.; Duplat, D.; Christides, J.; Arnault, I.; Auger, J. Aroma analysis of fresh and preserved onions and leek by dual solid-phase microextraction-liquid extraction and gas chromatography-mass spectrometry. *J. Chromatogr. A* **2002**, *963*, 89−93.
(35) Liu, P.; Yang, B.; Kallio, H. Characterization of phenolic compounds in Chinese hawthorn (*Crataegus pinnatifida* Bge. var. *major*) fruit by high performance liquid chromatography-electrospray ionization mass spectrometry. *Food Chem.* **2010**, *121*, 1188−1197.
(36) Liu, P.; Kallio, H.; Lü, D.; Zhou, C.; Yang, B. Quantitative analysis of phenolic compounds in Chinese hawthorn (*Crataegus* spp.) fruits by high performance liquid chromatography-electrospray ionisation mass spectrometry. *Food Chem.* **2011**, *127*, 1370−1377.
(37) Fan, J.; Ding, X.; Gu, W. Radical-scavenging proanthocyanidins from sea buckthorn seed. *Food Chem.* **2007**, *102*, 168−177.
(38) Rösch, D.; Mugge, C.; Fogliano, V.; Kroh, L. W. Antioxidant oligomeric proanthocyanidins from sea buckthorn (*Hippophae rhamnoides*) Pomace. *J. Agric. Food Chem.* **2004**, *52*, 6712−6718.

behavior was greatly altered, influencing both PAC degree of polymerization (DP) and ratios of "A-type" to "B-type" interflavan bonds. The research reported here shows how matrix-assisted laser desorption/ionization time-of-flight mass spectrometry (MALDI-TOF MS) can be used to characterize PAC fractions that differ as a result of prior SFE extraction.

In the present research, we investigated how PAC fractions with and without prior SFE affect ExPEC agglutination and enterocyte cell invasion, which is relevant for urinary tract health because PAC are not absorbed in the gastrointestinal tract. The implication is that if bacteria are agglutinated, their surface virulence factors, such as P fimbriae, will not be available to interact with ligands on gut epithelial cells, thus reducing their invasivity. For the first time, we have unraveled how the structural heterogeneity of PAC, namely, DP and ratios of "A-type" to "B-type" interflavan bonds, can influence PAC bioactivity in relation to UTI.

MATERIALS AND METHODS

Chemicals and Reagents. Ethanol (200 proof) was obtained from Decon Laboratories Inc. (King of Prussia, PA, USA). The reagent 4-(dimethylamino)cinnamaldehyde (DMAC) was purchased from Acros Organics (Geel, Belgium). Sterilized water, thiamin hydrochloride, 2,5-dihydroxybenzoic acid, and Triton 100X were purchased from Sigma-Aldrich (St. Louis, MO, USA). Sephadex LH-20 was purchased from GE Healthcare (Uppsala, Sweden). Tryptose and dextrose were obtained from BD (Sparks, MD, USA). Fetal bovine serum (FBS) was purchased from Atlanta Biologicals (Lawrenceville, GA, USA). Cellgro's Dulbecco's phosphate-buffered saline (PBS) with calcium and magnesium was from Mediatech, Inc. (Manassas, VA, USA). HyClone Dulbecco's PBS without calcium and magnesium and Hyclone Roswell Park Memorial Institute medium (RPMI-1640) were obtained from Thermo Scientific (South Logan, UT, USA). Caco-2 cells ATCC HTB-37 were obtained from ATCC (Manassas, VA, USA). All other chemicals were from Fisher Scientific (Fair Lawn, NJ, USA).

Samples. Cranberry fruits (*V. macrocarpon* Ait. cv. 'Stevens') were obtained from the United Cranberry Growers Cooperative (Wausau, WI, USA). The fruits were homogenized to a fine powder by blending with liquid nitrogen, followed by freeze-drying. The fruit powder was stored at −80 °C until extraction.

Isolation of Proanthocyanidins. *Isolation of Cranberry Proanthocyanidins with No Prior Supercritical Fluid Extraction (CE_{NSFE}).* The PAC extraction procedure was adapted from our previous work.[23] Cranberries were blended with liquid nitrogen and freeze-dried as powder. Cranberry powder (100 g) was extracted with 70% aqueous acetone (400 mL) in an ultrasonic bath for 15 min. The extract was centrifuged at 400*g* at 15 °C for 10 min, and the supernatant was collected. The extraction was repeated two additional times, and the supernatants were combined. After filtration with cellulose paper, acetone was removed by rotary evaporation under vacuum at 35 °C, and the remaining suspension was solubilized in ethanol. The extract was then centrifuged at 13416*g* at 0 °C for 10 min to eliminate insoluble material. The cranberry extract supernatant (CE_{NSFE}) was used to isolate PAC by chromatography on Sephadex LH-20 as described below (Figure 1).

Isolation of Cranberry Proanthocyanidins with Prior Supercritical Fluid Extraction (CE_{SFE}). SFE of freeze-dried cranberry powder was performed on a pilot scale SFE (DynaSep, Newark, DE, USA) composed of a 2 L extraction vessel and twin separators 1 and 2 (1 L each). One hundred and fifty grams of cranberry powder was loaded into the extraction vessel, and the remaining volume was displaced with glass marbles. Extraction temperature (40 °C) and pressure (65.5 MPa) were maintained constant. The pressure and temperature of separators 1 and 2 were set at 9.7 MPa and 40 °C and 5.5 MPa and 20 °C, respectively. The supercritical CO_2 fluid flow rate was maintained at 125 g/min with a solvent to feed ratio (w/w) of 80 during dynamic extraction (cycle 1). After collection of the extracts on separators 1 and 2, ethanol modifier (30%, w/w based on the starting material initial weight) was added to the residue in the extractor at the bottom with an air-driven pump at the start of extraction with no soak time at 62.1 MPa and 40 °C (cycle 2). The extracts on both separators were collected. Residual defatted material was extracted with 70% aqueous acetone, as described for CE_{NSFE}, and the cranberry extract supernatant (CE_{SFE}) was used to isolate PAC by chromatography on Sephadex LH-20 as described below (Figure 1).

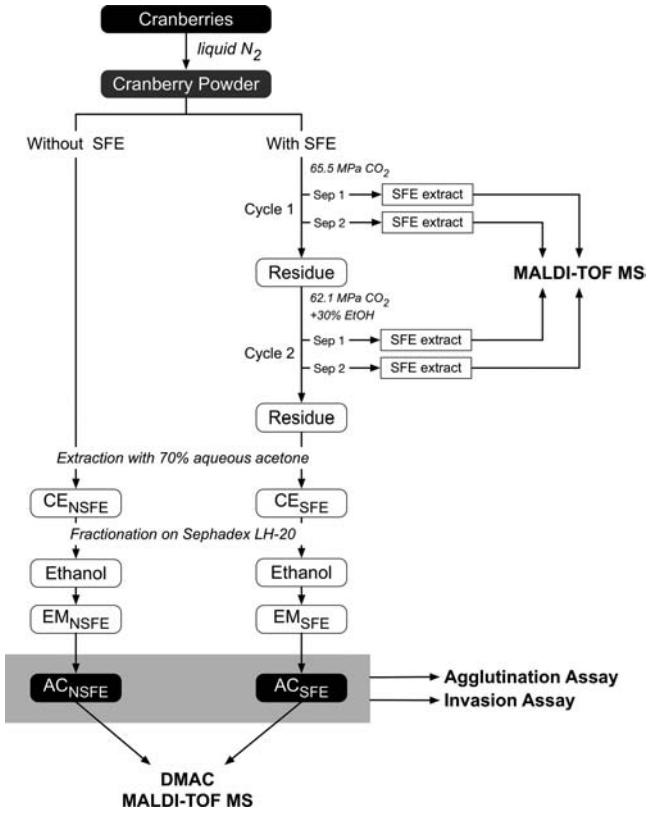

Figure 1. Flow diagram illustrating the isolation of proanthocyanidins from cranberries with and without prior supercritical fluid extraction (SFE). "CE" stands for cranberry extract; "EM" and "AC" correspond to ethanol/methanol (1:1) and 80% acetone fractions from Sephadex LH-20, respectively. Each of these abbreviations is followed by the respective treatment in subscript, either with prior SFE ($_{SFE}$) or with no prior SFE ($_{NSFE}$).

Proanthocyanidin Isolation. Both CE_{NSFE} and CE_{SFE} were loaded on different glass columns (2.5 cm i.d. × 60 cm length; Kontes, Chromaflex) packed with Sephadex LH-20 that was previously swollen and washed in water and equilibrated with ethanol for 45 min at a flow rate of 4 mL/min as previously described.[3] The columns were eluted with ethanol, followed by ethanol/methanol (1:1) and 80% aqueous acetone. The ethanol/methanol (1:1) fractions with no prior SFE (EM_{NSFE}) and with prior SFE (EM_{SFE}) and the 80% aqueous acetone fractions with no prior SFE (AC_{NSFE}) and with prior SFE (AC_{SFE}) were characterized by MALDI-TOF MS (Figure 1).

Characterization of Supercritical Fluid Extraction Fractions. Fractions collected after SFE with CO_2 (cycle 1) and CO_2 and ethanol (cycle 2) in separators 1 and 2 were evaporated to dryness and solubilized in 2 mL of chloroform/methanol (2:1) and isopropanol/acetonitrile (3:2) for cycles 1 and 2, respectively. Half a microliter of these extracts was mixed with 1 μL of 2,5-dihydroxybenzoic acid (50.0 mg/mL in ethanol) and analyzed by MALDI-TOF MS, and spectra were collected as described below (Figure 1).

Characterization of Proanthocyanidin Fractions. An understanding of the natural abundance of C, H, and O isotopes allowed us to develop a method to determine the ratios of "A-type" to "B-type" interflavan bonds in cranberry PAC. On the basis of theoretical relative

dx.doi.org/10.1021/jf502296b | J. Agric. Food Chem. 2014, 62, 7730−7737

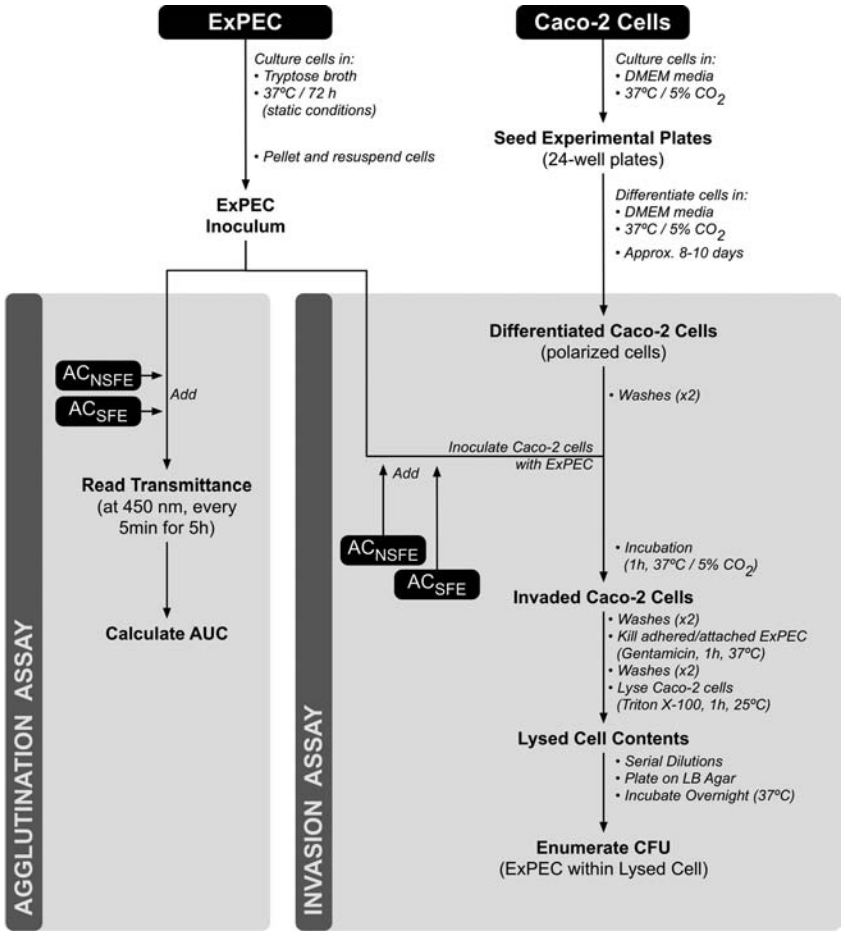

Figure 2. Flow diagram illustrating the methodological approach to evaluating bioactivity of cranberry proanthocyanidins 80% acetone fractions isolated with (AC_{SFE}) and without (AC_{NSFE}) prior supercritical fluid extraction on agglutination and invasion assays.

intensities of each PAC and absolute intensities detected in MALDI-TOF MS per DP, we used matrix algebra to calculate the ratios of each type of interflavan bond per DP as previously described.[24] Deconvolution of MALDI-TOF MS spectra was applied to determine the percentage of "A-type" interflavan bonds in cranberry PAC fractions with and without prior SFE (EM_{NSFE}, EM_{SFE}, AC_{NSFE}, and AC_{SFE}). An aliquot of each fraction was evaporated to dryness and suspended in 20 μL of ethanol to a final concentration of approximately 17 ppm of purified PAC, as quantified by the DMAC method, as previously published by our group. Two hundred and ten microliters of 0.1% DMAC (w/v) was added to 70 μL of standards and samples, and the maximum absorbance at 640 nm detected over 1 h was used to calculate PAC concentration.[23] An aliquot (0.5 μL) of each fraction was then mixed with 1 μL of 2,5-dihydroxybenzoic acid (50.0 mg/mL in ethanol) in three different wells on the stainless steel MALDI target (Figure 1). Mass spectra were collected on a Bruker ULTRAFLEX-III MALDI TOF/TOF mass spectrometer (Billerica, MA, USA). Analyses were performed in positive reflectron mode. Spectra were the sum of different locations in each well, accumulating a total of 500 shots to minimize intrawell variability, and deflection was set at 550 Da. The deconvolution method, which is based on the relative intensity of PAC isotope patterns[24] obtained in reflectron mode, was used to calculate the percentage of "A-type" bonds in PAC oligomers with a DP of 3−8.

Bacterial and Gut Epithelial Cell (Enterocyte) Cultures. The strain of ExPEC (strain 5011) used in this study was isolated from a woman with recurrent UTI at the University of Wisconsin Hospital and Clinics. The selected strain was found in both the gastrointestinal and urinary tracts and expresses fimH and papA, the adhesins of type 1 and P fimbriae, respectively. Type 1 fimbriae play an important role in early attachment of ExPEC to uroepithelial cells in the lower genitourinary tract, whereas P fimbriae bind to kidney cells in the upper genitourinary tract via digalactoside receptors.[25] Furthermore, P fimbriae expression is an important virulence factor for ExPEC colonization of the gut[26] and is critical for attachment of *E. coli* to epithelial cells in the urinary tract, colon, and ileum.[27,28] Strain 5011 was cultured under static conditions in tryptose broth at 37 °C, and the concentration of the inoculum was adjusted on the basis of the optical density at 450 nm as previously reported.[3] Caco-2 cells were cultured in Dulbecco's modification of Eagle's medium (DMEM) supplemented with 10% FBS (v/v), 1% L-alanyl-L-glutamine (v/v), 1% penicillin/streptomycin (v/v), and 1% nonessential amino acids (v/v) at 37 °C with 5% CO_2 atmosphere. Cells were allowed to differentiate for 8−10 days after reaching confluency, with medium changes every 2−3 days[3] (Figure 2).

Bacterial Agglutination Assay. ExPEC stock solutions (50 μL) were added to microcuvettes to provide a final ExPEC concentration of 5×10^8 colony-forming units (CFU)/mL. PAC fractions AC_{NSFE} and AC_{SFE} were added at 0, 6, 12, 29, 58, and 116 ppm of purified PAC (final concentration). PBS containing calcium and magnesium was added to bring the final reaction volume to 1.0 mL.[3] Transmittances at 450 nm were read every 5 min for 5 h on a Beckman DU 640 spectrophotometer (Schaumburg, IL, USA). The area under the transmittance curve (AUC) was calculated for each concentration as a function of each PAC fraction to agglutinate ExPEC strain 5011 over the length of the assay (Figure 2).

Invasion Assay. The invasion assay was based on our previously published method.[3] Bacteria were added to 5 mL tubes to reach a multiplicity of infection of 100 (8.0×10^7 bacterial CFU and 8.0×10^5 Caco-2 cells per well). PBS containing calcium and magnesium and PAC treatments (0, 6, 12, 29, 58, and 116 ppm of purified PAC) were added to a total volume of 75 μL, gently mixed, and incubated for 10

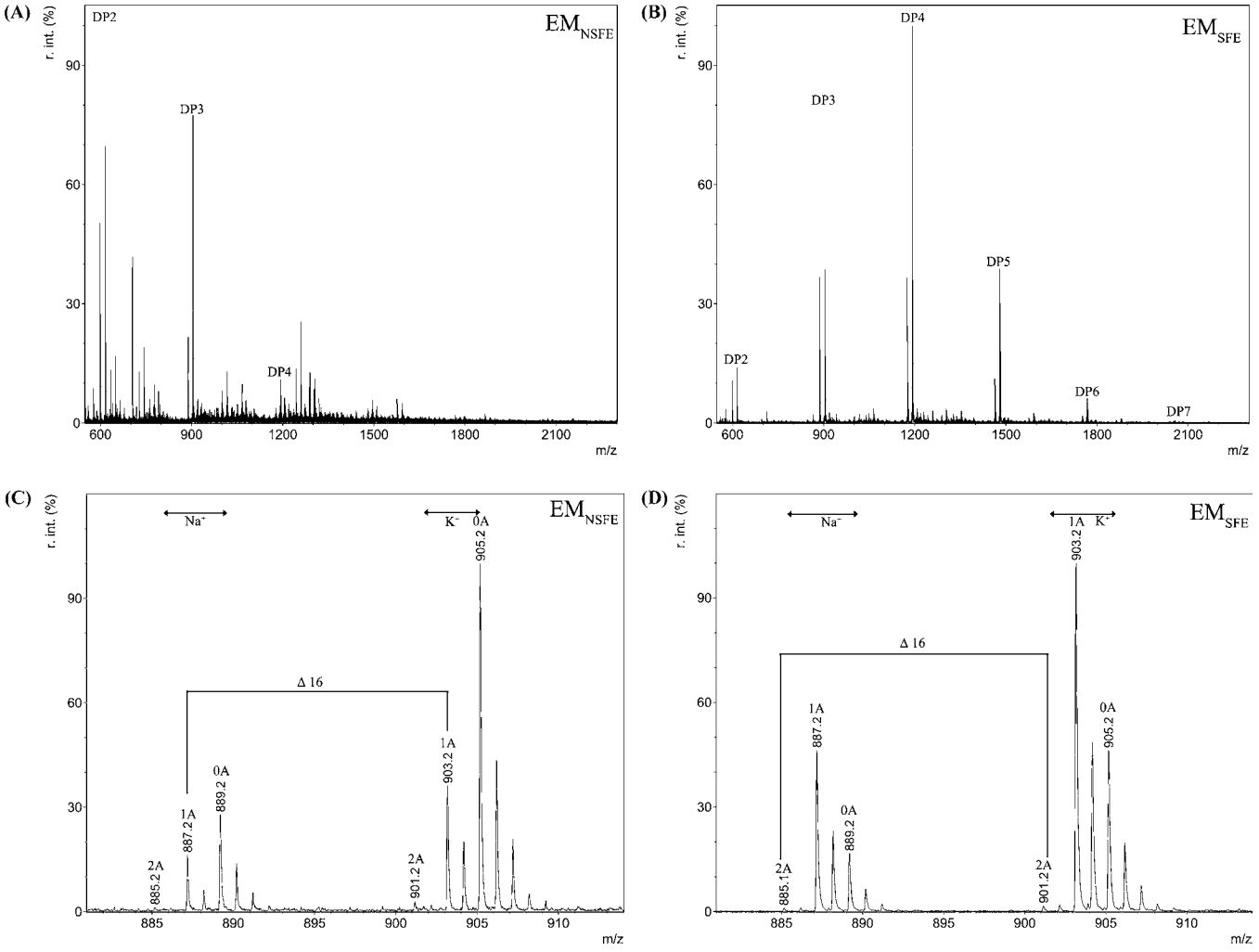

Figure 3. Mass spectra obtained with MALDI-TOF MS in positive reflectron mode for (A) EM_{NSFE}, (B) EM_{SFE}, and (C) EM_{NSFE} and (D) EMsfe fractions, displaying proanthocyanidin (PAC) trimers interflavan bonds. "r.int." and "DP" correspond to relative intensity and degree of polymerization, respectively.

min, followed by addition of 2.425 mL of RPMI medium supplemented with 5% FBS (v/v). After 1 h of bacterial invasion, cells were washed twice with PBS containing calcium and magnesium. Extracellular bacteria were killed by incubating the cells with gentamicin (100 μg/mL) at 37 °C for 1 h. Caco-2 cells were washed twice with PBS without calcium and magnesium and lysed with 1 mL/well Triton for 30 min. Dilutions of well contents were plated (100 μL) in duplicate on LB plates to enumerate the CFU of ExPEC that invaded Caco-2 cells[3] (Figure 2).

Data and Statistical Analysis. All data are reported as the mean ± standard deviation of at least three replicates. mMass version 3.9.0[29] was used for mass spectra analysis, and SAS was used for AUC calculation using the trapezoidal method (version 9.3; SAS Institute Inc., Cary, NC, USA). Statistical analysis was done using JMP Pro (version 10.0.0; SAS Institute Inc.), setting α = 0.05. Results were analyzed with two-way ANOVA models with interaction between the independent variables "treatment" and "concentration" to assess significant differences. The dependent variables were AUC and $\arcsin[\sqrt{(\%\ \text{invasion}/100)}]$ for the agglutination and invasion assays, respectively. ANOVA post hoc analysis was performed using the *t* test.

RESULTS

Effect of Supercritical Fluid Extraction on Proanthocyanidins Elution Profile on Sephadex LH-20. Cranberry PAC were not detected in SFE fractions from cycles 1 and 2 when analyzed by MALDI-TOF MS (data not shown). The remaining fruit residue was submitted to extraction and Sephadex LH-20 chromatography to isolate PAC.[23] PAC with DP between 2 and 4 could be detected in the EM_{NSFE} fraction (Figure 3A), whereas in the EM_{SFE} fraction, PAC up to DP = 7 were detected (Figure 3B). Pretreatment with SFE affected the distribution of PAC interflavan bonds within a specific DP. For instance, in EM_{NSFE}, in PAC trimers, the distribution was 2.3% of two "A-type", 32.5% of one "A-type", and 65.2% of zero "A-type" (Figure 3C). In EM_{SFE}, the distribution for trimers was 1.5% of two "A-type", 81.3% of one "A-type", and 17.2% of zero "A-type" (Figure 3D). Therefore, more PAC with one "A-type" interflavan bonds were eluted from the Sephadex LH-20 column with ethanol/methanol when the cranberries had been previously treated with SFE.

In AC_{NSFE}, PAC had a DP between 3 and 12 as detected with MALDI-TOF MS in reflectron mode (Figure 4A). In AC_{SFE}, the same DP range was detected but the distribution was skewed toward PAC with higher DP as shown in the MALDI-TOF MS spectra (Figure 4B).

The deconvolution method[24] was applied only to PAC with DP between 3 and 8 because the signal-to-noise ratio was <3.0 for oligomers with a higher DP (Table 1). PAC do not ionize as $[M]^+$ but attach to sodium and potassium ions, forming alkali metal adducts,[30] which creates PAC peaks that differ by 16

dx.doi.org/10.1021/jf502296b | J. Agric. Food Chem. 2014, 62, 7730−7737

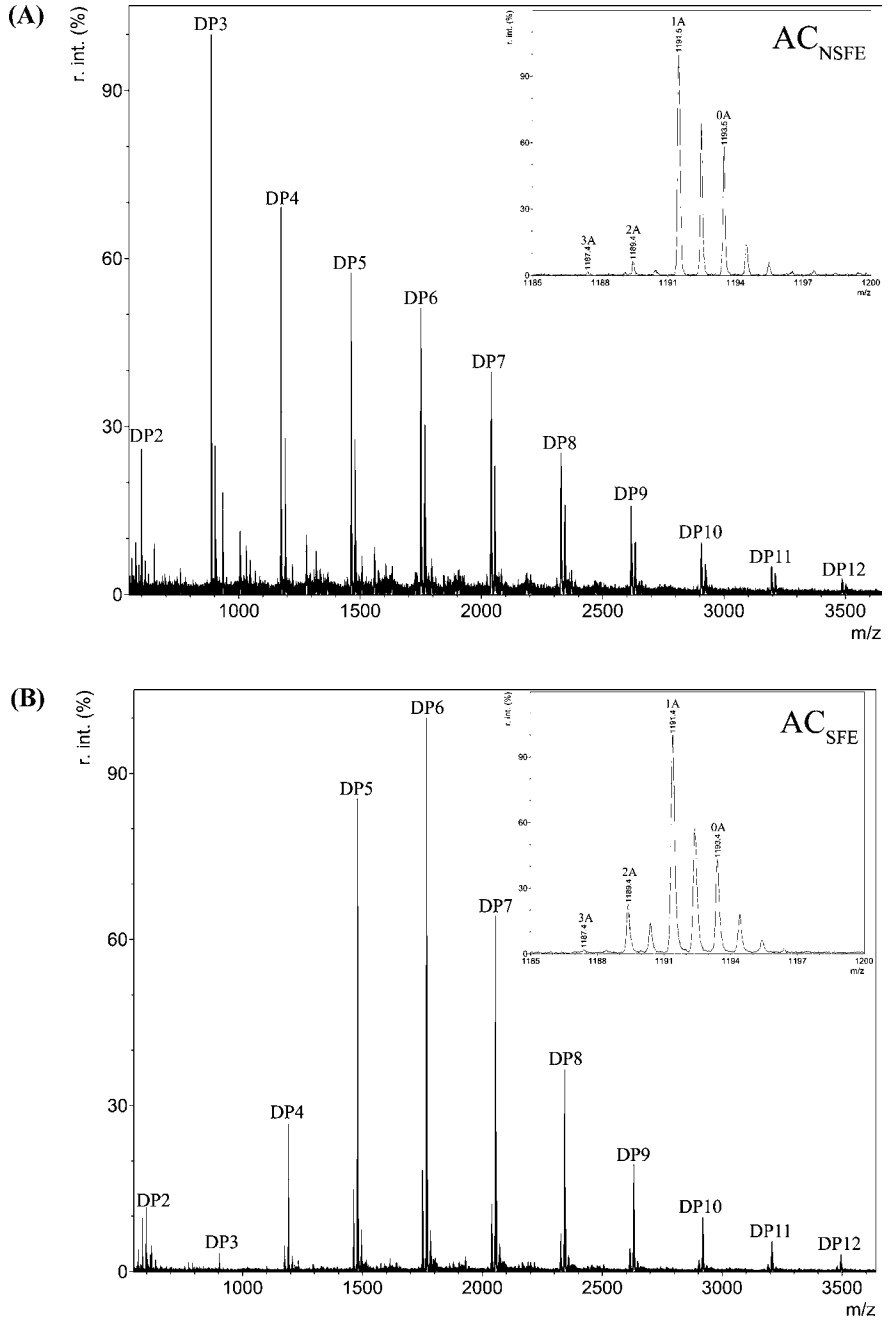

Figure 4. Mass spectra obtained with MALDI-TOF MS in positive reflectron mode for the (A) AC_{NSFE} and (B) AC_{SFE} fractions. "r.int." and "DP" correspond to relative intensity and degree of polymerization, respectively. (Inset) Enlarged spectrum to assist with visualizing the isotopic distribution of potassium adducts of proanthocyanidin (PAC) tetramers.

mass units (Figure 3C,D). Both adducts were analyzed by the deconvolution method. PAC with at least one "A-type" interflavan bond had similar amounts in AC_{NSFE} (median = 92.9%) and AC_{SFE} fractions (median = 92.7%). However, the spectra showed differences in the percentages of two and three "A-type" interflavan bonds: the percentage of PAC with two or three "A-type" bonds was higher in AC_{SFE} for oligomers with a DP between 3 and 7 (Table 1). For instance, AC_{SFE} showed a higher abundance of PAC tetramers with two "A-type" interflavan bonds compared to AC_{NSFE} (insets in Figure 4).

The median percentage of PAC across all DP with two or three "A-type" bonds was 26.1% for AC_{NSFE} and 33.7% for AC_{SFE}. When these percentages were compared per each DP, PAC with two or three "A-type" interflavan bonds were 2-, 4-, and 14-fold higher in AC_{SFE} than in AC_{NSFE} for pentamers, tetramers, and trimers, respectively.

Bacterial Agglutination Assay. The agglutination assay showed clear dose−response curves, which were normalized to time zero of the experiment as previously reported.[3] Results show that both AC_{NSFE} and AC_{SFE} fractions significantly increased agglutination, when compared to control (p value < 0.0001). As PAC concentration increased, transmittance increased, which demonstrated that more bacteria have agglutinated and precipitated. The AUC is an indicator of the ability of different PAC to agglutinate ExPEC; higher AUC corresponds to a higher agglutination.[3] AC_{SFE} had a

dx.doi.org/10.1021/jf502296b | J. Agric. Food Chem. 2014, 62, 7730−7737

Table 1. Percentage of Proanthocyanidins (PAC) with 1, 2, and 3 "A-Type" Interflavan Bonds per Degree of Polymerization (DP) in Cranberry 80% Acetone Fractions without (AC_{NSFE}) and with Prior (AC_{SFE}) Supercritical Fluid Extraction[a]

	PAC with one "A-type" interflavan bond		PAC with two or three "A-type" interflavan bonds	
DP	AC_{NSFE}	AC_{SFE}	AC_{NSFE}	AC_{SFE}
3	91.9 ± 2.7	70.3 ± 5.1	1.7 ± 0.7	19.7 ± 3.9
4	82.6 ± 3.2	72.3 ± 4.6	5.4 ± 0.7	19.9 ± 3.1
5	77.1 ± 4.3	68.8 ± 4.1	13.1 ± 3.3	23.2 ± 2.8
6	56.5 ± 5.2	49.3 ± 3.8	39.0 ± 3.5	44.1 ± 1.2
7	47.9 ± 2.5	40.5 ± 3.6	51.7 ± 1.9	56.3 ± 3.6
8	37.4 ± 4.6	38.9 ± 3.0	60.1 ± 0.6	59.5 ± 1.8
median	66.8	59.0	26.1	33.7

[a]The results are expressed as the average of three independent wells ± standard deviation on the MALDI-TOF MS plate.

significantly greater effect on ExPEC agglutination than AC_{NSFE} (p value = 0.0055). ExPEC agglutination was 137, 40, 3, 9, and 9% higher for 6, 12, 29, 58, and 116 ppm of purified PAC, respectively, when AC_{SFE} was compared with AC_{NSFE} (Figure 5A).

Invasion Assay. The Caco-2 invasion assay showed dose–response curves with a statistically significant effect of the concentration (p value < 0.0001) and prior SFE (p value = 0.0017). Our results show that cranberry PAC from AC_{SFE} were more effective in inhibiting ExPEC invasion of enterocytes than AC_{NSFE} (Figure 5B). ExPEC invasion was lower by 19, 20, 13, 11, and 6% at 6, 12, 29, 58, and 116 ppm of PAC, respectively, when AC_{SFE} was compared with AC_{NSFE}. The greater inhibition of enterocyte invasion by PAC from AC_{SFE} was statistically significant for all concentrations except for 116 ppm. The higher inhibition was more pronounced for lower PAC concentrations as the p values for 6, 12, 29, and 58 ppm of PAC were 0.0017, 0.0024, 0.0151, and 0.0262, respectively.

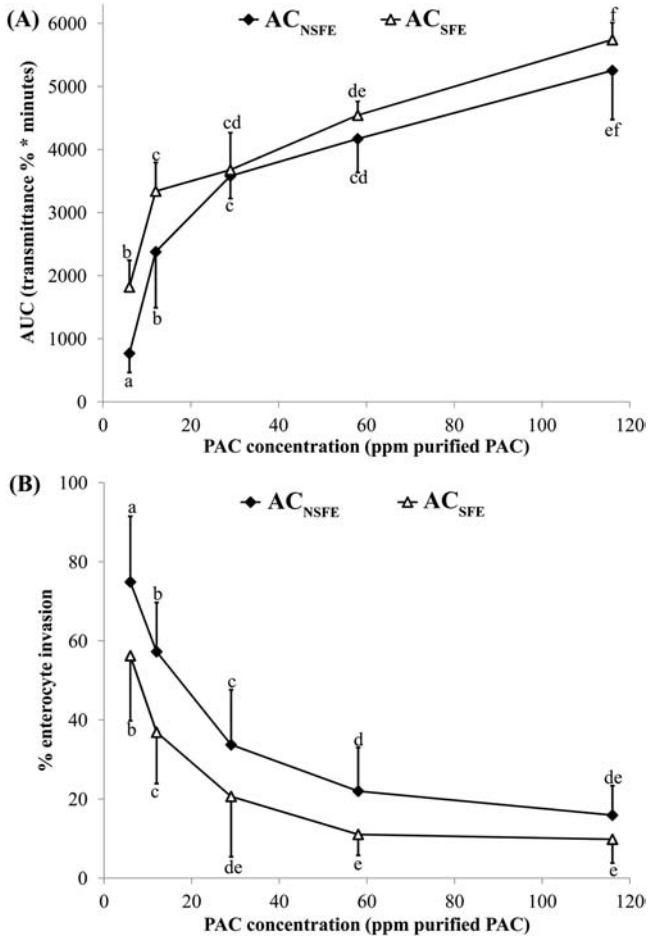

Figure 5. (A) Area under the curve (AUC) obtained for the ExPEC agglutination assay with increasing concentrations of cranberry proanthocyanidins (PAC) in AC_{NSFE} and AC_{SFE} fractions. (B) Dose–response curves of AC_{NSFE} and AC_{SFE} fractions on the effect of PAC inhibition of ExPEC invasion of enterocytes. PAC concentrations are expressed in parts per million of purified PAC as quantified by the 4-(dimethylamino)cinnamaldehyde (DMAC) method.[23] The results are expressed as the average of three independent assays ± standard deviation. Different letters correspond to significant differences at p < 0.05.

DISCUSSION

Effect of Supercritical Fluid Extraction on Proanthocyanidins Elution Profile on Sephadex LH-20. In this work, we initially investigated the potential of SFE, with and without modifiers, to extract PAC from cranberries. The use of CO_2 in cycle 1 generated yellow extracts, and the subsequent addition of ethanol to CO_2 in cycle 2 generated red extracts in separators 1 and 2. MALDI-TOF MS spectra of these extracts showed multiple peaks that corresponded to lipophilic compounds in the yellow extracts and phenolic compounds in the red extracts, including anthocyanins (data not shown). These results are in agreement with previous work in which anthocyanins have been extracted from cherries,[31] elderberries,[32] and grapes[33] using CO_2 and ethanol under supercritical conditions. CO_2 is the most commonly used solvent for SFE[34] and can replace organic solvents in laboratory and industrial extractions of nonpolar compounds. However, for more polar compounds, the addition of modifiers is necessary. For instance, catechin is not extracted with SFE unless a modifier is used.[35]

Although research indicates that PAC monomers,[18] dimers,[19] and trimers[20] can be extracted from grape seeds with SFE using CO_2 and modifiers, our work showed that SFE is not able to extract PAC with DP >2 in cranberries, as analyzed by MALDI-TOF MS. Cranberry PAC have high molecular weight and are amphiphilic, and our results demonstrate that PAC with DP >2 are not good candidates for extraction with SFE even when modifiers are used. Nonetheless, we discovered that prior extraction of cranberries with SFE removed polar and amphiphilic components and altered the composition of PAC fractions from Sephadex LH-20 chromatography, affecting the ratios of "A-type" to "B-type" interflavan bonds and DP in PAC fractions. Although the ethanol fractions from Sephadex LH-20 chromatography were not analyzed by MALDI-TOF MS, we assume that the ethanol fraction with no prior SFE treatment contained lower amounts of PAC dimers than the ethanol fraction with prior SFE treatment. Consequently, EM_{NSFE} contained a larger proportion of PAC with DP 2 compared to EM_{SFE}. Our results also showed that AC_{SFE} contained more oligomers with two and three "A-type" interflavan bonds and contained PAC with higher DP than AC_{NSFE} because PAC with lower DP and only one "A-type" interflavan bonds were eluted in EM_{SFE}. More than 92% of PAC in AC_{SFE} and AC_{NSFE} had at least one "A-type" interflavan bond, which is in agreement with

dx.doi.org/10.1021/jf502296b | J. Agric. Food Chem. 2014, 62, 7730–7737

our previous work in which 91 and 95% of PAC isolated from cranberry press cake and fruits, respectively, had at least one "A-type" interflavan bond.[3,24]

The higher amounts of PAC with two and three "A-type" interflavan bonds and the higher DP in AC_{SFE} compared to AC_{NSFE} prompted the interest in studying the impact of these PAC structural differences on ExPEC agglutination and Caco-2 cell invasion. These studies were conducted only with AC_{NSFE} and AC_{SFE} because MALDI-TOF MS showed that these fractions did not contain other components, whereas EM_{NSFE} and EM_{SFE} spectra contained m/z peaks that did not correspond to PAC.

Bacterial Agglutination Assay. For any given PAC concentration, AC_{SFE} had higher agglutination ability than AC_{NSFE}. The differences described here were not as striking as when cranberry "A-type" PAC were compared with apple "B-type" PAC.[3] Bacterial agglutination prevents the specific adhesion of ExPEC to gut epithelial cells and therefore can decrease enterocyte invasion and subsequent gut colonization by ExPEC, possibly preventing earlier steps of UTI and other extra-intestinal infections.[3]

Invasion Assay. In this work, we were able to generate dose−response curves with physiologically relevant PAC concentrations for both AC_{NSFE} and AC_{SFE} fractions.[3] Our results show that AC_{SFE} was more efficient in inhibiting invasion than AC_{NSFE} and that enterocyte invasion rate was reduced to 9% when compared to the control at 116 ppm of PAC. This effect may be related to the higher amount of PAC with two and three "A-type" interflavan bonds and the shift toward PAC with higher DP as detected by MALDI-TOF MS in the AC_{SFE} fraction.

PAC isolation with prior SFE extraction removed non-PAC components, which greatly altered the chromatographic behavior of PAC on Sephadex LH-20. The generated cranberry PAC fractions contained a higher number of "A-type" interflavan bonds and contained PAC with higher DP. These results are the first in the literature to suggest that the number of "A-type" interflavan bonds influences bioactivity.

SFE can be used as a prior step in PAC isolation to manipulate the ratios of "A-type" to "B-type" PAC and obtain formulations enriched in PAC with multiple "A-type" interflavan bonds. Our results show that the bioactivity of cranberry PAC is related to DP and ratios of "A-type" and "B-type" interflavan bonds. These ratios are highly variable in cranberry products. For instance, the range in content of PAC trimers with "A-type" was between 0 and 1579 μg/g in cranberry powders.[36] Our results also suggest that MALDI-TOF MS deconvolution[24] is useful for assessing cranberry PAC bioactivity.

AUTHOR INFORMATION

Corresponding Author

*(J.D.R.) Phone: (608) 263-4310. Fax: (608) 262-5157. E-mail: jdreed@wisc.edu.

Funding

This research was funded by the National Institute of Food and Agriculture, U.S. Department of Agriculture, ID WIS01519, the Reed Research Group Multi-Donor Fund, United Cranberry Growers Cooperative, and a collaborative effort of Complete Phytochemical Solutions, LLC. R.P.F. is the recipient of a BD fellowship (SFRH/BD/73067/2010) from Fundação para a Ciência e a Tecnologia, Portugal.

Notes

The authors declare the following competing financial interest(s): Jess D. Reed and Christian G. Krueger have ownership interest in Complete Phytochemical Solutions, LLC, and in full disclosure their affiliation with this company is acknowledged in the author affiliation.

ACKNOWLEDGMENTS

We thank the United Cranberry Growers Cooperative for providing cranberry samples, Standard Process Inc. for use of the SFE equipment, Peter Crump for statistical consulting, and Dr. Walt Hopkins for kindly providing *E. coli* strain 5011.

ABBREVIATIONS USED

SFE, supercritical fluid extraction; AC_{NSFE}, Sephadex LH-20 fraction eluted with 80% acetone with no prior SFE; AC_{SFE}, Sephadex LH-20 fraction eluted with 80% acetone with prior SFE; AUC, area under the curve; CE_{NSFE}, cranberry extract with no prior SFE; CE_{SFE}, cranberry extract with prior SFE; CFU, colony-forming units; DMAC, 4-(dimethylamino)-cinnamaldehyde; DP, degree of polymerization; EM_{NSFE}, Sephadex LH-20 fraction eluted with ethanol/methanol (1:1) with no prior SFE; EM_{SFE}, Sephadex LH-20 fraction eluted with ethanol/methanol (1:1) with prior SFE; ExPEC, extraintestinal pathogenic *Escherichia coli*; FBS, fetal bovine serum; MALDI-TOF MS, matrix-assisted laser desorption/ionization time-of-flight mass spectrometry; PAC, proanthocyanidins; PBS, phosphate-buffered saline; UTI, urinary tract infections

REFERENCES

(1) Foo, L. Y.; Lu, Y.; Howell, A. B.; Vorsa, N. The structure of cranberry proanthocyanidins which inhibit adherence of uropathogenic P-fimbriated *Escherichia coli* in vitro. *Phytochemistry* **2000**, *54*, 173−181.

(2) Howell, A. B.; Reed, J. D.; Krueger, C. G.; Winterbottom, R.; Cunningham, D. G.; Leahy, M. A-type cranberry proanthocyanidins and uropathogenic bacterial anti-adhesion activity. *Phytochemistry* **2005**, *66*, 2281−2291.

(3) Feliciano, R. P.; Meudt, J. J.; Shanmuganayagam, D.; Krueger, C. G.; Reed, J. D. Ratio of "A-type" to "B-type" proanthocyanidin interflavan bonds affects extra-intestinal pathogenic *Escherichia coli* invasion of gut epithelial cells. *J. Agric. Food Chem.* **2014**, *62*, 3919−3925.

(4) Porter, M. L.; Krueger, C. G.; Wiebe, D. A.; Cunningham, D. G.; Reed, J. D. Cranberry proanthocyanidins associate with low-density lipoprotein and inhibit in vitro Cu^{2+}-induced oxidation. *J. Sci. Food Agric.* **2001**, *81*, 1306−1313.

(5) Reed, J. Cranberry flavonoids, atherosclerosis and cardiovascular health. *Crit. Rev. Food Sci. Nutr.* **2002**, *42*, 301−316.

(6) Koo, H.; Duarte, S.; Murata, R. M.; Scott-Anne, K.; Gregoire, S.; Watson, G. E.; Singh, A. P.; Vorsa, N. Influence of cranberry proanthocyanidins on formation of biofilms by *Streptococcus mutans* on saliva-coated apatitic surface and on dental caries development in vivo. *Caries Res.* **2010**, *44*, 116−126.

(7) Feng, G.; Klein, M. I.; Gregoire, S.; Singh, A. P.; Vorsa, N.; Koo, H. The specific degree-of-polymerization of A-type proanthocyanidin oligomers impacts *Streptococcus mutans* glucan-mediated adhesion and transcriptome responses within biofilms. *Biofouling* **2013**, *29*, 629−640.

(8) Janecki, A.; Kolodziej, H. Anti-adhesive activities of flavan-3-ols and proanthocyanidins in the interaction of group A-streptococci and human epithelial cells. *Molecules* **2010**, *15*, 7139−7152.

(9) Burger, O.; Ofek, I.; Tabak, M.; Weiss, E. I.; Sharon, N.; Neeman, I. A high molecular mass constituent of cranberry juice inhibits *Helicobacter pylori* adhesion to human gastric mucus. *FEMS Immunol. Med. Microbiol.* **2000**, *29*, 295−301.

(10) Su, X.; Howell, A. B.; D'Souza, D. H. The effect of cranberry juice and cranberry proanthocyanidins on the infectivity of human enteric viral surrogates. *Food Microbiol.* **2010**, *27*, 535−540.
(11) Krueger, C. G.; Reed, J. D.; Feliciano, R. P.; Howell, A. B. Quantifying and characterizing proanthocyanidins in cranberries in relation to urinary tract health. *Anal. Bioanal. Chem.* **2013**, *405*, 4385−4395.
(12) Krenn, L.; Steitz, M.; Schlicht, C.; Kurth, H.; Gaedcke, F. Anthocyanin- and proanthocyanidin-rich extracts of berries in food supplements − analysis with problems. *Pharmazie* **2007**, *62*, 803−812.
(13) Sarnoski, P. J.; Johnson, J. V.; Reed, K. A.; Tanko, J. M.; O'Keefe, S. F. Separation and characterisation of proanthocyanidins in Virginia type peanut skins by LC-MS^n. *Food Chem.* **2012**, *131*, 927−939.
(14) Herrero, M.; Cifuentes, A.; Ibañez, E. Sub- and supercritical fluid extraction of functional ingredients from different natural sources: plants, food-by-products, algae and microalgae: a review. *Food Chem.* **2006**, *98*, 136−148.
(15) Souza Machado, B. A.; Pereira, C. G.; Nunes, S. B.; Padilha, F. F.; Umsza-Guez, M. A. Supercritical fluid extraction using CO_2: main applications and future perspectives. *Sep. Sci. Technol.* **2013**, *48*, 2741−2760.
(16) Wijngaard, H.; Hossain, M. B.; Rai, D. K.; Brunton, N. Techniques to extract bioactive compounds from food by-products of plant origin. *Food Res. Int.* **2012**, *46*, 505−513.
(17) Khoddami, A.; Wilkes, M.; Roberts, T. Techniques for analysis of plant phenolic compounds. *Molecules* **2013**, *18*, 2328−2375.
(18) Yilmaz, E. E.; Özvural, E. B.; Vural, H. Extraction and identification of proanthocyanidins from grape seed (*Vitis vinifera*) using supercritical carbon dioxide. *J. Supercrit. Fluids* **2011**, *55*, 924−928.
(19) Murga, R.; Ruiz, R.; Beltran, S.; Cabezas, J. L. Extraction of natural complex phenols and tannins from grape seeds by using supercritical mixtures of carbon dioxide and alcohol. *J. Agric. Food Chem.* **2000**, *48*, 3408−3412.
(20) Ashraf-Khorassani, M.; Taylor, L. T. Sequential fractionation of grape seeds into oils, polyphenols, and procyanidins via a single system employing CO_2-based fluids. *J. Agric. Food Chem.* **2004**, *52*, 2440−2444.
(21) Bhagdeo, M.; Ashraf-Khorassani, M.; Taylor, L. T. Analysis of supercritical CO_2 extractables from cranberry seeds. *Modern Extraction Techniques*; American Chemical Society: Washington, DC, USA, 2006; No. 926, pp 36−50.
(22) Laroze, L.; Díaz-Reinoso, B.; Moure, A.; Zúñiga, M.; Domínguez, H. Extraction of antioxidants from several berries pressing wastes using conventional and supercritical solvents. *Eur. Food Res. Technol.* **2010**, *231*, 669−677.
(23) Feliciano, R. P.; Shea, M. P.; Shanmuganayagam, D.; Krueger, C. G.; Howell, A. B.; Reed, J. D. Comparison of isolated cranberry (*Vaccinium macrocarpon* Ait.) proanthocyanidins to catechin and procyanidins A2 and B2 for use as standards in the 4-(dimethylamino)cinnamaldehyde assay. *J. Agric. Food Chem.* **2012**, *60*, 4578−4585.
(24) Feliciano, R. P.; Krueger, C. G.; Shanmuganayagam, D.; Vestling, M. M.; Reed, J. D. Deconvolution of matrix-assisted laser desorption/ionization time-of-flight mass spectrometry isotope patterns to determine ratios of A-type to B-type interflavan bonds in cranberry proanthocyanidins. *Food Chem.* **2012**, *135*, 1485−1493.
(25) Kaper, J. B.; Nataro, J. P.; Mobley, H. L. T. Pathogenic *Escherichia coli*. *Nat. Rev. Microbiol.* **2004**, *2*, 123−140.
(26) Nowrouzian, F. L.; Adlerberth, I.; Wold, A. E. Enhanced persistence in the colonic microbiota of *Escherichia coli* strains belonging to phylogenetic group B2: role of virulence factors and adherence to colonic cells. *Microbes Infect.* **2006**, *8*, 834−840.
(27) Lee, Y. M.; Dodson, K. W.; Hultgren, S. J. Adaptor function of PapF depends on donor strand exchange in P-pilus biogenesis of *Escherichia coli*. *J. Bacteriol.* **2007**, *189*, 5276−5283.
(28) Adlerberth, I.; Hanson, Å. L.; Svanborg, C.; Svennerholm, A. M.; Nordgren, S.; Wold, A. E. Adhesins of *Escherichia coli* associated with extra-intestinal pathogenicity confer binding to colonic epithelial cells. *Microb. Pathogenesis* **1995**, *18*, 373−385.
(29) Strohalm, M.; Kavan, D.; Novak, P.; Volny, M.; Havlicek, V. mMass 3: A cross-platform software environment for precise analysis of mass spectrometric data. *Anal. Chem.* **2010**, *82*, 4648−4651.
(30) Krueger, C. G.; Vestling, M. M.; Reed, J. D. Matrix-assisted laser desorption/ionization time-of-flight mass spectrometry of heteropolyflavan-3-ols and glucosylated heteropolyflavans in sorghum [*Sorghum bicolor* (L.) Moench]. *J. Agric. Food Chem.* **2002**, *51*, 538−543.
(31) Serra, A. T.; Seabra, I. J.; Braga, M. E. M.; Bronze, M. R.; de Sousa, H. C.; Duarte, C. M. M. Processing cherries (*Prunus avium*) using supercritical fluid technology. Part 1: Recovery of extract fractions rich in bioactive compounds. *J. Supercrit. Fluids* **2010**, *55*, 184−191.
(32) Seabra, I. J.; Braga, M. E. M.; Batista, M. T.; de Sousa, H. C. Effect of solvent (CO_2/ethanol/H2O) on the fractionated enhanced solvent extraction of anthocyanins from elderberry pomace. *J. Supercrit. Fluids* **2010**, *54*, 145−152.
(33) Ghafoor, K.; Park, J.; Choi, Y.-H. Optimization of supercritical fluid extraction of bioactive compounds from grape (*Vitis labrusca* B.) peel by using response surface methodology. *Innovative Food Sci. Emerging Technol.* **2010**, *11*, 485−490.
(34) Rawson, A.; Tiwari, B. K.; Brunton, N.; Brennan, C.; Cullen, P. J.; O'Donnell, C. P. Application of supercritical carbon dioxide to fruit and vegetables: extraction, processing, and preservation. *Food Rev. Int.* **2012**, *28*, 253−276.
(35) Berna, A.; Cháfer, A.; Montón, J. B.; Subirats, S. High-pressure solubility data of system ethanol (1) + catechin (2) + CO_2 (3). *J. Supercrit. Fluids* **2001**, *20*, 157−162.
(36) Sánchez-Patán, F.; Bartolomé, B.; Martín-Alvarez, P. J.; Anderson, M.; Howell, A.; Monagas, M. Comprehensive assessment of the quality of commercial cranberry products. Phenolic characterization and in vitro bioactivity. *J. Agric. Food Chem.* **2012**, *60*, 3396−3408.

Chemicals and Standards. HPLC-grade acetonitrile (Carlo-Erba) and formic acid (Merck, Darmstadt, Germany) were purchased from Merck (Darmstadt, Germany). Water was permuted using a reverse osmosis Milli-Q system (Millipore, Molsheim, France). Chlorogenic acid, caffeic acid, metformin (dimethyl-biguanide), cytochalasin B, and tolbutamide were provided by Sigma-Aldrich (St. Quentin Fallavier, France).

Burdock Root Extraction. The dried burdock roots were crushed into a fine powder that was placed into a cellulose cartridge suspended in a glass graduated cylinder. Then, a sequential extraction was performed by "soaking", i.e., pouring slowly different solutions on the powder using a peristaltic pump. The pump can extend each extraction for 12 h in a closed circulation. The extraction was started with an aqueous solution (50 mM Tris-HCl at pH 8, 150 mM NaCl, and 2 mM EDTA) and continued with a 70% ethanolic solution [ethanol/water, 70/30 (v/v)] for 48 h. The filtrate was then treated by chloroform (0.5:1; v/v) in a "bulb" glass decanter. The alcoholic phase was collected and dried in a Rotavapor apparatus before storage at −20 °C. Before use, the powder was solubilized in 20% ethanol. Sugar, protein, and phenolic compounds content was measured by the method of Dubois et al.,[13] the Bradford method,[14] and the method of Singh et al.,[15] respectively.

GC−MS and LC−MS Analysis of Compounds. *GC−MS Analysis.* Gas chromatography was performed using a Focus GC oven (Thermo) fitted with a mass spectrometer as detector. The column system used was a TG-5MS (30 m × 0.25 mm i.d., 0.25 μm d_f) supplied by Thermo. The column was connected to a split/splitless injector. The GC conditions were as follows: the oven was temperature-programmed for 70 °C, initially held for 1 min, then raised at 10 °C/min to 300 °C and held for 5 min. The column flow was 1.2 mL·min^{-1} helium. Injections of 2 μL were performed in splitless mode with a splitless time of 2 min. The injector temperature was 200 °C. The mass spectrometer used was a DSQII (Thermo) with EI source (70 eV). The scan range was 40−500 Da. A scan speed of 3000 amu/s was used. The source and transfer line temperature were held at 250 and 310 °C, respectively. The data were processed using the Xcalibur system. Identifications were performed using the NIST library.

LC−MS Analysis. In a first step, high-resolution mass spectrometry (HRMS/MS) was performed to characterize elemental composition of parent and fragment ions. Abundance of each compound was assessed in a second step with a diode array detector (DAD) coupled with a second HPLC−ESI−MS. For the first step, chromatographic separation was carried out on Acquity H-Class ultrahigh performance liquid chromatography (UPLC) system (Waters Corp., Milford, MA), equipped with a 100/2 Nucleoshell RP18 2.7 μm column (Macherey-Nagel). The mobile phase consisted of permuted water (solvent A) and acetonitrile (solvent B), both phases acidified by 0.1% (v/v) formic acid. The extract was then characterized using a Synapt G2-S high definition mass spectrometry system (Waters Corp., Milford, MA) equipped with electrospray ionization. Mass spectra were acquired in the positive and negative ionization mode with a capillary voltage of 1 kV. The TOF mass analyzer was calibrated using phosphoric acid in 1:1 (v:v) acetonitrile:H_2O from 50 to 1200 m/z to obtain mass accuracy within 3 ppm. The Synapt parameters were optimized as follows: the sample cone was set at 20 V, the source and desolvation temperature were set at 120 and 600 °C, respectively. Each sample was processed with MassLynx (V4.1) software.

In the second step, absorbance spectra were acquired using a Waters 996 photodiode array detector. Chromatographic separation was carried out on a XTerra MS C_{18} column (100 × 2.1 mm, 3.5 μm) heated at 30 °C (Gecko 2000, Cluzeau Info Labo, France). Gradient was performed at a 210 μL·min^{-1} flow rate using a binary HPLC pump (Waters 1525 μ, Waters, Manchester, UK); it was composed of permuted water (solvent A) and acetonitrile (solvent B), both acidified by 0.1% (v/v) formic acid. The analysis was performed on a Micromass ZQ ESCi multimode ionization mass spectrometer (Micromass Ltd, Manchester, UK) equipped with an electrospray ionization ion source. Absorbance spectra were acquired using a Waters 996 photodiode array detector. Sensitivity of the mass spectrometer was optimized using a chlorogenic acid standard. For peak assignment, we took as references LC−MS/MS characterizations from Lin and Harnly,[11] Jaiswal and Kuhnert,[16] and Matura et al.[7] Compounds were identified by their retention times, UV absorbance spectra, and MS fragmentation pattern and numbered in conformity with the IUPAC numbering system.[17] Isomers were assigned by using the appropriate standards from Sigma-Aldrich (chlorogenic acid, caffeic acid). Since other caffeoylquinic acid derivatives were not commercially available, they were identified by comparison with chromatograms of *Arnica montana* L. flower extract and of the leaf extract from *Coffea canephora*, *Ilex paraguariensis*, *Cynaria scolymus* L. The compound concentrations were calculated by integrating chromatogram peak areas at 326 nm (maximal absorbance of CGA) and expressed as equivalent absorbance of the authentic chlorogenic acid standard (Sigma-Aldrich). Calibration curves were performed by dilution of stock solutions (10^{-3} M) in aqueous methanol (30/70, v/v), stored at −4 °C during experiments.

L6 Myocyte Culture and [^{3}H]-2-Deoxyglucose Uptake. The experimental procedure used has been previously described by Tousch et al.[12] On the day of the experiment, cells were first starved during 4 h in DMEM supplemented with 0.1% BSA alone and then incubated during 1 h in KRB, 0.1% BSA, 5 mM glucose supplemented with or without 100 nM insulin,[18] DBRE at 50 or 100 μg·mL^{-1}, or CGA (100 μg·mL^{-1}) and cytochalasin B (CCB) (1 μM), used as pharmacological controls. Cells were incubated in 1 mL of KRB containing 0.5 μCi [^{3}H]deoxyglucose per well. Uptake was stopped by three washings in cold PBS, and cells were lysed in 0.1 N NaOH. Radioactivity was measured and the total protein concentration was evaluated by a Bradford assay.[14] Results are expressed in cpm·mg protein^{-1}·min^{-1}.

Hepatocyte Culture and Glucose Output Test. Hepatocytes were isolated from male Wistar rats (180−260 g) fed ad lib using a two-step perfusion technique, as described by Seglen.[19] Cells were cultivated on collagen-coated 12-well plates in basal medium (William's E containing 11.1 mM glucose, 100 U·mL^{-1} penicillin, 100 μg·mL^{-1} streptomycin) supplemented with 6% FCS at a cell density of 830 000 cells/well. Four hours after initial plating, the medium was replaced with a basal medium supplemented with 100 nM dexamethasone, and plates were incubated for 24 h. Hepatocytes were loaded in glycogen with a 20 h incubation in loading medium: William's E containing 11.1 mM glucose, 100 U·mL^{-1} penicillin, 100 μg·mL^{-1} streptomycin supplemented with 100 nM dexamethasone, 13.9 mM glucose, and 100 nM insulin. After the loading period, hepatocytes were washed three times with PBS and incubated for 3 h in buffer [117.6 mM NaCl, 5.4 mM KCl, 0.82 mM $MgSO_4$, 1.5 mM KH_2PO_4, 20.0 mM Hepes, 9.0 mM $NaHCO_3$, 0.1% (w/v) BSA, 2.25 mM $CaCl_2$ (pH 7.4)][20] without or with DBRE at 50 or 100 μg·mL^{-1} or CGA at 50 μg·mL^{-1} in the presence of 100 nM glucagon (stimulating conditions). After 3 h incubation, supernatants were collected and frozen at −20 °C until glucose quantification.

Glucose release (nmol/well) was measured using a glucose oxidase kit (Megazyme, Wicklow, Ireland). Results are presented as the percentage of glucagon stimulation values.

In Vitro Measurement of Hepatic Glucose 6-Phosphatase Activity. Commercial liver microsomes (BD Biosciences, Le Pont de Claix, France) were used to quantify glucose 6-phosphatase activity. In the standard glucose 6-phosphatase assay, microsome suspension samples (2 μg of proteins by assay) were incubated for 30 min at 30 °C in the buffer containing 20 mM of glucose 6-phosphate.[21] The reaction was stopped by the addition of 1 mL of malachite green color reagent and incubated during 5 min before measuring optical density at 660 nm with NaH_2PO_4 (1−20 nmol) taken as standard. The integrity of microsomes was checked with 0.1% Triton X100 to measure the activity of the catalytic subunit of glucose 6-phosphatase after membrane disruption as previously described by Murataliev and Vufson.[22] The effects of DBRE (50 and 100 μg·mL^{-1}) and CGA (50 μg·mL^{-1}) were tested. The results are expressed as P_i (nmol·h^{-1}).

β-Cell Culture and Measurement of Insulin Release. The experimental procedure on rat insulinoma-derived INS-1 β-cells[23] has been previously described by Tousch et al.[12] For incubation experiments, cells were first washed twice and incubated for 60 min

Table 1. LC−MS Fingerprint with Fragmentation of DBRE Compounds[a]

peak	t_R (min)[b]	parent ion mol. form.[c]	parent ion theor mass(m/z)[d]	Δppm[e]	parent ion $[M - H]^-$	fragmentation data (m/z, relative intensity) $[M - H]^-$
P1	10.7	$C_{16}H_{17}O_9$	353.0878	1.6	353.088	191 (100),179 (67), 93 (64)
P2	11.6	$C_{16}H_{17}O_9$	353.0878	0.5	353.087	179 (75), 161 (10), 135 (19), 85 (25)
P3	16.2	$C_{16}H_{17}O_9$	353.0878	1.3	353.099	191 (100), 85 (12)
P4	19.2	$C_{16}H_{17}O_9$	353.0878	−1.9	353.087	173 (100), 191 (34), 179 (75), 135 (26)
P5	27.0	$C_{25}H_{23}O_{12}$	515.1195	−1.3	515.120	353 (100), 299 (37), 255 (28), 203 (61), 179 (3), 173 (19)
P6	29.5	$C_{29}H_{27}O_{16}$	631.1305	2 5	631.132	515 (85), 469 (100), 353 (95), 307 (5), 191 (10), 179 (12), 93 (20)
P7	30.4	$C_{33}H_{31}O_{20}$	747.1414	−0.2	747.141	631 (82), 515 (32), 469 (100), 353 (98), 307 (95), 191 (70), 179 (100), 161 (95), 93 (99)
P8	31.3	$C_{25}H_{23}O_{12}$	515.1195	2.1	515.120	353 (100), 191 (12), 179 (9), 85 (10)
P9	30.5	$C_{29}H_{27}O_{16}$	631.1305	0.9	631.130	515 (38), 469 (92), 353 (100), 307 (100)
P10	31.4	$C_{38}H_{33}O_{18}$	777.1672	−0.7	777.167	615 (100), 515 (52), 453 (92), 353 (5)
P11	32.6	$C_{29}H_{27}O_{16}$	631.1305	2.1	631.131	515 (100), 469 (91), 353 (100), 191 (95), 179 (15), 161 (11), 135 (8), 111 (10)
P12	34.4	$C_{33}H_{31}O_{20}$	747.1414	1.1	747.141	631 (100), 469 (70), 335 (13), 453 (15), 191 (27), 161 (18), 135 (3), 93 (58)
P13	34.8	$C_{29}H_{27}O_{16}$	631.1305	−1.0	631.129	515 (12), 469 (10), 353 (100), 335 (5), 191 (30), 179 (9), 161 (11), 93 (6)
P14	35.2	$C_{29}H_{27}O_{15}$	615.1355	−1.0	615.134	515 (15), 453 (25), 353 (100), 335 (5), 191 (25), 127 (14), 93 (12), 85 (10)
P15	35.4	$C_{33}H_{31}O_{20}$	747.1414	1.0	747.141	631 (15), 469 (17), 335 (19), 453 (100), 191 (62), 161 (31), 93 (52)
P16	35.6	$C_{25}H_{23}O_{12}$	515.1195	1.0	515.120	353 (100), 191 (10), 173 (25), 179 (10)
P17	36.0	$C_{33}H_{31}O_{19}$	731.1433	1.9	731.146	631 (8), 615 (32), 515 (31), 469 (45), 453 (12), 353 (100), 307 (18), 179 (41), 173 (36), 135 (8)
P18	36.7	$C_{33}H_{31}O_{19}$	731.1433	−1.6	731.145	631 (7), 615 (21), 515 (12), 469 (100), 453 (28), 353 (100), 307 (35), 134 (38)
P19	36.9	$C_{33}H_{31}O_{20}$	747.1414	−1.0	747.144	631 (5), 469 (100), 453 (50), 353 (20), 191 (300), 135 (170), 85 (120)
P20	37.3	$C_{33}H_{31}O_{19}$	731.1433	−1.2	731.146	631 (7), 615 (100), 569 (31), 515 (21), 469 (18), 453 (65), 307 (35)
P21	37.6	$C_{29}H_{27}O_{15}$	615.1355	−0.3	615.135	515 (10), 453 (54), 353 (100), 335 (28), 191 (32)
P22	38.1	$C_{33}H_{31}O_{20}$	747.1414	−2.8	747.139	631 (2), 453 (100), 469 (25), 335 (18), 191 (120), 173 (42), 161 (61), 93 (150)
*P*23	39.0	$C_{28}H_{32}O_{19}$	793.4000	−1.8	793.160	677 (100), 631 (2), 515 (55), 469 (100), 353 (2), 307 (25), 191 (85), 161 (95), 93 (99)
P24	39.2	$C_{33}H_{31}O_{18}$	715.1516	−2.7	715.149	615 (15), 515 (60), 453 (100), 353 (2), 191 (95), 161 (80), 93 (99)
P25	40.3	$C_{38}H_{33}O_{19}$	793.4000	−1.5	793.160	677 (1), 631 (22), 515 (23), 469 (100), 353 (12), 335 (25), 307 (6), 191 (99), 161 (95), 93 (85)
P26	42.2	$C_{38}H_{33}O_{18}$	777.1672	−2.6	777.165	615 (11), 515 (3), 453 (45), 353 (100), 191 (67), 179 (85), 161 (99)
P27	42.7	$C_{34}H_{29}O_{15}$	677.1512	−2.6	677.150	615 (11), 515 (3), 453 (45), 353 (100), 191 (67), 179 (85), 161 (99)

[a]Peaks obtained in DBRE are listed in the order of elution. with their names, molecular formulas, retention times (t_R), precursor ions, and fragmentation data of hydroxycinnamoylquinic acids. [b]t_R (min): retention time in minutes. [c]Mol. form.: molecular formula. [d]Theo. mass: theoretical monoisotopic mass of precursor ion $[M - H]^-$. [e]Δppm: mass tolerance expressed in parts per million.

in glucose-free KRB, BSA (0.1%). They were then washed once again with the same medium and incubated for 60 min in KRB, BSA (0.1%) with glucose at 2.8, 5.6, and 11.2 mM. We investigated the effects of DBRE at 50 or 100 $\mu g \cdot mL^{-1}$, in the presence of 5.6 mM glucose. Tolbutamide was used at 200 μM as a control insulinotropic drug. Insulin released in the medium was determined by FRET technology with the HTRF Insulin-Kit (Cis-Bio International). Fluorescence levels were measured on a RUBY star instrument (BMG LABTECH). Results are expressed in $ng \cdot mL^{-1}$.

Animals. Experiments were performed in male Wistar rats (280−320 g) obtained from Charles River Laboratories (L'Arbresle, France) and maintained on a 12 h/12 h light−dark schedule. The protocols have been reviewed and approved (2009/11/03) by the Animal Care and Use Committee Languedoc-Roussillon (CEEA-LR-0920 and CEEA-LR-0921).

Glucose Tolerance Test. Two experimental sets were carried out. The first four groups received, during 4 days, daily intraperitoneal (ip) administrations of DBRE at 0.75 or 3 $mg \cdot kg^{-1}$ or metformin at 100 $mg \cdot kg^{-1}$ as a pharmacological positive control or saline (controls). On the fourth day, fasted rats were submitted to an intraperitoneal glucose tolerance test (IPGTT; 1 $g \cdot kg^{-1}$). In the second set, the animals were divided into three groups; they received four daily oral administrations of either DBRE at 3 or 15 $mg \cdot kg^{-1}$ or saline (controls). On the fourth daily administration, an oral glucose tolerance test (OGTT; 3 $g \cdot kg^{-1}$) was performed.

Blood samples were collected from the tail vein, at different times before and after glucose administration. After centrifugation at 4 °C, plasma glucose levels were measured by the glucose oxidase method[24] and plasma insulin concentrations using a radioimmunological method.[25]

Data Analysis. In vitro data are expressed as means ± SD and in vivo data as means ± SEM. Multiple group comparisons were performed by analysis of variance (ANOVA) followed by Fisher's protected least significant difference test at $^*p < 0.05$ or $^{**}p < 0.01$, using the Stat Graphics software.

For in vivo experiments, plasma glucose and insulin values are expressed in $mmol \cdot L^{-1}$ and $ng \cdot mL^{-1}$, respectively. The areas under the curve (AUCs) for the first 60 min (IPGTT) or 120 min (OGTT) were also evaluated.

RESULTS

GC−MS and LC−MS Chemical Analysis. The global composition of DBRE (percent of weight) was as follows: 12% of glucidic compounds, 86% of phenolic compounds, 0.8% proteins, and 1.2% others. The total phenolic content is 150 mg/g of dry plant material.

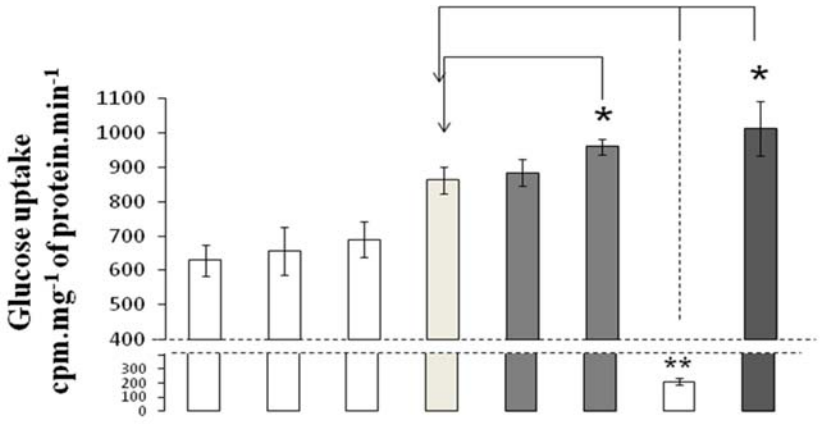

Insulin (100 nM)	-	-	-	+	+	+	+	+
DBRE (µg.mL^{-1})	-	50	100	-	50	100	-	-
CCB (1 µM)	-	-	-	-	-	-	+	-
CGA (100 µg.mL^{-1})	-	-	-	-	-	-	-	+

Figure 1. Effect of DBRE (50 or 100 μg·mL^{-1}) on glucose uptake in L6 muscle cells without or in the presence of 100 nM insulin. CGA (100 μg·mL^{-1}) and CCB (1 μM) were used as control pharmacological compounds. Values are means (±SD) of six independent experiments (n = 24 for each condition). *p < 0.05, **p < 0.01 versus insulin (100 nM) alone.

GC−MS and LC−MS allowed us to assign and characterize all substances except sugars. The data obtained by LC−MS analysis are shown in Tables 1 and 2. The GC−MS chemical monitoring allowed the detection of 27 hydroxycinnamic acids, of which 19 have been previously described by Lin and Harnly[11] and Jaiswal and Kuhnert;[16] hence, our analysis allowed us to identify eight other additional isomers in our original extract.

The chemical analysis of DBRE has been performed by LC−MS and GC−MS. LC−MS analysis revealed the presence of a large majority of dicaffeoylquinic acid derivatives (75.4%). Four maloyl-dicaffeoylquinic acid isomers were identified by their parent ion (m/z 631.129) and m/z 469.099 fragment, corresponding to [maloyl−caffeoylquinic acid−H] after the loss of one caffeoyl group. The three peaks P6, P9, and P11 have been previously observed by Jaiswal and Kuhnert.[16] Among them, 1,5-di-*O*-caffeoyl-4-*O*-maloylquinic acid (peak P11) is the most abundant DBRE compound and contributes to 44% of chlorogenic acid equivalent absorbance.

1,4-*O*-Dicaffeoylquinic acid (peak P5) and 1,5-*O*-dicaffeoylquinic acid (cynarin, peak P16) represent respectively 1 and 3%. P5 and P16 correspond to the two major dicaffeoylquinic acids of *Cynaria scolymus* leaf extract (i.e., 1,4-di-*O*-caffeoylquinic acid and 1,5-di-*O*-caffeoylquinic acid. Likewise, peak P8 corresponds to the 3,5-dicaffeoylquinic acid peak of *Coffea robusta* and *Ilex paraguariensis* leaf extracts.

DBRE is poor in monocaffeoylquinic acids (m/z 353.098 [M − H], peaks P1−P4), representing 12%, of which 7% is chlorogenic acid (5-*O*-caffeoylquinic acid, named CGA and used as " authentic standard" in in vitro experiments, peak P3).

Effect of DBRE on Glucose Uptake in L6 Myocytes. In the absence of insulin, DBRE has no effect on glucose uptake by L6 myocytes (Figure 1). In the presence of insulin (100 nM), glucose uptake increased from 629 to 862 cpm·mg^{-1}·min^{-1} (i.e., +37%, p < 0.01). Addition of DBRE (100 μg·mL^{-1}) significantly increased insulin-induced glucose uptake (+16%, p < 0.05). CGA induced a similar increase (p < 0.05), whereas CCB provoked a drop in glucose uptake (p < 0.01).

Effect of DBRE on Hepatic Glucose Output. Glucagon (100 nM)-induced glucose release reached 450 ± 30 nmol glucose/well (100%) (Figure 2A). The presence of 50 or 100 μg·mL^{-1} DBRE induced a significant non-concentration-dependent decrease (p < 0.01). Similar results were obtained with CGA at 50 μg·mL^{-1} (p < 0.05).

Effect of DBRE on Hepatic Glucose 6-Phosphatase Activity. DBRE induced a significant inhibition of glucose 6-phosphatase activity on hepatic microsomal fractions (Figure 2B). A similar inhibitory effect was observed in the presence of 50 and 100 μg·mL^{-1} DBRE or 50 μg·mL^{-1} CGA (p < 0.01).

Effect of DBRE on INS-1 β-Cells Insulin Release. As expected, increasing glucose concentration in the medium from 2.8 to 5.6 and 11.2 mM resulted into a clear and significant glucose-dependent stimulation of insulin release (Figure 3). Tolbutamide also induced a clear insulinotropic effect. In the presence of 5.6 mM glucose, addition of DBRE at 50 μg·mL^{-1} did not modify insulin release. However, a slight but significant (p < 0.05) reduction in insulin release occurred for the higher 100 μg·mL^{-1} concentration.

Glucose Tolerance Test. After four daily DBRE (0.75 or 3 mg·kg^{-1}) or metformin (100 mg·kg^{-1}) ip administrations, basal glucose and insulin levels were not found to be significantly modified (Table 3A). IPGTTs clearly show that DBRE at 0.75 mg·kg^{-1} is able to reduce the increase in plasma glucose (p < 0.05) from minute 10 to 30. A similar effect was observed in metformin-treated rats. These results are corroborated by AUCs for the first 60 min. Glucose-induced insulin response was significantly reduced (p < 0.05) by DBRE at 0.75 mg·kg^{-1}. In contrast, in rats treated with the higher DBRE dose (3 mg·kg^{-1}) no significant effect could be observed.

After four daily oral administrations of DBRE at 3 or 15 mg·kg^{-1}, basal glucose and insulin levels were not found to be modified (Table 3B). Oral glucose tolerance tests bring evidence that DBRE at 15 mg·kg^{-1} is able to significantly

dx.doi.org/10.1021/jf500926v | J. Agric. Food Chem. 2014, 62, 7738−7745

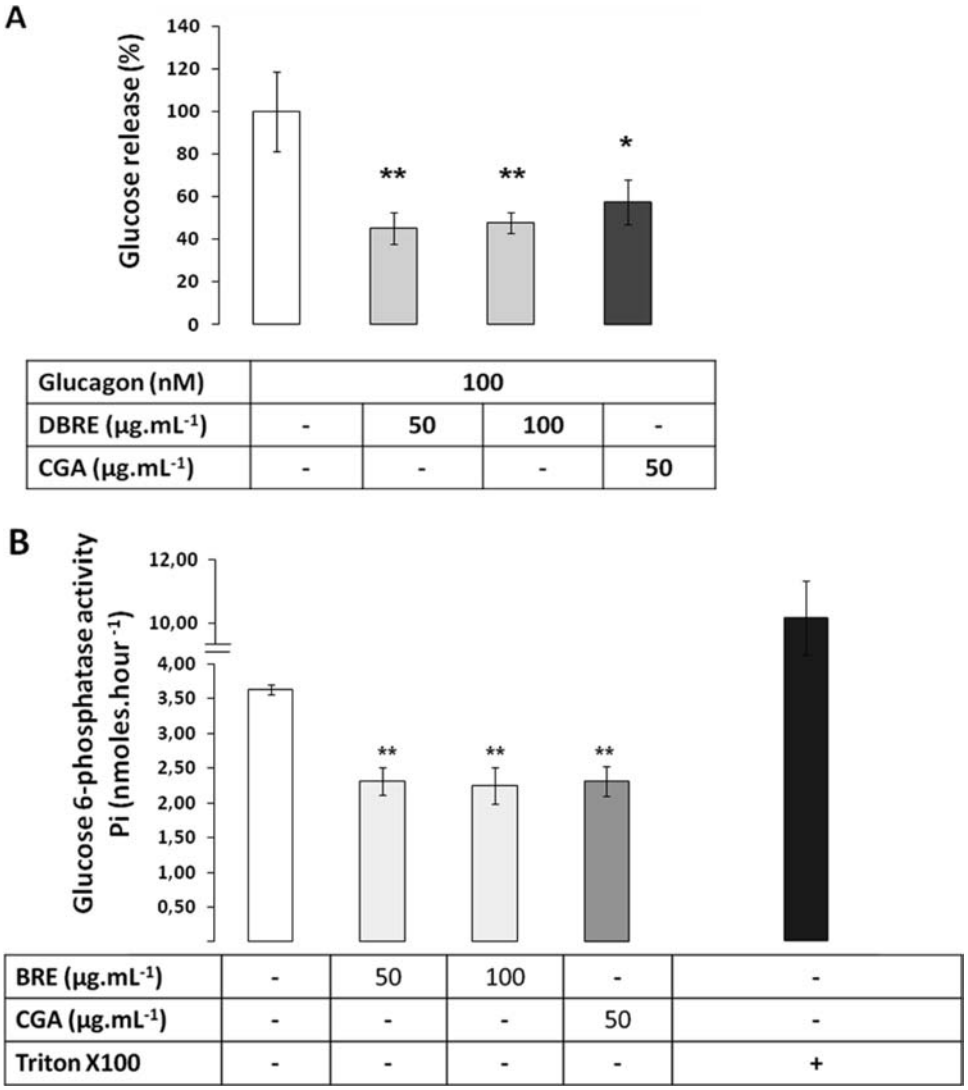

Figure 2. Effect of DBRE at 50 or 100 $\mu g \cdot mL^{-1}$ on glucagon-induced glucose release from rat isolated hepatocytes (A) and on glucose 6-phosphatase activity of liver microsomes (B). CGA (50 $\mu g \cdot mL^{-1}$) was used as control. For panel A, results are expressed as percent of glucose release in the presence of glucagon alone. Data are means (±SD) of three independent experiments (n = 14 values for each condition). *p < 0.05 and **p < 0.01 versus glucagon alone (100% effect). For panel B, results are expressed as P_i nmol·h^{-1}. Data are means (±SD) of three experiments (n = 9 for each condition). **p < 0.01.

reduce hyperglycemia from minute 60 to 90 (p < 0.05) (Table 3B). Interestingly, a clear increase in insulin response to oral glucose preceded the reduction in hyperglycemia at 30 min (p < 0.05) and 60 min (p < 0.01). AUCs for the first 120 min confirm this observation. No significant change could be observed for DBRE at 3 $mg \cdot kg^{-1}$.

DISCUSSION

Our extraction procedure allowed us to get an original polyphenol-rich extract of dried burdock roots. The total phenolic content is 150 mg/g of dry plant material, in comparison with 28.7 mg/g of dry plant material in the hydro-methanolic (70:30, v/v) burdock root extract obtained by Ferracane et al.[8]. The chemical analysis of DBRE by GC−MS and LC−MS led to the identification of 27 caffeoylquinic acids derivatives and notably 1,5-di-*O*-caffeoyl-4-*O*-maloylquinic (44%) and monocaffeoylquinic acid (CGA) (7%). DBRE differs clearly from the extracts obtained by Ferracane et al.,[8] Lin and Harnly,[11] and Jaiswal and Kuhnert.[16] These differences are largely due to our sequential partitioned extraction procedure but also could be due at the plant growth geographic conditions and also the burdock genotypes, as was shown by Liu at al.[26] None of the six lignans previously described in burdock roots were present in DBRE. Likewise, no fructan, terpen, or lipid could be detected.

Our in vitro experiments bring evidence that DBRE is able to increase glucose uptake in myocytes (L6 cells) in the presence of insulin, pointing to an insulin-sensitizing effect of the extract. Upon stimulation of glucose production by glucagon in rat isolated hepatocytes, DBRE induced a strong decrease in glucose release which was paralleled by a significant decrease in glucose 6-phosphatase activity. These results are in agreement with previous studies investigating CGA effects.[10,12] In contrast, in the presence of glucose (5.6 mM), DBRE (100 $\mu g \cdot mL^{-1}$) significantly decreased insulin release by INS-1 β-cells. This result is in discordance with the presence of CGA, which has been described as an insulinotropic compound,[12] suggesting that in DBRE another compound is present that is able to counteract and reverse the CGA effect.

dx.doi.org/10.1021/jf500926v | J. Agric. Food Chem. 2014, 62, 7738−7745

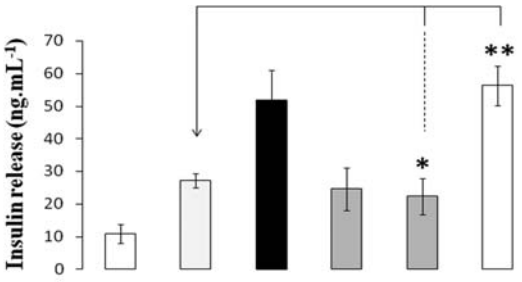

Glucose (mM)	2.8	5.6	11.2	5.6		5.6
DBRE (μg.mL^{-1})	-	-	-	50	100	-
Tolbutamide (μM)						200

Figure 3. Effect of DBRE on insulin release in the INS-1 β-pancreatic cell line. DBRE (50 and 100 μg·mL^{-1}) or tolbutamide (200 μM) as a positive control were tested in the presence of 5.6 mM glucose. Data are means (±SD) of six independent experiments; they are expressed as ng·mL^{-1} (n = 24) for each experimental condition. *p < 0.05, **p < 0.01 versus 5.6 mM glucose.

Our in vivo data obtained after IP subchronic treatments clearly show that DBRE (0.75 mg·kg^{-1}) improves IP glucose tolerance, an effect that occurs together with a decrease in insulin secretion. These data confirm and extend in vivo and in vitro experiments pointing to an insulin sensitizing effect. It is noteworthy that similar results could be obtained with metformin, another well-known insulin-sensitizing agent. At the higher dose (3 mg·kg^{-1}), DBRE was ineffective, which suggests probably an adverse effect, as already described for pro-oxidants, showing once again and emphasizing the importance of avoiding high dosages upon treatments with polyphenols.[27,28] It is interesting to note that a treatment of diabetic db/db mice with a rich caffeolyquinic acid extract of *Pandanus tectorius* for 3 weeks induced an antihyperglycemic effect by insulin-sensitizing action.[29] Concerning oral repeated administrations of DBRE, our extract, at the dose of 15 mg·kg^{-1}, remained able to improve oral glucose tolerance. A similar beneficial effect on plasma glucose levels has been previously reported in rats with orally ingested synthetic CGA (3.5 mg·kg^{-1});[30] these authors ascribed the reduced increase in plasma glucose to a possible reduced glucose intestinal absorption. From a physiological point of view, it is worthy to mention that a tricaffeoylquinic acid (3,4,5-tri-*O*-caffeoylquinic acid) present in the brazilian propolis exerts an antihyperglycemic effect through the inhibition of intestinal maltase activity.[31] Anyhow, our experiments bring evidence that subchronic oral DBRE administrations result in a clear increase of glucose-induced insulin response. Previous studies have reported that heavy coffee (with CGA as the chief polyphenol present) consumption is associated with increased plasma levels of GLP-1.[32] We therefore suggest that the increased insulin response and the beneficial effect on oral glucose tolerance could be due to a DBRE-induced increase in incretin activity, all the more since insulin response to glucose is not modified after repeated ip DBRE administrations, which is also in line with the absence of insulinotropic effect in vitro on INS cells.

In conclusion, we realized and chemically characterized an extract of dried Burdock roots (DBRE). Our data demonstrate that the original set of caffeoylquinic acid compounds present in DBRE at 86% displays both in vitro and in vivo compelling antihyperglycemic properties with potential therapeutic relevance. However, further investigations are required to address and understand the specific role of each caffeoylquinic acid compound, in the beneficial effects of DBRE.

Table 2. Concentrations of Each Compound Were Calculated by Integrating Peak Areas of Chromatograms at 326 nm (maximal absorbance of CGA) and Are Expressed as Equivalent Absorbance of the Authentic Chlorogenic Acid Standard at 10^{-3} M

peak	t_R (min)	name	Abs_{326}	ref
P1	10.7	1-*O*-caffeoylquinic acid	0.38	11
P2	11.6	3-*O*-caffeoylquinic acid	4.08	11
P3	16.2	5-*O*-caffeoylquinic acid	7.52	11, 16
P4	19.2	4-*O*-caffeoylquinic acid	0.06	11
P5	27.0	1,4-di-*O*-caffeoylquinic acid	0.97	11, 16
P6	29.5	1,5-di-*O*-caffeoyl-3-*O*-maloylquinic acid	4.17	16
P7	30.4	dimaloyl-dicaffeoylquinic acid isomer 1	0.00	
P8	31.3	3,5-di-*O*-caffeoylquinic acid	2.95	11, 16
P9	30.5	1,4-di-*O*-caffeoyl-3-*O*-maloylquinic acid	0.95	16
P10	31.4	succinoyl-tricaffeoylquinic acid isomer	0.24	
P11	32.6	1,5-di-*O*-caffeoyl-4-*O*-maloylquinic acid	43.95	16
P12	34.4	1,3-di-*O*-caffeoyl-4,5-di-*O*-maloylquinic acid	1.18	16
P13	34.8	maloyl-dicaffeoylquinic acid isomer	0.32	
P14	35.2	1,5-di-*O*-caffeoyl-3-*O*-succinoylquinic acid	12.29	7, 11, 16
P15	35.4	1,4-di-*O*-maloyl-3,5-di-*O*-caffeoylquinic acid	1.83	16
P16	35.6	1,5-di-*O*-caffeoylquinic acid	2.96	7, 11, 16
P17	36.0	dicaffeoyl-succinoyl-malonylquinic acid isomer 1	0.44	
P18	36.7	dicaffeoyl-succinoyl-malonylquinic acid isomer 2	0.48	
P19	36.9	dimaloyl-dicaffeoylquinic acid isomer 2	0.03	
P20	37.3	1,5-di-*O*-caffeoyl-3-*O*-succinoyl-4-*O*-maloylquinic acid	0.45	16
P21	37.6	1,5-di-*O*-caffeoyl-4-*O*-succinoylquinic acid	1.23	7, 11, 16
P22	38.1	dimaloyl-dicaffeoylquinic acid isomer 3	0.09	
P23	39.0	maloyl-tricaffeoylquinic isomer	2.18	
P24	39.2	1,5-di-*O*-caffeoyl-3,4-di-*O*-succinoylquinic acid	2.08	16
P25	40.3	1,3,5-tri-*O*-caffeoyl-4-*O*-maloylquinic acid	7.04	
P26	42.2	1,3,5-tri-*O*-caffeoyl-4-*O*-succinoylquinic acid	1.40	7, 11, 16
P27	42.7	1,3,5-tri-*O*-caffeoylquinic acid	0.73	11

AUTHOR INFORMATION

Corresponding Author

*Tel: +33 4 11 75 94 89. Fax: +33 4 11 75 95 47. E-mail: jacqueline.milhau@univ-montp1.fr; UFR des Sciences Pharmaceutiques et Biologiques, Centre de Pharmacologie et Innovation dans le Diabète, EA7288, 15 avenue Charles Flahault, B.P. 14491, 34093 Montpellier cedex 5, FRANCE.

Notes

The authors declare no competing financial interest.

ACKNOWLEDGMENTS

Excellent technical support from Yves Baissac is acknowledged. We sincerely thank Dr. Gérard Ribes, Dr. René Gross, and Prof. Pierre Petit for consenting to give us some precious scientific advice.

Table 3. Effects of DBRE on Glycemia and Insulinemia during either an Intraperitoneal Glucose Tolerance Test (IPGTT) (A) or an Oral Glucose Tolerance Test (OGTT) (B) in Wistar Rats[a]

(A) Intraperitoneal Glucose Tolerance Test[b]								
	0 min	10 min	20 min	30 min	60 min	90 min	120 min	AUCs (60 min)
glycemia ($mmol·L^{-1}$)								
controls	5.3 ± 0.1	10.3 ± 0.9	10 ± 0.8	9.7 ± 0.5	7.7 ± 0.5	6.3 ± 0.6	7.1 ± 0.2	538 ± 31
DBRE, 0.75 $mg·kg^{-11}$	5.6 ± 0.2	6.3 ± 0.5*	5.7 ± 0.4*	7 ± 0.3*	6.8 ± 0.8	6.3 ± 0.6	5.9 ± 0.4	390 ± 20*
DBRE, 3 $mg·kg^{-1}$	5.4 ± 0.2	10.3 ± 0.6	8.7 ± 0.9	7.7 ± 0.9	7.9 ± 0.7	7.3 ± 0.4	6.2 ± 0.2	488 ± 29
metformin, 100 $mg·kg^{-1}$	5.7 ± 0.2	7.9 ± 0.5*	7.8 ± 0.7*	7.1 ± 0.7*	7.1 ± 0.6	5.8 ± 0.2	6.3 ± 0.4	434 ± 25*
insulinemia ($ng·mL^{-1}$)								
controls	0.3 ± 0.1	3.3 ± 0.6	1.7 ± 0.4	1.2 ± 0.4	1.7 ± 0.7	1.3 ± 0.4	1.0 ± 0.4	102 ± 27
DBRE, 0.75 $mg·kg^{-1}$	0.6 ± 0.2	1.8 ± 0.5*	1.1 ± 0.2	0.8 ± 0.3	0.7 ± 0.1	0.9 ± 0.3	1.0 ± 0.2	60 ± 13*
DBRE, 3 $mg·kg^{-1}$	0.3 ± 0.1	2.4 ± 0.4	1.2 ± 0.3	0.9 ± 0.3	1.2 ± 0.3	0.9 ± 0.2	1.1 ± 0.2	76 ± 10
metformin, 100 $mg·kg^{-1}$	0.4 ± 0.1	2.5 ± 0.1	1.9 ± 0.4	1.2 ± 0.3	1.0 ± 0.3	1.3 ± 0.4	1.3 ± 0.4	87 ± 15

(B) Oral Glucose Tolerance Test[c]								
	0 min	15 min	30 min	60 min	90 min	120 min	180 min	AUCs (120 min)
glycemia ($mmol·L^{-1}$)								
controls	5.2 ± 0.3	8.6 ± 0.5	9.5 ± 0.8	8.7 ± 0.5	8.0 ± 0.3	8.1 ± 0.2	6.1 ± 0.3	1002 ± 50
DBRE, 3 $mg·kg^{-1}$	4.9 ± 0.3	8.4 ± 0.4	8.0 ± 0.4*	8.3 ± 0.3	8.0 ± 0.2	7.2 ± 0.3	5.6 ± 0.1	938 ± 31
DBRE, 15 $mg·kg^{-1}$	5.7 ± 0.2	7.6 ± 0.6	8.4 ± 0.5*	8.3 ± 0.2*	8.3 ± 0.2	7.7 ± 0.3	6.1 ± 0.2	962 ± 34
insulinemia ($ng·mL^{-1}$)								
controls	0.5 ± 0.3	2.6 ± 0.3	1.7 ± 0.6	1.7 ± 0.3	0.7 ± 0.2	0.9 ± 0.3	0.6 ± 0.1	169 ± 23
DBRE, 3 $mg·kg^{-1}$	0.4 ± 0.1	2.5 ± 0.3	1.5 ± 0.2	1.3 ± 0.2	1.5 ± 0.3	0.8 ± 0.2	0.7 ± 0.2	170 ± 15
DBRE, 15 $mg·kg^{-1}$	0.4 ± 0.1	3.1 ± 0.2*	3.6 ± 0.6**	1.8 ± 0.3	1.4 ± 0.2	1.2 ± 0.6	1.1 ± 0.4	244 ± 5*

[a]Values are means (±SEM) expressed in $mmol·L^{-1}$. [b]Time courses of plasma glucose ($mmol·L^{-1}$) and plasma insulin ($ng·mL^{-1}$) during IPGTTs (1 $g·kg^{-1}$) in rats previously treated by intraperitoneal DBRE (0.75 and 3 $mg·kg^{-1}$), saline, or metformin (100 $mg·kg^{-1}$) during 4 days; $n = 5$ for each experimental condition. AUCs were calculated for the first 60 min. *$p < 0.05$. [c]Time courses of plasma glucose ($mmol·L^{-1}$) and plasma insulin ($ng·mL^{-1}$) during OGTTs (3 $g·kg^{-1}$) in rats treated with oral DBRE (3 and 15 $mg·kg^{-1}$) or saline during 4 days; $n = 5$ for each experimental condition. AUCs were calculated for the first 120 min. *$p < 0.05$, **$p < 0.01$.

REFERENCES

(1) Cicero, A. F.; Derosa, G.; Gaddi, A. What do herbalist suggest to diabetic patients in order to improve glycemic control? Evaluation of scientific evidence and potential risks. *Acta Diabetol.* **2004**, *41*, 91−98.

(2) Bradley, P. (Ed.) *British Herbal Compendium*; British Herbal Medicine Association: Dorset, England, 1992; Vol. *1*, pp 46−49.

(3) Chan, Y. S.; Cheng, L. N.; Wu, J. H.; Chan, E.; Kwan, Y. W.; Lee, S. M.; Leung, G. P.; Yu, P. H.; Chan, S. W. A review of the pharmacological effects of *Arctium lappa* (burdock). *Inflammopharmacology* **2011**, *19*, 245−54.

(4) Lu, L. C.; Zhou, W.; Li, Z. H.; Yu, C. P.; Li, C. W.; Luo, M. H.; Xie, H. Effects of arctiin on streptozotocin-induced diabetic retinopathy in Sprague−Dawley rats. *Planta Med.* **2012**, *78*, 1317−23.

(5) Pourghassem Gargari, B.; Dehghan, P.; Aliasgharzadeh, A.; Jafar-abadi, M. A. Effects of high performance inulin supplementation on glycemic control and antioxidant status in women with type 2 diabetes. *Diabetes Metab. J.* **2013**, *37*, 140−148.

(6) Ivorra, M. D.; Paya, M.; Villar, A. Effect of beta-sitosterol-3-beta-D-glucoside on insulin secretion in vivo in diabetic rats and in vitro in isolated rat islets of Langerhans. *Pharmazie* **1990**, *45* (4), 271−273.

(7) Maruta, Y.; Kawabata, J.; Niki, R. Antioxidative caffeoylquinic acid derivatives in the roots of burdock (*Arctium lappa* L.). *J. Agric. Food Chem.* **1995**, *43*, 2592−2595.

(8) Ferracane, R.; Graziani, G.; Gallo, M.; Fogliano, V.; Ritieni, A. Metabolic profile of the bioactive compounds of burdock (*Arctium lappa*) seeds, roots and leaves. *J. Pharm. Biomed. Anal.* **2010**, *51*, 399−404.

(9) Lin, L.-Z.; Harnly, J.; Zhang, R.-W.; Fan, X.-E.; Chen, H.-J. Quantitation of the hydroxycinnamic acid derivatives and the glycosides of flavonols and flavones by UV absorbance after identification by LC−MS. *J. Agric. Food Chem.* **2012**, *60*, 544−553.

(10) Arion, W. J.; Canfield, W. K.; Ramos, F. C.; Schindler, P. W.; Burger, H. J.; Hemmerle, H.; Schubert, G.; Below, P.; Herling, A. W. Chlorogenic acid and hydroxylnitro-benzaldehyde: New inhibitors of hepatic glucose 6-phosphatase. *Arch. Biochem. Biophys.* **1997**, *339*, 315−322.

(11) Lin, L.-Z.; Harnly, J. M. Identification of hydroxycinnamoyl-quinic acids of *Arnica* flowers and burdock roots using a standardized LC-DAD-ESI/MS profiling method. *J. Agric. Food Chem.* **2008**, *56*, 10105−10114.

(12) Tousch, D.; Lajoix, A.-D.; Hosy, E.; Azay-Milhau, J.; Ferrare, K.; Jahannault, C.; Cros, G.; Petit, P. Chicoric acid, a new compound able to enhance insulin release and glucose uptake. *Biochem. Biophys. Res. Commun.* **2008**, *377*, 131−135.

(13) Dubois, M.; Gilles, K. A.; Hamilton, J. K.; Rebers, P. A.; Smith, F. Colorimetric method for determination of sugars and related substances. *Anal. Chem.* **1956**, *28*, 350−356.

(14) Bradford, M. M. A dye binding assay for protein. *Anal. Biochem.* **1976**, *72*, 248−254.

(15) Singh, R. P.; Murthy, K. N. C.; Jayaprakasha, G. K. Studies on the antioxidant activity of pomegranate (*Punica granatum*) peel and seed extracts using in vitro models. *J. Agric. Food Chem.* **2002**, *50*, 81−86.

(16) Jaiswal, R.; Kuhnert, N. Identification and characterization of five new classes of chlorogenic acids in burdock (*Arctium lappa* L.) roots by liquid chromatography/tandem mass spectrometry. *Food Funct.* **2011**, *2*, 63−71.

(17) IUPAC. IUPAC Commission on the Nomenclature of Organic Chemistry (CNOC) and IUPAC-IUB Commission on Biochemical Nomenclature (CBN). Nomenclature of cyclitols. Recommendations. *Biochem. J.* **1976**, *153*, 23−31.

(18) Wang, P. H.; Moller, D.; Flier, J. S.; Nayak, R. C.; Smith, R. J. Coordinate regulation of glucose transporter function, number, and gene expression by insulin and sulfonylureas in L6 rat skeletal muscle cells. *J. Clin. Invest.* **1989**, *84*, 62−67.

(19) Seglen, P. O. Preparation of isolated rat liver cells. *Methods Cell. Biol.* **1976**, *13*, 29−83.
(20) Andersen, B.; Rassov, A.; Westergaard, N.; Lundgren, K. Inhibition of glycogenolysis in primary rat hepatocytes by 1,4-dideoxy-1,4-imino-D-arabinitol. *Biochem. J.* **1999**, *342*, 545−550.
(21) Arden, S. D.; Zahn, T.; Steegers, S.; Webb, S.; Bergman, B.; O'Brien, R. M.; Hutton, J. C. Molecular cloning of a pancreatic islet-specific glucose-6-phosphatase catalytic subunit-related protein. *Diabetes* **1999**, *48*, 531−542.
(22) Murataliev, M. B.; Vulfson, E. N. The effect of 1-cyclohexyl-3-(2 morpholinoethyl) carbodiimide on the rat liver microsomal glucose-6-phosphatase system. *Eur. J. Biochem.* **1986**, *160*, 401−405.
(23) Asfari, M.; Janjic, D.; Meda, P.; Li, G.; Halban, P. A.; Wollheim, C. B. Establishment of 2-mercaptoethanol-dependant differentiated insulin-secreting cell lines. *Endocrinology* **1992**, *130*, 167−178.
(24) Trinder, P. Determination of blood glucose using an oxidase-peroxydase system with a non-carcinogenic chromogen. *J. Clin. Pathol.* **1969**, *22*, 158−161.
(25) Herbert, V.; Law, K. S.; Gottlieb, C. W.; Bleicher, S. J. Coated charcoal immunoassay of insulin. *J. Clin. Endocrinol. Metab.* **1965**, *25*, 1375−1384.
(26) Liu, J.; Cai, Y.-Z.; Wong, R. N. S.; Lee, C. K.-F.; Tang, S. C. W.; Sze, S. C. W.; Tong, Y.; Zhang, Y. Comparative analysis of caffeoylquinic acids and lignans in roots and seeds among various burdock (*Arctium lappa*) genotypes with high antioxidant activity. *J. Agric. Food Chem.* **2012**, *60* (16), 4067−4075.
(27) Mennen, L. I.; Walker, R.; Bennetau-Pelissero, C.; Scalbert, A. Risks and safety of polyphenol consumption. *Am. J. Clin. Nutr.* **2005**, *81* (suppl), 326S−9S.
(28) Martin, K. R.; Appel, C. L. Polyphenols as dietary supplements: A double-edged sword. *Nutr. Diet.* **2010**, *2* (suppl), 1−12.
(29) Wu, C.; Zhang, X.; Zhang, X.; Luan, H.; Sun, G.; Sun, X.; Wang, X.; Guo, P.; Xu, X. The caffeoylquinic acid-rich *Pandanus tectorius* fruit extract increases insulin sensitivity and regulates hepatic glucose and lipid metabolism in diabetic db/db mice. *J. Nutr. Biochem.* **2014**, *25*, 412−419.
(30) Bassoli, B. K.; Cassolla, P.; Borba-Murad, G. R.; Constantin, J.; Salgueiro-Pagadigorria, C. L.; Bazotte, R. B.; da Silva, R. S.; de Souza, H. M. Chlorogenic acid reduces the plasma glucose peak in the oral glucose tolerance test: Effects on hepatic glucose release and glycaemia. *Cell Biochem. Funct.* **2008**, *26* (3), 320−328.
(31) Matsui, T.; Ebuchi, S.; Fujise, T.; Abesundara, K. J. M.; Doi, S.; Yamada, H.; Matsumoto, K. Strong antihyperglycemic effects of water-soluble fraction of Brazilian propolis and its bioactive constituent, 3,4,5-tri-*O*-caffeoylquinic acid. *Biol. Pharm. Bull.* **2004**, *27* (11), 1797−1803.
(32) Mc Carty, M. F. A chlorogenic acid-induced increase in GLP-1 production may mediate the impact of heavy coffee consumption of diabetes risk. *Med. Hypotheses* **2005**, *64*, 848−853.

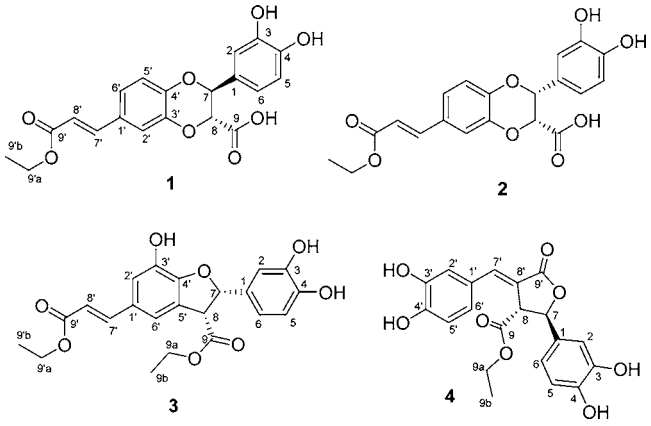

Figure 1. Structures of compounds **1**−**4**.

IR spectra were recorded on a Bruker IFS-66/S FT-IR spectrometer (Bruker, Karlsruhe, Germany). Circular dichroism (CD) spectra were measured on a Jasco J-715 spectropolarimeter (Jasco, Easton, MD, USA). Ultraviolet (UV) spectra were recorded with a Shimadzu UV-1601 UV−visible spectrophotometer (Shimadzu, Tokyo, Japan). High-resolution (HR)-electrospray ionization (ESI) mass spectra were recorded on a SI-2/LCQ DecaXP liquid chromatography (LC)-mass spectrometer (Thermo Scientific, West Palm Beach, FL, USA). Nuclear magnetic resonance (NMR) spectra were recorded on a Varian UNITY INOVA 500 NMR spectrometer (Varian, Palo Alto, CA, USA) operating at 500 MHz (^{1}H) and 125 MHz (^{13}C), with chemical shifts given in ppm (δ). Preparative high performance liquid chromatography (HPLC) used a Gilson 306 pump (Gilson, Middleton, WI, USA) with a Shodex refractive index detector (Shodex, New York, NY, USA). Column chromatography was performed with a silica gel 60 (Merck, 70−230 mesh and 230−400 mesh) and RP-C_{18} silica gel (Merck, 230−400 mesh). The packing material for molecular sieve column chromatography was Sephadex LH-20 (Pharmacia, Uppsala, Sweden). Merck precoated silica gel F_{254} plates and reversed-phase (RP)-18 F_{254s} plates (Merck, Darmstadt, Germany) were used for thin-layer chromatography (TLC). Spots were detected on TLC under UV light or by heating after spraying with anisaldehyde-sulfuric acid.

Plant Material. The seeds of *P. nil* were purchased at Kyungdong herbal market, Seoul, Korea, in July 2006, and were identified by one of the authors (K. R. Lee). A voucher specimen (SKKU 2006-7) has been deposited in the herbarium of the School of Pharmacy, Sungkyunkwan University, Suwon, Korea.

Extraction and Isolation. Air-dried *P. nil* seeds (10 kg) were extracted with 50% EtOH (3 × 4 L, on each of 3 days) at room temperature and filtered. The filtrate was evaporated under reduced pressure using a rotavapor to obtain the EtOH extract (1.4 kg), which was suspended in distilled H_2O (7.2 L) in a separatory funnel to be partitioned in sequence with *n*-hexane, chloroform ($CHCl_3$), ethyl acetate (EtOAc), and butanol (*n*-BuOH), which yielded 10, 7, 10, and 550 g of dried organic fractions, respectively. A bioactivity-guided fractionation method was used for isolation work. Each fraction was tested for cytotoxic activity against A549, SK-OV-3, SK-MEL-2, and HCT-15 human tumor cell lines using a sulforhodamine B (SRB) bioassay, which proved that the EtOAc-soluble fraction showed the strongest activity (IC_{50}: 28.74, 23.45, 10.32, and 17.81 μM, respectively against A549, SK-OV-3, SK-MEL-2, and HCT-15 cells). The most active EtOAc-soluble fraction (10 g) was chromatographed on the open-column of silica gel (230−400 mesh, 300 g) eluting with $CHCl_3$/methanol (MeOH) (10:1 → 1:1, gradient system) to give six fractions (A−F). Each fraction obtained from the EtOAc-soluble fraction was further tested for cytotoxic activity against the four aforementioned cell lines to identify the active fraction. Fractions B, D, and F displayed activity: fraction B (IC_{50}: 5.31, 3.10, 8.39, and 6.11 μM, respectively, against A549, SK-OV-3, SK-MEL-2, and HCT-15), fraction D (IC_{50}: 40.24, 33.97, 12.60, and 20.37 μM, respectively), and fraction F (IC_{50}: 48.92, 27.09, 15.74, and 19.40 μM, respectively). Fraction B (2.5 g) was chromatographed further on the open-column of RP-C_{18} silica gel (230−400 mesh, 150 g) eluting with MeOH/H_2O (3:2 → 4:1, gradient system) to give seven subfractions (B1−B7). Fraction B7 (50 mg) was purified by semipreparative normal-phase HPLC (*n*-hexane/EtOAc, 1:1), using an Apollo Silica column (250 mm × 10 mm i.d., 5 μm, Alltech, Nicholasville, KY, USA) to give **3** (24 mg, t_R = 16.0 min). Fraction D (2.5 g) was applied to an RP-C_{18} silica gel open-column chromatograph (60% MeOH) to yield six subfractions (D1−D6). Fraction D2 (340 mg) was passed through a Sephadex LH-20 column eluted with 100% MeOH and further purified by semipreparative reversed-phase HPLC (30% MeCN), using an Econosil RP-18 column (250 mm × 10 mm i.d., 10 μm, Alltech, Nicholasville, KY, USA) to give **4** (16 mg, t_R = 15.0 min). Fraction F (3.6 g) was passed through a Sephadex LH-20 column and eluted with CH_2Cl_2/MeOH (1:1) to obtain four subfractions (F1−F4). Finally, fraction F3 (700 mg) was purified by semipreparative reversed-phase HPLC (18% MeCN) to yield **1** (20 mg, t_R = 18.0 min) and **2** (13 mg, t_R = 18.5 min).

*Pharbilignanol A (**1**).* White amorphous powder. $[\alpha]_D^{25}$ −9.1 (*c* 0.80, MeOH). UV (MeOH) λ_{max} (log ε): 259 (4.05), 306 (3.62) nm. CD (MeOH): $[\theta]_{220}$ −2810, $[\theta]_{234}$ +3140, $[\theta]_{282}$ +1530. IR (KBr) ν_{max}: 3361, 2946, 2833, 1726, 1630, 1610, 1511, 1451, 1370, 1033, 670 cm^{-1}. For ^{1}H (500 MHz) and ^{13}C (125 MHz) NMR spectroscopic data, see Table 1. Electrospray ionization (ESI)-MS (positive-ion mode) *m*/*z*: 409 $[M + Na]^+$. High-resolution (HR)-ESIMS (positive-ion mode) *m*/*z*: 409.0902 $[M + Na]^+$ (calcd for $C_{20}H_{18}NaO_8$, 409.0899).

Table 1. ^{1}H (500 MHz) and ^{13}C NMR (125 MHz) Data of Compounds 1−2 in CD_3OD[a]

	1		2	
position	δ_C	δ_H	δ_C	δ_H
1	130.0		129.9	
2	115.7	6.88 d (2.0)	116.1	6.84 d (2.0)
3	145.2		144.7	
4	146.2		146.1	
5	116.3	6.74 d (8.5)	116.2	6.63 d (8.5)
6	120.3	6.76 dd (8.5, 2.0)	120.8	6.73 dd (8.5, 2.0)
7	78.2	5.16 d (6.0)	77.4	5.59 d (3.5)
8	81.0	4.53 d (6.0)	78.2	4.68 d (3.5)
9	174.5		173.4	
1′	129.1		129.7	
2′	117.5	7.15 d (2.0)	117.5	7.15 d (2.0)
3′	146.7		146.9	
4′	147.1		147.2	
5′	118.6	6.96 d (8.0)	118.9	7.02 d (8.0)
6′	123.2	7.11 dd (8.0, 2.0)	122.9	7.11 dd (8.0, 2.0)
7′	146.2	7.58 d (16.0)	146.4	7.58 d (16.0)
8′	116.7	6.34 d (16.0)	117.0	6.35 d (16.0)
9′	169.2	169.2		
9′a	61.6	4.22 q (7.0)	61.6	4.22 q (7.0)
9′b	14.7	1.32 t (7.0)	14.7	1.32 t (7.0)

[a] δ is in ppm, and *J* values are in parentheses. The assignments were based on ^{1}H,^{1}H−COSY, HMQC, and HMBC experiments.

*Pharbilignanol B (**2**).* White amorphous powder. $[\alpha]_D^{25}$ −15.6 (*c* 0.35, MeOH). UV (MeOH) λ_{max} (log ε): 259 (4.05), 306 (3.63) nm. CD (MeOH): $[\theta]_{234}$ −2610, $[\theta]_{250}$ +2530, $[\theta]_{288}$ −890. IR (KBr) ν_{max}: 3361, 2947, 2833, 1727, 1630, 1608, 1507, 1450, 1355, 1033, 670 cm^{-1}. For ^{1}H (500 MHz) and ^{13}C (125 MHz) NMR spectroscopic data, see Table 2. ESIMS (positive-ion mode) *m*/*z*: 409 $[M + Na]^+$. HR-ESIMS (positive-ion mode) *m*/*z*: 409.0906 $[M + Na]^+$ (calcd for $C_{20}H_{18}NaO_8$, 409.0899).

Table 2. ^{1}H (500 MHz) and ^{13}C NMR (125 MHz) Data of Compounds 3−4[a]

	3[b]		4[c]	
position	δ_C	δ_H	δ_C	δ_H
1	132.0		132.5	
2	113.0	6.84 d (2.0)	113.4	6.74 d (2.5)
3	144.0		147.0	
4	144.3		147.3	
5	115.6	6.77 d (8.0)	116.7	6.78 d (8.0)
6	118.7	6.70 dd (8.0, 2.0)	118.4	6.67 dd (8.0, 2.5)
7	87.1	5.97 d (8.0)	82.5	5.59 d (3.0)
8	55.6	4.21 d (8.0)	54.6	4.24 dd (3.0, 2.0)
9	170.8		172.0	
9a	62.1	4.25 q (7.0)	63.2	4.19 q (7.0)
9b	14.1	1.27 t (7.0)	14.4	1.20 t (7.0)
1′	128.7		126.8	
2′	116.4	6.97 br s	118.2	7.06 d (2.0)
3′	140.3		150.1	
4′	148.5		146.9	
5′	125.6		116.7	6.83 d (8.0)
6′	117.5	7.03 br s	125.5	6.99 dd (8.0, 2.5)
7′	144.9	7.52 d (16.0)	142.4	7.59 d (2.5)
8′	115.6	6.21 d (16.0)	119.8	
9′	168.1		173.8	
9′a	60.8	4.25 q (7.0)		
9′b	14.2	1.32 t (7.0)		

[a] δ is in ppm, and J values are in parentheses. The assignments were based on ^{1}H,^{1}H−COSY, HMQC, and HMBC experiments. [b] ^{1}H and ^{13}C NMR data were recorded in $CDCl_3$. [c] ^{1}H and ^{13}C NMR data were recorded in CD_3OD.

*Pharbilignanol C (**3**).* White amorphous powder. $[\alpha]_D^{25}$ −26.3 (*c* 0.65, MeOH). UV (MeOH) λ_{max} (log ε): 229 (4.23), 256 (3.98), 322 (3.75) nm. CD (MeOH): $[\theta]_{212}$ +3630, $[\theta]_{234}$ +4570, $[\theta]_{254}$ +8870, $[\theta]_{279}$ −1210, $[\theta]_{335}$ +4820. IR (KBr) ν_{max}: 3356, 2947, 2832, 1723, 1690, 1603, 1512, 1451, 1350, 1275, 1033, 670 cm^{-1}. For ^{1}H (500 MHz) and ^{13}C (125 MHz) NMR spectroscopic data, see Table 2. ESIMS (positive-ion mode) *m*/*z*: 415 $[M + H]^+$. HR-ESIMS (positive-ion mode) *m*/*z*: 415.1388 $[M + H]^+$ (calcd for $C_{22}H_{23}O_8$, 415.1393).

*Pharbilignanol D (**4**).* White amorphous powder. $[\alpha]_D^{25}$ +27.7 (*c* 0.40, EtOH). UV (MeOH) λ_{max} (log ε): 258 (4.03), 310 (3.74) nm. CD (MeOH): $[\theta]_{211}$ +2160, $[\theta]_{231}$ +4550, $[\theta]_{245}$ +4710, $[\theta]_{263}$ −5020, $[\theta]_{276}$ +6780. IR (KBr) ν_{max}: 3361, 2947, 2833, 1734, 1642, 1604, 1526, 1450, 1294, 1202, 1032, 670 cm^{-1}. For ^{1}H (500 MHz) and ^{13}C (125 MHz) NMR spectroscopic data, see Table 2. ESIMS (positive-ion mode) *m*/*z*: 387 $[M + H]^+$. HR-ESIMS (positive-ion mode) *m*/*z*: 387.1087 $[M + H]^+$ (Calcd for $C_{20}H_{19}O_8$, 387.1080).

Cell Cultures. All tumor cell cultures were maintained using RPMI1640 cell growth medium (Gibco, Carlsbad, CA, USA) supplemented with 5% fetal bovine serum (FBS) (Gibco), 100 units/mL penicillin, and 100 mg/mL streptomycin. The human tumor cell lines, A549 (nonsmall cell lung carcinoma), SK-OV-3 (ovary malignant ascites), SK-MEL-2 (skin melanoma), and HCT-15 (colon adenocarcinoma) were provided by the National Cancer Institute (NCI). BV2 murine microglia cells were generously provided by Dr. E. Choi from Korea University (Seoul, Korea) and were maintained in Dulbecco's modified Eagle's medium (DMEM) supplemented with 5% FBS, 100 units/mL penicillin, and 100 mg/mL streptomycin. All cells were incubated at 37 °C in a humidified incubator with 5% CO_2.

Cytotoxicity Assessment. The cytotoxicity of the isolates (**1**−**4**) against cultured human tumor cell lines was evaluated by the SRB method. The assays were performed at the Korea Research Institute of Chemical Technology. Each tumor cell line was inoculated over standard 96-well flat-bottom microplates and then incubated for 24 h at 37 °C in a humidified atmosphere of 5% CO_2. The attached cells were then incubated with the serially diluted samples. After continuous exposure to the compounds for 48 h, the culture medium was removed from each well, and the cells were fixed with 10% cold trichloroacetic acid at 4 °C for 1 h. After washing with tap water, the cells were stained with 0.4% SRB dye and incubated for 30 min at room temperature. The cells were washed again and then solubilized with 10 mM unbuffered Tris base solution (pH 10.5). The absorbance was measured spectrophotometrically at 520 nm with a microtiter plate reader. Doxorubicin (Sigma-Aldrich, St. Luuis, Mo, USA; ≥98% purity) was used as the positive control. Doxorubicin had IC_{50} values against A549, SK-OV-3, SK-MEL-2, and HCT15 of 0.02, 0.02, 0.03, and 0.08 μM, respectively.

Measurement of Nitric Oxide (NO) Production and Cell Viability in Lipopolysaccharide (LPS)-Activated BV-2 Cells. Murine microglia BV-2 cells were plated in wells of a 96-well plate (3×10^4 cells/well). After 24 h, cells were pretreated with samples for 30 min and then stimulated with 100 ng/mL LPS for another 24 h. Nitrite in the culture media, a soluble oxidation product of NO, was measured by the Griess reaction. The supernatant (50 μL) was harvested and mixed with an equal volume of Griess reagent (1% sulfanilamide and 0.1% *N*-1-naphthylethylenediamine dihydrochloride in 5% phosphoric acid). After 10 min, the absorbance at 540 nm was measured using a microplate reader (Emax, Molecular Device, Sunnyvale, CA, USA). Graded sodium nitrite solutions were used as standards to calculate nitrite concentration. Cell viability was measured using a 3-[4,5-dimethylthiazol-2-yl]-2,5-diphenyltetrazolium bromide (MTT) colorimetric assay. The NO synthase inhibitor, N^G-monomethyl-L-arginine (L-NMMA, Sigma-Aldrich), served as the positive control.

RESULTS AND DISCUSSION

Isolation and Structural Elucidation of Compounds. Air-dried seeds of *P. nil* were extracted with 50% aqueous EtOH. The hydroethanolic extract showed considerable cytotoxicity against some human tumor cell lines using the SRB bioassay. The hydroethanolic extract was subjected to solvent-partition into *n*-hexane, chloroform, ethyl acetate, and *n*-butanol fractions. The ethyl acetate fraction showed the strongest activity and was subjected to separation and purification by successive column chromatography over silica gel and Sephadex LH-20, and semipreparative HPLC, which resulted in the isolation and identification of four new lignans, named pharbilignans A−D (**1**−**4**) (Figure 1).

Pharbilignan A (**1**) was isolated as a white, amorphous powder. Its HR-ESIMS at *m*/*z* 409.0902 $[M + Na]^+$ (calcd for $C_{20}H_{18}NaO_8$, 409.0899) and NMR spectroscopic data (Table 1) established the molecular formula as $C_{20}H_{18}O_8$, implying the existence of 12 of unsaturation. The UV absorption maxima at 259 and 306 nm were indicative of a lignan skeleton.[14] The IR absorption bands of **1** were characteristic of hydroxy (3361 cm^{-1}), carbonyl (1726 cm^{-1}), and aromatic ring (1610 and 1451 cm^{-1}) functional groups. The ^{1}H NMR spectrum of **1** showed signals attributable to a deshielded benzylic oxymethine proton at δ_H 5.16 (H-7) and an oxygenated proton at δ_H 4.53 (H-8), implying the linkage of two phenylpropanoid units via a 1,4-dioxane bridge.[15,16] Detailed inspection of the ^{1}H and ^{13}C NMR spectra (Table 1) of **1** showed that the signals were similar to those of americanol A[15] and were almost identical to those of 7-[(1*E*)-2-carboxyethenyl]-3-(3,4-dihydroxyphenyl)-2,3-dihydro-1,4-benzodioxin-2-carboxylic acid, except for the presence of an ethoxy group in **1**.[16,17] The skeleton was confirmed by heteronuclear multiple bond correlation (HMBC), showing correlations from H-7 (δ_H 5.16) to C-2, C-6, C-9, and C-4′ and correlations from H-8 (δ_H 4.53) to C-1, and C-3′. The HMBC correlation between H-9′a (δ_H 4.22) and

dx.doi.org/10.1021/jf501470k | J. Agric. Food Chem. 2014, 62, 7746−7752

C-9′ (δ_C 169.2) indicated the presence of an ethoxy group at C-9′ (Figure 2).

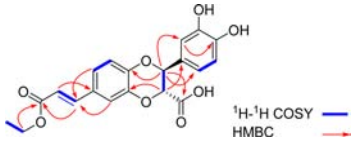

Figure 2. Key ^{1}H−^{1}H COSY (blue line) and HMBC (red arrow) correlations of **1**.

It is difficult to determine whether benzodioxane-type neolignans belong to the americanol or isoamericanol type. Recently, it was reported that the chemical shift differences between H-2′ and H-5′ in the ^{1}H NMR spectra measured in CD_3OD allow for an unambiguous identification of the isomeric structures.[15,16] The ^{1}H NMR spectrum of **1** showed a large difference of 0.19 ppm between H-2′ (δ_H 7.15) and H-5′ (δ_H 6.96), consistent with that of the americanol type.[15,16] Difference nuclear Overhauser effect (NOE) experiments were used to assign the structure, where significant long-range NOE enhancements could be observed between H-2′ and H-8 and between H-5′ and H-7, confirming the americanol type. Additionally, the americanol type of **1** was supported by a small difference of 0.4 ppm between C-3′ (δ_C 146.7) and C-4′ (δ_H 147.1) in the ^{13}C NMR data of **1**.[15,16] The coupling constant ($J_{7,8}$ = 6.0 Hz) between H-7 and H-8, and nuclear Overhauser effect spectroscopy (NOESY) correlation (H-6/H-8) indicated a *trans*-relationship of H-7/H-8 on the 1,4-benzodioxane ring.[17,18] The absolute configuration of the C-7 and C-8 was designated as *S* and *R*, respectively, on the basis of CD data ($[\theta]_{220}$ −2810, $[\theta]_{234}$ +3140, $[\theta]_{282}$ +1530), which was in good agreement with the configuration reported in the literature.[19] Therefore, the structure of **1** was established as depicted in Figure 1.

Pharbilignan B (**2**) was obtained as a white, amorphous powder. Its molecular formula $C_{20}H_{18}O_8$ (12 of unsaturation) was derived by HR-ESIMS *m*/*z* 409.0906 $[M + Na]^+$ (calcd for $C_{20}H_{18}NaO_8$, 409.0899). The similarity of UV and IR absorption bands in **1** and **2** suggested that **2** had the same lignan skeleton as **1**. The ^{1}H and ^{13}C NMR spectra (Table 1) of **2** also showed a similarity with those of **1**, except for the chemical shifts of C-7 and C-8 in **2** (δ_H 5.59, H-7; δ_C 77.4, C-7 and δ_H 4.68, H-8; δ_C 78.2, C-8). Thus, compound **2** is an isomer of **1** with a 1,4-dioxane bridge. A large difference of 0.13 ppm between H-2′ (δ_H 7.15) and H-5′ (δ_H 7.02) and a small difference of 0.3 ppm between C-3′ (δ_C 146.9) and C-4′ (δ_H 147.2) in the NMR data of **2** indicated that compound **2** should be americanol type **1**.[15,16] A relatively small coupling constant ($J_{7,8}$ = 3.5 Hz) between H-7 and H-8 suggested a *cis*-configuration of H-7 and H-8 in the molecule.[17,18] The absolute configuration of the C-7 and C-8 was assigned on the basis of CD data ($[\theta]_{234}$ −2610, $[\theta]_{250}$ +2530, $[\theta]_{288}$ −890), allowing the assignment of 7*R* and 8*R* configurations, respectively.[20] Accordingly, the structure of **2** was elucidated as depicted in Figure 1.

Pharbilignan C (**3**) was isolated as a white, amorphous powder. It had the molecular formula $C_{22}H_{22}O_8$ with 12 of unsaturation, as deduced by HR-ESIMS *m*/*z* 415.1388 $[M + H]^+$ (calcd for $C_{22}H_{23}O_8$, 415.1393). The UV absorption maxima at 256 and 322 nm indicated a lignan skeleton for **3**.[14] The IR absorption bands of **3** exhibited the presence of hydroxy (3356 cm^{-1}), carbonyl (1723 cm^{-1}), and aromatic ring (1603 and 1451 cm^{-1}) moieties. The ^{1}H and ^{13}C NMR data for C-7 and C-8 in **3** (δ_H 5.97, H-7; δ_C 87.1, C-7; and δ_H 4.21, H-8; δ_C 55.6, C-8) supported that compound **3** was a dihydro[*b*]-benzofuran-type neolignan, and the ^{1}H and ^{13}C NMR spectra (Table 2) of **3** were very similar to those of caffeicin F, except for the presence of two ethoxy groups, indicating that compound **3** was an analogue of caffeicin F with two ethoxy groups as a side chain.[18] The structure was verified by an HMBC experiment showing correlations from H-7 (δ_H 5.97) to C-2, C-6, C-9, and C-4′ and from H-8 (δ_H 4.53) to C-1, C-4′, and C-6′. The HMBC correlations H-9a/C-9 (δ_C 170.8) and H-9′a/C-9′ (δ_C 168.1) allowed the assignment of an ethoxy group at C-9 and the other ethoxy group at C-9′ (Figure 3).

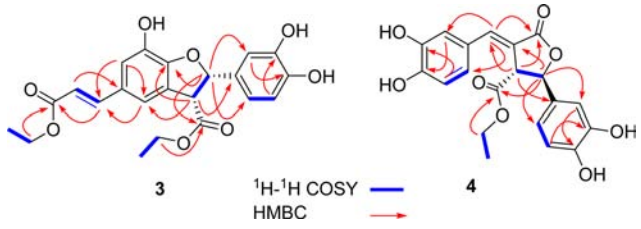

Figure 3. Key ^{1}H−^{1}H COSY (blue line) and HMBC (red arrow) correlations of **3** and **4**.

The relative configuration at H-7 and H-8 was established on the basis of their coupling constant ($J_{7,8}$ = 8.0 Hz), which was consistent with a *cis*-configuration of H-7 and H-8 in **3**.[21] This arrangement was also supported by a NOESY correlation between H-7 and H-8 but the lack of NOESY correlations between H-7 and H-9a or between H-8 and H-2/H-6. Finally, the positive Cotton effect at 254 nm in the CD spectrum of **3** suggested the absolute configuration at C-7 as 7*S*.[22,23] This analysis also determined an 8*R* configuration based on the relative stereochemistry previously determined as *cis*-configuration between H-7 and H-8. Therefore, the structure of **3** was assigned the structure depicted in Figure 1. A survey of the literature revealed that an epimer of **3** with the 7*S*,8*S*-form was synthesized previously.[24]

Pharbilignan D (**4**) had the molecular formula $C_{20}H_{18}O_8$, with 12 of unsaturation, deduced by HR-ESIMS *m*/*z* 387.1087 $[M + H]^+$ (calcd for $C_{20}H_{19}O_8$, 387.1080). The ^{1}H and ^{13}C NMR spectra (Table 2) of **4** were similar to those of phellinsin A, except for the presence of an ethoxy group, which suggested that compound **4** was the same lignan-type as phellinsin A.[25] The lignan skeleton was verified by HMBC correlations of H-7/C-2, C-6, C-9, C-8′, and C-9′; H-8/C-1, C-7′, and C-9′; and H-7′/C-8, C-2′, C-6′, and C-9′ (Figure 3). The presence of an ethoxy group at C-9 in **4** was confirmed by the HMBC correlation of H-9a/C-9. The geometry of the double bond at C-7′ was established to be *E* on the basis of the chemical shift of H-7′ (δ_H 7.59) and the long-range coupling constant ($J_{7',8}$ = 2.5 Hz).[26,27] This was confirmed by the NOESY experiment where the correlations between H-8 (δ_H 4.24) and H-2′ (δ_H 7.06)/ H-6′ (δ_H 6.99) are shown. Furthermore, a *trans*-configuration of H-7 and H-8 was concluded by the relatively small coupling constant ($J_{7,8}$ = 2.5 Hz), combined with a NOESY correlation between H-8 and H-2/H-6.[26,27] The configurations of C-7 and C-8 were assigned as 7*R** and 8*R** on the basis of the optical rotation value of **4** ($[\alpha]_D^{25}$ +27.7).[27] Moreover, its CD spectrum showed Cotton effects at 231 and 263 nm ($[\theta]_{231}$ +4550, $[\theta]_{263}$ −5020). According to the above

dx.doi.org/10.1021/jf501470k | J. Agric. Food Chem. 2014, 62, 7746−7752

Table 3. Cytotoxic Activities of Compounds 1−4 against Four Cultured Human Tumor Cell Lines Using the SRB Assay

	IC_{50} (μM)[a]			
compd	A549	SK-OV-3	SK-MEL-2	HCT-15
1	>30.0	27.45 ± 0.75	15.23 ± 1.30	19.84 ± 0.13
2	>30.0	22.67 ± 2.15	17.64 ± 0.52	21.72 ± 1.18
3	1.42 ± 0.38	0.16 ± 0.03	0.20 ± 0.11	0.14 ± 0.07
4	>30.0	21.59 ± 0.83	13.77 ± 0.28	16.52 ± 1.20
doxorubicin[b]	0.02 ± 0.003	0.02 ± 0.002	0.03 ± 0.007	0.08 ± 0.008

[a]IC_{50} value of compounds against each tumor cell line. The IC_{50} value was defined as the concentration (μM) that caused 50% inhibition in cell growth in vitro. Data are expressed as the mean ± SD of three distinct experiments [b]Doxorubicin as a positive control.

analysis, the structure of **4** was elucidated as depicted in Figure 1.

It was likely that compounds **1**−**4** were artifacts of the isolation procedure because 50% EtOH was used as the solvent for extraction. In order to verify that compounds **1**−**4** are authentic natural products, another supply of the plant was obtained and extracted with MeOH and EtOAc, respectively. The resulting extracts were tested using LC-MS analyses, alone and coinjected with the pure compounds **1**−**4**. Compounds **1**−**4** were all identified on the HPLC chromatogram of the crude extracts. The increase in peak areas corresponding to **1**−**4** supported that these compounds are indeed naturally occurring metabolites.

Evaluation of Antitumor Activity. All isolated compounds (**1**−**4**) were evaluated for antitumor activity by determining their inhibitory effects on four human tumor cell lines including A549 (nonsmall cell lung carcinoma), SK-OV-3 (ovary malignant ascites), SK-MEL-2 (skin melanoma), and HCT-15 (colon adenocarcinoma) using a SRB bioassay.[28] The results (Table 3) showed that all tested lignans had consistent cytotoxicity against the SK-OV-3, SK-MEL-2, and HCT-15 cell lines but not A549, with IC_{50} values of 0.14 to 27.45 μM. In particular, compound **3** exhibited the most potent cytotoxicity against the A549, SK-OV-3, SK-MEL-2, and HCT-15 cell lines with IC_{50} values of 1.42 ± 0.38, 0.16 ± 0.03, 0.20 ± 0.11, and 0.14 ± 0.07 μM, respectively, which was slightly less active but comparable to that of the positive control, doxorubicin.

The data obtained in this biological test suggested that the dihydrobenzofuran-type lignan, the skeleton of compound **3**, could be a promising class for antitumor agents toward human tumor cell lines. A series of such synthetic dihydrobenzofuran lignans and related derivatives have been explored for their potential antitumor and antiproliferative activities.[24,29] In our previous search for bioactive compounds from Korean natural resources, 3-(β-D-glucopyranosyloxymethyl)-2-(4-hydroxy-3-methoxyphenyl)-5-(3-hydroxypropyl)-7-methoxydihydrobenzofuran, (7*S*,8*R*)-dihydrodehydrodiconiferyl alcohol, and (7*S*,8*R*)-dehydrodiconiferyl alcohol 4-*O*-β-D-glucopyranoside, belonging to the dihydrobenzofuran-type lignan, were identified as minor constituents in Korean traditional medicines.[30−32] However, none exhibited a promising cytotoxic effect in the previously used human tumor cell lines (IC_{50} > 30.0 μM). This result was in agreement with the structure−activity relationship (SAR) analysis of dihydrobenzofuran lignans for antitumor activity in human tumor cell lines, where it was reported that (i) apparently, methylation of the hydroxyl group in two aromatic moieties reduces the activity, (ii) reduction of the double bond in the C_3 side chain causes a decrease in the activity, and (iii) reduction of the ester functionality to a primary alcohol leads to loss in the activity.[29] The SAR analysis suggests that the dihydrobenzofuran-type lignan, compound **3**, which contains the ethyl ester functionality and the double bond in the side chain, but no methoxyl group, yields the greatest cytotoxicity against all tumor cell lines presently examined. However, the dihydrobenzofuran-type lignan has been reported to have a pharmacophore for inhibitors of tubulin polymerization binding at the colchicine site, which can lead to the display of antimitotic and potential antitumor properties.[29] Particularly, methyl(*E*)-3-{2-(3,4-dihydroxyphenyl)-7-hydroxy-3-methoxycarbonyl-2,3-dihydro-1-benzofuran-5yl}prop-2-enoate, which is very similar to compound **3** with the only difference being the replacement of methyl ester functionality, was recently determined to be a potential antitumor agent by causing G2/M arrest and apoptosis involving the mitochondrial controlled pathway.[33]

Progression of cancer is associated with inflammatory responses.[34] Inflammatory gene expression is often negatively correlated with cancer stage and prognosis.[35−37] Nonsteroidal anti-inflammatory drugs are effective for cancer prevention, further supporting a role for inflammation in tumor progression.[38] On the basis of the expanded understanding that an anti-inflammatory agent could be a potential antitumor molecule, we evaluated the anti-inflammatory activities of the isolates (**1**−**4**) through the measurement of nitrite, a soluble oxidation product of NO, in the culture medium using the Griess reaction in LPS-activated BV-2 microglial cells.[39] BV-2 has both the phenotypic and functional properties of reactive microglia cells and is activated following stimulation by various agents including LPS.[40,41] Activated BV-2 cells exhibit various inflammatory responses including the production of the proinflammatory factor NO.[42] Among the tested compounds, compound **3** showed significant inhibitory effects on LPS-stimulated NO production with an IC_{50} of 12.8 μM in BV-2 microglial cells at 20 μM without cytotoxicity, which actually is more potent than N^G-monomethyl-L-arginine (L-NMMA), an inducible NO synthase (iNOS) inhibitor (IC_{50} value of 17.7 μM).[39] The rest of the compounds did not show any significant inhibitory effects on NO production in the range of 1 to 20 μM. Toxicity induced by overproduction of NO, when it becomes chronic, can lead to enhanced cell replication that is a risk factor for many cancers,[43] and oxidative damage to DNA by NO has been associated with the development of cancer.[44] Compound **3** thus could be a potential antitumor agent via the inhibition of NO formation.

In conclusion, it appears that lignans **1**−**4** isolated from the most active EtOAc fraction are at least partially responsible for the antitumor effect of the crude EtOH extract of the morning glory seeds. Among them, pharbilignan C (**3**) is the most promising by virtue of the most potent cytotoxicity in various human tumor cell lines and anti-inflammatory activity involving the inhibited production of NO.

■ ASSOCIATED CONTENT

Supporting Information

NMR data for compounds **1**−**4**. This material is available free of charge via the Internet at http://pubs.acs.org.

■ AUTHOR INFORMATION

Corresponding Author

*Tel: 82-31-290-7710. Fax: 82-31-290-7730. E-mail: krlee@skku.edu.

Funding

This research was supported by the Global Leading Technology Program of the Office of Strategic R&D Planning (OSP) funded by the Ministry of Knowledge Economy, Republic of Korea (10039303).

Notes

The authors declare no competing financial interest.

■ ACKNOWLEDGMENTS

We thank Drs. E. J. Bang, S. G. Kim, and J. J. Seo at the Korea Basic Science Institute for their aid in the NMR and MS spectra measurements.

■ REFERENCES

(1) Kitts, D. D.; Yuan, Y. V.; Wijewickreme, A. N.; Thompson, L. U. Antioxidant activity of the flaxseed lignan secoisolariciresinol diglycoside and its mammalian lignan metabolites enterodiol and enterolactone. *Mol. Cell. Biochem.* **1999**, *202*, 91−100.

(2) Cornwell, T.; Cohick, W.; Raskin, I. Dietary phytoestrogens and health. *Phytochemistry* **2004**, *65*, 995−1016.

(3) Magee, P. J.; Rowland, I. R. Phyto-oestrogens, their mechanism of action: current evidence for a role in breast and prostate cancer. *Br. J. Nutr.* **2004**, *91*, 513−531.

(4) Kim, K. H.; Ha, S. K.; Kim, S. Y.; Youn, H. J.; Lee, K. R. Constituents of *Limonia acidissima* inhibit LPS-induced nitric oxide production in BV-2 microglia. *J. Enzyme Inhib. Med. Chem.* **2010**, *25*, 887−892.

(5) Kim, K. H.; Moon, E.; Kim, S. Y.; Lee, K. R. Lignans from the tuber-barks of *Colocasia antiquorum* var. *esculenta* and their antimelanogenic activity. *J. Agric. Food Chem.* **2010**, *58*, 4779−4785.

(6) Kim, K. H.; Choi, J. W.; Ha, S. K.; Kim, S. Y.; Lee, K. R. Neolignans from *Piper kadsura* and their anti-neuroinflammatory activity. *Bioorg. Med. Chem. Lett.* **2010**, *20*, 409−412.

(7) Kim, K. H.; Kim, H. K.; Choi, S. U.; Moon, E.; Kim, S. Y.; Lee, K. R. Bioactive lignans from the rhizomes of *Acorus gramineus*. *J. Nat. Prod.* **2011**, *74*, 2187−2192.

(8) Kim, K. H.; Ha, S. K.; Choi, S. U.; Kim, S. Y.; Lee, K. R. Bioactive phenolic constituents from the seeds of *Pharbitis nil*. *Chem. Pharm. Bull.* **2011**, *59*, 1425−1429.

(9) Bensky, D.; Gamble, A. *Chinese Herbal Medicine*, revised ed.; Materia Medica; Eastland Press: Seattle, WA, 1993; p 121.

(10) Lee, T. H.; Choi, J. J.; Kim, D. H.; Choi, S.; Lee, K. R.; Son, M.; Jin, M. Gastroprokinetic effects of DA-9701, a new prokinetic agent formulated with Pharbitis Semen and Corydalis Tuber. *Phytomedicine* **2008**, *15*, 836−843.

(11) Kawasaki, T.; Okabe, H.; Nakatsuka, I. Studies on resin glycosides. I. Reinvestigation of the components of pharbitin, a resin glycoside of the seeds of *Pharbitis nil* CHOISY. *Chem. Pharm. Bull.* **1971**, *19*, 1144−1149.

(12) Ono, M.; Noda, N.; Kawasaki, T.; Miyahara, I. Resin glycosides. VII.: Reinvestigation of the component organic and glycosidic acids of pharbitin, the crude ether-insoluble resin glycoside ("convolvulin") of Pharbitidis Semen (seeds of *Pharbitis nil*). *Chem. Pharm. Bull.* **1990**, *38*, 1892−1897.

(13) Yokota, T.; Murofushi, N.; Takahashi, N.; Tamura, S. Gibberellins in immature seeds of *Pharbitis nil*. Part II. Isolation and structures of novel gibberellins, gibberellins A_{26} and A_{27}. *Agric. Biol. Chem.* **1971**, *35*, 573−582.

(14) Kim, Y. L.; Chin, Y. W.; Kim, J. Two new neolignans from the aerial parts of *Rodgersia podophylla*. *Chem. Pharm. Bull.* **2005**, *53*, 103−104.

(15) Waibel, R.; Benirschke, G.; Benirschke, M.; Achenbach, H. Sesquineolignans and other constituents from the seeds of *Joannesia princeps*. *Phytochemistry* **2003**, *62*, 805−811.

(16) Takahasi, H.; Yanagi, K.; Ueda, M.; Nakade, K.; Fukuyama, Y. Structures of 1,4-benzodioxane derivatives from the seeds of *Phytolacca americana* and their neuritogenic activity in primary cultured rat cortical neurons. *Chem. Pharm. Bull.* **2003**, *62*, 805−811.

(17) Matsumoto, K.; Takahashi, H.; Miyake, Y.; Fukuyama, Y. Convenient syntheses of neurotrophic americanol A and isoamericanol A by HRP catalyzed oxidative coupling of caffeic acid. *Tetrahedron Lett.* **1999**, *40*, 3185−3186.

(18) Cilliers, J. J. L.; Singleton, V. L. Characterization of the products of nonenzymic autoxidative phenolic reactions in a caffeic acid model system. *J. Agric. Food Chem.* **1991**, *39*, 1298−1303.

(19) Kim, T. H.; Ito, H.; Hayashi, K.; Hasegawa, T.; Machiguchi, T.; Yoshida, T. Aromatic Constituents from the Heartwood of *Santalum album* L. *Chem. Pharm. Bull.* **2005**, *53*, 641−644.

(20) Arnoldi, A.; Merlini, L. Asymmetric synthesis of 3-methyl-2-phenyl-1,4-benzodioxanes. Absolute configuration of the neolignans eusiderin and eusiderin C and D. *J. Chem. Soc. Perkin Trans. I* **1985**, *1985*, 2555−2557.

(21) Wada, H.; Kido, T.; Tanaka, N.; Murakami, T.; Saiki, Y.; Chen, C. M. Chemical and chemotaxonomical studies of ferns. LXXXI. Characteristic lignans of Blechnaceous ferns. *Chem. Pharm. Bull.* **1992**, *40*, 2099−2101.

(22) Murata, T.; Sasaki, K.; Sato, K.; Yoshizaki, F.; Yamada, H.; Mutoh, H.; Umehara, K.; Miyase, T.; Warashina, T.; Aoshima, H.; Tabata, H.; Matsubara, K. Matrix metalloproteinase-2 inhibitors from *Clinopodium chinense* var. *parviflorum*. *J. Nat. Prod.* **2009**, *72*, 1379−1384.

(23) Yuen, M. S. M.; Xue, F.; Mak, T. C. W.; Wong, H. N. C. On the absolute structure of optically active neolignans containing a dihydrobenzo[*b*]furan skeleton. *Tetrahedron* **1998**, *54*, 12429−12444.

(24) Mierta, S. V.; Dyckb, S. V.; Schmidtc, T. J.; Brund, R.; Vlietincka, A.; Lemiereb, G.; Pieters, L. Antileishmanial activity, cytotoxicity and QSAR analysis of synthetic dihydrobenzofuran lignans and related benzofurans. *Bioorg. Med. Chem.* **2005**, *13*, 661−669.

(25) Hwang, E. I.; Yun, B. S.; Kim, Y. K.; Kwon, B. M.; Kim, H. G.; Lee, H. B.; Jeong, W. J.; Kim, S. U. Phellinsin A, a novel chitin synthases inhibitor produced by *Phellinus* sp. PL3. *J. Antibiot.* **2000**, *53*, 903−911.

(26) Wan, X.; Liu, H.; Huang, X.; Luo, J.; Kong, L. Biotransformation of caffeic acid by *Momordica charantia* peroxidase. *Can. J. Chem.* **2008**, *86*, 821−830.

(27) Dall'Acqua, S.; Viola, G.; Piacente, S.; Cappelletti, E. M.; Innocenti, G. Cytotoxic constituents of roots of *Chaerophyllum hirsutum*. *J. Nat. Prod.* **2004**, *67*, 1588−1590.

(28) Skehan, P.; Storeng, R.; Scudiero, D.; Monks, A.; MaMahon, J.; Vistica, D.; Warren, J. T.; Bokesch, H.; Kenney, S.; Boyd, M. R. New colorimetric cytotoxicity assay for anticacer-drug screening. *J. Natl. Cancer Inst.* **1990**, *82*, 1107−1112.

(29) Pieters, L.; Van Dyck, S.; Gao, M.; Bai, R.; Hamel, E.; Vlietinck, A.; Lemiere, G. Synthesis and biological evaluation of dihydrobenzofuran lignans and related compounds as potential antitumor agents that inhibits tubilin polymerization. *J. Med. Chem.* **1999**, *42*, 5475−5481.

(30) Kim, K. H.; Lee, K. H.; Choi, S. U.; Kim, Y. H.; Lee, K. R. Terpene and phenolic constituents of *Lactuca indica* L. *Arch. Pharm. Res.* **2008**, *31*, 983−988.

(31) Park, C. H.; Kim, K. H.; Lee, I. K.; Lee, S. Y.; Choi, S. U.; Lee, J. H.; Lee, K. R. Phenolic constituents of *Acorus gramineus*. *Arch. Pharm. Res.* **2011**, *34*, 1289−1296.

(32) Kim, K. H.; Moon, S. R.; Kim, C. S.; Woo, K. W.; Choi, S. U.; Lee, K. R. Lignan glucosides form *Sinomenium acutum* rhizomes. *Biosci. Biotechnol. Biochem.* **2013**, *77*, 2144−2147.
(33) Bose, J. S.; Gangan, V.; Prakash, R.; Jain, S. K.; Manna, S. K. A dihydrobenzofuran lignan induces cell death by modulating mitochondrial pathway and G2/M cell cycle arrest. *J. Med. Chem.* **2009**, *52*, 3184−3190.
(34) Rakoff-Nahoum, S. Why cancer and inflammation? *Yale J. Biol. Med.* **2006**, *79*, 123−130.
(35) Chang, H. Y.; Sneddon, J. B.; Alizadeh, A. A.; Sood, R.; West, R. B.; Montgomery, K.; Chi, J. T.; van de Rijn, M.; Botstein, D.; Brown, P. O. Gene expression signature of fibroblast serum response predicts human cancer progression: similarities between tumors and wounds. *PLoS Biol.* **2004**, *2*, E7.
(36) Galon, J.; Costes, A.; Sanchez-Cabo, F.; Kirilovsky, A.; Mlecnik, B.; Lagorce-Pagès, C.; Tosolini, M.; Camus, M.; Berger, A.; Wind, P.; Zinzindohoué, F.; Bruneval, P.; Cugnenc, P. H.; Trajanoski, Z.; Fridman, W. H.; Pagès, F. Type, density, and location of immune cells within human colorectal tumors predict clinical outcome. *Science* **2006**, *313*, 1960−1964.
(37) Wang, W. S.; Chen, P. M.; Wang, H. S.; Liang, W. Y.; Su, Y. Matrix metalloproteinase-7 increases resistance to Fas-mediated apoptosis and is a poor prognostic factor of patients with colorectal carcinoma. *Carcinogenesis* **2006**, *27*, 1113−1120.
(38) Ulrich, C. M.; Bigler, J.; Potter, J. D. Non-steroidal anti-inflammatory drugs for cancer prevention: promise, perils and pharmacogenetics. *Nat. Rev. Cancer* **2006**, *6*, 130−140.
(39) Reif, D. W.; McCreedy, S. A. N-nitro-L-arginine and N-monomethyl-L-arginine exhibit a different pattern of inactivation toward the three nitric oxide synthases. *Arch. Biochem. Biophys.* **1995**, *320*, 170−176.
(40) Blasi, E.; Barluzzi, R.; Bocchini, V.; Mazzolla, R.; Bistoni, F. Immortalization of murine microglial cells by a v-raf/v-myc carrying retrovirus. *J. Neuroimmunol.* **1990**, *27*, 229−237.
(41) Dheen, S. T.; Kaur, C.; Ling, E. A. Microglial activation and its implications in the brain diseases. *Curr. Med. Chem.* **2007**, *14*, 1189−1197.
(42) Hanisch, U. K. Microglia as a source and target of cytokines. *Glia* **2002**, *40*, 140−155.
(43) Ames, B. N.; Gold, L. S. Too many rodent carcinogens: mitogenesis increases mutagenesis. *Science* **1990**, *249*, 970−971.
(44) Tamir, S.; Tannenbaum, S. R. The role of nitric oxide (NO.) in the carcinogenic process. *Biochim. Biophys. Acta* **1996**, *1288*, F31−F36.

diffusion method.[25] The minimum inhibitory concentration (MIC) value of RHSE was 0.822% (v/v). The in vivo antibacterial activity of RHSE (1.0%, v/v) was also examined in a *Salmonella*-infected Balb/c mouse model. Mice infected with a sublethal dose of the pathogens were administered intraperitoneally a 1.0% solution of RHSE at four 12 h intervals during the 48 h experimental period. The results showed that RHSE antimicrobial potency approached that of the standard medical antibiotic vancomycin and that the combination of RHSE and vancomycin acted synergistically against the foodborne bacteria. The inclusion of RHSE (1.0% v/w) as part of a standard mouse diet fed for 2 weeks decreased mortality of 10 mice infected with lethal doses of *Salmonella*. Photomicrographs of histological changes in liver tissues show that RHSE also protected the liver against *Salmonella*-induced pathological necrosis lesions. These beneficial results suggest that RHSE has the potential to complement wood-derived smokes as an antimicrobial flavor formulation for use in human food and animal feeds.

Because RHSE inhibited *Salmonella* in culture and in vivo, expectations are that it might protect the mice against *Salmonella* LPS-induced murine endotoxemia (sepsis). The objective of this study was to determine whether this is the case.

MATERIALS AND METHODS

Test Compounds. *Salmonella enterica* LPS and D-galactosamine (GalN) were purchased from Sigma-Aldrich (St. Louis, MO, USA). All reagents were of analytical grade and used without further purification. The RPMI 1640 medium, Hank's Balanced Salt Solution (HBSS), fetal bovine serum (FBS), and other cell culture reagents were obtained from Hyclone Laboratories (Logan, UT, USA). The enzyme kit for glutamic-oxaloacetic transaminase/glutamic-pyruvic transaminase (GOT/GPT) was the product of Asan Pharmaceutical Co. (Seoul, Korea). The ELISA kit for the quantification of tumor necrosis factor-α (TNF-α) was obtained from Biosource USA (Camarillo, CA, USA).

Chemicals. The rice hull liquid smoke extract (RHSE) was obtained from Daewon GSI (Waegwan, Korea). The industrial production of the commercially available RHSE, characterized chemical components, and beneficial bioactivities in chemical and cell assays were described in our previous publication in this journal.[22] GC/MS analysis showed that the rice hull extract contained 161 characterized aliphatic, aromatic, and heterocyclic compounds. The aqueous extract was acidic, had a specific gravity of 1.007, and contained 0.026% solids. The in vitro antioxidative activity of the extract as determined by the DPPH assay was similar to that of the widely used food antioxidant BHT (butylated hydroxytolune).

Animals and Treatment. The protocol for the mice studies was approved by the Ethics Committee for Animal Care and Use, Ajou University, Republic of Korea. All experiments were performed in compliance with the relevant laws and institutional guidelines. Five-week-old female BALB/c mice were purchased from Orient Bio Inc. (Seoul, Korea) and were hosted under a 12 h light/dark cycle at 20−22 °C and relative humidity of 50 ± 10%. The mice were fed freely a pelletized commercial chow diet obtained from Orient Bio Inc. (catalogue no. 5L79) and sterile tap water during the entire period. After acclimation for 1 week, the mice were then divided into three groups (n = 10), avoiding any intergroup difference in body weight. The endotoxemic shock assay in a murine model was carried out following the method of Yun et al.,[26] with modification. Briefly, two groups of mice each (PBS-treated control and RHSE-treated experimental group) were fed a pelletized commercial chow diet without and with RHSE (1.0%, v/w) during the entire experimental period. After 14 consecutive days of RHSE administration, the control and experimental mice were injected with LPS and GalN (5 μg/kg and 700 mg/kg, respectively) via an intraperitoneal (ip) route. To determine the survival rate, lethal dose of LPS and GalN (20 μg/kg and 700 mg/kg, respectively) were employed. The mice were observed for 60 h after the LPS and GalN challenge. Apart from the determination of the survival rate, the other experiments were carried out 4 h after challenge of a sublethal dose of the LPS and GalN (5 μg/kg and 700 mg/kg, respectively). The mice were sacrificed by CO_2 asphyxia, and livers and kidneys from each group were excised and weighed. The blood from the three groups of mice was collected by cardiac puncture and allowed to clot at room temperature for 30 min. Subsequently, the blood was subjected to centrifugation at 2000g for 30 min. The separated serum was stored at −20 °C until use.

Histology of Liver Tissue. For histological analysis, the liver tissue of the mice was fixed with paraformaldehyde (4%) in phosphate buffer (0.5 M; pH 7.4). The tissue was rinsed with water, dehydrated with ethanol, and embedded in paraffin. The tissues were sectioned into samples (4 μm) and mounted onto glass slides. The sections were then dewaxed using xylene and ethanol and stained with hematoxylin and eosin Y (H&E) to reveal the hemorrhagic necrosis in the liver. Histological changes were observed under a light microscope at ×100 magnification.

Serum Nitrite and Nitrate Levels. Serum nitrite and nitrate levels were measured primarily following the method of Misko et al.,[27] with some modification. Briefly, serum was filtered through an Ultrafree-MC microcentrifuge filter unit (Millipore, Bedford, MA, USA) for 1 h at 14000 rpm to remove the hemoglobin released by cell lysis. The serum (50 μL) was incubated in a reaction mixture [40 mM Tris Cl, 40 μM reduced β-nicotinamide adenine dinucleotide phosphate, 40 μM flavin adenine dinucleotide, and nitrate reductase 0.05 U/mL at pH 7.9] at 37 °C for 15 min. Reduced samples were incubated with an equal volume of Griess reagent [1% sulfanilamide and 0.1% *N*-(1-naphthyl)ethylenediamine dihydrochloride in 5% phosphoric acid] at room temperature for 15 min. The absorbance at 570 nm was recorded using a microplate reader (model 550, Bio-Rad). The total nitrate/nitrite concentration was determined by comparison with a reduced sodium nitrate standard curve.

TNF-α and Serum Transaminase. TNF-α level was determined using an enzyme-linked immunosorbent assay (ELISA) kit specific for murine TNF-α according to the manufacturer's instruction. After the termination of all reactions, the absorbance of the chromophore at 420 nm was measured using a microplate reader. The activities of serum enzymes glutamic-oxaloacetic transaminase (GOT) and glutamine-pyruvic transaminase (GPT) were estimated using a commercial colorimetric kit. Briefly, appropriately diluted serum (200 μL) was added to the reaction solution (0.1 mL; L-asparaginic acid and α-ketoglutaric acid mixture). The resultant mixture was incubated at 37 °C for 30 min (GPT) or 60 min (GOT), and 2,4-dinitrophenylhydrazine (1 mL) was added. After incubation at room temperature for 20 min, 0.4 N sodium hydroxide (10 mL) was added, and the absorbance of the solution was measured at 505 nm using a microplate reader.

Antioxidant Enzyme Activities in Mouse Liver. The liver tissue was homogenized in 10 volumes of phosphate-buffered saline (PBS) on ice for 30 s using a power-driven Polytron homogenizer (Pro Scientific, Monroe, CT, USA). The homogenate was centrifuged at 9000g at 4 °C for 20 min. The supernatant was recovered and used to measure two antioxidant enzyme activities, catalase and superoxide dismutase. For the catalase activity assay at time zero, each supernatant (1.8 mL) was mixed with PBS (0.2 mL) containing hydrogen peroxide (10 mM). The reaction mixture (1 mL) was immediately added to a cuvette and placed into a UV−vis spectrophotometer (model V-550, Jasco, Tokyo, Japan). The enzyme activity was observed via degradation of hydrogen peroxide as determined by a decrease in UV light absorbance at 240 nm over time. The measurement of absorbance was taken at 15 s intervals after the addition of the homogenate to the hydrogen peroxide buffer. Units of catalase activity per milligram of protein were calculated following the method of Nandi et al.[28] For the superoxide dismutase (SOD)-like activity assay, the supernatant (100 μL) was mixed with a homogenizing buffer (1.5 mL; 50 mM Tris, 10 mM EDTA, pH 8.5), then pyrogallol (100 μL; 7.2 mM) was added, and the reaction mixture was incubated at 25 °C for 10 min. The reaction was terminated by adding 1 M HCl (50 μL), and the absorbance was then measured at 420 nm. One unit was

defined as the amount of enzyme that inhibited the oxidation of pyrogallol by 50%. The activity was expressed as units per milligram of protein.[29]

Myeloperoxidase (MPO) Activity. MPO activity was assayed according to the method of Bralley et al.[30] Briefly, the supernatants recovered from lung and kidney tissue homogenates (30 μL) were added to the reaction mixture (200 μL) consisting of 100 μL of PBS (80 mM phosphate, 140 mM NaCl, pH 5.4), 85 μL of PBS2 (220 mM phosphate, 140 mM NaCl, pH 5.4), and 0.017% H_2O_2 (15 μL). The reaction was started by adding tetramethylbenzidine (18.4 μM) in aqueous dimethylformamide (8%; 20 μL) and was left standing for 3 min at 37 °C. The reaction was stopped by the addition of sodium acetate buffer (30 μL; 1.46 M; pH 3.0). The absorbance (OD) of the supernatant was then read in a microplate reader at 655 nm for 30 min. The reaction rate (change in OD/time) was derived from an initial slope of the curve. A calculation curve was used to show the rate of reaction plotted against the concentration of a standard human MPO preparation.

Serum Urea Nitrogen and Creatinine. The concentration of urea nitrogen and creatinine were determined using the commercial QuantiChrom creatinine assay kit and QuantiChrom urea assay kit, respectively (Bioassay System, Hayward, CA, USA).

Statistical Analysis. Results are expressed as the mean ± SD of three independent experiments. Significant differences between means were determined by ANOVA test using the Statistical Analysis Software package SAS (Cary, NC, USA). $P < 0.05$ is regarded as significant.

RESULTS AND DISCUSSION

Dose Selection. The reason why we did not assess the dose-related mortality in mice is because (a) in previous studies, we found that 1% to be the optimal dose for expressing maximum levels of anti-inflammatory activities, including inhibition of NO production and release of anti-inflammatory cytokines and protection of cell viabilities without any side effects both in vitro and in mice; and (b) we also used 1% of the rice hull extract to protect *Salmonella*-infected mice against mortality. The present complementary study shows that the 1% concentrations also protected the mice against endotoxemia.

Effects of RHSE on Weights and Histopathology of Mouse Liver. Figure 1 shows that the induction of endotoxemia by LPS/GalN resulted in a significant increase in liver weight as well as in the formation of hemorrhagic lesions in the liver tissues. By contrast, no apparent hepatic injury was observed in the vehicle-treated control group. As anticipated, RHSE treatment through dietary administration (1%, v/w) markedly blocked the hemorrhagic liver injury as well as hepatomegaly induced by a lethal dose of the LPS/GalN challenge. These results demonstrate strongly that RHSE protected the mice against injury of a major organ associated with endotoxemia.

Effects of RHSE on Antioxidant Enzyme Activities in Mouse Liver. To find out whether reactive oxygen species (ROS) level is a crucial factor for the incidence of liver injury associated with LPS/GalN-induced endotoxemia, the activity of hepatic antioxidant enzymes including catalase and SOD-like enzymes was evaluated in the control and experimental mice groups.

Table 1 shows that in the liver of LPS/GalN-treated mice, the dietary administration of RHSE induced a significant suppression of the catalase and SOD-like enzyme activities from 24.53 to 7.18 U/mg protein (~71% change) and from 18.65 to 8.49 U/mg protein (54% change), respectively. These results show that dietary administration of RHSE reduced oxidative damage in the liver induced by the LPS/GalN challenge.

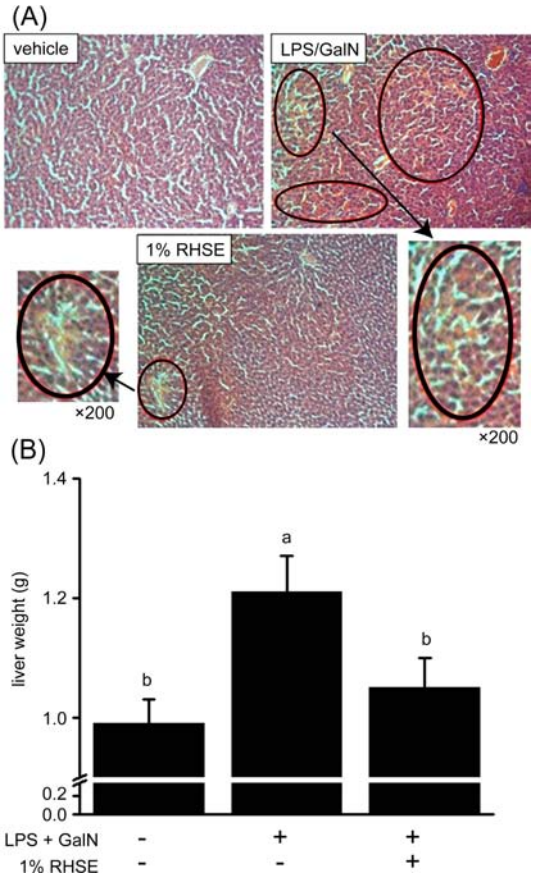

Figure 1. Modulation of liver injury in LPS/GalN-induced endotoxemic mice by administration of diet supplemented with RHSE (1.0%, v/w). (A) Liver sections from LPS/GalN (5 μg/kg/700 mg/kg)-administered mice show disorganized hepatic architecture, intense cellular necrosis, and marked hemorrhagic lesions compared with the liver section of vehicle-treated mice. Dietary administration of RHSE markedly ameliorated LPS/GalN-induced liver damage. (B) Increase in liver weight by LPS/GalN injection was reversed by dietary administration of RHSE. Mice were sacrificed 4 h after LPS/GalN treatment, and the livers were weighed. Each liver specimen was fixed with 4% paraformaldehyde, and sections were stained with hematoxylin and eosin (H&E). Magnification, ×100 for each of the three treatments, and ×200 for the magnified sections. Circular areas indicate local hemorrhage and necrosis regions. Bars not sharing a common letter are significantly different between groups at $p < 0.05$.

Table 1. Effects of RHSE on Antioxidant Catalase and Superoxide Dismutase (SOD)-Like Enzyme Activities in LPS/GalN-Induced Endotoxemic Mouse Liver[a]

sample	catalase activity (U/mg protein)	SOD-like activity (U/mg protein)
vehicle	3.12 ± 0.28 a	4.77 ± 0.32 a
LPS/GalN (5 μg/kg/700 mg/kg)	24.5 ± 2.0 b	18.7 ± 1.5 b
RHSE (1.0%, v/w) dietary administration	7.18 ± 0.43 c	8.49 ± 0.69 c

[a]Data are expressed as the mean ± SD ($n = 10$). Values in each column with the same letter are not significantly different between groups at $p < 0.05$.

Effects of RHSE on Liver Transaminase Enzyme Activities in Mouse Serum. Figure 2 shows that, compared

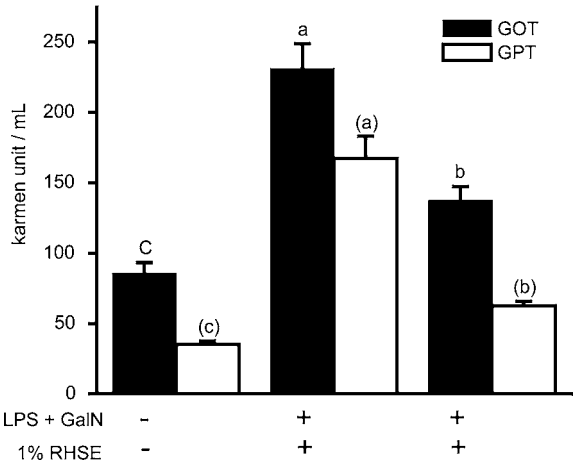

Figure 2. Effect of dietary administration of RHSE (1.0%, v/w) on glutamic-oxaloacetic/glutamic-pyruvic transaminases (GOP/GTP) in LPS/GalN-induced endotoxemic mice. The mice were pretreated with RHSE for 2 weeks through dietary administration before the LPS/GalN treatment. Mice were sacrificed 4 h after LPS/GalN (5 μg/kg/700 mg/kg) treatment, and blood was collected to produce serum. Bars not sharing a common letter are significantly different between groups at $p < 0.05$.

with the normal control group, the liver enzyme levels of the transaminase GOT and GPT, primary enzymes that serve as an index of hepatic injury, increased significantly in the serum of the LPS/GalN-treated mice. In the mice fed an RHSE-supplemented diet (1.0% v/w), GOT and GPT activities decreased substantially from 231.7 to 137.3 U/mL (~41% change) and from 167.3 to 62.8 U/mL (~63% change), respectively. These results show that RHSE protected the liver against necrotic injury associated with endotoxemia.

Effects of RHSE on TNF-α and Nitrite Concentrations in Mouse Serum. Table 2 shows that TNF-α and nitrite/nitrate levels in the serum of LPS/GalN-induced endotoxemic mice were markedly increased compared with those observed in the normal control mice group (~7.8- and 20.2-fold increases, respectively). The dietary administration of RHSE significantly decreased the TNF-α and nitrite/nitrate concentrations from 401.6 to 156.2 pg/mL (~61% change) and from 19.3 to 3.2 μM (~83% change), respectively. These results show that RHSE protected the treated mice against increased production of nitrite/nitrate, a source of bioactive nitric oxide (NO), and TNF-α, a critical factor associated with the cause of the endotoxemia syndrome.

Table 2. Effects of RHSE on Tumor Necrosis Factor-α (TNF-α) and Nitrite Concentrations in Mouse Serum[a]

sample	TNF-α (pg/mL)	nitrite (μM)
vehicle	51.3 ± 3.9 a	0.951 ± 0.021 a
LPS/GalN (5 μg/kg/700 mg/kg)	401 ± 26 b	19.3 ± 1.1 b
RHSE (1.0%, v/w) dietary administration	156 ± 14 c	3.205 ± 0.053 c

[a]Data are expressed as the mean ± SD (n = 10). Values in each column with the same letter are not significantly different between groups at $p < 0.05$.

Effects of RHSE on Lung and Kidney Injuries in Endotoxemic Mouse. The evidence of necrotic cell injuries in the lung and kidney in LPS/GalN challenged endotoxemia was further confirmed by the observed decreases in the MPO enzyme activity induced by RHSE (Table 3). The results in Table 3 show that RHSE treatment via the oral route markedly decreased the MPO activities from 12.6 to 4.3 U/g protein (~66% change) in the lung and from 6.8 to 2.5 U/g protein (~63% change) in the kidney, respectively.

The protective effect of RHSE treatment against LPS/GalN-induced renal injury was also evaluated by measuring creatinine and urea nitrogen concentrations in the serum. Table 3 also shows that creatinine and urea nitrogen levels in the serum of endotoxemic mice were significantly greater than those in normal mice group (~1.7- and ~4-fold increases, respectively), indicating the association of endotoxemia with the release of these amino acid metabolites from the damaged kidney. By contrast, RHSE administration via the oral route significantly lowered LPS/GalN-triggered increases in creatinine and urea nitrogen levels by up to 35.6% and 62.0%, respectively. The present study shows that RHSE neutralized the toxic effect of the LPS-induced endotoxin by reducing the expression of the cytokine TNF-α and production of ROS.

Effects of RHSE on Mortality of Endotoxemic Mice. To determine the therapeutic effects of RHSE on life expectancy, a lethal dose of LPS/GalN was used to induce sepsis and to determine the protection by RHSE against mortality. Each group of 10 mice was fed on a diet supplemented with RHSE (1%, v/w) during the entire experimental period. Figure 3 shows that mice treated with a lethal dose of LPS/GalN all died after 50 h. By contrast, the group treated with RHSE through dietary administration survived >60 h. These observations demonstrate strikingly the potential of RHSE to protect mice against sepsis-induced lethality, presumably via down-regulating the production of the pro-inflammatory cytotoxic factors such as reactive oxygen radicals, cytokines, and nitric oxide.

Mechanistic Aspects. We previously reported[22−25] that the extract elicited changes in the expression of seven genes and two biomarkers [(prostaglandin E2 (PGE2) and leukotriene-4 (LTB4)] associated with inflammation. The extract also inhibited generation of NO through inhibition of inducible nitric oxide synthase (iNOS) gene expression and suppressed

Table 3. Effects of RHSE on Lung and Kidney Injuries in LPS/GalN-Induced Endotoxemic Mice Assessed by Changes in Myeloperoxidase, Creatinine, and Blood Urea Nitrogen (BUN) Concentrations[a]

sample	myeloperoxidase (U/g protein)		BUN (mg/dL)	creatinine (mg/dL)
	lung	kidney		
vehicle	2.922 ± 0.093 a	1.86 ± 0.11 a	0.334 ± 0.018 a	14.2 ± 1.1 a
LPS/GalN (5 μg/kg/700 mg/kg)	12.59 ± 0.89 b	6.83 ± 0.23 b	0.582 ± 0.033 b	56.9 ± 4.4 b
RHSE (1.0%, v/w) dietary administration	4.32 ± 0.12 c	2.51 ± 0.18 c	0.375 ± 0.021 c	21.6 ± 1.5 c

[a]Data are expressed as the mean ± SD (n = 10). Values in each column with the same letter are not significantly different between groups at $p < 0.05$.

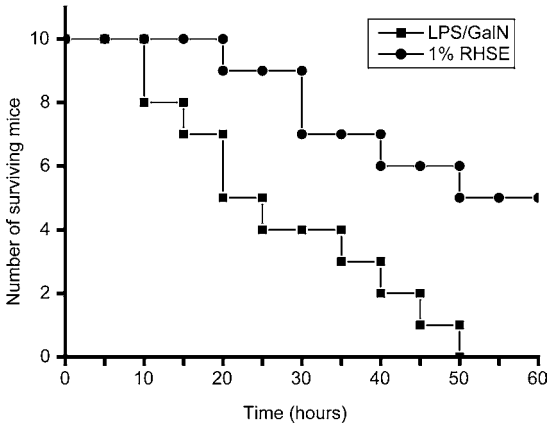

Figure 3. Histogram showing the effect of dietary administration of RHSE (1.0%, v/w) on LPS/GalN-induced endotoxemia induced lethality. BALB/c mice were fed RHSE-supplemented diet for 2 weeks and then challenged ip with a lethal dose of LPS/GalN (20 μg and 700 mg per kg body weight). RHSE was then again administered through the same route during the entire experimental period. Plotted values are mean values of triplicate determinations.

the inflammatory reaction through inhibition of pro-inflammatory gene expressions, including tumor necrosis factor-α (TNF-α), interleukin-1β (IL-1β), and interleukin-6 (IL-6) and increased the production of interferon-γ (IFN-γ) produced by the spleen, suggesting that it stimulated the immune system.

In the present study, we report that the extract suppressed the production of TNF-α, confirming its anti-inflammatory properties as well as the antioxidative enzymes catalase and superoxide dismutase, suggesting that the beneficial effects might also be associated with inhibition of cell-damaging reactive oxygen species (ROS).

On the basis of the mentioned biomarkers, it seems that the antiendotoxemia mechanism might involve suppression of production of NO, cytokines TNF-α, IL-β, and IL-6, and the eicasinoids PGE2 and LTB4, and the inhibition of ROS, thus blocking the observed organ injuries caused by endotoxin-induced acute inflammation.

Related Studies. There have been other recent reports of natural compounds that have antiendotoxemia properties and they are described briefly here, in context of the present study.

We found that a polysaccharide isolated from the liquid culture of *Lentinus edodes* (Shiitake) mushroom mycelia containing black rice bran did not inhibit the growth of *Salmonella* in vitro but did protect mice against LPS-GalN-induced liver, lung, and kidney injuries and inflammation and enhanced the survival of the toxic shock-induced mice by blocking oxidative stress and TNF-α production, suggesting that the novel polysaccharide has the potential to serve as a new functional food.[31]

Other researchers recently reported that flucoidan, a sulfated polysaccharide from the brown alga *Fucus evanescens*, increased resistance to LPS, increased the survival time, and prevented endotoxin-induced damage in mice through the inhibition of pro-inflammatory cytokines (TNF-α and IL-6), attenuation of microcirculatory disorders, and regulation of the immune system.[32]

The administration of the plant phenolic antioxidant chlorogenic acid is reported to prevent mortality of mice induced by endotoxemia and polymicrobial sepsis through modulation of cytokine and chemokine release, suppression of immune cell apoptosis, and enhanced bacterial elimination without apparent adverse effects, suggesting the need for the evaluation of this and other plant antioxidants as potential therapeutic agents.[10] Similar promising results have been reported with the phenolic antimicrobial carvacrol, a natural compound present in oregano oil, which is used as a salad dressing.[33]

It has also been shown that the antimicrobial and anti-inflammatory natural phenolic compound 3,4,5-trihydroxybenzoic acid protected mice against LPS-induced endotoxemia and associated symptoms and biomarkers.[34]

Interestingly, cocoa (*Theobroma cacao*), a polyphenol-rich food added to a high-fat diet reduced metabolic endotoxemia and adipose tissue inflammation in mice by modulating eicosanoid metabolism.[35]

Another murine study showed that a bactericidal peptide derived from zebra fish phosvitin inhibited LPS-induced tumor necrosis factor (TNF-α) and interleukin (IL-1β) in mice and increased the survival of endotoxemic mice and thus has the potential for the clinical treatment of LPS-induced sepsis.[36]

The antioxidant ascorbic acid (vitamin C) inhibited alcohol-induced endotoxemia in guinea pigs, suggesting that the vitamin has the potential to decrease endotoxemia symptoms by reducing small intestinal bacterial overgrowth (SIBO) and the activation of NF-kB and the synthesis of cytokines.[37]

Acute and chronic consumption of red wine, a rich source of antioxidant and antimicrobial flavonoids,[38] by middle-aged men increased the *Bifidobacterium* and *Prevotella* gut microbiota that correlated negatively with LPS concentration.[39] A similar beneficial effect was observed with the wine polyphenolic compounds resveratrol[40] and quercetin.[41]

Gossypol, an anti-inflammatory compound present in cotton seeds, seems to be a promising therapeutic agent for the treatment of lung injury, owing to its ability to protect mice against LPS-induced acute lung injury and to inhibit the NF-kB and MAPKs signaling pathways.[42]

The antiendotoxemia efficacy of plant phenolic antioxidants mentioned above at the cellular level might be due to their ability to counteract the adverse effects associated with the reduction in the LPS-induced murine hepatic level of the glutathione (GSH) antioxidant that protect liver tissues against injury.[43] It needs to be emphasized, however, that other properties of some proposed antiendotoxemia compounds such as those of gossypol, which is reported to inhibit male spermatogenesis,[44] might reduce their potential value in endotoxemia therapy. Other nonfood related proposed compounds and plant extracts also need to be evaluated for possible toxicity. These considerations suggest that food-related compounds that are considered generally accepted as safe (GRAS) might have advantages over others that need to be evaluated further for possible safety.

In summary, the results of the present and cited studies show that, because the commercially available rice hull liquid smoke extract exhibits antiallergic, antidiabetic, antiendotoxemia, and antimicrobial properties, it has the potential to serve as an antimicrobial food preservative and might contribute to the prevention and therapy of several chronic diseases. Because the chemical nature of the large number of individual compounds in the rice hull smoke extract varied widely, we do not know which individual compound or combination of compounds might be responsible for the observed bioactivity. Future studies should determine the bioactivities of individual compounds isolated from the liquid rice hull extract and the

possible synergism of combinations of the extract, compounds isolated from the extract, and other bioactive food compounds and extracts that have been shown to exhibit beneficial in vivo effects. Such dietary combinations, in which the individual components might exert their effect by different mechanisms, might act as multifunctional foods with therapeutic potential and might make it possible to use lower amounts of each component. It is also necessary to demonstrate that the liquid rice hull smoke is safe. Our in vitro, ex vivo, and in vivo previous and present studies are designed to contribute to this assessment.

AUTHOR INFORMATION

Corresponding Authors

*For S.H.N.: phone, 82-31-219-2619; fax, 82-31-219-1615; E-mail, shnam@ajou.ac.kr.

*For M.F.: phone, 01-510-559-5615; fax, 01-510-559-6162; E-mail, Mendel.Friedman@ars.usda.gov.

Notes

The authors declare no competing financial interest.

ACKNOWLEDGMENTS

We thank Carol E. Levin for assistance with the preparation of the manuscript.

ABBREVIATONS USED

BHT, butylated hydroxytoluene; BPP, pro-processed polymer; BUN, blood urea nitrogen; ELISA, enzyme-linked immunoassay; FBS, fetal bovine serum; GalN, D-galactosamine; GOT, glutamic-oxaloacetic transaminase; GPT, glutamic-pyruvic transaminase; GRAS, generally accepted-as-safe; GSH, reduced glutathione; HBSS, Hank's Balanced Salt Solution; HMGB1, high mobility group box-1 protein; HPAEC-PAD, high performance liquid chromatography with pulsed amperometric detection; IFN-γ, interferon-γ; IL-6, interleukin-6; LPS, lipopolysaccharide; MAPK, mitogen activated protein kinase; MIC, minimum inhibitory concentration; MPO, myeloperoxidase; p-NPP, *p*-nitrophenyl phosphate; PBS, phosphate saline buffer; RHSE, rice hull smoke extract; SIBO, small intestinal bacterial overgrowth; SOD, superoxide dismutase; TNF-α, tumor necrosis factor-α

REFERENCES

(1) Hurley, J. C.; Guidet, B.; Offenstadt, G.; Maury, E. Endotoxemia and mortality prediction in ICU and other settings: underlying risk and co-detection of gram negative bacteremia are confounders. *Crit. Care* **2012**, *16*, R148.

(2) Hurley, J. C.; Opal, S. M. Prognostic value of endotoxemia in patients with Gram-negative bacteremia is bacterial species dependent. *J. Innate Immun.* **2013**, *5*, 555−64.

(3) Samraj, R. S.; Zingarelli, B.; Wong, H. R. Role of biomarkers in sepsis care. *Shock* **2013**, *40*, 358−365.

(4) King, E. G.; Bauza, G. J.; Mella, J. R.; Remick, D. G. Pathophysiologic mechanisms in septic shock. *Lab. Invest.* **2014**, *94*, 4−12.

(5) Lew, W. Y.; Bayna, E.; Molle, E. D.; Dalton, N. D.; Lai, N. C.; Bhargava, V.; Mendiola, V.; Clopton, P.; Tang, T. Recurrent exposure to subclinical lipopolysaccharide increases mortality and induces cardiac fibrosis in mice. *PLoS One* **2013**, *8*, e61057.

(6) Hurley, J. C. Diagnosis of endotoxemia with gram-negative bacteremia is bacterial species dependent: a meta-analysis of clinical studies. *J. Clin. Microbiol.* **2009**, *47*, 3826−3831.

(7) Ostrowski, S. R.; Berg, R. M.; Windelov, N. A.; Meyer, M. A.; Plovsing, R. R.; M?ller, K.; Johansson, P. I. Coagulopathy, catecholamines, and biomarkers of endothelial damage in experimental human endotoxemia and in patients with severe sepsis: a prospective study. *J. Crit. Care* **2013**, *28*, 586−596.

(8) Storka, A.; Fuhrlinger, G.; Seper, M.; Wang, L.; Jew, M.; Leisser, A.; Wolzt, M. *E. coli* endotoxin modulates the expression of Sirtuin proteins in PBMC in humans. *Mediators Inflammation* **2013**, *2013*, 876943.

(9) Yanai, H.; Matsuda, A.; An, J.; Koshiba, R.; Nishio, J.; Negishi, H.; Ikushima, H.; Onoe, T.; Ohdan, H.; Yoshida, N.; Taniguchi, T. Conditional ablation of HMGB1 in mice reveals its protective function against endotoxemia and bacterial infection. *Proc. Natl. Acad. Sci. U. S. A.* **2013**, *110*, 20699−20704.

(10) Lee, C. H.; Yoon, S. J.; Lee, S. M. Chlorogenic acid attenuates high mobility group box 1 (HMGB1) and enhances host defense mechanisms in murine sepsis. *Mol. Med.* **2012**, *18*, 1437−1448.

(11) Yoo, C. H.; Yeom, J. H.; Heo, J. J.; Song, E. K.; Lee, S. I.; Han, M. K. Interferon beta protects against lethal endotoxic and septic shock through SIRT1 upregulation. *Sci. Rep.* **2014**, *4*, 4220.

(12) McPherson, D.; Griffiths, C.; Williams, M.; Baker, A.; Klodawski, E.; Jacobson, B.; Donaldson, L. Sepsis-associated mortality in England: an analysis of multiple cause of death data from 2001 to 2010. *BMJ Open* **2013**, *3*, e002586.

(13) O'Brien, J. M.; Lu, B.; Ali, N. A.; Levine, D. A.; Aberegg, S. K.; Lemeshow, S. Insurance type and sepsis-associated hospitalizations and sepsis-associated mortality among US adults: A retrospective cohort study. *Crit. Care* **2011**, *15*, R130.

(14) Kavanagh, K.; Wylie, A. T.; Tucker, K. L.; Hamp, T. J.; Gharaibeh, R. Z.; Fodor, A. A.; Cullen, J. M. Dietary fructose induces endotoxemia and hepatic injury in calorically controlled primates. *Am. J. Clin. Nutr.* **2013**, *98*, 349−357.

(15) Foo, K. Y.; Hameed, B. H. Utilization of rice husk ash as novel adsorbent: a judicious recycling of the colloidal agricultural waste. *Adv. Colloid Interface Sci.* **2009**, *152*, 39−47.

(16) Salanti, A.; Zoia, L.; Orlandi, M.; Zanini, F.; Elegir, G. Structural characterization and antioxidant activity evaluation of lignins from rice husk. *J. Agric. Food Chem.* **2010**, *58*, 10049−10055.

(17) Garabal, J. I.; Rodriguez-Alonso, P.; Franco, D.; Centeno, J. A. Chemical and biochemical study of industrially produced San Simon da Costa smoked semi-hard cow's milk cheeses: effects of storage under vacuum and different modified atmospheres. *J. Dairy Sci.* **2010**, *93*, 1868−1881.

(18) Morey, A.; Bratcher, C. L.; Singh, M.; McKee, S. R. Effect of liquid smoke as an ingredient in frankfurters on *Listeria monocytogenes* and quality attributes. *Poult. Sci.* **2012**, *91*, 2341−2350.

(19) Montazeri, N.; Himelbloom, B. H.; Oliveira, A. C.; Leigh, M. B.; Crapo, C. A. Refined liquid smoke: a potential antilisterial additive to cold-smoked sockeye salmon (*Oncorhynchus nerka*). *J. Food Prot.* **2013**, *76*, 812−819.

(20) Van Loo, E. J.; Babu, D.; Crandall, P. G.; Ricke, S. C. Screening of commercial and pecan shell-extracted liquid smoke agents as natural antimicrobials against foodborne pathogens. *J. Food Prot.* **2012**, *75*, 1148−1152.

(21) Cadwallader, K. R. Wood Smoke Flavor. In *Handbook of Meat, Poultry and Seafood Quality*; Nollet, L. M. L., Boylston, T., Eds. Blackwell Publishing: Ames, IA, 2007; pp 201−210.

(22) Kim, S. P.; Yang, J. Y.; Kang, M. Y.; Park, J. C.; Nam, S. H.; Friedman, M. Composition of liquid rice hull smoke and anti-inflammatory effects in mice. *J. Agric. Food Chem.* **2011**, *59*, 4570−4581.

(23) Yang, J. Y.; Kang, M. Y.; Nam, S. H.; Friedman, M. Antidiabetic effects of rice hull smoke extract in alloxan-induced diabetic mice. *J. Agric. Food Chem.* **2012**, *60*, 87−94.

(24) Yang, J. Y.; Moon, E.; Nam, S. H.; Friedman, M. Antidiabetic effects of rice hull smoke extract on glucose-regulating mechanism in type 2 diabetic mice. *J. Agric. Food Chem.* **2012**, *60*, 7442−7449.

(25) Kim, S. P.; Kang, M. Y.; Park, J. C.; Nam, S. H.; Friedman, M. Rice hull smoke extract inactivates *Salmonella* Typhimurium in laboratory media and protects infected mice against mortality. *J. Food Sci.* **2012**, *77*, M80−M85.

(26) Yun, S. S.; Kim, S. P.; Kang, M. Y.; Nam, S. H. Inhibitory effect of curcumin on liver injury in a murine model of endotoxemic shock. *Biotechnol. Lett.* **2010**, *32*, 209−214.
(27) Misko, T. P.; Schilling, R. J.; Salvemini, D.; Moore, W. M.; Currie, M. G. A fluorometric assay for the measurement of nitrite in biological samples. *Anal. Biochem.* **1993**, *214*, 11−16.
(28) Nandi, D.; Mishra, M. K.; Basu, A.; Bishayi, B. Protective effects of interleukin-6 in lipopolysaccharide (LPS)-induced experimental endotoxemia are linked to alteration in hepatic anti-oxidant enzymes and endogenous cytokines. *Immunobiology* **2010**, *215*, 443−451.
(29) Aebi, H. Catalase in vitro. *Methods Enzymol.* **1984**, *105*, 121−126.
(30) Bralley, E. E.; Greenspan, P.; Hargrove, J. L.; Wicker, L.; Hartle, D. K. Topical anti-inflammatory activity of *Polygonum cuspidatum* extract in the TPA model of mouse ear inflammation. *J. Inflammation* **2008**, *5*, 1.
(31) Kim, S. P.; Park, S. O.; Lee, S. J.; Nam, S. H.; Friedman, M. A polysaccharide isolated from the liquid culture of *Lentinus edodes* (Shiitake) mushroom mycelia containing black rice bran protects mice against a *Salmonella* lipopolysaccharide-induced endotoxemia. *J. Agric. Food Chem.* **2013**, *61*, 10987−10994.
(32) Kuznetsova, T. A.; Besednova, N. N.; Somova, L. M.; Plekhova, N. G. Fucoidan extracted from *Fucus evanescens* prevents endotoxin-induced damage in a mouse model of endotoxemia. *Mar. Drugs* **2014**, *12*, 886−98.
(33) Feng, X.; Jia, A. Protective effect of carvacrol on acute lung injury induced by lipopolysaccharide in mice. *Inflammation* **2014**, *37*, 1091−1101.
(34) Lee, J. W.; Bae, C. J.; Choi, Y. J.; Kim, S. I.; Kwon, Y. S.; Lee, H. J.; Kim, S. S.; Chun, W. 3,4,5-Trihydroxycinnamic acid inhibits lipopolysaccharide (LPS)-induced inflammation by Nrf2 activation in vitro and improves survival of mice in LPS-induced endotoxemia model in vivo. *Mol. Cell. Biochem.* **2014**, *390*, 143−153.
(35) Gu, Y.; Yu, S.; Park, J. Y.; Harvatine, K.; Lambert, J. D. Dietary cocoa reduces metabolic endotoxemia and adipose tissue inflammation in high-fat fed mice. *J. Nutr. Biochem.* **2014**, *25*, 439−445.
(36) Ding, Y.; Liu, X.; Bu, L.; Li, H.; Zhang, S. Antimicrobial-immunomodulatory activities of zebrafish phosvitin-derived peptide Pt5. *Peptides* **2012**, *37*, 309−313.
(37) Abhilash, P. A.; Harikrishnan, R.; Indira, M. Ascorbic acid suppresses endotoxemia and NF-κB signaling cascade in alcoholic liver fibrosis in guinea pigs: a mechanistic approach. *Toxicol. Appl. Pharmacol.* **2014**, *274*, 215−224.
(38) Friedman, M. Antibacterial, antiviral, and antifungal properties of wines and winery byproducts in relation to their flavonoid content. *J. Agric. Food Chem.* **2014**, *62*, 6025−6042.
(39) Clemente-Postigo, M.; Queipo-Ortuño, M. I.; Boto-Ordoñez, M.; Coin-Aragüez, L.; Roca-Rodriguez, M. D. M.; Delgado-Lista, J.; Cardona, F.; Andres-Lacueva, C.; Tinahones, F. J. Effect of acute and chronic red wine consumption on lipopolysaccharide concentrations. *Am. J. Clin. Nutr.* **2013**, *97*, 1053−1061.
(40) Sebai, H.; Sani, M.; Yacoubi, M. T.; Aouani, E.; Ghanem-Boughanmi, N.; Ben-Attia, M. Resveratrol, a red wine polyphenol, attenuates lipopolysaccharide-induced oxidative stress in rat liver. *Ecotoxicol. Environ. Saf.* **2010**, *73*, 1078−1083.
(41) Chang, Y. C.; Tsai, M. H.; Sheu, W. H.; Hsieh, S. C.; Chiang, A. N. The therapeutic potential and mechanisms of action of quercetin in relation to lipopolysaccharide-induced sepsis in vitro and in vivo. *PLoS One* **2013**, *8*, e80744.
(42) Liu, Z.; Yang, Z.; Fu, Y.; Li, F.; Liang, D.; Zhou, E.; Song, X.; Zhang, W.; Zhang, X.; Cao, Y.; Zhang, N. Protective effect of gossypol on lipopolysaccharide-induced acute lung injury in mice. *Inflammation Res.* **2013**, *62*, 499−506.
(43) Tomasi, M. L.; Ryoo, M.; Yang, H.; Iglesias Ara, A.; Ko, K. S.; Lu, S. C. Molecular mechanisms of lipopolysaccharide-mediated inhibition of glutathione synthesis in mice. *Free Radical Biol. Med.* **2014**, *68*, 148−58.
(44) Wang, X.; Howell, C. P.; Chen, F.; Yin, J.; Jiang, Y. Gossypol—a polyphenolic compound from cotton plant. *Adv. Food Nutr. Res.* **2009**, *58*, 215−63.

MATERIALS AND METHODS

Chemicals. Porcine pancreas α-amylase, amylose, amylopectin, and acarbose were purchased from Sigma-Aldrich Co., Ltd. (St. Louis, MO). α-(2-Chloro-4-nitrophenyl)-β-1,4-galactopyranosylmaltoside (Gal-G2-α-CNP) was purchased from Toyobo Co., Ltd. (Osaka, Japan). Vitexin, isovitexin, orientin, and isoorientin were purchased from Shifeng Biological Technology Co., Ltd. (Shanghai, China), and their structures are shown in Figure 1. Soluble starch was purchased

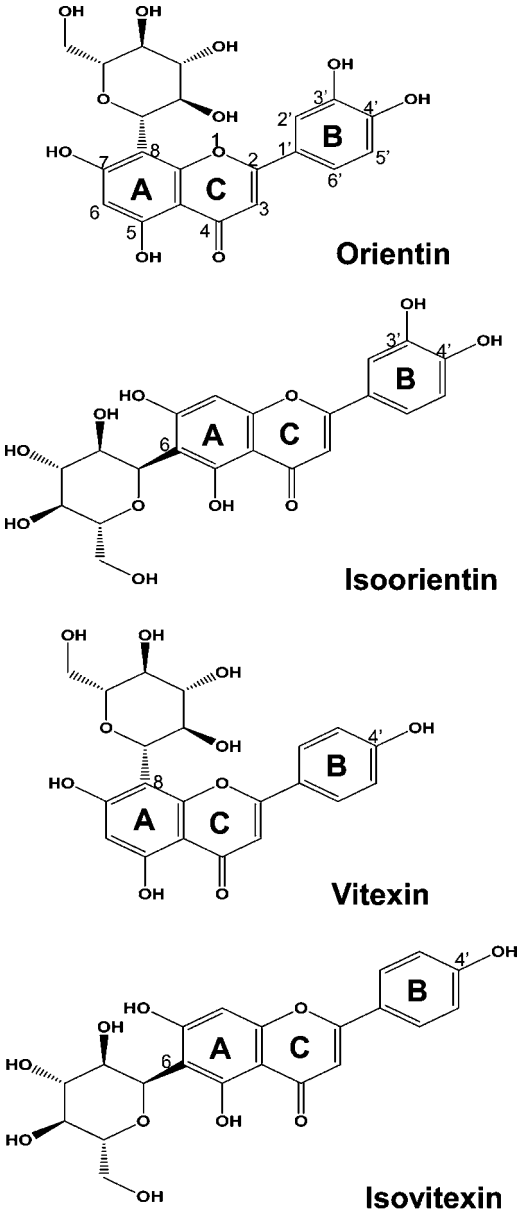

32

Figure 1. Structures of four *P. edulis* leaf flavonoids. The parent nucleus of flavonoid is composed of A, B, and C rings.

from Sinopharm Chemical Reagent Co., Ltd. (Shanghai, China). 2-Chloro-4-nitrophenol (CNP) was purchased from Energy Chemical (Shanghai, China). Acetonitrile (HPLC-grade) was provided by Tedia Co. Inc. (Fairfield, OH).

Preparation of the Main Solutions. Iodine solution:[26,31] 1.5 g of potassium iodide was dissolved to 25 mL of distilled water, and then 0.635 g of iodine was added. Finally, the solution was adjusted to 50 mL by distilled water. Starch suspension:[26,31] 10 mg of soluble starch was suspended in 1 mL of boiling water and water bathed at 90 °C for 30 min to make the starch swell. Then 7.5 mL of 50 mM KCl−HCl (pH 2.0) buffer was added followed 30 min later by 7.5 mL of 100 mM sodium phosphate buffer (pH 7.1) (the final pH was 6.8). They were used to simulate the pH of the stomach and duodenum. Last, the suspension was homogenized by a glass homogenizer. The preparation of amylose and amylopectin suspensions was the same as that of soluble starch suspensions.

Sample Preparation. *P. edulis* leaves were collected in Anji County (the bamboo hometown of China) during the winter and identified by Pei-xin Zhang of the Anji Forestry Bureau. The pregrounded *P. edulis* leaves were extracted with 50% ethanol (1:10, w/v) with a 1 h sonic treatment (DT series, Xingzhi Co., Ltd., Ningbo, China) and intermittent stirring. The extract was concentrated to 1/10 of the original volume by a rotary evaporator (RE-52A, Shanghai Jingke Co. Ltd., Shanghai, China). Then it was stored in a 4 °C refrigerator for 12 h to flocculate and filter some macromolecular compounds. After that, the solution was sequentially fractioned by petroleum ether, EtOAc, and 1-butanol. All these extracts were dried to obtain the petroleum ether fraction, EtOAc fraction, 1-butanol fraction, and residual fraction. The 1-butanol fraction was subjected to an AB-8 macroporous adsorption resin (polystyrene resin, weak polarity, 0.3−1.25 mm particle size) for further purification. The purification was carried out in a glass column (1.4 cm × 40 cm) wet-packed with washed AB-8 resin. The sample was dissolved in water. After all the sample was loaded, the column was first washed by 6 BV (bed volumes) of water to remove the impurities which could not adsorb tightly. Then the column was desorbed by 2 BV of 40% ethanol (v/v) solution at a speed of 2 BV/h.

Determination and Quantification of the Main Bioactive Components. The Shimadzu HPLC system (Shimadzu Corp., Tokyo, Japan) equipped with an Agilent Eclipse Plus C18 column (250 mm × 4.6 mm, particle size of 5 mm, Agilent Technologies Inc., Santa Clara, CA) was used. The mobile phase was phosphoric acid−water (0.3:99.7, v/v; A) and acetonitrile (B). The gradient elution condition was 15−25% B in 0−35 min. The flow rate was set as 1.0 mL/min. The signal was monitored at 330 nm. A Thermo LCQ-Deca HPLC-MS (Thermo Fisher Scientific Inc., San Jose, CA) fitting with an ESI (electrospray ionization) interface and negative ion mode was also used for determining the main bioactive components. For quantitative analysis, the calibration curves of orientin, isoorientin, vitexin, and isovitexin were obtained at a concentration of 6.25−200 μg/mL (n = 6).

Measurement and Kinetics Assay of α-Amylase Inhibitory Activity. The measurement of α-amylase inhibitory activity was carried out by using the method described previously.[32,33] Briefly, 20 μL of *P. edulis* flavonoids at different concentrations (final concentrations were 9, 18, 36, and 72 μg/mL) were mixed with 10 μL of 200 μg/mL α-amylase and 70 μL sodium phosphate buffer (pH 6.8). After intensive shaking for mixing, 100 μL of 5 mM Gal-G2-α-CNP solution was added to start the reaction. After 10 min of incubation at 37 °C, the absorbance of released CNP was monitored at 405 nm by a Bio-Tek Power Wave XS2 microwell plate reader (Bio-Tek Instruments, Winooski, VT). To further explore their inhibitory character, we performed kinetic analysis by using Lineweaver−Burk plots. The K_i value of competitive inhibition was obtained from the least-squares regression line of the slopes of Lineweaver−Burk plots versus the corresponding [I]. The derivation formulas are

$$V = \frac{V_{max}[S]}{K_m\left(1 + \frac{[I]}{K_i}\right) + [S]} \quad \text{and}$$

$$\frac{1}{V} = \frac{K_m}{V_{max}}\left(1 + \frac{[I]}{K_i}\right)\frac{1}{[S]} + \frac{1}{V_{max}} \tag{1}$$

$$\text{slope} = \frac{K_m}{V_{max}}\left(1 + \frac{[I]}{K_i}\right) \quad \text{and} \quad \text{slope} = \frac{K_m}{V_{max}K_i}[I] + \frac{K_m}{V_{max}} \tag{2}$$

$-K_i$ = intercept of eq 2 on x axis

Thermal Stability. First, the standard solutions of the four flavonoids were mixed. Second, we placed a certain volume of the mixed standard into a tube. The tube was sealed by plastic tape and heated at 100 °C for 2 h. Last, we detected the samples without and with heat treatment by HPLC and calculated the concentration alteration of our four flavonoids according to their peak areas.

Molecular Modeling. The three-dimensional structures of orientin, isoorientin, vitexin, and isovitexin were downloaded from the National Centre for Biotechnology Information PubChem compound database (http://pubchem.ncbi.nlm.nih.gov/). The three-dimensional structure of substrate Gal-G2-α-CNP was constructed by using ChemBio3D Ultra 12.0 software (Cambridge Soft Corp., Cambridge, U.K.). The crystal structure of the pig pancreatic α-amylase protein complex (PDB code 1WO2) was retrieved from the RCSB Protein Data Bank (http://www.rcsb.org). Then docking was carried out by using the Autodock v4.2 program (Scripps Research Institute, La Jolla, CA). The Lamarckian Genetic Algorithm was used to run the docking. First, we did a blind docking in which the grid box covers the whole receptor protein. Then a smaller grid box that mainly covers the site of the best cluster of blind docking was set for doing an accurate docking. After docking, cluster analysis based on the root-mean-square deviation (RMSD) value was performed. The tolerance of RMSD was set as 2.0. The lowest energy conformation of the most populated cluster was considered as the most reliable solution. The interaction analysis was carried out by using Pymol 0.99 (DeLano Scientific LLC, San Carlos, CA), YasaraView v13.9.8 (YASARA Biosciences, Vienna, Austria), and Ligplus v1.4.5 (EMBL-EBI, Cambridge, U.K.).

Interaction between Flavonoids and Starch and Their Influence on Starch Digestion. The interaction between *P. edulis* flavonoids and starch was studied by using the spectroscopic method described previously.[26,31] Briefly, 25 μL of flavonoid was added to 0.9 mL of soluble starch suspension (the final concentrations of flavonoid were 9, 18, and 36 μg/mL). After vortexing, 0.1 mL of iodine solution was added to the suspension. Then the absorption spectrum of the starch−iodine complex was measured from 500 to 900 nm by using a UV-1800 spectrophotometer (Shimadzu, Tokoyo, Japan). The absorption spectra of the amylose−iodine complex and the amylopectin−iodine complex were obtained in the same way as that of the soluble starch−iodine complex. The digestion of starch was also studied by using the spectroscopic method.[26,31] Briefly, 25 μL of flavonoid was added to 0.9 mL of starch suspension (the final concentrations of flavonoid were 9, 18, and 36 μg/mL), and then 10 μL of 0.5 mg/mL α-amylase was added to the suspension. After the suspension was incubated for 5 min at 37 °C, 0.1 mL of iodine solution was added to terminate the digestion and color the residual starch. The degree of digestion was estimated by the difference spectrum (ΔA) of the starch−iodine complex after and before digestion.

X-ray Diffraction (XRD). The sample preparation and detection parameters were the same as those described in previous reports.[29,34] Soluble starch and resin-purified extract (10:1, w/w) were mixed first, and then deionized water was added (10:1, v/w, based on starch). The mixture was water bathed at 90 °C with vigorous stirring for 60 min. Then it was stored at 4 °C for 3 days (at room temperature more than 10 days is needed to achieve the same degree of retrogradation) and freeze-dried last. A D/MAX 2550 rotating anode X-ray powder diffractometer (Rigaku, Tokoyo, Japan) equipped with a copper tube at 40 kV and 100 mA with Cu Kα radiation (λ = 0.154 nm) was used for crystalline analysis. The diffractograms were detected in the angle range from 5° to 50° (2θ) with a step size of 0.02°. The MDI Jade 5.0 software (Materials Data Inc., Livermore, CA) was used to analyze the diffractograms. The relative crystallinity was calculated by using the following equation: relative crystallinity (%) = $100A_c/(A_c + A_a)$, where A_c is the area of the crystal peak and A_a is the area of the amorphous peak.

Scanning Electron Microscopy (SEM). The sample was fixed on a silver specimen holder using double-sided adhesive and sputtered with gold in a vacuum evaporator to make the sample conductive. Then the sample was investigated with an S-3400N scanning electron microscope (Hitachi, Tokoyo, Japan) with a 15 kV accelerating voltage.

Statistical Analysis. All experiments were repeated three times. Statistical analysis was carried out by using one-way analysis of variance in SPSS 18.0 (SPSS, Chicago, IL); $p < 0.05$ was considered to be statistically significant.

RESULTS AND DISCUSSION

α-Amylase Inhibition Ability and Yield of *P. edulis* Leaf Extract Fractions. The α-amylase inhibition ability and the yield of several *P. edulis* leaf extract fractions are listed in Table 1. The EtOAc fraction and 1-butanol fraction exhibited stronger α-amylase inhibitory activity than the other fractions,

Table 1. α-Amylase Inhibition Ability and Yield of Each Fraction

extract	IC_{50} (μg/mL)	yield (%)
ethanol extract	591.8	6.96 ± 0.33
petroleum ether fraction	>800	0.97 ± 0.04
EtOAc fraction	318.1	0.33 ± 0.04
1-butanol fraction	354.1	0.93 ± 0.06
residual fraction	>800	4.36 ± 0.32
resin-purified extract	206.7	0.63 ± 0.03

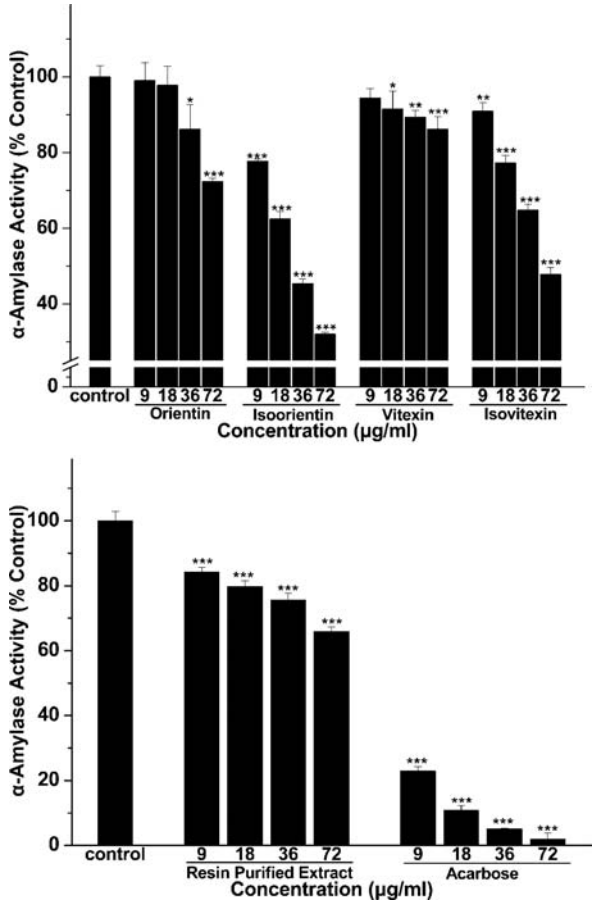

Figure 2. α-Amylase inhibitory activity of *P. edulis* leaf flavonoids, resin-purified extract, and acarbose. Values are normalized to controls (100%) and expressed as the mean ± SD of three experiments. One asterisk means $p < 0.05$, two asterisks mean $p < 0.01$, and three asterisks mean $p < 0.001$ compared to the control group.

dx.doi.org/10.1021/jf501931m | J. Agric. Food Chem. 2014, 62, 7760−7770

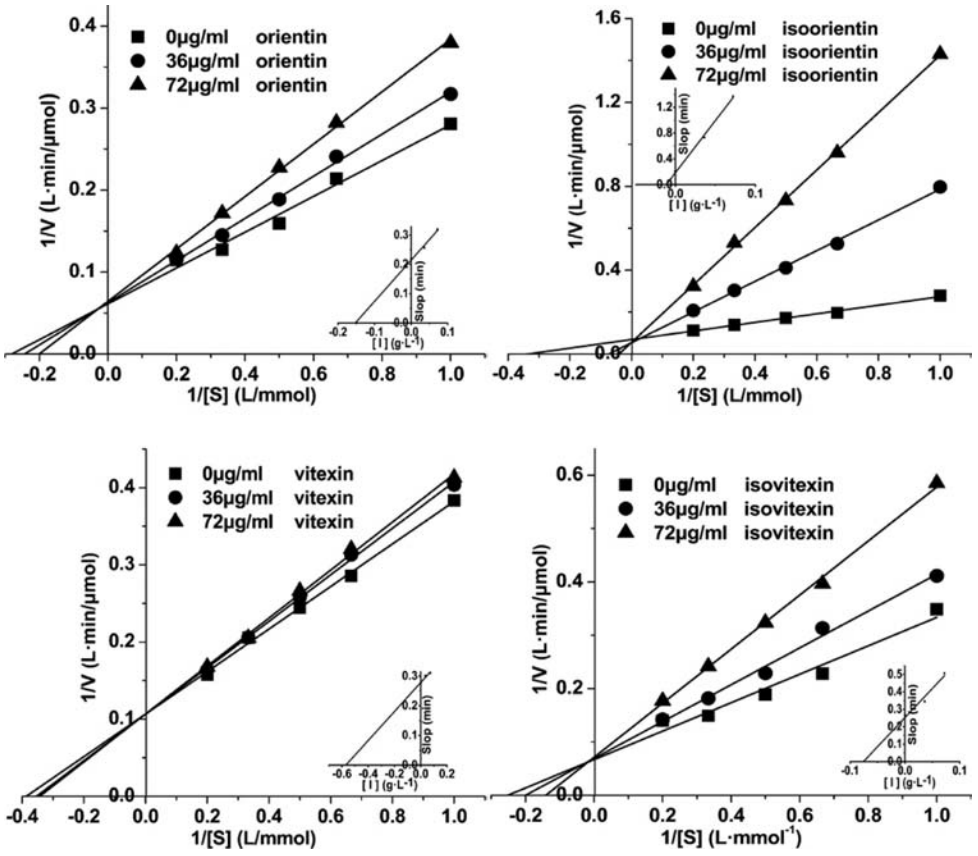

Figure 3. Lineweaver−Burk plots of *P. edulis* leaf flavonoids. The concentrations of *P. edulis* leaf flavonoids were respectively 0, 36, and 72 μg/mL. The concentrations of Gal-G2-CNP were respectively 1, 1.5, 2, 3, and 5 mM. The insets ([I] versus the corresponding slope of Lineweaver−Burk plots) were used to calculate the K_i value.

Table 2. Inhibitory Type, K_i, and IC_{50} of *P. edulis* Leaf Flavonoids and Resin-Purified Extract against α-Amylase

ligand	inhibitory type	K_i (μg/mL)	IC_{50} (μg/mL)
orientin	competitive	152.6	>270
isoorientin	competitive	11.5	29.9
vitexin	competitive	569.6	>270
isovitexin	competitive	75.8	65.3
resin-purified extract			206.7

but the yield of the EtOAc fraction is just one-third of the yield of the 1-butanol fraction and the EtOAc fraction is barely soluble in water. When loading the resin column, the materials must be dissolved in water, so the 1-butanol fraction is more suitable than the EtOAc fraction to be subjected to the AB-8 macroporous adsorption resin column for further purification. The obtained resin-purified extract exhibited the strongest α-amylase inhibitory activity.

Determination and Quantitation of the Main Bioactive Components. From the HPLC spectrum of the resin-purified extract (Supporting Information), we found two peaks were significantly higher than the other peaks. The two peaks might be the main α-amylase inhibitory components of the resin-purified extract. From the ultraviolet spectra (Supporting Information) of the two peaks, we found their maximum absorbances were near 270 and 340 nm, which suggested that these compounds might be flavonoids. According to the published data[12,17] and by further comparing the retention times, ultraviolet spectra, and m/z values with those of our standards, peaks 7, 8, 9, and 10 were identified as isoorientin ($[M - H]^-$, m/z 447.0), orientin ($[M - H]^-$, m/z 447.0), vitexin ($[M - H]^-$, m/z 431.1), and isovitexin ($[M - H]^-$, m/z 431.0), respectively (Supporting Information). Using the calibration curve, the concentrations of orientin, isoorientin, vitexin, and isovitexin were respectively 12.64, 87.15, 4.82, and 9.33 mg/g in the resin-purified extract. We were going to further affirm their α-amylase inhibitory activity. However, there might be other compounds with potent α-amylase inhibitory activity in the ethyl acetate fraction. We will try to purify them by silica gel column chromatography and Sephadex LH-20 column chromatography in the future.

α-Amylase Inhibitory Activities of the Four Flavonoids and Their Structure−Activity Relationships. As shown in Figure 2, all four flavonoids can dose-dependently inhibit α-amylase, and the inhibitory effect of isoorientin and isovitexin is stronger than the inhibitory effect of many other phytochemicals such as hesperidin, naringin, neohesperidin, nobiletin,[28] andrographolide,[35] cyanidin, cyanidin 3-glucoside,[36] myricetin, quercetin, luteolin, kaempferol, and baicalein[19] (the comparison of their IC_{50} values is given in the Supporting Information). However, their inhibitory effect is weaker than that of the positive drug acarbose.

All the four flavonoids are flavone *C*-glycosides. Unlike flavone *O*-glycosides, flavone *C*-glycosides will not be hydrolyzed to their aglycon by β-glucosidase in the small intestine.[37] Therefore, the four flavonoids can contact α-amylase which is located in the intestine. According to the two HPLC spectra without and with heat treatment (Supporting Information), the concentration alterations of isoorientin, orientin, vitexin, and

dx.doi.org/10.1021/jf501931m | J. Agric. Food Chem. 2014, 62, 7760−7770

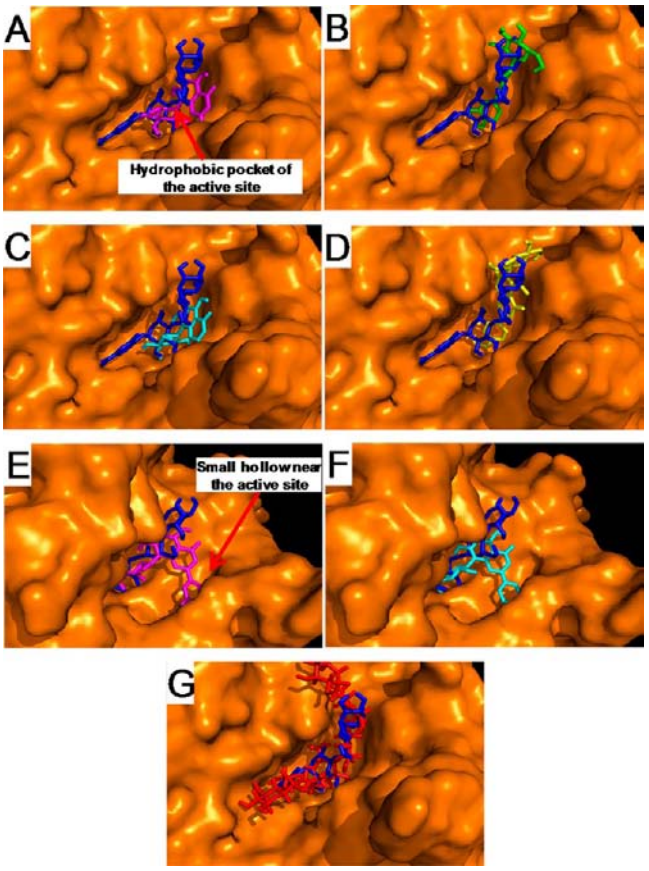

Figure 4. Surface representations of docked ligands on α-amylase with the superimposition of substrate Gal-G2-CNP. The big orange background is the surface of α-amylase (PDB code 1WO2), the dark blue molecule is synthetic substrate Gal-G2-CNP, the pink molecule is orientin, the green molecule is isoorientin, the light blue molecule is vitexin, the yellow molecule is isovitexin, and the red molecule is the positive drug acarbose.

isovitexin are respectively 6.6%, 1.8%, 9.3%, and 8.0% after heat treatment. This indicates that the four flavonoids will not be easily destroyed during food processing. However, many phytochemicals such as anthocyanin[38] and hypericin[39] are extremely unstable under heating, even under lighting.

The Lineweaver−Burk plots of the four flavonoids are given in Figure 3. They all have an intersection at the *y* axis which indicates their inhibitory types are all competitive. Their K_i and IC_{50} values are given in Table 2. Their inhibitory sequence is isoorientin > isovitexin > resin-purified extract > orientin > vitexin, and the differences between their effects are very significant. This is an interesting phenomenon because the structures of the four flavonoids are highly similar. Two speculations can be elicited from this phenomenon: (1) Flavone *C*6-glycosides have stronger α-amylase inhibitory activity than flavone *C*8-glycosides (because the IC_{50} of isoorientin is less than that of orientin and the IC_{50} of isovitexin is less than that of vitexin). (2) The *C*3′-hydroxyl on the B ring is important for the α-amylase inhibitory activity (because the IC_{50} of isoorientin is less than that of isovitexin).

Speculation 2 can be supported by the previous work of Tadera et al.[19] They found that the inhibitory activity of flavonoid is positively related to the number of hydroxyls on the B ring. For speculation 1, we have not found any literature support, but we tried to explain it by using molecular docking in the following subsection.

Molecular Docking between *P. edulis* Flavonoids and α-Amylase. Molecular docking was used to stimulate the binding mode of the ligand and receptor according to the "lock" and "key" principle. Here we used molecular docking to analyze why the four *P. edulis* flavonoids have highly similar structures but exhibit greatly different α-amylase inhibitory activities.

Figure 4 illustrates that all four flavonoids bind at the active site of α-amylase, which is a large hydrophobic pocket on the surface of α-amylase.[40] They all occupy the binding position of substrate Gal-G2-CNP more or less. Among them, isooreintin (B) and isovitexin (D) cover a large part of the binding position of the substrate, but oreintin (A) and vitexin (C) cover a smaller part. Therefore, isoorientin and isovitexin can more effectively cause steric hindrance to hinder the binding of the substrate. This is consistent with our experimental result that isoorientin and isovitexin exhibit much stronger inhibitory activity than orientin and vitexin. In fact, when the glucose links at C8 (orientin, vitexin), a corner of less than 90° will exist inside the flavonoid molecule and lead the three-dimensional structure of the flavonoid to look like a "V". Molecules with a "V" structure (orientin and vitexin) are easily trapped in a small hollow near the active site of α-amylase (which is veiled in Figure 4A,C, but is clear in Figure 4E,F). When the glucose links at C6 (isoorientin, isovitexin), the structure of the flavonoid is linear. Molecules with a linear structure are more similar to the substrate and fit the active site of amylase better. Additionally, we downloaded the X-ray crystal structure of the porcine pancreatic α-amylase−acarbose complex (Figure 4G) which was derived from an X-ray diffraction experiment and not in silico docking as ours was. We find that the positive drug acarbose almost fully occupies the binding position of the substrate. This is why its inhibitory effect is stronger than that of our flavonoids.

Besides geometry complementarity, the binding strength between the ligand and receptor is also important.[41] In Table 3, we summarize the H-bond, π−π, and hydrophobic interactions

Table 3. H-Bond, π−π, and Hydrophobic Interactions between Our Flavonoids and the Residues of α-Amylase[a]

	hydrogen bond	π−π interaction	hydrophobic interaction
orientin	**Asp300**, His299, Gly304, His305	Trp58, Trp59, His305	**Glu233**, **Asp300**, Trp58, Trp59, Tyr62, His299, Arg303, Gly304, His305, Asp356
isoorientin	**Asp197**, **Glu233**,Gln63, Val163, Arg195	Trp58, Trp59, Tyr62, Arg195, His299	**Asp197**, **Glu233**, **Asp300**,Trp58, Trp59, Tyr62, Gln63, Val163, Arg195, Ala 198, His299
vitexin	**Asp300**, His299, Gly304, His305	Trp58, Trp59, His305	**Glu233**, **Asp300**,Trp58, Trp59, Tyr62, His299, Arg303, Gly304, His305, Asp356
isovitexin	**Asp197**, Gln63, Val163, Arg195	Trp58, Tyr62, Arg195, His299	**Asp197**, **Asp300**,Val51, Trp58, Trp59, Tyr62, Gln63, Val163, Leu165, Arg195, His299

[a]The bold-font residues (Asp197, Glu233, Asp300) are the residues which play the key role in cutting the starch chain.

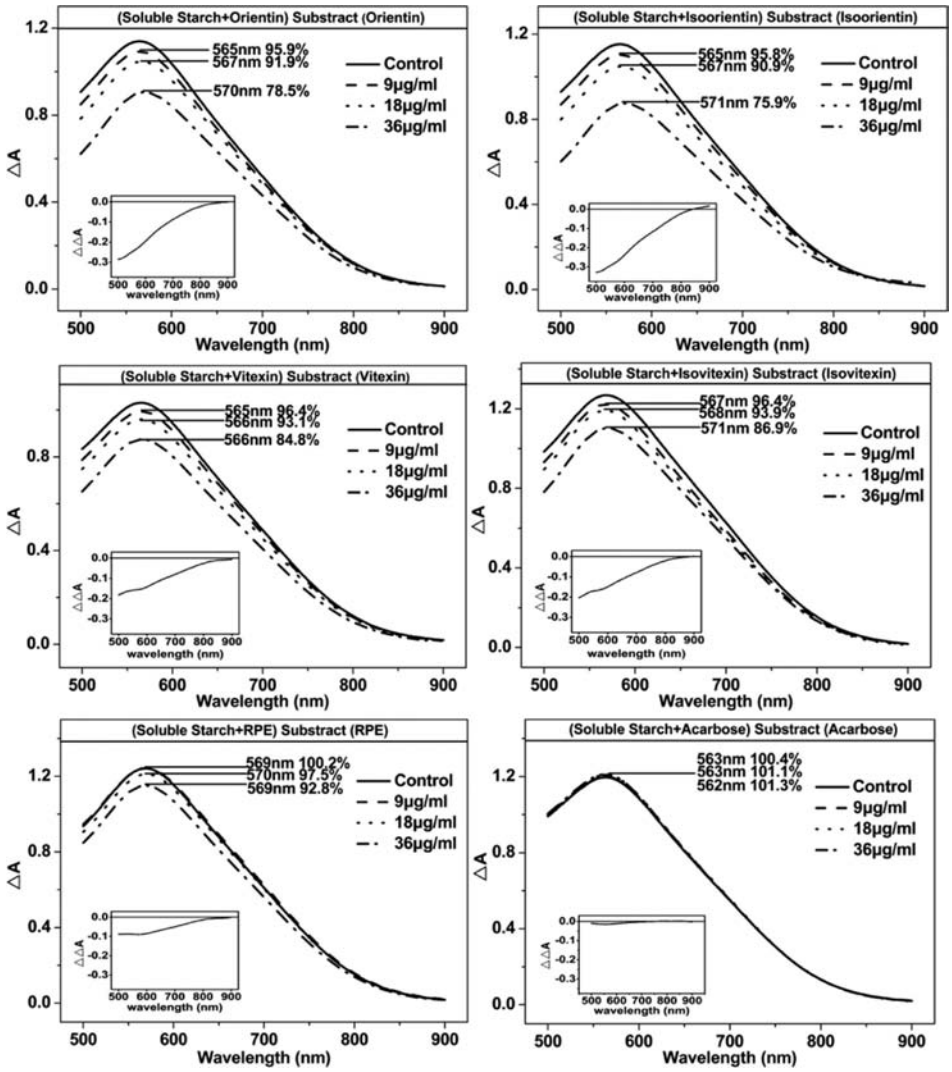

Figure 5. Interactions between *P. edulis* leaf flavonoids, resin-purified extract, acarbose, and soluble starch. $\Delta A = A$(soluble starch + compound + iodine) − A(compound + iodine): (A) orientin added, (B) isoorientin added, (C) vitexin added, (D) isovitexin added, (E) resin-purified extract (RPE) added, (F) acarbose added. The control for each panel is no addition of compound. Inset: $\Delta\Delta A$ spectrum, which is the curve of 36 μg/mL compound minus the curve of the control. The percentage on the right side of each curve is the peak ΔA value of the curve divided by the peak ΔA value of the control curve.

between flavonoids and the residues of α-amylase. Their interacting graphs are also given in the Supporting Information (Figures S4−S6). We find that, due to the extra 3′-hydroxyl, isoorientin forms more H-bonds with α-amylase than isovitexin, and two of them are formed with key residues. (The active site of α-amylase contains three key acidic residues, Asp197, Glu233, and Asp300. They work together to cleave the starch chain.[40,42]) This explains why isoorientin exhibited stronger inhibitory activity than isovitexin.

***P. edulis* Leaf Extracts Bind with Starch and Affect Its Digestibility.** Some small molecular phytochemicals can affect the digestibility of starch through binding with starch.[25,26,28] Here we used a spectroscopic method[26,31] to investigate whether *P. edulis* extracts bind with starch and further affect its digestibility. The ΔA curve of Figure 5 was obtained through subtraction of the absorption curve of flavonoid + iodine from the absorption curve of starch + flavonoid + iodine (the control is absence of flavonoid). Figure 5 shows that the ΔA curves decline with an increase of our flavonoids and resin-purified extract, but do not decline with an increase of acarbose. This indicates that orientin, isoorientin, vitexin, isovitexin, and resin-purified extract can bind with starch, but the positive drug acarbose cannot. According to the percentages on the right side of each curve, the binding strength order of our compounds is isoorientin ≈ orientin > vitexin ≈ isovitexin > resin-purified extract > acarbose.

The $\Delta\Delta A$ spectrum at the left bottom of each picture was obtained through subtraction of the ΔA curve of the control from the ΔA curve of 36 μg/mL flavonoid. Unlike the $\Delta\Delta A$ curves of naringin and neohesperidin[28] which have a distinct peak at 600 nm but are nearly zero at 500 nm, the $\Delta\Delta A$ curves of our flavonoids do not have a distinct peak at 600 nm but show a significant negative value at 500 nm. This indicates they mainly bind with amylopectin because the λ_{max} of the amylopectin−iodine complex is between 500 and 540 nm but the λ_{max} of the amylose−iodine complex is between 540 and 660 nm.[43]

The influence of *P. edulis* leaf extracts on the formation of the amylopectin−iodine complex and amylose−iodine complex was also tested (Supporting Information). The decline of the ΔA

dx.doi.org/10.1021/jf501931m | J. Agric. Food Chem. 2014, 62, 7760−7770

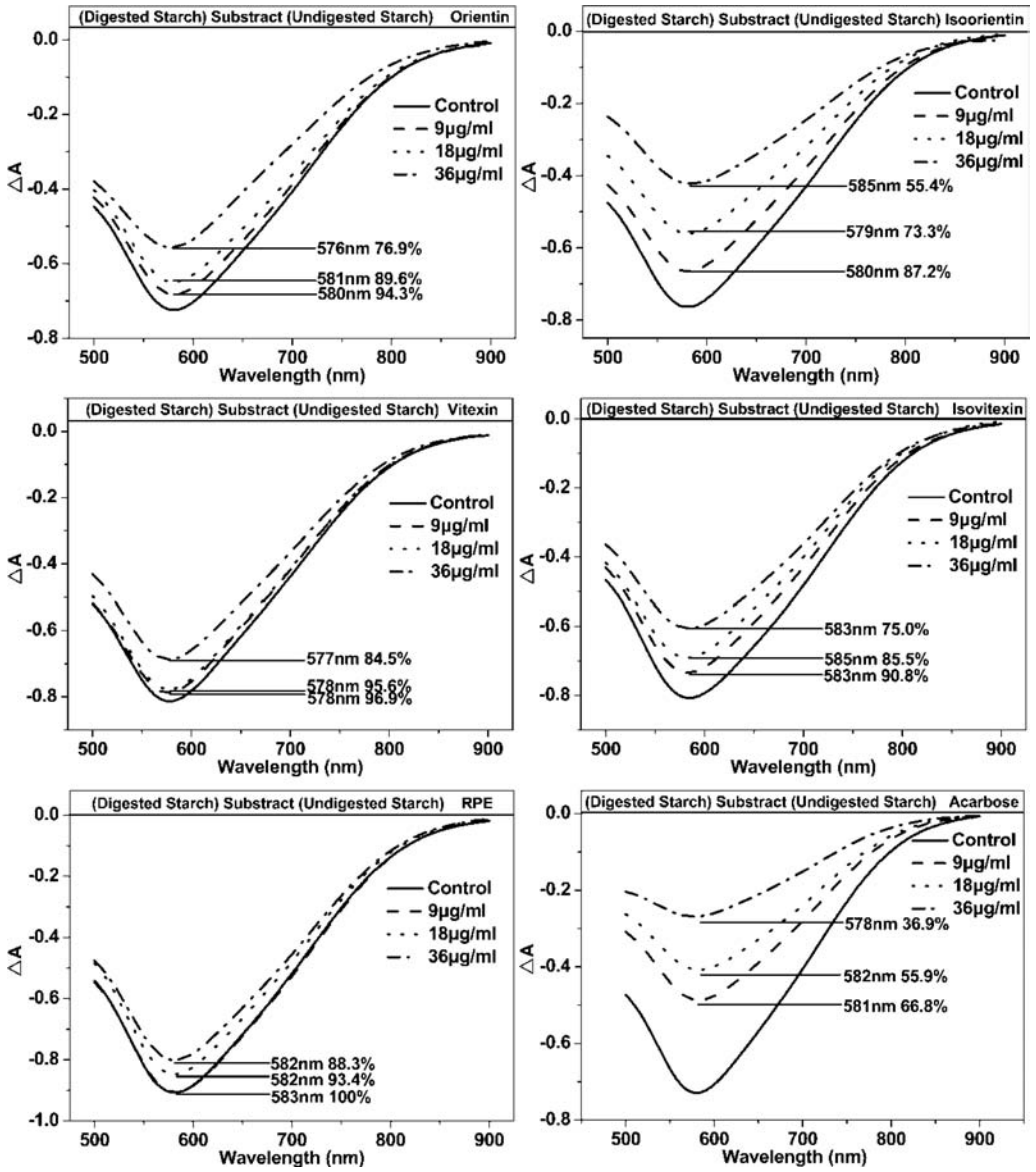

Figure 6. Effect of *P. edulis* leaf flavonoids, resin-purified extract, and acarbose on the digestion of soluble starch: (A) orientin added, (B) isoorientin added, (C) vitexin added, (D) isovitexin added, (E) resin-purified extract added, (F) acarbose added. $\Delta A = A$(digested starch−iodine complex) − A(undigested starch−iodine complex). The control for each panel is no addition of compound. The percentage at the right side of each curve is the peak ΔA value of the curve divided by the peak ΔA value of the control curve.

curve of amylopectin−iodine is more significant than the decline of the ΔA curve of amylose−iodine. This confirms the conclusion induced from the $\Delta\Delta A$ spectra of Figure 5 that *P. edulis* flavonoids mainly bind with amylopectin. Additionally, the amylopectin−iodine complex shows a peak around 535 nm, and the amylose−iodine complex shows a peak around 605 nm. The peak of the soluble starch−iodine complex is between them (around 565 nm, Figure 5) due to soluble starch being composed of amylopectin and amylose.

The ΔA curve of Figure 6 was obtained through subtraction of the absorption curve of the undigested starch−iodine complex from the absorption curve of the digested starch−iodine complex (addition of iodine after incubation with α-amylase). The less the starch was digested, the higher the ΔA value (negative). Figure 6 illustrates that the ΔA curve rises with an increase of our compounds. This indicates that our compounds can inhibit the digestion of soluble starch. The order of their effect was acarbose > isoorientin > isovitexin ≈ orientin > vitexin > resin-purified extract. However, this is different from the α-amylase inhibitory order we obtained from Figure 2 (the substrate was Gal-G2-CNP, a small molecule which was used to exclude the influence of the interaction between starch and our compounds), that is, acarbose > isoorientin > isovitexin > resin-purified extract > orientin > vitexin, and the gap between orientin and isovitexin and the gap between acarbose and isoorientin are narrowed when starch is used as the substrate. If these compounds simply inhibited the activity of α-amylase, whether using Gal-G2-CNP or starch as the substrate, the orders of their inhibitory effect should be the same. Therefore, we speculate that the effect of *P. edulis* extracts on the digestion of starch is not only due to the inhibition of α-amylase. Maybe they can further affect the digestibility of starch through binding with it. Two studies can support our speculation: One study found that due to the binding of rutin, epicatechin dimethylgallate, and fatty acids the glycemic index of buckwheat flour is lower than that of wheat flour.[26]

dx.doi.org/10.1021/jf501931m | J. Agric. Food Chem. 2014, 62, 7760−7770

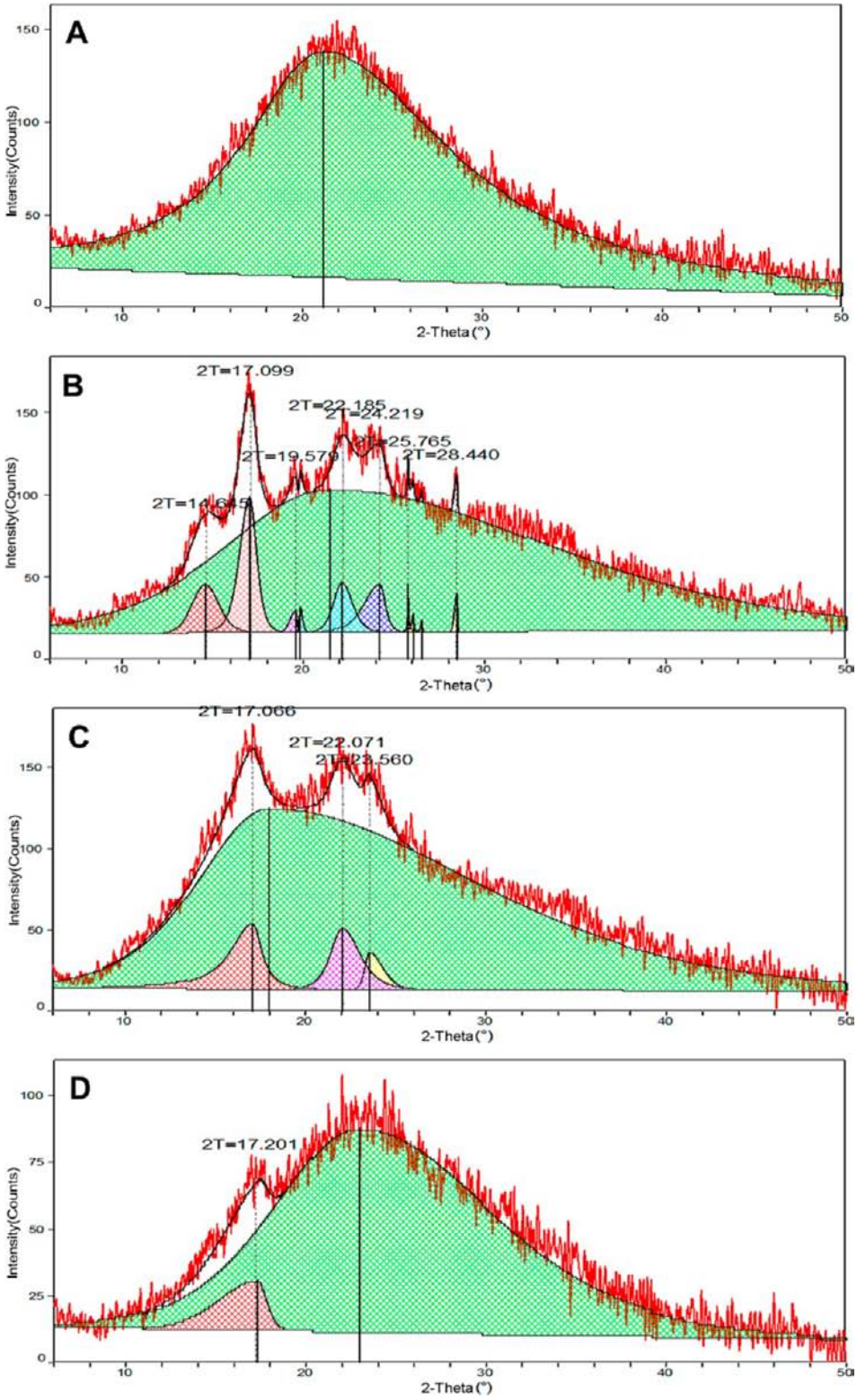

Figure 7. X-ray diffractograms of starch: (A) resin-purified extract, (B) natural soluble starch, (C) retrograded starch, and (D) retrograded resin-purified extract−starch complex. The red jagged line is the original diffractogram. The green area represents the amorphous peak obtained by fitting. The other colored areas represent the crystal peaks obtained by fitting.

The other study found that the resistant starch content of the quercetine−starch complex was sharply higher than that of common starch.[44] We had known that the binding strength between our compounds and starch was different: isoorientin ≈ orientin > vitexin ≈ isovitexin > resin-purified extract > acarbose. Therefore, the inhibitory order change when using starch as the substrate was due to the different binding strengths of these compounds with starch. Why can the binding retard the digestion of starch? Many researchers hold the view that some compounds can bind with starch through occupation

dx.doi.org/10.1021/jf501931m | J. Agric. Food Chem. 2014, 62, 7760−7770

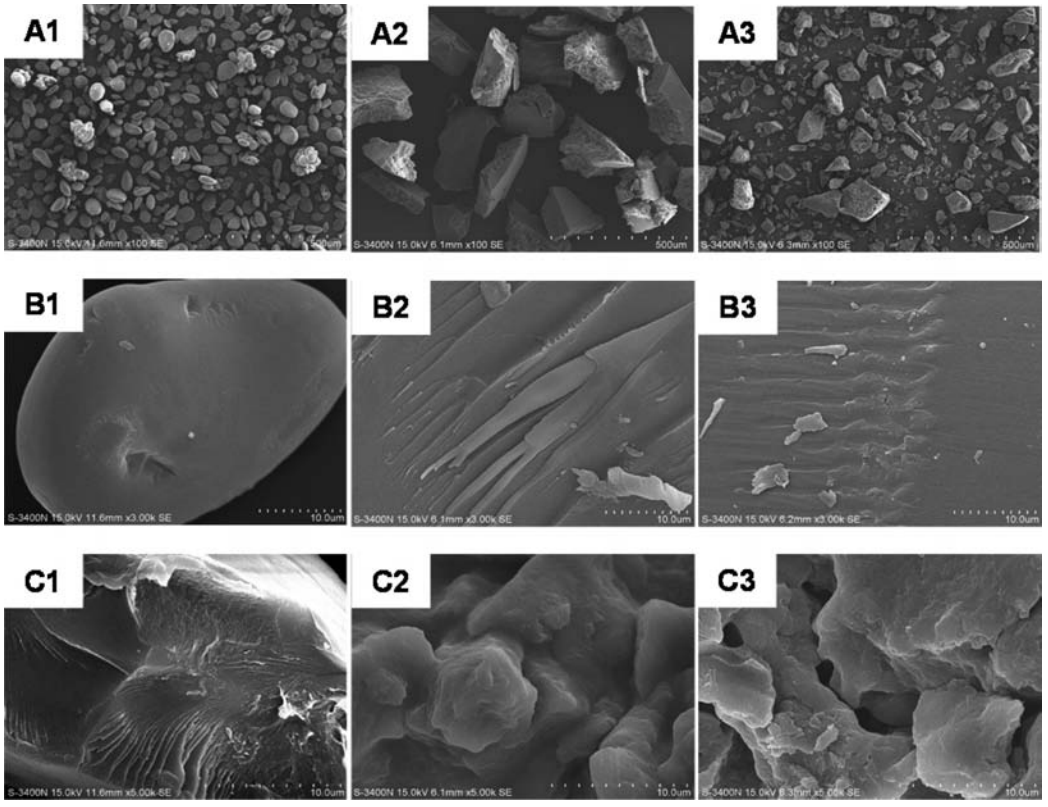

Figure 8. SEM images of starch. Panels A1, B1, and C1 are natural soluble starch (without gelatinization and retrogradation), and their magnifications are respectively 100×, 3000×, and 5000×. Pictures A2, B2, and C2 are retrograded starch (without addition of resin-purified extract), and their magnifications are respectively 100×, 3000×, and 5000×. Pictures A3, B3, and C3 are the retrograded resin-purified extract−starch complex, and their magnifications are respectively 100×, 3000×, and 5000×. B1, B2, and B3 are the outside surface. C1,C2, and C3 are the fracture surface.

of the hydrophobic helical structure of starch. The occupation of the hydrophobic helical structure will disturb the combination of starch and amylase.[26−28]

Influence of *P. edulis* Extract on the Physical Properties of Starch. In the cooking process, well-ordered starch polymers will be broken into free starch chains; this is called gelatinization. During cooling, these free starch chains will reassociate and re-form crystalline domains; this is called retrogradation. Retrogradation will markedly increase the rigidity and shorten the shelf life of starch-based food.[45] To further prove the binding between *P. edulis* leaf extract and starch, we investigated whether the resin-purified extract can influence the retrogradation of starch by using X-ray diffraction and scanning electron microscopy.

Figure 7A is the X-ray diffractogram of the resin-purified extract which does not have any crystal peak. This means that the resin-purified extract is amorphous. Figure 7B is the X-ray diffractogram of natural soluble starch (without heating and cooling treatment). It exhibits a typical B-type crystalline structure (according to X-ray diffractograms, the crystalline form of starch can be classified as A, B, C, and V[46]) with peaks close to 17.2°, 22.2°, and 24.0°. Parts C and D of Figure 7 are the diffractograms of retrograded starch and the retrogradated resin-purified extract−starch complex. We find three crystal peaks in Figure 7C, but only one crystal peak (17.2°) in Figure 7D. Their crystallinities are respectively 8.99% and 4.93%. This indicates that, once we added the resin-purified extract, the retrogradation of starch was retarded.

The mechanism of retrogradation is the reassociation of starch chains through hydrogen bonds. Phenolic compounds which contain many reactive hydroxyls can disturb the formation of H-bonds between starch chains through formation of H-bonds with starch.[29,30] Researchers had confirmed that the greater the number of OH groups in the plasticizer, the better the plasticizer reduces the crystallization of starch.[47] Some other researchers hold the view that, during boiling, phenolic compounds and starch can form covalent bonds which can further retard the crystallization of starch.[48]

Scanning electron microscopy was used to investigate the morphology difference between natural soluble starch, retrogradated starch, and the retrogradated resin-purified extract−starch complex. In Figure 8A1,A2,A3 (100×), the shape of natural soluble starch is an elliptic granule (A1) whose diameter is about 50 μm; the retrogradated starch (A2) and retrogradated resin-purified extract−starch complex (A3) are irregularly shaped agglomerates whose long axes respectively vary between 200 and 250 μm and betwen 50 and 150 μm. From Figure 8B1,B2,B3 (3000×), we find that the surface of natural starch is smooth (B1), but there are many apophyses on the surface of retrogradated starch and the retrogradated resin-purified extract−starch complex (B2, B3). Parts C1, C2, and C3 (5000×) of Figure 8 are the faultages of these starches. The natural starch showed a very dense faultage which indicates its compact interior structure (C1), while on the faultages of retrogradated starch and the retrogradated resin-purified extract−starch complex there are many irregular bulges (C2, C3). Inside the faultage of the retrogradated resin-purified

extract−starch complex (C3), we also find some cracks and cavities. The cracks and cavities illustrate the crystalline texture of the retrogradated resin purified extract−starch complex is less compact than that of retrogradated starch. This indicates that *P. edulis* leaf extract can interact with starch and retard the retrogradation of starch. This is similar to the result of another study that the gel matrix of a wheat starch−pomegranate peel extract complex is looser than that of common starch.[30]

In conclusion, our studies provide scientific support for the further use of *P. edulis* leaf extract as a functional food additive that can adjust postprandial hyperglycemia and prolong the shelf life of starch-based food. Furthermore, our study on the structure−activity relationship of flavone *C*-glycosides can be applied to drug design. In the future, the influence of bamboo leaf extract on the glucose transporter of small intestinal brush border cells deserves further study, because it is the last step in the generation of blood glucose.[49] We hope our study can attract more attention to this bamboo leaf resource and benefit diabetes research and hardworking bamboo farmers in the future.

■ ASSOCIATED CONTENT

Supporting Information

Comparison of the IC_{50} values of isoorientin, isovitexin, and other compounds (Table S1), HPLC spectrum (Figure S1) and HPLC−MS spectrum (Figure s2) of the resin-purified extract, HPLC spectra of the mixed standard without and with heat treatment (Figure S3), hydrogen bond interaction networks (Figure S4), $\pi-\pi$ interaction networks (Figure S5), and hydrophobic interaction networks (two-dimensional) (Figure S6) between *P. edulis* flavonoids and α-amylase, and interactions between *P. edulis* leaf flavonoids and amylopectin (Figure S7) and amylose (Figure S8). This material is available free of charge via the Internet at http://pubs.acs.org.

■ AUTHOR INFORMATION

Corresponding Author

*E-mail: luyanhua@ecust.edu.cn. Phone: +86-21-64251185. Fax: +86-21-64251185.

Funding

This work was supported by the Fundamental Research Funds for the Central Universities and partially supported by the Shanghai Leading Academic Discipline Project (Grant B505) and the National Special Fund for State Key Laboratory of Bioreactor Engineering (Grant 2060204).

Notes

The authors declare no competing financial interest.

■ ABBREVIATION USED

Gal-G2-CNP, α-(2-chloro-4-nitrophenyl)-β-1,4-galactopyranosylmaltoside

■ REFERENCES

(1) Guariguata, L.; Whiting, D.; Hambleton, I.; Beagley, J.; Linnenkamp, U.; Shaw, J. Global estimates of diabetes prevalence for 2013 and projections for 2035 for the IDF Diabetes Atlas. *Diabetes Res. Clin. Pract.* **2013**, *103*, 137−149.

(2) Stumvoll, M.; Goldstein, B. J.; van Haeften, T. W. Type 2 diabetes: principles of pathogenesis and therapy. *Lancet* **2005**, *365*, 1333−1346.

(3) Pekkanen, J.; Tuomilehto, J.; Qiao, Q.; Jousilahti, P.; Lindström, J. Glucose tolerance and mortality: comparison of WHO and American Diabetes Association diagnostic criteria. *Lancet* **1999**, *354*, 617−621.

(4) Ahmed, N. Advanced glycation endproducts—role in pathology of diabetic complications. *Diabetes Res. Clin. Pract.* **2005**, *67*, 3−21.

(5) Peng, X.; Zheng, Z.; Cheng, K.-W.; Shan, F.; Ren, G.-X.; Chen, F.; Wang, M. Inhibitory effect of mung bean extract and its constituents vitexin and isovitexin on the formation of advanced glycation endproducts. *Food Chem.* **2008**, *106*, 475−481.

(6) Hsiao, S.-H.; Liao, L.-H.; Cheng, P.-N.; Wu, T.-J. Hepatotoxicity associated with acarbose therapy. *Ann. Pharmacother.* **2006**, *40*, 151−154.

(7) Chiasson, J.-L.; Josse, R. G.; Gomis, R.; Hanefeld, M.; Karasik, A.; Laakso, M. Acarbose treatment and the risk of cardiovascular disease and hypertension in patients with impaired glucose tolerance: the STOP-NIDDM trial. *JAMA, J. Am. Med. Assoc.* **2003**, *290*, 486−494.

(8) Neuser, D.; Benson, A.; Brückner, A.; Goldberg, R. B.; Hoogwerf, B. J.; Petzinna, D. Safety and tolerability of acarbose in the treatment of type 1 and type 2 diabetes mellitus. *Clin. Drug Invest.* **2005**, *25*, 579−587.

(9) Yilmazer-Musa, M.; Griffith, A. M.; Michels, A. J.; Schneider, E.; Frei, B. Grape seed and tea extracts and catechin 3-gallates are potent inhibitors of α-amylase and α-glucosidase activity. *J. Agric. Food Chem.* **2012**, *60*, 8924−8929.

(10) Lu, B.; Wu, X.; Tie, X.; Zhang, Y.; Zhang, Y. Toxicology and safety of anti-oxidant of bamboo leaves. Part 1: acute and subchronic toxicity studies on anti-oxidant of bamboo leaves. *Food Chem. Toxicol.* **2005**, *43*, 783−792.

(11) Lu, B.; Wu, X.; Shi, J.; Dong, Y.; Zhang, Y. Toxicology and safety of antioxidant of bamboo leaves. Part 2: developmental toxicity test in rats with antioxidant of bamboo leaves. *Food Chem. Toxicol.* **2006**, *44*, 1739−1743.

(12) Zhang, Y.; Jiao, J.; Liu, C.; Wu, X.; Zhang, Y. Isolation and purification of four flavone C-glycosides from antioxidant of bamboo leaves by macroporous resin column chromatography and preparative high-performance liquid chromatography. *Food Chem.* **2007**, *107*, 1326−1336.

(13) Panee, J.; Liu, W.; Lin, Y.; Gilman, C.; Berry, M. J. A novel function of bamboo extract in relieving lipotoxicity. *Phytother. Res.* **2008**, *22*, 675−680.

(14) Nam, J. S.; Chung, H. J.; Jang, M. K.; Jung, I. A.; Park, S. H.; Cho, S. I.; Jung, M. H. Sasa borealis extract exerts an antidiabetic effect via activation of the AMP-activated protein kinase. *Nutr. Res. Pract.* **2013**, *7*, 15−21.

(15) Jung, S. H.; Lee, J. M.; Lee, H. J.; Kim, C. Y.; Lee, E. H.; Um, B. H. Aldose reductase and advanced glycation endproducts inhibitory effect of *Phyllostachys nigra*. *Biol. Pharm. Bull.* **2007**, *30*, 1569−1572.

(16) Choi, Y.-J.; Lim, H.-S.; Choi, J.-S.; Shin, S.-Y.; Bae, J.-Y.; Kang, S.-W.; Kang, I.-J.; Kang, Y.-H. Blockade of chronic high glucose-induced endothelial apoptosis by *Sasa borealis* bamboo extract. *Exp. Biol. Med.* **2008**, *233*, 580−591.

(17) Zhang, Y.; Bao, B.; Lu, B.; Ren, Y.; Tie, X.; Zhang, Y. Determination of flavone C-glucosides in antioxidant of bamboo leaves (AOB) fortified foods by reversed-phase high-performance liquid chromatography with ultraviolet diode array detection. *J. Chromatogr., A* **2005**, *1065*, 177−185.

(18) Ying, Z. Natural functional extract of bamboo leaves-bamboo leaf anthoxanthin. *China Food Addit.* **2002**, *3*, 54−66.

(19) Tadera, K.; Minami, Y.; Takamatsu, K.; Matsuoka, T. Inhibition of α-glucosidase and α-amylase by flavonoids. *J. Nutr. Sci. Vitaminol.* **2006**, *52*, 149−153.

(20) Ali Asgar, M. Anti-diabetic potential of phenolic compounds: a review. *Int. J. Food Prop.* **2013**, *16*, 91−103.

(21) Cao, H.; Chen, X. Structures required of flavonoids for inhibiting digestive enzymes. *Anti-Cancer Agents Med. Chem.* **2012**, *12*, 929−939.

(22) Tsujita, T.; Shintani, T.; Sato, H. α-Amylase inhibitory activity from nut seed skin polyphenols. 1. Purification and characterization of almond seed skin polyphenols. *J. Agric. Food Chem.* **2013**, *61*, 4570−4576.

(23) Hanhineva, K.; Törrönen, R.; Bondia-Pons, I.; Pekkinen, J.; Kolehmainen, M.; Mykkänen, H.; Poutanen, K. Impact of dietary polyphenols on carbohydrate metabolism. *Int. J. Mol. Sci.* **2010**, *11*, 1365−1402.
(24) Perera, A.; Meda, V.; Tyler, R. Resistant starch: a review of analytical protocols for determining resistant starch and of factors affecting the resistant starch content of foods. *Food Res. Int.* **2010**, *43*, 1959−1974.
(25) Thompson, L. U.; Yoon, J. H. Starch digestibility as affected by polyphenols and phytic acid. *J. Food Sci.* **1984**, *49*, 1228−1229.
(26) Takahama, U.; Hirota, S. Fatty acids, epicatechin-dimethylgallate, and rutin interact with buckwheat starch inhibiting its digestion by amylase: implications for the decrease in glycemic index by buckwheat flour. *J. Agric. Food Chem.* **2010**, *58*, 12431−12439.
(27) Cohen, R.; Orlova, Y.; Kovalev, M.; Ungar, Y.; Shimoni, E. Structural and functional properties of amylose complexes with genistein. *J. Agric. Food Chem.* **2008**, *56*, 4212−4218.
(28) Shen, W.; Xu, Y.; Lu, Y. H. Inhibitory effects of *Citrus* flavonoids on starch digestion and antihyperglycemic effects in HepG2 cells. *J. Agric. Food Chem.* **2012**, *60*, 9609−9619.
(29) Wu, Y.; Chen, Z.; Li, X.; Li, M. Effect of tea polyphenols on the retrogradation of rice starch. *Food Res. Int.* **2009**, *42*, 221−225.
(30) Zhu, F.; Cai, Y.-Z.; Sun, M.; Corke, H. Effect of phytochemical extracts on the pasting, thermal, and gelling properties of wheat starch. *Food Chem.* **2009**, *112*, 919−923.
(31) Takahama, U.; Hirota, S. Inhibition of buckwheat starch digestion by the formation of starch/bile salt complexes: possibility of its occurrence in the intestine. *J. Agric. Food Chem.* **2011**, *59*, 6277−6283.
(32) Morishita, Y.; Iinuma, Y.; Nakashima, N.; Majima, K.; Mizuguchi, K.; Kawamura, Y. Total and pancreatic amylase measured with 2-chloro-4-nitrophenyl-4-*O*-β-D-galactopyranosylmaltoside. *Clin. Chem.* **2000**, *46*, 928−933.
(33) Kandra, L.; Gyémánt, G.; Zajácz, Á.; Batta, G. Inhibitory effects of tannin on human salivary α-amylase. *Biochem. Biophys. Res. Commun.* **2004**, *319*, 1265−1271.
(34) Liu, J.; Wang, M.; Peng, S.; Zhang, G. Effect of green tea catechins on the postprandial glycemic response to starches differing in amylose content. *J. Agric. Food Chem.* **2011**, *59*, 4582−4588.
(35) Subramanian, R.; Asmawi, M. Z.; Sadikun, A. In vitro α-glucosidase and α-amylase enzyme inhibitory effects of *Andrographis paniculata* extract and andrographolide. *Acta Biochim. Polym.* **2008**, *55*, 391−398.
(36) Akkarachiyasit, S.; Charoenlertkul, P.; Yibchok-anun, S.; Adisakwattana, S. Inhibitory activities of cyanidin and its glycosides and synergistic effect with acarbose against intestinal α-glucosidase and pancreatic α-amylase. *Int. J. Mol. Sci.* **2010**, *11*, 3387−3396.
(37) Nmeth, K.; Plumb, G. W.; Berrin, J.-G.; Juge, N.; Jacob, R.; Naim, H. Y.; Williamson, G.; Swallow, D. M.; Kroon, P. A. Deglycosylation by small intestinal epithelial cell-glucosidases is a critical step in the absorption and metabolism of dietary flavonoid glycosides in humans. *Eur. J. Nutr.* **2003**, *42*, 29−42.
(38) Gradinaru, G.; Biliaderis, C. G.; Kallithraka, S.; Kefalas, P.; Garcia-Viguera, C. Thermal stability of *Hibiscus sabdariffa* L. anthocyanins in solution and in solid state: effects of copigmentation and glass transition. *Food Chem.* **2003**, *83*, 423−436.
(39) Wirz, A.; Meier, B.; Sticher, O. Stability of hypericin and pseudohypericin in extract solutions of *Hypericum perforatum* and in standard solutions. *Pharm. Ind.* **2001**, *63*, 410−415.
(40) Buisson, G.; Duee, E.; Haser, R.; Payan, F. Three dimensional structure of porcine pancreatic alpha-amylase at 2.9 A resolution. Role of calcium in structure and activity. *EMBO J.* **1987**, *6*, 3909−3916.
(41) Lo Piparo, E.; Scheib, H.; Frei, N.; Williamson, G.; Grigorov, M.; Chou, C. J. Flavonoids for controlling starch digestion: structural requirements for inhibiting human α-amylase. *J. Med. Chem.* **2008**, *51*, 3555−3561.
(42) Rydberg, E. H.; Li, C.; Maurus, R.; Overall, C. M.; Brayer, G. D.; Withers, S. G. Mechanistic analyses of catalysis in human pancreatic α-amylase: detailed kinetic and structural studies of mutants of three conserved carboxylic acids. *Biochemistry* **2002**, *41*, 4492−4502.
(43) Wang, J.; Li, Y.; Tian, Y.; Xu, X.; Ji, X.; Cao, X.; Jin, Z. A novel triple-wavelength colorimetric method for measuring amylose and amylopectin contents. *Starch/Stärke* **2010**, *62*, 508−516.
(44) Zhang, L.; Yang, X.; Li, S.; Gao, W. Preparation, physicochemical characterization and in vitro digestibility on solid complex of maize starches with quercetin. *LWT—Food Sci. Technol.* **2011**, *44*, 787−792.
(45) Karim, A. A.; Norziah, M.; Seow, C. Methods for the study of starch retrogradation. *Food Chem.* **2000**, *71*, 9−36.
(46) Zobel, H. Starch crystal transformations and their industrial importance. *Starch/Stärke* **1988**, *40*, 1−7.
(47) Smits, A.; Kruiskamp, P.; Van Soest, J.; Vliegenthart, J. The influence of various small plasticisers and malto-oligosaccharides on the retrogradation of (partly) gelatinised starch. *Carbohydr. Polym.* **2003**, *51*, 417−424.
(48) Takahama, U.; Tanaka, M.; Hirota, S. Proanthocyanidins in buckwheat flour can reduce salivary nitrite to nitric oxide in the stomach. *Plant Foods Hum. Nutr.* **2010**, *65*, 1−7.
(49) de la Garza, A. L.; Etxeberria, U.; Lostao, M. a. P.; San Román, B.; Barrenetxe, J.; Martínez, J. A.; Milagro, F. n. I. Helichrysum and grapefruit extracts inhibit carbohydrate digestion and absorption, improving postprandial glucose levels and hyperinsulinemia in rats. *J. Agric. Food Chem.* **2013**, *61*, 12012−12019.

This study aimed to evaluate in vivo hyperuricemic activity of brown adlay and in vitro xanthine oxidase inhibitory effects of several adlay seed-derived products (i.e., polished adlay, brown adlay, adlay bran, and adlay hull). Comparison on the profiles of free and bound phenolics and antioxidant activities of the extracts derived from these adlay seed products was also performed to elucidate the potential association between in vitro or in vivo bioactivities and the intrinsic phytochemials in the adlay products.

MATERIALS AND METHODS

Chemicals. 2,2′-Azobis (2-methylpropionamidine) dihydrochloride (AAPH), fluorescein sodium salt, Trolox, allopurinol, xanthine, xanthine oxidase, uric acid, nitro blue tetrazolium (NBT), protocatechuic acid, chlorogenic acid, vanillic acid, caffeic acid, *p*-coumaric acid, ferulic acid, and Folin-Ciocalteu reagent were purchased from Sigma Chemical Co. (St. Louis, MO, USA). Acetonitrile and methanol were obtained from Merck (Darmstadt, Germany). All the solvents for high-performance liquid chromatography (HPLC) analyses were of HPLC grade. All the other chemicals used were of analytical grade.

Plant Material. Air-dried polished adlay, brown adlay, adlay bran, and adlay hull were purchased from Shenlong adlay cooperative (Fujian, China) in August 2013. All the materials were ground into fine powder with a laboratory mill (FW100, Taisite Instrument Co., Ltd., Tianjin, China). The materials were stored at room temperature in a desiccator until use.

Extraction of Free Phenolic Compounds. Free phenolic compounds of polished adlay, brown adlay, adlay bran, and adlay hull were extracted using the method of Zhang et al.[24] with slight modification. Briefly, 5 g of adlay flour was mixed with 50 mL of acidified methanol (95% methanol:1 M HCl = 85:15 v/v) for 2 h. The obtained mixture was then centrifuged at 2000g for 10 min. The supernatant was collected, and the residue pellet was re-extracted twice with 50 mL of the acidified methanol. All the resultant supernatants were combined and dried via evaporation in a rotary evaporator under reduced pressure at 45 °C. The dried extracts containing free phenolics were redissolved in methanol and stored at −20 °C until further use.

Extraction of Bound Phenolic Compounds. Bound phenolic compounds of polished adlay, brown adlay, adlay bran, and adlay hull were extracted following the method of Zhang et al.[24] with slight modification. Briefly, the bound phenolics herein refer to those in the residue pellets that resulted from the centrifugation steps of the free phenolic extraction (as described in the paragraph above). These residue pellets were combined, homogenized, and a portion of the combined pellet was then mixed with an aliquot (50 mL) of 2 M sodium hydroxide. The resultant mixture was allowed to stand in capped 100-mL conical flasks at room temperature for 2 h before being centrifuged at 2000g for 10 min. The supernatant was collected, neutralized with concentrated hydrochloric acid, washed with hexanes (to remove lipids), and then extracted six times with ethyl acetate. The resultant ethyl acetate fractions were combined and evaporated to dryness. The dried extracts containing bound phenolics were redissolved in methanol and stored at −20 °C until further use.

Effects of Brown Adlay Extract on Serum Uric Acid Levels in Oxonate-Induced Hyperuricemic Rats. Adult male Sprague−Dawley rats (weight 150−250 g) were purchased from the Laboratory Animal Center of the Guangzhou University of Chinese Medicine (Guangzhou, China). Rats were housed one per cage with minimal suffering, kept in a room controlled at 22−24 °C and with a 12:12-h light/dark cycle, and given a standard laboratory diet and distilled water *ad libitum* before the actual studies. This study was carried out strictly following the Guide for the Care and Use of Laboratory Animals of the National Institutes of Health. The protocol used in this study was approved by the Committee on the Ethics of Animal Experiments of Jinan University (Permit SCXK (yue) 2013-0020).

For the hyperuricemia study, potassium oxonate (a uricase inhibitor) was used to induce acute hyperuricemia following the procedure of Li et al.[9] with some modifications. Sixty rats were randomly assigned to four equal groups (i.e., $n = 15$ per group). Group one consisted of rats who consumed distilled water only (untreated or non- hyperuricemic group). Group two was rats who received 2 g/kg potassium oxonate, administrated by oral gavage once a day for 7 consecutive days before distilled water only. Group three rats were given 2 g/kg potassium oxonate, administrated by oral gavage once a day for 7 consecutive days before allopurinol (50 mg/kg). Group four rats received 2 g/kg potassium oxonate, administrated by oral gavage once a day for 7 consecutive days before dried brown adlay extract containing combined free phenolic and bound phenolic extracts, 166 mg/kg. On the 10th day of the treatment, whole blood sample was collected after final administration and centrifuged to separate serum for serum uric acid, creatinine, and urea nitrogen determination.

The concentrations of serum uric acid, creatinine, and urea nitrogen were measured by enzymatic colorimetric methods using a Varioskan Flash spectral scan multimode plate reader (Thermo Fisher Scientific, Thermo Electron Co., Waltham, MA, USA).

Determination of Total Phenolic Content. Total phenolic content was determined following the method of Singleton and Rossi.[25] Briefly, 200 μL of each sample was transferred to a 10-mL volumetric flask, to which 0.5 mL of undiluted Folin-Ciocalteu reagent was added. Then 1.5 mL of 20% (w/v) Na_2CO_3 was added and the volume of the mixture was brought up to 10 mL with distilled water, before 2 h of incubation at 40 °C and subsequent absorbance measurements at 760 nm. Total phenolic content was calculated based on the calibration curve of gallic acid standard and expressed as mg gallic acid equiv/100 g sample.

Phenolic Profiling by HPLC. HPLC analysis was carried out using a Waters 600 HPLC system (Waters, Milford, MA, USA) equipped with an Agilent XDB-C18 column (250 × 4.6 mm i.d., 5 μm, Santa Clara, CA, USA). Samples were separated using a gradient elution with the mobile phase consisting of 0.1% (v/v) formic acid (A) and acetonitrile (B). The gradient conditions were 95% A in 0−5 min; 95−90% A in 5−10 min; 90−80% A in 15−20 min; 80−70% A in 20−45 min; 70−50% A in 45−50 min; 50−95% A in 50−55 min; 95% A in 55−65 min. The flow rate was set at 1.0 mL/min. The detection wavelength was 280 nm. The samples for analysis were filtered through a 0.22-μm nylon membrane prior to injection to HPLC.

Determination of In Vitro Xanthine Oxidase Inhibitory Activity. Xanthine oxidase activity was determined by measuring the formation of uric acid from xanthine according to the method of de Araújo et al.[7] All solutions were prepared in 50 mM phosphate buffer (pH 7.4). Fifty microliters of a test sample and 50 μL of xanthine oxidase (0.1 U/mL) were added in a well of a 96-well microplate, and the mixture was preincubated at 37 °C for 5 min before an aliquot (150 μL) of 0.42 mM xanthine was added. The resultant mixture was incubated at 37 °C for 60 min and then the enzymatic reaction was stopped by adding 80 μL of 1 M hydrochloric acid. Then dilution by ten times with buffer was performed and the diluted mixture was filtered through a 0.22-μm nylon membrane for HPLC analysis. For HPLC analysis, a Marchal C18 column (250 × 4.6 mm i.d., 5 μm, Guangzhou, China), and an isocratic mobile phase (i.e., 95% A in 0−10 min) consisting of 10 mM NaH_2PO_4−Na_2HPO_4 buffer (pH 5.5) (A) and methanol (B) were used. The flow rate was set at 1.0 mL/min and the detection wavelength was 290 nm. Phosphate buffer (50 mM, pH 7.4) was used as a negative control. Allopurinol was used as a positive control.

$$\begin{aligned}&\text{percent xanthine oxidase inhibition ratio}(\%)\\&\quad=(\text{uric acid content of negative control reaction}\\&\qquad-\text{uric acid content of sample reaction})/\text{uric acid content of}\\&\qquad\text{negative control reaction}\times 100\end{aligned}\tag{1}$$

IC_{50} value refers to the required allopurinol content (μg/mL) when the xanthine oxidase activity inhibition ratio is 50%. Xanthine oxidase inhibition activity value (μg of allopurinol equiv/100 g of dry wt) refers to the required allopurinol content (μg) when xanthine oxidase inhibition activity of allopurinol is equal to 100 g test sample. A higher

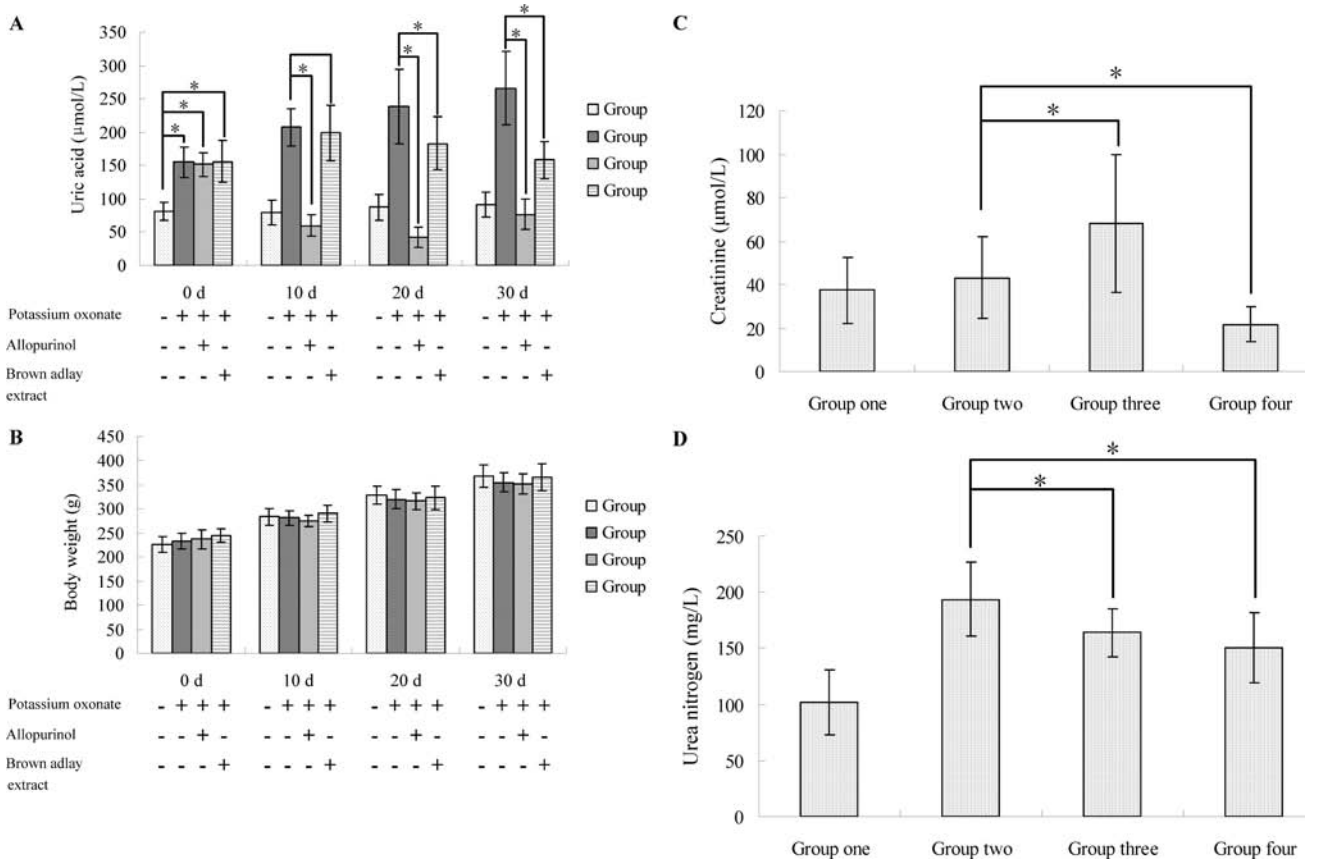

Figure 1. Effect of brown adlay extract on (A) rat serum uric acid, (B) rat body weight, (C) rat creatinine levels, and (D) rat urea nitrogen levels. All values are mean ± standard deviation (SD, $n = 15$) of 15 independent experiments. Asterisk (*) indicates $p < 0.05$.

xanthine oxidase inhibition activity value indicates a stronger xanthine oxidase inhibition activity of the sample.

DPPH Radical Scavenging Activity Assay. DPPH radical scavenging activity was determined by the method of Blois with some modifications.[26] One hundred microliters of a test sample was added in a well of a 96-well microplate. Then, 100 μL of 0.2 mM DPPH was added. The mixture was shaken, and then left to stand for 30 min at 25 °C. The absorbance was measured at 517 nm. All the above measurements were performed on a Varioskan Flash spectral scan multimode plate reader (Thermo Fisher Scientific). The absorbance of the negative control was obtained by replacing the sample with ethanol. The absorbance of the blank was obtained by replacing DPPH with ethanol. Trolox was used as a positive control.

$$\text{DPPH radical scavenging activity}(\%) = (1 - (\text{absorbance}_{\text{sample}} - \text{absorbance}_{\text{blank}}) / \text{absorbance}_{\text{negative control}}) \times 100 \quad (2)$$

DPPH radical scavenging activity value (μmol of Trolox equiv/100 g of dry wt) refers to the required Trolox content (μmol) when DPPH radical scavenging activity of Trolox is equal to 100 g sample. A higher DPPH radical scavenging activity value indicates a stronger DPPH radical scavenging activity of the sample.

Oxygen Radical Absorbance Capacity (ORAC) Assay. The ORAC assay was conducted using our published method.[27] All solutions were prepared in 75 mM phosphate buffer (pH 7.4). Twenty-five microliters of a test sample was added in a well of a 96-well microplate, and then 75 μL of fluorescein sodium salt (0.159 μM) was added. The mixture was preincubated for 10 min at 37 °C. Finally, 100 μL of 38.25 mM AAPH was added before analysis. The fluorescence was measured every 60 s for 4200 s. The reaction was carried out at a constant temperature of 37 °C. All the above measurements were performed on a Varioskan Flash spectral scan multimode plate reader (Thermo Fisher Scientific) with an excitation wavelength of 485 nm and an emission wavelength of 530 nm. Phosphate buffer (75 mM, pH 7.4) was used as a negative control. Trolox was used as a positive control.

Oxygen radical absorbance capacity value was calculated using the regression equation between Trolox concentration and the net area under curve (AUC).

$$\text{AUC} = 0.5(f_0 + f_n) + (f_1 + f_2 + \cdots + f_i + \cdots + f_{n-1}) \quad (3)$$

Where f_0 is the initial fluorescence and f_i is the fluorescence reading at any time. The net AUC is calculated as follows:

$$\text{Net AUC} = \text{AUC}_{\text{sample}} - \text{AUC}_{\text{negative control}} \quad (4)$$

Oxygen radical absorbance capacity value (μmol of Trolox equiv/100 g of dry wt) refers to the required Trolox content (μmol) when oxygen radical absorbance capacity of Trolox is equal to 100 g sample. A higher oxygen radical absorbance capacity value indicates a stronger oxygen radical absorbance capacity of the sample.

Superoxide Radical Scavenging Assay. Superoxide radicals were generated using the method of Wu et al.[28] All solutions were prepared in 50 mM phosphate buffer (pH 7.4). Twenty microliters of a test sample, 180 μL of 0.6 mM NBT solution, and 20 μL of 3 mM xanthine were mixed in a well of a 96-well microplate, to which 20 μL of xanthine oxidase (0.1 U/mL) was added to initiate the reaction. Such a mixture was incubated at 37 °C for 30 min before its absorbance was measured at 560 nm using a Varioskan Flash spectral scan multimode plate reader (Thermo Fisher Scientific). Phosphate buffer (50 mM, pH 7.4) was used as a negative control. Trolox was used as a positive control.

dx.doi.org/10.1021/jf501952e | J. Agric. Food Chem. 2014, 62, 7771−7778

$$\text{Superoxide radical scavenging activity}(\%) = ((\text{absorbance}_{\text{negative control}} - \text{absorbance}_{\text{sample}}) / \text{absorbance}_{\text{negative control}}) \times 100 \quad (5)$$

Superoxide radical scavenging activity value (μmol of Trolox equiv/100 g of dry wt) refers to the required Trolox content (μmol) when superoxide radical scavenging activity of Trolox is equal to 100 g sample. A higher superoxide radical scavenging activity value indicates a stronger superoxide radical scavenging activity of the sample.

Statistical Analysis. All the determinations were carried out in triplicate, and the experimental results were expressed as means ± SD. Statistical analysis was performed by SPSS 11 (SPSS Inc., Chicago, IL, USA). The probabilities of less than 5% ($p < 0.05$) were considered significant.

RESULTS AND DISCUSSION

Effects of Brown Adlay Extract on Serum Uric Acid Levels of Oxonate-Induced Hyperuricemic Rats. On day 0, the serum uric acid levels of potassium oxonate-treated groups including groups two (154.8 μmol/L), three (151.4 μmol/L), and four (155.9 μmol/L) were much higher than those of control group (group one, 81.5 μmol/L) after potassium oxonate treatment (Figure 1A). The serum uric acid levels of potassium oxonate-treated group two (265.7 μmol/L) steadily increased over 30 days, a phenomenon different from those of the control group (91.8 μmol/L) and the other groups treated with allopurinol (76.3 μmol/L) or brown adlay extract (158.3 μmol/L). Potassium oxonate is an uricase inhibitor and can drastically increase the serum uric acid levels causing hyperuricemia in rats. Allopurinol and brown adlay extract effectively decreased the serum uric acid levels of oxonate-induced hyperuricemic rats. Allopurinol is well-known as an effective xanthine oxidase inhibitor for treating hyperuricemia.[29] Thus, it is predicted that the brown adlay extract would act as a potential agent to prevent and treat hyperuricemia through lowering the serum uric acid levels.

Figure 1B shows that the brown adlay extract did not exert any adverse effect on rat body weight. The body weights of all groups increased gradually over 30 days, and there was no significant difference in body weight among the four groups at the same observation time point. Figure 1C and D further revealed the effects of different oral administrations on the serum creatinine and urea nitrogen levels of rats. The oxonate treatment did not significantly change ($p < 0.05$) the serum creatinine but caused considerably increased urea nitrogen in rats (group one vs group two). The administration of allopurinol did not lead to significant change ($p < 0.05$) in serum creatinine and urea nitrogen of oxonate-treated rats (group two vs group three). However, the brown adlay extract considerably reduced the serum creatinine (group four vs the other 3 groups), although the effects of brown adlay extract and allopurinol similarly influenced the urea nitrogen of oxonate-treated rats (both exerted significantly lowering effects). Although the brown adlay extract was not as effective as allopurinol for decreasing the serum uric acid levels of oxonate-induced hyperuricemic rats during the observation period (30 days), the brown adlay extract (a natural agent) could possess full benefits over an extended supplementation period. Thus, the brown adlay extract could be superior to allopurinol and possess the renal protective effect on hyperuricemic rats.

Phenolic Contents of Polished Adlay, Brown Adlay, Adlay Bran, and Adlay Hull. As shown in Table 1, total phenolic content of adlay bran (751 mg of gallic acid equiv/100 g of dry wt) was highest among all the test samples.

Table 1. Comparison of Total Phenolic Contents of Polished Adlay, Brown Adlay, Adlay Bran, and Adlay Hull[a]

	total phenolic content (mg of gallic acid equiv/100 g of dry wt)		
sample	free	bound	total
polished adlay	59 ± 4 d	8 ± 1 d	67 ± 5 d
brown adlay	109 ± 3 c	11 ± 2 c	120 ± 4 c
adlay bran	503 ± 21 a	248 ± 4 a	751 ± 25 a
adlay hull	274 ± 16 b	117 ± 18 b	391 ± 21 b

[a]Values with different letters in column show significant difference from one another ($p < 0.05$).

The total phenolic contents (Table 1) decreased in the order of adlay bran > adlay hull > brown adlay > polished adlay, with adlay bran having 2−11 times as much as the other adlay samples. The free and bound phenolic contents of adlay bran were the highest, respectively, among all the test samples. Adlay hull was ranked the second highest in all the free, bound, and total phenolic contents. The free and bound phenolic contents of adlay bran were 8.5 times and 29 times higher than those of polished adlay. These results suggest that the bran and hull are the most important sources for providing phenolic antioxidants of the adlay seed. The free phenolic contents contributed largely to the total phenolic contents of all the test samples: ∼88% for polished or brown adlay, and ∼68% for adlay bran or hull, respectively. The bound phenolic contents accounted for about 30% of the total phenolic contents of adlay bran and hull; thereby the role of the bound phenolic compounds became more important for adlay bran and hull, compared to polished or brown adlay.

HPLC chromatograms (Figure 2) of the free and bound phenolic extracts from polished adlay, brown adlay, adlay bran, and adlay hull were determined. Protocatechuic acid, chlorogenic acid, vanillic acid, caffeic acid, *p*-coumaric acid, and ferulic acid were used as standards according to the previous studies.[14,16] The phenolic profiles of the free phenolic extracts largely resembled, although the concentrations of individual phenolics varied with, the type of adlay sample. More significant differences were observed among the bound phenolic profiles of all the test samples. The concentrations of identified phenolics are listed in Table 2. Although chlorogenic acid, *p*-coumaric acid, and an unknown compound (retention time at 28.5 min, λ = 254 nm) were the most abundant in the free phenolic extracts, ferulic acid and *p*-coumaric acid were dominant in the bound phenolic extracts (except for adlay hull, i.e., *p*-coumaric acid and chlorogenic acid). According to Table 2, the varieties of phenolic compounds in the free phenolic extracts of the test samples were superior to those in the bound phenolic extracts of the test samples.

Yao et al.[17] reported the total phenolic content in the ethanol extract of adlay bran as 358 mg/100 g, a result much lower than that detected in the present study (751 mg/100 g). This result could be associated with the lower contents of ferulic acid, *p*-coumaric acid, and caffeic acid in the study of Yao et al.[17] Chung et al. were unable to detect *p*-coumaric acid and chlorogenic acid in their adlay bran ethanol extract due to low contents, a result disagreeing with the present study.[16] These variations were related to the different extraction methods or

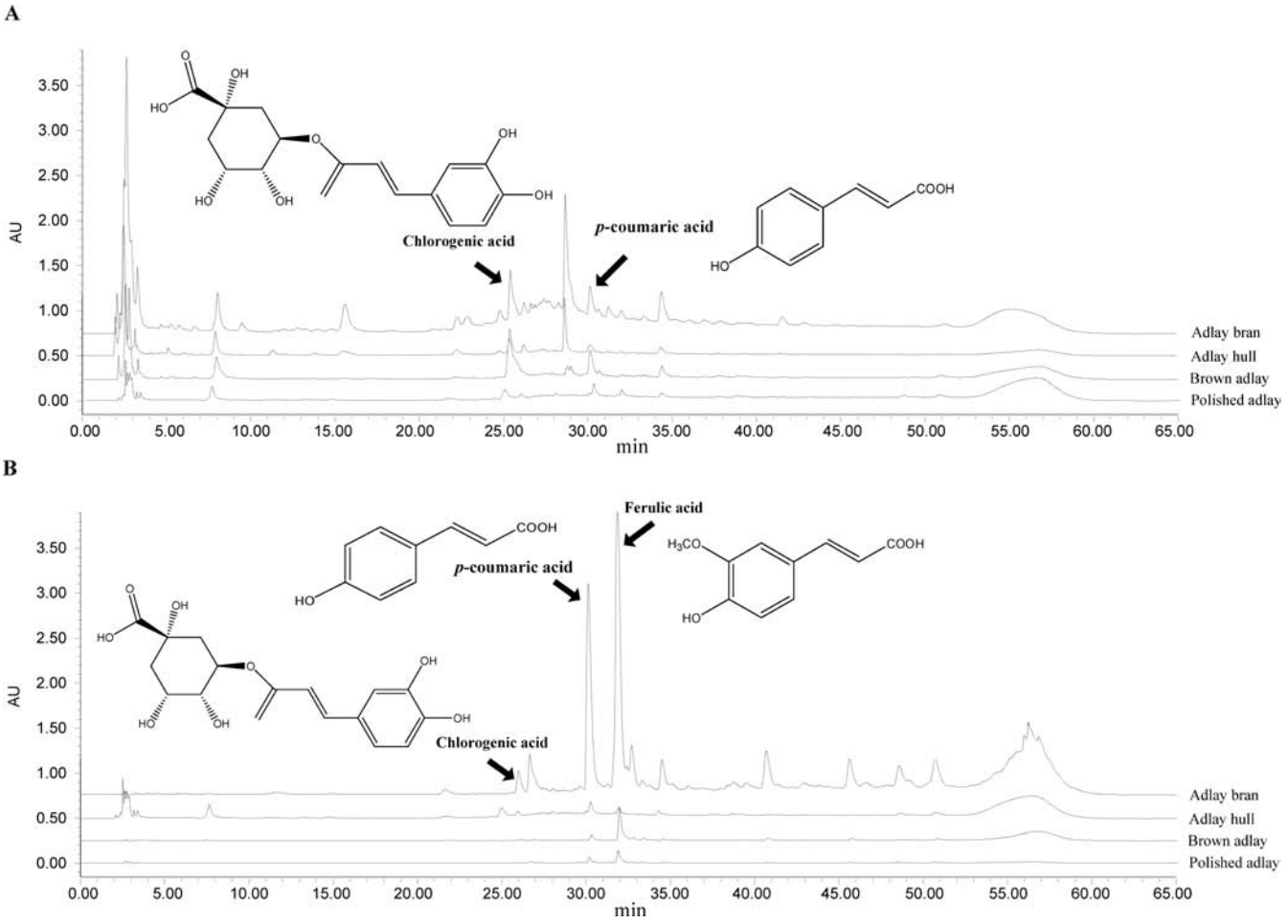

Figure 2. HPLC profiles of (A) free and (B) bound phenolic compounds in polished adlay, brown adlay, adlay bran, and adlay hull.

Table 2. Identified Phenolics in the Extracts from Polished Adlay, Brown Adlay, Adlay Bran, and Adlay Hull[a]

	amount of identified phenolic compounds (mg/100 g of dry wt)							
	polished adlay		brown adlay		adlay bran		adlay hull	
	free	bound	free	bound	free	bound	free	bound
protocatechuic acid	0.15 ± 0.02 bc	ND	0.19 ± 0.02 b	ND	0.49 ± 0.03 a	0.12 ± 0.02 c	0.48 ± 0.03 a	0.13 ± 0.02 c
chlorogenic acid	20.5 ± 2.35 a	ND	21.6 ± 1.98 a	ND	23.5 ± 2.56 a	0.09 ± 0.01 d	15.3 ± 1.43 b	3.91 ± 0.32 c
vanillic acid	0.46 ± 0.24 d	0.06 ± 0.01 d	1.21 ± 0.12 c	0.07 ± 0.01 d	5.38 ± 0.57 a	0.14 ± 0.02 d	1.88 ± 0.16 b	ND
caffeic acid	0.29 ± 0.18 d	0.16 ± 0.02 d	1.04 ± 0.11 c	0.18 ± 0.02 d	3.11 ± 0.28 b	5.15 ± 0.48 a	1.25 ± 0.12 c	0.39 ± 0.03 d
p-coumaric acid	3.84 ± 0.31 b	1.42 ± 0.23 b	1.21 ± 0.12 b	1.51 ± 0.13 b	7.36 ± 0.68 b	81.1 ± 7.96 a	5.26 ± 0.47 b	5.92 ± 0.56 b
ferulic acid	0.29 ± 0.04 b	2.95 ± 0.29 b	0.21 ± 0.02 b	3.24 ± 0.38 b	1.23 ± 0.12 b	38.7 ± 3.65 a	1.44 ± 0.17 b	1.58 ± 0.17 b

[a]Values with different letters in row show significant difference from one another ($p < 0.05$). ND, not detected.

adlay origin. Quite a few traditional extraction methods led to underestimated total phenolic contents due to the failure of recognizing the bound phenolics.[22] However, these bound phenolics could be of biological importance, e.g. the bound phytochemicals could exert their health benefits after their release by microflora in colon.[23,30]

In Vitro Xanthine Oxidase Inhibitory Activities of Polished Adlay, Brown Adlay, Adlay Bran, and Adlay Hull. In vitro xanthine oxidase inhibitory activities of extracts from four adlay materials, as well as their major phenolic compounds (i.e., chlorogenic acid, *p*-coumaric acid, and ferulic acid) are shown in Table 3. Allopurinol was used as a positive control (IC_{50} value = 4.75 ± 0.13 μg/mL). The adlay seed extracts were capable of inhibiting xanthine oxidase. The free phenolic extracts showed stronger xanthine oxidase inhibitory activities than the corresponding bound phenolic extracts. The free, bound, and total phenolic extracts of adlay bran or polished adlay possessed the greatest or lowest xanthine oxidase inhibitory activities in corresponding extract categories. The bran layer of adlay contributed largely to the xanthine oxidase inhibitory activity. Xanthine oxidase can oxidize xanthine or hypoxanthine, and produce uric acid and reactive oxygen species. Excess accumulation of uric acid causes gout.[19,31] As shown in an earlier section, the brown adlay extract significantly lowered the serum uric acid levels thus having potential agent for preventing and treating hyperuricemia. Therefore, the protective and therapeutic effects of brown adlay extract on oxonate-induced hyperuricemic rats may be attributed (i.e., at

dx.doi.org/10.1021/jf501952e | J. Agric. Food Chem. 2014, 62, 7771−7778

Table 3. Inhibitory Effects on Xanthine Oxidase Activity of Polished Adlay, Brown Adlay, Adlay Bran, Adlay Hull (μg of Allopurinol equiv/100 g of dry wt) and Standard Compounds (μg of Allopurinol equiv/g)[a]

sample	xanthine oxidase inhibition activity value		
	free	bound	total
polished adlay	135 ± 7 d	32 ± 2 c	167 ± 8 d
brown adlay	312 ± 14 c	36 ± 2 c	348 ± 16 c
adlay bran	607 ± 32 a	301 ± 15 a	908 ± 46 a
adlay hull	486 ± 21 b	255 ± 11 b	741 ± 31 b
chlorogenic acid		176 ± 7	
p-coumaric acid		17976 ± 10	
ferulic acid		18637 ± 11	

[a]Values with different letters in column show significant difference from one another ($p < 0.05$).

least partially) to the xanthine oxidase inhibitory activities of the test adlay samples.

The in vitro xanthine oxidase inhibitory activities of three purified phenolic chemicals were in this descending order: ferulic acid > *p*-coumaric acid > chlorogenic acid. Chlorogenic acid had ∼100 times weaker in vitro xanthine oxidase inhibitory activity per gram, compared to ferulic acid and *p*-coumaric acid. Therefore, the contribution of chlorogenic acid to the detected in vitro xanthine oxidase inhibitory activities of the free phenolic extracts could be very small, although chlorogenic acid was abundant in the free phenolic extracts (i.e., variations in the concentrations of their chlorogenic acid and other phenolics were <18 times). Therefore, in vitro xanthine oxidase inhibitory activities of the free phenolic extracts mainly came from *p*-coumaric acid (the other dominant phenolic compound) or other phenolic compounds and their interactive effects. For the bound phenolic extracts, *p*-coumaric acid and ferulic acid could have contributed largely to the detected in vitro xanthine oxidase inhibitory activities. However, Yoshizumi et al. found that the in vitro xanthine oxidase inhibitory activity of *p*-coumaric acid (IC_{50} value >100 μM) was weak.[32] The different results may be attributed to the different test methods. In addition, Nile and Park reported that ferulic acid possessed good in vitro inhibition effect on xanthine oxidase (IC_{50} value = 8.2 μM).[33] This result was consistent with that obtained in the present study.

It is worth noting the similarity in chemical structure between *p*-coumaric acid/ferulic acid and xanthine/uric acid, which suggest the possibility of acting as substrates (just as allopurinol) for xanthine oxidase. When phenolic compounds with low molecular weight came into the xanthine oxidase pocket, these phenolics may act as a "plug" causing subsequent inhibition of uric acid formation.[28] Therefore, low molecular weight *p*-coumaric acid and ferulic acid could effectively inhibit the xanthine oxidase activity. Chlorogenic acid has about 2-fold molecular weight and an extra 6-C ring compared to *p*-coumaric acid and ferulic acid. Thus, chlorogenic acid was possibly too large for xanthine oxidase pocket, leading to weak xanthine oxidase inhibitory activity.

Antioxidant Activities of Polished Adlay, Brown Adlay, Adlay Bran, and Adlay Hull. The antioxidant activities as DPPH radical scavenging activities, oxygen radical absorbance capacities, or superoxide radical scavenging activities of various adlay samples are listed in Table 4. Although the mechanisms of DPPH radical scavenging activity, oxygen radical absorbance capacity, and superoxide radical

Table 4. Antioxidant Activities of Polished Adlay, Brown Adlay, Adlay Bran, Adlay Hull (μmol of Trolox equiv/100 g of dry wt) and Standard Compounds (mol of Trolox equiv/mol)[a]

sample	DPPH radical scavenging activity value			oxygen radical absorbance capacity value			superoxide radical scavenging activity value		
	free	bound	total	free	bound	total	free	bound	total
polished adlay	110.51 ± 0.33 c	38.58 ± 0.36 c	149.09 ± 0.87 c	1930.83 ± 263.57 d	197.06 ± 6.12 d	2127.89 ± 268.67 d	97.05 ± 7.0 d	33.15 ± 0.42 c	130.20 ± 7.26 d
brown adlay	149.62 ± 1.67 c	45.01 ± 0.11 c	194.57 ± 2.93 c	3872.56 ± 202.19 c	913.49 ± 62.82 c	4786.05 ± 260.13 c	199.98 ± 13.27 c	60.18 ± 2.91 c	260.16 ± 15.73 c
adlay bran	873.81 ± 1.76 a	304.12 ± 10.61 a	1177.91 ± 15.62 a	22123.03 ± 1297.34 a	13128.19 ± 903.47 a	35251.22 ± 2198.72 a	741.04 ± 34.74 a	227.51 ± 13.97 a	968.55 ± 45.57 a
adlay hull	381.94 ± 4.40 b	200.94 ± 3.20 b	582.76 ± 11.76 b	14164.64 ± 885.99 b	5207.34 ± 82.58 b	19371.98 ± 965.37 b	363.81 ± 18.48 b	102.41 ± 4.83 b	466.22 ± 21.61 b
chlorogenic acid		2.75 ± 0.10			3.88 ± 0.14			0.47 ± 0.02	
p-coumaric acid		0.79 ± 0.03			3.67 ± 0.11			0.34 ± 0.02	
ferulic acid		0.67 ± 0.03			2.03 ± 0.08			0.08 ± 0.01	

[a]Values with different letters in column show significant difference from one another ($p < 0.05$).

dx.doi.org/10.1021/jf501952e | J. Agric. Food Chem. 2014, 62, 7771−7778

scavenging activity assays differ, the results of these three assays agreed with one another. The antioxidant activities were in the order of adlay bran > adlay hull > brown adlay > polished adlay, with the antioxidant activity values of the former two being much higher than those of the latter two. The free phenolic extracts exhibited stronger antioxidant activities than the bound phenolic extracts, indicating that the adlay samples with a higher total phenolic content possessed greater antioxidant activities. Moreover, the antioxidant activities of three phenolic compounds decreased in this order: chlorogenic acid > *p*-coumaric acid > ferulic acid. Chlorogenic acid is a dihydroxycinnamic acid with two hydroxy groups in ortho in aromatic ring, which is responsible for its greater antioxidant activity.

The DPPH radical scavenging activity assay, mainly based on an electron transfer reaction with marginal hydrogen atom transfer, is a rapid method and quite often used for evaluating antioxidant activity.[34] The ORAC assay is also popular because of its biologically relevant free radicals.[35] Furthermore, Lavelli et al. reported that xanthine oxidase is one of the major reactive oxygen species of enzymatic sources.[5] Excess reactive oxygen species could lead to a variety of pathophysiological phenomena, such as inflammation, aging, atherosclerosis, cancer, rheumatoid arthritis, hepatotoxicity, and reperfusion injury.[19] In the present study, the scavenging activities of the adlay samples for the superoxide radical generated by the xanthine/xanthine oxidase system were determined using an enzymatic assay.

The test adlay samples, as well as three purified phenolic chemicals, all inhibited the xanthine oxidase activity. *p*-Coumaric acid was found to have good xanthine oxidase inhibitory activity and superoxide radical scavenging activity, suggesting that *p*-coumaric acid is a xanthine oxidase inhibitor and can impart additional superoxide radical scavenging activity. Therefore, the superoxide radical scavenging activity of the adlay seed might be associated with their xanthine oxidase inhibitory activity. In comparison, chlorogenic acid with weak xanthine oxidase inhibitory activity still exhibited the strongest superoxide radical scavenging activity, i.e. a good superoxide radical scavenger with weak inhibitory activity on xanthine oxidase. Ferulic acid with strong xanthine oxidase inhibitory activity had the weakest superoxide radical scavenging activity, i.e. ferulic acid is a good xanthine oxidase inhibitor with weak superoxide radical scavenging activity. These different activity patterns were due to the different chemical structures of chlorogenic acid, *p*-coumaric acid, and ferulic acid.[8] Additionally, chlorogenic acid can be cleaved into caffeic acid and quinic acid in the body by an esterase enzyme in the colonic microflora. And caffeic acid can be metabolized to the form of glucuronide and sulfate conjugates.[36,37] Ferulic acid (FA) can be absorbed along the entire gastrointestinal tract and be metabolized into a number of metabolites (especially FA-glucuronide, FA-sulfate, and FA-sulfoglucuronide).[38] *p*-Coumaric acid is absorbed throughout the digestive tract. However, it seems to be less metabolized. Therefore, *p*-coumaric acid may have great health benefits.[39]

In conclusion, the results of this study provide strong in vitro and in vivo evidence to support the notion that polished adlay, brown adlay, adlay bran, and adlay hull could be active ingredients for functional food applications. Adlay seed and derived materials contained significant amounts of free or bound phenolics, possessing strong DPPH radical scavenging activities, oxygen radical absorbance capacities, and antioxidant activities in scavenging xanthine/xanthine oxidase-derived superoxide radicals. Adlay seed and derived materials could be used as effective radical scavengers and inhibitors of reactive oxygen species-generating enzyme. Therefore, seed and derived materials, especially the adlay bran, have positive future potential and could be potential raw materials for food and nutraceutical products to prevent and treat hyperuricemia.

AUTHOR INFORMATION

Corresponding Author

*E-mail: felzlin@scut.edu.cn; phone: +86 20 87113914; fax: +86 20 87113914.

Funding

This research was supported by the financial support from Twelfth five-year National Key Technology R&D Program of China (Project 2012BAD37B08-01), Science and Technology Planning Project of Guangdong Province, China (Project 2011B030500004), and Fundamental Research Funds for the Central Universities (Project 2014ZB0010).

Notes

The authors declare no competing financial interest.

REFERENCES

(1) Becker, M. A.; Schumacher, H. R.; Wortmann, R. L.; MacDonald, P. A.; Eustace, D.; Palo, W. A.; Streit, J.; Joseph-Ridge, N. Febuxostat compared with allopurinol in patients with hyperuricemia and gout. *New Engl. J. Med.* **2005**, *353*, 2450−2461.

(2) Tung, Y. T.; Hsu, C. A.; Chen, C. S.; Yang, S. C.; Huang, C. C.; Chang, S. T. Phytochemicals from *Acacia confusa* heartwood extracts reduce serum uric acid levels in oxonate-induced mice: Their potential use as xanthine oxidase inhibitors. *J. Agric. Food Chem.* **2010**, *58*, 9936−9941.

(3) Arafat, O. M.; Tham, S. Y.; Sadikun, A.; Zhari, I.; Haughton, P. J.; Asmawi, M. Z. Studies on diuretic and hypouricemic effects of *Orthosiphon stamineus* methanol extracts in rats. *J. Ethnopharmacol.* **2008**, *118*, 354−360.

(4) Lavelli, V. Antioxidant activity of minimally processed red chicory (*Cichorium intybus* L.) evaluated in xanthine oxidase-, myeloperoxidase-, and diaphorase-catalyzed reactions. *J. Agric. Food Chem.* **2008**, *56*, 7194−7200.

(5) Lavelli, V.; Peri, C.; Rizzolo, A. Antioxidant activity of tomato products as studied by model reactions using xanthine oxidase, myeloperoxidase, and copper-induced lipid peroxidation. *J. Agric. Food Chem.* **2000**, *48*, 1442−1448.

(6) Lin, J. K.; Chen, P. C.; Ho, C. T.; Lin-Shiau, S. Y. Inhibition of xanthine oxidase and suppression of intracellular reactive oxygen species in HL-60 cells by theaflavin-3,3′-digallate, (−)-epigallocatechin-3-gallate, and propyl gallate. *J. Agric. Food Chem.* **2000**, *48*, 2736−2743.

(7) de Araújo, M. E. M. B.; Moreira Franco, Y. E.; Alberto, T. G.; Sobreiro, M. A.; Conrado, M. A.; Priolli, D. G.; Frankland Sawaya, A. C. H.; Ruiz, A. L. T. G.; de Carvalho, J. E.; de Oliveira Carvalho, P. Enzymatic de-glycosylation of rutin improves its antioxidant and antiproliferative activities. *Food Chem.* **2013**, *141*, 266−273.

(8) Cos, P.; Ying, L.; Calomme, M.; Hu, J. P.; Cimanga, K.; Van Poel, B.; Pieters, L.; Vlietinck, A. J.; Berghe, D. V. Structure−activity relationship and classification of flavonoids as inhibitors of xanthine oxidase and superoxide scavengers. *J. Nat. Prod.* **1998**, *61*, 71−76.

(9) Li, J. M.; Zhang, X.; Wang, X.; Xie, Y. C.; Kong, L. D. Protective effects of cortex fraxini coumarines against oxonate-induced hyperuricemia and renal dysfunction in mice. *Eur. J. Pharmacol.* **2011**, *666*, 196−204.

(10) Prasad, K. N.; Chew, L. Y.; Khoo, H. E.; Kong, K. W.; Azlan, A.; Ismail, A. Antioxidant capacities of peel, pulp, and seed fractions of *Canarium odontophyllum* Miq. fruit. *J.Biomed. Biotechnol.* **2010**, No. 871379.

(11) Prasad, N.; Yang, B.; Kong, K. W.; Khoo, H. E.; Sun, J.; Azlan, A.; Ismail, A.; Romli, Z. B. Phytochemicals and antioxidant capacity from Nypa fruticans Wurmb. fruit. *Evid.-Based Compl. Alt. Med.* **2013**, No. 154606.
(12) Chen, H. J.; Chung, C. P.; Chiang, W.; Lin, Y. L. Anti-inflammatory effects and chemical study of a flavonoid-enriched fraction from adlay bran. *Food Chem.* **2011**, *126*, 1741−1748.
(13) Huang, D. W.; Chung, C. P.; Kuo, Y. H.; Lin, Y. L.; Chiang, W. Identification of compounds in adlay (*Coix lachryma-jobi L. var. ma-yuen* Stapf) seed hull extracts that inhibit lipopolysaccharide-induced inflammation in raw 264.7 macrophages. *J. Agric. Food Chem.* **2009**, *57*, 10651−10657.
(14) Chung, C. P.; Hsu, H. Y.; Huang, D. W.; Hsu, H. H.; Lin, J. T.; Shih, C. K.; Chiang, W. Ethyl acetate fraction of adlay bran ethanolic extract inhibits oncogene expression and suppresses DMH-induced preneoplastic lesions of the colon in F344 rats through an anti-inflammatory pathway. *J. Agric. Food Chem.* **2010**, *58*, 7616−7623.
(15) Lin, L. J.; Hsiao, E. S. L.; Tseng, H. S.; Chung, M. C.; Chua, A. C. N.; Kuo, M.-E.; Tzen, J. T. C. Molecular cloning, mass spectrometric identification, and nutritional evaluation of 10 coixins in adlay (*Coix lachryma-jobi* L.). *J. Agric. Food Chem.* **2009**, *57*, 10916−10921.
(16) Chung, C. P.; Hsia, S. M.; Lee, M. Y.; Chen, H. J.; Cheng, F.; Chan, L. C.; Kuo, Y. H.; Lin, Y. L.; Chiang, W. Gastroprotective activities of adlay (*Coix lachryma-jobi L. var. ma-yuen* Stapf) on the growth of the stomach cancer AGS cell line and indomethacin-induced gastric ulcers. *J. Agric. Food Chem.* **2011**, *59*, 6025−6033.
(17) Yao, H. T.; Lin, J. H.; Chiang, M. T.; Chiang, W.; Luo, M. N.; Lii, C. K. Suppressive effect of the ethanolic extract of adlay bran on cytochrome P-450 enzymes in rat liver and lungs. *J. Agric. Food Chem.* **2011**, *59*, 4306−4314.
(18) Lee, M. Y.; Lin, H. Y.; Cheng, F.; Chiang, W.; Kuo, Y. H. Isolation and characterization of new lactam compounds that inhibit lung and colon cancer cells from adlay (*Coix lachryma-jobi L. var. ma-yuen* Stapf) bran. *Food Chem. Toxicol.* **2008**, *46*, 1933−1939.
(19) Kuo, C. C.; Shih, M. C.; Kuo, Y. H.; Chiang, W. Antagonism of free-radical-induced damage of adlay seed and its antiproliferative effect in human histolytic lymphoma U937 monocytic cells. *J. Agric. Food Chem.* **2001**, *49*, 1564−1570.
(20) Vinson, J. A.; Hao, Y.; Su, X.; Zubik, L. Phenol antioxidant quantity and quality in foods: Vegetables. *J. Agric. Food Chem.* **1998**, *46*, 3630−3634.
(21) Vinson, J. A.; Su, X.; Zubik, L.; Bose, P. Phenol antioxidant quantity and quality in foods: Fruits. *J. Agric. Food Chem.* **2001**, *49*, 5315−5321.
(22) Adom, K. K.; Liu, R. H. Antioxidant activity of grains. *J. Agric. Food Chem.* **2002**, *50*, 6182−6187.
(23) Liu, R. H. Whole grain phytochemicals and health. *J. Cereal Sci.* **2007**, *46*, 207−219.
(24) Zhang, M. W.; Zhang, R. F.; Zhang, F. X.; Liu, R. H. Phenolic profiles and antioxidant activity of black rice bran of different commercially available varieties. *J. Agric. Food Chem.* **2010**, *58*, 7580−7587.
(25) Singleton, V. L.; Rossi, J. Colorimetry of total phenolics with phosphomolybdic-phosphotungstic acid reagents. *Am. J. Enol. Vitic.* **1965**, *16*, 144−158.
(26) Blois, M. S. Antioxidant determinations by the use of a stable free radical. *Nature* **1958**, *181*, 1199−1200.
(27) Lin, L.; Zhao, H.; Dong, Y.; Yang, B.; Zhao, M. Macroporous resin purification behavior of phenolics and rosmarinic acid from *Rabdosia serra* (MAXIM.) HARA leaf. *Food Chem.* **2012**, *130*, 417−424.
(28) Wu, N.; Zu, Y.; Fu, Y.; Kong, Y.; Zhao, J.; Li, X.; Li, J.; Wink, M.; Efferth, T. Antioxidant activities and xanthine oxidase inhibitory effects of extracts and main polyphenolic compounds obtained from *Geranium sibiricum* L. *J. Agric. Food Chem.* **2010**, *58*, 4737−4743.
(29) Lin, K. W.; Chen, Y. T.; Yang, S. C.; Wei, B. L.; Hung, C. F.; Lin, C. N. Xanthine oxidase inhibitory lanostanoids from *Ganoderma tsugae*. *Fitoterapia* **2013**, *89*, 231−238.
(30) Andreasen, M. F.; Kroon, P. A.; Williamson, G.; Garcia-Conesa, M. T. Intestinal release and uptake of phenolic antioxidant diferulic acids. *Free Radical Biol. Med.* **2001**, *31*, 304−314.
(31) Lin, S. M.; Wu, J. Y.; Su, C.; Ferng, S.; Lo, C. Y.; Chiou, R. Y. Y. Identification and mode of action of 5-hydroxymethyl-2-furfural (5-HMF) and 1-methyl-1,2,3,4-tetrahydro-β-carboline-3-carboxylic acid (MTCA) as potent xanthine oxidase inhibitors in vinegars. *J. Agric. Food Chem.* **2012**, *60*, 9856−9862.
(32) Yoshizumi, K.; Nishioka, N.; Tsuji, T. The xanthine oxidase inhibitory activity and hypouricemia effect of the propolis in rats. *Yakugaku Zasshi* **2005**, *125*, 315−321.
(33) Nile, S. H.; Park, S. W. Antioxidant, α-glucosidase and xanthine oxidase inhibitory activity of bioactive compounds from maize (*Zea mays* L.). *Chem. Biol. Drug Des.* **2014**, *83*, 119−125.
(34) Prior, R. L.; Wu, X.; Schaich, K. Standardized methods for the determination of antioxidant capacity and phenolics in foods and dietary supplements. *J. Agric. Food Chem.* **2005**, *53*, 4290−4302.
(35) Prior, R. L.; Hoang, H.; Gu, L.; Wu, X.; Bacchiocca, M.; Howard, L.; Hampsch-Woodill, M.; Huang, D.; Ou, B.; Jacob, R. Assays for hydrophilic and lipophilic antioxidant capacity (oxygen radical absorbance capacity (ORACFL)) of plasma and other biological and food samples. *J. Agric. Food Chem.* **2003**, *51*, 3273−3279.
(36) Plumb, G. W.; Garcia-Conesa, M. T.; Kroon, P. A.; Rhodes, M.; Ridley, S.; Williamson, G. Metabolism of chlorogenic acid by human plasma, liver, intestine and gut microflora. *J. Sci. Food Agric.* **1999**, *79*, 390−392.
(37) Nardini, M.; Forte, M.; Vrhovsek, U.; Mattivi, F.; Viola, R.; Scaccini, C. White wine phenolics are absorbed and extensively metabolized in humans. *J. Agric. Food Chem.* **2009**, *57*, 2711−2718.
(38) Zhao, Z.; Moghadasian, M. H. Chemistry, natural sources, dietary intake and pharmacokinetic properties of ferulic acid: A review. *Food Chem.* **2008**, *109*, 691−702.
(39) Garrait, G.; Jarrige, J. F.; Blanquet, S.; Beyssac, E.; Cardot, J. M.; Alric, M. Gastrointestinal absorption and urinary excretion of *trans*-cinnamic and *p*-coumaric acids in rats. *J. Agric. Food Chem.* **2006**, *54*, 2944−2950.

of the Japanese rice wine "sake". Herein, we describe the extraction of the adsorbed components from the used activated charcoal and their subsequent evaluation as pol inhibitors. This work culminated in the isolation of a potent inhibitor of mammalian pol, which was also investigated for its anti-inflammatory and antiallergic activities. Finally, we have provided a detailed discussion of the way in which bioactive compounds can be isolated from waste products to provide potential anti-inflammatory/antiallergic agents.

MATERIALS AND METHODS

Chemicals and Materials. The used activated charcoal, which is an industrial waste product generated during the manufacture of sake (trade name: Kuromatsu-Hakushika), was obtained from Tatsuuma-Honke Brewing Co. Ltd. (Nishinomiya, Japan). Tyrosol (**1**), which is also known as 4-(2-hydroxyethyl)phenol, 3-hydroxytyrosol (**2**), and 3,4-dihydroxyphenyl acetic acid (**3**) were purchased from Sigma-Aldrich Inc. (St. Louis, MO, U.S.A.). These compounds were of purchased as the analytical grade and purified by high-performance liquid chromatography. A chemically synthesized DNA template, poly(dA), was purchased from Sigma-Aldrich Inc., and a customized oligo$(dT)_{18}$ DNA primer was produced by Sigma-Aldrich Japan K.K. (Ishikari, Japan). The radioactive nucleotide [^{3}H]-labeled 2′-deoxythymidine-5′-triphosphate (dTTP; 43 Ci/mmol) was obtained from Moravek Biochemicals Inc. (Brea, CA, U.S.A.). Precoated Silica-Gel 60 plates (10 × 20 cm^2, 0.25 mm layer thickness) for thin-layer chromatography (TLC) were purchased from Merck (Darmstadt, Germany). All of the other reagents used in the current study were purchased from Nacalai Tesque Inc. (Kyoto, Japan) as the analytical grade.

Instrumental Analyses. ^{1}H- and ^{13}C-nuclear magnetic resonance (NMR) were recorded on a Bruker DRX600 (Bruker Biospin GmbH, Rheinstetten, Germany). Mass spectra were obtained on an esquire6000-TR (Bruker Daltonics, Billerica, MA, U.S.A.).

Enzymes. Pol α was purified from calf thymus by immuno-affinity column chromatography according to the method described by Tamai et al.[14] Recombinant rat pol β was purified from *Escherichia coli* JMpβ5 according to the procedure reported by Date et al.[15] The human pol γ catalytic gene was cloned into the pFastBac vector. A histidine-tagged enzyme was subsequently expressed using the BAC-TO-BAC HT Baculovirus Expression System (Life Technologies, Frederick, MD, U.S.A.) according to the manufacturer's instructions and purified over ProBound resin (Invitrogen Japan, Tokyo Japan).[16] Human pols δ and ε were purified by the nuclear fractionation of human peripheral blood cancer cells (Molt-4) using the second subunit of pol δ and ε-conjugated affinity column chromatography, respectively.[17] A truncated form of human pol η (residues 1−511) tagged with His_6 at its C-terminal was expressed in *E. coli* cells and purified as previously described by Kusumoto et al.[18] A recombinant mouse pol ι tagged with His_6 at its C-terminal was expressed and purified by nickel−nitriloacetic acid (Ni−NTA) column chromatography as previously described.[19] A truncated form of pol κ (residues 1−560) with a His_6 residue tag attached to its C-terminal was overexpressed in *E. coli* and purified according to the method described by Ohashi et al.[20] Recombinant human His-pol λ was overexpressed and purified according to the method described by Shimazaki et al.[21] Recombinant human His-pol μ was overexpressed in *E. coli* BL21 and purified by Glutathione Sepharose 4B column chromatography (GE Healthcare Bio-Science Corp., Piscataway, NJ, U.S.A.) according to the method described by Shimazaki et al.[21] for the preparation of pol λ. Pol α from the higher plant cauliflower inflorescence was purified according to the methods reported by Sakaguchi et al.[22] Recombinant rice (*Oryza sativa* L. cv. Nipponbare) pol λ tagged with His_6 at its C-terminal was expressed in *E. coli* and subsequently separated from the cells according to the method described by Uchiyama et al.[23] Calf TdT, *Taq* pol, T4 pol, T7 RNA polymerase, and T4 polynucleotide kinase were purchased from Takara Bio Inc. (Kyoto, Japan). The Klenow fragment of pol I from *E. coli* was purchased from Worthington Biochemical Corp. (Freehold, NJ, U.S.A.). Purified human placenta DNA topoisomerases I and II were purchased from TopoGen Inc. (Columbus, OH, U.S.A.). Bovine pancreas deoxyribonuclease I was obtained from Stratagene Cloning Systems (La Jolla, CA, U.S.A.).

Measurement of Pol Activity. The compositions of the reaction mixtures used for calf pol α, rat pol β, plant pol α, and the prokaryotic pols have been described previously elsewhere.[24,25] The reaction mixtures used for human pol γ, as well as human pols δ and ε have been described previously by Umeda et al.[16] and Ogawa et al.,[26] respectively. The reaction mixtures used for mammalian pols η, ι, and κ were the same as that used for pol α, whereas those used for human pols λ and μ, and plant pol λ were the same as that of pol β. For the pol reactions, poly(dA)/oligo$(dT)_{18}$ (A/T, 2/1) and dTTP were used as the DNA template-primer and nucleotide (dNTP; 2′-deoxynucleoside-5′-triphosphate) substrates, respectively. For the TdT reactions, oligo$(dT)_{18}$ (3′-OH) and dTTP were used as the DNA primer and nucleotide substrates, respectively.

The compounds to be tested were dissolved in freshly distilled dimethyl sulfoxide to various concentrations, and the resulting solutions were sonicated for 30 s. For microliter aliquots were of the solutions were then mixed with 16 μL of each enzyme (0.05 units) in 50 mM Tris-HCl (pH 7.5), containing 1 mM dithiothreitol, 50% glycerol (v/v), and 0.1 mM ethylenediaminetetraacetic acid, and the resulting mixtures were held at 0 °C for 10 min. Eight microliter aliquots of the inhibitor-enzyme mixtures were then added to 16 μL of the enzyme standard reaction mixture and incubated at 37 °C for 60 min, except for *Taq* pol, which was incubated at 74 °C for 60 min. Activity in the absence of the inhibitor was considered to be 100%, and the relative activity was determined for each inhibitor concentration. One unit of pol activity was defined as the amount of each enzyme required to catalyze the incorporation of 1 nmol of dTTP into the synthetic DNA template-primers in 60 min at 37 °C under standard reaction conditions.[24,25]

Other DNA Metabolic Enzyme Assays. The activities of T7 RNA polymerase, human DNA topoisomerases I and II, mouse IMP dehydrogenase (type II), T4 polynucleotide kinase, and bovine deoxyribonuclease I were measured using standard assay protocols according to the manufacturers' specifications, as described by Nakayama and Saneyoshi,[27] Yonezawa et al.,[28] Mizushina et al.,[29] Soltis and Uhlenbeck,[30] and Lu and Sakaguchi,[31] respectively.

Animals. Female ICR mice (6 weeks old with a body weight in the range of 25−27 g) were obtained from Japan SLC, Inc. (Hamamatsu, Japan), and maintained on a standard moderate fat (MF) diet (Oriental Yeast Co. Ltd., Osaka, Japan), with water provided ad libitum. Mice that had been bred in-house with free access to food and water were used for all of the experiments in the current study. All of the mice were maintained under a 12-h light/dark cycle and housed at room temperature (25 °C). This study was approved by the Institutional Animal Care and Use Committee of Kobe Gakuin University and was performed in accordance with the guidelines outlined in the Care and Use of Laboratory Animals of Kobe Gakuin University. The animals were anesthetized with pentobarbital before undergoing cervical dislocation.

Measurement of Anti-Inflammatory Activity. The mouse inflammatory test was performed according to Gschwendt's method.[32] Briefly, an acetone solution of the compound of interest (500 μg in 20 μL) or 20 μL of acetone as a vehicle control was applied to the inner part of the mouse ear. Thirty minutes after the test compound was applied, a TPA solution (0.5 μg/20 μL of acetone) was applied to the same part of the ear. TPA was also applied to the other ear of the same mouse as a control. After 7 h, a disk (6 mm diameter) was obtained from the ear and weighed. The inhibitory effect (IE) was then determined as the ratio of the weights of the two ear disks, as follows:

$$\mathrm{IE} = [(\text{TPA only}) - (\text{tested compound plus TPA})] / [(\text{TPA only}) - (\text{vehicle})] \times 100$$

Measurement of Anti-Anaphylactic Activity. The PCA reaction was conducted according to the method described by Sato et al.[33] Mice were sensitized by an intradermal injection of 0.1 μg of

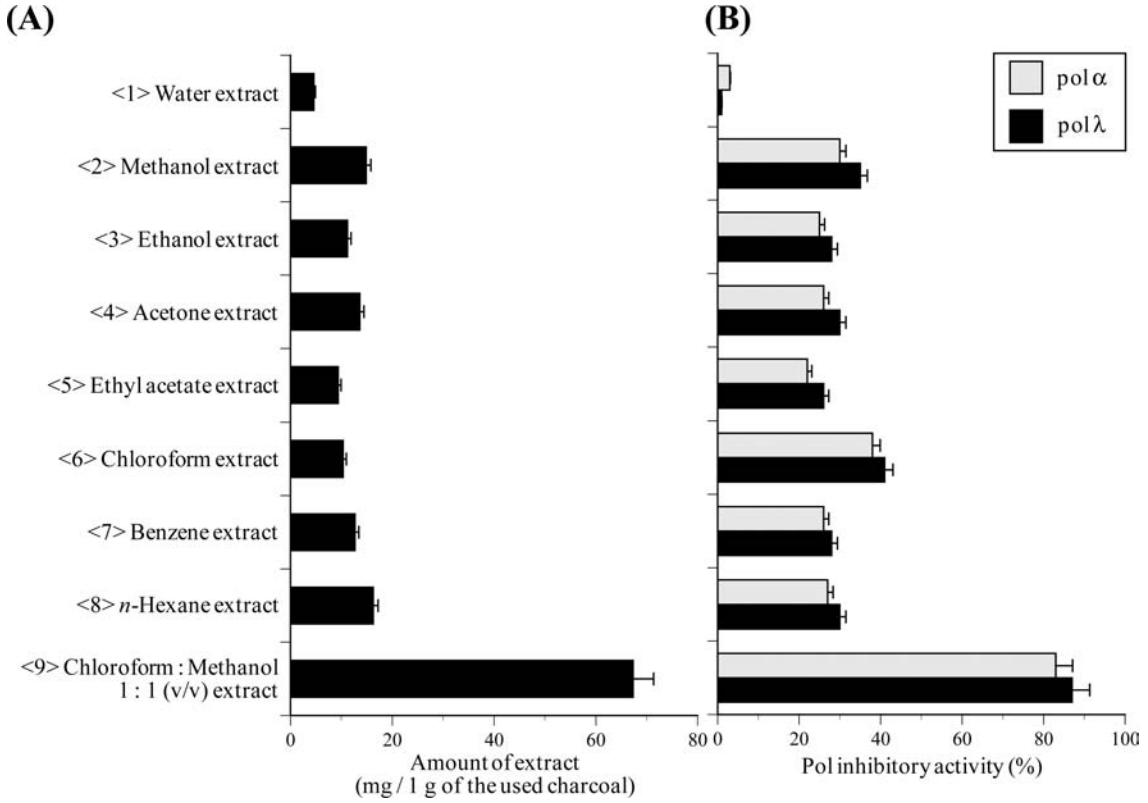

Figure 1. Extraction of the absorbed materials from the used activated charcoal generated during the sake-brewing process with different organic solvents. (A) Amount of extract collected from the used activated charcoal by the nine organic solvents. Data are shown as the mean values ± SD of three independent experiments. (B) Inhibitory activity of calf pol α and human pol λ by 100 μg/mL of extract collected from the used activated charcoal by the nine organic solvents. Data are shown as the mean values ± SD of three independent experiments.

antidinitrophenyl (DNP) IgE in their ear. Four hours later, the mice were intravenously challenged with 0.2 mL (1 mg/mL) of DNP-labeled human serum albumin containing 2% Evans blue dye. A test compound (100 mg/kg) or saline was also administered orally 2 h prior to the antigen challenge, with saline being used as a control. The mice were subsequently sacrificed, and their ears removed and weighed 30 min after the challenge. The ears were then dissolved in 200 μL of 1 N KOH, and the resulting solutions were incubated overnight at 37 °C. To measure the amount of Evans blue dye present in the exudates, the dissolved tissue solution was added to 400 μL of a 5:13 (v/v) mixture of acetone and 0.6 N phosphoric acid, and the optical density of the resulting solution was measured at 620 nm. The amount of dye in the exudates was calculated from an Evans blue standard curve, and the results expressed as a percentage for the mean amount of exudate dye from the treated mice. These data were then compared with those from the controls.

Statistical Analysis of Animal Experiments. All data of animal experiments such as anti-inflammatory and antiallergic activities are expressed as the means ± SD of six independent determinations for each experiment. Statistical significance between each experimental group was analyzed using Student's *t* test, and a level of probability of 0.01 and 0.05 was used as the criterion of significance.

RESULTS AND DISCUSSION

Extraction of Absorption Components from the Used Activated Charcoal Derived from Sake-Brewing Process. The Japanese rice wine "sake" is made from fermented rice. The fermentation process for the production of this wine involves the conversion of starch to sugar using the fungus *Aspergillus orizae*, whereas the brewing process uses the yeast *Saccharomyces cerevisiae*. During sake production, the fermented sake (i.e., irekuchi-sake) becomes colored and off-flavored, and is consequently treated with activated charcoal to remove the colors and off-flavors. The resulting activated charcoal-treated sake is known as "sumikuchi-sake", and this material is subsequently packaged and distributed as a commercial product. The used activated charcoal, however, is treated as an industrial waste product and disposed of accordingly. The aim the current study was to identify bioactive compounds that had been adsorbed onto the activated charcoal during the manufacture of sumikuchi-sake, and evaluate these compounds in terms of their pol-inhibitory activities. In this way, it could be possible to recycle these byproducts and find alternative industrial/medical applications for these materials.

We investigated the extraction of the absorbed materials from the used activated charcoal using nine different organic solvent systems, including (1) water, (2) methanol, (3) ethanol, (4) acetone, (5) ethyl acetate, (6) chloroform, (7) benzene, (8) *n*-hexane, and (9) a 1:1 (v/v) mixture of chloroform and methanol (Figure 1). Solvents (1) to (8) have been listed in order of their hydrophilicity. Five-hundred milligrams of the used activated charcoal was added to 1 mL of each organic solvent, and the resulting mixtures were shaken and vortex-mixed for 10 min, before being centrifuged at 10 000*g* for 10 min to separate the organic extract from the charcoal. Extract from solvent system (9) was very yellow in color, and the extract from solvent (4) was only slightly yellow in color. In contrast, the extracts from all of the other solvents remained colorless. The amounts of adsorbed material extracted from 1 g of used activated charcoal by the different organic solvents are shown in Figure 2A. The amount of material extracted by solvent system (9) was more than 4-fold greater than that of

dx.doi.org/10.1021/jf502095p | J. Agric. Food Chem. 2014, 62, 7779−7786

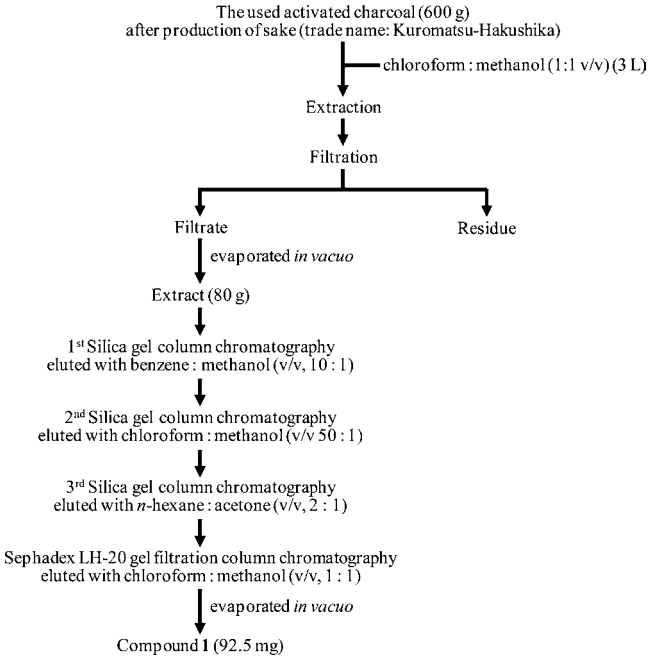

Figure 2. Method for purification of compound **1**, a mammalian pol inhibitor, from the used activated charcoal generated during the sake-brewing process.

any other organic solvent. Solvent system (9) therefore exhibited the best extraction efficiency of all of the solvents tested toward the used activated charcoal. The inhibitory activities of the extracts of nine organic solvent toward mammalian pols was investigated, using pol α and pol λ as a representative DNA replicative pol and DNA repair/recombination-related pol, respectively.[4,5] The inhibitory activity of calf pol α and human pol λ against 100 μg/mL of each extract is shown in Figure 1B. Among the nine extracts tested, solvent system (9) showed the strongest inhibition of both pols α and λ, with inhibitory activities of 83.0 and 87.2%, respectively. The extracts of solvent system (2) to (8) slightly inhibited the pol activity, but solvent system (1) had no effect on the activity, suggesting that water-soluble (i.e., hydrophilic) components of the absorbed materials from the used activated charcoal did not have the inhibitory activities of mammalian pols.

Isolation of a Mammalian Pol Inhibitor from the Absorption Extract of the Used Activated Charcoal. The materials extracted from the used activated charcoal with solvent system (9) exhibited potent inhibitory activity toward mammalian pol, and the decision was taken to purify this extract to isolate and identify the compound responsible for this inhibitory activity. Briefly, a large portion of used activated charcoal (600 g) was extracted with a 1:1 (v/v) mixture of chloroform and methanol (3 L), and the resulting extract was evaporated to dryness to give a residue (80 g), which was subjected to purification by column chromatography over silica gel eluting with a 10:1 (v/v) mixture of benzene and methanol. The active fractions (1.15 g) were then combined and purified by column chromatography over silica gel eluting with a 50:1 (v/v) mixture of chloroform and methanol. Once again, the active fractions (310 mg) were combined and purified by column chromatography over silica gel eluting with a 2:1 (v/v) mixture of *n*-hexane and acetone. Finally, the active fractions (123 mg) were combined and purified by column chromatography over Sephadex LH-20 eluting with a 1:1 (v/v) mixture of chloroform and methanol to give compound **1** as a white powder (92.5 mg), which was confirmed to be an inhibitor of mammalian pol (Figure 2). The yield and 50% inhibitory concentration (IC_{50}) for human pol λ activity of the purification steps are shown in Table 1. Since the extract of solvent system (9) was stronger pol λ inhibitor than the active fraction of first silica gel column chromatography, the extract of solvent system (9) should contain several pol inhibitory compounds.

Table 1. Purification Steps of Compound 1 from the Used Activated Charcoal after Production of Sake

step of purification	yield (mg)	IC_{50} value for pol λ (μg/mL)
extract of chloroform: methanol (1:1 v/v)	80 000	55.3
active fraction of first silica gel column chromatography	1150	66.8
active fraction of second silica gel column chromatography	310	18
active fraction of third silica gel column chromatography	123	6.5
active fraction of LH-20 gel filtration column chromatography (compound **1**)	92.5	4.7

Determination of the Structure of Compound 1 Purified from the Used Activated Charcoal Derived from the Sake-Brewing Process. Compound **1** purified from the used activated charcoal was identified as tyrosol [4-(2-hydroxyethyl)phenol] by spectroscopic analyses, including 1D/2D NMR and MS. These spectroscopic data were consistent with those reported previously in the literature for the same compound.[34] Two tyrosol (**1**) analogues were also prepared, including 3-hydroxytyrosol (**2**) and 3,4-dihydroxyphenyl acetic acid (**3**) (Figure 3), and all three of these compounds were used in the next part of the study.

Effects of Tyrosol (1) and Its Analogues (2 and 3) on the Activities of Various Pols and Other DNA Metabolic Enzymes. Tyrosol (**1**), 3-hydroxytyrosol (**2**), and 3,4-dihydroxyphenyl acetic acid (**3**) were evaluated in terms of

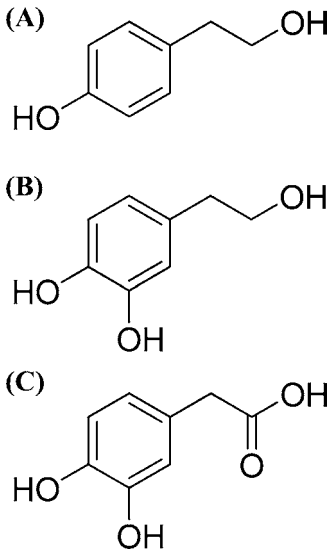

Figure 3. Structure of compound **1**, which was obtained from the absorption extract of the used activated charcoal generated during the sake-brewing process, and two related compounds. Compound **1**, tyrosol [4-(2-hydroxyethyl)phenol]; compound **2**, 3-hydroxytyrosol; and compound **3**, 3,4-dihydroxyphenyl acetic acid.

dx.doi.org/10.1021/jf502095p | J. Agric. Food Chem. 2014, 62, 7779−7786

Table 2. IC_{50} Values of Tyrosol (1) and Its Analogues (2 And 3) towards Various Pols and other DNA Metabolic Enzymes[a]

enzymes	IC_{50} values (μM)				
	tyrosol (1)	3-hydroxytyrosol (2)	3,4-dihydroxyphenylacetic acid (3)	aphidicolin	curcumin
[1] mammalian pols					
[A-family]					
human pol γ	42.0 ± 2.5	>200	>200	>200	>200
[B-family]					
calf pol α	40.7 ± 2.4	>200	>200	19.6 ± 1.0	>200
human pol δ	42.6 ± 2.6	>200	>200	13.3 ± 0.7	>200
human pol ε	42.8 ± 2.5	>200	>200	16.2 ± 0.8	>200
[X-family]					
rat pol β	36.0 ± 2.1	>200	>200	>200	>200
human pol λ	34.3 ± 2.0	>200	>200	>200	7.0 ± 1.0
human pol μ	37.5 ± 2.2	>200	>200	>200	>200
calf TdT	38.1 ± 2.2	>200	>200	>200	>200
[Y-family]					
human pol η	44.4 ± 2.6	>200	>200	>200	>200
mouse pol ι	46.1 ± 2.7	>200	>200	>200	>200
human pol κ	45.2 ± 2.5	>200	>200	>200	>200
[2] plant pols					
cauliflower pol α	>200	>200	>200	25.0 ± 1.3	>200
rice pol λ	>200	>200	>200	>200	>200
[3] prokaryotic pols					
E. coli pol I	>200	>200	>200	>200	>200
Taq pol	>200	>200	>200	>200	>200
T4 pol	>200	>200	>200	>200	>200
[4] other DNA metabolic enzymes					
human topo I	>200	>200	>200	>200	>200
human topo II	>200	>200	>200	>200	>200
mouse IMP dehydrogenase (type II)	>200	>200	>200	>200	>200
T4 polynucleotide kinase	>200	>200	>200	>200	>200
bovine deoxyribonuclease I	>200	>200	>200	>200	>200

[a]Compounds **1**–**3** and positive controls (aphidicolin and curcumin) were incubated with each pol (0.05 U) and other DNA metabolic enzymes. Enzyme activity in the absence of the compound was considered to be 100%. Data are shown as the mean values ± SD of three independent experiments.

their inhibitory activities toward various pols and other DNA metabolic enzymes. The purities of these compounds were determined to be greater than 98% by NMR analysis (data not shown).

Tyrosol (**1**) exhibited inhibitory activity toward 11 mammalian pols, including pols belonging to family A (human pol γ), family B (calf pol α, human pol δ, and human pol ε), family X (rat pol β, human pol λ, and human pol μ), and family Y (human pol η, mouse pol ι, and human pol κ),[4,5] with IC_{50} values of 42.0, 40.7–42.8, 34.3–38.1, and 44.4–46.1 μM, respectively (Table 2). Tyrosol (**1**) strongly inhibited the activities of X-family pols, with human pol λ being the most sensitive of all 11 of the mammalian pols tested toward this compound. Aphidicolin, a known inhibitor of pols α, δ, and ε,[1] and curcumin, a specific inhibitor of pol λ,[35] showed stronger pol inhibitory activity than tyrosol (**1**).

In contrast, 3-hydroxytyrosol (**2**) and 3,4-dihydroxyphenyl acetic acid (**3**) had no effect on any of these pols, indicating that the presence of a hydroxyl group at the 3-position tyrosol was having an adverse impact on its inhibitory activity toward mammalian pols, and that the whole structure of tyrosol (**1**) may be essential to its inhibitory activity. When activated DNA (bovine deoxyribonuclease I-treated DNA) was used as the DNA template-primer substrate instead of synthesized DNA [poly(dA)/oligo$(dT)_{18}$ (A/T = 2/1)], and dNTP was used as the nucleotide substrate instead of dTTP, the inhibitory effects of these compounds did not change (data not shown).

None of these three compounds exhibited any influence over the activities of the plant pols, including cauliflower pol α and rice pol λ. Furthermore, none of these compounds exhibited inhibitory activity toward prokaryotic pols, such as the Klenow fragment of *E. coli* pol I, *Taq* pol and T4 pol, or DNA metabolic enzymes, such as T7 RNA polymerase, human DNA topoisomerases I and II, mouse IMP dehydrogenase (type II), T4 polynucleotide kinase, and bovine deoxyribonuclease I (Table 2). On the basis of these results, tyrosol (**1**) can be classified as a selective inhibitor of mammalian pols. Given that tyrosol (**1**), which is an absorption component of the activated charcoal waste generated during the manufacture of sake, is an inhibitor of the mammalian pol species is of great interest.

Specific assays were used to determine whether the tyrosol (**1**)-induced inhibition was dependent on the binding of tyrosol (**1**) to DNA or to the enzyme. The extent of the interaction between tyrosol (**1**) and dsDNA was investigated based on the thermal transition of dsDNA by measuring the melting temperature (T_m) of dsDNA in the presence of an excess amount of tyrosol (**1**) (200 μM) using a spectrophotometer equipped with a thermoelectric cell holder. A thermal transition of T_m was not observed within the compound concentration range used in the assay. In contrast, a typical intercalating compound used as a positive control (ethidium bromide, 15

dx.doi.org/10.1021/jf502095p | J. Agric. Food Chem. 2014, 62, 7779–7786

μM) produced a clear thermal transition (data not shown). To determine whether the inhibitory effect of tyrosol (**1**) was caused by nonspecific adhesion to mammalian pols or its selective binding to specific sites, we proceeded to investigate whether an excessive amount of nucleic acid [poly(rC)] or protein [bovine serum albumin (BSA)] abrogated the effects of tyrosol (**1**). Poly(rC) and BSA had little to no effect on the pol-inhibitory activity of tyrosol (**1**) (data not shown), which suggested that this compound was binding selectively to the pol molecule. These observations indicated that tyrosol (**1**) was not acting as a DNA intercalating agent, and that it was exerting its inhibitory activity by binding directly to selected pol enzymes.

Effect of Tyrosol (1) and Its Analogues (2 and 3) on TPA-Induced Inflammation In Vivo. In our previous pol inhibitor studies, we observed a relationship between pol λ inhibitors and their ability to suppress TPA-induced inflammation.[6,7,9,35,36] With this in mind, we used an in vivo mouse ear inflammatory test in the current study to examine the anti-inflammatory activities of tyrosol (**1**), 3-hydroxytyrosol (**2**), and 3,4-dihydroxyphenyl acetic acid (**3**). The application of TPA (0.5 μg) to the mouse ear induced edema resulted in a 241% increase in the weight of the ear disk 7 h after application. As shown in Figure 4, pretreatment with 500 μg of tyrosol (**1**) had

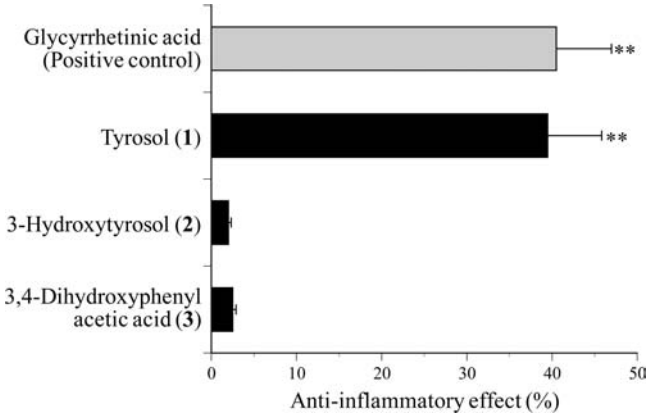

Figure 4. Anti-inflammatory activities of tyrosol (**1**) and its analogues (**2** and **3**) toward TPA-induced edema in a mouse ear model. Each compound (500 μg) was applied individually to one ear of a mouse, and TPA (0.5 μg) was applied 30 min later to both ears. Edema was evaluated after 7 h. The inhibitory effect is expressed as the percentage of edema. Data are shown as the mean values ± SD of six independent experiments. ** $P < 0.01$ versus controls.

a 55% anti-inflammatory effect, whereas 3-hydroxytyrosol (**2**) and 3,4-dihydroxyphenyl acetic acid (**3**) had no effect. The in vivo anti-inflammatory effects of these compounds therefore displayed a similar trend to that observed for their in vitro inhibitory effects toward mammalian pols (Table 2). The anti-inflammatory effect of glycyrrhetinic acid, which is a known anti-inflammatory agent, was very similar to that of tyrosol (**1**), and it was therefore concluded that tyrosol (**1**) was at least as effective as this benchmark compound.

Effect of Tyrosol (1) and Its Analogues (2 and 3) on Anti-Allergic Activity In Vivo. The IgE-mediated PCA reaction can be used as an in vivo tool to study the mechanism of the immediate hypersensitivity reaction. As shown in Figure 5, tyrosol (**1**) inhibited the PCA reaction in mice by 79.4%, when it was used at a dose of 100 mg/kg. In contrast, 3-hydroxytyrosol (**2**) and 3,4-dihydroxyphenyl acetic acid (**3**) had very little impact on the reaction. The antiallergic effects of

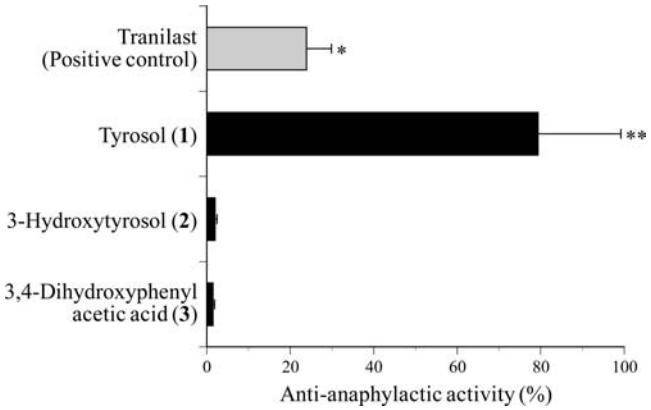

Figure 5. Antiallergic activities of tyrosol (**1**) and its analogues (**2** and **3**) measured by mouse PCA reaction. Each compound (100 mg/kg) was orally administered to the mice, and the IgE-dependent PCA reaction was investigated. Inhibition of anaphylactic activity by the vehicle control was taken as 0%. Data are shown as the mean values ± SD of six independent experiments. ** $P < 0.01$ and * $P < 0.05$ versus controls.

these compounds were therefore of the same order of magnitude as their in vitro inhibitory effects toward the mammalian pols (Table 2). Tranilast, which is a commonly used antiallergic drug that targets mast cell degranulation and inhibits the PCA reaction, caused 23.9% inhibition in this PCA reaction assay at a dose of 100 mg/kg (Figure 5). The inhibitory effect of tyrosol (**1**) was 3.3-fold greater than that of tranilast, which suggested that tyrosol could potentially be used as an antiallergic compound. Antiallergic effect by PCA experiment using rat of dorsal skin was same tendency as that using mouse ear (the inhibitory effect of 100 mg/kg tyrosol (**1**) was 2.6-fold greater than that of 100 mg/kg tranilast).

In addition to causing inflammation, TPA influences cell proliferation and exhibits tumor-promoting activity.[12] Anti-inflammatory agents are therefore expected to suppress DNA replication/repair/recombination in nuclei in relation to the action of TPA. Given that pol is related to repair/recombination,[1−3] our finding that it is a molecular target of tyrosol (**1**), which selectively inhibited mammalian pol activity (Table 2), is in agreement with this expected mechanism of anti-inflammatory/antiallergic action. Recently, we found that there is the positive correlation between inflammatory cytokines induction, such as TNF-α by lipopolysaccharide and expression of pol λ,[37] which has been implicated in 5′-deoxyribose-5-phosphate (dRP)-lyase activity,[38] V(D)J recombination,[39] translesion synthesis,[40] and base excision repair,[41] in cultured mouse macrophage RAW264.7 cells; thus, not only DNA polymerization activity, but also the protein expression of pol λ is likely to be important in inflammation. However, detailed mechanisms describing the way in which tyrosol (**1**) inhibits mammalian pols, such as pol λ, as well as the way in which it elicits it anti-inflammatory effects, remain unclear, and further studies are currently underway in our laboratory to elucidate these mechanisms.

Sake-byproduct is formed during fermentation of *Orzya sativa* to produce the Japanese rice wine "sake". This contains fermentation products of fungus (*Aspergillus oryzae*) and yeast (*Saccharomyces cerevisiae*) using rice tissues such as endosperm, bran, and germ, and this byproduct is an unused resource containing novel bioactive compounds. Therefore, we focused on the absorption extract, collected from the used activated

charcoal, of sake-byproduct. Activated charcoal is a form of carbon that is processed in such a way as to introduce multiple small, low-volume pores that are designed to increase the surface area available for adsorption or chemical reactions. These pores can also bind to low molecular weight compounds containing benzene rings, although very little is known about the molecular mechanism involved in adsorption of different materials by activated charcoal. Tyrosol (**1**) is produced from tyrosine during the fermentation of yeast,[42] and is therefore present in the fermented sake. Tyrosol (**1**) is a derivative of phenethyl alcohol, which is known as a natural phenolic antioxidant. As an antioxidant, tyrosol (**1**) can protect cells against injuries caused by oxidation.[43] To the best of our knowledge, this study represents the first reported account of tyrosol (**1**) being used to inhibit the activities of mammalian pols. These results suggest that the used activated charcoal generated as a waste product during sake production could be used as a good source of tyrosol (**1**) for its anti-inflammatory/antiallergic activities. This compound could also be used as an effective nutritional supplement because of its anti-inflammatory and antiallergic effects, which could lead to significant improvements in human health. The tyrosol (**1**)-enriched fraction of the used activated charcoal generated during the sake-brewing process, or purified tyrosol (**1**), could potentially be used in functional foods or cosmetics to deliver anti-inflammatory/antiallergic properties.

AUTHOR INFORMATION

Corresponding Author

*Phone: +81-78-974-1551 (ext. 3232). Fax: +81-78-974-5689. E-mail: mizushin@nutr.kobegakuin.ac.jp.

Notes

The authors declare no competing financial interest.

ACKNOWLEDGMENTS

We are grateful for the following donations: calf pol α from Dr. M. Takemura of Tokyo University of Science (Tokyo, Japan); rat pol β and human pols δ and ε from Dr. K. Sakaguchi of Tokyo University of Science (Chiba, Japan); human pol γ from Dr. M. Suzuki of Nagoya University School of Medicine (Nagoya, Japan); mouse pol η and human pol ι from Dr. F. Hanaoka of Gakushuin University (Tokyo, Japan) and Dr. C. Masutani of Nagoya University (Nagoya, Japan); human pol κ from Dr. H. Ohmori of Kyoto University (Kyoto, Japan); and human pols λ and μ from Dr. O. Koiwai of Tokyo University of Science (Chiba, Japan). This study was supported in part by the Ministry of Education, Culture, Sports, Science and Technology (MEXT, Japan)-Supported Program for the Strategic Research Foundation at Private Universities, 2012−2016. Y.M. received Grant-in-Aids for Scientific Research (C) (No. 24580205) from MEXT.

REFERENCES

(1) Kornberg, A.; Baker, T. A. *DNA Replication*, 2nd ed.; Freeman, W. D., Ed.; University Science Books: Sausalito, CA, 1992; Chapter 6, pp 197−225.

(2) Bebenek, K.; Kunkel, T. A. *DNA Repair and Replication*. In *Advances in Protein Chemistry*; Yang, W., Ed.; Elsevier: San Diego, CA, 2004; pp 137−165.

(3) Hubscher, U.; Maga, G.; Spadari, S. Eukaryotic DNA polymerases. *Annu. Rev. Biochem.* **2002**, *71*, 133−163.

(4) Lange, S. S.; Takata, K.; Wood, R. D. DNA polymerases and cancer. *Nat. Rev. Cancer* **2011**, *11*, 96−110.

(5) Loeb, L. A.; Monnat, R. J., Jr. DNA polymerases and human disease. *Nat. Rev. Genet.* **2008**, *9*, 594−604.

(6) Mizushina, Y. Specific inhibitors of mammalian DNA polymerase species. *Biosci. Biotechnol. Biochem.* **2009**, *73*, 1239−1251.

(7) Mizushina, Y. Screening of novel bioactive compounds from food components and nutrients. *J. Jpn. Soc. Nutr. Food Sci.* **2011**, *64*, 377−384.

(8) Mizushina, Y.; Kamisuki, S.; Kasai, N.; Ishidoh, T.; Shimazaki, N.; Takemura, M.; Asahara, H.; Linn, S.; Yoshida, S.; Koiwai, O.; Sugawara, F.; Yoshida, H.; Sakaguchi, K. Petasiphenol: A DNA polymerase λ inhibitor. *Biochemistry* **2002**, *41*, 14463−14471.

(9) Mizushina, Y.; Hirota, M.; Murakami, C.; Ishidoh, T.; Kamisuki, S.; Shimazaki, N.; Takemura, M.; Perpelescu, M.; Suzuki, M.; Yoshida, H.; Sugawara, F.; Koiwai, O.; Sakaguchi, K. Some anti-chronic inflammatory compounds are DNA polymerase λ-specific inhibitors. *Biochem. Pharmacol.* **2003**, *66*, 1935−1944.

(10) Hecker, E. *Carcinogenesis*; Raben Press: New York, 1978; pp 11−48.

(11) Fujiki, H.; Sugimura, T. *Adv. Cancer Res.*; Academic Press, Inc.: London, UK, 1987; pp 223−264.

(12) Nakamura, Y.; Murakami, A.; Ohto, Y.; Torikai, K.; Tanaka, T.; Ohigashi, H. Suppression of tumor promoter-induced oxidative stress and inflammatory responses in mouse skin by a superoxide generation inhibitor 1′-acetoxychavicol acetate. *Cancer Res.* **1995**, *58*, 4832−4839.

(13) Mitoshi, M.; Kuriyama, I.; Nakayama, H.; Miyazato, H.; Sugimoto, K.; Kobayashi, Y.; Jippo, T.; Kanazawa, K.; Yoshida, H.; Mizushina, Y. Effects of essential oils from herbal plants and citrus fruits on DNA polymerase inhibitory, cancer cell growth inhibitory, antiallergic, and antioxidant activities. *J. Agric. Food Chem.* **2012**, *60*, 11343−11350.

(14) Tamai, K.; Kojima, K.; Hanaichi, T.; Masaki, S.; Suzuki, M.; Umekawa, H.; Yoshida, S. Structural study of immunoaffinity-purified DNA polymerase α-DNA primase complex from calf thymus. *Biochim. Biophys. Acta* **1988**, *950*, 263−273.

(15) Date, T.; Yamaguchi, M.; Hirose, F.; Nishimoto, Y.; Tanihara, K.; Matsukage, A. Expression of active rat DNA polymerase β. *E. coli. Biochem.* **1998**, *27*, 2983−2990.

(16) Umeda, S.; Muta, T.; Ohsato, T.; Takamatsu, C.; Hamasaki, N.; Kang, D. The D-loop structure of human mtDNA is destabilized directly by 1-methyl-4-phenylpyridinium ion (MPP^+), a parkinsonism-causing toxin. *Eur. J. Biochem.* **2000**, *267*, 200−206.

(17) Oshige, M.; Takeuchi, R.; Ruike, R.; Kuroda, K.; Sakaguchi, K. Subunit protein-affinity isolation of *Drosophila* DNA polymerase catalytic subunit. *Protein Expr. Purif.* **2004**, *35*, 248−256.

(18) Kusumoto, R.; Masutani, C.; Shimmyo, S.; Iwai, S.; Hanaoka, F. DNA binding properties of human DNA polymerase η: Implications for fidelity and polymerase switching of translesion synthesis. *Genes Cells* **2004**, *9*, 1139−1150.

(19) Braithwaite, E. K.; Kedar, P. S.; Stumpo, D. J.; Bertocci, B.; Freedman, J. H.; Samson, L. D.; Wilson, S. H. DNA polymerases β and λ mediate overlapping and independent roles in base excision repair in mouse embryonic fibroblasts. *PLoS One* **2010**, *5*, No. e12229.

(20) Ohashi, E.; Murakumo, Y.; Kanjo, N.; Akagi, J.; Masutani, C.; Hanaoka, F.; Ohmori, H. Interaction of hREV1 with three human Y-family DNA polymerases. *Genes Cells* **2004**, *9*, 523−531.

(21) Shimazaki, N.; Yoshida, K.; Kobayashi, T.; Toji, S.; Tamai, T.; Koiwai, O. Over-expression of human DNA polymerase λ in *E. coli* and characterization of the recombinant enzyme. *Genes Cells* **2002**, *7*, 639−651.

(22) Sakaguchi, K.; Hotta, Y.; Stern, H. Chromatin-associated DNA polymerase activity in meiotic cells of lily and mouse. *Cell Struct. Funct.* **1980**, *5*, 323−334.

(23) Uchiyama, Y.; Kimura, S.; Yamamoto, T.; Ishibashi, T.; Sakaguchi, K. Plant DNA polymerase λ, a DNA repair enzyme that functions in plant meristematic and meiotic tissues. *Eur. J. Biochem.* **2004**, *271*, 2799−2807.

(24) Mizushina, Y.; Tanaka, N.; Yagi, H.; Kurosawa, T.; Onoue, M.; Seto, H.; Horie, T.; Aoyagi, N.; Yamaoka, M.; Matsukage, A.; Yoshida, S.; Sakaguchi, K. Fatty acids selectively inhibit eukaryotic DNA

polymerase activities in vitro. *Biochim. Biophys. Acta* **1996**, *1308*, 256−262.
(25) Mizushina, Y.; Yoshida, S.; Matsukage, A.; Sakaguchi, K. The inhibitory action of fatty acids on DNA polymerase β. *Biochim. Biophys. Acta* **1997**, *1336*, 509−521.
(26) Ogawa, A.; Murate, T.; Suzuki, M.; Nimura, Y.; Yoshida, S. Lithocholic acid, a putative tumor promoter, inhibits mammalian DNA polymerase β. *Jpn. J. Cancer Res.* **1998**, *89*, 1154−1159.
(27) Nakayama, C.; Saneyoshi, M. Inhibitory effects of 9-β-D-xylofuranosyladenine 5′-triphosphate on DNA-dependent RNA polymerase I and II from cherry salmon (*Oncorhynchus masou*). *J. Biochem. (Tokyo)* **1985**, *97*, 1385−1389.
(28) Yonezawa, Y.; Tsuzuki, T.; Eitsuka, T.; Miyazawa, T.; Hada, T.; Uryu, K.; Murakami-Nakai, C.; Ikawa, H.; Kuriyama, I.; Takemura, M.; Oshige, M.; Yoshida, H.; Sakaguchi, K.; Mizushina, Y. Inhibitory effect of conjugated eicosapentaenoic acid on human DNA topoisomerases I and II. *Arch. Biochem. Biophys.* **2005**, *435*, 197−206.
(29) Mizushina, Y.; Dairaku, I.; Yanaka, N.; Takeuchi, T.; Ishimaru, C.; Sugawara, F.; Yoshida, H.; Kato, N. Inhibitory action of polyunsaturated fatty acids on IMP dehydrogenase. *Biochimie* **2007**, *89*, 581−590.
(30) Soltis, D. A.; Uhlenbeck, O. C. Isolation and characterization of two mutant forms of T4 polynucleotide kinase. *J. Biol. Chem.* **1982**, *257*, 11332−11339.
(31) Lu, B. C.; Sakaguchi, K. An endo-exonuclease from meiotic tissues of the basidiomycete *Coprinus cinereus*: Its purification and characterization. *J. Biol. Chem.* **1991**, *266*, 21060−21066.
(32) Gschwendt, M.; Kittstein, W.; Furstenberger, G.; Marks, F. The mouse ear edema: A quantitatively evaluable assay for tumor promoting compounds and for inhibitors of tumor promotion. *Cancer Lett.* **1984**, *25*, 177−185.
(33) Sato, H.; Kobayashi, Y.; Hattori, A.; Suzuki, T.; Shigekawa, M.; Jippo, T. Inhibitory effects of water-soluble low-molecular-weight β-(1,3−1,6) D-glucan isolated from *Aureobasidium pullulans* 1A1 strain black yeast on mast cell degranulation and passive cutaneous anaphylaxis. *Biosci. Biotechnol. Biochem.* **2012**, *76*, 84−88.
(34) Chu, Y. H.; Chen, C. J.; Wu, S. H.; Hsieh, J. F. Inhibition of xanthine oxidase by *Rhodiola crenulata* extracts and their phytochemicals. *J. Agric. Food Chem.* **2014**, *62*, 3742−3749.
(35) Mizushina, Y.; Hirota, M.; Murakami, C.; Ishidoh, T.; Kamisuki, S.; Shimazaki, N.; Takemura, M.; Perpelescu, M.; Suzuki, M.; Yoshida, H.; Sugawara, F.; Koiwai, O.; Sakaguchi, K. Some anti-chronic inflammatory compounds are DNA polymerase λ-specific inhibitors. *Biochem. Pharmacol.* **2003**, *66*, 1935−1944.
(36) Mizushina, Y.; Takeuchi, T.; Kuramochi, K.; Kobayashi, S.; Sugawara, F.; Sakaguchi, K.; Yoshida, H. Study on the molecular structure and bio-activity (DNA polymerase inhibitory activity, anti-inflammatory activity and anti-oxidant activity) relationship of curcumin derivatives. *Curr. Bioactive Compounds* **2007**, *3*, 171−177.
(37) Mizushina, Y.; Nishiumi, S.; Nishida, M.; Yoshida, H.; Azuma, T.; Yoshida, M. Inhibition of repair-related DNA polymerases by vitamin Ks, their related quinone derivatives and associated inflammatory activity (Review). *Int. J. Oncol.* **2013**, *42*, 793−802.
(38) Ramadan, K.; Shevelev, I. V.; Maga, G.; Hubscher, U. DNA polymerase λ from calf thymus preferentially replicates damaged DNA. *J. Biol. Chem.* **2002**, *277*, 18454−18458.
(39) Nick McElhinny, S. A.; Havener, J. M.; Garcia-Diaz, M.; Juarez, R.; Bebenek, K.; Kee, B. L.; Blanco, L.; Kunkel, T. A.; Ramsden, D. A. A gradient of template dependence defines distinct biological roles for family X polymerases in nonhomologous end joining. *Mol. Cell* **2005**, *19*, 357−366.
(40) Maga, G.; Villani, G.; Crespan, E.; Wimmer, U.; Ferrari, E.; Bertocci, B.; Hubscher, U. 8-Oxo-guanine bypass by human DNA polymerases in the presence of auxiliary proteins. *Nature* **2007**, *447*, 606−608.
(41) Markkanen, E.; van Loon, B.; Ferrari, E.; Parsons, J. L.; Dianov, G. L.; Hubscher, U. Regulation of oxidative DNA damage repair by DNA polymerase λ and MutYH by cross-talk of phosphorylation and ubiquitination. *Proc. Natl. Acad. Sci. U.S.A.* **2012**, *109*, 437−442.
(42) Ghosh, S.; Kebaara, B. W.; Atkin, A. L.; Nickerson, K. W. Regulation of aromatic alcohol production in *Candida albicans*. *Appl. Environ. Microbiol.* **2008**, *74*, 7211−7218.
(43) Giovannini, C.; Straface, E.; Modesti, D.; Coni, E.; Cantafora, A.; De Vincenzi, M.; Malorni, W.; Masella, R. Tyrosol, the major olive oil biophenol, protects against oxidized-LDL-induced injury in Caco-2 cells. *J. Nutr.* **1999**, *129*, 1269−1277.

Three varieties of olive fruit (Mission, Manzanillo, and Lucca) were harvested (1−2 kg) from the Arai Olive Co., Ltd. in October, November, and December 2011 on Shodoshima Island, Kagawa Prefecture, Japan, for quantitatively measuring target chemicals during maturation.

Chemicals and Reagents. Dulbecco's modified Eagle's medium (D-MEM), phosphate-buffered saline (PBS) (−), and Triton X-100 were obtained from Wako Pure Chemical Industries, Ltd. (Osaka, Japan). Fetal bovine serum (FBS) was obtained from Equitech-Bio (Kerrville, TX). Antibiotic−antimycotic 100× was obtained from Invitrogen (Grand Island, NY). Mouse monoclonal anti-dinitrophenyl (DNP) antibody, albumin dinitrophenyl (HSA), Tyrode's salt solution, and *p*-nitrophenyl-2-acetamido-2-deoxy-β-D-glucopyranoside (*p*-NAG) were obtained from Sigma-Aldrich (St. Louis, MO). Bovine serum albumin (BSA) was obtained from Jackson ImmunoResearch Laboratories (West Grove, PA). Verbascoside, hydroxytyrosol, oleuropein, and luteolin were purchased from Extrasynthèse (Genay, France) and used without further purification.

Preparation of the Media and Samples. DMEM including 10% FBS and 1% antibiotic−antimycotic 100× was used as a base medium. Modified Tyrode's (MT) buffer was prepared by dissolving *N*-2-hydroxyethylpiperazine-*N*′-2-ethanesulfonic acid (HEPES) (4.76 g/L) and BSA (1 g/L) in Tyrode's salt solution. Anti-DNP IgE solution (antibody) was prepared by diluting mouse monoclonal anti-DNP antibody with the base medium (50 ng/mL). HSA solution (antigen) was prepared by dissolving HSA in MT buffer (2.5 μg/mL). The samples tested were dissolved in dimethyl sulfoxide (DMSO), and the solutions were added to MT buffer (final DMSO concentration was adjusted at 0.1%).

Extracts from Olive Fruit. Olive fruit (2.3 kg, Mission variety, December 2009) was crushed using a hand mixer. The crushed olives were then transferred to a 100% cotton bag, and the fruit juice and oil were separated from the pomace by compression. The pomace was then soaked in 100% methanol (700 mL) 3 times. The total methanol extracts (2.1 L) were obtained after the extraction. The oil separated from the methanol extracts was recovered again from hexane extracts by partition with 100% methanol and 100% hexane. Both solvents were removed under vacuum. Finally, 69 g of olive pomace extract was obtained from the methanol solution.

Extraction Using the Quick, Easy, Cheap, Effective, Rugged, and Safe (QuEChERS) Method. In quantitative comparison of olive metabolites in different varieties and seasons, the extraction was performed by the QuEChERS method that was usually used in residual agricultural chemicals analysis.[22,23] Olive fruit (100 g) was chopped in a food processor. A total of 10 g of the chopped sample was placed into a polypropylene centrifuge tube (50 mL), and 10 mL of acetonitrile was then added. The mixture was homogenized for 3 min. A total of 1 g of sodium chloride, 1 g of trisodium citrate dihydrate, 0.5 g of disodium hydrogen citrate sesquihydrate, and 4 g of anhydrous magnesium sulfate were added to the solution, and the mixture was immediately hand-shaken for 1 min. Finally, the mixture was centrifuged at 3000 rpm for 5 min. Hexane (10 mL) was added to the recovered acetonitrile layer to remove the remaining oil and chlorophylls. The acetonitrile extract obtained was dried using an evaporator with a vacuum pump. Solid acetonitrile extract (205.35 mg) was obtained from 10 g of green Mission olive in October 2011.

Fractionation of the Methanol Extracts from the Olive Pomace. The fractionation was performed by an Amberlite XAD-7 column according to Goto et al.,[24] who applied for the separation of anthocyanins. The separation of the olive pomace extracts (34.5 g) using an Amberlite XAD-7 column was started from 20% methanol (500 mL), and then 2 L each of 40% methanol, 60% methanol, 80% methanol, and 100% methanol were applied to the column in this order, as shown in Figure 1. Eluents (950 mL each of fractions 1−9) were collected using column chromatography. Each extract was dried under vacuum.

Isolation of 2-Hydroxy-3-ethylidene-5-(methoxycarbonyl)-3,4-dihydro-2*H*-pyran-4-acetic Acid 2-(3,4-Dihydroxyphenyl)-ethyl Ester (3,4-DHPEA-EA) and Elenolic Acid from Fractions 7 and 4. To isolate 3,4-DHPEA-EA, fraction 7 (50 mg) was purified using a high-performance liquid chromatography (HPLC) 5 μm

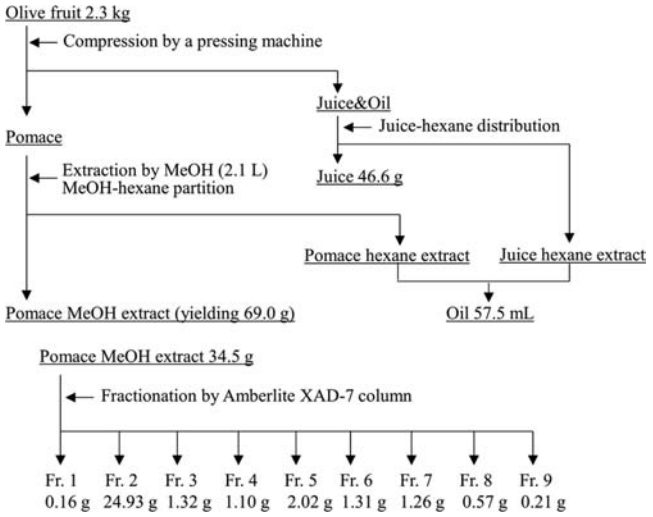

Figure 1. Extraction and fractionation from the Mission variety of green olive fruit harvested in December 2009.

octadecylsilane (ODS) column with a mixture of 16% acetic acid and 20% acetonitrile in water at a flow rate of 1 mL/min and an ultraviolet (UV) wavelength of 290 nm. Finally, 20 mg of pure 3,4-DHPEA-EA with 97% purity was isolated after drying under vacuum. To isolate elenolic acid, 50 mg of fraction 4 was purified using a HPLC 5 μm ODS column with a mixture of 8% acetic acid and 10% acetonitrile in water at a flow rate of 1 mL/min and at an UV wavelength of 250 nm. Finally, 10 mg of pure elenolic acid with 90% purity was isolated after drying under vacuum.

Physical data of 3,4-DHPEA-EA: UV λ_{max}, 243 and 279 nm; electrospray ionization−mass spectrometry (ESI−MS) (intensity of fragment ions), *m*/*z* 137 (100), 158 (68), 213 (57), 225 (30), 229 (12), 379 (72, $[M + H]^+$, $C_{19}H_{23}O_8$; found, 379.1373; calculated, 379.1393).

Physical data of elenolic acid: UV λ_{max}, 243 nm; ESI−MS (intensity of fragment ions), *m*/*z* 95 (80), 127 (100), 139 (65), 165 (30), 209 (11), 241 (70, $[M-H]^-$, $C_{11}H_{13}O_6$; found, 241.0708; calculated, 241.0712).

Nuclear magnetic resonance (NMR) data of 3,4-DHPEA-EA and elenolic acid are shown in Table 1.

Analytical HPLC. The HPLC analysis was performed by the following conditions according to Asada et al.[25] The HPLC system was comprised of a 250 × 4.6 mm COSMOSIL $5C_{18}$-AR II column, coupled to a JASCO MD 2010 Plus photodiode array (PDA) detector and double JASCO PU-980 pumps. Chromatograms were obtained from UV absorbance at 290 nm. The column temperature was set at 40 °C. The flow rate was 1 mL/min. The mobile phase used was a mixture of 2% acetic acid, 2.5% acetonitrile, and 1.5% phosphoric acid in water (A) and a mixture of 20% acetic acid, 25% acetonitrile, and 1.5% phosphoric acid in water (B). The total analytical time was 41 min, and the gradient was performed as follows: from 100 to 0% A for 35 min, and 0% A was kept for 5 min. For preparative HPLC, the HPLC system consisted of a 10 × 250 mm Develosil 5 μm ODS column, coupled to a JASCO 875-UV detector (290 nm for 3,4-DHPEA-EA and 250 nm for elenolic acid) with a JASCO PU-980 pump at 1 mL/min. For the preparative HPLC, non-volatile phosphoric acid was removed from the solvents described above. Hydroxytyrosol, 3,4-DHPEA-EA, elenolic acid, luteolin, verbascoside, and oleuropein were dissolved in dimethyl sulfoxide and then diluted to prepare a standard solution (0.067−0.5 μg/mL) for making the calibration curve of each chemical.

Hydrolysis of 3,4-DHPEA-EA. The hydrolysis of 3,4-DHPEA-EA was performed by hydrochloric acid according to the study by Davidek et al.[26] Fraction 7 extract (50 mg) containing 3,4-DHPEA-EA was dissolved in 1 mL of 1% HCl aqueous solution and left for 24 h at room temperature. The product and 3,4-DHPEA-EA were quantitatively monitored using a HPLC 5 μm ODS column.

Table 1. Chemical Shifts (δ) of Compounds 3 and 6 and Literature Data of Elenolic Acid and 3,4-DHPEA-EA

							reference data[a]					
	compound 3			compound 6			elenolic acid[31]			(5S,8R,9S)-3,4-DHPEA-EA[33]		
atom	δ ^{1}H (ppm)	J (Hz)	δ ^{13}C (ppm)	δ ^{1}H (ppm)	J (Hz)	δ ^{13}C (ppm)	δ ^{1}H (ppm)		δ ^{13}C (ppm)	δ ^{1}H (ppm)	J (Hz)	δ ^{13}C (ppm)
1	9.61	s	199.74	9.47	d, J = 1.38	200.36	9.60	s	199.40	9.45	d, J = 1.5	201.34
3	7.62	s	156.97	7.55	d, J = 0.72	155.92	7.63	s	156.66	7.51	d, J = 1.3	154.75
4			106.45			106.37			105.90			107.11
5	3.35	dd, J = 2.76, 11.04	27.90	3.36	m, J = 0.72, 3.42, 4.80, 8.94	26.97	3.35	m	28.90	3.29	m, J = 1.3, 3.7, 4.9, 9.7	26.70
6	a 2.27	dd, J = 11.04, 16.50	38.35	a 2.52	dd, J = 8.94, 15.78	37.17	a 2.32	dd	37.80	a 2.51	dd, J = 9.7, 15.9	37.28
	b 2.95	dd, J = 2.76, 16.50		b 2.86	dd, J = 3.42, 15.78		b 2.85	dd		b 2.76	dd, J = 3.7, 15.9	
7			176.09			172.03			170.20			172.49
8	4.20	q, J = 6.90	69.66	4.43	quin, J = 5.52, 6.84	70.81	4.20	q	69.62	4.53	quin, J = 5.0, 6.7	71.05
9	2.64	s	50.96	2.54	d, J = 1.38, 4.80, 5.52	54.29	2.69	s	50.96	2.54	dt, J = 1.5, 4.9, 5.0	54.33
10	1.56	d, J = 6.90	17.96	1.36	d, J = 6.84	19.36	1.49	d	17.88	1.34	d, J = 6.7	19.17
11			167.18			167.72			167.34			167.65
12	3.70	s	51.50	3.71	s	51.69	3.75	s	51.48	3.65	s	51.42
1′				4.25	m, J = 6.18	65.32				4.21	dt, J = 6.7, 14.6	65.50
2′				2.79	dt, J = 6.18	34.25				2.76	t, J = 6.7	34.39
3′						130.27						130.55
4′				6.74	d, J = 1.38	116.10				6.69	d, J = 2.1	116.38
5′						142.95						145.10
6′						143.65						144.20
7′				6.76	d, J = 8.28	115.26				6.72	d, J = 8.1	115.85
8′				6.58	dd, J = 1.38, 8.28	121.14				6.56	d, J = 2.1, 8.1	121.19

[a]NMR data of compounds 3 and 6 with elenolic acid and (5S,8R,9S)-3,4-DHPEA-EA.

β-Hexosaminidase Release Assay of RBL-2H3 Cells. For the amount of β-hexosaminidase release by basophilic leukemia cells, RBL-2H3 was determined using a previous method with some modifications.[4,27] RBL-2H3 were obtained from RIKEN BioResource Center Cell Bank (Ibaraki, Japan). The RBL-2H3 cells in the base medium (DMEM containing 10% FBS and 1% antibiotic−antimycotic 100×) were dispensed into a 24-well plate (2.5×10^5 cells/well) and were incubated overnight at 37 °C under a humidified 5% CO_2 atmosphere. After the cells were washed with 1 mL of PBS, they were incubated with 500 μL of antibody solution (mouse monoclonal anti-DNP antibody, 50 ng/mL dissolved in base medium) for 2 h of sensitization. A test sample solution of 490 μL was added to the well after washing twice with 500 μL of MT buffer (Tyrode's salt solution containing 1 g/L BSA and 4.76 g/L HEPES). The MT buffer was used as a control instead of the sample. The test sample was dissolved in DMSO and diluted with MT buffer (the final concentration of DMSO was set at 0.1%). After 10 min of incubation, albumin dinitrophenyl (10 μL, final concentration of 50 ng/mL) was added to each well and the cells were incubated for 30 min to evoke allergic reactions (degranulation). The reaction was stopped by cooling in an ice bath for 10 min. The supernatant (50 μL) was transferred to a 96-well plate and incubated with 100 μL of substrate (3.3 mM *p*-nitrophenyl-2-acetamide-2-deoxy-β-D-glucopyranoside) in 0.1 M citrate buffer (pH 4.5) at 37 °C for 25 min. The reaction was terminated by adding 100 μL of stop solution (2 M glycine buffer at pH 10.0). The absorbance (OD) was measured at 405 nm using a microplate reader (Thermo Scientific Multiskan FC, Yokohama, Japan). The gaining OD reflects β-hexosaminidase release. The calculation was performed using eqs 1 and 2 shown below. To obtain a valid value, the factors that are not typically induced by samples need to be excluded. In "blank", neither antibody solution nor sample was added to the cells to confirm spontaneous β-hexosaminidase release from the cells. In "control", MT buffer instead of samples was added to the cells to confirm β-hexosaminidase release from the cells in conditions without a sample. In "total", the cells were lysed in 0.1% Triton X-100 in MT buffer to confirm the total amount of β-hexosaminidase contained in the cells. In "sample", both antibody solution and samples were added to the cells to confirm β-hexosaminidase release from the cells in these conditions.

$$\text{ratio of } \beta\text{-hexosaminidase release (\%)} = \frac{(\mathrm{OD}_{\text{control}} \text{ or } \mathrm{OD}_{\text{sample}} - \mathrm{OD}_{\text{blank}})}{(\mathrm{OD}_{\text{total}} - \mathrm{OD}_{\text{blank}})} \times 100 \quad (1)$$

$$\beta\text{-hexosaminidase release (\%)} = \frac{\mathrm{OD}_{\text{sample}} - \mathrm{OD}_{\text{blank}}}{(\mathrm{OD}_{\text{control}} - \mathrm{OD}_{\text{blank}})} \times 100 \quad (2)$$

The ratio of β-hexosaminidase release of "control" should be greater than 25%.

β-Hexosaminidase Inhibitory Activity Assay. β-Hexosaminidase inhibitory activity was measured according to previous methods, with some modifications.[10−12] RBL-2H3 cells were grown in base medium. The cells were lysed in 0.1% Triton X-100 (5.0×10^5 cells/mL). The cell lysate (25 μL) was transferred to a 96-well plate. The tested solutions were diluted in different concentrations with MT buffer and then added to the sample well (25 μL); MT buffer was added to the control well (25 μL). Following that, 100 μL of 0.1 M citrate buffer (pH 4.5) containing 3.3 mM *p*-NAG (substrate) was added to each well and incubated for 25 min at 37 °C. The reaction was stopped by adding 100 μL of 2 M glycine buffer (the stop buffer solution) at pH 10.0 to each well. The absorbance (OD) of each reaction was measured at 405 nm using a microplate reader (Thermo Scientific Multiskan FC, Yokohama, Japan). The inhibitory activity of β-hexosaminidase was calculated using the following equation:

$$\beta\text{-hexosaminidase inhibitory (\%)} = \left(1 - \frac{\mathrm{OD}_{\text{sample}}}{\mathrm{OD}_{\text{control}}}\right) \times 100 \quad (3)$$

dx.doi.org/10.1021/jf502151b | J. Agric. Food Chem. 2014, 62, 7787−7795

NMR Analysis. ^{1}H, ^{13}C, distortionless enhancement by polarization transfer (DEPT)-45, DEPT-90, DEPT-135, correlated spectroscopy (COSY), heteronuclear correlation (HETCOR), and heteronuclear multiple-bond connectivity (HMBC) NMR spectra were recorded with a 600 MHz JNM-ECA spectrometer, dissolving samples in deuterated chloroform with tetramethylsilane (TMS, Isotec, Taiyo Nippon Sanso Corp., Ltd., Tokyo, Japan) as an internal standard.

Mass Spectrometry (MS) Analysis. Mass spectra of 3,4-DHPEA-EA and elenolic acid were measured using liquid chromatography/electrospray ionization quadrupole time-of-flight mass spectrometry (LC/ESI-Q-TOF-MS) analysis using an Acquity UPLC/Xevo QTof MS system (Waters). Chromatographic separations were conducted using an Acquity UPLC BEH C_{18} (1.7 μm, 2.1 × 50 mm) column (Waters). The instrument was operated with ESI source in negative-ion mode (elenolic acid) and positive-ion mode (3,4-DHPEA-EA).

Statistical Analysis. Statistical analysis was carried out using EZR (version 1.23) with the Tukey test [one-way analysis of variation (ANOVA)]. The values represents the mean ± standard deviation (SD) in triplicates at least. Significant differences was set at $p < 0.05$.

RESULTS AND DISCUSSION

Isolation and Identification of Antiallergic Active Compounds. The pomace portion showed significant suppression of β-hexosaminidase release (Figure 2) compared to the oil and juice. Therefore, the pomace extracts were further separated into nine fractions with an Amberlite XAD-7 column

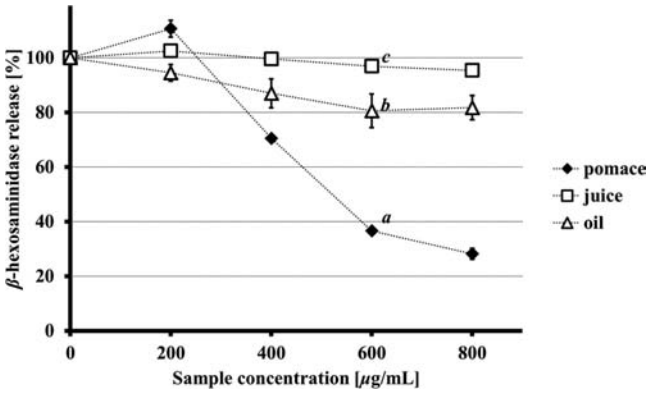

Figure 2. Antiallergic activity of olive extracts, such as pomace, oil, and juice, of Mission green olive fruit. Each value represents the mean ± SD ($n = 4$). Means with different letters are significantly different ($p < 0.05$).

chromatograph using solvents from 20% methanol to 100% methanol stepwise, as shown in Figure 1. The residues from pomace, oil, and juice were 69.0 g, 46.6 g, and 57.5 mL, respectively. Antiallergic activities of each fraction at the 200 μg/mL concentration found that fraction 7 exhibited the lowest β-hexosaminidase release (12.8 ± 5.3%), followed by fraction 6 (39.2 ± 2.1%), with significant differences ($p < 0.05$), while other fractions exhibited β-hexosaminidase release over 65% (Figure 3). Thus, fractions 1−3 did not show any antiallergic activity. On the other hand, fractions 4, 5, 8, and 9 showed some activity.

The nine fractions of the pomace extracts, the oil, and the juice were analyzed using HPLC, and the retention times and UV spectra obtained from a PDA detector were compared to known authentic and commercially available chemicals, as shown in Figure 4. There were large numbers of major peaks of chemicals (compounds **1**−**6**) in the pomace of the olive fruit (Figure 4A), but there were none of those substances in the oil

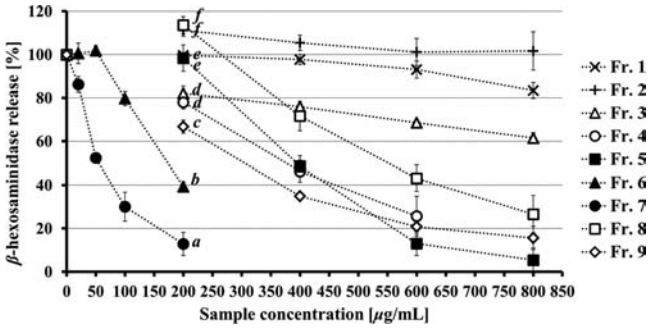

Figure 3. Antiallergic activity of each fraction of Amberlite XAD-7 column chromatography. Each value represents the mean ± SD ($n = 4$). Means with different letters are significantly different ($p < 0.05$).

and juice. Thus, hydroxytyrosol (**1**), which has significant antioxidant[28] and whitening[20,21] activities, was found in fractions 2 and 3 as a main chemical (Figure 4B). Verbascoside (**2**) was found in fractions 4 and 5. Oleuropein (**4**), which is a major compound in olive leaves, was found in fractions 4 and 5. A small amount of luteolin (**5**), which has been reported in many papers[10,29,30] as one of the most powerful antiallergic compounds, was detected in fractions 8 and 9.

Fractions 6 and 7, which had significant antiallergic activity, showed a marked peak as compound **6**. The antiallergic active compound in these two fractions was newly determined by MS spectra and NMR analyses.

Determination of the Structure of the Antiallergic Active Substance, Compound 6. Compound **3** in fraction 4 was purified using a 5 μm ODS preparative HPLC column. Mass spectra data of compound **3** showed the molecular ion at m/z 241.0708 ($[M - H]^-$, negative-ion mode) using high-resolution HPLC−TOFMS, giving the molecular formula as $C_{11}H_{14}O_6$ for compound **3**. ^{13}C NMR (DEPT) and ^{1}H NMR data made it possible to assign 11 carbon, 14 hydrogen, and 6 oxygen atoms in the molecule. ^{13}C NMR signals at 167.18, 176.09, and 199.74 ppm indicated two carboxylic acid or ester groups and carbonyl aldehyde. These data explain the existence of 5 oxygen and 3 carbon atoms in the molecule. ^{13}C NMR signals at 106.45 ppm (C) and 156.97 ppm (CH) indicated one double bond (C═CH−). Furthermore, DEPT analysis of signals at 69.66 and 51.50 ppm supported the existence of methoxy and methine groups with oxygen. Because two carboxylic acid or ester groups were found in the molecule, the methoxy group at position 12 should be part of the ester group (−COOMe). The methine group should not be the part of ester but part of the ether group. Other fragments of the molecule were one methyl group, one methylene group, and two methine groups.

The partial structure of fragment a in Figure 7 clarified the linkage of the partial structure of compound **3** from the $^{1}H-^{1}H$ COSY spectrum. Thus, the CH−O− group at position 8 was connected to one methyl group (at position 10 on the molecule), and one methine group (position 9) was coupled with one aldehyde group. The methine group at position 9 was related to the methine group at position 5 and then followed by the methylene group at position 6. Finally, one carboxylic acid at position 7 of the partial structure of fragment a was determined by HMBC data, as shown in Figure 7. Thus, HMBC measurement determined that the 176.09 ppm carbon signal (COO−) showed a strong cross-peak with the 2.27 and 2.95 ppm signals at H-6a and H-6b (C-6, 38.35 ppm ^{13}C NMR, methylene group).

For the partial structure of fragment b, HMBC data showed a strong correlation between the 167.18 ppm carbon signal

dx.doi.org/10.1021/jf502151b | J. Agric. Food Chem. 2014, 62, 7787−7795

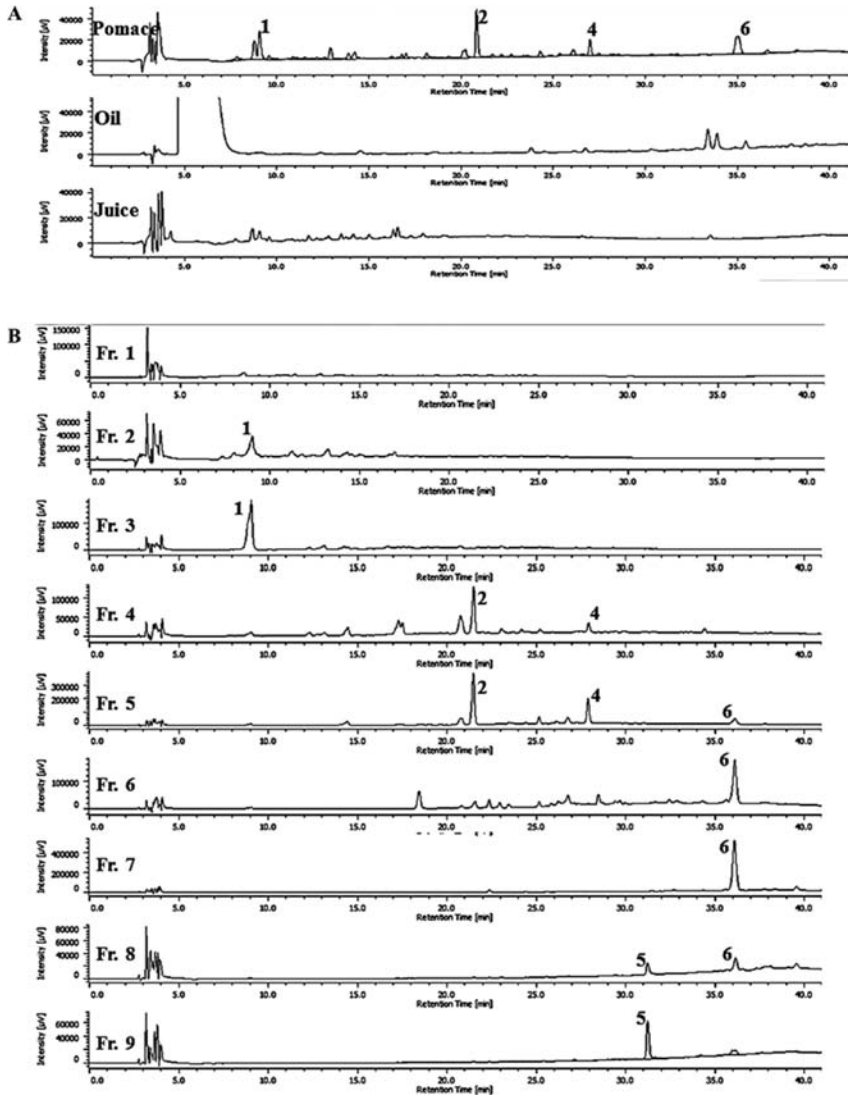

Figure 4. (A) HPLC chromatograms of extracts of pomace, oil, and juice. (B) HPLC chromatograms of nine fractions (λ = 290 nm). Compounds **1**, **2**, **4**, and **5** were identified as hydroxytyrosol, verbascoside, oleuropein, and luteolin, respectively, by comparing their retention times and UV spectra of each peak to those of authentic compounds.

(COOMe) at position 11 and the 7.62 ppm signal at H-3 (C-3, 156.97 ppm ^{13}C NMR) and the 3.35 ppm signal at H-5 (C-5, 27.90 ppm ^{13}C NMR). Furthermore, the COOMe group (fragment b) at position 11 was connected with C═CH− (Figure 7A) in the same manner. Finally, when fragments a and b are combined, the molecular formula of compound **3** was confirmed to be elenolic acid by comparing the MS spectra, spectra of ^{1}H and ^{13}C NMR,[31] and UV spectra (λ_{max} of elenolic acid = 239 nm)[32] (Figure 6).

Compound **6** (50% purity at 290 nm) in fraction 7 was hydrolyzed using 1% HCl for 24 h at room temperature to give elenolic acid and hydroxytyrosol (Figure 5A). The percentage of hydroxytyrosol calculated by standard curve was 24.3% in fraction 7 after hydrolysis. Elenolic acid was detected at 250 nm and found in a small amount in the hydrolysate and also in fractions 3−5 (Figure 5B).

Compound **6** should be an ester of hydroxytyrosol and elenolic acid because compound **3** and hydroxytyrosol were released by acid hydrolysis (Figure 5A). The chemical structure of compound **6** was determined by interpreting the mass spectra data and ^{1}H and ^{13}C NMR spectra, individually. The mass spectra data of compound **6** showed the molecular ion at m/z 379.1373 ([M + H]$^{+}$, positive-ion mode) using high-resolution HPLC−TOFMS, giving the molecular formula as $C_{19}H_{22}O_8$ for compound **6**. This molecular weight corresponds to the dehydrated compound of compound **3** ($C_{11}H_{14}O_6$) and hydroxytyrosol ($C_8H_{10}O_3$). Because the HMBC spectrum of compound **6** showed cross-peaks between C-7 and H-1′ (Figure 7B), compound **6** should be 3,4-DHPEA-EA.[32,33]

Antiallergic Active Compounds in Olive Pomace. Table 2 shows the antiallergic activities among the metabolites identified in olive pomace. Luteolin showed the highest antiallergic activity and is expressed as IC_{50} at 0.752 ± 0.1 μg/mL. The second highest activity was observed with 3,4-DHPEA-EA, with IC_{50} at 33.5 ± 0.6 μg/mL. Because the activities of hydroxytyrosol and elenolic acid were weaker than 3,4-DHPEA-EA, the ester linkage of the two molecules should enhance the antiallergic activity several times.

Furthermore, the antiallergic activity of 3,4-DHPEA-EA was 30 times greater than that of oleuropein. It was reported that the glycoside linkage decreased the activity because many flavonoids show greater activity in the aglycone of flavonoids.

dx.doi.org/10.1021/jf502151b | J. Agric. Food Chem. 2014, 62, 7787−7795

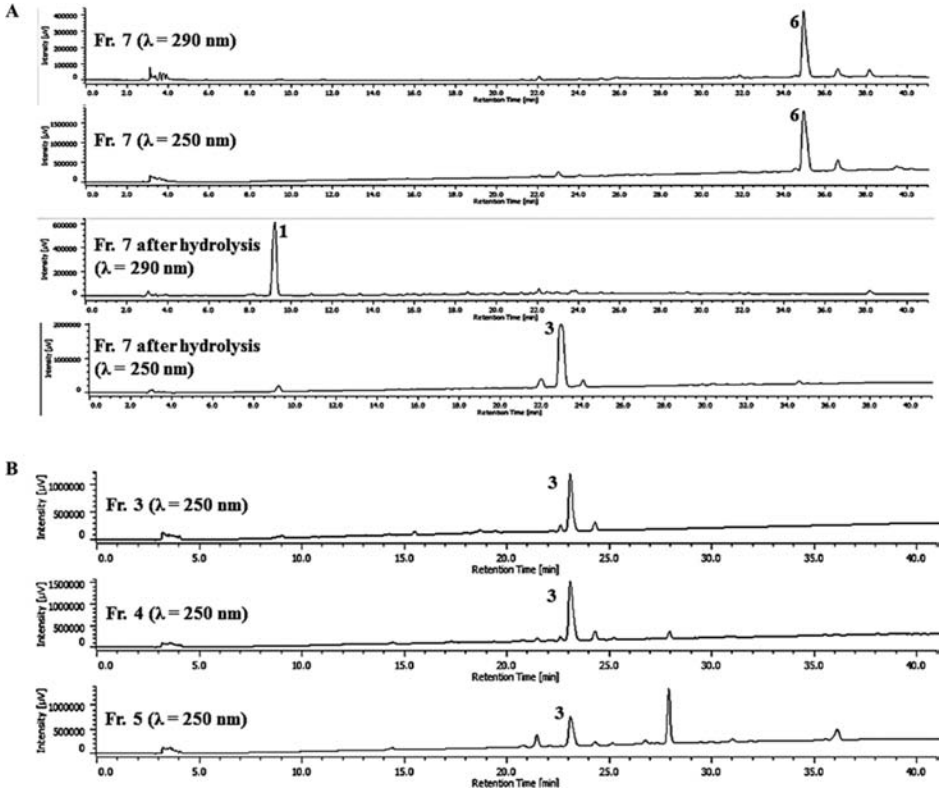

Figure 5. (A) HPLC chromatograms of fraction 7 before and after hydrolysis (λ = 250 and 290 nm). (B) HPLC chromatograms of fractions 3−5 (λ = 250 nm).

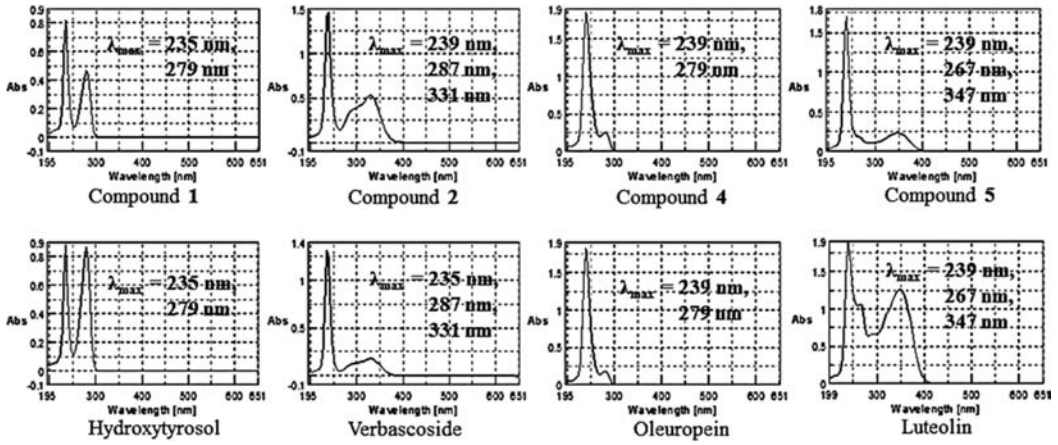

Figure 6. UV absorption spectra of the antiallergic substance in olive from the PDA detector of HPLC analyses. Sources of UV spectra: compound **1** (from fraction 3), compounds **2** and **4** (from fraction 5), and compound **5** (from fraction 9). λ_{max} of each compound is as follows: compound **1**, 235 and 279 nm; hydroxytyrosol, 235 and 279 nm; compound **2**, 239, 287, and 331 nm; verbascoside, 235, 287, and 331 nm; compound **4**, 239 and 279 nm; oleuropein, 239 and 279 nm; compound **5**, 239, 267, and 347 nm; and luteolin, 239, 267, and 347 nm.

The antiallergic activities of 3,4-DHPEA-EA (secoiridoid aglycone) and oleuropein (its glucoside) in olive pomace were consistent with those of flavonoids reported elsewhere.[10,34]

Each metabolite was tested for the enzyme inhibition rate of hexosaminidase itself. No enzyme inhibition was observed. Therefore, each metabolite inhibits the release of hexosaminidase from RBL-2H3 cells but did not inhibit the activity of hexosaminidase.

Finally, the total antiallergic activities of the isolated compounds were compared among all metabolites, as shown in Table 2. 3,4-DHPEA-EA showed significant antiallergic activity because of its low IC_{50} and was more abundant in the olive pomace than in luteolin. *p*-Hydroxyphenyl ethanol-decarboxymethyl elenolic acid ester dialdehyde [oleocanthal, *p*-HPEA-EDA, 3-(2-oxoethyl)-4-formyl-4-hexenoic acid 4-hydroxyphenethyl ester], one of the anti-inflammatory substances,[16] and 3,4-dihydroxyphenyl ethanol-decarboxymethyl elenolic acid ester dialdehyde [3,4-DHPEA-EDA, 3-(2-oxoethyl)-4-formyl-4-hexenoic acid 3,4-dihydroxyphenethyl ester] are secoiridoid compounds in some olives. In further research, we identified oleocanthal and 3,4-DHPEA-EDA in only trace amounts in the pomace of Japanese Mission olive (data not shown; retention times of 3,4-DHPEA-EDA and oleocanthal were 25.6 and 31.2 min under the same analytical conditions shown in Figure 4, respectively).

dx.doi.org/10.1021/jf502151b | J. Agric. Food Chem. 2014, 62, 7787−7795

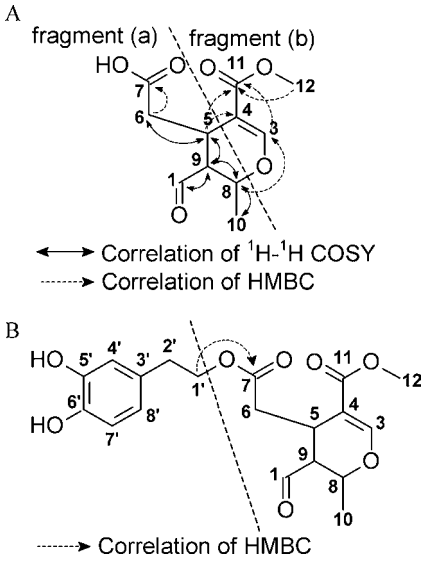

Figure 7. Chemical structure of (A) compound **3** and (B) compound **6** in olive.

The bioavailability of 3,4-DHPEA-EA and luteolin requires further study, especially in terms of antiallergic activity and the absorption rate of chemicals.[13] 3,4-DHPEA-EA is soluble in ethanol, diethyl ether, or other organic solvents, but luteolin can be resolved only in ethanol or ethanol containing water but not in diethyl ether. There may be big differences in solubility, absorption efficiency, and affinity of 3,4-DHPEA-EA and luteolin in neutral aqueous solution and physiological pH in the small intestine. Therefore, actual bioavailability in humans should be further studied.

Comparison of Active Chemicals in Three Kinds of Olive Fruit Using the QuEChERS Method. The QuEChERS method is commonly used to quantitatively analyze food residues and agrochemicals. The operation for solvent extraction, moisture removal, and recovery of agrochemicals can be performed simply and quickly. It is also suitable for a series of analyses of several samples.[22,23] Therefore, the QuEChERS method to analyze the active chemicals in olive pomace was selected as an appropriate extraction procedure for samples (about 10 g) of three varieties of olive leaves in different seasons. The comparative analysis of the antiallergic substances in olive fruit is shown in Table 3. Of the three varieties used in this study, the green olive fruit of the Mission variety in October had the highest concentration of 3,4-DHPEA-EA (50.33 ± 1.18 mg/10 g of olive fruit) as determined by quantitative analysis using ODS−HPLC and then decreased with the change in seasons. On the other hand, the amounts of hydroxytyrosol and elenolic acid increased when the harvesting period was delayed to November or December. To obtain efficient amounts of antiallergic substances, early harvest in October at the green stage of maturation was found to be the most important factor. Indeed, the antiallergic activities (IC_{50} values) of the fruit extracts harvested in October, November, and December were 138.91 ± 8.53 μg/mL for the October sample, 247.85 ± 3.34 μg/mL for the green sample in November, 337.71 ± 10.03 μg/mL for red sample in November,

Table 2. Comprehensive Antiallergic Activities of Substances Found in Olive Pomace Extract

compound	IC_{50} [μg/mL (μM)]	enzyme inhibition (%)[a]	amount (mg/kg)[b]	total activity[c]	active unit[d]
3,4-DHPEA-EA (**6**)	33.5 ± 0.6 (88.7)	0.5 ± 1.7	1854	55343	350
elenolic acid (**3**)	377.9 ± 1.6 (1561.6)	18.4 ± 4.3	902	2386	15.1
luteolin (**5**)	0.752 ± 0.1 (2.6)	3.8 ± 0.8	1.04	1382	8.74
hydroxytyrosol (**1**)	305.3 ± 15.2 (1980.9)	0.9 ± 0.9	140	458	2.89
oleuropein (**4**)	891.2 ± 6.1 (1648.8)	0.7 ± 7.5	346	388	2.45
verbascoside (**2**)	788.0 ± 29.2 (1261.7)	15.7 ± 5.5	125	158	1.00

[a]Values indicate enzyme inhibition (%) against β-hexosaminidase. Sample concentrations: hydroxytyrosol, 800 μg/mL; verbascoside, 800 μg/mL; luteolin, 2 μg/mL; 3,4-DHPEA-EA, 50 μg/mL; oleuropein, 800 μg/mL; and elenolic acid, 600 μg/mL. Each value represents the mean ± SD (n = 4). [b]The amount was calculated and shown from green Mission olive harvested in December 2009. [c]Total activity was estimated using the following formula: total activity = amount (mg/kg)/IC_{50} (mg/mL). [d]Active unit was calculated on the basis of the relative intensity of total activity (total activity of verbascoside was defined as 1.00).

Table 3. Amount of Hydroxytyrosol Derivative and Elenolic Acid in QuEChERS Extract Olive Harvest in 2011[a]

month	October			November		December
variety	Manzanillo	Mission	Lucca	Mission		Mission
color		green		green	red	red
extract from 10 g of olives						
weight (mg)	181.33	205.35	116.33	134.88	126.53	164.96
yield (%)	1.81	2.05	1.16	1.34	1.26	1.64
hydroxytyrosol						
amount in 100 mg of extract (mg)	2.59 ± 0.02	2.45 ± 0.05	1.04 ± 0.02	6.00 ± 0.03	7.01 ± 0.12	4.48 ± 0.01
amount in 10 g of fruits (mg)	4.71 ± 0.03	5.04 ± 0.09	1.21 ± 0.02	8.04 ± 0.03	8.84 ± 0.15	7.35 ± 0.01
elenolic acid						
amount in 100 mg of extract (mg)	2.48 ± 0.05	3.05 ± 0.04	3.29 ± 0.01	6.82 ± 0.04	9.53 ± 0.01	5.11 ± 0.02
amount in 10 g of fruits (mg)	4.51 ± 0.08	6.27 ± 0.07	3.83 ± 0.01	9.15 ± 0.04	12.01 ± 0.01	8.39 ± 0.03
3,4-DHPEA-EA						
amount in 100 mg of extract (mg)	18.29 ± 0.09	24.50 ± 0.58	12.39 ± 0.08	12.71 ± 0.13	7.50 ± 0.02	0.69 ± 0.02
amount in 10 g of fruits (mg)	33.18 ± 0.17	50.33 ± 1.18	14.42 ± 0.09	17.04 ± 0.17	9.46 ± 0.02	1.14 ± 0.03

[a]Each value represents the mean ± SD (n = 3).

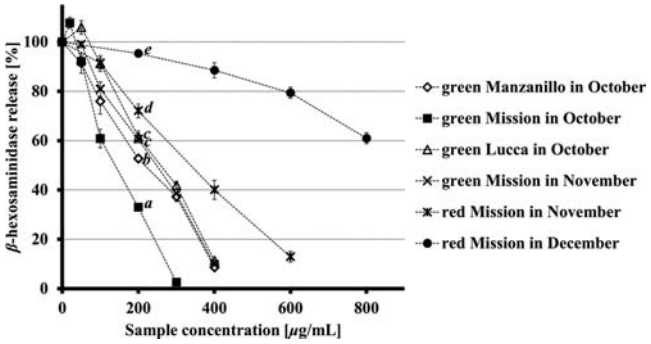

Figure 8. Difference in antiallergic activity of different olive varieties and harvesting seasons. Each value represents the mean ± SD ($n = 4$). Means with different letters are significantly different ($p < 0.05$).

and 919.83 ± 23.25 μg/mL for the December sample, as shown in Figure 8. Antiallergic activities of methanol extracts at the 200 μg/mL concentration in different harvesting time were conducted and then concluded that green Mission in October exhibited the lowest β-hexosaminidase release (32.9 ± 0.5%), followed by green Manzanillo in October (52.6 ± 1.2%), with significant differences ($p < 0.05$) (Figure 8) in the earlier harvest time, the greater antiallergic activity, and the higher concentration of 3,4-DHPEA-EA. The antiallergic activities of the olive fruit extracts depended upon the amount of 3,4-DHPEA-EA.

In conclusion, 3,4-DHPEA-EA was found as an antiallergic active substance in olive pomace. To increase the consumption of olive oils, olive oil manufacturers need to consider the utility of olive juice and pomace. The Japanese Mission variety contained a higher amount of 3,4-DHPEA-EA as a major component of the pomace fraction and also as a major antiallergic substance.

AUTHOR INFORMATION

Corresponding Author

*Telephone: +81-87-891-3104. Fax: +81-87-891-3021. E-mail: tamura@ag.kagawa-u.ac.jp.

Notes

The authors declare no competing financial interest.

ACKNOWLEDGMENTS

The authors are grateful to Dr. Hisashi Nishiwaki for measuring the ESI−MS spectra of elenolic acid and 3,4-DHPEA-EA.

ABBREVIATIONS USED

3,4-DHPEA-EA, 2-hydroxy-3-ethylidene-5-(methoxycarbonyl)-3,4-dihydro-2*H*-pyran-4-acetic acid 2-(3,4-dihydroxyphenyl)ethyl ester; oleocanthal, 3-(2-oxoethyl)-4-formyl-4-hexenoic acid 4-hydroxyphenethyl ester; 3,4-DHPEA-EDA, 3-(2-oxoethyl)-4-formyl-4-hexenoic acid 3,4-dihydroxyphenethyl ester; UV, ultraviolet; DEPT, distorsionless enhancement by polarization transfer; COSY, correlated spectroscopy; HETCOR, heteronuclear correlation; HMBC, heteronuclear multiple-bond connectivity

REFERENCES

(1) Hadley, C. Food allergies on the rise? Determining the prevalence of food allergies, and how quickly it is increasing, is the first step in tackling the problem. *EMBO Rep.* **2006**, *11*, 1080−1083.

(2) Priftis, K. N.; Anthracopoulos, M. B.; Nikolaou-Papanagiotou, A.; Mantziou, V.; Paliatsos, A. G.; Tzavelas, G.; Nicolaidou, P.; Mantzouranis, E. Increased sensitization in urban vs. rural environment—Rural protection or an urban living effect? *Pediatr. Allergy Immul.* **2007**, *18*, 209−216.

(3) Morissette, G.; Lodge, R.; Bouthillier, J.; Marceau, F. Receptor-independent, vacuolar ATPase-mediated cellular uptake of histamine receptor-1 ligands: Possible origin of pharmacological distortions and side effects. *Toxicol. Appl. Pharmacol.* **2008**, *229*, 320−331.

(4) Shimoda, H.; Tanaka, J.; Yamada, E.; Morikawa, T.; Kasajima, N.; Yoshikawa, M. Anti type I allergic property of Japanese butterbur extract and its mast cell degranulation inhibitory ingredients. *J. Agric. Food Chem.* **2006**, *54*, 2915−2920.

(5) Zhu, F.; Asada, T.; Sato, A.; Koi, Y.; Nishiwaki, H.; Tamura, H. Rosmarinic acid extract for antioxidant, antiallergic, and α-glucosidase inhibitory activities, isolated by supramolecular technique and solvent extraction from *Perilla* leaves. *J. Agric. Food Chem.* **2014**, *62*, 885−892.

(6) Burda, S.; Oleszek, W. Antioxidant and antiradical activities of flavonoids. *J. Agric. Food Chem.* **2001**, *49*, 2774−2779.

(7) Ruby, A. J.; Kuttan, G.; Dinesh Babu, K.; Rajasekharan, K. N.; Kuttan, R. Anti-tumour and antioxidant activity of natural curcuminoids. *Cancer Lett.* **1995**, *94*, 79−83.

(8) Adams, B. K.; Ferstl, E. M.; Davis, M. C.; Herold, M.; Kurtkaya, S.; Camalier, R. F.; Hollingshead, M. G.; Kaur, G.; Sausville, E. A.; Rickles, F. R.; Snyder, J. P.; Liotta, D. C.; Shoji, M. Synthesis and biological evaluation of novel curcumin analogs as anti-cancer and anti-angiogenesis agents. *Bioorg. Med. Chem.* **2004**, *12*, 3871−3883.

(9) Vidya Priyadarsini, R.; Senthil Murugan, R.; Maitreyi, S.; Ramalingam, K.; Karunagaran, D.; Nagini, S. The flavonoid quercetin induces cell cycle arrest and mitochondria-mediated apoptosis in human cervical cancer (HeLa) cells through p53 induction and NF-κB inhibition. *Eur. J. Pharmacol.* **2010**, *649*, 84−91.

(10) Matsuda, H.; Morikawa, T.; Ueda, K.; Managi, H.; Yoshikawa, M. Structural requirements of flavonoids for inhibition of antigen-induced degranulation, TNF-α and IL-4 production from RBL-2H3 cells. *Bioorg. Med. Chem.* **2002**, *10*, 3123−3128.

(11) Matsuda, H.; Morikawa, T.; Managi, H.; Yoshikawa, M. Antiallergic principles from *Alpinia galanga*: structural requirements of phenylpropanoids for inhibition of degranulation and release of TNF-α and IL-4 in RBL-2H3 cells. *Bioorg. Med. Chem. Lett.* **2003**, *13*, 3197−3202.

(12) Matsuda, H.; Tewtrakul, S.; Morikawa, T.; Nakamura, A.; Yoshikawa, M. Anti-allergic principles from Thai zedoary: structural requirements of curcuminoids for inhibition of degranulation and effect on the release of TNF-α and IL-4 in RBL-2H3 cells. *Bioorg. Med. Chem.* **2004**, *12*, 5891−5898.

(13) Walle, T. Abosrption and metabolism of flavonoids. *Free Radical Biol. Med.* **2004**, *36*, 829−837.

(14) Lipinski, C. A.; Lombardo, F.; Dominy, B. W.; Feeney, P. J. Experimental and computational approaches to estimate solubility and permeability in drug discovery and development settings. *Adv. Drug Delivery Rev.* **1997**, *23*, 3−25.

(15) Harai, N.; Takagi, M. Manufacturing of olive leaf tea. *Jpn. Kokai Tokkyo Koho*, JP 2006-191854A, 20060727, 2006.

(16) Beauchamp, G. K.; Keats, R. S. J.; Morel, D.; Lin, J.; Pika, J.; Han, Q.; Lee, C.; Smith, A. B.; Breslin, P. A. S. Ibuprofen-like activity in extra-virgin olive oil. *Nature* **2005**, *437*, 45−46.

(17) McDonald, S.; Prenzler, P. D.; Antolovich, M.; Robards, K. Phenolic content and antioxidant activity of olive extracts. *Food Chem.* **2001**, 73−84.

(18) Gonzalez-Santiago, M.; Martın-Bautista, E.; Carrero, J. J.; Fonolla, J.; Baro, L.; Bartolome, M. V.; Gil-Loyzaga, P.; Lopez-Huertas, E. One-month administration of hydroxytyrosol, a phenolic antioxidant present in olive oil, to hyperlipemic rabbits improves blood lipid profile, antioxidant status and reduces atherosclerosis development. *Atherosclerosis* **2006**, *188*, 35−42.

(19) Romero, C.; Medina, E.; Vargas, J.; Brenes, M.; Castro, A. D. In vitro activity of olive oil polyphenols against *Helicobacter pylori*. *J. Agric. Food Chem.* **2007**, *55*, 680−686.

(20) Peak, M. J.; Peak, J. G. Hydroxy radical quenching agents protect against DNA breakage caused by both 365-nm UVA and by gamma radiation. *Photochem. Photobiol.* **1990**, *51*, 649−652.

(21) Tyrrell, R. M.; Pidoux, M. Singlet oxygen involvement in the inactivation of cultured human fibroblasts by UVA (334 nm, 365 nm)

and near-visible (405 nm) radiations. *Photochem. Photobiol.* **1989**, *49*, 407−412.
(22) Payá, P.; Anastassiades, M.; Mack, D.; Sigalova, I.; Tasdelen, B.; Oliva, J.; Barba, A. Analysis of pesticide residues using the quick, easy, cheap, effective, rugged, and safe (QuEChERS) pesticide multiresidue method in combination with gas and liquid chromatography and tandem mass spectrometric detection. *Anal. Bioanal. Chem.* **2007**, *389*, 1697−1714.
(23) Lehotay, S. J.; Son, K. A.; Kwon, H.; Koesukwiwata, U.; Fu, W.; Mastovska, K.; Hoh, E.; Leepipatpiboon, N. Comparison of QuEChERS sample preparation methods for the analysis of pesticide residues in fruits and vegetables. *J. Chromatogr., A* **2010**, *1217*, 2548−2560.
(24) Goto, T.; Kondo, T.; Tamura, H.; Kawahori, K.; Hattori, H. Structure of platyconin, a diacylated anthocyanin isolated from the Chinese bell-flower *Platycodon grandiflorum*. *Tetrahedron Lett.* **1983**, *24*, 2181−2184.
(25) Asada, T.; Tamura, H. Isolation of bilberry anthocyanidin 3-glycosides bearing *ortho*-dihydroxyl groups on the B ring by forming an aluminum complex and their antioxidant activity. *J. Agric. Food Chem.* **2012**, *60*, 10634−10640.
(26) Davidek, J.; Velisek, J.; Kubelka, V.; Janicek, G.; Simicova, Z. Glycerol chlorohydrins and their esters as products of the hydrolysis of tripalmitin, tristearin and triolein with hydrochloric acid. *Z. Lebensm.-Unters. Forsch.* **1980**, *171*, 14−17.
(27) Sugiura, Y.; Torii, T.; Matsuda, K.; Yamada, Y. Anti-allergic effects of extracts from commercial products of cooked burdock. *Food Sci. Technol. Res.* **2009**, *15*, 423−426.
(28) Visioli, F.; Bellomo, G.; Galli, C. Free radical-scavenging properties of olive oil polyphenols. *Biochem. Biophys. Res. Commun.* **1998**, *247*, 60−64.
(29) Cheong, H.; Ryu, S. Y.; Oak, M. H.; Cheon, S. H.; Yoo, G. S.; Kim, K. M. Studies of structure activity relationship of flavonoids for the anti-allergic actions. *Arch. Pharm. Res.* **1998**, *21* (4), 478−480.
(30) Kimata, M.; Shichijo, M.; Miura, T.; Serizawa, I.; Inagaki, N.; Nagai, H. Effects of luteolin, quercetin and baicalein on immunoglobulin E-mediated mediator release from human cultured mast cells. *Clin. Exp. Allergy* **2000**, *30*, 501−508.
(31) Briante, R.; La Cara, F.; Pia Tonziello, M.; Febbraio, F.; Nucci, R. Antioxidant activity of the main bioactive derivatives from oleuropein hydrolysis by hyperthermophilic β-glycosidase. *J. Agric. Food Chem.* **2001**, *49*, 3198−3203.
(32) Inarejos-Garcia, A. M.; Androulaki, A.; Salvador, M. D.; Fregapane, G.; Tsimidou, M. Z. Discussion on the objective evaluation of virgin olive oil bitterness. *Food Res. Int.* **2009**, *42*, 279−284.
(33) Perez-Trujillo, M.; Gomez-Caravaca, A. M.; Segura-Carretero, A.; Fernandez-Gutierrez, A.; Parella, T. Separation and identification of phenolic compounds of extra virgin olive oil from *Olea europaea* L. by HPLC-DAD-SPE-NMR/MS. Identification of a new diastereoisomer of the aldehydic form of oleuropein aglycone. *J. Agric. Food Chem.* **2010**, *58*, 9129−9136.
(34) Itoh, T.; Ohguchi, K.; Nakajima, C.; Oyama, M.; Iinuma, M.; Nozawa, Y.; Akao, Y.; Ito, M. Inhibitory effects of flavonoid glycosides isolated from the peel of Japanese persimmon (*Diospyros kaki Fuyu*) on antigen-stimulated degranulation in rat basophilic leukemia RBL-2H3 cells. *Food Chem.* **2011**, *126*, 289−294.

Table 1. ^{1}H and ^{13}C NMR Data for 1−3 (CD_3OD)

	1[a]		2[b]		3[b]	
position	δ_C	δ_H	δ_C	δ_H	δ_C	δ_H
1	132.4		132.4		132.4	
2	109.2	6.96 (1H, d, 1.6)	109.3	6.97 (1H, d, 1.8)	109.2	6.97 (1H, d, 1.8)
3	147.8		147.8		147.8	
4	146.5		146.5		146.5	
5	114.8	6.79 (1H, d, 8.0)	114.9	6.80 (1H, d, 8.1)	114.9	6.79 (1H, d, 1.8)
6	118.4	6.85 (1H, dd, 8.0, 1.6)	118.4	6.86 (1H, dd, 8.1, 1.8)	118.4	6.85 (1H, dd, 8.1, 1.8)
7	89.0	5.66 (1H, d, 6.4)	89.0	5.67 (1H, d, 6.4)	89.1	5.66 (1H, d, 6.4)
8	53.2	3.61 (1H, m)	53.1	3.60 (1H, m)	53.1	3.61 (1H, m)
9	63.1	3.88 (2H, m)	63.1	3.90 (1H, m)	63.1	3.90 (1H, m)
				3.86 (1H, m)		3.86 (1H, m)
1′	129.1		128.7		128.7	
2′	112.9	7.57 (1H, br s)	112.9	7.59 (1H, br s)	112.9	7.59 (1H, br s)
3′	144.2		144.4		144.2	
4′	153.0		153.4		153.4	
5′	131.3		129.3		129.3	
6′	118.7	7.66 (1H, br s)	119.0	7.67 (1H, br s)	119.0	7.67 (1H, br s)
7′	198.2		198.2		198.2	
8′	40.5	3.21 (1H, t, 6.0)	74.2	5.15 (1H, t, 5.2)	74.2	5.14 (1H, t, 5.2)
9′	57.5	3.97 (2H, t, 6.0)	64.8	3.93 (1H, m)	64.8	3.92 (1H, m)
				3.79 (1H, m)		3.79 (1H, m)
3-OCH_3	55.0	3.85 (3H, s)	55.0	3.84 (3H, s)	55.0	3.83 (3H, s)
3′-$OCHH_3$	55.3	3.93 (3H, s)	55.4	3.93 (3H, s)	55.4	3.93 (3H, s)

[a]NMR spectroscopic data were recorded at 400 MHz (^{1}H NMR) and 100 MHz (^{13}C NMR). [b]NMR spectroscopic data were recorded at 300 MHz (^{1}H NMR) and 75 MHz (^{13}C NMR).

dimethylthiazol-2-yl)-2,5-diphenyltetrazolium bromide (MTT) were purchased from Sigma-Aldrich (St. Louis, MO, USA). Cell culture medium [Dulbecco's modified Eagle's medium (DMEM)], penicillin/streptomycin, fetal bovine serum (FBS), and all other materials required for culturing cells were purchased from Gibco BRL, Life Technologies (Grand Island, NY, USA).

Apparatus. Optical rotations were measured on a JASCO P-1020 polarimeter (Jasco Co., Tokyo, Japan). The UV spectra were measured on a Shimadzu UV-1700 spectrometer. The CD spectra were obtained using an MOS 450 detector from BioLogic. The FT-IR spectra were recorded using a Bruker IFS-55 spectrometer. HRESIMS experiments were performed on a MicroTOF spectrometer (Bruker Co., Karlsruhe, Germany). 1D NMR (^{1}H and ^{13}C) spectra were recorded on Bruker ARX-300, Bruker DPX-400, and Bruker AV-600 instruments (Bruker Co., Billerica, MA, USA); 2D NMR (HMBC, HSQC, and NOESY) spectra were recorded on Bruker DPX-400 and Bruker AV-600 instruments. High-performance liquid chromatography (HPLC) preparation was performed on a Waters 1525 instrument (UV 2549 detector) using a YMC C18 column (250 mm × 10 mm, 5 μm). GC was carried out using an Agilent 7890A gas chromatograph (Agilent Technologies, Inc., Santa Clara, CA, USA) equipped with an HP-5 capillary column (30 m × 320 mm × 0.25 μm).

Plant Material. The seeds of *P. tomentosa* were collected from Liaoning province of China on July 18, 2012. The plant material was identified by Prof. Jin-Cai Lu (Department of Traditional Chinese Materia Medica, Shenyang Pharmaceutical University). A voucher specimen (no. 20120718) has been deposited in the Herbarium of Shenyang Pharmaceutical University, Liaoning, People's Republic of China.

Extraction and Isolation. The dried and powdered seeds of *P. tomentosa* (15 kg) were refluxed three times 70% EtOH. Then, the aqueous alcohol solution was evaporated under reduced pressure to obtain the EtOH extract (650 g). This extract was suspended in H_2O and partitioned successively with petroleum ether, EtOAc, and *n*-BuOH. All fractions were tested in antioxidant (scavenging activities on DPPH and ABTS$^{\bullet+}$) and anti-inflammatory assays, and the ethyl acetate extract was found to exhibit the strongest activities of all these fractions. The ethyl acetate fraction (70 g) was subjected to a polyamide CC and eluted successively with MeOH/H_2O (30:70, 50:50, 70:30, 100:0, v/v) to yield four fractions (fractions 1−4). Fraction 1 (15 g) was separated on an ODS CC (4.0 × 50.0 cm) by gradient elution with MeOH/H_2O (30:80−100:0, v/v) to give four fractions (fractions 1-1−1-4). Fraction 1-1 (4 g) was subjected to a silica gel CC (2.5 × 50.0 cm) and eluted using a gradient of CH_2Cl_2/MeOH (40:1−3:1) to give five fractions (fractions 1-1-1−1-1-5). Fraction 1-1-4 was isolated by preparative HPLC using CH_3CN/H_2O (20:80, v/v; 8 mL/min) to afford **6** (17.4 mg, t_R = 15.8 min), **5** (18.5 mg, t_R = 18.1 min), **15** (70.4 mg, t_R = 25.6 min), and **16** (30.9 mg, t_R = 27.4 min). Fraction 1-2 (5 g) was loaded on a silica gel column CC (2.5 × 50.0 cm) using CH_2Cl_2/MeOH (50:1−5:1, v/v) as eluant to give six fractions (fractions 1-2-1−1-2-6). Fraction 1-2-2 was chromatographed on a Sephadex LH-20 column eluting with MeOH/H_2O (1:1) and then purified by semipreparative HPLC using MeOH/H_2O (34:66, v/v; 2.5 mL/min) to obtain **14** (13.3 mg, t_R = 15.7 min), **2** (9.3 mg, t_R = 22.5 min), **3** (8.9 mg, t_R = 22.7 min), **12** (14.1 mg, t_R = 24.7 min), and **13** (9.8 mg, t_R = 27.0 min). Fraction 1-2-3 was separated on an ODS CC (4.0 × 50.0 cm) with MeOH/H_2O (10:90−100:0, v/v) to give three fractions (fractions 1-2-3-A−1-2-3-C). Fraction 1-2-3-A was further isolated by semipreparative HPLC using MeOH/H_2O (40:60, v/v; 3.0 mL/min) to obtain **4** (12.7 mg, t_R = 23.0 min), **7** (25.2 mg, t_R = 25.7 min), **1** (18.3 mg, t_R = 29.2 min), and **11** (14.3 mg, t_R = 31.7 min). Fraction 1-2-3-B was purified by semipreparative HPLC using CH_3CN/H_2O (25:75, v/v; 3.5 mL/min) to obtain **10** (50.5 mg, t_R = 19.3 min), **8** (24.9 mg, t_R = 30.1 min), and **9** (36.4 mg, t_R = 30.2 min).

*Prunustosanan AI (**1**):* colorless oil; $[\alpha]_D^{20}$ −16.5 (*c* 0.13, MeOH); UV (MeOH) λ_{max} (log ε) 228 (0.53), 287 (0.30); CD [MeOH, nm ($\Delta\varepsilon$)] 223 (−3.43), 281 (−2.61); IR (KBr) V_{max} 3451, 1641, 1600, 1510, 1464, 1384, 1326, 1272, 1162, 1119, 1032 cm^{-1}; HRESIMS at *m*/*z* 397.1257 [M + Na]$^+$ (calcd for $C_{20}H_{22}O_7Na$, 397.1263); ^{1}H and ^{13}C NMR, see Table 1.

*Prunustosanan AII (**2**):* colorless oil; $[\alpha]_D^{20}$ −19.7 (*c* 0.17, MeOH); UV (MeOH) λ_{max} (log ε) 232 (0.23), 287 (0.14); CD [MeOH, nm ($\Delta\varepsilon$)] 224 (−4.73), 282 (−1.31); [$Mo_2(OAc)_4$]-induced CD [DMSO, nm ($\Delta\varepsilon$)] 310 (−0.94); IR (KBr) V_{max} 3441, 1641, 1600, 1516, 1464, 1430, 1384, 1329, 1125, 1034 cm^{-1}; HRESIMS at *m*/*z* 413.1218 [M +

dx.doi.org/10.1021/jf502171z | J. Agric. Food Chem. 2014, 62, 7796−7803

Table 2. ^{1}H and ^{13}C NMR Data for 4−6 (CD_3OD)

	4[a]		5[b]		6[b]	
position	δ_C	δ_H	δ_C	δ_H	δ_C	δ_H
1	133.4		132.7		138.4	
2	109.2	6.96 (1H, d, 2.0)	102.9	6.72 (1H, br s)	102.6	6.80 (1H, br s)
3	147.7		147.9		153.3	
4	146.1		135.0		134.8	
5	114.7	6.78 (1H, d, 8.0)	147.9		153.3	
6	118.3	6.84 (1H, dd, 8.0, 2.0)	102.9	6.72 (1H, br s)	102.6	6.80 (1H, br s)
7	87.5	5.54 (1H, d, 6.4)	87.8	5.61 (1H, d, 6.0)	87.4	5.68 (1H, d, 6.0)
8	54.1	3.50 (1H, m)	52.0	3.65 (1H, m)	52.2	3.65 (1H, m)
9	63.3	3.85 (2H, m)	71.1	4.23 (1H, dd, 10.8, 6.0)	71.2	4.27 (1H, dd, 9.6, 6.0)
				3.76 (1H, m)		3.75 (1H, m)
2‴					83.4	4.02 (1H, t, 4.8)
1‴,3‴					60.7	3.74 (4H, dd, 4.8, 1.2)
1′	134.1		135.6		135.8	
2′	112.8	6.80 (1H, br s)	112.8	6.73 (1H, br s)	112.9	6.74 (1H, br s)
3′	143.8		143.8		143.9	
4′	146.8		146.1		146.0	
5′	128.9		127.7		127.7	
6′	116.3	6.80 (1H, br s)	116.8	6.78 (1H, br s)	116.8	6.75 (1H, br s)
7′	50.6	2.93 (1H, m)	31.5	2.62 (2H, t, 7.8)	31.5	2.62 (2H, t, 7.8)
8′	63.6	3.77 (1H, m)	34.4	1.81 (2H, m)	34.4	1.81 (2H, m)
9′	63.7	3.86 (2H, m)	60.8	3.55 (2H, t, 6.6)	60.8	3.55 (2H, t, 6.6)
3-$OCHH_3$	55.0	3.85 (3H, s)	55.3	3.81 (3H, s)	55.4	3.82 (3H, s)
5-$OCHH_3$			55.3	3.81 (3H, s)	55.4	3.82 (3H, s)
3′-$OCHH_3$	55.4	3.89 (3H, s)	55.4	3.86 (3H, s)	55.5	3.87 (3H, s)
Glc-1″			103.2	4.39 (1H, d, 7.8)	103.2	4.39 (1H, d, 7.8)
Glc-2″			73.8	3.23 (1H, m)	73.8	3.22 (1H, m)
Glc-3″			76.9	3.35 (1H, m)	76.9	3.35 (1H, m)
Glc-4″			70.1	3.28 (1H, o[c])	70.2	3.28 (1H, o[c])
Glc-5″			76.7	3.29 (1H, o[c])	76.7	3.28 (1H, m)
Glc-6″			61.4	3.87 (1H, m)	61.4	3.84 (1H, m)
				3.67 (1H, m)		3.65 (1H, m)

[a]NMR spectroscopic data were recorded at 400 MHz (^{1}H NMR) and 100 MHz (^{13}C NMR); [b]NMR spectroscopic data were recorded at 600 MHz (^{1}H NMR) and 150 MHz (^{13}C NMR); [c]"o" refers to overlapped signals.

$Na]^+$ (calcd for $C_{20}H_{22}O_7Na$, 413.1207); ^{1}H and ^{13}C NMR, see Table 1.

*Prunustosanan AIII (**3**):* colorless oil; $[\alpha]_D^{20}$ −6.3 (*c* 0.09, MeOH); UV (MeOH) λ_{max} (log ε) 227 (0.32), 285 (0.18); CD [MeOH, nm ($\Delta\varepsilon$)] 223 (−5.15), 287 (−2.54); [$Mo_2(OAc)_4$]-induced CD [DMSO, nm ($\Delta\varepsilon$)] 309 (+1.48); IR (KBr) V_{max} 3442, 1641, 1512, 1463, 1384, 1327, 1268, 1131, 1031 cm^{-1}; HRESIMS at *m*/*z* 413.1206 $[M + Na]^+$ (calcd for $C_{20}H_{22}O_7Na$, 413.1207); ^{1}H and ^{13}C NMR, see Table 1.

*Prunustosanan AIV (**4**):* colorless oil; $[\alpha]_D^{20}$ −14.1 (*c* 0.11, MeOH); UV (MeOH) λ_{max} (log ε) 231 (1.24), 280 (0.34); CD [MeOH, nm ($\Delta\varepsilon$)] 228 (−4.23), 281 (−3.18); [$Mo_2(OAc)_4$]-induced CD [DMSO, nm ($\Delta\varepsilon$)] 310 (−0.39); IR (KBr) V_{max}: 3396, 1605, 1513, 1464, 1424, 1384, 1268, 1157, 1133, 1030 cm^{-1}; HRESIMS at *m*/*z* 399.1431 [M +Na]$^+$ (calcd for $C_{20}H_{24}O_7Na$, 399.1414); ^{1}H and ^{13}C NMR, see Table 2.

*Prunustosananside AI (**5**):* colorless oil; $[\alpha]_D^{20}$ −7.5 (*c* 0.19, MeOH); UV (MeOH) λ_{max} (log ε) 230 (1.54), 281 (0.57); CD [MeOH, nm ($\Delta\varepsilon$)] 226 (−0.96), 274 (0.83); IR (KBr) V_{max} 3419, 1606, 1515, 1499, 1463, 1384, 1327, 1272, 1211, 1126, 1075, 1032 cm^{-1}; HRESIMS at *m*/*z* 575.2089 [M +Na]$^+$ (calcd for $C_{27}H_{36}O_{12}Na$, 575.2099); ^{1}H and ^{13}C NMR, see Table 2.

*Prunustosananside AII (**6**):* colorless oil; $[\alpha]_D^{20}$ −19.3 (*c* 0.21, MeOH); UV (MeOH) λ_{max} (log ε) 231 (0.48), 279 (0.18); CD [MeOH, nm ($\Delta\varepsilon$)] 230 (−3.48), 283 (−2.57); IR (KBr) V_{max} 3406, 1605, 1515, 1499, 1463, 1430, 1384, 1327, 1272, 1211, 1125, 1074, 1032 cm^{-1}; HRESIMS at *m*/*z* 649.2464 [M +Na]$^+$ (calcd for $C_{20}H_{22}O_7Na$, 649.2467); ^{1}H and ^{13}C NMR, see Table 2.

Acid Hydrolysis and Derivatization of Compounds 5 and 6. Each compound (4.0 mg) was hydrolyzed with 2 M HCl (5.0 mL), heated for 4 h at 95 °C, and extracted with EtOAc (3 × 4.0 mL). Then, the aqueous layer was concentrated in vacuo to appropriate volume, the solution was examined by TLC (EtOAc/BuOH/H_2O/HOAc, 4:4:1:1) and compared with authentic samples, and glucose was detected. The remaining aqueous layer was evaporated to dryness to give a residue, which was dissolved in pyridine (1.0 mL), and then L-cysteine methyl ester hydrochloride (2.0 mg) was added to the solution. The mixture was heated at 60 °C for 2 h, and 0.5 mL of tremethylsilyimidazole (TMSI) was added, followed by heating at 60 °C for 2 h. The reaction product was subjected to GC analysis with flame ionization detection. The column temperature was raised from 120 to 280 °C at the rate of 8 °C/min, and the carrier gas was N_2 (1.4 mL/min); the injection temperature was 250 °C and the injection volume, 1 mL. The absolute configuration of the monosaccharide were confirmed to be D-glucose by comparison of the retention times of its Me_3Si ethers with that of standard sample (t_R = 20.1 min).

DPPH Radical Scavenging Assay. The DPPH radical scavenging activity of samples was measured using a published method[20] with some modifications. The samples with different concentrations (0.1−100 μM) in EtOH (100 μL) were added to 0.2 mM DPPH in EtOH (150 μL). The mixture was shaken vigorously and then immediately incubated in darkness for 1 h. The absorbance of the reaction solution was determined in a Varioskan Flash (Thermo Scientific, Waltham, MA, USA) at 515 nm. Trolox, a stable antioxidant, was used as a positive reference. The DPPH radical scavenging activity in terms of the percentage of sample was calculated as follows: DPPH scavenging

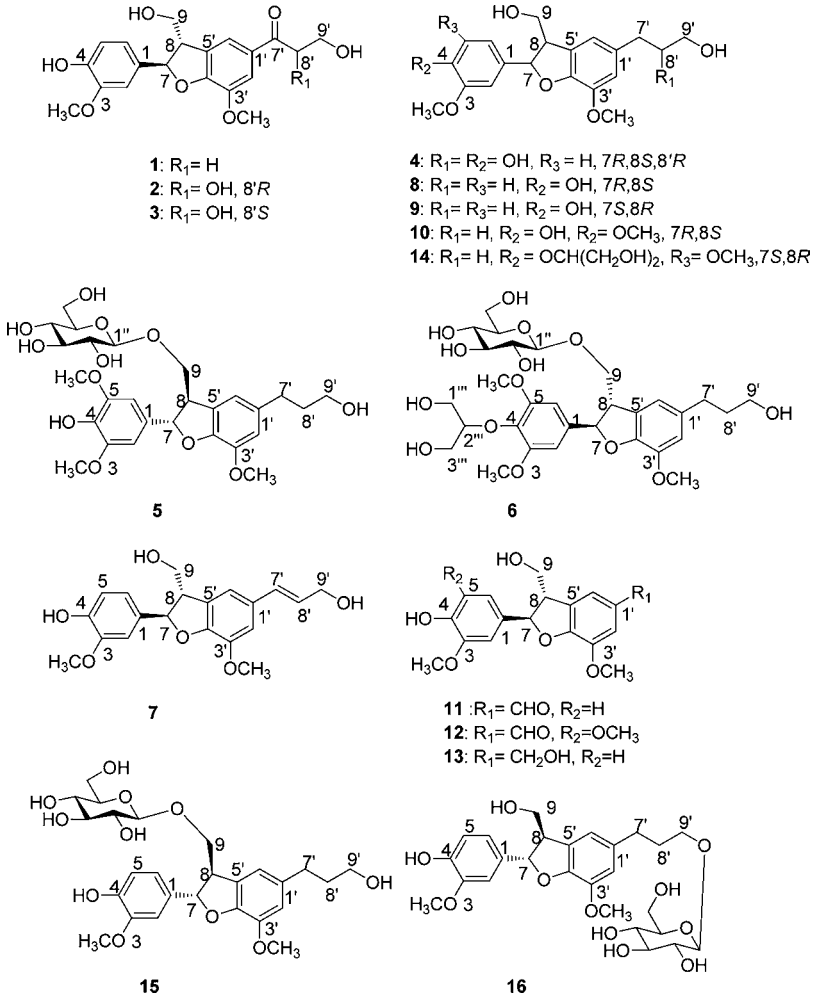

Figure 1. Structures of compounds **1**−**16**.

activity (%) = $[1 - (S - S_B)/(C - C_B)] \times 100\%$, where S, S_B, C, and C_B are the absorption of the sample, the blank sample, the control, and the blank control, respectively. Tests were performed in triplicate.

ABTS Radical Scavenging Activity Assay. The total antioxidant capacity was evaluated using an improved ABTS radical cation ($ABTS^{\bullet+}$) decolorization assay with some modifications.[21] $ABTS^{\bullet+}$ was produced by reacting 7 mM stock solution of $ABTS^{\bullet+}$ with 2.45 mM potassium persulfate (final concentration) and allowing the mixture to stand in the dark at room temperature for 16 h before use. The $ABTS^{\bullet+}$ solution was diluted with ethanol, to an absorbance of 0.7 ± 0.02 at 734 nm. An ethanolic solution (100 μL) of different concentrations of samples (0.1−100 μM) or trolox standard at various concentrations was mixed with 150 μL of diluted $ABTS^{\bullet+}$ solution. After reaction at room temperature for 10 min, the absorbance was measured at 734 nm using a Varioskan Flash (Thermo Scientific). The $ABTS^{\bullet+}$ scavenging ability was calculated using the formula $ABTS^{\bullet+}$ scavenging activity (%) = $[1 - (S - S_B)/(C - C_B)] \times 100$, where S, S_B, C, and C_B are the absorption of the sample, the blank sample, the control, and the blank control, respectively. Tests were performed in triplicate.

Cell Culture and Viability Assay. BV-2 cells, a mouse microglia cell line, were cultured in DMEM containing 5% fetal bovine serum (FBS), 100 U/mL penicillin, and 100 mg/mL streptomycin. BV-2 cells were plated at a density of 4×10^5/mL and maintained at 37 °C in a humidified atmosphere containing 5% CO_2. MTT assays were used to determine cell viability. Briefly, BV-2 cells were treated with the various concentrations of neolignan samples (0.1−100 μM) for 1 h and then stimulated with LPS (100 ng/mL) for 24 h. Then, the cells were incubated with a solution of 0.25 mg/mL MTT followed by incubation for 4 h at 37 °C and 5% CO_2. Supernatant was removed, and the formation of formazan was observed by monitoring the signal at 540 nm using a Varioskan Flash (Thermo Scientific).

NO-Releasing Assay. NO produced by the cells was determined by assaying the levels of NO_2^- using the Griess reagent. BV-2 cells were preincubated in 96-well plates at a density of 4×10^5 cells/well overnight and were then treated with different concentrations of the isolated compounds (0.1−100 μM) for 30 min. After 100 ng/mL LPS stimulation for 24 h, 100 μL of culture supernatant was mixed with the same volume of Griess reagent (1% sulfanilamide/0.1% *N*-(1-naphthyl)ethylenediamine dihydrocholoride/2.5% phosphoric acid). The absorbance was recorded at 540 nm on a Varioskan Flash (Thermo Scientific). NO concentration was calculated with reference to a standard curve of sodium nitrite produced using known concentrations.[22]

RESULTS AND DISCUSSION

Compound **1** was obtained as a colorless oil. The HRESIMS at m/z 397.1257 $[M + Na]^+$ indicated the molecular formula of $C_{20}H_{22}O_7$. The UV spectrum showed absorbances at λ_{max} 228 and 287 nm, and the IR spectral data indicated the presence of OH (3451 cm^{-1}), CO (1641 cm^{-1}), and aromatic rings (1600, 1510, and 1464 cm^{-1}).[23] The ^1H NMR spectrum of **1** showed the presence of a 1,3,4-trisubstituted benzene ring [δ 6.96 (1H, d, J = 1.6 Hz), 6.85 (1H, dd, J = 8.0, 1.6 Hz), and 6.79 (1H, J = 8.0 Hz)], a 1,3,4,5-tetrasubstituted benzene ring [δ 7.66 (1H, br s) and 7.57 (1H, br s)], and a sequence of methine−methine−methylene [CH(O)−CH(Ph)−CH_2O] successively coupled in

dx.doi.org/10.1021/jf502171z | J. Agric. Food Chem. 2014, 62, 7796−7803

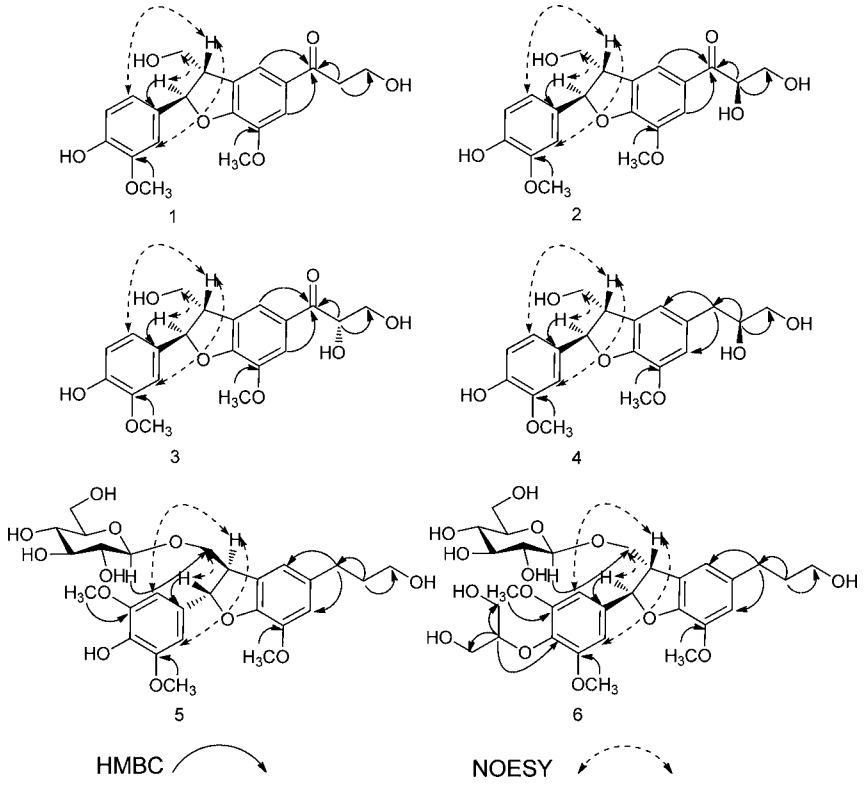

Figure 2. Key HMBC and NOESY correlations of compounds **1**−**6**.

this order [5.66 (1H, d, J = 6.4 Hz), 3.61 (1H, m) and 3.88 (2H, m)] in addition to two methoxyl groups at δ 3.93 (3H, s) and 3.85 (3H, s). The ^{13}C NMR spectrum of **1** (Table 1) showed 20 carbon signals including 2 methoxy groups, 12 aromatic units, a carbonyl carbon, and 5 aliphatic carbons. Careful comparison of the NMR data of **1** (Table 1) with those of known neolignans[24,25] revealed that compound **1** is a dihydrobenzofuran neolignan with oxidation of C-7′, which was confirmed by HMBC correlations (Figure 2) of H-8′ at δ 3.21 with C-7′, C-9′ and of H-9′ at δ 3.97 with C-7′ and C-9′. The relative stereochemistry of H-7 and H-8 was established as a trans relationship based on the $J_{7,8}$ coupling constant (6.4 Hz)[26] and NOESY cross peaks (Figure 2) H-7/H$_2$-9, H-8/H-2, and H-8/H-6.[27] As a negative Cotton effect at 281 nm ($\Delta\varepsilon$ = −2.61) was observed, 7*R* and 8*S* configurations were indicated.[27] On the basis of the above evidence, the structure of **1** was established as (7*R*,8*S*)-3,3′,5-trimethoxy-4′,7-epoxy-8,5′-neolignan-7′-one-4,9,9′-triol and named prunustosanan AI.

Compound **2** was also obtained as a colorless oil, with $C_{20}H_{22}O_8$ as its molecular formula, indicated by HRESIMS at m/z 413.1218 [M + Na]$^+$. The IR spectroscopic data of **2** showed absorptions for hydroxy (3441 cm^{-1}), carbonyl (1641 cm^{-1}), and aromatic groups (1600, 1516, and 1464 cm^{-1}).[23] Detailed comparison of ^{13}C NMR spectral data of **2** with those of **1** (Table 1) revealed signals at δ_C 40.5 and 57.5, moving downfield by δ_C 33.7 and 7.3, which were assigned to C-8′ and C-9′, respectively, indicating that one proton of H-8′ was substituted by a hydroxyl group. HMBC correlations (Figure 2) confirmed the structure and allowed the unambiguous assignment of its NMR data. The coupling constant $J_{7,8}$ (6.4 Hz) in the ^{1}H NMR of **2**, as well as the NOESY correlations (Figure 2) of H-7/H$_2$-9, H-8/H-2, and H-8/H-6, suggested a relative trans configuration.[26,27] In the CD spectrum, a negative Cotton effect at 282 nm indicated the 7*R*,8*S* configuration for **2**.[27] Additionaly, the absolute configuration of the vicinal diol (8′-OH and 9′-OH) moiety in **2** was determined by the induced CD spectra of its in situ complex with $Mo_2(OAc)_4$ in DMSO solution (Snatzke's method).[28,29] On the basis of the empirical helicity rule relating the sign of the Cotton effect of the diagnostic O−C−C−O moiety, the negative Cotton effect at 310 nm indicated an 8′*R* configuration. Accordingly, the structure of **2** was identified as (7*R*,8*S*,8′*R*)-3,3′,5-trimethoxy-4′,7-epoxy-8,5′-neolignan-7′-one-4,9,8′,9′-tetraol and named prunustosanan AII.

Compound **3** was proposed to have the molecular formula $C_{20}H_{22}O_8$ on the basis of HRESIMS. The IR and NMR spectroscopic data were in good agreement with those of **2** (Table 1), suggesting that the planar structure and relative configuration of **3** was the same as that of compound **2**. The CD spectrum showed a negative Cotton effect ($\Delta\varepsilon_{287}$ = −2.54), which indicated the absolute configurations of **3** to be 7*R*,8*S* configuration.[27] The 8′*S* configuration was supported by a positive Cotton effect at 310 nm in the $Mo_2(OAc)_4$-induced CD spectrum of **3**.[28,29] Thus, compound **3** was defined as an optical isomer of **2** and assigned as (7*R*,8*S*,8′*S*)-3,3′,5-trimethoxy-4′,7-epoxy-8,5′-neolignan-7′-one-4,9,8′,9′-tetraol, named prunustosanan AIII.

Compound **4** gave the positive HRESIMS m/z 399.1431 [M + Na]$^+$ (calcd for $C_{20}H_{24}O_7Na$, 399.1414), consistent with the molecular formula $C_{20}H_{24}O_7$. The ^{13}C NMR spectral data of **4** were very similar to those of **3**, except for the reduction of a carbonyl group (δ_C 198.2) on C-7′ in **4**. This difference was supported by the HMBC correlations (Figure 2) of H-7′/C-1′, C-2′, C-6′, and C-8′. The relative configurations of compound **4** were defined by the $J_{7,8}$ value (6.4 Hz) and NOESY spectrum (Figure 2).[26,27] The positive Cotton effect at 281 nm in the CD spectrum of **4** justified a 7*R*,8*S* configuration[27] as shown in Figure 1. In addition, the configuration of 8′-OH was confirmed

dx.doi.org/10.1021/jf502171z | J. Agric. Food Chem. 2014, 62, 7796−7803

using Snatzke's method: the negative Cotton effect at 310 nm in the induced CD spectrum of the complex of **4** with $Mo_2(OAc)_4$ indicated an 8′*R* configuration.[28,29] Consequently, the structure of **4** was undoubtedly elucidated as (7*R*,8*S*,8′*R*)-3,3′,5-trimethoxy-4′,7-epoxy-8,5′-neolignan-4,9,8′,9′-tetraol, named prunustosanan AIV.

The molecular formula of **5** was determined as $C_{27}H_{36}O_{12}$ by the $[M + Na]^+$ ion peak at *m*/*z* 575.2089 in the HRESIMS. The IR spectrum of **5** showed absorption for hydroxyl (3419 cm^{-1}), aromatic (1606 and 1515 cm^{-1}), and glycosidic (1075 and 1032 cm^{-1}) functions.[23,30] The NMR data of **5** (Table 2) were very similar to those of a known neolignan glucoside.[31] The anomeric proton signal at δ_H 5.62 (1H, d, J = 7.0 Hz, H-1″) in the ^{1}H NMR spectrum and six sugar carbon signals at δ_C 103.2 (C-1″), 73.8 (C-2″), 76.9 (C-3″), 70.1 (C-4″), 76.7 (C-5″), and 61.4 (C-6″) demonstrated that the sugar was β-D-glucose.[32,33] Furthermore, acid hydrolysis of **5** gave D-glucose. The position of the glucoside linkage was confirmed at C-9 by HMBC experiments (Figure 2), which showed long-range correlations between the 1″-proton and 9-carbon. The relative configuration of compound **5** was suggested to be relative trans according to the $J_{7,8}$ value of 6.0 Hz. This was verified by NOE correlations (Figure 2) of H-7/H_2-9 and H-8/H-6 and H-8/H-2 in the NOESY spectrum of **5**.[26,27] In addition, the CD spectrum of **5** showed a positive Cotton effect at 274 nm ($\Delta\varepsilon$ = 0.83), indicating that the absolute configuration of **5** was the (7*S*,8*R*) configuration.[31] Therefore, **5** was proposed to be (7*S*,8*R*)-3,3′,5-trimethoxy-4′,7-epoxy-8,5′-neolignan-7′-one-4,9,9′-triol 4-*O*-β-D-glucopyranoside, a neolignan glucoside prunustosananside AI.

Compound **6** showed the $[M + Na]^+$ ion peak at *m*/*z* 649.2464 in the positive-ion mode HRESIMS, indicating the molecular formula $C_{30}H_{42}O_{14}$. The IR spectrum of **6** showed the presence of aromatic (1605 and 1515 cm^{-1}) and glycosidic groups (1074 and 1032 cm^{-1}).[23,30] Comparison of its NMR data with those of **5** (Table 2) disclosed their extreme similarity. The main difference observed in the ^{13}C NMR spectrum of **6** was due to the presence of a 1,2,3-propanetriol moiety [δ_C 83.4 (C-2‴) and 60.7 (C-1‴and C-3‴)], which was confirmed by HMBC correlations (Figure 2) from H-2‴ to C-4, C-1‴, and C-3‴. Acid hydrolysis of **6** afforded glucose. Combined with its ^{1}H and ^{13}C NMR data, the configurations of the anomeric carbons of sugars were determined to be β-D for glucose.[32,33] The absolute configuration of glucose was further determined by acid hydrolysis and comparison with an authentic sample. The position of the glucoside linkage was confirmed at C-9 by HMBC experiments (Figure 2), which showed long-range correlations between the 1″-proton and 9-carbon. The trans relationship between H-7 and H-8 was inferred from their coupling constant ($J_{7,8}$ = 6.0 Hz), which was further verified by the NOE correlations (Figure 2) between H-7 and H_2-9 and between H-8 and H-2,6.[26,27] The CD spectrum showed a negative Cotton effect (283 nm, $\Delta\varepsilon$ = −2.57), which suggested a 7*R*,8*S* configuration.[27] According to the accumulated evidence above, the structure of **6** was designated (7*R*,8*S*)-3,3′,5-trimethoxy-4-(1‴,3‴-dihydroxy-2‴-propyloxyl)-4′,7-epoxy-8,5′-neolignan-7′-one-4,9,9′-triol 4-*O*-β-D-glucopyranoside and had been accorded the trivial name prunustosananside AII.

The other known compounds were identified as (*E*)-3-[(2*R*,3*S*)-2,3-dihydro-3-hydroxymethyl-7-methoxy-2-(4′-hydroxy-3′-methoxyphenyl)-1-benzo[*b*]furan-5-yl]-2-propen-1-ol (**7**),[34] (−)-7*R*,8*S*-dihydrodehydroconiferyl alcohol (**8**),[35] rel-(2α,3β)-7-*O*-methylcedrusin (**9**),[24] (+)-7*R*,8*S*-5-methoxydihydrodehydroconiferyl alcohol (**10**),[36] ficusal (**11**),[23] phenylcoumaran-α′-aldehyde (**12**),[37] 2-(4-hydroxy-3-methoxyphenyl)-3-methyl-5-hydroxymethyl-7-methoxycoumaran (**13**),[38] sakuraresinol (**14**),[39] dihydrodehydrodiconiferyl alcohol 9-*O*-β-D-glucopyranoside (**15**),[40] and dihydrodehydrodiconiferyl alcohol 9′-*O*-β-D-glucopyranoside (**16**)[40] by analyses of their ^{1}H and ^{13}C NMR and ESI-MS data in combination with the comparison of their data with the reported values.

Neolignans are a class of secondary metabolites produced by oxidative dimerization of two phenylpropanoid units. Neolignans exhibit a wide range of pharmacological effects, particularly antioxidant and anti-inflammatory activities.[41−43]

The antioxidant activities of **1**−**16** were evaluated by their ability to scavenge DPPH and ABTS radicals (Table 3).

Table 3. Antioxidant and Anti-inflammatory Activities of Compounds 1−16

compd	DPPH (IC_{50}, μM)[a]	ABTS (IC_{50}, μM)[a]	anti-inflammatory activity (IC_{50}, μM)[a]
1	>100	47.1 ± 2.7	>100
2	>100	46.4 ± 3.1	>100
3	>100	48.4 ± 4.1	>100
4	>100	57.1 ± 2.9	58.7 ± 3.0
5	42.6 ± 1.8	74.5 ± 3.9	34.7 ± 2.1
6	>100	>100	>100
7	>100	40.4 ± 1.8	4.4 ± 0.5
8	>100	33.7 ± 2.6	50.3 ± 2.6
9	>100	31.5 ± 2.3	48.4 ± 1.7
10	57.0 ± 2.3	43.0 ± 3.8	60.1 ± 4.9
11	>100	45.9 ± 2.8	4.8 ± 0.7
12	59.5 ± 3.5	56.2 ± 2.3	26.4 ± 1.4
13	>100	28.1 ± 1.1	44.3 ± 1.9
14	>100	>100	>100
15	>100	67.5 ± 5.9	>100
16	>100	51.4 ± 3.1	>100
trolox	39.2 ± 1.2	38.4 ± 0.8	nd[b]
mino	nd[b]	nd[b]	19.7 ± 1.5

[a]IC_{50} values represent the means ± SD of three parallel measurements. [b]nd, not determined.

Compounds **5**, **10**, and **12** showed moderate DPPH radical scavenging activities with IC_{50} values of 42.6 ± 1.8, 57.0 ± 2.3, and 59.5 ± 3.5 μM, respectively, whereas the other compounds (IC_{50} > 100 μM) did not display significant DPPH radical scavenging activity (Table 3). These results are comparable to those of previously isolated neolignan in other studies.[44,45] Zhao et al. reported that two new neolignan glycosides (IC_{50} > 100 μM) from *Pittosporum glabratum* were inactive in the DPPH radical scavenging assay.[46] A comparison of the structures of **5**, **10**, and **12** with those of **15**, **8**, and **11** indicated that additional methoxy groups at C-5 positions appeared to increase the antioxidant activity of the dihydrobenzofuran neolignans. In the ABTS assay, most of the isolated compounds showed significant antioxidant activity, with compounds **8** (IC_{50} = 33.7 ± 2.6 μM), **9** (IC_{50} = 31.5 ± 2.3 μM), and **13** (IC_{50} = 28.1 ± 1.1 μM) being the most potent, whereas compounds **1**−**4**, **7**, **10**−**12**, **15**, and **16** also showed moderate ABTS radical scavenging activities, comparable with that of the standard compound trolox with an IC_{50} value of 38.4 ± 0.8 μM (Table 3). Comparison of the structure of **6** with that of **5** or the structure of **10** with that of **14** showed

dx.doi.org/10.1021/jf502171z | J. Agric. Food Chem. 2014, 62, 7796−7803

that the antioxidant activity declined sharply when a hydroxyl group on the benzene ring was replaced by a 1,2,3-propanetriol group. This fact indicated that the free phenolic hydroxyl was crucial for the antioxidant activity, which was consistent with previous observations.[47,48]

In this investigation, we further evaluated the anti-inflammatory activity of the isolated compounds **1**−**16** using exposure to LPS-induced NO production in murine microglia BV-2 cell line. NO is a gaseous signaling molecule that plays key roles in immune and inflammatory responses and neuronal transmission in the brain.[49] Under normal conditions, NO has neuroprotective and antioxidant effects. However, excess production of NO from activated microglia causes a number of neurodegenerative diseases.[50] Inhibitors of NO production can be considered as potential anti-inflammatory agents. As shown in Table 3, compounds **4**, **5**, and **7**−**13** reduced NO levels in LPS-stimulated BV-2. In particular, the activities of **7** and **11** were more potent than that of the positive control, mino (IC_{50} = 19.7 ± 1.5 μM), in inhibiting NO production with IC_{50} values of 4.4 ± 0.5 and 4.8 ± 0.7 μM, respectively. The observed NO inhibitory activities appear to be somewhat correlated to their structures. For example, with regard to the results for compounds **8**, **9** and **11**−**13**, it appeared that shortening of the side chain might be important for the higher activity. Interestingly, comparing the structures and inhibitory activities of compound **7** with those of compounds **8** and **9**, it appeared that the double bond at C-7 may increase the inhibition of NO production. In addition, the inflammatory activity of one pair of isomers, **8** and **9**, was similar, which led us to conclude that the absolute configuration of the compounds might have little or no inhibitory effect on NO production. The cytotoxicity of compounds **1**−**16** to BV-2 cells was measured by an MTT assay. The results obtained indicated that the compounds exerted no cytotoxic effect at concentrations up to 100 μM and that the cell viability was >95% (see Table S1 in the Supporting Information), suggesting that compounds **1**−**16** do not affect normal cell growth.

In conclusion, this study reports the structures of 16 neolignans isolated from the active fraction of *P. tomentosa* seeds, along with their antioxidant and anti-inflammatory activities. Compounds **5**, **10**, and **12** showed moderate activity against DPPH, and compounds **8**, **9**, and **13** exhibited significant ABTS free radical scavenging activity (IC_{50} = 28.1−33.7 μM). Furthermore, compounds **7** and **11** exhibited remarkable NO inhibition with IC_{50} values of 4.4 ± 0.5 and 4.8 ± 0.7 μM, respectively, compared with the standard anti-inflammatory drug, mino, at 19.7 ± 1.5 μM. The results obtained in our study provide a potential justification for the use of the seeds from *P. tomentosa* industrial byproducts as a valuable source of raw material for new antioxidant and anti-inflammatory agents.

■ ASSOCIATED CONTENT

Supporting Information

UV, CD, IR, NMR, and HRESIMS data for compounds **1**−**6** and effect of compounds **1**−**16** on growth of BV-2 cells. This material is available free of charge via the Internet at http://pubs.acs.org.

■ AUTHOR INFORMATION

Corresponding Author

*(S.J.S.) Phone: +8621 23986510. Fax: +8621 23986510. E-mail: songsj99@163.com.

Notes

The authors declare no competing financial interest.

■ ACKNOWLEDGMENTS

We thank Wen Li and Yi Sha of Shenyang Pharmaceutical University for recording the NMR spectra.

■ ABBREVIATIONS USED

HPLC, high-performance liquid chromatography; GAS, gas chromatograph; NMR, nuclear magnetic resonance spectrometry; COSY, correlation spectroscopy; HSQC, heteronuclear single-quantum coherence; HMBC, heteronuclear multiple-bond correlation; NOESY, nuclear Overhaser effect spectroscopy; ESI, electrospray ionization; MS, mass spectrometry; UV, ultraviolet spectrometry; CD, electronic circular dichroism; IR, infared absorption spectrum

■ REFERENCES

(1) Pradhan, A. Obesity, metabolic syndrome, and type 2 diabetes: inflammatory basis of glucose metabolic disorders. *Nutr. Rev.* **2007**, *65*, 152−156.

(2) Lee, Y. J.; Han, S. B.; Nam, S. Y.; Oh, K. W.; Hong, J. T. Inflammation and Alzheimer's disease. *Arch. Pharm. Res.* **2010**, *33*, 1539−1556.

(3) Coussens, L. M.; Werb, Z. Inflammation and cancer. *Nature* **2002**, *420*, 860−867.

(4) Hensley, K.; Robinson, K. A.; Gabbita, S. P.; Salsman, S.; Floyd, R. A. Reactive oxygen species, cell signaling, and cell injury. *Free Radical Biol. Med.* **2000**, *28*, 1456−1462.

(5) Kris-Etherton, P. M.; Lefevre, M.; Beecher, G. R.; Gross, M. D.; Keen, C. L.; Etherton, T. D. Bioactive compounds in nutrition and health-research methodologies for establishing biological function: the antioxidant and anti-inflammatory effects of flavonoids on atherosclerosis. *Annu. Rev. Nutr.* **2004**, *24*, 511−538.

(6) Sogi, D. S.; Siddiq, M.; Greiby, I.; Dolan, K. D. Total phenolics, antioxidant activity, and functional properties of 'Tommy Atkins' mango peel and kernel as affected by drying methods. *Food Chem.* **2013**, *141*, 2649−2655.

(7) Fazio, A.; Plastina, P.; Meijerink, J.; Witkamp, R. F.; Gabriele, B. Comparative analyses of seeds of wild fruits of *Rubus* and *Sambucus* species from southern Italy: fatty acid composition of the oil, total phenolic content, antioxidant and anti-inflammatory properties of the methanolic extracts. *Food Chem.* **2013**, *140*, 817−824.

(8) Hasnaoui, N.; Wathelet, B.; Jiménez-Araujo, A. Valorization of pomegranate peel from 12 cultivars: dietary fibre composition, antioxidant capacity and functional properties. *Food Chem.* **2014**, *160*, 196−203.

(9) Jing, P.; Ye, T.; Shi, H. M.; Sheng, Y.; Slavin, M.; Gao, B. Y.; Liu, L. W.; Yu, L. Antioxidant properties and phytochemical composition of China-grown pomegranate seeds. *Food Chem.* **2012**, *132*, 1457−1464.

(10) Liu, Y. B.; Kakani, R.; Nair, M. G. Compounds in functional food fenugreek spice exhibit anti-inflammatory and antioxidant activities. *Food Chem.* **2012**, *131*, 1187−1192.

(11) Mueller, D.; Triebel, S.; Rudakovski, O.; Richling, E. Influence of triterpenoids present in apple peel on inflammatory gene expression associated with inflammatory bowel disease (IBD). *Food Chem.* **2013**, *139*, 339−346.

(12) Huang, Y. S.; Ho, S. C. Polymethoxy flavones are responsible for the anti-inflammatory activity of citrus fruit peel. *Food Chem.* **2010**, *119*, 868−873.

(13) Zhang, Q.; Yan, G.; Dai, H.; Zhang, X.; Li, C.; Zhang, Z. Characterization of Tomentosa cherry (*Prunus tomentosa* Thunb.) genotypes using SSR markers and morphological traits. *Sci. Hortic.* **2008**, *118*, 39−47.

(14) Wang, S.; Zhang, C. Y.; C, X. The anti-inflammation activity of volatile oil of cherry seeds. *J. New Chinese Med.* **2012**, *44*, 139−140.

(15) Sun, J. B.; Wang, J.; Liu, C. Y.; Qi, Z. W.; Cao, C. W.; Qiao, Y. Y.; Zhang, J.; Zhang, C. Y. Chemical composition of volatile oils from *Prunus tomentosa* Thunb's shell and kernel. *J. Jilin Univ. (Sci. Ed.)* **2013**, *51*, 145−147.
(16) Gao, H. S.; Shi, P. B.; Zhang, J. C. Study on technique of producing serial Nanking cherry wines. *Food Sci.* **2006**, *27*, 378−381.
(17) Lin, Y. F. Production technology of *Prunus tomentosa* Thunb. juice carbonic acid drink. *Trans. CSAE* **2003**, *19*, 226−229.
(18) Zhang, C. Y.; Shao, S. H.; Shi, Y. L. Effects on frostbite and inflammation dependablity of Chang Bai *Prunus tomentosa* Thunb. total flavone. *Chinese J. Immunol.* **2010**, *11*, 977−981.
(19) Kim, S. K.; Kim, H. J.; Choi, S. E.; Park, K. H.; Choi, H. K.; Lee, M. W. Anti-oxidative and inhibitory activities on nitric oxide (NO) and prostaglandin E_2 (COX-2) production of flavonoids from seeds of *Prunus tomentosa* Thunberg. *Arch. Pharm. Res.* **2008**, *31*, 424−428.
(20) Wu, S. B.; Wu, J.; Yin, Z.; Zhang, J.; Long, C.; Kennelly, E. J.; Zheng, S. Bioactive and marker compounds from two edible dark-colored myrciaria fruits and the synthesis of jaboticabin. *J. Agric. Food Chem.* **2013**, *61*, 4035−4043.
(21) Wu, S. B.; Dastmalchi, K.; Long, C.; Kennelly, E. J. Metabolite profiling of jaboticaba (*Myrciaria cauliflora*) and other dark-colored fruit juices. *J. Agric. Food Chem.* **2012**, *60*, 7513−7525.
(22) Wang, X. J.; Li, L.; Yu, S. S.; Ma, S. G.; Qu, J.; Liu, Y. B.; Li, Y.; Wang, Y.; Tang, W. Five new fawcettimine-related alkaloids from *Lycopodium japonicum* Thunb. *Fitoterapia* **2013**, *91*, 74−81.
(23) Li, Y. C.; Kuo, Y. H. Four new compounds, ficusal, ficusesquilignan A, B, and ficusolide diacetate from the heart wood of *Ficus microcarpa*. *Chem. Pharm. Bull.* **2000**, *48*, 1862−1865.
(24) Seidel, V.; Bailleul, F.; Waterman, P. G. Novel oligorhamnosides from the stem bark of *Cleistopholis glauca*. *J. Nat. Prod.* **2000**, *63*, 6−11.
(25) Huang, X. X.; Zhou, C. C.; Li, L. Z.; Peng, Y.; Lou, L. L.; Liu, S.; Li, D. M.; Ikejima, T.; Song, S. J. Cytotoxic and antioxidant dihydrobenzofuran neolignans from the seeds of *Crataegus pinnatifida*. *Fitoterapia* **2013**, *91*, 217−223.
(26) Xiao, H. H.; Dai, Y.; Wong, M. S.; Yao, X. S. New lignans from the bioactive fraction of *Sambucus williamsii* Hance and proliferation activities on osteoblastic-like UMR106 cells. *Fitoterapia* **2014**, *94*, 29−35.
(27) Xiong, L.; Zhu, C.; Li, Y.; Tian, Y.; Lin, S.; Yuan, S.; Hu, J.; Hou, Q.; Chen, N.; Yang, Y.; Shi, J. G. Lignans and neolignans from *Sinocalamus affinis* and their absolute configurations. *J. Nat. Prod.* **2011**, *74*, 1188−1200.
(28) Frelek, J.; Geiger, M.; Voelter, W. Transtion metal complexes as auxiliary chromophores in chiroptical studies on carbohydrates. *Curr. Org. Chem.* **1999**, *3*, 117−146.
(29) Di Bari, L.; Pescitelli, G.; Pratelli, C.; Pini, D.; Salvadori, P. J. Determination of absolute configuration of acyclic 1,2-diols with $Mo_2(OAc)_4$. 1. Snatzke's method revisited. *J. Org. Chem.* **2001**, *66*, 4819−4825.
(30) Yokosuka, A.; Mimaki, Y.; Sashida, Y. Steroidal saponins from *Dracaena surculosa*. *J. Nat. Prod.* **2000**, *63*, 1239−1243.
(31) Wang, Y. H.; Sun, Q. Y.; Yang, F. M.; Long, C. L.; Zhao, F. W.; Tang, G. H.; Niu, H. M.; Wang, H. A.; Huang, Q. Q.; Xu, J. J.; Ma, L. J. Neolignans and caffeoyl derivatives from *Selaginella moellendorffii*. *Helv. Chim. Acta* **2010**, *93*, 2467−2477.
(32) Kostova, I.; Dinchev, D. Saponins in *Tribulus terrestris*-chemistry and bioactivity. *Phytochem. Rev.* **2005**, *4*, 111−137.
(33) Agrawal, P. K.; Jain, D. C.; Gupta, P. K.; Thakur, R. S. Carbon-13 NMR spectroscopy of steroidal sapogenins and steroidal saponins. *Phytochemistry* **1985**, *24*, 2479−2496.
(34) Yuen, M. S. M.; Xue, F.; Mak, T. C. W.; Wong, H. N. C. On the absolute structure of optically active neolignans containing a dihydrobenzo[*b*]furan skeletont. *Tetrahedron* **1998**, *54*, 12429−12444.
(35) Jiang, J. S.; Feng, Z. M.; Wang, Y. H.; Zhang, P. C. New phenolics from the roots of *Symplocos caudata* WALL. *Chem. Pharm. Bull.* **2005**, *53*, 110−113.
(36) Li, L.; Seeram, N. P. Maple syrup phytochemicals include lignans, coumarins, a stilbene, and other previously unreported antioxidant phenolic compounds. *J. Agric. Food Chem.* **2010**, *58*, 11673−11679.
(37) Toshiaki, U.; Fumiaki, N.; Takayoshi, H. Lignin degradation by *Phanerochaete chrysosporium*: metabolism of a phenolic phenylcoumaran substructure model compound. *Arch. Microbiol.* **1982**, *131*, 124−128.
(38) Miyakoshi, T.; Chen, C. L. ^{13}C NMR spectroscopic studies of phenylcoumaran and 1,2-diarylpropane type lignin model compounds. *Holzforschung* **1992**, *46*, 39−46.
(39) Yoshinari, K.; Shimazaki, N.; Sashida, Y.; Mimaki, Y. Flavanone xyloside and lignans from *Prunus jamasakura* bark. *Phytochemistry* **1990**, *29*, 1675−1678.
(40) Otsuka, H.; Hirata, E.; Shinzato, T.; Takeda, Y. Isolation of lignan glucosides and neolignan sulfate from the leaves of *Glochidion zeylanicum* (Gaertn) A. Juss. *Chem. Pharm. Bull.* **2000**, *48*, 1084−1086.
(41) Yang, X. W.; He, H. P.; Du, Z. Z.; Liu, H. Y.; Di, Y. T.; Ma, Y. L.; Wang, F.; Lin, H.; Zuo, Y. Q.; Li, L.; Hao, X. J. Tarennanosides A−H, eight new lignan glucosides from *Tarenna attenuata* and their protective effect on H_2O_2-induced impairment in PC12 cells. *Chem. Biodivers.* **2009**, *6*, 540−550.
(42) Sadhu, S. K.; Khatun, A.; Phattanawasin, P.; Ohtsuki, T.; Ishibashi, M. Lignan glycosides and flavonoids from *Saraca asoca* with antioxidant activity. *J. Nat. Med.* **2007**, *61*, 480−482.
(43) Zhang, Y. L.; Zeng, W. M.; Wang, H. R.; Zhu, L.; Xu, H. L.; Kuang, H. X. Antioxidant lignans from *Dryopteris fragrans*. *Chin. Tradit. Herbal Drugs* **2008**, *39*, 343−346.
(44) Chin, Y. W.; Chai, H. B.; Keller, W. J.; Kinghorn, A. D. Lignans and other constituents of the fruits of *Euterpe oleracea* (açai) with antioxidant and cytoprotective activities. *J. Agric. Food Chem.* **2008**, *56*, 7759−7764.
(45) Shen, C. C.; Hong, K. Y.; Chen, J.; Zhang, L. J.; Lin, Z. H.; Huang, H. T.; Cheng, H. L.; Kuo, Y. H. Antioxidant and anti-nitric oxide components from *Quercus glauca*. *Chem. Pharm. Bull.* **2012**, *60*, 924−929.
(46) Zhao, H.; Nie, T.; Guo, H.; Li, J.; Bai, H. Two new neolignan glycosides from *Pittosporum glabratum* Lindl. *Phytochemistry Lett.* **2012**, *5*, 240−243.
(47) Abdel-Mageed, W. M.; Backheet, E. Y.; Khalifa, A. A.; Ibraheim, Z. Z.; Ross, S. A. Antiparasitic antioxidant phenylpropanoids and iridoid glycosides from *Tecoma mollis*. *Fitoterapia* **2012**, *83*, 500−507.
(48) Hamerski, L.; Bomm, M. D.; Silva, D. H. S.; Young, M. C. M.; Furlan, M.; Eberlin, M. N. Phenylpropanoid glucosides from leaves of *Coussarea hydrangeifolia* (Rubiaceae). *Phytochemistry* **2005**, *66*, 1927−1932.
(49) Karpuzoglu, E.; Ahmed, S. A. Estrogen regulation of nitric oxide and inducible nitric oxide synthase (iNOS) in immune cells: implications for immunity, autoimmune diseases, and apoptosis. *Nitric Oxide* **2006**, *15*, 177−186.
(50) Hämäläinen, M.; Lilja, R.; Kankaanranta, H.; Moilanen, E. Inhibition of iNOS expression and NO production by anti-inflammatory steroids reversal by histone. deacetylase inhibitors. *Pulm. Pharmacol. Ther.* **2008**, *21*, 331−339.

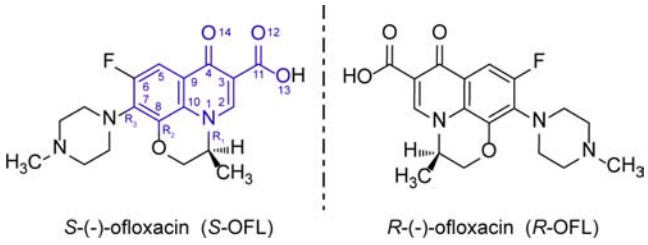

Figure 1. Chemical structures of ofloxacin stereoisomers. The common structure of QNs is labeled in blue.

animal byproducts and environmental samples with a simple, cost-effective, and high-throughput analysis method.

In this study, ofloxacin isomers with a stereogenic center were chosen as a model while predicting the epitopes of small molecules. The ofloxacin isomers were conjugated to bovine serum albumin (BSA) to form immunogens using the carbodiimide method. Two monoclonal antibodies (mAbs) were raised by BALB/c mice immunization, cell fusion, and hybridoma selection. Then, the enantioselectivity and specificity of mAbs were characterized using indirect competitive ELISA (icELISA). On the basis of the CR data, the epitopes of the ofloxacin enantiomers were predicted by both a hologram quantitative structure−activity relationship (HQSAR) method and a comparative molecular field analysis (CoMFA) method. The conformational structures of epitope on the carrier protein were modeled for explaining the experimental phenomenon and providing a theoretical guide for hapten design.

MATERIALS AND METHODS

Chemicals and Apparatus. *R*-(+)-Ofloxacin (*R*-OFL), *S*-(−)-ofloxacin (*S*-OFL), *S*-(−)-ofloxacin methyl ester (*S*-OFLM), and *R*-(+)-ofloxacin methyl ester (*R*-OFLM) were obtained from Daicel Chiral Technologies Company (Shanghai, China). Racemic ofloxacin (rac-OFL), pefloxacin (PEF) mesylate, gatifloxacin (GAT), norfloxacin (NOR) hydrochloride, sarafloxacin hydrochloride (SAR), garenoxacin (GAR), clinafloxacin (CLI), rufloxacin (RUF), ciprofloxacin hydrochloride (CIP), enrofloxacin (ENR), prulifloxacin (PRU), lomefloxacin (LOM), tosufloxacin (TOS), sparfloxacin (SPA), difloxacin (DIF), pazufloxacin (PAZ), marbofloxacin (MAR), moxifloxacin (MOX), pipemidic acid (PIP), nalidixic acid (NAL), and oxolinic acid (OXO) were purchased from Veterinary Medicine Supervisory Institute of China (Beijing, China). The structure of QNs is shown in Figure S1 of the Supporting Information. BSA, ovalbumin (OVA), 1-(3-(dimethylamino)propyl)-3-ethyl carbodiimide (EDC), 2,4,6-trinitrobenzene-1-sulfonic acid (TNBS), complete and incomplete Freund's adjuvant, horseradish peroxidase−immunoglobulin G (HRP−IgG), 3,3′,5,5′-tetramethylbenzidine (TMB), the culture media RPMI-1640, hypoxanthine−aminopterin−thymidine (HAT), hypoxanthine−thymidine (HT), and poly(ethylene glycol) (PEG) 2000 were purchased from Sigma-Aldrich (St. Louis, MO). All of the chemicals and organic solvents, which were analytical grade or better, were obtained from a local chemical supplier (Yunhui Trade Co., Ltd., Guangzhou, China). Deionized water was prepared using a Milli-Q water purification system (Millipore, Bedford, MA).

A total of 96 microtiter plates for ELISA were obtained from Yunpeng Technology Development Co., Ltd. (Xiamen, China). Female BALB/c mice, 6−8 weeks old, were provided by the Guangdong Medical Laboratory Animal Center (Guangzhou, China).

Buffers. Carbonate−bicarbonate buffer (CBS, 50 mmol/L, pH 9.6) is used as the coating buffer. Phosphate-buffered saline with Tween 20 (PBST) contains 10 mmol/L phosphate buffer, 0.8% saline solution, and 0.05% Tween 20 (pH 7.4). The phosphate−citrate buffer is a 40 mmol/L solution of sodium citrate (pH 5.5). The substrate solution contains 0.01% tetramethylbenzidine (TMB) and 0.004% H_2O_2 in citrate buffer.

Apparatus and Software. Ultraviolet−visible (UV−vis) spectra were recorded on a UV-160A Shimadzu spectrophotometer (Kyoto, Japan). The washing steps were carried out using a DEM-III microplate washer (Tuopu Analytical Instrument, Beijing, China). The absorbance readings were carried out at 450 nm with a Multiskan MK3 microplate reader (Thermo Fisher Scientific, Pittsburgh, PA). The competitive curves were analyzed with a four-parameter equation using the OriginPro 8.0 software (OriginLab Corporation, Northampton, MA).

Preparation of Hapten−Protein Conjugates. The haptens of the ofloxacin enantiomers containing a carboxylic acid group on dihydroquinoline were synthesized and bound to carrier proteins using the carbodiimide method to prepare the immunogenic agents.[25] BSA and OVA were used as carrier proteins for the immunogens and coating antigens, respectively. *R*-OFL and *S*-OFL were coupled to BSA separately for immunogens (*R*-OFL−BSA and *S*-OFL−BSA) and to OVA for coating antigens (*R*-OFL−OVA and *S*-OFL−OVA). The hapten−protein conjugates were prepared using the carbodiimide method with modifications. The hapten (10 mg) was dissolved with BSA or OVA (15 mg) in 0.9% normal saline (1.5 mL). EDC (30 mg) was added slowly to the hapten solution, and the mixture was stirred at room temperature for 30 min. The hapten−carrier protein conjugates were dialyzed against phosphate-buffered saline (PBS) at 4 °C for 72 h and then characterized with UV−vis spectrometry.

Preparation of mAbs. *Immunization.* The immunization protocol was similar to those previously described.[9] Briefly, eight BALB/c female mice were randomly separated into two equal groups, which were immunized with *S*-OFL−BSA and *R*-OFL−OVA, respectively. All of the mice aged 6−8 weeks were immunized intraperitoneally with the immunogens (50 μg for each mouse) at 2 week intervals. Blood samples were taken from the mice to detect the presence of antibodies against *R*-OFL or *S*-OFL using icELISA in a homologous conjugate-coated format on the eighth day after each immunization, starting 49 days after the first injection. The mouse that exhibited the best titer and inhibition rate for each hapten was selected as the donor of spleen cells for hybridoma production. Each selected mouse received a final intraperitoneal injection with 100 μg of immunogen, and the mice were sacrificed for cell fusion in the third day after the final injection. All experiments involving animals were performed in compliance with the relevant protective and administrant laws for laboratory animals of China and were conducted with the approval of the Institutional Authority for Laboratory Animal Care.

Cell Fusion, Hybridoma Selection, and Cloning. The fusion of SP2/0 cells (saved in our laboratory) and spleen cells was performed with PEG 2000 to produce hybridoma cells. The positive hybridomas were selected and cloned by limited dilution. After the fourth subcloning, monoclonal hybridomas possessing *S*-OFL or *R*-OFL enantioselectivity were selected to intraperitoneally inject to each pretreated mice. After 10 days, ascites fluids were obtained. They were first purified by sequential precipitation with caprylic acid and ammonium sulfate[26] and then purified using a protein-G column. The concentrations of purified mAbs were determined with UV−vis spectrometry. The isotype of mAbs were identified using IsoQuick Strips (Sigma-Aldrich).

icELISA Protocol. The ELISA was established on the basis of the common protocol of icELISA.[9] A total of 96 microtiter plates were coated with 100 μL of the coating antigen at the optimal dilution in CBS overnight at 4 °C, and then they were washed 2 times with PBST solution. Each well was blocked with 150 μL of 5% skim milk in PBS buffer for 3 h at 37 °C. After five washes, the plates were added with different concentrations of ofloxacin standard solutions (50 μL/well) and an appropriate concentration of antibody solutions (50 μL/well), both of which were diluted in PBST solution. Afterward, the plates were incubated for 40 min at 37 °C. After washing 5 times with PBST solution, the plates were incubated with 100 μL/well of HRP−IgG (diluted 1:5000 in PBST) for 30 min at 37 °C. After five washes, 100 μL of TMB solution was added to each well and incubated at 37 °C for 10 min; the color development was stopped by adding 50 μL/well of 2 mol/L H_2SO_4, and the absorbance was recorded at 450 nm (A_{450}). The concentrations of antibodies and coating antigens had been

optimized using checkerboard titration and standard curves. The conditions that resulting in the smallest IC_{50} were chosen as the optimized conditions ($1.0 < A_{max\ 450\ nm} < 1.2$). The 50% inhibition value (IC_{50}) was obtained from the four-parameter logistic equation of the sigmoidal curve[27] using OriginPro 8.0 (OriginLab Corporation, Northampton, MA).

CR Study. The specificity of the mAbs was determined using 24 ofloxacin analogues under optimized icELISA conditions. The CR values were calculated according to the following equation:

$$CR\ (\%) = IC_{50(\text{ofloxacin isomer, }\mu\text{mol/L})}/IC_{50(\text{analyte, }\mu\text{mol/L})} \times 100$$

HQSAR. All molecular modeling calculations were conducted with Sybyl 7.3 software package (Tripos, Inc., St. Louis, MO) running on a personal computer. The sketched QN structures were optimized to global low-energy conformations using the standard Tripos force field with an 8 Å cutoff for non-bonded interactions in conjunction with Gasteiger–Hückel charges,[28] a 0.005 kcal mol^{-1} $Å^{-1}$ termination gradient, and a dielectric constant of 4. A database containing ofloxacin stereoisomers and its analogues was established using the Sybyl 7.3 software package. Hologram lengths, atom count in fragments, and information sources were optimized, and the best model with the least standard error was selected. In both HQSAR and CoMFA models, pIC_{50} values ($pIC_{50} = -\log IC_{50}$) in homologous format were chosen as dependent variables, while the HQSAR or CoMFA descriptors were chosen as independent variables. The HQSAR descriptors (independent variables) were related to pIC_{50} (dependent variable) using partial least-squares (PLS) analysis. Fragment contribution to pIC_{50} was illustrated by encoded colors.

CoMFA. The optimal structures obtained above were put into a database. A database including all of the QN molecules previously sketched and optimized was built. The common structure of the QNs (4-oxo-4,7-dihydroquinoline-3-carboxylic acid nucleus) was chosen as the basis for the alignment. Experimental pIC_{50} (dependent variable) and CoMFA descriptors (independent variables) were correlated by PLS analysis with a leave-one-out (LOO) cross-validation and no cross-validation, respectively. The favored and disfavored contour maps could be visually investigated.

Hapten–Carrier Conjugate Modeling. The chiral hapten–carrier conjugate was modeled by Sybyl 7.3. BSA was chosen as the model for the carrier protein, and the crystal structure of BSA [Protein Data Bank (PDB) ID: 4F5S] was obtained from the PDB. BSA was composed of two chains: chain A and chain B. A substructure containing 80 amino acids (AA) at the N terminus of chain A was chosen as the BSA mimic. The carboxyl groups from the ofloxacin isomers were randomly coupled with amino groups, forming a new amido linkage. The conformational structures of ofloxacin isomer–BSA conjugate mimics were optimized using staged minimization: first the ligands, then the side chains, then the biopolymer without C-α, and finally, minimize all. The weighted root-mean-square (RMS) distances of carbon atoms between the free and conjugated ofloxacin isomers were measured using the Fit Atoms module of Sybyl 7.3. The distances from the chiral carbon of the ofloxacin isomers to the nearest atom from the carrier protein residues were also measured.

RESULTS AND DISCUSSION

Production of mAbs. Ofloxacin isomers are small molecules (MW = 361.37 < 1000) that must be conjugated to a carrier protein to elicit an immune response. Through the free carboxylic acid on the ofloxacin isomer, the molecule was conjugated with BSA or OVA using EDC. The BSA conjugates (*S*-OFL–BSA and *R*-OFL–BSA) were used as immunogens, and the OVA conjugates (*S*-OFL–OVA, *R*-OFL–OVA, and rac-OFL–OVA)were used as coating antigens.

Two groups (four mice in each group) of mice were immunized with conjugates *S*-OFL–BSA and *R*-OFL–BSA, respectively. The mouse that showed the highest titer of antiserum and the best inhibition with corresponding hapten in icELISA in each group was selected for monoclonal antibody production. After cell fusion and four rounds of limited dilution screening, hybridomas named WR1 (obtained from the *R*-OFL–BSA immunizing group) and MS1 (obtained from the *S*-OFL–BSA immunizing group) that can secrete the highest specificity antibodies against the corresponding ofloxacin isomer (*R*-OFL and *S*-OFL, respectively) were obtained. Finally, mAbs were obtained from WR1 and MS1 by ascites production and purified using a protein-G sepharose column. The isotypes of mAb-WR1 and mAb-MS1 were all IgG1/κ.

Enantioselectivity of Antibodies. Competitive ELISA can be divided in general into homologous and heterologous formats. In homologous icELISA (Ho-icELISA) formats, the same hapten is used for immunization and assay purposes, whereas in heterologous icELISA (He-icELISA) formats, the immunizing hapten and the competitor hapten (coating antigen hapten) differ in their molecular structures (e.g., ofloxcin isomer).

icELISA using OVA conjugate as the coating antigen was applied to investigate the enantioselectivity and sensitivity of the obtained mAbs to ofloxacin stereoisomers. The optimal concentration of mAbs and coating antigens by checkerboard titration is shown in Table S1 of the Supporting Information. In Ho-icELISA, the optimized concentrations of *R*-OFL–OVA, mAb-WR1, *S*-OFL–OVA, and mAb-WS1 were 250.0, 40.0, 250.0, and 5.5 μg/L, respectively. Ho-icELISA results showed that mAb-WR1 selectively recognizes *R*-OFL and mAb-MS1 selectively recognizes *S*-OFL (Figure 2). The sensitivity (IC_{50}) of mAb-WR1 to *R*-OFL (0.0344 μmol/L) is higher than that of *S*-OFL (0.3988 μmol/L) (Figure 2a and Table 1). Concurrently, the sensitivity of mAb-MS1 to *S*-OFL (0.0018 μmol/L) is higher than that of *R*-OFL (0.0096 μmol/L) (Figure 2b and Table 1). Both mAbs predominately have enantioselectivity to the corresponding ofloxacin isomer.

The effect of He-icELISA on enantioselectivity was also investigated. The results showed that icELISA based on heterologous coating antigens have no obvious effect on enantioselectivity of mAb-WR1 and mAb-MS1 (Table 2). For mAb-WR1, both the CR values of *S*-OFL in Ho-icELISA and He-icELISA were about 8%. Concurrently, for mAb-MS1, both the CR values of *S*-OFL in Ho-icELISA and He-icELISA were about 18%. Above all, we can conclude that the enantioselectivity of mAbs was not affected by the heterologous coating reaction model and the enantioselectivity of mAbs (mAb-WR1 and mAb-MS1) would be the intrinsic property of its own.

Sensitivity and Specificity of Antibodies. The sensitivity and specificity data showed that mAb-WR1 and mAb-MS1 have a high sensitivity and specificity (Table 1). In Ho-icELISA of mAb-WR1 and mAb-MS1, 24 analytes were employed for the CR study. The IC_{50} of mAb-WR1 to *R*-OFL is 10 times larger than that of mAb-MS1 to *S*-OFL. That is to say, the sensitivity of mAb-MS1 is higher than that of mAb-WR1. A similar rule was also found in other antibodies, including anti-serum against ofloxacin stereoisomers in our studies. It seems that different enantiomers may be different in immunogenicity, especially in sensitivity.

The CR studies showed that both mAb-WR1 and mAb-MS1 have a relatively high specificity (Table 1). Except for *S*-OFLM, *R*-OFLM, RUF, GAR, and MAR, the CR values of other QNs are lower than 2% or even not detected (ND). The CR values of PAZ (ND for mAb-WR1 and 0.2% for mAb-MS1) and DIF (0.7% for mAb-WR1 and 1.0% for mAb-MS1) were much lower, although they have a little bit of difference in R1, R2 (oxazine ring), or R3 (piperazinyl ring) groups compared to

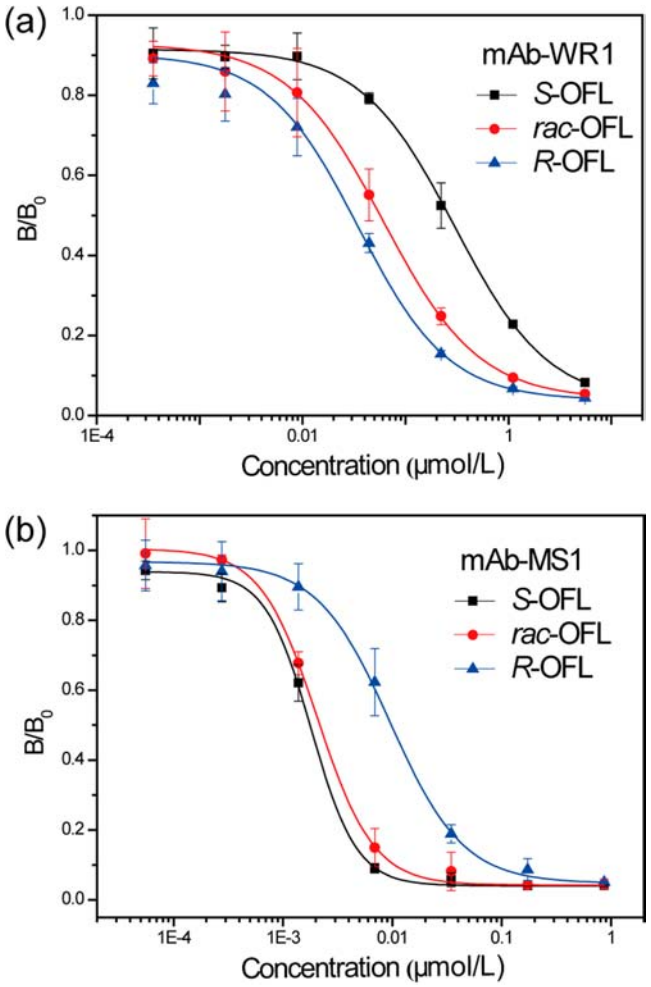

Figure 2. Enantioselectivity of (a) mAb-WR1 and (b) mAb-MS1 by icELISA using the homologous coating antigen.

ofloxacin enantiomers. This result indicated that R1, R2, and R3 were critical in the hapten−antibody interaction.

However, what properties and how groups affected the hapten−antibody recognition from the quantitative perspective were still unknown. Thus, 2D- and 3D-QSAR were performed to explore deeper insights.

HQSAR Analysis. HQSAR is a technique that employs fragment fingerprints as predictive variables of biological activity or other structural-related data.[29] Although HQSAR model generation deals with the 2D structure-directed fragment fingerprints, information on chirality is included in model development and suitable for chiral recognition investment. The model development was performed using parameters: atom (A), bond (B), connection (C), chirality (Ch), hydrogen (H), and donor/acceptor (DA). The HQSAR technique gives us straightforward clues about the individual atomic contribution to the biological activity through the different color codes. As far as we know, this is the first time to perform HQSAR for hapten−antibody chiral recognition.

In HQSAR analysis, the correlation between descriptors (molecular hologram, "bins") and biological activity of the antibody (pIC_{50}) was performed by PLS with cross-validation. The parameters and statistical results of HQSAR for mAb-WR1 and mAb-MS1 are shown in Table 3. For mAb-WR1, on the basis of optimized hologram parameters (the best length was 307; fragment size was 4−7; and information sources were A, B, C, and Ch), the established HQSAR model showed high correlation (r^2_{ncv} = 0.95) and predictive ability (r^2_{cv} = 0.68). For mAb-MS1, the HQSAR modeling in the absence of NOR (NOR is an outlier in the data set) was obtained, and under the optimized hologram parameters (best length was 199; fragment size was 4−7; and information sources were A, B, C, H, Ch, and DA), the results showed high correlation (r^2_{ncv} = 0.96) and predictive ability (r^2_{cv} = 0.56). In both of the HQSAR models, parameter Ch played an important role in modeling. In the absence of parameter Ch (other parameters are shown in Table 3), the value of r^2_{cv} was only 0.41 (for mAb-WR1) and 0.42 (for mAb-MS1). In other words, in this study, the chirality of the

Table 1. Enantioselectivity, Sensitivity, and Specificity of mAb-WR1 and mAb-MS1 in Homologous Format (n = 3)

	mAb-WR1		mAb-MS1	
analytes	IC_{50}[a]	CR (%)	IC_{50}	CR (%)
S-OFL	0.3988	8.6	0.0018	100.0
rac-OFL	0.0610	56.4	0.0020	90.0
R-OFL	0.0344	100.0	0.0096	18.8
S-OFLM	0.0398	86.4	0.0001	1800.0
R-OFLM	0.0025	1376.0	0.0079	22.8
RUF	0.0327	105.2	0.0026	69.2
GAR	0.0244	141.0	0.0065	27.7
MAR	0.5041	6.8	0.0097	18.6
NOR	6.5761	0.5	0.1697	1.1
DIF	4.9749	0.7	0.1742	1.0
ENR	5.8431	0.6	0.3328	0.5
PEF	5.6943	0.6	0.4923	0.4
CLI	8.9403	0.4	0.2713	0.7
LOM	5.6923	0.6	6.1420	<0.1
GAT	5.2418	0.7	ND	ND
MOX	ND[b]	ND	0.5235	0.3
TOS	ND	ND	0.6627	0.3
PAZ	ND	ND	1.0490	0.2
CIP	ND	ND	29.7993	<0.1
SAR	ND	ND	12.6117	<0.1
SPA	ND	ND	ND	ND
PIP	ND	ND	ND	ND
NAL	ND	ND	ND	ND
PRU	ND	ND	ND	ND
OXO	ND	ND	ND	ND

[a]IC_{50} values are in units of μmol/L. [b]ND represented not detected (or IC_{50} > 150 μmol/L).

Table 2. Effect of Heterologous icELISA on Enantioselectivity of mAb-WR1 and mAb-MS1 (n = 3)

antibody versus coating antigen	analytes	IC_{50} (μmol/L)	CR (%)
mAb-WR1 versus *S*-OFL−OVA	*S*-OFL	0.6336	9.1
	rac-OFL	0.1132	51.1
	R-OFL	0.0579	100.0
mAb-WR1 versus rac-OFL−OVA	*S*-OFL	1.6860	6.0
	rac-OFL	0.2818	36.1
	R-OFL	0.1018	100.0
mAb-MS1 versus *R*-OFL−OVA	*S*-OFL	0.0019	100.0
	rac-OFL	0.0021	90.5
	R-OFL	0.0104	18.3
mAb-MS1 versus rac-OFL−OVA	*S*-OFL	0.0022	100.0
	rac-OFL	0.0025	88.0
	R-OFL	0.0123	17.9

dx.doi.org/10.1021/jf404449n | J. Agric. Food Chem. 2014, 62, 7804−7812

Table 3. Summary of HQSAR Parameters and Statistical Results for mAb-WR1 and mAb-MS1

	mAb-WR1	mAb-MS1
model[a]	A, B, C, and Ch	A, B, C, H, Ch, and DA
r^2_{cv} [b]	0.68	0.56
r^2_{ncv} [c]	0.95	0.96
SEE[d]	0.36	0.38
ONC[e]	6	5
best length	307	199
fragment size	4−7	4−7

[a]Fragment distinction: A, atom; B, bond; C, connection; H, hydrogen; Ch, chirality; and DA, donor and acceptor. [b]r^2_{cv} = cross-validated correlation coefficient after the LOO procedure. [c]r^2_{ncv} = correlation coefficient. [d]SEE = standard error of the estimate. [e]ONC = optimum number of components.

molecule played an important part in hapten−antibody recognition.

An atomic contribution map for chiral recognition based on HQSAR analysis was shown by encoded color (Figure 3 and Figure S3 of the Supporting Information). Red and orange contours indicate negative contribution to the hapten−antibody recognition. On the contrary, green and yellow regions represent positive contribution to the antigen−antibody interaction. The white color stands for intermediate contribution to activity, and the cyan color represents the common structure of QNs. The atomic contribution maps of HQSAR told us the following: (i) The chiral center was green, which indicated that the chiral center played an important role in chiral recognition. (ii) With the decrease of the CR vale, the color of the oxazine ring and the piperazinyl ring turned from green to red, gradually. The color contour on the oxazine ring and the piperazinyl ring reflected the sensitivity of each QN to some extent. This phenomenon implied that the epitope of ofloxacin isomers may be mainly composed of the oxazine ring and the piperazinyl ring and antibodies recognize haptens from the side of the oxazine and piperazinyl rings. (iii) The greened (or yellowed) methoxy group of *R*-OFLM and *S*-OFLM showed that mAb-WR1 and mAb-MS1 recognize the hapten−carrier linking group during antigen−antibody interaction. (iv) The common structure also played a role in the hapten−antibody interaction.

CoMFA. Besides HQSAR, a 3D-QSAR method (CoMFA) was performed to investigate the hapten−antibody interaction. CoMFA is based on the ligand structure, making the spatial alignment crucial when determining the accuracy of these approaches. In this study, the structures of the QNs were aligned into a lattice box by fitting with a 4-oxo-4,7-dihydroquinoline-3-carboxylic acid skeleton as a common structure (Figure 1). The aligned QNs are shown in Figure 4.

The statistical results obtained from standard CoMFA models are given in Table 4. In the model of mAb-WR1, PLS analysis showed a high cross-validation correlation

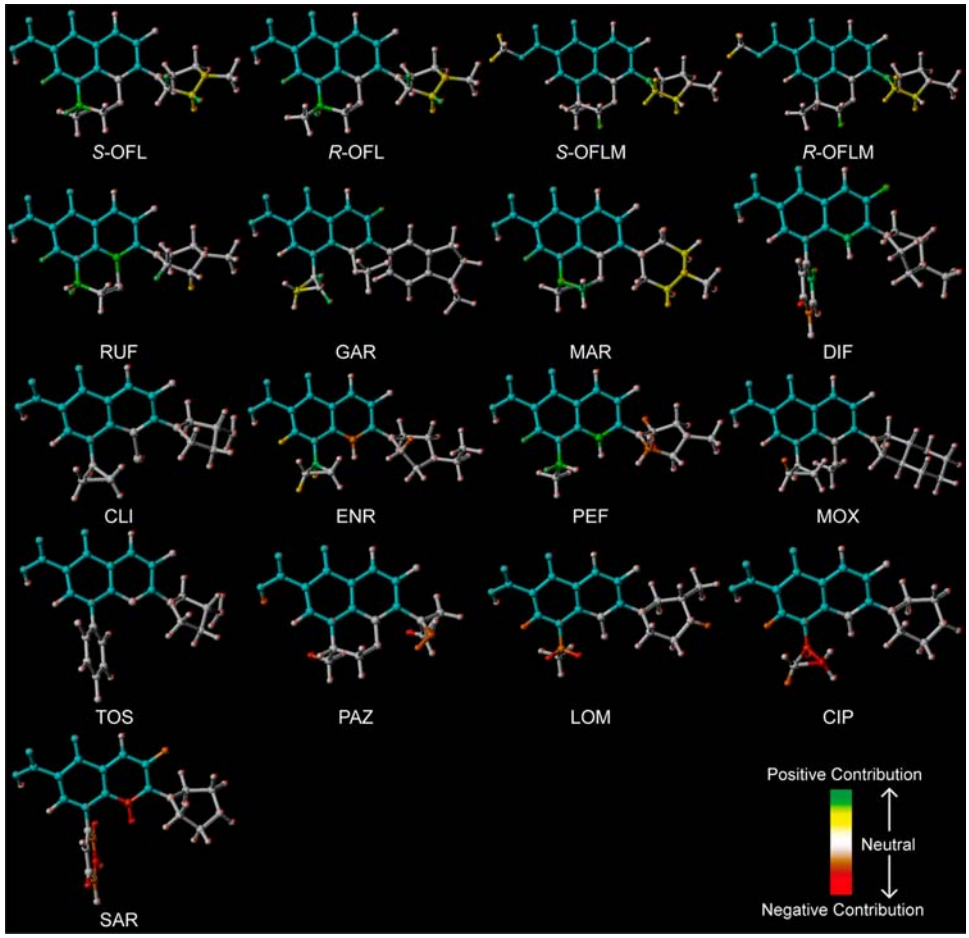

Figure 3. Atomic contribution map for chiral recognition based on HQSAR analysis of mAb-WR1. Red and orange contours represent negative contribution; green and yellow contours are for positive contribution; and the cyan contour represents the common backbone of QNs.

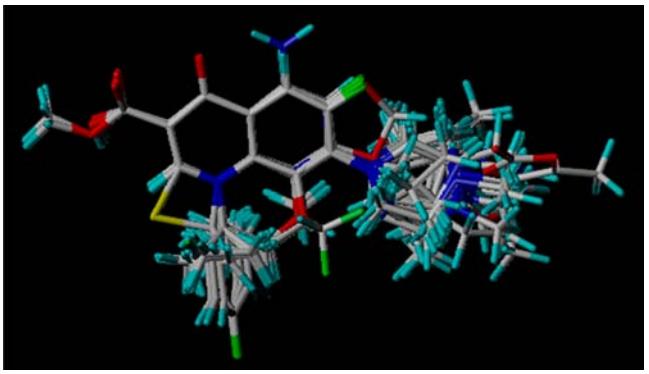

Figure 4. Molecular alignment of all molecules based on the common structure of QNs.

Table 4. Summary of CoMFA Statistical Results for mAb-WR1 and mAb-MS1

	mAb-WR1	mAb-MS1
r^2_{cv} [a]	0.52	0.51
r^2_{ncv} [b]	0.89	0.96
ONC[c]	3	4
SEE[d]	0.46	0.34
F value	28.04	76.74
probability of $r^2 = 0$	<0.001	<0.001
field contribution		
steric	0.73	0.78
electrostatic	0.27	0.22

[a] r^2_{cv} = cross-validated correlation coefficient after the LOO procedure. [b] r^2_{ncv} = correlation coefficient. [c] ONC = optimum number of components. [d] SEE = standard error of the estimate.

coefficient (r^2_{cv}) value of 0.52 with three components. NOR is an outlier in the data set of mAb-MS1 because of its high residual value (1.64). The CoMFA model of mAb-MS1 in the absence of NOR resulted in an ideal r^2_{cv} (0.51). Normally, the r^2_{cv} is used as a criterion for both the robustness and predictive ability of the model. In many cases, a high r^2_{cv} value (usually >0.50) is considered an indicator or the ultimate proof to show that the model is accurate or reliable.[30] The final CoMFA model was generated using non-cross-validated PLS analysis to give a high non-cross-validated correlation coefficient (r^2_{ncv} = 0.89 for mAb-WR1 and 0.96 for mAb-WR1). A model with a correlation coefficient value greater than 80% ($r^2_{ncv} \geq 0.80$), a large *F* value, and a small standard error of the estimate (SEE) has good predictability.[31] The low (usaually <0.05) value of probability of $r^2 = 0$ means that the QSAR models were statistically significant. The field contribution showed that multiple fields (steric and electrostatic fields) co-effected chiral recognition. Correlations between the experimental and predicted pIC_{50} values for those analytes according to CoMFA analyses were reported in Figure S4 of the Supporting Information. The high statistical parameters (adjusted $r^2 = 0.88$ for the mAb-WR1 model and adjusted $r^2 = 0.90$ for the mAb-MS1 model) showed an acceptable statistical correlation and predictability in both the mAb-WR1 and mAb-MS1 models.

The CoMFA contour maps of mAb-WR1 (panels a and b of Figure 5) and mAb-MS1 (panels c and d of Figure 5) in combination with *R*-OFL are shown in Figure 5. The interaction maps were found mainly around the oxazine and piperazinyl rings, indicating that this moiety has great influence on the hapten−antibody recognition. In other words, the epitope of the ofloxacin enantiomers were mainly located in the side of the oxazine ring and the piperazinyl ring, coinciding with the HQSAR results. This epitope would be recognized by immune molecules [such as a major histocompatibility complex (MHC), B cell receptor (BCR), T cell receptor (TCR), antibody, etc.] during an immune response.

In the steric contour map (panels a and c of Figure 5), the green contours refer to sterically favored regions, while the yellow contours indicate sterically disfavored regions. The yellow contours near the chiral center showed that steric hindrance may be the real reason for chiral recognition during immune response (panels a and c of Figure 5). The green contour beside the oxazine ring showed that the conformational structures of this ring also influence the antibody−antigen recognition (Figure 5a). The large green contour near the methyl group of the piperazinyl ring indicated that a steric

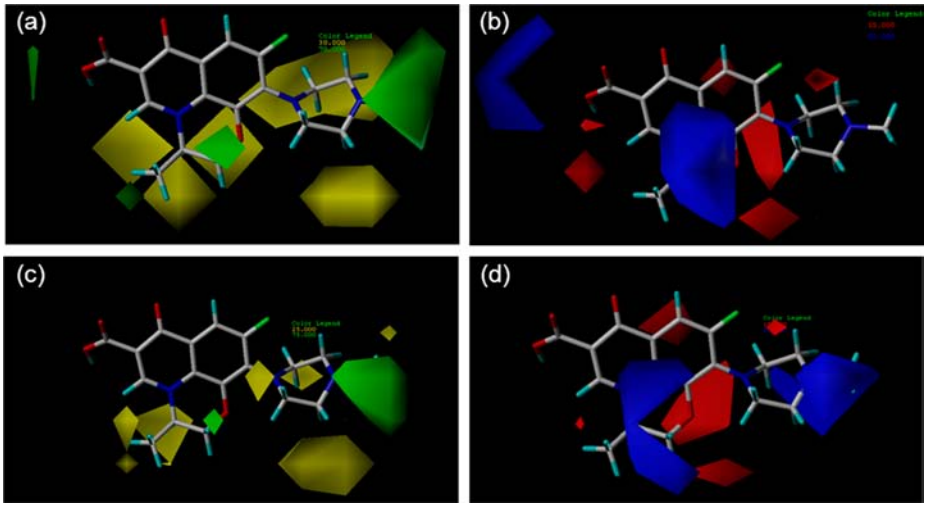

Figure 5. CoMFA contour plots of steric and electrostatic properties in combination with *R*-OFL. (a) Steric contour plot of the mAb-WR1 model. (b) Electrostatic contour plot of the mAb-WR1 model. (c) Steric contour plot of the mAb-MS1 model. (d) Electrostatic contour plot of the mAb-MS1 model. Green and yellow contours refer to sterically favored and disfavored regions, respectively, and blue and red contours refer to regions where positively and negatively charged substituents are favored, respectively.

dx.doi.org/10.1021/jf404449n | *J. Agric. Food Chem.* 2014, 62, 7804−7812

bulky group, such as a methyl group, in this region favors the ofloxacin–antibody interaction (panels a and c of Figure 5). The planar isoindole group of GAR forms a 3D conformation similar to the conformation of methyl piperazine, possibly explaining why GAR has a high CR value. The yellow contours near the piperazinyl ring showed that the steric bulky group on the flank of the piperazinyl ring would not be favorable toward antigen–antibody recognition. GAT has a similar conformational structure with GAR, except for the 2-methylpiperazine structure, but the CR value of GAT is much smaller than that of GAR, possibly owing to the steric hindrance of the *meta*-methyl on the flank of the piperazinyl ring.

In the electrostatic contour map (panels b and d of Figure 5), a positive-charge-favorable region is indicated in a blue color and a negative-charge-favorable region is indicated in a red color. One large blue contour map is observed at the position of stereogenic carbon, showing that positively charged substituents in this position are favored for antibody recognition. The blue contour beside the piperazinyl ring showed that the C–C bonds in piperazine provide a positive electrostatic potential, favoring antibody–antigen interactions. In the model of mAb-WR1, green and blue contours were found near the carboxyl group of *R*-OFL, which indicated that mAb-WR1 may recognize the linker of ofloxacin conjugates.

The HQSAR and CoMFA studies consistently showed that both antibodies recognize ofloxcin isomers from the side of the oxazine and piperazinyl ring moiety, and this moiety is an important part of the epitope. The predicted epitope of the ofloxacin enantiomer can be easily observed by overlay contour maps of CoMFA (Figure 6). From the composition of the predicted epitope, it is clear that the epitope of ofloxacin isomers may be mainly composed of the oxazine ring and the piperazinyl ring. The common structure of QNs also plays a part in the hapten–antibody interaction. Therefore, the enantioselective mAbs recognize not only the chiral center but also the other parts of the molecule. In other words, the enantioselectivity of the antibodies against the ofloxacin optical isomers requires additional recognition sites on hapten. From the analysis above, we conclude that the predicted epitope model can explain the binding character of mAbs.

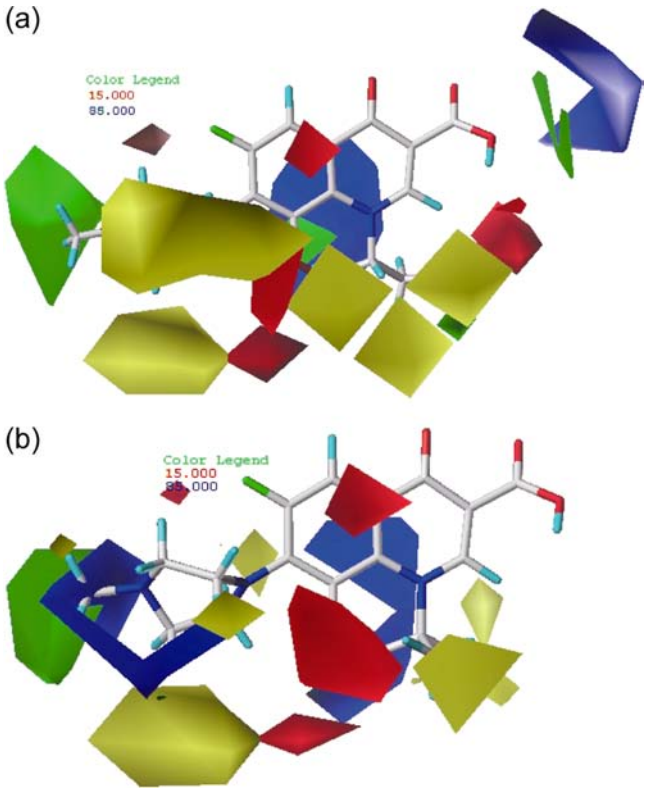

Figure 6. Predicted epitope of ofloxacin enantiomers in immune response (*R*-OFL as a reference molecule): (a) mAb-WR1 and (b) mAb-MS1.

Chiral Conjugate Modeling. Few reports detail the conformational changes of hapten–carrier conjugates during the development of immunoassays for small molecules. Initially, modeling the 3D conformations of the hapten–carrier conjugate was not feasible because of the complex structure of the conjugate. Xu et al.[32] designed three generic haptens containing both the *O*,*O*-diethyl thiophosphate moiety and a benzene ring using three different linkers. The conformational structure and electrostatic potential isosurfaces of the hapten–lysine conjugates were modeled to explain the observed CR of the organophosphorus pesticides to the different monoclonal antibodies. However, the generated model failed to consider the effects of the tertiary structure of the carrier protein. These features might cause interactions between the hapten and the carrier protein.

To investigate the conformational structure of the ofloxacin isomers on the carrier protein, we modeled the 3D structures of ofloxacin isomers conjugating to BSA mimics (see Figure S5 of the Supporting Information). The models showed that the conjugated ofloxacin enantiomers remained upright on the carrier protein surface, and the epitope does not interact with the amino acid residues of the carrier protein (Figure 7). This conformation is advantageous when obtaining the immunogenicity of chiral ofloxacin. The results obtained from the fit atom analysis showed that the conjugated ofloxacin isomers and the corresponding free ofloxacin isomers have identical geometries at their minimum energy level. The RMS distance values for the carbon atoms between the free ofloxacin isomers and the conjugated ofloxacin isomers are only 0.003 19 and 0.000 46 Å, respectively, proving that the geometry of the ofloxacin isomers is not significantly affected by conjugation. Similarly, the electrostatic potential distribution is almost the same in both the free and conjugated molecules.

The way of conjugation may influence the chiral recognition of the antibody. The distance between the stereogenic center and the adjacent amino acid on the carrier protein is only 5.60 Å for *S*-OFL and 5.52 Å for *R*-OFL (Figure 7). The short distance between the stereogenic center and the carrier protein may influence the exposure of the stereogenic center during immune responses, possibly producing antibodies with a relative enantioselectivity. On the basis of the epitope model on the carrier protein, we conclude that two methods may improve the enantioselectivity of the antibodies against the ofloxacin isomers: (i) introducing an appropriate linker, such as ethylenediamine (EDA) or 1,4-diaminobutane, between the hapten and carrier protein may increase the exposure of the stereogenic center, enhancing the enantioselectivity, and (ii) novel immunogens, such as desmethyl levofloxacin (CAS registry number 117707-40-1) and its enantiomer, linked to the carrier protein through the piperazine moiety at the R_3 position would sully the expose of the stereogenic center of ofloxacin. Desmethyl levofloxacin is an analogue of *S*-OFL that has one less methyl group on the piperazine ring compared to *S*-OFL. The novel immunogens may also improve the enantioselectivity

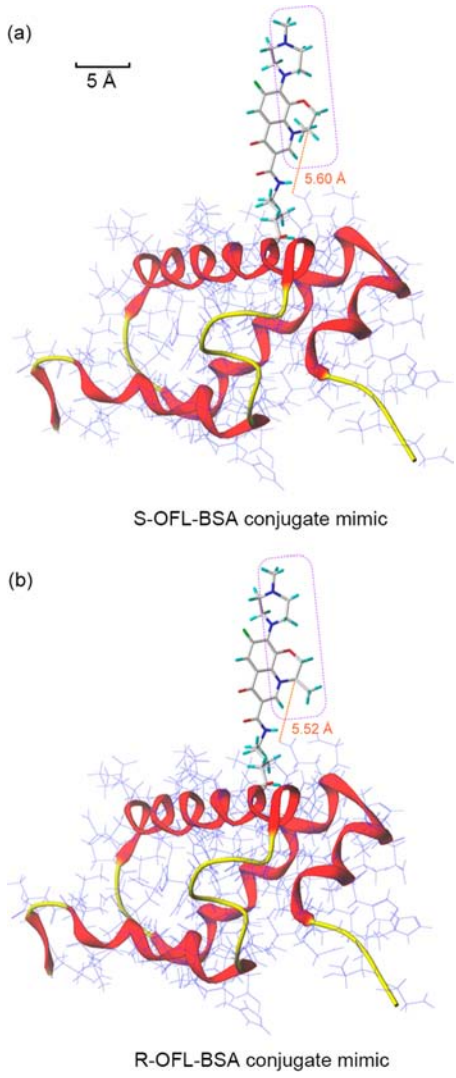

Figure 7. Conformational analysis of ofloxacin isomers coupled with BSA mimics. The elements are presented in the following manner: green, fluorine; red, oxygen; blue, nitrogen; white, carbon; and light blue, hydrogen.

of the antibodies against the ofloxacin isomers. Further studies of those attempts are currently in progress in our laboratory.

Except for the predicted epitope, the other moiety of hapten is also fully exposed on the surface of the carrier protein; this moiety is the common structure of QNs. According to the study above, none of the mAbs would recognize haptens from the side of the common structure. The structure of nalidixic acid (NAL) is almost the same as the common structure of QNs (4-oxo-4,7-dihydroquinoline-3-carboxylic acid nucleus); however, the anti-sera does not recognize this molecule at all. This case also supports the conclusion above. The predicted hapten epitope of ofloxacin isomers would explain why the antibody raised from ofloxacin has high specificity and is not suitable for a generic immunoassay of QNs.

In summary, we synthesized two chiral immunogens based on ofloxacin enantiomers to produce enantioselective mAbs with high sensitivity and specificity. The enantioselectivity of the mAbs is not affected by the heterologous coating format. Molecular modeling methods, such as HQSAR and CoMFA, were performed to determine the epitope of the ofloxacin enantiomers. The different modeling results consistently showed that the epitope of chiral immunogen is primarily composed of oxazine and piperazinyl rings and mAbs recognize the hapten from the side of this moiety. (i) The stereogenic center plays an important role in immune response by generating steric hindrance. (ii) The mAbs may recognize the hapten−carrier linking group during the antigen−antibody interaction. (iii) The common structure of QNs also plays a role in the hapten−antibody interaction. (iv) The unique conformational structures of the oxazine and piperazinyl rings are also essential for the epitope. (v) In addition to the stereogenic center, other auxiliary groups are needed for recognition. The predicted epitope can well explain the enantioselectivity and specificity of the obtained mAbs. Modeling the chiral immunogens showed that conjugated ofloxacin enantiomers remain upright on the carrier protein surface and that the epitope has no interaction with the amino acid residues of the carrier protein. The relative enantioselectivity of mAbs may be due to the short distance between the stereogenic center and carrier proteins. The short distances possibly influence the exposure of the stereogenic center toward immune responses.

Molecular modeling methods, such as HQSAR and CoMFA, provide a simple, efficient, and general way for predicting the epitopes of small organic molecules. Predicting the epitope of hapten would elucidate the physiochemical principles that govern the molecular recognition during the immune response. The epitope prediction method presented in this study should make the redesign of the hapten or its conjugate possible, obtaining antibodies with an improved enantioselectivity, specificity, or other desired characteristics and promoting the development of an immunoassay for determination of small molecules. This study also highlights the power of molecular-modeling-based analyses, providing insights into antibody−hapten recognition and the rational design of a hapten−protein conjugate.

■ ASSOCIATED CONTENT

Supporting Information

Structures of QNs (Figure S1), optimized ELISA conditions (in bold) of two mAbs with three coating antigens using the checkerboard titration method (Table S1), correlation ship between observed and predicted pIC_{50} in the HQSAR model (Figure S2), atomic contribution map for chiral recognition based on HQSAR analysis of mAb-WR1 (Figure S3), correlation ship between observed and predicted pIC_{50} in the CoMFA model (Figure S4), and conformational and electrostatic potential analysis of ofloxacin isomers, which coupled with BSA mimics (Figure S5). This material is available free of charge via the Internet at http://pubs.acs.org.

■ AUTHOR INFORMATION

Corresponding Authors

*Telephone 86-20-85283448. Fax: 86-20-85280270. E-mail: hongtao@scau.edu.cn.

*Telephone: 86-20-85283925. E-mail: ymsun@scau.edu.cn.

Funding

This work was supported by the Guangdong Natural Science Foundation (S2013030013338), the Ph.D. Programs Foundation of the Ministry of Education of China (20114404130002), the Science and Technology Achievements Transformation Projects of Guangdong Higher Education Institutes

(Cgzhzd0808), and the National Spark Program (2011GA780024).

Notes

The authors declare no competing financial interest.

REFERENCES

(1) Raman Suri, C.; Boro, R.; Nangia, Y.; Gandhi, S.; Sharma, P.; Wangoo, N.; Rajesh, K.; Shekhawat, G. Immunoanalytical techniques for analyzing pesticides in the environment. *TrAC, Trends Anal. Chem.* **2009**, *28*, 29−39.

(2) Spinks, C. A. Broad-specificity immunoassay of low molecular weight food contaminants: New paths to Utopia! *Trends Food Sci. Technol.* **2000**, *11*, 210−217.

(3) Toldrá, F.; Reig, M. Methods for rapid detection of chemical and veterinary drug residues in animal foods. *Trends Food Sci. Technol.* **2006**, *17*, 482−489.

(4) Song, J.; Wang, R. M.; Wang, Y. Q.; Tang, Y. R.; Deng, A. P. Hapten design, modification and preparation of artificial antigens. *Chin. J. Anal. Chem.* **2010**, *38*, 1211−1218.

(5) Hofstetter, O.; Hofstetter, H.; Schurig, V.; Wilchek, M.; Green, B. S. Antibodies can recognize the chiral center of free α-amino acids. *J. Am. Chem. Soc.* **1998**, *120*, 3251−3252.

(6) Wang, Q.; Haughey, S. A.; Sun, Y. M.; Eremin, S. A.; Li, Z. F.; Liu, H.; Xu, Z. L.; Shen, Y. D.; Lei, H. T. Development of a fluorescence polarization immunoassay for the detection of melamine in milk and milk powder. *Anal. Bioanal. Chem.* **2011**, *399*, 2275−2284.

(7) Wang, Z.; Zhu, Y.; Ding, S.; He, F.; Beier, R. C.; Li, J.; Jiang, H.; Feng, C.; Wan, Y.; Zhang, S. Development of a monoclonal antibody-based broad-specificity ELISA for fluoroquinolone antibiotics in foods and molecular modeling studies of cross-reactive compounds. *Anal. Chem.* **2007**, *79*, 4471−4483.

(8) Xu, Z. L.; Dong, J. X.; Wang, H.; Li, Z. F.; Beier, R. C.; Jiang, Y. M.; Lei, H. T.; Shen, Y. D.; Yang, J. Y.; Sun, Y. M. Production and characterization of a single-chain variable fragment linked alkaline phosphatase fusion protein for detection of *O*,*O*-diethyl organophosphorus pesticides in a one-step enzyme-linked immunosorbent assay. *J. Agric. Food. Chem.* **2012**, *60*, 5076−5083.

(9) Xu, Z. L.; Shen, Y. D.; Zheng, W. X.; Beier, R. C.; Xie, G. M.; Dong, J. X.; Yang, J. Y.; Wang, H.; Lei, H. T.; She, Z. G. Broad-specificity immunoassay for *O*,*O*-diethyl organophosphorus pesticides: Application of molecular modeling to improve assay sensitivity and study antibody recognition. *Anal. Chem.* **2010**, *82*, 9314−9321.

(10) Yuan, M.; Na, Y.; Li, L.; Liu, B.; Sheng, W.; Lu, X.; Kennedy, I.; Crossan, A.; Wang, S. Computer-aided molecular modeling study on antibody recognition of small molecules: An immunoassay for triazine herbicides. *J. Agric. Food. Chem.* **2012**, *60*, 10486−10493.

(11) Bader, A. N.; Grubor, N. M.; Ariese, F.; Gooijer, C.; Jankowiak, R.; Small, G. J. Probing the interaction of benzo[*a*]pyrene adducts and metabolites with monoclonal antibodies using fluorescence line-narrowing spectroscopy. *Anal. Chem.* **2004**, *76*, 761−766.

(12) Omelyanenko, V. G.; Jiskoot, W.; Herron, J. N. Role of electrostatic interactions in the binding of fluorescein by anti-fluorescein antibody 4-4-20. *Biochemistry* **1993**, *32*, 10423−10429.

(13) Ramakrishnan, M.; De Melo, F. A.; Kinsey, B. M.; Ladbury, J. E.; Kosten, T. R.; Orson, F. M. Probing cocaine−antibody interactions in buffer and human serum. *PloS One* **2012**, *7*, No. e40518.

(14) Van Oss, C. Hydrophobic, hydrophilic and other interactions in epitope−paratope binding. *Mol. Immunol.* **1995**, *32*, 199−211.

(15) Wang, Z.; Luo, P.; Cheng, L.; Zhang, S.; Shen, J. Hapten−antibody recognition studies in competitive immunoassay of α-zearalanol analogs by computational chemistry and Pearson Correlation analysis. *J. Mol. Recognit.* **2011**, *24*, 815−823.

(16) Delaunay-Bertoncini, N.; Pichon, V.; Hennion, M. C. Experimental comparison of three monoclonal antibodies for the class-selective immunoextraction of triazines: Correlation with molecular modeling and principal component analysis studies. *J. Chromatogr. A* **2003**, *999*, 3−15.

(17) Holtzapple, C. K.; Carlin, R. J.; Rose, B. G.; Kubena, L. F.; Stanker, L. H. Characterization of monoclonal antibodies to aflatoxin M1 and molecular modeling studies of related aflatoxins. *Mol. Immunol.* **1996**, *33*, 939−946.

(18) Benjamin, D. C.; Berzofsky, J. A.; East, I. J.; Gurd, F. R.; Hannum, C.; Leach, S. J.; Margoliash, E.; Michael, J. G.; Miller, A.; Prager, E. M. The antigenic structure of proteins: A reappraisal. *Annu. Rev. Immunol.* **1984**, *2*, 67−101.

(19) Engen, J. R.; Smith, D. L. Peer reviewed: Investigating protein structure and dynamics by hydrogen exchange MS. *Anal. Chem.* **2001**, *73*, 256 A−265A.

(20) Geysen, H. M.; Meloen, R. H.; Barteling, S. J. Use of peptide synthesis to probe viral antigens for epitopes to a resolution of a single amino acid. *Proc. Natl. Acad. Sci. U. S. A.* **1984**, *81*, 3998−4002.

(21) Jemmerson, R.; Paterson, Y. Mapping epitopes on a protein antigen by the proteolysis of antigen−antibody complexes. *Science* **1986**, *232*, 1001−1004.

(22) Suckau, D.; Köhl, J.; Karwath, G.; Schneider, K.; Casaretto, M.; Bitter-Suermann, D.; Przybylski, M. Molecular epitope identification by limited proteolysis of an immobilized antigen−antibody complex and mass spectrometric peptide mapping. *Proc. Natl. Acad. Sci. U. S. A.* **1990**, *87*, 9848−9852.

(23) Amit, A.; Mariuzza, R.; Phillips, S.; Poljak, R. Three-dimensional structure of an antigen−antibody complex at 2.8 Å resolution. *Science* **1986**, *233*, 747−753.

(24) Norrby, S. Side-effects of quinolones: Comparisons between quinolones and other antibiotics. *Eur. J. Clin. Microbiol. Infect. Dis.* **1991**, *10*, 378−383.

(25) Staros, J. V.; Wright, R. W.; Swingle, D. M. Enhancement by *N*-hydroxysulfosuccinimide of water-soluble carbodiimide-mediated coupling reactions. *Anal. Biochem.* **1986**, *156*, 220−222.

(26) Perosa, F.; Carbone, R.; Ferrone, S.; Dammacco, F. Purification of human immunoglobulins by sequential precipitation with caprylic acid and ammonium sulphate. *J. Immunol. Methods* **1990**, *128*, 9−16.

(27) Hennion, M. C.; Barcelo, D. Strengths and limitations of immunoassays for effective and efficient use for pesticide analysis in water samples: A review. *Anal. Chim. Acta* **1998**, *362*, 3−34.

(28) Gasteiger, J.; Marsili, M. Iterative partial equalization of orbital electronegativity—A rapid access to atomic charges. *Tetrahedron* **1980**, *36*, 3219−3228.

(29) Lowis, D. R. HQSAR: A new, highly predictive QSAR technique. *Tripos Tech. Notes* **1997**, *1*, 1−10.

(30) Alexander, G.; Alexander, T. Beware of q2! *J. Mol. Graphics Modell.* **2002**, *20*, 269−276.

(31) Xu, Z. L.; Xie, G. M.; Li, Y. X.; Wang, B. F.; Beier, R. C.; Lei, H. T.; Wang, H.; Shen, Y. D.; Sun, Y. M. Production and characterization of a broad-specificity polyclonal antibody for *O*,*O*-diethyl organophosphorus pesticides and a quantitative structure−activity relationship study of antibody recognition. *Anal. Chim. Acta* **2009**, *647*, 90−96.

(32) Xu, Z. L.; Wang, H.; Shen, Y. D.; Nichkova, M.; Lei, H. T.; Beier, R. C.; Zheng, W. X.; Yang, J. Y.; She, Z. G.; Sun, Y. M. Conformational changes of hapten−protein conjugates resulting in improved broad-specificity and sensitivity of an ELISA for organophosphorus pesticides. *Analyst* **2011**, *136*, 2512−2520.

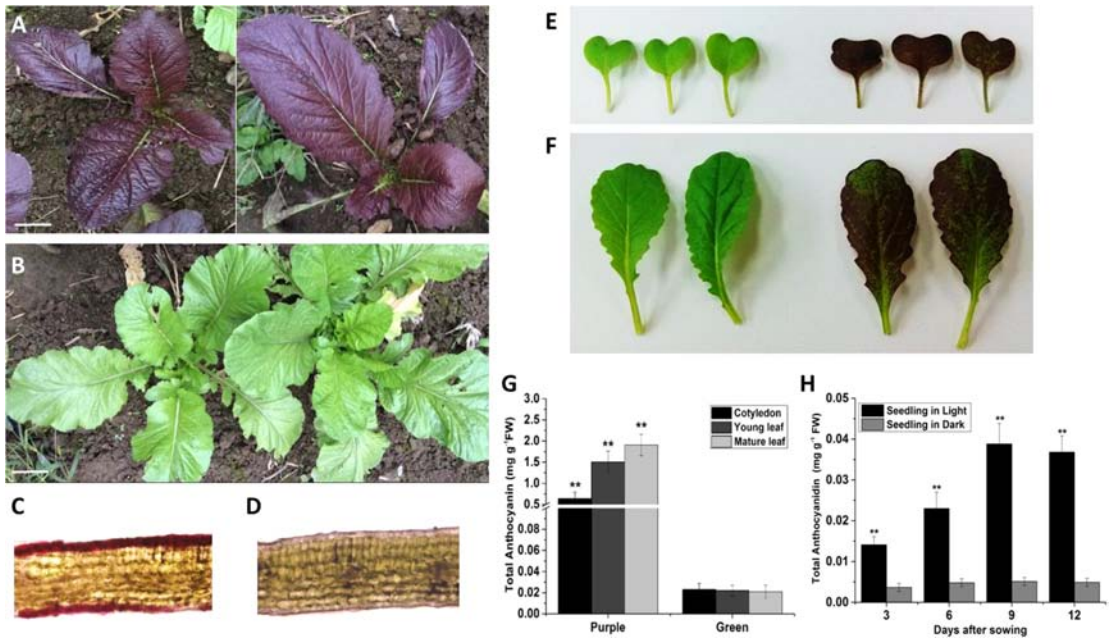

Figure 1. Phenotype of purple cultivar "Zi Ying" and green cultivar "Lv Ying" and total anthocyanin content. (A) Phenotype of purple tumorous stem mustard, at 4 months of growth. (B) Phenotype of green tumorous stem mustard, at 4 months of growth. (C and D) Free-hand section of leaf samples of panels A and B examined under a light microscope, respectively. (E and F) Phenotype of cotyledons (14 days) and young leaves (45 days) of purple cultivar "Zi Ying" and green cultivar "Lv Ying", respectively. (G) Total anthocyanin content of cotyledons (14 days), young leaves (45 days), and mature leaves (120 days) of purple cultivar "Zi Ying" and green cultivar "Lv Ying". (H) Total anthocyanin content of seedlings (3, 6, 9, and 12 DAS) of purple cultivar. The data represent the mean from three replicates with three biological repeats. (**) $p < 0.01$ between the wild type and others by the *t* test. Error bars indicate standard error (SE).

biosynthetic genes, leading to the anthocyanin accumulation in purple cauliflower and red cabbage.[19,20] In *Arabidopsis*, anthocyanin accumulation in vegetative tissues has been shown to be mediated by four MYB proteins, production of anthocyanin pigment 1 (PAP1), PAP2, MYB113, and MYB114, as well as bHLH protein, transparent testa 8 (TT8).[21−23] Furthermore, MYB transcription factors are central players in the coordinated activation of sets of genes specific for the anthocyanin and tannin pathways.[24] R2R3-MYB and bHLH transcription factors regulate anthocyanin biosynthesis in gentian flowers.[25] In *Petunia*, R2R3-MYB transcription factors are developmentally and environmentally regulated to control complex floral and vegetative pigmentation patterning.[26] *Rc* encodes a bHLH protein conditioning red pericarp in rice.[27] Although the MYB transcription factors require a bHLH in regulating anthocyanin biosynthesis in *Arabidopsis*,[28] MYB proteins can act directly in activating transcription in maize.[29]

The anthocyanin biosynthetic pathway is also regulated by environmental factors, such as light and temperature, as well as internal factors, such as plant hormones, other secondary metabolites, and nutrients.[30] Light acts as an essential stimulus and also modulates the intensity of the pigment by affecting the regulatory and structural genes involved in anthocyanin biosynthesis.[31] Research in eggplant showed that anthocyanin synthesis was induced in the hypocotyl tissues when the seedlings were grown under purple light with an ultraviolet (UV) light supplement.[32] The apple gene *MdMYB1* was shown to regulate anthocyanin biosynthesis in response to sunlight.[33] In *Arabidopsis*, a genome-wide analysis suggests that *PAP1* and *PAP2* play a major role in the induction of the anthocyanin biosynthesis transcriptional cluster by high light stress.[34] Recently, Cevallos-Casals and Cisneros-Zevallos observed that the duration and amount of light applied during sprouting strongly affected the mechanisms of flavonoid and anthocyanin biosynthesis.[35]

Along with economic development, demand by people for high-quality vegetables is increasing. In addition to common leaf color vegetables, especially those vegetables with novel leaf or flower color have broad prospects for development and use. Tumorous stem mustard (*Brassica juncea* var. *tumida* Tsen et Lee), a native cruciferous vegetable crop in Asia countries, is a very important fresh and processed vegetable in winter and spring. In the domestication history of mustard, lots of morphological and physiological changes have been preserved on the basis of human selection. The purple tumorous stem mustard (*B. juncea* var. *tumida* Tsen et Lee) is a mutation of the *B. juncea* (Cruciferae) crop containing an inflated tumorous stem and abundant anthocyanin accumulation in leaves. The swollen succulent stems are used as raw material for pickled products, which are very popular for their special flavor and nutritional value.[36] In addition, because of abundant anthocyanins in its leaves, purple tumorous stem mustard can be also used in many important fields, such as the health protection, pharmaceutical, and cosmetic industries. Although radishes and other root crops containing anthocyanins are used as plants for natural pigment extraction, it will take a long time to collect the fully mature organs with anthocyanins, which is limited by the plant developmental stages. However, leaves of purple tumorous stem mustard remain bright fuchsia in the whole life of plants. Therefore, purple tumorous stem mustard can be used as a better resource for natural pigment. In summary, purple tumorous stem mustard attracts more and more attention because of its wide applications in food, pharmaceutical, and cosmetic industries. In recent years, most studies about purple tumorous stem mustard are focused on the cultivations. The molecular regulatory mechanism of antho-

cyanin biosynthesis and the anthocyanin composition and content in purple tumorous stem mustard remain unclear.

In this study, the anthocyanin content and composition of the mature leaf of purple tumorous stem mustard were detected. To investigate the mechanism of the anthocyanin biosynthesis in the purple tumorous stem mustard, the expression of structural and regulatory genes were detected in two genotype cultivars, purple cultivar "Zi Ying" and green cultivar "Lv Ying". The effect of light on anthocyanin accumulation of "Zi Ying" was also investigated.

MATERIALS AND METHODS

Plant Materials and Growth Conditions. To analyze the influence of genotype on anthocyanin productions, two cultivars of tumorous stem mustard, "Zi Ying" and "Lv Ying", were selected in this study based on different phenotype appearances. The seeds were sowed on September 1, 2012, transplanted into plastic pots after 20 days, colonized on October 10, 2012, and managed routinely. For light and dark treatment, the seeds were surface-sterilized using 70% (v/v) ethanol for 1 min, rinsed 3 times with sterile water, then washed in 1% sodium hypochlorite solution for 12−15 min, and rinsed 8 times with sterile water. The sterilized seeds were divided into two sets germinated on 1/2MS medium in a growth chamber under light (16 h of light/8 h of dark) or dark (24 h of dark) conditions at 25 °C, 60% humidity, and 440 μmol m^{-2} s^{-1} light intensity. For biological replicates, we used three plastic boxes for each single treatment, placed 80 seeds per box, and harvested sprouts in each plastic box at 3, 6, 9, and 12 days after sowing (DAS).

Microscopic Analysis of Anthocyanin Distribution in Tumorous Stem Mustard. Young fresh leaves of the "Zi Ying" cultivar underwent microscopic observation and analysis [Figure 1C with an optical microscope (Leica-DMI4000B)]. Observations were repeated three times for each sample.

RNA Extraction and Quantitative Real-Time Reverse Transcription Polymerase Chain Reaction (qRT-PCR) Analysis. When the color of "Zi Ying" leaf turned to brilliant purple, the mature leaves of both "Zi Ying" and "Lv Ying" cultivars were collected for the treatments and sprouts in each box at 3, 6, 9, and 12 days after sowing were harvested for RNA isolation. Total RNA was extracted from samples for three biological repeat using RNAiso Plus (TaKaRa). Then, 1−2 μg of total RNA was used to synthesis the complementary DNA (cDNA) through reverse transcriptase (M-MuLV RT) (Promega) with Oligo-dT18 primer. The synthesized cDNAs were diluted 1 times with RNase/DNase-free water. qRT-PCR analysis was carried out using the CFX96 real-time system (C1000 Thermal Cycler, Bio-Rad). All reactions were performed using the SYBR Premix Go *Taq* II kit (Promega, China) in a 10 μL total sample volume (5.0 μL of 2× SYBR Premix Go *Taq* II, 0.5 μL of primers, 1.0 μL of cDNA, and 3.5 μL of ddH_2O). To remove the effect of genomic DNA and the template from the environment, no template control (NTC) and no reverse transcription control (NRT) were performed. Three replications for each sample were used, and standard curves were run simultaneously. Melting curve analysis of qRT-PCR samples revealed that there was only one product for each gene primer reaction. The PCR products were sequenced to confirm the specific amplification. A house-keeping gene *BjEF-1-α*[37] was used as an internal standard in tissues. Expression of genes from the green cultivar were set to 1. PCR primers are shown in Table 1S of the Supporting Information.

Chemicals. The anthocyanin cyanidin-3-glucoside chloride for external standards was purchased from Phytolab (Germany). High-performance liquid chromatography (HPLC)-grade methanol (MeOH) and formic acid were bought from Sigma. HPLC-grade water was prepared from distilled water using a Milli-Q system (Millipore Laboratory, Bedford, MA). All of the other solvents were provided from Aldrich (St. Louis, MO).

Anthocyanin Extraction and High-Performance Liquid Chromatography−Electrospray Ionization−Tandem Mass Spectrometry (HPLC−ESI−MS/MS) Analysis. Anthocyanins were extracted and separated by HPLC following the improved procedure described by Wu and Prior.[38] Samples (100 mg) were extracted in 1 mL of methanol/H_2O/acetic acid (85:15:0.5) for 10 min at room temperature and centrifuged at 12000*g* for 10 min. The supernatants were collected and filtered through a 0.2 μm polytetrafluoroethylene (PTFE) syringe filter to remove cell debris. The samples were then analyzed by Waters 2795 HPLC (Waters, Milford, MA), equipped with a variable wavelength detector. The results were analyzed by Waters 2795 HPLC ChemStation software. The chromatographic separation was performed on a Zorbax Stablebond Analytical SB-C18 column (4.6 × 150 mm, 5 μm, Waters). The injection volume was 10 μL. Elution was performed using mobile phase A (aqueous 2% formic acid solution) and mobile phase B (methanol). The detection was at 520 nm, and the column oven temperature was set at 40 °C. The flow rate was 1 mL/min. The gradient program is described as follows: 0−2 min, 10−20% B; 2−40 min, 20−55% B; 40−45 min, 55−60% B; 45−60 min, 90% B; and 60−65 min, 10% B. Quantification of the different anthocyanins was based on peak areas and calculated as equivalents of the external standards. All contents were expressed as milligrams per gram of dry weight. Low-resolution electrospray mass spectrometry was performed with a solariX ion trap mass spectrometer (Bruker Daltoniks, Billerica, MA). The experimental conditions were as follows: ESI interface, nebulizer, 50 psi; dry gas, 15.0 psi, dry temperature, 320 °C; MS/MS, scan from m/z 200 to 2000; ion trap, scan from m/z 200 to 2000; source accumulation, 50 ms; ion accumulation time, 300 ms; flight time to acquire cell, 1 ms; smart parameter setting (SPS), compound stability, 50%; and trap drive level, 60%.

Total Anthocyanin Analysis. The total anthocyanin content in samples was measured with a pH-differential spectrum method.[39] The mature leaves or seedlings (100 mg) were frozen in liquid nitrogen and immediately crushed into powder. Samples were treated separately with 2 mL of pH 1 buffer solution (50 mM KCl and 150 mM HCl) and 2 mL of pH 4.5 buffer solution (400 mM sodium acetate and 240 mM HCl). The mixtures were centrifuged at 12000*g* for 20 min at 4 °C. Then, absorbance of the solutions was measured at 520 nm using diluted supernatants. The anthocyanin content was calculated according to the equation: amount [mg g^{-1} of fresh weight (FW)] = $(A_1 - A_2) \times 484.8/24\,825 \times$ dilution factor, where A_1 represents the absorbance of supernatants gathered from pH 1.0 buffer solution at 520 nm, A_2 represents the absorbance of supernatants gathered from pH 4.5 buffer solution at 520 nm, 484.8 represents the molecular mass of cyanidin-3-glucoside chloride, and 24 825 is its molar absorptivity at 520 nm. Each sample was analyzed in triplicate, and the results were expressed as the average of the three measurements.

Statistical Analysis. Data were analyzed by Origin 8.6 (OriginLab) software, using the *t* test to assess significant differences among the means.

RESULTS AND DISCUSSION

Influence of Genotype on Anthocyanin Concentrations. Two cultivars, "Zi Ying" and "Lv Ying", were investigated to study the influence of genotype on anthocyanin biosynthesis. During the seedling stage, cotyledons of the "Zi Ying" cultivar began to show a punctate purple and the purple area gradually increased with plant growing. When four true leaves were present, 80−90% area of the leaves showed purple. Later all leaves turned purple gradually. Under the same growth conditions, the leaves of "Lv Ying" cultivar remain green in the whole growth process, no purple was seen (panels A and B of Figure 1). The anthocyanin content in "Zi Ying" and "Lv Ying" was measured with a pH-differential spectrum method. At the seedling stage, the anthocyanin content of cotyledon of "Zi Ying" was up to 0.61 mg g^{-1} of FW. Higher amounts of anthocyanins were detected in young leaves of "Zi Ying" (1.52 mg g^{-1} of FW). The highest level of anthocyanin accumulation (1.929 mg g^{-1} of FW) was found in mature leaves of "Zi Ying"

Table 1. Anthocyanin Levels (mg g^{-1} of Dry Weight) in the Two Cultivars (Purple and Green) (n = 3)

peak number[a]	anthocyanin	cultivar	
		purple	green
1	cyanidin 3-feruloylsophoroside-5-glucoside[b]	0.042 ± 0.000	nd[c]
2	cyanidin 3-caffeoylsinapoylsophoroside-5-glucoside[b]	0.01 ± 0.001	nd
3	cyanidin 3-hydroxyferuloylcaffeoylsophoroside-5-malonylglucoside	0.070 ± 0.001	nd
4	cyanidin 3-feruloylsophoroside-5-malonylglucoside	0.286 ± 0.002	nd
5	cyanidin 3-caffeoylsophoroside-5-malonylglucoside	0.063 ± 0.002	nd
6	cyanidin 3-feruloylsophoroside-5-malonylglucoside	0.090 ± 0.001	nd
7	cyanidin 3-*p*-coumaroylsophoroside-5-glucoside[b]	0.031 ± 0.001	nd
8	cyanidin 3-caffeoylferuloylsophoroside-5-gIucoside[b]	0.006 ± 0.001	nd
9	cyanidin 3-caffeoylsinapoylsophoroside-5-malonylglucoside	0.032 ± 0.002	nd
10	cyanidin 3-diferuloylsophoroside-5-glucoside[b]	0.236 ± 0.002	nd
11	cyanidin 3-*p*-coumaroylsophoroside-5-malonylglucoside	0.308 ± 0.003	nd
12	cyanidin 3-feruloylcaffeoylsophoroside-5-malonylglucoside	0.270 ± 0.001	nd
13	cyanidin 3-*p*-coumaroylferuloylsophoroside-5-glucoside[b]	0.037 ± 0.002	nd
14	cyanidin 3-feruloylsinapoylsophoroside-5-malonyldiglucoside	0.076 ± 0.001	nd
15	cyanidin 3-*p*-coumaroylsinapoylsophoroside-5-malonyldiglucoside	0.127 ± 0.001	nd
16	cyanidin 3-feruloylsinapoylsophoroside-5-malonylglucoside[b]	0.858 ± 0.001	nd
17	cyanidin 3-*p*-coumaroylferuloylsophoroside-5-malonyldiglucosid	0.214 ± 0.001	nd
18	cyanidin 3-diferuloylsophoroside-5-malonylglucoside	0.694 ± 0.001	nd
19	cyanidin 3-*p*-coumaroyltriglucoside-5-malonylglucoside	0.398 ± 0.002	nd
20	cyanidin 3-di-*p*-coumaroylsophoroside-5-malonylglucoside	0.068 ± 0.001	nd
total		3.916 ± 0.025	nd

[a]Peak number corresponds to elution order by HPLC analysis in Figure S1 of the Supporting Information. [b]Known *Brassica* anthocyanins (most were identified with the reference anthocyanin in the database). [c]nd = not detected.

(panels E−G of Figure 1), a level comparable to that found in blueberries.[40] On the contrary, low amounts of anthocyanins were detected at various stages in the "Lv Ying" grown under the same conditions, which is consistent with their phenotype. Microscopic examination of sections of young leaf tissues revealed that the purple pigments accumulated in both upper and lower epidermal layers in "Zi Ying" samples, while no pigments were present in the "Lv Ying" samples (panels C and D of Figure 1).

Qualitative and Quantitative Analyses of Anthocyanins in Purple Tumorous Stem Mustard. To examine the composition and relative content of anthocyanins in "Zi Ying", the anthocyanins were extracted and analyzed by HPLC−ESI−MS/MS. The elution profile of purple cultivar is shown in Figure 1S of the Supporting Information. There were 20 major peaks detected in the extracts of "Zi Ying". The individual peaks were putatively identified through comparison of the retention time and spectrum character to the published data[38,41−43] and listed in Table 1S of the Supporting Information. The content of each individual anthocyanin in "Zi Ying" was calculated and shown in Table 1. All of these anthocyanins were cyanidin 3-diglucoside-5-glucoside and derivatives with different acylated groups bound to diglucoside (Table 1 and see Figure 1S of the Supporting Information). The anthocyanins showing the highest levels were cyanidin 3-feruloylsinapoylsophoroside-5-malonylglucoside (m/z 1241) and cyanidin 3-diferuloylsophoroside-5-malonylglucoside (m/z 1211) of 0.858 and 0.694 mg g^{-1} of dry weight, respectively. It was reported that 67 anthocyanins were identified from red mustard greens (*B. juncea* Coss variety) using an ultrahigh-performance liquid chromatography−photodiode array−electrospray ionization−high-resolution tandem mass spectrometry operated in the MS^n mode (UHPLC−PDA−ESI−HRMS/MS^n) profiling method,[43] and cyanidin 3-feruloylsinapoylsophoroside-5-malonyldiglucoside (m/z 1403) and cyanidin 3-*p*-coumaroylsinapoylsophoroside-5-malonyldiglucoside (m/z 1373) were found as the major anthocyanins in red mustard greens. Different numbers and types of anthocyanins identified in purple tumorous stem mustard are different from those in red mustard greens, which might be owing to the different varieties and methods.

Analysis of Sprouts Grown under Light and Dark Conditions. In our study, we find that the color of the upper epidermis is deeper than the lower epidermis, which may be attributed to the different light intensities in the upper and lower surfaces of the "Zi Ying" leaves (Figure 1C). Previous studies on apple and pear showed that anthocyanin biosynthesis was light-induced and restricted in fruit skin.[33,44] Therefore, the experiment of light and dark treatments of "Zi Ying" seedlings was performed. Cotyledons grown under light conditions were purple, whereas cotyledons grown under dark conditions were yellow. The anthocyanin contents in seedlings of "Zi Ying" grown under light conditions were all significantly higher than the anthocyanin contents in seedlings of "Zi Ying" grown under dark conditions from 3 to 12 DAS (Figure 1H). These results are consistent with those findings in radish and buckwheat sprouts,[31,45] which indicates that the light is essential for anthocyanin synthesis in the "Zi Ying" cultivar.

Expression of Anthocyanin Biosynthetic Genes. To determine the relationship between anthocyanin accumulation and the expression of anthocyanin biosynthetic genes, the transcripts of anthocyanin structural genes were examined in the mature leaves between the purple cultivar "Zi Ying" and the green cultivar "Lv Ying".

The expressions of phenylpropanoid pathway genes *PAL* and *C4H* and anthocyanin biosynthetic genes *CHS*, *CHI*, *F3H*, *F3′H*, *DFR*, *ANS*, and *UFGT* are shown in Figure 2. All structural genes in "Zi Ying" were dramatically upregulated in comparison to those in "Lv Ying". Early structural gene *CHS* was upregulated about 149-fold, while transcript levels of late structural genes *F3H*, *F3′H*, *DFR*, and *ANS* in the purple

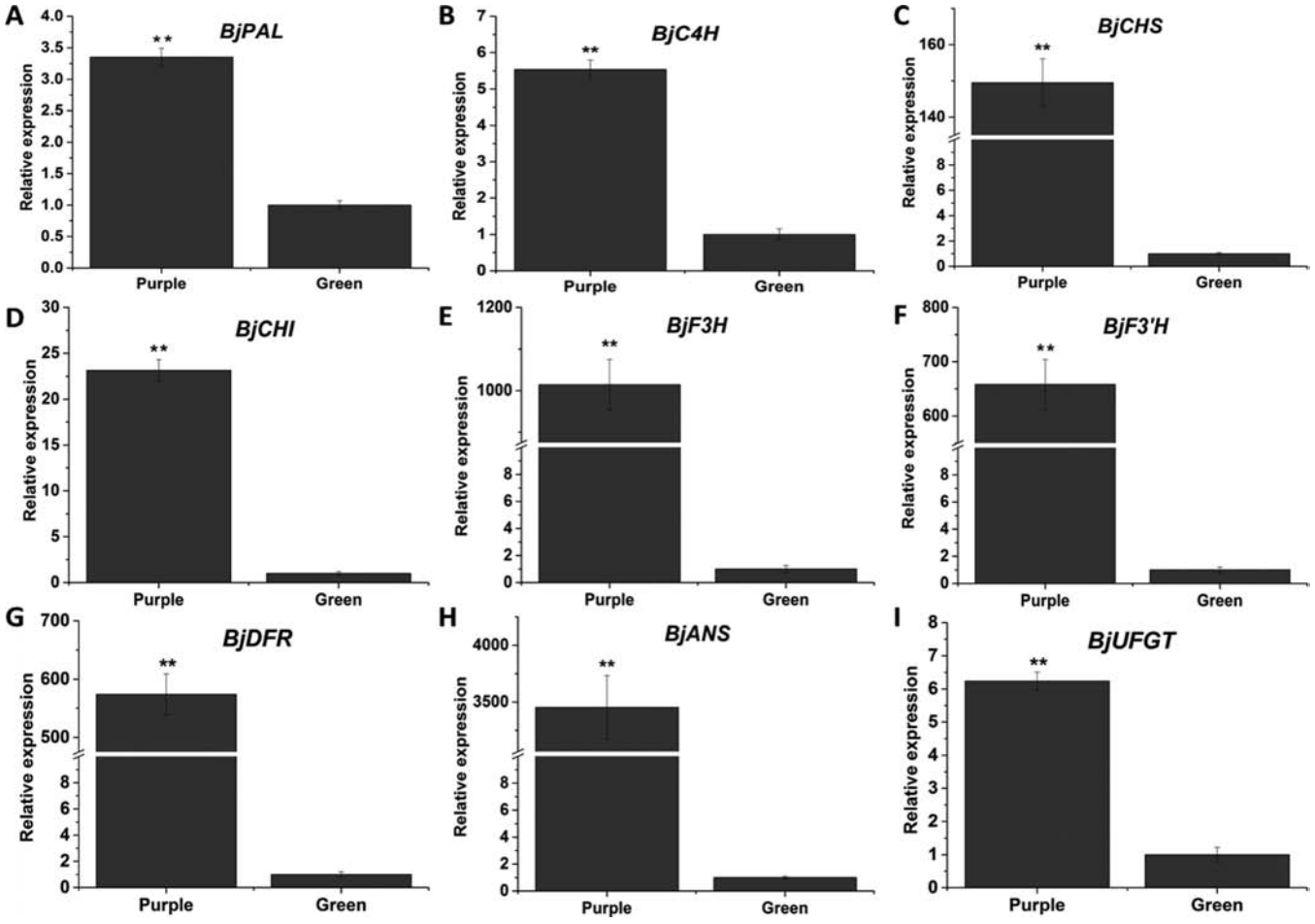

Figure 2. Expression analysis of anthocyanin synthesis genes under normal growth conditions. Expression analysis of (A) *BjPAL*, (B) *BjC4H*, (C) *BjCHS*, (D) *BjCHI*, (E) *BjF3H*, (F) *BjF3′H*, (G) *BjDFR*, (H) *BjANS*, and (I) *BjUFGT* in mature leaves of purple cultivar "Zi Ying" and green cultivar "Lv Ying", respectively. The data represent the mean from three replicates with three biological repeats. (**) $p < 0.01$ between the wild type and others by the *t* test. Error bars indicate SE. Relative expression was normalized using the housekeeping gene *BjEF1* (GO479260). The expression level of genes in the green cultivar were set to 1.

cultivar were approximately 1020-, 660-, 572-, and 3450-fold higher than those in the green cultivar, respectively. In addition, the expression levels of *PAL*, *C4H*, *CHI*, and *UFGT* in "Zi Ying" were about 3.3-, 5.5-, 22.6-, and 6.2-fold higher than those in the green cultivar, respectively. Despite the absence of visual anthocyanin pigmentation in green cultivars, low expression levels of all of these structural genes were observed (Figure 2), which was consistent with the previous reports in other plant species.[46,47] These results illustrate that the high expression levels of biosynthetic genes are strongly associated with the high intensity of anthocyanin pigments in purple tumorous stem mustard.

A number of plants that show constitutive accumulation of high levels of anthocyanins have been studied. In purple-fleshed apple, the transcript levels of anthocyanin biosynthetic genes were significantly higher throughout fruit development than those found in white-fleshed apple.[48] Similarly, examination of seven sweet potato cultivars revealed that the high anthocyanin accumulation in purple sweet potato also showed high-level expression of the structural genes.[49] In *pap1*-D *Arabidopsis*, the increased anthocyanin production throughout the plant was associated with upregulation of the entire biosynthetic pathway genes.[19,23] It appears that purple tumorous stem mustard shares very similar upregulation of structural genes in mediating anthocyanin accumulation to those high anthocyanin accumulating plants.

Furthermore, previous studies have reported that *RsCHS*, *RsCHI*, and *RsDFR* mRNAs were not expressed in the dark, but their expression was induced in seedlings exposed to light up to day 6.[50] *FtPAL*, *Ft4CL*, *FtF3H*, *FtDFR*, and *FtANS* show higher transcript levels in both seeds and sprouts from 2 to 10 DAS, and most genes in the flavonoid biosynthetic pathway are upregulated at 2 DAS under light/dark or dark culture.[45] In our light-treated seedlings, except the upstream pathway gene *BjPAL*, the transcript levels of structural genes were all higher in light-treated sprouts than those in the dark (Figure 4). The transcript levels of all of these genes were highest at nearly 3 and 6 DAS, except *BjC4H*, which had no change in light conditions from 3 to 12 DAS. It is noteworthy that, in light-treated sprouts, the transcript levels of *BjF3′H* and *BjANS* were about 1200- and 120-fold higher than those in the dark treated at 6 DAS, respectively. At 3 DAS, the transcript levels of *BjF3H* of light-treated sprouts were about 60-fold higher than those in the dark. In addition, except *BjPAL*, all other genes are hardly detected in the dark-treated seedlings. Moreover, anthocyanin contents in light-treated seedlings of "Zi Ying" were all significantly higher than those in dark-treated seedlings from 3 to 12 DAS (Figure 1H). These results are completely

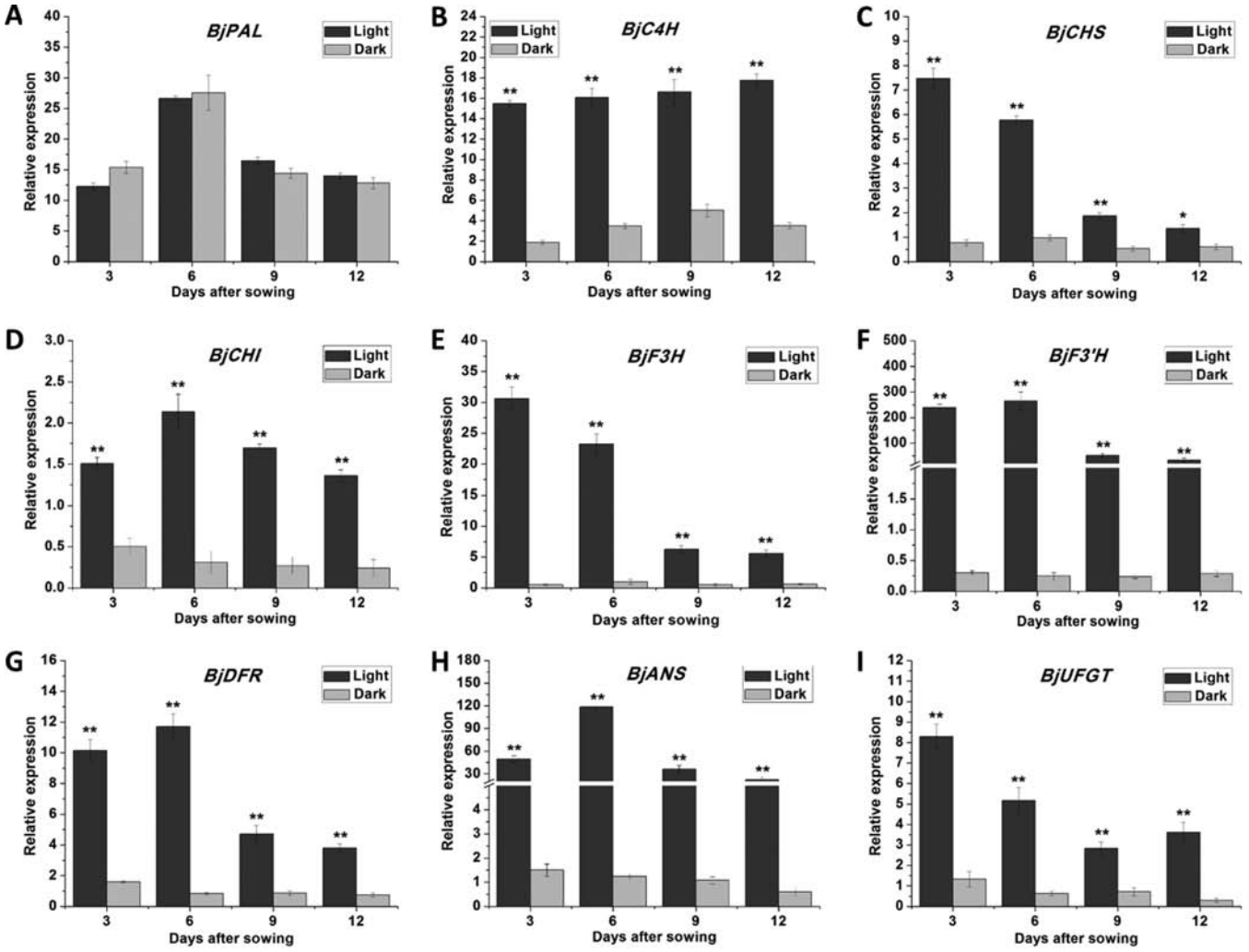

Figure 3. Expression analysis of anthocyanin synthesis genes of seedlings under light and dark growth conditions. Expression analysis of (A) *BjPAL*, (B) *BjC4H*, (C) *BjCHS*, (D) *BjCHI*, (E) *BjF3H*, (F) *BjF3′H*, (G) *BjDFR*, (H) *BjANS*, and (I) *BjUFGT* in seedlings of 3−12 DAS of purple cultivar "Zi Ying" grown in light and dark conditions. The data represent the mean from three replicates with three biological repeats. (**) $p < 0.01$ between the wild type and others by the *t* test. Error bars indicate SE. Relative expression was normalized using the housekeeping gene *BjEF1* (GO479260).

consistent with their phenotype and further illustrate that the expression level of structural genes is closely related to the anthocyanin accumulation in purple tumorous stem mustard.

Expression of Anthocyanin Biosynthetic Regulatory Genes. On the extensive studies of *Arabidopsis*, grape, apple, *Petunia*, pears, and strawberry, more and more evidence show that plants are often fond of the way of regulating anthocyanin biosynthesis by transcriptional control of anthocyanin biosynthetic genes.[4,12]

MYB transcription factors, bHLH proteins, and WD40 proteins are known to participate in regulating anthocyanin biosynthesis. In this work, the transcripts of *BjMYB1*, *BjMYB2*, *BjMYB3*, *BjMYB4*, *BjTT8*, and *BjTTG1* (homologues of *AtPAP1*, *AtPAP2*, *AtMYB113*, *AtMYB114*, *AtTT8*, and *AtTTG1*, respectively) were analyzed. As shown in Figure 4, these genes had a consistent expression trend, and their expression was elevated in the "Zi Ying" variety. Among them, the expression levels of MYB transcription factors *BjMYB1*, *BjMYB2*, *BjMYB3*, and *BjMYB4* were increased by approximately 2.9, 2.3, 1.8, and 5.9 times, respectively. *BjTTG1* exhibited only a small increase (1.4-fold) in the purple cultivar. It is noteworthy that *BjTT8* was increased by up to 80-fold in "Zi Ying". These results suggest that upregulation of *BjMYB1*, *BjMYB2*, *BjMYB3*, *BjMYB4*, and *BjTT8* expression is likely to activate the structural genes (*F3H*, *F3′H*, *DFR*, and *ANS*) of anthocyanin biosynthesis, and *BjTT8* is likely a critical gene to control the anthocyanin biosynthetic pathway in "Zi Ying". This is likely the general mechanism underlying anthocyanin production responsible for the purple leaves of purple tumorous stem mustard. This regulation mechanism is similar to that in red cabbage.[19]

Moreover, in the light- and dark-treated seedlings, the transcript levels of *BjMYB1*, *BjMYB2*, *BjMYB3*, and *BjMYB4* were 16.5-, 14.2-, 1.73, and 15.5-fold higher in the light than those in the dark treated at 9 DAS, respectively (Figure 5). *BjTTG1* was also induced in the seedling stage, but there was no significant difference between the light and dark conditions. These results indicated that MYB transcription factors may participate in the regulation of anthocyanin accumulation in seedlings of purple cultivar and *BjTTG1* might not account for the transcriptional activation of anthocyanin structural genes in purple tumorous stem mustard in the light. In addition, the transcript levels of *BjTT8* in the light-treated seedlings were approximately 85-, 80-, and 240-fold higher than those in the

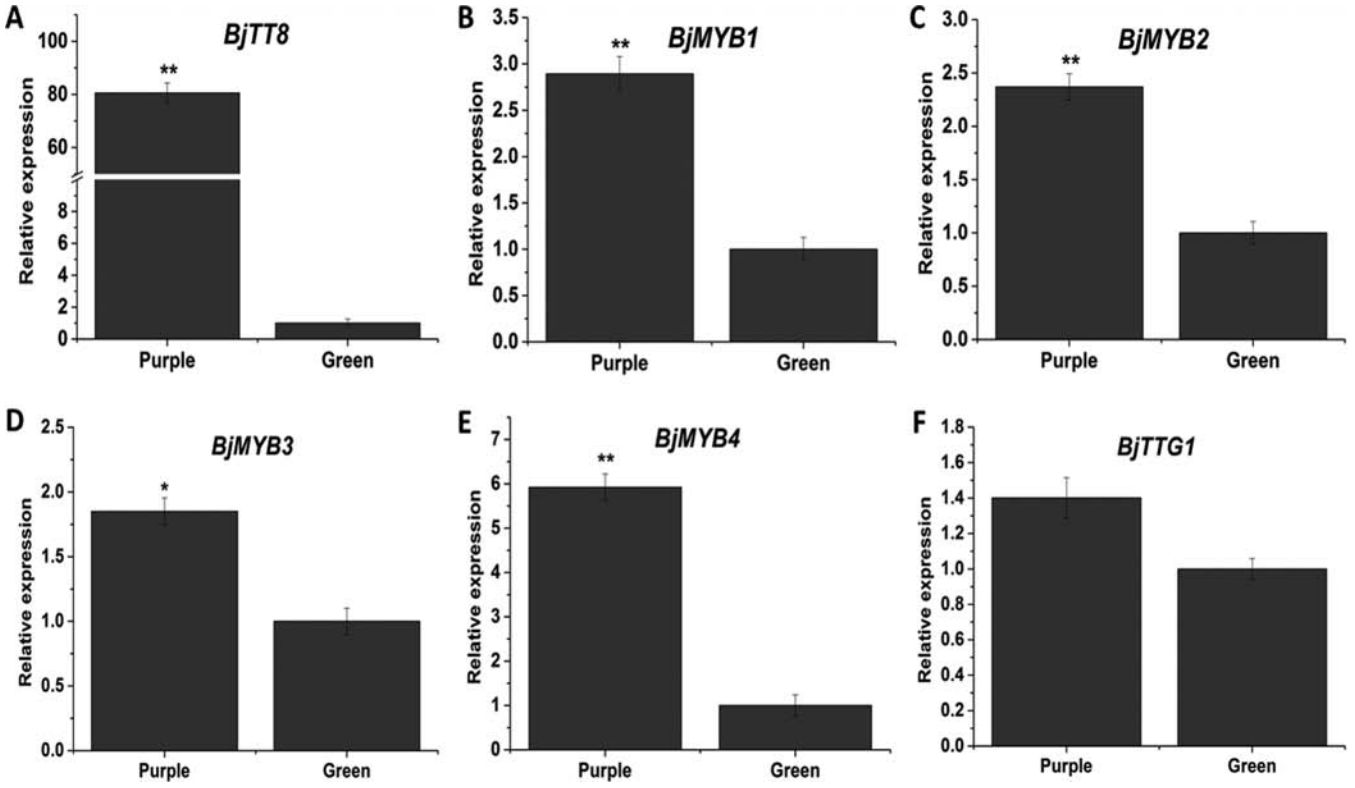

Figure 4. Expression analysis of anthocyanin regulatory genes under normal growth conditions. Expression analysis of (A) *BjTT8*, (B) *BjMYB1*, (C) *BjMYB2*, (D) *BjMYB3*, (E) *BjMYB4*, and (F) *BjTTG1* in mature leaves of purple cultivar "Zi Ying" and green cultivar "Lv Ying", respectively. The data represent the mean from three replicates with three biological repeats. (∗) $p < 0.05$ and (∗∗) $p < 0.01$ between the wild type and others by the *t* test. Error bars indicate SE. Relative expression was normalized using the housekeeping gene *BjEF1* (GO479260). The expression level of genes in the green cultivar were set to 1.

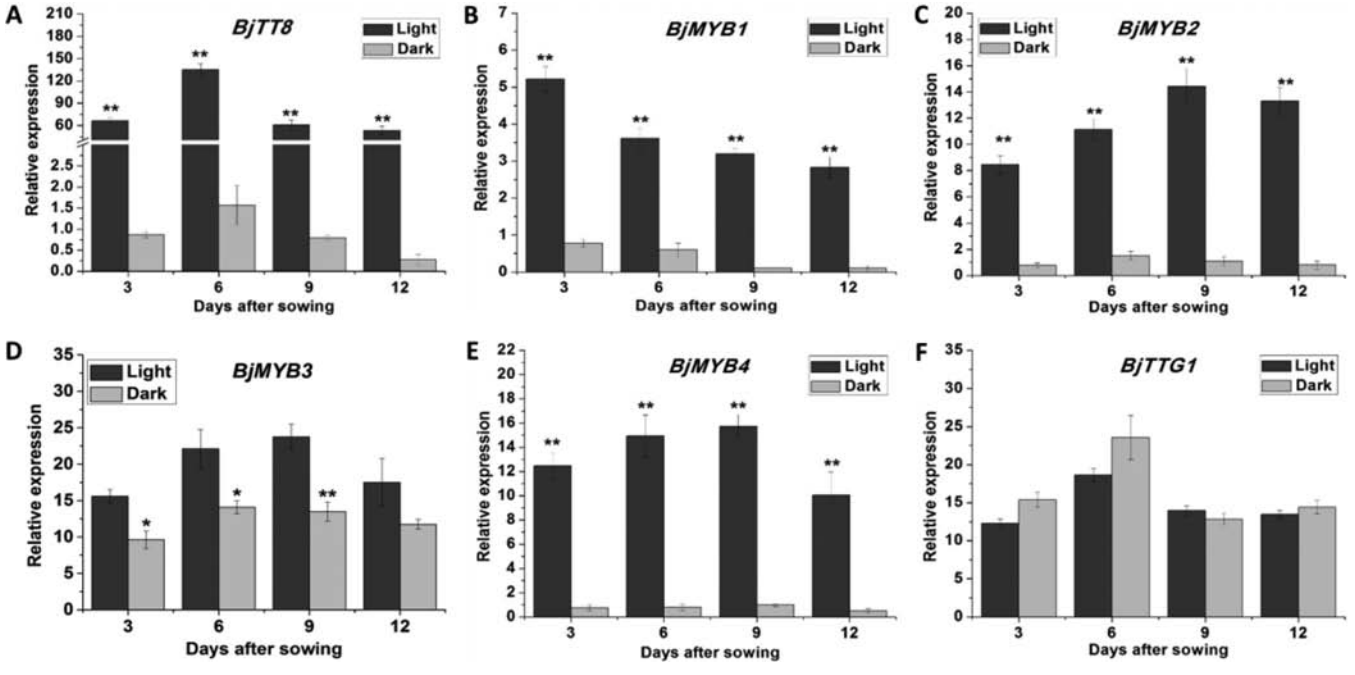

Figure 5. Expression analysis of anthocyanin regulatory genes of seedlings under light and dark growth conditions. Expression analysis of (A) *BjTT8*, (B) *BjMYB1*, (C) *BjMYB2*, (D) *BjMYB3*, (E) *BjMYB4*, and (F) *BjTTG1* in seedlings of 3−12 DAS of purple cultivar "Zi Ying" grown in light and dark conditions, respectively. The data represent the mean from three replicates with three biological repeats. (∗) $p < 0.05$ and (∗∗) $p < 0.01$ between the wild type and others by the *t* test. Error bars indicate SE. Relative expression was normalized using the housekeeping gene *BjEF1* (GO479260).

dx.doi.org/10.1021/jf501790a | J. Agric. Food Chem. 2014, 62, 7813−7821

dark-treated seedlings at 6, 9, and 12 DAS, respectively. The upregulation of *BjTT8* in purple cultivar is as extreme as that in purple cauliflower and red cabbage,[19,20] suggesting that *BjTT8* may be a very important regulatory factor, regulating accumulation of anthocyanins in purple tumorous stem mustard. On the basis of these results, we can speculate that mustard, cabbage, and cauliflower may have the same way of regulating the anthocyanin accumulation.

In conclusion, our research investigated the anthocyanin composition and transcriptional analysis of flavonoid structural and regulatory genes in purple tumorous stem mustard. The results suggest that cyanidin is characterized as the major anthocyanin in the purple tumorous stem mustard, and the upregulation of *BjMYB* genes and *BjTT8* likely triggers anthocyanin accumulation. Because of its extreme upregulation, *BjTT8* is likely a key gene to control the anthocyanin accumulation in the "Zi Ying" cultivar. To clarify the role of *BjMYB* genes and *BjTT8* in anthocyanin production in purple tumorous stem mustard, future studies through genetic analysis and candidate gene approach should be carried out.

■ ASSOCIATED CONTENT

Supporting Information

Major structure of anthocyanins and HPLC profiles of anthocyanins in purple tumorous stem mustard (Figure 1S), sequence alignment and phylogenetic analysis of *Brassica* TT8s (Figure 2S), primers used for qRT-PCR (Table 1S), and data on anthocyanin identification in purple tumorous stem mustard (Table 2S). This material is available free of charge via the Internet at http://pubs.acs.org.

■ AUTHOR INFORMATION

Corresponding Author

*Telephone/Fax: 0086-23-65112674. E-mail: chenguoping@cqu.edu.cn.

Funding

This work was supported by the National Natural Science Foundation of China (30871709, 31100089, and 31171968) and the Fundamental Research Funds for the Central Universities (CDJXS10232209).

Notes

The authors declare no competing financial interest.

■ ABBREVIATIONS USED

PAL, phenylalanine ammonia lyase; C4H, cinnamate 4-hydroxylase; CHS, chalcone synthase; CHI, chalcone isomerase; F3H, flavanone 3-hydroxylase; F3′H, flavonoid 3′-hydroxylase; DFR, dihydroflavonol reductase; ANS, anthocyanidin synthase; UFGT, UDP-glucose:flavonoid 3-*O*-glucosyltransferase; HPLC, high-performance liquid chromatography; ESI−MS/MS, electrospray ionization−tandem mass spectrometry; qRT-PCR, quantitative real-time reverse transcription polymerase chain reaction

■ REFERENCES

(1) Kong, J.-M.; Chia, L.-S.; Goh, N.-K.; Chia, T.-F.; Brouillard, R. Analysis and biological activities of anthocyanins. *Phytochemistry* **2003**, *64*, 923−933.

(2) Castañeda-Ovando, A.; Pacheco-Hernández, M. d. L.; Páez-Hernández, M. E.; Rodríguez, J. A.; Galán-Vidal, C. A. Chemical studies of anthocyanins: A review. *Food Chem.* **2009**, *113*, 859−871.

(3) Jackman, R. L.; Yada, R. Y.; TUNG, M. A.; Speers, R. Anthocyanins as food colorants—A review. *J. Food Biochem.* **1987**, *11*, 201−247.

(4) Harborne, J. B.; Williams, C. A. Advances in flavonoid research since 1992. *Phytochemistry* **2000**, *55*, 481−504.

(5) Chou, P.-h.; Matsui, S.; Misaki, K.; Matsuda, T. Isolation and identification of xenobiotic aryl hydrocarbon receptor ligands in dyeing wastewater. *Environ. Sci. Technol.* **2007**, *41*, 652−657.

(6) Bridle, P.; Timberlake, C. Anthocyanins as natural food colours-selected aspects. *Food Chem.* **1997**, *58*, 103−109.

(7) Lila, M. A. Anthocyanins and human health: An in vitro investigative approach. *Biomed. Res. Int.* **2004**, *2004*, 306−313.

(8) Chen, P.-N.; Chu, S.-C.; Chiou, H.-L.; Kuo, W.-H.; Chiang, C.-L.; Hsieh, Y.-S. Mulberry anthocyanins, cyanidin 3-rutinoside and cyanidin 3-glucoside, exhibited an inhibitory effect on the migration and invasion of a human lung cancer cell line. *Cancer Lett.* **2006**, *235*, 248−259.

(9) Hou, D.-X. Potential mechanisms of cancer chemoprevention by anthocyanins. *Curr. Mol. Med.* **2003**, *3*, 149−159.

(10) Brown, C.; Wrolstad, R.; Durst, R.; Yang, C.-P.; Clevidence, B. Breeding studies in potatoes containing high concentrations of anthocyanins. *Am. J. Potato Res.* **2003**, *80*, 241−249.

(11) McGhie, T.; Hall, H.; Ainge, G.; Mowat, A. Breeding *Rubus* cultivars for high anthocyanin content and high antioxidant capacity. *Proceedings of the 8th International Rubus and Ribes Symposium*; Dundee, U.K., July 4−8, 2001; pp 495−500.

(12) Grotewold, E. The genetics and biochemistry of floral pigments. *Annu. Rev. Plant Biol.* **2006**, *57*, 761−780.

(13) Winkel-Shirley, B. Flavonoid biosynthesis. A colorful model for genetics, biochemistry, cell biology, and biotechnology. *Plant Physiol.* **2001**, *126*, 485−493.

(14) Broun, P. Transcriptional control of flavonoid biosynthesis: A complex network of conserved regulators involved in multiple aspects of differentiation in *Arabidopsis*. *Curr. Opin. Plant Biol.* **2005**, *8*, 272−279.

(15) Koes, R.; Verweij, W.; Quattrocchio, F. Flavonoids: A colorful model for the regulation and evolution of biochemical pathways. *Trends Plant Sci.* **2005**, *10*, 236−242.

(16) Dixon, R. A.; Xie, D. Y.; Sharma, S. B. Proanthocyanidins—A final frontier in flavonoid research? *New Phytol.* **2005**, *165*, 9−28.

(17) Goodrich, J.; Carpenter, R.; Coen, E. S. A common gene regulates pigmentation pattern in diverse plant species. *Cell* **1992**, *68*, 955−964.

(18) Schwinn, K.; Venail, J.; Shang, Y.; Mackay, S.; Alm, V.; Butelli, E.; Oyama, R.; Bailey, P.; Davies, K.; Martin, C. A small family of MYB-regulatory genes controls floral pigmentation intensity and patterning in the genus *Antirrhinum*. *Plant Cell* **2006**, *18*, 831−851.

(19) Yuan, Y.; Chiu, L. W.; Li, L. Transcriptional regulation of anthocyanin biosynthesis in red cabbage. *Planta* **2009**, *230*, 1141−1153.

(20) Chiu, L.-W.; Zhou, X.; Burke, S.; Wu, X.; Prior, R. L.; Li, L. The purple cauliflower arises from activation of a MYB transcription factor. *Plant Physiol.* **2010**, *154*, 1470−1480.

(21) Nesi, N.; Debeaujon, I.; Jond, C.; Pelletier, G.; Caboche, M.; Lepiniec, L. The TT8 gene encodes a basic helix−loop−helix domain protein required for expression of DFR and BAN genes in *Arabidopsis* siliques. *Plant Cell* **2000**, *12*, 1863−1878.

(22) Payne, C. T.; Zhang, F.; Lloyd, A. M. GL3 encodes a bHLH protein that regulates trichome development in *Arabidopsis* through interaction with GL1 and TTG1. *Genetics* **2000**, *156*, 1349−1362.

(23) Borevitz, J. O.; Xia, Y.; Blount, J.; Dixon, R. A.; Lamb, C. Activation tagging identifies a conserved MYB regulator of phenylpropanoid biosynthesis. *Plant Cell* **2000**, *12*, 2383−2393.

(24) Dixon, R. A.; Liu, C.; Jun, J. H. Metabolic engineering of anthocyanins and condensed tannins in plants. *Curr. Opin. Biotechnol.* **2013**, *24*, 329−335.

(25) Nakatsuka, T.; Haruta, K. S.; Pitaksutheepong, C.; Abe, Y.; Kakizaki, Y.; Yamamoto, K.; Shimada, N.; Yamamura, S.; Nishihara, M. Identification and characterization of R2R3-MYB and bHLH tran-

scription factors regulating anthocyanin biosynthesis in gentian flowers. *Plant Cell Physiol.* **2008**, *49*, 1818−1829.
(26) Albert, N. W.; Lewis, D. H.; Zhang, H.; Schwinn, K. E.; Jameson, P. E.; Davies, K. M. Members of an R2R3-MYB transcription factor family in *Petunia* are developmentally and environmentally regulated to control complex floral and vegetative pigmentation patterning. *Plant J.* **2011**, *65*, 771−784.
(27) Sweeney, M. T.; Thomson, M. J.; Pfeil, B. E.; McCouch, S. Caught red-handed: *Rc* encodes a basic helix−loop−helix protein conditioning red pericarp in rice. *Plant Cell* **2006**, *18*, 283−294.
(28) Gonzalez, A.; Zhao, M.; Leavitt, J. M.; Lloyd, A. M. Regulation of the anthocyanin biosynthetic pathway by the TTG1/bHLH/Myb transcriptional complex in *Arabidopsis* seedlings. *Plant J.* **2008**, *53*, 814−827.
(29) Grotewold, E.; Drummond, B. J.; Bowen, B.; Peterson, T. The Myb-homologous *P* gene controls phlobaphene pigmentation in maize floral organs by directly activating a flavonoid biosynthetic gene subset. *Cell* **1994**, *76*, 543−553.
(30) Mol, J.; Jenkins, G.; Schäfer, E.; Weiss, D.; Walbot, V. Signal perception, transduction, and gene expression involved in anthocyanin biosynthesis. *Crit. Rev. Plant Sci.* **1996**, *15*, 525−557.
(31) Park, W. T.; Kim, Y. B.; Seo, J. M.; Kim, S.-J.; Chung, E.; Lee, J.-H.; Park, S. U. Accumulation of anthocyanin and associated gene expression in radish sprouts exposed to light and methyl jasmonate. *J. Agric. Food Chem.* **2013**, *61*, 4127−4132.
(32) Toguri, T.; Umemoto, N.; Kobayashi, O.; Ohtani, T. Activation of anthocyanin synthesis genes by white light in eggplant hypocotyl tissues, and identification of an inducible P-450 cDNA. *Plant Mol. Biol.* **1993**, *23*, 933−946.
(33) Takos, A. M.; Jaffé, F. W.; Jacob, S. R.; Bogs, J.; Robinson, S. P.; Walker, A. R. Light-induced expression of a MYB gene regulates anthocyanin biosynthesis in red apples. *Plant Physiol.* **2006**, *142*, 1216−1232.
(34) Vanderauwera, S.; Zimmermann, P.; Rombauts, S.; Vandenabeele, S.; Langebartels, C.; Gruissem, W.; Inzé, D.; Van Breusegem, F. Genome-wide analysis of hydrogen peroxide-regulated gene expression in *Arabidopsis* reveals a high light-induced transcriptional cluster involved in anthocyanin biosynthesis. *Plant Physiol.* **2005**, *139*, 806−821.
(35) Cevallos-Casals, B. A.; Cisneros-Zevallos, L. Impact of germination on phenolic content and antioxidant activity of 13 edible seed species. *Food Chem.* **2010**, *119*, 1485−1490.
(36) Sun, Q.; Zhou, G.; Cai, Y.; Fan, Y.; Zhu, X.; Liu, Y.; He, X.; Shen, J.; Jiang, H.; Hu, D. Transcriptome analysis of stem development in the tumourous stem mustard *Brassica juncea* var. *tumida* Tsen et Lee by RNA sequencing. *BMC Plant Biol.* **2012**, *12*, 53.
(37) Zhang, B.; Hu, Z.; Zhang, Y.; Li, Y.; Zhou, S.; Chen, G. A putative functional MYB transcription factor induced by low temperature regulates anthocyanin biosynthesis in purple kale (*Brassica oleracea* var. *acephala* f. tricolor). *Plant Cell Rep.* **2012**, 1−9.
(38) Wu, X.; Prior, R. L. Identification and characterization of anthocyanins by high-performance liquid chromatography−electrospray ionization−tandem mass spectrometry in common foods in the United States: Vegetables, nuts, and grains. *J. Agric. Food Chem.* **2005**, *53*, 3101−3113.
(39) Rapisarda, P.; Fanella, F.; Maccarone, E. Reliability of analytical methods for determining anthocyanins in blood orange juices. *J. Agric. Food Chem.* **2000**, *48*, 2249−2252.
(40) Gao, L.; Mazza, G. Quantitation and distribution of simple and acylated anthocyanins and other phenolics in blueberries. *J. Food Sci.* **1994**, *59*, 1057−1059.
(41) Arapitsas, P.; Turner, C. Pressurized solvent extraction and monolithic column−HPLC/DAD analysis of anthocyanins in red cabbage. *Talanta* **2008**, *74*, 1218−1223.
(42) McDougall, G. J.; Fyffe, S.; Dobson, P.; Stewart, D. Anthocyanins from red cabbage—Stability to simulated gastrointestinal digestion. *Phytochemistry* **2007**, *68*, 1285−1294.
(43) Lin, L.-Z.; Sun, J.; Chen, P.; Harnly, J. UHPLC−PDA−ESI/HRMS/MS n analysis of anthocyanins, flavonol glycosides, and hydroxycinnamic acid derivatives in red mustard greens (*Brassica juncea* Coss variety). *J. Agric. Food Chem.* **2011**, *59*, 12059−12072.
(44) Feng, S.; Wang, Y.; Yang, S.; Xu, Y.; Chen, X. Anthocyanin biosynthesis in pears is regulated by a R2R3-MYB transcription factor PyMYB10. *Planta* **2010**, *232*, 245−255.
(45) Li, X.; Thwe, A. A.; Park, N. I.; Suzuki, T.; Kim, S. J.; Park, S. U. Accumulation of phenylpropanoids and correlated gene expression during the development of tartary buckwheat sprouts. *J. Agric. Food Chem.* **2012**, *60*, 5629−5635.
(46) Feyissa, D. N.; Løvdal, T.; Olsen, K. M.; Slimestad, R.; Lillo, C. The endogenous GL3, but not EGL3, gene is necessary for anthocyanin accumulation as induced by nitrogen depletion in *Arabidopsis* rosette stage leaves. *Planta* **2009**, *230*, 747−754.
(47) Palapol, Y.; Ketsa, S.; Lin-Wang, K.; Ferguson, I. B.; Allan, A. C. A MYB transcription factor regulates anthocyanin biosynthesis in mangosteen (*Garcinia mangostana* L.) fruit during ripening. *Planta* **2009**, *229*, 1323−1334.
(48) Espley, R. V.; Hellens, R. P.; Putterill, J.; Stevenson, D. E.; Kutty-Amma, S.; Allan, A. C. Red colouration in apple fruit is due to the activity of the MYB transcription factor, MdMYB10. *Plant J.* **2007**, *49*, 414−427.
(49) Mano, H.; Ogasawara, F.; Sato, K.; Higo, H.; Minobe, Y. Isolation of a regulatory gene of anthocyanin biosynthesis in tuberous roots of purple-fleshed sweet potato. *Plant Physiol.* **2007**, *143*, 1252−1268.
(50) Song, J. Y.; Lee, J. S.; An, C. S. Expression of CHS, CHI, and DFR genes in response to light in small radish seedlings. *J. Plant Biol.* **1998**, *41*, 277−282.

from the fresh fruiting bodies of *P. giganteus* and to compare its properties with those of other fungal FAEs.

MATERIALS AND METHODS

Materials. Wheat bran and corn bran were processed as described by Wang and Ou.[16] Fresh fruiting bodies of the mushroom *P. giganteus* were purchased from a local market. DEAE-cellulose and Q-Sepharose were obtained from Sigma Chemical Co., St. Louis, MO, USA. A Hypersil ODS C18 column was from Agilent Technologies Co., Santa Clara, CA, USA. Superdex 75 HR 10/30 was from GE Healthcare. *p*-Nitrophenyl stearate, palmitate, caproate, butyrate, and acetate were purchased from Sigma. Methyl *p*-coumarate (MpCA), caffeate (CA), ferulate (MFA), and ferulic acid (FA) were obtained from Apin Chemicals Ltd., Abingdon, UK. Xylanase was obtained from Sigma. E-FAERU (a commercial FAE) was purchased from Megazyme, Wicklow, Ireland.

Purification Scheme. Fresh fruiting bodies of the mushroom *P. giganteus* (800 g) were homogenized in distilled water (2 mL/g) using a Waring blender followed by centrifugation (8000*g*, 15 min). Tris-HCl buffer (pH 8.2) was added to the resulting supernatant until the concentration of Tris-HCl buffer was 10 mM. The supernatant was then applied on a DEAE-cellulose column (5 cm × 20 cm) previously equilibrated with 10 mM Tris-HCl buffer (pH 8.2). Following elution of unadsorbed proteins in fraction D1, adsorbed proteins were desorbed sequentially with 50, 150, and 300 mM NaCl in the same buffer, to produce fractions D2, D3, and D4, respectively. Fraction D3, which exhibited FAE activity, was dialyzed prior to ion exchange chromatography on a 3 cm × 20 cm column of Q-Sepharose in 10 mM Tris-HCl buffer (pH 7.2).

Following elution of unadsorbed proteins in fraction D3Q1, adsorbed proteins were desorbed from the column with a linear 0–1 M NaCl concentration gradient in the same buffer. The active fraction (D3Q2) was dialyzed and then resolved by ion exchange chromatography on a 1 cm × 10 cm DEAE-cellulose column in 10 mM sodium phosphate buffer (pH 6.8).

Following removal of the unadsorbed proteins from the DEAE-cellulose column in fraction D3Q2D1, adsorbed proteins were desorbed with 1 M NaCl in the same buffer. Fraction D3Q2D1 with activity was further purified on a gel filtration Superdex G-75 HR10/30 column by fast protein liquid chromatography (FPLC) using an AKTA purifier and was eluted with 0.2 M NH_4HCO_3 buffer (pH 8.5). The second adsorbance peak (D3Q2D1S2) from the Superdex G-75 column represented the purified FAE.

Assay for Esterolytic Activity. *p*-Nitrophenyl butanoate (*p*NPB) was used as substrate. The test sample (5 μL) was mixed with 195 μL of 50 mM sodium phosphate buffer (pH 6.0) and 5 μL of 50 mM *p*NPB in isopropanol. The increase of absorbance was monitored at 37 °C at 415 nm for 20 min. One unit of enzyme activity was defined as 1 μmol of *p*-nitrophenol released within 1 min under the assay conditions. FAE activity was determined with a modified assay employing MFA as substrate.[17] The assay was conducted at 30 °C for 10 min in 100 mM 3-(*N*-morpholino)propanesulfonic acid (MOPS) buffer (pH 5.0) containing 50 μM MFA, and then the decrease of the MFA was determined at 340 nm. One unit (U) of enzymatic activity was defined as the amount of enzyme that catalyzes the release of 1 μmol min^{-1} FA under the assay conditions. All determinations were performed in triplicate. Release of the FA was also detected by HPLC on a Hypersil ODS C18 column. Detection was achieved at 320 nm on the basis of calibration curves prepared using standard FA and MFA. Elution was conducted with 45/55% (v/v) methanol/sodium formate (10 mM) at a flow rate 0.3 mL min^{-1}.

Molecular Mass Determination. SDS-PAGE was carried out using a 12% resolving gel and a 5% stacking gel.[18] Staining of the gel with Coomassie brilliant blue was performed at the end of electrophoresis. The electrophoretic mobility of the FAE was compared with those of molecular mass standards, and the molecular mass of the FAE was determined from a calibration curve. Gel filtration by FPLC on a Superdex G-75 column, which had previously been calibrated with molecular mass standards, was also employed to ascertain the molecular mass of the FAE from a calibration curve.

Mass Spectrometry of the Purified FAE. The purified FAE band was excised from SDS–polyacrylamide gel, dried, and digested with trypsin. The resulting peptides were extracted and purified according to standard protocols. Then the peptides were analyzed by high-performance liquid chromatography combined with an LTQ Orbitrap mass spectrometer (HPLC-LTQ Orbitrap MS). The amino acid sequences were manually deduced and used for blast searches in public protein primary sequence databases (www.ncbi.nlm.nih.gov/BLAST.cgi).[19]

Substrate Specificities and Kinetics. Substrate preferences for the purified FAE against hydroxycinnamate ester derivatives were determined using the standard assay in the presence of the following esters at 50 μM concentration: methyl ferulate (MFA), methyl *p*-coumarate (MpCA), and methyl caffeate (MCA). Activities toward fatty acid nitrophenyl esters with different chain lengths, including *p*-nitrophenyl acetate, butyrate, caproate, caprylate, palmitate, and stearate, were determined by following a published standard method. The Michaelis–Menten constants (K_m) and maximal velocity (V_{max}) of the *P. giganteus* FAE based on different MFA concentrations (50, 100, 200, 300, 500, and 900 μM) were determined using the Lineweaver–Burk plot. All determinations were conducted in triplicate at pH 4.0 and 40 °C. The reciprocals of the enzyme reaction velocities were plotted on the vertical axis, and the reciprocal of the substrate concentrations were plotted on the horizontal axis to generate the Lineweaver–Burk plot for calculation of K_m and V_{max}.

Biochemical Properties. To determine the optimal temperature, the standard FAE activity assay using MFA as substrate was run at 20, 30, 40, 50, 60, 70, 80, and 90 °C. MOPS buffer was used as the assay buffer. In the thermostability assay, the enzyme solution was exposed for 120 min to various temperatures ranging from 20 to 80 °C before cooling to 25 °C. The activity remaining was then determined. Triplicate determinations were conducted.

The pH optimum of the enzyme was measured using the standard FAE activity assay above, but in a series of McIlvaine buffers (mixtures of 0.1 M citric acid and 0.2 M sodium hydrogen phosphate) in the pH range from pH 2.0 to 8.0 instead of MOPS buffer (pH 5.0). Reaction conditions were the same as those described above for activities toward MFA.

Effects of Metal Ions. For studying how metal ions affect the enzyme activity, the purified enzyme solution was exposed to metal ions, such as Pb^{2+}, Al^{3+}, Zn^{2+}, Mg^{2+}, Cu^{2+}, K^{+}, Mn^{2+}, Ca^{2+}, and Cd^{2+} ions at 5 mM concentration, at 4 °C for 2 h before the standard FAE assay using MFA as substrate was performed. The control sample was maintained in the absence of metal ions.

Enzymatic Degradation of Different Cereal Brans. Enzymatic hydrolyses were performed in 100 mM MOPS buffer (pH 5) in an incubator at 37 °C with shaking. Wheat bran (100 mg) and corn bran (100 mg) were incubated with 0.02 U/mg FAE, in the absence and also in the presence of xylanase (0.6 U/mg) in a final volume of 1.0 mL. At the end of the incubation, the reaction mixture was boiled for 3 min to terminate the reaction. After cooling and centrifugation (13000 *g*, 5 min), the FA released into the supernatant was subjected to HPLC analysis by using a Hypersil ODS C18 column. E-FAERU (a commercial FAE from rumen microorganism) was used as a positive control. The dosage and the reaction conditions of this enzyme were identical to those for FAE from *P. giganteus*.

Alkali Hydrolysis of the Substrates. To determine the total alkali-extractable FA of the substrate, 1.5 mL of 2 M NaOH was added to 100 mg of substrate. Incubation was carried out at 37 °C for 24 h. The supernatant obtained following centrifugation was neutralized using 6 M HCl. Determination of the FA content measured using HPLC was then carried out as described above.

RESULTS

Purification of FAE. The FAE from *P. giganteus* was purified to homogeneity by employing three successive ion

exchange chromatography steps and a gel filtration step, resulting in 10.1% recovery of activity (Table 1).

Table 1. Yields and FAE Activities at Each Purification Step (from 800 g of *Panus giganteus* Fresh Fruiting Bodies)

purification step	yield (mg)	specific activity (U/mg)	total activity (U)	recovery (%)	purification fold
crude extract	15680	1.3	20384	100	1
DEAE-cellulose	765.5	17.4	13320	65.3	13.4
Q-Sepharose	163.4	35.7	5833	28.6	27.5
DEAE-cellulose	28.3	93.7	2652	13.0	72.1
Superdex 75 on FPLC	12.1	170.0	2057	10.1	130.8

Upon chromatography on the ion exchanger DEAE-cellulose, the *P. giganteus* extract was separated into an unadsorbed fraction D1 and three adsorbed fractions, D2, D3, and D4, eluted at 50, 150, and 300 mM NaCl, respectively. Fraction D3, which contained FAE activity, was then fractionated into two peaks, D3Q1 and D3Q2, on a Q-Sepharose column. The unadsorbed fraction (D3Q1) was devoid of FAE activity. High FAE activity was found in the adsorbed fraction (D3Q2). Subsequently, D3Q2 was resolved on DEAE-cellulose into an unadsorbed fraction, D3Q2D1, and a large adsorbed fraction, D3Q2D2. D3Q2D1 was then fractionated into two peaks of about the same size after gel filtration on Superdex 75. FAE activity was confined to the second fraction, D3Q2D1S2.

Determination of Molecular Mass and Internal Amino Acid Sequence. Fraction D3Q2D1S2 appeared as a single 61 kDa band as determined by SDS-PAGE and as a single 61 kDa peak upon rechromatography on Superdex 75 (data not shown). The data indicate that the purified FAE is a monomeric enzyme (Figure 1).

Several internal sequences of the purified FAE were elucidated. Database search using BLAST indicated that two peptides, VEMNAAPGVDL and GTAAGDNVV, showed some homology with FAEs from other microorganisms (Table 2).

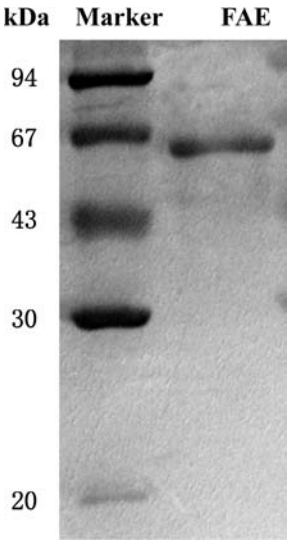

Figure 1. Molecular mass of *Panus giganteus* FAE by SDS-PAGE: left lane, molecular mass standards (from top downward, phosphorylase *b* (94 kDa), bovine serum albumin (67 kDa), ovalbumin (43 kDa), carbonic anhydrase (30 kDa), soybean trypsin inhibitor (20 kDa)); right lane, *P. giganteus* FAE.

Table 2. Comparison of the Internal Amino Acid Sequences of *Panus giganteus* FAE with Those of Other Microbial FAEs

accession no.	microorganism	peptide
	Peptide 1	
this study	*Panus giganteus*	**VEMNAAPGVDL**
WP014670826.1	*Streptomyces hygroscopicus*	**MNPGVDL**SPAA
WP009774585.1	*Janibacter* sp.	SC**MNPGVD**K
XP007600389.1	*Colletotrichum fioriniae*	AV**MAARGVDL**
EQB57686.1	*Colletotrichum gloeosporioides*	**VEM**FD**AADGV**E
XP002341414.1	*Talaromyces stipitatus*	FRLFL**APGVD**H
CCT67738.1	*Fusarium fujikuroi*	LRLFL**APGVD**H
ENH67953.1	*Fusarium oxysporum*	LRLFL**APGVD**H
	Peptide 2	
this study	*Panus giganteus*	**GTAAGDNVV**
XP002476624.1	*Postia placenta*	**GTQAGDNVV**
YP006442683.1	*Mycobacterium chubuense*	**GQAAGDNVV**
WP021612423.1	*Actinomyces* sp.	AM**AAGDDVV**
EJT76105.1	*Gaeumannomyces graminis*	**GTAA**SNN**IV**
GAA86475.1	*Aspergillus kawachii*	**GTDTGDNLV**
CCD54784.1	*Botrytis cinerea*	HNGR**GDNVV**
WP020275788.1	*Streptomyces afghaniensis*	**STADGGNVV**

Substrate Specificities and Kinetics. The purified FAE was allowed to react with hydroxycinnamic acid methyl esters and fatty acid nitrophenyl esters with different chain lengths. The relative activities were calculated and are shown in Table 3.

Table 3. Activities (Mean ± SD, $n = 3$) of the Purified *Panus giganteus* FAE on Different Substrates

substrate	relative activity (%)
methyl ferulate	100.00
methyl caffeate	65.32 ± 2.46
methyl coumarate	53.17 ± 2.84
p-nitrophenyl acetate	62.44 ± 4.01
p-nitrophenyl butyrate	38.30 ± 3.58
p-nitrophenyl caproate	15.09 ± 2.00
p-nitrophenyl palmitate	nd[a]
p-nitrophenyl stearate	nd

[a]nd, not detected.

The enzyme expressed the highest activity toward methyl ferulate, but it was about 35% less active on methyl caffeate and 47% less active on methyl coumarate. The FAE enzyme also showed activity toward short-chain fatty acid nitrophenyl esters: 62.44 ± 4.01% active on *p*-nitrophenyl acetate, 38.30 ± 3.58% active on *p*-nitrophenyl butyrate, and 15.09 ± 2.00% active on *p*-nitrophenyl caproate. There was no activity toward the long-chain substrates.

The K_m and V_{max} values for the purified *P. giganteus* FAE with MFA as substrate were determined by using the Lineweaver–Burk plot to measure the decreasing level of MFA at pH 4.0 and 40 °C. The K_m and V_{max} for the enzyme were estimated to be 0.36 mM and 18.97 U mg^{-1} protein, respectively.

Characteristics of *P. giganteus* FAE Activity. FAE had its optimal temperature at 40 °C. At 20 °C, 68% of the activity remained, and at 90 °C, 45% activity was left (Figure 2a). FAE activity was completely abolished when the enzyme was boiled for 10 min (data not shown). *P. giganteus* FAE was stable at

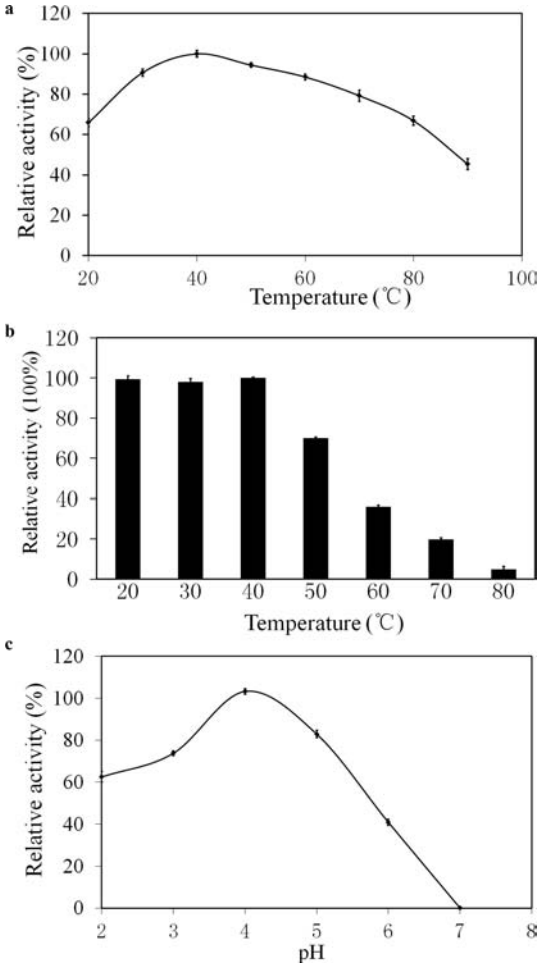

Figure 2. Effects of pH and temperature on *Panus giganteus* FAE: (a) effects of temperature on activity of *P. giganteus* FAE; (b) thermostability of *P. giganteus* FAE; (c) effects of pH on activity of *P. giganteus* FAE. Results represent the mean ± SD (n = 3).

20−40 °C, and 70% residual activity was detected after incubation of the enzyme at 50 °C for 120 min (Figure 2b).

The optimal pH value of the purified FAE was pH 4.0, and 60% of the activity remained at pH 2.0, whereas the enzyme activity declined sharply as the pH was increased. Negligible FAE activity was detected at pH 7.0, whereas no activity was discerned at pH 8.0 (Figure 2c).

The sensitivity of *P. giganteus* FAE to several metal ions is shown in Table 4. The purified enzyme activity was inhibited to different degrees in the presence of metal ions: >60% inhibition in the presence of Mn^{2+}, Ca^{2+}, and Cd^{2+} ions; >40% inhibition by K^{+}, Al^{3+} Zn^{2+}, Mg^{2+}, and Cu^{2+} ions; and 20% inhibition by Pb^{2+} ions.

Table 4. Effects of Different Metal Ions (5 mM) on the Activity (Mean ± SD, n = 3) of Purified *Panus giganteus* FAE

metal ion	residual activity (%)	metal ion	residual activity (%)
Pb^{2+}	84.36 ± 3.06	K^{+}	43.04 ± 2.73
Al^{3+}	60.27 ± 2.33	Mn^{2+}	38.38 ± 2.97
Zn^{2+}	55.30 ± 3.49	Ca^{2+}	32.60 ± 3.03
Mg^{2+}	54.79 ± 2.16	Cd^{2+}	31.53 ± 2.44
Cu^{2+}	52.62 ± 3.11		

Enzyme Activity on Cereal Brans. Wheat bran and corn bran were selected for their high contents of FAs. The total amount of FA was first determined after alkaline hydrolysis and by HPLC analysis. Wheat bran and corn bran contained about 2.16 and 13.85 mg/g FA, respectively (Table 5). Before the action of the enzymes, no free FAs could be detected. Only 1% of the total FA was released from wheat bran, whereas no free FA was released from corn bran when hydrolyzed with xylanase alone. Without the help of accessory enzymes, 8.1 and 0.3% of the total FA was released, respectively, from wheat bran and corn bran with purified FAE. To investigate the action of purified FAE in synergism with xylanase, they were added to the reaction of substrates at the same time, and it was found that the release amount of FA from wheat bran and corn bran was significantly increased (51.9 and 1% of the total FA, respectively) (Table 5). No free FA was released from corn bran, and 5.3% of the total FA was released from wheat bran when hydrolyzed with E-FAERU alone. Under the combined action of E-FAERU and xylanase, 43.3 and 1.1% of the total FA were released from wheat bran and corn bran, respectively (Table 5).

DISCUSSION

FAE was first detected in cultures of *S. olivochromogenes*;[20] since then, many FAEs have been isolated from fungi but rarely from mushrooms. Recently it has been reported that FA was detected in the broth of mycelial culture of four kinds of edible mushrooms.[21] A new FAE was isolated from the mycelial culture of the edible mushroom *Pleurotus sapidus*.[22]

In the present study, we have purified a novel FAE from *P. giganteus* with a chromatographic procedure involving DEAE-cellulose, Q-Sepharose, DEAE-cellulose, and gel filtration on Superdex 75. The procedure employed in the present study was useful for isolating *P. giganteus* FAE. The chromatographic behavior of *P. giganteus* FAE on ionic exchangers was similar to that of *Sporotrichum thermophile*[23] and *Aspergillus niger* FAE.[24] They were adsorbed only on anionic exchangers, such as DEAE-cellulose and Q-Sepharose.

The specific activity of purified FAE was 170.0 U/mg, which was significantly higher than that of FAEs from other fungi, most of which ranged from 0.001 to 36.7 U/mg.[14] The purified FAE was a monomeric protein with a molecular mass of 61 kDa. Its molecular weight was similar to that of FAEs from the mushroom *P. sapidus* (55 kDa)[22] and also close to those of other fungi, such as *Fusarium oxysporum* (62 kDa), *A. niger* (63 kDa), and *Penicillium pinophilum* (57 kDa). *P. giganteus* FAE was larger in molecular mass than FAEs reported from *A. tubingensis* (36 kDa) and *F. oxysporum* (27 kDa) and smaller than FAEs from *A. niger* (120 kDa) and *A. awamori* (112 kDa).[14]

Due to the lack of a significant homology to known microbial FAEs, the purified FAE was likely a novel enzyme. Previous research has also shown that the homology of FAE was low between species.[25,26] For instance, *P. sapidus* FAE, the only FAE from macrofungi, also showed no significant homology to any of the published FAE sequences.[22]

The activity of the purified FAE on the synthetic methyl esters declined with decreasing degree of substitution: it preferred methyl ferulate over methyl caffeate and was least active on methyl coumarate. It also displayed activity toward various *p*-nitrophenyl esters with short chain lengths, and the activity decreased as the number of carbon atoms increased, which was similar to the esterases reported from mushrooms

Table 5. Alkaline and Enzymatic Hydrolysis of Ferulic Acid from Cereal Brans[a]

	ferulic acid (μg/100 mg substrates)					
		enzymatic extraction				
substrate	alkaline extract	xylanase	*pg*FAE	*pg*FAE + xylanase	E-FAERU	E-FAERU + xylanase
wheat bran	216.3 ± 7.5	2.3 ± 0.2	17.6 ± 0.7	112.2 ± 2.9	11.5 ± 0.4	93.7 ± 1.8
corn bran	1385.5 ± 96.0	nd	4.7 ± 0.1	13.7 ± 0.3	nd	15.5 ± 0.5

[a]Data represent the mean ± SD (n = 3); nd, not detected. *pg*FAE, *Panus giganteus* FAE; E-FAERU, a commercial FAE as positive control.

species, such as *S. crispa*,[27] *A. vaginata* var. *vaginata*, *Tricholoma terreum*,[28] and *Lycoperdon perlatum*,[29] and showed specificity toward short-chain fatty acids such as *p*-nitrophenyl butyrate and *p*-nitrophenyl acetate. Apparently, this specificity study suggests that the enzyme is an esterase and not a lipase.

The present FAE manifested an optimal temperature at 40 °C, which was similar to those of FAEs reported from *A. niger*, *F. oxysporum*, and *A. awamori*,[14] whereas it was lower than that of FAE from *P. sapidus* (50 °C).[22] *P. giganteus* FAE was stable at 20−40 °C. This feature can be successfully employed in applications that require a moderate temperature, such as in the production of pharmaceuticals and in the extraction of free phenolic acids. The purified FAE displayed an acidic pH optimum at pH 4.0, which is in accordance with human gastrointestinal pH values. Owing to its high catalytic efficiency under acidic conditions, the purified FAE was more valuable than most other fungal FAEs in many biotechnological applications such as used as functional food and animal feed additives.

The FAE in this study was very sensitive to metal ions. It had some similarities to other mushroom esterases. Esterase activity in the mushroom *S. crispa* could be inhibited by the addition of Zn^{2+} and K^{+} ions.[27] Addition of Zn^{2+} and Fe^{2+} ions could inhibit the esterase activity in the mushroom *Volvariella volvacea*.[30] Addition of Cd^{2+} and Mn^{2+} ions inhibited the esterase activity in the mushroom *T. terreum*.[28] On the other hand, the addition of Ca^{2+}, Fe^{2+}, and Mn^{2+} ions produced stimulatory effects on esterase activity in the mushroom *L. perlatum*.[29] K^{+} and Al^{3+} ions had no effect on esterase activity in the mushroom *A. vaginata* var. *vaginata*.[28]

The present study suggests that FA can be recovered from corn bran and wheat bran by using the purified FAE alone. The percent recovery of FA in wheat bran was higher than those of E-FAERU and FAEs reported in the literature. It has been shown that AnFae alone releases a maximum of 4% of the FA present in wheat bran.[31] The amount of FA released from wheat bran was greatly enhanced (51.9% of total FA) by the synergistic action of xylanase, which was consistent with the published data. This could be because xylanolytic enzymes can degrade long-chain feruloylated xylooligosaccharides to shorter-chain feruloylated xylooligosaccharides, which are more easily hydrolyzed,[31] whereas the purified FAE could release FAs from corn bran to much less extent and to only 1% of the total amount even with the addition of xylanase. The small extent of hydrolysis in corn bran could be attributed to the number of substitutions on the heteroxylan backbone, the presence of extensively branched xylose, and the existence of a linkage between arabinose and xylose in the vicinity of the ferulic acid group.[31] The abundance of ferulic dimers in corn bran restricts enzymatic degradation.[32] The amount of FA released from corn bran by E-FAERU was slightly higher than that by the purified FAE in the presence of xylanase. However, the E-FAERU was from a rumen microorganism, which is anaerobic and difficult to propagate, and hence its further development is limited and it is not easy to widen the field of application. In comparison, *P. giganteus* is a cultivated edible mushroom, which is easy to culture and absolutely safe, and so FAE from *P. giganteus* will have broader prospects of application.

AUTHOR INFORMATION

Corresponding Authors

*(H.W.) Phone: +86 10 62732578. Fax: +86 10 62732578. E-mail: hxwang1957@gmail.com.

*(T.B.N.) E-mail: b021770@mailserv.cuhk.edu.hk.

Funding

This work was financially supported by National Grants of China (Biomass dissociation and low-molecular fragment green monomerization and transformation, 2010CB732202).

Notes

The authors declare no competing financial interest.

REFERENCES

(1) Ou, S. Y.; Kwok, K. C. Ferulic acid: pharmaceutical functions, preparation and applications in foods. *J. Sci. Food Agric.* **2004**, *84*, 1261−1269.

(2) Fazary, A. E.; Ju, Y. H. Feruloyl esterases as biotechnological tools: current and future perspectives. *Acta Biochem. Biophys. Sin.* **2007**, *39*, 811−828.

(3) Liu, R. H. Whole grain phytochemicals and health. *J. Cereal Sci.* **2007**, *46*, 207−219.

(4) Mathew, S.; Abraham, T. M. Ferulic acid: an antioxidant found naturally in plant cell walls and feruloyl esterases involved in its release and their applications. *Crit. Rev. Biotechnol.* **2004**, *24*, 59−83.

(5) Palafox-Carlos, H.; Ayala-Zavala, Z. F.; González-Aguilar, G. A. The role of dietary fiber in the bioaccessibility and bioavailability of fruit and vegetable antioxidants. *J. Food Sci.* **2011**, *76*, 6−15.

(6) Wang, J.; Sun, B. G.; Cao, Y. P.; Wang, C. T. Wheat bran feruloyl oligosaccharides enhance the antioxidant activity of rat plasma. *Food Chem.* **2011**, *123*, 472−476.

(7) Faulds, C. B.; Williamson, G. The role of hydroxycinnamates in the plant cell wall. *J. Sci. Food Agric.* **1999**, *79*, 393−395.

(8) Oosterveld, A.; Beldman, G.; Voragen, A. G. Oxidative cross-linking of pectic polysaccharides from sugar beet pulp. *Carbohydr. Res.* **2000**, *328*, 199−207.

(9) Topakas, E.; Stamatis, H.; Biely, P.; Kekos, D.; Macris, B. J.; Christakopoulos, P. Purification and characterization of a feruloyl esterase from *Fusarium oxysporum* catalyzing esterification of phenolic acids in ternary water−organic solvent mixtures. *J. Biotechnol.* **2003**, *102*, 33−44.

(10) Mackenzie, C. R.; Bilous, D.; Schneider, H.; Johnson, K. G. Induction of cellulolytic and xylanolytic enzymes in *Streptomyces* spp. *Appl. Environ. Microbiol.* **1987**, *53*, 2835−2839.

(11) Wang, X. K.; Geng, X.; Egashira, Y.; Sanada, H. Purification and characterization of a feruloyl esterase from the intestinal bacterium *Lactobacillus acidophilus*. *Appl. Environ. Microbiol.* **2004**, *70*, 2367−2372.

(12) Abeijón Mukdsi, M. C.; Haroc, C.; González, S. N.; Medina, R. B. Functional goat milk cheese with feruloyl esterase activity. *J. Funct. Foods* **2013**, *5*, 801−809.

(13) Sigoillot, C.; Camarero, S.; Vidal, T.; Record, E.; Asther, M.; Perez-Boada, M.; Martinez, M. J.; Sigoillot, J. C.; Asther, M.; Colom, J. F.; Martinez, A. T. Comparison of different fungal enzymes for bleaching high-quality paper pulps. *J. Biotechnol.* **2005**, *115*, 333−343.
(14) Topakas, E.; Vafiadi, C.; Christakopoulos, P. Microbial production, characterization and applications of feruloyl esterases. *Process Biochem.* **2007**, *42*, 497−509.
(15) Wong, W. L.; Abdulla, M. A.; Chua, K. H.; Kuppusamy, U. R.; Tan, Y. S.; Sabaratnam, V. Hepatoprotective effects of *Panus giganteus* (Berk.) Corner against thioacetamide- (TAA-) induced liver injury in rats. *Evidence-Based Complement. Altern. Med.* **2012**, DOI: 10.1155/2012/170303.
(16) Wang, Y.; Ou, S. Y. Preparation of xylooligosaccharides from wheat bran. *J. Hunan Agric. Univ.* **2009**, *35*, 441−445 (in Chinese).
(17) Ralet, M. C.; Faulds, C. B.; Williamson, G.; Thibault, J. F. Degradation of feruloylated oligosaccharides from sugar-beet pulp and wheat bran by ferulic acid esterases from *Aspergillus niger*. *Carbohydr. Res.* **1994**, *263*, 257−269.
(18) Laemmli, U. K.; Favre, M. Maturation of head of bacteriophage-T4. *J. Mol. Biol.* **1973**, *80*, 575−599.
(19) Wang, S. X.; Liu, Y.; Zhang, G. Q.; Zhao, S.; Xu, F.; Geng, X. L.; Wang, H. X. Cordysobin, a novel alkaline serine protease with HIV-1 reverse transcriptase inhibitory activity from the medicinal mushroom *Cordyceps sobolifera*. *J. Biosci. Bioeng.* **2012**, *113*, 42−47.
(20) Faulds, C. B.; Williamson, G. Purification and characterization of 4-hydroxy-3-methoxy cinnamic acid esterase from *Streptomyces olivochromogenes*. *J. Gen. Microbiol.* **1991**, *137*, 2339−2345.
(21) Xie, C. Y.; Gu, Z. X.; You, X.; Liu, G.; Tan, Y.; Zhang, H. Screening of edible mushrooms for release of ferulic acid from wheat bran by fermentation. *Enzyme Microb. Technol.* **2010**, *46*, 125−128.
(22) Linke, D.; Matthes, R.; Nimtz, M.; Zorn, H.; Bunzel, M.; Berger, R. G. An esterase from the basidiomycete *Pleurotus sapidus* hydrolyzes feruloylated saccharides. *Appl. Microbiol. Biot.* **2013**, *97*, 7241−7251.
(23) Topakas, E.; Stamatis, H.; Biely, P.; Christakopoulos, P. Purification and characterization of a type B feruloyl esterase (StFAE-A) from the thermophilic fungus *Sporotrichum thermophile*. *Appl. Microbiol. Biot.* **2004**, *63*, 686−690.
(24) Hegde, S.; Muralikrishna, G. Isolation and partial characterization of alkaline feruloyl esterases from *Aspergillus niger* CFR 1105 grown on wheat bran. *World J. Microbiol. Biotechnol.* **2009**, *25*, 1963−1969.
(25) Crepin, V. F.; Faulds, C. B.; Connerton, I. F. A non-modular type B feruloyl esterase from *Neurospora crassa* exhibits concentration-dependent substrate inhibition. *J. Biochem.* **2003**, *370*, 417−427.
(26) Shin, H. D.; Chen, R. R. A type B feruloyl esterase from *Aspergillus nidulans* with broad pH applicability. *Appl. Microbiol. Biotechnol.* **2007**, *73*, 1323−1330.
(27) Chandrasekaran, G.; Kim, G. J.; Shin, H. J. Purification and characterisation of an alkaliphilic esterase from a culinary medicinal mushroom *Sparassis crispa*. *Food Chem.* **2011**, *124*, 1376−1381.
(28) Ertunga, N. S.; Cakmak, U.; Colak, A.; Faiz, O.; Sesli, E. Characterisation of esterolytic activity from two wild mushroom species, *Amanita vaginata* var. *vaginata* and *Tricholoma terreum*. *Food Chem.* **2009**, *115*, 1486−1490.
(29) Colak, A.; Camedan, Y.; Faiz, O.; Sesli, E.; Kolcuoglu, Y. An esterolytic activity from a wild edible mushroom *Lycoperdon perlatum*. *J. Food Biochem.* **2009**, *33*, 482−499.
(30) Liu, X.; Ding, S. Molecular characterization of a new acetyl xylan esterase (AXEII) from edible straw mushroom *Volvariella volvacea* with both de-*O*-acetylation and de-*N*-acetylation activity. *FEMS Microbiol. Lett.* **2009**, *295*, 50−56.
(31) Faulds, C. B.; Williamson, G. Release of ferulic acid from wheat bran by a ferulic acid esterase (FAE-III) from *Aspergillus niger*. *Appl. Microbiol. Biotechnol.* **1995**, *43*, 1082−1087.
(32) Saulnier, L.; Vigouroux, J.; Thibault, J. F. Isolation and partial characterization of feruloylated oligosaccharides from maize bran. *Carbohydr. Res.* **1995**, *272*, 241−253.

Table 1. Presence of CPFA Detected by GC-MS Analysis in Milk Samples[a]

	no. of samples	no. of samples positive to CPFA[b]	percentage of CPFA in positive samples	
			mean ± SD[c]	min − max[c]
raw bulk milk of different origin				
Lombardy (Italy)	6	6	0.080 ± 0.009	0.065−0.093
Veneto (Italy)	5	5	0.028 ± 0.009	0.014−0.039
Emilia Romagna (Italy)	2	2	0.038 ± 0.006	0.030−0.045
Piedmont (Italy)	2	2	0.067 ± 0.002	0.062−0.070
Austria	2	1	0.065 ± 0.001[d]	
Germany	5	2	0.039 ± 0.002	0.030−0.045
commercial cow milk samples (Parma market, Italy)	6	4	0.06 ± 0.03	0.031−0.105
goat milk (Parma market, Italy)	6	0	nd	
sheep milk (Parma farms, Italy)	6	0	nd	
yak milk (China)	10	0	nd	

[a]Results are reported as mean ± SD, minimum and maximum for homogeneous groups of samples. [b]Positivity for values ≥0.01% of the total fat content. [c]With respect to the total chromatographic area of fatty acid methyl esters. [d]Mean ± SD of replicate analyses of the only positive sample.

survey on the presence of CPFA in dairy samples from different animal sources such as milk, cheeses, yogurt, other fermented milks, and butter, in order to obtain a deeper knowledge on the mechanisms involved in the transfer of CPFA from the bacterial cell walls to milk fat.

MATERIALS AND METHODS

Sampling. *Milk Samples (Table 1).* Samples of bovine bulk milk were collected from stables in different Italian regions (Lombardy, Veneto, Emilia Romagna, Piedmont), Austria, and Germany and provided by Parmalat Spa. Six different brands of commercial milks, two of them coming from Italian alpine regions, were purchased on the market, together with six samples of goat milk. Six samples of sheep milk were from local farms (Parma). Additionally, ten samples of yak (*Bos grunniens*) milk coming from China were provided by Animal Science Department of Qinghai University, China.

Yogurt and Fermented Milk (Table 2). Parmalat Spa (Parma, Italy) provided the experimental milks fermented with the following combination of microorganisms. Fermentations were conducted at 42 °C for 12 h.

Trial A: *Bifidobacterium infantis* + *Lactobacillus acidophilus*

Trial B: *Lactobacillus paracasei*

Trial C: *Lactobacillus bulgaricus* + *Streptococcus thermophilus (Yogurt)*

Trial D: *Lactococci*

Each milk sample was analyzed before the addition of bacteria, after the inoculum, and then sampled at 10, 20, 30 days of the shelf life (stored refrigerated at 4 °C). Two series of experiments were conducted, utilizing bulk milk samples collected in winter or in summer.

Cheese Samples. A total of 125 cheese samples were analyzed for their CPFA content. Samples of grated Parmigiano-Reggiano (10 samples) and Grana Padano cheeses (10 samples) were purchased on the market. Additionally, 15 samples of certified Grana Padano and 15 samples of certified Parmigiano-Reggiano were provided by Consorzio del Formaggio Parmigiano-Reggiano (Reggio Emilia, Italy). Ten samples of Asiago cheese from lowland and from highland farms were provided by Padua University (Italy). Other cheese samples coming from milk of different species (cow, goat, and sheep) having different production technologies (Table 3) were purchased on the market.

Butter. Seven samples of commercial butter were purchased on the market, including one sample from a farm producing milk for Parmigiano-Reggiano cheese, one from an alpine farm, and one from goat milk.

Sample Preparation for GC-MS Analysis of Milk Fat and Cheese. Ten grams of milk/fermented milk was mixed for 1 min with 1 mL of 33% ammonia (Carlo Erba, Milan, Italy). The mixture was then extracted twice with 20 mL of hexane/acetone (2/1 v/v) (Sigma-Aldrich, Saint Louis, MO, USA) in a separatory funnel; the organic phase was then recovered and evaporated to dryness under vacuum. As regards the cheese analysis, 0.5 g of grated sample was stirred with a hexane/acetone mixture (20 mL, 4/1 v/v) and then filtered on paper. The organic phase was evaporated to dryness. Butter was directly submitted to the following steps.

Table 2. Presence of CPFA Detected by GC-MS Analysis in Fermented Milk Samples[a]

	percentage of CPFA[b]	
	winter starting milk	summer starting milk
Pasteurized Milk		
	0.038 ± 0.005	0.043 ± 0.003
Milk Fermented with *Bifidobacterium infantis* + *Lactobacillus acidophilus*		
zero time	0.044 ± 0.004	0.044 ± 0.005
10 days	0.042 ± 0.003	0.036 ± 0.004
20 days	0.041 ± 0.005	0.047 ± 0.001
30 days	0.037 ± 0.003	0.052 ± 0.006
Milk Fermented with *Lactobacillus paracasei*		
zero time	0.039 ± 0.002	0.042 ± 0.004
10 days	0.037 ± 0.002	0.039 ± 0.003
20 days	0.040 ± 0.003	0.044 ± 0.005
30 days	0.038 ± 0.003	0.047 ± 0.004
Milk Fermented with *Lactobacillus bulgaricus* + *Streptococcus thermophilus* (Yogurt)		
zero time	0.038 ± 0.002	0.042 ± 0.005
10 days	0.036 ± 0.004	0.041 ± 0.004
20 days	0.043 ± 0.004	0.047 ± 0.003
30 days	0.030 ± 0.003	0.039 ± 0.004
Milk Fermented with Lactococci		
zero time	0.040 ± 0.004	0.041 ± 0.004
10 days	0.035 ± 0.003	0.038 ± 0.003
20 days	0.036 ± 0.004	0.051 ± 0.006
30 days	0.034 ± 0.003	0.045 ± 0.004

[a]Results are reported as mean ± SD of replicate analysis. [b]With respect to the total chromatographic area of fatty acid methyl esters.

100 mg of fat recovered was dissolved in hexane (5 mL) and mixed for 1 min with 2 mL of KOH 5% (Carlo Erba, Milan, Italy) in methanol (Sigma-Aldrich, Saint Louis, MO, USA). After phase separation, the superior organic phase was injected (1 μL, split mode) on an Agilent Technologies 6890N gas chromatograph (Agilent Technologies, Palo Alto, CA, USA) coupled to an Agilent Technologies 5973 mass spectrometer (Agilent Technologies, Palo Alto, CA, USA). A low-polarity capillary column (SLB-5 ms, Supelco, Bellefonte, PA, USA) was used. The chromatogram was recorded in the scan mode (40−500 m/z) with a programmed temperature from 40 to 280 °C. Peak identity of CPFA was confirmed by comparison

dx.doi.org/10.1021/jf4057204 | J. Agric. Food Chem. 2014, 62, 7828−7832

Table 3. Presence of CPFA Detected by GC-MS Analysis in Cheese and Butter Samples[a]

cheese	no. of samples	no. of samples positive to CPFA[b]	percentage of CPFA in positive samples	
			mean ± SD[c]	range[c]
cow cheeses				
Parmigiano-Reggiano (Emilia Romagna, Italy)	15	0	nd	
Grana Padano (Lombardy, Italy)	15	15	0.15 ± 0.04	0.06−0.23
commercial grated Parmigiano-Reggiano (Emilia Romagna, Italy)	10	0	nd	
commercial grated Grana Padano (Lombardy, Italy)	10	10	0.08 ± 0.01	0.06−0.10
Taleggio (Lombardy, Italy)	2	2	0.06 ± 0.02	0.044−0.086
Gorgonzola (Lombardy, Italy)	3	3	0.15 ± 0.09	0.047−0.251
Bitto Valtellina (Lombardy, Italy)	2	0	nd	
cheeses from Piedmont (Italy)	4	4	0.07 ± 0.04	0.046−0.130
Fontina (Aosta Valley, Italy)	6	0	nd	
Montasio (Friuli Venezia Giulia, Italy)	3	3	0.08 ± 0.03	0.042−0.106
Asiago (Veneto, Italy)	10	5	0.04 ± 0.02	0.014−0.066
Mascarpone (Italy)	3	3	0.08 ± 0.05	0.022−0.130
Camoscio (Italy)	3	3	0.09 ± 0.04	0.048−0.138
Emmenthal (Switzerland)	4	0	nd	
Sbrinz (Switzerland)	2	0	nd	
Gruyere (Switzerland)	4	0	nd	
Emmenthal (French)	2	2	0.039 ± 0.001	0.038−0.041
Brie (French)	3	3	0.036 ± 0.009	0.025−0.047
Commercial cheeses (Netherland)	2	2	0.029 ± 0.001	0.028−0.030
sheep cheeses				
Pecorino (Tuscany, Sardinia, Lazio, Italy)	13	0	nd	
Roquefort (French)	2	0	nd	
Ricotta (Italy)	2	0	nd	
goat cheeses				
commercial goat cheese (Italy)	3	0	nd	
Quatre feuilles (French)	2	0	nd	
commercial butters (Italy)	7	4	0.04 ± 0.02	0.018−0.067

[a]Results are reported as mean ± SD, minimum and maximum for homogeneous groups of samples. [b]Positivity for values ≥0.01%. [c]With respect to the total chromatographic area of fatty acid methyl esters.

with bacterial acid methyl ester (BAME) mix standard containing cyclopropane fatty acid methyl esters (Sigma-Aldrich, Saint Louis, MO, USA). Content of CPFA was reported as relative percentage response area (%) of the corresponding peak (evidenced in Figure 2) with respect to the total chromatographic area from GC-MS analysis of the other main methyl esters of fatty acids (including C4:0, C6:0, C8:0, C10:1, C10:0, C11:0, C12:1, C12:0, C13:0, C14:0iso, C14:1, C14:0, C15:0iso, C15:0anteiso; C15:1, C15:0, C16:0iso, C16:1, C16:0, C17:0iso, C17:0anteiso, C17:1, C17:0, C18:2, C18:1, C18:0, C18:2cla, C19:1, C19:0, C20:4, C20:3, C20:1, C20:0, C21:0, C22 PUFA, C22:0, C23:0, C24:0).

Data Analysis. Data are obtained as duplicate analysis of two independent sample extractions and are presented as mean ± SD of groups of homogeneous samples. The range (minimum and maximum value) of CPFA was also provided. Positivity or negativity of samples to CPFA was defined on the basis of the threshold of 0.01% (CPFA with respect to total chromatographic area of fatty acid methyl esters); this value corresponds to the experimental detection limit, calculated at a signal-to-noise ratio >3. For fermented milk samples, one-way ANOVA and post hoc Tukey-HSD tests at a p level = 0.05 (n = 4) were performed to detect an eventual effect of fermentation and shelf life on CPFA content. All the statistical analyses were performed utilizing SPSS statistical software (Version 20.0, SPSS Inc., Chicago, Illinois, USA).

RESULTS AND DISCUSSION

Milk Samples. We previously showed that 80 samples of milk from cows fed with maize silage were found positive for the presence of CPFA (0.08 to 0.12%). In contrast, 140 samples of milk from cows fed with forage without maize silages were all negative.[9] In this paper, we extend the investigation on the presence of CPFA to about 50 other milk samples, comprising commercial milk samples, bulk raw milk collected from different regions of Italy, countries of the European Union, and China, and milk from different animal species. The content of CPFA detected in cow milk varies greatly according to region of origin, and different trademarks (Table 1). The majority of the cow milk samples collected resulted positive to CPFA, reflecting a large use of ensiled products in cows' feeding. The collections of milk from Austria and Veneto (Italy) areas show values of CPFA lower than those collected in Emilia Romagna and Lombardy (Brescia, Milan, Reggio Emilia). Among commercial cow milk samples, the two samples negative to CPFA come from mountain regions. Goat, sheep, and yak milks analyzed were all negative to CPFA, indicating that the feeding system is fundamental for the presence of these fatty acids in milk; in fact, these animals are usually fed with pasture grass or, during the winter, with hay.

Fermented Milks. CPFA are reported to be present in large amount in cytoplasmic membrane fatty acids of LAB as *Lactobacillus bulgaricus*, *Lactobacillus helveticus*, *Lactobacillus acidophilus*,[15−17] and *Lactobacillus casei*,[18] so it would be expected that they were released in fermented products in significant amounts. To confirm this hypothesis, experimental fermented milks were prepared inoculating different combinations of microorganisms, as reported in Materials and Methods.

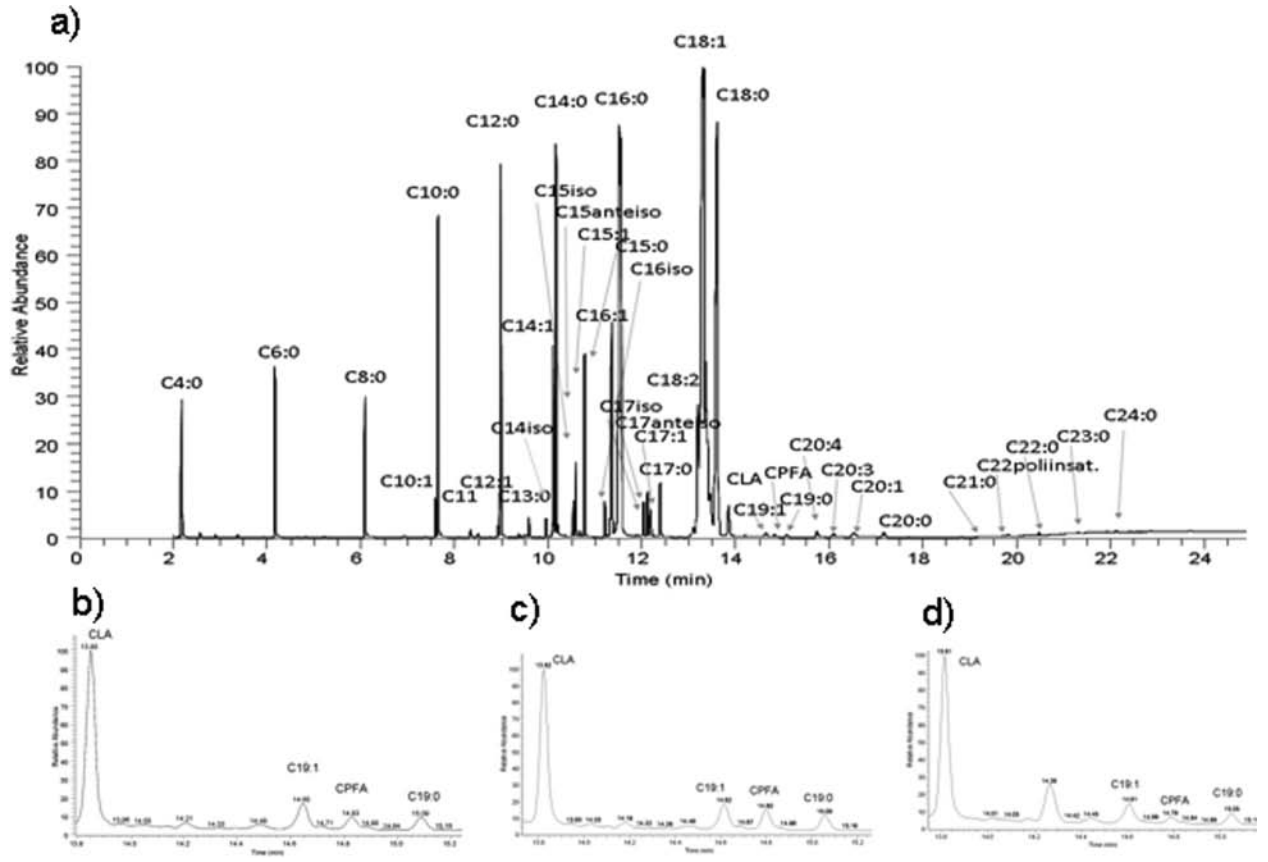

Figure 2. (a) GC-MS chromatogram of Grana Padano cheese sample fatty acid methyl esters on a SLB5 capillary column and details of the elution zone of CPFA for (b) Grana Padano, (c) milk from Lombardy, and (d) commercial butter. The CPFA peak corresponds to the sum of dihydrosterculic and lactobacillic acid.

Fermented milk samples were tested for the content of CPFA and compared with the content in the starting milk (Table 2). Results showed that starting bulk milks for yogurt/fermented milk productions were positive to CPFA, containing mean percentages of CPFA of 0.041%, with no significant differences (ANOVA test, $p > 0.05$) between milk collected in summer (0.043%) and milk collected in winter (0.038%). Fermented milks and yogurt maintained the percentages of CPFA present in the starting milk; in fact, the CPFA contents of fermented products are not significantly different (Tukey multiple comparisons, p level 0.05, $n = 4$) from starting milk, in all the experiments conducted with different microorganisms. Moreover, CPFA content does not change during the shelf life of the products. These results demonstrate that the most common microorganisms tested and utilized for yogurt or fermented milks production (*Bifidobacterium infantis*, *Lactobacillus acidophilus*, *Lactobacillus paracasei*, *Lactobacillus bulgaricus*, *Streptococcus thermophilus*, and Lactococci) are not able to release significant amounts of CPFA in the medium and to incorporate them in triglycerides. Therefore, we can conclude that the amount of CPFA found in fermented milks derives only from their initial content in milk and not from the fermentation process.

Cheeses. Many different kinds of cheeses were analyzed, focalizing the attention on two important Italian PDO hard cheeses, i.e., Parmigiano-Reggiano and Grana Padano. The results showed that all the samples of Parmigiano-Reggiano (both commercial grated products and samples certified from Consorzio del Formaggio Parmigiano-Reggiano) are negative to CPFA, while samples of Grana Padano tested are all positive (Table 3). Results obtained for these two cheeses reinforce the hypothesis that the CPFA presence in milk derives from the incorporation in milk triglycerides of the cellular bacterial fatty acids detected in the ensiled products.[9] In fact, the product specifications for Parmigiano-Reggiano[19] prohibit the use of silages for feeding cows, while the specification rules for Grana Padano[20] allow the use of silages. Consequently, the control of CPFA in milk fat could be considered as a quality parameter for cheese productions that prohibit the use of silage feeding. Cheeses coming from mountain regions as Swiss cheeses (Emmenthal, Gruyere) and Aosta Valley (Fontina, Italy) were negative to CPFA, indicating that the use of ensiled forages is infrequent.

Goat and sheep cheeses (fresh or seasoned, from several Italian regions) are exempt of CPFA, confirming data reported for milk of these two species.

The absence of CPFA in Parmigiano-Reggiano, as well as in other cheeses reported in Table 3, confirms the hypothesis that lactic acid bacteria are not able to release detectable amounts of CPFA in dairy products during manufacturing and seasoning steps.

Butter. Among the seven commercial butters analyzed, four were positive to CPFA, showing variable CPFA contents (Table 3), and three were negative. The negative samples were butter declared of alpine origin, butter produced from milk for Parmigiano-Reggiano production, and goat butter, further confirming data reported for goat milk and cheese.

dx.doi.org/10.1021/jf4057204 | J. Agric. Food Chem. 2014, 62, 7828−7832

Due to the limited number of butter samples analyzed, further studies are needed to confirm these results.

Summarizing, our results suggest that the presence of CPFA in milk and dairy products is derived from their presence in silage forages, where CPFA can be released by bacteria during silage fermentation conditions. On the contrary, lactic acid bacteria, ubiquitous in fermented milk and cheeses, seem not to be able to release CPFA in the conditions of milk fermentation. Therefore, CPFA can be considered interesting molecular markers, able to distinguish milk from dairy cows fed with silage-based diet from milk from cows fed with hay-based diets.

The analysis of CPFA can be a useful tool of the quality control for PDO cheeses, such as Parmigiano-Reggiano, whose specifications of production do not allow the use of silages, as well as a marker to differentiate high quality dairy products such as milk, cheese, and yogurt from alpine regions, where cattle feeding is based only on pasture and hay. Further analytical work on feed is in progress to confirm the presence of CPFA in all ensiled feeds.

AUTHOR INFORMATION

Corresponding Author

*Tel: +39 0521 905407. Fax: +39 0521 905472. E-mail: augusta.caligiani@unipr.it.

Notes

The authors declare no competing financial interest.

REFERENCES

(1) Vickery, J. Fatty acid composition of seed oils from 10 plant families with particular reference to cyclopropene and dihydrosterculic acids. *J. Am. Oil Chem. Soc.* **1980**, *57*, 87−91.

(2) Gaydou, E. M.; Ralaimanarivo, A.; Bianchini, J. P. Cyclopropanoic fatty acids of litchi (litchi-chinensis) seed oil—A reinvestigation. *J. Agric. Food Chem.* **1993**, *41*, 886−888.

(3) Grogan, D. W.; Cronan, J. E. Cyclopropane ring formation in membrane lipids of bacteria. *Microbiol. Mol. Biol. Rev.* **1997**, *61*, 429−441.

(4) Russell, N. J.; Evans, R. I.; Ter Steeg, P. F.; Hellemons, J.; Verheul, A.; Abee, T. Membranes as a target for stress adaptation. *Int. J. Food Microbiol.* **1995**, *28*, 255−261.

(5) Shabala, L.; Ross, T. Cyclopropane fatty acids improve *Escherichia coli* survival in acidified minimal media by reducing membrane permeability to H^+ and enhanced ability to extrude H^+. *Res. Microbiol.* **2008**, *159*, 458−461.

(6) Gómez Zavaglia, A.; Disalvo, A. E.; De Antoni, L. G. Fatty acid composition and freeze-thaw resistance in Lactobacilli. *J. Dairy Res.* **2000**, *67*, 241−247.

(7) Ehrmann, M. A.; Vogel, R. F. Molecular taxonomy and genetics of sourdough lactic acid bacteria. *Trends Food Sci. Technol.* **2005**, *16*, 31−42.

(8) Montanari, C.; Sado Kamdem, S. L.; Serrazanetti, D. I.; Etoa, F. X.; Guerzoni, M. E. Synthesis of cyclopropane fatty acids in *Lactobacillus helveticus* and *Lactobacillus sanfranciscensis* and their cellular fatty acids changes following short term acid and cold stresses. *Food Microbiol.* **2010**, *27* (4), 493−502.

(9) Marseglia, A.; Caligiani, A.; Comino, L.; Righi, F.; Quarantelli, A.; Palla, G. Cyclopropyl and ω-cyclohexyl fatty acids as quality markers of cow milk and cheese. *Food Chem.* **2013**, *140* (4), 711−716.

(10) Johnson, L. M.; Harrison, J. H.; Davidson, D.; Mahanna, W. C.; Shinners, K. Corn silage management: effectts of hybrid, maturity, inoculation, and mechanical processing on fermentation characteristics. *J. Dairy Sci.* **2003**, *86*, 287−308.

(11) Lin, C. J.; Bolsen, K. K.; Brent, B. E.; Fung, D. Y. C. Epiphytic lactic-acid bacteria succession during the pre-ensiling and ensiling periods of alfalfa and maize. *J. Appl. Bacteriol.* **1992**, *73*, 375−387.

(12) Stevenson, D.; Muck, R.; Shinners, K.; Weimer, P. Use of real time PCR to determine population profiles of individual species of lactic acid bacteria in alfalfa silage and stored corn stover. *Appl. Microbiol. Biotechnol.* **2006**, *71*, 329−338.

(13) Rossi, F.; Dellaglio, F. Quality of silages from Italian farms as attested by number and identity of microbial indicators. *J. Appl. Microbiol.* **2007**, *103*, 1707−1715.

(14) Brusetti, L.; Borin, S.; Mora, D.; Rizzi, A.; Raddadi, N.; Sorlini, C.; Daffonchio, D. Usefulness of length heterogeneity-PCRfor monitoring lactic acid bacteria succession during maize ensiling. *FEMS Microbiol. Ecol.* **2006**, *56*, 154−164.

(15) Rizzo, A. F.; Korkeala, H.; Mononen, I. Gas chromatography analysis of cellular fatty acids and neutral monosaccharides in the identification of lactobacilli. *Appl. Environ. Microbiol.* **1987**, *53*, 2883−2888.

(16) Guillot, A.; Obis, D.; Mistou, M. Y. Fatty acid membrane composition and activation of glycine-betaine transport in *Lactococcus lactis* subjected to osmotic stress. *Int. J. Food Microbiol.* **2000**, *55*, 47−51.

(17) Béal, C.; Fonseca, F.; Corrieu, G. Resistance to freezing and frozen storage of *Streptococcus thermophilus* is related to membrane fatty acid composition. *J. Dairy Res.* **2001**, *84*, 2347−2356.

(18) Broadbent, J. R.; Larsen, R. L.; Deibel, V.; Steele, J. L. Physiological and Transcriptional Response of *Lactobacillus casei* ATCC 334 to Acid Stress. *J. Bacteriol.* **2010**, *5*, 2445−2458.

(19) Regulation (EU) N. 794/2011.

(20) Regulation (EU) N. 584/2011.

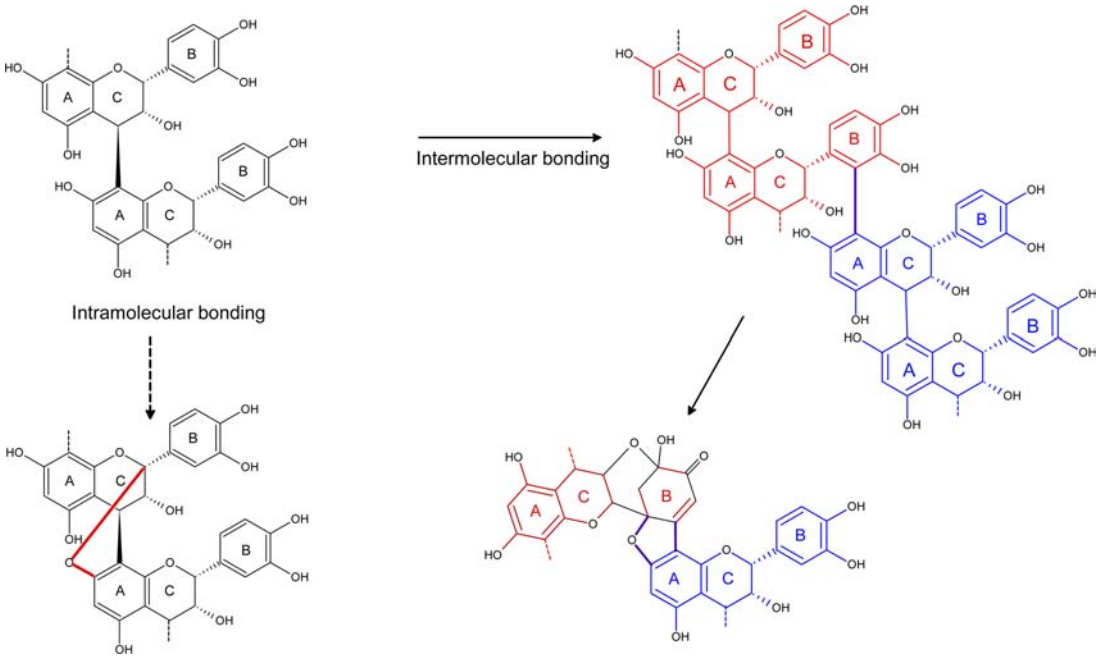

Figure 1. Examples of chemical structures of oxidized tannins. According to current knowledge on monomers and dimers, the creation of new bonds may occur on the same macromolecule (intramolecular bonding) leading to the formation of an A-type tannin or between two macromolecules (intermolecular bonding). In the case of intermolecular reactions, the new bond is formed between A and B rings. Further oxidation may lead to additional cyclization between rings A and B.

and 10 g/L) for DP14 tannins. At high concentrations, we observed an increase of the weight average molecular weight of tannins upon autoxidation, attributed to intermolecular reactions.[16] Our results also suggested that the concentration of tannins during autoxidation could play a key role in the competition intermolecular reaction versus intramolecular reaction.[15] Working with oxidized tannins, Zanchi et al.[17] observed only the formation of intramolecular bonds, but they worked in more dilute conditions and separated the fractions on chromatographic supports prior to SAXS experiments.

Our present objectives were as follows: (i) to confirm that tannins are semiflexible polymers, working with a broader range of tannin fractions, from DP6 to DP80; (ii) to assess the impact of oxidation on the conformation of tannins; and (iii) to determine the key parameters that rule the formation of intermolecular or intramolecular bonds upon autoxidation reactions, especially the impact of the initial DP and concentration of tannins.

To answer these questions, six different fractions of native apple tannins were studied, and kinetics of oxidation were monitored with two different DP for forty days and at two different concentrations. These concentrations, 0.1 and 5 g/L, were chosen as representative of white and red wine conditions, respectively. Apple condensed tannins were first studied instead of grape condensed tannins due to their simpler structure.

MATERIALS

Deionized water was obtained with a Milli-Q system (Millipore, Billerica, MA, USA). Chemicals (solvents, organic acids, and reagents) were of analytical grade and purchased from VWR and Merck (Hohenbrunn, Germany). Freeze-dried powder of apple (*Malus domestica*) cortex tissues were kindly prepared and provided by S. Guyot (Unité de Recherches Cidricoles, INRA Rennes, France), and different apple tannin fractions were purified as described before.[18,16] These fractions are referred to as DPX, with X being the number average molecular weight determined by depolymerization methods, coupled with HPLC analysis.[15] These native fractions were used to get the relationship between the average DP and the scattering intensity at null Q obtained from SAXS experiments.

Apple tannin fractions were oxidized at pH 3.5 (which is considered as a relevant pH in enology) to study the effect of concentration on oxidation mechanisms (intra- vs intermolecular reactions), according to the procedure described before,[16] either in dilute (0.1 g/L) or concentrated (5 g/L) solutions. Typically, native tannins were dissolved in deionized water, the pH of which was adjusted to 3.5 with trifluoroacetic acid. The solutions were centrifuged (100 000*g*, 90 min, 20 °C) to remove insoluble species. The supernatants were stirred at 25 °C in sealed vials to prevent any additional oxygen intake. At low concentrations, typically 10 mg of tannins (34.5 μmoles of flavanol units) was dissolved in 100 mL of buffer containing 26 μmoles of oxygen and put in a 125 mL flask (headspace of 25 mL corresponding to ∼215 μmoles of O_2): in these conditions, O_2 was in large excess (almost 7 equiv). At higher concentrations, typically 15 mg of tannins (52 μmoles) was dissolved in 3 mL of buffer containing 0.78 μmoles of O_2. The volume of the vials was 10 mL; thus, the headspace was 7 mL (60 μmoles of O_2), resulting in a slight excess of oxygen (1.2 equiv). Oxidation was followed by UV−visible spectroscopy and depolymerization reactions after 7, 14, 26, and 40 days.

Oxidations were stopped after 7, 14, 26, and 40 days; samples were pulled, freeze-dried, and kept under argon, in sealed vials, protected from light to avoid further oxidation and at −80 °C. Samples will be referred to as DPXox dil or conc (for dilute or concentrated oxidation) yd, with y being the duration of oxidation in days. For example, DP6ox conc 40d stands for an initially DP6 tannin fraction oxidized for 40 days at a concentration of 5 g/L.

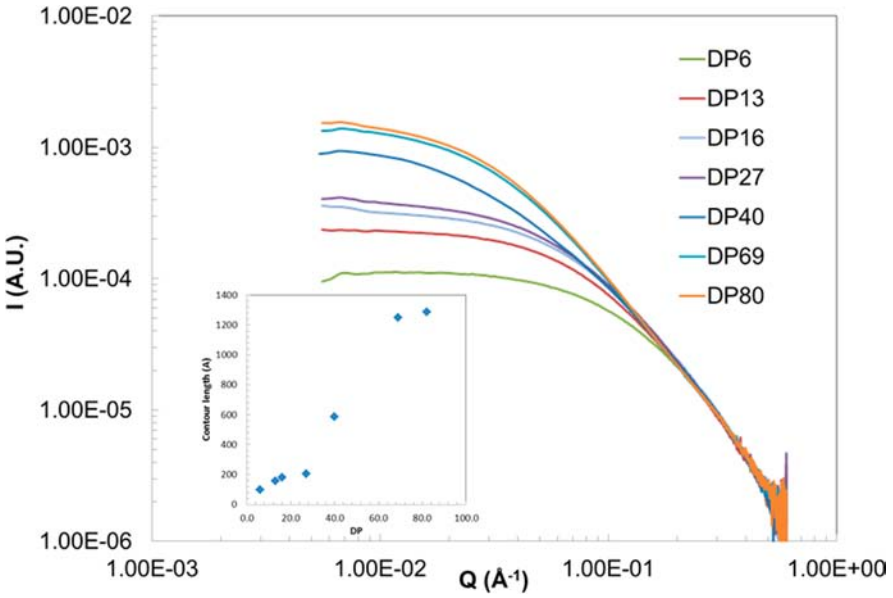

Figure 2. SAXS intensity (normalized by concentration) of native tannins in the log I−log Q representation. DP40 results[16] were included in the graph. In the insert: the persistence length L obtained for the native tannin fractions by fitting SAXS spectra with the WLC model[21] increases linearly with DPn up to DP40.

METHODS

UV−Visible Spectroscopy. UV−visible experiments were carried out on a UV−visible UV Safas mc^2 spectrophotometer at 25 °C. Spectra of the native and oxidized fractions were recorded in ethanol, from 250 to 700 nm.

Depolymerization of Tannins and HPLC-DAD Analysis. Depolymerization was carried out with 100 μL of tannin solution (at a concentration of 1g/L in methanol) combined with 100 μL of a solution of nucleophile (0.8% v/v thioglycolic acid solution in 0.2 M HCl in methanol). The mixture was heated at 90 °C for 6 min and then cooled in cold ice. HPLC analysis followed the conditions described by Vernhet et al.[15] The DPn was calculated as the ratio between the summed molar concentrations of all released monomer constitutive units and the summed molar concentrations of terminal constitutive units.

Small-Angle X-ray Scattering. SAXS experiments were performed on the beamline SWING, at Synchrotron Soleil (Saint-Aubin, France). The incident beam energy was 10.5 keV (λ = 1.18 Å), and the distance from the sample to the Aviex CCD detector was 1500 mm. The corresponding scattering vector $Q = 4\pi \sin\theta/\lambda$ ranged from 0.007 to 0.575 Å^{-1}, where 2θ is the scattering angle and λ is the incident wavelength. Experiments were performed at 25 °C. Several successive frames (typically 10) of 1 s each were recorded for both the sample and the solvent (EtOH). It was checked that X-rays did not cause any damage to the polyphenol molecules by comparing successive frames. The average intensity and experimental error of each set of frames were subsequently computed. Scattering from the solvent was measured and subtracted from the corresponding intensity the of tannin solution.

The SAXS data were analyzed according to classical formulas for scattering from dispersions of particles or macromolecules in a homogeneous solvent.[14] For such dispersions, the intensity can be decomposed as a product of the intensity scattered by a single particle and a structure factor that describes interferences arising from different particles:

$$I(Q) = N_p(\rho_p - \rho_s)^2 V_p^2 P(Q) S(Q) \quad (1)$$

where ρ_p is the electron density of the particles and ρ_s is that of the solvent, V_p is the volume of a particle, N_p is the number of particles per unit volume, $P(Q)$ is the form factor of particle, and $S(Q)$ is the structure factor that describes the pair correlations between the positions of all particles. If the sample is a dilute solution, where the relative positions of the particles are not correlated, then $S(Q) = 1$ at all Q values. If the sample is a dilute solution of polydisperse macromolecules, the intensity scattered in the $Q \to 0$ limit is proportional to a weight average of the molecular weight M_w, or the DP, and the polymer concentration C:

$$I(Q \to 0) \propto M_w C(\rho_p - \rho_s)^2 \quad (2)$$

The form factor $P(Q)$ represents the shape of the particle and its internal electron density distribution. For macromolecules that behave like freely jointed chains, the form factor is given by the Debye scattering function[19] as a function of the reduced parameter $x = (QR_g)^2$ where R_g is the radius of gyration of the macromolecules:

$$P(x) = 2(e^{-x} + x - 1)^2/x^2 \quad (3)$$

Different models exist in the literature for particles or polymers. Scattering curves were fitted with the Sasfit software,[20] using different form factors: flexible chains fitted with eq 3; wormlike chain (WLC),[21] defined by three parameters: the contour length L of the semiflexible wormlike structure, its Kuhn length b, which is the length of the statistical segment or twice the persistence length, and the radius of gyration of the cross section of the chain, R_{cs}; self-similar branched polymers fitted with the Fisher−Burford (FB) approximation,[22] with two parameters that are the radius of gyration R_g and the self-similarity exponent D_f, also called the fractal dimension. The fractal dimension is a value that gives information on the polymer structure: for instance, D_f = 1.67 for a linear swollen polymer, 2 for a polymer in θ solvent and a swollen branched polymer, and 2.29 for a randomly branched ideal polymer.[23] In addition to the latter model, the impact of the chain thickness was accounted for in the Fisher−Burford model, using the following equation:

$$P_{FB,R_{cs}}(Q) = P_{FB}(Q) e^{-Q^2 R_{cs}^2/2} \quad (4)$$

where $P_{FB}(Q) = (1 + ({}^2/_3 D_f)x^2)^{-D_f/2}$ is the form factor calculated with the Fisher−Burford equation, whereas $P_{FB,R_{cs}}(Q)$ is the form factor obtained when the chain cross-section radius of gyration R_{cs} is taken into account.

dx.doi.org/10.1021/jf501441j | J. Agric. Food Chem. 2014, 62, 7833−7842

Table 1. Scattered Intensities Extrapolated to $Q \rightarrow 0$ I_0/C and Structural Parameters Derived from the Scattering Curves Using the Gaussian, Wormlike Chain, and Fischer–Burford Models[a]

	Gaussian			WLC					Fisher–Burford			
fraction	I_0/C	R_g (Å)	χ^2	I_0/C	L	b	R_{cs}	χ^2	I_0/C	R_g	D_f	χ^2
DP6	1.20×10^{-4}	15.6	36	1.08×10^{-4}	97	14.4	4.1	10	1.22×10^{-4}	15.8	2.63	11
DP13	2.70×10^{-4}	22.3	56	2.71×10^{-4}	158.3	17.9	4.9	12	2.79×10^{-4}	23.44	2.43	11.0
DP16	3.07×10^{-4}	24.6	103	3.03×10^{-3}	179.5	19.8	5.1	33	3.12×10^{-4}	27.15	2.31	26.4
DP27	3.90×10^{-4}	26.7	99	3.93×10^{-4}	203	20	5.3	46.6	4.00×10^{-4}	28.7	2.35	19.7
DP40[b]	*7.20 × 10⁻⁴*	*42.2*	*180*	*7.75 × 10⁻⁴*	*585*	*16.9*	*4.5*	*76*	*8.50 × 10⁻⁴*	*57*	*1.91*	*44.9*
DP69	1.30×10^{-3}	51.9	254	1.28×10^{-3}	1250	7.5	6.3	400	1.30×10^{-3}	57.2	2.25	17.6
DP80	1.60×10^{-3}	53.7	271	1.64×10^{-3}	1286	8	6.7	400	1.67×10^{-3}	58.2	2.28	11.5

[a] R_g: radius of gyration; L: contour length; b: Kuhn length; R_{cs}: radius of cross section; D_f: fractal dimension; χ^2 values are an indication of the quality of the fit. [b] Data taken from ref 16.

RESULTS AND DISCUSSION

As already described in previous papers,[14,15] we expected SAXS to provide information on the conformation of tannins and on the structural changes induced by autoxidation.[7,8,24] The conformation of native apple tannins was studied first. Then, changes induced by autoxidation were studied using two different techniques.

Conformation of Native Tannins. The conformation of native tannins was previously studied using mainly fractions of DP9 (from grape seeds) and DP40 (from apple parenchyma). In this paper, we studied six additional apple tannin fractions including higher molecular weight tannins (DP69 and DP80). The main constitutive unit in apple condensed tannins is (−)-epicatechin (95%), (+)-catechin being only present as the terminal unit.[25] The average DPs of the fractions, determined using acid-catalyzed depolymerization of the fractions in the presence of a nucleophilic reagent, were 6, 13, 16, 27, 69, and 80. The yields of the depolymerization reaction were in the range 65–80%. SAXS measurements were done in ethanol at 25 °C because it is considered as a good or θ solvent for native and oxidized tannins. SAXS intensities of all the native fractions are plotted on the Figure 2.

According to eq 2, I_0 is proportional to the weight average molecular weight M_w, and therefore, a relation with the number average molecular weight M_n calculated from the DPn obtained through the depolymerization method was expected. We obtained a linear relation between intensities from SAXS and molecular weights from depolymerization methods:

$$\frac{I_0}{c} = 3 \times 10^{-5} \times M_n \tag{5}$$

The correlation coefficient was 0.97. This is not excellent, probably because of discrepancies between the number average and the weight average molecular weights brought by a slight polydispersity of the fractions with the highest degree of polymerization. In the next section, the SAXS intensities from oxidized tannins will be compared with those of native tannins, and this relation will be used to evaluate their average molecular weights.

Geometrical parameters and scattered intensities at $Q \rightarrow 0$ were determined by fitting the curves with the Gaussian, WLC, and Fisher–Burford models (Table 1). The quality of the fit was evaluated with the χ^2 values: the best fits were the ones with the lowest χ^2 values. Concerning the structural parameters, best fits were obtained with the WLC model up to DP27, whereas the best results were obtained with the Fisher–Burford model for DP69 and DP80, which can be implemented using the cross-section radius, as explained in the next section. Results obtained previously with a DP40 tannin fraction[16] have been included in the results. Also, for this fraction, the best fits were obtained with the Fisher–Burford model.

The radius of gyration R_g of a linear macromolecular chain is expected to increase with the DP according to the following equation:

$$R_g = a\mathrm{DP}^{\nu} \tag{6}$$

where ν is the Flory coefficient and a is the length of the monomer unit.

Plotting ln R_g as a function of ln DP yielded ln R_g = 1.816 + 0.517 ln DP, with a correlation coefficient of 0.97. In our conditions, a equals ∼6.15 Å, which is in the same order of magnitude as results obtained by Martinez et al. using molecular modeling.[26] For polymers in θ conditions, ν equals 0.5, whereas it is 0.6 for a polymer in good solvent. With ν equals 0.517, we are somewhere in between. This can be partly explained by the fact that we do not work with monodisperse fractions and/or the fact that we work with macromolecules that are linear within the range 6–40 (less than one decade) and/or the fact that the polymer adopts an intermediate behavior.

Using the WLC model to fit SAXS spectra (Table 1), we obtained a value of the persistence length in the range 7.5–10 Å for DPs up to 40, whereas the radius of cross section was nearly 4.5–5 Å. These values were consistent with what we observed previously for a DP40,[15,16] and a good linear relationship was found between the contour length L and the DPn (insert in the Figure 2). The length per monomer L/DPn obtained from these values (12 Å) is consistent with the dimensions of the monomeric units.[26] However, for DP69 and DP80, this relationship was no longer observed: the persistence length dropped suddenly, along with an increase in R_{cs}, and the quality of the fit also dropped: the WLC model was no longer suitable for these two fractions.

Fisher–Burford fits were improved after considering that macromolecular chains have a thickness (Table 2). Up to DP40, the fractal dimensions and the cross-section radius remained constant. For DP69 and DP80, the fractal dimension increased to 2.20 and 2.25, suggesting denser objects: in the case of polymers, it could indicate the presence of ramifications.[23] In addition, the R_g values found for these two molecular weight fractions did not increase compared to the DP40 values (Table 1). The presence of ramifications was confirmed by the Kratky plots of the scattering curve (Figure 3): a point of inflection was observed with the DP69 and DP80,

Table 2. Scattered Intensities Extrapolated to $Q \rightarrow 0$ I_0/C, Radius of Gyration R_g, Fractal Dimension D_f, and Cross-Section Radius R_{cs} of Apple Tannin Fractions, χ^2 Values Are an Indication of the Quality of the Fit

fraction	I_0/C	R_g	D_f	R_{cs}	χ^2
DP6	1.20×10^{-4}	16.0	2.0	2.6	14.9
DP13	2.79×10^{-4}	24.6	2.0	2.5	13.1
DP16	3.20×10^{-4}	27.9	2.0	2.5	9.8
DP27	4.20×10^{-4}	31.1	2.0	2.5	16.1
DP40[a]	*8.60×10^{-4}*	*60.5*	*1.7*	*2.8*	*13.5*
DP69	1.30×10^{-3}	56.5	2.25	1.5	43.5
DP80	1.59×10^{-3}	59	2.2	1.0	58.1

[a]Data taken from ref 16.

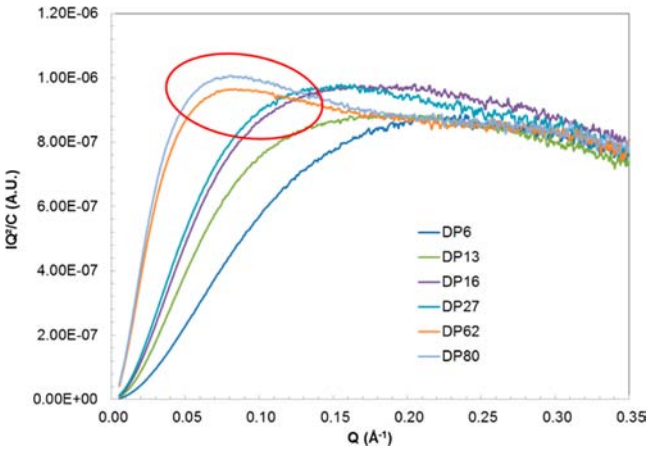

Figure 3. Kratky plots of native tannins fractions. The inflection points observed with DP62 and DP80 are consistent with branched and/or star polymers.

which is consistent with the appearance of branched macromolecules. This is in agreement with the results obtained by Zanchi et al.[17] using ab initio modeling and Gasbor on apple parenchyma tannins having DPs of 75 and 150.

To summarize, results obtained here and in previous experiments are consistent with the fact that tannins extracted from apple parenchyma (i.e., epicatechin polymers) were linear macromolecules up to DP~40 and became more or less branched at higher DPs. However, it was previously shown that oxidation can induce branching,[16] and thus, the fact that branching is due to oxidation cannot be ruled out, whether it takes place *in planta* or during extraction.

Oxidized Tannins. SAXS experiments were performed on oxidized fractions in order to get information on (i) the evolution of the molecular weight of tannins upon oxidation and (ii) the branching versus elongation of macromolecules. Especially, we wanted to check the impact of the initial tannin DP and concentration. The two tannin fractions used were the DP6 and DP16, autoxidized either at 0.1 or 5 g/L. These concentrations were chosen to emphasize the concentration effect: intramolecular reactions were expected to be favored at low concentration, because in these conditions, a macromolecular chain has more chances to react with itself rather than with its neighbors. On the contrary at higher concentrations, the formations of both inter- and intramolecular bonds are expected. UV−visible spectra (Figure S1, Supporting Information) exhibited typical changes usually observed upon oxidation of tannins, that is, the appearance of humps at 320 and 420 nm.

In parallel, the yields of the acid-catalyzed depolymerization reaction dropped (Table 3). This was attributed to the absence of cleavage of new covalent bonds created by oxidation[12] and was used to evaluate the extent of tannin oxidation, as described later.

Oxidation in "Concentrated" Systems. During oxidation, the visual aspect of solutions evolved: apparition of color changes and of a slight haze after 40 days. After centrifugation, tannins in the pellet were freeze-dried and weighed; they represented about 5%, except for DP6 after 40 days where they represented nearly 20%. They were disregarded for further experiments.

The proportion of decrease of depolymerization yield was calculated as

$$\left(1 - \frac{\text{depolymerization yield after } n \text{ days}}{\text{initial depolymerization yield}}\right) \times 100 \quad (7)$$

As observed in previous papers,[15,16] the DPn calculated from depolymerization experiments (Table 3) slightly decreased during autoxidation whereas the yield of the reaction drastically dropped (roughly −30% and −50%, respectively, for DP6 and DP16 after 26 and 40 days). As previously stated, this is attributed to the formation of new bonds, resistant to depolymerization. This means that one-third to one-half of the interflavonoid bonds underwent chemical reactions. Dimers and trimers released from the nondepolymerization of these bonds, which can be considered as oxidation markers, have been identified using UPLC/ESI-MS^n.[13] However their separation and quantification remains a challenge.

SAXS curves are shown in Figure 4 (DP6) and in Figure 5 (DP16). Intensities normalized by the concentration increased with the time of oxidation, indicating that the weight average molecular weight of tannins increased. The scattering curves were fitted with the same models as previously (Table 4). For the DP6 tannins, the best results were obtained with the WLC and Fisher−Burford models. The contour length increased with the ratio I_0/C, which is proportional to the actual DPw. The persistence length $b/2$ was 7.5 ± 0.4 Å, and the cross section

Table 3. Number Average Degree of Polymerization (DPn), Yield of Depolymerization Reaction during Oxidation at High Concentrations (5 g/L^{-1}), and Decrease of Yield Compared to Day 0

	DP6			DP16		
time of oxidation	DPn	depolymerization yield (%)	decrease of yield (%)	DPn	depolymerization yield (%)	decrease of yield (%)
0 days	6.0 ± 0.1	78.0 ± 1		15.4 ± 0.8	67 ± 3	
7 days	5.9 ± 0.1	56.0 ± 4	28			
14 days	5.9 ± 0.1	57.0 ± 4	27	16.5 ± 0.1	41 ± 1	39
26 days	5.8 ± 0.1	51.5 ± 5	34	16.5 ± 0.2	32 ± 1	53
40 days	5.6 ± 0.2	52.0 ± 4	33	15.0 ± 0.7	33 ± 3	51

dx.doi.org/10.1021/jf501441j | J. Agric. Food Chem. 2014, 62, 7833−7842

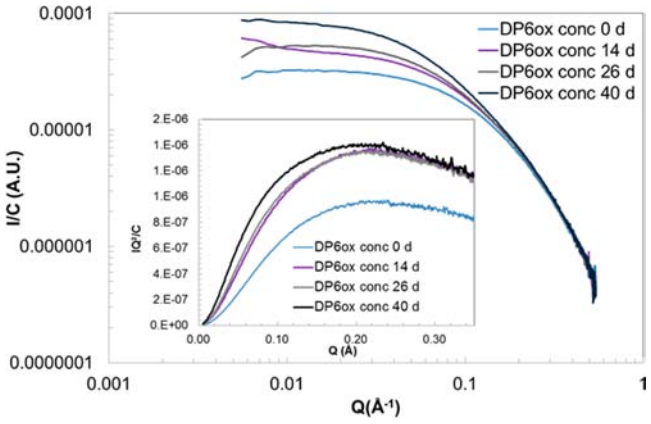

Figure 4. SAXS intensity (normalized by concentration) of native and oxidized DP6 in concentrated solutions (5 g/L) at different times of oxidation in the log I–log Q representation. Kratky plots are displayed in an insert.

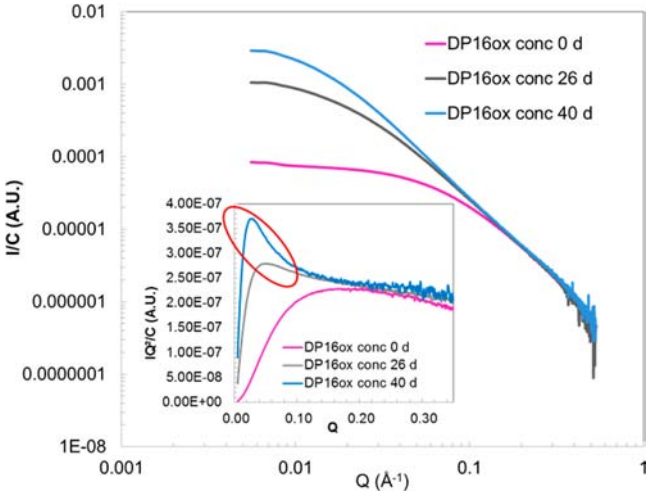

Figure 5. SAXS intensity (normalized by concentration) of native and oxidized DP16 in concentrated solutions (5 g/L) at different times of oxidation in the log I–log Q representation. Kratky plots are displayed in an insert.

was roughly 4 Å, like with linear native tannins. Parameters determined from the Fisher–Burford model with cross section were consistent with a linear polymer (D_f = 2) with a constant cross section. Kratky plots (insert in Figure 4) confirmed that polymers "grew" in a linear way, probably due to mainly end to end reaction (extension). After 40 days of oxidation, I_0/C increased by a factor 3.5, so was the molecular weight according to eq 2, resulting in a DP roughly equals to 21.

For the DP16, poor results were obtained with the WLC models: this can be explained by the fact that polymers are no longer linear, as confirmed by the Kratky plots (insert in the Figure 5), typical of branched macromolecules. Parameters determined from the Fisher–Burford model with or without cross section (Table 4) were consistent with branched polymers (D_f > 2.2[23]). This suggests that, in this case, intermolecular reactions took place in an end-to-middle way, as already observed with DP40.[16] After 40 days of oxidation, I_0/C increased by a factor 35, so was M_w.

The main differences observed between DP6 and DP16 concerned (i) end-to-end reactions with the shorter native tannins, leading to slightly longer linear macromolecules, versus

Table 4. Fitting Parameters for DP6 and DP16 Tannins Oxidized at 5 g/L[a]

	DP6												DP16											
	WLC					Fisher–Burford with cross section					Fisher–Burford					Fisher–Burford with cross section								
oxidation time (days)	I_0/C	L	b	R_{cs}	χ^2	I_0/C	R_g	D_f	R_{cs}	χ^2	I_0/C	R_g	D_f	χ^2	I_0/C	R_g	D_f	R_{cs}	χ^2
0	1.08×10^{-4}	97	14.4	4.1	10	1.20×10^{-4}	16.0	2.0	2.6	14.9	3.12×10^{-4}	26.4	2.36	26.4	3.20×10^{-4}	27.9	2.0	2.5	9.8
14	2.59×10^{-4}	128.6	14.7	4.1	49	2.20×10^{-4}	19	2.0	2.5	55.1	2.34×10^{-3}	99.2	2.2	16.1	2.30×10^{-3}	98.0	2.2	1	181.2
26	2.60×10^{-4}	144	15.8	4.2	36.4	2.67×10^{-4}	21.5	2.0	2.5	32.5	6.01×10^{-3}	106.5	2.2	92	6.00×10^{-3}	106.6	2.2	1.5	101.3
40	3.84×10^{-4}	181	19.0	4.2	49.4	4.0×10^{-4}	27.2	1.92	2.5	30.4	1.09×10^{-2}	150.0	2.39	31	1.22×10^{-2}	161.0	2.35	1	104.0

[a]Scattered intensities extrapolated to $Q \rightarrow 0$ I_0/C, and structural parameters derived from the scattering curves using the WLC, Fisher–Burford, and Fisher–Burford with cross section models. R_g: radius of gyration; L: contour length; b: Kuhn length; R_{cs}: radius of cross section are given in angströms; D_f: fractal dimension. χ^2 values are an indication of the quality of the fit.

dx.doi.org/10.1021/jf501441j | J. Agric. Food Chem. 2014, 62, 7833–7842

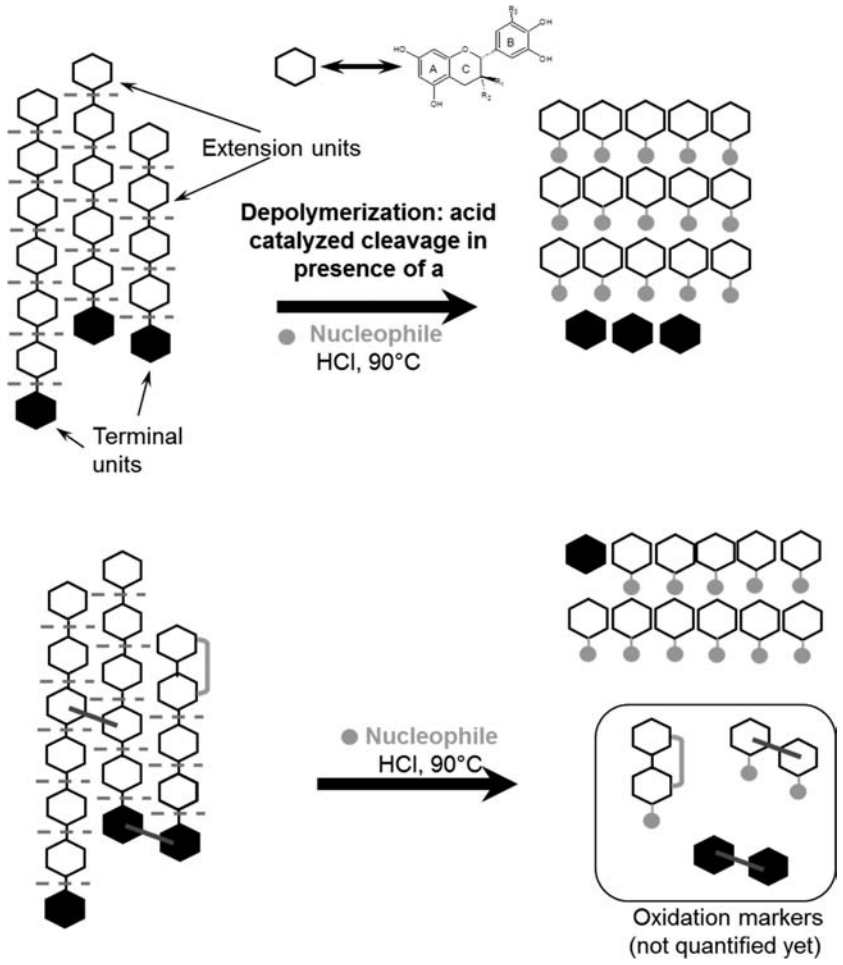

Figure 6. Illustration of the evolution of the thiolysis yields when non-cleavable oxidation bonds are created. In this example, the thiolysis yield decreases by 33%, with 22% attributed to the formation of intermolecular bonds and 11% attributed to the formation of intramolecular bonds.

Table 5. Number Average Degree of Polymerization (DPn), Yield of Depolymerization Reaction during Oxidation at Low Concentration (0.1 g/L), and Decrease of Yield Compared to Day 0

	DP6			DP16		
time of oxidation	DPn	depolymerization yield (%)	decrease of yield (%)	DPn	depolymerization yield (%)	decrease of yield (%)
0 days	6.0 ± 0.1	78.0 ± 1		15.4 ± 0.8	67 ± 3	
7 days	5.8 ± 0.1	38.0 ± 1	51	*a*	*a*	*a*
14 days	5.8 ± 0.1	35.0 ± 1	55	14.0 ± 0.1	47 ± 5	30
26 days	4.9 ± 0.1	33.0 ± 2	58	*b*	*b*	*b*
40 days	4.6 ± 0.1	29.0 ± 4	63	12.3 ± 0.7	11 ± 3	84

[a]No data available because of bacterial growth. [b]No data available because samples could not be dissolved in ethanol.

end-to-middle connections with longer native tannins leading to branched macromolecules; this can be explained by the ratio between terminal and extension units (when the chain is longer, it has more chances to react with an extension unit than with a terminal unit); and (ii) the competition between intermolecular and intramolecular reactions.

Indeed, the yields of the depolymerization reaction indicated that 30% of the units had reacted for DP6 versus 50% for DP16 (Table 3). Oxidation reactions can be related to the formation of either intramolecular or intermolecular bonds. Coupled with SAXS results, the different yields indicated that the ratio of intermolecular versus intramolecular reactions was totally different for the two tannins: for DP6, the weight average molecular weight increased by a factor 3.5, whereas it increased by a factor 35 with DP16.

These results can be used to evaluate the proportions of inter- and intramolecular bonds created during oxidation. Indeed, if during oxidation the average degree of polymerization DPn increased by a factor x, it means that $(x - 1)$ non-cleavable interflavonoid bonds were created in average, also meaning that $2(x - 1)$ flavanol units became non-quantitatively analyzed (Figure 6). Thus, the percentage of monomers involved in intermolecular bonds, is expected to be

$$\rho = \frac{2(x-1)}{nx} \times 100 \quad (8)$$

dx.doi.org/10.1021/jf501441j | J. Agric. Food Chem. 2014, 62, 7833−7842

With our values (x = 3.5 for DP6 and x = 35 for DP16), we would have expected a loss of yield of 24% and 12%, respectively, (actual values: 30% and 50%). This means that, for DP6, intermolecular bonds represent about 80% of the newly formed bonds, whereas they represent 24% for DP16. This is probably due to the fact that longer chains have more possibilities to have adjacent monomers and thus have more possibilities to form intramolecular bonds.

Oxidation in "Dilute" Systems. During oxidation, the color of solutions changes (Figure S1, Supporting Information), and as observed in concentrated conditions, the DPn obtained from depolymerization decreased (Table 5). This decrease was more pronounced than in concentrated conditions and associated with a dramatic drop of the yield of the depolymerization reaction: −63% and −84%, respectively, for DP6 and DP16 after 40 days, meaning that only 37% and 16% of the initial interflavonoid bonds remained unreacted. It was much less than what was observed at higher concentrations: 70% of unreacted interflavonoid bonds for DP6, 50% for DP16. This is likely due to the ratio between oxygen and tannins, which is much higher in the case of dilute solutions (7 equiv of O_2 vs 1.2) and thus favors more oxidation reactions.

SAXS curves are shown in Figures 7 (DP6) and 8 (DP16). Intensities normalized by the concentration increased with the

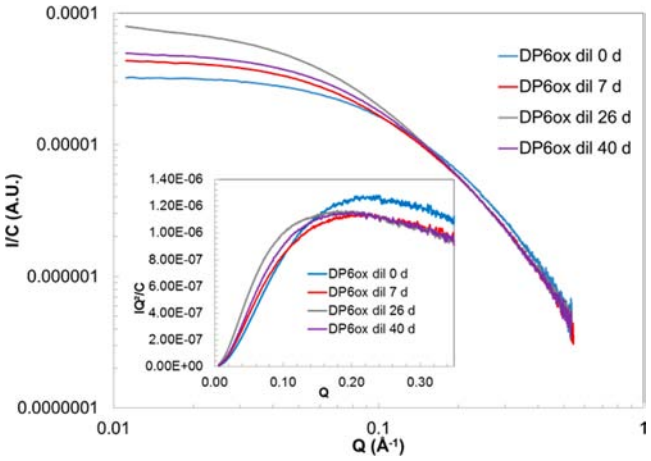

Figure 7. SAXS intensity (normalized by concentration) of native and oxidized DP6 in dilute solutions (0.1 g/L) at different times of oxidation in the log I−log Q representation. Kratky plots are displayed in an insert.

time of oxidation until day 26, indicating that the weight average molecular weight of tannins increased, before dropping at day 40. The scattering curves were fitted with the same models as previously (Tables 6 and 7).

For the DP6 tannins, the best results were obtained with the Fisher−Burford models, with or without cross section, depending on the oxidation time. However, results obtained with the WLC were correct and showed that the persistence length $b/2$ evolved when the oxidation time increased and was 10.5 Å at 26 days. The cross section was still in the range 4.1−5 Å. Parameters determined from the Fisher−Burford model with cross section are consistent with a linear polymer ($D_f \sim 2$) with a constant cross section. However, at longer oxidation times, the fractal dimension slightly increased. The weight average molecular weight did not increase regularly: it was surprisingly higher after 26 days than after 40 days. After 40 days, the M_w was increased by a factor of 2 in dilute solution, instead of 3.5

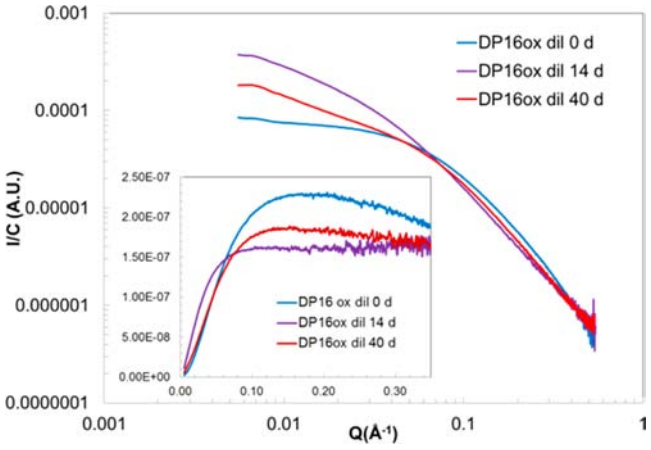

Figure 8. SAXS intensity (normalized by concentration) of native and oxidized DP16 in concentrated solutions (5 g/L) at different times of oxidation in the log I−log Q representation. Kratky plots are displayed in an insert.

when tannins were more concentrated. It is also worth noting that the depolymerization yield decreased by 63% versus 33% in concentrated solutions: more interflavonoid bonds were modified, but they led to the formation of more intramolecular bonds. According to eq 8, if only intermolecular reactions had occurred, we would have observed a decrease of the depolymerization yield of 16%. Thus, roughly 47% of the uncleavable bonds are due to intramolecular reactions ($^1/_4$ intermolecular, $^3/_4$ intramolecular).

For the DP16 tannins, the best results were obtained with the Fisher−Burford models, with or without cross section, depending on the oxidation time. However, χ^2 values are higher than with DP6. This may be due to the presence of aggregates (even though samples were filtered) or to a high heterogeneity of the sample, making curve fitting more difficult. Parameters determined from the Fisher−Burford model with cross section were consistent with a linear polymer ($D_f \sim 2$) but with a slightly decreasing fractal dimension. This could reflect the local stiffening of (some of) the macromolecules: indeed the fractal dimension for rods is 1.[23]

The weight average molecular weight did not evolve regularly as already observed with DP6 and was higher after 14 days than after 40 days. However, with the sample oxidized 14 days, nearly 30% of the tannins were lost upon filtration prior to SAXS experiments, and thus, its composition may not be representative of the total fraction. It is also worth noting that problems of redissolution in ethanol were observed with the fraction oxidized during 26 days and that no measurement could be performed. This might be an indication of the formation of intermediate species, having different solubilities in ethanol. After 40 days, no loss upon filtration was observed, and the M_w increased by a factor 1.6, instead of 35 when tannins were oxidized at a higher concentration. The depolymerization yield decreased by 84% instead of 51% in concentrated solutions (Table 6): more interflavonoid bonds were modified, but they mainly led to the formation of intramolecular bonds. According to eq 8, if only intermolecular reactions had occurred, we would have observed a decrease of the depolymerization yield of less than 5% instead of 84%. Thus 6% of the uncleavable bonds can be attributed to intermolecular reactions and 94% to intramolecular reactions.

dx.doi.org/10.1021/jf501441j | J. Agric. Food Chem. 2014, 62, 7833−7842

Table 6. Fitting Parameters for DP6 Tannins Oxidized at 0.1 g/L[a]

	WLC					Fisher–Burford				Fisher–Burford with cross section				
oxidation time (days)	I_0/C	L	b	R_{cs}	χ^2	I_0/C	R_g	D_f	χ^2	I_0/C	R_g	D_f	R_{cs}	χ^2
0	1.08×10^{-4}	97	14.4	4.1	10	1.20×10^{-4}	16.0	2.59	11	1.20×10^{-4}	16.0	2.00	2.6	14.9
7	2.04×10^{-4}	133	16.0	4.3	21.6	2.10×10^{-4}	20.6	2.35	18.9	2.10×10^{-4}	20.6	2.00	2.5	16.0
26	3.60×10^{-4}	174	21.0	5.0	18.3	3.50×10^{-4}	26.9	2.27	12.9	3.70×10^{-4}	27.6	2.05	2.3	37.9
40	2.18×10^{-4}	140	16.8	4.6	15.6	2.43×10^{-4}	21.3	2.43	13.0	2.40×10^{-4}	21.3	2.10	2.5	11.9

[a]Scattered intensities extrapolated to $Q \rightarrow 0$ I_0/C and structural parameters derived from the scattering curves using the Gaussian, WLC, and Fischer–Burford models. R_g: radius of gyration; L: contour length; b: Kuhn length; R_{cs}: radius of cross section; D_f: fractal dimension; χ^2 values are an indication of the quality of the fit.

Table 7. Fitting Parameters for DP16 Tannins Oxidized at 0.1 g/L[a]

	WLC					Fisher–Burford				Fisher–Burford with cross section				
oxidation time (days)	I_0/C	L	b	R_{cs}	χ^2	I_0/C	R_g	D_f	χ^2	I_0/C	R_g	D_f	R_{cs}	χ^2
0	3.03×10^{-4}	179.5	19.8	5.1	33	3.12×10^{-4}	26.4	2.36	26.4	3.20×10^{-4}	27.9	2.0	2.5	9.8
14	8.90×10^{-4}	789.0	24.2	5.4	98	9.80×10^{-4}	78.8	1.9	47.8	1.09×10^{-3}	83.0	1.9	2.0	102.4
40	4.90×10^{-4}	280.0	25.0	5.0	214	5.30×10^{-4}	41.6	1.97	157.0	5.20×10^{-4}	40.8	1.9	2.0	164.0

[a]Scattered intensities extrapolated to $Q \rightarrow 0$ I_0/C and structural parameters derived from the scattering curves using the Gaussian, WLC, and Fischer–Burford models. R_g: radius of gyration; L: contour length; b: Kuhn length; R_{cs}: radius of cross section; D_f: fractal dimension; χ^2 values are an indication of the quality of the fit.

To summarize our results, we confirmed that usual analytical methods (depolymerization followed by HPLC analysis) provide information that must be cautiously interpreted when dealing with autoxidized tannins. Indeed, upon oxidation, conversion yields dramatically decrease, meaning that the proportion of identified monomers can be as low as 10%. The decrease of conversion yield is by itself an indicator for tannin oxidation and should be indicated.

Using SAXS allowed determination of the conformations of native tannins and evidence of conformational changes upon oxidation. Native tannins can be considered as wormlike chains (or semiflexible polymers) having a relatively short persistence length (7.5–10 Å) and a cross section in the range 4.5–5 Å. However, for chains having more than 40 monomers, results indicated some degree of branching. Upon oxidation, several scenarios were observed (also summarized in Table 8) depending on the initial tannin concentration and its initial degree of polymerization:

Table 8. Proportions of Oxidation Bonds Created Either Intermolecularly or Intramolecularly

tanin fraction	intermolecular bonds (%)	intramolecular bonds (%)
DP6ox conc 40d	80 (end to end)	20
DP16ox conc 40d	24 (end to middle)	76
DP6ox dil 40d	25	75
DP16ox dil 40d	6	94

(i) Increase of the weight average molecular weight of tannins but no conformational changes (the chains are getting longer, but no polymer branching is observed) in the case of DP6 tannins. In this case, intermolecular and intramolecular reactions occur, but it is worth noting that the proportion of intramolecular reactions is higher when the concentration is lower: in dilute solutions a chain has more chances to react with itself than with a faraway neighbor.

(ii) Huge increase of the weight average molecular weight (X35), with the formation of branched macromolecules with DP16 tannins oxidized at high concentrations: in this case, intermolecular reactions are favored, and as the ratio extension units/terminal units is higher than with DP6, the probability for the chains to react end-to-middle increases.

(iii) In the case of dilute solutions of DP16, a relative stagnation of the molecular weight (X1.7 compared to X35) and slight decrease of the fractal dimension were observed, possibly accounting for the partial stiffening of macromolecules in connection with (mainly) intramolecular reactions

The impact of the initial concentration and DP of condensed tannins on autoxidation mechanisms was evidenced: oxidation in dilute and concentrated solutions leads to the formation of different structures, the solubility of which is very different. Concentrations (0.1 and 5 g/L) were chosen to mimic those of condensed tannins in white and red wines. However, it must be kept in mind that these results apply to the simple model systems considered first: apple tannin fractions (mainly epicatechin subunits) with different DP, given oxygen/flavanol unit ratios, water acidified to pH 3.5. When dealing with complex systems such as wine, the initial DP of condensed tannins is polydispersed, and the constitutive units of grape tannins include not only epicatechin and catechin, but also epigallocatechin and epicatechin-gallate. The reactivity of the latter may be different and influence structural changes. Further studies will have to consider this complexity. Last, but not least, other modified tannins are formed, for instance ethyl-linked tannins and anthocyanins/tannins adducts.

■ ASSOCIATED CONTENT

Supporting Information

UV–visible spectra of native and oxidized tannins. This material is available free of charge via the Internet at http://pubs.acs.org.

AUTHOR INFORMATION

Corresponding Author

*Phone: 33 (0)4 99 61 20 23; fax: 33 (0)4 99 61 28 57; e-mail: poncetc@supagro.inra.fr.

Notes

The authors declare no competing financial interest.

ACKNOWLEDGMENTS

We acknowledge the Synchrotron SOLEIL for provision of synchrotron radiation facilities, and we thank Pierre Roblin for assistance in using beamline SWING, Hélène Fulcrand, Laetitia Mouls and Virginie Hugouvieux for help in fruitful discussions.

REFERENCES

(1) Singleton, V.; Noble, A. C. In *Advance in Food Research*; Chichester, C. O., Ed.; American Chemical Society: Washington, DC, 1976; pp 47−70.

(2) Flanzy, C. *Oenologie - Fondements Scientifiques et Technologiques*; Technique Lavoisier: Paris, 1998; p 1311.

(3) Cheynier, V.; Duenas-Paton, M.; Salas, E.; Maury, C.; Souquet, J. M.; Sarni-Manchado, P.; Fulcrand, H. Structure and properties of wine pigments and tannins. *Am. J. Enol. Vitic.* **2006**, *57*, 298−305.

(4) Dueñas, M.; Fulcrand, H.; Cheynier, V. Formation of anthocyanin−flavanol adducts in model solutions. *Anal. Chim. Acta* **2006**, *563*, 15−25.

(5) Fulcrand, H.; Duenas, M.; Salas, E.; Cheynier, V. Phenolic reactions during winemaking and aging. *Am. J. Enol. Vitic.* **2006**, *57*, 289−297.

(6) Matthews, S.; Mila, I.; Scalbert, A.; Donnelly, D. M. X. Extractable and non-extractable proanthocyanidins in barks. *Phytochemistry* **1997**, *45*, 405−410.

(7) Rigaud, J.; Perez-Ilzarbe, X.; Ricardo da Silva, J. M.; Cheynier, V. Micro method for the identification of proanthocyanidin using thiolysis monitored by high-performance liquid chromatography. *J. Chromatogr.* **1991**, *540*, 401−405.

(8) Souquet, J.-M.; Cheynier, V.; Brossaud, F.; Moutounet, M. Polymeric proanthocyanidins from grape skins. *Phytochemistry* **1996**, *43*, 509−512.

(9) Kennedy, J. A.; Taylor, A. W. Analysis of proanthocyanidins by high-performance gel permeation chromatography. *J. Chromatogr. A* **2003**, *995*, 99−107.

(10) Guyot, S.; Vercauteren, J.; Cheynier, V. Structural determination of colourless and yellow dimers resulting from (+)-catechin coupling catalysed by grape polyphenoloxidase. *Phytochemistry* **1996**, *42*, 1279−1288.

(11) Kusano, R.; Tanaka, T.; Matsuo, Y.; Kouno, I. Structures of epicatechin gallate trimer and tetramer produced by enzymatic oxidation. *Chem. Pharm. Bull. (Tokyo)* **2007**, *55*, 1768−1772.

(12) Tanaka, T.; Matsuo, Y.; Kouno, I. A novel black tea pigment and two new oxidation products of epigallocatechin-3-*O*-gallate. *J. Agric. Food Chem.* **2005**, *53*, 7571−7578.

(13) Mouls, L.; Fulcrand, H. UPLC-ESI-MS study of the oxidation markers released from tannin depolymerization: Toward a better characterization of the tannin evolution over food and beverage processing. *J. Mass Spectrom.* **2012**, *47*, 1450−1457.

(14) Pedersen, J. S. Analysis of small-angle scattering data from colloids and polymer solutions: modeling and least-squares fitting. *Adv. Colloid Interface Sci.* **1997**, *70*, 171−210.

(15) Vernhet, A.; Dubascoux, S.; Cabane, B.; Fulcrand, H.; Dubreucq, E.; Poncet-Legrand, C. Characterization of oxidized tannins: Comparison of depolymerization methods, asymmetric flow field-flow fractionation and small-angle X-ray scattering. *Anal. Bioanal. Chem.* **2011**, *401*, 1559−1569.

(16) Poncet-Legrand, C.; Cabane, B.; Bautista-Ortin, A.-B.; Carrillo, S.; Fulcrand, H.; Pérez, J.; Vernhet, A. Tannin oxidation: Intra- versus intermolecular reactions. *Biomacromolecules* **2010**, *11*, 2376−2386.

(17) Zanchi, D.; Konarev, P. V; Tribet, C.; Baron, A.; Svergun, D. I.; Guyot, S. Rigidity, conformation, and solvation of native and oxidized tannin macromolecules in water-ethanol solution. *J. Chem. Phys.* **2009**, *130*, 245103.

(18) Poncet-Legrand, C.; Cartalade, D.; Putaux, J.-L.; Cheynier, V.; Vernhet, A. Flavan-3-ol aggregation in model ethanolic solutions: Incidence of polyphenol structure, concentration, ethanol content, and ionic strength. *Langmuir* **2003**, *19*, 10563−10572.

(19) Debye, P. Molecular-weight determination by light scattering. *J. Phys. Chem.* **1947**, *51*, 18−32.

(20) Kohlbrecher, J. SASfit: A program for fitting simple structural models to small angle scattering data. http://sans.web.psi.ch/SANSSoft/sasfit.pdf, 2009.

(21) Pedersen, J. S.; Schurtenberger, P. Scattering functions of semiflexible polymers with and without excluded volume effects. *Macromolecules* **1996**, *29*, 7602−7612.

(22) Fisher, M. E.; Burford, R. J. Theory of critical-point scattering and correlations. I. The Ising model. *Phys. Rev.* **1967**, *156*, 583.

(23) Beaucage, G. Small-angle scattering from polymeric mass fractals of arbitrary mass-fractal dimension. *J. Appl. Crystallogr.* **1996**, *29*, 134−146.

(24) Matthews, S.; Mila, I.; Scalbert, A.; Pollet, B.; Lapierre, C.; duPenhoat, C.; Rolando, C.; Donnelly, D. M. X. Method for estimation of proanthocyanidins based on their acid depolymerization in the presence of nucleophiles. *J. Agric. Food Chem.* **1997**, *45*, 1195−1201.

(25) Guyot, S.; Marnet, N.; Laraba, D.; Sanoner, P.; Drilleau, J.-F. Reversed-phase HPLC following thiolysis for quantitative estimation and characterization of the four main classes of phenolic compounds in different tissue zones of a french cider apple variety (*Malus domestica* Var. Kermerrien). *J. Agric. Food Chem.* **1998**, *46*, 1698−1705.

(26) Martinez, S. Inhibitory mechanism of mimosa tannin using molecular modeling and substitutional adsorption isotherms. *Mater. Chem. Phys.* **2002**, *77*, 97−102.

Preparation of the Modified "in Bean" Green Coffee Models. Modified "in bean" models enriched with CGA were prepared using a previously developed method[16] with small modifications. Brazil arabica green coffee beans were initially freeze-dried until constant weight (6% weight loss). For the preparation of the chlorogenic acid-enriched coffee model (CGAcoffee), to 100 g of the freeze-dried green coffee beans was added 200 mL of a CGA aqueous solution (1.5 g/200 mL), and the mixture was shaken for 16 h at 4 °C. After incorporation, the coffee beans were washed with distilled water for removal of the surface-adhering solution and freeze-dried. As a control, 100 g of freeze-dried coffee beans was immersed in 200 mL of water under the same conditions.

Roasting of Coffee Bean Model Samples. Prior to roasting, all samples (original freeze-dried coffee, water control, and CGAcoffee) were adjusted to the same moisture of 6% by spraying enough water and checking coffee weight after 1 week. Then, the coffee beans (40 g) were roasted at 200 °C during approximately 5 min to obtain an organic roast loss of 8%.

Preparation of Coffee Brews and Isolation of the High Molecular Weight Material (HMWM). Roasted coffee beans were ground (250−450 μm), and infusions were prepared by extraction of 25 g of powdered coffee with 800 mL of water at 80 °C during 20 min. After filtration and vacuum concentration to 200 mL, 50 mL of coffee infusion was freeze-dried to calculate the total soluble solids. The other 150 mL was extensively dialyzed at 4 °C (six water renewals, MW cutoff 12−14 kDa). After dialysis, the retentate was freeze-dried, giving the HMWM.

Fractionation of the HMWM by Graded Precipitation in Ethanol. For the fractionation of HMWM for each coffee infusion, the method previously developed[20] was used with a modification;[16] for complete solubilization of the freeze-dried HMWM, a solution of 6 M urea was used. The HMWM was then precipitated by the addition of absolute ethanol. The material was recovered in the 50% ethanol solution (Et50) and in the 75% ethanol solution (Et75). It was resolubilized in water and dialyzed (six water renewals, MW cutoff 12−14 kDa). After dialysis, the retentate was freeze-dried. The material soluble in the 75% ethanol (EtSn) fraction was recovered after concentration, dialysis, and freeze-drying.

Chlorogenic Acids and Caffeine Content of Green and Roasted Coffees. CGA were extracted overnight from green and roasted ground coffees (1 g) with 100 mL of a solution of methanol/water (70:30 v/v) containing 0.5% Na_2SO_3 with constant stirring (125 rpm) in the dark. To the solution was added 1 mL of veratric acid as internal standard (100 mg/mL, in methanol). After filtration of the coffee powder, the colloidal material present in the extracts was precipitated by the addition of 1 mL of Carrez I and II solutions.[21] The extracts were analyzed by HPLC (Dionex, Ultimate 3000) by injection of 25 μL of the sample on a reversed-phase HPLC column (C18-ACE; 25 cm length, 0.45 cm internal diameter, and 5 μm particle diameter). Eluent A was a 5% formic acid aqueous solution, and eluent B was methanol. The eluent program was as follows: 0−5 min, 5% eluent B; 5−45 min, 40% B; 45−65 min, 70% B; 65−75 min, 5% B. The column temperature was set at 25 °C, and the flow was 0.8 mL/min. The eluent was continuously monitored from 200 to 600 nm with a photodiode array detector (PDA-100, Dionex). The identification of caffeine and 5-caffeoylquinic acid was made by comparison of their retention times and UV−vis spectra with those of pure standards analyzed under the same conditions. The other caffeoylquinic acids (CQA) and cinnamoyl-1,5-γ-quinolactones (CQL) were tentatively identified by comparison of their retention times and UV−vis spectra with those of the literature.[22] CGA were quantified by the internal standard method using a 5-CQA calibration curve. Caffeine was quantified using the same methodology and a caffeine calibration curve.

Characterization of Coffee Bean Samples and Fractions. Green and roasted coffee and coffee models were characterized regarding their sucrose, glucose, and fructose contents by high-performance anion exchange chromatography.[23] Total sugars content was determined by anion exchange chromatography after Saeman and acid hydrolysis.[20] Protein content was determined according to the Dumas method (PRIMACS, carbon−nitrogen/protein analyzer, Skalar, The Netherlands) by multiplying the nitrogen content by 6.25. The melanoidin content of fractions was determined by the K_{mix} at 405 nm as previously described.[4]

Color of Roasted Coffee Powder. Roasted coffee powder colors obtained for the original, control, and "in bean" CGAcoffee model were directly measured with a Minolta chroma meter (model CR-400, Minolta, Tokyo, Japan). The equipment was set up for illuminant D65 and 10° observer. The equipment was calibrated with a white standard (L^* = 97.71, a+* = −0.59, and b^* = 2.31), and each sample was put on a Petri dish and read in five different locations. Numerical values of chroma (C^*), hue (h), and color difference (ΔE^*) were calculated according to the following formulas:

$$h^* = \tan^{-1}\left(\frac{b^*}{a^*}\right)$$

$$C^* = (a^{*2} + b^{*2})^{1/2}$$

$$\Delta E^* = [(\Delta L^*)^2 + (\Delta a^*)^2 + (\Delta b^*)^2]^{1/2}$$

Total Phenolic Groups Content. The total phenolic groups content of the coffee samples was determined with the Folin−Ciocalteu reagent.[4] For all coffee samples, a 0.33 or 1 mg/mL solution was prepared. To 1 mL of the coffee sample solution was added 0.5 mL of Folin−Ciocalteu reagent. After mixing of the sample, 1 mL of a saturated Na_2CO_3 solution was added, and filtered demineralized water was added to reach a total volume of 10 mL. After 1 h of reaction, the absorbance of the sample was measured at 725 nm. 5-CQA was used as reference.

Adsorbed Phenolic Compounds. For determination of coffee melanoidins adsorbed phenolic compounds, a 5 mg/mL solution of coffee melanoidins was analyzed by direct injection (100 μL) on a RP-HPLC according to the method described previously for CGA determination. For determination of the effect of melanoidins in the determination of free phenolic compounds, melanoidin solutions (5 mg/mL) were spiked with different concentrations of 5-CQA and incubated overnight at room temperature. Each solution was analyzed by RP-HPLC as described previously, and the areas were compared with that of aqueous solutions of 5-CQA with the same concentrations.

Alkaline Saponification. For determination of ester-linked phenolic compounds, melanoidins were subjected to alkaline saponification by using a procedure that prevented oxidation of phenolic compounds.[24] To 750 μL of the melanoidin solution (12 mg/mL) was added 750 μL of a 2 M NaOH solution containing 2% (w/w) ascorbic acid and 20 mM ethylenediaminetetraacetic acid. After incubation for 1 h at 30 °C, the mixture was quenched to pH ≈1 with 330 μL of 5 M HCl to precipitate most of the coffee material, preventing precipitation during further analysis. The mixture was stored for 2 h at 4 °C, the precipitate was removed by centrifugation, and the supernatant was analyzed by reversed-phase HPLC. Experiments were performed at least in duplicate. The identification of caffeic, ferulic, and 4-hydroxycinnamic acids was made by comparison of their retention times and UV−vis spectra with that of pure standards analyzed under the same conditions. Caffeic, ferulic, and 4-hydroxycinnamic acids were quantified by external calibration.

Alkaline Fusion. In a nickel crucible were weighed 1 g of solid NaOH and 100 mg of zinc dust, and, after fusion of the mixture at 350 °C,[6,25] 5 mg of HMWM was added (or 5 mg of melanoidin fractions). After 10 s, the nickel crucible was removed and rapidly cooled on ice. The fusion cake was solubilized by adding 6 M HCl, and 200 μL of internal standard solution was added (3,4-dimethoxybenzoic acid, 1 mg/mL) and acidified to pH 1−2 with 6 M HCl. The acidic mixture was extracted four times with 30 mL of diethyl ether. After evaporation of the organic solvent, carefully and with protection, the residue was derivatized and analyzed by GC-EI/MS. Samples were derivatized with 0.5 mL of pyridine and 0.5 mL of *N*,*O*-bis(trimethylsilyl)-trifluoroacetamide and heated at 70 °C for 30 min. After cooling to room temperature, the silyl derivatives of phenolic compounds were

Table 1. Soluble Sugar, Caffeine, and Protein Contents (Grams per 100 g, Dry Basis) of Original, Control, and "in Bean" Green and Roasted[a] Coffee Models

coffee	glucose	fructose	sucrose	total	caffeine	protein[b]
green						
original	0.018 ± 0.001	0.60 ± 0.00	7.45 ± 1.32	8.07 ± 1.32	1.37 ± 0.01	14.0 ± 0.9
control	0.018 ± 0.001	0.59 ± 0.00	5.78 ± 1.10	6.39 ± 1.10	1.12 ± 0.02	14.1 ± 0.7
CGAcoffee	0.017 ± 0.001	0.58 ± 0.00	5.08 ± 0.98	5.69 ± 0.99	1.07 ± 0.05	14.0 ± 1.1
roasted						
original	0.018 ± 0.001	0.008 ± 0.002	0.64 ± 0.06	0.66 ± 0.07	1.42 ± 0.15	9.5 ± 0.7
control	0.018 ± 0.001	0.019 ± 0.001	0.99 ± 0.02	1.07 ± 0.05	1.23 ± 0.12	12.3 ± 0.9
CGAcoffee	0.017 ± 0.001	0.032 ± 0.025	3.07 ± 0.07	3.16 ± 0.02	1.11 ± 0.07	11.8 ± 0.5

[a]Not corrected for weight loss during roasting. [b]$(N_{total} - N_{caffeine}) \times 6.25$.

Table 2. Chlorogenic Acid (CGA) Composition of Original, Control, and "in Bean" Green and Roasted[a] Coffee Model (Grams per 100 g, Dry Basis)

	green			roasted		
CGA	original	control	CGAcoffee	original	control	CGAcoffee
3-CQA	0.53 ± 0.02	0.44 ± 0.03	0.44 ± 0.01	0.48 ± 0.04	0.43 ± 0.02	0.53 ± 0.00
5-CQA	3.36 ± 0.02	2.92 ± 0.17	3.34 ± 0.20	1.04 ± 0.10	1.12 ± 0.07	1.07 ± 0.02
4-CQA	0.007 ± 0.001	0.001 ± 0.001	0.006 ± 0.002	0.17 ± 0.03	0.20 ± 0.02	0.11 ± 0.00
total CQA	3.90 ± 0.03	3.37 ± 0.20	3.79 ± 0.20	1.70 ± 0.16	1.75 ± 0.11	1.72 ± 0.02
1-FQA	0.01 ± 0.00	0.01 ± 0.00	0.01 ± 0.00	0.01 ± 0.00	0.01 ± 0.00	0.01 ± 0.00
3-FQA	0.70 ± 0.05	0.60 ± 0.07	0.63 ± 0.05	0.76 ± 0.02	0.69 ± 0.04	0.88 ± 0.01
5-FQA	0.05 ± 0.01	0.04 ± 0.00	0.04 ± 0.00	nd	nd	nd
4-FQA	0.003 ± 0.005	0.003 ± 0.004	0.003 ± 0.004	nd	nd	nd
total FQA	0.77 ± 0.06	0.65 ± 0.07	0.68 ± 0.06	0.77 ± 0.02	0.69 ± 0.04	0.89 ± 0.01
3-CoQA	nd	nd	nd	nd	nd	nd
5-CoQA	0.007 ± 0.001	0.008 ± 0.003	0.006 ± 0.002	nd	nd	nd
4-CoQA	0.04 ± 0.02	0.03 ± 0.02	0.03 ± 0.02	nd	nd	nd
total CoCQA	0.05 ± 0.02	0.04 ± 0.02	0.03 ± 0.02	nd	nd	nd
3-CQL	nd	nd	nd	0.04 ± 0.02	0.04 ± 0.00	0.04 ± 0.00
4-CQL	nd	nd	nd	0.09 ± 0.03	0.09 ± 0.01	0.09 ± 0.00
3-FQL	nd	nd	nd	0.01 ± 0.00	0.01 ± 0.00	0.04 ± 0.05
4-FQL	nd	nd	nd	0.02 ± 0.01	0.02 ± 0.00	Nd
1-FQL	nd	nd	nd	0.04 ± 0.01	0.06 ± 0.00	0.03 ± 0.03
total FQL	nd	nd	nd	0.08 ± 0.02	0.09 ± 0.01	0.07 ± 0.02
3,4-diCQA	0.18 ± 0.00	0.16 ± 0.02	0.31 ± 0.01	0.01 ± 0.00	0.01 ± 0.00	nd
3,5-diCQA	0.30 ± 0.01	0.26 ± 0.05	0.48 ± 0.01	0.07 ± 0.01	0.07 ± 0.01	0.06 ± 0.02
total diCQA	0.48 ± 0.01	0.42 ± 0.07	0.79 ± 0.02	0.08 ± 0.01	0.08 ± 0.01	0.06 ± 0.02
total (CGA)	5.19 ± 0.13a	4.48 ± 0.09ab	5.43 ± 0.20bc	2.53 ± 0.19	2.52 ± 0.16	2.67 ± 0.00

[a]Not corrected for weight loss during roasting. Identical letters in the same row are significantly different.

analyzed by GC-MS (Agilent) and quantified by GC-FID (PerkinElmer) using a DB-1 column (30 m length, 0.23 mm internal diameter, and 0.2 μm film thickness) and injecting 1 μL in splitless mode (time of splitless, 0.75 min). Both the injector and the transfer line were set at 250 °C. The initial column temperature was 70 °C, held for 1 min, increasing at 5 °C/min until 250 °C. The MS source temperature was set at 180 °C, and the electron ionization energy was set at 70 eV, with scans from m/z 40 to 600. Retention times and electron impact ionization spectra of pure standards were used to identify the following compounds: 3,4-dihydroxybenzoic acid, hydroquinone, catechol, gallic acid, benzoic acid, 2-hydroxybenzoic acid, 4-hydroxybenzoic acid, 2,3-dihydroxybenzoic acid, and 3,5-dihydroxybenzoic acid. Other phenolic compounds were identified by comparison of their mass spectra with those of the Wiley mass spectra database (Wiley 8). Quantification was performed by the internal standard method using 3,4-dimethoxybenzoic acid as the internal standard.

Statistical Analysis. All chemical analyses of green coffees, roasted coffees, soluble solids, HMWM, and fractions obtained by ethanol fractionation of the HMWM were performed in duplicate unless otherwise stated. Significant differences ($p < 0.05$) in chemical composition were analyzed by one-way ANOVA using the software Statistica 8.0 (StatSoft, Inc., Tulsa, OK, USA). A Newman−Keuls post hoc test was performed for detecting significantly different means ($p < 0.05$). For calculating the correlation between the phenolic compounds determined by the Folin−Ciocalteau method and those released by alkaline saponification, the nonparametric Spearman correlation coefficient (ρ) and the parametric Pearson correlation coefficient (r) were used.

dx.doi.org/10.1021/jf501510d | J. Agric. Food Chem. 2014, 62, 7843−7853

Table 3. Total Sugar[a] Composition (Grams per 100 g, Dry Basis) of Original, Control, and "in Bean" Green and Roasted Coffee Models[b]

	Ara	Man	Gal	Glc	$Glc_{polymeric}$	total	$total_{polymeric}$
green							
original	1.71 ± 0.04	22.7 ± 0.2	12.7 ± 0.2	11.2 ± 1.0	7.61	48.3 ± 1.1	44.7
control	1.86 ± 0.81	26.3 ± 7.9	13.2 ± 2.2	9.81 ± 3.58	6.60	51.2 ± 4.5	48.0
CGAcoffee	2.12 ± 0.44	30.8 ± 2.2	14.7 ± 0.7	10.3 ± 1.3	7.44	57.9 ± 4.6	55.0
ANOVA	0.758	0.359	0.412	0.835		0.169	
roasted							
original	1.62 ± 0.20	18.0 ± 2.5	7.61 ± 1.01	8.41 ± 1.23	8.07	35.7 ± 5.0	35.4
control	1.99 ± 0.27	20.3 ± 2.2	8.86 ± 1.18	9.30 ± 0.80	8.75	40.4 ± 4.4	39.9
CGAcoffee	1.92 ± 0.05	20.6 ± 0.4	9.37 ± 0.07	10.2 ± 0.2	8.60	42.0 ± 1.1	40.4
ANOVA	0.276	0.444	0.276	0.259		0.370	

[a]Values expressed in anhydrosugar residues. [b]Not corrected for weight loss during roasting.

RESULTS AND DISCUSSION

With the purpose of studying the effect of the green coffee CGA content, if any, in the incorporation of phenolic compounds into coffee melanoidins, a modified "in bean" model coffee was produced by enrichment of the freeze-dried coffee beans with a CGA mixture isolated and purified from green coffee beans. The procedure for production of the modified "in bean" coffee model was performed at 4 °C to minimize side reactions. This was a modification from our previous work, in which the incorporation was performed at room temperature.[16]

Chemical Characterization of Green and Roasted Coffee Samples and Model. *Green Coffee.* As can be seen in Table 1, the sucrose hydrolysis was significantly lowered in this new protocol when compared to the previous one, when a significant sucrose hydrolysis was observed.[16] Original green coffee had a total soluble sugar content of 8.1%, mainly composed of sucrose (92%) and low amounts of glucose and fructose (Table 1), which is in accordance with the literature values.[26] For the control coffee there was a decrease of 20% of total soluble sugar content when compared with the original green coffee, only due to the decrease in sucrose. For the CGAcoffee model the amounts of sucrose, fructose, and glucose are similar to those of the control coffee (Table 1). This decrease in the amount of soluble sugars can be due to leaching of compounds during the incorporation process and contrasts with the previous procedure at room temperature,[16] when all of the solution was incorporated into coffee beans.

The amount of caffeine present in the original coffee was significantly higher than that present in control and CGAcoffee model, but the protein content of the coffees, estimated on the basis of the nitrogen content after correction for caffeine nitrogen, was not significantly different (Table 1).

The amount of total CGA in the CGAcoffee model was significantly higher (21% higher) than that present in control coffee, showing that the incorporation process was successful (Table 2). As observed for the soluble sugars, control coffee contained a significantly lower amount of CGA. The CGA profiles were similar in all coffees, with 5-CQA as the most abundant, representing, on average, 64% of the total CGA.

The sugar composition of green coffee polysaccharides was determined by subtracting from the total sugar content the contribution of glucose and sucrose present as soluble sugars (Table 3). The sugar content was in accordance with the known sugar composition of coffee cell wall polysaccharides,[16,27,28] not significantly different for the original, control, and CGAcoffee model.

The results presented showed that this new protocol for production of the modified "in bean" model coffees results in fewer changes in the chemical composition of control coffee in relation to the original coffee when compared with the original protocol,[16] being more suitable for the study of the incorporation of selected compounds into green coffee beans prior to the roasting process.

Roasted Coffee. Original, control, and CGAcoffee model coffees were roasted to 8.0 ± 0.5% of organic matter loss, and their chemical composition was determined. After the roasting process, losses of 92% of the total soluble sugar content of the original coffee, 84% for the control, and only 44% for the CGAcoffee model were observed (Table 1). This difference in total soluble sugar loss may be due to the higher content of CGA in the CGAcoffee model that might be preferentially lost during the roasting process (further discussed below). The decrease in the total soluble sugar in roasted original and control coffees are similar to that described in the literature.[16,29] The caffeine level remained unchanged, and the protein content of roasted coffees decreased between 20 and 38% (Table 1).

The amount of total CGA also decreased during the roasting process in all coffee models (Table 2). For the original and CGAcoffee model, the amount of total CGA decreased 55%, and a decrease of 48% was observed for control coffee. This decrease is in accordance with a coffee submitted to a degree of roast of 8%.[30]

The content of polymeric sugars had also a significant decrease after the roasting process (Table 3). All coffee samples behaved similarly, with an average decrease of 28% in the content of total polymeric sugars, in accordance with the literature.[31,32] For all coffees, when calculated for the equivalent weight of green coffee, the polymeric glucose levels were maintained or decreased slightly. For all other sugars, when calculated for the equivalent weight of green coffee, there was observed a decrease (17% for arabinose, 30% for mannose, and 41% for galactose).

The identical degradation profile of the studied coffee constituents led to the conclusion that the freeze-drying of green coffee beans and their immersion in water did not change significantly the behavior and properties of coffee during the roasting process.

During the roasting process, browning reactions occur, contributing to the coffee brown color formation. By visual inspection of the interior of roasted coffee beans, an even distribution of the brown color could be observed. The CIELAB color space used to characterize the coffee powders

Table 4. Yield and Chemical Composition (Grams per 100 g, Dry Basis) of the High Molecular Weight and Resulting Ethanol-Precipitated Fractions of the Original, Control, and "in Bean" Coffee Models

	g/100 g coffee	g/100 g HMWM	Ara	Man	Gal	Glc	total	protein	$K_{mix405\ nm}$	MBI	phenolics[a]
original											
soluble solids	22.5								0.75 ± 0.03		
HMWM	2.39		11.1 ± 0.3a	20.2 ± 0.3	19.8 ± 0.7a	0.50 ± 0.09a	51.6 ± 1.3	9.9 ± 0.3a	1.40 ± 0.05a	3.63	4.59 ± 0.24a
Et50		34.8	3.9 ± 0.9	30.1 ± 3.0	9.4 ± 2.0	0.53 ± 0.09	44.0 ± 0.3	2.3 ± 0.1	0.85 ± 0.01	1.58	1.16 ± 0.10
Et75		12.5	14.2 ± 0.6	11.6 ± 0.2	32.8 ± 2.6	0.50 ± 0.07	59.1 ± 3.4	12.1 ± 0.5	0.82 ± 0.02	2.85	1.69 ± 0.20
EtSn		52.7	16.8 ± 1.2	5.5 ± 0.4	23.8 ± 1.2	1.63 ± 1.48	47.7 ± 4.4	14.3 ± 0.4	1.37 ± 0.11	3.61	5.36 ± 0.33
control											
soluble solids	14.9								0.74 ± 0.08		
HMWM	3.73		11.5 ± 1.3b	17.1 ± 1.9	17.2 ± 1.9b	0.45 ± 0.15ab	46.2 ± 5.2	14.1 ± 0.8ab	0.89 ± 0.00ab	2.24	4.50 ± 0.61b
Et50		32.7	2.7 ± 0.1	34.9 ± 1.1	4.85 ± 0.22	1.54 ± 1.27	44.0 ± 0.2	5.2 ± 0.2	0.89 ± 0.03	1.75	1.57 ± 0.04
Et75		16.8	19.2 ± 3.8	7.9 ± 1.7	30.4 ± 5.5	0.49 ± 0.08	57.9 ± 11.0	12.3 ± 0.5	0.56 ± 0.02	1.88	1.93 ± 0.13
EtSn		50.5	16.7 ± 1.8	4.0 ± 0.4	20.4 ± 2.2	0.44 ± 0.05	41.6 ± 4.4	14.6 ± 0.3	1.07 ± 0.19	2.44	7.28 ± 0.18
CGAcoffee											
soluble solids	18.4								0.70 ± 0.00		
HMWM	3.86		5.94 ± 0.6ab	20.1 ± 2.0	12.5 ± 1.3ab	−ab	38.6 ± 4.0	18.9 ± 1.0ab	1.27 ± 0.15b	2.99	6.19 ± 0.36ab
Et50	1.44	37.3	1.70 ± 0.4	38.7 ± 9.2	3.5 ± 0.8	1.02 ± 0.28	44.9 ± 10.1	4.8 ± 0.4	0.56 ± 0.09	1.11	1.55 ± 0.16
Et75	0.26	6.7	11.3 ± 1.7	11.1 ± 1.9	25.3 ± 3.7	1.13 ± 0.31	48.7 ± 7.6	14.7 ± 0.5	0.88 ± 0.13	2.40	3.13 ± 0.27
EtSn	2.16	56.0	13.2 ± 0.9	3.5 ± 0.2	14.8 ± 0.3	0.87 ± 0.48	32.3 ± 1.5	27.9 ± 0.7	1.27 ± 0.07	3.19	8.20 ± 0.45
ANOVA			0.0121	0.234	0.0296	0.0277	0.0940	0.0030	0.0234		0.049

[a]Phenolics measured by the Folin−Ciocalteu method and expressed as 5-CQA equivalents. Identical letters in the same column are significantly different.

dx.doi.org/10.1021/jf501510d | J. Agric. Food Chem. 2014, 62, 7843−7853

showed that the C^* value (chroma) of the CGAcoffee model was significantly higher than that of the control, showing that the incorporation of CGA increased the color intensity of the resulting roasted coffee. Furthermore, this increase is related to a significant increase of the b^* value for the CGAcoffee model, showing that the CGAcoffee model had a yellower color than that presented by the control.

Chemical Composition of Coffee Infusions and HMWM. Coffee infusions were prepared from the original, control, and CGAcoffee model, and the HMWM was isolated from each coffee infusion. The amount of soluble solids extracted from control coffee was lower (33% less) than that extracted for the original coffee (Table 4). For the CGAcoffee model an increase of 23% was observed in the amount of soluble solids in relation to control coffee. However, using the $K_{mix\ 405}$ values for estimating the melanoidins present in soluble solids, it can be observed that the incorporation of CGA did not significantly increase the $K_{mix\ 405}$ value of the soluble solids in relation to the control.

The chemical composition of the HMWM isolated from coffee infusions prepared from the original, control, and CGAcoffee model is shown in Table 4. The main component of all the HMWM was the carbohydrates (39−52%), with no significant differences between the coffees, followed by the protein (10−19%), with CGAcoffee model containing a higher amount of protein when compared to the control (+34%). The amount of phenolic compounds was also significantly higher for the CGAcoffee model when compared to the control (+38%), with the latter presenting a similar amount of phenolic compounds to that present in the original coffee HMWM. From these results it is evident that the incorporation of CGA in the "in bean" model resulted in an increase in the amount of phenolic compounds and protein in the HMWM.

The original coffee HMWM presented a significantly higher $K_{mix\ 405\ nm}$ value when compared to control coffee that also presented a significantly lower $K_{mix\ 405\ nm}$ value than the CGAcoffee model. In fact, the proportion of $K_{mix\ 405\ nm}$, indicative of the brown color of the HMWM, in relation to the $K_{mix\ 405\ nm}$ of the soluble solids was higher for the CGAcoffee model (37%), being the lowest for the control coffee (19%). By subtracting the percentage of carbohydrates and protein present in the HMWM, the amount of unknown material can be calculated. The results show that it is similar for all coffees and has an average value of 60%. Also, and as previously observed,[16] there is no trend between the amount of unknown material and the color of the HMWM determined by the $K_{mix\ 405\ nm}$ value. Using the melanoidin browning index (MBI), calculated by dividing the $K_{mix\ 405\ nm}$ values by the relative amount of unknown material,[16] which corresponds to the absorbance at 405 nm by unit amount of unknown material (Table 4), it can be seen that the enrichment of CGAcoffee with CGA increased by 33% the MBI. These observations allow inferring that the CGA have a significant influence on the color of the HMWM, although not increasing significantly the amount of unknown material.

Profiling Phenolic Compounds in Coffee HMWM. To evaluate the different natures of phenolic compounds present in the HMWM, either adsorbed, ester-linked, or in condensed form, as well the effect of the green coffee CGA levels in the phenolic compounds profile, the HMWM was subjected to alkaline saponification and alkaline fusion.

Adsorbed Phenolic Compounds. The amount of adsorbed phenolic compounds was determined by direct injection of the HMWM solutions on an RP C-18 column. To determine the possible influence of the HMWM matrix on the determination of phenolic compounds, a solution containing 5 mg/L HMWM and different amounts of 5-CQA was compared to the amount determined by injection of the same amounts of 5-CQA in water. The regression line obtained by representing the amount determined in water in relation to the amount determined in the presence of HMWM was $y = 0.9962x + 0.2584$ with $r = 0.9998$, indicating that the presence of HMWM did not interfere in the determination of phenolic compounds by RP-HPLC. The direct injection of HMWM showed the presence of intact CGA acids in all HMWMs (Figure 1a), mainly 5-CQA, although the presence of diCQA and 3CQA could also be detected (not shown). The amount of adsorbed CGA ranged from 0.1 to 0.7 mmol/100 g HMWM.

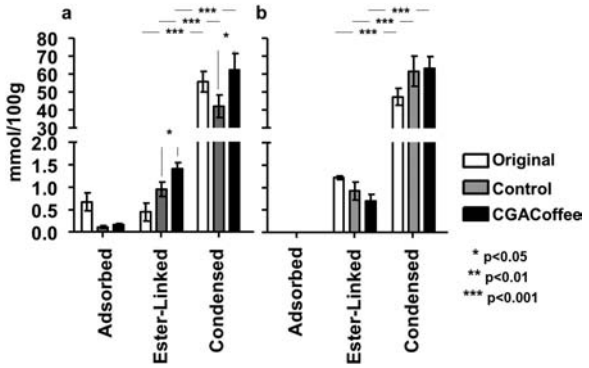

Figure 1. Profile of phenolic compounds present in (a) original, control, and CGAcoffee model HMWM; (b) original, control, and CGAcoffee model 75% ethanol soluble melanoidin population.

Ester-Linked Phenolic Compounds. The presence of ester-linked phenolic compounds in the HMWM from original, control, and CGAcoffee was determined after saponification. This procedure, known to release ester-linked phenolic compounds,[33] allowed the release of simple phenolic compounds from the HMWM, including caffeic, ferulic, and coumaric acids (Figure 2). Caffeic acid was the main cinnamic acid detected in all analyzed HMWMs. These simple phenolic compounds released by alkaline saponification have their origin in the adsorbed CGA present but also, probably, in the CGA incorporated into melanoidins, with structures where the cinnamic acids are esterified and maintain unchanged their structure. The amount of phenolic compounds released by saponification ranged from 1.1 to 1.6 mmol/100 g, which was significantly higher than that found adsorbed in the HMWM. For calculating the amount of ester-linked phenolic compounds in the HMWM, the amount of simple phenolics released by saponification was subtracted from the amount of adsorbed phenolics (Figure 1a). As can be observed, the amount of ester-linked phenolic compounds present in the HMWM ranged from 0.5 to 1.4 mmol/100 g. The values are in the range of those found in a previous study,[15] although lower values have been reported[14] or even not detected after alkaline hydrolysis,[6,9] probably due to their oxidation during extraction.[24] The amount of ester-linked phenolic compounds present in the CGAcoffee model was significantly higher than that present in the HMWM of control, showing that the incorporation of phenolic compounds in the CGAcoffee resulted in a significantly higher amount of ester-linked phenolic compounds in the HMWM.

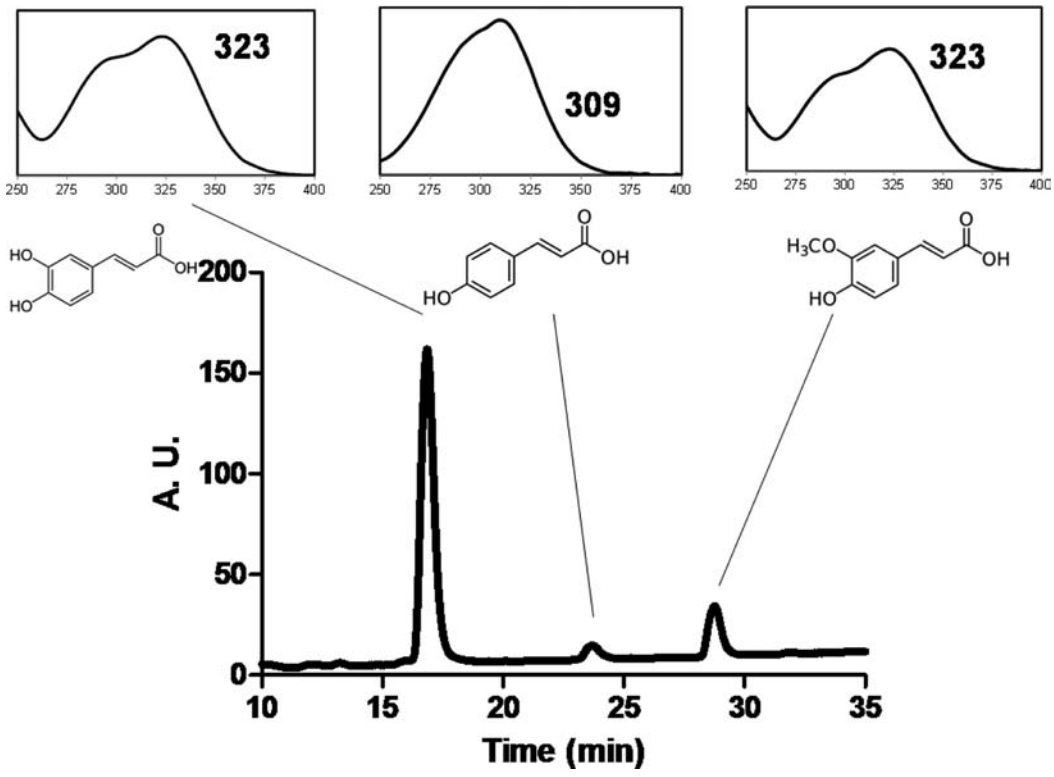

Figure 2. Phenolic compounds ester linked to the HMWM.

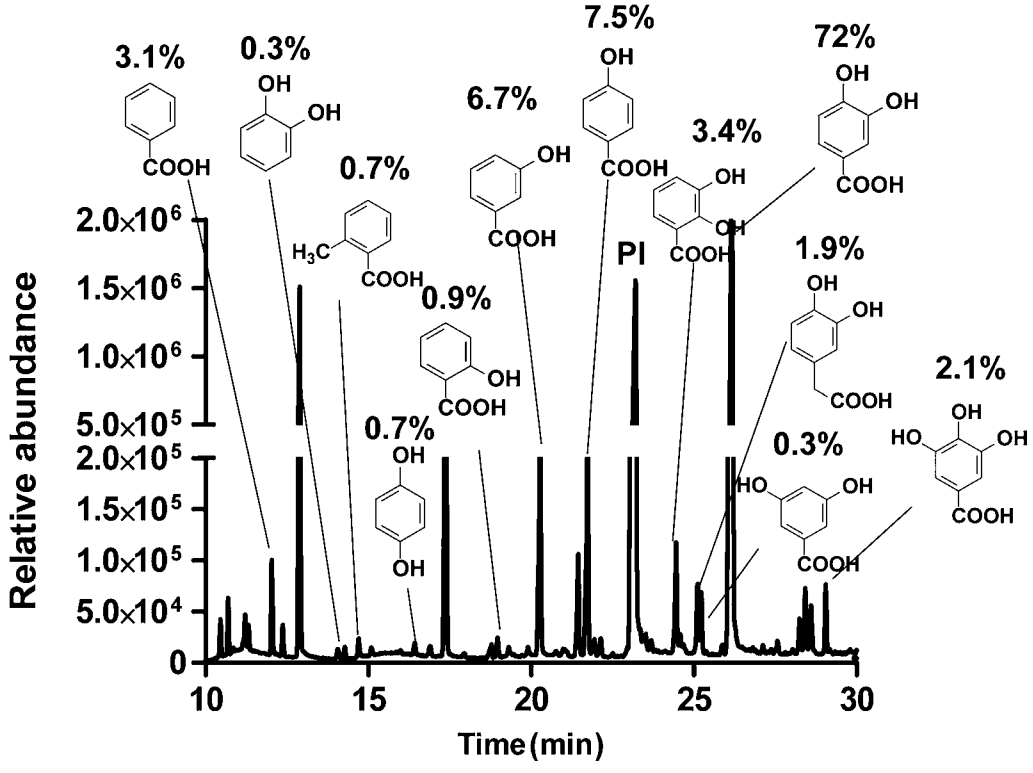

Figure 3. Nature and relative abundance of phenolic compounds released by alkaline fusion of the high molecular weight material recovered from the "in bean" CGAcoffee model.

Condensed Phenolic Compounds. For determining the amount of condensed phenolic compounds present in the HMWM, the samples were subjected to alkaline fusion. As can be observed in Figure 3, more than 10 simple phenolic compounds were released from the HMWM after alkaline fusion. 3,4-Dihydroxybenzoic acid was the most abundant phenolic compound in all samples. The abundance of the different phenolic compounds, expressed as the relative areas,

dx.doi.org/10.1021/jf501510d | J. Agric. Food Chem. 2014, 62, 7843−7853

was not significantly different for the different HMWMs studied. The amount of phenolic compounds released by alkaline fusion was significantly higher than the amount of phenolic compounds released by alkaline saponification by a factor of approximately 40 times and ranged from 42 to 62 mmol/100 g. These values are in the range of those reported by Nunes et al.[16] and Nunes and Coimbra[6] for HMWMs isolated from coffee infusions and higher than those found by Takanake et al.[9] for a zinc chelating fraction isolated from instant coffee. The low abundance of esterified phenolic compounds if compared to condensed phenolics present in coffee melanoidins is in accordance with the results of Gniechwitz et al.,[10] who performed an NMR analysis of an isolated intact melanoidin fraction and could not observe HSQC signals diagnostic for intact caffeic acid moieties. When the amount of phenolic compounds present in condensed form was calculated by subtracting the amount of phenolic compounds released by alkaline fusion from that released by alkaline saponification, it can be observed that the amount of phenolic compounds present in condensed form in the HMWM recovered from the CGAcoffee was significantly higher than that present in control. As observed for the ester-linked phenolic compounds, the incorporation of phenolic compounds in CGAcoffee model also increased the amount of condensed phenolic structures in the HMWM (Figure 1a). Expressing the amount of condensed phenolic structures in equivalent weight of caffeic acid, it can be concluded that the HMWM contained 7.5 g of condensed phenolics/100 g for control coffee, 10.0 g/100 g for the original coffee, and 11.2 g/100 g for the CGAcoffee model, showing that these condensed phenolic structures are an important component of the HMWM. In fact, the contribution of these condensed phenolic structures to the overall weight of the HMWM can be higher as some of the phenolic compounds bound to the HMWM seem to remain esterified with quinic acid after roasting.[14]

Mechanism and Efficiency of Alkaline Fusion. The alkaline fusion method is known to release phenolic compounds from condensed structures such as lignin and humic acids.[25] Nevertheless, there is a lack of knowledge about the nature of linkages between phenolic compounds cleaved by alkaline fusion and the efficiency of their cleavage. To have a deeper insight into which types of linkages are cleaved by alkaline fusion and to what extent, a series of standard phenolic compounds containing aryl-ether linkages (8-*O*-4-dehydrodiferulic acid), stilbene-type linkages (8,5(noncyclic)-dehydrodiferulic acid), and biphenyl linkages (5,5-dehydrodiferulic acid) between ferulic acids were subjected to alkaline fusion. The phenolic compounds containing aryl-ether linkages and stilbene-type linkages were quantitatively cleaved by alkaline fusion, yielding only 3,4-dihydroxybenzoic acid, catechol, and hydroquinone. Nevertheless, the phenolic compound containing biphenyl type linkage was not quantitatively recovered from the alkaline fusion, being recovered only 19% of the original phenolic compound. This result may show that this type of linkage is more resistant to alkaline fusion. Also, it is possible that the phenolic compounds released were of different nature or that they were lost during the alkaline fusion, not allowing their recovery.

Fractionation of the HMWM by Ethanol Precipitation. The HMWM of roasted coffee infusions is composed by a mixture of thermally transformed galactomannans and arabinogalactans and by a diversity of melanoidin populations presenting different physical properties and chemical composition, including melanogalactomannans, melanoarabinogalactans, and melanoidins containing low amounts of carbohydrates.[6,7] These macromolecules can be roughly separated by ethanol precipitation. Galactomannans and melanogalactomannans can be obtained by precipitation in 50% ethanol solutions (Et50), arabinogalactans and melanoarabinogalactans can be obtained by precipitation in 75% ethanol solutions (Et75), and a second melanoarabinogalactan fraction and the melanoidins with low amounts of carbohydrates remain soluble in 75% ethanol solutions (EtSn). The yield and chemical composition of the fractions obtained by ethanol fractionation are shown in Table 4. For all coffees, the amount of material recovered was highest on the EtSn fraction (53%, on average) followed by the Et50 fraction (35%), and the Et75 fraction accounted for the lowest amount (13%). This distribution of the different melanoidin populations is in accordance with previous ethanol fractionation procedures in Arabica and Robusta coffees.[6,16,20,34,35] The amount of protein recovered in the fractions isolated from the different coffees increased significantly with the increase of the ethanol concentration, in accordance with Bekedam et al.[4] The amount of protein recovered in the EtSn and Et75 fractions from CGAcoffee was significantly higher than that of control. The phenolic compounds present in the each fraction also increased with the increase in ethanol solubility, being also observed a significantly higher amount of total phenolics in the Et75 and EtSn fractions recovered from CGAcoffee when compared to control. A significant correlation between the amount of protein and phenolic compounds present in the ethanol fractions ($r = 0.830$, $p < 0.05$) was also observed. When the percentage of phenolic compounds present in each fraction is calculated in relation to the amount of phenolic compounds present in the HMWM, it can be observed that the phenolic compounds present in the EtSn fraction represent nearly 83% of the HMWM phenolic compounds, followed by the Et50 fraction (15%) and the Et75 (12%). These results show that the melanoidin population soluble in ethanol contained the majority of the phenolic compounds incorporated into the HMWM during roasting, which is in accordance with Nunes et al.[16] and Bekedam et al.[4] The MBI increased for all coffee fractions with the increase of their solubility in ethanol. For the Et75 and EtSn fractions recovered from the CGAcoffee model, an average of 30% increase in the MBI was observed. In these fractions, the amounts of protein and phenolic compounds are significantly higher for CGAcoffee model when compared to the control. Also, a significant correlation between the phenolic compounds and MBI ($r = 0.674$, $p < 0.05$) is observed. The amount of phenolic compounds was also significantly correlated with the color of the different melanoidin populations ($r = 0.782$, $p < 0.05$), a significant correlation between the amount of protein and MBI ($r = 0.749$, $p < 0.05$) being also observed.

As the melanoidin populations soluble in 75% ethanol contained the majority of the phenolic compounds present in the HMWM, the nature of the phenolic compounds present in these melanoidin populations was further studied (Figure 1b). The EtSn fraction did not contain adsorbed phenolic compounds, which can be explained by the experimental procedure used, including dialysis and urea solubilization, probably resulting in the loss of the adsorbed phenolics. The amount of ester-linked phenolic compounds was in the range of that found for the HMWM, and there was no significant difference between the amounts of ester-linked phenolics for

the three coffees studied. The amount of condensed phenolic compounds present in the EtSn fraction was significantly higher, by a factor of 60, than the ester-linked phenolic compounds. The amount of condensed phenolic compounds present in the CGAcoffee model was, on average, higher than that present in the control coffee (Figure 1b). Nevertheless, it was not significantly different, probably due to the higher variability obtained in the analysis, as the total phenolic acids measured by the Folin−Ciocalteu colorimetric method were significantly higher. There was observed a significant correlation between the amount of phenolic compounds released by alkaline fusion and that determined by the colorimetric Folin−Ciocalteu method (ρ = 0.886, p < 0.05), although this correlation was not significantly linear (r = 0.767, p < 0.075). The Folin−Ciocalteu colorimetric method measures the sample's reducing capacity, which includes, among others, phenolic compounds.[36] However, this assay is also sensitive to the presence of proteins, ascorbic acid, and other reducing compounds.[37,38] In fact, melanoidins produced from model systems containing only sugar and amino acids are known to possess reducing capacity,[39] showing that proteins or reducing Maillard reaction products such as reductones present in the material can contribute to the reducing power of the solution, resulting in an overestimation of the amount of phenolic compounds present when measured by the Folin−Ciocalteu method. Nevertheless, as the reducing power of 5-CQA is 21 times higher, on a weight basis, than that of bovine serum albumin (BSA), protein interference should be comparably low (although the actual interference clearly depends on the amino acid composition of the proteins). Also, it is certainly harder to estimate the contribution of Maillard reaction products to the reducing power of the actual coffee sample. Nevertheless, although the application of the Folin−Ciocaultau method can have drawbacks, it is widely used for accessing the presence of phenolic compounds in coffee melanoidins, and the results obtained in this work show that it can be used as an indicator for phenolic compounds present.

Fate of CGA during Roasting, Contribution to Melanoidin Formation, and Potential Health Effects. The amount of phenolic compounds incorporated in coffee melanoidins, determined by the alkaline fusion method, ranged from 10 to 13 mol/100 mol of the CGA content present in green coffee. When the amount of phenolic compounds incorporated in coffee melanoidins was calculated in relation to the amount of phenolic compounds lost during roasting, the values ranged from 18 to 33 mol/100 mol. From these values it can be observed that the incorporation of phenolic compounds into the HMWM is a significant pathway of CGA degradation during roasting. When the amount of phenolic compounds incorporated in the HMWM is expressed as caffeic acid, it represents, on average, 23 g/100 g of the material not accounted for by polysaccharides and proteins. These results show that the phenolic compounds incorporated into coffee melanoidins represent a significant proportion of the previously described unknown material. The correlation found between the amount of phenolic compounds present in the different melanoidin populations and the K_{mix} color as well the MBI shows that the incorporation of phenolic compounds has an impact on the color of melanoidins. Although the structure of phenolic compounds present in the coffee melanoidins cannot be deduced from the data obtained from the methods applied, the data showed that they can be connected by aryl-ether, stilbene-type linkages, and biphenyl linkages, as these can be cleaved by alkaline fusion. The presence of phenolic compounds besides 3,4-dihydroxybenzoic acid, catechol, and hydroquinone in the alkaline fusion may represent different linkages or phenolic compounds transformed during roasting with structural features different from caffeic acid, but not yet available to be determined. The detection of 4-hydroxybenzoic acid in the alkaline fusion medium may represent the incorporation of coumaric acid in coffee melanoidins. The relative contribution of ferulic acid and caffeic acid to the amount of phenolic compounds incorporated into coffee melanoidins cannot be deduced due to the observed demethylation of phenolic compounds during alkaline fusion.[16] Further work is needed to disclose the structural details of the condensed phenolic compounds present in coffee melanoidins. The correlation between proteins and phenolic compounds in the different melanoidin populations suggests that the incorporation of phenolic compounds in coffee melanoidins is related to the amount of proteins. This can be explained by the easy cross-link between phenolic compounds through quinoidal structures and amino acids such as lysine and cysteine present in proteins.[40−42] The condensation of phenolic compounds during roasting has been shown to occur, but only low molecular weight structures have been found.[43−45] These might represent the starting point of the reaction that, on further reaction with proteins and also possibly with polysaccharides, incorporates these compounds into coffee melanoidins. As condensed phenolic structures are present in light-roasted coffee,[6] the incorporation process seems to occur as soon as the roasting starts, and this is in agreement with the data obtained from Smrke et al.[46] The presence of phenolic compounds in coffee melanoidins, mainly in condensed form, may be an explanation for the high antioxidant activity described for coffee melanoidins.[47,48] The association of these condensed phenolic structures with indigestible polysaccharides and melanoidins present in coffee HMWM may also be one of the reasons for the observed association between coffee consumption and the antioxidant capacity of feces from healthy subjects.[49] The presence of these condensed phenolic structures can act as a "radical-sponge" in the gastrointestinal tract (stomach and small and large intestine), as those described for other antioxidant dietary fibers when associated phenolic compounds are present.[50] Studies on the impact of gut microorganisms on the antioxidant activity of melanoidins are rare, but it was demonstrated, for example, that after a 24 h in vitro fermentation of high-molecular weight coffee fractions with gut microorganisms, roughly 25% of the original antioxidant activity was still present.[13] Due to the relatively high amount of phenolic compounds that can reach the gut, especially the large intestine, the fact that they are linked to the coffee dietary fiber deserves further study.

■ ASSOCIATED CONTENT

Ⓢ Supporting Information

Additional figures and tables. This material is available free of charge via the Internet at http://pubs.acs.org.

■ AUTHOR INFORMATION

Corresponding Author

*(F.M.N.) E-mail: fnunes@utad.pt. Phone: +351259350242.

Funding

We appreciate the financial support provided to the project PTDC/QUI-QUI/100044/2008, to the Research Unit in Vila

Real (PEst-OE/QUI/UI0616/2014), and to the QOPNA Research Unit 62/94 (Project PEst-C/QUI/UI0062/2013; FCOMP-01-0124-FEDER-037296) by the Foundation for Science and Technology (FCT) and COMPETE.

Notes

The authors declare no competing financial interest.

REFERENCES

(1) Ledl, F.; Schleider, E. New aspects of the Maillard reaction in foods and in the human body. *Angew. Chem., Int. Ed. Engl.* **1990**, *29*, 565−594.

(2) Hofmann, T.; Bors, W.; Stettmaier, K. Radical-assisted melanoidin formation during thermal processing of foods as well as under physiological conditions. *J. Agric. Food Chem.* **1999**, *47*, 391−396.

(3) Fogliano, V.; Morales, F. J. Estimation of dietary intake of melanoidins from coffee and bread. *Food Funct.* **2011**, *2*, 117−123.

(4) Bekedam, E. K.; Schols, H. A.; van Boekel, M. A.; Smit, G. High molecular weight melanoidins from coffee brew. *J. Agric. Food Chem.* **2006**, *54*, 7658−7666.

(5) Bekedam, E. K.; De Laat, M. P. F. C.; Schols, H. A.; Van Boekel, M. A. J. S.; Smit, G. Arabinogalactan proteins are incorporated in negatively charged coffee brew melanoidins. *J. Agric. Food Chem.* **2007**, *55*, 761−768.

(6) Nunes, F. M.; Coimbra, M. A. Melanoidins from coffee infusions. Fractionation, chemical characterization, and effect of the degree of roast. *J. Agric. Food Chem.* **2007**, *55*, 3967−3977.

(7) Nunes, F. M.; Coimbra, M. A. Role of hydroxycinnamates in coffee melanoidin formation. *Phytochem. Rev.* **2010**, *9*, 171−185.

(8) Silván, J. M.; Morales, F. J.; Saura-Calixto, F. Conceptual study on Maillardized dietary fiber in coffee. *J. Agric. Food Chem.* **2010**, *58*, 12244−12249.

(9) Takenaka, M.; Sato, N.; Asakawa, H.; Wen, X.; Murata, M.; Homma, S. Characterization of a metal-chelating substance in coffee. *Biosci, Biotechnol., Biochem.* **2005**, *69*, 26−30.

(10) Gniechwitz, D.; Reichardt, N.; Ralph, J.; Blaut, M.; Steinhart, H.; Bunzel, M. Isolation and characterisation of a coffee melanoidin fraction. *J. Sci. Food Agric.* **2008**, *88*, 2153−2160.

(11) Morales, F. J.; Somoza, V.; Fogliano, V. Physiological relevance of dietary melanoidins. *Amino Acids* **2012**, *42*, 1097−1109.

(12) Moreira, A. S. P.; Nunes, F. M.; Domingues, M. R.; Coimbra, M. A. Coffee melanoidins: structures, mechanisms of formation and potential health impacts. *Food Funct.* **2012**, *3*, 903−915.

(13) Reichardt, N.; Gniechwitz, D.; Steinhart, H.; Bunzel, M.; Blaut, M. Characterization of high molecular weight coffee fractions and their fermentation by human intestinal microbiota. *Mol. Nutr. Food Res.* **2009**, *53*, 287−299.

(14) Bekedam, E. K.; Schols, H. A.; van Boekel, M. A.; Smit, G. Incorporation of chlorogenic acids in coffee brew melanoidins. *J. Agric. Food Chem.* **2008**, *56*, 2055−2063.

(15) Perrone, D.; Farah, A.; Donangelo, C. M. Influence of coffee roasting on the incorporation of phenolic compounds into melanoidins and their relationship with antioxidant activity of the brew. *J. Agric. Food Chem.* **2012**, *60*, 4265−4275.

(16) Nunes, F. M.; Cruz, A. C. S.; Coimbra, M. A. Insight into the mechanism of coffee melanoidin formation using modified "in bean" models. *J. Agric. Food Chem.* **2012**, *60*, 8710−8719.

(17) Jilek, M. L.; Bunzel, M. Dehydrotriferulic and dehydrodiferulic acid profiles of cereal and pseudocereal flours. *Cereal Chem.* **2013**, *90*, 507−514.

(18) Amorim, H. V.; Josephson, V. R. Water soluble protein and nonprotein components of Brazilian green coffee beans. *J. Food Sci.* **1975**, *40*, 1179−1184.

(19) Hulme, A. C. The isolation of chlorogenic acid from the apple fruit. *Biochem. J.* **1953**, *53*, 337−340.

(20) Nunes, F. M.; Coimbra, M. A. Chemical characterization of the high molecular weight material extracted with hot water from green and roasted arabica coffee. *J. Agric. Food Chem.* **2001**, *49*, 1773−1782.

(21) Trugo, L. C.; Macrae, R. A study of the effect of roasting on the chlorogenic acid composition of coffee using HPLC. *Food Chem.* **1984**, *15*, 219−227.

(22) Farah, A.; de Paulis, T.; Moreira, D. P.; Trugo, L. C.; Martin, P. R. Chlorogenic acids and lactones in regular and water decaffeinated arabica coffees. *J. Agric. Food Chem.* **2006**, *54*, 374−381.

(23) Abraão, A. S.; Lemos, A. M.; Vilela, A.; Sousa, J. M.; Nunes, F. M. Influence of osmotic dehydration process parameters on the quality of candied pumpkins. *Food Bioprod. Process.* **2013**, *91*, 481−494.

(24) Nardini, M.; Cirillo, E.; Natella, F.; Mencarelli, D.; Comisso, A.; Scaccini, C. Detection of bound phenolic acids: prevention by ascorbic acid and ethylenediaminetetraacetic acid of degradation of phenolic acids during alkaline hydrolysis. *Food Chem.* **2002**, *79*, 119−124.

(25) Batistic, L.; Mayaudon, J. Étude chromatographic des acides phénoliques et des phenols obtenus par la fusion alcaline des acides humiques. *Plant Soil* **1970**, *33*, 473−477.

(26) Murkovic, M.; Derler, K. Analysis of amino acids and carbohydrates in green coffee. *J. Biochem. Biophys. Methods* **2006**, *69*, 25−32.

(27) Fischer, M.; Reimann, S.; Trovato, V.; Redgwell, R. J. Polysaccharides of green Arabica and Robusta coffee beans. *Carbohydr. Res.* **2001**, *330*, 93−101.

(28) Oosterveld, A.; Harmsen, J. S.; Voragen, A. G. J.; Schols, H. A. Extraction and characterization of polysaccharides from green and roasted *Coffea arabica* beans. *Carbohydr. Polym.* **2003**, *52*, 285−296.

(29) Hughes, W. J.; Thorpe, T. M. Determination of organic acids and sucrose in roasted coffee by capillary gas chromatography. *J. Food Sci.* **1987**, *52*, 1078−1083.

(30) Perrone, D.; Donangelo, R.; Donangelo, C. M.; Farah, A. Modeling weight loss and chlorogenic acids content in coffee during roasting. *J. Agric. Food Chem.* **2010**, *58*, 12238−12243.

(31) Redgwell, R. J.; Trovato, V.; Curti, D.; Fischer, M. Effect of roasting on degradation and structural features of polysaccharides in arabica coffee beans. *Carbohydr. Res.* **2002**, *337*, 421−431.

(32) Oosterveld, A.; Voragen, A. G. J.; Schols, H. A. Effect of roasting on the carbohydrate composition of *Coffea arabica* beans. *Carbohydr. Polym.* **2003**, *54*, 183−192.

(33) Robbins, R. J. Phenolic acids in foods: an overview of analytical methodology. *J. Agric. Food Chem.* **2003**, *51*, 2866−2887.

(34) Nunes, F. M.; Coimbra, M. A. Chemical characterization of galactomannans and arabinogalactans from two arabica coffee infusions as affected by the degree of roast. *J. Agric. Food Chem.* **2002**, *50*, 1429−1434.

(35) Nunes, F. M.; Coimbra, M. A. Chemical characterization of the high molecular weight material extracted with hot water from green and roasted robusta coffee as affected by the degree of roast. *J. Agric. Food Chem.* **2002**, *50*, 7046−7052.

(36) Huang, D.; Ou, B.; Prior, R. L. The chemistry behind antioxidant capacity assays. *J. Agric. Food Chem.* **2005**, *53*, 1841−1856.

(37) Waterhouse, A. L. Determination of total phenolics. In *Current Protocols in Food Analytical Chemistry*; Wrolstad, R. E., Ed.; Wiley: Hoboken, NJ, USA, 2001.

(38) Singleton, V. L.; Orthofer, R.; Lamuela-Raventós, R. M. Analysis of total phenols and other oxidation substrates and antioxidants by means of Folin-Ciocalteu reagent. *Methods Enzymol.* **1999**, *299*, 152−178.

(39) Homma, S.; Terasawa, N.; Kubo, T.; Yoneyama-Ishii, N.; Aida, K.; Fujimaki, M. Changes in chemical properties of melanoidin by oxidation and reduction. *Biosci., Biotechnol., Biochem.* **1997**, *61*, 533−535.

(40) Rawel, H. M.; Rohn, S.; Kroll, J. Characterisation of 11S protein fractions and phenolic compounds from green coffee beans under special consideration of their interactions − a review. *Dtsch. Lebensm. Rundsch.* **2005**, *101*, 148−160.

(41) Montavon, P.; Mauron, A. F.; Duruz, E. Changes in green coffee protein profiles during roasting. *J. Agric. Food Chem.* **2003**, *51*, 2335−2343.

(42) Ali, M.; Homann, T.; Rawel, H.; Kreisel, J.; Khalil, M.; Puhlmann, R.; Kruse, H.-P. Characterization and modeling of the

interactions between coffee storage proteins and phenolic compounds. *J. Agric. Food Chem.* **2012**, *60*, 11601−11608.
(43) Stadler, R. H.; Welti, D. H.; Stampfli, A. A.; Fay, L. B. Thermal decomposition of caffeic acid in model systems: identification of novel tetraoxygenated phenylindan isomers and their stability in aqueous solution. *J. Agric. Food Chem.* **1996**, *44*, 898−905.
(44) Frank, O.; Blumberg, S.; Kunert, C.; Zehentbauer, G.; Hofmann, T. Structure determination and sensory analysis of bitter-tasting 4-vinylcatechol oligomers and their identification in roasted coffee by means of LC-MS/MS. *J. Agric. Food Chem.* **2007**, *55*, 1945−1954.
(45) Jaiswal, R.; Matei, M. F.; Golon, A.; Witt, M.; Kuhnert, N. Understanding the fate of chlorogenic acids in coffee roasting using mass spectrometry based targeted and non-targeted analytical strategies. *Food Funct.* **2012**, *3*, 976−984.
(46) Smrke, S.; Opitz, S. E. W.; Vovk, I.; Yeretzian, C. How does roasting affect the antioxidants of a coffee brew? Exploring the antioxidant capacity of coffee via on-line antioxidant assays coupled with size exclusion chromatography. *Food Funct.* **2013**, *4*, 1082−1092.
(47) Borrelli, R. C.; Visconti, A.; Mennella, C.; Anese, M.; Fogliano, V. Chemical characterization and antioxidant properties of coffee melanoidins. *J. Agric. Food Chem.* **2002**, *50*, 6527−6533.
(48) Delgado-Andrade, C.; Rufián-Henares, J. A.; Morales, F. J. Assessing the antioxidant activity of melanoidins from coffee brews by different antioxidant methods. *J. Agric. Food Chem.* **2005**, *53*, 7832−7836.
(49) Garsetti, M.; Pellegrini, N.; Baggio, C.; Brighenti, F. Antioxidant activity in human faeces. *Br. J. Nutr.* **2000**, *84*, 705−710.
(50) Saura-Calixto, F. Antioxidant dietary fiber product: a new concept and a potential food ingredient. *J. Agric. Food Chem.* **1998**, *46*, 4303−4306.

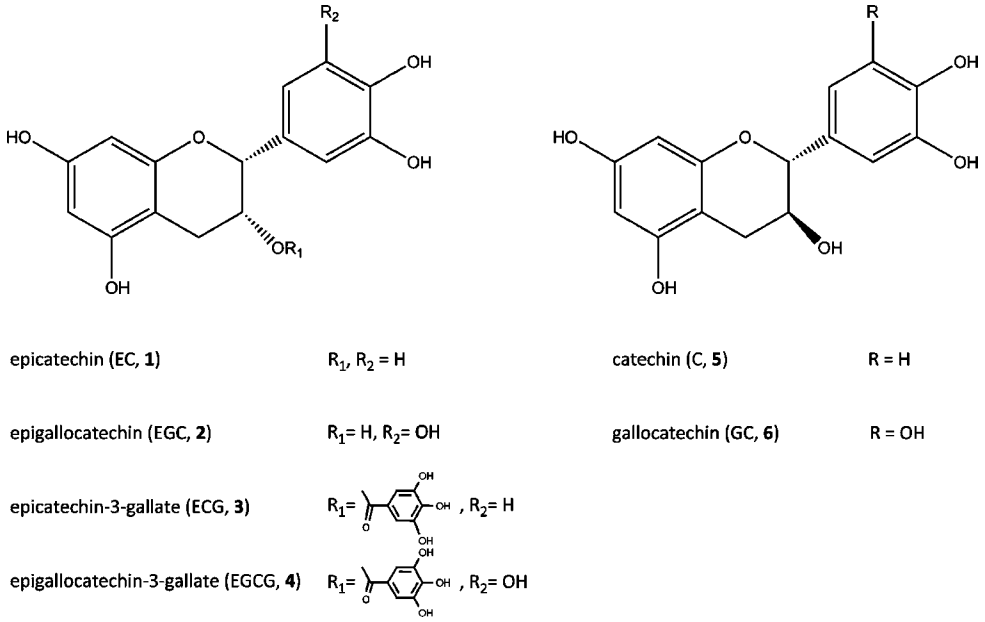

Figure 1. Chemical structures of the six most common flavan-3-ols **1**−**6** in green tea.

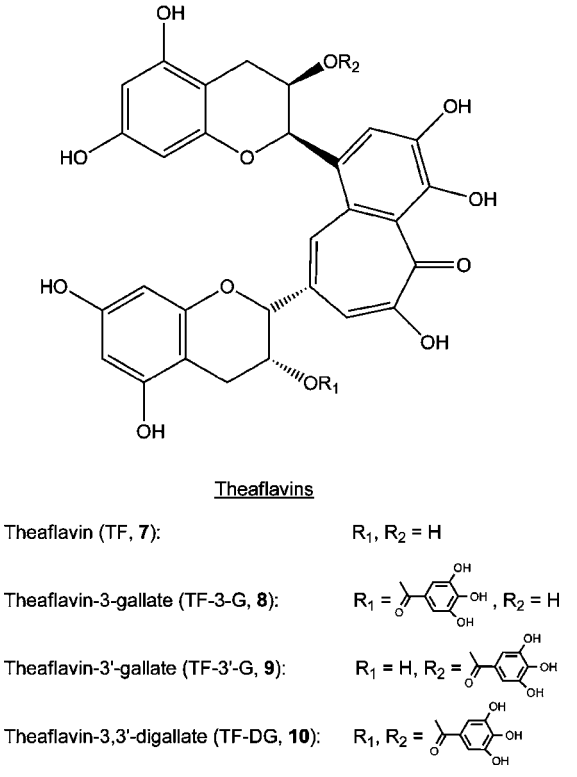

Figure 2. Structures of theaflavin and its gallate esters: theaflavin **7**, theaflavin 3-gallate **8**, theaflavin 3′-gallate **9**, and theaflavin 3,3′-digallate **10**.

Several groups were able to synthesize and isolate a number of oxidation products, such as theaflavins, theasinensins, and theanaphthoquinone, using model fermentations with green tea leaves.[14−17]

In an approach to gather information about the enzymatically catalyzed oxidative reactions which are almost solely responsible for the differences between a black and a green tea, we decided to employ model fermentations. Based on a system reported by Bonnely et al., polyphenol-free leaves of *Camellia sinensis* with active enzymes were used to oxidize selected combinations of flavan-3-ols.[18] As an alternative approach model oxidations using horseradish POD enzyme without matrix were carried out. Analytical techniques such as HPLC-DAD and LC-ESI-MS^n were employed for analysis and obtained results compared with the literature.

MATERIALS AND METHODS

Chemicals. The following chemicals were used: ethylenediaminetetracetic acid disodium salt dihydrate (>99%, Fluka Chemie GmbH, Buchs, Switzerland), L-(+)-ascorbic acid (≥99%, VWR BDH Prolabo, Leuven, Belgium), MES (2-(*N*-morpholino)ethanesulfonic acid; EGA Chemie, Steinheim, Germany), Triton X-100 (AppliChem GmbH, Darmstadt, Germany), benzamidine hydrochloride (AppliChem). Peroxidase from horseradish (lyophilized powder, 52 units/mg solid) was obtained from Sigma-Aldrich Chemie GmbH (Steinheim, Germany) as well as (−)-epicatechin and (+)-catechin hydrate with purities of 90% and 98%, respectively. The following solvents were used: acetonitrile (for HPLC, HPLC super gradient grade, ≥99.9%, VWR International S.A.S., Fontenay-sous-Bois, France; for LC-MS, LC-MS grade, ≥99.95%, Carl Roth GmbH & Co. KG, Karlsruhe, Germany), methanol (HPLC gradient grade, 100.0%, VWR International S.A.S.), MTBE (for synthesis, ≥99.5%, Carl Roth), chloroform (p.a., ≥99.99%, stabilized with amylene, Fisher Scientific, Loughborough, U.K.), acetic acid (for HPLC, HPLC grade, ≥99.7%, Fisher Scientific; for LC-MS, LC-MS grade, ≥99.7%, Fisher Scientific), petroleum ether (technical grade, distilled before use). All water used in the experiments was of Nanopure quality (Werner Reinstwassersysteme, Leverkusen, Germany). For identification of monitored compounds ((+)-C, EC, ECG, EGC, EGCG, TF, TF-3-G, TF-3′-G, TF-DG, and gallic acid) isolated and spectroscopically characterized compounds were used as reference.

Isolation of EGCG, EGC, and ECG. For the isolation of EGCG, EGC, and ECG, an instant white tea (Hälssen & Lyon GmbH, Hamburg, Germany) and an extract enriched with flavanols (Sunphenon 80SK, Taiyo International, Inc., Minneapolis, MN, USA) were used.

The isolation was carried out by HSCCC using MTBE/ACN/H_2O (2/2/3, v/v/v) in tail-to-head mode on a triple coil machine (total volume 850 mL, Pharma-Tech Research Corp. model CCC-1000, Baltimore, MD, USA), allowing the separation of 2 g of source material per run. Fractions containing EGCG and ECG showed a

dx.doi.org/10.1021/jf501591j | J. Agric. Food Chem. 2014, 62, 7854−7861

chromatographic purity of 85−95% at 278 nm, whereas the EGC fraction needed additional purification via column chromatography on Sephadex LH-20 using chloroform/methanol/petroleum ether (1/2/1, v/v/v) as reported by Robertson and Bendall to yield a chromatographic purity (λ = 278 nm) of around 90%.[5]

The Model Fermentation (Oxidation) Setup. The model fermentation system that was used for our experiments is based on a publication by Bonnely et al.[18] However, to meet our requirements, modifications were necessary:

Fresh tea leaves with active endogenous enzymes were described as source material and were sourced and processed by the Bangalore/India group locally. By using acetone as extraction solvent large volumes could be avoided as described originally when doing the extraction with water. The obtained freeze-dried powder was shipped to the German lab for the model fermentation work, where it was tested for enzymatic activity. To check whether the removal of flavan-3-ols was successful, the leaf powder was extracted according to ISO 14502-2 and the obtained solution was analyzed via HPLC-DAD (see Determination of Remaining Flavanols).[19] Further adjustments were made with regard to scale, temperature regulation, and selection of inert gas.

Preparation of Flavanol Free Tea Leaf Material. Fresh tea leaves (400 g) were stored overnight at −80 °C and ground while cooled with liquid nitrogen to a fine powder. Cold acetone (500 mL) was mixed with the powder in a steel container stored in an ice bath. The suspension was mixed with a Silverson mixer for 15 min and immediately filtrated over vacuum (Whatman Filter Paper No. 40). The residue was washed with cold acetone, and the extraction with acetone was repeated three more times before water−acetone mixtures (500 mL each) were used in the following order:

$$75\%\ \text{acetone} \rightarrow 50\%\ \text{acetone} \rightarrow 25\%\ \text{acetone} \rightarrow 50\%\ \text{acetone} \rightarrow 75\%\ \text{acetone}$$

Finally the powder was washed again with cold acetone and freeze-dried.

Determination of Remaining Flavanols. The freeze-dried leaf powder (40 mg) was extracted with 1 mL of 70% methanol$_{(aq)}$ for 10 min at 70 °C. The extract was separated from the leaves via centrifugation (Hermle Labortechnik GmbH, Typ Z383, Wehingen, Germany), and the remaining leaves were extracted two more times. 210 μL of a stabilizing solution (12.5 mg of EDTA and 12.5 mg of ascorbic acid are dissolved in water and made up to 50 mL) were added to the combined extracts. After microfiltration this solution was analyzed via HPLC-DAD (see HPLC-DAD Analysis of Flavanols and Thearubigins).

Determination of Enzyme Activity. The determination of the enzyme activity was carried out according to the literature.[18] Briefly, 100 mg of polyphenol free tea leaf material was suspended with 3 mL of enzyme buffer (488 mg of 2-(*N*-morpholino)ethanesulfonic acid (MES), 1.42 g of sodium sulfate, 7.83 mg of benzamidine hydrochloride, and 150 μL of Triton X-100 made up to 50 mL with water and the pH value set to 5.5 with 2.5 M sodium hydroxide), stirred on ice for 30 min, and centrifuged at 3000 rpm for 20 min and the upper phase (enzyme extract) separated from the leaves.

50 μL of the enzyme extract was given into a cuvette, 1.38 mL of sodium phosphate-citrate buffer (100 mM, pH 5.5) and 75 μL of (+)-catechin solution (60 mM) were added, and the extinction was monitored during the next 30 min at 400 nm against water. For measurement of PPO activity, this was done at 40 °C; for POD activity, at 30 °C and after addition of 25 μL of 1.5% hydrogen peroxide.

Blanks were taken by adding 100 μL of stop solution (acetonitrile, acetic acid, water; 60/10/30, v/v/v) to the solution before incubation at 30/40 °C.

The rate of quinone formation was calculated as μA/min from the linear part of the monitored curves and set into relation with the dry weight of the enzyme extract. The latter was determined after 24 h of dialysis (14 kDa dialysis tube Visking, cellulose type 20/32 in., Carl Roth) and lyophilization of the residue.

$$\text{EA}\left[\frac{\mu\text{A}}{\text{min}\cdot\text{g}}\right] = \frac{\text{rate}\left[\frac{\mu\text{A}}{\text{min}}\right]}{\text{dry weight [g]}}$$

Fermentation (Oxidation) Procedure. The following solutions were used during the model fermentation experiments:

stop solution: 60 mL of acetonitrile and 10 mL of glacial acetic acid made up to 100 mL with water
hydrogen peroxide: 1.5% (aq)
stabilizing solution: see Determination of Remaining Flavanols

The polyphenol-free tea leaf powder (500 mg) was given into a 250 mL three-necked flask, 10 mL of water and a stir bar were added, and the flask was put into a water bath (Julabo Labortechnik GmbH, model MP-PA/KÜ, Seelbach, Germany) connected to a thermostat (Lauda Dr. R. Wobser GmbH & Co. KG, model RC 6, Lauda-Königshofen, Germany). The following step depended on the enzymes used in the oxidation process; for PPO catalyzed oxidations the suspension was sparged with synthetic air (20.5 vol % O_2, 79.5 vol % N_2). To use PPO and POD 1.95 mL of H_2O_2 solution was added in addition to the synthetic air flow. This resulted in a concentration of about 8 mmol/L H_2O_2 and about 0.25 mmol/L O_2 in a total volume of 100 mL. For the use of POD only, 1.95 mL of hydrogen peroxide solution was added and the whole fermentation (oxidation) process was carried out in an argon atmosphere.

Selected flavanols (for most experiments: 60 mg each) were dissolved in 70−110 mL of water and brought to the correct temperature. To start the oxidation process, this solution was given into the reaction flask and, thus, brought into contact with the enzymes of the tea leaf powder.

Samples (2 mL) were taken at various times, and stop solution (0.7 mL) was added immediately. These samples were split, and 158 μL of stabilizing solution was added to one half. After microfiltration (Rotilabo Mini-Tip syringe filter, PTFE membrane, 0.45 μm, ⌀ 15 mm; Carl Roth), the samples with added stabilizers were used for HPLC-DAD analysis while samples without stabilizers were used for measurement via HPLC-MS^n.

The reactions were stopped after 5−7 h.

Alternative Oxidation Using Peroxidase from Horseradish. EC and EGCG (50 mg each) were dissolved in 96 mL of water in a 250 mL three-necked flask. Hydrogen peroxide solution (1.95 mL, 1.5%) was added and the solution sparged with synthetic air. For the investigation of tea leaf matrix effects, 1.5 g of commercially available green tea leaves was extracted (3× for 15 min with 100 mL of 70% methanol$_{(aq)}$ at 40 °C while stirring) to remove flavanol content and freeze-dried, and 0.5 g was added to the solution. As enzymes are inactivated by heat in green tea manufacture, these leaves should not contain enzyme activity. This was verified as described above (see Determination of Enzyme Activity). For the binding of free metal cations 0.2 mL of an EDTA solution (1%) was added as well. The reaction was started by addition of 4 mL of fresh horseradish POD solution (0.5 mg/4 mL). The reaction was carried out at room temperature, and the sampling procedure was done as described above (see Fermentation (Oxidation) Procedure). After 5 h the reaction was stopped.

HPLC-DAD Analysis of Flavanols and Thearubigins. For HPLC analysis the following equipment was employed: Agilent Technologies (Waldbronn, Germany) series 1100 HPLC consisting of autosampler, binary pump, column oven, and DAD detector. The measurement was performed using a modified system from ISO-14502-2:2002: flow, 1.0 mL/min; temperature, 35 ± 0.5 °C; column, Luna 5 μm Phenyl-Hexyl, 250 × 4.6 mm (Phenomenex, Aschaffenburg, Germany); injection volume, 20 μL; mobile phase, A = 9% acetonitrile in 2% acetic acid$_{(aq)}$ and 20 μg/mL EDTA, B = 80% acetonitrile in 2% acetic acid$_{(aq)}$ and 20 μg/mL EDTA; gradient elution, 0% B, 0−15 min; 0−32% B, 15−30 min; 32% B, 30−35 min; 32%−100% B, 35−36 min; 100% B, 36−45 min; 100%−0% B, 45−46 min; equilibration time, 20 min; detection, diode array (λ = 278 and 354 nm).[19]

HPLC-DAD Analysis of Theaflavins. The separation of theaflavins was achieved on an Agilent Technologies series 1200

HPLC consisting of autosampler, binary pump, column oven, and DAD detector via the following system: flow, 2.0 mL/min; temperature, 30 ± 0.5 °C; column, Zorbax Eclipse XDB C-18, 150 × 4.6 mm, 3.5 μm (Agilent Technologies); injection volume, 10 μL; mobile phase, A = 2% acetic acid$_{(aq)}$ and 20 μg/mL EDTA, B = 2% acetic acid in acetonitrile and 20 μg/mL EDTA; gradient, isocratic at 20% B; detection, diode array (λ = 274 nm).

Analysis via HPLC-ESI-MS^n. The separation via HPLC was performed on an Agilent Technologies series 1100 HPLC consisting of binary pump and DAD detector with a series 1200 autosampler: flow, 0.25 mL/min; temperature, RT; column, Luna 3 μm Phenyl-Hexyl, 150 × 2 mm (Phenomenex); injection volume, 5 μL; mobile phase, A = 9% acetonitrile in 2% acetic acid$_{(aq)}$, B = 80% acetonitrile in 2% acetic acid$_{(aq)}$; gradient elution, 0% B, 0−15 min; 0−32% B, 15−30 min; 32% B, 30−35 min; 32%−100% B, 35−36 min; 100% B, 36−45 min; 100%−0% B, 45−46 min; equilibration time, 20 min; detection, diode array (λ = 278 nm).

The analysis via ESI-MS^n was done on a Bruker Daltonics (Bremen, Germany) HCT PTM Discovery System electrospray ionization ion trap mass spectrometer using the following parameters: ion mode, alternating; scan, 100−1000 m/z; nebulizer, 60.00 psi; dry gas, 11 L/min; 365 °C; capillary, −/+ 3500 V.

RESULTS AND DISCUSSION

Advantages and Drawbacks of the Model System. The main advantage of this approach is the use of the tea leaf matrix and its endogenous enzymes, making it more authentic than other systems that often employ isolated enzymes from other plant sources, such as POD from horseradish. This way, the influence of secondary/minor compounds of tea and possibly also reactions of additional enzymes besides PPO and POD have to be taken into account. Furthermore, the system offers the possibility to freely select the enzymes and their substrates (flavanols) that are used during the oxidation process. This provides the opportunity to investigate the influence of various factors as well as it simplifies—at least to a degree—the highly complex processes.

However, this being only a model system, there are also limitations to this experimental setup. For example, the presence of water that is used in the model system is much higher than during authentic tea manufacture. Moreover, the addition of hydrogen peroxide (8 mM) is probably higher than the amount that is formed during authentic fermentation conditions which may affect the enzyme activity and give rise to reactions other than enzymatic oxidation.[20]

Influence of Temperature and Water Amount. In Figure 3 the strong effect of the temperature on the enzyme activity and hence the reaction speed is presented. First

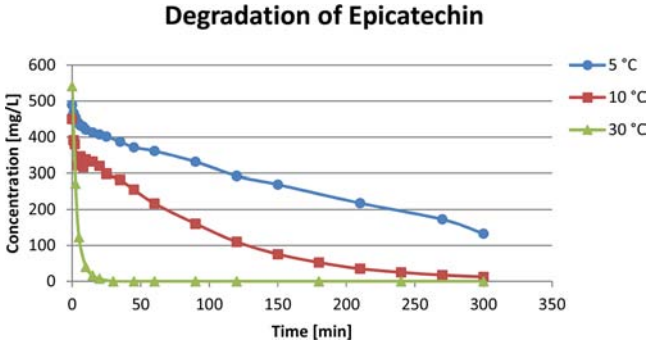

Figure 3. Influence of temperature on the degradation of EC during model fermentations (oxidations) with EC and EGCG at 5, 10, and 30 °C.

experiments were carried out at 30 °C leading to a rapid degradation of flavanols and a fast formation of TFs and TRs. As one aim of the study was to understand the time course of the reaction, a lower temperature (5 °C) was employed to slow down the reaction. It can be observed much more clearly now that for example the reaction of POD with EGCG is much faster than with PPO or POD with EC.

To study whether or not the amount of added water has an influence on the reactions, model oxidations using 45, 60, and 80 mL of water were carried out. It was found that the degree of dilution with water had no significant effect on the oxidation process (data not shown). However, the use of less water would have been more authentic and thus preferable but was not possible due to practical reasons, especially the sampling process.

Color Development. In Figure S1 in the Supporting Information photographs are given of the reaction mixture of ECG and EGC at 5 °C during an oxidation with PPO and POD from the start and after 1 and 4 h. The color change of the reaction mixture from a pale yellow to orange and finally to brown can be clearly observed. The colorless flavanols and the pale yellow tea leaf powder used as starting material (the latter is also shown as dry material in Figure S1 in the Supporting Information) are (partially) converted to colored material. Indeed upon freeze-drying the reaction mixture, a brownish residual powder, also shown in Figure S1 in the Supporting Information, was obtained. This is similarly observed in green tea oxidation to black tea.

Degradation of Flavanols. Immediately after the start of the oxidation procedure with both enzymes active and two or more flavanols present, a depletion of the flavanol content is observed. The individual flavanols were converted with different speed: EGC ≈ EGCG > ECG > EC > (+)-C. This is probably due to a higher affinity of the enzymes to 3′-hydroxylated and gallated flavanols. This observation is consistent with those reported by Muthumani and Kumar and the finding of Robertson that PPO oxidizes gallocatechins more rapidly than simple catechins.[6,21] It was also reported that PPO prefers flavanols carrying no gallate ester as substrate.[22] This contradiction may be explained by the oxidative behavior of the EC-quinone. For example in an oxidation of EC and ECG, EC gets preferentially oxidized by PPO to its corresponding *o*-quinone, which in turn oxidizes ECG to the ECG-quinone.[14,22,23] As this step is associated with the recovery of EC, the EC concentrations would appear to be almost constant. Following this theory a more rapid decrease of the EC content is expected after total consumption of the galloylated flavanol. This was not observed in our experiments; in fact, the rate of degradation of EC remained unchanged.

Formation of Theaflavins and Thearubigins. In Figure 4 is shown the formation of the expected theaflavin products in three experiments as measured via HPLC-DAD. In each experiment a mixture of two flavanols (60 mg each) was fermented in the presence of the leaf powder. As expected, a fast generation of the theaflavin that corresponds to the selected pair of flavanols was observed. Also differences in quantities, reaction speed, and stability of the formed theaflavin can be observed. E.g., the combination of both gallated EGCG and ECG gives a low product yield and a much slower reaction while stability is good compared to the combination of EGCG with nongallated EC. This is in agreement with the previous statement that EC is a good substrate for the PPO enzyme and its formed quinone readily reacts with the gallated EGCG. The

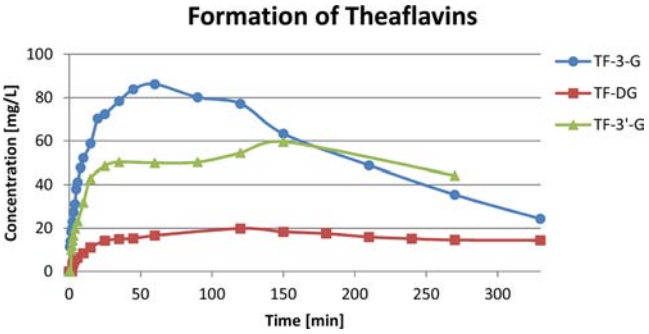

Figure 4. Formation of theaflavins during model oxidations with different combinations of flavanols at 5 °C: TF-3-G from EGCG + ECG; TF-3′-G from ECG + EGC; and TF-DG from EGCG + ECG.

formed quinone of EGCG and any quinone of EC subsequently react efficiently to the product. However, as part of the product site in the TF-3-G is nongallated, it might react further, although more slowly, with the enzyme, resulting in degradation not possible in the TF-DG, which indeed gives a more stable product be it on much lower concentration. The higher stability of TF-DG and TF-3′-G may also hint to the 3′-site as being more suitable for further oxidation of PPO/POD as it is protected by gallate.

In Table 1 is presented an overview of all theaflavins formed by PPO and POD enzymatic oxidation of seven different

Table 1. Combinations of Flavanols Used in Model Fermentations (Oxidations) and Thereof Generated Theaflavins As Detected via HPLC-DAD[a]

combination of flavanols	products
epicatechin + epigallocatechin	**theaflavin**
epigallocatechin 3-gallate + epicatechin	**theaflavin 3-gallate**, theaflavin
epigallocatechin 3-gallate + epicatechin 3-gallate	**theaflavin 3,3′-digallate**, theaflavin 3-gallate
epigallocatechin 3-gallate + (+)-catechin	**neotheaflavin 3-gallate**, neotheaflavin
epigallocatechin + epicatechin 3-gallate	**theaflavin 3′-gallate**, theaflavin
epigallocatechin + epigallocatechin 3-gallate	no theaflavins formed
epicatechin + epicatechin 3-gallate	no theaflavins formed[b]

[a]Products written in boldface letters are the primary product. [b]Small amounts of TF-3-G found via LC-MS, probably due to impurities in the isolated ECG used as substrate.

combinations of flavanols tested. It can be seen that the reaction of two flavanols with either both trihydroxylated or both dihydroxylated B-rings leads to no TF formation. Also, if only a single flavanol was treated with the enzymes, no TF formation was observed. This is in accordance with the pathway of TF formation that requires one *o*-dihydroxylated and one *vic*-trihydroxylated B-ring to give the characteristic benzotropolone moiety.[14]

Figure S2 in the Supporting Information shows the course of formation of TF, TF-3-G, TF-3′-G, and TF-DG in a fermentation (oxidation) of the four main epicatechins together (EC, ECG, EGC, EGCG; each 30 mg/100 mL). Theaflavin was the primary oxidation product within the group of theaflavins, whereas the galloylated derivatives showed significantly lower concentrations. This is different from the relatively balanced ratio of TF, TF-3-G, TF-3′-G, and TF-DG in authentic black tea and can in part be explained by the large proportion of nongallated flavanols, which show the highest molar concentrations in the model reaction, compared to green tea leaves. Even so, the dominance of theaflavin hints to a promoted oxidative degallation in the model fermentation system in addition to the possible presence of tannase activity.[22,24]

Apart from the TFs, an unresolved hump appears in the HPLC chromatograms (data not shown). As there is currently no reliable method of quantitation, the area (λ = 278 nm) of the hump, exclusive of all peak areas on top of it, was used to get an idea about the amount of generated TRs. As can be seen in Figure 5, the TR hump takes a sharp rise in the first minutes

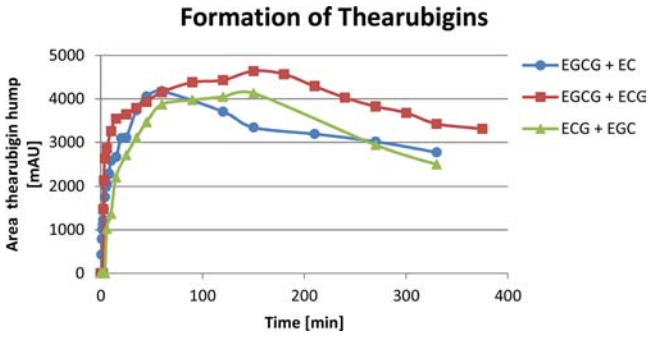

Figure 5. Development of the of the thearubigin hump (λ = 278 nm) during three model oxidation experiments with different combinations of flavanols.

of the fermentation process and slows down afterward to reach a maximum around 100 min. In the subsequent course of the oxidation process the area decreases slightly. This may be the result either of a degradation of the TRs or, perhaps more likely, of ongoing conversions (oxidations) that adversely affect their absorbance.

TF concentrations increased rapidly after the start but decreased after reaching a maximum. TRs were also formed early but during most model fermentations reached their maximum area at a later time compared to TFs. This confirms the assumption that TFs are partially an intermediate product in tea manufacture and may be converted into other species, such as thearubigins, during the oxidation.

Influence of Enzymes. All results described above were obtained through oxidations with both enzymes, PPO and POD. The enzyme activities were determined as described above (see Determination of Enzyme Activity) and showed values of 52 μA/min·g for the polyphenoloxidase and 149 μA/min·g for the peroxidase. These activities lie in a similar range compared to the literature.[18] An up to five times higher activity of the POD compared to PPO has also been reported earlier.[23] However, with a prolonged storage time a decrease in the enzyme activities was noticed and could be compensated by an increased temperature.

As the model fermentation system allows selecting single enzymes, a number of experiments with pairs of two flavanols were conducted to analyze their specific impact on the oxidation process.

Influence of Enzymes on Flavanol Degradation. In Figure 6 is shown that, in PPO-driven oxidations (absence of H_2O_2), EGCG was clearly the preferred substrate and showed an exponential degradation curve (above), whereas the concentration of all other flavanols, with EC shown, decreased more slowly and nearly linearly (below). It was observed that the total consumption of one flavanol did not have any effect on

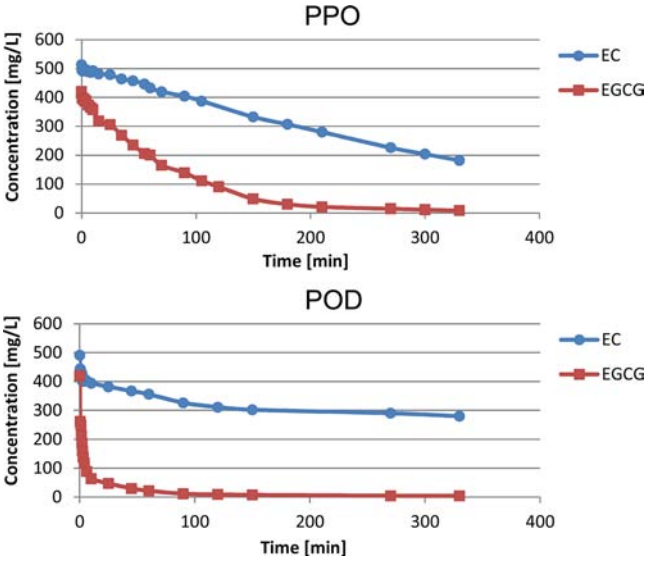

Figure 6. Course of flavanol degradation during model fermentations with EC and EGCG using PPO (above) and POD (below) at 5 °C.

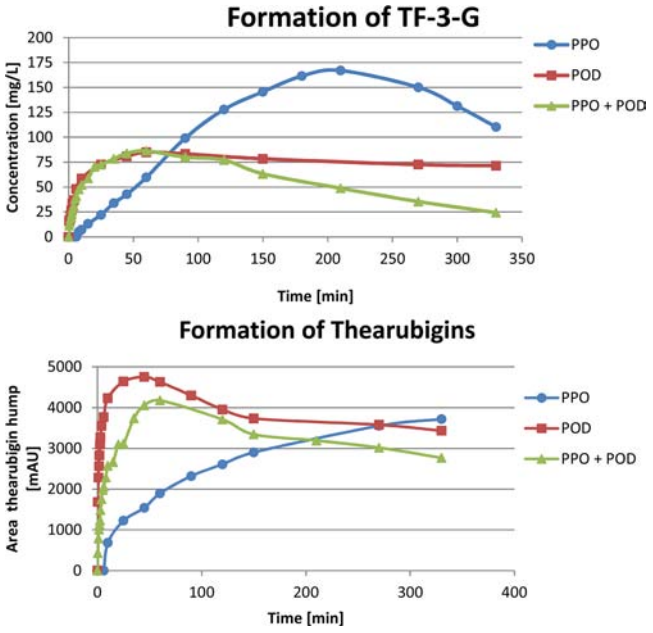

Figure 7. Influence of enzyme selection on the formation of theaflavin 3-gallate (above) and thearubigins (below, area at λ = 278 nm) during model fermentations with EC and EGCG at 5 °C.

the degradation of the remaining one. Also it was found that, in the presence of hydrogen peroxide and an inert atmosphere, the POD enzyme becomes active, while PPO activity is negligible and degraded gallocatechins (EGC, EGCG) faster over the flavanols which have 2 OH in the B-ring. In this case the conversion of one flavanol seems to be dependent on the presence of a second reactant. E.g., in Figure 6 it can also be seen that, after complete depletion of EGCG, the conversion speed of the remaining flavanol, in this case EC, slowed down dramatically and its concentration remained almost constant. Similar observations were made when other flavanols with dihydroxylated B-rings (ECG, (+)-C) were used, indicating that the tea leaf peroxidase does not react with this group of flavanols.

It could be argued that O_2 might be available by decomposition of H_2O_2 which gives rise to a PPO activity. However, by calculation of possible oxygen concentration it was assumed that PPO activity would be negligible. As the monitored results from oxidations using POD only are clearly distinct from those using PPO (also in combination with POD), it was confirmed that the inactivation of PPO in the model fermentation system was successful.

Enzymes on Formation of Theaflavins and Thearubigins. The complexity of the reactions and the large number of (possibly confounding) variables hampers the finding of general dependencies and affinities of the enzymes. Even so, it was observed throughout all oxidation experiments that those using only PPO yielded higher concentrations in TFs. Figure 7 shows the influence of the enzymes on the formation of theaflavin 3-gallate and thearubigins in an oxidation of EC and EGCG (each 60 mg). When POD was active, the concentrations of TFs were lower and the TR area was larger. The observed nonreactivity of POD with flavanols carrying dihydroxylated B-rings may lead to the conclusion that TFs can be formed from one quinone and one nonquinone flavanol. This should be further investigated. In summary PPO catalyzes a slow but constant formation of theaflavins which gives final concentrations twice as high as in the presence of POD. POD seems to preferentially catalyze reactions leading to TR formation.

pH Value and Release of Gallic Acid. Initially the pH of the model fermentation solutions was around 6.5. During the course of a model oxidation the pH value decreased due to the release of gallic acid, but did not fall under 5.0. The pH values were in accordance with those reported in the literature as suitable for PPO and POD.[22,23,25] Hence, the setup can be used without any buffer systems.

In Figure S3 in the Supporting Information it can be seen that the release of gallic acid was found to be fastest and highest in oxidations with PPO only. This is in accordance with the reported ability of PPO to catalyze the degallation of flavanols; however, if POD was present (alone or in combination with PPO) the release of gallic acid was significantly lower.[22] POD does therefore seem to stand in competition with PPO.

Influence of Tea Leaf Matrix. Two model fermentations (oxidations) using commercially available POD from horseradish as enzyme and a combination of EC and EGCG as its substrates were carried out. To investigate possible matrix effects of tea leaves 0.5 g of flavanol- and caffeine-free Chinese green tea leaves with inactive enzymes were added to one of the two setups. It can be drawn from Figure 8 that the presence of tea leaves leads to a degradation of TF-3-G after it has reached its maximum concentration. This was not the case when tea leaves were absent.

From this observation it is assumable that matrix effects play a crucial role in the manufacture of a black tea. The reasons are not quite clear. The catalyzing effect of transition-metal ions, obtained after denaturing the redox enzymes, e.g., in membrane structures, would be a conceivable explanation. Yet, a repetition of the experiment using EDTA as chelating agent against transition-metal cations displayed the same degradation of TF-3-G and, thus, effectively rules out this option.

Results Obtained by HPLC-ESI-MS^n. Selected samples from the model fermentation experiments were analyzed using HPLC-ESI-MS^n. Mass chromatograms were measured in negative ion mode. A list of some m/z values with corresponding fragment ions and assigned substances is given

dx.doi.org/10.1021/jf501591j | J. Agric. Food Chem. 2014, 62, 7854−7861

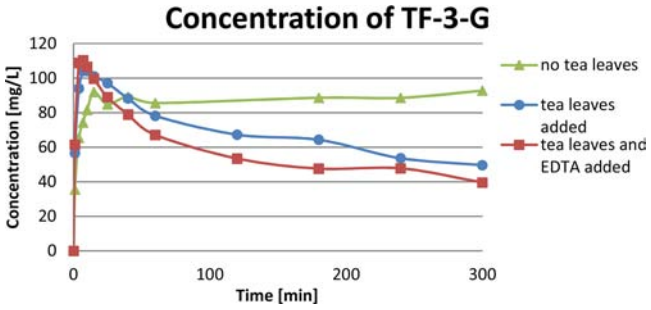

Figure 8. Concentration of TF-3-G during model fermentations with EC and EGCG using horseradish POD at 20 °C with or without addition of an extracted tea leaf matrix.

in Table 2. It can be seen that the model oxidation experiments led to the formation of oxidation products that are also found in black tea samples. Notably, the formation of theaflavate A, a benzotropolone-type dimer derived from ECG, was observed in the mass spectra at m/z of 851 in negative ion mode and also found in HPLC chromatograms with absorption maxima at 232, 280, and 402 nm.[26] As expected, this compound was present only in model oxidations using ECG as substrate. A preference on the use of either PPO or POD was not observed.

Table 2. Masses Found in Samples from Model Fermentations (Oxidations) and Assignment to Tea Compounds Reported in the Literature[11]

retention time [min]	m/z $[M-H]^-$	fragment ions m/z $[M-H]^-$	compound
2.0–2.2	191	173	quinic acid
2.7–3.0	169	125	gallic acid
6.1–6.4	305	261/219/179	EGC
7.5–7.7	289	245/205/203	(+)-C
9.4–10.1	353	217/173	CQA
14.2–14.7	289	245/227/205	EC
18.9–19.9	457	305/169/125	EGCG
24.7–25.9	579	561/533/517/413	oolongtheanin
29.1–29.4	441	289/245/205/169	ECG
32.9–33.0	427	383/227	theaflavic acid
33.2–34.8	563	545/379/241	TF
34.4–34.7	715	563/545/241	Neo-TF-G
34.6	533	515/471/305	theanaphthoquinone
35.8–36.2	715	563/527/371	TF-G
36.4	867	715/563/527/389	TF-DG
37.2	851	579	theaflavate A

Similar to the HPLC-DAD chromatograms, a broad hump-shaped figure was visible in the total ion chromatogram, representing the TRs (data not shown). To interpret this complex data, the oxidative cascade hypothesis by Kuhnert et al. was consulted and it was searched for masses corresponding to one of the oxidation series, e.g., the theaflavin-monogallate series.[11]

The intensities of signals that belonged to the m/z value of one oxidative stage, for example after the first formal insertion of one oxygen (= TF-G+O), were added and compared to those of the other oxidative stages. It was observed that in most model oxidations a tendency exists that m/z values corresponding to higher oxidative stages had lower intensities. This is in accordance with the oxidative cascade hypothesis that describes the stepwise formation of these oxidized species.

These different stages of oxidation were also compared at various time points of the fermentation process. Again a tendency was found that in the beginning the intensities of the lower oxidation stages are comparably high and decrease during the course of a fermentation, whereas the higher stages of oxidation show a more or less constant increase.

This observation is illustrated in Table 3 with arrows showing tendencies of signal intensity changes (green = increase, red = decrease) and may be seen as a qualified confirmation of the oxidative cascade hypothesis that has been postulated as the main mechanism in TR formation. However, as the intensities were taken as sums of several individual signals that could only be assigned by their m/z value (due to low quality MS^2 spectra), these results have to be treated with caution.

■ ASSOCIATED CONTENT

Supporting Information

Color development during a model fermentation experiment (Figure S1), formation of theaflavins during a model oxidation of EC, ECG, EGC, and EGCG (Figure S2), and influence of enzyme selection on the release of gallic acid during an oxidation of ECG and EGC (Figure S3). This material is available free of charge via the Internet at http://pubs.acs.org.

Table 3. Measured Signal Intensities of Masses Assumingly Belonging to the Different Stages of the Theaflavin-Monogallates Undergoing the Hypothetical Oxidative Cascade

Time point of sampling [min]	*Intensity TF-G* $C_{36}H_{28}O_{15}$ $C_{36}H_{26}O_{15}$ $C_{36}H_{24}O_{15}$	*Intensity TF-G+O* $C_{36}H_{28}O_{16}$ $C_{36}H_{26}O_{16}$ $C_{36}H_{24}O_{16}$	*Intensity TF-G+2O* $C_{36}H_{28}O_{17}$ $C_{36}H_{26}O_{17}$ $C_{36}H_{24}O_{17}$	*Intensity TF-G+3O* $C_{36}H_{28}O_{18}$ $C_{36}H_{26}O_{18}$ $C_{36}H_{24}O_{18}$	*Intensity TF-G+4O* $C_{36}H_{28}O_{19}$ $C_{36}H_{26}O_{19}$ $C_{36}H_{24}O_{19}$
1.5	8.15×10^5	3.38×10^5	2.52×10^5	2.11×10^5	1.95×10^5
4	9.81×10^5	3.60×10^5	2.31×10^5	2.55×10^5	2.86×10^5
20	1.67×10^6	3.75×10^5	3.08×10^5	2.79×10^5	2.19×10^5
60	1.89×10^6	3.50×10^5	3.09×10^5	2.99×10^5	2.25×10^5
90	1.18×10^6	3.14×10^5	3.14×10^5	2.87×10^5	2.85×10^5
210	4.00×10^5	3.60×10^5	2.90×10^5	2.62×10^5	2.93×10^5

dx.doi.org/10.1021/jf501591j | J. Agric. Food Chem. 2014, 62, 7854–7861

AUTHOR INFORMATION

Corresponding Author

*E-mail: u.stodt@tu-braunschweig.de. Phone: +049-(0)531-391-7220. Fax: +049-(0)531-391-7230.

Notes

The authors declare no competing financial interest.

ABBREVIATIONS USED

(+)-C, (+)-catechin; EC, (−)-epicatechin; ECG, (−)-epicatechin gallate; EGC, (−)-epigallocatechin; EGCG, (−)-epigallocatechin gallate; TF, theaflavin; TF-3-G, theaflavin 3-gallate; TF-3′-G, theaflavin 3′-gallate; TF-DG, theaflavin 3,3′-digallate; TR, thearubigin; EDTA, ethylenediaminetetraacetic acid; HSCCC, high-speed countercurrent chromatography; HPLC, high-performance liquid chromatography; DAD, diode array detector; p.a., pro analysi; RT, room temperature; CQA, 3-caffeoylquinic acid; MTBE, methyl *tert*-butyl ether

REFERENCES

(1) Engelhardt, U. H.. Chemistry of Tea. In *Reference Module in Chemistry, Molecular Sciences and Chemical Engineering*; Reedijk, J., Ed.; Elsevier: Waltham, MA, 2013. DOI: 10.1016/B978-0-12-409547-2.02784-0.

(2) Ryan, L.; Petit, S. Addition of whole, semiskimmed, and skimmed bovine milk reduces the total antioxidant capacity of black tea. *Nutr. Res. (N.Y.)* **2010**, *30*, 14−20.

(3) Chen, H.; Shurlknight, K.; Leung, T.; Sang, S. Structural identification of theaflavin trigallate and tetragallate from black tea using liquid chromatography/electrospray ionization tandem mass spectrometry. *J. Agric. Food Chem.* **2012**, *60*, 10850−10857.

(4) Suzuki, T.; Yamazaki, N.; Sada, Y.; Oguni, I.; Moriyasu, Y. Tissue distribution and intracellular localization of catechins in tea leaves. *Biosci., Biotechnol., Biochem.* **2003**, *67*, 2683−2686.

(5) Robertson, A.; Bendall, D. S. Production and HPLC analysis of black tea theaflavins and thearubigins during *in vitro* oxidation. *Phytochemistry* **1983**, *22*, 883−887.

(6) Robertson, A. Effects of catechin concentration on the formation of black tea polyphenols during *in vitro* oxidation. *Phytochemistry* **1983**, *22*, 897−903.

(7) Opie, S. C.; Clifford, M. N.; Robertson, A. The formation of thearubigin-like substances by in-vitro polyphenol oxidase-mediated fermentation of individual flavan-3-ols. *J. Sci. Food Agric.* **1995**, *67*, 501−505.

(8) Kuhnert, N.; Clifford, M. N.; Müller, A. Oxidative cascade reactions yielding polyhydroxy-theaflavins and theacitrins in the formation of black tea thearubigins: Evidence by tandem LC-MS. *Food Funct.* **2010**, *1*, 180−199.

(9) Roberts, E. A. H.; Cartwright, R. A.; Oldschool, M. The phenolic substances of manufactured tea. I.—Fractionation and paper chromatography of water-soluble substances. *J. Sci. Food Agric.* **1957**, *8*, 72−80.

(10) Kuhnert, N. Unraveling the structure of the black tea thearubigins. *Arch. Biochem. Biophys.* **2010**, *501*, 37−51.

(11) Kuhnert, N.; Drynan, J. W.; Obuchowicz, J.; Clifford, M. N.; Witt, M. Mass spectrometric characterization of black tea thearubigins leading to an oxidative cascade hypothesis for thearubigin formation. *Rapid Commun. Mass Spectrom.* **2010**, *24*, 3387−3404.

(12) Kutyrev, A. A.; Moskva, V. V. Nucleophilic reactions of quinones. *Russ. Chem. Rev.* **1991**, *60*, 72−88.

(13) Ngure, F. M.; Wanyoko, J. K.; Mahungu, S. M.; Shitandi, A. A. Catechins depletion patterns in relation to theaflavin and thearubigins formation. *Food Chem.* **2009**, *115*, 8−14.

(14) Tanaka, T.; Kouno, I. Oxidation of tea catechins: chemical structures and reaction mechanism. *Food Sci. Technol. Res.* **2003**, *9*, 128−133.

(15) Sang, S.; Lambert, J. D.; Tian, S.; Hong, J.; Hou, Z.; Ryu, J.-H.; Stark, R. E.; Rosen, R. T.; Huang, M.-T.; Yang, C. S.; Ho, C.-T. Enzymatic synthesis of tea theaflavin derivatives and their anti-inflammatory and cytotoxic activities. *Bioorg. Med. Chem.* **2004**, *12*, 459−467.

(16) Sang, S.; Tian, S.; Stark, R. E.; Yang, C. S.; Ho, C.-T. New dibenzotropolone derivatives characterized from black tea using LC/MS/MS. *Bioorg. Med. Chem.* **2004**, *12*, 3009−3017.

(17) Tanaka, T.; Mine, C.; Kouno, I. Structures of two new oxidation products of green tea polyphenols generated by model tea fermentation. *Tetrahedron* **2002**, *58*, 8851−8856.

(18) Bonnely, S.; Davis, A. L.; Lewis, J. R.; Astill, C. A model oxidation system to study oxidised phenolic compounds present in black tea. *Food Chem.* **2003**, *83*, 485−492.

(19) ISO/CD-14502−2:2002, Tea - Methods for determination of substances characteristic of green and black tea - Part 2: Determination of catechins in green tea - Method using high performance liquid chromatography.

(20) Jiang, Y.; Miles, P. W. Generation of H2O2 during enzymic oxidation of catechin. *Phytochemistry* **1993**, *33* (1), 29−34.

(21) Muthumani, T.; Senthil Kumar, R. S. Influence of fermentation time on the development of compounds responsible for quality in black tea. *Food Chem.* **2007**, *101*, 98−102.

(22) Coggon, P.; Moss, G. A.; Sanderson, G. W. Tea catechol oxidase: Isolation, purification and kinetic characterization. *Phytochemistry* **1973**, *12*, 1947−1955.

(23) Finger, A. In-vitro studies on the effect of polyphenol oxidase and peroxidase on the formation of polyphenolic black tea constituents. *J. Sci. Food Agric.* **1994**, *66*, 293−305.

(24) Ding, Z.; Kuhr, S.; Engelhardt, U. Influence of catechins and theaflavins on the astringent taste of black tea brews. *Z. Lebensm.-Unters. Forsch.* **1992**, *195*, 108−111.

(25) Haslam, E. Thoughts on thearubigins. *Phytochemistry* **2003**, *64*, 61−73.

(26) Wan, X.; Nursten, H. E.; Cai, Y.; Davis, A. L.; Wilkins, J. P. G.; Davies, A. P. A new type of tea pigment − from the chemical oxidation of epicatechin gallate and isolated from tea. *J. Sci. Food Agric.* **1997**, *74*, 401−408.

MATERIALS AND METHODS

Materials. Normal cornstarch (NC) was purchased from COFOO Biochemical Energy Co. (Yushu, China). Pancreatin from porcine pancreas (catalog number P7545) and amyloglucosidase (catalog number A7095) were purchased from Sigma-Aldrich (St. Louis, MO). Glucose oxidase−peroxidase (GOPOD) assay kits were purchased from Megazyme International Ireland, Ltd. (Wicklow, Ireland). Lauric acid (LA) was purchased from Nanjing Chemical Co. (Nanjing, China). All other chemicals used in this study were of analytical grade and used without further treatments.

Preparation of LA-Complexed Starch. *Heating Starch Prior to the Addition of LA (HM).* NC was dried at 105 °C for 3 h, and the moisture content of the starch was 2.05%. Distilled water was added to the dried NC [40 g, dry basis (db)] and stirred vigorously to obtain starches with 10, 20, 30, 40, and 50% moisture contents. The moisturized starches were heated in a sealed stainless-steel reaction vessel at 80 °C for 12 h. LA [6 g, 15%, w/w, dry starch basis (dsb)] dissolved in ethanol (15 g, 35%, w/w, dsb) was then added to the prior heated starch at different moisture contents, stirred vigorously in the reaction vessel for 5 min, and then uncovered to evaporate ethanol at 80 °C. The final mixture was heated at 80 °C for another 2 h.

Adding LA to the Starch Prior to Heating (MH). LA (6 g, 15%, w/w, dsb) dissolved in ethanol (15 g, 35%, w/w, dsb) was added to the dried NC (40 g, db) and mixed vigorously. The mixture was heated without cover at 80 °C for 5 min to evaporate ethanol before being heated in a sealed stainless-steel reaction vessel at 80 °C for 2 h. Distilled water was then added to the mixture and stirred vigorously to obtain a mixture with 10, 20, 30, 40, and 50% moisture contents and then heated at 80 °C for 12 h.

All LA-complexed NC prepared using HM and MH were cooled to 25 °C, washed 3 times with 50% distilled water−ethanol mixture, and recovered by centrifugation (1500*g* for 10 min). The resulting precipitates, HM-NC represented LA-complexed NC prepared using HM and MH-NC represented LA-complexed NC prepared using MH, were dried at 40 °C overnight and subsequently ground to a fine powder. Control samples were prepared with the same procedure without adding LA.

Lipid Content. The lipid contents in the native NC and LA-complexed NC were determined according to previous reports.[19,20] Free lipid extraction was Soxhlet extracted with petroleum ether at 50 °C for 10 h. The total lipid content was determined after acid hydrolysis. Approximately 1.00 g of starch was accurately weighed and suspended in 10 mL of water. HCl (15 mL, 8.0 N) was added, and the mixture was heated in a boiling water bath for 25 min. After the addition of 50.0 mL of distilled water, the mixture was filtered through paper and washed with distilled water until the filtrate was neutral. The filter paper with the residue was dried at 40 °C overnight and then transferred to a defatted extraction thimble. The dried samples were Soxhlet-extracted with petroleum ether at 50 °C for 8 h. The recipients with the extracted fat were then dried at 110 °C to a constant weight. All samples were performed in duplicates.

Pasting Property. Each starch−LA complex sample (2.24 g, db) was suspended in deionized water to make a total weight of 28.0 g (8%, w/w) and then analyzed using a rapid visco analyzer (RVA, Newport Scientific, Sydney, Australia) following the method reported by Ai et al.[21] The pasting temperature and peak, breakdown, and setback viscosity were recorded.

Light Microscopy. Light micrographs were obtained using an Olympus BX-51 light microscope (Tokyo, Japan) with brightfield and polarized light. Starch powder was sprinkled on a glass slide and covered with a single drop of an aqueous glycerol solution (1:1 water/glycerol). The starch suspension was covered with a coverslip. Images were recorded at 500× magnification.

Scanning Electron Microscopy (SEM). Morphology of starch granules was studied using SEM (ZEISS EVO18, Germany) operated at 10 kV accelerating voltage. The native NC, control NC, and LA-complexed NC were mounted on aluminum stubs with double-sided sticky carbon tape and sputter-coated with a thin film of gold.

Wide-Angle X-ray Diffraction (XRD). The native NC and LA-complexed NC were equilibrated in a chamber with 100% relative humidity at 25 °C for 24 h prior to X-ray analysis. The X-ray diffractometer (D8 Advance, Bruker, Germany) was operated at 40 kV and 40 mA with Cu Kα radiation (λ = 0.154 nm). The starch powder was packed tightly in a rectangular glass cell and scanned over the range of 4−35° 2θ angles at a rate of 2°/min at 25 °C. The percentage crystallinity of the starch was calculated using the following equation:[22]

$$\text{crystallinity}\ (\%) = 100A_c/(A_c + A_a)$$

where A_c is the area of the crystalline peak and A_a is the area of the amorphous peak.

Differential Scanning Calorimetry (DSC). Thermal properties of starches were analyzed using a differential scanning calorimeter (Diamond DSC, PerkinElmer, Norwalk, CT). The native NC or the LA-complexed NC (2−5 mg, db) with deionized water (3×, w/w) was scanned from 10 to 120 °C at a rate of 10 °C/min in a sealed aluminum pan. The thermal properties were calculated using Pyris software (PerkinElmer). The analysis was performed in duplicate.

In Vitro Starch Digestibility. *In vitro* digestibility of the native NC and the LA-complexed NC was analyzed using the Englyst method as described by Englyst et al.,[23] with slight modification. Starch samples (1.00 g, db) were suspended in a sodium acetate buffer solution (20 mL, 0.1 M, pH 5.2), and five glass beads were added to 50 mL centrifuge tubes. The tubes were capped and mixed for 5 min. Samples were placed in a boiling water bath for 30 min and vortexed at 5 min intervals to prevent agglomeration of starch. The dispersion was equilibrated in a shaker water bath (160 strokes/min) at 37 °C for 30 min. The enzyme mixture containing porcine pancreatin and amyloglucosidase was added to each tube. The enzyme mixture was prepared by stirring 3 g of porcine pancreatin in 20 mL of deionized water in each of four tubes for 10 min and then centrifuging at 1500*g* for 10 min. The supernatant (54 mL) mixed with 6 mL of diluted amyloglucosidase solution and 4 mL of deionized water instead of invertase. Aliquots (1.00 mL) were taken at the end of 20 and 120 min reaction and mixed with 20 mL of ethanol (66%, v/v) to stop the enzyme reaction. Starch digestibility was determined using the GOPOD assay. Each sample was analyzed in duplicate.

Statistical Analysis. The mean values and differences were analyzed using Duncan's multiple-range test. Treatment means were tested separately for least significant difference (LSD) with SPSS 18.0 statistical software for Windows (SPSS, Inc., Chicago, IL). The significance level was set at $p < 0.05$.

RESULTS AND DISCUSSION

Thermal Properties. Thermal properties of the native NC and LA-complexed NC are listed in Table 1. The onset gelatinization temperature (T_o) increased from 63.4 to 78.2 °C for the HM-NC and from 61.7 to 69.5 °C for the MH-NC with the moisture content increased from 10 to 50%. There were two peaks observed in the HM-NC thermograms: peak I was attributed to the melting of the double-helical crystallite of amylopectin side chains; peak II was attributed to the melting of the amylose−LA complex. The MH-NC displayed two peaks when the moisture content was 10, 20, and 30%. The MH-NC, however, displayed three separate peaks at 40 and 50% moisture content (Table 1), in which the peak (41−44 °C) was attributed to the melting of free LA[12] and the other two peaks represented the same as those in the HM-NC. These results were consistent with higher free lipid contents in MH-NC prepared with 40 and 50% moisture contents (Table 2).

Except the starches treated with 10% moisture content, an increase in the onset gelatinization temperature in peak I suggested that the hydrothermal/LA treatments resulted in a more ordered crystalline structure. The HM-NC and MH-NC all exhibited decreases in the enthalpy change of peak I with the increase in the moisture content, which was attributed to the

dx.doi.org/10.1021/jf501606w | J. Agric. Food Chem. 2014, 62, 7862−7868

Table 1. Thermal Properties of the Native NC and LA-Complexed NC[a]

	melting of free LA				peak I				peak II			
sample[b]	T_o[c] (°C)	T_p[c] (°C)	T_c[c] (°C)	ΔH[c] (J/g)	T_o[c] (°C)	T_p[c] (°C)	T_c[c] (°C)	ΔH[c] (J/g)	T_o[c] (°C)	T_p[c] (°C)	T_c[c] (°C)	ΔH[c] (J/g)
NC					64.9 ± 0.6 a	70.3 ± 0.6 a	74.7 ± 0.7 a	12.2 ± 0.7 a				
HM-NC10%					63.4 ± 0.0 ab	68.9 ± 0.0 cd	73.7 ± 0.0 c	11.1 ± 0.3 a	88.1 ± 0.7 ac	98.6 ± 0.0 a	104.8 ± 0.5 d	2.0 ± 0.7 a
HM-NC20%					65.5 ± 0.9 a	70.3 ± 0.1 a	74.9 ± 0.1 a	11.9 ± 0.3 a	88.9 ± 0.2 ab	98.3 ± 0.2 a	103.9 ± 0.4 abd	1.9 ± 0.2 a
HM-NC30%					72.3 ± 0.1 d	78.1 ± 0.1 f	81.6 ± 0.2 d	10.7 ± 0.1 a	88.8 ± 0.2 bd	95.6 ± 0.7 bc	103.0 ± 0.1 abcd	2.4 ± 0.2 ac
HM-NC40%					77.6 ± 0.2 e	80.5 ± 0.2 g	83.2 ± 0.2 e	7.2 ± 0.2 d	88.3 ± 0.2 bd	95.3 ± 0.4 bc	102.4 ± 0.3 abc	2.8 ± 0.1 acd
HM-NC50%					78.2 ± 0.0 f	81.3 ± 0.1 g	83.9 ± 0.1 f	3.8 ± 0.6 e	88.5 ± 0.0 bd	95.2 ± 0.3 bc	102.3 ± 0.3 abc	2.6 ± 0.0 ac
MH-NC10%					61.7 ± 0.3 b	67.8 ± 0.0 b	72.5 ± 0.4 b	11.6 ± 1.2 a	88.9 ± 0.5 ab	97.8 ± 0.8 a	103.4 ± 0.9 abcd	1.6 ± 0.2 a
MH-NC20%					65.1 ± 1.9 a	68.2 ± 0.4 bc	72.5 ± 0.2 b	11.2 ± 1.3 a	88.8 ± 0.8 ab	97.1 ± 1.7 ab	103.4 ± 1.3 abcd	2.1 ± 0.1 ab
MH-NC30%					65.9 ± 1.4 a	69.2 ± 0.7 d	74.4 ± 0.5 ac	10.6 ± 0.3 ac	89.2 ± 0.2 b	98.1 ± 0.6 a	104.0 ± 0.6 bd	2.1 ± 0.2 ad
MH-NC40%	41.4 ± 0.2	42.4 ± 0.3	43.7 ± 0.4	2.1 ± 0.1	65.7 ± 0.3 a	69.9 ± 0.2 ad	73.6 ± 0.3 c	8.5 ± 0.2 cd	87.2 ± 0.2 cd	94.2 ± 0.1 c	101.9 ± 0.0 c	3.4 ± 0.0 c
MH-NC50%	41.6 ± 0.0	42.5 ± 0.1	43.8 ± 0.1	1.8 ± 0.9	69.5 ± 0.1 c	72.2 ± 0.1 e	75.3 ± 0.0 a	3.5 ± 1.2 e	86.8 ± 0.4 d	94.5 ± 0.1 c	101.8 ± 0.4 c	2.4 ± 0.9 ac

[a]All data are averages of two measurements with standard deviation. Means in a column with different letters are significantly different ($p < 0.05$) by the least significant difference (LSD) test. [b]Sample code: HM-NC, LA-complexed NC was prepared using heating starch prior to the addition of LA; MH-NC, LA-complexed NC was prepared using adding LA to the starch prior to heating; and 10, 20, 30, 40, and 50%, moisture contents of LA-complexed NC. [c]T_o, T_p, T_c, and ΔH are onset temperature, peak temperature, conclusion temperature, and enthalpy change, respectively.

Table 2. Lipid Content of the Native NC and LA-Complexed NC[a]

	lipid content (g/100 g of dry starch sample)		
sample[b]	acid hydrolyzed (total lipids, T)	petroleum ether extracted (free lipids, F)	$T - F$ (complexed lipids)
NC	0.98 ± 0.03 a	0.47 ± 0.08 a	0.51
HM-NC10%	1.98 ± 0.25 b	0.75 ± 1.00 b	1.22
HM-NC20%	1.91 ± 0.41 b	0.76 ± 0.29 b	1.15
HM-NC30%	2.50 ± 0.04 c	0.80 ± 0.52 b	1.69
HM-NC40%	2.80 ± 0.20 d	0.89 ± 0.18 bc	1.91
HM-NC50%	2.64 ± 0.36 cd	0.83 ± 0.01 bc	1.80
MH-NC10%	1.55 ± 0.04 e	0.52 ± 0.29 a	1.03
MH-NC20%	1.88 ± 0.01 b	0.53 ± 0.76 a	1.35
MH-NC30%	1.97 ± 0.72 b	0.59 ± 0.14 a	1.38
MH-NC40%	3.76 ± 0.23 f	1.40 ± 0.09 d	2.35
MH-NC50%	2.87 ± 0.01 d	1.13 ± 0.58 e	1.74

[a]The data are averages of two measurements with standard deviation. Means in a column with different letters are significantly different ($p < 0.05$) by the LSD test. [b]Sample code: HM-NC, LA-complexed NC prepared using heating starch prior to the addition of LA; MH-NC, LA-complexed NC prepared using adding LA to the starch prior to heating; and 10, 20, 30, 40, and 50%, moisture contents of LA-complexed NC.

loss of the double helices of amylopectin. The enthalpy change of peak II showed an increasing trend when the moisture content increased from 10 to 40% (Table 1), indicating increases in the formation of the amylose−LA complex. However, when the moisture content increased to 50%, the enthalpy change decreased. This could be attributed to substantial starch gelatinized when the moisture content increased to 50%, resulting in a viscous texture, which retarded the amylose−LA complex formation, which is consistent with the results of the lipid content. The content of complexed lipids of LA-complexed NC showed an increase when the moisture content was increased from 10 to 40% but a decrease when the moisture content was 50% (Table 2).

Morphology of NC and LA-Complexed NC. Morphology of the NC and the LA-complexed NC was studied using optical microscopy and scanning electron microscopy (Figures 1 and 2). Polarized light micrographs of the native NC showed a characteristic Maltese cross (image not show). LA-complexed NC, both prepared by HM or MH, showed that increasing numbers of granules lost the Maltese cross with the increase in the moisture content. HM-NC with a 50% moisture content was mostly gelatinized and showed few Maltese cross remaining, whereas MH-NC maintained more intact granules and Maltese cross even after heating with 50% moisture content. These results indicated that the starch gelatinized to a greater extent during heating without the presence of LA than that of LA-complexed NC.[24] In contrast, with the addition of LA prior to heating in the MH-NC, LA coated on the granule surface, complexed with amylose, impaired water movement into the granules, and retarded the gelatinization of the starch.

The structures of the control NC and LA-complexed NC studied using SEM are shown in Figure 2. The surface of native NC appeared smooth and exhibited pinholes on its surface (image not shown), which was consistent with the findings by Jane et al.[25] and Rocha et al.[26] Following the hydrothermal treatment, control NC with 40% moisture content was partially gelatinized and the granules were aggregated. When the moisture content increased to 50%, the control NC was

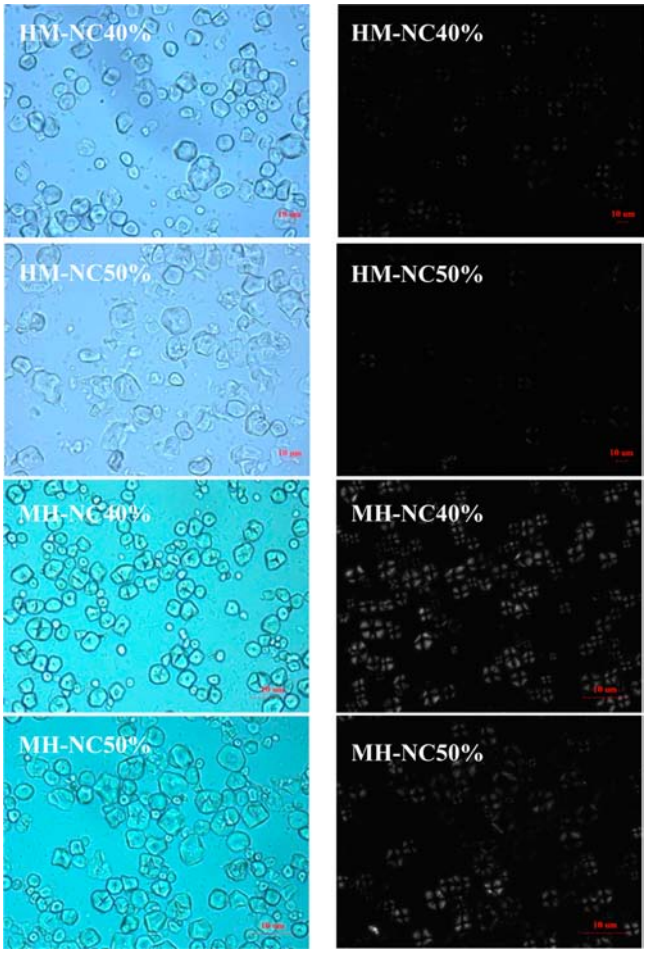

Figure 1. Light microscopic images of LA-complexed NC with brightfield and polarized light. Sample code: HM-NC, LA-complexed NC prepared using heating starch prior to the addition of LA; MH-NC, LA-complexed NC prepared using adding LA to the starch prior to heating; and 40 and 50%, moisture contents of LA-complexed NC.

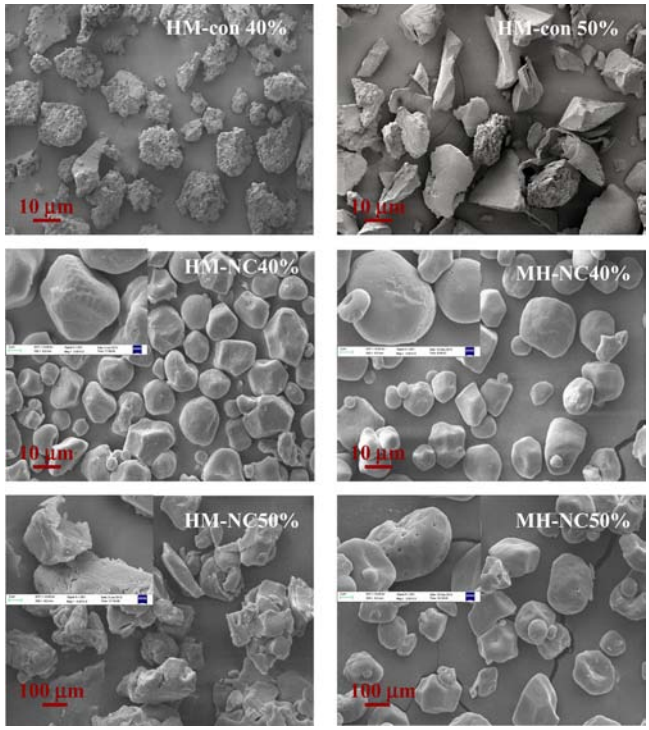

Figure 2. Morphology of the control NC and LA-complexed NC. Sample code: HM-con, control samples for HM-NC; HM-NC, LA-complexed NC prepared using heating starch prior to the addition of LA; MH-NC, LA-complexed NC prepared using adding LA to the starch prior to heating; and 40 and 50%, moisture contents of LA-complexed NC.

gelatinized and lost the shape of granules. Because HM control and MH control displayed similar images, only HM controls are shown. Following the hydrothermal/LA treatments, LA-complexed NC showed intact granular shape, except HM-NC with 50% moisture content, which was partially gelatinized and disrupted (Figure 2). The addition of LA retarded the gelatinization of starch granules, which was consistent with the results of DSC.

Wide-Angle XRD. XRD patterns and percentage crystallinity of the native NC and LA-complexed NC are shown in Figure 3. The native NC showed an A-type diffraction pattern.[27] The hydrothermal/LA treatments changed the X-ray pattern to a mixture of A- and V-type patterns. This change in diffraction pattern was attributed to the fact that the increasing moisture content increased the mobility of amylose and facilitated the formation of the amylose−LA complex. The peaks shown at 8°, 13°, and 20° reflected the V pattern of the amylose−LA complex.[12,28] The peak shown at 21.5° was the crystallites of LA,[29,30] which was only observed in MH-NC prepared with the moisture contents of 40 and 50%. The result was consistent with a melting peak of crystalline LA appearing in DSC thermograms of MH-NC prepared with 40 and 50% moisture contents (Table 1). These results could be attributed to the fact that, when the moisture content increased to 40 and 50% in the MH-NC process, it gave mobility for LA to segregate and merge to crystallize. At high moisture contents (40 and 50%) in the HM-NC process, however, starch was partially gelatinized and the viscosity of the gelatinized starch retarded the mobility of LA. Therefore, LA did not aggregate to crystallize.

The crystallinity of LA-complexed NC was attributed to the contents of free lipids, double-helix amylopectin, and single-helix amylose−LA complex and had a correlation with its corresponding enthalpy change in DSC thermograms. The crystallinity of HM-NC increased from 28.9 to 30.0% and then decreased to 28.2% (higher than native NC) when the moisture content increased from 10 to 30%. With a further increase in the moisture content (up to 50%), the crystallinity sharply decreased to 18.6%, which was consistent with the enthalpy change of gelatinization and the amylose−LA complex (Table 1). These results suggested that, when the moisture content increased to 10 and 30%, there was a heat−moisture treatment effect and amylose−LA complex formation (peak II in DSC thermograms) to improve the crystalline structure. When the moisture content was 40 and 50%, partial gelatinization took place, which was confirmed by the loss of Maltese cross (Figure 1). The crystallinity of MH-NC samples with the moisture content from 10 to 50%, however, decreased from 26.3 to 18.9%. It appears that heat−moisture treatment effect did not take place in starch with the presence of LA in MH-NC.

Pasting Properties. Pasting viscosity profiles of the native NC and LA-complexed NC are shown in Figure 4. The hydrothermal/LA treatments increased the pasting temperature of the starch and decreased the peak viscosity, which was consistent with reports in previous studies.[2,17,31,32] The pasting

dx.doi.org/10.1021/jf501606w | J. Agric. Food Chem. 2014, 62, 7862−7868

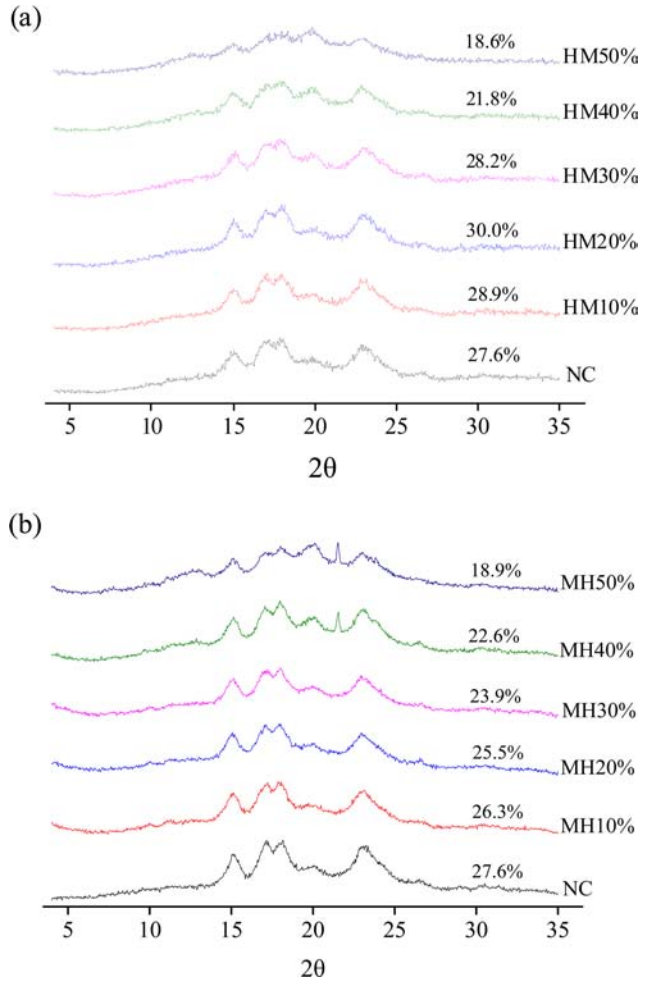

Figure 3. XRD patterns of the native NC and LA-complexed NC. Sample code: HM, heating starch prior to the addition of LA; MH, adding LA to the starch prior to heating; and 10, 20, 30, 40, and 50%, moisture contents of LA-complexed NC.

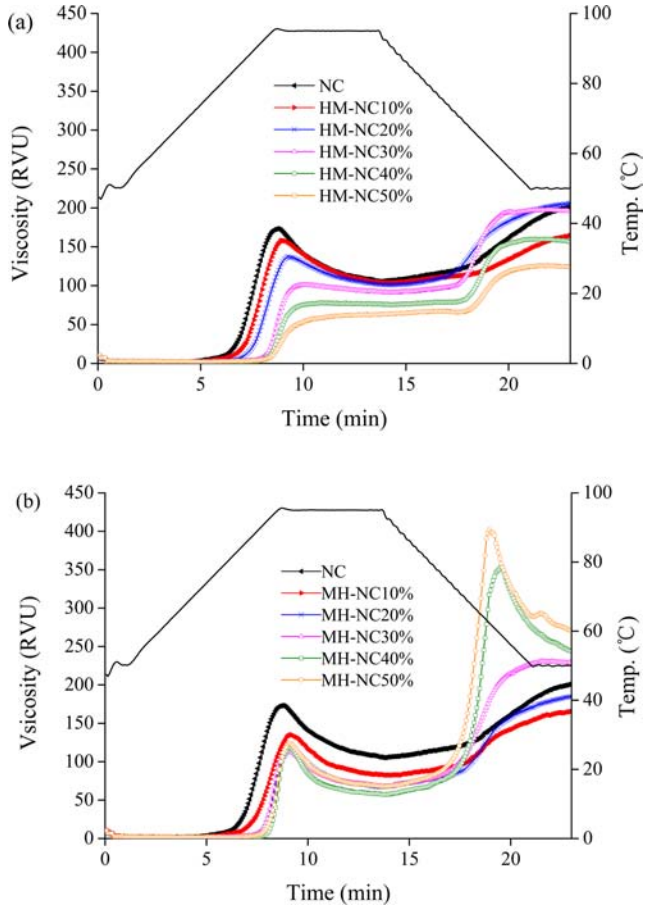

Figure 4. Pasting profiles of the native NC and LA-complexed NC: (a) pasting profiles of the native NC and HM-NC and (b) pasting profiles of the native NC and MH-NC. Sample code: HM-NC, LA-complexed NC prepared using heating starch prior to the addition of LA; MH-NC, LA-complexed NC prepared using adding LA to the starch prior to heating; and 10, 20, 30, 40, and 50%, moisture contents of LA-complexed NC.

temperature of HM-NC and MH-NC both showed increases when the moisture content increased from 10 to 50%. The peak viscosity of HM-NC decreased with an increase in the moisture content. For MH-NC, however, when the moisture content increased from 10 to 30%, the peak viscosity displayed the same trend as its counterparts in HM-NC. However, when the moisture content increased to 40 and 50%, the peak viscosity increased. The presence of the amylose−LA complex and ordered crystallites in LA-complexed NC restricted the swelling of starch granules and resulted in higher pasting temperature and lower peak viscosity.[2,33] These results were consistent with a high enthalpy change of the amylose−LA complex and free lipid (Table 1). When the moisture content was 40%, MH-NC showed a higher content of complexed lipids and free lipids than other LA-complexed NC (Table 2), which resulted in a higher pasting temperature and lower peak viscosity.

HM-NC displayed a decrease in the breakdown and setback viscosity when the moisture content increased from 10 to 50%. MH-NC showed the same trend of breakdown and setback viscosity as their counterparts in HM-NC when the moisture content increased from 10 to 30%. However, when the moisture content increased to 40 and 50%, MH-NC showed increases in the breakdown viscosity and drastic increases in the setback viscosity. The remarkable increase in the setback viscosity could result from the formation of the helical complex between amylose and free LA present in the samples. During the heating procedure of RVA, most starch and part of the amylose−LA complex were dissociated and there was sufficient amylose to complex with LA in the amylose−LA complex and free LA. When the procedure temperature was cooled from 95 to 50 °C, amylose, LA, and amylopectin formed a new amylose−LA complex and an amylose−amylopectin network, which increased the viscosity of MH-NC with moisture contents at 40 and 50%.

***In Vitro* Digestibility.** The contents of RDS, SDS, and RS in the native NC and LA-complexed NC are shown in Table 3. LA-complexed NC showed decreases in the RDS content and increases in the SDS and RS contents with increases in the moisture content. MH-NC was more resistant to the enzyme than that of HM-NC. The SDS content in MH-NC was much higher than that in the counterparts of HM-NC with greater moisture contents (10−50%).

The increase in SDS and RS contents in LA-complexed NC with greater moisture contents was attributed to the formation of the amylose−LA complex and more ordered crystallites, which had a positive relationship with enthalpy change, as shown in Table 1. The V−amylose complex is known to be resistant to enzyme hydrolysis.[2,6] The presence of the

dx.doi.org/10.1021/jf501606w | J. Agric. Food Chem. 2014, 62, 7862−7868

Table 3. RDS, SDS, and RS Contents in the Cooked Native NC and LA-Complexed NC[a]

sample[b]	RDS (%)	SDS (%)	RS (%)
NC	88.9 ± 0.6 a	5.0 ± 0.3 a	6.6 ± 0.2 a
HM-NC10%	81.1 ± 0.5 b	5.8 ± 0.2 a	13.0 ± 0.3 b
HM-NC20%	80.3 ± 0.3 b	5.7 ± 0.3 a	14.0 ± 0.0 bc
HM-NC30%	78.6 ± 0.1 c	6.0 ± 0.1 ab	15.4 ± 0.0 de
HM-NC40%	76.8 ± 0.1 d	7.5 ± 0.1 c	16.2 ± 0.3 e
HM-NC50%	74.8 ± 0.5 e	7.4 ± 0.9 bc	17.8 ± 0.4 f
MH-NC10%	78.7 ± 0.3 c	7.7 ± 0.7 cd	13.6 ± 0.3 b
MH-NC20%	77.1 ± 0.1 d	8.0 ± 0.6 cef	14.9 ± 0.7 cd
MH-NC30%	75.1 ± 0.8 e	9.0 ± 0.1 df	14.9 ± 0.2 cd
MH-NC40%	74.1 ± 0.5 e	9.5 ± 0.2 ef	16.0 ± 0.2 e
MH-NC50%	72.3 ± 0.6 f	10.2 ± 0.8 f	17.6 ± 0.2 f

[a]RDS, rapidly digestible starch; SDS, slowly digestible starch; and RS, resistant starch. The data are averages of two measurements with standard deviation. Means in a column with different letters are significantly different ($p < 0.05$) by the LSD test. [b]Sample code: HM-NC, LA-complexed NC prepared using heating starch prior to the addition of LA; MH-NC, LA-complexed NC prepared using adding LA to the starch prior to heating; and 10, 20, 30, 40, and 50%, moisture contents of LA-complexed NC.

amylose−LA complex restricted the swelling of starch granules, as shown in Figure 4, resulting in reduced starch hydrolysis.[1,16] Hasjim et al.[1] and Zhang et al.[12] used partially gelatinized debranched high amylose cornstarch complexed with lipids to produce highly resistant starch, which was attributed to a combination of amylose double-helical crystallite and the amylose−stearic acid complex. The SDS and RS contents in LA-complexed NC prepared in this study both increased. MH-NC with 40 and 50% moisture contents showed higher SDS content than that of other LA-complexed NC, indicating that more amylose−LA complex formed between amylose and free LA after cooking.

The diagram of the difference between the hydrothermal treatments of the two methods is shown in Figure 5. For HM-NC, starch granules swelled, partially gelatinized during the heating before adding LA, resulting in a viscous texture, and decreased the mobility of amylose. LA was then thoroughly mixed with the partially gelatinized starch and subjected to additional heating. When the moisture content was at 40 and 50%, most of the starch crystalline structure was lost. LA dispersed in the viscous starch could not move freely to form aggregate and crystallites, as shown by no melting peak of crystalline LA in DSC and XRD patterns (Table 1 and Figure 3). However, all HM-NC contained higher free lipids than that of NC in the lipid content (Table 2). For MH-NC, however, LA was added to the dried starch and heated in a sealed container at 80 °C for 2 h. LA coated on the surface of the granule, delayed water penetrate into starch granules, and retarded starch gelatinization. The mixture was then heated under different moisture contents for another 12 h. During this heating process, the increased moisture content facilitated mobility of amylose and LA to form a complex. The crystalline structure of the starch remained as shown in the polarized light micrographs of MH-NC (Figure 1). Some of the free LA aggregated and crystallized, as shown in the DSC thermograms and XRD patterns.

The physicochemical properties of the amylose−LA complex were influenced by the moisture content of starch and the order of adding LA to starch before or after heating at 80 °C. The presence of LA retarded the gelatinization of starch during heating. A high moisture content enhanced the mobility of amylose, amylopectin, and LA and promoted the formation of the amylose−LA complex. The formation of the amylose−LA complex was the key factors in decreasing the hydrolysis of starch. With increasing the moisture content, LA had a greater chance to complex with amylose. MH favored the formation of slowly digestible starch and resistant starch, especially when the moisture content was 40%. The results of this study may have potential application in starch food processing applications that desire a higher content of SDS or RS.

AUTHOR INFORMATION

Corresponding Author

*Telephone: +86-20-8711-3845. Fax: +86-20-8711-3848. E-mail: fechoh@scut.edu.cn.

Funding

The authors thank the financial support received from the National Natural Science Foundation of China (NSFC) (31130042 and 31101378), the Fundamental Research Funds for the Central Universities (2013ZZ0065), the Science and Technology Planning Project of Guangdong Province, China (2012A020602005 and 2012NL016), and the Department of Science and Information Technology of Guangzhou, China (2013J4500036).

Notes

The authors declare no competing financial interest.

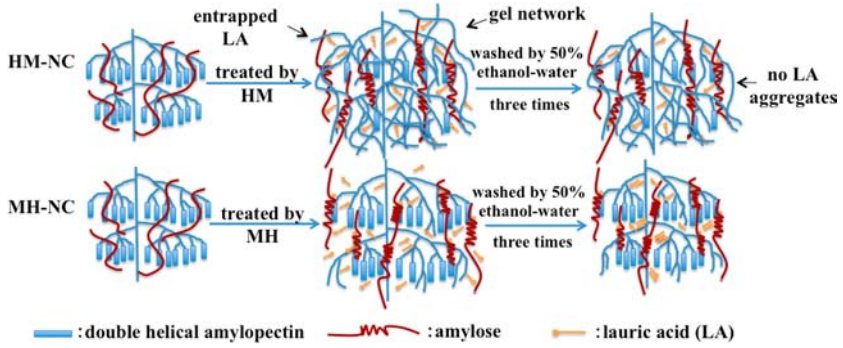

Figure 5. Schematic diagram of LA-complexed NC. Sample code: HM, heating starch prior to the addition of LA; MH, adding LA to the starch prior to heating; HM-NC, LA-complexed NC prepared using heating starch prior to the addition of LA; and MH-NC, LA-complexed NC prepared using adding LA to the starch prior to heating.

■ ACKNOWLEDGMENTS

The authors acknowledge the discussion and technical assistance of Joshua Lyte, Department of Food Science and Human Nutrition, Iowa State University.

■ ABBREVIATIONS USED

NC, normal cornstarch; LA, lauric acid; HM, heating starch prior to the addition of LA; MH, adding LA to the starch prior to heating; HM-NC, LA-complexed NC prepared by HM; MH-NC, LA-complexed NC prepared by MH; HM-con, control samples for HM-NC; RDS, rapidly digestible starch; RS, resistant starch; SDS, slowly digestible starch; SEM, scanning electron microscopy; XRD, X-ray diffraction; DSC, differential scanning calorimetry; T_o, onset temperature; T_p, peak temperature; T_c, conclusion temperature; ΔH, enthalpy change

■ REFERENCES

(1) Hasjim, J.; Lee, S.-O.; Hendrich, S.; Setiawan, S.; Ai, Y.; Jane, J. Characterization of a novel resistant-starch and its effects on postprandial plasma-glucose and insulin responses. *Cereal Chem.* **2010**, *87*, 257−262.

(2) Ai, Y.; Hasjim, J.; Jane, J. Effects of lipids on enzymatic hydrolysis and physical properties of starch. *Carbohydr. Polym.* **2013**, *92*, 120−127.

(3) Jane, J. Current understanding on starch granule structures. *J. Appl. Glycosci.* **2006**, *53*, 205−213.

(4) Okuda, M.; Aramaki, I.; Koeski, T.; Satoh, H.; Hashizume, K. Structural characteristics, properties, and in vitro digestibility of rice. *Cereal Chem.* **2005**, *82*, 361−368.

(5) Reed, M.-O.; Ai, Y.; Leutcher, J.-L.; Jane, J. Effects of cooking methods and starch structures on starch hydrolysis rates of rice. *J. Food Sci.* **2013**, *78*, H1076−H1081.

(6) Jane, J.; Robyt, J.-F. Structure studies of amylose−V complexes and retrograded amylose by action of α amylases, and a new method for preparing amylodextrins. *Carbohydr. Res.* **1984**, *132*, 105−118.

(7) Gelders, G. G.; Duyck, J. P.; Goesaert, H.; Delcour, J. A. Enzyme and acid resistant of amylose−lipid complexes differing in amylose chain length, lipid and complexation temperature. *Carbohydr. Polym.* **2005**, *60*, 379−389.

(8) Conde-Petit, B.; Escher, F.; Nuessli, J. Structural features of starch-flavor complexation in food model systems. *Trends Food Sci. Technol.* **2006**, *17*, 227−235.

(9) Bail, P.-L.; Rondeau, C.; Buléo, A. Structural investigation of amylose complexes with small ligands: Helical conformation, crystalline structure and thermostability. *Int. J. Biol. Macromol.* **2005**, *35*, 1−7.

(10) Cohen, R.; Orlova, Y.; Kovalev, M.; Ungar, Y.; Shimoni, E. Structural and functional properties of amylose complexes with genistein. *J. Agric. Food Chem.* **2008**, *56*, 4212−4218.

(11) Cohen, R.; Schwartz, B.; Peri, I.; Shimoni, E. Improving bioavailability and stability of genistein by complexation with high-amylose corn starch. *J. Agric. Food Chem.* **2011**, *59*, 7932−7938.

(12) Zhang, B.; Huang, Q.; Luo, F.-X.; Fu, X. Structural characterizations and digestibility of debranched high-amylose maize starch complexed with lauric acid. *Food Hydrocolloids* **2012**, *28*, 174−181.

(13) Nakazawa, Y.; Wang, Y.-J. Effect of annealing on starch−palmitic acid interaction. *Carbohydr. Polym.* **2004**, *57*, 327−335.

(14) Chang, F.; He, X.; Huang, Q. Effect of lauric acid on the V−amylose complex distribution and properties of swelled normal cornstarch granules. *J. Cereal Sci.* **2013**, *58*, 89−95.

(15) D'Silva, T. V.; Taylor, J. R. N.; Emmambux, M. N. Enhancement of the pasting properties of teff and maize starches through wet−heat processing with added stearic acid. *J. Cereal Sci.* **2011**, *53*, 192−197.

(16) Cui, R.; Oates, C. G. The effect of amylose−lipid complex formation on enzyme susceptibility of sago starch. *Food Chem.* **1999**, *65*, 417−425.

(17) Chang, F.; He, X.; Huang, Q. The physicochemical properties of swelled maize starch granules complexed with lauric acid. *Food Hydrocolloids* **2013**, *32*, 365−372.

(18) Putseys, J. A.; Lamberts, L.; Delcour, J. A. Amylose-inclusion complexes: Formation, identity and physico-chemical properties. *J. Cereal Sci.* **2010**, *51*, 238−247.

(19) Vasanthan, T.; Hoover, R. A comparative study of the composition of lipids associated with starch granule from various botanical sources. *Food Chem.* **1992**, *43*, 19−27.

(20) Eerlingen, R. C.; Cillen, G.; Delcour, J. A. Effect of endogenous lipids and added dodecyl sulphate on formation of resistant starch. *Cereal Chem.* **1999**, *71*, 170−177.

(21) Ai, Y.; Medic, J.; Jiang, H.; Wang, D.; Jane, J. Starch characterization and ethanol production of sorghum. *J. Agric. Food Chem.* **2011**, *59*, 7385−7392.

(22) Hermans, P. H.; Weidinger, A. Quantitative X-ray investigations on the crystallinity of cellulose fibers. *J. Appl. Phys.* **1948**, *19*, 491−506.

(23) Englyst, K. N.; Englyst, H. N.; Hudson, G. J.; Cole, T. J.; Cummings, J. H. Rapidly available glucose in foods: An in vitro measurement that reflects the glycemic response. *Am. J. Clin. Nutr.* **1999**, *69*, 448−454.

(24) Primo-Martín, C.; van Nieuwenhuijzen, N. H.; Hamer, R. J.; van Vliet, T. Crystallinity changes in wheat starch during the bread-making process: Starch crystallinity in the bread crust. *J. Cereal Sci.* **2007**, *45*, 219−226.

(25) Jane, J.; Kasemsuwan, T.; Leas, S.; Zobel, H.; Robyt, J. F. Anthology of starch granule morphology by scanning electron-microscopy. *Starch/Staerke* **1994**, *46*, 121−129.

(26) Rocha, T. S.; Felizardo, S. G.; Jane, J.; Franco, C. M. L. Effect of annealing on the semicrystalline structure of normal and waxy corn starches. *Food Hydrocolloids* **2012**, *29*, 93−99.

(27) Jane, J.; Chen, Y.-Y.; Lee, L. F.; Mcpherson, A. E.; Wong, K. S.; Radosavljevic, M.; Kasemsuwan, T. Effects of amylopectin branch chain length and amylose content. *Cereal Chem.* **1999**, *76*, 629−637.

(28) Chanvrier, H.; Uthayakumaran, S.; Appelqvist, I. A. M.; Gidley, M. J.; Gilbert, E. P.; López-Rubio, A. Influence of storage conditions on the structure, thermal behavior, and formation of enzyme-resistant starch in extruded starches. *J. Agric. Food Chem.* **2007**, *55*, 9883−9890.

(29) Tang, M. C.; Copeland, L. Analysis of complexes between lipids and wheat starch. *Carbohydr. Polym.* **2007**, *67*, 80−85.

(30) Zabar, S.; Lesmes, U.; Katz, I.; Shimoni, E.; Bianco-Peled, H. Structural characterization of amylose−long chain fatty acid complexes produced via the acidification method. *Food Hydrocolloids* **2010**, *24*, 347−357.

(31) Copeland, L.; Blazek, J.; Salman, H.; Tang, M. C. Form and functionality of starch. *Food Hydrocolloids* **2009**, *23*, 1527−1534.

(32) Guraya, H. S.; Kadan, R. S.; Champagne, E. T. Effect of rice starch−lipid complexes on in vitro digestibility, complexing index and viscosity. *Cereal Chem.* **1997**, *74*, 561−565.

(33) Krog, N. Influence of food emulsifiers on pasting temperature and viscosity of various starches. *Starch/Staerke* **1973**, *25*, 22−27.

Table 1. Chromaticity of Coffee Fruits Surface for Seven Cultivars of *Coffea arabica* at Three Stages of Ripening[a]

cultivar	ripening stage	chromaticity (r)	chromaticity (g)	chromaticity (b)	r/g ratio
Typica	unripe	0.38 ± 0.03i	0.46 ± 0.01bc	0.16 ± 0.03bcd	0.83
	semiripe	0.59 ± 0.05def	0.31 ± 0.05f	0.10 ± 0.02efg	1.93
	ripe	0.69 ± 0.06ab	0.17 ± 0.02h	0.14 ± 0.04cde	4.05
Bourbon	unripe	0.35 ± 0.01i	0.51 ± 0.02a	0.14 ± 0.02cde	0.67
	semiripe	0.54 ± 0.06fgh	0.35 ± 0.06def	0.11 ± 0.01efg	1.57
	ripe	0.65 ± 0.08bc	0.19 ± 0.03h	0.16 ± 0.05bcd	3.52
Mundo Novo	unripe	0.33 ± 0.02i	0.50 ± 0.01ab	0.17 ± 0.03abc	0.68
	semiripe	0.50 ± 0.03gh	0.37 ± 0.03d	0.13 ± 0.02de	1.35
	ripe	0.61 ± 0.05cde	0.20 ± 0.02gh	0.19 ± 0.03ab	3.04
Costa Rica	unripe	0.38 ± 0.01i	0.48 ± 0.02ab	0.13 ± 0.02cde	0.79
	semiripe	0.55 ± 0.03fgh	0.34 ± 0.04def	0.12 ± 0.02ef	1.62
	ripe	0.61 ± 0.04cd	0.20 ± 0.01gh	0.19 ± 0.03ab	3.13
Oro Azteca	unripe	0.36 ± 0.02i	0.47 ± 0.01bc	0.17 ± 0.02abcd	0.78
	semiripe	0.53 ± 0.04fgh	0.37 ± 0.04d	0.10 ± 0.02efg	1.44
	ripe	0.74 ± 0.04cd	0.19 ± 0.02gh	0.08 ± 0.02fg	3.94
Red Garnica	unripe	0.38 ± 0.01i	0.43 ± 0.01c	0.19 ± 0.02ab	0.89
	semiripe	0.49 ± 0.02h	0.32 ± 0.02ef	0.19 ± 0.01ab	1.52
	ripe	0.55 ± 0.02efg	0.24 ± 0.01g	0.21 ± 0.02a	2.30
Yellow Garnica	unripe	0.38 ± 0.02i	0.50 ± 0.01ab	0.12 ± 0.02ef	0.77
	semiripe	0.49 ± 0.02h	0.44 ± 0.01c	0.07 ± 0.02g	1.12
	ripe	0.57 ± 0.03def	0.36 ± 0.03de	0.07 ± 0.02g	1.60

[a]Data are presented as a mean value ± standard deviation; the same letter in a column means no significant differences (Tukey HDS test, $\alpha = 0.05$) between samples.

MATERIALS AND METHODS

Chemicals. Chlorogenic, caffeic, *p*-coumaric, ferulic, and ascorbic acids were obtained from Sigma-Aldrich (St. Louis, MO, USA); hexane, methanol, acetic acid, sodium hydroxide, and ethylenediaminetetraacetic acid (EDTA) were purchased from J. T. Baker (Phillipsburg, NJ, USA).

Plant Material. Coffee cherries from seven cultivars (Typica, Bourbon, Mundo Novo, Costa Rica, Oro Azteca, Red Garnica, and Yellow Garnica) were collected in December 2012 from a plantation in the municipality of Xico, Veracruz, Mexico (latitude 96°57′ N; longitude 19°25′ W; altitude ≈1135 m above sea level). Coffee fruits were harvested at three different stages of ripening (unripe, semiripe, and ripe). Identification of coffee cultivars and classification by ripening stage was performed by trained local personnel according to the physical characteristics of plants and fruits.

Samples were transported immediately under refrigeration to the laboratory and stored at 4 °C until processing (within 48 h). Fruits were manually pulped, and the obtained CP was dried in a tray dryer with forced aeration for 72 h at 25−40 °C. Dry CP was milled with a blade grinder and sieved to obtain a particle size of 0.15−0.84 mm (20−100 mesh).

CP from a commercial wet process (beneficio) located in the same region (Xico, Veracruz, Mexico) was used to standardize the methodology for HCA extraction. This CP was sun-dried for 72 h until reaching moisture content of <10%.

Physical Characterization of Coffee Fruits. Average weight, volume, and color of fruits were measured. Average weight was calculated from 100 fruits by triplicate. Average volume was measured by water displacement of 100 fruits in a 1 L graduated cylinder.

The external color of coffee fruits was evaluated by image analysis techniques. Pictures of at least 10 fruits per sample were obtained with a digital camera under standardized conditions of lighting and distance. Thereafter, the pictures were analyzed using the software Fiji (available at http://fiji.sc/Fiji). Average values R, G, and B were obtained and used to calculate the chromaticity parameters r, g, and b, using the following equations:

$$r = \frac{R}{R+G+B};\ g = \frac{G}{R+G+B};\ b = \frac{B}{R+G+B}$$

R, G, and B represent the red, green, and blue color intensity, respectively, and r, g, and b are the normalized trichromatic coefficients (intensity independents).[11]

Extraction of Soluble and Bound HCAs. Extraction of soluble HCAs was performed by successive extractions with hexane and methanol as previously reported.[4,10] First, 2 g (DW) of CP was put into a 125 mL Erlenmeyer flask. Then, sample was extracted three times with 20 mL of hexane for 30 min at 30 °C and 150 rpm. Hexane extracts were discarded, and the remaining solids were extracted three times with 20 mL of aqueous methanol (20:80, v/v) acidified with 1% (v/v) acetic acid. Methanolic extraction was carried out for 35 min at 55 °C with agitation at 100 rpm. Methanolic extracts were centrifuged (8000 rpm, 10 min), filtered through 0.22 μm regenerated cellulose membranes, and analyzed by HPLC.

To confirm the efficiency of the extraction of soluble HCAs, a sample of CP (from a commercial wet process) was submitted to successive methanolic extractions, and each extract was analyzed separately. The effect of hexane extraction was also investigated.

Bound HCAs were extracted by alkaline hydrolysis using a method described previously,[6,10] which was modified as follows: The solids obtained from hexane and aqueous methanol extractions were immediately hydrolyzed with 20 mL of NaOH at different concentrations (0.5, 1.0, and 2.0 M), with EDTA (10 mM) and ascorbic acid (1% w/v). Mixtures were incubated for 15, 30, 60, 120, and 240 min at 40 °C under constant agitation on an orbital shaker (150 rpm). Subsequently, the pH of the mixtures was adjusted to 3.0 ± 0.1 with 6 M HCl. Then, mixtures were filtered through a no. 2

fritted glass filter, the solid residues were extracted with 10 mL of distilled water, and the filtrates were combined and filtered through a 0.22 μm regenerated cellulose membrane and analyzed by HPLC. All extractions were under darkness by triplicate. The extracts obtained were kept at −18 °C and protected from light until analysis. At this stage, chlorogenic acid (compound **1**) was used as internal standard.

HPLC Analysis. Analysis of HCAs was carried out in a Shimadzu Prominence HPLC system (Shimadzu Corp., Kyoto, Japan) consisting of an LC-20AT pump, a DGU-20AS degasser, an SIL-20A HT autosampler, an SPD-M20A diode array detector, and a CTO-20A oven. Separation was performed using a Varian Polaris Amide C18 column (200 × 4.6 mm, 5 μm). An isocratic method was used with a mobile phase consisting of 35% (v/v) methanol, 1.25% (v/v) acetic acid, and 63.75% (v/v) water at a flow rate of 1 mL/min for 20 min. HCAs were detected at 320 nm. Quantitation was performed by the external standard method. Calibration curves were obtained for each compound in concentrations ranging from 0.025 to 0.5 mg/mL. Results were expressed as milligrams per gram of CP (dw).

Statistical Analysis. All extractions and analyses were carried out at least in triplicate, and the results are expressed as means ± standard deviation. Tukey's HSD test was used to compare the means and to reveal significant differences between samples (α = 0.05). Statistical analysis was performed using the statistical package JMP 9 (SAS Institute Inc., Cary, NC, USA).

RESULTS AND DISCUSSION

Physical Characterization of Coffee Fruits. Coffee cherries were classified by trained personnel at the plantation. Then, a physical characterization of fruit samples was carried out in the laboratory. Morphological differences between fruits of the same cultivar but at different ripening stage as well as differences between fruits at the same ripening stage but different cultivar (for some cultivars) were observed. These observations were confirmed by the physical characterization (Supporting Information Figures 1−3).

As expected, we observed a progressive increment of fruit size and weight for all cultivars as a function of ripening. We also observed significant differences between coffee fruits at the same ripening stage but from different cultivars. The larger and heavier fruits were the ripe coffee cherries of Oro Azteca cultivar, followed by the cherries of Mundo Novo and Costa Rica cultivars. The smaller and lighter ripe fruits belonged to the Bourbon cultivar.

Changes in the size and weight of coffee cherries during the ripening process have been previously described by several authors.[12−14] Physical differences (weight and volume) between coffee cherries from different cultivars are known by coffee growers and processors, but they are poorly described in the scientific literature.

Changes in color have been traditionally considered as the main criterion determining the ripening stage of coffee cherries. This characteristic is used to decide the beginning of the harvest.[15] We used image analysis techniques to measure the external color of coffee cherries and to establish differences between ripening stages of coffee fruits.

We observed a progressive increase in the red (r) component of the color as well as a decrease in the green (g) component for all coffee cultivars (Table 1). On the other hand, the blue component was the lowest for all coffee samples. Moreover, we did not observe the same trend in the change of the parameter b (blue) during ripening of the fruits of different cultivars. Therefore, we consider that the r (red) and g (green) chromaticity parameters should be used to evaluate color changes during ripening of coffee cherries.

Values of r increased from 0.335−0.387 for unripe fruits to 0.552−0.736 for ripe cherries. Values of g decreased from 0.427−0.514 for unripe fruits to 0.170−0.357 for ripe cherries. Another parameter that could be considered for assessing color change during ripening of coffee cherries is the ratio between r and g chromaticity parameters (r/g ratio). Values of r/g lower than 1 were obtained for unripe fruits. For semiripe fruits, r/g ratio values ranged between 1 and 2 (1.12−1.93), and for ripe fruits, values of r/g were >2 (2.30−4.06) except for the yellow cultivar (r/g = 1.60).

Several authors have studied the changes in the external color of coffee fruits using spectrophotometric[16−18] or computer vision techniques.[19] These methodologies allow obtaining reliable and reproducible measurements of fruit color. However, they require specialized equipment, which is not always available. Other authors have evaluated the color of coffee cherries by a subjective comparison with color reference charts.[15,20] Color charts are useful aids to compare colors, but they have some disadvantages. In this method color assessment depends on the visual abilities of judges. On the other hand, it is difficult to compare a uniformly colored card with the color of a nonhomogenous surface.[21] In all cases an increase in the red chromaticity and a decrease in green chromaticity have been observed.

Changes in external color can be explained by chemical changes in the exocarp (peel) during ripening. Exocarp persists as a green-colored tissue during most of the coffee fruit development. However, in the ripe state, it becomes red (or yellow, for some cultivars) as result of the decrease of chlorophyll and accumulation of anthocyans.[22]

Extraction of Soluble and Bound HCAs. The phenolic compounds of CP have been the subject of several studies.[4,6,8−10] The interest in these compounds is due to their biological activities (antioxidant, anti-inflammatory, anticarcinogenic, etc.).[6] Most of these studies are limited to the compounds extractable with aqueous methanol solutions.[4,8,9] However, significant amounts of phenolic compounds may remain in the solid residues after such extractions. For example, phenolic acids covalently bound to cell wall polysaccharides.[23]

In preliminary studies, it was found that the estimation of soluble and bound phenolic compounds in CP is strongly dependent on the methodologies used for their extraction and analysis. Thus, we decided to evaluate the conditions commonly used for the extraction of phenolic acids.

As a first step, we evaluated the effects of a hexane extraction followed by an aqueous methanolic (20:80, v/v) extraction on the recovery yield of soluble HCAs (Figure 1). It was calculated using compound **1**, because it was the main soluble HCA (93.8−98.8%). Figure 2 shows the amount of compound **1** extracted by four successive methanolic extractions with and without pretreatment with hexane. Because no compound **1** was detected from the fifth methanolic extraction, the amount of compound **1** obtained in the first four extractions was considered as the total soluble compound **1**, and this amount was used to calculate the extraction yield.

No significant differences were found between the yields of **1** obtained with or without treatment with hexane. Thus, hexane extraction does not affect HCA extraction, but it may help to remove less polar compounds such as carotenoids and other lipophilic compounds that can interfere with the chromatographic analysis of extracts.[4] Therefore, we decided to make three hexane extractions followed by three successive

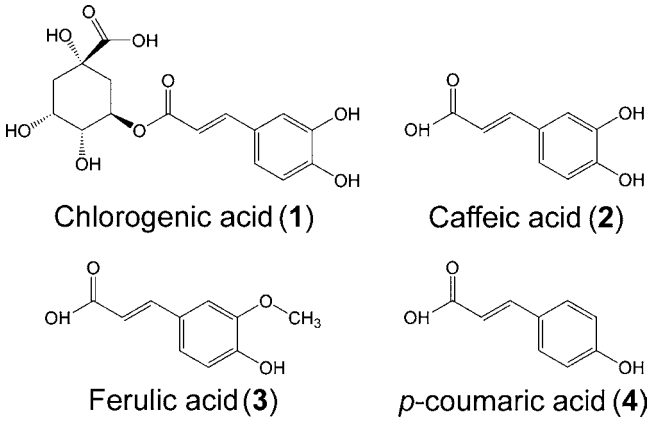

Figure 1. Structures of hydroxycinnamates analyzed in coffee pulp samples.

methanolic extractions for analytical purposes. In these conditions, >98% of **1** was recovered.

Several authors performed alkaline hydrolysis for the extraction of covalently bound phenolic acids. However, it is known that this alkaline hydrolysis led to important losses of phenolic compounds, particularly dihydroxy derivatives such as caffeic acid (**2**).[24]

Krygier et al.[25] reported 66.7% compound **2** lost after treatment with 2 M NaOH for 4 h under nitrogen atmosphere. To prevent loss of phenolic acids, Nardini et al.[24] proposed the addition of EDTA-ascorbate during alkaline hydrolysis. Under their assay conditions (2 M NaOH containing 10 mM EDTA and 1% ascorbic acid at 30 °C for 30 min), complete hydrolysis of compound **1** was achieved without any detectable loss of compound **2**.[24]

Preliminary studies showed significant loss of phenolic compounds during the alkaline hydrolysis of CP. Therefore, we decided to study the conditions of alkaline hydrolysis for recovery of HCAs from CP. The effect of different NaOH concentrations (in the presence of EDTA and ascorbic acid) and incubation times on the recovery of HCAs was evaluated.

Figure 3 shows the time course of compound **2** extraction during alkaline hydrolysis of CP using different NaOH concentrations. We observed an increase in the amount of **2** extracted during the first minutes of the reaction, followed by a decrease of this compound. This can be explained by the existence of at least two reactions: first, a hydrolysis reaction that breaks the covalent bond linking compound **2** to a cell wall polymer, and then a second reaction that transforms compound **2** to another compound, presumably by oxidation. The greatest amount of **2** was obtained using 2 M NaOH and incubating for 2 h at 40 °C. Therefore, we used these conditions for the analytical procedure. To confirm the efficiency of alkaline hydrolysis, compound **1** was used as internal standard. We added a known amount of compound **1** to CP (1 mg/g of CP). Then we subjected the CP to an alkaline hydrolysis as described above. In the proposed conditions, 90% of the expected compound **2** was recovered.

HCA Content in CP from Different *C. arabica* Cultivars. Information about the content and distribution of phenolic compounds in CP is often confusing and sometimes contradictory. Cultivar and degree of ripeness of the fruit can affect the content of phenolic compounds in CP. The ripening of coffee cherries occurs at the end of the physiological maturation of fruits. This process is characterized by a series of physical and chemical changes, such as increased weight and size and changes in color and in the content of sugars and phenolic compounds. Therefore, the ripening stage can significantly affect the HCAs content in CP samples.[15] Therefore, we analyzed the content of soluble and bound HCAs in CP as a function of ripening and cultivar of *C. arabica*.

The content of HCAs strongly depends on the ripening stage and cultivar (Figure 4). Total HCA (defined as the sum of soluble and bound compounds **1**–**4**) content increased during ripening of coffee fruit (from unripe to semiripe stage) for five cultivars. This is followed by a decrease in the HCA content at

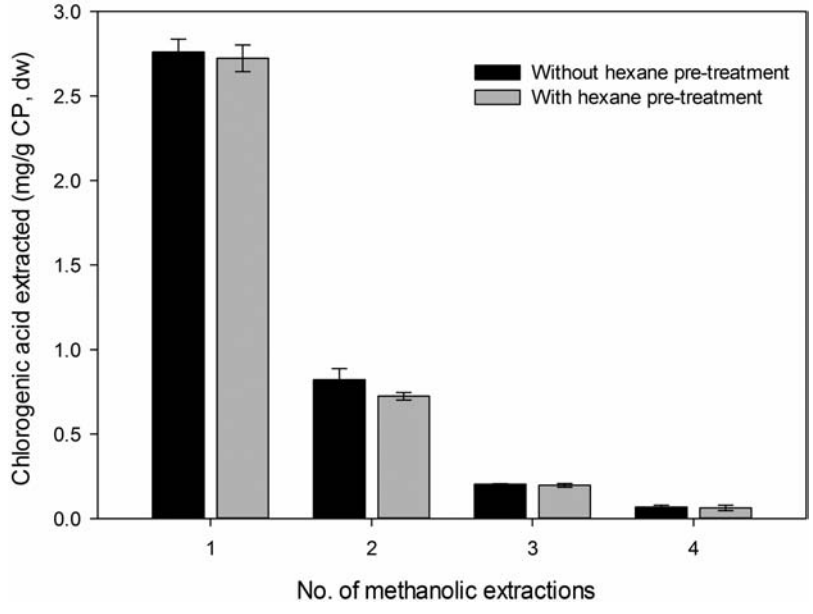

Figure 2. Extraction of chlorogenic acid from cofee pulp by succesive extractions with acidified aqueous methanol (data are presented as a mean value ± standard deviation).

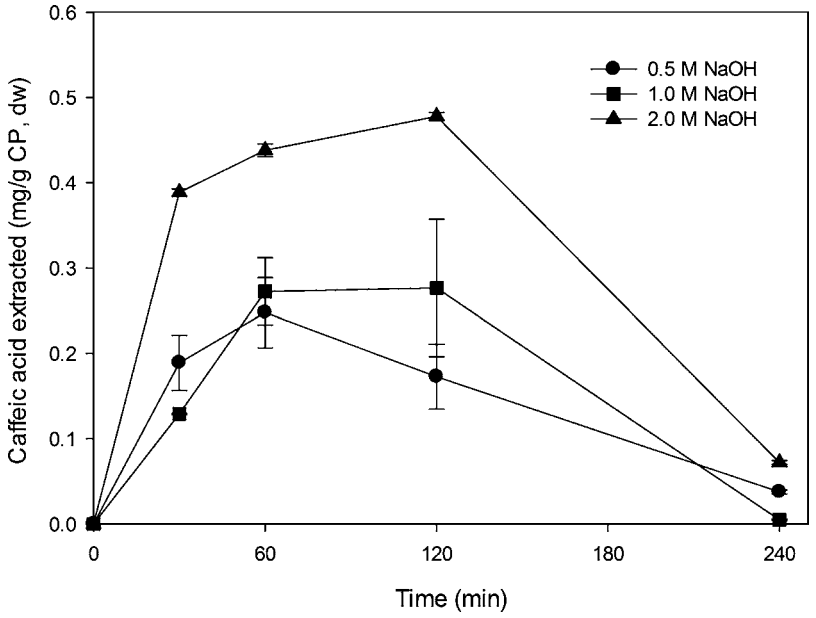

Figure 3. Time course of caffeic acid extraction during alkaline hydrolysis of coffee pulp with different concentrations of NaOH (in the presence of 1% ascorbic acid and 10 mM EDTA) (data are presented as a mean value ± standard deviation).

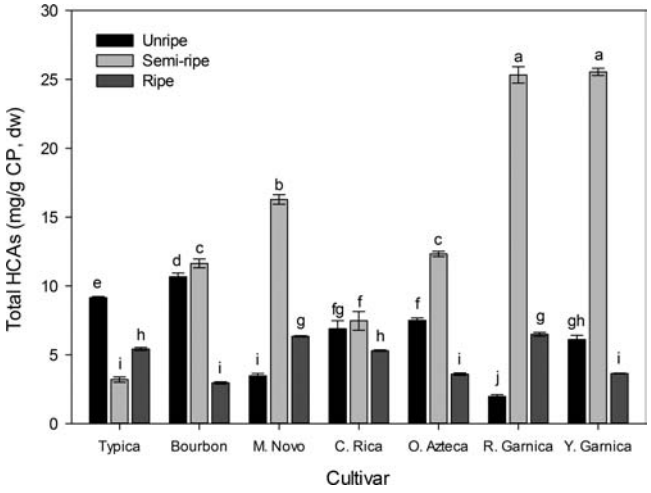

Figure 4. Content of total hydoxycinnamates in the pulp of coffee fruits from seven cultivars at three ripening stages (data are presented as a mean value ± standard deviation).

the end of ripening for six cultivars. For the Typica cultivar an inverse trend was observed.

These observations are different from that of Koshiro et al.[12] They studied the content of compound **1** in pulp and seeds of fruits of *C. arabica* and *C. canephora* at five different ripening stages. They found a progressive increase of **1** during the ripening of coffee fruit. They explained this increase by the continuous synthesis of **1** as suggested by the expression of three genes related to the biosynthesis of compound **1**. These differences in the pattern of accumulation of HCAs can be explained by differences in the presentation of results. Koshiro et al.[12] expressed the content of HCAs as milligrams per fruit. When they took into account the growth of the fruit and expressed the content of HCAs as milligrams per gram of pericarp (dw), they did not observe any increase in the content of **1** during maturation of coffee cherries.

On the other hand, Miljkovic et al.[26] patented a process for the extraction of a nutraceutical product from whole coffee cherry. They recommended the use of unripe or semiripe cherries because these fruits had a higher content of phenolics and compound **1** (from 6.7 to 8.6% w/w of **1**) with respect to the ripe cherries (1.3% w/w of **1**). These results are in agreement with our findings.

Puertas-Mejía et al.[27] studied the accumulation of phenolic compounds in the pericarp (pulp) of coffee fruits at five ripening stages. They found a progressive increase of anthocyanins during ripening (from unripe to overripe stage). Nevertheless, the semiripe stage showed the highest antioxidant capacity. They associated this observation with the presence of additional components with antioxidant activity.[27] These findings could suggest that this additional antioxidant activity could be associated with the presence of HCAs. Nevertheless, no antioxidant assays were carried out in this work.

The content of total HCAs in CP significantly differs from cultivar to cultivar. However, these differences also depend on the ripening stage (Figure 4). For the pulp of ripe fruits, Red Garnica and Mundo Novo cultivars presented the highest content of total HCAs (from 6.34 to 6.49 mg/g dw), followed for the pulp of Typica and Costa Rica cultivars (from 5.29 to 5.42 mg/g dw), and the Yellow Garnica, Oro Azteca, and Bourbon varieties presented the lowest content of total HCAs (from 2.96 to 3.64 mg/g dw). For the semiripe coffee we observed that pulp from Yellow and Red Garnica cultivars had a remarkably high content of HCAs (from 25.32 to 25.54 mg/g dw); on the other hand, the Typica cultivar presented a low content of these compounds (3.20 mg/g dw). All other cultivars had a higher content of HCAs than any sample of pulp from ripe cherries (from 7.45 to 16.68 mg/g dw). Finally, unripe cherries of Bourbon and Typica cultivars presented the highest content of HCAs, whereas the Mundo Novo and Red Garnica had the lowest content of these compounds.

Other authors have studied the content of phenolic compounds in CP from different cultivars. However, those studies are limited to the methanolic extracts from the pulp of

Table 2. Content of Soluble Hydroxycinnamates in Coffee Pulp Samples (in Milligrams per Gram of Coffee Pulp, dw Basis)[a]

cultivar	ripening stage	chlorogenic acid	caffeic acid	ferulic acid	*p*-coumaric acid	total soluble HCAs[b]	chlorogenic acid (%)
Typica	unripe	8.21 ± 0.07e	nd	0.18 ± 0.02ef	0.03 ± 0.00cdef	8.43 ± 0.08e	97.4
	semiripe	2.56 ± 0.18j	nd	0.06 ± 0.00j	0.02 ± 0.00efg	2.64 ± 0.19k	96.8
	ripe	4.59 ± 0.14i	nd	0.16 ± 0.00fgh	0.04 ± 0.00bc	4.79 ± 0.13j	95.9
Bourbon	unripe	9.77 ± 0.25d	nd	0.25 ± 0.00bc	0.04 ± 0.00bcde	10.05 ± 0.25d	97.1
	semiripe	10.84 ± 0.29c	nd	0.22 ± 0.02cd	0.05 ± 0.00abc	11.10 ± 0.32c	97.6
	ripe	2.26 ± 0.08j	nd	0.11 ± 0.00i	0.03 ± 0.00bcde	2.41 ± 0.09k	93.8
Mundo Novo	unripe	2.80 ± 0.17j	nd	0.02 ± 0.00k	0.03 ± 0.01bcde	2.85 ± 0.17k	98.2
	semiripe	15.27 ± 0.36b	nd	0.28 ± 0.01bc	0.05 ± 0.01abc	15.60 ± 0.37b	97.9
	ripe	5.56 ± 0.05gh	nd	0.16 ± 0.00fgh	0.04 ± 0.00bcd	5.76 ± 0.05hi	96.5
Costa Rica	unripe	6.08 ± 0.56fg	nd	0.14 ± 0.01hi	0.02 ± 0.00efg	6.23 ± 0.56fgh	97.5
	semiripe	6.70 ± 0.65f	nd	0.16 ± 0.00fgh	0.04 ± 0.03abc	6.91 ± 0.68f	97.0
	ripe	4.56 ± 0.05i	nd	0.17 ± 0.01fg	0.05 ± 0.00abc	4.78 ± 0.05j	95.4
Oro Azteca	unripe	6.62 ± 0.17f	nd	0.17 ± 0.01fg	0.02 ± 0.01efg	6.81 ± 0.17fg	97.2
	semiripe	11.45 ± 0.18c	nd	0.21 ± 0.00de	0.03 ± 0.00cde	11.69 ± 0.18c	97.9
	ripe	2.89 ± 0.09j	nd	0.15 ± 0.01ghi	0.04 ± 0.00bcde	3.07 ± 0.09k	94.0
Red Garnica	unripe	1.31 ± 0.15k	nd	0.04 ± 0.00jk	0.01 ± 0.00g	1.35 ± 0.15l	96.6
	semiripe	24.15 ± 0.62a	nd	0.39 ± 0.00a	0.06 ± 0.00a	24.60 ± 0.63a	98.2
	ripe	5.84 ± 0.13fgh	nd	0.04 ± 0.00jk	0.04 ± 0.00abc	5.93 ± 0.14ghi	98.5
Yellow Garnica	unripe	5.04 ± 0.36hi	nd	0.05 ± 0.00j	0.01 ± 0.00fg	5.11 ± 0.37ij	98.8
	semiripe	24.420 ± 0.256a	nd	0.42 ± 0.03a	0.05 ± 0.00ab	24.89 ± 0.28a	98.1
	ripe	3.01 ± 0.03j	nd	0.07 ± 0.00j	0.02 ± 0.00defg	3.10 ± 0.03k	97.2

[a]Data are presented as a mean value ± standard deviation; the same letter in a column means no significant differences (Tukey HDS test, $\alpha = 0.05$) between samples; values = 0.00 means = ≤0.005; nd, not detected. [b]Calculated as the sum of chlorogenic, caffeic, ferulic, and *p*-coumaric acids.

ripe cherries.[8,9] They found a content of HCAs from 3.98 to 16.20 mg/g (dw) for cultivars of *C. arabica* and *C. canephora*. Those values are higher than the results obtained in this paper for ripe CP (from 2.96 to 6.49 mg/g dw). Differences between the contents of HCAs could be related to the origin of coffee fruits (soil, climate, etc.) and agricultural practices.

Tables 2 and 3 show the content of soluble and bound HCAs for each cultivar at each ripening stage, respectively. The content of soluble HCAs is higher than the bound HCAs for all analyzed samples. The content of soluble HCAs represents around 81−97% of total HCAs for all samples except for unripe Red Garnica (soluble HCAs = 68%). This observation differs from previous papers that indicate that most of the HCAs in CP are covalently bound to the cell wall polysaccharides.[6,10,28]

Differences in distribution of soluble and bound HCAs can be related to the origin of the coffee fruits, ripening stage, extraction methodology, and number of consecutive extractions. Furthermore, under the extraction conditions, phenolic compounds may undergo different chemical reactions in the presence of the solvent used. This work has been shown that the amount of three consecutive extractions with aqueous methanol yields 98% of total compound **1** from CP (Figure 1).

In this paper, we confirmed the influence of cultivar and ripening on the content and distribution of soluble and bound HCAs, but we also observed that the extraction method affects the yields of these compounds. Thus, both fractions (soluble and bound) can be under- or overestimated when the extraction has been not exhaustive.

The main component of methanolic extracts of the seven cultivars was compound **1** (Table 2). Compound **1** represented around 94−99% of soluble HCAs for all analyzed samples (from 1.31 to 24.42 mg/g dw). These values are higher than those reported by other authors.[4,6,28] They found that **1** accounts for 80−84% of soluble HCAs. The content of **1** in the methanolic extracts of the pulp of ripe coffee cherries (2.2−5.8 mg/g dw) is within the range found by other authors.[4,6,8,9] These authors have reported a content of 2.3−9.7 mg/g of CP as determined by HPLC analysis of methanolic extracts. On the other hand, Labat et al.[29] reported a content of **1** of 3.6−27.0 mg/g CP. However, they did not describe the extraction and analysis conditions; they neither reported the origin of the plant material.

There is very less information on the content of **1** (and HCAs) in CP from cherries at different stages of ripeness. Koshiro et al.[12] reported the evolution of **1** and its isomers in pulp and seeds of coffee fruits during ripening. They found a continuous decrease of compound **1** from 10 mg/g CP (dw) for green mature fruits to 5−5.5 mg/g for ripe cherries of *C. arabica* cv. Tall Mokka. A similar trend was observed for fruits of *C. canephora*, but in that case, the content of compound **1** decreased from 30 to 10 mg/g CP (dw). In our results a decrease in compound **1** was also observed from unripe to ripe fruits for five of seven cultivars. Nevertheless, in our case an increase of compound **1** was observed in the semiripe fruits for six of seven cultivars.

Other HCAs identified in methanolic extracts were ferulic acid (**3**) and *p*-coumaric acid (**4**). Compound **3** was found at highly variable concentrations (0.02−0.41 mg/g dw), whereas compound **4** was found in small amounts (0.01−0.06 mg/g dw). Compound **2** was not detected in methanolic extracts.

Table 3. Content of Bound Hydroxycinnamates in Coffee Pulp Samples (in Milligrams per Gram of Coffee Pulp, dw Basis)[a]

cultivar	ripening stage	chlorogenic acid	caffeic acid	ferulic acid	*p*-coumaric acid	total bound HCAs[b]	caffeic acid (%)
Typica	unripe	0.06 ± 0.00c	0.64 ± 0.01b	0.03 ± 0.00cdef	0.03 ± 0.00cd	0.75 ± 0.02b	84.5
	semiripe	0.05 ± 0.00cd	0.45 ± 0.00fg	0.04 ± 0.00cd	0.02 ± 0.00fghijk	0.56 ± 0.00ijk	80.9
	ripe	0.08 ± 0.00a	0.47 ± 0.01f	0.04 ± 0.01b	0.03 ± 0.00cde	0.62 ± 0.02efgh	75.0
Bourbon	unripe	0.05 ± 0.00cd	0.54 ± 0.01e	0.02 ± 0.00jkl	0.02 ± 0.00kl	0.63 ± 0.01efg	85.4
	semiripe	0.05 ± 0.00cd	0.42 ± 0.01fghi	0.03 ± 0.00hijkl	0.02 ± 0.00ghijk	0.52 ± 0.00jk	81.0
	ripe	0.08 ± 0.00a	0.41 ± 0.01ghi	0.04 ± 0.00c	0.02 ± 0.00defghi	0.55 ± 0.01jk	73.4
Mundo Novo	unripe	0.04 ± 0.00d	0.54 ± 0.01e	0.03 ± 0.00defghi	0.02 ± 0.00defgh	0.64 ± 0.01efg	84.6
	semiripe	0.05 ± 0.01cd	0.58 ± 0.02cde	0.03 ± 0.00ijkl	0.02 ± 0.00hijk	0.67 ± 0.03cdef	85.5
	ripe	0.07 ± 0.00b	0.44 ± 0.01fg	0.04 ± 0.00cd	0.03 ± 0.00cde	0.58 ± 0.01ghij	76.7
Costa Rica	unripe	0.06 ± 0.00c	0.56 ± 0.02de	0.03 ± 0.00cde	0.03 ± 0.00ab	0.69 ± 0.02cde	81.6
	semiripe	0.05 ± 0.00cd	0.44 ± 0.01fg	0.03 ± 0.00ghijk	0.02 ± 0.00defg	0.54 ± 0.01jk	81.3
	ripe	0.08 ± 0.00a	0.37 ± 0.04i	0.04 ± 0.00cd	0.02 ± 0.00cdef	0.51 ± 0.04k	71.8
Oro Azteca	unripe	0.05 ± 0.00cd	0.61 ± 0.00bcd	0.03 ± 0.00fghij	0.02 ± 0.00defgh	0.71 ± 0.00bcd	85.4
	semiripe	0.04 ± 0.00d	0.53 ± 0.01e	0.02 ± 0.00kl	0.02 ± 0.00ijk	0.62 ± 0.01fghi	86.0
	ripe	0.08 ± 0.00a	0.38 ± 0.01hi	0.03 ± 0.00cdefg	0.02 ± 0.00efghijk	0.52 ± 0.01jk	73.0
Red Garnica	unripe	0.05 ± 0.00cd	0.53 ± 0.01e	0.03 ± 0.00cdefgh	0.03 ± 0.00bc	0.65 ± 0.02def	82.5
	semiripe	0.04 ± 0.00d	0.63 ± 0.02bc	0.02 ± 0.00jkl	0.02 ± 0.00jkl	0.72 ± 0.03bc	87.8
	ripe	0.06 ± 0.00c	0.45 ± 0.00fg	0.03 ± 0.00defghi	0.02 ± 0.00efghij	0.56 ± 0.00hijk	80.2
Yellow Garnica	unripe	0.05 ± 0.00cd	0.91 ± 0.05a	0.05 ± 0.00a	0.04 ± 0.00a	1.05 ± 0.05a	86.8
	semiripe	0.04 ± 0.00d	0.57 ± 0.01de	0.02 ± 0.00l	0.02 ± 0.00l	0.65 ± 0.02def	87.6
	ripe	0.05 ± 0.00cd	0.44 ± 0.02fgh	0.03 ± 0.00efghij	0.02 ± 0.00ghijk	0.54 ± 0.02jk	80.7

[a]Data are presented as a mean value ± standard deviation; the same letter in a column means no significant differences (Tukey HDS test, $\alpha = 0.05$) between samples; values = 0.00 means = ≤0.005. [b]Calculated as the sum of chlorogenic, caffeic, ferulic, and *p*-coumaric acids.

The main component after the alkaline hydrolysis was **2**, and it represented around 72−88% of bound HCAs (Table 3). Compound **2** is the most abundant HCA found in fruits. It is commonly esterified to sugars, organic acids, and lipids.[30] Compound **1** was found to be principally in the form of soluble ester (**1**) in CP, but also a significant amount of this acid was in the form of insoluble esters.

A small amount of **1** was detected in alkaline hydrolysates, probably due to an incomplete hydrolysis of phenolic compounds. Compounds **2** and **3** were found in the range of 0.016−0.052 mg/g CP (dw). These values of bound phenolic acids are lower than those reported by Torres-Mancera et al.[6] or Pérez-Morales et al.[28] They found contents of 0.083−0.108 mg of bound **3** and 0.079−0.094 mg of bound **2** per gram of CP (dw). These differences could be related to chemical differences between CP samples, maturity state, or the hydrolysis conditions such as time, temperature, and concentration as shown in Figure 3.

CP is a potential source of phenolic antioxidants and other bioactive compounds. However, available data of phenolic content in CP are widely variable. This study contributes to the understanding of the differences found in previous research on HCA extraction from CP. Furthermore, these findings suggest that unripe or semiripe coffee cherries, which are currently discarded as defective cherries, and fruits that remain on the coffee trees after harvest can be used as an inexpensive source of phenolic antioxidants, such as chlorogenic and caffeic acids.

■ ASSOCIATED CONTENT

Supporting Information

Figures showing the results of morphological characterization of coffee fruits and chromatograms of reference compounds and selected samples. This material is available free of charge via the Internet at http://pubs.acs.org.

■ AUTHOR INFORMATION

Corresponding Author

*(G.S.-C.) Phone: +52 55-58 04-4600. Fax: +52 55-580- 4499. E-mail: saucedo@xanum.uam.mx.

Notes

The authors declare no competing financial interest.

■ ABBREVIATIONS USED

CP, coffee pulp; HCAs, hydroxycinnamates; dw, dry weight

■ REFERENCES

(1) Aranda, E.; Duran, L.; Escamilla, E. Vermicomposting in coffee cultivation. In *Coffee: Growing, Processing, Sustainable Production*; Wintgens, J. N., Ed.; Wiley-VCH Verlag: Weinheim, Germany, 2004; pp 324−338.

(2) Esquivel, P.; Jiménez, V. M. Functional properties of coffee and coffee by-products. *Food Res. Int.* **2012**, *46*, 488−495.

(3) Murthy, P. S.; Naidu, M. M. Sustainable management of coffee industry by-products and value addition − a review. *Resour., Conserv. Recycl.* **2012**, *66*, 45−58.

(4) Ramirez-Coronel, M. A.; Marnet, N.; Kolli, V. S. K.; Roussos, S.; Guyot, S.; Augur, C. Characterization and estimation of proanthocyanidins and other phenolics in coffee pulp (*Coffea arabica*) by thiolysis-

high-performance liquid chromatography. *J. Agric. Food Chem.* **2004**, *52*, 1344−1349.
(5) Mateos, R.; Goya, L.; Bravo, L. Uptake and metabolism of hydroxycinnamic acids (chlorogenic, caffeic, and ferulic acids) by HepG2 cells as a model of the human liver. *J. Agric. Food Chem.* **2006**, *54*, 8724−8732.
(6) Torres-Mancera, M. T.; Cordova-López, J.; Rodríguez-Serrano, G.; Roussos, S.; Ramírez-Coronel, M. A.; Favela-Torres, E.; Saucedo-Castañeda, G. Enzymatic extraction of hydroxycinnamic acids from coffee pulp. *Food Technol. Biotechnol.* **2011**, *49*, 369−373.
(7) Torres-Mancera, M. T.; Baqueiro-Peña, I.; Figueroa-Montero, A.; Rodríguez-Serrano, G.; González-Zamora, E.; Favela-Torres, E.; Saucedo-Castañeda, G. Biotransformation and improved enzymatic extraction of chlorogenic acid from coffee pulp by filamentous fungi. *Biotechnol. Prog.* **2013**, *29*, 337−345.
(8) Ramirez-Martinez, J. R. Phenolic compounds in coffee pulp: quantitative determination by HPLC. *J. Sci. Food Agric.* **1988**, *43*, 135−144.
(9) Clifford, M. N.; Ramirez-Martinez, J. R. Phenols and caffeine in wet-processed coffee beans and coffee pulp. *Food Chem.* **1991**, *40*, 35−42.
(10) Arellano-González, M. A.; Ramírez-Coronel, M. A.; Torres-Mancera, M. T.; Pérez-Morales, G. G.; Saucedo-Castañeda, G. Antioxidant activity of fermented and nonfermented coffee (*Coffea arabica*) pulp extracts. *Food Technol. Biotechnol.* **2011**, *49*, 374−378.
(11) Bulanon, D. M.; Kataoka, T.; Ota, Y.; Hiroma, T. A color model for recognition of apples by a robotic harvesting system. *J. Jpn. Soc. Agric. Mach.* **2002**, *64*, 123−123.
(12) Koshiro, Y.; Jackson, M.; Katahira, R.; Wang, M. L.; Nagai, C.; Ashihara, H. Biosynthesis of chlorogenic acids in growing and ripening fruits of *Coffea arabica* and *Coffea canephora* plants. *Z. Naturforsch., C: Biosci.* **2007**, *62*, 731−742.
(13) Carvajal-Herrera, J. J.; Aristizábal-Torres, I. D.; Oliveros-Tascón, C. E. Evaluación de las propiedades físicas y mecánicas del fruto de café (*Coffea arabica* L. var. Colombia) durante su desarrollo y maduración. *Dyna* **2012**, *79*, 116−124.
(14) Geromel, C.; Ferreira, L. P.; Cavalari, A. A.; Pereira, L. F. P.; Guerreiro, S. M. C.; Vieira, L. G. E.; Leroy, T.; Mazzafera, P.; Marraccini, P. Sugar metabolism during coffee fruit development. *Proceedings of the 20th International Scientific Colloquium on Coffee*, Bangalore, India, Oct 11−15, 2004; International Scientific Association on Coffee: Paris, France, 2005; pp 651−655.
(15) Marín-López, S. M.; Arcilla-Pulgarín, J.; Montoya-Restrepo, E. C.; Oliveros-Tascón, C. E. Cambios físicos y químicos durante la maduración del fruto de café *Coffea arabica* L. var. Colombia. *Cenicafé* **2003**, *54*, 208−225.
(16) Aristizábal-Torres, I. D.; Carvajal-Herrera, J. J.; Oliveros-Tascón, C. E. Physical and mechanical properties correlation of coffee fruit (*Coffea arabica*) during its ripening. *Dyna* **2012**, *79*, 148−155.
(17) Carvajal-Herrera, J. J.; Aristizábal-Torres, I. D.; Oliveros-Tascón, C. E.; Mejía-Montoya, J. W. Colorimetría del fruto de café (*Coffea arabica* L.) durante su desarrollo y maduración. *Rev. Fac. Nac. Agron. (Medellin, Colomb.)* **2011**, *64*, 6229−6240.
(18) Ramos, P.; Valdés, C.; Gómez, E.; Sanz, J. R.; Solate, E. Características espectrales de la luz reflejada por frutos de café (*Coffea arabica*). *Rev. Colomb. Fis.* **2006**, *38*, 823−825.
(19) Sandoval-Niño, Z. L.; Prieto-Ortiz, F. A. Caracterización de café cereza empleando técnicas de visión artificial. *Rev. Fac. Nac. Agron. (Medellin, Colomb.)* **2007**, *60*, 4105−4127.
(20) Cárdenas, S. I. Caracterización morfológica y agronómica del grupo de café (*Coffea arabica* L.) del CATIE. M.Sc. thesis, Centro Agronómico Tropical de Investigación y Enseñanza (CATIE), Turrialba, Costa Rica, 2007.
(21) Hernández, B.; Sáenz, C.; Alberdi, C.; Alfonso, S.; Berrogui, M.; Diñeiro, J. M. Design and performance of a color chart based in digitally processed images for sensory evaluation of piquillo peppers (*Capsicum annuum*). *Color Res. Appl.* **2004**, *29*, 305−311.
(22) De Castro, R. D.; Marraccini, P. Cytology, biochemistry and molecular changes during coffee fruit development. *Braz. J. Plant Physiol.* **2006**, *18*, 175−199.
(23) Pérez-Jiménez, J.; Torres, J. L. Analysis of nonextractable phenolic compounds in foods: the current state of the art. *J. Agric. Food Chem.* **2011**, *59*, 12713−12724.
(24) Nardini, M.; Cirillo, E.; Natella, F.; Mencarelli, D.; Comisso, A.; Scaccini, C. Detection of bound phenolic acids: prevention by ascorbic acid and ethylenediaminetetraacetic acid of degradation of phenolic acids during alkaline hydrolysis. *Food Chem.* **2002**, *79*, 119−124.
(25) Krygier, K.; Sosulski, F.; Hoggs, L. Free, esterified, and insoluble-bound phenolic acids. 1. Extraction and purification procedure. *J. Agric. Food Chem.* **1982**, *30*, 330−334.
(26) Miljkovic, D.; Duell, B.; Miljkovic, V. Methods for coffee cherry products. U.S. Patent 7,754,263, July 13, 2010.
(27) Puertas-Mejía, M. A.; Rivera-Echeverry, F.; Villegas-Guzmán, P.; Rojano, B. A.; Pelaez-Jaramillo, C. Comparación entre el estado de maduración del fruto de café (*Coffea arabica* L.), el contenido de antocianinas y su capacidad antioxidante. *Rev. Cubana Plant. Med.* **2012**, *17*, 1−7.
(28) Pérez-Morales, G. G.; Ramírez-Coronel, A.; Guzmán-López, O.; Cruz-Sosa, F.; Perraud-Gaime, I.; Roussos, S.; Saucedo-Castañeda, G. Feruloyl esterase activity from coffee pulp in solid-state fermentation. *Food Technol. Biotechnol.* **2011**, *49*, 352−358.
(29) Labat, M.; Augur, C.; Rio, B.; Perraud-Gaime, I.; Sayadi, S. Biotechnological potentielities of coffee and similar with olive, two models of agroindustrial products rich in polyphenolic compounds: a review. In *Coffee Biotechnology and Quality*; Sera, T., Soccol, C. R., Pandey, A., Roussos, S., Eds.; Kluwer Academic Publishers: Dordrecht, The Netherlands, 2000; pp 517−531.
(30) Scalbert, A.; Williamson, G. Dietary intake and bioavailability of polyphenols. *J. Nutr.* **2000**, *130*, 2073S−2085S.

Comparative assessments should be made for differences in phenotype and genotype, market quality traits, and nutritional composition. Substantial equivalence was established by an iterative process as follows: If differences are not found, transgenic lines are considered substantially equivalent to their non-transgenic counterpart. However, if differences are found, then transgenic lines must be evaluated further to ensure that the changes fall within the range of natural variation among different varieties of the same species. This approach has been adopted by numerous studies on major biotechnology-derived field crops, which demonstrated compositional equivalence of transgenic crops to their non-transgenic counterpart.[7,12−17]

In the process of characterizing disease susceptibility and yield of Blight Blocker peanuts from 2004 to 2009, we collected a large amount of data on three transgenic peanut lines and their non-transgenic counterparts. These data included grade characteristics of kernels, fatty acid composition, mineral nutrient profiling, and constituents in peanut. The goal of this study was to assess the nutritional value of transgenic Blight Blocker peanut. Our specific objectives were to (1) compare the nutritional composition of transgenic Blight Blocker peanut lines and their non-transgenic counterparts, (2) investigate equivalence of individual components to determine if Blight Blocker peanut lines are compositionally equivalent to non-transgenic peanut, and (3) perform canonical discriminant analysis of all combined data to assess whether the introduction of a transgene caused significant unintended changes in transgenic lines when compared to their non-transgenic peanut.

MATERIALS AND METHODS

Transgenic Lines and Field Testing. Field testing of transgenic lines was approved by the Animal and Plant Health Inspection Service (APHIS) for comparing the T_4, T_5, and T_6 generations of N70, W73, and P39 in 2006, 2007, and 2008, respectively. Trials were conducted at the Tidewater Agricultural Research and Extension Center in Suffolk, VA, on a field site of Kenansville loamy sand. Transgenic lines and their corresponding non-transgenic parents were planted in a randomized complete block design with four replications. Transgenic lines and corresponding non-transgenic cultivars were planted in two 9.1 m rows/plot. Rows were spaced 0.9 m apart and planted at a rate of ca. 9.8 seed/m of row. Metam sodium 42% (Vapam, Amvac, Newport Beach, CA) at 26.8 kg of active ingredient/ha was applied 20.3 cm under each row with a coulter and trailing chisel shank for control of Cylindrocladium black rot of peanut on March 29 and April 7, 2006, April 19, 2007, and April 15, 2008. Disks and a bed shaper produced smooth beds measuring 64 cm wide and 10.2 cm high over treated rows. Standard practices for production of Virginia-type peanuts were followed throughout the growing season. These trials were harvested on October 31, 2006, November 2, 2007, and October 16, 2008.

Peanut Quality Characteristics. Peanut grade was determined using the United States Department of Agriculture (USDA) grading system for Virginia-type peanut.[18] A 2 kg sample of raw, in-shell peanuts was taken from thoroughly mixed pods harvested from each plot. Pod samples were processed by separating the foreign material, loose-shelled kernels, and pods. Foreign material and loose-shelled kernels were weighed, and their percentage was determined. The remaining intact pods were pre-sized using a set of sizing rollers prior to shelling. The fancy pods (FPP) were a percentage of in-shell peanuts that ride up to 13.5 mm spacing on the pod pre-sizer. Pod brightness (FPB) was measured using a Hunterlab D25-PC2 colorimeter equipped with the D25-2RL reduced area viewing for a L optical sensor (51 mm diameter sample area). The whole pods were shelled using a peanut sheller (Davidson and McIntosh). Size distribution of the shelled kernels was determined with a series of slotted screens prescribed by federal−state inspection standards for Virginia-type peanuts.[18] Extra-large kernels (ELK) were the percentage by weight of extra-large kernels that ride the 8.5 × 25.4 mm slotted screen; sound mature kernels (SMK) were the percentage by weight of kernels that ride the 6.0 × 25.4 mm slotted screen; sound splits (SS) were the percentage by weight of kernels that consist of undamaged split or broken kernels with size between 0.25 and 0.75 mm; total sound mature kernels (TSMK) were the sum of ELK, SMK, and SS; other kernels (OK, percentage by weight) were kernels from the shelled peanut that goes through the SMK screen; and damaged kernels (DK, percentage by weight) were kernels from the shelled peanut that are inedible because of decay, mold, insect damage, sprouting (>3.2 mm), discoloration or pitting darker than light yellow, freeze damaged, or skin discoloration (<25%).

Sample Preparation and Nutritional Composition Analysis. Peanut seed and hay samples harvested from the 2006, 2007, and 2008 field trials were used for compositional analysis. After pods were harvested, subsamples of peanut hay collected along each plot were mixed and pooled to produce a 1 kg sample. The hay samples were air-dried and kept in paper bags at ambient temperature until further analysis. After grading, a 500 g sample of SMK kernels was taken for milling. Aliquots of 50 g were ground to a homogeneous paste using a coffee grinder (Black and Decker CBG5, Miami Lakes, FL) at medium speed for 2 min. The milled samples were stored in airtight polythene bags at −20 °C until chemical analysis. A total of 1 g of subsamples of the milled kernels was used for mineral analysis, and a total of 10 g of subsamples was used to extract oil for analysis of fatty acid composition.

The samples were subjected to chemical analyses for 17 nutritional components that are considered the most important nutrients of peanut seeds for human consumption or in peanut hay for feed uses. Peanut seed samples were analyzed for levels of potassium, calcium, magnesium, sulfur, phosphorus, palmitic acid, stearic acid, oleic acid, linoleic acid, arachidic acid, eicosenoic acid, behenic acid, and lignoceric acid. Hay samples were analyzed for neutral detergent fiber (NDF), acid detergent fiber (ADF), and crude protein (CP). The compositional analyses were performed by accredited laboratories following good laboratory practices.[19] A control sample with known nutritional composition was included in each run of the methods. A limit of quantification (LOQ) was also estimated by the lowest quantitated standard or control sample.

Mineral Analysis. Levels of mineral elements (potassium, calcium, magnesium, sulfur, and phosphorus) in the seed sample were determined according to AOAC method 985.01.[20] Briefly, 1 g of the paste sample was dry-ashed at 550 °C in a furnace, and the ash dissolved in 0.5 N hydrochloric acid (HCl). The solution was filtered with Whatman filter paper No. 2 and brought to 100 mL with deionized water. The elements mentioned above were determined in triplicates at appropriate wavelengths using an inductively coupled plasma atomic emission spectrometer (ICP, Spectro Ciros, Fitchburgh, MA). The ICP instrument was calibrated and programed to analyze 30 samples for 10 elements in about 20 min. Each sample had a 24 s preflush with a 10 s integration time to read the element and background spectral lines, and there was approximately a 10 s rinse that occurred during the integration time. A quality control solution was read and verified after every tray of 30 samples. The concentration of each element was calculated by comparing the emission of the unknown sample to the emission of the standard control solution. Calcium and phosphorus each had a LOQ of 2.5 mg/kg of fresh weight (fw). The LOQ for potassium was 19.5 mg/kg of fw; the LOQ for magnesium was 7.6 mg/kg of fw; and the LOQ for sulfur was 13.5 mg/kg of fw. The measurements were converted to dry weight of sample for comparison.

Fatty Acid Profile. Peanut oil was extracted with the chloroform and methanol method described by Bligh and Dyer.[21] The oil content of the samples was determined by acid hydrolysis based on AOAC method 922.06.[22] Fatty acid methyl esters (FAMEs) were prepared according to the AOCS method Ce 2-66.[23] The fatty acid composition of all FAME samples was determined by gas chromatography (Agilent 6890N GC) using a J&W DB-225 GC capillary column (30 m × 0.252 mm inner diameter with 0.25 μm thickness; Chrom Tech, Inc., Apple

Table 1. Mineral and Fatty Acid Compositions, Forage Quality, and Grade Characteristics of Blight Blocker Peanut N70 and Its Non-transgenic Counterpart NC 7

	2006 field season		2007 field season		2008 field season	
component[a]	N70 mean[b] ± SE[c] (range)[d]	NC 7 mean ± SE (range)	N70 mean ± SE (range)	NC 7 mean ± SE (range)	N70 mean ± SE (range)	NC 7 mean ± SE (range)
calcium	632 ± 27 (505−771)	662 ± 46 (585−749)	518 ± 20 (439−619)	524 ± 20 (424−582)	466 ± 16 (334−563)	485 ± 23 (381−584)
potassium	7576 ± 84 (7166−8250)	7519 ± 145 7274−7742)	8521 ± 230 (7769−9502)	8560 ± 223 (7587−9840)	8651 ± 88 (8044−9301)	8930 ± 125 (8263−9506)
magnesium	1821 ± 22 (1715−1948)	1754 ± 38 (1653−1832)	1963 ± 36 (1787−2188)	1859 ± 69 (1790−1946)	1940 ± 21 (1812−2140)	1900 ± 30 (1805−1985)
phosphorus	3695 ± 69 (3327−4101)	3410 ± 120 (3160−3693)	4132 ± 141 (3640−4931)	3930 ± 195 (3632−4572)	4114 ± 66 (3587−4504)	4019 ± 93 (3701−4266)
sulfur	403 ± 13 (356−455)	429 ± 23 (334−478)	460 ± 21 (422−587)	467 ± 25 (397−573)	462 ± 16 (355−548)	456 ± 22 (360−599)
palmitic acid	9.2[e] ± 0.1 (8.9−9.5)	8.8 ± 0.1 (8.4−9.2)	9.5 ± 0.1 (9.1−10.3)	9.1 ± 0.1 (8.3−9.9)	9.0[e] ± 0.2 (8.7−9.3)	8.6 ± 0.1 (8.5−8.7)
stearic acid	3.2[e] ± 0.0 (3.0−3.4)	3.4 ± 0.1 (3.2−3.8)	3.4 ± 0.1 (3.3−3.6)	3.6 ± 0.2 (3.4−3.9)	3.3[e] ± 0.0 (3.2−3.5)	3.5 ± 0.0 (3.3−3.8)
oleic acid	55.1 ± 0.3 (53.5−57.1)	55.5 ± 0.5 (54.3−56.8)	56.6 ± 0.3 (54.9−57.6)	56.7 ± 0.3 (55.4−58.0)	57.4 ± 0.2 (55.8−58.6)	58.1 ± 0.3 (57.1−59.3)
linoleic acid	26.0 ± 0.2 (24.5−27.1)	25.6 ± 0.4 (24.6−26.4)	24.7 ± 0.3 (24.0−25.8)	25.1 ± 0.4 (24.0−26.2)	24.0 ± 0.1 (22.8−25.5)	23.8 ± 0.2 (22.8−24.6)
arachidic acid	1.5 ± 0.0 (1.5−1.6)	1.6 ± 0.0 (1.6−1.7)	1.5 ± 0.0 (1.3−1.6)	1.5 ± 0.0 (1.3−1.6)	1.5 ± 0.0 (1.5−1.6)	1.5 ± 0.0 (1.5−1.6)
eicosenoic acid	1.1 ± 0.0 (1.1−1.3)	1.1 ± 0.0 (1.0−1.2)	1.0 ± 0.0 (0.0−1.1)	1.0 ± 0.0 (0.8−1.0)	1.0 ± 0.0 (1.0−1.1)	1.0 ± 0.0 (0.9−1.0)
behenic acid	2.7 ± 0.1 (2.4−3.1)	2.7 ± 0.1 (2.6−2.9)	2.3 ± 0.1 (1.9−2.6)	2.2 ± 0.1 (1.7−2.4)	2.5 ± 0.1 (2.5−2.6)	2.4 ± 0.1 (2.3−2.5)
lignoceric acid	1.1 ± 0.0 (1.0−1.2)	1.1 ± 0.0 (1.1−1.2)	1.0 ± 0.0 (0.7−1.1)	1.0 ± 0.0 (0.8−1.1)	1.1 ± 0.0 (1.0−1.2)	1.1 ± 0.0 (1.0−1.1)
CP	8.1 ± 0.2 (7.2−9.2)	8.2 ± 0.3 (7.5−9.3)	5.7 ± 0.4 (4.8−6.9)	6.1 ± 0.7 (4.9−8.1)	7.8 ± 0.2 (7.1−8.3)	7.7 ± 0.2 (6.8−9.0)
ADF	46.5 ± 0.7 (42.3−49.5)	48.7 ± 1.3 (46.2−52.3)	35.0 ± 2.6 (28.1−47.9)	34.7 ± 2.5 (28.3−44.7)	46.1 ± 0.8 (40.9−51.0)	44.5 ± 1.1 (40.5−48.7)
NDF	50.2 ± 0.8 (45.3−53.3)	52.9 ± 1.4 (49.5−56.4)	38.0 ± 2.8 (30.5−52.2)	37.9 ± 2.5 (31.3−48.3)	51.1 ± 0.9 (45.1−56.3)	48.8 ± 1.3 (44.0−53.6)
FPP	20.5 ± 1.4 (14.0−29.0)	21.8 ± 2.4 (18.0−25.0)	18.1[e] ± 0.9 (15.0−23.0)	23.6 ± 3.2 (19.0−27.0)	16.4[e] ± 1.2 (9.0−29.0)	21.1 ± 1.7 (16.0−26.0)
FPB	38.7 ± 0.4 (36.6−40.9)	40.4 ± 0.8 (38.0−42.6)	38.5 ± 1.3 (34.5−43.7)	40.0 ± 2.8 (34.9−44.5)	43.5 ± 0.4 (40.7−47.4)	44.9 ± 0.6 (43.2−46.5)
ELK	54.7 ± 1.1 (50.0−61.0)	56.2 ± 1.9 (50.0−61.0)	53.4[e] ± 4.2 (49.0−58.0)	48.8 ± 1.2 (43.0−54.0)	53.6 ± 0.8 (49.0−59.0)	55.6 ± 1.1 (51.0−60.0)
SMK	70.2 ± 0.5 (68.0−73.3)	69.4 ± 0.9 (66.2−71.2)	67.6 ± 1.1 (65.0−70.5)	66.3 ± 0.6 (64.0−68.0)	66.0 ± 0.6 (60.6−70.9)	66.8 ± 0.8 (64.3−69.3)
SS	0.8 ± 0.2 (0.2−1.5)	1.3 ± 0.3 (0.2−2.0)	2.5 ± 0.4 (1.0−4.0)	2.5 ± 0.4 (1.0−5.0)	2.8 ± 0.3 (0.6−5.6)	2.9 ± 0.4 (1.9−3.9)
OK	1.1 ± 0.1 (0.7−1.9)	1.2 ± 0.2 (0.7−2.2)	1.1 ± 0.2 (0.5−2.0)	1.3 ± 0.1 (1.0−2.0)	1.4 ± 0.1 (0.7−1.9)	1.3 ± 0.1 (1.0−2.0)
DK	0.2 ± 0.1 (0.0−0.7)	0.3 ± 0.1 (0.0−0.6)	0.9 ± 0.2 (0.0−2.0)	0.6 ± 0.4 (0.0−1.0)	0.9 ± 0.1 (0.0−1.7)	0.6 ± 0.2 (0.1−1.2)

[a]Refer to the "Abbreviations Used" for a description. [b]Least-squares means of four replicate values. [c]The standard error (SE) of the least-squares mean. [d]Range denotes the lowest and highest values reported by others. [e]Value statistically different from the non-transgenic counterpart ($p \leq 0.05$).

dx.doi.org/10.1021/jf5016297 | J. Agric. Food Chem. 2014, 62, 7877−7885

Table 2. Mineral and Fatty Acid Compositions, Forage Quality, and Grade Characteristics of Blight Blocker Peanut W73 and Its Non-transgenic Counterpart Wilson

	2006 field season		2007 field season		2008 field season	
component[a]	W73 mean[b] ± SE[c] (range)[d]	Wilson mean ± SE (range)	W73 mean ± SE (range)	Wilson mean ± SE (range)	W73 mean ± SE (range)	Wilson mean ± SE (range)
calcium	748 ± 51 (576−872)	734 ± 51 (644−794)	626 ± 25 (580−740)	597 ± 33 (464−737)	586 ± 37 (480−733)	534 ± 27 (460−634)
potassium	7880 ± 123 (7610−8079)	7942 ± 123 (7665−8244)	8649 ± 289 (8081−9969)	8847 ± 252 (7972−9894)	9377 ± 239 (8413−10167)	9125 ± 185 (8832−9744)
magnesium	2013 ± 49 (1940−2154)	1906 ± 49 (1820−2031)	2000 ± 45 (1900−2112)	1915 ± 32 (1778−2078)	2166 ± 67 (2002−2592)	2015 ± 53 (1920−2183)
phosphorus	3946[e] ± 55 (3818−4049)	3705 ± 55 (3574−3811)	4110 ± 167 (3827−4710)	3975 ± 106 (3593−4374)	4500[e] ± 134 (4060−5187)	4138 ± 95 (3925−4372)
sulfur	372 ± 11 (345−412)	359 ± 11 (350−367)	412[e] ± 16 (387−450)	462 ± 45 (410−611)	484 ± 28 (384−640)	444 ± 39 (345−626)
palmitic acid	9.1 ± 0.1 (8.6−9.3)	9.4 ± 0.1 (9.3−9.7)	8.8 ± 0.1 (8.6−8.9)	8.9 ± 0.1 (8.7−9.5)	8.6 ± 0.0 (8.4−8.7)	8.6 ± 0.0 (8.4−8.9)
stearic acid	2.6 ± 0.1 (2.5−2.8)	2.7 ± 0.1 (2.5−2.9)	3.1 ± 0.1 (2.9−3.5)	3.2 ± 0.1 (2.9−3.5)	2.9 ± 0.0 (2.7−3.1)	2.9 ± 0.0 (2.9−3.2)
oleic acid	55.2 ± 0.7 (54.1−57.3)	55.0 ± 0.7 (53.4−56.5)	55.0 ± 0.5 (53.9−56.6)	54.7 ± 0.3 (53.5−55.9)	55.4 ± 0.2 (54.5−55.9)	55.6 ± 0.3 (54.7−56.6)
linoleic acid	27.4 ± 0.6 (25.8−28.1)	28.1 ± 0.6 (26.6−29.4)	26.9 ± 0.2 (25.7−27.8)	27.1 ± 0.3 (26.3−28.2)	26.6 ± 0.2 (26.1−27.4)	26.4 ± 0.3 (25.6−27.2)
arachidic acid	1.2 ± 0.0 (1.1−1.4)	1.2 ± 0.0 (1.1−1.2)	1.4 ± 0.0 (1.3−1.5)	1.4 ± 0.0 (1.3−1.5)	1.4 ± 0.0 (1.3−1.4)	1.4 ± 0.0 (1.4−1.5)
eicosenoic acid	1.1 ± 0.0 (1.1−1.2)	1.1 ± 0.0 (1.0−1.2)	1.1 ± 0.0 (1.1−1.3)	1.1 ± 0.0 (1.0−1.3)	1.2 ± 0.0 (1.2−1.2)	1.2 ± 0.0 (1.1−1.2)
behenic acid	2.1 ± 0.1 (2.0−2.5)	2.0 ± 0.1 (1.9−2.1)	2.4 ± 0.1 (2.1−2.6)	2.4 ± 0.1 (1.9−2.7)	2.6 ± 0.0 (2.5−2.7)	2.6 ± 0.0 (2.5−2.6)
lignoceric acid	1.0 ± 0.1 (0.9−1.2)	0.9 ± 0.1 (0.9−0.9)	1.2 ± 0.1 (0.9−1.3)	1.1 ± 0.1 (0.8−1.3)	1.3 ± 0.0 (1.2−1.4)	1.3 ± 0.0 (1.2−1.3)
CP	7.7[e] ± 0.1 (7.5−8.0)	8.5 ± 0.1 (8.3−8.9)	5.4 ± 0.4 (4.7−7.0)	6.1 ± 0.7 (5.2−7.9)	6.7 ± 0.2 (6.6−7.0)	7.3 ± 0.5 (6.8−8.3)
ADF	53.6 ± 1.1 (51.7−56.0)	54.0 ± 1.1 (51.5−56.6)	38.3 ± 2.6 (31.3−48.4)	38.5 ± 2.7 (31.3−50.1)	50.2 ± 0.6 (48.4−52.0)	49.2 ± 0.5 (48.4−49.9)
NDF	57.1 ± 1.3 (53.6−60.0)	56.8 ± 1.3 (53.7−59.4)	41.1 ± 2.8 (32.8−52.2)	41.0 ± 3.1 (32.9−53.2)	54.9 ± 0.8 (52.7−57.2)	53.8 ± 0.6 (52.8−54.6)
FPP	63.8[e] ± 1.9 (57.0−68.0)	52.3 ± 1.9 (50.0−55.0)	39.6 ± 5.5 (29.0−56.0)	37.6 ± 2.7 (27.0−43.0)	47.9 ± 1.8 (40.0−56.0)	41.0 ± 6.9 (34.0−46.0)
FPB	43.6 ± 1.2 (40.5−45.4)	46.5 ± 1.2 (43.2−49.0)	41.4 ± 2.3 (36.9−49.5)	41.0 ± 1.9 (33.3−47.0)	47.8 ± 0.8 (44.0−50.2)	47.8 ± 0.8 (44.8−51.6)
ELK	44.0 ± 1.8 (39.0−48.0)	40.3 ± 1.8 (37.0−44.0)	44.6 ± 2.8 (40.0−51.0)	42.4 ± 1.1 (36.0−44.0)	47.0 ± 1.9 (39.0−52.0)	45.6 ± 1.4 (38.0−49.0)
SMK	66.6 ± 1.1 (65.6−67.9)	64.2 ± 1.7 (63.2−65.4)	65.3 ± 1.5 (60.0−69.0)	63.4 ± 1.1 (58.0−67.0)	66.4 ± 1.3 (65.1−68.4)	64.1 ± 0.7 (58.3−67.5)
SS	1.0 ± 0.2 (0.4−1.4)	1.0 ± 0.2 (0.5−1.8)	2.3 ± 0.6 (1.0−5.0)	2.7 ± 0.8 (0.5−6.0)	1.7 ± 0.3 (1.2−2.2)	2.8 ± 0.9 (1.2−4.5)
OK	1.6 ± 0.1 (1.4−1.8)	1.9 ± 0.1 (1.6−2.4)	1.5 ± 0.2 (1.0−2.0)	1.6 ± 0.2 (1.0−3.0)	1.3 ± 0.2 (0.9−1.9)	1.7 ± 0.5 (0.6−2.8)
DK	1.3 ± 0.2 (0.8−1.9)	1.8 ± 0.2 (1.5−2.2)	0.8 ± 0.2 (0.0−1.5)	1.1 ± 0.3 (0.5−2.0)	0.9 ± 0.2 (0.0−2.2)	1.2 ± 0.2 (0.5−2.0)

[a]Refer to the "Abbreviations Used" for a description. [b]Least-squares means of four replicate values. [c]The standard error (SE) of the least-squares mean. [d]Range denotes the lowest and highest values reported by others. [e]Value statistically different from the non-transgenic counterpart ($p \leq 0.05$).

dx.doi.org/10.1021/jf5016297 | J. Agric. Food Chem. 2014, 62, 7877−7885

Table 3. Mineral and Fatty Acid Compositions, Forage Quality, and Grade Characteristics of Blight Blocker Peanut P39 and Its Non-transgenic Counterpart Perry

	2006 field season		2007 field season		2008 field season	
component[a]	P39 mean[b] ± SE[c] (range)[d]	Perry mean ± SE (range)	P39 mean ± SE (range)	Perry mean ± SE (range)	P39 mean ± SE (range)	Perry mean ± SE (range)
calcium	558 ± 46 (446–817)	621 ± 65 (502–760)	526 ± 25 (444–582)	529 ± 56 (425–683)	530 ± 22 (440–581)	536 ± 28 (424–642)
potassium	7404 ± 88 (7159–7936)	7556 ± 124 (7314–7753)	8324 ± 238 (7563–9371)	8598 ± 322 (7970–9482)	8592 ± 114 (7913–8996)	8554 ± 110 (7952–8901)
magnesium	1896 ± 31 (1746–2040)	1793 ± 44 (1757–1819)	1994[e] ± 51 (1873–2240)	1862 ± 39 (1801–1941)	2060 ± 39 (1864–2170)	1993 ± 45 (1770–2097)
phosphorus	3766 ± 100 (3360–4264)	3518 ± 141 (3335–3856)	4308[e] ± 353 (3752–5125)	3891 ± 137 (3636–4395)	4338 ± 85 (3909–4648)	4197 ± 93 (3739–4492)
sulfur	357 ± 8 (324–390)	356 ± 11 (345–367)	383 ± 9 (349–409)	392 ± 16 (351–434)	387 ± 23 (300–499)	403 ± 40 (300–499)
palmitic acid	9.9 ± 0.1 (9.6–10.2)	10.0 ± 0.1 (9.6–10.4)	9.8 ± 0.1 (9.6–10.2)	10.0 ± 0.2 (9.7–10.6)	9.7 ± 0.1 (9.5–9.8)	9.5 ± 0.2 (9.2–9.8)
stearic acid	2.2 ± 0.0 (2.1–2.4)	2.3 ± 0.1 (2.2–2.5)	2.6 ± 0.1 (2.3–2.7)	2.7 ± 0.2 (2.5–2.9)	2.6 ± 0.1 (2.5–2.8)	2.7 ± 0.1 (2.6–2.9)
oleic acid	49.2 ± 0.4 (47.7–51.1)	48.8 ± 0.5 (47.8–49.8)	49.9 ± 0.5 (48.4–52.1)	49.9 ± 0.4 (48.8–51.2)	50.7 ± 0.3 (49.6–51.5)	50.8 ± 0.5 (49.3–52.2)
linoleic acid	32.6 ± 0.4 (31.1–34.1)	32.8 ± 0.5 (31.9–34.0)	31.4 ± 0.5 (29.9–32.8)	31.3 ± 0.3 (30.6–32.3)	30.6 ± 0.3 (30.0–31.5)	30.5 ± 0.3 (29.2–32.0)
arachidic acid	1.1 ± 0.0 (1.1–1.2)	1.1 ± 0.0 (1.1–1.3)	1.2 ± 0.0 (1.1–1.3)	1.2 ± 0.0 (1.2–1.3)	1.2 ± 0.0 (1.2–1.3)	1.2 ± 0.0 (1.3–1.4)
eicosenoic acid	1.3 ± 0.0 (1.2–1.4)	1.2 ± 0.0 (1.2–1.3)	1.1 ± 0.0 (1.1–1.3)	1.1 ± 0.0 (1.0–1.3)	1.2 ± 0.0 (1.1–1.2)	1.2 ± 0.0 (1.1–1.2)
behenic acid	2.4 ± 0.1 (2.2–2.5)	2.4 ± 0.1 (2.1–2.7)	2.4 ± 0.1 (2.0–2.7)	2.4 ± 0.1 (1.9–2.7)	2.6 ± 0.0 (2.5–2.6)	2.6 ± 0.0 (2.5–2.5)
lignoceric acid	1.2 ± 0.0 (1.1–1.4)	1.2 ± 0.0 (1.1–1.4)	1.3 ± 0.1 (1.0–1.5)	1.3 ± 0.1 (0.9–1.4)	1.4 ± 0.0 (1.3–1.4)	1.4 ± 0.0 (1.3–1.5)
CP	7.4 ± 0.2 (6.5–8.3)	7.2 ± 0.3 (6.3–8.1)	5.3 ± 0.2 (4.8–6.3)	5.2 ± 0.2 (4.8–6.1)	7.1 ± 0.1 (6.8–7.5)	7.1 ± 0.1 (6.9–7.3)
ADF	44.5 ± 1.2 (40.0–48.8)	47.7 ± 1.7 (43.6–51.8)	33.1 ± 2.4 (25.3–43.4)	34.2 ± 2.6 (28.2–43.3)	47.2[e] ± 0.6 (45.5–48.8)	45.2 ± 0.8 (42.6–47.9)
NDF	47.5 ± 1.3 (42.7–51.3)	50.6 ± 1.8 (46.1–55.5)	35.6 ± 2.6 (27.2–46.8)	36.7 ± 2.8 (30.2–46.7)	52.1[e] ± 0.7 (49.5–54.5)	49.8 ± 1.2 (47.5–53.1)
FPP	56.8 ± 2.0 (45.0–66.0)	45.8 ± 2.8 (45.0–47.0)	51.3 ± 1.5 (50.0–53.0)	38.0 ± 10.2 (28.0–45.0)	47.1[e] ± 2.4 (43.0–51.0)	36.6 ± 1.5 (30.0–47.0)
FPB	45.9 ± 0.5 (44.6–47.9)	45.0 ± 0.7 (42.9–47.2)	41.1 ± 1.7 (36.7–47.4)	41.4 ± 1.9 (36.1–48.0)	48.4 ± 0.5 (47.3–51.0)	47.3 ± 0.8 (45.4–50.6)
ELK	48.1 ± 0.8 (45.0–52.0)	53.0 ± 1.1 (52.0–54.0)	44.8[e] ± 1.3 (40.0–51.0)	49.1 ± 2.0 (45.0–56.0)	45.4[e] ± 0.9 (42.0–48.0)	48.9 ± 2.1 (44.0–54.0)
SMK	71.9 ± 0.6 (69.5–73.4)	71.1 ± 0.9 (70.0–73.1)	68.3 ± 0.9 (63.0–70.0)	67.5 ± 0.7 (65.0–70.0)	65.1 ± 1.7 (45.9–69.1)	66.1 ± 1.9 (61.9–68.5)
SS	1.3 ± 0.3 (0.3–2.7)	1.9 ± 0.4 (1.2–3.1)	3.3 ± 0.7 (1.0–8.0)	2.4 ± 0.7 (1.0–5.0)	2.6 ± 0.4 (1.2–3.8)	2.6 ± 0.4 (1.3–4.8)
OK	1.5 ± 0.1 (1.0–1.8)	1.1 ± 0.2 (0.5–0.7)	1.2 ± 0.2 (0.0–2.0)	1.7 ± 0.4 (0.7–2.0)	1.3 ± 0.1 (0.8–1.7)	1.6 ± 0.1 (1.1–2.0)
DK	0.0 ± 0.0 (0.0–0.2)	0.0 ± 0.0 (0.0–0.1)	0.7 ± 0.3 (0.0–1.0)	1.0 ± 0.4 (0.0–4.0)	1.0 ± 0.3 (0.0–2.2)	1.0 ± 0.3 (0.3–2.3)

[a]Refer to the "Abbreviations Used" for a description. [b]Least-squares means of four replicate values. [c]The standard error (SE) of the least-squares mean. [d]Range denotes the lowest and highest values reported by others. [e]Value statistically different from the non-transgenic counterpart ($p \leq 0.05$).

dx.doi.org/10.1021/jf5016297 | J. Agric. Food Chem. 2014, 62, 7877–7885

Valley, MN). The oven temperature was initially set at 150 °C and held for 1 min, then increased at 10 °C/min to 175 °C, held for 10 min, then increased at 10 °C/min to 220 °C, and held for 8 min. The inlet and detector temperatures were 225 and 275 °C, respectively; the split ratio was 80:1; and a 1 μL injection volume was used. The hydrogen carrier gas flow rate was 1.9 mL/min. Hydrogen flow to the detector was 30 mL/min; airflow was 400 mL/min; and the flow of nitrogen makeup gas was 40 mL/min. Fatty acid peaks were identified using pure methyl ester standards (Nu-Check Prep, Inc., Elysian, MN). Methyl tricosanate (23:0) was used as an internal standard for quantification. The LOQ for all fatty acid components was 0.2 mg/g of fw. Data were integrated and quantified using a Chem DataStation (Agilent Technologies, Palo Alto, CA). All sample values were converted to percent total seed oil content. The iodine value, oleic/linoleic (O/L) ratio, percentage of total saturated, percentage of total long-chain saturated acids, and polyunsaturated/saturated (P/S) ratio were calculated using the following formulas:

$$\text{iodine value} = (\%\,\text{oleic})(0.8601) + (\%\,\text{linoleic})(1.7321) + (\%\,\text{eicosenoic})(0.7854)$$

$$\text{oleic/linoleic (O/L) ratio} = \%\,\text{oleic}/\%\,\text{linoleic}$$

$$\%\,\text{total saturated} = \%\,\text{palmitic} + \%\,\text{stearic} + \%\,\text{arachidic} + \%\,\text{benehic} + \%\,\text{lignoceric}$$

$$\text{polyunsaturated/saturated (P/S) ratio} = \%\,\text{polyunsaturated (linoleic)}/\%\,\text{total saturated}$$

$$\%\,\text{total long-chain saturated} = \%\,\text{arachidic} + \%\,\text{benehic} + \%\,\text{lignoceric}$$

Forage and Fiber Analysis. Hay samples were prepared according to AOAC method 922.02.[24] Peanut vines were chopped into 1.5 cm pieces and ground in a Wiley mill to pass 4−6 mm sieve, and ground powder samples were thoroughly mixed and kept in an airtight container until analysis. Dry matter was estimated by oven drying for 2 h at 135 °C according to AOAC method 930.15.[25] Crude protein (CP) and acid detergent fiber (ADF) were determined according to AOAC method 989.03 using a near-infrared reflectance spectroscope.[26] Neutral detergent fiber (NDF) was estimated by boiling the sample with neutral detergent solution, adding α-amylase, rinsing with acetone, and determining the percent ADF gravimetrically.[27] The LOQ for CP, ADF, and NDF was 0.1% fw.

Statistical Analysis. SAS software (SAS 9.2, SAS Institute, Inc., Cary, NC) was used to perform all statistical analyses. Percentage data were normalized by arcsine transformation. Data points that are outside of the ±5 studentized PRESS residual range (Proc GLM) were considered as outliers. No data point in this study was identified as an outlier. Standard error (SE) of the sample mean was computed by dividing the standard deviation by the square root of the number of sample values. A total of 21 different components were subjected to analysis of variation (ANOVA) to determine differences at $p \leq 0.05$ between three transgenic lines and their non-transgenic cultivars. Equivalence for a component investigated whether the differences in transgenic lines surpass the normal range of non-transgenic cultivars.[11,28] Equivalence was evaluated as follows: (1) equivalence was assumed if no significant difference was detected between transgenic lines and their corresponding non-transgenic cultivars; (2) if a significant difference was noted, then the range of the test values was compared to the range of test values compiled from the literature. Equivalence was assumed if the test values fell inside the reported range for non-transformed cultivars.[12,28]

The method as described above to infer equivalence from the absence of a significant difference had uncontrolled increased risks of false positive conclusion that is the assumption of non-equivalence.[12] Multivariate analysis, such as canonical discriminant analysis, can alleviate this problem and has proven to be a very powerful tool for assessing the relative pattern of the objects that have very similar properties.[13,29,30] The canonical discriminant analysis was a dimension-reduction technique that combined principal component analysis and canonical correlation.[31] Principal component analysis produced linear combinations of the original variables that were responsible for the highest variation. Canonical correlation generated canonical discriminant functions that contained the highest multiple correlations with each group and best summarized variation between population groups. These canonical functions were orthogonal to each other, even though the original variables were highly correlated.[32] These canonical discriminant functions differentiate groups by simultaneously considering the interrelationships of all variables in the data set and the dependent variables (peanut lines). The pooled within canonical structure and pooled within class standardized canonical coefficients were used to estimate the relative contributions of each variable to the canonical discriminant functions. Mahalanobis distance (D^2) is the difference between centroid values (the mean value of the canonical discriminant function) of groups and has the power of justifying any correlations that might exist between original variables. Therefore, it is a quantitative measure of the distance between groups. Mahalanobis distance (D^2) is calculated as

$$D^2 = (\bar{X}_1 - \bar{X}_2)' S^{-1} (\bar{X}_1 - \bar{X}_2)$$

where $\bar{X}_1$ and $\bar{X}_2$ are the estimated mean vectors in given groups and S^{-1} is the inverse of the pooled sample variance and covariance matrix.

RESULTS AND DISCUSSION

Mineral and Fatty Acid Compositions of Peanut Seeds. No significant differences in five major mineral elements were observed across all 3 years between transgenic line N70 and the non-transgenic parent NC 7 (Table 1), indicating that they had a very similar mineral composition. For transgenic line W73 and non-transgenic parent Wilson, statistical differences were observed only in sulfur in 2007 and in phosphorus in 2006 and 2008 (Table 2). Transgenic line P39 had slightly higher magnesium and phosphorus contents than those of the non-transgenic parent Perry in 2007 (Table 3). However, magnesium and phosphorus levels in P39 were similar to those of their corresponding non-transgenic parent cultivars in other years, suggesting that the elevated and/or reduced values in a field season were likely caused by the environmental variations among three growing seasons. Moreover, the values were always within the reported ranges of conventional peanut cultivars[7,33] and were not sufficient to cause any nutritional or health concerns.

The fatty acid composition of transgenic lines was similar to that of their non-transgenic counterparts. For example, oleic (47.7−59.3%) and linoleic (22.8−34.1%) acids are two major components of fatty acid in peanuts, and there were no statistical differences in oleic and linoleic acids between each of the three transgenic lines and their non-transgenic parents across all three field seasons (Tables 1−3). Furthermore, transgenic lines W73 and P39 showed no statistical differences in all eight fatty acid components tested from those of their corresponding parents (Tables 2 and 3). Although N70 had slightly higher palmitic acid or lower stearic acid than that of non-transgenic parent NC 7 in 2006 and 2008 (Table 1), the differences were marginally small and the measured values were in agreement with previously reported ranges of conventional peanut cultivars.[7,33,34]

Grade Characteristics and Peanut Hay Constituents. The grade characteristics and peanut hay constituents of transgenic lines were similar to those of their corresponding non-transgenic counterparts (Tables 1−3). In comparison to non-transgenic cultivar NC 7, N70 had a slightly higher

percentage of extra-large kernels in 2007 but a lower percentage of fancy pods in 2007 and 2008 (Table 1). The statistical difference between W73 and its non-transgenic parent Wilson was observed only in the percentage of fancy pods and crude proteins in 2006 (Table 2). P39 had a slightly higher percentage of ADF and fancy pods but a lower percentage of extra-large kernels than its non-transgenic parent Perry in 2008 (Table 3). These minor differences mostly occurred in only one field season and were unlikely to be biologically meaningful.

Canonical Discriminant Analysis. Results from canonical discriminant analysis clearly demonstrated that transgenic lines N70, W73, and P39 were substantially equivalent to their non-transgenic parents NC 7, Wilson, and Perry, respectively (Figure 1). A total of five canonical discriminant functions were generated to discriminate six peanut lines. Each canonical discriminant function was an optimal linear combination of trait variables and was uncorrelated to the others. The variance associated with the first three canonical discriminant functions accounted for 98% of the total variance among six peanut lines (Table 4). Canonical correlation measures the strength of relationships between canonical discriminant function and peanut lines. The significant ($p < 0.0001$) correlation between peanut lines and the first three canonical discriminant functions (r_c = 0.997, 0.946, and 0.748, respectively) indicated that these three canonical functions can explain the differentiation of peanut lines. Despite the fact that the first three canonical discriminant functions had the highest power to separate six peanut lines, transgenic lines N70, W73, and P39 cannot be separated out from their non-transgenic parent cultivars (Figures 1 and 2). Transgenic lines derived from the same parent were grouped together with the parent cultivar and distinctly separated from other cultivars and their transgenic derivatives.

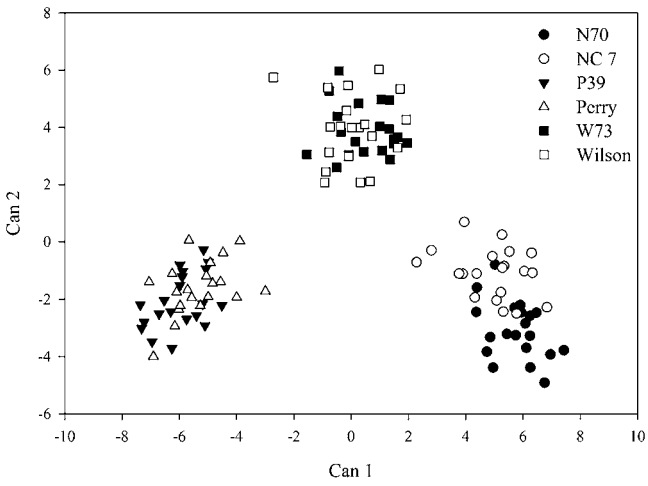

Figure 1. Scatterplot of three transgenic lines and non-transgenic parents by the score of the first two canonical discriminant functions.

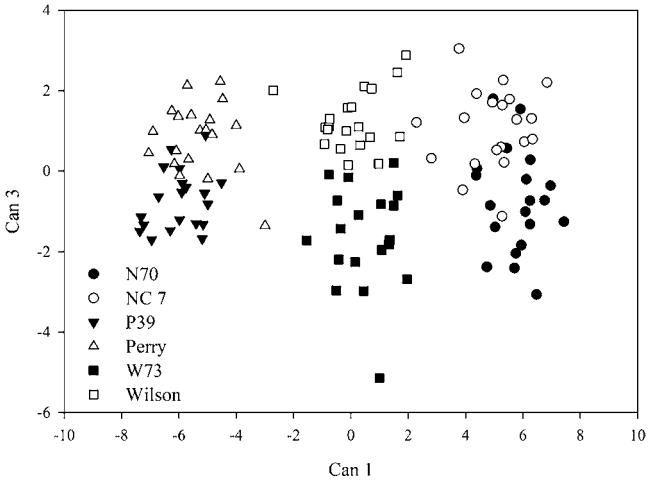

Figure 2. Scatterplot of three transgenic lines and non-transgenic parents by the score of the first and third canonical discriminant functions.

Canonical structures measure correlations between canonical variables and the original variables. These can be interpreted as the relative contribution of each variable to each canonical function.[32] The first canonical discriminant function had the highest correlations with the O/L ratio (0.5717), followed by the P/S ratio (−0.5384), percentage of sound splits (0.2140), percentage of fancy pods (0.1832), and percentage of extra-large kernels (0.1371) (Table 5). The second function was dominated by a large loading from the percentage of total saturated (−0.3766), followed by the percentage of extra-large kernels (−0.2787), calcium (0.1498), percentage of sound mature kernels (−0.1429), and magnesium (0.1119). The third function was most highly correlated with magnesium (−0.3872) and phosphorus (−0.2928). These functions indicated that six peanut lines differ mostly in variables of the O/L ratio, polyunsaturated/total saturated ratio, percentage of total saturated, percentage of fancy pods, percentage of extra-large kernels, percentage of sound mature kernels, and elements of calcium, magnesium, and phosphorus.

Results from canonical discriminant analysis presented a composite picture of how six peanut lines were related to each other in a multi-dimensional space by separating the among-population effect from the within-population variation caused by the environment. Mahalanobis distance (D^2) from the

Table 4. Canonical Discriminant Analysis with CANDISC Procedure

canonical variable[a]	canonical correlation[b]	proportion[c]	cumulative proportion[d]	likelihood ratio[e]	F value	Pr > F
1	0.9974	0.6745	0.6745	0.0012	13.86	<0.0001
2	0.9455	0.2657	0.9401	0.0272	7.50	<0.0001
3	0.7478	0.0399	0.9801	0.2563	3.11	<0.0001
4	0.5495	0.0136	0.9937	0.5815	1.80	0.0074
5	0.4086	0.0063	1.0000	0.8330	1.24	0.2521

[a]Canonical variable represents a linear combination of the subset of original variables in the data set. [b]Canonical correlation measures the strength of correlation between the canonical variable and original variables in the data set. [c]Proportion means that percentage of the total variations in the data set can be explained by that canonical variable. [d]Cumulative proportion is the sum of proportions for previous canonical variables. [e]Likelihood ratio is the ratio testing the hypothesis that the given canonical correlation and all smaller canonical correlations are equal to zero in the population.

Table 5. Canonical Structure and the Standardized Coefficients of the First Three Canonical Discriminant Functions

	pooled within canonical structure			pooled within-class standardized coefficients		
component[a]	can1	can2	can3	can1	can2	can3
calcium	−0.0049	0.1498	−0.0835	0.3419	0.4842	0.3468
potassium	0.0188	0.1028	0.0133	0.0597	1.3691	1.4296
magnesium	−0.0340	0.1119	−0.3872	0.3549	−0.0663	−0.4719
phosphorus	−0.0318	0.0368	−0.2928	−0.4483	−0.8838	−1.5439
sulfur	0.0989	0.0448	0.0458	0.2455	−0.0390	0.1732
OLR	0.5717	0.0925	0.0143	1.0243	−3.1351	0.4815
IV	−0.0200	0.0144	−0.0009	1.2558	−0.1898	−0.6185
TS	0.0115	−0.3766	0.0887	0.3917	−3.0573	0.3979
PSR	−0.5384	0.0659	−0.0486	−0.7930	−3.4657	0.7667
TLCS	−0.0412	−0.0472	−0.0798	−0.0680	0.5949	0.0826
NDF	0.0108	0.0831	−0.0426	−1.8490	−7.0292	−2.4706
ADF	0.0070	0.0944	−0.0381	1.5468	7.5886	1.9125
CP	0.0493	0.0008	0.1301	−0.3538	−0.3832	1.2006
FPB	−0.0725	0.0708	0.0216	0.0154	−0.0479	0.1509
FPP	0.1832	−0.0339	−0.0422	0.1041	0.1058	−0.1532
ELK	0.1371	−0.2787	0.0807	−0.0519	−0.3734	0.0998
SMK	−0.0083	−0.1429	−0.1238	0.0940	−0.0235	−0.1595
SS	−0.214	−0.0210	0.1269	−0.1749	0.0682	0.6495

[a]Refer to the "Abbreviations Used" for a description.

canonical discriminant analysis measured similarity or genetic distance that indicates the extent of separation among peanut lines. The distance D^2 between each pair of transgenic line and its non-transgenic parent was several-fold smaller than the distances of other pairwise combinations, indicating the similarity between transgenic lines and their corresponding parent. For example, the distance D^2 from N70 to its non-transgenic parent NC 7 was 9.9, and the distances D^2 from N70 to Wilson, W73, Perry, and P39 were 86.5, 78.0, 129.3 and 140.7, respectively. Similarly, the distance D^2 from W73 to non-transgenic parent Wilson was 10.3, and the distances D^2 from W73 to NC 7, Perry, and P39 were 51.9, 72.6, and 80.4, respectively. Finally, the distance D^2 from P39 to non-transgenic parent Perry was 6.9, and the distances D^2 from P39 to NC 7 and Wilson were 124.4 and 76.8, respectively.

This research has provided strong evidence that insertion and expression of an oxalate oxidase gene in peanut did not cause substantial changes in grade characteristics nor mineral and fatty acid contents of kernels or constituents in peanut hay. Statistically significant differences ($p < 0.05$) were rarely observed in comparisons of a transgenic line to its corresponding non-transformed parent cultivar in a growing season (Tables 1−3). However, for the comparisons observed to be significantly different between transgenic lines and their non-transformed counterparts, the variations were usually small and within the range of natural variability of conventional-bred peanut cultivars.[7,33] Significant differences in growing conditions among three field seasons were likely responsible for the observed compositional variations. In addition, compositional differences among the non-transgenic lines in the study were much greater than the differences seen between each transgenic and paired non-transgenic counterpart. More importantly, such small compositional variations did not diminish the nutritional value of peanut kernels and hay. Additional results from canonical discriminant analysis also demonstrated the compositional similarity between transgenic crops and their corresponding non-transformed parent cultivars.

In conclusion, this study provided multiple-year data on chemical composition and grade characteristics in different climates and agronomic conditions. No biologically meaningful unintended compositional or quality effects were found between the transgenic lines and their paired non-transgenic counterparts, and the composition of transgenic lines was within the known range of the non-transgenic peanut. Results clearly indicated that insertion and expression of an oxalate oxidase gene in peanut did not cause substantial unintended changes in chemical composition in seeds or hay constituents. Therefore, this study provides strong evidence for concluding substantial equivalence in quality and compositional traits among transgenic lines expressing oxalate oxidase and their non-transformed parent cultivars.

AUTHOR INFORMATION

Corresponding Author

*Telephone: 540-231-7876. E-mail: egrabau@vt.edu.

Funding

Funding was provided by the National Peanut Board, Virginia Peanut Growers' Association, Virginia Agricultural Council, and USDA, Southern Region IPM Program.

Notes

The authors declare no competing financial interest.

ACKNOWLEDGMENTS

The authors thank Dr. Ben Corl for fatty acid and mineral analyses of peanut kernels, Dr. Chris Teutsch for analysis of constituents in peanut hay, and B. Keeling, S. Byrum, E. Hobbs, and J. Hampton for technical assistance in the laboratory and field.

ABBREVIATIONS USED

OLR, O/L ratio; IV, iodine value; TS, percentage of total saturated; PSR, ratio of polyunsaturated/total saturated; TLCS, percentage of total long-chain saturated; NDF, percentage of neutral detergent fiber; ADF, percentage of acid detergent fiber; CP, percentage of crude protein; FPP, percentage of fancy pods; FPB, fancy pod brightness; ELK, percentage of extra-large kernels; SMK, percentage of sound mature kernels; SS,

percentage of sound splits; OK, percentage of other kernels; DK, percentage of damaged kernels; can1, first canonical function; can2, second canonical function; can3, third canonical function

REFERENCES

(1) Beute, M. K.; Porter, D. M.; Hadley, B. A. Sclerotinia blight of peanut in North Carolina and Virginia and its chemical control. *Plant Dis. Rep.* **1975**, *59*, 697−701.

(2) Wadsworth, D. F. Sclerotinia blight of peanut in Oklahoma and occurrence of the sexual stage of the pathogen. *Peanut Sci.* **1979**, *6*, 77−79.

(3) Phipps, P. M. An assessment of environmental conditions preceding outbreaks of Sclerotinia blight on peanut in Virginia. *Peanut Sci.* **1995**, *22*, 90−93.

(4) Smith, F. D.; Phipps, P. M.; Stipes, R. J. Fluazinam: A new fungicide for control of Sclerotinia blight and other soilborne pathogens of peanut. *Peanut Sci.* **1992**, *19*, 115−120.

(5) Partridge-Telenko, D.; Hu, J.; Livingstone, D.; Shew, B.; Phipps, P. M.; Grabau, E. Sclerotinia blight resistance in Virginia-type peanut transformed with a barley oxalate oxidase gene. *Phytopathology* **2011**, *101*, 786−793.

(6) Chenault, K. D.; Burns, J. A.; Melouk, H. A.; Payton, M. E. Hydrolase activity in transgenic peanut. *Peanut Sci.* **2002**, *29*, 89−95.

(7) Jonnala, R.; Dunford, N.; Dashiell, K. New high oleic peanut cultivars grown in the southwestern US. *J. Am. Oil Chem. Soc.* **2005**, *85*, 125−128.

(8) Livingstone, D. M.; Hampton, J. L.; Phipps, P. M.; Grabau, E. A. Enhancing resistance to *Sclerotinia minor* in peanut by expressing a barley oxalate oxidase gene. *Plant Physiol.* **2005**, *137*, 1354−1362.

(9) Hollowell, J. E.; Shew, B. B. Oxalic acid production by nine isolates of *Sclerotinia minor*. *Proc. Am. Peanut Res. Ed. Soc.* **2001**, *33*, 24.

(10) Zhou, F.; Zhang, Z.; Gregersen, P. L.; Mikkelsen, J. D.; Neergaard, E. D.; Collinge, D. B.; Thordal-Christensen, H. Molecular characterization of the oxalate oxidase involved in the response of barley to the powdery mildew fungus. *Plant Physiol.* **1998**, *117*, 33−41.

(11) van der Voet, H.; Perry, J.; Amzal, B.; Paoletti, C. A statistical assessment of differences and equivalences between genetically modified and reference plant varieties. *BMC Biotechnol.* **2011**, *11*, 15 DOI: 10.1186/1472-6750-11-15.

(12) Oberdoerfer, R. B.; Shillito, R. D.; De Beuckeleer, M.; Mitten, D. H. Rice (*Oryza sativa* L.) containing the bar gene is compositionally equivalent to the non-transgenic counterpart. *J. Agric. Food Chem.* **2005**, *53*, 1457−1465.

(13) Garcia-Ruiz, C.; Garcia, C.; Cifuentes, A.; Marina, L. Characterization and differentiation of diverse transgenic and non-transgenic soybean varieties from CE protein profiles. *Electrophoresis* **2007**, *28*, 2314−2323.

(14) Hamilton, K. A.; Pyla, P. D.; Breeze, M.; Olson, T.; Li, M.; Robinson, E.; Gallagher, S. P.; Sorbet, R.; Chen, Y. Bollgard II cotton: Compositional analysis and feeding studies of cottonseed from insect-protected cotton (*Gossypium hirsutum* L.) producing the Cry1Ac and Cr2Ab2 proteins. *J. Agric. Food Chem.* **2004**, *52*, 6969−6976.

(15) Catchpole, G. S.; Beckmann, M.; Enot, D. P.; Mondhe, M.; Zywicki, B.; Taylor, J.; Hardy, N.; Smith, A.; King, R. D.; Kell, D. B.; Fiehn, O.; Draper, J. Hierarchical metabolomics demonstrates substantial compositional similarity between genetically modified and conventional potato crops. *Proc. Natl. Acad. Sci. U.S.A.* **2005**, *102*, 14458−14462.

(16) Obert, J. C.; Ridley, W. P.; Schneider, R. W.; Riordan, S. G.; Nemeth, M. A.; Trujillo, W. A. The composition of grain and forage from glyphosate tolerant wheat MON71800 is equivalent to that of conventional wheat (*Triticum aestivum* L.). *J. Agric. Food Chem.* **2004**, *52*, 1375−1384.

(17) Herman, R. A.; Phillips, A. M.; Collins, R. A.; Taglani, L. A.; Claussen, F. A.; Graham, C. D.; Bickers, B. L.; Harris, T. A.; Prochaska, L. M. Compositional equivalence of Cry1F corn event TC6275 and conventional corn (*Zea mays* L.). *J. Agric. Food Chem.* **2004**, *52*, 2726−2734.

(18) United States Department of Agriculture (USDA). *Minimum Quality and Handling Standards for Domestic and Imported Peanuts Marketed in the United States (67e-CFR 57140)*; USDA: Washington, D.C., 2008; Code of Federal Regulations 7 CFR Part 996.

(19) United States Environmental Protection Agency (U.S. EPA). *Federal Insecticide, Fungicide and Rodenticide Act: Good Laboratory Practice Standards*; U.S. EPA: Washington, D.C., 1999; Code of Federal Regulations 40 CFR Part 160.

(20) AOAC International. AOAC method 985.01—Metals and other elements in plants and pet foods. In *Official Methods of Analysis*; Horwitz, W., Ed.; AOAC International: Gaithersburg, MD, 2000.

(21) Bligh, E. G.; Dyer, W. J. A rapid method of total lipid extraction and purification. *Can. J. Biochem. Physiol.* **1959**, *37*, 911−917.

(22) AOAC International. AOAC method 922.06—Fat in flour. In *Official Methods of Analysis*; Horwitz, W., Ed.; AOAC International: Gaithersburg, MD, 2000.

(23) American Oil Chemists' Society (AOCS). Official method Ce 2-66, preparations of methyl esters of fatty acids. In *Official Methods and Recommended Practices*; AOCS: Champaign, IL, 1997.

(24) AOAC International. AOAC method 922.02—Preparation of sample. In *Official Methods of Analysis*; Horwitz, W., Ed.; AOAC International: Gaithersburg, MD, 2000.

(25) AOAC International. AOAC method 930.15—Moisture in animal feed. In *Official Methods of Analysis*; Horwitz, W., Ed.; AOAC International: Gaithersburg, MD, 2000.

(26) Goering, H. K.; Van Soest, P. J. Forage and fiber analyses. *Agriculture Handbook No. 379*; Agricultural Research Service (ARS), United States Department of Agriculture (USDA): Washington, D.C., 1970.

(27) AOAC International. AOAC method 989.03—Fiber (acid detergent) and protein (crude) in animal feed and forages: Near-infrared reflectance spectroscopic method. In *Official Methods of Analysis*; Horwitz, W., Ed.; AOAC International: Gaithersburg, MD, 2000.

(28) McCann, M. C.; Rogan, G. J.; Fitzpatrick, S.; Trujillo, W. A.; Sorbet, R.; Hartnell, G. F.; Riodan, S. G.; Nemeth, M. A. Glyphosate-tolerant alfalfa is compositionally equivalent to conventional alfalfa (*Medicago sativa* L.). *J. Agric. Food Chem.* **2006**, *54*, 7187−7192.

(29) Jiao, Z.; Si, X.; Li, G.; Zhang, Z.; Xu, X. Unintended compositional changes in transgenic rice seeds (*Oryza sativa* L.) studied by spectral and chromatographic analysis coupled with chemometrics methods. *J. Agric. Food Chem.* **2010**, *58*, 1746−1754.

(30) Le Gall, G.; Colquhoun, I.; Davis, A.; Collins, G.; Verhoeyen, M. Metabolite profiling of tomato (*Lycopersicon esculentum*) using ^{1}H NMR spectroscopy as a tool to detect potential unintended effects following a genetic modification. *J. Agric. Food Chem.* **2003**, *51*, 2447−2456.

(31) Barcikowski, R.; Stevens, J. P. A Monte Carlo study of the stability of canonical correlations, canonical weights, and canonical variate-variable correlations. *Multivar. Behav. Res.* **1975**, *10*, 353−364.

(32) Cruz-Castillo, J. G.; Ganeshanandam, S.; MacKay, B. R.; Lawes, G. S.; Lawoko, C. R. O.; Woolley, D. J. Applications of canonical discriminant analysis in horticultural research. *HortScience* **1994**, *29*, 1115−1119.

(33) Derise, N. L.; Lau, H. A.; Ritchie, S. J.; Murphy, E. W. Yield, proximate composition and mineral element content of three cultivars of raw and roasted peanuts. *J. Food Sci.* **1974**, *39*, 264−266.

(34) Rodrigues, A. C.; Ströher, G. L.; Freitas, A. R.; Visentainer, J. V.; Oliveira, C. C.; de Souza, N. E. The effect of genotype and roasting on the fatty acid composition of peanuts. *Food Res. Int.* **2011**, *44*, 187−192.

susceptible to Maillard induced chemical changes, proteolytic and other non-Maillard chemical changes were observed during storage compared to corresponding changes in conventional UHT milk.

MATERIAL AND METHODS

Chemical References. Decane (99%), tetradecane (99%), dodecane (99%), 2-methylbutanal (95%), hexanal (98%), heptanal (95%), octanal (99%), furfural (98%), nonanal (95%), decanal (98%), 2-butanone (99%), 2-pentanone (99%), 2-hexanone (99.5%), 2-heptanone (98%), 2-octanone (98%), 2-nonanone (99%), 6-methyl-5-heptene-2-one (99%), 6,10-dimethyl-5,4-undecadien-2-one (97%), 2-undecanone (99%), dimethyl disulfide (98%), dimethyl trisulfide (98%) 4-methyl-1-pentanol (97%), toluene (99.5%), styrene (99%). 2-methylfuran (98%), 2-ethylfuran (99%), 2-pentylfuran (97%), fluorescamine (4-phenylspiro[furan-2(3*H*),19-phthalan]-3,39-dione) (99%), and D_2O containing 0.025% sodium trimethylsilyl-[2,2,3,3-$^2H_4$]-1-propionate were obtained from Sigma-Aldrich Inc. (Steinheim, Germany). Trichloroacetic acid, HCl, and water-free acetone were from Merck (Darmstadt, Germany).

Milk Samples. Milk for the study was produced at a commercial Danish dairy plant (Arla Foods, Esbjerg, Denmark) (Figure 1). Three types of milk (conventional indirect UHT (CONVI), lactose-hydrolyzed direct UHT (LHD), and lactose-hydrolyzed indirect UHT (LHI)) were produced (Table 1). The milk was UHT-treated using either direct heat treatment (LHD) (steam is injected into the milk to heat it followed by flash cooling[12]) (140−145 °C for 2−3 s) or indirect heat treatment (CONVI, LHI) (a tubular heat exchanger is used to heat the milk, followed by slow cooling[12]) (140−145 °C for 2−3 s) and packaged aseptically in 1 L Tetra Brik cartons. Lactose in the lactose-hydrolyzed milk (LHD, LHI) was removed (approximately 40% of initial lactose content) before heat treatment using ultra- and nanofiltration. The remaining lactose was enzymatically hydrolyzed (LHD, LHI), after heat treatment, by the addition of lactase (Maxilact LAG 5000, DSM, Limburg, The Netherlands).

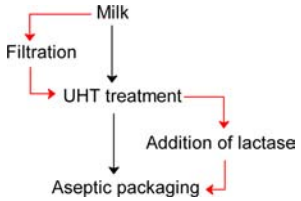

Figure 1. Flowchart of production of lactose-hydrolyzed UHT milk (red) and conventional UHT milk (black).

After transportation to the laboratory, the milk samples were stored in an air-conditioned room at a constant temperature of 22 °C. At days 7, 14, 21, 28, 45, 60, 90, 120, 150, 180, 210, 240, and 270 after production, two milk cartons were picked and frozen and stored at −20 °C until analysis. Milk for the NMR spectroscopy analysis and fluorescamine determination was filtered using Amicon Ultra 0.5 mL 10 kDa (Millipore, Bedford, MA, USA) spin filters at 10000*g* for 15 min to remove residual lipids and protein prior to freezing. After frozen storage, the milk samples and filtrates were randomized and thawed in 4 °C before final analyses.

Determination of Volatile Compounds by Dynamic Headspace Sampling and GC-MS. The volatile compounds were extracted using dynamic headspace sampling and analyzed by gas chromatography−mass spectrometry (GC-MS) according to the procedure described by Jansson et al.[13] The volatile compounds were isolated on adsorbent traps (Tenax TA, 200 g Tenax TA, 35/60 mesh (Markes International Limited, LIantrisant, UK)) and desorbed (250 °C, 15 min) into a cold trap (U-TIIGCP, Markes International Limited) using a thermal desorption system (ultra-UNITY, Markes International Limited) and subsequently injected onto a gas chromatograph (Finnigan trace GC ultra, Thermo, Waltham, MA, USA) using a CP-Wax 52CB column (50 m × 0.25 mm, film thickness = 0.25 μm (Varian, Palo Alto, CA, USA)).

To identify the separated volatile compounds, a single-quadrupole mass spectrometer (Finnigan Trace dual-stage quadrupole (DSQ), Thermo) was used. The mass spectrometer scanned over a mass to charge (m/z) of 45−350 (1.61 scans/s) in TIC mode, and specific m/z values were detected in SIM mode (Table 2). The volatile compounds were identified using an MS database (NIST MS search 2.0, 2011) and verified by comparison of mass spectral data and retention times with those of authentic reference compounds.

Table 2. Overview of Retention Time (t_R), Identified and Verified Volatile Compounds, and m/z Ions Scanned with GC-MS SIM Mode

t_R (min)	volatile compound	m/z
4.84	3,3-dimethylhexane	
6.18	2-methylfuran	82
6.87	2-butanone	
7.05	2-methylbutanal	86
8.22	2-ethylfuran	81
9.20	2-pentanone	
10.12	decane	
12.14	toluene	
14.48	dimethyl disulfide	
15.47	2-hexanone	
15.50	hexanal	82
27.37	2-heptanone	
27.38	heptanal	70
30.48	dodecane	
32.69	2-pentylfuran	95
34.84	styrene	
36.75	2-octanone	
36.94	octanal	
39.07	6-methyl-5-heptene-2-one	
40.12	dimethyl trisulfide	
40.75	2-nonanone	
40.95	nonanal	
41.14	tetradecane	
42.91	furfural	
43.42	decanal	
45.25	2-undecanone	170
48.90	6,10-dimethyl-5-undecadien-2-one	

Table 1. Overview of Milk Types Included in the Study, Heat Treatments, and Lactose Levels[a]

	milk	enzymatic hydrolysis	heat treatment	filtration	level of lactose (% of original level)	amount of lactose (% w/w)
CONVI	conventional UHT	−	indirect	−	100	5
LHD	lactose-hydrolyzed direct UHT	+	direct	+	<1	0.01
LHI	lactose-hydrolyzed indirect UHT	+	indirect	+	<1	0.01

[a]All milks contained 1.5% w/w fat and 3.5% w/w protein.

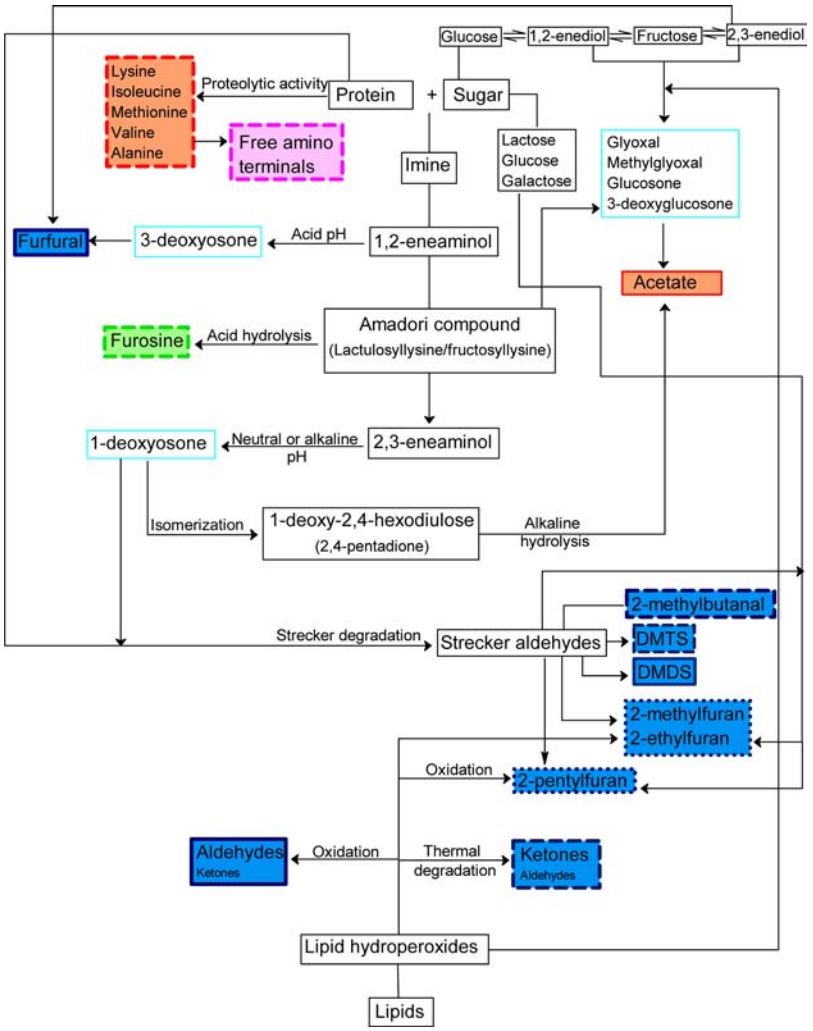

Figure 2. Overview of compounds identified in the milk originating from the Maillard reaction, lipid oxidation, and proteolytic activity analyzed with GC-MS (blue rectangles), NMR (orange rectangles), HPLC (green rectangles), and fluorescamine assay (pink rectangle). A dashed outline indicates increase of compounds in lactose-hydrolyzed UHT milk, a dotted outline indicates increase of compounds in conventional UHT milk, a solid outline indicates no difference between lactose-hydrolyzed and conventional UHT milk during storage.

A total of 15 identified volatile compounds were quantified using external standard curves prepared in duplicates in UHT milk. For each standard curve, the regression equation, limit of detection (LOD), and limit of quantification (LOQ) were calculated from the standard error of the *y*-intercept and the slope of the linear regression (Table 2).[14,15]

Determination of Furosine by RP-HPLC. Furosine formation was determined in milk after acid hydrolysis by RP-HPLC as described previously in ISO 18329:2004 (IDF 193:2004)[16] with some modifications. One milliliter of milk was mixed with 3 mL of 10 M HCl in screw-cap tubes, and nitrogen was bubbled through the samples for 2 min. The tubes were closed and heated at 110−115 °C for 18 h. After heating, the samples were cooled and filtered through a filter paper (Black Ribbon 589/1, Schleicher & Schuell MicroScience GmbH, Dassel, Germany), and 2 mL of filtrate was filtered through a 0.45 μM disposable filter, diluted 5 times in 3 M HCl, and transferred into HPLC vials. Furosine detection was performed on a Dionex 300DX system (Dionex, Germering, Germany) with a DAD detector and using a Supelco Supercosil LC-8 column (Sigma-Aldrich Inc.) with isocratic elution with 0.06 M sodium acetate buffer at a flow rate of 1 mL/min. The injection volume was 10 μL, and the DAD detection (UV) was at 280 nm.

Determination of Free Amino Acids Using ^{1}H NMR Spectroscopy. Determination of free amino acids was performed using ^{1}H NMR spectroscopy analysis according to a method adapted from Sundekilde er al.[17] The milk filtrates were thawed, and 400 μL was mixed with 200 μL of D_2O containing 0.025% sodium trimethylsilyl-[2,2,3,3-$^2H_4$]-1-propionate (TSP) as internal chemical shift reference. A Bruker Avance III 600 spectrometer (Bruker Biospin, Rheinstetten, Germany) equipped with a 5 mm TXI probe was used for the analyses. The sample sequence was randomized prior to acquisition. Standard one-dimensional spectra were acquired using a single 90° pulse experiment with a relaxation delay of 5 s. Water suppression was achieved by irradiating the water peak during the relaxation delay, and a total of 64 scans were collected into 32K data points scanning a spectral width of 12.15 ppm. All ^{1}H spectra were initially referenced to the TSP signal at 0 ppm. Prior to Fourier transformation the data were multiplied by a 0.3 Hz line-broadening function. The proton NMR spectra were phase and baseline corrected manually using Topspin 3.2 (Bruker Biospin). Amino acid concentrations were calculated for valine, methionine, isoleucine, alanine, and acetate using Chenomx software (Chenomx NMR suite 7.7, Edmonton, Canada).

Determination of Free Amino Terminals by Fluorescamine Assay. The level of free amino terminals in the milk was determined according to the method of Dalsgaard et al.[18] An amount of 75 μL of milk was mixed with 75 μL of 24% trichloroacetic acid (24 g TCA/100 mL water) and placed on ice for 30 min to accelerate protein precipitation. The precipitated mixture was centrifuged (17049*g* for 20 min). A total of 37.5 μL of supernatant was then added to 1130 μL of 0.1 M borate buffer and 375 μL of fluorescamine solution (0.2 mg/mL fluorescamine in water free acetone), and 250 μL was then transferred

to each well in a microtiter plate. The analysis was carried out, 18 min after the addition of the fluorescamine, on a Synergy 2 Multi-Mode microplate reader (Holm & Halby, Brøndby, Denmark) with excitation at 390 nm and emission at 480 nm. Quantification was achieved by calculating leucine equivalents using an external leucine standard curve prepared as follows. A 0.1 M leucine stock solution was made (327.5 mg of leucine in 25 mL of 1 mM HCl), and from the stock solution six different concentrations were made (0.00050–0.0030 M leucine) and mixed with 10 mL of 1 mM HCl and analyzed as the milk samples.

Statistical Analysis. To identify significant effects of milk type, storage time, and degree of increase in concentration on the quantified volatile compounds, furosine, and free amino acids, regressions were made by a linear model (lm) followed by a one-way analysis of variance (ANOVA). In addition, a linear mixed model (lme) and a generalized linear mixed model (lmer), least-squares means (LSMEANS), and Tukey's honest significant difference (α = 0.05) test was performed using the software R (version 3.0.2, R Foundation for Statistical Computing, Vienna, Austria).

RESULTS

GC-MS, NMR, furosine, and fluorescamine analyses were conducted on industrially produced conventional UHT milk (100% lactose) and lactose-hydrolyzed UHT milk (<1% of original level of lactose) throughout a storage period of 9 months at 22 °C. The lactose-hydrolyzed UHT milk was heated with 60% of the original level lactose, which was subsequently hydrolyzed to glucose and galactose by the addition of lactase. The compounds detected in the milk by the different analytical approaches are summarized in Figure 2.

Furosine. The development of furosine levels in the milk after acid hydrolysis was found to be significantly affected by milk type. A significantly higher initial level of furosine was observed in CONVI milk (p < 0.001) (Figure 3) compared to

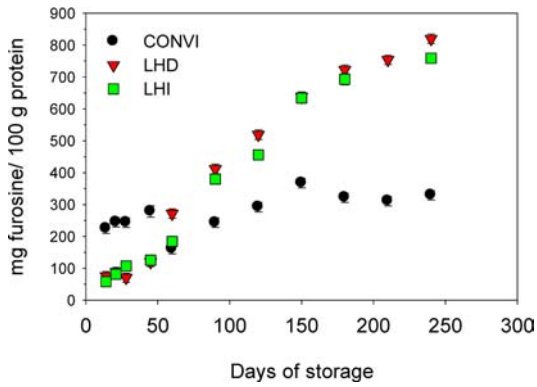

Figure 3. HPLC analysis of furosine in conventional indirect UHT milk (CONVI), lactose-hydrolyzed direct UHT milk (LHD), and lactose-hydrolyzed indirect UHT milk (LHI) during storage.

LHD milk and LHI milk; however, after approximately 60 days, furosine levels started to increase in LHD milk and LHI milk, whereas in CONVI milk furosine levels were constant throughout the storage period. After 270 days of storage, the furosine content was about 2.5 times higher in lactose-hydrolyzed milk than in conventional milk.

GC-MS. A total of 27 volatile compounds were extracted from the headspace sampling and identified using GC-MS (Table 2), and of these 15 were quantified (Table 3). The remaining 12 identified compounds (Tables 2 and 3) were constant throughout the storage period for all milk types and were therefore not quantified.

Notably, the levels of the five ketones quantified were significantly higher in conventional UHT milk (p < 0.001) than in lactose-hydrolyzed milk in the initial phase of the storage period by a factor of 4–5 (Figure 3). All of the quantified ketones followed a similar trend during storage for all milk types, and a significant (p < 0.001) increase in the concentration of ketones was observed during storage (Figure 4). However, for 2-pentanone (p < 0.001), 2-heptanone (LHD, p = 0.016; LHI, p = 0.006), and 2-nonanone (LHD, p < 0.001; LHI, p < 0.001) the formation rate significantly increased at a higher extent for lactose-hydrolyzed milk compared with conventional milk (Figure 4A–C; Supporting Information). In addition, the formation rate of 2-undecanone increased significantly more in LHD than in CONVI (p = 0.029) and LHI (p = 0.023) milks. 2-Nonanone was the only ketone for which a difference between direct and indirect heat treatment could be observed during storage and a higher formation rate was seen in LHD (p = 0.0012) milk compared with LHI milk. 2-Octanone did not appear before 90 days in lactose-hydrolyzed milk, whereas it was observed already at day 14 in conventional milk. A higher formation rate in the level of 2-octanone was observed in CONVI (p = 0.0224) milk compared to LHD milk during storage (Figure 4D).

With the exception of 2-methylbutanal, no significant change in the concentration was observed for the quantified aldehydes during storage (Figure 5). Notably, the concentration of 2-methylbutanal was almost constant in CONVI milk during the 9 month storage period, whereas its concentration (Figure 5D; Supporting Information) increased tremendously after 150 days of storage in LHD (p < 0.001) and LHI (p < 0.001) milk. In addition, it was observed that the level of 2-methylbutanal significantly increased more in LHI (p < 0.001) milk than in LHD milk from day 200.

Heterocycles 2-methylfuran and 2-ethylfuran exhibited a pattern similar to that of the ketones, and a significant increase in their concentrations was observed for all of the milk types during storage (p < 0.001) (Figure 6A,B; Supporting Information). The increase in concentration of the two furans during the storage period was significantly higher in CONVI (p < 0.001) milk compared with the lactose-hydrolyzed milk, and the concentration of 2-ethylfuran increased more in LHI (p = 0.012) milk compared with LHD milk. A different pattern was observed for 2-pentylfuran (Figure 6C). Whereas a significant increase in the concentration of 2-pentylfuran was observed in CONVI (p < 0.001) milk during the storage period, the concentration remained almost constant in LHD and LHI milk.

Dimethyl trisulfide (DMTS) increased in LHD and LHI milk up to 50 days of storage, followed by a decrease to below the initial concentration. In CONVI milk a higher initial concentration of DMTS was observed than in LHD and LHI milks; however, the concentration decreased rapidly during storage, and a low and constant concentration of approximately 0.2 μg/kg milk was reached after approximately 50 days of storage (Figure 7). Dimethyl disulfide (DMDS) was constant throughout the storage period for all milk types (data not shown).

Analysis of Amino Acids by NMR. Four free amino acids, isoleucine, alanine, methionine, and valine (Figure 8), were identified and quantified by ^{1}H NMR spectroscopy. The levels of alanine (LHD, p < 0.001; LHI, p < 0.001), isoleucine (LHD, p = 0.002; LHI, p < 0.001), and valine (LHD, p < 0.001; LHI, p < 0.001) increased in lactose-hydrolyzed milk, whereas they remained constant in the conventional milk throughout the

Table 3. Regression Equations, Limits of Detection (LOD), Limits of Quantification (LOQ), and Coefficients of Determination (R^2) for Calibration Curves in 1.5% Fat UHT Milk

compound	calibration concn (μg/kg)	LOD (μg/kg)	LOQ (μg/kg)	regression eq	R^2
aldehydes					
2-methylbutanal	3.06−10.69	0.82	2.50	$y = 0.07x$	0.993
hexanal	2.29−15.97	2.10	6.35	$y = 0.046x$	0.970
nonanal	3.93−19.64	3.66	11.08	$y = 0.0308x - 0.0448$	0.967
furfural	2.27−68.21	0.84	2.53	$y = 0.0212x$	0.999
decanal	4.07−16.23	1.05	3.18	$y = 0.0346x$	0.997
ketones					
2-pentanone	4.01−64.07	1.72	5.20	$y = 0.1474x$	0.997
2-heptanone	8.04−80.36	3.25	9.84	$y = 0.3954x$	0.997
2-nonanone	7.64−61.10	5.60	16.96	$y = 0.1534x$	0.988
2-octanone	1.61−20.07	0.45	1.35	$y = 0.3196x + 0.0718$	0.999
2-undecanone	16.25−48.75	3.35	10.15	$y = 0.0029x$	0.995
furans					
2-methylfuran	5.74−28.68	5.09	15.44	$y = 0.2506x - 1.4156$	0.969
2-ethylfuran	4.51−18.06	1.27	3.85	$y = 4.711x$	0.996
2-pentylfuran	5.37−26.86	2.92	8.84	$y = 0.5085x - 0.3116$	0.991
sulfides					
DMDS	1.04−10.39	0.58	1.77	$y = 2.3148x + 0.8038$	0.997
DMTS	1.17−35.22	0.56	1.69	$y = 0.5219x$	0.999

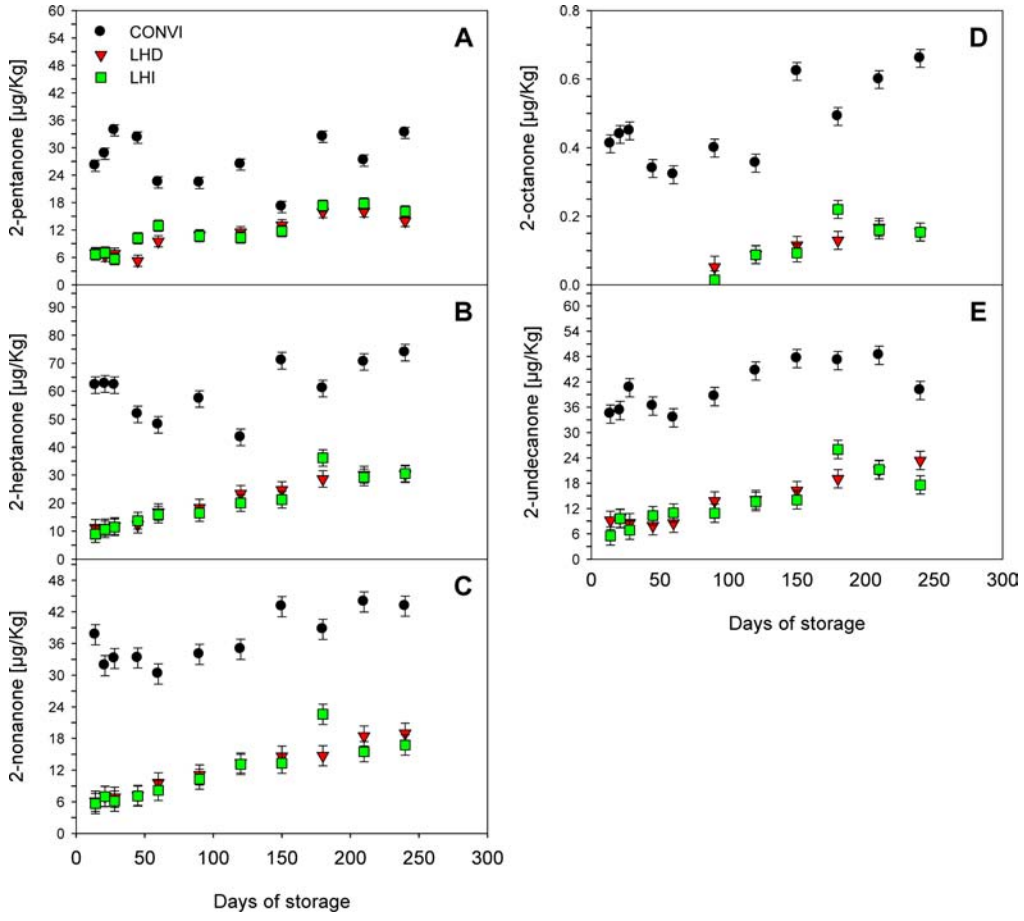

Figure 4. GC-MS analysis of (A) 2-pentanone, (B) 2-heptanone, (C) 2-nonanone, (D) 2-octanone, and (E) 2-undecanone in conventional indirect UHT milk (CONVI), lactose-hydrolyzed direct UHT milk (LHD), and lactose-hydrolyzed indirect UHT milk (LHI) during storage.

storage period (Figure 8A,B,D; Supporting Information). Methionine content was initially significantly higher in CONVI (p = 0.0011) compared to LHI milk (Figure 8C; Supporting Information). Throughout the storage period methionine levels in CONVI and LHD milk decreased to the level of LHI milk.

In addition to the four amino acids, acetate was also quantified by ^{1}H NMR spectroscopy (Figure 9; Supporting Information). The level of acetate significantly increased in

dx.doi.org/10.1021/jf501671z | J. Agric. Food Chem. 2014, 62, 7886−7896

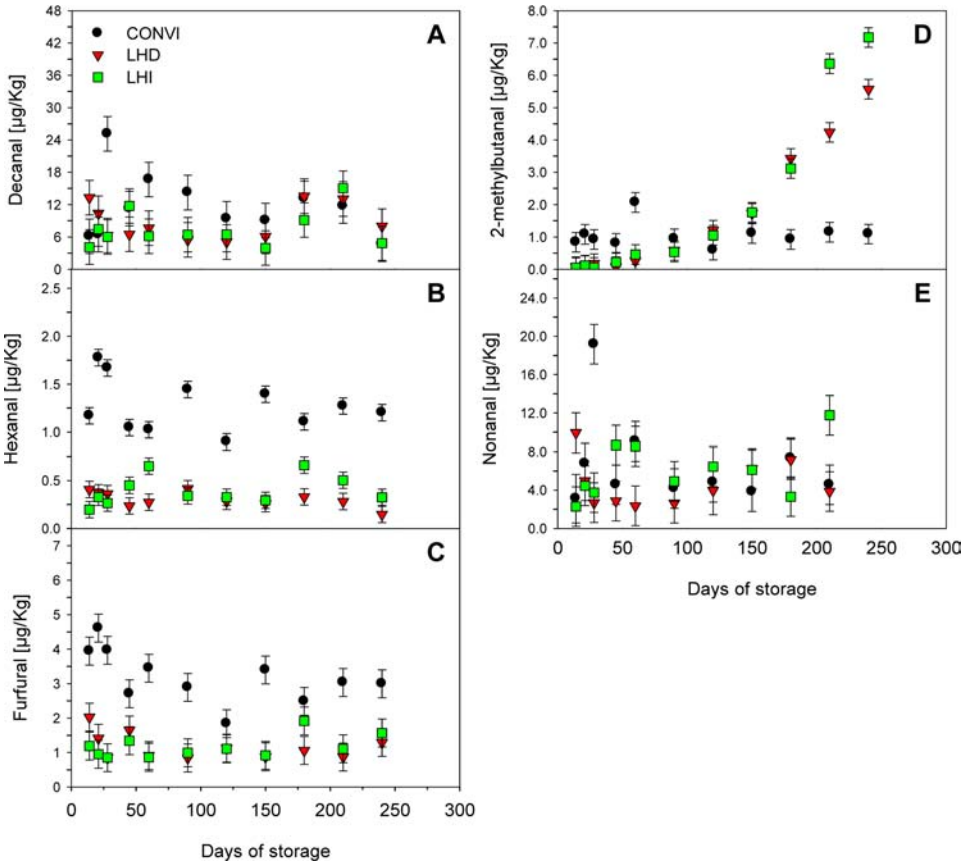

Figure 5. GC-MS analysis of (A) decanal, (B) hexanal, (C) furfural, (D) 2-methylbutanal, and (E) nonanal in conventional indirect UHT milk (CONVI), lactose-hydrolyzed direct UHT milk (LHD), and lactose-hydrolyzed indirect UHT milk (LHI) during storage.

lactose-hydrolyzed milk (LHD, $p = 0.028$; LHI, $p = 0.0336$) during storage, whereas the increase in conventional milk during storage was not significant.

Analysis of Free Amino Terminals by Fluorescamine Assay. Slightly higher initial levels of free amino terminals and amino groups of lysine side chains were observed in the CONVI milk compared with lactose-hydrolyzed milk (Figure 10). However, the level of free amino terminals, expressed as leucine equivalents, significantly increased in the lactose-hydrolyzed milk ($p < 0.001$), whereas it remained rather constant in the conventional milk during storage (Figure 10; Supporting Information). After 270 days of storage, the level of free amino terminals was about 2 times higher in lactose-hydrolyzed milk than in conventional milk. No differences were observed between LHD and LHI milks.

DISCUSSION

In the present study volatile compounds, Amadori products as determined by furosine levels, levels of free amino acids, and levels of amino terminals, and proteolysis were analyzed in lactose-hydrolyzed and conventional UHT milk to elucidate the detailed chemical changes during a 9 month storage period (Figure 2).

Maillard Reaction Products. An increase in the level of furosine was observed in all milk types during the 9 month storage, which demonstrates a continuous formation of its precursors, lactulosyllysine and fructosyllysine (Figures 2 and 3). During the first 60 days of storage lactose-hydrolyzed milk was characterized by a significantly lower furosine level than conventional milk. This was likely due to the removal of approximately 40% of lactose prior to the UHT treatment in the lactose-hydrolyzed milk, resulting in lower levels of carbohydrates during the UHT treatment and lower levels of Maillard reactions in the initial storage period. This indicates that furosine precursors were formed during the heat treatment. However, during storage, the formation rate was significantly higher in lactose-hydrolyzed milk compared to conventional milk. This is consistent with the fact that the monosaccharides polymerize more progressively[19] than disaccharides. This finding reveals that despite lower carbohydrate levels, the Maillard reaction proceeds more rapidly and to a greater extent in lactose-hydrolyzed milk during storage. Previous studies have followed the development of furosine in lactose-hydrolyzed and conventional milk for up to 4 months and showed significant increases in furosine during storage.[4,20] Messia et al. investigated the formation of furosine in lactose-hydrolyzed and conventional indirect UHT milk during 4 months of storage at 20 °C and found higher values of furosine in the former.[4] The concentrations of furosine found in the lactose-hydrolyzed milk at production and after storage for 4 months were 234 and 562 mg/100 g protein, respectively, whereas the corresponding concentrations found in the conventional milk were 235 and 310 mg/100 g protein, respectively. These results are quantitatively consistent with the results in the present study for the same storage period, temperature, and milk type. However, this study shows that it is important to follow the development of furosine for longer than 4 months (Figure 3). Tossavainen and Kallionen investigated furosine content in three milk types: nonhydrolyzed, hydrolyzed, and lactose-reduced-hydrolyzed (similar to the lactose-hydrolyzed milk in

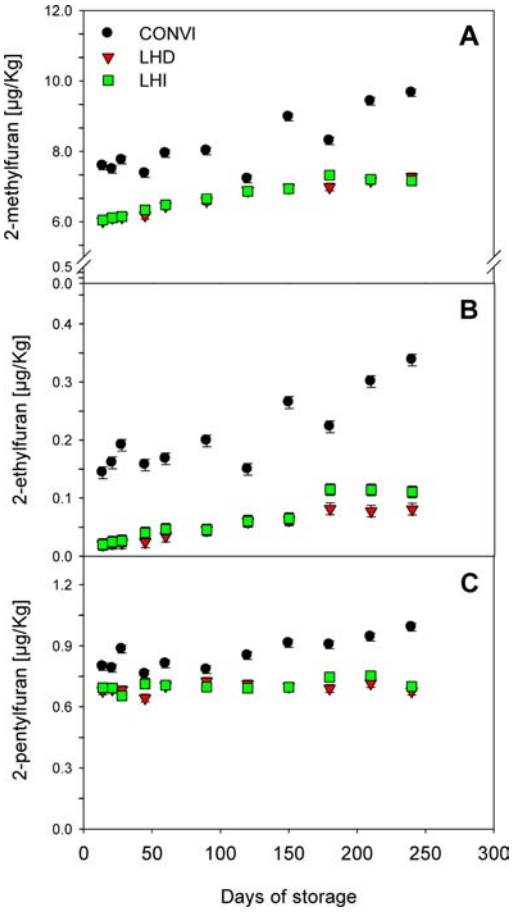

Figure 6. GC-MS analysis of (A) 2-methylfuran, (B) 2-ethylfuran, and (C) 2-pentylfuran in conventional indirect treated UHT milk (CONVI), lactose-hydrolyzed direct UHT milk (LHD), and lactose-hydrolyzed indirect UHT milk (LHI) during storage.

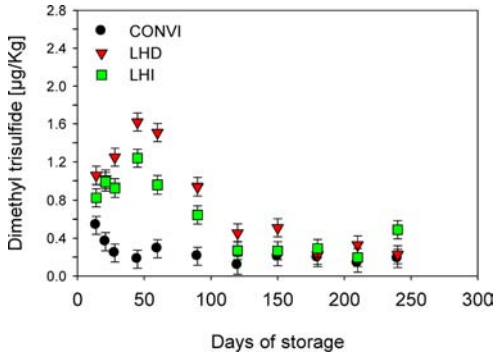

Figure 7. GC-MS analysis of dimethyl trisulfide in conventional indirect UHT milk (CONVI), lactose-hydrolyzed direct UHT milk (LHD), and lactose-hydrolyzed indirect UHT milk (LHI) during storage.

the present study) UHT milk stored for 12 weeks.[7] Tossavainen and Kallionen found a 2.5-fold higher level of furosine in the lactose-reduced-hydrolyzed milk and lactose-hydrolyzed milk, respectively, compared with the nonhydrolyzed milk and concluded that the content of furosine was dependent on both the amount and type of sugar. In the present study it was observed that the content of furosine was dependent on the amount of sugar the first 90 days and that type of sugar was important after 90 days of storage. It was also revealed that the level of furosine in conventional and lactose-hydrolyzed UHT milk is very dependent on the storage period. This has implications for understanding storage-induced deterioration of milk quality.

A very similar formation pattern was observed for the furosine generation and the Maillard reaction product, 2-methylbutanal (Figure 5D). After initially being observed at a lower concentration in LHI and LHD, which is consistent with total carbohydrate content, accumulation of 2-methylbutanal was found to occur more rapidly and to a much greater extent in lactose-hydrolyzed milk. This observation is in good agreement with the current understanding of the Maillard–Strecker degradation pathway. The volatile 2-methylbutanal is a Strecker degradation aldehyde[21] and is formed when isoleucine reacts with dicarbonyl compounds in the milk. The increased concentration of 2-methylbutanal in lactose-hydrolyzed compared to conventional UHT milk can be ascribed to the type of sugar (lactose, glucose, and galactose) available in the milk. Kato et al. studied protein polymerization and browning in a model system consisting of ovalbumin, glucose, and lactose and concluded that glucose accelerates the protein polymerization as well as the Amadori degradation.[19] Kato et al. also concluded that the Amadori compounds formed from lactose were less prone to degradation into aldehyde compounds compared with the Amadori compounds from glucose. Intriguingly, in the present study it could be observed that the free amino acid and precursor for Strecker degradation, isoleucine, increased during storage in lactose-hydrolyzed milk, whereas it remained constant in conventional milk (Figure 8A). This finding is probably related to a higher level of proteolysis in lactase-treated milk and could be due to unwanted side activities of the enzyme preparation. Balagiannis et al. investigated the formation of 2-methylbutanal and observed that the sugar concentration, the Amadori rearrangement, the rate of dicarbonyl formation, and the amount of isoleucine were the limiting steps of its formation.[21] The simultaneous increase of isoleucine, furosine, and 2-methylbutanal in lactose-hydrolyzed milk after approximately 100–150 days of storage indicates that the level of isoleucine and the Amadori rearrangement is important for the formation of 2-methylbutanal, which, in addition to the lower reactivity of lactose with proteins and the nondetectable formation of isoleucine, explains the absence of a formation of 2-methylbutanal in the conventional UHT milk.

Furfural is formed in the 3-deoxyosone pathway in the early Maillard reaction, which is favored by acidic pH. However, furfural may be a precursor of the formation of furan derivatives in the Maillard reaction.[22] Berg observed that furfural was formed in milk in very small concentrations after heating and that the level of furfural increased with increasing heat load.[23] In the present study, furfural was identified and quantified, and it was found that furfural remained almost constant at a concentration of 0.8–6 μg/kg (8.3–62.4 μmol/kg) throughout the storage period. This concentration is higher than the concentration detected by Berg, who reported 0.68 μmol furfural/kg in UHT milk.[23] This difference is possibly due to differences in the UHT treatment or differences in the sensitivity of the applied GC-MS method. The results in the present study indicate that no formation of furfural is taking place during storage at room temperature, likely due to the nonpreferred pathway at normal milk pH.

Acetate, identified by NMR spectroscopy in the present study (Figure 9), is a major degradation product of sugars in the Maillard reaction. In neutral and basic pH, acetate is formed

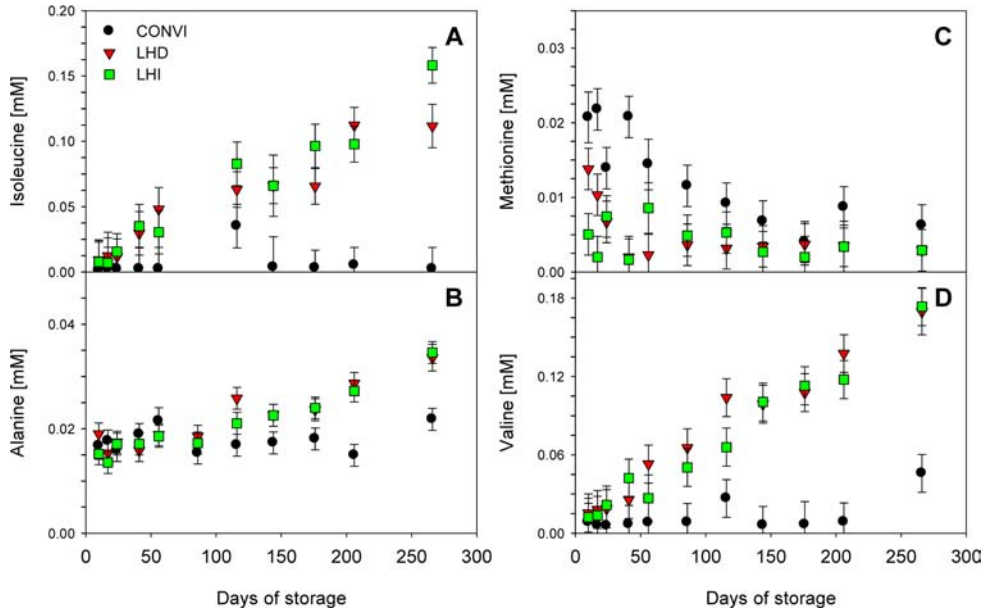

Figure 8. NMR spectroscopic analysis of (A) isoleucine, (B) alanine, (C) methionine, and (D) valine in conventional indirect treated UHT milk (CONVI), lactose-hydrolyzed direct UHT milk (LHD), and lactose-hydrolyzed indirect UHT milk (LHI) during storage.

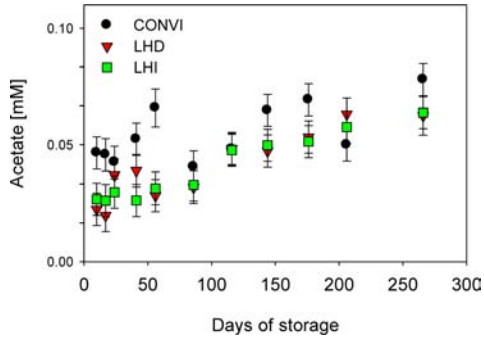

Figure 9. NMR spectroscopic analysis of acetate in conventional indirect UHT milk (CONVI), lactose-hydrolyzed direct UHT milk (LHD), and lactose-hydrolyzed indirect UHT milk (LHI) during storage. Acetate significantly increased for LHD and LHI during storage: significance level for LHD (p = 0.0275), LHI (p = 0.0336).

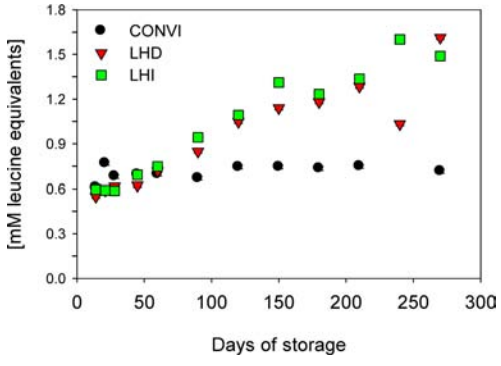

Figure 10. Concentration of free amines in conventional indirect UHT milk (CONVI), lactose-hydrolyzed direct UHT milk (LHD), and lactose-hydrolyzed indirect UHT milk (LHI) determined by fluorescamine assay during storage.

primarily from C2−C3 β-cleavage of the 1-deoxyosone isomerization product 1-deoxy-2,4-hexodiulose (2,4-pentadione).[24,25] Acetate is a stable end product of this pathway and considered as a marker for the 2,3-enolization in the Maillard reaction.[24] In addition, acetate can also be formed directly from sugar fragmentation.[25] In the present study the level of acetate increased during storage for all of the milk types, and no significant difference was found between the milk types (Figure 9). The accumulation of acetate in the milk during storage indicates that a continuous formation is taking place throughout storage and that the degradation of the respective Amadori compound (fructosyllysine in lactose-hydrolyzed milk and lactulosyllysine in conventional milk) occurs throughout storage, leading to a continuous formation of the dicarbonyls, which are included in Strecker degradation in the Maillard reaction (Figure 2). The comparable increase of acetate in lactose-hydrolyzed and conventional milk indicates that the same level of Amadori compound degradation is present in both milk types. Kato et al. observed that Amadori compounds from lactose were more difficult to degrade compared with the Amadori compounds from glucose, which could explain the lower level of Strecker aldehydes such as 2-methylbutanal in conventional milk in the present study.[19] However, contrary to Kato et al., the present study indicates that the 2,3-enolization from the Amadori compounds to 1-deoxyosone is similar in conventional and lactose-hydrolyzed UHT milk and that the hindrance for further degradation to aldehydes is taking place after this step in the Maillard reaction cascade (Figure 2).

2-Methylfuran and 2-ethylfuran increased significantly during storage in all milk types (Figure 6), but a larger increase was seen in CONVI milk compared with LHD and LHI milks. The furans 2-methylfuran and 2-ethylfuran are Strecker aldehyde (acetaldehyde and lactaldehyde) products as well as sugar and protein degradation products.[26,27] The higher content of furans in the conventional milk indicates that the formation of furans is favored by lactose, and not glucose and galactose. This suggestion is supported by a recent published work by Owczarek-Fendor et al., who investigated furan formation in starch-based systems containing various carbohydrates and proteins, heated at 130 °C for 30 min, at different pH values.[28] The study revealed that lactose and lactose−protein systems

dx.doi.org/10.1021/jf501671z | J. Agric. Food Chem. 2014, 62, 7886−7896

generated higher amounts of furan at pH 6 compared with glucose and fructose systems.

Thermal Degradation and Oxidation Products. In addition to 2-methylbutanal, four other aldehydes were quantified. The nonsystematic variation in aldehydes could potentially be ascribed to the low concentration of these compounds. During thermal processing fatty acids may undergo thermal degradation reactions, including isomerization, cyclization, and cleavage, and aldehydes are mainly formed by oxidation of fatty acids;[29,30] straight-chain aldehydes are the most important markers for fat oxidation.[31] Vazquez-Landaverde et al. observed that aldehydes were not affected by heat to the same extent as ketones.[2] Valero et al. found a small increase in aldehydes during 120 days of storage.[3] Jeon et al. investigated the effect of addition of ascorbic acid, acting as antioxidant, on the formation of aldehydes in UHT milk and found that the addition of ascorbic acid reduced the formation of aldehydes.[32] Osada and Shibamoto investigated the antioxidative activity of volatile extracts from Maillard model systems and observed that the combined effect of many compounds produced in the Maillard reaction possessed an antioxidative effect that decreased the oxidation of hexanal.[33] Thus, in the present study, an antioxidant activity from the advanced Maillard reaction products[34] or peptides and proteins,[35] formed from proteolysis, may inhibit the formation of aldehydes. This could explain the low level of change observed for the aldehydes during storage in all milk types. However, the low level of aldehydes may also indicate a low level of oxidation in the milk.

During storage a significant increase in the concentration of ketones was observed in the milks (Figure 4). Ketones are derived from fatty acids through β-oxidization[30,36] and are primarily formed by thermal degradation.[29] The ketones are known to be temperature-dependent, and increased levels of ketones have been observed in milk exposed to higher temperatures.[2] The present study revealed that both the level and the formation rate of ketones were affected by milk type. Whereas the level of ketones was higher in conventional UHT in the beginning of the storage period, the levels of 2-pentanone, 2-heptanone, and 2-nonanone increased significantly higher in the lactose-hydrolyzed compared to conventional milk. In addition, a higher increase in 2-undecanone was observed in LHD milk compared with CONVI milk. These findings indicate that the thermal degradation of the fatty acids is more pronounced in lactose-hydrolyzed milk than conventional UHT milk. However, because the heat treatments applied were similar, the exact mechanism remains unknown.

A significant increase in 2-pentylfuran was found in CONVI milk during storage, whereas this compound was found to be constant in lactose-hydrolyzed milk (Figure 6C). Overall, 2-pentylfuran is formed from oxidation of unsaturated lipids.[27,37] A possible explanation for the increased formation of 2-pentylfuran in the conventional UHT milk compared with the lactose-hydrolyzed milk may be a higher antioxidant activity in the lactose-hydrolyzed milk due to an increased Maillard reaction[34,38] or increased proteolytic activity[35] forming antioxidative compounds.The antioxidative compounds may decrease the oxidation of the unsaturated lipids present in the milk and thereby the furan formation.

When β-lactoglobulin is heat-denatured, methionine and cysteine are exposed to further reactions, such as oxidation and Maillard reactions, and Strecker degradation. The Strecker degradation of methionine may lead to the formation of methional, which further oxidizes to DMDS and DMTS,[36,39] and in the present study, DMTS apparently was formed after or during heat treatment in all milk types. In lactose-hydrolyzed milk the DMTS concentration increased further during storage and then decreased rapidly after approximately 50 days (Figure 7), whereas an immediate decrease was observed in the conventional UHT milk. In addition, it was observed that methionine decreased in lactose-hydrolyzed milk, which could indicate that methionine was degraded to DMTS in the initial part of the storage period. However, for the conventional UHT milk, methionine first increased followed by a slow decrease, and the decrease could not be correlated to any simultaneous formation of DMTS. Sulfides and sulfur-containing amino acids are very reactive, and the decrease of these compounds during storage is mainly thought to be due to degradations and oxidations.[40,41] Because of observations of increased levels of free amino acids or peptides in lactose-hydrolyzed milk during storage (Figure 8A,C,D), a similar observation was expected with methionine; however, no increase was observed. This may be explained by the specificity of the proteolytic enzyme, which may not cleave methionine or methionine-containing peptides, or rapid degradation of exposed methionine residues, which would prevent its detection in the NMR.

Protein Hydrolysis during Storage. In the present study ^{1}H NMR spectroscopy was used to determine amino acids acting as precursors in Maillard reaction and also to determine acetic acid, which can be formed during the Maillard reaction. In addition to methionine and isoleucine already discussed, alanine and valine were quantified in the milk by ^{1}H NMR spectroscopy. This quantification revealed that these amino acids increased significantly in lactose-hydrolyzed milk during storage, whereas they remained constant at a lower level in the conventional milk (Figure 8B,D). In addition, an increase in the level of free amino terminals, obtained from the fluorescamine assay, was observed in lactose-hydrolyzed milk compared to conventional UHT milk in Figure 10. These results demonstrate a higher proteolytic activity in lactose-hydrolyzed milk compared to conventional milk. An increased level of free amino terminals and amino groups of lysine side chains in lactose-hydrolyzed milk may contribute considerably to the higher level of Maillard reaction products in the lactose-hydrolyzed milk. An increased Maillard reaction decreases lysine availability in lactose-hydrolyzed milk, and therefore the protein nutrition value may be lower in this type of milk. A lower protein availability might pose a challenge when aiming at decreased malnutrition in countries with a high prevalence of lactose intolerance. Thus, it is of interest to optimize the production of lactose-hydrolyzed milk to avoid high levels of Maillard reactions and thereby maintain a high nutritional value of the milk. The increased level of free amino acids and amino terminals (Figures 8 and 9) in lactose-hydrolyzed milk during storage indicates that the proteolytic activity is more pronounced than the Maillard reaction activity. Tossavainen and Kallioinen analyzed proteolytic activity in lactose-hydrolyzed and unhydrolyzed UHT milk directly after production and after 4 weeks of storage and observed a higher proteolytic activity in the hydrolyzed UHT milk compared to the unhydrolyzed UHT milk, which is in agreement with the present study.[10] The higher proteolytic activity is probably due to the proteolytic side effect of the added lactase enzyme preparation, which gives rise to substrates for the Maillard reaction and thereby an increased risk for milk quality deterioration during storage.

Effect of Heat Treatment. In addition to the effect of lactose hydrolysis, the effects of heat treatment were also elucidated in the present study as two different types of heat treatments were included: a direct and an indirect heat treatment. However, no differences in detection in furosine content or free amino terminals were observed between direct and indirect heat-treated lactose-hydrolyzed milks. Higher furosine levels in conventional indirect UHT milk compared with conventional direct UHT milk have been reported in previous studies.[1,42] The levels of 2-nonanone and 2-undecanone increased more in LHD than in LHI milk, which is contrary to the observation of Perkins et al., who found an increased total amount of ketones in indirect heat-treated conventional UHT milk, compared with the direct heat-treated milk. The significantly higher increases in 2-methylbutanal and 2-ethylfuran during storage in LHI compared with LHD milk could be explained by the different heat loads from direct and indirect heat treatments.[2] To the best of our knowledge, no studies comparing direct and indirect heat treatments of lactose-hydrolyzed milk, where lactose is removed and hydrolyzed after heat treatment, have been reported.

The present study, which included several complementary analyses, shows that the type of carbohydrate has a greater impact on the Maillard reaction, heat load indicators such as furosine, and total concentration of ketones, compared to the impact of different heat treatments (direct and indirect UHT). The formation of 2-methylbutanal and furosine was considerably higher in lactose-hydrolyzed milk compared with conventional UHT milk after a 9 month storage period. In addition, an increase in free amino acids and free amines increased tremendously in lactose-hydrolyzed milk, whereas they remained constant in conventional UHT milk. Residual proteolytic activity from the lactase-enzyme preparation may be responsible for the higher levels of free amino acids observed in lactose-hydrolyzed UHT milk. This study reveals that lactose-hydrolyzed UHT milk, compared to conventional UHT milk, is more vulnerable to reactions that can impair the milk quality, primarily the Maillard reaction and proteolysis but, to some extent, also oxidation.

■ ASSOCIATED CONTENT

Supporting Information

Overview of storage and effects on the amount of volatile compounds in lactose-hydrolyzed direct UHT milk (LHD), lactose-hydrolyzed indirect UHT milk (LHI), and conventional indirect UHT milk (CONVI). This material is available free of charge via the Internet at http://pubs.acs.org.

■ AUTHOR INFORMATION

Corresponding Author

*(H.C.B.) E-mail: HanneC.Bertram@agrsci.dk. Phone: +45 871 58353.

Present Addresses

△(S.N.) University of Toronto, 555 University Avenue, Toronto, Ontario, Canada.

▽(A.S.) O. Kavli AB, Armborstvägen 7, 12444 Älvsjö, Sweden.

Funding

The present study is part of the Ph.D. work of T.J. and was financially supported by Arla Foods Amba, Food Future Innovation (FFI), Danish Dairy Research Foundation, and Aarhus University.

Notes

The authors declare no competing financial interest.

■ ACKNOWLEDGMENTS

We are thankful for the excellent technical assistance of Birgitte Foged and Hanne S. Møller.

■ ABBREVIATIONS USED

CONVI, conventional indirect UHT milk; DMDS, dimethyl disulfide; DMTS, dimethyl trisulfide; DSQ, dual-stage quadrupole; ESL, extended shelf life; HCl, hydrochloric acid; HPLC, high-pressure liquid chromatography; GC-MS, gas chromatography−mass spectrometry; LHD, lactose-hydrolyzed direct UHT milk; LHI, lactose-hydrolyzed indirect UHT milk; LME, linear mixed model; LSMEANS, least-squares means; LOD, limit of detection; LOQ, limit of quantification; NMR, nuclear magnetic resonance; TIC, total ion current; SIM, selected-ion monitoring; UHT, ultra-high temperature; UV, ultraviolet

■ REFERENCES

(1) Datta, N.; Elliott, A. J.; Perkins, M. L.; Deeth, H. C. *Aust. J. Dairy Technol.* **2002**, *57*, 211−227.

(2) Vazquez-Landaverde, P. A.; Velazquez, G.; Torres, J. A.; Qian, M. C. *J. Dairy Sci.* **2005**, *88*, 3764−3772.

(3) Valero, E.; Villamiel, M.; Miralles, B.; Sanz, J.; Martinéz-Castro, I. *Food Chem.* **2001**, *72*, 51−58.

(4) Messia, M. C.; Candigliota, T.; Marconi, E. *Food Chem.* **2007**, *104*, 910−917.

(5) Ingram, C. J. E.; Mulcare, C. A.; Itan, Y.; Thomas, M. G.; Swallow, D. M. *Hum. Genet.* **2009**, *124*, 579−591.

(6) Harju, M.; Kallioinen, H.; Tossavainen, O. *Int. Dairy J.* **2012**, *22*, 104−109.

(7) Tossavainen, O.; Kallioinen, H. *Milchwissenschaft* **2008**, *63*, 22−26.

(8) Naranjo, G. B.; Pereyra Gonzales, A. S.; Leiva, G. E.; Malec, L. S. *Food Chem.* **2013**, *141*, 3790−3795.

(9) Kato, Y.; Matsuda, T.; Kato, N.; Watanabe, K.; Nakamura, R. *J. Agric. Food Chem.* **1986**, *34*, 351−355.

(10) Tossavainen, O.; Kallioinen, H. *Milchwissenschaft−Milk Sci. Int.* **2007**, *62*, 410−415.

(11) Reineccius, G. In *Flavor Chemistry and Technology*; Taylor & Francis Group: Boca Raton, FL, USA, 2006; pp 108−139.

(12) Bylund, G. *Dairy Processing Handbook*, 2nd ed.; Tetra Pak Processing Systems: Malmö, Sweden, 2003; pp 227−246.

(13) Jansson, T.; Jensen, S.; Eggers, N.; Clausen, M. R.; Larsen, L. B.; Ray, C.; Sundgren, A.; Andersen, H. J.; Bertram, H. C. *Dairy Sci. Technol.* **2014**, *94*, 311−325.

(14) Dolan, J. W. *LCGC North Am.* **2009**, *27*, 224−230.

(15) Dolan, B. J. W. *LCGC North Am.* **2009**, *27*, 306−312.

(16) International Organization for Standardization, International Dairy Federation. International Standard ISO 18329, 2004.

(17) Sundekilde, U. K.; Poulsen, N. A.; Larsen, L. B.; Bertram, H. C. *J. Dairy Sci.* **2013**, *96*, 290−299.

(18) Dalsgaard, T. K.; Nielsen, J. H.; Larsen, L. B. *Mol. Nutr. Food Res.* **2007**, *51*, 404−414.

(19) Kato, Y.; Matsuda, T.; Kato, N.; Nakamura, R. *J. Agric. Food Chem.* **1988**, 806−809.

(20) Evangelisti, F.; Calcagno, C.; Nardi, S.; Zunin, P. *J. Dairy Res.* **1999**, *66*, 237−243.

(21) Balagiannis, D. P.; Parker, J. K.; Pyle, D. L.; Desforges, N.; Wedzicha, B. L.; Mottram, D. S. *J. Agric. Food Chem.* **2009**, *57*, 9916−9922.

(22) Whitfield, F. B.; Mottram, D. S.; Brock, S.; Puckey, D. J.; Salter, L. J. *J. Sci. Food Agric.* **1988**, *42*, 261−272.

(23) Berg, H. *Reactions of Lactose during Heat Treatment of Milk: A Quantitative Study*; Agricultural University: Wageningen, The Netherlands, 1993; pp 1−176.
(24) Davídek, T.; Devaud, S.; Robert, F.; Blank, I. *J. Agric. Food Chem.* **2006**, *54*, 6667−6676.
(25) Brands, C. M.; van Boekel, M. a. *J. Agric. Food Chem.* **2001**, *49*, 4667−4675.
(26) Limacher, A.; Kerler, J.; Davidek, T.; Schmalzried, F.; Blank, I. *J. Agric. Food Chem.* **2008**, *56*, 3639−3647.
(27) Perez Locas, C.; Yaylayan, V. A. *J. Agric. Food Chem.* **2004**, *52*, 6830−6836.
(28) Owczarek-Fendor, A.; De Meulenaer, B.; Scholl, G.; Adams, A.; Van Lancker, F.; Eppe, G.; De Pauw, E.; Scippo, M.-L.; De Kimpe, N. *Food Chem.* **2012**, *133*, 816−821.
(29) Nawar, W. W.; Cancel, I. E.; Fagerson, I. S. *J. Dairy Sci.* **1962**, *45*, 1172−1177.
(30) Hawke, J. C. *J. Dairy Res.* **1966**, *33*, 225−243.
(31) Hall, G.; Andersson, J.; Lingnert, H.; Olofsson, B. *J. Food Qual.* **1985**, *7*, 153−190.
(32) Jeon, I. J.; Thomas, E. L.; Reineccius, G. A. *J. Agric. Food Chem.* **1978**, *26*, 1183−1188.
(33) Osada, Y.; Shibamoto, T. *Food Chem.* **2006**, *98*, 522−528.
(34) Gu, F.; Kim, J. M.; Hayat, K.; Xia, S.; Feng, B.; Zhang, X. *Food Chem.* **2009**, *117*, 48−54.
(35) Clausen, M. R.; Skibsted, L. H.; Stagsted, J. *J. Agric. Food Chem.* **2009**, *57*, 2912−2919.
(36) Belitz, H.-D.; Grosch, W.; Schieberle, P. *Food Chemistry*, 4th ed.; Belitz, H.-D., Schieberle, P., Eds.; Springer: Berlin, Germany, 2001; Vol. 73, pp 158−402.
(37) Zhang, Y.; Guo, S.; Liu, Z.; Chang, S. K. C. *J. Agric. Food Chem.* **2012**, *60*, 7457−7462.
(38) Morales, F. J.; Jiménez-pérez, S. *Food Chem.* **2001**, *72*, 119−125.
(39) Pripis-Nicolau, L.; de Revel, G.; Bertrand, A.; Maujean, A. *J. Agric. Food Chem.* **2000**, *48*, 3761−3766.
(40) Al-Attabi, Z. *Volatile Sulphur Compounds in UHT Milk*; School of Land, Crop, and Food Sciences, The University of Queensland: St. Lucia, QLD, Australia, 2009; Vol. 49.
(41) Min, D. B.; Boff, J. M. *Compr. Rev. Food Sci. Food Saf.* **2002**, *1*, 58−72.
(42) Elliott, A. J.; Dhakal, A.; Datta, N.; Deeth, H. C. *Aust. J. Dairy Technol.* **2003**, *58*, 3−10.

during the sun-drying season. (3) Experiment 3 (AT): alternating temperatures of 40 and 15 °C every 12 h, simulating the average temperatures in the central hours of the day and night during the traditional sun-drying. The grapes were introduced at 15 °C with the temperature being increased to 40 °C and remained constant during the first 12 h, and then the conditions changed and the temperature started to decrease to 15 °C again and so on.

The three experiments were finished at the end of 48 h. During the drying process, reducing sugar concentration of the grapes was measured using a refractometer model Atago Master. After the drying, the whole bunches of raisins were pressed on a vertical press similar to industrial models. The maximum pressure reached in each of the two pressing cycles was 300 bar. The resulting musts were centrifuged at 3000 rpm, filtered, and analyzed in triplicate.

Dry matter (dm) was determined by placing a known amount of grape in a stove and measuring the weight loss until a constant weight was observed.

The moisture contents (kilograms water/kilograms dry matter) at any time of drying (Mt) were registered. The moisture ratio (MR) and drying rate (DR) of grapes during experiments were calculated using the following equations:[15]

$$\mathrm{MR} = \frac{M_t}{M_0} \quad \mathrm{DR} = \frac{M_{t+\Delta t} - M_t}{\Delta t}$$

Where M_t, M_0, and $M_{t+\Delta t}$ are the moisture content at any time of drying, initial moisture content, and moisture content at $t + \Delta t$, respectively, and t is time (hours).

Spectrophotometric Determinations. Absorbances at 420 and 520 nm were made on a PerkinElmer (Waltham, MA) Lambda 25 spectrophotometer, using quartz cells of 1 mm light paths. Samples were previously passed through Millipore (Billerica, MA) HA filters of 0.45 μm pore size. All measurements were corrected for a path length of 1 cm. Hue was calculated as the relationship between absorbance at 420 nm and absorbance at 520 nm.

Anthocyanins Analysis. For the extraction and fractionation of anthocyanins, the method proposed by Marquez et al.[14] was used. A volume of 2 mL of wine was passed through a Sep-Pak C18 cartridge packed with 900 mg of material (Long Body Sep-Pak Plus, Water Associates, Milford, MA) that was previously activated with 5 mL of methanol and washed with aqueous 0.01% (v/v) HCl. The cartridge was successively washed with 10 mL of 0.01% aqueous HCl and 5 mL of ethyl acetate, and the anthocyanins were recovered with 5 mL of methanol acidified to a pH 2 with HCl. Anthocyanin samples were concentrated on a vacuum centrifuge thermostated at 35 °C and passed through a filter of 0.45 μm pore size for injection into a P4000 HPLC instrument from Spectra-Physics (San Jose, CA).

Anthocyanins were identified by comparing their retention times with those for standards, recording UV spectra on a Spectra-Physics UV6000LP diode array spectrophotometer and calculating the UV absorbance ratios for samples and standards simultaneously coinjected one at a time.[14] Identification was confirmed by HPLC-ESI-MS on an AQA quadrupole mass spectrometer from ThermoQuest Finningan. The instrument was operated in both the negative and positive ion modes. The ion spray voltage was −4 kV, and the orifice voltage was −60 V. Mass data were acquired in the scan mode (by scanning the m/z range 150 to 1066 at 1.2 intervals) and the multiple ion mode (by using mass ranges around specific m/z values). The compounds were quantified by comparison with a calibration curve obtained from the malvidin-3-glucoside.

Antioxidant Activity. The DPPH assay was realized for the antioxidant activity determination. The wines were diluted with a solution containing 12% ethanol, and an aliquot of 200 μL was placed in a cell with 3 mL of a 45 mg/L solution of DPPH in methanol. A blank (200 μL dilution sample and 3 mL methanol), a control sample (200 μL of 12% ethanol in water and 3 mL of DPPH solution), and a Trolox standard (200 μL of 80 mg/L Trolox solution and 3 mL of DPPH solution) were also prepared in parallel. The absorbances at 517 nm of the control sample and blank were measured, and the absorbances of the standard and samples were measured after 10 min of incubation. The antioxidant activity, expressed in millimoles of Trolox (mmol TE) per liter, were calculated as follows:

$$\text{antioxidant activity of sample (mmol TE/L)} = (0.32A_1{*}\text{wine dilution factor})/A_2$$

$$A_1 = \text{absorbance}_{\text{control(t=0)}} - \text{absorbance}_{\text{sample}}$$

$$A_2 = \text{absorbance}_{\text{control(t=0)}} - \text{absorbance}_{\text{standard(t=10)}}$$

$$A_{\text{sample}} = \text{absorbance}_{\text{sample(t=10)}} - \text{absorbance}_{\text{blank(t=0)}}$$

Statistical Analysis. The results for the three controlled drying samples were subjected in triplicate to principal component analysis (PCA), and the anthocyanins compounds were subjected to analysis of variance (ANOVA) in triplicate, using the Statgraphics computer package version 5.0 from Statistical Graphics Corp.

RESULTS AND DISCUSSION

Figure 1 shows the changes in the moisture ratio against the dehydration time in the chamber under controlled conditions.

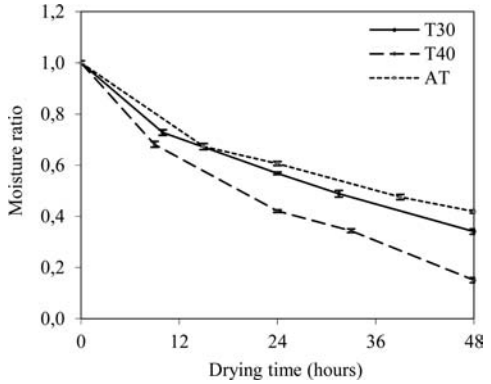

Figure 1. Changes in moisture ratio during the three controlled dehydration experiments at 30 °C (T30), 40 °C (T40), and alternating temperatures between 40 and 15 °C (AT).

As can be seen, the moisture ratio, determined as the relation between the moisture content at each time compared with the initial moisture content, decreased during the drying process. The drying at 40 °C constant temperature (T40) showed the lowest values during the study time with a final value of 0.150, 56, and 64% lower than the drying at 30 °C and alternating temperatures, respectively, which suggested that this drying was the fastest. The last two processes presented similar drying kinetics, with the drying with alternating temperatures which presented the highest values of moisture ratio (0.419).

Changes in the drying rate in function of the total weight of the control sample are shown in Figure 2. As can be seen, the rate decreased during the raisining time, with the rate faster at the beginning in the three assays when the grape weight was higher. The dehydration rate reached low values in the last hours. Also, for the same sample weight, the controlled dehydration at a constant temperature of 40 °C took place at a higher rate, which would agree with the previous results. Then the drying at a constant temperature of 30 °C and the dehydration with alternating temperatures was the slowest.

The absorbances at 420 and 520 nm and the hues were measured with the aim of evaluating the influence of the temperature on the color of musts from the dried grapes (Figure 3). The absorbance at 420 nm could be considered as an index of the brown color of the musts, A_{520} as the red color index and the hue is the relation between the two (A_{420}/A_{520}).

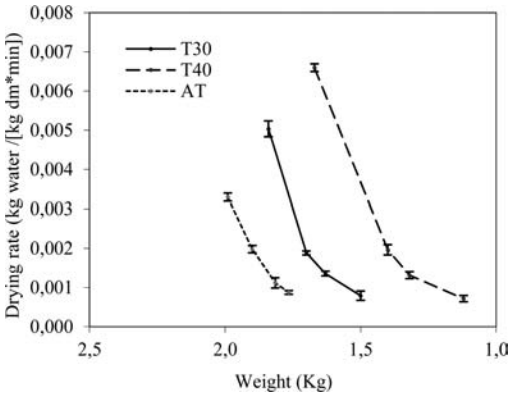

Figure 2. Variation of drying rate (kg water/[kg dm min]) as a function of the grape weight during the three controlled dehydration experiments at 30 °C (T30), 40 °C (T40), and alternating temperatures between 40 and 15 °C (AT).

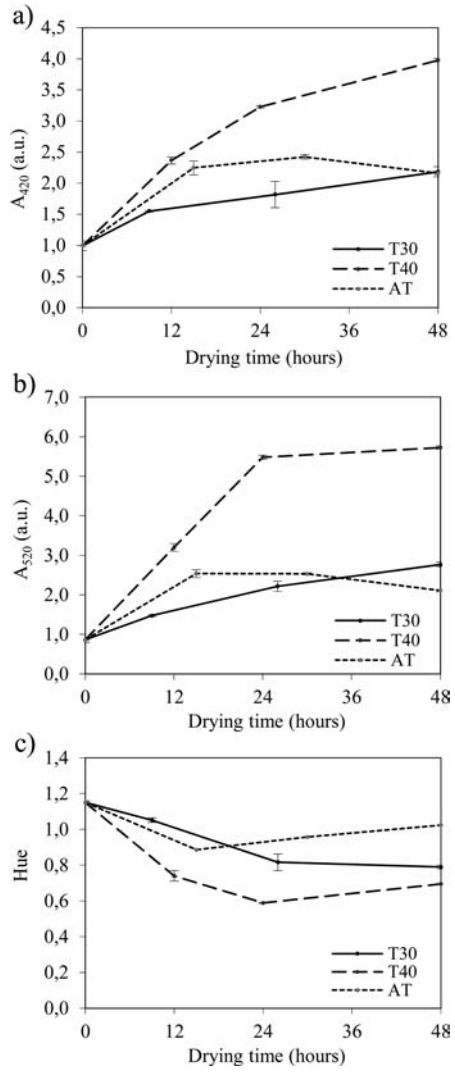

Figure 3. Changes in (a) absorbance at 420 nm (a.u.), (b) absorbance at 520 nm (a.u.), and (c) hue during the three controlled dehydration experiments at 30 °C (T30), 40 °C (T40), and alternating temperatures between 40 and 15 °C (AT).

As can be seen, an increase of absorbance at 420 nm in the three drying process took place (Figure 3a), indicating an increase in the brown color of the musts as a consequence of the grape raisining. The final values were similar in AT and T30 and, with the value of the drying at a constant temperature of 40 °C, the highest (3.98 au). The synthesis of pigments with these colors has been demonstrated by other authors[16] and can be caused by enzymatic and nonenzymatic reactions, with the necessary presence of oxygen in some of them. On one hand, the brown pigments called melanins are formed by the enzymatic activity of the polyphenoloxidases,[17] when the enzymes contact with the phenolic compounds. On other hand, the browning is known due to the Maillard reaction, a nonenzymatic reaction which induces the formation of colored compounds called melanoidins from free carbonyl and amino groups.[18] However, the latter reaction is particularly effective at temperatures above 50 °C,[19] so the synthesized pigments in the three drying assays under controlled conditions were mainly from enzymatic browning reactions.

The absorbance at 520 nm also increased during the three processes (Figure 3b), indicating a rise of the red color of the musts. The drying at 40 °C (T40) had a marked increase during the first 24 h, reaching a final value of 5.73 au. As a result, the must obtained in this process presented the reddest color, so the presence of red pigments, especially anthocyanins, was higher. These compounds could be extracted from the skins during the drying process, as a consequence of cell damage caused by heat during the dehydration process at high temperatures.[15] Because of this, the colored compounds, found naturally in grape skins, would diffuse to the pulp and later move to the must, conferring a red color. In the AT assay, the absorbance at 520 nm increased during the first 30 h and then decreased. This is an indication of the different behavior of the red compounds due to the temperature changes during the grape dehydration process. From the data, it might be thought that the colored compounds would be extracted from the skins at first, but then they could be degraded, reducing the absorbance at 520 nm.

Figure 3c shows a different reduction in the hue values during the three drying processes. In the alternating temperature assay (AT), the hue decreased to 15 h of drying and then increased. In the T40 assays, the minimum value was reached at 24 h, whereas in the T30 assay the decrease was continued to the end of the study but very slowly in the late hours. The decrease in the hue would be due to a higher increase in the A520 than in the A420, indicating that in the musts the red colors dominated the brown colors. Throughout the study, the musts from T40 showed the smallest hue values and, consequently, the reddest colors; on the contrary, the musts from AT were the most browning.

Then, the anthocyanin profile of the three musts, obtained during grapes drying at different temperatures, was studied (Table 1). The glucosides, acetylglucosides, and coumaroylglucosides of the delphinidin, cyanidin, petunidin, peonidin, and malvidin anthocyanins, in addition to the caffeoylglucoside of malvidin were quantified. Before the drying experiments, 11 of these monomers were found in the grapes, with glucosylated monomers of the main family, with a percentage of 91.6%, followed by the family of acetylglucosides (4.3%), and coumaroylglucosides (1.2%). The three controlled drying processes resulted in an increase in the concentration of anthocyanins in the first hours, reaching the maximum for most of the compounds at 15 h in AT, 24 h in T40, and 48 h in T30. The final values of all families showed significant differences. In this regard, the T40 assay resulted in a final concentration of

Table 1. Anthocyanin Concentrations (mg/L) and Homogeneous Groups during the Three Controlled Dehydration Experiments at 30 °C (T30), 40 °C (T40), and Alternating Temperatures between 40 and 15 °C (AT)[a]

	initial	T30			T40			AT		
hours	0	9	26	48	12	24	48	15	30	48
Dp-glc	0.933 ± 0.070^{a}	1.92 ± 0.042^{b}	2.50 ± 0.229^{bc}	2.89 ± 0.065^{c}	9.82 ± 0.350^{d}	16.3 ± 0.651^{e}	11.3 ± 0.404^{f}	2.74 ± 0.463^{c}	0.687 ± 0.069^{a}	0.481 ± 0.095^{a}
Cn-glc	0.587 ± 0.034^{bc}	0.693 ± 0.021^{c}	0.620 ± 0.121^{c}	0.598 ± 0.102^{bc}	4.01 ± 0.211^{d}	7.28 ± 0.169^{e}	6.68 ± 0.229^{f}	0.580 ± 0.101^{cd}	0.303 ± 0.051^{ab}	0.173 ± 0.025^{a}
Pt-glc	2.09 ± 0.091^{a}	3.38 ± 0.075^{b}	4.78 ± 0.420^{c}	5.84 ± 0.215^{c}	15.0 ± 0.519^{d}	25.2 ± 0.709^{e}	19.0 ± 0.862^{f}	5.37 ± 0.996^{c}	1.61 ± 0.114^{a}	1.12 ± 0.044^{a}
Pn-glc	3.93 ± 0.080^{bc}	3.50 ± 0.261^{b}	3.72 ± 0.450^{bc}	4.73 ± 0.130^{c}	9.98 ± 0.101^{d}	16.5 ± 0.115^{e}	17.4 ± 1.35^{e}	3.93 ± 0.744^{bc}	1.10 ± 0.092^{a}	1.29 ± 0.095^{a}
Mv-glc	26.0 ± 0.404^{a}	37.3 ± 0.379^{b}	53.7 ± 3.99^{cd}	58.1 ± 0.972^{d}	95.0 ± 2.22^{e}	149 ± 5.68^{f}	128 ± 8.30^{g}	45.6 ± 8.03^{bc}	18.9 ± 1.46^{a}	24.5 ± 2.42^{a}
	33.6 ± 0.630^{ab}	**46.7 ± 0.440^{bc}**	**65.3 ± 5.13^{de}**	**72.2 ± 1.42^{e}**	**134 ± 2.56^{f}**	**214 ± 7.18^{g}**	**182 ± 11.9^{h}**	**58.2 ± 10.3^{cd}**	**22.6 ± 1.61^{a}**	**27.5 ± 2.60^{a}**
Dp-acglc	n.d.	n.d.	n.d.	n.d.	2.61 ± 0.187^{a}	4.98 ± 0.229^{b}	5.37 ± 0.209^{c}	n.d.	n.d.	n.d.
Cn-acglc	n.d.	0.379 ± 0.070^{a}	0.594 ± 0.044^{b}	1.10 ± 0.012^{d}	2.26 ± 0.041^{e}	4.22 ± 0.029^{f}	4.25 ± 0.089^{f}	0.834 ± 0.118^{c}	0.301 ± 0.031^{a}	0.315 ± 0.044^{a}
Pt-acglc	0.268 ± 0.038^{a}	0.337 ± 0.025^{a}	0.474 ± 0.067^{b}	0.963 ± 0.049^{d}	2.88 ± 0.058^{e}	5.49 ± 0.036^{f}	5.02 ± 0.021^{g}	0.812 ± 0.077^{c}	0.277 ± 0.007^{a}	0.366 ± 0.048^{ab}
Pn-acglc	0.165 ± 0.023^{a}	0.208 ± 0.020^{a}	0.136 ± 0.009^{a}	0.445 ± 0.060^{b}	4.71 ± 0.099^{c}	7.16 ± 0.160^{d}	6.46 ± 0.155^{e}	0.276 ± 0.116^{ab}	0.062 ± 0.108^{a}	0.157 ± 0.010^{a}
Mv-acglc	1.13 ± 0.015^{a}	2.51 ± 0.085^{b}	2.61 ± 0.347^{b}	2.76 ± 0.091^{b}	8.45 ± 0.685^{c}	13.5 ± 0.416^{d}	11.6 ± 0.404^{e}	2.62 ± 0.510^{b}	1.12 ± 0.138^{a}	1.22 ± 0.197^{a}
	1.56 ± 0.020^{a}	**3.43 ± 0.060^{b}**	**3.81 ± 0.430^{bc}**	**5.26 ± 0.090^{d}**	**21.0 ± 0.874^{e}**	**35.3 ± 0.798^{f}**	**32.7 ± 0.445^{g}**	**4.54 ± 0.200^{cd}**	**1.76 ± 0.220^{a}**	**2.06 ± 0.240^{a}**
Cn-coumglc	0.181 ± 0.001^{a}	0.074 ± 0.071^{a}	n.d.	n.d.	2.41 ± 0.052^{b}	4.61 ± 0.172^{c}	4.52 ± 0.173^{c}	n.d.	0.162 ± 0.022^{a}	0.176 ± 0.171^{a}
Pt-coumglc	n.d.	0.105 ± 0.004^{a}	0.185 ± 0.012^{ab}	0.253 ± 0.027^{ab}	4.69 ± 0.022^{e}	7.45 ± 0.051^{f}	6.39 ± 0.136^{g}	0.332 ± 0.12^{bc}	0.529 ± 0.064^{d}	0.451 ± 0.039^{cd}
Pn-coumglc	n.d.	n.d.	n.d.	0.096 ± 0.003^{a}	2.51 ± 0.035^{b}	5.15 ± 0.040^{c}	5.01 ± 0.096^{c}	0.372 ± 0.571^{a}	0.262 ± 0.027^{a}	0.143 ± 0.026^{a}
Mv-coumglc	0.248 ± 0.029^{a}	0.323 ± 0.008^{a}	0.332 ± 0.006^{a}	0.850 ± 0.075^{a}	10.8 ± 0.241^{b}	18.0 ± 0.289^{c}	14.8 ± 0.737^{d}	0.837 ± 0.074^{a}	0.789 ± 0.100^{a}	0.501 ± 0.034^{a}
	0.430 ± 0.030^{a}	**0.500 ± 0.080^{a}**	**0.520 ± 0.010^{a}**	**1.20 ± 0.080^{ab}**	**20.5 ± 0.312^{c}**	**35.2 ± 0.163^{d}**	**30.7 ± 1.14^{e}**	**1.54 ± 0.660^{b}**	**1.74 ± 0.070^{b}**	**1.27 ± 0.170^{ab}**
Mv-cafglc	0.298 ± 0.017^{a}	0.484 ± 0.068^{ab}	0.294 ± 0.018^{a}	0.619 ± 0.069^{bcd}	4.01 ± 0.098^{e}	7.67 ± 0.116^{f}	8.35 ± 0.251^{g}	0.812 ± 0.033^{d}	0.538 ± 0.041^{bc}	0.735 ± 0.062^{cd}
Total	**35.9 ± 0.665^{a}**	**51.2 ± 0.415^{b}**	**69.9 ± 5.58^{c}**	**79.3 ± 1.63^{c}**	**179 ± 3.62^{d}**	**292 ± 8.22^{e}**	**254 ± 12.8^{f}**	**65.1 ± 10.0^{bc}**	**26.6 ± 1.74^{a}**	**31.6 ± 2.76^{a}**

[a]Dp, delphinidin; Cn, cyanidin; Pt, petunidin; Pn, peonidin; Mv, malvidin; glc, glucoside; acglc, acetylglucoside; coumglc, coumaroylglucoside; cafglc, caffeoylglucoside. n.d. = not detected. Values in the same row with different superscript letters are significantly different, $p = 0.01$.

dx.doi.org/10.1021/jf502235b | J. Agric. Food Chem. 2014, 62, 7897−7902

total anthocyanins of 254 ± 12.8 mg/L compared to the concentrations of 79.3 ± 1.64 and 31.6 ± 2.76 mg/L obtained for T30 and AT, respectively, so the anthocyanin concentration was significantly higher when the process took place at a high and constant temperature. At the end of the drying processes, the glucoside derivatives represented a percentage of 91.0% in T30, followed by AT and T40 with values of 87.0 and 71.6%, respectively, indicating that the percentage of the glucosides derivatives decreased more markedly in the drying at 40 °C. The acetylglucosides represented 6.63, 12.9, and 6.52% in T30, T40, and AT, respectively, and this family increased their representation in the final musts. The coumaroylglucosides derivatives represented 1.51, 12.1, and 4.02% and, finally, the caffeoylglucoside derivative 0.7, 3.28, and 2.33% in T30, T40, and AT, respectively. These derivatives increased more markedly in the dryings at 40 °C and alternating temperatures.

The drying at 40 °C was the process that showed major differences; greater similarities in the processes carried out at 30 °C and alternating temperatures were found. Specifically, the final values of most compounds in the AT assay showed no significant differences with the initial values, indicating that this drying did not alter significantly the content in anthocyanins. Nevertheless, the assays at constant temperature increased the final content of all the anthocyanin families, with the final values at 40 °C the highest. Due to the difference found in the three experiments being very marked, especially in the case of T40, the temperature had an important influence on the extraction of these compounds.

To explain the changes in color and anthocyanin composition after the three dehydration processes, a possible hypothesis based on different temperature conditions has been proposed. At first, when the temperature was constant and high during the process, the water evaporation through the berries was continuous, so this evaporation could reduce the molecular oxygen diffusion to the berry, which is necessary in the browning reactions. At the same time, the dehydration would cause cell damage in berries, with consequent skin breakage. Structural changes in the cell are irreversible and can improve the diffusion of compounds from the skin to the pulp, especially polyphenols. The anthocyanins are the main polyphenols in the grape skins, so the drying should increase the concentration of red compounds in the pulp and prevent the formation of brown compounds.

In the process with alternating temperature, when the temperature was maintained at 40 °C, a water evaporation from the berries occurred, reducing the oxygen entry. However, when the temperature was lowered to 15 °C, the water evaporation stopped and the oxygen could enter more easily through the berry skins. Also, the low temperature favored the oxygen solubilization. In this moment, the oxygen presence could cause browning reactions, increasing the musts hue and the brown color. Concurrently, the red color could be decreased because the anthocyanins could be substrates of different reactions. In this regard, it is demonstrated that anthocyanins are substrates in the browning reactions, but they can also participate in several direct condensation reactions with themselves or with tannins, in condensation reactions with flavanols, through or not a bridge methylmethyne[20,21] and/or copigmentation reactions.[22]

Finally, the hypothesis could also explain the higher concentration of anthocyanins reached in the process at 40 °C (T40) compared with the drying at 30 °C (T30). The higher temperature used in the first process could cause more damage to the grape skins, favoring a greater compound transfer to the pulp. In addition, the hindrance to the oxygen diffusion was minor at 30 °C compared with that at 40 °C, so there were higher concentrations of oxygen in the pulp of grapes dried at 30 °C and, consequently, the reactions involving anthocyanins were more favored. Most likely, both processes occurred simultaneously during the T30 drying. On the one hand, the temperature of 30 °C used damaged cells skin but not as much as 40 °C. Furthermore, the anthocyanins, which were diffused to the pulp, reduced their concentration because they would take part in polymerization or condensation reactions with tannins, with other anthocyanins, or with flavanols,[15,23] as well as in copigmentation reactions.[24]

In recent years, there has been a growing interest in winemaking products due to their antioxidant properties and beneficial effects in the prevention of various diseases.[25] Therefore, the evolution of the antioxidant activity was studied during the three controlled dehydration experiments (Figure 4). As can be seen, the antioxidant activity increased in the

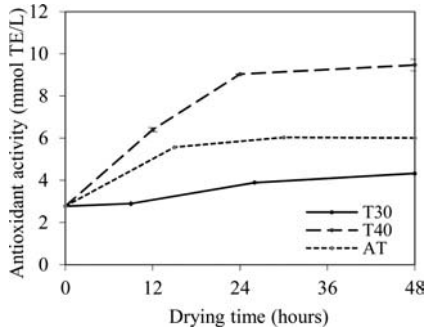

Figure 4. Changes in antioxidant activity (mmol TE/L) during the three controlled dehydration experiments at 30 °C (T30), 40 °C (T40), and alternating temperatures between 40 and 15 °C (AT).

three experiments, with the higher increments measured during the drying at 40 °C (T40), with the highest final value (9.5 mmol TE/L). The increments in the other dryings were 1.6 and 2.2 for T30 and AT, respectively, reaching final values of 4.3 and 6.0 mmol TE/L for the same tests.

Figure 5 shows a principal component analysis performed with the data of color, anthocyanin concentration, and

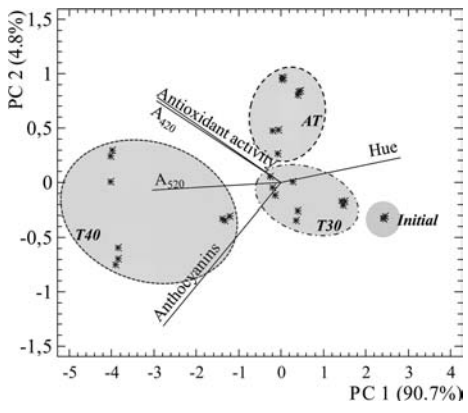

Figure 5. Principal component analysis: biplot representation of must samples and statistical variables during the three controlled dehydration experiments at 30 °C (T30), 40 °C (T40), and alternating temperatures between 40 and 15 °C (AT).

dx.doi.org/10.1021/jf502235b | J. Agric. Food Chem. 2014, 62, 7897−7902

antioxidant activity during the three controlled drying experiments. The first two components jointly explained 95.5% of the total variance of the process, with PC1 the most important with 90.7%. This component influenced all the studied parameters with similar factors, with the hue the one with a positive influence (0.4325). The other four influenced negatively on PC1 with factors of −0.4674 for A_{520}, −0.4542 for A_{420}, −0.4518 for antioxidant activity, and −0.4290 for the anthocyanins concentration. Under this component, the samples corresponding to T30 and AT differed statistically from T40, which experienced the most marked changes during drying. As a result, the final must of T40 was the most different from the initial must and presented higher absorbance values, anthocyanins, and antioxidant activity and the lowest values of hue. Consequently, dehydration at a constant temperature of 40 °C would be the most suitable if the desire is to obtain musts with an important red color and high concentration of antioxidant compounds.

In conclusion, the temperature used during the controlled dehydration of red grapes influenced the color and composition of the final musts. When the temperature was high and constant during the assay, an important extraction of anthocyanins from the skins to the pulp was obtained, as a result of damage caused by the water evaporation of berries. Consequently, the musts presented an increase in red color and antioxidant activity. At lower temperatures, the water evaporation decreased, facilitating the oxygen diffusion into the berries, and resulting in degradation reactions of anthocyanins, which caused a loss of red color.

AUTHOR INFORMATION

Corresponding Author

*E-mail: jmerida@uco.es. Tel: +34 957 218 612. Fax: +34 957 212 146.

Notes

The authors declare no competing financial interest.

REFERENCES

(1) Doymaz, I.; Ozdemir, O. Effect of air temperature, slice thickness and pretreatment on drying and rehydration of tomato. *Int. J. Food Sci. Technol.* **2013**, *49* (2), 558−564.

(2) Ruiz, M. J.; Zea, L.; Moyano, L.; Medina, M. Aroma active compounds during the drying of grapes cv. Pedro Ximénez destined to the production of sweet sherry wine. *Eur. Food Res. Technol.* **2010**, *230*, 429−435.

(3) Pangavhane, D. R.; Sawhney, R. L. Review of research and development work on solar dryers for grape drying. *Energy Convers. Manage.* **2002**, *43*, 45−61.

(4) Cortés, S.; Salgado, J. M.; Rivas, B.; Torrado, A. M.; Domínguez, J. M. Fermentation kinetics and chemical characterisation of Vino Tostado, a traditional sweet wine from Galicia (NW Spain). *J. Sci. Food Agric.* **2010**, *90*, 121−131.

(5) Paronetto, L.; Dellaglio, F. Amarone: A modern wine coming from an ancient production technology. *Adv. Food Nutr. Res.* **2011**, *63*, 285−306.

(6) Doymaz, I.; Smail, O. Drying characteristics of sweet cherry. *Food Bioprod. Process.* **2011**, *89* (1), 31−38.

(7) Serratosa, M. P.; López-Toledano, A.; Mérida, J.; Medina, M. Changes in color and phenolic compounds during the raisining of grape cv. Pedro Ximénez. *J. Agric. Food Chem.* **2008**, *56*, 2810−2816.

(8) Bellicontro, A.; De Santis, D.; Botondi, R.; Villa, I.; Mencarelli, F. Different postharvest dehydration rates affect quality characteristics and volatile compounds of Malvasia, Trebbiano and Sangiovese grapes for wine production. *J. Sci. Food Agric.* **2004**, *84*, 1791−1800.

(9) Barbanti, D.; Mora, B.; Ferrarini, R.; Tornielli, G. B.; Cipriani, M. Effect of various thermo-hygrometric conditions on the withering kinetics of grapes used for the production of "Amarone" and "Recioto" wines. *J. Food Eng.* **2008**, *85*, 350−358.

(10) Bellincontro, A.; Nicoletti, I.; Valentini, M.; Tomas, A.; De Santis, D.; Corradini, D.; Mencarelli, F. Integration of nondestructive techniques with destructive analyses to study postharvest water stress of winegrapes. *Am. J. Enol. Vitic.* **2009**, *60*, 57−65.

(11) Serratosa, M. P.; López-Toledano, A.; Medina, M.; Mérida, J. Drying of Pedro Ximénez grapes in chamber at controlled temperature and with dipping pretreatments. Changes in the color fraction. *J. Agric. Food Chem.* **2008**, *56*, 10739−10746.

(12) Serratosa, M. P.; López-Toledano, A.; Millán, C.; Medina, M.; Mérida, J. Changes of ochratoxin A in grapes inoculated with Aspergillus carbonarius and subjected to chamber-drying under controlled conditions. *J. Agric. Food Chem.* **2010**, *58*, 11907−11912.

(13) Serratosa, M. P.; Márquez, A.; López-Toledano, A.; Medina, M.; Mérida, J. Differences in browning index and CIELAB coordinates of the two grape drying processes, traditional sun-drying and chamber-drying and during the ageing of Pedro Ximenez sweet wine. *J. Life Sci.* **2011**, *5*, 974−980.

(14) Marquez, A.; Serratosa, M. P.; López-Toledano, A.; Mérida, J. Colour and phenolic compounds in sweet red wines from Merlot and Tempranillo grapes chamber-dried under controlled conditions. *Food Chem.* **2012**, *130*, 111−120.

(15) Marquez, A.; Serratosa, M. P.; Merida, J. Anthocyanin evolution and color changes in red grapes during their chamber drying. *J. Agric. Food Chem.* **2013**, *61* (41), 9908−9914.

(16) Karadeniz, F.; Durst, R. W.; Wrolstad, R. E. Polyphenolic composition of raisins. *J. Agric. Food Chem.* **2000**, *48*, 5343−5350.

(17) Cheynier, V.; Moutounet, M. Oxidative reactions of caffeic acid in model systems containing polyphenol oxidase. *J. Agric. Food Chem.* **1992**, *40*, 2038−2044.

(18) Kim, J. S.; Lee, Y. S. Effect of reaction pH on enolization and racemization reactions of glucose and fructose on heating with amino acid enantiomers and formation of melanoidins as result of the Maillard reaction. *Food Chem.* **2008**, *108*, 582−592.

(19) Oliveira, C. M.; Silva Ferreira, A. C.; De Freitas, V.; Silva, A. M. S. Oxidation mechanisms occurring in wines. *Food Res. Int.* **2011**, *44*, 1115−1126.

(20) Pissarra, J.; Lourenço, S.; González-Paramás, A. M.; Mateus, N.; Santos-Buelga, C.; De Freitas, V. Formation of new anthocyanin-alkyl/aryl-flavanol pigments in model solutions. *Anal. Chim. Acta* **2004**, *513*, 215−221.

(21) Marquez, A.; Serratosa, M. P.; Merida, J. Pyranoanthocyanin derived pigments in wine: Structure and formation during wine-making. *J. Chem.* **2013**, *2013*, Article ID 713028, 1−15.

(22) Boulton, R. The copigmentation of anthocyanins and its role in the color of red wine: a critical review. *Am. J. Enol. Vitic.* **2001**, *52*, 67−87.

(23) Pissarra, J.; Lourenço, S.; Gonzalez-Paramas, A. M.; Mateus, N.; Santos-Buelga, C.; De Freitas, V. Formation of new anthocyanin-alkyl/aryl-flavanol pigments in model solutions. *Anal. Chim. Acta* **2004**, *513*, 215−221.

(24) Boulton, R. The copigmentation of anthocyanins and its role in the color of red wine: A critical review. *Am. J. Enol. Vitic.* **2001**, *52*, 67−87.

(25) Arts, I. C. W.; Hollman, P. C. H. Polyphenols and disease risk in epidemiologic studies. *Am. J. Clin. Nutr.* **2005**, *81*, 317S−325S.

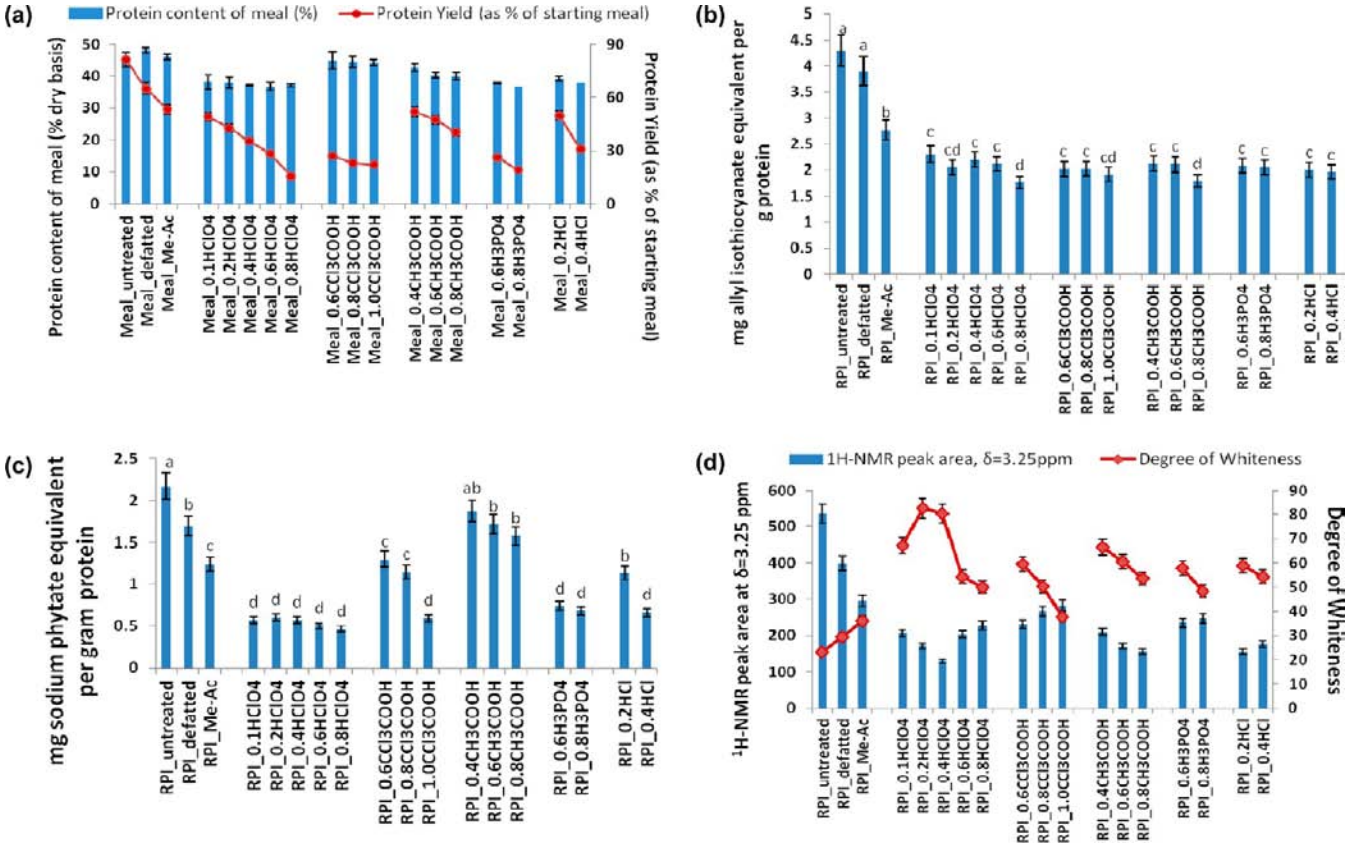

Figure 1. (a) Protein content of rapeseed meals treated with different solvents and their corresponding protein yield; impact of solvent treatment on (b) AITC, (c) phytates, and (d) sinapine content and degree of whiteness of the produced isolates.

equal to or higher than that of the solvent system having only methanol and acetone mixture (Me-Ac, 1:1 v/v). This criterion was fulfilled by 15 different solvent systems containing Me-Ac (1:1 v/v) in combination with different acids: 0.1, 0.2, 0.4, 0.6, or 0.8% perchloric acid ($HClO_4$); 0.6, 0.8, or 1.0% trichloroacetic acid (CCl_3COOH); 0.4, 0.6, or 0.8% acetic acid (CH_3COOH); 0.6 or 0.8% phosphoric acid (H_3PO_4); and 0.2 or 0.4% hydrochloric acid (HCl). As such, samples used for the preparation of protein isolates included (i) meal without any solvent treatment as control (untreated), (ii) meal treated with diethyl ether for removing lipids (defatted), (iii) defatted meal treated with Me-Ac (1:1 v/v) without any added acid, and (iv) defatted meal treated with Me-Ac (1:1 v/v) added with various concentrations of different acids as stated above.

Preparation of Solvent-Treated Meals. Meal (1 g) was treated with 10 mL of different solvents (mentioned above) according to earlier protocol.[3]

Preparation of Protein Isolate from Untreated or Solvent-Treated Meals. Meal (20 g) was extracted with water (meal/solvent ratio = 1:20 (w/v)) at room temperature for 1 h under constant agitation (200 rpm) in an orbital shaker (Sartorius Stedin Biotech, CERTOMAT IS) and then centrifuged at 4 °C (Sigma 3-18K centrifuge) to get aqueous extract. The pellet was re-extracted as before with NaOH solution at pH 11. Both extracts were combined, to which ammonium sulfate was added up to 85% saturation.[4] The resulting precipitate was redispered in water, adjusted to pH 7, dialyzed against Milli-Q water, and finally freeze-dried to obtain rapeseed protein isolate (RPI).

The respective meal and its corresponding isolate are denoted on the basis of the solvent used for their processing (mentioned in Figure 1a,b). Protein purity of all the isolates was >80% (dry basis), based on Kjeldahl nitrogen (N × 6.25). The yield was calculated as follows:

$$\%\ \text{protein yield} = \frac{\text{wt of protein isolate} \times \%\ \text{protein in isolate}}{\text{wt of starting meal} \times \%\ \text{protein in starting meal}} \times 100 \quad (1)$$

Quantification of Antinutritional Compounds. Sinapine content was determined according to the method developed by Wanasundara et al.[5] Freeze-dried protein was extracted with 99.8% methanol (1:20, w/v) in a round-bottom flask for 48 h with stirring. The extract was filtered through cotton wool, concentrated under vacuum, to which internal standard (*N*,*N*-dimethylformamide) was added, and then resuspended in deuterium oxide (1 mL). Proton NMR signals were recorded at 400 MHz using a JEOL ^{1}H NMR system. Singlet peak at δ 3.25 ppm was identified as phenylpropanoid ester (sinapic acid ester or sinapine).

Protocols for estimating phytates, glucosinolates, and AITC are the same as those reported earlier.[3]

Analytical Methods. Color was determined with a Hunter Lab colorimeter (Ultrascan, VIS-Hunter Associates Laboratory, Reston, VA, USA). The majority of the isolates displayed a similar off-white color (Supporting Information Figure S1). However, upon dissolution in water, their solution showed a light brown color of different intensities, an observation that was consistent with a previous paper.[6] Therefore, following the protocol of Xu and Diosady,[6] colorimetric evaluation was performed by scanning their aqueous solution (7 mg/mL). Measured values were expressed as L (lightness), a (redness/greenness), and b (yellowness/blueness) color units. Whiteness was calculated as follows:[7]

$$\text{degree of whiteness} = 100 - [(100 - L)^2 + a^2 + b^2]^{1/2} \quad (2)$$

Ultraviolet (UV)−visible (vis) spectroscopy was performed on a UV−vis CECIL 7400 spectrophotometer (Aquarius, 7000 series) by scanning an aqueous protein solution (2 mg/mL).

dx.doi.org/10.1021/jf5023803 | J. Agric. Food Chem. 2014, 62, 7903−7914

Free sulfhydryl group (SH) and disulfide bond (SS) were assayed according to the methods of Tang et al.[8] and Deng et al.[9] Surface hydrophobicity (S_0) was measured by using the SDS binding method.[10,11]

Intrinsic fluorescence spectra were recorded in a PerkinElmer LS55 fluorescence spectrophotometer (PerkinElmer Corp., Boston, MA, USA) using a 2 mg/mL protein solution and background calibrated with Milli-Q water. To minimize the contribution of tyrosine residues, the solution was excited at 290 nm.[4]

Fourier transform infrared (FTIR) spectroscopy was carried out on solid samples according to the KBr pelleting method using a PerkinElmer Spectrum-100 model.

Differential scanning calorimetry (DSC) was performed in a DSC-60 (Shimadzu, Kyoto, Japan), using 5 mg of freeze-dried sample according to the methods of Manamperi et al.[12] and Li et al.[13] Denaturation temperature (T_d) and enthalpy (ΔH) were acquired from the thermogram using TA-60WS software (Shimadzu).

Sodium dodecyl sulfate−polyacrylamide gel electrophoresis (SDS-PAGE) was performed in a Bio-Rad vertical electrophoresis system (Bio-Rad Laboratories, Hercules, CA, USA) with 12% separating and 5% stacking gels (12.5 cm × 14 cm and 0.75 mm thickness), following the procedure provided by the manufacturer. Freeze-dried samples (4 g/L) were solubilized in either nonreducing or reducing (2% β-mercaptoethanol (β-ME)) buffer solution, heated for 5 min in boiling water, and then centrifuged at 10000 rpm for 3 min prior to loading. Fifteen microliters of each sample was loaded onto a gel lane. A constant current of 45 mA per gel was applied for 1 h (approximately), stained with Coomassie Brilliant Blue (0.125%) in 25% methanol and 10% acetic acid, and then destained with 40% methanol and 10% acetic acid. A GelDoc system equipped with Vilber Lourmat image analysis software was used for scanning the gel. Premixed protein markers (high range, catalog no. 623110375001730; and medium range, catalog no. 623112375001730, Genei, Bangalore, India) [myosin (205 kDa), phosphorylase *b* (98 kDa), bovine serum albumin (68 kDa), ovalbumin (44 kDa), glutathione-*S*-transferase (29 kDa), and lysozyme (16 kDa)] were used for molecular weight (MW) comparison. Nondenaturing polyacrylamide gel electrophoresis (native-PAGE) was performed on 7% separating gel and 3% stacking gel. The main differences from the SDS-PAGE assay were the absence of SDS and β-ME in the procedure and no thermal treatment before electrophoresis.

Protein solubility (at neutral pH) was measured according to the Lowry method using bovine serum albumin as standard.[14,15] Results were expressed as percentage of the nitrogen protein in the starting isolates (determined by Kjeldahl).

Foaming capacity (FC) and stability (FS) were evaluated according to the protocol of Hassan et al.[16] Emulsion capacity (EC) and stability (ES) were also studied according to the methodology of Hassan et al.[16] after incorporation of a slight modification from Kalashnikova et al.[17] Oil-in-water (o/w) emulsions were prepared by blending soybean oil with aqueous protein solution (7 mg/mL) at a ratio of 3:7 (v/v). The mixture was sonicated to form an emulsion using an ultrasonic water bath (Labotec Inc., Nottingham, UK) for 10 min. Fifteen microliters of the resulting emulsion was added to 1 mL of distilled water and stirred gently, and then a single drop was poured onto a glass slide and observed via light microscope (BX51 Olympus). Droplet diameter (μm) was measured by ImageJ software, and average droplet diameter (d_{43}) is expressed as[18]

$$d_{43} = \frac{\sum n_i d_i^4}{\sum n_i d_i^3} \tag{3}$$

where n_i is the number of droplets of diameter d_i.

Statistical Analyses. All analyses were performed in triplicate, and the mean value was calculated. Analysis of variance and separation of means were carried out by Tukey's HSD test, using SPSS software (version 16.0, SPSS Inc., Chicago, IL, USA) and considered significantly different at $p < 0.05$.

RESULTS AND DISCUSSION

Untreated or treated meals were first analyzed by Kjeldahl process for checking their protein content and to evaluate whether the treatments led to any protein loss. The protein content of the treated meals was within a range (36.7−48.1%) similar to that of the control (44.8%) (Figure 1a). Marginal increases in the protein level of defatted and Me-Ac-treated meals were expected, due to leaching of lipids and nitrogen-free compounds. A slight reduction of protein content in $HClO_4$- and H_3PO_4-treated meals may be due to the removal of nonprotein nitrogen in the form of glucosinolates, triamine compounds such as betaine, choline, sinapine, and free amino acids. As the use of nitrogen content to estimate protein levels of oilseeds and meal has been the norm for the oilseed industry,[5] greater elimination of these nitrogen-containing components by the acidified solvents reduced the crude protein level in such meals. This may also be the reason for the decreasing trend of protein content in CCl_3COOH- and CH_3COOH-treated meals with increasing acid concentration. Overall, the actual protein loss from the meal during solvent treatment was minimal due to the presence of a high concentration of nonpolar solvents (methanol and acetone), instead of any aqueous medium, which ensures negligible protein dissolubility. Unfortunately, the treatments diminished protein yield, which dropped almost linearly from by >81% to 15.6% with the rise in acid concentration, indicating dramatic decreases in protein solubility and denaturation. It seems highly likely that the acidified organic solvents (acetone in particular) produced a dehydrating effect and underwent different interactions with the proteins, leading to nonextractable complexes/aggregates. Pretreatment of rapeseed/canola meal with a two-phase solvent system ($CH_3OH/NH_3/H_2O$/hexane) also resulted in a similar reduction in protein yield.[19]

Effect on Antinutritional Factors. Glucosinolate level was undetectable in all of the isolates (<0.15 μg sinigrin equivalent/g protein), indicative of its complete elimination or rapid degradation into AITC[3] during processing. Defatting and successive treatment with Me-Ac mixture led to a progressive decrease in AITC content of the respective isolate (Figure 1b). Isolates from acid-treated meals were characterized by a lower content of AITC as compared to untreated RPI ($p < 0.05$), the extent of decrease being almost similar for any such isolate. With regard to phytates, a distinct decreasing trend with increasing acid concentration was found, confirming that each treatment indeed removed some phytates from the meal and, thus, from the isolates (Figure 1c). The phytate level of all the isolates were well below the value reported for soy protein isolate containing flour-type infant foods (>230 mg/100 g), estimated using Wade reagent.[20] Samples from $HClO_4$-treated meals presented the lowest value (0.47−0.57 mg/g), which supported our earlier findings that $HClO_4$ helps in maximum removal of phytates among the tested acids.[3]

Phenolic compounds (chiefly sinapine, choline ester of sinapic acid) are important factors when rapeseed protein is considered for use in food formulations,[1] as they are found to cause unacceptable darkening. As anticipated, successive treatment with higher levels of acids resulted in remarkable reduction in sinapine content (Figure 1d), manifested from their NMR peak area (Supporting Information Figure S2). Sinapine level in RPI_untreated (as 100%) was considerably higher than that of RPI_defatted (74.8%) and RPI_Me-Ac (55.3%). For isolates from $HClO_4$- (RPI_0.6$HClO_4$ and

dx.doi.org/10.1021/jf5023803 | J. Agric. Food Chem. 2014, 62, 7903−7914

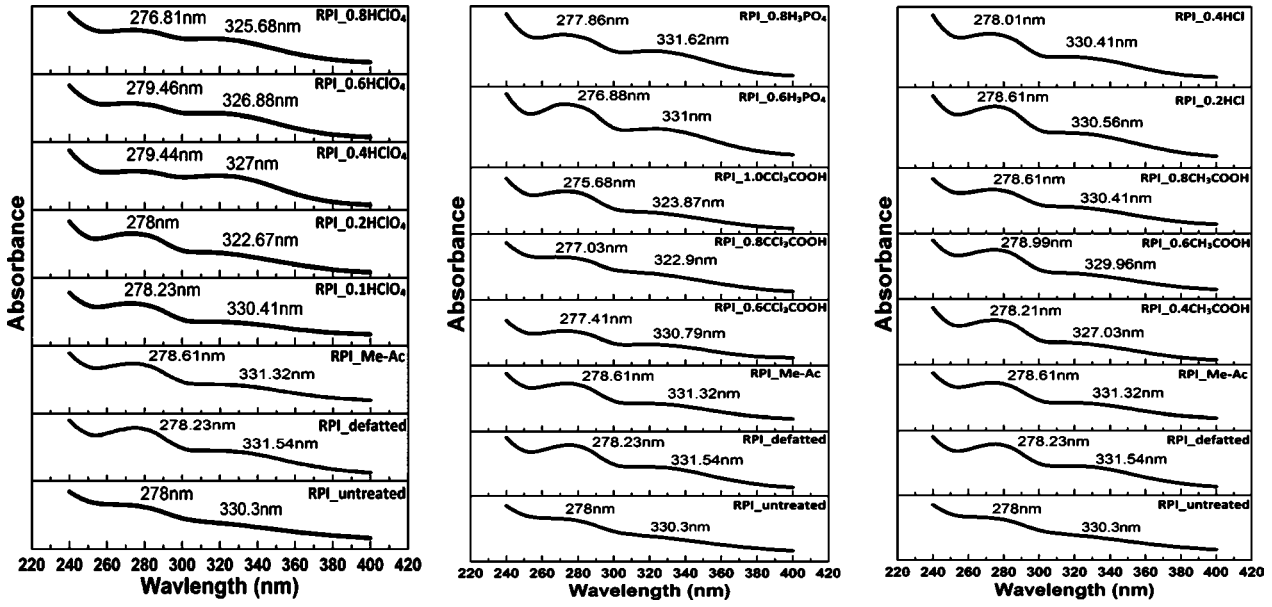

Figure 2. UV absorption spectra of soluble proteins in Milli-Q water from different meals.

RPI_0.8$HClO_4$), CCl_3COOH-, and H_3PO_4-treated meals, the increase in sinapine was mainly contributed by preferential association of polyphenols with some specific proteins to form protein−polyphenol complexes, which can be augmented to a great extent by the presence of denatured proteins. The higher acid concentration used in this study denatures protein (discussed later). Denatured protein provides additional binding sites for phenolic compounds.[21] Charlton et al.[22] proved that intermolecular binding between polyphenols and protein/peptides is dominated by stacking of polyphenolic rings onto planar hydrophobic surfaces and is strengthened by multiple cooperative bindings of phenolic rings. When the coating is sufficiently extensive to provide polyphenol bridges, precipitation occurs. Such polyphenols may readily oxidize into color-forming quinones during protein extraction in an alkaline medium, which cannot be eliminated later.[15] This is an indirect indication that such isolates with high phenolic content or their oxidized forms would possess darker appearance (as shown in Figure S1 in the Supporting Information). The above-stated reasons probably accounted for the observed general increase in degree of whiteness of the isolates with decrease in their sinapine content (Figure 1d), except for the samples obtained from CH_3COOH-treated meals, in which the decrease in sinapine paralleled the decrease in whiteness value. The exact reason for this discrepancy could not be deduced. RPI_0.2H-ClO_4 and RPI_0.4$HClO_4$ had the highest values, which can be ascribed to their least sinapine content. Compared to the extent of decrease in sinapine (1.3−4.1-fold), the extent of increase in whiteness (1.3−3.6-fold) was slightly less. Data indicated that the influence of the treatment with acidic organic solvents on the whiteness of the isolates was mainly due to the reduction in protein-bound polyphenols or their oxidized forms; however, too intensive treatments to remove phenolics may not give a satisfactory lighter product.

Effect on Physicochemical Properties. UV spectra of the protein solutions showed similar profiles irrespective of the acid used for treating the meal (Figure 2). Strong UV absorbances in tryptophan (>290 nm) and phenylalanine (<275 nm) regions were not detected. The spectra mainly revealed changes in the position of peak maxima in the tyrosine region (275−290 nm), which give evidence of rearrangement in the protein structure. Tyrosine peak maxima of RPI_defatted and RPI_Me-Ac showed a red shift with reference to RPI_untreated. Proteins obtained from the meals treated with $HClO_4$ (0.1−0.6%), CH_3COOH, and HCl also presented a red shift with respect to the control. This bathochromic effect could be attributed to a more polar environment of tyrosine residues.[23] Among others, RPI_0.8$HClO_4$ and the proteins recuperated from CCl_3COOH- and H_3PO_4-treated meals produced a shift of the maxima to lower wavelengths (blue shift) in comparison to the control. The appearance of a blue shift could be due to the exposure of chromophores present at the interface of the subunits or from the interior of the molecule due to unfolding or dissociation, followed by rapid reaggregation or non-native refolding of denatured molecules.[24] A second weaker peak within 322−332 nm was seen in all spectra. Absorbance in this region may correspond to the residual phenolic compounds (mainly sinapic acid or sinapine) complexed with rapeseed proteins.[25] Phenolics in rapeseed bind to the protein through a variety of mechanisms in aqueous media, including hydrogen bonding, covalent binding, hydrophobic interactions, and ionic binding.[1] The impact of the various acids on structural changes of phenolics and their cross-linking with protein might be different in each case, in terms of degree and site/domain of interaction,[7] which could be one of the possible reasons for the slight differences in the position of this second absorption band. Thus, the extent of structural changes due to denaturation and complexation differs for each protein sample.

Figure 3a shows free SH and SS contents of the isolates. Treatment with acidified solvents affected their number as opposed to that of untreated meal protein ($p < 0.05$). SH groups of CH_3COOH-, H_3PO_4-, and HCl-treated samples were comparable to those of RPI_defatted and RPI_Me-Ac, whereas the level markedly increased in $HClO_4$-treated ones. The increase can be ascribed to the higher removal of polyphenols from such samples and subsequent exposure of SH groups. Covalent attachment of the phenolic compounds to protein via its hydroxyl and carbonyl groups are known to cause the blocking of amino and thiol groups.[8,26] A drastic reduction of SH in CCl_3COOH-treated samples was possibly because most

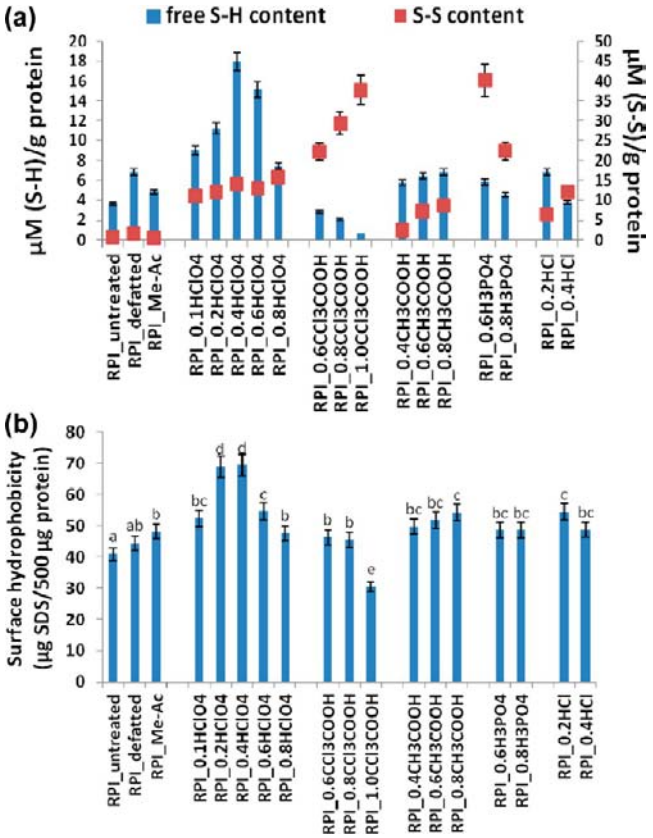

Figure 3. (a) Free sulfhydryl and disulfide content; (b) surface hydrophobicity of isolates prepared from different meals.

or all of the available free SH groups had reacted. It is worth noting that the nature of aggregates, that is, spatial distribution and accessibility of SH groups, might also play an important role in causing such differences.[27,28] In the case of SS content, all of the acid-treated samples showed much higher values compared to the control, with special emphasis to CCl_3COOH-(51.5−30.4-fold increase) and H_3PO_4-treated (54.9−30.6-fold increase) ones. The presence of such a high amount of S−S in these samples clearly explains their poor solubility/dispersibility and high aggregate formation, as observed in SDS-PAGE and FTIR results. It is feasible to believe that the formation of the S−S bond was in agreement with the decrease in thiol content.[27] Organic solvent treatment followed by alkaline extraction induced unfolding of protein and subsequent exposure of SH groups from the interior of protein molecules, which possibly underwent oxidation to form S−S linkages. Also, the conformation of protein is severely compromised in the presence of higher acid concentration, which then competes with the formation of non-native intermolecular interactions giving rise to the S−S bond.[29] Although this supposition seems to be suitable for explaining the rise in S−S content in the majority of the samples, in the case of $HClO_4$-treated isolates, the presence of high SH group content was not accompanied by an increase in S−S level. This may possibly be due to the presence of very low phenolic compounds in these samples: factually, it has been suggested that plant polyphenols are oxidized to quinones. Quinones may then form peroxides under extreme conditions, which are highly reactive oxidizing agents, and could facilitate oxidation of thiol and amino acid residues and polymerization of proteins, that is, favoring S−S formation.[30]

S_0 is an indicator of the number of hydrophobic groups on the protein surface that are in contact with the polar aqueous

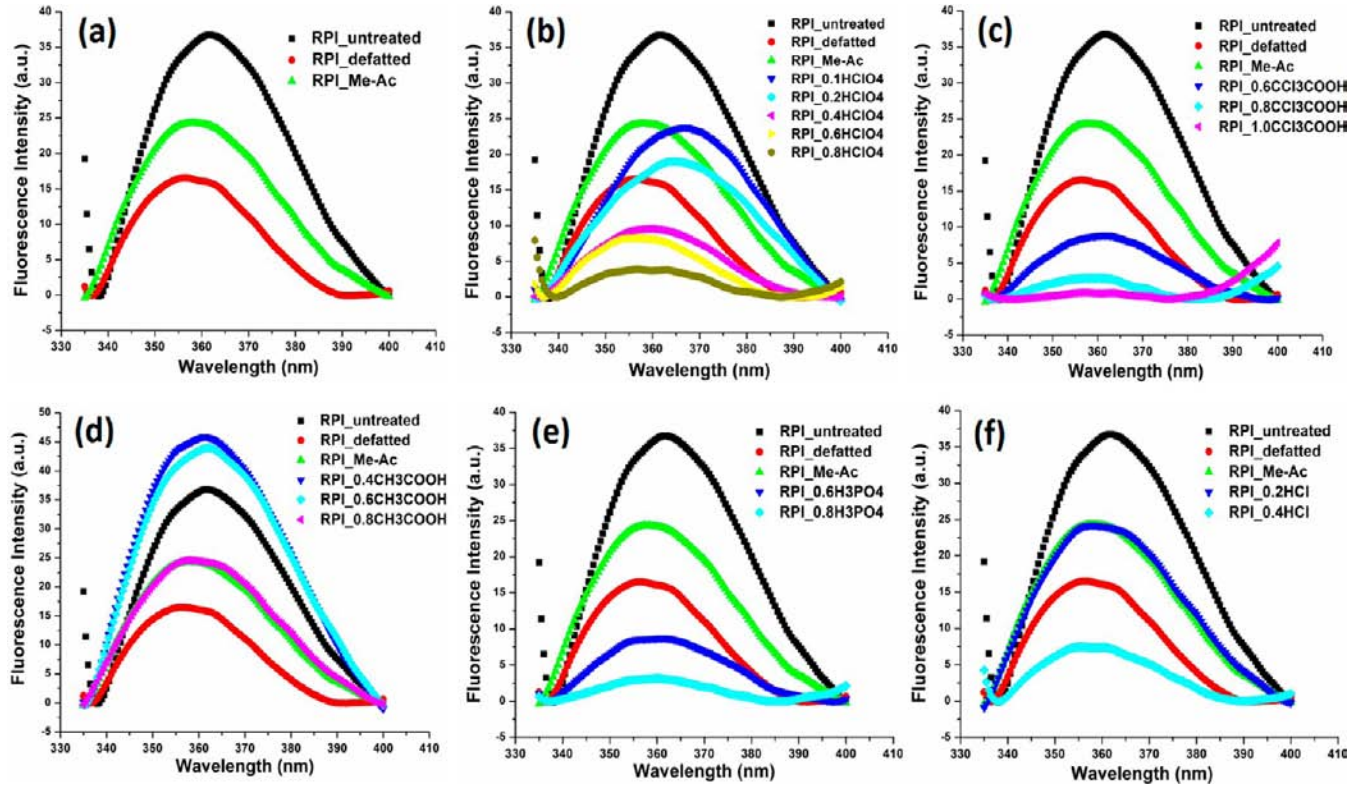

Figure 4. Comparative representation of emission fluorescence spectra of isolates from different solvent-treated meals (excitation at 290 nm).

dx.doi.org/10.1021/jf5023803 | J. Agric. Food Chem. 2014, 62, 7903−7914

environment. In other words, the level of protein unfolding can be measured by its S_0 value. Overall, S_0 of oilseed proteins is known to be significantly higher than those of other food proteins.[31] S_0 slightly increased at low acid treatment (0.1−0.4% $HClO_4$ and 0.4−0.8% CH_3COOH), presumably due to partial unfolding and subsequent uncovering of more buried hydrophobic moieties such as the thiol group (Figure 3b). Further application of a higher concentration of acids might have caused greater extent of conformational changes, promoting hydrophobic interactions between the unfolded and/or dissociated molecules to form rapid aggregation, thus causing restricted access to buried hydrophobic moieties.[27,28] Markedly lower S_0 values of such samples corroborates this supposition.[32] Again, many researchers proposed that complexation of protein with polyphenols reduces hydrophobicity.[26] Acidified solvent treatment initiates the unfolding of the native protein structure and exposes the hydrophobic groups to interaction with the residual polyphenols, thus blocking the reactive residues. This might account for the low S_0 values in samples having high sinapine content.

The intrinsic fluorescence emission spectrum of protein is usually dominated by tryptophan (Trp) and provides sensitive detection of tertiary conformation of the protein involved. Emission spectra of all the isolates are collectively shown in Figure S3 in the Supporting Information, and the spectra of protein samples from each type of acid used are segregated individually (Figure 4) along with RPI_untreated, RPI_defatted, and RPI_Me-Ac for ease of comparison. Spectra of the isolates are typical of those generally obtained for Trp-containing proteins. The emission maximum (λ_{max}) of Trp buried within the protein is expected below 330 nm,[33] and that of pure napin is reported at 333 ± 1 nm.[23] However, RPI_untreated showed λ_{max} at around 362 nm. This discrepancy may be due to the presence of a mixture of proteins in the isolate, instead of a pure fraction. Exposure of Trp residues on the protein surface, possibly fostered by heat generated during mechanical oil pressing in concert with alkaline protein extraction technique, might have led to such deviation. Solvent-exposed Trp is mostly observed above 335 nm,[33] which was apparent in all of the tested samples. Changes in λ_{max} are likely to occur in response to polyphenol binding.[34] Except for RPI_0.4CH_3COOH and RPI_0.6CH_3COOH, the isolates presented dramatic reductions in fluorescence intensity to a varying extent compared to RPI_untreated, together with a blue shift in λ_{max} (movement toward lower wavelengths) in the case of the majority of the samples. Indeed, the emission intensity in RPI_defatted and RPI_Me-Ac reduced by 2.2- and 1.5-fold, respectively. This implies less polar surroundings of Trp; that is, Trp residues are shielded from bulk water medium or moved closer to the more hydrophobic core.[35] A plausible explanation for the lower fluorescence intensity in the isolates from acid-treated meals could be the more compact tertiary conformation of protein. It is well-known that exposure of protein to organic solvent and/or acidic condition leads to perturbations in its native structure (partial or complete unfolding). Upon rehydration by solvents such as ethanol, methanol, water, and dimethyl sulfoxide, the protein probably refolds back[36] to compete with the formation of non-native intra/intermolecular interactions or aggregation, as discussed earlier. This phenomenon possibly resulted in burial/confinement of the fluorophores once again into the nonpolar environment.[24] This statement is partly in agreement with the FTIR result. In Figure 4b, emission intensity decreased up to ≈9.6-fold with the successive increase in $HClO_4$ concentration, indicating a quenching effect of the acid. This was also seen with other tested acids (HCl, H_3PO_4, and CCl_3COOH). Apart from the acids, the presence of various degrees of polyphenols in the isolates can contribute to the observed quenching effect. A red shift in λ_{max} was observed in RPI_0.1$HClO_4$ and RPI_0.2$HClO_4$, which suggests that the Trp surrounding became more polar; that is, the chromophores are more exposed to the hydrophilic environment. Further increase in $HClO_4$ concentration caused a blue shift in λ_{max}. Use of CH_3COOH in the treatment solvent did not shift λ_{max} significantly in the case of RPI_0.4CH_3COOH and RPI_0.6CH_3COOH, although an increase in their intensities was noted with respect to RPI_untreated. A lack of spectral shift pinpoints that Trp is not exposed to any change in polarity. However, their enhancement in intensity could be explained by the positive overall net charge of protein molecules under acidic condition (eq 4) because of which the sensitive areas in the backbone of protein molecule acquire more like charges, causing internal repulsion, or perhaps lose charges that were previously involved in attractive forces holding the protein structure together.[35] This in turn leads to a less compact structure, increasing the possibility of exposure or accessibility of more buried fluorophores, thereby enhancing emission intensity.

$$\underset{\text{low pH}}{H_3N^+CHRCOOH} \overset{H^+}{\rightleftharpoons} \underset{\text{zwitterion}}{H_3N^+CHRCOO^-} \overset{OH^-}{\rightleftharpoons} \underset{\text{high pH}}{H_2NCHRCOO^-} \quad (4)$$

FTIR spectroscopic patterns of the proteins were nearly identical, with no significant differences in the major bands (Figure 5a). Amide B band (≈3100 cm^{-1}) originates from N−H stretching of protein vibrations, with contribution from O−H stretching of intermolecular H-bonding. Amide I band (within 1600−1700 cm^{-1}) arises predominantly from C═O stretching vibrations (70−85%), whereas the amide II region (within 1500−1600 cm^{-1}) represents N−H bending vibrations (40−60%) coupled to C−N stretching vibration (18−40%). Spectral changes in the amide I region have been widely used for the conformational analysis of the secondary structure of proteins. Therefore, secondary structure quantitations were performed by Gaussian curve fitting of the spectra in the amide I region (Supporting Information Figure S4) using OriginPro software (version 8.0, OriginLab Corp., Northampton, MA, USA). Peak positions were assigned at those positions where the second-order derivative had local minima. Bands were assigned to various elements of secondary structure (α-helix, β-sheet, and others), and the data are compiled in Table S5 in the Supporting Information. The correlation coefficient (adj R^2) between the original and fitted spectra was ≥0.998, and the error of estimate (chi-square value) was ≤1.08×10^{-5}. The percentage of each secondary structure was calculated from the integrated areas of the component bands. Schmidt et al.[23] studied rapeseed napin and found that the protein is primarily composed of α-helices (45−57.9%) and β-sheets (7−15.3%) as a function of pH 3−12. He et al.[2] also showed that native rapeseed protein comprises 43.6% α-helix and 25.8% β-sheet (β-strand + β-turn). These data are consistent with the result presented in Table S5 in the Supporting Information. The α- and β-contents of RPI_untreated, RPI_deftatted, and RPI_Me-Ac were found to vary minimally, which strongly suggests structural similarity between these samples. Estimated α:β ratio decreased with increasing acid concentration ($p < 0.05$) (Figure

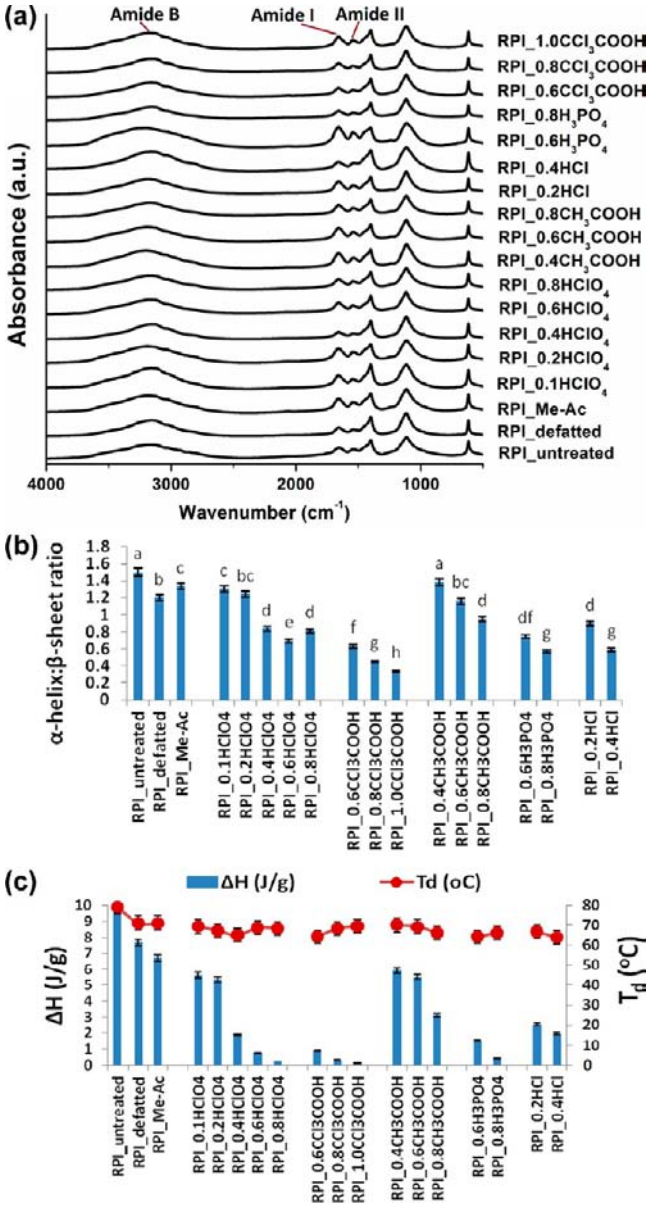

Figure 5. (a) FTIR spectra; (b) estimated ratio of α-helical to β-sheet conformation; and (c) thermal transition characterization of isolates from different meals.

5b). This clearly reflects that acidic solvents induced an increase in β-sheet formation (non-native protein aggregates) accompanied by a decrease in α-helical conformation (indicative of organized native structure), the effect being much stronger on proteins recuperated from CCl_3COOH-treated meals. These results complement the findings of Ayutsede et al.,[37] who reported formic acid treatment to increase β-sheet with a concomitant decrease in α-helix of silk protein. β-Sheet probably arises at the expense of α-helix (partial unfolding of α-helices and subsequent aggregation).[27]

ΔH reflects the extent of ordered structure of protein as the transition from native to denatured state takes place, and T_d provides information on the temperature needed to unfold the structure.[38] Thermograms of the majority of the samples displayed one broad endothermic peak (not shown), possibly corresponding to the overlapping denaturation of 12S (cruciferin) and 2S (napin) rapeseed proteins.[13] A progressive decrease in ΔH from 9.82 to 6.7 J/g with defatting followed by Me-Ac treatment revealed solvent-induced protein unfolding (Figure 5c). Regardless of the acid type, proteins from meals treated with higher acid concentration exhibited very low ΔH, confirming denaturation and more disordered conformation, the effect being higher in RPI_0.8$HClO_4$, RPI_0.8CCl_3COOH, RPI_1.0CCl_3COOH, and RPI_0.8H_3PO_4, which were denatured almost completely (having a flat trace with negligible sign of transition). It could be speculated that the native structure of RPI_untreated had not been completely lost with acidified solvent treatment; proteins from meals treated with lower acid level partially conserved their native structure (manifested by their higher ΔH), especially in RPI_0.1$HClO_4$, RPI_0.2$HClO_4$, RPI_0.4CH_3COOH. and RPI_0.6CH_3COOH. It is feasible to believe that treating the meal with low acidic solvent exposes protein to conditions of minimum harshness and, therefore, yields a protein with least structural aberrations. The current enthalpy data are somewhat comparable to those reported by He et al.[2] With regard to T_d, solvent-treated species presented lower values ($p < 0.05$) in comparison with RPI_untreated, in agreement with the generally described unfolding effect of organic solvents on protein. Unlike ΔH, the T_d of the samples varied within a narrow range of 64−79.5 °C. This observation is partly similar to that reported for buckwheat protein isolates obtained from organic solvent-treated flours,[8] for which the T_d value of 13S globulin was found to be nearly unaffected by the removal of polyphenols with cold organic solvents; however, ΔH was found to increase significantly. In Figure 5c, T_d decreased as the amount of $HClO_4$, CH_3COOH, and HCl increased, although a slight increase was seen in RPI_0.6$HClO_4$ and RPI_0.8$HClO_4$. On the contrary, the isolates from CCl_3COOH- and H_3PO_4-treated meals underwent a steep rise in T_d with increasing acid level. Taking into account the data from FTIR, higher T_d can be expected due to the tendency of proteins to aggregate into a more compact moiety after unfolding, especially in a highly denaturing condition. As a comparison, ΔH and T_d values of rapeseed protein obtained in this study were inferior to those reported earlier.[13,39,40] Partial protein denaturation due to commercial oil expression and alkaline extraction procedure could explain this difference. In addition, most authors perform DSC analysis of protein solution in different ionic strength buffers instead of dry protein powder, which in turn causes remarkable differences in thermal properties[41] due to the stabilizing effect of salt (nonspecific charge-shielding effect)[38] and water.[42]

Of 18 tested samples, native-PAGE of only 10 samples could be traced (Figure 6a). High MW proteins (>205 kDa) were caught at the top of the lanes as smears. Electrophoretograms of these isolates did not present any detectable difference from the control, precluding that these samples are relatively native-like. Remaining samples did not enter the separating gel and are presumed to be complex(es) of very high MW, perhaps due to protein aggregation. The MW of cruciferin, one of the major canola/rapeseed proteins, was reported to be in the range of 230−240 kDa,[39] whereas other studies suggest its MW above 300 kDa.[43] Because MWs of the proteins could not be calculated according to their mobility by native-PAGE, the samples were further analyzed by SDS-PAGE. Examining the gel in Figure 6b shows that the very same samples, which presented diffused bands in native-PAGE, also yielded similar electrophoretic patterns under nonreducing condition (without β-ME), except RPI_0.4HCl and RPI_0.4$HClO_4$, and contained mainly globulin (cruciferin) subunits, which were composed of

dx.doi.org/10.1021/jf5023803 | J. Agric. Food Chem. 2014, 62, 7903−7914

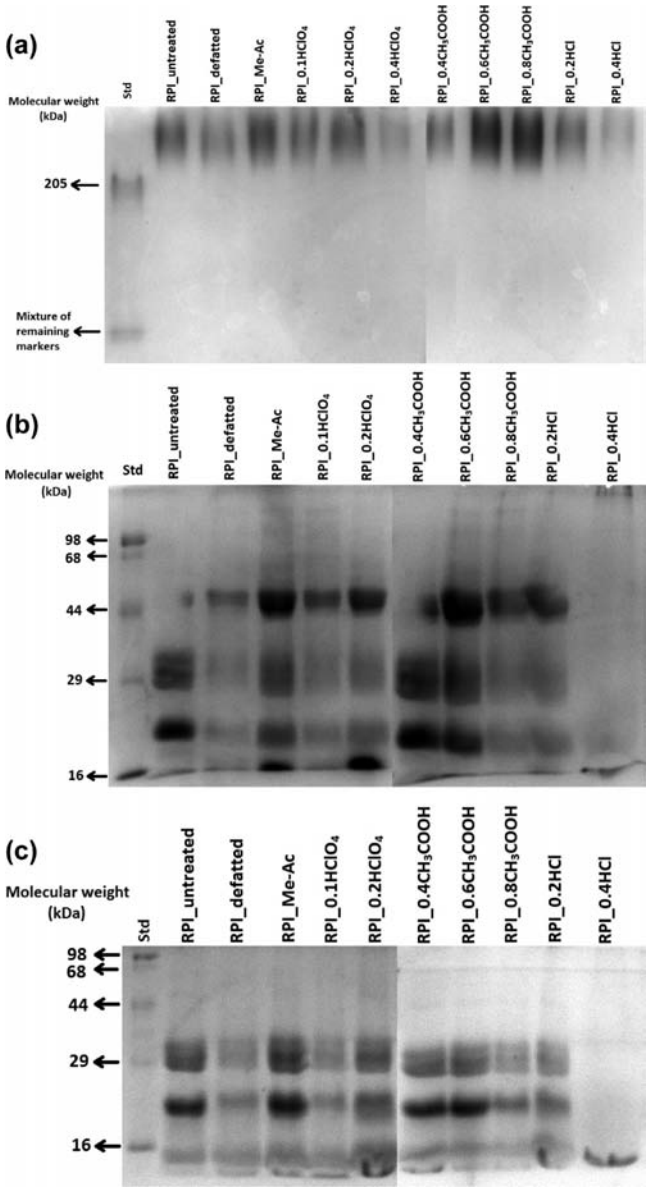

Figure 6. (a) Native-PAGE; (b) nonreducing and (c) reducing SDS-PAGE profiles of isolates from different solvent-treated meals.

bands with MW above 20 kDa (56−49.6, 35−28, and 20.2−19.2 kDa), and albumin (napin) subunits (ranging from 15.9 to 14.8 kDa). This result is consistent with earlier papers.[13,39] Aluko and McIntosh[44] also reported four major polypeptide bands in canola with MWs of 16, 18, 30, and 53 kDa in nonreducing SDS-PAGE. RPI_0.4HCl gave feeble bands of high MW aggregates, seen as smears at the top, and RPI_0.4HClO$_4$ failed to enter the resolving gel. Upon addition of β-ME to cleave SS bonds (reducing condition), the bands within 56−49.6 and 15.9−14.8 kDa disappeared and concomitantly two additional bands with estimated MWs of 13.9−12.5 and 10 kDa appeared (Figure 6c). The latter (10 kDa) probably corresponds to dissociated napin components (reported MW is 10−9.5 kDa).[39,40] The disappearance of canola protein bands having MWs of 59, 53, and 47.5 kDa in the presence of β-ME has been shown earlier.[39,44] Under reducing condition, cruciferin dissociated into acidic (37.8−28.5 kDa) and basic (21.4−20 kDa) polypeptides, in agreement with a previous study.[40] The protein profile of RPI_0.4HCl exhibited changes compared to the pattern described under nonreducing condition, displaying fewer bands having lower MW (≈11.7 kDa). Therefore, the high MW aggregate of this isolate detected in Figure 6b was stabilized by S−S linkages. Dissociation followed by reaggregation after acidic treatment (pH ≤3) has been reported in a number of oilseed proteins.[24] Surprisingly, in the case of the remaining samples, even after the addition of β-ME, diminished concentrations of soluble aggregates were able to enter the gel, which suffered pronounced decreases in band intensity (Supporting Information Figure S6). The coincidental occurrence of polymerized proteins at the bottom of the loading wells and at the junction between stacking and resolving gels was clearly noticeable. Protein denaturation in such samples was clearly reflected by the diffusive and unresolved bands of very low electrophoretic mobility. It is apparent that the results follow the trend observed in FTIR (predominance of β-sheet formation), and the formed aggregates are not soluble in buffer used for electrophoresis. These moieties are more likely stabilized by covalent bonds in addition to SS linkages. Covalent bonding occurring locally in the deep protein structure, especially in highly denatured state, cannot be excluded.[38] The assumption that most of the S−S cross-links are located deep or hidden in the hydrophobic core due to conformational change or protein folding in a manner that limits the accessibility of the reducing agent (β-ME) may also corroborate such a result.[27,38]

Effect on Functional Properties. Protein solubility (at neutral pH) of RPI_untreated (as 100%) was reduced to 80 and 94% in RPI_defatted and RPI_Me-Ac, respectively (Figure 7a). The slightly higher value of the latter could be due to hydration of protein caused by alcohol (methanol), preventing a severe dehydrating effect on the protein.[45] The decrease in solubility with increasing acid concentration can be ascribed to a number of factors: First, it may be a consequence of solvent-induced protein denaturation or due to the varying level of residual antinutrients remaining associated with protein. It is well-known that increasing the level of phytates and/or polyphenols in protein products decreases N solubility.[46,47] However, despite the highest level of phytates and polyphenols in RPI_untreated, it shows maximum solubility because of the partial native state of proteins from pristine rapeseed meal as well as differences in the nature of phytate−protein complexes or phenolic−protein complexes in the protein from pristine meal compared with the isolates from solvent-treated meals.[47] Second, varying degrees of physicochemical changes caused by the solvents may be responsible for these deviations, such as nonavailability or blocking of the residual thiol groups leading to sustained insolubility. Floris et al.[28] proved that the insoluble aggregate is the result of SH group oxidation and not the result of SH/SS exchange reactions. It was demonstrated that SH/SS rearrangement takes place in the aqueous environment, and reshuffling of S−S groups, which can occur when free SH groups are present, is very important in the process of protein resolubilization.[28] Thus, it is difficult to ascertain which influence would play a predominant role, or their concerted effects may dictate the solubility property of different isolates.

Proteins, being amphiphilic, show a strong tendency at fluid interfaces (reducing interfacial tension), which allows them to play a major role in the formation and stabilization of emulsion and foam. Literature data on rapeseed protein-stabilized foams and emulsions are conflicting. As reviewed by Moure et al.,[48] EA and ES of rapeseed/canola protein (concentrates and isolates) widely range from 28.3 to 54% and from 5 to 71%,

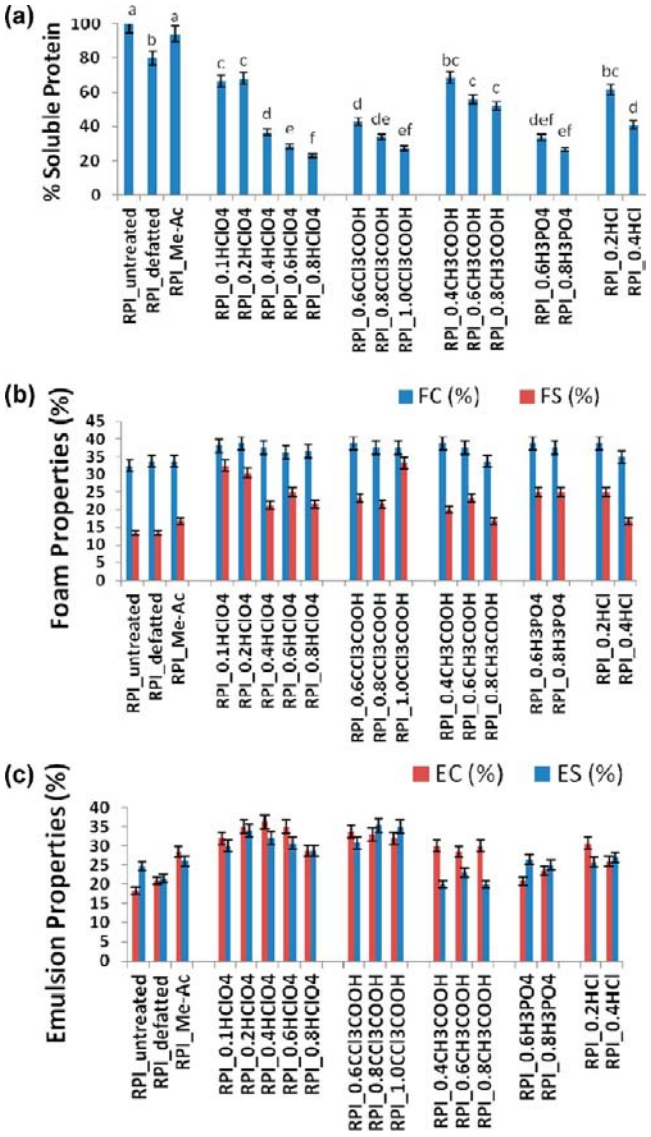

Figure 7. (a) Protein solubility (at pH 7.0); (b) foaming capacity (FC) and stability (FS); and (c) emulsion capacity (EC) and stability (ES) of isolates from different meals.

respectively. In the case of FC and FS, the respective value varies from 43.3 to 211.9% and from 8.2% to 74.7%. Dispersion interactions between proteins and the oil–water interface are always attractive, whereas those between proteins and the air–water interface are generally repulsive. Because of this difference, proteins are adsorbed much more readily at the oil–water interface than at the air–water interface.[49] Thus, the emulsification behavior of a protein may not be analogous to its foaming ability. Apparently, proteins from meals treated with lower concentrations of acids showed slightly higher ability to form foam (Figure 7b), which can be partly ascribed to their higher S_0 and solubility.[48] Highly ordered proteins possess poorer FC than ones that have disordered structure,[49] due to their inability to migrate into the air–water interface of gas bubbles to facilitate a more cohesive film. This might be the cause for inferior FC and FS in untreated sample. Thus, structural and conformational features of protein as a whole rather than solubility alone appear to be the primary determinants for foaming properties.[47] For RPI_0.1HClO$_4$ and RPI_0.2HClO$_4$, a pronounced increase in FS was found (Figure 7b), which seems to be related with their high SH content. Introduction of thiol groups in protein has been shown to increase FS significantly, promoted by SH/SS interchange reaction at the interface,[49] which provides a highly viscoelastic film resisting coalescence. In contrast, CCl_3COOH-treated samples, although with very low SH group content, showed improved stability, the influence being very pronounced in RPI_1.0CCl_3COOH. This was tentatively attributed to the presence of high protein aggregates, which could behave as surface-active solid particles begetting a Pickering foam.[50] Such particles could attract each other, increasing jamming in the fluid interstices between bubbles and the formation of a firmer shell.[50]

EC was found to vary within 18.32–36.28%, with all treated samples showing higher values than the untreated one (Figure 7c). This is because solvent-induced partial denaturation of protein generally improves surface activity.[49] Reduction in S_0 and/or high level of phenolics in RPI_untreated and RPI_defatted impeded their emulsion properties.[26] Excessive denaturation may impair EC by rendering the protein insoluble, as a highly rigid protein cannot unfold/reorient at the interface rapidly and, thus, may not form the film around the oil droplets effectively. This may be the probable reason for decreased EC in samples obtained from high acid-treated meals. EC of such samples may also be affected by their S_0 and solubility,[48] although a high solubility is not a prerequisite for good interfacial properties.[49] Usually EC shows a positive correlation with S_0; the greater the number of hydrophobic patches on a protein's surface, the higher is the probability of its adsorption and retention at the interface, albeit highly hydrophobic proteins may precipitate and cause instability.[49] As reflected in Figures 3b and 7c, EC and ES of proteins from treated meals partly paralleled their S_0. An exception to this observation was the TCA-treated samples, which showed highest ES. The increase in acid level in the processing treatment did not present any close relationship with ES. CH_3COOH-treated samples showed the least stability, which may be due to their high phytate content. Our observation is in line with those of Dev and Mukherjee.[47]

In light of the differences among the wide number of systems available, the results of a single method can give only a reductive suggestion of the emulsion properties of the sample. For that reason, morphological changes occurring in the droplets of emulsions stabilized by different isolates were visualized. At t = 0 h (Figure 8a), the emulsion droplet morphology stabilized by RPI_untreated compares well with those of RPI_defatted, RPI_Me-Ac, RPI_0.1HClO$_4$, and RPI_0.2HClO$_4$. Although a smaller droplet size was found in the emulsions stabilized by RPI_0.4HClO$_4$ and RPI_0.6HClO$_4$, insoluble protein aggregates were visible in the matrix. Such aggregates were also detected in emulsions formed by CCl_3COOH-treated samples. Poor emulsifying properties of H_3PO_4 and HCl-treated samples can be anticipated from their flocculated droplets with large diameters. This is congruent with their EC values. At t = 24 h, the droplets displayed a significant level of flocculation (Figure 8b). The spherical shape of oil droplets was severely distorted; the burst of large droplets dominated, and some emulsion collapsing was observed, such as those stabilized by defatted and CH_3COOH- and HCl-treated samples. These phenomena seem to denote their inferior ES. Interestingly, the droplet diameters were initially larger in emulsions formed by CCl_3COOH-treated samples, but their stabilities were found to be outstanding, although these

dx.doi.org/10.1021/jf5023803 | J. Agric. Food Chem. 2014, 62, 7903–7914

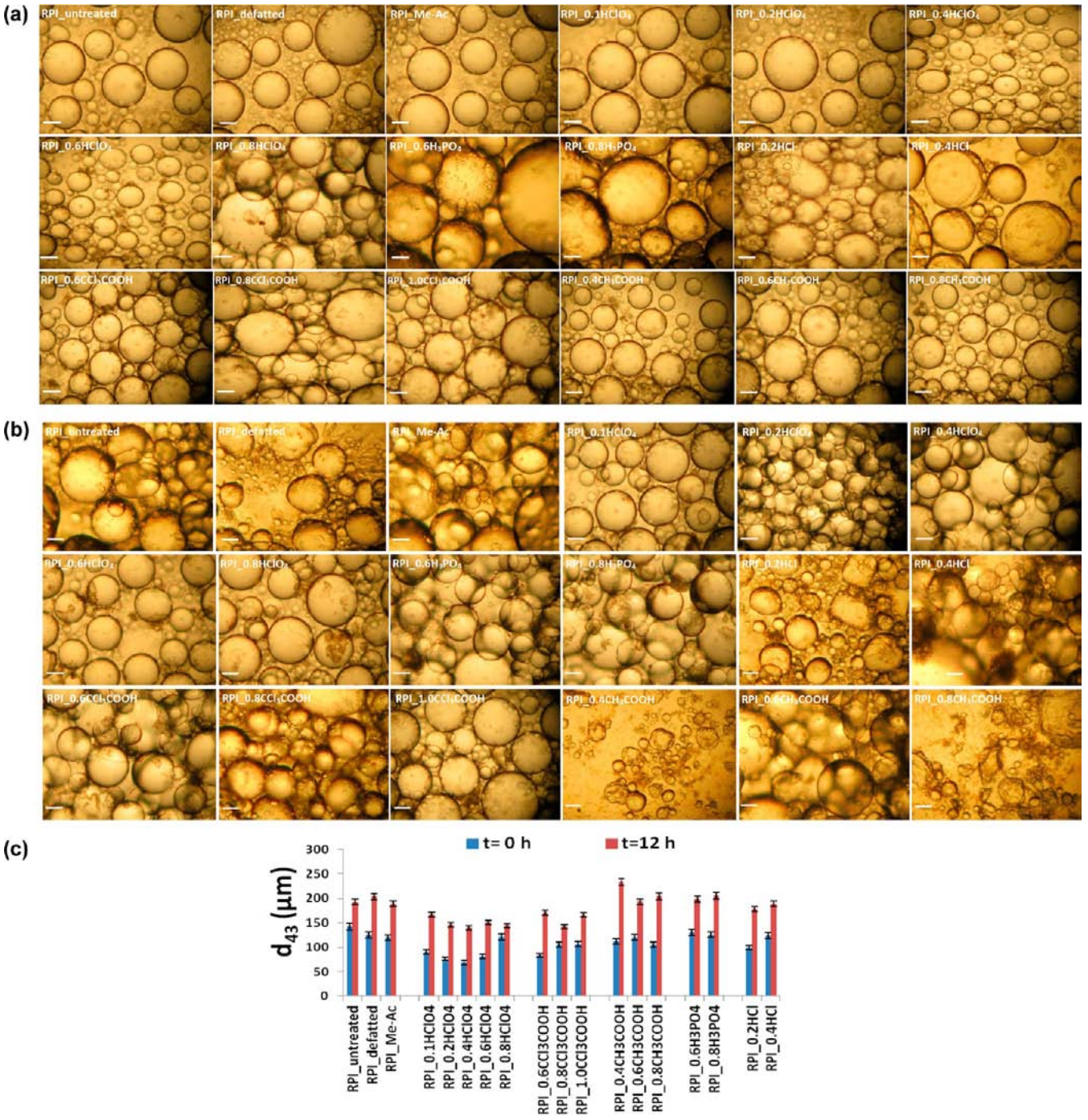

Figure 8. Optical micrographs of the o/w emulsions stabilized by protein isolates from different meals at (a) t = 0 h and (b) t = 24 h (scale bar represents 55 μm); (c) impact of different isolates on the average droplet size (d_{43}) of o/w emulsions stored at 25 °C for t = 0 h and t = 12 h.

samples possessed very low S_0 and protein solubility. This vast improvement can be attributed to insoluble protein aggregates, which were mainly located at the junction between oil droplets, favoring network stabilization by retarding droplet coalescence. However, the intense color of these isolates should be taken into account when considering their potential applications.

Additionally, changes in droplet/particle size of these emulsions (denoted by d_{43}) are shown in Figure 8c. Emulsifying ability of a surfactant can be assessed by d_{43}; the smaller the particle size, the better the ability. At t = 0 h, emulsion from all solvent-treated samples presented comparatively smaller particle sizes, indicating higher EA, which is due to their S_0. Except RPI_0.8HClO$_4$, perchloric acid-treated samples had lower d_{43} values compared to others. The droplet size of emulsions decreased markedly when HClO$_4$ concentration increased from 0.1 to 0.4%; however, further increase in acid level produced larger sizes. This can be related to their S_0 and soluble protein content.[49] The initial increase in hydrophobicity facilitated enhanced interaction between the oil and aqueous phases.[14] As the acid level increased, a point was reached where the unfolded polypeptide chains reconstructed (SS linkages with polymerization), which made it prone to aggregation rather than to adsorb onto the interface.[14] When the soluble protein amount is limited, there is no longer

dx.doi.org/10.1021/jf5023803 | J. Agric. Food Chem. 2014, 62, 7903−7914

sufficient protein to fully stabilize the droplet interface, and therefore larger particles may be formed as a result of coalescence or bridging flocculation. In the case of emulsions stabilized by other protein samples, larger particle sizes were observed. The decreased S_0 might have precluded the migration of such proteins to the interface. A similar trend in d_{43} values was observed for these systems at t = 12 h, so the factors accounting for emulsion droplet sizes during storage may be similar to those stated previously. Overall, the particle size of emulsions gradually increased with increasing storage time, due to individual droplet growth (Ostwald ripening) or droplet aggregation (flocculation or coalescence).[26] At t = 24 h, the studied emulsions presented a significant amount of ruptured/collapsed droplets, because of which their d_{43} values could not be calculated. Taken together, these data suggest that an efficient method to stabilize the oil−water or air−water interface consists in using protein from a meal treated with low acidic solvents, having an intermediate degree of hydrophobicity.

In summary, the efficiency of the removal of polyphenols and phytates from protein with $HClO_4$-acidified solvent was much better than that with other acids, but the extent of AITC removal was similar for all acids tested. Isolates were essentially free of glucosinolates. The solvent treatment lowered protein yield and its solubility; conversely, their color and interfacial properties were enhanced, but the results did not necessarily match those obtained from highly acidified solvent-treated meals because the mechanism of denaturation and structural changes caused by different solvent systems were not the same. The treatment also resulted in distinct changes in proteins' secondary and tertiary conformations; especially, higher levels of acid led to detrimental effects of protein unfolding and aggregation, which seemed to be more likely consecutive events. Such aggregation-prone conformation tended to enhance thermal stability (higher T_d). From a calorimetric point of view, meals treated with lower levels of acids seemed to consist of considerably structure-preserved proteins relative to the control. Further evidence that these samples have not undergone appreciable denaturation comes from their electrophoretic patterns. It is evident that 0.2% $HClO_4$ in Me-Ac (1:1 v/v) constitutes a valid extraction mixture, giving results that are either higher than or comparable to the other solvents tested, and also does not affect the protein much, as is shown by its physicochemical and functional features. Further investigation should be undertaken to improve the technofunctional properties of such isolates.

■ ASSOCIATED CONTENT

Supporting Information

Photographs of freeze-dried protein isolates; ^{1}H NMR spectra highlighting sinapine content; collective representation of emission fluorescence spectra of isolates; Gaussian curve-fitting of amide I region of FTIR spectra and calculated percentage of secondary protein structures in the isolates; reducing SDS-PAGE patterns of proteins from CCl_3COOH and H_3PO_4-treated meals; fluorescence quenching measurements in isolates from $HClO_4$-treated meals; hemocompatibility of the isolates recuperated from untreated and solvent-treated meals. This material is available free of charge via the Internet at http://pubs.acs.org.

■ AUTHOR INFORMATION

Corresponding Author

*(C.L.M.) Phone: +91 3712 267008 (5702). Fax: +91 3712 267005. E-mail: charu@tezu.ernet.in.

Funding

M.D.P. is thankful to DST-INSPIRE Programme, India, for a meritorious fellowship.

Notes

The authors declare no competing financial interest.

■ REFERENCES

(1) Thiyam, U.; Claudia, P.; Jan, U.; Alfred, B. De-oiled rapeseed and a protein isolate: characterization of sinapic acid derivatives by HPLC−DAD and LC−MS. *Eur. Food Res. Technol.* **2009**, *229*, 825−831.

(2) He, R.; He, H.-Y.; Chao, D.; Ju, X.; Aluko, R. Effects of high pressure and heat treatments on physicochemical and gelation properties of rapeseed protein isolate. *Food Bioprocess Technol.* **2013**, DOI:10.1007/s11947-013-1139-z (accessed July 6, 2013).

(3) Das Purkayastha, M.; Das, S.; Manhar, A. K.; Deka, D.; Mandal, M.; Mahanta, C. L. Removing antinutrients from rapeseed press-cake and their benevolent role in waste cooking oil-derived biodiesel: conjoining the valorization of two disparate industrial wastes. *J. Agric. Food Chem.* **2013**, *61*, 10746−10756.

(4) Liu, Y.; Zhao, G.; Ren, J.; Zhao, M.; Yang, B. Effect of denaturation during extraction on the conformational and functional properties of peanut protein isolate. *Innovative Food Sci. Emerging. Technol.* **2011**, *12*, 375−380.

(5) Wanasundara, J. P. D.; Abeysekara, S. J.; McIntosh, T. C.; Falk, K. C. Solubility differences of major storage proteins of Brassicaceae oilseeds. *J. Am. Oil Chem. Soc.* **2012**, *89*, 869−881.

(6) Xu, L.; Diosady, L. L. Removal of phenolic compounds in the production of high-quality canola protein isolates. *Food Res. Int.* **2002**, *35*, 23−30.

(7) Balange, A. K.; Benjakul, S. Effect of oxidised phenolic compounds on the gel property of mackerel (*Rastrelliger kanagurta*) surimi. *Lebensm. Wiss. Technol.* **2009**, *42*, 1059−1064.

(8) Tang, C.-H.; Wang, X.-Y.; Liu, F.; Wang, C.-S. Physicochemical and conformational properties of buckwheat protein isolates: influence of polyphenol removal with cold organic solvents from buckwheat seed flours. *J. Agric. Food Chem.* **2009**, *57*, 10740−10748.

(9) Deng, Q.; Wang, L.; Wei, F.; Xie, B.; Huang, F. H.; Huang, W.; Shi, J.; Huang, Q.; Tian, B.; Xue, S. Functional properties of protein isolates, globulin and albumin extracted from *Ginkgo biloba* seeds. *Food Chem.* **2011**, *124*, 1458−1465.

(10) Hiller, B.; Lorenzen, P. C. Surface hydrophobicity of physicochemically and enzymatically treated milk proteins in relation to techno-functional properties. *J. Agric. Food Chem.* **2008**, *56*, 461−468.

(11) Hiller, B.; Lorenzen, P. C. Effect of phosphatase/transglutaminase treatment on molar mass distribution and techno-functional properties of sodium caseinate. *Lebensm. Wiss. Technol.* **2009**, *42*, 87−92.

(12) Manamperi, W. A. R.; Wiesenborn, D. P.; Chang, S. K. C.; Pryor, S. W. Effects of protein separation conditions on the functional and thermal properties of canola protein isolates. *J. Food Sci.* **2011**, *76* (3), E266−E273.

(13) Li, N.; Qi, G.; Sun, X. S.; Stamm, M. J.; Wang, D. Physicochemical properties and adhesion performance of canola protein modified with sodium bisulfite. *J. Am. Oil Chem. Soc.* **2012**, *89*, 897−908.

(14) Wu, H.; Wang, Q.; Maa, T.; Ren, J. Comparative studies on the functional properties of various protein concentrate preparations of peanut protein. *Food Res. Int.* **2009**, *42*, 343−348.

(15) Salgado, P. R.; Drago, S. R.; Ortiz, S. E. M.; Petruccelli, S.; Andrich, O.; González, R. J.; Mauri, A. N. Production and characterization of sunflower (*Helianthus annuus* L.) protein-enriched

products obtained at pilot plant scale. *Lebensm. Wiss. Technol.* **2012**, *45*, 65−72.
(16) Hassan, H. M. M.; Afify, A. S.; Basyiony, A. E.; Ahmed Ghada, T. Nutritional and functional properties of defatted wheat protein isolates. *Aust. J. Basic Appl. Sci.* **2010**, *4* (2), 348−358.
(17) Kalashnikova, I.; Bizot, H.; Cathala, B.; Capron, I. New Pickering emulsions stabilized by bacterial cellulose nanocrystals. *Langmuir* **2011**, *27*, 7471−7479.
(18) Winuprasith, T.; Suphantharika, M. Microfibrillated cellulose from mangosteen (*Garcinia mangostana* L.) rind: preparation, characterization and evalution as an emulsion stabilizer. *Food Hydrocolloids* **2013**, *32*, 383−394.
(19) Naczk, M.; Diosady, L. L.; Rubin, L. J. Functional properties of canola meals produced by a two-phase solvent extraction system. *J. Food Sci.* **1985**, *50* (6), 1685−1688.
(20) Park, H.-R.; Ahn, H.-J.; Kim, S.-H.; Lee, C.-H.; Byun, M.-W.; Lee, G.-W. Determination of the phytic acid levels in infant foods using different analytical methods. *Food Control* **2006**, *17*, 727−732.
(21) Siebert, K. J.; Carrasco, A.; Lynn, P. Y. Formation of protein-polyphenol haze in beverages. *J. Agric. Food Chem.* **1996**, *44*, 1997−2005.
(22) Charlton, A. J.; Baxter, N. J.; Khan, M. L.; Moir, A. J. G.; Haslam, E.; Davies, A. P.; Williamson, M. P. Polyphenol/peptide binding and precipitation. *J. Agric. Food Chem.* **2002**, *50*, 1593−1601.
(23) Schmidt, I.; Renard, D.; Rondeau, D.; Richomme, P.; Popineau, Y.; Axelos, M. A.-V. Detailed physicochemical characterization of the 2S storage protein from rape (*Brassica napus* L.). *J. Agric. Food Chem.* **2004**, *52*, 5995−6001.
(24) Sripad, G.; Narasinga Rao, M. S. Effect of acid pH on the 11S protein of sunflower seed. *J. Agric. Food Chem.* **1987**, *35*, 668−672.
(25) Rybarczyk, A.; Chavan, U. D.; Amarowicz, R. Separation of rapeseed globulin by micellar electrokinetic chromatography (MEKC) − a short report. *Polym. J. Food Nutr. Sci.* **2007**, *57* (3), 353−356.
(26) Aewsiri, T.; Benjakul, S.; Visessanguan, W.; Eun, J.-B.; Wierenga, P. A.; Gruppen, H. Antioxidative activity and emulsifying properties of cuttlefish skin gelatin modified by oxidised phenolic compounds. *Food Chem.* **2009**, *117*, 160−168.
(27) Byaruhanga, Y. B.; Emmambux, M. N.; Belton, P. S.; Wellner, N.; Ng, K. G.; Taylor, J. R. N. Alteration of kafirin and kafirin film structure by heating with microwave energy and tannin complexation. *J. Agric. Food Chem.* **2006**, *54*, 4198−4207.
(28) Floris, R.; Bodnár, I.; Weinbreck, F.; Alting, A. C. Dynamic rearrangement of disulfide bridges influences solubility of whey protein coatings. *Int. Dairy J.* **2008**, *18*, 566−573.
(29) Estey, T.; Kang, J.; Schwendeman, S. P.; Carpenter, J. F. BSA degradation under acidic conditions: a model for protein instability during release from PLGA delivery systems. *J. Pharm. Sci.* **2006**, *95* (7), 1626−1639.
(30) Duodu, K. G.; Taylor, J. R. N.; Belton, P. S.; Hamaker, B. R. Factors affecting sorghum protein digestibility. *J. Cereal Sci.* **2003**, *38* (2), 117−131.
(31) Karaca, A. C.; Low, N.; Nickerson, M. Emulsifying properties of canola and flaxseed protein isolates produced by isoelectric precipitation and salt extraction. *Food Res. Int.* **2011**, *44*, 2991−2998.
(32) Hojilla-Evangelista, M. P.; Evangelista, R. L. Functional properties of protein from *Lesquerella fendleri* seed and press cake from oil processing. *Ind. Crop Prod.* **2009**, *29*, 466−472.
(33) Abugoch, L. E.; Romero, N.; Tapia, C. A.; Silva, J.; Rivera, M. Study of some physicochemical and functional properties of quinoa (*Chenopodium quinoa* Willd) protein isolates. *J. Agric. Food Chem.* **2008**, *56*, 4745−4750.
(34) Skrt, M.; Benedik, E.; Podlipnik, Č.; Ulrih, N. P. Interactions of different polyphenols with bovine serum albumin using fluorescence quenching and molecular docking. *Food Chem.* **2012**, *135*, 2418−2424.
(35) Kwaambwa, H. M.; Maikokera, R. A fluorescence spectroscopic study of a coagulating protein extracted from *Moringa oleifera* seeds. *Colloids Surf., B* **2007**, *60*, 213−220.
(36) Sirotkin, V. A.; Zinatullin, A. N.; Solomonov, B. N.; Faizullin, D. A.; Fedotov, V. D. Calorimetric and FTIR-spectroscopic study of solvent effect on the state of dry solid bovine pancreatic α-chymotrypsin immersed in anhydrous organic solvents. *Biocatal.−2000: Fundam. Appl.* **2000**, *41* (6), 37−42, http://www.chem.msu.su/eng/journals/vmgu/00add/37.pdf.
(37) Ayutsede, J.; Gandhi, M.; Sukigara, S.; Micklus, M.; Chen, H.-E.; Ko, F. Regeneration of *Bombyx mori* silk by electrospinning. Part 3: Characterization of electrospun non-woven mat. *Polymer* **2005**, *46*, 1625−1634.
(38) Mession, J.-L.; Sok, N.; Assifaoui, A.; Saurel, R. Thermal denaturation of pea globulins (*Pisum sativum* L.)−molecular interactions leading to heat-induced protein aggregation. *J. Agric. Food Chem.* **2013**, *61*, 1196−1204.
(39) Wu, J.; Muir, A. D. Comparative structural, emulsifying, and biological properties of 2 major canola proteins, cruciferin and napin. *J. Food Sci.* **2008**, *73* (3), C210−C216.
(40) Salleh, M. R. B. M.; Maruyama, N.; Adachi, M.; Hontani, N.; Saka, S.; Kato, N.; Ohkawa, Y.; Utsumi, S. Comparison of protein chemical and physicochemical properties of rapeseed cruciferin with those of soybean glycinin. *J. Agric. Food Chem.* **2002**, *50*, 7380−7385.
(41) Tandang, M. R. G.; Adachi, M.; Inui, N.; Maruyama, N.; Utsumi, S. Effects of protein engineering of canola procruciferin on its physicochemical and functional properties. *J. Agric. Food Chem.* **2004**, *52*, 6810−6817.
(42) Paredes-López, O. Safflower proteins for food use. In *Developments in Food Proteins−7*; Hudson, B. J. F., Ed.; Elsevier Applied Science: New York, 1991; pp 1−33.
(43) Dong, X.-Y.; Guo, L.-L.; Wei, F.; Li, J.-F.; Jiang, M.-L.; Li, G.-M.; Zhao, Y.-D.; Chen, H. Some characteristics and functional properties of rapeseed protein prepared by ultrasonication, ultrafiltration and isoelectric precipitation. *J. Sci. Food Agric.* **2011**, *91*, 1488−1498.
(44) Aluko, R. E.; McIntosh, T. Polypeptide profile and functional properties of defatted meals and protein isolates of canola seeds. *J. Sci. Food Agric.* **2001**, *81*, 391−396.
(45) Sodini, G.; Canella, M. Acidic butanol removal of color-forming phenols from sunflower meal. *J. Agric. Food Chem.* **1977**, *25* (4), 822−825.
(46) Rawel, H. M.; Kroll, J.; Rohn, S. Reactions of phenolic substances with lysozyme−physicochemical characterisation and proteolytic digestion of the derivatives. *Food Chem.* **2001**, *72* (1), 59−71.
(47) Dev, D. K.; Mukherjee, K. D. Functional properties of rapeseed protein products with varying phytic acid contents. *J. Agric. Food Chem.* **1986**, *34*, 775−780.
(48) Moure, A.; Sineiro, J.; Domínguez, H.; Parajo, J. C. Functionality of oilseed protein products: a review. *Food Res. Int.* **2006**, *39*, 945−963.
(49) Damodaran, S. Protein stabilization of emulsions and foams. *J. Food Sci.* **2005**, *70* (3), R54−R66.
(50) Manzocco, L.; Panozzo, A.; Nicoli, M. C. Effect of pulsed light on selected properties of egg white. *Innovative Food Sci. Emerging Technol.* **2013**, *18*, 183−189.

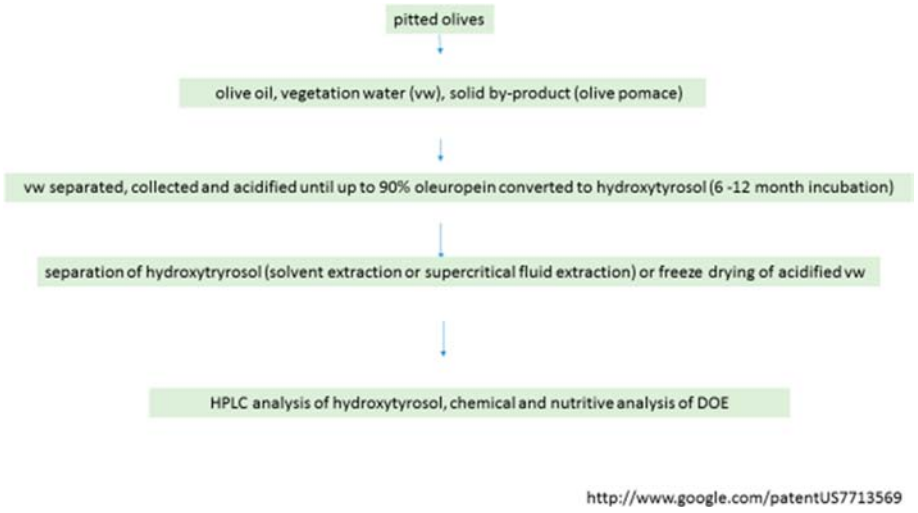

Figure 1. One of many variations for the production of dried olive extract with hydroxytyrosol.

retard lipid oxidation during processing and storage of post-mortem tissue and further processed poultry products.[22,23]

DOE is a certified organic, generally recognized as safe (GRAS), and Kosher agricultural byproduct from the production of olive oil[24] (Figure 1). As delineated in Table 1, the solid olive oil extract (olive oil pulp) is 98−99% water-soluble and contains 2.5% (minimum) hydroxytyrosol, more than contained in extra virgin olive oil. Therefore, DOE as an agricultural byproduct, potentially, could be administered (in vivo) to poultry to retard lipid oxidation in post-mortem poultry meat, high in unsaturated fatty acids that degenerate and produce free radicals during processing and storage.

Table 1. Nutritive Analysis of DOE[a]

carbohydrate	64.4%
fat	20.0%
ash	11.4%
simple and polyphenols	8.82%
protein	4.4%
hydroxytyrosol	2.5% (minimum)
lead	<1.0 ppm
heavy metals	<10.0 ppm

[a]Bitter, 2007 (see ref 24).

Myricetin, a bioflavonoid extract from the bark powder of the bayberry tree (*Myrica cerifera*), has anticancerous properties, is antimutagenic, and has therapeutic effects for heart disease and diabetes.[25,26] Although myricetin has been evaluated for it pharmacological effectiveness, its antioxidative capacity when added to foods containing unsaturated fatty acids has received less attention. Like hydroxytyrosol, myricetin is water-soluble and scavenges $OH^{\bullet}$ and O_2^- radicals.[26,27] Thus, this free radical scavenger may be another effective antioxidant in poultry products.

DOE and myricetin may be among several antioxidants that could be added to poultry to promote growth, retard disease, and prevent oxidation in post-mortem tissue. Therefore, a study was conducted to (1) assess the capacity of DOE to enhance the growth of poultry, (2) determine the effectiveness of DOE (administered in vivo) as an antioxidant in post-mortem tissue and further processed meat, and (3) compare the in vitro antioxidative capacities of hydroxytyrosol and myricetin.

MATERIALS AND METHODS

DOE (2.5% hydroxytyrosol) was obtained gratis from CreAgri, Inc. (Hayward, CA). 2,2-Diphenylpicrylhydrazyl and myricetin (95%) were purchased from Thermo Fisher Scientific Acros Organics (Fair Lawn, NJ, USA). Acetic acid, butan-1-ol, methanol, HCl, sodium dodecyl sulfate, and thiobarbituic acid were obtained from Chemical Stores (University of California, Davis, CA, USA). NaCl was obtained from Morton Salt (Chicago, IL, USA). All chemicals were at least reagent grade.

Unvaccinated chicks and commercial feed were from Ellenwood Hatchery (Foster Farms, Livingston, CA, USA) and the Foster Farm Feed Mill, respectively.

Administration of DOE Treatments. The Institutional Animal Care and Use Committee (University of California, Davis, CA, USA) approved the protocol for the study. Feed and water were administered ad libitum throughout the feeding trial to Arbor Acres Crosses reared under 12 h of light and 12 h of darkness. One-day-old chicks (276) were fed a commercial starter diet and water during acclimatization for 1 week. At the beginning of the second week, chicks were randomized into 12 pens (each at 2.13 m^2) of 24 birds each. The experimental design was 3 diets × 2 blocks (pens) × 2 replications.

Commercial diets were provided as starter for week 1, grower for weeks 3−5, and finisher for week 6. Throughout the experiment, broilers were provided water containing DOE as follows: no DOE as a control, 6 mg of DOE per bird per day, or 12 mg of DOE per bird per day.[24] For weeks 1 and 2, water for the control and that with antioxidant was provided fresh each day in 0.946 L containers. For weeks 3−6, water was provided in 18.93 L containers. Broilers completely consumed water with DOE during the first 4 h of light (8:00 a.m. to 12:00 p.m.). All containers, including the control, were rinsed several times before the addition of fresh water that broilers consumed during the remainder of the lit period.

Enhancement of Growth, Detection of Disease, and Defects. Body weights (BW) for 12 broilers from each pen were recorded each week. Quantities of added feed were recorded. Adverse effects were not expected due to feeding of DOE, a GRAS substance. However, as a precautionary measure, two birds per pen were sacrificed at the end of the study and examined for disease and growth defects at the California Animal Health and Food Safety Laboratory (University of California, Davis, CA, USA). Laboratory findings (two samples per bird) were reported for bacteriological, histological, immunological, parasitological, toxicological, and virological analyses.

Preparation of Samples from Thigh Meat of Broilers Fed DOE. After 6 weeks, birds were harvested at Grimaud Farms (Stockton, CA, USA). Birds were frozen at −28.8 °C for approximately 24 h and transported to the laboratory, where they were frozen at −40 °C until thighs were removed and further

Table 2. Effect of DOE on Body Weight, Feed Consumption, and Feed Conversion[a]

	BW[b,c] (kg)					
treatment[d]	1 week	3 weeks	5 weeks	6 weeks	feed consumption (kg)	feed conversion[c]
control	0.14	1.32	2.42	3.36	5.62 ± 0.64	1.67
6 mg	0.14	1.35	2.41	3.31	5.39 ± 0.48	1.63
12 mg	0.14	1.34	2.39	3.29	5.46 ± 0.49	1.65

[a]Feed and water were provided ad libitum. [b]Means (12 observations) within a row lacking a common letter differ ($P \leq 0.05$). [c]Calculated value. [d]DOE was administered at 6 or 12 mg per bird per day in water from 8:00 a.m. to 12:00 p.m. each day.

Table 3. Absorbance Values from Thigh Meat Treated with Two Levels of in Vitro DOE and Myricetin

	treatment[a]				
processing condition[b]	control	H1	H2	M1	M2
fresh	0.07 ± 0.02a	0.08 ± 0.02a	0.07 ± 0.01a	0.06 ± 0.02a	0.07 ± 0.01a
heated	0.13 ± 0.04a	0.14 ± 0.04a	0.11 ± 0.02ab	0.06 ± 0.01b	0.07 ± 0.01b
NaCl/heated/stored	0.20 ± 0.04a	0.15 ± 0.02b	0.13 ± 0.04b	0.06 ± 0.01c	0.06 ± 0.02c

[a]H1 and H2, addition of 0.025% (w/w) and 0.05% (w/w) of DOE, respectively; M1 and M2, addition of 0.025% (w/w) and 0.05% (w/w) of myricetin, respectively. Means (six observations) within rows lacking a common letter differ ($P \leq 0.05$). [b]Samples (approximately 25 g) from right thighs of two broilers from each treatment across each replication were thawed, pooled, and ground. Samples (3 g) from each mixture were ground for approximately 1 min and analyzed immediately as fresh or boiled (37.8 °C) in boiling bags, cooled (30 min), and analyzed as heated. NaCl/heated/stored samples were the same as heated samples with the addition of 1.0% (w/w) NaCl in 7 mL of deionized distilled water before grinding and heating followed by storage in aluminum pouches for 2 days at −12.22 °C for 24 h before analysis.

processed. Samples (approximately 25 g) from right thighs of two broilers from each treatment across block (pen) and replication were thawed in aluminum pouches for 24 h at −12.22 °C, pooled, and ground in a food processor (Cuisinart, model DLC-7 Super Pro, Norwich, CT, USA) for 2 min. After initial processing, samples (3 g) were ground for approximately 1 min and analyzed immediately as fresh. Heated samples were boiled (37.8 °C) in boiling bags and cooled (30 min) before analysis. NaCl/heated/stored samples were treated in the same manner as heated samples with the addition of 1.0% (w/w) NaCl in 7 mL of deionized distilled water before grinding and heating followed by storage in aluminum pouches at −12.22 °C for 72 h before analysis. The experimental design was 3 treatments (from the feeding experiment) × 3 processing conditions × 3 samples × 2 replications. This design produced six samples for each treatment by processing condition.

In Vitro Addition of DOE and Myricetin. Thigh samples of control broilers from the feeding trial were processed as above. Control samples (3 g) did not contain antioxidants. Antioxidants at 0.025% (w/w) and 0.05% (w/w) of DOE or myricetin in 7 mL of deionized distilled were added during grinding for 1 min.[8,10,22] NaCl (1.0% w/w) was added with antioxidants where indicated. H1 and H2 denote samples containing 0.025% (w/w, 1.875×10^{-5}g) and 0.05% (w/w, 3.75×10^{-5}g) of hydroxytyrosol (2.5% in DOE, Table 1), respectively. M1 and M2 denote samples containing 0.025% (w/w, 7.125×10^{-4}g) and 0.05% (w/w, 1.425×10^{-3}g) of myricetin, respectively. The actual quantity of myricetin was greater than that of hydroxytyrosol because DOE (containing hydroxytrosol) and myricetin were inadvertently added to post-mortem tissue without attention to differences in purity of the two antioxidants.

Determination of Absorbance Values To Indicate Levels of Lipid Oxidation. Absorbance values were used to indicate levels of lipid oxidations in samples based on consistent standard curves. The method of Cuendet et al.[28] was used to determine 2,2-diphenylpicrylhydrazyl (DPPH) at 517 nm (DV 1700 Pharma spectrophotometer, Shimadzu Scientific Instruments, Jiangsu, China) for samples from birds administered DOE. All in vitro and in vivo samples were analyzed by using methods of Fasseas et al.[29] at 532 nm to obtain absorbance values to approximate the level of lipid oxidation (thiobarbituric acid reactive substances, TBARS).

Statistical Analysis. Data were analyzed by ANOVA.[30] Means were evaluated using Turkey's Student *t* test, and significance of means was determined at $P \leq 0.05$.

RESULTS

In Vivo Effect of DOE. Table 2 shows that feed consumption, BW, and feed conversion were not affected ($P \leq 0.05$) by the addition of DOE. Results showing absorbance values for TBARS revealed no significant change for fresh, heated, and NaCl/heated/stored samples (data not shown).

Similarly, DPPH results (data not shown) showed no effect ($P \leq 0.05$) for DOE.

Detection of Disease and Defects. Results indicated that birds had no unusual lesions in the tissue of brains, hearts, inactive ovaries, intestinal tracts, kidneys, livers, or peripheral nerves. There were no abnormalities in the growth plates except for one control bird. Mixed lymphoid infiltration indicated that all broilers (unvaccinated) were affected with low levels of Marek's Herpes virus.

In Vitro Effect of DOE and Myricetin. As indicated by statistical similarity of absorbance values in Table 3, there was no effect of antioxidants in fresh samples ($P \leq 0.05$). For heated samples, H2 produced intermediate absorbency values; control and H1 had significantly higher values than M1 and M2.

NaCl/heated/stored samples had absorbance values ranked as M1 = M2 < H1 = H2 < control ($P \leq 0.05$). As noted above, 3 g samples contained 38 times more myricetin than hydroxytyrosol.

DISCUSSION

Visual observations indicated that birds readily consumed the agricultural byproduct, DOE, in water during the time allotted. As a GRAS substance it did not enhance the growth of broilers, nor was it detrimental when fed to them. These results are similar to those of Paiva-Martins et al.[31] and Botsoglou et al.,[32] who found that pigs and turkeys, respectively, fed olive leaves did not exhibit enhanced weight gain; however, these investigators reported significantly greater oxidative stability for meat from pigs and turkeys fed olive leaves. Paiva-Martins et al.[31] stored meat from pigs for 8 days at 4 °C. They attributed the lowered peroxide values and conjugated dienes to the higher α-tocopherol concentration in fat of meat from pigs fed

olive leaves. However, the significantly more stable oxidative stability of the meat from pigs fed olive leaves could be associated with the α-tocopherol and hydroxytyrosol contents as well.[32] Olive leaves (10 g/kg) fed to turkeys lowered lipid oxidation of stored muscle as compared to oregano, although it was not as effective as α-tocopheryl acetate at 300 mg/kg.[33]

As a highly effective radical scavenger, hydroxytyrosol in DOE could potentially retard lipid deterioration in chicken thigh meat as reported for turkey meat. However, in our study, it did not reduce lipid oxidation in post-mortem tissue as has been found with in vivo administration of α-tocopherol in the diets of broilers and consumption of olive oil leaves by turkeys.[21,22,32] Medina[33] showed that hydoxytyrosol is more effective in emulsions having short−medium lipophilic chains (acetate, butyrate, or octanoate). These investigators suggested that short−medium chains helped to position hydroxytyrosol in the interface of the fish oil emulsions, whereas longer chains did not. It is also known that the fatty acid content of both chicken and turkey meat can be altered significantly by the composition of the diet.[19,20] The fatty acid content of leaves fed by Botsoglou et al. was not reported; however, it is not likely that the composition of the turkey and broiler meat changed to such an extent as to affect the oxidative capacity of the antioxidant in turkey as compared to chicken meat.

It is likely that the antioxidative capacity of DOE provided in vivo is related to its solubility of >95% in water.[24] According to Vissers et al., hydroxytyrosol is highly water-soluble as well. Absorption of hydroxytyrosol by birds was not determined in our study; however, if it did occur, some of the antioxidant was likely excreted in the urine.[5] Although not measured in our study, the residual remaining in the tissue of broilers that did not consume water with DOE for 4−6 h prior to processing may have been negligible. In comparison, antioxidants in olive leaves are associated with oil (fatty acids) that may be readily maintained in the membranes to retard lipid deterioration during processing and storage.

When DOE and myricetin were added to post-mortem thigh meat, they were not further stabilized to prevent their deterioration. The effectiveness of these antioxidants in reducing absorbance (retarding lipid oxidation) was observed. Overall, myricetin showed greater capacity to decrease lipid deterioration in poultry products ($P \leq 0.05$, Table 3). Inadvertently, myricetin was added to post-mortem tissue at the same concentrations as that recommended by the manufacturer for DOE. Upon closer inspection, it was noted that DOE contained ∼2.5% hydroxytyrosol compared to myricetin at 95% purity. Thus, the actual ratio of antioxidants added to poultry meat samples was 38:1 for myricetin and hydroxytyrosol. H2 reduced absorbance for NaCl/heated/stored samples by 35% compared to M2 at 70%. On the basis of these results, hydroxytyrosol at $^{1}/_{38}$ the concentration reduced absorbance values half as well as that of myricetin. On the basis of this observation, if hydroxytyrosol were added to post-mortem poultry thigh tissue or further processed products at the same quantity as myricetin, it would be a more effective antioxidant. Further investigation to determine the potency of each antioxidant when equal quantities are added to unprocessed tissue and processed poultry meat is warranted.

AUTHOR INFORMATION

Corresponding Author

*(A.J.K.) E-mail: ajking@ucdavis.edu. Phone: (530) 752-3530.

Notes

The authors declare no competing financial interest.

REFERENCES

(1) Brenes-Balbuena, M.; Garcia-Garcia, P.; Garrido-Fernandez, A. Phenolic compounds related to the black color formed during the processing of ripe olives. *J. Agric. Food Chem.* **1992**, *40*, 1192−1196.

(2) Robards, K. Strategies for the determination of bioactive phenols in plants, fruit and vegetables. *J. Chromatogr., A* **2003**, *1000*, 657−692.

(3) Allouche, N.; Fki, I.; Sayadi, S. Toward a high yield recovery of antioxidants and purified hydroxtyrosol from olive mill wastewaters. *J. Agric. Food Chem.* **2003**, *52*, 267−272.

(4) Pellegrini, N.; Serafini, M.; Colombi, B.; Del Rio, D.; Salvatore, S.; Blanchi, M.; Brighenti, F. Total antioxidative capacity of plant foods, beverages and oils consumed in Italy assessed by three different *in vitro* assays. *J. Nutr.* **2003**, *133*, 2812−2819.

(5) Bonoli, M.; Montanucci, M.; Toschi, T. G.; Lercker, G. Fast separation and determination of tyrosol, hydroxytyrosol and other phenolic compounds in extra-virgin olive oil by capillary zone electrophoresis with ultraviolet-diode array detection. *J. Chromatogr., A* **2003**, *1011*, 163−172.

(6) Igna, I.; Volf, I.; Popa, V. A critical review of methods for characterization of polyphenolic compounds in fruit and vegetables. *Food Chem.* **2011**, *226*, 1821−1835.

(7) Aeschbach, R.; Loliger, J.; Scott, B. C.; Butler, J.; Hallwell, B.; Aruoma, D. I. Antioxidant actions of thymol, carvacrol, 6-gingerol, zingerone and hydroxytyrosol. *Food Chem. Toxicol.* **1994**, *32*, 31−36.

(8) Saija, A.; Trombetta, D.; Tomaino, A.; Lo Casio, R.; Princi, P.; Uccella, N.; Bonina, F.; Castelli, F. In vitro evaluation of the antioxidant activity and biomembrane interaction of the plant phenols oleuropein and hydroxytyrosol. *Int. J. Pharm.* **1998**, *166*, 123−133.

(9) Visioli, F.; Galli, C.; Plasmati, E.; Viappiani, S.; Hernandez, A.; Colombo, C.; Sala, A. Olive phenolhydroxytyrosol prevents passive smoking-induced oxidative stress. *Circulation* **2000**, *102*, 2169−2117.

(10) Gordon, M. H.; Palva-Martins, F.; Almeida, M. Antioxidant activity of hydroxytryrosol acetate compared with that of other olive oil polyphenols. *J. Agric. Food Chem.* **2001**, *49*, 2480−2488.

(11) Tuck, K. L.; Freeman, M. P.; Hayball, P. J.; Stretch, G. L.; Stupans, L. The *in vitro* fate of hydroxytyrosol and tyrosol antioxidant phenolic constituents of olive oil, after intravenous and oral dosing of labeled compounds in rats. *J. Nutr.* **2001**, *131*, 1993−1996.

(12) D'Angelo, S.; Manna, C.; Magliardi, V.; Mazzoni, O.; Morrica, P.; Capasso, G.; Galletti, P.; Zappia, V. Pharmcokinetics and metabolism of hydroxytyrosol, a natural antioxidant from olive oil. *Drug Metab. Dispersion* **2001**, *29*, 1492−1498.

(13) Visioli, F.; Poli, A.; Gall, C. Antioxidant and other biological activities of phenols from olives and olive oil. *Med. Res. Rev.* **2002**, *22*, 65−67.

(14) Lamuela-Raventós, R. M.; Gimeno, E.; Fitó, M.; Castellote, A.-I.; Covas, M.; De La Torre-Baronat, M. C.; López-Sabater, M. C. Interaction of olive phenol antioxidant components with low-density lipoprotein. *Biol. Res.* **2004**, *37*, 247−252.

(15) Solomon, A.; Golubowicz, S.; Yablowicz, Z.; Grossman, S.; Bergman, M.; Gottlieb, H. E.; Altman, A.; Kerem, Z.; Flaishman, M. A. Antioxidant activities and anthocyanin content of fresh fruits of common fig (*Ficus carica* L.). *J. Agric. Food Chem.* **2006**, *54*, 7717−7723.

(16) Vazquez-Anon M.; Bowman, G. R. Antioxidant combination for use in feed rations to increase milk production. Patent 7910604, March 22, 2011.

(17) IOC (International Olive Council). The antioxidant properties of the olive oil; www.internationaloliveoil.org/estaticos/view/89-the-antioxidant-properites-of-the-olive-oil (accessed July 2012).

(18) Varriale, E. Hydroxytyrosolflipper.diff.org/app/items/info/4333 (accessed September 2012).

(19) Vissers, M. N.; Zock, P. L.; Katan, M. B. Bioavailability and antioxidant effects of olive oil phenols in humans: a review. *Eur. J. Clin. Nutr.* **2004**, *58*, 955−965.

(20) Rietjens, S. J.; Bast, A.; Haenen, G. R. M. M. New insights into controversies on the antioxidant potential of the olive oil antioxidant hydroxytyrosol. *J. Agric. Food Chem.* **2007**, *55*, 7609−7614.
(21) Chow, K. C. Fatty acids in poultry and egg products. In *Fatty Acids in Foods and Their Health Implications*, 3rd ed.; Chow, K. C., Ed.; CRC Press: New York, 2008; pp 127−130.
(22) King, A. J.; Uijttenboogaart, T.; deVries, A. W. α-Tocopherol, β-carotene and ascorbic acid as antioxidants in stored poultry muscle. *J. Food Sci.* **1995**, *60*, 1009−1012.
(23) King, A. J.; Zeidler, G. Tomato pomace may be a good source of vitamin E in broiler diets. *Calif. Agric.* **2004**, *58*, 59−62.
(24) Bitter, C. Personal Correspondence, Hayward, CA, USA, 2007.
(25) Catus Botanics. Myricetin, bayberry extract, cactus botanics, 2006; www.cactusbotanics.com/Products/Bayberry.htm (accessed July 2012).
(26) Ong, K. C.; Kkoo, H. E. Review: biological effects of myricetin. *Gen. Pharmacol.* **1977**, *29*, 121−126.
(27) Choi, D. H.; Li, C.; Choi, J. S. Effects of myricetin, an antioxidant, on the pharmacokinetics of losartan and its active metabolite, EXP-3174, in rats: possible role of cytochrome P450 3A4, cytochrome P450 2C9 and P-glycoprotein inhibition by myricetin. *J. Pharm. Pharmacol.* **2010**, *62*, 908−914.
(28) Cuendet, K.; Hostettmann, K.; Potterat, O. Iridoid glucosides with free radical scavenging properties from *Fagraea blumei*. *Helv. Chim. Acta* **1997**, *80*, 1144−1152.
(29) Fasseas, M. K.; Mountzouris, K. C.; Tarantilis, P. A.; Polissiou, M.; Zervas, G. Antioxidant activity in meat treated with oregano and essential oils. *Food Chem.* **2008**, *106*, 1188−1194.
(30) SAS Institute. *SAS/STAT User's Guide*, version 9.1; SAS Institute, Inc.: Cary, NC, USA, 2004.
(31) Paiva-Martins, F.; Barbosa, S.; Pinheiro, V.; Mourão, J. L. The effect of olive leaves supplementation on the feed digestibility, growth performances of pigs and quality of pork meat. *Meat Sci.* **2009**, *82*, 438−443.
(32) Botsoglou, E.; Govaris, A.; Moulas, A.; Botsoglou, N. Oxidative stability and microbial growth of turkey breast fillets during refrigerated storage as influenced by feed supplementation with olive leaves, oregano and/or α-tocopheryl acetate. *Br. Poult. Sci.* **2010**, *51*, 760−768.
(33) Medina, I.; Lois, S.; Alcantara, D.; Lucas, R.; Morales, C. Effect of lipophilization of hydroxytyrosol on its antioxidant activity in fish oils and fish oil-in-water emulsions. *J. Agric. Food Chem.* **2009**, *57*, 9773−9779.

beam- and γ-irradiation on the total aerobic bacteria and yeasts/molds in garlic samples was also evaluated.

MATERIALS AND METHODS

Garlic Samples and Irradiation Treatments. Garlic samples were purchased from retail markets in Daegu, South Korea. The samples were harvested in two different regions including Korea and China. The crushed garlics were originally vacuum-packed in polyethylene bags (packaging sizes: Korea, 500 g; and China, 1 kg) and stored at −18 °C. The bag units containing the samples were divided into two equal sets and labeled with the specific irradiation dose/type. Furthermore, the samples were placed in insulated polystyrene boxes and individually carried to the irradiation processing plants. The transportation was done under a frozen state at −20 °C. One set of samples was irradiated under γ-rays ^{60}Co radiation source (100 kCi point source AECL, IR-79, MDS Nordion International Co. Ltd., Ottawa, ON, Canada) at the Korea Atomic Energy Research Institute, Jeongeup, South Korea. Likewise, electron beam (e-beam) irradiation was performed on the second set of samples using an e-beam accelerator (Model ELV-4, acceleration voltage of 2.5 MeV, Fujifilm, Tokyo, Japan) stationed at EB-TECH Co., Daejeon, South Korea. The irradiation was performed at room temperature with doses of 0, 1, 4, and 7 kGy. The dose rate was 2.5 kGy/h from both radiation sources. The bags were rotated crosswise while receiving the radiation treatments. A ceric/cerous dosimeter (Harwell, Didcot, UK) was used to verify the absorbed dose in e-beam irradiated samples. On the other hand, an alanine dosimeter (Bruker Instruments, Rheinstetten, Germany) was used to confirm the absorbed dose in γ-irradiated samples. The samples were stored at −18 °C until required for further analysis. All of the planned experiments were replicated three times and completed within 2 weeks.

Total Aerobic Bacteria and Yeasts/Molds Count. Garlic samples were analyzed for the total aerobic bacteria and yeasts/molds count. Briefly, 5 g of the crushed garlic was mixed with 45 mL of sterile peptone water. Serial dilutions in peptonized water were made and plated on plate count agar (Difco Lab, Franklin Lakes, NJ, USA) for the total aerobic bacteria and on potato dextrose agar (Difco Lab), acidified by means of sterile 10% solution of tartaric acid, for yeasts and molds. To count total aerobic bacteria, plates were incubated at 37 °C for 24−48 h. Plate reading and colony count determinations were performed according to the Bacteriological Analytical Manual Online.[15] Yeasts and molds colonies were counted 5 days after incubation at 30 °C. Colonies were counted, and the count was described as colony-forming units per gram (CFU/g). All plating was performed in triplicates to ensure accuracy.

DEFT/APC Analysis. The DEFT method calculates the total number of contaminating microorganisms in a food sample regardless of viability. On the other hand, the APC method enumerates the number of viable microorganisms that can form colonies on an agar plate. A reduction of viable microbiological counts in irradiated food could be a potential screening parameter.[9] The first step includes membrane filtration to capture the microorganisms, followed by its staining with a fluorochrome acridine orange. Then the membrane is rinsed after staining and fixed on a microscope slide for counting with an epifluorescent microscope. The method is quick and full analysis can be completed in 25−30 min. The sample preparation, performance, and calculations were done according to EN 13783[9] followed by different scientists.[16,17]

Electronic Nose Analysis. A zNose (Electronic Sensor Technology, Newbury Park, CA, USA) equipped with a surface acoustic wave (SAW) sensor and VaporPrint (Misrosense 4.88) software was used to evaluate the volatile compound profiles of non-irradiated and irradiated garlic. Principal component analysis (PCA) was applied to understand the trend in distribution of the numerical data.

Photostimulated Luminescence Analysis. PSL photon counts (PCs) registered in 60 s were measured by a SURRC PPSL irradiated food screening system (SURRC, Glasgow, UK). Samples were distributed into 50 mm diameter Petri dishes (Bibby Sterilin type 122, Glasgow, UK). Sample preparation, handling, and the sensitivity of the instrument were tested at the start of each set of measurements using a reference light source. The PCs were analyzed with respect to lower and upper threshold limits. The accumulated PCs were classified as "'negative'" (T1 = 700 counts/60 s), "'intermediate'" (between 700 and 5000 counts/60 s), or "'positive'" (T2 = 5000 counts/60 s).[7] PSL measurements were performed under subdued light conditions in accordance with EN 13751[7] recommendations.

Thermoluminescence Analysis. The silicate minerals were separated from the non-irradiated and irradiated garlic samples by a density gradient method. TL measurements were made by a 4500 TL Reader (Harshaw, Erlangen, Germany) equipped with controlled-temperature ramping and automatic reheating facility at the Centre for Instrumentation, Kyungpook National University. The TL glow curves (glow 1) were recorded on both irradiated and non-irradiated samples with a reading time of 80 s and a heating range of 50−400 °C at a linear heating rate of 5 °C/s. The TL oven was purged under a continuous nitrogen flux (2 mL/min) to reduce spurious TL signals. Each sample disk containing tested minerals was subjected to a re-irradiation step at a standard dose of 1 kGy for normalization of the glow 1 results. The second TL glow curve (glow 2) was recorded to obtain the integrated TL signal ratios (TL_1/TL_2). Mineral isolation, sample preparation, and TL measurements were performed according to EN 1788.[8]

Statistical Analysis. Origin 8.0 (Microcal Software Inc., Northampton, MA, USA) and SAS program (version 9.3, SAS Institute, Cary, NC, USA) were used for data analysis. All analyses were performed in triplicates, and values were reported as the means (±SD).

RESULTS AND DISCUSSION

Effect of Irradiation on Total Aerobic Bacterial and Yeasts/Molds Count. The counts of total bacteria and yeasts/molds from countable plates are given in Figure 1. No significant differences in aerobic bacterial and yeasts/molds count were observed among two sources of untreated crushed garlics. The non-irradiated samples from China or Korea contained a relatively moderate population of aerobic bacteria, that is, approximately 10^5 CFU/g. Treatment with irradiation, either e-beam or γ-rays, unequivocally reduced the microbial population with dose increment from 1 to 7 kGy in a logarithmic manner. These results illustrate that the counts of total aerobic bacteria were reduced by 2-logarithmic cycles by a γ-ray dose of 4 kGy. Furthermore, a dose of 7 kGy was enough to reduce the bacterial count to nondetectable levels in locally harvested samples. In contrast, the count of aerobic bacteria was still high (10^4 CFU/g) in imported garlic samples. No considerable changes in bacterial count were observed in samples from China after the e-beam treatment. In general, the effect of both irradiation treatments on total aerobic bacterial count was almost similar on all examined samples. However, the garlic samples of domestic origin showed a little more sensitivity to the irradiation disinfestation as shown in Figure 1. The total aerobic bacterial values of untreated samples of the present study are equivalent to counts reported by Hong and Kim[12] for crushed garlic harvested in Korea.

Similarly, the initial yeasts/molds count in untreated samples was about 10^5 CFU/g as shown in Figure 1B. The yeasts/molds count decreased significantly with increasing irradiation dose. Irradiation treatment at 4 kGy effectively reduced the plate count of yeasts/molds to about 10^2 CFU/g in both types of samples. Further γ-ray application at 5 kGy dose completely decontaminated the locally produced garlic samples. On the other hand, e-beam irradiation succeeded in reducing the fungal count only by 1 log CFU/g by using a higher dose of 7 kGy. Therefore, the effect of γ-irradiation was more pronounced on

dx.doi.org/10.1021/jf500200r | J. Agric. Food Chem. 2014, 62, 7920−7926

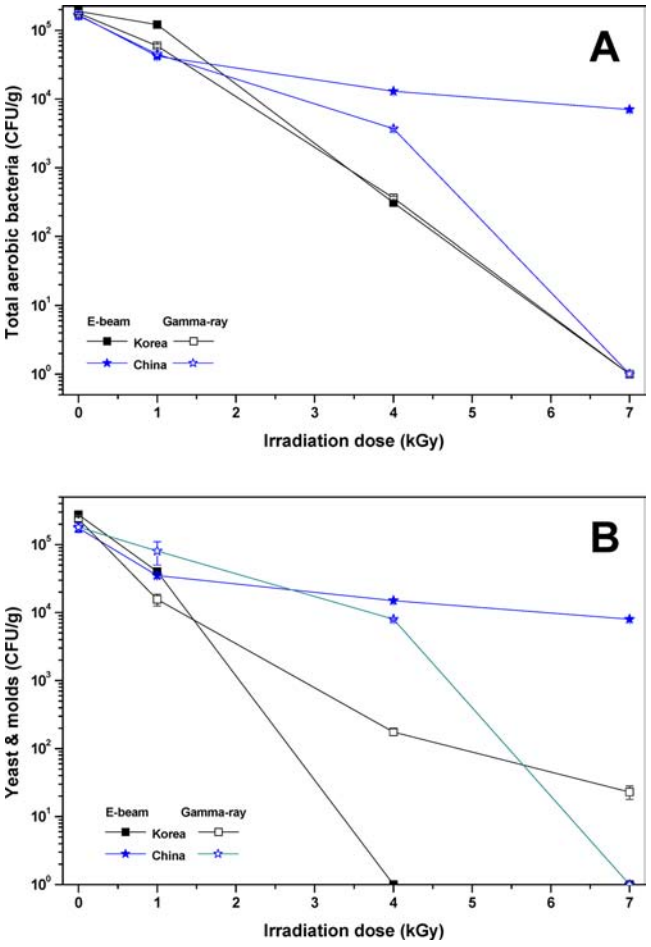

Figure 1. Total aerobic bacteria (A) and yeasts/molds (B) counts of electron beam- and γ-irradiated frozen crushed garlic produced in Korea and China.

the yeast and mold loads in all samples corresponding to total aerobic count. Comparable reductions in the microflora resulting from ionizing radiations were reported by Pezzutti et al.[18] for dehydrated garlic sold in the Argentinean retail market. Irradiation exposure between 5 and 10 kGy reduced the microbial load to acceptable levels in dehydrated garlic.

Microbial contamination of the vegetables may occur during production, harvesting, and distribution processes. In addition, the degree of contamination depends on the environmental conditions from growing to marketing and the physiological condition of the product.[19] The microbiological results in the present study indicated that the frozen crushed garlic samples available in the Korean market from both sources were hygienically safe for human consumption. The count of the total aerobic bacteria in frozen processed foods should not exceed 10^6 CFU/g according to the microbiological specifications established by the Ministry of Food and Drug Safety, South Korea.[20] It is worth noting that garlic, either freeze-dried or fresh-crushed, also has high antibacterial properties.[21] A review of different studies confirmed the presence of potential foodborne pathogens such as *Salmonella*, *Escherichia coli*, *Clostridium perfringens*, *Bacillus cereus*, and toxigenic molds in powdered garlic grown/processed in different countries.[22] Additionally, a given irradiation dose will be able to destroy a certain proportion of the microbial population regardless of the number of microorganisms present. This characteristic of irradiation implies that the higher the initial population of spoilage microorganism, the higher the population will be after the irradiation treatment depending upon several other factors. Furthermore, and of course, if spoilage has already initiated, radiation processing can do nothing to reverse it.[1]

Screening Analyses. The garlic samples were screened for their irradiation status using three different types of screening techniques based on microbiological, chemical, and physical principles.

Microbial Population Characterization by DEFT/APC Analysis. Prior to decontamination treatment, the microbial counts measured by DEFT and APC were of similar order due to the presence of microbes in the samples. However, there is a significant reduction in the APC count as compared to the DEFT count after the application of a decontamination treatment such as irradiation.[10,16]

The DEFT and APC values of non-irradiated and irradiated garlic samples are shown in Figure 2. Moderate APC count

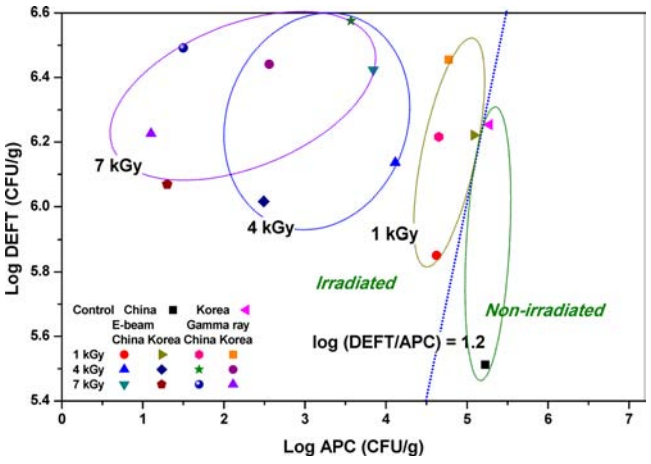

Figure 2. Logarithmic microbial counts of non-irradiated and electron beam- and γ-irradiated frozen crushed garlic produced in Korea and China.

(>10^5 CFU/g) was detected in the untreated samples from both sources. The DEFT count remained almost unchanged despite the irradiation treatment. On the other hand, APC values (mesophilic bacteria) progressively decreased with the dose increment either by e-beam or γ-ray processing. There was a clear reduction of mesophilic bacterial population (viable microorganisms) to the level of 10^2 CFU/g on exposure to 4 kGy γ-irradiation. The log DEFT/APC ratio was determined for each sample. The log DEFT/APC ratio of garlic samples increased with the gradual increase in the irradiation dose. For example, the log DEFT/APC ratio of non-irradiated sample from China was 1.05, whereas it was 1.27 for 1 kGy irradiated samples. In general, the log DEFT/APC ratio was <1.2 for non-irradiated samples, whereas irradiated samples showed >1.2 logarithmic units. Therefore, DEFT/APC analysis provided clear separation of the non-irradiated and irradiated garlic samples of both origins. On the basis of the present results, it is suggested that a DEFT/APC ratio of 1.2 logarithmic units could be used as a standard for the screening of frozen crushed garlic samples available in the Korean market as non-irradiated or irradiated.

Oh et al.[23] successfully evaluated the applicability of the DEFT/APC method for the screening of irradiated spices produced in Korea. Other studies showed that a clear screening

of the different irradiated (0−10 kGy) spices is possible by studying changes in microbial profile employing DEFT/APC methods.[17] Previously, the DEFT/APC method gave satisfactory screening results to indicate irradiation treatment of minimally processed vegetables. In general, a log DEFT/APC difference of around 2.0 is required for the useful application of this technique. However, the main drawback of the DEFT/APC method is that it not specific to irradiation treatment.[16]

E-Nose Screening Analysis. Irradiation can alter the odor profile of a food. Gardner and Bartlett[24] initially reported that the volatile profiles of samples based on the odor patterns are more useful indicators rather than the specific volatile compounds during E-nose analysis. The differences and similarities of odor patterns among different samples have been represented by the distinct fingerprint of the volatile profile.[25]

Figure 3 shows the PCA of irradiated garlic samples using E-nose measurement. A prominent screening of the irradiated samples was observed depending on the irradiation dose. It was clear that there were large differences in odor patterns between irradiated and non-irradiated garlics. In the case of the irradiated samples, different electronic fingerprints were observed in comparison with the non-irradiated ones, establishing the possibility of detection of the irradiated samples. PCA helped further to understand the trend in distribution of the numerical data.[26] Published studies have reported the use of E-nose analysis for irradiated spices,[17] fresh mushrooms,[26] and anchovy sauce.[25] Radiation-induced changes in odor pattern on food cannot be considered as radiation-specific detection markers, and the results need to be confirmed by a validated technique.[17]

Photoluminescence Screening Analysis. The development of a PSL novel screening has been aimed at resolving the practical limitations of laborious mineral separation in the TL method. Many foods are contaminated with mineral debris, which can store energy in charge carriers at structural, interstitial, or impurity sites upon irradiation. The PSL technique employs light rather that heat as a stimulus for liberating the trapped energy induced by radiation in solid materials. However, false-positive and false-negative results may be observed on the basis of the quality and quantity of the minerals present on the surface of the food sample.[7]

All non-irradiated garlic samples gave PCs in the negative PSL range [<700 photon counts/60 s (PCs)]. The PSL counts of non-irradiated samples were 327.1 ± 106.4 and 283.6 ± 95.6, harvested in China and Korea, respectively. All irradiated samples from China gave PCs in the positive range (>5000 PCs), thereby easily screening them out as irradiated. Furthermore, the PSL response was linear with the absorbed irradiation doses for imported samples (Table 1). On the contrary, the irradiated garlic samples from Korea exhibited a rather unusual behavior. Table 1 shows either intermediate or false-negative PSL counts were recorded for γ- or e-beam-treated domestic samples. The PCs of 1 and 4 kGy γ-irradiated garlics from Korea were 625.5 ± 306.3 and 1511.6 ± 923.4, respectively. According to European standard protocol (EN 13751),[7] negative calibrated PSL results are indicative of insufficient PSL sensitivity. Therefore, the varying results from our data emphasize the application of PSL as a screening analysis.

This behavior was in agreement with that reported by Cutrubinis et al.[13] for the PSL screening analysis of γ-irradiated (25, 50, and 100 Gy) garlic bulbs collected from the Brazilian,

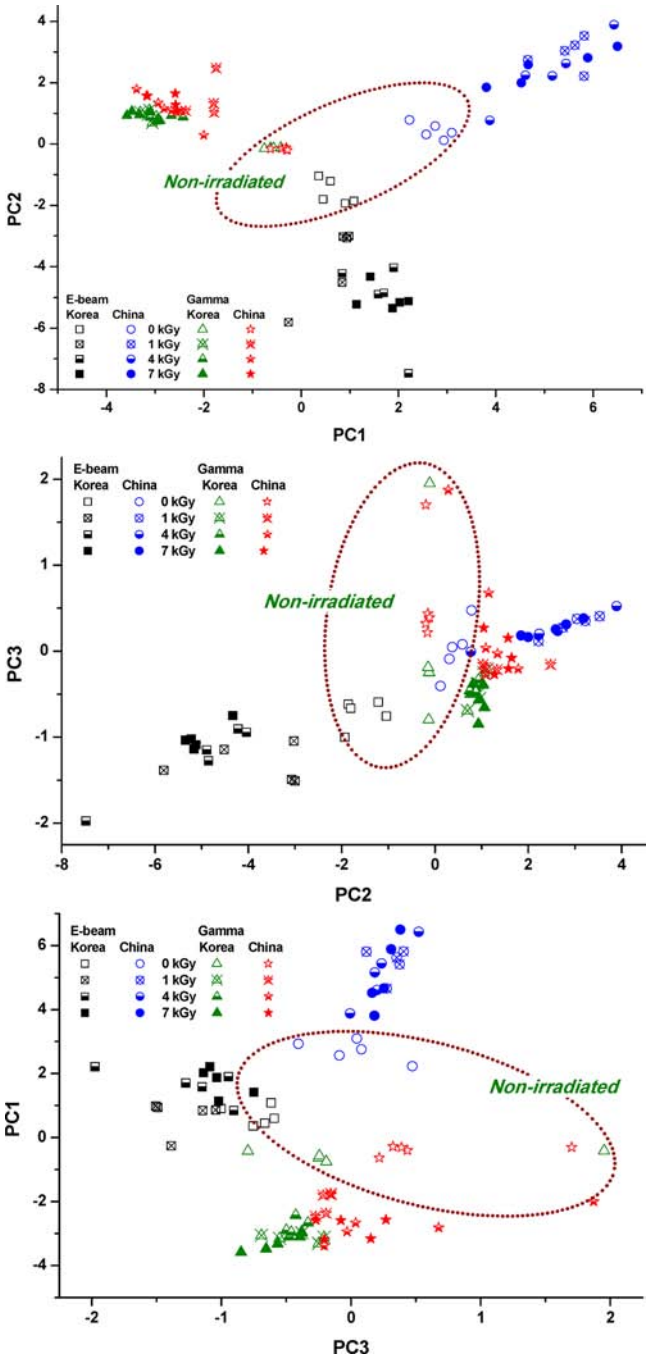

Figure 3. Principal component analysis of E-nose determinations on non-irradiated and electron beam- and γ-irradiated frozen crushed garlic produced in Korea and China.

German, and Romanian markets. The PSL technique showed limitations as PCs values were found below the lower threshold limit, possibly due to the low dose or irradiation. PSL sensitivity relies on the quantity and type of minerals within the individual sample.[7] Therefore, the insufficient PSL screening in domestic garlic bulbs can be ascribed to the presence of a low amount of silicate minerals.

Ahn et al.[27] studied how different light conditions (natural light, artificial light, and dark room) can affect the PCs values for irradiated garlic bulbs during storage. In general, the PCs of all garlic samples decreased as storage time proceeded. The control garlic samples showed intermediate PSL PCs at day 0

dx.doi.org/10.1021/jf500200r | J. Agric. Food Chem. 2014, 62, 7920−7926

Table 1. Photostimulated Luminescence Properties of Electron Beam- and γ-Irradiated Frozen Crushed Garlic Produced in China and Korea

		photon count/60 s[a]	
radiation source	dose (kGy)	garlic sample produced in China	garlic sample produced in Korea
electron beam	0	329.1 ± 122.7 (−)[b] bx	251.5 ± 118.3 (−) bx
	1	11603.2 ± 18512.2 (+) abxy	395.4 ± 116.4 (−) abxy
	4	3105.0 ± 786.2 (M) abxy	345.9 ± 149.6 (−) abxy
	7	17412.9 ± 23747.8 (+) axy	466.8 ± 226.7 (−) axy
γ-ray	0	327.1 ± 106.4 (−) bx	283.6 ± 95.6 (−) cx
	1	13840.3 ± 17732.8 (+) bx	625.5 ± 306.3 (−) cy
	4	14124.8 ± 4281.1 (+) bx	1511.6 ± 923.4 (M) by
	7	35612.3 ± 25533.9 (+) ax	2488.5 ± 1291.1 (M) ay

[a]Mean ± SD (n = 10). Values within the same row with different letters (a–c) are significantly different at $p < 0.05$. Values within the same column with different letters (x, y) are significantly different at $p < 0.05$. [b]Threshold value: T_1 = 700, T_2 = 5000, (−) <T_1, T_1 < (M) < T_2, (+) > T_2.

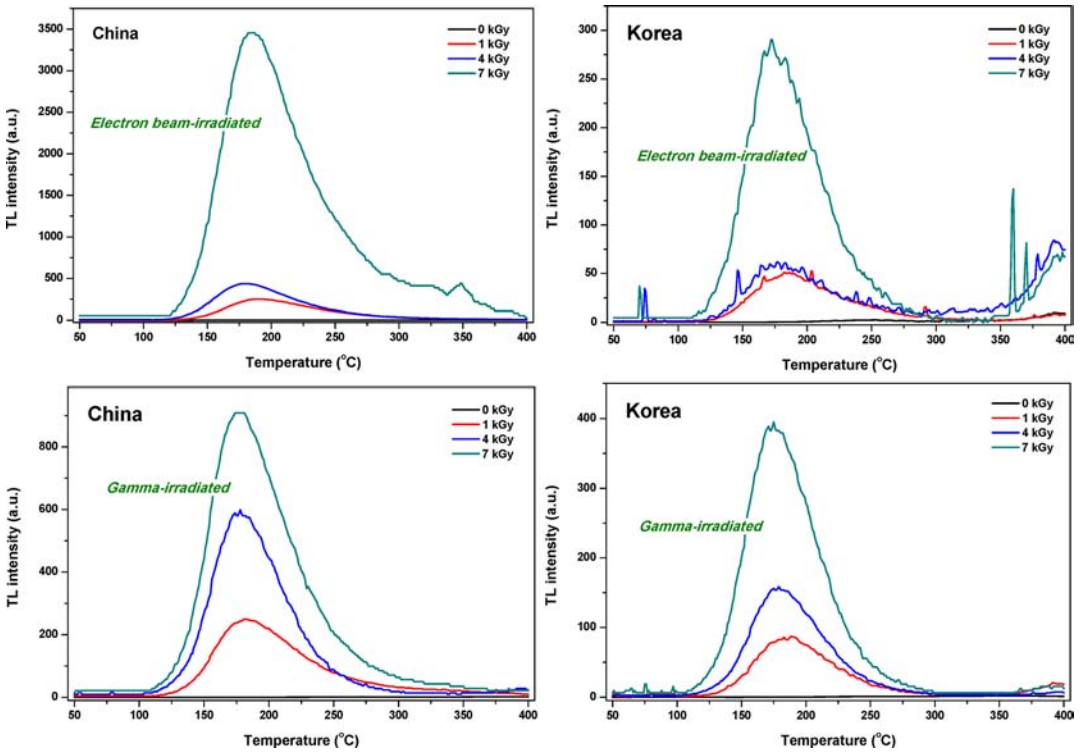

Figure 4. Thermoluminescence glow curves of minerals separated from electron beam- and γ-irradiated frozen crushed garlic produced in Korea and China.

that decreased upon different storage conditions. In another study, Ahn et al.[17] found unsatisfactory PSL screening values during the analysis of irradiated powder samples of different spices and fresh paprika. The presence of a low quantity of the minerals in food samples and insensitivity to light stimulation could lead to poor PSL output. Despite varying results, PSL is a versatile technology to get a valuable indication about the irradiation status of various food stuffs. However, there is a need to confirm the results obtained from the PSL method using a more validated technique that can ensure the irradiation status of the suspected samples.[5,7]

Confirmation Analysis. *Thermoluminescence Characteristics of Isolated Minerals.* The TL technique offers the possibility of a very accurate identification of non-irradiated and irradiated inorganic dust, that is, quartz or feldspar.

During irradiation, free charge carriers, namely, electrons and holes, are produced in the crystals, which may be trapped by localized states within the band gap. The physical process of TL is based on the emission of light photon upon recombination of the opposite charge carriers when stimulated by thermal means. The emitted light is detected by a sensitive photon counter and amplified using a photomultiplier tube. The light intensity is finally recorded as a function of temperature to construct the TL glow curve.[4,8]

All of the irradiated garlics from different origins of production were reliably detected by the TL method. The TL spectra of minerals from garlic samples produced in China and Korea are shown in Figure 4. Minerals separated from irradiated samples produced TL glow curves in the recommended temperature interval between 150 and 250 °C. The TL glow curves from irradiated samples peaked at approximately 180 °C with high intensity. Furthermore, there were no interference signals at around 180 °C. The glow curve structure was very clear with well-defined peaks. In addition,

the TL intensity was proportional to dose level and the origin of cultivation. Garlic from China comparatively produced TL glow curves with high intensity at all irradiation doses. Thus, the difference in intensity may be related to the mineral composition. All of the non-irradiated garlics produced a residual geologically derived TL signal (natural TL) of maximum peak at approximately 300 °C or above with low intensity regardless of the area of production (Figure 4).

Normalization of TL glow curves through a re-irradiation step with a standard dose of 1 kGy can greatly improve the reliability of TL results. The TL glow ratio (Tl_1/TL_2) was calculated for all samples as shown in Figure 5. The TL ratio

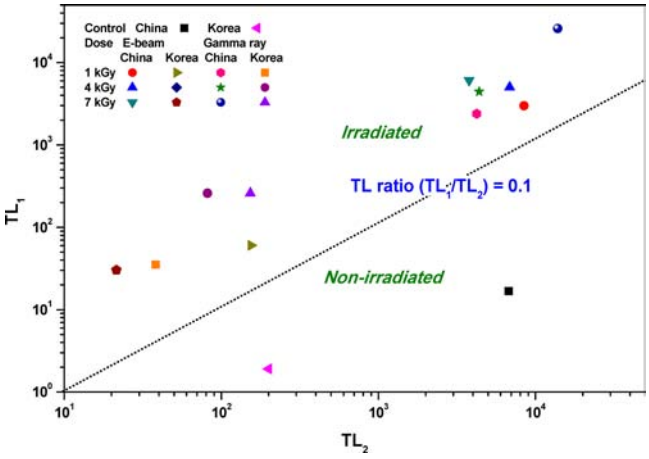

Figure 5. TL ratio (TL_1/TL_2) of inorganic dust minerals separated from electron beam- and γ-irradiated frozen crushed garlic produced in Korea and China.

was less than threshold value of 0.1 for the non-irradiated garlic samples produced in China and Korea. On the other hand, all irradiated samples regardless of their origin and type of irradiation treatment gave a TL ratio of >0.1 that increased with the given dose (Figure 5). Therefore, the clear identification of irradiated samples was guaranteed by the analysis of shape and intensity of the first TL glow curve and TL ratios.

Cutrubinis et al.[13] reported the limited availability of an amount of silicate minerals from the garlic bulbs. However, TL analysis successfully detected the irradiation status of the garlic bulb samples obtained from three different countries. Recently, Ahn et al.[28] investigated the effect of storage time under different light conditions on the TL properties of garlic bulbs cultivated in two different regions of Korea. A typical TL glow curve of high intensity with a maximum peak in the temperature range of 160−185 °C was prominent in all irradiated garlic samples. Additionally, no difference in the shapes of TL glow curves was experienced in all irradiated samples irrespective of the origin of cultivation. However, a significant difference in intensity was recorded relating to the origin of the cultivation. Furthermore, there was a time-dependent decrease during 2 years of storage in TL intensities and TL ratios for all irradiated samples. Kim et al.[29] applied the TL technique to identify different spice blends containing small amounts of different irradiated (0, 1, and 10 kGy) spice powders, such as red pepper, garlic, or ginger. Upon analysis, the blends containing even the lowest 0.5% irradiated garlic component gave typical TL glow curves that could be interpreted as positive. Ahn et al.[17] also discussed the TL method as a reliable confirmatory technique to identify different irradiated spices. The authenticity of TL for the identification of irradiated foods has been confirmed by various studies.[3,4,6,30]

In conclusion, the frozen crushed garlics of different origins of production available in the Korean market were hygienically safe according to the set microbiological quality standards. In general, γ-irradiation resulted in greater reduction in total bacterial or yeasts/molds count in garlics regardless of their origin of harvest. Therefore, irradiation processing may satisfy the demand of consumers for high-quality minimally processed garlic.

AUTHOR INFORMATION

Corresponding Author

*((J.-H.K.) Phone: +82 53 950 5775. Fax: +82 53 950 6772. E-mail: jhkwon@knu.ac.kr.

Funding

This research was supported in 2013 by a grant (10162KFDA995) from the Ministry of Food and Drug Safety, Republic of Korea.

Notes

The authors declare no competing financial interest.

REFERENCES

(1) WHO. Practical applications of food irradiation. In *Food Irradiation − A Technique for Preserving and Improving the Safety of Food*; WHO/FAO: Geneva, Switzerland, 1988; pp 33−43.

(2) Molins, R. A.; Motarjemi, Y.; Käferstein, F. K. Irradiation: a critical control point in ensuring the microbiological safety of raw foods. *Food Control* **2001**, *12*, 347−356.

(3) Arvanitoyannis, I. S.; Tserkezou, P. Legislation on Food Irradiation. In *Irradiation of Food Commodities: Techniques, Applications, Detection, Legislation, Safety and Consumer Opinion*, 1st ed.; Arvanitoyannis, I. S., Ed.; Academic Press: London, UK, 2010; pp 673−698.

(4) Chauhan, S. K.; Kumar, R.; Nadanasabapathy, S.; Bawa, A. S. Detection methods for irradiated foods. *Compr. Rev. Food Sci. Food Saf.* **2009**, *8*, 4−16.

(5) Shahbaz, H. M.; Ahn, J. J.; Akram, K.; Kwon, J. H. Screening methods for the identification of irradiated foods: a review. *Curr. Res. Agric. Life Sci.* **2013**, *31*, 1−10.

(6) Akram, K.; Ahn, J. J.; Kwon, J. H. Analytical methods for the identification of irradiated foods. In *Ionizing Radiation: Applications, Sources and Biological Effects*; Belotserkovsky, E., Ostaltsov, Z., Eds.; Nova Science Publishers: New York, 2012; pp 1−36.

(7) EN13751. *Foodstuffs−Detection of irradiated food using photostimulated luminescence*; European Committee of Standardization (CEN), Brussels, Belgium, 2009.

(8) EN1788. *Foodstuffs−Thermoluminescence detection of irradiated food from which silicate minerals can be isolated*; European Committee of Standardization (CEN), Brussels, Belgium, 2001.

(9) EN13783. *Foodstuffs−Detection of irradiated food using direct epifluorescent filter technique/aerobic plate count (DEFT/APC)*; European Committee of Standardization (CEN), Brussels, Belgium, 2001.

(10) Corzo-Martinez, M.; Corzo, N.; Villamiel, M. Biological properties of onions and garlic. *Trends Food Sci. Technol.* **2007**, *18*, 609−625.

(11) FAO. STAT data; http://faostat3.fao.org (accessed July 11, 2014).

(12) Hong, S. I.; Kim, D. M. Storage quality of chopped garlic as influenced by organic acids and high-pressure treatment. *J. Sci. Food Agric.* **2001**, *81*, 397−403.

(13) Cutrubinis, M.; Delincee, H.; Bayram, G.; Villavicencio, A. C. H. Germination test for identification of irradiated garlic. *Eur. Food Res. Technol.* **2004**, *219*, 178−183.

(14) IAEA Food Authorization Database. http://nucleus.iaea.org/ifa/FoodAuthorisationDisplay.aspx (accessed July 11, 2014).
(15) Bacteriological Analytical Manual Online. http://www.fda.gov/Food/FoodScienceResearch/LaboratoryMethods/ucm063346.htm (accessed July 11, 2014).
(16) Araújo, M. M.; Duarte, R. C.; Silva, P. V.; Marchioni, M.; Villavicencio, A. L. C. H. Application of the microbiological method DEFT/APC to detect minimally processed vegetables treated with gamma radiation. *Radiat. Phys. Chem.* **2009**, *78*, 691−693.
(17) Ahn, J. J.; Akrama, K.; Kwak, J. Y.; Jeong, M. S.; Kwon, J. H. Reliable screening of various foodstuffs with respect to their irradiation status: a comparative study of different analytical techniques. *Radiat. Phys. Chem.* **2013**, *91*, 186−192.
(18) Pezzutti, A.; Marucci, P. L.; Sica, M. G.; Matzkin, M. R.; Croci, C. A. Gamma-ray sanitization of Argentinean dehydrated garlic (*Allium sativum* L.) and onion (*Allium cepa* L.) products. *Food Res. Int.* **2005**, *38*, 797−802.
(19) Zagory, D. Effects of post-processing handling and packaging on microbial populations. *Postharvest Biol.Technol.* **1999**, *15*, 313−321.
(20) Ministry of Food and Drug Safety. *Food Code*; Seoul, Korea, 2012; pp 3-1-1−3-1-2.
(21) Guo, J. J.; Kuo, C. M.; Chuang, Y. C.; Hong, J. W.; Chou, R. L.; Chen, T. I. The effects of garlic-supplemented diets on antibacterial activity against *Streptococcus iniae* and on growth in orange-spotted grouper *Epinephelus coioides*. *Aquaculture* **2012**, *364/365*, 33−38.
(22) McKee, L. H. Microbial contamination of spices and herbs: a review. *LWT−Food Sci. Technol.* **1995**, *28*, 1−11.
(23) Oh, K. N.; Lee, S. Y.; Lee, H. J.; Kim, K. E.; Yang, J. S. Screening of gamma irradiated spices in Korea by using a microbiological method (DEFT/APC). *Food Control* **2003**, *14*, 489−494.
(24) Gardner, J. W.; Bartlett, P. N. A brief history of electronic noses. *Sens. Actuator B−Chem.* **1993**, *18*, 211−220.
(25) Kim, J. H.; Ahn, H. J.; Yook, H. S.; Kim, K. S.; Rhee, M. S.; Ryu, G. H.; Byun, M. W. Color, flavor, and sensory characteristics of gamma-irradiated salted and fermented anchovy sauce. *Radiat. Phys. Chem.* **2004**, *69*, 179−187.
(26) Akram, K.; Ahn, J. J.; Yoon, S. R.; Kim, G. R.; Kwon, J. H. Quality attributes of *Pleurotus eryngii* following gamma irradiation. *Postharvest Biol. Technol.* **2012**, *66*, 42−47.
(27) Ahn, J. J.; Kim, G. R.; Akram, K.; Kim, J. S.; Kwon, J. H. Effect of storage conditions on photostimulated luminescence of irradiated garlic and potatoes. *Food Res. Int.* **2012**, *47*, 315−320.
(28) Ahn, J. J.; Kim, G. R.; Akram, K.; Kim, J. S.; Kwon, J. H. Changes in thermoluminescence properties of minerals separated from irradiated potatoes and garlic during long-term storage under different light conditions. *Eur. Food Res. Technol.* **2012**, *235*, 75−82.
(29) Kim, B. K.; Akram, K.; Kim, C. T.; Kang, N. R.; Lee, J. W.; Ryang, J. H.; Kwon, J. H. Identification of low amount of irradiated spices (red pepper, garlic, ginger powder) with luminescence analysis. *Radiat. Phys. Chem.* **2012**, *81*, 1220−1223.
(30) Shahbaz, H. M.; Akram, K.; Ahn, J. J.; Kwon, J. H. Investigation of radiation-induced free radicals and luminescence properties in fresh pomegranate fruits. *J. Agric. Food Chem.* **2013**, *61*, 4019−4025.

Table 1. 96 h LC_{50}, 96 h EC_{50} (Malformation), Teratogenic Index (TI; LC_{50}/EC_{50}), Mortality–Malformation No Observable Effects Concentration (NOEC), Lowest Observable Effect Level (LOEC), and Minimum Concentration To Inhibit Growth (MCIG) for Acrylamide, Furan, and L-Cysteine[a]

					mortality		malformation		
clutch	total embryos	LC_{50} (mmol/L)	EC_{50} (mmol/L)	TI	NOEC (mmol/L)	LOEC	NOEC (mmol/L)	LOEC	MCIG (mmol/L)
				Acrylamide					
April 1, 2013	280	1.879 (1.692–2.099)	0.702 (0.625–0.792)	2.7	2.0	2.5	1.0	2.0	0.5
April 22, 2013	280	2.136 (2.011–2.263)	1.161 (1.007–1.356)	1.8	2.0	2.5	1.0	2.0	1
June 10, 2013	280	1.466 (1.306–1.641)	0.780 (0.674–0.917)	1.9	2.0	2.5	0.5	1.0	0.5
Aug 2, 201313	280	2.080 (1.843–2.381)	1.134 (0.992–1.314)	1.8	2.0	2.5	0.5	1.0	0.5
average		**1.890**	**0.944**	**2.0**					
				Furan					
Aug 6, 2012	400	53.94 (49.51–59.36)	44.41 (39.13–51.82)	1.2	20	30	20	30	30
Aug 13, 2012	400	38.81 (36.11–41.70)	27.30 (24.25–31.14)	1.4	30	40	20	30	30
Sept 20, 2012	400	37.92 (34.60–41.50)	47.20 (41.04–56.60)	0.8	40	50	20	30	30
average		**43.56**	**39.64**	**1.1**					
				L-Cysteine					
Aug 6, 2012	760	42.40 (37.04–49.83)	39.71 (33.96–50.04)	1.1	54	90	27	54	27
Aug 13, 2012	760	49.01 (44.49–55.15)	40.46 (34.49–51.13)	1.2	n.c.	42	64	85	64
Sept 10, 2012	760	34.14 (30.08–39.48)	35.68 (33.06–41.17)	1.0	33	42	27	33	33
average		**41.85**	**38.62**	**1.1**					

[a]Numbers in parentheses are the 95% Fieller bounds. Numbers for acrylamide are from interaction experiments.

On the basis of the available data, Moro et al.[10] concluded that both genotoxicity and chronic cytotoxicity seem to contribute to furan-induced tumor formation.[8,29−31] Reported efforts to reduce or prevent the formation of furan in foods include the use of polyphenolic compounds and plant extracts[32] and modification of food-processing conditions.[33,34] In a previous study, we reported that the amino acid L-cysteine and the tripeptide glutathione protected frog embryos against acrylamide-induced malformation (birth defects) of fetuses and that *N*-acetyl-L-cysteine protected against acrylamide-induced mortality but not against malformations.[35] In related studies, we also reported that other food ingredients protected embryos against potato glycoalkaloid-induced teratogenesis.[36−38]

Because acrylamide and furan can be formed concurrently during heat processing of numerous foods, the objectives of this study were (a) to define possible cumulative adverse and beneficial effects using the frog embryo teratogenesis assay-*Xenopus* (FETAX) of acrylamide, furan, and L-cysteine individually and the combinations of L-cysteine and acrylamide, acrylamide and furan, furan and L-cysteine, and acrylamide, furan, and L-cysteine; (b) to analyze mathematically and graphically the interactions of these compounds in the ex vivo environment that might optimize the protection by L-cysteine against adverse effects; and (c) to depict the effect of exposure to the food ingredients on the appearance of the frog embryos.

MATERIALS AND METHODS

Materials. The following compounds were obtained from Sigma (St. Louis, MO, USA): L-cysteine (catalog no. C7352); acrylamide (catalog no. A3553); human chorionic gonadotropin (catalog no. CG5); MS-222 (catalog no. E10521); calcium sulfate (catalog no. C-3771); magnesium sulfate (catalog no. M-7506); sodium bicarbonate (catalog no. S8875); potassium chloride (catalog no. P-5405); calcium chloride (catalog no. C-1016); and sodium chloride (catalog no. S7653). Furan was obtained from Aldrich-Sigma (St. Louis, MO, USA; catalog no. 185922).

Animal Care and Husbandry. *Xenopus* frogs were purchased from *Xenopus* I, Inc. (Dexter, MI, USA) and housed in a glass aquaria recirculation system with 2−4 frogs per 10 gallons of dechlorinated tap water. Human chorionic gonadotropin (250−600 IU) was injected in the dorsal lymph sac of both male and female frogs to induce breeding. Breeding pairs were placed in false-bottom breeding chambers, and embryos were collected the next morning. The jelly coat was removed by swirling the embryos for 1−3 min in a 2% L-cysteine solution (pH 8.1). Embryos were then rinsed and placed into sorting dishes. Embryos were double sorted into test dishes of 20 embryos per 8 mL of test solution in plastic disposable 60 × 15 mm Petri dishes. The negative control was FETAX solution (0.625 g/L NaCl, 0.086 g/L $NaHCO_3$, 0.03 g/L KCl, 0.015 g/L $CaCl_2$, 0.006 g/L $CaSO_4{\cdot}2H_2O$, and 0.075 g/L $MgSO_4$ in distilled ASTM type I water).[39] Frogs were not bred more than once every 2 months.

FETAX Assay Procedures. FETAX was used to determine acrylamide toxicity and teratogenesis according to the American Society for Testing Materials (ASTM) Guide for FETAX and our earlier studies with teratogenic glycoalkaloids.[40−47] Stock solutions of acrylamide and of test compounds were made in FETAX solution. Appropriate dilutions were made to achieve final concentrations. Each day of the 4 day test, new solutions were placed into 60 mm covered plastic Petri dishes with

various concentrations of test compounds dissolved in FETAX solution. At 24, 48, and 72 h, all solutions were prepared and replaced in the dishes. Dead embryos were removed, and live embryos counted. The embryos were cultured in the dark at 24 °C. At 96 h, surviving (stage 46) embryos were identified to verify embryos had reached the proper stage of development. Stage 46 embryos possess hind-limb buds and tightly coiled guts but do not yet feed. At the end of 96 h, the mortality was determined and embryos were anesthetized with MS-222. Malformed survivors, dead embryos, and the developmental stage were observed under a dissecting microscope and recorded according to the *Atlas of Malformations*.[48] Embryos were photographed with an Olympus Stylus 720sw on macro setting for growth measurements, and detailed photographs were taken of selected embryos using Pro Reg digital camera attached to a Nikon dissection microscope. As a measure of growth, head−tail length was measured by following body contour using a computer equipped with digitizing software Image Pro Plus.

Malformations were determined by observing embryos under a dissecting microscope for abnormal survivors, developmental stage, and dead embryos. *Xenopus laevis* embryos are transparent and allow for easy determination of gut, heart, head, axial, and other internal and external malformations. The malformations are quantitatively scored on a standard score sheet and tallied. The data were recorded according to American Society of Testing Material (ASTM) guidelines.[40] The total number of abnormal tadpoles divided by the total number of living tadpoles multiplied by 100 is the percentage malformed from each dish. The 96 h LC_{50} (concentration causing 50% lethality) and 96 h EC_{50} (concentration inducing malformation or gross malformations in 50% of surviving embryos) were calculated using probit analysis from Systat 13 software. The teratogenic index (TI) was calculated as the 96 h LC_{50} divided by the 96 h EC_{50} (malformation). The minimum concentration to inhibit growth (MCIG) was calculated using ANOVA with the post hoc Bonferroni test using Systat 13 software.

Individual Toxicity Experimental Design and Analysis (Acrylamide, Furan, and L-Cysteine). For concentration−response studies of toxic effects on embryos, four negative controls (4 replicates of 20 embryos in 60 × 15 mm Petri dishes) and various test concentrations (2 replicates of 20 embryos in 60 × 15 mm Petri dishes each) of chemical ranging 0.5 to 80 mM were tested. Each experiment was repeated three times. Each experiment used between 280 and 480 embryos. Previously tested acrylamide[34] had the fewest concentrations, as detailed experiments have previously been carried out as indicated by the total number of embryos for each test (Table 1). The furan and L-cysteine data were independent definitive assays as these chemicals had not been tested in the FETAX assay. The acrylamide experiments were the acrylamide positive controls for the interaction experiments. All data were analyzed according to FETAX methods above.

Interaction Experiments of Binary and Ternary Mixtures. On the basis of data from the individual experiments above, binary and trinary mixtures were calculated such that estimated ratios for mixtures could be created. For acrylamide/L-cysteine, the ratios attempted were 0TU:1TU, 1TU:0TU, 1TU:1TU, 1TU:3TU, 3TU:1TU, and 19TU:1TU. For furan/acrylamide and furan/L-cysteine, the ratios used were 0TU:1TU, 1TU:0TU, and 1TU:1TU. For acrylamide/furan/L-cysteine, the ratios used were 0TU:0TU:1TU, 0TU:1TU:0TU, 1TU:0TU:0TU, and 10TU:4TU:1TU. Once appropriate mixtures were made, they were tested with the standard FETAX to determine the 96 h LC_{50}, EC_{50}, and TI for each of the interaction ratios. For each clutch of embryos single-chemical toxicity measurements were taken to determine the clutch-specific 96 h LC_{50} for each individual experiment. Each mixture study was repeated two times.

Toxic Unit Conversion. A toxic unit (TU) is defined as the 96 h LC_{50} = 1 TU for mortality. Toxic unit conversion allowed for the two compounds to be normalized to toxicity and, thus, a correlation could be studied for mixtures. A hypothetical example calculation is shown below:

96 h LC_{50} for compound *X*: 1 mmol/L

96 h LC_{50} for compound *Y*: 2 mmol/L

96 h LC_{50} for a mixture containing a ratio of 1 mmol/L *X* : 2 mmol/L *Y* is (i.e., 1 TU:1 TU) 0.5 mmol of *X*: 1 mmol of *Y*

$$\text{TU of } X = [0.5 \text{ mmol/L (amount of } X \text{ in mixture)}]/[1 \text{ mmol/L } (LC_{50} \text{ of } X)] = 0.5$$

$$\text{TU of Y} = [1 \text{ mmol/L (amount of } Y \text{ in mixture)}]/[2 \text{ mmol/L } (LC_{50} \text{ of Y})] = 0.5$$

The toxic units add (0.5 + 0.5 =1) and would indicate concentration additive response.

The TU values for the each component of the mixture were plotted on an isobole diagram to demonstrate the interaction of the two compounds. Generally, such diagrams are divided into three major regions relating to the types of interactions possible: synergism, additive effects, and antagonism. The area of the graph below the diagonal line connecting 1 TU of axis *X* to 1 TU of axis *Y* shows increasing synergism as the points approach the origin. Concentration addition is indicated by the diagonal line connecting 1 TU of axis *X* to 1 TU of axis *Y*. Points found between the lines connecting 1 TU to 1 TU and within the squares formed by these two points from their respective axis show response additive interactions. Points outside this box indicate antagonistic interactions.

RESULTS

Controls. Each experimental trial contained 4 replicates of 20 embryos as controls. These 80 embryos represented the genetic effects of the clutch absent exposure to the compound of study. A 96 h control mortality >10% represents a poor-quality clutch. All control groups had <10% mortality at 96 h. Control malformations were within the range of 1.3−6.9% with an average of 3.9%, well below the 10% acceptable for FETAX. The average control lengths were between 0.93 and 1.13 cm. The control data indicate an acceptable test for the FETAX assay.

Individual Toxicity Experiments. L-Cysteine had an average 96 h LC_{50} of 41.85 mM and ranged between 34.14 and 49.01 mM (Table 1). The average 96 h EC_{50} (malformation) was 38.62 mM and ranged between 35.68 and 40.46 mM (Table 1). A typical concentration−response curve for L-cysteine (Figure 1) indicated a fairly sharp mortality curve. The malformation curve (Figure 1) indicates a threshold effect at around 15 mM but does not increase in effect even near mortality concentrations. The teratogenic index ranged from 1.0 to 1.2. There was considerable variability in the no observable effect concentration (NOEC), lowest observable effect concentration (LOEC), and minimum concentration to inhibit growth (MCIG) concentrations for L-cysteine. We observed tank effects where one replicate of a concentration would have 100% mortality and the other replicate, 0% mortality. Here were very few abnormalities (Chart 1B).

Furan had an average 96 h LC_{50} of 43.56 mM, which ranged from 37.92 to 53.94 mM (Table 1). Furan had an average 96 h EC_{50} (malformation) of 39.64 mM and ranged from 27.30 to 47.20 mM. The teratogenic index ranged from 0.8 to 1.2. A typical concentration response curve for a single experiment (Figure 2) showed both mortality and malformation curves increased in a consistent manner for furan. The vertical lines indicate the 96 h LC_{50} and 96 h EC_{50} values. The NOEC for malformation was consistently the lowest end point of 20 mM. A typical growth curve (Figure 2) indicated furan at 40 mM caused a significant decrease in length by approximately 90% of the 96 h LC value. Furan caused minor edema and tail abnormities (Chart 1C). The most interesting malformation was abnormal cell

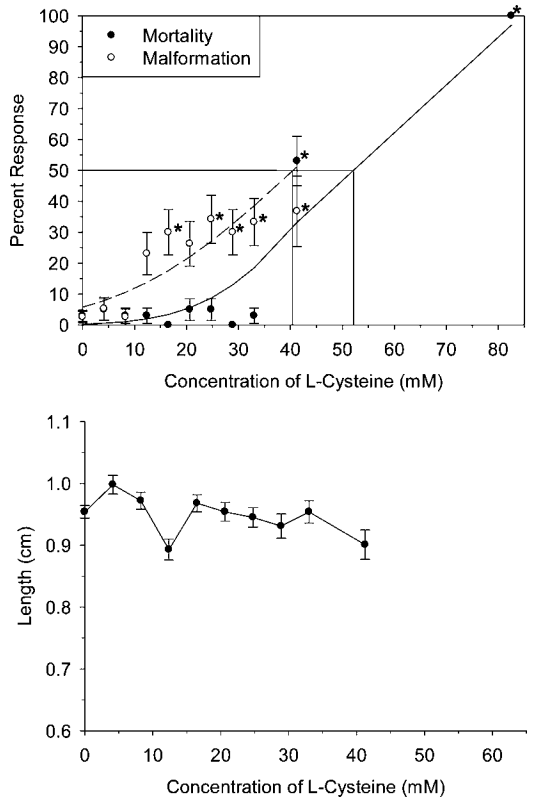

Figure 1. Dose–response mortality and malformation data for a representative trial of L-cysteine (top panel); change in embryo length in a representative trial with exposure to L-cysteine (bottom panel). Error bars are the standard error of the mean. (*) Significant differences from controls, $p \leq 0.05$. There were two replicates for each concentration; controls had four replicates. Regression lines (top panel) are PROBIT estimates. The line from the 50% effect indicates EC_{50} (malformation) and LC_{50} estimates.

growth seen near the otic vesicle (Chart 1D). This was seen consistently, but at a low frequency (<20%).

The average 96 h LC_{50} for acrylamide was 1.890 mM and ranged from 1.466 to 2.136 mM (Table 1). The average 96 h EC_{50} (malformation) was 0.944 mM and ranged from 0.702 to 1.161 mM (Table 1). The teratogenic index ranged from 1.8 to 2.7 (Table 1). The mortality and malformation NOEC and LOEC were very consistent. The MCIG was often at the lowest concentration tested, 0.5 mM, and may indicate the MCIG may be lower. The high concentrations of acrylamide caused tail abnormalities and edema in the ocular, cardiac, and abdominal regions. Severe gut abnormalities were also observed (Chart 2C).

Binary Interaction Experiments. The 96 h LC_{50} and 96 h EC_{50} values for furan and L-cysteine (Tables 2 and 3) indicate that there were some differences between these clutches and clutches reported earlier (Table 1). These are the positive controls for the interaction experiments and used fewer concentrations because these were performed concurrently with mixture studies. In particular, L-cysteine seems to indicate less toxicity (higher 96 h LC_{50} values). The 96 h LC_{50} values for the interaction of furan with acrylamide and L-cysteine in Table 2 with 95% Fieller bound for each component indicate a good consistency. The TI showed the highest value for furan/acrylamide 1:1 mixture (Table 2). The TI for furan/L-cysteine interaction indicated a reduction of TI with the mixture. The interactions plotted on an isobole diagram showed furan/L-cysteine (1:1) points were near the concentration addition line

Chart 1. (A) Normal Control Larvae; (B) Typical Normal Larvae Found in 41 mM L-Cysteine; (C) Typical Malformation Found in 60 mM Furan Larvae; (D) Zoomed in Section of a 60 mM Furan Embryo Showing Abnormal Cell Growth near the Otic Vesicle

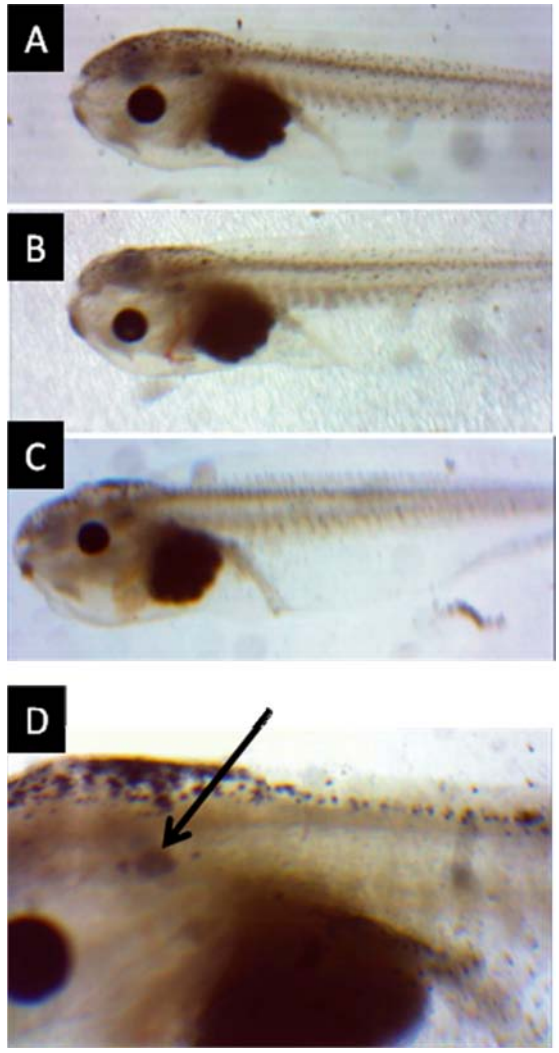

(Figure 3). Furan/acrylamide (1:1) shows points very close to the antagonism on the edge of response addition (Figure 3).

Furan/L-Cysteine Combinations. Interestingly, furan and L-cysteine have similar 96 h LC_{50} values in millimolar (Table 1). This means that the 1:1 TU interaction used had nearly identical concentrations of furan and L-cysteine for its 96 h LC_{50} values, furan/L-cysteine (37.10:36.320 and 24.75:25.69), as shown in Table 2. The TI values for both furan and L-cysteine and the mixtures were close to 1. The points on the isobole diagram (Figure 3) indicate that furan and L-cysteine are concentration additive as the open circles are close to the diagonal line indicating concentration addition. The 96 h EC_{50} (malformation) values showed the same pattern as the 96 h LC_{50} values. There were very few malformations, and they were not severe with very little edema and loose gut coiling (Chart 2B).

Furan/Acrylamide Combinations. The 96 h LC_{50} values for the furan/acrylamide mixtures were fairly close to one another. Furan was less toxic to the clutch of embryos on June 10, 2013. This reduction in toxicity was also seen in the 1:1 furan/acrylamide mixture. Interestingly, the two isobole points (solid

dx.doi.org/10.1021/jf5013743 | J. Agric. Food Chem. 2014, 62, 7927–7938

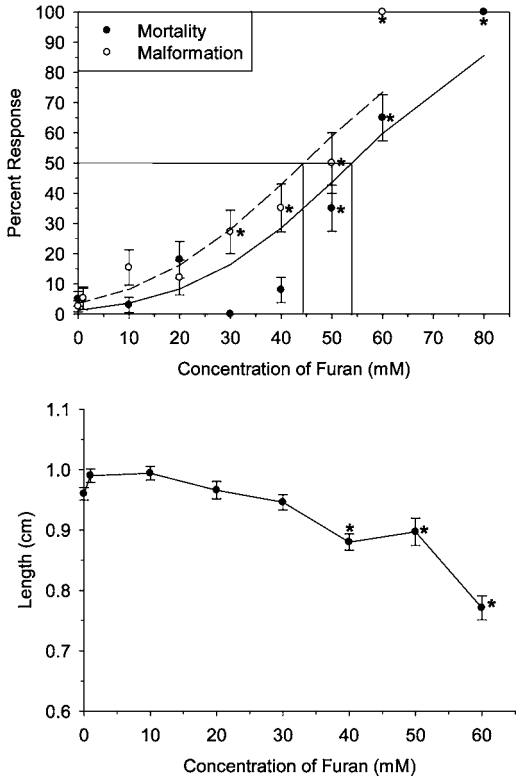

Figure 2. Dose−response mortality and malformation data for a representative trial of furan (top panel); change in embryo length in a representative trial with exposure to furan (bottom panel). Error bars are the standard error of the mean. (∗) Significant differences from controls, $p \leq 0.05$. There were two replicates for each concentration; controls had four replicates. Regression lines (top panel) are PROBIT estimates. The line from the 50% effect indicates EC_{50} (malformation) and LC_{50} estimates.

circles) in Figure 3 show a very close relationship, even with embryos that were responding differently. The furan/acrylamide mixture showed an increase in teratogenic index up to 5.1, indicating that this mixture would be more teratogenic than either furan or acrylamide alone. This also indicates that the interaction on the 96 h EC_{50} (malformation) is most likely different from for the mortality. Although there was increase in the TI, this mixture primarily showed acrylamide-like malformations, that is, notochord curving, with mortality appearing to be directly related to concentration addition (Chart 2E).

Acrylamide/L-Cysteine Combinations. Four different mixtures of acrylamide/L-cysteine were tested with increasing concentrations of acrylamide to L-cysteine ratios of 1:3, 1:1, 3:1, and 19:1 (Table 3; Figure 4). As the ratio of L-cysteine was reduced, the average 96 h LC_{50} value showed an increase in the amount of acrylamide (in the mixtures) from 0.663 mM (1:3) to 43.32 mM (19:1). The 96 h EC_{50} (malformation) also showed the amount of acrylamide increased from 0.742 (1:3) to 10.86 mM (19:1). The differences in the changes in the 96 h LC_{50} and 96 h EC_{50} (malformation) values in the 19:1 ratio of acrylamide/L-cysteine resulted in an increase in TI to an average of 4.3 (Table 3) for the 19:1 mixture. The isobole plots (Figure 4) showed the 19:1 ratio (open triangles) indicated a dramatic antagonism with low amounts of L-cysteine. The 1:3 acrylamide/L-cysteine ratio showed a response addition (solid circles), which indicates that acrylamide does not affect L-cysteine toxicity. As mixtures increase, the ratios of acrylamide to L-cysteine exhibit greater

Chart 2. (A) Normal Control Larvae; (B−F) Typical Abnormal Larvae at High Concentrations of the Following Treatments: (B) Furan/L-Cysteine (1:1); (C) Acrylamide; (D) Acrylamide/L-Cysteine (19:1); (E) Furan/Acrylamide (1:1); (F) Acrylamide/Furan/L-Cysteine (12:4:1)

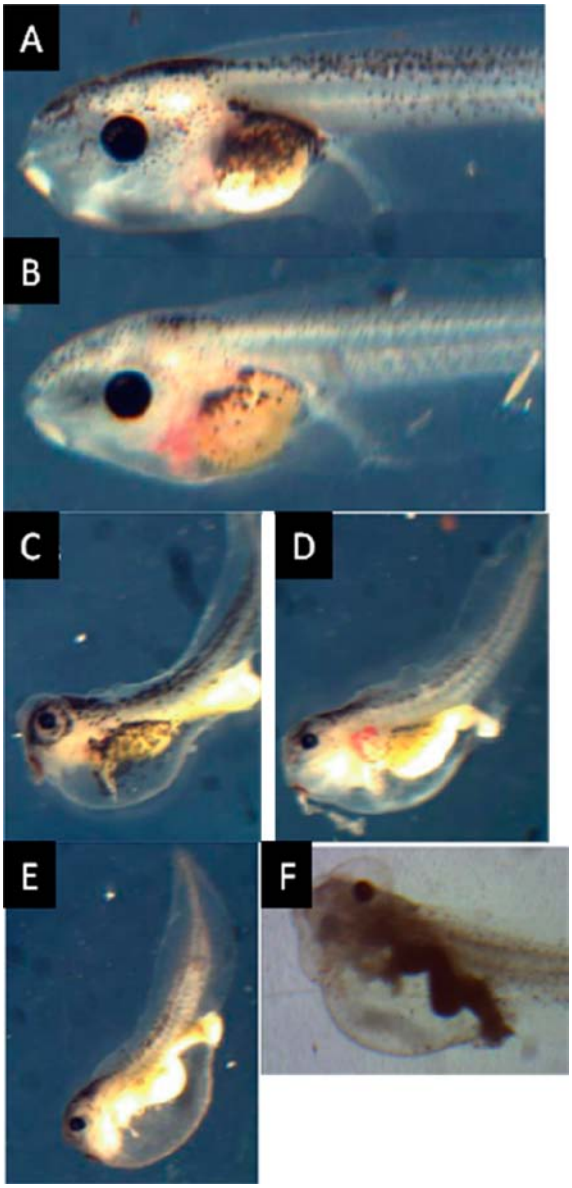

antagonism as indicated by the progression of points. The typical malformations seen were edema, gut coiling, and tail abnormalities similar to those of acrylamide (Chart 2D).

Furan/Acrylamide/L-Cysteine Combinations. The clutches of embryos used showed consistency with individual experiments reported in Table 1 (Table 4). Furan and L-cysteine were slightly less toxic (96 h LC_{50} were higher) but were within approximately 2-fold range. The 96 h EC_{50} (malformation) did not show as much increase as the 96 h EC_{50} for furan, which caused furan to have a slightly increased TI of 1.4 (Table 4). The three-way (10:4:1) mixtures show high consistency between the two experiments (Table 4). The two experiments did not have malformations until very high concentrations were reached. This resulted in a very low average TI of 0.6 for the mixture and in a very high variability in the 96 h EC_{50} data. The malformations

dx.doi.org/10.1021/jf5013743 | J. Agric. Food Chem. 2014, 62, 7927−7938

Table 2. 96 h LC_{50}, 96 h EC_{50}, and Teratogenic Index (TI; 96 h LC_{50}/96 h EC_{50}) Values for Furan, Acrylamide, L-Cysteine, and the 1:1 Binary Mixtures for Furan/Acrylamide and Furan/L-Cysteine[a]

	96 h LC_{50} mmol/L (95% Fieller bounds)			96 h EC_{50} mmol/L (95% Fieller bounds)			
	furan	acrylamide	L-cysteine	furan	acrylamide	L-cysteine	TI
furan							
April 22, 2013	45.10 (40.15−50.72)			51.86 (41.72−72.22)			0.9
June 10, 2013	94.11 (81.98−116.4)			66.83 (57.16−82.60)			1.4
acrylamide							
April 22, 2013		2.136 (2.011−2.263)			1.161 (1.007−1.356)		1.8
June 10, 2013		1.466 (1.306−1.641)			0.780 (0.674−0.917)		1.9
L-cysteine							
April 22, 2013			68.95 (63.91−74.92)			72.13 (58.12−104.2)	1.0
Aug 2, 2013			61.17 (55.70−67.56)			70.61 (56.62−100.5)	0.9
furan/acrylamide (1:1 TU)							
April 22, 2013	40.49 (36.58−46.03)	2.056 (1.858−2.338)		14.59 (12.77−16.80)	0.741 (0.648−0.853)		2.8
June 10, 2013	68.18 (58.59−81.64)	1.56 (1.340−1.868)		13.28 (11.29−15.66)	0.674 (0.573−0.795)		5.1
average	**54.34**	**1.808**		**13.94**	**0.708**		**3.95**
furan/L-cysteine (1:1 TU)							
April 22, 2013	37.10 (34.38−40.36)		36.32 (33.67−39.52)	55.40 (41.03−101.7)		54.25 (40.18−99.56)	0.7
Aug 2, 2013	24.75 (22.32−27.46)		25.69 (23.18−34.01)	24.75 (22.32−27.46)		25.69 (23.17−28.50)	1.0
average	**30.93**		**31.01**	**40.08**		**39.97**	**0.85**

[a]Dates represent clutches of embryos for each experiment.

seen were typical of acrylamide with facial and abdominal edema, tail abnormalities, and severe gut abnormalities (Chart 2F).

DISCUSSION

Individual Experiments. *Furan.* Furan average values for 96 h LC_{50} and 96 h EC_{50} (43.56, 39.64, respectivly) were relatively high. By comparison, in the fathead minnow, behavioral effects were reported in the 28−31 day juvenile fathead minnow test at concentrations a low as 1.044 mM.[49] This is most likely due to the short duration of the FETAX. In this assay, we were determining the relative risk of furan causing birth defects. Due to the low TI (0.8−1.4) and the lack of significant abnormalities (Chart 1D), furan appears to not be teratogenic in the FETAX test. However, we did note the development of abnormal cell growths in several embryos that may indicate tumor formation if the test had been longer. This would agree with mammilian studies that show furan-induced tumorigenicity.[50]

L-Cysteine. L-Cysteine toxicity was studied to compare toxic unit analysis of the three test compounds. These results indicate that L-cysteine had a very low TI between 1.0 and 1.2, suggesting little or no teratogenic potential from L-cysteine. Within the first 24 h, L-cysteine delayed hatching; however, growth data showed no inhibition of growth at 96 h. We did observe tank effects that seemed to be related to pH in individual Petri dishes. This proved challenging because the pH range for the study became very small. In agreement with the present study, other studies found that L-cysteine seems to be toxic and becomes unstable when exposed to neonatal rats.[51]

Interaction Experiments. *Furan/L-Cysteine.* Furan and L-cysteine showed very similar millinolar 96 h LC_{50} and 96 h EC_{50} (malformation) values in individual testing, with an average of 43.56 mM for furan compared to 41.85 mM for L-cysteine (Table 1). Some variability was seen in the clutches used for the interaction study. The two experiments with furan/L-cysteine indicated very close to concentration addition behavior, with one point falling below the diagonal line and the other falling above the line (Figure 3, open circles). The 95% confidence intervals indicated a normal amount of variability around these points. With the points being this close, either a concentration addition or response addition effect is expected for this mixture ratio (1:1). Because of the differences in the compounds, we believe that this is more indicative of a response addition rather than the two acting in a concentration manner. The similarities of the 96 h LC_{50} and EC_{50} may explain this. As malformations of both mixture compounds lean toward GI tract stunting, no conclusions could be made with as to which chemical was causing the malformation; most likely it was both. It seems that furan and L-cysteine show additive activities.

Furan/Acrylamide Combinations. The furan/acrylamide (1:1) mixtures were interesting in that the two points were very consistently right on the box formed by the 1 toxic unit for the *X* and *Y* axes (solid circles, Figure 3). This border is where response addition and potential antagonisms are indicated. Because it is possible that both chemicals can affect the same individual, if they were to do so almost exactly for both tests, these results would be expected. However, it is more likely this indicates a weak antagonism for this mixture. The TI values of 2.8

Table 3. 96 h LC_{50}, 96 h EC_{50}, and Teratogenic Index (TI; 96 h LC_{50}/96 h EC_{50}) Values for Acrylamide/L-Cysteine Binary Mixtures of Toxic Units 1:3, 1:1, 3:1 19:1[a]

		LC_{50} (mmol/L, average and range)		EC_{50} (mmol/L, average and range)		
	clutch	acrylamide	cysteine	acrylamide	cysteine	TI
acrylamide	April 1, 2013	1.879 (1.692−2.099)		0.702 (0.624−0.792)		2.7
	April 22, 2013	2.136 (2.011−2.263)		1.161 (1.007−1.356)		1.8
L-cysteine	April 1, 203		42.59 (nc)		41.16 (nc)	1.0
	April 22, 2013		68.95 (63.91−74.92)		72.13 (58.12−104.2)	1.0
acrylamide + L-cysteine (1:3 TU)	April 1, 2013	0.487 (0.443−0.534)	28.66 (26.07−31.43)	0.608 (0.466−1.003)	35.85 (27.39−59.02)	0.8
	April 22, 2013	0.839 (0.747−0.942)	48.22 (42.93−54.17)	nc	nc	<1
	average	**0.663**	**38.44**	**0.724**	**42.03**	**0.9**
acrylamide + L-cysteine (1:1 TU)	April 1, 2013	2.037 (1.861−2.280)	38.71 (35.36−43.32)	3.049 (2.337−5.078)	57.94 (44.40−96.29)	0.7
	April 22, 2013	2.525 (2.272−3.008)	47.97 (43.17−57.15)	10.75 (nc)	207.3 (nc)	0.2
	average	**2.281**	**43.34**	**6.900**	**132.6**	**0.3**
acrylamide + L-cysteine (3:1 TU)	April 1, 2013	2.541 (2.139−2.987)	16.40 (13.80−19.28)	6.996 (nc)	45.14 (nc)	0.4
	April 22, 2013	25.94 (18.74−12.15)	166.6 (120.3−384.8)	18.18 (14.98−25.82)	116.7 (96.21−165.8)	1.4
	average	**14.14**	**91.48**	**12.59**	**80.92**	**1.1**
acrylamide + L-cysteine (19:1 TU)	April 1, 2013	50.97 (35.13−113.5)	51.43 (35.45−114.5)	12.56 (10.93−14.36)	12.57 (11.02−14.48)	4.1
	April 22, 2013	43.32 (39.09−49.65)	43.94 (39.66−50.37)	9.256 (8.125−10.70)	9.390 (8.242−10.85)	4.7
	average	**43.31**	**43.94**	**10.86**	**10.98**	**4.3**

[a]Dates represent clutches of embryos. nc, not calculable.

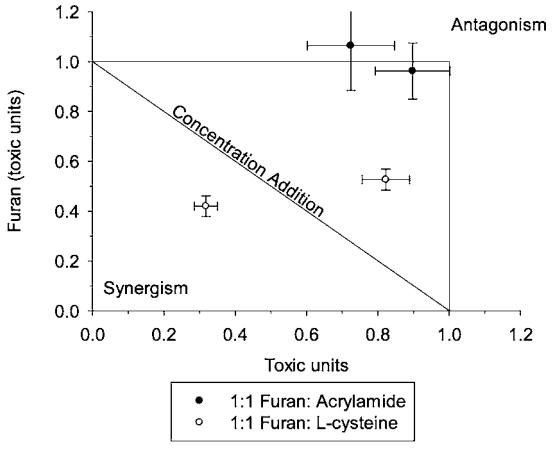

Figure 3. Toxic unit comparison 1:1 of furan/acrylamide and furan/L-cysteine (isobole diagram). Error bars indicate 95% confidence intervals. The *y*-axis is furan. The *x*-axis for the solid circles is acrylamide. The *x*-axis for the open circles is L-cysteine. Each point represents an individual experiment.

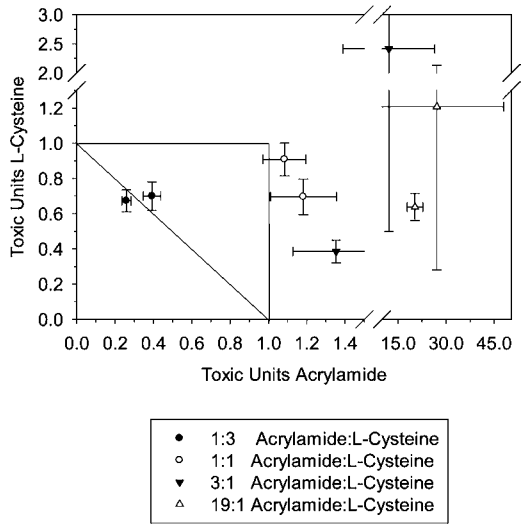

Figure 4. Toxic unit comparison of acrylamide and cysteine binary mixtures. The *x*-axis and *y*-axis were cut to be able to show all of the points.

dx.doi.org/10.1021/jf5013743 | J. Agric. Food Chem. 2014, 62, 7927−7938

Table 4. 96 h LC_{50}, 96 h EC_{50}, and Teratogenic Index (TI; 96 h LC_{50}/96 h EC_{50}) Values for Furan, Acrylamide, L-Cysteine, and the Three-Component Mixture of Acrylamide/Furan/L-Cysteine[a]

	LC_{50} (mmol/L, average and range)			EC_{50} (mmol/L, average and range)			
	furan	acrylamide	cysteine	furan	acrylamide	cysteine	TI
furan							
June 10, 2013	94.11 (81.98−116.4)			66.83 (57.16−82.60)			1.4
Aug 2, 2013	77.91 (71.20−86.77)			37.10 (34.38−40.36)			1.4
acrylamide							
June 10, 2013		1.466 (1.306−1.641)		0.780 (0.674−0.917)			1.9
Aug, 2, 2013		2.080 (1.843−2.381)		1.134 (0.992−1.314)			1.8
L-cysteine							
June 10, 2013			64.70 (55.61−76.57)			98.19 (75.25−157.7)	0.6
Aug 2, 2013			61.17 (55.70−67.56)			70.61 (56.62−100.5)	0.9
acrylamide/furan/L-cysteine (10:4:1TU)							
June 10, 2013	32.28 (25.93−38.13)	1.389 (1.116−1.640)	5.241 (4.211−6.190)	105 (nc)	5.01 (nc)	32.4 (nc)	0.3
Aug 2, 2013	32.53 (28.72−37.10)	1.399 (1.235−1.596)	5.281 (4.662−6.023)	57.78 (34.98−498.9)	2.485 (1.51−21.46)	9.380 (5.680−80.99)	0.6
average	**32.41**	**1.394**	**5.261**	**54.82**	**1.823**	**13.77**	**0.6**

[a]Dates represent clutches of embryos for each experiment. nc, not calculable.

and 5.1 for the mixture of furan and acrylamide indicate this mixture is more teratogenic than acrylamide alone. This also indicates that the 96 h EC_{50} (malformation) altered differently from the 96 h LC_{50}, suggesting the mortalities and malformations were being caused by separate mechanisms. The malformations seen were predominantly those associated with acrylamide (Chart 2E). This may indicate that the effects on acrylamide toxicity may be indirect rather than a direct interaction of furan with acrylamide.

Acrylamide/L-Cysteine. Early experiments showed that L-cysteine reduced the toxicity and teratogenicity of acrylamide at a single concentration of acrylamide with an approximately equal molar amount of L-cysteine.[35] These experiments were to determine the effect of different ratios of acrylamide/L-cysteine based on toxicity units and how much protective effect could be measured. The acrylamide/L-cysteine ratios of 1:3, 1:1, and 3:1 are standardly used for experiments investigating interactions using isobole diagrams. The 19:1 acrylamide/L-cysteine combination was chosen because that would have been approximately equal molar concentrations as seen in the single-component experiments reported earlier. These mixtures show an increasing amount of antagonisms as the amount of L-cysteine is reduced, indicating that L-cysteine toxicity was being observed in the 1:3 mixture (solid circles). For the 19:1 acrylamide/L-cysteine combination, open triangles showed extreme antagonism at nearly 30 toxic units on the acrylamide axis even with the wide error bars. The change in TI was also unexpected, increasing to nearly 5 in the 19:1 acrylamide/L-cysteine mixture. This again indicates separate mechanisms from the mortality end point. As expected, all of the abnormalities seen were very similar to those caused by acrylamide (Chart 2D).

Acrylamide/Furan/L-Cysteine Mixture. The three-way mixture was tested at a 10:4:1 ratio of acrylamide/furan/L-cysteine to determine if the binary mixtures could predict the toxicity of the trinary mixture. On the basis of the binary mixtures we would expect to see severe antagonism based on the 19:1 acrylamide to L-cysteine mixture. Two surprising events occurred with the trinary mixture. First, instead of severe antagonism, a minor antagonism (black dots Figure 5) seems indicated. The expectation was for the sample points to be within the green line, indicating antagonism. Although they are close, it does not appear to be as antagonistic as expected. The second surprise was the change in TI to <1 (Table 4). With both L-cysteine and furan

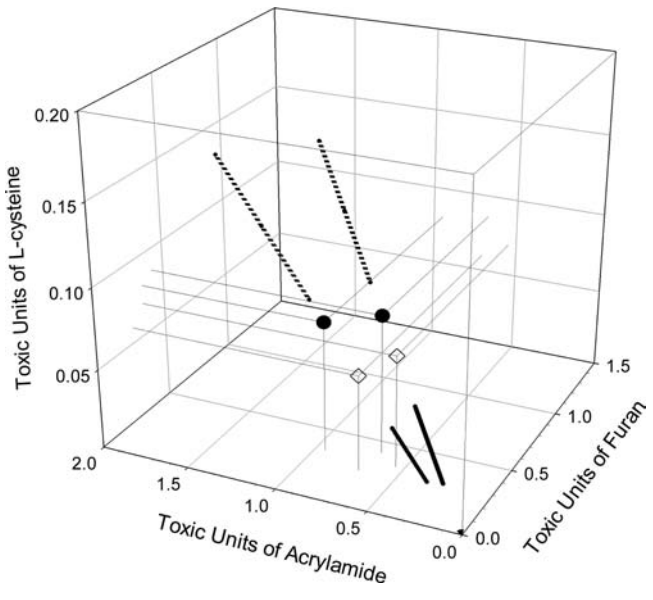

Figure 5. Three-way toxic unit comparison of furan, acrylamide, and L-cysteine. Experimental values are represented by black circles. For purposes of comparison, calculated synergism is indicated by solid lines, calculated concentration response addition by open diamonds, and calculated antagonism by dashed lines.

dx.doi.org/10.1021/jf5013743 | J. Agric. Food Chem. 2014, 62, 7927−7938

(Tables 2 and 3) there is an increase in TI with added acrylamide. These results imply that an interaction in metabolic pathways between acrylamide and furan adversely affects the beneficial effects of L-cysteine.

Mechanistic Aspects. *Acrylamide.* In vivo, cytochrome P-450 enzymes transform acrylamide to the reactive epoxide glycidamide, which can react with free NH_2 and SH functional groups of hemoglobin, enzymes, and DNA and lead to carcinogenesis, teratogenesis, and neurotoxicity. The protein adduct and DNA adduct chemistry of acrylamide and related conjugated vinyl compounds offers a mechanistic explanation and insight into the pathogenesis of certain human neurodegenerative diseases.[52,53] Nucleophilic SH-containing compounds such as L-cysteine and reduced glutathione might prevent the in vivo alkylations by reacting with (blocking) the electrophilic (double bond and epoxide) sites of acrylamide and glycidamide, as illustrated in Figure 6A. The detailed

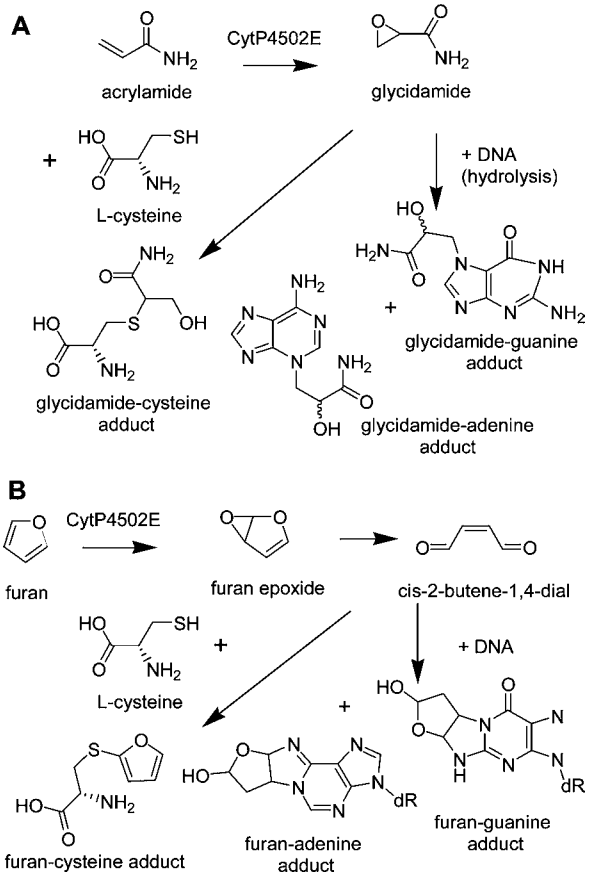

Figure 6. Comparison of biological alkylations of L-cysteine and DNA by acrylamide and furan via epoxide intermediates. Adapted from refs 10, 14, 16, 35,57, and 66−70.

chemistry of these transformations is extensively discussed elsewhere.[14,16] It is relevant to note that the human liver carcinogen aflatoxin B_1 that is present in some foods is also reported to react with DNA NH_2 groups via a reactive epoxide intermediate and that L-cysteine inhibited its toxicity.[54]

Furan. Furan is also metabolically activated by cytochrome P-450 to the reactive and toxic metabolite *cis*-2-butene-1,4-dial (O═CH—CH═CH—CH═O), which can form adducts with proteins and nucleic acid residues of DNA as illustrated in Figure 6B. The indicated chemical changes have been postulated to cause the observed genotoxicity and hepatocarcinogenicity.[1,10,23,29,30,55−59] As far as we know, unlike acrylamide, furan does not seem to be neurotoxic. The results of the present study show that it also does not seem to be teratogenic in the ex vivo frog embryo teratogenesis assay. Why these two biological alkylating agents induce different pathogenesis is not known. Moreover, it is also not known if the combined consumption of acrylamide and furan that may be present in heat-processed foods (Table 1) will act additively or synergistically in inducing liver carcinogenesis and whether the reported >3-fold up-regulation by furan compounds of oxidoreductases in *Escherichia coli* bacteria[60] also takes place in humans.

SUMMARY AND RESEARCH NEEDS

The amino acid L-cysteine, commercially used as a dough additive to improve rheology by rearranging the structure of gluten proteins via sulfhydryl−disulfide interchange and to increase bread volume after baking,[61,62] seems to continue to act as an inhibitor of malformations in the three-component mixture. However, the sum effect of these compounds leads to higher mortality than the two-compound mixtures would imply. The interactions indicate several conclusions: (a) L-cysteine is highly effective in inhibiting acrylamide toxicity at very low concentrations of L-cysteine to acrylamide, in particular, the reduction of severe acrylamide malformations (i.e., edema, facial, and gut coiling); even at very high concentrations of acrylamide the beneficial effect was dramatic; (b) L-cysteine seems to interact in a response addition with furan; (c) acrylamide and furan appear to have a less than additive response (antagonism); and (d) the activity of the three-component mixture of acrylamide, furan, and L-cysteine was similar to that of the binary mixture of acrylamide and furan, without nearly as much antagonism as seen with acrylamide and L-cysteine alone. This result demonstrates the weakness of two-compound mixtures.

More complex interactions may occur with the addition of another degree of complexity, but the added degree of complexity also makes it difficult to observe the consequences of complete interactions among the components of the mixture. It seems that toxicities observed from furan and acrylamide individually may not be able to predict toxicities of mixtures; specific combinations found in different foods need to be tested to assess the safety of a particular set of processing conditions (processing treatments including cooking, pressure cooking, slow cooking, baking, frying, microwaving, grilling, roasting, and sautéing).

We found that for acrylamide alone, the lowest toxic dose for the frog embryos was ~0.7 mmol/L or ~49.8 μg/L. However, an attempt to relate these concentration exposures of the embryos to human dietary intake is difficult, in view of reported wide variation in the consumption of acrylamide by different populations. For example, Wong et al.[63] found that the mean and the 95th percentile exposure to dietary acrylamide of the Hong Kong population were 0.213 and 0.538 μg/kg, respectively, and the Joint FAO/WHO Expert Committee on Food Additives[64] concluded that whereas the average consumer daily intake was on the order of 1 μg/kg body weight, high acrylamide consumer intake was 4 times higher, or ~240 μg for a person weighing 60 kg. The situation is even more complicated because of adverse effects induced with increasing concentrations. Thus, Obón-Santacana et al.[65] observed increasing relative risk for type I endometrial cancer in a set of women with increasing acrylamide intake, with an upper quintile median of 44 μg/day. Our results indicate that L-cysteine has the potential to

overcome adverse effects in individuals consuming the indicated amounts of acrylamide.

Continuing these trials to discover the limit of inhibition between L-cysteine and acrylamide might be valuable, but the scale seen here may already limit the need. The three-component study analyzed here forms the basis for a novel quantitative method of addressing interactions among bioactive naturally occurring and processing-induced food ingredients. More research is needed to determine how to best use the data. We reported similar conclusions on the interaction results of two potato glycoalkaloids, α-chaconine and α-solanine, obtained with the aid of FETAX.[45] Whether folic acid and glucose-6-phosphate, which protected the frog embryos against α-chaconine-induced malformations, would also protect the embryos against acrylamide-induced teratogenicity also merits study. A largely unexplored area is the content of both acrylamide and furan in the same processed food.

AUTHOR INFORMATION

Corresponding Author

*(J.R.R.) E-mail: jrayburn@jsu.edu.

Funding

We thank the Jacksonville State University (JSU) Biology Department and JSU faculty research grants for partial funding for this research.

Notes

The authors declare no competing financial interest.

ACKNOWLEDGMENTS

We thank Rachel Lester and Kristin Carlisle for their technical assistance with this project. We are most grateful to Carol E. Levin for facilitating the preparation of the manuscript.

REFERENCES

(1) Perez Locas, C.; Yaylayan, V. A. Origin and mechanistic pathways of formation of the parent furan − a food toxicant. *J. Agric. Food Chem.* **2004**, *52*, 6830−6836.

(2) Märk, J.; Pollien, P.; Lindinger, C.; Blank, I.; Märk, T. Quantitation of furan and methylfuran formed in different precursor systems by proton transfer reaction mass spectrometry. *J. Agric. Food Chem.* **2006**, *54*, 2786−2793.

(3) Senyuva, H. Z.; Gökmen, V. Potential of furan formation in hazelnuts during heat treatment. *Food Addit. Contam.* **2007**, *24*, 136−142.

(4) Limacher, A.; Kerler, J.; Davidek, T.; Schmalzried, F.; Blank, I. Formation of furan and methylfuran by Maillard-type reactions in model systems and food. *J. Agric. Food Chem.* **2008**, *56*, 3639−3647.

(5) Morehouse, K. M.; Nyman, P. J.; McNeal, T. P.; DiNovi, M. J.; Perfetti, G. A. Survey of furan in heat processed foods by headspace gas chromatography/ mass spectrometry and estimated adult exposure. *Food Addit. Contam., Part A* **2008**, *25*, 259−264.

(6) Crews, C.; Roberts, D.; Lauryssen, S.; Kramer, G. Survey of furan in foods and coffees from five European Union countries. *Food Addit. Contam., Part B* **2009**, *2*, 95−98.

(7) Capuano, E.; Fogliano, V. Acrylamide and 5-hydroxymethylfurfural (HMF): a review on metabolism, toxicity, occurrence in food and mitigation strategies. *LWT−Food Sci. Technol.* **2011**, *44*, 793−810.

(8) European Food Safety Authority. Update on furan levels in food from monitoring years 2004−2010 and exposure assessment. *EFSA J.* **2011**, *9*, article 2347.

(9) Arisseto, A. P.; Vicente, E.; Furlani, R. P.; Ueno, M. S.; Pereira, A. L.; Toledo, M. C. Occurrence of furan in commercial processed foods in Brazil. *Food Addit. Contam., Part A* **2012**, *29*, 1832−1839.

(10) Moro, S.; Chipman, J. K.; Wegener, J.-W.; Hamberger, C.; Dekant, W.; Mally, A. Furan in heat-treated foods: formation, exposure, toxicity, and aspects of risk assessment. *Mol. Nutr. Food Res.* **2012**, *56*, 1197−1211.

(11) Pérez-Palacios, T.; Petisca, C.; Henriques, R.; Ferreira, I. M. P. L. V. O. Impact of cooking and handling conditions on furanic compounds in breaded fish products. *Food Chem. Toxicol.* **2013**, *55*, 222−228.

(12) Pye, C.; Crews, C. Furan in canned sardines and other fish. *Food Addit. Contam., Part B* **2014**, *7*, 43−45.

(13) Mills, C.; Mottram, D. S.; Wedzicha, B. L. Acrylamide. In *Process-Induced Food Toxicants: Occurrence, Formation, Mitigation, and Health Risks*; Stadler, R. H., Lineback, D. R., Eds.; Wiley: Hoboken, NJ, USA, 2009; pp 23−50.

(14) Friedman, M. Chemistry, biochemistry, and safety of acrylamide. A review. *J. Agric. Food Chem.* **2003**, *51*, 4504−4526.

(15) Friedman, M. Biological effects of Maillard browning products that may affect acrylamide safety in food. *Adv. Exp. Med. Biol.* **2005**, *561*, 135−156.

(16) Friedman, M.; Levin, C. E. Review of methods for the reduction of dietary content and toxicity of acrylamide. *J. Agric. Food Chem.* **2008**, *56*, 6113−6140.

(17) Lineback, D. R.; Coughlin, J. R.; Stadler, R. H. Acrylamide in foods: a review of the science and future considerations. *Annu. Rev. Food Sci. Technol.* **2012**, *3*, 15−35.

(18) Beland, F. A.; Mellick, P. W.; Olson, G. R.; Mendoza, M. C. B.; Marques, M. M.; Doerge, D. R. Carcinogenicity of acrylamide in B6C3F1 mice and F344/N rats from a 2-year drinking water exposure. *Food Chem. Toxicol.* **2013**, *51*, 149−159.

(19) Nixon, B. J.; Stanger, S. J.; Nixon, B.; Roman, S. D. Chronic exposure to acrylamide induces DNA damage in male germ cells of mice. *Toxicol. Sci.* **2012**, *129*, 135−145.

(20) Mariotti, M.; Granby, K.; Fromberg, A.; Risum, J.; Agosin, E.; Pedreschi, F. Furan occurrence in starchy food model systems processed at high temperatures: effect of ascorbic acid and heating conditions. *J. Agric. Food Chem.* **2012**, *60*, 10162−10169.

(21) Han, J.-S.; Kozukue, N.; Young, K.-S.; Lee, K.-R.; Friedman, M. Distribution of ascorbic acid in potato tubers and in home-processed and commercial potato foods. *J. Agric. Food Chem.* **2004**, *52*, 6516−6521.

(22) Friedman, M.; Gumbmann, M. R.; Ziderman, I. I. Nutritional value and safety in mice of proteins and their admixtures with carbohydrates and vitamin C after heating. *J. Nutr.* **1987**, *117*, 508−518.

(23) Van Lancker, F.; Adams, A.; Owczarek-Fendor, A.; De Meulenaer, B.; De Kimpe, N. Mechanistic insights into furan formation in Maillard model systems. *J. Agric. Food Chem.* **2011**, *59*, 229−235.

(24) Scholl, G.; Scippo, M.-L.; De Pauw, E.; Eppe, G.; Saegerman, C. Estimation of furan contamination across the Belgian food chain. *Food Addit. Contam., Part A* **2011**, *29*, 172−179.

(25) Scholl, G.; Humblet, M.-F.; Scippo, M.-L.; De Pauw, E.; Eppe, G.; Saegerman, C. Risk assessment of Belgian adults for furan contamination through the food chain. *Food Addit. Contam., Part A* **2011**, *29*, 345−353.

(26) Scholl, G.; Huybrechts, I.; Humblet, M.-F.; Scippo, M.-L.; De Pauw, E.; Eppe, G.; Saegerman, C. Risk assessment for furan contamination through the food chain in Belgian children. *Food Addit. Contam., Part A* **2012**, *29*, 1219−1229.

(27) Scholl, G.; Humblet, M.-F.; Scippo, M.-L.; De Pauw, E.; Eppe, G.; Saegerman, C. Preliminary assessment of the risk linked to furan ingestion by babies consuming only ready-to-eat food. *Food Addit. Contam., Part A* **2013**, *30*, 654−659.

(28) Jackson, A. F.; Williams, A.; Recio, L.; Waters, M. D.; Lambert, I. B.; Yauk, C. L. Case study on the utility of hepatic global gene expression profiling in the risk assessment of the carcinogen furan. *Toxicol. Appl. Pharmacol.* **2014**, *274*, 63−77.

(29) Bakhiya, N.; Appel, K. E. Toxicity and carcinogenicity of furan in human diet. *Arch. Toxicol.* **2010**, *84*, 563−578.

(30) Ding, W.; Petibone, D. M.; Latendresse, J. R.; Pearce, M. G.; Muskhelishvili, L.; White, G. A.; Chang, C.-W.; Mittelstaedt, R. A.; Shaddock, J. G.; McDaniel, L. P.; Doerge, D. R.; Morris, S. M.; Bishop, M. E.; Manjanatha, M. G.; Aidoo, A.; Heflich, R. H. In vivo genotoxicity

of furan in F344 rats at cancer bioassay doses. *Toxicol. Appl. Pharmacol.* **2012**, *261*, 164−171.
(31) FDA. Foodborne Illness and Contaminants, Chemical Contaminants: Furan. http://www.fda.gov/Food/FoodborneIllnessContaminants/ChemicalContaminants/ucm2006786.htm (accessed Dec 19, 2013).
(32) Oral, R. A.; Dogan, M.; Sarioglu, K. Effects of certain polyphenols and extracts on furans and acrylamide formation in model system, and total furans during storage. *Food Chem.* **2014**, *142*, 423−429.
(33) Anese, M.; Suman, M. Mitigation strategies of furan and 5-hydroxymethylfurfural in food. *Food Res. Int.* **2013**, *51*, 257−264.
(34) Anese, M.; Manzocco, L.; Calligaris, S.; Nicoli, M. C. Industrially applicable strategies for mitigating acrylamide, furan, and 5-hydroxymethylfurfural in food. *J. Agric. Food Chem.* **2013**, *61*, 10209−10214.
(35) Rayburn, J. R.; Friedman, M. L-Cysteine, *N*-acetyl-L-cysteine, and glutathione protect *Xenopus laevis* embryos against acrylamide-induced malformations and mortality in the frog embryo teratogenesis assay. *J. Agric. Food Chem.* **2010**, *58*, 11172−11178.
(36) Rayburn, J. R.; Bantle, J. A.; Qualls, C. W., Jr.; Friedman, M. Protective effects of glucose-6-phosphate and NADP against α-chaconine-induced developmental toxicity in *Xenopus* embryos. *Food Chem. Toxicol.* **1995**, *33*, 1021−1025.
(37) Friedman, M.; Burns, C. F.; Butchko, C. A.; Blankemeyer, J. T. Folic acid protects against potato glycoalkaloid α-chaconine-induced disruption of frog embryo cell membranes and developmental toxicity. *J. Agric. Food Chem.* **1997**, *45*, 3991−3994.
(38) McWilliams, M. L.; Blankemeyer, J. T.; Friedman, M. The folic acid analogue methotrexate protects frog embryo cell membranes against damage by the potato glycoalkaloid α-chaconine. *Food Chem. Toxicol.* **2000**, *38*, 853−859.
(39) Dawson, D. A.; Bantle, J. A. Development of a reconstituted water medium and preliminary validation of the Frog Embryo Teratogenesis Assay-*Xenopus* (FETAX). *J. Appl. Toxicol.* **1987**, *7*, 237−244.
(40) Bantle, J. A.; Sabourin, T. D. Standard guide for conducting the frog embryo teratogenesis assay-*Xenopus* (FETAX). *Environmental Assessment, Risk Management, and Correction Action*; ASTM Interntional: Philadelphia, PA, USA, 1991; VOl. 11.06, pp 111
(41) Bantle, J. A.; Finch, R. A.; Burton, D. T.; Fort, D. J.; Dawson, D. A.; Linder, G.; Rayburn, J. R.; Hull, M.; Kumsher-King, M.; Gaudet-Hull, A. M.; Turley, S. D. FETAX interlaboratory validation study: Phase III − Part 1 testing. *J. Appl. Toxicol.* **1996**, *16*, 517−528.
(42) Friedman, M.; Rayburn, J. R.; Bantle, J. A. Developmental toxicology of potato alkaloids in the frog embryo teratogenesis assay-*Xenopus* (FETAX). *Food Chem. Toxicol.* **1991**, *29*, 537−547.
(43) Friedman, M.; Rayburn, J. R.; Bantle, J. A. Structural relationships and developmental toxicity of *Solanum* alkaloids in the frog embryo teratogenesis assay-*Xenopus*. *J. Agric. Food Chem.* **1992**, *40*, 1617−1624.
(44) Rayburn, J. R.; Bantle, J. A.; Friedman, M. Role of carbohydrate side chains of potato glycoalkaloids in developmental toxicity. *J. Agric. Food Chem.* **1994**, *42*, 1511−1515.
(45) Rayburn, J. R.; Friedman, M.; Bantle, J. A. Synergistic interaction of glycoalkaloids α-chaconine and α-solanine on developmental toxicity in *Xenopus* embryos. *Food Chem. Toxicol.* **1995**, *33*, 1013−1019.
(46) Bantle, J. A.; Finch, R. A.; Fort, D. J.; Stover, E. L.; Hull, M.; Kumsher-King, M.; Gaudet-Hull, A. M. Phase III interlaboratory study of FETAX − Part 3. FETAX validation using 12 compounds with and without an exogenous metabolic activation system. *J. Appl. Toxicol.* **1999**, *19*, 447−472.
(47) Dumont, J. N.; Bantle, J. A.; Linder, G. The history and development of FETAX (ASTM standard guide, E-1439 on conducting the frog embryo teratogenesis assay-*Xenopus*). *ASTM Spec. Tech. Publ.* **2003**, *1443*, 3−22.
(48) Bantle, J. A. ASTM Committee E-47 on Biological Effects and Environmental Fate. Subcommittee E47.01 on Aquatic Toxicology. *Atlas of Abnormalities: A Guide for the Performance of FETAX*; Oklahoma State University: Stillwater, OK, USA, 1991; p 68.
(49) Call, D. J.; Brooke, L. T.; Ahmad, N.; Vaishnav, D. D. Aquatic pollutant hazard assessments and development of a hazard prediction technology by quantitative structure-activity relationships. In *Second Quarterly Report, U.S. EPA Cooperative Agreement No. CR 809234-01-0, Center for Lake Superior Environmental Study*; University of Wisconsin: Superior, WI, USA, 1981.
(50) Moser, G. J.; Foley, J.; Burnett, M.; Goldsworthy, T. L.; Maronpot, R. Furan-induced dose-response relationships for liver cytotoxicity, cell proliferation, and tumorigenicity (furan-induced liver tumorigenicity). *Exp. Toxicol. Pathol.* **2009**, *61*, 101−111.
(51) White, R. D.; Wilson, D. M.; Glosson, J. A.; Madsen, D. C.; Rowe, W. B.; Goldberg, D. I. Toxicity evaluations of L-cysteine and procysteine, a cysteine prodrug, given once intravenously to neonatal rats. *Toxicol. Lett.* **1993**, *69*, 15−24.
(52) Martyniuk, C. J.; Feswick, A.; Fang, B.; Koomen, J. M.; Barber, D. S.; Gavin, T.; LoPachin, R. M. Protein targets of acrylamide adduct formation in cultured rat dopaminergic cells. *Toxicol. Lett.* **2013**, *219*, 279−287.
(53) LoPachin, R. M.; Gavin, T. Molecular mechanism of acrylamide neurotoxicity: lessons learned from organic chemistry. *Environ. Health Perspect.* **2012**, *120*, 1650−1657.
(54) Friedman, M.; Rasooly, R. Review of the inhibition of biological activities of food-related selected toxins by natural compounds. *Toxins (Basel)* **2013**, *5*, 743−775.
(55) Chen, L.-J.; Hecht, S. S.; Peterson, L. A. Identification of *cis*-2-butene-1,4-dial as a microsomal metabolite of furan. *Chem. Res. Toxicol.* **1995**, *8*, 903−906.
(56) Chen, L.-J.; Hecht, S. S.; Peterson, L. A. Characterization of amino acid and glutathione adducts of *cis*-2-butene-1,4-dial, a reactive metabolite of furan. *Chem. Res. Toxicol.* **1997**, *10*, 866−874.
(57) Byrns, M. C.; Predecki, D. P.; Peterson, L. A. Characterization of nucleoside adducts of *cis*-2-butene-1,4-dial, a reactive metabolite of furan. *Chem. Res. Toxicol.* **2002**, *15*, 373−379.
(58) Peterson, L. A.; Cummings, M. E.; Chan, J. Y.; Vu, C. C.; Matter, B. A. Identification of a *cis*-2-butene-1,4-dial-derived glutathione conjugate in the urine of furan-treated rats. *Chem. Res. Toxicol.* **2006**, *19*, 1138−1141.
(59) Carrette, L. L.; Madder, A. A synthetic oligonucleotide model for evaluating the oxidation and crosslinking propensities of natural furan-modified DNA. *ChemBioChem* **2014**, *15*, 103−107.
(60) Wang, X.; Miller, E. N.; Yomano, L. P.; Shanmugam, K. T.; Ingram, L. O. Increased furan tolerance in *Escherichia coli* due to a cryptic *ucpA* gene. *Appl. Environ. Microbiol.* **2012**, *78*, 2452−2455.
(61) Zhang, H.-H.; Li, Q.; Claver, I. P.; Zhu, K.-X.; Peng, W.; Zhou, H.-M. Effect of cysteine on structural, rheological properties and solubility of wheat gluten by enzymatic hydrolysis. *Int. J. Food Sci. Technol.* **2010**, *45*, 2155−2161.
(62) Pecivová, P.; Pavlínek, V.; Hrabe, J.; Valäsek, P.; Bouda, L. Impact of reducing and oxidising agents on the wheat flour dough dynamic rheological properties. *Acta Univ. Agric. Silvic. Mendelianae Brun.* **2011**, *59*, 191−198.
(63) Wong, W. W.; Chung, S. W.; Lam, C. H.; Ho, Y. Y.; Xiao, Y. Dietary exposure of Hong Kong adults to acrylamide: results of the first Hong Kong Total Diet Study. *Food Addit. Contam., Part A* **2014**, *31*, 799−805.
(64) FAO/WHO. Toxicological and intake evaluations and recommendations on specific contaminants: section on acrylamide. In *Summary and conclusions of the 64h meeting of the Joint FAO/WHO Expert Committee on Food Additives*; Rome, Italy, 2005; pp 7−17.
(65) Obón-Santacana, M.; Kaaks, R.; Slimani, N.; Lujan-Barroso, L.; Freisling, H.; Ferrari, P.; Dossus, L.; Chabbert-Buffet, N.; Baglietto, L.; Fortner, R. T.; Boeing, H.; Tjønneland, A.; Olsen, A.; Overvad, K.; Menéndez, V.; Molina-Montes, E.; Larrañaga, N.; Chirlaque, M. D.; Ardanaz, E.; Khaw, K. T.; Wareham, N.; Travis, R. C.; Lu, Y.; Merritt, M. A.; Trichopoulou, A.; Benetou, V.; Trichopoulos, D.; Saieva, C.; Sieri, S.; Tumino, R.; Sacerdote, C.; Galasso, R.; Bueno-de-Mesquita, H. B.; Wirfält, E.; Ericson, U.; Idahl, A.; Ohlson, N.; Skeie, G.; Gram, I. T.; Weiderpass, E.; Onland-Moret, N. C.; Riboli, E.; Duell, E. J. Dietary intake of acrylamide and endometrial cancer risk in the European Prospective Investigation into Cancer and Nutrition cohort. *Br. J. Cancer* **2014**, DOI: 10.1038/bjc.2014.328.

(66) Von Tungeln, L. S.; Churchwell, M. I.; Doerge, D. R.; Shaddock, J. G.; McGarrity, L. J.; Heflich, R. H.; Da Costa, G. G.; Marques, M. M.; Beland, F. A. DNA adduct formation and induction of micronuclei and mutations in B6C3F1/Tk mice treated neonatally with acrylamide or glycidamide. *Int. J. Cancer* **2009**, *124*, 2006−2015.
(67) Kotova, N.; Jurén, T.; Myöhänen, K.; Cornelius, M.; Abramsson-Zetterberg, L.; Backman, J.; Menzel, U.; Rydberg, P.; Kronberg, L.; Vähäkangas, K.; Segerbäck, D. ^{32}P-HPLC analysis of *N*1-(2-carboxy-2-hydroxyethyl)deoxyadenosine: a DNA adduct of the acrylamide-derived epoxide glycidamide. *Toxicol. Lett.* **2011**, *207*, 18−24.
(68) Watzek, N.; Bohm, N.; Feld, J.; Scherbl, D.; Berger, F.; Merz, K. H.; Lampen, A.; Reemtsma, T.; Tannenbaum, S. R.; Skipper, P. L.; Baum, M.; Richling, E.; Eisenbrand, G. N7-glycidamide-guanine DNA adduct formation by orally ingested acrylamide in rats: a dose-response study encompassing human diet-related exposure levels. *Chem. Res. Toxicol.* **2012**, *25*, 381−390.
(69) Lu, D.; Peterson, L. A. Identification of furan metabolites derived from cysteine-*cis*-2-butene-1,4-dial-lysine cross-links. *Chem. Res. Toxicol.* **2010**, *23*, 142−151.
(70) Gates, L. A.; Lu, D.; Peterson, L. A. Trapping of *cis*-2-butene-1,4-dial to measure furan metabolism in human liver microsomes by cytochrome P450 enzymes. *Drug Metab. Dispos.* **2012**, *40*, 596−601.

Table 1. Screening of Various Tetrazolium Dyes for Suitability for Detecting Caffeine Using Cdh

Tetrazolium dyes	Reduction with Cdh and Caffeine [a]		Background Color [b]	Retail price from Sigma (in $/ mg)[c]
Iodonitrotetrazolium Chloride (INT)	Yes	Dark Red	No	0.042
Tetrazolium Blue Chloride (TB)	No		No	0.018
Thiazolyl Blue Tetrazolium Bromide (MTT)	Yes	Dark Blue	Yes	0.071
Tetrazolium Violet (TV)	No		No	0.036
Nitro Blue Tetrazolium (NBT)	Yes	Purple	Yes	0.170
Tetranitro blue Tetrazolium Chloride (TNBT)	Yes	Black	Yes	0.362

[a]Screening was performed with 8−10 U (40−50 μg) of Cdh and 100 ppm caffeine per assay as described in the Materials and Methods. The incubation time was 30 min to differentiate between various dyes. [b]Color of the dye in potassium phosphate buffer (pH 7.5) without addition of the test sample and enzyme. [c]The price calculation is based on the largest pack size available to get the lowest price from www.sigmaaldrich.com. Respective product catalog numbers are I10406-25G, T4375-25G, M2128-10G, T0138-10G, N6876-5G, and T4000-1G (accessed March 24, 2014) .

Several attempts have been made to develop a suitable assay for caffeine detection and/or measurement.[28−36] However, none of these tests meet the attributes required for a suitable diagnostic test, such as speed of detection, ability to detect in commercial/natural fluids, and sensitivity of detection. In the present work, we report a novel enzyme, caffeine dehydrogenase (Cdh), which is highly suitable for detection of caffeine and potential development of a diagnostic test. In the presence of a tetrazolium dye such as INT, Cdh is able to detect caffeine in less than 1 min with a sensitivity of 1−5 ppm. In addition, this enzyme-based test is able to detect decaffeinated beverages instantly. Spiked caffeine as low as 5−20 ppm can be detected in mother's milk with no interference from milk components. Last, but not least, caffeine can be detected quantitatively in pharmaceuticals, nearly matching the reported values as detected by high-performance liquid chromatography (HPLC).

MATERIALS AND METHODS

Chemicals and Test Samples. Caffeine, DNase I, iodonitrotetrazolium chloride (INT), tetrazolium blue chloride (TB), tetrazolium blue tetrazolium bromide (MTT), tetrazolium violet (TV), nitro blue tetrazolium (NBT), and tetranitro blue tetrazolium (TNBT) were purchased from Sigma-Aldrich (St. Louis, MO). Yeast nitrogen base without amino acids and without ammonium sulfate (YNB) was purchased from ForMedium (Norfolk, U.K.). HPLC-grade methanol and acetonitrile were obtained from Sigma-Aldrich. Coffee, soft drinks, and pharmaceuticals were obtained from local outlets. Nursing mother's milk was obtained from the Mother's Milk Bank of Iowa (University of Iowa Children's Hospital).

Media and Growth Conditions. Strain CBB1 was grown in M9 mineral salts medium[37] with 2.5 g/L caffeine and 4 g/L YNB at 30 °C with shaking at 200 rpm. Cell growth was monitored by measuring the optical density at 600 nm (OD_{600}). Cells were harvested at late log phase by centrifugation (13800*g* for 10 min at 4 °C) as described by Yu et al.[37] Cell pellets were washed twice with 50 mM potassium phosphate (KP_i) buffer (pH 7.5) and frozen at −80 °C until required.

Purification of Caffeine Dehydrogenase from *Pseudomonas* sp. CBB1. All purification procedures were performed at 4 °C using an automated fast protein liquid chromatography system (AKTA Design, Amersham Pharmacia Biotech) as described by Yu et al.[37] Chromatography columns and column resins were from Amersham Biosciences, Piscataway, NJ. An Amicon Ultra-15 (30K) ultrafiltration membrane (Millipore, Bedford, MA) was used for concentration and buffer exchange of the protein fractions containing caffeine dehydrogenase activity. About 8 g of frozen cells were thawed and suspended in 30 mL of 50 mM KP_i buffer (pH 7.5), and DNase I was added to a final concentration of 10 μg/mL. The cells were lysed using a chilled French press in two cycles at 138 MPa. Unbroken cells and debris were removed from the lysate by centrifugation (20400*g* for 20 min at 4 °C), and the supernatant was designated the crude cell extract (CCE). A 4.0 M solution of ammonium sulfate was added dropwise to the CCE to obtain a final ammonium sulfate concentration of 0.8 M with constant stirring. After incubation with shaking on ice for 1 h, the mixture was centrifuged at 20400*g* for 20 min at 4 °C to remove precipitated proteins. The supernatant was loaded onto a 40 mL (bed volume) Phenyl Sepharose high-performance column (Amersham) preequilibrated with 50 mM KP_i buffer (pH 7.5) containing 0.8 M ammonium sulfate. Unbound proteins were washed from the column with 40 mL of 50 mM KP_i buffer containing 0.8 M ammonium sulfate. Bound proteins were eluted with a 200 mL reverse gradient of ammonium sulfate (0.8−0 M in KP_i buffer) at a rate of 1 mL/min. The column was then washed with 40 mL of 50 mM KP_i buffer (pH 7.5), followed by 40 mL of water at the same flow rate, to elute hydrophobic proteins tightly bound to the column. Fractions containing caffeine dehydrogenase were identified by the spectrophotometric enzyme activity assay as described below. Caffeine dehydrogenase was eluted from the column during the final wash step with water. The protein concentration was determined by Bradford[38] using bovine serum albumin (BSA) as the standard with a dye reagent purchased from Bio-Rad.

Enzyme Assays. A spectrophotometric activity assay based on caffeine-specific reduction of NBT was developed to monitor the purification of caffeine dehydrogenase as described by Yu et al.[37] A typical 1 mL reaction mixture contained an appropriate amount of enzyme (usually 1−10 μg), 0.5 mM caffeine, and 0.5 mM NBT in 50 mM KP_i buffer (pH 7.5). Caffeine dehydrogenase activity was determined by monitoring with a UV/vis spectrophotometer (Shimadzu UV-2450) the increase in absorbance at 566 nm (extinction coefficient of 15 500 M^{-1} cm^{-1}) due to formazan production. One unit of enzyme activity was defined as reduction of 1 nmol of NBT/min at 25 °C and pH 7.5. All colorimetric assays in 96-well plates were carried out at room temperature and 400 rpm. The final reaction volume of 200 μL/well contained 0.5 mM tetrazolium dye in 50 mM KP_i buffer (pH 7.5). Reaction was started with addition of the appropriate amount of enzyme.

Analytical Procedures and Test Sample Preparation. Identification and quantification of caffeine in test samples was conducted with a Shimadzu LC-20AT HPLC system equipped with an

SPD-M20A photodiode array detector and a Hypersil BDS C18 column (4.6 by 125 mm) as described by Yu et al.[39] A 20% methanol/80% water/0.5% acetic acid (20:80:0.5, v/v/v) mixture was used as the isocratic mobile phase with a flow rate of 0.5 mL/min. Prior to testing of the drugs, one tablet from each of the listed pharmaceuticals (Table 2) was powdered separately, dissolved in 50 mM KP_i buffer (pH 7.5), and diluted appropriately to bring the caffeine concentration range to 5−50 ppm. Correspondingly, a reference color chart was prepared using 50 mM KP_i buffer (pH 7.5) by spiking known concentrations of pure caffeine purchased from Sigma Chemicals and developing the shades of red color using the Cdh-based detection test in the range of 0−50 ppm. The caffeine concentration in the diluted samples was determined in triplicate using HPLC as described previously.[39] The coffee extract used in the validation test was obtained by boiling 10 g of coffee powder for 10 min with 200 mL of deionized water and filtering using filter paper. The HPLC method was employed to determine the caffeine content in the extract, in soft drinks, and in pharmaceutical samples.

RESULTS

Testing Various Tetrazolium Dyes for the Best Visual Suitability. Several commercially available tetrazolium dyes were screened as electron acceptors in Cdh-based caffeine detection. Two critical attributes were (i) rapid reduction in the presence of Cdh and caffeine to give a bright-colored product and (ii) low or no background (minimum nonenzymatic reduction). Six tetrazolium dyes were tested at 0.5 mM as described in the Materials and Methods. As shown in Table 1, the enzyme in the presence of caffeine reduced all dyes except TB and TV. Of the four dyes that showed activity, MTT and TNBT showed a strong background color (Table 1), which made it difficult to distinguish between reaction and no reaction (data not shown). On the other hand, INT had no background color and produced shades of light pink to dark red proportional to the caffeine concentration. NBT upon reduction produced shades of dark blue to dark purple which were readily distinguishable from the light yellow background color. INT was found to be the most suitable dye for Cdh-based detection of caffeine. It also was the lowest priced dye (Table 1). NBT was chosen as a backup for INT. Previously, a 1:1 stoichiometry between caffeine and tetrazolium dye was established (Figure 1).[37] Hence, the dye concentration was fixed at 0.5 mM. This ensured that the dye-dependent color formation was not the limiting factor for caffeine detection.

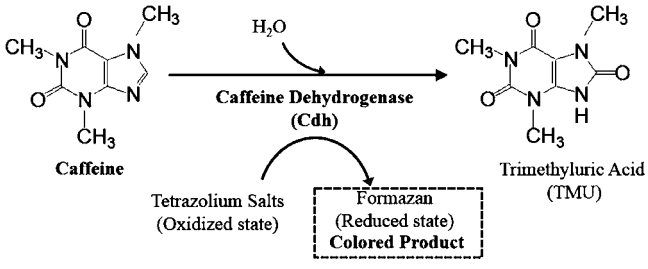

Figure 1. Reaction catalyzed by Cdh: oxidation of caffeine to TMU with concomitant reduction of tetrazolium dyes to formazans.

Cdh Required for Detection of Caffeine in 1 min. It is important that the Cdh-based detection of caffeine produced a visible color fast, i.e., within 1 min, at the lowest detection limit of caffeine. In applications such as detection of caffeine in breast milk, 5 ppm is deemed as the safe upper limit on the basis of the assumption that a mother consumes 500 mg of caffeine (100 mg higher than the safe upper limit set by the FDA for adults/day[25] and about 1−1.5% of it partitioning into breast milk in 1 h).[39] Hence, 5 ppm caffeine was fixed as the lower limit for detection at varying enzyme load, and the corresponding time required for maximum color development was determined (Figure 2). As expected, increasing the enzyme load decreased the time required for color development exponentially (Figure 2). On this basis, for maximum color development within a threshold of 1 min, the minimum enzyme load for the present study was fixed at 20 U. While this enzyme load is adequate for further validation of Cdh-based caffeine detection in a microtiter plate, the actual enzyme load in a commercial diagnostic kit may have to be higher to compensate for loss of activity due to (i) immobilization of Cdh in a test strip, (ii) formulation of the enzyme, and (iii) shelf life of the enzyme and the dye. These parameters will have to be further optimized during the development of a commercial diagnostic kit, such as a dipstick test. The color development in a diagnostic kit with a threshold detection of 1 min should also be independent of the caffeine concentration in the test sample. This will also demand a higher enzyme load than 20 U.

First-Level Attributes for Cdh-Based Caffeine Detection. The first-level attributes for further validation of the test with real-world samples (caffeinated and caffeine-containing beverages, nursing mother's milk, and pharmaceuticals) were set as (i) a minimum enzyme load of 20 U Cdh, (ii) INT as the dye due to no background color, (iii) an optimal dye concentration of 0.5 mM (equal to 97.1 ppm), (iv) visible pink color at 5 ppm caffeine to readily differentiable shades of red at 20, 100, and ≫100 ppm, and (v) a threshold time of 1 min for detection. The above conditions were used for caffeine detection in various samples in a 96-well microtiter plate in a total reaction volume of 200 μL.

Validation of Cdh for Caffeine Detection: Color Development at 5 ppm Caffeine (Lowest Limit). As discussed previously, 0−5 ppm was designated as the safe range for caffeine in breast milk on the basis of FDA guidelines and the literature.[25,40] Thus, the lowest detection limit for the Cdh-based test should be 5 ppm. The color development for the Cdh-based test in buffer at 1 ppm caffeine is shown in the inset of Figure 2. A light pink color is clearly distinguishable within 1 min of reaction time at a level lower than the safe limit of caffeine. There is no background in the control where caffeine is absent. These results establish that the Cdh-based test can detect caffeine as low as 1 ppm within the threshold time. Thus, detecting caffeine at 5 ppm should not be a limitation. However, this result needs to be validated with "real-world samples". These samples are different in that they are finished products in complex formulations. Detection of caffeine in buffer under optimized conditions may not translate to the commercial samples. Interfering components in the formulations, the pH of the test solution, and the background color of the test sample (such as cola, coffee, milk, etc.) are some of the issues. Hence, for further validation of Cdh for caffeine detection, three different categories of commercial samples were chosen. These include (i) pharmaceuticals formulated with caffeine, (ii) caffeinated and caffeine-free beverages, and (iii) milk samples, including breast milk (spiked with caffeine).

Estimation of Caffeine in Pharmaceuticals. The first validation for Cdh-based detection of caffeine was done with pharmaceuticals containing caffeine. Caffeine is added in the final formulation of a number of drugs, although it is not an active ingredient in most of these drugs.[41] Thus, estimating the caffeine in pharmaceuticals would be an excellent validation of

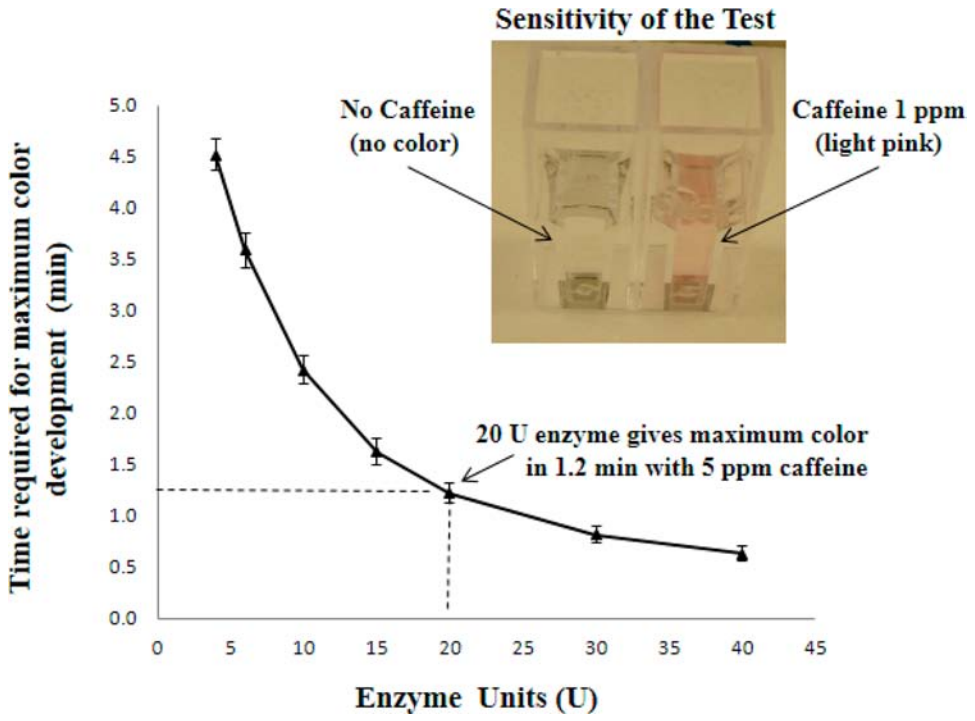

Figure 2. Cdh assay with varying amounts of enzyme at a fixed concentration of caffeine (5 ppm). Inset: color development with Cdh at 1 ppm caffeine. The control reaction on the left has no caffeine, only INT. The color development time was 1 min.

Table 2. Validation of Cdh-Based Caffeine Estimation for Six Pharmaceuticals[c]

Name of the Drug	Manufacturer Specified Caffeine amount per tablet (in mg)	Caffeine after dilution (in ppm)[a]	As determined by (in ppm)		Color developed by Cdh-based test (in triplicate)
			HPLC	Cdh-based Test[b]	
Diurex (Diuretic)	50	25	25.1 ± 0.1	30	
Menstrual Relief (Pain Reliever)	60	30	29.7 ± 0.3	30	
Vanquish (Pain Reliever)	33	33	31.2 ± 0.6	30	
Midol (Pain Reliever)	60	6	5.7 ± 0.2	5	
Excedrin (Pain Reliever)	65	6.5	5.6 ± 0.4	5	
Vivarin (Stimulant)	200	20	19.4 ± 0.7	20	
Color Reference Chart (Caffeine Concentration in ppm)			0	5 10 20 30 40 50	

[a]Sample preparation and dilutions were done as described in the Materials and Methods. [b]The test was carried out with 20 U of Cdh per assay in potassium phosphate buffer (pH 7.5) at room temperature (22 °C). Approximate value estimated by visually comparing the color obtained within 1 min (last column) with the reference color chart with various concentrations of spiked caffeine in 50 mM KP_i buffer (pH 7.5) (last row). [c]A reference color chart for caffeine concentration in the range of 0−50 ppm is shown at the bottom of the table.

the suitability of Cdh toward development of a diagnostic test. Caffeine concentrations in the drug formulations are given in the label. This was further confirmed by HPLC before estimation of the caffeine levels in these drugs using Cdh. Six commercially available pharmaceuticals were chosen, namely, Diurex (a diuretic), Menstrual Relief, Vanquish, Midol, and Excedrin (pain relievers), and Vivarin (a stimulant). After appropriate dilution, the caffeine concentration was measured in triplicate in these pharmaceutical samples using Cdh (last column in Table 2). A reference chart was created with standard caffeine at various concentrations, to visibly determine approximate caffeine levels in the pharmaceutical samples. As shown in Table 2, the caffeine concentration from the Cdh test matched reasonably with the HPLC estimates. The Cdh test gave credible estimations in the range of 5−50 ppm. The components in the drug formulations did not interfere with Cdh for color development. Also, color development was within the threshold time of 1 min.

Determination of Caffeine in Commercial Beverages (Coffee and Soft Drinks). The second validation of Cdh for caffeine diagnosis was performed with beverages such as coffee and soft drinks and their decaffeinated counterparts. For this, two sets of caffeine-containing beverages were selected. Set 1 was regular coffee from Dunkin' Donuts, 50% decaffeinated

Table 3. Cdh-Based Caffeine Detection: Validation Using Various Caffeinated and Noncaffeinated Beverages

Type of Beverage	Manufacturer specified caffeine content (ppm)[a]	As determined by HPLC (ppm)[b]	Cdh-based caffeine Detection Test
Coffee			Blank[c] Assay
Dunkin Donut (Regular)	NA	601.6 ± 21.4	
Folgers (50% Decaffeinated)	NA	331.6 ± 5.9	
Dunkin Donut (Decaffeinated)	NA	20.4 ± 1.3	
Soft Drinks (Caffeine free vs Regular)[d]			Caffeine Free Regular
Coca-Cola	96.4	83.3 ± 4.2	
Pepsi	107	96.1 ± 5.6	
Mountain Dew	152	142 ± 9.4	

[a]Powdered coffee from Dunkin' Donuts and Folgers does not have the manufacturer-specified caffeine content in the label. [b]Caffeine values reported for coffee are based on brewing methods described in the Materials and Methods followed by analysis with HPLC in triplicate. [c]Dye (in buffer) added to the sample without enzyme. [d]For soft drinks, the caffeine contents are based on the manufacturer's specifications and HPLC analysis.

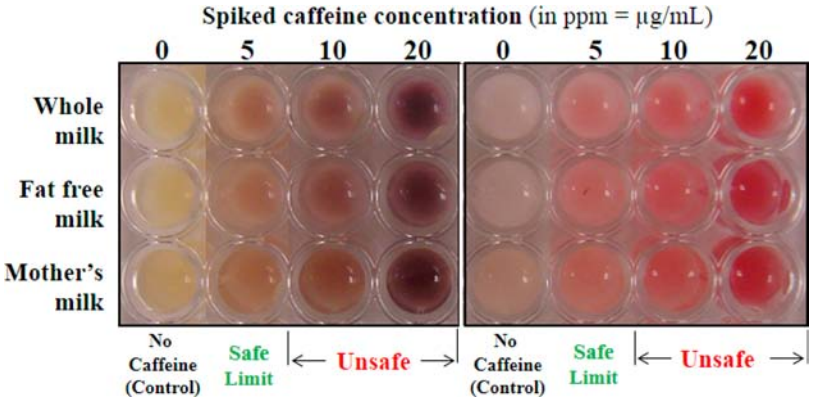

Figure 3. Cdh-based detection of caffeine in 1 min, with milk samples spiked with the alkaloid as indicated. Commercially available whole milk and fat-free milk were used for the test. Nursing mother's milk was obtained from the Mother's Milk Bank of Iowa, University of Iowa Children's Hospital. The left panel is the NBT-based test and the right panel the INT-based test.

coffee from Folgers, and decaffeinated coffee from Dunkin' Donuts, with caffeine concentrations of about 600, 330, and 20 ppm, respectively (Table 3). Set 2 was regular Coca-Cola with a caffeine concentration of 96.4 ppm, caffeine-free cola (zero caffeine), regular Pepsi with a caffeine concentration of 107 ppm, caffeine-free Pepsi, regular Mountain Dew with a caffeine concentration of 152 ppm, and caffeine-free Diet Mountain Dew (Table 3). The caffeine content of soft drinks from the label on the cans is also shown in Table 3. The caffeine content on the label and that determined by HPLC were comparable (Table 3). Beverages listed in Table 3 were analyzed for caffeine using Cdh. The objective here was qualitative, i.e., to differentiate among the presence, the absence, and a low level of caffeine in decaffeinated coffee. The fact that many of these beverages have a background color was a concern; caffeine-dependent color formation should still be readily differentiable relative to the background. The results of the Cdh test with the beverages are shown in Table 3. There was intense color production with caffeinated and 50% decaffeinated coffee (Table 3). In contrast, the color was light with decaffeinated coffee (~20 ppm caffeine). The background color of the coffee extracts did not interfere with Cdh in terms of clearly and instantly differentiating decaffeinated beverages from their caffeinated counterparts. Interestingly, the color is distinguishably lighter in 50% decaffeinated coffee (330 ppm caffeine) relative to regular coffee (600 ppm caffeine), although the commercial relevance of this is not clear. Ingredients present in these beverages such as sugar, added chemicals, coloring agents, etc. did not interfere with the Cdh-based test. These results further affirmed that Cdh is highly suitable and robust toward developing a diagnostic test and can quickly differentiate caffeinated drinks from decaffeinated or noncaffeinated counterparts. This test could be very useful to avoid human errors in restaurants and other outlets when all these beverages are served in nonlabeled cups.

Detection of Caffeine in Breast Milk. Cdh-based caffeine diagnosis would be of great value for rapidly detecting caffeine levels in nursing mother's milk. Caffeine is highly restricted for

dx.doi.org/10.1021/jf501598c | J. Agric. Food Chem. 2014, 62, 7939−7946

Table 4. Comparison of the Attributes of Reported Caffeine Detection Methods with Those of Cdh-Based Caffeine Detection

	attribute				
detection method	in situ	time of detection	sensitivity	method of detection	commercial availability
bacterial cell based[28]	no (DO probe)	>3 min	100 ppm	digital	no
lipid polymer membrane based[31]	no (electrode)	<30 s	NA[a]	digital	no
fluorescent dye based[32]	yes (test strips)	20 min	100 ppm	visual (green)	no
enzyme based[29]	yes (test strips)	NA	NA	digital/visual	no
antibody based (FPIA)[34]	no	2 min	parts per billion	digital	not applicable
antibody based (D+Caf)[43]	yes (test strips)	<60 s	112 ppm	visual (blue)	discontinued[b]
Cdh enzyme based (current work)	yes	<60 s	1−5 ppm	visual (pink to shades of red)	work in progress

[a]Data not available. [b]Does not work with milk and sugared drinks. The test has to be done before addition of milk and sugar to coffee.

pregnant women and infants as documented earlier.[25,26] The potential teratogenic effect of excess caffeine on infants was also documented.[27] Hence, Cdh-based caffeine detection was tested with various milk samples spiked with caffeine. Milk is a complex mixture of proteins, fat, sugars, and other ingredients, including calcium and vitamin D. In addition, nursing mother's milk has immunoglobulins, metal ions, cofactors, hormones, and other biochemicals. The present test must not have any interference from these components. The results of the Cdh-based caffeine detection with various milk samples (spiked with caffeine) are shown in Figure 3. For this specific test, both INT and NBT were used, assuming that there might be nonspecific reduction of one or both dyes due to metal ions and other biological components in milk. The Cdh-based test scored very well in all the tests. Both dyes were able to differentiate no caffeine (0 ppm) and a safe level (5 ppm) and unsafe levels (>20 ppm) of caffeine (based on FDA regulations) in all milk samples, especially mother's milk. The complex components in the milk did not interfere with caffeine detection and the rapidity of color development. Clearly, the test is suitable to determine if the caffeine level is safe before an infant is nursed. There is a light background color in nursing mother's milk with the INT dye at "0" caffeine (Figure 3). This might be due to very low level reduction of the dye by milk components in this specific sample. Nevertheless, this does not interfere with the speed or the ability of Cdh to determine the safe and unsafe levels of caffeine in milk.

DISCUSSION

Need for a Caffeine Diagnostic Test. Caffeinated drinks and other products are growing in number and caffeine content in the form of energy drinks and even items such as chewing gum and jelly beans that children consume. This unregulated growth of caffeinated products has caught the FDA's attention and has also resulted in a move toward regulating caffeinated products.[21,22] In addition, the FDA has set guidelines for caffeine consumption for normal adults and pregnant women;[25] guidelines/restriction limits for infants and teenagers are currently under consideration by the FDA.[22] Thus, there is a real need for a rapid diagnostic test at the consumer level. Several attempts, using different approaches, have been made to develop caffeine detection/diagnostic tests and are compared in Table 4.

Caffeine Dehydrogenase, an Ideal Candidate for Caffeine Detection. Cdh (EC 1.17.5.2; systematic name caffeine:ubiquinone oxidoreductase) catalyzes the first step of caffeine degradation via the C-8 oxidation pathway.[37,42] It is non nicotinamide adenine dinucleotide (NAD) dependent, but needs a stoichiometric amount of an electron acceptor such as NBT or quinone (Q_0) as an electron sink.[37] The enzyme is easily purified for caffeine detection and potential development of a diagnostic test. The optimized procedure gave a 48.6% yield with a specific activity of 210 units/mg of protein. Previously, Cdh was shown to be highly specific for caffeine with a K_m of 3.7 ± 0.9 μM, with a 50-fold less preference for the closest analogue theobromine and very slight or no activity with other di- and monomethylxanthines and xanthine.[37] Thus, none of these compounds interfered with the color development with caffeine in 1 min (data not shown). The enzyme is robust in terms of activity at temperatures ranging from 15 to 60 °C with a linear increase in activity with temperature.[37] This makes the enzyme suitable for measuring the caffeine content in a number of cold and moderately hot beverages. The enzyme has activity over a broad pH range (6−8) as previously reported[37] and in the present work with commercial beverages in the pH range of 3−7. Cdh also has other suitable attributes for development of a diagnostic test, such as (i) in situ (on-the-spot) detection, (ii) a speed of detection of 1 min or less (Figure 2), (iii) easy visualization for both semiquantitative and qualitative detection (Tables 2 and 3), and (iv) a caffeine sensitivity to the level of 5−20 ppm (the FDA safe limit in nursing mother's milk is 5 ppm, and decaffeinated beverages have 20 ppm caffeine).

Comparison of the New Cdh-Based Caffeine Detection with Other Reported Caffeine Detection Methods. Detection of caffeine in various laboratories including quality control is traditionally done by the well-established LC−MS/MS[34] or HPLC method.[37,39] However, this method is tedious, instrument-intensive, expensive, and time-consuming and is not practical for a rapid diagnostic test. Various caffeine detection methods/diagnostic tests that have been reported are compared in Table 4 with respect to their attributes. These methods range from those using live bacterial whole cells[28] and enzymes[29,30] and antibody-based methods[34−36] to other nonbiological methods using lipid/polymer membranes[31] and fluorescent dyes.[32,33] The immobilized bacterial cell based assay is an electrode based amperometric test in which a dissolved oxygen (DO) probe measures oxygen depletion as a function of caffeine metabolism.[28] This method has major deficiencies such as bulky electronic instrumentation and a low response time (more than 3 min) and sensitivity (>100 ppm). Similarly, the lipid/polymer membrane based method (also known as the electronic tongue) is also an electrode based amperometric test.[31] This method is rapid (response time of less than 1/2 min), but has other drawbacks similar to those of the bacterial cell based method. None of these tests are commercially available. Recently, two other methods were reported based on binding of fluorescent dyes to caffeine on a thin-layer chromatography (TLC) plate and visualization using UV light.[32,33] Although these methods are simple compared to the bacterial cell based method, the test failed to meet criteria

such as rapid detection (more than 20 min for color development) and sensitivity (cannot detect <100 ppm). Thus, none of the previously reported caffeine detection/diagnostic tests have the right attributes for consumer use.

The antibody methods described for caffeine detection are based on caffeine-specific monoclonal antibodies (mAb's).[34,35] One such method is a fluorescence polarization immunoassay (FPIA) which, although fast (2 min) and highly sensitive (parts per billion range), is instrument-intensive (Table 4) and thus unsuitable for at-home-type tests.[34] On the other hand, an anti-caffeine, mAb-based colorimetric test (D+Caf) met most of the required attributes except sensitivity (Table 4), which was found to be about 20 mg/6 oz of fluid (~112 ppm).[43] Also, these D+Caf strips were not able to detect caffeine in beverages in the presence of milk and sugar.[43] The enzymatic method known for caffeine detection is based on either xanthine oxidase[29] or alkaline phosphatase.[30] Notable drawback of this method is a lack of specificity of xanthine oxidase to caffeine. Thus, while several attempts have been made to develop a caffeine detection test, none of them meet the required attributes needed for an at-home test in terms of sensitivity, rapidity of detection, and ability to detect the alkaloid in various commercial formulations and cocktails.

Suitability of Cdh for Rapid Diagnosis of Caffeine. Cdh-based caffeine detection is highly suitable for development of a rapid diagnostic test. Cdh has high specificity for caffeine.[37] The sensitivity for caffeine detection by Cdh is 1 ppm, well below the 5 ppm sensitivity required. The detection time for the alkaloid is 1 min. Last, but not the least, this enzyme readily detects caffeine in commercial beverages, in nursing mother's milk, and in sugared drinks. The inherent pH variation of the samples did not affect the speed of color development. With nursing mother's milk, the Cdh-based test is able to detect safe and unsafe levels of caffeine in 1 min (Figure 3). This will be very useful for nursing mothers where FDA limits the safe level of caffeine at 5 ppm. To the best of our knowledge, there is no rapid diagnostic test for caffeine that is commercially available for testing nursing mother's milk. Cdh-based caffeine detection is also applicable for readily differentiating decaffeinated products (Table 3). Various additives in commercial caffeinated drinks do not interfere with detection of caffeine in the rapid Cdh test. One exception is tea; flavonoids and phenolic components in this beverage interfere with Cdh-based detection of caffeine. Last, but not least, the Cdh detection test is applicable to rapidly estimating caffeine in several drug formulations. The values obtained from the Cdh test with a standard color chart are in the range determined by HPLC (Table 2). Again, the formulation components in the drug do not interfere with the test. It is tempting to propose that the Cdh-based caffeine estimation could be useful for quality control laboratories, including in pharmaceutical formulations, to establish the caffeine concentration for labeling. It will be faster, easier, simpler, and cheaper compared to the laborious, time-consuming, and expensive HPLC procedures. Cdh-based caffeine detection is robust and versatile in terms of development of a commercial diagnostic test for various applications ranging from qualitative tests (yes/no caffeine levels, safe/unsafe caffeine levels) to quality control estimations for caffeine in drug formulations.

Future Plans for the Cdh-Based Test. A Cdh-based commercial diagnostic kit has to be simple, such as litmus paper or pH paper (may be a dipstick-type test), like a glucose detection kit and portable. This will enable rapid on the spot detection by consumers and enable quick decisions based on the result. The expectation of the end user of such a test may not be accurate detection of caffeine concentration, but to know the safety range to make decisions. Examples of such diagnostic tests in the market are digital readout of approximate blood sugar levels for diabetics[44] and qualitative yes/no pregnancy tests.[45] The next phase of work includes, but is not limited to, (i) development of a dipstick by immobilizing Cdh and INT dye on a test strip, (ii) determination of the shelf life of Cdh and dye for speed of caffeine detection and sensitivity at various temperatures, (iii) formulation of Cdh for maximum activity/shelf life and appropriate enzyme loading to compensate activity loss during storage, (iv) quality control to ensure consistent performance of the diagnostic test, and (v) production of a well-calibrated reference color chart to facilitate the semiquantitative caffeine determination (5−100 ppm) and a chart coded as safe−moderate−unsafe.

AUTHOR INFORMATION

Corresponding Author

*Phone: 319-335-4900. Fax: 319-339-4901. E-mail: manisubramanian@uiowa.edu.

Present Address

[§]C.L.Y.: Proteomics Facility, Carver College of Medicine, University of Iowa, 355 Eckstein Medical Research Building, Iowa City, IA 52242.

Funding

This research was supported by University of Iowa Research Funds.

Notes

The authors declare no competing financial interest.

ACKNOWLEDGMENTS

We thank the Mother's Milk Bank of Iowa, University of Iowa Children's Hospital, for supplying frozen nursing mother's milk used in the current work.

ABBREVIATIONS USED

ICO, International Coffee Organization; FDA, Food and Drug Administration; Cdh, caffeine dehydrogenase; INT, iodonitrotetrazolium chloride; TB, tetrazolium blue chloride; MTT, tetrazolium blue tetrazolium bromide; TV, tetrazolium violet; NBT, nitro blue tetrazolium; TNBT, tetranitro blue tetrazolium; YNB, yeast nitrogen base; HPLC, high-performance liquid chromatography; KP_i, potassium phosphate buffer; CCE, crude cell extract; mAb's, monoclonal antibodies

REFERENCES

(1) Ashihara, H.; Crozier, A. Caffeine: A Well-Known but Little Mentioned Compound in Plant Science. *Trends Plant Sci.* **2001**, *6*, 407−413.

(2) Barone, J. J.; Roberts, H. R. Caffeine Consumption. *Food Chem. Toxicol.* **1996**, *34*, 119−129.

(3) Sivak, A. Coffee Consumption and Cancer. In *Caffeinated Beverages: Health Benefits, Physiological Effects, and Chemistry*; Parliment, T. H., Ho, C. T., Schieberle, P., Eds.; ACS Symposium Series *754*; American Chemical Society: Washington, DC, 2000; pp 64−70.

(4) Juliano, L. M.; Griffiths, R. R. Caffeine. In *Substance Abuse: A Comprehensive Textbook*; Lowinson, J. H., Ruiz, P., Millman, R. B., Eds.; Lippincott Williams & Wilkins: Philadelphia, PA, 2005; pp 403−420.

(5) Energy Fiend Home Page. http://www.energyfiend.com (accessed March 24, 2014).
(6) Dash, S. S.; Gummadi, S. N. Catabolic Pathways and Biotechnological Applications of Microbial Caffeine Degradation. *Biotechnol. Lett.* **2006**, *28*, 1993−2002.
(7) Daly, J. W. Caffeine Analogs: Biomedical Impact. *Cell. Mol. Life Sci.* **2007**, *64*, 2153−2169.
(8) Stavric, B. Methylxanthines: Toxicity to Humans. 2. Caffeine. *Food Chem. Toxicol.* **1998**, *26*, 645−662.
(9) Spiller, G. A. Basic Metabolism and Physiological Effects of the Methylxanthines. In *Caffeine*; Spiller, G. A., Ed.; CRC: Boca Raton, FL, 1998; pp 225−232.
(10) International Coffee Organization. Monthly Coffee Market Report—September 2013. http://www.ico.org/documents/cy2012-13/cmr-0913-e.pdf (accessed March 24, 2014).
(11) Pohler, H. Caffeine Intoxication and Addiction. *J. Nurse Pract.* **2010**, *6*, 49−52.
(12) Fredholm, B. B.; Battig, K.; Holmen, J.; Nehlig, A.; Zvartau, E. E. Actions of Caffeine in the Brain with Special Reference to Factors That Contribute to Its Widespread Use. *Pharmacol. Rev.* **1999**, *51*, 83−133.
(13) Eteng, M. U.; Eyong, E. U.; Akpanyung, E. O.; Agaiang, M. A.; Aremu, C. Y. Recent Advances in Caffeine and Theobromine Toxicities: A Review. *Plant Foods Hum. Nutr.* **1997**, *51*, 231−243.
(14) Gunja, N.; Brown, J. A. Energy Drinks: Health Risks and Toxicity. *Med. J. Aust.* **2012**, *196*, 46−49.
(15) Schmidt, A.; Karlson-Stiber, C. Caffeine Poisoning and Lactate Rise: An Overlooked Toxic Effect? *Acta Anaesthesiol. Scand.* **2008**, *52*, 1012−1014.
(16) van Dam, R. M. Coffee Consumption and Risk of Type 2 Diabetes, Cardiovascular Diseases, and Cancer. *Appl. Physiol. Nutr. Metab.* **2008**, *33*, 1269−1283.
(17) McGee, M. B. Caffeine Poisoning in a 19-Year-Old Female. *J. Forensic Sci.* **1980**, *25*, 29−32.
(18) Garriott, J. C.; Simmons, L. M.; Poklis, A.; Mackell, M. A. Five Cases of Fatal Overdose from Caffeine Containing "Look-Alike" Drugs. *J. Anal. Toxicol.* **1985**, *9*, 141−143.
(19) Mrvos, R. M.; Reilly, P. E.; Dean, B. S.; Krenzelok, E. P. Massive Caffeine Ingestion Resulting in Death. *Vet. Hum. Toxicol.* **1989**, *31*, 571−572.
(20) Reissig, C. J.; Strain, E. C.; Griffiths, R. R. Caffeinated Energy Drinks—A Growing Problem. *Drug Alcohol Depend.* **2009**, *99*, 1−10.
(21) Tomson, B. Caffeinated Snacks Draw FDA Scrutiny. *Wall Street Journal*, May 1, 2013, p B8.
(22) U.S. Food and Drug Administration. FDA To Investigate Added Caffeine, May 2013. http://www.fda.gov/ForConsumers/ConsumerUpdates/ucm350570.htm (accessed March 24, 2014).
(23) Esterl, M. Drink's Possible Ties to Death Are Probed. *Wall Street Journal*, Nov 14, 2012, Business section, http://online.wsj.com/news/articles/SB10001424127887323551004578119790449286544 (accessed online March 24, 2014).
(24) Esterl, M. Monster Beverage under Fire. *Wall Street Journal*, May 6, 2013. http://online.wsj.com/news/articles/SB10001424127887323826804578466780766004340 (accessed March 24, 2014).
(25) U.S. Food and Drug Administration. Medicines in My Home: Caffeine and Your Body. htttp://www.fda.gov/downloads/Drugs/ResourcesForYou/Consumers/BuyingUsingMedicineSafely/UnderstandingOver-the-CounterMedicines/UCM205286.pdf (accessed March 24, 2014).
(26) Stefanidou, E. M.; Caramellino, L.; Patriarca, A.; Menato, G. Maternal Caffeine Consumption and Sine Causa Recurrent Miscarriage. *Eur. J. Obstet. Gynecol. Reprod. Biol.* **2011**, *158*, 220−224.
(27) Whalley, K. Neural Development: Coffee Disrupts Brain Development. *Nat. Rev. Neurosci.* **2013**, *14*, 666.
(28) Sarath Babu, V. R.; Patra, S.; Karanth, N. G.; Kumar, M. A.; Thakur, M. S. Development of a Biosensor for Caffeine. *Anal. Chim. Acta* **2007**, *582*, 329−334.
(29) Scherl, M.; Scherl, J.; Fiedler, S. B. Detection of Caffeine in Beverages. U.S. Patent 5,610,072, Mar 11, 1997.
(30) Akyilmaz, E.; Turemis, M. An Inhibition Type Alkaline Phosphatase Biosensor for Amperometric Determination of Caffeine. *Electrochim. Acta* **2010**, *55*, 5195−5199.
(31) Shen, H.; Habara, M.; Toko, K. Development of Caffeine Detection Using Taste Sensor with Lipid/Polymer Membranes. *Sens. Mater.* **2008**, *20*, 171−178.
(32) Luisier, N.; Ruggi, A.; Steinmann, S. N.; Favre, L.; Gaeng, N.; Corminboeuf, C.; Severin, K. A Ratiometric Fluorescence Sensor for Caffeine. *Org. Biomol. Chem.* **2012**, *10*, 7441−7636.
(33) Rochat, S.; Steinmann, S. N.; Corminboeuf, C.; Severin, K. Fluorescence Sensing of Caffeine in Water with Polysulfonated Pyrenes. *Chem. Commun.* **2011**, *47*, 10584−10586.
(34) Oberleitner, L.; Grandke, J.; Mallwitz, F.; Resch-Genger, U.; Garbe, L. A.; Schneider, R. J. Fluorescence Polarization Immunoassays for the Quantification of Caffeine in Beverages. *J. Agric. Food Chem.* **2014**, *62*, 2337−2343.
(35) Franco, E. J.; Sonneson, G. J.; DeLegge, T. J.; Hofstetter, H.; Horn, J. R.; Hofstetter, O. Production and Characterization of a Genetically Engineered Anti-Caffeine Camelid Antibody and Its Use in Immunoaffinity Chromatography. *J. Chromatogr., B: Anal. Technol. Biomed. Life Sci.* **2010**, *878*, 177−186.
(36) Graham, A. Q.; Hathaway, C.; Geisberg, M. S. Caffeine Detection via Internally Referenced Two Part Assay. U.S. Patent 8,137,984, Mar 20, 2012.
(37) Yu, C. L.; Kale, Y.; Gopishetty, S.; Louie, T. M.; Subramanian, M. A Novel Caffeine Dehydrogenase in *Pseudomonas* sp. Strain CBB1 Oxidizes Caffeine to Trimethyluric Acid. *J. Bacteriol.* **2008**, *190*, 772−776.
(38) Bradford, M. M. A Rapid and Sensitive Method for the Quantitation of Microgram Quantities of Protein Utilizing the Principle of Protein-Dye Binding. *Anal. Biochem.* **1976**, *72*, 248−254.
(39) Yu, C. L.; Louie, T. M.; Summers, R.; Kale, Y.; Gopishetty, S.; Subramanian, M. Two Distinct Pathways for Metabolism of Theophylline and Caffeine Are Coexpressed in *Pseudomonas putida* CBB5. *J. Bacteriol.* **2009**, *191*, 4624−4632.
(40) Tyrala, E. E.; Dodson, W. E. Caffeine Secretion into Breast Milk. *Arch. Dis. Child.* **1979**, *54*, 787−800.
(41) Durrant, K. L. Known and Hidden Sources of Caffeine in Drug, Food, and Natural Products. *J. Am. Pharm. Assoc.* **2002**, *42*, 625−637.
(42) Mohanty, S. K.; Yu, C. L.; Das, S.; Louie, T. M.; Gakhar, L.; Subramanian, M. Delineation of the Caffeine C-8 Oxidation Pathway in *Pseudomonas* sp. Strain CBB1 via Characterization of a New Trimethyl Acid Monooxygenase and Genes Involved in Trimethyluric Acid Metabolism. *J. Bacteriol.* **2012**, *194*, 3872−3882.
(43) D+Caf Caffeine Test Strips Review. http://abouttesting.testcountry.com/2009/12/dcaf-caffeine-test-strips-review.html (accessed March 24, 2014).
(44) Clarke, W. L.; Cox, D.; Gonder-Frederick, L. A.; Carter, W.; Pohl, S. L. Evaluating Clinical Accuracy of Systems for Self-Monitoring of Blood Glucose. *Diabetes Care* **1987**, *10*, 622−628.
(45) Crane, M. M. Diagnostic Test Device. U.S. Patent 3,579,306, May 18, 1971.

Table 1. Type, Origin and Trade Name of the Samples[a]

no.	type	origin	trade name	no.	type	origin	trade name
1	bacteria-type douchi	Hunan	LinSanLin	31	gray sufu	Beijing	WangZhiHe
2		Yunnan	YunZhiNan	32		Sichuan	LinJiangSi
3		Guizhou	ShuiXiangZi	33		Hunan	#
4		Guizhou	LaoGanMa	34		Hunan	#
5		Chongqing	#	35		Chongqing	#
6		Chongqing	#	36	red sufu	Guizhou	LaoGanMa
7		Yunnan	SanChuanBan	37		Beijing	WangZhiHe
8		Sichuan	XinFan	38		Beijing	WangZhiHe
9		Yunnan	ShanLiXiang	39		Beijing	WangZhiHe
10	aspergillus-type douchi	Guangzhou	YangFan	40		Beijing	LaoCaiChen
11		Guangzhou	YangFan	41	White sufu	Chongqing	ZhongZhou
12		Guangzhou	YangFan	42		Chongqing	DouXiaoDe
13		Guangzhou	YangFan	43		Sichuan	LinJiangSi
14		Guangzhou	YangFan	44		Guangxi	GuRong
15		Guangzhou	YangJiang	45		Chongqing	ZhongZhou
16		Guangzhou	YangJiang	46		Chongqing	XianJia
17		Guangzhou	YangJiang	47		Chongqing	ZhongZhou
18		Guangzhou	YangJiang	48		Chongqing	GanShui
19		Hunan	LiuYang	49		Chongqing	DouXiaoDe
20	mucor-type douchi	Guangxi	HuangYaoGuZhen	50		Sichuan	WeiDuiWei
21		Guangxi	HuangYaoGuZhen	51		Sichuan	WeiDuiWei
22		Guangxi	HuangYaoGuZhen	52		Sichuan	QiaoPai
23		Shandong	WeiYiZhai	53		Beijing	LaoCaiChen
24		Yongchuan,Chongqing	WaiZuMu	54		Chongqing	GanShui
25		Yongchuan,Chongqing	QinMei	55		Sichuan	QiaoPai
26		Yongchuan,Chongqing	AnJun	56		Beijing	WangZhiHe
27		Yongchuan,Chongqing	WuJianFang	57		Chongqing	GanShui
28		Yongchuan,Chongqing	JunYi	58		Beijing	WangZhiHe
29		Yongchuan,Chongqing	JiaTai	59		Yunnan	ShiFangZhi
30		Yongchuan,Chongqing	YongLai	60		Chongqing	ZhuJiangQiao
				61		Chongqing	DouXiaoDe
				62		Beijing	LaoCaiChen
				63		Chongqing	XianJia

[a]Among them, the same brands are composed of different flavor; "#" expressing home-fermented.

Fermented soya beans (or douchi) and fermented bean curd (or sufu) are the most typical traditional fermented soy products. Both are made by microbial fermentation beginning with soybean as raw material. On the basis of the microorganisms used, fermented soya beans can be classified into aspergillus-type douchi, mucor-type douchi, and bacterial-type douchi. Similarly, fermented bean curd can be divided into three main types according to the differences of the dressing mixture, which are white sufu, gray sufu, and red sufu, respectively. During the fermentation process both of fermented soya beans and fermented bean curd, microorganisms are involved, such as some type of yeast, lactic acid bacteria (bending *Lactobacillus casei* and lactobacillus), bacillus, streptococcus, *Staphylococcus aureus*, etc., some of which could produce decarboxylase.[26,27] In short, because of the existence of biogenic amine precursors, the process is bound to generate biogenic amines in an appropriate environment. Therefore, this study seeks to determine what biogenic amines occur in commercially available fermented soy products, and to evaluate the safety of biogenic amines. We hope to also provide advice so people can safely eat fermented soy products.

MATERIALS AND METHODS

Samples and Standards of BAs. Thirty fermented soya bean samples (9 bacteria-type douchi, 10 aspergillus-type douchi, 11 mucor-type douchi.) and 33 fermented bean curd samples (5 gray sufu, 5 red sufu, and 23 white sufu) were purchased from retail markets and supermarkets in China. Specific descriptions of the samples (region of origin, types, and trade names) are listed in Table 1. Standard amines, including putrescine (Put, ≥98%), cadaverine (Cad, 98%), spermidine (Spd, ≥98%), tryptamine (Try, ≥98%), β-phenethylamine (β-Phe, ≥98%), histamine (His, ≥99%), tyramine (Tyr, ≥98%) and spermine (Spm, ≥98%) were purchased from the Sigma-Aldrich Corporation in the United States. Dansyl chloride (≥98%) was bought from Tedia Company in the United States.

Apparatus. High performance liquid chromatograph (Agilent1260), with UV-detector and Agilent XDB-C18 (250 × 4.6 mm^2, 5 μm) column; an ultrasonic bath KQ5200DB; an Eppendorf centrifuge table high speed; an ultrapure water Milli-Q; water bath temperature oscillator, and a syringe filter 0.22 μm.

Sample and Standard Preparation. Five grams of each sample was extracted with approximately 20 mL of 0.4 M perchloric acid (Sigma), placed in the ultrasonic bath for 30 min, and then centrifuged for 5 min at 5000 rpm, taking supernatants on standby.

Standard stock solutions of the eight biogenic amines were prepared separately at 1 mg/mL concentration in 0.4 M $HClO_4$. Working solutions, containing all the amines at 3.0−100 mu g/mL concentrations, were prepared by diluting the standard stock solution.[28]

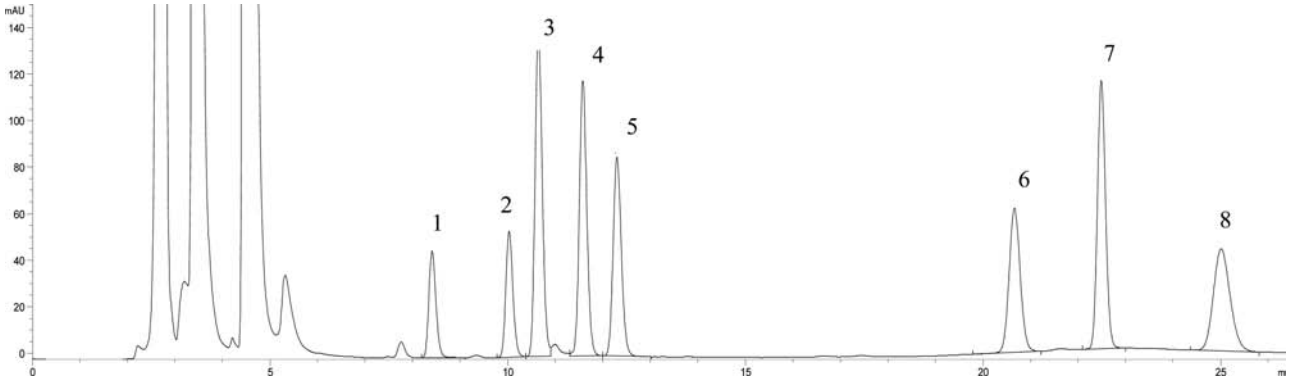

Figure 1. Chromatogram of derivatives of biogenic amines standards (70 μg/mL). (1) Tryptamine, (2) β-phenylethylamine, (3) putrescine, (4) cadaverine, (5) histamine, (6) tyramine, (7) spermidine, and (8) spermine. The peaks that are omitted have no meaning. As shown, the peaks of the 8 standard derivatives are shown later and flagged as 1, 2, 3, 4, 5, 6, 7, and 8.

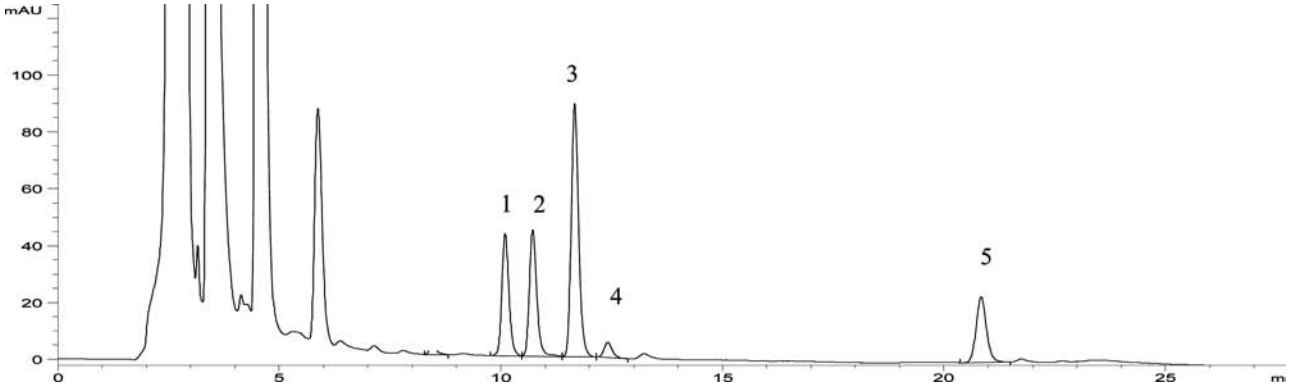

Figure 2. Chromatogram of derivatives of biogenic amines in one of the fermented soya beans. (1) β-Phenylethylamine, (2) putrescine, (3) cadaverine, (4) histamine, and (5) tyramine.

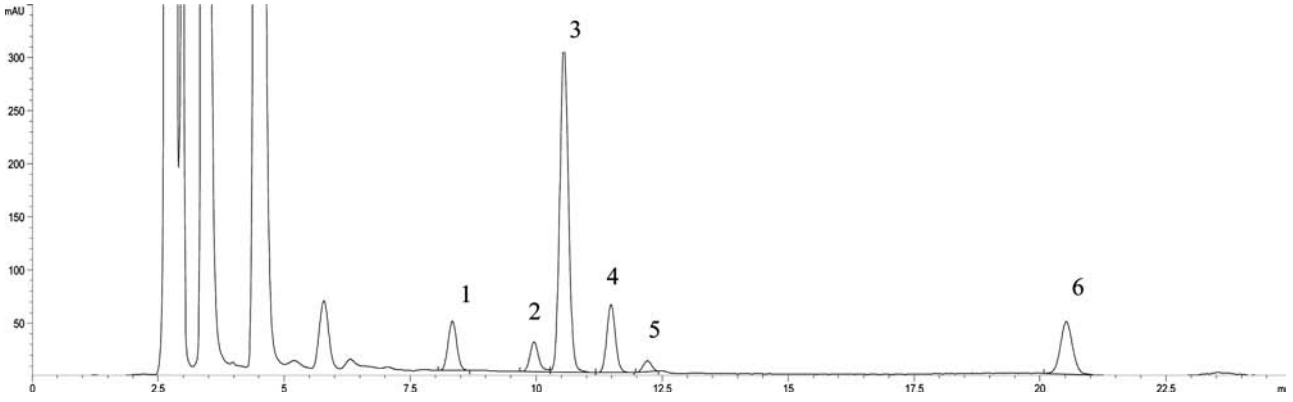

Figure 3. Chromatogram of derivatives of biogenic amines in one of the fermented bean curd samples. (1) tryptamine, (2) β-phenylethylamine, (3) putrescine, (4) cadaverine, (5) histamine, and (6) tyramine.

Derivatization. One milliliter of a sample solution was mixed with 200 μL of 2 M sodium hydroxide and 300 μL of saturated sodium carbonate. Under the alkaline conditions, the mixture was derivatized by the addition of 2 mL dansyl chloride solution (10 mg/mL in acetone). After incubation for 30 min at 40 °C in darkness, 100 mL of aqueous ammonia was added to remove any residual Dansyl chloride. The volume was adjusted to 5 mL with acetonitrile. Finally, the supernatant was filtered through 0.22 μm pore-size filters prior to HPLC analysis.

Chromatographic Conditions. Column temperature = 30 °C, flow rate = 1.0 mL/min, injected volume = 5 μL, detection wavelength (λ) = 254 nm were used. The mobile phase was a gradient elution program with a binary mixture of acetonitrile and H_2O. Each HPLC run took about 30 min, and the column was conditioned again with a mixture of 65% solvent A and 35% solvent B.

Statistical Analysis. All the tests were repeated three times, using Excel 2007 version for analysis and data processing.

RESULTS

Chromatograms of Standard BAs and Sample. Through the elution procedure, each BAs was detected in turn. The representative HPLC chromatogram and peak identification recorded for mixer of standard BAs, a fermented soya bean sample, and a fermented bean curd are shown in Figures 1, 2, and 3, respectively.

dx.doi.org/10.1021/jf501772s | J. Agric. Food Chem. 2014, 62, 7947−7954

Table 2. Contents of Biogenic Amines in Samples[a]

	biogenic amines ($mg \cdot kg^{-1}$)								
	Trp	Phe	Put	Cad	His	Tyr	Spd	Spm	total content
1	ND	ND	32.12 ± 0.30	ND	ND	ND	ND	ND	32.12
2	ND	ND	26.92 ± 0.31	ND	ND	ND	ND	ND	26.92
3	ND	ND	ND	ND	ND	ND	19.51 ± 1.43	ND	19.51
4	ND	ND	27.56 ± 1.03	ND	ND	ND	ND	ND	27.56
5	ND	ND	15.67 ± 0.74	ND	ND	ND	ND	ND	15.67
6	ND	ND	34.94 ± 1.07	ND	ND	ND	ND	ND	34.94
7	ND	ND	25.27 ± 2.13	ND	ND	ND	ND	ND	25.27
8	ND	ND	14.08 ± 1.03	ND	ND	ND	74.92 ± 1.66	ND	89.00
9	ND	ND	21.11 ± 0.55	ND	ND	ND	ND	ND	42.22
10	ND	16.77 ± 0.88	51.58 ± 4.39	ND	152.42 ± 4.60	180.14 ± 5.97	ND	ND	400.91
11	ND	ND	34.82 ± 9.11	ND	100.17 ± 1.86	159.38 ± 6.64	ND	ND	294.37
12	ND	28.37 ± 0.63	139.85 ± 3.98	ND	255.36 ± 12.91	183.06 ± 3.44	ND	ND	606.64
13	ND	ND	44.36 ± 1.77	ND	122.63 ± 4.51	139.93 ± 2.30	ND	ND	306.92
14	ND	79.00 ± 4.36	120.10 ± 1.54	ND	478.77 ± 8.79	252.08 ± 1.27	ND	ND	929.97
15	ND	ND	28.27 ± 0.62	ND	14.76 ± 1.01	ND	ND	ND	43.03
16	ND	ND	26.49 ± 1.53	ND	18.94 ± 0.57	ND	ND	ND	45.43
17	ND	ND	29.84 ± 2.68	ND	24.47 ± 1.48	57.85 ± 1.63	ND	ND	112.17
18	ND	ND	36.00 ± 1.64	ND	18.45 ± 1.51	ND	ND	ND	54.45
19	ND	ND	38.03 ± 1.58	ND	19.03 ± 1.10	ND	ND	ND	57.07
20	69.56 ± 1.87	736.64 ± 26.32	276.03 ± 8.41	672.33 ± 51.46	52.80 ± 4.03	250.21 ± 3.24	ND	ND	2057.56
21	ND	25.14 ± 2.25	249.01 ± 8.10	222.94 ± 2.81	83.87 ± 1.64	86.77 ± 7.65	ND	ND	667.74
22	ND	135.66 ± 8.37	267.59 ± 9.32	243.08 ± 13.07	102.09 ± 2.27	170.12 ± 5.16	ND	ND	918.53
23	ND	ND	36.71 ± 2.42	18.30 ± 1.53	20.62 ± 1.22	ND	23.47 ± 1.34	ND	99.10
24	ND	17.56 ± 0.40	83.14 ± 10.20	ND	ND	ND	ND	ND	100.70
25	ND	ND	48.93 ± 4.50	ND	ND	ND	ND	ND	48.93
26	ND	ND	54.75 ± 1.79	10.28 ± 0.99	ND	20.04 ± 0.83	ND	ND	80.82
27	ND	ND	48.77 ± 1.10	ND	ND	ND	ND	ND	48.77
28	ND	ND	48.97 ± 0.79	ND	ND	35.91 ± 2.76	ND	ND	84.87
29	ND	ND	54.30 ± 3.77	ND	ND	ND	ND	ND	54.30
30	ND	ND	39.42 ± 1.10	5.14 ± 0.49	ND	17.90 ± 1.33	16.15 ± 0.27	ND	83.74
31	ND	ND	124.32 ± 6.49	19.33 ± 0.36	16.85 ± 0.67	15.58 ± 0.84	ND	ND	176.10
32	ND	ND	25.16 ± 1.11	10.01 ± 0.75	174.36 ± 3.43	34.44 ± 0.92	ND	ND	243.96
33	ND	ND	234.12 ± 2.37	23.11 ± 1.11	120.78 ± 1.06	26.00 ± 2.11	ND	ND	304.01
34	ND	ND	123.79 ± 1.26	34.33 ± 2.67	12.11 ± 1.41	12.79 ± 1.66	ND	ND	183.02
35	ND	ND	205.57 ± 1.11	32.12 ± 1.26	17.43 ± 2.77	14.55 ± 1.26	ND	ND	269.67
36	ND	ND	11.38 ± 0.18	ND	ND	ND	ND	ND	11.38
37	ND	ND	19.93 ± 0.55	5.47 ± 0.07	ND	ND	ND	ND	25.41
38	ND	ND	13.16 ± 0.23	11.00 ± 0.15	ND	ND	ND	ND	24.16
39	ND	ND	15.95 ± 2.37	ND	7.82 ± 0.30	39.07 ± 2.63	ND	ND	62.83
40	ND	ND	13.57 ± 0.84	14.36 ± 0.31	ND	ND	ND	ND	27.93
41	463.45 ± 3.60	238.88 ± 1.62	907.79 ± 9.35	235.12 ± 3.39	41.39 ± 0.90	330.12 ± 7.05	ND	ND	2216.76
42	147.20 ± 4.86	125.34 ± 2.97	922.98 ± 24.19	308.44 ± 3.03	45.95 ± 4.03	370.38 ± 13.70	ND	ND	1920.29
43	124.82 ± 1.58	136.98 ± 4.53	542.16 ± 8.63	47.33 ± 1.06	14.28 ± 0.75	357.50 ± 29.90	ND	ND	1223.08
44	163.57 ± 0.60	8.73 ± 0.17	911.26 ± 24.12	102.14 ± 5.09	145.70 ± 0.94	167.91 ± 13.59	ND	ND	1499.29
45	394.61 ± 0.77	245.84 ± 2.88	1024.10 ± 5.33	242.31 ± 1.06	68.82 ± 1.26	431.27 ± 33.30	ND	ND	2406.95
46	70.41 ± 0.89	13.89 ± 0.39	361.81 ± 11.37	12.92 ± 0.83	6.07 ± 0.20	265.37 ± 22.99	ND	ND	730.48
47	118.71 ± 4.10	341.03 ± 11.26	580.05 ± 11.12	72.56 ± 0.84	23.18 ± 0.15	213.82 ± 6.55	ND	ND	1349.36
48	118.82 ± 6.20	100.77 ± 3.05	475.68 ± 37.69	137.17 ± 10.35	34.28 ± 3.27	336.07 ± 14.17	ND	ND	1202.80
49	126.11 ± 3.59	52.38 ± 0.48	919.57 ± 23.54	ND	304.16 ± 13.39	388.15 ± 25.29	ND	ND	1790.37
50	237.63 ± 3.77	66.69 ± 1.13	1147.32 ± 17.45	88.72 ± 1.40	161.68 ± 4.51	270.32 ± 10.10	ND	ND	1972.36
51	256.08 ± 4.58	27.83 ± 0.12	920.93 ± 25.61	32.28 ± 1.76	312.24 ± 6.93	410.72 ± 8.24	ND	ND	1960.07
52	185.28 ± 2.47	9.52 ± 0.80	585.06 ± 8.50	76.67 ± 5.07	164.59 ± 4.03	549.34 ± 19.63	ND	ND	1570.46
53	240.81 ± 8.99	36.14 ± 1.45	764.70 ± 26.95	26.46 ± 1.49	160.45 ± 6.68	269.23 ± 20.11	ND	ND	1497.79
54	91.51 ± 5.49	25.27 ± 1.29	411.40 ± 21.53	36.64 ± 2.58	9.42 ± 0.78	239.75 ± 13.43	ND	ND	813.99
55	246.74 ± 5.01	52.62 ± 4.22	1075.92 ± 9.74	82.61 ± 3.26	312.11 ± 16.51	388.41 ± 22.39	ND	ND	2158.41
56	228.33 ± 10.64	39.24 ± 1.63	172.90 ± 6.21	3.37 ± 0.29	20.30 ± 1.38	222.01 ± 12.50	ND	ND	686.14
57	54.47 ± 2.71	53.35 ± 2.81	316.86 ± 2.44	260.86 ± 21.87	164.30 ± 16.03	223.56 ± 11.59	ND	ND	1073.39
58	121.80 ± 0.68	51.90 ± 3.68	471.18 ± 9.34	51.40 ± 2.33	415.38 ± 6.15	380.62 ± 15.20	ND	ND	1492.27
59	51.95 ± 0.66	38.66 ± 0.39	224.34 ± 2.60	152.61 ± 0.20	6.08 ± 0.46	152.27 ± 6.79	ND	ND	625.92

dx.doi.org/10.1021/jf501772s | J. Agric. Food Chem. 2014, 62, 7947−7954

Table 2. continued

	biogenic amines ($mg \cdot kg^{-1}$)								
	Trp	Phe	Put	Cad	His	Tyr	Spd	Spm	total content
60	322.56 ± 24.98	73.28 ± 5.30	907.02 ± 61.64	35.23 ± 2.97	265.48 ± 19.98	257.59 ± 14.96	ND	ND	1861.16
61	70.13 ± 3.53	73.00 ± 1.31	409.78 ± 2.81	210.94 ± 3.38	58.85 ± 3.77	361.47 ± 20.83	ND	ND	1184.17
62	208.83 ± 16.18	6.84 ± 0.41	578.23 ± 42.55	88.08 ± 7.72	54.39 ± 4.08	33.11 ± 2.24	ND	ND	969.48
63	188.23 ± 7.59	47.62 ± 2.12	671.36 ± 13.99	71.38 ± 3.37	32.58 ± 2.15	330.57 ± 6.60	ND	ND	1341.74

[a]Trp: tryptamine, Phe: β-phenethylamine, Put: Putrescine, Cad: cadaverine, His: histamine, Tyr: tyramine, Spd: spermidine, and Spm: spermine. 1−30: fermented soya bean, 31−63: fermented bean curd, 1−9: Bacterial-type douchi, 10−19: Aspergillus-type douchi, 20−30: Mucor-type douchi, 31−35: Gray sufu, 36−40: Red sufu, 41−63: White sufu, and ND expressed not detected.

As shown in Figure 1, all BAs were detected in 30 min. The effect of the useful peak's separation was good. The retention time of tryptamine, β-phenethylamine, putrescine, cadaverine, histamine, tyramine, spermine, and spermine were 8.374, 9.994, 10.606, 11.536, 12.257, 20.595, 12.257, and 20.595 min, respectively. In addition, at the beginning of the chromatogram, a few peaks were omitted, whose value were so high that the useful ones were not present.

Type of BA in the Samples. Through the HPLC method, all samples were tested, the results showed in Table 2. The types of BAs can decide whether the food is safety, so this part had introduced the types of BAs, to evaluate the safety of the samples in brief.

Tryptamine, β-phenethylamine, putrescine, cadaverine, histamine, tyramine, and spermidine were detected in fermented soya bean samples, the content range was 69.56, 16.77−736.64, 14.08−276.03, 5.14−672.33, 14.76−478.77, 17.90−252.08, and 16.15−74.92 mg/kg, respectively. The types of BA was no obvious regularity, and had nothing to do with the fermentation type. The 1st, 2nd, 4th∼7th, 9th, 25th, 27th, and 29th samples only detected putrescine; the 3rd sample only detected spermidine; the 8th sample detected putrescine and spermidine; the 10th, 12th, and 14th samples detected β-phenethylamine, putrescine, histamine, and tyramine; the 11th, 13th, and 17th samples detected putrescine, histamine, and tyramine; the 15th, 16th, 18th, and 19th samples detected putrescine and histamine; the 20th sample detected six kinds of BAs except spermidine and spermine; the 21st and 22nd samples detected five kinds of BAs excepte tryptamine, spermidine, and spermine; the 23th sample detected putrescine, cadaverine, histamine, and spermidine; the 24th sample detected β-phenethylamine and putrescine; the 26th sample detected putrescine, cadaverine and tyramine; the 28th sample detected putrescine and tyramine; the 30th sample detected putrescine, cadaverine, tyramine, and spermidine. In conclusion, the BAs' types were different in fermented soya beans, and the BAs' types were less than three there were in 22 samples. Among these, only putrescine existed in all samples, histamine, and tyramine were detected in 14 and 12 samples, respectively, closely following putrescine. Therefore, putrescine, histamine, and tyramine might be regard as safety indexes of fermented soya bean samples contaminated by BAs.

Alternatively, tryptamine, β-phenethylamine, putrescine, cadaverine, histamine, and tyramine were detected in fermented bean curd, the content range was 51.95−463.45, 6.84−341.03, 11.38−1147.32, 3.37−308.44, 6.07−415.38, and 12.76−549.34 mg/kg, respectively. Compared with fermented soya beans, the type of BA was more regular in fermented bean curd, and had something with the differences of the dressing mixture. First, putrescine, cadaverine, histamine, and tyramine were detected in gray sufu (the 31st∼35th samples). Second, there were a little difference in red sufu (the 36th∼40th samples), the 36th sample only detected putrescine; the 37th, 38th, and 40th samples detected putrescine and cadaverine; the 39th sample detected putrescine, histamine, and tyramine. At last, there were tryptamine, β-phenethylamine, putrescine, cadaverine, histamine, and tyramine detected in all white sufu samples except the 49th sample, and the 49th sample detected tryptamine, β-phenethylamine, putrescine, histamine, and tyramine. As above, there were a few differences of BAs' types among gray, red, and white sufu samples. It could be speculated that white sufu was most dangerous among the sufu samples.

Safety of the BAs in the Samples. *Safety of the Total BAs in Samples.* As shown in Table 2, the total BAs content was between 15.67−89.00, 43.03−929.97, and 48.77−2057.56 mg/kg, the median was 27.56, 203.27, and 84.87 mg/kg in bacterial-type, aspergillus-type, and mucor-type douchi samples, respectively. The total BAs content was more than 900 mg/kg only in the 14th, 20th, and 22nd samples. As mentioned before, the total BAs content in food should not be more than 900 mg/kg,[7,8] and when the total BAs content reached 1000 mg/kg in food, they would cause great harm to human health.[9] So the sample would be considered unsafe when the total BAs content were more than 900 mg/kg. In conclusion, it was observed that the total BAs content was within the relative safety range in most fermented soya bean samples except the 14th, 20th, and 22nd sample.

However, the total BAs content range was 625.92−2406.95, 11.38−62.83, and 176.10−404.01 mg/kg, the median was 1492.27, 25.41, and 243.96 mg/kg in white, red, and gray sufu samples, respectively. The total BAs content was less than 900 mg/kg in gray and red sufu, while which was more than 900 mg/kg in 19 white sufu samples (all samples except the 46th, 54th, 56th, and 59th sample), accounting for 82.61% of the total number of white sufu samples. According to the total BAs content in samples and the related knowledge of toxicology. It is worth noting that the total BAs content was in a relatively safe range in gray and red sufu samples, but was in a dangerous concentration range in part white sufu samples, which could cause a safety risk.[8−10]

Safety of Histamine in the Samples. Histamine was detected in 10 aspergillus-type and 4 mucor-type douchi samples, respectively. The content was 14.76−478.77 and 20.62−102.09 mg/kg, the median was 62.32 and 68.33 mg/kg, the detection rate was 100% and 36.36%, respectively. Histamine's content was more than 50 mg/kg in 5 aspergillus-type (the 10th−14th sample) and 1 mucor-type (the 22th sample) douchi sample, accounting for 50% and 25%, respectively. As mentioned before, the maximum allowable

concentration of histamine were 50−100 mg/kg in food.[11] So the sample would be considered unsafe when the total content of BAs were more than 50 mg/kg. Therefore, the high histamine's concentration in part aspergillus-type and mucor-type douchi samples could cause a potential safety hazard.[15−17]

Similarly, histamine was detected in 23 white, 5 gray, and 1 red sufu samples, the content range was 6.07−415.38, 12.11−174.36, and 12.11 mg/kg, the median was 58.85, 17.43, and 7.82 mg/kg, respectively. Among the samples, histamine's content was more than 50 mg/kg in two gray (the 32nd and 33rd samples) and 13 white (the 44th, 45th, 49th∼53rd, 55th, 57th, 58th, and 60th∼62nd sample) sufu samples, accounting for 40% and 56.52%, respectively. According to the related knowledge of toxicology, the content of histamine was high in some white and gray sufu samples, resulting in health problems.[15−17]

Safety of Tryptamine, β-Phenethylamine, and Tyramine in Samples. Tyramine was detected in 6 aspergillus-type and 6 mucor-type douchi samples, the content range was 57.85−252.08 and 17.90−250.21 mg/kg, the median was 169.76 and 61.34 mg/kg, the detection rate was 60% and 54.54%, respectively. Tyramine's content was more than 100 mg/kg in 5 aspergillus-type (the 10th∼14th samples) and 2 mucor-type (the 20th and 22nd samples) douchi samples, accounting for 83.33% and 33.33%, respectively. β-Phenethylamine was detected in 3 aspergillus-type and 4 mucor-type douchi samples, the content was 16.77−79.00 and 17.56−736.64 mg/kg, the median was 28.37 and 80.40 mg/kg, the detection rate was 30% and 36.36%, respectively. As mentioned before, Tyramine could cause migraines or induce severe poisoning symptoms when ingested more than 100 mg orally or 1080 mg/kg respectively, the maximum allowable range was 100−800 mg/kg in food.[18] So the sample would be considered unsafe when the content of tyramine was more than 100 mg/kg. Obviously, the content of tyramine and β-phenethylamine were a little high in part aspergillus-type and mucor-type douchi samples, which would pose a safety risk.

Besides, tryptamine and β-phenethylamine were detected in 23 white sufu samples, the content range were 51.95−463.45 and 6.84−341.03 mg/kg, the median were 163.57 and 52.38 mg/kg, and the detection rate were both 76.67%, respectively. Tyramine was detected in one red, all white, and all gray sufu samples, the contents were ispermidinen the ranges 33.11−549.34, 39.07, and 12.79−34.44 mg/kg, the median was 330.12, 39.07, and 15.58 mg/kg, respectively. Tyramine's content was more than 100 mg/kg in 22 white sufu samples (except the 62nd sample). As a result, the detection of tyramine, β-phenethylamine, and tyramine made them some certain safety hidden danger in white sufu samples.[18−20]

Safety of Putrescine, Cadabverine, and Spermidine in Samples. Putrescine was detected in all samples except the third sample, the content range was 26.49−139.85, 39.42−276.03, and 39.42−42.22 mg/kg, the median was 37.02, 54.30, and 27.24 mg/kg in aspergillus-type, mucor-type, and bacterial-type douchi samples, respectively; cadaverine was detected in 6 mucor-type douchi samples, the content range was 6.03−672.33 mg/kg, the median was 120.62 mg/kg; spermine was detected in 2 mucor-type and 2 bacterial-type douchi samples, the content was 16.15−23.47 and 19.51−74.92 mg/kg, the median was 19.81 and 47.21 mg/kg, respectively. As mentioned above, the toxicity of cadaverine, putrescine, spermidine, and spermine is not obvious relatively, but they can interact with nitrite to form carcinogenic nitrosamine, and can inhibit other toxic BAs' metabolism to make their toxicity higher.[22] Furthermore, putrescine's detection rate was the highest among all the BAs, and the concentration was also highest in most of the samples, in consideration of the addition of the synergy between BAs, it was still considered that the existence of putrescine was a potential safety hazard in fermented soya beans. Similarly, the cadaverine and spermidine were considered in a safe range concentration in fermented soya bean samples.

However, putrescine was detected in all fermented bean curd samples, the content range was 172.90−1147.32, 11.38−19.93 and 25.16−234.12 mg/kg, the median was 585.06, 13.57, and 124.32 mg/kg in white, red, and gray sufu samples, respectively. The detection rate was the highest among all the BAs, and the concentration was also the highest in most samples. Meanwhile, putrescine's concentration was more than 900 mg/kg in 9 white sufu samples (the 41st, 42nd, 44th, 45th, 49th∼51st, 55th, and 60th sample), which made the total BAs content out of the safe limit. Similarly, cadaverine was detected in 22 white, 3 red, and 5 gray sufu samples, the content was 3.37−308.44, 5.47−14.36, and 10.01−34.33 mg/kg, the median was 79.64, 11.00, and 23.11 mg/kg, respectively, the detection rate was just lower than putrescine. As a result, the existence of putrescine and cadaverine was a certain safety hidden danger in some white and gray sufu samples.

Safety of the Samples. In summary, because of BAs, several fermented soya bean and fermented bean curd samples had some potential safety risk. On the one hand, the content of histamine and tyramine had exceeded their limit level for the 10th∼14th aspergillus-type douchi samples, and the total BAs content of the 14th sample was more than 900 mg/kg, therefore it could be considered that the 10th∼14th samples had some obvious safety risk; the 20th and 22nd samples were unsafe because the content of total BAs, histamine, and tyramine were more than their limit level; histamine's content was 83.87 mg/kg in the 21th sample, which could pose safety risk. In conclusion, there were 8 samples (the 10th−14th, and 20th−22nd samples) unsafe for fermented soya beans.

On the other hand, first, the red sufu samples (the 36th∼40th samples) were relatively safe. Second, among the gray sufu samples (the 31st∼35th samples), the 32nd and 33rd samples were unsafe for their high histamine concentration. Finally, as mentioned above, all the white sufu samples (the 41st∼63rd samples) had some unsafe factors. Namely, the total BAs content had exceeded 900 mg/kg in 19 samples except the 46th, 54th, 56th, and 59th samples; the tyramine's content was more than 100 mg/kg in all except the 62th samples; the histamine's content was more than 50 mg/kg in 13 samples (the 44th, 45th, 49th∼53rd, 55th, 57th, 58th, and 60th∼62nd samples). So all of the white sufu samples were unsafe. As a whole, there were 21 samples (the 32nd, 33rd, and 41st∼63rd samples) unsafe for fermented bean curds.

DISCUSSION

Safety of Fermented Soya Products. Looking from the results, there were 8 samples unsafe for fermented soya beans. The 32nd and 33rd gray sufu sample were unsafe for their high histamine's concentration, and all the white sufu samples were unsafe. Therefore, the content of BAs should be limited in all the fermented soy products.

However, the experimental results were just a preliminary evaluation; there still needs to be a more in-depth study to

realize the safety limit of each BA in the fermented soya products, like the histamines in fish products.

Safety of Other Foods. The BAs have been detected in many foods, such as cheese, fish, fish products, dairy products, pork, and sausages, and so forth. From the related research, most of the BAs content were in a relatively safe range in pork and sausages;[29−36] the histamines content was more than 100 mg/kg in some sausages,[29,31] which could cause a safety hazard; putrescine and cadaverine could be not only used as the spoilage indicators of chilled pork, but also might reflect the spoilage degree in pork;[34] some BAs content had reached the level of threat to human health in some fish products,[37−41] and the highest content of tryptamine, β-phenethylamine, putrescine, cadaverine, histamine, tyramine, spermidine, and spermine was 517.2,[40] 219.0,[40] 420,[37] 969.4,[40] 2500,[37] 456.2,[40] 51.98,[41] and 53.30[41] mg/kg respectively, which could pose a safety risk; almost all the BAs content had reached the level of threat to human health in cheese,[42−46] the highest contents of tryptamine, β-phenethylamine, putrescine, cadaverine, histamine, tyramine, spermidine, and spermine were 312.2,[45] 312.2,[46] 986.0,[43] 2127.6,[43] 1157.9,[45] 1771.3,[43] 340.0,[46] and 449.6[46] mg/kg respectively, which were obviously dangerous factors.

As above, the content of BAs has exceeded the safety limit in these foods, and there were very few scholars having evaluated the safety of them. So it must be emphasized that the foods which contain a large number of BAs should be detected to evaluate whether they are safe, and if not, the content of BAs should be limited.

Toxicity of BAs. The toxicity of BAs was not discussed in the current study, but there still needs to be a more in-depth study to realize the toxicology of BAs deeply and comprehensively, such as the toxic effect of each BA, the safety range of each BA, and the synergy among them, and so forth.

■ ASSOCIATED CONTENT

Ⓢ Supporting Information

Elution gradient of mobile phase for separation of derivatives of biogenic amines (Table S1); regression equations, correlation coefficients, linearity range, detection limits, and recovery of biogenic amines derivatives (Table S2). This material is available free of charge via the Internet at http://pubs.acs.org.

■ AUTHOR INFORMATION

Corresponding Author

*E-mail: xiaowend@sina.com.

Notes

The authors declare no competing financial interest.

■ REFERENCES

(1) Askar, A.; Treptow, H. Biogenous amines in foodstuffs. Occurrence, importance and determination. *Verlag Eugen Elmer* **1986**.

(2) Brink, B.; Damirik, C.; Joosten, H. M. L. J. Occurrence and formation of biologically active amines in foods. *Int. J. Food Microbiol.* **1990**, *11*, 73−84.

(3) Halász, A.; Baráth, Á.; Simon-Sarkadi, L.; Holzapfel, W. Biogenic amines and their production by microorganisms in food. *Trends Food Sci. Technol.* **1994**, *5*, 42−49.

(4) Saaid, M.; Saad, B.; Hashim, N. H. Determination of biogenic amines in selected Malaysian food. *Food Chem.* **2009**, *113*, 1356−1362.

(5) Parente, E.; Matuscelli, M.; Gadrini, F. Evdufion of microbial populations and bingenic amines production in dry sausages produced in southern Italy. *J. Appl. Microbiol.* **2001**, *90*, 882−89l.

(6) Onal, A. A review: Current analytical methods for the determination of biogenic amines in foods. *Food Chem.* **2007**, *103* (4), 1475−1486.

(7) ten Brink, B.; Damink, C.; Joosten, H. M. L. J. Occurrence and formation of biologically active amines in foods. *Int. J. Food Microbiol.* **1990**, *11*, 73−84.

(8) Spanjer, M. C.; van Roode, B. A. S. W. Towards a regulatory limit for biogenic amines in fish, cheese and sauerkraut. *DeWare(n)-Chemicus* **1991**, *21*, 139−167.

(9) Santos, M. H. S. Biogenic amines in foods. *Int. J. Food Microbiol.* **1996**, *29*, 213−231.

(10) Shukla, S.; Park, H. K.; Kim, J. K.; Kim, M. Determination of biogenic amines in Korean traditional fermented soybean paste. *Food Chem. Toxicol.* **2010**, *48*, 1191−1199.

(11) Maijala, R.; Eerola, S. Contaminant lactic acid bacteria of dry sausages produce histamine and tyramine. *Meat Sci.* **1993**, *35*, 387−395.

(12) Tripathi, T.; Khan, A. A.; Shahid, M.; Khanc, H. M.; Siddiquia, M.; Khand, R. A.; Mahdie, A. A.; Malikc, A. Biochemical and histopathological evaluation of histamine receptors (H1R, H2R, H3R, and H4R)-agonist in rabbits. *Exp. Toxicol. Pathol.* **2013**, *65*, 271−275.

(13) Wu, T. S.; Gan, X. L.; Zhou, S. L.; Ge, M.; Zhang, Z.; Hei, Z. Q. Histamine at low concentrations aggravates rat liver BRL-3A cell injury induced by hypoxia/reoxygenation through histamine H2 receptor in vitro. *Toxicol. In Vitro* **2013**, *27*, 3778−3786.

(14) Tripathi, T.; Shahid, M.; Khan, H. M.; Khan, R. A.; Siddiqui, M.; Mahdi, A. A. The Influence of histamine H1-receptor on liver functions in immunized rabbits. *Saudi J. Biol. Sci.* **2011**, *18*, 411−418.

(15) Keles, N.; Arican, R. Y.; Coskun, M.; Elpek, G. O. Histamine induces the neuronal hypertrophy and increases the mast cell density in gastrointestinal tract. *Exp. Toxicol. Pathol.* **2012**, *64*, 713−716.

(16) Tang, T.; Qian, K.; Shi, T. Y.; Wang, F.; Li, J. Q.; Cao, Y. S.; Hu, Q. B. Monitoring the contents of biogenic amines in sufu by HPLC with SPE and pre-column derivatization. *Food Control* **2011**, *22*, 1203−1208.

(17) Shalaby, A. R. Significance of biogenic amines to food safety and human health. *Food Research International.* **1996**, *29*, 675−690.

(18) Nout, M. J. R. Fermented foods and food safety. *Food Res. Int.* **1994**, *27*, 291−298.

(19) Mazumder, M. K.; Rajib, P.; Anupom, B. β-Phenethylamine-A Phenylalanine Derivative in Brain-Contributes to Oxidative Stress by Inhibiting Mitochondrial Complexes and DT-Diaphorase: An In Silico Study. *CNS Neurosci. Ther.* **2013**, *19*, 596−602.

(20) Ma, G. Y.; Bavadekar, S. A.; Schaneberg, B. T.; Khan, I. A.; Feller, D. R. Effects of Synephrine and β-Phenethylamine on Human α-Adrenoceptor Subtypes. *Planta Medica* **2010**, *76*, 981−986.

(21) Shalaby, A. R. Significance of biogenic amines to food safety and human health. *Food Res. Int.* **1996**, *29*, 675−690.

(22) Rauscher-Gabernig, E.; Gabernig, R.; Brueller, W.; Grossgut, R.; Bauer, F.; Paulsen, P. Dietary exposure assessment of putrescine and cadaverine and derivation of tolerable levels in selected foods consumed in Austria. *Eur. Food Res. Technol.* **2012**, *235*, 209−220.

(23) Tasic, T.; Ikonic, P.; Mandic, A.; Jokanovic, M.; Tomovic, V.; Savatic, S.; Petrovic, L. Biogenic amines contents in traditional dry fermented sausage petrovska klobasa as possible indicator of good manufacturing practice. *Food Control* **2012**, *23*, 107−112.

(24) Zhai, H. L.; Yang, X. Q.; Lai, H.; Li, L. H.; Xia, G. B.; Cen, J. W.; Hui, H. H.; Hao, S. X. Biogenic amines in commercial fish and fish products in southern China. *Food Control* **2012**, *25*, 303−308.

(25) Til, H. P.; Falke, H. E.; Prinsen, M. K.; Willems, M. I. Acute and subacute toxicity of tyramine, spermidine, spermine, putrescine and cadaverine in rats. *Food Chem. Toxicol.* **1997**, *35*, 337−348.

(26) Halásza, A.; Barátha, Á.; Simon-Sarkadib, L.; Holzapfel, W. Biogenic amines and their production by microorganisms in food. *Trends Food Sci. Technol.* **1994**, *5*, 42−49.

(27) Wang, R. Z. *Fremented Bean Curd in China (In Chinese)*; Chinese Light Industry Press: Beijing, 2009, pp 1−10.

(28) Önal, A.; Tekkeli, S. E. K.; Önal, C. A review of the liquid chromatographic methods for the determination of biogenic amines in food. *Food Chem.* **2013**, *138*, 509−515.
(29) Rabie, M. A.; Peres, C.; Malcata, F. X. Evolution of amino acids and biogenic amines throughout storage in sausages made of horse, beef and turkey meats. *Meat Sci.* **2014**, *96*, 82−87.
(30) Leggio, A.; Belsito, E. L.; Marco, R. D.; Di Gioia, M. L.; Liguori, A.; Siciliano, C.; Spinella, M. Dry Fermented Sausages of Southern Italy: A Comparison of Free Amino Acids and Biogenic Amines between Industrial and Homemade Products. *J. Food Sci.* **2012**, *77*, 170−175.
(31) Mey, E. D.; Klerck, K. D.; Maere, H. D.; Dewulf, L.; Derdelinckx, G.; Peeters, M. C.; Fraeye, I.; Heyden, Y. V.; Paelinck, H. The occurrence of *N*-nitrosamines, residual nitrite and biogenic amines in commercial dry fermented sausages and evaluation of their occasional relation. *Meat Sci.* **2014**, *96*, 821−828.
(32) Kurt, S.; Zorba, Ö. Biogenic amine formation in Turkish dry fermented sausage (sucuk) as affected by nisin and nitrite. *J. Sci. Food Agric.* **2010**, *90* (15), 2669−2674.
(33) Tasić, T.; Ikonić, P.; Mandić, A.; Jokanović, M.; Tomović, V.; Savatić, S.; Petrović, L. Biogenic amines content in traditional dry fermented sausage Petrovská klobása as possible indicator of good manufacturing practice. *Food Control* **2012**, *23*, 107−112.
(34) Li, M. Y.; Tian, L.; Zhao, G. M. Formation of biogenic amines and growth of spoilage-related microorganisms in pork stored under different packaging conditions applying PCA. *Meat Sci.* **2013**, *96*, 843−850.
(35) Rosinská, D.; Lehotay, J. Influence of temperature on production of biogenic amines in pork, beef, and poultry and their HPLC determination after postcolumn derivatizatiom. *J. Liquid Chromatogr. Relat. Technol.* **2014**, *37*, 609−619.
(36) Delgado-Pando, G.; Cofrades, S.; Ruiz-Capillas, C.; Triki, M.; Jiménez-Colmenero, F. Enriched *n*-3 PUFA/konjac gel low-fat pork liver pâté: Lipid oxidation, microbiological properties and biogenic amine formation during chilling storage. *Meat Sci.* **2012**, *92*, 62−767.
(37) Prester, L. Biogenic amines in fish, fish products and shellfish: a review. *Food Addit. Contam.* **2011**, *28*, 1547−1560.
(38) Koral, S.; Tufan, B.; Ščavničar, A.; Kočar, D.; Pompe, M.; Köse, S. Investigation of the contents of biogenic amines and some food safety parameters of various commercially salted fish products. *Food Control* **2013**, *32*, 597−606.
(39) Hu, Y.; Huang, Z. Y.; Li, J.; Yang, H. Concentrations of biogenic amines in fish, squid and octopus and their changes during storage. *Food Chem.* **2012**, *135*, 2604−2611.
(40) Köse, S.; Koral, S.; Tufan, B.; Pompe, M.; Scavniçar, A.; Koçar, D. Biogenic amine contents of commercially processed traditional fish products originating from European countries and Turkey. *Eur. Food Res. Technol.* **2012**, *235*, 669−683.
(41) Zhai, H. L.; Yang, X. Q.; Li, L. H.; Xia, G. B.; Cen, J. W.; Huang, H.; Hao, S. X. Biogenic amines in commercial fish and fish products sold in southern China. *Food Control* **2012**, *25*, 303−308.
(42) Andic, S.; Genccelep, H.; Kosea, S. Determination of Biogenic Amines in Herby Cheese. *Int. J. Food Prop.* **2010**, *13* (6), 1300−1314.
(43) Schirone, M.; Tofalo, R.; Fasoli, G.; Perpetuini, G.; Corsetti, A.; Manetta, A. C.; Ciarrocchi, A.; Suzzi, G. High content of biogenic amines in Pecorino cheeses. *Food Microbiol.* **2013**, *34*, 137−144.
(44) Schirone, M.; Tofalo, R.; Visciano, P.; Corsetti, A.; Suzzi, G. Biogenic Amines in Italian Pecorino Cheese. *Front. Microbiol.* **2012**, *3*, 171.
(45) Mayer, H. K.; Fiechter, G.; Fischer, E. A new ultra-pressure liquid chromatography method for the determination of biogenic amines in cheese. *J. Chromatogr. A* **2010**, *1217* (19), 3251−3257.
(46) Loizzo, M. R.; Menichini, F.; Picci, N.; Puoci, F.; Spizzirri, U. G.; Restuccia, D. Technological aspects and analytical determination of biogenic amines in cheese. *Trends Food Sci. Technol.* **2013**, *30*, 38−55.

aspects of the interaction have been studied, the calorimetric studies to elucidate the thermodynamics of the interaction have not yet been performed. Thus, the present work elucidates the thermodynamics of the interaction of amaranth with two homologous serum proteins using isothermal titration calorimetry (ITC) and differential scanning calorimetry (DSC) techniques.

MATERIALS AND METHODS

Materials. HSA (0.99 mass fraction purity, essentially fatty acid and globulin free), BSA (0.99 mass fraction purity, essentially fatty acid and globulin free), and amaranth (dye content of 85−95%) were procured from Sigma-Aldrich Co. LLC (St. Louis, MO). All of the experiments were performed in 10 mM citrate−phosphate buffer at pH 7.0, unless otherwise mentioned, where the serum albumins are in the normal (or N) form. The concentrations of HSA and BSA samples were spectrophotometrically determined using molar absorption coefficient values (ε) of 3.66×10^4 and 4.38×10^4 M^{-1} cm^{-1}, respectively, at 280 nm.[28] The concentration of the dye was also determined spectrophotometrically using the ε value of 2.56×10^4 M^{-1} cm^{-1} reported in the literature.[25] All of the buffer salts were of analytical grade. The aforementioned citrate−phosphate buffer was prepared in triple-distilled and deionized water. All of the solutions were filtered through filters with a pore size of 0.22 μM (Millipore India Pvt. Ltd., Bangalore, India).

ITC. Thermodynamic characterization of the amaranth−serum albumin interaction was performed on a MicroCal VP-ITC calorimeter (MicroCal LLC, Northampton, MA). The protein solutions were prepared by dialyzing against the buffer. The dye solution was prepared in the buffer. Both the dye and protein solutions were extensively degassed prior to the titrations. The titrant, amaranth solution, was loaded into the rotating injector syringe, and the serum protein solution was placed in the calorimeter cell. The programmable dye−protein titration was controlled by the Origin 7.0 software (MicroCal) of the unit. The autocontrolled rotating syringe (351 rpm) injected 10 μL aliquots of the dye solution into the protein solution (1.4235 mL) at intervals of 240 s. This time interval was sufficient enough for the heat signal to return to the baseline after each heat spike generation. The duration of each injection was fixed at 10 s, and the initial delay before the first injection was 60 s. To correct for the thermal effect because of mixing and dilution, appropriate control experiments were performed by injecting an identical volume of the same concentration dye solutions into the experimental buffer alone. The integrated heat change was analyzed by means of nonlinear regression using the Origin software of the unit. The resulting corrected injection heats were then plotted against the molar ratio (χ) of amaranth/serum protein and fitted to a model for single binding sites. The binding equilibrium constant (K), standard molar enthalpy change ($\Delta_r H^\circ$), and stoichiometry value "N" were obtained from the analysis of the titration curve. The values of the standard molar Gibbs energy change ($\Delta_r G^\circ$) and standard molar entropic contribution ($T\Delta_r S^\circ$) were then calculated using the relationships

$$\Delta_r G^\circ = -RT \ln(K) = T\Delta_r S^\circ - \Delta_r H^\circ \quad (1)$$

where R is the gas constant (8.314 472 J K^{-1} mol^{-1}) and T is the temperature in kelvin (298.15 K). The thermodynamic parameters presented are averages of triplicate measurements. Periodic calibration of the ITC unit for volume of the calorimetric chamber, heat exchange, and injected volumes of titrant were performed. Furthermore, to ensure the accuracy of the calorimetric results, water−water dilution experiments were performed as per criteria of the manufacturer that the mean energy per injection was less than 5.46 μJ and the standard deviation was less than 0.063 μJ. Chemical calibration of the unit was performed with propan-1-ol of three different concentrations, 2, 5, and 10%, as proposed by Adão et al.[29]

DSC. The change in excess heat capacity ($\Delta_r C_p^\circ$) as a function of the temperature "T" was measured in a VP-DSC microcalorimeter (MicroCal LLC). The temperature difference between the reference and sample cell was measured and converted to power. This data channel is referred to as the differential power (DP) between the reference and sample cell. Calibration of this signal was performed electrically by administering a known quantity of power through a resistive heater element located in the sample cell and then measuring the actual deflection of the DP data signal. The samples were incubated at 303.15 K for 10 min and scanned from 306.15 to 363.15 K at approximately 30 psi pressure at a scan rate of 50 K h^{-1}. Prior to sample scans, the DSC unit was thermally stabilized by repeated buffer scans under an identical scan rate and in the same temperature range. Typically around 10−12 scans were needed to attain the baseline stability. A total of 40 μM of the serum protein solution was scanned in the aforementioned temperature range to obtain the DSC thermogram of the unbound protein. Thereafter, the serum proteins were incubated with the azo dye solution for 10 min to ensure complete complex formation and then scanned in the same temperature range to obtain the thermogram of the bound form. The thermograms were analyzed with the Origin software built-in with the unit. The non-2-state (cursor initiation) model of curve fitting was employed to fit the raw DSC thermograms. Each experiment was repeated 3 times with separate fillings. The C_p° of the protein solution was measured with respect to the C_p° of the buffer. The C_p° at a constant pressure is a temperature derivative of the enthalpy

$$C_p^\circ = \left(\frac{\partial H}{\partial T}\right)_P \quad (2)$$

and hence, the calorimetric enthalpy change (ΔH_{cal}) can be calculated by integration of C_p°. The transition temperature (T_m) is the temperature at which the excess heat capacity reaches its maximum value. Calibration of the DSC unit was performed with built-in calibration heaters, whereas the temperature calibration was performed using the MicroCal standards.

RESULTS AND DISCUSSION

Elucidation of the Thermodynamics of the Complexation from ITC Studies. ITC is the most efficient tool to thermodynamically characterize the ligand−protein binding phenomenon.[30,31] The thermodynamics of the binding reaction are characterized by the equilibrium constant, the stoichiometry of the reaction, the standard molar Gibbs energy change, the standard molar enthalpy change, the standard molar entropy change, and the standard molar heat capacity change ($\Delta_r C_p^\circ$). ITC directly measures the equilibrium constant for the binding reaction by measuring the heat evolved on complexation of a ligand with protein. Thus, the distinct advantage of this protocol is that, from a single experiment, we can obtain the values of the equilibrium constant, the stoichiometry of the reaction (N), and the standard molar enthalpy change of binding. The standard molar Gibbs energy change and the standard molar entropy change of binding may be subsequently calculated using the standard relationships described above. The temperature dependence of the values of $\Delta_r H^\circ$, obtained by performing the titration at varying temperatures, permits the calculation of $\Delta_r C_p^\circ$.

Figure 2 presents the ITC thermograms for the binding reaction of amaranth to BSA and HSA at 298.15 K. It can be seen that the ITC thermograms were characterized by negative peaks in the plot of power versus time, suggesting the binding reaction to be exothermic. Each heat spike in the thermogram corresponds to an injection of the dye into the respective serum protein solution. It was corrected for heat effects resulting from dilution and mixing by subtracting the corresponding control heats derived from the injection of an identical amount of the amaranth into the buffer alone. The resulting corrected heats for amaranth−protein complexation were plotted as a function

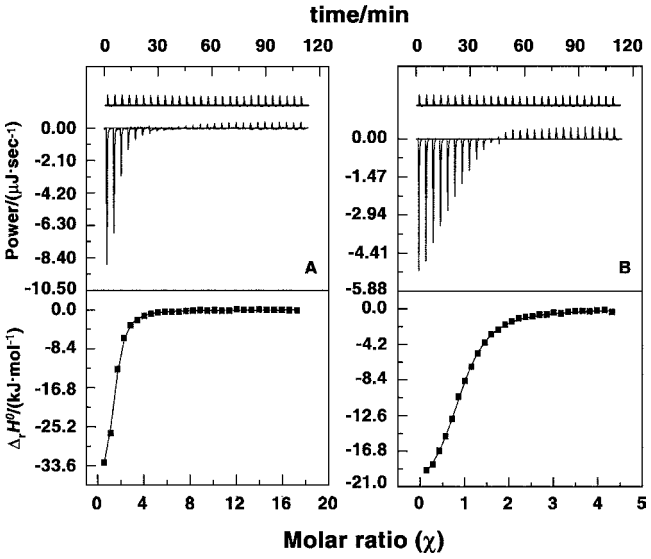

Figure 2. ITC thermograms for the titration of amaranth with (A) BSA and (B) HSA at 298.15 K. The top panels represent the raw data for the sequential injection of the amaranth solution into the serum proteins along with the corresponding dilution profiles (curves on the top offset for clarity). The bottom panels show the integrated heat data after correction of heat of dilution. The data points (■) reflect the experimental injection heats, while the solid lines represent the calculated fit of the data.

of the molar ratio of amaranth/protein. The data points in the bottom panels of Figure 2 represent the experimental injection heats, whereas the solid lines are the calculated best fits of the experimental data. The data points were fitted with a Levenberg–Marquardt nonlinear least-squares curve fitting algorithm to calculate the values of K, N, and $\Delta_r H°$. At T = 298.15 K, the equilibrium constant for the binding reaction of amaranth to BSA and HSA was calculated to be $(5.79 \pm 0.07) \times 10^5$ and $(1.76 \pm 0.05) \times 10^5$ M^{-1}, respectively. This value is in good agreement with that reported in an earlier structural study.[9] The magnitude of the equilibrium constant suggested that amaranth has a stronger binding affinity for BSA in comparison to HSA. The N values for the binding reaction were calculated to be 1.28 ± 0.07 and 0.91 ± 0.03, respectively, for BSA and HSA. Thus, a 1:1 complexation scenario may be envisaged for the association of amaranth to both the serum proteins. The analysis of the ITC thermograms yielded the value of $\Delta_r H°$ to be -40.00 ± 0.04 and -22.59 ± 0.03 kJ mol^{-1}, respectively, for BSA and HSA at T = 298.15 K. Thus, the magnitude of $\Delta_r H°$ was higher for BSA in comparison to HSA. The strengthening of the H bonds in the low dielectric macromolecular interior of the serum albumins in conjunction with van der Waals interactions introduced as a consequence of the hydrophobic effect account for the observed negative $\Delta_r H°$ values.[32]

Using the aforementioned standard relationship, the values of $\Delta_r G°$ for the complexation of amaranth with BSA and HSA were evaluated to be -32.89 ± 0.07 and -29.94 ± 0.05 kJ mol^{-1}, respectively. Thus, the binding of amaranth to BSA over HSA was favored by an additional Gibbs energy change of 2.95 kJ mol^{-1} (in absolute values). The entropy contributions for the binding reactions were calculated to be -7.11 ± 0.03 and 7.35 ± 0.02 kJ mol^{-1}, respectively. Thus, it can be observed that the binding reaction in the case of HSA was driven by both negative standard molar enthalpy change and positive standard molar entropy contributions. However, for BSA, the binding reaction was entirely driven by negative standard molar enthalpic contribution. The standard molar entropic contribution was unfavorable, but the magnitude of the standard molar enthalpic contribution was large enough to overcome this unfavorable entropy term and make the overall reaction feasible. It is also noteworthy that the binding reaction was enthalpy-dominated for both the serum proteins.

Influence of the Ionic Strength of the Medium upon Binding and Parsing of the Standard Molar Gibbs Energy Change. Salt-dependent ITC studies provide further insights into the molecular forces driving the binding reaction. To have knowledge about the role of the polyelectrolytic forces governing the complexation phenomena, salt dependence of the binding was studied as a function of four different Na^+ concentrations, viz., 10, 20, 30, and 50 mM, by ITC experiments. The thermodynamic parameters obtained from these salt-dependent ITC studies are collated in Table 1. Upon increasing the salt concentration, the K value progressively decreased for both the serum proteins (Table 1). The K value decreased from $(5.79 \pm 0.07) \times 10^5$ to $(5.02 \pm 0.07) \times 10^5$ M^{-1} upon increasing the salt concentration from 10 to 20 mM. Upon further increasing the salt concentration to 30 mM, the K value decreased to $(4.51 \pm 0.06) \times 10^5$ M^{-1}, and finally, at 50 mM, the K value was $(3.51 \pm 0.05) \times 10^5$ M^{-1}. Thus, the K value decreased 1.65 times upon increasing the salt concentration from 10 to 50 mM. For HSA, also the K value decreased upon increasing the ionic strength of the medium. The K value reduced from $(1.76 \pm 0.05) \times 10^5$ to $(1.29 \pm 0.04) \times 10^5$ M^{-1} upon increasing $[Na^+]$ from 10 to 20 mM. At 30 and

Table 1. Thermodynamic Parameters for the Association of Amaranth with BSA and HSA from ITC at Different Salt Concentrations[a]

protein	c(NaCl) (mM)	K ($\times 10^{-5}$, M^{-1})	N	$\Delta_r H°$ (kJ mol^{-1})	$T\Delta_r S°$ (kJ mol^{-1})	$\Delta_r G°$ (kJ mol^{-1})	$\Delta_r G°_t$ (kJ mol^{-1})	$\Delta_r G°_{pe}$ (kJ mol^{-1})
BSA	10	5.79 ± 0.07	1.28 ± 0.07	−40.00 ± 0.04	−7.11 ± 0.03	−32.89 ± 0.07	−29.43 ± 0.07	−3.46 ± 0.07
	20	5.02 ± 0.07	1.14 ± 0.06	−38.72 ± 0.04	−6.18 ± 0.03	−32.54 ± 0.07	−29.60 ± 0.07	−2.94 ± 0.07
	30	4.51 ± 0.06	0.98 ± 0.04	−36.94 ± 0.04	−4.67 ± 0.02	−32.27 ± 0.06	−29.64 ± 0.06	−2.63 ± 0.06
	50	3.51 ± 0.05	0.89 ± 0.03	−33.77 ± 0.04	−2.12 ± 0.01	−31.65 ± 0.05	−29.40 ± 0.05	−2.25 ± 0.05
HSA	10	1.76 ± 0.05	0.91 ± 0.03	−22.59 ± 0.03	7.35 ± 0.02	−29.94 ± 0.05	−25.50 ± 0.05	−4.44 ± 0.05
	20	1.29 ± 0.04	0.94 ± 0.03	−22.18 ± 0.03	6.99 ± 0.01	−29.17 ± 0.04	−25.40 ± 0.04	−3.77 ± 0.04
	30	1.12 ± 0.04	0.99 ± 0.04	−22.04 ± 0.03	6.78 ± 0.01	−28.82 ± 0.04	−25.44 ± 0.04	−3.38 ± 0.04
	50	0.94 ± 0.03	1.09 ± 0.05	−21.99 ± 0.02	6.40 ± 0.01	−28.39 ± 0.03	−25.50 ± 0.03	−2.89 ± 0.03

[a]All of the data in this table are derived from ITC experiments conducted in citrate–phosphate buffer of different $[Na^+]$ at pH 7.0 and 298.15 K. The standard uncertainties associated with K, N, $\Delta_r H°$, $T\Delta_r S°$, $\Delta_r G°$, $\Delta_r G°_t$, and $\Delta_r G°_{pe}$ are 6, 5, 4, 2, 6, 6, and 6%, respectively, for BSA. Similarly, the standard uncertainties associated with K, N, $\Delta_r H°$, $T\Delta_r S°$, $\Delta_r G°$, $\Delta_r G°_t$, and $\Delta_r G°_{pe}$ are 4, 4, 3, 1, 4, 4, and 4%, respectively, for HSA.

dx.doi.org/10.1021/jf5025278 | J. Agric. Food Chem. 2014, 62, 7955–7962

50 mM [Na^+], the K values were calculated to be (1.12 ± 0.04) × 10^5 and (0.94 ± 0.03) × 10^5 M^{-1}, respectively. Thus, for HSA, the K value decreased around 1.87 times upon increasing the ionic strength of the medium from 10 to 50 mM. However, the stoichiometry values remained largely unchanged with increasing the ionic strength of the medium. The N values suggested that 1:1 complexation occurs between amaranth and the serum proteins, irrespective of the salt concentration of the medium. However, the magnitude of Δ_rH° decreased with an increasing ionic strength of the medium for both BSA and HSA. This decrease is probably due to shielding of the macromolecule by the sodium ions, which prevented the dye molecules from coming in contact with the serum albumins. The magnitude of Δ_rG° also decreased with an increase in the ionic strength of the medium. At 10 mM [Na^+], Δ_rG° was calculated to be −32.89 ± 0.07 and −29.94 ± 0.05 kJ mol^{-1}, respectively, for BSA and HSA. However, at 50 mM, it was reduced to −31.65 ± 0.05 and −28.39 ± 0.03 kJ mol^{-1}. Thus, the value of Δ_rG° decreased by 1.24 and 1.55 kJ mol^{-1} (in absolute values) for BSA and HSA, respectively, upon increasing [Na^+] from 10 to 50 mM. There is a standard relationship that correlates the variation of the equilibrium constant with the sodium ion concentration[33,34]

$$\Delta_rN(\text{ion}) = \left(\frac{\partial \log K}{\partial \log[Na^+]}\right)_{T,P} = -z\phi \quad (3)$$

where Δ_rN(ion) represents the number of ions released upon binding of the azo dye, z is the apparent charge of the bound dye, and φ is the fraction of [Na^+] bound per anion. The plot of the variation of log K as a function of log [Na^+] yielded straight lines (Figure 3). The slopes of these plots were calculated to be

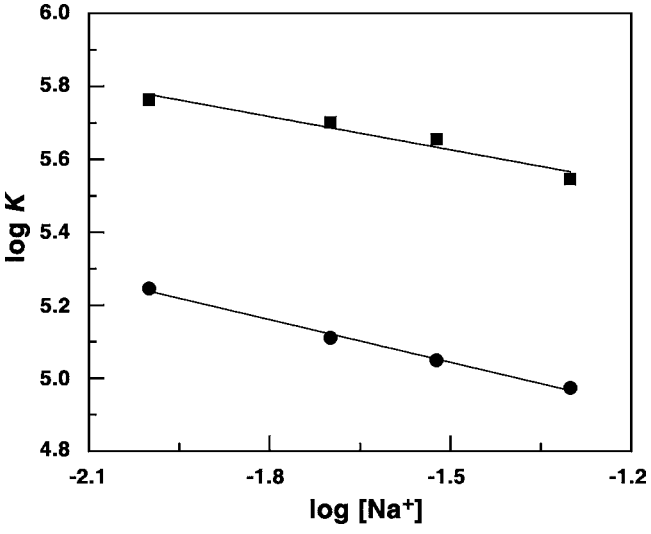

Figure 3. Plot of log K against log [Na^+] for the binding of amaranth to BSA (■) and HSA (●).

−0.303 and −0.389 for BSA and HSA, respectively. Hence, a sharper decrease in the K values was observed for HSA in comparison to BSA. The dependence of K upon [Na^+] enabled Δ_rG° to be partitioned into two components, viz., the non-polyelectrolytic component ($\Delta_rG^\circ_t$) and the polyelectrolytic component ($\Delta_rG^\circ_{pe}$) (Figure 4)

$$\Delta_rG^\circ = \Delta_rG^\circ_t + \Delta_rG^\circ_{pe} \quad (4)$$

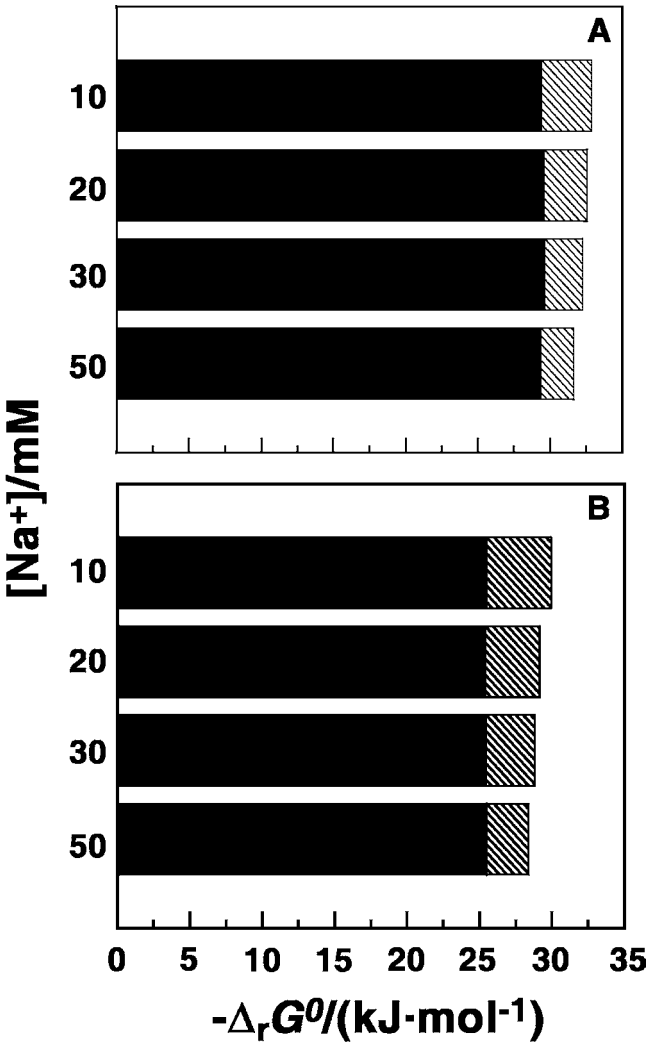

Figure 4. Partitioned polyelectrolytic ($\Delta_rG^\circ_{pe}$) (hatched) and non-polyelectrolytic ($\Delta_rG^\circ_t$) (black) contributions to the standard molar Gibbs energy (Δ_rG°) at different Na^+ concentrations for the complexation of (A) BSA and (B) HSA with amaranth.

The $\Delta_rG^\circ_{pe}$ at any given [Na^+] can be calculated quantitatively using the relationship[35,36]

$$\Delta G^\circ_{pe} = -z\phi RT \ln([Na^+]) \quad (5)$$

The $\Delta_rG^\circ_{pe}$ term accounts for the contribution arising from coupled polyelectrolytic forces, such as the release of condensed counterions upon binding of the synthetic azo dye amaranth. The $\Delta_rG^\circ_t$ term accounts for the contribution arising from other non-polyelectrolytic sources, such as van der Waals interaction, $\pi-\pi$ stacking, H bonding, and hydrophobic transfer. For BSA, $\Delta_rG^\circ_{pe}$ at 10, 20, 30, and 50 mM [Na^+] was −3.46 ± 0.07, −2.94 ± 0.07, −2.63 ± 0.06, and −2.25 ± 0.05 kJ mol^{-1}, respectively. Similarly, $\Delta_rG^\circ_{pe}$ was −4.44 ± 0.05, −3.77 ± 0.04, −3.38 ± 0.04, and −2.89 ± 0.03 kJ mol^{-1} for HSA at 10, 20, 30, and 50 mM [Na^+], respectively. $\Delta_rG^\circ_t$ contribution was calculated from the difference between Δ_rG° and $\Delta_rG^\circ_{pe}$. At 10, 20, 30, and 50 mM [Na^+], $\Delta_rG^\circ_t$ was calculated to be −29.43 ± 0.07, −29.60 ± 0.07, −29.64 ± 0.06, and −29.40 ± 0.05, kJ mol^{-1}, respectively, for amaranth−BSA complexation. Similarly, for the amaranth−HSA binding reaction, the magnitude of $\Delta_rG^\circ_t$ was calculated to be −25.50 ± 0.05, −25.40 ± 0.04, −25.44 ± 0.04, and −25.50 ± 0.03 kJ

dx.doi.org/10.1021/jf5025278 | J. Agric. Food Chem. 2014, 62, 7955−7962

Table 2. Thermodynamic Parameters for the Association of Amaranth with BSA and HSA from ITC at Different Temperatures[a]

protein	T (K)	K ($\times 10^{-5}$, M^{-1})	N	$\Delta_r H^\circ$ (kJ mol^{-1})	$T\Delta_r S^\circ$ (kJ mol^{-1})	$\Delta_r G^\circ$ (kJ mol^{-1})	$\Delta_r C_p^\circ$ (kJ K^{-1} mol^{-1})
BSA	283.15	7.23 ± 0.08	0.91 ± 0.03	−27.77 ± 0.03	3.99 ± 0.05	−31.76 ± 0.08	−0.73 ± 0.06
	293.15	6.12 ± 0.08	0.97 ± 0.04	−35.24 ± 0.04	−2.76 ± 0.04	−32.48 ± 0.08	
	298.15	5.79 ± 0.07	1.28 ± 0.07	−40.00 ± 0.04	−7.11 ± 0.03	−32.89 ± 0.07	
	303.15	2.67 ± 0.05	0.89 ± 0.03	−41.84 ± 0.04	−10.35 ± 0.01	−31.49 ± 0.05	
HSA	283.15	3.03 ± 0.05	0.96 ± 0.04	−14.73 ± 0.02	14.98 ± 0.03	−29.71 ± 0.05	−0.60 ± 0.06
	293.15	2.28 ± 0.05	0.98 ± 0.04	−19.82 ± 0.02	10.25 ± 0.03	−30.07 ± 0.05	
	298.15	1.76 ± 0.05	0.91 ± 0.03	−22.59 ± 0.03	7.35 ± 0.02	−29.94 ± 0.05	
	303.15	1.29 ± 0.04	1.24 ± 0.07	−27.19 ± 0.03	2.47 ± 0.01	−29.66 ± 0.04	

[a]The standard uncertainties associated with K, N, $\Delta_r H^\circ$, $T\Delta_r S^\circ$, $\Delta_r G^\circ$, and $\Delta_r C_p^\circ$ are 7, 4, 4, 3, 7, and 6%, respectively, for BSA. Similarly, the standard uncertainties associated with K, N, $\Delta_r H^\circ$, $T\Delta_r S^\circ$, $\Delta_r G^\circ$, and $\Delta_r C_p^\circ$ are 5, 4, 2, 2, 5, and 6%, respectively, for HSA.

mol^{-1}, respectively. Thus, although large in magnitude, the non-polyelectrolytic component remained largely invariant with changing salt concentrations. However, the polyelectrolytic component decreased in magnitude with the increase in $[Na^+]$. At the highest salt concentration studied, viz., 50 mM $[Na^+]$, the ΔG°_{pe} term accounted for only 7 and 10% of the total standard molar Gibbs energy change for BSA and HSA, respectively. Hence, for both serum proteins, the binding reaction was dominated by non-polyelectrolytic forces, which accounted for ∼90% of the total standard molar Gibbs energy change. Thus, the dissection of the standard molar Gibbs energy into polyelectrolytic and non-polyelectrolytic components unequivocally established the dominant role played by non-polyelectrolytic forces in the protein−dye complexation process.

Temperature Dependence of the Enthalpy: Determination of Heat Capacity Changes. To gain additional insights into the forces controlling the binding reaction of amaranth with serum albumins, temperature-dependent ITC studies were performed at four different temperatures, viz., 283.15, 293.15, 298.15, and 303.15 K. The pH of the solutions remained unchanged in this temperature range studied. The thermograms for amaranth−protein complexation were found to be sigmoidal at all four temperatures studied. The binding reaction was exothermic at all of the temperatures, yielding negative peaks in the plot of power versus time. The thermodynamic data derived from temperature-dependent ITC studies are collated in Table 2. The K values decreased, $\Delta_r H^\circ$ values became more negative with their magnitudes increasing, and the $T\Delta_r S^\circ$ values also decreased with the rise in the temperature. However, the magnitude of $\Delta_r G^\circ$ remained largely unaltered with the temperature. The variations in the thermodynamic parameters with increasing the temperature are graphically represented in Figure 5. From the N values, it was clearly established that 1:1 complexation occurs between amaranth and the serum proteins, irrespective of the temperature. The standard molar specific heat capacity changes were derived from a plot of $\Delta_r H^\circ$ versus T at a constant pressure, using the following relationship:

$$\Delta_r C_p^{\,0} = [\partial(\Delta_r H^\circ)/\partial T]_p \quad (6)$$

The variation of $\Delta_r H^\circ$ with T afforded straight lines, the slopes of which resulted in values of −0.73 ± 0.06 and −0.60 ± 0.06 kJ K^{-1} mol^{-1}, respectively, for the complexation of amaranth with BSA and HSA (Figure 6). Many ligand−protein and ligand−nucleic acid interactions have been characterized by such negative $\Delta_r C_p^\circ$ values.[28,32,37] Besides, negative $\Delta_r C_p^\circ$ values are often associated with alterations in hydrophobic or polar group hydration and suggest that the binding reaction is dominated by hydrophobic interactions. The $\Delta_r C_p^\circ$ value is lower for HSA compared to BSA, indicating differences in the

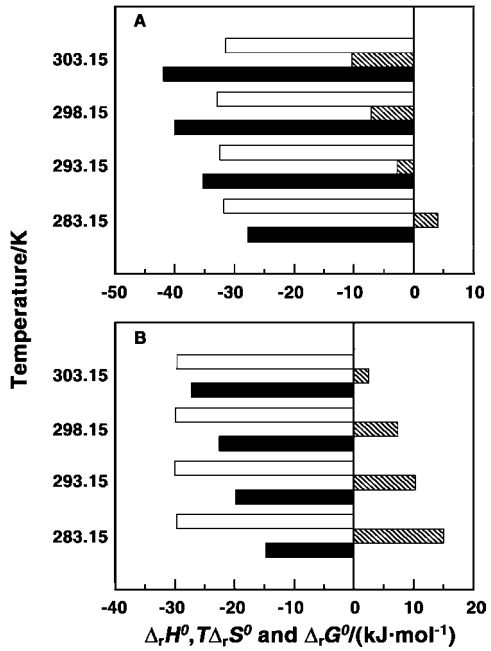

Figure 5. Variation of $\Delta_r G^\circ$ (white), $T\Delta_r S^\circ$ (hatched), and $\Delta_r H^\circ$ (black) with temperature for the complexation of amaranth with (A) BSA and (B) HSA.

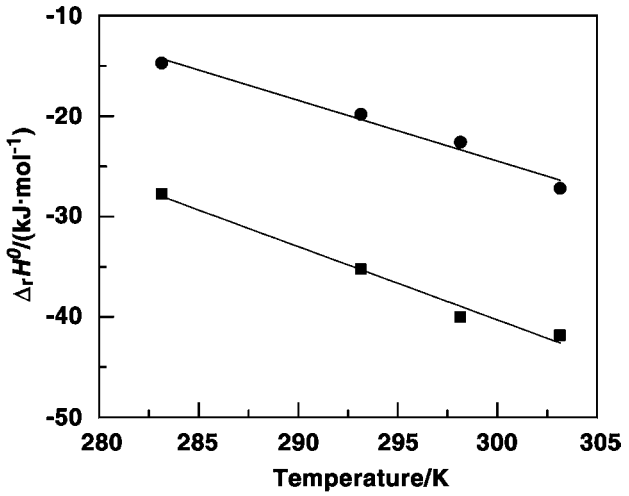

Figure 6. Plot of variation of $\Delta_r H^\circ$ as a function of the temperature for the complexation of BSA (■) and HSA (●) with amaranth.

dx.doi.org/10.1021/jf5025278 | J. Agric. Food Chem. 2014, 62, 7955−7962

release of structured water upon complexation with amaranth. It is also an indicator of the different extent of hydrophobic interactions in the two systems studied. First, it is pertinent to note that the non-zero negative values of $\Delta_r C_p^\circ$ suggest temperature dependence of $\Delta_r H^\circ$ and establish the involvement of hydrophobic forces in the complexation process. Second, the calculated values of $\Delta_r C_p^\circ$ fall well within the range that is frequently observed for biomolecular interactions.[28,38] The magnitude of the $\Delta_r C_p^\circ$ value for amaranth−BSA complexation is slightly higher than that for amaranth−HSA complexation, indicating slight conformational differences in the complexation process and also differences in the disruption of the protein-bound water molecules and counterions. Besides, the removal of water molecules from hydrophobic interfaces, owing to electrostatic interaction, may also be responsible for the negative $\Delta_r C_p^\circ$ term. The negative $\Delta_r C_p^\circ$ values calculated for amaranth−serum protein complexation appears to denote that the binding is specific and accompanied by burial of the nonpolar surface area.[39,40] The standard molar Gibbs energy contribution ($\Delta_r G^\circ_{hyd}$) from the hydrophobic transfer step of binding was calculated using the Records relationship,[41] $\Delta_r G^\circ_{hyd} = (80 \pm 10)\Delta_r C_p^\circ$. The $\Delta_r G^\circ_{hyd}$ value for amaranth−BSA complexation was calculated to be −58.40 kJ mol^{-1}, which is slightly higher than that calculated for amaranth−HSA complexation, viz., −48.00 kJ mol^{-1}.

Enthalpy−Entropy Compensation (EEC). EEC is a characteristic phenomenon of many ligand−protein interactions.[28,42] EEC has been regarded as a natural consequence of finite $\Delta_r C_p^\circ$ values by Cooper et al.[43] They suggested that EEC is a consequence of quantum confinement effects, multiple weak non-covalent interactions, and limited free energy windows, which give rise to thermodynamic homeostasis that may be of evolutionary and functional advantage because it enables adaptation to harsher environments.[43] EEC is also linked with solvent reorganization, accompanying biomolecular interactions.[44−46] The $\Delta_r H^\circ$ values increased in magnitude, whereas the $T\Delta_r S^\circ$ term decreased with increasing the temperature. However, the $\Delta_r G^\circ$ values remained almost unaltered with changing the temperature. The $\Delta_r H^\circ$ and $T\Delta_r S^\circ$, both of which are strong functions of T, compensated one another to make the overall $\Delta_r G^\circ$ temperature invariant. Linearity of the relationship of $\Delta_r H^\circ$ with $T\Delta_r S^\circ$ with slope close to unity suggests complete compensation, and this occurs in systems with $\Delta_r C_p^\circ \neq 0$ and $\Delta_r C_p^\circ > \Delta_r S^\circ$. $\Delta_r H^\circ$ and $\Delta_r G^\circ$ were plotted as a function of $T\Delta_r S^\circ$, and the slopes of the plot of $\Delta_r H^\circ$ versus $T\Delta_r S^\circ$ were deduced to be 1.01 ± 0.05 and 0.99 ± 0.06, respectively, for BSA and HSA (Figure 7). Linear relationship between $\Delta_r H^\circ$ and $T\Delta_r S^\circ$ with slope close to unity suggested complete EEC in the two protein−dye systems studied.

DSC Studies. DSC is an effective and reliable tool for monitoring protein folding−unfolding.[30,47] To monitor the effect of the azo dye amaranth on the thermal stability of the two homologous serum proteins, the DSC thermograms of excess heat capacity versus temperature were analyzed with Origin 7.0 software. It was found that both the serum proteins, BSA and HSA, unfolded cooperatively, exhibiting a single endothermic peak with melting temperatures of 327.61 and 328.85 K, respectively (Figure 8). The binding reaction with amaranth resulted in remarkable enhancement of the thermal stability of both the serum proteins. Upon binding to amaranth, the thermal denaturation temperature (T_m) of BSA and HSA was enhanced to 335.56 and 341.01 K, respectively (Figure 8).

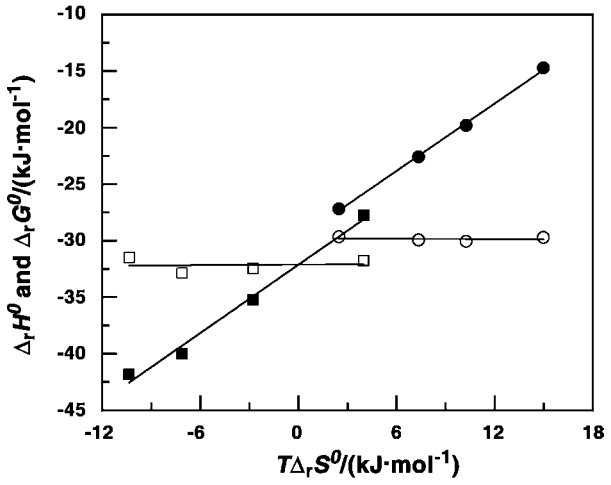

Figure 7. Plot of variation of $\Delta_r H^\circ$ (closed symbols) and $\Delta_r G^\circ$ (open symbols) as a function of $T\Delta_r S^\circ$ for the binding of amaranth to BSA (■ and □) and HSA (● and ○).

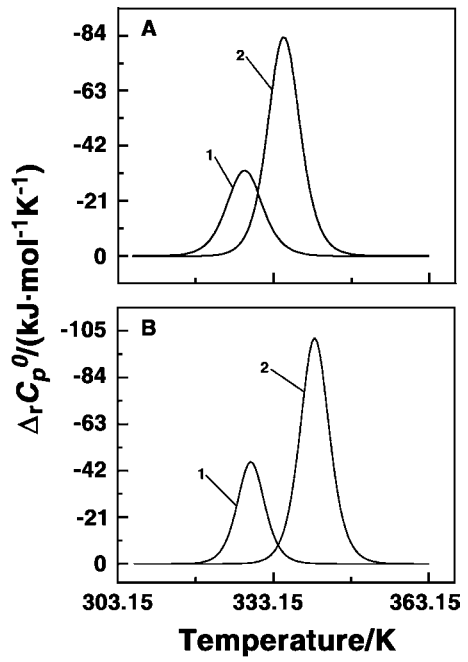

Figure 8. DSC thermograms of (A) BSA and (B) HSA. Curves 1 and 2 represent the free protein and amaranth−protein complexes, respectively.

Thus, the two homologous serum proteins, BSA and HSA, were stabilized (ΔT_m) by 7.95 and 12.16 K, respectively. In addition to the T_m values, the DSC thermograms upon analysis also afforded the calorimetric transition enthalpy ($\Delta_r H_{cal}$). The value of $\Delta_r H_{cal}$ is model-independent and has no relation with the nature of the transition. It is pertinent to mention here that there was no significant change in the shape of the DSC thermograms, which enabled us to conclude that the denaturation process was not altered but only shifted to higher temperatures in the presence of the dye. The $\Delta_r H_{cal}$ value increased from 296.52 ± 0.08 kJ mol^{-1} in the unbound form to 683.76 ± 0.15 kJ mol^{-1} in the bound form for BSA. For HSA, the magnitude of $\Delta_r H_{cal}$ enhanced from 321.30 ± 0.14 kJ mol^{-1} in the unbound form to 759.36 ± 0.16 kJ mol^{-1} in the bound form. Thus, $\Delta_r H_{cal}$ increased by 387.24 ± 0.07 and 438.06 ±

dx.doi.org/10.1021/jf5025278 | J. Agric. Food Chem. 2014, 62, 7955−7962

0.02 kJ mol^{-1}, respectively, for BSA and HSA upon binding to amaranth.

The present study presents a detailed description of the thermodynamics of the interaction of the toxic food colorant amaranth with two homologous serum proteins. These microcalorimetric investigations lend deeper insights into the thermodynamics of the interaction of the toxic food additives with the serum proteins, which may prove critical in realizing the toxic and hazardous effects of food colorants on biological systems.

AUTHOR INFORMATION

Corresponding Author

*Telephone: +91-33-2499-5723/2472-4049. Fax: +91-33-2472-3967. E-mail: gskumar@iicb.res.in and/or gsk.iicb@gmail.com.

Funding

This work was supported by the network project BIOCERAM (ESC0103) of the Council of Scientific and Industrial Research (CSIR), Government of India.

Notes

The authors declare no competing financial interest.

ACKNOWLEDGMENTS

The authors extend their thanks to all of the members of the Biophysical Chemistry Laboratory for their cooperation and help and to the anonymous reviewers for their critical and judicious evaluation of the manuscript and helpful suggestions.

REFERENCES

(1) Sanchez-Prado, L.; Lompart, M.; Lores, M.; Garcma-Jares, C.; Bayona, J. M.; Cela, R. Monitoring the photochemical degradation of triclosan in waste water by UV light and sunlight using solid-phase microextraction. *Chemosphere* **2006**, *65*, 1338−1347.

(2) Ratna; Padhi, B. S. Pollution due to synthetic dyes toxicity & carcinogenicity studies and remediation. *Int. J. Environ. Sci.* **2012**, *3*, 940−955.

(3) Chen, H. Recent advances in azo dye degrading enzyme research. *Curr. Protein Pept. Sci.* **2006**, *7*, 101−111.

(4) Weisburger, J. H. Comments on the history and importance of aromatic and heterocyclic amines in public health. *Mutat. Res.* **2002**, *506*−*507*, 9−20.

(5) Umbuzeiro, G. A.; Freeman, H. S.; Warren, S. H.; Oliveira, D. P.; Terao, Y.; Watanabe, T.; Claxton, D. L. The contribution of azo dyes to the mutagenic activity of Cristais river. *Chemosphere* **2005**, *60*, 55−64.

(6) Puvaneswari, N.; Muthukrishnan, J.; Gunasekaran, P. Toxicity assessment and microbial degradation of azo dyes. *Indian J. Exp. Biol.* **2006**, *44*, 618−626.

(7) Chowdhury, G. Human health perspectives on environmental exposure to benzidine: A review. *Chemosphere* **1996**, *32*, 267−291.

(8) Mpountoukas, P.; Pantazaki, A.; Kostareli, E.; Christodoulou, P.; Kareli, D.; Poliliou, S.; Mourelatos, C.; Lambropoulou, V.; Lialiaris, T. Cytogenetic evaluation and DNA interaction studies of the food colorants amaranth, erythrosine and tartrazine. *Food Chem. Toxicol.* **2010**, *48*, 2934−2944.

(9) Zhang, G.; Ma, Y. Mechanistic and conformational studies on the interaction of food dye amaranth with human serum albumin by multispectroscopic methods. *Food Chem.* **2013**, *136*, 442−449.

(10) Nevado, J. J. B.; Cabanillas, C. G.; Salcedo, A. M. C. Simultaneous spectrophotometric determination of three food dyes by using the first derivative of ratio spectra. *Talanta* **1995**, *42*, 2043−2051.

(11) King-Thom, C. Mutagenicity and carcinogenicity of aromatic amines metabolically produced from azo dyes. *J. Environ. Sci. Health, Part C: Environ. Carcinog. Ecotoxicol. Rev.* **2000**, *18*, 51−74.

(12) Ishidate, M., Jr.; Sofuni, T.; Yoshikawa, K.; Hayashi, M.; Nohmi, T.; Sawada, M.; Matsuoka, A. Primary mutagenicity screening of food additives currently used in Japan. *Food Chem. Toxicol.* **1984**, *22*, 623−636.

(13) Carter, D. C.; He, X.; Munson, S. H.; Twigg, P. D.; Gernert, K. M.; Broom, M. B.; Miller, T. Y. Three-dimensional structure of human serum albumin. *Science* **1989**, *244*, 1195−1198.

(14) Kratochwil, N. A.; Huber, W.; Muller, F.; Kansy, M.; Gerber, P. R. Predicting plasma protein binding of drugs: A new approach. *Biochem. Pharmacol.* **2002**, *64*, 1355−1374.

(15) Ghuman, J.; Zunszain, P. A.; Petitpas, I.; Bhattacharya, A. A.; Otagiri, M.; Curry, S. Structural basis of the drug-binding specificity of human serum albumin. *J. Mol. Biol.* **2005**, *353*, 38−52.

(16) Pan, X.; Qin, P.; Liu, R.; Wang, J. Characterizing the interaction between tartrazine and two serum albumins by a hybrid spectroscopic approach. *J. Agric. Food Chem.* **2011**, *59*, 6650−6656.

(17) Pan, X. R.; Liu, R. T.; Qin, P. F.; Wang, L.; Zhao, X. C. Spectroscopic studies on the interaction of acid yellow with bovine serum albumin. *J. Lumin.* **2010**, *130*, 611−617.

(18) Foster, J. F. *Albumin Structure, Function and Uses*; Pergamon Press: Oxford, U.K., 1977; p 53.

(19) He, X. M.; Carter, D. C. Atomic structure and chemistry of human serum albumin. *Nature* **1992**, *358*, 209−215.

(20) Peters, T., Jr. *All about Albumins. Biochemistry, Genetics and Medical Applications*; Academic Press: San Diego, CA, 1996; p 9.

(21) Dockal, M.; Carter, D. C.; Rücker, F. The three recombinant domains of human serum albumin. Structural characterization and ligand binding properties. *J. Biol. Chem.* **1999**, *274*, 29303−29310.

(22) Huang, B. X.; Kim, H. Y.; Dass, C. Probing three-dimensional structure of bovine serum albumin by chemical cross-linking and mass spectrometry. *J. Am. Soc. Mass Spectrom.* **2004**, *15*, 1237−1247.

(23) Sudlow, G.; Birkett, D. J.; Wade, D. N. The characterization of two specific drug binding sites on human serum albumin. *Mol. Pharmacol.* **1975**, *11*, 824−832.

(24) Sudlow, G.; Birkett, D. J.; Wade, D. N. Further characterization of specific drug binding sites on human serum albumin. *Mol. Pharmacol.* **1976**, *12*, 1052−1061.

(25) Murakami, K. Equilibrium and kinetic studies of the binding of tri- and tetra-anionic ligands to bovine serum albumin. *Biophys. Chem.* **1991**, *41*, 253−261.

(26) Yoon, J.-H.; McKenzie, D.; Prichard, F. E. The binding of food dyes with human serum albumin. *Arch. Pharmacal Res.* **1996**, *19*, 269−274.

(27) Sun, W.; Jiao, K.; Wang, X.; Lu, L. Electrochemical studies of the reaction between albumin and amaranth and its analytical application. *J. Electroanal. Chem.* **2005**, *578*, 37−43.

(28) Basu, A.; Suresh Kumar, G. Study on the interaction of the toxic food additive carmoisine with serum albumins: A microcalorimetric investigation. *J. Hazard. Mater.* **2014**, *273*, 200−206.

(29) Adão, R.; Bai, G.; Loh, W.; Bastos, M. Chemical calibration of isothermal titration calorimeters: An evaluation of the dilution of propan-1-ol into water as a test reaction using different calorimeters, concentrations and temperatures. *J. Chem. Thermodyn.* **2012**, *52*, 57−63.

(30) Bernazzani, L.; Ferrari, C.; Gianni, P.; Mollica, V.; Tombari, E. Calorimetric investigation on the interaction of sodium taurodeoxycholate with human serum albumin. *Thermochim. Acta* **2013**, *555*, 7−16.

(31) Damian, L. Isothermal titration calorimetry for studying protein−ligand interactions. *Methods Mol. Biol.* **2013**, *1008*, 103−118.

(32) Ross, P. D.; Subramanian, S. Thermodynamics of protein association reactions: Forces contributing to stability. *Biochemistry* **1981**, *20*, 3096−3102.

(33) Manning, G. S. The molecular theory of polyelectrolyte solutions with applications to the electrostatic properties of polynucleotides. *Q. Rev. Biophys.* **1978**, *11*, 179−246.

(34) Record, M. T., Jr.; Anderson, C. F.; Lohman, T. M. Thermodynamic analysis of ion effects on the binding and conformational equilibria of proteins and nucleic acids: The roles of

ion association or release, screening, and ion effects on water activity. *Q. Rev. Biophys.* **1978**, *11*, 103−178.
(35) Record, M. T., Jr.; Spolar, R. S. In *The Biology of Nonspecific DNA−Protein Interactions*; Revzin, A., Ed.; CRC Press: Boca Raton, FL, 1990; p 33.
(36) Record, M. T., Jr.; Ha, H. H.; Fisher, M. A. Analysis of equilibrium and kinetic measurements to determine thermodynamic origins of stability and specificity and mechanism of formation of site-specific complexes between proteins and helical DNA. *Methods Enzymol.* **1991**, *208*, 291−343.
(37) Basu, A.; Suresh Kumar, G. Minor groove binding of the food colorant carmoisine to DNA: Spectroscopic and calorimetric characterization studies. *J. Agric. Food Chem.* **2014**, *62*, 317−326.
(38) Liu, C. C.; Richard, A. J.; Datta, K.; LiCata, V. J. Prevalence of temperature-dependent heat capacity changes in protein−DNA interactions. *Biophys. J.* **2008**, *94*, 3258−3265.
(39) Spolar, R. S.; Record, M. T., Jr. Coupling of local folding to site-specific binding of proteins to DNA. *Science* **1994**, *263*, 777−784.
(40) O'Brien, R.; DeDecker, B.; Fleming, K. G.; Sigler, P. B.; Ladbury, J. E. The effects of salt on the TATA binding protein−DNA interaction of a hyperthermophilic archaeon. *J. Mol. Biol.* **1998**, *279*, 117−125.
(41) Ha, J. H.; Spolar, R. S.; Record, M. T., Jr. Role of the hydrophobic effect in stability of site-specific protein-DNA complexes. *J. Mol. Biol.* **1989**, *209*, 801−816.
(42) Olsson, T. S.; Ladbury, J. E.; Pitt, W. R.; Williams, M. A. Extent of enthalpy−entropy compensation in protein−ligand interactions. *Protein Sci.* **2011**, *20*, 1607−1618.
(43) Cooper, A.; Johnson, C. M.; Lakey, J. H.; Nöllmanna, M. Heat does not come in different colours: Entropy−enthalpy compensation, free energy windows, quantum confinement, pressure perturbation calorimetry, solvation and the multiple causes of heat capacity effects in biomolecular interactions. *Biophys. Chem.* **2001**, *93*, 215−230.
(44) Sharma, S.; Bharadwaj, S.; Surolia, A.; Podder, S. K. Evaluation of the stoichiometry and energetics of carbohydrate binding to *Ricinus communis* agglutinin: A calorimetric study. *Biochem. J.* **1998**, *333*, 539−542.
(45) Williams, B. A.; Chervenak, M. C.; Toone, E. J. Energetics of lectin−carbohydrate binding. *J. Biol. Chem.* **1992**, *267*, 22907−22911.
(46) Gupta, D.; Cho, M.; Cummings, R. D.; Brewer, C. F. Thermodynamics of carbohydrate binding to galectin-1 from Chinese hamster ovary cells and two mutants. A comparison with four galactose-specific plant lectins. *Biochemistry* **1996**, *35*, 15236−15243.
(47) Waldron, T. T.; Murphy, K. P. Stabilization of proteins by ligand binding: Application to drug screening and determination of unfolding energetics. *Biochemistry* **2003**, *42*, 5058−5064.

Table 1. Potato Cultivars for Wound Healing Study

cultivar	flesh	periderm russeting	skin
Norkotah Russet	white	russeted and netted	dark tan
Atlantic	white	lightly netted to heavily scaled	white
Chipeta	white	small russeted areas	light to buff
Yukon Gold	light yellow	smooth, finely flaked, yellowish white	yellowish

methodological and agricultural standpoints: high performance liquid chromatography (LC-MS) and nuclear magnetic resonance (NMR) may offer more robust characterization of the healing tissue extracts, and cultivar comparisons could show metabolite differences that reveal the molecular underpinnings of russeted skin character and/or wound-induced stress response.

In turn, the oxidative stress due to wounding can unleash the production of antioxidant compounds, which are present in the native skin of potato and have already found practical use as preservatives in the food industry.[3] Antioxidant evaluation of a purple potato cultivar using a diphenyl picrylhydrazyl (DPPH$^{\bullet}$) scavenging assay showed that the activity increased as a result of wounding,[15] but a trend of decreasing DPPH$^{\bullet}$ scavenging activity was reported in a wounded Norkotah Russet sample.[16] This inconsistency could reflect a shortcoming of the DPPH$^{\bullet}$ assay, whereby steric hindrance could compromise assessments of scavenging activities for larger phytochemical constituents. Thus, the current experimental design couples LC-MS and NMR metabolite profiling for four cultivars, at day 3 and day 7 after wounding, with broadly applicable extended-duration scavenging assays using 2,2′-Azinobis (3-ethylbenzothiazoline-6-sulfonic acid ammonium salt) (ABTS$^{\bullet+}$).[17] By coordinating information on chemical composition and antioxidant activity, the long-term goal is to develop improved methods that ensure rapid and complete wound healing for various potato cultivars while also providing a rich source of chemical compounds with potential application as functional foods.[3,18,19]

MATERIALS AND METHODS

Reagents. HPLC-MS grade acetonitrile, water, chloroform and methanol (J. T. Baker, Phillipsburg, NJ) and formic acid (Sigma-Aldrich, St. Louis, MO) were used for LC-MS/MS and time-of-flight (TOF-MS) analysis. 2,2′-Azinobis (3-ethylbenzothi-azoline-6-sulfonic acid ammonium salt) (ABTS), 6-hydroxy-2,5,7,8 tetramethylchromane-2-carboxylic acid (TCI, Tokyo, Japan), and potassium peroxosulfate (Sigma-Aldrich, St. Louis, MO) were utilized in the antioxidant assay.

Plant Material. Potato tuber cultivars from the 2011 crop year were provided by Joe Nuñez, University of California Cooperative Extension (Davis, CA). Table 1 summarizes the differences in overall phenotypic characteristics that were used in making these selections.

Sample Preparation. Freshly harvested potato tubers were peeled, and the internal flesh tissues were sectioned longitudinally with a mandolin slicer to obtain slices about 5 mm thick. The central part of the tuber was set aside to avoid the internal medulla. Slices were placed on wet cellulose filter paper and left for 3 or 7 days of healing on wire netting supports within closed plastic boxes at 25 °C. Water was added at the bottom of the boxes to maintain humidity; healing proceeded in the dark. The brown surface layer of wound-healing tissue was collected carefully using a flat spatula, making efforts to avoid flesh (parenchyma) contamination. The samples were harvested at 3 and 7 days after wounding, representing the early healing tissue in which the suberized closing layer and the wound periderm were developing, respectively. Harvested wound periderm samples were frozen immediately in liquid nitrogen and stored at −80 °C until processed. For processing, samples were ground under liquid nitrogen, freeze-dried, and again stored at −80 °C.[20]

The samples were prepared for chemical analysis using a modification of the method employed by Choi et al., which enables concurrent extraction and partitioning of polar and nonpolar constituents and has become an established protocol for metabolomic studies of plant materials.[20,21] Samples of 10 mg (dry weight) each were placed in jn glass vials (Microliter Analytical Supplies, Suwanee, GA) and extracted with 2 mL of 60% (v/v) methanol−water by pan ultrasonication (Branson Ultrasonics, Danbury, CT) for 1 min, followed by addition of 2 mL chloroform and sonication again for 1 min. Each extract was then incubated at room temperature in a shaker for 10 min, followed by tabletop centrifugation (Beckman Coulter, Fullerton, CA) at 3000 rpm to produce three separate phases: soluble polar, soluble nonpolar, and an interphase of suspended particulates. Six replicate extracts were prepared per cultivar for each wound-healing time point (day 3 and day 7). The upper soluble polar extracts were removed carefully with a glass Pasteur pipet and dried under a flow of nitrogen for a few hours. This phase was selected for the current analysis.

NMR. Aliquots of the polar extract were dried and reconstituted using a 100 mM pH 7.4 phosphate buffer in D_2O that contained the internal standard DSS (0.01 mg/mL). Spectra were recorded using a Bruker AVANCE PLUS spectrometer (Bruker Biospin, Karlsruhe, Germany) operating at a ^{1}H frequency of 800 MHz and equipped with a cryomicroprobe that accommodates 1.7 mm o.d. sample tubes (Norell, Landisville, NJ). Acquisition of the spectra was achieved using TOPSPIN version 3.1 software and an NMR SAMPLEJET accessory for automated sample changing. ^{1}H NMR data were collected for the polar extracts at 298 K with a constant receiver gain, using 512 scans with 4 initial "dummy" scans, a recycle delay of 1.0 s between acquisitions, and presaturation of the residual water signal set to a chemical shift of 4.695 ppm. The spectral window after Fourier transformation and signal conditioning was 14 ppm defined by 32K data points.

LC-MS. Liquid chromatography was conducted with a Shimadzu UFLC (Shimadzu U.S.A., Canby, OR) equipped with two LC-20 AD pumps, a SIL-20AC automatic injector, a CBM-20A communication bus module and a CTO-20AC column oven. The separations were carried out using a 150 × 4.6 mm i.d., 3.0 μm AscentisR C18 column (Supelco Analytical, Bellefonte, PA). Each analysis was performed by injecting a 10 μL sample into the column and eluting at 35 °C with a flow rate of 0.4 mL/min. Six replicate extracts per cultivar were analyzed for each wound-healing time point, and each sample was injected twice. The mobile phase was composed of 0.1% aqueous formic acid (A) and 0.1% formic acid in acetonitrile (B) using a program of nonlinear gradient elution: 2% B (0−5 min), 2−10% B (5−8 min), 10−15% B (8−13 min), 15% B (13−25 min), 15−30% B (25−28 min), 30−40% B (28−50 min), and 40−100% B (50−60 min).

The LC system was interfaced to an Applied Biosystems 4000 Q Trap mass spectrometer (Applied Biosystems, Foster City, CA) for LC-MS/MS measurements. The source type was electrospray ionization (ESI) and the source temperature was 300 °C. Mass spectra were acquired in both positive and negative modes over the range m/z 100−1300. Full scan, MS^2, and MS^3 data were collected using these settings. The optimized declustering potentials were 66 V in the positive mode and −140 V in the negative mode; chlorogenic acid and rutin, compounds reported previously in potatoes,[9,11,22] were used as reference standards. Analyst 1.4.2 software was used for data processing.

Fractionation of the Extracts. The polar extracts were fractionated using an Agilent 1200 series HPLC-PDA liquid

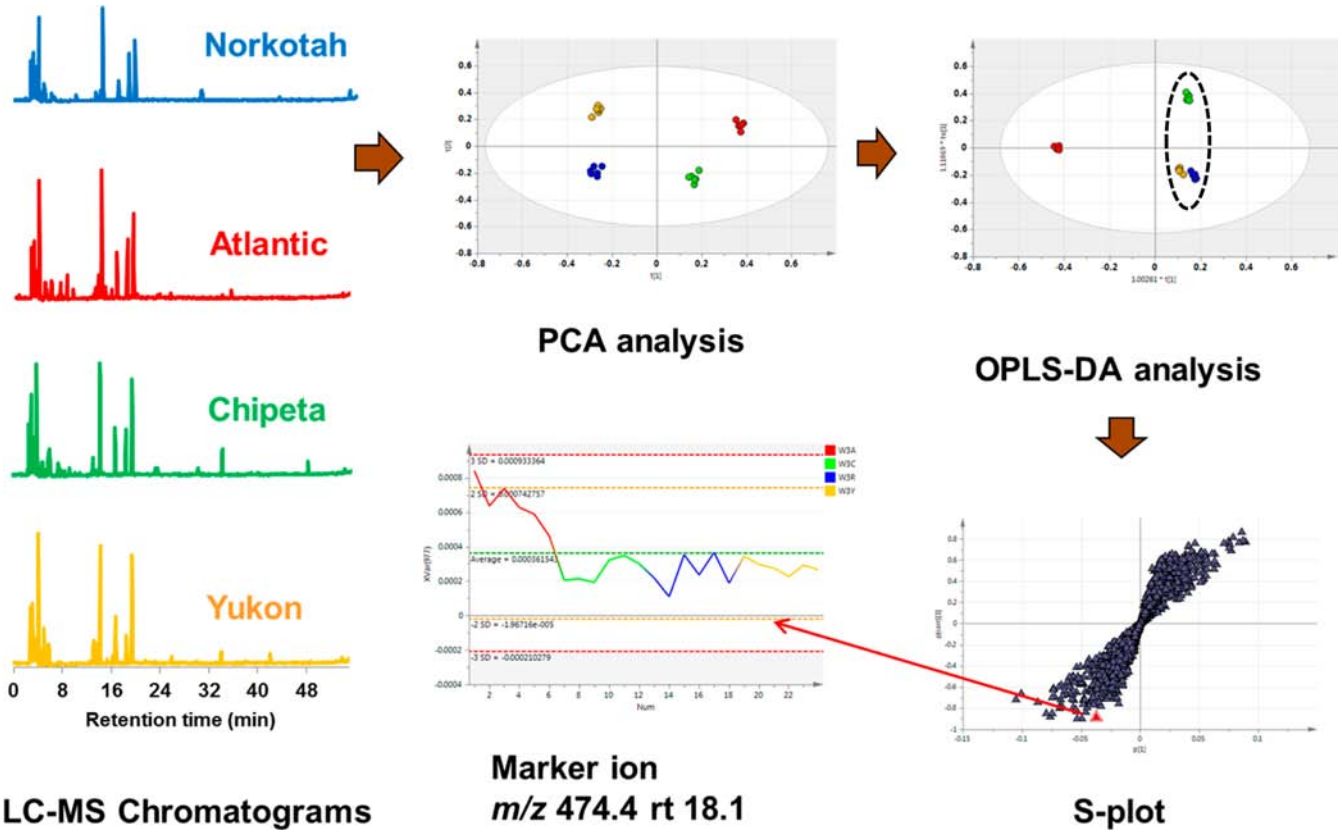

Figure 1. Schematic representation of the experimental design, including typical data and statistical multivariate analyses including PCA, OPLS-DA and S-plot analysis of liquid chromatography - mass spectrometry (LC-MS) data (total ion current (TIC) chromatograms in positive mode), leading to the detection of marker ions. Stacked LC-MS chromatograms of the polar extracts each represent average data from six biological replicates from day 3 potato wound periderm samples, color coded for Norkotah Russet (blue), Atlantic (red), Chipeta (green), and Yukon Gold (gold). Statistical procedures are detailed in the text.

chromatography system (Agilent Technologies, Santa Clara, CA) equipped with a G1322A degasser, G1311A quaternary pump, G1316A thermostatically controlled chamber, G1315B diode array detector, and G1364C analytical fractionator. The mobile phase composition, flow rate, gradient, and column were as described above. Fractions were collected at 30-s intervals throughout a 60 min chromatographic run. This fractionation protocol was repeated several times to generate sufficient material that could be concentrated and analyzed by TOF-MS to obtain the exact mass of the compounds under investigation.

TOF-MS. Chromatographic fractions from the polar extracts were injected directly into a Waters LCT premier XE TOF mass spectrometer (Micromass, Manchester, U.K.) using a Harvard 11 Plus Single Syringe Pump (Harvard Apparatus, Holliston, MA) equipped with an ESI interface and controlled by MassLynx V4.1 software. Mass spectra were acquired in both positive and negative modes over the range m/z 100−1300. The capillary voltages were set at 4000 V for both acquisition modes. Nitrogen gas flowing at 300 L/h was used for both the nebulizer and in desolvation. The desolvation temperature was 150 °C, and the source temperature was 80 °C. For the dynamic range enhancement (DRE) lockmass, a solution of leucine enkephalin (Sigma-Aldrich, St. Louis, MO) was infused by a secondary reference probe at 200 pg/mL in acetonitrile/water (1:1 v/v) containing 0.1% formic acid with the help of a second LC pump (Waters 515 HPLC). The reference mass was determined once every five scans for both positive and negative data collection; both types of ESI data were collected using a scan time of 0.2 s and an interscan time of 0.01 s.

ABTS$^{\bullet+}$ Scavenging. The ABTS$^{\bullet+}$ scavenging activity was assessed according to the method described by Re et al.[17] with minor modifications. ABTS$^{\bullet+}$ was generated by reacting an aqueous ABTS solution (7 mM) with $K_2S_2O_8$ (2.45 mM) in the dark for 12−16 h at ambient temperature and adjusting the absorbance at 734 nm to 0.70 (±0.02) with ethanol. To a 2 μL aliquot of the periderm extract of interest was added 198 μL of ABTS$^{\bullet+}$ reagent; the absorbance was recorded at 734 nm after initial mixing and subsequently at 5 min intervals (45 min in total) using a Spectra$_{max}$ microplate reader (Molecular Devices, Sunnyvale, CA). The percentage inhibition values for different concentrations were calculated using the following equation:

$$\left[\frac{(\mathrm{Abs}_{\mathrm{control}}) - (\mathrm{Abs}_{\mathrm{sample}})}{(\mathrm{Abs}_{\mathrm{control}})}\right] \times 100 \quad (1)$$

A plot of percentage inhibition versus concentration was made for the reference standard, 6-Hydroxy-2,5,7,8-tetramethylchroman-2-carboxylic acid (Trolox). On the basis of this plot, the Trolox equivalent antioxidant capacity (TEAC, μmol Trolox/g dried sample) values were calculated for each extract.

Preprocessing of NMR Data. For metabolite profiling analysis, MESTREC software version 4.9.9.9 (Mestrelab Research, Escondido, CA) was used to correct the phase and baseline of each spectrum and to remove the spectral region containing the remaining water signal. The spectra were then subjected to binning and integrated in 0.04 ppm regions. The integrated area of each bin/bucket was normalized with respect to the area of all bins.

Preprocessing of LC-MS Data. MZmine version 2.4 (VTT Technical Research Center, Helsinki, Finland and Turku Center for Biotechnology, Turku, Finland) was used to filter the spectra according to retention time and m/z range. Spectral deconvolution and feature detection were followed by peak alignment and data normalization.[23] The region of the chromatogram between 0 and 4

dx.doi.org/10.1021/jf501330h | J. Agric. Food Chem. 2014, 62, 7963−7975

Table 2. Biomarkers for Polar Extracts of Wound-Healing Potato Periderms

Compound No.	$[M+H]^+$ or $[M+Na]^+$ ions exact masses (formula, error)[a]	MS/MS Fragment ions (positive mode) (m/z)[b]	Biomarker Formula and Molecular Weight	Structural Formula	Cultivar-Specific Marker[e]	Day 7 Time-Point Marker[f]	References
Identified Constituents							
Phenolic amines							
1	531.3167 $[M+H]^+$ ($C_{28}H_{43}N_4O_6$ -3.0ppm)	413, 367, 310 266, 257, 222, 184, 165, 123	**Kukoamine isomer** *N*,*N*-bis (dihydrocaffeoyl) spermine $C_{28}H_{42}N_4O_6$[c,d] 530.3104	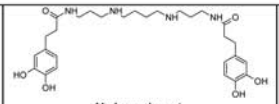 Kukoamine A 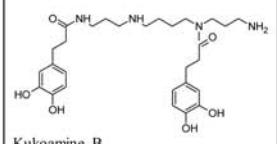 Kukoamine B 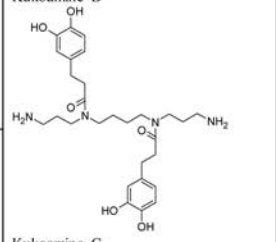 Kukoamine C 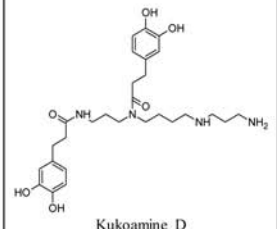 Kukoamine D	Atlantic (Wd3) Norkotah Russet (Wd3)	+	10, 11, 45
2	531.3180 $[M+H]^+$ ($C_{28}H_{43}N_4O_6$ 0.6ppm)	413, 367, 310 266, 257, 222, 184, 165, 123	**Kukoamine isomer** $C_{28}H_{42}N_4O_6$[c,d] 530.3104		Atlantic (Wd3) Norkotah Russet (Wd3)		10, 11
3	265.1534 $[M+H]^+$ ($C_{14}H_{21}N_2O_3$ -6.8ppm)	162, 149, 134, 117	**Feruloyl putrescine** $C_{14}H_{20}N_2O_3$[c,d] 264.1474	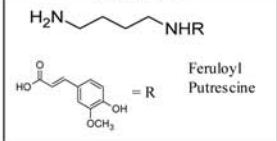 Feruloyl Putrescine	Atlantic (Wd3) Yukon (Wd7)		10, 45, 46
4	265.1553 $[M+H]^+$ ($C_{14}H_{21}N_2O_3$ 0.4ppm)	162, 149, 134, 117	**Feruloyl putrescine isomer** $C_{14}H_{20}N_2O_3$[c,d] 264.1474	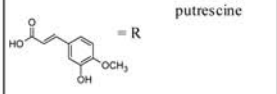 Isoferuloyl putrescine	Atlantic (Wd3) Norkotah Russet (Wd3)	+	10, 46
5	474.2582 $[M+H]^+$ ($C_{25}H_{36}N_3O_6$ -4.6ppm)	457, 293, 236, 222, 165, 137, 123	**N^1,N^4-bis (dihydrocaffeoyl) spermidine** $C_{25}H_{35}N_3O_6$ 473.2526	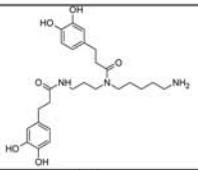	Atlantic (Wd3)	+	10, 11, 45
6	638.3086 $[M+H]^+$ ($C_{34}H_{44}N_3O_9$ 1.3ppm)	474, 293, 236, 222, 165, 137, 123	**N^1,N^4,N^8-tris(dihydrocaffeoyl) spermidine** $C_{34}H_{43}N_3O_9$ 637.2999	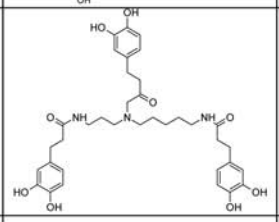	Norkotah Russet (Wd3) Atlantic (Wr3) Chipeta (Wd7)		10, 11
7	314.1386 $[M+H]^+$ ($C_{18}H_{20}NO_4$ -1.9ppm)	177, 159, 149, 145, 134, 125, 121, 117	**Feruloyl tyramine** $C_{18}H_{19}NO_4$[c] 313.1392	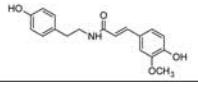	Norkotah Russet (Wd3, Wd7)		11, 24, 26

dx.doi.org/10.1021/jf501330h | J. Agric. Food Chem. 2014, 62, 7963−7975

Table 2. continued

Compound No.	$[M+H]^+$ or $[M+Na]^+$ ions exact masses (formula, error)[a]	MS/MS Fragment ions (positive mode) (m/z)[b]	Biomarker Formula and Molecular Weight	Structural Formula	Cultivar-Specific Marker[e]	Day 7 Time-Point Marker[f]	References
Identified Constituents							
Phenolic amines							
8	251.1398 $[M+H]^+$ ($C_{13}H_{19}N_2O_3$ 0.8ppm)	235, 175, 163, 145, 135, 117	**Caffeoyl putrescine** $C_{13}H_{18}N_2O_3$ 250.1317	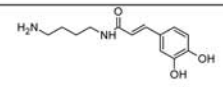	**Atlantic (Wd3)**		*10, 11*
9	235.1471 $[M+H]^+$ ($C_{13}H_{19}N_2O_2$ 10.2ppm)	218, 179, 147, 119	**Coumaryl putrescine** $C_{13}H_{18}N_2O_2$ 235.134	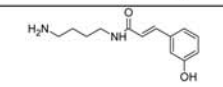	**Atlantic (Wd7) Chipeta (Wd7)**		*11*
10	695.3613 $[M+H]^+$ ($C_{37}H_{51}N_4O_9$ 6.2ppm)	677, 531, 457, 386, 293, 276, 222, 165, 123	**N^1,N^5,N^{10} tris(dihydrocaffeoyl) spermine** $C_{37}H_{50}N_4O_9$[c] 694.3578	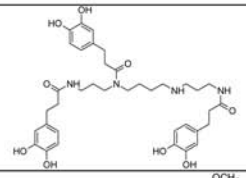	**Norkotah Russet (Wd7) Yukon (Wd7)**		*10, 11*
11	625.2567 $[M+H]^+$ ($C_{36}H_{37}N_2O_8$ 2.7ppm)	488, 460, 351, 323, 308, 291, 265, 250, 237, 201, 191	**Grossamide** $C_{36}H_{36}N_2O_8$[g] 624.2471	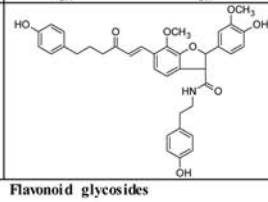		+	*24*
Flavonoid glycosides							
12	449.1089 $[M+H]^+$ ($C_{21}H_{21}O_{11}$ 1.1ppm)	413,413, 329,287	**Kaempferol hexoside** $C_{21}H_{20}O_{11}$ 448.1006	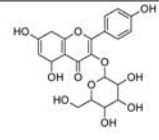	**Yukon (Wd3, Wd7)**	+	*45*
13	611.1628 $[M+H]^+$ ($C_{27}H_{31}O_{16}$2. 6ppm)	449, 413, 383, 329, 287	**Kaempferol dihexoside** $C_{27}H_{30}O_{15}$	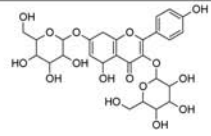	**Yukon (Wd3)**		*9, 12*
14	595.1513 $[M+H]^+$ ($C_{30}H_{27}O_{13}$1 3.3ppm)	449,431, 413, 359, 329, 290, 287, 270	**Potengriffioside** $C_{30}H_{26}O_{13}$ 594.1373	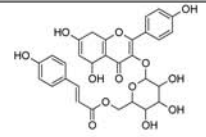	**Yukon Wd7 Norkotah Russet (Wd3)**		*27*
Phenolic acids							
15	355.1012 $[M+H]^+$ ($C_{16}H_{19}O_9$ -4.8ppm)	215, 163, 145, 135	**Chlorogenic acid** 3-Caffeoylquinic acid $C_{16}H_{18}O_9$[e] 354.0951	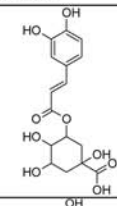	**Yukon (Wd3, Wd7) and Norkotah Russet (Wd3, Wd7)**	+	*9, 47-49*
16	369.1165 $[M+H]^+$ ($C_{17}H_{21}O_9$ -5.7ppm)	327, 251, 215, 195, 175, 132	**Feruloylquinic acid** $C_{17}H_{20}O_9$ 368.1107	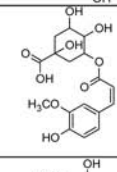	**Norkotah Russet (Wd3, Wd7)**		*11, 45, 50*
17	217.0465 $[M+Na]^+$ ($C_{10}H_{10}O_4$ -5.5ppm)	173, 155, 127	**Ferulic acid** $C_{10}H_{10}O_4$[g] 194.0579	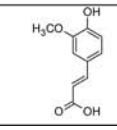	**Yukon (Wd3)**	+	*9*

dx.doi.org/10.1021/jf501330h | *J. Agric. Food Chem.* 2014, 62, 7963−7975

Table 2. continued

Compound No.	$[M+H]^+$ or $[M+Na]^+$ ions exact masses (formula, error)[a]	MS/MS Fragment ions (positive mode) (m/z)[b]	Biomarker Formula and Molecular Weight	Structural Formula	Cultivar-Specific Marker[e]	Day 7 Time-Point Marker[f]	References
Identified Constituents							
Phenolic acids							
18	691.1805 $[M+H]^+$ ($C_{32}H_{34}O_{17}$ -10ppm)	377, 355, 195	**Caffeoylquinic acid dimer** $C_{32}H_{34}O_{17}$[h] 690.1796	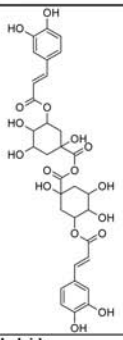	Atlantic (Wd3, Wd7) and Chipeta (Wd3, Wd7)		47
Glycoalkaloids							
19	852.5095 $[M+H]^+$ ($C_{45}H_{74}NO_{14}$ -1.6ppm)	707, 561, 398, 380, 366	**Chaconine** $C_{45}H_{73}NO_{14}$[c] 851.5031	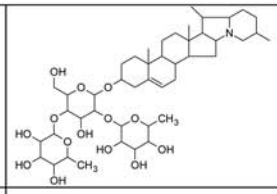	Chipeta (Wd7)	+	9, 12, 51
20	916.4995 $[M+H]^+$ ($C_{45}H_{74}NO_{18}$ -9.7ppm) 938.4602 $[M+Na]^+$ ($C_{45}H_{73}NO_{18}Na$ +13.1ppm)	894, 852, 834, 818, 734, 707	**Solanidene triol Solatriose** $C_{45}H_{73}NO_{18}$ 915.4828	(structure not reported)	Chipeta (Wd3)		12
21	884.4924 $[M+H]^+$ ($C_{45}H_{74}NO_{16}$ -9.2ppm)	866, 738,720, 704, 414, 396, 380, 378, 253	**Leptinine II** $C_{45}H_{73}NO_{16}$ 883.4929	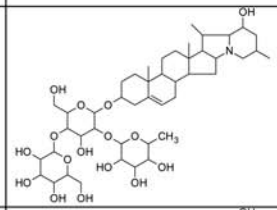	Norkotah Russet (Wd3)		12
22	868.4992 $[M+H]^+$ ($C_{45}H_{74}NO_{15}$ -7.6ppm)	850, 722, 704, 558, 414, 396, 378, 253	**Leptinine I** $C_{45}H_{73}NO_{15}$ 867.4980	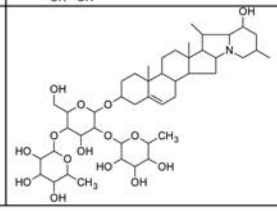		+	12
Incompletely Identified Constituents							
23	527.2870	253, 236, 165,123	Spermine derivative		Yukon Gold (Wd3, Wd7)	+	
24	486.4414	222, 177, 165, 123, 117			Chipeta (Wd7)		

[a]Exact mass data obtained from MS-TOF analysis. [b]Fragmentation data obtained from LC-MS/MS analysis using a 4000Q Trap instrument. [c]Also among the biomarkers identified in native periderms of these four cultivars (Huang et al., unpublished observations). [d]Isomeric compounds which were distinguished from each other by their retention times and the intensities of their mass fragmentation peaks. [e]The wound healing time point is denoted by Wd3 or Wd7, and color coded depending on the cultivar(s) specific for the biomarker. The coloring scheme denotes Atlantic (red), Chipeta (green), Norkotah Russet (blue), or Yukon Gold (gold). [f]Marker compounds found in all four cultivars that are specific to day 7 post wounding, which is associated with nascent wound periderm development. The (+) sign indicates that the compound in question is a marker for the day 7 time point. [g]Also among the metabolites identified in native periderms of these four cultivars (Huang et al., unpublished observations). [h]This compound can be distinguished from gas-phase dimer ions produced as artifacts during MS analysis: the observed m/z value of its molecular ion differs from a simple doubling of chlorogenic acid due to loss of water consequent with dimer formation.

min, which contains primary metabolites reported previously,[14] was not included in the current PCA analysis.

Multivariate Data Analysis. Principal component analysis (PCA) of the normalized data from NMR and MS experiments was carried

out using Simca-P+ software version 13.0 (Umetricas, Umeå, Sweden) and Pareto scaling.[20] In addition, the data were subjected to orthogonal partial least-squares discriminate analysis (OPLS-DA), in which data from a particular cultivar were assigned to one class that was then compared with another class comprising the remaining cultivars. The corresponding S-plots displayed extreme "wings" that yielded chemical shifts or mass-to-charge (m/z) ratios of the biomarkers that contribute to compositional differences among the tissue samples (Figure 1). These variables were evaluated individually using variable line plots to ascertain if the markers were unique to a particular cultivar at a specified wounding time point (Figure 1).

Tentative Metabolite Structural Identification. The markers were then characterized using mass and fragmentation data (MS, MS/MS and MS/MS/MS) from the 4000Q Trap and the exact mass values from the TOF-MS instrument, respectively. The marker compounds were identified tentatively by comparison of these data with published MS results using SciFinder Scholar and online databases such as PubChem, ChemSpider and Metlin.

To check the consistency of the MS-based identifications with observed NMR data for the extract mixtures, ACD software (ACD Laboratories, Toronto, Canada) was first used to simulate the NMR spectra of the identified markers. The simulated ^{1}H spectra of each compound were checked against the chemical shift list derived for biomarkers by OPLS-DA and S-plot analysis of the experimental NMR data for extract mixtures. For example, a biomarker compound for the Atlantic day 3 extract was tentatively identified as bis (dihydrocaffeoyl) spermidine, compound **5**, (474.4 m/z; 18.1 min) (Figure 1 and Table 2). The simulated ^{1}H chemical shifts for this MS-derived biomarker were compared with marker shifts derived from the experimentally observed NMR data for the extract mixture.

RESULTS AND DISCUSSION

Metabolic Fingerprinting. Visual inspection of the stacked ^{1}H NMR spectra for wound-healing tissue extracts from various cultivars at days 3 and 7 (Figure 2 and Supporting Information (SI) Figure S1, respectively) shows good consistency among the six replicates for each cultivar, a high degree of instrumental reproducibility, and modest but clear differences among the four cultivars. A more rigorous multivariate analysis of the data provides essential unbiased confirmation of these differences. The PCA-associated score plots for the NMR data (Figure 3) demonstrate that the polar

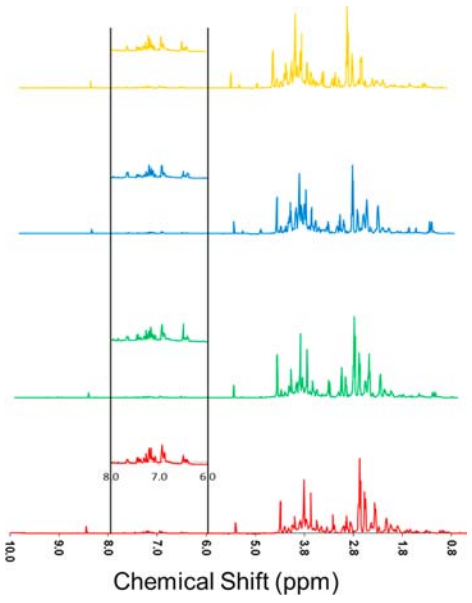

Figure 2. Stacked 800 MHz ^{1}H nuclear magnetic resonance (NMR) spectra, showing average data from six biological replicates of polar extracts from day 3 potato wound periderm samples, color coded for Yukon Gold (gold), Norkotah Russet (blue), Chipeta (green), and Atlantic (red). Vertical expansions of the aromatic and multiple-bonded region between 6.0 and 8.0 ppm are shown in each inset.

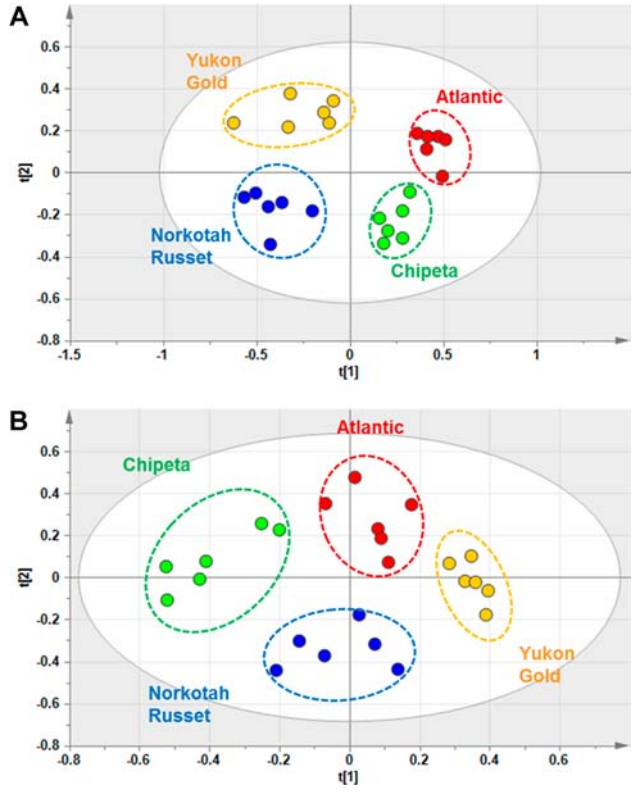

Figure 3. PCA score plots for the NMR data from extracts of day 3 (A) and day 7 (B) wound-healing samples, color coded for Atlantic (red), Chipeta (green), Norkotah Russet (blue), and Yukon Gold (gold) potato periderms.

metabolites for each of the four cultivars form distinct and nonoverlapping clusters, more distinct at day 3 compared with day 7 post wounding. To compare the metabolic profiles at different wound-healing time points, PCA was carried out for day-3 and day-7 NMR data together; the resulting score plot (Figure 4) shows a clear separation of metabolites at the two time points according to PC1. Again, a closer convergence of the clusters for each cultivar is evident at day 7.

In an analogous fashion, Figure 2 and SI Figure S2 demonstrate consistency among LC-MS experiments on nominally identical samples and distinct signatures for each of the four cultivars and wound-healing time points. Even more definitively than via NMR data, score plots obtained from PCA analysis of the LC-MS experiments show polar metabolite differences among the clusters corresponding to Russet Norkotah, Atlantic, Chipeta, and Yukon Gold cultivars (Figure 5). As compared with day 3 (Figure 5A), the convergent trend of metabolite compositions at day 7 is demonstrated by both the LC-MS score plot (Figure 5B) and the overall PCA analysis for both healing time points (Figure 6), again aligning with the NMR-derived multivariate analysis (Figures 3 and 4). This convergence of metabolite profiles with time, which has been observed previously in GC-MS-based multivariate analysis of Russet Burbank periderms,[14] could reflect common biosynthetic pathways associated with wounding in the four cultivars.

dx.doi.org/10.1021/jf501330h | J. Agric. Food Chem. 2014, 62, 7963−7975

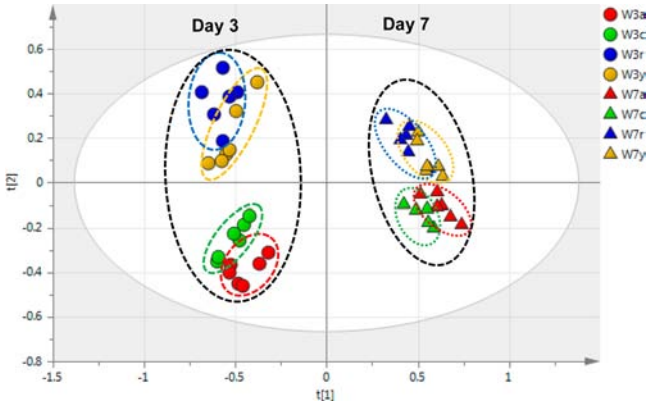

Figure 4. PCA score plot for the overall NMR data from extracts of the four cultivars at both day 3 (circles) and day 7 (triangles) post wounding (W). The samples are coded for Atlantic (red, a), Chipeta (green, c), Norkotah Russet (blue, r), and Yukon Gold (gold, y).

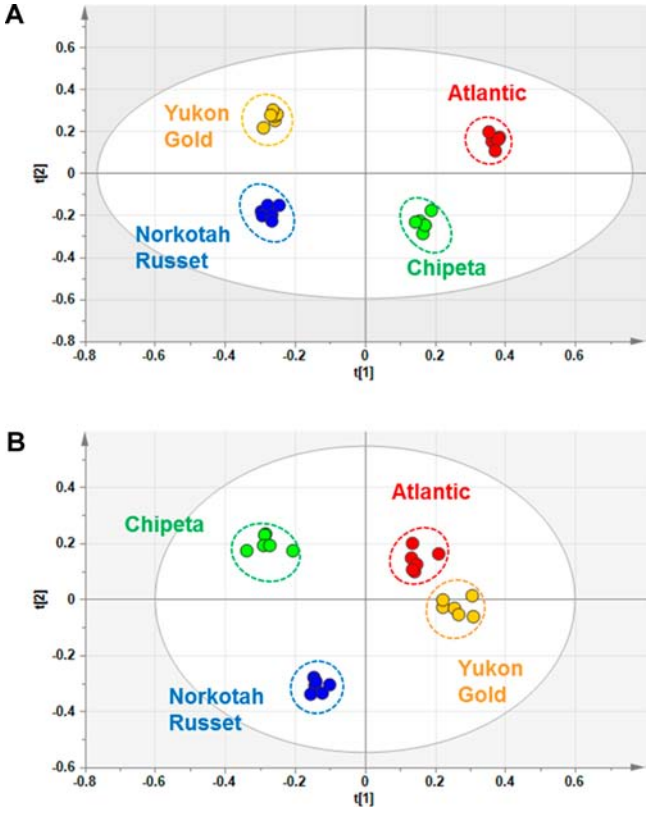

Figure 5. PCA score plots for the LC-MS data from extracts of day 3 (A) and day 7 (B) potato wound-healing samples, color coded for Atlantic (red), Chipeta (green), Norkotah Russet (blue), and Yukon Gold (gold).

That is, if the initially distinct metabolite pools for the four cultivars accumulate a common set of phytochemicals associated with wound induction, these common metabolites will become increasingly dominant at later healing stages.

OPLS-DA analyses and their corresponding S-plots, illustrated in Figure 1, provide chemical insight into the basis for variations in metabolic profiles. In particular, it is possible to identify the NMR chemical shifts and/or MS ions corresponding to metabolites ("biomarkers") that accumulate or are specific for a particular cultivar or wound-healing time point from the extremes of the S-plots. By comparing the marker ions

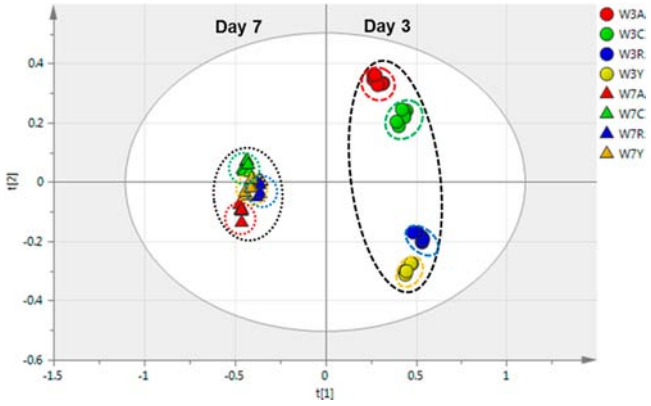

Figure 6. PCA score plot for the overall LC-MS data from extracts of the cultivars at both day 3 (circles) and day 7 (triangles) post wounding (W). The periderm samples are coded for Atlantic (red, a), Chipeta (green, c), Norkotah Russet (blue, r), and Yukon Gold (gold, y).

with published MS data using SciFinder Scholar (https://scifinder.cas.org/scifinder) or other online databases, it was possible to tentatively identify the polyphenolic amines, flavonoid glycosides, phenolic acids, and glycoalkaloids listed in Table 2. A total of 22 of 24 biomarkers were identified by MS/MS and MS-TOF methods. As noted in the Materials and Methods section, early eluting primary metabolites were excluded from the current PCA analysis.

Biomarkers for Cultivar Type. The majority of the identified biomarkers for Atlantic and Norkotah Russet varieties, at both days 3 and 7 post wounding, are polyphenolic amines. Conversely, most of the polyphenolic amine biomarkers are found in the Atlantic and Norkotah Russet cultivars (Table 2). Polyphenolic amines have been claimed previously to offer resistance to potato pathogens such as *Phytophthora infestans* and *Streptomyces scabies*.[24−26] Therefore, accumulation of these antimicrobial compounds can offer protection at the wound site and aid in development of an effective moisture barrier.

The polyphenolic amine biomarkers include derivatives of spermine, spermidine, tyramine, and putrescine. Among these compounds, markers for closing layer formation include kukoamine isomers (**1**, **2**), feruloyl putrescine and its isomer (**3**, **4**), N^1, N^4-bis (dihydrocaffeoyl) spermidine (**5**), N^1,N^4,N^8-tris (dihydrocaffeoyl) spermidine (**6**), feruloyl tyramine (**7**) and caffeoyl putrescine (**8**) for the Atlantic and/or Norkotah Russet cultivars.[24] By contrast, other phenolic amines are found as biomarkers for these cultivars only after the closing layer has been formed and wound periderm formation has been initiated: coumaryl putrescine (**9**) for Atlantic and N^1,N^4,N^{12} tris-(dihydrocaffeoyl)spermine (**10**) for Norkotah Russet, respectively. Feruloyl tyramine (**7**) is a Norkotah Russet marker at both day 3 and day 7 time points. Compounds **6**, **9**, and **10** are also markers for the day 7 wound-healing time point in Chipeta or Yukon Gold cultivars. The polyphenolic amine biomarkers listed in Table 2 have been reported previously in the flesh of potato tubers.[10,11] Feruloyl tyramine and related compounds are associated with the lesions and heavier skins formed by scab-infected potato tubers.[24,26] (The phenolic amine Grossamide (**11**), which is not a cultivar marker but is upregulated for all four cultivars, is discussed in the following section.) One additional unidentified biomarker (**23**) can be classified as a spermine derivative from its MS data. Finally, several of the

polyphenolic amines in Table 2 were also identified in native periderms (tuber skin) from these four potato cultivars (noted as [a] for biomarkers, [e] for nonbiomarker metabolites; Huang et al., unpublished observations).

Kaempferol glycosides (**12**−**14**) are detected as biomarkers for Norkotah Russet and Yukon Gold. Most of the glycosides are present in Yukon Gold. All glycoside compounds have been reported in potato peels[9] with the exception of Potengriffioside (**14**), which was isolated from *Solanum crinitum* Lam. tubers.[27] One common potato phenolic metabolite that is identified as a biomarker for Yukon Gold and Norkotah Russet is chlorogenic acid (**15**). Feruloyl quinic acid (**16**) is a marker specific to Norkotah Russet at days 3 and 7; ferulic acid itself (**17**), which plays an integral role in suberin formation,[28,29] is a marker for the day 3 extracts of Yukon Gold. Both **15** and **17** have been reported previously in the polar extracts from wound-healing Russet Burbank potato periderms.[14] Finally, the Atlantic and Chipeta cultivars exhibit a caffeoylquinic acid dimer biomarker (**18**) in both 3- and 7-day wound-healing samples.

Glycoalkaloids, compounds **19**−**22**, are identified as biomarkers for Chipeta and Norkotah Russet cultivars. Chaconine (**19**) and solanidine solatriose (**20**) are detected in day 3 and day 7 Chipeta samples, respectively, whereas Leptinine II (**21**) is a marker for day 3 Norkotah Russet polar extracts. Leptinine I (**22**) is a marker for day 7 extracts in all four cultivars and should thus be viewed as a marker associated with this later time point of wound-induced healing. The glycoalkaloids chaconine, leptinine II, leptinine I, and solanidine solatriose have been reported previously in the tubers of Norkotah Russet potatoes.[12] Chaconine has also been reported to be present in potato peels of diverse cultivars.[9,12] Taken together, the glycoalkaloid compounds are viewed as an important class of potato biomarkers because of their demonstrated role in resistance to pests and pathogens.[30] However, they also show concentration-dependent toxicity in organisms ranging from fungi to humans.[31,32] Due to their structural similarity to steroidal hormones, glycoalkaloids are considered additionally to be promising intermediates in the production of contraceptives and steroidal anti-inflammatory drugs.[3] Glycoalkaloids have been reported to have a wide range of bioactivities, including anticancer, anti-inflammatory, anti-nociceptive, and antipyretic effects.[32]

Biomarkers for Wound-Healing Time Point. Although the current comparisons are limited to day-3 and day-7 time points, a prior extended time course study of healing Russet Burbank tubers reported a significantly different polar metabolic profile at day 0, the onset of wound induction.[14] OPLS-DA and S-plot analysis of day-3 and day-7 wound-induced metabolite data for the four cultivars permits the identification of compounds that are more abundant at day 7, the healing time point related to the development of the nascent wound-healing periderm.[5,6] These compounds include several classes of phytochemical substances: polyphenolic amines, flavonoid glycosides, phenolic acids and glycoalkaloids. A kukoamine isomer (**1**), feruloyl putrescine isomer (**4**), N^1,N^4 bis(dihydrocaffeoyl) spermidine (**5**), grossamide (**11**), kaempferol hexoside (**12**), chlorogenic acid (**15**), ferulic acid (**17**), chaconine (**19**) leptinine I (**22**), spermine derivative (**23**) were all identified as markers specific to the day-7 healing time point., Thus, compounds produced in significantly larger quantities at the day-7 time point compared with day 3 can be associated with wound periderm development. Indeed, phenolic amines and glycoalkaloids similar to **1**, **4**, **5**, **11**, **19**, and **22** have been reported to offer resistance against microbes, insects, and herbivores.[25,33] Therefore, their accumulation during wound periderm formation could be part of the protective mechanism against infections.

The current results complement a prior GC-MS study of wound-healing samples from Russet Burbank potato periderms, in which the majority of the identified constituents were primary metabolites but phenolic compounds such as chlorogenic acid, ferulic acid, *iso*-chlorogenic acid, caffeic acid, and coniferyl alcohol were also reported.[14] No phenolic amines, flavonoid glycosides, or glycoalkaloids were identified in the earlier work, presumably because silylation produced species that exceeded the detectable m/z ratio, were only partially derivatized, or underwent side reactions rather than the desired formation of volatile derivatives.[34]

Methodological Challenges for Biomarker Identification. As shown in Figures 3−6, robust multivariate analyses can be conducted for polar periderm extracts using either NMR or LC-MS data; chemical shifts and mass-to-charge ratios of markers for cultivar type or wound-healing time point can also be extracted from S-plots in OPLS-DA analyses (Figure 1). For each of the 22 MS-derived biomarkers identified by comparison with published mass spectral data (TOF, LC-MS, and mass fragmentation) for potatoes or related plant species, we were able to simulate an NMR spectrum; the prediction could then be cross-checked against biomarker chemical shifts that had been determined from the wings of the corresponding NMR-derived S-plots. This situation is illustrated by the biomarkers for the Yukon Gold day 7 extract: for feruloyl putrescine (**3**), N^1,N^4,N^{12} tris(dihydrocaffeoyl spermine (**10**), kaempferol hexoside (**12**), potengriffioside (**14**), and chlorogenic acid (**15**), the MS-based identifications and associated NMR spectral simulations were supported by observed biomarker chemical shifts (e.g., 7.68, 7.48, 7.44, 7.32, 7.28, 7.20, 7.16, 7.04, 7.00, 6.96, 6.88, 6.84, 6.76, 6.72, 6.60, 6.56, 6.52, 6.40, 5.32, 4.26, 4.22, 3.90, 3.86, 3.82, 3.70, 3.38, 3.34, 3.30, 3.10, 2.22, 1.54, and 1.14 ppm).

For biomarkers such as **23**, however, the MS ion could not be identified because no published literature was available; it was possible to deduce its compound class from the associated MS^n fragments and to validate that supposition from the NMR-derived biomarkers. Such novel compounds then remain to be isolated and elucidated using standard but lengthy spectroscopic procedures. Even more seriously, LC-MS could miss an oligomeric biomarker i.e., give a false negative result, if the compound fails to ionize and thus goes undetected. Either previously unreported MS marker ions or biomarkers that do not ionize in MS experiments should be evident if analysis of the NMR data reveals marker shifts that fail to match the predictions for MS-identified compounds.

Although ^{1}H NMR methods have a broader detection range,[35] they suffer from considerably lower molar sensitivity than MS. A pitfall associated with this limitation is illustrated by the observed marker shifts at 5.40 and 5.44 ppm, which are consistent with NMR spectra predicted for the leptinine II glycoalkaloid (**21**), a metabolite that is accessible by LC-MS but does not satisfy biomarker criteria for the Yukon Gold day-7 polar periderm extract. The limited sensitivity of NMR could render this compound unobservable in the remaining cultivar samples, producing a false positive among the NMR-derived biomarkers. Finally, NMR-based identification of individual metabolites in an extract mixture is also challenged by incomplete spectral resolution, even when multidimensional

experiments are conducted. Although a number of promising NMR-based metabolomic identification approaches have been proposed in recent years,[36] they remain limited by the complexity of plant extract mixtures and the scope of current structural data libraries.

Complications such as those illustrated above reflect incomplete structural databases for plant-derived materials as well as limited MS ionization and NMR sensitivity capabilities, respectively, arguing for use of a conservative dual-method analysis to improve the completeness of the resulting structural profile for constituent metabolites.

ABTS$^{\bullet+}$ Scavenging Activity of Wound-Healing Extracts. As noted above, the oxidative stress associated with tuber wounding and the potential of potato-derived antioxidant compounds as food preservatives[3] together motivate quantitative assessments of such compounds in potato cultivar samples. Polar extracts of day 3 and day 7 tissue samples were screened for their free radical scavenging activities. All extracts exhibited scavenging activity, and their activities increased with incubation time (Figures 7 and 8). Thus, it may be deduced

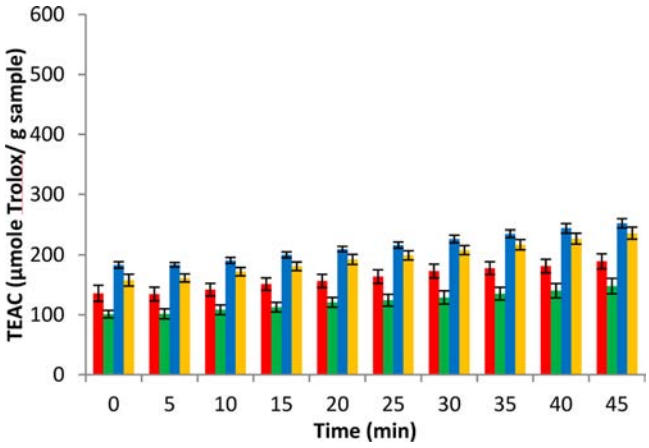

Figure 7. ABTS$^{\bullet+}$ scavenging activity of polar extracts from day 3 potato wound periderm samples expressed as TEAC (μmol Trolox/g dried sample), color coded for Atlantic (red), Chipeta (green), Norkotah Russet (blue), and Yukon Gold (gold). Values are expressed as mean ± standard error of the mean (n = 6). The assay is described fully in the text.

that the cultivars contain slow- as well as fast-acting antioxidants, underscoring the need for an assay such as ABTS$^{\bullet+}$ that measures the scavenging capability of the extracts over an extended period of time.[17] The assay has additional advantages such as absence of steric hindrance, a broad pH range, and minimal spectral interference from other natural products,[37,38] distinguishing the current investigation from previous antioxidant research on extracts from potato peels.[15,18,19]

At day 3, the order of activity among the cultivars was as follows: Yukon Gold ≈ Norkotah Russet (not significantly different, $P > 0.05$) > Atlantic > Chipeta. The order of activity was changed at day 7, to Yukon Gold > Norkotah Russet > Atlantic > Chipeta. Overall, the extracts of Yukon Gold stood out for their high scavenging activity, displaying the highest rates especially after 7 days of wound healing. Although the scavenging capability for most varieties is achieved early during closing layer development and maintained at comparable levels as a functional periderm barrier begins to develop, the Yukon Gold variety nearly doubles its scavenging activity at day 7. This

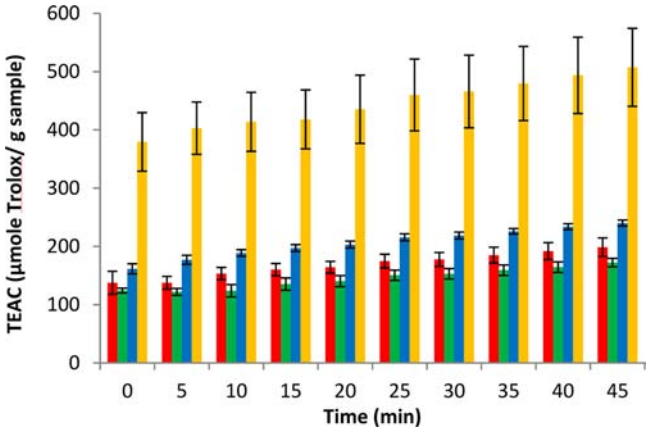

Figure 8. ABTS$^{\bullet+}$ scavenging activity of polar extracts from day 7 potato wound periderm samples expressed as TEAC (μmol Trolox/g dried sample), color coded for Atlantic (red), Chipeta (green), Norkotah Russet (blue), and Yukon Gold (gold). Values are expressed as mean ± standard error of the mean (n = 6). Note that the large standard error of the mean for Yukon day 7 extracts corresponds to a percent error that is similar to the other extracts.

increase in activity could be attributed to the accumulation of antioxidant metabolite(s) during wound periderm development, where the measured extract activity will represent the net effect of potentiation, synergism and antagonism among components of a mixture of antioxidants. The presence of biomarkers such as kaempferol hexoside (**12**), potengriffioside (**14**), and chlorogenic acid (**15**), which have established antioxidant activities,[39,40] could account for the high activity measured in the Yukon Gold extracts. At day 3, extracts of both Yukon Gold and Norkotah Russet demonstrate similar high scavenging activity so that analogously, antioxidant biomarkers such as kaempferol dihexoside (**13**) potengriffioside (**14**) chlorogenic acid (**15**), feruloylquinic acid (**16**) and ferulic acid (**17**)[41,42] could be responsible for their robust scavenging activities.

It is also instructive to compare the current antioxidant results with a prior study of unprocessed, baked and chipped tubers from Yukon Gold and Atlantic cultivars. The ABTS$^{\bullet+}$ scavenging activities, reported as TEAC values for extracts of those three preparations,[43] were much smaller than values measured herein for both day-3 and day-7 wound-healing tissue extracts from the same cultivars (Table 3). This trend persists even when the previously reported fresh-weight assessments are expressed commensurately to our dry-weight values: the scavenging activities of unprocessed tubers (presumably flesh and skin together) are ∼4−8 times lower than our late-time point wound sample, for instance. Although a portion of these differences may reflect variations in methodology, the most potent factors are likely to involve our focus on wound-healing tissues and wound induction.

The significantly higher activity observed for the current samples thus supports the potential of wound periderms as sources of antioxidants. Among the studied cultivars, Yukon Gold followed by Norkotah Russet may prove to be of highest value for future industrial applications. Moreover, time-dependent trends in antioxidant assessment can be viewed as a useful tool to monitor the wound-healing process in these potato cultivars.

Table 3. Comparison of ABTS$^{\bullet+}$ Scavenging Activities of Tissue Extracts from Atlantic and Yukon Cultivars[a]

cultivar	baked[c]	chipped[c]	unprocessed[c]	dry unprocessed[d]	dry wound periderm day 3	dry wound periderm day 7
Atlantic[b]	1.13 ± 0.12	0.09 ± 0.00	5.75 ± 0.02	57.5	189.28 ± 12.56	198.48 ± 16.01
Yukon Gold	2.30 ± 0.22	0.12 ± 0.00	6.59 ± 0.00	65.9	235.78 ± 9.51	507.38 ± 66.91

[a]The scavenging activities of the samples are expressed as TEAC (μmol Trolox/g dried sample). [b]The values are expressed as mean ± standard error of the mean (n = 6). [c]Published TEAC values were measured for tubers.[43] [d]Adjusted by estimating that the tissue is 90%-by-weight water.

CONCLUSIONS AND PROSPECTUS

The current study is the first report of secondary plant metabolites including phenolic amines, flavonoid glycosides, phenolic acids, and glycoalkaloids as biomarkers for closing layer formation and wound periderm initiation from four potato cultivars with distinctive russeting patterns. Analysis of polar extracts from these materials serves to identify 22 of 24 biomarker compounds that discriminate among the potato cultivars and between healing time points, also revealing the complementary strengths of LC-MS and NMR profiling approaches.

The most heavily russeted Norkotah Russet and Atlantic cultivars are especially rich in polyphenolic amine biomarkers, compounds with established resistance to potato pathogens.[24−26] During suberized closing layer formation (3 days healing), the polyphenolic amine markers are found preferentially in polar periderm extracts from the russeted and netted cultivars, namely Norkotah Russet and Atlantic; that marker class appears at the later day-7 wound-healing time point, if at all, for the smoother Yukon Gold and Chipeta varieties. At the day-7 time point after wound periderm formation has been initiated,[44] both NMR and LC-MS multivariate analyses show significant convergence of the polar metabolite compositions for the four cultivars, suggesting a common wound-healing response which could be compatible with the similar up-regulation patterns reported for cell wall and cell cycle genes during potato tuber wound healing for contrasting potato genotypes and after different harvests.[5] Among the biomarkers for the extracts at day 7, during the formation of the suberized waterproofing barrier, we find polyphenolic amines and glycoalkaloids that are known to confer protection against potato pathogens, pests and herbivores.[25,32] Analysis of the corresponding nonpolar extracts and developing polymeric solids, which can provide complementary information on tissue metabolism after wound induction, will be presented elsewhere.

The presence of antioxidant polyphenolic amine, flavonoid glycoside, and phenolic acid constituents among the biomarkers provides a molecular rationale for the robust radical scavenging activity measured in developing wound periderm extracts from cultivars such as Yukon Gold and Norkotah Russet during wound healing. Nonetheless, the unique rise in day-7 scavenging capability for the Yukon Gold periderm extracts reveals the possible roles of multiple metabolites and the likely interplay of potentiating, synergistic, and antagonistic effects on antioxidant activity. The antioxidants in potato peel have great potential as preservatives in the food industry.[3] As wound periderm formation is initiated, a variety of biomarkers including phenolic amines and glycoalkaloids are found to accumulate; their protective capabilities hold promise for improvements in agricultural productivity.[32,33] In addition glycoalkaloids can be potential intermediates for the production of contraceptive and steroidal anti-inflammatory drugs,[3] and they possess wide ranging bioactivities of interest in drug discovery research.[32] Thus, in addition to the agricultural significance of closing layer and wound periderm formation in potatoes, the antioxidant and biological activities of the newly identified wounding biomarkers make them potentially interesting to the food and pharmaceutical industries.

ASSOCIATED CONTENT

Supporting Information

Figures S1 and S2, overlaid NMR spectra and LC-MS chromatograms of day 7 wound periderm extracts from Norkotah, Atlantic, Chipeta, and Yukon Gold cultivars, respectively. This material is available free of charge via the Internet at http://pubs.acs.org.

AUTHOR INFORMATION

Corresponding Author

*Phone: +1 212 650 8916; fax: +1 212 650 8719; e-mail: rstark@ccny.cuny.edu.

Notes

The authors declare no competing financial interest.

ACKNOWLEDGMENTS

The authors are pleased to acknowledge the New York Structural Biology Center, a STAR center supported by the New York State Office of Science, Technology, and Academic Research and the U.S. National Institutes of Health (2G12 RR03060 from the National Center for Research Resources and 8G12MD007603 from the National Institute on Minority Health and Health Disparities), for providing access to the 800 MHz NMR spectrometer with cryomicroprobe. Dr. Lijia Yang provided expert technical assistance and access to the LC-MS/MS and LC-TOF instruments. Prof. David Jeruzalmi provided generous access to the microplate reader. Joe Nuñez (University of California Cooperative Extension) kindly provided the tubers for these analyses. Financial support for this work came from the U.S. National Science Foundation (MCB-0843627, 1411984, and 0741914 to R.E.S.) and a mobility grant from the Spanish Ministry of Education (JC2010-0147 to O.S.).

REFERENCES

(1) Spooner, D. M.; McLean, K.; Ramsay, G.; Waugh, R.; Bryan, G. J. A single domesication for potato based on multilocus amplified fragment length polymorphism genotyping. *Proc. Nat'l. Acad. Sci.* **2005**, *102*, 14694−14699.

(2) Smith, A. F. *Potato: A Global History*; Reaktion Books: London, 2012.

(3) Schieber, A.; Saldana, M. D. A. Potato peels: A source of nutritionally and pharmacologically interesting compounds-A review. *Food* **2008**, *3*, 23−29.

(4) Varns, J. L.; Schaper, L. A.; Preston, D. A. Potato losses during the first three months of storage for processing. *Am. Potato J.* **1985**, *62*, 91−99.

(5) Neubauer, J. D.; Lulai, E. C.; Thompson, A. L.; Suttle, J. C.; Bolton, M. D. Wounding coordinately induces cell wall protein, cell cycle and pectin methyl esterase genes involved in tuber closing layer and wounding periderm development. *J. Plant Physiol.* **2012**, *169*, 586−595.

(6) Lulai, E. C.; Corsini, D. L. Differential deposition of suberin phenolic and aliphatic domains and their roles in resistance to infection during potato tube (*Solanum tuberosum* L.) wound healing. *Physiol. Mol. Plant P.* **1998**, *53*, 209−222.
(7) Ginzberg, I.; Barel, G.; Ophir, R.; Tzin, E.; Tanami, Z.; Muddarangappa, T.; de Jong, W.; Fogelman, E. Transcriptomic profiling of heat-stress response in potato periderm. *J. Exp Bot.* **2009**, *60*, 4411−4421.
(8) Love, S. L.; Werner, B. K.; Pavek, J. J. Selection for individual traits in the early generations of a potato breeding program dedicated to producing cultivars with tubers having long shape and russet skin. *Am. Potato J.* **1997**, *74*, 199−213.
(9) Ieri, F.; Innocenti, M.; Andrenelli, L.; Vecchio, V.; Mulinacci, N. Rapid HPLC/DAD/MS method to determine phenolic acids, glycoalkaloids and anthocyanins in pigmented potatoes (*Solanum tuberosum* L.) and correlations with variety and geographical origin. *Food Chem.* **2011**, *125*, 750−759.
(10) Parr, A. J.; Mellon, F. A.; Colquhoun, I. J.; Davis, H. E. Dihydrocaffeoyl polyamines (kukoamine and allies) in potato (*Solanum tuberosum*) tubers detected during metabolite profiling. *J. Agric. Food Chem.* **2005**, *56*, 6949−6958.
(11) Narvaez-Cuenca, C.-E.; Vincken, J.-P.; Zheng, C.; Gruppen, H. Diversity of (dihydro) hydroxycinnamic acid conjugates in Columbian potato tubers. *Food Chem.* **2013**, *139*, 1087−1097.
(12) Shakya, R.; Navarre, D. A. LC-MS analysis of solanidane glycoalkaloids diversity among tubers of four wild potato species and three cultivars (*Solanum tuberosum*). *J. Agric. Food Chem.* **2008**, *56*, 6949−6958.
(13) Yang, M.; Bernards, M. A. Wound-induced metabolism in potato (*Solanum tuberosum*) tubers. *Plant Sig. Behav.* **2006**, *1*, 59−66.
(14) Yang, W.-L.; Bernards, M. A. Metabolite profiling of potato (*Solanum tuberosum* L.) tubers during wound-induced suberization. *Metabol.* **2007**, *3*, 147−159.
(15) Reyes, L. F.; Cisneros-Zevallos, L. C. Wounding stress increases the phenolic content and antioxidant capacity of purple-flesh potatoes (*Solanum tuberosum* L.). *J. Agric. Food Chem.* **2003**, *51*, 5296−5300.
(16) Reyes, L. F.; Villarreal, J. E.; Cisneros-Zevallos, L. The increase in antioxidant capacity after wounding depends on the type of fruit or vegetable tissue. *Food Chem.* **2007**, *101*, 1254−1262.
(17) Re, R.; Pellegrini, N.; Pannala, A.; Yang, M.; Rice-Evans, C. Antioxidant activity applying an improved ABTS radical cation decolorization assay. *Free Radical Biol. Med.* **1999**, *26*, 1231−1237.
(18) Ji, X.; Rivers, L.; Zielinski, Z.; Xu, M.; MacDougall, E.; Stephen, J.; Zhang, S.; Wang, Y.; Chapman, R. G.; Keddy, P.; Robertson, G. S.; Kirby, C. W.; Embleton, J.; Worrall, K.; Murphy, A.; De Koeyer, D.; Tai, H.; Yu, L.; Charter, E.; Zhang, J. Quantitative analysis of phenolic components and glycoalkaloids from 20 potato clones and in vitro evaluation of antioxidant, cholesterol uptake, and neuroprotective activities. *Food Chem.* **2012**, *133*, 1178−1187.
(19) Nara, K.; Miyoshi, T.; Honma, T.; Koga, H. Antioxidant activity of bound-form phenolics in potato peels. *Biosci. Biotechnol. Biochem.* **2006**, *70*, 1489−1491.
(20) Kim, H. K. C.; Y, H.; Verpoorte, R. NMR-based metabolomics analysis of plants. *Nat. Protoc.* **2010**, *5*, 536−549.
(21) Choi, H.-K.; Choi, Y. H.; Verberne, M.; Lefeber, A. W. M.; Erkelens, C.; Verpoorte, R. Metabolic fingerprinting of wild type and transgenic tobacco plants by ^{1}H NMR and multivariate analysis technique. *Phytochemistry* **2004**, *65*, 857−864.
(22) Navarre, D. A.; Pillai, S. S.; Shakya, R.; Holden, M. J. HPLC profiling of phenolics in diverse potato genotypes. *Food Chem.* **2011**, *127*, 34−41.
(23) Katajamaa, M.; Miettinen, J.; Orešič, M. MZmine: Toolbox for processing and visualization of mass spectrometry based molecular profile data. *Bioinformatics* **2006**, *22*, 634−636.
(24) King, R. R.; Calhoun, L. A. Characterization of cross-linked hydroxycinnamic acid amides isolated from potato common scab lesions. *Phytochemistry* **2005**, *66*, 2468−2473.
(25) Back, K. Hydroxycinnamic acid amides and their possible utilization for enhancing agronomic traits. *Plant Pathology J.* **2001**, *17*, 123−127.
(26) King, R. R.; Calhoun, L. A. A feruloyltyramine trimer isolated from potato common scab lesions. *Phytochemistry* **2010**, *71*, 2187−2189.
(27) Cornelius, M. T. F.; de Carvalho, M. G.; da Silva, T. M. S.; Alves, C. C. F.; Siston, A. P. N.; Alves, K. Z.; Sant'Anna, C. M. R.; Neto, M. B.; Eberlin, M. N.; Braz-Filho, R. Other chemical constituents isolated from *Solanum crinitum* Lam. (Solanaceae). *J. Braz. Chem. Soc.* **2010**, *21*, 2211−2219.
(28) Bernards, M. A. Demistifying suberin. *Can. J. Bot.* **2002**, *80*, 227−240.
(29) Graca, J.; Santos, S. Suberin: A biopolyester of plant's skin. *Macromol. Biosci.* **2007**, *7*, 128−135.
(30) Savarese, S.; Andolfi, A.; Cimmino, A.; Carputo, D.; Frusciante, L.; Evidente, A. Glycoalkaloids as biomarkers for recognition of cultivated, wild and somatic hybrids of potato. *Chem. Biodiver.* **2009**, *6*, 437−446.
(31) Valcarcel, J.; Reilly, K.; Gaffney, M.; O' Brien, N. Effect of genotype and environment on the glycoalkaloid content of rare, heritage and commercial potato variaties. *J. Food Sci.* **2014**, *79*, T1039−T1048.
(32) Milner, S. E.; Brunton, N. P.; Jones, P. W.; O' Brien, N. M.; Collins, S. G.; Maguire, A. R. Bioactivities of glycoalkaloids and their aglycones from *Solanum tuberosum*. *J. Agric. Food Chem.* **2011**, *59*, 3454−3484.
(33) Bassard, J.-E.; Ulmann, P.; Bernier, F.; Werck-Reichhart, D. Phenolamides: Bridging polyamine to the phenolic metabolism. *Phytochemistry* **2010**, *71*, 1808−1824.
(34) Halket, J. M.; Waterman, D.; Przyborowska, A. M.; Patel, R. K. P.; Fraser, P. D.; Bramley, P. M. Chemical derivatization and mass spectral libraries in metabolite profiling by GC/MS and LC/MS/MS. *J. Exp. Bot.* **2005**, *56*, 219−243.
(35) van der Kooy, F.; Maltese, F.; Choi, Y. H.; Kim, H. K.; Verpoorte, R. Quality control of herbal material and phytopharmaceuticals with MS and NMR based metabolic fingerprinting. *Planta Med.* **2009**, *75*, 763−775.
(36) Robinette, S.; Zhang, F.; Bruschweiler-Li, L.; Bruschweiler, R. Web server based complex mixture analysis by NMR. *Anal. Chem.* **2008**, *80*, 3606−3611.
(37) Magalhaes, L. M.; Segundo, M. A.; Reis, S.; Lima, J. L. F. C. Methodological aspects about in vitro evaluation of antioxidant properties. *Anal. Chim. Acta* **2008**, *613*, 1−19.
(38) Prior, R. L.; Wu, X.; Schaich, K. Standardized methods for the determination of antioxidant capacity and phenolics in foods and dietary supplements. *J. Agric. Food Chem.* **2005**, *53*, 4290−4302.
(39) Shafek, R. E.; Shafik, N. H.; Michael, H. N. Antibacterial and antioxidant activities of two new kaempferol glycosides isolated from *Solenostemma argel* stem extract. *Asian J. Plant Sci.* **2012**, *11*, 143−147.
(40) Amakura, Y.; Yoshimura, M.; Yamakami, S.; Yoshida, T. Isolation of phenolic constituents and characterization of antioxidant markers from sunflower (*Helianthus annuus*) seed extract. *Phytochem. Lett.* **2013**, *6*, 302−305.
(41) Hadjipavlou-Litina, D.; Garnelis, T.; Athanassopoulos, C. M.; Papaioannou, D. Kukoamine A analogs with lipoxygenase inhibitory activity. *J. Enz. Inhib. Med. Chem.* **2009**, *24*, 1188−1193.
(42) Mozdzan, M.; Szemraj, J.; Rysz, J.; Stolarek, R. A.; Nowak, D. Antioxidant activity of spermine and spermidine re-evaluated with oxidizing systems involving iron and copper ions. *Int. J. Biochem. Cell B* **2006**, *38*, 69−81.
(43) Madiwale, G. P.; Reddivari, L.; Stone, M.; Holm, D. G.; Vanamala, J. Combined effects of storage and processing on the bioactive compounds and pro-apoptotic properties of color-fleshed potatoes in human colon cancer. *J. Agric. Food Chem.* **2012**, *60*, 11088−11096.
(44) Morris, S. C.; Forbes-Smith, M. R.; Scriven, F. M. Determination of optimum conditions for suberization, wound periderm formation, cellular desiccation and pathogen resistance in

wounded *Solanum tuberosum* tubers. *Physiol. Mol. Plant P.* **1989**, *36*, 177−190.
(45) Wu, S.-B.; Meyer, R. S.; Withaker, B. D.; Litt, A.; Kennelly, E. J. A new liquid chromatography-mass spectrometry based strategy to integrate chemistry, morphology, and evolution of eggplant species. *J. Chrom. A* **2013**, *1314*, 154−172.
(46) Matsuda, F.; Morino, K.; Ano, R.; Kuzawa, M.; Wakasa, K.; Miyagawa, H. Metabolic flux analysis of the phenylpropanoid pathway in elicitor-treated potato tuber tissue. *Plant Cell Physiol.* **2005**, *46*, 454−466.
(47) Clifford, M. N.; Wu, W.; Kirkpatrick, J.; Jaiswal, R.; Kunhnert, N. Profiling and characterization by liquid chromatography/multi-stage mass spectrometry of the chlorogenic acids in *Gardeniae fructus*. *Rapid Commun. Mass Sp.* **2010**, *24*, 3109−3120.
(48) Panusa, A.; Zuorro, A.; Lavecchia, R.; Marrosu, G.; Petrucci, R. Recovery of natural antioxidants from spent coffee grounds. *J. Agric. Food Chem.* **2013**, *61*, 4162−4168.
(49) Jaiswal, R.; Matei, M. F.; Golon, A.; Witt, M.; Kunhnert, N. Understanding the fate of chlorogenic acids in coffee roasting using mass spectrometry based targeted and non-targeted analytical strategies. *Food Funct.* **2013**, *3*, 976−984.
(50) Gomez-Romero, M.; Segura-Carretero, A.; Fernandez-Gutierrez, A. Metabolite profiling and quantification of phenolic compounds in methanol extracts of tomato fruit. *Phytochemistry* **2010**, *71*, 1848−1864.
(51) Mader, J.; Harshadrai, R.; Kroh, L. W. Composition of phenolic compounds and glycoalkaloids α-Solanine and α-Chaconine during commercial potato processing. *J. Agric. Food Chem.* **2009**, *57*, 6292−6297.

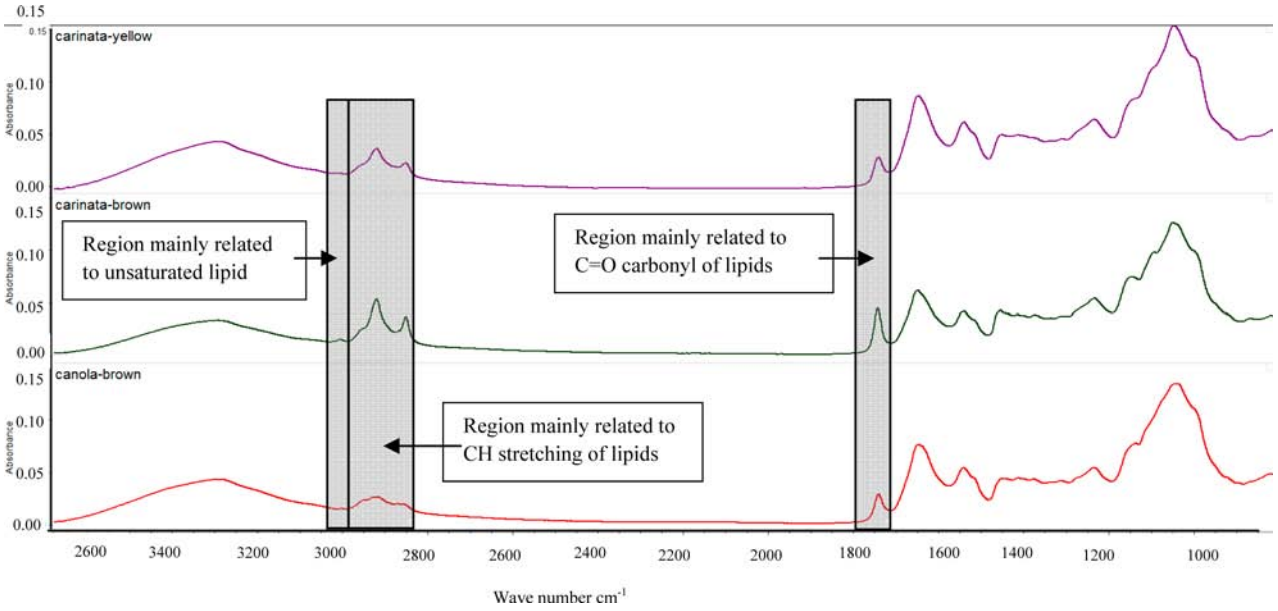

Figure 1. Typical ATR-FT/IR molecular spectrum of *B. carinata* seeds and canola seed (as a reference control) in the mid-IR region ca. 4000−800 cm^{-1}.

unsaturated lipid bands (ULB), and lipid ester C═O carbonyl (LECC) using ATR-FT/IR spectroscopy, between the yellow-seeded and brown-seeded *B. carinata*. Canola seeds were used as a reference. The second objective was to determine the relationship between the molecular spectral data and the contents of oil, fatty acid and glucosinolate profiles, total polyphenols, and condensed tannins in the oilseed.

MATERIALS AND METHODS

Seed Sampling and Processing. Seeds from newly developed yellow-seeded (AAC A100) and brown-seeded (110915EM) lines of *B. carinata* were evaluated in the present study. These two carinata lines were bred for the industrial oil market using traditional pedigree breeding methods. Canola seed with a brown seed coat was used as a reference. Samples (n = 4) from all seed types were obtained from plots at the Saskatoon Research Centre experimental farm of Agriculture and Agri-Food Canada (AAFC) and from contra-season research plots in the central region of Chile during the winter of 2010/2011. Each seed type was obtained from two replicate plots in each location.

For wet chemical and spectral analysis, seeds were ground in a coffee grinder (PC770, Loblaws Inc., Toronto, Canada) for 10 s, then chilled, and reground for another 10 s.

Oil Content and Fatty Acid Profile Determination. The samples (~0.500 g) were analyzed for oil content according to the standard procedure of AOAC (method 920.39).[18] Fat from the ground oilseeds (~0.375 g) was extracted with chloroform/methanol (2:1 v/v) according to the method of Folch et al.[19] with slight modification as described by Khan et al.[20] Tridecanoic acid (C13:0) was used as an internal standard. The fatty acids were separated and quantified using gas chromatography as described by Khan et al.[21] All samples were analyzed in duplicate and repeated if error exceeded the acceptable level of each analysis.

Determination of Glucosinolates, Polyphenols, and Condensed Tannins. All seed samples (~0.100 g) were analyzed for glucosinolate profile according to the official method of the Canadian Grain Commission.[22] The method of Slinkard and Singleton[23] was used to analyze the contents of total polyphenols in samples (~1.00 g). The HCl−butanol procedure as described by Reed[24] was used to analyze the content of condensed tannins in the seeds (~0.050 g). All samples were analyzed in duplicate and repeated if error exceeded the acceptable level of each analysis.

Lipid Molecular Structure by ATR-FTIR Spectroscopy. The lipid-related molecular structural band intensities (Figure 1) of each sample were generated in the mid-IR region (ca. 4000−800 cm^{-1}) with 128 co-added scans at a spectral resolution of 4 cm^{-1} in a transmission mode, using a JASCO FT/IR 4200 with ATR (JASCO Corp., Tokyo, Japan). Each sample was run six times. The spectral data were collected with JASCO Spectra Manager II software, and the lipid-related spectral band intensities were quantified using OMNIC 7.2 software (Madison, WI, USA). The lipid-related functional bands including asymmetric CH_3 (CH_3-as, ca. 2959 cm^{-1}), asymmetric CH_2 (CH_2-as, ca. 2921 cm^{-1}), symmetric CH_3 (CH_3-s, ca. 2871 cm^{-1}), symmetric CH_2 (CH_2-s, ca. 2853 cm^{-1}), ULB (ca. 3008 cm^{-1}), and LECC (ca. 1744 cm^{-1}) were identified according to published methodologies.[15,25,26] The asymmetric and symmetric CH_3 and CH_2 stretching bands were identified in the CH region (ca. 2999−2800 cm^{-1}) of the original spectra, using the second-derivative and Fourier self-deconvolution functions of the OMNIC 7.2 software. The spectral peak height, area, and their ratios were calculated from the original spectra.

Multivariate Spectral Analysis. Agglomerative hierarchical cluster analysis (AHCA) and principal component analysis (PCA), as described in detail earlier,[27−30] were performed on the overall data of lipid-related spectral bands, to visualize and classify the differences in the inherent molecular structures of lipids among the three types of oilseeds. The overall spectral data of CH_3 and CH_2 asymmetric and symmetric stretchings (ca. 2999−2800 cm^{-1}), ULB (ca. 3035−2991 cm^{-1}), and LECC (ca. 1788−1707 cm^{-1}) regions were used for multivariate analyses. The AHCA results are presented as dendrograms using the linkage distance method and Ward's algorithm cluster method without prior parametrization. The PCA results are presented as a scatter plot between the first principal factor and the second principal factor, based on loading scores. These analyses were carried out using Statistica software (version 8, StatSoft Inc., Tulsa, OK, USA).

Statistical Analysis. Data on the oil content, fatty acid and glucosinolate profiles, polyphenols, and condensed tannins and univariate lipid spectral data were statistically analyzed using the Mixed Model procedure of the Statistical Analysis System (SAS version 9.2, SAS Institute Inc., Cary, NC, USA). The following model was used:

$$Y_{ijk} = \mu + F_i + S(F)_j + e_{ijk}$$

Table 1. Oil Content and Fatty Acid Profile in the Yellow- and Brown-Seeded *B. carinata* with Comparison to Canola Seeds

	carinata					contrast, *P* value	
	yellow[a]	brown[a]	canola brown[a]	SEM[b]	*P* value	carinata vs canola	carinata (yellow vs brown)
oil, % DM	41.36b	39.45b	46.27a	0.36	0.002	0.001	0.03
total fatty acids, mg/g oil	913.21	914.34	912.33	1.98	0.780	0.590	0.710
fatty acids profile, % total fatty acids							
C14:0, myristic acid	0.07	0.05	0.06	0.01	0.36	0.671	0.202
C16:0, palmitic acid	3.07	2.73	3.79	0.09	0.01	0.004	0.091
C16:1n-7, palmitoleic acid	0.19b	0.18b	0.33a	0.01	0.001	0.001	0.352
C17:0, margaric acid	0.12b	0.10c	0.13a	0.00	<0.001	<0.001	<0.001
C18:0, stearic acid	1.07b	0.94b	1.91a	0.03	0.001	<0.001	0.043
C18:1n-9, oleic acid	8.67b	7.44b	61.73a	0.66	<.001	<0.001	0.282
C18:1, octadecenoic acid	0.77b	0.65b	2.63a	0.04	0.001	<0.001	0.163
C18:2n-6, linoleic acid	15.0b	14.7b	18.4a	0.13	0.001	<0.001	0.281
C18:3n-3, α-linolenic acid	12.7a	12.1a	7.88b	0.32	0.003	<0.001	0.260
C20:0, arachidic acid	0.91a	0.91a	0.63b	0.01	<.0.001	<0.001	1.000
C20:1, eicosenoic acid	8.73a	7.54b	1.37c	0.03	<0.001	<0.001	<0.001
C20:2n-6, eicosadienoic acid	0.98a	0.91b	0.08c	0.00	<0.001	<0.001	0.002
C20:3n-3, eicosatrienoic acid	0.17	0.15	ND[c]	0.01	0.110		
C22:0, behenic acid	0.79b	0.87a	0.34c	0.01	<0.001	<0.001	0.005
C22:1n-9, erucic acid	41.3b	45.0a	0.12c	0.07	<0.001	<0.001	<0.001
C22:2n-9, docosadienoic acid	0.63b	0.79a	ND	0.01	0.002		
C22:2n-6, docosadienoic acid	1.42b	1.64a	ND	0.01	0.004		
C24:0, lignoceric acid	0.58b	0.64a	0.14c	0.01	<.001	<0.001	0.014
C24:1n-9, nervonic acid	2.04a	1.94b	0.13c	0.01	<0.001	<0.001	0.022
total SFA[d]	6.60ab	6.25b	6.99a	0.07	0.01	0.01	0.043
total MUFA[e]	61.60b	62.72b	66.33a	0.54	0.02	0.01	0.253
total PUFA[f]	30.91a	30.32a	26.42b	0.43	0.01	0.004	0.422
total n-3 fatty acids	12.92a	12.20a	7.88b	0.32	0.003	0.001	0.251
total n-6 fatty acids	17.42b	17.30b	18.52a	0.14	0.01	0.01	0.700
total n-9 fatty acids	61.32	62.73	63.33	0.59	0.19	0.16	0.200

[a]Means with different letters in the same row are significantly different ($P < 0.05$). [b]SEM, standard error of the mean. [c]ND, not determined. [d]Saturated fatty acids. [e]Monounsaturated fatty acids. [f]Polyunsaturated fatty acids.

Y_{ijk} is the observation of the dependent variable *ijk*; μ is the population mean; F_i was a fixed effect of seed type (i = 3; yellow-seeded *B. carinata*, brown-seeded *B. carinata*, and canola seed); $S(F)_j$ is the random effect of seed source (location: Saskatoon, Canada, vs Chile) nested within seed; e_{ijk} is the random error associated with the observation *ijk*. Statistical significance was declared and detected at $P < 0.05$.

The strength of relationships between the oil content, fatty acid and glucosinolate profiles, condensed tannins, and the lipid-related functional band intensities in the oilseeds was analyzed by the PROC CORR procedure of SAS using the Pearson correlation method. Multiple regression analyses, with stepwise variable selection, were performed using the PROC REG procedure of SAS to determine the lipid molecular spectral features that can be used to estimate oil content, fatty acid composition, glucosinolates, polyphenols, and condensed tannins in the oilseeds. The independent variables tested include CH_3-as, CH_2-as, CH_3-s, CH_2-s, ULB, and LECC. All variables left in the final model were significant at the 0.05 level.

RESULTS AND DISCUSSION

Oil Content and Fatty Acid Profile. The results of oil content and fatty acid profile of yellow-seeded and brown-seeded *B. carinata* in comparison with canola seeds are presented in Table 1. In the *Brassica* family, oil content, ranging from 17 to >40%, is one of the most important features of the seed.[31] The oil contents varied among the seed types, and canola seeds had higher ($P = 0.02$) oil content than the carinata. The yellow-seeded line had 1.91% higher ($P = 0.03$) oil content than the brown-seeded line, which could be related to their larger seed size and thinner seed coat, which results in a relatively greater proportion of cotyledons and endosperm (oil containing mass) and a smaller proportion seed coat (fiber-containing mass) compared to the brown-seeded varieties.[32] Getinet et al.[32] argued that the yellow-seeded lines should be further developed for high seed weight and oil and protein contents in future breeding projects. The oil content of *B. carinata* seeds observed in this study is approximately 2−14 units higher than the values reported in previous studies.[2,13,33] This could be related to the recent progress in achieving the breeding targets of the *B. carinata* seed improvement programs, which has been focused on increasing the oil content of the seeds at the expense of other nutrients such as protein and fiber.[32,33] In agreement with our findings, Taylor et al.[13] observed lower oil contents in *B. carinata* seed compared to canola seed cultivated at three different locations in western Canada.

The total fatty acid content, as a proportion of the oil, did not differ among the oilseeds (Table 1). However, the fatty acid composition of the oil, particularly long-chain fatty acids, differed among the oilseeds. The brown-seeded *B. carinata* had lower ($P < 0.05$) contents of C17:0, C20:1, C20:2n-6, C24:1n-9, and total saturated fatty acids and higher ($P < 0.05$) contents of C22:0, C22:1n-9, and C24:0 than the yellow-seeded line (Table 1). Little information could be found on the comparison of fatty acid profile of yellow- and brown-seeded *B. carinata* lines; however, all of the individual fatty acid proportions of *B. carinata* seed were within the ranges reported by Velasco et al.[34] and Warwick et al.[2] for *B. carinata* germplasm in Germany

Table 2. Contents of Glucosinolates, Polyphenols, and Condensed Tannins in the Yellow- and Brown-Seeded Carinata with Comparison to Canola Seeds

	carinata					contrast, *P* value	
	yellow[a]	brown[a]	canola brown[a]	SEM[b]	*P* value	carinata vs canola	carinata (yellow vs brown)
glucosinolates, μmol/g[c]							
allyl glucosinolate	83.40	84.41	ND[d]	1.92	0.750		
3-butenyl glucosinolate	0.50	0.80	2.25	0.43	0.120	0.061	0.661
4-pentenyl glucosinolate	ND	0.10	0.30	0.07	0.180		
2-OH-3-butenyl glucosinolate	0.65b	1.50b	4.75a	0.55	0.030	0.012	0.352
2-OH-4-pentenyl glucosinolate	0.10	0.10	0.15	0.03	0.460	0.250	1.000
CH_3-thiobutenyl glucosinolate	ND	ND	0.15	0.05			
phenylethyl glucosinolate	ND	ND	0.10	0.00			
CH_3-thiopentenyl glucosinolate	ND	ND	0.10	0.00			
3-CH_3-indolyl glucosinolate	0.10b	0.10b	0.40a	0.00	<0.001	<0.001	1.000
4-OH-3-CH_3-indolyl glucosinolate	2.35b	1.95b	4.80a	0.30	0.01	0.011	0.423
total glucosinolates	87.0a	88.9a	12.9b	2.10	0.002	<0.001	0.583
total polyphenols, mg/g	6.65a	6.58a	5.71b	0.11	0.010	0.012	0.672
condensed tannins, % DM[e]	0.28	0.30	0.27	0.01	0.210	0.193	0.201

[a]Means with the different letters in the same row are significantly different ($P < 0.05$). [b]SEM, standard error of the mean. [c]Until otherwise stated. [d]ND, not detected. [e]DM, dry matter.

Table 3. Lipids CH_3 and CH_2 Asymmetric and Symmetric Stretching Band, Unsaturated Band, and Carbonyl Ester C═O Stretching Band Profiles in the Yellow- and Brown-Seeded Carinata with Comparison to Canola Seeds, Revealed Using Infrared Molecular Spectroscopy

	carinata					contrast, *P* value	
	brown[a]	yellow[a]	canola brown[a]	SEM[b]	*P* value	carinata vs canola	carinata (yellow vs brown)
CH_3 and CH_2 stretching profiles[c]							
CH_3 asymmetric (CH_3-as) height	0.011a	0.011a	0.008b	0.0003	<0.001	<0.001	0.800
CH_2 asymmetric (CH_2-as) height	0.037a	0.033a	0.010b	0.0012	<0.001	<0.001	0.030
CH_3 symmetric (CH_3-s) height	0.011a	0.011a	0.008b	0.0002	<0.001	<0.001	0.750
CH_2 symmetric (CH_2-s) height	0.023a	0.020a	0.006b	0.0009	<0.001	<0.001	0.030
CH_3 and CH_2 stretching area	2.417a	2.277a	1.052b	0.0667	<0.001	<0.001	0.150
unsaturated lipid bands (ULB) profiles[d]							
ULB height	0.001a	0.001a	0.000b	0.0002	<0.001	<0.001	1.000
ULB area	0.023a	0.021a	0.001b	0.0022	<0.001	<0.001	0.550
lipid ester C═O carbonyl (LECC) profiles[e]							
LECC height	0.031a	0.029a	0.016b	0.0017	<0.001	<0.001	0.340
LECC area	0.677a	0.641a	0.363b	0.0375	<0.001	<0.001	0.500
spectral ratio profile							
height ratio of CH_3-as:CH_2-as	0.305b	0.337b	0.800a	0.0226	<0.001	<0.001	0.310
height ratio of CH_3-as:CH_3-s	0.997b	1.000b	1.068a	0.0156	0.004	0.001	0.900
height ratio of CH_3-s:CH_2-s	0.493b	0.556b	1.298a	0.0489	<0.001	<0.001	0.370
height ratio of CH_2-as:CH_2-s	1.608	1.646	1.723	0.0334	0.060	0.030	0.440
height ratio of asymmetric:symmetric	1.406a	1.414a	1.351b	0.0117	0.001	<0.001	0.630
area ratio of ULB:CH stretchings	0.000	0.000	0.000	0.0001	0.260	0.100	1.000
area ratio of LECC:CH stretchings	0.013	0.013	0.015	0.0009	0.200	0.100	0.820
height ratio of ULB:LECC	0.038a	0.044a	0.005b	0.0048	0.020	0.010	0.450
area ratio of ULB:LECC	0.031a	0.032a	0.003b	0.0027	0.010	0.003	0.940

[a]Means with the different letters in the same row are significantly different ($P < 0.05$). [b]SEM, standard error of the mean. [c]Lipid data measured in IR absorbance units; CH_3 and CH_2 stretching peak baseline, 2999−2800 cm^{-1} with CH_3-as, CH_2-as CH_3-s, and CH_2-s peaks centered at 2959, 2921, 2871, and 2853 cm^{-1}, respectively, and their peak regions were ca. 2959−2955, 2932−2919, 2873−2871, and 2860−2851 cm^{-1}, respectively. [d]Unsaturated lipid bands (ULB) peak baseline, ca. 3035−2991 cm^{-1}; peak region was ca. 3009−3003 cm^{-1}. [e]Lipid ester C═O carbonyl (LECC) peak baseline, ca. 1788−1707 cm^{-1}; peak region was ca. 1745−1738 cm^{-1}.

and western Canada, respectively. The *B. carinata* seed oil was quite different from canola seed oil in almost all individual fatty acid contents. The largest differences between *B. carinata* and canola seed were observed in the contents (% of total fatty acids) of C18:1n-9, C18:3n-3, and C22:1n-9 (Table 1). During the biosynthesis of fatty acids in plants, the C18:0 fatty acids are first desaturated to C18:1n-9, which is then elongated to C22:1n-9 or desaturated to C18:3n-3 by the "prokaryotic pathway" (in plastids) and the "eukaryotic pathway" (in the endoplasmic reticulum) by different fatty acid elongases and desaturases.[35−38] C18:1n-9 is the main precursor of these two biosynthetic pathways. The significantly higher levels C22:1n-9 in *B. carinata* seed in our study showed that C18:1n-9 had been extensively and preferentially elongated to C22:1n-9 compared

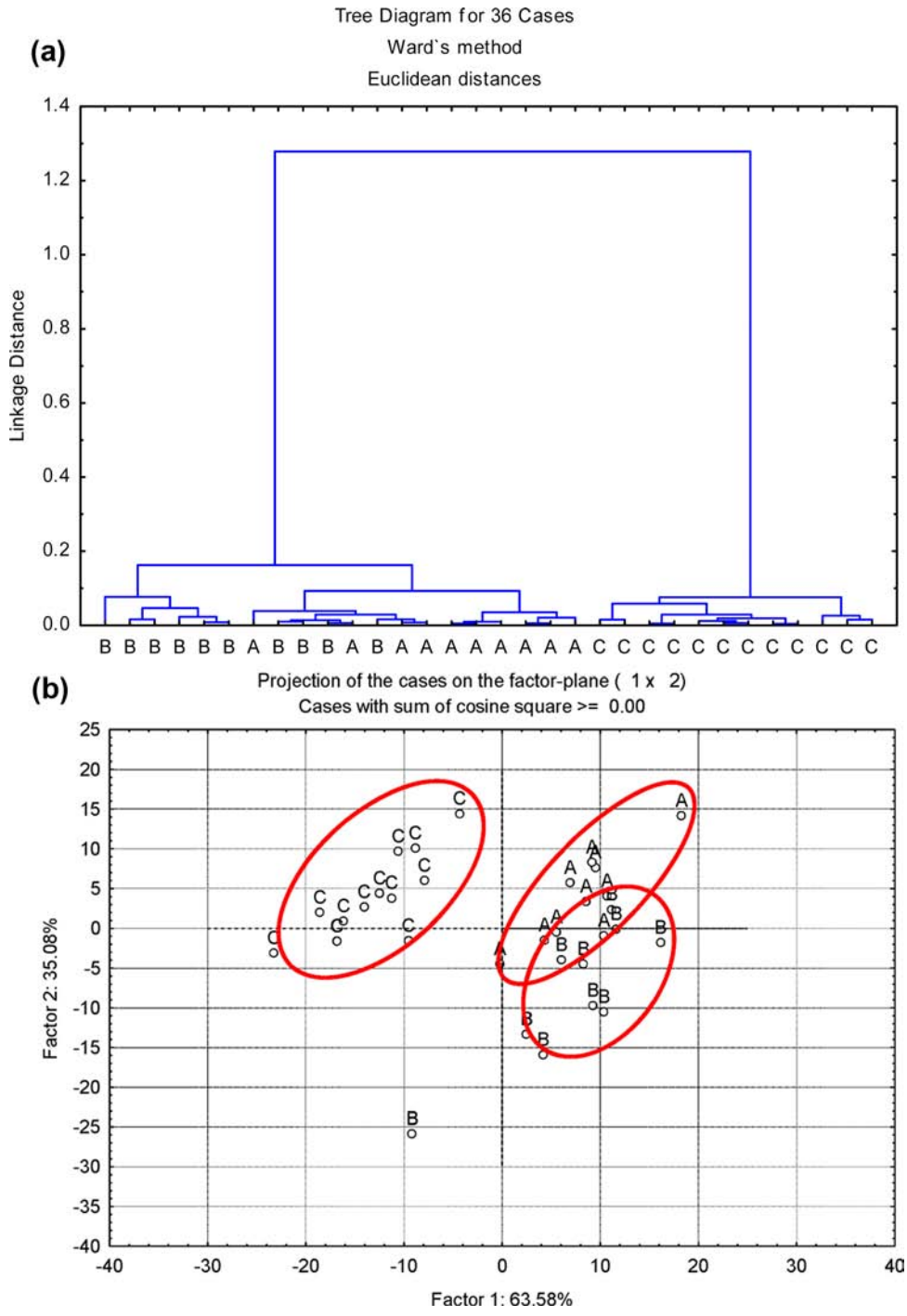

Figure 2. Agglomerative hierarchical cluster analysis (CLA) dendrograms (a) and principal component analysis (PCA) scatter plot (b) visualizing the differences in CH_3 and CH_2 asymmetric and symmetric stretching (2999−2800 cm^{-1}) bands among different oilseeds: A, yellow-seeded *B. carinata*; B, brown-seeded *B. carinata*; C, canola seed.

to in canola seed. Moreover, C18:1n-9 is also preferentially desaturated to C18:3n-3 in *B. carinata* seed. Although not suitable for human consumption, oilseeds bearing a high content of C22:1n-9 could be used as a valuable feedstock for biodiesel production[6,8] and for other industrial applications such as plastics, lubricants, and cosmetics products.[9,39,40] Environmental conditions such as differences in growing season and temperature can influence the oil content and fatty acid compositions;[3,41,42] our study revealed consistent differences in the oilseeds grown in western Canada and contra-season (data not shown). Across the oilseeds, C16:0 (2.73−3.79%) was the major saturated fatty acid, followed by C18:0, C20:0, C22:0, and C24:0, and only small amounts (<0.1%) of C14:0 and C17:0 were detected in the oilseeds. No differences were observed between the yellow-seeded and brown-seeded *B. carinata* ($P > 0.05$) in the contents of total n-3, n-6, and n-9 fatty acids. However, the contents of total n-3 and n-6 fatty acids were 1.6 ($P = 0.001$) and 0.9 times ($P = 0.01$) higher in *B. carinata* seed than those in canola seed.

Glucosinolates, Polyphenols, and Condensed Tannins. Table 2 presents the contents of glucosinolates, polyphenols, and condensed tannins in the yellow-seeded and

dx.doi.org/10.1021/jf502209x | J. Agric. Food Chem. 2014, 62, 7977−7988

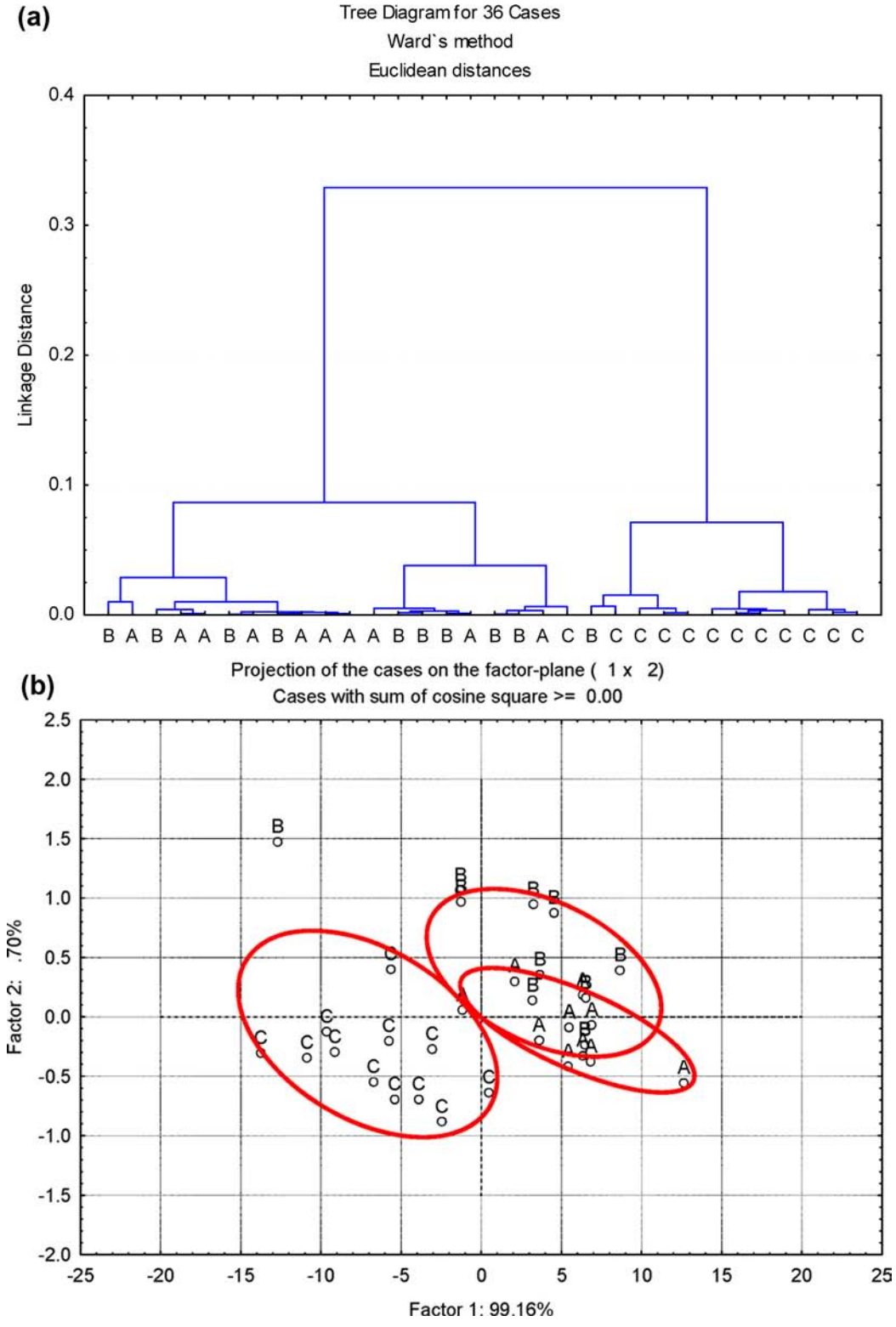

Figure 3. Agglomerative hierarchical cluster analysis (CLA) dendrograms (a) and principal component analysis (PCA) scatter plot (b) visualizing the differences in the unsaturated lipid (3035−2991 cm^{-1}) bands among different oilseeds: A, yellow-seeded *B. carinata*; B, brown-seeded *B. carinata*; C, canola seed.

brown-seeded *B. carinata* in comparison with canola. The total glucosinolate content was markedly higher ($P < 0.001$; 87.0−88.9 vs 12.96 μmol/g) in *B. carinata* seed compared to canola. Glucosinolates are a group of sulfur-containing glycosides produced by plants in the *Brassica* family. To our knowledge, more than 130 types of glucosinolates have been identified so far, starting from 170 years ago when sinigrin was first found in mustard (*Brassica juncea*). Within this large glucosinolate family, allyl glucosinolates usually account for >95% of the total alkenyl glucosinolate,[43,44] which is the sum of allyl, 3-butenyl, 4-pentenyl, 2-OH-3-butenyl, and 2-OH-4-pentenyl in *B. carinata* seed. In our study, allyl glucosinolates accounted for

dx.doi.org/10.1021/jf502209x | J. Agric. Food Chem. 2014, 62, 7977−7988

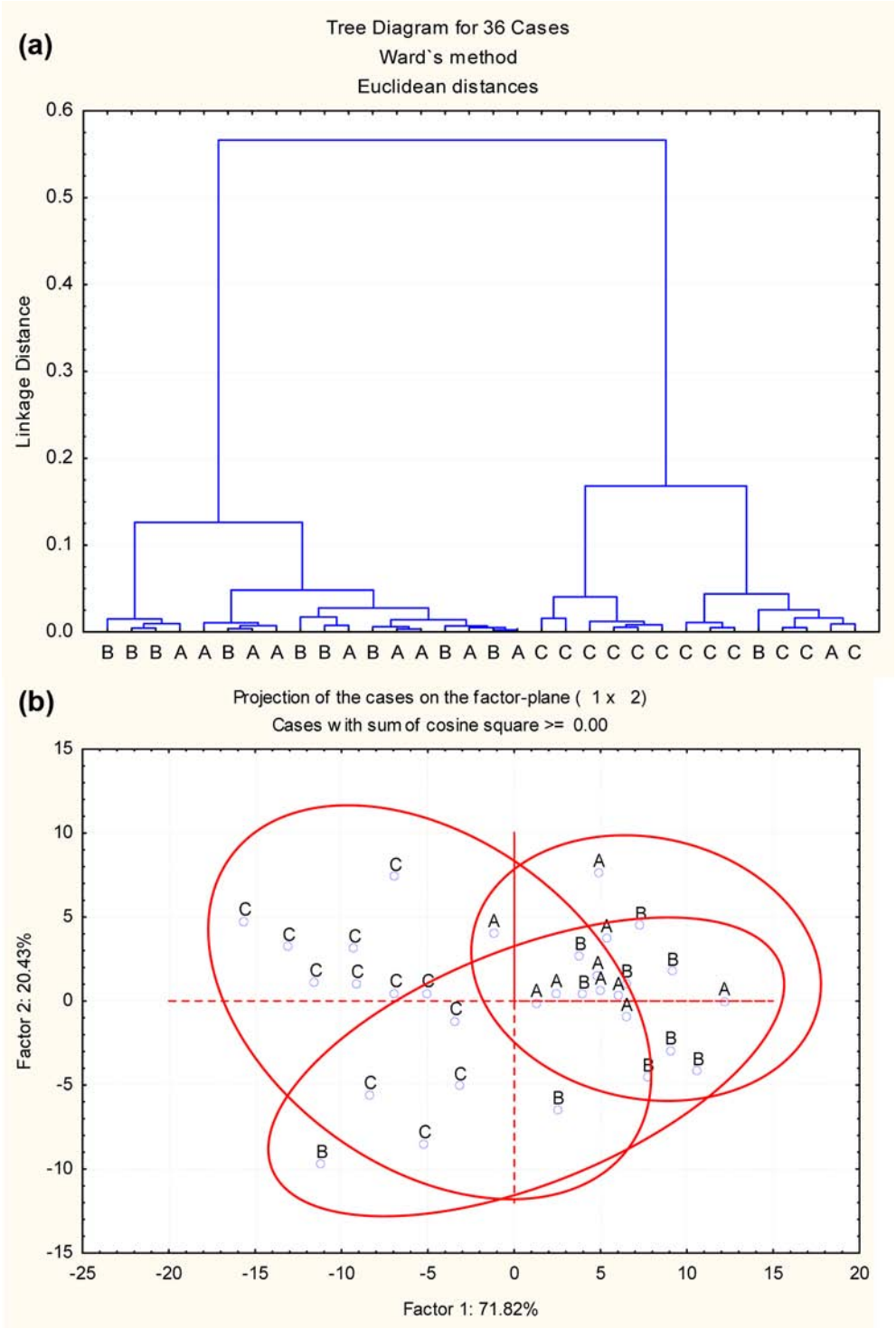

Figure 4. Agglomerative hierarchical cluster analysis (CLA) dendrograms (a) and principal component analysis (PCA) scatter plot (b) visualizing the differences in the lipid ester C═O carbonyl (1788−1707 cm^{-1}) bands among different oilseeds: A, yellow-seeded *B. carinata*; B, brown-seeded *B. carinata*; C, canola seed.

97.1−98.5% of total alkenyl glucosinolates in *B. carinata* seed, which was consistent with earlier observations.[2,13] The total and individual glucosinolate contents were not different ($P > 0.05$) between the yellow- and brown-seeded lines of *B. carinata*. However, canola seed had higher contents of 2-OH-3-butenyl, 3-CH_3-indolyl, and 4-OH-3-CH_3-indolyl than the *B. carinata* seed. Moreover, no allyl glucosinolate could be detected in canola seed, which resulted in its markedly lower content of total glucosinolates in canola as compared to *B. carinata* seed. The total glucosinolate content of the canola seed was, however, close to the average values (9−12 μmol/g) recorded in western Canada.[45]

On average, the content of total polyphenols was 13% higher ($P = 0.01$) in *B. carinata* seed than in canola seed. The presence of higher amounts of glucosinolates and phenolic compounds limits the usage of oilseeds and oilseed meals as a food or feed-

dx.doi.org/10.1021/jf502209x | J. Agric. Food Chem. 2014, 62, 7977−7988

Table 4. Coefficients of Correlation (Pearson)[a] between Lipid-Related Structural Characteristics and the Contents of Fatty Acid, Glucosinolates, Polyphenols, and Condensed Tannins in *B. carinata* and Canola Seeds

	CH_3 and CH_2 stretching area	ULB area[b]	LECC area[c]	area ratio of ULB:CH stretching	area ratio of LECC:CH stretching	area ratio of ULB:LECC
EE, % DM	−0.97**	−0.95**	−0.96**	−0.87*	0.70	−0.92*
total fatty acids, mg/g	0.42	0.49	0.44	0.48	−0.46	0.48
fatty acids, % total fatty acids						
C14:0, myristic acid	0.08	0.08	0.13	0.000	0.19	0.10
C16:0, palmitic acid	−0.97**	−0.96**	−0.94**	−0.93**	0.83*	−0.94**
C16:1n-7, palmitoleic acid	−0.99***	−0.99***	−0.98***	−0.97**	0.80*	−0.99***
C17:0, margaric acid	−0.81	−0.79	−0.80*	−0.72	0.58	−0.73
C18:0, stearic acid	−0.99***	−0.98**	−0.98**	−0.92**	0.75	−0.96**
C18:1n-9, oleic acid	−0.99***	−0.98**	−0.98**	−0.94**	0.79	−0.98**
C18:1, octadecenoic acid	−0.99***	−0.99***	−0.98**	−0.96**	0.82*	−0.98***
C18:2n-6, linoleic acid	−0.99***	−0.99***	−0.98**	−0.97**	0.82*	−0.99***
C18:3n-3, α-linolenic acid	0.95**	0.94**	0.95**	0.89**	−0.71	0.95**
C20:0, arachidic acid	0.99***	0.98**	0.97**	0.96**	−0.83*	0.98**
C20:1, eicosenoic acid	0.97**	0.96**	0.95**	0.94**	−0.79	0.97**
C20:2n-6, eicosadienoic acid	0.98***	0.97**	0.98**	0.95**	−0.80	0.98**
C20:3n-3, eicosatrienoic acid	−0.54	0.01	−0.02	0.000	0.32	0.46
C22:0, behenic acid	0.99***	0.98**	0.97**	0.95**	−0.80	0.97**
C22:1n-9, erucic acid	0.99***	0.98***	0.98**	0.95**	−0.79	0.98**
C22:2n-9, docosadienoic acid	0.82	0.38	0.41	0.000	0.08	−0.13
C22:2n-6, docosadienoic acid	0.81	0.35	0.38	0.000	0.05	−0.15
C24:0, lignoceric acid	0.99***	0.98**	0.97**	0.94**	−0.80	0.97**
C24:1n-9, nervonic acid	0.99***	0.97**	0.97**	0.94**	−0.80	0.98**
total SFA[d]	−0.91*	−0.91*	−0.91*	−0.86*	0.73	−0.87*
total MUF[e]	−0.89*	−0.88*	−0.89*	−0.82*	0.64	−0.89*
total PUFA[f]	0.94**	0.92**	0.94**	0.86*	−0.67	0.92**
total n-3 fatty acids	0.96**	0.94**	0.95**	0.90*	−0.71	0.95**
total n-6 fatty acids	−0.99***	−0.99***	−0.97**	−0.99***	0.84*	−0.99***
total n-9 fatty acids	−0.52	−0.50	−0.54	−0.43	0.24	−0.52
glucosinolates, μmol/g						
allyl	0.649	0.85	0.93	−0.40	0.93	0.58
3-butenyl	−0.806	−0.79*	−0.83*	−0.69	0.44	−0.78
2-OH-3-butenyl	−0.890*	−0.88*	−0.89*	−0.813*	0.61	−0.88*
2-OH-4-pentenyl	−0.513	−0.50	−0.58	−0.34	0.02	−0.46
3-CH_3-indolyl	−0.990**	−0.97**	−0.96*	−0.95*	0.88*	−0.96*
4-OH-3-CH_3-indolyl	−0.951**	−0.93**	−0.95**	−0.86*	0.67	−0.91*
total glucosinolates	0.996***	0.99***	0.98***	0.95**	−0.80	0.99***
total polyphenols, mg/g	0.951**	0.95**	0.97**	0.85*	−0.66	0.94**
condensed tannins, % DM	0.652	0.63	0.60	0.61	−0.72	0.59

[a]Significance levels are represented as *, $P < 0.5$; **, $P < 0.01$; **, $P < 0.001$; coefficients with no stars are not significant ($P > 0.05$). [b]ULB, unsaturated lipid bond. [c]LECC, lipid ester C═O carbonyl. [d]Saturated fatty acids. [e]Monounsaturated fatty acids. [f]Polyunsaturated fatty acids.

grade protein source.[46] Therefore, the oil from *B. carinata* seed with the higher content of glucosinolates and phenolic compounds is more suitable for a wide range of other inedible industrial applications, such as for the production of bioethanol, biodiesel, and biolubricants,[6−9,13] whereas the meal can be used as a biopesticide to control nematodes in potatoes and turf grasses. The contents of condensed tannins did not differ ($P > 0.05$) among the oilseeds and averaged 0.28% DM.

Spectral Features of Lipid Molecular Structures. Table 3 shows data on the intrinsic molecular structural characteristics of lipids in terms of CH_3 and CH_2 bands and ULB and LECC bands in yellow- and brown-seeded *B. carinata* in comparison with canola. The frequencies of all lipid-related spectral bands reported here for the three types of oilseeds were similar to the values reported previously for other feeds.[15,47] The asymmetric CH_2 and symmetric CH_2 peak heights were significantly higher ($P = 0.03$) in yellow-seeded than in brown-seeded *B. carinata*. All other peaks area, height, and height ratios did not differ between these two lines of *B. carinata* (Table 3). However, the absorbed peak intensities in the regions of asymmetric and

Table 5. Multiple Regressions with Variable Selection Analysis To Find the Most Important Variables To Predict Contents of Oil (EE), Fatty Acids, and Some Chemical Components Using Lipid-Related Spectral Parameters Obtained from ATR-FTIR Spectroscopy in *B. carinata* and Canola Seeds

predicted variable (Y)	regression ($Y = a + b_1 \times x_1 + b_2 \times x_2 + ...$)[a]	R^2	RSD[b]	P value
EE, % DM	$Y = 62.66 - 11.58 \times$ A_CH $- 336.58 \times$ R_LECC_CH $+ 292.02 \times$ R_ULB_LECC	0.99	0.13	0.001
fatty acids profile, % total fatty acids				
C16:0, palmitic acid	$Y = 4.55 - 0.71 \times$ A_CH	0.93	0.14	0.002
C16:1n-7, palmitoleic acid	$Y = 0.44 - 0.11 \times$ A_CH	0.99	0.01	<0.001
C18:0, stearic acid	$Y = 2.62 - 0.69 \times$ A_CH	0.98	0.07	<0.001
C18:1n-9, oleic acid	$Y = 104.02 - 40.76 \times$ A_CH	0.98	4.06	<0.001
C18:1, octadecenoic acid	$Y = 4.16 - 1.47 \times$ A_CH	0.99	0.08	<0.001
C18:2n-6, linoleic acid	$Y = 21.34 - 2.76 \times$ A_CH	0.99	0.10	<0.001
C18:3n-3, α-linolenic acid	$Y = 4.45 - 3.37 \times$ A_CH	0.91	0.79	0.003
C20:0, arachidic acid	$Y = 0.41 - 0.21 \times$ A_CH	0.98	0.02	<0.001
C20:1, eicosenoic acid	$Y = 0.81 + 229.72 \times$ R_ULB_LECC	0.94	0.96	0.001
C20:2n-6, eicosadienoic acid	$3Y = -0.60 + 0.65 \times$ A_CH	0.97	0.09	<0.001
C22:0, behenic acid	$Y = -0.06 + 0.38 \times$ A_CH	0.99	0.03	<0.001
C22:1n-9, erucic acid	$Y = -34.19 + 32.88 \times$ A_CH	0.99	2.24	<0.001
C24:0, lignoceric acid	$Y = -0.23 + 0.36 \times$ A_CH	0.99	0.03	<0.001
C24:1n-9, nervonic acid	$Y = -1.33 + 1.41 \times$ A_CH	0.97	0.18	<0.001
total SFA	$Y = 7.04 - 29.12 \times$ A_ULB	0.83	0.16	0.010
total MUFA	$Y = 69.27 - 2.99 \times$ A_CH	0.80	1.13	0.020
total PUFA	$Y = 23.26 + 3.10 \times$ A_CH	0.88	0.87	0.010
total n-3 fatty acids	$Y = 4.32 + 3.49 \times$ A_CH	0.91	0.81	0.003
total n-6 fatty acids	$Y = 18.66 - 42.57 \times$ R_ULB_LECC	0.99	0.07	<0.001
glucosinolates, μmol/g				
3-butenyl	$Y = 4.04 - 5.08 \times$ A_LECC	0.69	0.60	0.040
2-OH-3-butenyl	$Y = 8.70 - 11.42 \times$ A_LECC	0.80	1.00	0.020
4-OH-3-CH_3-indolyl	$Y = 6.82 - 1.97 \times$ A_CH	0.90	0.48	0.004
total glucosinolates	$Y = 20.45 - 24.82 \times$ A_LECC	0.83	1.96	0.010
total polyphenols, mg/g	$Y = 4.64 + 2.98 \times$ A_LECC	0.94	0.14	0.002

[a] A_CH, CH_3, and CH_2 stretching area; R_LECC_CH, area ratio of lipid ester C═O carbonyl to CH stretching; R_ULB_LECC, area ratio of unsaturated lipid to lipid ester C═O carbonyl; A_ULB, unsaturated lipid area; A_LECC, lipid ester C═O carbonyl area. [b] RSD, residual standard deviation.

symmetric stretching vibrations of CH_3 and CH_2 groups were much higher ($P < 0.001$) in *B. carinata* seed than those in canola. This can also be seen in Figure 1 (ca. 2959−2853 cm^{-1}), suggesting differences in the lipid molecular structures of *B. carinata* and canola seed. The tiny bands (ca. 3035−2991 cm^{-1}) and another strong band (ca. 1788−1707 cm^{-1}), highlighted in Figure 1 indicate the ULB and LECC bands[48,49] in the oilseeds. The ULB and LECC bands did not differ between the two types of *B. carinata* ($P > 0.05$); however, the peak height and area of these bands were higher ($P < 0.001$) in *B. carinata* than those in canola seed. The absorbed peak intensities of CH groups, ULB, and LECC in canola seed found in our study were much weaker than those reported by Abeysekara et al.,[15] which might be related to the inherent differences in seed types used in the two studies. To date, few studies have evaluated genetic modification in nutritional value of *B. carinata*;[12,13,42] however, studies on lipid molecular structural characteristics of yellow- and brown-seeded *B. carinata* are scarce. Therefore, no direct comparisons with other studies could be made. However, our results were somewhat consistent with the findings of Yu et al.,[50] who observed no structural differences in lipid-related molecular structural characteristics between the yellow- and brown-seeded canola. A number of studies have shown that molecular structural characteristics of biopolymers are highly related to their concentration, digestibility, and metabolic characteristics.[51,52] Consequently, lipid molecular structures could be used to explain the differences in oil content and composition, digestion, and utilization between *B. carinata* seed and canola seed. The spectral ratios of CH_3-as to CH_2-as, CH_3-as to CH_3-s, CH_3-s to CH_2-s, and CH_2-as to CH_2-s did not differ between yellow-seeded and brown-seeded *B. carinata*. However, these ratios were 6−62% lower ($P < 0.05$) than those observed in canola, whereas the height ratios of asymmetric to symmetric and ULB to LECC as well as area ratio of ULB to LECC were 1−10 times higher ($P < 0.05$) than those of canola. These findings indicated that lipid structural makeup of the seed tissues differed between *B. carinata* and canola seed.

Discriminating and Classifying Differences in Lipid Molecular Structures. The dendograms of AHCA analysis and biplots of PCA can distinguish and classify the overall differences in lipid molecular structures in the regions of the CH stretchings (ca. 2999−2800 cm^{-1}; Figure 2), ULB (ca. 3035−2991 cm^{-1}; Figure 3), and LECC band (ca. 1788−1707 cm^{-1}; Figure 4). The AHCA dendograms showed that the lipid molecular spectra of both yellow-seeded and brown-seeded *B. carinata* were fully distinguished from canola at a linkage distance of <0.2 within the region of CH stretchings (Figure 2a), and at a linkage distance of <0.1 within the region of ULB (Figure 3a). Similarly, the PCA biplots showed that the spectra of canola were grouped into separate ellipses from both types of *B. carinata* seeds in the region of CH stretchings (Figure 2b) and ULB (Figure 3b). These findings demonstrated differences in the inherent molecular structures of lipids between *B.*

dx.doi.org/10.1021/jf502209x | J. Agric. Food Chem. 2014, 62, 7977−7988

carinata and canola seeds. Such differences can influence lipids digestion, metabolism, and their industrial applications. However, the PCA and AHCA graphs showed that the yellow-seeded and brown-seeded *B. carinata* seeds could not be discriminated from each other in the regions of CH stretchings and ULB. Moreover, both AHCA dendograms and PCA biplots could not distinguish the lipid molecular spectra of the three types of oilseeds within the LECC region, indicating some structural similarities among them in this region. Although no published studies are available for comparison of lipid inherent molecular structures in the yellow-seeded and brown-seeded *B. carinata*, such differences have been reported for yellow-seeded and brown-seeded canola.[15]

Correlations between Lipid Molecular Spectral Intensity Profiles and Oil Content, Fatty Acid Composition, and Chemical Compound Factors. Table 4 shows the coefficients of correlation (Pearson) and their significance level between the lipid molecular spectral parameters and the contents of oil, fatty acids, glucosinolates, condensed tannins, and polyphenols in *B. carinata* and canola seeds. The data showed that the oil content had strong negative correlations ($P < 0.05$) with lipid-related molecular spectral intensities, namely, the CH_3 and CH_2 stretching area ($r = -0.966$), ULB area ($r = -0.950$), LECC area ($r = -0.964$), area ratio of ULB to CH stretching ($r = -0.867$), and area ratio of ULB to LECC ($r = -0.917$). No significant ($P > 0.05$) relationship was observed between the lipid-related structural parameter and the contents (% of total FA) of C14:0, C17:0, C20:3n-3, C22:2n-9, C22:2n-6, and total n-9 fatty acids. Except for the LECC:CH area ratio, a significant negative correlation ($P < 0.05$; $r > -0.82$) was observed between the lipid molecular structural parameters and the contents (% of total FA) of C16:0, C16:1n-7, C18:0, C18:1n-9, C18:1, C18:2n-6, total saturated fatty acids, total monounsaturated fatty acids, and total n-6 fatty acids. Except for the LECC:CH area ratio, significant ($P < 0.05$; $r > 0.86$) positive correlations were observed between the lipid molecular structural parameters and the contents (% of total FA) of C18:3n-3, C20:0, C20:1, C20:2n-6, C22:0, C20:1n-9, C24:0, C24:1n-9, total polyunsaturated fatty acids, and total n-3 fatty acids. Among other chemical compounds, the contents of 2-OH-3-butenyl, 3-CH_3-indolyl, 4-OH-3-CH_3-indolyl, total glucosinolates, and total polyphenols strongly ($P < 0.05$; $r > 0.813$) correlated with the spectral intensities of CH_3 and CH_2 stretching area, ULB area, and LECC area, area ratio of ULB to CH stretchings, and area ratio of ULB to LECC. Although other studies[52,53] have demonstrated that food/feed nutrient quantity and digestibility could be predicted from protein- and carbohydrate-related molecular spectral features, our study demonstrated for the first time the lipid-related molecular spectral intensities had close relationships with chemical compositions of *Brassica* oilseeds.

Regression Analysis of Lipid Molecular Spectral Parameters and the Contents of Oil, Fatty Acids, Glucosinolates, and Polyphenols. Table 5 shows the multiple regression equations, based on lipid-related spectral parameters, and their predictive power for estimation of the contents of oil, fatty acids, glucosinolates, and polyphenols in the oilseeds. The equations gave a high degree of fit for all of the parameters mentioned in Table 5. The results showed that oil content could be predicted from spectral data on CH stretching area, area ratio of LECC to CH stretchings, and area ratio of ULB to LECC with high accuracy ($R^2 = 0.990$). The equations further showed that the ratio of ULB to LECC could be used to estimate the contents of C20:1 ($R^2 = 0.941$) and total n-6 fatty acids ($R^2 = 0.991$), whereas all other mentioned fatty acids can be estimated from CH stretchings area with a good degree of fit ($R^2 \geq 0.800$; Table 5). The contents of 3-butenyl, 2-OH-3-butenyl, total glucosinolates, and total polyphenols can be estimated ($R^2 \geq 0.689$) from LECC area, whereas the 4-OH-3-CH_3-indolyl concentration in oilseeds can be estimated with relatively good accuracy ($R^2 = 0.831$) from the area of CH stretchings. The high predictive powers for functional fatty acids such as C21:1n-9 and glucosinolates could have important practical implications for breeders and the food/feed industries for selecting appropriate seed types. FTIR-ATR molecular spectroscopy is a fully established non-destructive technique, which can directly and rapidly analyze a large number of feed samples. Earlier studies[16,52,53] suggested that the spectral band intensities can be used as an indicator for the quantitative differences in biopolymers such as protein and carbohydrates among different feeds, which is also supported by the findings of the present study. However, it is pertinent that these prediction equations were derived from limited data based on a small number of samples. Further study is required to obtain predictive equations based on a large number of samples of diverse origin to validate the findings of the current study.

In summary, brown-seeded *B. carinata* had significantly lower ($P < 0.05$) oil content, C17:0, C20:1, C20:2n-6, C24:1n-9, and total saturated fatty acids, and significantly higher ($P < 0.05$) content of C22:0, C22:1n-9, and C24:0 than yellow-seeded *B. carinata*. However, the glucosinolate, polyphenols, and condensed tannins contents were not different. There were marked differences between *B. carinata* and canola seed in oil content, fatty acid profile, glucosinolate profile, and polyphenols. ATR-FTIR spectroscopy can be used to quantify lipid-related spectral band intensities. Compared with the brown *B. carinata* seed, the yellow seeds were markedly lower in peak heights of asymmetric CH_2 and symmetric CH_2, and no changes were found in other spectral parameters. The absorbed peak intensities of CH stretchings and ULB and LECC bands of *B. carinata* strains were remarkably higher than those observed in canola. The multivariate analyses showed no significant differences in the lipid molecular structures between the yellow and brown *B. carinata* lines, whereas both types of *B. carinata* seed were fully distinguished from canola in the regions of CH stretchings and ULB. The lipid-related spectral band intensities were strongly correlated to oil content, fatty acids, glucosinolates, and polyphenols. Therefore, regression equations were developed that gave relatively high predictive power for the estimation of oil ($R^2 = 0.990$); all measured fatty acids ($R^2 \geq 0.800$), except C14:0, C20:3n-3, C22:2n-9, and C22:2n-6; a few individual glucosinolates, namely, 3-butenyl, 2-OH-3-butenyl, 4-OH-3-CH_3- indolyl; and total glucosinolates ($R^2 \geq 0.686$) and total polyphenols ($R^2 = 0.935$). However, further study is required to obtain predictive equations based on a large number of samples with diverse sources to validate the findings of the current study.

AUTHOR INFORMATION

Corresponding Author

*(P.Y.) Phone: (306) 966-4132. Fax: (306) 966-4151. E-mail: Peiqiang.yu@usask.ca.

Funding

The Chair (Professor Peiqiang Yu) research programs have been financially supported by the Ministry of Agriculture

Strategic Research Chair Program, NSERC (Discovery Grant and CRD grant), SaskCanola, ADF-Saskatchewan, and Thousand-Talent-People Program in Tianjin.

Notes

The authors declare no competing financial interest.

■ ACKNOWLEDGMENTS

We are grateful to Zhiyuan Niu (University of Saskatchewan) for assistance in chemical analysis and spectral data collection.

■ REFERENCES

(1) Belayneh, H.; Riley, K. W.; Tadesse, N.; Getinet, A. The response of three oil seed *Brassica* species to different planting dates and seed rates in highlands of Ethiopia. *Eth. J. Agric. Sci.* **1983**, *5*, 22−33.

(2) Warwick, S. I.; Gugel, R. K.; McDonald, T.; Falk, K. C. Genetic variation of Ethiopian mustard (*Brassica carinata* A. Braun) germplasm in western Canada. *Genet. Resour. Crop Evol.* **2006**, *53*, 297−312.

(3) Pan, X.; Caldwell, C. D.; Falk, K. C.; Lada, R. The effect of cultivar, seeding rate and applied nitrogen on *Brassica carinata* seed yield and quality in contrasting environments. *Can. J. Plant Sci.* **2012**, *92*, 961−971.

(4) Getinet, A.; Rakow, G.; Raney, J. P.; Downey, R. K. Development of zero erucic acid Ethiopian mustard through an interspecific cross with zero erucic acid Oriental mustard. *Can. J. Plant Sci.* **1994**, *74*, 793−795.

(5) Velasco, L.; Nabloussi, A.; De Haro, A.; Fernández-Martínez, J. M. Development of high-oleic, low-linolenic acid Ethiopian-mustard (*Brassica carinata*) germplasm. *Theor. Appl. Genet.* **2003**, *107*, 823−830.

(6) Bouaid, A.; Martinez, M.; Aracil, J. Production of biodiesel from bioethanol and *Brassica carinata* oil: oxidation stability study. *Bioresour. Technol.* **2009**, *100*, 2234−2239.

(7) Vicente, G.; Martínez, M.; Aracil, J. Optimization of *Brassica carinata* oil methanolysis for biodiesel production. *J. Am. Oil Chem. Soc.* **2005**, *82*, 899−904.

(8) Cardone, M.; Mazzoncini, M.; Menini, S.; Rocco, V.; Senatore, A.; Seggiani, M.; Vitolo, S. *Brassica carinata* as an alternative oil crop for the production of biodiesel in Italy: agronomic evaluation, fuel production by transesterification and characterization. *Biomass Bioenergy* **2003**, *25*, 623−636.

(9) Nieschlag, H. J.; Wolff, L. A. Industrial uses of high erucic oils. *J. Am. Oil Chem. Soc.* **1971**, *48*, 723−727.

(10) Ma, D. W. L.; Wierzbicki, A. A.; Field, C. J.; Clandinin, M. T. Preparation of conjugated linoleic acid from safflower oil. *J. Am. Oil Chem. Soc.* **1999**, *76*, 729−730.

(11) Robbelen, G.; Thies, W. Variation in rapeseed glucosinolates and breeding for improved meal quality. In *Brassica Crops and Wild Allies*; Tsunoda, S., Hinata, K., Gomez-Campo, C., Eds.; Japan Scientific Societies Press: Tokyo, Japan, 1980; pp 285−299.

(12) Getinet, A.; Rakow, G.; Raney, J. P.; Downey, R. K. Glucosinolate conent in interspecific crosses of *Brassica carinata* with *B. juncea* and *B. napus*. *Plant Breed.* **1997**, *116*, 39−46.

(13) Taylor, D. C.; Falk, K. C.; Palmer, C. D.; Hammerlindl, J.; Babic, V.; Mietkiewska, E.; Jadhav, A.; Marillia, E.; Francis, T.; Hoffman, T.; Giblin, E. M.; Katavic, V.; Keller, W. A. *Brassica carinata* − a new molecular farming platform for delivering bio-industrial oil feedstocks: case studies of genetic modifications to improve very long-chain fatty acid and oil content in seeds. *Biofuels, Bioprod. Bioref.* **2010**, *4*, 538−561.

(14) Nabloussi, A.; Márquez-Lema, A.; Fernández-Martínez, J. M.; Velasco, L. Novel seed oil types of Ethiopian mustard with high levels of polyunsaturated fatty acids. *Ind. Crops Prod.* **2008**, *27*, 359−363.

(15) Xin, H.; Falk, K. C.; Yu, P. Studies on *Brassica carinata* seed. 1. Protein molecular structure in relation to protein nutritive values and metabolic characteristics. *J. Agric. Food Chem.* **2013**, *42*, 10118−10126.

(16) Xin, H.; Falk, K. C.; Yu, P. Studies on *Brassica carinata* seed. 2. Carbohydrate molecular structure in relation to carbohydrate chemical profile, energy values, and biodegradation characteristics. *J. Agric. Food Chem.* **2013**, *42*, 10127−10134.

(17) Abeysekara, S.; Samadi; Yu, P. Response and sensitivity of lipid related molecular structure to wet and dry heating in canola tissue. *Spectrochim. Acta Part A: Mol. Biomol. Spectrosc.* **2012**, *90*, 63−71.

(18) AOAC. *Official Methods of Analysis*; Association of Official Analytical Chemists: Washington, DC, USA, 1990.

(19) Folch, J.; Lee, M.; Sloane Stanley, G. H. A simple method for the isolation and purification of total lipids from animal tissues. *J. Biol. Chem.* **1957**, *226*, 497−509.

(20) Khan, N. A.; Cone, J. W.; Hendriks, W. H. Stability of fatty acids in grass and maize silages after exposure to air during the feed out period. *Anim. Feed Sci. Technol.* **2009**, *154*, 183−192.

(21) Khan, N. A.; Cone, J. W.; Pellikaan, W. F.; Khan, M. A.; Struik, P. C.; Hendriks, W. H. Changes in fatty acid content and composition in silage maize during grain filling. *J. Sci. Food Agric.* **2011**, *91*, 1041−1049.

(22) Daun, J. K.; McGregor, D. I. Glucosinolate analysis of rapeseed (canola). *Methods of the Canadian Grain Commission*; Grain Research Laboratory, Agriculture Canada, Canadian Grain Commission: Winnipeg, Canada, 1981, revised 1983.

(23) Slinkard, K.; Singleton, V. L. Total phenol analysis: automation and comparison with manual methods. *Am. J. Enol. Vitic.* **1977**, *28*, 49−55.

(24) Reed, J. D. Relationships among phenolics, insoluble proanthocyanidins and fiber in East African browse species. *J. Range Manage.* **1986**, *39*, 5−7.

(25) Himmelsbach, D. S.; Khalili, S.; Akin, D. E. FT-IR microspectroscopic imaging of flax (*Linum usitatissimum* L.) stems. *Cell. Mol. Biol.* **1998**, *44*, 99−108.

(26) Yu, P. Study the sensitivity of molecular functional groups to bioethanol processing in lipid biopolymer of co-products using DRIFT molecular spectroscopy. *Spectrochim. Acta Part A: Mol. Biomol. Spectrosc.* **2011**, *82*, 1−7.

(27) Yu, P. Applications of hierarchical cluster analysis (CLA) and principal component analysis (PCA) in feed structure and feed molecular chemistry research, using synchrotron-based Fourier transform infrared (FTIR) microspectroscopy. *J. Agric. Food Chem.* **2005**, *53*, 7115−7127.

(28) Liu, N.; Yu, P. Molecular clustering, interrelationships and carbohydrate conformation in hull and seeds among barley cultivars. *J. Cereal Sci.* **2011**, *53*, 379−383.

(29) Jackson, M.; Mantsch, H. H. Infrared spectroscopy ex vivo tissue analysis. In *Encyclopedia of Analytical Chemistry*; Meyers, R. A., Ed.; Wiley: Chichester, UK, 2000; pp 131−156.

(30) Miller, L. M. Infrared microsperctroscopy and imaging; available at http://nslsweb.nsls.bnl.gov/nsls/pubs/nslspubs/imaging0502/irxrayworkshopintroduction.ht (accessed Oct 2002).

(31) Kumar, P. R.; Tsunoda, S. Variation in oil content and fatty acid composition among seeds from the Cruciferae. In *Brassica Crops and Wild Allies*; Tsunoda, S., Hinata, K., Gomez-Campo, C., Eds.; Japan Scientific Societies Press: Tokyo, Japan, 1980; pp 235−252.

(32) Getinet, A.; Rakow, G.; Downey, R. K. Agronomic performance and seed quality of Ethiopian mustard in Saskatchewan. *Can. J. Plant Sci.* **1996**, *76*, 387−392.

(33) Lohaus, G.; Moellers, C. Phloem transport of amino acids in two *Brassica napus* L. genotypes and one *B. carinata* genotype in relation to their seed protein content. *Planta* **2000**, *211*, 833−840.

(34) Velasco, L.; Goffman, F. D.; Becker, H. C. Variability for the fatty acid composition of the seed oil in a germplasm collection of the genus *Brassica*. *Genet. Resour. Crop Evol.* **1998**, *45*, 371−382.

(35) Harwood, J. L. Recent advances in the biosynthesis of plant fatty acids. *Biochim. Biophys. Acta* **1996**, *1301*, 7−56.

(36) Ohlrogge, J. B.; Jaworski, J. G. Regulation of fatty acid synthesis. *Annu. Rev. Plant Physiol. Plant Mol. Biol.* **1997**, *48*, 109−136.

(37) Baud, S.; Lepiniec, L. Regulation of de novo fatty acid synthesis in maturing oilseeds of *Arabidopsis*. *Plant Physiol. Biochem.* **2009**, *47*, 448−455.

(38) Baud, S.; Lepiniec, L. Physiological and developmental regulation of seed oil production. *Prog. Lipid Res.* **2010**, *49*, 235−249.
(39) Sontag, N. O. V. Erucic, behenic: feedstocks of the 21st century. *INFORM* **1991**, *2*, 449−463.
(40) Taylor, D. C.; Barton, D. L.; Giblin, E. M.; Mackenzie, S. L.; Van den Berg, C. G. J.; McVetty, P. B. E. Microsomal lysophosphatidic acid aciltransferase from a *Brassica oleracea* cultivar incorporates erucic acid into the sn-2 position of seed triacylglycerols. *Plant Physiol.* **1995**, *109*, 409−420.
(41) Velasco, L.; Fernández-Martínez, J. M.; De Haro, A. Determination of the fatty acid composition of the oil in intact-seed mustard by near-infrared reflectance spectroscopy. *J. Am. Oil Chem. Soc.* **1997**, *74*, 1595−1602.
(42) Zanetti, F.; Vamerali, T.; Mosca, G. Yield and oil variability in modern varieties of high-erucic winter oilseed rape (*Brassica napus* L. var. *oleifera*) and Ethiopian mustard (*Brassica carinata* A. Braun) under reduced agricultural inputs. *Ind. Crops Prod.* **2009**, *30*, 265−270.
(43) Gland, A.; Röbbelen, G.; Thies, W. Variation of alkenyl glucosinolates in seeds of *Brassica* species. *Z. Pflanzenztichtg.* **1981**, *87*, 96−110.
(44) Getinet, A.; Rakow, G.; Raney, J. P. Glucosinolate content variation in *Brassica carinata A.* Braun germpiasm grown at Holetta, Ethiopia. *Cruciferae Newsl.* **1996**, *18*, 84−85.
(45) Canadian Grain Commission. *Quality of Western Canadian Canola Varieties*; Winnipeg, MB, Canada, 2011.
(46) Kozlowska, H.; Naczk, M.; Shahidi, F.; Zadernowski, R. Phenolic acids and tannins in rapeseed and canola. In *Rapeseed and Canola: Production, Chemistry, Nutrition and Processing Technology*; Shahidi, F., Ed.; Van Nostrand Reinhold: New York, 1990; pp 193−210.
(47) Wetzel, D. L.; LeVine, S. M. Imaging molecular chemistry with infrared microscopy. *Science* **1999**, *285*, 1224−1225.
(48) Wetzel, D. L.; Eilert, A. J.; Pietrzak, L. N.; Miller, S. S.; Sweat, J. A. Ultraspatially resolved synchrotron infrared microspectroscopy of plant tissue *in situ*. *Cell. Mol. Biol.* **1998**, *44*, 145−167.
(49) Marinkovic, N. S.; Huang, R.; Bromberg, P.; Sullivan, M.; Toomey, J.; Miller, L. M.; Sperber, E.; Moshe, S.; Jones, K. W.; Chouparova, E.; Lappi, S.; Franzen, S.; Chance, M. R. Center for synchrotron biosciences' U2B beamline: an international resource for biological infrared spectroscopy. *J. Synchrotron Radiat.* **2002**, *9*, 189−197.
(50) Yu, P.; Christensen, C. R.; Christensen, D. A.; McKinnon, J. J. Ultrastructural-chemical makeup of yellow-seeded (*Brassica rapa*) and brown-seeded (*Brassica napus*) canola within cellular dimensions, explored with synchrotron reflection FTIR microspectroscopy. *Can. J. Plant Sci.* **2005**, *85*, 533−541.
(51) Khan, N. A.; Booker, H.; Yu, P. Molecular structures and metabolic characteristics of protein in brown and yellow flaxseed with altered nutrient traits. *J. Agric. Food Chem.* **2014**, *62*, 6556−6564.
(52) Yu, P.; Nuez-Ortín, W. G. Relationship of protein molecular structure to metabolisable proteins in different types of dried distillers grains with solubles: a novel approach. *Br. J. Nutr.* **2010**, *104*, 1429−1437.
(53) Peng, Q.; Khan, N. A.; Wang, Z.; Yu, P. Moist and dry heating-induced changes in protein molecular structure, protein subfractions, and nutrient profiles in camelina seeds. *J. Dairy Sci.* **2014**, *97*, 446−457.

approach using cellulase and protease treatment has been commercialized by Tang et al.[17] Enzymatic hydrolysis of carbohydrates has been commonly used to improve the feed quality, such as digestibility and bioavailability, of rapeseed press cake,[18,19] but it is also a potential technology to facilitate rapeseed protein extraction. A patent by Kvist et al.[20] reports 83% total protein extraction yield into four fractions from wet-milled rapeseed press cake after treatment with pectinase, β-glucanase, and hemicellulase enzymes, without the addition of proteases.

Although rapeseed protein extraction has been studied extensively, deeper understanding of the protein−carbohydrate interactions and the impact of processing on press cake cell wall structure could open up new possibilities for efficient protein release. Rapeseed cell walls are composed of a strongly interconnected network of polysaccharides, where xyloglucan, xylan, and pectic polysaccharides cross-link with cellulose and each other through noncovalent and sometimes covalent interactions.[8,21] Meanwhile, the majority of rapeseed protein is stored in protein bodies inside cells that are surrounded by these cell walls.[5,22] Transmission electron micrographs have shown partial disruption of rapeseed cell structure during cold pressing,[16] and Srivastava et al.[23] reported a correlation between microstructural changes and oil extraction yield after enzyme treatment of rapeseeds. However, a respective correlation for structural changes and protein extraction is yet to be established.

The aim of this study was to determine the effects of polysaccharide hydrolases on cell wall disintegration and protein extractability from two rapeseed press cakes obtained by cold pressing of intact *B. rapa* and partially dehulled *B. napus* seeds.

MATERIALS AND METHODS

Rapeseed press cakes. Two rapeseed press cakes were used as raw materials for mechanical and enzymatic processing. The intact press cake (6.8% moisture) was obtained from Kankaisten Öljykasvit Oy (Turenki, Finland) after cold pressing of oil from *B. rapa* L. seeds at 50−60 °C, pelletizing, and air-drying. The dehulled press cake (6.6% moisture) was received from Kroppenstedter Ölmühle Walter Doepelheuer GmbH (Kroppenstedt, Germany) after cold pressing of partially dehulled *B. napus* L. seeds and drying.

Enzymes. Three enzyme products were used: Pectinex Ultra SP-L and Celluclast 1.5L from Novozymes A/S (Bagsvaerd, Denmark) and Depol 740L from Biocatalysts Ltd. (Cardiff, United Kingdom). Their protein concentration was quantified using a DC Protein Assay Kit (Bio-Rad, Hercules, CA). Activity profiles of the enzyme preparations, including β-glucanase,[24] β-glucosidase,[25] *endo*-1,3(4)-β-glucanase, polygalacturonase,[26] xylanase,[27] and protease[28] activity, were determined (Table 1). The polysaccharide hydrolase assays were performed at 40 °C, pH 6 and the protease assay at 30 °C, pH 5.5.

Mechanical Pretreatment. Rapeseed press cakes were dry-milled at 17 800 rpm using a 100 UPZ-II fine impact mill (Hosokawa Alpine Ag, Ausburg, Germany). Prior to dry milling, the pelletized, intact press cake was ground at 1000 rpm at room temperature using an SM 300 cutting mill (Retsch, Düsseldorf, Germany).

Enzymatic Treatments. Dry-milled intact and dehulled rapeseed press cakes were treated with Pectinex, Depol, and Celluclast for 0, 4, and 48 h at an enzyme dosage of 10 mg protein/g dry substrate. On the basis of the temperature optima obtained from the manufacturer of the enzymes, the incubation temperature was 50 °C for Depol and Celluclast and 30 °C for Pectinex. The enzymatic treatments were performed in duplicate in 25 mL volume at 10% (w/v) consistency in distilled water containing 0.02% (w/v) sodium azide as an antimicrobial agent. After the treatment, liquid fractions were separated from the residual solids by centrifugation for 15 min at 3220*g*. The liquid fractions were stored in aliquots at −20 °C prior to analysis. The residual solid fractions obtained from 48 h hydrolysis were freeze-dried and weighed.

Table 1. Protein Concentration and Activities of Pectinex Ultra SP-L, Depol 740L, and Celluclast 1.5L[a]

	Pectinex Ultra SP-L	Depol 740 L	Celluclast 1.5L
protein concn (mg/mL)	61	48	170
activity (nkat/mg protein)			
endo-1,3(4)-β-glucanase (EC 3.2.1.6)	135	223	158
β-glucosidase (EC 3.2.1.21)	0.07	10	1.3
cellulase (EC 3.2.1.4)	22	23	112
polygalacturonase (EC 3.2.1.15)	2876	0.2	1.6
endo-1,4-β-xylanase (EC 3.2.1.8)	7.0	288	52
protease	0.3	0.6	nd

[a]Polysaccharide hydrolase activities were determined at pH 6 and protease activity at pH 5.5; nd = not detected.

Analysis of the Liquid Fractions from Enzymatic Treatments. Protein hydrolysis was monitored by reducing SDS−PAGE on a Criterion TGX, stain-free precast 18% gel (Bio-Rad, Hercules, CA). Molecular weights of the protein bands were determined on the basis of the migration of recombinant 10−250 kDa Precision Plus Protein standards (Bio-Rad). The protein bands were identified by correspondence of the band molecular weights with known molecular weights of the major rapeseed proteins. Monosaccharides (glucose, fructose, galactose, rhamnose, arabinose, xylose, and mannose), uronic acids, and sucrose in the 48-h enzymatic hydrolysates were identified directly by high-performance anion-exchange chromatography with pulse amperometric detection (HPAEC-PAD) using a ICS-3000 ion chromatography system equipped with a CarboPac PA1 column (Dionex, Sunnyvale, CA).[29] Likewise, monosaccharide profiles of extracted polysaccharides were analyzed by HPAEC-PAD after secondary hydrolysis of the 48-h enzymatic hydrolysates.[29,30] The secondary hydrolyses were performed in duplicate in 4% sulfuric acid for 1 h at 120 °C.

Compositional Analysis of Rapeseed Press Cakes and Solid Fractions after Enzymatic Treatment. Protein concentration was determined in duplicate by Kjeldahl total nitrogen analysis (N × 6.25), according to the method by Kane.[31] Ash content of the press cakes was quantified gravimetrically after combustion for 23 h at 550 °C in an N 11 muffle furnace in triplicate (Nabertherm GmbH, Lilienthal, Germany). For total lipid content, the dry-milled press cakes were defatted by heptane extraction for 5 h in a Soxhlet apparatus. Total lipid content was determined by gravimetrical analysis of the heptane-extracted dry mass. To extract water-soluble carbohydrates, the heptane-defatted press cakes were mixed with water at 10% (w/v) consistency, 60 °C for 2 h in duplicate. Water-soluble mono- and disaccharides were analyzed from the water extracts by HPAEC-PAD. Monosaccharide profiles of water-soluble polysaccharides were determined by HPAEC-PAD after acid hydrolysis of the water extracts in 4% sulfuric acid.[29,30]

The water-extracted and enzyme-treated press cakes were analyzed for insoluble polysaccharides and lignin. The press cakes were remilled and hydrolyzed in triplicate with 70% sulfuric acid for 1 h at 30 °C followed by hydrolysis with 4% sulfuric acid for 50 min at 120 °C. The released neutral monosaccharides were analyzed by HPAEC-PAD.[29,30] Acid-soluble lignin was measured spectrophotometrically at 215 and 280 nm[32] from the acid hydrolysates, and acid-insoluble lignin was determined as the weight of the acid hydrolysis residues. Ash content of the acid hydrolysis residue was quantified gravimetrically after combustion and subtracted from the acid-insoluble lignin. Additionally, insoluble noncellulosic polysaccharides were determined after dilute acid hydrolysis of the water-extracted and enzyme-treated press cakes in triplicate with 4% sulfuric acid for 1 h at 120 °C. Cellulose content was calculated as the difference of glucose in the total and noncellulosic polysaccharides. Digestible starch content of the press cakes was determined enzymatically according to the method of

McCleary et al.[33] β-Glucan content was determined enzymatically according to the work of Munck et al.[34]

Microstructure of the Rapeseed Press Cakes before and after Enzymatic Hydrolysis. The press cakes were prepared for microscopy according to the method of Holopainen-Mantila et al.[35] As an exception, the press cakes before enzyme treatment were not embedded in 2% agar prior to fixation. The sections were stained with 0.1% (w/v) aqueous Acid Fuchsin (BDH Chemicals Ltd., Poole, United Kingdom) in 1.0% acetic acid for 1 min and with 0.01% (w/v) aqueous Calcofluor White (Fluorescent brightener 28, Aldrich, Germany) for 1 min. When the stained sections were examined with a fluorescence microscope (excitation λ 400−410 nm, emission λ >455 nm), glucans in intact cell walls appear blue (Calcofluor) and proteins appear red (Acid Fuchsin).[36,37] Additionally, the sections were stained with 0.2% (w/v) Ruthenium Red (Fluka Chemie AG, Buchs, Switzerland) in water for 2 h. Ruthenium Red associates with the carboxyl groups of galacturonic acid residues and thus shows pectins as red in bright-field illumination.[38,39] The sections were imaged with an Olympus BX-50 microscope (Olympus Corp., Tokyo, Japan). Micrographs were obtained using a PCO SensiCam CCD color camera (PCO AG, Kelheim, Germany) and the cell^P imaging software (Olympus). Images taken from replicate sample blocks were examined and representative images were selected for publication.

Protein extraction yield was expressed as the proportion of total nitrogen that was lost from the solid fraction during 48-h enzymatic and reference treatments. The yield represents the average of two Kjeldahl total nitrogen analysis results from two parallel reactions. Carbohydrate extraction yield was expressed as the proportion of total press cake carbohydrates (monosaccharides, sucrose, or polysaccharides) that were recovered in the liquid fraction after 48-h enzymatic and reference treatments. Extracted polysaccharides were calculated as the difference of the monosaccharide concentration before and after secondary acid hydrolysis. Two replicate secondary acid hydrolyses and HPLC analyses were performed for each of the two parallel reactions; thus, the carbohydrate yields represent the average of four parallel analysis results.

RESULTS AND DISCUSSION

Chemical Composition of Intact and Dehulled Rapeseed Press Cakes. Differences in the chemical composition of the intact and dehulled rapeseed press cakes were identified. The intact *B. rapa* press cake consisted of 36% crude protein, 19% acid-soluble and insoluble lignin, 12% crude oil, and 7% ash, on a dry matter basis (Table 2). In the dehulled *B. napus* press cake, the protein and oil concentrations were higher, whereas the proportion of lignin and ash was expectedly lower. The values were consistent with earlier reports for cold-pressed *B. rapa*[9] and *B. napus*[1] press cakes. Compositional differences between the intact *B. rapa* and dehulled *B. napus* press cake were expected to result rather from the removal of lignin-rich hulls than from species-related variation.[40] Dehulling reduces the carbohydrate and lignin content and enriches protein and ash in rapeseed press cake,[4] whereas equally processed, solvent-extracted *B. rapa* and *B. napus* meals have been reported to possess similar chemical composition despite the species variation.[8,12]

Both press cakes contained 35% of carbohydrates as quantified from the total neutral monosaccharides recovered after acid hydrolysis. A substantial portion of the carbohydrates consisted of water-soluble mono- and disaccharides (Table 2). Glucose originated mainly from sucrose and cellulose, while starch and β-glucan accounted for less than 0.3% of the dry matter (Table 3). The *B. napus* press cake contained more sucrose and other water-soluble sugars and less cellulose than the *B. rapa* press cake (Tables 2 and 3). Monosaccharide profiles of the press cakes (Table 2) were consistent with the rapeseed polysaccharide composition comprising cellulose, xyloglucan, xylan, and pectic polysaccharides, including homogalacturonan, rhamnogalacturonan, arabinan, and arabinogalactan.[8,9] Pectin-derived uronic acids could not be quantified from the press cakes before enzyme treatment due to their degradation during secondary acid hydrolysis.

Table 2. Chemical Composition of the Intact *B. rapa* and Dehulled *B. napus* Rapeseed Press Cakes (PC) and Solid Fractions Obtained from Treatment at 30 °C without Enzyme Addition (no 30) or with Pectinex (P)[a]

	concentration (% dm)					
	intact *B. rapa* press cake			dehulled *B. napus* press cake		
	PC	no 30	P	PC	no 30	P
protein	35.9	30.7	32.3	40.1	29.6	31.4
carbohydrates	35.4	21.0	9.3	34.5	20.7	8.2
monosaccharide composition						
glucose	14.7	9.4	5.0	14.4	9.2	4.2
arabinose	5.8	4.8	1.5	4.8	5.1	1.4
galactose	3.9	2.1	0.9	3.9	2.1	0.8
xylose	2.3	2.5	0.6	1.9	2.6	0.8
fructose	7.4	0.6	0.4	8.6	0.7	0.5
mannose	0.8	1.0	0.7	0.5	0.5	0.3
rhamnose	0.5	0.5	0.2	0.4	0.5	0.2
water-soluble carbohydrates	15.7	na	na	18.7	na	na
monosaccharides and sucrose	13.7			16.7		
polysaccharides	1.9			2.0		
insoluble carbohydrates	19.8	21.0	9.3	15.8	20.7	8.2
lignin	18.8	17.3	23.5	13.7	11.8	19.8
acid-insoluble lignin	13.5	12.7	19.4	8.2	8.3	15.8
acid-soluble lignin	5.3	4.6	4.0	5.5	3.6	3.9
oil	11.8	13.9	20.5	16.7	20.5	28.2
ash	7.0	na	na	5.6	na	na

[a]na = not analyzed. Standard deviations were <12% of the measured values from at least two parallel analyses.

Table 3. Composition of Glucose Polysaccharides in Intact *B. rapa* and Dehulled *B. napus* Rapeseed Press Cakes[a]

	content (% dm)	
	intact *B. rapa* press cake	dehulled *B. napus* press cake
sucrose	11.7	13.8
cellulose	5.2	1.6
starch	0.2	0.2
β-glucan	0.1	0.1

[a]Standard deviations <15% of the measured values (N = 2).

Microstructure of Intact and Dehulled Rapeseed Press Cakes. Rapeseed press cakes and solid fractions obtained after enzymatic treatment of the intact press cake were analyzed by microscopy to visualize the cell structure as well as integrity and localization of polysaccharides and proteins and to understand the effects of enzymatic treatment. In thin sections of the press cakes, structures originating from seed coat (hull) and embryo including cotyledons of the rapeseed were

dx.doi.org/10.1021/jf501802e | J. Agric. Food Chem. 2014, 62, 7989−7997

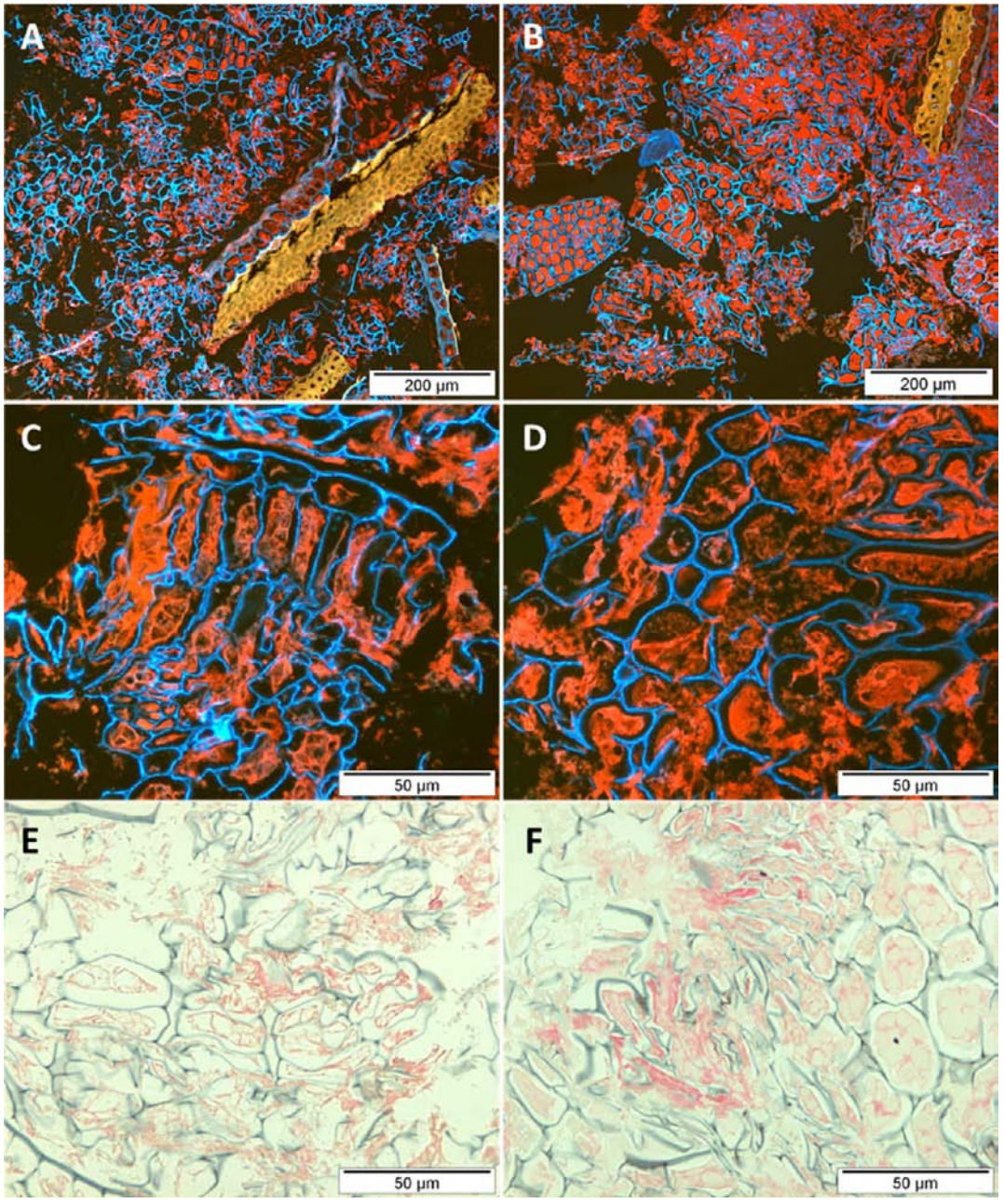

Figure 1. Micrographs of press cakes obtained from cold pressing of intact *B. rapa* seeds (A, C, E) and partially dehulled *B. napus* seeds (B, D, F). The sections were stained with Calcofluor White and Acid Fuchsin (A–D), showing cell wall glucans as blue and proteins as red, and with Ruthenium Red (E, F), showing pectins as red.

recognized (Figure 1A,B). Seed coat fragments were detected in all samples both before and after the enzymatic treatment and appear in some of the selected micrographs. Staining of the press cakes with Calcofluor White visualized cellulose and other β-linked glucans[41] in the cell walls of embryo and seed coat, whereas staining with Acid Fuchsin showed the proteins inside the embryonic cells. Cold pressing had partially disrupted the structure of embryonic cell walls (shown as blue) and protein bodies (shown as red) (Figure 1A–D). Dry milling caused further fragmentation of the embryonic cell walls without noticeable effect on proteins (Figure 3A). No clear difference was observed in the cell wall fluorescence of the two press cakes. However, proteins seemed to form more compact structures in the dehulled press cake than in the intact press cake (Figure 1A,B). Such variation in the packing density of protein bodies was not observed in intact *B. rapa* and dehulled *B. napus* seeds obtained before oil pressing (data not shown).

Pectins were visualized by staining with Ruthenium Red, which binds to the pectin polygalacturonan backbone.[39] Pectins were abundant in the seed coat (Figure 2C) and detected in smaller amounts in the embryonic cell walls (data not shown). Pectins were more intensely stained by Ruthenium Red in the seed coat than in the embryo, which may be related to differences in their composition: pectins in rapeseed hulls have been reported to contain substantially more galacturonic acid than pectins in the embryo.[3] In addition to the cell wall pectins, networks stained by Ruthenium Red were observed inside the embryo cells (Figure 1E,F), suggesting the presence of

dx.doi.org/10.1021/jf501802e | J. Agric. Food Chem. 2014, 62, 7989–7997

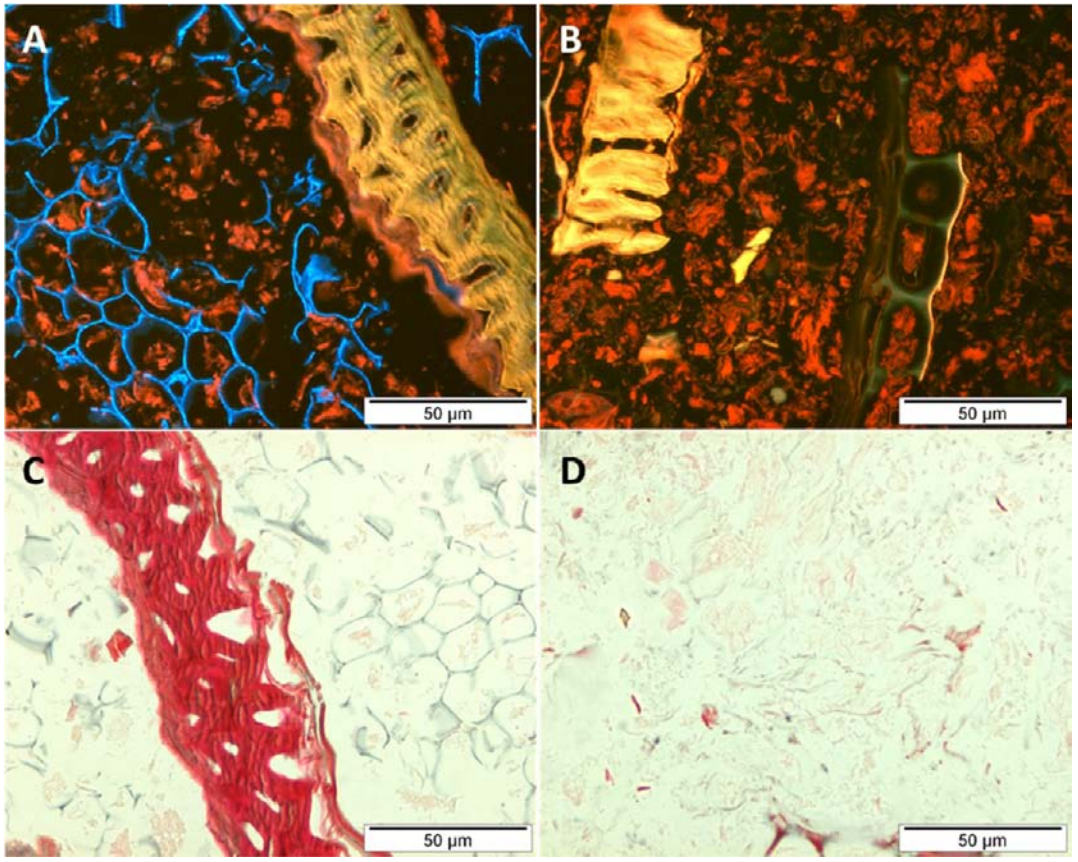

Figure 2. Micrographs of the solid fractions obtained from treatment of intact *B. rapa* press cake at 30 °C without enzyme addition (A, C) or with Pectinex (B, D). The sections were stained with Calcofluor White and Acid Fuchsin (A, B), showing cell wall glucans as blue and proteins as red, and with Ruthenium Red (C, D), showing pectins as red. Panels A–C include fragments of the seed coat.

intracellular pectin-type material. These networks were colocalized with proteins in the cells (shown by Acid Fuchsin staining in Figure 1C,D). Intracellular pectic polysaccharides have not been reported in rapeseed, but their presence was recently detected in the olive pistil.[42]

Enzymatic Hydrolysis of Rapeseed Carbohydrates. The commercial enzyme product Pectinex Ultra SP-L hydrolyzed the rapeseed carbohydrates most effectively, solubilizing up to 75% of the carbohydrates (Figure 4) and causing complete degradation of the embryonic cell walls, as shown by microscopy (Figure 2). The total carbohydrate hydrolysis yield was higher than in the study reported by Pustjens et al.,[18] who extracted 64% of the total carbohydrates in solvent-extracted *B. napus* meal during 4.75 h hydrolysis with amyloglucosidase and proteases. The higher yield is most probably explained by longer hydrolysis time and a better targeted enzyme product used in our study.

According to the sugar profiles of the 48-h enzymatic hydrolysates, carbohydrates were released almost exclusively as monosaccharides into the liquid fractions (Table 4). Release of galacturonic acid by Pectinex indicated hydrolysis of pectin (homogalacturonan, rhamnogalacturonan), whereas the release of galactose and arabinose by both Pectinex and Depol suggested hydrolysis of other pectic polysaccharides (arabinan and arabinogalactan). Substantial amounts of fructose and glucose were released as a result of sucrose hydrolysis during all enzymatic and reference treatments at 50 °C (Table 4). Respectively, the sucrose content in these hydrolysates was remarkably lower or nondetectable in comparison to the 30 °C reference treatments. Sucrose hydrolysis at 50 °C suggests that rapeseed contains an endogenous fructosyltransferase (i.e., invertase) with enhanced activity at above 30 °C. On the other hand, the high fructosyltransferase activity of Pectinex[43] was obviously responsible for the hydrolysis of sucrose into glucose and fructose at 30 °C.

The three commercial enzyme preparations were selected on the basis of the correspondence of their activity profiles with rapeseed carbohydrate composition. The Pectinex Ultra SP-L product contains a variety of activities that target the rapeseed cell walls. According to enzyme activity assays, it is rich in polygalacturonase, which is responsible for the release of galacturonic acid from pectins. The preparation also contains *endo*-β-1,4-galactanase, active on arabinogalactan,[44] and β-glucanase, which hydrolyzes glucans (cellulose and xyloglucan in rapeseed). High β-glucanase and endoxylanase activities in the Depol 740L product hydrolyzed the cellulose, xyloglucans, and xylan. However, due to the lack of polygalacturonase activity in Depol, no galacturonic acid was released from pectin. Celluclast 1.5L, which contained *endo*-1,3(4)-β-glucanase and β-glucanase (EC 3.2.1.4) as its main activities, was expected to hydrolyze cellulose and xyloglucan.

Effects of Enzymatic Treatment on the Microstructure of Rapeseed Press Cakes. Light microscopy of the solid fractions obtained after enzyme treatment of the intact press cake revealed differences in cell wall and pectin stainability after each treatment. Enzyme action was mainly detected in the cell walls of the embryo, which forms the major part of the seed and where most of rapeseed protein is stored.[5,22] By comparison,

dx.doi.org/10.1021/jf501802e | J. Agric. Food Chem. 2014, 62, 7989–7997

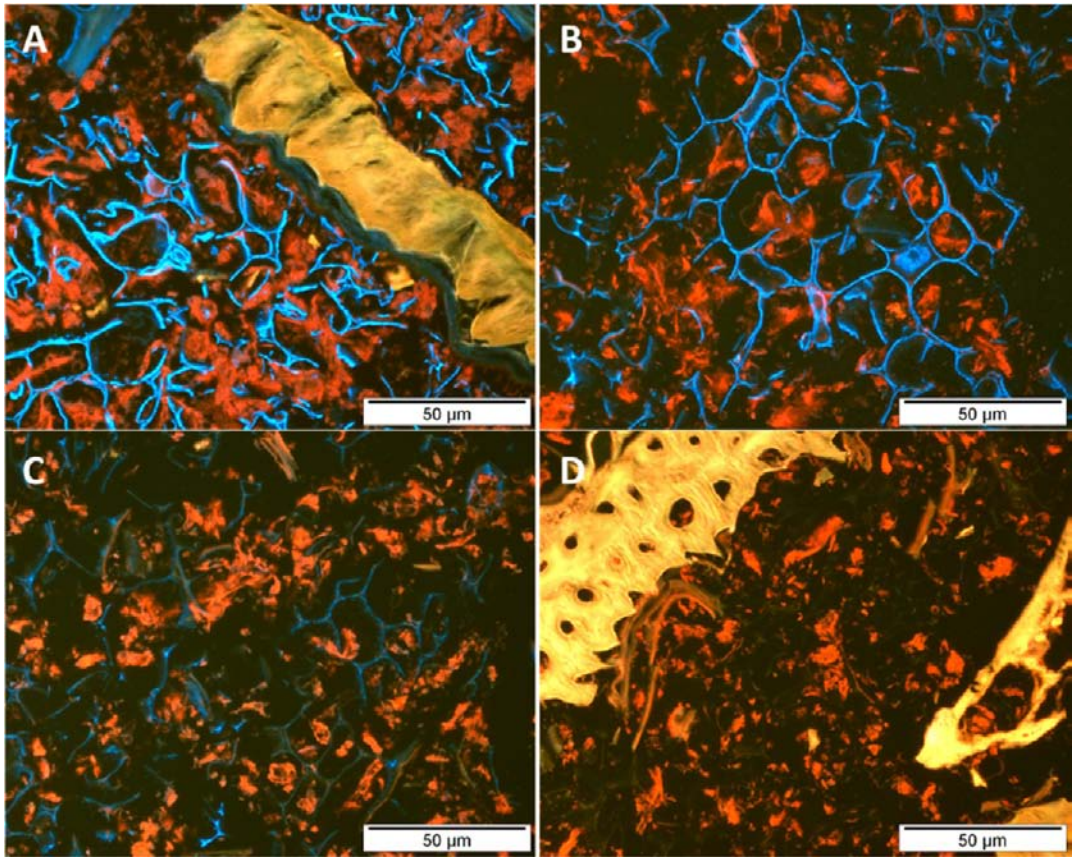

Figure 3. Micrographs of the intact *B. rapa* press cake after dry-milling (A) and of the solid fractions obtained from treatment of the press cake at 50 °C without enzyme addition (B), with Celluclast (C) or with Depol (D). The sections were stained with Calcofluor White and Acid Fuchsin, showing cell wall glucans as blue and proteins as red. Panels A and D include fragments of the seed coat.

the seed coat fragments were mostly unaffected by the enzymes. The embryonic cell walls were stainable with Calcofluor after the reference treatment but not after the Pectinex treatment (Figure 2A,B), suggesting complete cell wall glucan hydrolysis at least on the surface of the cell walls. The cell walls were likewise detected in the bright-field image of the reference sample but not in the Pectinex-treated sample (Figure 2C,D). According to Ruthenium Red staining, the seed coat pectins were still present after the Pectinex treatment (data not shown). The Ruthenium Red-stained networks inside the embryo cells were also detectable in both the Pectinex-treated and the reference sample, but their staining intensity had been reduced, suggesting partial hydrolysis of this pectin-type material. The substantial effect of Pectinex on the press cake microstructure was obviously caused by the hydrolysis of pectins and pectic polysaccharides, which are among the main rapeseed carbohydrates[3,8,45]

Depol had a strong disruptive effect on the cell wall structure, despite the lower carbohydrate extraction yield in comparison to that of Pectinex. Similarly, as after Pectinex treatment, the embryonic cell walls were no longer stainable with Calcofluor after Depol treatment (Figure 3D). However, while Pectinex degraded the embryonic cell walls completely, skeletons of the cell walls were still detectable after Depol treatment. This suggests that complete cell wall degradation by Depol may have been hindered by its inability to hydrolyze pectin. Proteins in the Depol-treated solids seemed more degraded and scattered than after other treatments (Figure 3D), indicating partial protein hydrolysis by the minor protease activity in Depol (Table 1).

In the Celluclast-treated solids (Figure 3C), cell wall stainability with Calcofluor was only slightly reduced in comparison to the reference sample (Figure 3B). Since cellulose and xyloglucan are among the major components of rapeseed cotyledon cell walls, the weak impact of Celluclast suggests that cellulase accessibility may be limited by the interconnections of cellulose with other polysaccharides.[8] The data indicates that efficient disintegration of rapeseed embryonic cell walls requires targeting of both glucans and pectic polysaccharides.

Protein Extractability from Rapeseed Press Cakes. Protein extractability was generally higher from the dehulled *B. napus* press cake than from the intact *B. rapa* press cake. Even without enzyme addition, 48% of the protein in the dehulled press cake was extractable in 50 °C water, whereas the corresponding yield was 34% from the intact press cake (Figure 4). Proteins have been previously reported to be more soluble in solvent-extracted *B. napus* meals than in the respective *B. rapa* meals,[46] but the effects of genetic variation on protein extractability are not yet well understood. Upstream processes such as seed drying and dehulling are presumably the main cause of variation in rapeseed protein extractability. Tighter protein compaction observed in the cold-pressed, dehulled *B. napus* press cake than in intact *B. rapa* press cake suggests that protein solubility had been better retained during cold pressing of dehulled seeds. It is well-known that excess heat used to facilitate seed drying or oil pressing may cause denaturation and

dx.doi.org/10.1021/jf501802e | J. Agric. Food Chem. 2014, 62, 7989−7997

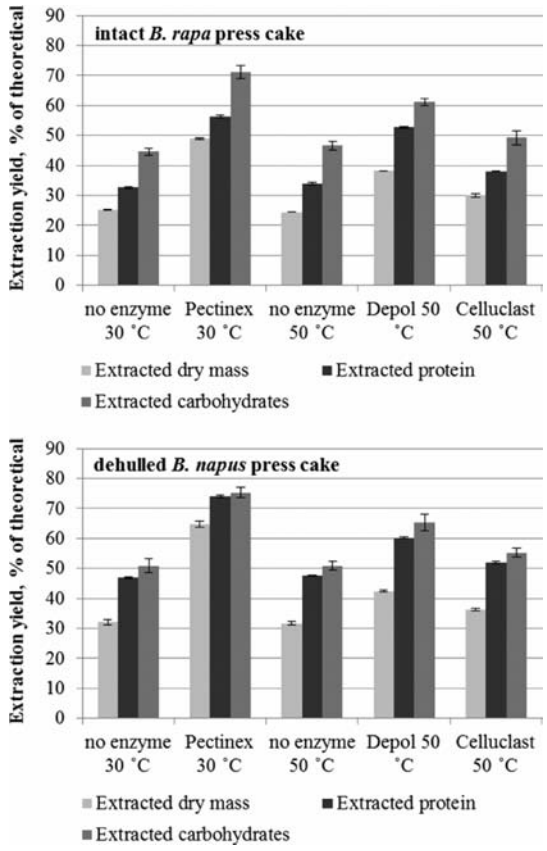

Figure 4. Effect of enzymatic treatment on extraction of proteins and carbohydrates from intact *B. rapa* and dehulled *B. napus* press cakes, in comparison to reference treatment without enzyme addition (no enzyme) at 30 or 50 °C. The press cakes were treated with Pectinex, Depol, and Celluclast for 48 h at 30 or 50 °C. Error bars represent standard deviations of at least two parallel reactions.

alteration of the proteins, reducing their solubility,[5] but denaturation may also occur due to mechanical force during cold pressing. For example, protein solubility has been previously reported to decrease during screw pressing of oil from flaked, cooked rapeseeds.[2] Cold pressing of intact seeds may require harsher conditions than pressing of dehulled seeds, which could have had a negative impact on protein solubility.

All enzyme treatments enhanced protein release from the press cakes. Pectinex increased protein extraction most, by 73% from the intact press cake and by 58% from the dehulled press cake in comparison to reference treatments without enzyme addition (Figure 4). In total, 56 and 74% of the protein in the intact and dehulled press cakes were extracted during the 48-h Pectinex treatment. The resulting liquid fraction from Pectinex treatment contained 39−54% of protein (as calculated from dry mass and protein concentration of the solid fraction) and 47−49% of carbohydrates per dry weight. SDS−PAGE analysis of the liquid fractions showed strong protein bands in the area of 20−30 kDa, corresponding to the subunits of rapeseed cruciferins (Figure 5). The small protein bands of 5−7 kDa corresponded to the subunits of napins, whereas 35−50 kDa bands observed after enzyme treatments originated from the enzymes. According to SDS−PAGE, the proteins remained mostly unhydrolyzed during Celluclast and Pectinex treatments. However, some of the bands corresponding to 20−30 kDa cruciferin subunits were hydrolyzed into 12−15 kDa fragments when the press cakes were treated with Depol due to the minor protease activity.

In the present work, combined structural and chemical characterization of rapeseed press cake and its enzymatically treated soluble and insoluble fractions provided understanding on how polysaccharide hydrolysis facilitates rapeseed protein extraction. Enzymatic hydrolysis of pectic polysaccharides (i.e., homogalacturonan, rhamnogalacturonan, arabinan and arabinogalactan) enhanced disintegration of the rapeseed embryonic cell walls, which facilitated protein extraction from cold-pressed rapeseed press cake. The presence of intracellular pectin-type networks colocalized with protein in the cotyledons and embryo was revealed, and such networks are proposed to affect protein release. However, more research on their presence and interactions with rapeseed storage proteins is needed. Our data supports the utilization of pectin-degrading enzymes for rapeseed press cake disassembly and subsequent fractionation and suggests that, in addition to the cell walls, the intracellular

Table 4. Concentration of Released Monosaccharides, Uronic Acids, Surcose, and Polysaccharides (glucose, fructose, galactose, rhamnose, arabinose, xylose and mannose) in the Liquid Fractions Obtained from Treatment of Intact *B. rapa* and Dehulled *B. napus* Rapeseed Press Cakes with Pectinex (P), Depol (D), and Celluclast (C) and without Enzyme Addition at 30°C (no 30) and 50°C (no 50)[a]

	concentration (g/L)									
	intact *B. rapa* press cake					dehulled *B. napus* press cake				
	no 30	P	no 50	D	C	no 30	P	no 50	D	C
glucose	5.4	9.1	6.2	7.1	6.8	4.2	9.9	6.3	6.7	6.9
fructose	6.4	6.7	7.1	6.3	6.5	4.3	6.6	6.6	5.5	6.3
galactose	0.8	2.0	1.2	1.5	1.3	1.4	2.5	1.7	2.2	1.9
rhamnose	0.0	0.1	0.0	0.0	0.0	0.0	0.1	0.0	0.0	0.0
arabinose	0.1	3.9	0.1	3.7	0.2	0.1	3.7	0.1	3.1	0.2
xylose	0.0	0.5	0.0	0.1	0.1	0.0	0.4	0.0	0.2	0.2
mannose	0.0	0.1	0.1	0.1	0.1	0.1	0.2	0.1	0.1	0.1
galacturonic acid	0.1	0.6	0.0	0.1	0.0	0.0	0.5	0.0	0.0	0.0
methyl glucuronic acid	0.4	0.3	0.1	0.1	0.0	0.1	0.2	0.0	0.1	0.0
glucuronic acid	0.0	0.0	0.0	0.0	0.0	0.0	0.0	0.0	0.1	0.0
sucrose	0.3	0.0	0.0	0.0	0.0	5.5	0.0	1.5	2.3	1.7
polysaccharides	2.7	2.9	2.0	2.9	2.6	1.9	2.6	1.4	2.6	1.8

[a]Standard deviations were <12% of the measured values from at least two parallel reactions.

dx.doi.org/10.1021/jf501802e | J. Agric. Food Chem. 2014, 62, 7989−7997

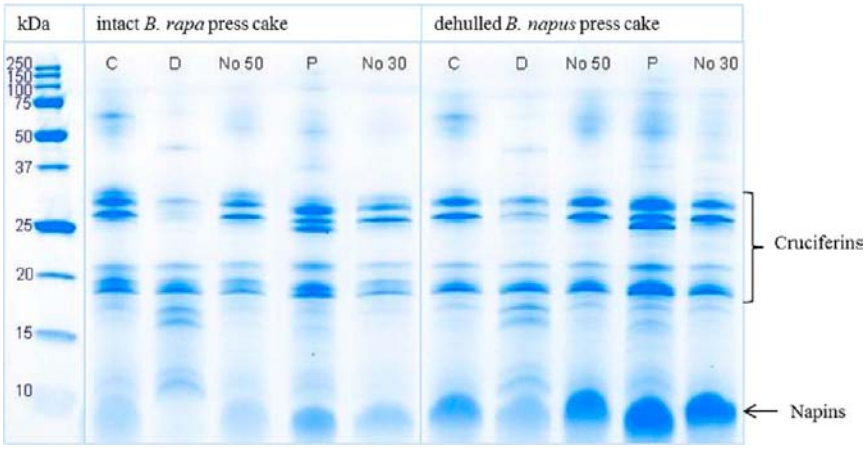

Figure 5. SDS−PAGE patterns of proteins released during enzymatic treatment of intact and dehulled rapeseed press cakes. The materials were hydrolyzed for 48 h with Celluclast (C), Depol (D), and Pectinex (P) at an enzyme dosage of 10 mg protein/g dry substrate. No enzyme was added in the reference treatments carried out at 50 °C (No 50) and 30 °C (No 30).

matrix should be targeted for enhanced protein release. Once qualified for technological functionality, rapeseed protein concentrates produced by enzyme-aided extraction may find use in food, feed, and cosmetic applications.

AUTHOR INFORMATION

Corresponding Author

*Phone: +358 20 722 4514. Fax: +358 20 722 7071. E-mail: katariina.rommi@vtt.fi.

Funding

The research leading to these results has received funding from the European Community's Seventh Framework Programme FP7/2007-2013 under grant agreement no. 289170−APROPOS. Funding from Academy of Finland to K.P. is likewise gratefully acknowledged.

Notes

The authors declare no competing financial interest.

ACKNOWLEDGMENTS

The authors wish to thank Kankaisten Öljykasvit Oy, Kroppenstedter Ölmühle Walter Doepelheuer GmbH, and IGV Institut für Getreideverarbeitung GmbH for rapeseed press cakes. The authors thank Mari Raulio, Juhani Sibakov, and Atte Mikkelson at the VTT Technical Research Centre of Finland for cooperation in the rapeseed microscopy mechanical pretreatment, and carbohydrate analytics and VTT's experienced technical staff for their valuable experimental work.

REFERENCES

(1) Schöne, F.; Kirchheim, U.; Schumann, W.; Lüdke, H. Apparent digestibility of high-fat rapeseed press cake in growing pigs and effects on feed intake, growth and weight of thyroid and liver. *Anim. Feed Sci. Technol.* **1996**, *62*, 97−110.

(2) Mustafa, A. F.; Christensen, D.; McKinnon, J.; Newkirk, R. Effects of stage of processing of canola seed on chemical composition and in vitro protein degradability of canola meal and intermediate products. *Can. J. Anim. Sci.* **2000**, *80*, 211−214.

(3) Shahidi, F. *Canola and Rapeseed: Production, Chemistry, Nutrition and Processing Technology*; Van Nostrand Reinhold: New York, 1990; 355 pp.

(4) Mustafa, A. F.; Christensen, D.; McKinnon, J. Chemical characterization and nutrient availability of high and low fiber canola meal. *Can. J. Anim. Sci.* **1996**, *76*, 579−586.

(5) Wanasundara, J. Proteins of *Brassicaceae* oilseeds and their potential as a plant protein source. *Crit. Rev. Food Sci. Nutr.* **2011**, *51*, 635−677.

(6) Ghodsvali, A.; Khodaparast, M. H.; Vosoughi, M.; Diosady, L. L. Preparation of canola protein materials using membrane technology and evaluation of meals functional properties. *Food Res. Int.* **2005**, *38*, 223−231.

(7) Bell, J.; Keith, M. A. Survey of variation in the chemical composition of commercial canola meal produced in Western Canadian crushing plants. *Can. J. Anim. Sci.* **1991**, *71*, 469−480.

(8) Pustjens, A. M.; Schols, H. A.; Kabel, M. A.; Gruppen, H. Characterisation of cell wall polysaccharides from rapeseed (*Brassica napus*) meal. *Carbohydr. Polym.* **2013**, *98*, 1650−1656.

(9) Ghosh, P.; Ghosal, P.; Thakur, S.; Lerouge, P.; Loutelier-Bourhis, C.; Driouich, A.; Ray, B. Cell wall polysaccharides of *Brassica campestris* seed cake: isolation and structural features. *Carbohydr. Polym.* **2004**, *57*, 7−13.

(10) Gaspar, Y.; Johnson, K. L.; McKenna, J. A.; Bacic, A.; Schultz, C. J. The complex structures of arabinogalactan−proteins and the journey towards understanding function. *Plant Mol. Biol.* **2001**, *47*, 161−176.

(11) Anderson, J. W.; Baird, P.; Davis, R. H., Jr; Ferreri, S.; Knudtson, M.; Koraym, A.; Waters, V.; Williams, C. L. Health benefits of dietary fiber. *Nutr. Rev.* **2009**, *67*, 188−205.

(12) Simbaya, J.; Slominski, B.; Rakow, G.; Campbell, L.; Downey, R.; Bell, J. Quality characteristics of yellow-seeded *Brassica* seed meals: Protein, carbohydrates and dietary fiber components. *J. Agric. Food Chem.* **1995**, *43*, 2062−2066.

(13) Slominski, B. A.; Campbell, L. D. Non-starch polysaccharides of canola meal: quantification, digestibility in poultry and potential benefit of dietary enzyme supplementation. *J. Sci. Food Agric.* **1990**, *53*, 175−184.

(14) Bérot, S.; Compoint, J. P.; Larré, C.; Malabat, C.; Guéguen, J. Large scale purification of rapeseed proteins (*Brassica napus* L.). *J. Chromatogr. B: Anal. Technol. Biomed. Life Sci.* **2005**, *818*, 35−42.

(15) Sari, Y. W.; Bruins, M. E.; Sanders, J. P. Enzyme assisted protein extraction from rapeseed, soybean, and microalgae meals. *Ind. Crops Prod.* **2013**, *43*, 78−83.

(16) Niu, Y. X.; Li, W.; Zhu, J.; Huang, Q.; Jiang, M.; Huang, F. Aqueous enzymatic extraction of rapeseed oil and protein from dehulled cold-pressed double-low rapeseed cake. *Int. J. Food Eng.* **2012**, *8*, 1−14.

(17) Tang, Q. N. *Protein concentrates and isolates, and processes for the production thereof.* 2010, US 2010/0136173 A1.

(18) Pustjens, A. M.; de Vries, S.; Gerrits, W.; Kabel, M.; Schols, H.; Gruppen, H. Residual carbohydrates from in vitro digested processed rapeseed (*Brassica napus*) meal. *J. Agric. Food Chem.* **2012**, *60*, 8257−8263.

(19) Meng, X.; Slominski, B. A.; Nyachoti, C. M.; Campbell, L. D.; Guenter, W. Degradation of cell wall polysaccharides by combinations of carbohydrase enzymes and their effect on nutrient utilization and broiler chicken performance. *Poult. Sci.* **2005**, *84*, 37−47.
(20) Kvist, S.; Carlsson, T.; Lawther, J. M.; Basile, F. Process for the fractionation of oilseed press cakes and meals. 2005, US2005/0136162 A1.
(21) Keegstra, K.; Talmadge, K. W.; Bauer, W. D.; Albersheim, P. The structure of plant cell walls: III. A model of the walls of suspension-cultured sycamore cells based on the interconnections of the macromolecular components. *Plant Physiol.* **1973**, *51*, 188−197.
(22) Hu, Z.; Hua, W.; Zhang, L.; Deng, L.; Wang, X.; Liu, G.; Hao, W.; Wang, H. Seed structure characteristics to form ultrahigh oil content in rapeseed. *PLoS One* **2013**, *8*, 1−10.
(23) Srivastava, B.; Agrawal, Y. C.; Sarker, B. C.; Kushwaha, Y. P.; Singh, B. P. Effect of enzyme extract on rapeseed microstructure and oil recovery. *J. Food Sci. Technol.* **2004**, *41*, 88−91.
(24) Zurbriggen, B.; Bailey, M.; Penttilä, M.; Poutanen, K.; Linko, M. Pilot scale production of a heterologous *Trichoderma reesei* cellulase in *Saccharomyces cerevisiae*. *J. Biotechnol.* **1990**, *13*, 267−278.
(25) Bailey, M. J.; Nevalainen, K. M. Induction, isolation and testing of stable *Trichoderma reesei* mutants with improved production of solubilizing cellulase. *Enzyme Microb. Technol.* **1981**, *3*, 153−157.
(26) Bailey, M. J.; Pessa, E. Strain and process for production of polygalacturonase. *Enzyme Microb. Technol.* **1990**, *12*, 266−271.
(27) Bailey, M. J.; Biely, P.; Poutanen, K. Interlaboratory testing of methods for assay of xylanase activity. *J. Biotechnol.* **1992**, *23*, 257−270.
(28) Lowry, O. H.; Rosebrough, N.; Farr, A.; Randall, R. Protein measurement with the Folin phenol reagent. *J. Biol. Chem.* **1951**, *193*, 265−275.
(29) Hausalo, T. Analysis of wood and pulp carbohydrates by anion exchange chromatography with pulsed amperometric detection. *Proceedings of the 8th International Symposium on Wood and Pulping Chemistry. June 6−9, 1995, Helsinki, Finland*; 1995; pp 131−136.
(30) Sluiter, A.; Hames, B.; Ruiz, R.; Scarlata, C.; Sluiter, J.; Templeton, D.; Crocker, D. Determination of structural carbohydrates and lignins in biomass. In *Laboratory Analytical Procedure (LAP)*; National Renewable Energy Laboratory: Golden, CO, 2008; 18 pp.
(31) Kane, P. F. $CuSO_4$−TiO_2 as Kjeldahl digestion catalyst in manual determination of crude protein in animal feeds. *J. Assoc. Off. Anal. Chem.* **1986**, *69*, 664−666.
(32) Goldschmid, O. Ultraviolet spectra. In *Lignins: Occurrence, Formation, Structure and Reactions*; Sarkanen, K. V., Ludwig, C. H., Eds.; John Wiley & Sons: New York, 1971; Chapter 6, pp 241−298.
(33) McCleary, B. V.; Gibson, T. S.; Mugford, D. C. Measurement of total starch in cereal products by amyloglucosidase-alpha-amylase method: Collaborative study. *J. AOAC Int.* **1997**, *80*, 571−579.
(34) Munck, L.; Jorgensen, K. G.; Ruud-Hansen, J.; Hansen, K. T. The EBC methods for determination of high molecular weight β-glucan in barley, malt, wort and beer. *J. Inst. Brewing* **1989**, *95*, 79−82.
(35) Holopainen-Mantila, U.; Marjamaa, K.; Merali, Z.; Käsper, A.; de Bot, P.; Jääskeläinen, A.; Waldron, K.; Kruus, K.; Tamminen, T. Impact of hydrothermal pre-treatment to chemical composition, enzymatic digestibility and spatial distribution of cell wall polymers. *Bioresour. Technol.* **2013**, *138*, 156−162.
(36) Fulcher, R. G.; Wong, S. J. Inside cereals—A fluorescence microchemical view. In *Cereals for Food and Beverages*; Inglett, G. E., Munck, L., Eds.; Academic Press: New York, 1980; pp 1−26.
(37) Maeda, H.; Ishida, N. Specificity of binding of hexopyranosyl polysaccharides with fluorescent brightener. *J. Biochem.* **1967**, *62*, 276−278.
(38) Hanke, D. E.; Northcote, D. H. Molecular visualization of pectin and DNA by ruthenium red. *Biopolymers* **1975**, *14*, 1−17.
(39) Hou, W. C.; Chang, W. H.; Jiang, C. M. Qualitative distinction of carboxyl group distributions in pectins with ruthenium red. *Bot. Bull. Acad. Sin.* **1999**, *40*, 115−119.
(40) Eriksson, I.; Westerlund, E.; Åman, P. Chemical composition in varieties of rapeseed and turnip rapeseed, including several samples of hull and dehulled seed. *J. Sci. Food Agric.* **1994**, *66*, 233−240.
(41) Herth, W.; Schnepf, E. The fluorochrome, calcofluor white, binds oriented to structural polysaccharide fibrils. *Protoplasma* **1980**, *105*, 129−133.
(42) Suárez, C.; Zienkiewicz, A.; Castro, A.; Zienkiewicz, K.; Majewska-Sawka, A.; Rodríguez-García, M. Cellular localization and levels of pectins and arabinogalactan proteins in olive (*Olea europaea* L.) pistil tissues during development: Implications for pollen−pistil interaction. *Planta* **2013**, *237*, 305−319.
(43) Ghazi, I.; Fernandez-Arrojo, L.; Garcia-Arellano, H.; Ferrer, M.; Ballesteros, A.; Plou, F. Purification and kinetic characterization of a fructosyltransferase from *Aspergillus aculeatus*. *J. Biotechnol.* **2007**, *128*, 204−211.
(44) Luonteri, E.; Laine, C.; Uusitalo, S.; Teleman, A.; Siika-Aho, M.; Tenkanen, M. Purification and characterization of *Aspergillus* β-d-galactanases acting on β-1,4- and β-1,3/6-linked arabinogalactans. *Carbohydr. Polym.* **2003**, *53*, 155−168.
(45) Siddiqui, I. R.; Wood, P. J. Carbohydrates of rapeseed: A review. *J. Sci. Food Agric.* **1977**, *28*, 530−538.
(46) Aluko, R. E.; Mcintosh, T. Polypeptide profile and functional properties of defatted meals and protein isolates of canola seeds. *J. Sci. Food Agric.* **2001**, *81*, 391−396.

which fruits are regarded as a functional mixture of water-soluble compounds from the fruit flesh and lipophilic constituents of the cuticle.[14] Nevertheless, current knowledge of the triterpenoid composition and content in grape cuticular waxes remains limited.[15]

Cuticle biosynthesis during fruit development has been primarily investigated from a morphological or quantitative perspective.[7] However, a limited number of studies have reported the compositional alterations in individual cuticular components during fruit development. These reports revealed substantial differences in time-dependent changes, in particular, constituents that are dependent on the type of fruit, indicating that these studies require case-by-case investigation. Moreover, alterations in a limited number of compounds, for example, proanthocyanidins,[16] polysaccharides,[17] and sterols,[18,19] that are present in the cuticle and the whole "skin" during grape berry development have been investigated.

The presence of several triterpenoids in grape berry cuticular waxes has been reported in several studies.[15,19] However, a complete identification of the triterpenoids in grape berry cuticular waxes has not been reported, although the number of identified compounds continues to increase due to the chemical diversity of grapevines. Therefore, the aim of this study was to determine the composition and content of triterpenoids in cuticular waxes of grape berries of the following eight cultivars that are characteristic of the Upper Rhine Valley: the white varieties Chasselas, Gewurztraminer, Muscat d'Alsace, Riesling, Sylvaner, Pinot auxerrois, and Pinot gris; and the red variety Pinot noir. Moreover, to enhance the understanding of the compositional and functional evolution of cuticular waxes during fruit development, alterations in the triterpenoid content were examined at three different phenological stages: young grapes, grapes at véraison (the onset of ripening), and mature grapes.

MATERIALS AND METHODS

Plant Material. Randomly selected bunches of eight grape cultivars (Chasselas, Gewurztraminer, Muscat d'Alsace, Pinot auxerrois, Pinot gris, Pinot noir, Riesling, and Sylvaner) were collected in vineyards in Ingersheim, Ammerschwihr, and Katzenthal in the Upper Rhine Valley in the summer of 2011 at three different stages corresponding to young grapes (denoted T1, collected on June 27), grapes at véraison (denoted T2, collected on July 25), and mature grapes (denoted T3, collected on August 22). T1 corresponded to stage 75 (berries pea-sized, bunches hang) of the BBCH scale,[20] T2 to stage 79 (berry touch complete), and T3 to stage 89 (berries ripe for harvest). The replicate samples of fruits (4−5 g for T1, 6−7 g for T2, and 11−13 g for T3) were prepared from different pooled sample sets of 20−25 g.

Chemicals and Standards. All solvents used for extraction and analysis were of analytical grade. Authentic standards of α-amyrin and ursolic acid methyl ester were purchased from Roth (Karlsruhe, Germany); β-amyrin, lupeol, oleanolic acid, campesterol, cholesterol, sitosterol, and stigmasterol were purchased from Sigma-Aldrich (Steinheim, Germany). α-Amyrenone and β-amyrenone were obtained by oxidation of the α-amyrin and β-amyrin standards with chromium trioxide-pyridine in dichloromethane.[21]

Extraction and Fractionation of Cuticular Waxes. Each sample of entire fruit was extracted by incubation in 40 mL of chloroform with gentle stirring for 30 s at room temperature. The extracts were decanted and evaporated to dryness. After weighing, the obtained wax extracts (masses of approximately 3.7 mg for T1 samples, 5.0 mg for T2, and 8.8 mg for T3) were separated by preparative thin layer chromatography on 20 cm × 20 cm glass plates coated with a 0.25 mm layer of silica gel 60G (Merck, Darmstadt, Germany) in the solvent system $CHCl_3$/MeOH (97:3, v/v) into three fractions: (i) free (nonesterified) steroids and neutral triterpenes (alcohols, aldehydes, and ketones); (ii) triterpene acids; and (iii) triterpenoid (sterol and triterpene) low-polarity esters. The individual fractions were localized on plates by comparison with standards of oleanolic acid, sitosterol, α-amyrin, and sitosterol palmitate and were visualized by spraying the appropriate area on the plate with 50% H_2SO_4, followed by heating with a hot-air stream. Fractions were eluted from the gel in at least 10 volumes of diethyl ether relative to the volume of the isolated gel, with the average recovery of individual triterpenoids of 96−98%.[22] The fractions containing free neutral triterpenes and steroids (R_F 0.3−0.9) were directly analyzed using GC-MS, whereas fractions containing triterpene acids (R_F 0.2−0.3) were first methylated with diazomethane, and fractions containing triterpenoid (triterpene and sterol) low-polarity esters (R_F 0.9−1) were subjected to alkaline hydrolysis.

Methylation of Triterpene Acids. Nitrosomethylurea (2.06 g) was added to a mixture of 20 mL of diethyl ether and 6 mL of 25% aqueous KOH, and the organic layer was washed with water (3 × 50 mL) and separated from the aqueous layer. Samples containing triterpene acids (not more than 10 mg) were dissolved in 2 mL of the obtained solution of diazomethane in diethyl ether and incubated at 2 °C for 24 h.

Alkaline Hydrolysis. The ester fraction was subjected to alkaline hydrolysis using 10% NaOH in 80% MeOH at 80 °C for 3 h. Subsequently, 5 volumes of water was added to each hydrolysate, adjusted to neutral pH with 5% CH_3COOH, and the obtained mixtures were extracted with diethyl ether (3 × 10 mL). These extracts were fractionated using preparative TLC as previously described. Subsequently, fractions containing free triterpene alcohols and sterols were directly analyzed using GC-MS, whereas triterpene acid fractions were methylated prior to this analysis.

Identification and Quantitation of Triterpenoids using GC-MS/Flame Ionization Detector (FID). An Agilent Technologies 7890A gas chromatograph (Perlan Technologies, Warsaw, Poland) equipped with a 5975C mass spectrometric detector was used for qualitative and quantitative analyses. Samples dissolved in diethyl ether/methanol (5:1, v/v) were applied (in a volume of 1−4 μL) using 1:10 split injection. All samples were analyzed in triplicate. The column used was a 30 m × 0.25 mm i.d., 0.25 μm, HP-5MS (Agilent Technologies, Santa Clara, CA, USA). Helium was used as the carrier gas at a flow rate of 1 mL/min. The following parameters were employed: column temperature, 280 °C; inlet and FID temperature, 290 °C; MS transfer line temperature, 275 °C; quadrupole temperature, 150 °C; ion source temperature, 230 °C; EI, 70 eV; m/z range, 33−500; FID gas (H_2) flow, 30 mL/min (hydrogen generator); and air flow, 400 mL/min. Individual compounds were identified by comparing their mass spectra with library data from Wiley 9th ed. and NIST 2008 Lib. SW version 2010 or previously reported data and by comparison of their retention times and corresponding mass spectra with those of authentic standards, when available. Quantitation was performed using an external standard method based on calibration curves determined for the following representative triterpenoid classes: α-amyrin, oleanolic acid methyl ester, and sitosterol.

Separation by High-Performance Liquid Chromatography (HPLC). Chromatographic analysis of samples containing a mixture of α-amyrin and lupeol was performed using a chromatographic system (Shimadzu, Shim-pol, Izabelin, Poland) equipped with two LC-10AT pumps, a CTO-10AS oven, and an SPD-10A spectrophotometer set at 200 and 254 nm. A 250 mm × 4.6 mm i.d., 4 μm, Synergi Max-RP 80-Å column (Phenomenex, Torrance, CA, USA) was used. All data were acquired and processed using Shimadzu CLASS-VP version 5.032 chromatography data system software. The mobile phase (flow rate of 0.6 mL/min) was 100% acetonitrile (isocratic system), and separation was performed at 30 °C. Quantitative analysis of α-amyrin and lupeol was based on the relative ratios of their peak areas.[22]

Statistical Analysis. Data are presented as the means ± standard deviations of three independent samples analyzed in triplicate. The data were subjected to one-way analysis of variance (ANOVA), and the differences between means were evaluated using Duncan's multiple-range test. Statistical significance was considered at $p < 0.05$.

Table 1. Masses of Cuticular Wax Extracts Obtained from Grapes at Three Phenological Stages[a]

	average water content (%)			mg/g dry wt ± SD[b]		
cultivar	T1	T2	T3	T1	T2	T3
Chasselas	82	91	85	6.0 ± 0.6 a	7.6 ± 0.9 a	3.5 ± 0.2 b
Gewurztraminer	86	89	83	5.7 ± 0.3 a	8.6 ± 0.3 b	5.5 ± 0.9 a
Muscat d'Alsace	76	92	86	3.5 ± 0.4 a	8.3 ± 1.3 b	3.8 ± 0.4 a
Pinot auxerrois	82	91	85	5.4 ± 0.5 a	6.5 ± 0.3 b	4.4 ± 0.3 c
Pinot gris	75	88	78	4.6 ± 0.4 a	7.9 ± 2.3 b	4.7 ± 0.9 a
Pinot noir	78	90	81	4.1 ± 0.6 a	7.7 ± 1.9 b	5.0 ± 0.9 a
Riesling	79	89	81	4.9 ± 0.4 a	7.6 ± 0.9 b	3.9 ± 0.4 c
Sylvaner	72	91	84	3.4 ± 0.5 a	7.8 ± 0.8 b	3.9 ± 0.4 a

[a]T1, young grapes; T2, grapes at véraison; T3, mature grapes. [b]Values are expressed as the means of three independent samples. Values in a row not sharing a common letter are significantly different ($p < 0.05$).

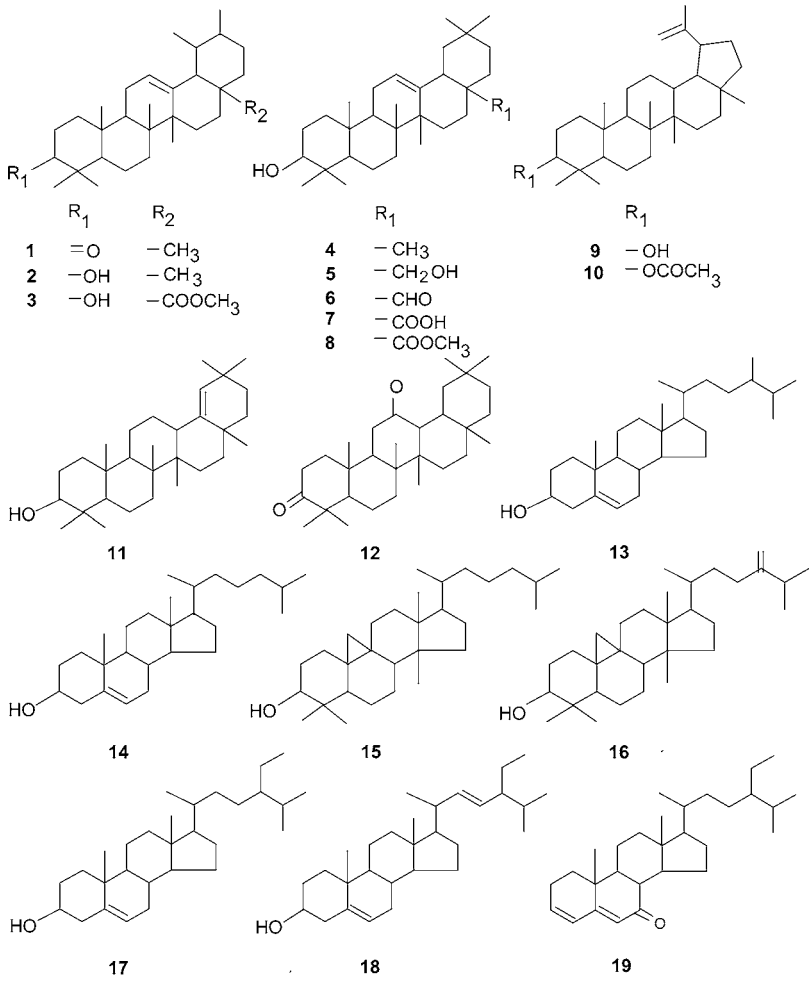

Figure 1. Chemical structures of triterpenoids identified in grape cuticular waxes: α-amyrenone, **1**; α-amyrin, **2**; ursolic acid methyl ester, **3**; β-amyrin, **4**; erythrodiol, **5**; oleanolic aldehyde, **6**; oleanolic acid, **7**; oleanolic acid methyl ester, **8**; lupeol, **9**; lupeol acetate, **10**; germanicol, **11**; 3,12-oleandione, **12**; campesterol, **13**; cholesterol, **14**; cycloartanol, **15**; 24-methylenocycloartanol, **16**; sitosterol, **17**; stigmasterol, **18**; stigmasta-3,5-dien-7-one, **19**.

RESULTS AND DISCUSSION

Cuticular wax extracts were obtained by incubation of fresh entire grapes in chloroform with gentle stirring for 30 s. Despite potential incomplete recovery (up to 73% of the cuticular wax, depending on the plant species[23]), this brief, gentle method of extraction is commonly applied because it precludes solvent penetration across the cuticle and prevents contamination by compounds originating from deeper tissues such as the epidermis, collenchyma, or parenchyma.[15,22] The masses of the obtained extracts are summarized in Table 1.

The development of the grape berry involves several phases, and each growth period is characterized by distinct physiological processes, which may be reflected in different chemical compositions.[16,24] In this study, the amount of chloroform-soluble cuticular waxes, which is expressed per 1 g of berry dry weight, was found to be highest at the véraison

dx.doi.org/10.1021/jf502033s | J. Agric. Food Chem. 2014, 62, 7998−8007

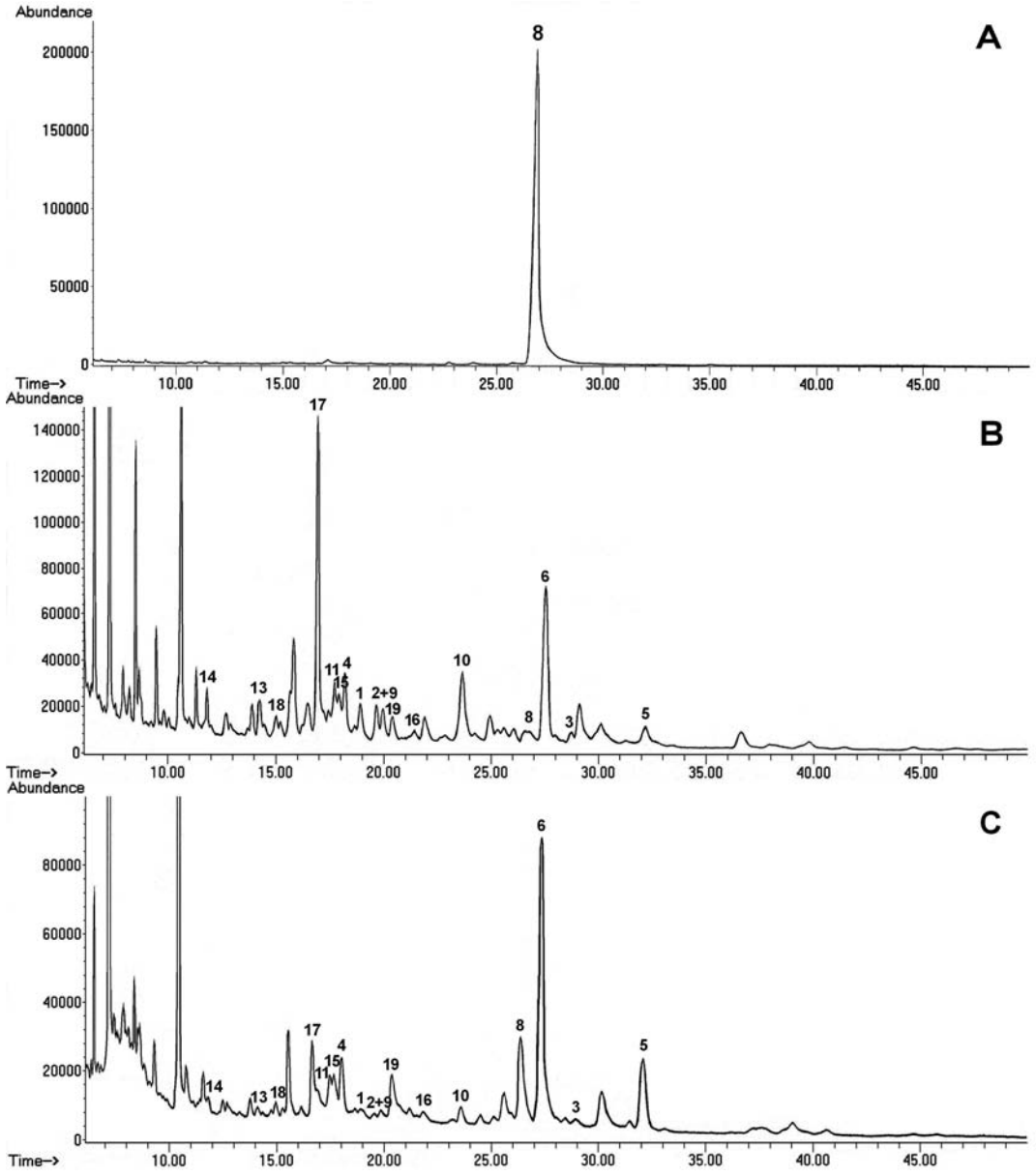

Figure 2. GC-FID chromatograms of the fraction containing methyl esters of triterpene acids obtained from cuticular waxes of Riesling young grapes (A) and the fractions containing sterols and neutral triterpenes (alcohols, aldehydes, and ketones) from cuticular waxes of Gewurztraminer and Sylvaner mature grapes (B, C). Peaks are numbered according to Figure 1.

stage (T2). The increase in the amount of wax extract from young grapes (T1) to grapes at véraison (T2) can be >2-fold, as observed for Muscat d'Alsace and Sylvaner. With berry ripening (T3), the amount of chloroform-soluble waxes sharply decreases for cultivars such as Chasselas, Gewurztraminer, Pinot auxerrois, and Riesling to a level below that of young grapes (T1). However, this decrease does not necessarily reflect a dramatic decrease in the amount of these waxes on the berry surface during ripening. The lower levels of extracted wax per 1 g of T3 berry dry weight are caused by the increase in the dry weight of the berry due to chemical changes that are characteristic for maturing and ripening fruit, that is, the accumulation of anthocyanin pigments, other phenolic compounds, and, primarily, substantial levels of sugars. The different stages of berry development can also be reflected in changes in the water content. The young grapes (T1) contained the lowest amount of water, which ranged from 72 to 86%. The grapes at véraison stage (T2), which are entering the period of rapid cell expansion and tissue softening, contained the highest amount of water (88−92%). In the mature grapes (T3), the amount of water decreased to 78−85% due to the accumulation of sugars and other compounds and the growing density of mesocarp cells; however, these phenomena may occur from the evaporative loss of water. Indeed, the observed water content in grapes at different developmental stages may depend on external conditions that influence water availability; for example, periods of dryness or high humidity can considerably modify the water content in grape berries at various stages of development.[24]

Identification of Triterpenoids in Grape Cuticular Waxes. The obtained chloroform extracts of grape cuticular waxes were separated into three fractions using preparative TLC. The fractions containing free (nonesterified) steroids and neutral triterpenes, triterpene acids after methylation, and

dx.doi.org/10.1021/jf502033s | J. Agric. Food Chem. 2014, 62, 7998−8007

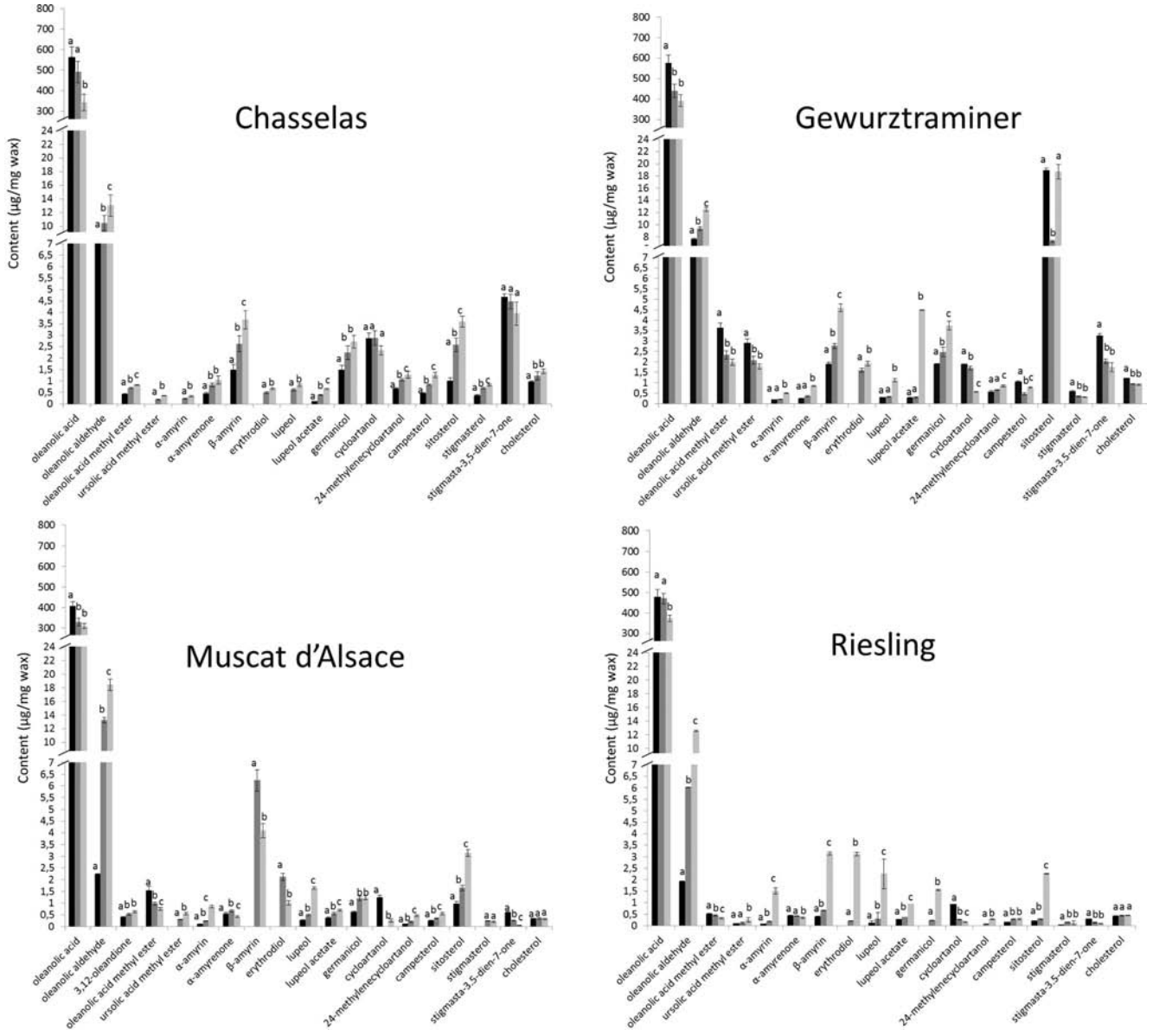

Figure 3. Triterpenoid content in the grape berry waxes of Chasselas, Gewurztraminer, Muscat d'Alsace, and Riesling at three phenological stages (black bars, young grapes; dark gray bars, grapes at véraison; light gray bars, mature grapes). The results are expressed as the means of three independent samples. The results for each triterpenoid not sharing a common letter are significantly different ($p < 0.05$).

triterpenoids released from their hydrolyzed esters were individually subjected to GC-MS/FID analysis. The chemical structures of the triterpenoid compounds identified in grape cuticular waxes are shown in Figure 1.

The only significant peak with a relative retention time of 2.29 (relative retention time values are relative to cholesterol, for which the retention time is set to 1) detected in the fractions containing triterpene acids after methylation obtained from cuticular waxes of grapes of all evaluated cultivars was identified as oleanolic acid methyl ester. A representative GC-FID chromatogram is shown in Figure 2A. By contrast, the chromatograms of the fractions containing steroids and neutral triterpenes (triterpene alcohols, aldehydes, and ketones) were much more complex, containing several peaks of various t_R and relative intensity. The representative chromatograms are shown in Figure 2B,C. The principal peak with a relative t_R of 2.35 was associated with oleanolic aldehyde, **6**, and its identification was confirmed by comparison with mass spectra from the Wiley-NIST library and with previously reported data.[25] Additional significant peaks, with relative t_R of 1.44 and 1.55, were identified as sitosterol, **17**, and β-amyrin, **4**, respectively. Certain smaller peaks present in all chromatograms were associated with other steroids, that is, cholesterol, **14**, campesterol, **13**, stigmasterol, **18**, and stigmasta-3,5-dien-7-one, **19**, as well as triterpene alcohols, that is, germanicol (olean-18-en-3-ol), **11**, α-amyrin, **2**, and lupeol, **9**, forming one common peak with a relative t_R of 1.68, cycloartanol, **15**, and its derivative 24-methylenecycloartanol, **16**, erythrodiol, **5**, and the triterpene ketone α-amyrenone, **1**. In addition to free triterpenoids, three triterpenoid esters, that is, lupeol acetate, **10**, and the naturally occurring methyl esters of oleanolic acid, **8**, and ursolic acid, **3**, which cofractionated with free neutral triterpenoids due to a similar chromatographic mobility, were also identified in the chromatograms of all cultivars. Moreover, the triterpene diketone 3,12-oleandione (relative t_R of 2.1), **12**, was exclusively detected in the fraction obtained from the wax

dx.doi.org/10.1021/jf502033s | J. Agric. Food Chem. 2014, 62, 7998−8007

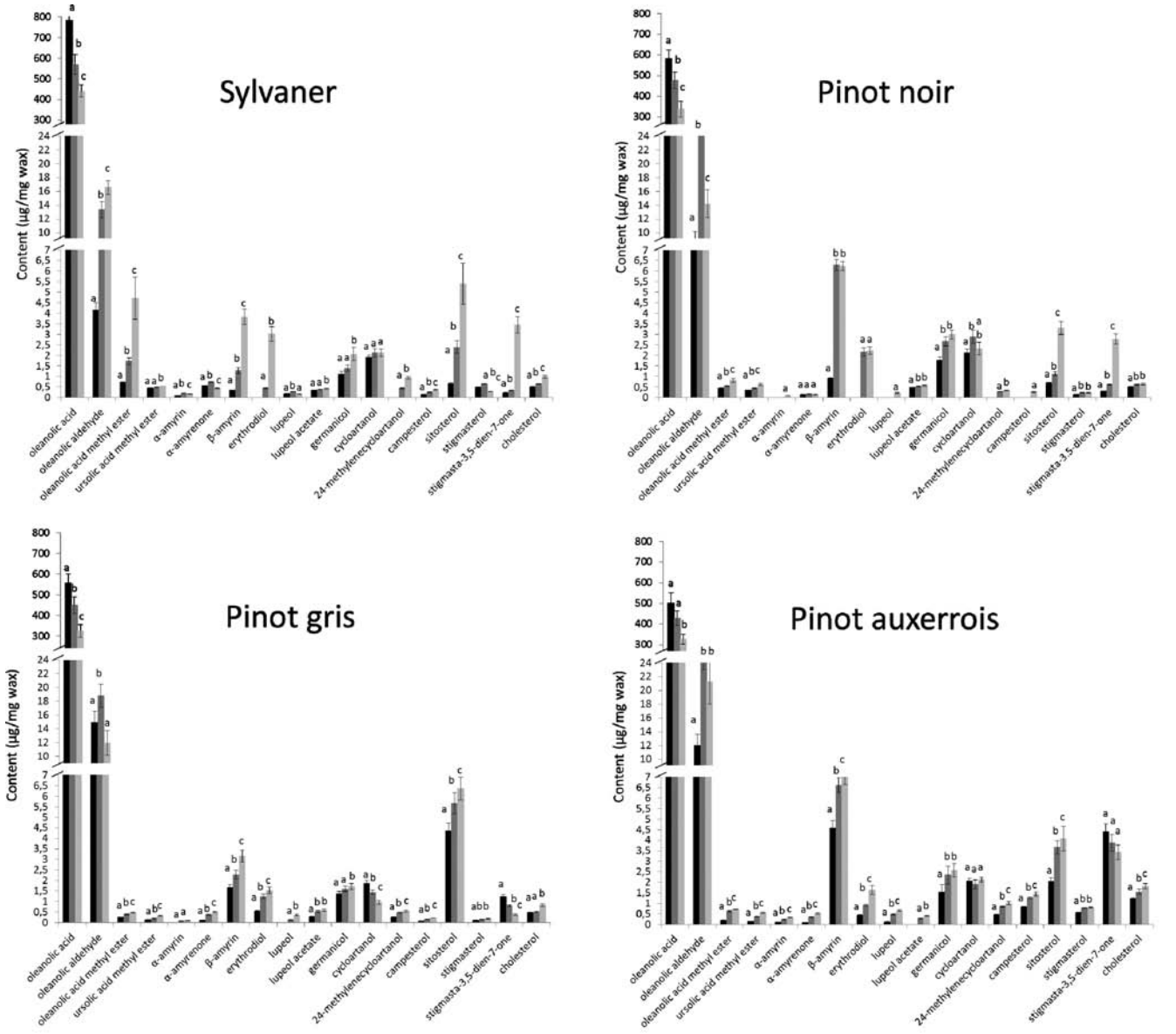

Figure 4. Triterpenoid content in the grape berry waxes of Sylvaner, Pinot noir, Pinot gris, and Pinot auxerrois at three phenological stages (black bars, young grapes; dark gray bars, grapes at véraison; light gray bars, mature grapes). The results are expressed as the means of three independent samples. The results for each triterpenoid not sharing a common letter are significantly different ($p < 0.05$).

extract of T1 Muscat d'Alsace samples. Other peaks that have not been numbered were in most cases identified as hydrocarbons typically occurring in plant cuticular waxes.

Chromatograms of the fractions obtained following alkaline hydrolysis of low-polar esters revealed only the presence of some aliphatic compounds and did not contain detectable peaks of any triterpenoids.

Thus, according to GC-MS analysis, the major triterpenoid profile of cuticular waxes of grapes from the eight examined cultivars exhibits the following composition: (i) one triterpene acid occurring in a free (nonesterified) form, oleanolic acid; (ii) two esters of triterpene acids, oleanolic and ursolic methyl esters; (iii) six monohydroxy alcohols, α-amyrin, β-amyrin, cycloartanol, 24-methylenecycloartanol, germanicol, and lupeol; (iv) one acetyl ester of a triterpene monohydroxy alcohol, lupeol acetate; (v) one dihydroxy alcohol, erythrodiol; (vi) one aldehyde, oleanolic aldehyde; (vii) one ketone, α-amyrenone; and (viii) five steroids, campesterol, cholesterol, sitosterol, stigmasterol, and stigmasta-3,5-dien-7-one.

The presence of oleanolic acid (which is a triterpene acid that contains an oleanane-type carbon skeleton that is very common in higher plants) in grape berry wax was known as early as 1938.[26] Notably, the triterpene acid ursolic acid, an isomer of oleanolic acid that differs in the position of methyl groups at C29 and C30, which contains an ursane-type skeleton, was found in grape waxes only as methyl esters rather than as free forms. Thus, it can be concluded that triterpenoids derived from the oleanane skeleton are predominant in *V. vinifera* species, comprising sequential oxidation products of the precursor β-amyrin that contain additional hydroxymethyl and carbonyl groups (i.e., erythrodiol and oleanolic aldehyde) and can proceed to the final product that contains a carboxylic group (oleanolic acid), which can undergo additional esterification. In contrast to the presence of different oleanane triterpenoids, the series of ursane compounds is unexpectedly

dx.doi.org/10.1021/jf502033s | J. Agric. Food Chem. 2014, 62, 7998−8007

incomplete, beginning with the alcohol and the ketone α-amyrin and α-amyrenone, respectively, and ending with ursolic acid (which is immediately esterified), whereas the intermediate compounds uvaol and ursolic aldehyde were not detected. In the cultivars studied herein, triterpenoids that contain a lupane-type carbon skeleton, which is the third most commonly found triterpene skeleton in plants, were represented only by the precursor of the series, lupeol, which was present as a free form and as an acetyl ester. Neither betulin (lupane dihydroxy alcohol) nor betulinic acid was found in grape waxes except for the samples of young (T1) Muscat d'Alsace grapes, in which a negligible peak of betulinic acid methyl ester was detected. However, the presence of betulin and betulinic acid has been previously reported in grapes of the California raisin cultivar Thompson seedless.[27]

According to our results and those previously reported, the presence of oleanolic acid, oleanolic aldehyde, erythrodiol, and lupeol, as well as sterols, that is, campesterol, cholesterol, sitosterol, and stigmasterol, in grape cuticular wax appears to be a common feature in all *V. vinifera* cultivars studied to date.[15] Our current results also revealed the presence of α- and β-amyrins, α-amyrenone, cycloartanol, 24-methylenecycloartanol, and germanicol, an oleanane monohydroxy alcohol with a double bond between C18 and C19, which can be synthesized in addition to β-amyrin by a multifunctional triterpenoid synthase.[28] These compounds have not been previously described in grape cuticular wax, perhaps due to the genuine absence of these compounds in other cultivars, but most probably because of their presence at low levels that are difficult to detect. The presence of certain other triterpenoids, for example, betulin and betulinic acid, is rather restricted to specific cultivars, for example, Thompson seedless grapes.[27] Additionally, the presence of the diketone 3,12-oleandione reported in this study appears to be characteristic for Muscat d'Alsace.

Triterpenoid Content in Grape Cuticular Waxes and Its Evolution during Fruit Ripening. Although the utilized method of wax extraction does not allow the 100% yield that is necessary for absolute quantitation, this study enables the evaluation of the relative changes in the content of pentacyclic triterpenes and steroids at three stages of fruit development: young grapes (T1), grapes at véraison (T2), and mature grapes (T3). The quantitative determination of individual triterpenoids identified in cuticular wax extracts of grapes of the eight evaluated cultivars are presented in Figures 3 and 4.

The total triterpenoid content in 1 mg of cuticular wax extract was the highest in young grapes (T1 samples) and significantly differed among the evaluated cultivars, ranging from the lowest levels of 42 and 48% of the wax extract mass in Muscat d'Alsace and Riesling, respectively, to 62% in Gewurztraminer and nearly 80% in Sylvaner, which exhibited the highest level of triterpenoids of all cultivars evaluated in this study. All Pinot cultivars exhibited relatively similar levels of triterpenoids in T1 samples (53−59%), which were comparable to those in Chasselas (58%). During subsequent phases of fruit development, the total triterpenoid content decreased, and in mature grapes (T3 samples), the total triterpenoid content ranged from 34% in Muscat d'Alsace to 45 and 49% of the wax extract mass in Gewurztraminer and Sylvaner, respectively. This decrease in triterpenoid content was particularly sharp in Pinot gris, Sylvaner, and Pinot noir (the level in respective T3 samples decreased by 41, 39, and 38% compared with the level in T1 samples). In Muscat d'Alsace and Riesling, the initial triterpenoid content decreased by only 18 and 15%, respectively, during fruit ripening.

The most abundant triterpenoid present in grape cuticular waxes of all cultivars was oleanolic acid, as previously reported in numerous studies.[15] A molecular model of the three-dimensional arrangement of oleanolic acid and aliphatic constituents of cuticular wax (e.g., *n*-hexacosanol) was proposed to explain the organization of the grape berry cuticle characterized by such a high abundance of a single triterpene acid.[29] In our study, oleanolic acid constituted on average 92% of the total triterpenoids in all cultivars. The level of oleanolic acid was highest in young grapes (T1) and ranged from 406 ± 22 μg/mg of wax extract in Muscat d'Alsace to 782 ± 58 μg/mg in Sylvaner; this level subsequently decreased during fruit maturation to 309 ± 12 μg/mg in Muscat d'Alsace and 440 ± 30 μg/mg in Sylvaner (Figures 3 and 4).

The total neutral triterpenoid (pentacyclic triterpenes and steroids) content in 1 mg of cuticular wax extract was low in comparison to oleanolic acid and ranged from 5.25 μg/mg of wax extract in T1 Riesling samples to 53.6 μg/mg in T3 Gewurztraminer samples. In contrast to oleanolic acid, the levels of neutral triterpenoids tended to increase during fruit development, although not in an identical manner in all cultivars. In Chasselas, Muscat d'Alsace, Riesling, and Sylvaner, this increase was constant from T1 to T3, with a final neutral triterpenoid content that was 4- or 5-fold higher in the waxes of mature grapes compared with young fruits (a particularly substantial increase was observed in Muscat d'Alsace, Riesling, and Sylvaner). For all Pinot cultivars, the highest total neutral triterpenoid content was observed at véraison (T2), and this level subsequently slightly decreased during the last stage of ripening. Unexpectedly, in Gewurztraminer, the total level of neutral triterpenoids was lowest in grapes of the T2 samples.

Among neutral triterpenoids, oleanolic aldehyde was the most abundant triterpenoid, except for Gewurztraminer, in which this compound was second to sitosterol. Indeed, in Gewurztraminer, oleanolic aldehyde constituted only 3% of all triterpenoids, whereas in other cultivars, the level of oleanolic aldehyde was higher, up to 6% of all triterpenoids in T2 samples of Pinot auxerrois and Pinot noir. The oleanolic aldehyde content increased during fruit development in grape waxes of all cultivars except for the three Pinot cultivars in which the highest concentration was observed at véraison (Figure 4). Considerable levels (>1 μg/mg of wax extract) of β-amyrin, erythrodiol (except for Chasselas), and germanicol were detected in all evaluated cultivars. The levels of β-amyrin and its derivative erythrodiol, which contains an additional hydroxyl group, were altered in a similar manner in all cultivars. The highest levels of erythrodiol were observed in T3 samples of Chasselas, Gewurztraminer, Pinot auxerrois, Pinot gris, Riesling, and Sylvaner and at véraison in Pinot noir and Muscat d'Alsace (Figures 3 and 4). Moreover, the level of germanicol increased uniformly in grape wax extracts of all cultivars during fruit ripening. Additional pentacyclic triterpenoids and their esters, that is, α-amyrin, α-amyrenone, lupeol, lupeol acetate, and ursolic acid methyl ester, were found at only low levels (up to 0.2% of total triterpenoids) in all cultivars.

The total steroid content generally increased during fruit development, reaching the highest level in the cuticular wax extract of mature grapes (5% of all triterpenoids in T3 samples of Gewurztraminer). As previously reported,[15,18,19] sitosterol was the most abundant phytosterol in the grape waxes of all cultivars, following campesterol and stigmasterol. Among the

evaluated cultivars, Gewurztraminer grape wax contained the highest level of sitosterol, constituting 4% of the total triterpenoids in T3 samples. Interestingly, the level of sitosterol was lowest at véraison in Gewurztraminer, in contrast to the other cultivars in which it increased relatively uniformly during grape maturation. In Chasselas and all Pinot cultivars, the sitosterol content linearly increased during fruit development; in Muscat d'Alsace and Sylvaner the level of sitosterol nearly doubled after véraison, and in Riesling, the level of sitosterol exhibited a sharp, 8-fold increase during fruit maturation (Figures 3 and 4). In addition to typical phytosterols (i.e., sitosterol, campesterol, and stigmasterol), grape cuticular wax extracts also contained small amounts of cholesterol, which is not considered a typical plant sterol, although it is commonly found in plant cuticular waxes.[30] The steroid ketone stigmasta-3,5-dien-7-one, also commonly found in plant cuticular waxes,[23,31] was the most abundant in Chasselas, exceeding the level of sitosterol and constituting 1% of the total triterpenoids in T3 samples. The level of stigmasta-3,5-dien-7-one decreased during fruit ripening in all cultivars except Sylvaner and Pinot noir. Finally, in all evaluated cultivars, the level of cycloartanol, which is the precursor of sterols, decreased during fruit maturation in all cultivars, whereas the amount of its derivative, 24-methylenecycloartanol, increased.

Previous studies on the evolution of phytosterol content in grape skins reported a decrease in the level of phytosterols either during the last stage of maturity[18] or during the transition from pre-véraison to véraison.[19] However, in these studies, phytosterol content was expressed per dry weight of fruits rather than per mass of the wax extract. Therefore, according to chemical changes that occur during fruit development, the relative content of compounds can be lowered due to an increase in the dry weight caused by the accumulation of sugars and other metabolites associated with grape maturation.

In this study, a considerable decrease in the level of oleanolic acid was observed during fruit development. It is unlikely that oleanolic acid, once accumulated in cuticular waxes, is either transported back to the cell or undergoes additional chemical transformations. Hence, this decrease could be explained by an increase in the level of aliphatic constituents of cuticular waxes and, consequently, by the dilution of oleanolic acid in the grape wax extract mass. It was previously demonstrated that the composition of grape cuticular waxes was altered during fruit development, with an increase in waxy deposits and a simultaneous decrease in the thickness of the cuticle.[32] It can be assumed that with the growing size of the berry and the increase in water content during fruit ripening, some aliphatic hydrophobic compounds (primarily hydrocarbons[32]) are accumulated in surface layers of the cuticle to prevent the uncontrolled loss of water. It is commonly believed that triterpenoid constituents do not participate in the protection against water loss, and a high level of triterpenoids in cuticular wax is not positively correlated with water impermeability.[15] However, as recently demonstrated for Fuyu persimmon fruit,[33] triterpenoids affect the mechanical properties of the fruit cuticle and endow its toughness by functioning as a nanofiller, that is, filling the gaps in the cutin matrix with low-ordered crystals. Moreover, a decrease in the oleanolic acid content could explain the growing susceptibility of berries to fungal diseases during maturation. The compositional changes in cuticular components has been suggested to influence the susceptibility to *Botrytis cinerea* infection in grapes.[32] Additional studies are necessary to confirm the possible role of biologically active triterpenoids, which are known for their antibacterial, antifungal, and antiparasitic properties[15] in grape resistance to pathogens.

The initially very high level of triterpenoids in cuticular waxes followed by a gradual decrease in this level during fruit development has also been demonstrated for other fruits, for example, sweet cherry (*Prunus avium*) fruit;[34] however, it is not a general rule in fruit ontogeny. In contrast, triterpenoids were shown to be progressively accumulated during olive fruit development, and the profile of these compounds was altered according to the different phases in its long maturation.[35] The evolution of triterpenoid content in grape berry is also of interest in terms of the metabolic pathways of these compounds. In young grapes, the rapid biosynthesis of high levels of oleanolic acid occurs, encompassing the entire sequence of oxidation of the precursor, β-amyrin. Intriguingly, in T2 and T3 samples, the final reaction appears to be terminated, and intermediates, including oleanolic aldehyde and erythrodiol, begin to be accumulated in larger quantities. The metabolic behavior of phytosterols appears to be more readily accounted for. At fruit developmental phases involving growth by cell division and consecutive synthesis of membranes, the level of these compounds "wasted" for accumulation in surface waxes is relatively low. During the stages of water and sugar accumulation, the excess steroids can be exported into cuticular waxes and accumulate there at more substantial levels.

The results presented in this study were obtained from samples collected during only one vegetative season. However, the similar patterns of changes in triterpenoid content observed in eight grape cultivars might suggest that this phenomenon is general, although the relative levels of individual compounds can vary in consecutive years due to the influence of external abiotic and biotic stimuli (e.g., meterological conditions, pathogen infections).

In recent years, studies that have investigated the constituents in grape skins have been of increasing importance due to the possible utilization of winemaking byproducts, as well as unripe green grapes collected during "green harvesting" to reduce the yield of vineyards.[36] The high level of oleanolic acid in grape pomace and green grapes makes these two agro-industrial waste residues an economically advantageous alternative source of this compound. One of the first reported methods was extraction of a freeze-dried grape pomace macerate of red grape Nerello Mascalese with ethyl acetate for obtaining oleanolic acid with a yield of 0.16% of pomace dry weight.[37] However, other triterpenoid constituents present in grape cuticular waxes, for example, triterpene alcohols or phytosterols, may also be worthwhile to obtain from pomace.[15,19,37]

Oleanolic acid is known to have numerous pharmacological properties including anticancer, antidiabetogenic, antimicrobial, and hepatoprotective effects; therefore, the high abundance of this compound in grape berry cuticular wax can contribute to health benefits ascribed to fresh grape consumption, for example, the reduction of the incidence of type 2 diabetes and the prevention of liver disorders.[15,38] Both oleanolic acid and oleanolic aldehyde obtained from Thompson seedless raisins were demonstrated to display significant antimicrobial activity against oral pathogens associated with human dental carries and periodontal diseases,[27] which makes the raisins a healthy alternative to widely consumed sugary snack foods.[39]

In conclusion, this study examining the triterpenoid profile of fruit cuticular waxes of eight *V. vinifera* cultivars enhances the knowledge of the chemical diversity of grapevines. The profile of identified triterpenoids comprises compounds commonly present at significant levels in all grape cultivars studied to date, that is, oleanolic acid, oleanolic aldehyde, erythrodiol, lupeol, and phytosterols (campesterol, sitosterol, and stigmasterol). We also identified compounds that have been rarely or not previously reported in grape berry waxes, for example, α- and β-amyrins, α-amyrenone, cycloartanol, 24-methylenecycloartanol, germanicol, and 3,12-oleandione. The triterpenoid content in cuticular waxes exhibits characteristic alterations during fruit development, with early deposition of high levels of oleanolic acid and its gradual decrease, which is not entirely compensated by the concomitant slight increase in the level of neutral triterpenoids. Termination of oleanolic acid biosynthesis may result in the modulation of the mechanical toughness of the cuticle and a decrease in disease resistance, features that typically appear in numerous fruits during ripening and storage.

■ ASSOCIATED CONTENT

Supporting Information

GC-MS data of triterpenoids identified in grape berry cuticular waxes (Table 1S), calibration data for quantitative determination of identified triterpenoids (Table 2S), triterpenoid content in grape berry waxes at three phenological stages (Table 3S), and identification of 3,12-oleandione based on comparison of the mass spectra (Figure 1S). This material is available free of charge via the Internet at http://pubs.acs.org.

■ AUTHOR INFORMATION

Corresponding Author

*(A.S.) Phone: +48 22 55 43 316. Fax: +48 22 55 43 221. E-mail: szakal@biol.uw.edu.pl.

Funding

Research subject carried out with the use of CePT infrastructure financed by the European Union, the European Regional Development Fund within the Operational Programme “Innovative economy” for 2007−2013.

Notes

The authors declare no competing financial interest.

■ ACKNOWLEDGMENTS

We thank Jean-Marc Bertsch and Hubert Straub for their kind permission for fruit collection in their vineyards.

■ REFERENCES

(1) Iriti, M.; Faoro, F. Bioactivity of grape chemicals for human health. *Nat. Prod. Commun.* **2009**, *4*, 611−634.
(2) Yadav, M.; Jain, S.; Bhardavi, A.; Naqpal, R.; Puniva, M.; Tomar, R.; Singh, V.; Parkesh, O.; Prasad, G. B.; Marotta, F.; Yadav, H. Biological and medicinal properties of grapes and their bioactive constituents: an update. *J. Med. Food* **2009**, *12*, 473−484.
(3) Ali, K.; Maltese, F.; Choi, Y. H.; Verpoorte, R. Metabolic constituents of grapevine and grape-derived products. *Phytochem. Rev.* **2010**, *9*, 357−378.
(4) Beveridge, T. H. J.; Girard, B.; Kopp, T.; Drover, J. C. G. Yield and composition of grape seed oils extracted by supercritical carbon dioxide and petroleum ether: varietal effects. *J. Agric. Food Chem.* **2005**, *53*, 1799−1804.
(5) El Gengaihi, S.; Ella, F. M. A.; Hassan, E. M.; Shalaby, E. A.; Baker, D. H. A. Phytochemical investigation and radical scavenging activity of wastes of some grape varieties grown in Egypt. *Global J. Pharmacol.* **2013**, *7*, 465−473.
(6) González-Centeno, M. R.; Jourdes, M.; Femenia, A.; Simal, S.; Roselló, C.; Teissedre, P. L. Characterization of polyphenols and antioxidant potential of white grape pomace byproducts (*Vitis vinifera* L.). *J. Agric. Food Chem.* **2013**, *61*, 11579−11587.
(7) Lara, I.; Belge, B.; Goulao, L. F. The fruit cuticle as a modulator of postharvest quality. *Postharvest Biol. Technol.* **2014**, *87*, 103−112.
(8) Buschhaus, C.; Jetter, R. Composition differences between epicuticular and intracuticular wax substructures: how do plants seal their epidermal surfaces? *J. Exp. Bot.* **2011**, *62*, 841−853.
(9) Sawai, S.; Saito, K. Triterpenoid biosynthesis and engineering in plants. *Front. Plant Biotechnol.* **2011**, *2*, 25.
(10) Xu, R.; Fazio, G. C.; Matsuda, S. P. T. On the origins of triterpenoid skeletal diversity. *Phytochemistry* **2004**, *65*, 261−291.
(11) Patočka, J. Biologically active pentacyclic triterpenes and their current medicine signification. *J. Appl. Biomed.* **2003**, *1*, 7−12.
(12) Petronelli, A.; Pannitteri, G.; Testa, U. Triterpenoids as new promising anticancer drugs. *Anti-Cancer Drugs* **2009**, *20*, 880−892.
(13) Yadav, V. R.; Prasad, S.; Sung, B.; Kannappan, R.; Aggarwal, B. B. Targeting inflammatory pathways by triterpenoids for prevention and treatment of cancer. *Toxins* **2010**, *2*, 2428−2466.
(14) Liu, R. H. Health benefits of fruits and vegetables are from additive and synergistic combination of phytochemicals. *Am. J. Clin. Nutr.* **2003**, *78*, 517S−520S.
(15) Szakiel, A.; Pączkowski, C.; Pensec, F.; Bertsch, C. Fruit cuticular waxes as a source of biologically active triterpenoids. *Phytochem. Rev.* **2012**, 263−284.
(16) Kennedy, J. A.; Hayasaka, Y.; Vidal, S.; Waters, E. J.; Jones, G. P. Composition of grape skin proanthocyanidins at different stages of berry development. *J. Agric. Food Chem.* **2001**, *49*, 5348−5355.
(17) Vicens, A.; Founard, D.; Williams, P.; Sidhoum, L.; Moutounet, M.; Doco, T. Changes in polysaccharide and protein composition of cell walls in grape berry skin (cv. Shiraz) during ripening and over-ripening. *J. Agric. Food Chem.* **2009**, *57*, 2955−2960.
(18) Le Fur, Y.; Hory, C.; Bard, M. H.; Olsson, A. Evolution of phytosterols in Chardonnay grape berry skins during last stages of ripening. *Vitis* **1994**, *33*, 127−131.
(19) Ruggiero, A.; Vitalini, S.; Burlini, N.; Bernasconi, S.; Iriti, M. Phytosterols in grapes and wine, and effects of agrochemicals on their levels. *Food Chem.* **2013**, *141*, 3473−3479.
(20) Lorenz, D. H.; Eichhorn, K. W.; Bleiholder, H.; Klose, R.; Meier, U.; Weber, E. Phenological growth stages of the grapevine (*Vitis vinifera* L. ssp. *vinifera*) − codes and descriptions according to the extended BBCH scale. *Aust. J. Grape Wine Res.* **1995**, *1*, 100−110.
(21) Tojo, G.; Fernández, M. *Oxidation of Alcohols to Aldehydes and Ketones*; Springer: Berlin, Germany, 2006; pp 1−97.
(22) Szakiel, A.; Pączkowski, C.; Huttunen, S. Triterpenoid content of berries and leaves of bilberry *Vaccinium myrtillus* from Finland and Poland. *J. Agric. Food Chem.* **2012**, *60*, 11839−11849.
(23) Santier, S.; Chamel, A. Reassessment of the role of cuticular waxes in the transfer of organic molecules through plant cuticles. *Plant Physiol. Biochem.* **1998**, *36*, 225−231.
(24) Conde, C.; Silva, P.; Fontes, N.; Dias, A. C. P.; Tavares, R. M.; Sousa, M. J.; Agasse, A.; Delrot, S.; Gerós, H. Biochemical changes throughout grape berry development and fruit and wine quality. *Food* **2007**, *1*, 1−22.
(25) Dagna, L.; Gasparini, G.; Icardi, M. L.; Sessia, E. Study of some components of the unsaponifiable fraction in the skin of grapes. *Am. J. Enol. Vitic.* **1982**, *33*, 201−206.
(26) Radler, F.; Horn, D. H. S. The composition of grape cuticle wax. *Aust. J. Chem.* **1965**, *18*, 1059−1069.
(27) Rivero-Cruz, J. F.; Zhu, M.; Kinghorn, A. D.; Wu, C. D. Antimicrobial constituents of Thompson seedless raisins (*Vitis vinifera*) against selected oral pathogens. *Phytochem. Lett.* **2008**, *1*, 151−154.
(28) Basyuni, M.; Oku, H.; Tsujimoto, E.; Kinjo, K.; Baba, S.; Takara, K. Triterpene synthases from the Okinawan mangrove tribe, Rhizophoraceae. *FEBS J.* **2007**, *274*, 5028−5042.

(29) Casado, C. G.; Heredia, A. Structure and dynamics of reconstituted cuticular waxes of grape berry cuticle (*Vitis vinifera* L.). *J. Exp. Bot.* **1999**, *50*, 175−182.
(30) Noda, M.; Tanaka, M.; Seto, Y.; Aiba, T.; Oku, C. Occurrence of cholesterol as a major sterol component in leaf surface lipids. *Lipids* **1988**, *23*, 439−444.
(31) Szakiel, A.; Niżyński, B.; Pączkowski, C. Triterpenoid profile of flower and leaf cuticular waxes of heather *Calluna vulgaris*. *Nat. Prod. Res.* **2013**, *27*, 1404−1407.
(32) Comménil, P.; Brunet, L.; Audran, J. C. The development of the grape berry cuticle in relation to susceptibility to bunch rot disease. *J. Exp. Bot.* **1997**, *48*, 1599−1607.
(33) Tsubaki, S.; Sugimura, K.; Teramoto, Y.; Yonemori, K.; Azuma, J. Cuticular membrane of *Fuyu* persimmon fruit is strengthened by triterpenoid nano-fillers. *PLoS One* **2013**, *8*, 1−12.
(34) Peschel, S.; Franke, R.; Schreiber, L.; Knoche, M. Composition of the cuticle of developing sweet cherry fruit. *Phytochemistry* **2007**, *68*, 1017−1025.
(35) Stiti, N.; Triki, S.; Hartmann, M. A. Formation of triterpenoids throughout *Olea europaea* fruit ontogeny. *Lipids* **2007**, *42*, 55−67.
(36) Rubio, M.; Alvarez-Ortí, M.; Alvarruiz, A.; Fernández, E.; Pardo, J. Characterization of oil obtained from grape seeds collected during berry development. *J. Agric. Food Chem.* **2009**, *57*, 2812−2815.
(37) Amico, V.; Napoli, E. M.; Renda, A.; Ruberto, G.; Spatafora, C.; Tringali, C. Constituents of grape pomace from the Sicilian cultivar 'Nerello Mascalese'. *Food Chem.* **2004**, *88*, 599−607.
(38) Liu, T.; Zhao, J.; Li, H. B.; Ma, L. Evaluation of anti-hepatitis viral activity of *Vitis vinifera* L. *Molecules* **2010**, *15*, 7415−7421.
(39) Wu, C. D. Grape products and oral health. *J. Nutr.* **2009**, *39*, 1818−1823.